Canadian Journal of Chemistry
Published by
THE NATIONAL RESEARCH COUNCIL OF CANADA

Journal canadien de chimie
Publié par
LE CONSEIL NATIONAL DE RECHERCHES DU CANADA

Volume 57 Number 1 January 1, 1979 Volume 57 numéro 1 1 janvier 1979

Complexes of substituted benzothiazoles. 1. Cobalt(II), copper(II), and zinc(II) complexes of 2,2′-*o*-phenylenebisbenzothiazole; a potential N or S donor ligand

JOHN CHARLES THOMAS RENDELL AND LAURENCE KENNETH THOMPSON[1]
Department of Chemistry, Memorial University of Newfoundland, St. John's, Nfld., Canada A1B 3X7

Received July 4, 1978

JOHN CHARLES THOMAS RENDELL and LAURENCE KENNETH THOMPSON. Can. J. Chem. **57**, 1 (1979).

A series of cobalt(II), copper(II), and zinc(II) complexes of the title ligand are reported. 1:1 complexes of cobalt and zinc, $M(OBT)X_2$ (M = Co, Zn; X = Cl, Br, I, NCS), have four-coordinate pseudo-tetrahedral stereochemistries while for copper (X = Cl, Br), distorted square geometries are suggested. Six-coordinate 1:1 derivatives are also obtained for cobalt and copper, $M(OBT)(NO_3)_2$ (M = Co, Cu), while the 1:2 derivative $Cu(OBT)_2(ClO_4)_2 \cdot 2H_2O$ may be square planar. OBT appears to coordinate as an N_2 donor in all cases. Preliminary X-ray data confirm a distorted square CuN_2Cl_2 structure for the copper chloride complex. Hydrogen bonded chloroform solvate molecules appear to be present in three cobalt complexes (X = Cl, Br, NCS).

JOHN CHARLES THOMAS RENDELL et LAURENCE KENNETH THOMPSON. Can. J. Chem. **57**, 1 (1979).

On décrit une série de complexes du cobalt(II), du cuivre(II) et du zinc(II) avec le coordinat ci-dessus. Les complexes 1:1 du cobalt et du zinc, $M(OBT)X_2$ (M = Co, Zn; X = Cl, Br, I, NSC), sont tétracoordonnés et possèdent une structure pseudo-tétraédrique, tandis qu'une géométrie carrée déformée est proposée dans le cas du cuivre (X = Cl, Br). On obtient également des composés 1:1 hexacoordonnés du cobalt et du cuivre, $M(OBT)(NO_3)_2$ (M = Co, Cu), alors que le composé 1:2 $Cu(OBT)_2(ClO_4)_2 \cdot 2H_2O$ pourrait être plan carré. Dans tous les cas, le coordinat OBT joue le rôle de donneur N_2. Les données préliminaires de diffraction des rayons X confirment la structure plane carrée CuN_2Cl_2 du complexe chloré du cuivre. Trois complexes du cobalt (X = Cl, Br, NCS) semblent renfermer des molécules du solvant, le chloroforme, retenues par liaisons hydrogène.

[Traduit par le journal]

Introduction

The current surge of interest in metalloprotein model systems has revealed that imidazole nitrogen and thioether sulphur functional groups are likely to be involved in coordination to copper in both Type I and Type III copper metalloproteins (ref. 1 and references therein). Benzothiazole has heterocyclic sulphur and pseudo-imidazole functional groups, the former being a poor Lewis base. Studies on the complexes of benzothiazole and 2-substituted benzothiazoles (R = NH_2, CH_3, Cl) (2–8) reveal that with first row transition element ions (M = Fe, Co, Ni, Cu, Zn) benzothiazole is *N*-bonded, except in a few cases involving bridging benzothiazole (4) in which it is assumed to behave as a bidentate ligand involving both N and S donation. The polyfunctional benzothiazole ligand 2,6-(dibenzothiazol-2-yl)pyridine (9) has been shown to behave as an N_3 donor, rather like 2,2′,2″-terpyridyl, in its complexes with manganese(II), iron(II), and nickel(II). The ligand 2-(*o*-hydroxyphenyl) benzothiazole behaves as an NO donor to copper(II) (10).

Studies on the cobalt(II), copper(II), and zinc(II) complexes of the ligand 2,2′-*o*-phenylenebisbenzo-

[1]To whom all correspondence should be addressed.

0008-4042/79/010001-07$01.00/0

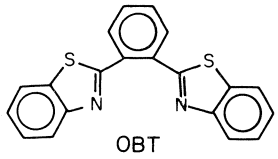

FIG. 1. 2,2′-*o*-Phenylenebisbenzothiazole.

thiazole (OBT) (Fig. 1) reveal that OBT behaves as an N_2 donor. Reaction of the ligand (OBT) with cobalt(II), copper(II), and zinc(II) salts in ethanol or acetone leads to a series of tetrahedral, octahedral, and square complexes whose structures have been established by electronic, vibrational, and esr spectra, magnetism and conductance data, and an X-ray structure.

Experimental

Electronic spectra were recorded on a Cary 17 spectrometer, infrared spectra were obtained with a Perkin-Elmer model 283 spectrometer, and electron spin resonance spectra were recorded at −196°C on a Varian E-3 X-band spectrometer, the magnetic field strength being calibrated with an nmr probe and with Mn(II) in MgO powder. Magnetic susceptibilities were obtained at room temperature by the Faraday method with a Cahn model #7600 Faraday Magnetic Susceptibility system, coupled to a Cahn gram electrobalance and conductance data were obtained with a General Radio Company bridge with impedance comparator and a constant temperature bath adjusted to 25°C. Microanalyses were carried out in part in the Chemistry Department at Memorial University with a Perkin-Elmer model #240 Elemental Analyzer and by Atlantic Microlab, Inc., Atlanta, Georgia. Metal analyses were determined by Atomic Absorption with a Varian Techtron AA-5, after digestion of the samples in concentrated HNO_3 or aqua-regia.

Metal Complexes of OBT

OBT was synthesized according to the procedure of Rai and Braunwarth (11). Hydrated or anhydrous metal salts were employed.

$Co(OBT)X_2(CHCl_3)_n$ ($X = Cl, Br, NCS$; n = 1; $X = I$, n = 0) $Co(OBT)(NO_3)_2 \cdot 2H_2O$

Stoichiometric amounts of the appropriate metal salt and OBT were dissolved separately in hot ethanol and the solutions were mixed and stirred with heating for 15 min. The resulting solutions were filtered and reduced in volume to induce crystallization. Some difficulty was encountered in obtaining crystals and it was found that addition of acetonitrile to concentrated solutions of the complexes resulted in the formation of crystalline products. Recrystallization was effected from chloroform and the complexes were dried under vacuum.

$Cu(OBT)X_2$ ($X = Cl, Br, NO_3$)

Stoichiometric amounts of the appropriate metal salt and OBT were dissolved separately in hot ethanol and the solutions were mixed. Crystalline products were obtained rapidly, which proved to be fairly insoluble in most solvents. The chloro- and bromo-compounds were recrystallized from dichloromethane and dried under vacuum while the nitrato-complex was recrystallized from chloroform.

$Cu(OBT)_2(ClO_4)_2 \cdot 2H_2O$

Stoichiometric amounts of the metal salt and OBT were dissolved separately in hot ethanol containing about 5% triethylorthoformate. On mixing the solutions a light khaki green precipitate was obtained which was washed with an ethanol/triethylorthoformate mixture and dried under vacuum.

$Zn(OBT)X_2(acetone)_n$ ($X = Cl, Br$, n = 1; $X = I, NCS$, n = 0)

Stoichiometric amounts of the metal salt and OBT were dissolved separately in hot acetone and the solutions were mixed. Crystalline products were obtained and were dried under vacuum.

Analytical data for the complexes are given in Table 1.

Results and Discussion

Cobalt Complexes

The cobalt complexes $Co(OBT)X_2$ (X = Cl, Br, NCS, I) exhibit electronic spectra, both in solution and in the solid state, typical of pseudo-tetrahedral cobalt(II) (Table 2). The splitting of the three components of ν_2 is quite large, falling in the range 3130–3850 cm^{-1}, suggesting a crystal field of lower symmetry than T_d. Systems of the type CoL_2Br_2 (L = 4Etpy, 2Etpy) have comparable spectra with large splittings of ν_2 (12). The general similarity between the spectra and ligand field parameters of the OBT complexes and Co(benzothiazole)X_2 (X = Cl, Br, I) (7) and Co(benzimidazole)X_2 (X = Cl, Br, I, NCS) (13) coupled with the absence of any intense bands, which could possibly be associated with sulphur-to-metal charge transfer, suggests that in these systems OBT coordinates as a bidentate ligand via two nitrogen atoms. The iodo-complex displayed a high intensity band around 22 500 cm^{-1}, both in the solid state and in solution; this is assigned to I → Co charge transfer (14).

The pink cobalt nitrate complex, $Co(OBT)(NO_3)_2 \cdot 2H_2O$, has an electronic spectrum typical of a pseudo-octahedral system (Table 2). Two moderately intense bands are observed, and the spectrum bears a close resemblance to that of $Co(\alpha\text{-picoline})_2(NO_3)_2$, a six-coordinate pseudo-octahedral complex with bidentate nitrate groups (15). Again it appears that OBT is behaving as a bidentate N_2 donor.

Conductance measurements in nitromethane (Table 3) indicate that the cobalt complexes are all essentially non-ionised in solution at 10^{-3} *M*. The iodo-complex exhibits the highest molar conductance indicating a small degree of dissociation. It was noted that this complex was somewhat more sensitive than the others to hydrolysis in wet solvents. The cobalt nitrate complex appears to be a non-electrolyte in freshly prepared nitromethane solution but on standing some dissociation occurred (approximately 20 mho mol^{-1} cm^2 after 12 h). Magnetic moments (Table 3) are typical for pseudo-tetrahedral cobalt(II) systems, with the exception of the chloride complex which has a moment somewhat higher than one

TABLE 1. Analytical and other data

Compound	Colour	Found				Calcd			
		C	H	N	M	C	H	N	M
$Co(OBT)Cl_2 \cdot CHCl_3$	Blue	41.9	2.28	4.71	10.2	42.5	2.19	4.72	9.93
$Co(OBT)Br_2 \cdot CHCl_3$	Blue	36.9	1.96	3.81	8.49	36.9	1.90	4.10	8.64
$Co(OBT)I_2$	Green	36.3	1.82	3.98	8.69	36.5	1.83	4.26	8.98
$Co(OBT)(NCS)_2 \cdot CHCl_3$	Blue	43.0	2.11	8.60	9.00	43.2	2.04	8.77	9.23
$Co(OBT)(NO_3)_2 \cdot 2H_2O$	Pink	42.0	2.31	9.72	10.8	42.6	2.84	9.95	10.5
$Cu(OBT)Cl_2$	Green	50.2	2.54	5.82	13.3	50.2	2.51	5.85	13.3
$Cu(OBT)Br_2$	Dark purple	42.2	2.15	4.95	11.5	42.3	2.12	4.94	11.2
$Cu(OBT)(NO_3)_2$	Blue	45.1	2.30	10.5	11.9	45.2	2.26	10.5	12.1
$Cu(OBT)_2(ClO_4)_2 \cdot 2H_2O$	Buff-green	48.6	2.55	5.71	6.64	48.7	2.84	5.68	6.43
$Zn(OBT)Cl_2 \cdot (CH_3)_2CO$	White	50.9	3.13	5.11	12.4	51.3	3.34	5.20	12.1
$Zn(OBT)Br_2 \cdot (CH_3)_2CO$	White	43.9	2.62	4.56	10.2	44.0	2.87	4.46	10.4
$Zn(OBT)I_2$	White	36.4	1.93	4.10	9.20	36.2	1.81	4.22	9.86
$Zn(OBT)(NCS)_2$	White	50.3	2.50	10.5	12.2	50.6	2.30	10.7	12.4

would expect for systems of this type (3, 4, 13). The higher magnetic moment (5.18 BM) associated with the nitrato complex confirms the pseudo-octahedral nature of this system (15, 16).

The infrared spectra of all the cobalt complexes show a general similarity where vibrations associated with the ligand are concerned. A sharp band of medium intensity in the range 2985–2995 cm^{-1} is assigned to CH stretch (ν_1, A_1) in chloroform (Table 4) in the complexes $Co(OBT)X_2 \cdot CHCl_3$ (X = Cl, Br, NCS). In addition, a strong band around 740 cm^{-1} in these complexes is assigned to a chloroform deformation mode (ν_5, E). These bands are absent in the cobalt iodide complex and also in the copper and zinc halide complexes. Chloroform exhibits the ν_1 band at 3034 cm^{-1} in the vapour phase, while the ν_5 band occurs in the range 760–770 cm^{-1} for the gaseous or liquid phases. Shifts in these bands in the cobalt OBT complexes from their free solvent positions are consistent with a hydrogen bonded chloroform molecule and it is assumed that the coordinated anions act as acceptor sites (ref. 17 and references therein). Prolonged drying of these complexes under vacuum at moderate temperatures does not remove the solvent molecule.

The complex $Co(OBT)(NCS)_2 \cdot CHCl_3$ exhibits two bands due to CN stretch (2070, 2058 cm^{-1}) which are associated with two isothiocyanates in an approximately C_{2v} environment. A low energy band at 473 cm^{-1} (Table 4) can be assigned to NCS bending in an *N*-bonded thiocyanate (18). The ligand has a fairly rich spectrum in the far infrared region but in general the observed bands are not affected very much by coordination. Other bands below 350 cm^{-1} can be associated with metal–ligand vibrations (Table 4) (3, 4, 19).

The cobalt nitrate complex exhibits nitrate fundamentals (20) and combination bands (21) typical of bidentate nitrate, in keeping with the proposed monomeric nature of the complex (Table 4). Absorptions at 290, 268 cm^{-1} are tentatively assigned to Co—O stretch (3). It is apparent from the high energy region of the spectrum that water is present in this compound, even after prolonged drying. However, it is assumed that the water molecules occupy lattice sites and are not coordinated to the metal.

Copper Complexes

The electronic spectra of the copper complexes (Table 2) can be divided into two groups according to the presence or absence of moderately intense bands in the range 19 000 – 25 000 cm^{-1}. The complexes $Cu(OBT)X_2$ (X = Cl, Br) are characterized by absorptions at 17 000 cm^{-1} or below whose intensities are too low to be associated with charge transfer transitions and are assigned to *d–d* transitions. Bands of much higher intensity are found in the range 19 000 – 25 000 cm^{-1} and it is suggested that these are associated with ligand-to-metal charge transfer transitions. The nitrate complex does not exhibit bands above 17 000 cm^{-1} which can be associated with charge transfer and although the perchlorate complex has a fairly intense shoulder around 24 000 cm^{-1}, this may well be associated with a *d–d* transition.

Benzothiazole complexes $Cu(benzothiazole)_2X_2$ (X = Cl, Br) are reported by two groups to exhibit *d–d* bands in the range 12 500 – 13 700 cm^{-1} in the solid state, associated with polymeric, halogen bridged pseudo-octahedral structures (3, 4). Higher energy bands above 20 000 cm^{-1} are reported but are not discussed and it is assumed that in these complexes the benzothiazole acts as a nitrogen donor ligand. 2-(*o*-Hydroxyphenyl)benzothiazole (PBS) has been shown to form a *trans*-planar CuN_2O_2 complex in which the benzothiazole groups are nitrogen

TABLE 2. Electronic spectra (cm^{-1})*

Compound		$^4T_1(F) \leftarrow {}^4A_2$ (ν_2)			$^4T_1(P) \leftarrow {}^4A_2$ (ν_3)				$10Dq$ (cm^{-1})	B (cm^{-1})	β
$Co(OBT)Cl_2 \cdot CHCl_3$	a	5700	7140	9300		15310	16950				
	b	5720(30)	7120(85)	9350(40)		15550(481)	17240(281)		4220	704	0.73
$Co(OBT)Br_2 \cdot CHCl_3$	a	5540	6800	8930	15040	15700	16500				
	b	[5460](34)	6780(117)	8810(37)	14930(740)	15400(609)	16530(372)		4120	687	0.71
$Co(OBT)I_2$	a	[5260]	6370	8440	13900	14800	15630	22500			
	b	[5200](34)	6430(165)	8330(56)	13900(946)	14700(850)	15600(565)	22700(1400)	3890	649	0.67
$Co(OBT)(NCS)_2 \cdot CHCl_3$	a	[6600]	8000	10300		16000	17540				
	b	[6350](49)	8000(140)	10200(73)	[15150](780)	15550(1020)	17640(314)		4860	649	0.67

Compound		$^4T_{2g} \leftarrow {}^4T_{1g}$ (ν_1)		$^4T_{1g}(P) \leftarrow {}^4T_{1g}$ (ν_3)	$10Dq$ (cm^{-1})	B (cm^{-1})	β
$Co(OBT)(NO_3)_2 \cdot 2H_2O$	a	9620		18700			
	c	8900(15)		19050(96)	9880	760	0.82
		d–d		$\pi X \rightarrow Cu$			
$Cu(OBT)Cl_2$	a	13600	17200	[24100]			
	b	13600(74)	[14800](73)	24100(511)			
	d	13700(70)	[14800](62)	23900(500)			
$Cu(OBT)Br_2$	a	[13400]	[16500]	19200			
	b	[13300](214)		18500(570)			
	d	13000(232)	[16100](362)	19400(595)			
$Cu(OBT)(NO_3)_2$	a	[13800]	16300				
	b	[13300](30)	16100(24)				
$Cu(OBT)_2(ClO_4)_2 \cdot 2H_2O$	a	[16700]	[24000]				
	d	[16000](86)	[23000](300)				

*Labels mean the following: *a*, mull transmittance spectrum (room temperature); *b*, solution in chloroform; *c*, solution in acetone; *d*, solution in nitromethane; [ ], shoulder; ( ), molar extinction coefficient.

TABLE 3. Magnetic moment and conductance data

Compound	M* (mho mol^{-1} cm^2)	μ (BM)† (room temperature)
$Co(OBT)Cl_2 \cdot CHCl_3$	5.33	4.85
$Co(OBT)Br_2 \cdot CHCl_3$	10.0	4.66
$Co(OBT)I_2$	23.0	4.67
$Co(OBT)(NCS)_2 \cdot CHCl_3$	7.22	4.44
$Co(OBT(NO_3)_2 \cdot 2H_2O$	4.0	5.18
$Cu(OBT)Cl_2$	22.2	1.92
$Cu(OBT)Br_2$	45.1	1.87
$Cu(OBT)(NO_3)_2$	34.1	1.98
$Cu(OBT)(ClO_4)_2 \cdot 2H_2O$	196	1.99

*Solvent nitromethane at approximately 10^{-3} M (25°C).
†Magnetic moment measured in solid state by Faraday method.

bound. A *d–d* band occurs around 17 000 cm^{-1} and bands at 22 700 and 24 100 cm^{-1} are assigned to $\pi^* \leftarrow \pi$ or $\pi^* \leftarrow$ n intraligand transitions (10).

The copper nitrate complex exhibits an electronic spectrum which is essentially the same in both solid state and solution (Table 2) and is typical of a pseudo-octahedral system of the type $CuL_2(NO_3)_2$ (L = α-picoline, quinoline, isoquinoline) (15). OBT is assumed to behave as an N_2 donor. The mull transmittance spectrum of the perchlorate complex, $Cu(OBT)_2(ClO_4)_2 \cdot 2H_2O$ shows a *d–d* band at 16 700 cm^{-1} and a more intense high energy shoulder at 24 000 cm^{-1}. Square coplanar CuN_4 systems would be expected to exhibit two major transitions at fairly high energy with the higher energy band appearing at 20 000 cm^{-1} or higher. $Cu(LE)_2(ClO_4)_2$ (LE = 1,2-bis(2′-pyridyl)ethane) is assumed to have a square planar CuN_4 structure and exhibits bands at 18 200 and 21 600 cm^{-1} (22). $Cu(LP)_2(ClO_4)_2$ (LP = 1,2-bis(2′-imidazolin-2′-yl) benzene) has bands at 16 000 and 21 000 cm^{-1} attributable to a CuN_4 square planar structure.[2] The large separation in energy between the two bands observed in the spectrum of the perchlorate complex of OBT can be rationalised in terms of a square CuN_4 system in which axial perturbation is either reduced to a minimum or absent. Molecular models suggest that a *trans* arrangement of two OBT ligands about a square planar metal centre would effectively block both axial sites. As an alternative explanation the band at 24 000 cm^{-1} could be associated with a $\pi^* \leftarrow \pi$ or $\pi^* \leftarrow$ n intraligand transition while the lower energy absorption at 16 700 cm^{-1} could be assigned to a *d–d* transition in a *cis*-octahedral species involving two coordinated water molecules (infrared data suggest the possibility of coordinated water).

Recent reports of copper thioether complexes and their relation to 'blue' copper proteins (1, 23, 24) indicate that σ(S)→Cu LM charge transfer bands for thioether systems occur as fairly intense bands in the range 22 000 – 31 000 cm^{-1}. Copper complexes of 2,5-dithiahexane and 3,6-dithiaoctane have charge transfer bands of moderate intensity in the range 22 000 – 26 000 cm^{-1}, assigned to S→Cu charge transfer (25). Complexes with less polarizable amine type ligands, e.g. $Cu(en)_2^{2+}$ and its alkylated derivatives (26, 27) exhibit σ(N)→Cu charge transfer absorptions at ca. 40 000 cm^{-1}. OBT can be considered as a bis-imidazole (N_2) or as a bis-sulphur donor (S_2) or as a mixed ligand if NS coordination takes place. As a sulphur donor ligand it would perhaps be expected to exhibit S→Cu charge transfer at comparable energies to those mentioned previously. It is probably unwise to compare imidazoles with simple amines but it is unlikely that N→Cu charge transfer for imidazole systems would occur below 30 000 cm^{-1}. In a recent paper describing copper complexes of the tripod ligand tris(2-benzimidazylmethyl) amine, no bands below 30 000 cm^{-1} could be associated with imidazole N→Cu charge transfer (28).

The halide complexes exhibit fairly intense bands at 24 100 cm^{-1} (Cl) and 19 200 cm^{-1} (Br) in their solid state spectra which are assigned to π-halogen→Cu charge transfer (29, 30). Lower energy bands for the chloro complex at 13 600 cm^{-1} and 17 200 cm^{-1} are assigned to *d–d* transitions associated with a four coordinate species having an almost square arrangement of donor atoms. Solution studies on this species indicate the presence of the charge transfer band but a shift to lower energy of the *d–d* bands. This can be interpreted in terms of the pseudo-square solid state species becoming more tetrahedral in solution. The bromo complex exhibits an intense band at ca. 19 000 cm^{-1} both in the solid state and in solution, which is assigned to a πBr → Cu charge transfer transition while lower energy bands at 16 000 and 13 000 cm^{-1} can again be associated with *d–d* transitions in a four-coordinate species with a stereochemistry in between square and tetrahedral.

Although the charge transfer bands in the halide complexes fall in a range consistent with S→Cu charge transfer, this assignment has been excluded because of the large difference in energy observed for this band in the chloro- and bromo-derivatives and their otherwise general similarity. Recent X-ray data[3] confirm this assignment and show that the complex $Cu(OBT)Cl_2$ has an almost square planar CuN_2Cl_2 structure (Fig. 2).

Conductance measurements (Table 3) on the copper complexes indicate the perchlorate complex to be a 1:2 electrolyte in nitromethane, while the halide and nitrate complexes appear to be largely non-

[2]Unpublished observations.

[3]R. G. Ball and J. Trotter. Private communication.

TABLE 4. Infrared data (cm^{-1})*

Compound	ν(M—X)	ν(M—N)	νCN(NCS)	$CHCl_3$ $\nu_1(A_1)$	$CHCl_3$ $\nu_5(E)$
$Co(OBT)Cl_2 \cdot CHCl_3$	344, 326	214		2995	744
$Co(OBT)Br_2 \cdot CHCl_3$	255, 249(sh)			2985	742
$Co(OBT)I_2$	238, 231	222, 215			
$Co(OBT)(NCS)_2 \cdot CHCl_3$	333, 313, 298	222, 218	2070, 2058	2990	741
$Cu(OBT)Cl_2$	319, 309				
$Cu(OBT)Br_2$	259, 240				
$Zn(OBT)Cl_2 \cdot (CH_3)_2CO$	321, 295	214			
$Zn(OBT)Br_2 \cdot (CH_3)_2CO$	243, 225	218			
$Zn(OBT)I_2$		212			
$Zn(OBT)(NCS)_2$	327, 302(sh), 291	213	2070(br)		

Compound	Bidentate nitrate	$(\nu_1 + \nu_4)$	ν(M—O)
$Co(OBT)(NO_3)_2 \cdot 2H_2O$	1500, 1280, 806	1768, 1714	290, 268(sh)
$Cu(OBT)(NO_3)_2$	1496, 1275, 809	1753, 1713	322, 305(sh)

Compound	ClO_4^- $\nu_3(T_2)$	ClO_4^- $\nu_4(T_2)$
$Cu(OBT)_2(ClO_4)_2 \cdot 2H_2O$	1080	620

*Infrared spectra obtained as Nujol or hexachlorobutadiene mulls between KBr or CsI plates.

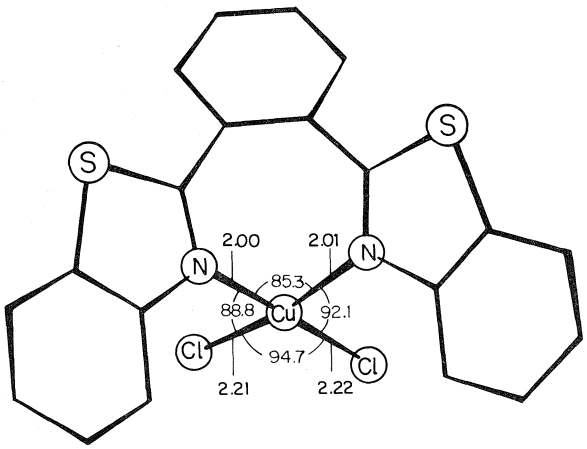

FIG. 2. X-ray structure of $Cu(OBT)Cl_2$. Dihedral angle 9.8°.

ionised. Storing of nitromethane solutions of the halide complexes for extended periods of time induced decomposition of these systems. Magnetic moments (Table 3) appear to be normal for systems of this type.

Copper halogen stretching vibrations have been identified in the far infrared spectra (Table 4) of the halide complexes, suggesting an approximately C_{2v} environment for these groups around the copper centre. Lorenz *et al.* (10) observed a band in the infrared spectrum of $Cu(PBS)_2$ at 352 cm^{-1} which was assigned to Cu—N stretch for a nitrogen bound benzothiazole. No such band was observed in the spectra of the copper halide derivatives of OBT and between 240 and 370 cm^{-1} the only bands observed were those due to copper halogen stretching. Nitrate fundamentals and combination bands (20, 21) indicate bidentate nitrate groups for the complex $Cu(OBT)(NO_3)_2$ and low energy bands at 322, 305 cm^{-1} are assigned to Cu—O stretch.

Electron spin resonance parameters are summarised in Table 5. Frozen glass spectra in nitromethane of the nitrate and perchlorate complexes are typical of axial species. Resolvable nitrogen superhyperfine splitting is observed in the case of the nitrate complex but is absent in the perchlorate derivative. In contrast the room temperature spectrum of the perchlorate complex in nitromethane shows nitrogen superhyperfine splitting while the nitrato derivative does not. Spin Hamiltonian parameters are similar to those for $Cu(MeIm)_4(ClO_4)_2$ and $Cu(LP)_2(ClO_4)_2$ (Table 5) in nitromethane, although values of $g_{\|}$ are somewhat higher than those expected for a CuN_4 chromophore and suggest mixed NO in plane donor atoms, which would certainly be the case for the nitrate complex.[2]

Frozen glass spectra for the halide complexes in dichloromethane gave rather poorly defined signals at 77 K with little evidence for copper hyperfine splitting. Room temperature powder spectra are consistent with distorted square four-coordinate systems. The spectra are characterised by narrow line widths (15–18 G at half height in the $g_{\perp}$ region) and while no splitting due to copper nuclear spins is apparent only two resonance peaks are clearly re-

TABLE 5. Electron spin resonance data

Compound		$g_{\parallel}$	$g_{\perp}$	g_0	$\lvert A_{\parallel}\rvert$†	$\lvert A_{\perp}\rvert$†	A_0	$\langle g \rangle$
$Cu(OBT)(NO_3)_2$	$MeNO_2$, 77 K	2.286	2.058		205	3‡		
	$MeNO_2$, *RT*			2.134			66	
	Powder	2.229	2.099					
$Cu(OBT)_2(ClO_4)_2 \cdot 2H_2O$	$MeNO_2$, 77 K	2.275	2.063		182	34		
	$MeNO_2$, *RT*			2.099			83	
	Powder	2.198	2.050		185			
$Cu(MeIm)_4(ClO_4)_2$*	$MeNO_2$, 77 K	2.256	2.055		192	35		
$Cu(LP)_2(ClO_4)_2$*	$MeNO_2$, 77 K	2.219	2.044		160	47		
$Cu(OBT)Cl_2$	CH_2Cl_2, 77 K							2.052
	Powder	2.144	2.074					
$Cu(OBT)Br_2$	CH_2Cl_2, 77 K							2.060
	Powder	2.161	2.044					

*Unpublished observations.
†All hyperfine coupling constants in units 10^{-4} cm^{-1}.
‡Opposite sign to $A_{\parallel}$. $A_{\perp}$, $g_{\perp}$estimated via $3A_0 = 2A_{\perp} + A_{\parallel}$, $3g_0 = 2g_{\perp} + g_{\parallel}$ using $g_{\parallel}$, $A_{\parallel}$ at 77 K, g_0, A_0 at 300 K.

solved. Narrow line widths have been observed in the solid state spectra of sulphur bound systems, e.g., $Cu(3,5\text{-dithiahexane})_2(BF_4)_2$ (31), but clearly in this case we are dealing with a nitrogen bound system. Other CuN_2Cl_2 systems, e.g., Cu[2-(2-dimethylaminoethyl)pyridine]Cl_2 (32), Cu(sparteine)Cl_2 (33), have similar solid state spectra but larger g values, in keeping with the more tetrahedral nature of these complexes.

Zinc Complexes

Analytical and infrared spectral data confirm the four-coordinate pseudo-tetrahedral nature of these systems. Metal halogen vibrations compare with those observed for both the cobalt and copper halide complexes and metal–ligand vibrations, associated with metal–nitrogen stretch, are observed as fairly strong bands in the range 212–218 cm^{-1}.

Acknowledgements

We thank the National Research Council of Canada for financial support for this study and in particular for the purchase of the Cary 17 Spectrophotometer. We are also indebted to the Chemistry Department at the University of British Columbia for the use of esr facilities.

1. A. R. AMUNDSEN, J. WHELAN, and B. BOSNICH. J. Am. Chem. Soc. **99**, 6730 (1977).
2. M. GOODGAME and M. J. WEEKS. J. Chem. Soc. A, 1156 (1966).
3. R. A. FORD, G. HALKYARD, and A. E. UNDERHILL. Inorg. Nucl. Chem. Lett. **4**, 507 (1968).
4. E. J. DUFF, M. N. HUGHES, and K. J. RUTT. J. Chem. Soc. A, 2354 (1968).
5. N. N. Y. CHAN, M. GOODGAME, and M. J. WEEKS. J. Chem. Soc.A, 2499 (1968).
6. E. J. DUFF, M. N. HUGHES, and K. J. RUTT. J. Chem. Soc. A, 2101 (1969).
7. M. J. M. CAMPBELL, D. W. CARD, and R. GRZESKOWIAK. Inorg. Nucl. Chem. Lett. **5**, 39 (1969).
8. M. J. M. CAMPBELL, D. W. CARD, R. GRZESKOWIAK, and M. GOLDSTEIN. J. Chem. Soc. A, 672 (1970).
9. S. E. LIVINGSTONE and J. D. NOLAN. J. Chem. Soc. Dalton, 218 (1972).
10. D. R. LORENZ, T. M. BARBARA, and J. R. WASSON. Inorg. Nucl. Chem. Lett. **12**, 65 (1976).
11. C. RAI and J. B. BRAUNWARTH. J. Org. Chem. **26**, 3634 (1961).
12. A. B. P. LEVER and S. M. NELSON. J. Chem. Soc. A, 859 (1966).
13. M. GOODGAME and F. A. COTTON. J. Am. Chem. Soc. **84**, 1543 (1962).
14. P. DAY and C. K. JØRGENSEN. J. Chem. Soc. 6226 (1964).
15. A. B. P. LEVER. Inorg. Chem. **4**, 1042 (1965).
16. A. B. P. LEVER, B. S. RAMASWAMY, S. H. SIMONSEN, and L. K. THOMPSON. Can. J. Chem. **48**, 3076 (1970).
17. A. W. ADDISON and R. D. GILLARD. J. Chem. Soc. Dalton, 2002 (1973).
18. I. BERTINI and A. SABATINI. Inorg. Chem. **5**, 1025 (1966).
19. R. J. H. CLARK and C. S. WILLIAMS. Inorg. Chem. **4**, 350 (1965).
20. K. NAKAMOTO. Infrared spectra of inorganic and coordination compounds. 2nd ed. Wiley-Interscience, New York. 1970.
21. A. B. P. LEVER, E. MANTOVANI, and B. S. RAMASWAMY. Can. J. Chem. **49**, 1957 (1971).
22. M. KEETON, A. B. P. LEVER, and B. S. RAMASWAMY. Can. J. Chem. **48**, 3185 (1970).
23. T. E. JONES, D. B. RORABACHER, and L. A. OCHRYMOWYCZ. J. Am. Chem. Soc. **97**, 7485 (1975).
24. V. M. MISKOWSKI, J. A. THICH, R. SOLOMON, and H. J. SCHUGAR. J. Am. Chem. Soc. **98**, 8344 (1976).
25. E. W. AINSCOUGH, A. M. BRODIE, and K. C. PALMER. J. Chem. Soc. Dalton, 2375 (1976).
26. H. YOKOI and T. ISOBE. Bull. Chem. Soc. Jpn. **42**, 2187 (1969).
27. B. P. KENNEDY and A. B. P. LEVER. J. Am. Chem. Soc. **95**, 6907 (1973).
28. L. K. THOMPSON, B. S. RAMASWAMY, and R. D. DAWE. Can. J. Chem. **56**, 1311 (1978).
29. A. B. P. LEVER. J. Chem. Ed. **51**, 612 (1974).
30. B. D. BIRD and P. DAY. J. Chem. Phys. **49**, 392 (1968).
31. U. SAKAGUCHI and A. W. ADDISON. Submitted for publication.
32. R. B. WILSON, J. R. WASSON, W. E. HATFIELD, and D. J. HODGSON. Inorg. Chem. **17**, 641 (1978).
33. S.-N. CHOI, R. D. BEREMAN, and J. R. WASSON. J. Inorg. Nucl. Chem. **37**, 2087 (1975).

Sensitized photolysis of bis(acetylacetonato)copper(II); general reaction pattern

GONZALO BUONO-CORE, KIYOSHI IWAI, and YUAN L. CHOW
Department of Chemistry, Simon Fraser University, Burnaby, B.C., Canada V5A 1S6

AND

TOHRU KOYANAGI, ARITSUNE KAJI, AND JUN-ICHI HAYAMI
Department of Chemistry, Faculty of Science, Kyoto University, Kyoto, Japan

Received June 5, 1978

GONZALO BUONO-CORE, KIYOSHI IWAI, YUAN L. CHOW, TOHRU KOYANAGI, ARITSUNE KAJI, and JUN-ICHI HAYAMI. Can. J. Chem. **57**, 8 (1979).

Bis(acetylacetonato)copper(II) was sensitized by some ketones with a wide range of triplet energies to undergo photodecomposition to give the same products as that obtained in the direct photolysis but with much better efficiency. Other sensitizers such as fluorenone and aromatic hydrocarbons failed to sensitize the reaction. There exists no correlation of the sensitizer triplet energies with the sensitization results. This, and rapid quenching processes, indicated that the classical energy transfer process was unlikely. The sensitization process by an electron transfer within an encounter complex was proposed to explain the decomposition of $Cu(acac)_2$; the calculated free energy changes (ΔG) associated with the electron transfer from the available data support the proposal. Chemical reactions of excited state anthracene and 1-cyanonaphthalene with $Cu(acac)_2$ may also occur. Irradiation of $Cu(acac)_2$ in the presence of triphenylphosphine and benzophenone led to an excellent yield of $Cu(acac)(PPh_3)_2$ without causing precipitation of copper(I) complexes.

GONZALO BUONO-CORE, KIYOSHI IWAI, YUAN L. CHOW, TOHRU KOYANAGI, ARITSUNE KAJI et JUN-ICHI HAYAMI. Can. J. Chem. **57**, 8 (1979).

On a sensibilisé du bis(acétylacétonato) cuivre(II) par quelques cétones couvrant une gamme étendue d'énergies d'états triplets provoquant une photodécomposition conduisant aux mêmes produits que par photolyse directe mais avec une meilleure efficacité. D'autres sensibilisateurs comme la fluorénone et des hydrocarbures aromatiques n'ont pas réussi à sensibiliser la réaction. Il n'existe aucune corrélation entre les énergies triplet des sensibilisateurs et les résultats des sensibilisation. Ce résultat et le fait que le processus d'extinction est rapide indiquent que le transfert classique d'énergie est peu probable. Le processus de sensibilisation par un transfert d'électron à l'intérieur d'un complexe de rencontre a été proposé pour expliquer la décomposition du $Cu(acac_2)$; les changements calculés d'énergie libre (ΔG) associée avec les transferts d'électrons disponibles à partir de données publiées sont en accord avec les propositions. Il peut aussi se produire des réactions chimiques entre les états excités de l'anthracène et du cyano-1 naphtalène avec le $Cu(acac)_2$. L'irradiation du $Cu(acac)_2$ en présence de triphénylphosphine et de benzophénone conduit à un excellent rendement du $Cu(acac)(PPh_3)_2$ sans provoquer de précipitation de complexes du cuivre(I).

[Traduit par le journal]

In connection with other research projects we have undertaken investigations of photochemical decomposition of bis(acetylacetonato)copper(II) (**1**) in organic solvents. While there are many photochemical studies of other first row transition metal β-diketonate complexes (1, 2), only one report (3) on photodecomposition of copper(II) β-diketonate complexes can be found in the literature. This and other studies (1, 4–6) of copper compounds use direct irradiation of solutions and have reported observations of reduction of copper(II) to copper(I) or metallic copper. Direct photodecomposition of copper(II) β-diketonates in alcohols, however, occurs only by irradiation of the charge transfer band of the ligand-to-metal type (CTTM) (3) at 230–250 nm and gives low quantum yields of <0.04. These studies have led the authors to propose the following mechanism

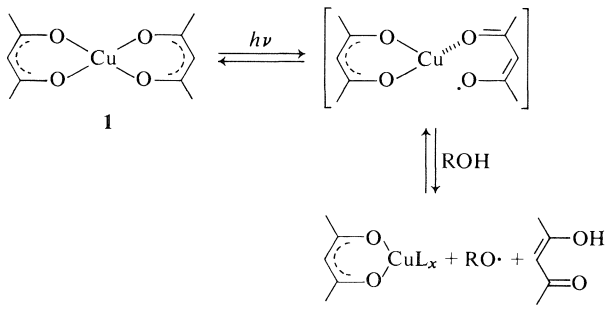

1

where L is a ligand derived from solvent. The copper(I) complex thermally decomposes to Cu^0 as reported previously (7). Noting earlier studies

0008-4042/79/010008-09$01.00/0

that transition metal complexes have marked activity as quenchers for the triplet states of organic molecules (8–10), we have decided to investigate the sensitized photodecomposition of bis(acetylacetonato)copper(II) in detail. In a recent publication (4) it was briefly mentioned that benzophenone and acetophenone sensitize the photodecomposition of polyfluorinated copper β-ketoacetonates. The general reaction pattern is reported here.

Results

In preliminary experiments methanol solutions of bis(acetylacetonato)copper(II), $Cu(acac)_2$, were irradiated in a conventional immersion type quartz photocell. This apparatus was clearly unsatisfactory because of the deposition of black precipitates followed by the formation of lustrous metallic copper mirrors, both of which obstructed the incident light. Nevertheless, we confirmed several features of the photodecomposition reported (3), e.g., (*i*) the blue colour of $Cu(acac)_2$ disappeared slowly under nitrogen to form metallic copper with a quartz but not a Pyrex filter, (*ii*) the photolysate, on exposure to air, was slowly converted to a blue solution of $Cu(acac)_2$, and (*iii*) under oxygen, the Cu(II) complex was irreversibly decomposed on irradiation.

In order to avoid the deposition problems, an apparatus as shown in Fig. 1 was designed in which the solution was irradiated from overhead with Hanovia Mercury lamp (SH 616 A0130, 140 W). This set-up proved to be satisfactory for semi-quantitative experiments, although it may not be a suitable apparatus for accurate quantitative studies. Since $Cu(acac)_2$ in alcohol solutions absorbs light strongly at λ_{max} 293 nm (ε, 23 500) which tails to the 370 nm region with $\varepsilon \sim 600$ at 330 nm, concentrations for the sensitizations were adjusted so that sensitizers absorb part or all of the incident light energy. Irradiation of a methanol solution of $Cu(acac)_2$ (5.7 mmolar) containing 6.3 mmolar of benzophenone under nitrogen gave a suspension of black precipitate in 3 h with concurrent discharge of the blue colour. On continued irradiation, the suspension changed to lustrous copper particles suspended in a colourless solution (or gave a copper mirror) in 18 h. The progress of the photoreaction was monitored by following the decrease of the absorption band of $Cu(acac)_2$ at 630 nm. The yield of copper was determined by colorimetry to be quantitative. The colourless solution contained acetylacetone (78%), as determined by high pressure liquid chromatography (HPLC) and uv spectroscopy, and formaldehyde (50% as its 2,4-DNPH); benzophenone was recovered quantitatively and the absence of benzpinacol was ascertained. Irradiation of an ethanol solution of $Cu(acac)_2$ in the absence of benzophenone through a quartz filter under similar conditions took more than 24 h to cause a 10% decrease in the intensity of the band at 630 nm.

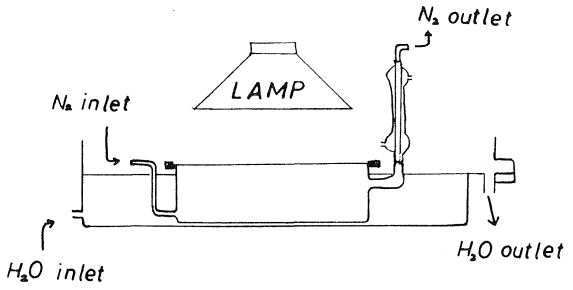

FIG. 1. Photolysis apparatus.

The metallic copper suspension, obtained after photolysis, was stable under nitrogen. However, on exposure to air it dissolved slowly and reverted quantitatively to give $Cu(acac)_2$ with the original concentration. This occurred more rapidly under oxygen purging; in both cases benzophenone was recovered nearly quantitatively. The suspension of the black precipitate in the transparent solution also reverted quantitatively to the original $Cu(acac)_2$ solution under oxygen and to half of the original $Cu(acac)_2$ concentration under nitrogen as determined by uv spectroscopy; metallic copper was also deposited in the latter case.

The effect of solvent was such that the sensitized photodecomposition of $Cu(acac)_2$ in ethanol caused appearance of the black precipitate within 30–40 min and in isopropanol within 15 min. In both cases copious amounts of the black suspension were formed rapidly as irradiation proceeded. The suspension was transformed to metallic copper (100% and 98%, respectively) on prolonged irradiation in 3 and 1 h, respectively. The yields of acetylacetone were analysed to be 84% and 76%, and the oxidation products of the solvents, acetaldehyde and acetone, were determined to be 38% and 69%, respectively. Benzophenone was recovered in high yields in both cases.

Under similar conditions, the benzophenone-sensitized photodecomposition of $Cu(acac)_2$ in tetrahydrofuran solution followed a similar pattern, i.e., disappearance of the 630 nm band in 1.5 h and complete reduction to Cu^0 in 6 h. However, oxidation products of THF could not be isolated. In benzene and chloroform the photodecomposition occurred very slowly but the colour changed to deep green and was not pursued further. The pattern of photo-

chemical changes in 1:1 mixtures of benzene–methanol or chloroform–methanol were the same as those observed in the alcohol solutions.

In the presence of $<0.1\ M$ 1,3-pentadiene, benzophenone-sensitized photodecompositions of $Cu(acac)_2$ ($6 \times 10^{-3}\ M$) were not retarded, but when the concentration of the diene was 0.15 or 0.70 M, the black precipitate was formed in lesser amounts. In the presence of $1.14 \times 10^{-2}\ M$ triethylamine the photodecomposition was not retarded, and benzophenone was not consumed. When the photodecomposition was carried out in methanol in the presence of 0.6 M cyclohexene, dicyclohexenyl was formed, as shown by tlc and vpc analyses, together with the formation of a copper mirror and recovered benzophenone.

As the primary photodecomposition product was the black precipitate, its identity was investigated. Its ready disporportionation to $Cu(acac)_2$ and Cu^0 appeared to be similar to the behaviour of a cuprous complex, $Cu(acac)\cdot 2.5NH_3$, prepared by Nast *et al.* (7). The black precipitate when treated with ethanol solution of triphenylphosphine under nitrogen gave a white crystalline compound analyzing as $Cu(acac)(PPh_3)_2$. Benzophenone sensitized photolysis of $Cu(acac)_2$ in the presence of triphenylphosphine gave a colourless, clear solution without formation of the black precipitate. From this photolysate the above crystalline compound (94%), acetylacetone (80%) and acetaldehyde (42% as 2,4-DNPH) were obtained. The compound was not formed in the dark. It exhibited identical ir and nmr data as those of $Cu(acac)(PPh_3)_2$ reported in the literature (11).

Other sensitizers were investigated in order to gain an insight to the mechanism of the photodecomposition. The results are summarized in Table 1. Photodecomposition of $Cu(acac)_2$ could be sensitized by anthrone, benzophenone, biacetyl, and xanthone (shown in order of decreasing efficiency). In all these sensitized decompositions the black precipitate, metallic Cu, and acetylacetone were formed in nearly stoichiometric yields and the sensitizers were recovered almost quantitatively. Vapour phase chromatographic analyses of the recovered anthrone and biacetyl showed small peaks that were assumed to be minor photoproducts of the sensitizers as they are known to decompose photolytically (12). Other sensitizers shown in Table 1 failed to photodecompose $Cu(acac)_2$ as indicated by uv and visual observation. Except in a few cases to be described below, the sensitizers were recovered quantitatively and no acetylacetone or black precipitate was obtained.

Fluorenone failed to sensitize the photodecomposition of $Cu(acac)_2$ in methanol or isopropyl alcohol on prolonged irradiation. Although in the latter solvent the absorption maximum at 630 nm was shown to shift to ~680 nm, no product other than the starting material was recovered from the photolysate in either solvent. Photolysis of a methanol solution containing $Cu(acac)_2$ and anthracene immediately precipitated the dimer of the latter (13). On prolonged irradiation the dimer was obtained in 70% yield and 60% of the $Cu(acac)_2$ was recovered. Trace amounts of other unidentified products were also detected by vpc but no acetylacetone was obtained. In the phenothiazine sensitized photodecomposition only 60% of $Cu(acac)_2$ was recovered and trace amounts of other products were detected by tlc. While prolonged photolysis gave a dark brown solution, phenothiazine was recovered in ~80% yield.

An attempted sensitization with 1-cyanonaphthalene did not cause reduction to the black precipitate but proceeded slowly to show a 15% decrease of the optical density at 630 nm and deposited a small amount of blue precipitate. The ir and melting point were identical with the compound obtained by reaction of $Cu(acac)_2$ in methanolic KOH solution for which structure **2** was assigned from ir, uv, and visible spectra (14). The authors (14) determined the magnetic moment to be 0.75 BM. The paramagnetic nature was shown by broad nmr and esr signals. The elemental analysis of our product indicated an empirical formula of $Cu(acac)OCH_3$. The ir spectrum showed, in addition to the ir peaks of $Cu(acac)_2$, absorption at 2820, 1070, and 560 cm^{-1} (but no absorption above 3000 cm^{-1}), indicating the presence of a methoxide moiety. A chloroform solution of the blue precipitate was evaporated to give a residue which showed an identical ir (KBr) spectrum to that of $Cu(acac)_2$. The mass spectrum of the blue precipitate showed *m/e* peaks at 386, 355, 324, and 261 (100%) corresponding to M^+, $M^+ - [OCH_3]$, $M^+ - 2[OCH_3]$, and $M^+ - [Cu(OCH_3)_2]$. The fragmentation pattern below *m/e* 263 was very similar to that of $Cu(acac)_2$. Structures **3** and **4** besides **2** could be suggested for the compound; **4**, however, appears to satisfy the mass spectral data better than the others.

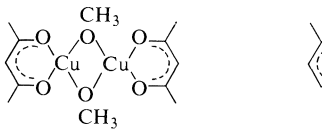

2

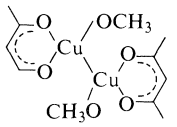

3

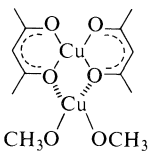

4

TABLE 1. Sensitized decomposition of $Cu(acac)_2$ 3.2–5.7 × 10^{-3} M

Sensitizer	Concentration (M × 10^3)	Solvent	E_T[c] (kcal/mol)	$E_{(A/A^-)}$[b] (V)	ΔG (kcal/mol)	Result[a]
Benzophenone	6.4	EtOH,MeOH, IPA,THF	69	−1.72	−1.3	+
Anthrone	3.8	EtOH	72	−1.09	−19.3	+
Biacetyl	470	EtOH	57	−1.0[e]	−6.4	+
Xanthone	12.7	MeOH	74	−1.65	−7.1	+
Fluorenone	5.5	MeOH,IPA	53	−1.37[e]	+6.4	−
1-Cyanonaphthalene	6.5	EtOH,IPA	57.5[d]	−2.33[d]	+23.8[d]	−
p-Dicyanobenzene	8.5	MeOH	70.1[d]	−2.00[d]	+4.8[d]	−
Acetylacetone	900	EtOH	—	−1.68	—	−
Anthracene	5.6	MeOH	43	−1.92	+29.1	−
Pyrene	4.2	EtOH	48	−2.09	+27.9	−
Phenanthrene	11.4	EtOH	66	−2.44	+21.8	−
Perylene	0.33	EtOH	35	−1.67	+31	−
Carbazole	5.0	EtOH	70	—	—	−
Phenothiazine	5.0	EtOH	62[f]	—	—	−

[a]The progress of reactions was followed by uv spectroscopy at 630 nm and the recovered materials were analysed by vpc, tlc, and in some cases by isolation. The details are described in the results.
[b]Unless specified otherwise, $E_{(A/A^-)}$ in dimethylformamide (38).
[c]The triplet energies were quoted from ref. 39.
[d]The $E_{(A/A^-)}$ was obtained in CH_3CN as reported in ref. 24. If E_s = 89.4 kcal/mol was used for the calculation, ΔG = −8.1 kcal/mol.
[e]Quoted from ref. 26.
[f]The approximate E_T calculated from the triplet absorption maximum at 460 nm (33).

Discussion

The results described above show that certain carbonyl compounds sensitize the photodecomposition of $Cu(acac)_2$ much more efficiently than direct photodecomposition. The product patterns in both cases are the same, i.e., acetylacetone and a copper(I) acetylacetonate complex are the primary photoproducts. The latter thermally disproportionates to Cu^0 and $Cu(acac)_2$ under nitrogen or is oxidized to $Cu(acac)_2$ under oxygen. Heterogeneity of the reaction can be avoided by running the photolysis in the presence of triphenylphosphine whereby the intermediate copper(I) complex could be intercepted to form soluble $Cu(acac)(PPh_3)_2$; this provides a direct proof that a copper(I) complex is the primary photoproduct. Since in the presence of 0.1 M acetylacetone, where the incident light is mostly absorbed by acetylacetone (see Table 1), $Cu(acac)_2$ does not decompose, it is concluded that the slow direct photodecomposition is not catalysed by acetylacetone. The reaction pathway can be expressed by reactions [1]–[4] where S* is an excited state sensitizer.

[1] $Cu(acac)_2 + S^* \longrightarrow Cu(acac) +$ 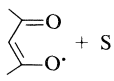 $+ S$

5

[2] $Cu(acac) + xL \longrightarrow Cu(acac)L_x$

[3] $Cu(acac) + 2PPh_3 \longrightarrow Cu(acac)(PPh_3)_2$

[4] $Cu(acac)L_x \xrightarrow{N_2} Cu(acac)_2 + Cu^0 + xL$

Since disproportionation of the copper(I) complex as in reaction [4] is rather slow in the solvents used in comparison to photodecomposition of $Cu(acac)_2$ (see reactions [1] and [2]) the black precipitate always appears first followed by the slow appearance of metallic copper. In ethanol or propanol, the photodecomposition of reactions [1] and [2] occurs much faster as seen by the rapid disappearance of the blue colour of the $Cu(acac)_2$ solution and immediate heavy deposition of the black precipitate. In the presence of triphenylphosphine the step of reaction [4] is circumvented and the sensitized photodecomposition occurs rapidly under homogeneous conditions. Provided that triphenylphosphine does not affect the rate of reaction [1], these conditions might allow quantitative studies of the sensitized photodecomposition in a homogeneous solution.

Stoichiometrically, the reduction of copper(II) to copper(0) via copper(I) in the sensitized photodecomposition must be coupled with the oxidation reaction of alcohols to carbonyl compounds. The mechanism of the oxidation might be related to the way an acetylacetonate ligand acquires a hydrogen to form acetylacetone. That the redox processes take place by radical mechanism is suggested by the following observations. Firstly, poor H-atom donating solvents, such as benzene and chloroform, do not promote the photoreduction. Secondly, the sensitized photoreduction occurs in alcohols with a decreasing order of efficiency of isopropyl alcohol > ethanol > methanol, which coincides with the efficiency order (15) in which these alcohols donate an α-hydrogen (but not hydroxy hydrogen) (3) by a radical mechanism. Finally, the formation of dicyclohexenyl in the sensitized photodecomposition of

$Cu(acac)_2$ in the presence of cyclohexene is consistent only with a radical mechanism. Therefore the yet unproven acetylacetonatoxy radical **5** might be suggested as the reactive intermediate in mediating the oxidation reaction by abstraction of an α-hydrogen of alcohols as shown in reactions [5] and [6]. Further, if a competing electron transfers from Cu(acac) to **5** is assumed to occur (reaction [7]), it is possible to explain the order of the photoreduction efficiency in these alcohols.

[5] $\mathbf{5} + RCH_2OH \rightarrow CH_3COCH_2COCH_3 + R\dot{C}HOH$

[6] $2R\dot{C}HOH \rightarrow RCH_2OH + RCH{=}O$

[7] $\mathbf{5} + Cu(acac) \rightarrow Cu(acac)_2$

Various mechanisms could operate in the sensitization step of reaction [1]. A hydrogen atom transfer from alcohol to $Cu(acac)_2$ mediated by the triplet state sensitizer as in reactions [8] and [9] is attractive in view of the well established reaction pattern of the benzophenone triplet state (16).

[8] $^*(C_6H_5)_2CO + RCH_2OH \rightarrow (C_6H_5)_2\dot{C}OH + R\dot{C}HOH$

[9] $(C_6H_5)_2\dot{C}OH + Cu(acac)_2 \rightarrow (C_6H_5)_2CO + Cu(acac) + acacH$

This mechanism, however, suffers inconsistency in that the H-abstraction by the benzophenone triplet is fairly slow ($k = 1.8 \times 10^6\ M^{-1}\ s^{-1}$ from isopropanol) and readily quenched by 1,3-pentadiene (16).

The direct photodecomposition has been speculated to occur by an internal redox process arising from the excitation of the charge-transfer or the ligand-to-metal band (CTTM) at 243 nm ($E \sim 119$ kcal/mol), based on which the acetylacetonatoxy radical **5** has been proposed as the intermediate (3). Since $Cu(acac)_2$ shows no emission, the energy levels of its excited states are unclear. While the sensitized photodecomposition might be assumed to proceed from a yet undefined excited state of $Cu(acac)_2$ by an internal redox mechanism similar to that proposed for direct photolysis, evidence as shown in Table 1 is against a classical triplet energy transfer mechanism (17) from excited states of the sensitizers to the ground state of $Cu(acac)_2$. For example, the order of sensitization efficiency, i.e., anthrone > benzophenone > biacetyl > xanthone, does not agree with the order of the lowest triplet energies of the sensitizers. It is also apparent none of these ketones has a singlet state energy high enough to successfully activate the CTTM band transition for $Cu(acac)_2$.

There are many investigations on the mechanism of sensitized reactions in metal complexes (18–21). It was found that (18–21) the luminescent excited state of polypyridineruthenium(II) complexes is quenched by various metal ions or complexes by either electron transfer or energy transfer mechanisms depending on the nature of the quenchers. In particular, this state of the ruthenium(II) complexes can act as an electron donor as well as an acceptor for a wide range of quenchers. On the other hand, Wilkinson (22) and others (23) have observed that the quenching efficiencies of the triplet states of organic compounds by iron and other coordination complexes are dependent on the relative energy levels of interacting states, from which energy transfer is put forward as the mechanism of quenching. While reinterpretation of Wilkinson's results (22) by an electron transfer mechanism might reveal more details, the present sensitized decomposition is not likely to occur by energy transfer for reasons given.

From the results of kinetic flash photolysis investigations Hammond and co-workers (24) have recognized that some transition metal complexes quench triplet states of a variety of sensitizers efficiently and that k_q are not correlated with the sensitizer triplet energy levels. The rate constants are $k_q \geq 10^9\ M^{-1}\ s^{-1}$ with very little variation. They have concluded that either the complexes have low lying excited states to which they can be promoted by energy transfer or with these complexes quenching does not involve energy transfer (24). In the present case, the former assumption is untenable from the pattern as shown in Table 1. An extremely high quenching rate of benzophenone excited states by $Cu(acac)_2$ is evident in the present investigation. The inefficient retardation of benzophenone-sensitized $Cu(acac)_2$ decomposition by 1,3-pentadiene indicates that the sensitization process is much faster than the quenching of the lowest triplet benzophenone by the diene, the rate constant (25) of which has been calculated to be $3.75 \times 10^9\ M^{-1}\ s^{-1}$. Triethylamine, which quenches triplet state benzophenone at a rate constant (26) of $2.3 \times 10^9\ M^{-1}\ s^{-1}$, does not retard the sensitized $Cu(acac)_2$ decomposition at all. Both observations indicate that an excited state benzophenone is quenched by $Cu(acac)_2$ with a rate constant at least an order of magnitude higher than these constants, or say $\sim 3 \times 10^{10}\ M^{-1}\ s^{-1}$. Such a rate constant is in the region of the diffusion-controlled bimolecular encounter rate constant (27), in methanol at 20°C $k_{diff} = 1.8 \times 10^{10}\ M^{-1}\ s^{-1}$. Since the uv spectrum of a methanol solution containing $Cu(acac)_2$ and benzophenone is essentially a composite of the individual uv spectra, formation of a ground state complex is not evident.

The sensitization of reaction [1] is thought to occur by electron transfer from the ligand of $Cu(acac)_2$ to excited states of the sensitizers (S*) via an unspecified encounter complex (and/or exciplex) as shown in reactions [10] and [11]. The free energy

change (ΔG) associated with the electron transfer in the encounter complex (reaction [10]) is represented by reaction [12] in which $E_{(D/D^+)}$ is the oxidation potential of the donor, $E_{(A/A^-)}$ the reduction potential of the acceptor, and ΔE_{0-0} the excited state energy of the acceptor in the present case (26, 29). The coulombic attraction term $e_0^2/\varepsilon\alpha$ in a polar medium with encounter distance of ca. 7 Å is small and is omitted in the calculation. Reaction [12] has been proposed by Rehm and Weller (28) from kinetic analysis of quenching and has been successfully applied by others (26, 29) to account for sensitization by electron transfer.

[10] $Cu(acac)_2 + S^* \rightleftarrows [Cu(acac)_2\text{---}S^*]$
Encounter complex
$\rightleftarrows Cu(acac)_2{}^{+\bullet}\text{---}S^{-\bullet}$
Solvated ion pair

[11] $Cu(acac)_2{}^{+\bullet}\text{---}S^{-\bullet} \rightarrow Cu(acac)_2{}^{+\bullet} + S^{-\bullet}$

[12] $\Delta G(\text{kcal/mol}) = 23.06[E_{(D/D^+)} - E_{(A/A^-)} - e_0^2/\varepsilon\alpha] - E_{0-0}$

In the present case, $E_{(D/D^+)}$ of $Cu(acac)_2$ is calculated (26, 30) from its ionization potential (IP = 7.75 eV) (31). These calculations (Table 1) show that the electron transfer to the triplet state of the first four ketones is spontaneous but to other sensitizers it is not, in general agreement with the observed experimental results. In polar alcoholic solvents, the electron transfer is complete as in reaction [10] and the ion pair separation of reaction [11] is probably facilitated wherefrom reactions of the individual radical ions may be observed.

The subsequent reactions of these radical ions remain a matter of conjecture at present. Among various possibilities reactions [13]–[14] might be proposed to conclude the photoreduction in analogy to those proposed for sensitized addition to olefins (29).

[13] $Cu(acac)_2{}^{+\bullet} \rightarrow Cu(acac)^+ + \mathbf{5}$

[14] $Cu(acac)^+ + S^{-\bullet} \rightarrow Cu(acac) + S$

In addition to the quenching process described so far, excited states of anthracene and 1-cyanonaphthalene (and probably of fluorenone) in alcohols appear to undergo unknown and slower chemical reactions to cause consumption of $Cu(acac)_2$ and/or to give other products, such as $[Cu(acac)(OCH_3)]_2$, rather than the reduction products. These reactions were not studied further but must occur at comparable rates to the photoreduction. Fluorenone has been shown to possess a $\pi \rightarrow \pi^*$ transition as its lowest triplet state and to be photostable in alcohols (32). Formation of the dimer from photolysis of anthracene has been well known for some time (13). The singlet excited state of 1-cyanonaphthalene is a good electron acceptor from β-phenylalkyl ethers and diphenylethylene and has been successfully used to sensitize photoreaction of these substrates (29). It should be mentioned that in the photolysis of 1-cyanonaphthalene and $Cu(acac)_2$, 1,3-pentadiene (0.3 M) did not retard the formation of $[Cu(acac)(OCH_3)]_2$.

The triplet states of fluorenone and anthracene have been shown to be quenched by $Cu(acac)_2$ in benzene solution at rate constants of 1.0×10^9 and 0.6×10^9 M^{-1} s^{-1}, respectively, as determined by flash photolysis (24). As fluorenone is photostable in alcoholic solution (32), we could not observe the extent of quenching by $Cu(acac)_2$ using stationary state methods. The reason for quenching of these excited states without decomposition of $Cu(acac)_2$ is not immediately clear. If the proposed mechanism for the sensitized $Cu(acac)_2$ decomposition is accepted, it might suggest that, in fluorenone and anthracene sensitization, the solvated ion pairs are readily decayed to the ground state through the reverse electron transfer.

In methanol solution the phenothiazine triplet state has been shown to be quenched by electron transfer to metal ions to give phenothiazine cation radical and the reduced metal ions provided the reduction potentials of the latter are favorable (33); the quenching rate constant by Cu^{2+} ion was determined to be 6×10^9 M^{-1} s^{-1} in methanol. The failure to photolytically reduce $Cu(acac)_2$ by phenothiazine photosensitization suggests that reduction of the complex by the direct electron transfer to the metal does not occur. The free energy change associated with the direct electron transfer from the triplet excited state phenothiazine or carbazole to $Cu(acac)_2$ are calculated from reaction [12] to be −37 and −27 kcal/mol, respectively. The negative experimental results might be taken as an indication that this mode of electron transfer is not operating.

In summary, there are compelling reasons to believe that excited states of these organic sensitizers are quenched by $Cu(acac)_2$ by accepting one electron from $Cu(acac)_2$ and/or by entering other chemical reactions with $Cu(acac)_2$: operation of the classical energy transfer is unlikely.

Experimental

Melting points (mp) were determined on a Fisher-Johns apparatus and were uncorrected. Infrared spectra (ir) were obtained with a Perkin-Elmer 457 spectrophotometer, ultraviolet and visible spectra with a Cary 17 spectrophotometer, mass spectra with a Hitachi-Perkin-Elmer RMU-6E instrument, and nmr spectra with a Varian A56/60 spectrometer in $CDCl_3$ using TMS as an internal standard. Vapour phase

chromatographic analyses were performed on a Varian 1200 (flame ionization detector) with a 10% SE-30 (6 ft × 1/8 in.) column. The gas chromatographic – mass spectra (gc–ms) used a 20% SE-30 (10 ft × 1/8 in.) column in a Varian 1400 which was directly coupled to the mass spectrometer. High pressure liquid chromatography was carried out with a Varian Model LC-4010-1 using a Porasil C-400 (37–75 μ) column. Elemental analyses were carried out by M. K. Yang on a Perkin-Elmer 240 microanalyzer.

Materials

Sensitizers were commercially available and purified by recrystallization, vacuum sublimation, or combinations of both. $Cu(acac)_2$ was prepared by the known method (34) and recrystallized from benzene. Solvents were previously distilled and stored over molecular sieves. Tetrahydrofuran (THF) was distilled from lithium aluminum hydride and stored over sodium. Nitrogen gas (Union Carbide of Canada) was scrubbed with a Fieser's solution and dried with sulfuric acid before being introduced to the reaction vessel.

Photolysis Procedure

The photolysis apparatus (Fig. 1) consisted of a cylindrical vessel fitted with a condenser, a Pyrex plate cover, and a gas inlet tube. A solution of $Cu(acac)_2$ (~100 mg) and sensitizer in 100 ml of solvent under nitrogen was irradiated with a 140 W Hanovia mercury lamp (SH 616 A 0130) at running water temperature. The progress of the reaction was followed by examining the decrease in the visible absorption of $Cu(acac)_2$ at ~630 nm. After photolysis copper was filtered and determined, after dissolution in HNO_3 (1:1), by colorimetric methods (35). The filtrate was distilled, the first fraction being collected with a receiver (cooled on a dry ice – methanol bath) containing a 2,4-DNPH solution. The yellow precipitate was filtered and recrystallized to afford the 2,4-DNPH of volatile carbonyl compounds. The second fraction containing the major part of the solvent was analyzed by HPLC to give only one peak which had the same retention times with acetylacetone. The concentration of acetylacetone was calculated from its uv absorption at λ_{max} 273 nm. The residue was analyzed by vpc or tlc. Sensitizers and/or products were separated when possible by preparative tlc or column chromatography on silica gel.

Benzophenone Sensitization

(a) In Methanol

A solution of $Cu(acac)_2$ (150 mg, 0.57 mmol), benzophenone (112 mg, 0.64 mmol) in methanol (100 ml) was irradiated to give a black solid after ~3 h. Irradiation for 18 h gave metallic copper suspension. The filtered solution showed no absorption at 630 nm. Copper (98%) was separated by filtration using a sintered glass funnel. A cold trap containing 15 ml of 2,4-DNPH solution was used to trap volatile compounds during filtration. A yellow precipitate was filtered out, washed, and dried under vacuum to give the 2,4-dinitrophenylhydrazone of formaldehyde (55 mg, 46%); the solid was recrystallized from methanol:H_2O, mp 166–168°C (lit. mp 166°C) (36). The filtrate was evaporated in a flash evaporator to give a solid (107 mg, 96%); mp 48–50°C; the ir spectrum superimposable with that of benzophenone. The distillate was analysed by HPLC to give one peak corresponding to acetylacetone. The uv spectrum of the distillate with 100-fold dilution showed λ_{max} 273 nm, O.D. = 0.52. The yield of acetylacetone was estimated from the O.D. (0.76 mmol, 67%). A similar photolysis was run in the presence of cyclohexene (250 mg). Copper was filtered. The solvent in the filtrate was evaporated to a small volume. Both tlc and vpc analysis showed the presence of benzophenone and dicyclohexenyl.

(b) In Ethanol

A solution of $Cu(acac)_2$ (120 mg, 0.46 mmol), benzophenone (112 mg, 0.64 mmol) in ethanol (100 ml) was irradiated to give a black solid after 1 h. After 3 h metallic copper suspension was observed and the absorption at 630 nm of a filtered aliquot disappeared. Usual work-up of the photolysate gave copper (100%), acetylacetone (0.77 mmol, 84%), and benzophenone (104 mg, 93%), the 2,4-DNPH of acetaldehyde (29 mg, 28%); mp 146–148°C; lit. mp 147°C (ref. 36, p. 320).

(c) In Isopropyl Alcohol

A solution of $Cu(acac)_2$ (50 mg, 0.19 mmol), benzophenone (112 mg, 0.64 mmol) in isopropyl alcohol (100 ml) was photollyzed to give a black solid after 15 min. After 1 h copper suspension was formed and no absorption at 630 nm was observed. Copper (98.4%) was filtered out and determined by the usual method (35). The filtrate was distilled (3 ml) into a receiver containing a 2,4-DNPH solution to give a solid (33 mg, 73%) which was recrystallized from ethanol–H_2O to give the 2,4-DNPH of acetone; mp 124–126.5°C (lit. mp 126°C) (37). The remainder was flash evaporated to give benzophenone (98 mg, 88%). HPLC analysis of the distillate showed the presence of acetylacetone (0.29 mmol, 76%) as determined by the O.D. at λ_{max} 273 nm.

(d) In THF

A solution of $Cu(acac)_2$ (200 mg, 0.77 mmol), benzophenone (164 mg, 0.94 mmol) in THF (100 ml) was irradiated to give a black solid after 3.5 h. After 7 h metallic copper was formed and the absorption at 630 nm disappeared. Copper (43 mg, 89%) was filtered. The filtrate was flash evaporated to give a yellow oil (214 mg). Analysis by vpc showed the presence of benzophenone and two minor compounds which were not identified. Acetylacetone (0.94 mmol, 61%) was determined by the O.D. at 273 nm.

(e) In the Presence of PPh_3

A solution of $Cu(acac)_2$ (100 mg, 0.38 mmol), benzophenone (112 mg, 0.64 mmol), and PPh_3 (240 mg, 0.92 mmol) in ethanol (100 ml) was irradiated for 2 h to give a colorless solution. The absorption at 630 nm had disappeared. The solution was distilled and the distillate was worked up as usual to give acetaldehyde (42%) and acetylacetone (80%). The residue was treated with ether and filtered to give a white solid (242 mg, 92%); mp 176–179°C; ir (Nujol) 1598, 1583, 1508, 745, and 700 cm^{-1}; nmr ($CDCl_3$) δ 1.76 (s, 6H), 5.08 (s, 1H), and 7.21 (s, 30H). The ir and nmr spectra were identical with those of $Cu(acac)(PPh_3)_2$ (37). *Anal.* calcd. for $C_{41}H_{37}CuO_2P_2$: C 71.65, H 5.4; found: C 71.76, H 5.5. Preparative tlc of the residue on silica gel (elution with CH_2Cl_2) gave benzophenone (109 mg, 97%) and PPh_3 (43 mg, 0.16 mmol).

Fluorenone Sensitization

(a) In Methanol or Isopropyl Alcohol

A solution of $Cu(acac)_2$ (100 mg, 0.38 mmol) and fluorenone (200 mg, 1.10 mmol) in 100 ml of solvent was irradiated for 28 h. The visible spectra of the photolysate showed no decrease of O.D. at 630 nm. After work-up $Cu(acac)_2$ and fluorenone were recovered.

1-Cyanonaphthalene Sensitization

(a) In Methanol

$Cu(acac)_2$ (100 mg, 0.38 mmol) in methanol (100 ml) was irradiated in the presence of 1-cyanonaphthalene (100 mg, 0.65 mmol) for 48 h. A blue solid (15 mg) was filtered off, washed with methanol, and dried under vacuum; mp 205–209°C; ir (KBr) 2820, 1590, 1530, 1400, 1360, 1275, 1070, 1025, 775, 560, and 460 cm^{-1}; ms (%) 386 (M^+, 0.6), 355 (1.0), 324 (20.4), 261 (100), 246 (75), 231 (56), 225 (6.4), and 43 (41). *Anal.* calcd. for $C_6H_{13}O_3Cu_2$: C 37.21, H 5.16; found: C

36.81, H 5.04. $[Cu(acac)(OMe)]_2$ was prepared by the method of Bertrand and Kaplan (14) and was identical, by ir and mass spectra, to the product obtained above. After work-up of the filtrate 76 mg of $Cu(acac)_2$ were recovered. Analysis by vpc indicated that 1-cyanonaphthalene was recovered unchanged.

(b) In Ethanol or THF

Solutions were irradiated for 48 h. After the usual work-up, the starting materials were quantitatively recovered.

Photolysis in the Presence of Other Sensitizers

Xanthone

A solution of $Cu(acac)_2$ (100 mg, 0.38 mmol) and xanthone (250 mg, 1.27 mmol) in methanol (100 ml) was irradiated for 48 h to give metallic copper suspension. A 50% decrease was observed in the 630 nm band. The usual work-up of the solution gave copper (48%) and acetylacetone (30%) determined as before. $Cu(acac)_2$ and xanthone were recovered in 40% and 96%.

Biacetyl

A solution of $Cu(acac)_2$ (100 mg, 0.38 mmol) and biacetyl (5 g, 48 mmol) in ethanol (120 ml) was irradiated to give a black solid after 1 h. After 6.5 h metallic copper was formed and no absorption was observed at 630 nm. Copper was filtered and determined as usual in 81% yield. The filtrate was analyzed by vpc to show two major and five minor peaks. The major peaks were shown to be biacetyl and acetylacetone by peak matching.

Anthrone

A solution of $Cu(acac)_2$ (100 mg, 0.38 mmol) and anthrone (86 mg, 0.45 mmol) in ethanol (120 ml) was irradiated to give a black solid after 15 min. Irradiation for 3.5 h gave metallic copper suspension and the solution showed no absorption at 630 nm. Filtration attempts were unsuccessful due to the colloidal nature of copper. The solution was flash evaporated to give a red–brown solid (99 mg). After treatment with ether, copper (92%) was filtered and determined as usual. The filtrate was evaporated to give a yellow solid (74 mg). Treatment with acetone (10 ml) gave an unidentified white solid (12 mg); mp 136–142°C; ir (KBr) ~3500, 1470, 1190, 1035, 780, 740, 700, 670, 650, and 640 cm^{-1}. The vpc of the filtrate showed one major peak, matching in retention time with anthrone, and one unidentified minor peak. Acetylacetone (68%) was determined from the distillate.

Anthracene

A solution of $Cu(acac)_2$ (100 mg, 0.38 mmol) and anthracene (100 mg, 0.56 mmol) in methanol (100 ml) was photolyzed to give white crystals after 15 min. Irradiation for 28 h showed an ~60% decrease in absorption at 630 nm. Formation of copper was not observed. The solution was filtered to give anthracene dimer (76 mg, 76%); mp 274–276°C (lit. mp 275°C) (13); ir (Nujol) 1300, 1220, 1160, 945, 820, 770, 760, and 680 cm^{-1}; ms (%), 356 (M^+, 4.5) and 178 (100). The filtrate was flash evaporated to give a blue solid (120 mg). Analysis by tlc on silica gel (elution with CH_2Cl_2) showed two major spots (R_f ~0.95 and 0.15) and one minor spot (R_f ~0.5). Preparative tlc on silica gel (elution with CH_2Cl_2) gave $Cu(acac)_2$ (85 mg, 85%), anthracene (18 mg, 18%), and an unidentified solid (8 mg) with ir (KBr), 2940, 1720, 1680, ~1600, 1450, 1290, 920, 740, 695, and 670 cm^{-1}.

Phenothiazine

A solution of $Cu(acac)_2$ (100 mg, 0.38 mmol) and phenothiazine (120 mg, 0.6 mmol) in ethanol (120 ml) was irradiated for 48 h to give a dark brown solution. The absorption at 630 nm decreased about 80%. The solution was flash evaporated to give a brown solid (176 mg). After treatment with acetone (20 ml) a blue solid (56 mg) was separated; the ir spectrum was superimposable with that of $Cu(acac)_2$. Analysis of the filtrate by vpc showed only one peak corresponding to phenothiazine by comparison with authentic sample.

Carbazole, Phenanthrene, Pyrene, Perylene, and Acetylacetone

A solution of $Cu(acac)_2$ (100 mg, 0.38 mmol) and the sensitizer in ethanol (120 ml) was photolyzed for 24 h. No decrease was observed in the absorption of the 630 nm band. After work-up the unchanged starting materials were recovered.

Acknowledgements

This research project was carried out in part by Y. L. Chow and the research group of Kyoto University during the former's visit at the University, January–April 1976. Y. L. Chow wishes to thank the Kyoto University 70th Anniversary Memorial Foundation for a generous award and the research group of Professor Kaji for discussion and hospitality.

The authors are grateful to the National Research Council of Canada for financial support of this research project. Grateful acknowledgement is made to Dr. R. K. Pomeroy for helpful discussion and suggestions.

1. V. Balzani and V. Carassity. Photochemistry of coordination compounds. Academic Press, New York. 1970. Chapt. 13.
2. R. L. Lintvedt. *In* Concepts of inorganic photochemistry. *Edited by* A. W. Adamson and P. D. Fleischauer. John Wiley and Sons, New York. 1975. Chapt. 7.
3. H. D. Gafney and R. L. Lintvedt. J. Am. Chem. Soc. **93**, 1623 (1971).
4. V. I. Saloutin, K. I. Pashkevich, and I. Ya. Postovskii. Bull. Acad. Sci. U.S.S.R., Chem. Sci. Part 2, **26**, 882 (1977).
5. G. A. Shagisultanova. Russ. J. Inorg. Chem. **11**, 510 (1966).
6. J. Y. Morimoto and B. A. DeGraff. J. Phys. Chem. **79**, 326 (1975).
7. R. Nast, R. Mohr, and C. Schultz. Chem. Ber. **96**, 2127 (1963).
8. W. M. Moore, G. S. Hammond, and R. P. Foss. J. Am. Chem. Soc. **83**, 2789 (1961).
9. J. A. Bell and H. Linschitz. J. Am. Chem. Soc. **85**, 528 (1963).
10. G. S. Hammond and R. P. Foss. J. Phys. Chem. **68**, 3739 (1964).
11. (*a*) D. Gibson, B. F. G. Johnson, and J. Lewis. J. Chem. Soc. A, 367 (1970); (*b*) W. Henderson, A. J. Carty, G. J. Palenic, and G. Schreiber. Can. J. Chem. **49**, 761 (1971).
12. W. G. Bentrude and K. R. Darnall. Chem. Commun. 811 (1968).
13. E. J. Bowen and D. W. Turner. Trans. Faraday Soc. **51**, 475 (1955).
14. J. A. Bertrand and R. I. Kaplan. Inorg. Chem. **4**, 1657 (1965).
15. A. J. Cessna, S. E. Sugamori, R. W. Yip, M. P. Lau, R. S. Snyder, and Y. L. Chow. J. Am. Chem. Soc. **99**, 4044 (1977).
16. N. J. Turro. Molecular photochemistry. Benjamin, New York. 1967. p. 137; J. A. Howard. Adv. Free Radical Chem. **4**, 49 (1970).

17. J. A. BARLTROP and J. D. COYLE. Excited states in organic chemistry. John Wiley and Sons, London. 1975. p. 125.
18. C. T. LIN, W. BÖTTCHER, M. CHOU, C. CREUTZ, and N. SUTIN. J. Am. Chem. Soc. **98**, 6536 (1976) and references therein.
19. H. JURIS, M. T. GANDOLFI, M. F. MANFRIN, and V. BALZANI. J. Am. Chem. Soc. **98**, 1047 (1976).
20. T. J. MEYER. Israel J. Chem. **15**, 200 (1977).
21. A. R. GUTIERREZ, T. J. MEYER, and P. G. WHITTEN. Mol. Photochem. **7**, 349 (1976).
22. F. WILKINSON and A. FARMILO. J. Chem. Soc. Faraday II, 604 (1976); F. WILKINSON. Pure Appl. Chem. **41**, 661 (1975).
23. T. OHNO and S. KATO. Bull. Chem. Soc. Jpn. **42**, 3385 (1969).
24. A. J. FREY, R. S. H. LIU, and G. S. HAMMON. J. Am. Chem. Soc. **88**, 4783 (1966); W. M. MOORE, G. S. HAMMOND, and R. P. FOSS. J. Am. Chem. Soc. **83**, 2789 (1961).
25. G. S. HAMMOND and P. A. LEERMAKERS. J. Phys. Chem. **66**, 1148 (1962).
26. J. B. GUTTENPLAN and S. G. COHEN. J. Am. Chem. Soc. **94**, 4040 (1972); Tetrahedron Lett. 2163 (1972); M. FEDORONKO, J. KONIGSTEIN, and K. LINEK. Coll. Czeck. Chem. Commun. **32**, 3998 (1967).
27. S. L. MUROV. Handbook of photochemistry. Marcel Dekker, Inc., New York. 1973. Section 3.
28. D. REHM and A. WELLER. Ber. Bunsenges. **73**, 834 (1969).
29. D. R. ARNOLD and A. J. MAROULIS. J. Am. Chem. Soc. **98**, 5931 (1976); A. J. MAROULIS, Y. SHIGEMITSU, and D. R. ARNOLD. J. Am. Chem. Soc. **100**, 535 (1978).
30. L. A. HULL, G. T. DAVIS, D. H. ROSENBLATT, and C. K. MANN. J. Phys. Chem. **73**, 2142 (1969).
31. H. F. HOLTZCLAW, JR., R. L. LINTVEDT, H. F. BAUNGARTEN, R. G. PARKER, M. M. BURSEY, and R. F. ROGERSON. J. Am. Chem. Soc. **91**, 3774 (1969).
32. G. A. DAVIS, P. A. CARAPILLUCCI, K. SZOC, and J. P. GRESSOR. J. Am. Chem. Soc. **91**, 2264 (1969).
33. S. A. ALKAITIS, G. BECK, and M. GRÄTZEL. J. Am. Chem. Soc. **97**, 5723 (1975).
34. E. W. BERG and J. T. TRUEMPER. J. Phys. Chem. **64**, 487 (1960).
35. N. H. FURMAN. Standard methods of chemical analysis. Vol. I. 6th ed. D. Van Nostrand Co., New Jersey. 1962. p. 408.
36. R. L. SKINNER, R. C. FUSON, and D. Y. CURTIN. The systematic identification of organic compounds. 5th ed. John Wiley and Sons, New York. 1965.
37. D. GIBSON, B. F. G. JOHNSON, and J. LEWIS. J. Chem. Soc. A, 367 (1970).
38. C. K. MANN and K. K. BARNES. Electrochemical reactions in non-aqueous solutions. M. Dekker, New York. 1970.
39. J. G. CALVERT and J. N. PITTS, JR. Photochemistry. John Wiley and Sons, New York. 1966.

Milieux hyperbasiques: Synthèse de cyclanones α-cyanées par cyclisation anionique d'amides-nitriles

MARC LARCHEVEQUE ET PATRICK MULOT

Laboratoire de Synthèse Organique associé au C.N.R.S., Université Pierre et Marie Curie, tour 44–45, 4, place Jussieu 75230, Paris Cédex 05, France

Reçu le 28 mars

MARC LARCHEVEQUE et PATRICK MULOT. Can. J. Chem. **57**, 17 (1979).

Les amides ω-cyanés sont aisément préparés par action d'un cyanure alcalin sur un amide ω-halogéné. Sous l'action des dialkylamidures de lithium en solution dans l'éther, ils conduisent à la formation exclusive d'un anion en α du groupe cyano. Celui-ci peut alors réagir sur la fonction amide pour conduire à des cyclanones α-cyanées diversement substituées.

MARC LARCHEVEQUE and PATRICK MULOT. Can. J. Chem. **57**, 17 (1979).

ω-Cyano *N,N*-disubstituted amides are conveniently prepared from halogenated amides by treatment with alkaline cyanides. By reacting them with powerful bases such as lithium dialkylamides in ether, these cyano amides may be metallated in α position to the cyano group only. When they are warmed up, the anions react with the amide group to afford α-cyano cyclanones by an intramolecular cyclisation.

Introduction

Les cyclisations de Dieckmann et de Thorpe–Ziegler ont été fréquemment utilisées en chimie organique pour préparer des cyclanones diversement substituées (1). Ces réactions sont, malgré tout, d'un emploi relativement limité en synthèse car elles sont difficilement applicables aux composés dissymétriques. Les produits de départ sont en effet, dans ce cas, d'un accès difficile; de plus, on isole en général après réaction des mélanges car la différence d'acidité entre les hydrogènes en α des fonctions F_0 et F_0' (**1**, $F_0 = F_0'$ = ester ou nitrile) qui est due à la présence d'un groupe R électrodonneur, est trop faible pour conduire à la formation d'un anion unique (2). D'autre part, la réversibilité de cette réaction (qui peut être contrôlée dans certains cas (3)) contribue également à la complexité de la réaction.

$$F_0—CH_2—(CH_2)_n—CHR—F_0'$$

1

Au cours de notre travail, nous avons essayé d'accroître le champ d'application de ces réactions et de remédier à leurs inconvénients en utilisant des composés porteurs de deux fonctions F_0 et F_0' différentes. Nous avons fait appel aux ω-cyano amides et nous proposons une méthode qui permet d'accéder directement à partir de ces composés à des cyclanones α-cyanées par cyclisation anionique.

Préparation des amides ω-cyanés

L'intérêt présenté par l'emploi de ces amides est double: (*i*) il existe une différence de pK_a assez importante entre les hydrogènes en α des deux fonctions; il est donc possible dans des conditions bien définies d'arracher un hydrogène plutôt que l'autre et d'effectuer ensuite une cyclisation anionique; (*ii*) les amides ω-cyanés dissymétriques sont aisément accessibles à partir des amides chlorés. Ceux-ci sont obtenus suivant une méthode déjà décrite par condensation d'un dérivé chloro-bromé sur un carbanion d'amide (4). On passe ensuite à l'amide-nitrile par action du cyanure de sodium dans le DMSO.

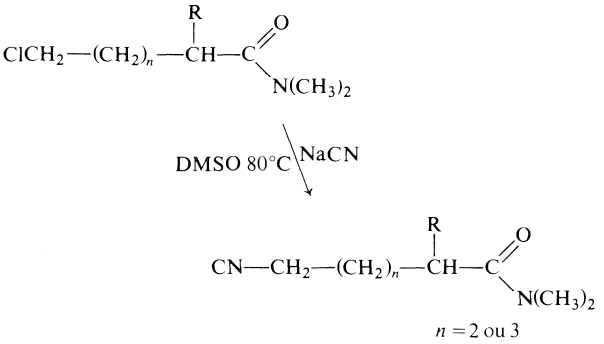

La réaction s'effectue avec de bons rendements (tableau 1) pourvu que l'on opère dans le DMSO. En milieu alcoolique on observe de nombreuses réactions parasites.

Cyclisation basique des amides ω-cyanés

La réaction de cyclisation nécessite la formation d'un carbanion qui puisse ensuite s'additionner sur l'amide par réaction intramoléculaire. Le milieu utilisé pour effectuer une telle opération doit donc être suffisamment basique pour former le carbanion en α du nitrile ($pK_a \sim 25$) en quantité appréciable

0008-4042/79/010017-04$01.00/0

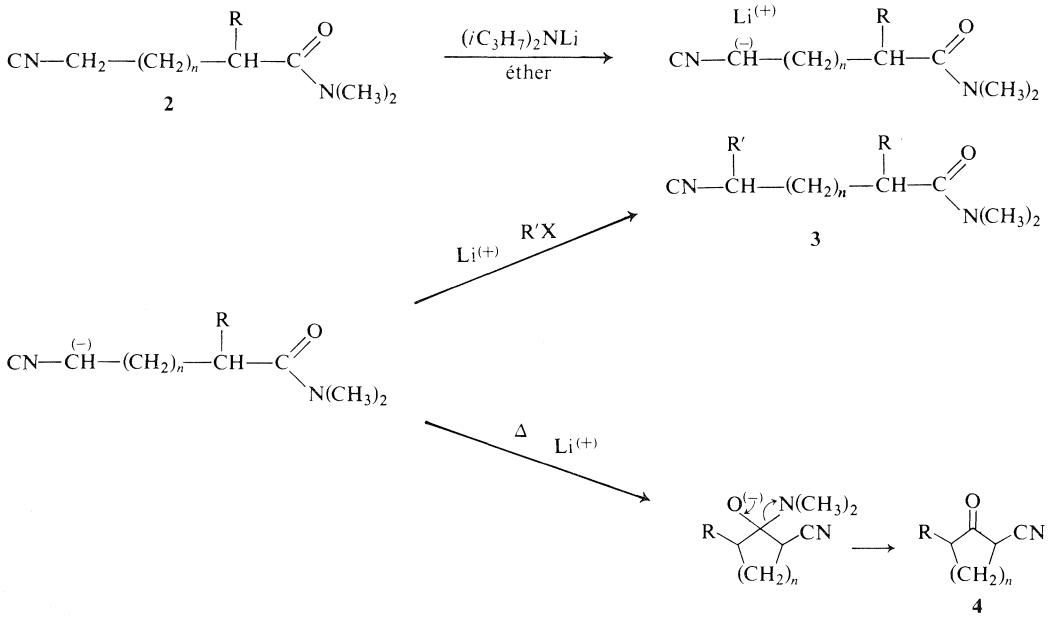

sans pour autant l'être trop, ce qui conduirait également à l'attaque en α de l'amide ($pK_a \sim 29$).

L'hydrure de sodium est à éviter: il n'est pas assez réactif et l'hétérogénéité du milieu ne favorise pas la formation du carbanion en α du groupe cyano. Par contre, les "amidures activés" (Li—Et_2NH—C_6H_6—HMPT) qui servent à préparer les amides ω-chlorés sont trop réactifs; ils conduisent à une proportion notable de goudrons indistillables. Nous avons finalement choisi les dialkylamidures de lithium en solution dans l'éther. Ceux-ci donnent avec les amides nitriles **2** une réaction propre contrairement à ce que l'on observe lorsqu'on opère dans le THF.

La température joue un rôle important et il est nécessaire d'additionner la base à température relativement basse si l'on veut éviter des réactions parasites d'auto-condensation du carbanion: on opère en général vers −40°C. On observe dans ces conditions uniquement la formation du carbanion en α du nitrile. Celui-ci peut ensuite, si on laisse le milieu réactionnel se réchauffer vers −20°C, réagir sur la fonction amide; on isole alors après hydrolyse acide les cétones α-cyanées **4** avec de bons rendements (tableau 2). Il devrait également, en théorie, être possible de piéger cet anion par un électrophile convenable (par exemple un dérivé halogéné) de façon à obtenir le nitrile-amide bisubstitué **3**. En opérant dans l'éther nous avons effectivement observé cette réaction, mais nous n'avons jamais réussi, quelle que soit la température du milieu réactionnel, à dépasser

TABLEAU 1. Synthèse d'amides ω-cyanés

R	*n*	Rendement (%)
CH_3	2	89
C_2H_5	2	79
$(CH_3)_2CH$	2	77
$(CH_3)_2CHCH_2$	2	75
CH_3	3	75
C_2H_5	3	77
$(CH_3)_2$ CH	3	76

TABLEAU 2. Synthèse de cyclanones α-cyanées

R	*n*	Cétone α-cyanée	Rendement (%)[a]
CH_3	2	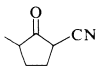	78
C_2H_5	2	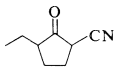	87
iC_3H_7	2	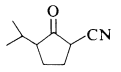	65
iC_4H_9	2	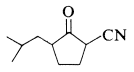	68
CH_3	3	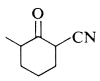	71
C_2H_5	3	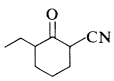	72
iC_3H_7	3	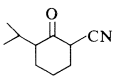	65

[a]Les rendements sont donnés en produits isolés.

un rendement de 25% en produit **3**. La réaction de substitution nucléophile s'effectue trop lentement sur le dérivé halogéné (surtout en milieu éther) pour concurrencer la réaction de cyclisation.

Celle-ci permet donc de préparer les cycles pentagonaux et hexagonaux avec de bons rendements. Par contre, les diverses tentatives faites pour l'appliquer aux cyclobutanones ont échoué: la réaction des amides γ-cyanés (**2**, $n = 1$) avec les dialkylamidures de lithium en solution dans l'éther ne fournit que des goudrons.

Nous avons observé que les dérivés obtenus sont particulièrement acides. Ils sont en fait isolés après hydrolyse sous forme de sels **5** et il est nécessaire de traiter ceux-ci par l'acide chlorhydrique à 50% pour libérer les céto-nitriles. Il faut noter que ces composés ne se présentent pas toujours sous forme cétonique. Ils sont partiellement énolisés et on isole fréquemment des mélanges contenant une forte proportion de composés **6**. Celle-ci dépend de la

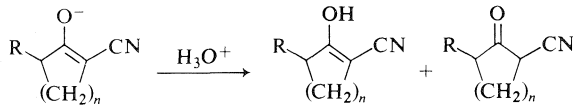

5 **6** **4**

nature du radical R et elle est particulièrement élevée dans le cas des cycles cyclopentaniques où elle peut dépasser 80%. Ce résultat est en désaccord avec celui de Kulp *et al.* (5) qui isole, lors de la synthèse de cyano-5 dialkyl-2,2 cyclopentanones, des composés ne comportant qu'une seule bande CN à 2250 et une bande CO à 1750 cm^{-1}. Par contre, les cyano-2 cyclohexanones se présentent presque exclusivement sous forme cétonique.

Nous avons indiqué ci-dessus que nous n'avions pas réussi à préparer les amides-nitriles **3** avec de bons rendements: il n'est donc pas possible dans ces conditions de synthétiser directement les α-cyano cyclanones α,α′-disubstituées **7**. On peut néanmoins les préparer par alkylation ultérieure des α-cyano cyclanones monosubstituées **4**. Ces composés analogues aux dérivés de la série malonique peuvent en effet être très aisément métallés. Nous avons vérifié que cette alkylation s'effectuait avec de bons rendements.

Le traitement par l'hydrure de sodium dans l'éther suivi d'une addition d'iodure de méthyle conduit à l'obtention d'un mélange de composé **7** (R = C_2H_5, R′ = CH_3) et de produit α,α′-dialkylé dans la proportion 85:15 (rendement global, 87%). Ainsi, il est possible par cette méthode d'accéder à des composés polyfonctionnels qui sont, particulièrement en série cyclopentanique, des intermédiaires de synthèse intéressants.

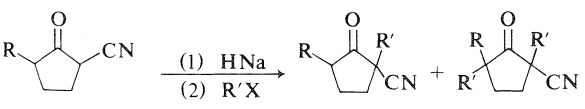

4 **7**

Partie expérimentale

La structure des différents produits a été confirmée par infrarouge et rmn. Les spectres infrarouges ont été effectués sur un spectrophotomètre Perkin Elmer 457 sous forme de film. Les spectres rmn ont été enregistrés sur un appareil Perkin Elmer R 24 à 60 MHz dans le tétrachlorure de carbone et en utilisant le tétraméthyl silane comme référence interne. La pureté des produits a été contrôlée par cpv (colonne SE 30 de 2.5 m). Les analyses centésimales sont correctes à ±0.25% pour le carbone et ±0.35% pour l'hydrogène.

Amides ω-chlorés

Cette réaction est décrite dans la réf. 4. Cependant les produits suivants n'avaient pas été synthétisés.

Chloro-5 méthyl-2 N,N-*diméthyl pentanamide*—rendement 75%; pé 126°C/13 Torr; ir: 1640 cm^{-1} (C=O); rmn δ: 1.07 (3H, d, J = 6.0 Hz, CH_3), 1.67 (4H, m, CH_2), 2.67 (6H, d, J = 8.0 Hz, $N(CH_3)_2$), 3.51 (2H, t, J = 6.0 Hz, $ClCH_2$).

Chloro-5 éthyl-2 N,N-*diméthyl pentanamide*—rendement 84%; pé 144°C/13 Torr; ir: 1645 cm^{-1} (C=O); rmn δ: 0.84 (3H, t, J = 6.0 Hz, CH_3), 1.55 (6H, m, CH_2), 2.97 (6H, d, J = 8.0 Hz, $N(CH_3)_2$), 3.47 (2H, t, J = 6.2 Hz, $ClCH_2$).

Chloro-5 isopropyl-2 N,N-*diméthyl pentanamide*—rendement 73%; pé 86°C/0.1 Torr; ir: 1640 cm^{-1} (C=O); rmn δ: 0.89 (6H, d de d, J = 6.0 Hz, $(CH_3)_2CH$), 1.62 (4H, m, CH_2), 2.96 (6H, d, J = 7.3 Hz, $N(CH_3)_2$), 3.12 (2H, m, $ClCH_2$).

Chloro-5 isobutyl-2 N,N-*diméthyl pentanamide*—pé 113°C/0.5 Torr; ir: 1645 cm^{-1} (C=O); rmn δ: 0.89 (6H, d, J = 6.0 Hz, $(CH_3)_2CH$), 3.00 (6H, d, J = 8.6 Hz, $N(CH_3)_2$), 3.47 (2H, t, $ClCH_2$).

Chloro-6 éthyl-2 N,N-*diméthyl hexanamide*—pé 109°C/0.8 Torr; ir: 1640 cm^{-1} (C=O); rmn δ: 0.89 (3H, t, J = 6.0 Hz, CH_3), 1.1–1.9 (8H, m, CH_2), 3.00 (6H, d, J = 9.0 Hz, $N(CH_3)_2$), 3.51 (2H, t, J = 6.6 Hz, $ClCH_2$).

Chloro-6 isopropyl-2 N,N-*diméthyl hexanamide*—pé 103°C/0.5 Torr; ir: 1650 cm^{-1} (C=O); rmn δ: 0.80 (6H, d de d, J = 6.6 Hz, $(CH_3)_2CH$), 1.1–2.0 (8H, m, CH_2), 3.00 (6H, d, J = 8.3 Hz, $N(CH_3)_2$), 3.52 (2H, t, J = 6.5 Hz, $ClCH_2$).

Amides-nitriles

Mettre dans un réacteur 0.3 mol de cyanure de sodium pulvérisé et 90 cm^3 de DMSO distillé sur hydrure de calcium. Chauffer à 90°C et additionner lentement 0.22 mol d'amide ω-chloré. Laisser chauffer le milieu réactionnel jusqu'à 120°C (environ 15 min). Refroidir, filtrer et distiller.

Méthyl-2 cyano-5 N,N-*diméthyl pentanamide*—pé 104°C/0.5 Torr; ir: 2240 (C≡N), 1635 cm^{-1} (C=O); rmn δ: 1.07 (3H, d, J = 6.0 Hz, CH_3), 2.37 (4H, m, CH_2CO et CH_2CN), 3.00 (6H, d, J = 9.0 Hz, $N(CH_3)_2$).

Ethyl-2 cyano-5 N,N-*diméthyl pentanamide*—pé 117°C/0.8 Torr; ir: 2240 (C≡N), 1630 cm^{-1} (C=O); rmn δ: 0.84 (3H, t, J = 7.3 Hz, CH_3), 2.38 (4H, m, CH_2CO et CH_2CN), 3.00 (6H, d, J = 9.2 Hz, $N(CH_3)_2$).

Isopropyl-2 cyano-5 N,N-*diméthyl pentanamide*—pé 128°C/0.05 Torr; ir: 2240 (C≡N), 1635 cm^{-1} (C=O); rmn δ: 0.91 (6H, d, J = 7.3 Hz, $(CH_3)_2CH$), 2.38 (4H, m, CH_2CO et CH_2CN), 3.00 (6H, d, J = 9.0 Hz, $N(CH_3)_2$).

Isobutyl-2 cyano-5 N,N-*diméthyl pentanamide*—pé 136°C/0.1 Torr; ir: 2245 (C≡N), 1640 cm^{-1} (C=O); rmn δ: 0.89

(6H, d, J = 6.0 Hz, $(CH_3)_2CH$), 2.33 (4H, m, CH_2CO et CH_2CN), 3.00 (6H, d, J = 9.8 Hz, $N(CH_3)_2$).

Méthyl-2 cyano-6 N,N-*diméthyl hexanamide*—pé 119°C/0.01 Torr; ir: 2245 (C≡N), 1640 cm^{-1} (C=O) rmn δ: 0.92 (3H, d, J = 6.0 Hz, CH_3), 2.30 (4H, m, CH_2CO et CH_2CN) 2.94 (6H, d, J = 9.0 Hz, $N(CH_3)_2$).

Ethyl-2 cyano-6 N,N-*diméthyl hexanamide*—pé 119°C/0.01 Torr; ir: 2255 (C≡N), 1640 cm^{-1} (C=O); rmn δ: 0.88 (3H, t, J = 6.2 Hz, CH_3), 2.37 (4H, m, CH_2CO et CH_2CN), 3.00 (6H, d, J = 9.0 Hz, $N(CH_3)_2$).

Isopropyl-2 cyano-6 N,N-*diméthyl hexanamide*—pé 124°C/0.08 Torr; ir: 2240 (C≡N), 1640 cm^{-1} (C=O); rmn δ: 0.89 (6H, d, J = 6.5 Hz, $(CH_3)_2CH$), 2.31 (4H, m, CH_2CO et CH_2CN), 3.00 (6H, d, J = 8.00 Hz, $N(CH_3)_2$).

α-Cyano cyclanones

Préparer 0.05 mol de diisopropylamidure de lithium par addition de butyllithium sur la diisopropylamine à 0°C. A −40°C couler goutte à goutte l'amidure préparé sur l'amidenitrile dissous dans 20 cm^3 d'éther. Le milieu réactionnel se prend en masse, mais redevient homogène dès que l'on revient à température ambiante. Après avoir agité 3 h à température ambiante, hydrolyser avec 5 cm^3 d'eau glacée. Le milieu réactionnel se prend à nouveau en masse. Filtrer, laver le précipité à l'éther, puis le dissoudre dans une solution à 50% d'acide chlorhydrique. Une couche organique relargue. Décanter, laver la couche aqueuse à l'éther, sécher la couche organique, chasser les solvants. Ne pas distiller car les produits sont très fragiles.

Cyano-2 méthyl-5 cyclopentanone—ir: 2245 et 2205 (C≡N), 1750 (C=O), 1630 cm^{-1} (C=C); rmn δ: 1.09 (3H, m, CH_3), 1.3–2.5 (5H, m, CH_2), 3.0–3.5 (1H, m, CH et OH).

Cyano-2 éthyl-5 cyclopentanone—ir: 2240 et 2200 (C≡N), 1745 (C=O), 1640 cm^{-1} (C=C); rmn δ: 0.95 (3H, d de t, CH_3), 1.31–1.90 (6H, m, CH_2), 1.95–2.52 (2H, m, CH et OH).

Cyano-2 isopropyl-5 cyclopentanone—ir: 2250 (C≡N), 1750 cm^{-1} (C=O); rmn δ: 0.91 (6H, m, $(CH_3)_2CH$), 1.6–2.5 (6H, m, CH_2), 3.0–3.5 (1H, m, CN—CH—CO).

Cyano-2 isobutyl-5 cyclopentanone—ir: 2240 (C≡N), 1735 cm^{-1} (C=O); rmn δ: 1.03 (6H, d, $(CH_3)_2CH$), 1.65–2.05 (8H, m, CH_2), 3.3–3.5 (1H, m, CN—CH—CO).

Cyano-2 méthyl-6 cyclohexanone—ir: 2240 (C≡N), 1720 cm^{-1} (C=O); rmn δ: 1.04 (3H, d de d, J = 6.0 Hz, CH_3), 1.64–2.70 (7H, m, CH_2), 3.3–3.6 (1H, m, CO—CH—CN).

Cyano-2 éthyl-6 cyclohexanone—ir: 2240 (C≡N), 1720 cm^{-1} (C=O); rmn δ: 0.98 (3H, d de d, J = 7.0 Hz, CH_3), 1.4–2.6 (9H, m, CH_2), 3.3–3.6 (1H, m, CO—CH—CN).

Cyano-2 isopropyl-6 cyclohexanone—ir: 2245 (C≡N), 1720 cm^{-1} (C=O); rmn δ: 0.94 (6H, d, $(CH_3)_2CH$), 1.5–2.6 (8H, m, CH_2), 3.2–3.7 (1H, m, CO—CH—CN).

Cyano-2 éthyl-5 méthyl-2 cyclopentanone

Additionner goutte à goutte 0.05 mol de cyano-2 éthyl-2 cyclopentanone sur une suspension de 0.05 mol d'hydrure de sodium dans du THF (25 cm^3). Maintenir la température en-dessous de 30°C. Agiter 3 h puis additionner lentement 0.05 mol d'iodure de méthyle dilué dans 10 cm^3 de THF. Chauffer ½ h à 50°C; hydrolyser; extraire à l'éther. Laver la coucher organique à l'hyposulfite; sécher sur sulfate de magnésium. On isole un mélange de produit monoalkylé et bisalkylé qui est purifié par distillation sous vide poussé. La chromatographie gazeuse (colonne SE 30 de 3 m chargée à 10%) et la rmn du ^{13}C indiquent une composition de 85:15 en produit mono- et bisalkylé.

1. J. P. Schaefer et J. J. Bloomfield. Org. React. **15**, 1 (1967).
2. (*a*) W. S. Johnson et A. R. Jones. J. Am. Chem. Soc. **72**, 2395 (1950); (*b*) N. J. Leonard et R. C. Sentz. J. Am. Chem. Soc. **74**, 1704 (1952).
3. G. Nee et B. Tchoubar. C.R. Acad. Sci. Ser. C, **280**, 1145 (1975).
4. Th. Cuvigny, P. Hullot, M. Larcheveque et H. Normant. (*a*) C.R. Acad. Sci., Ser. C, **278**, 1105 (1974); (*b*) Can. J. Chem. **54**, 1098 (1976).
5. S. S. Kulp, J. Molnar, P. J. Miller et S. T. Herman. J. Org. Chem. **36**, 2203 (1971).

Structure and bonding in cyclic phosphoramidates as determined by carbon-13 magnetic resonance[1]

GERALD W. BUCHANAN AND FREDERICK G. MORIN
Department of Chemistry, Carleton University, Ottawa, Ont., Canada K1S 5B6

Received June 15, 1978

GERALD W. BUCHANAN and FREDERICK G. MORIN. Can. J. Chem. **57**, 21 (1979).

^{13}C chemical shifts and ^{13}C–^{31}P couplings are reported for 11 cyclic phosphoramidates of ring sizes from four to nine. Vicinal couplings are compared with those of carbocyclic analogs and provide insight regarding the degree of nitrogen lone pair delocalization into the N—P bond. For six-membered and larger rings, there appears to be nearly complete lone pair delocalization, i.e., a trigonal planar nitrogen atom. In azetidine derivatives the nitrogen lone pair remains localized, giving rise to a highly puckered ring conformation. Pyrrolidine derivatives are viewed as having a nitrogen with a partially delocalized electron pair.

GERALD W. BUCHANAN et FREDERICK G. MORIN. Can. J. Chem. **57**, 21 (1979).

On rapporte les déplacements chimiques ^{13}C et les constantes de couplage ^{13}C–^{31}P de onze phosphoramidates cycliques dont la grandeur du cycle varie de quatre à neuf. On compare les couplages vicinaux à ceux des analogues carbocycliques et on obtient ainsi des informations relatives au degré de délocalisation de la paire d'électrons non-partagée de l'azote dans la liaison N—P. Dans le cas des cycles à six chaînons ou plus, il semble que la délocalisation de la paire d'électrons non-partagée soit complète, à savoir que l'atome d'azote adopte une forme planaire bigonale. Dans les dérivés de l'azétidine, la paire d'électrons non-partagée de l'azote reste localisée provoquant un plissement du cycle. On considère que la paire d'électrons non-partagée de l'azote dans les dérivés de la pyrrolidine est partiellement délocalisée.

[Traduit par le journal]

Introduction

Since the advent of commercially available ^{13}C Fourier Transform spectrometers, the application of ^{13}C–heteronuclear spin coupling to structural analysis has been widespread. Coupling interactions between ^{13}C and ^{31}P seem particularly useful. In these laboratories, attention has been paid to the study of carbocyclic hydroxy phosphonates (1, 3, 4) and phosphonates (2) via ^{13}C chemical shifts and ^{13}C–^{31}P couplings through one to five bonds.

When a nitrogen atom is bonded to phosphorus, the interesting question arises as to the degree of nitrogen lone pair delocalization into the N—P bond (below).

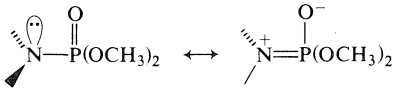

(*a*) (*b*)

In cyclic systems, vicinal ^{13}C–^{31}P couplings are known to depend on the dihedral angle between the coupled atoms, at least to a first approximation (5, 6).

If the ring nitrogen atom becomes trigonal planar (resonance form (*b*) above), then the dihedral angles from ^{31}P to vicinal ring carbons will be substantially altered, relative to the case (*a*) of a pyramidal nitrogen. With the expectation that the degree of nitrogen lone pair delocalization should be, to some extent, a function of ring size, we have synthesized a series of cyclic phosphoramidates with ring sizes from four to nine. Conformational conclusions are based on both coupling and chemical shift arguments.

Results and Discussion

Spectral Assignments

Routinely the ^{13}C spectra were recorded using complete ^{1}H noise decoupling. Subsequently the single frequency off-resonance decoupling procedure was employed to identify CH_3, CH_2, CH, and quaternary carbons. Selective ^{1}H decoupling was occasionally used, and the effects of molecular symmetry were often valuable assignment aids.

Chemical Shifts

The ^{13}C shieldings for **1**–**11** are presented in Table 1, with the corresponding structures and numbering scheme shown in Fig. 1. In Table 1, values in parentheses indicate uncertain assignments. For compounds **3**, **4**, and **8**, the OCH_3 groups are diastereotopic (7) and have small chemical shift differences (ca. 0.1–0.2 ppm).

For the piperidine derivatives, **1** and **5**, the ^{13}C shifts alone do not permit detailed structural con-

[1]Presented in part at the 4th International Meeting on Nuclear Magnetic Resonance Spectroscopy, York, England, July 2–7, 1978.

0008-4042/79/010021-06$01.00/0

TABLE 1. ^{13}C shifts for cyclic phosphoramidates (δ from TMS ±0.1)*

Compound	Position									
	C-2	C-3	C-4	C-5	C-6	C-7	C-8	C-9	CH_3	OCH_3
1	45.8	26.3	24.6	26.3	45.8					52.8
2	45.2	34.8	31.2	34.8	45.2				22.3	53.3
3	52.4	31.5	33.3	26.0	45.3				19.3	53.2
										53.1
4	47.1	31.1	19.1	26.6	39.5				16.7	53.0
										53.1
5	46.5	26.5	24.9	26.5	46.5					53.5
6	47.2	26.7	26.7	47.2						53.2
7	49.6	18.5	49.6							53.6
8	58.3	26.7	45.7						23.5	53.3
										53.5
9	47.9	30.6	27.3	27.3	30.6	47.9				53.0
10	48.2	28.3	25.1	27.0	25.1	28.3	48.2			52.8
11	48.8	27.6	(24.6)	(26.0)	(26.0)	(24.6)	27.6	48.8		52.9

*0.2–0.3 *M* solutions in $CDCl_3$.

clusions. It is interesting to note, however, that introduction of the $-P(O)(OCH_3)_2$ group on N induces only minor shifts (<1 ppm) at each carbon relative to piperidine itself (8). From this result it can be suggested that there is no appreciable contribution in **1** and **5** from a chair form in which the phosphorus is axial, since this would be expected to shield C-3,5. In the cyclohexyl compound (2) the $-P(O)(OCH_3)_2$ is sterically bulky, $-\Delta G^0$ being in excess of 3.0 kcal/mol. Additionally, it is clear that substitution of S for O (**5** vs. **1**) has little effect.

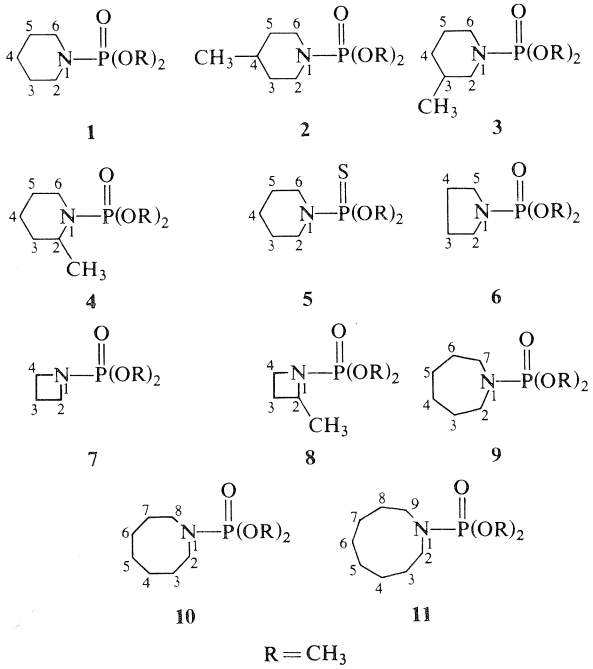

FIG. 1. Structures and numbering scheme for phosphoramidates.

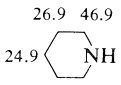

For compound **2**, the CH_3 at C-4 is suggested to be equatorial. This follows from comparison of the C-2,6 shifts in **1** and **2**. Since these are only 0.6 ppm different, it is clear the CH_3 is not axial to any large extent, since the γ shielding would be manifest at C-2,6 relative to **1**. One can calculate the CH_3 substituent effects to be α_{eq} = 6.6 ppm (deshielding) and β_{eq} = 8.5 ppm (deshielding). These values are not greatly different from those of methylcyclohexane (9): α_{eq} = 5.6 ppm and β_{eq} = 8.9 ppm. Similar conformational arguments apply to the 3-CH_3 compound **3**, where again no notable γ shielding is present compared to **1** and an equatorial CH_3 is likely.

By contrast, results for **4** are clearly indicative of an axial CH_3 at C-2. Both ring carbons which are potentially γ-*gauche* to an axial 2-CH_3 are shielded relative to **1**: namely C-6 by 6.3 ppm and C-4 by 5.5 ppm. Also, C-2 of **4** is deshielded by only 1.3 ppm compared to **1**, i.e., α_{ax} = +1.3 ppm. Thus the α effect of an axial CH_3 in **4** is very similar to that in the methyl cyclohexanes (9), where α_{ax} = +1.4 ppm, whereas α_{eq} = +5.6 ppm.

Further discussion regarding the degree of nitrogen lone pair delocalization, and hence the overall ring geometry, will follow in the coupling constant section.

^{13}C shieldings for pyrrolidine (10) are indicated below. Substitution of the $-P(O)(OCH_3)_2$ function for H on the nitrogen (compound **6**) causes essentially no shift at C-2,5 and only a small deshielding (1 ppm) at C-3,4. These results are not interpretable in terms of a definite conformation for **6** but they do rule out an envelope form with pyramidal nitrogen,

having an axial or quasi-axial dimethylphosphono group, since there is no upfield shift at C-3,4.

For the azetidines **7** and **8**, substitution of the CH_3 at C-2 of **8** induces downfield shifts of the expected magnitude (11) at the α and β positions (i.e., C-2 and C-3, respectively) relative to **7**. Interestingly, C-4 of **8** is shielded by 3.9 ppm relative to **7**, which suggests an axial CH_3 in a puckered azetidine ring. Further discussion will be presented to support this view in the coupling constant section.

In the seven-membered ring compound **9**, the shifts are again not greatly different from those of the simple amine (12) below. The nearly identical shifts at C-2 probably reflect offsetting deshielding β effects (by phosphorus) and shielding γ effects (by oxygen) in all the phosphoramidates compared to the parent amines.

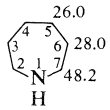

Coupling Constants

Geminal and vicinal ^{13}C–^{31}P couplings are presented in Table 2. In all materials, geminal J values of 5.8 ± 0.2 Hz were noted between ^{31}P and the OCH_3 carbon but since these values were essentially invariant, they are not included in the table. All the other geminal couplings are rather small, i.e., less than 4.5 Hz, and trends are difficult to extract from the data. The vicinal J values, however, show a rather spectacular variation with ring size and can, we feel, give insight into both ring geometry and the degree of nitrogen lone pair delocalization in these molecules.

For compound **1**, a vicinal J of 4.6 Hz is found between ^{31}P and ^{13}C via the P—N—$C_{2,6}$—$C_{3,5}$ path. This is a remarkably low value in light of the 16.2 Hz coupling in the corresponding carbocyclic phosphonate below (2).

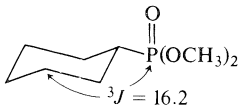

There are three possible sources for this dramatic reduction of ^3J, which are as follows: (*i*) contribution from an axial —$P(O)(OCH_3)_2$ group in a ring with a pyramidal nitrogen; (*ii*) a reduction owing to the influence of the more electronegative nitrogen (vs. carbon) in the coupling path; and (*iii*) a trigonal nitrogen, which reduces the dihedral angles relative to the case of pyramidal nitrogen.

Possibility (*i*) can be ruled out from our low temperature experiments (to −120°C) in which the spectra are essentially identical to those obtained at room temperature. Also, couplings for the compound below (only one isomer can be synthesized) are nearly identical to those for **1**.

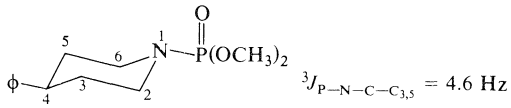

14

The findings of Morr *et al.* (13) indicate that the presence of an N atom in the coupling path does not cause large reductions of $^3J_{PNCC}$ relative to $^3J_{PCCC}$. For the cyclophosphate (below), via the path P—N—$C_{3'}$—$C_{2'}$, θ = 180° and ^3J = 10.6 Hz. Since ^3J values for **1**–**5** are ca. 4 Hz, it is unreasonable to propose that the dihedral angles (θ) for **1**–**5** are also near 180°.

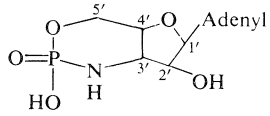

Accordingly, for **1**–**5** we envisage a flattened chair conformation with a trigonal planar nitrogen atom (below), which renders the overall ring geometry akin to that of cyclohexanone. The dihedral angle for the paths P—N—$C_{2,6}$—$C_{3,5}$ is about 120° leading to reduced ^3J values ranging from 3.6 to 4.8 Hz. The

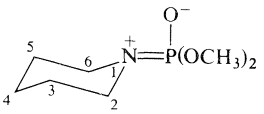

recent work (6) in which a plot of $^3J_{CP}$ vs. dihedral angle was illustrated for phosphonates, predicts a ^3J of ca. 4 Hz for θ = 120°, in excellent agreement with our findings. The coupling from ^{31}P to C-4 in the model compound below (θ = 120°) is 3.9 Hz (6).

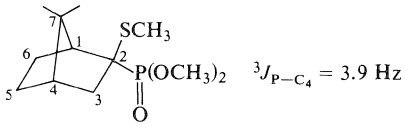

It might be argued that the S—CH_3 group has a perturbing effect on ^3J in this model but we have recently found[2] that an S—CH_3 has essentially no influence on $^3J_{CP}$, for a given dihedral angle, relative to a hydrogen substituent.

[2]G. W. Buchanan and J. H. Bowen. Unpublished observations.

TABLE 2. Geminal and vicinal ^{13}C–^{31}P couplings in phosphoramidates (±0.1 Hz)

	Geminal		Vicinal	
Compound	Path	^2J	Path	^3J
1	P—N—$C_{2,6}$	2.0	P—N—C—$C_{3,5}$	4.6
2	P—N—$C_{2,6}$	2.0	P—N—C—$C_{3,5}$	4.8
3	P—N—C_2	1.3	P—N—C—C_3	4.3
	P—N—C_6	1.6	P—N—C—C_5	4.8
4	P—N—C_2	2.5	P—N—C—C_3	4.7
	P—N—C_6	2.6	P—N—C—C_5	3.6
			P—N—C—CH_3	1.4
5	P—N—$C_{2,6}$	1.6	P—N—C—$C_{3,5}$	4.8
6	P—N—$C_{2,5}$	4.5	P—N—C—$C_{3,4}$	9.0
7	P—N—$C_{2,4}$	2.4	P—N—C—C_3	18.0
8	P—N—C_2	1.9	P—N—C—C_3	20.4
	P—N—C_4	1.1	P—N—C—CH_3	nr*
9	P—N—$C_{2,7}$	4.0	P—N—C—$C_{3,6}$	3.7
10	P—N—$C_{2,8}$	3.7	P—N—C—$C_{3,7}$	3.3
11	P—N—$C_{2,9}$	3.3	P—N—C—$C_{3,8}$	3.6

*nr is < 0.6 Hz.

The case of the azetidine derivatives **7** and **8** is in sharp contrast to that of the piperidine derivatives **1**–**5**. Comparison of $^3J_{CP}$ for **7** with that of its carbocyclic analog (**12**) shows nearly identical values of 18–19 Hz. In **7** and **8**, the resonance form in which

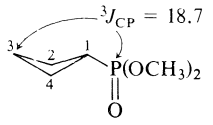

12

nitrogen is trigonal planar will be much less favourable than in **1**–**5** owing to increased bond angle strain in the four-membered ring. In fact, the ^3J of 18.7 in **12** indicates close to 180° dihedral angle between ^{31}P and C-3 (2, 6), i.e., a highly puckered cyclobutane ring. The close correspondence in **7** and **8** would indicate that the azetidine is also highly puckered, with an essentially pyramidal nitrogen atom. In **8**, the tendency of the axial CH_3 and the equatorial —$P(O)(OCH_3)_2$ groups to minimize their steric interactions will lead to increased puckering and accordingly a slightly larger $^3J_{CP}$ in **8** (20.4 Hz) than in **7**, since the P—N—$C_{2,4}$—C_3 angle will expand to near 180° as the P—N—C_2—CH_3 angle opens to near 90°. This latter expansion is reflected in the non-resolvable (<0.6 Hz) ^3J between the CH_3 and ^{31}P in **8**. We therefore formulate the preferred conformation of **8** as shown below.

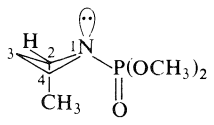

8

An alternative to a highly puckered azetidine ring which would also give rise to a dihedral angle of 180°, is a planar structure. Recent theoretical studies on the structure of azetidine itself, however, indicate that a planar form is of considerably higher energy than the puckered conformer (14). Electron diffraction studies on azetidine (15) give a large puckering angle of 33°. Substitution of the sterically bulky dimethylphosphono group on N should, if anything, increase the degree of puckering, and thus we favor an interpretation based on a highly puckered, rather than a planar four-membered ring.

For the pyrrolidine derivative **6**, $^3J_{P-N-C-C_{3,4}}$ is 9.0 Hz compared to 12.3 Hz for the carbocyclic system **13** shown below. In view of the results for the

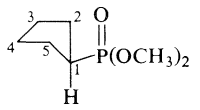

$^3J_{P-C-C-C_{3,4}}$ = 12.3

13

four- and six-membered rings, we suggest that the five-membered analog is an intermediate case. The significant reduction of 3.3 Hz for ^3J in **6** vs. **13** could result from a minor (ca. 25%) contribution from the resonance form with a trigonal planar nitrogen, with the major contribution being the tetrahedral nitrogen moiety. The $P(O)(OCH_3)_2$ group will be equatorial, predominantly.

For the seven-, eight-, and nine-membered rings (**9**, **10**, **11**, respectively), ^3J values are in the narrow range of 3.3 to 3.7 Hz. Although the carbocyclic analogs were synthesized, the ^3J values could not be extracted from the spectra owing to peak overlap. Shift reagents were not added since these would

likely alter the conformations and render comparisons of data meaningless. The only materials related to **9**, **10**, and **11** are the carbocyclic hydroxy phosphonates (3), which exhibit $^3J_{P-C-C-C}$ values of 10.9, 8.8, and 6.7 Hz, respectively, for seven-, eight-, and nine-membered ring compounds. The considerably smaller values in **9** → **11** seem to indicate trigonal nitrogen, since values for hydroxy phosphonates are known to be appreciably lower (3–4 Hz) than for phosphonates of similar geometry (1–3). It seems reasonable that these larger rings should be able to accommodate a trigonal planar nitrogen and thus the ^3J values for **9–11** are rather close to those of **1–5**.

Infrared Spectroscopy as a Probe for N Lone Pair Delocalization

For a series of acyclic phosphoramidates, $(OR)_2P(O)NHR$, and thiophosphoramidates, $(OR)_2P(S)NHR$, the P—N vibration occurs in the range 953–965 cm^{-1} (25). This is intermediate between that for a single bond (ca. 700 cm^{-1}) and a double bond (ca. 1300 cm^{-1}) and accordingly it is suggested that there is partial double bond character in the N—P bonds.

In the materials examined here, no clear trends emerge from the infrared spectral data. Interpretations are complicated by the fact that P=O stretching occurs very near the position of P=N stretching (ca. 1300 cm^{-1}).

We propose, therefore, that $^{13}C-^{31}P$ vicinal coupling constitutes a valuable addition to available techniques for monitoring nitrogen lone pair delocalization into N—P bonds.

Experimental

Spectra

^{13}C spectra were obtained via previously described techniques (1), on a Varian XL-100-12 NMR spectrometer, operating at 25.16 MHz, for compounds **1**—**11** and **13**. A Varian CFT-20 instrument was employed in the case of **12**, with a 2000 Hz sweep width and 8K data points.

Materials

For amines of ring size of five and above, the following general procedure was used to prepare the *N*-dimethylphosphono derivatives. To a solution of amine (2 equiv.), CCl_4 (1 equiv.) in an equal volume of ether at 0–5°C was added dimethyl phosphite (1 equiv.) dropwise with stirring. The reaction mixture was stirred at room temperature for ½ h, the hydrochloride salt filtered, the solvent evaporated and the residue distilled. Compounds obtained in this fashion were:

Compound ***1***—bp 85–90°C/3 Torr, n_D^{20} 1.4513 (lit. (16) bp 119°C/15 Torr, n_D^{20} 1.4528).

Compound ***2***—bp 100–102°C/2.5 Torr, n_D^{20} 1.4509. *Anal.* calcd. for $C_8H_{18}NO_3P$: C 46.37, H 8.76, N 6.76, P 14.95, O 23.16; found: C 46.31, H 8.59, N 6.82, P 14.87.

Compound ***3***—bp 91–92°C/2 Torr, n_D^{20} 1.4519. *Anal.* found: C 45.98, H 8.72, N 6.73, P 15.01.

Compound ***4***—bp 92–94°C/4 Torr, n_D^{20} 1.4554. *Anal.* found: C 46.22, H 8.72, N 6.74, P 14.63.

Compound ***6***—bp 90–93°C/3 Torr, n_D^{20} 1.4498 (lit. (17) bp 56–57°C/0.6 Torr, n_D^{20} 1.4498).

Compound ***9***—bp 94–96°C/1.5 Torr, n_D^{20} 1.4620. *Anal.* calcd. for $C_8H_{18}NO_3P$: C 46.37, H 8.76, N 6.76, P 14.95, O 23.16; found: C 46.31, H 8.52, N 6.81, P 14.79.

Compound ***10***—bp 112–115°C/3 Torr, n_D^{20} 1.4662. *Anal.* calcd. for $C_9H_{20}NO_3P$: C 48.86, H 9.11, N 6.33, P 14.00, O 21.69; found: C 48.70, H 9.18, N 6.25, P 14.34.

Compound ***11***—bp 111–112°C/4 Torr, n_D^{20} 1.4714. *Anal.* calcd. for $C_{10}H_{22}NO_3P$: C 51.05, H 9.43, N 5.95, P 13.17, O 20.40; found: C 51.27, H 9.31, N 5.80, P 13.11.

N-*Dimethylphosphonoazetidine (****7****)*

This compound was prepared as follows. 1-Azido-3-iodopropane (1.0 g, 4.7 mmol), prepared from acrolein by the published method (18), and 0.58 g (4.7 mmol) of trimethyl phosphite were stirred in 75 ml of pentane at room temperature for 5 days. Extra phosphite (2.0 mmol total) was added occasionally. After the pentane was evaporated off, the residue was distilled to yield **7**, bp 66°C/2 Torr (lit. (19) bp 108–109 °C/11 Torr).

N-*(Dimethylphosphono)-2-methylazetidine (****8****)*

This was synthesized from 2.25 g 3-azido-1-iodobutane (0.01 mol) (18) and 1.55 g trimethyl phosphite (0.0125 mol) in 75 ml pentane. The mixture was stirred for 3 days at room temperature and the excess phosphite removed under vacuum. The residue was judged pure by ^1H and ^{13}C nmr.

N-*(Dimethylthiophosphono)piperidine (****5****)*

This compound was prepared as follows. To 4.0 g piperidine (0.047 mol) in 50 ml anhydrous ether at 0°C was added dropwise 3.52 g (0.22 mol) dimethyl chlorothiophosphate with stirring. The mixture was stirred at room temperature for 1 h, filtered, concentrated, and distilled (bp 68–72°C/1.5 Torr, n_D^{20} 1.5002 (lit. (20) bp 80°C/3.0 Torr.).

*Dimethylphosphonocyclobutane (****12****)*

This compound was prepared by methods previously described (2), from cyclobutanone via cyclobutane-1,1-dithiol (21) and subsequently the methyl thiophosphonate (22), which was desulfurized using Raney nickel. For **12**, n_D^{20} 1.4440 (lit. (23) n_D^{25} 1.4442).

*Cyclopentyl Phosphonate (****13****)*

Dimethyl phosphite (11.0 g, 0.1 mol) in 30 ml toluene was brought to reflux in a 100 ml three-necked flask equipped with an efficient condenser and dropping funnel. To this was added a slurry of 4.09 g cyclopentene (0.06 mol) and 0.366 g dibenzoyl peroxide (0.0015 mol). Reflux was continued for 3 h and the toluene and excess dimethyl phosphite were removed under vacuum. The resultant 1.3 g sample was chromatographed on silica gel with ether as solvent to give the product with ^1H nmr identical to that of the literature (23); n_D^{20} 1.4521 (lit. (23) n_D^{25} 1.4511).

N-*Dimethylphosphono-4-phenylpiperidine (****14****)*

To 4-phenylpiperidine (2.0 g, 12.4 mmol), triethylamine (1.57 g, 15.5 mmol) and carbon tetrachloride (2.38 g, 15.5 mmol) in 40 ml anhydrous ether, maintained at 5°C, was added dropwise dimethyl phosphite (1.57 g, 14.3 mmol). The reaction mixture was stirred overnight, filtered and the solvent removed by rotary evaporation. The resultant oil slowly crystallized. Recrystallized from ethanol–hexane, mp 72–73°C; ^1H nmr ($CDCl_3$) δ: 7.23 (s, aromatic, 5H), 3.7 (d, J = 11.5 Hz, CH_3O—P, 6H), 3.4–3.9 (m, 2H), 2.3–3.1 (m, 3H), 1.6–2.0 (m, 4H).

Acknowledgements

G.W.B. thanks the National Research Council of Canada for financial aid. We thank Richard Ozubko for examining the ^{13}C spectrum of **12** and Catherine Cousineau for the synthesis of this material.

1. G. W. Buchanan and C. Benezra. Can. J. Chem. **54**, 231 (1976).
2. G. W. Buchanan and J. H. Bowen. Can. J. Chem. **55**, 604 (1977).
3. G. W. Buchanan and F. G. Morin. Can. J. Chem. **55**, 2885 (1977).
4. G. I. Birnbaum, G. W. Buchanan, and F. G. Morin. J. Am. Chem. Soc. **99**, 6652 (1977).
5. L. Ernst. Org. Magn. Reson. **9**, 35 (1977).
6. J. Thiem and B. Meyer. Org. Magn. Reson. **11**, 50 (1978).
7. K. Mislow and M. Raban. Top. Stereochem. **1**, 1 (1967); **2**, 199 (1967).
8. G. E. Ellis and R. G. Jones. J. Chem. Soc. Perkin II, 437 (1973).
9. D. K. Dalling and D. M. Grant. J. Am. Chem. Soc. **89**, 6612 (1967).
10. L. F. Johnson and W. C. Jankowski. Carbon-13 spectra. Spectrum 84. Wiley-Interscience, New York, NY. 1972.
11. J. B. Stothers. Carbon-13 nmr spectroscopy. Academic Press, New York, NY. 1972. p. 123.
12. T. Pehk and E. Lippmaa. Eesti NSV Tead. Akad. Toim. Keem. Geol. **17**, 291 (1968).
13. M. Morr, M-R. Kula, and L. Ernst. Tetrahedron, **31**, 1619 (1975).
14. J. Catalan, O. Mo, and M. Yanez. J. Mol. Struct. **43**, 251 (1978).
15. V. S. Mastryukov, O. V. Dorofeeva, and L. V. Vilkov. J. Mol. Struct. **34**, 99 (1976).
16. J. Chaymol. C. R. Acad. Sci. **249**, 1240 (1959).
17. N. P. Grechkin and L. N. Grishina. Izv. Akad. Nauk SSSR, Ser. Khim. **7**, 1608 (1969).
18. A. Hassner and J. E. Galle. J. Org. Chem. **41**, 2273 (1976).
19. N. P. Grechkin and L. N. Grishina. Dokl. Akad. Nauk SSSR, **162**, 1063 (1965).
20. R. G. Cooks and A. F. Gerrard. J. Chem. Soc. B, 1327 (1968).
21. C. Fournier, B. Lemaire, B. Braillon, D. Paquer, and M. Vayeux. Org. Magn. Reson. **10**, 20 (1977).
22. Z. Yoshida, S. Yoneda, and T. Kawase. Chem. Lett. 279 (1975).
23. R. S. Marmor and D. Seyferth. J. Org. Chem. **36**, 128 (1971).
24. R. Mathis, M. J. Khemdoudi, T. Bouisson, M. Barthelat, and F. Mathis. C. R. Acad. Sci. Ser. C, **281**, 437 (1975).

^{13}C and ^{1}H nuclear magnetic resonance spectroscopy of C-19 and 6β-methyl substituted steroids: long-range shift effects in conformational analysis

KATHERINE NÁSFAY SCOTT[1] AND THOMAS HAROLD MARECI

Veterans Administration Hospital, and Department of Radiology, University of Florida, Gainesville, FL 32610, U.S.A.

Received April 13, 1978

KATHERINE NÁSFAY SCOTT and THOMAS HAROLD MARECI. Can. J. Chem. **57**, 27 (1979).

^{13}C and ^{1}H nmr spectra were obtained and assigned for nine C-19 substituted cholest-5-enes, three 6β-substituted 19-norcholest-5(10)-enes, and several related steroids. ^{13}C chemical shift effects have previously not been studied in either C-19 substituted steroids or in cholest-5(10)-enes. In the present study, substituent effects on the ^{13}C chemical shifts of the α, β, γ, and δ carbons were evaluated in detail. Although the substituent in C-19 substituted and 6β-methyl substituted steroids is less rigidly oriented with respect to the rest of the molecule than in ring-substituted steroids, similar shift effects were observed. In cholest-5-enes the observed ^{13}C and ^{1}H shift effects and the temperature dependence of the ^{13}C shifts indicate that the preferred orientation of the C-19 substituent is *anti* to C-1. The relative stabilities of the rotamers can be attributed to the orientation of the C-19 substituent with respect to the double bond. This interpretation is supported by the fact that the preferred orientation of the iodine in 6β-iodomethyl-19-norcholest-5(10)-en-3β-ol has the same spacial relationship with respect to the double bond, i.e., *gauche* to C-5 and C-7.

KATHERINE NÁSFAY SCOTT et THOMAS HAROLD MARECI. Can. J. Chem. **57**, 27 (1979).

On a enregistré les spectres rmn de ^{13}C et de ^{1}H et fait les attributions pour neuf cholestènes-5 substitués en C-19, trois nor-19 cholestènes-5(10) substitués en 6β et plusieurs stéroides apparentés. Les effets de déplacement chimique de ^{13}C n'ont encore fait l'objet d'une étude ni pour les stéroides substitués en C-19, ni pour les cholestènes-5(10). Dans le présent travail, on évalue en détail les effets des substituants sur les déplacements chimiques de ^{13}C des carbones α, β, γ et δ. Bien que le substituant dans les stéroides substitués en C-19 ou sur le groupe méthyle en position 6β, soit orienté moins rigidement par rapport au reste de la molécule que dans les stéroides substitués sur le cycle, on a observé des effets de déplacement semblables. Dans les cholestènes-5, les effets de déplacement de ^{13}C et de ^{1}H et l'influence de la température sur les déplacements de ^{13}C indiquent que le substituant en C-19 adopte une orientation préférentielle *anti* par rapport à C-1. On peut attribuer les stabilités relatives des rotamères à l'orientation du substituant en C-19 par rapport à la double liaison. Cette interprétation est renforcée du fait que l'orientation préférentielle de l'iode dans l'iodométhyl-6β nor-19 cholestén-5(10) ol-3β possède la même relation spatiale par rapport à la double liaison, soit *gauche* par rapport à C-5 et C-7.

[Traduit par le journal]

Introduction

Since steroids are rigid structures, long-range effects of substituents on ^{13}C chemical shifts have previously been correlated with the spacial relationship between the carbons and the ring substituent. Substituents γ-*gauche* or -eclipsed to a given carbon produce shielding; when *anti* to the carbon the effect is generally deshielding (ref. 1 and references cited therein). The direction and the magnitude of the shifts depends on the degree of substitution of the intervening carbons. This conclusion has also been reached from theoretical considerations (2). In ring-substituted hydroxy steroids, methyl-*trans*-decalols, and methylnorbornanols, substituents in the *syn*-axial configuration substantially deshield δ carbons (3–5). Deshielding of carbons four bonds from the substituent is not peculiar to hydroxy substituents or cyclic systems, but has also been observed for methyl substituents and acyclic compounds (6, 7). However, the crowded *syn*-axial δ configuration has ca. 3 kcal/mol interaction energy (8); therefore, more stable orientations of the substituent are favored and deshielding δ effects are seldom observed in acyclic systems.

The γ and δ effects are of very obvious utility in stereochemical assignment of rigid systems. In addition, since these γ and δ effects are frequently quite substantial (2 ppm or larger), it seemed to us that they might be utilized for conformational analysis of less rigid systems which have rotation of the sub-

[1]Author to whom correspondence may be addressed.

0008-4042/79/010027-11$01.00/0

stituent about one bond. Accordingly we examined substituent effects in some C-19 and 6β-methyl substituted steroids.

The effect of introducing substituents at the C-19 methyl of steroids has previously not been investigated (9). Rotation of the methyl group about the bond between C-10 and C-19 allows for various orientations of the C-19 substituent relative to the rest of the molecule. An nmr investigation of C-19 substituted steroids could show whether substituent effects in this less rigid system follow the trends established for substitution on the steroid ring and whether these effects could be used to establish any orientational preference of the substituent. For this reason we report ^{13}Cmr and ^{1}Hmr data on the several C-19 substituted cholest-5-enes and related steroids shown in Fig. 1. We examined several 19-hydroxy substituted cholest-5-enes, since the effect of hydroxy substitution has been most widely studied in steroids. Because we wanted to study conformational effects, bulky substituents, such as iodo and *p*-toluenesulfonyl, were also examined. Our results show that the preferred orientation for the C-19 substituent is *anti* to C-1. We attribute the relative stabilities of the rotamers in the cholest-5-enes to the orientation of the C-19 substituent with respect to the double bond. To test this interpretation, we also investigated the orientational preference of a different double-bonded steroid, 6β-iodomethyl-19-norcholest-5(10)-en-3β-ol.

^{131}I labelled **4***a* and **8***a* are two adrenal radioimaging agents approved for human use and are thus of considerable biological and radiopharmaceutical interest.

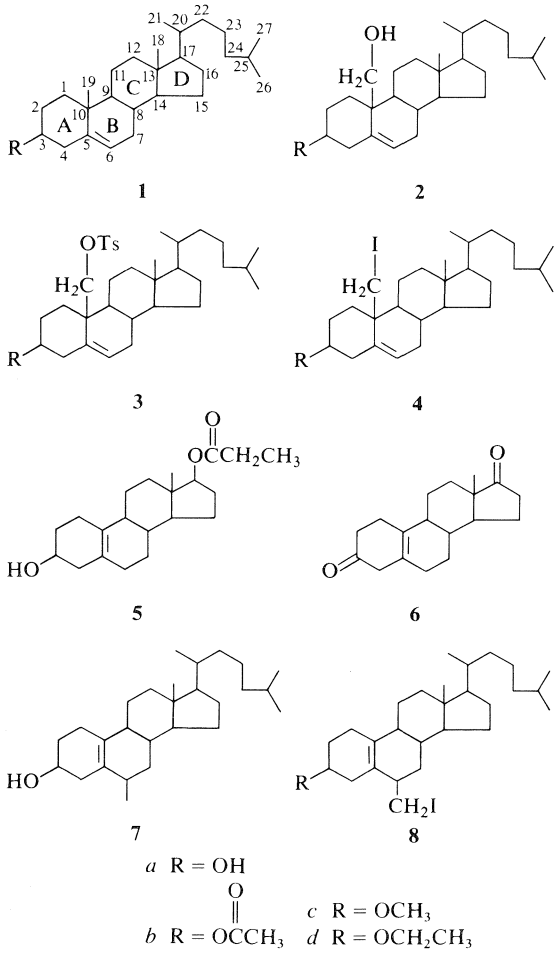

FIG. 1. Compounds studied: **1***a*, cholest-5-en-3β-ol; **2***b*, cholest-5-en-3β,19-diol 3-acetate; **3***a*, cholest-5-ene-3β,19-diol 19-*p*-toluenesulfonate; **4***a*, 19-iodocholest-5-en-3β-ol; **5**, estr-5(10)-ene-3β,17β-diol 17-propionate; **6**, estr-5(10)-ene-3β,17β-dione; **7**, 6β-methyl-19-norcholest-5(10)-en-3β-ol; **8***a*, 6β-iodomethyl-19-norcholest-5(10)-en-3β-ol.

Results and Discussion

A. ^{13}C Nuclear Magnetic Resonance

Spectral Assignments

The ^{13}C chemical shifts obtained in this study are summarized in Table 1. Chemical shifts for **1***a*, **1***b*, and **1***c* have been reported previously (10–13). The chemical shifts in Table 1 for these compounds agree with the literature values to 0.6 ppm or better, which is in the range expected for solvent and concentration effects. Our assignments for **1***a*, **1***b*, and **1***c* agree with those originally reported (10–13) except for the reversal of the assignments of C-12 and C-16, as noted for cholesterol (14) and some cholestanes (15) and later confirmed for several related steroids (16–19).

In assigning the remaining compounds, it was assumed that the D ring and the C-17 side chain were least affected by substitution. Indeed, these resonances changed little in the cholesterol series of compounds and were assigned on this basis. The expected shifts of the remaining carbons for each of the compounds were predicted from the observed shifts of appropriate model compounds and from known substituent effects. Agreement between observed and predicted shifts was sufficient to permit preliminary assignment. Then the specific assignments were confirmed by establishing the type of carbon (methyl, methylene, methine, quaternary) by a combination of low power broadband decoupling (LPBBD) or single frequency off-resonance decoupling (SFORD) of the protons. Unequivocal assignment of all but a few resonances could be achieved by the above procedure. Ambiguities in assignment remained only for those few resonances for which the spectrum contained close-lying resonances of carbons with the same number of attached hydrogens or where the SFORD spectra did not establish the num-

TABLE 1. ^{13}C chemical shifts[a]

Carbon	1*a*	1*b*	1*c*	2*b*	2*c*	3*a*[b]	3*b*[b]	3*c*[b]	4*a*	4*b*	4*c*	4*d*	5	6	7	8*a*	8*c*
1	37.5	37.1	37.5	33.3[c]	33.6[c]	32.8[c]	32.7	32.9[c]	37.6	37.3	37.4	37.6	22.7	25.0	24.6	24.5	24.6
2	31.7	27.8	28.3	28.0	28.6	31.6	27.9	28.3	31.7	28.1	28.3	28.9	31.3	39.1	31.3	30.8	27.2
3	71.7	73.9	80.7	73.5	80.2	71.4	73.3	79.9	71.2	73.0	79.7	78.3	66.1	210.4	67.2	66.6	75.7
4	42.3	38.2	39.0	38.3	38.9	42.3	38.2	38.8	42.2	38.2	38.6	39.3	39.3	44.7	38.8	38.8	35.7
5	141.0	139.6	141.2	134.8	135.9	134.6	133.5	134.8	136.5	135.4	136.5	136.9	124.6	127.0	129.4	125.5	125.4[d]
6	121.7	122.6	121.7	127.9	127.3	127.1	128.1	127.0	125.5	126.6	125.4	125.4	30.1	32.2	35.2	43.4	43.3
7	32.0	31.9	32.3	31.3	31.5	31.6	31.5	31.6	31.2	31.2	31.2	31.3	25.2	27.7	34.8[d]	31.8	31.7
8	32.0	31.9	32.3	33.1[c]	33.7[c]	33.1[c]	32.7	33.1[c]	31.9	31.9	31.9	32.0	38.9	38.9	34.0[d]	33.6	33.5
9	50.4	50.1	50.7	50.4	50.7	50.4	50.2	50.5	51.4	51.3	51.4	51.5	46.4	46.5	47.0	47.6	47.7
10	36.6	36.6	37.2	41.5	42.1	40.2	40.2	40.7	38.5	38.6	38.8	39.1	129.7	130.9	130.0	133.9	134.2
11	21.3	21.3	21.4	21.8	22.0	22.0	22.0	22.0	22.2	22.2	22.2	22.3	26.9	26.0	26.3	25.7	25.5
12	40.0	39.8	40.2	40.1	40.3	40.2	40.2	40.3	40.1	40.0	40.1	40.1	37.5	30.8	40.8	40.0	40.4
13	42.5	42.3	42.6	42.5	42.7	42.6	42.5	42.6	42.7	42.7	42.7	42.8	43.4	48.3	43.4	43.3	43.2
14	57.0	56.8	57.2	57.6	57.9	57.5	57.3	57.7	57.8	57.7	57.8	57.9	49.9	50.4	55.5	55.0	54.9
15	24.4	24.3	24.5	24.1	24.3	24.2	24.3	24.2	24.2	24.2	24.2	24.3	23.3	21.6	24.0	23.8	23.8
16	28.4	28.3	28.3	28.0	28.4	28.3	28.4	28.3	28.3	28.3	28.3	28.4	28.0[c]	35.9	28.6	28.5	28.4
17	56.4	56.2	56.6	56.2	56.4	56.5	56.3	56.5	56.3	56.2	56.3	56.3	82.8	220.1	56.8	56.6	56.6
18	11.9	11.9	12.0	12.2	12.3	12.1	12.1	12.1	12.4	12.3	12.4	12.4	12.4	14.1	12.5	12.4	12.4
19	19.5	19.3	19.5	62.7	62.9	70.1	69.9	70.1	11.4	10.8	11.1	11.4			20.6[e]	11.9[f]	12.1[f]
20	36.0	35.9	36.0	35.8	36.0	36.0	36.0	36.0	35.9	35.9	35.9	36.0			36.2	36.0	36.0
21	18.8	18.7	18.9	18.7	18.8	18.9	18.9	18.9	18.7	18.8	18.8	18.8			18.9	18.8	18.7
22	36.4	36.3	36.5	36.2	36.5	36.5	36.5	36.5	36.3	36.4	36.3	36.4			36.6	36.4	36.3
23	24.1	23.9	24.2	23.9	24.1	24.2	24.1	24.2	24.0	24.0	24.0	24.1			24.2	24.1	24.0
24	39.7	39.6	39.8	39.5	39.7	39.8	39.8	39.8	39.6	39.6	39.6	39.7			39.9	39.8	39.7
25	28.1	28.0	28.3	28.0	28.2	28.3	28.4	28.3	28.1	28.1	28.1	28.2			28.3	28.2	28.2
26	22.6	22.6	22.4	22.6	22.6	22.6	22.6	22.7	22.6	22.6	22.6	22.7			22.7	22.7	22.6
27	22.9	22.8	22.6	22.8	22.9	22.9	22.8	22.9	22.8	22.8	22.9	22.9			22.9	22.9	22.9
C=O		170.0		170.4			170.5			170.2			174.7				
CH_2												63.4	27.8[c]				
CH_3		21.1	55.6	21.3	55.7		21.4	55.6		22.3	55.6	15.8	9.3				55.7

[a]In ppm from TMS.
[b]Aromatic C-2′ and C-6′ at 128.1, C-3′ and C-5′ at 129.9. Aromatic C-1′ and C-4′ of too low intensity to de detected. Aromatic methyl at 21.6.
[c]Close-lying assignments within the same column may be reversed.
[d]Or 124.1.
[e]6β-Methyl.
[f]6β-Iodomethyl.

ber of attached hydrogens. Possible alternative assignments are indicated in Table 1.

The expected chemical shifts of the individual compounds were predicted as follows: The shifts of **2***b* and of **2***c* were predicted from the observed shifts of **1***b* and **1***c* and the —OH substituent effect observed in 2,2-dimethyl-1-propanol (11*b*, 20). The observed steroid shifts of **3** were very similar to those of **2***b* and **2***c* and were assigned on this basis. We determined the shifts for *p*-toluenesulfonyl chloride (C-1′ 141.8; C-2′, C-6′ 127.1; C-3′, C-5′ 130.3; C-4′ 146.9; CH_3 21.8) and this permitted the assignment of the tosyl resonances of **3**. The shifts of **4** were predicted from the observed shifts of **1** and the iodine substituent effect observed for 1-iodopentane (11*c*, 21).

To facilitate our assignment of **8***a*, which is the first ^{13}Cmr assignment of a 5(10)-ene steroid, we obtained and assigned spectra **5**, **6**, **7**, and **8***c*. Compound **7** was obtained by $LiAlH_4$ reduction of **8***a* and **8***c* was obtained by methylating **8***a*. Since there are major discrepancies among the previously reported ^{1}Hmr data for **8***a* (22–25), we report the assignment of the ^{13}Cmr spectrum of this compound in somewhat more detail to show that ^{13}Cmr unequivocally confirms the structure as 6β-iodomethyl-19-norcholest-5(10)-en-3β-ol. Each of **7**, **8***a*, and **8***c* shows the same eight resonances as those observed for the C-17 side chain in all the other cholesterol compounds of this series and these resonances were assigned to C-20 through C-27. The chemical shifts of C-18 and the C- and D-ring carbons of **7**, **8***a*, and **8***c* were predicted from the observed shifts of **1***a* and the effect of the removal of the C-19 methyl. This effect was obtained by comparing the shifts of testosterone and 19-nortestosterone (10, 11*a*, 19). The agreement between observed and predicted shifts was 0.1–1.0 ppm. The larger deviations, which occurred for the C-ring carbons, undoubtedly reflect the additional structural differences in the A and B rings between **1***a* and compounds **7**, **8***a*, and **8***c*.

The principal differences between the ^{13}Cmr spectrum of **8***a* and its isomer, **4***a*, occur in the A- and B-ring resonances, which means that the structural differences between **4***a* and **8***a* must be in the A and B rings. By LPBBD we showed that both olefinic carbons of **8***a* had no directly attached hydrogens; therefore, the double bond had to be either between C-5 and C-10 or C-9 and C-10. In the ^{1}Hmr spectrum of **8***a*, the CH_2I protons form the AB part of an ABX pattern, confirming that the CH_2I is attached to a CH carbon. Therefore, the C=C(CH_2I) possibility for quaternary olefinic carbons could be eliminated. In the ^{13}Cmr spectrum of 5α-pregn-9(10)-ene-16α-methyl-17α,21-diol-3,20-dione 21-acetate, we obtained olefinic resonances at 145.6 and 117.0 ppm for the C-9 to C-10 double bond. According to the CH_2I substituent effects observed in **4**, the attachment of CH_2I anywhere on the A or B rings could not have changed these olefinic shifts to those observed in **8***a* (125.5 and 133.9 ppm), thus the C-9 to C-10 double bond possibility for **8***a* is eliminated.

We then assigned ^{13}Cmr spectra of **5** (an authentic sample (26) was kindly provided by Prof. S. G. Levine for this purpose) and of **6**. The C- and D-ring carbon shifts of **6** were predicted from the observed shifts of 19-norandrost-4-ene-3,17-dione (10, 11, 19). The propionate side-chain carbons of **5** could easily be identified from the corresponding shifts (27.9 and 9.2 ppm) which we obtained for isopropyl propionate. The shifts of C-18 and the C- and D-ring carbons of **5** were predicted from the shifts of testosterone 17-acetate (10, 11*a*) and the effect of the removal of the 19-methyl. The A- and B-ring carbons of **5** and **6** could then be matched carbon by carbon and assigned if the effect of carboxylation at C-3 was added to the observed shifts of **5**. This effect was obtained by comparing the observed shifts of cholestan-3β-ol with those of cholestan-3-one (10, 11*a*,*b*, 19).

Once we had assigned the spectra of **5** and **6**, the A- and B-ring resonances of **7** could be predicted by adding the 6β-methyl effect (4) to the observed shifts of **5**. The shifts of **8***a* were then obtained by adding the iodine substituent effect to the observed shifts of **7**. Carbons 2, 3, and 4 of **8***a* were further identified by comparison with **8***c*, which gave the same resonances as **8***a*, except C-3 was deshielded by 9.1 ppm and C-2 and C-4 were shielded by 3.6 and 3.1 ppm, respectively. Thus, by the above detailed analysis of the ^{13}Cmr spectra of the five compounds **5**, **6**, **7**, **8***a*, and **8***c*, we could unequivocally confirm that the structure for **8***a* is as indicated.

Effect of Oxygen or Iodine Substitution α and β Effects

The ^{13}C chemical shift effects of oxygen or iodine substitution are summarized in Table 2. Hydroxylation at C-19 deshields the α carbon by 43.4 ppm and the β carbon by 4.9 ppm. These shift effects are similar to the 41.4 and 5.0 ppm deshieldings observed for the α and β carbons of 2,2-dimethyl-1-propanol (11*b*, 20). Tosylation at C-19 gives 50.6 and 3.6 ppm deshielding of the α and β carbons, respectively. Thus the *p*-toluenesulfonyl substituent deshields the α carbon 7.2 ppm more and the β carbon 1.3 ppm less than the OH. Although these effects are smaller, they are analogous to the changes observed between the shifts of ethyl sulfate (69.6 and 14.5 ppm, ref. 12*b*) and ethanol (57.3 and 17.9 ppm, refs. 11*b* and 20).

The α carbon in each of the iodine substituted

TABLE 2. Effect of oxygen or iodine substitution on ^{13}C chemical shifts[a]

Substituent	Compounds[b]	α C-19	β C-10	γ C-1	γ C-5	γ C-9	δ C-2	δ C-4	δ C-6	δ C-8	δ C-11	ε C-3	ε C-7	ε C-12	ε C-14
—OH	**2***b* − **1***b*	+43.4	+4.9	−3.8	−4.8	+0.3	+0.2	+0.1	+5.3	+1.2	+0.5	−0.4	−0.6	+0.3	+0.8
	2*c* − **1***c*	+43.4	+4.9	−3.9	−5.3	0.0	+0.3	−0.1	+5.6	+1.4	+0.6	−0.5	−0.8	+0.1	+0.7
	(A[c] − B[c])	(+41.4)	(+5.0)	(−4.9)											
—OTs	**3***a* − **1***a*	+50.6	+3.6	−4.7	−6.4	0.0	−0.1	0.0	+5.4	+1.1	+0.7	−0.3	−0.4	+0.2	+0.5
	3*b* − **1***b*	+50.6	+3.6	−4.4	−6.1	+0.1	+0.1	0.0	+5.5	+0.8	+0.7	−0.6	−0.4	+0.4	+0.5
	3*c* − **1***c*	+50.6	+3.5	−4.6	−6.4	−0.2	0.0	−0.2	+5.3	+0.8	+0.6	−0.8	−0.7	+0.1	+0.5
	(C[c] − D[c])	(+63.7)	(+8.6)												
—I	**4***a* − **1***a*	−8.1	+1.9	+0.1	−4.5	+1.0	0.0	−0.1	+3.8	−0.1	+0.9	−0.5	−0.8	+0.1	+0.8
	4*b* − **1***b*	−8.5	+2.0	+0.2	−4.2	+1.2	+0.3	0.0	+4.0	0.0	+0.9	−0.9	−0.7	+0.2	+0.9
	4*c* − **1***c*	−8.4	+1.6	−0.1	−4.7	+0.7	0.0	−0.4	+3.7	−0.4	+0.8	−1.0	−1.1	−0.1	+0.6

Substituent	Compounds	α 6-Me	β C-6	γ C-5	γ C-7	δ C-4	δ C-10	δ C-8	ε C-1	ε C-3	ε C-9	ε C-14
—I	**8***a* − **7**	−8.7	+8.2	−3.9	−3.0	0.0	+3.9	−0.4	−0.1	−0.6	+0.6	−0.5
	(E[c] − F[c])	(−6.5)	(+11.3)	(−1.2)		(−0.2)			(+1.0)			

[a]In ppm from TMS. Positive substituent effects indicate a downfield shift. Values in parentheses are known substituent effects in model compounds.
[b]Chemical shifts of the two compounds that were compared to obtain the substituent effects.
[c]A is 2,2-dimethyl-1-propanol, refs. 11*b* and 20; B is 2,2-dimethylpropane, refs. 11*b* and 20; C is ethyl sulfate, ref. 12*b*; D is ethane, refs. 27 and 11*d*; E is 1-iodopentane, refs. 21 and 11*c*; F is pentane, refs. 21 and 11*c*.

steroids is shielded by about the same extent (8.1 to 8.7 ppm), which is about 2 ppm larger than the 6.5 shielding observed in 1-iodopentane. The reason for the larger shielding in the steroids is not apparent. The β carbon in the cholest-5-enes is deshielded by 1.6 to 2.0 ppm and in the 5(10)-ene by 8.2 ppm. These values are smaller than the 11.3 ppm deshielding of the β carbon in 1-iodopentane (21, 11*c*). The lesser shielding of the β carbons in the steroids can be attributed to the greater degree of substitution for C-6 in **8***a* and particularly C-10 in **4**. Decreased β substituent effects with increased branching were first observed for norbornyl derivatives (28) and then confirmed for the decalols (3*b*) and for various steroids (3*b*, 5, 29).

γ *Effects*

In C-19 substituted steroids, rotation about the C-10 to C-19 bond gives the staggered rotamers, **I**, **II**, and **III** (Fig. 2). The rotamers are nonequivalent and may have unequal population. For the 6β-iodomethyl compounds rotation about the iodomethyl to C-6 bond yields the staggered rotamers, **A**, **B**, and **C** (Fig. 2). At room temperature, none of the rotamers are 'frozen out' and the observed chemical shift is a rotationally averaged shift. However, from the observed ^{13}C and ^{1}H chemical shifts we were able to establish the relative populations of the rotamers.

A recent reinterpretation of the γ effect (30) and the data on hydroxy steroids in ref. 5 show that large (2.3 to 8.3 ppm) upfield γ-*gauche* effects are possible if the substituent removes a 1,3-diaxial proton–proton interaction. If no such interaction is removed by the substituent, the γ-*gauche* effect will be much smaller (0.1 to 0.9 ppm). In the present compounds, 1β-H gives a 1,3-diaxial type interaction with the C-19 protons and 7β-H with the 6β-methyl protons. These interactions are removed by the substituent only in rotamer **II** and rotamer **A**, respectively. The

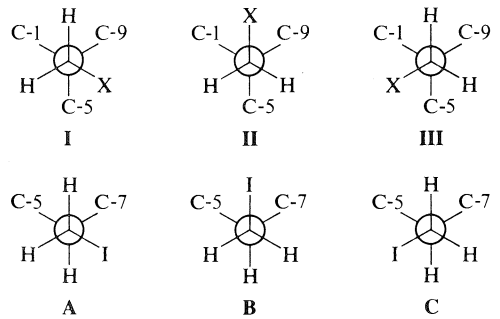

FIG. 2. Upper row: The three staggered rotamers (**I**, **II**, and **III**) of the C-19 CH_2X group in C-19 substituted cholest-5-enes. The C-19 to C-10 bond is into the plane of the paper. Lower row: The three staggered rotamers (**A**, **B**, and **C**) of the 6β-iodomethyl group of 6β-iodomethyl-19-norcholest-5(10)-en-3β-ol. The 6β-iodomethyl to C-6 bond is into the plane of the paper.

substantial shielding (−3.8 to −4.7 ppm) of C-1 in the 19-O compounds shows that rotamer **II** is appreciably populated in these compounds, whereas the lack of shielding effect on C-1 (−0.1 to +0.2 ppm) indicates that rotamer **II** is not well populated in the 19-I compounds. (The difference in relative populations of the 19-I and 19-O compounds will be discussed in subsequent sections.) The 3.0 ppm shielding of C-7 in **8** shows that rotamer **A** has appreciable population.

Since C-5 has no hydrogen, the large shielding (−3.9 to −6.4 ppm) of this carbon cannot be accounted for by the removal of the 1,3-diaxial interaction but must be due to linear electric field shift effects. (See subsequent sections.)

δ *Effects*

In 10-methyl-*trans*-decalols, methylnorbornanols, and some hydroxy steroids, larger positive (+2 ppm or greater) δ substituent effects were observed for carbons in the *syn*-axial conformation relative to the OH (3, 4). In 31 monohydroxylated cholestanes and androstanes, about 80 examples of interaction between the OH and the δ carbon were examined (5). Of the five possible orientations, $\delta_1 - \delta_5$ (3*b*, 5), only the δ_1 *syn*-axial configuration showed large (2.0 to 3.8 ppm) deshielding effects (5). Although most of the observed interactions were between OH and CH_3, several interactions were between OH and ring methylene carbons (e.g., 1β-OH and C-11).

In the present series of 19-O compounds, C-6 is consistently strongly deshielded (5.3 to 5.6 ppm). C-6 is δ_1 relative to the 19-O only in rotamer **I**. (See Table 3.) Thus the strong deshielding of C-6 in the compounds indicates that rotamer **I** has appreciable population. In this configuration, C-8 too is δ_1 to the 19-O. Indeed, C-8 is the only other δ carbon which shows a substantial deshielding (0.8 to 1.4 ppm).

In the present 19-O compounds, the δ_1 effect on C-6 is larger and on C-8 somewhat smaller than the 1.4 to 3.8 ppm deshielding effects previously observed in ring-substituted steroids, methyl-*trans*-decalols, and methylnorbornanols (3–5). Some of the deshielding of C-6 may be due to linear electric field shift (LEFS) effects (31, 32), since these effects can be substantial on sp^2 carbons (33, 34). The oxygen–carbon bond acts as a dipole, polarizing the charge distribution of the C=C in such a manner as to shield the carbon closer to the polar group and deshield the carbon farther away. Using eqs. [2]–[4] of ref. 33*a*, we estimated the LEFS on C-5 and C-6 in the 19-OH compounds. The appropriate distances and angles were obtained from molecular models, dipole moments from ref. 35, and LEF coefficients from ref. 33*b*. The LEFS thus estimated for C-5 and C-6 in the rotamers are: **I** −4.8 and 1.0; **II** −1.7 and 1.4;

III −0.1 and 0.6 ppm, respectively. Since the value of the LEF coefficient may involve errors up to a factor of 2 (33*b*), clearly these LEFS are only estimates. Nonetheless, they account for a substantial part of the observed shift effect on C-5 but only for a fraction of the observed effect on C-6. The LEFS suggest that **I** is most populated.

There are additional reasons why the δ_1 effect on C-6 is large. First, the sp^2 hybridized C-6 does not necessarily experience the same δ_1 effect as the sp^3 hybridized carbons. Whether the δ_1 effect on sp^2 carbons is generally larger than on sp^3 carbons cannot be stated at this time, since the present series of compounds and those in ref. 9 represent the only report of δ_1 effects on sp^2 carbons. Second, in monohydroxylated cholestanes and androstanes, smaller δ_1 effects were observed for the more rigid molecules and also for larger OH to δ_1 carbon distances (5). Indeed, the very small (−0.1 and +0.4 ppm) δ_1 effect on C-7 in the 15β-hydroxyl compounds was attributed to the considerably larger (ca. 30%) than usual internuclear distance between the oxygen and δ_1 carbon. In rotamer **I** of the 19-O compounds, the C-8 to O internuclear distance has the usual (2.5 ± 0.2 Å) value, whereas the C-6 to O internuclear distance is considerably larger (3.1 ± 0.2 Å). However, there is reason to believe (see the following two paragraphs) that the preferred orientation of the substituent is not precisely *anti* C-1 but slightly rotated toward the C-5 eclipsed position. This would increase the substituent to C-8 distance and account for the lower δ_1 effect on this carbon.

Recently, a shorter T_1 (hence slower rotation rate) was observed for the C-19 methyl in androst-5-ene than in androstan-17-one (36) and was attributed to a lower energy of the preferred conformer in the 5-ene. In the 17-ketone, the C-19 methyl group has *syn*-axial interactions with the axial protons on carbons 2, 4, 6, 8, and 11. In the 5-ene, the interaction with the axial proton on C-6 has been removed; this is believed to account for the lower energy of the preferred rotamer in this compound.

In the present work, the stability of one staggered rotamer over another is most probably due to the presence of the C=C. Since C-6 has no H, the bulky substituent (OH or I) in **I** experiences fewer nonbonded proton interactions, which accounts for the lower energy. Furthermore, the nonbonded interaction between the substituent and 8β-H can be decreased if the substituent is slightly rotated toward the C-5 eclipsed position and since there is no 6β-H, this will *not* result in an increased interaction between the substituent and the 6β-H.

Thus we postulate that because of the double bond, the nonbonded interaction between the substituent and the 8β-H in **I** is less severe than the interaction between the substituent and 11β-H in **II**. And furthermore that it is much less than the combined nonbonded interactions between the substituent and the axial protons on C-2 and C-4 in **III**. If this is so, then the relative populations of the rotamers should be **I** > **II** ≫ **III**. Furthermore, the more bulky the substituent on C-19, the more rotamer **I** would be stabilized, relative to rotamer **II**. This may well explain why rotamer **II** is populated for the 19-O compounds but not for the 19-I compounds. (The covalent radius of iodine is almost twice that of oxygen.)

For the 6β-iodomethyl compound similar considerations would predict that the nonbonded interaction between the substituent and 8β-H in **B** is less severe than the interaction between the substituent and 4β-H in **C**. Hence **B** would be of lower energy than **C**. But because there are no δ_1 interactions in rotamer **A**, this rotamer may be of lowest energy. We will give experimental evidence in subsequent paragraphs to show that the relative populations of rotamers **I**, **II**, **III** and of **A**, **B**, **C** are indeed as predicted.

The strong deshielding of C-6 in the 19-I compounds and of C-10 in **8***a* is consistent with the δ_1 interaction between these carbons and iodine, if the most populated rotamers are **I** and **B**, respectively. Since C-8 is also δ_1 to the iodine in these rotamers, the much smaller substituent effect at C-8 most likely arises from the slight rotation of the substituent toward the C-5 eclipsed position, as previously discussed for the 19-O compounds. The difference in iodine substituent effect between C-8 and C-6 is identical to the difference in oxygen substituent effect between these carbons.

The lack of deshielding effects at C-2 and C-4 for the 19-substituted compounds and at C-4 for **8** shows the absence of δ_1 interaction for these carbons, hence negligible population of rotamers **III** and **C**. (See Table 3.) Thus by the analysis of all the γ and δ effects, we established that the rotamers with appreciable populations are **I** for the 19-I compounds, **I** and **II** for the 19-O compounds, and **A** and **B** for **8**.

TABLE 3. Spacial relationship[a] between the substituent and the δ carbon in the staggered rotamers[b]

	C-19 substituted				6β-Methyl substituted		
δ carbon	**I**[b]	**II**[b]	**III**[b]	δ carbon	**A**[b]	**B**[b]	**C**[b]
C-2	δ_2	δ_3	δ_1	C-4	δ_5	δ_3	δ_1
C-4	δ_3	δ_2	δ_1	C-8	δ_3	δ_1	δ_2
C-6	δ_1	δ_2	δ_3	C-10	δ_2	δ_1	δ_3
C-8	δ_1	δ_3	δ_2				
C-11	δ_3	δ_1	δ_2				

[a]The spacial relationship between the substituent and the δ carbon is designated by δ_1 to δ_5 (refs. 3*b* and 5).
[b]The rotamers **I**, **II**, **III** and **A**, **B**, **C** are shown in Fig. 2.

TABLE 4. Temperature dependence of the C-19 hydroxy and of the 6β-iodomethyl iodine substituent effect on ^{13}C shifts[a]

	α		β		γ		δ	
Substituent	Carbon	Δ ppm	Carbon	Δ ppm	Carbon	Δ ppm	Carbon	Δ ppm
—OH[b]	C-19	−0.36	C-10	−0.16	C-1	+0.05	C-2	+0.13
					C-5	−0.08	C-4	−0.17
					C-9	−0.04	C-6	+0.10
							C-8	+0.24
							C-11	−0.56
−I[c]	6β-Me	+0.37	C-6	+0.39	C-5	−0.04	C-4	+0.19
					C-7	−0.11	C-8	−0.15
							C-10	+0.11

[a]All compounds 0.5 *M* in $CDCl_3$.
[b]Substituent effect at +34°C (shifts of **2***b* − shifts of **1***b*) subtracted from substituent effect at −20°C (shifts of **2***b* − shifts of **1***b*).
[c]Substituent effect at +34°C (shifts of **10***a* − shifts of **9**) subtracted from substituent effect at −20°C (shifts of **10***a* − shifts of **9**). Positive values indicate increased deshielding at −20°C. Spectra were run at 3500 Hz sweep width, therefore, the shifts are known with ±0.04 ppm precision.

We then examined the temperature dependence of the 19-hydroxy substituent effect to establish whether rotamer **I** or **II** is of lower energy. Similarly, the temperature dependence of the 6β-iodomethyl iodine substituent effect was used to establish the relative population of rotamers **A** and **B**.

Temperature Dependence of the C-19 Hydroxy and of the 6β-Iodomethyl Iodine Substituent Effects

^{13}C spectra were obtained for compounds **1***b*, **2***b*, **7**, and **8***a* over the temperature range of +34 to −20°C. The solubilities in chloroform decreased to such an extent that it was not practical to obtain spectra below −20°C. Thus the conformational equilibrium could be studied only in the fast exchange limit. This generally provides only a first approximation to the equilibrium (11*e*); therefore, the relative rotamer populations obtained in this manner should be considered indicative rather than conclusive.

By comparing the chemical shifts at +34 and −20°C, the temperature dependences shown in Table 4 were obtained. As expected, the temperature dependence of the substituent effects over the 54°C temperature range was small; however, many of the observed effects were 4 to 14 times as large as the experimental error, and therefore can be considered significant. The α and β effects show substantial changes, which are not readily analyzable, since these effects are a composite of inductive, resonance, and steric effects (11*b*, 20).

The temperature dependence of the hydroxy γ effects is only on the order of the experimental error. The hydroxy δ effects are larger (2 to 14 times as large as the experimental error). If rotamer **I** is of lower energy, then decreasing the temperature should further increase the population of rotamer **I** relative to rotamer **II**. Inspection of Table 3 and the expected shifts of the δ carbons (δ_1 strong deshielding, δ_2 moderate deshielding, δ_3 and δ_4 very small effect, δ_5 moderate shielding (5)) allows us to predict deshielding of C-2, C-6, C-8 and shielding of C-4 and C-11 at lower temperature. This is indeed the experimentally observed trend.

For **8***a* the temperature dependence of the δ effects is smaller and of the γ effect slightly larger than for **2***b*. Half of these effects (at C-4 and C-10) indicate that rotamer **B** is of lower energy, whereas the other two effects (at C-7 and C-8) indicate that rotamer **A** is of lower energy. This can only be interpreted to mean that neither **A** nor **B** predominates. Thus from the careful consideration of the γ and δ substituent effects and their temperature dependence, the following relative rotamer populations are indicated: **I** > **II** ≫ **III** and **A** ~ **B** ≫ **C**. These relative populations are consistent with the hypothesis that it is the presence of the double bond in these compounds which accounts for the relative energies of the rotamers. Moreover, since the energy of **B** is comparable to that of **A**, the stabilizing effect of the double bond is substantial.

Recent data on three 19-hydroxy-4-en-3-one steroids (9) show strong shielding of C-5 and strong deshielding of C-4. More importantly, C-2 is now moderately shielded (+0.6 to +1.2 ppm). These shifts indicate that rotamer **III** has an appreciable population; that is, the 19-OH has the same orientation with respect to the C=C as it did in the 5-ene steroids.

X-ray crystallography showed the 19-OH conformation to be **III** for 19-hydroxyandrost-4-ene-3,17-dione but to be out-of-ring (rather than **I**) for androst-5-ene-3β,17β,19-triol 17-*p*-bromobenzoate (37). The discrepancy between the X-ray and our data for the 5-ene may indicate conformational differences between the crystalline form and the solution, or interaction between the 19-OH and the bulky 17β substituent, or both. However, when there are two substituents on C-19, as in [19-*R*]- and [19-*S*]-19-methylandrost-5-ene-3β,17β,19-triol, the methyl was in the over-B-ring position. The fact that both

TABLE 5. Proton chemical shifts[a]

Proton	1*a*	1*b*	1*c*	2*b*	2*c*	3*a*	3*b*	3*c*	4*a*	4*b*	4*c*	7	8*a*	8*c*
3-H	3.55	4.61	3.07	4.61	3.0	3.54	4.57	3.0	3.5	4.60	3.0	3.9	4.0	3.4
—$OCOCH_3$		2.02		2.02			2.01			2.03				
—OCH_3			3.35		3.35			3.30			3.36			3.35
6-H	5.34	5.37	5.35	5.75	5.75	5.58	5.59	5.56	5.63	5.65	5.63	—[b]	—[b]	—[b]
18-CH_3	0.69	0.68	0.69	0.74	0.74	0.55	0.55	0.62	0.78	0.78	0.80	0.69	0.70	0.71
19-CH_3	1.01	1.02	1.01									—[b,c]		
—CH_2X				3.85	3.83	4.15	4.15	4.12	3.60	3.59	3.60		3.48[d]	3.48[d]
				3.62	3.58	3.99	3.99	3.98	3.30	3.31	3.30		3.06[d]	3.05[d]
21-CH_3	0.93	0.92	0.93	0.92	0.92	0.90	0.90	0.89	0.92	0.93	0.93	0.92	0.92	0.92
26-, 27-CH_3	0.86	0.86	0.86	0.86	0.86	0.86	0.86	0.86	0.86	0.86	0.86	0.86	0.86	0.87

[a]In ppm from tetramethylsilane.
[b]Could not be assigned.
[c]6β-Methyl.
[d]6β-Iodomethyl.

TABLE 6. Substituent effects on proton chemical shifts[a]

Substituent	Compounds[b]	3β-H	6β-H	18-CH_3	19-CH_2		21-CH_3	OCH_3
19-OH	2*b* − 1*b*	0.00	+0.38	+0.06	+2.83	+2.60	0.00	
	2*c* − 1*b*	0.0	+0.40	+0.05	+2.82	+2.57	−0.01	0.00
19-OTs	3*a* − 1*a*	−0.01	+0.24	−0.14	+3.14	+2.98	−0.03	
	3*b* − 1*b*	−0.04	+0.22	−0.13	+3.13	+2.97	−0.02	
	3*c* − 1*c*	0.0	+0.21	−0.07	+3.11	+2.97	−0.04	−0.05
19-I	4*a* − 1*a*	0.0	+0.29	+0.09	+2.59	+2.29	−0.01	
	4*b* − 1*b*	−0.01	+0.28	+0.10	+2.57	+2.29	+0.01	
	4*c* − 1*c*	0.0	+0.28	+0.11	+2.58	+2.30	0.00	+0.01
3β-$OCOCH_3$[c]	1*b* − 1*a*	+1.06	+0.03	−0.01			−0.01	
	3*b* − 3*a*	+1.03	+0.01	0.00	0.00	0.00	0.00	
	4*b* − 4*a*	+1.1	+0.02	0.00	−0.01	+0.01	+0.01	
3β-OCH_3[d]	1*c* − 1*a*	−0.48	+0.01	0.00			0.00	
	3*c* − 3*a*	−0.5	−0.02	+0.07	−0.03	−0.01	−0.01	
	4*c* − 4*a*	−0.5	0.00	+0.02	0.00	0.00	+0.01	

[a]In ppm. Positive values indicate downfield shift. Substitution had no effect (±0.01 ppm) on the chemical shifts of the 26-CH_3, the 27-CH_3 and the 3β-$OCOCH_3$ protons.
[b]Chemical shifts of the two compounds that were compared to obtain the substituent effects.
[c]Acylation of the 3β-OH.
[d]Methylation of the 3β-OH.

diastereomers have the bulkier methyl group in the over-B-ring position suggests that this is the least energy conformation (37).

B. ^1H *Nuclear Magnetic Resonance*

Spectral Assignments

In the ^{1}Hmr spectra only the 3-H, 6-H, and methyl protons were assigned. The results are summarized in Table 5. The spectral assignments relied heavily on previously published steroidal assignments (38). We have previously published the ^{1}Hmr data for compounds **4***a* and **8***a* elsewhere (25), but have included them in Table 5 for the sake of completeness. Our observed ^{1}Hmr data for **8***a* agree with those reported by Kojima and co-workers (22, 24) but not with those of Basmadjian *et al.* (23). The peak positions and intensities reported by Basmadjian *et al.* are not possible for steroids containing the C-20 cholestane side chain (25, 38*a*, 39, 40).

Substituent Effects on Proton Chemical Shifts

The more important effects of substitution on the proton chemical shifts are summarized in Table 6. The largest substituent effect is the nonequivalence of the 19-CH_2 protons in all the C-19 substituted compounds. This nonequivalence is the result of the rotationally averaged chemical shifts of the protons in the three rotamers shown in Fig. 2. Since the rotamers are different, the rotationally averaged chemical shifts of the protons will be different, even if the rotamers were of equal probability. Therefore, the observed nonequivalence of the 19-CH_2 protons does not yield any information about the relative population of the rotamers. However, the nonequivalence of the protons confirms that the rotamers are sufficiently different to cause appreciable (0.2 ppm) chemical shift difference.

The 19-OH deshields the 18-CH_3 by 0.06 ppm. Since the 18-CH_3 is many bonds removed from the 19-OH substituent, the effect must be long range in nature, such as magnetic anisotropy and dipole–dipole interactions. Both of these effects are inversely proportional to the cube of the distance between the affected proton and the substituent (38*b*). Table 7

TABLE 7. Effect of β-hydroxy substitution on C-18 methyl proton chemical shifts

Substituent	18-H[a] (ppm) Ref. 38c	Ref. 41	r[b] (Å)
6β-OH	+0.042	+0.033	4.8
7β-OH	+0.033	+0.022	4.2
8β-OH	+0.183		2.0
11β-OH	+0.242	+0.242	2.0
12β-OH	+0.067		2.6

[a]Relative to unsubstituted androstane. Positive values indicate downfield shift.
[b]Approximate (±0.2 Å) distance from the oxygen nucleus to the nearest proton of the C-18 methyl, as measured from molecular models. The same distance in the rotamers of **2** is **I**, 3.1 Å; **II**, 3.1 Å; **III**, 5.1 Å.

shows some of the previously observed (38*c*, 41) effects of B- and C-ring β-OH substitution on the 18-CH_3. This table also contains the approximate distance from the oxygen nucleus to the nearest proton in the 18-CH_3 and this distance in the three rotamers of Fig. 2. Only the 12β-OH substituent effect of 0.067 ppm is comparable to the 0.06 ppm effect observed for the 19-OH substituent. The 8β- and 11β-OH effects are much larger because of their close proximity to the 18-CH_3 and the 6β- and 7β-OH effects are smaller because of the larger distance. It is noteworthy that only in rotamers **I** and **II** is the distance comparable to the distance in the 12β-OH compound. The distance in rotamer **III** is considerably larger and would yield smaller substituent effects than observed. Therefore, the 19-OH substituent effects on the 18-CH_3 proton chemical shifts further support the conclusion reached from ^{13}C chemical shift effects that rotamers **I** and **II** predominate at room temperature. Furthermore, the 0.38 to 0.40 ppm deshielding of the 6β-H by the 19-OH suggests close proximity of the oxygen and the 6β-H and, hence, the predominance of rotamer **I**.

The 19-I substituent effect on the proton chemical shifts are comparable to those of the 19-OH substituent. This suggests that for the 19-I substituted compounds, also, rotamer **I** predominates. The 19-OTs substituent deshields the methyl protons at C-18 and C-21, and also the 3β-*O*-methyl of **3***c*, undoubtedly because of the ring current effect of the aromatic ring. However, because the deshielding effect of the aromatic ring can extend to distances of several ring radii (42), and because the *p*-toluenesulfonyl substituent group is internally flexible, no statement can be made from the ^1Hmr data about the relative population of the rotamers in the 19-OTs compounds.

Conclusions

Since this is the first investigation of long-range shift effects in the conformational analysis of substituted methyls in steroids, it remains to be seen whether this method is generally applicable. However, the present study shows the feasibility of utilizing γ and δ effects for conformational analysis of some steroid derivatives even when the rotamers are rapidly interconverting. The method should be applicable to short side chain conformers in other rigid ring systems and, to a more limited extent, to highly branched acyclic compounds. A large shielding γ effect is expected for rotamers in which the substituent removes a 1,3-diaxial proton–proton interaction. The δ_1 interaction will act as an indicator by deshielding carbons in rotamers with appreciable population. Moreover, if the carbons δ_1 to the substituent have protons to give nonbonded interaction with the substituent, the rotamer is expected to be destabilized in proportion to the number of these interactions. Thus the observed γ and δ effects may establish which rotamers are appreciably populated. In the case of more than one highly populated rotamer, the temperature dependence of these shift effects may establish the relative stabilities of the rotamers.

Experimental

Nuclear Magnetic Resonance

Nuclear magnetic resonance spectra were obtained with a Bruker model HX-90 spectrometer equipped with a fast Fourier transform system using a Nicolet model 1083 computer. Proton spectra were obtained at 90.00 MHz and ^{13}C spectra at 22.63 MHz spectrometer operating frequencies. The samples were dissolved in a stock solution of deuteriochloroform which contained 5% by volume hexafluorobenzene (the fluorine signal served as the field-frequency stabilization signal) and tetramethylsilane in 1% by volume concentration for ^1Hmr spectra and 10% by volume concentration for ^{13}Cmr spectra. Solution concentrations ranged from 0.05 to 2.0 *M* and were dictated by the amount of sample available. The ^{13}Cmr shifts could be determined with 0.05 ppm precision and ^1Hmr shifts with 0.01 ppm precision, except for 0.1 ppm precision for the very broad H-3 resonance.

Materials

Compounds **1***a*, **1***b*, **6**, and 5α-pregn-9(10)-ene-16α-methyl-17,21-diol-3,20-dione 21-acetate were commercially available. An authentic sample of **5** (26) was kindly supplied by Dr. S. G. Levine.

The remaining compounds were synthesized by known methods in the following sequence: **1***b* → 5α-bromo-cholestan-3β,6β-diol 3-acetate (43–46) → 5α-bromo-6β,19-oxidocholestan-3β-ol 3-acetate (43, 44, 46, 47) → **2***b* (43, 44, 48); **2***b* → **3***b* (43–45); **3***b* → **4***b* (44, 49); **3***a* and **4***a* were prepared from **3***b* and **4***b*, respectively (43, 44); **4***a* → **8***a* (25); **8***a* → **7** (22).

Compound **1***c*, was synthesized by the action of perchloric acid on **1***a* in trimethylorthoformate (43, 50). The same method was also used to prepare **8***c* from **8***a*. Compound **4***c* was similarly prepared from **4***a* by the use of triethyl orthoformate (43). The reaction sequence for the remaining 3β-methoxy derivatives, **2***c*–**4***c*, started with **1***c* and was as for the 3-acetates described in the previous paragraph (43).

All compounds tested gave satisfactory elemental analyses and had melting points as reported in the literature. All solid compounds were found to be spectroscopically pure by ^{13}Cmr and ^1Hmr. Compounds **7**, **8***a*, and **8***c* were oils. High pressure liquid chromatographic separation of **8***a*, as previously de-

scribed, yielded a pale yellow glass, which was shown by ^{13}Cmr to be >98 mol% pure (25). Compounds **7** and **8***c* were not purified by high pressure liquid chromatography but the impurities detected by ^{13}Cmr and ^{1}Hmr did not interfere with the spectroscopic analysis, except possibly for the assignment of C-5 in **8***c* (see Table 1).

Acknowledgments

Financial support was provided by the Medical Research Service of the Veterans Administration. We are indebted to Drs. H. L. Holland, P. R. P. Diakow, and G. J. Taylor for letting us use some of their data before publication. This led to a reassignment of C-1 and C-7 in our 19-O compounds and aided the discussion of results for the 5-ene compounds. We thank Dr. S. G. Levine for providing a sample of **5** and Dr. J. A. Owoyale for the syntheses of the 3β-methoxy and 3β-ethoxy derivatives. We are greatly indebted to Dr. M. W. Couch for the syntheses of all other compounds and to Dr. C. M. Williams for initiating the research project.

1. W. H. Ayer, L. M. Browne, S. Fung, and J. B. Stothers. Org. Magn. Reson. **11**, 73 (1978).
2. K. Seidman and G. E. Maciel. J. Am. Chem. Soc. **99**, 659 (1977); D. J. Gorenstein. J. Am. Chem. Soc. **99**, 2254 (1977).
3. (*a*) S. H. Grover, J. P. Guthrie, J. B. Stothers, and C. T. Tan. J. Magn. Reson. **10**, 227 (1973); (*b*) S. H. Grover and J. B. Stothers. Can. J. Chem. **52**, 870 (1974); (*c*) J. B. Stothers, C. T. Tan, and K. C. Teo. J. Magn. Reson. **20**, 570 (1975); (*d*) J. B. Stothers, C. T. Tan, and K. C. Teo. Can. J. Chem. **54**, 1211 (1976).
4. J. W. Blunt. Aust. J. Chem. **28**, 1017 (1975).
5. H. Eggert, C. L. Van Antwerp, N. S. Bhacca, and C. Djerassi. J. Org. Chem. **41**, 71 (1976).
6. L. P. Lindeman and T. Q. Adams. Anal. Chem. **43**, 1245 (1971).
7. J. G. Batchelor, J. Magn. Reson. **18**, 212 (1975).
8. P. J. Flory. Statistical mechanics of chain molecules. John Wiley and Sons, New York, NY. 1969. Chapt. 3.
9. H. L. Holland, P. R. P. Diakow, and G. J. Taylor. Can. J. Chem. This issue.
10. H. J. Reich, M. Jautelat, M. T. Messe, F. J. Weigert, and J. D. Roberts. J. Am. Chem. Soc. **91**, 7445 (1969).
11. J. B. Stothers. Carbon-13 nmr spectroscopy. Academic Press, New York, NY. 1972. (*a*) pp. 439–451; (*b*) pp. 140–141; (*c*) p. 133; (*d*) p. 56; (*e*) pp. 420–432.
12. L. F. Johnson and W. C. Jankowski. Carbon-13 nmr spectra. John Wiley and Sons, New York, NY. 1972. (*a*) Spectrum No. 494; (*b*) Spectrum No. 13.
13. H. H. Mantsch and I. C. P. Smith. Can. J. Chem. **51**, 1384 (1973).
14. W. B. Smith, D. L. Davenport, J. A. Swanzy, and G. A. Pate. J. Magn. Reson. **12**, 15 (1973).
15. H. Eggert and C. Djerassi. J. Org. Chem. **28**, 3788 (1973).
16. D. Leibfritz and J. D. Roberts. J. Am. Chem. Soc. **95**, 4996 (1973).
17. R. J. Abraham and J. R. Monasterios. J. Chem. Soc. Perkin Trans. **2**, 662 (1974).
18. R. J. Cushley and J. D. Filipenko. Org. Magn. Reson. **8**, 308 (1976).
19. J. W. Blunt and J. B. Stothers. Org. Magn. Reson. **8**, 439 (1977).
20. J. D. Roberts, F. J. Weigert, J. I. Kroschwitz, and H. J. Reich. J. Am. Chem. Soc. **92**, 1338 (1970).
21. T. D. Brown. Ph.D. Thesis, University of Utah, Salt Lake City, UT. 1965.
22. M. Kojima, M. Maeda, H. Ogawa, K. Nitta, and T. Ito. J. Chem. Soc. Chem. Commun. 47 (1975).
23. G. P. Basmadjian, K. R. Hetzel, R. D. Ice, and W. H. Beierwaltes. J. Labelled Compounds, **11**, 427 (1975).
24. M. Maeda, M. Kojima, H. Ogawa, K. Nitta, and T. Ito. Steroids, **26**, 241 (1975).
25. K. N. Scott, M. W. Couch, T. H. Mareci, and C. M. Williams. Steroids, **28**, 295 (1976).
26. S. G. Levine, N. H. Eudy, and C. F. Leffler. J. Org. Chem. **31**, 3995 (1966).
27. H. Spiesecke and W. G. Schneider. J. Chem. Phys. **35**, 722 (1961).
28. J. B. Grutzner, M. Jautelat, J. B. Dence, R. A. Smith, and J. D. Roberts. J. Am. Chem. Soc. **92**, 7107 (1970).
29. N. S. Bhacca, D. D. Giannini, W. S. Jankowski, and M. E. Wolff. J. Am. Chem. Soc. **95**, 8421 (1973).
30. H. Beierbeck and J. K. Saunders. Can. J. Chem. **54**, 2985 (1976).
31. A. D. Buckingham. Can. J. Chem. **38**, 300 (1960).
32. J. Feeney, L. H. Sutcliffe, and S. M. Walker. Mol. Phys. **11**, 117 (1966).
33. (*a*) J. G. Batchelor, J. H. Prestegard, R. J. Cushley, and S. R. Lipsky. J. Am. Chem. Soc. **95**, 6358 (1973); (*b*) J. G. Batchelor. J. Am. Chem. Soc. **97**, 3410 (1975).
34. H.-J. Schneider, G. Gschwendtner, and U. Buchheit. J. Magn. Reson. **26**, 175 (1977).
35. V. I. Minkin, O. A. Osipov, and Y. A. Zhdanov. Dipole moments in organic chemistry. Plenum Press, New York, NY. 1970. Chapt. III.
36. J. W. ApSimon, H. Beierbeck, and J. K. Saunders. Can. J. Chem. **53**, 338 (1975).
37. Y. Osawa, K. Shibata, D. Rohrer, C. Weeks, and W. L. Duax. J. Am. Chem. Soc. **97**, 4400 (1975).
38. N. S. Bhacca and D. H. Williams. Applications of nmr spectroscopy in organic chemistry. Holden-Day, San Francisco, CA. 1964. (*a*) pp. 7 and 35; (*b*) p. 24 and references cited; (*c*) pp. 20–22.
39. N. S. Bhacca, L. F. Johnson, and J. N. Shoolery. High resolution nmr spectra catalog. Vol. 1. Varian Associates, Palo Alto, CA. 1962. Spectrum No. 363.
40. N. S. Bhacca, D. P. Hollis, L. F. Johnson, and E. A. Pier. High resolution nmr spectra catalog. Vol. 2. Varian Associates, Palo Alto, CA. 1963. Spectrum No. 698.
41. W. Arnold, W. Meister, and G. Englert. Helv. Chim. Acta, **57**, 1559 (1974).
42. C. E. Johnson, Jr. and F. A. Bovey. J. Chem. Phys. **29**, 1012 (1958); J. W. Emsley, J. Feeney, and L. H. Sutcliffe. High resolution nuclear magnetic resonance spectroscopy. Vol. 1. Pergamon Press, London, England. 1965. pp. 595–604.
43. J. A. Owoyale. Ph.D. Dissertation, University of Florida, Gainesville, FL. 1975.
44. M. W. Couch, K. N. Scott, and C. M. Williams. Steroids, **27**, 451 (1976).
45. M. Akhtar and D. H. R. Barton. J. Am. Chem. Soc. **86**, 1528 (1964).
46. D. R. James and C. W. Shoppee. J. Chem. Soc. 4224 (1954).
47. R. M. Moriarty and T. D. J. D'Silva. Tetrahedron, **21**, 547 (1965).
48. J. Kalvoda, K. Heusler, J. Ueberwasser, G. Anner, and A. Wettstein. Helv. Chim. Acta, **46**, 1361 (1963).
49. R. E. Counsell, V. V. Ranade, R. J. Blair, W. H. Beierwaltes, and P. A. Weinhold. Steroids, **16**, 317 (1970).
50. J. P. Dusza, J. P. Joseph, and S. Bernstein. Steroids, **8**, 495 (1966).

C-Stannane derivatives of carbohydrates[1]

LAURANCE D. HALL, PAUL R. STEINER,[2] AND DIANE C. MILLER
Department of Chemistry, University of British Columbia, Vancouver, B.C., Canada V6T 1W5

Received June 7, 1978

LAURANCE D. HALL, PAUL R. STEINER, and DIANE C. MILLER. Can. J. Chem. **57**, 38 (1979).

Triphenyltin lithium (**1**) was reacted separately with 1,2:3,5-di-*O*-methylene-6-*O*-tosyl-α-D-glucofuranose (**2**), with methyl 2,3-anhydro-4,6-*O*-benzylidene-α-D-allopyranoside (**4**), and with methyl 2,3-anhydro-4,6-*O*-benzylidene-α-D-mannopyranoside (**6**), to form in each case a sugar–stannane derivative having a stable carbon–tin bond. These products have been studied by ^{1}H and ^{13}C nmr spectroscopy.

LAURANCE D. HALL, PAUL R. STEINER et DIANE C. MILLER. Can. J. Chem. **57**, 38 (1979).

On a fait réagir le triphénylstannyl lithium (**1**) avec le di-*O*-méthylène-1,2:3,5 *O*-tosyl-6 α-D-glucofurannose (**2**), avec l'anhydro-2,3 *O*-benzylidène-4,6 α-D-allopyrannoside de méthyle (**4**) et avec l'anhydro-2,3 *O*-benzylidène-4,6 α-D-mannopyrannoside de méthyle (**6**); on a obtenu dans chacun des cas un dérivé sucre–stannane comportant une liaison carbone–étain stable. On a étudié ces produits au moyen de la spectroscopie rmn de ^{1}H et du ^{13}C.

[Traduit par le journal]

Introduction

Organotin compounds are finding (3) an ever increasingly wide range of industrial applications in areas ranging from the formation of wood preservation and marine antifouling paints, to food packaging (where they are used as stabilizers in polyvinylchloride films). Prompted by the fact that carbohydrate derivatives can be either water soluble or, when suitably substituted, soluble in organic media, we have investigated the synthesis of sugar–tin conjugates in which a tin moiety is covalently coupled to a sugar via a tin–carbon bond. It might be anticipated that such derivatives could have interesting biological properties resulting from the combined presence of the sugar and metal moieties; there is some basis for this speculation in the form of sucrose–triaryltin conjugates which have recently been shown[3] to be effective in marine antifouling paints.

From a more academic standpoint there is also a need for organo–tin materials which have defined conformations in solution to serve as models for further (4) evaluating the stereospecific dependencies of various spectroscopic parameters of tin, particularly scalar, spin–spin couplings. The success of such measurements is dependent both on the molecule having a conformation which can be determined with reasonable confidence using 'conventional' methods and an nmr spectrum which is sufficiently well resolved to enable transitions from the subspectra of the two molecules which are substituted by a magnetic isotope of tin (^{117}Sn, 7.54% or ^{119}Sn, 8.62%) to be detected in the presence of the substantially higher abundance of molecules which bear a nonmagnetic tin isotope (83.62%). As will be seen later, although the sugar derivatives we have synthesized are not perfectly satisfactory, they nevertheless provide an abundance of interesting data. In the following discussion, we describe the routes to the synthesis of derivatives having an organotin (specifically, in this case, a triphenyltin) moiety attached to either a primary, or a secondary, carbon atom of a sugar. We also document the use of ^{1}H and ^{13}C nmr to evaluate the primary structure and the solution conformation of these substances.

Results and Discussion

Synthesis

The two synthetic routes reported here both involve nucleophilic attack on a suitably activated sugar substrate by triphenyltin lithium (**1**) from triphenyltin chloride and lithium metal by the method of Tamborski *et al.* (5).

Synthesis of a sugar substituted at a primary centre is exemplified by the reaction of triphenyltin lithium (**1**) with 1,2:3,5-di-*O*-methylene-6-*O*-tosyl-α-D-glucofuranose (**2**). Thin-layer chromatography showed that the reaction was essentially completed after 2 h and work-up, as described in the Experimental, afforded a colourless crystalline product **3** in 43% yield, mp 108–110°C. The elemental microanalytical data and ^{1}H nmr parameters indicated that **3** has the structure (1,2:3,5-di-*O*-methylene-α-D-glucofuranos-6-yl) triphenylstannane. Important in the latter interpretation was the observation of the characteristically

[1]For preliminary communications, see refs. 1 and 2.

[2]Present address, Western Forest Products Laboratory, 6620 N.W. Marine Drive, Vancouver, B.C.

[3]L. Hough. Private communication.

0008-4042/79/010038-06$01.00/0

intense resonances of the protons of the triphenyl moiety and the pronounced high-field shift of the protons attached to the same carbon as the triphenyltin moiety; in benzene-d_6, the H-6 resonances of the tin product **3** were at τ 8.5 whereas those of 1,2:3,5-di-*O*-methylene-α-D-glucofuranose (**8**) came at ca. τ 6.65; see Experimental for Fig. 1 caption.

Attention was next directed to the more challenging problem of attaching a tin substituent to a secondary carbon centre. To our pleasant surprise we found that the triphenyltin lithium (**1**) reacted

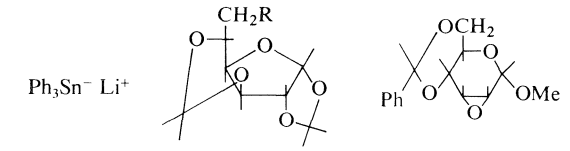

1 **2** R = OTs; **3** R = $SnPh_3$ **4**

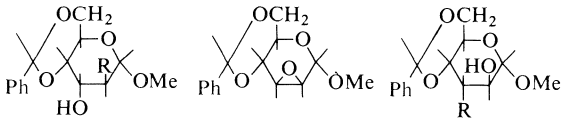

5 R = $SnPh_3$ **6** **7** R = $SnPh_3$

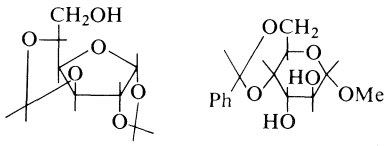

8 **9**

almost instantaneously with methyl 2,3-anhydro-4,6-*O*-benzylidene-α-D-allopyranoside (**4**). A colourless solid product was obtained after conventional work-up, in 75% yield, mp 67–69°C, which was subsequently identified as (methyl 4,6-*O*-benzylidene-α-D-altropyranoside-2-yl) triphenylstannane (**5**). In like fashion, methyl 2,3-anhydro-4,6-*O*-benzylidene-α-D-mannopyranoside (**6**) gave in 94% yield (methyl 4,6-*O*-benzylidene-α-D-altropyranoside-3-yl) triphenylstannane (**7**), mp 166–168°C.

Nuclear Magnetic Resonance Spectra and Conformational Properties

Proton Data

The ^1H chemical shifts and coupling constants for the triphenyltin derivatives **3**, **5**, and **7** are summarized in Table 1 together with, for comparison purposes, the data for 1,2:3,5-di-*O*-methylene-α-D-glucofuranose (**8**) and methyl 4,6-*O*-benzylidene-α-D-altropyranoside (**9**).

That the parameters for the ring protons of **3** and **8** are so closely similar implies that both derivatives have similar solution conformations, probably ap-

TABLE 1. Chemical shifts (τ values) and multiplet splittings (Hz) for methyl 4,6-*O*-benzylidene-α-D-altropyranosides and 1,2:3,4-di-*O*-methylene-α-D-glucofuranoses in deuteriobenzene solutions

Compound	H-1	H-2	H-3	H-4	H-5	H-6	H-6′	OMe	Aromatic protons	Benzyl proton
3	4.14	5.75	6.05	6.32	5.59	8.37	8.68		2.6	[a]
	$J_{1,2}$3.8	$J_{2,3}$0	$J_{3,4}$2.4	$J_{4,5}$2.3	$J_{5,6}$11.3	$J_{6,6'}$−13.3	$J_{5,6'}$ 6.1			
5	4.82	6.93	5.14	6.01	5.47	5.65	6.23	7.35	2.48	4.64[b]
	$J_{1,2}$0.5	$J_{2,3}$2.6	$J_{3,4}$2.5	$J_{4,5}$9.1	$J_{5,6}$ 4.7	$J_{6,6'}$−10.3	$J_{5,6'}$ 8.8			
7	5.63	8.58	7.26	5.55	6.03	6.45	6.09	7.19	2.80–2.17	4.57[c]
	$J_{1,2}$0	$J_{2,3}$2.1	$J_{3,4}$5.9	$J_{4,5}$8.8	$J_{5,6}$11.4	$J_{6,6'}$−11.8	$J_{5,6'}$ 4.8			
8	4.14	5.59	5.96	6.21	6.07	6.65				[d]
	$J_{1,2}$3.75	$J_{2,3}$0	$J_{3,4}$2.6	$J_{4,5}$1.9	$J_{5,6}$ 5.3	$J_{6,6'}$ −6	$J_{5,6'}$ 0			
9	5.68	6.02	6.32	6.13	5.84	5.87	6.38	7.07	2.56	4.57[e]
	$J_{1,2}$0	$J_{2,3}$	$J_{3,4}$2.9	$J_{4,5}$9.5	$J_{5,6}$7	$J_{6,6'}$−11.5	$J_{5,6'}$11.7			

[a] O, H, X, H 5.31 and 5.60.
[b] —OH 6.38, $J_{OH,3}$ = 8.7 Hz.
[c] —OH 5.84, $J_{OH,2}$ = 3.6 Hz.
[d] O, H, X, H 5.25, 5.33, 5.40; —OH 2.83.
[e] —OH-2 7.26, $J_{OH,2}$ = 7.5 Hz; —OH-3 5.44, $J_{OH,3}$ ~1 Hz.

proximating to the $^3T_2$ conformation shown in **A**. More interesting are the very substantial differences between the two sets of parameters for the protons associated with C-5 and C-6. It seems reasonable to ascribe the change in the geminal coupling from −6 Hz for **8** to −13.3 Hz for **3** to the difference in 'electronegativity' between —OH and —$SnPh_3$ substituents. In the absence of adequate reference data it is not sensible to attempt a quantitative interpretation of the vicinal ^1H–^1H couplings. Nevertheless we depict below in **B**, **C**, and **D** the three noneclipsed rotamers about the C-5—C-6 bond of **3** with the corresponding rotamers for **8** depicted in **E**, **F**, and **G**. From the data given in Table 1, it appears **3** favours either rotamer **B** or **D** and examination of molecular models suggests that rotamer **B** is the more favoured because of the substantial steric interaction in **D** between the sugar ring and the triphenyltin moiety.

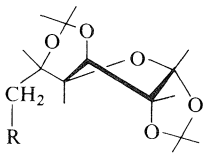

A

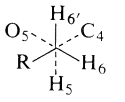

B R = $SnPh_3$
E R = OH

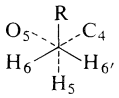

C R = $SnPh_3$
F R = OH

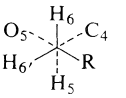

D R = $SnPh_3$
G R = OH

We had anticipated that opening of the epoxide ring of **4** would occur by nucleophilic attack on C-2 and this was confirmed by the finding that the H-2 resonance of **5** was shifted to high field (τ 6.93) of the other ring protons; see Experimental for Fig. 2 caption. The vicinal, ring proton coupling constants for **5** are close to those reported by Coxon (6) for derivatives of methyl 4,6-*O*-benzylidene-α-D-altropyranoside (**9**) and measured by us for **9** itself. Without repeating here Coxon's earlier discussion, it is clear that the triphenyltin moiety of **5** has seriously perturbed the pyranose ring from the $^4C_1$ conformation depicted in **H**.

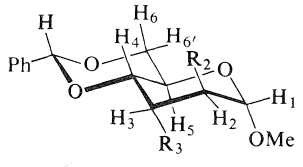

H

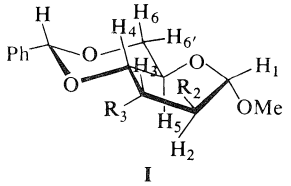

I

That the triphenyltin moiety of **7** was attached to C-3 was evidenced by the high-field shift of H-3, thus confirming that the ring-opening of **6** had also followed the expected course. Although the vicinal ^1H–^1H couplings serve to confirm that this product has the α-D-altropyranose configuration it is noteworthy that $J_{3,4}$ is substantially larger (5.9 Hz) than the equivalent coupling of either **5** (2.5 Hz) or **9** (2.9 Hz). It is tempting to simply ascribe this differential to an electronegativity effect of the tin moiety, yet, if that were so, it is difficult to understand why a similar enhancement is not also observed for $J_{2,3}$, which is, if anything, smaller (2.1 Hz) for **7** than for **8**. An alternative explanation is that the pyranose ring is distorted by steric interaction involving the triphenyltin moiety towards the skew conformation, $^OS_5$, depicted in **I**; this conformational change would diminish the dihedral angle between H-3 and H-4 and this would be accompanied by an increase in $J_{3,4}$. In the absence of more comprehensive reference data is is clearly not fruitful to pursue this point too far. Nevertheless, it seems more than coincidental that whereas the H-3 resonance of **5** appears to have a normal shift, the H-2 resonance of **7** is shifted to high field by ca. 2 ppm. A field shift of this magnitude clearly reflects a substantial interaction between the H-2 proton and the ring current of the aromatic rings of the triphenyltin moiety.

Carbon-13 Data

Assignments of the ^{13}C nmr spectra were based on the selective proton decoupling technique summarised in the Experimental and the ^{13}C shifts for derivatives **3**, **5**, and **7** are summarised in Table 2. These data are unexceptional. That the carbon which bears the tin substituent is invariably the higher-field resonance suggests that this is a reliable criterion for assigning positional isomerisation in this class of sugar–tin conjugates, more reliable in fact than the analogous ^1H shifts, see Experimental for Fig. 3 caption.

Tin Coupling Constants

The remainder of this discussion will be concerned with the coupling constants between the two magnetic isotopes of tin and suitably disposed ^1H and ^{13}C nuclei and with their stereospecific dependencies.

It proved to be very difficult to detect in either the 100 MHz or 270 MHz proton spectra of derivatives **3**, **5**, and **7** any satellites arising from coupling with the ^{117}Sn and ^{119}Sn nuclei, mainly because the satellite transitions were for the most part obscured by the transitions of the protons of those molecules substituted by a nonmagnetic tin isotope. The only clearly resolved tin couplings in the spectra of **5** are with H-1 (25.8 Hz) and with H-2 (73.4 Hz) and for **3** with H-3 (56.2 Hz).

In contrast to the ^1H spectra, the ^{13}C resonances were sufficiently well dispersed, even at 20 MHz,

TABLE 2. ^{13}C chemical shifts (ppm) for methyl 4,6-*O*-benzylidene-α-D-altropyranosides and 1,2:3,4-di-*O*-methylene-α-D-glucofuranoses in deuteriobenzene solutions

Compound	C-1	C-2	C-3	C-4	C-5	C-6	—OCH_3	O H / O H	Benzy
3	105.09	83.59	75.39	80.68	71.47	14.95		96.33 85.79	
5	101.91	38.61	69.37	79.19	59.32	68.64	54.76		102.41
7	101.1	70.81	35.29	77.15	64.32	69.35	53.74		100.56

TABLE 3. ^{13}C-Sn coupling constants (Hz) for tin–sugar derivatives

Compound	n	$^1J(^{119}Sn–^{13}C_n)$	n	$^1J(^{117}Sn–^{13}C_n)$	n	$^2J(Sn–^{13}C_n)$[a]	n	$^3J(Sn–^{13}C_n)$
3	6	372	6	348	5	−24	4	60
5	2	340	2	323	1	−14.8	4	0
					3	−9.6		
7	3	392	3	376	2	−10.1	1	32.8
					2	−32	5	15.7

[a]Sign assumed by analogy with the literature (12).

for the $^{117}Sn–^{119}Sn$ satellite transitions to be readily detectable; see Experimental for Fig. 4 caption. The various coupling constants obtained from the spectra of derivatives **3**, **5**, and **7** are summarised in Table 3. Although it was simple to separately resolve the ^1J couplings of the ^{117}Sn and ^{119}Sn nuclei, the ^2J and ^3J couplings were too small and both the latter sets of data given in Table 3 are averaged values. The magnitudes of these data are in general agreement with values previously reported (4, 5) for cycloalkyl derivatives of tin; thus the ^1J couplings should be larger than the ^3J couplings which should in turn be larger than the ^2J couplings.

The literature data for ^3J ($^{13}C–Sn$) couplings are concisely summarised in Fig. 2, with the familiar (7) cos function being given in [1]; see Experimental for Fig. 5 caption. Although the solution conforma-

$$[1] \qquad J_{obs} = 30.4 - 7.6 \cos\theta + 25.2 \cos 2\theta$$

tions of the derivatives **3** and **7** are by no means as well defined as we had originally hoped, it is instructive to compare their ^3J ($^{13}C–Sn$) couplings, as well as those of **5**, with the data of Fig. 2; as we shall see the conformations previously proposed for all three derivatives appear to be consistent with the observed couplings.

Let us start with the C-2 substituted derivative **5** for which a $^4C_1$ chair conformation **H** had been previously proposed. The coupling between the tin and C-4 substituents cannot be precisely determined, but must lie between 0 and 0.3 Hz. According to the data of Fig. 5 this implies a dihedral separation between the C-4—C-3 and C-2—Sn bonds of 70–100°; conformation **H** would require a dihedral angle of ~95°.

Turning now to the C-3 substituted derivative **7** for which the $^OS_5$ conformation **I** had been suggested, we note that we now have two ^3J couplings to consider, the coupling with C-1 (32.8 Hz) which we must ascribe to a dihedral angle of ca. 130 or 35°, and the coupling with C-5 (15.7 Hz) which should correspond to an angle of ca. 110 or 58°. Since it is impossible to distort a pyranose ring to achieve a dihedral angle of 35°, the C-1 coupling must correspond to the dihedral angle of 130°. Because of the *trans*-fused junction between the pyranose and benzylidene rings limits the extent of possible conformational distortion for the pyranose ring, it is impossible to obtain a dihedral angle between the C-3—Sn and C-4—C-5 bonds of less than ~50°, we must assume that the C-5 coupling corresponds to a dihedral angle of 112°, it happens that the $^OS_5$ conformation **I** previously nominated for **7** would require this angle to be 112°.

Conformational assignments for acyclic derivatives which ignore conformational time averaging are necessarily simplistic so the discussion of the ^3J coupling between C-4 and the tin substituent of **3** cannot be expected to be definitive. Yet the observed coupling (ca. 60 Hz), which can only correspond to a large dihedral angle, is in excellent agreement with the previous assignment of **B** as being the favoured rotamer about the C-5—C-6 bond.

Conclusions

As we noted in the Introduction, we were somewhat disappointed that the tin derivatives **3**, **5**, and **7** did not all have undistorted conformations, since this appeared, at first, to vitiate the major reason for this project. Nevertheless, the agreement between

the conformations deduced by 'conventional' proton nmr methods and the angles based on the ^{13}C—Sn couplings described previously in the literature, and here, provides a compelling, albeit less direct, substantiation for the basic premise that sugar–metal derivatives do provide convenient model systems for heteronuclear nmr studies.

As a final comment we draw attention to the fact that the axial triphenyltin substituent at C-3 but not that at C-2, results in deformation of the conformation of the pyranose ring. This is a perfectly reasonable finding but it has an important implication, namely, that it would now appear to be very worthwhile to evaluate the conformational preferences of other substituents attached to the C-3 position of this altroside system to evaluate their ability to cause conformational distortions. Included in this category could be any of the following: $—C(Me)_3$, $—C(Ph)_3$, $—X(Me)_3$, and $—X(Ph)_3$ where X = Si, Sn, Pb, or P^V.

Experimental

All solutions were concentrated under reduced pressure using a Buchi rotary evaporator. All melting points were determined using a Hoover Unimelt (6406-K) instrument and are uncorrected. All optical rotations were determined for acetone solutions using a Perkin-Elmer 141 polarimeter.

Thin-layer chromatography (tlc) was performed on silica gel G (Merck) using toluene–ether (1:2) and detection by charring with H_2SO_4. All reactions were performed in anhydrous solvents under an atmosphere of dry nitrogen; solvents were dried, distilled, and then stored over molecular sieves.

Triphenyltin chloride (95+ %) was obtained from Alfa Products (Danvers, MA) and was used after recrystallisation from methanol–chloroform and drying at 80°C using Drierite as the dessicant at ca. 0.8 Torr for 24 h. Lithium metal rods (technical grade) were obtained from Fisher Scientific Co., Chemical Manufacturing Division (Fair Lawn, NJ).

Proton nmr spectra were measured at 100 MHz with a Varian XL-100 (15) spectrometer fitted with a Varian 620L (16K) computer; and at 270 MHz with the prototype of a home-built spectrometer based on a Bruker WP-60 console, a Nicolet 1080 computer (16K), a Nicolet 293 pulse controller unit, a Diablo Disk, and an Oxford Instruments Superconducting solenoid. The 270 MHz radiofrequency was derived from the Bruker Console by mixing with the output of a Hewlett Packard frequency synthesiser using a mixing technique developed in this laboratory (8).

Carbon-13 nmr spectra were measured with a CFT-20 spectrometer. The selective proton decoupling experiments used a heteronuclear decoupler, described previously (9); see Fig. 6 caption below.

Nuclear Magnetic Resonance Spectra

Detailed nmr spectra of certain of the materials discussed in this manuscript have been placed in the Depository of Unpublished Data.[4] The full captions of those figures are listed below to provide the reader with a summary of the spectral information which is available. Fig. 1. Continuous-wave ^1H nmr spectrum (100 MHz) of (1,2:3,5-di-*O*-methylene-α-D-glucofuranose-6-yl) triphenylstannane (**3**) (at top) and of 1,2:3,5-di-*O*-methylene-α-D-glucofuranose (**8**) (at bottom), both measured in benzene-d_6 solutions. The peak marked * is from an impurity. Fig. 2. Fourier transform ^1H nmr spectrum (270 MHz) of (methyl 4,6-*O*-benzylidene-α-D-altropyranoside-2-yl) triphenylstannane **5** in benzene-d_6 solution, showing the spectral assignments and the ^1H–Sn coupling constants. Fig. 3. Natural abundance ^{13}C nmr spectra in benzene-d_6 solutions (ca. 0.3 m) of *A*, (1,2:3,5-di-*O*-methylene-α-D-glucofuranose-6-yl) triphenylstannane (**3**) and *B*, 1,2:3,5-di-*O*-methylene-α-D-glucofuranose (**8**). Fig. 4. Natural abundance ^{13}C nmr spectrum of (methyl 4,6-*O*-benzylidene-α-D-altropyranoside-2-yl) triphenylstannane (**5**) in acetone-d_6 solution (0.3 *M*) showing the normal resonances and the tin satellites of the C-1, C-2, and C-3 resonances. (PW 7; PD 0; NT 80 000; AT 1.023 s.) Fig. 5. Magnitudes of $^3J(^{119}Sn–^{13}C)$ coupling constants plotted as a function of the dihedral angle between the $^{119}Sn—^{13}C—C$ bonds. (This diagram is reproduced by permission of the authors of ref. 4.) Fig. 6. Natural abundance ^{13}C nmr spectra of (methyl 4,6-*O*-benzylidene-α-D-altropyranoside-2-yl) triphenylstannane (**5**) benzene-d_6 solution (0.3 m); *A*, with complete proton decoupling and *G*, with the decoupler gated off during the spectral acquisition. The spectra *B*–*F* show the effect of selective irradiation of individual proton resonances.

Preparation of Triphenyltin Lithium

NOTE: It was found that the reaction to form triphenyltin lithium worked well only when the surface of the lithium metal was very clean. It was found necessary to clean the metal surface in dry methanol and then to quickly rinse the piece of metal in dry tetrahydrofuran before adding it to the solvent in the reaction vessel.

Following the procedure of Tamborski *et al.* (6), 2.5 g, (6.5×10^{-3} mol) of triphenyltin chloride in ca. 15 ml tetrahydrofuran was added to a well-stirred solution containing lithium shavings (0.55 g, 0.08 mol) and tetrahydrofuran. Within about 15 min, heat was evolved and the reaction mixture became a dark olive-green colour. The solution was stirred for 1–2 h. after which time it was filtered through glass wool and immediately used for the following reactions. Yields for this reaction have been reported (4, 5) to be 50–75%.

Preparation of (1,2:3,5-Di-O-methylene-α-D-glucofuranose-6-yl) Triphenylstannane (3)

Triphenyltin chloride (2.5 g, 6.5×10^{-3} mol) in tetrahydrofuran were reacted with an excess of lithium metal in the manner described above, for 2 h, filtered through glass wool and added, dropwise, to a stirred solution of 1,2:3,5-di-*O*-methylene-6-*O*-tosyl-α-D-glucofuranose (10) (1.5 g, 4.2×10^{-3} mol) in tetrahydrofuran (25 ml). After 4 h, tlc indicated that all the tosylate had reacted. The reaction mixture was then poured into water (250 ml) and neutralized with ammonium chloride. The mixture was extracted with chloroform (3 × 5 ml) and the chloroform solution dried over magnesium sulfate, after which the solvent was removed under reduced pressure. Any contaminating hexaphenylditin was precipitated by adding cold anhydrous diethyl ether and filtering off the crystals. The ether was then evaporated to yield a white crystalline material which was subsequently identified as **3**; yield, after one recrystallization (benzene – light petroleum, bp 30–60°C was 1 g (43.5%), mp 108–110°C, $[\alpha]_D^{25}$ +60.00° (*c* 2.37). *Anal.* calcd. for $C_{26}H_{26}O_5Sn$: C 58.13, H 4.88; found: C 57.90, H 4.86.

Preparation of (Methyl 4,6-O-Benzylidene-α-D-altropyranoside-2-yl) Triphenylstannane (5)

Triphenyltin chloride (2.5 g, 6.5×10^{-3} mol) and lithium metal (0.5 g, 0.08 mol) were reacted as described above, filtered, and added, dropwise, to a stirred solution of methyl

[4]Copies are available, at a nominal charge, from the Depository of Unpublished Data, CISTI, National Research Council of Canada, Ottawa, Ont., Canada K1A 0S2.

2,3-anhydro-4,6-*O*-benzylidene-α-D-allopyranoside (11) (1.0 g, 3.78×10^{-3} mol) in tetrahydrofuran (ca. 25 ml). The reaction appeared to be instantaneous, as the dark olive-green colour of the triphenyltin lithium disappeared immediately upon addition; however, to ensure complete reaction, the mixture was stirred for 1 h. After work-up, as described for **3**, 2.6 g (75% yield) of a crystalline compound was obtained, subsequently identified as **5**, mp 67–69°C, $[\alpha]_D^{25}$ +5.91° (*c* 2.15). *Anal.* calcd. for $C_{32}H_{32}O_5Sn$: C 62.47, H 5.24; found: C 63.88, H 5.31.

Preparation of (Methyl 4,6-O-Benzylidene-α-D-altropyranoside-3-yl) Triphenylstannane (7)

Triphenyltin chloride (1.25 g, 3.25×10^{-3} mol) was reacted with lithium metal shavings (0.55 g, 0.08 mol) in the manner described above, filtered, and added, dropwise, to a stirred solution of methyl 2,3-anhydro-4,6-*O*-benzylidene-α-D-mannopyranoside (11) (0.37 g, 0.6×10^{-3} mol) in tetrahydrofuran (ca. 25 ml). After work-up, as for **3**, a foamy syrup was obtained. This syrup solidified after 12 h under vacuum; yield 0.81 g (94%), mp 166–168°C, $[\alpha]_D^{25}$ +91.0° (*c* 1.97). *Anal.* calcd. for $C_{32}H_{32}O_5Sn$: C 62.47, H 5.24; found: C 62.01, H 5.40.

Acknowledgments

It is a pleasure to thank the National Research Council of Canada for their support of this work via operating grants to L.D.H. (A 1905). Funds for the components of the 270 MHz nmr spectrometer came from the University of British Columbia (Chemistry Department and the President's Emergency Research Equipment Fund).

1. L. D. HALL, D. C. MILLER, and P. R. STEINER. Carbohydr. Res. **52**, C1 (1976).
2. P. R. STEINER. Ph.D. Thesis, Chemistry Department, University of British Columbia, Vancouver, B.C. 1971; D. C. MILLER. M.Sc. Thesis, Chemistry Department, University of British Columbia, Vancouver, B.C. 1977.
3. P. SMITH and L. SMITH. Chem. Br. 208 (1975).
4. H. G. KUIVILA, J. L. CONSIDINE, R. H. SARMA, and R. J. MYNOTT. J. Organomet. Chem. **111**, 179 (1976).
5. C. TAMBORSKI, F. C. FORD, and E. J. SOLOSKI. J. Org. Chem. **28**, 181 (1962).
6. B. COXON. Tetrahedron, **21**, 3481 (1965).
7. D. DODDRELL, I. BURFITT, W. KITCHING, M. BULLPIT, R. J. MYNOTT, J. L. CONSIDINE, H. G. KUIVILA, and R. H. SARMA. J. Am. Chem. Soc. **96**, 1640 (1974).
8. A. G. MARSHALL, L. D. HALL, M. HATTON, and J. SALLOS. J. Magn. Reson. **13**, 392 (1974).
9. R. BURTON and L. D. HALL. Can. J. Chem. **49**, 59 (1970); V. G. GIBB and L. D. HALL. Carbohydr. Res. **55**, 239 (1977).
10. O. T. SCHMIDT, A. DISTELMAIER, and H. REINHARD. Chem. Ber. **86**, 741 (1955).
11. C. J. ROBERTSON and C. J. GRIFFITH. J. Chem. Soc. 1193 (1935); D. A. PRINS. Helv. Chim. Acta, **29**, 1 (1946).
12. R. C. POLLER. Chemistry of organotin compounds. Academic Press, New York, NY. 1970.

Some reactions of a 4-(1-chloroethyl)-1,4-dihydropyridine

BRIAN GREGORY,[1] ERIC BULLOCK, AND TENG-SONG CHEN

Department of Chemistry, Memorial University of Newfoundland, St. John's, Nfld., Canada A1B 3X7

Received July 5, 1978

BRIAN GREGORY, ERIC BULLOCK, and TENG-SONG CHEN. Can. J. Chem. **57**, 44 (1979).

The preparation of dimethyl 4-(1-chloroethyl)-1,4-dihydro-2,6-dimethylpyridine-3,5-dicarboxylate and its reaction with nucleophilic reagents are described. Potassium cyanide, potassium succinimide, or methanolic triethylamine gave, stereospecifically, 4,5-dihydroazepines in which substituents at C(4) and C(5) are *trans*, whereas potassium thiocyanate afforded only the corresponding 4-(1-thiocyanatoethyl)-1,4-dihydropyridine. Sodium hydrosulfide afforded a mixture of 8-thia-2-azabicyclo[3.2.1]oct-3-ene-4,7-diesters epimeric at C(7), whereas potassium carbonate in aqueous dimethyl sulfoxide yielded an 8-oxa-2-azabicyclo-[3.2.1]oct-3-ene-4,7-diester. The stereochemistry of these bicyclic compounds is established using nmr spectroscopy. In acid media, dimethyl 2,5,7-trimethylazepine-3,6-dicarboxylate and a 4-methoxy-4,5-dihydroazepine rearranged to give 1,4-dihydropyridine derivatives; a mechanism for this ring contraction is suggested.

BRIAN GREGORY, ERIC BULLOCK et TENG-SONG CHEN. Can. J. Chem. **57**, 44 (1979).

On décrit la préparation du (chloro-1 éthyl)-4 dihydro-1,4 diméthyl-2,6 pyridinedicarboxylate-3,5 de diméthyle et ses réactions avec des réactifs nucléophiles. Le cyanure de potassium, le sel de potassium de la succinimide ou la triéthylamine éthanolique conduisent d'une façon stéréospécifique aux dihydro-4,5 azépines dans lesquelles les substituants en C(4) et en C(5) sont *trans*; toutefois le thiocyanate de potassium ne fournit que la (thiocyanato-1 éthyl)-4 dihydro-1,4 pyridine. L'hydrosulfure de sodium conduit à un mélange de thia-8 aza-2 bicyclo-[3.2.1] octène-3 diesters-4,7 épimères en C(7) alors que le carbonate de potassium dans le diméthylsulfoxyde aqueux fournit une oxa-8 aza-2 bicyclo[3.2.1] octène-3 diester-4,7. On a déterminé la stéréochimie de ces composés bicycliques à l'aide de la spectroscopie rmn. En milieu acide, le triméthyl-2,5,7 azépinedicarboxylate-3,6 de diméthyle et une méthoxy-4 dihydro-4,5 azépine se transforment pour donner des dérivés dihydro-1,4 pyridines; on suggère un mécanisme pour cette contraction de cycle.

[Traduit par le journal]

Studies, by us and others, show that the rearrangement reactions of 4-chloromethyl-1,4-dihydropyridines e.g., **1** or **2**, with nucleophilic reagents have afforded useful routes to several different heterocyclic ring systems (1 and references therein). As part of some related work, we required the 4-(1-chloroethyl)-1,4-dihydropyridine **3**, in which the carbon bearing the potential leaving group, chlorine, is labelled by attachment of a methyl group. Such a compound is clearly useful for stereochemical and mechanistic studies of some of these nucleophile-induced rearrangement reactions and is the subject of the present report.

Reaction of 1,2-dichloropropyl ethyl ether with methyl 3-aminocrotonate gave, in moderate yield, the chloroethyl compound **3** whose spectroscopic properties were in accord with the assigned structure. In particular, the ^{1}Hmr spectrum contained a three-proton doublet at δ 1.34 and a one-proton partly obscured double quartet at δ 4.02 which arise from the methyl and methine protons, respectively, of the chloroethyl group, and the ultraviolet (2, 3) and infrared spectra (2) were typical of Hantsch-type dihydropyridines. The mass spectrum was, however, temperature dependent. At reasonably low temperatures, the compound behaved as a typical 1,4-dihydropyridine and showed a base peak due to a pyridinium cation formed by loss of chloroethyl radical (cf. ref. 4). As the inlet temperature was increased, ions arising from loss of hydrogen chloride from the molecular ion became increasingly important and the mass spectrum then resembled that of the azepine **15**.

Reaction of the chloroethyl compound **3** with sodium cyanide in dimethyl sulfoxide gave, after chromatography, methyl 4-cyano-2,5-dimethylpyrrole-3-carboxylate and a less soluble product **9** whose long wavelength ultraviolet absorption maximum appeared at a shorter wavelength and was more intense than that of the starting dihydropyridine, a characteristic of 4,5-dihydroazepines (2). The ^{1}Hmr spectrum showed, in addition to singlets due to methyl groups at C(2) and C(7), methyl esters and NH, a three-proton doublet at δ 0.94, a one-proton multiplet at δ 3.73, and a one-proton doublet at δ 4.34 due to the CH_3—CH—CH(CN)—

[1]Author to whom all correspondence should be addressed.

0008-4042/79/010044-09$01.00/0

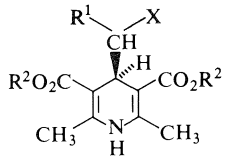

1 $R^1 = H, R^2 = CH_3, X = Cl$
2 $R^1 = H, R^2 = CH_2CH_3, X = Cl$
3 $R^1 = CH_3, R^2 = CH_3, X = Cl$
4 $R^1 = CH_3, R^2 = CH_3, X = Br$
5 $R^1 = CH_3, R^2 = CH_3, X = OCH_3$
6 $R^1 = CH_3, R^2 = CH_3, X = SCN$

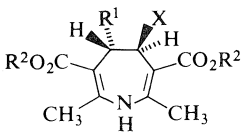

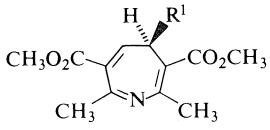

7 $R^1 = H, R^2 = CH_3, X = CN$
8 $R^1 = H, R^2 = CH_2CH_3, X = CN$
9 $R^1 = CH_3, R^2 = CH_3, X = CN$
10 $R^1 = CH_3, R^2 = CH_3, X = OCH_3$

14 $R^1 = H$
15 $R^1 = CH_3$

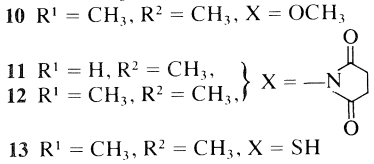

11 $R^1 = H, R^2 = CH_3$,
12 $R^1 = CH_3, R^2 = CH_3$,
} $X = -N$ (succinimino)

13 $R^1 = CH_3, R^2 = CH_3, X = SH$

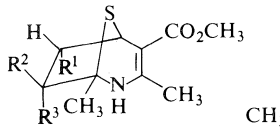

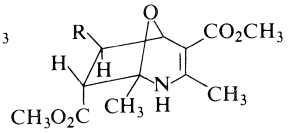

18 $R^1 = CH_3, R^2 = H, R^3 = CO_2CH_3$
19 $R^1 = CH_3, R^2 = CO_2CH_3, R^3 = H$
20 $R^1 = H, R^2 = H, R^3 = CO_2CH_3$
21 $R^1 = H, R^2 = CO_2CH_3, R^3 = H$

22 $R = CH_3$
23 $R = H$

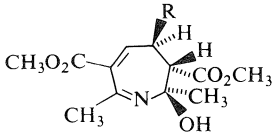

24 $R = CH_3$
25 $R = H$

system. Further, the doublet at δ 4.34 showed a coupling of 6.2 Hz which is consistent with the protons at C(4) and C(5), and therefore the cyano and methyl substituents on these carbon atoms having a *trans* relationship.[2] Since no *cis* isomer was detected, either the reaction had occurred stereospecifically to give the *trans* isomer or alternatively any *cis* isomer formed had been converted to the *trans* isomer through base-catalysed formation of a carbanion at C(4). To distinguish between these possibilities, dihydroazepines having groups incapable of stabilization of a carbanion at C(4) have been prepared. Thus when the chloroethyl compound **3** was solvolyzed in methanol containing triethylamine, the 4-methoxy-4,5-dihydroazepine **10** was obtained. The presence in the ^{1}Hmr spectrum of a doublet, $J = 6.6$ Hz, at δ 4.60 again confirmed the *trans* configuration of substituents at C(4) and C(5). Similarly the chloroethyl compound **3** reacted with potassium succinimide in ethanol to give the *trans*-4-succinimino compound[3] **12** (the doublet at δ 5.31 showed $J = 6.0$ Hz). The ring expansion reactions of the chloroethyl compound **3** are thus stereospecific. From a study of the kinetics of the reaction of cyanide ion with 4-chloromethyl-1,4-dihydropyridines, e.g. **1**, Eisner and co-workers (5) have suggested a ring-expansion mechanism which involves elimination to form an intermediate azepine, e.g. **14**, followed by 1,4-addition of hydrogen cyanide. The azepine **14** was shown to be converted to racemic 4-cyano-4,5-dihydroazepine **7** (only one enantiomer is shown for convenience) by the action of cyanide ion (5). Similarly, we have shown that the reaction of the 2,5,7-trimethylazepine **15** with potassium cyanide in methanol occurs, in this case, stereospecifically to give racemic *trans*-4-cyano-4,5-dihydroazepine **9** in good yield, along with a lesser amount of the *trans*-4-methoxy compound **10**. The trimethylazepine **15** used in this experiment was obtained by the action of sodium ethoxide in ether or potassium carbonate in dimethyl sulfoxide on the chloroethyldihydropyridine **3**, or by pyrolysis of the methoxy- or succiniminodihydroazepines **10** and **12**, respectively. At ambient temperatures, the nmr spectrum of **15** showed extreme broadening of the C(4)-methyl resonance in the δ 0.55–1.15 region. At 80°C, however, a sharp spectrum was obtained which showed in addition to singlets due to methyl esters and methyl groups at C(2) and C(7), a doublet at δ 0.88 ($J = 7.0$ Hz), a multiplet at δ 2.88, and a doublet at δ 5.23 ($J = 7.0$ Hz).

Earlier we have shown that diethyl 4-cyano-4,5-dihydro - 2,7 - dimethylazepine - 3,6 - dicarboxylate **8** may be converted in alkaline media to ethyl 4-cyano-2,5-dimethylpyrrole-3-carboxylate and ethyl acrylate (2). Accordingly, when the cyano compound **9** was

[2]In related 4,5-dihydroazepines, values of J_{AX} and J_{BX} of 6.0–8 and 0–1.6 Hz, respectively, have been reported. Examination of Dreiding models reveals approximate dihedral angles for H_A—C—C—H_X and H_B—C—C—H_X of 158 and 80°, respectively. If the substituent at C(4) occupies a pseudo-equatorial configuration, then H_A is *trans* to H_X whereas H_B is *cis* to H_X providing that the Karplus relationship is obeyed.

[3]Reaction of the chloromethyl compound **1** with potassium succinimide gave the corresponding succinimino compound **11** (see Experimental).

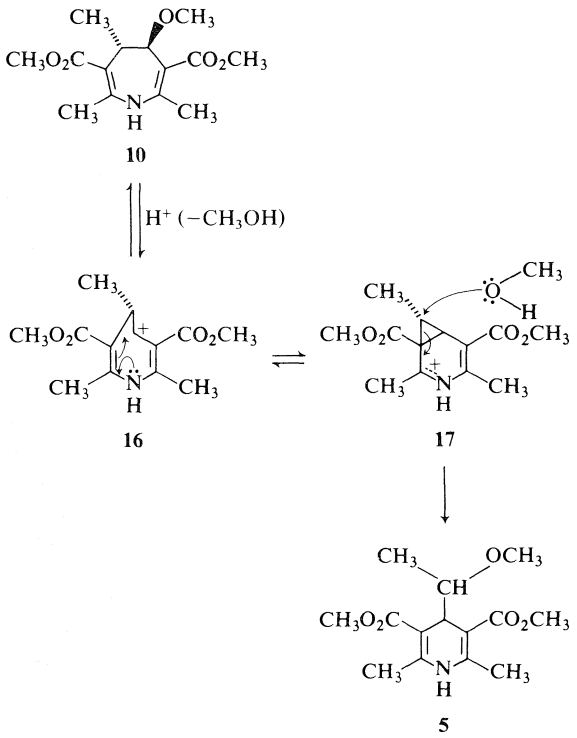

SCHEME 1

treated with potassium hydroxide in methanol, the products obtained were methyl crotonate, methyl 3-aminobutyrate, and methyl 4-cyano-2,5-dimethylpyrrole-3-carboxylate. The formation of methyl crotonate provides confirmation that the unsaturated ester originates from the ring carbon atoms C(5), C(6) and the ester group at C(6), and is in agreement with the postulated mechanism (6) which involves the formation of an intermediate 2-azabicyclo[3.2.0]heptene. The 3-aminobutyrate probably arises by Michael addition of ammonia, formed by competing base-catalysed hydrolysis of dihydroazepine **9** to methyl crotonate. When the cyanodihydroazepine **9** was treated with aqueous methanolic silver nitrate, the products included a furo[2,3-*b*]pyridine, a pyrrolo[2,3-*b*]pyridine, and a 2-oxo-1,2,3,4-tetrahydropyridine derivative (7).

Reaction of the methoxydihydroazepine **10** with methanolic hydrogen chloride yielded the methoxyethyldihydropyridine **5** (58%), the chloroethyldihydropyridine **3** (30%), and dimethyl 2,6-dimethylpyridine-3,5-dicarboxylate (5%). The formation of **5** is envisaged as proceeding via a carbonium ion mechanism as outlined in Scheme 1. Thus acid-catalyzed loss of methanol is believed to give a resonance-stabilized homoallyl–allyl carbonium ion **16** which is in equilibrium with the resonance-stabilized cyclopropylcarbinyl-type carbonium ion **17**.[4] Nucleophilic attack on **17** by methanol, as shown, would afford the methoxyethyl compound **5**, whereas competitive attack by chloride ion on the same cation would give the chloroethyl compound **3**. The conversion of cyclopropylcarbinyl compounds to homoallyl compounds in acidic media has precedent in the reaction of cyclopropylcarbinols with hydrochloric acid (8) and the acid-catalysed conversion of 3,5-cyclocholestan-6-yl compounds to cholesteryl derivatives (9 and references therein). The mechanism shown in Scheme 1 is essentially the reverse of a plausible mechanism for ring expansion of dihydropyridines **1**–**4** involving homoallylic participation and electron release from nitrogen. The origin of dimethyl 2,6-dimethylpyridine-3,5-dicarboxylate is not clear at the present time but it is believed to involve the action of oxygen on the methoxyethyl compound **5** in the presence of acid.[5] When the methoxydihydroazepine **10** in ether was reacted with hydrobromic acid, the bromoethyl compound **4** was formed in high yield. Similarly the 4*H*-azepine **15** reacted with concentrated hydrochloric or hydrobromic acids to give the chloroethyl and bromoethyl compounds **3** and **4**, respectively. In this case it is considered that the carbonium ion **16** is generated by *N*-protonation of the 4*H*-azepine. Acid-catalysed ring contraction of related azepine derivatives has been reported by Anderson and Johnson (6).

The reactions of the chloroethyl compound **3** with some sulfur nucleophiles have been examined. Thus reaction with potassium thiocyanate in methanol afforded the 4-(1-thiocyanatoethyl)-1,4-dihydropyridine **6** in good yield. Retention of the dihydropyridine ring system in such substitution reactions is rare and has been reported in examples involving iodide ion (5) or thiourea (1) only.

Reaction of the chloroethyl compound **3** with sodium hydrosulfide in ethanol afforded two isomeric products. Each product showed a base peak in the mass spectrum at *m/e* 185 owing to loss of methyl crotonate, peaks due to saturated and un-

[4]For convenience, we have represented this mechanism as proceeding via an equilibrating pair of carbonium ions **16** and **17**. We have no evidence at the present time which allows a choice between this and the corresponding nonclassical carbonium ion.

[5]When diethyl 2,6-dimethyl-4-methoxymethyl-1,4-dihydropyridine-3,5-dicarboxylate was allowed to stand in chloroform containing a trace of hydrogen chloride in the presence of air, the methoxymethyl substituent was eliminated and diethyl 2,6-dimethylpyridine-3,5-dicarboxylate was formed (B. Gregory, unpublished observations). This is reminiscent of the mass spectral fragmentation of this compound and may involve a radical reaction. 4-Alkyl-1,4-dihydropyridines do not behave in this way.

saturated esters in the infrared spectrum, and ultraviolet spectra in accord with the presence of an alkyl 1,4,5,6-tetrahydronicotinate chromophore (10). These spectroscopic properties and the ^{1}Hmr spectra were consistent with the formulation of the isomers as dimethyl 1,3-dimethyl-8-thia-2-azabicyclo[3.2.1]-oct-3-ene-4,7-dicarboxylate stereoisomers. The formation of such products clearly involves sulfhydryl-induced ring expansion to give, by analogy with the cyanide and methoxide reactions, the *trans*-4-thiol **13**. Michael addition of the thiol group or its conjugate base to C(7) of the unsaturated ester would give, after protonation, the *exo*- and *endo*-7-methoxycarbonyl compounds **18** and **19**. In addition to singlets due to methyl esters and methyl groups at C(1) and C(3), the ^{1}Hmr spectrum of each isomer showed a three-proton doublet, a one-proton multiplet, and two one-proton doublets consistent with the presence of the CH—CH(CH_3)—CH system. For each isomer, the lower field doublet (lowered by presence of adjacent sulfur, and due to the proton at C(5)) exhibited similar coupling constants (J = 4.7 and 4.8 Hz) showing that the stereochemistry at C(6) was similar in the two compounds, and confirming that the methyl at C(6) has an *endo* configuration.[6] The higher melting, less soluble major component and the lower melting, more soluble minor component showed doublets at δ 2.55 (J = 7.4 Hz) and δ 3.16 (J = 3.0 Hz), respectively. Examination of Dreiding molecular models of **18** and **19** shows dihedral angles between C(6)-H and C(7)-H of 120 and 0°, respectively. Using the Karplus curve, the higher melting isomer is therefore assigned the *endo*-7-methoxycarbonyl structure **18** and the lower melting isomer consequently has the *exo*-7-methoxycarbonyl structure **19**. The lower melting isomer **19** was easily epimerised to the more stable compound **18** using sodium methoxide in refluxing dioxan. Ashby and Eisner (11) obtained the 8-thia-2-azabicyclo[3.2.1]oct-3-ene **20**[7] but no *exo*-7-methoxycarbonyl isomer **21**, by the action of potassium hydrosulfide on the chloromethyl compound **1**. It would therefore appear that the steric requirement of the *endo*-6-methyl group is responsible for some degree of stabilization of the *exo*-7-methoxycarbonyl compound **19**.

Prolonged treatment of the chloroethyl compound **3** with potassium carbonate in aqueous dimethyl sulfoxide afforded, in low yield, a crystalline product $C_{13}H_{19}NO_5$ whose infrared and ultraviolet spectra closely resembled those of the foregoing sulfur bridge compounds **18–20** and left little doubt that it was an oxygen bridged analogue. In addition to singlets due to nonequivalent methyl esters, two methyls attached to sp^2 and sp^3 carbon atoms, and a three-proton doublet (methyl at C(5)), the ^{1}Hmr spectrum showed one-proton signals at δ 2.55 (doublet J = 3.9 Hz), 2.93 (double quartet, J = 7.0, 3.9 Hz), 4.61 (singlet), and 4.63 (broad singlet due to NH). The multiplicity of the δ 2.93 signal and the low field position of the δ 4.61 signal leave no doubt that these signals are caused by hydrogens attached at C(6) and C(5), respectively, and the signal at δ 2.55 must therefore be due to hydrogen at C(7). The singlet nature of the hydrogen at C(5) is explainable only if the methyl at C(6) occupies an *exo* position, allowing the proton at C(6) to have an *endo* configuration and giving a dihedral angle[8] near 90°. The *endo* and *exo* bonds at C(7) make dihedral angles of approximately 0 and 120° at the *endo* hydrogen at C(6); the observed interproton coupling constant of 3.9 Hz is more consistent with a dihedral angle of 120° (cf. J = 7.4 and 3.0 Hz for **18** and **19**, respectively). The methoxycarbonyl group at C(7) is therefore assigned an *endo* configuration and the stereochemistry of the compound is therefore that shown in **22**. In dihydroazepines **9**, **10**, and **12** and the sulfur bridged compounds **18** and **19**, the attacking nucleophile has occupied a position *trans* to the methyl group on the adjacent carbon atom. The *cis* relationship between oxygen bridge and methyl at C(6) in compound **22** may mean that a different mechanism is involved in its formation, e.g., elimination with ring expansion to give the azepine **15** followed by attack of hydroxide at C(2) to give **24** and intramolecular Michael addition of the hydroxyl to C(5). 8-Oxa-2-azabicyclo[3.2.1]octene derivatives[9] have not, to our knowledge, been reported previously, although it has been suggested (14) that the properties of a compound formulated as **25** by Anderson and Johnson (15) are in better agreement with the oxygen bridged structure **23**. The reported (15) spectroscopic properties of this compound show many similarities to those of compound **22**.

The electron-impact-induced fragmentations of **18**, **19**, and **22** were very similar, although some differences were observed. The major fragmentation pathways for **18** and **19** are shown in Scheme 2 and

[6]The dihedral angle between the hydrogen at C(5) and an *endo*-hydrogen at C(6) is close to 90° and would therefore be expected to result in a coupling constant close to zero.

[7]This structure was later confirmed in an X-ray study (12) although some reassignment of ^{1}Hmr signals was necessary.

[8]The dihedral angle between the C(5)-H bond and the *exo* bond at C(6) is approximately 34°; if the proton at C(6) had an *exo* configuration a coupling constant of about 5 Hz would be expected by analogy with compounds **18** and **19**.

[9]An 8-oxa-2-azabicyclo[3.2.1]octane is known (13).

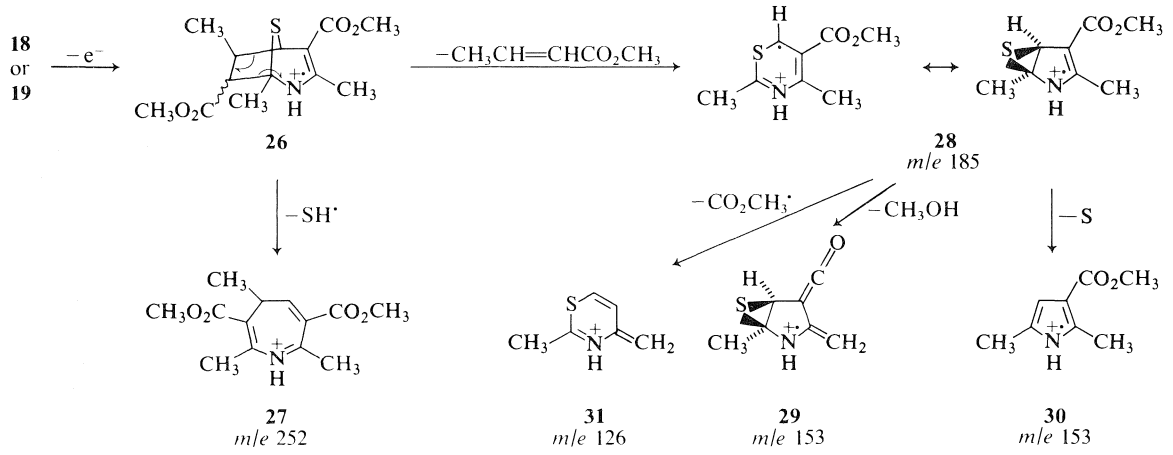

SCHEME 2

TABLE 1. Accurate mass measurements on compounds **18** and **22**

Compound	Ion structure	Ion composition	Mass	
			Found	Required
18	**27**	$C_{13}H_{18}NO_4$	252.1243	252.1236
	28	$C_8H_{11}NO_2S$	185.0511	185.0510
	29	C_7H_7NOS	153.0256(major)	153.0248
	30	$C_8H_{11}NO_2$	153.0785(minor)	153.0790
	31	C_6H_8NS	126.0375(major)	126.0378
	—	—	126.0078(minor)	—
22	$M - CO_2CH_3\cdot - CH_3OH$	$C_{10}H_{12}NO_2$	178.0869(minor)	178.0868
	Unknown	$C_{10}H_{10}O_3$	178.0632(major)	178.0630
	32	$C_8H_{11}NO_3$	169.0741	169.0739
	33	$C_7H_8NO_3$	154.0521(major)	154.0504
	34	$C_8H_{10}O_3$	154.0664(minor)	154.0630

are supported by accurate mass measurements (see Table 1). The prominent ion at *m/e* 252 results from loss of hydrosulfide radical from **26** and may have structure **27**. Loss of methyl crotonate (cf. ref. 11) from the molecular ion **26** yields a resonance-stabilized cation **28** which subsequently loses methanol, sulfur, or methoxycarbonyl radical to yield ions **29**, **30**, or **31**, respectively. Ions formed by successive loss of methoxycarbonyl and methanol are observed at *m/e* 226 and 194 but this is a relatively minor pathway.

In the case of **22**, the base peak again arises by loss of methyl crotonate to give ion **32** (see Scheme 3); an abundant ion $C_7H_8NO_3$ may arise by loss of methyl from **32** and may be represented by **33**. In addition to expected loss of methoxyl radical, methoxycarbonyl radical, or methoxycarbonyl radical and methanol to give ions at *m/e* 238, 210, and 178, a further pathway results in the formation of a minor ion $C_8H_{10}O_3$ and may be represented by structure **34**. This latter pathway would appear to be initiated by loss of a lone pair electron from the bridge oxygen of **22**. Although it is well known that thioethers have lower ionization potentials than ethers (16 and references therein), the failure of the sulfur bridged compounds **18** and **19** to fragment by such a pathway may be explained by the lesser ability of sulfur to stabilize an adjacent carbonium ion resulting in the decreased importance of α cleavage in thioethers relative to ethers (17). An example of a compound containing both ether and thioether groups has been reported to fragment by initial loss of an electron from oxygen despite the ionization potential values (18).

The 4-succinimino-4,5-dihydroazepine **11** showed activity at 100 mg/kg po in an antihypertensive assay using spontaneously hypertense rats. However, no hypotensive activity was observed in conscious normotensive rats (100 mg/kg po), a normotensive anesthetized dog (up to 10 mg/kg iv), or a renal hypertensive dog (25 mg/kg, po).

Experimental

Details concerning spectral measurements, analyses, etc., are provided in an earlier publication (1). Vapour phase chromatography measurements were obtained using a Beck-

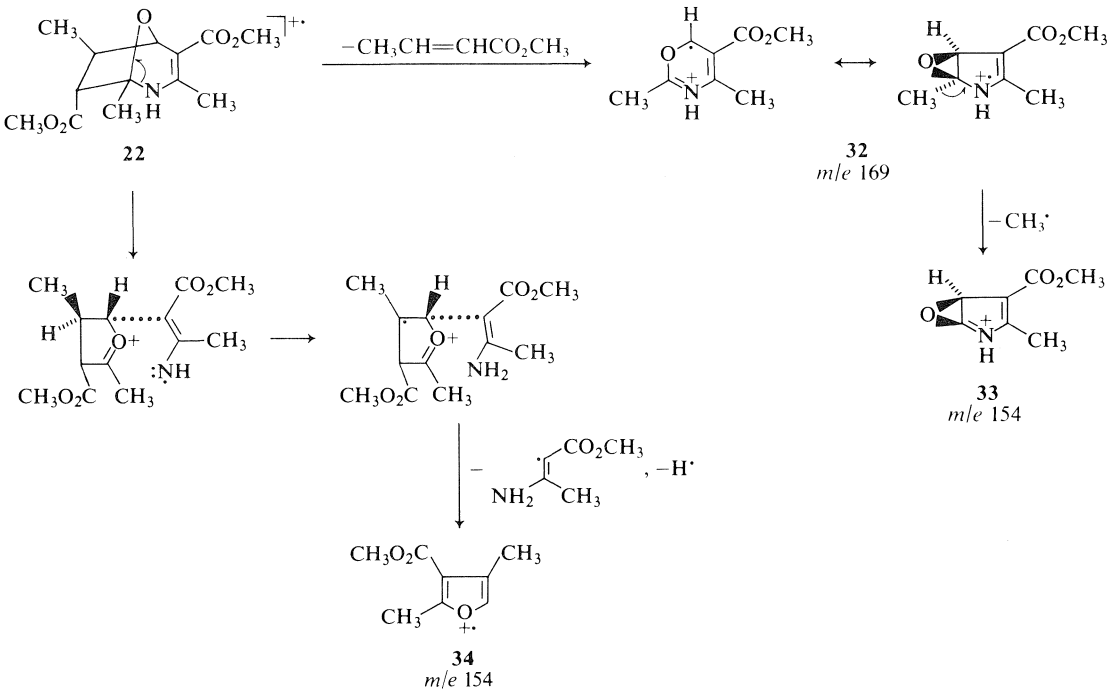

SCHEME 3

man GC-2A gas chromatograph equipped with column No. 70007 (Carbowax 4000 dioleate on C-22 Firebrick) operated at 70°C and 12 psi pressure of helium. Accurate mass measurements were obtained using a Varian MAT 311 mass spectrometer. Spin decoupling experiments were performed using a Bruker WP80DS Fourier Transform nmr spectrometer.

Dimethyl 4-(1-Chloroethyl)-1,4-dihydro-2,6-dimethylpyridine-3,5-dicarboxylate (3)

A mixture of 1,2-dichloropropyl ethyl ether (40 mL) and methyl 3-aminocrotonate (48 g) in benzene (50 mL) was stirred at room temperature for 2 days. Water (300 mL) and ether (300mL) were added, and after shaking, the organic layer was collected. The aqueous layer was extracted with ether (3 × 300 mL) and the combined ether extract was then washed with water (2 × 50 mL), dried ($MgSO_4$), filtered, and evaporated. Crystallization from benzene yielded colorless crystals of **3** (18.2 g, 30%), mp 169–170°C; ir ν_{max}: 3429 (NH, free), 3318 (NH, bonded), 1697 (unsaturated ester), 1649 cm^{-1} (C=C); uv λ_{max} (ε): 232 (16 850), 339 nm (7300); ^{1}Hmr δ: 1.34 (d, J = 6.6 Hz, CH_3—CHCl—), 2.38 (s, methyls at C(2), C(6)), 3.78 (s, methyl esters), 4.02 (partly obscured double q, J = 5.0, 6.6 Hz, —CHCl—CH_3), 4.41 (d, J = 5.0 Hz, H at C(4)), 6.22 (s, NH); ms *m/e*: 287 (<1%, M^+, ^{35}Cl), 224(100), 220(34), 219(41), 192(99.5), 191(33), 160(82), and 132(51). *Anal.* calcd. for $C_{13}H_{18}ClNO_4$: C 54.26, H 6.31, N 4.87, Cl 12.32; found: C 54.44, H 6.08, N 4.80, Cl 12.28.

Dimethyl 4-Cyano-4,5-dihydro-2,5,7-trimethylazepine-3,6-dicarboxylate (9)

(*a*) The chloroethyl compound **3** (4.0 g) and sodium cyanide (1.6 g) in dimethyl sulfoxide (30 mL) were stirred at room temperature for 48 h. After addition of water (200 mL) the reaction mixture was extracted with ether (3 × 200 mL). The ether solution was washed with water (2 × 30 mL) and the solvent evaporated under reduced pressure to give a pale yellow solid (3.5 g) which tlc revealed to be two components. Recrystallization from ether – petroleum ether afforded the less soluble cyano compound **9** as white prisms (2.41 g, 63%), mp 147–148.5°C; ir ν_{max}: 3416 (NH, free) 2246 (C≡N), 1709 (unsaturated ester), 1696 (unsaturated ester), and 1633 cm^{-1} (C=C); uv λ_{max} (ε): 229 (14 400), 326 nm (16 300); ^{1}Hmr (Varian HA 100) δ: 0.94 (d, J = 6.8 Hz, methyl at C(5)), 2.34 (s, methyl at C(7)), 2.39 (s, methyl at C(2)), 3.73 (m, signal obscured by singlets at δ 3.73, 3.74, C(5)-H), 3.73 and 3.74 (s, s, methyl esters), 4.34 (d, J = 6.2 Hz, C(4)-H), 6.17 (s, NH); the doublets due to H at C(4) and methyl at C(5) became singlets on irradiation at 373 Hz; ms *m/e*: 278(26, M^+), 247(35), 179(100), 159(21), 121(21), 119(26), 118(28), 42(28). *Anal.* calcd. for $C_{14}H_{18}N_2O_4$: C 60.42, H 6.52, N 10.07; found: C 60.31, H 6.37, N 9.96.

The more soluble component was obtained by removal of solvent from the mother liquor and recrystallization from benzene to give methyl 4-cyano-2,5-dimethylpyrrole-3-carboxylate as white prisms (0.58 g, 23%), mp 180.5–181.5°C; ir ν_{max}: 3435 (NH, free), 3251 (NH, bonded), 2233 (aryl C≡N), 1710 cm^{-1} (aryl ester); uv λ_{max} (ε): 211 (15 000), 263 nm (8700); ^{1}Hmr δ: 2.35 and 2.47 (s, s, methyls at C(2), C(5)), 3.80 (s, methyl ester); ms *m/e*: 178 (66, M^+), 163(53), 147(100), 146(47), 145(32), 118(32), and 42(44). *Anal.* calcd. for $C_9H_{10}N_2O_2$: C 60.67, H 5.66, N 15.71; found: C 60.75, H 5.88, N 15.71.

(*b*) The 4*H*-azepine **15** (0.310 g) and potassium cyanide (0.150 g) in methanol (25 mL) were stirred for 10 h at room temperature. The mixture was then poured into ice water (100 mL) and extracted with ether (3 × 60 mL). The ether extract was washed with water (3 × 15 mL), dried ($MgSO_4$), filtered, and evaporated under reduced pressure. The residue was recrystallized from ether – petroleum ether to give the cyano compound **9** (0.085 g). The mother liquor was evaporated and the residue separated by preparative tlc on silica gel G to yield more cyano compound **9** (0.172 g; total yield 75%) and the methoxy compound **10** (0.016 g; 5%); both were identical with the authentic compounds.

Base-catalyzed Rearrangement of Cyanodihydroazepine ***9***

To the cyano compound **9** (300 mg) in methanol (10 mL) was added potassium hydroxide (65 mg) in methanol (2 mL) and the solution heated under reflux on the steam bath for 2 h. Most of the methanol was then distilled off slowly and the rest was distilled under reduced pressure and collected in a Dry Ice cooling trap. The distillate was separated, using vapour phase chromatography, into methyl crotonate, identified by its retention time and mass spectrum and a second component. This latter product, formed in trace amounts, was identified as ethyl 3-aminobutyrate by comparison of retention time and infrared and mass spectra with authentic material.

The residue from the distillation was dissolved in methanol (5 mL) and poured into ice water (50 ml). The precipitate was collected and recrystallized from benzene to give white prisms, mp 180–181°C, shown to be identical with the methyl 4-cyano-2,5-dimethylpyrrole-3-carboxylate which was obtained in the preparation of the 4-cyano-4,5-dihydroazepine **9**.

*Dimethyl 4,5-Dihydro-4-methoxy-2,5,7-trimethylazepine-3,6-dicarboxylate (**10**)*

The chloroethyl compound **3** (3.1 g) and triethylamine (1.5 mL) in methanol (250 mL) were heated in an oil bath at 50°C for 48 h. Methanol was then removed on the rotary evaporator and the residue was treated with ether and water. After separation the ether layer was washed with water, dried ($MgSO_4$), filtered, and evaporated. The residue was recrystallized from ether – petroleum ether to give colorless prisms **10** (2.65 g, 87%), mp 157–159°C; ir ν_{max}: 3418 (NH), 1701 (unsaturated ester), 1634 cm^{-1} (C=C); uv λ_{max} (ε): 231 (12 750), 325 nm (15 550); ^{1}Hmr (Varian HA 100) δ: 0.77 (d, J = 6.8 Hz, methyl at C(5)), 2.29, 2.36 (s, s, methyls at C(7) and C(2)), 3.29 (s, *O*-methyl), 3.55 (partly obscured double q, J = 6.6 and 6.8 Hz, C(5)-H), 3.72 (s, methyl esters), 4.60 (d, J = 6.6 Hz, C(4)-H), and 5.68 (s, NH); the multiplicity of the signal at δ 3.55 was confirmed by irradiation at 462 Hz when the multiplet at δ 3.55 collapsed to a clearly discernible q (J = 6.8 Hz); irradiation at 356 Hz decoupled doublets due to H at C(4) and methyl at C(5) to singlets; ms *m/e*: 283 (10, M^+), 252(15), 251(33), 236(23), 220(35), 219(38), 192(100), 191(28), 176(25), 160(64), 132(40). *Anal.* calcd. for $C_{14}H_{21}NO_5$: C 59.36, H 7.47, N 4.94; found: C 59.15, H 7.60, N 4.87.

Reaction of Dimethyl 4,5-Dihydro-4-methoxy-2,5,7-trimethylazepine-3,6-dicarboxylate ***10*** *with Methanolic Hydrogen Chloride*

To the methoxydihydroazepine **10** (300 mg) in dry methanol (5 mL) was added 0.2 *M* methanolic hydrogen chloride solution (10 mL). The solution was stirred at room temperature for 0.5 h, then evaporated under reduced pressure and the excess hydrogen chloride removed by adding dry ether and evaporating *in vacuo* three times. The residue was separated by preparative tlc on silica gel G.

The band of highest R_F exhibited the light blue fluorescence characteristic of Hantsch dihydropyridines under ultraviolet light. Elution, evaporation and crystallization from benzene afforded dimethyl 4-(1-chloroethyl)-1,4-dihydro-2,6-dimethylpyridine-3,5-dicarboxylate **3** (92 mg, 30%), mp 165–167°C, which was shown to be identical with authentic material by comparison of ir, uv, ^{1}Hmr, and mass spectra.

The second band yielded dimethyl 4-(1-methoxyethyl)-1,4-dihydro-2,6-dimethylpyridine-3,5-dicarboxylate **5** (175 mg, 58%), mp 127–129°C; ir ν_{max}: 3430 (NH, free), 3306 (NH, bonded), 1696 (unsaturated ester), 1650 cm^{-1} (C=C); uv λ_{max} (ε): 233.5 (14 050) 347 nm (6700); ^{1}Hmr δ: 0.97 (d, J = 6.5 Hz, CH_3—CH), 2.31 (s, methyls at C(2), C(6)), 3.16 (partly obscured double q, J = 5.0 and 6.5 Hz, C*H*—CH_3), 3.31 (s, methoxyl), 3.76 (s, methyl esters), 4.34 (d, J = 5.0 Hz, C(4)-H), 6.31 (s, NH); ms *m/e*: 283 (0.0006, M^+), 225(22), 224(100), 192(24). *Anal.* calcd. for $C_{14}H_{21}NO_5$: C 59.36, H 7.47, N 4.94; found: C 59.32, H 7.49, N 5.05.

The last band was eluted using methanol and, after passage through a short column of basic alumina and sublimation *in vacuo*, afforded white prisms of dimethyl 2,6-dimethylpyridine-3,5-dicarboxylate (12 mg, 5%), mp 98–99°C (lit. (19) mp 100–102°C).

*Dimethyl-4-(1-Bromoethyl)-1,4-dihydro-2,6-dimethylpyridine-3,5-dicarboxylate (**4**)*

To the methoxydihydroazepine **10** (200 mg) in ether (50 mL) was added concentrated hydrobromic acid (0.5 mL) in a separatory funnel. The mixture was shaken for 5 min and the ether layer was washed with water (3 × 5 mL). After removal of ether the residue was recrystallized from benzene – petroleum ether to give the bromoethyl compound **4** as white prisms (213 mg; 91%), mp 164–165°C; ir ν_{max}: 3431 (NH, free), 3320 (NH, bonded), 1700 (unsaturated ester), 1653 cm^{-1} (C=C); uv λ_{max} (ε): 233 (14 550), 333 nm (7050); ^{1}Hmr δ: 1.54 (d, J = 6.8 Hz, CH_3—CHBr), 2.38 (s, methyls at C(2), C(6)), 3.77 (s, methyl esters), 4.14 (partly obscured double q, J = 5.2 and 6.8 Hz, C*H*Br—CH_3), 4.43 (d, J = 5.2 Hz, H at C(4)), 6.09 (s, NH); ms *m/e*: 251(26), 224(94), 220(27), 219(40), 192(93), 191(25), 160(82), 149(34), 132(50). *Anal.* calcd. for $C_{13}H_{18}NO_4Br$: C 47.00, H 5.46, N 4.22, Br 24.05; found: C 47.07, H 5.55, N 4.37, Br 24.18.

*Dimethyl 4,5-Dihydro-2,5,7-trimethyl-4-succiniminoazepine-3,6-dicarboxylate (**12**)*

The chloroethyl compound **3** (2.87 g) was added to a stirred solution of potassium succinimide (1.4 g) in absolute ethanol (60 mL) at room temperature. After 48 h the solvent was removed under reduced pressure and the residue recrystallized from chloroform – ether – petroleum ether to give the succinimino compound **12** as white prisms (2.58 g; 74%), mp 180–181°C; ir ν_{max}: 3410 (NH), 1701 (unsaturated ester and succinimino carbonyls), 1623 cm^{-1} (C=C); uv λ_{max} (ε): 235 (10 450), 328 nm (14 650); ^{1}Hmr (Varian HA 100) δ: 0.97 (d, J = 7.2 Hz, methyl at C(5)), 2.18 (s, methyl at C(7)), 2.46 (s, methyl at C(2)), 2.51 (s, —CH_2—CH_2— of succinimino group), 3.35 (double q, J = 6.0 and 7.2 Hz, H at C(5)), 3.63 (s, methyl esters), 5.31 (d, J = 6.0 Hz, H at C(4)), 5.91 (s, NH); the C(5)-H multiplet became a doublet (J = 6.0 Hz) on irradiation at 99 Hz; the C(4)-H doublet and C(5)-CH_3 doublet became singlets on irradiation at 336 Hz, and the C(5)-H multiplet became a quartet on irradiation at 534 Hz; ms *m/e*: 350 (5, M^+), 251(57), 236(19), 220(33), 219(51), 192(100), 191(32), 179(26), 176(24), 160(79), 132(49). *Anal.* calcd. for $C_{17}H_{22}N_2O_6$: C 58.27, H 6.33, N 8.00; found: C 58.05, H 6.45, N 7.84.

*Dimethyl 4,5-Dihydro-2,7-dimethyl-4-succiniminoazepine-3,6-dicarboxylate (**11**)*

In a similar manner, the chloromethyl compound **1** (3.0 g) and potassium succinimide (1.4 g) in absolute ethanol (80 mL) gave, after recrystallisation from chloroform – petroleum ether, the succinimino compound **11** as white prisms (2.78 g, 75%), mp 192.5–193.5°C; ir ν_{max}: 3410 (NH), 1705 (ester and imide carbonyls), 1622 cm^{-1} (C=C); uv λ_{max} (ε): 235 (11 800) 330 nm (13 800); ^{1}Hmr (Varian HA 100) δ: 2.23 (s, methyl at C(7)), 2.40 (dd, J = 1.0, 14.0 Hz, H at C(5)), 2.44 (s, methyl at C(2)), 2.52 (s, succinimino methylene groups), 3.22 (dd, J = 6.5, 14.0 Hz, H at C(5)), 3.61 (s, methyl ester), 3.64 (s, methyl ester), 5.52 (dd, J = 1.0, 6.5 Hz, H at C(4)), 5.78 (s, NH); ms *m/e*: 336 (6, M^+), 237(66), 206(31), 205(35), 179(40),

178(100), 177(21), 146(97), 118(42), 99(47), 59(35), 56(42). *Anal.* calcd. for $C_{16}H_{20}N_2O_6$: C 57.14, H 5.99, N 8.33; found: C 57.05, H 6.09, N 8.22.

*Dimethyl 2,4,7-Trimethyl-4*H*-azepine-3,6-dicarboxylate (**15**)*

(*a*) The chloroethyldihydropyridine **3** (2.5 g) was stirred with powdered anhydrous potassium carbonate (2.0 g) in dimethyl sulfoxide (35 mL) at room temperature for 5 h and then poured into cold water (120 mL). The product was extracted with ether (3 × 50 mL) and the ether extract was washed with water (3 × 20 ml) and dried ($MgSO_4$). After removal of solvent, the residue was distilled from a Späth tube at 110–115°C (bath temperature) and 0.03 Torr to give the 4*H*-azepine **15** as a pale yellow oil (1.8 g, 82%); ir ν_{max}: 1723 and 1702 cm^{-1} (unsaturated esters); uv λ_{max} (ε): 213 (8200), 295 nm (7150); ^{1}Hmr (CCl_4) at room temperature: δ 0.55–1.15 (v br., centred at 0.85, nuclear methyl), 2.05–2.45 (br, centred at 2.25, nuclear methyl), 2.40 (s, nuclear methyl), 3.75 and 3.78 (s, s, methyl esters); ^{1}Hmr at 80°C; δ 0.88 (d, J = 7.0 Hz, methyl at C(4)), 2.20 and 2.38 (s, s, methyls at C(2) and C(7)), 2.88 (m, H at C(4)), 3.73 and 3.76 (s, s, methyl esters), and 5.23 (d, J = 9.0 Hz, H at C(5)); ms *m/e*: 251 (34, M^+), 236(13), 220(28), 219(47), 192(100), 191(34), 176(24), 160(90), 159(21), and 132(47). *Anal.* calcd. for $C_{13}H_{17}NO_4$: C 62.13, H 6.82, N 5.57; found: C 62.08, H 6.75, N 5.73.

(*b*) The reaction of sodium ethoxide in dry ether with the chloroethyl compound **3** afforded the 4*H*-azepine **15** (yield 76%).

(*c*) The 5-methyl-4-succinimino-4,5-dihydroazepine **12** (150 mg) was pyrolyzed at 175–180°C in a sublimation tube containing small glass beads to increase the residence time. The product was then distilled at the same temperature and 0.03 Torr to give a colorless oil **15** (82 mg, 76%) which had identical ir, uv, ^{1}Hmr, and ms with the product of preparation *a*.

(*d*) The 4-methoxy-5-methyl-4,5-dihydroazepine **10** (100 mg) was pyrolyzed at 160°C, using the same experimental technique as that of preparation *c*, to give the 4*H*-azepine **15** (65 mg; 73%) as a colorless oil.

Reactions of the 4H*-Azepine*

(*a*) To the 4*H*-azepine **15** (450 mg) in ether (50 mL) was added concentrated hydrochloric acid (1 mL). The reaction mixture was shaken for 5 min and then ice water (10 mL) added. The ether layer was separated, washed with water (3 × 5 mL), dried ($MgSO_4$), filtered, and evaporated. The residue was crystallized twice from benzene to give white crystals of the chloroethyl compound **3** (435 mg, 84%), mp 168–169°C.

(*b*) To the 4*H*-azepine **15** (220 mg) in ether (50 mL) was added concentrated hydrobromic acid (0.5 mL). After shaking for 5 min, the reaction was worked up as above to give white prisms of the bromoethyl compound **4** (246 mg, 85%), mp 164–165°C, after recrystallization from benzene – petroleum ether.

*Dimethyl 1,4-Dihydro-2,6-dimethyl-4-(1-thiocyanatoethyl)-pyridine-3,5-dicarboxylate (**6**)*

A solution of the dihydropyridine **3** (1.4 g) and potassium thiocyanate (0.6 g) in methanol (50 mL) was heated under reflux for 2 h. The solution was evaporated *in vacuo* and the residue dissolved in ether (80 mL). The ether solution was washed with water (3 × 10 mL), dried ($MgSO_4$), concentrated to 10 mL, and petroleum ether added to yield the product (1.31 g, 87%), mp 142–145°C. After two recrystallizations from ether – petroleum ether, the thiocyanato compound **6** was obtained as white prisms, mp 149–150.5°C; ir ν_{max}: 3428 (NH free), 3306 (NH, bonded), 2154 (thiocyanate), 1699 cm^{-1} (unsaturated ester); uv λ_{max} (ε): 233 (17 350), 341 nm (6700) ^{1}Hmr δ: 1.38 (d, J = 7.2 Hz, CH_3—CH), 2.39 (s, methyls at C(2), C(6)), 3.36 (double q, J = 5.0 and 7.2 Hz, C*H*—CH_3), 3.79 (s, methyl esters), 4.42 (d, 5.0 Hz, H at C(4)), and 6.91 (s, NH); ms *m/e*: 251(37), 224(60), 220(31), 192(100), 191(30), 160(64), 132(38). *Anal.* calcd. for $C_{14}H_{18}N_2O_4S$: C 54.18, H 5.85, N 9.03, S 10.33; found: C 54.10, H 5.81, N 8.97, S 10.39.

*Dimethyl 1,3,6-Trimethyl-8-thia-2-azabicyclo[3.2.1]oct-3-ene-4,7-dicarboxylate (**18** and **19**)*

The chloroethyl compound **3** (1.5 g) was added to a solution of sodium hydrosulfide (0.8 g) in ethanol (50 mL) and the mixture heated to 65°C on a water bath for 5 h. After cooling, the reaction mixture was poured into cold water (200 mL) containing ammonium chloride (5 g) and the solution was extracted with ether (3 × 200 mL). After washing with water (3 × 30 mL) and drying ($MgSO_4$), the ether extract was evaporated to dryness. The residue was recrystallized from benzene – petroleum ether to give the 6-*endo*-methyl-7-*endo*-methoxycarbonyl isomer **18** as colorless prisms (0.78 g, 52%), mp 163–164°C; ir ν_{max}: 3408 (NH, free), 3307 (NH, bonded), 1737 (saturated ester), 1689 cm^{-1} (unsaturated ester); uv λ_{max} (ε): 231 (2850), 291 nm (12 900); ^{1}Hmr δ: 1.06 (d, J = 7.0 Hz, methyl at C(6)), 1.77 (s, methyl at C(1)), 2.30 (s, methyl at C(3)), 2.55 (d, J = 7.4 Hz, H at C(7)), 3.04 (m, J = 4.8, 7.0 and 7.4 Hz, H at C(6)), 3.74 (s, methyl esters), 4.68 (d, J = 4.8 Hz, H at C(5)), and 4.99 (s, NH); ms *m/e*: 285 (55, M^+), 252(30), 226(19), 220(16), 194(26), 185(100), 153(86), 126(60), 84(42), 59(33), and 42(37). *Anal.* calcd. for $C_{13}H_{19}NO_4S$: C 54.72, H 6.71, N 4.91, S 11.24; found: C 54.59, H 6.54, N 4.78, S 11.34.

From a second crop, needles of the more soluble 6-*endo*-methyl-7-*exo*-methoxycarbonyl isomer **19** were separated by hand from a trace of **18** and recrystallized from benzene – petroleum ether to give the pure product **19** (0.51 g, 34%), mp 144–146°C; ir ν_{max}: 3423 (NH, free), 3322 (NH, bonded), 1734 (saturated ester), and 1687 cm^{-1} (unsaturated ester); uv λ_{max} (ε): 293.5 nm (13 550); ^{1}Hmr δ: 0.99 (d, J = 6.5 Hz, methyl at C(6)), 1.83 (s, methyl at C(1)), 2.31 (s, methyl at C(3)), 3.09 (m, J = 3.0, 4.7, and 6.5 Hz, H at C(6)), 3.16 (d, overlapping signal at δ 3.09, J = 3.0 Hz, H at C(7)), 3.70 (s, methyl esters), 4.77 (d, J = 4.7 Hz, H at C(5)), and 5.09 (s, NH); ms *m/e*: 285 (71, M^+), 252(64), 226(14), 220(40), 194(13), 185(100), 153(98), 126(55), 84(11), 59(29), and 42(30). *Anal.* calcd. for $C_{13}H_{19}NO_4S$: C 54.72, H 6.71, N 4.91, S 11.24; found: C 54.60, H 6.64, N 5.05, S 11.09.

The lower melting, more soluble isomer was converted to the higher melting, less soluble, more stable epimer by refluxing with sodium methoxide in dioxane for 5 h.

*Dimethyl 1,3,6-Trimethyl-8-oxa-2-azabicyclo[3.2.1]oct-3-ene-4,7-dicarboxylate (**22**)*

A stirred mixture of the chloroethyl compound **3** (3 g) and potassium carbonate (1.5 g) in dimethyl sulfoxide (40 mL) and water (15 mL) was heated at 65°C in the dark and under a nitrogen pressure of 50 Torr for 3 days. After cooling the reaction mixture was poured into aqueous ammonium chloride (300 mL, 1%) and the product extracted into chloroform (3 × 25 mL). The chloroform extract was washed with water (3 × 10 mL), dried ($MgSO_4$), filtered, evaporated, and the residue crystallized from aqueous dioxane to give colorless prisms of the bicyclic compound **22** (0.92 g, 33%), mp 173–175°C; ir ν_{max}: 3522 (NH), 1742 (saturated ester), 1690 (unsaturated ester), 1606 cm^{-1} (C=C); uv λ_{max} (CH_3OH) (ε): 288 nm (15 000); ^{1}Hmr δ: 1.11 (d, J = 7.0 Hz, methyl at C(6)), 1.70 (s, methyl at C(1)), 2.09 (s, methyl at C(3)), 2.55 (d, J = 3.9 Hz, H at C(7)), 2.93 (double q, J = 7.0 Hz,

3.9 Hz, H at C(6)), 3.62 (s, methyl ester), 3.64 (s, methyl ester), 4.61 (s, H at C(5)), 4.63 (br, s, NH); spin decoupling resulted in the expected changes in multiplicity of signals at δ 1.11, 2.55, and 2.93; ms *m/e*: 269(37, M^+), 238(22), 210(34), 194(16), 178(54), 169(100), 168(24), 164(25), 154(76), 150(22), 136(32), 122(22), 43(36), 42(31). *Anal.* calcd. for $C_{13}H_{19}NO_5$: C 57.98, H 7.11, N 5.20; found: C 57.97, H 6.98, N 5.12.

Acknowledgements

The authors wish to thank Memorial University of Newfoundland and the National Research Council of Canada for financial support and Memorial University for the award of a Fellowship to one of us (T.S.C.). In addition the authors wish to express their gratitude to Dr. W. Snedden for accurate mass measurements, Dr. C. R. Jablonski for spin decoupling experiments on compound **22**, and Dr. M. A. Davis and Ayerst Research Laboratories, Montreal, for the pharmacological evaluation of compound **11**.

1. E. Bullock, B. Gregory, and M. T. Thomas. Can. J. Chem. **55**, 693 (1977).
2. P. J. Brignell, E. Bullock, U. Eisner, B. Gregory, A. W. Johnson, and H. Williams. J. Chem. Soc. 4819 (1963).
3. P. J. Brignell, U. Eisner, and P. G. Farrell. J. Chem. Soc. B, 1083 (1966).
4. G. Schroll, S.-P. Nygaard, S.-O. Lawesson, A. M. Duffield, and C. Djerassi. Ark. Kemi, **29**, 525 (1968).
5. P. J. Brignell, U. Eisner, and H. Williams. J. Chem. Soc. 4226 (1965).
6. M. Anderson and A. W. Johnson. J. Chem. Soc. 2411 (1965).
7. B. Gregory, E. Bullock, and T. S. Chen. Can. J. Chem. **55**, 4061 (1977).
8. P. Bruylants and A. Dewael. Bull. Cl. Sci. Acad. R. Belg. **14**, 140 (1928).
9. S. Winstein and E. M. Kosower. J. Am. Chem. Soc. **81**, 4399 (1959).
10. K. Tsuda, Y. Satch, N. Ikekawa, and H. Mishima. J. Org. Chem. **21**, 800 (1956).
11. J. Ashby and U. Eisner. J. Chem. Soc. C, 1706 (1967).
12. U. Eisner, M. Z. Haq, J. Flippen, and I. Karle. J. Chem. Soc. Perkin I, 357 (1972).
13. H. Paulsen and K. Todt. Chem. Ber. **100**, 512 (1967).
14. U. Eisner and J. Kuthan. Chem. Rev. **72**, 1 (1972).
15. M. Anderson and A. W. Johnson. J. Chem. Soc. C, 1075 (1966).
16. G. Condé-Caprace and J. E. Collin. Org. Mass Spectrom. **2**, 1277 (1969).
17. B. G. Keyes and A. G. Harrison. J. Am. Chem. Soc. **90**, 5671 (1968).
18. D. J. Pasto. J. Heterocycl. Chem. **6**, 175 (1969).
19. T. J. Bergen and R. M. Kellogg. J. Org. Chem. **36**, 978 (1971).

Fumaritine *N*-oxide, an alkaloid of *Fumaria kralikii* Jord.

H. G. KIRYAKOV

Department of Chemistry and Biochemistry, Medical Faculty, 4000 Plovdiv, Bulgaria

AND

DONALD W. HUGHES, BALA C. NALLIAH, AND DAVID B. MACLEAN

Department of Chemistry, McMaster University, Hamilton, Ont., Canada L8S 4M1

Received July 24, 1978

H. G. KIRYAKOV, DONALD W. HUGHES, BALA C. NALLIAH, and DAVID B. MACLEAN. Can. J. Chem. **57**, 53 (1979).

Alkaloid F_k-5, isolated from *F. kralikii*, has been shown to be fumaritine *N*-oxide. The structure was established by ^1H and ^{13}C nmr and by mass spectrometry and confirmed by reduction of F_k-5 to fumaritine. The ^{13}C spectra of fumaritine and its *N*-oxide are discussed.

H. G. KIRYAKOV, DONALD W. HUGHES, BALA C. NALLIAH et DAVID B. MACLEAN. Can. J. Chem. **57**, 53 (1979).

On a montré que l'alcaloïde F_k-5 isolé du *F. kralikii* est le *N*-oxyde du fumaritine. On a déduit la structure en se basant sur des spectres rmn du ^1H et du ^{13}C et sur la spectrométrie de masse; on l'a confirmée par réduction du F_k-5 en fumaritine. On discute des spectres rmn du ^{13}C de la fumaritine et de son *N*-oxyde.

[Traduit par le journal]

An examination of the alkaloids of *Fumaria kralikii* Jord. has recently been reported (1). Five alkaloids of established structure, 1-adlumine, protopine, cryptopine, *d*-parfumine, and fumarofine were obtained. In addition *O*-methylfumarofine (2) was isolated for the first time from nature and a new alkaloid, designated F_k-5, was reported. The authors considered F_k-5 might be a member of the spirobenzylisoquinoline group of alkaloids but there was no direct evidence to this effect.

Alkaloid F_k-5 (**1**) (mp 204°C) was a polar compound, eluted from an alumina column with 10% methanol in benzene. It contained a broad band (2500–3500 cm^{-1}) in its ir spectrum indicative of a strongly hydrogen-bonded compound. The authors reported that in its ^1H nmr spectrum in DMSO there were two aromatic singlets and an aromatic AB quartet. The presence of one methoxy, one methylenedioxy, and one *N*-methyl group was also apparent.

We report here further studies on the alkaloid that have led to the elucidation of its structure. The mass spectrum showed a weak molecular ion at *m/e* 371 corresponding in composition to $C_{20}H_{21}NO_6$. The molecular ion had fragment ion peaks corresponding to the loss of oxygen, water, and CH_3O. The most intense ion appeared at *m/e* 192 corresponding in composition to $C_{11}H_{14}NO_2$. Ions of this composition are frequently found in isoquinoline alkaloids, including spirobenzylisoquinolines (3), that have the structural feature **a**. The mass spectrum

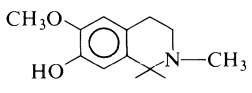

a

however did not provide other structural information.

In this study the ^1H nmr spectrum (Table 1) was reexamined in DMSO-d_6 and also in alkaline D_2O in which the alkaloid was readily soluble in contrast to its behaviour in DMSO. The solubility in base is in agreement with the presence of a phenolic hydroxyl as inferred above. Although the DMSO spectrum was similar to that previously reported (1), three additional resonances were found in the low field region. There was a broad singlet at 8.81 ppm which was attributed to a hydrogen-bonded phenolic proton. A pair of doublets was also observed at 6.40 and 5.33 ppm with a coupling constant of 7.6 Hz. The addition of D_2O to this sample removed the signals at 8.81 and 5.33 ppm and caused the doublet at 6.40 ppm to collapse to a sharp singlet. This result indicated the presence of a secondary alcohol function.

The high field region of the alkaline D_2O spectrum had two singlets of area three at 3.73 and 3.11 δ that were assigned to methoxy and *N*-methyl groups, respectively. The chemical shift of the *N*-methyl resonance suggested that it was bonded to a quaternary nitrogen. In the high field region there was also an AB quartet with the signals centred at 3.90 and 3.34 δ, with a coupling constant of 15.5 Hz. Four

0008-4042/79/010053-04$01.00/0

TABLE 1. ^{1}H chemical shifts and coupling constants for F_k-5 and fumaritine[a]

Protons	F_k-5 DMSO	F_k-5 Alkaline D_2O[b]	Fumaritine $CDCl_3$[c]
	(*a*) Chemical shifts		
H-1	6.27	6.15	6.47
H-4	6.68	6.65	6.59
H-11	6.76	6.89	6.74
H-12	6.80	6.89	6.58
H-8	6.40	6.23	5.42
H-13	4.05[d]	3.90, 3.34	3.29
OCH_3	3.72	3.73	3.85
NCH_3	2.87	3.11	2.41
9,10-OCH_2O—	5.95	5.92	5.95
C-8-OH	5.33		
C-2-OH	8.81		
	(*b*) Coupling constants		
J_{H-8}, OH	7.6		
$J_{11,12}$	7.9		
J_{AB}, H-13	16.7	15.5	

[a]Spectrum recorded at 90 MHz; chemical shifts are in ppm relative to internal TMS; coupling constants in Hz.
[b]Spectrum recorded at 100 MHz; chemical shifts are in ppm relative to DSS using *tert*-butyl alcohol-OD as an internal reference.
[c]Spectrum recorded at 100 MHz using TMS as an internal reference.
[d]High field portion of the AB quartet was partially obscured by the HDO peak.

TABLE 2. ^{13}C chemical shifts for F_k-5 and fumaritine

Carbon	F_k-5[a]	Fumaritine[b]
1	117.4	111.2
2	156.8	144.2
3	153.0	146.4
4	112.9	112.9
4a	118.2	127.4
5	27.6	23.3
6	64.8	47.6
8	77.2	82.3
8a	124.2	125.5
9	145.4	144.2
10	148.6	147.5
11	110.9	108.9
12	117.9	113.3
12a	135.3	135.0
13	38.8	44.0
14	90.6	74.5
14a	127.2	127.9
3 OCH_3	57.4	56.0
9,10 OCH_2O	103.1	101.6
NCH_3	53.7	38.1

[a]Solvent: D_2O + 2 drops 40% NaOD.
[b]Solvent: $CDCl_3$.

other protons also absorbed in this region giving a complex pattern. The low field region of the spectrum had a pair of overlapping doublets centred at 5.92 δ, assigned to a methylenedioxy group, and four singlets in the region 6.1–6.9 ppm, one of which integrated for two protons giving a total of five protons in this region. In view of the DMSO spectra, four of the five signals are very likely aromatic in character. We were however unable to interpret these data in terms of a unique structure for the alkaloid despite the relatively simple spectrum.

The ^{13}C nmr spectrum (both broad-band and off-resonance were recorded) was however more revealing; the data are recorded in Table 2 in terms of the structure eventually deduced for the alkaloid. In the aliphatic region of the spectrum the methoxy and *N*-methyl resonances were readily assigned by virtue of their residual coupling in the off-resonance spectrum and the assignments were confirmed by selective proton decoupling. There were three signals assigned to methylenes at 27.6, 38.0, and 64.8 ppm, a methine at 77.2 ppm and a quaternary carbon at 90.6 ppm. The presence of a quaternary carbon centre was the first evidence from the present study in support of the premise enunciated earlier (1) that F_k-5 might be a spirobenzylisoquinoline alkaloid. In the low field region of the spectrum there was a signal at 103.1 assigned to the methylene of a methylenedioxy group and twelve signals attributed to aromatic carbons. Four of these signals were at significantly lower field than the others and were assigned to aromatic carbons bonded to oxygen, four others were bonded to hydrogen, and the remaining four were fully substituted.

A consideration of these data led us to conclude that F_k-5 was an *N*-oxide either of fumaritine (4) (Fig. 1) or an isomer of fumaritine in which the phenolic hydroxy and methoxy group are interchanged or an isomer in which the hydroxyl function has a different configuration, or both. Accordingly we treated F_k-5 with SO_2, a reagent known to convert *N*-oxides to tertiary amines (5), and isolated the resulting product. Examination revealed that the reduction product was indeed fumaritine **2** by comparison of its spectroscopic properties with those of an authentic specimen.

The ^{13}C nmr spectrum of fumaritine was recorded and the data are shown in Table 2 along with those of F_k-5. Signals were assigned by comparing the spectra to those of alkaloids previously studied (6, 7). Except for the resonances assigned to C-8 and C-13 the chemical shift assignments are very similar to those of ochrobirine and yenhusomine both of which have saturated five-membered rings (7). The fact that C-8 resonates at lower field may be a consequence of the substitution pattern of the five-membered ring (8). Carbon-13, which does not carry an OH function, was identified from the off-resonance spectrum and was found at lower field than the methylene in ochotensimine (7). In ochotensimine

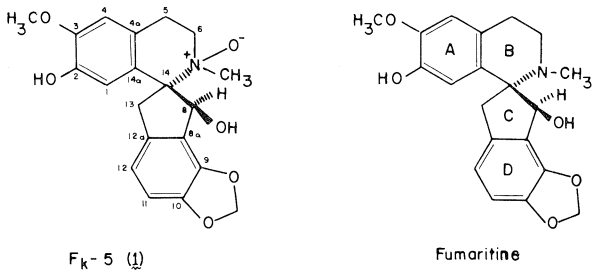

FIG. 1. Structures of F_k-5 (**1**) and fumaritine (**2**).

the methylene at C-8 may be shielded through a steric interaction with the aromatic substituent at C-9.

The ^{13}C spectrum of fumaritine *N*-oxide differs from fumaritine in several important respects. The conversion of the nitrogen to its *N*-oxide has the most pronounced effect on the neighboring carbon atoms, namely the *N*-methyl, the quaternary carbon at C-14, and the methylene at C-6. The chemical shift changes are of the same order as those observed for the *N*-oxides of *N*-methylpiperidine (9), the *Nuphar* alkaloids (10), and strychnine (11). These changes are attributed to the combined inductive effect of the positively charged *N*-atom and the β-substituent effect of the oxygen. The changes observed for the aromatic resonances of ring A of F_k-5 relative to fumaritine at C-1, C-2, C-3, and C-4a may be attributed to the change from phenoxide to phenol at C-2. The ^{13}C chemical shifts of guaiacol are known (12) and are reproduced in the accompanying formulas (Fig. 2) along with those of the anion of guaiacol obtained in basic D_2O. The changes observed for this acid–base pair are very similar to those found in ring A of F_k-5 (spectrum was recorded in alkaline D_2O) relative to fumaritine itself, a similar acid–base pair. One may therefore be reasonably confident of the assignments recorded in Table 2.

By making use of selective proton decoupling experiments it was possible to correlate proton resonances in F_k-5 with the ^{13}C resonances. In this way it was found that the signal at 6.23 was associated with the proton at C-8 geminal to the OH function, that the two protons at 6.89 were at C-11 and C-12, and that the signals at 6.15 and 6.65 were associated with the protons at C-1 and C-4, respectively. In Table 1 the chemical shifts are recorded

FIG. 2. The ^{13}C chemical shifts of guaiacol and its anion.

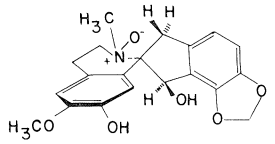

FIG. 3. Proposed conformation of fumaritine *N*-oxide (F_k-5).

of those protons of F_k-5 and fumaritine that have been established.

To determine the configuration of the nitrogen substituents in F_k-5, a series of nOe experiments were performed. Previous studies on sibiricine (13) which has the same substituents and configuration at C-8 produced a 25% enhancement of the H-8 resonance when the N—CH_3 was irradiated. Irradiation of the methoxy group in fumaritine (4) resulted in a 24% nOe for H-4. Several experiments on two samples of F_k-5 in alkaline D_2O produced a 20% nOe for H-4 during irradiation of the OCH_3 group whereas a less than 5% change in peak intensity was observed for H-8 when the N—CH_3 was irradiated. These results not only provided additional confirmation of the assignment of H-4 but also indicated a large internuclear separation between the NCH_3 and H-8. Of the possible configurations and conformations about the nitrogen that were examined from molecular models, the one with the methyl in a pseudoaxial position directed away from H-8 (Fig. 3) appears to fit the above data.

Experimental

The ^{13}C nuclear magnetic resonance spectra were recorded on a Bruker WH-90 Fourier transform spectrometer at 22.62 MHz and a temperature of +35°C. Sample concentrations ranged from 0.14 to 0.92 *M* in either D_2O (using DMSO as an external reference) or $CDCl_3$ (using TMS as an internal reference). Spectra were recorded over a 6000 Hz sweep width using 16K data points (1.359 s acquisition time). A pulse width of 3.4 μs (15.6° pulse angle) was used. The alkaloid spectra were obtained in 6000 to 50000 scans.

^1H nuclear magnetic resonance spectra and nOe experiments were performed on a Varian HA-100 spectrometer in the frequency sweep mode. The concentration of F_k-5 in the nOe sample was 0.16 *M* in alkaline D_2O (glass distilled) which also contained 2 mmol EDTA. The sample was sealed under vacuum after three freeze–pump–thaw cycles. *tert*-Butyl alcohol-OD was used as an internal reference and lock in the aqueous samples. The chemical shifts are reported in ppm downfield from DSS (2,2-dimethyl-2-silapentan-5-sulphonate). In the fumaritine samples $CDCl_3$ and TMS were used as solvent and reference, respectively. The ^1H spectra of F_k-5 in DMSO-d_6 were recorded at 90 MHz on a Bruker WH-90 Fourier transform spectrometer. Sample concentration was approximately 0.06 *M*. Spectra were obtained in 32 scans using a pulse width of 3.0 μs (67.5° pulse angle). The sweep width was 1200 Hz in 8K data points (3.411 s acquisition time). TMS was used as an internal reference.

Mass spectra were determined on a C.E.C. 21-110B mass spectrometer at an ionizing voltage of 80 eV and a source temperature of 200–250°C. The high resolution spectra were

recorded on plates and accurate mass measurements were made by using perfluorokerosene as a marker (14). The composition of all ions discussed in this paper have been checked by high resolution mass spectrometry and agree with calculated values within ± 0.005 amu. Infrared spectra were obtained on a Perkin-Elmer 283 spectrometer.

Reduction of N-*Oxide (5)*

Sulphur dioxide was bubbled through an aqueous solution of F_k-5 (90 mg in 5 ml H_2O). The progress of the reaction was followed by observing the precipitation of the free amine which redissolved as the solution became more acidic. The reaction mixture was then neutralized and extracted repeatedly with CH_2Cl_2. The extracts were dried and evaporated to produce a compound as a foam which gave spectral data identical with fumaritine; ^1H nmr: see Table 1; ir ($CHCl_3$) ν_{max}: 3550, 2880, 1590, 1275, 1100 cm^{-1}.

Acknowledgements

The work done at McMaster University was supported by grants from the National Research Council of Canada. We wish to thank Prof. N. Mollov, Institute of Organic Chemistry, Bulgarian Academy of Sciences, for his interest and encouragement.

1. H. G. Kiryakov and P. P. Panov. C.R. Acad. Bulg. Sci. **29**, 677 (1976).
2. C. K. Yu, J. K. Saunders, D. B. MacLean, and R. H. F. Manske. Can. J. Chem. **49**, 3020 (1971).
3. C. K. Yu and D. B. MacLean. Can. J. Chem. **49**, 3025 (1971).
4. D. B. MacLean, R. A. Bell, J. K. Saunders, C.-Y. Chen, and R. H. F. Manske. Can. J. Chem. **47**, 3593 (1969).
5. A. R. Katritzky and J. M. Lagowski. Chemistry of the heterocyclic *N*-oxides. Academic Press, New York, NY. 1971.
6. D. W. Hughes, H. L. Holland, and D. B. MacLean. Can. J. Chem. **54**, 2252 (1976).
7. D. W. Hughes, B. C. Nalliah, H. L. Holland, and D. B. MacLean. Can. J. Chem. **55**, 3304 (1977).
8. R. G. S. Ritchie, N. Cyr, B. Korsch, H. J. Koch, and A. S. Perlin. Can. J. Chem. **53**, 1424 (1975).
9. J. B. Stothers. Carbon-13 nmr spectroscopy. Academic Press, New York, NY. 1972.
10. R. T. Lalonde, T. N. Donvito, and A. I.-M. Tsai. Can. J. Chem. **53**, 1714 (1975).
11. E. Wenkert, H. T. A. Cheung, H. E. Gottlieb, M. C. Koch, A. Rabaron, and M. M. Plat. J. Org. Chem. **43**, 1099 (1978).
12. R. A. Archer, D. W. Johnson, E. W. Hagaman, L. N. Moreno, and E. Wenkert. J. Org. Chem. **42**, 490 (1977).
13. R. H. F. Manske, R. Rodrigo, D. B. MacLean, D. E. F. Gracey, and J. K. Saunders. Can. J. Chem. **47**, 3585 (1969).
14. K. Biemann. Pure Appl. Chem. **9**, 95 (1964).

The molecular and crystal structure of [Pt(diethylenetriamine)(guanosine)]$(ClO_4)_2$

R. MELANSON AND F. D. ROCHON

Département de chimie, Université du Québec à Montréal, C.P. 8888, Montréal (Qué.), Canada H3C 3P8

Received May 11, 1978

R. MELANSON and F. D. ROCHON. Can. J. Chem. **57**, 57 (1979).

The crystal structure of [Pt(diethylenetriamine)(guanosine)]$(ClO_4)_2$ has been determined by X-ray diffraction. The crystals are orthorhombic, space group $P2_12_12_1$, with $a = 12.486(6)$, $b = 13.444(7)$, $c = 14.678(11)$ Å, and $Z = 4$. The structure was refined by block-diagonal least-squares analysis to a conventional R factor of 0.050 and a weighted $R_w = 0.045$.

The coordination around the platinum atom is square planar. Guanosine is bonded to platinum through N(7). The purine planar ring makes an angle of 62.7° with the platinum coordination plane. The structure is stabilized by hydrogen bonding.

R. MELANSON et F. D. ROCHON. Can. J. Chem. **57**, 57 (1979).

La structure cristalline de [Pt(diéthylènetriamine)(guanosine)]$(ClO_4)_2$ a été déterminée par diffraction des rayons-X. Les cristaux appartiennent au groupe d'espace orthorhombique $P2_12_12_1$, avec $a = 12.486(6)$, $b = 13.444(7)$, $c = 14.678(11)$ Å et $Z = 4$. Les coordonnées atomiques et les facteurs thermiques anisotropes ont été affinés par moindres-carrés (matrice diagonale) jusqu'à $R = 0.050$ et $R_w = 0.045$.

La coordination autour de l'atome de platine est plane. La guanosine est liée au platine par l'atome N(7). Le plan du groupement purine fait un angle de 62.7° avec le plan de coordination du platine. La structure cristalline est stabilisée par des ponts hydrogènes.

Introduction

Recently we have started a study of the molecular and crystal structure of a series of platinum nucleoside complexes (1). Guanosine is believed to play an important role in the interaction of platinum antitumour drugs with DNA. In a recent communication (2, 3) the crystal structure of the [Pt(ethylenediamine)-(guanosine)$_2$]$^{2+}$ cation was reported. Intermolecular hydrogen bonding between the —NH_2 group of the ethylenediamine ligand and the carbonyl group of the guanine was observed. The authors suggested that this hydrogen bonding might be important in the Pt—DNA interaction in view of the fact that anti-tumour activity of *cis*-[Pt(amine)$_2$X$_2$] complexes decreases markedly along the series $NH_3 \sim NH_2R > NHR_2 \gg NR_3$ (4).

The present compound [Pt(diethylenetriamine)-(guanosine)]$(ClO_4)_2$ was studied partly to determine the role of the C=O group, if any, on the amine ligand.

Experimental

[Pt(dien)(guanosine)]$(ClO_4)_2$ (where dien = diethylenetriamine) was prepared by the following method. $AgClO_4$ was added to an aqueous solution of [Pt(dien)Cl]Cl and mixed. After filtering the AgCl precipitate, guanosine was added in a 1:1 proportion to the solution which consisted of [Pt(dien)-H_2O]$(ClO_4)_2$. The mixture was stirred and then filtered. The aqueous solution was allowed to evaporate slowly. Crystals of [Pt(dien)(guanosine)]$(ClO_4)_2$ were then obtained.

A set of precession photographs indicated the $P2_12_12_1$ space group in the orthorhombic system. The cell parameters were calculated by least-squares refinement of the setting angles of 15 independent peaks centered on a Syntex P$\bar{1}$ diffractometer using graphite monochromatized MoKα radiation.

Crystal Data

$PtCl_2C_{14}H_{26}N_8O_{13}$ mw = 780.40

Orthorhombic $P2_12_12_1$, $a = 12.487(6)$, $b = 13.444(7)$, $c = 14.678(11)$ Å, $Z = 4$, $V = 2464(2)$ Å^3, $D_m = 2.09(2)$ g cm^{-3} (flotation), $D_x = 2.103$ g cm^{-3}, λMoK$\alpha = 0.71069$ Å, μMoK$\alpha = 62.9$ cm^{-1}, and $T = 22$°C.

Collection and Reduction of Intensity Data

The intensity data were collected from a crystal having 9 faces with approximate dimensions of 0.15 × 0.20 × 0.25 mm. A total of 4023 independent reflections were measured in the region of $2\theta < 60°$ by the $2\theta/\theta$ scan technique using MoKα radiation. During the data collection, three standard reflections were measured after every 47 reflections. Their variations were less than 2% from their respective means. The reflections for which the intensity was less than $2.5\sigma(I)$ were considered as unobserved. The standard deviation $\sigma(I)$ was calculated as already described (5). An absorption correction based on the equations of the crystal faces was applied to the 2501 observed reflections. The transmission factors varied from 0.441 to 0.504. The data were then corrected for the Lorentz and polarization effects. The scattering factors of Cromer and Waber (6) were used for platinum, chlorine, oxygen, nitrogen, and carbon, those of Stewart *et al.* (7) were used for hydrogen. The anomalous dispersion terms (8) of platinum and chlorine were included in the calculations.

Structure Determination

The position of the platinum atom was easily located from the three-dimensional Patterson map. The positions of all the other atoms, except the hydrogen atoms, were obtained by structure factor and Fourier map calculations. The refinement of the parameters was carried out by block-diagonal least-squares methods. In the early stages of refinement, unit weight was assigned to all observed reflections. Later, individual weights w according to the equation $1/w = a + bF_o + cF_o^2$ were calculated. The constants of the equation were adjusted

0008-4042/79/010057-05$01.00/0

to make the distribution of $w|\Delta F|^2$ almost constant with respect to $|F_o|$ and sin θ/λ ($a = 35.589$, $b = -0.4508$, and $c = 0.00154$). The hydrogen atoms in the diethylenetriamine ligand and on the carbon atoms and on N(1) in the guanosine moiety were fixed at their calculated position[1] (C—H distance = 0.95 Å and N—H distance = 0.85 Å) and assigned isotropic temperature factors of 6.0 Å^2. The refinement of the scale factor, the coordinates and anisotropic temperature factors of all the non-hydrogen atoms converged to $R = \Sigma||F_o| - |F_c||/\Sigma|F_o| = 0.050$ and $R_w = [\Sigma w(|F_o| - |F_c|)^2/\Sigma w|F_o|^2]^{1/2} = 0.045$. The final difference Fourier map did not show peaks higher than ± 0.8 e Å^{-3}. Attempts to find, on the final difference Fourier map, the hydrogen atoms that could not be calculated, were not successful. The torsion angles within the ribose segment, confirmed the expected *D*-configuration of the molecule. The *R* factor for the other enantiomorphic structure was much higher (0.062) indicating that the coordinates of Table 1 correspond to the absolute structure.

The calculations were carried out with a Cyber 73 computer and the programs used have already been described (5). A table of observed and calculated structure factors is available.[1]

Results and Discussion

The refined atomic parameters are listed in Table 1. A list of the anisotropic temperature factors is available.[1] A labelled stereoscopic view of the ion [Pt(dien)guanosine)]$^{2+}$ is shown in Fig. 1. (The size of the ellipsoids corresponds to a 50% probability.) The bond lengths within the ions are shown on Fig. 2, and the bond angles on Fig. 3.

As expected, guanosine is bonded to the platinum atom through the N(7) atom. The coordination around the platinum atom is square planar. The weighted best plane was calculated through the five atoms. The deviations from this plane are: Pt, −0.002; N(4), 0.0807; N(5), −0.0045; N(6), 0.0746; and N(7), 0.057 Å. The angles around platinum are close to the expected 90° and 180° but there are some distorsions. The N(4)—Pt—N(5) and N(5)—Pt—N(6) angles (84.7°) are smaller than the N(4)—Pt—N(7) and N(6)—Pt—N(7) angles (98.2, 92.4°). The N(4)—Pt—N(6) angle (168.5°) is also smaller than expected. A slight strain caused by the tridentate ligand is responsible for these deviations from the ideal square planar coordination. The Pt—N bond lengths (1.97–2.04 Å) are normal and agree well with the published results (1–3, 5, 9–11). The four methylene groups of the dien ligand all lie on one side of the plane of the nitrogen atoms.

The purine ring is planar. The weighted best plane was calculated through the nine atoms. The deviations from this plane are: N(7), −0.012; N(9), 0.028; N(3), −0.008; N(1), 0.002; C(8), −0.020; C(4), −0.013; C(5), 0.015; C(6), 0.015; and C(2), −0.011 Å. The deviations of the substituents on the ring are as follows: N(2), −0.101; O(6), 0.024; and C(1′), −0.067 Å (esd = 0.014 to 0.021 Å). Since N(2) plays an important role in the hydrogen bonding system of the crystal, it might explain the slight non-planarity of the substituent. The purine planar ring makes an angle of 62.7° with the platinum coordination plane.

The bond lengths in the purine ring vary from 1.29 to 1.46 Å. They are similar to those found in guanosine rings mentioned in a review by Voet and Rich (12). They are almost identical to those found in guanosine dihydrate (13). The bond angles also seem normal and agree well with the published results mentioned above. The bond angles within the five-member ring vary from 105 to 111°. In the six-membered ring, the range is from 111° to 128°. As

TABLE 1. Final structure parameters (× 10^4). The estimated standard deviations are given in parentheses

Atom	*x*	*y*	*z*
Pt	3611.6(5)	6872.2(4)	6184.9(5)
Cl(1)	3531(5)	906(3)	8707(4)
Cl(2)	1676(4)	4996(4)	4113(4)
N(4)	3626(14)	6846(12)	4832(12)
N(5)	4359(10)	8198(12)	6041(13)
N(6)	3621(15)	7190(9)	7498(12)
N(7)	2859(10)	5550(10)	6399(10)
N(9)	2544(11)	3938(10)	6513(10)
N(3)	853(11)	3931(11)	7287(11)
N(1)	238(12)	5594(12)	7546(13)
N(2)	−725(14)	4201(13)	8055(15)
C(1)	4203(19)	7723(20)	4472(14)
C(3)	4080(19)	8549(16)	5125(16)
C(7)	4083(16)	8776(15)	6853(16)
C(9)	4218(16)	8121(20)	7668(15)
C(8)	3245(13)	4676(11)	6238(14)
C(4)	1714(13)	4393(13)	6909(11)
C(5)	1892(14)	5396(11)	6805(12)
C(6)	1091(15)	6094(13)	7157(11)
C(2)	117(17)	4554(10)	7612(12)
C(1′)	2776(10)	2854(10)	6486(12)
C(2′)	1789(12)	2309(10)	6095(16)
C(3′)	2391(14)	1358(12)	5725(12)
C(4′)	3492(15)	1740(12)	5469(12)
C(5′)	3662(20)	1896(16)	4463(14)
O(6)	1120(10)	7001(8)	7135(10)
O(2′)	997(10)	2042(9)	6717(11)
O(3′)	2428(10)	583(8)	6387(10)
O(1′)	3631(12)	2685(7)	5920(9)
O(5′)	2829(16)	2478(13)	4080(11)
O(1)	2501(14)	481(13)	8598(19)
O(2)	4212(14)	314(14)	9187(16)
O(3)	3955(14)	1082(13)	7820(13)
O(4)	3426(14)	1817(13)	9169(15)
O(5)	2752(13)	4691(11)	4122(12)
O(7)	1270(22)	4900(26)	3287(14)
O(8)	1555(18)	5919(13)	4428(20)
O(9)	1129(21)	4392(22)	4719(22)

[1]Lists of structure factors, calculated hydrogen positions, and anisotropic thermal parameters are available, at a nominal charge, from the Depository of Unpublished Data, CISTI, National Research Council of Canada, Ottawa, Ont., Canada K1A 0S2.

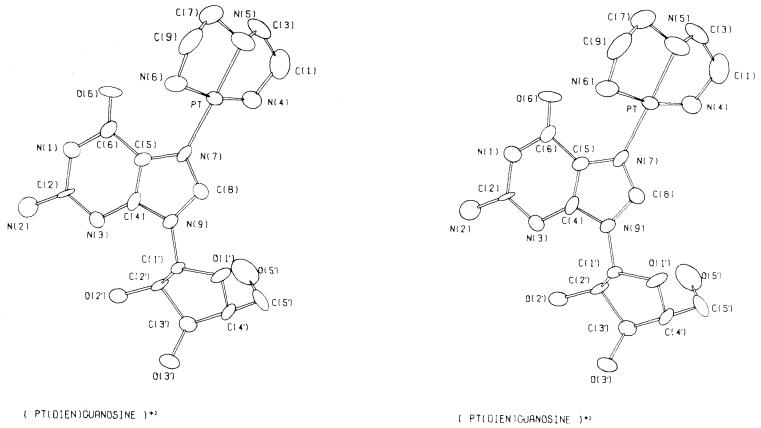

FIG. 1. Stereoscopic view of the $[Pt(dien)(guanosine)]^{2+}$ ion.

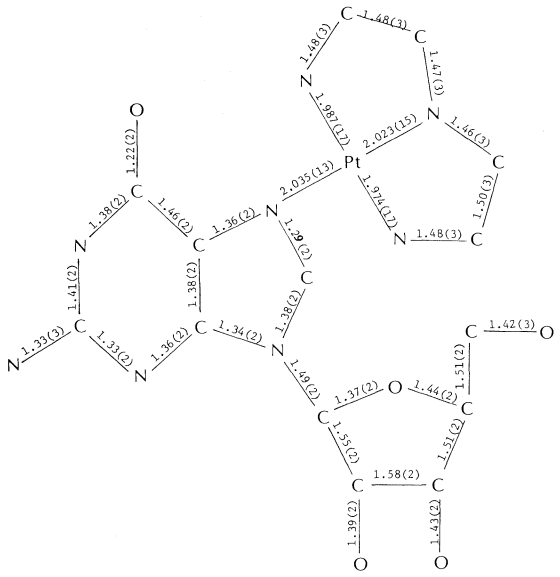

FIG. 2. Bond lengths within the $[Pt(dien)(guanosine)]^{2+}$ ion.

Singh has pointed out (14), the internal ring angle at a nitrogen atom is greater if the N atom is covalently bound to an extra-annular H atom than if the N atom has no extra-annular attachment. Here C(6)—N(1)—C(2) = 126° while C(2)—N(3)—C(4) = 113°.

The glycosyl bond is normal (1.49 Å) (12). The angles in the ribose ring are close to the tetrahedral values. O(1′), C(1′), C(3′), and C(4′) are coplanar within 2σ and C(2′) is 0.57 Å distant from that plane on the same side as C(5′) and N(9). This corresponds to the C(2′) *endo* conformation. The dihedral angle between the purine and the ribose planes is 30.3°.

The torsion angles within the ribose group are listed in Table 2. The conventions suggested by Sundaralingam (15) and Trueblood and co-workers (16, 17) have been used. The torsion angle O(1′)-C(1′)N(9)C(8), ϕ_{CN}, is −17° and defines an *anti* conformation about the glycosidic bond. The C(5′)—O(5′) bond is in a *gauche–gauche* conformation relative to the ribose group: $\phi_{OO} = -68$ and $\phi_{OC} = 51°$.

The bond lengths and the bond angles in the perchlorate ions are shown in Table 3. The distances vary from 1.32 to 1.42 Å. The standard deviations are quite large (0.016 to 0.030 Å), probably because the thermal parameters of the oxygen atoms are fairly large. The bond angles are close to the tetrahedral values (106 to 111°).

A packing diagram is shown in Fig. 4. In most nucleoside crystal structures, base stacking plays a very important role. In this structure base stacking

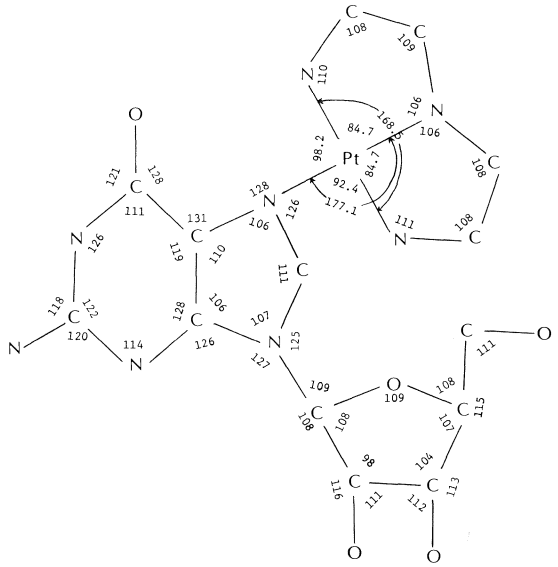

FIG. 3. Bond angles within the $[Pt(dien)(guanosine)]^{2+}$ ion.

TABLE 2. Torsion angles in the ribose group*

Atoms	Angle (deg)	
O(1′)C(1′)N(9)C(8)	−17	ϕ_{CN} (*anti*)
O(1′)C(1′)N(9)C(4)	173	
O(1′)C(4′)C(5′)O(5′)	−68	ϕ_{OO} (*gauche*)
C(3′)C(4′)C(5′)O(5′)	51	ϕ_{OC} (*gauche*)
C(2′)C(1′)O(1′)C(4′)	−28	τ_0
C(3′)C(2′)C(1′)O(1′)	37	τ_1
C(4′)C(3′)C(2′)C(1′)	−31	τ_2
O(1′)C(4′)C(3′)C(2′)	18	τ_3
C(1′)O(1′)C(4′)C(3′)	6	τ_4
O(2′)C(2′)C(3′)O(3′)	−31	

*The conventions suggested by Sundaralingam (15) and Trueblood and co-workers (16, 17) have been used.

is not a very important packing factor since the perchlorate ions are located between the bases. Hydrogen bonding is probably the predominant packing effect in this structure. The most important hydrogen bonds are listed in Table 4. All the hydrogens attached to the oxygen and nitrogen atoms in the guanosine group are involved in strong hydrogen bonds. O(2′)—H of each ribose group is intramolecularly hydrogen-bonded to N(3). The two other hydroxyl groups O(3′)—H and O(5′)—H are involved in hydrogen bonds with the perchlorate ions. N(1) and N(2) also play an important role in the system, forming intermolecular hydrogen bonds, N(1)—H with O(2′) and N(2)$\begin{smallmatrix}\text{H}\\\text{H}\end{smallmatrix}$ with both O(3′) and O(6). The role of the diethylenetriamine ligand in the hydrogen bonding system is doubtful. The most probable hydrogen bonds are shown in Table 4. The longer distances and the less favourable angles, especially those involving platinum, seem to suggest that these bonds are weaker.

In the crystal structure of the [Pt(ethylenediamine)-(guanosine)$_2$]$^{2+}$ cation (2, 3), the authors observed an intermolecular hydrogen bond between the carbonyl group of guanine and the —NH_2 group of ethylenediamine. The distance was 2.78 Å indicating a strong interaction. The bond angle was not given, but it appeared very favourable. The authors

TABLE 3. Bond distances and bond angles in ClO_4^-

Bond	Distance (Å)	Bond	Distance (Å)
Cl(1)—O(1)	1.42(2)	Cl(2)—O(5)	1.41(2)
Cl(1)—O(2)	1.36(2)	Cl(2)—O(7)	1.32(2)
Cl(1)—O(3)	1.42(2)	Cl(2)—O(8)	1.33(2)
Cl(1)—O(4)	1.41(2)	Cl(2)—O(9)	1.39(3)

Bonds	Angle (deg)	Bonds	Angle (deg)
O(1)—Cl(1)—O(2)	113(1)	O(5)—Cl(2)—O(7)	110(1)
O(1)—Cl(1)—O(3)	108(1)	O(5)—Cl(2)—O(8)	112(1)
O(1)—Cl(1)—O(4)	109(1)	O(5)—Cl(2)—O(9)	107(1)
O(2)—Cl(1)—O(3)	110(1)	O(7)—Cl(2)—O(8)	111(2)
O(2)—Cl(1)—O(4)	109(1)	O(7)—Cl(2)—O(9)	110(2)
O(3)—Cl(1)—O(4)	109(1)	O(8)—Cl(2)—O(9)	106(2)

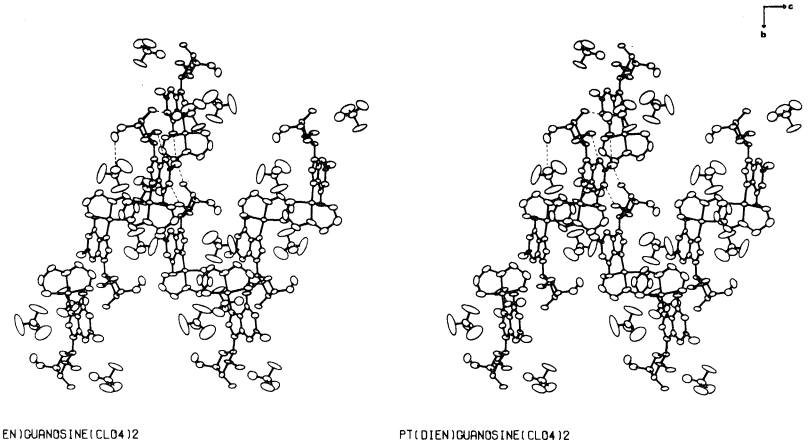

FIG. 4. Stereoscopic diagram of the packing of [Pt(dien)(guanosine)]$(ClO_4)_2$.

TABLE 4. Distances and angles involved in hydrogen bonds

Atoms	Transformation (on third atom)	Distance (Å)	Atoms	Angle (deg)
O(2′)—H...N(3)	x, y, z	2.68(2)	C(2′)—O(2′)...N(3)	90(1)
O(3′)—H...O(3)	x, y, z	2.92(2)	C(3′)—O(3′)...O(3)	110(1)
O(5′)—H...O(5)	x, y, z	2.98(2)	C(5′)—O(5′)...O(5)	124(1)
N(1)—H...O(2′)	$-x, \frac{1}{2} + y, 1\frac{1}{2} - z$	2.71(2)	C(6)—N(1)...O(2′)	105(1)
			C(2)—N(1)...O(2′)	129(1)
N(2)—H...O(3′)	$-x, \frac{1}{2} + y, 1\frac{1}{2} - z$	2.94(2)	C(2)—N(2)...O(3′)	119(1)
N(2)—H...O(6)	$-x, y - \frac{1}{2}, 1\frac{1}{2} - z$	3.01(2)	C(2)—N(2)...O(6)	116(1)
Possible hydrogen bonds involving the dien ligand:				
N(5)—H...O(8)	$\frac{1}{2} + x, 1\frac{1}{2} - y, 1 - z$	3.07(2)	C(7)—N(5)...O(8)	101(1)
			C(3)—N(5)...O(8)	83(1)
			Pt—N(5)...O(8)	141(1)
N(6)—H...O(6)	x, y, z	3.18(2)	C(9)—N(6)...O(6)	126(1)
			Pt—N(6)...O(6)	79(1)
N(6)—H...O(5′)	$\frac{1}{2} - z, 1\frac{1}{2} - y, \frac{1}{2} + z$	2.98(2)	C(9)—N(6)...O(5′)	93(1)
			Pt—N(6)...O(5′)	142(1)
			N(6)...O(6)...N(2)	96(1)

suggested that this hydrogen bonding could be an important factor in the Pt–DNA interaction since the anti-tumour activity of *cis*-[Pt(amine)$_2$X$_2$] decreases in the order $NH_3 \sim NH_2R > NHR_2 \gg NR_3$.

In the present structure, the carbonyl group of guanosine (O(6)) would be strongly intermolecularly hydrogen bonded with the amino group of guanosine (N(2)). It might also form a weaker intramolecular hydrogen bond with the $-NH_2$ of diethylenetriamine (N(6)). The angle N(6)...O(6)...N(2) is 96°.

It is therefore difficult at the moment to evaluate the importance of hydrogen bonding between the amine ligand and the nucleoside in the Pt—DNA interaction. More data are needed before attempting to discuss in detail this possible mechanism of interaction of platinum drugs.

Acknowledgments

The authors are grateful to the National Research Council of Canada and the Cancer Research Society Inc. for financial support, to Dr. P. C. Kong for the synthesis of the compound, and to Johnson Matthey and Co. Limited for the loan of potassium chloroplatinite.

1. R. MELANSON and F. D. ROCHON. Inorg. Chem. **17**, 679 (1978).
2. R. W. GELLERT and R. BAU. J. Am. Chem. Soc. **97**, 7379 (1975).
3. R. BAU, R. W. GELLERT, S. M. LEHOVEC, and S. LOUIE. J. Clin. Hematol. Oncol. **7**, 51 (1977).
4. M. J. CLEARE and J. D. HOESCHELE. Bioinorg. Chem. **2**, 187 (1973).
5. R. MELANSON and F. D. ROCHON. Can. J. Chem. **53**, 1139 (1975).
6. D. T. CROMER and J. T. WABER. Acta Crystallogr. **18**, 104 (1965).
7. R. F. STEWART, E. R. DAVIDSON, and W. T. SIMPSON. J. Chem. Phys. **42**, 3175 (1965).
8. D. T. CROMER. Acta Crystallogr. **18**, 17 (1965).
9. S. LOUIE and R. BAU. J. Am. Chem. Soc. **99**, 3874 (1977).
10. R. E. CRAMER and P. L. DAHLSTROM. J. Clin. Hematol. Oncol. **7**, 330 (1977).
11. C. J. L. LOCK, J. BRADFORD, R. FAGGIANI, R. A. SPERANZINI, G. TURNER, and M. ZVAGULIS. J. Clin. Hematol. Oncol. **7**, 63 (1977).
12. D. VOET and A. RICH. Prog. Nucl. Acid. Res. Mol. Biol. **10**, 183 (1970).
13. V. THEWALT, C. E. BUGG, and R. E. MARSH. Acta Crystallogr. B, **26**, 1089 (1970).
14. C. SINGH. Acta Crystallogr. **19**, 861 (1965).
15. M. SUNDARALINGAM. Biopolymers, **7**, 821 (1969).
16. J. DONOHUE and K. N. TRUEBLOOD. J. Mol. Biol. **2**, 363 (1960).
17. E. SHEFTER and K. N. TRUEBLOOD. Acta Crystallogr. **18**, 1067 (1965).

Conformational dissymmetry. Circular dichroism of amino acid and peptide complexes

E. A. SULLIVAN[1]

Lash Miller Chemical Laboratories, University of Toronto, Toronto, Ont., Canada M5S 1A1

Received May 26, 1978

E. A. SULLIVAN. Can. J. Chem. **57**, 62 (1979).

A number of Pd(II) and Pt(II) complexes of amino acids and dipeptides have been isolated and characterized. The solution and solid-state circular dichroism of the amino acid complexes show a fairly consistent pattern, which is opposite to that shown by the dipeptide complexes. Some of the problems associated with the interpretation of the spectra in terms of spectroscopic assignment and structural features are discussed.

E. A. SULLIVAN. Can. J. Chem. **57**, 62 (1979).

On a isolé et caractérisé un certain nombre de complexes du Pd(II) et du Pt(II) avec des acides aminés et des dipeptides. Le dichroïsme circulaire, à l'état solide et en solution, des complexes avec les acides aminés présente des caractéristiques cohérentes; ceci est à l'opposé du comportement des complexes des dipeptides. On discute de quelques-uns des problèmes associés avec l'interprétation des spectres en termes d'attributions spectroscopiques et de caractéristiques de structures.

[Traduit par le journal]

The circular dichroism associated with the *d–d* transitions of amino acid and peptide complexes has been the study of extensive investigation, the impetus for which stems ultimately from an interest in the nature of metal–protein binding. Most studies have concentrated on the square coplanar species formed with Ni(II) and Cu(II) (1), which are labile in solution. Wide limits of conformational flexibility are allowed to coordinated amino acid ligands (2), a fact which complicates the unresolved problem of identifying the particular (chiral) stereochemical features which generate the optical activity in the *d*-electron transitions (1, 3–5).

Although some studies, involving solution-generated species of Pd(II) with amino acid derivatives, have been reported (6), this paper describes the circular dichroism of a number of amino acid and dipeptide complexes of Pd(II) and Pt(II), all of which have been isolated and characterized. The spectra were recorded in solution and also in KBr matrices in order to determine the effects on the circular dichroism in various environments.

Results

In Figs. 1 and 2 are shown the absorption and circular dichroism spectra of the mono amino acid complexes of Pd(II) and Pt(II) respectively, and in Fig. 3 the spectra of the bis-amino acid complexes of Pd(II). All the aqueous spectra of the mono complexes were determined in 0.2 *M* KCl in order to suppress standing concentrations of aquo species which are rapidly and extensively formed in the absence of Cl^- ions. The solid-state linear absorption spectra are very similar to those obtained in solution, except that the charge-transfer bands tend to shift to lower energies.

The solution absorption spectra of the Pd(II) and Pt(II) mono- and bis-amino acid complexes usually show two discernible major components; in the case of $[Pt(S\text{-ala})Cl_2]^-$, the bands occur at 30 600 cm^{-1} and 34 000 cm^{-1}. In the Pd(II) amino acid complexes the bands are less distinct, the solution spectra usually consisting of a broad composite band with a shoulder on the low energy side; for the mono complexes the shoulder occurs near 24 000 cm^{-1} and for the bis complexes, near 28 000 cm^{-1}. In similar Pd(II) and Pt(II) ammine complexes the lower energy component of the *d*-electron manifold has been identified as the $d_{xy} \rightarrow d_{x^2-y^2}$ spin-allowed transition while the higher energy component was assigned to the spin-allowed $d_{xz},d_{yz} \rightarrow d_{x^2-y^2}$ promotion (6, 7). The same assignments will be applied to the amino acid complexes, and will be referred to as the *A* and *E* transitions respectively. Ideally, each transition requires to be identified and assigned and then the corresponding components compared for a series of compounds. As will be seen from the present data, extensive overlap between components generally precludes unambiguous assignments.

Whatever the actual assignment of the shoulder band in the solution absorption spectra of the mono and bis complexes, if it corresponds to the same transition for these complexes, then there is a fairly consistent CD sign pattern, both in solution and the

[1]Present address: Faculty of Engineering Science, University of Western Ontario, London, Ont., Canada N6A 5B7.

0008-4042/79/010062-05$01.00/0

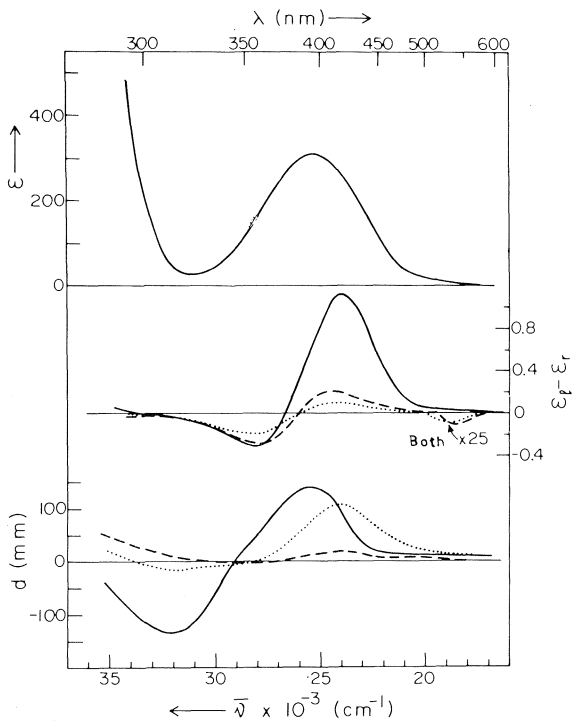

FIG. 1. The circular dichroism spectra of K[Pd(*S*-ala)Cl_2] (···), K[Pd(*S*-ser)Cl_2] (---), and K[Pd(*S*-pro)Cl_2] (—) in 0.2 *M* KCl aqueous solutions (middle) and in 1% KBr matrices (bottom). The top diagram is the absorption spectrum of K[Pd(*S*-pro)Cl_2] in 0.2 *M* KCl solution; the other complexes show similar spectra. In the middle diagram, the triplet region of both the *S*-serine and *S*-alanine complexes are × 25.

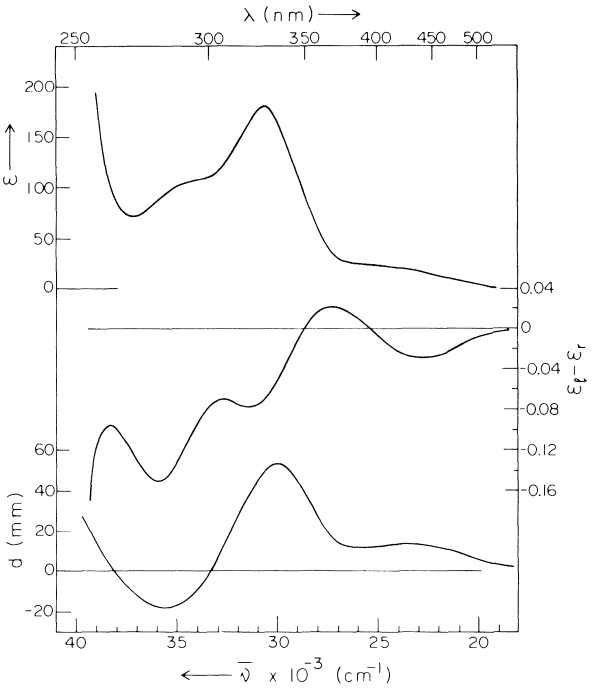

FIG. 2. The absorption (top) and circular dichroism spectra (middle) of K[Pt(*S*-ala)Cl_2] in 0.2 *M* KCl aqueous solution. The bottom diagram refers to the spectrum in a 1% KBr matrix.

solid state. Thus, at the same energy position corresponding to the shoulder in the solution absorption spectra, the CD spectra of all the complexes show a positive band in the solid state and in solution. For the Pt(II) mono complex, however, this region of the solution CD shows a negative band; some Pd(II) amino acid amide complexes also show this behaviour, the sign of the band depending on the particular solvent (8). In the region of the *E* transition, the amino acid complexes all show negative CD although the position of the band varies between complexes, particularly for the solid-state spectra. It is notable that the proline mono complex with its fixed δ-conformation and chiral (*S*) nitrogen atom shows by far the strongest CD. Strong positive CD in the region of the *A* transition (and negative CD in the region of the *E*) has been associated with the vicinal effect of a chiral nitrogen atom in the *S*-absolute configuration (9). Although the circular dichroism of the proline complex retains the same form in the solid, the two (solid-state) bands are displaced to higher energies compared to the seemingly corresponding bands in solution.

The two isomers of [Pd(*S*-ala)$_2$] slowly equilibrate in aqueous solution and the rate constant k, for the approach to equilibrium, as well as the equilibrium constant K, has been determined spectrophotometrically at 30°C in neutral water solution.

$$\textit{trans}\text{-[Pd(}S\text{-ala)}_2\text{]} \rightleftharpoons \textit{cis}\text{-[Pd(}S\text{-ala)}_2\text{]}$$

For the composite constant $k = 1.1 \times 10^{-4}\ s^{-1}$ and $K = 6.0$, reflecting 86% of the *cis*-isomer at equilibrium. The equilibration is remarkably clean, since both the pairs of near ultra-violet isosbestic and isodichroic points are maintained throughout 5 half-lives of reaction.

The isomerism has been tentatively assigned on the basis of the relative intensities of the *d–d* bands of the two isomers. Considering only the donor atom symmetry, the *trans*-isomer is centrosymmetric, while the *cis* is not, hence the latter is expected to have the more intense spectrum (Fig. 3). In the Pd(II) bis-glycinato complexes, the *cis*-isomer has the greater absorptivity (10).

The circular dichroism spectra of the two isomers in water solution are nearly identical and the pattern

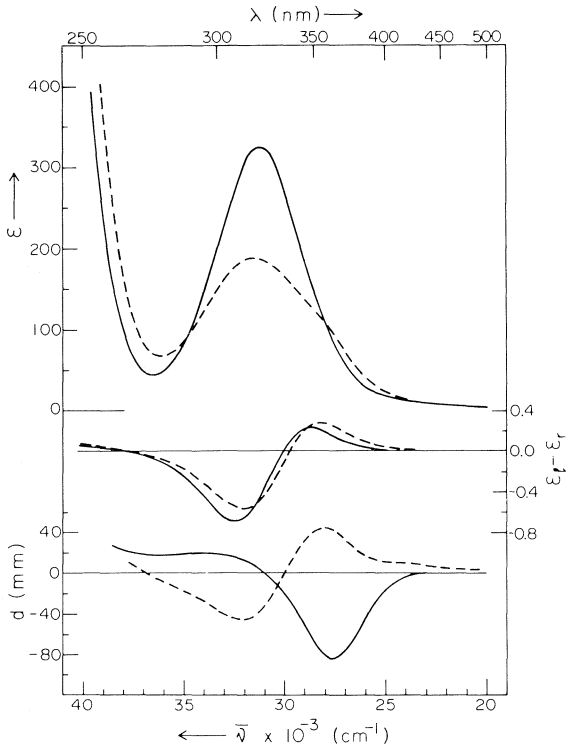

FIG. 3. The absorption and circular dichroism spectra of *cis*-[Pd(*S*-ala)$_2$] (—) and *trans*-[Pd(*S*-ala)$_2$] (---) in water solutions. The bottom diagram refers to spectra in 1% KBr matrices.

is the same as that observed for the mono *L*-amino acid complexes in solution. Unlike the *trans*-species and the mono complexes, however, the *cis*-[Pd(*S*-ala)$_2$] species in the solid state shows an almost enantiomorphic spectrum.

The spectra of the dipeptide complexes Cs[Pd(gly-*S*-ala)Cl] and Cs[Pd(*S*-alagly)Cl] are shown in Figs. 4 and 5. Upon dissolution in water, both complexes immediately aquate to give the species [Pd(dipeptide)H_2O] in dilute solution. Beer's law is obeyed exactly, for concentrations between 2×10^{-3} and 1×10^{-4} *M* in complex, and the addition of Cl^- ions results immediately in new spectra which are shifted to the red as would be expected if the aquo ligand is replaced by chloride. Further addition of KCl to 0.2 *M* KCl solutions of the complexes does not affect the spectra.

The circular dichroism spectra of the chloro complexes in 0.2 *M* KCl solution show three spin-allowed circular dichroism bands; the negative bands at 27 000 cm^{-1} and 25 500 cm^{-1} for the [Pd(*S*-alagly)Cl]$^-$ and [Pd(gly-*S*-ala)Cl]$^-$ ions, respectively, are assigned to the *A* transition and the higher energy couplets to a split *E* band. (At 22 500 cm^{-1}, the [Pd(*S*-alagly)Cl]$^-$ ion shows an additional

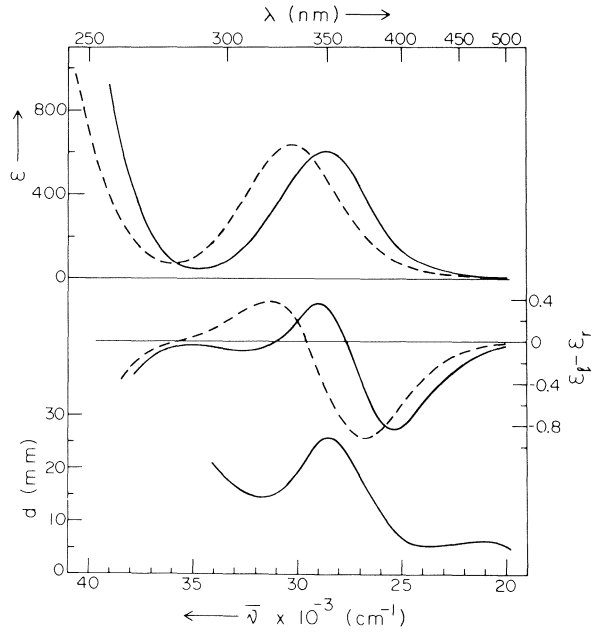

FIG. 4. The absorption and circular dichroism spectra of Cs[Pd(gly-*S*-ala)Cl] in 0.2 *M* KCl aqueous solution (—), and of [Pd(gly-*S*-ala)H_2O] in water (---). The bottom diagram refers to the Cs[Pd(gly-*S*-ala)Cl] complex dispersed in a 1% KBr matrix.

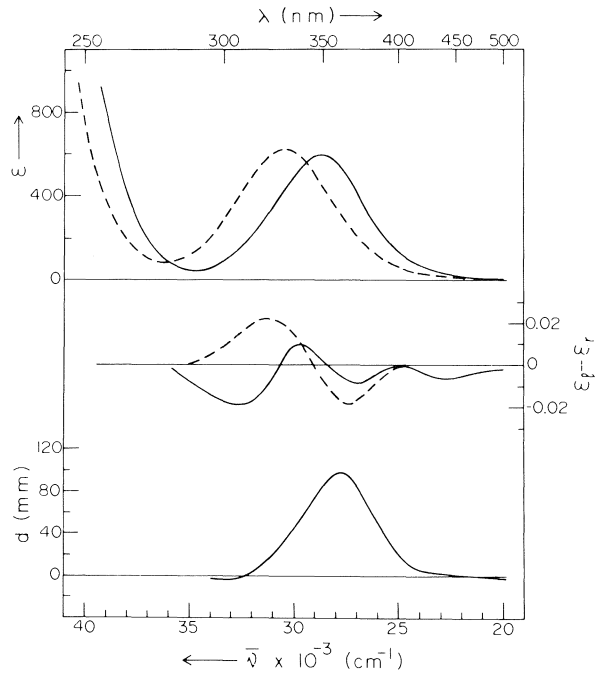

FIG. 5. The absorption and circular dichroism spectra of Cs[Pd(*S*-alagly)Cl] (—) in 0.2 *M* KCl aqueous solutions and of [Pd(*S*-alagly)H_2O] (---) water solution. The bottom spectrum refers to a 1% KBr matrix of Cs[Pd(*S*-alagly)Cl].

negative band which is assigned to a spin-forbidden transition.) Apparently, the effective symmetry of the chloro complexes is low enough for the *E* band to lose its degeneracy. In the solid state, each chloro complex shows a positive band which is difficult to associate with any of the corresponding CD bands shown in solution.

In the CD spectra of the aquo complexes, the lower energy (negative) bands probably represent *A* transitions (in part at least), but since there is no indication of the effective symmetry of these complexes, the assignment of the higher energy (positive) band is uncertain. If the *E* band is split, it is not resolved.

Discussion

The spectra of the complexes described in this investigation differ somewhat in intensity from those obtained from previous solution studies (6). This is perhaps not surprising, in view of the uncertainty as to the identity of species in (equilibrium) mixtures of reactants.

Spectroscopic assignments are also uncertain, but CD patterns for the series of complexes may be compared. Thus, the CD spectra of the mono and bis complexes of Pd(II) and Pt(II) are quite similar. Despite the variety of ring conformations and sidechain dispositions available to chelated amino acids (2), the solution CD of the complexes are remarkably similar to those of analogous diamine complexes (11).

The solid-state CD spectrum of *cis*-[Pd(*S*-ala)$_2$] and the solution CD spectra of the aquo dipeptides are very similar, if the positions of the respective maxima in the solution absorption spectra are matched. Notably, however, these CD spectra are almost enantiomorphic to the solid-state CD of the *trans*-isomer and the solution CD of both *cis*- and *trans*-isomers, even though all four complexes have the same donor atoms (2N, 2O). For the various complexes, differing effective donor atom symmetries could perhaps provide a rationalization for this behaviour. In the solid state, the effective symmetry of the *trans*-isomer might be approximately D_{4h} (although formally D_{2h}) and that of the *cis*-isomer could be C_{2v} or lower. The structures of a number of *cis*-bis complexes of Cu(II) and Pd(II) show axial orientations of amino acid sidechains (12, 13), so perhaps crystal packing requirements could result in low effective symmetry for such complexes. In that case it might not be unreasonable to expect the solid-state CD of the *cis*-isomer to resemble that of the aquo dipeptide complexes (if the effective symmetry of the complexes were the same and for ligands with the same absolute configuration), and yet at the same time differ from that of the *trans*-isomer and the solution species.

It is difficult to rationalize the consistencies in the CD spectra of the mono and bis amino acid complexes and the 'reversed' pattern of the aquo dipeptide complexes in terms of either the vicinal effect of chiral carbon atoms (3), conformation of ligands (4), donor atom distortions (5), or the disposition of C_α-sidechains (1). Furthermore, sign patterns may be determined largely by the effective symmetry of the complexes (14). Whatever the origins of optical activity in chiral metal complexes, until some of the more fundamental problems are resolved, the use of circular dichroism to probe the metal coordination in complicated structures such as metallo-enzymes, requires extreme caution.

Experimental Section

Absorption spectra were measured on a Unicam 800A spectrophotometer, and solution CD spectra were obtained with a Roussel-Jouan Dichrographe II. KBr discs (1% in complex in 100 mg total sample) were prepared as described elsewhere (5). The solid-state CD spectra were obtained with a Durrum JASCO J-20 spectrophotometer with a SS-20 CD attachment; the ordinate units are deflection in mm for a sensitivity of 5 mdeg cm^{-1}. The kinetics of the *cis–trans* isomerization of [Pd(*S*-ala)$_2$] were followed at 318 nm using a Cary 16 spectrophotometer.

In this article we use the abbreviations: *S*-alaH = *L*-alanine; *S*-serH = *L*-serine; *S*-proH = *L*-proline; *S*-alaglyH$_2$ = *L*-alanylglycine; gly-*S*-alaH$_2$ = glycyl-*L*-alanine.

K[Pt(*S*-ala)Cl$_2$] was prepared by the published method (15).

The K[Pd(*L*-amino acid)Cl$_2$] complexes were prepared by the following aqueous reaction:

$$PdCl_2 + \begin{matrix} KAc \\ \text{or} \\ K_2CO_3 \end{matrix} + L\text{-amino acid} \rightarrow K[Pd(L\text{-amino acid})Cl_2] + HAc$$

where Ac = acetate. The products were precipitated with ethanol (or acetone for the alanine complex) and recrystallized from water by the same precipitating agent.

*K[Pd(*S*-ala)Cl$_2$]*

Anal. calcd. for K[Pd($C_3H_6NO_2$)Cl$_2$]: C 11.8, H 2.0, N 4.6, Cl 23.3; found: C 12.0, H 2.0, N 4.7, Cl 23.2.

*K[Pd(*S*-ser)Cl$_2$]*

Anal. calcd. for K[Pd($C_3H_6NO_3$)Cl$_2$]: C 11.2, H 1.9, N 4.4, Cl 22.1; found: C 11.2, H 2.0, N 4.4, Cl 22.0.

*K[Pd(*S*-pro)Cl$_2$]*

Anal. calcd. for K[Pd($C_5H_8NO_2$)Cl$_2$]: C 18.2, H 2.4, N 4.2, Cl 21.4; found: C 18.3, H 2.7, N 4.2, Cl 21.3.

[Pd(*S*-ala)$_2$] precipitates as a yellow solid when a solution of PdCl$_2$, *L*-alanine, and excess LiCl is slowly neutralized with NaHCO$_3$.

trans-[*Pd(*S*-ala)$_2$*]

The crude product (1 g) from above was dissolved in boiling water (50 ml). The solution was filtered and set aside at 25°C for 2 days. The *trans*-isomer separated as large yellow plates; mp 150–155°C (dec.). The aqueous filtrate was retained.

Anal. calcd. for [Pd($C_3H_6NO_2$)$_2$]: C 25.5, H 4.3, N 9.9; found: C 25.6, H 4.2, N 9.8.

cis-[*Pd(*S*-ala)$_2$*]

To the above filtrate was added ethanol (250 ml) and then ether (250 ml) and the mixture was set aside at 0°C for 12 h. The crude product (0.4 g) was collected and then stirred in

water (20 ml) at 15°C for 15 min. The mixture was filtered and ethanol (150 ml) was added to the filtrate. Upon scratching the sides of the flask, the *cis*-isomer began to form. After allowing the solution to stand at 0°C for 12 h, the yellow needles were collected. They were recrystallized from cold water by the addition of ethanol (0.25 g). mp 230°C (dec.).

Anal. found: C 25.6, H 4.2, N 9.9.

The dipeptide complexes Cs[Pd(dipeptide)Cl] were prepared by neutralizing with $CsCO_3$ a solution containing stoichiometric amounts of $PdCl_2$ and the dipeptide, then precipitating the crude product with ethanol and acetone. The complexes were recrystallized from a small volume of water by careful addition of ethanol and acetone. The pure complexes were deposited as small needles, of a yellow to orange-yellow colour.

Cs[Pd(gly-S-ala)Cl]

Anal. calcd. for $Cs[Pd(C_5H_8N_2O_3)Cl]$: C 14.3, H 1.9, N 6.7, Cl 8.5; found: C 14.9, H 2.0, N 6.7, Cl 8.7.

Cs[Pd(S-alagly)Cl]

Anal. calcd. for $Cs[Pd(C_5H_8N_2O_3)Cl]$: C 14.3, H 1.9, N 6.7, Cl 8.5; found: C 14.4, H 2.1, N 6.9, Cl 8.8.

Acknowledgements

This work was supported in part by the National Research Council of Canada. The author wishes to thank Dr. B. Bosnich for advice and assistance at all stages of this investigation.

1. J. W. Chang and R. B. Martin. J. Phys. Chem. **73**, 4277 (1969); J. M. Tsangaris and R. B. Martin. J. Am. Chem. Soc. **92**, 4255 (1970).
2. H. C. Freeman. Adv. Protein Chem. **22**, 257 (1967); J. R. Gollogly, C. J. Hawkins, and C. L. Wong. Inorg. Nucl. Chem. Lett. **6**, 215 (1970).
3. C. J. Hawkins and C. L. Wong. Aust. J. Chem. **23**, 2237 (1970).
4. K. W. Wellman, W. Mungall, T. G. Mecca, and C. R. Hare. J. Am. Chem. Soc. **89**, 3647 (1967).
5. B. Bosnich and J. Harrowfield. J. Am. Chem. Soc. **94**, 3425 (1972).
6. E. W. Wilson and R. B. Martin. Inorg. Chem. **9**, 528 (1970); E. W. Wilson and R. B. Martin. Inorg. Chem. **10**, 1197 (1971).
7. J. Chatt, G. A. Gamlen, and L. E. Orgel. J. Chem. Soc. 486 (1958); D. S. Martin, M. A. Tucker, and A. J. Kassman. Inorg. Chem. **4**, 1682 (1965); P. Day, A. F. Orchard, A. J. Thomson, and R. J. P. Williams. J. Chem. Phys. **42**, 1973 (1965); A. J. McCaffery, P. N. Schatz, and P. J. Stephens. J. Am. Chem. Soc. **90**, 5730 (1968).
8. T. Komorita, J. Hidaka, and Y. Shimura. Bull. Chem. Soc. Jpn. **42**, 1782 (1969); **41**, 854 (1968).
9. C. J. Hawkins. Chem. Commun. 777 (1969); L. J. DeHayes, M. Parris, and D. H. Busch. Chem. Commun. 1398 (1971); B. Bosnich and E. A. Sullivan. Inorg. Chem. **14**, 2768 (1975).
10. J. S. Coe and J. R. Lyons. J. Chem. Soc. A, 829 (1971).
11. H. Ito, J. Fujita, and K. Saito. Bull. Chem. Soc. Jpn. **40**, 2584 (1967).
12. R. D. Gillard, R. Mason, N. C. Payne, and G. B. Robertson. J. Chem. Soc. A, 1864 (1969); C. M. Weeks, A. Cooper, and D. A. Norton. Acta Crystallogr. **25**B, 443 (1969).
13. T. C. Jarzab, C. R. Hare, and D. A. Langs. Cryst. Struct. Commun. **3**, 395 (1973).
14. F. S. Richardson. J. Chem. Phys. **54**, 2453 (1971); Inorg. Chem. **10**, 2121 (1971).
15. H. Ley and K. Ficken. Ber. Dtsch. Chem. Ges. **45**, 377 (1912).

Circular dichroism of palladium(II) and platinum(II) diamine complexes

E. A. SULLIVAN[1]

Lash Miller Chemical Laboratories, University of Toronto, Toronto, Ont., Canada M5S 1A1

Received May 27, 1978

E. A. SULLIVAN. Can. J. Chem. **57**, 67 (1979).

An identifiable relationship exists between the absolute configuration of chiral diamine ligands and the circular dichroism of their complexes with palladium(II) and platinum(II). Complexes which contain simple *C*-substituted diamines with the *R*-absolute configuration show positive circular dichroism in the region associated with the $^1A_{1g} \rightarrow {}^1E_g$ transition, both in solution and the solid state. There is no general consistency in the sign of the $^1A_{1g} \rightarrow {}^1A_{2g}$ transition, and only for solution does the sign of the net circular dichroism show a correlation with the absolute configuration of the ligands.

E. A. SULLIVAN. Can. J. Chem. **57**, 67 (1979).

Il existe une relation qui peut être identifiée entre la configuration absolue de ligands diaminés chiraux et le dichroïsme circulaire de leurs complexes avec le palladium(II) et le platine(II). Les complexes qui comportent des diamines simples, substitués sur le *C* et de configuration absolue *R*, présentent un dichroïsme circulaire positif dans la région associée à la transition $^1A_{1g} \rightarrow {}^1E_g$ tant en solution qu'à l'état solide. Il n'y a pas de relation générale pour le signe de la transition $^1A_{1g} \rightarrow {}^1A_{2g}$ et l'on ne retrouve qu'en solution une relation entre le dichroïsme circulaire net et la configuration absolue des ligands.

[Traduit par le journal]

Ligand field CD spectra provide an empirical basis for differentiation between the various kinds of dissymmetric stereochemical features in chiral metal complexes (1). Attempts have been made to correlate absolute configuration of metal complexes with features in the CD spectra but no agreement has been reached as to whether absolute configuration should be correlated with the sign of specific bands (2–4) or with the net CD over the whole *d*-electron manifold (5). In order to assess the general applicability of such correlations, the solution and solid-state CD spectra of a series of diamine complexes of Pd(II) and Pt(II) have been examined. These complexes were chosen because they are sufficiently stable to be sure of the species present.

Spectroscopic assignments have been established for Pd(II) and Pt(II) complexes (6), and the approximate location of these transitions (3, 6) is shown in Fig. 1. The two *d–d* excitations which are both magnetic dipole allowed and spin allowed (i.e. $d_{xy} \rightarrow d_{x^2-y^2}$ and $d_{xz,yz} \rightarrow d_{x^2-y^2}$) will be subsequently referred to as the *A* and *E* transitions respectively.

Typical linear absorption spectra and CD spectra for solution and the solid state are shown in Figs. 2–5. The solid-state spectra of Pt(*R*-pn)Cl_2 (Fig. 4) are not typical, but resemble the behaviour of Pt(en)Cl_2 in which cooperative effects dominate the spectrum (7). The position of the absorption band

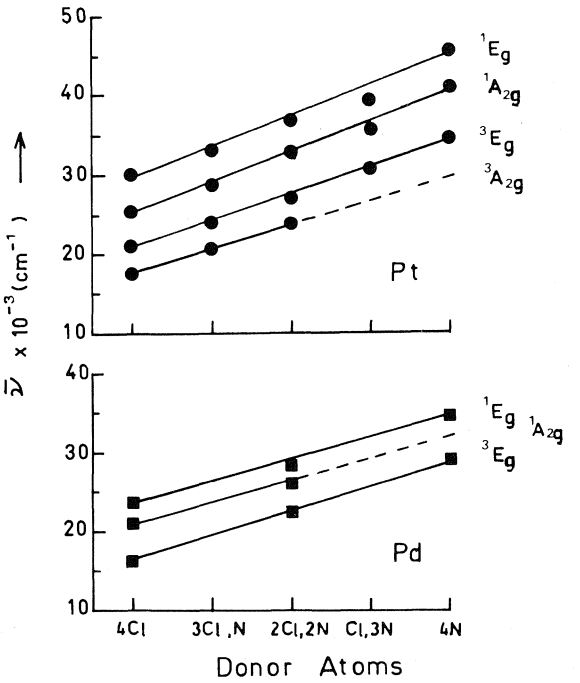

FIG. 1. Absorption energies for *d–d* transitions in chloroammine complexes of Pt(II) and Pd(II). From the data of Chatt *et al.* (6) and Ito *et al.* (3).

maxima in the linear absorption spectra of the Pt(II) complexes are generally unaffected by changes in the media, but the absorption spectra of the Pd(II) complexes consist of a composite band, the maximum

[1]Present address: Faculty of Engineering Science, University of Western Ontario, London, Ont., Canada N6A 5B7.

0008-4042/79/010067-04$01.00/0

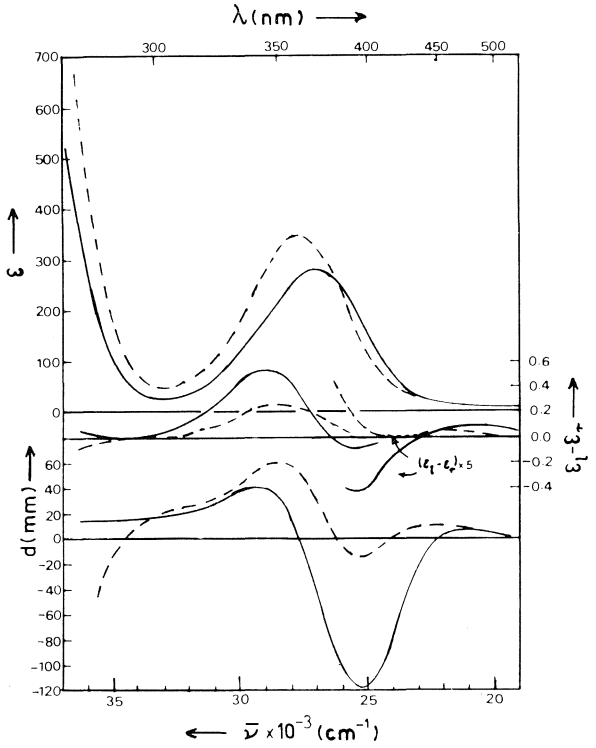

FIG. 2. Absorption and CD spectra of [Pd(*R*-pn)Cl_2] (—) and [Pd(*R*,*R*-dmtn)Cl_2] (---) in 0.2 *M* KCl. Bottom curves are the solid-state CD spectra.

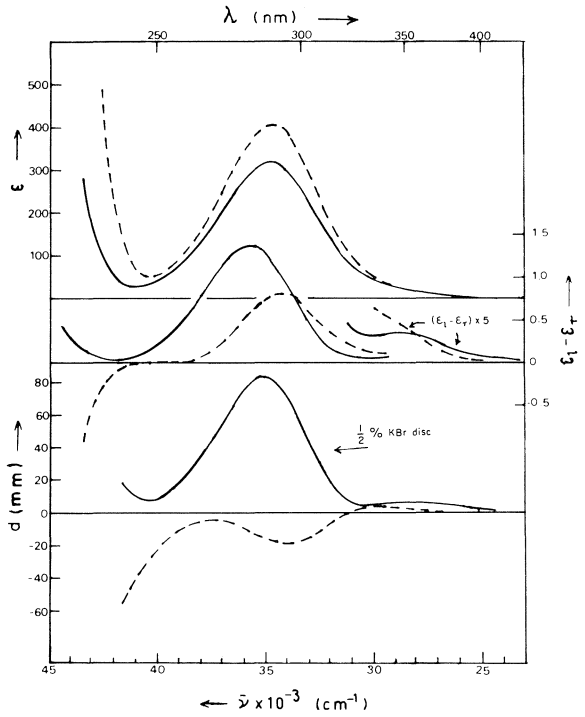

FIG. 3. Absorption and CD spectra of [Pd(*R*-pn)$_2$]$Cl_2 \cdot H_2O$ (—) and [Pd(*R*,*R*-dmtn)$_2$]$Cl_2 \cdot H_2O$ (---) in water. Bottom curves are the solid-state CD spectra.

of which varies considerably according to the medium. Thus for Pd(*R*-pn)Cl_2, the solution maximum occurs at 27 100 cm^{-1} (for 0.2 *M* KCl solution), whereas in a KBr disc or a Nujol mull it occurs at 25 700 – 26 000 cm^{-1}. However, despite these large apparent shifts (which probably reflect changes in the relative intensity of the components under the absorption manifold), the positions of the corresponding extrema in the solution and solid-state CD spectra do not change. These extrema occur at frequencies which correspond to the expected positions of the *A* and *E* components, as determined by Gaussian analysis of the solution absorption spectra (3, 6). With the bis-complexes, unambiguous assignments are not always possible, owing to extensive overlap between components. The CD signs associated with the regions of the *A* and *E* transitions are summarized in Table 1.

The experimental results for Pd(II) and Pt(II) complexes show, as in the case of octahedral Co(III) complexes (4), that there is no general consistency in the sign of the *A* band, regardless of whether the spectra are obtained from solution or the solid state. Moreover, it is doubtful whether the net CD sign can in general (8) give a reliable indication of absolute configuration, since it can be envisaged that component band intensities alone could determine the net sign of a composite band of overlapping transitions. Table 1 shows that the net CD sign obtained from the solid-state spectra exhibits a variable sign. The sign of the net CD of the solution spectra does show consistent behaviour for the present series of complexes, as in an impressive number of other cases (9), and may therefore serve as a useful index of absolute configuration, but this consistency may also result if the rotational strength associated with a particular transition dominates the solution CD spectrum. Such is the case for the *E* band in complexes of Pd(II) and Pt(II) (3), as well as other metals such as Co(III) and Rh(III) (2, 10). Indeed, the sign of the *E* band is the one consistent feature in the present series of complexes, when this band can be identified.

Both in solution and the solid state, complexes which contain simple (*C*-substituted) diamines with the *R*-absolute configuration show positive CD in the region associated with the *E* transition; this relationship is obtained irrespective of whether the chelate rings carry aliphatic or aromatic substituents.

It has been noted previously (3) that for a number of metal complexes in which the chelate rings are fixed in the λ-conformation, positive CD is associated with the *E* band (3) and that this sign persists for

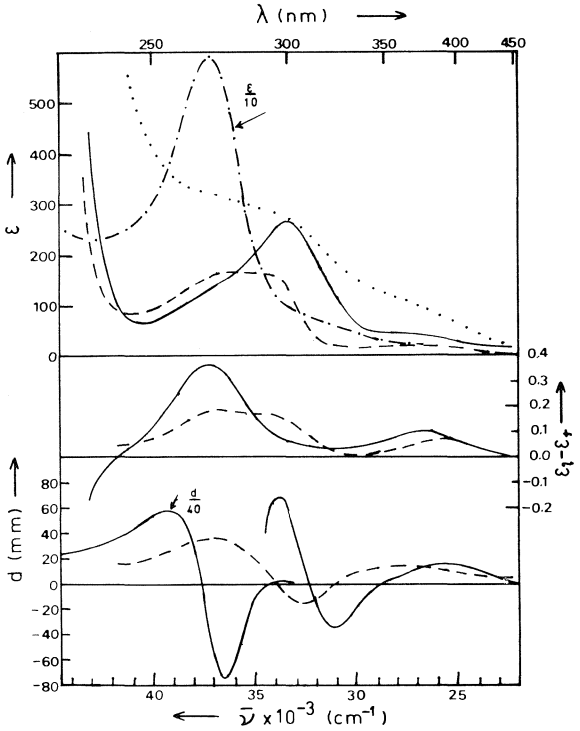

FIG. 4. Solution absorption and CD spectra of [Pt(*R*-pn)Cl_2] (—) and [Pt(*R*,*R*-dmtn)Cl_2] (fresh solution) (---) in 2 *M* HCl; relative solid-state absorption spectra of [Pt(*R*-pn)Cl_2] (·····) and [Pt(*R*,*R*-dmtn)Cl_2] (···). Bottom curves are the solid-state CD spectra.

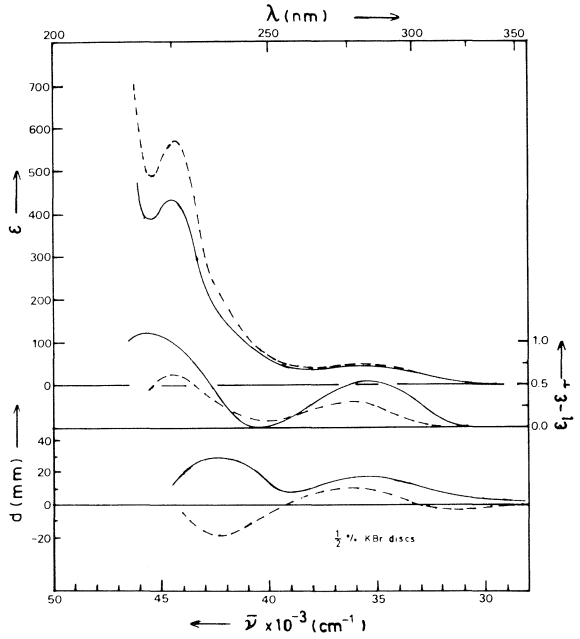

FIG. 5. Absorption and CD spectra of [Pt(*R*-pn)$_2$]Cl_2·H_2O (—) and [Pt(*R*,*R*-dmtn)$_2$]Cl_2 (---) in water. Bottom curves are the solid-state CD spectra.

different solvents and for the solid state (4). This investigation extends the results to a wider range of complexes and ligands and suggests that the sign of the *E* band (if it can be determined unambiguously) may be a useful and quite general criterion of absolute configuration.

Experimental

Absorption spectra were measured on a Unicam 800A spectrophotometer and the solution CD spectra were obtained with a Roussel-Jouan Dichrographe II. The solid-state spectra were obtained with a Durrum JASCO J-20 spectrophotometer with a SS-20 CD attachment. The CD for the solid state is reported in terms of the deflection *d*, in mm, at a sensitivity of

TABLE 1. Signs of the circular dichroism for Pt(II) and Pd(II) complexes

		Solution[e]			Solid state[e]		
Complex	Solvent	*E*	*A*	Net	*E*	*A*	Net
[Pd(*R*-pn)Cl_2]	0.2 *M* KCl	+	−	+	+	−	−
[Pd(*R*,*R*-dmtn)Cl_2]	0.2 *M* KCl	+	(+)	+	+	−	+
[Pd(*R*-phenen)Cl_2]	[a]				+	−	−
[Pd(*R*,*R*-stien)Cl_2]	[a]				+	−	+
[Pd(*R*-pn)$_2$]Cl_2	Water	+	[b]	+	+	[b]	+
[Pd(*R*,*R*-dmtn)$_2$]Cl_2	Water			+[c]			−[c]
[Pd(*R*,*R*-stien)$_2$]Cl_2	Methanol	+	[b]	+	+	[b]	+
[Pd(*R*,*R*-stien)$_2$]$(NO_3)_2$	Methanol	+	−	+	+	[b]	+
[Pt(*R*-pn)Cl_2]	2 *M* HCl	+	[b]	+			[d]
[Pt(*R*,*R*-dmtn)Cl_2]	2 *M* HCl	+	+	+	+	−	+
[Pt(*R*-pn)$_2$]Cl_2	Water	+	(+)	+			+[c]
[Pt(*R*,*R*-dmtn)$_2$]Cl_2	Water	+	(+)	+			−[c]
[Pt(*R*-pn)$(NH_3)_2$]Cl_2	Water	+	(+)	+	+	(+)	+
[Pt(*R*,*R*-dmtn)$(NH_3)_2$]Cl_2	Water	+	(+)	+	+	[b]	+

[a]Complex insoluble in water; solvolyses in dipolar aprotic solvents.
[b]Sign uncertain; band obscured.
[c]Composite band.
[d]Solid-state effects dominate spectrum; assignments uncertain.
[e]Parentheses denote most probable sign.

5 mdeg cm^{-1}. KBr discs contained 1% of complex in 100 mg of total sample, unless otherwise stated.

Abbreviations for the diamines are as follows: *R*-pn = (−)-1,2-diaminopropane; *R,R*-dmtn = (−)-2,4-diaminopentane; *R*-phenen = (−)-1,2-diaminophenylethane; *R,R*-stien = (+)-1,2-diamino-1,2-diphenylethane (stilbenediamine).

The ligands *R*-pn, *R,R*-dmtn, and *R,R*-stien were prepared according to methods described in the literature (4). During the preparation of *R*-phenen (11) partial racemization occurred. The ligand was resolved via the (+)-tartrate salt and the resolving agent was removed by the method of Bailar *et al.* (12). The absolute configuration of the ligands has been established by absolute crystal structure determinations (13), or by chemical correlations (14). The general preparation for the complexes has been previously reported (15).

Analyses

[*Pd*(R,R-*dmtn*)Cl_2]
Anal. calcd. for $C_5H_{14}N_2Cl_2Pd$: C 21.5, H 5.1, N 10.0, Cl 25.4; found: C 21.4, H 5.1, N 9.9, Cl 25.1.

[*Pd*(R,R-*dmtn*)$_2$]$Cl_2 \cdot H_2O$
Anal. calcd. for $C_{10}H_{30}N_4OCl_2Pd$: C 30.0, H 7.7, N 14.0, Cl 17.7; found: C 30.4, H 7.7, N 14.6, Cl 17.4.

[*Pd*(R-*phenen*)Cl_2]
Anal. calcd. for $C_8H_{12}N_2Cl_2Pd$: C 30.6, H 3.9, N 8.9, Cl 22.6; found: C 30.5, H 3.9, N 8.9, Cl 22.7.

[*Pd*(R,R-*stien*)Cl_2]
Anal. calcd. for $C_{14}H_{16}N_2Cl_2Pd$: C 43.2, H 4.1, N 7.2, Cl 18.2; found: C 43.2, H 4.3, N 7.2, Cl 18.1.

[*Pd*(R,R-*stien*)$_2$]$Cl_2 \cdot 2H_2O$
Anal. calcd. for $C_{28}H_{36}N_4O_2Cl_2Pd$: C 52.7, H 5.7, N 8.8, Cl 11.2; found: C 52.7, H 5.7, N 8.7, Cl 10.9.

[*Pd*(R,R-*stien*)$_2$]$(NO_3)_2$
Anal. calcd. for $C_{28}H_{32}N_6O_6Pd$: C 51.3, H 4.9, N 12.8; found: C 51.3, H 5.1, N 12.7.

[*Pt*(R,R-*dmtn*)Cl_2]
Anal. calcd. for $C_5H_{14}N_2Cl_2Pt$: C 16.3, H 3.8, N 7.6, Cl 19.3; found: C 16.4, H 3.7, N 7.5, Cl 19.5.

[*Pt*(R,R-*dmtn*)$(NH_3)_2$]$Cl_2 \cdot H_2O$
Anal. calcd. for $C_5H_{22}N_4OCl_2Pt$: C 14.3, H 5.3, N 13.3; found: C 14.4, H 5.4, N 13.4.

[*Pt*(R,R-*dmtn*)$_2$]Cl_2
Anal. calcd. for $C_{10}H_{28}N_4Cl_2Pt$: C 25.5, H 6.0, N 11.9; found: C 25.5, H 6.1, N 11.8.

1. B. E. Douglas. *In* Coordination chemistry. *Edited by* S. Kirschner. Plenum Press, New York. 1969. pp. 29–41.
2. C. J. Hawkins and E. Larsen. Acta Chem. Scand. **19**, 185 (1965); **19**, 1969 (1965).
3. H. Ito, J. Fujita, and K. Saito. Bull. Chem. Soc. Jpn. **40**, 2584 (1967).
4. B. Bosnich and J. MacB. Harrowfield. J. Am. Chem. Soc. **94**, 3425 (1972).
5. F. S. Richardson. J. Chem. Phys. **54**, 2453 (1971).
6. J. Chatt, G. A. Gamlen, and L. E. Orgel. J. Chem. Soc. 486 (1958); D. S. Martin, M. A. Tucker, and A. J. Kassman. Inorg. Chem. **4**, 1682 (1965); P. Day, A. F. Orchard, A. J. Thomson, and R. J. P. Williams. J. Chem. Phys. **42**, 1973 (1965); A. J. McCaffery, P. N. Schatz, and P. J. Stephens. J. Am. Chem. Soc. **90**, 5730 (1968).
7. D. S. Martin, L. D. Hunter, R. Kroening, and R. F. Coley. J. Am. Chem. Soc. **93**, 5433 (1971).
8. B. Bosnich and J. MacB. Harrowfield. Inorg. Chem. **14**, 828 (1975).
9. E. W. Wilson and R. B. Martin. Inorg. Chem. **10**, 1197 (1971) and references therein.
10. S. K. Hall and B. E. Douglas. Inorg. Chem. **7**, 533 (1968).
11. L. Arpesella, A. La Manna, and M. Grassi. Gazz. Chim. Ital. **85**, 1354 (1955).
12. J. C. Bailar, H. B. Jonassen, and A. D. Gott. J. Am. Chem. Soc. **74**, 3131 (1952).
13. Y. Saito and H. Iwasaki. Bull. Chem. Soc. Jpn. **35**, 1131 (1962); A. Kobayashi, F. Marumo, and Y. Saito. Acta Crystallogr. B**29**, 2443 (1973).
14. R. Meric and J.-P. Vigneron. Tetrahedron Lett. 2059 (1974); R. Lukes, J. Kovar, and K. Blaha. Coll. Czech. Chem. Commun. **23**, 1367 (1958).
15. B. Bosnich and E. A. Sullivan. Inorg. Chem. **14**, 2768 (1965).

Use of scaled-particle theory in the assessment of the Ph_4As^+/Ph_4B^- assumption for single ions

MICHAEL H. ABRAHAM AND ASADOLLAH NASEHZADEH
Chemistry Department, University of Surrey, Guildford, Surrey, England

Received May 17, 1978

MICHAEL H. ABRAHAM and ASADOLLAH NASEHZADEH. Can. J. Chem. **57**, 71 (1979).

A novel method for the assessment of the Ph_4As^+/Ph_4B^- assumption for free energies of transfer of single ions has recently been suggested by Treiner, and used by him to deduce that the assumption is not valid for transfers between water, propylene carbonate, sulpholane, dimethylsulphoxide, *N*-methyl-2-pyrrolidone, and perhaps also dimethylformamide. The basis of the method is the estimation of the free energy of cavity formation by scaled-particle theory, together with the hypothesis that the free energy of interaction of Ph_4As^+ (or Ph_4B^-) with solvent molecules is the same in all solvents, $\Delta G_t^0(\text{int}) = 0$. It is shown in the present paper that (*a*) whether or not the Ph_4As^+/Ph_4B^- assumption applies to transfer to a given solvent depends on which other solvent is taken as the reference solvent in Treiner's method, (*b*) the calculation of the cavity free energy term by scaled-particle theory and by the theory of Sinanoglu – Reisse – Moura Ramos (SRMR) yields values so different that the method cannot be considered reliable, (*c*) the calculation of cavity enthalpies and entropies for Ph_4As^+ or Ph_4B^- by scaled-particle theory yields results that are chemically not reasonable, (*d*) the hypothesis that $\Delta G_t^0(\text{int}) = 0$ conflicts with SRMR theory, and (*e*) the conclusions reached by Treiner are not in accord with recent work that in general supports the Ph_4As^+/Ph_4B^- assumption for solvents that are rejected by Treiner.

MICHAEL H. ABRAHAM et ASADOLLAH NASEHZADEH. Can. J. Chem. **57**, 71 (1979).

Treiner a récemment proposé une méthode nouvelle destinée à étudier la validité de l'hypothèse Ph_4As^+/Ph_4B^- pour les énergies libres de transfert des ions simples. Faisant appel à cette méthode, cet auteur a déduit que l'hypothèse n'est pas applicable aux transferts entre l'eau, le carbonate de propylène, le sulfolane, la diméthylsulfoxyde, la *N*-méthylpyrrolidone-2 et peut être aussi la diméthylformamide. Cette méthode se fonde, d'une part, sur une estimation de l'énergie libre de formation d'une lacune, selon la théorie des sphères rigides et, d'autre part, sur l'hypothèse à l'effet que l'énergie libre d'interaction de Ph_4As^+ (ou Ph_4B^-) avec les molécules de solvant demeure la même dans tous les solvants, soit $\Delta G_t^0(\text{int}) = 0$. Dans le présent travail, on démontre (*a*) que l'hypothèse Ph_4As^+/Ph_4B^- peut s'appliquer ou ne pas s'appliquer au transfert dans un solvant donné, tout dépend de la nature de l'autre solvant qui sert de solvant de référence selon la méthode de Treiner, (*b*) que les valeurs de l'énergie libre des lacunes calculées selon la théorie des sphères rigides d'une part, et selon la théorie de Sinanoglu–Reisse–Moura Ramos (SRMR) diffèrent à un point tel qu'on ne peut se fier à la méthode, (*c*) que les enthalpies et les entropies des lacunes pour Ph_4As^+ et Ph_4B^- telles que calculées selon la théorie des sphères rigides ne sont pas chimiquement raisonnable, (*d*) que l'hypothèse à l'effet que $\Delta G_t^0(\text{int}) = 0$ est en contradiction avec la théorie SRMR et (*e*) que les conclusions de Treiner sont en désaccord avec les travaux récents qui, d'une manière générale.

[Traduit par le journal]

Introduction

There is now available a large quantity of data on the thermodynamics of transfer of neutral combinations of ions between various solvents (1–4). For many purposes it is convenient to separate the thermodynamic parameters into cationic and anionic contributions through single-ion transfer values, using some extra-thermodynamic assumption in order to assign these single-ion values. Parker and co-workers (5–7) have extensively examined a number of such assumptions, and have suggested that the Ph_4As^+/Ph_4B^- assumption is the most reliable to date. On this basis, they assigned single-ion values for free energies, enthalpies, and entropies of transfer from water to a number of nonaqueous solvents. Concurrently with the studies of Parker, a number of other workers (8–10) used the correspondence plot method to assign single-ion entropies of transfer, also from water to nonaqueous solvents. Abraham (1) pointed out that the above two methods of assigning single-ion entropies of transfer yielded results in reasonable agreement with each other for transfers between water and many nonaqueous solvents, although for transfers between water and alcohols the two methods disagreed (4) by about 7 cal K^{-1} mol^{-1}. Quite recently, Treiner (11) put

0008-4042/79/010071-06$01.00/0

forward a novel method of examining the Ph_4As^+/Ph_4B^- assumption through the use of scaled-particle theory as outlined by Pierotti (12). Treiner concluded that for free energies of transfer, the Ph_4As^+/Ph_4B^- assumption was valid for transfers from water to methanol, ethanol, acetonitrile, and formamide but was not valid for transfer to dimethylformamide (DMF), dimethylsulphoxide (DMSO), sulpholane, propylene carbonate (PC), or *N*-methylpyrrolidone (NMPy). These conclusions of Treiner are so different from those of Parker (5–7) and of Abraham and Namor (1, 4) that we thought it useful to re-examine Treiner's method and to investigate the application of Treiner's method to enthalpy and entropy data. Results on entropies should be extremely interesting because the correspondence plot method leads to a quite independent set of single ion entropies of transfer which for many solvents agrees with the Ph_4As^+/Ph_4B^- assumption.[1]

Results using Scaled-particle Theory

(A) Free Energy of Transfer of Ph_4As^+ and Ph_4B^-

The free energy of solution of a hard-sphere solute in a given solvent is obtained through eq. [1]

$$[1] \quad \Delta G_s^0 = \Delta G^0(\text{cav}) + RT \log (RT/V) + \Delta G^0(\text{int})$$

where ΔG^0(cav) is the work required to create a suitably sized cavity in the solvent, calculated by scaled-particle theory, $RT \log (RT/V)$ is a correction term, and ΔG^0(int) is the energy of interaction of the solute with the surrounding solvent molecules. For transfer of the solute from a reference solvent 1 to another solvent 2, the free energy of transfer is given by eq. [2].

$$[2] \quad \Delta G_t^0 = \Delta G_t^0(\text{cav}) + RT \log (V_1/V_2) + \Delta G_t^0(\text{int})$$

Treiner set ΔG_t^0(int) = 0 in eq. [2], calculated ΔG_t^0 for a solute of diameter 8.4 Å (the diameter of Ph_4As^+ or Ph_4B^-), and then compared the resulting values with the observed free energies of transfer. He suggested that if calculated and observed values agreed to within about 30% the Ph_4As^+/Ph_4B^- assumption could be regarded as valid, but if the difference was greater than 30% the assumption should not be used.

We adopt a slightly different procedure that takes into account the electrostatic contribution to the free energy of transfer of a charged solute, as calculated by the recent theory of Abraham and Liszi (14). We write therefore

$$[3] \quad \Delta G_t^0 = \Delta G_t^0(\text{cav}) + \Delta G_t^0(\text{int}) + \Delta G_t^0(\text{elec})$$

For simplicity we include in the term ΔG_t^0(cav) the calculated cavity term together with the correction term $RT \log (V_1/V_2)$. We then calculate ΔG_t^0(cav) and ΔG_t^0(elec), we take ΔG_t^0 as the observed value, and we then deduce the value of the remaining term ΔG_t^0(int). Treiner's criterion corresponds to the situation that if the deduced value of $\Delta G_t^0(\text{int}) \leq \sim 3$ kcal mol^{-1}, the Ph_4As^+/Ph_4B^- assumption is valid, but if $\Delta G_t^0(\text{int}) > \sim 3$ kcal mol^{-1} the assumption should not be used. Details of the calculation are in Table 1 for the solvents that Treiner studied plus the additional solvents 1-propanol, acetone, 1,2-dichloroethane (1,2-DCE), and 1,1-dichloroethane (1,1-DCE).[2] As expected, our calculations lead to the same results as found by Treiner. For transfers from water to methanol, ethanol, 1-propanol, formamide, and acetonitrile, the interaction term is small enough to take the Ph_4As^+/Ph_4B^- assumption as valid; for all the other solvents the assumption (on Treiner's hypothesis) must be questioned. We stress that our criterion based on the actual value of the interaction term leads in general to the same conclusions as does Treiner's (percentage) criterion. We used the actual value because workers (5–7) are interested in whether the assumption holds to within a given value rather than to within a given percentage value.

A difficulty not pointed out by Treiner is that choice of reference solvent is completely arbitrary. In Table 1 we also recalculate all results to acetonitrile as a reference solvent. It now appears that for transfers to solvents water, ethanol, 1-propanol, formamide, acetone, and 1,1-DCE the Ph_4As^+/Ph_4B^- assumption is valid (on Treiner's hypothesis), and for transfers to the other solvents the assumption is questionable. Clearly, by altering the reference solvent, it is possible to obtain quite different values for ΔG_t^0(int) and hence quite different conclusions as to the validity of the Ph_4As^+/Ph_4B^- assumption.

Even more serious is Treiner's basic hypothesis that ΔG_t^0(int) = 0 for transfer of Ph_4As^+ and Ph_4B^-.[3] We can see no reason why this interaction term should be zero. The Ph_4As^+/Ph_4B^- assumption, for free energies of transfer, is simply that:

$$[4] \quad \Delta G_t^0 \text{ for } Ph_4As^+ = \Delta G_t^0 \text{ for } Ph_4B^-$$

[1]Recent work by Gritzner (13) shows that when bisphenylchromium(I)/bisphenylchromium(II) is used as a reference redox system, single-ion free energies of transfer from acetonitrile to methanol, DMF, DMSO, NMPy, and to some extent PC, agree well with values calculated using the Ph_4As^+/Ph_4B^- assumption.

[2]Values of $\Delta G_t^0(Ph_4As^+ + Ph_4B^-)$ recently found by Kim (18) agree very well with those in Table 1.

[3]This is the fundamental hypothesis used by Treiner. Thus only if the deduced value of ΔG_t^0(int) is zero or small (say < 3 kcal mol^{-1}) is the Ph_4As^+/Ph_4B^- assumption considered to be reasonable.

TABLE 1. Free energies of transfer from water or from acetonitrile for the Ph_4As^+ (or Ph_4B^-) ion with cavity terms calculated by scaled-particle theory, in kcal mol^{-1} at 298 K[a]

			ΔG_t^0 from water				ΔG_t^0 from acetonitrile	
Solvent	ρ[b]	σ[c]	Cavity[d]	Electrical[e]	Interaction[f]	Total (observed)[g]	Interaction[h]	Total (observed)[h]
Water	0.9917	2.76	0	0	0	0	2.2	8.4
Methanol	0.7868	3.59	−9.2	1.6	1.6	−6.0	3.8	2.4
Ethanol	0.7851	4.36	−7.2	2.3	−0.7	−5.6	1.5	2.8
1-Propanol	0.7997	4.71	−9.7	2.9	−0.1	−6.9	2.1	1.5
Formamide	1.1292	3.63	−7.9	0.9	0.8	−6.2[i]	3.0	2.2
Acetonitrile	0.7768	4.12	−8.0	1.8	−2.2	−8.4	0	0
Dimethylformamide	0.9443	4.98	−5.8	2.4	−6.6	−10.0	−4.4	−1.6
Dimethylsulphoxide	1.0961	5.05	1.8	2.1	−13.6	−9.7	−11.4	−1.3
Sulpholane	1.2660	5.76	6.6	2.3	−18.8	−9.9[i]	−16.6	−1.5
Propylene carbonate	1.1920	5.40	0.4	2.2	−12.0	−9.4[i]	−9.8	−1.0
N-Methylpyrrolidone	1.0279	5.69		2.8		−10.5[i]		−2.1
Acetone	0.7844	4.86	−6.5	2.8	−5.1	−8.8	−2.9	−0.4
1,2-Dichloroethane	1.2458	5.08	−4.6	4.2	−8.3	−8.7	−6.1	−0.3
1,1-Dichloroethane	1.1680	5.07	−7.8	4.3	−3.9	−7.4	−1.7	1.0

[a]All free energies refer to the mol fraction scale, and are for Ph_4As^+ or Ph_4B^-.
[b]Solvent density.
[c]Solvent diameter in Å.
[d]This is the combined term $[\Delta G_t^0(\text{cav}) + RT \log (V_1/V_2)]$, calculated for a solute of diameter 8.4 Å.
[e]Calculated by the method of Abraham and Liszi for a solute of diameter 8.4 Å.
[f]Determined from interaction = total − cavity − electrical.
[g]Taken from refs. 1 and 4 unless indicated, and corrected to the $Ph_4As^+ = Ph_4B^-$ convention.
[h]Obtained through rearrangement of the values in the previous two columns.
[i]From ref. 2.

Now since the diameters of the two species are equal, the terms $\Delta G_t^0(\text{cav})$ and $\Delta G_t^0(\text{elec})$ will be the same for the two species, and we are left with:

[5] $\Delta G_t^0(\text{int})$ for $Ph_4As^+ = \Delta G_t^0(\text{int})$ for Ph_4B^-

It is not clear why these interaction terms should be small or zero in order for the Ph_4As^+/Ph_4B^- assumption to apply. If, however, the $\Delta G_t^0(\text{int})$ terms can take any value, then there is no basis for Treiner's criterion at all. Thus in Table 1 it could be argued, for example, that the Ph_4As^+/Ph_4B^- assumption applies to PC and that for this solvent the interaction term happens to be particularly large.

(B) Enthalpy of Transfer of Ph_4As^+ and Ph_4B^-

The enthalpy of solution of a hard-sphere solute is given by eq. [6]

[6] $\Delta H_s^0 = \Delta H^0(\text{cav}) - RT + \alpha pRT^2 + \Delta H^0(\text{int})$

where αp is the coefficient of thermal expansion of the solvent. If we include the electrostatic energy of a charged solute, the resulting expression for the transfer of a solute is eq. [7]

[7] $\Delta H_t^0 = \Delta H_t^0(\text{cav}) + \Delta H_t^0(\text{int}) + \Delta H_t^0(\text{elec})$

where for simplicity the term $\Delta H_t^0(\text{cav})$ now includes $(\alpha p_2 RT^2 - \alpha p_1 RT^2)$. Details of the calculations are in Table 2 with water as the reference solvent. If Treiner's hypothesis applies also to enthalpies, then $\Delta H_t^0(\text{int})$ should be zero or small (say again <3 kcal mol^{-1}) for the Ph_4As^+/Ph_4B^- assumption to be valid. Use of such a hypothesis results in the extraordinary situation that for transfer from water to every solvent in Table 2, the Ph_4As^+/Ph_4B^- assumption cannot be valid. Clearly, the use of scaled-particle theory plus the hypothesis that $\Delta H_t^0(\text{int})$ should be zero for Ph_4As^+ and Ph_4B^- does not lead to any meaningful results.

(C) Entropy of Transfer of Ph_4As^+ and Ph_4B^-

Combination of the equations for free energy and enthalpy will yield an expression for the entropy of transfer of a charged solute. There is, however, an important proviso in that, as applied by Pierotti, the entropy of interaction is taken as zero. Thus if $\Delta S_s^0(\text{int}) = 0$ it follows that $\Delta S_t^0(\text{int}) = 0$; the final expression for ΔS_t^0 becomes:

[8] $\Delta S_t^0 = \Delta S_t^0(\text{cav}) + \Delta S_t^0(\text{elec})$

Since there are no unknown interaction terms in eq. [8], it should be possible, if scaled-particle theory really does apply to solutes such as Ph_4As^+ and Ph_4B^-, to calculate values of ΔS_t^0. Details are in Table 3 with water as the reference solvent. There is total disagreement between all the calculated and observed values, so that for transfers from water it is now clear that scaled-particle theory cannot account for the entropy term. It is possible by choice of some other reference solvent to obtain agreement for a few transfers, but in general these results demonstrate that scaled-particle theory is of little use in

TABLE 2. Enthalpies of transfer from water for the Ph_4As^+ (or Ph_4B^-) ion with cavity terms calculated by scaled-particle theory, in kcal mol^{-1} at 298 K

Solvent	$\alpha p \times 10^3$[a]	$\Delta H_t^0(Ph_4As^+$ or $Ph_4B^-)$ Cavity[b]	Electrical[c]	Interaction[d]	Total[e]
Water	0.257	0	0	0	0
Methanol	1.123	5.5	0.3	−6.2	−0.4
Ethanol	1.063	8.6	0.6	−9.2	0.0
1-Propanol	0.935	5.2	0.4	−5.2	+0.4
Formamide	0.746	3.3	0.7	−4.1	−0.1[f]
Acetonitrile	1.390	10.5	1.1	−14.1	−2.5
Dimethylformamide	0.589	5.0	1.4	−11.1	−4.7
Dimethylsulphoxide	1.009	22.2	1.8	−26.8	−2.8
Sulpholane	0.683	22.0	1.8	−26.3	−2.5[f]
Propylene carbonate	1.863	42.5	1.8	−47.9	−3.6[f]
N-Methylpyrrolidone			1.8		−4.2[f]
Acetone	1.369	14.7	1.2	−19.9	−4.0
1,2-Dichloroethane	1.194	15.9	0.2	−21.5	−5.4
1,1-Dichloroethane	1.327	12.6	0.7	−17.8	−4.5

[a]Solvent coefficient of thermal expansion, in K^{-1}.
[b]This is the combined term $\Delta H_t^0(cav) + \alpha p_2 RT^2 - \alpha p_1 RT^2$.
[c]Calculated by the method of Abraham and Liszi.
[d]Determined from interaction = total − cavity − electrical.
[e]Taken from refs. 1 and 4 unless indicated, and corrected to the $Ph_4As^+ = Ph_4B^-$ convention.
[f]Reference 2.

TABLE 3. Calculation of entropies of transfer from water for the Ph_4As^+ (or Ph_4B^-) ion with cavity terms calculated by scaled-particle theory, in cal K^{-1} mol^{-1} at 298 K

Solvent	Cavity[a]	Electrical[b]	Total calculated[c]	Total observed[d]
Water	0	0	0	0
Methanol	49	−4	45	19
Ethanol	53	−6	47	19
1-Propanol	50	−8	42	24
Formamide	38	−1	37	20
Acetonitrile	62	−3	59	20
Dimethylformamide	36	−3	33	18
Dimethylsulphoxide	68	−1	67	23
Sulpholane	52	−2	50	25
Propylene carbonate	141	−1	140	20
N-Methylpyrrolidone		−3		21
Acetone	71	−6	65	16
1,2-Dichloroethane	69	−13	56	11
1,1-Dichloroethane	69	−12	57	10

[a]From the cavity terms in Tables 1 and 2.
[b]Calculated by the theory of Abraham and Liszi (13).
[c]The sum of the cavity and electrical terms.
[d]From the observed values in Tables 1 and 2.

attempts to calculate entropy changes for Ph_4As^+ and Ph_4B^-.

Results using the Sinanoglu – Reisse – Moura Ramos (SRMR) Method

A quite different method of obtaining cavity terms was suggested by Halicioglu and Sinanoglu (15) and applied recently by Reisse and Moura Ramos (16). These latter workers make no attempt to calculate the interaction term but deduce this term from the expression:

$$[9] \qquad \Delta P_t^0(\text{int}) = \Delta P_t^0 - \Delta P_t^0(\text{cav})$$

where $P = G$, H, or S. We use exactly the same procedure as Reisse and Moura Ramos to calculate the cavity terms and, like these workers, then deduce the interaction term from eq. [9]. In the SRMR method, the molar volume of the solute is used, rather than its diameter, and we took values given by Millero (17) of $\bar{V} = 245.6$ ml mol^{-1} for Ph_4As^+ and $\bar{V} = 295.6$ ml mol^{-1} for Ph_4B^-. Although the cavity terms differ a little in these two cases, the differences from one solvent to another are negligible. We give in Table 4 the results for Ph_4As^+, but these can be taken as being the same as those for Ph_4B^- within

TABLE 4. Free energies of transfer from acetonitrile of Ph_4As^+ with cavity terms calculated by the SRMR method, in kcal mol^{-1} at 298 K[a]

Solvent	Cavity[b]	Electrical[c]	Interaction[d]	Total (observed)[c]
Water	19.1	−1.8	−8.9	8.4
Methanol	−1.6	−0.2	4.2	2.4
Ethanol	−2.2	0.5	4.5	2.8
1-Propanol	−2.0	1.1	2.4	1.5
Formamide	12.9	−0.9	−9.8	2.2
Acetonitrile	0	0	0	0
Dimethylformamide	2.1	0.6	−4.3	−1.6
Dimethylsulphoxide	5.6	0.3	−7.2	−1.3
Sulpholane	1.3	0.5	−3.3	−1.5
Propylene carbonate[e]	7.4	0.4	−8.8	−1.0
N-Methylpyrrolidone[e]	3.2	1.0	−6.3	−2.1
Acetone	−3.3	1.0	1.9	−0.4
1,2-Dichloroethane	−0.8	2.4	−1.9	−0.3
1,1-Dichloroethane	−3.5	2.5	2.0	1.0

[a]Values for Ph_4B^- ($\bar{V}$ = 282.6 ml mol^{-1}) are almost identical to those for Ph_4As^+ ($\bar{V}$ = 295.6 ml mol^{-1}).
[b]Calculated by the method of Reisse and Moura Ramos (16).
[c]From Table 1.
[d]Determined from interaction = total − cavity − electrical.
[e]Approximate calculated values.

TABLE 5. Comparison of cavity terms for Ph_4As^+ calculated by scaled-particle theory[a] and SRMR theory

	Scaled-particle theory (σ = 8.4 Å)			SRMR theory ($\bar{V}$ = 295.6 ml mol^{-1})		
Solvent	ΔG_t^0	ΔH_t^0	ΔS_t^0	ΔG_t^0	ΔH_t^0	ΔS_t^0
Water	8.0	−10.5	−62	19.1	26.7	25
Methanol	−1.2	−5.0	−13	−1.6	−3.1	−5
Ethanol	0.8	−1.9	−9	−2.2	−3.4	−5
1-Propanol	−1.7	−5.3	−12	−2.0	−3.2	−4
Formamide	0.1	−7.2	−24	12.9	19.9	23
Acetonitrile	0	0	0	0	0	0
Dimethylformamide	2.2	−5.5	−26	2.1	11.7	32
Dimethylsulphoxide	9.8	11.7	6	5.6	8.6	10
Sulpholane	14.6	11.5	−10	1.3	−1.8	−11
Propylene carbonate[b]	8.4	32.0	79	7.4	3.2	−14
N-Methylpyrrolidone[b]				3.2	4.8	5
Acetone	1.5	4.2	9	−3.3	−3.7	−2
1,2-Dichloroethane	3.4	5.4	7	−0.8	−0.9	0
1,1-Dichloroethane	0.2	2.1	7	−3.5	−5.6	−7

[a]The terms on the scaled-particle theory are ΔG_t^0(cav) + $RT \log (V_1/V_2)$ and ΔH_t^0(cav) + $\alpha p_2 RT^2 - \alpha p_1 RT^2$; ΔG_t^0 and ΔH_t^0 in kcal mol^{-1} and ΔS_t^0 in cal K^{-1} mol^{-1}.
[b]SRMR calculated values are approximate ones.

about 0.1 kcal mol^{-1}. In the case of SRMR theory, it is difficult to take into account contributions due to solvent reorganisation. Since this effect will be much more important for water than for any other solvent, the SRMR calculation for water will be less reliable than calculations for other solvents.[4] We therefore took acetonitrile as the reference solvent in Table 4; the results in Table 1 provide a direct comparison between SRMR calculation and scaled-particle theory. For transfers from acetonitrile to several solvents there are considerable differences in the ΔG_t^0(cav) terms as calculated by the two methods (see Table 5). The SRMR results (Table 4) can be interpreted using the approach of Reisse and Moura Ramos to the effect that there are, indeed, large variations in ΔG_t^0(int) with change of solvent so that, contrary to Treiner's hypothesis, ΔG_t^0(int) cannot be regarded as small or zero for Ph_4As^+ or Ph_4B^-.

In Table 5 we compare the calculated cavity terms in free energy, enthalpy, and entropy on the two

[4]We note also that the term used by Sinanoglu to correct for loss of translational entropy of the solute in solution, R ln [V(gas)/$\bar{V}$(solvent)], overestimates the translational entropy in solution, since the available volume in solution is less than the solvent molar volume, $\bar{V}$. However, for transfer from one solvent to another there is so much cancellation that values of ΔG_t^0(cav) and ΔS_t^0(cav) are not greatly affected by errors in this term. We are grateful to Professor Reisse for clarifying this point.

theories. There are such differences in the values calculated by the two methods that it seems quite unrealistic to attempt deductions as to the validity of the Ph_4As^+/Ph_4B^- assumption on the basis of calculated cavity terms.

In our view all the above considerations suggest that the validity of the Ph_4As^+/Ph_4B^- assumption cannot usefully be investigated by the method of Treiner, and we cannot see any basis for the previous rejection of the assumption. It is of interest that quite recently Kim (18) has strongly supported the Ph_4As^+/Ph_4B^- assumption, in terms of free energy, for the very solvents rejected by Treiner (11).

Although several workers (19, 20) have applied scaled-particle theory to the transfer of large ions and have obtained reasonable agreement between the calculated cavity term and the observed free energy (19) or enthalpy (20) of transfer, it is noticeable that such agreement is always limited to transfers between water and aqueous organic mixtures. For example, Treiner (11) calculated ΔG_t^0(cav) for the transfer of Ph_4As^+ from water to aqueous ethanol and found good agreement with the observed ΔG_t^0 value. But inspection of Table 1 shows that for transfer from water to ethanol itself, the two terms differ by 1.6 kcal mol^{-1} and for the corresponding enthalpy function the terms differ by no less than 8.6 kcal mol^{-1} (Table 2). It seems clear that in non-aqueous solvents, scaled-particle theory cannot usefully be applied to transfers of large ions. Whether or not the agreement observed in the more aqueous media is an artifact is a matter of opinion. We note that Tenne and Ben-Naim (21), in connection with calculations on free energy, state that it is impossible to apply scaled-particle theory alone for mixtures of water and ethanol.

Acknowledgements

We thank Professor J. Reisse and Dr. J. J. Moura Ramos for their helpful comments on their method of calculating cavity terms.

1. M. H. Abraham. J. Chem. Soc. Faraday Trans. I, **69**, 1375 (1973).
2. B. G. Cox, G. R. Hedwig, A. J. Parker, and D. W. Watts. Aust. J. Chem. **27**, 477 (1974).
3. M. H. Abraham, A. F. D. de Namor, and R. A. Schulz. J. Soln. Chem. **5**, 529 (1976).
4. M. H. Abraham and A. F. D. de Namor. J. Chem. Soc. Faraday Trans. I, **74**, 2101 (1978).
5. R. Alexander, A. J. Parker, J. H. Sharp, and W. E. Waghorne. J. Am. Chem. Soc. **94**, 1148 (1972).
6. B. G. Cox and A. J. Parker. J. Am. Chem. Soc. **95**, 402 (1973).
7. J. W. Diggle and A. J. Parker. Electrochim. Acta, **18**, 975 (1973).
8. B. Jakuszewski and S. Taniewska-Osińska. Soc. Sci. Lodz. Acta Chim. **4**, 17 (1959); **7**, 31 (1961); **8**, 11 (1962).
9. C. M. Criss, R. P. Held, and E. Luksha. J. Phys. Chem. **72**, 2970 (1968).
10. C. M. Criss. J. Phys. Chem. **78**, 1000 (1974).
11. C. Treiner. Can. J. Chem. **55**, 682 (1977).
12. R. A. Pierotti. Chem. Rev. **76**, 717 (1976).
13. G. Gritzner. Inorg. Chim. Acta, **24**, 5 (1977).
14. M. H. Abraham and J. Liszt. J. Chem. Soc. Faraday Trans. I, **74**, 1604 (1978); In press.
15. T. Halicioglu and O. Sinanoglu. Ann. N.Y. Acad. Sci. **158**, 308 (1969).
16. J. J. Moura Ramos, M. Lemmers, R. Ottinger, M.-L. Stein, and J. Reisse. J. Chem. Res. (S) 56 (1977); (M) 0658 (1977).
17. F. J. Millero. Chem. Rev. **71**, 147 (1971).
18. J. I. Kim. J. Phys. Chem. **82**, 191 (1978).
19. C. Treiner, P. Tzias, M. Chemla, and G. M. Poltoratskii. J. Chem. Soc. Faraday Trans. I, **72**, 2007 (1976).
20. N. Desrosiers and J. Desnoyers. Can. J. Chem. **54**, 3800 (1976).
21. R. Tenne and A. Ben-Naim. J. Chem. Phys. **67**, 4632 (1977).

Fast reaction kinetics of the binding of bromide to iron(III) studied on a high pressure laser temperature jump apparatus[1]

BRIAN B. HASINOFF

Department of Chemistry and the Faculty of Medicine, Memorial University of Newfoundland, St. John's, Nfld., Canada A1B 3X7[2]

and

University Chemical Laboratory, University of Kent at Canterbury, Canterbury, Kent, England

Received April 12, 1978

BRIAN B. HASINOFF. Can. J. Chem. **57**, 77 (1979).

The kinetics of the binding of Br^- to Fe(III) were studied as a function of $[H^+]$ and $[Br^-]$ on a high pressure laser temperature jump apparatus up to 2.76 kbar. At constant $[H^+]$ the pseudo first order rate constant for formation of $FeBr^{2+}$ showed little dependence on pressure or on $[Br^-]$ over the range 0.02 to 1.9 *M*. The results were interpreted by a mechanism in which Fe^{3+} and $FeOH^{2+}$ react with Br^- to form ion pairs prior to formation of their inner sphere complexes. The kinetic activation volume for the conversion of the Fe^{3+},Br^- ion pair to $FeBr^{2+}$ appears to be quite negative, consistent with an associative interchange (I_a) mechanism.

BRIAN B. HASINOFF. Can. J. Chem. **57**, 77 (1979).

On a étudié la cinétique de la liaison du Br^- au Fe(III) en fonction de $[H^+]$ et de $[Br^-]$ à l'aide d'un appareil à saut de température activé par un laser à haute pression opérant jusqu'à 2.76 kbar. A $[H^+]$ constante, la constante de vitesse de pseudo premier ordre pour la formation du $FeBr^{2+}$ n'est que faiblement influencée par la pression ou la $[Br^-]$ à des concentrations allant de 0.02 à 1.9 *M*. On a enterprété les résultats en termes d'un mécanisme dans lequel le Fe^{3+} et le $FeOH^{2+}$ réagissent avec le Br^- pour former des paires d'ions avant la formation de leurs complexes de sphères internes. Il semble que le volume d'activation cinétique pour la conversion de la paire d'ions Fe^{3+}, Br^- en $FeBr^{2+}$ soit assez négative; ceci est en accord avec un mécanisme d'échange associatif (I_a).

[Traduit par le journal]

High pressure kinetic studies of the reaction of Fe^{3+} with Cl^- (1) and with NCS^- (2) have provided evidence for the existence of an associative interchange mechanism for ligand substitution. In contrast, the more labile $FeOH^{2+}$ species is thought to undergo ligand substitution by a dissociative interchange mechanism. Previous high pressure kinetic studies of ligand binding to Co^{2+}, Ni^{2+}, Zn^{2+}, and Cu^{2+} (3, 4) yielded results consistent with a dissociative interchange mechanism as suggested by Eigen and Wilkins (5).

This study extends the Fe(III) pressure work to another anionic ligand, Br^-. Product yield, kinetic and spectrophotometric experiments have been independently used to evaluate an ion pair formation constant for reaction of Fe(III) and Br^- (6). Earlier kinetic studies (7, 8) indicated the $[H^+]^{-1}$ dependence of the reaction rate but did not include the effect of ion pairing. It must be noted that the extent of formation of $FeBr^{2+}$ cannot be made large under reasonable conditions and it is necessary to construct an interpretation from judicious combinations of values derived from both equilibrium and kinetic experiments. The direct analysis of the more uncertain parts of the kinetics produce parameters in agreement with the constraints imposed by combined considerations and, consequently, are most probably significant.

Experimental

Reagents

All reagents ($Fe(NO_3)_3$, NaBr, $NaClO_4$, $HClO_4$, and $Cu(NO_3)_2$) were of analytical reagent grade. Solutions of HBr, $HClO_4$, and NaOH were determined by titration. The total ionic strength in the reaction solutions was kept constant by the addition of $NaClO_4$ to solutions containing NaBr and $HClO_4$ or to solutions containing HBr, $HClO_4$, and NaOH. $Fe(NO_3)_3$ was 5.0 m*M* in all solutions. The rate and equilibrium constants are on a molality scale reduced to molarity at 1 bar.

Apparatus

The high pressure ruby laser temperature jump apparatus and the analysis of the exponential relaxation curves have been described (1, 3). A 1.6°C temperature jump was produced in the thermostatted (±0.1°C) reaction solution by absorbing the 694 nm laser radiation with 0.02 *M* $Cu(NO_3)_2$. Representative oscilloscope traces of the relaxation process are shown in Fig. 1. Experiments conducted on a joule heating temperature jump apparatus (Messanlagen, Göttingen) at 400 nm with a 5°C jump indicated the absence of any effect of

[1]This work has been supported in part by the National Research Council of Canada, Grant No. A9430 and the Science Research Council (Great Britain), Grant No. B/SR/8667.

[2]Present address.

0008-4042/79/010077-06$01.00/0

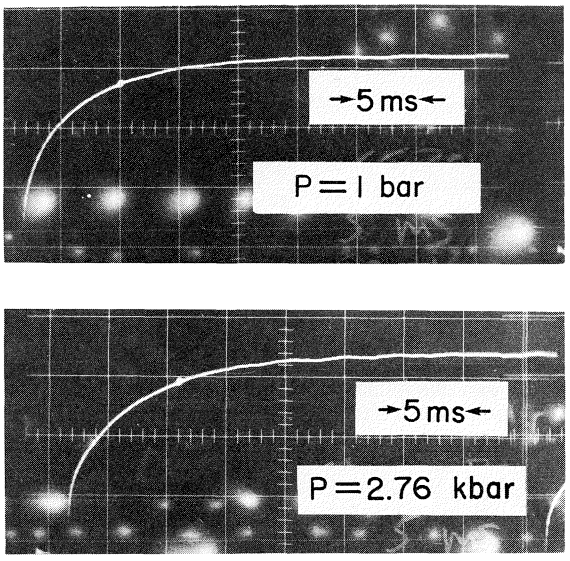

FIG. 1. Oscilloscope traces of voltage vs. time for the relaxation observed for the reaction of Fe(III) and Br^- at 1 bar and 2.76 kbar with $[H^+] = 0.525\ M$, $[Br^-] = 1.9\ M$, $[Fe(III)]_\Sigma = 5.0\ mM$, $T = 25.0°C$, and $\mu = 2.0\ M$. The temperature jump of 1.6°C was produced by a ruby laser. The large horizontal divisions are 5 ms.

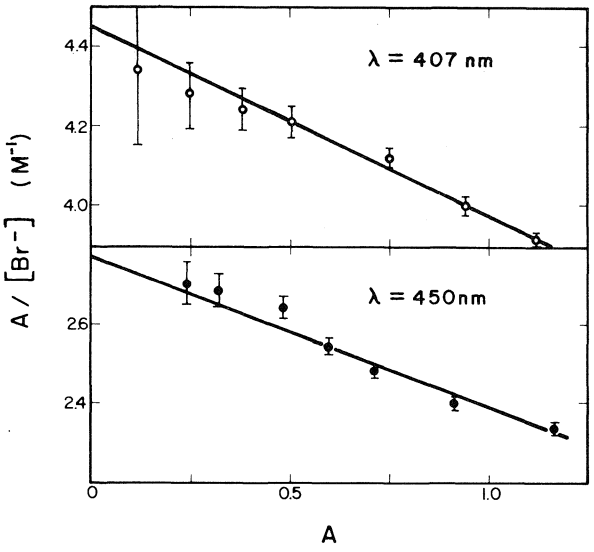

FIG. 2. $A/[Br^-]$ vs. A observed for the reaction of Fe(III) and $[Br^-]$ at 25.0°C with $[H^+] = 2.00\ M$ and $\mu = 2.0\ M$ and $[Fe(III)]_\Sigma$ held constant at 5.0 mM. The slopes yield K (eq. [1]). The solid straight lines are from weighted linear least-squares analyses. The error bars are the standard deviations used in the weighted linear least-squares analyses; assuming an error in A of 0.0025.

$Cu(NO_3)_2$. Only a single exponential relaxation process was detected in a search over a wide range of sweep speeds. Thus any kinetic contribution from higher Fe(III) bromide complexes can be ruled out. An interference filter or a blue colored glass filter of maximum transmission in the region of maximum $FeBr^{2+}$ absorption (408 nm) provided monochromatic light for the photometric detector. A Unicam SP8000 spectrophotometer with a thermostatted cell block was used for equilibrium measurements at 1 bar. Changes in light transmission with pressure were measured with a 10-turn off-set potentiometer.

Results

Equilibrium

The binding of Br^- to Fe(III) may be interpreted in terms of

$$[1] \qquad K = [FeBr^{2+}]_\Sigma/[Fe^{3+}]_\Sigma[Br^-]$$

where $[FeBr^{2+}]_\Sigma$ includes all inner sphere complex absorbing species and $[Fe^{3+}]_\Sigma$ includes all other non-absorbing species including outer sphere complexes. Absorbances, A, were used to determine K by plotting $A/[Br^-]$ vs. A (Fig. 2) similar to (6) and yielded from linear least-squares slopes, K's of $0.38 \pm 0.04\ M^{-1}$ and $0.48 \pm 0.03\ M^{-1}$ at 450 nm and 407 nm, respectively. This indicates only small outer sphere complexation. Previous determinations of K at 25°C have yielded values of $0.37\ M^{-1}$ ($\mu = 1.0\ M$) (6); $0.61\ M^{-1}$ ($\mu = 1.2\ M$) (9); and $0.5 \pm 0.2\ M^{-1}$ ($\mu = 1.092$) (10). The agreement is reasonable considering the low stability of the complex.

Using an average K of $0.43\ M^{-1}$ in eq. [1] and the absorbance at 440 nm at 1 bar the product of molar absorptivity and path length was calculated for $FeBr^{2+}$. Assuming this product remains, to a first approximation, constant with pressure, from the absorbances observed at higher pressures values of K were determined. From solutions with $[Br^-]$ of 0.2 M and 0.5 M, K's were determined at each pressure and their average values plotted in Fig. 3 as log K. The variation of the equilibrium constant with pressure is related to the molar volume of the reaction, ΔV, by (11)

$$[2] \qquad \Delta V = -RT\,(\partial \ln K/\partial P)_T$$

Since the K data of Fig. 3 show significant curvature, the data were least-squares fit to an equation of the form $\log K = a + bP + cP^2$ yielding: log K at 0 bar of -0.370 ± 0.002, from b and eq. [2] at 0 bar $\Delta V = 8.1 \pm 0.2\ cm^3\ mol^{-1}$, and from c and the derivative of eq. [2] $(\partial\Delta V/\partial P)_T = -2.3 \pm 0.2\ cm^3\ mol^{-1}\ kbar^{-1}$. Also plotted in Fig. 3 is the pressure variation of log K_a obtained at a single $[H^+]$ of $7.1 \times 10^{-3}\ M$ for the reaction $Fe^{3+} \rightleftharpoons FeOH^{2+} + H^+$ where $K_a = [FeOH^{2+}][H^+]/[Fe^{3+}]$ but at $\mu = 1.5\ M$ and 24.2°C and $\lambda = 325$ nm. The absorbance changes observed were small (from 0.18 at 1 bar to 0.15 at 2.76 kbar). A density correction for the pressure dependence of the molar absorptivity was not made as in ref. 2 ($\Delta V_a = 3.0 \pm 0.5\ cm^3\ mol^{-1}$ at

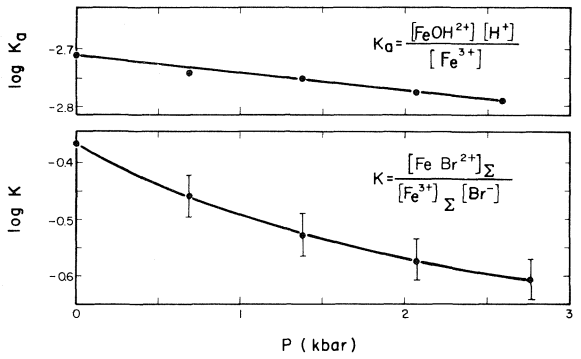

FIG. 3. Plots of log K_a and log K vs. pressure. Values of K_a were determined from absorbance measurements at 325 nm at 24.2°C and $\mu = 1.5$ *M*. Values of K were obtained at 440 nm at 25.0°C, $[H^+] = 1.00$ *M* and $\mu = 2.0$ *M*. The solid lines are least-squares calculated. Their slopes yield their respective volumes of reaction. The error bars are average standard deviations from the averaged K's.

25°C and $\mu = 0.2$ *m*) since it is well known that both density changes and band shifts can cause changes in molar absorptivities. A least-squares fit to the equation $\log K_a = a + bP$ yielded $\Delta V_a = 1.6 \pm 0.1$ cm^3 mol^{-1} and $a = -2.715 \pm 0.004$. A density correction alone to the molar absorptivities would yield a slightly higher ΔV_a, close to that in ref. 2.

Kinetic

The kinetics of the binding of Br^- to Fe(III) were studied on a stopped flow apparatus at wavelengths from 400 to 500 nm at a constant $[H^+] = 2.00$ *M* and with $[Br^-]$ varying from 0.02 to 1.43 *M*. The single exponential process characterized by the pseudo first order rate constant for approach to equilibrium, k_{obs}, showed little or no $[Br^-]$ dependence (Table 1) as previously reported (6); thus it is dominated by dissociation. The joule heating temperature jump experiments (Table 1), with $[H^+] = 1.00$ *M* and $[Br^-]$ varying from 0.05 to 1.90 *M*, yielded similar results. The lack of $[Br^-]$ dependence

TABLE 1. Rate constants and reciprocal relaxation times for the reaction of Fe(III) and Br^- at 25.0°C and ionic strength 2.0 *M*

Joule heating temperature jump[a]		Stopped flow[b]	
$[Br^-]$ (*M*)	τ^{-1} (s^{-1})	$[Br^-]$ (*M*)	k_{obs} (s^{-1})
0.05	127	0.02	37.0
0.10	120	0.05	49.3
0.20	123	0.10	53.4
0.50	123	0.20	54.4
1.00	126	0.50	50.4
1.00[c]	132	1.00	50.9
1.90	120	1.43	47.3

[a]Average standard deviation on τ^{-1} is 6 s^{-1}, $[H^+] = 1.00$ *M*.
[b]Average standard deviation on k_{obs} is 2 s^{-1}, $[H^+] = 2.00$ *M*.
[c]Solution also contained 0.02 *M* $Cu(NO_3)_2$.

of the rates was confirmed by linear least-squares analyses. Slopes of k_{obs} and the reciprocal relaxation times, τ^{-1} vs. $[Br^-]$, were both zero within one standard deviation.

In the reaction of Br^- with Fe(III) the reactions of Fe^{3+} and $FeOH^{2+}$ with Br^- to form an ion pair prior to formation of their respective inner sphere complexes may be usefully considered as resolvable steps.

[3]
$$\begin{array}{ccccc} Fe^{3+} + Br^- & \xrightleftharpoons{K_1} & Fe^{3+},Br^- & \underset{k_{-1}}{\overset{k_1}{\rightleftharpoons}} & FeBr^{2+} \\ \Big\uparrow\Big\downarrow K_a & & \Big\uparrow\Big\downarrow K_b & & \Big\uparrow\Big\downarrow K_c \\ FeOH^{2+} + Br^- & \xrightleftharpoons{K_2} & FeOH^{2+},Br^- & \underset{k_{-2}}{\overset{k_2}{\rightleftharpoons}} & FeOHBr^+ \end{array}$$

where $K_b = [FeOH^{2+},Br^-][H^+]/[Fe^{3+},Br^-]$; $K_c = [FeOHBr^+][H^+]/[FeBr^{2+}]$; $K_1 = [Fe^{3+},Br^-]/[Fe^{3+}][Br^-]$; and $K_2 = [FeOH^{2+},Br^-]/[FeOH^{2+}][Br^-]$. With $[Br^-] \gg [Fe(III)]_\Sigma$ and $[H^+] \gg K_a$, K_b, K_c, K_aK_2/K_1 and fast proton and ion pair equilibria, both the reciprocal relaxation time and k_{obs} obtained by mixing are given by:

$$[4] \quad k_{obs} = \frac{K_1[Br^-]}{1 + K_1[Br^-]}\left(k_1 + \frac{k_2K_b}{[H^+]}\right) + k_{-1} + \frac{k_{-2}K_c}{[H^+]}$$

From a consideration of eqs. [1] and [3] it is readily seen (6, 12) that the equilibrium constant of eq. [1] is an apparent equilibrium constant only and as such is a composite of the rate and equilibrium constants of eq. [3]. Yet it behaves as a simple equilibrium (eq. [1]). At high $[H^+]$ this apparent equilibrium constant is, in terms of the ion pair equilibrium and ion pair – inner sphere rate constants, given by

$$[5] \quad K = K_1(k_1/k_{-1} + 1)$$

and from eq. [3]

$$[6] \quad k_{-2}K_c = k_{-1}k_2K_b/k_1$$

combining eqs. [4]–[6] yields:

$$[7] \quad k_{obs} = \left(\frac{K_1}{K - K_1}\right)\left(k_1 + \frac{k_2K_b}{[H^+]}\right) \times \left(\frac{1 + K[Br^-]}{1 + K_1[Br^-]}\right)$$

$$[8] \quad k_{obs} = \left(k_{-1} + \frac{k_{-2}K_c}{[H^+]}\right)\left(\frac{1 + K[Br^-]}{1 + K_1[Br^-]}\right)$$

It is useful at this point to qualitatively examine the significance of the data of Table 1. The lack of

TABLE 2. Rate data for the reaction of Fe(III) with Br^- obtained by laser temperature jump at 25.0°C and ionic strength 2.0 M[a]

	k_{obs} (s^{-1})							
	$[H^+] = 1.925\ M$ $[Br^-] = 1.90\ M$		$[H^+] = 1.925\ M$ $[Br^-] = 0.50\ M$		$[H^+] = 0.525\ M$ $[Br^-] = 1.90\ M$		$[H^+] = 0.525\ M$ $[Br^-] = 0.50\ M$	
P (kbar)	Expt.	Pred.	Expt.	Pred.	Expt.	Pred.	Expt.	Pred.
0.001	64.0	64.1	65.6	61.0	165	172	181	164
0.69	61.1	65.4	62.9	61.3	147	172	184	161
1.38	59.9	66.6	67.1	61.1	152	171	184	157
2.07	63.5	67.2	65.1	60.0	159	168	179	150
2.76	66.2	71.8	71.7	62.7	154	176	184	153

[a]Predicted values of k_{obs} are those obtained from the parameters of Table 3 substituted in eq. [7].

any observable $[Br^-]$ dependence on the rates indicates that only the terms of eq. [4] containing the dissociation rate constants k_{-1} and k_{-2} for the inner sphere complexes make any measurable contribution to k_{obs}; thus $k_{obs} \simeq k_{-1} + k_{-2}K_c/[H^+]$. Further, from eq. [8], for k_{obs} to show a lack of $[Br^-]$ dependence K and K_1 must be similar in value. It is important to realize that this conclusion can also be reached from product yield experiments (6) where $K_1 = 0.83K$ can be obtained. From eq. [5], then, $k_1/k_{-1} = 0.2$. These relationships are of importance for the analysis which follows.

Taking logarithms and differentiating eq. [5] gives

$$[9] \quad \Delta V = \Delta V_1 + (\Delta V_1^{\ddagger} - \Delta V_{-1}^{\ddagger}) \frac{k_1/k_{-1}}{k_1/k_{-1} + 1}$$

where the activation volume (11) is

$$\Delta V^{\ddagger} = -RT(\partial \ln k/\partial P)_T$$

The laser temperature jump relaxation data obtained at pressures up to 2.76 kbar are given in Table 2. It is worth noting that k_{obs} does not show an appreciable dependence on pressure. This conclusion was confirmed by linear least-squares analysis. The apparent $\Delta V^{\ddagger}$, $-RT(\partial \ln k_{obs}/\partial P)$, is zero within one standard deviation in three out of four cases. Since $k_{obs} \simeq k_{-1} + k_{-2}K_c/[H^+]$ the conclusion may be reached that neither k_{-1} nor $k_{-2}K_c$ have much of a pressure dependence and hence have small activation volumes. (This conclusion is further reinforced from the pressure dependence of k_{-1} obtained from extrapolations to $1/[H^+] = 0$ yielding an average $\Delta V_{-1}^{\ddagger}$ of -2 ± 1 cm^3 mol^{-1}.) This result may be combined with the equilibrium results to yield further information. From eq. [9] at 0 bar with $\Delta V = 8.1$ cm^3 mol^{-1}, $k_1/k_{-1} = 0.2$ and $\Delta V_{-1}^{\ddagger} = -2$ cm^3 mol^{-1} it is seen that $\Delta V_1 + 0.17\Delta V_1^{\ddagger} = 6$ cm^3 mol^{-1}. But without knowledge of ΔV_1 the value of $\Delta V_1^{\ddagger}$ cannot be obtained. However, it is well known that the formation of an ion pair between two oppositely charged ions leads to a decrease in electrostriction (11) with a consequent increase in the volume of electrostricted water. This conclusion is reinforced by theory (14) and has also been confirmed experimentally. Reaction volumes for the ion pairs following are: 10 ± 3 cm^3 mol^{-1} for Be^{2+},SO_4^{2-} (12) at 25°C and $\mu = 1.0\ M$; 16 ± 0.5 cm^3 mol^{-1} for $Co(NH_3)_6^{3+}$,SO_4^{2-} (13) at 30°C and $\mu = 0.1\ m$. If in fact ΔV_1 for Fe^{3+},Br^- is larger than 6 cm^3 mol^{-1}, as would seem likely, then $\Delta V_1^{\ddagger}$ must be negative.

An alternative and more quantitative analysis of the data of Table 2 is as follows. Substitution of $k = k_0 \exp(-P\Delta V^{\ddagger}/RT)$ with k_0 the rate constant at 0 bar and the equivalent equilibrium constant expression in eq. [7] yields k_{obs} as a function of four variables ($[H^+]$, $[Br^-]$, P, and K) and five parameters (k_1 and k_2K_b at 0 bar, and $\Delta V_1^{\ddagger}$, $\Delta V_{2b}^{\ddagger}$, and ΔV_1) if K_1 at 1 bar is fixed from $K_1 = 0.83K = 0.36\ M^{-1}$. The best fit values are given in Table 3. Since eq. [7] by virtue of its $K - K_1$ term is more sensitive to physically reasonable values of K_1 (K must be larger than K_1 at all pressures) the parameters of eq. [8] were obtained from a four-parameter analysis using the value of ΔV_1 obtained from the non-linear least-squares analysis of eq. [7]. The initial parameter estimates for the iterative non-linear procedure were obtained graphically and from linear least-squares methods. The non-linear confidence limits on the parameters are somewhat more conservative than the standard deviations listed in Table 3. For example the non-linear confidence limits yield an upper and lower bound of $\Delta V_1^{\ddagger}$ of -11 and -23 cm^3 mol^{-1}. Overall the relative standard deviation of the fit is 3%.

The non-linear computer analysis must be viewed in its proper perspective in assessing the reliability of the parameters obtained. The first point to be made in this regard is that five parameters are being determined from only 20 data points which statistically is a fairly small number. It must also be remembered

TABLE 3. Activation and reaction volumes for the reaction of Fe(III) and Br^- at 25.0°C and ionic strength 2.0 M[a]

Parameter	$\Delta V^{\ddagger}$ or ΔV ($cm^3\ mol^{-1}$)	Value of parameter at 0 bar[b]	Reaction step
k_1	-19 ± 4	$4.4\pm1.6\ s^{-1}$	$Fe^{3+},Br^- \rightarrow FeBr^{2+}$
k_{-1}	-2 ± 4	$22\pm7\ s^{-1}$	$FeBr^{2+} \rightarrow Fe^{3+},Br^-$
k_2K_b	-15 ± 3	$15\pm2\ M\ s^{-1}$	—
$k_{-2}K_c$	2 ± 2	$72\pm9\ M\ s^{-1}$	—
K_1	11 ± 1	$0.36\ M^{-1}$	$Fe^{3+} + Br^- \rightleftharpoons Fe^{3+},Br^-$
K_a[c]	1.6 ± 0.1	$1.9\times10^{-3}\ M$	$Fe^{3+} \rightleftharpoons FeOH^{2+} + H^+$
K	8.1 ± 0.2[d]	$0.43\pm0.07\ M^{-1}$	—

[a]All errors quoted are standard deviations from non-linear least-squares analysis only and do not represent the reliability of the individual parameters.
[b]At $[H^+] = 1.00\ M$, $P = 1$ bar, and low $[Br^-]$ these parameters predict $k_{obs} = 94 \pm 11\ s^{-1}$ which compares to $k_{obs} = 105\ s^{-1}$ (6) at $\mu = 1.00\ M$ and 22°C; $k_{obs} = 82 \pm 16\ s^{-1}$ (7) at $\mu = 1.7\ M$ and 22°C; and $k_{obs} = 220 \pm 40\ s^{-1}$ (8) at $\mu = 1.2\ M$ and 25°C.
[c]At 24.2°C and $\mu = 1.5\ M$.
[d]At 0 bar.

that the accuracy of the temperature jump method is not as high as some other kinetic methods. A second point is that the analysis assumes that the activation and reaction volumes of eqs. [7] and [8] do not vary with P. This is probably a reasonable assumption but nevertheless is an assumption that is introduced without any knowledge as to its validity. Introduction of compressibility terms would increase the number of parameters from 5 to an unacceptable 8. A third and even more general point is that the parameters are very dependent on the model used. While eq. [3] is a reasonable and generally accepted mechanism for ligand substitution, inclusion of further intermediates in eq. [3], solvent separated ion pairs, for example, would necessarily lead to different rate expressions than those used. Nonetheless, the parameters do meet the constraints outlined in the paragraphs above which explored the qualitative features of this difficult reaction.

Discussion

The results of the qualitative analysis of the kinetics described in the Results section lead to a number of firm qualitative conclusions. One is that the lack of $[Br^-]$ dependence on the rate is due to the relatively large size of the last two terms of eq. [4]. Further, the pressure dependence of k_{obs} is small leading to the conclusion that $\Delta V_{-1}^{\ddagger}$ is small. Consideration of these facts with knowledge of the volume of reaction ΔV leads to the further conclusion that $\Delta V_1^{\ddagger}$ is negative *if* ΔV_1 is larger than 6 $cm^3\ mol^{-1}$.

All of these qualitative conclusions are confirmed by the non-linear least-squares quantitative analysis which combines both kinetic and equilibrium data and which is subject to the qualifications given in the Results section. The value of $\Delta V_1 = 11\ cm^3\ mol^{-1}$ determined from eq. [7] for formation of the Fe^{3+},Br^- ion pair is positive as might be expected (11) for a reaction leading to a loss of electrostricted water. The magnitude of ΔV_1 is reasonable in comparison to similar reactions (12, 13) but is somewhat larger than the theoretical value of 5.4 $cm^3\ mol^{-1}$ (but at $\mu = 0\ M$) obtained from the Hemmes equation (1, 14). In the absence of a direct measurement of ΔV_b and ΔV_c the significance of the composite activation volumes for k_2K_b and $k_{-2}K_c$ is unknown.

A negative activation volume is usually indicative of bond formation in the transition state (11). The volume of a partially bonded species in the transition state would be less than a ion paired non-bonded species. Thus, the $\Delta V_1^{\ddagger}$ of $-19\ cm^3\ mol^{-1}$ indicates an associative process for substitution of Br^- into the inner coordination sphere of Fe^{3+}. The negative activation volumes for Br^-, Cl^-, and NCS^- substitution on Fe^{3+} contrast sharply to positive activation volumes found for substitution on $FeOH^{2+}$ by Cl^- of $7.8 \pm 1\ cm^3\ mol^{-1}$ (1) and by NCS^- of $6.6\ cm^3\ mol^{-1}$ (2) which are due to dissociative loss of water in the transition state (5).

The activation volume ($\Delta V_1 + \Delta V_1^{\ddagger}$) of the product K_1k_1 of $-8 \pm 4\ cm^3\ mol^{-1}$ compares to that obtained from the Cl^- (1) study of $-4.5 \pm 1.1\ cm^3\ mol^{-1}$ and $\sim 0\ cm^3\ mol^{-1}$ (individual determinations ranged from -4.9 to $4.4\ cm^3\ mol^{-1}$) for NCS^- (2). The previous indirect determinations of $\Delta V_1^{\ddagger}$ for the reaction of Fe^{3+} with Cl^- (1) of $-9.9\ cm^3\ mol^{-1}$ and with NCS^- (2) of $-1.2\ cm^3\ mol^{-1}$ were also taken to indicate an associative ligand substitution reaction.

Further evidence for the associative character of ligand substitution on Fe^{3+} is afforded by comparing the formation rate constants (the product K_1k_1) of Cl^-, Br^-, and NCS^-. All are singly charged unprotonated ligands and thus minimize ambiguity as to which protonated species is reactive. Thus, K_1k_1 for

NCS^- (2) is 122 $M^{-1}\,s^{-1}$, for Cl^- (1) 4.8 $M^{-1}\,s^{-1}$, and for Br^- 1.6 $M^{-1}\,s^{-1}$, almost an 80-fold variation. Generally dependence of a formation rate constant on the nature of the entering ligand is evidence for an associative reaction. The variation in K_1k_1 must be largely due to k_1 as K_1 would be expected to be relatively constant for ligands of the same charge type.

The reason for the change in mechanism from dissociative to associative in going from $FeOH^{2+}$ to Fe^{3+} may be due to the large charge of Fe^{3+} (15). The higher charge density of Fe^{3+} might be expected to raise the energy required to dissociate the cation–water bond, thus favouring an associative mechanism. Swaddle (16) has even suggested that there is a general change in mechanism (excluding cobalt), from dissociative interchange to associative interchange, in going from the divalent to the trivalent transition metals.

Acknowledgements

Suggestions by one of the referees for the presentation of this work and the advice and encouragement of Professor Edward F. Caldin are gratefully acknowledged.

1. B. B. Hasinoff. Can. J. Chem. **54**, 1820 (1976).
2. A. Jost. Ber. Bunsenges. Phys. Chem. **80**, 316 (1976).
3. E. F. Caldin, M. W. Grant, and B. B. Hasinoff. J. Chem. Soc. Faraday I, **68**, 2247 (1972).
4. M. W. Grant. J. Chem. Soc. Faraday I, **69**, 560 (1973).
5. M. Eigen and R. G. Wilkins. Mechanisms of inorganic reactions. Adv. Chem. Ser. No. **49**, 55 (1965).
6. D. W. Carlyle and J. H. Espenson. Inorg. Chem. **8**, 575 (1969).
7. P. Matthies and H. Wendt. Z. Phys. Chem. **30**, 137 (1961).
8. T. Yasunaga and S. Harada. Bull. Chem. Soc. Jpn. **42**, 2165 (1969).
9. M. W. Lister and D. E. Rivington. Can. J. Chem. **33**, 1603 (1955).
10. E. Rabinowitch and W. H. Stockmayer. J. Am. Chem. Soc. **64**, 335 (1942).
11. W. J. Le Noble. Prog. Phys. Org. Chem. **52**, 207 (1967).
12. W. Knoche, C. A. Firth, and D. Hess. Adv. Mol. Relaxation Processes, **6**, 1 (1974).
13. T. G. Spiro, A. Revesz, and J. Lee. J. Am. Chem. Soc. **90**, 4000 (1968).
14. P. Hemmes. J. Phys. Chem. **76**, 895 (1972).
15. F. Basolo and R. G. Pearson. Mechanisms of inorganic reactions. Wiley, New York. 1967. pp. 136–8.
16. T. W. Swaddle. Coord. Chem. Rev. **14**, 217 (1974).

Spectroscopic studies of mercury(II) acetate complexes of some tertiary phosphines[1]

ELMER C. ALYEA AND SHELTON A. DIAS

Guelph–Waterloo Centre for Graduate Work in Chemistry, Guelph Campus, University of Guelph, Guelph, Ont., Canada N1G 2W1

Received March 10, 1978

ELMER C. ALYEA and SHELTON A. DIAS. Can. J. Chem. **57**, 83 (1979).

Mercury(II) acetate complexes of the type $(R_3P)_nHg(OAc)_2$, where $n = 1$ and 2, and R_3P = $(p\text{-tolyl})_3P$, $(p\text{-F-}C_6H_4)_3P$, Ph_2MeP, Ph_2EtP, and $PhEt_2P$ have been prepared in good yields. Only the 1:1 adduct is formed with $(o\text{-tolyl})_3P$. Conductance measurements in nitromethane show that these complexes are non-electrolytes. The 1:1 adducts are monomeric in dichloroethane but the 1:2 adducts are extensively dissociated. Tentative assignments for ν(COO), ν(Hg—O), ν(Hg—P) are made from the infrared and Raman spectral data. The correlation of the coordination chemical shifts, $\Delta\delta(^{31}P)$, with the coupling constants $^1J(^{199}Hg\text{–}^{31}P)$ of the complexes is discussed with respect to the bulkiness and the basicity of the phosphine ligands.

ELMER C. ALYEA et SHELTON A. DIAS. Can. J. Chem. **57**, 83 (1979).

On a préparé, avec de bons rendements, des complexes de l'acétate mercurique du type $(R_3P)_nHg(OAc)_2$ où $n = 1$ et 2 et R_3P = $(p\text{-tolyl})_3P$, $(p\text{-F-}C_6H_4)_3P$, Ph_2MeP, Ph_2EtP et $PhEt_2P$. Il ne se forme que l'adduit 1:1 avec le $(o\text{-tolyl})_3P$. Des mesures de conductivité dans le nitrométhane montrent que ces complexes ne sont pas des électrolytes. Les adduits 1:1 existent sous forme de monomères dans le dichloroéthane; toutefois les adduits 1:2 sont fortement dissociés. On a proposé des attributions préliminaires pour les ν(COO), ν(Hg—O), ν(Hg—P) observées dans les spectres infrarouges et Raman. On discute de la corrélation qui existe entre les déplacements chimiques de coordination, $\Delta\delta(^{31}P)$, et les constantes de couplage, $^1J(^{199}Hg\text{–}^{31}P)$, des complexes en relation avec l'encombrement et la basicité des ligands phosphines.

[Traduit par le journal]

Introduction

Spectroscopic and structural studies in our laboratory have recently involved mercury(II) complexes of tertiary phosphines containing bulky substituents. The characterization of these complexes by solution measurements (1, 2) was often hampered by their low solubility, which is partly governed by the nature of the anion. The latter was shown, by X-ray analysis of $[(Cy_3P)Hg(NO_3)_2]_2$ (3) and $(Cy_3P)Hg(SCN)_2$ (4), to also determine the coordination geometry of the mercury atom. Subsequently we have found that mercury(II) acetate complexes of tertiary phosphines are much more soluble than the analogous halide complexes, enabling the present characterization in solution of complexes involving phenyl-substituted phosphines with a range of steric and electronic properties.

Relatively few complexes of mercury(II) acetate are known (see, for example, ref. 5) and there are only two reports (6) on complexes with a phosphine ligand.[2] The complex bis(trimethylphosphine)mercury(II) acetate was considered to contain two-coordinate mercury and ionic acetate groups (6*a*). However, the complex $(Bu_3^tP)Hg(OAc)_2$ was determined to have a monomeric trigonal bipyramidal structure (8*a*). Very recently we reported (2) that the complexes $(Ph_3P)_2Hg(OAc)_2$ (8*b*), $(Ph_3P)Hg(OAc)_2$ (8*b*), $(Cy_3P)_2Hg(OAc)_2$, $(Cy_3P)Hg(OAc)_2$, and $[(o\text{-tolyl})_3P]Hg(OAc)_2$ also have non-ionic structures. The effects of the carboxylate groups on the nature of the phosphine complexes of mercury(II) carboxylates have been investigated in an independent study (8*b*). In the present study, we report the vibrational and nmr spectroscopic investigation of a series of mono and bis tertiary phosphine – mercury(II) acetate complexes with a variety of tertiary phosphines.

Experimental

General Procedures

Mercury(II) acetate and tertiary phosphines were commercial samples. Solvents were purified and dried following standard procedures. Microanalyses were performed at M-H-W Laboratories, Garden City, Michigan. Melting points were determined with a Gallenkamp melting point apparatus in open capillary tubes and are uncorrected. Molecular weights were measured in dichloroethane solution using a Hitachi-Perkin-Elmer 115 osmometer. Conductivity measurements were obtained for nitromethane solutions with a Yellow Springs conductivity bridge using a conductivity cell with platinum electrodes.

[1]Presented in part at the American Chemical Society/Chemical Institute of Canada Joint Meeting, Montreal, P.Q., Canada, May/June 1977.

[2]Mercuration reactions are, however, more widely studied (7).

0008-4042/79/010083-08$01.00/0

TABLE 1. Melting points, analytical, conductance, and molecular weight data

Compound	Melting point (°C)[a]	Calcd. C%	Calcd. H%	Found C%	Found H%	Λ_m[b] (ohm^{-1} cm^{-2} mol^{-1})	Molecular weight[c]
$Hg(OAc)_2[(o\text{-tolyl})_3P]$	176–177	48.19	4.37	47.52	4.77	6.1	625 (623)
$Hg(OAc)_2[(p\text{-tolyl})_3P]$	179–180	48.19	4.37	48.26	4.32	10.1	—
$Hg(OAc)_2[(p\text{-tolyl})_3P]_2$[d]	164–165	55.76	4.98	55.55	4.92	10.1	—
$Hg(OAc)_2[(p\text{-F—}C_6H_4)_3P]$	198–200	41.62	2.86	42.95	3.09	8.1	—
$Hg(OAc)_2[(p\text{-F—}C_6H_4)_3P]_2$	186–187	50.51	3.18	50.35	3.12	7.5	—
$Hg(OAc)_2(MePh_2P)$	117–118	39.35	3.69	39.16	3.63	1.9	534 (519)
$Hg(OAc)_2(MePh_2P)_2$	138–139	50.11	4.49	49.94	4.51	11.0	357 (719)
$Hg(OAc)_2(EtPh_2P)$	140–142	40.57	3.97	40.37	3.85	0.8	613 (533)
$Hg(OAc)_2(EtPh_2P)_2$	146–148	51.44	4.86	51.65	4.88	3.4	—
$Hg(OAc)_2(Et_2PhP)$	100–102	34.68	4.37	34.63	4.52	21.0	—

[a]Decomposition occurs.
[b]For 10^{-3} *M* solutions in nitromethane.
[c]In 1,2-dichloroethane for ca. 5×10^{-3} *M* solutions.
[d]Isolated with one molecule of dichloromethane.

Infrared spectra were obtained with a Beckman IR-12 spectrophotometer; solid state spectra were recorded as Nujol and Halocarbon mulls between CsI plates whereas solution spectra were obtained using matched KBr cells of 0.2 mm path length. Raman spectra were obtained for samples sealed in capillaries with a Jarrell-Ash spectrometer using the 514.5 nm line of a Spectra-Physics 165 laser. ^1H nmr spectra were recorded on a Varian A-60 spectrometer with TMS as reference standard and ^{31}P nmr spectra were measured with a Bruker WP-60 FT spectrometer at 24.3 MHz using the side-band technique with 85% H_3PO_4 as reference in a concentric capillary.

Preparation of the Complexes

All of the mercury(II) acetate complexes were prepared by the general method already outlined for mercury(II) halide complexes of tertiary phosphines (1, 2). The suspension of mercury(II) acetate in ethanol, benzene, or dichloromethane disappeared immediately as it was allowed to react with either a 1:1 or 1:2 molar ratio of tertiary phosphine at ambient temperature under dry dinitrogen. The white solids obtained by evaporation of the solvent were normally recrystallized from dichloromethane/diethyl ether or dichloromethane/hexane. In the case of $(Et_2PhP)_2Hg(OAc)_2$, the product was obtained as a colourless viscous oil and its purity deduced from its ^1H nmr spectrum. The complex $(Ph_3P)Hg(OAc)_2$ was also formed by the reaction of methyl mercury acetate with Ph_3P in a 1:1 molar ratio in dichloromethane solution.[3] Product yields were in the 70–99% range. Although stable in the solid state towards decomposition on exposure to air and moisture, the products decomposed gradually with the deposition of metallic mercury upon standing in solution.

Results and Discussion

Some of the physical properties and the analysis of the new series of complexes are listed in Table 1. Tri(*o*-tolyl)phosphine forms only a 1:1 adduct with mercury(II) acetate. Attempts to prepare higher adducts using as much as sixfold excess of phosphine still afforded only the 1:1 adduct, but in slightly higher yields. This behavior parallels that previously reported (1) for mercuric halides and thiocyanate with tri(*o*-tolyl)phosphine and tris(*tert*-butyl)phosphine and clearly reflects the steric bulkiness of these phosphines. Tolman used CPK molecular models to define "cone angles" for phosphines; estimated values for $(o\text{-tolyl})_3P$, $Bu_3{}^tP$, and Ph_3P are 194°, 182°, and 145°, respectively (9). X-ray structural studies of several metal complexes give experimentally derived cone angles in relatively good agreement with Tolman's estimates, and further, provide a quantitative description of the steric requirements of the phosphine ligands in terms of a "ligand profile" (3, 4, 8*a*, 10, 11).

All of the complexes prepared in this study are white solids which are stable towards air in the solid state. However, in solution the stability appears to decrease as the number of alkyl substituents increases. The complex $Hg(OAc)_2(PPhEt_2)_2$ could not be obtained in a solid form but its purity was verified by ^1H nmr spectroscopy. Molecular weight determinations in dichloroethane show that the 1:1 adducts are monomeric whilst the 1:2 adducts undergo dissociation. Since all of the complexes are essentially non-electrolytes in nitromethane, the dissociation in solution must involve the following equilibrium:

$$[1] \qquad Hg(OAc)_2(PR_3)_2 \rightleftarrows Hg(OAc)_2(PR_3) + PR_3$$

Nuclear magnetic resonance studies, discussed below, confirmed the existence of equilibrium [1].

[3]The full characterization of $(Ph_3P)_nHg(OAc)_2$ ($n = 1, 2$) is described in the independent study of triphenylphosphine complexes of several substituted mercury acetates (8*b*).

TABLE 2. Infrared acetate group and Raman mercury–oxygen and mercury–phosphine stretching frequencies[a]

Compound	Solid state[b] ν_8[c]	Solid state[b] ν_8[d]	Solid state[b] $\Delta\nu$	Dichloromethane solution ν_8[c]	Dichloromethane solution ν_3[d]	Dichloromethane solution $\Delta\nu$	ν(Hg—O)	ν(Hg—P)
$Hg(OAc)_2[(o\text{-tolyl})_3P]$	1580vs	1392s	188	1570vs	1410s	160	202s	**150s**
$Hg(OAc)_2[(p\text{-tolyl})_3P]$	1615vs 1560vs	1403vs 1362m	205[e]	1595vs, sh 1575vs	1420s, br	165[e]	—	—
$Hg(OAc)_2[(p\text{-tolyl})_3P]_2$	1600vs 1580vs, sh	1375vs	215[e]	1575vs, br	1410s	165	—	—
$Hg(OAc)_2[(p\text{-F—}C_6H_4)_3P]$	1590vs, br	1370s	220	1712m 1586vs, br	1375m 1326s	386[f] 211[f]	223m	**165m**
$Hg(OAc)_2[(p\text{-F—}C_6H_4)_3P]_2$	1720m 1550s	1398s 1338m	382[f] 152[f]	1570vs, br	1335s	235	—	—
$Hg(OAc)_2(MePh_2P)$	1562vs	1376s	186	1575vs, br	1372vs	203	182s	**132m**
$Hg(OAc)_2(MePh_2P)_2$	1560vs	1380s	180	1570vs, br	1380vs, br	190	152s	**114s**
$Hg(OAc)_2(EtPh_2P)$	1560vs	1385m	175	1570vs, br	1375s, br	195	187s	**119s**
$Hg(OAc)_2(EtPh_2P)_2$	1562vs	1380s	182	1572vs	1380s	192	164s	**118m**
$Hg(OAc)_2(Et_2PhP)$	1578vs, br	1392s	186	1575vs, br	1408s	167	—	—
$Hg(OAc)_2(Et_2PhP)_2$	—	—	—	1570vs	1410s	160	—	—

[a]In cm^{-1}. Abbreviations: v, very; s, strong; m, medium; sh, shoulder; br, broad.
[b]Halocarbon or Nujol mulls.
[c]Asymmetric stretching frequency, $\nu_{asym}(COO)$.
[d]Symmetric stretching frequency, $\nu_{sym}(COO)$.
[e]An average value is estimated.
[f]Alternative values are possible.

Vibrational Spectral Studies

Spectroscopic measurements in solution were facilitated by the solubility of all the complexes in common organic solvents. The infrared study was mainly concerned with an attempt to determine the mode of coordination of the acetate group. The solid state and solution infrared absorptions associated with the asymmetric (ν_8) and the symmetric (ν_3) stretching frequencies of the acetate moiety for all the complexes are given in Table 2. Although assignment of the asymmetric stretch of the COO group could be made quite unequivocally, the assignment of the corresponding symmetric stretch was sometimes difficult due to the occurrence of methyl deformation frequencies and phosphine bands in the same region. Comparison of both solid and solution data with the spectra of the free phosphines or their mercury(II) halide complexes normally overcame any ambiguity in the assignment.

The acetate group is known to interact with a metal ion in the four following principle ways (12). In addition, types **3** and **4** occur less commonly with unsymmetrical modes of coordination. Infrared studies relating these modes of bonding of the acetate group to metals to changes in C—O frequencies have focused on the $\nu_{asym}(COO) - \nu_{sym}(COO)$ separation ($\Delta\nu$ or $\nu_8 - \nu_3$) (12–16). Though earlier work (15) suggested that the magnitude of $\Delta\nu$ was not a reliable criterion of the mode of acetate coordination, recent correlations of the infrared spectra of metal acetates with X-ray structural evidence for modes **2–4** show that qualitative application of this criterion is possible (12). Waddington and co-workers found that the divergence of $\Delta\nu$, as compared to the free ion value of 164 cm^{-1} for sodium acetate, was greatest for type **2** since in unidentate acetate groups the ν_8 and ν_3 frequencies correspond approximately to C=O and C—O; values of $\Delta\nu$ may exceed 500 cm^{-1} for some Group 4 acetates (12). Chelating bidentate acetate groups (type **3**) normally have $\Delta\nu$ less than 100 cm^{-1}, whilst the bridging mode of coordination (type **4**) leads to $\Delta\nu$ values nearer 150 cm^{-1}, i.e., similar to the free acetate value of $\Delta\nu$ (12). Obviously, intermediate situations with unsymmetrical modes of bonding are expected to give rise to $\Delta\nu$ values that are between those shown by types **2** and **3**, and a distinction from type **4** would not be possible from this infrared criterion alone.

In the present series of complexes, with the exception of the $(p\text{-F—}C_6H_4)_3P$ complexes, $\Delta\nu$ lies in the range 172–215 cm^{-1}. Since the conductance and molecular weight measurements rule out types **1** and **4** acetate interaction, we conclude that the

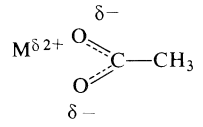

1

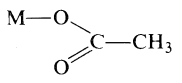

2

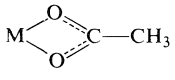

3

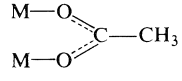

4

mode of coordination is intermediate between types **2** and **3**, i.e., unsymmetrically bidentate. The similarity of the solid state and solution values for the 1:1 complexes suggests that the structure is the same in both media. The change in $\Delta\nu$ values from the solid state to solution for the 1:2 complexes is compatible with their dissociation according to equilibrium [1]. An X-ray structural determination for $Hg(OAc)_2(PBu_3^t)$ (*8a*) ($\Delta\nu = 172\ cm^{-1}$) has confirmed that the mercury atom is in a distorted trigonal bipyramidal geometry by virtue of the acetate groups being unsymmetrically chelated and spanning axial and equatorial sites. Values of ca. 185 cm^{-1} for $\Delta\nu$ for nearly all of the 1:1 and 1:2 adducts thus indicate that the mode of acetate bonding is similar to that found by X-ray analysis. Exceptions to the normal value of $\Delta\nu$ for these complexes are observed for the two complexes involving $(p\text{-F—}C_6H_4)_3P$. The higher values of $\Delta\nu$ suggest that the oxygen atoms of the unsymmetrically bound acetate group are quite inequivalent, and indeed, for the 1:1 adduct in solution and the 1:2 solid adduct of $(p\text{-F—}C_6H_4)_3P$, two kinds of acetate groups are apparently present. Values of ca. 380 cm^{-1} for $\Delta\nu$ in these cases are compatible with unidentate coordination (type **2**) and it is noteworthy that $Hg(OAc)_2$ itself, for which two-coordination has been assigned (17), has $\Delta\nu = 270$ cm^{-1}. The only other complexes reported in this work which display splitting of the ν_3 and ν_8 modes are both $(p\text{-tolyl})_3P$ complexes. The separation of peaks in these instances are not clearly interpretable and may only arise from lattice effects or vibrational coupling, though inequivalent acetate groups are the more probable cause; similarly $Hg(OAc)_2(PBu_3^t)$, which has equivalent unsymmetrically bound acetate groups, has peaks assignable to ν_8 at 1575 cm^{-1}, 1560 cm^{-1}, and 1540 cm^{-1} (*6b*). At the same time, it is well to remember that $\Delta\nu$ for bridging acetate groups would also be expected to be near 150–200 cm^{-1} and thus dimeric structures in the solid state for the 1:1 adducts cannot be ruled out in the absence of an X-ray analysis.[4]

Raman spectra were obtained for most of the complexes in the region below 1800 cm^{-1}. Due to the difficulty in assigning the relatively weak ν_3 absorption, these spectra were of little assistance in making assignments of acetate bonding type. However, all of the spectra obtained show a strong bond in the range 223–164 cm^{-1} (Table 2) that can be assigned to the symmetric mercury–oxygen stretching frequency. This absorption occurs at 274 cm^{-1} in the Raman spectrum of $Hg(OAc)_2$ (17). Similarly, following our assignment in phosphine complexes of mercuric halides and thiocyanate (1), a strong to medium band in the range 150–114 cm^{-1} (Table 2) may be assigned to ν(Hg—P).

Nuclear Magnetic Resonance Spectral Studies

Table 3 lists the ^1H nmr spectral data for the complexes and the corresponding phosphines. In general, the phosphine resonances shift downfield upon coordination in both series of complexes; the shift is, expectedly, greater for the 1:1 series. A similar trend is exhibited by the acetate methyl signals. More interestingly, for both the 1:1 and 1:2 series, the acetate methyl signal appeared as a single peak and the phosphine groups produced a single set of absorptions. This observation prompted an investigation, to be discussed below, of the lability of these systems. A simple integration of the distinct acetate methyl signal against the aromatic signals afforded an immediate indication of the composition of a complex and its purity.

Phosphorus-31 nmr data are in Table 3. All of the 1:1 complexes except $Hg(OAc)_2(PPh_3)$ and $Hg(OAc)_2[P(p\text{-F—}C_6H_4)_3]$ showed ^{31}P spectra having two small satellite peaks due to coupling with mercury-199 nuclei ($I = 1/2$; natural abundance 16.8%). No splitting was observed for mercury-201 ($I = 3/2$; natural abundance 13.2%). The observation of a single broad peak and the absence of the expected triplet pattern of relative intensity of approximately 8:84:8 (18) for the two complexes mentioned above clearly indicate dissociation and exchange of the phosphine, which are fast on the nmr time scale. In the 1:2 series none of the complexes show the ^{199}Hg satellites at room temperature, which again shows the lability of the phosphine complexes on the nmr time scale. Observation of the ^{199}Hg–^{31}P coupling was made by recording the spectra at 183 K, which is consistent with the slowing down of the ligand exchange reaction via equilibrium [1].

Reduction of the temperature to observe the ^{199}Hg–^{31}P coupling also produced shifts of the ^{31}P signal and an increase in the value of $^1J(^{199}Hg\text{–}^{31}P)$ for complexes in both series (Table 3). The observation of changes in phosphorus chemical shifts with decreasing temperature is, at best, qualitative since 85% H_3PO_4 cannot be used as a reference at 183 K. On the other hand, the increase of the coupling constant with decrease in temperature is a significant result. For example, the value of $^1J(^{199}Hg\text{–}^{31}P)$ for $Hg(OAc)_2(PPh_3)_2$ increased from 5024 Hz at 230 K

[4] $Hg(OAc)_2(PCy_3)$, which shows peaks in the ν_8 region in the solid state at 1605 cm^{-1}, 1595 cm^{-1}, and 1575 cm^{-1}, has been determined to have a dimeric structure involving both bridging and unsymmetrically bidentate acetate groups (*11c*). X-ray analysis of $Hg(OAc)_2[(o\text{-tolyl})_3P]$ is also underway.

TABLE 3. Proton[a] and phosphorus-31[b] nuclear magnetic resonance data for the complexes[c]

Compound	Acetate-CH_3[d]	Phosphine peaks	Free phosphine peaks	Assignments	Chemical shift ppm (δ)[b]	Coordination chemical shift, ppm (Δδ)[e]	$^1J(^{199}Hg–^{31}P)$ Hz
$Hg(OAc)_2[(o\text{-tolyl})_3P]$	1.95	2.48	2.37, $4J(^{31}P–^1H) = 1$ Hz	$—CH_3$	13.7	45.9	8236
		6.84–7.83	6.56–7.29	$—C_6H_4—$	8.3(183 K)	40.5	8374
$Hg(OAc)_2(Ph_3P)$	1.82	7.33–8.03	7.07–7.63	$—C_6H_5$	30.2	36.0	—
					27.7(183 K)	33.5	8853
$Hg(OAc)_2(Ph_3P)_2$	1.59	7.08–7.85	7.07–7.63	$—C_6H_5$	29.4	35.2	—
					33.2(183 K)	39.0	5503
$Hg(OAc)_2[(p\text{-tolyl})_3P]$	1.95	2.42	2.33	$—CH_3$	29.4	38.0	8521
		7.21–7.83	6.97–7.48	$—C_6H_4—$	26.5(183 K)	35.1	8897
$Hg(OAc)_2[(p\text{-tolyl})_3P]_2$[f]	1.63	2.33	2.33	$—CH_3$	31.0	39.6	—
		6.89–7.85	6.97–7.48	$—C_6H_4—$	31.6(183 K)	40.2	5483
$Hg(OAc)_2[(p\text{-F}—C_6H_4)_3P]$	1.78	7.03–8.08	6.73–7.66	$—C_6H_4—$	26.5	37.7	—
					24.9(183 K)	36.1	8981
$Hg(OAc)_2[(p\text{-F}—C_6H_4)_3P]_2$	1.63	6.56–7.98	6.73–7.66	$—C_6H_4—$	26.1	37.3	—
					30.4(183 K)	41.6	5640
$Hg(OAc)_2(MePh_2P)$	1.83	2.44, $^2J(^{31}P–^1H) = 12.5$ Hz	1.58, $^2J(^{31}P–^1H) = 4.0$ Hz	$—CH_3$	18.9	47.0	8804
		7.33–8.01	7.10–7.68	$—C_6H_5$			
$Hg(OAc)_2(MePh_2P)_2$	1.83	2.26 (broad)	1.58	$—CH_3$	17.9	46.0	—
		7.17–8.09	7.10–7.68	$—C_6H_5$	21.5(183 K)	49.6	5801
$Hg(OAc)_2(EtPh_2P)$	1.92	0.94–1.61	0.75–1.50	$—CH_3$			
		2.38–3.15	1.77–2.43	$—CH_2—$	32.8	46.8	8477
		7.37–8.07	7.04–7.56	$—C_6H_5—$			
$Hg(OAc)_2(EtPh_2P)_2$	1.75	0.68–1.60	0.75–1.50	$—CH_3$			
		2.08–3.17	1.77–2.43	$—CH_2—$	32.2	46.8	—
		6.95–8.19	7.04–7.56	$—C_6H_5$	37.2(183 K)	51.2	5615
$Hg(OAc)_2(Et_2PhP)$	1.98	0.85–1.76	0.53–1.35	$—CH_3$			
		2.15–3.07	1.37–2.09	$—CH_2—$	38.8	56.5	8242
		7.40–8.17	6.75–7.67	$—C_6H_5$	39.8(183 K)	57.5	8608
$Hg(OAc)_2(Et_2PhP)_2$	1.94	0.35–1.75	0.53–1.35	$—CH_3$			
		2.07–3.03	1.37–2.09	$—CH_2—$	37.4	55.1	—
		6.94–8.24	6.75–7.67	$—C_6H_5—$	41.2(183 K)	58.9	5620

[a]In deuteriochloroform with TMS as internal standard; values are in ppm (δ).
[b]In dichloromethane with 85% H_3PO_4 as reference standard; positive chemical shifts are downfield.
[c]Measured at room temperature unless noted otherwise.
[d]Peak is singlet; occurs at 1.93 for $Hg(OAc)_2$ in dimethylsulfoxide-d_6.
[e]$\Delta\delta = \delta(\text{complex}) - \delta(PR_3)$.
[f]Peak due to dichloromethane also observed for the sample.

(2) to 5503 Hz at 183 K. Since the coupling constant should be independent of the rate of phosphine exchange, an explanation for the increased magnitude with decreasing temperature is not readily apparent. Further studies are needed to determine which one (or more) of the several factors (19) which influence $^1J(^{199}Hg–^{31}P)$ are important.

As expected, the 1:1 complexes show larger coupling constants (ca. 8500 Hz) than the corresponding 1:2 complexes (ca. 5500 Hz). As Grim previously explained for some $HgX_2(PR_3)_n$ (n = 1, 2) complexes (18), the greater values of $J(^{199}Hg–^{31}P)$ are explicable in terms of greater electron deficiency of mercury in the case of the 1:1 complexes. Similarly, the observed coupling constants and coordination chemical shifts are greater for these acetate complexes than for the corresponding halide complexes (2).

Two of the critically important factors that determine the magnitude of $\Delta\delta$ are the electronegativities of the substituents on the phosphorus atom and the bond angles between the substituents (19, 20). Parameters which reflect these factors are the basicities, given by pK_a values (21), and cone angles (9) of the phosphines. Consideration of the magnitude of the coordination chemical shift for the present complexes shows the importance of these factors. In both series of complexes, $\Delta\delta$ increases in magnitude from Ph_3P to Et_2PhP; the lowest $\Delta\delta$ values occur as expected for the complexes of Ph_3P, which has the lowest pK_a (2.73 as compared to 6.25 for Et_2PhP) and the least change in its C—P—C bond angles (20) in forming a complex. The greater values of $\Delta\delta$ for the $(p\text{-F—}C_6H_4)_3P$ complexes may initially seem surprising as fluorine is an electron-withdrawing substituent. However, the upfield position of the ^{31}P chemical shift of $(p\text{-F—}C_6H_4)_3P$ relative to Ph_3P perhaps indicates that electron density on phosphorus is greater, thus leading to greater σ-bond strength with mercury.

The relatively high value of $\Delta\delta$ for $Hg(OAc)_2$-[(*o*-tolyl)$_3$P] requires explanation, since the bulkiness of the phosphine should result in lower σ-interaction with mercury as compared to (*p*-tolyl)$_3$P, which would have similar basicity. The high $\Delta\delta$ value is anomalous and can be attributed to the unusually high resonance position of (*o*-tolyl)$_3$P itself. The latter effect, believed to be caused by an interaction of the ortho methyl groups with the phosphorus lone pair, would be lost upon coordination (9, 22). Consequently the "true" $\Delta\delta$ value for $Hg(OAc)_2$[(*o*-tolyl)$_3$P] would be much less than that observed for $Hg(OAc)_2(Ph_3P)$, as expected due to the large steric effect. The relatively low value (ppm) of $\Delta\delta$ for $Hg(OAc)_2(Bu_3^tP)$ (2) is much less than expected based on the basicity of Bu_3^tP, which would be near that reported for Me_3P (i.e., pK_a = 8.65) (21) because of the similar electronegativity of the methyl and *t*-butyl groups (23). The much lower $J(^{199}Hg–^{31}P_3)$ value for $Hg(OAc)_2(Bu_3^tP)$ must also be a consequence of the steric bulk of Bu_3^tP (θ = 182°) (9). Indeed, the C—P—C angles in $Hg(OAc)_2$-(Bu_3^tP) average 112° (8*a*) as compared to C—P—C angles near 104° for Ph_3P in its complexes (24). Preliminary ^{31}P nmr measurements for $Hg(OAc)_2$-$(PCy_3)_n$ (n = 1, 2) (2) also indicate that the large steric requirements of the phosphine lead to lower $\Delta\delta$ and $J(^{199}Hg–^{31}P)$ values than anticipated from the pK_a (9.6) of Cy_3P.

Ligand Exchange Studies

Several complexes were investigated by variable temperature ^1H and ^{31}P nmr spectral measurements to confirm the occurrence of ligand exchange. The observation of ^{199}Hg satellites at room temperature in the ^{31}P nmr spectra of most of the 1:1 complexes indicates that dissociation and exchange are not extensive. For example, the satellite peaks sharpen noticeably at 253 K as compared to room temperature in the spectrum of $Hg(OAc)_2$[(*o*-tolyl)$_3$P] in dichloromethane solution; at 183 K the side peaks are very sharp and $J(^{199}Hg–^{31}P)$ has increased only a small extent. We cannot comment on the significance of the upfield shift in $\Delta\delta$ because 85% H_3PO_4 is not useful as a standard at the low temperature. Addition of (*o*-tolyl)$_3$P in a 3:1 molar ratio to a dichloromethane solution of $Hg(OAc)_2$[(*o*-tolyl)$_3$P] at room temperature gives a ^{31}P nmr spectrum showing only a broad (half-width of 350 Hz) signal at -22.6δ. Cooling this solution to 183 K gives a spectrum with a peak at $+7.2\delta$ due to the complexed phosphine (but without satellite peaks) and a peak at -31δ due to the free phosphine. Dissociation is apparently only slight for the 1:1 complex but addition of free phosphine greatly enhances the exchange rate.

The ^{31}P nmr spectrum of $Hg(OAc)_2(PPh_3)_2$ in dichloromethane solution at room temperature showed only a broad (half-width 189 Hz) signal, and its position at $+29.4\delta$ is only slightly upfield from the signal of the 1:1 complex. Addition of free phosphine in 2:1 and 4:1 molar ratios gave spectra with peaks at $+5.6\delta$ (half-width 80 Hz) and -1.0δ (half-width 42 Hz) respectively. The gradual shift of the averaged signal (of bound and free phosphine) toward the resonance position of Ph_3P itself indicates that dissociation occurs, followed by rapid exchange according to equilibrium [1]. At 183 K, $Hg(OAc)_2$-$(PPh_3)_2$ in dichloromethane solution shows the expected triplet pattern, with $J(^{199}Hg–^{31}P)$ = 5503 Hz, and the main resonance peak at +33.2 Hz. Both

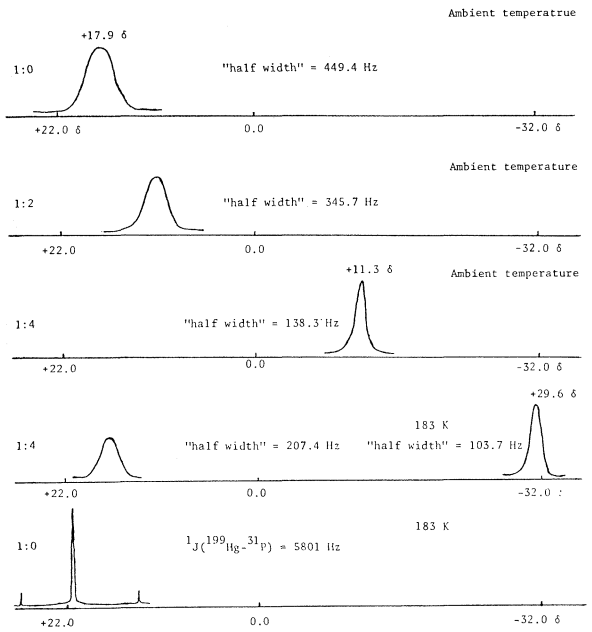

FIG. 1. Phosphorus-31 nmr exchange studies of $Hg(OAc)_2(PMePh_2)_2$ in dichloromethane solution; molar ratios for complex to phosphine are indicated.

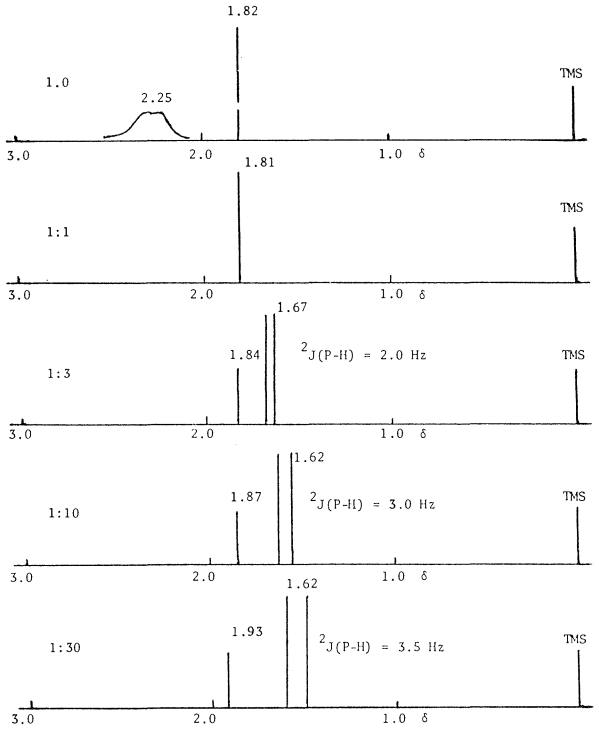

FIG. 2. Proton nmr exchange studies of $Hg(OAc)_2(PMePh_2)_2$ in deuteriochloroform solution at ambient temperature; molar ratios for complex to phosphine are indicated.

dissociation and exchange are retarded at the low temperature.

The most detailed investigation of exchange was performed on $Hg(OAc)_2(PMePh_2)_2$. The ^{31}P nmr studies are schematized in Fig. 1. The behaviour of this 1:2 complex closely parallels that found for $Hg(OAc)_2(PPh_3)_2$, in which dissociation is appreciable and phosphine exchange is fast on the nmr time scale. The ^1H nmr spectral results, obtained as a function of temperature and of methyldiphenylphosphine concentration, support the same conclusion. The ^1H nmr spectrum of $Hg(OAc)_2(PMePh_2)_2$ in deuteriochloroform is virtually unchanged from 243 K (broad singlet at 2.30δ, sharper singlet at 1.88δ) to 308 K (2.23δ, 1.83δ). However, sharpening of the broad singlet due to the methyl protons occurs at 323 K (half-width 13 Hz); the doublet observed at 333 K at 2.21δ ($^2J(^1H-^{31}P)$ = 10 Hz) probably arises from the increased proportion of $Hg(OAc)_2(PMePh_2)$ in solution at the higher temperature. Figure 2 illustrates the ^1H nmr spectra behaviour at ambient temperature as phosphine is added to a deuteriochloroform solution of $Hg(OAc)_2(PMePh_2)_2$. The resonance position of the methyl protons of the acetate groups remains a singlet near 1.85δ so that it is unlikely that higher phosphine–mercury complexes are formed in the presence of excess methyldiphenylphosphine. The complex itself at ambient temperature shows a broad peak at 2.25δ that moves upfield toward the free phosphine (methyl) position as increasing amounts of methyldiphenylphosphine are added. Throughout the addition of free phosphine, the phosphine methyl resonance position represents the weighted average in chemical shift and coupling constant of the resonances of complexes and free phosphine since rapid exchange is taking place. Similar exchange phenomena which only involve internal coupling have been discussed for $CH_3AuP(CH_3)_3$ (25), $Ni(PR_3)_4$ (26), and $(n\text{-}Bu_3PSe)_2HgX_2$ complexes (27).

Acknowledgements

We are grateful to the National Research Council of Canada for an operating grant. Raman spectra were obtained through the courtesy of Professor D. E. Irish, University of Waterloo. We also thank Dr. A. Woon-Fat for his assistance in obtaining the ^{31}P nmr spectra and Dr. C. A. Tolman for a preprint of his review.

1. E. C. ALYEA, S. A. DIAS, R. G. GOEL, and W. O. OGINI. Can. J. Chem. **55**, 4227 (1977).
2. E. C. ALYEA, S. A. DIAS, R. G. GOEL, W. O. OGINI, P. PILON, and D. W. MEEK. Inorg. Chem. **17**, 1697 (1978).
3. E. C. ALYEA, S. A. DIAS, G. FERGUSON, and R. J. RESTIVO. Inorg. Chem. **16**, 2329 (1977).
4. E. C. ALYEA, G. FERGUSON, and R. J. RESTIVO. J. Chem. Soc. Dalton, 1845 (1977).

5. (*a*) W. U. MALIK, P. K. SRIVASTAVA, and S. C. MEHTA. J. Ind. Chem. Soc. **45**, 486 (1969); (*b*) V. KOSI, M. ZUPAN, and D. HADZI. Vestn. Solv. Kem. Drus. **17**, 53 (1970); (*c*) C. A. MCAULIFFE. Transition metal complexes of phosphorus, arsenic, and antimony ligands. MacMillan, London. 1973.
6. (*a*) H. SCHMIDBAUR and K-H. RÄTHLEIN. Chem. Ber. **106**, 2491 (1973); (*b*) W. O. OGINI. M.Sc. thesis. University of Guelph, Guelph, Ont. 1976.
7. F. A. COTTON and G. WILKINSON. Advanced inorganic chemistry. 3rd ed. Interscience, New York. 1972. p. 525.
8. (*a*) P. J. ROBERTS, G. FERGUSON, R. G. GOEL, W. O. OGINI, and R. J. RESTIVO. J. Chem. Soc. Dalton, 253 (1978); (*b*) T. ALLMAN, R. G. GOEL, and P. PILON. Can. J. Chem. This issue.
9. C. A. TOLMAN. Chem. Rev. **77**, 313 (1977).
10. E. C. ALYEA, A. COSTIN, G. T. FEY, G. FERGUSON, R. G. GOEL, and R. J. RESTIVO. J. Chem. Soc. Dalton, 1294 (1975).
11. (*a*) G. FERGUSON, E. C. ALYEA, R. J. RESTIVO, and P. J. ROBERTS. Paper HN8 A.C.A. Spring Meeting, Asilomar, U.S.A., 1977; (*b*) G. FERGUSON, P. J. ROBERTS, E. C. ALYEA, and M. KHAN. Inorg. Chem. **18**, 2965 (1979); (*c*) E. C. ALYEA, S. A. DIAS, G. FERGUSON, and M. KHAN. 175th National Meeting of the American Chemical Society, Anaheim, CA. March 12–17, 1978, No. INOR 221.
12. N. W. ALCOCK, V. M. TRACY, and T. C. WADDINGTON. J. Chem. Soc. Dalton, 2243 (1976).
13. L. H. JONES and E. MCLAREN. J. Chem. Phys. **22**, 1796 (1954).
14. K. ITO and H. J. BERNSTEIN. Can. J. Chem. **34**, 170 (1956).
15. D. A. EDWARDS and R. N. HAYWARD. Can. J. Chem. **46**, 3443 (1968).
16. E. V. VAN DEN BERGHE, G. P. VAN DER KELEN, and J. ALBRECHT. Inorg. Chim. Acta, **2**, 89 (1968).
17. R. P. J. COONEY and J. R. HALL. J. Inorg. Nucl. Chem. **34**, 1519 (1972).
18. S. O. GRIM, P. J. LUI, and R. L. KEITER. Inorg. Chem. **13**, 342 (1974).
19. (*a*) L. S. MERIWETHER and J. R. LETO. J. Chem. Soc. **83**, 3192 (1961); (*b*) J. G. VERKADE. Coord. Chem. Rev. **9**, 1(1972/73).
20. B. E. MANN. J. Chem. Soc. Perkin II, 30 (1972).
21. (*a*) C. A. STREULI. Anal. Chem **32**, 985 (1960); W. A. HENDERSON, JR. and C. A. STREULI. J. Am. Chem. Soc. **82**, 5791 (1960).
22. S. O. GRIM and A. W. YANKOWSKY. J. Org. Chem. **42**, 1236 (1977).
23. J. E. HUHEEY. J. Phys. Chem. **69**, 3284 (1965).
24. M. R. CHURCHILL and T. A. O'BRIEN. J. Chem. Soc. A, 2970 (1968).
25. A. SHIOTANI, H.-F. KLEIN, and H. SCHMIDBAUR. J. Am. Chem. Soc. **93**, 1555 (1971).
26. C. A. TOLMAN, W. C. SEIDEL, and L. W. GOSSER. J. Am. Chem. Soc. **96**, 53 (1974).
27. S. O. GRIM, E. D. WALTON, and L. C. SATEK. Inorg. Chim. Acta, **27**, L115 (1978) and references therein.

Triphenylphosphine complexes of mercury(II) acetate and fluoroacetates. Preparation, characterization, and spectral studies[1]

TIM ALLMAN, RAM G. GOEL, AND PIERRE PILON

Guelph–Waterloo Centre for Graduate Work in Chemistry, University of Guelph, Guelph, Ont., Canada N1G 2W1

Received April 3, 1978

TIM ALLMAN, RAM G. GOEL, and PIERRE PILON. Can. J. Chem. **57**, 91 (1979).

Triphenylphosphine reacts with mercury(II) acetate and fluoroacetates to form complexes of the types $Ph_3PHg(O_2CR)_2$, $(Ph_3P)_2Hg(O_2CR)_2$, and $(Ph_3P)_3Hg(O_2CR)_2$, where R = CH_3, CH_2F, CHF_2, or CF_3. The 1:1 and 2:1 have been isolated and characterized by elemental analysis, molecular weight, and conductance measurements and by vibrational and nmr spectroscopic studies. The formation of the 3:1 complexes is inferred by ^{31}P nmr spectral measurements at 183 K. Both the 1:1 and 2:1 complexes are indicated to be monomeric molecular species in which the O_2CR groups are bidentately bonded to mercury. The Hg—O and Hg—P stretching frequencies for these complexes have been assigned by infrared and Raman spectral measurements. The ^{199}Hg–^{31}P spin–spin coupling constants and the ^{31}P coordination chemical shifts for the 1:1 as well as the 2:1 complexes increase in the order: $O_2CCH_3 < O_2CCH_2F < O_2CCHF_2 < OCCF_3$. Correlations between $^1J(^{199}Hg$–$^{31}P)$ values, ^{31}P coordination chemical shifts, and the pK_a values for the carboxylic acids are discussed.

TIM ALLMAN, RAM G. GOEL et PIERRE PILON. Can. J. Chem. **57**, 91 (1979).

La triphénylphosphine réagit avec l'acétate et les fluoroacétates mercuriques pour former des complexes de type $Ph_3PHg(O_2CR)_2$, $(Ph_3P)_2Hg(O_2CR)_2$ et $(Ph_3P)_3Hg(O_2CR)_2$ où R = CH_3, CH_2F, CHF_2 et CF_3. On a isolé les adduits 1:1 et 2:1 et on les a caractérisés grâce à leur analyse élémentaire, à leur poids moléculaire, à des mesures de conductivité et à des études de spectroscopies vibrationnelles et rmn. On a déduit que des complexes 3:1 se forment en se basant sur des mesures spectrales de rmn ^{31}P effectuées à 183 K. Il semble que les complexes 1:1 et 2:1 sont des espèces moléculaires monomères dans lesquelles les groupes O_2CR sont doublement lié au mercure. On a attribué les fréquences de vibration de valence Hg—O et Hg de ces complexes grâces à des mesures spectrales infrarouges et Raman. Les constantes de couplage spin–spin ^{199}Hg–^{31}P de même que les déplacements chimiques de coordination ^{31}P des complexes 1:1 et 2:1 augmentent dans l'ordre: $O_2CCH_3 < O_2CCH_2F < O_2CCHF_2 < OCCF_3$. On discute des corrélations entre les valeurs des $^1J(^{199}Hg$–$^{31}P)$, des déplacements chimiques de coordination ^{31}P et des valeurs des pK_a des acides carboxyliques.

[Traduit par le journal]

Introduction

Due to their electrophilic nature, mercury(II) carboxylates, particularly, the acetate and trifluoroacetate are important reagents for mercuration and oxomercuration reactions (1). However, the reactions of these active electrophiles with electron-pair donor ligands have received little attention.

In a recent investigation (2–5) on the tri-*tert*-butylphosphine complexes of zinc(II), cadmium(II), and mercury(II), the complex $Bu^t_3PHg(O_2CCH_3)_2$ (2, 4) was prepared. In contrast to the mercury(II) halide complexes, $Bu^t_3PHgX_2$ (2, 5), which have a dimeric tetrahedral structure, the acetate complex $Bu^t_3PHg(O_2CCH_3)_2$, has a monomeric pentacoordinate structure in the solid state as well as in solution (4). Crystal structure determination (4) showed that the acetate groups in $Bu^t_3PHg(O_2CCH_3)_2$ are bonded to the mercury in an asymmetrically bidentate manner giving rise to a distorted trigonal bipyramidal coordination around mercury. One oxygen atom of each CH_3CO_2 group is tightly bound in the equatorial plane of the mercury atom and the other oxygens form weak bonds above and below this plane. The only other reported phosphine complex of a mercury(II) carboxylate is $(Me_3P)_2Hg(O_2CCH_3)_2$ (6*a*) which has been assigned an ionic structure containing the linear $(Me_3P)_2Hg^{2+}$ cation and ionic acetates. In the present work, reactions of triphenylphosphine with mercury(II) acetate and haloacetates have been investigated. The preparation, characterization, and vibrational and magnetic resonance spectroscopic studies of the complexes prepared in this work are reported herein. Concurrent with this work, Alyea and Dias (6*b*) have investigated mercury acetate complexes of several other tertiary phosphines.

[1]Presented in part at the 2nd Joint Chemical Institute of Canada–American Chemical Society conference, Montreal, May 29–June 2, 1977.

0008-4042/79/010091-07$01.00/0

TABLE 1. Analytical, molecular weight, and conductance data

Compound	Melting point (°C)	%C		%H		Mol. wt.[a]		Molar conductance[c]
		Calcd.	Found	Calcd.	Found	Calcd.	Found	
$Ph_3PHg(O_2CCH_3)_2$	185[d]	45.47	45.45	3.62	3.67	580	614[b]	0.84
$Ph_3PHg(O_2CCH_2F)_2$	166[d]	42.82	42.68	3.08	2.83	616	650	0.95
$Ph_3PHg(O_2CCHF_2)_2$	151[d]	40.45	40.24	2.60	2.42	652	666	2.61
$Ph_3PHg(O_2CCF_3)_2$	169	38.34	38.61	2.18	2.24	688	711	5.99
$(Ph_3P)_2Hg(O_2CCH_3)_2$	190[d]	56.97	56.79	4.27	4.27	842	833[b]	5.86
$(Ph_3P)_2Hg(O_2CCH_2F)_2$	189[d]	54.63	54.83	3.87	3.64	878	862	10.96
$(Ph_3P)_2Hg(O_2CCHF_2)_2$	198[d]	52.48	52.25	3.50	3.36	914	932	12.76
$(Ph_3P)_2Hg(O_2CCF_3)_2$	221[d]	50.49	50.37	3.16	3.12	950	874	19.42

[a]In 1,2-dichloroethane at $\sim 10^{-2}$ M concentration.
[b]In chloroform at $\sim 10^{-2}$ M concentration.
[c]In ohm^{-1} cm^2 mol^{-1} at 25°C for 10^{-3} M solutions in nitromethane.
[d]Compound decomposed upon melting.

Results and Discussion

Triphenylphosphine reacts with mercury acetate and fluoroacetates to form 1:1, 2:1, and 3:1 complexes. However, the 3:1 complexes could not be isolated. Attempts to isolate complexes of mercury(II) chloroacetates were also unsuccessful due to the decomposition of mercury(II) chloroacetates. For example, the reaction of triphenylphosphine with mercury(II) trichloroacetate in 1:1 or 2:1 mole ratios afforded the complexes Ph_3PHgCl_2 or $(Ph_3P)_2HgCl_2$ as the sole mercury(II)-containing species.

The analytical, molecular weight, and conductance data for the complexes isolated in the present study are given in Table 1. All the compounds listed in Table 1 are air-stable, white crystalline solids. They are soluble in polar organic solvents, sparingly soluble in benzene, and insoluble in hexane or light petroleum ether. All the compounds decomposed on or near melting. The results of molecular weight measurements (Table 1) show that all the complexes exist as monomeric molecular species in 10^{-2} M solutions in 1,2-dichloroethane or chloroform.

The molecular weight measurements on 1,2-dichloroethane solutions of $(Ph_3P)_2Hg(O_2CCH_3)_2$, in the 10^{-2}–10^{-3} M concentration range, gave values in the 600 to 500 range indicating some dissociation of the complex according to the following equation:

$$(Ph_3P)_2Hg(O_2CCH_3)_2 \rightleftharpoons Ph_3PHg(O_2CCH_3)_2 + PPh_3$$

Molecular weight measurements for other complexes in this concentration range, however, showed no evidence for such a dissociation. Molar conductances for 10^{-3} M solutions of the complexes in dichloromethane were found to be less than 0.5 ohm^{-1} cm^2 mol^{-1}. Conductance measurements in nitromethane, however, show that the 2:1 complexes of mercury(II) fluoroacetates are ionized to the extent of 10 to 20%.

Vibrational Spectral Studies

The CO_2 stretching frequencies for both 1:1 and 2:1 complexes were assigned by comparing their infrared spectra with those of uncomplexed mercury(II) carboxylates and free triphenylphosphine. The observed CO_2 stretching frequencies for the complexes in the solid state as well as in dichloromethane are listed in Table 2. The data in Table 2 show that the CO_2 stretching frequencies in the solid state are not very different than those observed in solution. Therefore, the structures of the complexes do not appear to change in going from solid state to solution. The occurrence of more than one band in the region of antisymmetric CO_2 stretching frequency can be caused by coupling of vibrations of the two carboxylate groups. In view of the molecular nature of the complexes in solution, the possibility of ionic or carboxylate bridged polymeric structures can be ruled out. The antisymmetric CO_2 stretching frequency for a monodentately bonded carboxylate ligand (7–10) is significantly higher than the frequency for the free ion (7, 11, 12). Since the antisymmetric CO_2 stretching frequencies for the complexes listed in Table 2 are lower than those observed for monodentately bonded carboxylates (7–10), the carboxylate groups in all the complexes appear to act as chelating bidentate ligands. Two oxygen atoms of a chelating bidentate carboxylate ligand may be coordinated to a metal atom either symmetrically or unsymmetrically (9). Although it is difficult to distinguish between the symmetrically and asymmetrically bonded carboxylate groups by infrared spectroscopy, it is noteworthy that the CO_2 stretching frequency for the 2:1 complex $(Ph_3P)_2Hg(O_2CCH_3)_2$ are very similar to these observed for $Bu^t{}_3PHg(O_2CCH_3)_2$ which is known to contain asymmetrically bonded bidentate acetates (4). For the 1:1 complex, $Ph_3PHg(O_2CCH_3)_2$, the symmetric CO_2 stretching frequency is not significantly altered but

TABLE 2. Infrared and Raman spectral data[a]

Compound	νCO_2 (ir) Solid	νCO_2 (ir) Solution	νCO_2 (ir) Solid	νCO_2 (ir) Solution	$\Delta\nu$ (solution)	νHg—O (ir) (solid)	νHg—P (R) (solid)
$(Ph_3P)Hg(O_2CCH_3)_2$	1595sh, 1585s	1580s	1375ms	1379s	201	266ms	150s
$(Ph_3P)Hg(O_2CCH_2F)_2$	1620s	1620s	1383ms	1390ms	230	223m	154s
$(Ph_3P)Hg(O_2CCHF_2)_2$	1656s	1660s	1421m	1420m	240	182s	156s
$(Ph_3P)Hg(O_2CCF_3)_2$	1690s, 1665ms, 1650s	1675s	1405ms	1410m	265	178s	166s
$(Ph_3P)_2Hg(O_2CCH_3)_2$	1575sh, 1560s	1565s	1380ms	1382ms	183	223ms	135s
$(Ph_3P)_2Hg(O_2CCH_2F)_2$	1590s, 1605s	1600s	1400m	1400m	200	168s	140s
$(Ph_3P)_2Hg(O_2CCHF_2)_2$	1640s	1640s	1423m	1420m	220	162s	142s
$(Ph_3P)_2Hg(O_2CCF_3)_2$	1672s	1662s	1412m	1415m	247	158s	146s

[a]In cm^{-1}. Abbreviations: ir, infrared; R, Raman; v, stretching frequency; m, medium; s, strong; sh, shoulder.

the antisymmetric stretching frequency is increased by 15 cm^{-1}. Similar differences in the CO_2 stretching frequencies are observed between 1:1 and 2:1 complexes of fluoroacetates. These differences can arise due to the weakening of the Hg—O bonds in the 2:1 complexes. Thus, the 1:1 complexes can be assigned a five-coordinate structure and the 2:1 complexes can be assigned a six-coordinate structure.

The assignments for the Hg—O stretching frequencies for the complexes, in the solid state, can be made by comparing their infrared spectra with those of the mercury(II) carboxylates and free phosphine. For example, the infrared spectrum of mercury(II) acetate shows a strong band at 309 cm^{-1} due to the antisymmetric Hg—O stretching frequency[2] (13). This band is not present in the infrared spectrum of either $Ph_3PHg(O_2CCH_3)_2$ or $(Ph_3P)_2Hg(O_2CCH_3)_2$. For $Ph_3PHg(O_2CCH_3)_2$, a strong infrared band is observed at 267 cm^{-1} which can be assigned to a Hg—O stretching frequency since no band is observed in this region in the spectrum of triphenylphosphine (14). The Hg—O stretching frequencies for other complexes were assigned in a similar manner and the assigned frequencies are listed in Table 2. By comparing the Raman spectra of the solid complexes with those for the mercury(II) carboxylates and triphenylphosphine, the Hg—P stretching frequencies for the complexes can be assigned with reasonable confidence. The assigned values are listed in Table 2. The Hg—P stretching frequencies for a number of phosphine complexes of mercury(II) halides and pseudohalides have been determined (5) in this laboratory.[3] The values for the Hg—P stretching frequencies given in Table 2 are in complete accord with the Hg—P stretching frequencies for the mercury(II) halide and pseudohalide complexes of triphenylphosphine.[3]

Two trends are evident from the data on Hg—O and Hg—P stretching frequencies. First, in each series of complexes, the Hg—O stretching frequency decreases and the Hg—P stretching frequency increases as the electron withdrawing power of the carboxylate groups increases ($CH_3CO_2 < CH_2FCO_2 < CHF_2CO_2 < CF_3CO_2$). Second, for a given carboxylate, the Hg—O and the Hg—P stretching frequencies are higher for the 1:1 complex. The first observation is in accord with the fact that the more electron withdrawing carboxylate groups will give rise to weaker Hg—O bonds and will create a larger electron deficiency at the mercury which in turn will result in the strengthening of the Hg—P bond. The second trend is also consistent with the electroneutrality principle. The addition of another phosphine to the 1:1 complex will increase the electron density at the mercury atom making it a weaker Lewis acid.

Nuclear Magnetic Resonance Spectral Studies

The ^1H nmr spectra for the 1:1 as well as the 2:1 complexes, at ambient temperatures, showed a multiplet due to the phenyl protons and a singlet due to the acetyl or fluoroacetyl protons. The phenyl multiplet was shifted downfield from the multiplet observed for free triphenylphosphine.

The ^{31}P nmr spectral data for all the complexes studied in this work are listed in Table 3. As can be

[2]The vibrational spectra of mercury(II) acetate have been interpreted in terms of a centrosymmetric linear structure of C_{2h} skeletal symmetry (13).

[3]R. G. Goel and P. Pilon. Unpublished results.

TABLE 3. ^{31}P nmr spectral data[a]

Compound	J(Hg–P) (Hz)		δ (ppm)	
	183 K	Ambient temperature	183 K	Ambient temperature
$Ph_3PHg(O_2CCH_3)_2$	8852	—	27.7	30.2
$Ph_3PHg(O_2CCH_2F)_2$	9042	8793	29.1	31.1
$Ph_3PHg(O_2CCHF_2)_2$	9120	8944	30.1	31.3
$Ph_3PHg(O_2CCF_3)_2$	9150	9111	30.5	31.7
$(Ph_3P)_2Hg(O_2CCH_3)_2$	5472	—	33.5	29.4
$(Ph_3P)_2Hg(O_2CCH_2F)_2$	5794	—	35.6	33.7
$(Ph_3P)_2Hg(O_2CCHF_2)_2$	5909	5717	36.4	35.5
$(Ph_3P)_2Hg(O_2CCF_3)_2$	5970	5834	37.1	36.9
$(Ph_3P)_3Hg(O_2CCH_3)_2$	3249		31.2	
$(Ph_3P)_3Hg(O_2CCH_2F)_2$	3290		32.6	
$(Ph_3P)_3Hg(O_2CCHF_2)_2$	3300		33.6	
$(Ph_3P)_3Hg(O_2CCF_3)_2$	3305		34.5	
Ph_3P			−9.1	−5.6

[a]In dichloromethane at 183 K and an ambient temperatures, the positive δ values are downfield from external H_3PO_4 standard.

seen from the data in Table 3, the ^{31}P nmr spectra of $Ph_3PHg(O_2CCH_3)_2$, $(Ph_3P)_2Hg(O_2CCH_3)_2$, and $(Ph_3P)_2Hg(O_2CCH_2F)_2$, at ambient temperatures, consist of a single peak. The spectra of the remaining complexes showed a triplet consisting of a main peak and two satellite peaks due to ^{199}Hg—^{31}P spin–spin coupling.[4] These results show that the complexes $Ph_3PHg(O_2CCH_3)_2$, $(Ph_3P)_2Hg(O_2CCH_3)_2$, and $(Ph_3P)_2Hg(O_2CCH_2F)_2$, like the triphenylphosphine complexes of mercury(II) halides and pseudohalides, undergo a fast phosphine exchange at room temperature whereas the remaining complexes are non-labile on the nmr time scale. Satellites due to the ^{199}Hg—^{31}P spin–spin coupling were observed for all the complexes when the ^{31}P nmr spectra were measured at 183 K.

The data in Table 3 show that the $^1J(^{199}Hg–^{31}P)$ values at 183 K are higher than the values at ambient temperatures. The ^{199}Hg—^{31}P spin–spin coupling for the phosphine complexes of mercury(II) halides is also reported to increase with decreasing temperatures (15). The increase has been attributed to a decrease in the rate of phosphine exchange. However, we believe that further investigations are required to explain this phenomenon.

As shown by the data in Table 3, the $^1J(^{199}Hg–^{31}P)$ values for the 1:1 complexes are about 50% higher than those for the 2:1 complexes. Similar differences in the magnitudes of ^{199}Hg—^{31}P spin–spin coupling constants are observed between the 1:1 and 2:1 phosphine complexes of mercury(II) halides (16–18).

[4]Mercury has two isotopes, ^{199}Hg and ^{201}Hg, which have nuclear spins. ^{199}Hg has a spin of 1/2 and is present in 16.86% natural abundance, ^{201}Hg has a spin of 3/2 and is present in 13.24% natural abundance.

^{31}P nmr spectral data (17, 18) for mercury(II) halide complexes also show that both the $^1J(^{199}Hg–^{31}P)$ values and the coordination chemical shifts, Δδ (Δδ = δ (complex) − δ (free phosphine)), for the 1:1 complexes (which are dimeric) as well as for the 2:1 complexes (which are monomeric) increase with the electronegativity of the halogen. As shown in Fig. 1, the plots of $^1J(^{199}Hg–^{31}P)$ values for both 1:1 and 2:1 complexes against the pK_a values of the parent carboxylic acids give straight lines. The plots of $^1J(^{199}Hg–^{31}P)$ values against the coordination chemical shifts, Δδ (shown in Fig. 2), also give straight lines. The observed variations in the $^1J(^{199}Hg–^{31}P)$ values in each series of complexes, thus, clearly show that the magnitude of the ^{199}Hg—^{31}P spin–spin interaction is determined by the electron deficiency of mercury in the given mercury(II) carboxylate. Similarly, the magnitude of the coordination chemical shift in these complexes also appears to be determined by the electron withdrawing power of the carboxylate ligands. However, a comparison of the chemical shifts of the fluoroacetate complexes shows that for a given fluoroacetate the chemical shifts for the 2:1 complexes is higher than that for the 1:1 complex. Furthermore, the chemical shifts for the 3:1 complexes, $(Ph_3P)_3Hg(O_2CCH_2F)_2$, $(Ph_3P)_3Hg(O_3CCHF_2)_2$, and $(Ph_3P)_3Hg(O_2CCF_3)_2$, are significantly different whereas the $^1J(^{199}Hg–^{31}P)$ values for the three complexes are very similar (*vide infra*). Therefore, the correlations between coupling constants and coordination chemical shifts observed in the present work as well as in previous studies cannot be very meaningful.

In contrast to the mercury(II) halide complexes which contain four-coordinate mercury(II), the

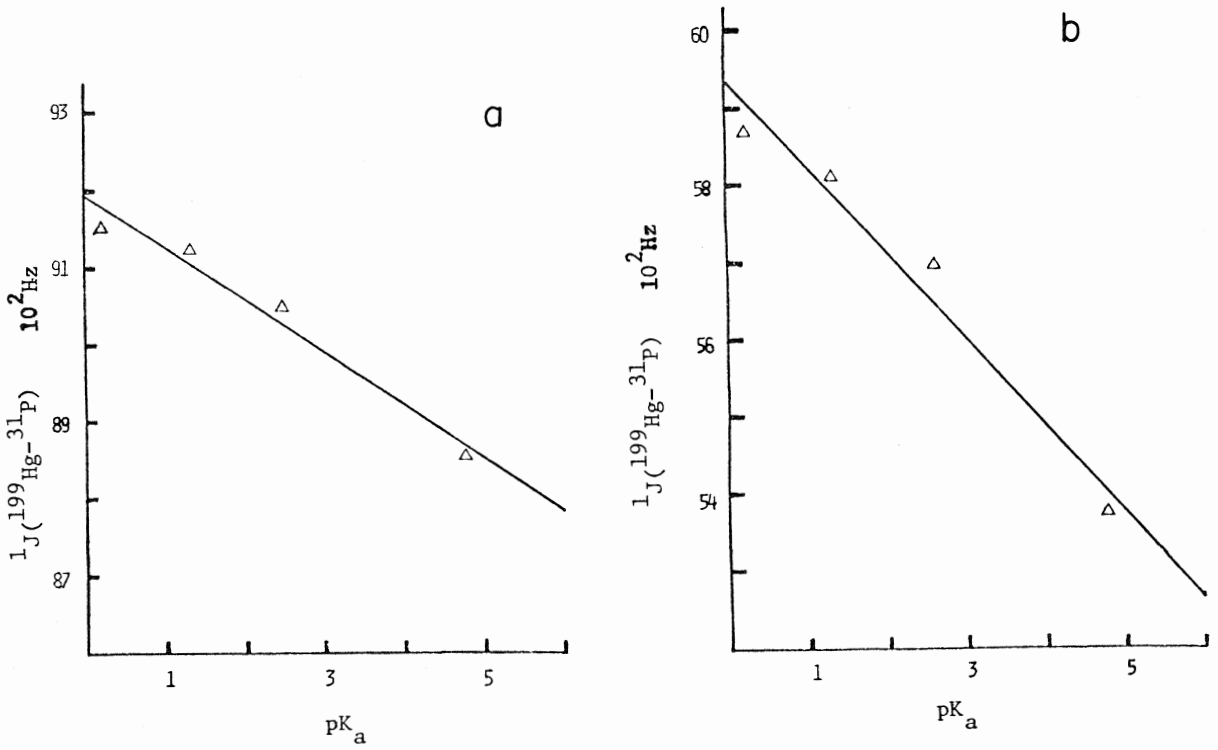

FIG. 1. Plot of $^1J(^{199}Hg–^{31}P)$ values of (*a*) 1:1 and (*b*) 1:2 complexes against the parent carboxylic acids.

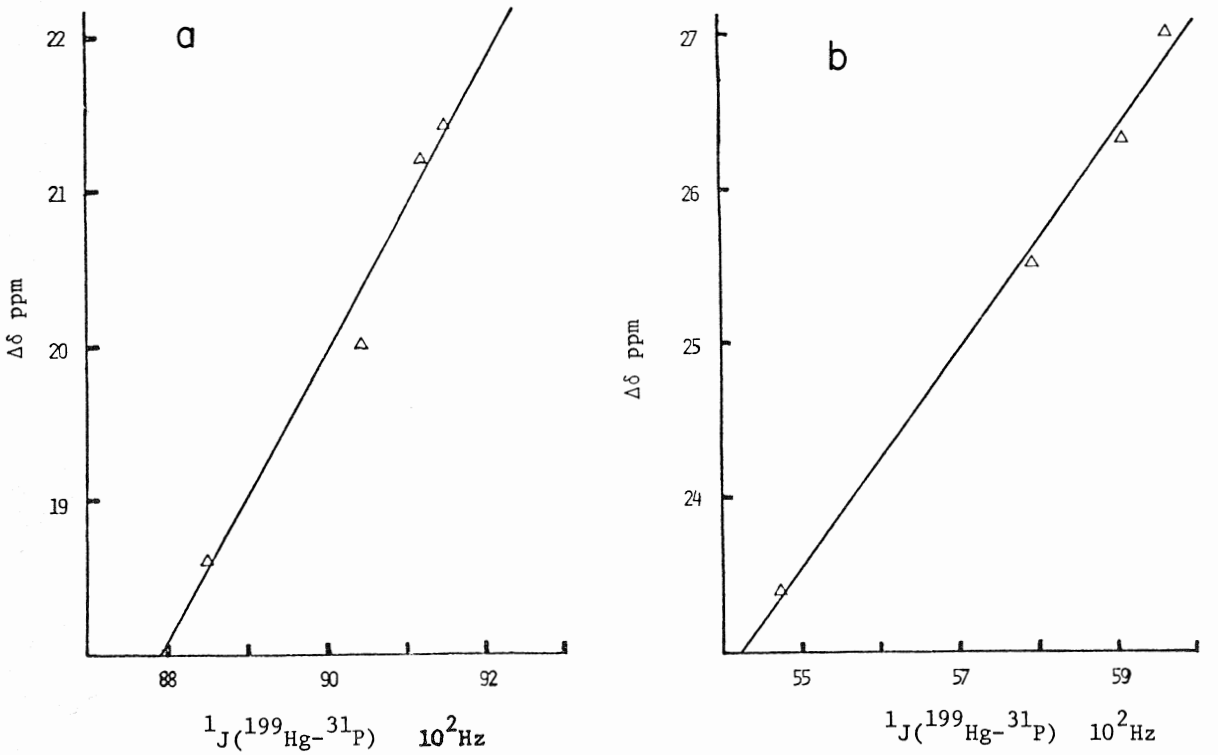

FIG. 2. Plot of $^1J(^{199}Hg–^{31}P)$ values of (*a*) 1:1 and (*b*) 1:2 complexes against the coordination chemical shifts, Δδ.

carboxylate complexes most likely contain five- and six-coordinate mercury. However, the $^1J(^{199}Hg–^{31}P)$ values for both types of carboxylate complexes are larger than those for the corresponding halide complexes. This is in accord with the stronger electrophilic character of mercury(II) carboxylates as compared with mercury(II) halides.

^{31}P nmr spectra of dichloromethane solutions of 2:1 complex containing excess triphenylphosphine, at ambient temperatures, consisted of a single broad line. However, the ^{31}P nmr spectra of these solutions, at 183 K, showed a triplet due to the 2:1 complex, a singlet due to free phosphine, and another triplet due to the formation of a new complex. For the given carboxylate, the chemical shifts and the $^{199}Hg–^{31}P$ coupling constants due to the new complex were invariant when the phosphine:mercury mole ratio was varied from 3 to 12. From the integration of the peaks it was established that the new complex contains three moles of phosphine per mole of mercury. No ^{31}P nmr evidence was found for the presence of any other phosphine containing species in solution. The $^1J(^{199}Hg–^{31}P)$ values and chemical shifts for the 3:1 complexes are listed in Table 3. The data in Table 3 show the $^1J(^{199}Hg–^{31}P)$ values for the 3:1 complexes $(Ph_3P)_3Hg(O_2CCH_2F)_2$, $(Ph_3P)_3Hg(O_2CCHF_2)_2$, and $(Ph_3P)_3Hg(O_2CCF_3)_2$ are invariant whereas the complex $(Ph_3P)_3Hg(O_2CCH_3)_2$ has a slightly smaller $^1J(^{199}Hg–^{31}P)$ value. We, therefore, conclude that the complexes $(Ph_3P)_3Hg(O_2CCH_2F)_2$, $(Ph_3P)_3Hg(O_2CCHF_2)_2$, and $(Ph_3P)_3Hg(O_2CCF_3)_2$ contain the three-coordinate cation, $(Ph_3P)_3Hg^{2+}$, whereas the complex $(Ph_3P)_3Hg(O_2CCH_3)_2$ is a penta-coordinated species in which the acetate anions are very weakly coordinated to the three coordinate $(Ph_3P)_3Hg^{2+}$ moiety.

The formation constants, K, for the 3:1 complexes were calculated by ^{31}P nmr measurements in dichloromethane and calculated values are listed in Table 4. The observed variations in the values of the formation constants for the 3:1 complexes are in accord with the variations in the electron withdrawing power of the carboxylate ligands. The failure to isolate these complexes is not surprising in view of the low values of their formation constants. The instability of the 3:1 complexes is most likely due to the relatively low basicity of triphenylphosphine (19). Work on the mercury(II) carboxylate complexes of more basic phosphines is in progress in our laboratory.

TABLE 4. Formation constants (K†) for the $(Ph_3P)_3Hg(O_2CCR)_2$ complexes at 183 K[a]

Complex	K†
$(Ph_3P)_3Hg(O_2CCH_3)_2$	1.66
$(Ph_3P)_3Hg(O_2CCH_2F)_2$	5.20
$(Ph_3P)_3Hg(O_2CCHF_2)_2$	22.70
$(Ph_3P)_3Hg(O_2CCF_3)_2$	1630

[a] K† = $[(Ph_3P)_3Hg(O_2CCR)_2]/[(Ph_3P)_2Hg(O_2CCR)_2][Ph_3P]$. Values calculated by using concentrations in mol/L. Estimated error in integration of the nmr signals is about 10%. At least five independent measurements were made to determine each K value.

Experimental

Materials

Triphenylphosphine (Eastman Kodak) was recrystallized twice from hot ethanol. Mercury(II) chloroacetates and fluoroacetates were prepared by the reaction of appropriate haloacetic acid with reagent grade mercury(II) oxide following the procedure of Deacon and Taylor (20). Reagent grade mercury(II) acetate was used without further purification. All the solvents were dried following standard procedure.

Physical Measurements

Elemental analyses were performed by M.H.W. Laboratories, Garden City, Michigan. Melting points were determined with a Gallenkamp melting point apparatus using open capillary tubes and are uncorrected. Molecular weights in 1,2-dichloromethane were determined with a Hitachi-Perkin-Elmer 115 osmometer. Molecular weights measurements in chloroform were performed at Galbraith Laboratories, Knoxville, TN. Conductance measurements were made at 25°C using a Yellow Springs Conductivity bridge and a conductivity cell with platinized platinum electrodes. Infrared spectra were recorded in the region 4000 to 300 cm^{-1} using a Beckman IR-12 spectrophotometer and in the region 400 to 150 cm^{-1} using a Perkin-Elmer 180 spectrophotometer. Spectra, in the solid state, were measured on mulls in Nujol and Halocarbon oil using KRS-5 or polythene discs. Sealed NaCl cells of 0.1 mm path length were used to record the spectra in solution. Raman spectra, in the solid state, were measured with a Jarrell-Ash spectrophotometer using the 5145 Å exciting line of an argon ion laser. The samples were sealed in glass capillary tubes. Attempts to obtain the Raman spectra, in solution, were not successful. The infrared and Raman frequencies are accurate to ± 3 cm^{-1}. ^{31}P nmr spectra were obtained on a Bruker HFX-60 Fourier transform spectrometer. ^1H nmr spectra were recorded with a Varian A60 spectrometer.

Preparation of 1:1 and 2:1 Complexes of Mercury(II) Acetate and Fluoroacetates

Mercury(II) acetate or fluoroacetate (2 mmol) and triphenylphosphine (2 mmol or 4 mmol) were dissolved separately in dry ethanol. The solution of triphenylphosphine was added dropwise, with stirring, to the solution of mercury(II) salt to give a clear solution. The solvent was removed with a rotary evaporator to give the desired product in quantitative yield. The product was dissolved in a minimum volume of dichloromethane and the solution was made cloudy by adding light petroleum ether dropwise. Upon cooling, white crystals were obtained which were filtered off and dried *in vacuo*.

Attempted Preparation of $(Ph_3P)_3Hg(O_2CCF_3)_2$

(*a*) Equimolar amounts of $(Ph_3P)_2Hg(O_2CCF_3)_2$ and triphenylphosphine were dissolved in dichloromethane. After stirring the solution for 1 h, the solvent was removed *in vacuo* at −78°C to give a white solid. The infrared spectrum of the solid in the CO_2 stretching frequency region was similar to that of $(Ph_3P)_2Hg(O_2CCF_3)_2$. Upon washing the solid with light petroleum ether it was readily separated into $(Ph_3P)_2Hg(O_2CCF_3)_2$ and Ph_3P.

(*b*) A dichloromethane solution containing equimolar amounts of 2:1 complex and triphenylphosphine was stirred for 1 h and then cooled to −95°C. Cold hexane (−95°C) was added dropwise, with stirring, to the cold solution (−95°C) to give a white precipitate which was allowed to stand for 1 h at −95°C and then filtered off. It was characterized to be $(Ph_3P)_2Hg(O_2CCF_3)_2$. Unreacted triphenylphosphine was recovered from the filtrate.

Attempted Preparation of Complexes of Mercury(II) Trichloroacetate

No reaction occurred when a suspension of mercury(II) trichloroacetate (1 mmol) in 50 ml ethanol was mixed with an ethanol solution of triphenylphosphine (2 mmol). Upon refluxing the mixture a clear solution was formed. White crystals of $(Ph_3P)_2HgCl_2$ were recovered in 90% yield upon cooling the solution. A similar reaction of $Hg(O_2CCCl_3)_2$ and Ph_3P in equimolar ratio afforded Ph_3PHgCl_2 in almost quantitative yield.

Acknowledgements

Thanks are due to the National Research Council of Canada for an operating grant (to R.G.G.), and to Dr. E. C. Alyea for a preprint of his paper on mercury(II) acetate complexes of other phosphines.

1. F. A. Cotton and G. Wilkinson. Advanced inorganic chemistry. 3rd ed. Interscience, New York. 1972. pp. 518 and 525 and references therein.
2. W. O. Ogini. M.Sc. Thesis. University of Guelph, Guelph, Ont. 1976.
3. R. G. Goel and W. O. Ogini. Inorg. Chem. **16**, 1968 (1977).
4. P. J. Roberts, G. Ferguson, R. G. Goel, W. O. Ogini, and R. J. Restivo. J. Chem. Soc. Dalton, 253 (1978).
5. E. C. Alyea, S. A. Dias, R. G. Goel, and W. O. Ogini. Can. J. Chem. **55**, 4227 (1977).
6. (*a*) H. Schmidbaur and K. H. Rathlein. Chem. Ber. **106**, 2491 (1973); (*b*) E. C. Alyea and S. A. Dias. Can. J. Chem. This issue.
7. K. Nakamoto. Infrared spectra of inorganic and coordination compounds. 2nd ed. Wiley Interscience, New York. 1970. p. 223.
8. R. G. Goel and D. R. Ridley. J. Organomet. Chem. **38**, 83 (1972).
9. N. W. Alcock, V. M. Tracy, and T. C. Waddington. J. Chem. Soc. Dalton, 2243 (1976), and references therein.
10. J. Catterick and P. Thornton. Adv. Inorg. Chem. Radiochem. **20**, 291 (1977), and references therein.
11. E. Spinner. J. Chem. Soc. 4217 (1964).
12. Sadtler Spectra Collection, Spectrum No. 14892.
13. R. P. J. Cooney and J. R. Hall. J. Inorg. Nucl. Chem. **34**, 1519 (1972).
14. K. Shobatake, C. Postmus, J. R. Ferraro, and K. Nakamoto. Appl. Spectrosc. **23**, 12 (1969).
15. S. O. Grim and D. P. Shah. Inorg. Nucl. Chem. Lett. **14**, 105 (1978).
16. A. Yamasaki and E. Fluck. Z. Anorg. Allg. Chem. **306**, 297 (1973).
17. S. O. Grim, P. J. Lui, and R. L. Keiter. Inorg. Chem. **13**, 342 (1974).
18. E. C. Alyea, S. A. Dias, R. G. Goel, W. O. Ogini, P. Pilon, and D. W. Meek. Inorg. Chem. **17**, 1697 (1978).
19. (*a*) C. A. Streuli. Anal. Chem. **32**, 985 (1960); (*b*) W. A. Henderson, Jr. and C. A. Streuli. J. Am. Chem. Soc. **82**, 5791 (1960).
20. G. B. Deacon and F. B. Taylor. Aust. J. Chem. **21**, 2675 (1968).

The dependence of ionization and excitation energies for the *cis*-azo group upon bond angle

N. Colin Baird

Department of Chemistry, University of Western Ontario, London, Ont., Canada N6A 5B7

Received June 14, 1978

N. Colin Baird. Can. J. Chem. **57**, 98 (1979).

Ab initio molecular orbital calculations using STO-3G and 4-31G basis sets have been performed for *cis*-HNNH and *cis*-CH_3NNCH_3 as a function of angle about the nitrogens, and for the cyclic molecules diazirine (**1***a*) and diazetine (**1***b*); in all cases the ground states of the neutral system and of the cation and anion and the first singlet excited state of the neutral molecule were studied. The optimum HNN angles for the cation and neutral excited $n_-\pi^*$ singlet state of HNNH are significantly larger than for the anion and neutral ground state. Thus the ionization energy and singlet excitation energies for *cis*-azo systems pass through a maximum in the region around a nitrogen angle of about 100°. The implications of these calculations to the excitation and photoelectron spectra of cyclic *cis*-azo compounds is discussed in some detail, as is the origin of the variation in stability with angle of the n_- molecular orbital. Due to the heavy involvement of carbon, the n_- MO in diazirine does not follow the angle trends established by the HNNH calculations.

N. Colin Baird. Can. J. Chem. **57**, 98 (1979).

On a effectué des calculs *ab initio* d'orbitales moléculaires faisant appel à des bases STO-3G et 4-31G pour le *cis*-HNNH et le *cis*-CH_3NNCH_3 en fonction de l'angle autour des azotes ainsi que pour des molécules cycliques comme la diazirine (**1***a*) et la diazétine (**1***b*); dans chacun des cas, on a étudié les états fondamentaux du système neutre, du cation et de l'anion ainsi que le premier état excité singulet de la molécule neutre. Les angles optimum HNN du cation et de l'état excité $n_-\pi^*$ singulet et neutre du HNNH sont beaucoup plus élevés que ceux de l'anion et de l'état fondamental neutre. Ainsi l'énergie d'ionisation et les énergies de l'excitation singulet des systèmes azo *cis* passent par un maximum pour un angle de l'azote d'environ 100°. On discute en détail des implications de ces calculs en relation avec les spectres photoélectroniques et d'excitation des composés azo *cis* de même que des origines de la variation de stabilité avec l'angle de l'orbitale moléculaire n_-. A cause de la forte implication du carbone, la OM n_- de la diazirine ne suit pas les tendances d'angle déterminé par les calculs du HNNH.

[Traduit par le journal]

Introduction

We have proposed that the substantial variations in the position of the uv–visible absorption maximum for the *cis*-azo chromophore are due primarily to changes in the CNN angle, since this angle determines the stability of n_-, the "lone pair" MO from which the lowest-energy excitation occurs (1). Recently Turro and co-workers have questioned this correlation since they claim ". . . there is no clear relationship of the absorption maxima of three-, four-, and five-membered ring compounds . . . with either the bond angle, the n_+–n_- orbital energy splitting, or the lowest ionization potential . . .", but rather agree with the conclusion (of Houk, Chang, and Engel (2)) that ". . . the wavelength of the n,π* absorption maximum is controlled more by factors which influence the energy of the π* orbital rather than the n_- orbital" (3). To attempt to resolve this controversy, we have undertaken to extend our calculations on *cis* —N=N— systems to angles less than 105° (the lower limit in our initial communication) and to improve the quality of the wavefunctions, as well as to study explicitly the positive and negative ions of such molecules and to investigate the relationships between excitation energy and ionization energy.

Method of Calculation

All calculations reported herein were generated using "*ab initio*" molecular orbital theory. The energies and wavefunctions for the open-shell species (i.e. the cations, the anions, and the $n_-\pi^*$ triplet state of the neutral molecules) were determined by the restricted open-shell theory of Roothaan (4). The MO's for the $^1(n_-\pi^*)$ state of HNNH and derivatives were taken as those determined for the $^3(n_-\pi^*)$ state; in this approximation the energy of the former exceeds that of the latter by twice $K_{n_-\pi^*}$, the exchange integral between the two orbitals. For the ground state of the neutral molecules, the Roothaan closed-shell method was used to determine the optimum single-determinant orbitals for the $...n_+^2\pi^2n_-^2(\pi^*)^0$ configuration. The energy of the ground state was then calculated by allowing this configuration to interact with the doubly-excited $...n_+^2\pi^2n_-^0(\pi^*)^2$ configuration. (The interaction between configurations increases with HNN angle, and peaks at 180°

0008-4042/79/010098-06$01.00/0

at which point the configurations are degenerate before interaction.) This extent of CI yields the correct degeneracy at 180° between the lowest two singlet states (if identical MO's are employed for both states).

The atomic orbital basis sets used in the calculations were the STO-3G and the 4-31G expansions (with standard molecular exponents) of Pople and co-workers (5). A few calculations were done with a basis in which six 1*s* "polarization functions" of exponent 0.5 and centred in the molecular plane were added to the usual minimal STO-3G basis centered on the atoms. Two of these six functions were placed 1.00 au from one nitrogen such as to make $\pm 120°$ angles with the NN axis, and similarly for two functions at the other nitrogen. The remaining two polarization functions were located ± 1.0 au above and below the midpoint of the NN bond.

The nitrogen–nitrogen and nitrogen–hydrogen bond distances in *cis*-HNNH (C_{2v} symmetry assumed) were fixed at the experimental values of 1.25 Å and 1.03 Å found for the *trans* isomer (6). (Alteration of these distances by a few hundredths of an Angstrom did not alter significantly the shapes of the energy curves discussed herein.) For *cis*-CH_3NNCH_3 and the cyclic systems, the NN separation was again taken as 1.25 Å, and the carbon–nitrogen distances were assumed to be 1.47 Å. The carbon–hydrogen distances in methyl groups were taken as 1.093 Å whereas those in ring systems were assumed to be 1.080 Å. The CC distance in the four-membered ring was chosen as 1.54 Å; the heavy-atom framework here and in all other systems was assumed planar. The HCH angles were taken as exactly tetrahedral in CH_3NNCH_3, and as 110° and 120° respectively in the four- and three-membered rings. C_{2v} symmetry was also assumed for all the carbon–nitrogen systems; the conformation in *cis*-CH_3NNCH_3 has the inplane hydrogens pointing inward (toward each other), since this is predicted by the calculations as the more stable conformation of this symmetry.

Results and Discussion

Theoretical Predictions

The variation in calculated energy (STO-3G) with bond angle about nitrogen is illustrated in Fig. 1 for the ground and lowest n_π* singlet excited state of planar, *cis*-diimide and for the ground states of the $HNNH^+$ and $HNNH^-$ ions.[1] The optimum bond angles for the ground states of the neutral molecule and anion are about 30° less than for the cation and excited HNNH singlet (see Table 1 for details).

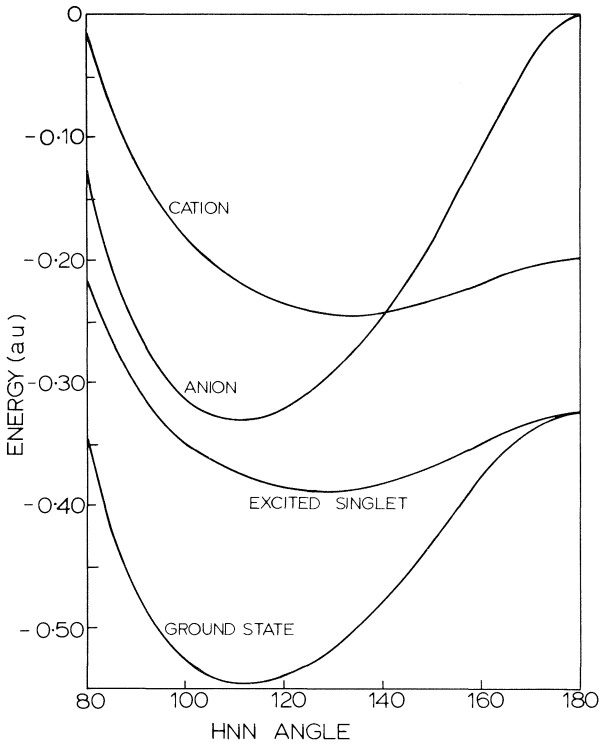

FIG. 1. STO-3G energy vs. HNN angle in *cis*-HNNH (offset by −109 au).

Clearly, the excitation energy to the n_π* singlet and the first ionization energy both should increase in magnitude continuously as the angle about nitrogen is bent away from linearity to about 110°, as obtained in our previous calculations for azomethane (1). However, for angles less than about 100°, the slope upwards of the ground state energy curve for HNNH is greater than that for either the excited singlet or the positive ion; thus *the excitation and ionization energies should decrease as the angle is decreased further toward 80°*. These effects are illus-

TABLE 1. Calculated bond angles in *cis*-HNNH systems

HNNH state	Angle (deg) when basis set = STO-3G	4-31G
Ground state (no CI)	112	115
Ground state (with CI)	112	115
n_π* singlet	128	135
Cation (ground state)	134	137
Anion (ground state)	111	115

[1]Note that electron capture to form the anion is predicted to be endothermic by these calculations, as is usual for *ab initio* calculations using Hartree–Fock–Roothaan theory.

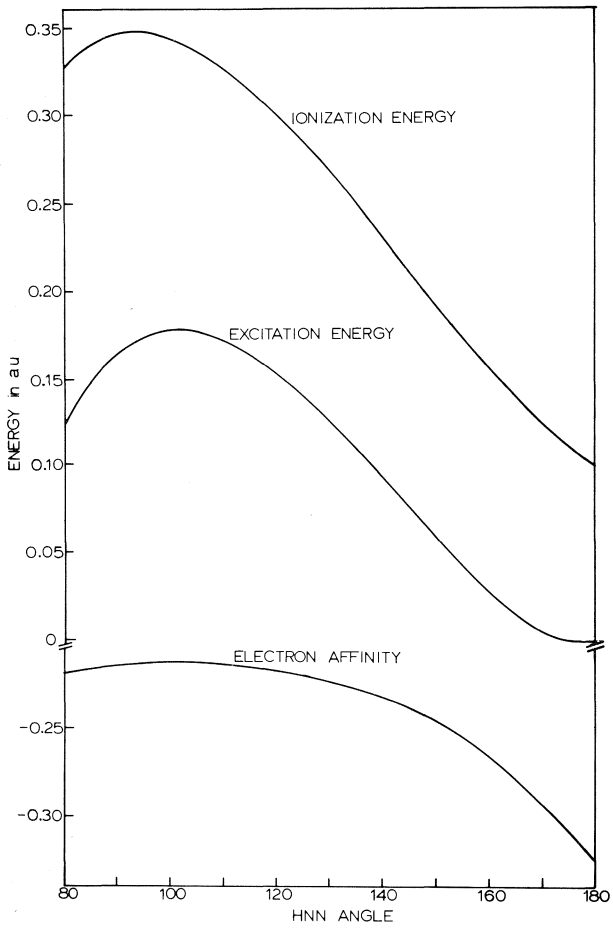

FIG. 2. Calculated (STO-3G) excitation energy to the $n_-\pi^*$ singlet state, ionization energy from the n_- MO, and electron affinity in *cis*-HNNH vs. HNN angle.

trated in the plots of excitation energy and ionization energy in Fig. 2; since the shapes of the curves are not altered significantly in changing the basis set from STO-3G to 4-31G, only the former are displayed. Preliminary calculations revealed that the shapes of these curves are essentially unchanged when the more expensive basis which includes polarization functions is employed; for reasons of economy, then, this basis was not used subsequently. Note also that on the basis of MINDO/2 calculations, Heilbronner and co-workers found the orbital energy for n_-, and the energy gap between the n_- and n_+ MO's, in HNNH both were minimum at angles of about 100° (7), in semiquantitative agreement with the present results.

One measure of the stability of the π^* orbital is the calculated electron affinity for HNNH; i.e. the energy difference between the ground states for the neutral and anionic species. From the plot of electron affinity versus angle in Fig. 2 it is clear that in the 80°–140° region at least, the stability of π^* varies rather less with angle than does that of n_-.

The correlation of excitation energy with ionization energy from STO-3G calculations is shown in Fig. 3; in the limit at 180° the curve becomes linear with a slope of unity. In the 105°–150° range the correlation is close to linear but the excitation energy increases only 0.7 times as fast as does the ionization energy as the bending is increased. The variation of excitation and ionization energies is a double-valued function in the 80°–105° region since the excitation energy peaks at a larger angle and falls more rapidly with decreasing angle thereafter than does the ionization energy.

In order to judge the relevance of these results for HNNH to *cis*-azoalkanes, STO-3G calculations for *cis*-azomethane at CNN angles of 130°, 150°, and 170°, and for the three- and four-membered rings **1***a* and **1***b* were performed; the results are summarized

1*a* **1***b*

in Table 2. The *difference* between each quantity and the corresponding value for *cis*-HNNH at the same HNN angle is given in parentheses below each entry. Obviously the excitation energy is virtually unaffected by the substitution of alkyl groups for the hydrogens, whereas the ionization energy is lessened by an almost constant factor of ~0.05 au (1.4 eV). The correlation of both properties with angle thus holds at least for the 80°–180° range. However, the magnitude of the substantial stabilization of the n_- "hole" in the cation may depend upon the nature of the alkyl group or ring involved. (In contrast, the π^* MO is at least 97% localized on the nitrogens in all the systems studied herein for both the excited state and the anion.)

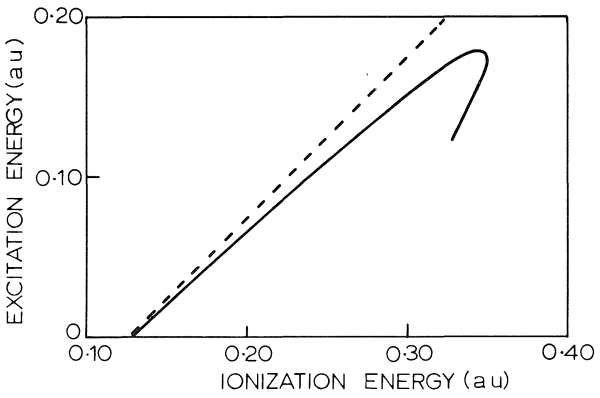

FIG. 3. Calculated (STO-3G) excitation energy vs. calculated ionization energy in *cis*-HNNH.

TABLE 2. Calculated energy differences (in au) for azoalkanes

Azoalkane system	CNN angle (deg)	Excitation energy	Ionization energy	Electron affinity
cis-$CH_3N{=}NCH_3$	170	0.0015	0.0713	−0.2763
		(−0.0048)	(−0.0612)	(−0.0245)
	150	0.0649	0.1438	−0.2358
		(+0.0038)	(−0.0526)	(−0.0094)
	130	0.1322	0.2223	−0.2175
		(+0.0050)	(−0.0498)	(−0.0057)
N=N ⌊⌋	95.7	0.1764	0.2997	−0.2024
		(+0.0014)	(−0.048)	(−0.009)
N=N ◺◿	64.8	0.1500	0.3462	−0.1691

Comparison with Experiment

To test our theoretical predictions, we considered the experimental data collected by Turro and co-workers (3) for the wavelength of highest transition probability and for the lowest ionization energy of nineteen cyclic azoalkanes. This data was characterized by the size of the (smallest) ring involved in each case and is summarized in Table 3 for 4-, 5-, and 6-membered rings. Clearly the wavelengths for the absorption maxima fall into three nonoverlapping groups, each of which is rather sharply defined in terms of the standard deviation. (Two systems listed by Turro and co-workers are not included in these averages. In one, their **8**, there is a carbonyl chromophore in the molecule as well. The interaction between the almost-degenerate —N=N— and —C=O excitations would account for the abnormally low wavelength of this system. Thus the ionization energy, but not the excitation energy, for **8** is included in the averages and standard deviations. The other, their **17**, contains a three-membered ring which may well alter the angle at —N=N—.) Thus the data clearly support our previous contention that the singlet–singlet excitation energy in *cis*-azoalkanes is controlled predominantly by the CNN angle. In addition, the prediction in the present calculations that the excitation energy should pass through a maximum value near a 100° bond angle is supported by the fact that the decrease in wavelength observed in going from six- to five-membered rings is not continued but rather reversed in going from five- to four-membered rings.

TABLE 3. Correlation of experimental data with ring size

Ring type[b]	Wavelength (nm) of absorption maximum[c]	Ionization energy for n_- MO (in eV)	Molecules in set[a]
4-Membered	351 ± 4	$8.9_4 \pm 0.1_0$	2, 3, 19
5-Membered	332 ± 7	$8.7_3 \pm 0.1_9$	4–7, 8,[d] 9, 16, 18
6-Membered	383 ± 10	$8.2_0 \pm 0.1_0$	10–13, 14,[e] 15

[a]All data are from ref. 3, and the numbering scheme refers to that used in the same paper.
[b]When the —N=N— unit is a component of two rings in the polycyclics, the molecule is listed under the smallest ring size involved as it is assumed primarily to determine the CNN angle.
[c]In hexane solution.
[d]Included only in ionization energy set; see text for discussion.
[e]No ionization energy is reported for **14** in ref. 3 and thus it is included only in the absorption calculations.

The correlation in Table 3 between ring size and ionization energy is consistent with the prediction that ionization energy should increase as the CNN angle decreases (at least down to about 92°). The distinction between the four- and five-membered ring groups is not clear-cut; the larger standard deviations here are not unexpected given the rather extensive delocalization of the "n_- hole" expected from the calculations (see above) for the cation. The lack of a reversal in order between the ionization energies for the four- and five-membered rings is consistent with the prediction (see Fig. 2) that this quantity peaks at an angle 5°–10° less than that for excitation energy. (The rough equality in ionization potentials implies the two systems probably lie on opposite sides of the peak.)

In Fig. 4 the wavelength of absorption maximum is plotted against ionization energy for the fifteen cyclic azoalkanes discussed in Table 3. Although the degree of scatter is large, the trends are not inconsistent with the hook-shaped, double-valued theoretical curve (Fig. 5).

The excitation and ionization energies predicted in Table 2 for the three-membered ("diazirine") ring clearly are much greater than expected from extrapolation of the curves in Fig. 2. (The HNNH calculations cannot be extended to angles lower than 80° since the hydrogen atom separation becomes equal to or less than that in H_2!). The large increase in ionization energy of 1.5 eV calculated in going from the four- to three-membered ring is of the same order of magnitude as that of 0.9 eV observed in the transition between the permethyl

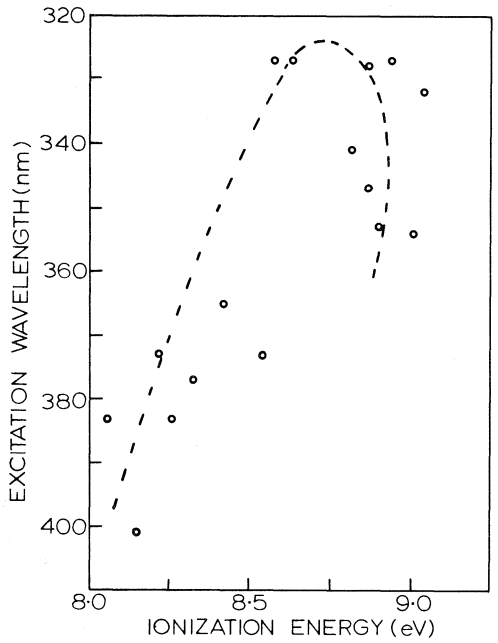

FIG. 4. Experimental excitation energy vs. experimental ionization energy for *cis*-azo systems.

derivatives of these rings (8). The calculated *decrease* of 0.4 eV in excitation energies for the same process is difficult to test due to the lack of experimental results for diazirines; however, it is clear that the excitation energies for the latter are equal to or less than those for four-membered rings. The breakdown in the excitation energy-ionization energy-bond angle correlations are due to the unusual electronic structure of the highly-strained three-membered rings. Inspection of the "n_-" MO for diazirine reveals it is actually more concentrated on carbon than on the nitrogens, and is really a bonding (rather than nonbonding) MO of the type Walsh described for cyclopropane:

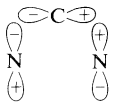

This qualitative difference in the nature of the highest-occupied orbital is the basis for our exclusion of three-membered rings containing —N=N— from the correlations discussed above; obviously the stability of this MO will be increased substantially due to its acquisition of substantial C—N bonding character.

The Stabilization of the n_- Orbital

At this stage it is useful to consider the variations in the electronic structure of the normal *cis*-azo chromophore which occur upon bending. As discussed above, most of the change in excitation

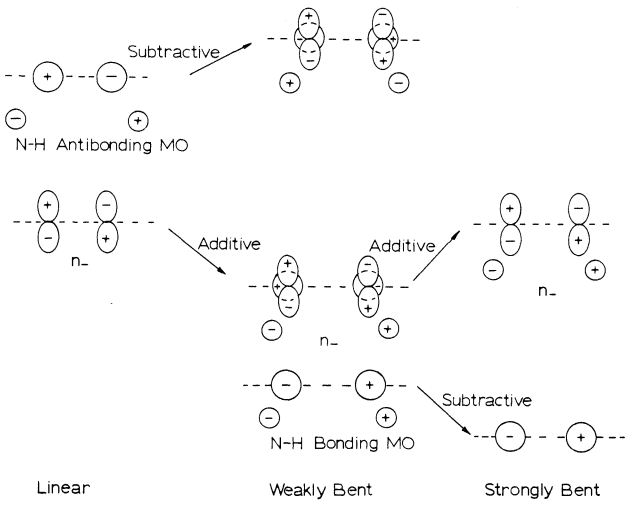

FIG. 5. Interaction of antisymmetric MO's in HNNH upon bending of HNN angle (schematic).

energies in the region of interest is caused predominantly by changes in stability of the n_- orbital. Overall this antibonding "lone pair" MO is stabilized by $\sim 5\frac{1}{2}$ eV by bending the HNN angle from linearity to 95°. This stabilization is due mainly to the acquisition of substantial $2s_N$ orbital character by n_- which, for reasons of symmetry, is completely $2p$ in character in the linear molecule.[2] The drain of $2s$ character into n_- comes mainly from the (empty) antisymmetric N—H antibonding MO and is depicted symbolically in Fig. 5. The calculated bond angles for the HNNH species (Table 1) agree with the Walsh-like view that n_- is stabilized significantly by bending, since the extent of bending is much less when n_- is only singly-occupied (cation and neutral molecule excited singlet) compared to when it is doubly-occupied (anion and neutral ground state). The variation with angle of the $2s_N$ character of n_- is graphically illustrated in Fig. 6 where the unpaired electron density in the $2s$ orbital of each nitrogen is plotted against HNN angle for both the cation and the $n_-\pi^*$ triplet state. For both states the contribution of $2s_N$ to n_- increases sharply as the HNN angle is bent from linearity, but the contribution peaks near an angle of 120° and declines thereafter. Again this behavior can be understood by considering the Walsh diagram involved. In particular, as n_- is stabilized by acquiring $2s_N$ character (from the N—H antibonding MO), its interaction with the antisymmetric combination of (filled) N—H *bonding* orbitals increases according to perturbation theory (since the strength of such interactions varies inversely as the

[2]For background to this type of perturbation theory discussion, see refs. 9 and 10.

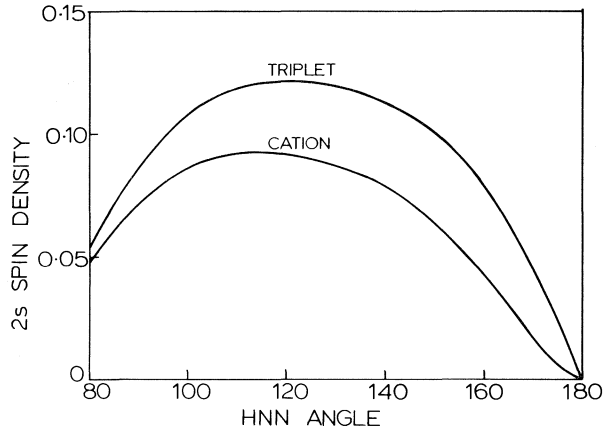

FIG. 6. Unpaired spin density (by STO-3G calculation) vs. HNN angle for triplet and cationic HNNH.

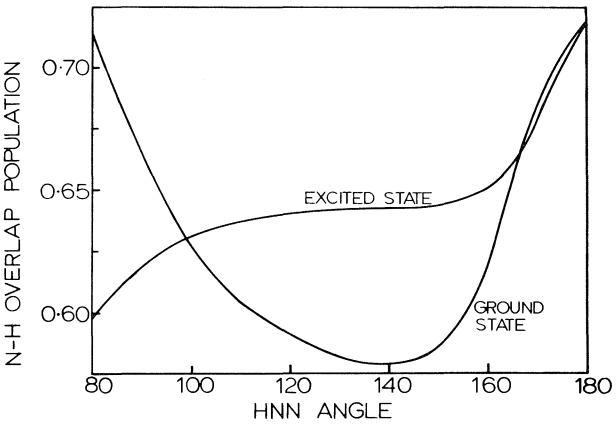

FIG. 7. Nitrogen–hydrogen overlap population vs. HNN angle in *cis*-HNNH.

energy gap between the original levels). Such interaction allows the lower, N—H bonding MO to steal $2s_N$ character from n_ and to donate to n_ some N—H bonding character (see bottom part of Fig. 7).

Both Houk *et al.* (2) and Turro and co-workers (3) have noted a correlation between ionization energy and the rate for decomposition of the singlet excited state (via N_2 extrusion). From their data it is clear that the rate is significantly smaller for those systems we classify in Table 3 as containing six-membered rings, compared to those which contain five- and four-membered rings. From the variations in N—H overlap population with angle illustrated in Fig. 7 one would expect the rates to decrease in the order of six- < five- < four-membered rings. The expectation of Turro and co-workers that excitation from n_ weakens the C—N bonds (3) is observed in the present calculations for HNNH and for the alkyl derivatives *only* for small angles (< 100°).

For reference, the total energies calculated for the molecules discussed herein are listed in Tables 4–6, available from the Depository of Unpublished Data.[3]

Conclusions

The analysis of the present calculations and of existing experimental spectra indicates that the excitation energy to the n_π* singlet state and the ionization energy from the n_ MO are determined primarily by the angle about the nitrogens in *cis*-azo molecules. Although the excitation energy and ionization energy versus angle curves are continuous, they peak at somewhat different angles in the 100° region, thus complicating correlations between the experimental parameters. An additional complication is the substantial delocalization of the hole in n_ through the molecule in the positive ions (but not the neutral excited state). Analysis of the MO's leads to the conclusion that the highest occupied MO in the three-membered diazirine ring (**1***a*) is different qualitatively from the n_ MO in the other systems considered and therefore one should not expect the properties of **1***a* to correlate smoothly with those of the larger rings.

Acknowledgements

Financial support of this research by the National Research Council of Canada and assistance with the calculations by Mrs. Rashmi Gupta are gratefully acknowledged. I would also like to thank Dr. N. J. Turro for providing a preprint of his publication and Ms. Kathleen Taylor for helpful discussions.

1. N. C. BAIRD, P. DE MAYO, J. R. SWENSON, and M. C. USSELMAN. J. Chem. Soc. Chem. Commun. 314 (1973).
2. K. N. HOUK, Y. M. CHANG, and P. S. ENGEL. J. Am. Chem. Soc. **97**, 1824 (1975).
3. M. J. MIRBACH, K-C. LIU, M. F. MIRBACH, W. R. CHERRY, N. J. TURRO, and P. S. ENGEL. J. Am. Chem. Soc. **100**, 5122 (1978).
4. C. C. J. ROOTHAAN. Rev. Mod. Phys. **32**, 179 (1960).
5. (*a*) W. J. HEHRE, R. F. STEWART, and J. A. POPLE. J. Chem. Phys. **51**, 2657 (1969); (*b*) R. DITCHFIELD, W. J. HEHRE, and J. A. POPLE. J. Chem. Phys. **54**, 724 (1971).
6. M. CARLOTTI, J. W. C. JOHNS, and A. TROMBETTI. Can. J. Phys. **52**, 340 (1974).
7. F. BROGLI, W. EBERBACH, E. HASELBACH, E. HEILBRONNER, V. HORNUNG, and D. M. LEMAL. Helv. Chim. Acta, **56**, 1933 (1973).
8. L. N. DOMELSMITH, K. N. HOUK, J. W. TIMBERLAKE, and S. SZILAGYI. Chem. Phys. Lett. **48**, 471 (1977).
9. C. C. LEVIN. J. Am. Chem. Soc. **97**, 5649 (1975).
10. W. CHERRY, N. EPIOTIS, and W. T. BORDEN. Acc. Chem. Res. **10**, 167 (1977).

[3]Complete set of data is available, at a nominal charge, from the Depository of Unpublished Data, CISTI, The National Research Council of Canada, Ottawa, Ont., Canada K1A 0S2.

Cobalt(II), nickel(II), and copper(II) complexes of di- and tetrapeptides containing tyrosine and glycine residues

MOHAMED S. EL-Ezaby,[1] JASSIM M. AL-HASSAN, NAMEK F. EWEISS, AND FARIDA AL-MASSAAD

Department of Chemistry, Faculty of Science, University of Kuwait, Kuwait

Received December 5, 1977[2]

MOHAMED S. EL-EAZBY, JASSIM M. AL-HASSAN, NAMEK F. EWEISS, and FARIDA AL-MASSAAD. Can. J. Chem. **57**, 104 (1979).

The solution equilibria of di- and tetrapeptides containing tyrosine and glycine residues have been investigated in absence and presence of cobalt(II), nickel(II), and copper(II) ions. The equilibrium constants have been determined by pH titration at 30°C and $\mu = 0.1$ *M* ($NaNO_3$) in 80% by weight DMSO – water mixed solvent. Protons are ionized from terminal (protonated amino and carboxyl) groups as well as from peptidic nitrogens. Complexes of 1:1 composition of metal ion – tetrapeptides were formed in quite a wide range of pH; also 1:1 complexes of the metal ions – dipeptides were formed in solution under the same conditions. Other higher complexes cannot be proved to form in the pH range studied. The complexes of these metal ions with glycine and *O*-Bzl-L-tyrosine were also studied under the same experimental conditions as control experiments and their equilibrium constants were calculated.

MOHAMED S. EL-EAZBY, JASSIM M. AL-HASSAN, NAMEK F. EWEISS et FARIDA AL-MASSAAD. Can. J. Chem. **57**, 104 (1979).

On a étudié l'équilibre en solution de di- et de tétrapeptides contenant des résidus de tyrosine et de glycine en l'absence et en présence d'ions cobalt(II), nickel(II) et cuivre(II). On a déterminé les constantes d'équilibre par titration de pH à 30°C et à une valeur de $\mu = 0.1$ *M* ($NaNO_3$) dans un solvant mixte contenant 80% en poids de DMSO dans H_2O. Les protons des groupes terminaux sont ionisés (les groupes amino et carboxyle protonés) de même que ceux des azotes peptidiques. Il y a formation de complexes de composition 1:1 d'ions métalliques:tétrapeptides sur un grand intervalle de pH; il y a aussi formation de complexes 1:1 d'ions métalliques:dipeptides en solution dans les mêmes conditions. On n'a pas pu mettre en évidence la formation de complexes plus élevés aux conditions de pH étudiées. On a aussi étudié les complexes de ces ions métalliques avec la glycine et la *O*-Bzl-L-tyrosine dans les mêmes conditions expérimentales comme expériences de contrôle; on a calculé leurs constantes d'équilibre.

[Traduit par le journal]

Introduction

Metal ions have been reported to play an important role in biological systems. Investigation of the reactions of some metal ions with compounds containing peptide groups in strongly alkaline solutions concluded that these reactions were due to ring formation by the metal ions with amino and peptidic nitrogens of the peptide under consideration (1). Confirmation of the existence of the metal–peptide linkage was reported from infrared studies (2, 3). In addition, considerable experimental evidence (4–7) indicated that the bonding of Cu(II) to serum albumin involves both the α-amino terminal plus one or more peptide nitrogen atoms.

Although the hydrogen atom in the peptide linkage is not very acidic, yet in the presence of some metal ions like Co(II), Ni(II), and Cu(II), the peptide group loses a proton and forms a metal–N(peptide) bond (8-11). However, Kim and Martell (8, 9) proposed the presence of copper bonds to the peptidic nitrogens without loss of the hydrogen ion. Further structural (12*a*) and spectral (13, 14) studies showed that the proton adds to the peptidic oxygen rather than to the peptidic nitrogen which is kinetically inert (11).

Generally, oligopeptide complexes with divalent metal ions like Pd(II), Cu(II), Ni(II), and Co(II) have a square-planar geometry (15). Other geometries found are either square-pyramidal (12*b*) or square-pyramidal with two co-ordinated water molecules (12*c*). On the other hand, dipeptides have the possibility of forming bis(dipeptide) complexes with an octahedral arrangement of donor groups (16).

It was reported (17) that the presence of the copper – amino acid complexes in human serum enhances the uptake of copper by liver tissues. This effect has also been seen in rapid transport of Cu(II) between plasma and cells in other systems (17, 18).

Because of the importance of the study of the kinetics and mechanism of the transfer of metal ions

[1]To whom correspondence should be addressed.

[2]Revision received June 29, 1978.

0008-4042/79/010104-09$01.00/0

between peptides and amino acids, we report in this work cobalt(II), nickel(II), and copper(II) complexes with di- and tetrapeptides containing *O*-Bzl-L-tyrosine and glycine residues.

The purpose of this study is to define the role of the peptidic as well as the terminal amino and carboxylic groups in the studied peptides with regards to chelation in isolation from the effect of the phenolic hydroxyl group of the tyrosyl residues. However, as a study of the fully unprotected same tyrosyl peptides would give some new information as to the influence of the phenolic group in the complexation reaction, it is our future intention to compare the results reported here with those to be obtained for the free fully unprotected same tyrosyl peptides.

Experimental

Reagents

Cobalt, nickel, and copper nitrates were a BDH product (AR grade). Aqueous stock solution (0.1 *F*) was standardized by EDTA titration. Commercial sodium nitrate was recrystallized twice from water. Stock solution (0.5 *F*) of sodium nitrate was prepared in 80% by weight dimethyl sulfoxide (DMSO) – water medium. Mixed 80% by weight DMSO (spectral grade) – water solvent was used as diluent. DMSO was checked titrimetrically for acidic and basic impurities prior to dilution with water.

Compound*		
Number	Formula	Abbreviation
Dipeptides		
1	Cl^-H^+-(*O*-Bzl)-L-Tyr-Gly-OH	D_1
2	Cl^-H^+-Gly-(*O*-Bzl)-L-Tyr-OH	D_2
3	Cl^-H^+-Gly-Gly-OH	D_3
4	Cl^-H^+-(*O*-Bzl)-L-Tyr-(*O*-Bzl)-L-Tyr-OH	D_4
Tetrapeptides		
5	Cl^-H^+-(*O*-Bzl)-L-Tyr-Gly-Gly-(*O*-Bzl)-L-Tyr-OH	T_1
6	Cl^-H^+-Gly-(*O*-Bzl)-L-Tyr-Gly-(*O*-Bzl)-L-Tyr-OH	T_2
7	Cl^-H^+-(*O*-Bzl)-L-Tyr-Gly-(*O*-Bzl)-L-Tyr-Gly-OH	T_3
8	Cl^-H^+-Gly-(*O*-Bzl)-L-Tyr-(*O*-Bzl)-L-Tyr-Gly-OH	T_4

*(*O*-Bzl)-L-Tyr = the phenolic OH function of L-tryosine is protected by benzyl group; Gly = glycine.

The dipeptides **1**–**4** and the tetrapeptides **5**–**8** were prepared and purified as described in literature (19). O-Bzl-L-tyrosine was prepared using the method of Wunsch *et al.* (20). Glycine, a BDH product, was used without further purification.

Because of solubility problems, accurately weighed amounts of the tetrapeptides, dipeptides, *O*-Bzl-L-tyrosine and glycine were dissolved in DMSO. The stock solutions were about 3×10^{-2} *F*. Equivalent amount of hydrochloride acid was only added to glycine.

Measurements

A Radiometer pH meter, model 63, equipped with Radiometer glass and reference electrodes types G 202 C and K 104, respectively, was used for pH titrations. The pH meter was standardized before use with Radiometer buffers of pH 4.00, 7.00, and 9.1. Solutions of ligand or of ligand and metal ion were titrated with standard carbonate-free sodium hydroxide solution (0.102 or 0.098 *F*) delivered from calibrated automatic burette type Metrohm Herisau Multi Dosimat E 415, accurate to ±0.005 ml. In each titration the initial volume of the solution was 25.0 ml. The ionic strength was adjusted to 0.10 by the addition of the concentrated sodium nitrate solution. In a typical titration, aliquots of ligand, metal ion, and sodium nitrate stock solution were mixed such that the solvent mixture was 80 wt.% DMSO – water (molar ratio nearly 1:1). The mixture was adjusted to 25.0 ml by adding the required amount of diluent. The temperature of the solution was maintained at 30.0°C in a tightly covered thermostated titration cell. The solution was mechanically stirred. A complete titration consisted of successive additions of 0.01–0.02 ml of the titrant. Half minute after each addition the stirring motor was stopped and the pH-meter reading was taken. The titration was continued until pH-meter could not be kept steady or reached pH 11.00. The range of the concentration of the metal ions and ligands were $(0.5–1.0) \times 10^{-3}$ *F* and $(0.495–2.0) \times 10^{-3}$ *F*, respectively.

Due to the probable uptake of oxygen by Co(II) complexes, their titrations in this study has been done under anaerobic (by flushing purified N_2 through the titration cell) and aerobic conditions. Titration results coincided in both cases at pH_0's less than 8.50. However, appreciable differences in the titration curves were observed at higher pH values; under aerobic conditions being slightly lower.

The pH-meter readings in 80 wt.% DMSO – water solution are converted to hydrogen ion concentration (H^+) by means of the widely used equation of Van Uitert and Haas (21), namely

$$[1] \qquad -\log [H^+] = pH_0 + \log U_H$$

where U_H is the correction factor for the solvent composition and ionic strength. For this purpose, readings were made on a series of solutions containing known amounts of nitric acid and sodium nitrate such that the ionic strength is equal to 0.10 in 80 wt.% DMSO – water medium in the pH range 1.00–4.00. In addition, readings of pH were taken for universal buffers (22) at the same solvent composition in the pH range 3.50–10.75. From the known stoichiometric $[H^+]$, a value of

log $U_H = 1.00 \pm 0.01$ was obtained for 80 wt.% DMSO – water medium of $\mu = 0.10$ at 30°C.

The ionic product of water in 80 wt.% DMSO – water medium at 30.0°C was determined potentiometrically (23). Potential measurements were made with the same pH-meter described above. The glass electrode used was the same as described above. The AgCl, Ag electrode was prepared from Radiometer (P 4011) silver Billet Electrode by electrolysis in chloride solution (0.1 *M*).

Cell A glass electrode/solution A: $HCl(C_1)$, $KNO_3(C_2)$,

in solvent S/AgCl, Ag

Most of the measurements began with cell A, containing a known volume of 80 wt.% DMSO – water solution of hydrochloric acid and potassium nitrate of known concentrations represented by C_1 and C_2. The same procedure was then followed with cell B,

Cell B glass electrode/solution B: NaOH (C_3), NaCl (C_4)

in solvent S/AgCl, Ag

that initially contained known volume of 80 wt.% DMSO – water with appropriate concentrations of sodium hydroxide and sodium chloride such that

$$C_1 + C_2 = C_3 + C_4$$

The equation used to calculate the equilibrium quotient is

$$[2] \quad pK_W = \frac{E_A - E_B}{K_2} + \log \frac{C_4}{C_3 C_1^2} \simeq -\log C_H C_{OH}$$

assuming that the activity of water to be unity in all solutions, where

$$E_A = K_1 + K_2 \log C_1^2 + K_2 \log (\gamma^{\pm})_A^2$$

$$E_B = K_1 + K_2 \log \frac{K_W C_4}{C_3} + K_2 \log (\gamma^{\pm})_B^2$$

where K_1 = standard potential of the cells, $K_2 = 58.6$ mV, and $\gamma^{\pm}$ = mean activity coefficient for the solute ions. The mean value of pK_W obtained was 15.04 ± 0.12.

The electronic spectra of the Co(II)–, Ni(II)–, and Cu(II)–tetrapeptides systems were taken at different pH values using Cary 17 spectrophotometer at room temperature (25 ± 1°C).

Results and Discussion

The reaction between the ligand, the divalent metal ions, and protons can be represented as follows:

$$[3] \quad jL + qM + rH \rightleftharpoons L_jM_qH_r \text{ (charges omitted)}$$

where L stands for the ligand, M stands for Co(II), Ni(II), or Cu(II), and *j*, *q*, and *r* are the stoichiometric coefficients.

Typical titration curves of the systems under consideration are shown in Fig. 1. In absence of metal ions the protonation and deprotonation equilibria are

$$[4] \quad L + H^+ \rightleftharpoons LH^+$$

$$\beta_{101} = \frac{[LH^+]}{[L][H^+]}$$

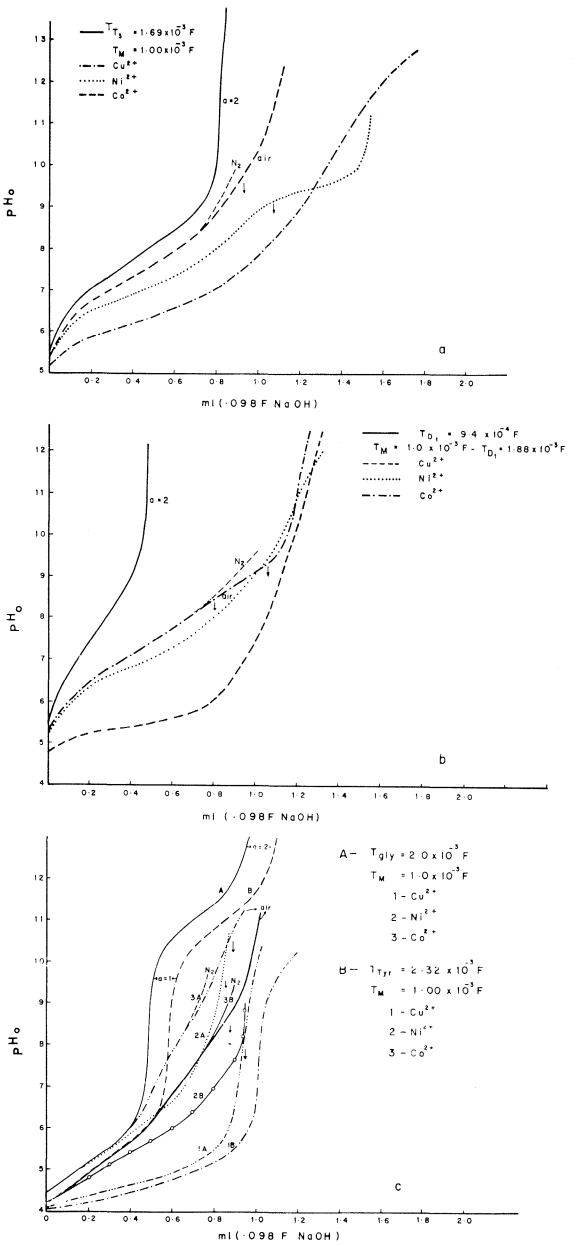

FIG. 1. Titration curves in absence and presence of the metal ions Cu^{2+}, Ni^{2+}, and Co^{2+}, (*a*) T_3 system, (*b*) D_1 system, (*c*) Gly and *O*-Bzl-L-Tyr systems.

$$[5] \quad L \rightleftharpoons LH_{-1} + H^+$$

$$\beta_{10-1} = \frac{[LH_{-1}][H^+]}{[L]}$$

The titration curves of dipeptides and tetrapeptides show only sharp inflection at *a* (the ratio of number of moles of base per number of moles of ligand) equal to 2 at pH_0 values greater than 10.0.

On the other hand, titration curves of the protonated *O*-Bzl-L-tyrosine and glycine show two inflections in the pH_0 range ~3.8–9.0 and the other at pH_0 values greater than 11.0. Programme MINIQUAD (24) and its modified version MINIQUAD 75 (25) were used to calculate the equilibrium constant of reactions [4] and [5]. The values are depicted in Table 1. By analogy to the acid–base equilibria of amino acids and their related compounds, one expects that reaction [4] deals with the protonation of the carboxylate group and reaction [5] with the deprotonation of the protonated amino group. Amide protons of dipeptides and tetrapeptides cannot be simply ionized even in strongly alkaline solution (26), a behaviour usually encountered by all peptides in absence of metal ions. The deprotonation constants of tetrapeptides can be arranged in the descending order of $T_3 > T_1 > T_4 > T_2$ and those of dipeptides in the order $D_4 > D_1 > D_2 > D_3$. These orders reflect the relative basicities of the amino groups in these compounds. The basic nature of the amino group in tetrapeptides and dipeptides is obviously lower than that in *O*-Bzl-L-tyrosine and glycine as evidenced from the log form of their deprotonation constant, Table 1. On the other hand, the protonation constants of the tetrapeptides and dipeptides are greater than those of *O*-Bzl-L-tyrosine and glycine. These differences in behaviour may be attributed to decrease in electronic density on the nitrogen of the amino group as the electronic transmission from the carboxylate group decreases in the presence of peptide linkages.

The Metal Ion Complexes of Tetrapeptides

Typical titration curves of the divalent metal ions – tetrapeptides systems are shown in Fig. 1*a*. Although no precipitation of any kind was observed in the copper(II) systems in the pH_0 range used, yet slight precipitation was observed at pH's > 9.6 in nickel(II) systems and > 10.6 in the cobalt(II) systems. During the titration the color of the solution changed considerably. Although clear inflections in the titration curves cannot be located, yet 4–5 moles of base per mole of copper(II) or nickel(II) and 3–4 moles of base per mole of cobalt(II) could be assumed to be consumed in these systems. MINIQUAD programmes have been used to test different models of equilibrium reactions (eq. [3]). The assessment was done by using the crystallographic R factor and X_i^2 values obtained by the forementioned programmes. In each case, the addition of one extra species gave an increased R value, a greater X_i^2 value, or both. The model which met these conditions is as follows:

$$LH^+ \rightleftharpoons L + H^+$$

[6] $$L + M^{2+} \rightleftharpoons MLH_{-1}^{+} + H^+$$

[7] $$L + M^{2+} \rightleftharpoons MLH_{-2}^{0} + 2H^+$$

[8] $$L + M^{2+} \rightleftharpoons MLH_{-3}^{-} + 3H^+$$

[9] $$L + M^{2+} \rightleftharpoons MLH_{-4}^{2-} + 4H^+$$

The log values of β_{jqr}'s for the equilibrium reactions [6]–[9] are listed in Table 1. Table 2*a*, on the other hand, shows the stepwise equilibria of M^{2+} tetrapeptide systems and their equilibrium constants.

From the order of arrangement of the deprotonation constants of the tetrapeptides in absence of metal ions, one expects that the order of the stability constants of their metal ions complex equilibria (MLH_{-1}^{+}) will be quite reversed, i.e. $T_2 > T_4 > T_1 > T_3$. This was found to be true in the systems of copper(II) complexes, in particular, and to a certain extent in the nickel(II) and cobalt(II) system. This conclusion indicates strongly that ring closure first occurs through coordination of the terminal groups of the tetrapeptides with copper(II). The situation is not quite clear in the cases of nickel(II) and cobalt(II) systems. Generally, the order of complexing of these metal ions with a particular tetrapeptide follows the Irving–Williams series (27) (Table 2*a*) which suggests high spin complexes in octahedral crystal field. In fact, it was not possible to detect complexes of compositions other than 1:1. This conclusion implies that coordination sites other than the C- or N-terminals may be involved in complex formation. The other coordination sites may be available through the nitrogen atom of the peptidic linkage. This type of linkage may facilitate deprotonation of the peptidic protons at lower pH values than it should be in absence of metal ions. This behaviour has been previously reported for other similar systems (17). The stepwise deprotonation constants of the MLH_{-1} complex show monotonic decrease in magnitude as they are deprotonated consecutively, Table 2*a*, a behaviour which may be interpreted as due to increase in electron density as peptidic protons dissociate.

It is also quite clear that the order of complexing ability of LH_{-2}, LH_{-3}, and LH_{-4} of a particular tetrapeptide follows also Irving–Williams series (27).

However, the log form of the deprotonation constants of MH_{-1}, MLH_{-2}, and MLH_{-3} of the divalent metal ion complexes, under consideration, do not follow a particular trend with respect to the type of the tetrapeptide. This is probably due to the effect of structure conformation of the tetrapeptide. However, the effect of sequence of each tetrapeptide does not seem to be clear. In the case of the depro-

TABLE 1. log β for the species $L_jM_qH_r$ at 30°C and μ = 0.10 *M* $NaNO_3$

(*a*) Tetrapeptides

				log $\beta_{jqr}(\pm S)$			
L	*j*	*q*	*r*	Ligand	Cu(II)	Ni(II)	Co(II)
T_1	1	0	1	6.32(0.02)			
	1	0	−1	−8.04(0.02)			
	1	1	−1		−1.26(0.07)	−2.22(0.03)	−2.53(0.05)
	1	1	−2		−7.23(0.06)	−10.15(0.08)	−10.83(0.11)
	1	1	−3		−13.88(0.08)	−18.30 —	−21.48(0.56)
	1	1	−4		−23.62(0.18)	−28.45(0.41)	—
T_2	1	0	1	6.20(0.01)			
	1	0	−1	−8.45(0.01)			
	1	1	−1		−1.13(0.02)	−2.16(0.05)	−3.06(0.04)
	1	1	−2		−7.42(0.04)	−9.93(0.13)	−12.60(0.08)
	1	1	−3		−14.60(0.05)	−18.92(0.14)	−22.96(0.10)
	1	1	−4		−24.42(0.10)	—	—
T_3	1	0	1	6.09(0.02)			
	1	0	−1	−7.60(0.02)			
	1	1	−1		−0.98(0.02)	−2.51(0.01)	−3.61(0.03)
	1	1	−2		−6.90(0.02)	−9.66(0.03)	−12.60(0.06)
	1	1	−3		−14.51(0.06)	−18.81(0.20)	−22.95(0.18)
	1	1	−4		−25.00(0.10)	—	—
T_4	1	0	1	5.83(0.02)			
	1	0	−1	−8.27(0.02)			
	1	1	−1		−1.32(0.03)	−1.79(0.02)	−2.89(0.03)
	1	1	−2		−7.72(0.06)	−8.12(0.03)	−11.18(0.06)
	1	1	−3		−14.60(0.07)	−16.36(0.07)	−21.80(0.22)
	1	1	−4		−24.21(0.14)	−25.35(0.07)	—

(*b*) Dipeptides

				log $\beta_{jqr}(\pm S)$			
L	*j*	*q*	*r*	Ligand	(CuII)	Ni(II)	Co(II)
D_1	1	0	1	5.93(0.02)			
	1	0	−1	−7.94(0.02)			
	1	1	−1		—	−2.86(0.05)	−4.15(0.09)
	1	1	−2		−4.34(0.01)	−11.29(0.11)	−12.79(0.14)
D_2	1	0	1	6.12(0.03)			
	1	0	−1	−8.64(0.03)			
	1	1	−1		—	−3.29(0.06)	−5.44(0.08)
	1	1	−2		−4.69(0.02)	−14.08(0.31)	−16.01(0.22)
D_3	1	0	1	6.11(0.03)			
	1	0	−1	−8.75(0.05)			
	1	1	−1		—	−3.36(0.08)	−5.68(0.11)
	1	1	−2		−3.75(0.09)		
D_4	1	0	1				
	1	0	−1	6.22(0.01)			
	1	1	−1	−7.29(0.01)	—	−2.96(0.02)	−4.02(0.05)
	1	1	−2		−3.37(0.05)	−10.53(0.04)	−12.15(0.06)
O-Bzl-L-Tyr	1	0	1	4.12(0.03)			
	1	0	−1	−10.52(0.05)			
	1	1	−1		0.56(0.01)	−2.51(0.09)	−3.60(0.08)
	2	1	−2		− 0.19(0.02)	−5.66(0.15)	−8.08(0.12)
Gly	1	0	1	4.27(0.02)			
	1	0	−1	−10.25(0.03)			
	1	1	−1		0.42(0.04)	−3.12(0.08)	−4.23(0.05)
	2	1	−2		−0.77(0.10)	−8.06(0.15)	−10.61(0.22)

tonation of $CuLH_{-1}$, the order of arrangement is $T_4 > T_2 > T_1 > T_3$, in the case of $CuLH_{-2}$ the order is $T_3 > T_2 > T_4 > T_1$, and in the case of $CuLH_{-3}$ the order is $T_3 > T_2 > T_1 > T_4$. The order of arrangement in the case of Ni(II) and Co(II) systems is not similar to that of the Cu(II) systems. This may be attributed to the difference in ionic radii of the former metal ions from the latter ions.

From the foregoing results, one cannot predict easily which peptide group will lose its proton first. However, it can be concluded that pentacoordinated complex species may be formed with the loss of all or some of the peptidic protons in addition to that of the terminal carboxylic group. It is not unreasonable to assume that water molecule or hydroxide ion may occupy the vacant hexacoordinate site of the metal ions.

Figure 2 shows a typical distribution diagram of various complex species at different pH values.

The electronic spectra of Co(II)–, Ni(II)–, and Cu(II)–tetrapeptides systems revealed the possible presence of different complex species at different pH values. In the Cu(II) system (Fig. 3), the spectra show hypsochromic shift with increase in intensity as pH increases in the 500–800 nm range. This was attributed to the *d–d* transition exhibited by copper(II) ions in possibly an octahedral field. The increase in intensity in the ligand bands (<430 nm) was explained as due to electronic transitions within the ligand as a result of metal ions perturbation. However, the spectra of Ni(II) and Co(II) were more or less similar to the ligand spectra except that the intensity is higher. A shoulder at ~400 nm and ~480 nm in case of Ni(II) and Co(II), respectively, was observed and attributed to the *d–d* transition in both cases.

The Metal Ion Complexes of the Dipeptides

Solutions of the Cu(II), Ni(II), and Co(II) exhibit various colors as their pH_0 increases in the course of titration. While no precipitation was observed in the Cu(II) systems in the pH_0 range used, colored precipitates in both Ni(II) and Co(II) systems were formed, depending on the system, initial concentrations of the reactants, and pH_0 of the medium. Typical titration curves of Cu(II), Ni(II), and Co(II) dipeptide systems are shown in Fig. 1*b*. Sharp inflections in these curves are noted at pH_0's > 6.0. These inflections correspond approximately to 3–4 moles of base to one mole of metal ions. The model which fits the experimental findings has been found to correspond to the following equilibrium reactions.

$$LH^+ \rightleftharpoons L + H^+$$

[10] $$L + M^{2+} \rightleftharpoons MLH_{-1}^{+} + H^+$$

[11] $$L + M^{2+} \rightleftharpoons MLH_{-2} + 2H^+$$

TABLE 2*a*. log β values for the stepwise equilibria of the complexes of the divalent metal ions with tetrapeptides*

Reaction	T_1			T_2			T_3			T_4		
	Co(II)	Ni(II)	Cu(II)	Co(II)	Ni(II)	Cu(II)	Co(II)	Ni(II)	Cu(II)	Co(II)	Ni(II)	Cu(II)
$LH_{-1}^{-} + M^{2+} \rightleftharpoons MLH_{-1}^{+}$	5.51	5.82	6.77	5.43	6.34	7.23	4.01	5.10	6.62	5.38	6.48	6.95
$MLH_{-1} \rightleftharpoons MLH_{-2}^{0} + H^+$	−8.30	−7.93	−5.97	−9.54	−6.77	−6.29	−8.99	−7.13	−5.92	−8.29	−6.33	−6.40
$MLH_{-2}^{0} \rightleftharpoons MLH_{-3}^{-} + H^+$	−10.65	−8.15	−6.65	−10.36	−9.00	−7.12	−10.35	−9.11	−7.60	−10.62	−8.11	−6.88
$MLH_{-3} \rightleftharpoons MLH_{-4}^{2-} + H^+$	—	−10.15	−9.74	—	—	−9.80	—	—	−10.50	—	−9.01	−9.60

*The log β of Cu(II) complexes with tetraglycine in aqueous solutions are 5.05, −5.60, −6.77, and −10.00, respectively (26). The log β of Ni(II) complexes with tetraglycine in aqueous solutions are 3.65, 3.30, −8.20, and −8.25 for the formation of MLH_{-1}, $M(LH_{-1})_2$, MLH_{-2}, and MLH_{-3}, respectively (26). The log β of Co(II) complexes with tetraglycine in aqueous solutions are 3.02, 2.47, for the formation of MLH_{-1} and $M(LH_{-1})_2$, respectively (26).

TABLE 2*b*. log β values for the stepwise equilibria of the complexes of the divalent metal ions with dipeptides*

Reaction	D_1			D_2			D_3			D_4		
	Co(II)	Ni(II)	Cu(II)	Co(II)	Ni(II)	Cu(II)	Co(II)	Ni(II)	Cu(II)	Co(II)	Ni(II)	Cu(II)
$LH_{-1}^{-} + M^{2+} \rightleftharpoons MLH_{-1}^{+}$	3.79	5.08	—	3.20	5.35	—	3.08	5.40	—	3.27	4.33	—
$MLH_{-1}^{+} \rightleftharpoons MLH_{-2}^{0} + H^+$	−8.64	−8.43	—	−10.57	−10.79	—	—	—	—	−8.13	−7.57	—
$L + M^{2+} \rightleftharpoons MLH_{-2} + 2H^+$	−12.79	−11.29	−4.34	−16.01	−14.08	−4.69	—	—	−3.75	−12.15	−10.53	−3.37

*The log β of Cu(II) complexes with diglycine in aqueous solutions are 4.96 and −3.90 for the formation of MLH_{-1} and MLH_{-2}, respectively (26). The log β of Ni(II) complexes with diglycine in aqueous solutions are 4.49, 3.42, and −9.35 for the formation of MLH_{-1}, $M(LH_{-1})_2$, and MLH_{-2}, respectively (26). The log β of Co(II) complexes with diglycine in aqueous solutions are 2.73 and 2.29 for the formation of MLH_{-1} and $M(LH_{-1})_2$, respectively (26).

TABLE 2*c*. log β values for the stepwise equilibria of the complexes of the divalent metal ions with *O*-Bzl-L tyrosine and glycine*

Reaction	*O*-Bzl-L-Tyrosine			Glycine		
	Co(II)	Ni(II)	Cu(II)	Co(II)	Ni(II)	Cu(II)
$LH_{-1}^- + M^{2+} \rightleftharpoons MLH_{-1}$	6.92	8.01	11.08	6.02	7.16	10.67
$LH_{-1}^- + MLH_{-1}^+ \rightleftharpoons M(LH_{-1})_2$	6.04	7.37	9.77	3.89	5.31	9.06

*The log β of Cu(II) complexes with glycine in aqueous solutions are 7.72 and 6.89, respectively (26). The log β of Ni(II) complexes with glycine in aqueous solutions are 5.55 and 4.62, respectively (26). The log β of Co(II) complexes with glycine in aqueous solutions are 4.77 and 4.22, respectively (26).

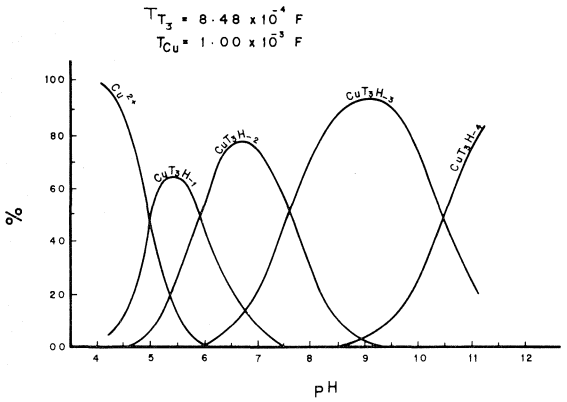

FIG. 2. Distribution diagram of the molecular species of T_3–Cu^{2+} system at various pH values.

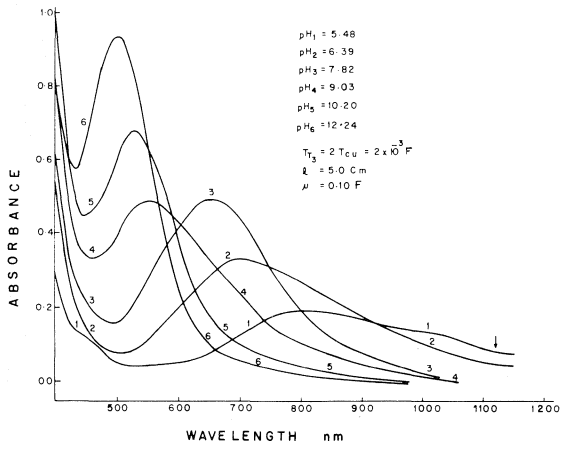

FIG. 3. Electronic spectra of T_3–Cu^{2+} system at different pH values.

The equilibrium constants of the reactions [10] and [11] are listed in Table 1. It is quite interesting to note that the constant of the equilibrium reaction [10] cannot be calculated for the Cu(II) system, contrary to the Ni(II) and Co(II) systems. This may be accounted for as due to the large polarizing power of the Cu(II) ions in comparison to that of Ni(II) and Co(II) ions; which facilitates loss of protons from the ligand, even that of the peptidic group. Few reports have discussed the loss of peptidic protons of dipeptides in presence of metal ions (8) in aqueous solutions. Metal–dipeptide complexes of 1:2 stoichiometry cannot be detected under the experimental conditions used in this work, similar to what have been found in the metal tetrapeptide systems. This conclusion is contrary to what one expects specially in Ni(II) and Co(II) systems where octahedral configuration is favourable. However, this can be attributed to the steric hindrance of the bulky *O*-Bzl-L-tyrosine residue in D_1, D_2, and D_4 in particular and/or the formation of neutral complex species incapable of attracting other ligand species in the mixed solvent under consideration. The order of arrangement of 1:1 complex of Ni(II) with the dipeptides follows the opposite order of arrangement of the deprotonation constants of the dipeptides, i.e., $D_3 > D_2 > D_1 > D_4$. This behaviour probably indicates that chelation occurs through the N and O terminals of the dipeptides similar to what have been shown for the Cu(II)–tetrapeptides systems. On the other hand Co(II) systems do not show this trend which may indicate that the N and O terminals are not simultaneously involved in the complex formation. The order of arrangement is $D_1 > D_4 > D_2 > D_3$, Table 2*b*. For a particular dipeptide, the order of stability of MLH_{-1} follows Irving–Williams series. Moreover, the order of the stability constants of the formation of MLH_{-2} shows the same sequence, i.e. Cu(II) > Ni(II) > Co(II) (Table 2*b*).

The Metal Ion Complexes of Glycine and O-*Bzl*-L-*Tyrosine*

Figure 1*c* shows typical titration curves of the divalent metal ions – glycine and *O*-Bzl-L-tyrosine systems. Sharp inflections were obtained at 2 moles of base per mole of metal ions for 1:1 metal-to-ligand ratios and four moles of base per mole of metal ions for 1:2 ratios. These were only observed in the copper(II) systems. Nickel(II) and cobalt(II) titration systems did not show such clear inflection points. However, 2–4 moles of base per mole of metal ions may be assumed to be consumed in these systems as the case of copper(II) systems. The model equilibrium reactions which successfully explained

these experimental data is as follows:

$$LH^+ \rightleftharpoons L + H^+$$

[12] $$L + M^{2+} \rightleftharpoons MLH_{-1} + H^+$$

[13] $$2L + M^{2+} \rightleftharpoons M(LH_{-1})_2 + 2H^+$$

Table 1 depicts the values of the stability constants of the equilibria [12] and [13] and Table 2*c* lists the corresponding stepwise constants. As was expected, the order of stability of the complexes follows that of Irving–Williams series. They are 2–4 units greater than those calculated for systems studied in aqueous solutions (26), which may be attributed to the solvent effect. The larger β values of the 1:1 complexes of glycine and *O*-Bzl-L-tyrosine compared to those of dipeptides and tetrapeptides are indicative of their stronger binding towards these metal ions. The formation of five-membered chelate complex is usually more favourable over other possibilities. However, the stability of the divalent metal complexes of dipeptides and tetrapeptides is enhanced more due to coordination with the peptidic nitrogen atoms. This enhancement, on the other hand, inhibits further chelation with other ligand molecules, a situation not encountered in the case of glycine and *O*-Bzl-L-tyrosine.

Conclusions

The observed difference in the log β_{101} value (Table 1) for Gly and *O*-Bzl-L-Tyr in 80 wt.% DMSO – water from the corresponding values in water only (Table 2*c*) is attributed to solvent effect. The higher electron density over the oxygen atom in DMSO compared to that in water renders the protonated amino group less electronegative and, consequently, the acidic proton of the carboxylic group will be more firmly held, i.e. log β_{101} is higher. On the other hand, solvation of the carboxylate ions of the dipolar species by water molecules and subsequent ease of abstraction of a proton from the terminal protonated amino group is not possible by an aprotic solvent as DMSO. This is confirmed by comparing the low values of log β_{10-1} of either Gly or *O*-Bzl-L-Tyr in 80 wt.% DMSO – water mixture with those in water only (Tables 1 and 2).

For the protonation equilibria in the case of di- and tetrapeptides, the same solvent effect is still operating, i.e., log β_{101} should be higher. Besides, one should also consider that as the protonated amino and carboxylic groups are now far apart from each other due to increase in chain length, the protonation constant in these ligands will be higher than the corresponding values in Gly or *O*-Bzl-L-Tyr systems (Tables 1 and 2).

For the deprotonation equilibria of di- and tetrapeptides, log β_{101} values are, as expected, higher than the corresponding values of Gly and *O*-Bzl-L-Tyr due to the effect of chain length. On the other hand, solvent effect has more or less no observed role.

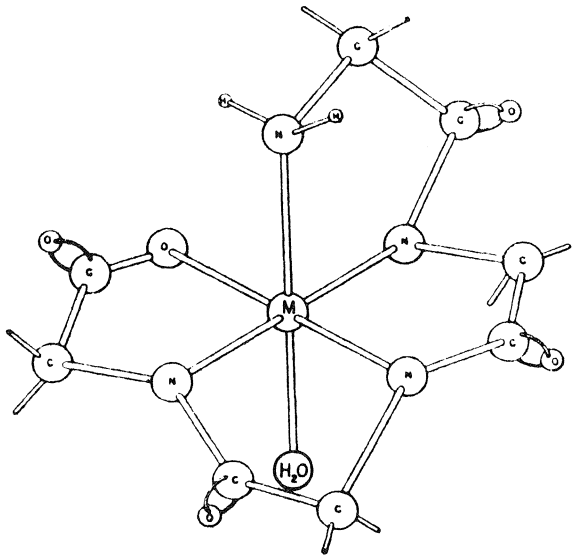

FIG. 4. Possible structure of the complex.

It is also clear that chelating properties of glycine and *O*-Bzl-L-tyrosine copper(II) ions are more pronounced than those of tetrapeptides, evidenced by the values of β_{11-1}. However, the enhanced loss of the peptidic protons by the metal ions probably increases the chelating effect of tetrapeptides over that of glycine and *O*-Bzl-L-tyrosine and even over that of dipeptides (cf. Table 2). Although the structures of these complexes have not been determined, it is not unreasonable to assume that they may have the structure shown in Fig. 4, in which penta-coordinated complex species is present. The vacant hexa-coordinate site may be occupied further by a water molecule or a hydroxide ion.

1. P. A. KOBER and A. B. HAW. J. Am. Chem. Soc. **38**, 457 (1916).
2. J. CHOUTEAU and H. LEONORMANT. C.R. Acad. Sci. Paris, **232**, 1479 (1951).
3. J. CHOUTEAU. C.R. Acad. Sci. Paris, **232**, 2314 (1951).
4. I. M. KOLTHOFF and B. R. WILLEFORD, JR. J. Am. Chem. Soc. **79**, 2956 (1957).
5. E. BRESLOW. J. Biol. Chem. **239**, 3252 (1964).
6. R. A. BRADSHAW, W. T. SHEARER, and F. R. N. GURD. J. Biol. Chem. **243**, 3817 (1968).
7. T. PETERS, JR. and F. A. BLUMENSTOCK. J. Biol. Chem. **242**, 1574 (1967).
8. M. K. KIM and A. E. MARTELL. Biochemistry, **3**, 1169 (1964).
9. M. K. KIM and A. E. MARTELL. J. Am. Chem. Soc. **88**, 914 (1966).
10. J. D. BELL, H. C. FREEMAN, A. M. WOOD, R. DRIVER, and W. R. WALKER. Chem. Commun. 1441 (1969).

11. M. T. BARNET, H. C. FREEMAN, D. A. BUCKINGHAM, I. N. HSU, and D. VAN DER HELM. Chem. Commun. 367 (1970).
12. H. C. FREEMAN. *In* Advances in protein chemistry. *Edited by* C. B. Anfinsen, M. L. Anson, J. T. Edsall, and F. M. Richards. Academic Press, New York. 1967. (*a*) p. 342; (*b*) pp. 348–349; (*c*) p. 404.
13. K. E. FALK, H. C. FREEMAN, T. JANSON, B. G. MALMSTROM, and T. VANNGARD. J. Am. Chem. Soc. **89**, 6071 (1967).
14. T. H. CRAWFORD and J. O. DALTON. Arch. Biochem. Biophys. **131**, 123 (1969).
15. M. S. MICHAILIDIS and R. B. MARTIN. J. Am. Chem. Soc. **91**, 4683 (1969).
16. H. C. FREEMAN, J. M. GUSS, and R. L. SINCLAIR. Chem. Commun. 485 (1968).
17. A. SASS-KORTASK, D. I. M. HARRIS, S. J. GOODMAN, M. HAWKE, and R. H. SMUKLER. Can. Med. Assoc. J. **92**, 368 (1965); D. I. M. HARRIS and A. SASS-KORTASK. J. Clin. Invest. **46**, 659 (1967).
18. P. Z. NEUMANN and M. SILVERBERG. Proc. Can. Fed. Biol. Soc. **8**, 49 (1965).
19. J. AL-HASSAN, J. S. DAVIES, and C. H. HASSALL. J. Chem. Soc. Perkin Trans. I, 2342 (1974).
20. E. WUNCH, G. FRIES, and A. ZWICK. Chem. Ber. **91**, 542 (1958).
21. L. G. VAN UITERT and C. G. HASS. J. Am. Chem. Soc. **75**, 451 (1953).
22. H. T. S. BRITTON. *In* Hydrogen ions: their determination and importance in pure and industrial chemistry. Vol. 1. 4th ed. Chapman and Hall, London. 1955. p. 365.
23. E. M. WOOLLEY, D. G. HARKOT, and L. G. HEPLER. J. Phys. Chem. **74**, 22 (1970).
24. A. SABATINI, A. VACCA, and P. GANS. Talanta, **21**, 53 (1974).
25. P. GANS, A. SABATINI, and A. VACCA. Inorg. Chim. Acta, **18**, 237 (1976).
26. L. G. SILLEN and A. E. MARTELL. *In* Stability constants of metal ion complexes. Spec. Publ. No. 17. 1964 and Supplement No. 1, Spec. Publ. No. 25. 1971. The Chemical Society, London.
27. H. IRVING and R. J. P. WILLIAMS. Nature, **162**, 746 (1948).

Ethylenediamine-*N*,*N*′-diacetic acid complexes with divalent manganese, zinc, cadmium, and lead: a thermodynamic study

R. J. GUALTIERI, W. A. E. MCBRYDE, AND H. K. J. POWELL

Guelph–Waterloo Centre for Graduate Work in Chemistry, University of Waterloo, Waterloo, Ont., Canada N2L 3G1

Received June 2, 1978

R. J. GUALTIERI, W. A. E. MCBRYDE, and H. K. J. POWELL. Can. J. Chem. **57**, 113 (1979).

The four protonation constants are reported for the dianion of ethylenediamine-*N*,*N*′-diacetic acid (H_2L), 25°C, I = 0.10 M (KNO_3), (log k_i = 9.60, 6.51, 2.12, 1.3). log K(potentiometric) and ΔH(calorimetric) data are reported for the formation of the complexes [ML], M = Mn^{2+}, Zn^{2+}, Cd^{2+}, and Pb^{2+} (log K = 6.87, 10.99, 9.16, and 10.66; ΔH = −2.9, −24.4, −16.7, and −28.0 kJ mol^{-1} respectively). The complexes [ZnL] and [PbL] undergo (aqua) proton dissociation reactions, [ML] + $H_2O \rightleftharpoons$ [ML(OH)] + H^+; log K_D = −10.56 and −11.02, ΔH_D = +60.7 and +38.5 kJ mol^{-1}, respectively. Potentiometric and nmr studies indicate that the ligand undergoes a slow (metal catalysed) hydrolysis or rearrangement in aqueous acid.

R. J. GUALTIERI, W. A. E. MCBRYDE et H. K. J. POWELL. Can. J. Chem. **57**, 113 (1979).

On rapporte les quatre constantes de protonation du dianion de l'acide éthylènediamine *N*,*N*′-diacétique (H_2L), à 25°C, I = 0.10 M (KNO_3), (log K_i = 9.60, 6.51, 2.12 et 1.3). On rapporte des données de log K(potentiométrique) et ΔH(calorimétrique) pour la formation des complexes [ML], M = Mn^{2+}, Zn^{2+}, Cd^{2+} et Pb^{2+} (log K = 6.87, 10.99, 9.16 et 10.66; ΔH = −2.9, −24.4, −16.7 et −28.0 kJ mol^{-1}, respectivement). Les complexes [ZnL] et [PbL] subissent des réactions de dissociation protonique (aqua), [ML] + $H_2O \rightleftharpoons$ [ML(OH)] + H^+; log K_D = −10.56 et −11.02, ΔH_D = +60.7 et +38.5 kJ mol^{-1}, respectivement. Des études rmn et potentiométriques indiquent qu'en milieu aqueux le ligand subit une hydrolyse lente (catalysée par les métaux) ou une transposition.

[Traduit par le journal]

Introduction

In the course of testing a new calorimetric system the complexing reactions of ethylenediamine-*N*,*N*′-diacetic acid (H_2L) with the divalent ions of Mn, Zn, Cd, and Pb were studied. The formation of the Mn, Zn, and Cd complexes (also Co, Ni) had been the subject of an earlier potentiometric and calorimetric study (1). However, this work did not consider the protonation reactions of the acetato groups in the zwitterion H_2L, $(-CH_2\overset{+}{N}H_2CH_2COO^-)_2$. Subsequent studies (2–4) have indicated log K values of ca. 2.4 and 1.8 for these reactions; thus the reaction $H_2L + H^+ \rightarrow H_3L^+$ will be important in the pH range in which NiL forms (2.5–3.5) and in which CoL and ZnL form (3.5–4.5). Further, McLendon *et al.* (5) have reported the formation of the species $[Co(HL)]^+$ (as well as [CoL] and $[CoL(OH)]^-$), and Schroeder and Johnson (3) reported $[M(HL)]^+$ (also [ML], $[ML(OH)]^-$, and $[M_2L]^{2+}$), M = Pb, Zn, although species $[M(HL)]^+$ were not reported by Degischer and Nancollas (1) for Co or Zn, nor for Ni which complexes at lower pH (6).

This work reports the four protonation constants for the diacetato anion L^{2-}, and enthalpy data for the formation of HL^- and H_2L. Log K and ΔH values are reported for the formation of [ML], M = divalent Mn, Zn, Cd, Pb, and of [ML(OH)], M = Zn, Pb. It was observed that solutions of the ligand and metal ions were not stable; for solutions kept at 25°C titration curves showed a steady increase in pH with time, especially at $\bar{n}_L > 0.8$. Nuclear magnetic resonance studies established that a slow decomposition or rearrangement of the ligand occurs in aqueous acid solution.

Experimental and Results

Materials

Ethylenediamine-*N*,*N*′-diacetic acid, EDDA (Aldrich 15, 818-6), was twice recrystallised from hot water. A sample of commercial EDDA required soxhlet extraction with 10% v/v methanol/ethanol (24 h) to remove adsorbed impurities before recrystallisation. The formula weight by titration against KOH, using Gran's plot to determine the end point was 176.6; calcd 176.2.

Stock solutions of $Mn(ClO_4)_2$, $Zn(NO_3)_2$, $Cd(NO_3)_2$, and $Pb(NO_3)_2$ were prepared from Analar grade reagents and acidified, ca. 2.5 × 10^{-3} M HNO_3. Stoichiometry was confirmed by titration against standard EDTA, using appropriate indicators and pH (7, 8).

pH Measurements

A Beckman Calomel electrode and Beckman E-2 glass electrode were used in conjunction with a Radiometer digital pH meter PHM 52. The electrodes were calibrated as a [H^+] probe by titration of HNO_3 into solutions of KNO_3 (p[H^+] 2.0–2.7), KNO_3/HNO_3 (p[H^+] 1.5–2.0), acetic acid (p[H^+] 3.7–5.8) (9), and potassium hydrogen phthalate (p[H^+] 4.0–

0008-4042/79/010113-06$01.00/0

TABLE 1. Thermodynamic data for protonation of $(-CH_2NHCH_2COO^-)_2$, 25°C, 0.1 *M* KNO_3

$\log k_1$	$\log k_2$	$\log k_3$	$\log k_4$	$\frac{\Delta H_1}{\text{kJ mol}^{-1}}$	$\frac{\Delta H_2}{\text{kJ mol}^{-1}}$	Reference
9.60±0.01	6.51±0.01	2.12±0.01	1.3±0.1	−33.2±0.1	−31.7±0.1	This work
9.62	6.55			−31.2	−30.6	1
9.63	6.55					5
9.67	6.57	2.32				2
9.57	6.48					31
9.58	6.59					21
9.59	6.69	2.37	1.85			4[a]

[a] 1 *M* $NaClO_4$.

5.9) (10), and of KOH into KNO_3 ($p[H^+]$ 10.8–11.8), μ = 0.10 *M* (KNO_3). All pH(measured) − $p[H^+]$ data were colinear within experimental error, the least-squares line for 90 data points being $pH_m = (1.012 \pm 0.001)p[H^+] + (0.037 \pm 0.003)$.

Ligand protonation was studied by titration of (*i*) HNO_3 (0.9944 *M*), or (*ii*) KOH (0.5475 *M*), from a Gilmont micrometer syringe into solutions of H_2L (ca. 3×10^{-3} *M*) and KNO_3 (*I* = 0.10 *M*). The step-wise protonation constants in Table 1 were computed from derived $\bar{n}_H$(obs) − pH data by use of the least-squares procedures detailed elsewhere (11). ($\bar{n}_H$ is the average number of protons bound per ligand molecule.) The protonation constants were determined for 5 titrations each of 50–60 data points in the range $\bar{n}_H$ 0.25–3.0; *R* factors (12) of ca. 0.25 were achieved and there were no systematic trends in the residuals, $\bar{n}_H$(obs) − $\bar{n}_H$(calcd) (13). (At $\bar{n}_H$ 3.0 the solution composition was 21% H_4L, 57% H_3L, 22% H_2L.)

Titration of KOH into solutions of ligand (ca. 4.3×10^{-3} *M*), metal salt (ca. 4.0×10^{-3} *M*), and KNO_3 gave titration curves with buffer regions (at pH 5.4–6.8, 3.3–4.5, 4.2–5.4, and 3.5–4.8 for Mn, Zn, Cd, and Pb, respectively) followed by end points corresponding to the addition of two moles of OH^- per mole of metal ion, i.e. the reaction

$$M(aq)^{2+} + H_2L + 2OH^- \rightarrow [ML] + 2H_2O$$

plus one mole of OH^- per mole of excess acid (HNO_3) and per mole of excess ligand. In each case a second buffer region followed at pH > 10. The Zn–EDDA and Pb–EDDA solutions were stable at high pH; Cd–EDDA solutions showed a downward drift in pH at pH > 10 and a gelatinous precipitate was apparent at pH 11. The Mn–EDDA solutions became increasingly sensitive to O_2 at high pH. Titration solutions under N_2 developed a pale amber colour at pH > 10; on exposure to air these solutions rapidly became deep amber and precipitated MnO_2. The two buffer regions were interpreted in terms of reactions [1] and [2], respectively. Values of $\log K_1$ and $\log K_D$ are given in Table 2.

$$[1] \qquad M(aq)^{2+} + L^{2-} \overset{K_1}{\rightleftharpoons} [ML]$$

$$[2] \qquad [ML] + H_2O \overset{K_D}{\rightleftharpoons} [ML(OH)]^- + H^+$$

All metal–ligand solutions were freshly prepared and/or stored at 4°C between titrations. Solutions (Zn, Cd) maintained at 25°C gave titration curves which displaced to higher pH at ca. 0.02 pH/12 h at $\bar{n}_L$ 0.2–0.8 and 0.1–0.3 pH/12 h at $\bar{n} > 0.9$.

Calorimetric Measurements

An LKB 8700-1 calorimeter was modified as follows. The polyethylene titrant coil was replaced by a glass titrant line (2 mm od) which entered the submerged outer container of the calorimeter via one of the support chimneys and had a single coil 7.5 cm in diameter inside this container. Titrant was delivered from a Gilmont micrometer syringe. Time-resistance measurements were effected by feeding the out-of-balance signal from the dc bridge into a Hewlett-Packard 419 A dc null voltmeter; the amplified signal was fed to a strip chart recorder (Hewlett-Packard Moseley 7101B). The precision of the system was estimated from electrical calibrations. The ratio of electrical heat input to measured resistance change (interpolated from the recorder trace and bridge settings before and after 'reaction') was reproducible to ±0.2% for reactions of 5–14 J. The accuracy of the system was checked by determining the enthalpy change for protonation of aqueous 2-amino-2-hydroxymethylpropane-1,3-diol (tris) with HCl; the mean and standard deviation of 7 measurements (measured heat change ca. 13 J) was −47.2 ± 0.2 kJ mol^{-1} (lit. (14, 15) −47.48 and −47.44 kJ mol^{-1}).

For the protonation of L^{2-}, buffered solutions of ligand (ca. 6.5×10^{-3}, $\bar{n}_H$ 0.2–0.3, *I* 0.10 *M* KNO_3) were titrated in the calorimeter with HCl (ca. 1 *M*). The determination of ΔH_i values from the measured heat changes (ca. 6.5–10 J, corrected for the heat of dilution of HCl titrant (16) and for the neutralization of OH^- (17) produced by reaction [3]), and the changes in solution composition between successive titration points, followed procedures detailed previously (18).

$$[3] \qquad H_2O + \text{ligand} \rightleftharpoons OH^- + \text{ligand,}H^+$$

The step-wise enthalpy changes given in Table 1 were determined from 12 data points (3 titrations).

For the complexes [ML] (and $[ML(OH)]^-$) calorimetric measurements involved titration of HNO_3 (ca. 1 *M*) into solutions of metal salt (ca. 6×10^{-3} *M*), EDDA (ca. 6.7×10^{-3} *M*), and KNO_3 (*I* = 0.10 *M*) buffered to appropriate pH by addition of KOH ($\bar{n}_L = 0.8$ or $[ML(OH)]^-/C_M = 0.3$); i.e. the enthalpy changes for (*i*) protonation,

$$[ML(OH)]^- + H^+ \rightarrow [ML]$$

and (*ii*) dissociation,

$$[ML] + nH^+ \rightarrow M(aq)^{2+} + H_nL^{(n-2)+}$$

of the complex were determined. Measurements were restricted to the composition range for which $[H_3L]/C_L < 0.02$, i.e. pH > 3.8 and $\bar{n}_L > 0$, 0.45, 0, and 0.3 for Mn, Zn, Cd, and Pb respectively. The composition of the calorimeter solution at each titration point was determined by solving the three mass balance equations (expressions for the stoichiometric concentrations, C_L, C_M, and C_H) for $[H^+]$ and [ligand]; the iterative procedure adopted was based on an initial estimate of $[H^+]$ obtained from a parallel titration on the calorimeter

TABLE 2. Thermodynamic data for the formation of complexes [M(EDDA)] and [M(EDDA)OH], M = Mn, Zn, Cd, Pb; 25°C, 0.1 *M* KNO_3

Metal	Reference	log K_1[a]	$-\Delta H_1$ / kJ mol^{-1}	ΔS_1 / J K^{-1} mol^{-1}	log K_D[b]	ΔH_D / kJ mol^{-1}	ΔS_D / J K^{-1} mol^{-1}
Mn	This work	6.85±0.05	2.9±0.4	122±2	(−11.5±0.1)		
	1	7.05	3.6±0.4				
Zn	This work	10.99±0.02	24.4±0.6	128±2	−10.56±0.04	60.7±0.4	2±2
	1	11.22	25.5±0.4				
	3	11.71					
Cd	This work	9.16±0.02	16.7±0.2	119±1			
	1	9.40	22.5±0.4				
	31	8.99					
Pb	This work	10.66±0.02	28.0±0.5	110±2	−11.02±0.02	38.5±0.6	−82±2
	32[c]	10.43					
	3	11.71					

[a]Reaction [1].
[b]Reaction [2].
[c]0.3. *M* $NaClO_4$.

solution. The measured heat changes were corrected for the heat of dilution of HNO_3 (19), for the neutralization of OH^- (17) (reaction [3]), and for the protonation of ligand not coordinated to the metal ion. The enthalpy changes for the well separated reactions [1] and [2], ΔH_1, ΔH_D, were calculated from $Q_{corr} = R\Delta H_i$ where R is the change in the number of moles of [ML] or $[ML(OH)]^-$, respectively, between successive titration points. Results (mean ± standard deviation, 6–10 data points) are given in Table 2.

Nuclear Magnetic Resonance Measurements

Nuclear magnetic resonance spectra were recorded on a Varian T-60 spectrometer for solutions of EDDA in D_2O/CF_3COOH at pH = 0.8 and 2.25, using TMS as external standard.

Discussion

Ligand Protonation

The first and second protonation reactions of the dianion $(—CH_2NHCH_2COO^-)_2$ have been studied by several workers and the log k_i values are similar to those reported in this study (Table 1). It is probable that discrepancies arise mainly from the method of estimating $[H^+]$ from the measured pH (11). In this work the electrode pair was calibrated directly as a $[H^+]$ probe, at the same ionic strength as for the titrations, by use of buffers for which $[H^+]$ could be calculated from known concentration quotients (CH_3COOH) (9) or from known thermodynamic equilibrium constants and activity coefficient expressions for individual ions (phthalic acid) (10), and by use of HNO_3 and KOH solutions of known stoichiometry. For KOH solutions $p[H^+]$ was calculated assuming $pK_w = 13.778$ for 0.10 *M* KNO_3 (20).

Yamada *et al.* (4) have reported values of log k_3 and log k_4 for carboxylate protonation of the zwitterion $(—CH_2\overset{+}{N}H_2CH_2COO^-)_2$ (2.37, 1.85, 1 *M* $NaClO_4$) while Schroeder and Johnson (3) and Harris and Martell (2) have reported values for log k_3 (1.54, 1 *M* $NaClO_4$, and 2.36, 0.10 *M* KNO_3, respectively). The measurement of log k values at low pH in aqueous solution is prone to large uncertainties in the calculations, and in this work measurements were restricted to pH ≥ 2.2, at which ≤21% of the ligand exists as H_4L^{2+}. Although our value of log k_4 carries a significant uncertainty the existence of this species in solution is confirmed by the low values of R (0.22%) and $\sigma_{\bar{n}}$ (±0.005) obtained in calculations; by assuming $k_4 = 0$, a value of log $k_3 = 2.31 \pm 0.02$ was obtained (in agreement with Harris and Martell (2)) but R (2.9%) and $\sigma_{\bar{n}}$ (±0.06) were significantly higher.

The values reported for ΔH_1 and ΔH_2 were derived from 11 titration points and the least-squares fitting of ΔH_i ($Q_{obs} = \alpha\Delta H_1 + \beta\Delta H_2$) gave a standard deviation of ±0.07 *J* in Q_{obs} (ca. 0.8%). Our results are ca. 15% higher than those of Silva and Samões (21) (temperature coefficient method) and ΔH_1 is ca. 6% higher than that reported by Degischer and Nancollas (1). No attempt was made to measure ΔH_3 and ΔH_4. It was anticipated that these enthalpy values for carboxylate protonation would be very small (22); subsequent calorimetric work on metal–EDDA species was limited to the pH range where $([H_3L] + [H_4L])/C_L < 0.02$.

Ligand Stability

It was observed that the pH of solutions of Zn or Cd and EDDA increased with time at 25°C. The pH increased by ca. 0.01–0.02/12 h in the composition range $\bar{n}_L = 0.1$–0.8, and by ca. 0.03 (Zn) or 0.1 (Cd)

at $\bar{n}_L = 0.9$. Solutions stored at 4°C gave reproducible titration curves after 12 and 24 h. The increase in pH, and decrease in calculated values of K_1, were consistent with either a rearrangement or hydrolysis of the ligand to give product(s) which were more basic and/or weaker complexing agents. An nmr study on a solution of EDDA in D_2O/CF_3COOH at pH 2.25 ($\bar{n}_H \sim 3.0$) established a slow reaction with a half-life of ca. 14 days at 25°C; zinc ions (Zn/EDDA ~ 1) increased the reaction rate ca. 1.5-fold. The resonance for N—CH_2—CH_2—N protons of EDDA broadened and split, indicating the non-equivalence of the two nitrogen atoms in the product species, while the resonance for —CH_2—COOH methylene protons split into two new downfield absorptions. An hydrolysis reaction to give glycollic acid and ethylenediamine-*N*-acetic acid, or an intramolecular condensation to give a cyclic amide, $\overline{CH_2CH_2NHCH_2CO}NCH_2COOH$, has products consistent with the observed pattern of nmr resonances. Comparison with the spectrum for glycollic acid in the reaction medium established that this was not a reaction product (glycollic acid resonance was ca. 1–2 Hz downfield from the low field —CH_2COOH resonance).

Metal Complexes

log *K* values for the formation of complexes [ML] and [ML(OH)] are given in Table 2 and compared with those reported by other workers. Individual values of log K_1 showed no drift in the range $\bar{n}_L$ 0.1–0.9 for freshly prepared solutions and thus it is unlikely that protonated species $[M(HL)]^+$ are formed. (For solutions aged at 25°C log K_1 decreased by ca. 0.21 as $\bar{n}_L$ increased from 0.1 to 0.9, an observation which would be consistent with formation of a protonated complex. It is possible that the postulates of species $[M(HL)]^+$, M = Co, Zn, Pb (3, 5), are based on data for aged solutions.) The published value (5) of log *K* ($[CoL] + H^+ \rightleftharpoons [Co(HL)]^+$) = 4.20 gives a value of log *K* ($Co(aq)^{2+} + HL^- \rightleftharpoons [Co(HL)]^+$) = 5.8 which is greater than log *K* for the cobalt(II)–glycinate complex (5.1) (23); one would expect bidentate HL (—$OOCH_2\overset{+}{N}H_2$-$CH_2CH_2NHCH_2COO^-$) to form a less stable complex than glycine cf. the relative stabilities of cobalt(II) complexes and amino acids $\overset{+}{N}H_3(CH_2)_x$-$CH(NH_2)COO^-$ (24). The published values of log *K* for $[M(HL)]^+$, M = Cu, Pb, Zn, give rise to a similar disparity with the data for glycine.

The log K_1 values reported here are uniformly lower (ca. 0.2) than those reported by Degischer and Nancollas (1). This discrepancy relates in part to their neglect of log k_3 (e.g. for Mn we calculate log $K_1 = 6.93 \pm 0.05$ by use of their log k_1 and log k_2) and in part to the different methods of estimating $[H^+]$ from pH_m (for a discussion on this point see ref. 11). The ΔI values reported for [MnL] and [ZnL] are in close agreement with those of Degischer and Nancollas (1), but the value for [CdL] is significantly different (this work, 5 titrations). Values for [PbL] and $[ML(OH)]^-$ have not been reported previously.

The entropy changes for formation of [ML] complexes are all similar; this could be interpreted as indicating a similar reaction for each metal ion, viz.

$$M(aq)^{2+} + L^{2-} \rightarrow [ML(H_2O)_x] + (6 - x)H_2O$$

However, the partial molal entropies of the reactant ions $M(aq)^{2+}$ are very different (−83.7, −106.5, −61.1, and +23 J K^{-1} mol^{-1} for Mn, Zn, Cd, and Pb respectively (25)). Assuming that the entropies for the larger, neutral, complex species [ML] may be less dissimilar, the sum

$$\Delta S + \bar{S}_{M(aq)^{2+}} (= (6 - x)\bar{S}_{H_2O} + \bar{S}_{[ML]} - \bar{S}_L)$$

can then be used to infer differences in the nature of the species $[ML(H_2O)_x]$. The values of $\Delta S + \bar{S}_{M(aq)^{2+}}$ for Mn, Zn, Cd, and Pb are 38, 22, 58, and 133 J K^{-1} mol^{-1}, respectively, suggesting that for Pb the term $(6 - x)H_2O$ is significantly larger, i.e. the Pb atom has a lower co-ordination number in the complex, probably four, as compared with six for the other ions. The difference of ca. 90 J K^{-1} mol^{-1} in $\Delta S + \bar{S}_{M(aq)^{2+}}$ for Pb and the other metals represents the contribution to ΔS from the release of *n* more water molecules from the co-ordination sphere of the Pb atom, i.e.

$$n\bar{S}_{H_2O} + \bar{S}_{[PbL]} - \bar{S}_{[ML(H_2O)_n]} \sim 90 \text{ J K}^{-1} \text{ mol}^{-1}$$

Given that $\bar{S}_{H_2O} = 70$ J K^{-1} mol^{-1} (16) a value of $n = 2$ would appear consistent with the experimental data.

The significantly different values of both ΔH_D and ΔS_D for the formation of $[ZnL(OH)]^-$ and $[PbL(OH)]^-$ afford further evidence for different structures for these two ions. The negative value of ΔS_D for $[PbL(OH)]^-$ would be consistent with the loss of entropy of a solvent water molecule ($[PbL] + H_2O \rightarrow [PbL(OH)]^- + H^+$; ΔS_D − 82 J K^{-1} mol^{-1}) in contrast to the deprotonation of a co-ordinated water molecule ($[ZnL(H_2O)_2] \rightarrow [ZnL(OH)H_2O]^- + H^+$; ΔS_D + 2 J K^{-1} mol^{-1}). The value of $\Delta S'$ for the reaction

$$[ML] + OH^- \rightarrow [ML(OH)]^-$$

is given by $\Delta S' = \Delta S_D + \Delta S_W$ where ΔS_W(= +80 J K^{-1} mol^{-1}) (16) is for the reaction $H^+ + OH^- \rightarrow H_2O$. The values are +82 and −2 J K^{-1} mol^{-1} for

TABLE 3. Comparison of some thermodynamic data for formation of ML complexes where L = aminopolycarboxylate or polyamine. The data are for $t \sim 25°C$, $\mu \sim 0.1$ ($-\Delta H$, in kJ mol^{-1}; ΔS in J K^{-1} mol^{-1})

Metal ion	Thermodynamic quantity	Value			
		EDTA	NTA	EDDA	TRIEN
Mn^{2+}	$\log K_1$[a]	13.6–14.0	7.4	6.85	4.9
	$-\Delta H_1$	19.2–21.8	−(4.8–6.0)	2.9	9.6
	ΔS_1	172–201	158–162	122	63
	$\log K_D$[b]		~ −12	−11.5	
Zn^{2+}	$\log K_1$[a]	16.3–16.7	10.4–10.7	10.99	11.9–12.1
	$-\Delta H_1$	18.8–23.4	3.5–3.6	24.4	35–37
	ΔS_1	230–247	190–192	128	105–113
	$\log K_D$[b]	−11	−10.45	−10.56	
Cd^{2+}	$\log K_1$[a]	16.4–16.6	9.5–9.8	9.16	10.8
	$-\Delta H_1$	38.1–42.2	−16.6	16.7	38
	ΔS_1	159–184	131	119	79
	$\log K_D$[b]			~ −12	
Pb^{2+}	$\log K_1$[a]	17.7–18.3	11.4–11.8	10.66	9.9
	$-\Delta H_1$	54.8–59.0	15.9	28	
	ΔS_1	141–159	164	110	
	$\log K_D$[b]			−11	

[a]Reaction [1].
[b]Reaction [2].

Zn and Pb respectively; these may be compared with values for complexes $[ML(H_2O)_n]^{2+}$ ($n \neq 0$) where L is a triamine ligand: M = Cu^{2+}, L = 3-azaheptane-1,7-diamine ($\Delta S' = +66$ J K^{-1} mol^{-1}) (26), 4-azaheptane-1,7-diamine (47) (ref. 27), 3-azahexane-1,6-diamine (58) (ref. 28); M = Zn^{2+}, L = 4-azaheptane-1,7-diamine (47), 3-azahexane-1,6-diamine (94) (ref. 28).

It is appropriate to compare the results of this work with comparable data for other aminopolycarboxylic acids. The extensive compilation by Wright, Holloway, and Reilley (29) deals mainly with ethylenediaminetetraacetic acid and structurally related ligands which are 6-dentate ligands. It is probably more suitable to compare a 4-dentate ligand where the number of bonds formed and solvent molecules displaced may be the same as for EDDA. In Table 3 are compiled data from standard sources (23, 30) showing such comparisons. As 4-dentate ligands NTA (one nitrogen, three oxygen donors) and TRIEN (four nitrogen donors) are listed. There are few obvious inferences to be drawn from this information. In all the cases listed EDDA stands intermediate between NTA and TRIEN, with clear evidence of the greater energy of the metal–nitrogen bonds as apparent in the greater enthalpy decreases in passing through the sequence NTA → EDDA → TRIEN. This is particularly the case with the d^{10} acceptor ions Zn^{2+} and Cd^{2+}. The near equivalence of $-\Delta G_1$ in passing from NTA to EDDA suggests an isokinetic relationship among the metal complexes of these two ligands, but further investigation is required before such speculation should be undertaken.

1. G. DEGISCHER and G. H. NANCOLLAS. Inorg. Chem. **9**, 1259 (1970).
2. W. R. HARRIS and A. E. MARTELL. Inorg. Chem. **15**, 713 (1976).
3. K. H. SCHROEDER and B. G. JOHNSON. Talanta, **21**, 671 (1974).
4. S. YAMADA, J. NAGASE, S. FUNAHASHI, and M. TANAKA. J. Inorg. Nucl. Chem. **38**, 617 (1976).
5. G. MCLENDON, R. J. MOTEKAITIS, and A. E. MARTELL. Inorg. Chem. **14**, 1993 (1975).
6. S. CHABEREK and A. E. MARTELL. J. Am. Chem. Soc. **74**, 6228 (1952).
7. A. I. VOGEL. Textbook of quantitative inorganic analysis. 3rd ed. Wiley, New York. 1968.
8. R. BELCHER and A. J. NUTTEN. Quantitative inorganic analysis. 2nd ed. Butterworths, London. 1960. p. 299.
9. H. S. HARNED and F. C. HICKEY. J. Am. Chem. Soc. **59**, 1284 (1937).
10. W. J. HAMER and S. F. ACREE. J. Res. Natl. Bur. Stand. **35**, 381 (1945); W. J. HAMER, G. D. PINCHING, and S. F. ACREE. J. Res. Natl. Bur. Stand. **35**, 539 (1945).
11. G. R. HEDWIG and H. K. J. POWELL. Anal. Chem. **43**, 1206 (1971).
12. A. VACCA, A. SABATINI, and M. A. GRISTINA. Coord. Chem. Rev. **8**, 45 (1972).
13. A. BRAIBANTI, F. DALLAVALLE, E. LAPORATI, and G. MORI. J. Chem. Soc. Dalton, 323 (1973).
14. I. GRENTHE, H. OTS, and O. GINSTRUP. Acta Chem. Scand. **24**, 1067 (1970).
15. G. OJELUND and I. WADSO. Acta Chem. Scand. **22**, 2691 (1968).
16. D. D. WAGMAN, W. H. EVANS, V. B. PARKER, I. HALOW,

S. M. BAILEY, and R. H. SCHUMM. Natl. Bur. Stand. Tech. Note 270-3 (1968).
17. J. J. CHRISTENSEN, R. M. IZATT, and J. D. HALE. J. Phys. Chem. **67**, 2605 (1963).
18. G. R. HEDWIG and H. K. J. POWELL. J. Chem. Soc. Dalton, 793 (1973).
19. R. C. WEAST (*Editor*). Handbook of chemistry and physics. 49th ed. The Chemical Rubber Co. 1969.
20. R. F. JAMESON and M. F. WILSON. J. Chem. Soc. Dalton, 2607 (1972).
21. J. J. R. F. SILVA and M. L. S. SIMÕES. Rev. Port. Quim. **11**, 54 (1969).
22. J. J. CHRISTENSEN, R. M. IZATT, and L. D. HANSEN. J. Am. Chem. Soc. **89**, 213 (1967).
23. L. G. SILLEN and A. E. MARTELL. Stability constants. Chem. Soc. Spec. Publ. Nos 17 and 25. Chemical Society, London. 1964 and 1971.
24. M. GOLD and H. K. J. POWELL. J. Chem. Soc. Dalton, 1418 (1976).
25. W. E. DASENT. Inorganic energetics. Penguin Library of Physical Sciences. 1970. p. 132.
26. M. GOLD and H. K. J. POWELL. J. Chem. Soc. Dalton, 230 (1976).
27. P. PAOLETTI, F. NUZZI, and A. VACCA. J. Chem. Soc. A, 1385 (1966).
28. R. BARBUCCI, L. FABBRIZZI, and P. PAOLETTI. J. Chem. Soc. Dalton, 2403 (1974).
29. D. L. WRIGHT, J. H. HOLLOWAY, and C. N. REILLEY. Anal. Chem. **37**, 884 (1965).
30. J. J. CHRISTENSEN, D. E. EATOUGH, and R. M. IZATT. Handbook of metal–ligand heats. Marcel Dekker Inc., New York. 1975.
31. L. C. THOMPSON. J. Inorg. Nucl. Chem. **24**, 1083 (1962).
32. M. KODAMA. Bull. Chem. Soc. Jpn. **47**, 1547 (1974).

The addition of 2,4-dinitrobenzenesulphenyl chloride to 1,3-disubstituted allenes: a reexamination

DENNIS G. GARRATT AND PIERRE BEAULIEU

Department of Chemistry, University of Ottawa, Ottawa, Ont., Canada K1N 9B4

Received June 29, 1978

DENNIS G. GARRATT and PIERRE BEAULIEU. Can. J. Chem. **57**, 119 (1979).

The reaction of 2,4-dinitrobenzenesulphenyl chloride with eight alkyl 1,3-disubstituted allenes in methylene chloride solution has been investigated. In contrast to earlier reports, attack by sulphur is found to occur exclusively at the central allenic carbon. The direction of approach of sulphenyl chloride leads preferentially to the formation of the *E* isomers in accord with the concept of steric approach control. The ratio of *E* to *Z* alkene is found to increase as the bulk of the substituent group *cis* to the arylthio group increases. We observe, however, very little regioselectivity with respect to which of the mutually perpendicular π bonds of the allene system is attacked, suggesting the presence of an effective mechanism for transmission of inductive effects to the more distant double bond.

DENNIS G. GARRATT et PIERRE BEAULIEU. Can. J. Chem. **57**, 119 (1979).

On a examiné la réaction du chlorure de dinitro-2,4 benzènesulfényle avec huit allènes dialkylés aux positions 1 et 3 dans le chlorure de méthylène. Contrairement à certains travaux antérieurs, on observe que l'atome de soufre attaque exclusivement le carbone allénique central. L'approche du chlorure de sulfényle se fait selon une direction qui conduit de préférence à la formation des isomères *E*, comme le prévoit le concept de contrôle par l'approche stérique. Il y a augmentation du rapport entre les alcènes *E* et *Z* lorsque la taille du substituant en position *cis* par rapport au groupe arylthio augmente. Cependant, on note très peu de régiosélectivité dans l'attaque des doubles liaisons π mutuellement perpendiculaires du système allénique. Ce fait laisse supposer qu'il existe un mécanisme efficace pour transmettre les effets inductifs à la double liaison la plus éloignée.

[Traduit par le journal]

It has been reported by Jacobs and Kammerer (1) that 2,4-dinitrobenzenesulphenyl chloride adds to 2,3-pentadiene, 2,3-hexadiene, and 3,4-heptadiene to give products of both type **I** and type **II** regio-

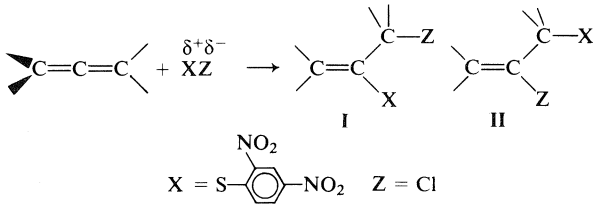

chemistry, the major adduct being of type **I** (eq. [1]). In contrast, no type **II** products were detected under similar reaction conditions from reactions involving 1,2-cyclononadiene, 1,2-cyclotridecadiene, or 1,3-di(1-adamantyl)allene. These results are at variance with those of others (2) which indicate that a given electrophile generally yields products of only one regiochemical type.

The anomalous nature of these results suggested to us that perhaps an alternative interpretation might be applicable. When the two substituents on a given terminal allenic carbon atom are different, there exist two possible directions of approach by the electrophile as shown in Scheme 1.

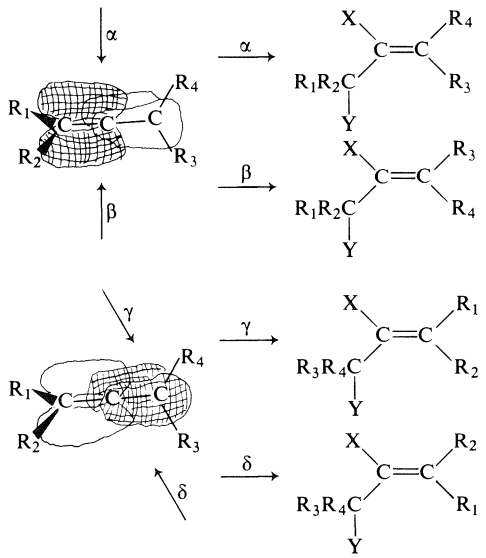

SCHEME 1

Because of the *orthogonality* of the π systems, this leads to a series of *E* and *Z* isomers. Thus in the general case, $R^1R^2C{=}C{=}CR^3R^4$, where $R^1 \neq R^2 \neq R^3 \neq R^4$, there exist eight possible addition products for an unsymmetric electrophile.

0008-4042/79/010119-09$01.00/0

TABLE 1. Kinetically controlled product distribution for the reaction of 2,4-dinitrobenzenesulphenyl chloride with a series of 1,3-disubstituted allenes in CH_2Cl_2

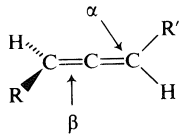

(*a*) Symmetric allenes

R = R′	*E*:*Z*
CH_3	64:36
C_2H_5	80:20
iC_3H_7	92: 8
—$(CH_2)_6$—	100: 0
—$(CH_2)_{10}$—	86:13

(*b*) Unsymmetric allenes

			E:*Z*	
R	R′	α:β	α	β
CH_3	C_2H_5	53:47	66:34	86:14
CH_3	iC_3H_7	52:48	65:35	95: 5
CH_3	tC_4H_9	42:58	69:31	100: 0

We wish to present experimental evidence which has a direct bearing upon this question.

Results

The addition of 2,4-dinitrobenzenesulphenyl chloride (DNBSC) to eight alkyl 1,3-disubstituted allenes, **1**–**8**, at ambient temperature in methylene chloride solution has been investigated. The kinetically controlled product distributions are given in Table 1.

RCH=C=CHR′

1 R = CH_3, R′ = CH_3

2 R = CH_3, R′ = C_2H_5

3 R = CH_3, R′ = iC_3H_7

4 R = CH_3, R′ = tC_4H_9

5 R = C_2H_5, R′ = C_2H_5

6 R = iC_3H_7, R′ = iC_3H_7

7 R,R′ = —$(CH_2)_6$—

8 R,R′ = —$(CH_2)_{10}$—

Although no variations in product ratios were observed during the course of the reaction, slow isomerizations were found to occur over a period of weeks. Analysis of ^1H and ^{13}C nmr spectra of the respective adducts suggests that these compounds are all formed via regiospecific attack of the arylthio moiety on the central allenic carbon giving mixtures of the isomeric *E* and *Z* alkenes.

For example, DNBSC reacts with 2,3-pentadiene, **1**, to give a 64:36 mixture of two adducts, **9** and **10**. The corresponding reaction with an unsymmetric allene, such as 2,3-hexadiene, yields four adducts. Spectral parameters are summarized in Tables 2–4.

The original assignments of **9** and **10**, by Jacobs and Kammerer (1), as 4-chloro-2-penten-3-yl and 3-chloro-2-penten-4-yl 2′,4′-dinitrophenyl sulphides (see structures **9′** and **11**, configuration undefined)

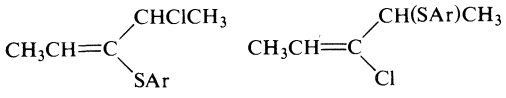

9′ **11**

as assigned by Jacobs

were based on the chemical shifts of the vinyl protons (H_3 of Table 2) and the methine protons (H_4 of Table 2) using $ClCH_2C(SAr)=CH_2$, the product of the reaction of DNBSC with propadiene, as the model system. An examination of the literature suggests that the isomeric 3,4-dichloro-2-pentenes may be better models. Byrd and Caserio (3) have reported the following ^1H nmr parameters: *E* isomer δ H_3 5.74, H_4 5.10; *Z* isomer δ H_3 5.93, H_4 4.67. A comparison of these values with those of Jacobs and Kammerer (1) and with those given in Table 2 indicates that our alternative assignments as *E*- and *Z*-4-chloro-2-penten-3-yl 2′,4′-dinitrophenyl sulphide are also consistent with the available data.

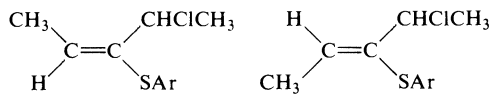

9 **10**

These regiochemical assignments are substantiated by the ^{13}C nmr chemical shifts of the methine carbons (C_3, Table 3). Thus Jacobs and Kammerer (1) assigned the major adduct **9** as that having a chlorine bonded to the methine carbon whereas the minor component of structure **11** would have the arylthio group bonded to the methine carbon. One would therefore expect the methine carbon of the major adduct to resonate at lower field because of the known dependence of ^{13}C chemical shifts on the relative electronegativities of the substituents (Cl 2.99; S 2.48). In contrast we observed resonances at δ 54.8 and 61.5. This, of course, might be interpreted in terms of a reversal of the initial assignments but model systems[1] such as *E*-2-(*RS*)-, 5-(*RS*)-, and *E*-2-(*RS*)-, 5-(*SR*)-5-chloro-3-hexen-2-yl 4′-chlorophenyl sulphide exhibit *CH*(SAr) carbon resonances at δ 45.4, 45.3, and *CH*$ClCH_3$ carbon resonances

[1]G. H. Schmid, S. Yeroshalmi, and D. G. Garratt. Unpublished results.

TABLE 2. The observed proton magnetic resonance parameters for the products of addition of 2,4-dinitrobenzenesulphenyl chloride to 1,3-disubstituted allenes

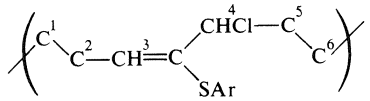

RCH=C(CHClR′)(SAr)			Chemical shifts and proton–proton coupling constants											
R	R′	Configuration	H_1	$^3J_{1,2}$	H_2	$^3J_{2,3}$	H_3	$^4J_{3,4}$	H_4	$^3J_{4,5}$	H_5	$^3J_{5,6}$	H_6	Other protons
CH_3	CH_3	*E*			2.11d	7.0	6.47q	≤0.2	5.21q	6.5	1.68			
		Z			1.90d	6.5	6.89qd	0.6	4.75qd	6.5	1.74			
C_2H_5	C_2H_5	*E*	1.13t	6.8	2.63q′	6.7	6.57t	≤0.2	5.07t	6.6	2.13q′	6.8	1.32t	
		Z	1.1t	7	2.6m		6.90t	0.5	4.62t		2.2m		1.3t	
iC_3H_7	iC_3H_7	*E*	1.16d	6.6	2.8m	10.2	6.15d	≃0.2	4.58d	9.8	2.2m	6.5	1.10d	
												6.5	0.97d	
		Z	1.18d	6.6		10	6.47dd	1.1	4.18dd	9	2.2m	6.5	1.12d	
												6.5	0.99d	
—$(CH_2)_6$—		*E*				8.5	6.68t		5.33dd	10.5	2.02m			1.0–1.8m(8H)
										3.0				
—$(CH_2)_{10}$—		*E*				8.5	6.39dd		5.05dd	9.2	2.0m			1.1–1.8m(12H)
						6.5				3.0				
		Z				7.0	6.72dd		4.75dd	10.5	2.0m			1.1–1.8m(12H)
						6.0				2.5				
CH_3	C_2H_5	*E*			2.14d	6.75	6.56q		4.96t	7.0	2.06q′		1.31t	
		Z			1.95d	6.65	6.89qd	0.5	4.62ddd	7.0			1.11t	
										6.0				
C_2H_5	CH_3	*E*	1.06t	7.5	2.54q′	7.5	6.42t		5.24q	6.5	1.72d			
		Z	1.11t	7.3			6.81td	0.5	4.78qd	6.8	1.77d			
CH_3	iC_3H_7	*E*			2.05d	7.2	6.51q		4.67d	9.6	2.3m	6.7	1.13d	
												6.7	1.02d	
		Z			1.92d	7.1	6.85q		4.30d	7.4	2.3m			
iC_3H_7	CH_3	*E*			2.8m	10.4	6.19d		5.42q	6.8	1.67d			
		Z			2.8m	7.8	6.84d		4.58q	6.6	1.73d			
CH_3	tC_4H_9	*E*			2.07d	7.2	6.63q		5.03s				1.14s	
		Z			1.95d	7.2	7.00q		4.43s				1.10s	
tC_4H_9	CH_3	*E*	1.34s				6.47s		5.67q	6.4	1.69d			

TABLE 3. Observed carbon-13 magnetic resonance parameters for the products of addition of 2,4-dinitrobenzenesulphenyl chloride to 1,3-disubstituted allenes

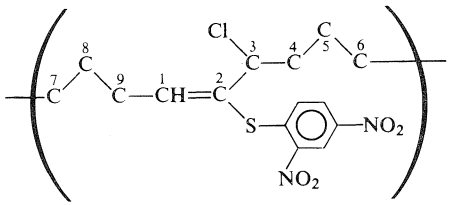

RCH=C(CHClR′)(SAr)			Chemical shift assignments														
												Aromatics					Other carbons
R	R′	Configuration	C_1	C_2	C_3	C_4	C_5	C_6	C_7	C_8	C_9	C_S	C_{oNO_2}	C_m	C_{pNO_2}	$C_{m'}$	C_o	
CH_3	CH_3	*E*	146.8	132.8	54.8	23.7					15.7	132.8	144.3	126.7	147.5	121.2	129.5	
		Z	142.0	131.9	61.5	24.5					15.7	132.0	143.4	126.9	144.7	121.7	128.6	
C_2H_5	C_2H_5	*E*	154.0	144.5	61.7	30.5	11.4			13.2	23.3		144.5	126.5	147.7	121.2	129.7	
		Z	149.5		68.1	30.9	11.2			12.9	23.7			126.8		121.7	129.0	
iC_3H_7	iC_3H_7	*E*	158.5		67.5	34.3	22.0			20.4	29.4		144.5	126.5	147.9	121.5	129.7	
		Z	155.3		72.7	33.8	21.8			20.9	30.2			126.6		121.2	129.3	
—$(CH_2)_6$—		*E*	152.1	144.2	60.0	36.8	27.7	23.6	25.5	26.7	30.1	130.2	144.5	126.3	147.7	121.3	130.4	
—$(CH_2)_{10}$—		*E*	153.9	144.6	59.3	36.8	27.8	27.0	27.2	27.4	28.5		144.6	126.6	147.5	121.3	130.0	26.2, 26.0, 24.5, 23.9
		Z	150.0		66.0	37.0	29.3	26.8	27.1	28.3	29.5			126.8		121.7	129.4	
CH_3	C_2H_5	*E*	147.2		61.5	30.5	11.4				15.9			126.5		121.4	129.5	
		Z	142.9		68.3	30.9	11.4				15.9			126.9		120.8	128.9	
CH_3	iC_3H_7	*E*	146.7		67.0	33.7	20.3 20.0				15.9			126.7		121.3	129.1	
		Z	142.7		73.4	33.3	20.7 21.3				15.9			126.9		121.6	128.7	
CH_3	tC_4H_9	*E*	148.0		69.8	38.4	27.5				17.1			126.6		121.2	128.7	
		Z	144.3		75.7	37.6	27.2				16.2			127.1		121.7	129.6	
C_2H_5	CH_3	*E*	153.5		55.1	24.2				13.2	23.3			126.6		121.8	129.9	
		Z	148.7		61.5	24.9				13.2	23.7			127.2		121.3	128.7	
iC_3H_7	CH_3	*E*	158.5		55.3	24.4				22.3 22.0	34.4			126.7		121.7	129.3	
		Z	155.2		61.0	24.8				21.7 21.3	34.3			127.0		121.9	128.7	
tC_4H_9	CH_3	*E*	161.1	148.4	55.3	24.0				30.6	35.2	131.4	144.3	126.5	148.7	121.2	129.0	

at δ 56.9, 56.8, therefore suggesting that both **9** and **10** have allylic chlorines. An examination of one bond coupling constants ($J_{3,3}$, Table 4) confirms this. Thus $J_{3,3}$ for **9** and **10** is, respectively, 151.6 and 150.6. These values are in the range expected for a carbon directly bonded to a halogen, e.g., CH_3Cl ^1J = 148.65, CH_3Br ^1J = 150.5, CH_3I ^1J = 150.3 vs. $(CH_3)_2S$ ^1J = 138.5 (4).

Further indication of the correctness of our assignments is found in the mass spectra of **9** and **10** which exhibit α cleavage with loss of a $CHClCH_3$ radial fragment from the molecular ion. No fragments were observed which could be rationalized in terms of the loss of a radical or formation of a cationic species of the formula $CH(SAr)CH_3$, as would have been anticipated from an adduct of structure **11**.

The assignment of configuration for **9** and **10** as *E* and *Z*, respectively, follows from several criteria based on ^1H and ^{13}C chemical shifts and coupling constants. From Table 2 it is seen that for trisubstituted alkenes of this type the chemical shift of the proton H_3 is shielded in the *E* isomer relative to that of the corresponding *Z* isomer and that H_4 is deshielded in the *E* isomer relative to that of the corresponding *Z* isomer. This trend is seen in the reported values of numerous other 3,4-disubstituted-2-pentenes (3, 5).

In accord with the available data for similarly substituted systems the allylic proton–proton coupling constant $^4J_{HC=CCH}$ (*cis*) is observed to be slightly larger than $^4J_{HC=CCH}$ (*trans*) thus allowing **10** to be assigned the *Z* configuration in agreement with the proton chemical shift data (6). One must take care in the interpretation of $^4J_{H,H}$ values, however, since they are quite small and change their stereochemical proportionality depending upon the nature of the remaining substituents used to define the alkene system (7).

Of more diagnostic value are vicinal carbon–proton coupling constants of the form $^3J_{CC=CH}$. The values for $^3J_{CC=CH}$ (*cis*) and $^3J_{CC=CH}$ (*trans*) are normally widely different, the ranges just overlapping, with the *trans* coupling being larger than the corresponding *cis* interaction (8). An examination of Table 4 indicates that $J_{3,1}$ ($\equiv {}^3J_{CC=CH}$) is in accord with our configurational assignments and thus reinforces our initial analysis.

These assignments are furthermore confirmed by the observed ^{13}C chemical shifts. The stereochemical dependence of ^{13}C chemical shifts is well documented (9). One of the most useful trends of this sort is the *γ-gauche* interaction, whereby the presence of a γ substituent oriented *cis* to the carbon under observation leads to a shielding relative to the corresponding system with the substituent oriented *trans*. Based on this criterion one expects the methine

TABLE 4. Carbon-13–proton coupling constants (in Hz)

$RCH{=}C(SAr)CHClR'$

R	R′	Configuration	$J_{1,1}$	$J_{1,3}$	$J_{1,9}$	$J_{3,3}$	$J_{3,4}$	$J_{3,1}$	$J_{4,4}$	$J_{4,3}$	$J_{4,5}$	$J_{9,9}$	$J_{9,1}$	$J_{m,m}$	$J_{m,m'}$	$J_{m',m'}$	$J_{m',m}$	$J_{o,o}$
CH_3	CH_3	*E*	159.2	6.9	3.0	151.6	4.3	9.1	129.4	2.8		128	2	172.0	5.0	173.9	4.6	171.7
		Z	154.2	6.8	4.2	150.6	4.5	2.4	129.9	2.3		128	2	172.5	5.4	174.9	4.9	171.2
C_2H_5	C_2H_5	*E*	156.4			147.8	4.6	10.4	127.5			127.9		173.7	4.9	171.8	4.8	171.3
		Z	152			152.7	4.5	3.1	127			127						
iC_3H_7	iC_3H_7	*E*				153.6	4.3	10.4	127.6			128.3		172.6	5.3	174.8	4.7	171.5
		Z																
	—$(CH_2)_6$—	*E*	170.0			149.5	4.1	6.0	134			130.8		171.9	5.5	174.3	4.6	172.0
	—$(CH_2)_{10}$—	*E*	157.6	6.9	3.8	149.5	4.0	6.8	133.3	2.9				171.9	5.4	174.0	4.7	171.9
		Z				147.5	4.4	2.3										
CH_3	C_2H_5	*E*	162.3	6.7	3.0	146.4	4.3	8.3	127	3.4		127.6	2.8	172.1	5.5	174.5	5.3	171.6
		Z	153	5.5	3.9	151.0	4.3	2.3	127			127.6		172.8	5.4	173.6	4.0	170.9
CH_3	iC_3H_7	*E*				151	4.0	9.8	129									
		Z				149	4.5	3.1										
CH_3	tC_4H_9	*E*	154.6	6.4	4.0	148	4.5	10.0	125.7*			128		172.0	5.3	174.5	4.4	171.8
		Z				151	4.0	1.8										
C_2H_5	CH_3	*E*	164.3			149.5	3.6	9.4	128.2	3.3		128.5	3	172.3	5.6	174.0	4.2	171.4
		Z							128.5	3.1		128						172.7
iC_3H_7	CH_3	*E*							128			129						
		Z				152	4.2	8.4										
tC_4H_9	CH_3	*E*	153.9			151.7	4.0	11.1	130.1	2.6		126.8*	4.6*	172.0	5.4	174.3	4.6	171.3

NOTE: Couplings marked with a * refer to the next carbon on the chain. Thus $J_{4,4}$ should read $J_{5,5}$ and $J_{9,9}$ as $J_{8,8}$ etc. Owing to problems of overlapping signals it was not possible to measure all coupling interactions between carbon and hydrogen.

carbon bonded to chlorine (C_3 of Table 3) to be shielded in the *E* isomer relative to the *Z* isomer. For example, C_3 of **9** resonates at δ 54.8 whereas C_3 of **10** resonates at 61.5. Little difference in chemical shifts would be expected for C_9 (see Table 3) in these isomers, since C_9 is always experiencing a *cis*-γ interaction.

Discussion

From our data is it clear that the regiochemistry of the reaction of 2,4-dinitrobenzenesulphenyl chloride with 1,3-disubstituted allenes corresponds to exclusive attack by sulphur on the central allenic carbon. In all cases the *E* isomer is found to be formed preferentially, in contrast to related studies of the halogenation and mercuration of acyclic 1,3-disubstituted allenes (see for example refs. 5*a–c* and 10). The ratio of *E* to *Z* alkene is found to increase as the bulk of the substituent group ($CH_3 < C_2H_5 < iC_3H_7 < tC_4H_9$) *cis* to the arylthio group increases. It is interesting to note, however, that the alkyl substituent on the double bond which is attacked does not affect this ratio to any degree. Furthermore we observe very little regioselectivity with respect to which of the mutually perpendicular π bonds of the allene system is attacked, suggesting the presence of an effective mechanism for the transmission of the inductive electron donation of the alkyl groups to the remote double bond.[2]

The reaction of sulphenyl halides with alkenes is generally considered to follow an Ad_E2 mechanism (11) similar to the one first proposed by Kharasch and Buess (12) as shown in Scheme 2. The first step is believed to be rate-determining formation of a thiiranium ion which subsequently undergoes nucleophilic attack by the halide ion in a fast step.

The mechanistic path for the analogous addition to allene is less clear. The observation of second-order kinetics for the reaction of DNBSC with phenylpropadiene (13) and for the reactions of benzene- and 4-chlorobenzenesulphenyl chlorides with propadiene and its six methyl-substituted derivatives (14) is in accord with the Ad_E2 mechanism.

The reaction of DNBSC with partially resolved 2,2-dimethyl-3,4-hexadien-1-ol has been reported (15) to give an optically active cyclic adduct **12**, consistent with the formation, during addition, of an unsymmetric intermediate such as the alkylidenethiiranium ion **13** or an alkylideneepisulphurane **14** (see Scheme 3) (16). The extent to which the reaction is truly stereospecific has, however, yet to be determined. The available data, therefore, although consistent with the proposed intermediates do not rule out the presence of alternative species, such as allylic carbonium ions, on the reaction coordinate.

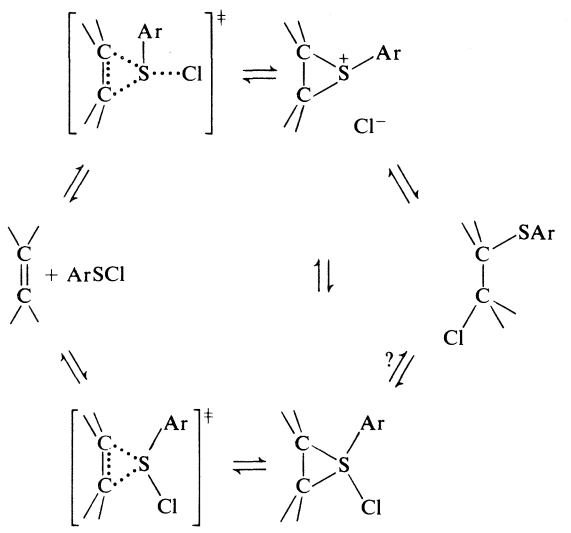

SCHEME 2

As can be seen from Scheme 1, a complicating factor in these studies is the presence of up to four competing reaction pathways, corresponding to the four independent modes of approach to the allenic system. Reducing the problem to one of only two competing pathways is, however, readily accomplished by examining the cases of symmetric allenes. In Scheme 4 a generalized reaction path for the additions is given. If one ignores for the time being the probable occurrence of a cyclic intermediate, such as **13′** or **14′**, the most likely species would be a nonplanar allylic carbonium ion **15**. One would anticipate however that **15** will undergo rapid bond rotation to give the resonance stabilized allylic ion, **16**.

If the activation energy for product formation is very small compared with the barrier height for interconversion among the allylic ions or for that matter between any of the proposed cyclic species, the ratio of products is equal to the ratio of the population of the starting states.

An examination of Scheme 4 indicates that such a scenario is equivalent to stating that the ratio of products corresponds to the percentage of attack on each face of the π system, or in other words reflects the direction of approach of the electrophile towards the allenic system. The same argument holds if one considers the nonplanar allylic ions or the alkylidenethiiranium ions, etc. Within the context of this

[2]Kinetic evidence for the transmission of substituent effects across both double bonds of allenes has recently been reported for the reaction of 4-chlorobenzenesulphenyl chloride and benzenesulphenyl chloride with the methyl-substituted allenes. See ref. 14.

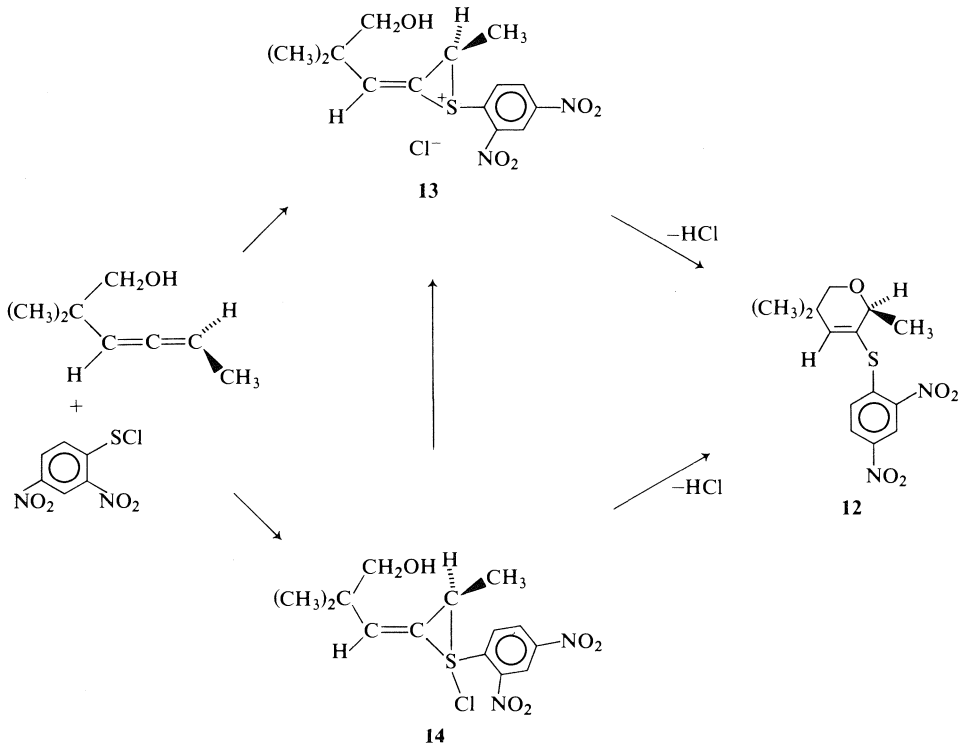

SCHEME 3

mechanism one would expect to observe 'steric approach control' where the steric interactions in the transition state are of the long range type between attacking reagent (DNBSC) and the substrate molecule (allene), which is in its ground state geometry (17).

Alternatively, if the activation energy of the reaction is large compared with the barrier to interconversion between intermediates of opposite configuration (for example, *E*- and *Z*-alkylidenethiiranium ions or *Z*,*Z*- and *E*,*Z*-allylic ions), the proportion of the products will in no way reflect the relative populations of the ground state configurations but will depend only on the activation energies of the processes leading to these products. Stated somewhat differently this implies that the ratio of two products formed from one starting material depends only on the difference in the free energy levels of the two transition states (18).

The available data appear to be in accord with the first scenario, our product distributions reflecting steric approach control. If the latter situation were of importance one would anticipate a predominance of the *Z* isomer under conditions where optical activity is conserved. For example, were the barrier to interconversion of the *E*- and *Z*-alkylidenethiiranium ions low, as a result of a fast reversible elimination–addition sequence, the activation energies for product formation would reflect the propensity for nucleophilic attack on the back side of the three-membered rings. Steric factors in such a case would be expected to favour attack on the less hindered *Z*-alkylidenethiiranium ion. The activation energy for attack on the ion of *Z* configuration should, therefore, be lower than the activation energy for attack on the *E* configuration leading to the preferential formation, stereospecifically, of *Z* alkenes. This is, however, the opposite to what we observed under conditions of kinetic control.

The presence of only one adduct from the reaction of DNBSC with 1,2-cyclononadiene, **7**, can now be rationalized in terms of steric hindrance to approach at one face of each double bond (Scheme 5). Studies using Dreiding models clearly indicate that attack on **7** to give the *Z* isomer would involve attack on the most hindered face of each double bond (i.e., from the inside of the ring). Similar results have been previously reported by Moore and Bertelson (16). The formation of both *E* and *Z* alkenes from 1,2-cyclotridecadiene, **8**, is indicative of the greater conformational flexibility of the 13 carbon ring system compared to rings of 9 or 10 carbons. Comparing the *E* to *Z* ratios for addition to 1,2-cyclotridecadiene, **8** (*E*:*Z* ≡ 86:13) and 3,4-heptadiene, **5** (*E*:*Z* ≡

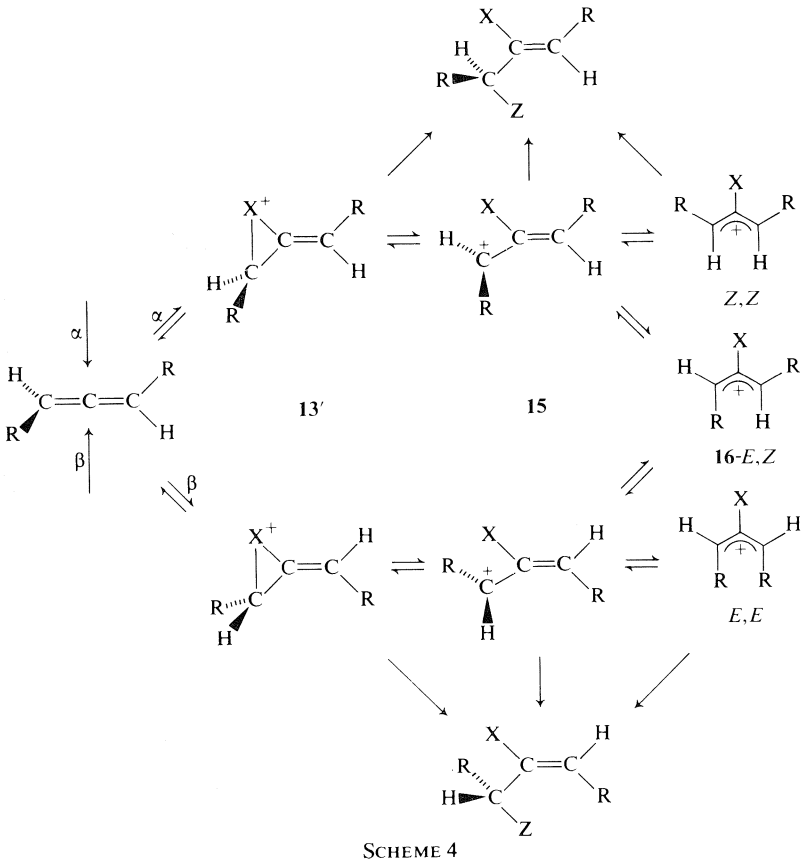

SCHEME 4

80:20) further indicate that the steric constraints imposed on **8** by its cyclic structure are no larger than those of the acyclic allene **5**.

Experimental

Proton and carbon-13 nmr spectra were run on Varian Associates HA-100 and FT80 spectrometers, respectively. Determination of carbon–proton coupling constants was based on first-order analysis of the fully coupled natural abundance ^{13}C spectra.

2,4-Dinitrobenzenesulphenyl Chloride

This was prepared by the method of Kharasch and co-workers (19).

Allenes

2,3-Pentadiene was commercially available from Chemical Samples Co.; 2,3-hexadiene, 3,4-heptadiene, 5-methyl-2,3-hexadiene, 5,5-dimethyl-2,3-hexadiene, 2,6-dimethyl–3,4-heptadiene, 1,2-cyclononadiene, and 1,2-cyclotridecadiene were prepared by the methods of Doering and LaFlamme (20), Skatteböl (21), and Moore and Ward (22).

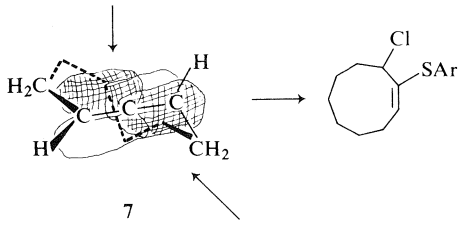

SCHEME 5

The Reaction of 2,4-Dinitrobenzenesulphenyl Chloride with Allenes

General Procedure

To a solution of 2,4-dinitrobenzenesulphenyl chloride (1.40 mmol) in 10 ml of anhydrous methylene chloride was added an equivalent (1.40 mmol) of the respective allene. The mixture was stirred at room temperature for a period of approximately 6 days until no further reaction was observed. After the solvent was evaporated, the residual oil which corresponded to a quantitative yield, was analyzed by ^1H and ^{13}C nmr and mass spectroscopy. No variation in product distribution was observed during the course of the reactions.

Acknowledgements

Continued financial support of the National Research Council of Canada and the University of Ottawa is gratefully acknowledged. We are also indebted to Mr. R. Capoor for technical assistance in recording some of the 100 MHz ^1H nmr spectra.

1. T. L. JACOBS and R. C. KAMMERER. J. Am. Chem. Soc. **96**, 6213 (1974).
2. (*a*) D. R. TAYLOR. Chem. Rev. **67**, 317 (1967); (*b*) M. V. MAVROV and V. F. KUCHEROV. Russ. Chem. Rev. **36**, 233 (1967); (*c*) M. C. CASERIO. Sel. Org. Transform. **1**, 259 (1970).

3. L. R. BYRD and M. C. CASERIO. J. Am. Chem. Soc. **92**, 5422 (1970).
4. (*a*) H. W. DOUGLAS. J. Chem. Phys. **45**, 3465 (1966); (*b*) P. HEAKE, W. B. MILLER, and D. A. TYSSLL. J. Am. Chem. Soc. **86**, 3577 (1964).
5. (*a*) W. L. WATERS, W. S. LINN, and M. C. CASERIO. J. Am. Chem. Soc. **90**, 6741 (1968); (*b*) M. C. FINDLAY, W. L. WALTERS, and M. C. CASERIO. J. Org. Chem. **36**, 275 (1971); (*c*) W. L. WATERS and E. F. KIEFER. J. Am. Chem. Soc. **89**, 6261 (1967).
6. M. BARFIELD and S. STERNHELL. J. Am. Chem. Soc. **94**, 1905 (1972).
7. (*a*) C. M. BANWELL, A. D. COHEN, N. SHEPPARD, and J. J. TURNER. Proc. Chem. Soc. 266 (1959); (*b*) R. A. HOFFMAN. Ark. Kimi, **17**, 1 (1961); (*c*) M. KARPLUS. J. Chem. Phys. **30**, 238 (1959); (*d*) S. STERNHELL. Rev. Pure Appl. Chem. **14**, 15 (1964).
8. (*a*) J. E. ANDERSON. Tetrahedron Lett. 4079 (1975); (*b*) G. L. KARABATSOR, J. D. GRAHAM, and F. M. VANE. J. Am. Chem. Soc. **84**, 37 (1962).
9. J. B. STOTHERS. Carbon-13 nmr spectroscopy. Academic Press, London. 1972. p. 55.
10. (*a*) A. V. FEDEROVA. J. Gen. Chem. USSR, **33**, 3508 (1963); (*b*) A. V. FEDEROVA and A. A. PETROV. J. Gen. Chem. USSR, **31**, 3273 (1961).
11. G. H. SCHMID and D. G. GARRATT. *In* The chemistry of functional groups, Supplement A: The chemistry of double-bonded functional groups. *Edited by* S. Patai. Wiley and Sons, London. 1977. pp. 828–858.
12. N. KHARASCH and C. M. BUESS. J. Am. Chem. Soc. **71**, 2724 (1949).
13. K. ILZAWA, T. OKUYAMA, and T. FUENO. J. Am. Chem. Soc. **95**, 4090 (1973).
14. G. H. SCHMID, D. G. GARRATT, and S. YEROSHALMI. J. Org. Chem. In press.
15. T. L. JACOBS, R. MACOMBER, and D. ZUCKER. J. Am. Chem. Soc. **89**, 7001 (1967).
16. W. R. MOORE and R. C. BERTELSON. J. Org. Chem. **27**, 4182 (1962).
17. (*a*) D. J. PASTO and B. LEPESKA. J. Am. Chem. Soc. **98**, 1091 (1976); (*b*) W. G. DAUBEN, G. J. FOUKEN, and D. S. NOYCE. J. Am. Chem. Soc. **78**, 2579 (1956); (*c*) E. C. ASHBY and S. A. NODING. J. Org. Chem. **42**, 264 (1977).
18. E. L. ELIEL. Stereochemistry of carbon compounds. McGraw-Hill, New York, NY. 1962. pp. 149–151, 237–239.
19. (*a*) D. LAWSON and N. KHARASCH. J. Org. Chem. **24**, 857 (1959); (*b*) N. KHARASCH, G. I. GLEASON, and C. M. BUESS. J. Am. Chem. Soc. **72**, 1796 (1950).
20. W. VON E. DOERING and P. M. LAFLAMME. Tetrahedron, **2**, 75 (1958).
21. L. SKATTEBOL. Acta Chem. Scand. **17**, 1683 (1963).
22. W. R. MOORE and H. R. WARD. J. Org. Chem. **27**, 4179 (1962).

Molecular reorientation in solid *sym*-triazine[1]

J. A. RIPMEESTER
Division of Chemistry, National Research Council of Canada, Ottawa, Ont., Canada K1A 0R9
AND
R. K. BOYD
Guelph–Waterloo Centre for Graduate Work in Chemistry, Guelph Campus, University of Guelph, Guelph, Ont., Canada N1G 2W1

Received June 14, 1978

J. A. RIPMEESTER and R. K. BOYD. Can. J. Chem. **57**, 128 (1979).

Molecular motion in solid *sym*-triazine was investigated using continuous wave and pulsed ^{1}H nmr methods between 290 and 350 K. In addition, the potential energy profile of the *sym*-triazine molecule as a function of orientation in the crystal lattice was calculated. From the nmr results, only one motional process was identified, in-plane reorientation of *sym*-triazine molecules with an activation energy of 15 kcal/mol. This is in agreement with the potential energy calculation which also shows that the reorientation takes place between equivalent sites.

J. A. RIPMEESTER et R. K. BOYD. Can. J. Chem. **57**, 128 (1979).

Opérant entre 290 et 350 K et faisant appel à des méthodes de rmn du ^{1}H pulsées et en fonction continue, on a étudié les mouvements moléculaires de la *sym*-triazène solide. De plus, on a calculé le profil du potentiel d'énergie de la molécule de *sym*-triazine en fonction de son orientation dans le réseau cristallin. Sur la base des données rmn, on a pu identifier un seul processus de mouvement, une réorientation dans le plan des molécules *sym*-triazine avec une énergie d'activation de 15 kcal/mol. Ce résultat est en accord avec le calcul d'énergie potentielle qui montre aussi que la réorientation se produit entre deux sites équivalents.
[Traduit par le journal]

Introduction

At ambient temperature and pressure, *sym*-triazine consists of transparent, easily sublimable crystals. These characteristics are some of the criteria used by Timmermans (1) to denote the class of 'plastic crystals.' Since general molecular reorientation and self-diffusion are other characteristics of plastic crystals, it was thought to be of interest to further investigate molecular motion in *sym*-triazine. Previously (2), threefold, in-plane reorientation was identified in both the high and low temperature phases of *sym*-triazine using ^{14}N nuclear quadrupole resonance, and motional rates were studied as far as the fade-out temperature near 280 K.

We have measured ^{1}H nmr linewidths and second moments between ~200 K and the melting point at 359 K and static and rotating frame ^{1}H spin–lattice relaxation times between ~280 and 340 K. In addition, the potential energy profile for the rotation of a *sym*-triazine molecule at its lattice site was calculated using an atom–atom approximation to the intermolecular forces.

Experimental

sym-Triazine was purchased from Aldrich Chemical Co. and was vacuum sublimed several times before use. Samples for the nmr measurements were prepared by sealing in Pyrex tubes small quantities of *sym*-triazine after outgassing by freeze–pump–thaw cycles. ^{1}H nmr lineshapes were recorded at a frequency of ~56 MHz using a marginal oscillator spectrometer with field modulation and lock-in detection. Second moments were calculated from the lineshape by a numerical integration procedure. ^{1}H spin–lattice relaxation times were measured at a frequency of 10 MHz using a Bruker SXP pulse nmr spectrometer; rotating frame relaxation times were made using a 90° pulse followed immediately by a variable length spin-locking pulse of amplitude 14 G.

The model used to estimate the potential energy profile for in-plane rotation of a *sym*-triazine molecule at its lattice site was identical in all essential respects to that used earlier (3) for the case of pyrazine. The charge distribution within the molecule was taken from published calculations (4). In addition, the nitrogen atom with its lone pair was simulated by an isoelectronic C—H group, with a bond length of 0.7 Å and a bond dipole moment of 2.2 D (3). Two sets of parameters for the C—C, C—H, and H—H potential energy functions were used; the first (5) is characterised by 'hard' repulsive contributions for H-atom interactions and the second (6) by 'softer' repulsions.

Results and Discussion

The potential energy profiles for the rotation of a *sym*-triazine molecule at its lattice site, calculated using the 'hard' and 'soft' repulsion parameters and the X-ray structure (7) of solid *sym*-triazine are shown in Fig. 1. They are qualitatively similar and show that the motion of the *sym*-triazine molecule consists of in-plane jumps of 120° between indis-

[1]NRCC No. 17065.

0008-4042/79/010128-03$01.00/0

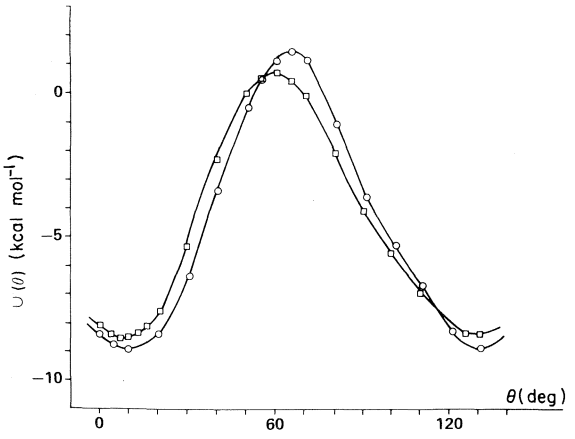

FIG. 1. Potential energy profile for the *sym*-triazine molecule on rotation in its molecular plane (circles, 'hard' repulsion parameters; squares, 'soft' repulsion parameters).

tinguishable orientations of the molecule with respect to the crystal lattice. The calculated activation energy for the thermally activated motion (twice the difference between potential minima and maxima (8, 9)) is 18 kcal/mol for the 'soft' repulsion parameters and 21 kcal/mol for the 'hard' repulsion model.

^{1}H nmr spectra, obtained between 200 and 340 K, were structureless, broad lines. Second moments calculated from suitably digitized lineshapes are shown in Fig. 2; motional narrowing is evident between 250 and 315 K. The limiting low and high temperature second moment values were 3.5 ± 0.1 and 0.72 ± 0.03 G^2, respectively. Theoretical second moments were calculated for two models. The first of these was a static model; Van Vleck's (10) equation was used to calculate the lattice sums using proton coordinates derived from a neutron diffraction study (11). Interactions of protons with other nuclei were neglected. The second model was a dynamic one, where the *sym*-triazine molecules were allowed to jump between the three potential wells evident from the potential energy profiles. Further details of calculations of this nature, made using the equations derived by Michel *et al.* (12), are given elsewhere (13); it suffices to give the results here. The theoretical second moments were 3.25 and 0.77 G^2 for the static and dynamic models, respectively, in good agreement with the limiting low and high temperature experimental second moments of 3.5 ± 0.1 and 0.72 ± 0.3 G^2.

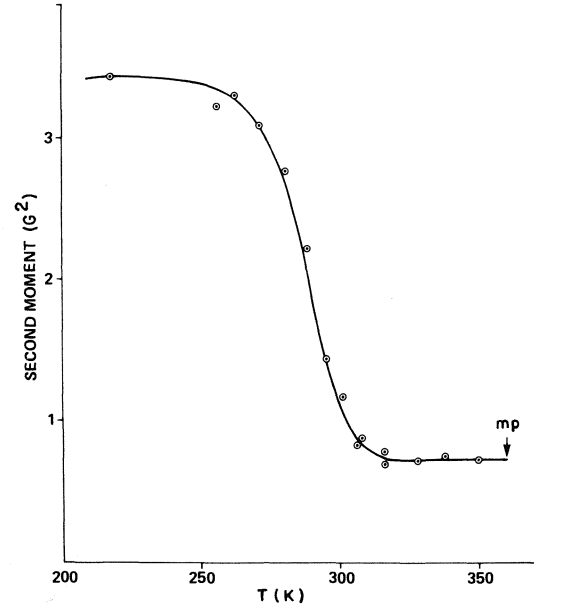

FIG. 2. ^{1}H second moments for solid *sym*-triazine shown as a function of temperature.

Figure 3 shows the static (T_1) and rotating frame ($T_{1\rho}$) spin–lattice relaxation times as a function of inverse temperature. T_1 decreases monotonically with increasing temperature, $T_{1\rho}$ has a minimum of 0.72 ms at 314 K. Spin–lattice relaxation, in this instance, is brought about by modulation of both intra- and inter-proton dipolar interaction by means

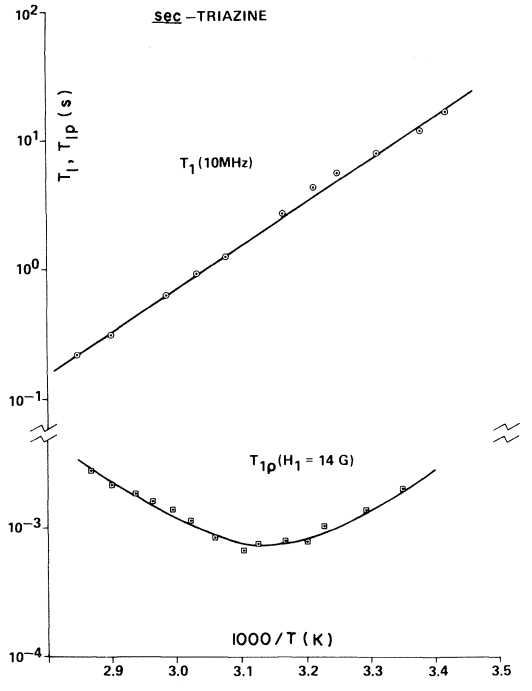

FIG. 3. Static and rotating frame (T_1 and $T_{1\rho}$, respectively) ^{1}H relaxation times of solid *sym*-triazine plotted as a function of inverse temperature (solid lines are calculated, see text).

of the threefold reorientations of *sym*-triazine molecules. The appropriate equations are (14);

$$T_1^{-1} = \frac{2}{3}\gamma^2\Delta M_2 \left\{\frac{\tau_c}{1 + \omega^2\tau_c^2} + \frac{4\tau_c}{1 + 4\omega^2\tau_c^2}\right\}$$

$$T_{1\rho}^{-1} = \frac{2}{3}\gamma^2\Delta M_2 \left\{\frac{2.5\tau_c}{1 + \omega^2\tau_c^2} + \frac{\tau_c}{1 + 4\omega^2\tau_c^2} + \frac{1.5\tau_c}{1 + 4\omega_1^2\tau_c^2}\right\}$$

where γ is the proton gyromagnetic ratio, ω is the radiofrequency used, and ΔM_2 is the portion of the second moment modulated by the motion. The motional correlation time τ_c is assumed to follow Arrhenius behaviour according to $\tau_c = \tau_0 \exp(\Delta E/RT)$ where ΔE is an activation energy. The solid lines in Fig. 2 were calculated with the following choice of parameters; $\Delta M_2 = 2.84$ G^2, $\tau_c = 6.62 \times 10^{-17} \exp(7550/T)$, indicating a reorientational activation energy of 15.0 kcal/mol. This ΔM_2 value, 2.84 G^2, is in good agreement with the value obtained by subtracting the limiting high temperature second moment from the limiting low temperature second moment, namely 2.75 G^2.

The activation energies indicated by the energy profile calculations are also in general agreement with the experimental value. The result obtained for the 'soft' repulsion model seems preferable in two respects. First, the calculated minimum in the potential profile is closer to the experimentally determined (7) crystallographic orientation than is the case for the 'hard' repulsion model; secondly, the calculated activation energy, ($\sim$18 kcal mol^{-1}) for the thermally activated motion is closer to the experimental value (15 kcal mol^{-1}) than the theoretical value ($\sim$21 kcal mol^{-1}) obtained using large repulsive parameters.

The two profiles (Fig. 1) do, however, agree on the main qualitative feature of the motion, viz. that it consists of in-plane jumps of 120°, between indistinguishable orientations of the molecule with respect to the crystal lattice. This is consistent with the observation of an ordered lattice of *sym*-triazine molecules by diffraction studies (7, 11). There should therefore by *no* thermal anomaly *directly* associated with the onset of this motion, since no disorder is thereby produced. The thermal transition previously observed (15) to occur between about 170 and 215 K involved a large-scale change in the crystal structure.

The qualitative feature of the crystal structure of *sym*-triazine, which accounts for in-plane motion by 120° jumps, is the same as that shown previously (16) to account for the difference in crystal packing between *sym*-triazine and benzene. In neither case are the electrostatic contributions of much importance; rather, any attempt to replace a nitrogen atom with its lone pair by a C—H group, e.g., substituting a benzene molecule for a triazine, in the *sym*-triazine lattice, results in short H---H and H---lone pair distances, with consequent large repulsive contributions to the total intermolecular potential energy. This is the basic reason (16) why benzene packs in the 'herring-bone' pattern, rather than in the 'parallel-stack' structure of *sym*-triazine; similarly, rotation of one *sym*-triazine molecule, by 60° in its plane, replaces all N lone pair groups by C—H groups. The discrepancy in the corresponding effective bond lengths ($\sim$0.7 Å as opposed to $>$1.0 Å) is sufficient, within the tight packing of the *sym*-triazine structure, to introduce large H—H repulsive interactions which dominate the potential energy of the rotated molecule.

Previously (2), threefold molecular reorientation of *sym*-triazine molecules has been identified at temperatures below $\sim$270 K using ^{14}N nqr measurements. In these studies (2), the activation energy for the motion was found to be 14 kcal/mol from spin–lattice relaxation measurements between 200 and 250 K and 15 kcal/mol from the exchange broadening contribution to spin–spin relaxation between $\sim$250 and 275 K. Thus the ^{14}N nqr values are in good agreement with the ^{1}H nmr value obtained between 290 and 350 K.

In concluding, we can state that all methods, including the diffraction (7, 11), ^{14}N nqr (2) and ^{1}H nmr measurements, as well as the potential calculations are consistent with a model where *sym*-triazine molecules reorientate in the plane of the molecule about the molecular threefold axis.

1. J. TIMMERMANS. J. Chem. Phys. **35**, 331 (1938); J. Phys. Chem. Solids, **18**, 1 (1961).
2. A. ZUSSMAN and M. ORON. J. Chem. Phys. **66**, 743 (1977).
3. W. E. SANFORD, R. K. BOYD, and J. A. RIPMEESTER. Mol. Cryst. Liq. Cryst. **46**, 121 (1978).
4. C. A. COULSON and A. STREITWIESER, JR. Dictionary of π-electron calculations. Freeman, San Francisco. 1965.
5. D. E. WILLIAMS. J. Chem. Phys. **45**, 3770 (1966).
6. D. E. WILLIAMS. Trans. Am. Crystallogr. Assoc. **6**, 21 (1970).
7. P. J. WHEATLY. Acta Crystallogr. **8**, 224 (1955).
8. W. R. BUSING. J. Phys. Chem. Solids. In press.
9. R. K. BOYD and C. A. FYFE. J. Phys. Chem. Solids. In press.
10. J. H. VAN VLECK. Phys. Rev. **74**, 1168 (1948).
11. P. COPPENS. Science, **158**, 1577 (1967).
12. J. MICHEL, M. DRIFFORD, and P. RIGNY. J. Chim. Phys. **67**, 31 (1970).
13. J. A. RIPMEESTER. Can. J. Chem. **54**, 3453 (1976).
14. S. ALBERT, H. S. GUTOWSKY, and J. A. RIPMEESTER. J. Chem. Phys. **56**, 2844 (1972).
15. P. COPPENS and T. M. SABINE. Mol. Cryst. **3**, 507 (1968).
16. R. MASON and A. I. M. RAE. Proc. R. Soc. A, **304**, 501 (1968).

Carbon-13 spectra of 2,5-dihydrothiophenes and their 1,1-dioxides

JOHN M. MCINTOSH

Department of Chemistry, University of Windsor, Windsor, Ont., N9B 3P4

Received June 23, 1978

JOHN M. MCINTOSH. Can. J. Chem. **57**, 131 (1979).

The complete carbon-13 nmr spectra of 16 alkylated 2,5-dihydrothiophenes and 10 sulfones derived from them are reported. No significant interactions between C-2 substituents and C-5 are noted and stereochemical determinations based on this γ effect are not possible. On oxidation to the sulfones, C-2 and C-5 are dramatically deshielded but C-3 and C-4 are shielded. A possible explanation for this effect is presented.

JOHN M. MCINTOSH. Can. J. Chem. **57**, 131 (1979).

On rapporte les spectres rmn du ^{13}C complets de 16 dihydro-2,5 thiophènes alkylés et de 10 sulfones qui en dérivent. On ne note aucune interaction importante entre les substituants en C-2 et en C-5; des déterminations de stéréochimie basées sur cet effet γ ne sont donc pas possibles. L'oxydation en sulfones provoque un déblindage important en C-2 et en C-5; les C-3 et C-4 sont blindés. On propose une explication possible de cet effet.

[Traduit par le journal]

Recently, we have been concerned with the preparation of substituted 2,5-dihydrothiophenes (**1**) and the utilization of these as precursors of conjugated dienes for use in the Diels–Alder reaction. Central to this problem is the question of the stereochemistry of **1**. Since the conversion to dienes ([1]) is known to be completely stereospecific, the stereochemistry of **1** controls both that of **3** and of the Diels–Alder products. We have previously determined the stereochemical composition of **1** by analysis of **3** (2) but a

[1] 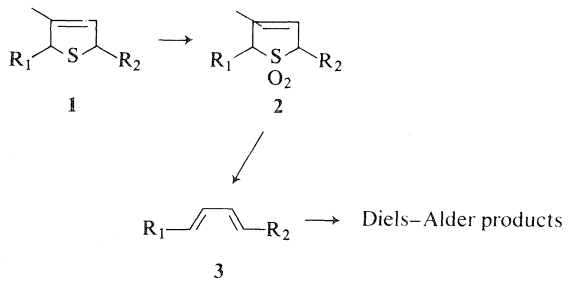

1 **2** **3**

direct method for this determination would be preferable. The ^{13}C nmr chemical shifts of organic compounds are well known to be extremely sensitive to steric effects (3) and therefore we have investigated the carbon spectra of a series of **1** and **2** to ascertain if predictable trends could be detected which would allow differentiation of stereoisomers.

Experimental

The compounds used were prepared as previously outlined (ref. 1 and references therein and refs. 4 and 5). ^{13}C nmr spectra were obtained as approximately 2 *M* solutions in $CDCl_3$ in 5-mm tubes on a Bruker CXP-100 instrument operating in the FT mode at 22.64 MHz and are reported in ppm downfield from TMS as internal standard. A flip angle of 36° was used and 3K–5K transients were collected for the noise-decoupled spectra. Single frequency off-resonance spectra required ca. 60K transients. In all cases the spectral width was 6000 Hz, quadrature detection was employed, and 8K data points were collected. Assignments of specific absorptions were made on the basis of off-resonance experiments, trends appearing within each series, and relative peak intensities. Where ambiguities exist, the absorptions are bracketed.

Results and Discussion

The spectra of **1** and **2** which bear only alkyl substitution are tabulated in Table 1. The stereochemistry of all these compounds was known from previous studies (2). Table 2 lists the spectra of some **1** and **2** which bear a carbomethoxy group at C-3.

Inspection of Table 1 (compounds **15**–**23**) reveals several trends. Carbon atoms attached directly to divalent sulfur absorb in the range of 39–60 ppm, depending on the degree of substitution. The α effect of a methyl group at C-2 falls in the range of 8–11 ppm, whether or not there is a substituent at C-3. (Compare **15**, **16**, **18**, **20** and **21**, **22**, **23**.) This value is in good agreement with the usual range of values in comparable hydrocarbons. The specific shifts are surprisingly close to similarly substituted cases which have considerably different molecular geometries (e.g., **4** (6), **5** (7)).

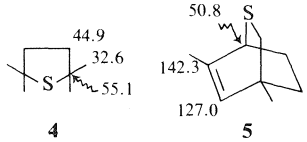

4 **5**

Neither the degree of substitution nor the relative stereochemistry at C-2 affects the chemical shift of C-5 significantly but the olefinic carbons are affected

0008-4042/79/010131-04$01.00/0

TABLE 1. ^{13}C spectra of alkylated 2,5-dihydrothiophenes and related sulfones

Compound (Ref.)	Structure	Chemical shifts[a,b] C-2	C-3	C-4	C-5	R-2	R-3	R-5	Other
15 (10)		39.1	128.8	128.8	39.1	—	—	—	—
16		57.9	(134.2)	(131.7)	49.4	31.8 CH_2 11.8 CH_3	—	25.1	—
17		57.1	132.3	132.3	57.1	31.8(CH_2) 12.0(CH_3)	—	31.8(CH_2) 12.0(CH_3)	—
18		52.0	141.3	129.1	47.7	25.4	14.8	28.8	—
cis-**19**		51.2	—	127.0	55.4	23.6	15.0	32.0(CH_2) 12.0(CH_3)	—
trans-**19**		51.0	—	127.0	55.0	22.7	15.0	31.4(CH_2) 11.8(CH_3)	—
20		60.3(s)	144.8(s)	128.0(d)	45.4(d)	30.8 31.9	12.4	24.8	—
21		37.5	118.6	145.0	53.3	—	—	—	
22		48.3(d)	125.5(d)	143.7(s)	54.9(d)	25.4(t)	—	—	
23		58.2	130.7	141.3	54.3	33.6 33.0	—	—	
24 (9)		55.5	123.2	123.2	55.5	—	—	—	—
25		66.1	(130.1)	(128.2)	60.2	22.6(CH_2) 11.6(CH_3)	—	13.3	
26	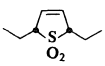	66.6	128.4	128.4	66.6	22.3(CH_2) 11.5(CH_3)	—	22.3(CH_2) 11.5(CH_3)	
27		56.2	113.2	140.5	64.1	—	—	—	
28		62.5	127.3	136.2	62.9	25.5	—	—	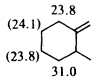

[a]Relative to internal TMS; values in parentheses may be interchanged.

in a manner analogous to the carbocyclic relatives (ref. 3, p. 78). Thus, the original aim of direct stereochemical analysis cannot be achieved.

For discussion purposes the chemical shifts of compounds **6**–**14** (3, 8, 9) are given in Fig. 1. From these data the following conclusions can be drawn. In both the saturated and unsaturated series, the α effect of divalent sulfur is deshielding (ca. −6 ppm), whereas the β-effect is deshielding in the saturated case ($\Delta\delta_{C\rightarrow S} = -5.8$) but shielding in the unsaturated one ($\Delta\delta_{C\rightarrow S} = +1.8$). This can be most conveniently rationalized on the basis of the differing molecular geometries of these ring systems. Compounds **9** and **10** have been shown (10, 11) to possess an essentially planar ring system whereas **6** and **7** are similar in shape to **8** (12). Appreciable *cis*-1,3-hydrogen γ interactions in **8** cause a shielding of the carbon atoms. When sulfur which lacks the hydrogens and has a considerably larger covalent radius than carbon is introduced, these 1,3 interactions are reduced, leading to the observed deshielding at C-3. Oxidation of **6** to **7** reintroduces these γ interactions resulting in little difference in the shifts of C-3 in **7** and **8** ($\Delta\delta_{C\rightarrow SO_2} = 0.4$). In the unsaturated series, distortion

TABLE 2. ^{13}C spectra of alkylated 3-carbomethoxy-2,5-dihydrothiophenes and related sulfones

Compound (Ref.)	Structure	Chemical shifts[a] C-2	C-3	C-4	C-5	COO*Me*	CO	Other
29	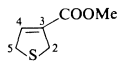	(37.2)	135.6	140.8	(39.0)	51.8	164.2	—
30	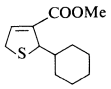	60.0(d)	137.7(s)	141.0(d)	37.0(t)	51.6(q)	164.1(s)	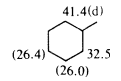
31	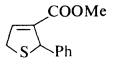	57.1	139.1	(141.3)	38.7	52.0	164.0	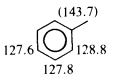
32	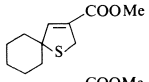	40.1	131.8	149.5	66.1	51.7	164.8	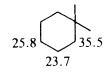
33	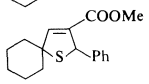	55.5	134.4	149.8	65.1	51.4	164.0	phenyl—143.0, 128.4, 127.5, 127.0 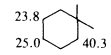
34	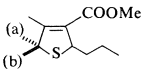	52.3(d)	130.1(s)	157.5(s)	60.4(s)	51.3(q)	166.7(s)	40.3(t), 21.0(t), 13.8(q)(CH_2—CH_2—CH_3), 31.7(q), 31.6(q) (CH_3 a,b), 12.7(q) (=C—CH_3)
35	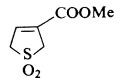	57.8(t)	129.7(s)	134.0(d)	55.0(t)	52.4(q)	162.7(s)	—
36	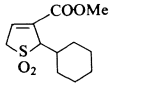	69.9(d)	134.7(s)	133.8(d)	56.8(t)	52.4(q)	163.4(s)	39.8(d), 30.0, 29.2, 26.6, 26.1
37	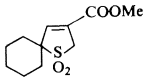	53.8(t)	126.6(s)	144.1(d)	68.8(s)	52.4(q)	163.2(s)	
38	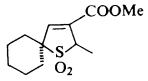	70.9(d)	131.9(s)	144.7(d)	68.5(s)	52.3(q)	163.2(s)	phenyl—135.6, 129.4, 128.8, 128.7 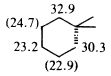
39	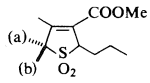	63.9	125.2	152.8	66.1	51.8	164.5	32.9, (19.3), 13.7 (CH_2—CH_2—CH_3), (21.0,) 23.2(CH_3b) 13.7(=C—CH_3)

[a]Relative to internal TMS; values in parentheses may be interchanged.

of the valence angle at C-3 by introduction of the large sulfur atom could account for the shielding at C-3 in **9** and further shielding is caused by introduction of a γ effect upon oxidation to **10**. The difference in magnitude of the shielding effect in the two series introduced by oxidation to the sulfones ($\Delta\delta_{S\rightarrow SO_2} = +6.2$ for the saturated system and +5.6 for the unsaturated one) can best be attributed to the differing ring geometries which result in reduced steric interactions in the planar system **10**. In the present work (Table 1) the same effects can be seen (compare **15–23** with **24–28**) where the shieldings ($\Delta\delta_{S\rightarrow SO_2}$) of C-3 and C-4 range from 3.5 to 5.5 ppm depending on the substitution pattern.

Whereas the effect of the introduction of S—O bonds on C-3 is different in the saturated and unsaturated systems, the data in Table 1 show that the same is not true for substituents at C-2. Previous

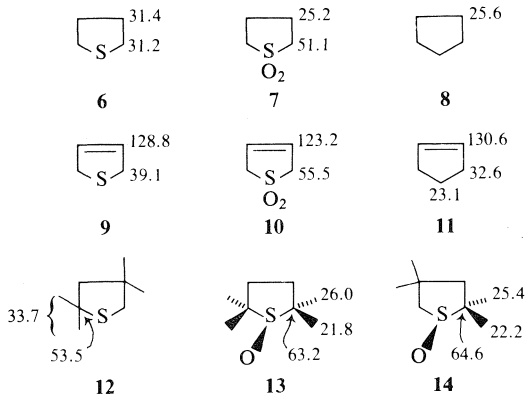

FIG. 1. The chemical shifts of compounds **6–14**.

TABLE 3. Chemical shift differences of 3-carbomethoxy-2,5-dihydrothiophenes and their sulfones

	$\Delta\delta_{S\rightarrow SO_2}$[a]			
Compounds	C-2	C-3	C-4	C-5
29–35	−20.6 −18.8	+5.9	+6.8	−16 −17.8
30–36	−9.9	+3.0	+7.2	−19.8
32–37	−13.7	+5.2	+5.4	−2.7
33–38	−15.4	+2.5	+5.1	−3.4

[a]A negative value indicates a deshielding effect.

work on the sulfoxides **13** and **14** (6) has shown that the C-2 methyl substituent *cis* to oxygen is strongly shielded ($\Delta\delta_{S\rightarrow SO} = 11$) but the effect on the *trans*-methyl group is smaller but still significant ($\Delta\delta_{S\rightarrow SO} = 8.3$). In the present work, all substituents at C-2 and C-5 are eclipsed with an S—O bond and this is reflected in shieldings of 8–12 ppm for methyl substituents (compare **16–25**, **17–26**, **23–28**) and 7.5–9.5 for methylene groups (compare **16–25**, **17–26**, **21–27**, **23–28**).

Turning to the data shown in Table 2, the same type of trends can be distinguished. Again the shielding of C-3 and C-4 are significant ($\Delta\delta_{S\rightarrow SO_2} =$ 2.5 to 7.2), the larger effect being uniformly at C-4. Also, although the effects of oxidation on C-2 and C-5 are approximately equal in **29** and **35**, the deshielding is affected dramatically by the degree and type of substitution. The data in Table 3 illustrate this point. No clear trend can be established from the available data. The chemical shift of the carbonyl group appears very insensitive to substitution at C-2.

In conclusion, the use of ^{13}C nmr to determine the stereochemical composition of 2,5-dihydrothiophenes does not appear to be feasible, presumably due to the planar ring which minimizes across-the-ring steric interactions. However, the chemical shift trends outlined may be useful in future structure determinations of sulfur heterocycles.

Acknowledgement

The assistance of the National Research Council of Canada in the form of a grant for the purchase of the ^{13}C spectrometer and operating grants is greatly appreciated.

1. J. M. McINTOSH and R. A. SIELER. Can. J. Chem. **56**, 226 (1978).
2. J. M. McINTOSH and G. M. MASSE. J. Org. Chem. **40**, 1294 (1975).
3. J. B. STOTHERS. Carbon-13 nmr spectroscopy. Academic Press, New York, NY. 1972.
4. J. M. McINTOSH, H. B. GOODBRAND, and G. M. MASSE. J. Org. Chem. **39**, 202 (1974).
5. J. M. McINTOSH and R. S. STEEVENSZ. Can. J. Chem. **52**, 1934 (1974).
6. R. T. LALONDE, C. F. WONG, A. I. TSAI, J. T. WROBEL, J. RUSZKOWSKA, K. KABZINKA, T. I. MARTIN, and D. B. MACLEAN. Can. J. Chem. **54**, 3860 (1976).
7. H. J. REICH and J. E. TREND. J. Org. Chem. **48**, 2637 (1973).
8. K. KABZINSKA. Bull. Acad. Pol. Sci. **24**, 363 (1976).
9. R. H. EVERHARDUS, B. GRÄFING, and L. BRANDSMA. Recl. Trav. Chim. Pays-Bas, **95**, 153 (1976).
10. W. H. GREEN and A. B. HARVEY. Spectrochim. Acta Part A, **25**, 723 (1969).
11. G. A. JEFFERY. Acta Crystallogr. **4**, 58 (1951).
12. J. B. LAMBERT, J. J. PAPAY, S. A. KHAN, K. A. KAPPAUF, and E. S. MAGYAR. J. Am. Chem. Soc. **96**, 6112 (1974).

Canadian Journal of Chemistry
Published by
THE NATIONAL RESEARCH COUNCIL OF CANADA

Journal canadien de chimie
Publié par
LE CONSEIL NATIONAL DE RECHERCHES DU CANADA

Volume 57 Number 2 January 15, 1979

Volume 57 numéro 2 15 janvier 1979

The molecular and crystal structure of tetrakis(4-methylpyridine)cobalt(II) hexafluorophosphate

RAYMOND M. MORRISON, ROBERT C. THOMPSON, AND JAMES TROTTER
Department of Chemistry, The University of British Columbia, Vancouver, B.C., Canada V6T 1W5

Received July 24, 1978

RAYMOND M. MORRISON, ROBERT C. THOMPSON, and JAMES TROTTER. Can. J. Chem. **57**, 135 (1979).

Crystals of tetrakis(4-methylpyridine)cobalt(II) hexafluorophosphate, $C_{24}H_{28}CoF_{12}N_4P_2$, are tetragonal, space group $I4_1/acd$, $a = 18.434(7)$, $c = 18.818(6)$ Å, $Z = 8$. The structure was solved by direct and Fourier methods. The positional and anisotropic thermal parameters were refined by full-matrix least-squares methods to $R = 0.072$ for 346 observed reflexions. The structure consists of discrete $[Co(4\text{-mepy})_4]^{2+}$ and PF_6^- ions. The structure of the cation is a distorted tetrahedron of 4-methylpyridine ligands around cobalt (crystal symmetry S_4) and that of the anion is a distorted octahedron of fluorines around phosphorus (crystal symmetry C_2).

RAYMOND M. MORRISON, ROBERT C. THOMPSON et JAMES TROTTER. Can. J. Chem. **57**, 135 (1979).

Les cristaux de l'hexafluorophosphate du tétrakis(méthyl-4 pyridine) cobalt(II), $C_{24}H_{28}CoF_{12}N_4P_2$, sont tétragonaux, groupe d'espace $I4_1/acd$, $a = 18.434(7)$, $c = 18.818(6)$ Å, $Z = 8$. On a résolu la structure par des méthodes directes et de Fourier. On a affiné les paramètres thermiques anisotrope et de position par la méthode des moindres carrés (matrice complète) jusqu'à une valeur de $R = 0.072$ pour les 346 réflexions observées. La structure comporte des ions $[Co(Me\text{-}4Py)_4]^{2+}$ et PF_6 séparés. La structure du cation implique un tétraèdre déformé comportant des ligands méthyl-4 pyridine autour du cobalt (symétrie cristalline S_4) alors que celle de l'anion implique un octaèdre déformé comportant des fluors autour du phosphore (symétrie cristalline C_2).

[Traduit par le journal]

Introduction

As a part of a study involving the synthesis and characterization of transition metal complexes containing anions of strong acids (1–4), we have synthesized a series of compounds, CoL_4A_2 (L = pyridine or 4-methylpyridine, A = PF_6^- or AsF_6^-). On the basis of spectral and magnetic data (3, 4), it was postulated that these compounds had structures involving tetrahedral coordination of neutral ligands around cobalt and non-coordinated anions. In order to confirm the structural assignments for this group of compounds and to determine more precisely the stereochemistry about cobalt and the arrangement of ions, we have now completed a single crystal X-ray diffraction study of $Co(4\text{-mepy})_4(PF_6)_2$.

Experimental

$Co(4\text{-mepy})_4(PF_6)_2$ was prepared as described previously (3). A saturated, filtered solution of the complex in a 1:1 mixture of dichloromethane and chloroform was allowed to evaporate slowly in an inert atmosphere chamber. After 1–2 weeks, the deep red-purple solution gave large elongated tetragonal crystals of the same color. The crystals were hygroscopic and were stored in the inert atmosphere chamber; however, the sealing of the crystals in Lindemann capillaries was done quickly in air and no apparent decomposition of the crystals was observed. The preliminary Weissenberg and precession photographs indicated a tetragonal space group and the systematic absences ($hkl: h + k + l = 2n + 1$; $hk0: h(k) = 2n + 1$; $0kl: l(k) = 2n + 1$; $hhl: l = 2n + 1$, $2h + l \neq 4n$) gave the space group as $I4_1/acd$ (D_{4h}^{20}, No. 142) (5).

The crystal chosen for data collection was mounted on a Datex-automated GE XRD-6 three-circle diffractometer equipped with a Mo-K_α ($\lambda = 0.7107$ Å) X-ray source with the

0008-4042/79/020135-04$01.00/0

c axis and the ϕ axis coincident. The unit cell parameters were determined by least-squares refinement on 12 manually centered reflections. Crystal data are: $C_{24}H_{28}CoF_{12}N_4P_2$, tetragonal, space group $I4_1/acd$, $a = 18.434(7)$ Å, $c = 18.818(6)$ Å, $V = 6395$ Å^3, $Z = 8$, $\rho_{calcd} = 1.50$ g cm^{-3}, $\mu = 7.60$ cm^{-1}.

Intensities were collected for $2\theta \leq 40°$, the scan range was $1.80 + 0.8$ (tan θ) with a speed of 2°/min, and the background was counted at the beginning and the end of each scan for 10 s. The strongest reflections were remeasured using a lesser current and extra zirconium filters and a second crystal (instrumental difficulties caused a delay of several months between the initial data collection and the remeasurement of the strong reflections; the second crystal was similar to the first, in size, shape, and orientation). The reflection 3 $\bar{3}$ 2, the intensity of which fluctuated randomly for the two crystals throughout data collection, was measured at intervals of 40 reflections and was used to scale the reflection data of the two crystals. The total number of independent reflections collected was 749. Lorentz and polarization factors were applied and standard deviations were calculated from $\sigma^2(I) = S + B + (0.04S)^2$ where S is the scan count and B is the background count. No absorption correction was made, since the absorption coefficient is low. A total of 347 reflections was considered observed with $I > 3\sigma(I)$ above the background.

Structure Determination

Although attempts to solve the structure with Patterson methods were unsuccessful, direct methods gave the solution. A total of 131 reflections with $E > 1.4$ and the computer programs TANS were used in the sign determining process. The starting set consisted of eight reflections, one for origin definition, five from Σ_1 relationships and two symbolic phases. Of the four sets generated, the one set which determined the phases of all reflections was used. The resulting E map gave cobalt at 8*a* (1/2,1/4,1/8, symmetry S_4) and phosphorus at 16*e* (0.10,0,1/4, symmetry C_2). Successive difference Fourier maps gave the position of the other ten non-hydrogen atoms; the resulting R value was 0.123 with isotropic temperature factors.

For the next three cycles of least-squares refinement, all atoms were given anisotropic temperature factors (symmetry constrained (6, 7) in the case of cobalt and phosphorus), a weighting scheme ($F_o \leq F^*$, $w = 1.0$; $F_o > F^*$, $w = F^*/F_o$; F^* = average $F_o = 80$) was employed, and the anomalous scattering (8) of cobalt and phosphorus was included. The values of R and R_w were 0.072 and 0.092 for 346 reflections (one reflection 4 −11 5 was considered poorly measured and is omitted, $F_o = 27.0$; $F_c = 2.0$). A subsequent cycle of least squares gave a maximum parameter shift of 0.024σ. The hydrogen atom positions were not determined. The observed and calculated structure factors have been placed in the Depository of Unpublished Data.[1] The final positional and thermal parameters are given in Tables 1 and 2.

TABLE 1. Final positional parameters (fractional $\times 10^4$) with estimated standard deviations in parentheses

Atom	x	y	z
Co	5000	2500	1250
P	1011(6)	0	2500
N	4185(7)	2280(10)	1929(8)
C1	4077(10)	2706(9)	2531(11)
C2	3567(11)	2511(14)	3046(11)
C3	3193(9)	1859(11)	2964(10)
C4	3286(11)	1454(10)	2356(12)
C5	3790(11)	1658(11)	1847(12)
C6	2657(11)	1656(11)	3543(10)
F1	397(11)	549(9)	2650(12)
F2	1584(9)	561(11)	2660(11)
F3	1008(12)	232(16)	1766(12)

Results and Discussion

The structure consists of distinct $[Co(4\text{-mepy})_4]^{2+}$ cations and PF_6^- anions. The closest contact between the cations and anions is 3.28(3) Å for F(2)...C(6), which is just less than the van der Waals contact distance of 3.35 Å for a fluoride and a methyl group (9). The closest contact between cobalt and the anions is 4.21(2) Å to F(1), which is well out of the range for interaction. Figure 1 shows a stereoview of the packing of the nearest anions about the cation. The Co...P distance is 5.499(4) Å and the P...Co...P angles are 100.54(2)° and 129.35(4)°. The other Co...P distances in the lattice are all greater than 8.0 Å.

Figure 2 shows a stereoview of the cation. The cobalt atom has crystallographic S_4 symmetry. The distortion of the cation from tetrahedral symmetry is shown by the compression along the S_4 axis and the orientation of the rings. The compression is shown by the N—Co—N angle of 101.2(9)° for one S_4 operation and 113.8(5)° for two successive S_4 operations. Tetrahedral symmetry would require both angles to be 109.47°. The atoms of the 4-methylpyridine moiety are planar within experimental error but the cobalt atom lies 0.28 Å out of this plane; the angle between the S_4 axis and the plane of the ring is 28°; tetrahedral symmetry (T_d) would require the angle to be 0° or 45°.

The bond lengths and angles are shown in Table 3. The values for the atoms of the ring are similar to those of pyridine derived from a microwave study (10) and 4-methylpyridine in other structures (ref. 11, for example). The values for the hexafluorophosphate anions are similar to those normally found for this anion. The thermal parameters indicate large thermal motion, as has been observed by other authors (11–18). As noted (17), this anion would be expected to have large temperature factors and show considerable apparent distortion due to it having nearly spherical symmetry.

Compounds of the type CoL_4A_2, where L is pyridine or a substituted pyridine and A is an anionic ligand such as perchlorate, tetrafluoroborate, trifluoroacetate, methylsulfate, or trifluoromethylsulfate (19–23) have pseudo-octahedral structures with *trans*-coordinated anions. Because of its very weak ligating ability, the PF_6^- anion is not coordinated to cobalt in $Co(4\text{-mepy})_4(PF_6)_2$, the co-

[1]Complete set of data is available, at a nominal charge, from the Depository of Unpublished Data, CISTI, National Research Council of Canada, Ottawa, Ont., Canada K1A 0S2.

TABLE 2. Final thermal parameters and their estimated standard deviations. Anisotropic thermal parameters ($U_{ij} \times 10^3$ Å^2)*

Atom	U_{11}	U_{22}	U_{33}	U_{12}	U_{13}	U_{23}
Co	82(2)	82	77(3)	0	0	0
P	157(9)	77(6)	76(7)	0	0	−2(6)
N	75(11)	99(12)	72(10)	−7(9)	−6(9)	11(9)
C1	95(15)	83(14)	85(14)	17(11)	−14(14)	−27(13)
C2	84(13)	111(16)	89(16)	−20(15)	19(12)	3(14)
C3	67(13)	76(14)	85(17)	−8(12)	−6(12)	13(13)
C4	96(19)	83(15)	88(16)	1(12)	5(14)	−32(14)
C5	74(14)	81(15)	100(16)	1(12)	19(13)	−11(12)
C6	116(17)	118(18)	92(15)	−33(13)	34(13)	16(12)
F1	217(20)	135(12)	328(25)	39(12)	75(18)	−5(14)
F2	189(19)	232(16)	283(25)	−102(14)	−41(16)	−36(18)
F3	292(27)	434(37)	143(17)	−18(24)	−24(17)	131(20)

*The anisotropic thermal parameters employed in the refinement are U_{ij} in the expression: $f = f^0 \exp(-2\pi^2 \Sigma_i \Sigma_j U_{ij} h_i h_j a_i^* a_j^*)$.

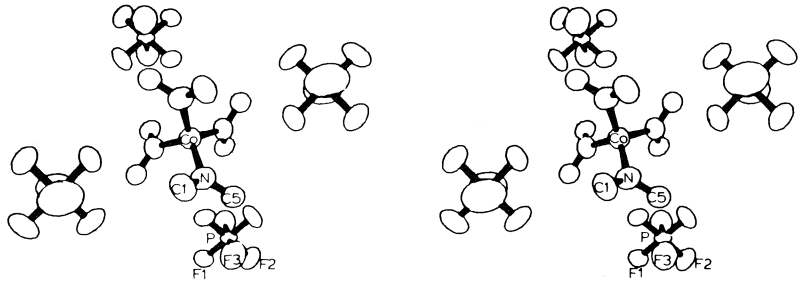

FIG. 1. Stereoview showing the packing of the anions about a cation. The atoms of anion and cation are drawn for 20% and 50% probabilities, respectively.

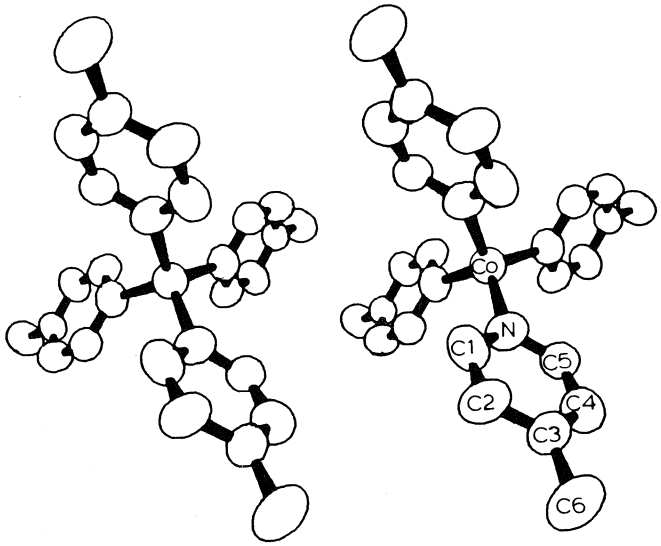

FIG. 2. Stereoview of the $[Co(4\text{-mepy})_4]^{2+}$ cation. All atoms drawn for 50% probability.

ordination sphere of cobalt being filled in this compound by a pseudo-tetrahedral array of the four 4-methylpyridine ligands. The CoN_4 chromophore found here has been observed previously, for example, with the anionic ligand, NCS^-, in the complexes, tetrakis(thiourea)mercury(II) tetrakis(isothiocyanato)cobaltate(II) (24), potassium tetrakis(isothiocyanato)cobaltate(II) trihydrate (25), tris(ethylenediamine)cobalt(III) tetrakis(isothiocyanato)cobaltate(II) nitrate (26), and 1,4-diphenyl-3-phenyl-

TABLE 3. Bond lengths and angles (estimated standard deviations in parentheses)

Bond	Distance (Å)
Co—N	2.01(1)
N—C1	1.39(2)
N—C5	1.37(2)
C1—C2	1.40(2)
C2—C3	1.40(3)
C3—C4	1.38(2)
C4—C5	1.39(2)
P—F1	1.54(2)
P—F2	1.51(2)
P—F3	1.45(2)
Bonds	**Angle (deg)**
N—Co—N′	113.8(5)
N—Co—N″	101.2(9)
F3—P—F2	89(1)
F3—P—F1	89(1)
F2—P—F1	92(1)
N—C1—C2	121(2)
C1—C2—C3	119(2)
C2—C3—C4	120(2)
C2—C3—C6	117(2)
C4—C3—C6	123(2)
C3—C4—C5	121(2)
C4—C5—N	121(2)
C5—N—C1	119(2)

amino-1,2,4-triazolium tetrakis(isothiocyanato)cobaltate(II) (27). The Co—N distances found in these compounds are 2.01(2), 1.949(7)–1.967(7),1.928(12)–1.966(15), and 1.952(5), respectively, compared to the value 2.01(1) Å found here for the $Co(4\text{-mepy})_4^{2+}$ species. Examples of complexes containing anionic bidentate ligands which also give CoN_4 chromophores are bis(*N-tert*-butylpyrrole-2-carboxyaldimino)cobalt(II) (28) and bis(dihydrobis(1-pyrazolyl)-borato)cobalt(II) (29); the Co—N distances in these compounds are 1.981(7)–2.066(8) and (average) 1.967(12) Å, respectively.

Acknowledgements

This research was supported by grants from the National Research Council of Canada and from the Natural, Applied, and Health Sciences Grants Committee of U.B.C. R.M.M. thanks the University Awards Committee for a MacMillan Family Fellowship and Dr. S. Rettig for many helpful discussions. We thank the University of British Columbia Computing Centre for assistance.

1. C. S. ALLEYNE and R. C. THOMPSON. Can. J. Chem. **52**, 3218 (1974).
2. A. L. ARDUINI, M. GARNETT, R. C. THOMPSON, and T. C. WONG. Can. J. Chem. **53**, 3812 (1975).
3. R. M. MORRISON and R. C. THOMPSON. Inorg. Nucl. Chem. Lett. **12**, 937 (1976).
4. R. M. MORRISON and R. C. THOMPSON. Can. J. Chem. **56**, 985 (1978).
5. International tables for X-ray crystallography. Vol. I. Birmingham, Kynoch Press. 1952.
6. H. A. LEVY. Acta Crystallogr. **9**, 679 (1956).
7. W. J. A. PETERSE and J. H. PALM. Acta Crystallogr. **20**, 147 (1966).
8. International tables for X-ray crystallography. Vol. III. Birmingham, Kynoch Press. 1962.
9. L. PAULING. The nature of the chemical bond. 3rd ed. Cornell University Press. 1960. p. 260.
10. B. BAK, L. HANSEN, and J. RASTRUP-ANDERSEN. J. Chem. Phys. **22**, 2013 (1954).
11. G. ALLEGRA, E. BENEDETTI, C. PEDONE, and S. L. HOLT. Inorg. Chem. **10**, 667 (1971).
12. B. R. DAVIS and J. A. IBERS. Inorg. Chem. **9**, 2768 (1970).
13. B. W. DAVIES and N. C. PAYNE. Can. J. Chem. **51**, 3477 (1973).
14. C. K. PROUT, T. S. CAMERON, and A. R. GENT. Acta Crystallogr. B**28**, 32 (1972).
15. F. C. MARCH and G. FERGUSON. Can. J. Chem. **49**, 3590 (1971).
16. M. NOLTE, E. SINGLETON, and M. LAING. J. Chem. Soc. Dalton, 1979 (1976).
17. K. PROUT, M. C. COULDWELL, and R. A. FORDER. Acta Crystallogr. B**33**, 218 (1977).
18. K. PROUT, S. R. CRITCHLEY, E. CANNILLO, and V. TAZZOLI. Acta Crystallogr. B**33**, 456 (1977).
19. D. H. BROWN, R. A. NUTTAL, J. MCAVOY, and D. W. A. SHARP. J. Chem. Soc. A, 892 (1966).
20. D. W. HERLOCKER and M. R. ROSENTHAL. Inorg. Chim. Acta, **4**, 501 (1970).
21. A. B. P. LEVER and D. OGDEN. J. Chem. Soc. A, 2041 (1967).
22. A. R. BYINGTON and W. E. BULL. Inorg. Chim. Acta, **21**, 239 (1977).
23. N. C. JOHNSON, J. T. TURK, and W. E. BULL. Inorg. Chim. Acta, **25**, 235 (1977).
24. A. KORCZYNSKI and A. PORAI-KOSHITS. Rocz. Chem. **39**, 1567 (1965).
25. M. G. B. DREW and A. HAMID BIN OTHMAN. Acta Crystallogr. B**31**, 613 (1975).
26. W. J. ROHRBAUGH and R. A. JACOBSON. Acta Crystallogr. B**33**, 3254 (1977).
27. S. CERRINI, M. COLAPIETRO, R. SPAGNA, and L. ZAMBONELLI. J. Chem. Soc. A, 1375 (1971).
28. C. H. WEI. Inorg. Chem. **11**, 1100 (1972).
29. L. J. GUGGENBERGER, C. T. PREWITT, P. MEAKIN, S. TROFIMENKO, and J. P. JESSON. Inorg. Chem. **12**, 508 (1973).

Complexes of the methyl tris(3,5-dimethylpyrazol-1-yl) gallate ligand, $MeGa(N_2C_5H_7)_3^-$, and its hydroxy derivative, $MeGa(N_2C_5H_7)_2(OH)^-$. Crystal and molecular structure of $[MeGa(N_2C_5H_7)_2(OH)]Mo(CO)_2(\eta^3\text{-}C_4H_7)$

KENNETH R. BREAKELL, STEVEN J. RETTIG, ALAN STORR, AND JAMES TROTTER

Department of Chemistry, University of British Columbia, Vancouver, B.C., Canada V6T 1W5

Received June 15, 1978

KENNETH R. BREAKELL, STEVEN J. RETTIG, ALAN STORR, and JAMES TROTTER. Can. J. Chem. **57**, 139 (1979).

The synthesis and coordinating properties of the tridentate tris-chelating ligand, methyl tris(3,5-dimethylpyrazol-1-yl)gallate, $MeGa(N_2C_5H_7)_3^-$, are described. Carbonyl and nitrosyl carbonyl compounds of manganese, molybdenum, and tungsten incorporating this ligand are detailed. The ready conversion of the above ligand to the less sterically demanding tris-chelating 'hydroxy' ligand $[MeGa(N_2C_5H_7)_2(OH)]^-$ occurs in attempted syntheses of the 'η^3-allyl' complexes, $[MeGa(N_2C_5H_7)_3]M(CO)_2$'$\eta^3$-allyl', (where M = Mo or W, 'η^3-allyl' = η^3-C_3H_5, η^3-C_4H_7). The tridentate chelating nature of this 'hydroxy' ligand is conclusively demonstrated in the crystal structure determination of the complex, $[MeGa(N_2C_5H_7)_2(OH)]$-$Mo(CO)_2(\eta^3\text{-}C_4H_7)$. Crystals of this complex are monoclinic, $a = 14.020(4)$, $b = 10.110(1)$, $c = 15.493(7)$ Å, $\beta = 111.58(3)°$, $Z = 4$, space group $P2_1/n$. The structure was solved by Patterson and Fourier syntheses and was refined by full-matrix least-squares procedures to a final R of 0.40 and R_w of 0.043 for 3374 reflections with $I \geq 3.5\sigma(I)$.

KENNETH R. BREAKELL, STEVEN J. RETTIG, ALAN STORR et JAMES TROTTER. Can. J. Chem. **57**, 139 (1979).

On décrit la synthèse et les propriétés coordinantes du ligand tridentate tris-chélatant, méthyl tris(diméthyl-3,5 pyrazolyl-1)gallate, $MeGa(N_2C_5H_7)_3^-$. On donne des détails concernant des composés carbonyl- et nitrosylcarbonyl du manganèse, du molybdène et du tungstène incorporant ce ligand. Le ligand ci-haut se transforme facilement en ligand "hydroxy" tris-chélatant stériquement moins empêché: $[MeGa(N_2C_5H_7)_2(OH)]^-$ lorsque l'on essaye de synthétiser les complexes "η^3-allyle", $[MeGa(N_2C_5H_7)_3]M(CO)_2$ "η^3-allyle" (où M = Mo ou W, "η^3-allyle" = $\eta^3C_3H_5$, η^3-C_4H_7). On a démontré d'une façon concluante la nature chélatante tridentate de ce ligand "hydroxy" à l'aide d'une détermination de la structure cristalline du complexe $[MeGa(N_2C_5H_7)_2(OH)]Mo(CO)_2(\eta^3\text{-}C_4H_7)$. Les cristaux de ce complexe sont monocliniques, $a = 14.020(4)$, $b = 10.110(1)$, $c = 15.493(7)$ Å, $\beta = 111.58(3)°$, $Z = 4$, groupe d'espace $P2_1/n$. On a résolu la structure par des synthèses de Patterson et de Fourier et on l'a affinée par la méthode des moindres carrés (matrice complète) jusqu'à une valeur finale de R de 0.40 et de R_w de 0.043 pour 3374 réflexions avec $I \geq 3.5\sigma(I)$.

[Traduit par le journal]

Introduction

Numerous examples of the coordination chemistry of tris(pyrazol-1-yl) borate ions, $RB(N_2C_3H_3)_3^-$, where R = H or alkyl, have been described (1). A recent paper (2) discussed a similar gallium ligand, $MeGa(N_2C_3H_3)_3^-$, and contrasted its coordinating ability with that of its boron analogues. A more electron-rich transition metal centre was created in the gallium complexes, with a greater degree of steric protection afforded the chelated metal. The introduction of methyl groups in the 3 or 3,5 positions of the pyrazolyl rings in the boron ligands led to some anomalous reactions in complex ions of the type $RB(N_2C_5H_7)_3Mo(CO)_3^-$ (3). The present paper describes the synthesis of the very sterically demanding gallium ligand, $MeGa(N_2C_5N_7)_3^-$ (incorporating three 3,5-dimethylpyrazolyl moieties), its coordinating ability in transition metal complexes, and its unusual propensity to convert to the less sterically demanding ligand, $MeGa(N_2C_5H_7)_2(OH)^-$, in some of its reactions. The tris-chelating nature of the latter system is confirmed conclusively in the X-ray crystal structure determination of the compound $[MeGa(N_2C_5H_7)_2(OH)]Mo(CO)_2(\eta^3\text{-}C_4H_7)$.

Experimental

Starting Materials

Air-sensitive materials were handled in a glove-box under an atmosphere of oxygen-free dry nitrogen or in a nitrogen-blanketed apparatus. Tetrahydrofuran (THF) was dried by refluxing over lithium aluminum hydride and was used immediately following distillation. Benzene was dried by refluxing over molten potassium prior to distillation. Sodium hydride (Alfa) and 3,5-dimethylpyrazole were used as supplied. Methyl gallium dichloride was prepared by a standard procedure (4) from gallium trichloride (5) and tetramethylsilane. Molybdenum and tungsten hexacarbonyls were used as supplied (Strem). Manganese pentacarbonyl bromide was pre-

0008-4042/79/020139-08$01.00/0

TABLE 1. Analytical and selected ir data

Compound	Analysis (%) Found C	Found H	Found N	Calcd C	Calcd H	Calcd N	ν_{CO} (cm^{-1}) Nujol	ν_{CO} (cm^{-1}) CH_2Cl_2	ν_{CO} (cm^{-1}) Cyclohexane	ν_{NO} (cm^{-1}) Nujol	ν_{NO} (cm^{-1}) CH_2Cl_2	ν_{OH} (cm^{-1}) Nujol
$[MeGa(N_2C_5H_7)_3]Mo(CO)_2NO$	39.3	4.4	18.0	39.2	4.4	17.8	2010 1905	2007 1914		1655	1650	
$[MeGa(N_2C_5H_7)_3]W(CO)_2NO$	34.1	3.8	14.8	33.8	3.8	15.3	1990 1880	1995 1891		1640 1620	1634	
$[MeGa(N_2C_5H_7)_3]Mn(CO)_3$	44.7	4.9	16.4	44.8	4.8	16.5	2022 1910					
$[MeGa(N_2C_5H_7)_2(OH)]Mo(CO)_2(\eta^3\text{-}C_4H_7)$	41.2	5.0	11.5	40.9	5.1	11.2	1910 1815 1795		1940 1850			3630
$[MeGa(N_2C_5H_7)_2(OH)]W(CO)_2(\eta^3\text{-}C_4H_7)$	35.0	4.2	9.4	34.8	4.3	9.5	1905 1790		1930 1837			3550
$[MeGa(N_2C_5H_7)_2(OH)]Mo(CO)_2(\eta^3\text{-}C_3H_5)$	40.3	4.8	11.4	39.6	4.7	11.6	1922 1825		1940 1850			3600

pared from dimanganese decacarbonyl (Strem) by a standard route (6). Allyl bromide and 2-methylallyl chloride were distilled under nitrogen prior to use, and isoamyl nitrite was used as purchased (MCB).

Preparative Details

Sodium Methyl Tris(3,5-dimethylpyrazol-1-yl)gallate $Na^+[MeGa(N_2C_5H_7)_3]^-$

$$MeGaCl_2 + 3Na^+(N_2C_5H_7)^- \xrightarrow[\text{r.t.}]{\text{THF}} Na^+[MeGa(N_2C_5H_7)_3]^- + 2NaCl$$

Methyl gallium dichloride (4.51 g, 29.0 mmol) in THF solution was treated with a 3-molar equivalent of sodium 3,5-dimethylpyrazolide (10.25 g, 86.9 mmol) in the same solvent. The mixture was stirred for 2 days and the white precipitate (NaCl) was then filtered off and washed with THF. The filtrate and the washings were made up to a standard volume and aliquots of the resulting solution were employed in subsequent reactions.

Preparation of $Na^+[MeGa(N_2C_5H_7)_3]M(CO)_3^-$ *Salts* $M = Mo, W$

$$Na^+MeGa(N_2C_5H_7)_3^- + M(CO)_6 \rightarrow Na^+[MeGa(N_2C_5H_7)_3]M(CO)_3^- + 3CO$$

In a typical reaction equimolar amounts of the gallium ligand solution and a THF slurry of the appropriate hexacarbonyl were mixed in a sealed bulb. The mixture was warmed for several days at ~80°C and the CO evolved then measured to confirm the completion of the reaction. The air-sensitive clear yellow solution of the tricarbonyl salt was then made up to standard volume and aliquots used in subsequent reactions.

Preparation of $[MeGa(N_2C_5H_7)_3]Mo(CO)_2NO$

To a THF solution of $Na^+[MeGa(N_2C_5H_7)_3]Mo(CO)_3^-$ was added an excess amount of isoamyl nitrite, and the resulting mixture was warmed briefly. Gas evolution was observed and from the product solution an orange-red material was obtained. This was recrystallized from benzene yielding well-formed orange-red crystals of the desired product. Analytical and ir data are reported in Table 1.

Preparation of $[MeGa(N_2C_5H_7)_3]W(CO)_2NO$

This compound was prepared in an identical manner to that described above using $Na^+[MeGa(N_2C_5H_7)_3]W(CO)_3^-$ as starting material and refluxing with an excess amount of isoamyl nitrate.

Preparation of $[MeGa(N_2C_5H_7)_3]Mn(CO)_3$

$$Na^+MeGa(N_2C_5H_7)_3^- + Mn(CO)_5Br \xrightarrow{\text{THF}} [MeGa(N_2C_5H_7)_3]Mn(CO)_3 + NaBr + 2CO$$

Equimolar amounts of the gallium ligand (1.78 g, 4.52 mmol) and manganese pentacarbonyl bromide (1.24 g, 4.52 mmol) were refluxed in THF solution until gas evolution had ceased. The solid isolated from the filtrate from the reaction mixture was recrystallized from benzene to yield an off-white crystalline material which pulverized to a chalky, white powder. Analytical and ir data are reported in Table 1.

Attempted Preparation of $[MeGa(N_2C_5H_7)_3]Mo(CO)_2(\eta^3\text{-}C_4H_7)$

To an aliquot of $Na^+[MeGa(N_2C_5H_7)_3]Mo(CO)_3^-$ solution an excess of 2- methylallyl chloride was added.

$$Na^+[MeGa(N_2C_5H_7)_3]Mo(CO)_3^- + \text{excess } C_4H_7Cl \xrightarrow[\text{reflux}]{\text{THF}} NaCl + CO + [MeGa(N_2C_5H_7)_3]Mo(CO)_2(\eta^3\text{-}C_4H_7)$$

As expected, CO evolution was observed and the reaction was deemed complete at the cessation of this evolution. The solid isolated from the filtrate from the reaction was recrystallized from benzene to give well-formed yellow crystals. The product was not the expected compound but the hydroxy derivative $[MeGa(N_2C_5H_7)_2(OH)]Mo(CO)_2(\eta^3\text{-}C_4H_7)$ (see Table 1).

Attempted Preparation of $[MeGa(N_2C_5H_7)_3]W(CO)_2(\eta^3\text{-}C_4H_7)$

Following the same procedure as described in the above reaction on intractable dark orange glue was obtained as product. An alternate route was therefore followed using $(MeCN)_3W(CO)_3$ as starting material (7).

$$[1]\quad (MeCN)_3W(CO)_3 + \text{excess } C_4H_7Cl \xrightarrow[\text{r.t.}]{\text{THF}} (MeCN)_2W(CO)_2(\eta^3\text{-}C_4H_7)(Cl) + MeCN + CO$$

$$[2]\quad (MeCN)_2W(CO)_2(\eta^3\text{-}C_4H_7)(Cl) + Na^+MeGa(N_2C_5H_7)_3^- \xrightarrow{\text{THF}} [MeGa(N_2C_5H_7)_3]W(CO)_2(\eta^3\text{-}C_4H_7) + 2MeCN + NaCl$$

An excess of 2-methylallyl chloride was added to a slurry of $(MeCN)_3W(CO)_3$ (1.125 g, 2.88 mmol) in THF at room temperature. The color of the mixture changed from yellow to red and the product was a clear solution. The gallium ligand (1.13 g, 2.88 mmol) in THF was added with a concomitant change of color to orange and the formation of a white precipitate. The isolated filtrate yielded a solid which gave well formed yellow crystals from benzene solution. These were not the expected compound but again a hydroxy derivative $[MeGa(N_2C_5H_7)_2(OH)]W(CO)_2(\eta^3\text{-}C_4H_7)$ (see Table 1).

Attempted Preparation of $[MeGa(N_2C_5H_7)_3]Mo(CO)_2(\eta^3\text{-}C_3H_5)$

Attempts to prepare this complex from $Na^+[MeGa(N_2C_5H_7)_3]Mo(CO)_3^-$ and excess C_3H_5Br were unsuccessful, an intractable sticky dark yellow material resulting from the reaction. However, employing $(MeCN)_3Mo(CO)_3$ (0.872 g, 2.88 mmol) as starting material and reacting with excess C_3H_5Br followed by an equivalent of $Na^+MeGa(N_2C_5H_7)_3^-$ (1.13 g, 2.88 mmol) ligand, a yellow solid was obtained from the resulting THF solution. This gave well formed yellow crystals from benzene solution. Again the product was a hydroxy compound, $[MeGa(N_2C_5H_7)_2(OH)]Mo(CO)_2(\eta^3\text{-}C_3H_5)$ (see Table 1), rather than the expected complex.

Spectra

Mass spectra were recorded on a Varian MAT CH4 Mass spectrometer at 70 eV with an ion source temperature of 100–180°C. Infrared spectra were recorded on a Perkin Elmer 457 spectrophotometer either as Nujol mulls or as solution spectra in cyclohexane or methylene chloride solvents. Proton nmr spectra were recorded in C_6D_6 solution on Varian XL-100 and Bruker WP-90 console 270 spectrometers. F.T. techniques were employed in recording the spectra of complexes of low solubility.

X-ray Crystallographic Analysis of $[MeGa(N_2C_5H_7)_2(OH)]Mo(CO)_2(\eta^3\text{-}C_4H_7)$

The crystal was mounted in a general orientation and had dimensions of ca. 0.36 × 0.48 × 0.53 mm. Unit-cell parameters were refined by least-squares on 2 sin θ/λ values for 24 reflections measured on a diffractometer with graphite monochromatized MoK_α radiation (λ = 0.71073 Å). Crystal data (at 21°C) are:

$C_{17}H_{25}GaMoN_4O_3$ fw = 499.07
Monoclinic, a = 14.020(4), b = 10.110(1), c = 15.493(7) Å, β = 111.58(3)°, V = 2042(1) Å^3, Z = 4, ρ_c = 1.623 g cm^{-3}, $F(000)$ = 1008, $\mu(MoK_\alpha)$ = 20.2 cm^{-1}. Absent reflections: $h0l$, $h + l \neq 2n$ and $0k0$, $k \neq 2n$ define uniquely the space group $P2_1/n$ (alternate setting of $P2_1/c$, C_{2h}^5, No. 14).

Intensities were measured with graphite monochromatized MoK_α radiation on an Enraf-Nonius CAD-4 diffractometer. A variable speed ω scan over a range of r = (0.80 + 0.45 tan θ) degrees in ω was employed. The scan was extended at both ends by r/4 for background measurement. Data were measured to 2θ = 60°. Crystal orientation was monitored every 150 reflections and the intensities of the 3 check reflections, measured every hour of X-ray exposure throughout the data collection, remained constant to within ±1.5%. After data reduction, an absorption correction was applied using the Gaussian integration method (8, 9). Transmission factors ranged from 0.429 to 0.510. Of the 5906 independent reflections measured, 3374 (57.1%) had intensities greater than 3.5σ(I) above background where $\sigma^2(I) = S + B + (0.04S)^2$ with S = scan count and B = normalized background count.

The positions of the Mo and Ga atoms were determined from the three-dimensional Patterson function and those of the O, N, and C atoms from a subsequent difference map. After full-matrix least-squares refinement of all non-hydrogen atoms with anisotropic thermal parameters to R = 0.059, a difference map gave the positions of all 25 hydrogen atoms which were included in subsequent cycles of refinement with isotropic thermal parameters.

The scattering factors of ref. 10 were used for non-hydrogen atoms and those of ref. 11 for hydrogen atoms. Anomalous scattering factors from ref. 12 were used for the Mo and Ga atoms. The weighting scheme $1/\sigma^2(F)$ where σ(F) is derived from the previously defined σ(I) gave uniform average values of $w(|F_o| - |F_c|)^2$ over ranges of $|F_o|$ and was employed in the final stages of refinement. An isotropic type I extinction correction (Lorentzian distribution) was applied (13–15); the final value of g was 1.0(1) × 10^4. Convergence was reached at R = 0.040 and R_w = 0.043 for 3374 reflections with $I \geq 3.5\sigma(I)$. For all 5906 reflections R = 0.091 and R_w = 0.050. On the final cycle of refinement the mean and maximum parameter shifts corresponded to 0.09 and 0.56σ respectively. The mean error in an observation of unit weight was 0.9591. A final difference map showed maximum fluctuations of −2.0 to 0.8 e Å^{-3} near the heavy atoms and was essentially featureless elsewhere. The final positional and thermal parameters appear in Tables 2 and 3 respectively.[1] Measured and calculated structure factors have been placed in the Depository of Unpublished Data.[1]

The ellipsoids of thermal motion are shown in Fig. 1. The thermal motion has been analysed in terms of the rigid-body modes of translation, libration, and screw motion (16) using the computer program MGTLS. The rms standard error in the temperature factors, σU_{ij} (derived from the least-squares analysis) is 0.0031 Å^2. Analysis of the entire molecule (rms ΔU_{ij} = 0.0057 Å^2) gave physically reasonable rigid-body parameters. The bond lengths have been corrected for libration (17) using shape parameters q^2 of 0.08 for all atoms involved. Corrected bond lengths appear in Table 4 along with the uncorrected values. Corrected bond angles do not differ by more than 0.15° from the uncorrected values in Table 5. Torsion angles in the three chelate rings are given in Table 6.

Results and Discussion

The integrity of the tris-chelating ligand MeGa-

[1]The structure factor table and Table 3 (thermal parameters) are available, at a nominal charge, from the Depository of Unpublished Data, CISTI, National Research Council of Canada, Ottawa, Ont., Canada K1A 0S2.

TABLE 2. Final positional parameters (fractional: O, N, and C × 10^4, Mo and Ga × 10^5, H × 10^3) with estimated standard deviations in parentheses. Equivalent positions: $\pm(x, y, z; 1/2 - x, 1/2 + y, 1/2 - z)$

Atom	x	y	z
Mo	36859(3)	52436(4)	21617(3)
Ga	48897(4)	24369(5)	21024(4)
O(1)	4430(3)	3371(4)	2914(3)
O(2)	2415(4)	7585(4)	1039(4)
O(3)	1611(3)	5362(4)	2450(4)
N(1)	3600(3)	2616(4)	1041(3)
N(2)	3033(3)	3729(4)	1047(3)
N(3)	5608(3)	3960(4)	1879(3)
N(4)	5000(3)	5087(4)	1638(3)
C(1)	3075(4)	1854(5)	305(3)
C(2)	2163(4)	2485(6)	−181(4)
C(3)	2157(4)	3637(5)	293(3)
C(4)	6405(4)	4098(5)	1588(4)
C(5)	6310(5)	5288(7)	1159(5)
C(6)	5425(4)	5875(5)	1178(4)
C(7)	5615(6)	760(7)	2376(6)
C(8)	3935(6)	5811(7)	3688(5)
C(9)	4750(4)	6263(5)	3455(4)
C(10)	4491(6)	7260(6)	2780(5)
C(11)	2933(4)	6700(5)	1432(4)
C(12)	2405(4)	5247(5)	2364(4)
C(13)	3477(6)	554(6)	141(6)
C(14)	1318(6)	4635(10)	56(6)
C(15)	7200(6)	3038(10)	1754(8)
C(16)	4962(7)	7166(7)	764(6)
C(17)	5826(5)	5723(7)	3873(5)
H(0)	413(4)	298(6)	305(4)
H(2)	165(4)	214(5)	−67(4)
H(5)	665(5)	557(6)	95(4)
H(7a)	537(5)	17(6)	256(5)
H(7b)	629(6)	91(7)	280(5)
H(7c)	582(6)	59(7)	199(5)
H(8a)	403(4)	502(5)	405(4)
H(8b)	339(5)	638(6)	365(4)
H(10a)	404(4)	791(5)	269(3)
H(10b)	493(4)	758(6)	250(4)
H(13a)	320(5)	31(6)	−46(5)
H(13b)	421(5)	51(6)	36(4)
H(13c)	326(5)	−7(6)	34(5)
H(14a)	74(5)	424(7)	−42(5)
H(14b)	145(6)	541(7)	−12(5)
H(14c)	112(6)	473(8)	52(6)
H(15a)	774(7)	330(9)	162(6)
H(15b)	692(5)	242(6)	135(5)
H(15c)	743(7)	283(10)	249(8)
H(16a)	528(6)	785(8)	113(6)
H(16b)	424(7)	720(9)	60(6)
H(16c)	493(6)	728(7)	16(6)
H(17a)	622(4)	630(5)	439(4)
H(17b)	624(4)	582(6)	345(4)
H(17c)	579(5)	477(7)	406(5)

$(N_2C_5H_7)_3^-$ has been proven by the isolation of the two nitrosyl complexes and the tricarbonyl manganese compound. In all three of these compounds the sterically demanding gallium ligand has the required space to occupy the three facial positions demanded by its geometry in the octahedral complexes. Attempted introduction of larger substituents into the $MeGa(N_2C_5H_7)_3M(CO)_3^-$ ions (M = Mo or W) does not yield the expected complexes but, instead, the observed hydroxy species, or intractable products. The origin of the 'OH' group in these complexes is puzzling since all solvents were dried and the 'yields' of 'OH' products were high and uncontaminated with the expected tris-chelate complexes. It is tempting to speculate abstraction of the 'OH' from the THF solvent but further studies will be necessary to establish this as its origin.

Infrared Spectra

Selected vibrations from the infrared spectra of the complexes are recorded in Table 1. It is noteworthy that the bands for the tungsten compounds are somewhat lower than the bands for the corresponding molybdenum compounds, a phenomenon which is becoming well documented (2, 3, 18, 19). Comparison of the ν_{CO} frequencies for the present 'η^3-allyl' complexes with the ν_{CO} frequencies of similar complexes (Table 7) bearing different uninegative 6-electron ligands indicates that the $[MeGa(N_2C_5H_7)_2(OH)]^-$ ligand creates a more electron-rich transition metal centre with consequent lowering of the ν_{CO} frequencies. The bond length data discussed below are consistent with these observations.

Mass Spectra

The six complexes listed in Table 1 were all sufficiently volatile and stable to give readily observable parent ion signals in their mass spectra. The results indicate the same monomeric nature for the products in the gas phase as is suggested by other evidence for the compounds in solution, and as has been demonstrated conclusively for the complex, $[MeGa(N_2C_5H_7)_2(OH)]Mo(CO)_2(\eta^3\text{-}C_4H_7)$, in the solid state by X-ray structural determination. In all six spectra the expected fragmentation patterns were observed (2) and the intensity ratios of the individual peaks in multi-peak signals agree closely with theoretical predictions based on the percentage isotope compositions of the contributing metal atoms.

^1H Nuclear Magnetic Resonance Spectra

Nitrosyl Complexes

The ^1H nmr spectra for the two nitrosyl compounds are reported in Table 8. In these complexes the three 3,5-dimethylpyrazolyl groups occupy two sets of positions and the H^4 proton and the Me^3 and Me^5 groups give two signals each in the predicted 2:1 intensity ratio.

Hydroxy Complexes

The main features recorded in these three spectra (Table 8) are explicable in terms of an octahedral

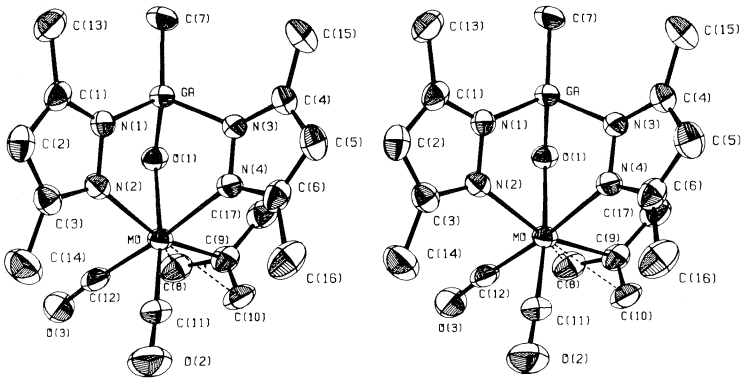

FIG. 1. Stereoview of $[MeGa(N_2C_5H_7)_2(OH)]Mo(CO)_2(\eta^3\text{-}C_4H_7)$. 50% thermal ellipsoids are shown. Hydrogen atoms have been omitted for the sake of clarity.

TABLE 4. Bond lengths (Å) with estimated standard deviations in parentheses

(*a*) Non-hydrogen atoms

	Length			Length	
Bond	Uncorrected	Corrected	Bond	Uncorrected	Corrected
Mo —O(1)	2.267(4)	2.272	N(1)—C(1)	1.345(6)	1.346
Mo —N(2)	2.237(4)	2.242	N(2)—C(3)	1.351(6)	1.353
Mo —N(4)	2.276 (4)	2.283	N(3)—C(4)	1.355(6)	1.356
Mo —C(8)	2.332(6)	2.334	N(4)—C(6)	1.345(6)	1.347
Mo —C(9)	2.260(5)	2.263	C(1)—C(2)	1.379(7)	1.381
Mo —C(10)	2.357(6)	2.359	C(1)—C(13)	1.490(8)	1.492
Mo —C(11)	1.917(5)	1.920	C(2)—C(3)	1.376(7)	1.378
Mo —C(12)	1.931(6)	1.933	C(3)—C(14)	1.489(8)	1.490
Ga —O(1)	1.866(4)	1.871	C(4)—C(5)	1.359(9)	1.361
Ga —N(1)	1.956(4)	1.962	C(4)—C(15)	1.500(9)	1.500
Ga —N(3)	1.939(4)	1.943	C(5)—C(6)	1.381(8)	1.382
Ga —C(7)	1.941(6)	1.941	C(6)—C(16)	1.497(9)	1.500
O(2)—C(11)	1.174(6)	1.174	C(8)—C(9)	1.398(8)	1.399
O(3)—C(12)	1.177(6)	1.177	C(9)—C(10)	1.405(8)	1.408
N(1)—N(2)	1.379(5)	1.382	C(9)—C(17)	1.505(8)	1.507
N(3)—N(4)	1.389(5)	1.392			

(*b*) Bonds involving hydrogen atoms

	Length	
Bond	Value	Mean
O—H	0.65(6)	
C(sp^2)—H	0.74–0.98(5–6)	0.89(8)
C(sp^3)—H	0.76–1.13(6–11)	0.92(9)

structure for the complexes in C_6D_6 solution similar to that demonstrated for $[MeGa(N_2C_5H_7)_2(OH)]$-$Mo(CO)_2(\eta^3\text{-}C_4H_7)$ in the solid state (see Fig. 1). Thus, the two 3,5-dimethylpyrazolyl groups are different and give two sets of signals for the H^4, Me^4, and Me^5 protons in all three spectra in the ratio of 1:1. The signals due to the protons on the η^3-2-methylallyl and η^3-allyl groups have been assigned following assignments for comparable complexes (21, 22) and also using assignments given in ref. 23. In addition to the expected couplings the H_{syn} protons display further splittings in all three spectra. The origin of these additional couplings may be partly the result of H_{syn}–H_{anti} *geminal* coupling although this is usually quite small ($\leq$1 Hz (24)). All three spectra clearly indicate that the 'n^3-allyl' groups are not undergoing rapid rotation about the M...'n^3-allyl' axis in solution, a process which would make both *syn* protons equivalent and both *anti* protons equivalent.

TABLE 5. Bond angles (deg) with estimated standard deviations in parentheses

(*a*) Non-hydrogen atoms

Bonds	Angle (deg)	Bonds	Angle (deg)
O(1) —Mo —N(2)	78.8(1)	Ga —N(3) —C(4)	133.4(4)
O(1) —Mo —N(4)	81.1(1)	N(4) —N(3) —C(4)	108.9(4)
O(1) —Mo —C(9)	84.0(2)	Mo —N(4) —N(3)	117.3(3)
O(1) —Mo —C(11)	173.3(2)	Mo —N(4) —C(6)	136.2(3)
O(1) —Mo —C(12)	101.3(2)	N(3) —N(4) —C(6)	106.2(4)
N(2) —Mo —N(4)	80.3(1)	N(1) —C(1) —C(2)	107.7(5)
N(2) —Mo —C(9)	161.1(2)	N(1) —C(1) —C(13)	121.9(5)
N(2) —Mo —C(11)	95.1(2)	C(2) —C(1) —C(13)	130.4(5)
N(2) —Mo —C(12)	89.2(2)	C(1) —C(2) —C(3)	106.8(5)
N(4) —Mo —C(9)	89.4(2)	N(2) —C(3) —C(2)	109.6(4)
N(4) —Mo —C(11)	100.7(2)	N(2) —C(3) —C(14)	123.4(5)
N(4) —Mo —C(12)	168.7(2)	C(2) —C(3) —C(14)	127.0(5)
C(9) —Mo —C(11)	102.5(2)	N(3) —C(4) —C(5)	108.1(5)
C(9) —Mo —C(12)	101.8(2)	N(3) —C(4) —C(15)	121.3(6)
C(11)—Mo —C(12)	75.7(2)	C(5) —C(4) —C(15)	130.6(6)
O(1) —Ga —N(1)	94.5(2)	C(4) —C(5) —C(6)	107.1(5)
O(1) —Ga —N(3)	92.9(2)	N(4) —C(6) —C(5)	109.6(5)
O(1) —Ga —C(7)	125.2(3)	N(4) —C(6) —C(16)	122.4(5)
N(1) —Ga —N(3)	99.0(2)	C(5) —C(6) —C(16)	128.0(6)
N(1) —Ga —C(7)	120.9(3)	Mo —C(8) —C(9)	69.5(3)
N(3) —Ga —C(7)	117.8(3)	Mo —C(9) —C(8)	75.1(3)
Mo —O(1)—Ga	106.5(2)	Mo —C(9) —C(10)	76.1(3)
Ga —N(1)—N(2)	115.2(3)	Mo —C(9) —C(17)	116.6(4)
Ga —N(1)—C(1)	134.9(3)	C(8) —C(9) —C(10)	114.3(6)
N(2) —N(1)—C(1)	109.7(4)	C(8) —C(9) —C(17)	123.8(6)
Mo —N(2)—N(1)	119.4(3)	C(10)—C(9) —C(17)	121.9(6)
Mo —N(2)—C(3)	134.3(3)	Mo —C(10)—C(9)	68.5(3)
N(1) —N(2)—C(3)	106.2(4)	Mo —C(11)—O(2)	173.5(5)
Ga —N(3)—N(4)	113.0(3)	Mo —C(12)—O(3)	173.7(5)

(*b*) Angles involving hydrogen atoms

Bonds	Angle (deg) Value	Mean
M—O—H	111(6), 113(6)	
C—C(*pz*)—H	125–128(3–6)	127(1)
C—C(allyl)—H	118–128(3–4)	123(4)
H—C(allyl)—H	105(5), 118(5)	
C—C(methyl)—H	104–118(3–6)	111(4)
H—C(methyl)—H	90–118(5–7)	108(8)

TABLE 6. Intra-annular torsion angles (deg) (groups correspond to the three unique chelate rings)

Bond	Observed	Bond	Observed
Mo —O(1)	44.9(2)	Mo —O(1)	−37.0(2)
O(1)—Ga	−47.9(2)	O(1)—Ga	51.4(2)
Ga —N(1)	28.4(3)	Ga —N(3)	−50.6(3)
N(1)—N(2)	5.2(3)	N(3)—N(4)	26.9(3)
N(2)—Mo	−30.2(2)	N(4)—Mo	6.0(2)
Mo —N(2)	52.5(2)		
N(2)—N(1)	5.2(3)		
N(1)—Ga	−65.2(3)		
Ga —N(3)	44.4(3)		
N(3)—N(4)	26.9(3)		
N(4)—Mo	−74.0(3)		

X-ray Crystallographic Analysis of $[MeGa(N_2C_5H_7)_2(OH)]Mo(CO)_2(\eta^3\text{-}C_4H_7)$

The crystallographic analysis of dicarbonyl-[methylbis(3,5-dimethylpyrazol-1-yl)hydroxygallato-(*N*(2),*N*(2)′,*O*)](η^3-2-methylallyl)molybdenum confirms the tridentate chelating nature of the $MeGa(N_2C_5H_7)_2(OH)^-$ ligand. Molecular models indicate that the steric crowding inherent in the $[MeGa(N_2C_5H_7)_3]Mo(CO)_2(\eta^3\text{-}C_4H_7)$ molecule is drastically reduced in the hydroxy complex $[MeGa(N_2C_5H_7)_2(OH)]Mo(CO)_2(\eta^3\text{-}C_4H_7)$ (Fig. 1). The Ga...Mo distance of 3.329(1) Å in the present study is considerably shorter than the distance of 3.67 Å found for $[MeGa(N_2C_3H_3)_3]Mo(CO)_2(\eta^3\text{-}C_3H_5)$ (2).

TABLE 7. Metal carbonyl stretching frequencies*

Compound	ν_{CO} (cm^{-1})	Reference
$(\eta^5\text{-}C_5H_5)Mo(CO)_2(\eta^3\text{-}C_3H_5)$	1970, 1963, 1903, 1889	20
$[HB(N_2C_3H_3)_3]Mo(CO)_2(\eta^3\text{-}C_3H_5)$	1959, 1874	18
$[MeGa(N_2C_3H_3)_3]Mo(CO)_2(\eta^3\text{-}C_3H_5)$	1948, 1860	2
$[MeGa(N_2C_3H_3)_3]Mo(CO)_2(\eta^3\text{-}C_4H_7)$	1949, 1863	2
$[MeGa(N_2C_5H_7)_2(OH)]Mo(CO)_2(\eta^3\text{-}C_3H_5)$	1940, 1850	This work
$[MeGa(N_2C_5H_7)_2(OH)]Mo(CO)_2(\eta^3\text{-}C_4H_7)$	1940, 1850	This work
$[MeGa(N_2C_5H_7)_2(OH)]W(CO)_2(\eta^3\text{-}C_4H_7)$	1930, 1837	This work

*Cyclohexane solutions.

TABLE 8. ^1H nmr data for the allyl and nitrosyl complexes in C_6D_6 solvent*

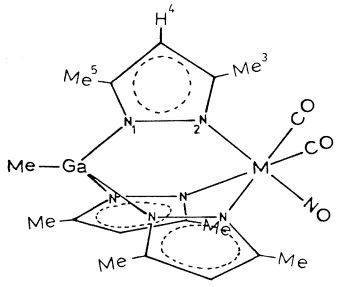

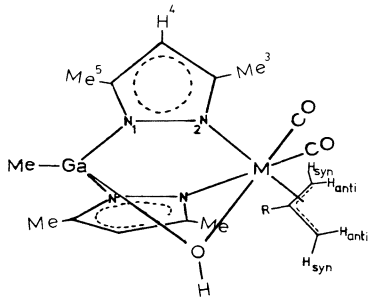

	Nitrosyl compounds		Allyl compounds		
τ_{ppm}	M = Mo	M = W	M = Mo R = Me	M = W R = Me	M = Mo R = H
H^4	4.38s(2) 4.56s(1)	4.43s(2) 4.61s(1)	4.41s(1) 4.54s(1)	4.46s(1) 4.57s(1)	4.43s(1) 4.53s(1)
Me^3, Me^5	7.34s(6), 8.08s(6) 7.59s(3), 8.18s(3)	7.27s(6), 8.11s(6) 7.52s(3), 8.24s(3)	6.85s(3), 8.19s(3) 7.64s(3), 8.28s(3)	6.83s(3), 8.24s(3) 7.63s(3), 8.34s(3)	6.82s(3), 8.18s(3) 7.58s(3), 8.28s(3)
H_{syn}			6.66d(1)† 7.25dd(1)‡	6.86d(1)† 7.36dd(1)‡	6.31dd(1)‡ 7.00m(1)§
H_{anti}			8.47s(1) 8.72s(1)	8.06s(1) 8.31s(1)	8.20d(1)‖ 8.70d(1)‖
R			8.44s(3)	8.31s(3)	6.48tt(1)¶
OH			10.18s(1)	9.83s(1)	10.56s(1)
Ga—Me	9.75s(3)	9.78s(3)	10.09s(3)	10.12s(3)	10.10s(3)

*τ(TMS) = 10 ppm, $\tau(C_6H_6)$ = 2.84 ppm, s = singlet, d = doublet, t = triplet, m = multiplet, dd = doublet of doublets, tt = triplet of triplets. Relative intensity of signals in parentheses.
†J = 4.5 Hz.
‡J = 4.5 Hz, 2 Hz.
§J = 4.5 Hz for major doublet, fine structure on doublet.
‖J = 8 Hz.
¶J = 4.5 Hz and 8 Hz.

The hydroxy bridge effectively creates much more space in positions *trans* to the 3,5-dimethylpyrazolyl groups in octahedral complexes. The Mo atom has distorted octahedral coordination geometry with the $\eta^3\text{-}C_4H_7$ group occupying an octahedral coordination site *trans* to a 'pyrazolyl' nitrogen atom and acting as a π-donating ligand (Mo—C = 2.334(6), 2.263(5), and 2.359(6) Å). The Mo—N distances (2.283(4) and 2.242(4) Å)) are significantly different, the bond *trans* to the $\eta^3\text{-}C_4H_7$ group being shorter (as expected). There is a small (1.7σ) difference between the two M—C(O) distances (1.920(5) and 1.933(6) Å), the shorter being *trans* to the OH bridge. The Mo—O bond length of 2.272(4) Å is rather long (for steric reasons).

Steric effects are the dominant factor in the bond length inequalities mentioned above as well as in the following notable features of the present structure. The 'pyrazolyl' ring *trans* to the 'allyl' group is planar (χ^2 = 2.25) with both methyl carbon atoms and both metal atoms significantly displaced from the mean plane (Mo, 0.0499(4), Ga, −0.0993(6),

C(13), −0.063(8), and C(14), −0.035(9) Å). The other 'pyrazolyl' group, *cis* to the 2-methylallyl, is severely distorted. The five-membered ring is significantly non-planar ($\chi^2 = 16.8$) and both metal atoms are considerably displaced from the mean plane (Mo, −0.2097(4), Ga, 0.6670(5) Å) while only one of the methyl carbons is out of plane (C(16), 0.071(8) Å). The torsion angle Ga[N(3)—N(4)]Mo, ideally zero, is 26.9(3)°, Ga[N(1)—N(2)]Mo is 5.2(3)°.

Relative to the structure of **1**, $[MeGa(N_2C_3H_3)_3]$-$Mo(CO)_2(\eta^3\text{-}C_3H_5)$, there are several notable differences. Both Mo—N distances lie between those in **1** (*cis*, 2.328(3) and 2.309(3), *trans*, 2.232(3) Å). Substitution of allyl by 2-methylallyl increases the central Mo—C(allyl) distance from 2.228(5) to 2.263(5) Å without changing the two other Mo—C(allyl) distances. All of the Mo—'allyl' distances in the present structure are in good agreement with those found for the related boron complex $[HB(N_2C_3H_3)_3]$-$Mo(CO)_2(\eta^3\text{-}C_4H_7)$ (24). The Mo—C(O) bonds are about 2σ shorter than those in **1** (1.936(5) and 1.948(5) Å) and significantly shorter than those in the boron complex (1.958(5) and 1.959(5) Å), at the same time the C—O distances are longer (mean values 1.176(2), 1.162(2), and 1.151(1) Å, respectively, for the present structure, **1**, and the boron complex). These data are consistent with the ν_{CO} ir values (Table 7 and ref. 2) and suggest that a more electron-rich Mo centre is created by the hydroxy ligand with consequent increased back bonding from the metal to the antibonding orbitals of the carbonyl groups. The M—C—O groupings are significantly more bent (173.5(5) and 173.7(5)°) than in **1** (177.2(5) and 176.5(5)°) and the OC—Mo—CO angle is reduced from 81.2(2)° to 75.7(2)°.

The coordination about the gallium atom is distorted tetrahedral. The two Ga—N bond lengths are significantly different (1.962(4) and 1.943(4) Å), the longer one being associated with the *trans* 'pyrazolyl' group which has the shorter Mo—N bond. Both Ga—N bonds are significantly longer than their counterparts in **1** (1.938(4), 1.922(4), and 1.917(3) Å). Other bond lengths in the molecule are as expected.

The trivalent oxygen atom has pyramidal coordination (mean angle at O(1) is 110.5°). The four carbon atoms of the $\eta^3\text{-}C_4H_7$ group are coplanar ($\chi^2 = 1.3$) but three of the four methylene hydrogen atoms are significantly displaced from the mean plane (H(8a), 0.18(5); H(8b), −0.40(6); H(10a), −0.39(5); H(10b), 0.11(6); Mo, 2.0126(4) Å). The crystal structure consists of discrete molecules, the shortest non-bonded distance between molecules being Ga...O(3) $[\frac{1}{2} - x, y - \frac{1}{2}, \frac{1}{2} - z]$, 3.222(4) Å.

Acknowledgements

We thank the National Research Council of Canada for financial support, Dr. S. Chan for nmr spectra, Mr. J. Nip for mass spectra, Mr. P. Borda for C, H, N analyses, and the University of British Columbia Computing Centre for assistance.

1. S. Trofimenko. Chem. Rev. **72**, 497 (1972).
2. K. R. Breakell, S. J. Rettig, D. L. Singbeil, A. Storr, and J. Trotter. Can. J. Chem. **56**, 2099 (1978).
3. S. Trofimenko. Inorg. Chem. **10**, 504 (1971).
4. H. Schmidbauer and W. Findeiss. Angew. Chem. Int. Ed. **3**, 696 (1964).
5. N. N. Greenwood and K. Wade. J. Chem. Soc. 1527 (1956).
6. R. B. King. Organometallic synthesis. Vol. 1. Academic Press, New York. 1965. p. 174.
7. D. P. Tate, W. R. Knipple, and J. M. Augl. Inorg. Chem. **1**, 433 (1962).
8. P. Coppens, L. Leiserowitz, and D. Rabinovich. Acta Crystallogr. **18**, 1035 (1965).
9. W. R. Busing and H. A. Levy. Acta Crystallogr. **22**, 457 (1967).
10. D. T. Cromer and J. B. Mann. Acta Crystallogr. Sect. A, **24**, 321 (1968).
11. R. F. Stewart, E. R. Davidson, and W. T. Simpson. J. Chem. Phys. **42**, 3175 (1965).
12. D. T. Cromer and D. Liberman. J. Chem. Phys. **53**, 1891 (1970).
13. P. J. Becker and P. Coppens. Acta Crystallogr. Sect. A, **30**, 129 (1974); **30**, 148 (1974); **31**, 417 (1975).
14. P. Coppens and W. C. Hamilton. Acta Crystallogr. Sect. A, **26**, 74 (1970).
15. F. R. Thornley and R. J. Nelmes. Acta Crystallogr. Sect. A, **30**, 748 (1974).
16. V. Schomaker and K. N. Trueblood. Acta Crystallogr. Sect. B, **24**, 63 (1969).
17. D. W. J. Cruickshank. Acta Crystallogr. **9**, 747 (1956); **9**, 754 (1956); **14**, 896 (1961).
18. S. Trofimenko. J. Am. Chem. Soc. **91**, 588 (1969).
19. K. S. Chong and A. Storr. Can. J. Chem. This issue.
20. R. B. King. Inorg. Chem. **5**, 2242 (1966).
21. A. Davidson and W. C. Rode. Inorg. Chem. **6**, 2124 (1967).
22. J. W. Faller and M. J. Incorvia. Inorg. Chem. **7**, 840 (1968).
23. M. L. Maddox, S. L. Stafford, and H. D. Kaesz. Adv. Organomet. Chem. **3**, 71 (1965).
24. E. M. Holt, S. L. Holt, and K. J. Watson. J. Chem. Soc. Dalton Trans. 2444 (1973).

Densities and kinematic viscosities of tetra-*n*-butylammonium iodide – nickel(II) chloride melts

NURUL ISLAM, ABDUL MAROOF, AND ISMAIL KOCHI[1]

Department of Chemistry, Aligarh Muslim University, Aligarh 202001, India

Received April 12, 1978

NURUL ISLAM, ABDUL MAROOF, and ISMAIL KOCHI. Can. J. Chem. **57**, 147 (1979).

Densities and kinematic viscosities of molten mixtures of nickel(II) chloride in tetra-*n*-butylammonium iodide have been measured as functions of temperature and composition. The data on the kinematic viscosity have been analyzed using both Arrhenius and non-Arrhenius type equations. The heat of activation, the entropy of activation, and the free energy of activation for viscous flow have been computed. At higher concentrations a slight tendency towards non-Arrhenius viscous behaviour is observed. The free energy of activation helps in describing the overall composition dependence of kinematic viscosity.

NURUL ISLAM, ABDUL MAROOF et ISMAIL KOCHI. Can. J. Chem. **57**, 147 (1979).

On a mesuré, en fonction de la température et de la composition, les densités et les viscosités cinématiques de mélanges fondus du chlorure de nickel(II) dans de l'iodure de tétra-*n*-butylammonium. On a analysé les données de viscosimétrie cinématique en faisant appel à des équations de type Arrhénius et à d'autres qui ne le sont pas. On a calculé la chaleur d'activation, l'entropie d'activation et l'énergie libre d'activation pour un écoulement visqueux. A des concentrations élevées, on a observé une tendance faible vers un comportement visqueux qui n'est pas du type Arrhénius. L'énergie libre d'activation permet de décrire la relation entre la composition globale et la viscosité cinématique.

[Traduit par le journal]

Introduction

There are two well known types of viscosity–temperature behaviour of liquids or molten salt systems, namely, Arrhenius and non-Arrhenius. In the higher temperature ranges the behaviour usually is Arrhenius and tends to non-Arrhenius as the temperature is lowered. There are established analytical expressions (1–5) to explain separately both of these types of behaviour. However, in a certain region of temperature both Arrhenius and non-Arrhenius behaviours may be expected to exist so that neither the Arrhenius nor the non-Arrhenius equation for the analysis of viscosity versus temperature data may apply. The non-Arrhenius viscous behaviour has also been found to increase with the supercooling of the system. Thus, at a particular temperature region in a binary molten mixture, the Arrhenius viscosity may change into non-Arrhenius as the solute concentration increases provided that the added solute causes an increase in the supercooling of the molten system. In order to further understanding of such anticipated shifts in Arrhenius or non-Arrhenius behaviour with respect to temperature as well as composition regions, measurements are reported in this paper of the viscosities of binary melts of nickel chloride and tetrabutylammonium iodide (TBAI).

Experimental

Tetra-*n*-butylammonium iodide (Fluka, AG) was used as solvent in the molten state. Anhydrous nickel chloride was prepared (6) from its recrystallized hexahydrate using purified thionyl chloride (Riedel). Preparation of samples and the measurements were made in a glycerol bath thermostatted to ± 0.1°C. During the preparation of samples the transference of salt was done in an inert atmosphere. The extent of solubility of $NiCl_2$ in tetraalkylammonium halide solvent was reported (7) as up to ~33 mol%. Densities were measured in a calibrated dilatometer of ~3.0 ml capacity with graduated stem of 0.01 ml divisions. Cannon-Ubbelohde viscometers of viscometer constants 0.0355 and 0.0286 cSt/s were used for viscosity measurements in the range 388–418 K. Accuracies of density and viscosity measurements were estimated to be $\pm 0.3\%$ and $\pm 0.1\%$, respectively.

Results and Discussion

The mean molecular weight and the mean molar volume of the TBAI + $NiCl_2$ melt decrease with increasing [$NiCl_2$] whereas a gradual increase has been observed in the case of the density, ρ. The densities of these binary molten mixtures also show a linear dependence on temperature (Table 1).

The kinematic viscosities, ν, of the molten mixtures under study obtained from the products of the viscometer constant and the times of fall are listed in Table 2 as functions of temperature and composition. Plots of the logarithms of the kinematic viscosities versus inverse temperature (Fig. 1) were found to be almost linear. However, the solutions of 23.99 and 30.12 mol% appear to have a tendency for slight

[1]Present address: Department of Chemistry, North-Eastern Hill University, Shillong 793003, India.

0008-4042/79/020147-04$01.00/0

TABLE 1. Computed parameters of density equation [ρ (g/cm^3) = $a - bt$ (°C)] for TBAI + $NiCl_2$ melts

Mol%	a	$b \times 10^3$	Standard deviation in density
4.62	1.2463	0.6754	0.00013
9.83	1.2619	0.7004	0.00008
14.17	1.2709	0.6616	0.00004
19.31	1.2832	0.6743	0.00020
23.99	1.2841	0.6753	0.00030
30.12	1.2914	0.6461	0.00030

TABLE 2. Kinematic viscosities (cm^2/s) of TBAI + $NiCl_2$ melts

T	ν at mol% =					
(K)	4.62	9.83	14.17	19.31	23.99	30.12
418	0.144	0.164	0.175	0.159	0.154	0.180
413	0.167	0.213	0.215	0.201	0.178	0.211
408	0.210	0.239	0.253	0.227	0.217	0.236
403	0.228	0.266	0.275	0.273	0.228	0.273
398	0.269	0.285	0.304	0.283	0.265	0.319
393	0.302	0.344	0.359	0.344	0.321	0.378
388	0.355	0.412	0.445	0.412	0.403	0.450

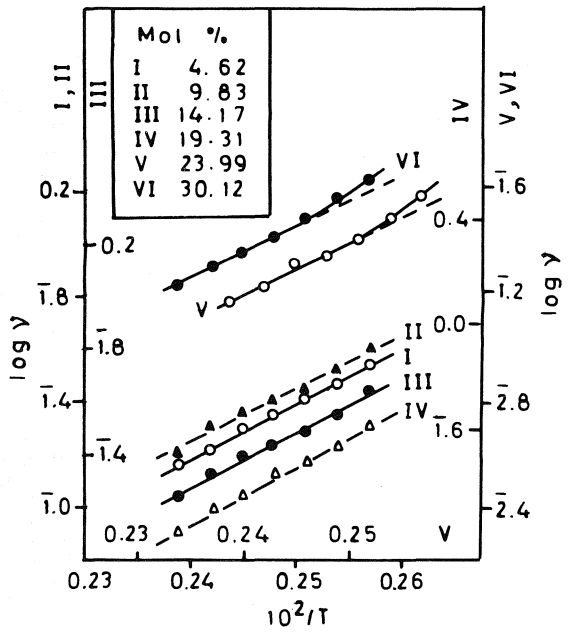

FIG. 1. Arrhenius plots for the kinematic viscosities of TBAI + $NiCl_2$ melts.

deviations from linearity particularly at lower temperatures. Similar plots have also been obtained with respect to absolute viscosities. The linearity of the Arrhenius plots in the case of mixtures of lower concentrations (4.62, 9.83, 14.17, and 19.13 mol%) may be visualized as due to two factors, namely, (*i*) the higher temperature range of the data, and (*ii*) less association of the type $\{[(C_4H_9)_4N^+]_2[NiCl_2I_2^{2-}]\}_x$ to form cluster-like structures in the molten system. The latter factor may also be considered as the cause for the solidification of molten mixtures of lower concentration encountered on cooling; the occurrence of such associations permitted supercooling of the two mixtures of higher concentration and probably caused deviations from Arrhenius behaviour (Fig. 1).

Assuming that the temperature dependence of viscosity is Arrhenius in all the molten mixtures (within the experimental temperature range), an attempt has been made to describe the viscosity data through the Eyring's expression (2). Recently Eyring's expression has been preferred over Andrade (1) equation owing to the fact that the activation free energy term in the exponential part enables an interpretation of the composition dependence of viscosity in liquid mixtures (8). However, in the present case, in order to account for the kinematic viscosity instead of absolute viscosity, η, Eyring's expression has been modified to

$$[1] \qquad \nu = \eta/\rho = (hN/\bar{M}) \exp [\Delta G^*/RT] = A \exp [\Delta H^*/RT]$$

where h is Planck's constant; N, Avogadro's number; $\bar{M}$, the mean molecular weight; ΔG^*, the free energy of activation; ΔH^*, the heat of activation; R, the gas constant; T, the absolute temperature; and $A = (hN/\bar{M}) \exp [-\Delta S^*/R]$; ΔS^* is the entropy of activation. The data on kinematic viscosity have been fitted to [1] by least-squares and the computed values of the parameters A and ΔH^* are given in Table 3. From the values of A the entropies of activation were computed using the expression

$$[2] \qquad \Delta S^* = R[\ln (hN/\bar{M}) - \ln A]$$

The values of ΔS^* so obtained are also included in Table 3.

It is apparent from Table 3 that the values of ΔS^* are positive, unlike the case during conductance flow

TABLE 3. Computed parameters of eq. [1] for TBAI + $NiCl_2$ melts

Mol%	ln A	ΔH^* (cal/mol)	Standard deviation in ν	ΔS^* (eu)
4.62	−13.67	9771.1	0.0062	4.50
9.83	−12.83	9217.6	0.0119	2.90
14.17	−13.13	9492.5	0.0125	3.56
19.31	−13.59	9812.2	0.0111	4.55
23.99	−14.05	10113.9	0.0131	5.53
30.12	−13.71	9967.2	0.0064	4.95

where negative values have usually been reported (9, 10). Positive values for ΔS^* during viscous flow were also reported (11) in the case of associated liquids. Such positive values of ΔS^* indicate that the flowing species attain higher entropy after activation. It may, therefore, be visualized that the viscous flow involves simpler flowing entities and that breaking of some bonds appears to take place before the initiation of flow in order to produce these flowing entities from the associated species.

An attempt has been made to account for a slightly non-Arrhenius viscous behaviour by least-squares fitting the kinematic viscosity data to an equation of the form

$$[3] \qquad \nu = A'T^n \exp [B/(T - T_0)]$$

where A', n, B, and T_0 are empirical constants. This equation has been reported (12) to describe the temperature dependence of the kinematic viscosities of organic liquids and was approximated from an expression based on the significant liquid structure theory.

The least-squares fitted values of the parameters of [3] are given in Table 4 along with the standard deviations in ν. It may, however, be noted that even though the linear plots of $\log(\nu/T^n)$ versus $1/(T - T_0)$ support the suitability of [3], too much significance should not be given to the computed parameters unless the deviation from Arrhenius behaviour is large.

The nature of composition dependence of kinematic viscosities of the present systems may be understood from Fig. 2. From 4.62 to 14.17 mol% an increase of ~20% in kinematic viscosity has been observed. It decreases by about 12% from 14.17 to 23.99 mol% and then increases by ~15% from 23.99 to 30.12 mol%. Accordingly, the kinematic viscosity isotherms show maxima at 14.17 mol% and minima at 23.99 mol%.

On the other hand, it is worthwhile to note the apparently invariant nature of ΔH^* and ΔG^* with concentration from Tables 3 and 5, respectively, as well as from the almost parallelism of the plots of log ν versus $1/T$ (Fig. 1). This implies that the composition dependence of kinematic viscosity is mainly

TABLE 4. Computed parameters of eq. [2] for TBAI + $NiCl_2$ melts

Mol%	A'	n	B	T_0	Standard deviation in ν
4.62	0.2238	−0.7026	649.3	249.2	0.0089
9.83	0.2344	−0.6537	624.5	247.8	0.0113
14.17	0.2292	−0.6597	637.4	248.7	0.0107
19.31	0.2241	−0.6851	650.7	249.5	0.0114
23.99	0.2181	−0.7111	658.9	251.3	0.0096
30.12	0.2195	−0.6782	652.8	250.9	0.0019

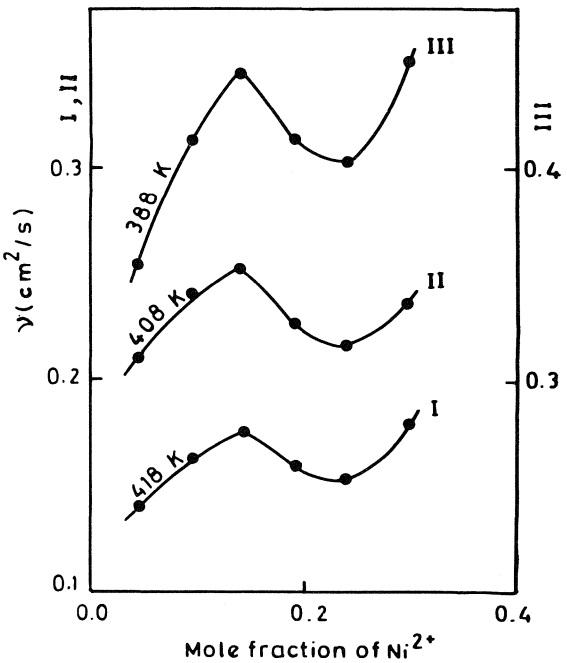

FIG. 2. Kinematic viscosity vs. composition isotherms for TBAI + $NiCl_2$ melts.

determined by that of the pre-exponential factor of [1] which in turn is related to the entropy of activation through [2]. Therefore, it may be visualized that the variation of ν with concentration is essentially guided by the entropy change involved in the breaking of associated species.

Furthermore, the variation of ν with concentration described above may also be viewed quantitatively through [1]. Equation [1], after accounting for the linear concentration dependence of log $(hN/\bar{M})$ (Fig. 3*a*), takes on the form

$$[4] \qquad \log \nu = \log A_0 + Qc + \Delta G^*/2.303RT$$

or

$$[5] \qquad \log \nu = \log A_0 + (\Delta G^* + Q'c)/2.303RT$$

where Q is the slope of the plot of log $(hN/\bar{M})$ versus composition; c, concentration in mole fraction; $Q' = 2.303RTQ$; and A_0 is the value of $(hN/\bar{M})$ for the pure solvent. The suitability of [5] to describe the concentration dependence of ν of the system under study is apparent from the linearity of the log ν versus $(\Delta G^* + Q'_c)$ isotherms drawn at 418 and 388 K (Fig. 3*b*). Similar isotherms may also be obtained at other experimental temperatures. Now, by considering ΔG^* as a composition independent factor [4] may be expressed as

$$[6] \qquad \log \nu = A' + Qc$$

where $A' = \log A_0 + \Delta G^*/2.303RT$. However, the

TABLE 5. Free energies of activation (cal/mol) for TBAI + $NiCl_2$ melts

T (K)	ΔG^* at mol% = 4.62	9.83	14.17	19.31	23.99	30.12
418	7902.3	8003.8	8004.8	7910.8	7800.8	7896.5
413	7911.4	8018.3	8022.5	7894.0	7828.4	7921.2
408	7933.9	8032.8	8040.4	7956.4	7856.0	7946.0
403	7956.4	8047.4	8058.1	7979.2	7883.6	7970.9
398	7979.0	8061.9	8076.0	8001.9	7911.4	7995.5
393	8001.5	8076.4	8093.7	8024.7	7939.1	8020.3
388	8023.9	8090.9	8111.6	8047.4	7966.7	8045.2

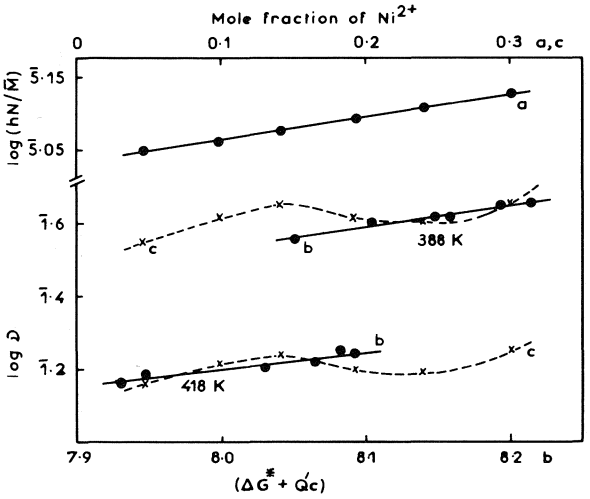

FIG. 3. (*a*) Plot of log $(hN/\bar{M})$ vs. mole fraction of Ni^{2+}; (*b*) plot of log ν vs. $(\Delta G^* + Q'_c)$; and (*c*) plot of log ν vs. mole fraction of Ni^{2+} for TBAI + $NiCl_2$ melts.

plots of log ν versus *c* are non-linear (Fig. 3*c*) which shows the inadequacy of [6] in describing the composition dependence of kinematic viscosity. This suggests that such a dependence of ν cannot be attributed to the changes in the pre-exponential factor alone. Therefore, although the change in ΔG^* with concentration is smaller, it appears to participate, along with the changes in the pre-exponential factor, in describing the overall dependence of kinematic viscosity on concentration.

Acknowledgements

Authors are thankful to The Head, Department of Chemistry, Aligarh Muslim University, Aligarh, for providing necessary research facilities. Financial assistance from University Grants Commission (New Delhi) to one of them (A.M.) is gratefully acknowledged.

1. E. N. ANDRADE. Nature, **125**, 309 (1930).
2. H. EYRING. J. Chem. Phys. **4**, 283 (1936).
3. A. K. DOOLITTLE. J. Appl. Phys. **22**, 7471 (1951).
4. M. H. COHEN and D. TURNBULL. J. Chem. Phys. **31**, 7164 (1959).
5. G. ADAMS and J. H. GIBBS. J. Chem. Phys. **43**, 139 (1965).
6. T. MOELLER. Inorganic synthesis. Vol. V. McGraw-Hill, New York. 1957. p. 153.
7. N. ISLAM, M. R. ISLAM, S. AHMAD, and B. WARIS. Appl. Spectrosc. **29**, 68 (1975).
8. D. E. GOLDSACK and R. FRANCHETTO. Can. J. Chem. **55**, 1062 (1977).
9. J. O. M. BOCKRIS, J. A. KITCHENER, S. IGNATOWICZ, and J. W. TOMLINSON. Trans. Faraday Soc. **48**, 75 (1952).
10. H. C. GAUR and S. K. JAIN. Indian J. Chem. **9**, 860 (1971).
11. R. H. EWELL and H. EYRING. J. Chem. Phys. **5**, 726 (1937).
12. L. D. EICHER and B. J. ZOWLINSKI. J. Phys. Chem. **76**, 3295 (1972).

Electrical conductance and thermal behaviour of some manganese(II) carboxylates

SAMUEL OLUYEMI ADEOSUN
Department of Chemistry, University of Ife, Ile-Ife, Nigeria

Received July 7, 1978

SAMUEL OLUYEMI ADEOSUN. Can. J. Chem. **57**, 151 (1979).

Data are presented on the heats of phase transitions and electrical conductances of the even chain length manganese(II) carboxylates from octanoate to octadecanoate inclusive. The total entropy change for the transition crystal → isotropic liquid is small indicating a high degree of aggregation in the isotropic liquid. This behaviour is similar to that of the cadmium carboxylates.

Plots of log specific conductivity against inverse temperature show curvature. Attempts to fit the data to the Vogel–Tammann–Fulcher equation

$$\kappa = A \exp [-C/(T - T_0)]$$

showed non-random deviations. Instead, the data were interpreted in terms of a simple dissociation equilibrium for which the enthalpy change is ~ 240 kJ mol^{-1}.

SAMUEL OLUYEMI ADEOSUN. Can. J. Chem. **57**, 151 (1979).

On rapporte des mesures de la chaleur de transition de phase et de la conductance électrique pour les composés du manganèse(II) avec les carboxylates à chaîne paire, depuis l'octanoate jusqu'à l'octadécanoate inclusivement. La transition cristal → liquide isotope ne produit qu'une faible variation totale d'entropie, ce qui dénote une formation importante d'agrégats dans le liquide isotope. On a noté un phénomène semblable pour les carboxylates de cadmium.

Quand on porte le logarithme de la conductivité spécifique en fonction de l'inverse de la température, on observe une courbure. On a tenté d'ajuster à ces données l'équation de Vogel–Tammann–Fulcher,

$$\kappa = A \exp [-C/(T - T_0)]$$

mais les écarts n'étaient pas aléatoires. Les données ont plutôt été interprétées en fonction d'un équilibre de dissociation simple faisant intervenir une variation d'entalpie de ~ 240 kJ mol^{-1}.
[Traduit par le journal]

Introduction

The electrical conductances of several molten metal carboxylates have been reported (1–4). The conductance behaviour of these compounds depends crucially on the nature of the metal ion. For example the Arrhenius plots for conductance of sodium and zinc carboxylates (2, 3) are linear while those of lead and cadmium (3, 4) show curvature. The curvature observed for the lead and cadmium soaps have been interpreted in terms of a simple dissociation equilibrium which is near completion at high temperatures.

Differential thermal analysis studies, coupled with optical observations on a hot-stage microscope, reveal that many metal carboxylates form mesophases (5–12). Mesophase formation in some divalent metal carboxylates has also been studied by Spegt, Luzzati, and co-workers (13–16) using X-ray diffraction technique. The number and type of mesophases formed by these soaps also vary with the nature of the metal ion as well as the carboxylate chain length. For example, it has been reported that lead(II) carboxylates form mesophases (11). The phase sequence for the dodecanoate and lower chain length soaps is crystal → $G_{(smectic)}$ → $V_{2(cubic\ isomorphous)}$ → liquid while for tetradecanoate and longer chain length soaps, the V_2 phase is absent and the G phase melts directly into the liquid phase. On the other hand, zinc soaps do not form mesophases but undergo solid → solid phase transitions only (12).

So far, no data have been reported in the literature on the electrical and thermal properties of any transition metal carboxylate and it would be of interest to see how the physical properties of transition metal soaps compare with those of the main group metals already studied. We have, therefore, examined the electrical and thermal properties of the even chain length manganese(II) carboxylates from octanoate to octadecanoate inclusive.

Experimental

Materials

The fatty acids were B.D.H. samples and were stated to have minimum 99% purity by glc assay. They were used without further purification. The manganese(II) chloride used was an Analar B.D.H. product.

Preparation of the Soaps

The soaps were prepared by matathesis in alcohol solution

0008-4042/79/020151-06$01.00/0

(1). The potassium soap was first prepared by the reaction of potassium metal with the stoichiometric amount of the acid in ethanol. The manganese soap was then obtained by the reaction of a stoichiometric amount of manganese(II) chloride in a minimum amount of water with the potassium soap in ethanol. The product was filtered, washed with water and acetone, and dried in a vacuum oven. The product was recrystallised from hot benzene. Infrared spectra showed that the soaps were dry and free of excess acid. The melting points and elemental analysis results for the soaps are shown in Table 1.

Lawrence (17) had earlier reported the preparation of manganese(II) octadecanoate for which he reported a melting point of 473 K. This value is much higher than the value of 392 K observed in the present study. However, we have shown that many of the products reported by some earlier workers are probably basic carboxylates. For example, we showed (4) that the samples of cadmium hexanoate and octanoate having extremely high melting points reported by Spegt and Skoulios (18) were basic carboxylates. It is therefore very likely that the manganese octadecanoate reported by Lawrence is a basic carboxylate. We believe that our samples are pure as indicated by the elemental analysis data in Table 1. It should be noted that Lawrence did not report elemental analysis data for his product.

Physical Measurements

Conductivities were measured in a cell with blackened platinum electrodes. The cell was joined to a socket which could be fitted with a vacuum tap. The cell was filled with the material, evacuated, and immersed in a furnace. The temperature of the furnace was controlled by a Pye-Ether Mini temperature controller, type 19–90B. Conductance measurements were made from about 10 K above the melting point of the material to just below its decomposition point using a Wayne–Kerr B224 conductivity bridge. Conductivities were measured upon heating the sample and upon cooling. The values obtained in both cases agree within experimental error. Duplicate runs also agree within experimental error. The cell constant was measured between each run using 0.01 Demal KCl solution.

DTA measurements were made on a Mettler TA 2000 Analyser which was calibrated with pure indium metal. The materials were premelted and about 20 mg samples were weighed into the standard aluminium crucibles of the analyser using a Kahn Electrobalance. The samples were then scanned at a heating rate of 1 K min^{-1}. Measurements were made in duplicate on at least three separate samples. Peak areas were determined by cutting and weighing the chart paper. Specific heats were determined by the method of base line displacement and optical observations were made on a polarising hot-stage microscope.

Results and Discussion

Quantitative DTA

The manganese(II) carboxylates show two DTA peaks except the octadecanoate which show three peaks. This observation is consistent with the fact that, in general, increase in carbon chain length in a homologous series of metal carboxylates results in an increase in the number of polymorphic phases present (19). The first polymorphic phase is described as phase I in Table 2 while the second polymorphic phase observed in manganese octadecanoate has been described as phase II.

On heating, the crystal first changed into a highly viscous phase which later passed into the isotropic liquid phase. However, visual observation under a hot-stage polarising microscope did not help in characterising the structures of the mesophases. No definite visible sign of changes in texture were observed at the phase transition temperatures when viewed under a hot-stage microscope.

TABLE 1. Melting points and elemental analyses

Carbon chain length	mp (K)	%C		%H	
		Theory	Found	Theory	Found
8	376–377	56.30	56.14	8.80	8.71
10	379–380	60.45	60.45	9.57	9.41
12	387–388	63.58	62.89	10.15	9.97
14	385	66.01	66.24	10.60	10.48
16	388–389	67.96	68.15	10.97	10.89
18	392	69.57	69.85	11.27	11.44

The thermodynamic data for the phase changes are summarised in Table 2 together with their standard errors. A noteworthy feature of the quantitative results is the increase in the total enthalpy and entropy changes with increasing chain length of the soaps. Figure 1 shows a plot of ΔS_{total} (i.e. the total entropy change accompanying the transition, crystal → isotropic liquid) against chain length of the soap. Although the plot is not accurately linear, it can be seen that ΔS_{total} is strongly chain length dependent, increasing with increasing chain length. This is consistent with the idea that the major step in the fusion process is the disordering of the hydrocarbon chains. The values of ΔS_{total} for the manganese carboxylates are significantly smaller than those of the corresponding lead and zinc carboxylates but close to those of the cadmium soaps. For example, the value of ΔS_{total} for manganese octadecanoate is 152 ± 4 J mol^{-1} K^{-1} while those of lead, zinc, and cadmium octadecanoates are, respectively, 311 ± 10, 256 ± 8, and 177 ± 5 J mol^{-1} K^{-1} (11, 12). This probably suggests that the isotropic liquid phases of manganese and cadmium carboxylates are more ordered than those of the lead and zinc carboxylates. We have earlier proposed that the cadmium carboxylates consist of cylindrical micelles in the liquid phase (12) while those of lead consist of spherical micelles (11). This is consistent with the extremely high values of the viscosities of the cadmium soaps (4) when compared to those of the lead compounds (20). It is, therefore, tempting to speculate that the liquid phase of the manganese carboxylates may also consist of cylindrical micelles similar to those of the cadmium carboxylates.

The values of the heat capacities of the manganese carboxylates in the solid phase are presented in Fig. 2. The values increase linearly with temperature suggesting that some subtle structural changes occur

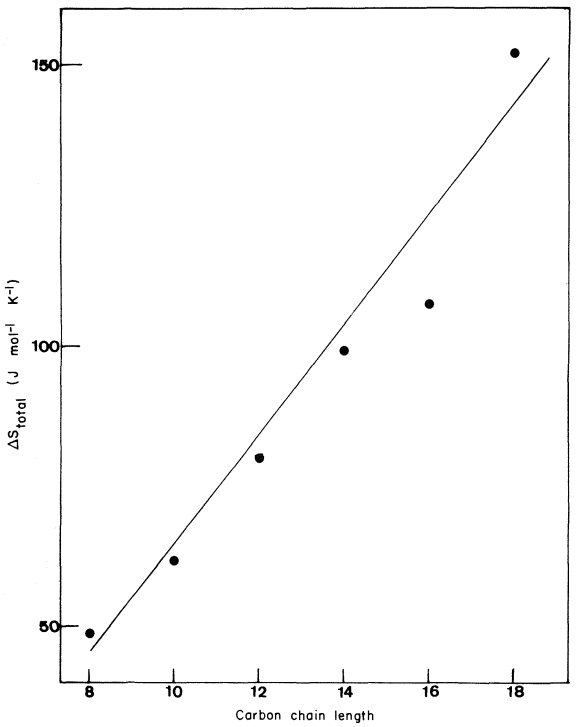

FIG. 1. Total entropy change for the process, crystal → liquid.

in the solid phase with increasing temperature. The heat capacity values in the liquid phase are also summarised in Table 3. The values are constant over the temperature range studied. The values of the heat capacities of the cadmium soaps have been included in Table 3 for comparison. It can be seen that the two sets of heat capacity data are not significantly different.

Electrical Conductance

The conductance data are presented in Fig. 3 where values of log κ are plotted against inverse temperature for all the compounds studied. Results of duplicate runs are also included in the plots. The specific conductances of the manganese carboxylates are bigger than those of zinc salts but smaller than the corresponding salts of lead and cadmium. For example, at 433 K the value of κ for manganese octadecanoate is 1.258×10^{-4} S m^{-1} while the values for lead, zinc, and cadmium octadecanoates are respectively, 1.201×10^{-2}, 2.511×10^{-5}, and 2.513×10^{-2} S m^{-1}.

One notable feature of the plots is that they show curvature. Similar curvature of Arrhenius plots has been observed in certain molten salt mixtures (21) and it has been suggested that such curvature may arise if the liquid is close to its ideal glass transition temperature. Cleaver *et al.* (22) observed non-linear

TABLE 2. Thermodynamic data for phase changes*

Carbon chain length	Crystal → phase I			Phase I → liquid			Phase I → phase II			Phase II → liquid		
	T(K)	ΔH	ΔS	T(K)	ΔH	ΔS	T(K)	ΔH	ΔS	T(K)	ΔH	ΔS
8	369.0	12.3±0.6	33.5±1.5	376.7	6.0±0.7	15.9±1.1	—	—	—	—	—	—
10	374.6	9.1±0.8	24.3±2.1	379.9	14.4±1.1	37.9±3.2	—	—	—	—	—	—
12	383.5	25.5±1.2	68.4±3.4	387.7	4.5±1.0	11.7±2.2	—	—	—	—	—	—
14	367.7	4.1±1.2	11.1±3.1	385.2	34.0±1.3	88.4±3.5	—	—	—	—	—	—
16	372.7	6.2±1.2	16.6±3.3	388.6	35.6±2.1	91.6±5.1	—	—	—	—	—	—
18	361.0	5.0±0.8	13.6±1.2	—	—	—	378.6	7.5±1.1	197±1.2	392.2	46.6±0.9	119.0±2.4

*Units of ΔH and ΔS are kJ mol^{-1} and J mol^{-1} K^{-1} respectively. Error in T is within ±0.2 K.

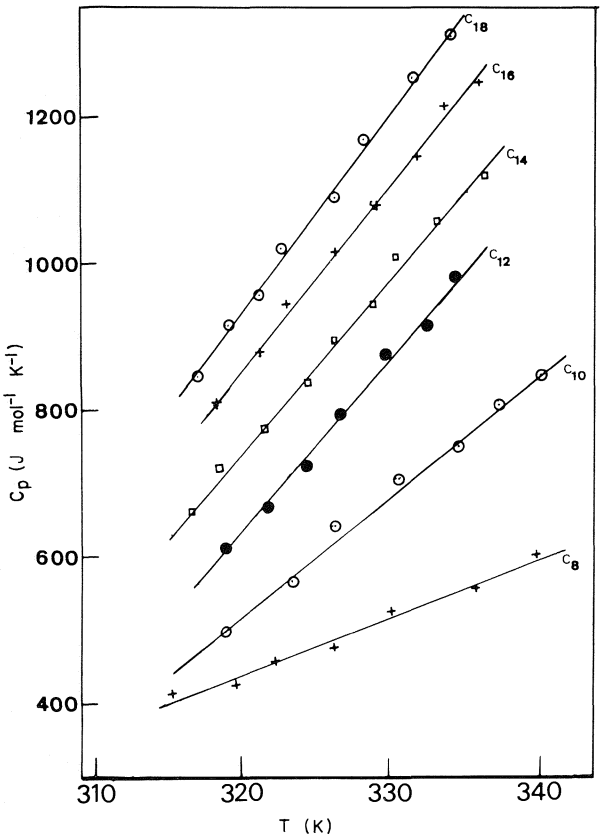

FIG. 2. Molar heat capacities of the solid manganese carboxylates.

Arrhenius plots for the conductance and viscosity of fused sodium polysulphides and fitted their data to the Vogel–Tammann–Fulcher equation:

$$[1] \qquad \kappa = A \exp [-C/(T - T_0)]$$

where A, C, and T_0 are constants. Angell (21) has interpreted T_0 as the temperature at which there is zero configurational entropy in the liquid phase and this has been identified with the ideal glass transition temperature.

We attempted to fit the conductance data of the manganese carboxylates to eq. [1] by using a computer program which systematically varied T_0 to find a minimum in the standard deviation of fits of $\log \kappa$ against $1/(T - T_0)$. In all cases, the standard deviations were non-random which suggests that our results cannot be adequately interpreted in terms of the glass-forming theory. Similar attempts to fit the conductance data of lead and cadmium carboxylates (which also show non-linear Arrhenius plots) to eq. [1] have been unsuccessful (3, 4). Instead, a simple dissociation theory has been proposed to explain the conductance behaviour of lead and cadmium carboxylates (3, 4). Following the model

TABLE 3. Specific heats of the liquid soaps

Carbon chain length	Temperature range (K)	C_p (J mol^{-1} K^{-1})	
		Manganese	Cadmium*
8	413–453	595 ± 25	—
10	413–458	724 ± 15	—
12	413–468	848 ± 20	909 ± 51
14	413–463	1145 ± 15	1220 ± 30
16	413–463	1320 ± 15	1400 ± 15
18	413–463	1475 ± 30	1500 ± 15

*Values are from ref. 12.

proposed for these bivalent metal carboxylates, it is proposed that manganese carboxylate dissociates according to the scheme

$$MnA_2 \rightleftharpoons Mn^{2+} + 2A^-$$

where the MnA_2 and A^- ions may be aggregated in the melt. Assuming that the major current carrier is the Mn^{2+} ion rather than the more bulky species, and that it moves by a simple activated process then the following expressions (3) can be obtained at low

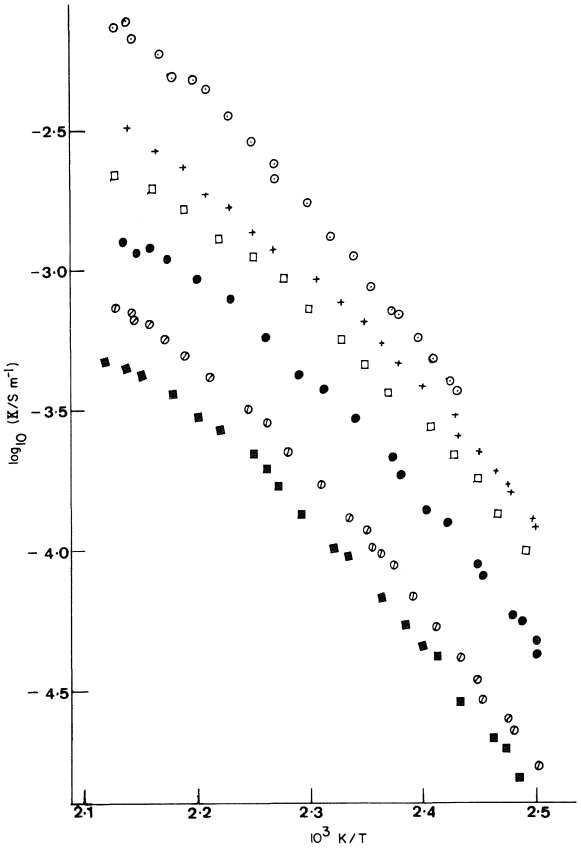

FIG. 3. Semilogarithmic plots of specific conductivity against inverse temperature for molten manganese carboxylates: ○, C_8; +, C_{10}; □, C_{12}; ●, C_{14}; ⊙, C_{16}; ■, C_{18}.

degrees of dissociation for the specific and equivalent conductance (λ).

$$[2] \qquad \log \kappa = \log Q - \frac{\Delta H^{\ddagger} + \Delta H/3}{2.303RT}$$

$$[3] \quad \log \lambda + \frac{\Delta H^{\ddagger} + \Delta H/3}{2.303RT} = \log \frac{NeA}{4} + \frac{\Delta S^{\ddagger} + \Delta S/3}{2.303RT}$$

where $\Delta H^{\ddagger}$, $\Delta S^{\ddagger}$, ΔH, and ΔS are the enthalpies and entropies of activation for movement of the Mn^{2+} ion and for the dissociation, respectively, and

$$[4] \quad \log Q = \log \frac{NeA}{2V_m} + \frac{1}{2.303R}(\Delta S^{\ddagger} + \Delta S/3)$$

where V_m is the molar volume of the soap. At low degrees of dissociation, a plot of $\log \kappa$ against $1/T$ should be linear with slope of $(\Delta H^{\ddagger} + \Delta H/3)/2.303R$, according to eq. [2]. Table 4 shows values of $\Delta H^{\ddagger} + \Delta H/3$ calculated from such plots. It can be seen that these values are reasonably constant within limits of experimental error and suggest that the major current carrier must be the same in all the carboxylates studied; most certainly the Mn^{2+} ion.

It is possible to have a rough idea of how the combined entropy term varies with chain length. The first term on the right hand side of eq. [3] is unlikely to be strongly chain length dependent. Thus a plot of the left hand side expression in eq. [3] against chain length will demonstrate the dependence of the combined entropy term, i.e., $\Delta S^{\ddagger} + \Delta S/3$ on the chain length of the carboxylate. Values of λ can be obtained from the specific conductance data (κ) but this requires knowledge of the molar volumes (V_m) of the manganese carboxylates. We attempted to measure V_m values for the manganese soaps by the same pycnometric technique used for the lead and zinc carboxylates (3). Unfortunately this method was not suitable for the manganese soaps because of the abnormally high viscosities of these compounds which made complete elimination of air bubbles in the melt extremely difficult. However, the molar volumes of corresponding carboxylates of lead, zinc, and cadmium differ by at most 0.5% from each other (3, 4). For example, values of V_m at 500 K for lead, zinc, and cadmium carboxylates are, respectively, 738.81×10^{-6}, 738.24×10^{-6}, and 737.00×10^{-6} m^3. It is, therefore, reasonable to assume that the molar volumes of the manganese soaps will not be significantly different from those of the other bivalent metal soaps. We have, therefore, computed values of λ for the manganese carboxylates using the molar volume data of the corresponding lead soaps. Figure 4 shows a plot of $\log \lambda + (\Delta H^{\ddagger} + \Delta H/3)/2.303RT$ against chain length. The slope of the plot shows that the entropy term decreases by 1.96 J K^{-1} per carbon atom. This value can be compared with those for zinc (1.86) and cadmium (1.60) carboxylates.

TABLE 4. Low temperature limiting slopes for conductance

Carbon chain length	$\Delta H^{\ddagger} + \Delta H/3$ (kJ mol^{-1})
8	98 ± 3
10	102 ± 4
12	100 ± 6
14	98 ± 3
16	99 ± 4
18	98 ± 4

According to the dissociation theory, the metal carboxylate is completely dissociated in the high temperature region. In this region, the plot of $\log k$ against $1/T$ should tend to a second linear portion with slope corresponding to $\Delta H^{\ddagger}$. Unfortunately this region was not reached before the manganese soaps started to decompose. However, it has been shown that the value of $\Delta H^{\ddagger}$ for Pb^{2+} ion, calculated in this manner, is in good agreement with that found for molten lead halides (3). The activation energy for conductance of manganese(II) chloride is 19.6 kJ mol^{-1} (23) which suggests that $\Delta H^{\ddagger}$ for

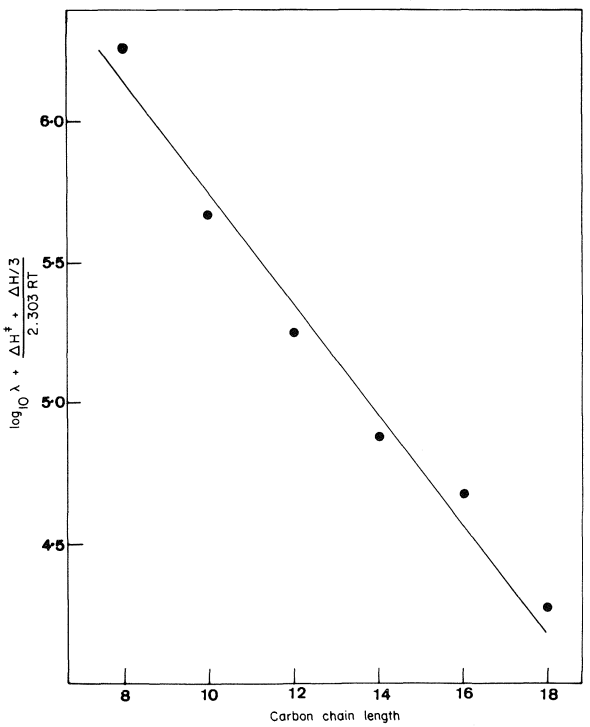

FIG. 4. The dependence of the entropy-containing term, $\log \lambda + (\Delta H^{\ddagger} + \Delta H/3)/2.303RT$ on carbon chain length of the manganese carboxylates.

Mn^{2+} ion must be close to this value. Using this value of $\Delta H^{\neq}$, the value of ΔH for the manganese carboxylates can be shown to be about 240 kJ mol^{-1}. This value is much higher than that obtained for the lead carboxylates ($\sim$88 kJ mol^{-1}) and slightly bigger than that of cadmium carboxylates ($\sim$190 kJ mol^{-1}), suggesting that the manganese–carboxylate bond is extremely strong.

Taken together with the DTA data, these results suggest that the structure of the manganese carboxylates in the melt is similar to that of the cadmium soaps for which cylindrical micelles have been postulated (12). Viscosity data (4) on the cadmium soaps show that the contribution of the methyl and head groups to the activation energy for viscous flow ($\sim$71 kJ mol^{-1}) is much bigger than that for the lead soaps ($\sim$15 kJ mol^{-1}) (20) which implies that a considerable amount of work must be done against coulombic and dipolar forces in the cadmium carboxylates to cause the movement of the unit of flow. It would, therefore, be useful to measure the viscosities of the manganese carboxylates. Unfortunately we were unable to obtain reliable viscosity data due to operational difficulties similar to those encountered with the molar volume measurements. However, visual observation suggests that the manganese carboxylate melts must have abnormally high viscosities.

Acknowledgment

The author is grateful to Messrs. O. Kehinde and O. Aiyemonisan for technical assistance.

1. S. M. Nelson and P. C. Pink. J. Chem. Soc. 4412 (1954).
2. J. J. Duruz, H. J. Michels, and A. R. Ubbelohde. Proc. R. Soc. A, 330 (1972); 1 (1972).
3. M. E. Ekwunife, M. U. Nwachukwu, F. P. Rinehart, and S. J. Sime. J. Chem. Soc. Faraday Trans. I, **71**, 1432 (1975).
4. S. O. Adeosun, W. J. Sime, and S. J. Sime. J. Chem. Soc. Faraday Trans. I, **72**, 2470 (1976).
5. J. J. Uruz, H. J. Michels, and A. R. Ubbelohde. Proc. R. Soc. A, 322 (1971); 281 (1971).
6. P. Ferloni and P. Franzosini. Gazz. Chim. Ital. **105**, 391 (1975).
7. M. J. Vold, H. Funakoshi, and R. D. Vold. J. Phys. Chem. **80**, 1753 (1976).
8. J. Roth, T. Meisel, K. Seybold, and Z. Halmos. J. Therm. Anal. **10**, 223 (1976).
9. T. Meisel, K. Seybold, Z. Halmos, J. Roth, and C. Melykuti. J. Therm. Anal. **10**, 419 (1976).
10. R. D. Vold. J. Am. Chem. Soc. **63**, 2915 (1941).
11. S. O. Adeosun and S. J. Sime. Thermochim. Acta, **17**, 351 (1976).
12. I. Konkoly -Thege, I. Ruff, S. O. Adeosun, and S. J. Sime. Thermochim. Acta. In press.
13. P. A. Spegt and A. E. Skoulios. Acta Crystallogr. **21**, 892 (1966).
14. V. Luzzati and P. A. Spegt. Nature, **215**, 701 (1967).
15. V. Luzzati, T. Gulik-Krzywicki, and A. Tardieu. Nature, **218**, 1031 (1968).
16. V Luzzati, A. Tardieu, and T. Gulik-Krzywicki. Nature, **217**, 1028 (1968).
17. A. S. C. Lawrence. Trans. Faraday Soc. **34**, 665 (1938).
18. P. A. Spegt and A. E. Skoulios. Acta Crystallogr. **16**, 301 (1963).
19. J. Roth, Z. Halmos, and T. Meisel. Thermal analysis, Vol. 2. Proc. Fourth ICTA, Budapest. 1974.
20. U. J. Ekpe and S. J. Sime. J. Chem. Soc. Faraday Trans. I, **72**, 1144 (1976).
21. C. A. Angell. J. Phys. Chem. **70**, 2793 (1966).
22. B. Cleaver, A. J. Davies, and M. D. Hames. Electrochim. Acta, **18**, 719 (1973).
23. G. J. Janz. Molten salts handbook. Academic Press. 1967. p. 291.

The crystal and molecular structure of 6,7-bis(methoxycarbonyloxy)-1,2,3,4-tetrahydroisoquinoline-[1,2-*c*]-oxazol-2-one-[3,4-*b*]-1-chloro-3-methoxycarbonyloxy-6,7-methylenedioxyindane

WINNIE WONG-NG AND S. C. NYBURG

Lash Miller Chemical Laboratories, University of Toronto, Toronto, Ont., Canada M5S 1A1

Received June 27, 1978

WINNIE WONG-NG and S. C. NYBURG. Can. J. Chem. **57**, 157 (1979).

A synthetic intermediate expected to be a *spiro*benzylisoquinoline bromo-derivative proved, on X-ray crystal structure analysis, to be the title compound, a chloro-derivative with the isoquinoline nitrogen ring-closed. Crystals belong to the monoclinic system, space group $P2_1/c$, $a = 13.68(2)$, $b = 10.81(2)$, $c = 22.12(4)$ Å, $\beta = 129.2(4)°$, $Z = 4$ molecules per cell. Intensity data were collected by diffractometer and the structure refined to a conventional R of 0.051.

WINNIE WONG-NG et S. C. NYBURG. Can. J. Chem. **57**, 157 (1979).

On croyait qu'un intermédiaire de synthèse était un dérivé bromé d'une *spiro*benzylisoquinoléine; une analyse de la structure cristalline par rayons-X a permis de prouver que l'intermédiaire est plutôt le composé mentionné dans le titre, un dérivé chloré dans lequel l'azote de l'isoquinoléine fait partie d'un cycle fermé. Les cristaux appartiennent au système monoclinique, groupe d'espace $P2_1/c$, $a = 13.68(2)$, $b = 10.81(2)$, $c = 22.12(4)$ Å, $\beta = 129.2(4)°$. $Z = 4$ molécules par maille. On a recueillie les données d'intensité à l'aide d'un diffractomètre et on a affiné la structure jusqu'à une valeur de R conventionnelle de 0.051.

[Traduit par le journal]

Introduction

One of the steps involved in the Pictet–Spengler route to *spiro*benzylisoquinoline alkaloids has typically been as follows:

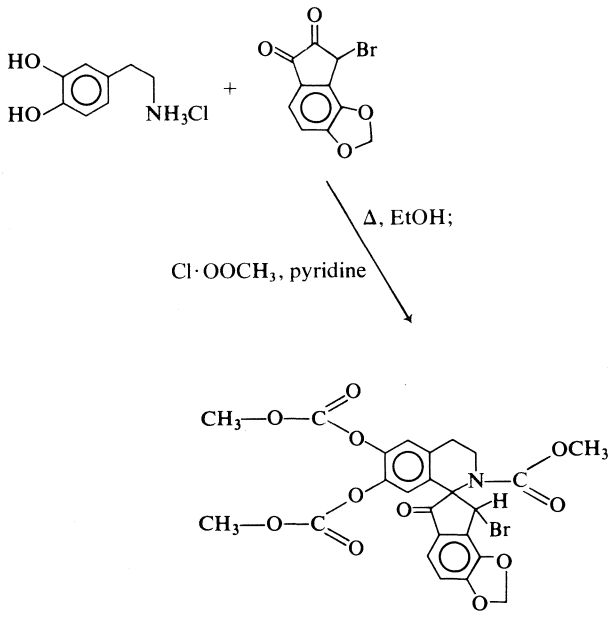

1

Since the local conformation is of interest a crystal structure analysis of the assumed material **1** was undertaken.

Experimental

Colourless crystals were kindly supplied by Professor S. McLean and from one of these a single fragment was cut ca. 0.31 × 0.18 × 0.48 mm. This was used for X-ray analysis.

Approximate cell dimensions and the systematic absences were established photographically. Refined cell dimensions were obtained from fourteen diffractometer-centered reflections. (The crystal proved to have neither the structure nor empirical formula of **1**. Full crystallographic data are given later.)

Intensity data were collected on a computer-automated four circle Picker diffractometer using Ni-filtered CuKα radiation and pulse height analyser in θ–2θ scan mode at 2° min^{-1} in the range $0 < \sin\theta < 0.87$. The scan range, adjusted for dispersion, was 2°, and a total of 3851 independent reflections was recorded with a standard at every 30 measurements. The standard intensity did not vary significantly. The standard deviation in raw intensity, $\sigma(I)$ was taken as $[a(\text{peak} + \text{background}) + aI^2 + 0.02I]$ where a = attenuation factor; thus $\sigma(F_o)$ was taken as $[(\sigma(I)/Lp) + 0.02F_o^4]^{1/2}/2F_o$ where Lp is the Lorentz-polarization factor and $0.02F_o^4$ makes some allowance for instrument instability. Absorption corrections were not made. The 2894 reflections having $F_o > 2\sigma(F_o)$ were taken as significant and used for structure analysis.

The 289 largest E values (> 1.5) were used in direct method routines MULTAN (1) and TANFOR[1]. Neither yielded intelligible results. All reflections with l odd are very weak implying heavy atoms at $y = \frac{1}{4}, \frac{3}{4}$. (Omitting l odd reflections and phasing only on E's with l even was not helpful; no chemical sense could be made of the peaks having false $P2_1/m$ symmetry.) The l odd and l even reflections were then separately normalised and, using MULTAN, and E map was obtained which was chemically intelligible but did not correspond to formula **1**. Attempts at refinement yielded consistently high R values.

[1]M. Drew. Local computer programme. Unpublished.

0008-4042/79/020157-03$01.00/0

Not until the putative bromine site was allowed to have variable occupancy was it clearly established to be chlorine. The molecular weights of the most promising chemical structure $C_{25}H_{20}NO_{13}Cl$ (577.61) and of the putative $C_{24}H_{20}NO_{11}Br$ (578.06) were too close for the measured density to be decisive. However, the mass spectrographic pattern of isotopic abundance confirmed that the former of the two empirical formulas was correct. Crystal data are as follows.

$C_{25}H_{20}NO_{13}Cl$ fw = 577.61
Monoclinic, $P2_1/c$, $a = 13.68(2)$, $b = 10.81(2)$, $c = 22.12(4)$ Å, $\beta = 129.2(4)°$, $V = 2534(28)$ Å^3, $Z = 4$, $\rho_o = 1.51$, $\rho_c = 1.50$ g cm^{-3}, 25°C, CuKα, $\lambda = 1.5418$ Å, μ(CuKα) = 14.91 cm^{-1}.

Refinement by full matrix anisotropic least-squares ORFLS[2] (using dispersion corrections $f' = 0.348$, $f'' = 0.702$ for chlorine) was uneventful. All hydrogen atom positions were allowed to vary but their isotropic temperature factors were fixed at $B = 6$ Å^2. The final unweighted R value was 0.051.

Final atomic coordinates are listed in Table 1. Observed and calculated structure factors and thermal parameters have been placed in the Depository of Unpublished Data.[3]

TABLE 1

(*a*) Atomic fractional coordinates ($\times 10^4$) for non-hydrogen atoms

Atoms	*x*	*y*	*z*
CL	−542(1)	2251(1)	2447(1)
C(1)	−1729(3)	2228(3)	1386(2)
C(2)	−2374(3)	1001(3)	1108(3)
C(3)	−3095(4)	409(3)	1252(2)
O(4)	−3403(3)	772(3)	1706(2)
C(5)	−4295(4)	−133(4)	1564(3)
O(6)	−4266(3)	−1150(3)	1163(2)
C(7)	−3616(4)	−738(3)	929(2)
C(8)	−3428(4)	−1336(3)	459(3)
C(9)	−2717(4)	−739(3)	300(2)
C(10)	−2211(3)	418(3)	625(2)
C(11)	−1462(3)	1178(3)	494(2)
O(12)	−2180(2)	1272(2)	−328(1)
C(13)	−1666(4)	1793(3)	−623(2)
O(14)	−697(3)	2331(3)	−274(2)
O(15)	−2486(3)	1587(2)	−1382(2)
C(16)	−2077(7)	1994(6)	−1816(3)
O(17)	−273(2)	655(2)	823(2)
C(18)	668(4)	1465(3)	1323(2)
O(19)	1748(3)	1272(3)	1609(2)
N(20)	201(3)	2427(3)	1459(2)
C(21)	916(4)	3570(4)	1810(2)
C(22)	483(4)	4498(4)	1166(3)
C(23)	−924(3)	4584(3)	597(2)
C(24)	−1496(3)	5670(3)	158(2)
C(25)	−2776(3)	5765(3)	−369(2)
O(26)	−3329(2)	6887(2)	−767(1)
C(27)	−3714(3)	6941(3)	−1497(2)
O(28)	−3555(3)	6146(2)	−1797(1)
O(29)	−4268(3)	8012(3)	−1783(2)
C(30)	−4660(5)	8300(5)	−2554(3)
C(31)	−3553(3)	4806(3)	−494(2)
O(32)	−4833(2)	5001(2)	−1064(1)
C(33)	−5652(3)	4539(3)	−995(2)
O(34)	−5426(3)	3881(3)	−486(2)
O(35)	−6779(2)	4960(3)	−1593(2)
C(36)	−7834(4)	4399(5)	−1704(3)
C(37)	−3025(3)	3711(3)	−82(2)
C(38)	−1705(3)	3608(3)	468(2)
C(39)	−1154(3)	2430(3)	954(2)

TABLE 1 (*Concluded*)

(*b*) Atomic fractional coordinates ($\times 10^3$) for hydrogen atoms

Atoms	*x*	*y*	*z*
H(1)	−227(5)	288(5)	129(3)
H(21a)	78(5)	387(5)	215(3)
H(21b)	191(5)	340(5)	214(4)
H(22a)	86(5)	529(5)	136(3)
H(22b)	78(5)	408(5)	89(3)
H(24)	−90(5)	642(5)	30(3)
H(37)	−365(5)	301(5)	−19(3)
H(9)	−393(5)	818(4)	−259(3)
H(30a)	−530(5)	755(5)	−296(3)
H(30b)	−525(5)	882(5)	−276(3)
H(30c)	−252(5)	−108(5)	−2(3)
H(8)	−379(5)	−210(5)	29(3)
H(5a)	−526(5)	35(5)	120(3)
H(5b)	−410(5)	−44(5)	202(3)
H(36a)	−779(5)	357(5)	−178(3)
H(36b)	−868(5)	493(5)	−223(3)
H(36c)	−764(5)	455(5)	−116(3)
H(16a)	−262(5)	166(6)	−219(3)
H(16b)	−103(5)	175(5)	−151(3)
H(16c)	−219(5)	290(5)	−190(3)

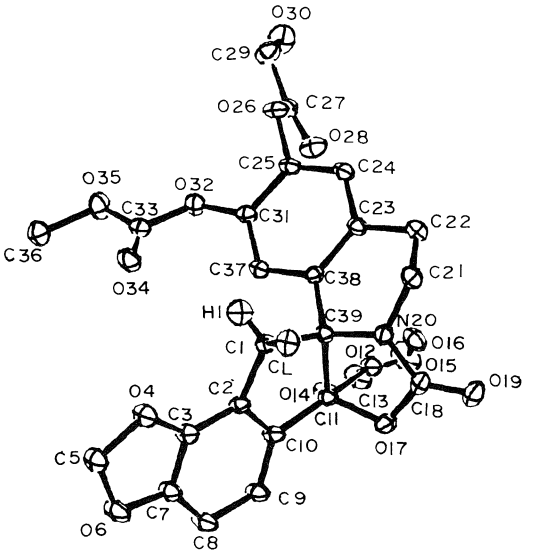

FIG. 1. ORTEP plot of the molecule showing 20% probability thermal ellipsoids. All hydrogen atoms except H(1) are omitted.

Discussion

The molecule has configuration **2**. An ORTEP

[2]R. D. Ellison. XFLS-3. An extensively modified version of ORFLS. Report ORNL. TM. 305. Oak Ridge National Laboratory (1962). Unpublished.

[3]Complete set of data may be obtained, at a nominal charge, from the Depository of Unpublished Data, CISTI, National Research Council of Canada, Ottawa, Ont., Canada K1A 0S2.

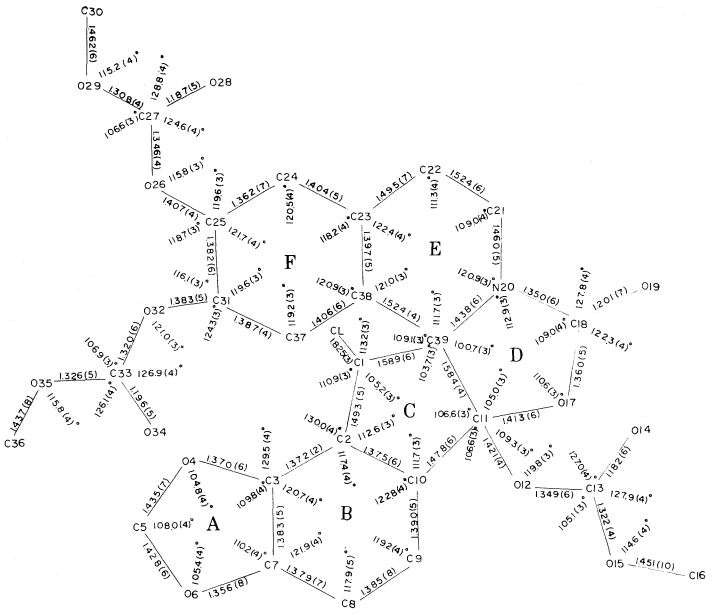

FIG. 2. Bond lengths (Å) and bond angles (deg).

plot with all hydrogen atoms except H(1) omitted is given in Fig. 1, and bond lengths and angles in Fig. 2.

The two striking differences in structure compared with the expected **1** are the replacement of bromine by chlorine and, instead of acetylation of N(20), its closure to form an oxazolone ring. (There is evidence, however, that a compound of type **1** is actually formed in the reaction but remains in solution.[4])

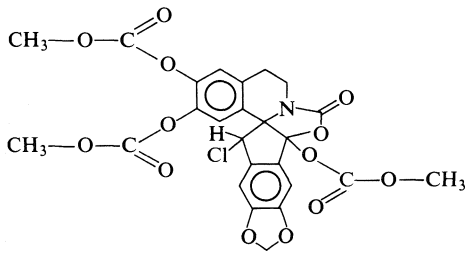

2

The chlorine atom lies *syn* to C(39)—N(20), C(39) itself being significantly out of the plane of ring F (0.090(4) Å) indicating some strain at C(38). C(5) is 0.183(5) Å out of the plane of ring B and the rest of ring A.

The two methoxycarbonyloxy groups at C(25) and C(31) lie at different angles to their adjacent planes, namely, 57.1(5)° and 84.4(3)°, respectively. In both cases there are hydrogen atoms close to the ketoxy oxygen atoms: O(28)—H(5) [x, $\frac{1}{2} - y$, $z - \frac{1}{2}$], 2.34(6) Å, O(34)—H(37) (intramolecular), 2.29(7) Å and O(34)—H(8) [$\bar{x} - 1$, $\bar{y}$, $\bar{z}$], 2.36(6) Å. The bond lengths in the three methoxycarbonyloxy groups are self-consistent, the C—O bonds adjacent to the central carbon atom being relatively short and the outer C—O bonds relatively long in each case.

Acknowledgment

We thank the National Research Council of Canada for support of this work.

1. G. GERMAIN, P. MAIN, and M. M. WOOLFSON. Acta Crystallogr. A**27**, 368 (1971).

[4]S. McLean. Private communication.

The preparation and characterisation of 1,1,2,2-tetramethyl-1,2-diacyloxyditin(IV) compounds

THOMAS BIRCHALL AND JAMES P. JOHNSON

Department of Chemistry, McMaster University, Hamilton, Ont., Canada L8S 4M1

Received July 28, 1978

THOMAS BIRCHALL and JAMES P. JOHNSON. Can. J. Chem. **57**, 160 (1979).

Reaction of hexamethylditin with haloacetic acids results in the production of 1,1,2,2-tetramethyl-1,2-diacyloxyditin(IV) compounds in good yield. Infrared, Raman, ^{1}H and ^{13}C nmr, and ^{119}Sn Mössbauer data have been interpreted in terms of a tetramethylditin species asymmetrically bridged by two acyloxy groups to give each tin a five-coordinate environment.

THOMAS BIRCHALL et JAMES P. JOHNSON. Can. J. Chem. **57**, 160 (1979).

La réaction de l'hexaméthylétain avec les acides haloacétiques conduit à la formation de composés tétraméthyl-1,1,2,2 diacyloxy-1,2 étain(IV) avec de bons rendements. On interprète les données de l'infrarouge, de Raman de la rmn du ^{1}H et ^{13}C et de Mössbauer du ^{119}Sn en termes d'espèces tétraméthyldiétain pontées d'une façon asymétrique par deux groupes acyloxy fournissant à chaque étain un environnement penta-coordonné.

[Traduit par le journal]

Introduction

Solvolysis of tetramethyl tin by strong acids leads to production of the $[(CH_3)_3Sn^+]$ and $[(CH_3)_2Sn^{2+}]$ ions which are strongly solvated in the reaction media (1). Isolation of $(CH_3)_3SnX$ and $(CH_3)_2SnX_2$ can be accomplished under appropriate conditions (2, 3). Several spectroscopic studies have been carried out, where $X = [RCOO^-]$, in order to establish the mode of coordination of the acetate to the central tin and hence the geometry about the tin atom (4–10). The five coordinate nature of tin in $R_3Sn(O_2CR)$ has been definitely established by X-ray crystallography, and the Sn—O axial bond lengths were found to be significantly different (11, 12).

In attempting solvolyses of hexamethylditin, we obtained nmr evidence for the presence of tetramethylditin species in solution. We now present details of the preparation and spectroscopic analyses for a number of ditin haloacetates. Compounds of this kind have been prepared before by the reaction of R_2SnH_2 ($R = C_6H_5$, *n*Bu) with carboxylic acids (13, 14). In the case of the $R_4Sn_2X_2$ systems there is uncertainty about the nature of the structures of these compounds in solution and in the solid state (15, 16). Our data are consistent with a five coordinate tin environment in solution and the solid state.

Experimental

Preparation

In a typical preparation 0.283 mol of trichloroacetic acid and 10 mL of chloroform were introduced under dry nitrogen into a two necked 100 mL flask containing a stirring bar. The flask was cooled in an acetone–ice bath. Hexamethylditin, 0.024 mol, was added via a 10 mL syringe through a rubber septum cap onto the stirred cold acid–chloroform mixture. An immediate slow but steady gas evolution occurred. After ~12 h the gas evolution had ceased and 90 mL of distilled water were added to the pale orange mixture which was allowed to warm to room temperature. The colour was discharged and the mixture was filtered through a fine glass frit under suction. The white solid was washed with 140 mL distilled water to give 12.963 g of product. Further work up of the filtrate yielded a further 1.173 g for a total yield of vacuum dried product of 95.1%.

A similar procedure was used for the preparation of the other compounds, all of which are white solids. No ditin species were obtained from the reactions with the $—CBr_3$, $—CH_3$, $—CH_2I$, or —CH acids. Analytical data are summarized in Table 1. Carbon and hydrogen were determined by Chemalytics Ltd. while Sn was determined gravimetrically by standard procedures (17).

Infrared spectra were recorded, as Nujol mulls, on a Perkin-Elmer 283 and a Nicolet 7000 F.T.I.R.; Raman spectra were recorded with a Spectro-Physics He/Ne (6328 Å) or an Ar ion (5145 Å) laser using a Spex 1400 spectrophotometer system; ^{1}Hmr spectra were obtained using a Varian H.A. 100, or E.M. 390 or a Bruker W.H. 90. This latter instrument was also used to obtain ^{13}Cmr spectra. Mössbauer spectra (^{119}Sn) were recorded using an Elscint AME 40 drive system operating in the constant acceleration mode with automatic folding of the triangular waveform. The transmitted radiation, through a Pd filter, was detected by a $Kr–CO_2$ (1 atm) proportional counter and fed to a Tracor-Northern multi-channel analyzer operating in the up-down multi-scaling mode. Samples were finely ground powders, intimately mixed with Apiezon N Grease, and sandwiched in a copper holder between thin aluminum foils. These samples contained ~10 mg natural tin/cm^{-2} and were rigidly held in a Liquid Transfer Cryotip system manufactured by Air Products and Chemicals Inc. The source was $Ca^{119}SnO_3$ obtained from Amersham-Searle, and was maintained at room temperature. Temperatures were monitored by means of a calibrated iron-doped gold chromel thermocouple and a Hewlett-Packard 419A DC null voltage detector. Spectra were computor fitted using a programme written by Stone (18) and modified by D. G. Grundy of the Department of Geology, McMaster University. The instru-

0008-4042/79/020160-07$01.00/0

TABLE 1. Analytical data for $(CH_3)_4Sn_2(O_2CR)_2$

R	Yield %	Melting point† (°C)	%Sn Calcd.	%Sn Found	%C Calcd.	%C Found	%H Calcd.	%H Found
CF_3	89	140(d)	45.34	44.74	18.35	18.37	2.31	2.27
CHF_2	12	131(d)	48.69	47.50*	19.71	19.51	2.89	2.43
CCl_3	87	150(d)	38.15	37.99*	15.44	14.90	1.94	1.68
$CHCl_2$	80	125(d)	42.90	42.72	17.36	17.55	2.55	2.39
CH_2Cl	61	158(d)	48.99	48.83*	19.83	20.06	3.33	3.10

*Single analysis.
†(d), decomposes at melting point.

ment was calibrated using a $^{57}Co/Rh$ source and a standard iron foil. All isomer shifts were measured relative to SnO_2 as zero.

Results and Discussion

Hexamethylditin can react with substituted acetic acids, with gaseous evolution, according to either [1] and/or [2].

[1] $(CH_3)_6Sn_2 \xrightarrow[-H_2]{RCOOH} (CH_3)_3Sn(O_2CR)$ **1**

$$\xrightarrow[-CH_4]{RCOOH} (CH_3)_2Sn(O_2CR)_2$$ **2**

[2] $(CH_3)_6Sn_2 \xrightarrow[-CH_4]{RCOOH} [(CH_3)_2Sn(O_2CR)]_2$ **3**

$$\xrightarrow[-H_2]{RCOOH} (CH_3)_2Sn(O_2CR)_2$$

Both pathways, if carried out under the most vigorous conditions, ultimately result in species **2**. These reactions can be monitored very conveniently by ^1H nmr and such a study allows one to chose the correct conditions so that the yield of **3** can be optimised.

The nature of **3** is of interest since a number of structures are possible (Fig. 1). The tin atoms could be four-coordinate, with monodentate acetate, as in **4**, or be five-coordinate as in **5**–**7**. In **5** the acetate groups bridge $(CH_3)_2Sn—Sn—(CH_3)_2$ units intermolecularly to give a polymeric structure. On the other hand, intramolecular bridging acetates could bond in a symmetric fashion, as indicated in **6**, or asymmetrically to give two C—O and two Sn—O distances as in **7**.

Infrared and Raman Spectra

The application of vibrational spectroscopy to structural elucidation is often fraught with difficulty, particularly when the molecules contain as many atoms as those discussed here. However, judicious use of infrared and Raman spectroscopies and simple group theoretical treatments can provide valuable

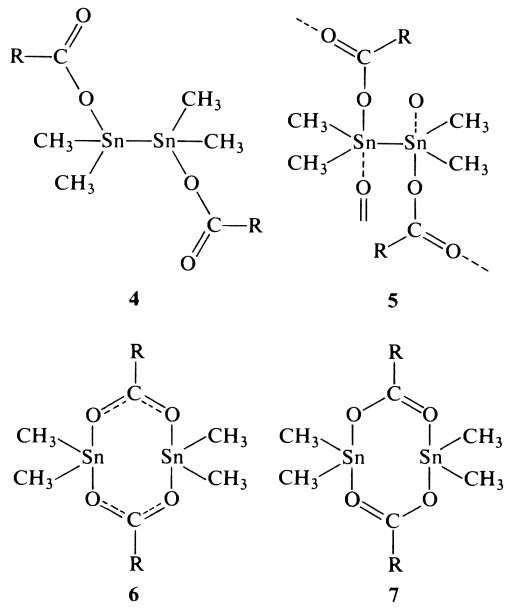

FIG. 1. Possible structures for $(CH_3)_4Sn_2(O_2CR)_2$.

structural information. In our initial investigations the presence of a tin–tin bond was established by nmr and is discussed below. Examination of the solid state Raman spectra of these compounds shows the presence of a strong vibration at $\sim 205\ cm^{-1}$, which is absent, or very weak, in the infrared spectra. The Raman spectrum of the $—CCl_3$ derivative in $CHCl_3$ also shows this strong band, which is polarized, and is assigned to the tin–tin stretch. The vibrational spectra are summarized in Table 2.

In order to simplify the assignment of the spectra we decided to treat the C_4Sn_2 moiety separately from the acyloxy unit. Twelve normal modes are expected from the C_4Sn_2. How these vibrational modes will be distributed between ir and Raman active modes will be determined by the overall symmetry of the molecule. Previous workers (7, 8) have established that the carbon–tin symmetric and asymmetric stretches

TABLE 2

Infra-Red and Raman Data for $(CH_3)_4Sn_2(O_2CR)_2$ *

CF_3		CHF_2		CCl_3		$CHCl_2$		CH_2Cl		ASSIGNMENT
IR	R	IR	R	IR	R	IR	R	IR	R	
									41(33)	LATTICE MODE
	100(25)				98(29)		104(15)		101(19)	$SnCH_3$ bend
	137(81)		149(30)	148 w	146(47)	140 m	145(52)	143 m	142(47)	$SnCH_3$ def.
150 m(b)			171(18)	167 w					166(15)	
		190 w(b)				181 m	182(12)	205 m	200(6)	
	204(64)		211(32)	212 w	(p)207(35)	210 w	204(32)		214(31)	ν sym. Sn-Sn (Ag)
265 w	267(1)	280 w(b)		275 w	225(8) 283(7)	262 m	279(14)	292 m	303(2)	ν sym Sn-O
310 w	307(1)	315 w(b)		355 w	303(3) 343(10)	350 m	347(1)	360 w		
440 m		380 w(b)			434(2)					
	506(2)	490 m(b)		450 m	475(3)	456 m	453(5)	490 m	479(2)	ν_{as} Sn-O
523 m		527 m		523 m		530 m		535 m		ν sym. Sn_2C_4 (Au)
	528(100)		531(100)		(p)530(100)		535(100)		538(100)	ν sym. Sn_2C_4 (Ag)
	546(40)		548(44)		548(50)		546(47)		544(52)	ν_{as} Sn_2C_4 (Bg)
552 m		555 m		553 m		552 m		550 m		ν_{as} Sn_2C_4 (Bu)
	599(1)	615 m(b)				630 m		575 w		
				686 s	685(4)	680 s		680 m		δ CO_2
727(s)	726(1)				750(11)	705 s(b)	705(1) 708(1)			
				750 s						ν C-Cl
770 m(b)								770 m(b)		
793 m		785 m(b)		780 s(b)		770 s(b)	771(7)	785 m(b)	782(7)	$Sn-CH_3$ rocking
		810 s	813(2)	840 s	835(5)	832 s	827(4)			
				848 s						δ CO_2
845 s	844(9)	950 m	932(8)	960 w	961(6)	950 m	947(7)	935 m	933(5)	ν C-C
1142 s(b)	1160(1)	1090s(b)	1110s(b)							ν C-F
	1190(14)		1192(30)	1190 w	1192(25)	1192 w	1190(26)	1180 w	1177(6) 1187(23)	$\delta(CH_3)$
1200 s(b)	1207(8)		1200(20)	1200 w	(p)1200(37)	1200 w	1197(36)	1195 w	1200(47)	$Sn-CH_3$ sym. def.
			1211(6)			1235 s	1223(1) 1240(1)	1250 s	1214(2)	ρC-H of R
		1330 s	1330(2)	1350 s(b)	1335(3)	1385 s	1378(3)	1390 s(b)	1389(2)	ν sym CO_2
1443 m	1443(6)	1340 m	1335(2)		1379(6)					
			1443(2)		1407(9)		1401(1)		1409(2)	$SnCH_3$ as. def.
1650 s(b)	1619(1)	1605 s(b)		1615 s(b)	1601(2)	1608 s	1543(1)	1583 s(b)		$\nu_{as}CO_2$
	2370(1)					2380 w	2440 w 2367(1)			
	2782(1)					2480 w	2780 w 2779(1)			ν CH_3
	2939(13)		2927(23)		(p)2927(22)		2920 w 2928(16)		2926(18)	ν sym CH_3
			2982(10)				3001(11)		2955(13)	ν C-H of R group
	3017(5)		3009(12)		3009(12)	3020 s	3009(32)		3002(11)	ν_{as} CH_3

*I.r. spectra were recorded as nujol mulls: Raman spectra were obtained from solid samples.

TABLE 3. Symmetric and asymmetric stretches (ir) of the $—CO_2$ group for $(CH_3)_4Sn_2(O_2CR)_2$, $(C_6H_5)_4Sn_2(O_2CR)_2$, and $(CH_3)_3Sn(O_2CR)$

	$(CH_3)_4Sn_2(O_2CR)_2$ solid*		$(C_6H_5)_4Sn_2(O_2CR)_2$ solid†		$(CH_3)_3Sn(O_2CR)$‡			
					Solid		Solution	
R	ν_{as}	ν_s	ν_{as}	ν_s	ν_{as}	ν_s	ν_{as}	ν_s
CF_3	1650	1443	1625	—	1680	1435	1720	1400
CCl_3	1615	1350	1610	1350	1655	1342	1702	1290
CHF_2	1605	1330	—	—	1630	1460	—	—
$CHCl_2$	1605	1380	1585	1385	1610	1380	1700	1324
CH_2Cl	1585	1390	1560	1395	1610	1380	1690	1335

*ν_{as} and ν_s have the same values in $CHCl_3$.
†Reference 15, ν_{as} and ν_s have the same values in $CHCl_3$.
‡Reference 5.

occur in the 520–550 cm^{-1} region of the spectrum. Two bands are present in this region in both the ir and Raman spectra of the molecules reported here. These can be assigned to the symmetric and asymmetric stretches associated with the $—SnC_2$ group. That these stretches in the ir are not identical to those in the Raman is apparent on close examination of Table 2. In all cases the symmetric stretch is at lower frequency in the ir than in the Raman, while the reverse is true for the asymmetric stretch. There is then mutual exclusion of bands in the ir and Raman, indicating the presence of an inversion centre in the molecule as a whole and a point group symmetry of C_{2h} is assigned. Five of the modes associated with the C_4Sn_2 moiety have been assigned on this basis in Table 2.

Comparison of these spectra in the acyloxy region with $(C_6H_5)_4Sn_2(O_2CR)_2$ and $(CH_3)_3Sn(O_2CR)$ allows identification of the ν_sCO_2 and $\nu_{as}CO_2$ modes. The relevant bands are compared in Table 3. Agreement between the three series of compounds is good for the solid state spectra suggesting that the acyloxy ligands are similarly bonded in all three types of molecules. In solution $(CH_3)_3Sn(O_2CR)$ has been shown to be largely monomeric (7, 8) but with some degree of association, while X-ray crystallography has shown that $\phi_4Sn_2(O_2CCH_3)_2$ (19) and $(CH_3)_3Sn(O_2CR)$ (11, 12) have bridging acyloxy groups which complete five-coordination about the tin atoms. The vibrational spectra of the ditin compounds strongly suggest that the acyloxy groups bridge the two tin atoms intramolecularly in these methyl derivatives, as has been established for the phenyl compound (19). The fact that, for the methyl and phenyl (15) compounds, neither ν_sCO_2 nor $\nu_{as}CO_2$ changes on going from the solid state to solution suggests that their structures are the same in the two phases. The difference between $\nu_{as}CO_2$ and ν_sCO_2 should reflect the difference in C—O bond strengths and hence the asymmetry of the acyloxy bridge. Examination of the data in Table 3 suggests that the most asymmetric situation should occur in the $—CCl_3$ and $—CHF_2$ cases, while the more symmetrically bonded cases should be $—CH_2Cl$ and $—CF_3$. The asymmetry in the C—O bonds should be reflected in the Sn—O distances.

Mössbauer Spectra

Tin-119 Mössbauer spectroscopy has proved extremely valuable in structural studies of organo–tin systems (20). We present such data for all of the compounds discussed in Table 4. No significant room temperature absorptions were observed for these compounds. All spectra appear as simple doublets (Fig. 2) having line widths of about 1 mm s^{-1}. The isomer shifts are slightly greater than those found for $(CH_3)_3Sn(O_2CR)$ (7, 9) systems but are very similar to the shifts for the $(C_6H_5)_4Sn_2(O_2CR)_2$ series (16). However, while the earlier workers (7, 9) report changes in isomer shift with different R groups, we find no such variation. This indicates that the *s* electron density at the tin nucleus does not change through our series of compounds.

Changes in the quadrupole splitting values do occur and, although these changes are small, the trend is to decreasing values as R becomes less electron withdrawing. A similar trend has been com-

TABLE 4. ^{119}Sn Mössbauer data for $(CH_3)_4Sn_2(O_2CR)_2$ at 77 K

	Isomer shift*	Quadrupole splitting*		Line width*	
R	δ	$\Delta_{measured}$	$\Delta_{calculated}$	Γ_1	Γ_2
CF_3	1.63	3.99	3.95	0.83	0.85
CHF_2	1.53	3.81	3.81	0.92	0.92
CCl_3	1.61	3.87	3.87	0.89	0.94
$CHCl_2$	1.59	3.84	3.81	0.84	0.84
CH_2Cl	1.63	3.63	†	1.03	1.10

*mm s^{-1} ± 0.03.
†This compound was used to derive a partial quadrupole splitting of − 0.807 mm s^{-1} for the $(CH_3)_2Sn(O_2CR)_2$ fragment.

mented upon in relation to the difference between the asymmetric and symmetric vibrations of the CO_2 group. The quadrupole splitting values are large, ~3.6–4.0 mm s^{-1}, and only slightly smaller than the corresponding values for the analogous $(C_6H_5)_4Sn_2(O_2CR)_2$ compounds (16). Such values are just those that would be predicted by the point charge model for a five-coordinate tin (21): the sign, which was not determined here, should be negative. This means that there is more electron density in the *xy* plane than there is along the *z* axis, which presumably contains the O—Sn—O atoms. Herber's criterion that $\Delta/\delta > 2.1$, for five-coordination (22) is also satisfied for these compounds. Calculation of the quadrupole splittings for these compounds using the approach of Bancroft *et al.* (23) gives excellent agreement with experiment, if five coordination is assumed. Finally, since $(C_6H_5)_4Sn_2(O_2CCH_3)_2$ has been shown to be monomeric and have five-coordinate tin atoms, we believe that tetramethyl derivatives reported here have the same basic structure.

It has been found that for $(CH_3)_3SnO_2CCH_3$ and $(CH_3)_3SnO_2CCF_3$, there is an increase in the quadrupole splitting of 0.54 mm s^{-1} from the former to the latter and the Sn—O distances are 2.205(3), 2.391(4), and 2.18(1) and 2.46(2) Å, respectively (12). The trifluoroacetate has somewhat more asymmetric bonds to the tin and in addition there is a slight increase in the average Sn—O distance, 2.32 Å for the $—CF_3$ compared to 2.298 Å for the $—CH_3$ compound. Although these differences are small they are paralleled by the trends in the quadrupole splitting. On the basis of the trends we observe in the quadrupole splittings for the $(CH_3)_4Sn_2(O_2CR)_2$ series we expect a similar increase in the average Sn—O distance from the monochloracetate to the trifluoracetate. We are presently trying to obtain crystallographic evidence for such changes.

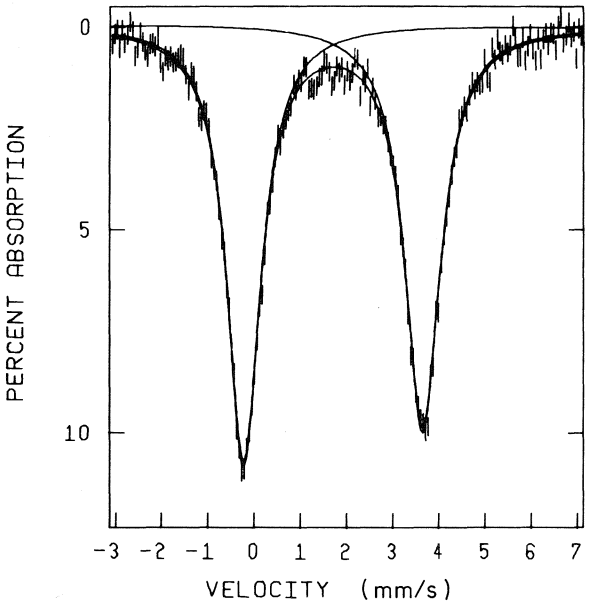

FIG. 2. ^{119}Sn Mössbauer spectrum of $(CH_3)_4Sn_2(O_2CCF_3)_2$ at 77 K.

Nuclear Magnetic Resonance Spectra

Nuclear magnetic resonance spectra (^{1}H and ^{13}C) have been recorded and the data are summarized in Table 5. The chemical shifts of the ^{1}H and ^{13}C nuclei follow the generally accepted trends and will not be commented upon further. All of the compounds show ^{117,119}Sn satellite peaks associated with the methyl groups confirming that the methyl groups are indeed bonded to tin. Furthermore, these satellites occur in two groups, those arising from $J_{^{117,119}Sn—C—^1H}$ and those from $J_{^{117,119}Sn—Sn—C—^1H}$: the ^{13}C spectra also show the same pattern. The coupling to the far tin indicates that the tin–tin bond is intact in solution. The tin–carbon and tin–hydrogen coupling constants vary slightly as the acyloxy groups are changed but there does not appear to be any systematic variation. Since $J_{Sn—C}$ is dependent upon the *s* character in the tin–carbon bond, the constant values for $J_{^{117,119}Sn—^{13}C}$ are consistent with the Mössbauer results where it was found that the isomer shift, which also depends on *s* character, remains unchanged throughout the series.

The magnitude of $J_{^{117,119}Sn—C—^1H}$ has been used to infer the coordination of the tin in $(CH_3)_3Sn(O_2CR)$ (4, 5, 9). Coupling constants in the range 55–60 Hz have been taken as an indication that the trimethyl tin acetate was monomeric and hence that the tin was four-coordinate in solution. However, other molecules containing the $(CH_3)_3Sn$ moiety in which the tin must be four-coordinate, e.g., $(CH_3)_3M—Sn(CH_3)_3$ (M = C, Si, Ge, or Sn), have $J_{^{119}Sn—C—^1H}$ ranging from 47–49 Hz. Recently, Mathiasch (24, 25) has reported nmr data for $(CH_3)_4Sn_2X_2$ (X = Cl, Br, I, H) which have four-coordinate tin atoms and the two-bond tin–hydrogen coupling constants range from 52.2–53.5 Hz, considerably lower than the coupling constants for the supposedly four-coordinate tin in $(CH_3)_3SnO_2CR$. It should be noted also that $J_{^{119}Sn—^{13}C}$ for $(CH_3)_4Sn_2X_2$ (23) range from 257 to 281 Hz and are much lower than the corresponding values (344 to 349 Hz) for the acyloxy compounds (Table 5). It would seem preferable to infer the geometry about the tin in the acyloxyditin compounds by comparing their nmr data with the ditin compounds of Mathiasch (24).

TABLE 5. Nuclear magnetic resonance data for $(CH_3)_4Sn_2(O_2CR)_2$ in $CDCl_3$

(*a*) Chemical shift (ppm)

Parameter	Value for R = CF_3	CHF_2*	CCl_3	$CHCl_2$	CH_2Cl
^1H (TMS = 0)					
δ_{CH_3}	0.82	0.75	0.82	0.73	0.70
δ_R	—	5.65	—	5.75	3.88
^{13}C (TMS = 0)					
δ_{CH_3}	−1.2	—	−0.9	−1.4	−1.7
δ_{CO}	166.7	—	171.2	174.8	178.2
δ_R	113.5	—	90.7	65.4	42.0
^{19}F ($CFCl_3$ = 0)					
δ_{CF_3}	76.76				

*Not sufficiently soluble for ^{13}C spectra to be recorded.

(*b*) Coupling constant (Hz)

Parameter	Value for R = CF_3	CHF_2	CCl_3	$CHCl_2$	CH_2Cl
$J_{^{117}Sn-C-^1H}$	57.5	58.5	59.0	58.4	57.9
$J_{^{119}Sn-C-^1H}$	60.2	61.0	61.7	60.8	60.5
$J_{^{117/119}Sn-Sn-C-^1H}$	13.2	13.5	13.9	13.5	13.2
$J_{^{13}C-^1H}$	133.8	—	133.8	133.4	132.9
$J_{^{117}Sn-^{13}C}$	331.5	—	328.7	333.9	340.5*
$J_{^{119}Sn-^{13}C}$	347.6	—	344.2	349.3	
$J_{^{117/119}Sn-Sn-^{13}C}$	75.5	—	78.7	79.4	77.2
$J_{^{19}F-^{13}C}$	284.5	—	—	—	—
$J_{^{19}F-C-^1H}$	—	55.5	—	—	—
$J_{^{19}F-C-^{13}C}$	37.7	—	—	—	—
$J_{^{13}C-^1H(R)}$	—	—	—	180.2	150.0

*Satellite doublets not resolved.

Because coupling constants for $(CH_3)_4Sn_2(O_2CR)_2$ are increased considerably over those for $(CH_3)_4Sn_2X_2$, we conclude that the five-coordination established in the solid state, for the acyloxy compounds, is maintained in solution. Simons and Graham (4) have shown that the addition of excess pyridine to solutions of $(CH_3)_3SnO_2CR$ results in an increase in $J_{^{119}Sn-C-^1H}$ from ~59 to 68 Hz, and this was taken as an indication of a change from four- to five-coordination about the tin. Addition of excess pyridine to solutions of $(CH_3)_4Sn_2(O_2CR)_2$ produces no significant change in $J_{^{119}Sn-C-^1H}$ (60.2 to 62.1 Hz). We take this as further confirmation of the five-coordinate tin environment in solution.

Conclusions

We have described a new preparative route to a series of tetramethyldiacyloxyditin(IV) compounds and examined these by a variety of spectroscopic methods. The compounds have been shown to have a planar tetramethylditin moiety in which the acyloxy ligand bridges both tin atoms: each tin is then five-coordinate. This structure persists in solution.

Acknowledgement

The National Research Council of Canada is thanked for financial support.

1. T. BIRCHALL, P. K. H. CHAN, and A. R. PERIERA. J. Chem. Soc. Dalton Trans. 2157 (1974).
2. P. A. YEATS, B. F. E. FORD, J. R. SAMS, and F. AUBKE. Chem. Commun. 791 (1969).
3. P. A. YEATS, J. R. SAMS, and F. AUBKE. Inorg. Chem. **10**, 1877 (1971).
4. P. B. SIMONS and W. A. G. GRAHAM. J. Organomet. Chem. **10**, 457 (1967).
5. E. V. VAN DEN BERGHE, G. P. VAN DER KELEN, and J. ALBRECHT. Inorg. Chim. Acta, **2**, 89 (1968).
6. B. F. E. FORD, B. V. LIENGME, and J. R. SAMS. J. Organomet. Chem. **19**, 53 (1969).
7. C. PODER and J. R. SAMS. J. Organomet. Chem. **19**, 67 (1969).
8. R. E. HESTER. J. Organomet. Chem. **23**, 127 (1970).
9. N. W. G. DEBYE, D. E. FENTON, S. E. ULRICH, and J. J. ZUCKERMAN. J. Organomet. Chem. **28**, 339 (1971).
10. T. N. MITCHELL. J. Organomet. Chem. **59**, 189 (1973).
11. N. W. ALCOCK and R. E. TIMMS. J. Chem. Soc. A, 1873 (1968); 1876 (1968).
12. H. W. CHIH and B. R. PENFOLD. J. Cryst. Mol. Struct. **3**, 285 (1973).

13. A. K. SAWYER and H. G. KUIVILA. J. Org. Chem. **27**, 610 (1962).
14. A. K. SAWYER and H. G. KUIVILA. J. Org. Chem. **27**, 837 (1962).
15. G. PLAZZOGNA, V. PERUZZO, and G. TAGLIAVINI. J. Organomet. Chem. **24**, 667 (1970).
16. M. DELMAS, J. C. MAIRE, Y. RICHARD, G. PLAZZOGNA, V. PERUZZO, and G. TAGLIAVINI. J. Organomet. Chem. **30**, C101 (1971).
17. R. OKAWARA and E. G. ROCHOW. J. Am. Chem. Soc. **82**, 3285 (1960).
18. G. M. BANCROFT, A. G. MADDOCK, W. K. ONG, R. M. PRINCE, and A. J. STONE. J. Chem. Soc. A, 1966 (1967).
19. G. BANDOLI, D. A. CLEMENTE, and C. PANATTONI. Chem. Commun. 311 (1971).
20. N. N. GREENWOOD and T. C. GIBB. Mössbauer spectroscopy. Chapman and Hall, London. 1971. p. 371 and references therein.
21. R. V. PARISH and C. E. JOHNSON. J. Chem. Soc. A, 1906 (1971).
22. R. H. HERBER, H. A. STOCKLER, and W. T. REICHLE. J. Chem. Phys. **42**, 2447 (1965).
23. G. M. BANCROFT, V. G. K. DAS, T. K. SHAM, and M. G. CLARK. J. Chem. Soc. Dalton Trans. 643 (1976).
24. B. MATHIASCH. J. Organomet. Chem. **141**, 295 (1977).
25. B. MATHIASCH. Inorg. Nucl. Chem. Lett. **13**, 13 (1977).

Molybdenum, tungsten, and manganese carbonyl compounds incorporating novel tridentate chelating dimethyl(1-pyrazolyl)(ethanolamino)gallate ligands

KENNETH S. CHONG AND ALAN STORR

Department of Chemistry, University of British Columbia, Vancouver, B.C., Canada V6T 1W5

Received May 18, 1978

KENNETH S. CHONG and ALAN STORR. Can. J. Chem. **57**, 167 (1979).

The coordinating properties of the tridentate tris-chelating ligand, $[Me_2Ga(OCH_2CH_2NH_2)(N_2C_3H_3)]^-$, and its three methyl substituted derivatives (methyl substitution on the amino nitrogen and the 3,5 positions of the pyrazolyl ring) have been studied in a series of molybdenum, tungsten, and manganese carbonyl compounds. Mixed allyl carbonyl and nitrosyl carbonyl compounds of both molybdenum and tungsten have been characterized, and a series of tricarbonyl manganese compounds studied. All the complexes are monomeric octahedral species having the tris-chelating ligands in *fac* coordination. Steric factors influence the arrangement of the three remaining groups in the mixed octahedral complexes (i.e. allyl carbonyl and nitrosyl carbonyl derivatives) and particular site preferences are inferred from spectroscopic measurements.

KENNETH S. CHONG et ALAN STORR. Can. J. Chem. **57**, 167 (1979).

On a étudié les propriétés de coordination du ligand tridentate tris-chélatant $[MeGa(OCH_2CH_2NH_2)(N_2C_3H_3)]^-$ et de trois de ses dérivés méthylés (substitution du méthyle sur l'azote de l'amine et sur les positions 3 et 5 du cycle pyrazolyle) avec une série de composés carbonylés du molybdène, du tungstène et du manganèse. On a caractérisé des composés mixtes allylcarbonyle et nitrosylcarbonyle du molybdène et du tungstène et on a étudié une série de composés du manganèse tricarbonyle. Tous les complexes sont des espèces octaédriques monomères portant les ligands tris-chélatants en coordination *fac*. Des facteurs stériques influencent la disposition des trois autres groupes dans les complexes octaédriques mixtes (comme dans les dérivés allylcarbonyle et nitrosylcarbonyle) et l'on a déduit des préférences particulières des sites à partir de mesures spectroscopiques.

[Traduit par le journal]

Introduction

A series of four anionic tridentate chelating ligands of the type **1** has been synthesized.

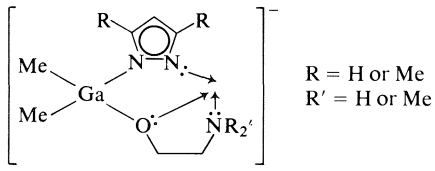

1

Previous reports dealt with octahedral complexes of the first row transition elements (Mn → Zn) incorporating the ligand **1** where R = H and R′ = H (1) and binuclear transition metal complexes (Co → Zn) using the ligand **1** where R = H and R′ = Me (2). The present account expands the study of these two ligands and introduces two additional ligands where R = Me, R′ = H, and R = Me, R′ = Me in **1**.

The coordinating properties of the four ligands have been investigated in a series of carbonyl, allyl carbonyl, and nitrosyl carbonyl compounds of molybdenum, tungsten, and manganese. The ligands are thought to occupy three *fac* positions in the octahedral complexes with the remaining positions occupied either by three carbonyl ligands or by two carbonyl ligands plus a nitrosyl or a 'η^3-allyl' ligand. The uninegative ligands, **1**, act as six electron donors and, as such, are compared with other six electron donors (viz. η^5-$C_5H_5^-$, $HB(N_2C_3H_3)_3^-$, and $MeGa(N_2C_3H_3)_3^-$) in similar carbonyl compounds. The effects of substitution of methyl for hydrogen on the 3,5 positions of the pyrazolyl moiety, on the amino nitrogen, and on the 2 position of the η^3-allyl group, are discussed.

Experimental

Starting Materials

Air sensitive materials were handled in a glove box under an atmosphere of oxygen-free, dry, nitrogen or in a nitrogen-blanketed apparatus. Tetrahydrofuran (THF) was dried by refluxing over lithium aluminum hydride and was used immediately following distillation. Benzene was dried by refluxing over molten potassium followed by distillation. Pyrazole and 3,5-dimethylpyrazole (K and K Laboratories) and sodium hydride (Alfa Inorganic) were used as supplied. Ethanolamine and *N,N*-dimethylethanolamine were refluxed over anhydrous $CaSO_4$ and distilled prior to use. Allyl bromide and 2-methallyl chloride were distilled under nitrogen prior to use. Molybdenum and tungsten hexacarbonyls were used as supplied (Strem). Manganese pentacarbonyl bromide was prepared from dimanganese decacarbonyl (Strem) by a standard route (3). Isoamyl nitrite (MCB) and Diazald (Aldrich) were used

0008-4042/79/020167-07$01.00/0

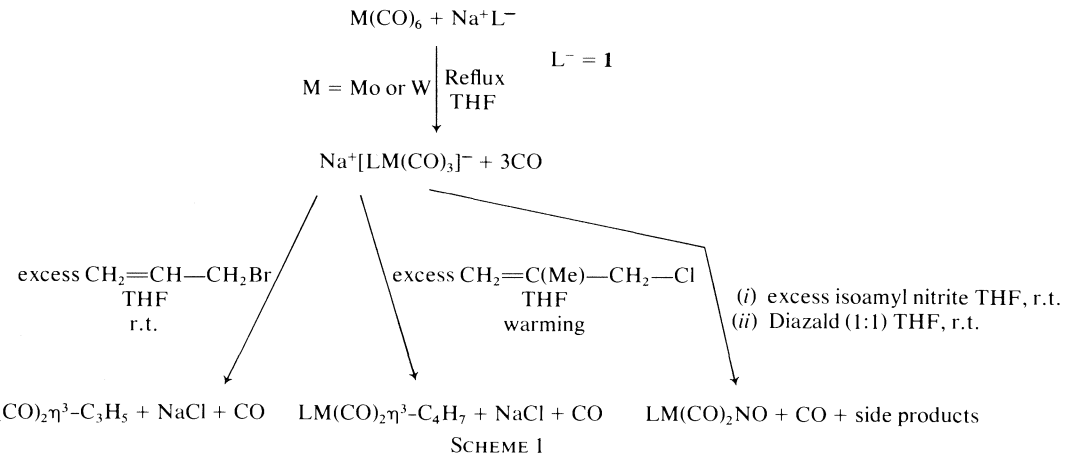

SCHEME 1

as purchased and gallium trimethyl was prepared as described previously (4).

Preparative Details

Ligand Synthesis

All four ligands were prepared as THF solutions by the same general route described previously for **1** where R = H, R′ = H (1), and where R = H, R′ = Me (2). These THF solutions of the ligands were employed in all subsequent reactions since isolation of the solid sodium salts of the ligands was impracticable. The THF solutions from the ligand syntheses were made up to standard volumes and accurately measured aliquots used in the preparations described below.

Preparations of Molybdenum and Tungsten Carbonyl Complexes

The general method employed for the preparation of these compounds (Scheme 1) was to react 1:1 molar ratios of the metal hexacarbonyls and the ligand sodium salts in THF to produce extremely air-sensitive yellow solutions of the sodium salts of the $LM(CO)_3^-$ ions. These solutions were then reacted with an excess of the appropriate 'allyl' halide, isoamylnitrite, or an equimolar amount of Diazald to produce the desired product. The crude materials isolated from THF solution were recrystallized from benzene solvent to give yields of approximately 50% for the 'allyl' compounds and the same approximate yield for the nitrosyl compounds if prepared using Diazald, but much lower yields of approximately 15% using isoamylnitrite. Analytical and selected ir data for the pure compounds are presented in Table 1. For a given ligand the stability of the compounds towards air was found to be nitrosyl > η^3-allyl > η^3-2-methallyl and W > Mo. Even in solution the tungsten nitrosyl compounds remained unchanged after exposure to air for several days. The production of the $LMo(CO)_3^-$ ions in solution required refluxing the reactant mixture for 24–48 h depending on the nature of the ligand. For the $LW(CO)_3^-$ ions even longer reaction times were necessary with reflux times of 70–100 h, not uncommon for reactions involving the more sterically demanding ligands. The second stage of the preparations were much more facile and frequently occurred at ambient temperatures (Scheme 1). The lower reactivity of $W(CO)_6$ compared with that of $Mo(CO)_6$ is further illustrated in our inability to prepare the tricarbonyl anion of tungsten incorporating the most sterically demanding ligand **1**, where R = Me and R′ = Me. The tungsten compound listed in Table 1 and bearing this ligand and a η^3-C_3H_5 group was prepared via an alternate route utilizing $(MeCN)_3W(CO)_3$ (5) as a starting material:

$$[1]\quad (MeCN)_3W(CO)_3 + \text{excess } C_3H_5Br \xrightarrow[\text{r.t.}]{\text{THF}} (MeCN)_2W(CO)_2(\eta^3\text{-}C_3H_5)Br + MeCN + CO$$

$$[2]\quad (MeCN)_2W(CO)_2(\eta^3\text{-}C_3H_5)Br + Na^+L^- \xrightarrow[\text{r.t.}]{\text{THF}} LW(CO)_2(\eta^3\text{-}C_3H_5) + NaBr + 2MeCN$$

where L^- = **1** (R = Me and R′ = Me). Attempts to prepare the analogous tungsten compound having a 'η^3-C_4H_7' ligand via the same route did not produce the desired complex.

Manganese Carbonyl Complexes

The four manganese tricarbonyl compounds were prepared directly from pentacarbonyl manganese bromide and the ligand salts in THF. The reaction mixtures were refluxed for ~16 h, the precipitated sodium bromide removed, and the crude products isolated from the THF solutions recrystallized from benzene solvent.

$$Mn(CO)_5Br + Na^+L^- \xrightarrow[\text{r.t.}]{\text{THF}} LMn(CO)_3 + NaBr + 2CO$$

Analytical and selected ir data are collected in Table 1 for these complexes. The compounds were considerably more air-sensitive than the molybdenum and tungsten compounds, with crystalline samples being noticeably oxidized after several hours' exposure to air

Spectra

Mass spectra were recorded on a Varian MAT CH4 mass spectrometer at 70 eV with an ion source temperature of 100–180°C. Infrared spectra were recorded on a Perkin-Elmer 457 spectrophotometer and ^{1}H nmr spectra on a Varian XL-100 spectrometer. For complexes of low solubility ^{1}H nmr spectra were obtained using FT techniques.

Results and Discussion

Analysis of mass spectral, ir, and ^{1}H nmr data (see below) for the complexes listed in Table 1, points to a monomeric octahedral structure for the whole

TABLE 1. Analytical data for complexes

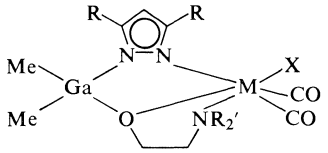

				Calculated (%)			Found (%)			ν_{CO} (cm^{-1})†	
M	R	R′	X	C	H	N	C	H	N	Cyclohexane	CH_2Cl_2
Mo	H	H	C_3H_5	34.3	4.8	10.0	34.4	4.8	9.9	1938, 1850	1928, 1832
Mo	H	H	C_4H_7	36.0	5.1	9.7	36.2	5.0	9.6	1938vs, 1851vs 1956s, 1842s 1966m, 1864m	1930, 1835
Mo	Me	H	C_3H_5	37.5	5.4	9.4	37.6	5.5	9.4	1935, 1847	
Mo	Me	H	C_4H_7	39.0	5.7	9.1	39.2	5.6	9.3	1933, 1840	
Mo	H	Me	C_3H_5	37.5	5.4	9.4	37.8	5.6	9.4	1934, 1848	
Mo	H	Me	C_4H_7	39.0	5.7	9.1	38.9	5.6	9.3	1929, 1841	
Mo	Me	Me	C_3H_5	40.4	5.9	8.8	40.2	6.1	9.1	1931, 1843	
Mo	Me	Me	C_4H_7	41.7	6.2	8.6	41.6	6.2	8.8	1928, 1838	
W	H	H	C_3H_5	28.4	4.0	8.3	28.5	3.9	8.3	‡	1916, 1816
W	H	H	C_4H_7	29.9	4.2	8.1	29.8	4.1	8.1	1928m, 1836m 1945w, 1854w	1918, 1817
W	Me	H	C_3H_5	31.4	4.5	7.8	31.5	4.5	7.7	1929, 1835	1916, 1813
W	Me	H	C_4H_7	32.8	4.8	7.6	32.9	5.0	7.4	1927, 1832	1913, 1813
W	H	Me	C_3H_5	31.4	4.5	7.8	31.4	4.5	8.0	1926, 1835	1916, 1814
W	H	Me	C_4H_7	32.8	4.8	7.6	32.7	4.8	7.9	1922, 1831	1909, 1809
W	Me	Me	C_3H_5	34.1	5.0	7.5	33.8	4.9	7.3	1924, 1832	1911, 1810
Mo	H	H	NO	26.4	3.7	13.7	27.0	3.6	13.6	‡	2020, 1920, (1645*)
Mo	H	Me	NO	30.2	4.4	12.8	30.6	4.4	12.6	‡	2020, 1920, (1647*)
Mo	Me	H	NO	30.2	4.4	12.8	30.4	4.3	12.8	‡	2018, 1918, (1640*)
Mo	Me	Me	NO	33.6	5.0	12.1	33.5	4.8	12.2	‡	2015, 1917, (1644*)
W	H	H	NO	21.8	3.0	11.3	22.2	3.0	11.5	‡	2001, 1898, (1627*)
W	H	Me	NO	25.2	3.6	10.7	25.9	3.7	10.3	‡	1998, 1894, (1626*)
W	Me	H	NO	25.2	3.6	10.7	25.6	3.6	10.6	‡	2000, 1898, (1625*)
W	Me	Me	NO	28.2	4.2	10.1	28.4	4.1	9.8	‡	1997, 1895, (1622*)
Mn	H	H	CO	32.8	4.1	11.5	32.7	4.1	11.7	2032, 1937, 1911	
Mn	H	Me	CO	36.6	4.9	10.7	36.6	5.0	10.7	2027, 1936, 1908	
Mn	Me	H	CO	36.6	4.9	10.7	36.7	4.7	10.7	2030, 1936, 1907	
Mn	Me	Me	CO	39.9	5.5	10.0	39.8	5.5	9.9	2024, 1934, 1902	

*ν_{NO} band.
†Reported ν_{CO} bands and ν_{NO} bands were all very strong. Relative ν_{CO} band intensities are given for the two compounds displaying isomers in cyclohexane solution. vs = very strong, s = strong, m = medium, w = weak.
‡Insoluble.

range of compounds studied. Further, it is proposed that the tridentate ligands are *fac* ligands in all the complexes. A schematic representation of a typical molybdenum complex, $[MeGa(N_2C_3H_3)(OCH_2CH_2NH_2)]Mo(CO)_2\eta^3\text{-}C_3H_5$, is shown in **2**.

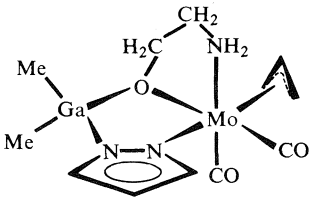

2

Infrared Spectra

$LMn(CO)_3$ Complexes

Three strong bands in the ν_{CO} region (see Table 1) for all four $LMn(CO)_3$ complexes indicate that the *unsymmetrical* ligand L occupies three facial positions in the octahedral structures, with the three CO groups occupying the remaining set of facial positions. A *mer* arrangement for L in these complexes would lead to two weak ν_{CO} bands and one strong ν_{CO} band in the ir spectra of the complexes (6).

$LM(CO)_2X$ Complexes (M = Mo or W; $X = \eta^3\text{-}C_3H_5$ or $\eta^3\text{-}C_4H_7$)

The ν_{CO} region of the ir spectra of these fifteen

complexes (see Table 1) showed, with two exceptions, two sharp strong bands of equal intensity, indicating a *cis* arrangement of the CO ligands in the complexes (6). This does not distinguish between a *mer* or *fac* arrangement for the ligand L about the central metal atom (1). However, molecular models indicate that the *fac* arrangement allows greater steric freedom to the X groups, particularly in the position *trans* to the pyrazolyl nitrogen (see **2**). The position *trans* to the amino nitrogen is slightly more crowded with the position opposite the oxygen atom least favored sterically. Evidence for the *fac* arrangement of L in the $LM(CO)_3^-$ ions is found in the ir spectra for these ions in THF solution. Two equally strong ν_{CO} bands are apparent with the one at lower frequency being much broader (unresolved *e* mode) than the higher frequency band (a_1 mode). A *fac* arrangement of the *unsymmetrical* ligand would be expected to give three strong ν_{CO} bands whereas a *mer* arrangement would give two weak bands and one strong band in the ν_{CO} region of the spectrum (6).

In the two complexes where more than two ν_{CO} bands occur in the ir spectra in cyclohexane solution (M = Mo or W; L where R = H, R′ = H; X = η^3-C_4H_7) the presence of more than one isomer is indicated. It is noteworthy that in CH_2Cl_2 solution these same complexes show but two ν_{CO} bands, an observation which suggests that the different isomers in cyclohexane solution may be due to different fixed orientations of the 'η^3-C_4H_7' group located in the same octahedral position, rather than two different positional isomers for the octahedral complexes. The effect of solvent on isomer distribution in this type of complex has been documented previously (7, 8).

Comparison of the ν_{CO} frequencies for the 'η^3-allyl' complexes incorporating the ligand **1** with the ν_{CO} frequencies of similar complexes bearing different uninegative 6-electron ligands indicates that the novel ligands described herein create a more electron-rich transition metal centre. The pertinent ν_{CO} values for the (ligand)$Mo(CO)_2\eta^3$-C_3H_5 series of compounds are listed in Table 2. The lower ν_{CO} values observed in the new complexes indicate an increased d_π–π^* back-bonding from the molybdenum atom to the carbon monoxide ligands when compared with the previously described systems. This presumably results from a more electron-rich transition metal centre which may be created by either an increased σ donation to the Mo atom from the new ligands, or may arise from reduced backbonding from the Mo atom to the L ligand acceptor orbitals. A combination of the two effects may well be responsible. The substitution of methyl groups for hydrogen atoms on the pyrazolyl (3,5 positions) and ethanolamino (nitrogen atom) moieties results in a slight decrease in the ν_{CO} values. This may reflect the inductive effect of these methyl groups with consequent increase in the σ-donor characteristics of the ligand system, although reduced back-bonding to L because of enhanced steric crowding and less favorable d_π–π orbital overlaps could also be an important factor.

TABLE 2. Carbonyl stretching frequencies for some $LMo(CO)_2\eta^3$-C_3H_5 complexes (cyclohexane solution)

L	ν_{CO} (cm^{-1})		Reference
η^5-C_5H_5	1970, 1963, 1903, 1889		9
$HB(N_2C_3H_3)_3$	1959	1874	10
$MeGa(N_2C_3H_3)_3$	1948	1860	7
1, R = H; R′ = H	1938	1850	This work
1, R = Me; R′ = Me	1931	1843	This work

As previously observed for similar complexes (7, 10, 11) the ν_{CO} bands in the tungsten compounds are approximately 10–20 cm^{-1} lower than those for the corresponding molybdenum compounds.

$LM(CO)_2NO$ Complexes (M = Mo or W)

The four molybdenum and four tungsten complexes reported in Table 1 displayed the expected ν_{CO} and ν_{NO} vibrations in their ir spectra (CH_2Cl_2 solutions). Two ν_{CO} bands are observed of approximately equal intensity but with the lower frequency band (asymmetric stretch) being much the broader of the two. Again a *cis* arrangement of the two CO ligands is suggested. One broad band is observed for the ν_{NO} stretching vibration in all the complexes. The ν_{CO} and ν_{NO} bands are 20 cm^{-1} lower in the W compounds than in the corresponding Mo derivatives, but within a particular series, changing the nature of L has little effect on the positions of the bands.

The presence of isomers so clearly demonstrated by the ^1H nmr spectra of these complexes in C_6D_6 solutions (see below) is not revealed by their ir spectra in CH_2Cl_2 solutions. Perhaps the different isomers give closely similar ir band positions and are therefore not detectable as separate entities by ir methods. It is, however, noteworthy that although of equal intensity the two ν_{CO} bands are very different in band width. The lower frequency ν_{CO} band is approximately three times broader (half-height band width) than the higher frequency ν_{CO} band. This phenomenon is not observed in the 'η^3-allyl' complexes discussed above where the two ν_{CO} bands are of equal intensity and sharpness.

^1H Nuclear Magnetic Resonance Spectra

$LM(CO)_2X$ Complexes (M = Mo or W; X = η^3-C_3H_5 or η^3-C_4H_7)

Selected ^1H nmr data for these compounds in

TABLE 3. ^{1}H nmr data for complexes in C_6D_6 solution*

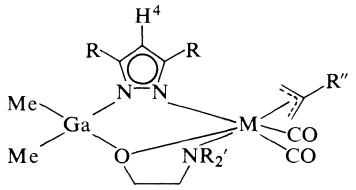

				τ (ppm)				
M	R	R′	R″	R	R′	R″	H^4	Ga—Me
Mo	H	H	H	2.53br, (2.9)			3.90t	10.03s, 10.39s
Mo	H	H	Me	2.34d, 2.75d		8.35s	3.80t	9.92s, 10.34s
Mo	Me	H	H	7.68s, 8.03s			4.33s	10.02s, 10.40s
Mo	Me	H	Me	7.62s 8.01s		8.33s	4.27s	9.93s, 10.39s
Mo	H	Me	H	2.67d, 2.91d	7.08s, 8.51s		3.97t	10.14s, 10.36s
Mo	H	Me	Me	2.75d, (2.9)	7.07s, 8.44s (br) (br)	8.65s	3.95t	10.05s, 10.35s (br) (br)
Mo	Me	Me	H	7.67s, 8.03s	7.05s, 8.29s		4.34s	10.06s, 10.33s
Mo	Me	Me	Me	7.22s, 8.08s	7.07s, 8.24s	8.60s	4.33s	9.98s, 10.34s
W	H	H	H	2.53br, 2.95d			4.00t	10.05s, 10.44s (br)
W	H	H	Me	2.36d, 2.89d		8.65s	3.93t	9.94s, 10.44s
				2.38d, 2.92d		(br)	4.01t	10.24s, 10.41s
W	Me	H	H	7.70s, 8.10s			4.39s	10.05s, 10.47s
W	Me	H	Me	7.60s, 8.09s		8.13s	4.34s	9.97s, 10.49s
W	H	Me	H	2.63d, 2.98d	6.97s, 8.58s		4.06t	10.15s, 10.39s
W	H	Me	Me	2.71d, 2.94d	6.93s, 8.43s	8.52s	4.03t	10.01s, 10.37s
W	Me	Me	H	7.67s, 8.09s	6.94s, 8.35s		4.38s	10.07s, 10.36s

*All τ values relative to $\tau(C_6H_6) = 2.84$ ppm, τ(TMS) = 10.00 ppm. $J_{HCCH} \simeq 2$ Hz (pyrazolyl ring). s = singlet, d = doublet, t = triplet, br = broad.

C_6D_6 solutions are listed in Table 3. In all of the molybdenum derivatives the spectra suggest the presence of one isomer for the octahedral complexes in solution. This would indicate either a fixed conformation for the 'η³-allyl' groupings or a fast rotation of these groupings about the Mo···'η³-allyl' axis. The former is most likely the correct interpretation but planned variable temperature ^{1}H nmr studies, above and below room temperature, should lead to a definitive answer. In one molybdenum compound (where R′ = Me, R″ = Me and R = H, see Table 2) the N—*Me* and Ga—*Me* signals were quite broad indicating the possibility of slow fluxionality for these groups in this complex. In the same complex, however, the R″ = Me signal and the pyrazolyl proton signals were quite sharp. The structure depicted in **2** is suggested for these complexes, with the 'η³-allyl' groups being in the sterically preferred position opposite the pyrazolyl moiety. The alternate arrangement most likely to occur would place the 'η³-allyl' groups opposite the amino nitrogen in the octahedral complexes, and indeed this arrangement may be preferred where the amino group is substituted and the pyrazolyl group unsubstituted. (See discussion below on 'nitrosyl' isomers.)

The spectra of the tungsten 'η³-allyl' complexes are very similar to their molybdenum counterparts with the exception of the compound where R = R′ = H and R″ = Me. For this particular complex two sets of signals for the pyrazolyl protons and the Ga—*Me* protons plus a broad R″ = Me signal indicate the presence of two distinguishable isomers in the C_6D_6 solution. As discussed in the ir section, it is probable that these two isomers correspond to different orientations of the η³-C_4H_7 group in the complex rather than to different positional isomers.

$LM(CO)_2NO$ Complexes (M = Mo or W)

Selected ^{1}H nmr data for these complexes in C_6D_6 solution are reported in Table 4. In all cases the presence of two isomers is suggested by the appearance of two sets of signals in the spectra. In contrast to the 'orientation isomers' postulated to explain the presence of two isomers in one of the tungsten 'η³-allyl' derivatives described above, the isomers

TABLE 4. ^{1}H nmr data for complexes in C_6D_6 solvent*

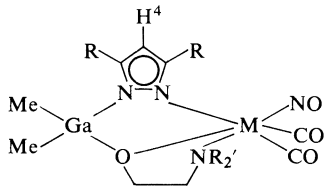

M	R	R′	τ (ppm) R	τ (ppm) R′	τ (ppm) H⁴	τ (ppm) Ga—Me	Approximate isomer ratio	Predicted position of NO substitution‡
Mo	H	H	2.34d†, 2.76d†,		3.81t†	9.99s, 10.32s	2	A
			2.76d†, 2.88d†		4.01t†	9.91s, 10.25s	1	B
Mo	H	Me	2.31d†, 2.75d†,	7.84s, 8.34s	3.83t†	10.01s, 10.23s	1	A
			2.71d†, 2.87d†	7.91s, 8.50s	4.02t†	9.91s, 10.19s	1	B
Mo	Me	H	7.64s, 8.00s		4.26s	9.93s, 10.27s	5	A
			7.95s, 8.06s		4.43s	9.82s, 10.21s	1	B
Mo	Me	Me	7.60s, 7.99s	7.84s, 8.21s	4.25s	10.06s, 10.19s	3	A
			7.79s, 8.10s	8.05s, 8.35s	4.43s	9.88s, 10.14s	1	B
W	H	H	2.29d†, 2.85d†,		3.88t†	9.99s, 10.38s	2	A
			2.72d†, 2.98d†		4.10t†	9.90s, 10.30s	1	B
W	H	Me	2.28d†, 2.84d†,	7.72s, 8.31s	3.89†	9.98s, 10.25s	1	A
			2.71d†, 2.98d†	7.72s, 8.47s	4.10†	9.86s, 10.20s	1	B
W	Me	H	7.62s, 8.04s		4.28s	9.94s, 10.32s	5	A
			7.93s, 8.11s		4.48s	9.80s, 10.24s	1	B
W	Me	Me	7.59s, 8.05s	7.67s, 8.20s	4.28s	10.03s, 10.28s	3	A
			7.67s, 8.11s	7.87s, 8.34s	4.48s	9.86s, 10.18s	1	B

*τ(TMS) = 10.00 ppm, τ(C_6H_6) = 2.84 ppm, s = singlet, d = doublet, t = triplet.
†$J \simeq 2$ Hz.
‡A = position opposite 'pyrazolyl' nitrogen. B = position opposite 'amino' nitrogen.

arising in the nitrosyl compounds must necessarily be positional isomers. The fact that only two sets of signals are observed in the spectra indicates that only two positions of the octahedral anions $LM(CO)_3^-$ are susceptible to NO substitution. Accepting that the ligand L is *fac*, the most favored positions for substitution, sterically, are first the position opposite the pyrazolyl nitrogen, and second the position opposite the amino nitrogen. The expected preference for substitution in the position opposite the pyrazolyl moiety is substantiated by the observed ratios for the two isomers in the solutions. Thus considering the ratios in Table 4 and using **2** it is straightforward to assign the two groups of proton signals to their respective positional isomers. It is noteworthy that only when the 'pyrazolyl' moiety is unsubstituted and the 'amino' nitrogen fully substituted do the two positions become equally favorably towards NO substitution. Conversely, when the 'pyrazolyl' moiety is substituted in the 3,5 positions, and the 'amino' nitrogen unsubstituted, NO substitution in the position opposite the 'pyrazolyl' nitrogen is favored over NO substitution in the position opposite the 'amino' nitrogen to the extent of 5:1. Attempts at separation of the two isomers for selected complexes by column chromatography have so far proved unsuccessful. If future attempts are more rewarding crystallographic structural studies will be carried out on the separated isomers to confirm the above predictions listed in Table 4.

Mass Spectra

The 27 complexes listed in Table 1 were all sufficiently volatile and stable to give readily observable parent ion signals in their mass spectra, which corresponded to monomer species in the vapour phase. The appearance of signals due to other ions in all of the spectra indicated fragmentation patterns which are predictable for the various complexes. The intensity ratios of the individual peaks in all multi-peak signals agreed closely with theoretical predictions based on the percentage isotope compositions of the contributing metal atoms. In all 27 spectra signals due to the five-membered ring ions, $\overline{M—\text{'pyrazolyl'}—Ga—O}^+$, were observed indicating a facile loss of the '$—CH_2—CH_2—NR_2$' moiety from the octahedral complexes, and the intrinsic stability of the five-membered ring system.

Currently under investigation are ligands incorporating amino thiols, in place of amino alcohols in

the present systems, and also ligands of higher denticity created by reacting suitable HX precursors with the $Me_3Ga(N_2C_3H_3)^-$ ion.

Acknowledgements

We thank the National Research Council of Canada for financial support, Mr. J. Nip for mass spectra, Dr. S. Chan for nmr spectra, and Mr. P. Borda for C, H, N analyses.

1. K. S. CHONG, S. J. RETTIG, A. STORR, and J. TROTTER. Can. J. Chem. **56**, 1212 (1978).
2. K. S. CHONG, S. J. RETTIG, A. STORR, and J. TROTTER. Can. J. Chem. **55**, 4166 (1977).
3. R. B. KING. Organometallic synthesis. Vol. 1. Academic Press, New York. 1965. p. 174.
4. A. STORR and B. S. THOMAS. Can. J. Chem. **48**, 3667 (1970).
5. D. P. TATE, W. R. KNIPPLE, and J. M. AUGL. Inorg. Chem. **1**, 433 (1962).
6. D. M. ADAMS. Metal–ligand and related vibrations. Edward Arnold Ltd., London. 1967. Chapt. 3.
7. K. R. BREAKELL, S. J. RETTIG, D. L. SINGBEIL, A. STORR, and J. TROTTER. Can. J. Chem. **56**, 2099 (1978).
8. J. W. FALLER and M. J. INCORVIA. Inorg. Chem. **7**, 840 (1968).
9. R. B. KING. Inorg. Chem. **5**, 2242 (1966).
10. S. TROFIMENKO. J. Am. Chem. Soc. **91**, 588 (1969).
11. S. TROFIMENKO. Inorg. Chem. **10**, 504 (1971).

The crystal and molecular structure of 1,4-diphenyl-2,2′,3,3′,5,5′,6,6′-octamethylcyclo-1,4-diphospha-2,3,5,6-tetrasilahexane, a phosphorus–silicon heterocycle

A. WALLACE CORDES AND PAUL F. SCHUBERT

Department of Chemistry, University of Arkansas, Fayetteville, AR 72701, U.S.A.

AND

RICHARD T. OAKLEY[1]

Department of Chemistry, University of Wisconsin, Madison, WI 53706, U.S.A.

Received June 6, 1978

A. WALLACE CORDES, PAUL F. SCHUBERT, and RICHARD T. OAKLEY. Can. J. Chem. **57**, 174 (1979).

The crystal structure of 1,4-diphenyl-2,2′,3,3′,5,5′,6,6′-octamethylcyclo-1,4-diphospha-2,3,5,6-tetrasilahexane, $(PhPSi_2Me_4)_2$, has been determined by single crystal X-ray diffraction. The crystals are monoclinic, space group $P2_1/c$, with $a = 9.866(1)$, $b = 11.921(1)$, and $c = 11.324(2)$ Å, $\beta = 104.31(1)°$, $Z = 2$, and $\rho_{calcd} = 1.15$ g/cm^3. The structure was solved by direct methods and was refined by full-matrix least-squares procedures to a final R of 0.060 and R_w of 0.078, for 1173 reflections with intensities greater than 3σ. The $(PhPSi_2Me_4)_2$ molecule lies on a crystallographic centre of symmetry, and the six-membered P_2Si_4 ring has a chair conformation with equatorial phenyl groups. The endocyclic angles at P (104.4(1)°) and Si (104.9(2)°) are intermediate between those found in cyclic hexaphosphine and hexasilane molecules, and the Si—Si and P—Si distances of 2.345(3) and 2.252(4) Å, respectively, correspond to single bond lengths, with no appreciable evidence for secondary $p\pi \rightarrow d\pi$ bonding between phosphorus and silicon. The Si—C (1.867(8) Å) and P—C (1.828(7) Å) bond lengths are also normal. The variations in the Si—P—C (101.6(2)°, 108.6(2)°), P—Si—C (range 106.2(3)–120.0(3)°), and Si—Si—C (range 105.8(3)–113.7(3)°) angles indicate that the positions of the exocyclic methyl and phenyl groups are influenced by both intra- and intermolecular steric forces.

A. WALLACE CORDES, PAUL F. SCHUBERT et RICHARD T. OAKLEY. Can. J. Chem. **57**, 174 (1979).

Faisant appel à la diffraction des rayons X par des monocristaux, on a déterminé la structure cristalline du diphényl-1,4 octaméthyl-2,2′,3,3′,5,5′,6,6′ cyclodiphospha-1,4 tétrasilahexane-2,3,5,6, $(PhPSi_2Me_4)_2$. Les cristaux sont monocliniques, groupe d'espace $P2_1/c$ avec $a = 9.886(1)$, $b = 11.921(1)$ et $c = 11.324(2)$ Å, $\beta = 104.31(1)$, $Z = 2$ et $\rho_{calcd} = 1.15$ g/cm^3. On a résolu la structure par des méthodes directes et on l'a affinée par la méthode des moindres carrés (matrice complète) jusqu'à une valeur finale R de 0.060 et R_w de 0.078 pour les 1173 réflexions avec des intensités plus grandes que 3σ. La molécule $(PhPSi_2Me_4)_2$ se trouve au centre de symétrie et le cycle à six chaînons P_2Si_4 adopte une conformation chaise avec les groupes phényles en position équatoriale. Les angles endocycliques au niveau du P (104.4(1)°) et du Si (104.9(2)°) sont intermédiaires entre ceux trouvés dans des molécules d'hexaphosphines et d'hexasilanes cycliques et les distances Si—Si et P—Si qui sont respectivement 2.345(3) et 2.252(4) Å correspondent à des longueurs de liaisons simples et l'on ne trouve aucune indication à l'effet qu'il existe une liaison secondaire $p\pi \rightarrow d\pi$ entre le phosphore et le silicium. Les longueurs des liaisons Si—C (1.867(8) Å) et P—C (1.828(7) Å) sont aussi normales. Les variations dans les angles Si—P—C (101.6(2)°, 108.6(2)°), P—Si—C (allant de 106.2(3)–120.0(3)°) et Si—Si—C (allant de 105.8(3) à 113.7(3)°) indiquent que les positions des groupes méthyles et phényles exocycliques sont influencées à la fois par des forces stériques intra- et intermoléculaires.

[Traduit par le journal]

Introduction

The molecular structures of a variety of homocyclic polysilanes $(R_2Si)_n$ (1, 2) and polyphosphines $(RP)_n$ (3–7) have been described, but to the present time there have been no reports concerning the structural characteristics of mixed phosphorus–silicon ring systems. We are currently investigating the physical and chemical properties of such compounds (8), and as a part of this work we have determined the crystal and molecular structure of 1,4-diphenyl-2,2′,3,3′,5,5′,6,6′-octamethylcyclo-1,4-diphospha-2,3,5,6-tetrasilahexane (**1**), the first such characterization of a compound containing an uncoordinated silylphosphine moiety.[2]

[1]Present address: Department of Chemistry, University of Calgary, Calgary, Alta., Canada T2N 1N4.

[2]NOTE ADDED IN PROOF: Since the submission of this article the structures of $P_4(SiMe_2)_3$ and $P_7(SiMe_3)_3$ have been reported (20).

0008-4042/79/020174-06$01.00/0

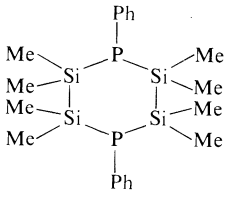

1

Experimental

Crystals suitable for X-ray work were obtained by slow cooling of a warm, saturated benzene/hexane (1:1) solution. The approximately cubic crystal used for all data collection had external faces roughly parallel to, and on the same side of the centre of, the 100, −100, 011, 0 −1 −1, 17 −1 0, −7 −3 8, and 230 faces at face-to-centre distances of 0.15, 0.15, 0.26, 0.26, 0.27, 0.24, and 0.25 mm, respectively. The crystal was sealed in a glass capillary under an atmosphere of nitrogen and mounted with the 001 reflection parallel to the ϕ axis of the diffractometer. A least-squares refinement of 15 values of 2 sin θ/λ for 2θ values between 50 and 87° (λCuK_α = 1.5418 Å) gave cell constants (at 22°C) of

$C_{20}H_{34}P_2Si_4$ fw = 448.78

a = 9.866(1), b = 11.921(1), c = 11.324(1) Å, β = 104.31(1)°, V = 1290.5 Å^3, and ρ_{calcd} (for Z = 2) = 1.15 g cm^{-3}.

The experimental density was not measured because of the extreme air sensitivity of the compound. Systematic absences uniquely indicated the space group $P2_1/c$; two molecules per unit cell in this space group require a centrosymmetric molecule.

Intensities were measured using Ni-filtered radiation on a manual GE-XRD-5 diffractometer. A θ–2θ scan ($2\theta_{max}$ = 120°) at 2° min^{-1} over 2° was used, with 10 s background counts taken at the end of the scan. Four reflections measured periodically indicated a 10% loss in intensity (of instrumental origins) on the third day of the six days of data collection; a simple correction was made for this situation. The μ value was 32.16 cm^{-1} for the crystal used; an absorption correction with summation points every 0.0075 cm gave a range of correction factors (for **1**) of 0.47 to 0.68. Of the 2042 reflections measured, 1173 had intensities greater than 3σ, where $\sigma^2(I)$ = scan + 9 background counts + $(0.05I)^2$. Seven of these reflections were excluded from the refinement data because of evidence for extinction.

The structure was solved by direct methods, and refined by Fourier and full-matrix least-squares procedures. The neutral atom scattering factors of ref. 9 were used for the refinement; anomalous dispersion corrections were made for phosphorus and silicon (10). All of the hydrogen atoms were located on difference maps. Positional parameters of all but two of the hydrogen atoms were refined in the least-squares treatment; two of the phenyl hydrogen atoms were constrained to calculated positions because of the unreasonable positions that they assumed when included in the least-squares matrix. The weighting scheme $w = 1/(2F_{min} + F_o + 2F_o^2/F_{max})$ for the full-matrix refinement (163 parameters, reflection/parameter ratio 7/1) gave a final R = 0.060, R_w = 0.078, a standard deviation of an observation of unit weight = 0.41, and no dependence of $\Delta F/\sigma(F)$ on either F or sin θ. On the final cycle of refinement all the non-hydrogen positional shifts were less than 0.09σ. A final difference Fourier gave a maximum peak of 0.45 e/Å^3, which is equal to 7% of the peak value for carbon on a regular Fourier map. Measured and calculated structure factors for the observed data have been placed in the Depository of Unpublished Data.[3]

Results and Discussion

The crystal structure of the title compound consists of discrete molecules of $(PhPSi_2Me_4)_2$. Figure 1 is an ORTEP drawing which shows a general view of the molecule and gives the crystallographic numbering scheme. Atomic coordinates are given in Table 1, and the anisotropic thermal parameters of the non-hydrogen atoms deposited in Table 2. The derived bond distance and valence angle information is presented in Tables 3 and 4. The six-membered P_2Si_4 ring exists in a chair conformation with a crystallographically imposed centre of symmetry, with no evidence of disorder.

Many of the structural features observed in $(PhPSi_2Me_4)_2$ are related to those found in the homocyclic molecules $(SiMe_2)_6$ (1) and $(PhP)_6$ (3)[4] and, for purposes of comparison, the valence, dihedral and torsion angles of the three molecules are listed in Table 5,[5] along with those expected for an idealized cyclohexane chair. All three molecules have chair conformations and, as in $(PhP)_6$, the phenyl groups on phosphorus in $(PhPSi_2Me_4)_2$ occupy equatorial positions. The degree of puckering of the chairs is significantly different and, as expected, is dependent on the size of the internal ring angles. Thus, in $(SiMe_2)_6$, where the endocyclic angle (111.9(5)°) is close to the tetrahedral value, the dihedral (131.8(2)°) and skeletal torsion (53.5(3)°) angles vary only slightly from those of the 'ideal' C_6H_{12} conformation. In $(PhP)_6$, the smaller ring angle leads to a more folded chair, with smaller dihedral (96.8(1)°) and larger torsion (85.0(1)°) angles. The geometry of the P_2Si_4 ring in $(PhPSi_2Me_4)_2$ then represents a compromise between those of the two homocyclic molecules; the valence, dihedral and torsion angles are all intermediate between the values found in the Si_6 and P_6 rings. The cross-ring distances Si(2)—Si(3) (3.550(3) Å), P(1)—Si(2′) (3.641(2) Å), and P(1)—Si(3′) (3.654(2) Å) are all slightly shorter than the sum of the van der Waals radii (4.20 and 3.90 Å for Si—Si and P—Si interactions, respectively) (11), and the equalization of the

[3]A copy of the observed and calculated structure factor table is available, at a nominal charge, upon request, from the Depository of Unpublished Data, CISTI, National Research Council of Canada, Ottawa, Ont., Canada K1A 0S2.

[4]The two forms of $(PhP)_6$ are nearly identical. The structural parameters of the trigonal modification, which include anisotropic thermal refinement, will be used throughout this discussion.

[5]Here and elsewhere in this paper, integers quoted in parentheses refer to estimated standard deviations for single-valued parameters, and indicate ranges of results for the averages of chemically equivalent parameters.

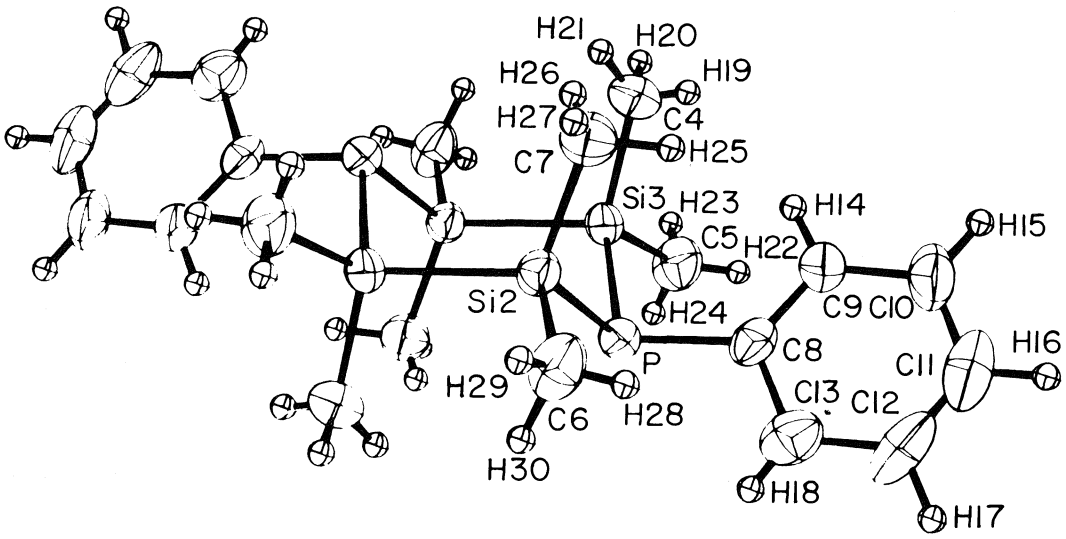

FIG. 1. An ORTEP drawing of the $(PhPSi_2Me_4)_2$ molecule, showing the atom numbering scheme used. Non-hydrogen thermal ellipsoids are drawn at the 50% probability level; hydrogen atoms have been given an isotropic β of 1.0 in this drawing in order to clarify the figure.

TABLE 1. Final atomic coordinates for non-hydrogen ($\times 10^4$) and hydrogen atoms ($\times 10^3$)

Atom	*x*	*y*	*z*
P(1)	1698(2)	4457(1)	6486(1)
Si(2)	1984(2)	4814(1)	4607(2)
Si(3)	121(2)	5741(1)	6735(2)
C(4)	361(9)	7249(6)	6386(8)
C(5)	38(11)	5637(8)	8361(7)
C(6)	3392(9)	3856(8)	4376(8)
C(7)	2514(9)	6283(7)	4357(8)
C(8)	3411(7)	4845(5)	7447(6)
C(9)	3808(8)	5921(6)	7895(7)
C(10)	5120(9)	6114(9)	8649(8)
C(11)	6073(8)	5296(10)	8959(8)
C(12)	5733(9)	4230(9)	8539(8)
C(13)	4401(9)	3999(7)	7802(7)
H(14)	313(10)	647(8)	762(9)
H(15)	543(11)	688(8)	896(9)
H(16)[a]	697	545	946
H(17)[a]	640	365	878
H(18)	416(10)	333(9)	756(9)
H(19)	105(11)	747(9)	676(10)
H(20)	−26(11)	777(9)	670(9)
H(21)	36(10)	756(8)	554(10)
H(22)	77(11)	577(8)	900(10)
H(23)	−71(10)	615(8)	858(9)
H(24)	−34(10)	498(8)	853(9)
H(25)	328(10)	647(8)	511(9)
H(26)	192(11)	674(9)	427(10)
H(27)	286(11)	635(9)	380(11)
H(28)	412(11)	395(9)	496(10)
H(29)	355(10)	384(9)	368(10)
H(30)	306(10)	308(9)	443(9)

[a]H(16) and H(17) were constrained to the positions given (see text). All hydrogen atoms were assigned isotropic thermal factors of β = 5.0.

endocyclic angles is probably necessary so as to increase an otherwise overly close Si(2)—Si(3) contact, and thereby minimize the repulsive interactions between the axial methyl groups (*vide infra*).

The differences in some of the chemically equivalent Si—Si—C and P—Si—C angles and the bent orientation of the phenyl group suggest that the methyl and phenyl group positions are strongly influenced by inter- and intramolecular steric forces. The angle of the phenyl group with respect to the P_2Si_4 ring is the most apparent distortion (Si(2)—P(1)—C(8) is 101.6(2)° and Si(3)—P(1)—C(8) is 108.6(2)°) and appears to be the result of the packing pattern as shown in the *xz* projection of Fig. 2. Although none of the intermolecular contacts are less than the sum of the corresponding van der Waals' separations (11), the three nearest C—C contacts (C_{10}—C_{11}, C_{10}—C_{12}, C_{11}—C_{11}), the shortest C—H contact (C_{10}—C_{18}), and one of the H—H intermolecular contacts (H_{15}—H_{18}) are all involved in the phenyl–phenyl packing and are indicated by dotted lines in Fig. 2. One of the axial (the C(4)) methyl groups also experiences a close intramolecular contact with the phenyl ring; the H(14)—H(19) distance is slightly less than the expected van der Waals' separation (2.40 Å) (11). The less pronounced rotation of the phenyl ring about the P—C bond than is found in $(PhP)_6$ (compare the P—P—C—C and Si—P—C—C torsion angles in Table 5) probably occurs to alleviate this phenyl–methyl repulsion. The equatorial C(5) methyl group appears to be slightly perturbed by a neigh-

TABLE 2. Anisotropic thermal parameters ($\times 10^4$) for non-hydrogen atoms[a]

β_{11}	β_{22}	β_{33}	β_{12}	β_{13}	β_{23}
97(2)	46(1)	56(2)	−2(1)	10(1)	0(1)
84(2)	55(1)	53(2)	5(1)	11(1)	−2(1)
96(2)	51(1)	49(2)	−2(1)	12(1)	−7(1)
146(11)	52(5)	103(9)	2(6)	24(8)	−4(6)
169(13)	97(7)	66(8)	11(8)	21(8)	−9(6)
123(10)	109(8)	72(8)	33(8)	17(7)	−11(6)
122(10)	73(6)	88(8)	−13(6)	24(7)	12(6)
96(8)	69(5)	55(6)	5(5)	9(5)	16(4)
125(10)	68(6)	83(8)	−16(6)	−12(7)	7(5)
150(12)	117(8)	82(8)	−47(9)	−26(8)	14(7)
101(10)	171(12)	80(8)	−23(9)	−3(7)	18(8)
112(11)	162(12)	97(9)	59(9)	1(8)	28(8)
138(10)	89(7)	88(8)	32(8)	31(8)	6(6)

[a]Estimated standard deviations are given in parentheses. Anisotropic thermal parameters are of the form exp $-(h^2\beta_{11} + k^2\beta_{22} + l^2\beta_{33} + 2hk\beta_{12} + 2hl\beta_{13} + 2kl\beta_{23})$.

TABLE 3

(*a*) Bond lengths (Å) between non-hydrogen atoms with esd's in parentheses

Bond	Distance	Bond	Distance	Bond	Distance
P(1)—Si(2)	2.256(2)	Si(2)—C(6)	1.866(9)	C(8)—C(9)	1.40(1)
P(1)—Si(3)	2.249(2)	Si(2)—C(7)	1.869(8)	C(9)—C(10)	1.38(1)
P(1)—C(8)	1.828(7)	Si(3)—C(4)	1.868(8)	C(10)—C(11)	1.34(1)
Si(2)—Si(3′)	2.345(3)	Si(3)—C(5)	1.866(9)	C(11)—C(12)	1.37(2)
				C(12)—C(13)	1.40(1)
				C(13)—C(8)	1.39(1)

(*b*) Non-bonded distances (Å) between atoms of P_2Si_4 ring, with esd's in parentheses[a]

Bond	Distance	Bond	Distance
P(1)—P(1′)	4.489(2)	Si(2)—Si(3)	3.550(3)
Si(2)—Si(2′)	4.247(3)	P(1)—Si(2′)	3.641(2)
Si(3)—Si(3′)	4.262(3)	P(1)—Si(3′)	3.654(2)

[a]Primed atom numbers designate atoms related by $-x, 1-y, 1-z$ to those with the unprimed number on Table 1.

TABLE 4. Bond angles (deg) between non-hydrogen atoms with esd's in parentheses[a]

Bonds	Angle	Bonds	Angle
Si(2)—P(1)—Si(3)	104.4(1)	C(4)—Si(3)—C(5)	108.1(4)
Si(3′)—Si(2)—P(1)	105.1(1)	C(6)—Si(2)—C(7)	107.9(4)
Si(2′)—Si(3)—P(1)	104.8(1)	P(1)—C(8)—C(9)	125.6(3)
Si(2)—P(1)—C(8)	101.6(2)	P(1)—C(8)—C(13)	117.9(5)
Si(3)—P(1)—C(8)	108.6(2)	C(8)—C(9)—C(10)	120.8(6)
P(1)—Si(2)—C(6)	106.7(3)	C(9)—C(10)—C(11)	122.0(9)
P(1)—Si(2)—C(7)	115.1(3)	C(10)—C(11)—C(12)	119.3(6)
P(1)—Si(3)—C(4)	120.0(3)	C(11)—C(12)—C(13)	120.3(6)
P(1)—Si(3)—C(5)	106.2(3)	C(12)—C(13)—C(8)	121.2(7)
Si(2′)—Si(3)—C(4)	105.8(3)	C(13)—C(8)—C(9)	116.4(7)
Si(2′)—Si(3)—C(5)	111.9(3)		
Si(3′)—Si(2)—C(6)	107.9(3)		
Si(3′)—Si(2)—C(7)	113.7(3)		

[a]Primed atom numbers designate atoms related by $-x, 1-y, 1-z$ to those with the unprimed number on Table 1.

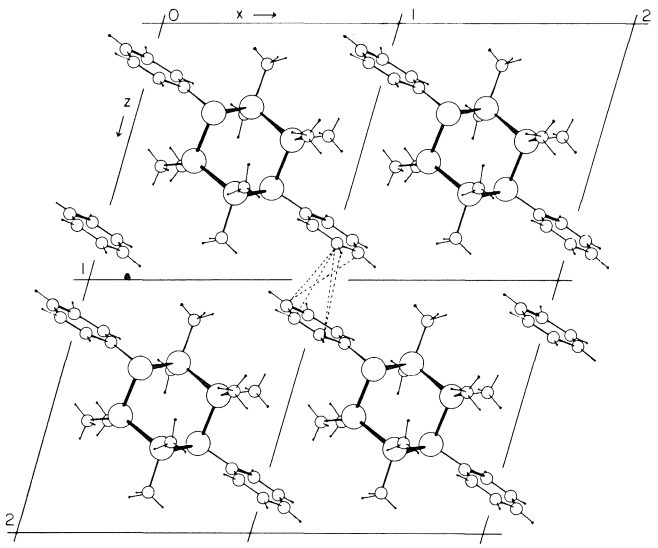

FIG. 2. The packing in the *xz* projection. Close intermolecular contacts (see text) are shown by the dotted lines. Only the molecules centered at $y = 0.5$ are shown.

TABLE 5. Ring parameters (deg) of $(PPhSi_2Me_4)_2$, P_6Ph_6, Si_6Me_{12}, and C_6H_{12}[a]

Parameter	Value			
	P_6Ph_6	$(PPhSi_2Me_4)_2$	Si_6Me_{12}	'Ideal' C_6H_{12}
(*A*) Bond angles of ring atoms	94.6(1)	104.4(1)[b] 104.9(2)[c]	111.9(5)	109.5
(*B*) Dihedral angles				
Chair back/chair seat	96.8(1)	114.8(1)[d] 114.3(1)[e]	131.8(2)	125.3
Phenyl group/XPX of ring	89.9(3)	79.7(2)		
(*C*) Torsion angles				
3 ring bonds	85.0(1)	70.0(1)[f] 70.7(1)[g]	53.5(3)	60
2 ring and 1 equatorial bond	175(1)	177.3(2)[h] 175.2(5)[i]	173.3(7)	180
2 ring and 1 axial bond		56.6(5)[i]	68(2)	60
1 ring and 2 equatorial bonds	76.4(3)	63.3(6)[j] 61.0(4)[k]	67(1)	60
1 ring, 1 axial, and 1 equatorial bond		58(1)[j] 58(1)[k]	51(2)	60
1 ring and 2 axial bonds		176.1(4)[k]	169(2)	180
1 ring, P—C(phenyl), and C—C(phenyl) bonds	42.7(1)[l] 53.3(1)[l]	23.0(1)[m] 86.3(1)[m]		

[a]Integers in parentheses give either esd's for single-valued parameters or indicate ranges of results for those angles which are averages of several chemically equivalent parameters.
[b]At P.
[c]At Si.
[d]SiPSi/SiSiSiSi.
[e]PSiSi/PSiPSi.
[f]SiPSiSi.
[g]PSiSiP.
[h]SiSiPC.
[i]PSiSiC.
[j]CPSiC.
[k]CSiSiC.
[l]P—P—C—C.
[m]Si—P—C—C.

bouring phenyl ring (H(23) to H(16) at $x - 1, y, z$ is 2.48 Å).

In contrast to $(SiMe_2)_6$, where the Si—Si—C angles are nearly equal, the Si—Si—C and P—Si—C angles in $(PhPSi_2Me_4)_2$ vary significantly (by 8 and 14°, respectively), probably as a result of both inter- and intramolecular interactions. The largest of these, the two P—Si—C(axial) angles, are caused by cross-ring axial–axial repulsions. The C—C distance for this contact is 3.679(3) Å, which is considerably

shorter than the 4.21 Å found in $(SiMe_2)_6$ and the van der Waals' distance (4.17 Å) for two methyl groups (11). In spite of these distortions, the mean C—Si—C angle (108.0(2)°) is similar to that in $(SiMe_2)_6$ (108.1(5)°), and the nearly equivalent Si—C bonds are only marginally shorter than in $(SiMe_2)_6$, where the axial (1.880(8) Å) and equatorial (1.897(12) Å) bonds are of unequal length. The P—C bond (1.828(7) Å) is slightly shorter than in $(PhP)_6$ (1.843(7) Å), the contraction probably being caused by the different geometries at phosphorus; the mean angle at phosphorus in $(PhPSi_2Me_4)_2$ (104(4)°) is greater than in $(PhP)_6$ (97(3)°), and the σ-bonds are expected to have a greater *s*-character associated with them. The phenyl ring is planar within experimental error ($\chi^2 = 4.7$), and the values of the mean C—C bond (1.38(4) Å) and C—C—C valence angle (120(2)°) are as expected.

The silicon–silicon distance of 2.345(3) Å corresponds to a normal single bond, the value being similar to those observed in $(SiMe_2)_6$ (2.338(6) Å) (1), $(OSi_2Me_4)_2$ (2.35 Å) (12), and silicon metal (2.352 Å) (13). The phosphorus–silicon bond length (2.252(4) Å) is close to the value obtained from vapour phase electron studies on $(H_3Si)_nP(Me_{3-n})$ ($n = 1, 3$) (2.245–2.249 Å) (14), but significantly shorter than in the recently determined structures of the cation $(Me_2P(SiMe_3)_2)^+$ (2.292(5) Å) (15) and the molybdenum complex $(CO)_4Mo(PPhH(Si_2Me_4)$-PPhH) (2.266(1) Å) (16), where the lone pair on phosphorus is coordinated directly to a competing acceptor centre. Although the shorter bonds in the free phosphines can be construed as the result of $p\pi$–$d\pi$ conjugation between phosphorus and silicon, as has been suggested to be the cause of the increased ionization potentials (17) and low inversion barriers (18) of such compounds, the effect is small, and must be viewed with caution. The shortening of the P—Si bond in $(PhPSi_2Me_4)_2$ by 0.035 Å from the normal single bond distance[6] is entirely consistent with the contraction expected from bond polarity contributions (19). However, similar effects should also be present in the complexed molecules, and changes in σ-hybridization between the 3- and 4-coordinate phosphorus atoms would be expected to shorten the bonds to the latter. The observed differences are thus hard to rationalize on a simple electronic basis, but in the absence of more detailed information from a wider selection of such compounds, it seems premature to speculate too deeply as to their cause. However, the results of the present work do confirm that the structural effects of P → Si π-bonding are small.

[6]Estimated by summing the covalent radii of phosphorus in $(PhP)_6$ and silicon in $(SiMe_2)_6$.

Acknowledgements

The authors are grateful to the National Research Council of Canada for a post-doctoral fellowship (to R.T.O.), to the National Science Foundation of the United States for an undergraduate fellowship (to P.F.S.), and to the University of Arkansas Research Committee for a computer research grant.

1. H. L. Carrell and J. Donohue. Acta Crystallogr. **28**B, 1566 (1972).
2. C. J. Hurt, J. C. Calabrese, and R. West. J. Organomet. Chem. **91**, 273 (1975).
3. J. J. Daly. (*a*) J. Chem. Soc. 4789 (1965); (*b*) J. Chem. Soc. A, 428 (1966).
4. J. J. Daly. J. Chem. Soc. 6147 (1964).
5. G. J. Palenik and J. Donohue. Acta Crystallogr. **15**, 564 (1962).
6. C. J. Spencer and W. N. Lipscomb. Acta Crystallogr. **14**, 250 (1961); **15**, 509 (1962).
7. J. C. J. Bart. Acta Crystallogr. **25**B, 762 (1969).
8. R. T. Oakley, D. A. Stanislawski, and R. West. J. Organomet. Chem. In press.
9. D. T. Cromer and J. T. Waber. International tables for X-ray crystallography. Kynoch Press. 1974.
10. D. T. Cromer. Acta Crystallogr. **18**, 17 (1965).
11. A. Bondi. J. Phys. Chem. **68**, 441 (1964).
12. T. Takano, N. Kasai, and M. Kakudo. Bull. Chem. Soc. Jpn. **36**, 585 (1963).
13. M. E. Straumans and E. Z. Aka. J. Appl. Phys. **23**, 330 (1952).
14. (*a*) B. Beagley, A. G. Robiette, and G. M. Sheldrick. J. Chem. Soc. A, 3002 (1968); (*b*) C. Glidewell, P. M. Pinder, A. G. Robiette, and G. M. Sheldrick. J. Chem. Soc. Dalton, 1402 (1972).
15. H. Schafer and A. G. MacDiarmid. Inorg. Chem. **15**, 848 (1976).
16. W. S. Sheldrick and A. Borkenstein. Acta Crystallogr. **33**B, 2916 (1977).
17. (*a*) S. Cradock, E. A. V. Ebsworth, W. J. Savage, and D. A. Whitehead. J. Chem. Soc. Faraday II, 934 (1972); (*b*) W. W. Dumont, H-J. Breunig, H. Schumann, H. Gotz, H. Juds, and F. Marschner. J. Organomet. Chem. **96**, 49 (1975).
18. (*a*) R. D. Baechler and K. Mislow. J. Am. Chem. Soc. **92**, 4758 (1970); (*b*) R. D. Baechler and K. Mislow. J. Am. Chem. Soc. **93**, 774 (1971); (*c*) A. Rauk, L. C. Allen, and K. Mislow. Ang. Chem. Int. Ed. **9**, 400 (1970); (*d*) R. D. Baechler and K. Mislow. Chem. Commun. 185 (1972); (*e*) K. Mislow. Trans. N.Y. Acad. Sci. **35**, 227 (1973).
19. (*a*) V. Schomaker and D. P. Stevenson. J. Am. Chem. Soc. **63**, 27 (1941); (*b*) M. L. Huggins. J. Am. Chem. Soc. **75**, 4126 (1953).
20. Von W. Honle and H. G. V. Schneering. Z. Anorg. Allg. Chem. **440**, 171 (1978).

Bis(ditertiaryphosphine) complexes of rhodium(I). Synthesis, spectroscopy, and activity for catalytic hydrogenation

BRIAN R. JAMES AND DEVINDER MAHAJAN

Department of Chemistry, University of British Columbia, Vancouver, B.C., Canada V6T 1W5

Received August 11, 1978

BRIAN R. JAMES and DEVINDER MAHAJAN. Can. J. Chem. **57**, 180 (1979).

Rhodium(I)–bis(ditertiaryphosphine) complexes of the general formula $Rh(P\frown P)_2Cl$ ($P\frown P = Ph_2P(CH_2)_nPPh_2$, $n = 1$–4, and (+)-diop (diop = 2,3-*O*-isopropylidene 2,3-dihydroxy-1,4-bis(diphenylphosphino)butane) have been prepared by treating $[Rh(cyclooctene)_2Cl]_2$ with the appropriate ditertiaryphosphine. The $n = 1$ and $n = 4$ and diop species are five-coordinate in the solid state and in non-polar solvents, while the $n = 2$ and 3 species contain ionic chloride. The cationic complexes $Rh(P\frown P)_2{}^+X^-$ were prepared from the $Rh(P\frown P)_2Cl$ species by adding AgX ($X = SbF_6$, PF_6, BF_4). Reaction of the chloro complexes with borohydride has yielded the hydrides, $HRh(P\frown P)_2$, for the $n = 2$ and 3 diphosphines, and for (+)-diop. ^1H and ^{31}P nmr, as well as visible spectral data, are presented: a solvent-dependent deshielding of *ortho* protons of the phenyl groups is observed in some of the complexes, and the ligand CH_2 protons are coupled to the rhodium in the $Rh(Ph_2PCH_2PPh_2)_2{}^+$ cation; the P atom in this bis(diphenylphosphino) ligand shows an usual high field shift on coordination to rhodium.

Preliminary kinetic data for catalytic hydrogenation of methylenesuccinic acid show that the cationic and hydrido complexes are more active than the corresponding chloro complexes, and that activity generally increases with increasing chain length of the diphosphine.

BRIAN R. JAMES et DEVINDER MAHAJAN. Can. J. Chem. **57**, 180 (1979).

On a préparé des complexes de bis(phosphines ditertiaires)rhodium(I) de formule générale $Rh(P\frown P)_2Cl$ ($P\frown P = Ph_2P(CH_2)_n PPh_2$, $n = 1$–4 et (+)-diop (diop = *O*-isopropylidène-2,3 dihydroxy-2,3 bis(diphénylphosphino)-1,4 butane) en faisant réagir le $[Rh(cyclooctène)_2Cl]_2$ avec la phosphineditertiaire appropriée. Les espèces où $n = 1$, $n = 4$ et diop sont pentacoordonnées à l'état solide et dans des solvants non-polaires alors que les espèces où $n = 2$ et $n = 3$ contiennent du chlorure ionique. On a préparé les complexes cationiques $Rh(P\frown P)_2{}^+X^-$ à partir des espèces $Rh(P\frown P)_2Cl$ auxquelles on a ajouté du AgX ($X = SbF_6$, PF_6, BF_4). La réaction des complexes chlorés avec le borohydrure conduit aux hydrures, $HRh(P\frown P)_2$, pour les diphosphines où $n = 2$ et 3 et pour le (+)-diop. On présente les spectres rmn ^1H et ^{31}P de même que les spectres dans le visible: dans quelques-un des complexes, on observe un déblindage des protons *ortho* des groupes phényles qui dépend du solvent et, dans le cation $Rh(Ph_2PCH_2PPh_2)_2{}^+$, les protons du CH_2 du ligand sont couplés au rhodium; l'atome de P de ce ligand bis(diphénylphosphino) subit un déplacement usuel vers les hauts champs par coordination avec le rhodium.

Des données cinétiques préliminaires concernant l'hydrogénation catalytique de l'acide méthylènesuccinique montrent que les complexes cationiques et hybrido sont plus actifs que les complexes chloro correspondants et que généralement l'activité augmente avec une augmentation de la longueur de la chaîne de la diphosphine.

[Traduit par le journal]

Introduction

Although the bis(ditertiaryphosphine) $Ph_2P(CH_2)_nPPh_2$ complexes of iridium(I) and iridium(III) have been studied fairly extensively (1–4), few details have been reported for the rhodium analogues. The $Rh(dpe)_2X$ complexes,[1] X = H, Cl, ClO_4, are well-known (5), and in terms of activation of small gas molecules and catalytic activity, the crystal structure of the cationic dioxygen complex $Rh(dpe)_2O_2{}^+PF_6{}^-$ has been reported (6). The $Rh(dpe)_2Cl$ complex is a 1:1 electrolyte in polar solvents (2, 5), and is ineffective as a catalyst for hydrogenation of olefinic substrates under mild conditions (2, 7). The $Rh(dpe)_2{}^+$ cation is unreactive toward H_2 (8, 9).

Our interest in these bis(diphenylphosphino) systems increased after our finding that an isolated $HRh[(+)\text{-diop}]_2$ complex was an efficient catalyst for asymmetric hydrogenation of certain prochiral olefinic carboxylic acids under mild conditions (10, 11). The illustrated diop ligand can be considered,

[1]Ligand abbreviations used for $Ph_2P(CH_2)_nPPh_2$: $n = 1$, bis(diphenylphosphino)methane or dpm; $n = 2$, 1,2-bis(diphenylphosphino)ethane or dpe; $n = 3$, 1,3-bis(diphenylphosphino)propane or dpp; $n = 4$, 1,4-bis(diphenylphosphino)butane or dpb. $P\frown P$ signifies generally a chelating diphosphine.

0008-4042/79/020180-08$01.00/0

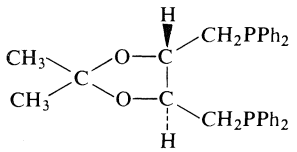

(+)-diop

for example, as a derivative of the dpb ligand, and this led us to look at the bis[$PPh_2(CH_2)_nPPh_2$] systems, including the hydrido, chloro, and cationic complexes, with a view to learning more of reactivity patterns generally as a function of *n*. Such data have appeared on the use of 1:1 rhodium(I)/$Ph_2P(CH_2)_nPPh_2$ hydrogenation catalysts formed *in situ* from rhodium(I) precursors (12), and, depending on the media, the catalysts may be neutral or cationic (13).

The synthesis and characterization of various bis(diphenylphosphino) complexes are reported in this paper along with some preliminary data concerning their catalytic activity for hydrogenation of the prochiral substrate, methylenesuccinic acid. We (11) and Kagan's group (14) have reported earlier on the characterization of the cationic complexes $Rh(diop)_2^+$ and $H_2Rh(diop)_2^+$, and Slack and Baird (15) reported on some *in situ* dpp and diop systems while our work was in progress. The luminescence of the $Rh[PPh_2(CH_2)_nPPh_2]_2^+$ cations (n = 1–3) has been discussed but no other details on the complexes were given (16, 17).

Experimental

All solutions were handled under an argon atmosphere using Schlenk techniques. Spectral grade solvents were stored over molecular sieves (BDH, type 5A) and were vacuum-degassed before use for synthetic procedures. Spectra were recorded on a Perkin-Elmer 202 or Cary 14 (for uv/vis), a Perkin-Elmer 457 (for ir, solid samples being run as Nujol mulls between CsI plates), a Varian T-60 (for ^1H nmr), and a Varian XL-100 in the Fourier transform mode (for ^1H nmr, and ^{31}P nmr at 40.5 MHz using a P_4O_6 capillary as external standard). Conductivity measurements were made either in nitromethane or in *N,N'*-dimethylacetamide (DMA) at 25°C using a Thomas Serfass conductivity bridge and cell. Microanalyses were performed by Mr. P. Borda of this department.

Rhodium(III) trichloride trihydrate was obtained from Johnson, Matthey Limited, silver salts from Alfa Inorganics and Cationics Inc., and the dpm, dpe, dpp, and (+)-diop ligands were Strem products. A literature method (18) was used to prepare dpb. All the diphosphines were recrystallized from hot ethanol before use.

The rate data were measured on a constant pressure gas-uptake apparatus described previously (19). The solvents for gas-uptake experiments were distilled before use; toluene and DMA were refluxed with CaH_2, and alcohols were refluxed with magnesium metal/iodine to remove traces of water and were stored under argon.

Preparation of Complexes

The cyclooctene dimer $[RhCl(C_8H_{14})_2]_2$ was prepared by a literature procedure (20); yields of 90% are obtained on leaving the reaction mixture for 10 days.

$Rh(dpe)_2Cl$ and $Rh(dpp)_2Cl$

A benzene solution (10 mL) of the phosphine (1.1 mmol, ~0.45 g) was added to a red, benzene solution (10 mL) of $[RhCl(C_8H_{14})_2]_2$ (0.25 mmol, 0.18 g). The precipitated yellow complex was washed with warm benzene and dried *in vacuo*. The complexes have been prepared previously by other methods (5, 16).

$Rh(dpm)_2Cl$

To a benzene solution (5 mL) of $[RhCl(C_8H_{14})_2]_2$ (0.30 mmol, 0.215 g) was added dpm (1.32 mmol, 0.50 g) in benzene (5 mL), and the resulting solution was freeze-dried. The residue obtained was recrystallized from CH_2Cl_2/ether to give orange needles.

$Rh(dpb)_2Cl$ and $Rh[(+)\text{-}diop]_2Cl$

A benzene solution (15 mL) of $[RhCl(C_8H_{14})_2]_2$ (0.30 mmol, 0.215 g) and phosphine (1.32 mmol, 0.56 g dpb or 0.66 g (+)-diop) was refluxed under Ar for 3 h. Concentration to a 5 mL volume, followed by addition of *n*-hexane, gave a yellow solid that was filtered, recrystallized from CH_2Cl_2/ether [$Rh(dpb)_2Cl$] or *n*-hexane [$Rh(diob)_2Cl$], and dried *in vacuo*.

$Rh(P\frown P)_2^+BF_4^-$

The complexes were prepared in each case from the corresponding chloro complex. For example, a mixture of a CH_2Cl_2 solution (5 mL) of $Rh(dpm)_2Cl$ (0.30 mmol, 0.27 g) and a methanol solution (5 mL) of $AgBF_4$ (0.30 mmol, 0.58 g) was stirred for 30 min. Removal of the AgCl and evaporation to dryness left a residue that was recrystallized from CH_2Cl_2/ether to give red crystals of $Rh(dpm)_2^+BF_4^-$. The dpb analogue was also red, while the dpe, dpp, and diop complexes were light orange.

$HRh(P\frown P)_2$

The literature method (5), involving treatment of the chloro complexes (0.50 mmol) with a 3 mole excess of sodium borohydride in ethanol (10 mL), was used in attempts to prepare the corresponding hydrides. The red dpe (5) and orange dpp complexes were recrystallized from benzene/ethanol, while the yellow diop complex (prepared earlier by a different route (21)) was recrystallized from *n*-hexane. Use of the dpm ligand yielded a deep red precipitate but this decomposed even under Ar, and we have been unable to characterize the compound. Borohydride reduction of $Rh(dpb)_2Cl$ yielded a mixture of complexes that have not been separated; borohydride species are almost certainly present as judged by ir bands in the 2340–2390 cm^{-1} region (22). Attempts to synthesize the $HRh(dpb)_2$ complex via the routes used to synthesize the diop analogue from $RhCl_3 \cdot 3H_2O$ (10, 11, 21) were similarly unsuccessful.

The yields of all the isolated complexes described in this section were in the 75–90% range.

Results and Discussion

Cleavage of the chloride bridge in $[RhCl(diene)]_2$ complexes by a Lewis base L, including monodentate phosphines, can yield both RhCl(diene)L and $Rh(diene)L_2^+Cl^-$ species, depending on the amount of L used and the polarity of the solvent used (23). Reaction of the diene dimer with 2 mol of a chelating diphosphine is assumed to yield RhCl(diphosphine) (solvent) or Rh(diene)(diphosphine)$^+$, de-

TABLE 1. Analytical and molar conductivity (Λ) data for the rhodium(I) complexes

Complex	Decomposition point (°C)[a]	Analysis %C Found	%C Calculated	%H Found	%H Calculated	Λ[b] (ohm^{-1} cm^2 mol^{-1})
$Rh(dpm)_2Cl$	97	62.03[c]	66.20	4.46	4.85	71
$Rh(dpe)_2Cl$	205–209	66.64	66.80	5.27	5.20	61
$Rh(dpp)_2Cl$	162–165	67.43	67.33	5.30	5.40	74 (49)[d]
$Rh(dpb)_2Cl$	108	65.66[e]	67.85	5.85	5.65	49
$Rh(diop)_2Cl$	79	64.97[e]	65.58	5.96	5.64	35
$Rh(dpm)_2{}^+BF_4{}^-$	124	61.50[f]	62.65	4.55	4.59	79
$Rh(dpe)_2{}^+BF_4{}^-$	273–276	61.40[f]	63.31	4.86	4.87	78
$Rh(dpp)_2{}^+BF_4{}^-$	180	63.14[f]	63.92	5.05	5.13	81
$Rh(dpb)_2{}^+BF_4{}^-$	169–173	63.22[f]	64.51	5.40	5.38	75
$Rh(diop)_2{}^+BF_4{}^-$	174–177	60.91[f]	62.74	5.09	5.40	78
$HRh(dpe)_2$	167	69.70	69.33	5.50	5.44	71 (2)[d]
$HRh(dpp)_2$	143–146	69.35	69.84	5.65	5.71	51 (12)[d]
$HRh(diop)_2$	128	66.70	67.64	6.28	6.00	4 (2)[d]

[a]Uncorrected, in air.
[b]10^{-3} M in CH_3NO_2 at 25°C under Ar.
[c]Complex hygroscopic.
[d]Value in DMA.
[e]Solids O_2-sensitive.
[f]Low carbon due to presence of CH_2Cl_2, detected in nmr; the calculated values are uncorrected.

pending on the solvent, and the cationic complexes are readily synthesized (12–15, 24–26). We have used the cyclooctene precursor $[RhCl(C_8H_{14})_2]_2$ to prepare the $Rh(P\frown P)_2Cl$ complexes (Table 1) via reaction [1].

$$[1]\quad [RhCl(C_8H_{14})_2]_2 + 4P\frown P \xrightarrow{C_6H_6} 2Rh(P\frown P)_2Cl + 4C_8H_{14}$$

While our studies were in progress, a report appeared (27) describing the synthesis of a $[RhCl(diop)(C_6H_6)]_2$ complex via a similar reaction, but using the bis(ethylene) dimer precursor with 2 mol of the diphosphine.

Reaction [1] at room temperature precipitates in analytically pure forms the dpe and dpp complexes, and probably the dpm complex but this is very hygroscopic and does not give satisfactory analytical data. The preparations are simpler than the ones reported earlier using rhodium(I) carbonyl precursors (5, 15, 28). Synthesis of the dpb and diop complexes via reaction [1] requires a refluxing procedure; the complexes are air-sensitive and this could explain the slightly low carbon analyses.

The $Rh(P\frown P)_2{}^+A^-$ complexes ($A^- = BF_4{}^-$, $PF_6{}^-$, $SbF_6{}^-$), readily prepared from the chloro complexes by treatment with Ag^+A^-, can be recrystallized from CH_2Cl_2/ether; the carbon analyses are somewhat low due to the presence of dichloromethane in the crystals (Table 1). Details are given for only the tetrafluoroborate complexes since these proved to have more convenient solubility properties for our catalytic studies (see below).

The borohydride method of Sacco and Ugo (5) was used to synthesize the $HRh(P\frown P)_2$ complexes from the chloro analogues. A presumedly dpm species decomposed spontaneously, at least at room temperature, and we were not able to isolate the dpb by this route or one developed by Robinson's group starting from rhodium trichloride (29). This latter method, in fact, proved to be unsatisfactory for all the hydrides, except $HRh(diop)_2$ (21).

Tables 1–3 report conductivity and spectroscopic data for the various complexes.

The molar conductivity data (Table 1) show that dpm, dpe, and dpp chloro complexes are 1:1 electrolytes in nitromethane, and the visible spectral data in methanol correspond also to those of the $BF_4{}^-$ salts (Table 2). The solid state spectra of the dpe and dpp chloro complexes also show absorption maxima at wavelengths similar to the solution values, indicating the same ionic structure in the solid state. These complexes have always been considered as ionic in the solid state with square planar cations (or approximately so (17)), and this appears to be based on electronic absorption and emission spectral data (16, 17, 30). The dpm complex, unlike the other two, is soluble in toluene and the visible absorption spectrum in this solvent and the solid state differs from that in methanol. We thus consider $Rh(dpm)_2Cl$ to be five-coordinate in the solid state and toluene. Detection of possible Rh—Cl stretching frequencies in the ir is prevented, due to absorption by the dpm (and dpe, dpp) ligands in the 400–280 cm^{-1} region. The dpb and diop chloro complexes also appear to be five-coordinate in the solid state and in non-polar

TABLE 2. Visible and high field ^{1}H nmr spectral data for the rhodium(I) complexes[a]

Complex	Medium	λ_{max} nm ($\varepsilon \times 10^{-3}$, M^{-1} cm^{-1})	τ[e]	J_{Rh-H} (Hz)	J_{P-H} (Hz)
$Rh(dpm)_2Cl$	Methanol	385 (3.8), 446 (3.5)			
	Toluene	406[b] (3.3)			
$Rh(dpe)_2Cl$	Methanol	406[b] (4.5)			
$Rh(dpp)_2Cl$	Methanol	410[b] (2.6)			
$Rh(dpb)_2Cl$	Methanol	435[c]			
	Toluene	420 sh (1.6)			
$Rh(diop)_2Cl$	Methanol	440[c]			
	Toluene	Continuum			
$Rh(dpm)_2{}^+BF_4{}^-$	Methanol	385 (3.7), 446 (3.5)			
$Rh(dpe)_2{}^+BF_4{}^-$	Methanol	407[d] (5.0)			
$Rh(dpp)_2{}^+BF_4{}^-$	Methanol	412[d] (2.8)			
$Rh(dpb)_2{}^+BF_4{}^-$	Methanol	435 (3.3)			
$Rh(diop)_2{}^+BF_4{}^-$	Methanol	442 (3.6)			
$HRh(dpe)_2$[f]	Toluene	406 (8.1)	20.1	10.0	18.0
$HRh(dpp)_2$[f]	Toluene	Continuum	19.8	8.0	20.8
$HRh(diop)_2$[f]	Toluene	355 (13.4)	21.0[g]	6.0	17.0

[a]Under Ar at room temperature.
[b]In solid state, ~410 nm.
[c]Intensity increases with time.
[d]In solid state, ~412 nm.
[e]In C_6D_6 at 25°C.
[f]ν(Rh—H) recorded in Nujol at 1900, 2100, and 2040 cm^{-1} for the dpe, dpp, and diop complexes, respectively.
[g]Incorrectly reported as 28.4 in refs. 10, 11, 21.

TABLE 3. ^{31}P and ^{1}H nmr data for the rhodium(I) complexes at 25°C

Complex	δ(P)[a]	J_{Rh-P}, Hz	δ(H)[b] aliphatic; phenyl[c]
$Rh(dpm)_2Cl$	+22.80[d]	115.3	3.4 m; 6.5 m, 7.2 m[b′]
	+17.38[e]	105.3	
$Rh(dpe)_2Cl$	−57.18[f]	134.2	2.15 m; 7.2 m[b]
$Rh(dpp)_2Cl$	−7.79[d]	132.3	1.8 m, 2.2m; 7.1 m[b]
$Rh(dpb)_2Cl$	See text		1.6 m, 2.0 m; 7.3 m[b]
$Rh(diop)_2Cl$	See text		1.10 s, 2.3 m, 3.6 m; 6.7 m, 7.2 m[b]
$Rh(dpm)_2{}^+BF_4{}^-$	+23.50[f]	117.0	5.1 m; 7.3 m[b] (4.85 m; 7.4 m, 7.6 m)[g]
$Rh(dpe)_2{}^+BF_4{}^-$	−57.22[f]	132.7	2.15 m; 7.25 m[b]
$Rh(dpp)_2{}^+BF_4{}^-$	−7.38[f]	130.5	1.85 m, 2.3 m; 7.2 m[b]
$Rh(dpb)_2{}^+BF_4{}^-$	−21.09[f]	132.0	1.7 m, 2.15 m; 7.15 m, 7.4 m[b]
$Rh(diop)_2{}^+BF_4{}^-$	−9.22[f,h]	140.0	1.10 s, 2.3 m, 3.8 m; 7.2 m, 7.4 m[b]
$HRh(dpe)_2$	−56.43[e]	142.5	2.2 m; 7.0 m, 7.6 m[b′]
$HRh(dpp)_2$	−18.26[e]	141.8	1.6 m, 2.1 m; 7.1 m, 7.7 m[b′]
$HRh(diop)_2$	−22.46[e]	146.0	1.26 s, 2.2 m, 3.4 m, 3.6 m; 7.0 m, 7.1 m, 7.5 m, 7.9 m[b′]

Free diphosphine	δ(H)[b] aliphatic; phenyl[c]
dpm	2.85 t; 7.3 m[b] (2.75 t; 7.0 m, 7.4 m)[b′]
dpe	2.1 t; 7.2 m[b] (2.2 m: 7.0 m, 7.3 m)[b′]
dpp	1.7 m, 2.2 m; 7.2 m[b] (1.55 m, 2.0 m; 7.1 m, 7.3 m)[b′]
dpb	1.5 m, 1.9 m; 7.1 m[b] (1.45 m, 1.8 m; 7.1 m, 7.4 m)[b′]
diop	1.28 s, 2.3 m, 3.8 m; 7.2 m[b]
	1.28 s, 2.4 m, 4.0 m; 7.0 m, 7.3 m[b′]

[a]Measured in ppm (upfield positive) from 85% H_3PO_4. Shifts (CH_2Cl_2 or $CDCl_3$) for the free ligands occur at +22.25(dpm), +12.51(dpe), +17.25(dpp), +15.95(dpb), and +22.50(diop).
[b]Measured in ppm (downfield positive) from TMS in $CDCl_3$(*b*) or C_6D_6(*b′*); s = singlet; t = triplet, m = multiplet.
[c]For phenyl region, lower shift when discernible is due to *m*- and *p*-protons, and the higher shift due to *o*-protons; for $HRh(diop)_2$, the 2 lower shifts are due to *m*-, *p*-protons, and the 2 higher shifts to *o*-protons.
[d]In CH_2Cl_2–acetone-d_6 (2:1 V/V).
[e]In C_6D_6.
[f]In CH_2Cl_2–C_6D_6 (2:1 V/V).
[g]In acetone-d_6.
[h]Corresponding values in CD_3OD were −9.12 (J_{Rh-P} 138.0), and in $CDCl_3$ −9.67 (J_{Rh-P} 140.1). In CD_3OD or acetone-d_6 at −60°C, a complex spectrum is obtained.

solvents; the conductivity data in nitromethane suggest incomplete dissociation of chloride, and their solubility in toluene (the corresponding fluoroborates being insoluble) is also consistent with coordinated chloride. Further, weak ir bands at 281 and 284 cm^{-1} for the dpb and diop complexes, respectively (not present in the BF_4^- analogues), are attributed to ν(Rh—Cl). The visible spectral data are solvent dependent and, in methanol, correspond to those of the cations, thus showing loss of ionic chloride in this medium. The absorption maximum in the cationic systems moves to higher wavelengths as *n* increases from 2 to 4. The dpm system is different in showing two maxima in the 380–450 nm region; 'anomalous' ^{31}P nmr shifts are also noted with this system (see below).

Measurement of the conductivity of the five-coordinate hydrides in nitromethane gave unexpectedly high values for the dpe and dpp complexes, while the diop species exhibited normal behaviour. All the hydrides were essentially non-conducting in polar DMA (31). Reaction of the hydrides with the nitromethane is indicated, and is being studied further, although the limited solubility of the complex and the extreme sensitivity of the solutions to oxygen present difficulties. Reaction of platinum metal hydride complexes with nitroalkanes is not unprecedented (32).

The hydride ligand of the $HRh(P\frown P)_2$ complexes is readily detected by ir, and the high field ^1H nmr, a well resolved doublet of quintets at room temperature (Table 2, Fig. 1), is consistent with four equivalent phosphorus atoms. The same nmr pattern with similar coupling constants (J_{Rh-H} 7 Hz, J_{P-H} 18 Hz) has been reported for $HRh[Ph_2P(CH_3)]_4$ at −60°C, and this was attributed to a tetragonal pyramid structure (33), although others have considered that a fluxional C_{3v} structure is more likely (34). The solid state structure of $HRh(PPh_3)_4$ with the hydrogen atom omitted is tetrahedral, and a threefold axis of symmetry implies that the hydrogen lies on this axis or must be randomly disordered in the crystal (35, 36). A recent structure determination of $HIr(dpe)_2$ shows it to be approximately trigonal bipyramidal with the hydride presumed to be at an axial site (37); the high field ^1H nmr is the quintet expected of a fluxional solution structure, and by analogy the $HRh(P\frown P)_2$ structures are likely to be similar.

The ^{31}P nmr signals (proton-decoupled for the hydrides) appear as sharp doublets at 25°C due to equivalent phosphorus atoms coupling to the rhodium (Table 3). No general trends are apparent, although the dpm ligand is different in undergoing upfield shifts on coordination to the metal. Such upfield shifts have been reported for both dpm and

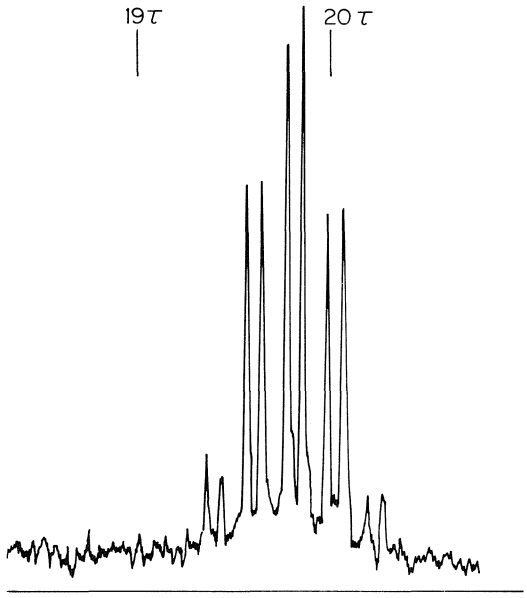

FIG. 1. High field ^1H nmr spectrum of $HRh(dpp)_2$ in C_6D_6 at 20°C.

dpp ligands in some iridium complexes (3), and the factors determining such shifts have been enunciated (38, 39). The substantially larger downfield shifts noted for the dpe complexes provide further examples of the large degree of deshielding apparent in five-membered ring systems (39). The data for the chloro and tetrafluoroborate complexes are consistent with the dpe and dpp complexes being ionic, and the variation of the ^{31}P chemical shift for $Rh(dpm)_2Cl$ with solvent is also consistent with ionic character in polar solvents and covalent character in benzene. Complex ^{31}P spectra were obtained at 25°C for the $Rh(dpb)_2Cl$ and $Rh(diop)_2Cl$ complexes in both C_6D_6 and CH_2Cl_2/acetone-d_6. Complications could arise by (*a*) partial ionization in the polar medium, (*b*) a more rigid five-coordinate structure (cf. the distorted trigonal bipyramidal structure of $HIr(dpe)_2$ (37)), since increasing chelate ring size leads to decreased fluxional behaviour (2, 3), (*c*) the occurrence of multinuclear species, which are becoming increasingly evident in rhodium–diphosphine chemistry (40, 41). The simple doublet pattern of $Rh(diop)_2{}^+BF_4{}^-$ in CD_3OD also gives way to a complex spectrum at −60°C; formation of associated species seems the most likely explanation. More detailed variable temperature nmr studies are in progress to help clarify the complications.

Data for the ^1H nmr in the phosphine region are given in Table 3. The shift of ligand protons on coordination is generally small except for the CH_2 protons of dpm which move downfield by ~0.6 and ~2.3 ppm in the $Rh(dpm)_2Cl$ and $Rh(dpm)_2{}^+BF_4{}^-$

complexes, respectively, the different shifts further confirming the non-ionic character of the chloro complex. These CH_2 resonances are somewhat solvent dependent (Table 3, footnote *g*), and appear as a sextet due to 'virtual coupling' with the rhodium (42). The *ortho* protons of the phenyl groups in the dpe and dpp complexes experience an anisotropic deshielding compared to the *meta* and *para* protons. The phenomenon is more apparent from data in benzene-d_6, since in $CDCl_3$ the phenyl absorption region is broad; for example, free dpe gives multiplets (3:2) at $\delta \sim 7.0$ (*meta,para*) and 7.3 (*ortho*), while in the $HRh(dpe)_2$ complex these absorptions appear at 7.0 and 7.6 ppm, respectively. Similar deshielding of *ortho* protons has been noted, for example (43), in some iridium alkyl complexes, $IrCl_2(CO)(PPh_3)_2$(alkyl), although a shielding of the *ortho* protons occurs in the *cis*-octahedral complexes $Ir(dpe)_2X_2^+$, X = O, S, Se (44), and in the $Rh(dpm)_2Cl$ complex reported here (Table 3).

The low field ^1H nmr of the $HRh(diop)_2$ complex is of interest (Fig. 2) in that the aromatic protons appear as four distinct multiplets of relative intensity 3:3:2:2 at δ7.0, 7.1 (*meta,para*) and δ7.5, 7.9 (*ortho*); the deshielding through coordination is again well demonstrated, and there are now two sets of phenyl groups. These very likely approximate an edge-face conformation, a geometry that has been demonstrated recently in several $Ph_2P\frown PPh_2$ complexes, including IrCl(COD)(diop) (45) and Rh(COD)(diphosphine)$^+$ species (46–48), where COD = 1,5-cyclooctadiene and diphosphine = 1,2-bis-[(anisole)(phenylphosphino)]ethane and 2,3-bis(diphenylphosphino)butane. The orientation of the phenyl groups appears critical for the high efficiency of such complexes as catalysts for asymmetric hydrogenation of prochiral olefinic substrates (13, 46, 48). All the complexes reported here are oxygen-sensitive in solution; in the solid state, only the chloride and fluoroborate complexes containing dpe and dpp are reasonably air-stable.[2]

Catalytic Hydrogenation

Some preliminary kinetic data for hydrogenation of methylenesuccinic acid to 2-methylsuccinic acid are summarized in Table 4.

In agreement with others (2, 7), we find that $Rh(dpe)_2^+Cl^-$ shows very low activity, and until our discovery of the activity of $HRh(diop)_2$ (10, 11), we and probably other workers, because of the early report (2), had not considered rhodium(I)–bis-(diphosphine) chelate complexes as likely catalysts; a

[2]The complexes $Rh(P\frown P)_2X_2$, $X_2 = O_2$ or CO, have been isolated in each case for dpm, dpe, and dpp, except for the dpe/CO system; details will be reported in a later paper.

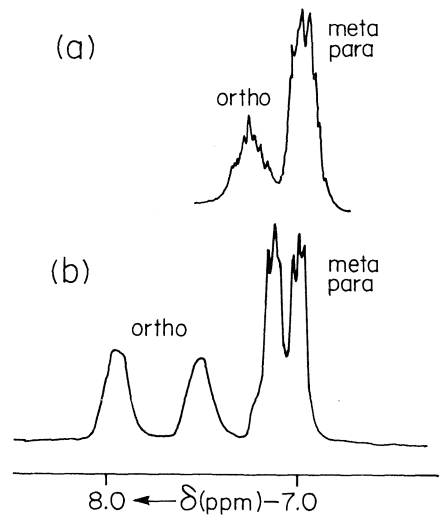

FIG. 2. ^1H nmr (phenyl region) of (*a*) diop, and (*b*) $HRh(diop)_2$ in C_6D_6 at 20°C.

reason was considered to be the difficulty in providing a vacant coordination site (49). Such complexes can clearly lead to quite high activity (Table 4), and in the case of $HRh(diop)_2$, the vacant site is thought to arise by one of the diphosphine ligands becoming monodentate (11, 50).

Initially surprising is that $Rh(dpe)_2^+BF_4^-$ shows about ten times the activity of $Rh(dpe)_2^+Cl^-$ under corresponding conditions, and a similar difference in behaviour is noted for the dpb complexes. Presumably chloride must coordinate and deactivate some intermediate (e.g. an alkyl) in the catalytic cycle. The activity of the $Rh(diop)_2^+$ cation, however, is essentially the same whether the associated anion be chloride or tetrafluoroborate. The cations generally are much less active in the polar and more strongly coordinating DMA.

The hydrides show activity comparable to that of the corresponding fluoroborate salts. The two species are interconvertible by the equilibria outlined in [2] (5, 11);

$$[2]\quad HRh(P\frown P)_2 + H^+ \rightleftharpoons H_2Rh(P\frown P)_2^+ \rightleftharpoons H_2 + Rh(P\frown P)_2^+$$

these are unimportant for the diop complex in butanol/toluene with the methylenesuccinic acid substrate used (11), but the dpe and dpp systems have not been studied in sufficient detail.

Comparison of the data for the fluoroborate salts at substrate concentrations $\geq 0.1\ M$ shows that catalytic activity increases with chain length, $n = 4$ (and diop) $> n = 3 > n = 2 > n = 1$. Kagan's group (12) reported a similar trend for rhodium(I)-*mono*diphosphine systems formed *in situ* from

TABLE 4. Catalytic hydrogenation of methylenesuccinic acid using the rhodium(I) complexes[a]

Complex	[Rh] × 10^3 (M)	[Substrate] (M)	Maximum rate × 10^6 (M s^{-1})	$t_{1/2}$ × 10^{-3}[b] (s)
$Rh(dpm)_2^+BF_4^-$	4.0	0.2	4.3	27
$Rh(dpe)_2Cl$	4.0	0.2	Very slow	72[c]
$Rh(dpe)_2^+BF_4^-$	4.0	0.2	9.6	10(6[c])
	4.0	0.2	Very slow[d]	72[e]
	4.0	0.1	9.3	5
	2.0	0.1	8.0	6
	2.0	0.05	6.8	4
	1.0	0.05	4.6	7
$HRh(dpe)_2$	4.0	0.1	7.9[f]	7
$Rh(dpp)_2^+BF_4^-$	2.0	0.05	31.6	2
	1.0	0.05	17.8	3
	1.0	0.1	25.4	4
$HRh(dpp)_2$	4.0	0.1	41[f]	3
$Rh(dpb)_2Cl$	2.0	0.1	18.2[g,h]	3
$Rh(dpb)_2^+BF_4^-$	2.0	0.1	130[g,h]	0.4
	2.0	0.1	13[d,g]	7
$Rh(diop)_2Cl$	1.0	0.1	—	0.6[f,g,i]
$Rh(diop)_2^+BF_4^-$	1.0	0.1	135	0.4[f,g,i]
$HRh(diop)_2$	1.0	0.1	150	0.4[f,g,i]

[a]Typical experiment involved 5 mL *n*-butanol, at 1 atm total pressure and 60°C.
[b]Approximate reaction time for 50% hydrogenation of the substrate.
[c]30% hydrogenation.
[d]In DMA.
[e]20% hydrogenation.
[f]In *n*-butanol/toluene (2.1 V/V).
[g]At 30°C.
[h]In ethanol.
[i]The *R*-(+)-2-methylsuccinic acid isolated had 48, 37, and 40% *ee* for the chloro, fluoroborate, and hydrido systems, respectively.

$[RhCl(C_2H_4)_2]_2$ for the hydrogenation of α-acetamidocinnamic acid in benzene/ethanol at 20°C, the $n = 1$ system being inactive; however, the $n = 6$ system had activity comparable to that for $n = 3$. Although these types of data are of use in designing better catalysts (including chiral ones), rationalizations to explain such trends, based solely on rate data measured at a set of convenient conditions, should not be attempted. These systems typically show saturation behaviour in their kinetics, that is, the rates level off at higher substrate and/or H_2 concentrations (11), and the rate vs. concentration profiles will vary for different systems. The limited data in Table 4 show that the rates for the $Rh(dpe)_2^+BF_4^-$ system are close to zero order in olefinic substrate and are fractional in catalyst, while for the $Rh(dpp)_2^+BF_4^-$ system the rates are close to first order in both substrate and catalyst. Detailed kinetic studies are necessary to elucidate the mechanisms, and then comparable rate constants can possibly be extracted by suitable analysis. In this particular case, we have found that while $Rh(dpe)_2^+$ does not form a dihydride at ambient conditions (as noted by others (8)), the dpp analogue readily gives an isolable *cis*-$H_2Rh(dpp)_2$ complex (51), and the mechanisms for catalytic hydrogenation may well differ. A quite different reactivity pattern has also been found, for example, for the monodiphosphine systems referred to above, when used to hydrogenate styrene in benzene ($n = 3 > n = 1$, $5 > n = 4 >$ diop $> n = 2$) (12).

The diop systems $Rh(diop)_2X$ (X = Cl, BF_4, H) all gave rise to similar optical enrichment in the 2-methylsuccinic acid product (Table 4, footnote *i*).

Acknowledgements

We thank the National Research Council of Canada for support of this research and Johnson, Matthey Ltd. for the loan of $RhCl_3 \cdot 3H_2O$.

1. L. VASKA and D. L. CATONE. J. Am. Chem. Soc. **88**, 5324 (1966).
2. K. A. TAYLOR. Adv. Chem. **70**, 195 (1968).
3. J. S. MILLER and K. G. CAULTON. J. Am. Chem. Soc. **97**, 1067 (1975).
4. M. J. HOPKINSON and J. F. NIXON. J. Organomet. Chem. **148**, 201 (1978).
5. A. SACCO and R. UGO. J. Chem. Soc. 3274 (1964).
6. J. A. MCGINNETY, N. C. PAYNE, and J. A. IBERS. J. Am. Chem. Soc. **91**, 6301 (1969).
7. Y. CHEVALIER. Docteur-Ingenieur Thesis, Paris, 1970; H. B. KAGAN and T. P. DANG. J. Am. Chem. Soc. **94**, 6429 (1972).
8. A. SACCO, M. ROSSI, and C. F. NOBILE. J. Chem. Soc. Chem. Commun. 589 (1966).
9. M. C. HALL, B. T. KILBOURN, and K. A. TAYLOR. J. Chem. Soc. A, 2539 (1970).

10. W. R. CULLEN, A. FENSTER, and B. R. JAMES. Inorg. Nucl. Chem. Lett. **10**, 167 (1974).
11. B. R. JAMES and D. MAHAJAN. Isr. J. Chem. **15**, 214 (1977).
12. J-C. POULIN, T-P. DANG, and H. B. KAGAN. J. Organomet. Chem. **84**, 87 (1975).
13. B. R. JAMES. Adv. Organomet. Chem. In press.
14. D. SINUO and H. B. KAGAN. J. Organomet. Chem. **114**, 325 (1976).
15. D. A. SLACK and M. C. BAIRD. J. Organomet. Chem. **142**, C69 (1977).
16. R. BRADY, W. V. MILLER, and L. VASKA. J. Chem. Soc. Chem. Commun. 393 (1974).
17. G. L. GEOFFROY, M. S. WRIGHTON, G. S. HAMMOND, and H. B. GRAY. J. Am. Chem. Soc. **96**, 3105 (1974).
18. P. RIGO, M. BRESSAN, and A. TURCO. Inorg. Chem. **7**, 1460 (1968).
19. B. R. JAMES and G. L. REMPEL. Discuss. Faraday Soc. **46**, 48 (1968); Can. J. Chem. **44**, 233 (1966).
20. A. VAN DER ENT and A. L. ONDERDELINDEN. Inorg. Synth. **14**, 92 (1973).
21. A. FENSTER, B. R. JAMES, and W. R. CULLEN. Inorg. Synth. **17**, 81 (1977).
22. D. G. HOLAH, A. N. HUGHES, and B. C. HUI. Can. J. Chem. **55**, 4048 (1977).
23. B. R. JAMES, R. H. MORRIS, and K. J. REIMER. Can. J. Chem. **55**, 2353 (1977), and references therein.
24. J. D. MORRISON, W. F. MASLER, and M. K. NEUBERG. Adv. Catal. **25**, 81 (1976).
25. R. R. SCHROCK and J. A. OSBORN. J. Am. Chem. Soc. **98**, 2134 (1976); **98**, 2143 (1976).
26. W. S. KNOWLES, M. J. SABACKY, B. D. VINEYARD, and D. J. WEINKAUFF. J. Am. Chem. Soc. **97**, 2567 (1975).
27. Y. CHAUVIN, D. COMMEREUC, and R. STERN. J. Organomet. Chem. **146**, 311 (1978).
28. J. CHATT and B. L. SHAW. J. Chem. Soc. A, 1437 (1966).
29. N. AHMAD, S. D. ROBINSON, and M. F. UTTLEY. J. Chem. Soc. Dalton Trans. 843 (1972).
30. R. BRADY, B. R. FLYNN, G. L. GEOFFROY, H. B. GRAY, J. PEONE, JR., and L. VASKA. Inorg. Chem. **15**, 1485 (1976).
31. W. J. GEARY. Coord. Chem. Rev. **7**, 81 (1971).
32. J. F. KNIFTON. J. Org. Chem. **40**, 519 (1975); **41**, 1200 (1976).
33. K. C. DEWHIRST, W. KEIM, and C. A. REILLY. Inorg. Chem. **7**, 546 (1968).
34. J. P. JESSON. Stereochemistry and stereochemical nonrigidity in transition metal hydrides. Transition metal hydrides. *Edited by* E. L. Muetterties. Marcel Dekker, New York. 1971. p. 110.
35. B. A. FRENZ and J. A. IBERS. Molecular structures of transition metal hydride complexes. Transition metal hydrides. *Edited by* E. L. Muetterties. Marcel Dekker, New York. 1971. p. 47.
36. R. W. BAKER and P. PAULING. J. Chem. Soc. Chem. Commun. 1495 (1969).
37. B-K. TEO, A. P. GINSBERG, and J. C. CALABRESE. J. Am. Chem. Soc. **98**, 3027 (1976).
38. J. F. NIXON and A. PIDCOCK. Ann. Rev. NMR Spect. **2**, 345 (1969).
39. P. E. GARROU. Inorg. Chem. **14**, 1435 (1975).
40. A. SANGER. J. Chem. Soc. Dalton Trans. 120 (1977).
41. J. HALPERN, D. P. RILEY, A. S. C. CHAN, and J. J. PLUTH. J. Am. Chem. Soc. **99**, 8055 (1977).
42. R. R. SCHROCK and J. A. OSBORN. J. Am. Chem. Soc. **93**, 2397 (1971).
43. M. A. BENNETT, R. CHARLES, and T. R. B. MITCHELL. J. Am. Chem. Soc. **100**, 2737 (1978).
44. A. P. GINSBERG and W. E. LINDSELL. Inorg. Chem. **12**, 1983 (1973).
45. S. BRUNIE, J. MAZAN, N. LANGLOIS, and H. B. KAGAN. J. Organomet. Chem. **114**, 225 (1976).
46. B. D. VINEYARD, W. S. KNOWLES, M. J. SABACKY, G. L. BACKMAN, and D. J. WEINKAUFF. J. Am. Chem. Soc. **99**, 5946 (1977).
47. R. G. BALL and N. C. PAYNE. Inorg. Chem. **16**, 1187 (1977).
48. M. D. FRYZUK and B. BOSNICH. J. Am. Chem. Soc. **99**, 6262 (1977).
49. B. R. JAMES. Homogeneous hydrogenation. Wiley, New York. 1973. p. 269.
50. B. R. JAMES, R. S. MCMILLAN, R. H. MORRIS, and D. K. W. WANG. Adv. Chem. Series, **167**, 122 (1978).
51. B. R. JAMES and D. MAHAJAN. To be published.

Dissolution of iron during the initial corrosion of carbon steel in aqueous H_2S solutions[1]

PARAM H. TEWARI AND ALLAN B. CAMPBELL

Research Chemistry Branch, Atomic Energy of Canada Limited, Whiteshell Nuclear Research Establishment, Pinawa, Man., Canada R0E 1L0

Received July 10, 1978

PARAM H. TEWARI and ALLAN B. CAMPBELL. Can. J. Chem. **57**, 188 (1979).

The dissolution of iron from carbon steel in aqueous H_2S solutions has been studied as a function of time and temperature at 0.1 MPa H_2S pressure using the rotating disc technique. The iron sulfide film formed on the disc surface has been identified by X-ray diffraction analysis. The solubility and dissolution rate of synthesized mackinawite, $FeS_{(1-x)}$, have also been determined to help establish the mechanism of release of iron from carbon steel corroding in aqueous H_2S solutions.

The rate data have been analysed by an equation for a joint chemical and transport controlled process. At 22°C and 0.1 MPa H_2S, the maximum rate of release of Fe^{2+}, obtained by extrapolating the data to infinite rotation speed, is 7.4 ± 0.5 μmol/m² s. This is similar to the dissolution rate determined for synthesized mackinawite powders, but is 20 times faster than the rate of dissolution for troilite and more than 1000 times faster than the dissolution rates for pyrrhotite and pyrite. Thus, troilite and iron sulfide phases that form subsequently are not major contributors to Fe^{2+} release during the corrosion of carbon steel.

At 22°C the diffusion coefficient for the $FeSH^+$ ion is (1.4 ± 0.2) × 10^{-9} m²/s and the activation energy of the diffusion process is 25 ± 7 kJ/mol. The chemical reaction occurring at the surface has an activation energy of 77 ± 14 kJ/mol.

It is concluded that the release of iron from corroding carbon steel is governed by the dissolution rate of mackinawite, the initial corrosion product. This dissolution is controlled by the chemical reaction between mackinawite and H^+ and by the transport of the complexed $FeSH^+$ from the interface to the bulk solution.

PARAM H. TEWARI et ALLAN B. CAMPBELL. Can. J. Chem. **57**, 188 (1979).

Faisant appel à la technique du disque rotatif, on a étudié la mise en solution du fer d'aciers au carbone dans des solutions aqueuses de H_2S en fonction du temps et de la température, à une pression de 0.1 MPa de H_2S. Grâce à une analyse par diffraction de rayons-X, on a identifié le film de sulfure de fer qui se forme à la surface du disque. On a aussi déterminé la solubilité et le taux de dissolution de mackinawite de synthèse, $FeS_{(1-x)}$, afin d'aider à déterminer le mécanisme de mise en liberté du fer à partir d'aciers au carbone soumis à une corrosion dans des solutions aqueuses de H_2S.

On a étudié les données de vitesse à l'aide d'une équation exprimant les processus contrôlés conjointement d'une façon chimique et par le transport. A 22°C et à une pression de 0.1 MPa de H_2S, le taux maximal de mise en liberté du Fe^{2+} que l'on obtient en extrapolant les données jusqu'à une vitesse de rotation infinie est égal à 7.4 ± 0.5 μmol/m² s. Cette valeur est semblable au taux de dissolution déterminé pour des poudres de mackinawite mais elle est 20 fois plus rapide que celle déterminée pour la dissolution de la troilite et plus de 1000 fois plus grande que les valeurs correspondantes pour la pyrrhotite et la pyrite. Donc les phases du troilite et de sulfure de fer qui se forment subséquemment ne contribuent pas d'une façon importante à la mise en liberté du Fe^{2+} au cours de la corrosion des aciers au charbon.

A 22°C, le coefficient de diffusion de l'ion $FeSH^+$ est (1.4 ± 0.2) × 10^{-9} m²/s et l'énergie d'activation du processus de diffusion est 25 ± 7 kJ/mol. L'énergie d'activation de la réaction chimique se produisant à la surface est 77 ± 14 kJ/mol.

On en conclut que la mise en liberté du fer par un acier au charbon soumis à une corrosion est déterminée par le taux de dissolution de la mackinawite, le produit de corrosion initial. Cette dissolution est contrôlée par la réaction chimique entre la mackinawite et H^+ et par le transport du $FeSH^+$ complexé de l'interface vers la solution.

[Traduit par le journal]

Introduction

Carbon steel exposed to aqueous H_2S solutions corrodes to give ferrous ions and hydrogen (1). Subsequently, a series of iron sulfides is formed (2–8), the first such corrosion product being mackinawite (3, 5), $FeS_{(1-x)}$. Cubic FeS (3, 6–8), troilite (hexagonal FeS), pyrrhotite ($Fe_{(1-x)}S$), and pyrite, FeS_2, can then form, depending on system conditions (3). We have shown that mackinawite is the most soluble phase among the various types of iron sulfide phases

[1]AECL No. 6264.

0008-4042/79/020188-09$01.00/0

formed (9); however, it changes to other phases quite easily. It thus seems desirable to compare the rate of Fe^{2+} release from carbon steel with dissolution rates of mackinawite. Accordingly, we now report the rate of release of Fe^{2+} in aqueous H_2S solutions during the initial corrosion (1–8 h) of carbon steel under conditions of controlled area and hydrodynamics. This release rate has been investigated at several temperatures and 0.1 MPa H_2S pressure by the rotating disc (10, 11) technique.

We have also measured the solubility and dissolution rates of mackinawite at various solution pH's. Such studies should help to determine if the dissolution of mackinawite is the chief pathway for the release of Fe^{2+} from carbon steel exposed to aqueous H_2S solutions. These studies are important in several applied areas, such as in the petroleum industry and Girdler-Sulfide (G.S.) heavy water plants.

Materials and Methods

Materials

Triple-distilled water containing less than 5×10^{-8} mol/kg iron was used in the experiments. All acidic solutions were made with analytical grade H_2SO_4. NaOH solutions were CO_2-free. Analytical grade reagents were used throughout.

Mackinawite was prepared electrochemically (8) using an all glass cell fitted with a carbon steel anode and a platinum cathode. A solution of 0.1 mol/kg NaOH was introduced into the cell and purged with nitrogen for 1 h before the passage of H_2S through the solution. A current of ~ 20 mA was passed through the solution while H_2S was bubbled continuously through the cell for 3 days. Air occlusion was avoided during the reaction. The mackinawite powder formed during the process was washed with deoxygenated water under a nitrogen atmosphere. The product was vacuum dried in a desiccator.

All samples were analysed by X-ray diffraction before and after the dissolution experiments to observe changes of phase, if any, during the experiments.

Apparatus

The rotating discs used in the study were made from carbon steel rod incorporating all the features recommended by Riddiford (11). The disc was fitted into the inset of the Teflon holder (Fig. 1). Immediately before a run, the exposed surface of the disc was ground to within 0.3 mm of the surrounding Teflon surface as described earlier (12). The release of Fe^{2+} was limited to a well defined area of the exposed surface of the carbon steel disc by painting the sides and part of the surface with polyurethane paint.

The bearing for the rotating assembly was designed to ensure minimum eccentricity of rotation of the disc ($< 1\%$ of the disc radius). Rotational velocities were measured using a stroboscope. The temperature was maintained to within ± 0.1°C of the desired value using a thermostatically controlled water bath.

All dissolution work was done in vessels that were degassed and kept oxygen-free. Since mackinawite was easily oxidized in air and the oxidized material later produced other phases of iron sulfides, dissolution work with mackinawite was always performed under N_2 to prevent its oxidation and subsequent transformation to other sulfides.

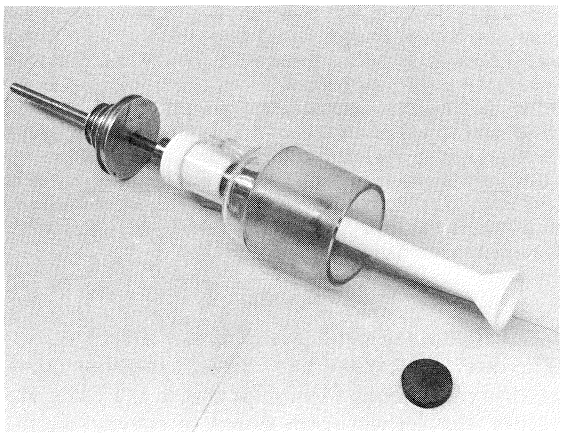

FIG. 1. Rotating disc assembly.

Method

After assembly of the reaction vessel, N_2 was bubbled through the solution for 1/2 h before introducing H_2S. The solutions were saturated with H_2S at room temperature before raising the temperature to any desired value. The temperature and H_2S pressure were allowed to reach equilibrium before the disc assembly was introduced for the start of the run.

The disc was rotated at a given speed between 10 to 85 radians/s (100–800 rpm), resulting in laminar flows with Reynolds number $\leq 10^4$. (The critical Reynolds number (11), when a transition from laminar to turbulent flow occurs, is $Re \simeq 2 \times 10^5$.)

Small aliquots of solution (< 4 g) were withdrawn at intervals from the reaction vessel for Fe^{2+} analysis without exposing the bulk solution to air. The total solution withdrawn for analysis was within 5–10% of the initial total volume. Hence the correction made in concentration change due to the withdrawn volume in samples was small and did not appreciably affect the calculation of rate of iron release.

Iron analyses were done by atomic absorption spectroscopy (detection limit $\simeq 6 \times 10^{-7}$ mol/kg) for samples containing more than 1 μg/g, and by colorimetry (Technicon Analyser) for samples containing less than 1 μg/g. In the latter (detection limit 2×10^{-8} mol/kg), iron is reduced to Fe^{2+} by hydroxylamine hydrochloride in a buffered solution of pH 5.4 before a colorimetric determination by 2,4,6-tri-2-pyridyl-*S*-triazine (TPTZ) reagent. The precision of Fe^{2+} determination was $\pm 12\%$ (2σ) in the concentration range less than 1 μg/g, and $\pm 5\%$ for concentrations > 1 μg/g.

To characterize the iron species being released from the disc, absorption spectra of dissolved iron were obtained using a Cary 17D spectrophotometer with a quartz cell. For comparison, spectra for ferrous solutions made by dissolving 99.999% pure iron in H_2SO_4 were also obtained at pH 1.0, 2.0, and 4.0 in the presence and absence of H_2S, with precautions taken to avoid oxidation of Fe^{2+} or H_2S by bubbling H_2 in the solution and by avoiding exposure to air.

The pH was measured with a Beckman research pH meter fitted with a combination pH and reference electrode. The equilibration time for the pH electrode was obtained for solutions of known acidity or basicity and, in most cases, was < 30 s except between pH 6 and 8 where it was almost 1 min. In solutions saturated with H_2S at 0.1 MPa, a prolonged and continuous exposure of the pH electrode to the H_2S environment was avoided because the performance of the electrode

deteriorated after long H_2S exposure due to silver sulfide precipitation at the tip. This presented no problem in the measurements, however, and the precision of the measured pH was always better than ± 0.01 units.

After the rate data were obtained, the disc was dismounted, washed, and stored in a vacuum desiccator. The morphology of the iron sulfide phases formed on the disc were determined by using a Cambridge Mark 2A Sterioscan electron microscope. Phase analyses of the various sulfides were performed with a Philips PW1050 X-ray diffractometer equipped with a diffracted beam monochromator.

Results

Rate of Release of Fe^{2+} from Carbon Steel

The rate of release of Fe^{2+} from a rotating carbon steel disc in aqueous H_2S solutions at 0.1 MPa H_2S pressure was derived from slopes of curves like that given in Fig. 2. At 22°C these rate data were remarkably reproducible (precision $\leq 5\%$) in contrast to the rate of dissolution data obtained from synthesized mackinawite powders (discussed later). The release rates of Fe^{2+} at 22°C at different rotation speeds are given in Table 1.

At higher temperatures, however, the rate data varied beyond the error in the analysis of iron ($\geq 10\%$). These variations were due to phase changes in mackinawite as observed by X-ray analysis, and also to peeling and rupture of the surface film and contribution from a second crystalline phase formed on the film (Figs. 3–4). Hence, interpretation of rate data at higher temperatures was not as reliable as at 22°C.

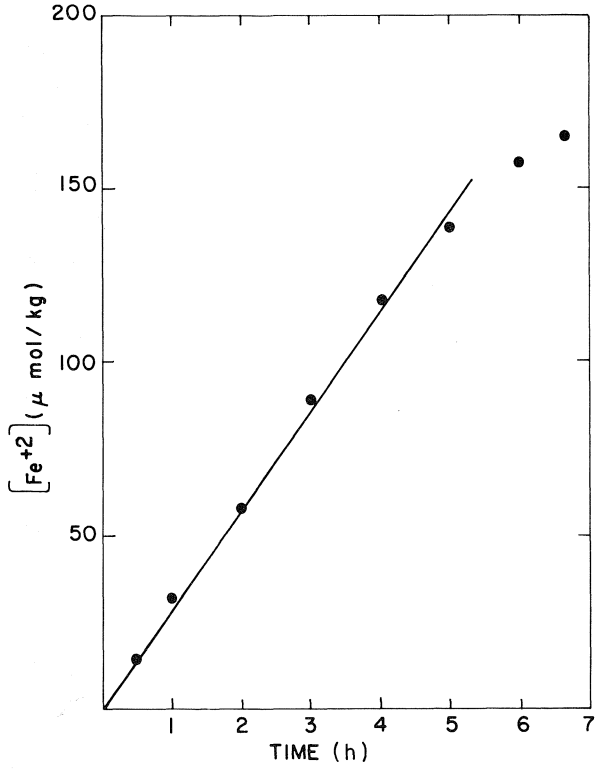

FIG. 2. Release of Fe^{2+} from rotating carbon steel discs as a function of time at 22°C and 0.01 MPa H_2S pressure.

TABLE 1. Release rate of Fe^{2+} from carbon steel discs in aqueous H_2S solutions at 0.1 MPa H_2S pressure and 22°C, at different speeds of rotation

ω (rad s^{-1})	Rate (μmol/m^2 s)
10.47	2.80
13.13	3.01
23.12	3.48
27.24	3.59
29.21	3.67
34.57	3.91
36.73	3.94
40.06	4.09
79.71	4.63
85.56	4.66

Solubility of Mackinawite

As explained earlier, solubility data for mackinawite are necessary in the discussion of the mechanism of Fe^{2+} release from carbon steel surfaces in aqueous H_2S solutions. Although mackinawite was always handled under N_2 to prevent oxidation and its subsequent transformation to other sulfides, analysis showed that some conversion had taken place. At 25°C and 0.1 MPa H_2S pressure, only in three runs out of 24, all with fresh batches of mackinawite with no detectable impurities, did the samples remain unchanged after the dissolution experiments. The others contained various amounts of other sulfides such as marcasite, greigite (Fe_3S_4), and pyrite.

The solubility data for mackinawite (Fig. 5) show significant scatter even in the runs where the major phase of the product, after dissolution, remained mackinawite. This variation was possibly due to phase changes on the surface although these could not be detected by X-ray diffraction analysis (detection limit $\sim 2\%$). At 25°C and 0.1 MPa H_2S pressure (with no added acid or base, pH $\sim$ 3.95), the observed solubility values ranged from 0.2×10^{-3} to 2.0×10^{-3} mol/kg. The true value could be even higher than 2.0×10^{-3} mol/kg since the unconverted phase would have a higher solubility.

The solubility of mackinawite at $T > 25$°C could not be accurately determined due to its rapid transformation to other sulfides at higher temperatures. Although the extremely poor reproducibility at $T > 25$°C precluded the possibility of obtaining accurate solubility data, it was concluded that mackinawite has a negative temperature coefficient of solubility.

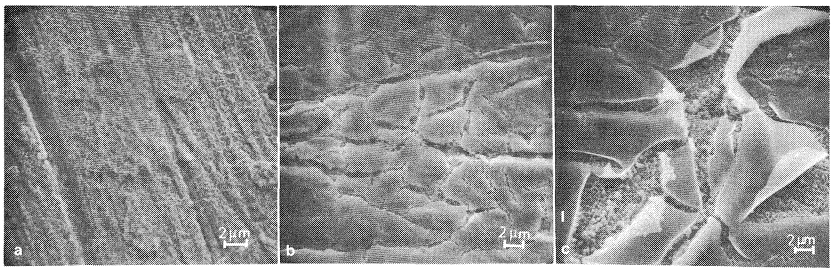

FIG. 3. Morphology of deposits on carbon steel discs exposed to aqueous H_2S solutions at 0.1 MPa H_2S pressure at 22°C. (*a*) Apparently smooth deposit of mackinawite with a preferred orientation. (*b*) Deposit with cracks which subsequently lead to peeling. (*c*) Peeling of deposits. The appearance of a fresh precipitation of cubic FeS phase is shown at location I.

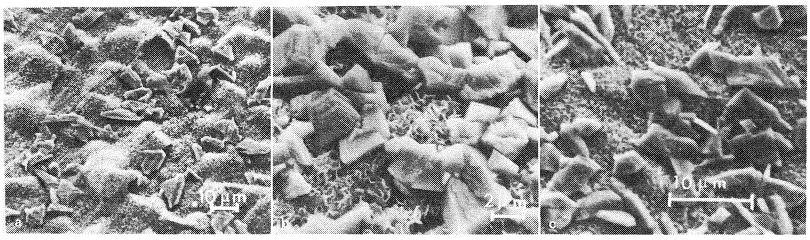

FIG. 4. Morphology of deposits on carbon steel discs exposed to aqueous H_2S solutions at 0.1 MPa H_2S pressure at 40 and 60°C. (*a*) Crystalline phase appearing on top of the first formed layer at 40°C. (*b*) Same crystals at a higher magnification. (*c*) Morphology of the disc surface at 60°C.

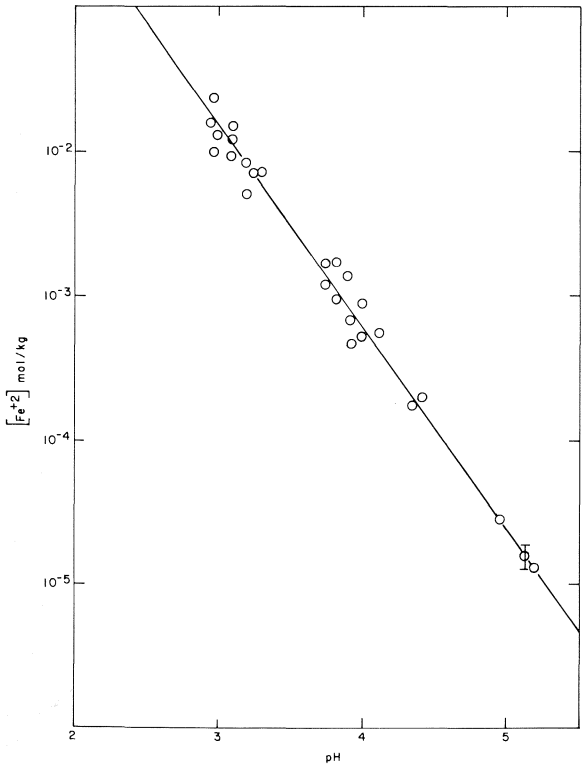

FIG. 5. Solubility of mackinawite at 25°C and 0.1 MPa H_2S pressure as a function of pH.

Stoichiometry of Reaction of Mackinawite with H^+

The kinetic order of the reaction between mackinawite and H^+ was determined by following the initial rates of dissolution at different acidities as described earlier (12) for troilite. The measurements were not accurate ($\pm 10\%$) since, in spite of precautions to avoid exposure to air, mackinawite converted to some extent to other less soluble iron sulfide phases as confirmed by X-ray analysis. From the initial slope of the curves of Fe^{2+} versus time, values of the negative logarithms of the rates were obtained and plotted against the pH of the solutions (Fig. 6). The slope of the line was 1.1 ± 0.1 showing R, the rate of dissolution of mackinawite, to be first order with respect to acid concentration. Therefore, $R = k[H^+]$, where k is the rate constant. The measured rate constant was $(1.2 \pm 0.2) \times 10^{-5}$ m/s, and this is similar to the rate constant for the release of Fe^{2+} from carbon steel discs determined at lower rotation speeds ($\sim 1.5 \times 10^{-5}$ m/s).

Morphology of Carbon Steel Surfaces Exposed to H_2S Solutions

After the kinetic studies, the products on the surface of the carbon steel discs were analysed by X-ray diffraction. At 22°C and 0.1 MPa H_2S pressure, the exposed surface of the discs had developed a black surface deposit which gave the characteristic diffraction pattern for mackinawite. Some of these deposits

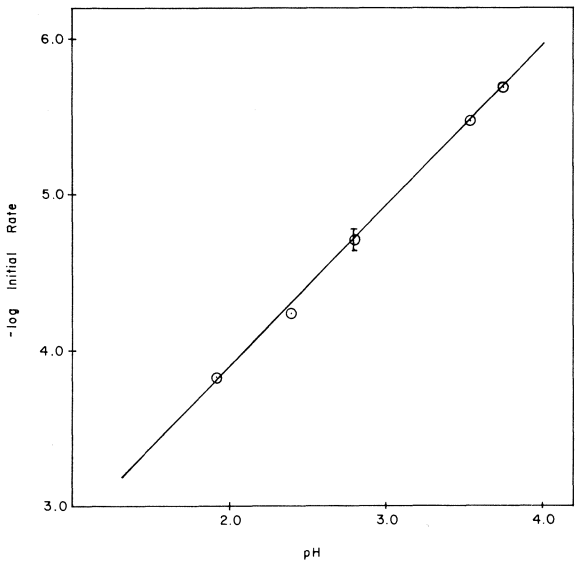

FIG. 6. Dependence of initial rate of dissolution of mackinawite on pH at 25°C.

had a preferred orientation and appeared smooth; however, the majority of these mackinawite films had cracks. Even the films which first appeared smooth developed cracks and were seen lifting and peeling off the surface as shown in Figs. 3 and 4. Peeling could be seen after exposures as short as 6 to 8 h.

The films formed on surfaces exposed to aqueous H_2S solutions at 40°C had mackinawite as the major phase, but these also contained some cubic FeS which always appeared as distinct crystals (Fig. 4). A similar crystalline appearance of cubic FeS has been observed in other studies (3, 7–8). There were fewer linear cracks in the surface film at 40°C, compared to those formed at 22°C. The large crystals appearing on top of the inner phase eventually covered the majority of the surface, but they were also observed to crack and fall off into the solution. In many cases, large numbers of these crystals appeared near an area where a hole was seen. It appeared that the raised areas in the first layer developed holes by cracks and, near the holes, crystals of cubic FeS developed by precipitation. At 60°C, the number of such crystals appearing on the top of the mackinawite phase was larger than that observed at 22 or 40°C, as is evident from Fig. 4*b* and *c*.

Absorption Spectra of Iron Solutions

Spectra of Ferrous Solutions in H_2SO_4

To characterize the iron ion being released from the carbon steel disc, spectra of ferrous solutions made by dissolving pure iron in H_2SO_4 solutions under H_2 atmosphere were obtained in the ultraviolet, visible, and infrared regions. Consistent with literature reports, a relatively intense peak (13) at 240 nm (molar extinction coefficient, $\varepsilon = 19.0$) and a weak peak (14) at 970 nm ($\varepsilon = 1.6$) are obtained for Fe^{2+} (or $[Fe_{(H_2O)_6}]^{2+}$) at pH 1.0 and 4.0 (Fig. 7).

Spectra of Ferrous Solutions in Aqueous H_2S

Since aqueous H_2S solutions have a very intense absorption at $\simeq$ 195 nm, any peak present at $\simeq$ 240 nm or lower is completely masked in the presence of H_2S. In aqueous H_2S solutions at pH 4.0 a peak at 330 nm, which is not present in solutions of iron in the absence of H_2S, is observed, suggesting the presence of species different from $[Fe_{(H_2O)_6}]^{2+}$ ($\varepsilon_{330\ nm} = 2.4$; compare curves *A* or *B* with *C* in Fig. 7).

The position of the peak at 970 nm does not change noticeably in H_2S solutions, but its intensity is very low ($\simeq 0.5$). A transient peak at 1155 nm, whose peak height is small but variable, was also sometimes observed. This peak, however, is likely due to some impurity in H_2S, since it was observed at times even in aqueous solutions of triply distilled water with no detectable iron. Since the intensity of the iron peak in the infrared region is very low, only peaks in the ultraviolet region were used for the characterization of iron species.

Spectra of Iron Ions from a Carbon Steel Disc in Aqueous H_2S

The absorption spectrum of dissolved iron from the carbon steel disc has a peak at 330 nm (Fig. 8, $\varepsilon_{330} = 2.4$), the same as that observed for iron solutions in aqueous H_2S at pH 4.0 (Fig. 7, Curve *C*).

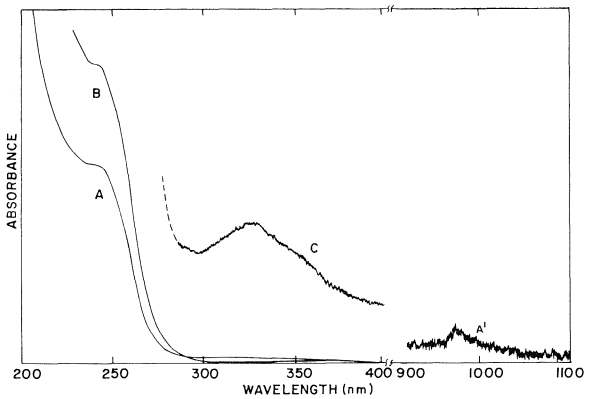

FIG. 7. Absorption spectra of ferrous solutions in H_2SO_4 acid at 25°C. *A*, Fe^{2+} in H_2SO_4, pH = 0.8, absorbance full scale 1.0, $Fe^{2+} = 1.97 \times 10^{-2}$ mol/kg, $\varepsilon_{240\ nm} = 19.0$, $\varepsilon_{970\ nm} = 1.6$. *B*, Fe^{2+} in H_2SO_4, pH = 3.9, absorbance full scale 0.5, $Fe^{2+} = 1.36 \times 10^{-2}$ mol/kg, $\varepsilon_{240\ nm} = 19.0$. *C*, dissolved iron in aqueous H_2S solution at pH = 3.95, absorbance full scale 0.02, $Fe^{2+} = 2.0 \times 10^{-3}$ mol/kg, $\varepsilon_{330\ nm} = 2.4$. *A'*, continuation of curve *A* in the infrared.

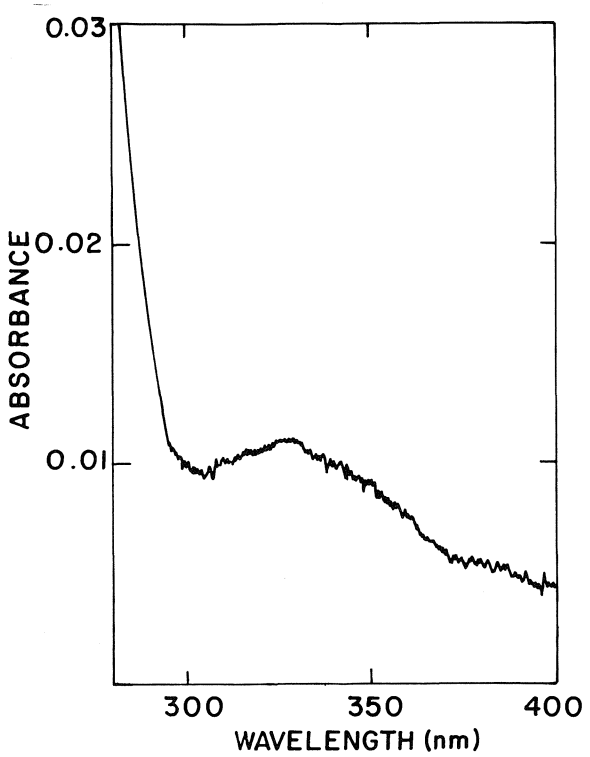

FIG. 8. Absorption spectra of dissolved iron from carbon steel in aqueous H_2S solutions (0.1 MPa) pH 3.95, Fe^{2+} = 5.3×10^{-3} mol/kg.

Discussion

Rate of Dissolution at Solid–Liquid Interfaces

The reaction between a solid and a solution giving dissolved species may comprise the following steps (11): (*a*) transport of the ions from the solution to the surface (in the present case H^+ or HS^-), (*b*) adsorption and chemical reaction at the solid surface, (*c*) desorption of the reaction products, and (*d*) transport of the products from the solid surface to the bulk solution. Steps (*a*) and (*d*) are transport controlled and are determined by the hydrodynamics of the system, whereas steps (*b*) and (*c*) are chemical processes at the surface and are termed chemical controlled.

According to Nernst theory (15–17), for transport controlled processes, the rate of dissolution, R, is given by

$$[1] \qquad R = \frac{DA}{V\delta}(c_s - c) = \frac{D}{\delta}(c_s - c)$$

where D = diffusion coefficient, A = area of the interface, c_s = solubility of the dissolving material at the given temperature, c = concentration of the solute at any time t, V = volume of solvent, δ = thickness of the Nernst diffusion layer.

According to Levich, for rotating discs in laminar flow (10, 11, 16),

$$\delta = 1.62D^{1/3}\gamma^{1/6}\omega^{-1/2}$$

where γ and ω are the kinematic viscosity and speed of rotation of the disc, respectively. Hence, the rate of dissolution or the flux of the ions diffusing away from the interface is

$$[2] \qquad R = 0.62D^{2/3}\gamma^{-1/6}\omega^{1/2}(c_s - c)$$

For dissolution of metals in acids with transport control, the concentration, c, is assumed to be zero (10, 18); then

$$[3] \qquad R = 0.62D^{2/3}\gamma^{-1/6}\omega^{1/2}[Fe^+]_{sat}$$

($c_s = [Fe^{2+}]_{sat}$ for the dissolving iron compound).

Equation [3] predicts that for a transport controlled process the rate of release of iron from the carbon steel disc is proportional to $\omega^{1/2}$ and that for a plot of R against $\omega^{1/2}$ the curve should pass through the origin. However, if the process of release of Fe^{2+} is not solely controlled by transport of materials to and from the disc, and the rate of surface reaction is also important, the equation for the rate under joint chemical and transport control is (10, 11)

$$[4] \qquad R^{-1} = R_\infty{}^{-1} + 1.62D^{-2/3}\gamma^{1/6}\omega^{-1/2}[Fe^{2+}]_{sat}{}^{-1}$$

where R, D, γ, and ω are the same as defined earlier, and R_∞ = the maximum dissolution rate at the interface (the chemical rate of dissolution), $[Fe^{2+}]_{sat}$ = saturation solubility of the dissolving iron sulfide formed at the interface.

Solubility data for mackinawite have been used since there is considerable evidence to show that this is the phase first formed during initial corrosion under these conditions (3), and our X-ray analysis of the disc surface has confirmed this conclusion.

The measured solubility of synthesized mackinawite powders in aqueous H_2S at 0.1 MPa pressure at 25°C is 2×10^{-3} mol/kg. The actual value may be slightly higher since the measurements are somewhat complicated by the conversion of mackinawite to other, less soluble, iron sulfide phases.

When the experimental data are analysed by eq. [4], the graph of R^{-1} vs. $\omega^{-1/2}$ is linear (Fig. 9). On the other hand, a graph of R vs. $\omega^{1/2}$ (eq. [3]) is not linear and the curve does not go through the origin. This shows that the rate of release of iron is not solely controlled by the transport of materials to and from the disc, but is controlled jointly by a chemical as well as a transport process.

Nature of the Iron Sulfide Film formed at the Interface and its Dissolution

Goeller and Rosenwald (19) have suggested that corrosion rates of iron under the influence of H_2S

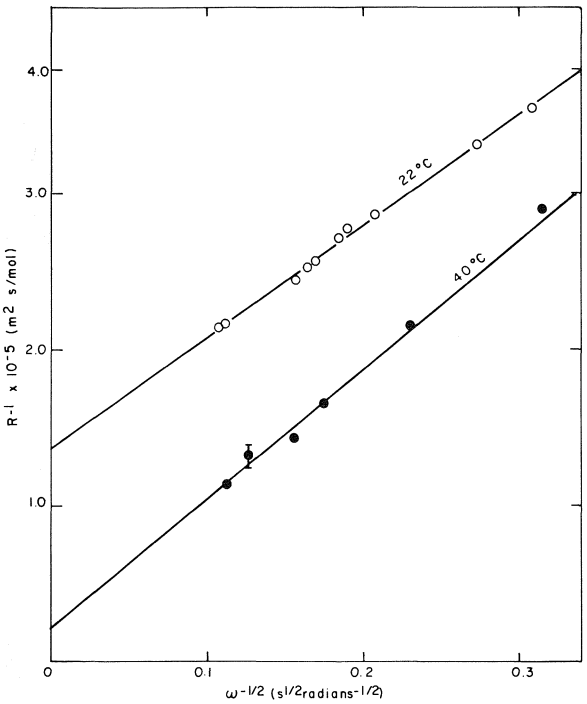

FIG. 9. A plot of R^{-1} vs. $\omega^{-1/2}$ at 22 and 40°C at 0.1 MPa H_2S pressure.

are controlled by mass transfer through an iron sulfide film, but have not specified which iron sulfide film is formed. The X-ray diffraction analyses of our corrosion films have confirmed that the initial film consists of mackinawite. Also, consistent with our postulate that mackinawite is the dissolving phase, the release rates of Fe^{2+} from carbon steel discs measured at lower rotation speeds (Table 1) are comparable to those measured from dissolving mackinawite powders at similar pH (2.8 μmol/m^2 s for carbon steel disc compared to $\simeq$ 2 μmol/m^2 s for mackinawite powder at $\simeq$ pH 3.9). At higher rotation speeds, Fe^{2+} release rates from the disc are higher than those measured from the dissolution rates of mackinawite, since the latter were severely restricted due to the low mixing speeds used in dissolving mackinawite powders.

The maximum release rate R_∞, obtained by extrapolating the release rate data for the discs to infinite rotation speed, is 7.4 $\pm$ 0.5 μmol/m^2 s at 22°C and 0.1 MPa H_2S pressure (Fig. 9). This release rate is $\simeq$ 20 times higher than that measured for troilite dissolution (9) (0.37 μmol/m^2 s), ruling out the latter as a major contributor to the Fe^{2+} release from the rotating disc. Furthermore, the rates of release of iron from the higher iron sulfides like pyrrhotite and pyrite (9) are at least 1000 times smaller ($\simeq 10^{-9}$–10^{-10} mol/m^2 s) than the observed release rates from the carbon steel disc. Thus, all higher iron sulfides can be eliminated as the cause of iron release.

Since the rate of dissolution of mackinawite is first order with respect to H^+, the rate constant k for the release of Fe^{2+} can be calculated from $k = R/[H^+]$, and at 22°C and $[H^+] = 1.23$ mol/m^3, $k = 6.0 \times 10^{-5}$ m/s.

Thermochemical Quantities and Diffusion Coefficient of Ferrous Ion

R_∞, the maximum rate of dissolution at 40°C (obtained from the intercept at $\omega^{-1/2} = 0$ in Fig. 9), is (4.8 $\pm$ 1.5) $\times 10^{-5}$ mol/m^2 s. From the two values of the intercepts at 22 and 40°C, the energy of activation of the chemical process is calculated to be 77 $\pm$ 14 kJ/mol. This value is consistent with the activation energy for the dissolution reactions of copper (20) and magnesium (21) in H_2SO_4, both of which are chemically controlled ($\simeq$ 63 kJ/mol for Cu and 55 kJ/mol for Mg).

The diffusion coefficients of the ferrous ion at 22 and 40°C have been calculated from the slope of the lines in Fig. 9 and eq. [4] by assuming that the kinematic viscosity of aqueous H_2S solutions is the same as that of water (89×10^{-6} m^2/s at 22 and 65×10^{-6} m^2/s at 40°C). This is consistent with the experimental observation of Murphy and Gaines Jr. (22) who observed little difference between the viscosity and density of water and H_2S saturated water up to 2.0 MPa pressure. The value of $[Fe^{2+}]_{sat}$ has been taken as 2×10^{-3} mol/kg at 22°C from our present results (Fig. 5) and 5×10^{-4} mol/kg at 40°C reported elsewhere (9). The values of D thus obtained are (1.4 $\pm$ 0.2) $\times 10^{-9}$ m^2/s and 2.7 $\times 10^{-9}$ m^2/s at 22 and 40°C, respectively.

The temperature dependence of the diffusion coefficient between 22 and 40°C gives E_A, the activation energy for the diffusion process, equal to 25 $\pm$ 7 kJ/mol. The reported (16) value for E_A is between 16–27 kJ/mol. Thus the thermodynamic data obtained from the results seem consistent with a joint chemical and diffusion process of iron release from carbon steel.

The derived diffusion coefficient at 22°C is higher than the literature (11, 23) values of $D_{Fe^{2+}}$ that range between 0.57×10^{-9} to 0.85×10^{-9} m^2/s. The difference between our value and the literature values for the diffusion coefficient for the iron ion is significant and is beyond the experimental error. Even if a much higher value of $[Fe^{2+}]_{sat}$ for mackinawite is chosen in calculating the diffusion coefficient (which would not be unreasonable since mackinawite changes to less soluble phases), our value of the diffusion coefficient remains significantly higher than the literature values.

The values reported in the literature for $D_{Fe^{2+}}$ are derived, however, for iron solutions containing 1.0 mol/kg perchloric acid or other more concentrated strong acids (11, 23), as compared to the aqueous H_2S solutions at 0.1 MPa pressure used in our experiments. Therefore, the reported values for the diffusion coefficient for Fe^{2+} are definitely for a different species than that observed in our experiments. As will be shown later, iron ions in aqueous H_2S solutions at pH 4.0 (the pH in our aqueous H_2S experiments) are different from the iron ions in pH 1.0 or more acidic solutions. Thus, a different diffusion coefficient is to be expected.

$FeSH^+$ species has been proposed in electrochemical studies of iron in aqueous H_2S solutions (24, 25), and by Pohl (26) for the formation of FeS troilite. Similarly $NiSH^+$ has been proposed in corrosion studies of nickel in H_2S solutions (27). Also, the existence of $PbSH^+$ and $ZnSH^+$ has been speculated in hydrothermal studies (28). No absorption spectra for such species have been reported, however, nor have their existence been confirmed experimentally by any other technique. Also, no values for the diffusion coefficients of either $NiSH^+$ or $FeSH^+$ are reported in the literature.

Kuehn and Taube (29) report the existence of $[Ru(NH_3)_5SH]^{2+}$ and $[Ru(NH_5)SH]^+$ from electrochemical evidence, but do not report absorption spectra because the species are unstable. Ramasami and Sykes (30) and Ardon and Taube (31) report the spectra of $CrSH^{2+}$ with peaks at 575 nm and 435 nm, but not the spectra for $CrSH^+$. They show that with the formation of the complex $CrSH^{2+}$, the peaks for Cr^{3+} shift to higher wavelengths; from 405 to 435 nm and from 560 to 575 nm, respectively.

Ehrenfreund and Leibenguth (13) have shown that ferrous solutions at pH $\leq$ 1.0 contain essentially Fe^{2+}, but at higher pH $FeOH^+$ species form with the appearance of a peak at $\sim$ 320 nm. In our studies, the absorption spectra for ferrous solutions contain an absorption band with a peak at 240 nm for Fe^{2+} ($\varepsilon_{240\ nm} = 19.0$) (Fig. 7), consistent with its reported spectrum (13). In aqueous H_2S solutions this 240 nm peak shifts to a higher wavelength, $\simeq$ 330 nm (Fig. 7*C*), and it is suggested that this is the absorption peak of $FeSH^+$. This is consistent with the reported shifts to higher wavelengths (13, 30, 31) in the peaks for Cr^{3+} and Fe^{2+} with the formation of $CrSH^{2+}$ and $FeOH^+$, respectively. The spectrum for the dissolved iron from the carbon steel discs in the aqueous H_2S also gives a peak at 330 nm, again suggesting $FeSH^+$ species in solution rather than Fe^{2+}. Thus, though literature confirmation for the spectrum of $FeSH^+$ is lacking, it is suggested that the dissolved iron species in H_2S solutions is $FeSH^+$.

Mechanism

According to our experimental data, formation of mackinawite on the surface of carbon steel exposed to aqueous H_2S solutions is very fast. Hence, the rate of release of iron is governed by the rate of dissolution of mackinawite formed on the carbon steel surface. The dissolution of mackinawite, in turn, is controlled by the chemical reaction between mackinawite and H^+ (adsorption reaction [5]), and by the transport of iron hydrosulfide ion ($FeSH^+$), desorbed from the mackinawite surface, into the bulk solution (eq. [7]). The kinetic data seem consistent with the following mechanism:

$$[5] \qquad FeS_{(mack)} + H^+ \overset{slow}{\rightleftharpoons} FeSH^+_{(ads)}$$

$$[6] \qquad FeSH^+_{(ads)} \overset{fast}{\rightleftharpoons} FeSH^+_{(desorb)}$$

$$[7] \qquad FeSH^+_{(desorb)} \overset{slow}{\rightleftharpoons} FeSH^+_{(soln)}$$

$$[8] \qquad FeSH^+_{(soln)} \overset{fast}{\rightleftharpoons} Fe^{2+}_{(soln)} + HS^-$$

where ads stands for adsorbed and desorb stands for desorbed. However, the following scheme with Fe^{2+} diffusing away from the interface into the bulk is also consistent with our data, i.e. kinetically indistinguishable from the first mechanism.

$$[9] \qquad FeS_{(mack)} + H^+ \overset{slow}{\rightleftharpoons} FeSH^+_{(ads)}$$

$$[10] \qquad FeSH^+_{(ads)} \overset{fast}{\rightleftharpoons} Fe^{2+}_{(ads)} + HS^-_{(ads)}$$

$$[11] \qquad Fe^{2+}_{(ads)} \overset{fast}{\rightleftharpoons} Fe^{2+}_{(desorb)}$$

$$[12] \qquad Fe^{2+}_{(desorb)} \overset{slow}{\rightleftharpoons} Fe^{2+}_{(soln)}$$

Either $FeSH^+$ or Fe^{2+} may be the diffusing species (eqs. [7] or [12]) in the transport process. We prefer eq. [7], with $FeSH^+$ diffusion, over eq. [12] because of the difference in the values of the diffusion coefficient of the diffusing species from that for Fe^{2+} given in the literature. Also, as discussed previously, absorption spectra suggest that $FeSH^+$ is the important species at pH 4.0 in aqueous H_2S solutions.

Iron release rates at higher temperatures and higher H_2S pressures are complicated by conversion of mackinawite to other phases. The morphology and erosion–corrosion behaviour of iron sulfides at 120°C and 1.6 MPa H_2S pressure, as a function of fluid velocity, will be discussed in a separate report (32).

Summary

The release rate of iron from carbon steel discs rotating in aqueous H_2S solution is governed by the

rate of dissolution of mackinawite, the first product of corrosion formed at the surface. The dissolution rate is controlled by the chemical reaction between mackinawite and hydrogen ion, and by the transport of iron hydrosulfide ions ($FeSH^+$) from the solid–liquid interface to the bulk solution. The maximum rate of release of iron at 22°C and 0.1 MPa H_2S pressure is 7.4 ± 0.5 μmol/m^2 s, which is $\simeq 20$ times higher than the measured dissolution rate of troilite and more than 1000 times higher than the dissolution rate of pyrrhotite and pyrite, ruling them out as major contributors to the iron release from carbon steel discs. At 22°C the diffusion coefficient of the complexed ferrous ion ($FeSH^+$) is $(1.4 \pm 0.2) \times 10^{-9}$ m^2/s and the activation energy for the diffusion process is 25 ± 7 kJ/mol. The chemical reaction occurring at the surface has an activation energy of 77 ± 14 kJ/mol.

Acknowledgements

The authors sincerely thank Drs. T. E. Rummery, N. Sagert, D. Shoesmith, P. Taylor, and A. Wikjord for helpful discussions and Mr. M. Duclos for X-ray diffraction analysis. Thanks are also due to Mr. H. D. Haworth for a literature search.

1. S. P. Ewing. Corrosion, **11**, 497t (1955).
2. J. C. Rowell. Corrosion of steel by hydrogen sulfide. Report Du Pont de Nemours. ESP-52-351 and DP-96.
3. A. G. Wikjord, T. E. Rummery, and F. E. Doern. To be published.
4. (*a*) A. G. Rozanov. Tra. Inst. Okeanol. Akad. Nauk SSSR, **63**, 172 (1973); (*b*) R. A. Berner. Science, **137**, 669 (1962); J. Geol. **72**, 293 (1964); (*c*) D. T. Rickard. Stockholm Contrib. Geol. **XX**:4, 67 (1969).
5. R. A. Berner. Science, **137**, 669 (1962).
6. R. DeMedicis. Rev. Chim. Mineral, **7**, 723 (1970); Science, **170**, 1191 (1970).
7. S. Takenow, H. Zoka, and T. Nhhara. Am. Minerol. **55**, 1639 (1970).
8. P. Taylor and D. Shoesmith. To be published.
9. P. H. Tewari, G. Wallace, and A. B. Campbell. Atomic Energy of Canada Limited, Report AECL-5960.
10. V. G. Levich. Physicochemical hydrodynamics. Prentice Hall Inc., Englewood Cliffs, NJ, USA. 1962.
11. A. C. Riddiford. Advances in electrochemistry and electrochemical engineering. *Edited by* P. Delahay. Interscience Publ. Inc., New York. **4**, 47 (1966).
12. P. H. Tewari and A. B. Campbell. J. Phys. Chem. **80**, 1844 (1976).
13. M. Ehrenfreund and J. L. Leibenguth. Bull. Soc. Chim. Fr. **7**, 2494 (1970); **8**, 2498 (1970).
14. (*a*) F. A. Cotton and M. D. Meyers. J. Am. Chem. Soc. **82**, 5023 (1960); (*b*) D. Sutton. Electronic spectra of transition metal complexes. McGraw-Hill, London. 1968. pp. 145–146; (*c*) C. K. Jorgenson. Absorption spectra and chemical bonding in complexes. Pergamon Press, London. 1962.
15. W. Nernst. Z. Phys. Chem. Leipzig, **47**, 52 (1904).
16. L. L. Bircumshaw and A. C. Riddiford. Q. Rev. **6**, 157 (1952).
17. P. J. Niebergall, G. Milosovich, and J. E. Goyan. J. Pharm. Sci. **52**, 236 (1963).
18. C. V. King. The surface chemistry of metals and semiconductors. *Edited by* H. C. Gates. John Wiley and Sons, New York. 1960. p. 357.
19. L. A. Goeller and R. H. Rosenwald. Ann. Univ. Ferrara, Ser. 5 (1970).
20. B. C.-Y. Lu and W. F. Graydon. Can. J. Chem. **32**, 153 (1954).
21. (*a*) D. D. Macdonald and D. Owen. Can. J. Chem. **49**, 3375 (1971); (*b*) D. A. Vermilyea. J. Electrochem. Soc. **116**, 1179 (1969).
22. J. A. Murphy and G. L. Gaines, Jr. J. Chem. Eng. Data, **19**, 359 (1974).
23. H. C. Kuo and D. Landoldt. Electrochim. Acta, **20**, 393 (1975).
24. T. P. Hoar and D. Havenhand. J. Iron Steel Inst. London, **113**, 239 (1936).
25. Z. A. Iofa, V. V. Batrakov, and B. Cho-Ngok. Zashch. Met. **1**, 55 (1965).
26. H. A. Pohl. J. Am. Chem. Soc. **76**, 2182 (1954).
27. M. Kesten. Corrosion, **32**, 94 (1976).
28. L. A. Kazmin and I. K. Karpov. Ezheg. Inst. Geokhim. Akad. Nauk SSSR, 319 (1972).
29. C. G. Kuehn and H. Taube. J. Am. Chem. Soc. **98**, 689 (1976).
30. T. Ramasami and A. G. Sykes. Inorg. Chem. **15**, 1010 (1976).
31. M. Ardon and H. Taube. J. Am. Chem. Soc. **89**, 366 (1967).
32. P. H. Tewari, M. G. Bailey, and A. B. Campbell. To be published.

The role of electron–phonon interaction and non-Gaussian transport in spectral changes of trapped electrons in glasses[1]

KOICHI FUNABASHI AND WILLIAM H. HAMILL

Department of Chemistry and Radiation Laboratory, University of Notre Dame, Notre Dame, IN 46556, U.S.A.

Received June 20, 1978

KOICHI FUNABASHI and WILLIAM H. HAMILL. Can. J. Chem. **57**, 197 (1979).

The continuous-time-random-walk (CTRW) model which was developed for electron scavenging reactions in polar glasses is extended to the phenomenon of spectral relaxation of electrons in shallow traps e_t^- in a wider range of systems. The central role of electron–phonon coupling in understanding the initial electron localization, the "pre-existing trap", and electron transfer processes are emphasized. The reactivity of e_t^- with scavengers, including protons, is discussed in terms of the theory of multi-phonon non-radiative transitions.

KOICHI FUNABASHI et WILLIAM H. HAMILL. Can. J. Chem. **57**, 197 (1979).

On a étendu le modèle de la marche aléatoire en temps continu (CTRW) qui avait été développé pour les réactions de piégeage d'électrons dans des verres polaires au phénomène de relaxation spectrale des électrons dans des pièges superficiels, e_t^-, dans un domaine plus large de systèmes On met en relief le rôle central du couplage électron–phonon pour la compréhension de la localisation initiale de l'électron, "le piège pré-existant", et les processus de transfert d'électrons. On discute de la réactivité des e_t^- avec les pièges, y compris les photons, en termes de la théorie des transitions non-radiatives multi-phonons.

[Traduit par le journal]

Introduction

The time dependence of optical absorption spectra for localized electrons in glasses involves two related problems. Since there are often at least two spectral regions (1, 2), visible and infrared, for the optical response of the localized electrons, one must first understand the physical origin of the spectral difference. Does the spectral difference represent two distinct localized states or alternatively reflect two distinguishable stages of a continuous dielectric relaxation process around the localized charge? A recent paper by Walker (3) deals with this interesting problem. For some aqueous glasses, Buxton, Gillis, and Klassen (BGK) (4) have demonstrated that the infrared (e_t^-) and visible (e_s^-) electrons belong to chemically distinguishable states because of the difference in their reactivities with electron scavengers, the fully solvated electron being more reactive.

The second problem is related to the time-dependent intensity of spectral response in each region. The decay mechanism which is commonly accepted among radiation chemists is that of electron tunneling between the acceptors and the initial trap sites, without involving any electron transport among the intermediate sites (5). We have suggested an alternative decay mode using the continuous-time-random-walk (CTRW) model (6).

The purpose of this work is to demonstrate that the CTRW model is applicable to both spectral relaxation and electron scavenging in a wider range of systems than those previously studied.

There are two objections to the tunneling mechanism. One is that the barrier-penetration model for tunneling is a "gross oversimplification" of the correct description of the two-site (i.e. a solvent trap and the acceptor) electron transfer process, according to Jortner (7). The second is that there is experimental evidence that electron scavenging is not a simple two-site electron transfer process, but requires electron transport involving both deep ("visible") and shallow ("infrared") traps (8). For the conversion $e_t^- \rightarrow e_s^-$, deep traps simulate the role of scavengers, as mentioned previously (9).

The correct description of the two-site electron transfer process has been given by the theory of non-radiative transitions (10–12). The same theory is also applicable to the electron jump process between two solvent traps in the description of electron transport. Although the relationship between the individual jump rate and the overall transport coefficient in disordered materials is quite complex (13), the magnitude and temperature dependence of the jump rate depend critically upon the nature of the electron–phonon interaction, in addition to the electronic tunneling factor. It is important to realize

[1]The research described herein was supported by the Office of Basic Energy Sciences of the Department of Energy. This is Document No. NDRL-1891 from the Notre Dame Radiation Laboratory.

0008-4042/79/020197-10$01.00/0

that, in the absence of electron–phonon interaction, electron localization itself does not take place, excluding the possibility of radiative transitions from quasi-free to localized states, and also the electron transfer between localized electron states does not take place. The electronic tunneling factor alone does not lead to physically meaningful electron transfer but gives only an oscillatory electron motion.

In polar molecular aggregates, the electron–phonon interaction may involve both long-range low-frequency medium modes and short-range high-frequency molecular modes. These interactions are operative uniformly throughout the system in the scale of intermolecular separation. Consequently, in the description of electron scavenging reactions, for example, it is difficult to accept the notion that a localized electron in the solvent is transferred (or "tunnels") directly to the scavenger molecule regardless of the separation distance.

If localized electrons are located at *special sites* of the system, such as F centers in ionic crystals or doped donors in semi-conductors (14), direct transfer to scavengers is a reasonable mechanism.

It is also important to distinguish the transient electron dynamics from that at thermal equilibrium, where the electron distribution function is given by the Boltzmann function. In the theoretical analysis of pulse-irradiated systems, we must cope initially with the electrons which are not necessarily in equilibrium with phonons, namely, with unrelaxed electrons. The transient currents of unrelaxed electrons are in general significantly large over an extended time period in amorphous solids, even though the long-time equilibrium currents are negligibly small.

In our understanding, the so-called visible and infrared electrons are not characterized simply by the difference in the degree of orientational polarization of surrounding medium, but are qualitatively different species in the sense that they could belong to different kinds of sites (e.g. alkane region and OH region in alcohols) or could be localized by different phonon modes (visible electrons by high-frequency intramolecular mode and ir electrons by low-frequency medium modes). However, both visible and ir electrons could deepen their trap depths by a small amount ($\sim$0.1 eV) by the orientational polarization at sufficiently high temperatures ($\gtrsim$77 K).

Electron hopping does not require "pre-existing traps". The electron moves concertedly with the localized deformation of the medium at low temperature. The configuration of the medium rearranges itself adiabatically by electron–phonon interaction. The electron remains localized throughout. Disorder of the medium ensures randomness among the sites and some produce much more deeply trapped electrons than most.

The notion of the pre-existing trap is a source of extensive misunderstanding in radiation chemistry. If the pre-existing trap is defined as a site at which there is no change of molecular configuration immediately before and after electron capture, then the non-radiative transition rate from the quasi-free state to the trapped state at such a site is negligibly small. When the molecular configuration of the acceptor site does not change upon electron capture there is an absence of electron–phonon interactions and there is no way to dissipate the excess electronic energy. Despite the dilemma in the definition of the pre-existing trap, our physical intuition tells us that electron localization in highly disordered materials, such as aqueous glasses, must be efficient and even activationless at low temperatures. A plausible argument for this intuition will be presented in a later section.

Finally, the diffusive motion (or hopping) of an electron in the CTRW model is not the same as classical diffusion in which the jump distance and the jump frequency are constant throughout the system. Reflecting the disordered structure of the system, the jump distance and the energy barrier fluctuate from site to site, causing a highly non-exponential decay, even under the assumption of usual first-order homogeneous kinetics (15). On a phenomenological level, this is equivalent to saying that the diffusion constant for the electron is time-dependent until all the electrons in the system settle down to the lowest levels at thermal equilibrium. The electron mobility at thermal equilibrium in aqueous glasses is expected to be negligibly small. Our model does provide for the finite *transient* mobility.

Rate Constant for Electron Scavenging

We present here a more detailed derivation for the electron scavenging rate expression according to the CTRW model from that obtained previously (6). The system of interest consists of trapped electrons and acceptor sites, e.g. scavenger molecules, whose concentration is far in excess of that of electrons. Assuming that the reaction is diffusion controlled, we are interested in calculating the number of electrons arriving at scavengers per unit time. Mathematically, this is equivalent to the problem of calculating the flux of walkers (scavengers) arriving at the origin (electron) for the first time. Since the position of the electron is fixed, diffusion motion of walkers (scavengers) corresponds practically to that of the electron itself.

Let us assume that each point of the lattice, taken arbitrarily as cubic, is initially occupied by a walker. Then the flux of the walkers arriving at the origin for the first time, $I(t)$, is related to the time-dependent

rate constant for scavenging, $k(t)$, which is defined as the same flux for unit concentration of walkers (scavengers), by

$$[1] \qquad I(t) = a^{-3}k(t)$$

where a is the lattice constant.

The number of trapped electrons at t, $n(t)$, is given by the usual first-order equation,

$$[2] \qquad n(t)/n_0 = \exp\left[-C_s \int_0^t k(t)\,dt\right]$$

where n_0 is the initial number of trapped electrons and C_s is the scavenger concentration.

The flux $I(t)$ may be calculated by the theory of random walk in the following way. If the jump time for each step is a constant τ, then [3] is obtained

$$[3] \qquad I(t) = \sum_{n,s} F_n(s)\delta(t - n\tau)$$

where $F_n(s)$ is the probability that the walker reaches the origin for the first time in n steps, starting from the lattice point s. The delta function in [3] indicates that walkers reach the origin only at times which are integral multiples of the jump time τ in this case. In order to generalize the flux calculation to the case of multiple-jump times, it is convenient to introduce the following generating functions,

$$[4] \qquad F(s,z) = \sum_{n=1}^{\infty} F_n(s)z^n$$

and

$$[5] \qquad P(s,z) = \sum_{n=0}^{\infty} P_n(s)z^n$$

where $P_n(s)$ is the probability that the walker is at the origin after n steps (not necessarily the first time), starting from the lattice point s. These generating functions satisfy the following equalities (16)

$$[6] \qquad F(s,z) = [P(s,z) - \delta_{s0}]/P(0,z)$$

and

$$[7] \qquad \sum_s P(s,z) = (1 - z)^{-1}$$

In the case of a single jump time τ, eq. [3] leads to essentially the same result (17) as that of the usual diffusion treatment, namely, $I(t)$ becomes time-independent after a few steps.

Let us now assume that at each lattice point the walker has a choice of jump time from a set of jump times, τ_1, τ_2, ..., with corresponding probabilities, C_1, C_2, ... Namely, the walker jumps to adjacent sites in jump time τ_i with probability C_i, which is normalized as

$$[8] \qquad \sum_i C_i = 1$$

In this case, the flux is given by

$$[9] \qquad I(t) = \sum_{n,s} \frac{n!\prod_i C_i^{n_i}}{\prod_i n_i!} F_n(s)\delta(t - \sum_i n_i\tau_i)$$

where

$$[10] \qquad \sum_i n_i = n$$

The summation over n in eq. [9] includes all possible combinations of n_i with the restriction [10]. Using the relationships

$$[11] \qquad \sum_{\{n_i\}} \frac{n!\prod_i C_i^{n_i}}{\prod_i n_i!} = \left(\sum_i C_i\right)^n = 1$$

and

$$[12] \qquad \delta\left(t - \sum_i n_i\tau_i\right) = \frac{1}{2\pi i} \times \int_{C-i\infty}^{C+i\infty} \exp\left[u\left(t - \sum_i n_i\tau_i\right)\right] du$$

eq. [9] can be written as

$$[13] \qquad I(t) = \frac{1}{2\pi i}\sum_{n,s} F_n(s) \times \int_{C-i\infty}^{C+i\infty} \left[\sum_i C_i\, e^{-u\tau_i}\right]^n e^{ut}\, du$$

At this point, let us assume that the jump time τ_i has a continuous spectrum so that

$$[14] \qquad \sum_i C_i\, e^{-u\tau_i} \rightarrow \int_0^{\infty} \psi(\tau)\, e^{-u\tau}\, d\tau$$

where $\psi(\tau)$ is a continuous jump – time distribution function. The rhs of [14] is the Laplace transform of $\psi(\tau)$, so that we define

$$[15] \qquad \phi(u) = \int_0^{\infty} \psi(\tau)\, e^{-u\tau}\, d\tau$$

Using eqs. [4], [13], [14], and [15],

$$[16] \qquad I(t) = \sum_{n,s} \frac{1}{2\pi i} \int F_n(s)[\phi(u)]^n e^{ut}\, du = \sum_s \frac{1}{2\pi i} \int F(s, \phi(u))\, e^{ut}\, du$$

Equation [16] is equivalent to

$$[17] \qquad I(u) = \int_0^{\infty} I(t)\, e^{-ut}\, dt = \sum_s F(s, \phi(u)) = \frac{1}{[1 - \phi(u)]P(0, \phi(u))} - 1$$

where, in the last step, eqs. [6] and [7] are used.

Since the generating function $P(s,z)$ is a property of the lattice, the effect of the disordered structure comes only from $\phi(u)$ or $\psi(t)$. By analyzing the transient photocurrents in amorphous films, Scher and Montroll (18) discovered that the following asymptotic form for $\psi(t)$ describes the experiment best,

$$[18] \quad \psi(t) \sim [At^{1+\alpha}\Gamma(1-\alpha)]^{-1} \qquad 0 < \alpha < 1$$

where Γ is the gamma function, A and α are constant parameters. The corresponding asymptotic form for $\phi(u)$ is given by

$$[19] \quad \phi(u) \sim 1 - u^{\alpha}/A \qquad z \to 1$$

Using eq. [16], one gets

$$[20] \quad P(0,z) \to 1.516 \qquad z \to 1$$

$$[21] \quad I(u) \sim \beta A u^{-\alpha} \qquad \beta = 0.659$$

The time-dependent flux has the form

$$[22] \quad I(t) \sim \frac{\beta A t^{\alpha-1}}{\Gamma(\alpha)}$$

Using eq. [1], the time-dependent scavenging rate constant is given by

$$[23] \quad k(t) \sim a^3 \beta A t^{\alpha-1}/\Gamma(\alpha) \equiv Bt^{\alpha-1}$$

Substituting eq. [20] into eq. [2], one gets

$$[24] \quad \ln \ln (n_0/n(t)) = \ln (BC_s/\alpha) + \alpha \ln t$$

Up to this point of derivation, the scavenging reaction is assumed to be diffusion-controlled. A more general model allows jumps to the reacting site which have probability p for reaction and probability $(1 - p)$ for survival to jump away from the reaction site. As far as the long-time asymptotic flux is concerned, this probability of reaction will simply scale down the magnitude of B in [24] (17). The parameter B therefore depends upon the nature of the solvent as well as that of the scavenger in general.

Equation [24] was the basis for analyzing the scavenging of trapped electrons in our previous work and will be applied to a wider class of systems and phenomena in this work.

The physical origin for the jump–time distribution [18] is the fluctuation in jump distances and trap depths. Scher and Montroll (18) neglected the latter fluctuation. Therefore, in the spirit of Scher and Montroll, the parameter α can be independent of temperature at sufficiently low temperatures because of the possibility of phonon-assisted tunneling. In general, one expects some kind of temperature dependence of α when the fluctuation in trap depth is included. It is not possible to predict the detailed form of temperature dependence without further specification of the statistical characteristics of the disordered structure itself. However, from the general structure of the continuous-time-random-walk, one can say that the temperature dependence of the decay kinetics will manifest itself on a relatively longer time scale of observation when the electrons in deeper traps begin to participate in the decay kinetics, while at earlier times the electrons can choose fast and easy passages towards the sink so that the temperature dependence is likely to be weak or even absent.

Experimentally, α is sensitive to the details of sample preparation and quantitative reproducibility from one laboratory to another is not to be expected. The preparation of glasses by plunging samples into liquid nitrogen and omission of annealing are probably responsible for much of the dispersion (small α) which has been observed.

In analyzing the decay of trapped electrons in deep traps, e_s^-, the sinks are the scavengers, while for the spectral relaxation of the electrons in shallow traps, e_t^-, the sinks are the deep traps themselves for undoped systems. As we demonstrate later, the reactivity of e_t^- with some scavengers is much less than that of e_s^-.

The preceding considerations apply to the recombination of coulombically correlated charge pairs but there is a superimposed time-dependent effect arising from the initial radial distribution. In the following section we have tried to avoid experimental results which involve this complication.

Experimental Evidence

There are many data in the early literature of trapped electrons in organic glasses which provide qualitative information for the electron transport process. Unfortunately the zero-time yield is usually unknown for γ irradiation. This problem is not serious for methyltetrahydrofuran (MTHF) at 77 K because decay of e_t^- is very slow in the undoped system. The epr data of Smith and Pieroni (19) can be fitted by eq. [24] but it is not clear whether the rate-controlling process involves trap-to-trap hopping or recombination of coulombically correlated charge pairs.

Partial but convincing support for the applicability of Scher–Montroll CTRW theory is provided by measurements of electron drift mobility in MTHF at 77 K by Huang *et al.* (20). Following 8 μs light pulses, the arrival of electrons at the anode tailed for ~250 μs after a nominal transit time of 130 μs. The basic requirement for application of S–M theory is satisfied since electrons must be trapped, detrapped, and retrapped. The initial traps are abundant and shallow and a distribution of trap depths assures a

gradual increase of trap depth. The transport is activated in the range 36–77 K with $E = 0.0035$ eV. There is little or no temperature dependence between 30 and 4 K.

Kevan (21) found that the photobleaching quantum efficiency in γ-irradiated MTHF is very small at >900 nm and maximizes at 520 nm, both at 4 K and 77 K, but the efficiency is still only ~0.2. The amplitudes of the maxima are substantially equal. This result implies that retrapping photoelectrons by the matrix is activationless in this range of temperature.

Time-dependent electron solvation in 32 mol% methanol – 68 mol% MTHF by Ogasawara *et al.* (22) following 40 ns pulses contains features of particular interest. One is that the system clearly contains a greater variety of traps than either pure component. Absorbance A is initially greatest at ~1250 nm and later is greatest at ~600 nm at 109 K. Another is that the absorbance decay is nearly first order at 116 K but deviates considerably beyond ~50% decay at 106 K. Also, there is optical evidence for intermediate solvation configurations. The authors concluded that the results did not support electron tunneling and accepted diffusive reaction of the electron with methanol clusters, involving more than one step. These features are qualitatively those needed for applying the CTRW model, although a somewhat lower temperature is certainly desirable. Data have been taken from the smooth curve reported for 106 K (22) and are presented in Fig. 1. The results suggest that after a short transition period, for which the decay seems to be nominally

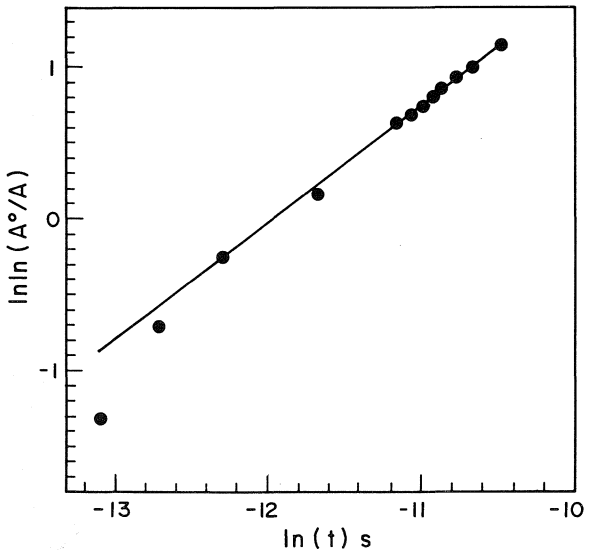

FIG. 1. The dependence of the optical absorbance A at 1250 nm on time for 32% methanol – 68% MTHF at 106 K from the data of Ogasawara *et al.* (22). The slope is 0.80.

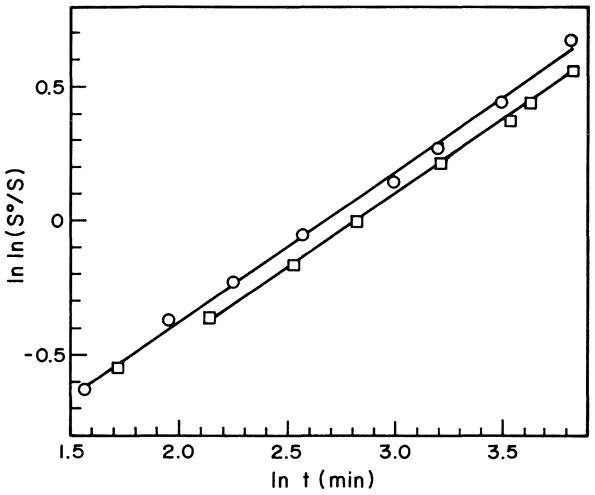

FIG. 2. The dependence of the epr signal amplitude S on time for 3MP containing 4.6 mol% trimethylamine and 2×10^{-2} mol% TMPD at 77 K following ^{60}Co-irradiation (●) and photo-ionization (■) from the work of Lin *et al.* (24). The slopes are 0.51.

first order, the decay does follow the CTRW model which is most clearly exhibited at long time.

There are few data for 3-methylpentane (3MP) in the range >1 s which are useful here but a simple qualitative demonstration of e_t^- migration is of interest. Photoionization of 2×10^{-3}% tetramethyl-*p*-phenylenediamine (TMPD) in 3MP with 0.20% biphenyl at 77 K was followed by linear increase in anion absorbance A with decrease in e_t^- absorbance. No measurable recombination occurred (23). The value of $A_0(e_t^-)$ cannot be estimated easily, but $A_\infty(\phi_2^-)$ can be. The plot of $\ln \ln A_\infty/(A_\infty - A_t)$ for ϕ_2^- vs. $\ln t$ (not shown) is adequately linear with $\alpha = 0.41$.

Lin *et al.* (24) used 3MP containing 4.6 mol% trimethylamine (to retard decay of e_t^-) with 0 and 2×10^{-2}% TMPD. After γ irradiations at 77 K, decay of e_t^- (measured by epr) is expected to arise almost entirely by impurity trapping on TMPD (23) and eq. [24] should apply. The decays of e_t^- following γ irradiation and photoionization are compared in Fig. 2. Signal amplitudes S were in arbitrary units and the zero of time used here is that reported. The decay is slower than for 3MP alone and only the comparison of the two curves is considered significant. The slope, $\alpha = 0.51$, is not affected by the mode of ionization.

Klassen, Gillis, and Teather (25) have measured spectral changes in 3MP and 3-methylhexane (3MH) at 76 K following pulsed irradiations. There was marked decay of absorbance at 2240 nm and there was no growth of absorbance at any wavelength for both systems. Since decay at 1500 nm, near the

maximum of the relaxed spectrum, was much less than that at 2240 nm, it is possible that the spectral relaxation consists of a transfer of e_t^- from shallow to deep traps. Using the data for 2240 nm, where there is little overlap from the relaxed spectrum, the results in Fig. 3 yield slopes of $\alpha = 0.11$ and 0.12 for undoped 3MP and 3MH from the curves in their Figs. 4 and 2, respectively.

In 3MP doped with 3.4 m*M* biphenyl, an electron trap, the slope for decay of 2240 nm absorption in Fig. 3 is 0.14. From the correlated growth at 410 nm due to biphenyl anion in Fig. 3, $\alpha = 0.10$. These data are taken from their Table 1, using $\text{Å} = 0.390$ at 2240 nm and $\text{Å} = 0.397$ at 410 nm. From this line and that for undoped 3MP, $\Delta \ln (BC/\alpha) = 0.42$, and $C(\text{biphenyl})/C(3\text{MP}) = 1.5$, or $C(3\text{MP}) = 5.2$ m*M*, where $C(3\text{MP})$ represents the "concentration" of self-trapping sites.

Decay of absorbance for e_t^- at 2240 nm in both doped and undoped 3MP and growth of the anion, both characterized by $\alpha = 0.11$, provides evidence that decay at 2240 nm involves migration by hopping on a rather long time scale.

Measurements of mobility in 3MP by time-of-flight correspond to a diffusion coefficient $\sim 10^{-4}$ cm^2/s (26). Consequently the states which contribute to the more mobile species are not those involved in the spectral decay just discussed. The two processes are qualitatively, but not quantitatively, similar. It must be remembered that only a quite small fraction of the electrons present contribute to the measured current. They occupy only the shallowest traps and observations are limited to events at $< 10^{-3}$ s.

After ~ 130 ns electron pulses at 76 K, Kevan observed that the absorbance at 1400 nm in C_2H_5OD decays linearly in $\ln(t)$ from $\sim 10^{-7}$ to $\sim 10^{-2}$ s (27). In C_2D_5OD + 20 mol% D_2O the decay at 1300 nm is very similar and the slopes are the same. Comparable results were obtained at 1800 nm and 1700 nm with slopes unchanged. Choosing the measurements at 1400 nm for C_2H_5OD and 1300 nm for C_2D_5OD + D_2O which are close to λ_{max}, the data are presented in Fig. 4 in terms of eq. [24] with slopes 0.28 and 0.22.

Miller *et al.* (28) have examined several undoped alcohols at 77 K in the range 10^{-7} to 10^2 s after pulsed irradiation. At the longest wavelength, 950 nm, the decay does not conform to eq. [24], suggesting that more than a single species of e_t^- is involved. The growth for ethanol at 550 nm has been chosen for examination because only one spectral component is expected, because there is an adequate range of absorbance and because there are no

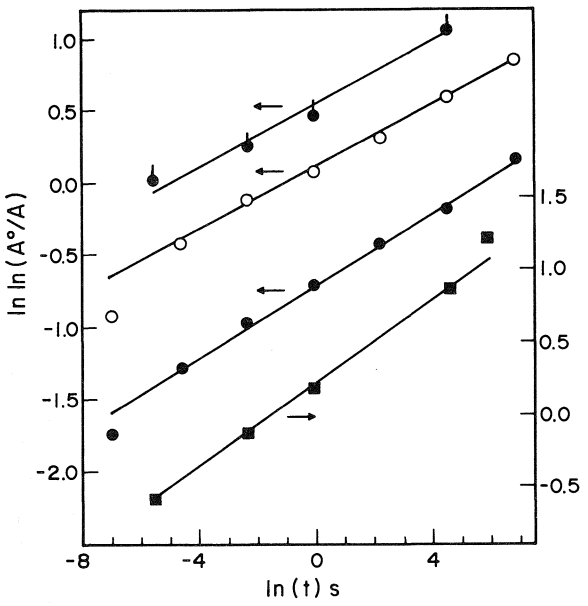

FIG. 3. The decay of absorbance in undoped 3MP (○) and 3MH (●) at 2400 nm and 76 K after pulsed irradiation. Similar data for 3MP containing 3.4 m*M* biphenyl at 2240 nm (■) and growth of biphenyl anion at 410 nm (◆), from the work of Klassen *et al.* (25). Slopes are 0.10, 0.11, 0.12, and 0.14 in order, top to bottom.

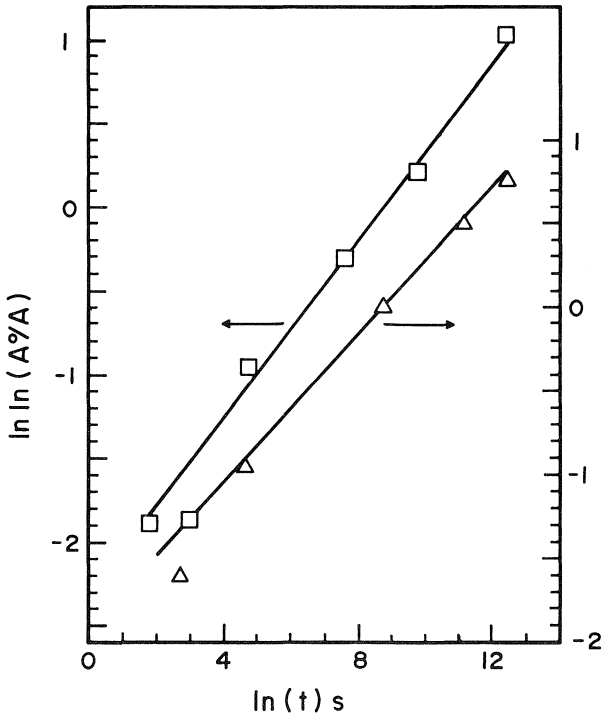

FIG. 4. The decay of absorbance of e_s^- at 1400 nm in C_2H_5OD (□) and at 1300 nm for C_2D_5OD + 20% D_2O (△), both at 76 K after ~130 ns pulsed irradiations, from the work of Kevan (27). The slopes are 0.28 and 0.22.

significant irregularities, such as appear for some of the other data. Results appear in Fig. 4.

Klassen *et al.* (29) have measured spectral shifts in ethanol at 76 K. Their results for decay of e_t^- at 1400 nm are not well described by eq. [24] when A_0 is taken as the measured value from their Fig. 3. For the yield at 200 ns after the onset of a 140 ns pulse, $G\varepsilon = 3.14 \times 10^4$ where G is the number of electrons per 100 eV and ε is the extinction coefficient in $M^{-1}\,cm^{-1}$. We find some improvement for $G\varepsilon = 4.2 \times 10^4$ at time zero. Results treated in this way, interpolated from their smooth curve, also appear in Fig. 5. The slope, 0.20, agrees adequately with the results from Miller *et al.* (27) with slope 0.18.

Data for decay of e_s^- at 750 nm in methanol/water (95/5) at 77 K, reported by Kevan (30), are included in Fig. 5.

Ogasawara and Kevan (31) have examined electron solvation kinetics in ethanol containing 0.1 M NaOH from 83 to 123 K by ruby laser photoionization of 5×10^{-4} M β-naphtholate. Decay at 123 K was simple first order. The more complicated decay at lower temperatures was attributed to a molecular reorientation mechanism. The results for growth of solvated electron absorption at 580 nm following ~20 ns ruby laser pulses appear in Fig. 6, for $A_\infty = 0.196$, at 108.0, 98.0, 92.8, 87.7, and 83.1 K (from top to bottom), the slopes being 0.134, 0.104, 0.099, 0.081, and 0.062. Although there are no data for 77 K, α is expected to be very much less than the values from Fig. 5. The difference is probably caused by the presence of 0.1 M NaOH and an increased dispersion of trap depths.

Data for decay of e_t^- in 1-propanol at 1300 nm and growth of e_s^- at 500 and 550 nm, all at 77 K, have already been published (9). For all alcoholic systems examined, $\alpha \simeq 0.2$ for both growth and decay, excepting Fig. 6.

Miller (*5a*) has measured the spontaneous decay of absorbance at 750 and 875 nm for undoped aqueous 6 M NaOH at 77 K following pulse irradiation. Some of this oscillator strength was transferred to the 400–500 nm region where there is no decay. Although A is approximately linear in ln t at both wavelengths, the slopes are not equal. These data are presented in Fig. 7 in terms of eq. [24]. The curves have the same intercept and are parallel with slope $\alpha = 0.11$. Therefore, one initial state, one final state. It has already been shown that nearly equal slopes have been obtained for decay at 550 nm and 77 K for the same matrix doped with electron acceptors (6). The value of α does not depend upon the

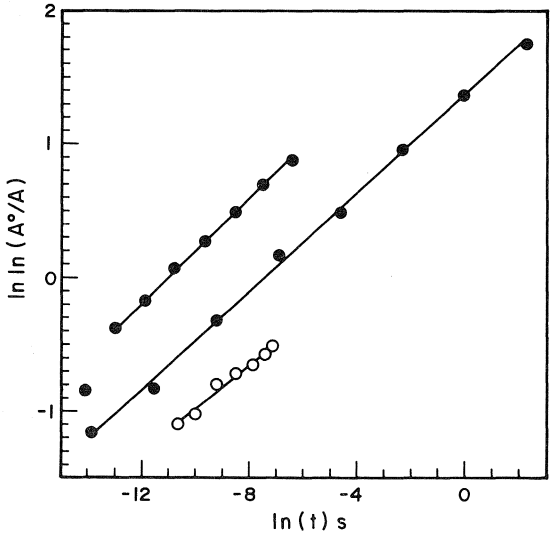

FIG. 5. The growth of optical absorbance of e_s^- in ethanol at 550 nm (●) from Miller *et al.* (28); decay of e_s^- in ethanol at 1400 nm (■) from Klassen *et al.* (29); decay of e_s^- in 95 methanol – 5 water at 750 nm (○) from Kevan (30), all at 77 K. The slopes are 0.20, 0.18, and 0.17, in order.

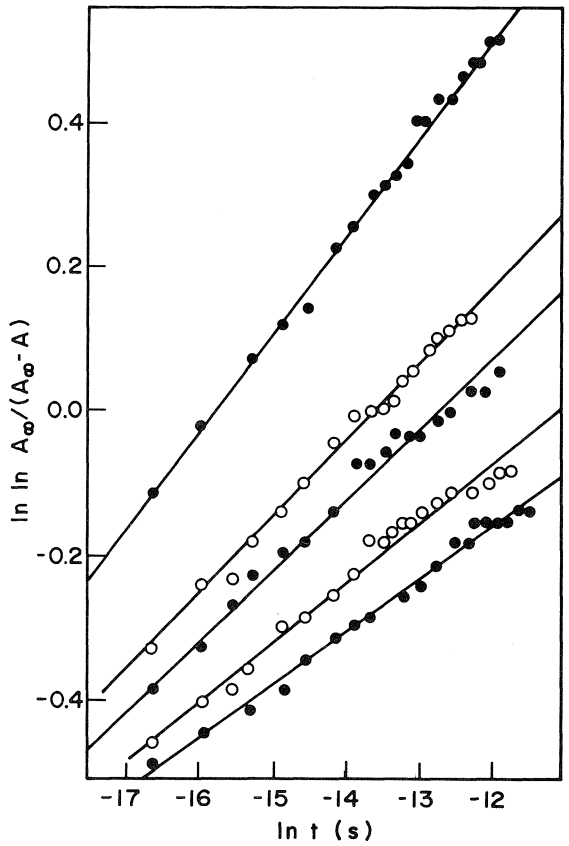

FIG. 6. The decay of e_s^- at 580 nm at 108.0, 98.0, 92.8, 87.7, and 83.1 K (top to bottom) in ethanol containing 0.1 M NaOH following ~20 ns ruby laser photoionization of 5×10^{-4} M β-naphtholate ion. The data are taken from the work of Ogasawara and Kevan (31).

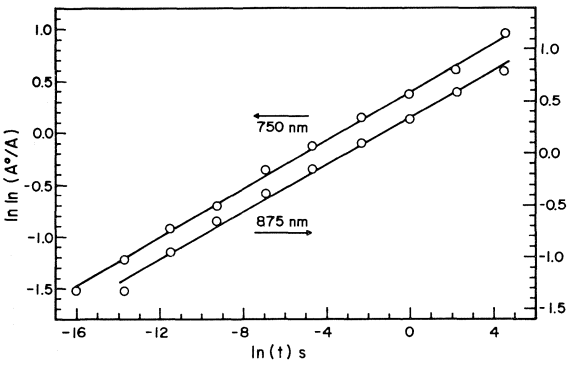

FIG. 7. The decay of e_s^- in 6 *M* NaOH at 750 nm and 875 nm at 77 K from the work of Miller (*5a*). The slopes are 0.12.

impurity or its concentration, although the rate of decay increases with increased concentration.

Pulse photoionization of γ-irradiated glassy 10 *M* NaOH has been used by Huang *et al.* (32) to measure electron mobility from transit times. Long current–time tails were attributed in part to weak trapping. The onset of this decrease was best resolved empirically on a log (time) scale. This evidence supports the dispersive hopping transport mechanism in alkaline glasses, including earlier work on trapped electron scavenging (6).

Discussion

Self-trapping Process in Disordered Media

The self-trapping process involves a radiationless transition from the quasi-free state to a localized electron state. In the Introduction, it was pointed out that the so-called static pre-existing trap cannot capture an electron non-radiatively. To elaborate in terms of a schematic diagram shown in Fig. 8*a*, the total energy of the system (i.e. an excess electron plus the medium) is plotted against the configuration coordinate which characterizes the inter- and intramolecular configurations around the trap. The pre-existing trap implies that the energy minima for the quasi-free state (curve I) and the trapped state (curve II) have the same equilibrium configuration R_0, and the same curvature. The transition rate for I → II would be zero, because the vibrational overlap is equal to zero due to the orthogonality of the vibrational wavefunctions. In order to have a finite transition rate, it is essential to destroy the orthogonality of the vibrational wavefunctions between the initial and final states. This can be achieved either by displacing the potential minimum of curve II with respect to that of I or changing the curvature (the force constant) of the curve II. In general, a finite coupling between the electron and the nuclear motion (i.e. electron–phonon coupling) causes both of these effects. For simplicity, assume that the only effect of the electron–phonon interaction is to shift the potential minimum ("displaced oscillator model"), as shown in Fig. 8*b*. Because of the non-orthogonality of vibrational wavefunctions for curves I and II, the transition rate is now non-vanishing. It can also be seen that the displaced oscillator model predicts a finite energy barrier (activation energy) for the self-trapping process. Toyozawa (33) has already pointed out the presence of a finite activation energy for self-trapping by a finite-range deformation potential. If the thermal trap depth, E_b of Fig. 8*b*, is constant throughout the system, self-trapping would be inefficient at low temperatures (~77 K) for a barrier height of ~2 kcal. When there is a fluctuation in the trap depth from site to site because of the disordered structure of the system, the crossing point of curves I and II can fall in the zero-point vibrational amplitude of curve I at certain sites, as shown by the dotted curve in Fig. 8*b*. The self-trapping process would be activationless and quite efficient. It depends upon the statistics of the energy level distribution for the localized states. Physically, this means that certain sites trap electrons much more efficiently than other sites which have a finite barrier. The essential physical feature which is required for these preferred trapping sites is provided by the disordered structure of the medium. Crystals at low temperature do not trap electrons efficiently.

The preceding discussion of non-radiative transitions to deeper traps has not included consideration of dipolar relaxation of the medium (34). Such a mechanism is quite plausible for localized electrons

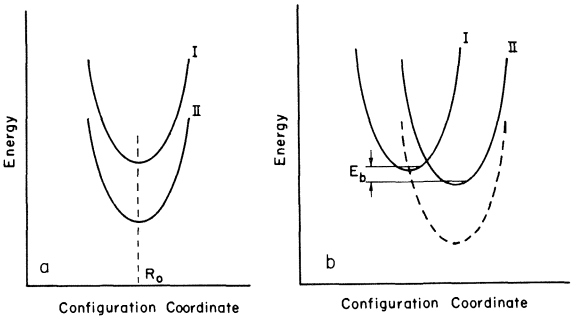

FIG. 8. (*a*) A schematic energy diagram for the quasi-free state I and the trapped state II, as a function of configuration coordinate. The transition probability for I → II is zero in this case. (*b*) A schematic energy diagram for the quasi-free state I and the trapped state II, when there is a finite electron phonon interaction at the trapping site. The transition probability for I → II is non-zero, due to the non-orthogonality of vibrational wavefunctions for I and II. Because of the energy fluctuation for the state II from site to site, there is a finite probability of finding a site where the curve crossing falls in the zero-point amplitude of curve I, as shown by the dotted curve. Such a site traps the quasi-free electron preferentially.

in liquids but it is not clear that it makes a measurable contribution in rigid glasses at low temperatures. Formation of e_s^- must be triggered by short-range electron–phonon interactions at preferred sites ("pre-existing traps") since they are observed at early time and low temperature. Relaxation of molecular configurations are expected on this time scale. The very small subsequent change in the visible spectrum, when it can be fully resolved at 77 K, requires either that dipolar relaxation is nearly complete at $\sim 10^{-8}$ s, or that it is not yet appreciable at $> 10^2$ s. Even if the former proves to be correct, our basic model for the primary localization mechanism is unaffected.

Reactivities of Localized Electrons

According to the work of BGK (4), electrons in shallow traps (the infrared electrons, e_t^-) in aqueous glasses do not react efficiently with some electron scavengers, while the solvated electrons (e_s^-) do react with the same scavengers at appreciable rates. For the same scavenger, the reaction of e_t^- is of course more exothermic than that of e_s^-. The electronic coupling matrix for e_t^- becomes smaller than that of e_s^- because of the diffuse electron wavefunction for e_t^-. Furthermore, the fact that e_t^- is weakly coupled with low-frequency medium modes ($1 \sim 10\ cm^{-1}$) and e_s^- is strongly coupled with both high-frequency molecular modes and the medium modes, in addition to the extra exothermicity for the e_t^- reaction, will make the scavenging rate for e_t^- even smaller compared to that for e_s^-.

BGK (4) also reported the similarly remarkable difference of reactivities of localized electrons with H_3O^+ in aqueous glasses. While e_t^- does not react detectably with H_3O^+, e_s^- reacts with H_3O^+ as expected. Although the same qualitative interpretation applies also for this case, one should not consider these reactions as simple electron transfer processes. Unlike other electron scavengers, the hydrated proton migrates through an efficient proton transfer from one water molecule to another. It is well-known that the reaction rate constants for proton transfer to anions are very large (35). It is tempting to suggest that the reaction mechanism for $e_s^- + H_3O^+ \rightarrow H + H_2O$ is also the proton transfer. However, the detailed nature of the reaction coordinate in the potential hypersurface for this reaction is not clear because of the limited information concerning the structural details of e_s^-. Nevertheless, it is qualitatively clear that such a possibility exists if the electron in a cavity is strongly coupled with high-frequency intramolecular vibrational modes, thereby resembling an anion, in addition to low-frequency solvent modes. On the other hand, if the electron is coupled weakly with low-frequency solvent modes only, as in the case of e_t^-, there is no effective way of dissipating the excess energy in the process of H atom formation. The details of electron–phonon coupling are also crucial in understanding some features of the absorption spectra of solvated electrons (e.g. width, temperature-dependence, isotope effect, etc.) (36).

It is to be noted that application of the barrier-penetration model to the reactions of e_s^- and e_t^- with electron scavengers or H_3O^+ would predict exactly the opposite result of what was observed by BGK (4).

The time-dependence of spectral intensity for trapped electrons can be explained quantitatively over at least several decades of time in a wide range of substances.

The apparent absence of reactivity for e_t^- with some scavengers, including protons, can be understood qualitatively in terms of the inherent inefficiency in converting a relatively large electronic energy into a large number of low-frequency phonons by radiationless transitions.

The central role of electron–phonon coupling is emphasized for understanding the initial electron localization, the meaning of the "pre-existing" trap, and electron transfer processes.

It is concluded that the so-called spectral relaxation for e_t^- in rigid glasses involves both electron transport among shallow traps and non-radiative transitions to deeper traps. Dipolar relaxation may occur subsequently but it does not affect the basic model.

1. H. HASE, M. NODA, and T. HIGASHIMURA. J. Chem. Phys. **54**, 2975 (1971).
2. G. V. BUXTON, H. A. GILLIS, and N. V. KLASSEN. Chem. Phys. Lett. **32**, 533 (1975).
3. D. C. WALKER. Can. J. Chem. **55**, 1987 (1977).
4. G. V. BUXTON, H. A. GILLIS, and N. V. KLASSEN. Can. J. Chem. **54**, 367 (1976).
5. (*a*) J. R. MILLER. J. Phys. Chem. **75**, 1070 (1975); (*b*) F. S. DAINTON, M. J. PILLING, and S. A. RICE. J. Chem. Soc. Faraday Trans. I, **71**, 568 (1975).
6. W. H. HAMILL and K. FUNABASHI. Phys. Rev. B**16**, 5523 (1977).
7. J. JORTNER. Can. J. Chem. **55**, 2132 (1977).
8. (*a*) G. V. BUXTON and K. G. KEMSLEY. J. Chem. Soc. Faraday Trans. I, **72**, 466 (1976); (*b*) J. H. BAXENDALE and P. H. G. SHARPE. Chem. Phys. Lett. **39**, 401 (1976); (*c*) H. A. GILLIS, G. G. TEATHER, and G. V. BUXTON. Can. J. Chem. **56**, 1889 (1978).
9. K. FUNABASHI and W. H. HAMILL. Chem. Phys. Lett. **56**, 175 (1978).
10. J. ULSTRUP and J. JORTNER. J. Chem. Phys. **63**, 4358 (1975).
11. N. R. KESTNER, J. LOGAN, and J. JORTNER. J. Phys. Chem. **78**, 2148 (1974).
12. R. KUBO and Y. TOYOZAWA. Prog. Theoret. Phys. **13**, 160 (1955).
13. V. AMBEGAOKAR, B. I. HALPERIN, and J. S. LANGER. Phys. Rev. B**4**, 2612 (1971).

14. D. G. THOMAS, J. J. HOPFIELD, and W. M. AUGUSTYNIAK. Phys. Rev. **140**, A202 (1965).
15. R. M. NOYES. Progress in reaction kintics. Vol. 1. *Edited by* G. Porter. Pergamon, New York. 1961. p. 129.
16. E. W. MONTROLL and G. H. WEISS. J. Math. Phys. **6**, 167 (1965).
17. W. H. HELMAN and K. FUNABASHI. J. Chem. Phys. **66**, 5790 (1977).
18. H. SCHER and E. W. MONTROLL. Phys. Rev. B**12**, 2455 (1975).
19. D. R. SMITH and J. J. PIERONI. Can. J. Chem. **43**, 876 (1965).
20. T. HUANG, I. EISELE, D. P. LIN, and L. KEVAN. J. Chem. Phys. **56**, 4702 (1972).
21. L. KEVAN. J. Phys. Chem. **76**, 3830 (1972).
22. M. OGASAWARA, L. KEVAN, and H. A. GILLIS. Chem. Phys. Lett. **49**, 549 (1977).
23. J. B. GALLIVAN and W. H. HAMILL. J. Chem. Phys. **44**, 2378 (1966).
24. J. LIN, K. TSUJI, and F. WILLIAMS. Chem. Phys. Lett. **1**, 66 (1967).
25. N. V. KLASSEN, H. A. GILLIS, and G. G. TEATHER. J. Phys. Chem. **76**, 3847 (1972).
26. Y. MARUYAMA and K. FUNABASHI. J. Chem. Phys. **56**, 2342 (1972).
27. L. KEVAN. J. Phys. Chem. **79**, 2847 (1975).
28. J. R. MILLER, B. E. CLIFFT, J. N. HINES, R. F. RUNOWSKI, and K. W. JOHNSON. J. Phys. Chem. **80**, 857 (1976).
29. N. V. KLASSEN, H. A. GILLIS, G. G. TEATHER, and L. KEVAN. J. Chem. Phys. **62**, 2474 (1975).
30. L. KEVAN. J. Chem. Phys. **56**, 838 (1972).
31. M. OGASAWARA and L. KEVAN. J. Phys. Chem. **82**, 378 (1978).
32. T. HUANG, I. EISELE, and L. KEVAN. J. Chem. Phys. **59**, 6334 (1973).
33. Y. TOYOZAWA. Polarons and excitons. *Edited by* C. G. Kuper and G. D. Whitfield. Plenum Press, New York. 1962. p. 211.
34. L. KEVAN. Advances in radiation chemistry. Vol. 4. *Edited by* M. Burton and J. L. Magee. John Wiley and Sons. 1973. p. 181.
35. M. EIGEN, W. KRUSE, G. MAASS, and L. DEMAYER. Progress in reaction kinetics. *Edited by* G. Porter. Pergamon, New York. 1961.
36. K. FUNABASHI, I. CARMICHAEL, and W. H. HAMILL. J. Chem. Phys. **69**, 2652 (1978).

The preparation and properties of some thioacylmethylenethiazolines and isothiazolines

D. M. McKINNON, M. E. HASSAN, AND M. S. CHAUHAN

Department of Chemistry, University of Manitoba, Winnipeg, Man., Canada R3T 2N2

Received June 1, 1978

D. M. McKINNON, M. E. HASSAN, and M. S. CHAUHAN. Can. J. Chem. **57**, 207 (1979).

Thiazoline-2-thiones and isothiazoline-3-thiones are converted into the 2- or 3-thiophenacylidene derivatives, respectively, by reaction with phenacyl bromide, treatment with pyridine, and thionation. The former compounds react with dimethyl acetylenedicarboxylate to form mono- and diadducts as well as some decomposition products. Attempts to demonstrate valency isomerism in the 3-thiophenacylideneisothiazoline derivatives were unsuccessful.

D. M. McKINNON, M. E. HASSAN et M. S. CHAUHAN. Can. J. Chem. **57**, 207 (1979).

On transforme les thiazolinethiones-2 et les isothiazolinethiones-3 respectivement en dérivés thio-2 (ou -3) phénacylidène par une réaction avec le bromure de phénacyle, suivie d'un traitement par la pyridine et d'une thionation. Les premiers composés réagissent avec l'acétylènedicarboxylate de méthyle pour former les mono- et les di-adduits de même que des produits de décomposition. Des essais tentés dans le but de démontrer l'existence d'une isomérie de valence conduisant à des dérivés thiophénacylidène-3 isothiazolines se sont avérés infructueux.

[Traduit par le journal]

Isothiazoline-3-thiones (**1**) are known to undergo cycloaddition reactions with dimethyl acetylenedicarboxylate to provide 2-thioacylmethylenethiazolines (**2**) (1), which react by further 1,4-cycloaddition reactions of the exocyclic thioacylmethylene group with the reagent to form thiopyranospirothiazole derivatives (**3**). Although under the conditions of this reaction none of the thiazoline intermediates **2** were isolated, two similar compounds, 2-thiophenacylidenethiazolines, were obtained via an alternative synthesis.

To provide some further information on the reaction of the 2-thioacylmethylenethiazolines (**2**) with acetylenic reagents, some other compounds have been synthesized from thiazoline-2-thiones by the procedure outlined below and allowed to react with dimethyl acetylenedicarboxylate.

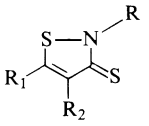

1

a R = Me, R_1 = Ph, R_2 = H
b R = R_1 = Ph, R_2 = H
c R = Me, R_1 = *p*Tol, R_2 = H
d R = Me, R_1 = R_2 = Ph

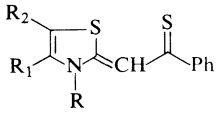

2

a R = R_1 = Ph, R_2 = H
b R = Me, R_1 = *p*Tol, R_2 = H
c R = Me, R_1 = R_2 = Ph
d R = Me, R_1 = Ph, R_2 = H
e R = Me, R_2 = Ph, R_1 = H
f R = Me, R_1, R_2 = (CH=CH)$_2$

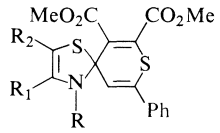

3

c R = Me, R_1 = R_2 = Ph
d R = Me, R_1 = Ph, R_2 = H
f R = Me, R_1, R_2 = (CH=CH)$_2$

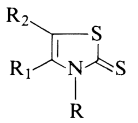

4

a R = R_1 = Ph, R_2 = H
b R = Me, R_1 = *p*Tol, R_2 = H
c R = Me, R_1 = R_2 = Ph
d R = Me, R_1 = Ph, R_2 = H
e R = Me, R_2 = Ph, R_1 = H
f R = Me, R_1, R_2 = (CH=CH)$_2$

A variety of thiazoline-2-thiones, mostly possessing aryl substituents (**4***a–e*), were prepared by reaction of the appropriate α-halogenated aldehydes or ketones with substituted dithiocarbamic acid salts according to known procedures (2). Some of these were new. In some cases, as described (2), the intermediate hydroxythiazolidinethiones were obtained initially but these dehydrated in sulfuric acid to the desired compounds. Another method of synthesis used in some cases (**4***d*, *e*) was the reaction of the α-halo aldehyde or ketone with methyl *N*-

0008-4042/79/020207-06$01.00/0

methyldithiocarbamate which afforded 3-methyl-2-methylthiothiazolium salts. The method is similar in concept to one for 1,3-dithiolium salts (3). The thione **4***f* was commercially available.

To allow elaboration of the thione function, these compounds were then allowed to react with phenacyl bromide to provide 2-phenacylthiothiazolium salts (**5**) which on treatment with anhydrous pyridine

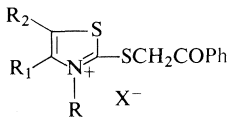

5

a R = Me, R_1 = Ph, R_2 = H, COPh = H, X = ClO_4
b R = Me, R_2 = Ph, R_1 = H, COPh = H, X = I

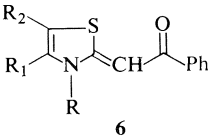

6

a R = R_1 = Ph, R_2 = H
b R = Me, R_1 = *p*Tol, R_2 = H
c R = Me, R_1 = R_2 = Ph
d R = Me, R_1 = Ph, R_2 = H
e R = Me, R_2 = Ph, R_1 = H
f R = Me, R_1, R_2 = (CH=CH)$_2$

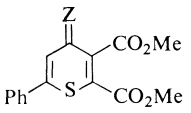

7

a Z = S
b Z = NMe
c Z = NPh

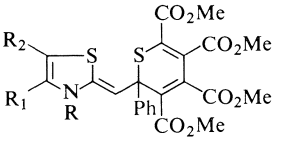

8

a R = R_1 = Ph, R_2 = H
c R = Me, R_1 = R_2 = Ph
d R = Me, R_1 = Ph, R_2 = H
e R = Me, R_2 = Ph, R_1 = H
f R = Me, R_1, R_2 = (CH=CH)$_2$

were converted into 2-phenacylidenethiazolines (**6***a–f*), according to the procedure of Knott (4). Yields were rather low and the products were contaminated with starting thiones, the result of simple dealkylation reactions of the 2-alkylthio salts **5**. Treatment of the compounds **6** with phosphorus pentasulfide afforded the desired 2-thiophenacylidenethiazolines (**2***a–f*).

In an earlier study (1) the reactions of 2-methyl-5-phenylisothiazoline-3-thione (**1***a*) with phenacylidenetriphenylphosphorane was reported to give a 2-thiophenacylidenethiazoline **2** via an unexpected 1,3-dipolar reaction. Comparison of the product from this reaction with the thiones **2***d* and **2***e* prepared above showed its identity with the former. Likewise the compound **2***b* was found to be identical to the reaction product of **1***a* with *p*-methylphenacylidenetriphenylphosphorane.

Also, treatment of 2,5-diphenylisothiazoline-3-thione (**1***b*) with phenacylidenetriphenylphosphorane gave a small yield of the thione **2***a* but 2-methyl-4,5-diphenylisothiazoline-3-thione (**1***d*) failed to react, possibly because of steric hindrance.

Treatment of the above 2-thioacylmethylenethiazolines **2** with dimethyl acetylenedicarboxylate was expected to yield spiran derivatives of type **3** as was found in the earlier study (1). Thus treatment of **2***f* with 1 equiv. of the ester afforded the expected monoadduct **3***f* as a yellowish oil. When the reaction was performed with 4 equiv. of the ester, another product was obtained in addition to the monoadduct **3***f*. On the bases of its spectral data and analysis this appears to be a diadduct. Both mono- and diadducts were isolated from a reaction of the thione **2***f* with 1 equiv. of the ester in dioxane, suggesting that the formation of the diadduct is dependent on solvent polarity. Treatment of the monoadduct with excess ester failed to give any diadduct, indicating that it is not formed from the monoadduct and that it is produced by a competing reaction. Although a number of possible structures could be advanced for the diadduct, we are inclined to favor a structure of type **8***f* on the basis of similar reactions of thiazolinethiones with the ester (5). This structure is consistent with its nmr spectrum.

Although similar results were obtained from 4,5-diphenyl-3-methyl-2-thiophenacylidenethiazoline (**2***c*) and dimethyl acetylenedicarboxylate to yield **3***c* and **8***c*, treatment of **2***d* with an equimolar quantity of the ester in boiling benzene afforded three products. The first two, which were oils, appear to be the thione **7***a* and the imine **7***b*, respectively. It appears likely that these may be formed via decomposition of a spiran intermediate of type **3***d*. Such decomposition would be possible by electron release from the thiopyran ring sulfur allowing ring opening of the thiazole ring, and has many similarities to reactions of other thiopyrans and related compounds (6, 7). The exact fate of the other parts of the spiran has not been determined.

The other product, which was crystalline, had analysis and spectral data corresponding to a diadduct **8***d*. Similar results were obtained from treatment of **2***e*, which gave **7***a*, **7***b*, and the diadduct **8***e* and from **2***a* which afforded **7***a* and **8***a*. Although **7***c* would also have been expected from the reaction we were unable to identify it in the products.

Applying the above method for conversion of a heterocyclic thione function to a thiophenacylidene function to the isothiazole series, it should be possible to prepare some compounds of the type **9** which are of some interest in studies on valency isomerism. These compounds have some structural features similar to 1,6,6a-S^{IV}-trithiapentalenes and although they do not possess the central atom capable of valency shell expansion that allows the particular symmetry properties of the latter and related isosteric compounds (8–11), it appeared possible that they might be capable of acquiring some symmetry by rapid valency tautomerism, similar to some examples described (12). For this study, compound **9***a* appeared suitable. Accordingly,

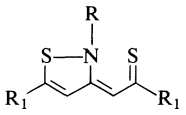

9

a R = Me, R_1 = *p*Tol
b R = Me, R_1 = Ph
c R = R_1 = Ph

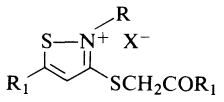

10

a R = Me, R_1 = *p*Tol, X = Br

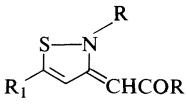

11

a R = Me, R_1 = *p*Tol

5-*p*-tolyl-1,2-dithiole-3-thione, prepared by the method of Thuillier and Vialle (13) with some modification, was converted by treatment with methyl iodide then methylamine into 2-methyl-5-*p*-tolylisothiazoline-3-thione (**1***c*), according to known methods (14, 15). Reaction of **1***c* with *p*-methylphenacyl bromide gave **10***a* which was converted into **9***a* by treatment with pyridine and thionation of the resulting ketone **11***a*. Compound **9***a* was obtained as stable red prisms. The nmr spectrum in deuteriochloroform exhibited the two *p*-tolyl methyl peaks as discrete singlets at 30°C. In 1,2,4-trichlorobenzene, over the temperature range 0 to 190°C, no coalescence of the peaks was observed, although at the higher range there was some approach of these values (to a difference of 0.3 τ). This indicates that the compound **9***a* has a rather high energy barrier to interconversion of the two identical valency tautomers, possibly because of the steric hindrance of the *N*-methyl group. The solution exhibited the original spectrum on cooling back to 0°C.

Similarly the thiones **1***a* and **1***b* were converted by reaction with phenacyl bromide, and following the above schemes, into **9***b* and **9***c*, respectively. These reactions are interesting in that although most isothiazolium salts appear to react preferentially at the ring sulfur atom with carbanions (14, 16), such a reaction is sterically impossible with the carbanions derived from the salts **10** (Scheme 1) and the subsidiary reaction site is favored.

It is obvious that compounds of the type **2**, **6**, and **8** could exist as geometrical isomers, with the thione, ketone, or the sulfide functions, respectively, being *cis* or *trans* to the thiazole ring sulfur. The involvement of *d* orbitals of this atom would certainly favor the *cis* geometry, as drawn, for the compounds of type **2** or **6** but for **8** the case is less certain.

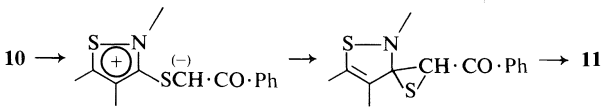

SCHEME 1

The nmr spectrum of **6***a* showed two doublets (J = 1.5 Hz) at 2.38 and 2.62 τ whereas that of **2***a* showed one doublet (J = 1.2 Hz) at 2.35 τ. The other signal is apparently buried in the aromatic proton signals. These signals in **6***a* are assigned, respectively, to the exocyclic methine proton and to the thiazoline ring proton since **6***f* shows a singlet at 2.46 τ. In **2***a* the assignments cannot be made with certainty. The magnitude of the J values are consistent with a five-bond all *trans* proton–proton coupling which would be given by *cis* geometries of the compounds **6***a* and **2***a*. Similar results were obtained from the other members of the series. Since the formation of the diadducts **8** only involves the thione function of **2**, it therefore appears likely that these may also have a *cis* geometry.

For compound **9** also, two geometrical isomers are possible but both coulombic and electronic effects favor the *cis* geometry.

Experimental

Thin-layer chromatography was performed on Camag silica gel D.S.F. 5, supplied by Terochem Laboratories. Development of plates, unless otherwise stated, was in benzene. Nuclear magnetic resonance spectra were obtained on a Varian 56/60A model spectrometer using, unless otherwise stated, deuteriochloroform containing tetramethylsilane as an internal standard. Silylation grade pyridine was used in reactions. Melting points were obtained on a precalibrated Thermopan apparatus.

*Preparation of Thiazoline-2-thiones (**4**)*

The general procedure described for other thiones (2) was used with the modification that the initially precipitated hydroxythiazolidinethiones were dissolved in 80% sulfuric acid. After ½ h, water was added and the thiones precipitated. These were recrystallized from benzene or ethanol as pale yellow or colorless needles. Three of these were new. The results are summarized below.

3,4-Diphenyl-4-thiazoline-2-thione (**4***a*) was obtained as pale yellow needles, mp 159°C (72%). *Anal.* calcd. for $C_{15}H_{11}NS_2$: C 66.91, H 4.09, N 5.20, S 23.79; found: C 66.77, H 4.00, N 4.86, S 23.51.

3-Methyl-4-*p*-tolyl-4-thiazoline-2-thione (**4***b*) was obtained as pale yellow needles, mp 110°C (60%). *Anal.* calcd. for $C_{11}H_{11}NS_2$: C 59.72, H 4.97, N 6.33, S 28.96; found: C 59.78, H 4.63, N 6.21, S 29.04.

4,5-Diphenyl-3-methyl-4-thiazoline-2-thione (**4***c*) was obtained as colorless needles, mp 178°C (65%). *Anal.* calcd. for $C_{16}H_{13}NS_2$: C 67.84, H 4.59, N 4.95, S 22.61; found: C 67.58, H 4.89, N 4.63, S 22.48.

Other thiazoline-3-thiones (**4***d–f*) were obtained by the method described (17) or by the procedure below or were commercially available.

*Preparation of 2-Methylthio-3-methyl-4-phenylthiazolium Perchlorate (**5**a)*

Methyl *N*-methyldithiocarbamate (1.21 g, 10 mmol) and

TABLE 1. Preparation of 2-phenacylidenethiazoles **6**

Compound	Yield (%)	Melting point (°C)	Formula	Analysis (%) Calculated C	H	N	S	Found C	H	N	S
6*a*	38	234	$C_{23}H_{17}NOS$	77.75	4.79	3.94	9.01	77.83	4.91	3.89	8.79
6*b*	28	164	$C_{19}H_{17}NOS$	74.26	5.53	4.56	10.42	74.11	5.59	4.58	10.44
6*c*	35	183	$C_{24}H_{19}NOS$	78.04	5.15	3.79	8.67	78.22	5.06	3.73	8.97
6*d*	40	124	$C_{18}H_{15}NOS$	73.72	5.12	4.78	10.92	73.62	5.01	4.66	10.55
6*e*	36	181	$C_{18}H_{15}NOS$	73.72	5.12	4.78	10.92	73.81	5.31	4.83	10.89
6*f**											

*Prepared before (4).

TABLE 2. Preparation of 2-thiophenacylidenethiazoles (**2**) by thionation of 2-phenacylidenethiazoles

Compound	Precursor	Yield (%)	Melting point (°C)	Formula	Analysis (%) Calculated C	H	N	S	Found C	H	N	S
2*a*	**6***a*	54	278–80	$C_{23}H_{17}NS_2$	74.39	4.58	3.77	17.25	74.11	4.62	3.83	16.99
2*b*	**6***b*	65	185*									
2*c*	**6***c*	45	167	$C_{24}H_{19}NS_2$	74.81	4.94	3.64	16.62	74.97	4.69	3.81	16.86
2*d*	**6***d*	63	144–145*									
2*e*	**6***e*	67	210	$C_{18}H_{15}NS_2$	69.85	4.85	4.53	20.62	70.01	4.65	4.51	20.73
2*f*	**6***f*	59	176–177†									

*Identical (mixture mp and ir) with an authentic sample (1).
†Literature (4) mp 175°C.

phenacyl bromide (1.99 g, 10 mmol) in ethanol (10 mL) were refluxed 24 h. The mixture was cooled and perchloric acid (0.5 mL) added. Dilution with ether afforded a pale yellow precipitate which recrystallised from acetic acid as colorless flakes, mp 132°C (81%). *Anal.* calcd. for $C_{11}H_{12}NS_2ClO_4$: C 41.05, H 3.73, N 4.35, S 19.95, Cl 11.04; found: C 40.79, H 3.69, N 4.28, S 19.62, Cl 10.89.

*Preparation of 3-Methyl-4-phenylthiazoline-2-thione (**4**d)*

The salt **5***a* (320 mg, 1 mmol) in pyridine (10 mL) was refluxed 10 min. Dilution with water and extraction with ether afforded the thione **4***d* identical (mixture mp and ir) with an authentic sample (2) (95%).

*Preparation of 2-Methylthio-3-methyl-5-phenylthiazolium Iodide (**5**b)*

α-Bromophenylacetaldehyde (1.99 g, 10 mmol) and methyl *N*-methyldithiocarbamate (1.21 g, 10 mmol) were treated as above to afford the perchlorate (**5***b*, X = ClO_4) as colorless flakes, mp 127°C (72%). Treatment of this with saturated aqueous potassium iodide solution afforded the iodide, identical with an authentic sample (17).

*Preparation of 3-Methyl-5-phenylthiazoline-3-thione (**4**e)*

This was prepared as described (17) from the methiodide (**5***b*).

*Preparation of 2-Phenacylidenethiazolines (**6**)*

Equimolar quantities of phenacyl bromide and the thiazoline-2-thiones (**4**) were allowed to react as described (4). The initially formed thiazolium salts **5** were washed with benzene to remove non-salt-like impurities, then treated with approximately five times by weight of dry pyridine, and refluxed until homogeneous. The mixtures were diluted with water and extracted with benzene. The benzene extracts were washed with dilute hydrochloric acid, water, and dried over magnesium sulfate. Evaporation gave solid products which were mixtures of phenacylidenethiazolines and thiazolinethiones. These were separated by chromatography. The results are summarized in Table 1.

*Preparation of 2-Thiophenacylidenethiazolines (**2**)*

The ketones **6** were treated with approximately twice their weight of phosphorus pentasulfide in refluxing benzene for 4 h. The solutions were filtered, washed with dilute sodium bicarbonate solution, and dried over magnesium sulfate. Evaporation yielded the thiones as red or orange crystals which were purified by chromatography. The results are summarized in Table 2.

Reaction of 2,5-Diphenylisothiazoline-3-thione with Phenacylidenetriphenylphosphorane

The thione (269 mg, 1 mmol) (1) and the phosphorane (380 mg, 1 mmol) were fused together under nitrogen at 180°C for 1½ h. The crude mixture was examined by tlc and a red band eluted. Work-up and crystallisation from benzene afforded 3,4-diphenyl-2-thiophenacylidenethiazoline (**2***a*) as red prisms, mp 278–280°C, identical (mixture mp) with those produced by the above method.

Reaction of 2-Methyl-4,5-diphenylisothiazoline-3-thione with Phenacylidenetriphenylphosphorane

The thione (15) with an equimolar quantity of the phosphorane were fused together as above. Although starting thione and triphenylphosphine oxide were recovered, no other products could be identified.

*Reaction of 2-Thiophenacylidenethiazolines (**2**) with Dimethyl Acetylenedicarboxylate in Benzene*

Reactions were performed in dry benzene under reflux for

7 h and under a nitrogen atmosphere using either equimolar quantities, or a threefold excess of ester. Evaporation of the solvent yielded oily residues which were examined by chromatography over silica gel using a benzene–chloroform 9:1 mixture as eluent. The order of elution of bands was thione (**7***a*), imine (**7***b*), monoadduct (**3**), and diadduct (**8**). The results of individual experiments are summarized below. Reactions in dioxane were performed similarly.

3-Methyl-2-thiophenacylidenebenzothiazoline (**2***f*) treated with 1 equiv. of dimethyl acetylenedicarboxylate afforded **3***f* as a yellowish oil (66%). *Anal.* calcd. for $C_{22}H_{19}NO_4S_2$: C 62.11, H 4.47, N 3.29, S 15.06; found: C 62.33, H 4.58, N 3.01, S 14.67. The nmr spectrum, τ: 7.20 and 6.45 (two 3H singlets, ester methyls), 6.22 (3H, s, *N*-methyl), 3.65 (1H, s), 2.41–3.29 (9H bands, aromatic protons); mass spectrum, M^+ calcd.: 425; found: 425.

Repeating the reaction with a threefold excess of the ester or using dioxane as a solvent gave **3***f* (51%) and **9***f* (19%) as orange plates, mp 161°C. *Anal.* calcd. for $C_{28}H_{25}NO_8S$: C 59.23, H 4.41, N 2.47, S 11.29; found: C 58.89, H 4.63, N 2.61, S 11.09. The nmr spectrum, τ: 7.8, 7.34, 6.65, 6.31 (four 3H singlets, the ester methyls), 6.15 (3H, s, *N*-methyl), 2.25–3.10 (10H bands, aromatic protons and exocyclic methine proton).

Treatment of **3***f* with the ester yielded only unchanged material.

3-Methyl-4,5-diphenyl-2-thiophenacylidenethiazoline (**2***c*) treated as above gave only **3***c* (40%) for a 1:1 ratio of reactants and gave **3***c* (18%) and **8***c* (26%) for a 1:4 ratio of reactants. Both of these products were oils and were not analysed. The mass spectra for **3***c* M^+ calcd.: 527; found: 527. For **8***c* M^+ calcd.: 669; found: 669.

3-Methyl-4-phenyl-2-thiophenacylidenethiazoline (**2***d*) treated as above afforded **7***a* as a yellow oil (30%), **7***b* as a yellow oil (22%), and **8***e* as red plates, mp 175–176°C (18%). *Anal.* calcd. for $C_{15}H_{12}O_4S_2$ (**7***a*): C 56.25, H 3.75, S 20.00; found: C 56.55, H 3.62, S 19.81. The mass spectrum, M^+ calcd.: 320; found: 320. *Anal.* calcd. for **7***b*: C 60.57, H 4.73, N 4.42, S 10.09; found: C 60.69, H 4.81, N 4.16, S 9.73. The mass spectrum M^+ calcd.: 317; found: 317. *Anal.* calcd. for $C_{30}H_{27}NS_2O_8$ (**8***d*): C 60.70, H 4.55, N 2.36, S 10.79; found: C 60.54, H 4.92, N 2.25, S 10.98. The mass spectrum, M^+ calcd.: 593; found: 593. The nmr spectrum, τ: 7.44, 6.94, 6.37, 6.10, 6.08 (five 3H singlets, methyl protons), 4.84 (1H, s, vinyl proton), 3.58 (1H, s, thiazoline proton), 2.41–2.78 (10H bands, aromatic protons).

3-Methyl-5-phenyl-2-thiophenacylidenethiazoline (**2***e*) treated as above gave **7***a* (19%) and **7***b* (26%). A third band afforded a diadduct **8***e* (32%) as orange plates, mp 182°C. *Anal.* calcd. for $C_{30}H_{27}NS_2O_8$: C 60.70, H 4.55, N 2.36, S 10.79; found: C 61.01, H 4.96, N 2.70, S 11.11. The mass spectrum, M^+ calcd.: 593; found: 593. The nmr spectrum, τ: 7.41, 6.89, 6.37, 6.42, 6.10, 6.07 (five 3H, s's, methyl protons), 4.82 (1H, s, vinyl proton), 3.56 (1H, s, thiazoline proton), 2.38–2.79 (10H bands, aromatic protons).

3,4-Diphenyl-2-thiophenacylidenethiazoline **2***a* treated as above gave a number of bands on examination by tlc. A rapidly eluted band gave **7***a* (11%). The third band afforded the diadduct **8***a* as brown prisms (31%), mp 196°C. *Anal.* calcd. for $C_{35}H_{29}NS_2O_8$: C 64.12, H 4.42, N 7.13, S 14.07; found: C 63.85, H 4.51, N 2.40, S 14.23. The mass spectrum M^+ calcd.: 655; found: 655. The nmr spectrum, τ: 6.08, 6.25, 6.41, 6.82 (four 3H s's, methyl protons), 4.72 (1H, s, vinyl proton), 3.76 (1H, s, thiazoline proton), 1.40–1.85 (15H bands, aromatic protons).

*Preparation of 2-Methyl-5-*p*-tolylisothiazoline-3-thione* **1***c*

This was made by the procedure of Thuillier and Vialle (13) except that thionation was effected in boiling benzene for 4 h. Work-up of the solution afforded 5-*p*-tolyl-1,2-dithiole-3-thione (70%), mp 120°C (lit. (13) mp 120°C). This thione was alkylated with methyl iodide in refluxing ethyl acetate. The resulting 3-methylthio-5-*p*-tolyl-1,2-dithiolium iodide on treatment with ethanolic methylamine solution (14, 15) afforded 2-methyl-5-*p*-tolylisothiazoline-3-thione (28%) as orange-yellow needles, mp 129–130°C from benzene. *Anal.* calcd. for $C_{11}H_{11}NS_2$: C 69.84, H 5.82, N 7.40, S 16.93; found: C 69.20, H 5.81, N 7.14, S 16.57. The mass spectrum, M^+ calcd.: 221; found: 221. The nmr spectrum, τ: 7.65 (3H, s, *C*-methyl protons), 6.31 (3H, s, *N*-methyl protons), 2.90 (1H, s, isothiazoline proton), 2.49–2.71 (4H bands, aromatic protons).

*Preparation of 2-Methyl-3-*p*-methylthiophenacylidene-5-*p*-tolylisothiazoline (***9***a)*

Equimolar quantities of **1***c* and phenacyl bromide were fused together gently for 10 min. The cooled product was extracted with hot benzene then the residue crystallised from ethanol as colorless needles, mp 175°C (63%). This product on treatment with pyridine as above afforded 3-*p*-methylphenacylidene-5-*p*-tolylisothiazoline (**11**) as pale yellow needles, mp 165°C (25%). The product was purified from thione contaminant by chromatography. Thionation with phosphorus pentasulfide in boiling benzene afforded a reddish oil which on chromatography gave **9***a* as red prisms, mp 161°C (42%). *Anal.* calcd. for $C_{20}H_{19}S_2N$: C 71.21, H 5.63, N 4.15, S 18.99; found: C 71.03, H 5.46, N 4.02, S 18.73. The mass spectrum M^+ calcd.: 337; found: 337. The nmr spectrum of **9***a* in $CDCl_3$, τ: 7.61, 7.52 (two 3H, s's, *p*-methyl protons), 6.32 (3H, s, *N*-methyl protons), 2.50 (1H, s, methine proton), 2.93–2.09 (9H bands, aromatic and isothiazole protons).

In 1,2,4-trichlorobenzene at 40°C the two *p*-methyl peaks were evident as two singlets at 7.51 and 7.60 τ. At 100°C, these were separated by 0.7 τ, and at 190°C, by 0.3 τ. No further temperature rise could be attempted owing to instrumental limitations.

*2-Methyl-3-thiophenacylidene-5-phenylisothiazoline (***9***b)*

This was made by the above procedure starting from **1***a* and phenacyl bromide. It was obtained as red needles, mp 160°C (18% overall yield from thione). *Anal.* calcd. for $C_{18}H_{15}NS_2$: C 69.90, H 4.85, N 4.53, S 20.71; found: C 70.25, H 4.66, N 4.55, S 20.93. The mass spectrum, M^+ calcd.: 309; found: 309.

*2,5-Diphenyl-3-thiophenacylidenethiazoline (***9***c)*

This was made by the above procedure starting from **1***b* and phenacyl bromide. Violet needles, mp 178°C (21% overall from the thione), were obtained. *Anal.* calcd. for $C_{23}H_{17}NS_2$: C 74.39, H 4.58, N 3.77, S 17.25; found: C 74.51, H 4.38, N 4.01, S 17.06. The mass spectrum, M^+ calcd.: 371; found: 371.

Acknowledgements

We wish to thank Mr. W. Buchannon and Mr. D. Buksak for the preparation of spectra, and the National Research Council of Canada for financial support.

1. M. S. CHAUHAN, M. E. HASSAN, and D. M. MCKINNON. Can. J. Chem. **52**, 1738 (1974).
2. W. J. HUMPHLETT and R. W. LAMON. J. Org. Chem. **29**, 2146 (1964).
3. D. LEAVER, W. A. H. ROBERTSON, and D. M. MCKINNON. J. Chem. Soc. 5104 (1962).
4. E. B. KNOTT. J. Chem. Soc. 916 (1955).
5. G. GUEDIN and J. VIALLE. Bull. Soc. Chim. Fr. 270 (1973).

6. E. I. G. BROWN, D. LEAVER, and D. M. MCKINNON. J. Chem. Soc. Perkin Trans. I, 1511 (1977).
7. A. GUENTHER and P. GABOR. Tetrahedron, **25**, 5995 (1969).
8. N. LOSACH. *In* Advances in heterocyclic chemistry. Vol. 13. Academic Press, New York, NY. 1971.
9. D. H. REID and J. D. SYMON. Chem. Commun. 1314 (1969).
10. I. H. POMERANTZ, L. J. MILLER, E. LUSTIG, D. MASTBROOK, E. HANSEN, R. BARRON, N. OATES, and J.-Y. TUNG CHEN. Tetrahedron Lett. 5307 (1969).
11. M. PERRIER and J. VIALLE. Bull. Soc. Chim. Fr. 4591 (1971).
12. M. S. CHAUHAN and D. M. MCKINNON. Can. J. Chem. **53**, 1336 (1975).
13. A. THUILLER and J. VIALLE. Bull. Soc. Chim. Fr. 1398 (1959).
14. D. M. MCKINNON and M. E. HASSAN. Can. J. Chem. **51**, 3081 (1973).
15. G. LE COUSTUMER and Y. MOLLIER. Bull. Soc. Chim. Fr. 3076 (1970).
16. D. M. MCKINNON, M. E. HASSAN, and M. S. CHAUHAN. Can. J. Chem. **55**, 1123 (1977).
17. G. KJELLIN and J. SANDSTRON. Acta Chem. Scand. **23**, 2879 (1969).

Allergenic α-methylene-γ-butyrolactones. A one-carbon degradation of isoalantolactone via Pummerer rearrangement of sulfoxides

JEAN-PIERRE CORBET AND CLAUDE BENEZRA

Laboratoire de Dermato-Chimie, Associé au CNRS, Université Louis Pasteur, Clinique Dermatologique, Hôpitaux de Strasbourg, 67005 Strasbourg, France

Received June 23, 1978

JEAN-PIERRE CORBET and CLAUDE BENEZRA. Can. J. Chem. **57**, 213 (1979).

Isoalantolactone and α-methylene-γ-butyrolactone were separately treated with NaSPh, transformed into sulfoxides, and rearranged under Pummerer conditions (Ac_2O + $(CF_3CO)_2O$). The Pummerer products were hydrolyzed, oxidized, and decarboxylated resulting in the formation of 13-norisoalantolactone (with migration of the *exo*-C(4) double bond into position C(4)—C(5)) on the one hand and of γ-butyrolactone on the other. The isomeric norisoalantolactone **17** is a starting material for the synthesis of ^{14}C-labelled alantolactone, **18**.

JEAN-PIERRE CORBET et CLAUDE BENEZRA. Can. J. Chem. **57**, 213 (1979).

L'isoalantolactone et l'α-méthylène-γ-butyrolactone ont été traitées séparément par NaSPh, oxydées dans les sulfoxydes correspondants et transposées dans les conditions de Pummerer (Ac_2O + $(CF_3CO)_2O$). Les produits de Pummerer ont été hydrolysés, oxydés et décarboxylés menant ainsi à la 13-norisoalantolactone (dans laquelle la double liaison en C(4) a migré en position C(4)—C(5) d'une part, à la γ-butyrolactone, d'autre part. La norisoalantolactone isomérisée **17** est un produit de départ pour la synthèse d'alantolactone marquée au ^{14}C, **18**.

In a general approach towards the mechanism of allergic contact dermatitis (ACD), we have undertaken the synthesis of ^{14}C-labelled allergens (1). α-Methylene-γ-butyrolactones seemed attractive models, since they are widespread in nature, especially in the *Compositae* family of plants and in liverworts such as *Frullania*. Two approaches have been chosen: (*a*) the synthesis of model compounds containing the α-methylene-γ-butyrolactone moiety; (*b*) introduction, through one-carbon degradation, of ^{14}C in natural sesquiterpene lactones. This paper describes this second type of approach.

Isoalantolactone **1** is a readily available lactone (isolated from *Inula helenium* as a commercial crude extract also containing an isomer, alantolactone). The initial idea was to attack the most reactive part of the molecule, the methylene group α to the lactone, and to reintroduce it (with a ^{14}C-labelled reagent) (Scheme 1).

Among several ways which have been attempted in this laboratory with varying success,[1] one seemed attractive: the Pummerer rearrangement of sulfoxides obtained via Michael addition (2, 3) to the conjugated lactone, followed by hydrolysis, oxidation, and decarboxylation (Scheme 2).

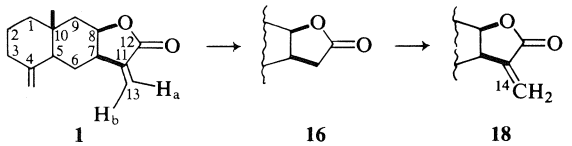

SCHEME 1

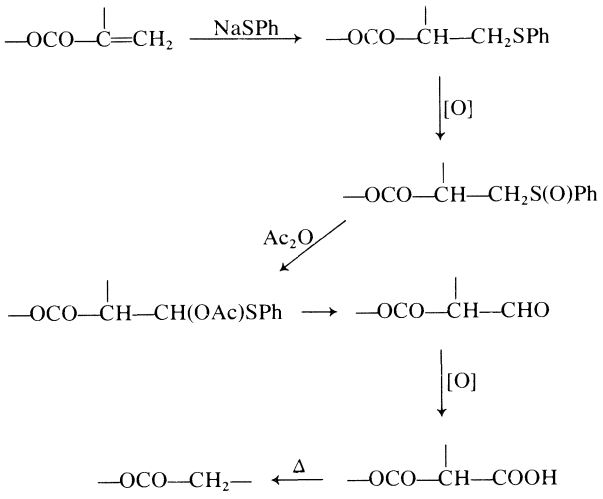

SCHEME 2

In order to understand the results for isoalantolactone, degradation of α-methylene-γ-butyrolactone (R = H) **2** (4) was attempted simultaneously.

Results and Discussion

Degradation of α-Methylene-γ-butyrolactone

Addition of sodium thiophenoxide to α-methylene-γ-butyrolactone **2** (R = H) gave the sulfide **3** which was oxidized (3) into diastereomeric sulfoxides **4** and

[1] J. L. Stampf, G. Schlewer, and C. Benezra. Unpublished results.

0008-4042/79/020213-05$01.00/0

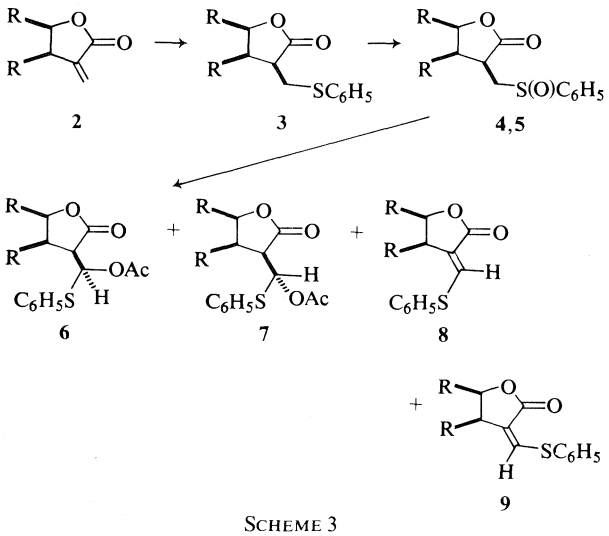

SCHEME 3

5 which were left as a mixture. Pummerer rearrangement of **4** + **5** was effected by using a mixture of Ac_2O and $(CF_3CO)_2O$ (5). This avoided heating with Ac_2O (6), which could have resulted in the thermal elimination of sulfenic acid, to give the starting α-methylene-γ-butyrolactone. This reaction gave, besides the normal Pummerer products **6** and **7**,[2] two vinyl sulfides: **8** and **9**.[3] The relative ratio of compounds **6**–**9** was approximately: 2:4:3:1. The mixture of compounds **6** and **7** was separated from **8** and **9** by column chromatography. A further separation by thin-layer chromatography gave pure **6** and **7**. Compounds **8** and **9** were analyzed as a mixture (Scheme 3).

The nmr spectra of compounds **6** and **7** (R = H) showed different coupling constants between the methine protons: —C*H*—CO— and —C*H*(OAc)SPh (3.3 Hz for isomer **6** and 6.7 Hz for isomer **7**). These results will be discussed later in the case of isoalantolactone.

Chloramine-T treatment (7) of compounds **6** and **7** gave the enol acetate **10** which was allowed to react with Ag_2O–NaOH (8), resulting in the formation of a carboxylic acid. Heating of the latter (9) gave γ-butyrolactone **11** (Scheme 4). Compound **10** was independently prepared from sodium α-hydroxymethylene-γ-butyrolactone (10) and acetyl chloride, in order to assign the configuration (*E* or *Z*) of **10**, obtained from **6** and **7**. No attempt was made to isolate the acid.

[2]For convenience of discussion, compounds **4** and **5** on the one hand, **6** and **7** on the other hand, are described with the configuration shown in the figures, even if these configurations have not been determined. In the case of α-methylene-γ-butyrolactone, compounds **4** and **5** have not been separated.

[3]Configurational assignment results from the nmr: the chemical shift of H(6) is δ 7.68 in isomer **8** (deshielding effect of the C=O group), while it is δ 7.12 in isomer **9** (no effect).

The same sequence of reactions was applied to isoalantolactone **1**. Only some differences will be noted.

Degradation of Isoalantolactone

The sulfoxides **4** and **5** (R = isoalantolactone residue, see **1**) were isolated and separated. With identical ir spectra, it is quite probable that the only difference is configuration at sulfur. The $—CH_2S(O)Ph$ group is β, as will be shown further in compounds **6** and **7**. The nmr spectra of **4** and **5** show interesting differences: in particular, the broad singlets due to ethylenic hydrogens at C(4) are located at δ 4.81 and 4.51 ppm in **4** and at 4.74 and 4.37 ppm in **5**. Assignment of configuration at S cannot be made at this stage.

The Pummerer reaction was attempted on the mixture of sulfoxides and also on each sulfoxide separately, both giving the same mixture of compounds **6**–**9** in a 1:4:5:1 ratio (as shown by nmr).

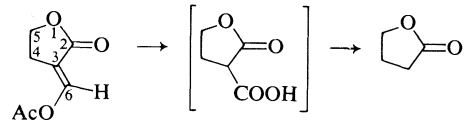

SCHEME 4

The vinyl sulfides **8** and **9** have the configuration shown in Scheme 3 (R = isoalantolactone residue). As observed in the case of the degradation of α-methylene-γ-butyrolactone, the nmr spectra of compounds **6** and **7** show notable differences, such as the H(11)–H(13) coupling constant which is 6.6 Hz in compound **6** and 10.7 Hz in isomer **7**.[2] This corresponds to favored conformations. Thus, isomer **6** has probably two *trans* hydrogens, as in **12**.

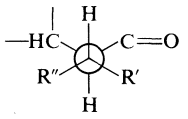

12

a R′ = SPh, R″ = OAc
b R′ = OAc, R″ = SPh

It is difficult to assess which of the *gauche* interactions C=O–SPh or C=O–OAc is the least favorable and therefore to assign configuration at C(13).

Sulfoxides **4** and **5** (R = isoalantolactone residue) separately gave the same products in the same ratio; this shows beyond any doubt that configuration at C(11) is the same in both sulfoxides and also in the sulfides, **3**. Indeed, the Pummerer intermediate **13** is achiral (11, 12).

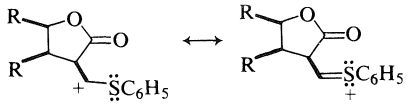

13

The H(7)–H(11) coupling constant is 6.6 Hz in compound **6** and 6.0 Hz in compound **7**. The similarity of these values implies the same configuration at C(11). They are also compatible with a β orientation of the —CH(OAc)SPh group. With an α orientation, the H(7)–H(11) dihedral angle is ~90°,[4] which would correspond to a ca 0 Hz coupling constant (13). Most Michael additions to the α-methylene group of alantolactone and isoalantolactone have been claimed to lead to the formation of β-derivatives (see for instance refs. 2 and 14).

Several reactions were attempted in order to hydrolyze the Pummerer products **6** and **7**.[5] Surprisingly, chloramine-T did not react at all and the reactants were recovered unchanged. This may be due to steric effects: according to the accepted mechanism of this reaction, chloramine-T attacks the sulfur atom. The approach might not be favorable, because of steric hindrance from the sesquiterpene skeleton.

Hydrolysis and further degradation was achieved by (*a*) oxidizing the sulfide group to a sulfoxide and (*b*) thermally eliminating sulfenic acid (3). The intermediate enol acetate **10** (R = isoalantolactone residue) was not isolated but was hydrolyzed and oxidized with an Ag_2O–NaOH mixture (8) and decarboxylated by heating (Scheme 5).

The base treatment opened the lactone ring to a hydroxy acid **15**. Ring closure to the lactone was achieved by *p*-toluenesulfonic acid treatment in CCl_4. This resulted in isomerization of norisoalantolactone **16** into lactone **17**, with migration of the *exo*-methylenic double bond from C_4 into ring A. Compound **17** has already been described and its transformation into alantolactone was made in several steps (17).

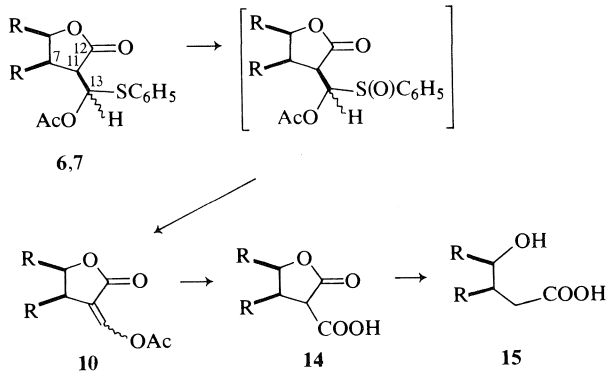

SCHEME 5

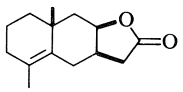

17

The sequence of reaction described in this paper provides, therefore, a means to achieve the synthesis of ^{14}C-labelled alantolactone **18**.

Experimental

Melting points were observed on a 510 Büchi apparatus and are uncorrected. Infrared spectra were recorded on a Beckman Acculab 1 spectrophotometer and absorptions are expressed in cm^{-1}. ^1H nuclear magnetic resonance spectra were recorded on a R 32 Perkin-Elmer (90 MHz), except when specified, using TMS as internal standard (δ 0); chemical shifts are given in δ ppm units, coupling constants in Hz. The combustion analyses were effected by the Centre de Microanalyses du CNRS. Mass spectra were recorded on 9000S LKB apparatus.

α-Methylene-γ-butyrolactone **2** (R = H) was prepared according to the method described in ref. 4 from α-(γ-butyrolactonylidene)triphenylphosphorane.

Isoalantolactone **1** was obtained pure from Helenin® (Sigma Products) by crystallization with a heptane–methanol mixture.

Addition of Sodium Thiophenoxide to α-Methylene-γ-butyrolactone: Sulfides 3 (R = H)

To a solution of sodium thiophenoxide in absolute ethanol (prepared from sodium (379 mg, 16.5 mmol) and thiophenol (4.49 g, 40.7 mmol) in 25 ml ethanol was added α-methylene-γ-butyrolactone (1.01 g, 10.3 mmol) in 40 ml absolute ethanol. The mixture was stirred at room temperature for 1.5 h. After hydrolysis, extraction with methylene chloride and washing of the combined extracts with water, drying with $MgSO_4$, and removing the solvent *in vacuo*, a crude mixture was obtained. This was chromatographed on a silica gel column (eluent: petroleum ether – ether 1:1), leading to sulfide **3** (1.97 g, 9.47 mmol; yield 92%); mp 60°C; ir ($CHCl_3$): 1765 (CO), 1580 (C_6H_5); nmr ($CDCl_3$): 1.8–3.0 (complex m, 4H, H(6) + H(4), 3.51 (complex m, 1H, H(3)), 4.0–4.4 (complex m, 2H, H(5)), 7.0–7.6 (complex m, 5H, aromatic); ms: 208 ($M^{\ddagger}$). *Anal.* calcd. for $C_{11}H_{12}O_2S$ (208): C 63.46, H 5.77; found: C 63.46, H 5.81.

[4]A referee has commented that the *cis* relationship between H-11 and H-7 (as shown by the 6.0–6.6 Hz coupling constant) could depend on the conformation of ring B. In the most stable conformation (chair), a *cis* H(11)–H(7) relationship corresponds, according to Dreiding models, to a ca. 30° angle (i.e., a ca. 7 Hz coupling) and a *trans* one to ca. 90° (i.e., a ca. 0 Hz coupling constant). A ring B boat conformation seems excluded because of steric hindrance. A third possibility is a twist-boat conformation: in this case, H(11)–H(7) dihedral angles are, respectively, ca. 150° (for an α orientation of the PhSCH(OAc) group, i.e., a coupling constant > 10 Hz) and 30° (for a β orientation, i.e., a coupling close to the one found). In conclusion, a β orientation of the PhSCH(OAc)—group seems well established, whatever the conformation of ring B.

[5]Several hydrolysis conditions were tried on the vinyl ethers **8** and **9**, with no success. (*a*) $TiCl_4$ treatment (15) resulted only in the migration of the C(4)=CH_2 bond into the C(4)=C(5) position. (*b*) It has been shown that vinyl thioethers with a homoallylic OH group could be hydrolyzed with $HgCl_2$ (16). The lactone group in **8** and **9** was opened by alkaline treatment and the resulting compounds were reacted with a CH_3CN–$HgCl_2$–H_2O mixture: the vinyl thioethers **8** and **9** were formed again (lactone ring closure catalyzed by the Lewis acid, $HgCl_2$). (*c*) Treatment of **8** + **9** with anhydrous HCl resulted only in the migration of the C(4)=CH_2 double bond into position C(4)—C(5). (*d*) The dithiane derivative (obtained through Michael addition of PhSNa to the **8** + **9** mixture) was treated with an aqueous mixture of $HgCl_2$–CH_3CN: the thioethers **8** and **9** were obtained again.

Oxidation of Sulfide **3**: *Sulfoxides* **4** + **5** (*R* = *H*)

A solution of sulfide **3** (1.77 g, 8.51 mmol) in methanol (120 ml) was reacted with sodium metaperiodate (2.36 g, 11.1 mmol) in water (50 ml) at room temperature for 2 days. The precipitate of sodium iodate was then filtered off, methanol removed *in vacuo*, and the remaining aqueous filtrate extracted with CH_2Cl_2. After the usual work-up, the crude sulfoxides were chromatographed on a silica gel column: compounds **4** and **5** coeluted (ethyl acetate) (1.68 g, 7.48 mmol; 88% yield.) The mixture crystallized slowly at room temperature; mp ~ 65°C; ir ($CHCl_3$): 1765(CO), 1580(Ph), 1025(SO); nmr ($CDCl_3$): 1.8–2.6 (m, 2H, H(4)), 2.7–3.6 (m, 3H, H(3) + H(6)), 4.0–4.6 (m, 2H, H(5)), 7.5–7.9 (m, 5H, aromatic); ms: 224 ($M^{\ddagger}$). *Anal.* calcd. for $C_{11}H_{12}O_3S$ (224): C 58.93, H 5.35; found: C 58.87, H 5.45.

Pummerer Rearrangement of Sulfoxides **4** + **5** (*R* = *H*): *Compounds* **6**–**9**

Trifluoroacetic anhydride (1.09 g, 9.3 mmol) was dissolved in acetic anhydride (6.25 ml) and kept standing for 5 hours at room temperature. The sulfoxide mixture (**4** + **5**, 1.40 g, 6.25 mmol) was then added and the resulting solution stirred for 2.5 h at room temperature. After removal of the anhydrides under reduced pressure, the residue was extracted with toluene. After usual work-up, chromatography of the residue on a silica gel column, 1.3 g of a mixture of compounds **6**–**9** was obtained. Compounds **6**, **7**, and **8** + **9** were further purified by thick-layer chromatography on silica gel coated plates. The relative ratio of compounds **6**–**9** was about 2:4:3:1, as shown by nmr.

Acetoxy sulfide **6**—ir($CHCl_3$): 1775 (CO lactone), 1755 (CO, AcO), 1580 (Ph); nmr ($CDCl_3$): 2.01 (s, 3H, CH_3CO), 2.2–2.7 (m, 2H, H(4)), 3.14 (dt, 1H, H(3), $J_{3,4}$ = 10, $J_{3,6}$ = 3.3), 4.0–4.6 (m, 2H, H(5)), 6.59 (d, 1H, H(6), $J_{6,3}$ = 3.3), 7.3–7.8 (m, 5H, aromatic).

Acetoxy sulfide **7**—ir ($CHCl_3$): 1770 (CO lactone), 1750 (CO, AcO), 1580 (Ph); nmr ($CDCl_3$): 2.11 (s, 3H, CH_3CO), 2.2–2.6 (m, 2H, H(4)), 3.0–3.3 (dt, 1H, H(3), $J_{3,6}$ = 6.7, $J_{3,4}$ = 10), 4.1–4.6 (m, 2H, H(5)), 6.41 (d, 1H, H(6), $J_{3,6}$ = 6.7), 7.3–7.8 (m, 5H, Ph).

Mixture of **6** + **7**—ms: 266 ($M^{\ddagger}$). *Anal.* calcd. for $C_{13}H_{14}O_4S$ (266): C 58.65, H 5.26; found: C 58.81, H 5.33.

Vinyl thioethers **8** + **9**— ir ($CHCl_3$): 1750 (CO lactone), 1625 (very strong, C=CSPh), 1580 (Ph); nmr ($CDCl_3$; 60 MHz): 2.84 (dt, 2H, H(3), $J_{4,6}$ = 3.0, $J_{4,5}$ = 7.5), 4.42 (t, 2H, H(5), $J_{5,4}$ = 7.7), 7.3–7.6 (m, 5H, Ph), 7.68 (t, 1H, H(6), $J_{4,6}$ = 3.0). Compound **9** showed a weak triplet at 7.12 ($J_{6,4}$ = 2.3). *Anal.* calcd. for $C_{11}H_{10}O_2S$ (206): C 64.08, H 4.85; found: C 64.22, H 4.96.

Hydrolysis of the Acetoxy Sulfides **6** + **7** (*R* = *H*): *Enol Acetate* **10**

The mixture of **6** + **7** (520 mg, 1.95 mmol) was treated with a solution of sodium *N*-chloro-*p*-toluenesulfonamide (chloramine-T, 1.1 g, 3.91 mmol) in an 85% aqueous solution of methanol (15 ml). The mixture was stirred for 5 min at room temperature and water was added. After usual work-up (with CH_2Cl_2), the residue was chromatographed on a silica gel column. The enol acetate **10** (eluent, petroleum ether – ether 25:75) was obtained in 63% yield (191 mg, 1.22 mmol). The compound crystallized slowly at 4°C; ir ($CHCl_3$): 3090 (C=C), 1780 (CO lactone), 1765 (CO, AcO), 1695 (C=C, sharp and strong); nmr ($CDCl_3$): 2.27 (s, 3H, CH_3CO), 2.99 (dt, 2H, H(4), $J_{4,5}$ = 7.3, $J_{4,6}$ = 2.8), 4.42 (t, 2H, H(5), $J_{5,6}$ = 7.3), 8.02 (t, 1H, H_a, $J_{4,a}$ = 2.8); ms: 156 ($M^{\ddagger}$).

The combustion analysis was not satisfactory, probably because the product is highly hygroscopic. To assess without ambiguity its structure and configuration, compound **10** was prepared by another route, as follows.

Preparation of Enol Acetate **10** (*R* = *H*) *from* γ-*Butyrolactone*

A solution of γ-butyrolactone (8.61 g, 100 mmol) and ethyl formate (7.41 g, 100 mmol) in anhydrous ethyl ether (25 ml) was added dropwise to a suspension of oil-free sodium hydride (2.52 g, 105 mmol) in ether (150 ml); 1 ml ethanol was added and the mixture was stirred at room temperature for 22 h. The resulting yellow-brown precipitate was filtered, washed with ether, and dried *in vacuo*. The sodium enolate was obtained in 97% yield (13.2 g, 97.0 mmol).

To a suspension of the sodium enolate (7.6 g, 55.8 mmol) in THF (100 ml) was added dropwise a solution of acetyl chloride (8.6 g, 110 mmol) in THF (150 ml). The mixture was heated under reflux for 4 h. After cooling, the NaCl precipitate was filtered off, the solvent removed *in vacuo* (this also eliminated excess acetyl chloride), and the residue chromatographed on a silica gel column, affording 3.36 g (21.5 mmol, 39% yield) of a compound whose spectra were identical with those reported for compound **10**. The nmr spectrum showed, in addition, a weak triplet centered at δ 7.46 ($J_{b,4}$ = 2.3); this corresponds to an isomer at C(6) (the *Z* isomer) and allowed us to assign configuration *E* to the major isomer.

Saponification and Oxidation of Enol Acetate **10**: *Formation of* γ-*Butyrolactone*

Enol acetate **10** (916 mg, 5.87 mmol) was treated with Ag_2O obtained from $AgNO_3$ (2.064 g, 12.1 mmol) and NaOH (6*N*, 5 ml). The mixture was stirred at room temperature for ca. 2 h and the black solid filtered off and washed with small portions of water. The aqueous layer was then refluxed for 4 h; after cooling, the solution was neutralized with HCl and water removed *in vacuo*; the resulting sodium chloride was washed several times with methylene chloride, methylene chloride was removed *in vacuo*, and the residue was chromatographed on a silica gel column. Thus, γ-butyrolactone, identical by ir and nmr spectra with an authentic sample, was obtained in an overall yield of 30% from enol acetate **10** (150 mg, 1.74 mmol).

Addition of Sodium Thiophenoxide to Isoalantolactone **1** (*R* = *isoalantolactone residue*): *Sulfide* **3**

A solution of isoalantolactone **2** (4.00 g, 17.2 mmol) in ethanol (50 ml) was added to a solution of sodium thiophenoxide in anhydrous ethanol (NaSPh was prepared from PhSH, 7.59 g, 68.9 mmol and sodium, 0.600 g, 26.1 mmol). The mixture was stirred at room temperature for 2 h and water was added. The white precipitate formed was filtered off and washed several times with small portions of heptane to eliminate the remainer of thiophenol. Pure sulfide **3** (5.47 g, 16.0 mmol) was thus obtained (93% yield); mp 138–139°C; ir ($CDCl_3$): 1770 (CO), 1645 (C(4)=CH_2), 1580 (Ph); nmr ($CDCl_3$): 0.81 (s, 3H, C(10)—CH_3), 2.9–3.1 (m, 2H, H(13)), 3.3–3.7 (m, 1H, H(11)), 4.3–4.6 (m, 1H, H(8)), 4.48 and 4.82 (2 broad s, 2H, C(4)=CH_2), 7.2–7.6 (m, 5H, Ph); ms: 342 ($M^{\ddagger}$). *Anal.* calcd. for $C_{21}H_{26}O_2S$ (342): C 73.68, H 7.60; found: C 73.54, H 7.71.

Oxidation of Sulfide **3** (*R* = *isoalantolactone residue*) *into Sulfoxides* **4** *and* **5**

A solution of sulfide **3** (2.94 g, 8.60 mmol) in 100 ml dioxane was treated with sodium metaperiodate (2.39 g, 11.2 mmol) in 50 ml water. After stirring the mixture for 2 days at 30°C, dioxane was removed *in vacuo* and the remaining aqueous phase worked up as usual with methylene chloride. The residue was chromatographed on a silica gel column, yielding a 1:1 mixture of sulfoxides **4** and **5** (2.62 g, 7.3 mmol, 85% yield). Pure compounds were obtained by thick-layer chromatography.

Sulfoxide **4**—mp 141°C; ir ($CHCl_3$): 1770 (CO), 1645 (C(4)=CH_2), 1030 (SO); nmr ($CDCl_3$): 0.78 (s, 3H,

C(10)—CH_3), 3.0–3.4 (m, 1H, H(11)), 3.16 (broad s, 2H, H(13)), 4.4–4.6 (m, 1H, H(8)), 4.51 and 4.81 (2 broad s, 2H, C(4)=CH_2), 7.5–7.8 (m, 5H, aromatic); ms: 358 ($M^{\ddagger}$).

Sulfoxide **5**—viscous oil; ir: identical with **4**; nmr ($CDCl_3$): 0.76 (s, 3H, C(10)—CH_3), 2.8–3.7 (m, 3H, H(13 + 11)), 4.56 (m, 1H, H(8)), 4.37 and 4.74 (2 broad s, 2H, C(4)=CH_2), 7.3–8.0 (m, 5H aromatic); ms: 358 ($M^{\ddagger}$).

Repeated combustion analyses gave unsatisfactory results: compounds **4** and **5** are extremely hygroscopic.

Pummerer Rearrangement of Sulfoxides ***4*** *+* ***5*** *(R = isoalantolactone residue). Compounds* ***6–9***

Trifluoroacetic anhydride (1.76 g, 8.36 mmol) was dissolved in Ac_2O (5.6 ml) and the resulting mixture was kept standing for 5 h at room temperature. This mixture was then added to sulfoxides **4** + **5** (2.01 g 5.61 mmol) and stirred for 2.5 h at room temperature. After removal of the excess anhydrides under reduced pressure, the residue was dissolved in toluene, washed with a $NaHCO_3$ solution, with water, and dried over $MgSO_4$. After removal of the solvent, a silica gel column chromatography afforded (eluent petroleum ether – ether 1:1) a mixture of compounds **6–9** (1.54 g) relative ratio as determined by nmr 1:4:5:1).

Compounds **6–9** were obtained in the same yield and with the same ratio from either **4** or **5**. Pure compounds were obtained by thick-layer chromatography.

α-Acetoxy sulfide ***6***—viscous oil; ir ($CHCl_3$): 3090 (C=C), 1770 (CO lactone), 1755 (CO, AcO), 1645 (C=C), 1580 (Ph); nmr ($CDCl_3$): 0.81 (s, 3H, C(10)—CH_3), 2.04 (s, 3H, CH_3CO), 3.22 (dd, 1H, H(11), $J_{11,13} = 6.6$, $J_{7,11} = 6.6$, this dd appears as a t), 4.48 (broad m, 1H, H(8)), 4.53 and 4.82 (2 broad s, 2H, C(4)=CH_2), 6.56 (d, 1H, H(13), $J_{11,13} = 6.6$), 7.3–7.8 (m, 5H, Ph).

α-Acetoxy sulfide ***7***—viscous oil; ir ($CHCl_3$): 3090 (C=C), 1770 (CO lactone), 1750 (CO, AcO), 1645 (C=C), 1580 (Ph); nmr ($CDCl_3$): 0.81 (s, 3H, C(10)—CH_3), 2.16 (s, 3H, CH_3CO), 3.05 (dd, 1H, H(11), $J_{11,13} = 10.7$, $J_{11,7} = 6.0$), 4.39 (m, 1H, H(8)), 4.56 and 4.86 (2 broad s, 2H, C(4)=CH_2), 6.45 (d, 1H, H(13), $J_{11,13} = 10.7$), 7.3–7.7 (m, 5H, aromatic).

Mixture of ***6*** *+* ***7***—ms: 400 ($M^{\ddagger}$). *Anal.* calcd. for $C_{23}H_{28}O_4S$ (400): C 69.00, H 7.00; found: C 69.13, H 6.95.

Vinyl sulfides ***8*** *+* ***9***—mp 178–179°C; ir ($CHCl_3$): 1740 (CO), 1645 (C=C), 1615 (very strong, C=CSPh), 1580 (Ph); nmr ($CDCl_3$): 0.78 (s, 3H, C(10)—CH_3, compound **9**), 0.84 (s, 3H, C(10)—CH_3, compound **8**), 2.9–3.3 (m, 1H, H(11)), 4.3–4.6 (m, 1H, H(8)), 4.48 and 4.77 (2 broad s, 2H C(4)=CH_2), 7.06 (d, 1H, H_b, compound **9**, $J_{b,7} = 1.0$), 7.1–7.6 (m, 5H, aromatic), 7.51 (d, 1H, H_a, $J_{a,7} = 1.2$, compound **8**); ms: 340 ($M^{\ddagger}$). *Anal.* calcd. for $C_{21}H_{24}O_2S$ (340): C 74.12, H 7.06; found: C 74.07, H 7.21.

Hydrolysis of Compounds ***6*** *+* ***7****: Formation of Compound* ***17***

A solution of α-acetoxy sulfides **6** + **7** (550 mg, 1.38 mmol) in a mixture of dioxan (20 ml) and benzene (2 ml) was treated with a solution of $NaIO_4$ (382 mg, 1.79 mmol) in water (8 ml). The mixture was heated with stirring at 40°C for 36 h. The precipitate of IO_3Na was filtered off and the solvent removed *in vacuo*. The residue was refluxed in toluene for 6 h, the solvent removed, the new residue dissolved in $CHCl_3$, and washed with water. The $CHCl_3$ extract was evaporated to dryness. Spectra showed that the major compound was the enol acetate **10** (R = isoalantolactone residue) and a hydroxymethylene lactone. This mixture was treated with Ag_2O (prepared from $AgNO_3$, 482 mg, 2.84 mmol and 2 ml of NaOH 6 *N*) with stirring at room temperature for 2 h. The black solid was filtered off and washed with small portions of ether. This was removed *in vacuo* and the remaining aqueous solution was refluxed for 4 h, neutralized with HCl 2 *N*, and extracted with $CHCl_3$ as usual. The ir spectrum of the residue thus obtained showed that the lactone had been opened in the base treatment into a hydroxy acid. The residue was therefore dissolved in CCl_4 containing catalytic amounts of *p*-toluenesulfonic acid and refluxed for 2 h. After usual work-up, the residue was chromatographed on a silica gel column yielding (eluent petroleum ether – ether 1:1) 100 mg (0.454 mmol, 33% yield from **6** + **7**) of lactone **17**. The ir and nmr spectra were identical with those reported by Marshall and Cohen (17); ir ($CHCl_3$): 1770 (CO), 1665 (C=C); nmr ($CDCl_3$): 1.13 (s, 3H, C(10)—CH_3), 1.65 (s, 3H, C(4)—CH_3), 4.56 (m, 1H, H(8)); ms: 220 ($M^{\ddagger}$).

Acknowledgements

We thank the I.N.S.E.R.M (Contrat libre 77-1-097-3) for financial support and the D.G.R.S.T for financial support and an "Allocation d'Etudes" to JPC.

1. G. Schlewer, J. L. Stampf, and C. Benezra. Can. J. Biochem. **56**, 153 (1978).
2. S. C. Srivastava, M. M. Mehra, G. K. Trivedi, and Bhattacharyya. Indian J. Chem. **9**, 512 (1971).
3. P. A. Grieco and M. Miyashita. J. Org. Chem. **40**, 1181 (1975).
4. P. A. Grieco and C. S. Pogonowski. J. Org. Chem. **39**, 1958 (1974).
5. R. Tanikaga, Y. Yabuki, N. Ono, and A. Kaji. Tetrahedron Lett. 2257 (1976).
6. P. A. Grieco and J. J. Reap. Tetrahedron Lett. 1097 (1974).
7. D. W. Emerson and H. Wynberg. Tetrahedron Lett. 3445 (1971).
8. N. Rabjohn (*Editor*). Organic synthesis. Coll. Vol. 4. John Wiley and Sons Inc., New York, NY. 1963. pp. 919–921.
9. J. Bus, H. Steinberg, and T. J. de Boer. Tetrahedron Lett. 1979 (1966).
10. A. D. Harmon and C. R. Hutchinson. J. Org. Chem. **40**, 3474 (1975).
11. C. R. Johnson and W. G. Phillips. J. Am. Chem. Soc. **91**, 682 (1969).
12. T. Numata and S. Oae. Tetrahedron, **32**, 2699 (1976).
13. M. Karplus. J. Chem. Phys. **30**, 11 (1959).
14. J. A. Marshall and N. Cohen. J. Org. Chem. **29**, 3727 (1964).
15. T. Mukaiyama, K. Kamio, S. Kobayashi, and H. Takei. Bull. Chem. Soc. Jpn. **45**, 3723 (1972).
16. A. J. Mura, J. G. Majetich, P. A. Grieco, and T. Cohen. Tetrahedron Lett. 4437 (1975).
17. J. A. Marshall and N. Cohen. J. Am. Chem. Soc. **88**, 3408 (1966).

Réduction catalytique de cétones α,β-éthyléniques à température modérée par $RhH(P\phi_3)_4$

D. BEAUPERE, P. BAUER ET R. UZAN

Laboratoire de Chimie Organique Physique, Université de Picardie, 33, rue Saint-Leu, 80039 Amiens, Cédex, France

Reçu le 12 mai 1978

D. BEAUPERE, P. BAUER et R. UZAN. Can. J. Chem. **57**, 218 (1979).

L'utilisation du catalyseur $RhH(P\phi_3)_4$ dans la réaction de réduction du système éthylénique de styryl cétones par le phényl-1 éthanol permet d'effectuer l'hydrogénation dès 50°C. A cette température, des effets de substituant dans les cétones α,β-éthyléniques ont pu être mis en évidence, montrant une augmentation de la vitesse initiale de réduction pour des groupes électronattracteurs et un effet inverse pour des groupes électrondonneurs. L'obtention d'une relation entre le potentiel de réduction électrochimique de ces cétones et leur vitesse d'hydrogénation suggère un transfert d'hydrogène vers la cétone par l'intermédiaire d'un ion hydrure.

D. BEAUPERE, P. BAUER, and R. UZAN. Can. J. Chem. **57**, 218 (1979).

The use of the catalyst $RhH(P\phi_3)_4$ in the reduction of the ethylenic system of styryl ketones by 1-phenylethanol permits the hydrogenation reaction to proceed at 50°C. Some substituent effects in the α,β-unsaturated ketones were demonstrated at this temperature. These showed an increase in the initial rate of reduction for electron-attracting groups and the inverse effect for electron-donating groups. The observation of a relation between the electrochemical reduction potential of these ketones and their rate of hydrogenation suggests a transfer of hydrogen to the ketone by a hydride ion intermediate.

[Journal translation]

Le transfert d'hydrogène entre un donneur tel qu'un alcool, un éther, une amine et un accepteur alcène ou une cétone, catalysé par les métaux de transition, permet de mettre en évidence l'influence électronique du donneur et du catalyseur. Dans la réduction de cétones α,β-éthyléniques à 180°C avec $RuCl_2(P\phi_3)_3$ l'étape lente est la déshydrogénation du donneur (1). Cette étape est précédée par la formation d'un complexe catalyseur–accepteur et des effets électroniques sont observés uniquement au niveau du donneur et du catalyseur. L'absence de tels effets au niveau de l'accepteur impliquerait que l'étape de transfert d'hydrogène à l'accepteur soit rapide. Ce résultat n'est pas généralisable aux observations faites lors de la réduction d'autres accepteurs (2, 3) où ces effets électroniques sont observés, il est vrai à des températures plus basses. Pour tenter de mettre en évidence de tels effets, nous avons recherché pour la réaction [1] un catalyseur

[1] $$\underset{A}{X\text{—}\phi\text{—}CH{=}CH\text{—}CO\text{—}R} + \underset{D}{\phi\text{—}CHOH\text{—}CH_3} \xrightarrow{C} X\text{—}\underset{P_{red}}{\phi\text{—}CH_2\text{—}CH_2}\text{—}CO\text{—}R + \underset{P_{ox}}{\phi\text{—}CO\text{—}CH_3}$$

permettant d'avoir des conditions expérimentales plus douces que celles utilisées précédemment (1).

Résultats

Pour la réaction de réduction de la benzalacétone en cétone saturée, le rendement et la température de la réaction dépendent du catalyseur. Si Sasson et Blum (1) réduisent en 1 h 95% de benzalacétone 0.4 *M* en solution dans l'alcool benzylique avec $RuCl_2(P\phi_3)_3$ (10^{-3} *M*) à 180°C, nous avons obtenu à une température voisine (170°C) un taux de réduction de l'ordre de 30% en 2 h de la même cétone (0.25 *M*) dans le prehnitène à l'aide du phényl-1 éthanol (0.25 *M*) en présence de $RhCl(P\phi_3)_3$ (0.01 *M*). Dès 50°C avec $RhH(P\phi_3)_4$ (10^{-2} *M*) nous sommes parvenus à réduire 71% de benzalacétone 0.25 *M* en 50 min par le phényl-1 éthanol 0.25 *M* dans le toluène.

L'évolution de cette dernière réaction est suivie par prélèvement et analyse cpv. Le taux de cétone réduite en fonction du temps est linéaire jusqu'à 50% de la réaction et la pente de cette droite permet la détermination graphique de la vitesse initiale v_i de la réaction avec une reproductibilité de l'ordre de 5%. Pour chaque cinétique les vitesses d'apparition du produit de réduction (P_{red}) et du produit d'oxydation (P_{ox}) sont les mêmes à ±5%.

Influence du donneur

Selon la nature de l'alcool D utilisé comme donneur, le produit P_{ox} peut être un aldéhyde ou une cétone, capables tous les deux de se complexer avec le catalyseur C et entrer ainsi en compétition avec l'accepteur A. Nous avons observé que cette complexation peut être suffisamment forte dans le cas d'un aldéhyde pour conduire à un empoisonnement du cata-

0008-4042/79/020218-04$01.00/0

TABLEAU 1. Vitesses initiales de réduction de *p*-X—ϕ—CH=CH—CO—R par ϕ—CHOH—CH_3[a] en présence de $RhH(P\phi_3)_4$[b] dans le toluène

A	[A] (*M*)	$v_i \times 10^4$ (mol L^{-1} min^{-1})	A	[A] (*M*)	$v_i \times 10^4$ (mol L^{-1} min^{-1})
ϕ—CH=CH—CO—CH_3	0.05	23	OMe-4—ϕ—CH=CH—CO—CH_3	0.05	18
	0.25	39	ϕ—CH=CH—CO—ϕ	0.05	8
	0.50	36	NO_2-4—ϕ—CH=CH—CO—ϕ	0.05	22
	1.5	32	Cl-3—ϕ—CH=CH—CO—ϕ	0.05	12
NO_2-4—ϕ—CH=CH—CO—CH_3	0.05	31	OMe-4—ϕ—CH=CH—CO—ϕ	0.05	7
	0.25	45	NMe_2-4—ϕ—CH=CH—CO—ϕ	0.05	4
	0.50	24	ϕ—CH=CH—CO—*t*Bu	0.05	4
	0.65	20	NO_2-4—ϕ—CH=CH—CO—*t*Bu	0.05	10
NMe_2-4—ϕ—CH=CH—CO—CH_3	0.05	12.5	ϕ—CH=CH—CO—*t*Bu[c]	0.05	25
	0.25	32	NO_2-4—ϕ—CH=CH—CO—*t*Bu[c]	0.05	50
	0.50	27	NMe_2-4—ϕ—CH=CH—CO—*t*Bu[c]	0.05	16
	0.65[d]	18			

[a]0.25 *M*.
[b]0.01 *M*.
[c]La température est de 70°C au lieu de 50°C.
[d]Limite de solubilité.

lyseur.[1] Cette constatation est parfaitement en accord avec les résultats de la littérature pour d'autres catalyseurs (4–6). C'est pourquoi nous avons préféré utiliser des alcools secondaires comme le phényl-1 éthanol (D) plutôt que des alcools primaires.

La vitesse de réduction de la benzalacétone augmente en fonction de la concentration de phényl-1 éthanol pour tendre, à partir d'une concentration en donneur égale à 2 *M*, vers une limite qui se situe à 75×10^{-4} *M* min^{-1}. L'allure de cette courbe est analogue à celle observée avec $RuCl_2(P\phi_3)_3$ (1); par contre, dans ce dernier cas, le palier est atteint moins rapidement.

Influence de l'accepteur

Les accepteurs étudiés sont du type X—ϕ—CH=CH—CO—R avec R = Me, ϕ, *t*Bu et X = NMe_2, OMe, H, Cl, NO_2. Pour ces composés, dont les résultats sont rassemblés tableau 1, on note une influence à la fois de X et de R sur la vitesse initiale de réduction: un substituant électronattracteur comme NO_2 dans le cas où R = ϕ multiplie approximativement par trois la vitesse initiale et un substituant électrondonneur comme NMe_2 la divise par deux.

Influence du catalyseur

Le pouvoir catalytique de C dépend fortement de la nature des ligands puisqu'à une température inférieure à 100°C seul $RhH(P\phi_3)_4$ présente une activité catalytique ce qui n'est pas le cas avec des catalyseurs chlorés tels que $RuCl_2(P\phi_3)_3$ ou $RhCl(P\phi_3)_3$. Avec $RhH(P\phi_3)_4$, la vitesse de la réaction est du premier ordre par rapport au catalyseur jusqu'à des concentrations voisines de la limite de solubilité. Ce résultat semble indiquer qu'à l'inverse de $RuCl_2(P\phi_3)_3$ (1) il n'y a pas formation de dimères ou de polymères avec $RhH(P\phi_3)_4$.

Discussion

En présence de $RhH(P\phi_3)_4$, le réduction de la double liaison des cétones éthyléniques peut donc être réalisée en catalyse homogène à des températures voisines de 50°C. Ces conditions extrêmement douces accroissent, en outre, le caractère régiosélectif de cette réaction. Ainsi la *p*-nitrobenzalacétone est réduite à plus de 90% en NO_2-4—ϕ—CH_2—CH_2—CO—CH_3 alors qu'à 180°C avec $RuCl_2(P\phi_3)_3$, au delà de 20% de réduction, le groupe nitro entre en compétition avec le système C=C. Ces conditions permettent également de mettre en évidence au niveau de l'accepteur des effets de substituant. Les résultats du tableau 1 montrent que lorsque R = Me, ϕ, *t*Bu, on observe une décroissance de la vitesse initiale et ce, quelle que soit la nature de X: c'est ainsi que la benzalacétone (R = Me) se réduit six fois plus vite que la benzalpinacolone (R = *t*Bu).

Une étude polarographique de ces mêmes cétones (7, 8) montre que le potentiel de demi-vague, caractéristique des effets polaires de substituant, diminue dans l'ordre ϕ, Me, *t*Bu. Par contre, pour la complexation de ces cétones avec le phénol (7, 9), les

[1]En effet la réduction du cinnamaldéhyde n'a pas lieu dans nos conditions expérimentales. De plus, la réduction de la benzalacétone est empêchée par l'introduction de cinnamaldéhyde.

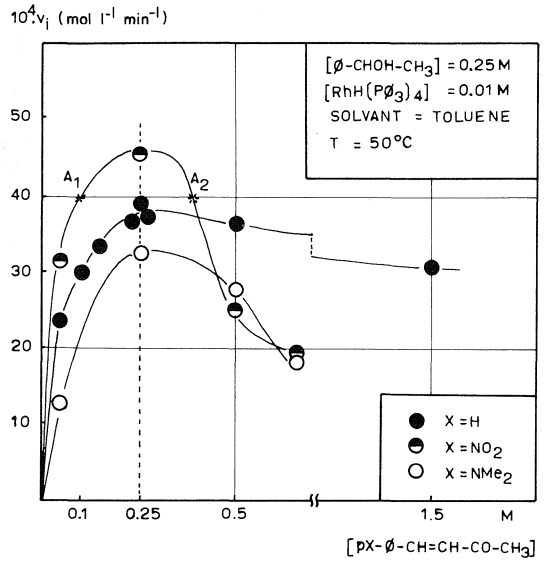

FIG. 1. Influence de la concentration en accepteur sur la vitesse de réduction de benzalacétones substituées.

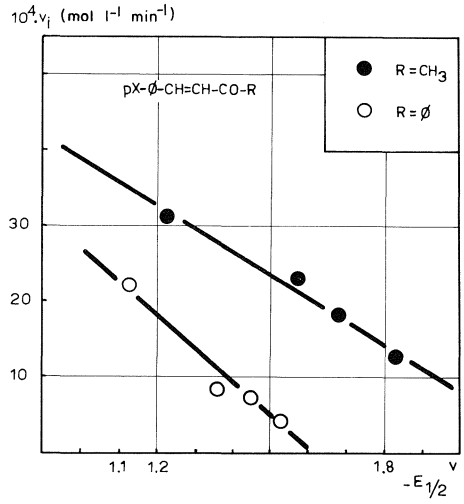

FIG. 2. Relations linéaires entre les vitesses initiales de réduction et les potentiels de réduction électrochimique pour les benzalacétones (R = Me) et les chalcones (R = ϕ).

$\Delta\nu_{OH}$, sensibles aux effets stériques, décroissent dans le même ordre que les vitesses initiales de réduction, montrant que l'influence de R est au moins partiellement d'origine stérique. Pour les composés dont le groupe R est maintenu constant, la vitesse initiale est influencée par le substituant X et par la concentration de l'accepteur (fig. 1). Pour des concentrations inférieures à 0.25 *M*, on constate qu'un groupe électrondonneur diminue la vitesse et qu'un substituant électronattracteur l'augmente. De tels effets qui n'ont jamais été mis en évidence antérieurement avec des composés analogues doivent permettre une nouvelle approche du processus de transfert d'hydrogène. En effet, il existe une tendance à la corrélation pour les benzalacétones (R = Me) et les chalcones (R = ϕ) entre les vitesses initiales de réduction et les potentiels de demi-vague (fig. 2). Comme en polarographie le potentiel de réduction correspond à l'arrivée d'un électron à la cétone, l'existence de cette corrélation implique que le transfert vers la cétone éthylénique engagé dans le complexe CDA (schéma 1) s'effectue par l'intermédiaire d'un ion hydrure. Les effets de substituant intéressent donc l'étape du transfert d'hydrogène: CDA → C + P_{red} + P_{ox}, cette hypothèse est confortée par les effets inverses observés au niveau du donneur (1, 10).

Pour des réactions de ce type trois mécanismes ont été proposés (schéma 1): la voie *1*, proposée par Imai *et al.* (13), dans laquelle la complexation du donneur D précéde celle de l'accepteur A; la voie *2* dans laquelle l'accepteur intervient avant le donneur (1, 14); enfin un mécanisme, suggéré par Sharf *et al.* (11, 12), dans lequel les deux voies sont concurrentielles. L'analyse des courbes de la fig. 1 permet de préciser la nature du mécanisme prépondérant dans la réaction envisagée ici. Pour des concentrations supérieures à 0.25 *M*, la vitesse décroît quand la concentration en accepteur augmente et cette décroissance est plus accentuée pour les dérivés nitré et aminé. Le fait d'observer, pour deux concentrations différentes de l'accepteur (points A_1 et A_2 de la fig. 1), des vitesses initiales identiques, implique l'apparition d'un nouveau phénomène intervenant au-delà de 0.25 *M* et qui vient progressivement s'opposer à l'effet normal de la concentration de l'accepteur. Comme [A_1] et [A_2] produisent au bout d'un temps *t* des concentrations égales en P_{red} et P_{ox}, ce phénomène peut être attribué au fait que [A_1] est inférieur à la concentration du donneur [D] et que [A_2] est supérieur à [D]. C'est donc qu'un accroissement de la concentration du complexe CA (schéma 1) diminue la vitesse de réduction. Ainsi dans le cas de la benzalacétone, il semble que le mécanisme passe principalement par la voie *1*, le complexe CA évoluant peu vers CAD par la voie *2*. Dans le cas des benzalacétones substituées, pour lesquelles on ob-

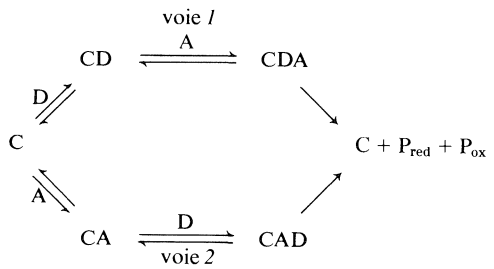

SCHÉMA 1

serve (fig. 1) une chute de la vitesse beaucoup plus importante, la voie *2* doit être pratiquement inexistante car les substituants NO_2 et NMe_2 s'associent fortement au catalyseur[2] empêchant la combinaison du donneur avec le complexe CA (2).

Conclusion

Les réactions de transfert d'hydrogène en catalyse homogène nécessitent fréquemment des conditions de température élevées, telles qu'elles restreignent fortement leur domaine d'application. L'utilisation de $RhH(P\phi_3)_4$ comme catalyseur des réactions de transfert entre le phényl-1 éthanol et les styryl cétones a permis d'opérer dans des conditions expérimentales plus douces et donc mieux adaptées à l'étude de ce type de réaction. C'est ainsi que la mise en évidence d'effets électroniques au niveau de l'accepteur suggère fortement que le transfert d'un ion hydrure constitue une étape importante de cette réaction. A 50°C, en présence de ce catalyseur, la régiosélectivité de la réaction est en outre considérablement accrue. Ces conditions permettent d'envisager l'extension de cette réaction à des structures thermiquement fragiles.

Partie expérimentale

La pureté des cétones éthyléniques préparées selon la littérature (15, 16) est vérifiée par cpv et spectroscopie rmn. Le toluène fraîchement distillé est gardé sur tamis moléculaire sous argon. Le phényl-1 éthanol Fluka, bidistillé après traitement par la dinitro-2,4 phényl hydrazine, est placé sous argon sur tamis moléculaire. $RhH(P\phi_3)_4$ est préparé selon la méthode de Levison et Robinson (17).

Exemple de cinétique

Un millilitre d'une solution dans le toluène de benzalacétone 0.25 *M* de phényl-1 éthanol 0.25 *M* et de $RhH(P\phi_3)_4$ 0.01 *M* est placé dans un tube en verre de 3 mL de contenance, rempli d'argon et fermé à l'aide d'une pastille en caoutchouc maintenue par un bouchon vissé. Ce tube est placé dans un bain thermostaté à 50°C et l'agitation est obtenue par un barreau aimanté préalablement placé à l'intérieur du tube. Des échantillons de 10 μL sont prélevés régulièrement, placés dans 40 μL d'acétone et analysés avec un chromatographe Varian 1400 muni d'un détecteur à ionisation de flamme et équipé d'une colonne DEGS 10%, 10 pieds à 160°C. La surface des pics est mesurée par un intégrateur LTT ICAP 5 et la méthode d'intégration est celle des facteurs de calibration spécifique (18).

[2]Dans la réduction des nitrobenzènes par les amines, Imai *et al.* (13) concluent que le groupe nitro se lie fortement au catalyseur ($RhCl_3$) et qu'il est alors nécessaire d'utiliser des amines qui s'associent également fortement pour réaliser la réduction.

1. Y. Sasson et J. Blum. J. Org. Chem. **40**, 1887 (1975).
2. H. Imai, J. Nishiguchi et K. Fukuzumi. J. Org. Chem. **42**, 431 (1977).
3. I. S. Shekoyan, G. V. Varnakova, V. N. Krutii, E. I. Karpeiskaya et V. Z. Sharf. Bull. Acad. Sci. USSR, Div. Chem. Sci. **24**, 2700 (1975).
4. J. A. Osborn, F. H. Jardine, J. F. Young et G. Wilkinson. J. Chem. Soc. A, 1711 (1966).
5. M. C. Baird, C. J. Nyman et G. Wilkinson. J. Chem. Soc. A, 348 (1968).
6. K. Ohno et J. Tsuji. J. Am. Chem. Soc. **90**, 99 (1968).
7. J. P. Seguin, D. Beaupere, P. Bauer et R. Uzan. Bull. Soc. Chim. Fr. **1–2**, 167 (1974).
8. J. P. Seguin, J. P. Doucet et R. Uzan. C. R. Acad. Sci. Sér. C, **278**, 129 (1974).
9. D. Beaupere, R. Uzan et J. P. Doucet. C. R. Acad. Sci. Sér. C, **278**, 187 (1974).
10. Y. Sasson, P. Albin et J. Blum. Tetrahedron Lett. 833 (1974).
11. V. Z. Sharf, L. Kh. Freidlin, I. S. Shekoyan et V. N. Krutii. Bull. Acad. Sci. USSR Pt 1, **26**, 758 (1977).
12. V. Z. Sharf, L. Kh. Freidlin et V. N. Krutii. Bull. Acad. Sci. USSR Pt. 1, **26**, 666 (1977).
13. H. Imai, T. Nishiguchi et K. Fukuzumi. J. Org. Chem. **39**, 1622 (1974).
14. C. Masters, A. A. Kiffen et J. P. Visser. J. Am. Chem. Soc. **98**, 1357 (1976).
15. H. Gilman et A. H. Blatt. Organic syntheses. Vol. 1. John Wiley and Sons, New York, NY. 1967. p. 78.
16. T. Nishimura. Bull. Chem. Soc. Jpn. **26**, 253 (1953).
17. J. J. Levison et J. D. Robinson. J. Chem. Soc. A, 2947, 1970.
18. R. Kaiser. Gaz chromatographie. Vol. 1. Butterworths, London. 1963. p. 182.

Nuclear analogs of β-lactam antibiotics. X. Synthesis of 2-substituted desthiocephalosporins[1]

TERRENCE WILLIAM DOYLE,[2,3] TERRY THOMAS CONWAY,[2] MICHAEL CASEY, AND GARY LIM

Bristol Laboratories of Canada, 100 Industrial Boulevard, Candiac, P.Q., Canada J5R 1J1

Received April 20, 1978

TERRENCE WILLIAM DOYLE, TERRY THOMAS CONWAY, MICHAEL CASEY, and GARY LIM. Can. J. Chem. **57**, 222 (1979).

The syntheses of the desthiocephem system from the enol **2** is described. Thus conversion of **2** to its triflate **3** followed by treatment with the sodium salts of malonate esters gave the cyclized products **4***a–c*. Azide reduction followed by coupling of phenoxyacetic acid and hydrogenolysis gave the acids **7** and **8**. Compound **15** was also prepared.

TERRENCE WILLIAM DOYLE, TERRY THOMAS CONWAY, MICHAEL CASEY et GARY LIM. Can. J. Chem. **57**, 222 (1979).

On décrit les synthèses du système desthiocephem à partir de l'énol **2**. Par conversion de **2** en son triflate **3**, puis un traitement avec les sels de sodium des esters malonates, on a obtenu les produits cyclisés **4***a–c*. La réduction de l'azide, puis le couplage avec l'acide phénoxyacétique et l'hydrogénolyse ont conduit aux acides **7** et **8**. On a également préparé le composé **15**.

[Traduit par le journal]

Over the past several years a number of reports on the preparation of nuclear analogs of the cephalosporins have appeared in the literature.[4] Previously we have reported (2)[5] the syntheses of a number of analogs (Fig. 1) in which the sulfur atom at 1 has been replaced by a methylene (or substituted carbon) and a hetero atom introduced in position 2. The syntheses of these analogs proceeded via the common intermediate **2**. Direct base treatment of the enol **2** gave the *O*-2-isocephem series whereas the preparation of the 2-isocephem (X = S) and *N*-2-isocephem systems proceeded via nucleophilic attack on the triflate **3** (or the corresponding mesylate). It occurred to us that treatment of **3** with appropriate carbon nucleophiles might well provide access to the desthiocephalosporins. At the time no reports of such analogs had appeared in the literature but about the time we were completing our own work a report appeared by Christensen and co-workers (3) of the synthesis of the 1-oxacephalosporin and 1-carbacephalosporin (=desthiocephalosporin) systems. These authors reported that the carbon analog exhibited activity approximately equal to that in the natural series. In this and the accompanying papers we should like to report our own results in this area.

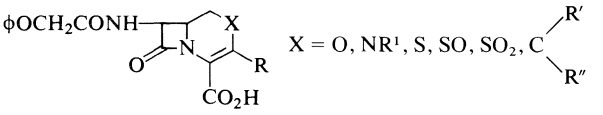

1

FIG. 1. Cephalosporin analogs.

Treatment of enol **2** in the presence of triethylamine with trifluoromethane sulfonic anhydride gave a high yield of the corresponding triflate **3** as a mixture of isomers (1). It proved possible to obtain one of the isomers as a crystalline solid at the expense of losing considerable amounts of product. The crude triflate was generally sufficiently pure to be used as such.

As we had anticipated, treatment of **3** with sodium dimethylmalonate in tetrahydrofuran gave the desired cyclized product **4***a* in 68% yield after chromatography. Similarly replacing the dimethyl malonate in the reaction with dibenzyl malonate or di-*tert*-butyl malonate gave the products **4***b* and **4***c* in 60 and 52% yields, respectively. The structures assigned to **4***a–c* were made on the basis of their elemental analyses and by comparison of their uv, ir, and nmr spectra with those of the earlier nuclear analogs synthesized in these laboratories. Examination of the proton nmr (Table 1) enables us to assign the conformation illustrated in Fig. 2 to these molecules.

Reduction of the azido function in **4***a* using triethylamine – hydrogen sulfide gave the amine **5***a* in 91% yield. Conversion of the amine **5***a* to the amide **6***a* proceeded in near quantitative yield using

[1]For Part IX of this series see ref. 5.

[2]To whom correspondence concerning this paper may be addressed.

[3]Present address: Bristol Laboratories, P.O. Box 657, Syracuse, NY 13201, U.S.A.

[4]For a brief review of some of these papers see ref. 2*a*.

[5]For a detailed argument concerning the conformations of these and similar analogs in solution see ref. 2*b*.

0008-4042/79/020222-05$01.00/0

TABLE 1. Nuclear magnetic resonance spectra[a]

Compound	Aromatic protons	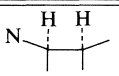		ArCH_2	CH_3	Other
3	7.40(s, 5H)	4.96(d) $J = 5$		5.20(d)[b] 5.40(d)[b] $J = 12$	2.27(s) 2.86(s, OMes) 2.47(s)[c] 2.90(s)[c]	4.45 (m, 3H, C*H*C*H*$_2$OMes)
4*a*	7.30(s, 5H)	4.84(d) $J = 5$		5.17(s)	2.06(s, 3H) 3.67(s, 6H)	2.65(1H, dd, $J_1 = 13$ $J_2 = 3.5$) 2.14 (1H, m)
4*b*	7.25(m, 15H)	4.73(d) $J = 5$	3.67(ddd) $J_1 = 11$ $J_2 = 5$ $J_3 = 3.5$	5.14(2H, s) 5.08(4H, s)	1.98(s)	2.66 (dd, $J_1 = 13$ $J_2 = 3.5$, 1H) 2.14 (m, 1H)
4*c*	7.27(m, 5H)	4.82(d)	3.75(ddd) $J_1 = 12$ $J_2 = 5$ $J_3 = 3.5$	5.19(2H, s)	2.12(s, 3H) 1.45(s, 9H)	2.59 (dd, 1H, $J_1 = 13, J_2 = 3.5$) 1.92(dd, 1H, $J_1 = 12, J_2 = 13$)
5*a*	7.30(s, 5H)	4.47(d) $J = 5$	3.64(ddd) $J_1 = 12$ $J_2 = 3.5$ $J_3 = 5$	5.21(2H, s)	3.71(s, 3H) 2.02(s, 3H)	2.68 (dd, 1H, $J_1 = 13$ $J_2 = 3.5$) 1.94 (dd, 1H, $J_1 = 13$ $J_2 = 12$) 1.68 (bs, 2H, NH_2)
5*b*	7.15(m, 15H)	4.30(d) $J = 5$	3.58(ddd) $J_1 = 12$ $J_2 = 3.5$ $J_3 = 5$	5.14(s, 2H) 5.09(s, 4H)	1.97(s, 3H)	1.92 (dd, $J_1 = 13$, $J_2 = 12$) 2.68 (dd, $J_1 = 13$, $J_2 = 3.5$) 1.50 (bs, 2H, NH_2)
6*a*	6.7–7.5(m, 11H)	5.36(dd) $J_1 = 5$ $J_2 = 8$	3.80(m)	5.80(s, 2H)	2.03(s, 3H) 3.67(s) 3.70(s)	4.46 (s, 2H, ϕOCH_2) 1.84 (dd, $J_1 = 13$ $J_2 = 12$) 2.51 (dd, $J_1 = 13$ $J_2 = 3.5$)
6*b*	6.6–7.5(m, 21H)	5.30(dd) $J_1 = 8$ $J_2 = 5.0$	3.75(m)	5.02(s, 2H) 5.05(s, 2H) 5.13(s, 2H)	1.95(s, 3H)	2.53 (m, 1H) 1.84 (m, 1H) 4.38 (s, 2H, ϕOCH_2)
7[d]	6.7–7.4(m, 5H) 8.67 $J \simeq 8$	5.37(d) $J = 5$	~3.7		3.69(s, 6H) 1.90(s, 3H)	4.50 (s, 2H, ϕOCH_2) 2.30 (m, 2H)
9	7.28(s)	4.87(d) $J = 5$	3.83(m)	5.22(s)	2.10(bs)	1–3 (bs, 2*H*)
10	7.27(s, 5H)	4.85(d) $J = 5$	3.90(m)	5.20(s)	2.10(s)	3.30 (bd, 1H, C*H*CO_2H) 1.70–2.6 (m 2H)
11	7.25(s, 5H)	4.85(d) $J = 5$	3.95(m)	5.13(s)	2.03(bs)	4.73 (bs, 1H, C*H*CO_2Bz) 2.60 (bd, $J \simeq 8$ Hz)
12	7.34(s, 5H)	4.90(d) $J = 5$	4.1(m)	5.23(s)	2.08(s) 3.70(s, OMe)	3.35 m(1H) 1.7–2.4(m, 2H)
13	7.35(s, 5H)	4.48(d) $J = 5$	~3.9(m)	5.26(s)	2.10(s) 3.73(s)	1.60 (bs, NH_2) 1.7–2.4 (m, 2H) 3.33 m (1H, bd, $J \simeq 6$)
14	7.30(s) 6.7–7.4(m, 11H)	5.34(dd) $J_1 = 6.5$ $J_2 = 5.0$	3.95(m)	5.20(s)	3.67(s, OMe) 2.06(s)	4.48 (s, 2H, ϕOCH_2) 1.5–2.3 (m, OH) 3.22 (m, 1H, bd $J = \sim 6$)
15	6.7–7.4(m, 6H)	5.35(m, 1H)	4.0(m, 1H)		3.72(s, OMe) 2.08(s)	4.55 (s, 2H, ϕOCH_2) 3.32 (m, 1H) 1.5–2.3 (m, 2H)

[a]Recorded at 60 MHz in $CDCl_3$ unless otherwise noted. The coupling constants are recorded in Hz.
[b]Arms of AB quartet.
[c]Minor isomer.
[d]DMSO-d_6.

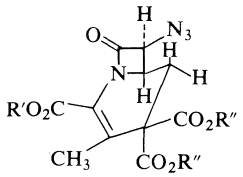

FIG. 2. Conformation of desthiocephalosporins.

2-ethoxy-*N*-ethoxycarbonyl-1,2-dihydroquinoline (EEDQ) and phenoxyacetic acid (4). Similarly **4***b* was converted to **5***b* and subsequently to **6***b*.

Hydrogenation of **6***a* over 10% palladium-on-carbon gave 3-methyl-2,2-biscarbomethoxy-7-β-phenoxyacetamido-Δ^3-desthiocephem-4-carboxylic acid **7** in 70% yield. Reduction of **6***b* over 10% palladium-on-carbon in acetic acid resulted in loss of all three benzyl functions and decarboxylation to give **8** in 44% yield.

To explore the synthesis of various 2-monosubstituted analogs the deesterification of **4***c* was studied next (Scheme 2). Treatment of **4***c* with trifluoroacetic acid at 60°C gave a foam the nmr spectrum of which was compatible with the diacid **9**. A solution of the foam in toluene was boiled at reflux for 10 min and evaporated to yield a mixture of the two compounds **10** and **11**, in a 3:1 ratio. Partial resolution of the mixture of acids was achieved by column chromatography on silica gel and the structural assignments made on the basis of their nmr spectra. The acid mixture was used as such in the next step. Thus treatment of the mixture with methyl chloroformate and triethylamine gave the methyl ester **12** in ~55% yield. The crude ester was reduced to the amine **13** using triethylamine – hydrogen sulfide and **13** was coupled to phenoxyacetic acid using EEDQ to give **14**. Hydrogenolysis of **14** gave the desired acid **15**. The stereochemistry of the carbomethoxy group in **14** and **15** was not determined owing to poor resolution of the nmr spectrum.

The biological activities of compounds **1**, **8**, and **15** were disappointingly low and will be discussed in full in a forthcoming structure–activity relationship paper.

Experimental

The infrared spectra were recorded on a Unicam Sp-200 G grating ir spectrophotometer. The nmr spectra were determined on a Varian A60-A spectrometer using tetramethylsilane as an internal standard. Melting points are uncorrected except where noted and were determined on a Gallenkamp melting point apparatus. The analyses were performed by Micro-Tech Laboratories, Skokie, IL.

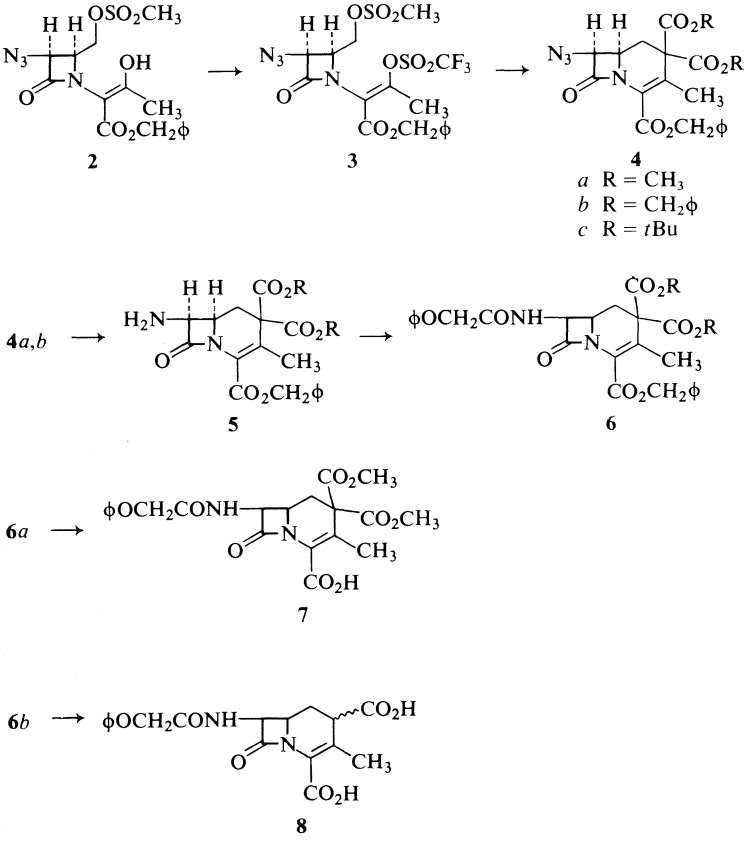

SCHEME 1

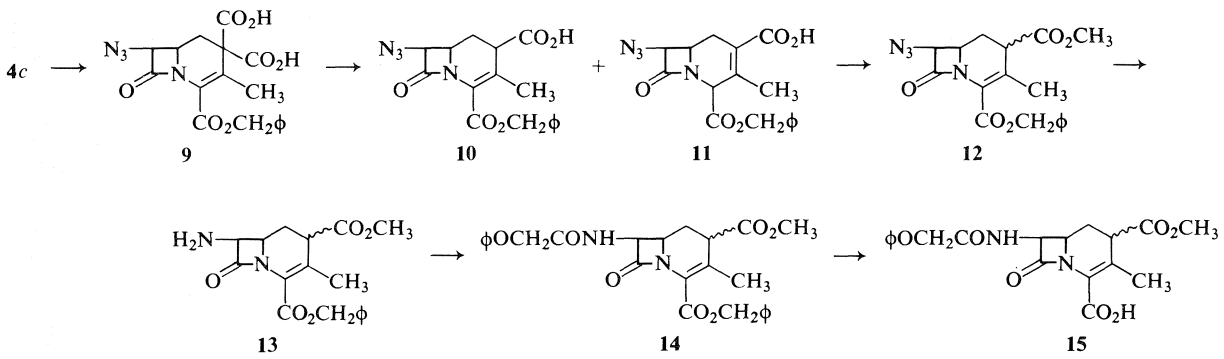

SCHEME 2

Preparation of Vinyl Triflate **3**

The enol **2** (48.0 g, 0.117 mol) was dissolved in 500 ml $CaCl_2$-dried CH_2Cl_2 and then cooled in an ice bath under N_2. Triflic anhydride (33.0 g, 19.5 ml, 0.117 mol) was added in one portion. A solution of triethylamine (11.8 g, 16.3 ml, 0.117 mol) in 80 ml CH_2Cl_2 was added dropwise over a period of 40 min. When the addition was complete, the ice bath was removed and the mixture stirred at 25°C for a further 45 min.

The mixture was poured into 300 ml ice–H_2O and washed with cold H_2O until the pH was ~6 (five or six washings were necessary). The CH_2Cl_2 solution was dried (Na_2SO_4) and evaporated to give a dark red oil (54.0 g) which was dissolved in 400 ml benzene and passed through a $1\frac{1}{2}$-in. pad of silica gel (15% water, w/w) (~150 g); the pad was washed with 1 ℓ of benzene. Evaporation of the benzene gave a yellow oil (38.3 g) which contained ~20% unreacted enol. Eluting the pad with 500 ml CH_2Cl_2 gave 5.42 g of a 40:60 mixture of triflate and enol. Further elution with 500 ml Et_2O gave 5.34 g of unreacted enol.

The yellow oil which contained the two isomeric triflates was triturated with 50 ml of absolute EtOH until there were no more large gummy particles. After cooling to 0°C for a few hours, the suspension was filtered to afford 19.5 g of a white powder consisting of one triflate isomer, mp 57–59°C; ir (neat): 2110, 1790, 1730, 1656 cm^{-1}; uv (EtOH) λ_{max}: 242 (ε 6360). *Anal.* calcd. for $C_{17}H_{17}F_3N_4O_9S_2$: C 37.67, H 3.14, N 10.33, S 11.82; found: C 37.40, H 3.12, N 10.43, S 11.73.

Preparation of Compounds **4**a–c

Compound **4**a

To a suspension of 225 mg (5.34 mmol) of sodium hydride (57% mineral oil dispersion washed three times with petroleum ether) in 2 ml dry tetrahydrofuran, under nitrogen, and cooled to 0–5°C, was added 1.32 g (2.43 mmol) of **3** and 282 mg (2.43 mol) of dimethylmalonate in 3 ml of dry tetrahydrofuran over 10 min. A red color developed and hydrogen was evolved. The reaction was stirred at 25°C for 1.5 h at the end of which time the reaction was complete as determined by thin-layer chromatography.

Five percent HCl was added to the reaction (pH 3.4) and was then distributed between ether and water. The organic phase was washed with water, dried (Na_2SO_4), and concentrated *in vacuo* to give **4***a* (1.02 g, 98%) as a yellow oil. The oil was chromatographed on silica gel (15% H_2O), developed with 1 volume hexane, and eluted with benzene. Pure **4***a* was obtained (688 mg, 66%); ir (neat): 2110, 1780, 1740, 1730, 1630 cm^{-1}; uv (EtOH) λ_{max}: 270 (ε 11 200).

Compound **4**b

Similarly treatment of 504 mg (11.95 mmol) of sodium hydride with 2.95 g (5.45 mmol) of **3** and 1.54 g (5.45 mmol) of dibenzyl malonate in THF gave 1.88 g (60%) of **4***b* as an oil after chromatography; ir (neat): 2110, 1780, 1740, 1730 cm^{-1}; uv (EtOH) λ_{max}: 270 (ε 10 967). *Anal.* calcd. for $C_{32}H_{28}N_4O_7$: C 66.12, H 4.86, N 9.65; found: C 66.68, H 4.99, N 9.31.

Compound **4**c

Treatment of 2.59 g (12 mmol) of di-*tert*-butyl malonate and 6.65 g (12 mmol) of **3** with 1.05 g (24 mmol) sodium hydride in tetrahydrofuran as in the previous examples gave, after the usual work-up, **4***c* as a light brown oil. Trituration of this oil with a small volume of ethanol induced crystallization to give 3.2 g (52%) of **4***c* as a colorless solid, mp 146–147°C after recrystallization from ether; ir ($CHCl_3$): 2110, 1780, 1725(s 1738) cm^{-1}; uv (EtOH) λ_{max}: 271 (ε 11 724). *Anal.* calcd. for $C_{26}H_{32}N_4O_7$: C 60.92, H 6.29, N 10.93; found: C 61.03, H 6.38, N 11.03.

Preparation of Compounds **5**a *and* b

Compound **5**a

The azide **4***a* (588 mg, 1.37 mmol) was dissolved in 10 ml methylene chloride and triethylamine (700 mg, 0.96 ml, 6.93 mmol) was added. Hydrogen sulphide was bubbled in slowly producing an orange-red color and complete reaction to a more polar (tlc) material after 45 min. The solution was concentrated *in vacuo* and the yellow residue distributed between ether and 10% HCl. The organic phase was washed once with 10% HCl which was then combined with the previous washings and extracted once with ether. The acidic solution was brought to pH 8 with solid $NaHCO_3$ (foams!) and saturated with NaCl precipitating the amine **5***a* as a thick oil which was extracted into CH_2Cl_2. The combined extracts were washed once with brine, dried (Na_2SO_4), and evaporated *in vacuo* leaving **5***a* (500 mg, 91%), which was used as such in the following reaction. A small amount of this material was converted to the hydrochloride salt (EtOH–HCl; Et_2O), mp 178–180°C; ir (free base, neat): 3410, 3350, 1770, 1740, 1725 cm^{-1}. *Anal.* calcd. for $C_{20}H_{22}N_2O_7 \cdot HCl$: C 54.73, H 5.28, N 6.38; found: C 54.10, H 5.41, N 6.26.

Compound **5**b

Treatment of 1.88 g (3.08 mmol) of **4***b* with triethylamine (6.16 mmol) and hydrogen sulfide as in the above example gave 1.07 g (100%) of **5***b* as an oil on work-up. The amine **5***b* was used as such in the subsequent reaction.

Preparation of Compounds **6**a *and* b

Compound **6**a

Amine **5***a* (350 mg, 0.87 mmol) was stirred in methylene chloride (20 ml) with phenoxyacetic acid (132 mg, 0.86 mmol) and EEDQ (220 mg, 0.89 mmol) until CO_2 evolution had ceased (80 min). The clear solution was washed with 1% $NaHCO_3$ (2 × 15 ml), 10% HCl (2 × 10 ml), brine (2 × 20 ml), dried (Na_2SO_4), and concentrated *in vacuo* to give **6***a* (480 mg, 103%) as a white foam. The material was chroma-

tographed on 10 g silica gel (15% H_2O) in $CHCl_3$–Et_2O (9:1). Pure **6***a* was isolated (480 mg, 103%) as a glassy solid; ir (smear): 3400, 1780, 1740, 1685, 1600, 1530, 1495 cm^{-1}; uv (EtOH) λ_{max}: 269 (ε 6778). *Anal.* calcd. for $C_{28}H_{28}N_2O_9$: C 61.64, H 5.35, N 5.13; found: C 61.37, H 5.26, N 5.02.

Compound **6**b

Amine **5***b* (1.8 g, 2.13 mmol) was stirred in CH_2Cl_2 (100 ml) with phenoxyacetic acid (471 mg, 3.1 mmol) and EEDQ (765 mg, 3.1 mmol) until CO_2 evolution had ceased (1.5 h). The solution was washed with 1% $NaHCO_3$ (2 × 15 ml), 10% HCl (2 × 10 ml), brine (2 × 20 ml), dried (Na_2SO_4), and concentrated *in vacuo* to give **6***b* (2.05 g) as a red oil. This material was chromatographed on SiO_2 (35 g, 15% H_2O) eluting with $CHCl_3$ to give white crystals (1.2 g) mp 134–135°C (corrected); ir (Nujol mull): 3320, 1770, 1725, 1680, 1550, 1495 cm^{-1}; uv (EtOH) λ_{max}: 269 (ε 14 556). *Anal.* calcd. for $C_{40}H_{35}N_2O_9$: C 69.85, H 5.12, N 4.07; found: C 69.51, H 5.33, N 3.94.

*3-Methyl-2,2-biscarbomethoxy-7-β-(phenoxyacetamido)-Δ³-desthiocephem-4-carboxylic Acid (***7***)*

Amide **6***a* (410 mg, 0.76 mmol) was dissolved in 60 ml EtOH – 8 ml THF and hydrogenated at 1 atm and 25°C over 10% Pd/C (410 mg); hydrogen uptake was complete at 10 min (27 ml, 145%). The catalyst was filtered off and washed with EtOH (50 ml) and evaporation of the filtrate left **7** (306 mg, 90%) as a clear oil. It was crystallized from acetone–pentane to give 237 mg (70%) of a white powder, mp 186–188°C (corrected); ir (Nujol mull): 3315, 3340, 2500–3600, 1785, 1755, 1725(1745s), 1665, 1600, 1550, 1500 cm^{-1}; uv (EtOH) λ_{max}: 267 (ε 9580). *Anal.* calcd. for $C_{21}H_{22}N_2O_9$: C 56.50, H 4.96, N 6.27; found: C 56.47, H 4.97, N 6.24.

*3-Methyl-7-β-(phenoxyacetamido)-Δ³-desthiocephem-2,4-dicarboxylic Acid (***8***)*

A mixture of amide **6***b* (270 mg, 0.39 mmol) and 10% Pd/C (270 mg) in glacial AcOH (10 ml) was hydrogenated at 1 atm and 25°C until H_2 uptake ceased. (More than the theoretical amount of H_2 was absorbed in all cases.) The catalyst was filtered off and the AcOH was evaporated at <1 Torr, 40–50°C water bath. The glassy residue was covered with benzene and reevaporated to remove the last traces of AcOH. The residue was crystallized by warming in water. The resulting white powdery crystals were dried *in vacuo* over P_2O_5 for 18 h (64 mg, 43.5%), mp 158–159°C (corrected); ir (Nujol mull): 3410, 3370, 2500–3600, 1775, 1750, 1725, 1715, 1685, 1650, 1600, 1525, 1500 cm^{-1}; uv (EtOH) λ_{max}: 268 (ε 5180). *Anal.* calcd. for $C_{18}H_{18}N_2O_7 \cdot \frac{1}{2}H_2O$: C 56.39, H 4.99, N 7.30; found: C 56.70, H 4.83, N 7.35.

Ester Cleavage of **4**c

A solution of 555 mg (1.085 mmol) of **4***c* in 15 ml of trifluoroacetic acid was placed on a rotary evaporator at 62°C and the solvent evaporated over a period of 5–10 min to give 425 mg of a foam the nmr spectrum of which indicated the complete loss of the *tert*-butyl signals. The foam was taken up in toluene and refluxed 10 min following which the toluene was evaporated to yield 380 mg (98.5%) of a white foam. The nmr spectrum of the crude material showed two methyl signals and two benzyl signals in a ratio of 3:1 indicating that decarboxylation of the diacid had occurred. The foam was chromatographed on 10 g silica gel (15% water w/w) using chloroform as eluent. The eluting solvent was gradually changed to ether. The earlier fractions gave material greatly enriched in compound **10**, the major isomer, while the column tailings were mostly compound **11**.

Preparation of Compound **14**

To a solution of 500 mg (1.4 mmol) of crude acid (3:1 mixture of **10** and **11**) in 25 ml methylene chloride was added 150 mg (1.5 mmol) of triethylamine. The solution was cooled to −10°C (ice–methanol) and 150 mg (1.6 mmol) methyl chloroformate in 2 ml CH_2Cl_2 was added dropwise. The solution was stirred 1.5 h. The solution was evaporated to dryness at reduced pressure and the residue partitioned between water and ether. The ethereal extracts were washed with 10% hydrochloric acid and then saturated sodium bicarbonate solution. Evaporation of the organic layer gave 300 mg crude methyl ester **12** which was used as such in the subsequent step. From the basic extracts, 120 mg of starting acid was recovered (mixture).

Reduction of 300 mg of crude ester using triethylamine (100 mg) – hydrogen sulfide gave, upon work-up (see preparation of **5***a*), 200 mg of **13** as an oil; ir (film): 3420, 3360, 1770, 1750, 1740, 1640 cm^{-1}.

Treatment of 172 mg (0.5 mmol) of the amine **13** with 76 mg (0.5 mmol) phenoxyacetic acid and 124 mg (0.5 mmol) EEDQ in 10 ml methylene chloride gave 220 mg (92%) of **14** as a white foam. Chromatography of this material on silica gel (15% water, w/w) using ether as eluent gave 200 mg of pure **14**, mp 57–58°C; ir ($CHCl_3$): 3430, 1770, 1740, 1695, 1600, 1590, 1525, 1495 cm^{-1}; uv (EtOH) λ_{max}: 268 (ε 12 900). *Anal.* calcd. for $C_{26}H_{26}N_2O_2 \cdot \frac{1}{2}H_2O$: C 64.06, H 5.58, N 5.75; found: C 64.31, H 5.52, N 5.60.

*3-Methyl-2-carbomethoxy-7-β-(phenoxyacetamido)-Δ³-desthiocephem-4-carboxylic Acid (***15***)*

Reduction of 100 mg (0.208 mmol) of **14** with 100 mg 10% Pd/C in 5 ml THF and 10 ml ethanol at 1 atm and 22°C for 3 h gave, after work-up (see preparation of **7**), 75 mg of a white powder, mp 84°C (dec.); ir ($CHCl_3$): 3420, 2500–3600, 1773, 1740, 1695, 1600, 1530, 1495 cm^{-1}; uv (EtOH) λ_{max}: 265 (ε 8150). *Anal.* calcd. for $C_{19}H_{20}N_2O_2 \cdot \frac{1}{2}H_2O$: C 57.43, H 5.33, N 7.04; found: C 57.87, H 5.60, N 6.61.

Acknowledgements

Partial financial support of this work by the National Research Council of Canada through its Industrial Research Assistance Plan is gratefully acknowledged. We also thank Dr. Bernard Belleau of McGill University for helpful discussions during the course of this work.

1. T. T. Conway, G. Lim, J. L. Douglas, M. Menard, T. W. Doyle, P. Rivest, D. Horning, L. R. Morris, and D. Cimon. Can. J. Chem. **56**, 1335 (1978).
2. (*a*) T. W. Doyle, B. Belleau, B. Luh, C. F. Ferrari, and M. P. Cunningham. Can. J. Chem. **55**, 468 (1977); (*b*) T. W. Doyle, B. Belleau, B. Luh, T. T. Conway, M. Menard, J. L. Douglas, D. T. Chu, G. Lim, L. R. Morris, P. Rivest, and M. Casey. Can. J. Chem. **55**, 2719 (1977); (*c*) T. W. Doyle, B. Y. Luh, D. T. Chu, and B. Belleau. Can. J. Chem. **55**, 484 (1977); (*d*) T. W. Doyle, J. L. Douglas, B. Belleau, J. Meunier, and B. Luh. Can. J. Chem. **55**, 2873 (1977).
3. L. D. Cama and B. G. Christensen. J. Am. Chem. Soc. **96**, 7582 (1974); R. N. Guthikonda, L. D. Cama, and B. G. Christensen. J. Am. Chem. Soc. **96**, 7584 (1974).
4. B. Belleau and G. Malek. J. Am. Chem. Soc. **90**, 1651 (1968).
5. T. T. Conway, J. L. Douglas, and D. E. Horning. Can. J. Chem. **56**, 2879 (1978).

Nuclear analogs of β-lactam antibiotics. XI. Synthesis of 3-methyl-7-β-(phenoxyacetamido)-Δ^3-desthiocephem-4-carboxylic acid[1]

TERRENCE WILLIAM DOYLE,[2,3] TERRY THOMAS CONWAY, GARY LIM, AND BING-YU LUH

Bristol Laboratories of Canada, 100 Industrial Boulevard, Candiac, P.Q., Canada J5R 1J1

Received April 20, 1978

TERRENCE WILLIAM DOYLE, TERRY THOMAS CONWAY, GARY LIM, and BING-YU LUH. Can. J. Chem. **57**, 227 (1979).

Treatment of the acid **3** with triethylamine in refluxing *tert*-butyl alcohol gave the decarboxylated product **4** which was isomerized to the desired Δ^3 isomer **5** using DBN. Reduction of the azido functions in **4** and **5** followed by coupling to phenoxyacetic acid and debenzylation gave the acids **11** and **8**, respectively. Attempts to prepare dienic cephalosporins failed. The halogenation of **4** and **5** was studied and is discussed.

TERRENCE WILLIAM DOYLE, TERRY THOMAS CONWAY, GARY LIM et BING-YU LUH. Can. J. Chem. **57**, 227 (1979).

Par traitement de l'acide **3** avec la triéthylamine dans l'alcool *tert*-butyle au reflux, on a obtenu le produit décarboxylé **4** qui, par isomérisation avec le DBN, a donné l'isomère Δ^3 attendu **5**. La réduction des fonctions azido dans **4** et **5**, puis le couplage subséquent à l'acide phénoxyacétique et la débenzylation ont conduit aux acides **11** et **8**, respectivement. Les tentatives pour préparer des céphalosporines diéniques ont échoué. On a étudié l'halogénation de **4** et de **5** et on discute de ces résultats.

[Traduit par le journal]

In the preceding paper of this series (1) we described the synthesis of some 2-substituted desthiocephalosporins from intermediates developed earlier for our syntheses of the *O*-2-isocephem (2*a*), *N*-2-isocephem (2*b*), and 2-isocephem (2*c*) systems (Fig. 1). In this paper we wish to report the synthesis of 7-β-phenoxyacetamido-3-methyl-Δ^3-desthiocephem-4-carboxylic acid **8**.

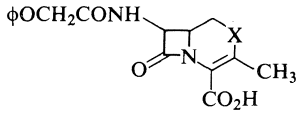

1

X = O, S, SO, SO_2, NMe, NCO_2Et, $C(CO_2R)_2$, $CH(CO_2R)$

FIG. 1. Cephalosporin analogs.

As we reported earlier trifluoroacetic acid effected cleavage of the diester **2** to give the corresponding diacid. As had been anticipated the diacid readily underwent decarboxylation to yield the monocarboxylic acid as a mixture of isomers **3**. We had expected that **3** would readily undergo a second decarboxylation to give either **4** or **5**. To our surprise even boiling **3** at reflux in toluene in the presence of acid gave no detectable amounts of either **4** or **5**. The conversion of **3** to **4** in 78% yield occurred readily in refluxing *tert*-butyl alcohol catalysed by triethylamine. No trace of **5** could be detected in the crude product. When **4** was treated with 1,5-diazabicyclo-[4.3.0]-5-nonene (DBN) a rapid quantitative conversion to **5** occurred. The structure assignments to **4** and **5** were amply supported by their ir, nmr, and uv spectra.

The fact that only the thermodynamically less stable **4** was formed upon decarboxylation of the anion of **3** implies that the reaction occurs with concomitant loss of the carboxyl group and migration of the double bond and not via the carbanion, **ii** (Fig. 2). Two explanations may be advanced for this: either rapid kinetic protonation of an initially formed anion or the involvement of an enolized ester anion form such as **i** which can be protonated at C4 rather than C2. That the latter explanation may be valid is supported by the work of Murphy and Koehler (3) on the preparation of Δ^2-cephalosporin esters (Fig. 3) via the ketene **iv** which adds alcohols to yield exclusively the Δ^2-cephem esters. Presumably the addition of alcohols proceeds via an intermediate very similar to if not identical to **i**.

With the desired Δ^3-desthiocephem at hand the conversion of **5** to 7-β-phenoxyacetamido-3-methyl-Δ^3-desthiocephem-4-carboxylic acid **8** was carried out. Reduction of the azido function using hydrogen sulfide – triethylamine (2*a*) gave the amine **6** in 91% yield. Treatment of **6** with phenoxyacetic acid and

[1]For Part X of this series see ref. 1.

[2]To whom correspondence concerning this paper may be addressed.

[3]Present address: Bristol Laboratories, P.O. Box 657, Syracuse, NY 13201, U.S.A.

0008-4042/79/020227-06$01.00/0

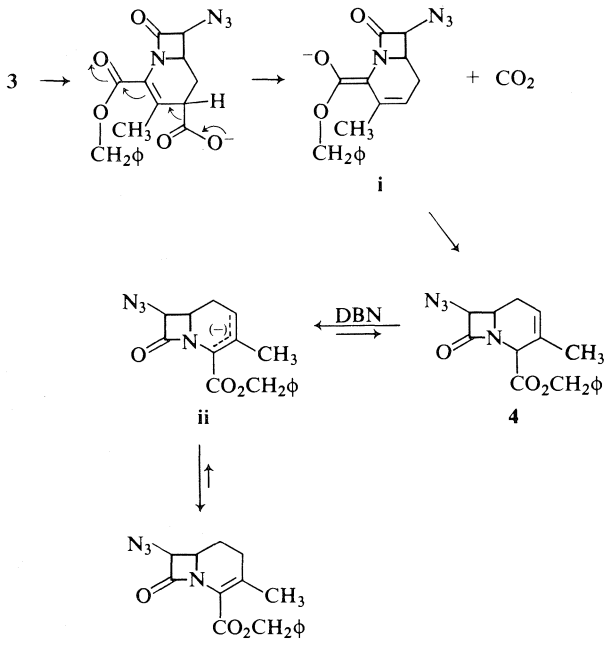

FIG. 2. Preparation of Δ^2- and Δ^3-desthiocephalosporin esters.

N-ethoxycarbonyl-2-ethoxy-1,2-dihydroquinoline (EEDQ) (4) gave the amide **7** in 68% yield. Finally removal of the benzyl ester was accomplished in 59% yield via hydrogenolysis over 10% palladium-on-carbon.

Similarly reduction of the azido function in **4** gave the amine **9** (86%). The coupling of phenoxyacetic acid to **9** using EEDQ proceeded in 95% yield to give **10**.

In view of the labile double bond in **10** removal of the benzyl function via hydrogenolysis was precluded. The saponification of the ester was modeled on the more available **4**. Thus treatment of **4** with 1 equiv. of 10% sodium hydroxide gave the acid **12** in 69% yield. We were unable to detect any **5** in the reaction thus indicating saponification to proceed more rapidly than isomerization. Similarly compound **10** was treated with 1% sodium hydroxide to give 7-β-phenoxyacetamido-3-methyl-Δ^2-desthiocephem-4-carboxylic acid **11** in 60% yield. These reactions are outlined in Scheme 1.

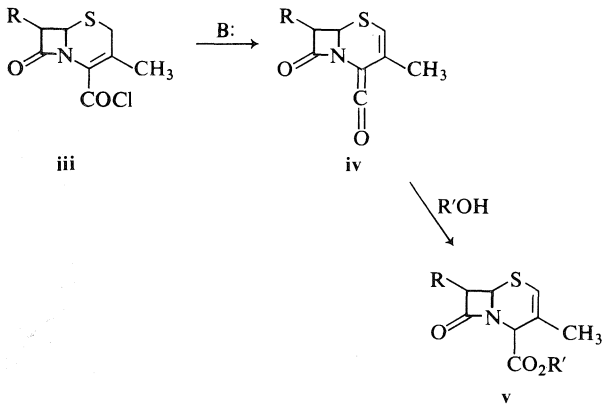

FIG. 3. Preparation of Δ^2-cephalosporin esters.

The ready access to compounds **4** and **5** led us to attempt the preparation of a desthiocephalosporin doubly unsaturated in the six membered ring or substituted with functionality other than carboxy groups at C2. The results obtained are outlined in Scheme 2.

Our first attempts involved treatment of **4** with NBS followed by treatment of the product with base to effect elimination to the diene. Thus upon treatment of **4** with NBS there was obtained a mixture of products. The nmr spectrum of the crude bromination mixture showed the presence of some starting material and at least two bromination products. The signals for the C3 methyl group and C4 protons was largely intact indicating bromination to have occurred at C1. Treatment of this crude mixture with triethylamine gave a mixture the nmr spectrum of which showed a singlet at 5.98 δ. Chromatography of the mixture led to recovery of **14** as an impure oil. Compound **14** proved to be relatively unstable and underwent rapid decomposition at ~25°C. The assignment of structure was made on the basis of the spectral data and the subsequent transformation of **14** to **5**. The nmr spectrum of **14** showed the proton α to the azide as a doublet at 5.05 δ (J = 5 Hz) and the C6 proton also as a doublet (J = 5 Hz) at 4.39 δ. The signals for the olefinic protons at C1 and C2 appeared together as a singlet at 5.98 δ integrating for two protons. The failure of the C1 proton to couple to the C6 proton is probably due to the fact that these protons are at ~75–80° dihedral angle to one another. The uv spectrum of **14** gave evidence of extended conjugation having a maxima at 322 nm (compared to 268 nm in **5**). All attempts to reduce the azido function in **14** to an amine failed. The use of hydrogen sulfide-triethylamine led to polymerization. When **14** was hydrogenated over 10% Pd/C the only characterizable product was **5** obtained in ~60% yield. All attempts to carry out formation of the dienic system via NBS bromination of **10** (or other suitable ester) and base treatment failed to give any detectable product.

Bromination of **4** proceeded readily to yield a dibromide **15** in quantitative yield. The nmr spectrum of **15** was compatible with a single product. The conversion of **15** to the desired **16** upon treatment with triethylamine was facile. The stereochemistry of the bromo group is that indicated in the scheme and is readily deduced from the nmr coupling constants to

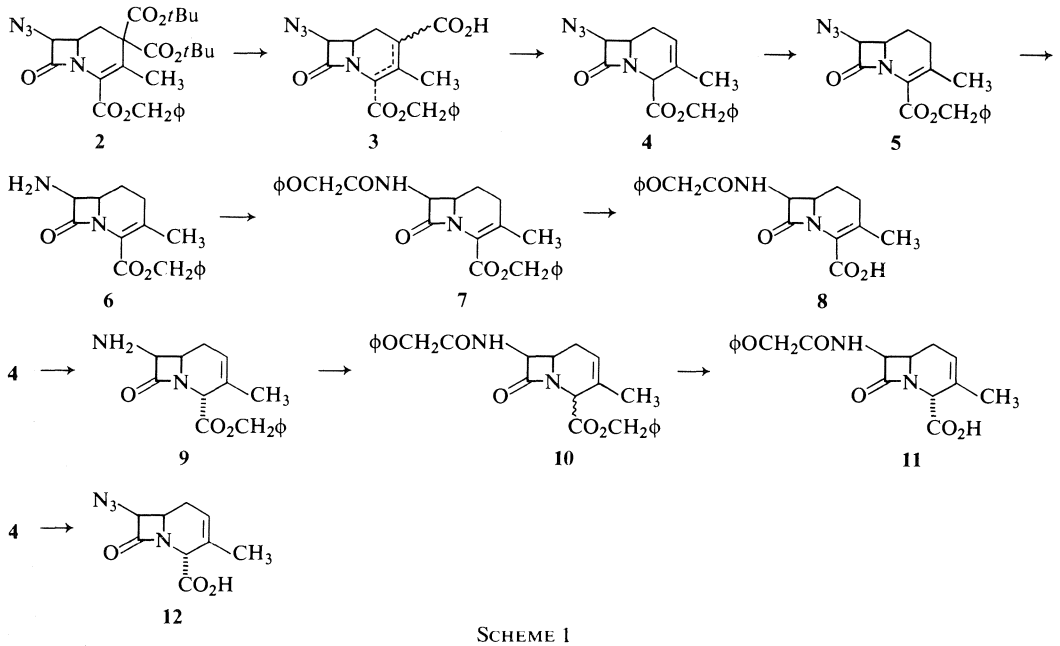

SCHEME 1

the C1 protons of the protons at C2 and C6. In our earlier work we have demonstrated that as in the natural series the molecule assumes the conformation shown in Fig. 4 (*2a–d*). The coupling constants of ~10.5 and 5 Hz between the C1-H_β and C6-H and between the C1-H_α and C6-H, respectively, confirm that as in the earlier work the desthiocephalosporins

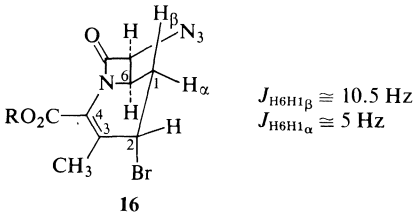

FIG. 4. Conformation of desthiocephalosporins.

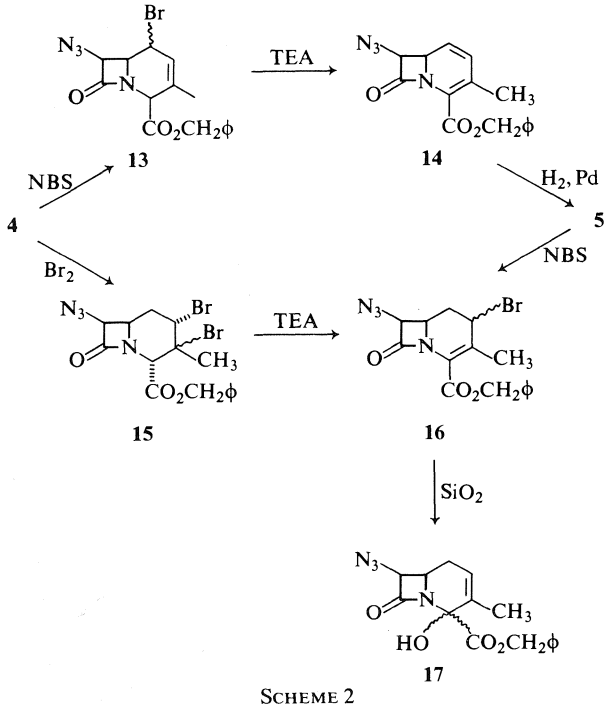

SCHEME 2

adopt the conformation shown. The appearance of the signal for the proton α to the bromine atom at 4.67 δ as a doublet of doublets with $J_1 = 3.5$, $J_2 = 2.5$ Hz is only compatible with the α configuration for the bromide. This also establishes the stereochemistry of the 2-bromo group in **15** as α. Compound **16** could also be prepared from **5** in near quantitative yield via treatment of **5** with NBS. The stereochemistry of **16** prepared from **5** was identical to that prepared via **15**.

Recently Macchia (5) and co-workers have reported the result of bromination of 2-cephems. As in our case they observed bromination to occur from the α face of the molecule. In their case however the entering bromide ended up at the C3 position owing to greater stabilization of charge in the bromonium ion by sulfur. Both *cis* and *trans* dibromides were obtained in their case (Fig. 5). In the case of the bromination of **4** only a single dibromide was formed. On mechanistic grounds the product might well be expected to be one of *trans* addition.

Attempts to displace the bromide **16** with various nucleophiles did not give well defined products so our

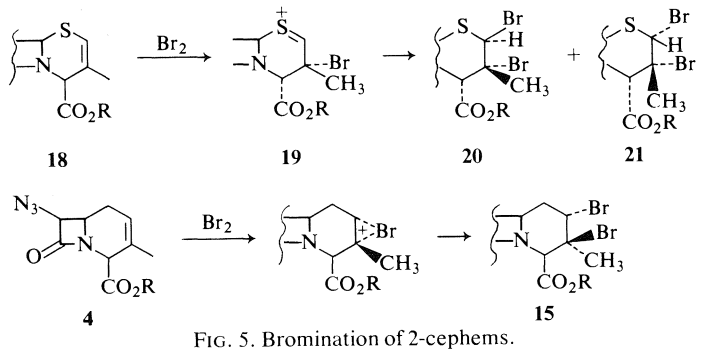

FIG. 5. Bromination of 2-cephems.

efforts along this line were abandoned. In one experiment attempted silica gel chromatography of **16** led to the rearranged alcohol **17** the structure of which was readily apparent from its spectral characteristics.

Compound **8** had antibiotic activity comparable to, although a bit weaker than the corresponding *O*-2-isocephem reported earlier (*2a*). A full discussion of the biological activities of **8** is reserved to a forthcoming structure activity paper.

Experimental

The infrared spectra were recorded on a Unicam SP-200G grating, ir spectrometer. The nmr spectra were determined on a Varian A60-A spectrometer using tetramethylsilane as an internal standard. Melting points are uncorrected and were determined on a Gallenkamp melting point apparatus. The analyses were performed by Micro-Tech Laboratories, Skokie, IL, U.S.A.

*Benzyl 3-Methyl-7-β-azido-Δ²-desthiocephem-4-carboxylate (**4**)*

A solution of 10.24 g (20 mmol) of **2** in 150 ml trifluoroacetic acid was evaporated at 50–60°C on a rotary evaporator at reduced pressure followed by pumping on a high vacuum pump (1 Torr). The residue was taken up in 100 ml chloroform and boiled at reflux for 20 min, following which the solution was washed three times with brine, dried over Na_2SO_4, filtered, and evaporated to dryness. The residual oil was taken up in 75 ml dry *tert*-butyl alcohol and 3 ml triethylamine was added. The solution was boiled at reflux for 30 min following which it was evaporated to dryness at reduced pressure. The residual oil was partitioned between ether (100 ml) and 1% NaOH (25 ml). The organic layer was washed with brine, 10% HCl, brine, and dried over Na_2SO_4. Filtration and evaporation of the filtrate yielded 4.84 g (77.5%) almost pure **4**. The oil was decolorized by passage through a pad of silica gel (Woelm) (15% water, w/w) with benzene. A small sample of the oil was sent for analysis; ir (film): 2110, 1770, 1750 cm^{-1}. *Anal.* calcd. for $C_{16}H_{16}N_4O_3$: C 61.53, H 5.16, N 17.94; found: C 61.69, H 5.27, N 17.96.

*Benzyl 3-Methyl-7-β-azido-Δ³-desthiocephem-4-carboxylate (**5**)*

To a solution of 480 mg (1.54 mmol) **4** in 25 ml CH_2Cl_2 was added 3 drops 1,5-diazabicyclo[4.3.0]-5-nonene (DBN). The solution was let stand 10 min at ambient temperature and washed with 10% HCl followed by brine. The solution was dried over Na_2SO_4, filtered, and evaporated to give 450 mg pure **5** which crystallized on trituration with a few drops of ether, mp 70.5–71.5°C (recrystallized from benzene – petroleum ether); ir ($CHCl_3$): 2110, 1770, 1725, 1635 cm^{-1}; uv (EtOH): λ_{max} 268 (ε 9250). *Anal.* calcd. for $C_{16}H_{16}N_4O_3$: C 61.53, H 5.16, N 17.94; found: C 61.39, H 5.17, N 18.19.

*Benzyl 3-Methyl-7-β-(phenoxyacetamido)-Δ³-desthiocephem-4-carboxylate (**7**)*

*Preparation of **6***

To a solution of 312 mg (1 mmol) **5** and 0.150 ml TEA in 20 ml CH_2Cl_2 was added a stream of H_2S gas over 2 min. The solution was observed to evolve N_2 and was let stand at 20°C until N_2 evolution ceased (30 min). The orange solution was evaporated to dryness at reduced pressure and the residue partitioned between ether and 10% HCl. The acidic layer was made basic with Na_2CO_3 and extracted into ether. The ethereal extracts were dried over Na_2SO_4, filtered, and evaporated to yield 260 mg (91%) pure amine **6**.

Side-chain Coupling

The oil from the above procedure 260 mg (0.91 mmol) was taken up in 20 ml CH_2Cl_2. To this was added 138 mg (0.91 mmol) phenoxyacetic acid followed by 225 mg (0.91 mmol) EEDQ. The solution was let stand 1.0 h at 25°C, washed with 10% HCl, dried over Na_2SO_4, filtered, and evaporated to give an oil. The oil was taken up in 5 ml ether and petroleum ether (30–60°C) was added to the cloud point. The solution was allowed to slowly evaporate over 18 h. The remaining solvent was decanted and the partially crystalline residue was triturated with ether (2 ml) and scratched. The crystals were isolated by filtration, mp 96–97°C (recrystallized from ether – petroleum ether). A total of 260 mg (68%) pure **7** were obtained; ir ($CHCl_3$): 3400, 3320, 1770, 1720, 1690, 1600, 1590, 1530, 1495 cm^{-1}; uv (EtOH): λ_{max} 269 (ε 12 750). *Anal.* calcd. for $C_{24}H_{24}N_2O_5$: C 68.56, H 5.75, N 6.66; found: C 68.28, H 5.80, N 6.57.

*3-Methyl-7-β-(phenoxyacetamido)-Δ³-desthiocephem-4-carboxylic Acid (**8**)*

A suspension of 200 mg (0.475 mmol) ester **7** and 100 mg 10% Pd/C in 25 ml ethylacetate was shaken 1.25 h at 45 psi under H_2. The suspension was filtered through Celite and evaporated to yield a semisolid glass which was triturated with 20 ml ether to induce crystallization. The solid was recrystallized from acetonitrile–ether to yield 92 mg (59%) pure acid, mp 184–185°C with decomposition (placed in melting point apparatus at 177°C, heating rate, 2°C/min); ir (Nujol mull): 3300, 2500–3600, 1770, 1685, 1620, 1600 cm^{-1}; uv (EtOH): λ_{max} 264 (ε 9050) shifts to λ_{max} 259 on addition of **1***d* TEA. *Anal.* calcd. for $C_{17}H_{18}N_2O_5$: C 61.81, H 5.49, N 8.48; found: C 61.63, H 5.52, N 8.61.

*Benzyl 3-Methyl-7-β-(phenoxyacetamido)-Δ²-desthiocephem-4-carboxylate (**10**)*

Reduction of 936 mg (3 mmol) of **4** using triethylamine (0.5 ml) – hydrogen sulfide in methylene chloride gave 712 mg (86%) of pure **9** after the usual work-up, mp 79–80°C (crystallized from ether); ir ($CHCl_3$): 3400, 1755, 1745 cm^{-1}. *Anal.* calcd. for $C_{16}H_{18}N_2O_3$: C 67.12, H 6.34, N 9.78; found: C 66.77, H 6.30, N 9.67.

TABLE 1. Nuclear magnetic resonance spectra[a]

Compound	Aromatic and vinyl protons	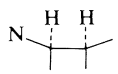		ARCH_2	CH_3	Other
4	7.20(s, 5H) 5.50(bm, 1H 2H)	4.70(d) $J = 4.5$	3.85(ddd) $J_1 = 7.5$ $J_2 = 4.5$ $J_3 = 6.5$	5.06(s, 2H)	1.65(bs, 3H)	4.55(bs, 1H, C*H*CO_2Bz) 2.15(m, 2H CH_2CH═)
5	7.34(m, 5H)	4.82(d) $J = 5$	3.66(dt) $J_1 = 10$ $J_2 = 5$	5.22(s, 2H)	2.02(s)	1.6–2.5(m, 2H)
6	7.35(m, 5H)	4.36(d) $J = 5$	3.59(ddd) $J_1 = 10$ $J_2 = 5$ $J_3 = 4.5$	5.23(s, 2H)	1.98(s)	1.3–2.5(m, 4H, NH_2 + —CH_2—)
7	7.36(s, 5H) 6.7–7.5(m, 5H)	5.38(dd) $J_1 = 7.5$ $J_2 = 5$	3.74(dt) $J_1 = 11$ $J_2 = 5$	5.22(s, 2H)	2.07(s)	1.2–2.4(m, 2H) 4.53(s, 2H, ϕOCH_2) 7.91(d, 1H, $J = 7.5$, N*H*)
8[b]	6.7–7.4(m, 5H)	5.35(dd) $J_1 = 7.5$ $J_2 = 5.0$	3.80(ddd) $J_1 = 10.5$ $J_2 = 5.0$ $J_3 = 4.5$		2.03(s)	1.6–2.5(m, 2H) 7.70(d, 1H, $J = 7.5$, N*H*) 9.08(bs, 1H, CO_2H)
9	7.22(s, 5H) 5.57(m, 1H)	4.31(d) $J = 4.5$	3.79(dt) $J_1 = 7.0$ $J_2 = 4.5$	5.08(s)	1.69(bs, 3H)	4.54(bs, C*H*, CO_2CH_2ϕ) 2.20(m, 2H) 1.50(bs, 2H, NH_2)
10	7.23(s, 5H) 6.7–7.4(m, 5H) 5.51(bs, 1H)	5.25(dd) $J_1 = 7.0$ $J_2 = 4.5$	3.95(dt) $J_1 = 7.0$ $J_2 = 4.5$	5.10(s)	1.68(bs)	7.64(d, 1*H*, N*H*, $J = 7.0$) 4.53(bs, 1*H*) 4.46(s, 2H, ϕOCH_2) 2.05(m, 2H)
11[b]	6.7–7.4(bs, 5H) 5.50(bs, 1H)	5.21(dd) $J_1 = 7.0$ $J_2 = 4.5$	4.0(dt) $J_1 = 7.0$ $J_2 = 4.5$		1.78(bs)	4.45(s, 3H, ϕOCH_2 + C*H*CO_2H) 2.05(m, 2H) 9.05(bs, 2H, CO_2H + N*H*)
12	5.61(m, 1H)	4.82(d) $J = 5$	3.93(dt) $J_1 = 7$ $J_2 = 5$		1.80(bs)	4.55(sb, C*H*CO_2H) 2.28(m, 2H)
14	7.24(s, 5H) 5.98(s, 2H)	5.05(d) $J = 5$	4.39(d, 1H) $J = 5$	5.18(s, 2H)	2.18(s)	
15	7.21(s, 5H)	4.81(d) $J = 5$	4.25(dt) $J_1 = 10$ $J_2 = 5$	5.05(s, 2H)	2.14(s)	4.74(s, 1H, C*H*CO_2Bz) 4.53(t, 1H, C*H*—Br, $J = 3$) 3.03(ddd, 1H, $J_1 = 14.5$, $J_2 = 10$, $J_3 = 3.0$) 1.8–2.5(m, 1H, obsc. by Me)
16	7.33(s, 5H)	4.93(d) $J = 5$	4.27(dt) $J_1 = 10.5$ $J_2 = 5$	5.21(s, 2H)	2.10(s)	2–2.5(m, 2H, CH_2) 4.67(dd, 1H, C*H*Br, $J_1 = 2.5$, $J_2 = 3.5$)
17	7.20(s, 5H) 5.66(m, 1H)	4.62(d) $J = 5$	3.71(ddd) $J_1 = 9.0$ $J_2 = 5$ $J_3 = 4.5$	5.01, 5.26[c] $J = 12$	1.61(m, 3H)	2.0–2.5(m, 2*H*) 4.70(s, 1H, OH)

[a]Recorded at 60 MHz in $CDCl_3$ unless otherwise noted. Coupling constants are in Hz.
[b]DMSO-d_6–$CDCl_3$.
[c]Arms of AB quartet.

The amine **9**, 712 mg (2.58 mmol) was treated with 378 mg (2.58 mmol) phenoxyacetic acid and 620 mg (2.58 mmol) EEDQ in 50 ml methylene chloride as in the previous example to yield 1.002 g (95%) of **10**, mp 95°C (corrected); ir ($CHCl_3$): 3430, 1775, 1750, 1695, 1600, 1595, 1525, 1495 cm^{-1}. *Anal.* calcd. for $C_{24}H_{24}N_2O_5$: C 68.56, H 5.75, N 6.66; found: C 68.49, H 5.82, N 6.47.

*3-Methyl-7-β-(phenoxyacetamido)-Δ²-desthiocephem-4-carboxylic Acid (**11**)*

To a solution of 210 mg (0.5 mmol) of **10** in 8 ml tetrahydrofuran was added 2 ml of 1% sodium hydroxide. The solution was stirred 30 min and diluted with 20 ml ether. The layers were separated and the organic layer washed three times with 10-ml aliquots of water. The combined aqueous layers were acidified with 10% HCl, saturated with sodium chloride, and extracted three times with methylene chloride. The extracts were dried over sodium sulfate and evaporated to yield 100 mg (60%) of the desired acid **11**, mp 157°C (corrected) with decomposition (recrystallized from ethanol–ether); ir (Nujol mull): 3300, 2500–3600, 1760, 1735, 1680, 1600, 1540, 1500 cm^{-1}. *Anal.* calcd. for $C_{17}H_{18}N_2O_5 \cdot \frac{3}{4}H_2O$: C 59.38, H 5.72, N 8.15; found: C 59.66, H 5.36, N 8.13.

*3-Methyl-7-β-azido-Δ²-desthiocephem-4-carboxylic Acid (**12**)*

Treatment of 1.75 g (5.6 mmol) of **4** in 30 ml tetrahydro-

furan with 22.5 ml of 1% sodium hydroxide as in the above example gave 857 mg (69%) of pure **12** after the usual work-up, mp 144–144.5°C (recrystallized from acetone – methylene chloride); ir ($CHCl_3$): 2500–3500, 2110, 1765, 1725(sh) cm^{-1}; *Anal.* calcd. for $C_9H_{10}N_4O_3$: C 48.64, H 4.54, N 25.22; found: C 48.65, H 4.59, N 25.33.

*Preparation of Compound **14***

A suspension of 624 mg (2 mmol) of **4** and 460 mg (2.58 mmol) *N*-bromosuccinimide in 20 ml carbon tetrachloride was boiled at reflux with irradiation from a sun lamp. After 30 min an aliquot was removed and checked by nmr for the presence of **4**. The reaction was continued an additional 15 min. The solution was cooled, washed with water, dried over sodium sulfate, and evaporated. The nmr spectrum showed traces of **4** and the presence of **13** in the reaction mixture. The sample was taken up in 25 ml methylene chloride and treated with 0.22 g of triethylamine. The solution was washed with 20 ml of water, dried over sodium sulfate, and evaporated. The oil was chromatographed on 50 g silica gel (15% water, w/w) with chloroform. The earlier fractions from the column yielded a material (~70 mg) the nmr spectrum of which was compatible with benzyl 3-bromomethyl-7-β-azido-Δ^2-desthiocephem-4-carboxylate. After a number of mixed fractions there was eluted 273 mg of impure **14** as an oil. Compound **14** was unstable being completely decomposed in a week. The assignment of structure is based on the ir, nmr, and uv spectra of **14**; ir ($CHCl_3$): 2110, 1780, 1770, 1720, 1600, 1585 cm^{-1}; uv (EtOH): λ_{max} 322 (ε 3550).

*Reduction of **14***

A solution of 250 mg of crude **14** in 20 ml ethyl acetate was hydrogenated over 10% Pd/C at atmospheric pressure and 25°C for 1 h. The solution was filtered and evaporated to yield an oil which was taken up in methylene chloride and chromatographed on 15 g silica gel (15% water, w/w) to give 145 mg of **5** identical in all respects with that obtained earlier.

*Benzyl 3-Methyl-2-α-bromo-7-β-azido-Δ^3-desthiocephem-4-carboxylate (**16**)*

*From **4***

To a solution of 1.78 g (5.7 mmol) of **4** in 50 ml methylene chloride was added an excess of bromine (3.2 g, 20 mmol). The solution was refluxed 20 minutes. A small aliquot was evaporated to dryness. The nmr spectrum of the residual oil was compatible with a single dibromide (see Table 1). To the solution was added 1.01 g (10 mmol) triethylamine. The solution was let stand 30 min, washed with water, 10% hydrochloric acid, and brine. After drying over sodium sulfate the solution was evaporated to dryness and the residual oil was triturated with ether. A total of 500 mg of pure **16** was obtained on filtration, mp 95.5–96°C; uv (EtOH): λ_{max} 284 nm (ε 6600). *Anal.* calcd. for $C_{16}H_{15}BrN_4O_3$: C 49.12, H 3.86, N 14.32, Br 20.42; found: C 49.01, H 3.91, N 14.43, Br 20.32.

*From **5***

To a solution of 106 mg of **5** in 10 ml carbon tetrachloride was added 60 mg *N*-bromosuccinimide and 2 mg benzoyl peroxide. The solution was brought to reflux for 30 min, cooled, washed with water, brine, and dried over sodium sulfate. The suspension was filtered and the filtrate evaporated to yield 137 mg (95%) of **16** identical in all respects with that obtained from **4**.

*Benzyl 3-Methyl-4-hydroxy-7-β-azido-Δ^2-desthiocephem-4-carboxylate (**17**)*

The mother liquors from the crystallization of **16** in the above experiment were chromatographed on 20 g silica gel (Woelm activity III) using methylene chloride as eluent. In addition to some **16** (450 mg) which eluted early a second material eluted from the column as an oil. The nmr spectrum (Table 1) was consistent for the material being **17**. *Anal.* calcd. for $C_{16}H_{16}N_4O_4$: C 58.53, H 4.91, N 17.07; found: C 58.41, H 5.02, N 16.93.

Acknowledgements

Partial financial support of this work by the National Research Council of Canada through its Industrial Research Assistance Plan is gratefully acknowledged. Many helpful discussions with Prof. Bernard Belleau during the course of this work are also gratefully acknowledged.

1. T. W. Doyle, T. T. Conway, M. Casey, and G. Lim. Can. J. Chem. **56**, 222 (1978).
2. (*a*) T. W. Doyle, B. Belleau, B-y. Luh, T. T. Conway, M. Menard, J. L. Douglas, D. T.-w. Chu, G. Lim, L. R. Morris, P. Rivest, and M. Casey. Can. J. Chem. **55**, 484 (1977); (*b*) T. W. Doyle, B-y. Luh, D. T.-w. Chu, and B. Belleau. Can. J. Chem. **55**, 2719 (1977); (*c*) T. W. Doyle, J. L. Douglas, B. Belleau, J. Meunier, and B-y. Luh. Can. J. Chem. **55**, 2873 (1977).
3. C. F. Murphy and R. E. Koehler. J. Org. Chem. **35**, 2429 (1970).
4. B. Belleau and G. Malek. J. Am. Chem. Soc. **90**, 1651 (1968).
5. A. Balsamo, P. Crotti, B. Macchia, F. Macchia, G. Nannini, E. Dradi, and A. Forgione. J. Org. Chem. **41**, 2150 (1976).

Facile syntheses of the enantiomers of sulcatol

BLAIR D. JOHNSTON AND KEITH N. SLESSOR[1]

Department of Chemistry, Simon Fraser University, Burnaby, B.C., Canada V5A 1S6

Received August 4, 1978

BLAIR D. JOHNSTON and KEITH N. SLESSOR. Can. J. Chem. **57**, 233 (1979).

The synthesis of *R*-(−)- and *S*-(+)-6-methyl-5-hepten-2-ol (sulcatol) from commercially available ethyl *S*-(−)-lactate via chiral methyloxiranes is reported. Both substances have crystalline intermediates in their synthetic routes insuring high optical purity. The necessity for a simple route to *S*-(+)-sulcatol results from the identification of this chiral substance in the pheromone complement of *Gnathotricus retusus*, a northwestern American timber pest.

BLAIR D. JOHNSTON et KEITH N. SLESSOR. Can. J. Chem. **57**, 233 (1979).

On rapporte la synthèse des *R*-(−)- et *S*(+)-méthyl-6 heptène-5 ols-2 (sulcatol) à partir du *S*(−)-lactate d'éthyle disponible commercialement et par l'intermédiaire de méthyloxirannes chirales. La synthèse de ces deux substances implique des intermédiaires cristallins qui assurent des puretés optiques élevées. La nécessité de trouver une voie simple permettant d'accéder au *S*(+)-sulcatol provient du fait que cette substance chirale a été identifiée dans le complément de la phéromone du *Gnathotricus retusus*, un insecte des bois du nord-ouest de l'Amérique.

[Traduit par le journal]

Introduction

Recent investigations[2] have shown that *S*-(+)-6-methyl-5-hepten-2-ol, *S*-(+)-sulcatol ((+)-**3**), is the aggregation pheromone of *Gnathotricus retusus*, a wood boring ambrosia beetle which attacks fallen and cut timber. The syntheses of sulcatol enantiomers (1, 2) devised for the elucidation of the role of the chiral pheromone complement in *G. sulcatus* (3) were clearly not applicable to the amounts necessary for *G. retusus* lab–field bioassays and future control programs. *R*-(+)- and *S*-(−)-Methyloxirane **2** appeared to be ideal synthons for the sulcatol enantiomers.

Seuring and Seebach (4) have identified the chiral pool as a convenient source of *S*-(−)-methyloxirane from the commercial ethyl *S*-(−)-lactate. A low melting crystalline intermediate enhances chiral purity but the crystallization is difficult. *R*-(+)-Methyloxirane, *R*-(+)-**2**, has been prepared by a fermentation method (5) with good results, although no crystalline intermediates provided the necessary insurance of optical purity. Diborane reduction of the carboxylate ester in the readily prepared, crystalline ethyl 2-*O*-*p*-toluenesulphonyl *S*-(−)-lactate **1** provided ideal access to *R*-(+)-**2**. With pure enantiomers of methyloxirane, prenylation provided the desired sulcatols **3**.

Stereospecific opening of methyloxiranes is well established (6) and recently regioselective alkylation

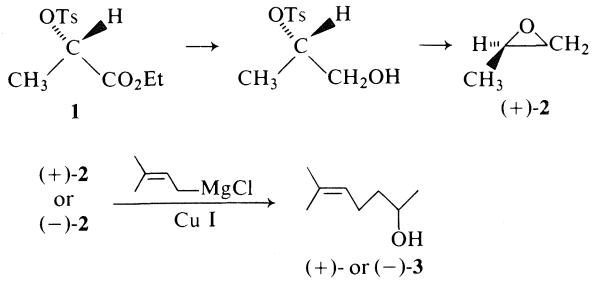

SCHEME 1

by allylic Grignard reagents has been achieved using copper(I) iodide catalysis (7). Recent syntheses of (+)-α-bisabolol (8) and *R*-(+)-recifeiolide (9) are examples of alkylation of chiral epoxides with no apparent racemization.

To insure the optical purity of the enantiomeric sulcatols, the crystalline *p*-nitrobenzoates **4** were prepared and recrystallized to constant melting point and optical rotation. Base hydrolysis of the esters regenerated the enantiomers of *S*-(+)- and *R*-(−)-**3**. The optical purity of the sulcatols was evident from the strong optical rotations of gc pure final products. To obtain optical rotations of sufficient accuracy, temperature control of the samples was necessary.

The utility of this work rests not only in the facile syntheses of chiral insect pheromones for pest

[1]Present address: Forest Pest Management Institute, Canadian Forest Service, Sault Ste Marie, Ont. P6A 5M7.

[2]Personal communication: Professor J. H. Borden, Pestology Centre, Department of Biological Sciences, Simon Fraser University.

0008-4042/79/020233-03$01.00/0

management but also in the availability of *R*-(+)-methyloxirane. The convenient synthesis of this synthon from a commercial product expands the usefulness of the chiral pool as a source of optically active reagents.

Experimental

General procedures and instrumentation were as described earlier (2). Melting and boiling points are uncorrected. The ethyl *S*-(−)-lactate was purchased from The Aldrich Chemical Co. and the cuprous iodide (purified grade) was obtained from Fisher Scientific.

S-*(−)-Methyloxirane* (S-*(−)*-**2**)

This compound was prepared by the method of Seuring and Seebach (4) via the crystalline *S*-(−)-1-*p*-toluenesulphonyl-2-propanol; $[\alpha]_D^{24}$ −14.2° (neat), bp 34°C/750 Torr. A linear dependence of $[\alpha]_D$ with temperature over the range α_{obs}^{14} −6.20° to α_{obs}^{32} −5.60° (0.4999-dm cell) was observed (lit. (4) $[\alpha]_D$ −12.5° (neat), bp 34°C/760 Torr. Nuclear magnetic resonance and ir spectra were identical with those of racemic propylene oxide (Aldrich ρ 0.83 g/mL).

S-*(+)-6-Methyl-5-hepten-2-ol* (S-*(+)*-**3**)

Magnesium (7.2 g, 300 mmol) was stirred with dry tetrahydrofuran (50 mL) under an N_2 atmosphere with ice-bath cooling. A solution of 1-chloro-3-methyl-2-butene (20.8 g, 200 mmol) in dry tetrahydrofuran (100 mL) was slowly added dropwise over a period of 1.5 h. After stirring for a further 1 h at ice-bath temperature the black suspension was filtered through a plug of glass wool into a clean, dry flask and again cooled in an ice-bath. Cuprous iodide (3.8 g, 20 mmol) was then added and a solution of *S*-(−)-**2** (5.8 g, 100 mmol) in dry tetrahydrofuran (50 mL) was dripped in over a period of 3 h with vigorous stirring. After a further 1 h the black suspension was poured into saturated aqueous ammonium chloride solution (300 mL) and extracted with ether (3 × 200 mL). The combined ether extracts were washed with water (75 mL) and saturated aqueous sodium chloride (75 mL), dried over anhydrous sodium sulphate, and evaporated to ~25 ml. After two vacuum distillations the yield of *S*-(+)-**3** was 9.4 g (75%), bp 85–86°C/20 Torr, $[\alpha]_D^{23}$ +17.4° (neat).

S-*(+)-6-Methyl-5-hepten-2-ol* p-*Nitrobenzoate* (S-*(+)*-**4**)

p-Nitrobenzoyl chloride (27.8 g, 150 mmol) was added to a solution of *S*-(+)-sulcatol (16.8 g, 131 mmol) in pyridine (200 mL). After stirring for 4 h at room temperature the solution was poured into water (500 mL) and extracted with ether (3 × 250 mL). The combined ether extracts were washed with 5% aqueous sodium bicarbonate (2 × 150 mL) and saturated aqueous sodium chloride (150 mL) solutions, dried over magnesium sulphate, filtered, and evaporated to a syrup which was co-evaporated twice with toluene (75 mL) to remove pyridine. The residue partially crystallized on cooling and was recrystallized from methanol (150 mL) to yield 32 g (88%) of light yellow needle-like crystals, mp 53–55°C. After two recrystallizations from methanol the derivative had mp 54–55°C, $[\alpha]_D^{22}$ +61.4° (*c* 5.01, $CHCl_3$). *Anal.* calcd. for $C_{15}H_{19}NO_4$: C 64.96, H 6.89, N 5.02; found: C 64.92, H 6.99, N 5.02.

Regeneration of S-*(+)-Sulcatol from the* p-*Nitrobenzoate* (*(+)*-**4**)

S-(+)-Sulcatol *p*-nitrobenzoate (29.5 g, 106 mmol) was dissolved in 2 *N* alcoholic sodium hydroxide (500 mL) and the solution stirred 20 h at room temperature, poured into water (1000 mL), and extracted with chloroform (3 × 250 mL). The chloroform extracts were dried over magnesium sulphate and evaporated to ~30 mL. Distillation, bp 74–75°C/12 Torr, yielded *S*-(+)-sulcatol (13 g, 95%), $[\alpha]_D^{24}$ +18.6° (neat), ρ^{24} 0.841 g/mL (observed), with a linear dependence of $[\alpha]_D$ with temperature over the range α_{obs}^{14} +8.07° to α_{obs}^{32} +7.58° (0.4999-dm cell), $[\alpha]_D^{23}$ +14.8° (*c* 4.96, EtOH) (lit. (1) $[\alpha]_D^{23}$ +14.4° (*c* 0.998, EtOH), lit. (2) $[\alpha]_D^{20}$ +13.96° (*c* 4.56, EtOH)).

*Ethyl 2-*p*-Toluenesulphonyl-*S*-(−)-lactate* (**1**)

Ethyl *S*-(−)-lactate (40 g, 0.34 mol) was dissolved in pyridine (400 mL) and cooled in an ice-bath to < 5°C. *p*-Toluenesulphonyl chloride (80 g, 0.42 mol) was added in small portions over a period of 10 min and the resulting yellow solution was kept for 24 h at −5°C. Small portions of ice (~1, ~5, and ~10 g) were then added, with a period of 15 min between additions, insuring that the temperature remained near 0°C. The solution was then poured into ice water (1 L) and extracted with chloroform (3 × 250 mL). The chloroform extracts were dried over anhydrous sodium sulphate and evaporated. The syrupy residue was taken up in petroleum ether (30–60°C) – $CHCl_3$ 10:1 (500 mL) and crystallized by rapid cooling in a Dry Ice – acetone bath to yield 66 g (71%) of the tosylate. Recrystallization from petroleum ether – $CHCl_3$ gave 60 g of pure tosylate **1**, mp 31°C, $[\alpha]_D^{23}$ −33.2° (*c* 5.05, $CHCl_3$). *Anal.* calcd. for $C_{12}H_{16}SO_5$: C 52.94, H 5.92; found: C 53.18, H 5.95.

R-*(+)-Methyloxirane* (R-*(+)*-**2**)

To 82 g (300 mmol) of **1** was added 1 *M* BH_3 in tetrahydrofuran (600 mL) and the solution stirred for 5 days at room temperature and 3 days at 40°C under N_2. The resulting cloudy solution was poured into water (1 L) and sodium carbonate (~5 g) was added to break the emulsion. The aqueous phase was extracted with ether (2 × 300 mL) and the combined ether extracts were washed with saturated aqueous sodium chloride (300 mL) and dried over magnesium sulphate. Filtration and evaporation at 0.01 Torr yielded 71 g of crude syrupy 2-*O*-*p*-toluenesulphonyl-1-propanol. This material was dripped into 100 mL of 50% KOH at 55°C. The *R*-(+)-methyloxirane which distilled out of the reaction flask was collected in a Dry Ice – acetone trap. Weak vacuum (200 Torr) was applied for 1/2 h to assist in collection of the product. A further distillation over KOH, bp 34–35°C/760 Torr, yielded 8.7 g of (+)-**2**, 50% based on **1**, $[\alpha]_D^{24}$ +13.9° (neat).

R-*(−)-6-Methyl-5-hepten-2-ol* (R-*(−)*-**3**)

This was prepared in exactly the same manner as *S*-(+)-**3** in 73% yield from *R*-(+)-**2**. Doubly distilled *R*-(−)-**3**, bp 85–86°C/20 Torr, exhibited a rotation of $[\alpha]_D^{24}$ −18.0° (neat). Purified via the *p*-nitrobenzoate, in the same way as the (+) enantiomer, *R*-(−)-**3** exhibited a rotation of $[\alpha]_D^{24}$ −18.5° (neat) and $[\alpha]_D^{23}$ −14.7° (*c* 5.02, EtOH) (lit. (1) $[\alpha]_D^{23}$ −14.5° (*c* 0.74, EtOH), lit. (2) $[\alpha]_D^{20}$ −13.89° (*c* 4.76, EtOH)).

R-*(−)-6-Methyl-5-hepten-2-ol* p-*Nitrobenzoate* (R-*(−)*-**4**)

This was prepared as described for *S*-(+)-**4**. Two recrystallizations yielded material of mp 54–55°C, $[\alpha]_D^{22}$ −61.2° (*c* 5.02, $CHCl_3$). *Anal.* calcd. for $C_{15}H_{19}NO_4$: C 64.96, H 6.89, N 5.02; found: C 64.95, H 6.88, N 5.06.

Acknowledgements

We thank Professor John Borden for his enthusiasm and encouragement of this work and the National Research Council of Canada (Operating A3785 and Co-op A0243 grants) for financial support.

1. K. MORI. Tetrahedron, **31**, 3011 (1975).
2. H. R. SCHULER and K. N. SLESSOR. Can. J. Chem. **55**, 3280 (1977).
3. J. H. BORDEN, L. CHONG, J. A. MCLEAN, K. N. SLESSOR, and K. MORI. Science, **192**, 894 (1976).
4. B. SEURING and D. SEEBACH. Helv. Chim. Acta, **60**, 1175 (1977).
5. C. C. PRICE and M. OSGAN. J. Am. Chem. Soc. **78**, 4787 (1956).
6. R. A. BENKESER. Synthesis, 347 (1971).
7. F. DERGUINI-BOUMECHAL, R. LORNE, and G. LINSTRUMELLE. Tetrahedron Lett. 1181 (1977).
8. A. KERGOMARD and H. VESCHAMBRE. Tetrahedron, **33**, 2215 (1977).
9. K. UTIMOTO, K. UCHIDA, M. YAMAYA, and H. NOZAKI. Tetrahedron Lett. 3641 (1977).

Tautomerization equilibria for phosphorous acid and its ethyl esters, free energies of formation of phosphorous and phosphonic acids and their ethyl esters, and pK_a values for ionization of the P—H bond in phosphonic acid and phosphonic esters

J. Peter Guthrie[1]

Department of Chemistry, University of Western Ontario, London, Ont., Canada N6A 5B7

Received June 2, 1978

J. Peter Guthrie. Can. J. Chem. **57**, 236 (1979).

From data in the literature the free energies of formation in aqueous solution of triethyl phosphite and diethyl phosphonate can be calculated as -138.4 ± 1.7 and -165.1 ± 2.0 kcal mol^{-1}, respectively. From these values, by application of free energy relations which we have published, the free energies of formation of the corresponding hydroxy compounds can be calculated and thence the equilibrium constants for tautomerization, which are $10^{7.2}$, $10^{8.7}$, and $10^{10.3}$ in favor of the tetracoordinate phosphonate tautomer for $P(OEt)_2OH$, $P(OEt)(OH)_2$, and $P(OH)_3$, respectively. Using estimated pK_a values for the tricoordinate phosphite species the tautomerization equilibria for the anions could also be calculated, as could the pK_a values from the P—H bonds: 13, 26, and 38 for $H—PO(OEt)_2$, $H—PO_2(OEt)^-$, and $H—PO_3^{2-}$, respectively.

J. Peter Guthrie. Can. J. Chem. **57**, 236 (1979).

En se basant sur des données de la littérature, on a calculé que les énergies libres de formation, en solution aqueuse, du phosphite de triéthyle et du phosphonate de diéthyle sont respectivement -138.4 ± 1.7 et -165.1 ± 2.0 kcal mol^{-1}. Utilisant ces valeurs et les relations d'énergie libre que nous avons publiées, on peut calculer les énergies libres de formation des composés hydroxylés correspondants ainsi que les constantes d'équilibre de la tautomérisation qui sont respectivement $10^{7.2}$, $10^{8.7}$ et $10^{10.3}$ en faveur du tautomère phosphonate tétracoordonné du $P(OEt)_2OH$, $P(OEt)(OH)_2$ et $P(OH)_3$. Faisant appel à des évaluations des valeurs de pK_a pour les espèces phosphites tricoordonnées, on peut aussi calculer l'équilibre de tautomérisation des anions de même que les valeurs de pK_a des liaisons P—H qui sont respectivement 13, 26 et 38 pour $H—PO(OEt)_2$, $H—PO_2(OEt)^-$ et $H—PO_3^{2-}$.

[Traduit par le journal]

Introduction

Phosphorous acid was one of the anomalous cases confusing the pattern of acidities shown by the inorganic oxy acids (1). The anomaly was removed by the recognition that phosphorous acid was not $P(OH)_3$, but rather $H—PO(OH)_2$, which normally acts as a dibasic acid (2).[2] Nevertheless, the tautomer $P(OH)_3$ must have some reality (although it may be much less stable than $HPO(OH)_2$) since its esters are well known. Furthermore, oxidation of phosphonate derivatives, $H—PO(OR)_2$ to phosphate derivatives demonstrably involves initial removal of the H bonded to P (4). Although the rate of exchange of this proton in dialkyl phosphonates has been measured (5), neither the pK_a of H directly bonded to phosphite P nor the equilibrium constant for the tautomerization is known.

Recently methods have been developed in this laboratory (6, 7) which permit these equilibrium constants to be evaluated. This paper reports a complete elucidation of the tautomeric equilibria for phosphorous acid and its mono and diethyl esters.

Results and Discussion

Thermodynamic Data

In Table 1 are found the thermodynamic quantities required for the compounds discussed in this paper. In some cases it was necessary to estimate quantities using accepted methods from the literature; these calculations are detailed under Calculations.

The heat of formation of diethyl phosphonate was calculated starting from results of Neale and Williams (8) who reported the difference in heats of formation for diethyl phosphonate and diethyl phosphate, both as the liquids. The heat of formation of diethyl phosphate in aqueous solution has recently been reported (7) and so it is possible to complete the calculation. The heat of solution of diethyl phosphate in aqueous KOH solution is known (8),

[1]Alfred P. Sloan Fellow, 1975–1979.

[2]This situation is recognized by an elaboration of nomenclature, not always followed for the parent acid: $P(OH)_3$ is phosphorous acid and its esters are alkyl phosphites; $HPO(OH)_2$ is phosphonic acid and its esters are alkyl phosphonates (3). Thus, on most of the occasions when one speaks of phosphorous acid, one should in fact refer to phosphonic acid; ordinarily there is no confusion but in the present paper the terms will be used only in the strict sense.

0008-4042/79/020236-04$01.00/0

TABLE 1. Thermodynamic quantities for compounds discussed in this paper[a]

(*a*) Compounds for which ΔG_f^0(aq) has not been reported

Compound	ΔH_f^0(g)[b]	S^0(g)[c]	ΔG_f^0(g)[b]	ΔH_v[b,d]	ΔH_f^0(l)[b]	ΔG_t[b,e]	ΔG_f^0(aq)[b]
$(EtO)_3P$	−195.9(1.3)[f]	127.62(2.0)[g]	−136.7(1.4)[h]	10.0 (1.0)[f]	−205.9 (1.0)[f]	−1.74(1.0)[i]	−138.4(1.7)[h]
$(EtO)_2PHO$	−206.4(1.9)[h]	108.13(2.0)[g]	−160.7(2.0)[h]	11.78(1.0)[i]	−218.14(1.61)[j]	−4.40(1.0)[i]	−165.1(2.0)[h]

(*b*) Compounds for which ΔG_f^0(aq) has been reported

Compound	ΔG_f^0(aq)[b]
H_2O	−56.69[k,l]
HPO_3H_2	−202.04(1.0)[j]
EtOH	−43.31[k]

(*c*) Compounds for which ΔG_f^0(aq) only was calculated in this work

Compound	ΔG_f^0(aq)
$P(OH)(OEt)_2$	−155.3(1.7)
$P(OH)_2(OEt)$	−171.8(1.8)
$P(OH)_3$	−187.8(1.8)
HPO(OH)(OEt)	−183.7(2.0)
$HPO(OH)_2$	−201.9(2.0)[m]

[a]At 25°C, standard states are ideal gas at 1 atm, pure liquid, and 1 *M* aqueous solution with an infinitely dilute reference state, unless otherwise noted; estimated standard deviations in parentheses. [b]In kcal mol^{-1}. [c]In cal deg^{-1} mol^{-1}. [d]Heat of vaporization. [e]Free energy of transfer, from gas at 1 atm to 1 *M* aqueous solution with an infinitely dilute reference state. [f]Reference 21. [g]Calculated by the method of atomic contributions; ref. 15; see Calculations. [h]Calculated from other values in this table. [i]Calculated as described in Calculations. [j]Calculated as described in the text. [k]Reference 22. [l]Standard state is the pure liquid. [m]This value is derived from ΔG_f^0 for $HPO(OEt)_2$ as described in the text; compare with the literature value in part *b* of this table.

the heat of ionization of diethyl phosphate is known (7), and the heat of ionization of water is known (9); by combining these quantities the heat of solution of diethyl phosphate in water to give a solution of the free acid can be calculated and so the heat of formation of the pure liquid can be obtained from the heat of formation of the ester in solution. Finally, the value of the heat of formation of liquid diethyl phosphonate can be calculated, giving the value in Table 1.

The free energy of formation of aqueous phosphonic acid was recalculated from the heat of formation given in the CATCH tables (10) and the entropy value given by Latimer (11).

Acidities

For the calculations reported below, it was necessary to have both the apparent pK_a values for phosphonic acid (i.e., for $HPO(OH)_2$) and the unobservable pK_a values for its tricoordinate tautomer $P(OH)_3$. For the latter, the values estimated by Kossiakoff and Harker (12) were employed. These authors used a simple electrostatic model which proved quite accurate for those acids where resonance is *not* important either in the acid or the anion. Their values for the first and second pK_a values for $P(OH)_3$ are used; the third pK_a (which they did not report) was estimated assuming that the electrostatic effect of going from the monoanion to the dianion is the same as that of going from the neutral acid to the monoanion with suitable allowance for symmetry effect. The pK_a values for the mono and diesters were estimated assuming that the effect of replacing OH by OEt is the same as the average value observed for phosphate esters (7) with suitable allowance for symmetry effects (13). These values may be found in Table 2.

Equilibria for Ester Hydrolysis

We have discovered (6, 7) and tested (13) a linear free energy relationship between free energies of hydrolysis of esters and the pK_a values of the corresponding acids which appears to work very well for those acids where resonance does not play an important role in determining the pK_a. This relationship states that for the reaction:

[1] $$X—OR + H—O—H \rightleftharpoons X—OH + H—OR$$

[2] $$\Delta G'' = -4.78(0.28) + 0.336(0.024)pK_a$$

where $\Delta G''$ is the standard free energy change in kcal mol^{-1} (with the standard state for water being the pure liquid) corrected for any steric or symmetry effects.[3] Using this relationship the free energies for the hydrolysis equilibria found in Table 3 were calculated. Steric effects should be very small for these equilibria; they were assumed to be the same as in the analogous orthoformate.

Tautomeric Equilibria

The free energy changes in Table 3, together with the free energies of formation in Table 1, permit the calculation of the free energy changes for the tautomeric equilibria, as shown in Table 4. The magnitude of the equilibrium constants is such that direct measurement is unlikely to be possible.

[3]$\Delta G''$ is used to indicate that what is calculated is the free energy change in the absence of steric or symmetry effects. These must now be added to get ΔG^0.

TABLE 2. pK_a values for the acids discussed in this paper[a]

Compound	pK_1	pK_2	pK_3
$P(EtO)_2OH$	6.1(0.9)[b]	—	—
$P(OEt)(OH)_2$	6.7(0.9)[b]	11.3(0.9)[b]	—
$P(OH)_3$	7.4(0.9)[c]	11.9(0.9)[c]	16.4(0.9)[b]
$HPO(OEt)OH$	0.9[b]	—	—
$HPO(OH)_2$	1.5[d]	6.79[d]	—
HPO_3^{2-}	38(2)[b]		
$HPO_2(OEt)^-$	26(2)[b]		
$HPO(OEt)_2$	13(2)[b]		

[a]In water at 25°C; estimated uncertainties in parentheses.
[b]Estimated as described in the text.
[c]Reference 12.
[d]Reference 23.

TABLE 3. Free energy changes for the hydrolysis reactions calculated using [2][a]

Reaction	ΔG^{0b}
$P(OEt)_3 + H_2O = HO—P(OEt)_2 + EtOH$	−3.53(0.35)
$P(OEt)_2(OH) + H_2O = (HO)_2POEt + EtOH$	−3.09(0.36)
$P(OEt)(OH)_2 + H_2O = (HO)_3P + EtOH$	−2.61(0.37)
$HPO(OEt)_2 + H_2O = HPO(OH)(OEt) + EtOH$	−5.14(0.33)
$HPO(OEt)(OH) + H_2O = HPO(OH)_2 + EtOH$	−4.84(0.28)

[a]In aqueous solution at 25°C.
[b]In kcal mol^{-1}; estimated uncertainties in parentheses.

TABLE 4. Tautomerization equilibria[a]

Equilibrium	ΔG^{0b}	log K
$P(OEt)_2OH = HPO(OEt)_2$	−9.8(2.6)	7.2(1.9)
$P(OEt)(OH)_2 = HPO(OEt)OH$	−11.9(2.6)	8.7(1.9)
$P(OH)_3 = HPO(OH)_2$	−14.1(2.1)	10.3(1.5)
$P(OEt)(OH)(O^-) = HP(O)_2OEt^-$	−19.8(2.9)	14.5(2.1)
$P(OH)_2(O^-) = HP(O)_2(OH)^-$	−22.1(2.3)	16.2(1.7)
$P(OH)(O^-)_2 = HP(O)_3^{2-}$	−29.1(2.5)	21.3(1.8)

[a]In aqueous solution at 25°C; estimated uncertainties in parentheses.
[b]In kcal mol^{-1}.

The only previous evaluation of a tautomeric equilibrium constant for phosphorous was the calculation of the equilibrium constant for tautomerism of hypophosphorous acid by Van Wazer (14), based on kinetic data, leading to a value of 10^{-12} for $K = [H—P(OH)_2]/[H_2PO(OH)]$. This value is rather similar to the value which we obtain for phosphorous acid.

pK_a for P—H Bonds

From the equilibrium constants for tautomerization and the pK_a values for O—H ionization found in Table 2, it is possible to calculate the pK_a values for P—H ionization. These values are also found in Table 2. The calculation is based upon Scheme 1 and was carried out for the cases where OR and OR′ are OEt and O^-. With a pK_a for $H—PO(OEt)_2$ in hand, it is possible to calculate a rate constant for the protonation of $:PO(OEt)_2^-$ from the published rate constant for proton abstraction by water (5); the value so calculated is $1.9 \times 10^8\ M^{-1}\ s^{-1}$.

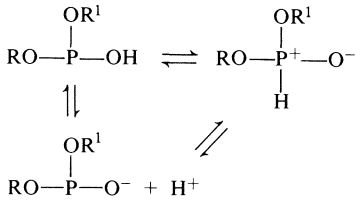

SCHEME 1

Calculations

Entropies of the gaseous esters were estimated by the method of atomic additivity of Benson and Buss (15); the only new parameter required was that for tetracoordinate phosphorous which was calculated, starting from the standard entropies of POF_3 and $POCl_3$ (16), as $-31.2(0.5)$ cal deg^{-1} mol^{-1}.

Solubilities of the esters were estimated from the parachors by the method of Deno and Berkheimer (17); for $P(OEt)_3$ the correction for hydrogen bonding (17) was assumed to be the same as for $HC(OEt)_3$, i.e., 3.34; the solubility of $P(OEt)_3$ is estimated as 0.149 M. The hydrogen bonding contribution for a PO group was taken as the difference in E_A between the value observed for $PO(OEt)_3$ and the value expected using $HC(OEt)_3$ as a model; this contribution amounted to 1.02. The value used for the solubility of $PO(OEt)_3$ was for ideal solutions derived from the free energy of transfer reported recently (2). Then for $HPO(OEt)_2$ the value for E_A was taken as that for PO plus two thirds of the value for $HC(OEt)_3$. This indirect procedure is necessary because of the high solubility of phosphate and phosphonate esters with small alkyl groups. The value obtained for the ideal solubility of diethyl phosphonate was 1.55 M.

The heat of vaporization of diethyl phosphonate was calculated from the slope of a plot of log p vs. $1/T$, using the vapor pressure data from Beilstein (18). The data are described by the line $\log p = 8.457 - 2571.4/T$, from which $\Delta H_v = 11.78$, kcal mol^{-1} in reasonable agreement with the value expected from the Wadsö equation (19), namely 12.7 kcal/mol. Page and Purnell (20) have reported a study of the vapor pressures of several phosphite esters, and give $\log p = 7.174 - 1988.5/T$ for diethyl phosphonate;[4] although this equation gives the boiling point at atmospheric pressure correctly, it is consistent with none of the data reported at lower pressures and leads to a heat of vaporization of 9.11 kcal mol^{-1}, which is far from the expected value.

The vapor pressure of diethyl phosphonate at 25°C was calculated from the equation reported above. The vapor pressure of triethyl phosphite was calculated from the boiling point using the heat of

[4]In the reference the slope was given as 1.9885 but this was assumed to be a typographical error.

vaporization (Table 1) and a value of -12 cal deg^{-1} mol^{-1} for the heat capacity of vaporization (24).

Free energies of transfer from the gas phase at one atmosphere to aqueous solution (standard state 1 *M* with an infinitely dilute reference state) were then calculated from the vapor pressures and the molar solubilities.

Experimental

The solubility of triethyl orthoformate (Aldrich; purity, 98% checked by nmr analysis) was determined in aqueous 0.1 *N* NaOH. The ortho ester was added to the solvent, the mixture was shaken vigorously to saturate the aqueous layer, centrifuged briefly, and then the organic layer was discarded. A known amount of dimethylformamide was added (Hamilton syringe) to serve as internal standard, and the concentration was determined by nmr analysis. The solubility was 0.225 ± 0.010 *M*.

Acknowledgements

I thank the National Research Council of Canada and the Alfred P. Sloan Foundation for financial assistance, and Patricia A. Cullimore for technical assistance.

1. F. A. Cotton and G. Wilkinson. Advanced inorganic chemistry. Interscience, New York, NY. 1962. p. 135.
2. (*a*) R. Wolf, R. Mathis-Noël, and F. Mathis. Bull. Soc. Chim. Fr. 124 (1960); (*b*) L. W. Daasch. J. Am. Chem. Soc. **80**, 5301 (1958); (*c*) C. F. Callis, J. R. Van Wazer, J. W. Shoolery, and W. A. Anderson. J. Am. Chem. Soc. **79**, 2719 (1957).
3. J. H. Fletcher, O. C. Dermer, and R. B. Fox. Nomenclature of organic compounds. Advances in Chemistry Series, 126, American Chemical Society, Washington, DC. 1973. p. 279.
4. (*a*) A. J. Kirby and S. G. Warren. The organic chemistry of phosphorus. Elsevier, London. 1967; (*b*) P. Nylen. Z. Anorg. Allg. Chem. **235**, 161 (1938).
5. P. R. Hammond. J. Chem. Soc. 1365 (1962).
6. J. P. Guthrie. Can. J. Chem. **53**, 898 (1975).
7. J. P. Guthrie. J. Am. Chem. Soc. **99**, 3991 (1977).
8. E. Neale and L. T. D. Williams. J. Chem. Soc. 2485 (1955).
9. J. W. Larson and L. G. Hepler. *In* Solute–solvent interactions. *Edited by* J. F. Coetzee and C. D. Ritchie. Dekker, New York, NY. 1969. p. 1.
10. G. Pilcher. CATCH tables for phosphorus compounds. University of Sussex, Brighton. 1972.
11. W. M. Latimer. The oxidation states of the elements and their potentials in aqueous solution. 2nd ed. Prentice Hall, Englewood Cliffs, NJ. 1952. p. 106.
12. A. Kossiakoff and D. Harker. J. Am. Chem. Soc. **60**, 2047 (1938).
13. J. P. Guthrie. Can. J. Chem. **56**, 2342 (1978).
14. J. R. Van Wazer. Phosphorus and its compounds. Vol. I. Interscience, New York, NY. 1958. p. 364.
15. S. W. Benson and J. H. Buss. J. Chem. Phys. **29**, 546 (1958).
16. S. W. Benson. Thermochemical kinetics. 2nd ed. Wiley, New York, NY. 1976.
17. N. C. Deno and H. E. Berkheimer. J. Chem. Eng. Data, **5**, 1 (1960).
18. Beilstein. Handbuch der organischen Chemie. **1**, 330; **1**(1), 169; **1**(2), 329; **1**(3) 1324; **1**(4) 1329.
19. I. Wadsö. Acta Chem. Scand. **20**, 544 (1966).
20. F. M. Page and J. H. Purnell. J. Chem. Soc. 621 (1958).
21. J. D. Cox and G. Pilcher. Thermochemistry of organic and organometallic compounds. Academic Press, New York, NY. 1970.
22. F. D. Rossini, D. D. Nagman, W. H. Evans, S. Levine, and J. Jaffe. Natl. Bur. Stand (U.S.) Cir. No. 500 (1952).
23. R. M. Smith and A. E. Martell. Critical stability constants. Vol. 4. Plenum Press, New York, NY. 1976.
24. S. W. Benson and G. D. Mendenhall. J. Am. Chem. Soc. **98**, 2046 (1976).

The enol content of simple carbonyl compounds: a thermochemical approach

J. Peter Guthrie[1] and Patricia A. Cullimore

Department of Chemistry, University of Western Ontario, London, Ont., Canada N6A 5B7

Received June 16, 1978

J. Peter Guthrie and Patricia A. Cullimore. Can. J. Chem. **57**, 240 (1979).

From the heats of hydrolysis of enol ethers, the heats of formation of the enol ethers, and thence the free energies of formation of the enol ethers in aqueous solution can be calculated. For this calculation it was necessary to determine the free energies of transfer from the gas phase to aqueous solution. By methods previously published it was possible to estimate the free energy change for the hypothetical hydrolysis reaction leading from the enol ether to the enol, which in turn made possible calculation of the free energy of formation of the enol. Finally the free energy change for enolization in aqueous solution could be calculated using the known free energy of formation of the corresponding keto tautomer. In this way the following were determined: carbonyl compound, $pK_{enol} = -\log([enol]/[keto])$: acetaldehyde, 5.3; propionaldehyde, 3.9; isobutyraldehyde, 2.8; acetone, 7.2; 2-butanone, 8.3; 3-pentanone, 7.8; cyclopentanone, 7.2; cyclohexanone, 5.7; acetophenone, 6.7.

J. Peter Guthrie et Patricia A. Cullimore. Can. J. Chem. **57**, 240 (1979).

Utilisant des chaleurs d'hydrolyse d'éthers énoliques, on a calculé les chaleurs de formation d'éthers énoliques ainsi que les énergies libres de formation d'éthers énoliques en solution aqueuse. Pour ces calculs, il est nécessaire de déterminer les énergies de transfert de la phase gazeuse à la solution aqueuse. Utilisant des méthodes décrites antérieurement, on a pu évaluer le changement d'énergie libre de la réaction d'hydrolyse hypothétique conduisant de l'éther énolique à l'énol; à partir de cette valeur, on a pu calculer l'énergie libre de formation de l'énol. Finalement on a pu calculer la variation d'énergie libre associée à l'énolisation en solution aqueuse en faisant appel à la valeur connue de l'énergie libre de formation du tautomère cétonique correspondant. De cette façon, on a pu déterminer les valeurs suivantes: composé carbonyle, $pK_{enol} = -\log([enol]/[cétol])$; acétaldéhyde, 5.3; propionaldéhyde, 3.9; isobutyraldéhyde, 2.8; acétone, 7.2; butanone-2, 8.3; pentanone-3, 7.8; cyclopentanone, 7.2; cyclohexanone, 5.7; acétophénone, 6.7.

[Traduit par le journal]

Introduction

Simple carbonyl compounds have a very small enol content; methods which work well for multifunctional compounds, such as halogen titration (1, 2), become very difficult to apply when the enol content falls to less than 1 ppm. The early literature contains reports of the enol content of simple compounds such as acetone (2, 3) but more recent work has shown the nature of the problems associated with the measurements (4, 5) and has led to the conclusion that for acetone in aqueous solution the amount of enol is too small to be measured by the halogen titration method, even in its most sensitive form (5).

There have been several attempts to apply thermochemical results to the problem of determining the enol content for compounds where it is not directly measurable. Sunner (6) estimated the heat of enolization of liquid acetone from the heat of hydrolysis of isopropenyl acetate, using *m*-cresyl acetate as a model. More recently Hine and Arata (7, 8) measured the heats of hydrolysis of three enol ethers and estimated the heat of enolization of the liquid ketones, using the enthalpy of hydrolysis of simple ethers as a model. These approaches suffer from the fact that they give only the enthalpy for the hypothetical pure liquid reaction, rather than the more useful free energy change for reaction in solution in a standard solvent. Furthermore they ignore the influence of the electronic nature of the ether upon the free energy or enthalpy change for the hydrolysis (9).

In this paper a new and general approach to the problem of determining the free energies of enolization will be presented. This approach is based upon previous studies of the effect of structure upon the free energy change in reaction [1] (9–13). Provided

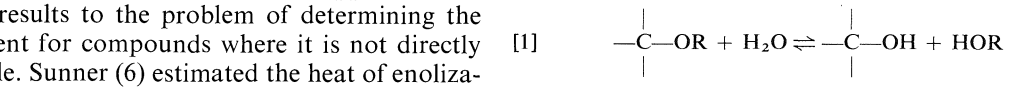

[1] $$-\overset{|}{\underset{|}{C}}-OR + H_2O \rightleftharpoons -\overset{|}{\underset{|}{C}}-OH + HOR$$

that the free energy of formation of the enol ether in aqueous solution can be determined and an estimate made of the pK_a of the enol, the free energy of formation of the enol can be calculated and so the free energy of enolization. The generality of the method comes not just from the possibility of

[1]Alfred P. Sloan Fellow, 1975–1979.

0008-4042/79/020240-09$01.00/0

preparing any enol ether and performing appropriate measurements but also from the possibility (once appropriate parameters have been evaluated) of calculating the free energy of formation by the methods of group additivity pioneered by Benson (14, 15).

Results

Thermodynamics of Enol Ethers

Heats of formation for several enol ethers were available in the literature; these values are found in Table 1, along with other thermodynamic quantities measured or calculated in this work. The heat of formation of α-methoxystyrene was determined by measuring its heat of hydrolysis. The experimental enthalpy data are found in Table 2, as are our data for 1-methoxycyclohexene and 2-methoxypropene which may be compared with the results of Hine and Arata (7, 8). These authors used quite different reaction conditions (aqueous tetrahydrofuran at 0°C) so that comparison is made for the ideal process involving pure liquid reagents and products at 25°C. Our results are seen to be in good agreement for 1-methoxycyclohexene and in fair agreement for 2-methoxypropene; since the latter compound is extremely volatile, we could easily have been subject to systematic errors from loss of substrate. In any case, the discrepancy is less than two standard deviations.

Heats of vaporization were estimated where necessary using the equation proposed by Wadsö (16); estimated values were checked for consistency with the available boiling point data at various pressures. Standard entropies for the gaseous compounds were calculated after Benson (14, 15), permitting calculation of free energies of formation in the gas phase. Free energies of transfer were calculated either from the solubilities and vapor pressures, using data derived as described in the Experimental or in the Calculations, and summarised in Table 3, or else were estimated by a modified version of the 'group additivity' method of Hine and Mookerjee (17) (corrected to give free energies in kcal mol^{-1} rather than dimensionless activity coefficients, with suitable allowance for both the change in units and the change in standard states). The results in Table 3 permit the determination of several new group contributions to the free energy of transfer suitable for enol ethers which should be useful for future applications of our method; these values are given in Table 4.

Equilibrium Constants for the Enol Ether – Enol Interconversion

Free energies for reaction [1] were initially shown to depend upon the electronic properties (as measured by the sum of the σ* values) of the substituents on the carbon bearing the OH or OR group (9). This

TABLE 1. Thermodynamic quantities for compounds discussed in this paper[a]

(*a*) Compounds for which free energies of formation in aqueous solution have not been reported previously

Compound	$\Delta H_f^0(g)$[b]	$S^0(g)$[c]	$\Delta G_f^0(g)$[b]	ΔH_v[b,d]	$\Delta H_f^0(l)$[d]	ΔG_t[b,e]	$\Delta G_f^0(aq)$[b]
CH_3CH_2CHO	−45.45(0.21)[f]	72.83(0.5)[g]	−30.68(0.20)[h]	7.09(0.10)[f]	−52.24(0.23)[f]	−1.54(0.1)[i]	−32.22(0.28)[h,j]
$CH_2{=}CH{-}O{-}CH_2CH_3$	−33.63(0.20)[f]	83.33(1.5)[k]	−12.48(0.49)[h]	6.35(0.30)[f]	−39.98(0.37)[f]	1.21(0.1)[i]	−11.27(0.50)[h]
$CH_3CH{=}CH{-}O{-}CH_3$(E)	−33.47(1.0)[k]	82.12(1.5)[k]	−11.81(1.10)[h]			1.02(0.5)[m,n]	−10.79(1.20)[h]
$CH_2{=}C(CH_3){-}OCH_3$	−35.79(1.01)[h]	81.06(1.5)[k]	−13.81(1.10)[h]	6.45(1.0)[o]	−42.25(0.11)[p]	1.26(0.1)[q,v]	−12.55(1.11)[h]
$CH_3COCH_2CH_3$	−57.02(0.29)[r]	81.11(0.20)[r]	−35.04(0.30)[r]			−1.82(0.1)[i]	−36.86(0.31)[h]
$(CH_3)_2CH{-}CHO$	−52.25(0.37)[f]	79.28(0.15)[k]	−29.74(0.58)[h]	7.54(0.30)[f]	−59.79(0.19)[f]	−0.71(0.1)[q,v]	−30.45(0.59)[h]
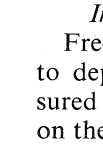	−46.03(0.40)[f]	78.97(1.5)[k]	−23.02(0.60)[h]	10.21(0.05)[f]	−56.24(0.40)[f]	−2.81(0.5)[s,v]	−25.83(0.78)[h]
$CH_2{=}C(CH_3){-}OCH_2CH_3$	−43.4(1.0)[t]	91.35(1.5)[h]	−14.78(1.10)[h]			+1.31(0.5)[m,n]	−13.47(1.21)[h]
$CH_3{-}C(OCH_3){=}CHCH_3$ (*E*?)[aa]	−39.9(1.0)[t]	89.64(1.5)[k]	−10.77(1.10)[h]			1.12(0.5)[m,n]	−9.65(1.21)[h]
$(CH_3)_2C{=}CH{-}OCH_3$	−41.85(1.0)[k]	89.67(1.5)[k]	−12.70(1.10)[h]			2.17(0.5)[m,n]	−10.53(1.20)[h]

TABLE 1 (*Concluded*)

(*a*) Compounds for which free energies of formation in aqueous solution have not been reported previously

Compound	ΔH_f^0(g)[b]	S^0(g)[c]	ΔG_f^0(g)[b]	ΔH_v[b,d]	ΔH_f^0(l)[d]	ΔG_t[b,e]	ΔG_f^0(aq)[b]
$CH_3CH_2COCH_2CH_3$	−61.65(0.21)[f]	89.28(1.5)[k]	−32.41(0.49)[h]	9.22(0.03)[f]	−70.87(0.20)[f]	−1.52(0.1)[u]	−33.93(0.50)[h]
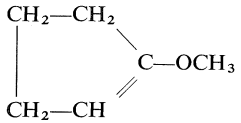	−30.32(1.09)[h]	88.01(1.5)[k]	−0.30(1.18)[h]	9.55(1.0)[o]	−39.87(0.43)[w]	+0.27(0.5)[m,n]	−0.03(1.28)[h]
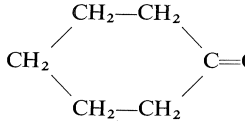	−54.04(0.52)[f]	79.89(1.5)[k]	−21.60(0.69)[h]	10.77(0.05)[f]	−64.81(0.51)[f]	−3.02(0.1)[q,v]	−24.62(0.69)[h]
$CH_3CH_2C(OCH_3)=CHCH_3$ (*E*?)[aa]	−44.66(1.0)[s]	99.45(1.5)[k]	−8.74(1.10)[h]			+1.44(0.5)[m,n]	−7.30(1.20)[h]
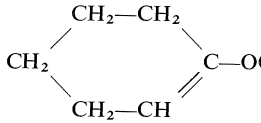	−39.43(1.09)[k]	93.13(1.5)[k]	−1.22(1.21)[h]	10.82(1.0)[o]	−50.25(0.54)[p]	+0.36(0.28)[q,v]	−0.86(1.24)[h]
$C_5H_5—C(OCH_3)=CH_2$	−4.00(1.04)[h]	99.62(1.5)[k]	23.78(1.15)[h]	12.83(1.0)[o]	−16.83(0.29)[q]	−0.56(0.3)[q,v]	23.22(1.21)[h]

(*b*) Compounds for which the free energy of formation in aqueous solution has been reported previously

Compound	ΔG_f^0(aq)
H_2O	−56.69[x]
CH_3OH	−41.88[x]
CH_3CH_2OH	−43.31[x]
CH_3CHO	−33.35(0.18)[y]
CH_3COCH_3	−38.40(0.19)[z]
$C_6H_5COCH_3$	−2.21(0.42)[z]

(*c*) Compounds for which only the free energy of formation aqueous solution has been calculated in this paper

Compound	ΔG_f^0(ag)	Compound	ΔG_f^0(aq)
$CH_2=CH—OH$	−26.1(0.7)	$CH_3—CH_2—C(OH)=CH—CH_3$	−23.2(1.3)
$CH_3—CH=CH—OH$	−27.0(1.3)	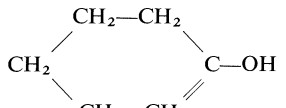	−16.8(1.4)
$CH_2=C(CH_3)—OH$	−28.6(1.3)		
$CH_3—CH=C(CH_3)—OH$	−25.6(1.4)		
$(CH_3)_2C=CH—OH$	−25.6(1.4)		
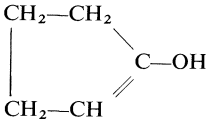	−16.0(1.4)	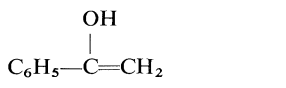	+6.9(1.3)

[a]At 25°C; standard states are ideal gas at 1 atm, pure liquid and 1 *M* aqueous solution with an infinitely dilute reference state, except that ΔG_f° (aq) for H_2O is taken as ΔG_f° (1). [b]In kcal mol^{-1}. [c]In cal deg^{-1} mol^{-1}. [d]Heat of vaporization. [e]Free energy of transfer from gas to aqueous solution. [f]Reference 41. [g]Reference 42. [h]Calculated from values in this table. [i]Calculated from data in ref. 17. [j]Equilibrium mixture of free aldehyde and covalent hydrate. [k]Calculated by the method of group contributions of ref. 15. [l]Calculated as described in the text; see Table 3. [m]Calculated using the group contributions of ref. 17 recalculated to give free energies of transfer rather than activity coefficients. [n]Some contributions were evaluated in this work; see text. [o]Estimated from the boiling point using the Wadsö equation (ref. 16). [p]Reference 8. [q]This work. [r]Reference 43. [s]Estimated as described under Calculations. [t]Reference 38. [u]Interpolated from data in ref. 44. [v]See Table 3. [w]Reference 7. [x]Reference 45. [y]Reference 46. [z]Reference 27. [aa]See Calculations for a discussion of stereochemical ambiguities.

TABLE 2. Calorimetric results[a]

Compound	ΔH_{rxn} Observed[b]	ΔH_{rxn} Ideal[c]	$\Delta H_f^0(l)$[d]
CH_3OH	−0.13(0.02)		
H_2O	−0.32(0.02)		
Ph—C(=CH_2)—OCH_3	−4.08(0.13)	−6.19(0.15)	−16.83(0.29)
Ph—CO—CH_3	+1.92(0.06)		
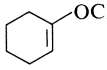	−3.25(0.23)	−3.44(0.23) (−3.26(0.17))[e]	−50.25(0.54)
	0.00(0.03)		
CH_3—C(=CH_2)—OCH_3	−4.87(0.26)	−5.24(0.27) (−5.75(0.11))[e]	−42.25(0.11)
CH_3—CO—CH_3	+0.18(0.07)		

[a]Heats of solution or reaction, measured in 0.1 *N* HCl in 75% methanol, 25% water (v/v) at 25°C; standard deviations in parentheses, enthalpies in kcal mol^{-1}.
[b]Observed heat of solution or reaction.
[c]Heat of hydrolysis for the ideal reaction of liquid enol ether with liquid water giving liquid products.
[d]Heat of formation of the liquid enol ether.
[e]Reference 8.

TABLE 3. Free energies of transfer[a]

Compound	Solubility[b]	Vapor pressure[c]	ΔG_t[d]
CH_3—C(=CH_2)—O—CH_3	0.082 ±0.005	526 ±15	1.26±0.10
CH_2=CH—OCH_2CH_3	0.0904 ±0.007[e]	525 ±10	1.21±0.10
$(CH_3)_2$CH—CHO	0.786 ±0.035	181 ±8	−0.71±0.10
	3.70 ±0.56	10.8±0.1	(−3.30[f]) −2.81±0.50[g]
	0.98 ±0.13	4.59±0.3	−3.02±0.10
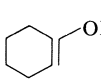	0.0043 ±0.005	6.02±2.8	0.36±0.28
Ph—C(=CH_2)—OMe	0.00173±0.0003	0.51±0.32	−0.56±0.37

[a]From the hypothetical ideal gas state at 1 atm to 1 *M* aqueous solution with an infinitely dilute reference state.
[b]This work unless otherwise noted; mole L^{-1}, solubility of the pure liquid in water.
[c]Calculated as described in the appendix; vapor pressure in Torr at 25°C for the pure liquid.
[d]In kcal mol^{-1}; conservative uncertainties of 0.1 kcal per mol^{-1} were assumed, except where error analysis led to larger values; calculated assuming that the vapor pressure of the pure liquid may be used for the partial pressure of the solute over a saturated solution.
[e]Reference 49.
[f]This value is derived from the observed solubility, but solutions above 1 *M* are certain to be nonideal; this value was not used.
[g]Estimated from ΔG_t for cyclohexanone, by subtracting the contribution for $[CH_2(C)_2]$.

approach cannot be applied to enol ethers in the absence of σ* values for alkylidene groups. More recently, in an extension of the method to phosphate derivatives it was shown that the free energy change for reaction [1] is linearly related to the pK_a of the OH species, provided that resonance does not make an important contribution to the acidity (13). Since it is intuitively clear that of the two contributing forms:

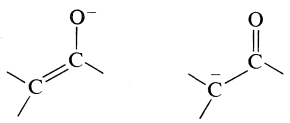

TABLE 4. New group contributions for enol ethers

Group	Contribution to ΔG_t[a] (kcal mol^{-1})
$[C_dH(O)] + [O(C)(C_d)]$	-2.28
$[C_d(C)(O)] + [O(C)(C_d)]$	-3.03 ± 0.12
$[C_d(C_B)(O)] + [O(C)(C_d)]$	-2.58

[a]Free energy of transfer from gas, 1 atm, to 1 *M* aqueous solution with an infinitely dilute reference state.

that with the negative charge on oxygen makes overwhelmingly the more important contribution to the resonance hybrid for an enolate ion, this latter relationship should be useful for reaction [1] applied to enol ethers, provided that the pK_a values of the enols can be estimated. Although it is clear that the pK_a for an enol must lie between that of an alcohol, ca. 16 and a phenol, ca. 10, no direct measurement is possible for any simple enol. Fortunately Novak and Loudon (18) have recently published an indirect evaluation of the pK_a for the enol of acetophenone as 11.0 ± 1.1. Since the free energy change for reaction [1] is rather insensitive to the pK_a value (13), estimated pK_a values need not be of high accuracy to be useful. For other enols, the pK_a values were estimated making the following two assumptions: for substituents on the β carbon of the enol the effect of the substituent is the same as for substitution at the *ortho* position of a phenol; for substituents at the α position of an enol the effect of the substituent is the same as for a saturated alcohol. Substituent effects were calculated from the observed pK_a values for *ortho*-substituted phenols (19) and from the linear free energy relationship shown to hold for alcohol pK_a values (20).

Using pK_a values estimated in this way and [1] the free energies of formation of the enols were calculated; these are found in Table 1. The pK_a values are found in Table 5, as are the equilibrium constants for enolization calculated from the free energies of formation of the enol and keto tautomers from Table 1.

Discussion

Our results for the enol content of a number of simple carbonyl compounds as well as results for the same compounds derived in a forthcoming paper by a completely independent method are found in Table 5, as are recent literature values for determinations of these equilibrium constants either by direct titration or by indirect kinetic arguments. For convenience in dealing with these very unfavorable equilibria, the equilibrium constants are expressed in terms of pK_{enol}, which is the negative logarithm of the equilibrium constant for formation of the enol tautomer from the keto tautomer.

Acetone and 3-pentanone are the two cases where enolization constants derived by our thermochemical method can be compared with unambiguous experimental values. The agreement is fairly good although the discrepancy for acetone is somewhat larger than is desirable. The value derived from the data of Dubois and Toullec (21, 22) is based upon the rate constants for halogenation (identical for chlorine, bromine, and iodine) under conditions where the rate determining step is reaction of enol with halogen, and a calculated value for the diffusion controlled rate constant. This calculated value should be close to $10^{10}\ M^{-1}\ s^{-1}$ on the basis of the Smolouchowski equation (23) but could vary as much as threefold from this value depending upon the probability of reaction occurring upon each collision (24). Any such effect would tend to make the true enol content larger than the calculated value.

The experimental values for the enolization constant derived from halogen titrations using extremely low halogen concentrations are in several cases in poor agreement with our thermochemical estimates. For acetone, no enol could be detected (5), so that pK_{enol} was necessarily greater than 6, which is consistent with our value of 7.2. For cyclohexanone the two methods are in good agreement. However, for cyclopentanone there is a serious disagreement. Hine and Arata (7, 8), reasoning from calculated enthalpies of enolization based upon their thermochemical results, also noted such a disagreement and argued that the results of Bell and Smith (5) appear to contradict various features of cycloalkanone chemistry. Our kinetic method (25) gives good agreement with the thermochemical method for both cycloalkanones. Two groups have measured the enol content of cyclopentanone using the same very sensitive technique and reported closely similar results (5, 18). To disregard such careful experimental work is disturbing to say the least, yet we are led to conclude that there is some systematic error in the method which leads at least part of the time to anomalously high enol contents being measured. The advantage of our methods, although they are less precise, is that they are based upon behavior of entire samples and not upon detection of the behavior of a tiny fraction of the sample.

The same difficulty arises in the case of acetophenone, where halogenation experiments (18) lead to a much larger enolization constant than our thermochemical method. On the other hand it must be pointed out that the value reported by Novak and Loudon (18) implies, as they stated, that the pK_a (keto) for acetophenone must be quite different from the normally accepted value of 19, whereas our value is in good agreement with this value.

TABLE 5. Comparison of various methods for determining the equilibrium constant for enolization[a]

Carbonyl compound	pK_a(enol)[b]	pK_{enol}[c]			
		Thermochemical[d]	Kinetic[e]	Equilibrium	Other
$CH_3—C(=O)—H$	11.1(1.0)	5.3(0.6)	4.7		
$CH_3CH_2—C(=O)—H$	11.4(1.0)	3.9(1.0)	3.9		
$(CH_3)_2CH—C(=O)—H$	11.7(1.0)	2.8(1.1)	2.7		
$CH_3—CO—CH_3$	11.8(1.0)	7.2(0.9)	7.0	>6[f,h]	8.84(0.9)[g]
$CH_3CH_2COCH_3$	12.1(1.0)	8.3(1.0)			
$CH_3CH_2COCH_2CH_3$	12.1(1.0)	7.8(1.0)			8.02(0.9)[g]
	12.1(1.0)	7.2(1.2)	6.7	4.9[f,h]	
	12.1(1.0)	5.7(1.1)	5.3	5.4[f,h]	
$Ph—CO—CH_3$	11.0(1.1)[i]	6.7(1.0)	6.6	4.7[j]	

[a]All in water at 25°C, values in parentheses are estimated standard deviations.
[b]Estimated as described in the text.
[c]K_{enol} = [enol]/[keto].
[d]This work.
[e]Calculated from rate constants for acid catalyzed enolization and for acid catalyzed hydrolysis of the corresponding enol ether; see ref. 25.
[f]Direct measurement by halogen titration.
[g]Calculated from second order rate constants for halogenation under conditions where halogenation is rate determining, using a calculated value for the rate of diffusion controlled reaction of enol and halogen; see text and refs. 21 and 22.
[h]Reference 5.
[i]Derived from a study of reactions of nucleophiles with α-acetoxystyrenes; ref. 18.
[j]Reference 18.

For the aldehydes, acetaldehyde, propionaldehyde, and isobutyraldehyde the thermochemical and the kinetic methods give very satisfactory agreement, although the high enol content predicted for isobutyraldehyde is somewhat surprising. This surprise is probably not justified, since for the aldehyde where one of the methyls in isobutyraldehyde is replaced by a phenyl the enol content in DMSO-d_6 at 60°C is 8.7% (26); phenyl stabilizes a double bond more than methyl but not dramatically more so. A measure of the greater stabilization by phenyl than by methyl is the ratio of equilibrium constants for dehydration of the aldol adducts of acetaldehyde and benzaldehyde, for the same carbon nucleophile (27). The average value for four such cases is 220, which may be compared with the ratio of the enolization constants for isobutyraldehyde (Table 5) and 2-phenylpropanal (26) which is 50.

Initially it had been hoped that the kinetics results of Salomaa and co-workers (28) could lead to an evaluation of the effect of halogen substituents upon enol stability. The published data do permit calculation of equilibrium constants for the acetal to enol ether conversion; unfortunately the equilibrium constant so calculated for acetaldehyde (which applies to solutions in ethanol) does not agree with the value calculated for aqueous solutions from the available thermochemical data. Either there are substantial free energy of transfer effects (which is not impossible since Abraham and Grellier (29) have shown that there are sizable free energies of transfer from water to ethanol for neutral organic compounds, (although no data are available for acetals or enol ethers) or else there is some systematic error in the procedure leading to the equilibrium constants. Since the discrepancies amount to several powers of 10 in enolization constant we have not reported any enolization constants for chloroacetaldehydes; the results of Salomaa and co-workers (28) clearly show a large enol stabilizing effect of chlorine.

Although the method which we use to derive enol free energies from the free energies of formation of the enol ethers is novel, the free energies of the enol ethers themselves and of the analogous ketones are based upon experimental enthalpies and well tested procedures for estimating standard entropies. Using the values from Table 1, the equilibrium constants for enol ether formation from the cycloalkanone and methanol are 9×10^{-9} M for cyclopentanone and 3×10^{-7} M for cyclohexanone. These equilibrium constants clearly reflect the relationship between the enolization constants which we derived from either

TABLE 6. Equilibrium constants for enol ether formation[a]

Carbonyl compound	Hydration[b]	Equilibrium constant: Acetal formation[c] (M^{-2})	Acetal to enol ether[c] (M)	Enol ether formation[d] (M^{-1})	Enol ether formation[e] (M^{-1})
CH_3CHO	1.06[f]	1.25×10^{-2} [f,k]	1.16×10^{-6} [g,h]	1.45×10^{-8} [k]	8.4×10^{-7} [k]
Cl—CH_2—CHO	37.0[h]	9.12×10^{-2} [i,h]	1.45×10^{-5} [g,k]	1.32×10^{-6} [k]	
Cl_2CH—CHO	1.48×10^{3} [i]	1.62×10^{1} [i,h]	8.66×10^{-3} [g,k]	1.39×10^{-1} [k]	
CH_3—CO—CH_3	1.4×10^{-3} [f]	7.2×10^{-6} [f,l]	1.12×10^{-3} [j,l]	8.00×10^{-9} [l]	8.3×10^{-9} [l]

[a]All equilibrium constants calculated with the standard states for water being the pure liquid of unit activity, even where the equilibrium constant was measured in an alcohol solvent.
[b]Dimensionless; K = [hydrate]/[carbonyl compound].
[c]Determined in alcohol solvent.
[d]Calculated from the equilibrium constant for acetal formation and for acetal to enol ether.
[e]Calculated from the free energy of formation data in Table 1.
[f]Reference 9 and references cited therein.
[g]Calculated from data in ref. 28, as described in the text.
[h]Reference 48.
[i]Estimated as described in the text.
[j]Reference 49.
[k]Ethanol as the alcohol.
[l]Methanol as the alcohol.

the thermochemical method or the kinetic method and are not consistent with the relative enol contents reported by Bell and Smith (5).

The thermochemical method for determining enolization constants has the disadvantage of being inherently imprecise but the advantage of being tied to experimental numbers of high reliability, by extrathermodynamic relations involving estimation of small free energy changes. It is confirmed by the close agreement observed with the kinetic method (25) which makes very different but also very plausible assumptions. This method also is subject to an inherent uncertainty based upon the imperfections of the model used; since methyl enol ethers and ethyl enol ethers do not hydrolyze at identical rates, they can not both be ideal models for the enol and in fact one expects that neither is much more than an approximate mode. Although both of our methods are subject to inherent imprecision, they seem to be in satisfactory agreement; this means that the problem of determining the enol content of carbonyl compounds can be considered as solved, since there are now a variety of unambiguous methods which can be employed: the kinetic method of Dubois and Toulec (21, 22); the kinetic method based upon Lienhard's observations (30), or our thermodynamic method (25). On the other hand, we are led to conclude that the halogen titration method, even in its most refined form, is not suitable for determining very small enol contents.

Calculations

Calculation of Vapor Pressures

For all but cyclohexanone (for which vapor pressure data were available in the Handbook of Chemistry and Physics (35), so that the vapor pressure at 25°C could be estimated by interpolation), vapor pressures at 25°C were estimated from the boiling point and the heat of vaporization (taken from Table 1), using a constant value for the heat capacity of vaporization of -12 cal/deg^{-1} mol^{-1} (36). The boiling points used were ethyl vinyl ether, 35.8°C (37*a*); 2-methoxypropene, 35.5°C (8); isobutyraldehyde, 64.2°C (37*b*); cyclopentanone, 131°C (35); 1-methoxycyclohexene, 140°C (8); and α-methoxystyrene, 193°C, corrected from a boiling point at 745 Torr (33). In all cases the predicted vapor pressures were checked by comparison with the rather sparse data on boiling points at reduced pressures in Beilstein.

Calculation of Thermodynamic Quantities

Entropies were estimated where necessary by the group equivalents method of Benson (15). It was necessary to estimate a few contributions not contained in the tables in ref. 15. The contribution for the group $[C_d(C)(O)]$ was assumed to be equal to that for $[C_d(C)_2]$; this approximation has been justified by Benson (15). Similarly the contribution for $[C_d(C_B)(O)]$ was taken as equal to that for $[C_d(C_B)(C)]$. For cyclopentanone and cyclohexanone the ring correction to S^0 was taken as that for the corresponding cycloalkane. For 1-methoxycyclopentene and 1-methoxycyclohexene the ring corrections were taken as those for the corresponding cycloalkenes.

There has been no experimental determination of the heat of formation of an enol ether of 3-pentanone. It was desirable to estimate this quantity in order to compare the thermochemical estimate of the enol content with the value reported by Dubois and Toullec (21, 22). In principle this should be straightforward, by Benson's method of group additivity (14, 15). However the values for the group contribu-

tions for enol ethers proposed by Eigenmann *et al.* (38) do not fit the experimental heats of formation (for 2-methoxypropene and 2-methoxy-2-butene) very well. Either the experimental values are in error or there is a destabilizing interaction in 2-methoxy-2-butene.[2] The latter explanation appears to be preferable. The reported heats of formation of 2-ethoxypropene and 2-methoxypropene are self consistent, differing by approximately the amount expected for an extra CH_2 group. If the free energy of formation of 2-methoxy-2-butene is estimated from that of 2-methoxypropene by taking the difference in group contributions between C_dH_2 and $C_dH(C)$ and $CH_3(C_d)$, the value so obtained is -13.16 and differs by 3.51 kcal mol^{-1} from the value based upon the experimental heat of formation. Furthermore this estimated value leads to a calculated $pK_{enol} = 5.98$, in poor agreement with the value of 7.96 derived from the results of Dubois and Toullec (21, 22) for 3-pentanone. The experimental heat of formation of 2-methoxy-2-butene leads to a calculated $pK_{enol} = 8.55$, in distinctly better agreement. Thus it seems plausible to conclude that there is a destabilizing interaction amounting to 3.51 kcal mol^{-1}. Taskinen (39) has shown that in 2-methoxy-2-butene, the preferred geometrical isomer has the methyl groups *cis*. The destabilizing interaction of 3.51 kcal mol^{-1} is considerably larger than the usual value of 1.0 kcal mol^{-1} for *cis* methyl groups (15) but there may be a buttressing effect of the methoxy group. If the free energy of formation of 3-methoxy-2-pentene is estimated starting from the free energy of formation of 2-methoxy-2-butene (using the value derived from the experimental heat of formation (38)), then a value of $pK_{enol} = 8.13$ is obtained which agrees very well with the observed value of 7.96. The assumption of no destabilizing effect leads to very poor agreement.

Experimental

Materials

2-Methoxypropene was prepared from the corresponding acetal by the procedure of Newman and Vanderzwan (31), bp 36–41°C (lit. (31) bp 37°C). 1-Methoxycyclohexene was prepared by heating cyclohexanone dimethyl acetal with a catalytic amount of *p*-toluenesulfonic acid in benzene and distilling out the methanol formed, bp 131°C (lit. (32) bp 137–142°C). α-Methoxystyrene was similarly prepared, using chlorobenzene as the solvent for the cracking (33), bp 90–93°C/17 Torr (lit. (33) bp 85–87°C/13 Torr). In all cases the enol ethers were purified by preparative gc using a Carbowax 20M column.

Calorimetry

Heats of reaction and solution were measured using an improved version of the simple Dewar calorimeter employed previously (34). Temperature changes were measured using a thermistor (Sargent Welch S-81670) with a Sargent Welch S-81601 bridge and a Heath SR 205 recorder. Electrical calibration was achieved using a Hewlett-Packard 6213A power supply to supply constant voltage across heater of ca. 10.1 Ω. The voltage drop across the heater was measured using a Simpson model C464 digital multimeter with a $3\frac{1}{2}$ figure display. The meter was also used to check the heater resistance. The heater consisted of a length of nichrome wire spot welded to copper leads; shrinkable polypropylene tubing was used to provide insulation; the leads extended below the surface of the liquid in the calorimeter.

The calorimeter was charged with 400 mL of solvent and brought to 25°C. The sample, usually 100 μL, was injected using a Hamilton syringe; the amount of the sample was determined by weighing before and after injection. Several electrical calibrations were performed for each run.

Solubility

The solubility of 2-methoxypropene was determined by nmr analysis of a saturated solution in 0.1 *N* NaOH, with 0.03 *M* *tert*-butyl alcohol as internal standard. The solubility of 1-methoxycyclohexene was too low for this method to be applicable. A saturated solution, 200 mL, in 0.1 *N* NaOH (purged with argon before adding the solute) separated from all undissolved solute was extracted four times using 5 mL portions of $CHCl_3$. The extracts were combined and made up to 25 mL with $CHCl_3$; a weighed amount of methyl benzoate was added as internal standard and the concentration of 1-methoxycyclohexene was determined by nmr analysis. This procedure permits an approximately 10-fold amplification before analysis and permits the use of nmr to determine solubility down to lower concentrations than would otherwise be practical. The solubility of α-methoxystyrene was too low even for this technique, and was determined by uv analysis. A sample (300 μL, measured using a 500 μL Hamilton syringe) of a saturated solution in 0.1 *N* NaOH was diluted to 10 mL using 0.1 *N* NaOH and the absorbance at 250 nm was measured. The extinction coefficient was determined to be 6680 ± 450.

[2]Although the heat of formation of 2-methoxy-2-butene probably refers to the *E* isomer, there is unfortunately some ambiguity. Dolliver *et al.* (40), who determined the heat of hydrogenation of 2-methoxy-2-butene, prepared it by what should be a stereospecific route from 2-butene, but identify the olefin only as 'purified butene-2,' with no comments concerning geometrical isomerism. Taskinen (39) found that *E*-2-methoxy-2-butene is 2.35 kcal mol^{-1} more stable than the *Z* isomer. Although it is most probable that the species studied by Dolliver *et al.* (40) is the *E* isomer or else a mixture, the possibility must exist that they studied the *Z* isomer, in which case there would be a systematic error of 2.35 kcal mol^{-1} in the free energies for 2-methoxy-2-butene and 3-methoxy-2-pentene.

Acknowledgements

We wish to thank the National Research Council of Canada, the Alfred P. Sloan Foundation and the Academic Development Fund of the University of Western Ontario for financial support of this research, and Dana Zendrowski for technical assistance.

1. K. H. Meyer. Chem. Ber. **45**, 2843 (1912); **47**, 826 (1914).
2. G. Schwarzenbach and C. Wittwer. Helv. Chim. Acta, **30**, 669 (1947).
3. A. Gero. J. Org. Chem. **19**, 1760 (1954).
4. J. E. Dubois and G. Barbier. Bull. Soc. Chim. Fr. 682 (1965).
5. R. P. Bell and P. W. Smith. J. Chem. Soc. B, 241 (1966).

6. S. SUNNER. Acta Chem. Scand. **11**, 1757 (1957).
7. J. HINE and K. ARATA. Bull. Chem. Soc. Jpn. **49**, 3085 (1976).
8. J. HINE and K. ARATA. Bull. Chem. Soc. Jpn. **49**, 3089 (1976).
9. J. P. GUTHRIE. Can. J. Chem. **53**, 898 (1975).
10. J. P. GUTHRIE. J. Am. Chem. Soc. **95**, 6999 (1973).
11. J. P. GUTHRIE. Can. J. Chem. **54**, 202 (1976).
12. J. P. GUTHRIE. J. Am. Chem. Soc. **96**, 3608 (1974).
13. J. P. GUTHRIE. J. Am. Chem. Soc. **99**, 3991 (1977).
14. S. W. BENSON and J. H. BUSS. J. Chem. Phys. **29**, 546 (1958).
15. S. W. BENSON. Thermochemical kinetics. 2nd ed. Wiley, New York, NY. 1976.
16. I. WADSÖ. Acta Chem. Scand. **20**, 544 (1966).
17. J. HINE and P. K. MOOKERJEE. J. Org. Chem. **40**, 292 (1975).
18. M. NOVAK and G. M. LOUDON. J. Org. Chem. **42**, 2494 (1977).
19. W. P. JENCKS and J. REGENSTEIN. *In* Handbook of biochemistry. 1st ed. *Edited by* Chemical Rubber Co., Cleveland, OH. 1968.
20. S. TAKAHASHI, L. A. COHEN, H. K. MILLER, and E. G. PEAKE. J. Org. Chem. **36**, 1205 (1971).
21. J. TOULLEC and J. E. DUBOIS. Tetrahedron, **29**, 2851 (1973).
22. J. E. DUBOIS and J. TOULLEC. Tetrahedron, **29**, 2859 (1973).
23. (*a*) M. V. SMOLUCHOWSKI. Z. Phys. Chem. **92**, 129 (1917); (*b*) M. EIGEN. Angew. Chem. Int. Ed. Engl. **3**, 1 (1964).
24. F. C. COLLINS. J. Colloid Sci. **5**, 499 (1955).
25. J. P. GUTHRIE. Can. J. Chem. In press.
26. H. AHLBRECHT, W. FUNK, and M. TH. REINER. Tetrahedron, **32**, 479 (1976).
27. J. P. GUTHRIE. Can. J. Chem. **56**, 962 (1978).
28. A. KANKAANPERÄ, P. SALOMAA, P. JUHALA, R. AALTONEN, and M. MATTSEN. J. Am. Chem. Soc. **95**, 3618 (1973).
29. M. H. ABRAHAM and P. L. GRELLIER. J. Chem. Soc. Perkin II, 1856 (1975).
30. G. E. LIENHARD and T. C. WANG. J. Am. Chem. Soc. **91**, 1146 (1969).
31. M. S. NEWMAN and M. C. VANDERZWAN. J. Org. Chem. **38**, 2910 (1973).
32. D. G. LINDSAY and C. B. REESE. Tetrahedron, **21**, 1673 (1965).
33. G. M. LOUDON, C. K. SMITH, and S. E. ZIMMERMAN. J. Am. Chem. Soc. **96**, 465 (1974).
34. J. P. GUTHRIE. Can. J. Chem. **55**, 3562 (1977).
35. R. C. WEAST (*Editor*). Handbook of chemistry and physics. 48th ed. Chemical Rubber Co., Cleveland, OH. 1967.
36. (*a*) S. W. BENSON and G. D. MENDENHALL. J. Am. Chem. Soc. **98**, 2046 (1976); (*b*) R. SHAW. J. Chem. Eng. Data, **14**, 461 (1969).
37. BEILSTEIN. Handbuch der organischen Chemie. (*a*) **1**(4) 2050; (*b*) **1**(4) 3262.
38. H. K. EIGENMANN, D. M. GOLDEN, and S. W. BENSON. J. Phys. Chem. **77**, 1687 (1973).
39. E. TASKINEN. J. Chem. Thermodyn. **6**, 345 (1974).
40. M. A. DOLLIVER, T. L. GRAHAM, G. B. KISTIAKOWSKY, E. A. SMITH, and W. E. VAUGHN. J. Am. Chem. Soc. **60**, 440 (1938).
41. J. D. COX and G. PILCHER. Thermochemistry of organic and organometallic compounds. Academic Press, New York, NY. 1970.
42. D. R. STULL, E. F. WESTRUM, JR., and G. C. SINKE. The chemical thermodynamics of organic compounds. Wiley, New York, NY. 1967.
43. J. CHAO and B. J. ZWOLINSKI. J. Phys. Chem. Ref. Data, **5**, 319 (1976).
44. P. GROSS, J. C. RINTELEN, and J. H. SAYLOR. J. Phys. Chem. **43**, 197 (1939).
45. F. D. ROSSINI, D. D. NAGMAN, W. H. EVANS, S. LEVINE, and I. JAFFE. Natl. Bur. Stand. (U.S.) Circ. No. 500 (1952).
46. J. P. GUTHRIE. Can. J. Chem. **52**, 2017 (1974).
47. P. GREENZAID, Z. LUZ, and D. SAMUEL. J. Am. Chem. Soc. **89**, 749 (1967).
48. J. TOULLEC and J. E. DUBOIS. Tetrahedron Lett. 1281 (1976).
49. P. SALOMAA and A. KANKAANPERA. Acta Chem. Scand. **20**, 1802 (1966).

The reactivity of $[C_3H_3^+]$ ions; a thermochemical study[1]

JOHN L. HOLMES

Chemistry Department, University of Ottawa, Ottawa, Ont., Canada K1N 9B4

AND

F. P. LOSSING

Division of Chemistry, National Research Council of Canada, Ottawa, Ont., Canada K1A 0R6

Received July 26, 1978

JOHN L. HOLMES and F. P. LOSSING. Can. J. Chem. **57**, 249 (1979).

The loss of halogen atom from the molecular ions of compounds of formulae C_3H_3Cl and C_3H_3Br produces the cyclopropenium cation as daughter ion. Each reaction takes place with appreciable reverse activation energy, most of which is partitioned into translational degrees of freedom of the products. In marked contrast, the iodo-analogues generate [propargyl]$^+$ as daughter ions at the thermochemical threshold (i.e. E_{rev} for these fragmentations is ~ 0). It is proposed that the reason for this behaviour lies in a large activation energy for the reaction [*cyclo*-$C_3H_3]^+ + I^\cdot \rightarrow [C_3H_3I]^{+\cdot}$.

JOHN L. HOLMES et F. P. LOSSING. Can. J. Chem. **57**, 249 (1979).

La perte de l'atome d'halogène par les ions moléculaires des composés de formule C_3H_3Cl et C_3H_3Br conduit au cation cyclopropénium comme ion-fille. Chaque réaction se produit avec une énergie d'activation inverse importante; on en attribue le maximum à des degrés de liberté de translation des produits. En opposition marquée, les analogues iodés donnent lieu au [propargyle]$^+$ comme ion-fille au seuil thermochimique (à savoir E_{rev} pour ces fragmentations est ~ 0). On croit que la raison de ce comportement est attribuable à une énergie d'activation élevée pour la réaction [*cycle* $C_3H_3]^+ + I^\cdot \rightarrow [C_3H_3I]^{+\cdot}$.

[Traduit par le journal]

Introduction

The simplest aromatic cation, cyclopropenium $[C_3H_3]^+$, has attracted considerable interest in recent years and its heat of formation now is well established. The appearance potentials (A.P.) for $[C_3H_3]^+$ fragment ions from a number of C_3H_4 and C_4H_6 hydrocarbons lead to ΔH_f values of 11.21 eV and 11.08 eV, respectively (1). These results, obtained by impact of monoenergetic electrons, are in good agreement with results from photoionisation studies (2–5) and photoelectron–photoion coincidence techniques (6). The slightly higher values for $\Delta H_f[C_3H_3]^+$ derived from C_3H_4 isomers arise from the small, common reverse activation energy of 0.1 eV (7) for the reaction $[C_3H_4]^{+\cdot} \rightarrow [C_3H_3]^+ + H^\cdot$. The mean $\Delta H_f = 11.1 \pm 0.1$ eV almost certainly corresponds to the cyclopropenium structure, because the isomeric propargyl cation, $[CH{\equiv}CCH_2]^+$, has been shown by experiment to have an appreciably higher $\Delta H_f = 12.2 \pm 0.1$ eV (1). Recent *ab initio* calculations using LCAO-SCF molecular orbital theory (8) are in agreement as to the greater stability of cyclopropenium, giving ΔH_f[*cyclo*-$C_3H_3]^+ = 10.98$ eV, with ΔH_f[propargyl]$^+$ 1.5 eV higher. These authors also calculated ΔH_f for six other $[C_3H_3]^+$ structures, all of which were much less stable than the propargyl cation and therefore were considered less likely to be encountered in experiment.

Metastable ion studies have shown that the formation of $[C_3H_3]^+$ from a variety of precursors frequently generates a metastable peak of composite shape (7, 9–12). For example, the reaction $[C_3H_5]^+ \rightarrow [C_3H_3]^+ + H_2$, yields a composite metastable peak comprising two dish-topped components. The broad component corresponds to the formation of cyclopropenium with a reverse activation energy of 1.2 eV and the other (narrow) component results from the formation of the propargyl cation, $[HC{\equiv}CCH_2]^+$, with a reverse activation energy of $\sim$0.5 eV (11). Formation of these two daughter ions has also been reported in a photoion–photoelectron coincidence study of the fragmentations of propargyl bromide and chloride (13).

In the present work we have measured the appearance potentials (A.P.) of $[C_3H_3]^+$ from C_3H_3X precursor molecules (where X = Cl, Br, I, and $[C_3H_3] = CH_3C{\equiv}C-$ or $HC{\equiv}C{-}CH_2-$). The translational energies released in the corresponding metastable fragmentations and the fraction of the reverse activation energy, E_{rev}, partitioned into translational degrees of freedom have been determined.

Results and Discussion

The ionisation potentials (I.P.) of C_3H_3X mole-

[1]NRCC No. 17066.

0008-4042/79/020249-04$01.00/0

TABLE 1. Energetics of the reactions $C_3H_3X \rightarrow [C_3H_3]^+ + X^\cdot$

Compound	I.P. (eV)	A.P.$[C_3H_3]^+$ (eV)	Apparent $\Delta H_f[C_3H_3]^+$	A.P.(calcd)[a] for $[cyclo\text{-}C_3H_3]^+$	A.P.(calcd)[a] for $[HC{\equiv}CCH_2]^+$	E_{rev} [a, b]	T_{min} [c]
CH_3CCCl	9.82	10.98	11.37	10.67	11.79	0.31	0.29
$CHCCH_2Cl$	10.68	11.00	11.39			0.32	
	10.68 (ref. 13)	11.02 (ref. 13)					
CH_3CCBr	9.60	10.90	11.91	10.06	11.18	0.84	0.35
$CHCCH_2Br$	10.48	10.88	11.89			0.82	
	10.42 (ref. 13)	10.94 (ref. 13)					
CH_3CCI	9.20	10.70	12.32	9.43	10.55	~0	0[e]
$CHCCH_2I$	>9.10[d]	10.50	12.12				

[a] $\Delta H_f[cyclo\text{-}C_3H_3]^+ = 11.07$ eV, $\Delta H_f[HC{\equiv}CCH_2]^+ = 12.2$ eV; all values ± 0.05 eV. ΔH_f of neutral pairs are taken as equal.
[b] A.P.(obs) − A.P.(calcd).
[c] Minimum energy partitioned into product translation.
[d] Contains ~ 2% iodoallene (see Experimental).
[e] Gaussian metastable peaks; $T_{0.5}(CH_3CCl) = 0.063$ eV, $T_{0.5}(HCCCH_2I) = 0.005$ eV.

cules and A.P. values for the $C_3H_3^+$ ions produced therefrom are presented in Table 1, together with the metastable peak measurements. The metastable peaks are shown in Fig. 1.

The observed I.P.'s are characteristic of electron removal from an acetylenic triple bond (14) for propargyl compounds (e.g. I.P.($CH_3C{\equiv}CH$) = 10.36 eV, I.P.($CH_3CH_2C{\equiv}CH$) = 10.18 eV) and for halogen ionisation in the case of the 1-halopropynes. For the apparent exception, propargyl iodide, the observed I.P. is no doubt too low because of the difficulty of preparing a sample of this compound completely free of its isomer, iodoallene (see Experimental); this impurity would certainly be expected to have an I.P. of ca. 9.1 eV.

The A.P. results for propargyl chloride agree well with previous data (13); it is the same for both chlorocompounds and lies well below that calculated for the propargyl ion and 0.32 eV above the calculated threshold for generation of $[cyclo\text{-}C_3H_3]^+$, see Fig. 2. The metastable peak for Cl$^\cdot$ loss is basically the same for both compounds and that for propargyl chloride is shown in Fig. 1. It should be noted that the metastable peak for 1-chloropropyne is of lower intensity than the above and also *appears* to contain a second (Gaussian) component situated in the centres of each 'dish'. However, this additional peak arises from a contribution from $[M—H]^+$—Cl from

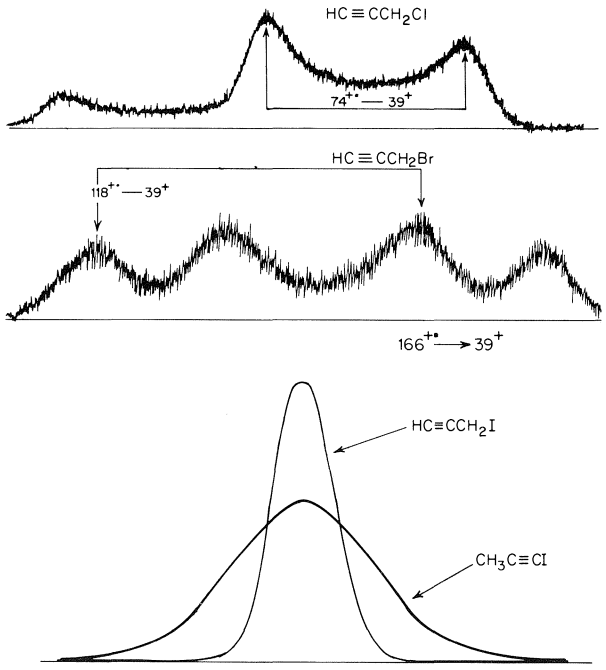

FIG. 1. Metastable peak shapes for the reaction $[C_3H_3X]^+ \rightarrow C_3H_3^+ + X^\cdot$. The *x*-axes do not have a common scale.

$[^{13}CC_2H_2Cl]^+$. The normal mass spectrum of 1-chloropropyne has an ion of appreciable abundance at *m/e* 73, $[C_3H_2Cl]^+$, and an intense metastable peak arises from the fragmentation $[C_3H_2Cl]^+ \rightarrow [C_3H_2]^{+\cdot} + Cl^{\cdot}$. The apparent second component described above also has a higher A.P. than the dished chlorine-atom-loss peak. The above observations may also account for the composite metastable peak reported by Sen-Sharma *et al.* (12) in their observations on propargyl chloride, although under our experimental conditions none was observable. The minimum energy released in the metastable fragmentation, 0.28 eV, was evaluated from the distribution of released energies (as described elsewhere (15)). It can be seen from the energy levels shown in Fig. 2 that the threshold daughter ion must be the cyclopropenium cation, and furthermore that the fragmentation has a reverse activation energy, E_{rev}, of 0.32 eV, about 90% of which is partitioned into translational energy of the products.

The bromo compounds also behaved similarly, generating a common dish-topped metastable peak and having a common A.P. for $[C_3H_3]^+$. Here, $E_{rev} = 0.83$ eV and a smaller fraction (~45%) is partitioned into product translational energy. Cyclopropenium again must be the threshold daughter ion (see Figs. 1 and 2).

In marked contrast, the A.P. for $[C_3H_3]^+$ from the iodo compounds corresponds very closely to the calculated threshold for [propargyl]$^+$. Furthermore, both metastable peaks are of Gaussian type (Fig. 2) and are associated with small energy releases; characteristic indeed, of fragmentations having zero E_{rev}. An explanation for the fragmentation behaviour of these molecules which fits all the observations is as follows.

Note from Table 1 that the activation energy for the reaction

$$[\text{halogen}]^{\cdot} + [cyclo\text{-}C_3H_3]^+ \rightarrow [C_3H_3X]^{+\cdot}$$

increases in the order $E_{iodo} > E_{bromo} > E_{chloro}$. It is suggested that E_{iodo} is *so large* that the fragmentation pathway of lowest energy for the C_3H_3I isomers becomes that leading to the propargyl cation, rather than that producing the more stable [cyclopropenium]$^+$.

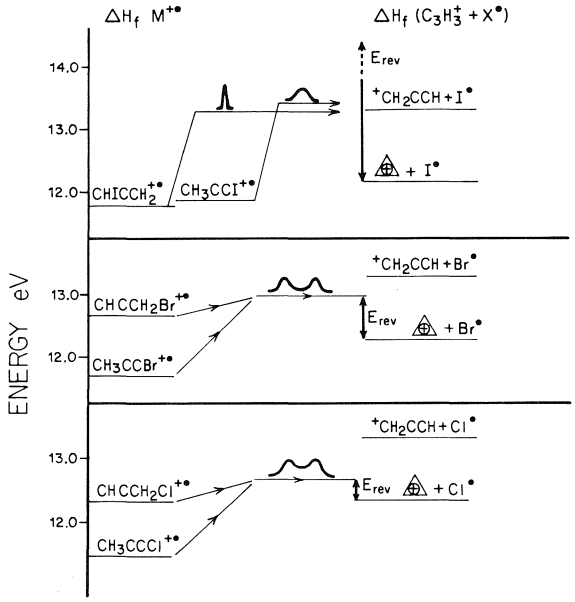

FIG. 2. Energy diagram for the reactions $[C_3H_3X]^{+\cdot} \rightarrow C_3H_3^+ + X^{\cdot}$. Metastable peak shapes are as illustrated above the transition arrows.

Experimental

Ionisation and appearance energies were measured using energy selected electrons in an apparatus which has previously been described (16, 17). Metastable peaks were measured on a Kratos-AEI MS902S Mass Spectrometer under conditions of good energy resolution (7). Propargyl chloride and bromide were obtained from Aldrich Co. Propargyl iodide was prepared by treating propargyl chloride with NaI in acetone (18), the Finkelstein reaction. This reaction was carried out at 0°C and purification was performed at the same temperature. In spite of these precautions a small amount of iodoallene (2–3%) was always produced. Any attempts to distill the product led to polymerisation and/or production of larger proportions of iodoallene. The halopropynes were prepared by the method of Smith and McLeod (19) (chloride), Cleveland and Murray (20) (bromide), and Grignard and Perichon (21) (iodide).

Acknowledgements

One of us (J.H.) thanks the National Research Council of Canada for financial assistance for this research. The authors are indebted to Dr. J. Krause and Dr. M. Dakubu for invaluable experimental assistance.

1. F. P. LOSSING. Can. J. Chem. **50**, 3973 (1972).
2. B. BREHM. Z. Naturforsch. **21a**, 196 (1966).
3. A. C. PARR and F. A. ELDER. J. Chem. Phys. **48**, 2659 (1968).
4. C. S. MATTHEWS and P. WARNECK. J. Chem. Phys. **51**, 854 (1969).
5. R. KRASSIG, D. REINKE, and H. BAUMGÄRTEL. Ber. Bunsenges. Ges. Phys. Chem. **78**, 425 (1974).
6. A. C. PARR, A. J. JASON, and R. STOCKBAUER. Int. J. Mass Spectrom. Ion Phys. **26**, 23 (1978).
7. J. L. HOLMES and J. K. TERLOUW. Org. Mass Spectrom. **10**, 787 (1975).
8. L. RADOM, P. C. HARIHARAN, J. A. POPLE, and P. VON R. SCHLEYER. J. Am. Chem. Soc. **98**, 10 (1976); **95**, 6531 (1973).
9. G. KHODADADI, R. BOTTER, and H. M. ROSENSTOCK. Int. J. Mass. Spectrom. Ion Phys. **3**, 397 (1969).
10. P. GOLDBERG, J. A. HOPKINSON, A. MATHIAS, and A. E. WILLIAMS. Org. Mass Spectrom. **3**, 1009 (1970).
11. J. L. HOLMES, A. D. OSBORNE, and J. K. TERLOUW. Org. Mass Spectrom. **10**, 867 (1975).

12. D. K. SEN-SHARMA, K. R. JENNINGS, and J. H. BEYNON. Org. Mass Spectrom. **11**, 319 (1976).
13. B. P. TSAI, A. S. WERNER, and T. BAER. J. Chem. Phys. **63**, 4384 (1975).
14. H. W. ROSENSTOCK, K. DRAXL, B. W. STEINER, and J. T. HERRON. J. Phys. Chem. Ref. Data, **6**, Suppl. 1 (1977).
15. J. L. HOLMES and A. D. OSBORNE. To be published.
16. K. MAEDA, G. P. SEMELUK, and F. P. LOSSING. Int. J. Mass Spectrom. Ion Phys. **1**, 395 (1968).
17. F. P. LOSSING and J. C. TRAEGER. Int. J. Mass Spectrom. Ion Phys. **19**, 9 (1976).
18. C. A. BUEHLER and D. E. PEARSON. Survey of organic synthesis. Wiley, New York. 1970. p. 339.
19. W. T. SMITH and G. L. MCLEOD. Org. Synth. **31**, 4 (1951).
20. F. F. CLEVELAND and J. M. MURRAY. J. Chem. Phys. **11**, 458 (1943).
21. V. GRIGNARD and H. PERICHON. Ann. Chim. **10**(5), 5 (1926).

Canadian Journal of Chemistry
Published by
THE NATIONAL RESEARCH COUNCIL OF CANADA

Journal canadien de chimie
Publié par
LE CONSEIL NATIONAL DE RECHERCHES DU CANADA

Volume 57 Number 3 February 1, 1979 Volume 57 numéro 3 1 février 1979

The electron spin resonance spectrum of $(CH_3)_3{}^{13}COO^{\cdot}$[1]

J. A. HOWARD
Division of Chemistry, National Research Council of Canada, Ottawa, Ont., Canada K1A 0R9

Received August 12, 1978

J. A. HOWARD. Can. J. Chem. **57**, 253 (1979).

The esr spectrum of $(CH_3)_3{}^{13}COO^{\cdot}$ has been observed in solution and the hyperfine interaction with the carbon-13 nucleus is 3.92 G.

J. A. HOWARD. Can. J. Chem. **57**, 253 (1979).

On a étudié le spectre rpe du radical $(CH_3)_3{}^{13}COO^{\cdot}$ en solution; on a évalué que l'interaction hyperfine avec le noyau du ^{13}C est égale à 3.92 G.

[Traduit par le journal]

Introduction

Alkylperoxy radicals have been extensively studied by electron spin resonance spectroscopy and *g*-factors, oxygen-17 and γ-hydrogen hyperfine coupling constants are well characterized (1–6). There has, however, been only one report of a carbon-13 hyperfine coupling constant (7) although central atom hyperfine coupling constants have been reported for vanadium (8), cobalt (9), manganese (9), and phosphorus (10–12) centred peroxy radicals while fluorine and hydrogen hyperfine couplings have been observed for $FOO^{\cdot}$ and $HOO^{\cdot}$ (13).

In this article we report the preparation of $(CH_3)_3{}^{13}COO^{\cdot}$ and the observation of its esr spectrum at low temperature.

Experimental

$(CH_3)_3{}^{13}COOH$ was prepared in about 40% yield from $(CH_3)_3{}^{13}CCl$, silver trifluoroacetate, and hydrogen peroxide by the method of Cookson *et al.* (14). $(CH_3)_3{}^{13}CCl$ (90% isotopic enrichment) was obtained from Merck, Sharpe and Dohme Canada Ltd.

Electron spin resonance spectra were recorded on a Varian E-4 spectrometer equipped with a variable temperature accessory. The microwave frequency was measured with a Systron-Donner Model 6016 frequency counter which also monitored the frequency of a proton magnetometer used to measure the magnetic field.

[1]NRCC No. 17093.

Results and Discussion

The esr spectrum shown in Fig. 1 was observed during photolysis of $(CH_3)_3{}^{13}COOH$ (0.2 *M*) and di-*tert*-butyl peroxide (0.2 *M*) in cyclopropane at low temperature (123 to 173 K) and consists of two lines 1.8 G wide, separated by 3.92 G and centred at $g = 2.0151$. At temperatures below 123 K the signal intensity did not decrease when the initiating light was switched off. Spectrum resolution was not as good above 173 K and the spectrum consists of a broad singlet ($\Delta H_{ms} = 7.5$ G) at 167 K. This spectrum can definitely be attributed to $(CH_3)_3{}^{13}COO^{\cdot}$ with the doublet arising because of interaction of the unpaired electron with the carbon-13 nucleus ($I = 1/2$) because *tert*-butylperoxy is the only radical that can be detected during low temperature photolysis of *tert*-butyl hydroperoxide (15).

Now it has been established that the unpaired electron on an alkylperoxy radical is confined almost entirely to a π orbital located on the two oxygen atoms with approximately 60% on the terminal oxygen and 40% on the inner oxygen (2). Since there is no direct mixing between the inner oxygen $2p_z$ orbital and the carbon 2*s* orbital the ^{13}C hyperfine interaction should be small. Negative spin density can, however, be induced onto the carbon atom via spin-polarization while hyperconjugation would produce positive spin density on this atom. The

0008-4042/79/030253-02$01.00/0

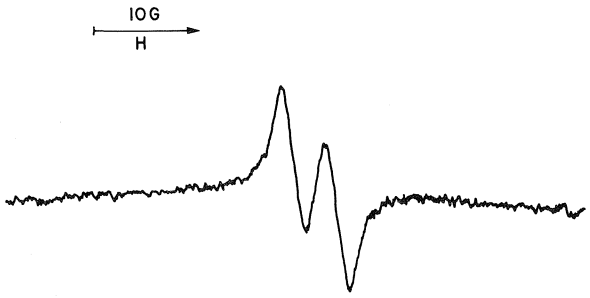

FIG. 1. Electron spin resonance spectrum of $(CH_3)_3{}^{13}COO^{\bullet}$ at 118 K in cyclopropane.

magnitude of the ^{13}C hyperfine splitting constant ($a_{^{13}C}$ = 3.92 G) divided by the value of A_0 (1339 G) for this atom (16) indicates that the 2*s* spin density at carbon is ca 0.003.

The value of $a_{^{13}C}$ for $(CH_3)_3{}^{13}COO^{\bullet}$ is smaller than $a_{^{13}C}$ = 6.15 G for $Cl_3{}^{13}COO^{\bullet}$ (7) which suggests a lower spin density at the central carbon atom in the former radical. This difference is consistent with the difference in electronegativity between the methyl and chlorine substituents. Thus the more electronegative chlorine will withdraw bonding electrons by an inductive mechanism leaving more unpaired spin density on the central carbon atom because of the essentially anti-bonding nature of the orbital occupied by the unpaired electron.

The value of the proton hyperfine coupling in $HOO^{\bullet}$ (13) is about 4 times larger than $a_{^{13}C}$ for $(CH_3)_3{}^{13}COO^{\bullet}$ even though $A_0(^{13}C)/A_0(^1H) \sim 2.63$. This implies that the *s* spin density on hydrogen is about 10 times larger than the 2*s* spin density on carbon which may reflect the difference in the polarizability of the electrons in the H—O and C—O bonds in these peroxy radicals.

Semi-empirical SCF-INDO calculations have proved useful for calculating the sign and magnitude of the spin density on the various atoms of free radicals. This method has in fact been applied to several alkylperoxy radicals by Biskupič and Valko (17). Not unexpectedly they calculate that the unpaired spin is almost entirely concentrated in a π orbital built from $2p_z$ orbitals on the terminal and inner oxygens. In addition they calculate that the total spin density on the central carbon atom is -0.0051 for $CH_3OO^{\bullet}$, -0.0053 for $C_2H_5OO^{\bullet}$, and -0.0052 for n-$C_4H_7OO^{\bullet}$. The INDO method would, therefore, be expected to give a value of -0.0052 for $(CH_3)_3COO^{\bullet}$ which is close to our estimated value of 0.003. The negative sign of the spin density does imply that spin-polarization overshadows hyperconjugation as a mechanism for inducing unpaired spin on the central atom in alkylperoxy radicals.

The INDO method also predicts a larger spin density on the proton in $HOO^{\bullet}$ (-0.0070) than on the carbon in $CH_3OO^{\bullet}$ although the ratio is much smaller than the ratio of the experimental spin densities. Values of a_H for $HOO^{\bullet}$ have, however, all been obtained in a powder or single crystal (13) and may not be directly comparable with $a_{^{13}C}$ for $(CH_3)_3COO^{\bullet}$ obtained in solution.

1. R. W. FESSENDEN and R. H. SCHULER. Adv. Rad. Chem. **2**, 1 (1970).
2. E. MELAMUD and B. SILVER. J. Phys. Chem. **77**, 1896 (1973).
3. K. ADAMIC, K. U. INGOLD, and J. R. MORTON. J. Am. Chem. Soc. **92**, 922 (1970).
4. J. A. HOWARD. Can. J. Chem. **50**, 1981 (1972).
5. J. E. BENNETT and R. SUMMERS. J. Chem. Soc. Faraday Trans. II, 1043 (1973).
6. T. J. KEMP and M. J. WELBOURN. Tetrahedron Lett. 87 (1974).
7. C. HESSE, N. LERAY, and J. RONCIN. Mol. Phys. **22**, 137 (1971).
8. M. C. R. SYMONS. J. Chem. Soc. A, 1889 (1970).
9. S. A. FIELDHOUSE, B. W. FULLAM, G. W. NEILSON, and M. C. R. SYMONS. J. Chem. Soc. Dalton, 567 (1974).
10. G. B. WATTS and K. U. INGOLD. J. Am. Chem. Soc. **94**, 2528 (1972).
11. A. G. DAVIES, D. GRILLER, and B. P. ROBERTS. J. Chem. Soc. Perkin II, 993 (1972).
12. J. A. HOWARD and J. C. TAIT. Can. J. Chem. **56**, 2163 (1978).
13. J. R. MORTON and K. F. PRESTON. Landolt-Börnstein, New Series, Vol. 9. *Edited by* H. Fischer and K.-H. Hellwege. Springer-Verlag. 1977. Part *a*.
14. P. G. COOKSON, A. G. DAVIES, and B. P. ROBERTS. J. Chem. Soc. Chem. Commun. 1022 (1976).
15. K. U. INGOLD and J. R. MORTON. J. Am. Chem. Soc. **86**, 3400 (1964).
16. J. R. MORTON and K. F. PRESTON. J. Magn. Reson. **30**, 577 (1978).
17. S. BISKUPIČ and L. VALKO. J. Mol. Struct. **27**, 97 (1975).

ρ as a quantitative measure of transition state structure

BO-LONG POH

School of Chemical Sciences, Universiti Sains Malaysia, Penang, Malaysia

Received August 25, 1977[1]

BO-LONG POH. Can. J. Chem. **57**, 255 (1979).

The values of the Brønsted exponent for several examples of nucleophilic substitution reactions, aromatic electrophilic substitution reactions, and hydrogen atom abstraction from toluene by free radicals have been calculated from the ρ values of the corresponding reactions. The magnitude of the Brønsted exponent is shown to indicate the degree of charge developed in the transition state structure.

BO-LONG POH. Can. J. Chem. **57**, 255 (1979).

En se basant sur les valeurs de ρ des réactions correspondantes, on a calculé les valeurs des exposants de Brønsted représentant plusieurs cas de réactions de substitutions nucléophiles, de réactions de substitutions aromatiques électrophiles et de réactions d'enlèvement d'atomes d'hydrogène du toluène par des radicaux libres. On a démontré que l'amplitude de l'exposant de Brønsted est une indication du développement de la charge dans la structure de l'état de transition.

[Traduit par le journal]

Introduction

We have been interested in understanding the success and failure of the common linear free energy correlations. In two earlier papers (1, 2) we have put forward a modified MacInnes equation and discussed its relationships with Taft (3), Brønsted (4), and Kirkwood–Westheimer (5) equations. In this paper we discuss the use of the ρ parameter as a quantitative measure of the charge developed in the transition state structure of a chemical reaction. Up to the present time only the Brønsted exponent (4, 6) has been used as a quantitative measure of transition state structure and the ρ parameter is commonly believed to give only a rough idea of the degree of charge developed in the transition state structure (7).

Results and Discussion

The Brønsted equation (4), which correlates the ionization constants of a given series of acids (or bases) with the rate constants of a reaction that is catalyzed by the same series of acids (or bases), is actually composed of two Hammett equations (1, 8, 9), one correlating ionization constants in reaction [1] and the other correlating rate constants in reaction [2].

$$[1] \qquad HA \underset{}{\overset{K}{\rightleftharpoons}} H^+ + A^-$$

$$[2] \qquad HA + S \xrightarrow[\text{slow}]{k} [S\text{---}H\text{---}A]^{\ddagger} \xrightarrow{\text{fast}} \text{Products}$$

The symbols HA and S denote acid and substrate respectively. The usual method of obtaining the value of the Brønsted exponent, α, is equivalent to calculating the ratio of the ρ values of reactions [1] and [2] for α is related to ρ_e (for the equilibrium process in reaction [1]) and ρ_r (for the rate process in reaction [2]) in the form of eq. [3] where *m* is the parameter defined earlier (1). For reactions in which the charge is located on the same atom in both the equilibrium and rate processes *m* is unity, eq. [3] reduces to eq. [4] (8).

$$[3] \qquad m\alpha = \rho_r/\rho_e$$

$$[4] \qquad \alpha = \rho_r/\rho_e$$

Since nucleophilic substitution reactions, aromatic electrophilic substitution reactions, and hydrogen abstraction from toluenes by free radicals are analogous to the reaction scheme shown in reaction [2] we can compute the values of α for these reactions from their ρ_r values if the ρ_e values of suitable reference series are available. We apply eq. [4] to several reactions and the reference series which provide the ρ_e values are given in Table 1. The values of α calculated are given in Table 2. These values have not been corrected for any temperature and solvent effects.[2] The α values of reactions [1], [2], and eq. [4]

[1]Revision received June 14, 1978.

[2]Solvent effects on ρ_e values are probably small because the reference equilibrium processes (Table 1) have their positive charge delocalised in the aromatic ring. Therefore, the values of α calculated without solvent corrections (Table 2) probably do not differ significantly from the corresponding true values. This view is supported by (*i*), the close agreement of the α values with Abraham's *z* values in Table 1 although the solvents differ and (*ii*), the large α value of reaction [13] in Table 2 (the value of 0.82 is close to the upper limit of 1) though ρ_r value is for aqueous medium and ρ_e for gas phase. Even when assuming that the true α value of reaction [13] is unity the ρ_e value for aqueous medium then differs from that for the gas phase by a maximum of 18% only.

0008-4042/79/030255-03$01.00/0

TABLE 1. Rate and reference equilibrium processes

Rate process	Reference equilibrium process	ρ_e	Reference
[1] Pyridines + EtI	Protonation of pyridines in water, 25°C	−6.01	8
[2] Solvolysis of $ArC(R)_2Cl$, R = alkyl, H [3] Hydrogen abstraction from $ArCH_3$	$ArCH(C_6H_5)OH + H^+ \rightleftharpoons Ar\overset{+}{C}H(C_6H_5) + H_2O$	−5.6	12[a]
[4] Electrophilic substitution in $ArCH_3$	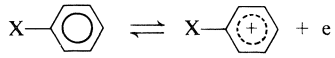	−14.7	13[b]
[5] Electrophilic substitution in thiophenes	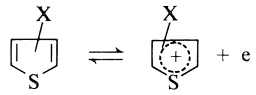	−16.5	13[c]

[a]The more appropriate reference equilibria should be the corresponding arylalkyl carbonium ion equilibria. But such data are lacking. However, their ρ_e values are estimated to be close to those of the arylmonophenyl carbonium ion equilibria given above (12).
[b]Data on the more appropriate reference equilibrium process (protonation of benzenes) are lacking. However, the above given equilibrium is a suitable reference series (13) since the aryl cation is a good model for the Wheland intermediate in aromatic electrophilic substitution reactions.
[c]Data on the more appropriate reference equilibrium process (ring protonation of thiophenes) are lacking. However, the above given equilibrium is a suitable reference series (13) for the same reason given in footnote *b*.

TABLE 2. Calculated Brønsted exponent, α, from eq [4]

Reaction	Solvent	Temperature (°C)	ρ_r	α	Reference
[1] Pyridines + EtI	$C_6H_5NO_2$	60	−2.94	0.49(0.42)[a]	15
[2] $ArCH_2Cl + H_2O$	48% EtOH	30	−2.18	0.39(0.40)[b]	16
[3] $ArCH(CH_3)Cl + H_2O$	H_2O–Dioxane	25	−4.3	0.77	17
[4] $ArC(CH_3)_2Cl + H_2O$	90% aqueous acetone	25	−4.62	0.83(0.85)[c]	18
[5] $ArCH_3$ + *t*-BuO·	C_6H_5Cl	45	−0.32	0.06	19
[6] $ArCH_3$ + ·Cl	CCl_4	40	−0.66	0.12	20
[7] $ArCH_3$ + ·CCl_3	C_6H_5Cl	80	−1.46	0.26	21
[8] $ArCH_3$ + ·Br	CCl_4	80	−1.37	0.24	22
[9] Ethylation of $ArCH_3$	CH_2ClCH_2Cl	25	−2.4	0.16	23
[10] Nitration of $ArCH_3$	CH_3COONO_2, $(CH_3CO)_2O$	25	−6.0	0.41	23
[11] Acetylation of $ArCH_3$	$C_2H_4Cl_2$	25	−9.1	0.62	23
[12] Chlorination of $ArCH_3$	CH_3COOH	25	−10.0	0.68	23
[13] Bromination of $ArCH_3$	CH_3COOH–H_2O	25	−12.1	0.82	23
[14] Mercuration of $ArCH_3$	CH_3COOH	25	−4.0	0.27	23
[15] Detritiation of $ArCH_3$	CF_3COOH–H_2O	25	−8.2	0.56	23
[16] Bromination of thiophenes	CH_3COOH–H_2O	25	−10.0	0.61	24
[17] Chlorination of thiophenes	CH_3COOH	25	−7.8	0.47	24
[18] Detritiation of thiophenes	CF_3COOH–CH_3COOH	25	−7.2	0.44	25
[19] Acetylation of thiophenes	CH_2ClCH_2Cl	25	−5.7	0.35	26
[20] Trifluoroacetylation of thiophenes	CH_2ClCH_2Cl	75	−7.4	0.45	24

[a]Charge developed on the nitrogen atom in the transition state of the reaction: pyridine + CH_3I; value taken from ref. 14.
[b]Charge developed on the methylene carbon atom in the transition state of solvolysis of benzyl chloride; value taken from ref. 14.
[c]Charge developed on the carbon atom in the transition state of solvolysis of *tert*-butyl chloride, value taken from ref. 14.

are in good agreement with the degree of charge developed in the transition state structures of the corresponding reactions. Therefore, the magnitude of α seems to give a quantitative measure of the degree of charge developed in the transition state structure, as we have suggested earlier (1). It is unfortunate that no data on the degree of charge developed in the transition state structures of the remaining reactions are available for comparison. It is worth noting that the α values of hydrogen abstraction reactions (reactions [5]–[8]) are small but, nevertheless, indicate polar character (10, 11). It must be cautioned that the above interpretation of α is not applicable to reactions in which ρ_r is a composite term (for example, acid-catalyzed hydrolysis of esters).

Acknowledgment

The author thanks Universiti Sains Malaysia for a short term research project grant.

1. B. L. POH. Can. J. Chem. **55**, 3721 (1977).
2. B. L. POH. Can. J. Chem. **56**, 747 (1978).
3. R. W. TAFT, JR. J. Am. Chem. Soc. **75**, 4231 (1953).
4. J. N. BRØNSTED and K. PEDERSEN. Z. Phys. Chem. **108**, 185 (1924).
5. J. G. KIRKWOOD and F. H. WESTHEIMER. J. Chem. Phys. **6**, 506 (1938); **6**, 513 (1938).
6. A. J. KRESGE. *In* Proton-transfer reactions. *Edited by* E. Caldin and V. Gold. Chapman and Hall, London. 1975.
7. K. B. WIBERG. Physical organic chemistry. John Wiley, New York. 1964. p. 407.
8. P. R. WELLS. Chem. Rev. **63**, 171 (1963).

9. L. P. HAMMETT. Physical organic chemistry. McGraw-Hill, New York. 1940.
10. E. S. HUYSER. Free radical chain reactions. Wiley-Interscience, New York. 1970. p. 7.
11. W. A. PRYOR. Free radicals. McGraw-Hill, New York. 1966. p. 170.
12. N. C. DENO and W. L. EVANS. J. Am. Chem. Soc. **79**, 5804 (1957).
13. P. LINDA, G. MARINO, and S. PIGNATARO. J. Chem. Soc. B, 1585 (1971).
14. M. H. ABRAHAM. *In* Progress in physical organic chemistry. Vol. 11. Interscience, New York. 1974.
15. A. FISCHER, W. J. GALLOWAY, and J. VAUGHAN. J. Chem. Soc. 3591 (1966).
16. H. H. JAFFE. Chem. Rev. **53**, 191 (1953).
17. C. MECHELYNCK-DAVID and P. J. C. FIERENS. Tetrahedron, **6**, 232 (1959).
18. H. C. BROWN and Y. OKAMOTO. J. Am. Chem. Soc. **79**, 1913 (1957).
19. H. SAKURAI and A. HOSOMI. J. Am. Chem. Soc. **89**, 459 (1967).
20. G. A. RUSSELL and R. C. WILLIAMSON, JR. J. Am. Chem. Soc. **86**, 2357 (1964).
21. E. S. HUYSER. J. Am. Chem. Soc. **82**, 394 (1960).
22. G. A. RUSSELL. J. Org. Chem. **23**, 1407 (1958).
23. L. M. STOCK and H. C. BROWN. *In* Advances in physical organic chemistry. Vol. 1. Academic Press, London. 1963.
24. S. CLEMENTI and G. MARINO. J. Chem. Soc. Perkin II, 71 (1972).
25. A. R. BUTLER and C. EABORN. J. Chem. Soc. B, 370 (1968).
26. S. CLEMENTI, P. LINDA, and M. VERGONI. Tetrahedron, **27**, 4667 (1971).

α,β-Epoxy sulfoxides and sulfones. Synthesis and some reactions

TONY DURST, KAM-CHUNG TIN, FRANCOIS DE REINACH-HIRTZBACH, JOHN M. DECESARE, AND M. DOMINIC RYAN

Department of Chemistry, University of Ottawa, Ottawa, Ont., Canada K1N 9B4

Received March 27, 1978

TONY DURST, KAM-CHUNG TIN, FRANCOIS DE REINACH-HIRTZBACH, JOHN M. DECESARE, and M. DOMINIC RYAN. Can. J. Chem. **57**, 258 (1979).

A number of α,β-epoxy sulfoxides and epoxy sulfones have been prepared via cyclization of α-chloro-β-hydroxy sulfoxides or phase-transfer catalyzed reaction between α-chloroalkyl sulfones and carbonyl compounds. Thermal and acid-catalyzed rearrangement of these epoxides resulted in migration of sulfinyl or sulfonyl groups to form β-carbonyl sulfoxides or sulfones. Upon treatment of the epoxy sulfones with $MgBr_2$ in ether, α-bromocarbonyl compounds were obtained in excellent yield. The reaction of epoxy sulfones with nucleophiles was also briefly investigated.

TONY DURST, KAM-CHUNG TIN, FRANCOIS DE REINACH-HIRTZBACH, JOHN M. DECESARE et M. DOMINIC RYAN. Can. J. Chem. **57**, 258 (1979).

On a préparé un certain nombre d'α,β-époxy sulfoxydes et d'époxy sulfones par cyclisation d'α-chloro β-hydroxy sulfoxydes ou par une réaction catalysée par transfert de phase entre des α-chloroalkyl sulfones et des composés carbonylés. Une transposition thermique ou acido-catalysée de ces époxydes provoque une migration des groupes sulfinyle ou sulfonyle avec formation de sulfoxydes ou de sulfones β-carbonylés. La réaction des époxysulfones avec du $MgBr_2$ dans l'éther fournit des composés α-bromo carbonylés avec d'excellents rendements. On a aussi étudié brièvement la réaction des époxy sulfones avec des nucléophiles.

[Traduit par le journal]

Synthesis

α,β-Epoxy sulfones have been prepared by two general routes: (*i*) epoxidation of α,β-unsaturated sulfones (1, 2), eq. [1], and, (*ii*) cyclization of halohydrin sulfones (3–7), eq. [2]. Several versions of the latter route have been described including Darzens-type (3) and phase-transfer-catalyzed reactions (4, 5) between α-halo sulfones and ketones or aldehydes, in which the halohydrin sulfones are intermediates converted *in situ* to the epoxy sulfones, and base-induced cyclizations of previously isolated halohydrin sulfones (6, 7).

Epoxy sulfoxides cannot be prepared by oxidation of α,β-unsaturated sulfoxides since all epoxidizing agents cause oxidation of the sulfur atom to the sulfone stage before epoxidation. These epoxides have been prepared by reaction of α-chloro sulfoxides with carbonyl compounds in the presence of K*t*OBu (8, 9) and by KOH-mediated cyclization of α-chloro-β-hydroxy sulfoxides (7).

[1] $RSO_2CR^1{=}CR^2R^3 \xrightarrow{[O]}$ 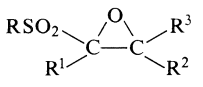

1 **2**

[2] 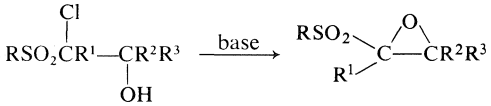

3

Zwanenburg and ter Wiel (1) reported that the epoxidation of the α,β-unsaturated sulfone **1** (R = R^2 = Ph, R^1 = R^3 = H) with basic hydrogen peroxide led only to the *trans*-epoxide **2**, irrespective of the stereochemistry of the starting olefin. More recently, Curci and Difuria (2) found that the stereoselectivity observed in the epoxidation of *cis*-**1** was dependent on the nature of the epoxidizing nucleophile. Thus *cis*-**1** and ClO^- gave exclusively *cis*-**2**, *m*-chloroperbenzoate gave a *cis–trans* ratio of 95:5, whereas basic H_2O_2 or basic *t*BuOOH yielded a 1:9 *cis–trans* mixture; the latter results essentially confirm the earlier report (1).

Vogt and Tavares (3) prepared several epoxy sulfones in good to excellent yield by reacting chloromethyl *p*-tolyl sulfone with aldehydes or ketones in the presence of KO*t*Bu. When benzaldehyde was used as the carbonyl component, the resulting epoxide had the *trans* geometry. Independently Bohlmann and Haffer (6) described the KOH induced cyclization of an α-chloro-β-hydroxy sulfone, having produced the intermediate **3** by oxidation of an α-chloro-β-hydroxy sulfide. Recently Makosza and co-workers (4) showed that α,β-epoxy sulfones are very simply prepared from α-chloro sulfones and carbonyl compounds under phase-transfer conditions with yields of 60–90% being obtained from chloromethyl *p*-tolyl sulfone and a variety of carbonyl components. Although we had developed a route to

0008-4042/79/030258-09$01.00/0

TABLE 1. Preparation of α-chloro-β-hydroxy sulfoxides and sulfones

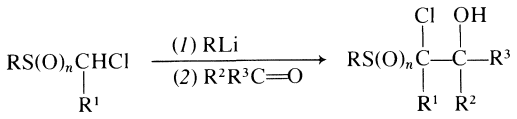

Entry	R	R^1	R^2	R^3	Yield (%) Sulfones **3**	Yield (%) Sulfoxides **6**
a	Ph	H	CH_3	CH_3	71	75
b	Ph	H	—$(CH_2)_5$—		94	79
c	Ph	H	Ph	Ph	0	68
d	Ph	H	Ph	H	94	—
e	Ph	CH_3	CH_3	CH_3	—	34, 70†
f	Ph	CH_3	—$(CH_2)_5$—		—	45, 72†
g	Ph	CH_3	Ph	Ph	—	68*
h	CH_3	H	(CH_2)—		78	15
i	CH_3	H	Ph	Ph	—	17*
j	nC_4H_9	nC_3H_7	CH_3	CH_3	—	66
k	nC_4H_9	nC_3H_7	—$(CH_2)_5$—		—	71
l	nC_4H_9	nC_3H_7	Ph	Ph	—	34*

*Isolated as the corresponding epoxy sulfoxide **9**.
†Using lithium diisopropyl amide (LDA) as base.

epoxy sulfones (see below) we have, in our recent work (5), used only the phase-transfer route and feel that it is the most practical and versatile approach to these compounds.

We had initially prepared a number of epoxy sulfones by cyclization of the chlorohydrin sulfones **3** with 5% KOH in methanol. The halohydrin sulfones were obtained via condensation of α-lithio-α-chloro sulfones with ketones or aldehydes at −70°C followed by quenching with H_2O at low temperature (eq. [3]). In some instances, Table 1, entries *g* and *l*, epoxy sulfones were formed directly by this procedure. One difficulty with this approach was that cleavage of **3** to its carbonyl and chloromethyl sulfone components competed, often to a major extent, with cyclization to the epoxide (see also ref. 6). This competing reaction is apparently more serious when R = Ph in **3** compared to when R = CH_3, probably because of the greater stability of **5** when R = Ph compared to R = CH_3.[1] The reversibility of **3** into its components is immaterial under the phase-transfer conditions.

An interesting aspect of the route outlined by [3] involved the preparation and trapping of the lithio derivative of chloromethyl methyl sulfone, i.e., **5** (R—CH_3, R^1 = H), without serious competition from the familiar Ramberg–Bäcklund reaction. In contrast to the behavior of chloromethyl methyl sulfone,

[3] 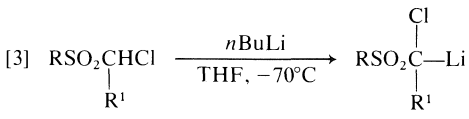

4 **5**

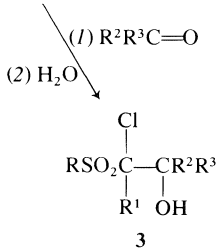

3

it was not possible to intercept a metallated derivative of 2-chlorothiane 1,1-dioxide. We did not attempt to isolate the possible by-products, 2-thia[2.1.0]bicyclohexane 2,2-dioxide or its decomposition product, cyclopentene. These results are summarized in Tables 1 and 2.

The phase-transfer technique (4) is also capable of providing epoxy sulfones starting from α-chloro sulfones, such as chloromethyl methyl sulfone, which have α′ hydrogens and are thus susceptible to the Ramberg–Bäcklund rearrangement. α-Chlorobenzyl benzyl sulfone, however, yielded only *trans*-stilbene and no condensation product upon attempted reaction with benzaldehyde under phase-transfer conditions (see Table 2).

The α-chloro-β-hydroxy sulfoxides **6**, prepared from the reaction of the α-chloro sulfoxides **7** with aldehydes and ketones (10), could be cyclized in very

[1]Bordwell *et al.* (25) have shown that $PHSO_2CH_3$ is more acidic by 2pK_a units than $CH_3SO_2CH_3$. One would expect a similar trend, for $PhSO_2CH_2Cl$ vs. $CH_3SO_2CH_2Cl$ and thus a greater stability for **5** when R = Ph than CH_3.

TABLE 2. Preparation of α,β-epoxy sulfoxides and sulfones

Series	R	R^1	R^2	R^3	Yield (%) Sulfoxide **9***	Yield (%) Sulfone **2**
a	Ph	H	CH_3	CH_3	91	10,* 94,† 93‡
b	Ph	H	$-(CH_2)_5-$		91	40,* 95‡
c	Ph	H	Ph	Ph	100§	0,*
d	Ph	H	Ph	H	—	0,* 92†
e	Ph	CH_3	CH_3	CH_3	96	—
f	Ph	CH_3	$-(CH_2)_5-$		99	76†
g	Ph	CH_3	Ph	Ph	68‖	—
h	CH_3	H	$-(CH_2)_5-$		96	94,* 72‡
i	CH_3	H	Ph	Ph	—	17‖
j	nC_4H_9	nC_3H_7	CH_3	CH_3	92	—
l	nC_4H_9	nC_3H_7	Ph	Ph	34‖	—
m	Ph	H		H	—	95†
n	Ph	CH_3		H	—	72†
o	Ph	CH_3	Ph	H	—	85†
p	CH_3	H	Ph	H	—	75†

*By cyclization of the corresponding chlorohydrin.
†Using phase-transfer catalysis.
‡Oxidation of the corresponding epoxy sulfoxide.
§Based on isolated yield of **11***c*.
‖The intermediate chlorohydrin was not isolated; yield based on overall reaction **4** → **3** → **9**.

high yield to α,β-epoxy sulfoxides **9** (eq. [4]). These substances were in several instances oxidized with *m*-chloroperbenzoic acid (MCPBA) to epoxy sulfones. Of considerable interest was the observation that the reactions of the α-lithio derivatives **7** derived from chloromethyl phenyl, chloromethyl methyl, and α-chlorobutyl sulfoxides yielded only one of the two diastereomeric products upon condensation with symmetrical ketones. The stereochemistry of these adducts has not been determined. The high stereoselectivity observed in the chloromethyl phenyl sulfoxide series initiated our investigations (11) into the nature and the reactions of α-sulfinyl carbanions (α-lithio sulfoxides).

The reaction of both chloromethyl methyl (9) and chloromethyl *p*-tolyl sulfoxides (8) with aldehydes in the presence of potassium *tert*-butoxide resulted in preferential formation of the *cis*-substituted epoxy sulfoxide (**9**, $R^1 = R^2 = H$), whereas similar preparations of epoxy sulfones normally gave *trans* epoxides (3).

The chlorohydrin sulfoxides **6** (Table 1) were prepared using *n*BuLi or CH_3Li to generate the lithio derivative **7**. In such a reaction displacement of the chloroalkyl function by the alkyl group of the RLi competes with α-metallation (11) thereby lowering the yield of the desired product. For example, treatment of α-chloroethyl phenyl sulfoxide with methyllithium followed by cyclohexanone gave the adducts **6***f* and **10** in a 45:55 ratio.

The interference from the displacement reaction

[4] 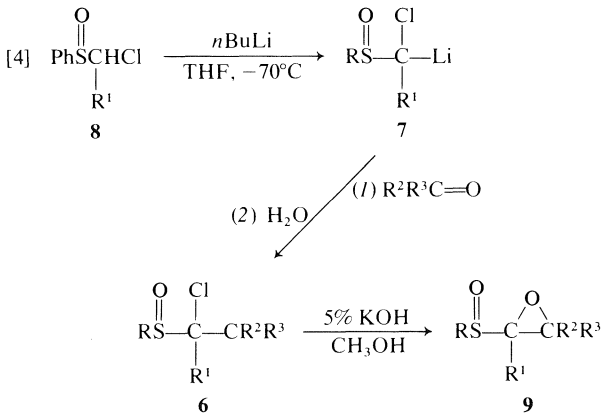

can be avoided if a nonnucleophilic base such as lithium diisopropyl amide (LDA) is employed. Thus the yields of the adducts **6***e* and **6***f* were raised from 34 and 45% to 72 and 70%, respectively, when the anion generating base was changed from CH_3Li to LDA.

BF_3-catalyzed and Thermal Rearrangements

The acid-catalyzed rearrangement of negatively substituted epoxides such as **2** and **9** to carbonyl compounds with concomitant migration of the

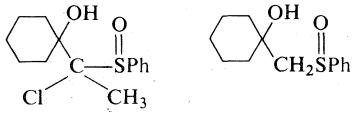

electronegative substituent (eq. [5]) has been well studied (see ref. 13*a* for X = Cl, *b* for X = COR, *c* for X = COOR, and *d* for X = P(O)(OCH$_3$)$_2$).

[5] 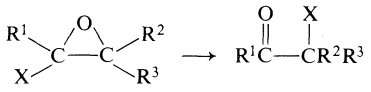

X = Cl, OAc, C(O)R, CO_2R, P(O)(OR)$_2$, S(O)R, SO_2R

In our hands, both the epoxy sulfoxides and sulfones when subjected to either $BF_3{\cdot}Et_2O$ treatment or heating in an inert solvent underwent the above rearrangement (7). In all cases studied phenylsulfonyl or phenylsulfinyl migration occurred with high preference over hydrogen migration in agreement with group migratory aptitudes observed in related systems (13). The temperature required for thermal rearrangement varied from less than 25°C in **2** or **9** ($R^2 = R^3 = Ph$) to greater than 130°C when $R^2 = R^3 =$ alkyl, as expected on the basis of the relative stability of the intermediate, e.g. **18**. For example, we were unable to isolate the epoxy sulfoxide **9***c*, the expected product from the reaction of **6***c* with methanolic KOH. Instead, benzhydryl phenyl sulfoxide **11**, the result of rearrangement of **9***c* to the aldehyde sulfoxide **12** and subsequent decarbonylation, was obtained in near quantitative yield. In agreement with this observation, attempted preparation of the epoxy sulfone **2***c* by the reaction of the unsaturated sulfone **13** with hot basic H_2O_2 resulted in the formation of benzhydryl phenyl sulfone **14**, presumably via a pathway analogous to that discussed for **11**. Tavares *et al.* (8) have succeeded in isolating the *p*-tolyl analogue of **2***c* and found that exposure of this substance to $BF_3{\cdot}Et_2O$ yielded the expected aldehyde sulfone.

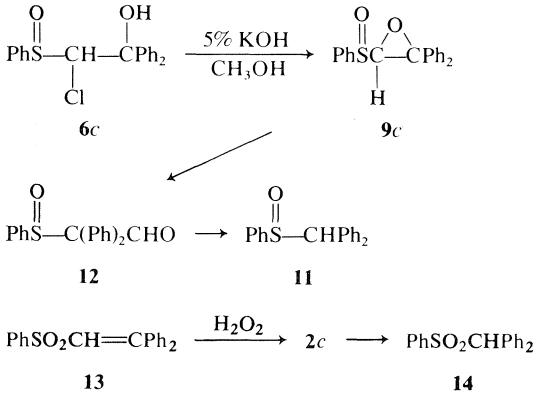

In the rearrangement of the epoxides **9***b* and **2***b* two products were isolated. The α,β-unsaturated aldehyde **15** was obtained from both starting materials and the α-formyl sulfoxide **16** and sulfone **17** from **9***b* and **2***b*, respectively. The formation of both types of products is easy to rationalize as shown below. In the thermolysis of **9***b*, the cyclohexencarboxaldehyde could also have arisen via the sulfenic acid elimination from **16** (14). Recently Reutrakul and Kanghae (15) have reported the thermolysis in refluxing toluene of a number of epoxy sulfoxides of the type **9***b* in which the carbocyclic ring varied in size from C_4 to C_8. α,β-Unsaturated aldehydes such as **15** were obtained 40–90% yield (15).

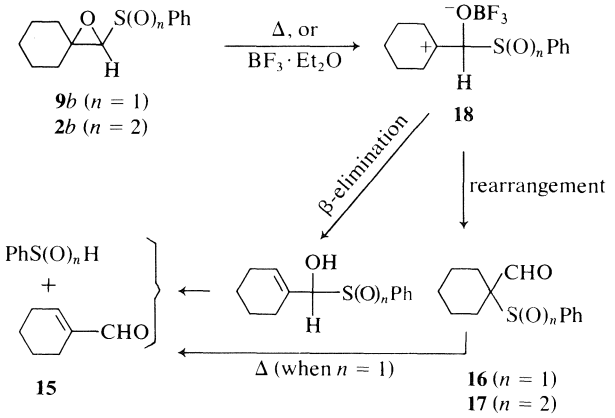

The above rearrangement of epoxy sulfones suggested a possible route to medium-size sulphur-containing rings via a one-carbon ring enlargement. Thus, the unsaturated sulfones **19** which are readily prepared from the corresponding parent cyclic sulfones, alkyllithiums, and benzophenone followed by dehydration, gave directly the expanded β-keto sulfones **20** in greater than 90% yield upon refluxing in $CHCl_3$ containing *m*-chloroperbenzoic acid. The spectroscopic properties of these compounds are in complete agreement with the structure assignments.

The six-membered ring sultone **21** likewise could be converted into the seven-membered β-keto sultone **22** (mp 150–151°C; ir: 1725, 1373, 1185, and 995 cm^{-1}; nmr: 1.8–2.6 (m, 2H), 3.02–3.35 (m, 2H), 4.62 (t, J = 5 Hz, 2H), and 7.2–7.6 (m, 10H)) in 24% isolated yield upon heating with trifluoroperacetic acid in CH_2Cl_2 for 30 min. The γ-sultone analogue of **21** could not be epoxidized and therefore not ring-expanded under identical conditions. Similarly, the α,β-unsaturated sulfonate ester $Ph_2C{=}CHSO_2OCH_3$ and sulfonamide $Ph_2C{=}CHSO_2N(CH_3)_2$ were unreactive toward pertrifluoroacetic acid.

Reaction with $MgBr_2$ and Grignard Reagents

Several electronegatively substituted epoxides (**23**) have been reported (16–18) to react with $MgBr_2$ according to [6]. It was expected that epoxy sulfones should behave in a similar manner and indeed they

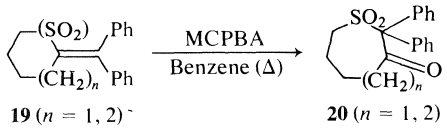

19 (n = 1, 2) **20** (n = 1, 2)

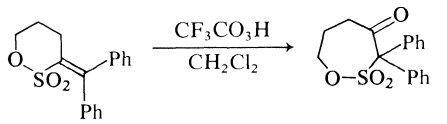

21 **22**

do. Thus seven different epoxy sulfones when reacted with $MgBr_2$ in ether at room temperature or below gave the expected α-bromocarbonyl compounds **24** in 80–90% isolated yields. These reactions were found to be exceptionally clean and the nmr spectra of the crude products which were obtained in almost quantitative yield were essentially identical with those of the purified materials. The results are shown in Table 3.

[6] 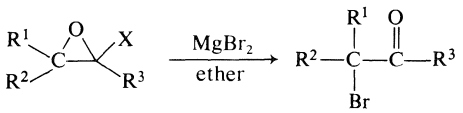

23 **24**

a X = CN (ref. 16)
b X = Cl (ref. 17)
c X = OAc (refs. 17, 18)
d X = SO_2Ph

Since the epoxy sulfones are conveniently prepared from α-chloro sulfones and ketones or aldehydes under phase-transfer conditions the overall synthetic transformation as represented by [7] represents a useful procedure for the introduction of both an acyl group and a Br atom at the original carbonyl carbon. The α carbon in the chlorosulfone thus serves as a masked nucleophilic acyl carbon.

[7] 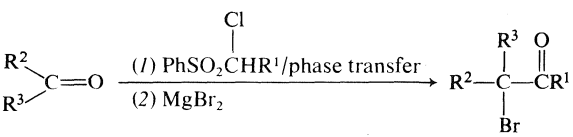

The epoxy sulfone route offers a number of advantages when compared to epoxy nitriles (16*a*) and chloro epoxides (see ref. 16*b* for the reactions of **23***a* with HCl) which can also be used to effect the overall transformation outlined in [7]. As mentioned above the epoxy sulfones are conveniently prepared using phase-transfer conditions whereas the synthesis of the chloro epoxides requires the generation of dichloromethyllithium in THF at −95°C. In addition, the epoxy sulfones are generally stable, easily purified, crystalline substances whereas the chloro epoxides are often not stable enough to be purified by distillation. Finally, the epoxy sulfone route is

TABLE 3. Preparation of α-bromo ketones and α-bromo aldehydes

Entry	α-Bromo derivative	Isolated yield (%)
a	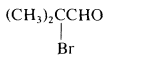	85
d	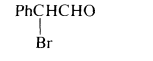	78
f	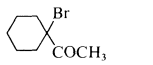	89
m	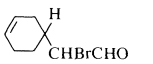	80
n	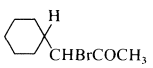	90
o	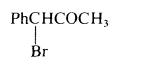	95

quite general and can quite easily be applied to the synthesis of both α-bromo ketones and α-bromo aldehydes since the required α-chloroalkyl phenyl sulfones are available by a number of simple routes.[2] Exposure of the epoxide **23** ($R^1 = R^3 = H$, $R^2 = Ph$, $X = SO_2PH$) to $FeCl_3$ in ether (20) resulted in an approximately equal mixture of α-chlorophenyl acetaldehyde and the α-formyl sulfone $PhCH(CHO)SO_2Ph$.

The reaction of several epoxy sulfones with Grignard reagents was also briefly investigated. Analysis of the crude products obtained from such reactions by infrared spectroscopy indicated the absence of carbonyl groups but showed strong O—H absorption. Thin-layer chromatography indicated the presence of a number of products presumably formed by reaction of several possible initial carbonyl-group containing intermediates with remaining Grignard reagents. These reactions were not further investigated.

Reactions with Nucleophilic Reagents

The ring opening of epoxy sulfones with nucleophiles would be expected to occur with complete regiospecificity at the carbon β to the sulfone group since S_N2 reactions α to a sulfonyl group are known to be extremely slow (21). The initial product of such a reaction, an α-hydroxy sulfone, is unstable and should fragment to a sulfinic acid and carbonyl compound (22). Up to the present only a few nucleophiles were found to be sufficiently reactive. For example PhS^- reacted with several epoxy sulfones to give α-phenylthio ketones and aldehydes

[2]Among the possible routes are (*i*) $PhSCH_2R$ + chlorinating agents followed by oxidation (19*a*); (*ii*) PhSH + RCHO + HCl (19*b*); and (*iii*) alkylation of $PhSO_2CH_2Cl$ with RX (4).

in good yield; no attempt was made to isolate phenyl sulfinic acid from these reactions. Azide and cyanide ion on the other hand were unreactive toward the epoxy sulfones on hand in solvents such as methanol or dimethylformamide. Reduction of the epoxide **2***d* with sodium borohydride furnished 2-phenylethanol, presumably by reduction of the initially formed carbonyl intermediate.

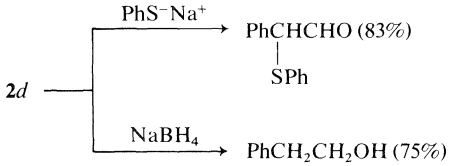

Experimental

General Comments

The organization of this section is as follows. All experiments pertaining to a particular epoxy sulfoxide or sulfone are gathered together. General descriptions are given for each of the major types of reaction and these are usually not repeated unless considered appropriate.

Nuclear magnetic resonance spectra were recorded as $CDCl_3$ solutions using Varian T-60 and HA-100 spectrometers; peak positions are given in δ units relative to TMS. Infrared spectra were obtained as films if liquid, or in $CHCl_3$ solution if solid, on a Beckman IR-20A spectrophotometer. Melting points and boiling points are uncorrected. Usual work-up involved partitioning the products between water and an organic solvent, generally CH_2Cl_2, drying the organic extracts, and evaporating the solvent under reduced pressure.

General Procedures

(I) Preparation of α-Chloro-β-hydroxy Sulfoxides or Sulfones

To a rapidly stirred solution of the α-chloro sulfoxide or sulfone in THF at −70°C under nitrogen atmosphere was added dropwise 1.1 equiv. of *n*BuLi in hexane or CH_3Li in ether. (As mentioned in the text the use of lithium diisopropylamide (LDA) is preferred (12).) The clear bright yellow or greenish-yellow solution was stirred for about 5 min at −70°C and then treated with the carbonyl component, neat if liquid or as a tetrahydrofuran solution if solid. The colour of the reaction mixture was generally discharged during this step. The reaction was then allowed to stir for a further 15–30 min at −70°C, poured into water, and worked up in the usual manner. The crude products were purified by recrystallization or column chromatography (Table 1).

The condensation reaction was carried out on a 1–25 mmol scale. The THF solutions were 0.1–0.25 *M* in carbanion solution.

(II) Conversion of Chlorohydrin Sulfoxides or Chlorohydrin Sulfones into the Corresponding Epoxides

The chlorohydrin sulfoxides or sulfones were dissolved in 10% methanolic KOH, about 1 mmol of substrate per 10 millilitres of solution, and stirred for 30–60 min at room temperature. The reaction mixture was then diluted with H_2O, extracted with CH_2Cl_2, and further worked up in the usual manner.

(III) Oxidation of Epoxy Sulfoxides to Epoxy Sulfones

This was carried out by allowing equimolar amounts of *m*-chloroperbenzoic acid and epoxy sulfoxide to react in a methylene chloride solution overnight. The reaction mixture was then washed with 5% NaOH, the organic layer dried with $MgSO_4$, and the solvent evaporated.

(IV) Preparation of Epoxy Sulfones using the Phase-transfer Technique

The following is a slight modification of the published procedure (5). The α-chloro sulfone and aldehyde, or ketone, were stirred at 0°C with 50% NaOH containing a few mol-% of benzyltriethylammonium chloride as catalyst until tlc showed the disappearance of either the α-chloro sulfone or the carbonyl component. If reaction periods of greater than 4 h were required then the reaction was carried out at room temperature. The epoxy sulfones were purified by silica gel chromatography or recrystallization.

(V) Reactions of Epoxy Sulfones with $MgBr_2$

An ethereal solution of $MgBr_2$ was prepared by reacting Mg with ethylene dibromide. To such a solution cooled to 5°C was added the epoxy sulfone. After completion of the reaction as judged by tlc (approximately 15–30 min), the ether layer was washed with ice water and the solvent dried and evaporated. The crude α-bromo ketone or α-bromo aldehyde was purified by chromatography on a short silica gel column using first hexane, which eluted any residual $BrCH_2CH_2Br$, and then 1:1 CH_2Cl_2–hexane to obtain the desired product.

Series a

Chloromethyl Phenyl Sulfone and Acetone

The chlorohydrin sulfone **3***a*, mp 82–83°C (CH_2Cl_2–pentane), was obtained in 71% yield according to method I. *Anal.* calcd. for $C_{10}H_{13}ClO_3S$: C 48.29, H 5.23, Cl 14.25, S 12.86; found: C 48.29, H 5.23, Cl 14.23, S 12.81.

Reaction of **3***a* (355 mg) with 0.5 g KOH in 10 mL of methanol for 10 min gave, after the usual work-up, 228 mg of a solid whose nmr indicated a 9:1 mixture of chloromethyl phenyl sulfone and the epoxy sulfone **2***a* (see below).

The epoxy sulfone **2***a* was also prepared in 94% yield starting with 1.25 g of $PhCH_2SO_2Cl$, 1.7 mL of acetone, 15 mL of 50% NaOH, 15 mL CH_2Cl_2, and 0.3 g of $PhCH_2\overset{+}{N}(CH_2CH_3)_3Cl^-$. These reagents were stirred first at 0°C for about 2 h, then overnight at room temperature. The yield of colorless granules, after chromatography, was 1.3 g, mp 72–74°C (ether–pentane); ir: 1305, 1145 cm^{-1}; nmr: 1.42 (s, 3H), 1.84 (s, 3H), 3.82 (s, 1H), 7.4–8.15 (m, 5H). *Anal.* calcd. for $C_{10}H_{12}O_3S$: C 56.60, H 5.70; found: C 56.83, H 5.56.

Compound **3***a* was also obtained upon oxidation of **9***a* (5.06 g) with 5.24 g of 85% MCPBA in 100 mL of CH_2Cl_2. The yield of **3***a* was 5.29 g (95%).

The chlorohydrin sulfoxide **6***a* was obtained in 75% yield via procedure I as colorless needles from CH_2Cl_2–pentane, mp 134–137°C; nmr: 1.58 (s, 6H), 2.87 (OH), 4.32 (s, 1H), 7.4–7.6 (m, 5H). *Anal.* calcd. for $C_{10}H_{13}ClO_2S$: C 51.61, H 5.63, Cl 15.24, S 13.77; found: C 51.16, H 5.59, Cl 15.87, S 13.60.

Reaction of 127 mg of **6***a* with 10 mL of 5% methanolic KOH for 15 min at room temperature yielded 96 mg (91%) of **9***a* as a colorless oil which was homogeneous on tlc; nmr: 1.41 (s, 3H), 1.72 (s, 3H), 3.66 (s, 1H), 7.4–7.8 (m, 5H). *Anal.* calcd. for $C_{10}H_{12}O_2S$: C 61.21, H 6.17; found: C 61.40, H 6.06.

Epoxy sulfone **2***a* (700 mg) was added to a twofold excess of $MgBr_2$ in 10 mL of ether, kept overnight, and then worked up. The nmr of the crude product showed only peaks for 2-bromo-2-methylpropanal (1.77 (s, 6H), 9.90 (s, 1H)) and the residual 1,2-dibromoethane used to generate $MgBr_2$. The estimated yield of α-bromo aldehyde was >85%.

Series b

Chloromethyl Phenyl Sulfone and Cyclohexanone

The chlorohydrin sulfone **3***b* was obtained in 94% yield

according to procedure I as colorless needles, mp 150–151°C (CH_2Cl_2–pentane). *Anal.* calcd. for $C_{13}H_{17}ClO_2S$: C 54.06, H 5.94, S 11.10, Cl 12.28; found: C 54.02, H 5.94, S 11.10, Cl 12.28.

Reaction of 206 mg of **3***b* with 0.5 g of KOH in 10 mL of methanol for 15 min gave 152 mg of a crude solid material whose nmr spectrum showed it to be a 4:6 mixture of the epoxy sulfone **2***b*, mp 56°C, and chloromethyl phenyl sulfone. Compound **2***b* had nmr peaks at 1.4–2.4 (m, 10H), 3.8 (s, 1H), 7.4–8.2 (m, 5H); ir: 1325, 1152 cm^{-1}. *Anal.* calcd. for $C_{13}H_{16}O_3S$: C 61.89, H 6.39; found: C 62.21, H 6.53. This compound was better prepared by MCPBA oxidation of the corresponding epoxy sulfoxide (see below).

Chloromethyl Phenyl Sulfoxide and Cyclohexanone

Addition of 3.80 mg (3.9 mmol) of cyclohexanone to 3.9 mmol of the α-lithio derivative of chloromethyl phenyl sulfoxide in 20 ml of THF gave, after work-up and recrystallization of the crude product, 844 mg (79%) of **6***b* as fluffy white needles, mp 169–171°C; ir: 3450, 1050 cm^{-1}; nmr: 1.5–2.2 (m, 10H), 2.7 (1H, OH), 4.31 (s, 1H), 7.4–7.7 (m, 5H). *Anal.* calcd. for $C_{13}H_{17}ClO_2S$: C 57.24, H 6.28, Cl 13.00, S 11.75; found: C 57.16, H 6.25, Cl 13.16, S 11.75.

Chlorohydrin sulfoxide **6***b* (90 mg, 0.33 mmol) was cyclized in 91% yield according to procedure II to **9***b*, colorless granules, mp 64–66°C (ether–pentane); ir: 1090, 1030 cm^{-1}; nmr: 1.4–2.3 (m, 10H), 3.6 (s, 1H), 7.4–7.8 (m, 5H). *Anal.* calcd. for $C_{13}H_{16}O_2S$: C 66.08, H 6.83, S 13.65; found: C 66.03, H 6.94, S 13.61.

MCPBA oxidation of **9***b* (200 mg) according to procedure III gave 202 mg of epoxy sulfone **2***b* (see above).

Thermal decomposition of **9**b—The epoxy sulfoxide **9***b* (822 mg) was heated in a micro distillation apparatus. The sulfoxide decomposed at about 190°C and 260 mg (62%) of Δ^1-cyclohexenecarboxaldehyde (ir: 2970, 1685, 1645 cm^{-1}; nmr: aldehyde proton, 9.48) distilled as a colorless liquid; mp of DNP 213–216°C (lit. (21) mp 213–214°C).

Acid-catalyzed rearrangement of **9**b—$BF_3{\cdot}Et_2O$ (0.45 mL) was added to a solution of 416 mg of epoxy sulfoxide in 20 mL of ether. The usual work-up after a 2-h reaction period gave a crude product which was separated on preparative tlc using 1:1 ether–pentane as eluent. Aldehyde sulfoxide **16** was obtained as a colorless oil, 149 mg, 36%. MCPBA oxidation afforded **17** (see below). In addition a 60% yield of Δ^1-cyclohexene carboxaldehyde was obtained.

Acid-catalyzed rearrangement of **2**b—To a solution of 300 mg of **2***b* in 25 mL of ether was added 0.4 mL of $BF_3{\cdot}Et_2O$. The reaction was refluxed for 1 h. The crude product showed a mixture of Δ^1-cyclohexenecarboxaldehyde and the aldehyde sulfone **17**. The sulfone **17** was obtained pure by preparative tlc (1:1 ether–pentane) as colorless plates, mp 66–67.5°C; ir: 1717, 1310, 1142 cm^{-1}; nmr: 0.7–2.5 (m, 10H), 7.3–7.9 (m, 5H), 9.67 (m, 1H). *Anal.* calcd. for $C_{13}H_{16}O_3S$: C 61.89, H 6.39, S 12.68; found: C 61.82, H 6.40, S 12.68.

Series c

Chloromethyl Phenyl Sulfoxide and Benzophenone

Using procedure I, the chlorhydrin sulfoxide **6***c* was obtained in 68% yield as colorless needles, mp 128–130°C (CH_2Cl_2–pentane); ir: 1060 cm^{-1}; nmr: 4.75 (OH), 5.36 (s, 1H), 7.2–7.8 (m, 15H). *Anal.* calcd. for $C_{20}H_{17}ClO_2S$: C 67.31, H 4.77, S 8.97, Cl 9.99; found: C 67.09, H 4.82, S 9.16, Cl 10.23.

The chlorohydrin sulfoxide **6***c* (180 mg) was heated in a mixture of 15 mL of H_2O, 5 mL of methanol, and 1 g of KOH until dissolution took place. On cooling 159 mg (99%) of colorless needles precipitated, mp 132–133°C (CH_2Cl_2–pentane); ir: 1045 cm^{-1}; nmr: 4.81 (s, 1H), together with an aromatic multiplet, 15H. The compound was identified as benzhydryl phenyl sulfoxide on the basis of its analysis (found: C 77.63, H 5.52, S 10.80) and oxidation to benzhydryl phenyl sulfone.

When the unsaturated sulfone **13** was refluxed overnight in a 1:1 CH_3OH – 30% H_2O_2–Na_2CO_3 mixture, benzhydryl phenyl sulfone was obtained in 83% isolated yield.

Series d

Chloromethyl Phenyl Sulfone and Benzaldehyde

Reaction of equimolar amounts of the lithio salt of chloromethyl phenyl sulfone in THF with benzaldehyde at −78°C according to procedure I furnished, in 94% yield, the chlorohydrin sulfone **3***d*. Recrystallization from CH_2Cl_2–pentane gave a single diastereoisomer, mp 129–130°C; *Anal.* calcd. for $C_{14}H_{13}ClO_3S$: C 56.66, H 4.41, S 10.80, Cl 11.9; found: C 56.45, H 4.16, S 10.79, Cl 12.15.

Attempted conversion of **3***d* to **2***d* by procedure II failed. Only the two components, $PhSO_2CH_2Cl$ and PhCHO, were obtained.

The epoxy sulfone **2***d* was prepared in 92% yield using the phase-transfer technique and stirring the reaction mixture for 1 h at ice-bath temperature; nmr: 4.18 (d, J = 1.5 Hz, 1H), 4.62 (d, J = 1.5 Hz, 11H), 7.2–8.2 (m, 10H). *Anal.* calcd. for $C_{14}H_{12}O_3S$: C 64.59, H 4.65, S 12.32; found: C 64.40, H 4.81, S 12.48.

To 25 mL of a $MgBr_2$ in ether solution prepared from 690 mg of Mg and 2.5 mL of $BrCH_2CH_2Br$ was added 1.10 g of the epoxide **2***d*. The reaction mixture was kept overnight and then worked up. Chromatography on silica gel yielded 642 mg (78%) of α-bromo aldehyde, **24***d*.

When **2***d* was stirred with an equimolar mixture of $FeCl_3$ in ether for 10 min (20) a 1:1 mixture of α-chlorophenylacetaldehyde and α-phenylsulfonylphenylacetaldehyde were obtained.

Reduction of **2***d* with $NaBH_4$ in ethanol at room temperature for 10 min gave, after work-up, 2-phenylethanol (75%) whereas reaction with PhS^-K^+ in methanol for 4 h afforded, after usual work-up and column chromatography, 83% of α-phenylthiophenylacetaldehyde; ir: 1685 cm^{-1}; nmr: 1.53–2.23 (m, 7H), 3.23–3.56 (m, 1H), 5.50–5.83 (m, 2H), 7.1–7.5 (m, 10H), 9.8 (d, J = 2 Hz, 1H).

Series e

α-Chloroethyl Phenyl Sulfoxide and Acetone

The crude products (2.67 g) obtained from 3.1 g of chloro sulfoxide and excess acetone (procedure I) were separated by chromatography. The less polar fraction, 1.36 g (34%), mp 105–107°C, was identified as **6***e*; ir: 3440, 1025 cm^{-1}; nmr: 1.48 (s, 3H), 4.18 (OH), 7.4–7.9 (m, 5H); $M^{\pm}$ 244 and 246 in 3:1 ratio. The more polar component, mp 116°C, was identical to the product obtained from the reaction of $PhS(O)CH_2Li$ and acetone (23).

Chlorohydrin sulfoxide **6***e* was better prepared using the following procedure. To a solution of 5 mmol of LDA, prepared from diisopropylamine and methyllithium, in 30 mL of dry THF at −70°C was added 955 mg, (5.0 mmol) of α-chloroethyl phenyl sulfoxide dissolved in 5 mL of THF. The reaction mixture was stirred for 5 min and then 490 mg of cyclohexanone was added. After a further 10 min, water was added and the reaction was worked up. The yield of **6***e* was 1.03 g (72%).

Reaction of **6***e* (630 mg) with 50 mL 10% methanolic KOH at 25°C for 30 min gave 514 mg (96%) of **9***e* as a colorless oil; ir: 1040 cm^{-1}; nmr: 1.52 (s, 3H), 1.63 (s, 3H), 1.81 (s, 3H),

7.4–7.9 (m, 5H). *Anal.* calcd. for $C_{11}H_{14}O_2S$: C 62.79, H 6.71; found: C 63.00, H 6.58.

Series f

α-Chloroethyl Phenyl Sulfone and Cyclohexanone

The epoxy sulfone **2***f* was obtained in 76% yield using phase-transfer conditions and a reaction time of 3 days, mp 79–80.5°C (ether–hexane). *Anal.* calcd. for $C_{14}H_{18}O_3S$: C 63.12, H 6.81, S 12.04; found: C 62.78, H 6.86, S 12.34. The CH_3 group occurred at 1.26 ppm.

The epoxy sulfone **2***f* (280 mg) was treated with $MgBr_2$ in ether at −30°C for 3 h. The yield of 1-bromo-1-acetylcyclohexane was 250 mg (89%).

Reaction of the α-chloroethyl phenyl sulfoxide (2.22 g) with 1.1 equiv. of CH_3Li followed by 1.77 g of cyclohexanone gave two components which were separated by fractional crystallization. From CH_2Cl_2–pentane was obtained 1.53 g (45%) of **6***f* as colorless plates, mp 163–164°C; ir: 3400, 1082, 1038 cm^{-1}; nmr: 0.8–2.4 (m, 10H), 1.46 (s, 3H), 3.4 (OH), 7.4–7.9 (m, 5H). *Anal.* calcd. for $C_{14}H_{19}ClO_2S$: C 58.64, H 6.63; found: C 58.52, H 6.79.

Recrystallization of the mother liquors from ether–pentane gave 1.55 g (55%) of **10**, identical with that produced from the reaction of $PhS(O)CH_2Li$ and cyclohexanone (23).

When LDA was used to generate the anion of α-chloroethyl phenyl sulfoxide rather than methyllithium, the yield of **6***f* was 70%. (See also the similar preparation of **6***e* above.)

The chlorohydrin sulfoxide **6***f* was converted in near quantitative yield into the epoxy sulfoxide **9***f*, mp 60–62°C (CH_2Cl_2–pentane); nmr: 1.31 (s, 3H), 1.4–2.5 (m, 10H), 7.4–7.8 (m, 5H); ir: 1045 cm^{-1}. *Anal.* calcd. for $C_{14}H_{18}O_2S$: C 67.18, H 7.25; found: C 67.05, H 7.32.

Series g

α-Chloroethyl Phenyl Sulfoxide and Benzophenone

Reaction of the lithio salt obtained from 2.47 g of the above sulfoxide with benzophenone (2.35 g) gave directly 2.73 g (68%) of the epoxide **9***g* after purification on basic Al_2O_3. The epoxide was obtained as a colorless oil having its parent ion at *m/e* 334; ir: 1078 and 1098 cm^{-1}; nmr: 1.2 (s, 3HO), 7.2–7.8 (m, 15H). In addition to **9***g*, 1.33 g of the hydroxy sulfoxide obtainable also from benzophenone and $PhS(O)CH_2Li$ was formed (23).

Series h

Chloromethyl Methyl Sulfone and Cyclohexanone

The chlorohydrin sulfone **6***h*, mp 73–74°C (ether–pentane), was obtained in 78% yield using procedure I; ir: 3520, 1315, 1126 cm^{-1}; nmr: 1.3–2.1 (m, 10H), 3.08 (s, 3H), 3.20 (OH), 4.67 (s, 1H); $M^{\ddagger}$ 226 and 228 (3:1).

The above chlorohydrin was converted in 94% yield to the epoxy sulfone **2***h*, colorless liquid; ir: 1320, 1145 cm^{-1}; nmr: 1.38–2.32 (m, 10H), 3.02 (s, 1H), 3.86 (s, 1H). *Anal.* calcd. for $C_8H_{14}O_2S$: C 55.14, H 8.10; found: C 55.01, H 7.99.

The chlorohydrin sulfoxide (**6***h*) was obtained in 15% isolated yield by reaction of cyclohexanone (830 mg) to the anion of chlormethyl methyl sulfoxide generated from 867 mg of sulfoxide and *n*BuLi, mp 144–146°C (ether–pentane); nmr: 1.4–2.1 (m, 10H), 2.65 (s, 3H), 2.94 (OH), 4.36 (s, 1H); ir: 3450, 1065 cm^{-1}. *Anal.* calcd. for $C_8H_{15}ClO_2S$: C 45.60, H 7.18, Cl 16.83, S 15.22; found: C 45.73, H 7.23, Cl 16.80, S 15.05.

The chlorohydrin sulfoxide **6***h* was converted in 94% yield to the epoxy sulfoxide (**9***h*); colorless oil having an ir band at 1035 cm^{-1}; nmr: 1.4–2.1 (m, 10H), 2.68 (s, 3H), 3.65 (1H). Oxidation with MCPBA afforded the sulfone **2***h*, identical with the one described above.

Series i

Chloromethyl Methyl Sulfoxide and Benzophenone

Benzophenone (1.31 g) was added to a solution of the lithio sulfoxide obtained by reacting 8.3 mmol of *n*BuLi with 807 mg of chloromethyl methyl sulfoxide. Usual work-up followed by recrystallization from ether–pentane gave 345 mg (17%) of the epoxy sulfoxide (**9***i*) resulting from cyclization of the intermediate chlorohydrin sulfoxide, mp 102.5–104°C; ir: 1160, 1135 cm^{-1}; nmr: 2.58 (s, 3H), 4.6 (s, 1H), 7.4–7.5 (m, 10H); ms *m/e* 258.

Series j, k, l

*Reactions of α-Lithio-*n*-butyl* n*-Butyl Sulfoxide with Ketones*

The above α-lithio salt was reacted according to procedure I with acetone, cyclohexanone, and benzophenone. The results were (*i*) chlorohydrin sulfoxide **6***j* (66%), colorless oil; nmr: 0.8–1.2 (m, 6H), 1.47 (s, 3H), 2.01 (s, 3H), 1.2–2.2 (m, 8H), 2.4–3.2 (m, 2H), 4.4 (OH); (*ii*) chlorohydrin sulfoxide **6***k* (71%), mp 88–90°C (ether–pentane); nmr: 0.8–2.4 (m, 18H), 2.6–3.3 (m, 2H), 3.08 (OH). *Anal.* calcd. for $C_{14}H_{27}ClO_2S$: C 57.06, H 9.17; found: C 57.21, H 9.25. The chlorohydrin sulfoxide **6***l* was not isolated, instead the epoxy sulfoxide **1** was obtained in 34% yield as a colorless powder, mp 74–75°C, after Al_2O_3 chromatography; nmr: 0.6–2.4 (m, 14H), 2.6–2.9 (m, 2H), 7.2–7.7 (m, 10H). *Anal.* calcd. for $C_{21}H_{26}O_2S$: C 73.66, H 7.66; found: C 73.63, H 7.46.

In the condensations involving cyclohexanone and benzophenone a 14 and 11% yield, respectively, of the condensation products expected from the reaction of $nBuS(O)CH_2^-Li^+$ and the ketones were obtained (12).

The chlorohydrin sulfoxide **6***j* was converted using method II into epoxy sulfoxide **9***j* in 92% yield, colorless oil; nmr: 0.8–1.2 (m, 6H), 1.2–2.2 (m, 8H), 1.50 (s, 3H), 1.62 (s, 3H), 2.5–2.8 (m, 2H). *Anal.* calcd. for $C_{11}H_{22}O_2S$: C 60.45, H 10.15; found: C 60.62, H 10.27.

Series m–p

The epoxy sulfones **2***m–p* were all prepared using the phase-transfer technique.

Compound **2**m—colorless oil; nmr: 1.2–2.3 (m, 7H), 3.5–3.7 (m, 1H), 4.01 (d, J = 2 Hz, 1H), 5.6 (s, 2H), 7.4–8.1 (m, 5H).

Reaction of **2***m* with $MgBr_2$ in ether furnished **24***m* as a colorless oil; ir: 1720 cm^{-1}; nmr: 1.3–2.5 (m, 7H), 3.14 (d of d, J = 7 and 4 Hz, 1H), 4.6 and 4.8 (m, 2H), and 9.41 (d, J = 4 Hz, 1H); ms *m/e*: 204 and 202 ($M^{\ddagger}$), 175 and 173 ($M^{\ddagger}$ − CHO), 150 and 148 ($M^{\ddagger}$ − C_4H_6), 123 ($M^{\ddagger}$ − Br).

Compound **2**n—mp 123–125°C; ir: 1145 (s), 1300 (s), 1310 (s) cm^{-1}; nmr: 1.60 (s, 3H), 1.4–2.4 (m, 7H), 3.6–3.8 (m, 1H), 5.7–5.8 (m, 1H), 7.5–8.0 (m, 5H). *Anal.* calcd. for $C_{15}H_{18}O_3S$: C 64.72, H 6.49; found: C 64.70, H 6.33.

Rearrangement of **2***n* with $MgBr_2$ gave **24***n* as a clear oil after chromatography; nmr: 1.2–2.6 (m, 7H), 2.19 (s, 3H), 3.12 (d, J = 7 Hz, 1H), 5.6–5.9 (m, 2H); ms *m/e*: 214 and 216 ($M^{\ddagger}$), 201 and 199 ($M^{\ddagger}$ − 15).

Compound **2**o—mp 98.5–99.5°C; ir: 1140 (s), 1300 (s), 1320 (s) cm^{-1}; nmr: 1.39 (s, 3H), 4.90 (s, 1H), 7.2–8.1 (m, 10H). *Anal.* calcd. for $C_{15}H_{14}O_3S$: C 65.63, H 5.14, S 11.69; found: C 65.71, H 5.06, S 11.87.

Rearrangement of **2***o* with $MgBr_2$ gave 1-bromo-1-phenyl-2-propanone; nmr: 2.12 (s, 3H), 5.43 (s, 1H), and 7.2–7.6 (m, 5H); $M^{\ddagger}$ at *m/e* 212 and 214.

Compound **2**p—colorless solid, mp 94–95°C; nmr: 3.00 (s, 3H), 4.22 (d, J = 2 Hz, 1H), 4.50 (d, J = 2 Hz, 1H), and

7.2–7.5 (m, 5H). *Anal.* calcd. for $C_9H_{10}O_3S$: C 54.54, H 5.05; found: C 54.42, H 5.17.

Preparation of ***22***

The unsaturated sultone **21** was prepared as described (24). To a solution of ~500 mg of per-trifluoroacetic acid in 25 mL of CH_2Cl_2 was added with stirring 882 mg of sultone **21** in 25 mL of CH_2Cl_2. The reaction mixture, which became yellow and cloudy, was refluxed for 30 min, then worked up by washing with 10% Na_2CO_3 and saturated NaCl solution. The crude black oil obtained upon evaporation of the organic solvents was chromatographed on Al_2O_3. β-Keto sultone **22**, mp 150–151°C was obtained in 24% yield, 34% based on recovered starting material; ir: 1725, 1375, 1185, 995 cm^{-1}; nmr: 1.8–2.3 (quintet, 2H), 3.0–3.3 (m, 2H), 4.64 (t, J = 6 Hz, 2H), 7.2–7.5 (m, 10H). *Anal.* calcd. for $C_{17}H_{16}O_4S$: C 64.55, H 5.10; found: C 64.38, H 3.58.

Preparation of ***19*** *(*n = *1,2)*

Thiane 1,1-dioxide or thiepane 1,1-dioxide were converted into the α-lithio derivative in the usual manner in THF at −70°C and reacted with benzophenone. The product was isolated and dehydrated to **19** by refluxing in benzene containing a trace of toluene sulfonic acid for 1 h. The overall yield in both instances approached 90%. Compound **19**, n = 1, showed peaks at δ 1.8–2.5 (m, 4H), 7.0–7.6 (m, 10H), and 2.6–3.0 (m, 2H), whereas that of **19**, n = 2, had peaks at 1.6–2.2 (m, 6H), 2.4–2.7 (m, 2H), 3.0–3.3 (m, 2H), and 7.0–7.4 (m, 10H).

The epoxidation rearrangement was carried out by refluxing the unsaturated sulfones with a four-fold excess in MCPBA in benzene overnight. The yield of **19***a* was 91% after column chromatography, mp 108°C (CH_2Cl_2–pentane); nmr: 1.1–3.2 (m, 8H), 7.0–7.7 (m, 10H); ir: 1725, 1315, 1123 cm^{-1} *Anal.* calcd. for $C_{18}H_{18}O_3S$: C 68.78, H 5.77; found: C 68.70, H 5.90.

Acknowledgement

The continued financial support of the National Research Council of Canada is greatly appreciated.

1. B. Zwanenburg and J. ter Wiel. Tetrahedron Lett. 935 (1970).
2. R. Curci and F. Difuria. Tetrahedron Lett. 4085 (1974).
3. P. F. Vogt and D. F. Tavares. Can. J. Chem. **47**, 2875 (1969).
4. A. Jończyk, K. Bańko, and M. Mąkosza. J. Org. Chem. **40**, 266 (1974).
5. F. de Reinach-Hirtzbach and T. Durst. Tetrahedron Lett. 3677 (1976).
6. F. Bohlmann and G. Haffer. Chem. Ber. **102**, 4017 (1969).
7. T. Durst and K.-C. Tin. Tetrahedron Lett. 2369 (1970).
8. D. F. Tavares, R. E. Estep, and M. Blezard. Tetrahedron Lett. 2373 (1970).
9. G. Tsuchihashi and K. Ogura. Bull. Chem. Soc. Jpn. **45**, 2023 (1972).
10. T. Durst. J. Am. Chem. Soc. **91**, 1034 (1969).
11. T. Durst and M. Molin. Tetrahedron Lett. 63 (1975).
12. T. Durst, M. J. LeBelle, R. Van den Elzen, and K.-C. Tin. Can. J. Chem. **52**, 761 (1974).
13. (*a*) R. N. McDonald and R. N. Steppel. J. Am. Chem. Soc. **91**, 782 (1969); (*b*) J. R. Williams, G. M. Sarkisian, J. Quigley, A. Hasiuk, and R. Vander Vennen. J. Org. Chem. **39**, 1028 (1974); (*c*) S. P. Singh and J. Kagan. J. Am. Chem. Soc. **91**, 6198 (1969); (*d*) C. E. Griffin and S. K. Kundu. J. Org. Chem. **34**, 1532 (1969).
14. B. M. Trost, T. N. Salzmann, and K. Hiroi. J. Am. Chem. Soc. **98**, 4887 (1976).
15. V. Reutrakul and W. Kanghae. Tetrahedron Lett. 1377 (1977).
16. (*a*) J. Cantacuzène, D. Ricard, and M. Thézé. Tetrahedron Lett. 1365 (1967); (*b*) G. Stork, W. S. Worrall, and J. J. Pappas. J. Am. Chem. Soc. **82**, 4315 (1960).
17. (*a*) A. Kirrmann, P. Duhamel, and M. R. Nouri-Birmorghi. Bull. Soc. Chem. Fr. 3264 (1964); (*b*) A. Kirrman and R. Nouri-Birmorghi. Bull. Soc. Chem. Fr. 3213 (1968); (*c*) J. Villieras, C. Bacquet, and J. F. Normant. J. Organomet. Chem. **40**, C1 (1972); (*d*) J. H. Taguchi, H. Yamamoto, and H. Nozaki. Tetrahedron Lett. 4661 (1972).
18. J. J. Riehl, P. Casara, and A. Fougerousse. C.R. Acad. Sci. Ser. C, **279**, 79 (1974); **279**, 113 (1974).
19. (*a*) F. G. Bordwell and B. M. Pitt. J. Am. Chem. Soc. **77**, 572 (1955); D. L. Tuleen and T. B. Stephens. J. Org. Chem. **34**, 31 (1969); (*b*) H. Bohme, H. Fischer, and R. Frank. Justus Liebigs Ann. Chem. **563**, 54 (1959).
20. J. Kagan, B. E. Firth, N. Y. Shih, and C. G. Boyajian. J. Org. Chem. **42**, 343 (1977).
21. F. G. Bordwell and W. T. Brannen, Jr. J. Am. Chem. Soc. **86**, 4645 (1964).
22. E. A. Braude and E. A. Evans. J. Chem. Soc. 3334 (1955).
23. T. Durst, K.-C. Tin, and M. J. V. Marcil. Can. J. Chem. **51**, 1704 (1973).
24. T. Durst and J. du Manoir. Can. J. Chem. **47**, 1230 (1969).
25. W. S. Matthews, J. E. Bares, J. E. Bartness, F. G. Bordwell, F. G. Cornforth, G. E. Drucker, Z. Margolin, R. J. McCallum, G. J. McCollum, and N. R. Vanier. J. Am. Chem. Soc. **97**, 7006 (1978).

The synthesis of peptides related to a conserved sequence found in histone H-1 and H-5. Their ability to act as substrates and inhibitors of exogenous protein kinases[1]

SANDRA L. KIELLAND, PONNAMPALAM MATHIAPARANAM,[2] LEWIS A. SLOTIN,[3] AND ROSS E. WILLIAMS[4]

Division of Biological Sciences, National Research Council of Canada, Ottawa, Ont., Canada K1A 0R6

Received May 29, 1978

SANDRA L. KIELLAND, PONNAMPALAM MATHIAPARANAM, LEWIS A. SLOTIN, and ROSS E. WILLIAMS. Can. J. Chem. **57**, 267 (1979).

Two peptides, H-Gly Ser Phe Lys-NH_2 and H-Gly Ser Phe Lys Leu-NH_2, whose sequence may be found in a conserved and phosphorylated site in histone H-1 have been synthesized. Their ability to act as substrates for several protein kinase preparations have been examined. In addition, their ability to inhibit the action of several protein kinases of muscle origin was also tested.

SANDRA L. KIELLAND, PONNAMPALAM MATHIAPARANAM, LEWIS A. SLOTIN et ROSS E. WILLIAMS. Can. J. Chem. **57**, 267 (1979).

On a synthétisé un tétrapeptide et un pentapeptide, H-Gly Ser Phe Lys-NH_2 et H-Gly Ser Phe Lys Leu-NH_2, ayant la séquence d'un site totalement conservé dans les histones H-1 et H-5. Il a été antérieurement démontré que ce site acceptait du phosphate pendant le fonctionnement de la cellule. On a examiné l'introduction du phosphate dans les peptides par quelques kinases de protéine, ainsi que l'inhibition par les peptides de l'activité enzymatique des kinases de protéines d'origine musculaire.

[Traduit par le journal]

Introduction

The lysine-rich histones H-1 and H-5[5] are believed to play an important role in the regulation of nuclear DNA transcription and condensation (1–5). Histone H-1 and H-5 fractions have been isolated from many different sources. The partial amino acid sequences of histone H-1 fractions from calf (6), rabbit (5, 7), sea urchin (8), and trout (9) have been reported. Partial amino acid sequences of the functionally-related histone H-5 found in chicken (10, 11), goose (12), duck (11), and pigeon (12) have also been reported.

The amino acid sequences of each of the histones may be subdivided into three regions: (*i*) the N-terminal region, composed of about 35–45 amino acid residues; (*ii*) the central region, composed of about 60–70 amino acid residues; (*iii*) the C-terminal region, composed of the remainder of the 190–225 amino acid residues. Although histone amino acid sequences tend to be highly conserved, only the central region of both these histones has been found to exhibit a high degree of homology (Fig. 1). In addition to being highly conserved this region has also been implicated in the observed salt-induced aggregation of histone H-1 in solution (13, 14), in the observed effect of histone H-1 phosphorylation on histone H-1 aggregation (15, 16), and in the observed phosphorylation of histone H-1 by a crude preparation of protein kinase from calf liver (17). The amino acid sequence of the phosphorylated peptide was reported to be (Thr, Ser, Gly_2, Ala)-Gly-Ser(PO_4)-Phe-Lys (18). This sequence is found in a very highly conserved section of the central region of both histones H-1 and H-5 (Fig. 1).

Bearing in mind the highly conserved nature of this section, its phosphorylation, its implication in chromosome condensation, and the observation that the phosphorylation by intracellular protein kinases may be controlled, in part, by the amino acid sequence surrounding the phosphorylated serine or threonine (19, 20) and, in part, by the secondary structure surrounding the site (21), we have prepared two peptide fragments related to this highly conserved and phosphorylated section of the central region of the histones H-1 and H-5. In this report we wish to describe the synthesis of these two fragments, their ability to act as substrates for four exogenous protein kinase preparations and their effect on the phosphorylation of purified calf thymus histone H-1 by three exogenous protein kinases from muscle.

Experimental

Chemicals used for synthesis and buffer preparation were

[1]NRCC No. 16949.

[2]NRCC Research Associate, 1977–present.

[3]NRCC Research Associate, 1975–1977. Present address: Ministry of State for Science and Technology, 270 Albert Street, Ottawa, Ont., Canada K1P 5G8.

[4]To whom correspondence should be addressed.

[5]Histone nomenclature is that agreed upon during a Ciba Foundation symposium (1, 2).

0008-4042/79/030267-07$01.00/0

Histone							Sequence		Ref.
Rabbit H-1	Thr	Leu	Val Glu Thr Lys	Gly	Thr	Gly Ala Ser Gly $\frac{\text{Ser}}{105}$ Phe Lys Leu	Asn Lys Lys	5, 7
Trout H-1	Thr	Leu	Val Glu Thr Lys	Gly	Thr	Gly Ala Ser Gly $\frac{\text{Ser}}{95}$ Phe Lys Leu	Asp Lys Lys	9
Sea urchin H-1	Ala	Leu	Lys Gln Val Thr	Gly	Thr	Gly Ala Ser Gly Ser Phe Lys Val	Gly Val Gly	8
Chicken H-5	Val	Leu	Lys Gln Thr Lys	Gly	Val	Gly Ala Gly $\frac{\text{Ser}}{92}$ Ser Phe Arg Leu	Ala Lys Ser	10, 11
Goose H-5	Val	Leu	Lys Gln Thr Lys	Gly	Val	Gly Ala Ser Gly $\frac{\text{Ser}}{93}$ Phe Arg Leu	Ala Lys Gly	12

FIG. 1. A highly conserved sequence in histones H-1 and H-5. Areas of sequence homology are boxed in and include functionally conserved residues, i.e., Lys → Arg. Where known, numbers are inserted to indicate the position of the -Gly Ser Phe Lys Leu- sequence in the histone.

reagent grade and were used as received unless otherwise noted. Solvents were purified as follows: Dimethylformamide (DMF) by distillation under reduced pressure from barium oxide (nitrogen purged system); 1,2-dimethoxyethane (DME) by distillation from lithium aluminum hydride (LAH); triethylamine (TEA) by distillation from barium oxide (nitrogen purged system); pyridine by distillation from *p*-toluenesulfonyl chloride and redistillation from LAH; water by resin deionization and distillation from glass; trifluoroacetic acid (TFA) by distillation from phosphorous pentoxide.

tert-Butyloxycarbonyl (Boc) amino acids and other amino acid derivatives were purchased from Beckman Instruments (Spinco Division) Toronto, Ont., Canada and Bachem Inc., Torrance CA, U.S.A. Disodium adenosine triphosphate, disodium glycerophosphoric acid, theophylline, ethyleneglycolbis(β-aminoethyl ether)-*N*,*N*′-tetraacetic acid (EGTA), 3′,5′-cyclic adenosine monophosphate (cAMP), crude calf thymus histone (lysine-rich histone fraction 1), and salmon protamine were purchased from Sigma Chemical Co., St. Louis MO, U.S.A. Protein kinases from rabbit skeletal muscle (peak I and peak II) and bovine cardiac muscle (peak II), isolated as crude fractions after DEAE-cellulose chromatography (22), were also purchased from Sigma Chemical Co. Biogel P-60 was purchased from Bio-Rad Inc., Mississauga, Ont., Canada. Cellulose chromatographic plates (MN300, 0.5 mm) were purchased from Analtech Inc., Newark, DE, U.S.A. Stoppered polypropylene vials, Whatman chromatographic paper (3 MM), Gelman Instant Thin-layer Chromatographic sheets (ITLC-SG) were purchased from either Fisher Scientific Ottawa, Ont., Canada or Canlab, Montreal, P.Q., Canada. Kemptide (Leu-Arg-Arg-Ala-Ser-Leu-Gly) was purchased from Peninsula Laboratories, San Carlos, CA, U.S.A. Amino acid analysis: Leu:Arg:Ala:Ser:Gly (2.15:2.04:1.08:1.00:1.00).

Calf thymus histone H-1 was purified by gel filtration on Biogel P-60 according to the published procedure of Böhm *et al.* (23, 24).

^{32}P-ATP(γ^{32}P adenosine triphosphate, tetra(triethylammonium) salt) (2–10 Ci/mmol) was purchased from New England Nuclear, Montreal, P.Q., Canada. Stock ^{32}P-ATP solutions were prepared as follows: the solution of labelled ATP (approximately 1 mCi) was diluted to 2.0 ml with incubation buffer. An aliquot (500 μl) was mixed before use with 2.5 ml of incubation buffer (^{32}P-ATP approximately 0.1 mCi/ml).

Elemental analyses were done on a Perkin-Elmer CHN analyzer, model 240. Amino acid analyses were done on a Beckman analyzer, model 120C equipped with a multisample inlet and automatic integrator. Samples for amino acid analysis were prepared by hydrolysis in 6 *N* HCl at 110°C for 24 h. Optical rotations were taken on a Perkin-Elmer polarimeter, model 141. Melting points were determined in an open capillary on a Gallenkamp melting point apparatus. Liquid scintillation counting was done on a Beckman counter LSC-250. Samples were prepared for counting in low potassium vials using 10 ml of a scintillation cocktail (8 g Omnifluor in 2 ℓ toluene–2-methoxyethanol (1:1, v/v)). A ^{14}C-^{32}P window was used in all cases in order to overcome energy profile shifts caused by quenching. Enzyme incubations were done in a Fisher-Versabath at 37.0 ± 0.5°C. High voltage electrophoresis was done in an apparatus equipped with a 20-cm water-cooled platen (10–15°C). Power for the apparatus was supplied by a Buchler high voltage supply. A 30 V/cm gradient was applied for 1–1.5 h to strips of paper (Whatman 3 MM) which had been equilibrated with citrate buffer (sodium citrate 0.05 *M*, citric acid 0.05 *M*, pH 3.5). After electrophoresis the strips were dried and cut into pieces (1 cm × 3 cm). The pieces were placed into vials and the radioactivity levels were determined.

Bovine Liver Protein Kinase Isolation

A crude fraction of protein kinase activity from an acetone powder of beef liver (animal weight less than 200 kg) was prepared by the procedures outlined by Langan (25). The crude fraction referred to here is that which was eluted at the calcium phosphate gel step. The protein kinase activity was eluted from the gel as described with 0.5 *M* phosphate buffer, pH 7.5, precipitated with $(NH_4)_2SO_4$ (75% saturation), collected and redissolved in 0.05 *M* phosphate buffer, pH 7.5. The preparation was dialyzed overnight at 4°C against several changes of 0.05 *M* phosphate buffer, pH 7.5. Protein concentration was determined spectrophotometrically (280 nm) to be 1.5 mg/ml (26, 27). Protein kinase activity was determined in the presence of cAMP and was found to be 12 ± 2 pmol ^{32}P incorporated per minute per milligram of protein (60 min assay, calf thymus histone H-1 (40 μg) as substrate).

Enzyme Assays

Substrate Activity

The peptide to be tested for substrate activity was incubated with either the bovine cardiac muscle or rabbit skeletal muscle enzyme preparations as in the following procedure: 50 μl γ-^{32}P ATP stock solution (0.1 mCi/ml), 5 μl c-AMP (from a 10 m*M* stock solution), 20 μl protein kinase enzyme preparation (bovine cardiac enzyme, 1 mg/ml stock solution; rabbit skeletal muscle, 2 mg/ml stock solution; bovine liver preparation, 1.5 mg/ml stock solution), and 5 μl of the peptide stock solution were incubated at 37°C for 1 h. Kemptide stock solutions used were approximately 30 m*M*. The other peptide stock solutions were approximately 30 m*M*. All solutions, save that of the peptide which was in water, contained the following buffer; buffer *A*: 50 m*M* β-glycerophosphoric acid disodium, 10 m*M* magnesium acetate tetrahydrate, 10 m*M* sodium

TABLE 2. Physical constants of intermediates in the synthesis of the tetra- and pentapeptides

Compound	Melting point (°C)	Specific rotation ($[\alpha]_D$) (deg)
Cbz Boc Phe Lys NH_2	162–163	−9.03 (*c* 2.26, MeOH)
OBzl Cbz Boc Ser Phe Lys NH_2	166–167	−14.11 (*c* 1.94, HOAc)
OBzl Boc Gly Ser Phe Lys NH_2	178–179	−6.74 (*c* 1.14, HOAcO)
H-Gly Ser Phe Lys-NH_2	—	−4.38 (*c* 1.88, H_2O)[a]
Cbz Boc Lys Leu NH_2	102–104	−36.1 (*c* 1.94, HOAc)
Cbz Boc Phe Lys Leu NH_2	164–165	−23.5 (*c* 1.99, HOAc)
OBzl Cbz Boc Ser Phe Lys Leu NH_2	184–185	−24.3 (*c* 2.02, HOAc)
OBzl Cbz Boc Gly Ser Phe Lys Leu NH_2	200–205	−16.7 (*c* 2.08, HOAc)
H-Gly Ser Phe Lys Leu-NH_2	—	−35.1 (*c* 4.3, H_2O)[b]

[a]Molar rotation (based on lysine concentration) $[M_D]$ −26.5 (c, 30.8 m*M*, H_2O).
[b]Molar rotation (based on lysine concentration) $[M_D]$ −341.9 (c, 43.8 m*M*, H_2O).

fluoride, 2 m*M* theophylline, and 0.3 m*M* EGTA, pH 7.0 (adjusted with 10% v/v HCl). Controls excluding the peptide and enzyme were run simultaneously. After the incubation period an aliquot (10 µl) was removed and applied to a strip of Whatman 3 MM chromatographic paper in preparation for high voltage electrophoresis as described above.

Inhibition Assays

The ability of the peptide to interfere with the phosphorylation of pure histone H-1 by protein kinase preparations was assessed as follows: 50 µl γ-^{32}P ATP stock solution (0.1 mCi/ml), 10 µl cAMP (from a 10 m*M* stock solution), 10 µl pure histone H-1 (from an 8 mg/ml stock solution), and either 10 µl of bovine cardiac muscle protein kinase preparation (from a 0.1 mg/ml stock solution) or 20 µl of rabbit skeletal muscle protein kinase preparation (from a 0.1 mg/ml stock solution). The total volume was made up to 200 µl with buffer. All stock solutions, save that of the histone which was made up in water, contained buffer *A*. The reaction mixture was incubated at 37°C and aliquots (10 µl) were removed at 5-min time intervals in order to determine the rate of incorporation of phosphorous into the histone H-1. Under all circumstances linear rates of incorporation were observed during the initial stages of the reaction. Phosphorous incorporation into protein was assayed using Gelman ITLC-SG strips and 20% trichloroacetic acid in 0.4 *M* KCl as irrigant (28). After irrigation, strips were heat-dried, the origins removed and deposited into vials in preparation for counting.

Peptide Syntheses

The elemental analysis of intermediate compounds are reported in Table 1.[6,7] The physical constants of the intermediate compounds are given in Table 2. Compounds were synthesized as given below.

[6]All analyses were within acceptable limits C ± 0.2%, H ± 0.2%, N ± 0.3%.

[7]Table 1 may be obtained, at a nominal charge, from the Depository of Unpublished Data, CISTI, National Research Council of Canada, Ottawa, Ont., Canada K1A 0S2.

Cbz
Boc Phe Lys-NH_2
Cbz

Boc Phe Lys OMe (20 g, 37 mmol, prepared as described previously (29)) was dissolved in cold (0°C) methanol (500 ml) and NH_3 bubbled in over a period of 1.5 h. The solution was then stoppered and placed in the refrigerator for 18 h. The solution was concentrated to dryness *in vacuo* and the residue recrystallized from ethyl acetate; yield 13.8 g (71%).

OBz Cbz
Boc Ser Phe Lys-NH_2
OBz

Boc Ser (4.43 g, 15 mmol) was dissolved in 100 ml DME–pyridine (95:5) and cooled to 0°C. *N*-Hydroxysuccinimide (15 mmol, 1.71 g) and DCC (15 mmol, 3.08 g) were added and the mixture stirred at 0°C for 6 h. The mixture was filtered and

Cbz

the filtrate concentrated *in vacuo*. Boc Phe Lys NH_2 (15 mmol, 7.9 g) was treated with trifluoroacetic acid–methylene chloride (1:1, 30 ml) and allowed to stand at room temperature for 2 h. The solution was then concentrated and the residue triturated with ether. The residue was dissolved in DME–DMF (1:1, 30 ml) and cooled to 0°C. Triethylamine (30 mmol, 4.2 ml) was

OBz

added followed by Boc Ser OSu in DME–DMF (1:1, 30 ml). The mixture was stirred overnight at 0°C and then concentrated. Water (100 ml) was added and the solution extracted with ethyl acetate (3 × 300 ml). The ethyl acetate was then washed with cold 0.1 *N* HCl (300 ml), 5% $NaHCO_3$ (cold, 300 ml), and cold water (300 ml). The ethyl acetate was dried over sodium sulfate, filtered and concentrated. The residue was recrystallized from ethyl acetate to yield 5.88 g (56%).

OBz Cbz
Boc Gly Ser Phe Lys-NH_2
OBz Cbz

Boc Ser Phe Lys NH_2 (0.35 g, 0.5 mmol) was treated with TFA–CH_2Cl_2 (3 mmol, 1:1) at room temperature for 2 h. The solution was concentrated and the residue triturated with

ether. The residue was dissolved in DME (5 ml) and cooled to 0°C. Triethylamine (0.5 mmol, 75 μl) was added followed by Boc Gly (0.5 mmol, 0.088 g) and EEDQ (0.5 mmol, 0.123 g) and the reaction stirred at 0°C overnight. After 20 min the mixture became a gummy paste. After 18 h the reaction was concentrated *in vacuo* and the residue washed with ether (3 × 50 ml), water (100 ml), and isopropanol (100 ml). The residue was then crystallized from methanol to yield 0.18 g (48%).

H-Gly Ser Phe Lys-NH_2
OBz Cbz

Boc Gly Ser Phe Lys NH_2 (0.1 g, 0.13 mmol) was treated with TFA–CH_2Cl_2 (2 ml, 1:1) at room temperature for 1 h. The reaction mixture was concentrated *in vacuo* and the residue triturated with ether. The residue was dissolved in methanol – acetic acid (10:1, 11 ml) and hydrogenated at room temperature and atmospheric pressure for 4 h over palladium oxide (Pd oxide). Analysis by tlc on cellulose in butanol – pyridine – acetic acid – water (15:10:3:12) and in butanol – acetic acid – water (5:2:3) showed a major ninhydrin positive spot at R_f 0.67 and 0.31, respectively. Preparative chromatography in the former solvent followed by elution with water gave, after filtration (Millipore, 0.45 μ), the required tetrapeptide (R_f 0.31); yield 0.062 mmol (42%). Amino acid analysis: Gly:Ser:Phe:Lys (0.97:0.97:1.01:1.00).

Cbz
Boc Lys Leu-NH_2
Cbz

Boc Lys DCHA (5.6 g, 10 mmol scale), HCl Leu OMe (1.8 g) were mixed in DME (50 ml). *N*-Hydroxysuccinimide (1.2 g) was added and the mixture was cooled to ice temperature, and stirred for 60 min. DCC (2.2 g) was added and the mixture stirred overnight during which time the ice coolant melted. Glacial acetic acid (2 drops) was added and the solution stirred for 5 min. CH_2Cl_2 (50 ml) was added and the precipitated dicyclohexylurea (DCU) was removed by filtration. The filtrate was evaporated, taken up in EtOAc, and washed with chilled acid (HCl), base ($NaHCO_3$), and water. The washed EtOAc was dried (Na_2SO_4) and evaporated (4.5 g). The residue was taken up in MeOH (200 ml), chilled to ice temperature, and NH_3 (gas) was blown in until the solution was saturated (15–20 min). The stoppered flask was kept 48 h at 4°C and the contents evaporated. The residue was crystallized from EtOAc–petroleum ether (bp 30–60°C); yield 3.85 g (88%).

Cbz
Boc Phe Lys Leu-NH_2
Cbz

Boc Lys Leu NH_2 (9.85 g, 20 mmol scale) was deblocked by treating with TFA–CH_2Cl_2 (1:1, v/v) (50 ml) for 30 min. The product was precipitated with ether (300 ml), washed with ether twice, and dried overnight under high vacuum. DMF–pyridine (9:1, v/v) (20 ml) and Boc Phe (4.94 g) were added to the residue and chilled to ice temperature. *N*-Hydroxysuccinimide (2.3 g), triethylamine (2.1 g), and DCC (4.3 g) were added and the solution stirred overnight during which time the ice coolant melted. Glacial acetic acid (2 drops) was added and the solution stirred for 5 min. The DCU precipitate was removed by filtration and the filtrate evaporated to dryness. The residue was taken up in EtOAc (4 ℓ) and washed with chilled acid (HCl), base ($NaHCO_3$), and water. The washed EtOAc was dried (Na_2SO_4) and evaporated. The residue was crystallized from EtOAc; yield 8.1 g (62%).

OBzl Cbz
Boc Ser Phe Lys Leu-NH_2
CBz

Boc Phe Lys Leu NH_2 (7.05 g, 10 mmol scale) was deblocked with TFA–CH_2Cl_2 (1:1, v/v) (50 ml) and the ether-insoluble product isolated as described above. DMF–pyridine
OBzl
(9:1, v/v) (100 ml), Boc Ser (3.2 g), and *N*-hydroxysuccinimide (1.3 g) were combined and the solution chilled in ice. DCC (2.3 g) was added and the solution stirred overnight during which time the ice coolant melted. The precipitated DCU was removed by filtration and the filtrate was added to a chilled solution of the above ether-soluble product in DMF–pyridine (9:1, v/v) (20 ml). Triethylamine (1.1 g) was added and the solution stirred for 48 h during which time the ice coolant melted. The solution was evaporated to dryness, taken up in cold EtOAc (10 ℓ), and washed with chilled acid (HCl), base ($NaHCO_3$), and water. The washed EtOAc was dried (Na_2SO_4), evaporated to 100 ml, filtered, and then evaporated to dryness. The residue was crystallized from MeOH–ether (1:40, v/v); yield 4.9 g (60%).

OBzl Cbz
Boc Gly Ser Phe Lys Leu-NH_2
OBzl Cbz

Boc Ser Phe Lys Leu NH_2 (2 g, 2 mmol scale) was deblocked with TFA–CH_2Cl_2 (1:1, v/v) (20 ml) and the ether-insoluble product isolated as described above. Boc Gly (1.8 g) was dissolved in chilled CH_2Cl_2 or DMF (10 ml) and DCC (1.01 g) was added. After stirring at ice temperature for 4 h the solution was filtered and added to the above ether-insoluble product dissolved in cold DMF (15 ml) containing pyridine (1 ml) and triethylamine (250 mg). The mixture was stirred for 4 days during which time the ice coolant melted. The solution was filtered and evaporated to dryness. The residue was crystallized from hot EtOAc (approximately 2 ℓ); yield 1.31 g (62%).

H-Gly Ser Phe Lys Leu-NH_2
OBzl Cbz

Boc Gly Ser Phe Lys Leu NH_2 (50 mg) was suspended in a stirred solution of trifluoroacetic acid (7.0 ml) containing a small amount of water (100 μl). The mixture was chilled in an ice bath and hydrogen bromide, which had been scrubbed with pure tetralin, was passed through the solution for 60 min. The reaction mixture was concentrated under reduced pressure (40°C) and anhydrous diethyl ether (approximately 150 ml) was added to the residue. The white solid which formed was collected by centrifugation, washed with diethyl ether (five times), and dried under high vacuum; yield 42.6 mg. Thin-layer chromatography on cellulose in ethyl acetate – pyridine – acetic acid – H_2O (20:10:3:5), v/v/v/v) showed one ninhydrin positive spot R_f 0.13; amino acid analysis: Gly:Ser:Phe:Lys:Leu (1.09:0.78 (0.96):0.96:1.00:1.05 (72 h)) (1.12:0.99(1.11):1.01:1.00:1.09 (48 h)). Figures in parentheses after serine are the ratios corrected for destruction of serine at the rate of 6% per 24-hour period. Paper electrophoretic mobility (citrate buffer pH 3.4, 30 V/cm, 5–10°C), R_{rel} 0.90 (relative to arginine).

Results and Discussion

Synthesis

Two peptides, related to the highly conserved sequence found in the central region of the H-1 and H-5 (Fig. 1), have been synthesized. They are I-H-Gly Ser Phe Lys-NH_2 and II-H-Gly Ser Phe Lys Leu-NH_2. They were synthesized by conventional methods according to Scheme 1A and 1B. Analyses and physical constants of the intermediates are given in Tables 1 and 2 respectively. Benzyloxycarbonyl (Cbz) blocking of the lysine ε-amino group, *tert*-butyloxycarbonyl (Boc) blocking of α-amino groups,

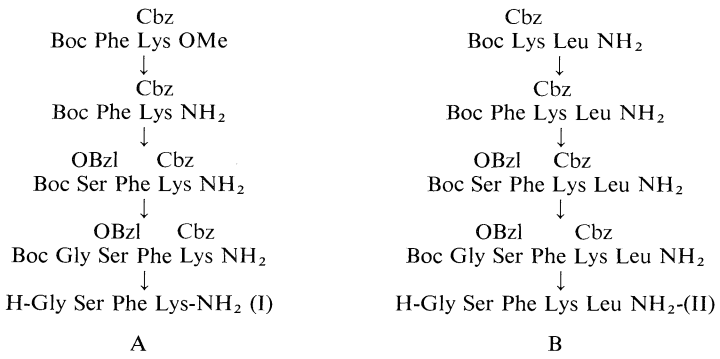

SCHEME 1

and *O*-benzyl (Bzl) group blocking of serine was used. Final deblockings of the fully blocked peptides were carried out either by catalytic hydrogenation or by treatment with HBr – trifluoroacetic acid – H_2O (30, 31). The tetrapeptide (I) was separated by thin-layer chromatography (tlc) on cellulose plates and isolated by extraction, filtration, and lyphilization. The pentapeptide product (II) was isolated by washing the fully deblocked material with ether. Homogeneity of the final products was assured by tlc and amino acid analyses.

Protein Kinase Substrate Activity

The two peptides which have been synthesized come from an area of histone H-1 which has been found to be phosphorylated by a crude preparation of calf liver protein kinase (17, 18). Both peptides were tested for their ability to act as substrates for the crude preparations of the peak II enzyme[8] activity from bovine cardiac muscle and the peak I and peak II enzyme activities from rabbit skeletal muscle. A peptide known to be a substrate of the enzymes was used as a control. This peptide, known as Kemptide (Leu-Arg-Arg-Ala-Ser-Leu-Gly), has been found to be a substrate of protein kinases (32). Peptides with similar structures have also been found in substrates of protein kinases (33–38). Work with these peptides and other substrates has suggested that a specific pattern of amino acids will be required in the peptide before it acquires the ability to act as a protein kinase substrate (19, 20, 33–38).

The two peptides and Kemptide were incubated separately with each of the crude muscle protein kinase preparations and the reaction products separated by electrophoresis. Phosphorous was incorporated readily into Kemptide by all protein kinase preparations. None of the muscle protein kinase preparations were able to incorporate measurable amounts of phosphorous into the tetrapeptide. Measurable amounts of phosphorous were, however, incorporated into the pentapeptide by the bovine cardiac muscle enzyme preparation. The results obtained with the crude peak II enzyme activity from bovine cardiac muscle are shown in Fig. 2*a*. Smaller, but still measurable, amounts of phosphorous were incorporated when the crude peak I and peak II enzyme activities from rabbit skeletal muscle were used.

The known structural requirements of the endogenous protein kinases (19, 20) and the ability of the pentapeptide to act as a phosphate acceptor suggest that there may have been a histone H-1 specific kinase present in calf liver, the tissue from which the phosphorylated peptide was originally isolated.

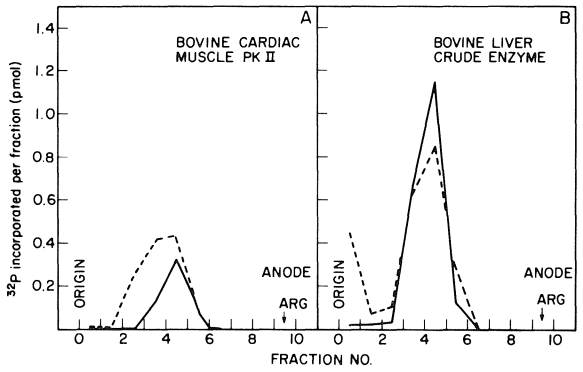

FIG. 2. The electrophoretic separation of the peptides after incubation with crude peak II protein kinase from bovine cardiac muscle and the crude protein kinase from beef liver. Radioactivity incorporated into the pentapeptide (II) (—) and Kemptide (---) by the crude peak II protein kinase from bovine cardiac muscle (Fig. 2*A*). Radioactivity incorporated into the pentapeptide (II) (—) and Kemptide (---) by the crude protein kinase from beef liver (Fig. 2*B*). Experimental conditions: incubation mixtures (180 μl) were 2.13×10^{-3} *M* in pentapeptide or 1.78×10^{-6} *M* in Kemptide. Incubations were carried out in buffer *A* at 37.5°C for 1 h with either crude bovine cardiac peak II protein kinase (20 μg) (Fig. 2*A*) or crude bovine liver protein kinase (30 μg) (Fig. 2*B*). An aliquot (10 μl) was electrophoresed in sodium citrate 0.05 *M*; citric acid 0.05 *M*, pH 3.5; voltage gradient, 30 V/cm; temperature, 10–15°C. Arg (=arginine) indicates the position of arginine after electrophoresis. Fraction number is equivalent to the distance migrated in centimetres.

[8]Peak numbers refer to the order of elution from a DEAE-cellulose column.

TABLE 3. Peptide inhibition of protein kinase phosphorylation of histone H-1

Peptide	Concentration[b] (*M*)	% inhibition of phosphate addition[a]		
		Bovine cardiac protein kinase, peak II[c]	Rabbit skeletal muscle protein kinase, peak I[d]	Rabbit skeletal muscle protein kinase, peak II[d]
H-Gly Ser Phe Lys-NH_2	1.50×10^{-3}	22±2	20±2	12±2
H-Gly Ser Phe Lys Leu-NH_2	2.13×10^{-3}	13±2	20±2	0
H-Leu Arg Arg Ala Ser Leu Gly-OH	2.28×10^{-3}	95	83	90
H-Leu Arg Arg Ala Ser Leu Gly-OH	1.78×10^{-6}	12±2	21±3	18±2

[a]Experimental conditions: buffer supplemented with cyclic AMP (10^{-6} *M*); incubation volume, 200 µl; temperature, 37°C; protein substrate, calf thymus histone H-1 (80 µg per assay); % inhibition is calculated as follows: $100\,(C_0 - C_p)/C_0\,100$ where $C_p = {}^{32}P$ counts incorporated in the presence of peptide and $C_0 = {}^{32}P$ counts incorporated in the absence of peptide. Errors (sd) indicated were determined from three or more experiments.
[b]Peptide concentrations are based on amino acid analyses and represent the final concentration in the assay.
[c]Incubation time, 10 min. Enzyme concentration, approximately 2 units per assay (approximately 1 µg per assay).
[d]Incubation time, 20 min. Enzyme concentration, approximately 4 units per assay (approximately 2 µg per assay).

Indeed, a histone H-1 specific kinase has been isolated from soyabean hypocotyls, but no indication of the distribution of the label within the histone was given (39). In addition, the distribution of Ser/Thr phosphorylated sites in rabbit thymus histone H-1 was recently shown to be influenced by the origin of the protein kinase preparation used for labelling (40).

When a crude preparation of protein kinase activity, isolated from bovine liver, was incubated with the pentapeptide substantial amounts of phosphate were incorporated into the peptide (Fig. 2*b*). This would suggest that this highly metabolically- and divisionally-active tissue may contain a highly site-specific histone H-1 kinase.

Inhibition Activity

Even though both peptides had very small or no substrate activity with the endogenous protein kinase preparations from muscle it is conceivable that they might be able to prevent the addition of phosphate to protein by binding at or near the substrate site. The ability of both peptides and Kemptide to inhibit the incorporation of phosphate into purified calf thymus histone H-1 by the exogenous enzymes was tested. Conditions were set up such that 2–3 phosphate groups of a total of 5–7 (41, 42) were incorporated into the histone during the time of the assay. The ability of the peptides to interfere with this incorporation was then tested. The results are given in Table 3. Kemptide was very effective at inhibiting the phosphorylation of histone H-1 by all the exogenous protein kinases. At 10^{-3} *M* it reduced incorporation by 80–90%. The tetra- and pentapeptides were also effective in inhibiting the reaction though not nearly to the same degree. Assays done with Kemptide showed that a 10–25% inhibition level could be achieved at 10^{-6} *M*, a concentration about a 1000-fold less than that of the two peptides. Some small differences between the tetra- and pentapeptides was noted. In general the pentapeptide was slightly less effective at inhibiting the enzymes. It also was unable to cause any inhibition of the rabbit skeletal muscle peak II protein kinase.

Although it is evident from the above results that the two peptides which have been synthesized are able to act as inhibitors of the endogenous enzymes studied, further work will be necessary before a full description of the actual mode of action of these peptides can be given.

Finally, two recent reports must be mentioned. It has recently been reported that several sequences surrounding serine-38 in calf thymus histone H-1 have been synthesized (43) and that this same serine-containing sequence, which is found only in the N-terminal section of calf thymus histone H-1, is able to act as a substrate for an endogenous protein kinase isolated from calf thymus nuclei (44). This peptide, Arg-Arg-Lys-Ala-Ser-Gly-Pro, has the same relationship of charged groups to the serine as in Kemptide and thus, fulfils not only the general requirements but also the specific requirements of protein kinases for recognition of primary amino acid sequences.

1. D. W. FITZSIMONS and G. E. W. WOLSTENHOLME (*Editors*). Ciba Foundation Symp. Structure Function Chromatin, **28**, 1 (1975).
2. E. M. BRADBURY. Methods Cell Biol. **16**, 179 (1977).
3. D. M. P. PHILIPS (*Editor*). Histones and nucleohistones. Plenum Press, New York, NY. 1971.
4. L. S. HNILICA. The structure and biological function of histones. CRC Press, Cleveland, OH. 1972.
5. S. C. ELGIN and H. WEINTRAUB. Ann. Rev. Biochem. **44**, 725 (1975).
6. S. C. RALL and R. D. COLE. J. Biol. Chem. **246**, 7175 (1971).
7. G. M. T. JONES, C. RALL, and R. D. COLE. J. Biol. Chem. **249**, 2548 (1974).

8. W. N. STRICKLAND, H. SCHALLER, M. STRICKLAND, and C. VAN HOLT. FEBS Lett. **66**, 322 (1976).
9. A. R. MACLEOD, N. C. W. WONG, and G. H. DIXON. Eur. J. Biochem. **78**, 281 (1977).
10. P. SAUTIERE, G. BRIAND, D. KMIECKE, O. LOY, G. BISERTE, A. GAREL, and M. CHAMPAGNE. FEBS Lett. **63**, 164 (1976).
11. V. SELIGY, C. ROY, M. DOVE, and M. YAGUCHI. Biochem. Biophys. Res. Commun. **71**, 196 (1976).
12. M. YAGUCHI, C. ROY, M. DOVE, and V. SELIGY. Biochem. Biophys. Res. Commun. **76**, 100 (1977).
13. E. M. BRADBURY, G. E. CHAPMAN, S. E. DANBY, P. G. HARTMAN, and P. L. RICHES. Eur. J. Biochem. **57**, 521 (1975).
14. P. G. HARTMAN, G. E. CHAPMAN, T. MOSS, and E. M. BRADBURY. Eur. J. Biochem. **77**, 45 (1977).
15. H. W. E. RATTLE, T. A. LANGAN, S. E. DANBY, and E. M. BRADBURY. Eur. J. Biochem. **81**, 499 (1977).
16. B. O. GLOTOV, L. G. NIKOLAEV, S. N. KUROCHKIN, and E. S. SEVERIN. Nucl. Acids Res. **4**, 1065 (1977).
17. T. A. LANGAN. Ann. N.Y. Acad. Sci. **185**, 166 (1971).
18. T. A. LANGAN. Fed. Proc. Fed. Am. Soc. Exp. Biol. **30**, 1089 (1971).
19. R. E. WILLIAMS. Science, **192**, 473 (1976).
20. H. G. NIMMO and P. COHEN. Adv. Cyclic Nucleotide Res. **8**, 145 (1977).
21. D. SMALL, P. Y. CHOU, and G. D. FASMAN. Biochem. Biophys. Res. Commun. **79**, 341 (1977).
22. A. G. GILMAN. Proc. Natl. Acad. Sci. U.S.A. **67**, 305 (1970).
23. E. L. BÖHM, W. N. STRICKLAND, M. STRICKLAND, B. H. THWAITS, D. R. VAN DER WESTHUIZEN, and C. VON HOLT. FEBS. Lett. **34**, 217 (1973).
24. C. VON HOLT and W. F. BRANDT. Methods Cell Biol. **16**, 205 (1977).
25. T. A. LANGAN. Science, **162**, 579 (1968).
26. O. WARBUNG and W. CHRISTIAN. Biochem. Z. **310**, 384 (1941).
27. E. LAYNE. Methods Enzymol. **3**, 447 (1975).
28. K.-P. HUANG and J. C. ROBINSON. Anal. Biochem. **72**, 593 (1976).
29. L. A. SLOTIN, D. R. LAUREN, and R. E. WILLIAMS. Can. J. Chem. **55**, 4257 (1977).
30. P. G. KATSOYANNIS and G. P. SCHWARTZ. Methods Enzymol. **47**, 501 (1977).
31. S. GUTTMANN and R. A. BOISSANNAS. Helv. Chim. Acta, **41**, 1852 (1958).
32. B. E. KEMP, D. A. GRAVES, and E. G. KREBS. Fed. Proc. Fed. Am. Soc. Exp. Biol. **35**, 1384 (1976).
33. B. E. KEMP, D. B. BYLUND, and E. G. KREBS. Proc. Natl. Acad. Sci. U.S.A. **72**, 3448 (1975).
34. P. O. DAILE, P. R. CARNEGIE, and J. D. YOUNG. Nature, **257**, 416 (1975).
35. P. O. DAILE, P. R. CARNEGIE, and J. D. YOUNG. Biochem. Biophys. Res. Commun. **61**, 852 (1975).
36. E. HUMBLE, L. BERGLAND, V. TITANJI, O. LJUNGSTROM, B. EDLUND, O. ZETTERQUIST, and L. ENGSTROM. Biochem. Biophys. Res. Commun. **66**, 614 (1975).
37. O. ZETTERQUIST, V. RAGNARSSON, E. HUMBLE, L. BERGLUND, and L. ENGSTROM. Biochem. Biophys. Res. Commun. **70**, 696 (1976).
38. B. E. KEMP, E. BENJAMINI, and E. G. KREBS. Proc. Natl. Acad. Sci. U.S.A. **73**, 1038 (1976).
39. P. P. C. LIN and J. L. KEY. Biochem. Biophys. Res. Commun. **73**, 396 (1976).
40. S. N. KUROCHKIN, I. N. TRAKHT, E. S. SEVERIN, and R. D. COLE. FEBS. Lett. **84**, 163 (1977).
41. P. HOHMANN, R. A. TOBEY, and L. R. GURLEY. J. Biol. Chem. **251**, 3685 (1976).
42. L. R. GURLEY, R. A. WALTERS, C. E. HILDEBRAND, P. G. HOHMANN, S. S. BARHAM, L. L. DEAVEN, and R. A. TOBEY. *In* International cell biology. *Edited by* B. R. Brinkley and K. R. Porter. Rockefeller University Press, New York, NY. 1977. p. 420.
43. V. A. SHIBNEV and O. D. TURAEV. Izv. Akad. Nauk SSSR Ser. Khim. 916 (1976).
44. A. H. POMERANTZ, V. G. ALLFREY, R. B. MERRIFIELD, and E. M. JOHNSON. Proc. Natl. Acad. Sci. U.S.A. **74**, 4261 (1977).

Nucleic acid related compounds. 29. Thionyl chloride reactions with adenine nucleosides. Course of nucleophilic displacements and a preferential route to the 2′-chloro-*arabino* isomer[1,2]

MORRIS J. ROBINS, PETER SPORNS, AND WOLFGANG H. MUHS[3]

Department of Chemistry, The University of Alberta, Edmonton, Alta., Canada T6G 2G2

Received August 14, 1978

MORRIS J. ROBINS, PETER SPORNS, and WOLFGANG H. MUHS. Can. J. Chem. **57**, 274 (1979).

A multistage sequence gave 5′-*O*-pivalyl-3′-*O*-methyladenosine (**2***e*) which was treated with thionyl chloride in hot pyridine to give the corresponding 2′-chloro-*arabino* product **3***a*. Hydrogenolysis using tri-*n*-butyltin hydride and deblocking gave 2′-deoxy-3′-*O*-methyladenosine (**3***b*). Analogous treatment of a mixture of 3′(2′),5′-di-*O*-acetyladenosines (**5***a*,*b*) with $SOCl_2$–pyridine gave the 3′-*O*-acetyl-2′-chloro-*arabino* (**6***a*) and 2′-*O*-acetyl-3′-chloro-*xylo* (**7***a*) derivatives in a ratio of ~3:2, respectively. Hydrogenolysis and deprotection gave 2′-deoxyadenosine (**6***c*) and 3′-deoxyadenosine (**7***c*) (~3:2) in ~45% overall yield from adenosine (based on recovered starting materials). This represents the first example of preferential external nucleophilic displacement at C-2′ (vs. C-3′) in an equilibrating purine ribonucleoside system. Treatment of 9-β-D-xylofuranosyladenine (**9**) with $SOCl_2$–HMPA gave the 5′-chloro-5′-deoxy product **10***a* rather than the previously suggested 2′-chloro-2′-deoxy derivative.

MORRIS J. ROBINS, PETER SPORNS et WOLFGANG H. MUHS. Can. J. Chem. **57**, 274 (1979).

Une longue série de réaction conduit à la *O*-pivalyl-5′ *O*-méthyl-3′ adénosine (**2***e*) qui par traitement avec du $SOCl_2$ dans la pyridine à chaud fournit le produit chloro-2 *arabino* correspondant **3***a*. Une hydrogénolyse à l'aide de l'hydrure de tri-*n*-butylétain suivie d'un déblocage donne la désoxy-2′ *O*-méthyl-3′ adénosine (**3***b*). Si l'on traite de la même manière un mélange de di-*O*-acétyl-3′(2′),5′ adénosine (**5***a*,*b*) avec du $SOCl_2$–pyridine, on obtient les dérivés *O*-acétyl-3′ chloro-2′ *arabino* (**6***a*) et *O*-acétyl-2′ chloro-3′ *xylo* (**7***a*) dans des rapports respectifs de ~3:2. Une hydrogénolyse suivie d'une déprotection conduit à un mélange de la désoxy-2′ adénosine (**6***c*) et de la désoxy-3′ adénosine (**7***c*) (dans un rapport de 3:2) avec un rendement global de 45% à partir de l'adénosine (et en se basant sur les produits récupérés). Ce sont les premiers exemples d'une substitution nucléophile externe préférentielle au niveau de C-2′ (vs. C-3′) dans une purine en équilibre d'un système ribonucléoside. La réaction de la β-D-xylofurannosyl-9 adénine (**9**) avec le $SOCl_2$–HMPA fournit le produit chloro-5′ désoxy-5′ (**10***a*) plutôt que le dérivé chloro-2 désoxy-2 suggéré antérieurement.

[Traduit par le journal]

Nucleophilic displacements at C-2′ of purine-type ribonucleosides using external nucleophiles have proven to be very difficult (1). Attempted substitutions of 2′-sulfonate esters have failed[4] (2). Reactions involving 'symmetrical' C-2′,C-3′ species such as 2′,3′-acyloxonium cation intermediates (3, 4) 2′,3′-anhydro (epoxide) structures (1, 3*d*, *h*, 4*d*), and 2′,3′-thiiranium (episulfonium) ions (1) in the *ribo* series have resulted in highly predominant or sometimes exclusive (1, 3*b*,*d*,*g*,*h*, 4*b*,*c*) formation of the 3′-substituted *xylo* products. This can be seen to result from the sterically (base at C-1′ *cis*-vicinal to the site of S_N2 attack at C-2′) and electronically (5) (C-2′ bonded to the electronegative *N*,*O*-acetal anomeric carbon) favored attack at C-3′.

We have explored some reactions of adenine nucleosides with thionyl chloride and now wish to report that replacement of the 2′-hydroxyl function by chlorine with inversion of configuration occurs, albeit in low to moderate yields with significant accompanying decomposition. The known favorable O-2′ ⇄ O-3′ equilibrium of adenosine acetate esters (6*a*) has been employed to provide the first noted preferential functionalization at C-2′ with an *external nucleophile*[5] by treatment of the equilibrium mixture with thionyl chloride – pyridine.

The 3′-*O*-methyl ether function was first chosen to provide a 'fixed' model compound for reaction at C-2′ since it exerts minimal steric and electronic

[1]For the previous paper in this series see ref. 30.

[2]Abstracted in part from the Ph.D. dissertation of P.S., University of Alberta, 1977.

[3]Postdoctoral Research Associate.

[4]M. J. Robins and J. R. McCarthy, Jr. Unpublished observations. Treatment of 2′-*O*-tosyl- (or *p*-nitrobenzenesulfonyl-) tubercidin with ethanethiolate in ethanol or dry DMF under various conditions resulted in formation of tubercidin by presumed nucleophilic attack on sulfonate sulfur.

[5]Formation of purine X-8 → C-2′ cyclonucleosides occurs readily by intramolecular nucleophilic attack of 8-*N*, *O*, or *S* substituents at C-2′ (7).

0008-4042/79/030274-09$01.00/0

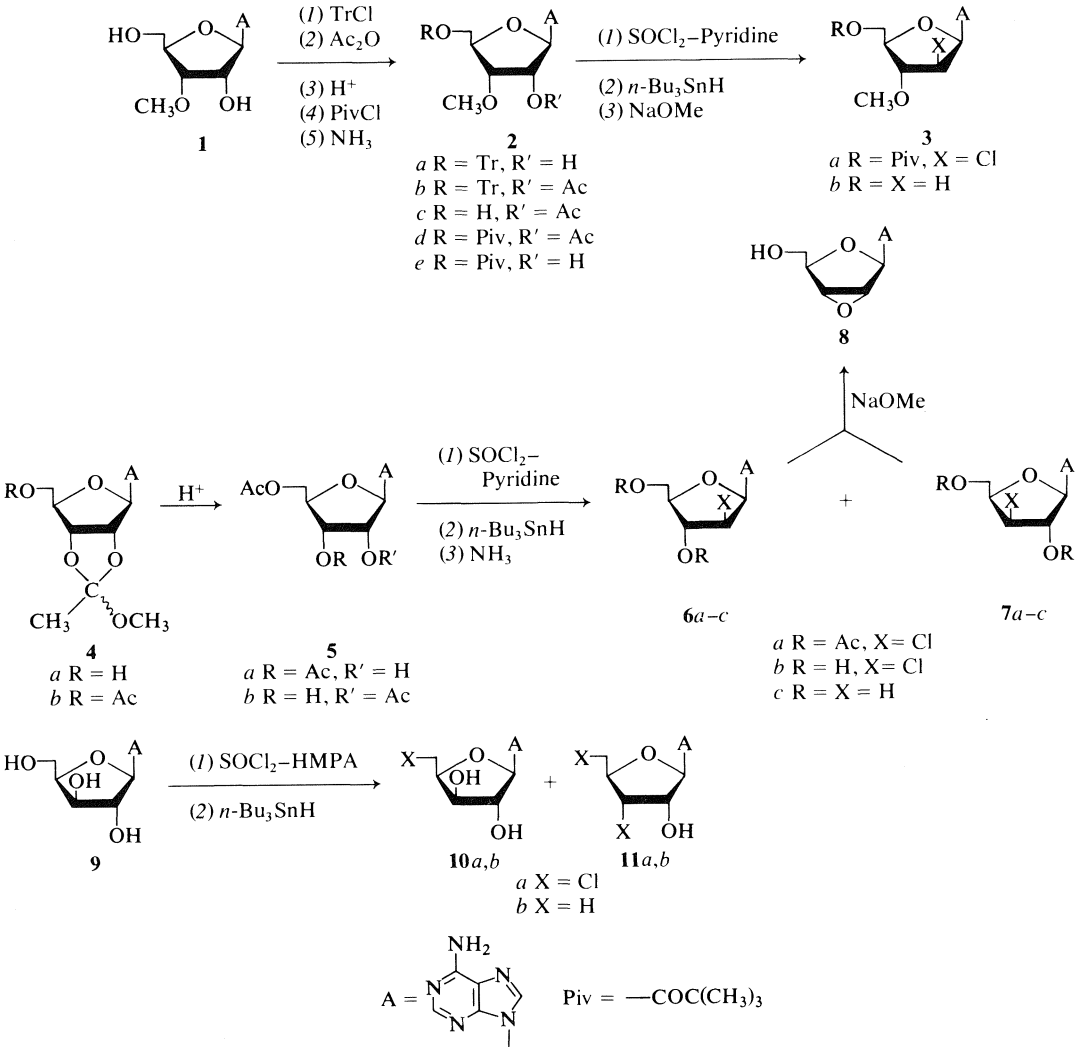

SCHEME 1

effects and is stable against migration or cleavage. Previous work in this laboratory has made 3′-*O*-methyladenosine (**1**) (and its 2′-*O*-methyl isomer) readily available (8). Selective blocking of **1** at O-5′ in high yield using pivalyl chloride was unsuccessful under several conditions as was selective deblocking of the 2′,5′-di-*O*-pivalyl derivative. Therefore, a multistage route was employed to prepare the desired O-5′ blocked model system.

Treatment of **1** (see Scheme 1) with triphenylmethyl chloride – pyridine gave 3′-*O*-methyl-5′-*O*-trityladenosine (**2***a*) in 66% yield (based on recovered **1**). Acetylation of **2***a* gave the 2′-*O*-acetyl derivative **2***b* which was detritylated in aqueous acetic acid to give 2′-*O*-acetyl-3′-*O*-methyladenosine (**2***c*) in 81% overall yield from **2***a*. Pivalylation of **2***c* gave the 2′-*O*-acetyl-5′-*O*-pivalyl derivative **2***d* plus some *N*-6,*O*-5′-dipivalylated material. Selective deacetylation (and *N*-6 depivalylation) occurred as expected using aqueous ethanolic ammonia to give the desired 3′-*O*-methyl-5′-*O*-pivalyladenosine (**2***e*) in 78% overall yield from **2***c*.

Treatment of **2***e* with thionyl chloride–pyridine under a variety of conditions (involving temperature, solvents, other tertiary organic bases, etc.) resulted in black mixtures from which ~20% maximum yields of 9-(2-chloro-2-deoxy-3-*O*-methyl-5-*O*-pivalyl-β-D-arabinofuranosyl)adenine (**3***a*) were isolated. The *arabino* configuration is suggested by the small coupling of H-2′ and H-3′ ($J_{2'-3'}$ ~ 1.6 Hz) which is indicative of *trans* orientation ($\phi_{H\text{-}2'\text{-}H\text{-}3'}$ ~ 115°) (9) on a five-membered ring (10). The

TABLE 1. ^{1}H nuclear magnetic resonance data[a]

Compound	Solvent[b]	H-8[c]	H-2[c]	6-NH_2[d]	H-1′ ($J_{1'-2'}$)[e]	H-2′ ($J_{2'-3'}$)	H-3′	H-4′	H-5′,5″	Other resonance peaks
2*a*	A	8.27	8.12	[f]	5.92(4.8)	4.90(4.5)	4.08[g]	4.08[g]	3.26	3.37 (s, 3, OCH_3), 5.55 (d, 1, 2′-OH), 7.31 (m, 17, 6-NH_2 & CPh_3)
2*b*	B	8.28	7.98	6.07	6.16(4.2)	5.93(~5)	4.38	4.24	3.36 3.55	2.34 (s, 3, OAc), 3.38 (s, 3, OCH_3), 7.30 (m, 15, CPh_3)
2*c*	A	8.20	8.18	7.36	6.15(5.8)	5.78(~5.5)	4.18[g]	4.18[g]	3.68	2.05 (s, 3, OAc), 3.35 (s, 3, OCH_3), 5.49 (br t, 1, 5′-OH)
2*d*	B	8.33	7.90	5.93	6.07(3.8)	5.93	4.33[g]	4.33[g]	4.33[g]	1.19 (s, 9, OPiv), 2.13 (s, 3, OAc), 3.41 (s, 3, OCH_3)
2*e*	B	8.28	7.83	6.20	5.95(4.8)	[f]	4.04	4.32[g]	4.32[g]	1.17 (s, 9, OPiv), 3.49 (s, 3, OCH_3), 4.85 (m, 2, H-2′ & 2′-OH)
3*a*	B	8.34	8.10	6.21	6.48(4.2)	4.61(1.6)	4.26[g]	4.26[g]	4.26[g]	1.20 (s, 9, OPiv), 3.47 (s, 3, OCH_3)
3*b*	A	8.33	8.14	7.36	6.26(8.5)[h]	2.77(5.0)	4.07[g]	4.07[g]	3.58	2.50 (m, 1, H-2″), 3.30 (s, 3, OCH_3), 4.07 (m, 1, 5′-OH)[g]
5*a*	A				5.95(5.9)	5.05(5.9)	5.16			
5*b*	A				6.17(4.2)	5.77(~5)	4.65			
10*a*	A	8.26	8.15	7.30	5.90(1.6)	4.39(1.6)	4.14	4.30	3.79[i] 3.94	5.95 (br s, 1, 3′-OH), 6.20 (d, 1, 2′-OH)
10*b*	A	8.23	8.14	7.27	5.91(1.5)	4.30[g]	4.30[g]	3.85	[f]	1.26 (d, $J_{5'-4'}$ = 6 Hz, 3, CH_3-5′) 5.92 (br s, 2, 2′ & 3′ OH's)
11*a*	A	8.34	8.14	7.28	6.03(4.6)	5.11(~5)	4.87	4.40	3.91[j] 4.06	6.29 (d, 1, 2′-OH)
11*b*	A	8.17	8.14	7.20	5.85(1.5)	4.63	2.04	4.42	[f]	1.31 (d, $J_{5'-4'}$ = 6 Hz, 3, CH_3-5′), 2.04 (m, 1, H-3″), 5.63 (br s, 1, 2′-OH)

[a]Chemical shifts in δ ppm from internal Me_4Si; 'apparent' coupling constants in (Hz).
[b]Solvent: A, Me_2SO-d_6; B, $CDCl_3$.
[c]Sharp singlets.
[d]Broad singlets.
[e]Doublets.
[f]See 'Other resonance peaks.'
[g]Overlapping multiplets.
[h]Doublet of doublets, $J_{1'-2''}$ = 6.5 Hz, $J_{2'-2''}$ = −14 Hz.
[i]$J_{4'-5'}$ = 5.1 Hz, $J_{4'-5''}$ = 7.4 Hz, $J_{5'-5''}$ = −11.3 Hz.
[j]$J_{4'-5'}$ = 4.7 Hz, $J_{4'-5''}$ = 6 Hz, $J_{5'-5''}$ = −11.7 Hz.

anomeric proton coupling constant ($J_{1'-2'} = 4.2$ Hz) is in agreement with a *cis* orientation of H-1′ and H-2′ with $\phi_{H\text{-}1'\text{-}H\text{-}2'} \sim 46°$ (9). These coupling–dihedral angle parameters are compatible with the indicated *arabino* structure **3***a* in an *S*-type furanose conformation (11). Replacement of hydroxyl by chloro with net inversion was determined chemically in the corresponding reactions with 3′(2′),5′-di-*O*-acetyladenosines (*vide infra*).

Hydrogenolysis of the chloro function from **3***a* proceeded smoothly using tri-*n*-butyltin hydride under free radical conditions (12). Deprotection of the resulting deoxy compound gave 3′-*O*-methyl-2′-deoxyadenosine (**3***b*) in ~19% overall yield from **2***e* without isolation of intermediate products. The structure of **3***b* was conclusively confirmed by elemental analyses, ^{1}H nmr (see Table 1) and mass spectral data.

With conversion of hydroxyl to chloro at C-2′ successfully demonstrated in the above 'fixed' model, we sought a blocked precursor which could be deprotected to give a free deoxynucleoside after functionalization and hydrogenolysis. Equilibration of O-2′- and O-3′-acyl nucleoside esters is known to favor the 3′-isomer substantially (6*a*). Since rapid equilibration in the $SOCl_2$–pyridine reaction mixture would occur, no advantage in the use of esterifying acids which give higher 3′:2′ ratios during selective crystallizations (6*b*) was anticipated. Therefore the easily accessible di-*O*-acetyl derivative mixture was employed.

Treatment of the mixed ortho ester 2′,3′-*O*-methoxyethylideneadenosine (**4***a*) (3*e*) with acetic anhydride and a catalytic amount of 4-*N*,*N*-dimethylaminopyridine (13) gave the corresponding 5′-*O*-acetyl derivative **4***b*. This diastereomeric product was treated with acetic acid (6*a*) to provide 3′,5′-di-*O*-acetyladenosine (**5***a*) and 2′,5′-di-*O*-acetyladenosine (**5***b*) in a ratio of ~63:37, respectively (by ^{1}H nmr).

The isomeric mixture **5***a*,*b* was heated with $SOCl_2$–pyridine. A black mixture resulted from which 38% of **5***a*,*b* was recovered and a 29% combined yield (by uv) of the 2′-chloro-*arabino*- (**6***a*) and 3′-chloro-*xylo*- (**7***a*) di-*O*-acetyl isomers was obtained in a ratio of ~3:2 (by nmr). Longer reaction times at elevated temperatures resulted in disappearance of starting material (**5***a*,*b*) without significant increases in the isolated yields of chloro isomers (**6***a*,**7***a*). A black insoluble polymeric material, which did *not* release uv absorbing materials (adenine chromophore) upon treatment with acid or base at reflux, separated from the reaction solution. Therefore, heating was terminated after 30 min and a conversion (**5***a*,*b* → **6***a*,**7***a*) of ~47% based on recovered starting material was obtained. The structures of **6***a*,**7***a* were confirmed by exact mass measurement of the molecular ions and the ~3:2 ratio by integration of the respective anomeric proton resonance peaks.

Treatment of **6***a*,**7***a* with aqueous ethanolic ammonia gave 9-(2-chloro-2-deoxy-β-D-arabinofuranosyl)adenine (**6***b*) and 9-(3-chloro-3-deoxy-β-D-xylofuranosyl)adenine (**7***b*) which were separated by column chromatography and identified by comparison with known samples (3*e*). Treatment of **6***a*,**7***a* with methanolic sodium methoxide gave 2′,3′-anhydroadenosine (**8**) (3*d*), which confirmed the exclusive formation of *trans*-2′,3′-chloro and -acetoxy products as demanded by an S_N2 process.

The possibility of 2′,3′-acetoxonium ion formation followed by attack at C-2′ or C-3′ by chloride ion exists in the conversion of **5***a*,*b* to **6***a*,**7***a*. However, significant intervention of such dioxolenium ion intermediacy is precluded by the observed 3′- to 2′-chloro isomer ratio (~2:3) since it is known that markedly predominant attack at C-3′ by chloride (>6:1) occurs in such reactions (3, 4). It may also be noted that the ratio of chloro isomers (**6***a*:**7***a*) obtained closely approximates the isomeric ratio of the corresponding precursor diacetates (**5***a*:**5***b*). Secondary alkyl chlorosulfite esters are known to undergo S_N2 or S_N1 (S_Ni ion pair collapse) processes with inversion or retention of configuration in the resulting chloro compound (see for example ref. 14 and references therein). The mechanism is affected by solvent changes and by heating in the absence of solvent. The inversion reaction (S_N2) would be expected to be favored using pyridine as solvent (14*c*) and, additionally, S_Ni ion pair collapse (S_N1) (14*b*) would be strongly inhibited in the nucleoside system (i.e., generation of carbonium ion character at C-2′ bonded to the electronegative *N*,*O*-acetal anomeric C-1′).

Hydrogenolysis of **6***a*,**7***a* gave the expected di-*O*-acetyl deoxynucleoside mixture as indicated by exact mass measurement of the molecular ions. Deprotection and anion exchange chromatography (15) gave 2′-deoxyadenosine (**6***c*) and 3′-deoxyadenosine (cordycepin) (**7***c*) in 25 and 17% overall yields (by uv, based on recovered starting material) from **5***a*,*b* without isolation of intermediates. Corresponding crystallized product yields were 17 and 11%.

A final aspect of the present work involved clarification of a previously reported study. Chlorination at C-5′ of nucleosides using neat thionyl chloride has been reported (16). The Vilsmeier–Haack reagent (SOX_2–DMF) (17) and the related (18) SOX_2–hexamethylphosphoric triamide (HMPA) reagent

(19, 20) have been employed to effect halogenation at C-5′ of nucleosides, with concomitant C-3′ (di)halogenation having been observed with 2′-deoxy nucleosides (20)

Hogenkamp noted that the product of treatment of 9-β-D-xylofuranosyladenine (**9**) with $SOCl_2$–HMPA failed to react with the reduced vitamin B_{12} product, cob(I)alamin (20*a*). This cobalt species was known to be nucleophilically unreactive with secondary alkyl halides. Therefore, Hogenkamp postulated the formation of a neutral cyclic 3′,5′-*O*-phosphorotriamidate intermediate from the HMPA reagent. This would be inert to replacement with chloride at C-5′ and allow formation of the 2′-chloro-2′-deoxynucleoside upon collapse of the cyclic pentacovalent phosphorus intermediate during aqueous processing. The absence of secondary hydroxyl replacement upon analogous treatment of ribonucleosides was rationalized on the basis of a 2′,3′-*O*-phosphorotriamidate protective intermediate. Since the 2′-deoxy nucleosides were not expected to form such a cyclic structure (i.e., no *cis*-diol system), accompanying onium activation and replacement at C-3′ could proceed. Steric effects were invoked to rationalize the selective primary (C-5′) chlorination of 9-β-D-arabinofuranosyladenine (20*a*).

The experimental conditions noted (20*a*) were applied by us to 9-β-D-xylofuranosyladenine (**9**). A 71% yield of a monochloro product (**10***a*) was obtained which had mass spectral peaks consistent with loss of CH_2Cl from the molecular ion and with formation of the BHCH=CHOH ion (2′-hydroxyl group present) (21). The ^1H nmr spectrum of this compound had downfield shifts of H-5′, H-5″, and H-4′ and had nmr properties consistent with N-3 → C-5′ cyclonucleoside formation upon heating the spectral sample at 100°C. The monochloro product also failed to exhibit complexing with borate (as evidenced by electrophoresis and paper chromatography) in contrast to the large effects of borate on the migrations of the 3′,5′-*cis*-diol starting material **9**. The structure of **10***a* was conclusively demonstrated by hydrogenolysis of the 5′-chloro group to provide a compound with melting point, ^1H nmr, and mass spectral properties in harmony with the known (22) 5′-deoxy-9-β-D-xylofuranosyladenine (**10***b*).[6] This raises an interesting question with respect to the observed lack of reactivity of this primary C-5′-alkyl chloride (with a sterically butressing *cis*-3′-hydroxyl group) with cob(I)alamin (20*a*).

An alternative explanation for the observed selectivity of replacement of hydroxyl by chloride in reactions of ribonucleosides with $SOCl_2$–HMPA (19, 20) is that only the activated primary 5′-onium group is readily subject to nucleophilic displacement by chloride ion at the ambient temperatures employed. Secondary (C-3′) substitution is known to proceed much more easily with 2′-deoxy nucleosides than with ribonucleosides (1). Sufficient energy is apparently available at room temperature to smoothly effect 3′,5′-dichloro-2′,3′,5′-trideoxynucleoside formation in the 2′-deoxy series (20*a*, *c*). In harmony with this interpretation is the observation that a small quantity (~4%) of a 3′,5′-dichloro product (**11***a*) was produced along with 71% of the 5′-chloro-*xylo* compound (**10***a*) under the standard conditions. Treatment of **9** at elevated temperatures or at ambient temperature for extended times with freshly distilled $SOCl_2$–HMPA reagents resulted in yields of greater than 50% of the 3′,5′-dichloro derivative[6] (presumed to be the inverted *ribo* diastereomer, **11***a*) along with reduced quantities of **10***a*. Compound **11***a* was considerably less stable than **10***a* and was obtained in only ~20% yield at 60°C. Hydrogenolysis of **11***a* gave a product whose ^1H nmr and mass spectral properties were compatible with its assignment as the known (23) 3′,5′-dideoxyadenosine (**11***b*).

The present study has demonstrated that external nucleophilic displacement reactions can be effected at C-2′ in purine ribonucleosides. Although the replacement yields are low to moderate, the facile free radical mediated hydrogenolysis of the chloro function results in overall C-2′ deoxygenation in yields which compare favorably with prior intramolecular (24) and acyloxonium (3*e*) routes as well as with 2-deoxy sugar, base coupling syntheses (25). Preferential displacement at C-2′ over C-3′ by an external nucleophile was observed for the first time in a 2′ ⇄ 3′ equilibrating adenosine system (resulting from the 3′-ester blocking function equilibrium predominance). Although deoxygenation of nucleosides at C-2′ can be effected more conveniently by direct free radical mediated routes[7] (26), nucleophilic displacement is necessary for the introduction of substituents required for modified structures presently under investigation. The selectivity for primary alcohol replacement at C-5′ appears now to be uniform for reactions of the diastereomeric pentofuranosyladenine nucleosides with $SOCl_2$–HMPA, although secondary (3′) replacement can occur upon extended treatment at ambient temperature or upon heating.

Experimental

Melting points were determined on a Reichert microstage apparatus and are uncorrected. Nuclear magnetic resonance spectra were recorded on Varian HA-100 and Bruker 90 spec-

[6]We have been informed by Dr. R. Mengel that they have independently made the same observations regarding the hydroxyl → chloro transformations of compound **9**.

[7]M. J. Robins and J. S. Wilson. Unpublished experiments.

trometers with Me_4Si as reference. Ultraviolet spectra were recorded on Cary 15 or Pye Unicam SP 1700 spectrophotometers. Optical rotations were determined with a Perkin Elmer Model 141 polarimeter using a 10-cm, 1-mL microcell. Mass spectra (ms) were determined by the mass spectrometry laboratory of this department on AEI MS-2, MS-9, or MS-50 instruments at 70 eV using a direct probe and are quoted as percentage relative intensity of the most intense ion at $m/e > 134$. Elemental analyses were determined by the microanalytical laboratory of this department or by Schwarzkopf Microanalytical Laboratory, Woodside, New York. Water of hydration when indicated was verified in the nmr spectrum. Thin-layer chromatography was performed on Eastman Chromatogram sheets (silica gel No. 13181, indicator No. 6060). Developed chromatograms were evaluated under 2537 Å light. Preparative scale tlc was performed on ~1-mm thick Merck silica gel GF 254 (20 × 20 cm) plates. Solvent system E (SSE) is the separated upper phase of EtOAc–*n*-propanol–H_2O 4:1:2 (by volume). Column chromatography was performed using J. T. Baker No. 3405 silica gel. Evaporations were carried out using a rotating evaporator with aspirator or oil pump vacuum at <40°C. Coevaporations were effected by adding the specified solvent and re-evaporating. 'Diffusion crystallization,' which has been modified in this laboratory (*3e, g*), was effected by allowing a concentrated solution of the nucleoside in the first mentioned (dissolving) solvent to stand in a desiccator containing a large volume of the second (diffusing) solvent in which the material is insoluble at room temperature and the resulting crystals were collected by filtration. Compounds reacted in dry pyridine as solvent were dried by repeated dissolution in and evaporation of dry pyridine. Pyridine was refluxed over and distilled from calcium hydride before use. HMPA was distilled and stored over 4 Å molecular sieves. Toluene was dried using sodium wire. DMF used for optical rotations was distilled from calcium hydride under reduced pressure at <40°C and stored over Linde 4A molecular sieves. Other solvents, pivalyl chloride, and $SOCl_2$ were of reagent purity and were distilled before use. Tri-*n*-butyltin hydride solution (~1 *M*) was prepared by the Holý modification (27) of the original procedure (28). The 3′-*O*-methyladenosine (**1**) (8) and 9-β-D-xylofuranosyladenosine (**9**) (*3d*) were prepared as described. Adenosine was purchased from Terochem Laboratories Ltd., Edmonton, Alberta.

*3′-O-Methyl-5′-O-triphenylmethyladenosine (**2**a)*

To a stirred solution of 6.36 g (22.6 mmol) of **1** in ~100 mL of dry pyridine was added 5.70 g (20.4 mmol) of triphenylmethyl chloride. The solution was heated, with exclusion of moisture, for 2 h at 100°C and then cooled. The solution was concentrated to ~50 mL and poured into 150 mL of cold saturated $NaHCO_3$–H_2O. The resulting mixture was extracted with $CHCl_3$. The organic phase was washed with saturated $NaHCO_3$–H_2O, dried (Na_2SO_4), evaporated, and coevaporated with dry toluene. The resulting yellow glass was treated with $CHCl_3$ and applied to a silica gel column (5.5 × 40 cm, 300 g) packed in $CHCl_3$. The column was washed with 4.2 L of $CHCl_3$ and eluted with MeOH–$CHCl_3$ (1:24). The first 1.5 L was discarded and the following 1.8 L was pooled and evaporated. Crystallization of the residue from acetone gave 5.92 g (50%) of **2***a*. The original aqueous $NaHCO_3$ layer and extracts were combined and continuously extracted with CH_2Cl_2 to recover 1.51 g of starting material, giving a 65.6% yield of **2***a* based upon recovered starting material. Pure **2***a* had mp 120–122°C; uv (MeOH) max 259 nm (ε 16 300), min 240 nm (ε 9000); ms (200°C) *m/e*: 523 (0.1, M), 280 (100, M − CPh_3), 243 (56, CPh_3), 165 (66, CPh_3 − Ph), 164 (21, BHCHO), 148 (7.5, BCH_2), 136 (55, B + 2H), 135 (16, B + H). *Anal.* calcd. for $C_{30}H_{29}N_5O_4$: C 68.82, H 5.58, N 13.38; found: C 68.79, H 5.78, N 13.61.

*2′-O-Acetyl-3′-O-methyladenosine (**2**c)*

To an ice-cold stirred solution of 8.1 g (15.5 mmol) of **2***a* in ~80 mL of dry pyridine was added 1.72 mL (15.5 mmol) of Ac_2O dropwise with exclusion of moisture. This solution was stirred for 18 h at 5°C and a further 0.15 mL of Ac_2O was added. After 2 h stirring at 5°C, the reaction was allowed to warm to 19°C and 0.5 mL of Ac_2O was added. After 1.5 h at 19°C, the reaction mixture was poured with stirring into 200 mL of ice water and extracted with $CHCl_3$. The combined organic phase was washed with cold 10% $NaHCO_3$–H_2O, H_2O, evaporated, and coevaporated with dry toluene to leave 8.45 g of 2′-*O*-acetyl-3′-*O*-methyl-5′-*O*-triphenylmethyladenosine (**2***b*) as a white amorphous solid; ms (200°C) *m/e*: 322 (37, M − CPh_3), 306 (2.5, M − $OCPh_3$), 243 (23, CPh_3), 220 (3, BHCH=CHOAc), 178 (7, BHCH=CHOH), 165 (100, CPh_3 − Ph), 164 (11, BHCHO), 148 (7.5, BCH_2), 136 (43, B + 2H), 135 (24, B + H).

The solid **2***b* (less 0.1 g) was dissolved in 100 ml of 80% aqueous HOAc and heated at 100°C for 15 min with stirring. The pale yellow solution was poured into 300 mL of cold H_2O and extracted with Et_2O. The combined organic phase was back-extracted with 10% HOAc. The combined aqueous layers were evaporated to dryness and the residue was crystallized from 98% EtOH to give 4.09 g (83%) of **2***c*, mp 214.5–215.5°C; uv (MeOH) max 259 nm (ε 14 300), min 227 nm (ε 1600); ms (200°C) *m/e*: 323 (2, M), 293 (6.5, MH − $CH_2O(5')$), 280 (0.3, M − Ac), 264 (5, M − OAc), 220 (24, BHCH=CHOAc), 189 (6.0, sugar), 178 (16.5, BHCH=CHOH), 164 (32, BHCHO), 148 (16, BCH_2), 146 (5, sugar − Ac), 136 (100, B + 2H), 135 (65, B + H). *Anal.* calcd. for $C_{13}H_{17}N_5O_5$: C 48.29, H 5.30, N 21.66; found: C 48.02, H 5.38, N 21.70.

*3′-O-Methyl-5′-O-pivalyladenosine (**2**e)*

To an ice-cold stirred solution of 3.9 g (12 mmol) of **2***c* in 125 mL of dry pyridine was added 2.3 mL (18 mmol) of pivalyl chloride dropwise with exclusion of moisture. The solution was stirred for 18 h at 5°C and poured into 300 mL of ice-water. The aqueous solution was extracted with $CHCl_3$. The combined organic extract was washed with cold 10% $NaHCO_3$–H_2O, H_2O, evaporated, and coevaporated with dry toluene and then 98% EtOH to give 5.09 g of 2′-*O*-acetyl-3′-*O*-methyl-5′-*O*-pivalyladenosine (**2***d*) as a white solid containing about 20% of 6-*N*-pivalyl-9-(2-*O*-acetyl-3-*O*-methyl-5-*O*-pivalyl-β-D-ribofuranosyl)adenine (by nmr). The major compound showed ms calcd. for $C_{18}H_{25}N_5O_6$: 407.1805; found: *m/e* 407.1816.

The solid residue (less 0.1 g) was then dissolved in 125 mL of 95% EtOH and 100 mL of concentrated NH_3–H_2O was added. This solution was stirred at 24°C for 1.5 h, evaporated to a small volume and partitioned between 150 mL of H_2O and 300 mL of $CHCl_3$. The $CHCl_3$ extract was washed with cold 10% $NaHCO_3$–H_2O, H_2O, and evaporated. The resulting oil was 'diffusion crystallized' from acetone (*n*-pentane, desiccator) and the resulting solid was recrystallized in the same manner to give 2.42 g of pure **2***e*. The mother liquors were treated with concentrated NH_3–H_2O as above and after analogous workup and crystallization yielded a further 0.87 g of **2***e*. The mother liquors from this crystallization were again processed to give a further 0.18 g for a total yield of 3.47 g (79%) of **2***e*. The pure material had mp 138–139°C; uv (MeOH) max 259 nm (ε 13 400), min 227 nm (ε 1800); ms (200°C) *m/e* 365 (0.5, M), 350 (8.5, M − CH_3), 280 (0.5, M − Piv), 264 (3, M − OPiv), 178 (5.5, BHCH=CHOH), 164 (100, BHCHO), 148 (9, BCH_2), 136 (89, B + 2H), 135 (51, B + H). *Anal.*

calcd. for $C_{16}H_{23}N_5O_5 \cdot 0.25\ H_2O$: C 51.95, H 6.40, N 18.94; found: C 51.80, H 6.66, N 19.09.

*9-(2-Chloro-2-deoxy-3-O-methyl-5-O-pivalyl-β-D-arabinofuranosyl)adenine (**3**a)*

To an ice-cold stirred solution of 0.5 g (1.35 mmol) of **2***e* in ~30 mL of dry pyridine was injected (through a septum) 0.5 mL (6.95 mmol) of $SOCl_2$ with exclusion of moisture. The resulting red solution was stirred for 30 min and after warming to room temperature was placed in a 120°C oil bath for 1 h. The cooled black mixture was poured into 150 mL of ice water and extracted with Et_2O. The combined organic phase was washed with cold 10% $NaHCO_3$–H_2O, H_2O, evaporated, and coevaporated with toluene. The dark brown residue was treated with hot 98% EtOH and filtered. On cooling a brown nonnucleoside precipitate separated and was filtered. The resulting solution was evaporated, the residue was dissolved in $CHCl_3$, and applied to a silica gel column (30 g) packed in and washed with $CHCl_3$. Elution was then begun with MeOAc. The first 165 mL was discarded and the following 130 mL was evaporated to give 109 mg (21%) of crude **3***a* which gave 86 mg (16.6%) of pure product in two crops upon 'diffusion crystallization' from acetone (*n*-pentane, desiccator). Pure **3***a* had mp 185–187°C; uv (MeOH) max 258 nm (ε 14 300), min 226 nm (ε 2500); ms (210°C) *m/e*: 383 (2.5, M), 368 (1.5, M − CH_3), 352 (1.5, M − OCH_3), 298 (12, M − Piv), 282 (25, M − OPiv), 220 (2, B + H + Piv), 214 (3.5, sugar − Cl), 196 (2.5, BHCH=CHCl), 164 (35, BHCHO), 136 (100, B + 2H), 135 (51, B + H). *Anal.* calcd. for $C_{16}H_{22}ClN_5O_4$: C 50.06, H 5.78, Cl 9.24, N 18.25; found: C 49.77, H 5.90, Cl 9.40, N 18.49.

*3′-O-Methyl-2′-deoxyadenosine (**3**b)*

To a solution of 75 mL of dry pyridine and 0.57 mL (7.92 mmol) of $SOCl_2$ in a 500-mL three-necked round bottomed flask, fitted with a mechanical stirrer, dropping funnel, dry N_2 flow and in an ice bath, was added dropwise over 15 min, 0.58 g (1.57 mol) of **2***e* in 100 mL of dry pyridine. The solution was stirred for 10 min and then was heated at 120°C for 1 h. The resulting black mixture was poured into 75 mL of ice water and extracted with $CHCl_3$. The combined organic phase was filtered, evaporated, and coevaporated with toluene. The black residue was treated with $CHCl_3$ and adsorbed on 3 g of silica gel which was applied to a dry-packed silica gel column (1.6 × 36 cm, 25 g). The column was developed with MeOH–$CHCl_3$ (1:19). The initial 25 mL of eluate was discarded and the next 50 mL was evaporated.

The resulting oil was mixed with 25 mL of dry benzene, 10 mg (6.1 mmol) of AIBN (α,α′-azobisisobutyronitrile), and 5 mL of tri-*n*-butyltin hydride solution in benzene (~5 mmol) (27). This orange mixture was heated at reflux for 1 h and another 10 mg of AIBN was added. After a further 2.75 h at reflux the pale yellow reaction mixture was cooled, concentrated to about one third volume and slowly added to 200 ml of *n*-pentane. The precipitate formed was filtered, dissolved in $CHCl_3$, and evaporated.

The resulting glass was dissolved in 25 mL of MeOH containing 1.25 g (54 mmol) of sodium. After stirring for 0.5 h, H_2O was added and the reaction was neutralized with HOAc. The MeOH was evaporated and the aqueous solution was extracted with MeOAc. The combined organic extract was evaporated and the residue partitioned between 50 mL of H_2O and 50 mL of *n*-pentane. The aqueous layer was washed with *n*-pentane, concentrated , and applied to a column (2.5 × 53 cm) of Dowex 1-X2(OH^-) resin packed in and eluted with H_2O. The first 460 mL of eluate was discarded. The following 490 mL contained 0.29 mmol (18.5% overall yield from **2***e*) of **3***b* by uv analysis. This solution was evaporated and the residue was 'diffusion crystallized' from 98% EtOH (*n*-pentane, desiccator) to give 59 mg (14%) of **3***b*, mp ~160–170°C (with resolidification and decomposition); $[\alpha]_D^{24}$ −25.4° (*c* 0.5, DMF); uv (H_2O) max 260 nm (ε 15 600), min 226 nm (ε 2600); ms (calcd. for $C_{11}H_{15}N_5O_3$: 265.1175; found *m/e*: 265.1172); ms (150°C) *m/e*: 265 (5, M), 250 (9, M − CH_3), 235 (11.5, MH − OCH_2(5′)), 235 (3.5, M − OCH_3), 164 (4.5, BHCHO), 162 (38, BHCH=CH_2), 136 (37, B + 2H), 135 (100, B + H), 131 (6, sugar). *Anal.* calcd. for $C_{11}H_{15}N_5O_3 \cdot 0.25\ H_2O$: C 48.97, H 5.79, N 25.97; found: C 48.89, H 5.85, N 25.88.

*Preparation of 2′-Deoxyadenosine (**6**c) and 3′-Deoxyadenosine (Cordycepin) (**7**c)*

To a stirred solution of 19.3 g (59.7 mmol) of **4***a* in 100 mL of dry pyridine cooled in a salt–ice bath was added 50 mg of 4-*N*,*N*-dimethylaminopyridine and 8 mL (85 mmol) of Ac_2O with exclusion of moisture. After stirring for 50 min, MeOH was added and the reaction was stirred for an additional 30 min, evaporated, and coevaporated with toluene, 98% EtOH, and CH_2Cl_2. An nmr spectrum of the residual amorphous solid (20.6 g) confirmed formation of the 5′-*O*-acetyl derivative (**4***b*) in a diastereomeric ratio (because of the methoxyethylidene moiety) of 3:2. Its mass spectrum contained the expected molecular ion, calcd. for $C_{15}H_{19}N_5O_3$: 365.1335; found: 365.1331.

This crude material was dissolved in 5% HOAc–H_2O (200 mL) and 98% EtOH (10 mL) and stirred at 24°C for 1 h. The reaction mixture was then evaporated and coevaporated with 98% EtOH and toluene. The solid glass (22.4 g) was a mixture of ~63% **5***a* and ~37% **5***b* (by nmr). Its mass spectrum contained the expected molecular ions, calcd. for $C_{14}H_{17}N_5O_6$: 351.1179; found: 351.1176.

A 0.93 g (2.6 mmol) sample of this mixture was dissolved in ~100 mL of dry pyridine. This solution was cooled to 4°C and added dropwise to a solution of 1.1 mL (15.3 mmol) of $SOCl_2$ in 75 mL of dry pyridine which was mechanically stirred in an ice bath under a flow of dry N_2 and exclusion of moisture. Stirring was continued for 20 min. The solution was then stirred vigorously in an oil bath for 30 min at 120°C. The resulting black mixture was poured into 50 mL of ice water and extracted with CH_2Cl_2. The combined organic phase was evaporated and coevaporated with toluene. The residue was adsorbed on 3 g of silica gel and applied to a silica gel column (1.8 × 20 cm, 25 g). The column was eluted with MeOH–CH_2Cl_2 (1:19). The first 40 mL of eluate was discarded and the next 70 mL contained product slightly contaminated with starting material. A further 480 mL of eluate contained starting material. Ultraviolet analysis indicated that 0.75 mmol of **6***a*,**7***a* and 1 mmol of starting **5***a*,*b* had been collected. The **5***a*,*b* was dissolved in CH_2Cl_2 and precipitated into *n*-pentane to yield 0.35 g of solid material. The yield of **6***a*,**7***a* less recovered starting material was 47%. An nmr spectrum ($CDCl_3$–D_2O) of the product indicated a ratio of **6***a* to **7***a* of ~3:2 (integration of δ 6.52 (d, $J_{1'-2'}$ = 3.9 Hz, 1, H-1′) to 6.24 (d, $J_{1'-2'}$ = 2.2 Hz, 1, H-1′), respectively). A mass spectrum of this mixture contained the expected molecular ions, calcd. for $C_{14}H_{16}{}^{35}ClN_5O_5$: 369.0841; found: 369.0841.

Mixed **6***a*,**7***a* (0.75 mmol) was dissolved in dry benzene (10 mL) and 25 mg (1.5 mmol) of AIBN and 12.5 mL of tri-*n*-butyltin hydride solution in benzene (~12.5 mmol) was added with stirring and exclusion of moisture. This mixture was heated at reflux for 4 h, concentrated to ~5 mL, and precipitated by slow addition to *n*-pentane (400 mL). A mass spectrum of the precipitate contained the expected molecular ions, calcd. for $C_{14}H_{17}N_5O_5$: 335.1230; found: 335.1227.

The precipitate was dissolved in 98% EtOH (25 mL) and

concentrated NH_3–H_2O (10 mL) and stirred for 23 h at room temperature. The solution was evaporated, dissolved in H_2O, and applied to a Dowex 1-X2(OH^-) column (72 × 2.2 cm). The column was eluted with 4 L of H_2O, 2 L of 10%, 1.6 L of 30%, 1.5 L of 60%, and 2 L of 90% MeOH–H_2O. The first 3.5 L of eluate was discarded and then 1.5 L of eluate containing pure **6***c* was collected. The continuing 1.1 L of uv transparent eluate was discarded and then 750 mL of eluate containing pure **7***c* was obtained. A further 2.5 L of uv transparent eluate was discarded and then 700 mL of eluate containing adenosine was collected. Analysis by uv showed 0.4 mmol (25%) of **6***c* plus 0.27 mmol (17%) of **7***c* (based on recovered **5***a,b*) and 0.047 mmol of adenosine. The solution containing pure **6***c* was evaporated and the residue was 'diffusion crystallized' from MeOH (Et_2O, desiccator) to give 67 mg (16.7%) of **6***c* (*3e*), mp 193.5–194°C; $[\alpha]_D^{24}$ −27.3° (*c* 0.7, H_2O); uv (H_2O) max 260 nm (ε 15 200), min 226.5 nm (ε 2200); ms (200°C) *m/e*: 251 (2.5, M). *Anal.* calcd. for $C_{10}H_{13}N_5O_3$: C 47.80, H 5.21, N 27.87; found: C 47.78, H 5.29, N 27.94.

The eluate containing **7***c* was evaporated and 'diffusion crystallized' from 98% EtOH (Et_2O, desiccator) to give 43 mg (11%) of **7***c* (*3e*), mp 210–211.5°C; $[\alpha]_D^{24}$ −46.5° (*c* 0.75, H_2O); uv (H_2O) max 260 nm (ε 14 600), min 227 nm (ε 2100); ms (185°C) *m/e*: 251 (4.5, M). *Anal.* calcd. for $C_{10}H_{13}N_5O_3$: C 47.80, H 5.21, N 27.87; found: C 47.57, H 5.26, N 27.89.

Evidence for the arabino *Configuration of* **6**a *and* xylo *Configuration of* **7**a

To a crude mixture of ~75 mg (0.2 mmol) of **6***a*,**7***a* (~3:2, prepared as given in the above procedure) was added 98% EtOH (10 mL) and concentrated NH_3–H_2O (5 mL). This solution was stirred for 3 h and the reaction mixture evaporated. EtOH (98%) was added and coevaporated to give a yellow glass which was applied to a silica gel column (1.4 × 17 cm, 35 g) wet packed in $CHCl_3$. The column was eluted with MeOH–$CHCl_3$ (1:9). The first 25 mL of eluate was discarded and the next 15 mL was collected. The following 12 mL was discarded and the next 20 mL was collected. The first 15 mL fraction contained **7***b* contaminated with a small amount of 2′,3′-anhydroadenosine (**8**) (*3d*) (epoxide formation was prevented by deblocking at 0°C or lower with MeOH saturated with NH_3). This material had an nmr spectrum (Me_2SO-d_6) identical to that of an authentic sample (*3e*).

The second fraction collected (20 mL) contained **6***b*. Some of this material crystallized directly from the eluate and had mp 242.5–243°C which was not depressed when mixed with an authentic sample of **6***b* (*3e*). This material also had nmr (Me_2SO-d_6) and ms (200°C) *m/e* 285 (1.5, M) identical to those of the authentic sample.

Both chloro samples **6***b* and **7***b* were converted to the epoxide **8** (*3d*) by treatment with NaOMe–MeOH. This further confirms the trans 'up' chloro and 'down' hydroxy configurations at the 2′ and 3′ positions.

*9-(5-Chloro-5-deoxy-β-D-xylofuranosyl)adenine (**10**a)*

To a solution of 0.1 mL of $SOCl_2$ in 1 mL of HMPA was added 100 mg (0.37 mmol) of **9** and stirring was continued for 12 h at room temperature. Ice water (1 mL) was added and the mixture was applied to a column (2 × 9 cm) of Amberlite IR-120(H^+) resin. The column was washed with 200 mL of H_2O and then eluted with 0.2 *N* NH_3–H_2O. Fractions (15 mL) 27–70 were pooled and evaporated. The residue was dissolved in MeOH, applied to two preparative tlc plates, and developed in SSE. The major band contained 77 mg (71%) of **10***a*. A faster migrating zone contained 4 mg (4%) of the dichloro derivative (**11***a*) and a slower migrating zone contained 3 mg (3%) of unreacted **9**. The major product was recrystallized from MeOH–Et_2O to give 55 mg of **10***a* as colorless crystals of mp 155–156°C; uv (H_2O) max 258 nm (ε 14 900) min 227 nm (ε 2100); ms *m/e*: 287 (2.5, M^+ [^{37}Cl]), 285.0628 (7.5, calcd. for M^+ [$C_{10}H_{12}{}^{35}ClN_5O_3$]: 285.0628), 250 (50, M − Cl), 236 (1.3, M − CH_2Cl), 194 (5, BCHOHCHOH), 178 (19, BHCH=CHOH), 164 (62, BHCHO), 148 (6.5, BCH_2), 136 (91, B + 2H), 135 (100, B + H). *Anal.* calcd. for $C_{10}H_{12}ClN_5O_3$: C 42.04, H 4.23, N 24.51; found: C 42.03, H 4.50, N 24.25.

Heating an nmr sample (Me_2SO-d_6–D_2O) of **10***a* in a boiling water bath resulted in the appearance of new peaks at δ 6.30 (s, 1, H-1′) and 8.47 & 8.70 (s & s, 1 & 1, H-8 & H-2). These resonances are indicative of formation of the corresponding N-3 → C-5′ cyclonucleoside (29).

*9-(3,5-Dichloro-3,5-dideoxy-β-D-ribofuranosyl)adenine (**11**a)*

To a solution of 53 mg (0.2 mmol) of **9** in 1 mL of freshly distilled HMPA was added 0.12 mL of freshly distilled $SOCl_2$ and stirring was continued for 9 days at room temperature. Ice water (2 mL) was added and the mixture was applied to a column (2 × 15 cm) of Amberlite IR-120(H^+) resin. The column was washed with 500 mL of 30% MeOH–H_2O, 300 mL of 50% MeOH–H_2O, and eluted with 1000 mL of 0.5 *N* NH_3 in 50% MeOH–H_2O. Fractions (20 mL) 40–70 were pooled and evaporated. The oily residue was diluted with 3 mL of MeOH, applied to two preparative tlc plates and developed in SSE. The major band contained 32 mg (54% by uv) of **11***a* and the minor slower migrating zone contained 15 mg (26% by uv) of **10***a*. Recrystallization of the major product from MeOH gave 26 mg (43%) of colorless crystals of **11***a* with mp ~200°C (dec.); uv (MeOH) max 258 nm (ε 15 300) min 226 nm (ε 1800); ms (150°C) *m/e*: 305.0258 (3.6, calcd. for M^+ ($C_{10}H_{11}{}^{35}Cl{}^{37}ClN_5O_2$): 305.0256), 303.0287 (7, calcd. for M^+ ($C_{10}H_{11}{}^{35}Cl_2N_5O_2$): 303.0290), 268 (16, M − Cl), 254 (1.4, M − CH_2Cl), 164 (62, BHCHO), 148 (2.7, BCH_2), 136 (95, B + 2H), 135 (100, B + H).

*9-(5-Deoxy-β-D-xylofuranosyl)adenine (**10**b)*

To a solution of 28 mg (0.1 mmol) of **10***a* in 1 mL of dry pyridine was added 0.15 mL of *N*,*O*-bis(trimethylsilyl)acetamide and stirring was continued for 1 h.

The solution was evaporated and the residue was dissolved in 2 mL of benzene. Several crystals of AIBN were added followed by 0.5 ml of *n*-Bu_3SnH in benzene (~0.5 mmol) and the mixture was heated for 4 h at reflux. After stirring overnight at room temperature, the mixture was evaporated. The oily residue was stirred for 1 h with 4 mL of 0.1 *N* NaOMe–MeOH, extracted with pentane, and applied to a column (2.5 × 7 cm) of Dowex 1-X2(OH^-) resin. The column was developed with 500 mL of H_2O, 1800 mL of 20% MeOH–H_2O, and 600 mL of 50% MeOH–H_2O. Fractions (15 mL) 111–180 contained 20 mg (80%) of **10***b*. Recrystallization of this product from MeOH gave **10***b* with mp 229–232°C (lit. (22) mp 229–231°C and 232–232.5°C); ms *m/e*: 251.1020 (calcd. for M^+ ($C_{10}H_{13}N_5O_3$): 251.1018).

*9-(3,5-Dideoxy-β-D-erythro-pentofuranosyl)adenine (3′,5′-Dideoxyadenosine) (**11**b)*

A solution of 20 mg of **11***a* in 10 mL of dry pyridine was treated with 0.4 mL of *N*,*O*-bis(trimethylsilyl)acetamide for 1 h at room temperature, evaporated, dissolved in 10 mL of dry benzene, and heated at reflux for 4.5 h with AIBN and 1 mL of *n*-Bu_3SnH solution. The solution was evaporated and the oily residue was processed as described above for the conversion **10***a* → **10***b*, using H_2O and then 25% MeOH–H_2O to develop the anion exchange column. Evaporation of appropriately pooled fractions gave 12 mg (77% by uv) of **11***b*; ms (200°C) *m/e*: 235.1069 (7.7, calcd. for M^+ ($C_{10}H_{13}N_5O_2$):

235.1069), 178 (21, BHCH=CHOH), 164 (100, BHCHO), 136 (68, B + 2H), 135 (93, B + H).

Acknowledgments

Generous financial support from the National Research Council of Canada (A5890), the National Cancer Institute of Canada, and The University of Alberta is gratefully acknowledged. We thank Dr. Y. Fouron for helpful discussions and for a sample of 9-β-D-xylofuranosyladenine.

1. L. Goodman. Basic principles in nucleic acid chemistry. Vol. I. *Edited by* P.O.P. Ts'o. Academic Press, New York, NY. 1974. pp. 129–141.
2. (*a*) A. Todd and T. L. V. Ulbricht. J. Chem. Soc. 3275 (1960); (*b*) D. Wagner, J. P. H. Verheyden, and J. G. Moffatt. J. Org. Chem. **39**, 24 (1974).
3. (*a*) M. J. Robins, R. Mengel, and R. A. Jones. J. Am. Chem. Soc. **95**, 4074 (1973); (*b*) M. J. Robins, J. R. McCarthy, Jr., R. A. Jones, and R. Mengel. Can. J. Chem. **51**, 1313 (1973); (*c*) M. J. Robins and R. A. Jones. J. Org. Chem. **39**, 113 (1974); (*d*) M. J. Robins, Y. Fouron, and R. Mengel. J. Org. Chem. **39**, 1564 (1974); (*e*) M. J. Robins, R. Mengel, R. A. Jones, and Y. Fouron. J. Am. Chem. Soc. **98**, 8204 (1976); (*f*) M. J. Robins, R. A. Jones, and R. Mengel. J. Am. Chem. Soc. **98**, 8213 (1976); (*g*) M. J. Robins, R. A. Jones, and R. Mengel. Can. J. Chem. **55**, 1251 (1977); (*h*) M. J. Robins, Y. Fouron, and W. H. Muhs. Can. J. Chem. **55**, 1260 (1977).
4. (*a*) A. F. Russell, S. Greenberg, and J. G. Moffatt. J. Am. Chem. Soc. **95**, 4025 (1973); (*b*) T. C. Jain, A. F. Russell, and J. G. Moffatt. J. Org. Chem. **38**, 3179 (1973); (*c*) T. C. Jain, I. D. Jenkins, A. F. Russell, J. P. H. Verheyden, and J. G. Moffatt. J. Org. Chem. **39**, 30 (1974); (*d*) F. W. Lichtenthaler, K. Kitahara, and K. Strobel. Synthesis, 860 (1974).
5. R. E. Parker and N. S. Isaacs. Chem. Rev. **59**, 737 (1959).
6. (*a*) H. P. M. Fromageot, B. E. Griffin, C. B. Reese, and J. E. Sulston. Tetrahedron, **23**, 2315 (1967); (*b*) J. H. van Boom, P. M. J. Burgers, C. A. G. Haasnoot, and C. B. Reese. Recl. Trav. Chim. Pays-Bas, **96**, 91 (1977).
7. M. Ikehara. Acc. Chem. Res. **2**, 47 (1969).
8. M. J. Robins, S. R. Naik, and A. S. K. Lee. J. Org. Chem. **39**, 1891 (1974); M. J. Robins, A. S. K. Lee, and F. A. Norris. Carbohydr. Res. **41**, 304 (1975).
9. M. Karplus. J. Chem. Phys. **30**, 11 (1959); R. J. Abraham, L. D. Hall, L. Hough, and K. A. McLauchlan. J. Chem. Soc. 3699 (1962).
10. R. U. Lemieux and D. R. Lineback. Ann. Rev. Biochem. **32**, 155 (1963); K. L. Rinehardt, Jr., W. S. Chilton, M. Hickens, and W. von Phillipsborn. J. Am. Chem. Soc. **84**, 3216 (1962).
11. C. Altona and M. Sundaralingam. J. Am. Chem. Soc. **94**, 8205 (1972); **95**, 2333 (1973).
12. H. G. Kuivila. Synthesis, 499 (1970); J. Farkaš and F. Šorm. Collect. Czech. Chem. Commun. **32**, 2663 (1967).
13. W. Steglich and G. Höfle. Angew. Chem. Int. Ed. Engl. **8**, 981 (1969); M. J. Robins, M. MacCoss, S. R. Naik, and G. Ramani. J. Am. Chem. Soc. **98**, 7381 (1976).
14. (*a*) E. S. Lewis and C. E. Boozer. J. Am. Chem. Soc. **74**, 308 (1952); (*b*) D. J. Cram. J. Am. Chem. Soc. **75**, 332 (1953); (*c*) J. K. Stille and F. M. Sonnenberg. J. Am. Chem. Soc. **88**, 4915 (1966).
15. C. A. Dekker. J. Am. Chem. Soc. **87**, 4027 (1965).
16. P. C. Srivastava, K. L. Nagpal, and M. M. Dhar. Experientia, **25**, 356 (1969); P. C. Srivastava and R. J. Rousseau. Carbohydr. Res. **27**, 455 (1973).
17. R. F. Dods and J. S. Roth. Tetrahedron Lett. 165 (1969); K. Kikugawa and M. Ichino. J. Org. Chem. **37**, 284 (1972).
18. J. F. Normant and H. Deshayes. Bull. Soc. Chim. Fr. 2854 (1972).
19. K. Kikugawa and M. Ichino. Tetrahedron Lett. 87 (1971).
20. (*a*) H. P. C. Hogenkamp. Biochemistry, **13**, 2736 (1974); (*b*) Y. Wang, H. P. C. Hogenkamp, R. A. Long, G. R. Revankar, and R. K. Robins. Carbohydr. Res. **59**, 449 (1977); (*c*) Y. Wang and H. P. C. Hogenkamp. J. Org. Chem. **43**, 998 (1978).
21. S. J. Shaw, D. M. Desiderio, K. Tsuboyama, and J. A. McCloskey. J. Am. Chem. Soc. **92**, 2510 (1970).
22. E. J. Reist, V. J. Bartuska, D. F. Calkins, and L. Goodman. J. Org. Chem. **30**, 3401 (1965).
23. E. J. Reist, D. F. Calkins, and L. Goodman. J. Org. Chem. **32**, 2538 (1967).
24. C. D. Anderson, L. Goodman, and B. R. Baker. J. Am. Chem. Soc. **81**, 3967 (1959); M. Ikehara and H. Tada. J. Am. Chem. Soc. **87**, 606 (1965); M. Ikehara and H. Tada. Chem. Pharm. Bull. **15**, 94 (1967); M. Ikehara and Y. Ogiso. Tetrahedron, **28**, 3695 (1972); A. Yamazaki, M. Akiyama, I. Kumashiro, and M. Ikehara. Chem. Pharm. Bull. **21**, 1143 (1973); T. Sowa and K. Tsunoda. Bull. Chem. Soc. Jpn. **48**, 3243 (1975).
25. H. Venner. Chem. Ber. **93**, 140 (1960); R. K. Ness and H. G. Fletcher, Jr. J. Am. Chem. Soc. **82**, 3434 (1960); C. Pedersen and H. G. Fletcher, Jr. J. Am. Chem. Soc. **82**, 5210 (1960); R. H. Iwamoto, E. M. Acton, and L. Goodman. J. Org. Chem. **27**, 3949 (1962); M. J. Robins and R. K. Robins. J. Am. Chem. Soc. **87**, 4934 (1965); M. J. Robins, T. A. Khwaja, and R. K. Robins. J. Org. Chem. **35**, 636 (1970).
26. D. H. R. Barton and R. Subramanian. J. Chem. Soc. Chem. Commun. 867 (1976).
27. A. Holý. Collect. Czech. Chem. Commun. **37**, 4072 (1972).
28. H. G. Kuivila and O. F. Beumel, Jr. J. Am. Chem. Soc. **83**, 1246 (1961).
29. L. B. Townsend. *In* Synthetic procedures in nucleic acid chemistry. Vol. 2. *Edited by* W. W. Zorbach and R. S. Tipson. Wiley-Interscience, New York, NY. 1973. pp. 328–329.
30. M. J. Robins and S. D. Hawrelak. Tetrahedron Lett. 3653 (1978).

Yields of excited states from thermolysis of some 1,2-dioxetanes[1]

KARL R. KOPECKY AND JOHN E. FILBY[2]

Department of Chemistry, University of Alberta, Edmonton, Alta., Canada T6G 2E1

Received April 7, 1978

KARL R. KOPECKY and JOHN E. FILBY. Can. J. Chem. **57**, 283 (1979).

The singlet $^1\Phi$ and triplet $^3\Phi$ excited state product yields produced on thermolysis in toluene of trimethyl- (**1**), tetramethyl- (**2**), *cis*-3, 4-butano-3,4-dimethyl- (**3**), and 3,4:3,4-dibutano-1,2-dioxetane (**4**) were determined to be as follows (dioxetane, °C, $^1\Phi$, $^3\Phi$): **1**, 40, 1.1×10^{-3}, 0.15; **2**, 45, 4.4×10^{-4}, 0.31; **3**, 26, 8.5×10^{-4}, 0.23; **4**, 24, 4.8×10^{-6}, 0.011. The reason for the low yield of excited states obtained from **4** is not known. Thermochemical calculation indicate that as much energy is available from thermolysis of **4** as is available from **2**.

Dioxetane-energized dimerization of acenaphthylene, accompanied by an intense yellow luminescence, produced mainly the *trans* dimer in 1–3% yield. Dioxetane-energized cyclization of 1-(2,4-dimethylphenyl)-1,2-propanedione produced 2-hydroxy-2,5-dimethylindan-1-one in 0.5–6% yields.

KARL R. KOPECKY et JOHN E. FILBY. Can. J. Chem. **57**, 283 (1979).

On a déterminé que les rendements des produits des états excités singulet $^1\Phi$ et triplet $^3\Phi$ obtenus lors de la thermolyse dans le toluène du triméthyl- (**1**), du tétraméthyl- (**2**), du *cis*-butano-3,4 diméthyl-3,4- (**3**) et du dibutano-3,4:3,4 dioxétanne-1,2 (**4**) sont les suivants: (dioxétanne, °C, $^1\Phi$, $^3\Phi$): **1**, 40, 1.1×10^{-3}, 0.15; **2**, 45, 4.4×10^{-4}, 0.31; **3**, 26, 8.5×10^{-4}, 0.23; **4**, 24, 4.8×10^{-6}, 0.011. On ne connait pas la raison des faibles rendements d'états excités obtenus dans le cas de **4**. Des calculs thermochimiques indiquent qu'il y a autant d'énergie disponible pour la thermolyse de **4** que de **2**.

La dimérisation de l'acénaphtylène activée par un dioxétanne est accompagnée par une luminescence jaune intense et conduit principalement au dimère *trans* avec un rendement de 1 à 3%. La cyclisation de la (diméthyl-2,4 phényl)-1 propanedione-2,5 conduit à l'hydroxy-2 diméthyl-2,5 indanone-1 avec des rendements de 0.5–6%.

[Traduit par le journal]

Introduction

Thermolysis of 1,2-dioxetanes yields carbonyl compounds in quantitative yield and is accompanied by luminescence, eq. [1] (1). The luminescence

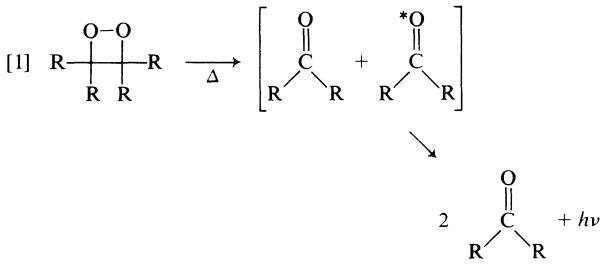

observed in aerated solutions of trimethyl-1,2-dioxetane **1** (1*a*) is evidence that a carbonyl product is formed in the excited singlet state. It was first thought that the singlet was the exclusive initial excited state product formed. However, it was soon shown that the triplet is by far the predominant initial excited state product by observing that thermolysis of **1** in the presence of acenaphthylene produces mainly the *trans* dimer of acenaphthylene, eq. [2] (2), the result of dimerization via the triplet state (3).

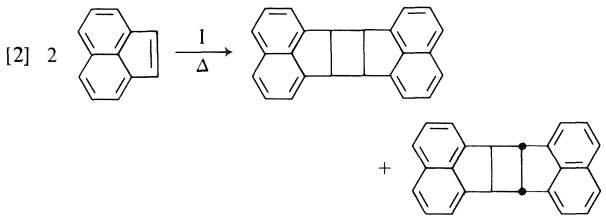

The luminescence from thermolysis of dioxetanes is enhanced by the presence of fluorescers, particularly by 9,10-dibromoanthracene DBA (4), which produces a much brighter luminescence than does 9,10-diphenylanthracene DPA even though the fluorescence efficiency of DBA, Φ_f(DBA) ~ 0.1, is much less than that of DPA, Φ_f(DPA) ~ 1. Energy transfer from triplet carbonyl to DBA produces excited singlet DBA fairly efficiently (5) whereas the same transfer to DPA produces only triplet DPA which does not fluoresce in solution. Thus, the more efficient luminescence with DBA is further evidence that the triplet is the predominant initial excited state product. This has been demonstrated in other

[1]This research was supported by the National Research Council of Canada.

[2]Holder of a Canadian Mortgage and Housing Fellowship, 1970–1971, and a National Research Council of Canada Scholarship, 1971–1973.

0008-4042/79/030283-06$01.00/0

ways (6) and most dioxetanes produce initially the triplet carbonyl product in far greater amount; for a review see ref. 7.

The quantitative determination of luminescence from dioxetane solutions containing DBA and DPA has been used to measure the yields of the initially formed triplet and singlet excited states, respectively (7, 8). The present paper reports our determination of the yields of excited states formed on thermolysis of **1**, tetramethyl-1,2-dioxetane **2**, *cis*-3,4-butano-3,4-dimethyl-1,2-dioxetane **3**, and 3,4:3,4-dibutano-1,2-dioxetane **4** by this method,

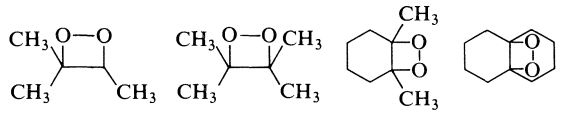

1 **2** **3** **4**

as well as the results of some energy transfer experiments to acenaphthylene and to 1-(2,4-dimethylphenyl)propane-1,2-dione **5**. This series of dioxetanes, containing mono-, di-, and tricyclic members, was chosen to study the effect of structure on the yield of excited state products formed.

Results

Our initial attempts to estimate excited state yields from the above dioxetanes involved energy transfer experiments to the photoreactive acceptors acenaphthylene and **5**. The dioxetane-energized cyclization of **5** to 2-hydroxy-2,5-dimethylindan-1-one **6**, eq. [3], was patterned after a similar reaction of

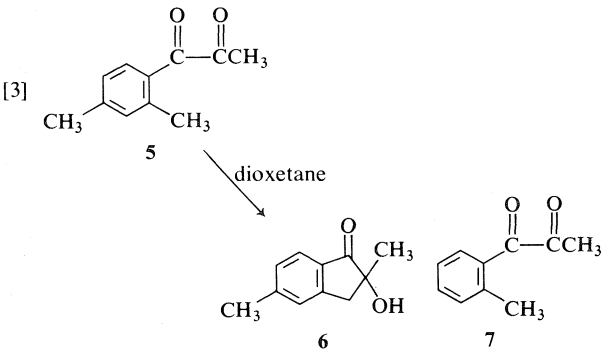

5 **6** **7**

1-(2-methylphenyl)propane-1,2-dione **7** (9). Since the preparation of **5** is much simpler than that of **7**, **5** was chosen for the present study.

Degassed benzene solutions 1 *M* in **2**, **3**, or **4** containing 1 *M* acenaphthylene or **5** were heated to ~90°C. The yield of acenaphthylene dimer, based on dioxetane used, was 2–3% from **2** and **3** and 1% from **4**. In all these reactions the *cis* to *trans* dimer ratio was ~0.1, indicating that mainly triplet energy transfer to acenaphthalene was occurring (2). The yields of **6** formed from **2**, **3**, and **4** were 6, 1, and 0.5%, respectively. Shortly after heating began all the reactions luminesced so brightly that the luminescence was clearly visible in ordinary room light for 5–10 s. It was not surprising to observe the greenish-yellow luminescence from **5** as 1,2-diketones are known to luminesce efficiently. However, the bright yellow luminescence from solutions containing acenaphthylene was completely unexpected since this compound fluoresces very weakly, if at all (10). This luminescence was not observed when the initial dioxetane concentration was less than 0.1 *M*.

The yields of acenaphthalene dimer obtained in the present study are about double those obtained previously using **1** under similar conditions (2) and the *cis* to *trans* dimer ratios of ~0.1 are lower than the value of ~0.3 obtained previously. It is not clear what the reasons for these discrepancies may be. The higher initial concentration of **1** used before, ~2 *M*, may have resulted in more wastage of dioxetane than in the present work (see below). At 25°C the triplet dimerization of acenaphthylene results in a *cis* to *trans* dimer ratio of ~0.25 in nonpolar solvents (3). The effect of temperature on this ratio is not known.

The yields of products formed in the above reactions are quite low. The quantum yield for the dimerization of triplet acenaphthylene is not known but that for cyclization of **5** must be ~0.8 (9). The low yield of **6** may be due to low yields of excited states formed from the dioxetanes and/or induced decomposition of the dioxetanes at the high concentration used by the excited state of **5** or of the initial carbonyl products (8, 11). Such a wastage of dioxetane does not occur in aerated solutions of DBA and DPA (8). Measurement of the light emitted from such solutions should be a more reliable method for determining the excited state yields (7).

The yields of excited singlet $^1\Phi$ and triplet $^3\Phi$ products from the dioxetanes **1**–**4**, Table 1, were determined from plots of the reciprocal of the light

TABLE 1. Yields of excited states formed on thermolysis of 1,2-dioxetanes[a]

Dioxetane	$^3\Phi$[b]	$^1\Phi \times 10^4$[c]
1	0.15	11
2	0.31	4.4
3	0.23	8.5
4	0.011	0.048

[a]The values given here differ somewhat from those previously published (8) because the spectrofluorimeter has been recalibrated and the luminescence intensities from solutions of some of the dioxetanes have been redetermined.
[b]Molecules of excited triplet ketone formed per molecule of dioxetane decomposed. Estimated errors ±25%.
[c]Molecules of excited singlet ketone formed per molecule of dioxetane decomposed. Estimated errors ±25%.

intensity vs. the reciprocal of the DBA and DPA concentrations, respectively (7, 8). The spectrofluorimeter used was calibrated with the luminol light standard (12). Use of this standard results in apparent excited state yields that are smaller by a factor of ~2.5 than those obtained on the basis of the radioactive light standard which is often used (7, 13). In fact, the yield of triplet acetone formed from **2** as determined in the present work is in the low end of the range of values, $^3\Phi \geq 0.2$–0.5, reported by others (7). The yield of singlet acetone is smaller by a factor of about 10 than most other determinations (7) but it is in very good agreement with recently reported values, $^1\Phi = 9 \times 10^{-4}$ at 72°C and 5×10^{-4} at 22°C (14).

Although the exact values of the excited state yields are uncertain the relative yields given in Table 1, using **2** as a reference point, should be meaningful. The yields of excited states formed from **1**, **2**, and **3** vary at most by a factor of about 2 but the tricyclic dioxetane **4** is only about 10^{-2} as efficient at forming the excited singlet and about a 30th as effective at forming triplet products as are the other dioxetanes. It can clearly be seen visually that the luminescence from solutions of **4** is much weaker than that from solutions of the other dioxetanes.

However, based on the sensitized dimerization of acenaphthylene and cyclization of **7** the efficiency of excited state formation from **4** is not so greatly different from those from the other dioxetanes. It is not obvious why the different methods of measurement should result in different relative excited state efficiencies. The yields determined by luminescence measurements using DPA and DBA should be the most accurate and the discussion will be based on these.

Discussion

Incorporation of the dioxetane ring into a bicyclic system as in **3** has little effect on the efficiency of excited state formation as compared with **2**. This has been observed already for the dioxetanes derived from 3,6-dioxacyclohexene (7) and 1,2-dimethylcyclopentene (15). But there certainly is an effect when the dioxetane ring is incorporated into the tricyclic system of **4**. It was thought initially that there might not be enough energy available (equal to the difference in the heats of formation of **4** and the ground state product plus the energy of activation for the thermolysis) on thermolysis of **4** to populate the excited singlet state of the product as a 10-membered ring is formed which might have considerable strain. However, cyclodecanone has been calculated to have only 3.6 kcal/mol of strain energy (16) and force-field calculations indicate that introduction of a second sp^2 center in cyclic molecules reduces the strain energy even further (17). Thus, 1,6-cyclodecanedione must be nearly strain free and thermochemical calculations (18) give a value of 93 kcal/mol for the energy available from **4**. This is essentially the same as is available from **2**. It was assumed that 1,6-cyclodecanedione was strain free and that the dioxetane ring of **4** had the same strain energy as does **2**.

Nor does the inefficiency of **4** appear to be due to its rigid structure which must restrict considerably the motions available during decomposition as compared to **1**, **2**, and **3**, for two other tricyclic dioxetanes, **8** and **9**, which also have rigid structures, are almost

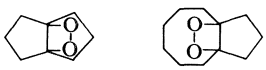

8 **9**

as efficient as **2** in the formation of excited states (19) Thus, the reason for the inefficiency of **4** must lie elsewhere and we are unable to offer an explanation.

It was suggested recently that the entropy of the overall reaction instead of the energy of activation should be considered in addition to the enthalpy of the reaction for calculating the energy available for population of excited states on thermolysis of dioxetanes (20). Monocyclic dioxetanes produce two molecules and the energy available as calculated in this way (20) is sufficient to produce excited singlet state products. However, the entropy of the reaction on thermolysis of the bicyclic **3** and especially the tricyclic dioxetanes is much less and the free energy of these reactions is not great enough to produce the excited singlet state of the product. The formation of excited singlet state from **3**, **8**, and **9** with the same efficiency as from **2** is experimental evidence that the original method (18) for the calculation of the energy available is correct. The original method also has been justified on thermodynamic grounds (21).

Experimental

The dioxetanes **1**–**4** were prepared as described (1*e*) and all had at least 99% of the theoretical active oxygen content.

1-(2,4-Dimethylphenyl)-1-(hydroxyazylene)propane

Treatment (22) of 2,4-dimethylpropiophenone (23) with 3-methyl-1-butyl nitrite gave an 87% yield of product, recrystallized from toluene, mp 104–105°C. *Anal.* calcd. for $C_{11}H_{13}NO_2$: C 69.09, H 6.85, N 7.33; found: C 69.31, H 6.96, N 7.49.

*1-(2,4-Dimethylphenyl)propane-1,2-dione (**5**)*

A mixture of 16 g sodium bisulfite and 1.9 g 1-(2,4-dimethylphenyl)-1-(hydroxyazylene) propane in 25 mL 50% aqueous ethanol was heated under reflux for 2 h. The solvent was evaporated and 25 mL water and 50 mL 6 *N* hydrochloric acid were added to the residue. The resulting mixture was extracted with 3 × 10 mL methylene chloride. The combined extracts were dried, concentrated, and the residue distilled to give

1.0 g (57%) of a yellow oil, bp 85–89°C/0.2 Torr, n_D^{21} 1.5382, which was crystallized from isopentane to give yellow needles, mp 16.5–17.5°C. *Anal.* calcd. for $C_{11}H_{12}O_2$: C 74.97, H 6.86; found: C 75.20, H 6.95.

*2-Hydroxy-2,5-dimethylindan-1-one (**6**)*

A stirred solution of 0.5 g of the above dione in 500 mL hexane was irradiated under a nitrogen atmosphere with a General Electric 'Sunlamp' until the yellow color had faded. The solvent was removed to leave a yellow oil which slowly deposited crystals at −10°C. These were crystallized from heptane to give white cubes, mp 84–85°C; ^{1}Hmr ($CDCl_3$): τ 2.29 (d, J = 8 Hz, 1H), 2.70 (s, 1H), 2.80 (d, J = 8 Hz, 1H), 6.8 (m, 2H), 7.66 (s, 1H), and 8.57 (s, 3H). *Anal.* calcd. for $C_{11}H_{12}O_2$: C 74.97, H 6.96; found: C 74.98, H 6.84.

cis- *and* trans-*Acenaphthylene Dimers*

These were formed by photolysis (3*b*) of purified (3*a*) acenaphthalene in cyclohexane and separated (3*b*) into the crude *cis*- and *trans* isomers. The *cis* dimer was dissolved in benzene and an equivalent amount of picric acid in a saturated benzene solution was added. After several hours splendid, deep red crystals of the picrate formed which were recrystallized from benzene and then decomposed with ammonia. The *cis* dimer was recrystallized from cyclohexane (activated charcoal) to yield white prisms, mp 231–232°C (lit. (3*b*) mp 231–233.5°C). The crude *trans* dimer was recrystallized several times from benzene until the melting point remained constant to give fine white needles, mp 320–321°C (lit. (3) mp 305–307°C). The extinction coefficients in cyclohexane used for analysis of the product mixtures were *cis* dimer, ε^{219} 1.44 × 10^5, ε^{225} 7.75 × 10^4 (lit. (3*b*) ε^{219} 1.27 × 10^5, ε^{225} 6.60 × 10^4); *trans* dimer, ε^{219} 7.50 × 10^4, ε^{225} 1.22 × 10^5 (lit. (3*b*) ε^{219} 7.38 × 10^4, ε^{225} 1.19 × 10^5).

Dioxetane Sensitized Dimerization of Acenaphthylene

Solutions of dioxetane and acenaphthylene in benzene were degassed by six freeze–thaw cycles at 0.005 Torr in clean Pyrex ampoules and sealed. The ampoules were then heated at 95°C in a water bath for 15 min. Bright yellow luminescence clearly visible in daylight was observed for about 10 s during thermolysis of solutions ~1 *M* in dioxetane. The ampoules were stored at 8°C for several days and opened. The crystals which had deposited were collected and washed with cold (0°C) pentane. The filtrate and washings were applied to a silica gel preparative tlc plate which was eluted twice in the dark with cyclohexane. The dimers, visualized under uv light as a purple line near the bottom of the plate, were isolated by extracting the silica gel for 8 h in a Soxhlet thimble with boiling benzene. The extract was evaporated to dryness and the residue repeatedly treated with 10 mL cyclohexane and evaporated. The residue was combined with the precipitated dimers and the product composition determined by uv analysis (3*b*). Blank solutions containing only acenaphthalene were handled in exactly the same way. The optical densities of solutions made up from the blank samples were negligible.

The *cis* dimer was shown to be stable to the isolation conditions. A solution of the *cis* dimer in C_6D_6 containing 1,4-dimethoxybenzene as internal standard was heated at 80°C for 4 h. Examination of the ^{1}H nmr spectra taken before and after heating revealed that no detectable decomposition had occurred.

*Dioxetane Sensitized Cyclization of 1-(2,5-Dimethylphenyl)-propane-1,2-dione (**5**)*

About 0.5 mL of benzene solutions 1 *M* in dioxetane and 1 *M* in **5** in clean test tubes were degassed with three freeze–thaw cycles under 0.005 Torr. The tubes were sealed and placed in a 95°C bath. After 1–2 min a bright green fluorescence lasting 10–15 s appeared. The samples were then cooled and some (4-methoxyphenyl)methanol was added as internal standard. The solutions were analyzed by gc at 190°C on a 5 ft × ¼ in. stainless steel column packed with 15% FFAP on 60–80 Chromosorb W. The gc instrument was calibrated by injecting solutions of internal standard and cyclized product **6** at known concentrations.

*Calibration of the Spectrofluorimeter and of a Solution of **2** Containing DBA*

Luminescence intensities from dioxetane solutions were measured using a Turner Model 430 spectrofluorimeter with the xenon lamp source turned off and using the 60 nm emission monochrometer band width. Solutions were placed in a 10 cm jacketed polarimeter type cell of 11 mL capacity with one end silvered. It was mounted in a specially made compartment with the unsilvered end ~2 cm from the entrance slit. Water from a constant temperature bath was circulated through the jacket and the internal temperature of the solution was measured with a calibrated thermometer.

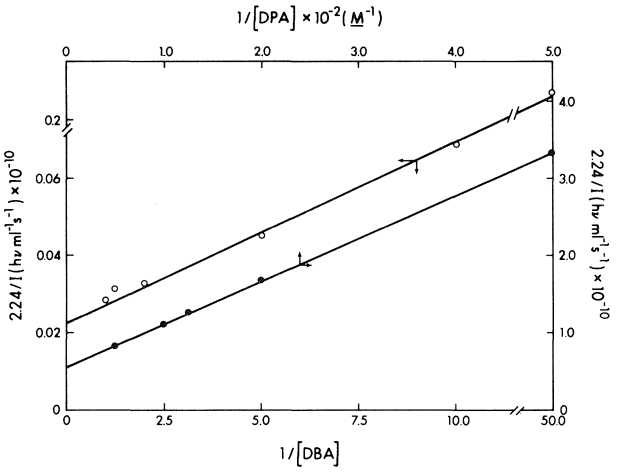

FIG. 1. Effect of DBA (○) and DPA (●) concentrations on the initial intensity of chemiluminescence from 1.50 × 10^{-3} *M* **1** in toluene at 40°C.

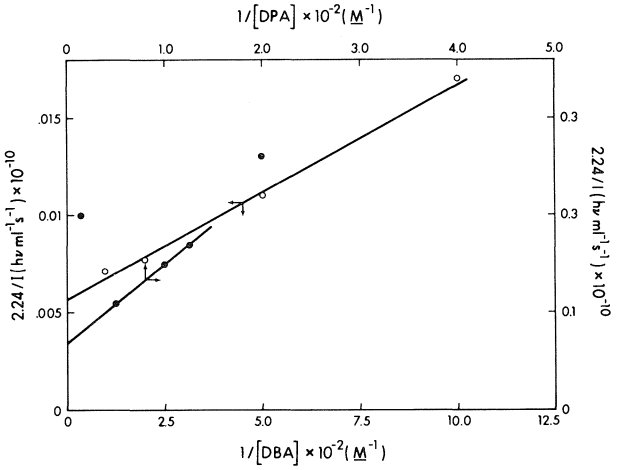

FIG. 2. Effect of DBA (○) and DPA (●) concentration on the initial intensity of chemiluminescence from 1.08 × 10^{-2} *M* **2** in toluene at 45°C.

TABLE 2. Parameters used in calculating yields of excited states formed on thermolysis of 1,2-dioxetanes

Dioxetane	I_∞(DBA)[a] ($h\nu$ mL^{-1} s^{-1})	I_∞(DPA)[a] ($h\nu$ mL^{-1} s^{-1})	Temperature (°C)	Dioxetane concentration ($M \times 10^3$)	$k_d \times 10^5$ [b] (s^{-1})	Φ_f(DBA)[c]
1	9.95×10^{10}	3.84×10^9	40	1.50	4.70	0.070
2	3.70×10^{11}	3.05×10^{10}	45	10.8	1.34	0.065
3	3.04×10^{10}	5.10×10^9	26	0.89	1.40	0.090
4	9.67×10^{10}	1.85×10^9	24	8.85	9.20	0.090

[a]Light emitted from dioxetane solutions, extrapolated to infinite fluorescer concentration.
[b]Rate of thermolysis of the dioxetanes, taken from ref. 1*e*.
[c]Fluorescence efficiencies at various temperatures were calculated as described (8).

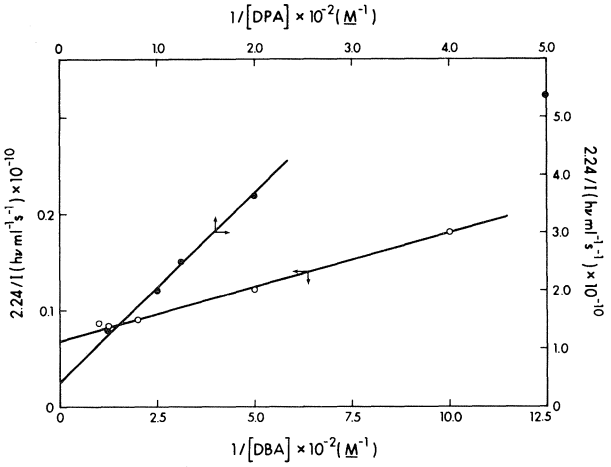

FIG. 3. Effect of DBA (○) and DPA(●) concentration on the initial intensity of chemiluminescence from 8.9×10^{-4} *M* **3** in toluene at 26°C.

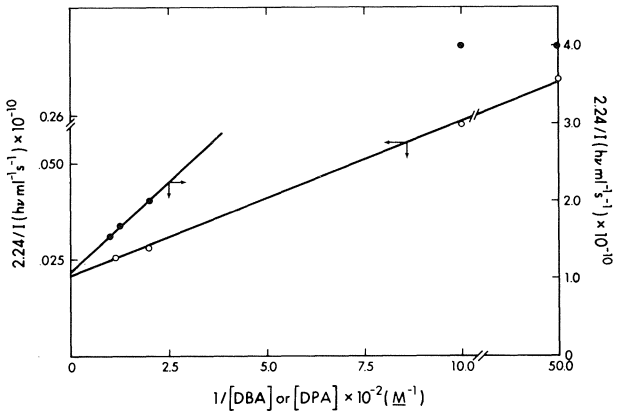

FIG. 4. Effect of DBA (○) and DPA(●) concentration on the initial intensity of chemiluminescence from 8.5×10^{-3} *M* **4** at 24°C.

The spectrofluorimeter was calibrated with the luminol light standard (12). Ten millilitres of a dry dimethyl sulfoxide solution of freshly prepared luminol (24) which had an optical density of 0.00163 at 360 nm and 1.0 mL of a solution of 0.1 *M* potassium *tert*-butoxide in *tert*-butyl alcohol were injected simultaneously into the cell through a light-tight septum. Injections could be completed within 3 s. The output from the spectrofluorimeter, with the emission wavelength setting at 484 nm, was recorded on a strip chart recorder. With a ×3 setting on the spectrofluorimeter and the recorder setting at 1 V and operating at 5 in./min the areas under the curves, measured with a planimeter, for four runs were 11.47, 11.15, 13.49, and 11.91 in.^{2}, average = 12.00 ± 0.49 in.^{2}. When 0.03 *M* potassium *tert*-butoxide was used the area was 12.01 in.^{2}. Two further determinations were made using 0.01 potassium *tert*-butoxide solution as base and the areas were measured to be 10.50 and 12.10 in.^{2}. The light intensity decreased much more slowly when the more dilute base was used, falling to 0.5% of the maximum intensity after 22 min with 0.01 *M* base as compared to six m with the 0.1 *M* base. The results indicate that all the light that was produced was detected even when 0.1 *M* base was used. The correct area under the curve was taken to be 12.00 ± 0.49 in.^{2}. With the emission wavelength setting at 450 nm (for maximum light intensity) and all other settings the same a toluene solution 6.87×10^{-4} *M* in **2** and 5×10^{-3} *M* in DBA at 44.8°C required 94.7 s to generate 12.00 in.^{2} under the output curve, a straight line. Using the light yield of $(9.75 \pm 0.7) \times 10^{14}$ photons per millilitre of luminol solution with optical density 1.00 (12) this dioxetane solution was emitting an apparent $(1.68 \pm 0.18) \times 10^{10}$ photons mL^{-1} s^{-1}. Correction factors (13*a*) to be applied to this value were obtained by graphical integration for the variable wavelength response of the photomultiplier tube (S-4 response), a factor of 0.84 for both DBA and DPA and for the relative amounts of light that passed through the slit from the solutions containing luminol, DBA and DPA, factors of 1.15 for DBA and 1.18 for DPA. The errors in the graphical integrations were estimated to be 5%. Applying the corrections for DBA to the apparent emission of the DBA solution above indicated that it was emitting $(1.63 \pm 0.26 \times 10^{10})$ photons mL^{-1} s^{-1}.

Excited State Yields from Dioxetanes

Plots of the reciprocal of the light intensity vs. the reciprocal of fluorescer concentration for dioxetane solutions in toluene are given in Figs. 1–4. The light intensities at infinite fluorescer concentration were obtained from the intercepts of the plots.

$$[4] \qquad {}^1\Phi = \frac{I_\infty(\mathrm{DPA})}{([\mathrm{D}] \times 10^{-3}) \times k_d \times (6.02 \times 10^{23}) \times 0.8}$$

$$[5] \qquad {}^3\Phi = \frac{I_\infty(\mathrm{DBA})}{\Phi_{T \to S} \times \Phi_f(\mathrm{DBA}) \times ([\mathrm{D}] \times 10^{-3}) \times k_d \times (6.02 \times 10^{23})}$$

The yields of excited singlet and triplet states formed on thermolysis of the 1,2-dioxetanes were calculated using [4] and [5], respectively. The parameters used in the calculations are listed and defined in Table 2 except for [D], the concentration of dioxetane and $\Phi_{T\rightarrow S}$, the efficiency with which triplet carbonyl compounds produces singlet DBA. This efficiency was assumed to be the same for all the carbonyl compounds produced from dioxetanes **1**–**4** and the value 0.2 determined for acetophenone (7) was used. The factor of 0.8 in [4] was used to correct for the fact that 20% of excited DPA molecules are quenched by oxygen in aerated solutions (8). The excited state yields are presented in Table 1 and the total error of each value is estimated to be ~25%. The errors consist of ~16% in the calibration of the spectrofluorimeter, ~5% in k_d and ~5% in the determination of the values of the intercepts of the plots of Figs. 1–4.

1. (*a*) K. R. KOPECKY and C. MUMFORD. Can. J. Chem. **47**, 709 (1969); (*b*) P. D. BARTLETT and A. P. SCHAAP. J. Am. Chem. Soc. **92**, 3223 (1970); (*c*) S. MAZUR and C. S. FOOTE. J. Am. Chem. Soc. **92**, 3225 (1970); (*d*) W. H. RICHARDSON and V. F. HODGE. J. Am. Chem. Soc. **93**, 3996 (1971); (*e*) K. R. KOPECKY, J. E. FILBY, C. MUMFORD, P. A. LOCKWOOD, and J.-Y. DING. Can. J. Chem. **53**, 1103 (1975).
2. (*a*) E. H. WHITE, J. WIEKO, and C. C. WEI. J. Am. Chem. Soc. **92**, 2167 (1970); (*b*) E. H. WHITE, P. D. WILDES, J. WIECKO, H. DOSHAN, and C. C. WEI. J. Am. Chem. Soc. **95**, 7050 (1973).
3. (*a*) I. HARTMANN, W. HARTMANN, and G. O. SCHENCK. Chem. Ber. **100**, 3146 (1967); (*b*) D. O. COWAN and R. L. E. DRISCO. J. Am. Chem. Soc. **92**, 6286 (1970).
4. E. H. WHITE, J. WIECKO, and D. F. ROSWELL. J. Am. Chem. Soc. **91**, 5194 (1969).
5. V. A. BELZAKOV and R. F. VASSIL'EV. Photochem. Photobiol. **11**, 179 (1970).
6. (*a*) N. J. TURRO and P. LECHTKEN. J. Am. Chem. Soc. **94**, 2886 (1972); (*b*) N. J. TURRO, H. C. STEINMETZER, and A. YETKA. J. Am. Chem. Soc. **95**, 6468 (1973); (*c*) N. J. TURRO, P. LECHTKEN, N. E. SHORE, G. SCHUSTER, H. C. STEINMETZER, and A. YETKA. Acc. Chem. Res. **7**, 97 (1974).
7. T. WILSON, *In* MPT Int. Rev. Sci., Chem. Kinet. Ser. 2. *Edited by* D. R. Herschbach. Butterworths, London. 1976. p. 265.
8. T. WILSON and A. P. SCHAAP. J. Am. Chem. Soc. **93**, 4126 (1971).
9. H. GUNSTEN and E. F. ULLMAN. Chem. Commun. 28 (1970).
10. (*a*) R. LIVINGSTON and S. K. WEI. J. Phys. Chem. **71**, 541 (1967); (*b*) T. D. SANTA CRUZ, D. L. AKINS, and R. L. BIRKE. J. Am. Chem. Soc. **98**, 1677 (1976).
11. P. LECHTKEN, A. YETKA, and N. J. TURRO. J. Am. Chem. Soc. **95**, 3027 (1973).
12. J. LEE and H. H. SELIGER. Photochem. Photobiol. **4**, 1015 (1965).
13. (*a*) J. W. HASTINGS and G. WEBER. J. Opt. Soc. Am. **53**, 1410 (1963); (*b*) J. W. HASTINGS and G. WEBER. Photochem. Photobiol. **4**, 1049 (1965).
14. W. ADAM, N. DURAN, and G. A. SIMPSON. J. Am. Chem. Soc. **97**, 5164 (1975).
15. N. J. TURRO, P. LECHTKEN, G. SCHUSTER, J. ORELL, H. C. STEINMETZER, and W. ADAM. J. Am. Chem. Soc. **96**, 1627 (1974).
16. (*a*) G. WOLFF. Helv. Chim. Acta, **55**, 1446 (1972); (*b*) H. K. EIGENMAN, D. M. GOLDEN, and S. W. BENSON. J. Phys. Chem. **77**, 1687 (1973).
17. N. L. ALLINGER, M. T. TRIBBLE, and M. A. MILLER. Tetrahedron, **28**, 1173 (1972).
18. (*a*) H. E. O'NEAL and W. H. RICHARDSON. J. Am. Chem. Soc. **92**, 6553 (1970); (*b*) H. E. O'NEAL and W. H. RICHARDSON. J. Am. Chem. Soc. **93**, 1828 (1971).
19. P. A. LOCKWOOD. Ph.D. Thesis. University of Alberta, Edmonton, Alta. 1977.
20. C. L. PERRIN. J. Am. Chem. Soc. **97**, 4419 (1975).
21. (*a*) E. LISSI. J. Am. Chem. Soc. **98**, 3386 (1976); (*b*) E. B. WILSON. J. Am. Chem. Soc. **98**, 3387 (1976).
22. W. H. HARTUNG and F. CROSALEY. *In* Org. Synthesis Coll. Vol. II. *Edited by* A. H. Blatt. John Wiley and Sons, Inc. New York. 1941. p. 363.
23. D. NIGHTINGALE and B. CARTON. J. Am. Chem. Soc. **62**, 280 (1940).
24. L. F. FIESER. Experiments in organic chemistry. 3rd ed. Heath, Boston. 1957. p. 199.

Dihydropyridines in synthesis and biosynthesis. I. Secodine and precursors of dehydrosecodine

JAMES P. KUTNEY, RODNEY A. BADGER, JOHN F. BECK, HERBERT BOSSHARDT, FATHY S. MATOUGH, VICENTE E. RIDAURA-SANZ, YING HUNG SO, RATTAN S. SOOD, AND BRIAN R. WORTH

Department of Chemistry, University of British Columbia, 2075 Wesbrook Place, Vancouver, B.C., Canada V6T 1W5

Received July 31, 1978

JAMES P. KUTNEY, RODNEY A. BADGER, JOHN F. BECK, HERBERT BOSSHARDT, FATHY S. MATOUGH, VICENTE E. RIDAURA-SANZ, YING HUNG SO, RATTAN S. SOOD, and BRIAN R. WORTH. Can. J. Chem. **57**, 289 (1979).

A synthesis of 16,17-dihydrosecodin-17-ol and of secodine is described. Various indole derivatives were elaborated to a series of pyridinium salts, potential precursors for 1,2- and 1,6-dihydropyridine compounds exemplifying the proposed biointermediate 'dehydrosecodine.'

JAMES P. KUTNEY, RODNEY A. BADGER, JOHN F. BECK, HERBERT BOSSHARDT, FATHY S. MATOUGH, VICENTE E. RIDAURA-SANZ, YING HUNG SO, RATTAN S. SOOD et BRIAN R. WORTH. Can. J. Chem. **57**, 289 (1979).

On décrit une synthèse du dihydro-16,17 sécodinol-17 et de la sécodine. On a transformé divers dérivés de l'indole en une série de sels de pyridinium qui sont des précurseurs possibles de composés dihydro-1,2 (et -1,6) pyridine et qui servent d'exemples pour les biointermédiaires suggérés pour la "déhydrosécodine."

[Traduit par le journal]

The possible role of dihydropyridines as late stage intermediates in indole alkaloid biosynthesis has been discussed for some years (see ref. 1 for a recent review). Wenkert (2) first speculated that such intermediates could be involved in the later stages of *Aspidosperma* and *Iboga* alkaloid biosynthesis and experimental evidence supporting such a proposal came forth from various investigations in different laboratories. Scott's experiments with germinated *Catharanthus roseus* seedlings (3–5) and our own studies with *C. roseus* plants (6) brought forward a rationale (Scheme 1) which invoked such systems (e.g., 'intermediate A'). Clearly such studies suggested, but did not prove, the role of dihydropyridines in these biosynthetic pathways. To provide more direct evidence in this direction a synthetic program was initiated in the hope that dihydropyridine systems could be made available

The expected instability of dihydropyridines led initially to the consideration of the more stable yet closely related tetrahydropyridines as model systems. To this end the synthesis of 16,17-dihydrosecodin-

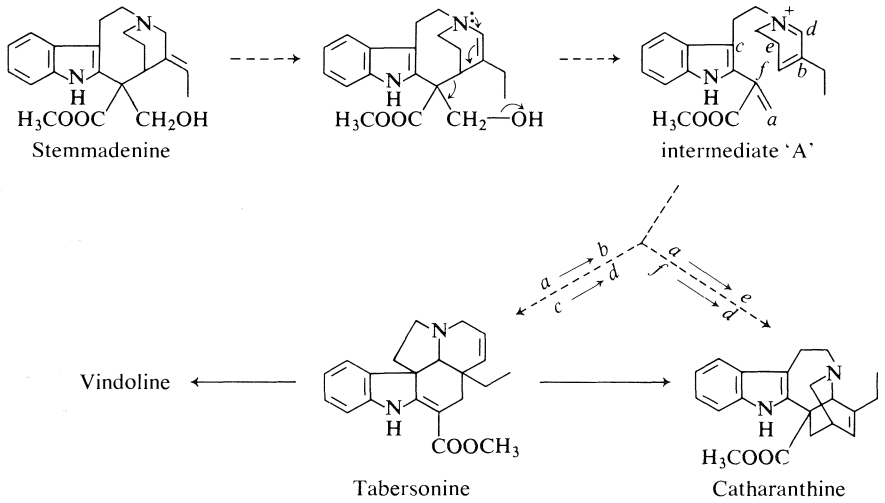

SCHEME 1. A possible rationale for the implication of intermediate 'A' in the biosynthesis of *Aspidosperma* and *Iboga* alkaloids.

0008-4042/79/030289-11$01.00/0

17-ol (**1**) and secodine (**2**) was finally completed and a large number of experiments, with radioactive-labelled forms of **1** and **2**, in various alkaloid bearing plants, carried out. Two recent reviews (7) provide a detailed account of these investigations and Scheme 2 summarises the most important features pertaining to the present discussion. Thus it was established that in three different plant species, containing very different alkaloids, *C. roseus* (catharanthine (**3**) and vindoline (**4**)), *Vinca minor* (vincamine (**5**)), and *Aspidosperma pyricollum* (apparicine (**6**)), secodine was incorporated *intact* with ^{14}C or ^{3}H labels retained except when tritium was located in the piperideine unit. In those cases significant loss (catharanthine, 61.5%; vindoline, 60%; apparicine, 50%) of the label was observed thereby suggesting a higher oxidised form of (**2**) as a more accurate representation of the biointermediate.

The importance of secodine and related dihydropyridines as possible intermediates in the biosynthesis of various indole alkaloid families necessitated considerable development of the chemistry of these systems. This report discusses our experiments in this area with reference to both biosynthetic and synthetic applications (8).

With a 'dehydrosecodine' (**7**) as an eventual goal it was necessary to evaluate methods for preparation and stabilisation of both the acrylic ester and dihydropyridine functions. The synthesis of secodine (9) (Scheme 3) provided the necessary experience

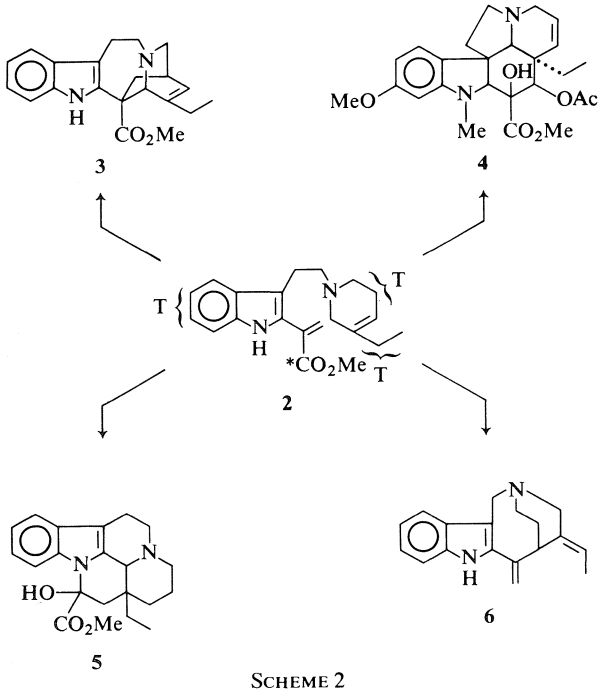

SCHEME 2

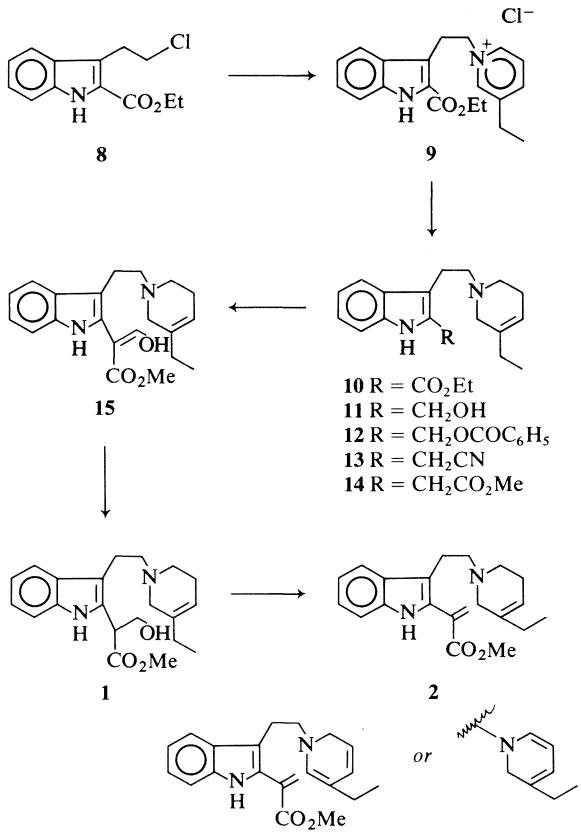

SCHEME 3

regarding generation of the labile indole acrylic ester moiety. The chloro ester **8** was available in large quantities by Japp–Klingemann reaction between diethyl γ-chloropropylmalonate (10) and benzenediazonium fluoroborate[1] and subsequent Fischer indole cyclisation. Condensation with 3-ethylpyridine afforded the salt **9** which on reduction with sodium borohydride gave the tetrahydropyridine **10**. Reduction of **10** with lithium aluminum hydride in tetrahydrofuran gave the primary alcohol **11** in 70% overall yield from **8**. Reaction of the corresponding benzoate with potassium cyanide in dimethylformamide provided the nitrile **13** which was solvolysed directly to the ester **14**. The conversion to 16,17-dihydrosecodin-17-ol (**1**) was similar to that reported by Battersby and Bhatnagar (11) and here formylation and careful reduction with sodium borohydride gave a 40% yield of **1**. At this point Smith and co-workers (12–14) had commented on the lability of secodine and in fact our initial attempts at dehydration of **1** met only with frustration.

[1]Alternative use of benzenediazonium chloride in large scale preparations proved quite hazardous.

Surprisingly, however, reaction with sodium hydride in benzene followed by *careful* work-up enabled a 61% isolation of the unstable secodine **2**. Studies with radiolabelled secodine revealed that 35% of the latter was transformed to presecamine and secamine (12–14) in 2 h at ambient temperature.

In view of the instability of secodine, the approach to 'dehydrosecodine' (**7**) necessitated either protection/stabilisation of the acrylic ester function and subsequent generation and trapping of the dihydropyridine moiety or alternatively, formation of the trapped dihydropyridine and then elaboration of the unsaturated ester. To adequately develop the chemistry of dihydropyridine units it was necessary to evaluate methods of their formation and trapping (15, 16) in the presence of a variety of functional groups (8). Thus pyridinium salts were chosen as the logical precursors of the corresponding dihydropyridines. Here we describe the preparation of simple pyridinium salts together with more complex alkaloid precursors containing this system.

The simplest model system (**16**) relevant to the present work was obtained by condensation between tryptophyl bromide and 3-ethylpyridine. The analogous product (**17**), now incorporating the acetic ester side chain, was available as outlined in Scheme 4. Exploitation of work reported by Plieninger (17) facilitated large scale preparations of the indole lactone (**18**) efficiently from butyrolactone. The action of dimethylamine readily afforded **19** which was reduced with lithium aluminum hydride to the corresponding tertiary amine. Reaction of the

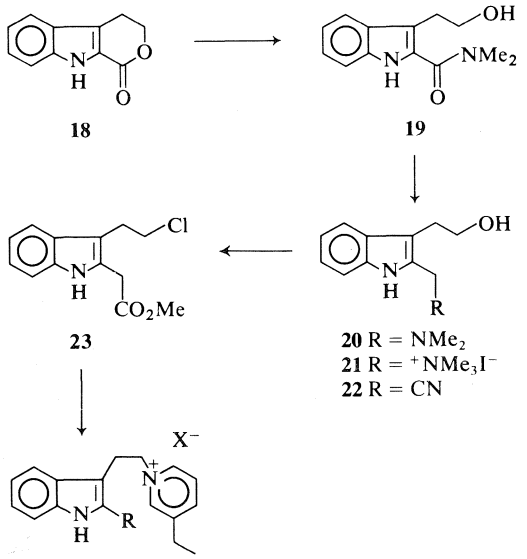

SCHEME 4

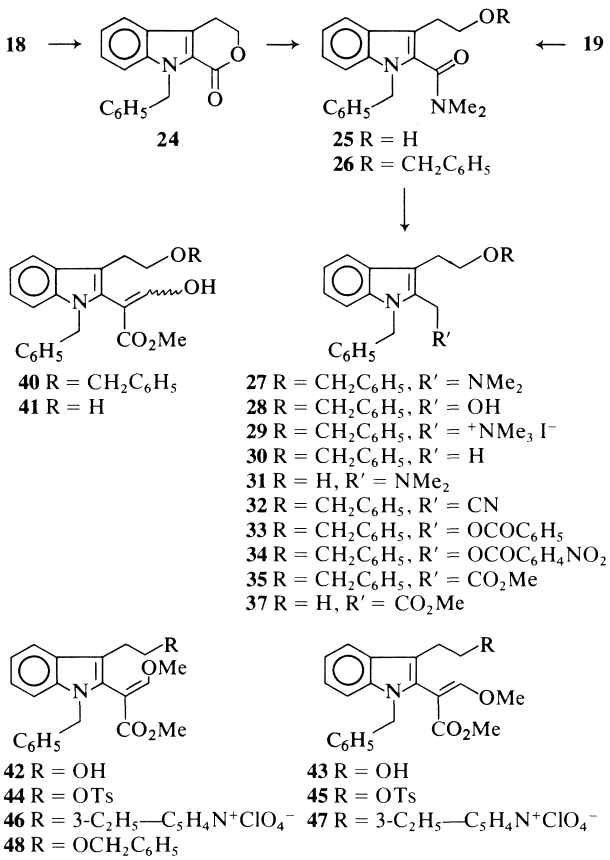

SCHEME 5

derived methiodide **21** with potassium cyanide in refluxing acetonitrile gave a high yield of the nitrile **22** which was solvolysed to the known (18) chloro ester **23**. Condensation with 3-ethylpyridine gave the salt, isolated as its perchlorate (**17**).

The salts **9**, **16**, and **17** now provided means of determining the formation and stability of trapped dihydropyridines in the presence of ester and indole groups and, via **17**, the possibility of elaborating an acrylic ester function in the presence of a preformed dihydropyridine. Subsequent investigations directed at the conversion of the ester side chain in **17** to the required acrylic ester met with difficulties. The instability of the latter system made isolation of intermediates virtually impossible, and it now appeared mandatory to provide stabilisation of the indole system before further elaboration.

N-Benzylation of the indole nucleus appeared to offer an appropriate means of stabilising the indole acrylic esters. Scheme 5 summarises the route employed. Ring opening of the protected indole lactone **24** and subsequent *O*-benzylation of the product provided **26** also available by dibenzylation of **19**. Reduction of **26** with lithium aluminum

hydride in tetrahydrofuran gave the required amine **27** as the minor component of a mixture with the primary alcohol **28**. Direct methylation, of the mixture, with methyl iodide in ethyl acetate gave a 48% yield of the methiodide salt **29**. Alternatively, borane reduction of **26** gave **27** in 58% yield together with the cleavage product **30**. At this point it was found that the hydroxy amide **25** was reduced cleanly, with lithium aluminum hydride, to the amine **31** without the complication of side products. Thus it was reasoned that an alkoxyaluminum hydride agent might provide similar improvements in the *O*-benzyl series. Indeed reduction of **26** with lithium *n*-butoxyaluminum hydride in tetrahydrofuran gave a 6.5:1 ratio of **27** and **28**. Direct methylation of this mixture gave an 82% yield of the salt **29**. As in the earlier sequence, displacement of triethylamine using potassium cyanide in acetonitrile proceeded efficiently to the corresponding nitrile **32**. Attempts to form **32** from the benzoate (**33**) or *p*-nitrobenzoate (**34**) were unsuccessful. Solvolysis of **32** with hydrogen chloride – moist methanol at reflux provided the debenzylated, chloro ester (**23**), whereas the use of acetyl chloride – methanol gave the ester (**35**) in 67% yield.

At this point elaboration to the model system (**36**) was readily accomplished by debenzylation to **37**, tosylation, iodination, and finally condensation of **39** with 3-ethylpyridine.

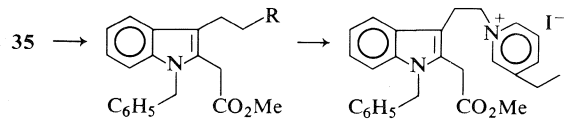

37 R = OH
38 R = OTs
39 R = I

36

Various methods of formation and protection of the acrylic ester function were investigated. The anion prepared from **35** and potassium diisopropylamide was allowed to react with methyl formate at ambient temperature to furnish the enol **40**, which on hydrogenolysis gave **41**. Methylation of **41** with diazomethane produced the *E*- and *Z*- enol ethers **42** and **43**, respectively. These ethers were more efficiently available from **35** by condensation with methyl formate, hydrogenolysis, and methylation without purification of the intermediates. In this manner a 58% yield of **42** and **43** was obtained. Each isomer formed a tosylate for eventual elaboration to the pyridinium systems **46** and **47**.

Analogous methylation of **40** did not yield the expected enol ether but gave instead two 'dimeric-type' products ($m/e \geq 838$) which were stable to quite vigorous acid conditions and were not affected by treatment with sodium borohydride. Furthermore these products were formed almost quantitatively on storage of **40** for several months, in the dark. Each of these dimers underwent apparent hydrogenolysis over Pd/C catalyst, to give in each case two products (m/e 658.3034, $C_{41}H_{42}N_2O_6$; m/e 700.3134, $C_{43}H_{44}N_2O_7$). Subsequently it was observed that the yield of the vinyl ethers **42** and **43** from the methylation of **41** was by no means reproducible and that the four desbenzyl 'dimers' mentioned above constituted up to 65% of the product mixture. The vinyl ether **42** was also available, although in poor yield, by acid-catalysed reaction of **41** in methanol for prolonged time periods at ambient temperature. Here, the major product (**37**) was presumably formed by Michael addition of methanol and subsequent retro-Aldol cleavage of the intermediate hemiacetal. Similarly **40** provided **48** and **35**. The consistent formation of 'dimeric' products, which were not further investigated, from the 3-hydroxyacrylic ester derivatives precluded this route as an efficient means of producing precursors containing the acrylic ester function. Moreover the expected enol ether hydrolysis was not observed when **42** was kept in dilute sulphuric acid for 18 h. Also the mild reduction process used earlier in the preparation of secodinol was ineffectual, even at ambient temperature, when applied to **40**.

Retrograde Michael reaction of β-amino lactones had proved efficient in the formation of α-methylene-γ-butyrolactone functions in certain sesquiterpenoids (19) and provided here a potential alternative for the generation of acrylic esters. In the event, condensation between the anion of **35** and the 1:1 adduct of dimethylformamide and dimethylsulphate gave the enamine **49**. Reduction of **49** with sodium cyanoborohydride gave directly the acrylic ester **50** together with the amine **51** which rapidly decomposed to **50** even below 0°C.

Alternatively, the stable enamine **52** was formed by heating **40** with piperidinium acetate in refluxing benzene. The use of piperidine in place of its salt gave variable ratios of **52** and **35**. Reduction of **52** with sodium cyanoborohydride and prolonged reflux in methanol afforded the required acrylic ester **50**. However, de-*O*-benzylation by hydrogenation over Pd/C catalyst was accompanied by saturation of the α,β-unsaturated ester to give **53**. Thus the enamine was hydrogenolysed to give the primary alcohol **54** which on reduction with sodium borohydride and subsequent base treatment produced the acrylic ester **55**. More efficiently, hydrogenation of **52** for prolonged periods followed by base treatment gave **55** directly. Reaction with *p*-toluenesulphonyl chloride and triethylamine in dichloromethane gave **56** which

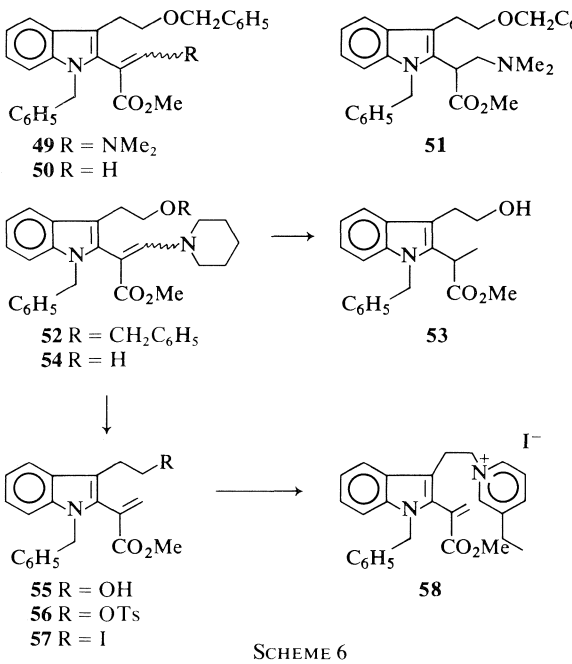

SCHEME 6

was converted to the primary iodide by the action of lithium iodide in refluxing acetone. Condensation of **57** with 3-ethylpyridine in the usual manner gave the required salt **58**. This final product, with the acrylic ester function stabilised by the *N*-benzyl group and containing the pyridinium progenitor of the dihydropyridine, appeared an ideal precursor of a dehydrosecodine (**7**).

Thus, in addition to the synthesis of secodine (**2**), a series of compounds, particularly **58**, of fundamental importance in the investigation of dihydropyridine systems such as **7**, was now in hand. Methods of generation and stabilisation of such systems are discussed in the accompanying publication.

Experimental

Melting points were determined on a Kofler block and are uncorrected. Ultraviolet (uv) spectra were recorded on a Cary 15 spectrophotometer in ethanol solution. The wavelengths of absorption maxima are reported in nanometers (nm) with log ε values in parentheses. Infrared (ir) spectra were measured on a Perkin Elmer model 710 or 457 spectrophotometer in chloroform solution. The absorption maxima are reported in wavenumbers (cm^{-1}), calibrated with respect to the absorption band of polystyrene at 1601 cm^{-1}. Proton magnetic resonance (^{1}Hmr) spectra were measured in deuteriochloroform ($CDCl_3$) solution at ambient temperature on either a Varian HA-100 or XL-100 spectrometer. Chemical shift values are given in the δ (ppm) scale relative to tetramethylsilane (TMS) used as internal standard. The integrated peak areas, signal multiplicities and proton assignments are given in parentheses. Low resolution mass spectra (ms) were determined on either an AEI-MS-902 or an Atlas CH-4B spectrometer. High resolution mass spectra were measured on an AEI-MS-902 instrument. Microanalyses were carried out by Mr. P. Borda of the Microanalytical Laboratory, University of British Columbia.

Thin-layer chromatography (tlc) utilized Merck silica gel G (according to Stahl) containing 2% fluorescent indicator. For preparative layer chromatography (plc), plates (20 × 20 or 20 × 60 cm) of 1-mm thickness were used. Visualization was effected by viewing under ultraviolet light and/or by colour reaction with ceric sulphate spray reagent. Column chromatography utilized Merck silica gel 60 (70–230 mesh) or Merck aluminum oxide 90 (neutral).

As a matter of routine, all reagents and solvents were recrystallised or distilled before use.

The Chloro Ester ***8***

Diethyl γ-chloropropylmalonate (10) (120 g) was added to a solution of sodium ethoxide (from 12 g of sodium) in dry ethanol and the mixture stirred at ambient temperature for 30 min in an atmosphere of nitrogen. Benzenediazonium fluoroborate (105 g) was added in small portions to the cooled solution such that the reaction mixture was kept below −2°C. Stirring was maintained at 0°C for 2 h and then at −10°C for 12 h. The mixture was poured into water (1 L) and extracted with ether. The extract was washed with water, brine, dried (Na_2SO_4), and concentrated *in vacuo*.

The crude product (190 g) and concentrated sulphuric acid (200 mL) were heated in refluxing dry ethanol (1 L) for 12 h. The cooled mixture was concentrated to ca. 500 mL *in vacuo*, poured onto crushed ice, and extracted with chloroform. The extract was washed successively with water, sodium carbonate solution, water, dried (Na_2SO_4), and concentrated *in vacuo*. The crude, semicrystalline material was chromatographed over alumina (grade III) with benzene–chloroform (1:1) to give the chloro ester **8** (yield 13–20%) as white plates from chloroform – petroleum ether; mp 131–132°C; uv λ_{max}: 296 (4.27), 229 (4.40); ir ν_{max}: 3250, 1670; ^{1}Hmr δ: 9.25 (1H, bs, —N*H*), 7.40 (4H, m), 4.46 (2H, q, J = 7 Hz, —$CO_2CH_2CH_3$), 3.50 (4H, m —CH_2CH_2Cl), 1.40 (3H, t, J = 7 Hz, —$CO_2CH_2CH_3$). *Anal.* calcd. for $C_{13}H_{14}NO_2Cl$: C 62.03, H 5.57, N 5.57, Cl 14.12; found: C 62.07, H 5.53, N 5.60, Cl 14.08.

The Salt ***9***

The chloro ester **8** (6.43 g) and 3-ethylpyridine (22 mL) were heated in a sealed tube at 120°C for 24 h. The mixture was poured into ether and the precipitate collected by filtration to give the pyridinium salt **9** (8.34 g, 91%); mp 87–89°C (methanol–ether); uv λ_{max}: 296 (4.20), 276 (3.90), 226 (4.35), 220 (4.30); ir ν_{max}: 3120–2880, 1701, 1250; ^{1}Hmr (CD_3OD) δ: 8.6–7.66 (4H, m, pyridinium-*H*), 7.44–6.82 (4H, m, indole-*H*), 4.26 (2H, q, J = 7 Hz, —$CO_2CH_2CH_3$), 2.60 (2H, q, J = 7 Hz, —CH_2CH_3), 1.37 (3H, t, J = 7 Hz, —$CO_2CH_2CH_3$), 1.02 (3H, t, J = 7 Hz, —CH_2CH_3); ms *m/e*: 358, 215, 187, 169, 129. This compound was hygroscopic and analysis was difficult.

The Tetrahydropyridine ***10***

A solution of sodium borohydride (25 g) in methanol (400 mL) was added slowly to the salt **9** (7.67 g) in methanol (275 mL) and triethylamine (8 mL). The mixture was stirred at ambient temperature for 2.5 h, diluted with water (100 mL), and the methanol removed *in vacuo*. The aqueous solution was adjusted to pH 2 with 6 *N* HCl, stirred at ambient temperature for 20 min, and then diluted with excess 10% sodium carbonate solution. The aqueous solution was extracted with dichloromethane, the extract washed with water, dried (Na_2SO_4), and concentrated *in vacuo* to give a thick gum (7 g); ^{1}Hmr ($CDCl_3$) δ: 5.5 (1H, bs, olefinic-*H*), 4.4 (2H, q, J = 7 Hz,

—$CO_2CH_2CH_3$). The crude product was homogeneous on tlc and was used as such for the next reaction.

The Alcohol ***11***

A solution of **10** (7 g) in dry tetrahydrofuran (70 mL) was added during 40 min to a suspension of lithium aluminum hydride (9 g) in dry tetrahydrofuran (350 mL) under a nitrogen atmosphere. The mixture was stirred at ambient temperature for 20 min then at reflux for 2 h. Normal work-up provided a light yellow gum (5.4 g) which was chromatographed on alumina to give the alcohol **11** (4.4 g, 70% from **8**); mp (methanol and sublimation) 108–110°C; uv λ_{max}: 292 (3.73), 284 (3.81), 274 (3.76), 223 (4.45); ir ν_{max}: 3340, 3180; ^{1}Hmr (CD_3OD) δ: 7.6–6.91 (4H, m, indole-*H*), 5.55 (1H, m, olefinic-*H*), 4.83 (2H, s, —CH_2OH), 1.00 (3H, t, J = 7 Hz, —CH_2CH_3); ms *m/e*: 284 (M^+), 174, 160, 142, 124. High resolution molecular weight determination, calcd. for $C_{18}H_{24}N_2O$: 284.188; found: 284.184. *Anal.* calcd. for $C_{18}H_{24}N_2O{\cdot}CH_3OH$: C 72.09, H 8.93, N 8.85; found: C 72.05, H 9.13, N 8.22.

The Benzoate ***12***

Benzoylation of **11** with benzoyl chloride in pyridine at 0°C gave **12**; mp (dichloromethane – petroleum ether) 110.5–112.5°C; uv λ_{max}: 293 (3.80), 284 (3.96), 274 (3.94), 224 (4.61); ir ν_{max}: 3000, 1715, 1455, 1260; ^{1}Hmr δ: 8.64 (1H, s, —N*H*), 8.0–7.0 (9H, m, aromatic-*H*), 5.42 (3H, bs, olefinic-*H* plus —$CH_2OCOC_6H_5$), 1.00 (3H, t, J = 7 Hz, —CH_2CH_3); ms *m/e*: 388 (M^+), 266, 170, 143, 124, 122. High resolution molecular weight determination, calcd. for $C_{25}H_{28}N_2O_2$: 388.216; found: 388.215. *Anal.* calcd. for $C_{25}H_{28}N_2O_2$: C 77.27, H 7.28, N 7.21; found: C 77.05, H 7.29, N 7.05.

The benzoate was also available (99% yield) by reaction of **11** with benzoyl chloride in tetrahydrofuran in the presence of anhydrous potassium carbonate, followed by chromatography on alumina.

The Nitrile ***13***

The benzoate **12** (2.0 g) and potassium cyanide (3.3 g) were stirred in dimethylformamide (60 mL) for 1 h under nitrogen. The temperature was raised gradually to 105–110°C over a period of 45 min, maintained at that temperature for 1 h, cooled, diluted with water (100 mL), and extracted with dichloromethane. The extract was washed with water, dried (Na_2SO_4), and concentrated *in vacuo*. Chromatography on alumina afforded **13** (0.95 g, 65%); mp (dichloromethane – petroleum ether) 135–137°C; uv λ_{max}: 291 (3.77), 281 (3.85), 274 (3.84), 221 (4.69); ir ν_{max}: 3160, 2900, 2256; ^{1}Hmr δ: 8.37 (1H, s, —N*H*), 7.54–7.00 (4H, m, indole-*H*), 5.42 (1H, m, olefinic-*H*), 3.8 (2H, s, —CH_2CN), 1.01 (3H, t, J = 7 Hz, —CH_2CH_3); ms *m/e*: 293 (M^+), 267, 169, 156, 124. High resolution molecular weight determination, calcd. for $C_{19}H_{23}N_3$: 293.189; found: 293.186. *Anal.* calcd. for $C_{19}H_{23}N_3$: C 77.75, H 7.92, N 14.32; found: C 77.65, H 7.86, N 14.16.

The Ester ***14***

A solution of the nitrile **13** (746 mg) and water (0.2 mL) in dry methanol (20 mL) was saturated, at 0°C, with HCl gas and then kept at ambient temperature for 60 h. The mixture was concentrated *in vacuo*, diluted with sodium bicarbonate solution, and extracted with dichloromethane. The extract was washed with water, dried (Na_2SO_4), and concentrated *in vacuo*. Chromatography on alumina gave the ester **14** (574 mg, 70%); mp (dichloromethane – petroleum ether) 85–87.5°C; uv λ_{max}: 292 (3.83), 283 (3.92), 274 (3.87), 223 (4.43); ir ν_{max}: 3000, 1728, 1460, 1245; ^{1}Hmr δ: 8.54 (1H, bs, —N*H*), 7.58–7.00 (4H, m, indole-*H*), 5.42 (1H, m, olefinic-*H*), 3.73 (2H, s, —$CH_2CO_2CH_3$), 3.66 (3H, s, —CO_2CH_3), 1.00 (3H, t, J = 7 Hz, —CH_2CH_3); ms *m/e*: 326 (M^+), 267, 202, 156, 144, 124. High resolution molecular weight determination, calcd. for $C_{20}H_{26}N_2O_2$: 326.199; found: 326.202. *Anal.* calcd. for $C_{20}H_{26}N_2O_2$: C 73.50, H 8.04, N 8.58; found: C 73.47, H 8.05, N 8.71.

The Enol ***15***

The ester **14** (50 mg) in dry benzene (3 mL) was added slowly to a suspension of excess sodium hydride (ca. 25 mg) in dry benzene (2 mL) and redistilled methyl formate (2 mL) under an atmosphere of dry nitrogen. The mixture was stirred at ambient temperature for 15 min and then at 35°C for 2 h. The mixture was cooled to ca. 0°C, diluted with methanol (3 drops), and crushed ice. The solution was adjusted to pH 2 with 2 *N* hydrochloric acid, diluted with sodium bicarbonate solution, and extracted with dichloromethane. The extract was washed with water, dried (Na_2SO_4), and concentrated *in vacuo* to afford the crude enol **15** as a white foam. This product was not purified but used directly for the next reaction.

16,17-Dihydrosecodin-17-ol ***1***

Sodium borohydride (50 mg) was added in small portions to a solution of the crude enol **15** (ca. 60 mg) in methanol (3 mL) at −30°C. The mixture was stirred at this temperature for 40 min. The excess hydride was destroyed by careful addition of 2 *N* HCl (2–3 drops). The mixture was diluted with water and the methanol removed *in vacuo*. The aqueous solution was acidified with 2 *N* HCl, then diluted with sodium bicarbonate solution, and extracted with chloroform. The extract afforded 68 mg of white foam. Chromatography on alumina gave **1** (22 mg, 40% from (**14**)); mp (dichloromethane) 131.5–132°C; uv λ_{max}: 292 (3.86), 284 (3.93), 274 (3.87), 222 (4.49); ir ν_{max}: 3400, 3050, 2900, 1718, 1465, 1235; ^{1}Hmr δ: 8.84 (1H, s, —N*H*), 7.52–7.00 (4H, m, indole-*H*), 5.39 (1H, bs, C(15)-*H*), 4.00 (4H, m, —$CHCH_2OH$), 3.63 (3H, s, —CO_2CH_3), 0.96 (3H, t, J = 7 Hz, —CH_2CH_3); ms *m/e*: 356 (M^+), 338, 326, 214, 202, 124. High resolution molecular weight determination, calcd. for $C_{21}H_{28}N_2O_3$: 356.209; found: 356.207. *Anal.* calcd. for $C_{21}H_{28}N_2O_3$: C 70.24, H 7.93, N 7.86; found: C 70.20, H 7.83, N 7.35.

Secodine ***2***

A solution of the alcohol **1** (20 mg) in dry benzene (2.5 mL) was added, all at once, to a suspension of sodium hydride (16 mg) in dry benzene (0.5 mL). The mixture was stirred at 40°C for 15 min, cooled, and quickly flushed through alumina (2 g, activity IV) with benzene. The eluate was quickly freeze dried to give secodine (**2**) (9.1 mg, 50%) as a light yellow gum; ^{1}Hmr δ: 9.11 (1H, bs, —N*H*), 7.60–7.00 (4H, m, indole-*H*), 6.45 (1H, d, J = 1 Hz, C(17)-*H*), 6.09 (1H, d, J = 1 Hz, C(17)-*H*), 5.42 (1H, m, C(15)-*H*), 3.80 (3H, s, —CO_2CH_3), 1.00 (3H, t, J = 7 Hz, —CH_2CH_3); ms *m/e*: 338 (M^+), 307, 251, 214, 154, 124.

The Amide ***19***

The indole lactone **18** and excess dimethylamine were stirred in dry methanol at ambient temperature for 48 h. The solvent was removed *in vacuo* and the residue crystallised from acetone–hexane to give the amide (**19**) (87.5%), mp 125–126°C; uv λ_{max}: 289 (4.31), 218 (4.75); ir ν_{max}: 3460, 3200, 1600; ^{1}Hmr δ: 5.92 (1H, s, D_2O exchangeable, —CH_2CH_2OH), 4.0 (2H, t, J = 6 Hz, —CH_2OH), 3.11 (2H, t, J = 6 Hz, —CH_2CH_2OH), 3.04 (6H, s, —$N(CH_3)_2$); ms *m/e*: 232 (M^+), 202 (100%), 158, 128. High resolution molecular weight determination, calcd. for $C_{13}H_{16}N_2O_2$: 232.1211; found: 232.1214.

The Amine ***20***

A solution of the amide **19** (32 g) in dry tetrahydrofuran

(200 mL) was added slowly to a suspension of lithium aluminum hydride (30 g) in dry tetrahydrofuran (750 mL) at 0°C under a nitrogen atmosphere. The mixture was heated under reflux for ca. 5 h, cooled, and quenched with saturated sodium sulphate solution. The mixture was filtered and the solids washed with hot ethyl acetate (ca. 2 L). The filtrate was evaporated and the residue recrystallised from ethyl acetate to give **20** (24.3 g, 84%); mp 140–142°C; uv λ_{max}: 290 (3.88), 281 (3.95), 274 (3.91), 222 (4.61); ir ν_{max}: 3470, 3400–3000; ^{1}Hmr δ: 8.70 (1H, bs, —N*H*), 4.29 (1H, bs, —O*H*), 3.84 (2H, t, J = 6 Hz, —CH_2OH), 3.49 (2H, s, —CH_2N(CH$_3$)$_2$), 3.01 (2H, t, J = 6 Hz, —CH_2CH$_2$OH), 2.20 (6H, s, —N(CH_3)$_2$); ms *m/e*: 218 (M^+), 174, 173, 144 (100%), 143, 132, 130, 115. *Anal.* calcd. for $C_{13}H_{18}N_2O$: C 71.53, H 8.31, N 12.83; found: C 71.39, H 8.15, N 12.79.

*The Methiodide **21***

A solution of iodomethane (27.2 g) in ethyl acetate (40 mL) was added to the amine **20** (24 g) in ethyl acetate (700 mL). The mixture was stirred at ambient temperature for 45 min then at 50°C for 1 h. The mixture was cooled and the precipitate collected by filtration. Recrystallisation from ethanol yielded **21** (35.7 g, 90%); mp 162–165°C; uv λ_{max}: 296 (3.68), 286 (3.93), 273 (4.02), 218 (4.72); ir ν_{max}: 3410, 3280; ^{1}Hmr ($CDCl_3$ + DMSO-d_6) δ: 10.84 (1H, s, —N*H*), 4.96 (2H, s, —CH_2N$^+$), 4.20 (2H, t, J = 6 Hz, —CH_2OH), 3.28 (9H, s, —$^+$N(CH$_3$)$_3$), 3.13 (2H, t, J = 6 Hz, —CH_2CH$_2$OH).

*The Nitrile **22***

The methiodide **21** (40 g) and potassium cyanide (30 g) were heated in refluxing acetonitrile (1 L) under nitrogen for 20 h. The mixture was cooled and filtered. The filtrate was evaporated and the residue filtered through alumina (grade III) with dichloromethane and then with ethyl acetate to give **22** (18.5 g, 87%) mp (benzene) 106–107°C; uv λ_{max}: 289 (3.79), 279 (3.90), 272 (3.89), 220 (4.58); ir ν_{max}: 3680, 3620, 3460, 2400; ^{1}Hmr δ: 8.29 (1H, bs, —N*H*), 3.84 (2H, s, —CH_2CN), 3.81 (2H, t, J = 6 Hz, —CH_2OH), 2.90 (2H, t, J = 6 Hz, —CH_2CH$_2$OH), 1.66 (1H, s, —OH); ms *m/e*: 200 (M^+), 182, 169, 142, 115, 77, 64. *Anal.* calcd. for $C_{12}H_{12}N_2O$: C 71.98, H 6.04, N 13.99; found: C 72.10, H 6.20, N 13.74.

*The Salt **17***

The chloro ester **23** (5.14 g) and freshly distilled 3-ethylpyridine (15 mL) were heated at 82°C for 18 h. The solution was cooled and diluted with ether. The ether was decanted and the residual oil chromatographed on alumina (grade V) with ethyl acetate. Evaporation of the eluate gave a thick oil which was dissolved in water (100 mL). A saturated solution of sodium perchlorate (25 mL) was added and the formed precipitate collected by filtration. Recrystallisation from methanol gave the perchlorate **17** (3.85 g, 44%), mp 140–141.5°C; uv λ_{max}: 289 (3.83), 280 (3.91), 271 (3.98), 265 (4.01), 219 (4.56); ir ν_{max}: 3350, 1740; ^{1}Hmr ($CDCl_3$ + DMSO-d_6) δ: 10.77 (1H, bs, —N*H*), 8.70 (1H, d, J = 6 Hz, C(6′)-*H*), 8.46 (1H, s, C(2′)-*H*), 8.19 (1H, d, J = 8 Hz, C(4′)-*H*), 7.79 (1H, dd, J = 8, 6 Hz, C(5′)-*H*), 4.81 (2H, t, J = 6.5 Hz, —CH$_2$C$H_2$$^+$N—), 3.83 (2H, s, —C$H_2CO_2CH_3$), 3.74 (3H, s, —OC$H_3$), 3.40 (2H, t, J = 6.5 Hz, —CH_2CH$_2$—$^+$N—), 2.60 (2H, q, J = 8 Hz, —CH_2CH$_3$), 1.01 (3H, t, J = 8 Hz, —CH$_2$CH_3). *Anal.* calcd. for $C_{20}H_{23}N_2ClO_6$: C 56.81, H 5.48, N 6.62; found: C 56.61, H 5.30, N 6.63.

*The Lactone **24***

A solution of the lactone **18** (18.7 g) in HMPA (40 mL) and tetrahydrofuran (30 mL) was added slowly to a suspension of potassium hydride (40 mL of 23% suspension) in HMPA (40 mL) and tetrahydrofuran (500 mL) at 0–5°C. Benzyl bromide (35 mL) was added at 0–5°C and stirring maintained at this temperature for 30 min then at ambient temperature for 2 h. The mixture was cooled in ice and excess hydride destroyed by the addition of alumina (grade III, 200 g) and the mixture stirred for 45 min. The solids were removed by filtration and the filtrate concentrated *in vacuo*. Chromatography on silica gel gave **24** (19.9 g, 67%) mp (ethyl acetate – hexane) 109–109.5°C; uv λ_{max}: 297 (4.55), 232 (4.64); ir ν_{max}: 1710; ^{1}Hmr δ: 7.7–7.0 (9H, m, aromatic-*H*), 5.76 (2H, s, —N—CH_2C$_6$H$_5$), 4.56 (2H, t, J = 6 Hz, —CH_2O—), 3.07 (2H, t, J = 6 Hz, —CH_2CH$_2$O—); ms *m/e*: 277 (M^+), 91 (100%). *Anal.* calcd. for $C_{18}H_{15}NO_2$: C 77.96, H 5.45, N 5.05; found: C 77.92, H 5.56, N 5.00.

*The Amide **25***

As described above for the preparation of **19**, **24** gave a 97% yield of **25**; mp (methanol–hexane) 93.5–94°C; uv λ_{max}: 287 (4.31), 215 (4.91); ir ν_{max}: 3280, 1630, 740–710; ^{1}Hmr δ: 6.8–7.8 (9H, m, aromatic-*H*), 5.28 (2H, s, —NCH_2C$_6$H$_5$), 3.78 (2H, t, J = 6 Hz, —CH$_2$CH_2OH), 2.93 (3H, bs, —CONCH_3), 2.95 (2H, m, —CH_2CH$_2$OH), 2.53 (3H, bs, —CONCH_3); ms *m/e*: 322 (M^+), 292 (100%), 291, 278, 277, 248, 247, 91. High resolution molecular weight determination, calcd. for $C_{20}H_{24}N_2O_2$: 322.168; found: 322.165. *Anal.* calcd. for $C_{20}H_{24}N_2O_2$: C 74.51, H 6.88, N 8.69; found: C 74.35, H 6.79, N 8.52.

*The Amide **26***

(*a*) As described for the preparation of **24**, **25** gave a 91% yield of **26** as a thick gum; uv λ_{max}: 287 (3.97), 215 (4.55); ir ν_{max}: 1630, 745, 700; ^{1}Hmr δ: 6.9–7.7 (14H, m, aromatic-*H*), 5.28 (2H, s, —NCH_2C$_6$H$_5$), 4.47 (2H, s, —OCH_2C$_6$H$_5$), 3.69 (2H, t, J = 7 Hz, —CH_2OCH$_2$C$_6$H$_5$), 3.04 (2H, t, J = 7 Hz, —CH_2CH$_2$O—), 2.89 (3H, bs, —CONCH_3), 2.44 (3H, bs, —CONCH_3); ms *m/e*: 412 (M^+), 291, 149, 91 (100%). High resolution molecular weight determination, calcd. for $C_{27}H_{28}N_2O_2$: 412.2151; found: 412.2159.

(*b*) A mixture of **19** (4.64 g), benzyl bromide (20 mL), and tetra-*n*-butylammonium iodide (7.2 g) was heated under reflux in 2 *N* KOH (40 mL) and toluene (65 mL) for 5 h. The mixture was cooled and extracted with ether. The extract was washed with brine, dried (Na_2SO_4), and evaporated. Chromatography on silica gel gave **26** (7.8 g, 95%) identical with that obtained above.

*Reductions of the Amide **26***

(*a*) A solution of the amide (**26**) (1.65 g) in dry tetrahydrofuran (10 mL) was added slowly to a suspension of lithium aluminum hydride (230 mg) in dry tetrahydrofuran (10 mL) at 0°C under nitrogen. The mixture was stirred at ambient temperature for 4 h, cooled, and excess hydride destroyed with $Na_2SO_4 \cdot 10H_2O$. The solids were removed by filtration and the filtrate concentrated *in vacuo*. Chromatography on silica gel afforded:

*The amine **27***—(150 mg, 9.5%); uv λ_{max}: 296, 285, 277, 225; ir ν_{max}: 1470, 1450, 1360, 740, 700; ^{1}Hmr δ: 6.8–7.7 (14H, m, aromatic-*H*), 5.50 (2H, s, —NCH_2C$_6$H$_5$), 4.48 (2H, s, —OCH_2C$_6$H$_5$), 3.67 (2H, t, J = 8 Hz, —CH$_2$CH_2O—), 3.19 (2H, s, —CH_2N(CH$_3$)$_2$), 3.09 (2H, t, J = 8 Hz, —CH_2CH$_2$O—), 2.11 (6H, s, —N(CH_3)$_2$); ms *m/e*: 398 (M^+), 354, 353, 352, 262, 232, 91 (100%). High resolution molecular weight determination, calcd. for $C_{27}H_{30}N_2O$: 398.2358; found: 398.2387.

*The alcohol **28***—(850 mg, 67%); uv λ_{max}: 297 (3.81), 286 (3.88), 279 (3.87), 225 (4.52); ir ν_{max}: 3400, 740, 700; ^{1}Hmr δ: 6.8–7.6 (14H, m, aromatic-*H*), 5.35 (2H, s, —NCH_2C$_6$H$_5$), 4.54 (2H, s, —CH_2OH), 4.38 (2H, s, —OCH_2C$_6$H$_5$), 3.66 (2H, t, J = 6 Hz, —CH$_2$CH_2O—), 3.06 (2H, t, J = 6 Hz, —CH_2CH$_2$O—), 2.82 (1H, bs, —O*H*); ms *m/e*: 371 (M^+),

250 (100%), 91. High resolution molecular weight determination, calcd. for $C_{24}H_{25}NO_2$: 371.1885; found: 371.1906.

(*b*) A solution of the amide **26** (3.0 g) in dry tetrahydrofuran (25 mL) was added slowly to a suspension of lithium aluminum hydride (928 mg) in dry tetrahydrofuran (20 mL) at 0–5°C under nitrogen. The mixture was stirred at ambient temperature for 18 h. Work-up as described above gave a thick oil (3.127 g) which was stirred with iodomethane (6 mL) in ethyl acetate (50 mL) for 40 h at ambient temperature. The solid material was collected by filtration and the filtrate evaporated to give **28** (1.26 g, 46%) identical with that obtained above. The solid was recrystallised from methanol – ethyl acetate to yield the methiodide **29** (2.12 g, 48%); mp 143–145.5°C (dec.); uv λ_{max}: 304 (3.71), 292 (3.89), 276 (4.01), 220 (4.68); ir ν_{max}: 1400, 1200, 1100, 1030, 860, 730, 690; ^{1}Hmr ($CDCl_3$ + DMSO-d_6) δ: 6.7–7.8 (14H, m, aromatic-*H*), 5.67 (2H, s, —N$CH_2C_6H_5$), 5.01 (2H, s, —$CH_2N(CH_3)_3$), 4.46 (2H, s, —O$CH_2C_6H_5$), 3.81 (2H, t, J = 6.5 Hz, —CH_2CH_2O—), 3.24 (11H, envelope, —N(CH_3)$_3$ and —CH_2CH_2O—). *Anal.* calcd. for $C_{28}H_{33}N_2OI$: C 62.22, H 6.15, N 5.18; found: C 62.21, H 6.30, N 5.12.

(*c*) A solution of borane–tetrahydrofuran (1.5 mL of 1 *N* solution) was added to the amide **26** (250 mg) in dry tetrahydrofuran (50 mL) at 0–5°C under a nitrogen atmosphere. The solution was refluxed for 1 h, diluted with triethylamine (1 mL), and reflux continued for 2 h. The mixture was cooled and concentrated *in vacuo*. The residue was dissolved in ethyl acetate, washed with 1 *N* ammonium hydroxide solution, water, brine, dried (Na_2SO_4), and concentrated *in vacuo*. Chromatography on silica gel gave the amine **27** (140 mg, 58%) identical with that prepared above.

(*d*) *n*-Butanol (8.4 mL) was added, over a period of 15 min, to a suspension of lithium aluminum hydride (3.5 g) in dry tetrahydrofuran (60 mL) at 0–5°C under nitrogen and the mixture stirred at ambient temperature for 1 h. A solution of the amide **26** (7.4 g) in dry tetrahydrofuran (100 mL) was added and the mixture stirred at ambient temperature for 4 h. Work-up as described above gave a mixture of **27** and **28** (6.5 g, ratio 6.5:1 by ^{1}Hmr).

This crude product was stirred in ethyl acetate (200 mL) with iodomethane (20 mL) for 18 h. The solid was collected by filtration and the filtrate evaporated to give **28** (0.91 g). Recrystallisation of the solid material from methanol – ethyl acetate gave the salt **29** (8.1 g, 82%).

The Nitrile 32

The salt **29** (18.5 g) and potassium cyanide (10 g) were stirred in refluxing acetonitrile (500 mL) for ca. 40 h. The mixture was cooled and filtered. The filtrate was washed with water (2×), brine (2×), dried, and concentrated *in vacuo*. Chromatography of the residue provided the nitrile **32** (10.6 g, 82%) as a thick gum; uv λ_{max}: 295 (3.84), 283 (3.93), 275 (3.93), 222 (4.59), ir ν_{max}: 2250, 740, 700; ^{1}Hmr δ: 6.8–7.7 (14H, m, aromatic-*H*), 5.40 (2H, s, —N$CH_2C_6H_5$), 4.44 (2H, s, —O$CH_2C_6H_5$), 3.69 (2H, s, —CH_2CN), 3.66 (2H, t, J = 6.5 Hz, —$CH_2OCH_2C_6H_5$), 3.04 (2H, t, J = 6.5 Hz, —CH_2CH_2O—); ms *m/e*: 380 (M^+), 289, 91 (100%). High resolution molecular weight determination, calcd. for $C_{26}H_{24}N_2O$: 380.1887; found: 380.1909.

Excess cyanide in the solid and aqueous washings was destroyed with a saturated solution of ferrous sulphate containing some ferric sulphate.

The Benzoate 33

Benzoyl chloride (3.5 mL) was added to a solution of the alcohol (**28**) (5.6 g) and triethylamine (10 mL) in tetrahydrofuran (200 mL) at 0–5°C and the mixture stirred at ambient temperature for 6 h. The mixture was partitioned between ether and saturated potassium bicarbonate solution. The organic layer was washed with water, brine, dried (Na_2SO_4), and evaporated. Recrystallisation of the residue from ethyl acetate – petroleum ether gave **33** (4.6 g, 64%); mp 90.5–92°C; uv λ_{max}: 300 (3.86), 275 (4.16), 225 (4.66); ir ν_{max}: 1710; ^{1}Hmr δ: 6.8–7.8 (19H, m, aromatic-*H*), 5.45 (2H, s, —$CH_2OCOC_6H_5$), 5.42 (2H, s, —N$CH_2C_6H_5$), 4.16 (2H, s, —O$CH_2C_6H_5$), 3.70 (2H, t, J = 7 Hz, —CH_2CH_2O—), 3.22 (2H, t, J = 7 Hz, —CH_2CH_2O—); ms *m/e*: 475 (M^+), 354 (100%), 232, 91. *Anal.* calcd. for $C_{32}H_{29}NO_3$: C 80.82, H 6.15, N 2.95; found: C 80.62, H 6.19, N 2.92.

The p*-Nitrobenzoate 34*

Similarly the use of *p*-nitrobenzoyl chloride gave **34** (54%); mp (ethyl acetate – hexane) 89–91°C; uv λ_{max}: 300 (3.96), 268 (4.30), 224 (4.63); ir ν_{max}: 1720, 1530, 1350; ^{1}Hmr δ: 8.07 (2H, d, J = 10 Hz, aromatic-*H*), 7.73 (2H, d, J = 10 Hz, aromatic-*H*), 6.8–7.7 (14H, m, aromatic-*H*), 5.57 (2H, s, —CH_2OCOAr), 5.46 (2H, s, —N$CH_2C_6H_5$), 4.50 (2H, s, —O$CH_2C_6H_5$), 3.75 (2H, t, J = 7 Hz, —CH_2CH_2O—), 3.26 (2H, t, J = 7 Hz, —CH_2CH_2O—); ms *m/e*: 520 (M^+), 399, 234, 167, 121, 91 (100%). *Anal.* calcd. for $C_{32}H_{28}N_2O_5$: C 73.83, H 5.42, N 5.38; found: C 73.91, H 5.63, N 5.23.

Solvolysis of the Nitrile 32

(*a*) A solution of the nitrile **32** (20 g) in dry methanol (400 mL) and water (4 mL), cooled to ca. 0°C was saturated with hydrogen chloride. The mixture was heated to reflux for 1 h, cooled, and concentrated *in vacuo*. The residue was partitioned between saturated sodium bicarbonate solution and dichloromethane. The organic layer was washed with water, brine, dried (Na_2SO_4 and K_2CO_3), and evaporated. Chromatography on silica gel afforded the ester (**23**) (8.8 g, 32%) identical with a sample prepared earlier.

(*b*) Reaction of the nitrile **32**, as described above in *a*, at ambient temperature for 72 h, gave after chromatography the ester **35** (67%) as a gum; uv λ_{max}: 295 (3.81), 287 (3.90), 277 (3.87), 224 (4.53); ir ν_{max}: 1735, 740, 700; ^{1}Hmr δ: 6.8–7.7 (14H, m, aromatic-*H*), 5.38 (2H, s, —N$CH_2C_6H_5$), 4.48 (2H, s, —O$CH_2C_6H_5$), 3.71 (2H, s, —$CH_2CO_2CH_3$), 3.68 (2H, t, J = 7 Hz, —CH_2CH_2O—), 3.43 (3H, s, —OCH_3), 3.08 (2H, t, J = 7 Hz, —CH_2CH_2O—); ms *m/e*: 413 (M^+), 312, 292, 91 (100%). High resolution molecular weight determination, calcd. for $C_{27}H_{27}NO_3$: 413.1989; found: 413.1950.

(*c*) Reaction as in *b* above, using acetyl chloride to generate hydrogen chloride in methanol also gave **35** in 67% yield.

The Ester 37

The ester **35** (2.0 g) was hydrogenated over 10% Pd/C (150 mg) in ethyl acetate (40 mL), methanol (40 mL), and 60% perchloric acid (1.6 mL) for 3 h. The mixture was filtered through Celite. The filtrate was diluted with ethyl acetate, washed with 5% sodium bicarbonate solution, dried (Na_2SO_4), and evaporated. Chromatography on silica gel gave the ester **37** (1.44 g, 92%); uv λ_{max}: 274 (3.40); ir ν_{max}: 3600, 1730; ^{1}Hmr δ: 6.9–7.7 (9H, m, aromatic-*H*), 5.37 (2H, s, —N$CH_2C_6H_5$), 3.90 (2H, t, J = 7 Hz, —CH_2CH_2OH), 3.78 (2H, s, —$CH_2CO_2CH_3$), 3.53 (3H, s, —OCH_3), 3.05 (3H, t, J = 7 Hz, —CH_2CH_2OH); ms *m/e*: 323 (M^+), 292, 131. High resolution molecular weight determination, calcd. for $C_{20}H_{21}NO_3$: 323.1516; found: 323.1543.

The Tosylate 38

The alcohol **37** (1.44 g), *p*-toluenesulphonic acid (2 g), and triethylamine (1 mL) were stirred in dichloromethane (50 mL) at ambient temperature for 24 h. The solvent was removed under reduced pressure and the residue chromatographed on silica gel to give starting material **37** (290 mg) and the tosylate **38** (1.5 g, 70%).

The Iodide ***39***

The crude tosylate **38** (1.5 g) and lithium iodide (400 mg) were heated in refluxing acetone (50 mL) for 19 h. The solvent was removed *in vacuo* and the residue chromatographed on silica gel to yield the iodide **39** (1.22 g, 90%).

The Pyridinium Salt ***36***

The crude iodide **39** (1.22 g) was heated at 45–50°C in 3-ethylpyridine (10 mL) for 17 h. The solvent was removed by aezeotropic distillation with water. The residue was partitioned between water and ethyl acetate. Evaporation of the aqueous layer gave the salt **36** (1.3 g, 85%); mp (acetone) 143–144°C; uv λ_{max}: 265 (4.0); ir ν_{max}: 1710; ^{1}Hmr δ: 9.12 (1H, d, J = 5 Hz, C(6′)-*H*), 8.74 (1H, s, C(2′)-*H*), 8.00 (1H, d, J = 7 Hz, C(4′)-*H*), 7.70 (1H, dd, J = 7, 5 Hz, C(5′)-*H*), 6.76–7.30 (9H, m, aromatic-*H*), 5.25 (2H, s, —NC*H*$_2$C$_6$H$_5$), 5.08 (2H, t, J = 6 Hz, —CH$_2$C*H*$_2$N—), 3.82 (2H, s, —C*H*$_2$CO$_2$CH$_3$), 3.48 (2H, t, J = 6 Hz, —C*H*$_2$CH$_2$N—), 3.49 (3H, s, —OC*H*$_3$), 2.56 (2H, q, J = 6 Hz, —C*H*$_2$CH$_3$), 0.90 (3H, t, J = 6 Hz, —CH$_2$C*H*$_3$). *Anal.* calcd. for C$_{27}$H$_{29}$N$_2$O$_2$I: C 60.00, H 5.37, N 5.19, I 23.52; found: C 59.64, H 5.40, N 5.13, I 23.40.

The Enol ***40***

Potassium diisopropylamide was prepared at −30 to 0°C from potassium hydride (5.5 mL of 20% dispersion in oil) and diisopropylamine (10 mL) in dry tetrahydrofuran (50 mL) and dry HMPA (5 mL). A solution of **35** (3.0 g) in dry tetrahydrofuran (10 mL) was added at −30°C. The mixture was stirred at this temperature for 15 min, at ambient temperature for 1 h, then cooled to −30°C. Dry methyl formate (50 mL) was added and the mixture stirred at ambient temperature for 18 h and diluted with water (100 mL), ethyl acetate (250 mL), and 1 *N* HCl (100 mL). The organic layer was washed with water, saturated sodium bicarbonate solution, brine, dried (Na_2SO_4), and concentrated *in vacuo*. Chromatography on silica gel gave the crude enol **40** (2.6 g) as a pale yellow crystalline solid satisfactory for use in further reactions. Recrystallisation from methanol gave pure **40** (2.1 g, 65%); mp 88–90°C; uv λ_{max}: 295 (4.01), 286 (4.12), 275 (4.17), 225 (4.45); ir ν_{max}: 3500–3000, 1665, 1605; ^{1}Hmr δ: 6.8–7.8 (16H, m, aromatic-*H*, olefinic-*H*, —O*H*), 5.11 (2H, s, —NC*H*$_2$C$_6$H$_5$), 4.46 (2H, s, —OC*H*$_2$C$_6$H$_5$), 3.64 (2H, t, J = 7 Hz, —CH$_2$C*H*$_2$O—), 3.35 (3H, s, —OC*H*$_3$), 2.95 (2H, t, J = 7 Hz, —C*H*$_2$CH$_2$O—); ms *m/e*: 441 (M$^+$), 320, 290, 289, 288, 91 (100%). *Anal.* calcd. for C$_{28}$H$_{27}$NO$_4$: C 76.17, H 6.16, N 3.17; found: C 76.16, H 6.00, N 3.35.

The Enol ***41***

The enol **40** (52 mg) and 10% Pd/C catalyst (11 mg) were stirred in methanol (5 mL) under one atmosphere of hydrogen at ambient temperature for 9 h. The mixture was filtered through Celite and the filtrate concentrated *in vacuo*. Chromatography on silica gel gave **40** (12 mg) and **41** (28 mg, 67%) as a clear gum; uv λ_{max}: 276, 225; ir ν_{max}: 3700–3200, 1665, 1610; ^{1}Hmr δ: 6.4–7.7 (12H, m, aromatic-*H*, olefinic-*H*, 2 × —O*H*), 5.11 (2H, bs, —NC*H*$_2$C$_6$H$_5$), 3.72 (2H, poorly resolved t, —CH$_2$C*H*$_2$OH), 3.36 (3H, bs, —OC*H*$_3$), 2.88 (2H, poorly resolved t, —C*H*$_2$CH$_2$OH); ms *m/e*: 351 (M$^+$), 320, 319, 292, 289, 288, 91 (100%).

The Ethers ***42*** *and* ***43***

Excess ethereal diazomethane was added at 0–5°C to a solution of **41** (55 mg) in ethyl acetate (2 mL). The solution was kept at this temperature for 12 h. Excess reagent and solvent were removed by passage of nitrogen. Chromatography of the residue provided **41** (16 mg) together with ethers **42** and **43**.

Ether ***42***—(12 mg, 21%); uv λ_{max}: 288 (3.86), 226 (4.56); ir ν_{max}: 3660, 3600, 3560, 1700, 1630; ^{1}Hmr δ: 7.69 (1H, s, olefinic-*H*), 7.0–7.6 (9H, m, aromatic-*H*), 5.16 (2H, s, —NC*H*$_2$C$_6$H$_5$), 4.86 (2H, t, J = 6 Hz, —CH$_2$C*H*$_2$OH), 3.69 (3H, s, —OC*H*$_3$), 3.57 (3H, s, —CO$_2$C*H*$_3$), 2.93 (2H, t, J = 6 Hz, —C*H*$_2$CH$_2$OH), 1.83 (1H, bs, —O*H*); ms *m/e*: 365 (M$^+$), 334 (100%), 91. High resolution molecular weight determination, calcd. for C$_{22}$H$_{23}$NO$_4$: 365.1627; found: 365.1627.

Ether ***43***—(6 mg, 11%); uv λ_{max}: 289 (3.89), 226 (4.56); ir ν_{max}: 3550, 1710, 1630; ^{1}Hmr δ: 6.9–7.8 (9H, m, aromatic-*H*), 6.52 (1H, s, olefinic-*H*), 5.24 (2H, s, —NC*H*$_2$C$_6$H$_5$), 3.88 (2H, t, J = 6 Hz, —CH$_2$C*H*$_2$OH), 3.79 (3H, s, —OC*H*$_3$), 3.51 (3H, s, —CO$_2$C*H*$_3$), 3.05 (2H, t, J = 6 Hz, —C*H*$_2$CH$_2$OH), 1.7 (1H, bs, —O*H*); ms *m/e*: 365 (M$^+$), 334 (100%), 91. High resolution molecular weight determination, calcd. for C$_{22}$H$_{23}$NO$_4$: 365.1627; found: 365.1628.

The Tosylates ***44*** *and* ***45***

The ether **42** (25 mg), *p*-toluenesulphonyl chloride (120 mg), and pyridine (150 μL) were stirred in chloroform (2 mL) initially at 0°C then at ambient temperature for 12 h. The mixture was diluted with chloroform, washed with water, sodium bicarbonate solution, brine, dried (Na_2SO_4), and concentrated. Chromatography on silica gel gave **44** (14 mg, 40%) as a clear oil; ir ν_{max}: 1705, 1630, 1360, 1190, 1175; ^{1}Hmr δ: 7.69 (1H, s, olefinic-*H*), 6.8–7.8 (13H, m, aromatic-*H*), 5.14 (2H, s, —NC*H*$_2$C$_6$H$_5$), 4.19 (2H, t, J = 8 Hz, —CH$_2$C*H*$_2$O—), 3.71 (3H, s, —OC*H*$_3$), 3.54 (3H, s, —CO$_2$C*H*$_3$), 3.01 (2H, t, J = 8 Hz, —C*H*$_2$CH$_2$O—), 2.40 (3H, s, —C$_6$H$_4$C*H*$_3$); ms *m/e*: 519 (M$^+$), 334, 155, 91 (100%). High resolution molecular weight determination, calcd. for C$_{29}$H$_{29}$NO$_6$S: 519.1893; found: 519.1891.

Similarly, **43** gave a 39% yield of **45**; uv λ_{max}: 285, 222; ir ν_{max}: 1710, 1630, 1360, 1190, 1175; ^{1}Hmr δ: 6.9–7.8 (13H, m, aromatic-*H*), 6.65 (1H, s, olefinic-*H*), 5.14 (2H, s, —NC*H*$_2$C$_6$H$_5$), 4.14 (2H, t, J = 7 Hz, —CH$_2$C*H*$_2$O—), 3.78 (3H, s, —OC*H*$_3$), 3.38 (3H, s, —CO$_2$C*H*$_3$), 3.01 (2H, t, J = 7 Hz, —C*H*$_2$CH$_2$O—), 2.30 (3H, s, —C$_6$H$_4$C*H*$_3$).

The Salts ***46*** *and* ***47***

The crude tosylates **44** and **45** obtained as described above from a mixture of **42** and **43** (1.98 g) were heated at 80°C in dry 3-ethylpyridine (4 mL) for 100 h. The excess solvent was removed *in vacuo* and the residue chromatographed on alumina (acidic, activity V) with ethyl acetate – methanol (95:5) to give the pure *E* isomer (300 mg) plus a mixture of *E* and *Z* isomers (400 mg). The *E* isomer was converted to the perchlorate (**46**) as described for the preparation of **17**; uv λ_{max}: 285 (3.90), 262 (4.03), 216 (4.59); ir ν_{max}: 1700, 1630; ^{1}Hmr δ: 8.67 (1H, d, J = 5 Hz, C(6′)-*H*), 8.24 (1H, bs, C(2′)-*H*), 8.06 (1H, bd, J = 7 Hz, C(4′)-*H*), 7.85 (1H, s, olefinic-*H*), 7.75 (1H, dd, J = 7, 5 Hz, C(5′)-*H*), 6.8–7.4 (9H, m, aromatic-*H*), 5.22 (2H, bs, —NC*H*$_2$C$_6$H$_5$), 4.86 (2H, 8 line m, —CH$_2$C*H*$_2$N$^+$—), 3.88 (3H, s, —OC*H*$_3$), 3.76 (3H, s, —CO$_2$C*H*$_3$), 3.42 (2H, bt, J = 6 Hz, —C*H*$_2$CH$_2$N$^+$), 2.56 (2H, q, J = 7 Hz, —C*H*$_2$CH$_3$), 0.95 (3H, t, J = 7 Hz, —CH$_2$C*H*$_3$). *Anal.* calcd. for C$_{29}$H$_{31}$N$_2$O$_7$Cl: C 62.76, H 5.63, N 5.05; found: C 62.37, H 5.93, N 4.60.

Methylation of ***40*** *and* ***41***

The crude enol **40** (44 mg) was dissolved in benzene (0.5 mL) and methanol (3 mL) saturated with hydrogen chloride. The mixture was kept in the dark at ambient temperature for 5 days. The solvent was removed *in vacuo* and the residue chromatographed on silica gel to give **35** (20 mg) together with **48** (8 mg); ir ν_{max}: 1700, 1630; ^{1}Hmr δ: 7.66 (1H, s, olefinic-*H*), 7.0–7.6 (14H, m, aromatic-*H*), 5.14 (2H, bs, —NC*H*$_2$C$_6$H$_5$), 4.56 (2H, s, —OC*H*$_2$C$_6$H$_5$), 3.62 (3H, s, —OC*H*$_3$), 4.50 (3H, s, —OC*H*$_3$), 3.02 (2H, dd, J = 8, 6 Hz,

—CH_2CH$_2$O—); ms *m/e*: 455 (M^+), 334, 163, 121, 105, 91 (100%).

Similarly, **41** gave **37** (40%) together with **42** (20%), identical with respective authentic samples.

The Enamine 49

A solution of the ester **35** (160 mg) in dry tetrahydrofuran (2 mL) was added to a solution of lithium diisopropylamide (0.84 mmol) in tetrahydrofuran (10 mL) and HMPA (0.13 mL) at −78°C under a nitrogen atmosphere. The solution was stirred at −78°C for 15 min then allowed to attain 0°C. The adduct of dimethylformamide and dimethyl sulphate (1:1, 1 g) was added and the mixture stirred at 0°C for 2 h. The mixture was diluted with water and extracted with ethyl acetate. The extract was washed with water, brine, dried (Na_2SO_4), and evaporated. Chromatography on silica gel gave **35** (68 mg) together with the enamine (**49**) (30%); mp (methanol) 112–113°C; ir ν_{max}: 1665, 1600; ^{1}Hmr δ: 7.71 (1H, s, olefinic-*H*), 7.0–7.7 (14H, m, aromatic-*H*), 5.12 (2H, q, J_{AB} = 16 Hz, N—CH_2C$_6$H$_5$), 4.48 (2H, s, —OCH_2C$_6$H$_5$), 3.64 (2H, m, —CH$_2$CH_2O—), 3.33 (3H, s, —CO$_2$CH_3), 2.92 (2H, m, —CH_2CH$_2$O—), 2.42 (6H, bs, —N(CH_3)$_2$); ms *m/e*: 468 (M^+, 100%), 347, 316, 256, 91. *Anal.* calcd. for $C_{30}H_{32}N_2O_3$: C 76.90, H 6.88, N 5.98; found: C 76.69, H 6.97, N 6.25.

The Acrylic Ester 50

Glacial acetic acid (8 drops) was added to a solution of the enamine **49** (50 mg) and sodium cyanoborohydride (50 mg) in methanol and tetrahydrofuran (1:1, 8 mL) and the mixture stirred under a nitrogen atmosphere for 18 h. The mixture was evaporated and the residue partitioned between saturated sodium bicarbonate solution and ethyl acetate. The extract was washed with water, brine, dried (Na_2SO_4), and concentrated *in vacuo*. The residue was chromatographed on silica gel to give the following compounds.

The acrylic ester 50—(16 mg, 35%); mp 87–89°C; uv λ_{max}: 276, 223; ir ν_{max}: 1720, 1615; ^{1}Hmr δ: 7.0–7.8 (14H, m, aromatic-*H*), 6.75 (1H, d, *J* = 2 Hz, olefinic-*H*), 5.89 (1H, d, *J* = 2 Hz, olefinic-*H*), 5.20 (2H, s, —NCH_2C$_6$H$_5$), 4.53 (2H, s, —OCH_2C$_6$H$_5$), 3.72 (2H, t, *J* = 7.5 Hz, —CH$_2$CH_2O—), 3.52 (3H, s, —CO$_2$CH_3), 3.05 (2H, t, *J* = 7.5 Hz, —CH_2CH$_2$O—); ms *m/e*: 425 (M^+), 304 (100%), 91. *Anal.* calcd. for $C_{28}H_{27}NO_3$: C 79.03, H 6.40, N 3.29; found: C 78.71, H 6.50, N 3.21.

The unstable amine 51—(8 mg); ^{1}Hmr δ: 6.8–7.6 (aromatic-*H*), 5.38 (2H, s, —NCH_2C$_6$H$_5$), 4.52 (2H, s, —OCH_2C$_6$H$_5$), 3.41 (3H, s, —CO$_2$CH_3), 2.03 (6H, s, —N(CH_3)$_2$).

The Enamine 52

The crude enol **40** (from 1.32 g of **35**) and piperidinium acetate (4 g) were heated in refluxing benzene (150 mL) for 17 h. The solution was cooled, washed with 5% sodium bicarbonate solution, water, brine, dried (Na_2CO_3), and concentrated. Chromatography on silica gel gave the enamine **52** (657 mg, 41% from **35**); uv λ_{max}: 283 (4.30); ir ν_{max}: 1670, 1590; ^{1}Hmr δ: 7.77 (1H, s, olefinic-*H*), 7.0–7.7 (14H, m, aromatic-*H*), 5.14 (2H, q, J_{AB} = 16 Hz, —NCH_2C$_6$H$_5$), 4.52 (2H, s, —OCH_2C$_6$H$_5$), 3.36 (3H, s, —OCH_3); ms *m/e*: 508 (M^+), 477, 449, 387, 296, 277, 224, 154, 91. High resolution molecular weight determination, calcd. for $C_{33}H_{36}N_2O_3$: 508.2716; found: 508.2727.

The Alcohol 53

Sodium cyanoborohydride (39 mg) was added to the enamine **52** (110 mg) in a 0.1 *M* solution of citric acid in methanol (10 mL). The pH of the solution was adjusted to 3.0 with 0.1 *M* aqueous disodium citrate, and the mixture stirred at ambient temperature for 16 h. The solution was then heated to reflux for 24 h, concentrated *in vacuo*, and the residue chromatographed on silica gel to give the acrylic ester **50** (10 mg). Hydrogenation of this product in methanol (10 mL) over 10% Pd/C (9 mg) as described for the preparation of **41**, gave **53** (10 mg); ^{1}Hmr δ: 6.8–7.7 (9H, m, aromatic-*H*), 5.30 (2H, bs, —NCH_2C$_6$H$_5$), 4.14 (1H, q, *J* = 7 Hz, —C*H*CH$_3$), 3.83 (2H, bt, *J* = 6 Hz, —CH$_2$CH_2OH), 3.34 (3H, s, —OCH_3), 1.40 (3H, d, *J* = 7 Hz, —CHCH_3); ms *m/e*: 337 (M^+), 319, 305, 278, 246, 156, 91.

The Alcohol 54

The enamine (**52**) (281 mg) was hydrogenated in methanol (30 mL) over 10% Pd/C (89 mg) for 3 h to give **54** (137 mg, 59%); ^{1}Hmr δ: 7.76 (1H, s, olefinic-*H*), 7.0–7.7 (9H, m, aromatic-*H*), 5.16 (2H, q, J_{AB} = 16 Hz, —NCH_2C$_6$H$_5$), 3.47 (3H, s, —OCH_3); ms *m/e*: 418 (M^+), 387.

The Acrylic Ester 55

(*a*) Sodium cyanoborohydride (41.5 mg) was added to a solution of crude **54** (135 mg) in methanol (76.5 mL) and 1 *M* citric acid in methanol (8.5 mL). The pH of the solution was adjusted to 3.0 with 0.1 *M* aqueous disodium citrate and stirring continued for 18 h. The solvents were removed *in vacuo* and the residue partitioned between sodium carbonate solution and ethyl acetate. The organic layer was dried (Na_2CO_3) and evaporated. The residue was heated in refluxing benzene for 18 h and chromatographed on silica gel to give **55** (104 mg, 96%); uv λ_{max}: 275 (3.30); ir ν_{max}: 3600, 1720; ^{1}Hmr δ: 6.9–7.7 (9H, m, aromatic-*H*), 6.75 (1H, d, *J* = 2 Hz, olefinic-*H*), 5.91 (1H, d, *J* = 2 Hz, olefinic-*H*), 5.20 (2H, s, —NCH_2C$_6$H$_5$), 3.88 (2H, t, *J* = 6 Hz, —CH$_2$CH_2OH), 3.58 (3H, s, —OCH_3), 3.00 (2H, t, *J* = 6 Hz, —CH_2CH$_2$OH), 1.62 (1H, bs, —O*H*); ms *m/e*: 335 (M^+), 304, 175, 143, 101, 91. High resolution molecular weight determination, calcd. for $C_{21}H_{21}NO_3$: 335.1516; found: 335.1541.

(*b*) As described above, the enamine **52** (657 mg) was hydrogenated in methanol (55 mL), ethyl acetate (55 mL), and perchloric acid (4 mL) over 10% Pd/C catalyst (378 mg) for 30 h. The mixture was filtered through Celite and the filtrate stirred vigorously with saturated sodium bicarbonate solution for 30 min. The aqueous layer was extracted with ethyl acetate and the combined organic layers washed with brine, dried (K_2CO_3), and evaporated. Chromatography on silica gel gave **55** (299 mg, 69%).

The Tosylate 56

Triethylamine (16 drops) was added to a solution of the crude alcohol (**55**) (65 mg) and *p*-toluenesulphonic acid (111 mg) in dichloromethane (8 mL) and the mixture stirred for 19 h. The solvent was removed *in vacuo* and the residue chromatographed on silica gel to give **55** (12 mg) together with the tosylate **56** (41 mg); ^{1}Hmr δ: 7.0–7.7 (13H, m, aromatic-*H*), 6.74 (1H, d, *J* = 2 Hz, olefinic-*H*), 5.84 (1H, d, *J* = 2 Hz, olefinic-*H*), 5.16 (2H, s, —NCH_2C$_6$H$_5$), 4.18 (2H, t, *J* = 7 Hz —CH$_2$CH_2O—), 3.56 (3H, s, —OCH_3), 3.04 (2H, t, *J* = 7 Hz, —CH_2CH$_2$O—), 2.36 (3H, bs, ArCH_3).

The Iodide 57

The crude tosylate **56** (41 mg) and lithium iodide (158 mg) were heated in refluxing, dry acetone (15 mL) for 19 h. The solvent was evaporated and the residue chromatographed on silica gel to yield **57** (35 mg, 94%); ^{1}Hmr δ: 6.9–7.7 (9H, m, aromatic-*H*), 6.80 (1H, d, *J* = 2 Hz, olefinic-*H*), 5.90 (1H, d, *J* = 2 Hz, olefinic-*H*), 5.22 (2H, bs, —NCH_2C$_6$H$_5$), 3.52 (3H, s, —OCH_3), 3.34 (4H, bs, —CH_2CH_2—); ms *m/e*: 445 (M^+), 318, 304, 149, 91.

The Pyridinium Salt 58

The crude iodide **57** (25 mg) was heated at 40°C in 3-ethylpyridine (4 mL) for 21 h. The solvent was removed by

azeotropic distillation with water, under reduced pressure. The residue was partitioned between water and benzene (vigorous stirring) and the layers separated. The organic layer gave a mixture (ca. 1:1) of **57** and **58** (9 mg). The aqueous layer afforded pure **58** (26 mg); mp 130–132°C; uv λ_{max}: 285 (3.70), 265 (3.85); ir ν_{max}: 1700; ^{1}Hmr δ: 9.15 (1H, d, J = 6 Hz, C(6′)-*H*), 8.61 (1H, s, C(2′)-*H*), 7.97 (1H, d, J = 8 Hz, C(4′)-*H*), 7.71 (1H, dd, J = 8, 6 Hz, C(5′)-*H*), 6.8–7.4 (9H, m, aromatic-*H*), 6.76 (1H, d, J = 2 Hz, olefinic-*H*), 6.00 (1H, d, J = 2 Hz, olefinic-*H*), 5.17 (2H, s, —N$CH_2C_6H_5$), 5.10 (2H, t, J = 6 Hz, —CH_2CH_2N—), 3.73 (3H, s, —OCH_3), 3.49 (2H, t, J = 6 Hz, —CH_2CH_2N—), 2.53 (2H, q, J = 7 Hz, —CH_2CH_3), 0.93 (3H, t, J = 7 Hz, —CH_2CH_3). *Anal.* calcd. for $C_{28}H_{29}N_2O_5I$: C 60.87, H 5.25, N 5.09, I 23.01; found: C 60.49, H 5.23, N 4.79, I 23.11.

Acknowledgements

The financial support of the National Research Council of Canada is gratefully acknowledged. One of us (V.E.R.) also acknowledges a fellowship from Consejo National de Ciencia y Technologia, Mexico, and F.S.M. is grateful to the University of El-Fateh, Tripoli, Libya for support during his leave from this institution.

1. J. P. KUTNEY. Heterocycles, **7**, 593 (1977).
2. E. WENKERT. J. Am. Chem. Soc. **84**, 98 (1962).
3. A. A. QURESHI and A. I. SCOTT. J. Chem. Soc. Chem. Commun. 948 (1968).
4. A. I. SCOTT, P. C. CHERRY, and A. A. QURESHI. J. Am. Chem. Soc. **91**, 4932 (1969).
5. A. I. SCOTT. Acc. Chem. Res. **3**, 151 (1970).
6. J. P. KUTNEY, C. EHRET, V. R. NELSON, and D. C. WIGFIELD. J. Am. Chem. Soc. **90**, 5929 (1968).
7. J. P. KUTNEY. Heterocycles, **4**, 169 (1976); **4**, 429 (1976).
8. J. P. KUTNEY, R. A. BADGER, W. R. CULLEN, R. GREENHOUSE, M. NODA, V. E. RIDAURA-SANZ, Y. H. SO, A. ZANAROTTI, and B. R. WORTH. Can. J. Chem. This issue.
9. R. S. SOOD. Ph.D. Thesis, University of British Columbia, Vancouver, B.C. 1970.
10. T. A. FAVORSKAYA and I. P. YAKOULEV. Zh. Obshch. Khim. **22**, 113 (1952); Chem. Abstr. **46**, 1119 (1952).
11. A. R. BATTERSBY and A. K. BHATNAGAR. J. Chem. Soc. Chem. Commun. 193 (1970).
12. G. A. CORDELL, G. F. SMITH, and G. N. SMITH. J. Chem. Soc. Chem. Commun. 189 (1970).
13. R. T. BROWN, G. F. SMITH, K. S. J. STAPLEFORD, and D. A. TAYLOR. J. Chem. Soc. Chem. Commun. 190 (1970).
14. G. A. CORDELL, G. F. SMITH, and G. N. SMITH. J. Chem. Soc. Chem. Commun. 191 (1970).
15. C. A. BEAR, W. R. CULLEN, J. P. KUTNEY, V. E. RIDAURA, J. TROTTER, and A. ZANAROTTI. J. Am. Chem. Soc. **95**, 3058 (1973).
16. J. P. KUTNEY, R. GREENHOUSE, and V. E. RIDAURA. J. Am. Chem. Soc. **96**, 7364 (1974).
17. H. PLIENINGER. Chem. Ber. **83**, 271 (1950).
18. E. WENKERT, K. G. DAVE, C. T. GNEWUCH, and P. W. SPRAGUE. J. Am. Chem. Soc. **90**, 5251 (1968).
19. T. KAWAMATA and S. INAYAMA. Chem. Pharm. Bull. **19**, 643 (1971).

Dihydropyridines in synthesis and biosynthesis. II.[1] Stable tricarbonylchromium(0) complexes[2]

JAMES P. KUTNEY, RODNEY A. BADGER, WILLIAM R. CULLEN, ROBERT GREENHOUSE, MASAKI NODA, VICENTE E. RIDAURA-SANZ, YING HUNG SO, ANTONIO ZANAROTTI, AND BRIAN R. WORTH

Department of Chemistry, University of British Columbia, 2075 Wesbrook Place, Vancouver, B.C., Canada V6T 1W5

Received July 31, 1978

JAMES P. KUTNEY, RODNEY A. BADGER, WILLIAM R. CULLEN, ROBERT GREENHOUSE, MASAKI NODA, VICENTE E. RIDAURA-SANZ, YING HUNG SO, ANTONIO ZANAROTTI, and BRIAN R. WORTH. Can. J. Chem. **57**, 300 (1979).

Controlled reduction of *N*-methyl-3-ethylpyridinium iodide afforded the corresponding 1,2-dihydropyridine which was stabilised by complexation to give 1,2- and 1,6-dihydro-3-ethyl-*N*-methylpyridinetricarbonylchromium(0). These stable, isomeric complexes were interrelated by thermal equilibration. Analogous sequences with more complex, alkaloid derivatives enabled formation, and stabilisation by complexation, of 1,2- and 1,6-dihydropyridines in the presence of other functions such as the indole unit and ester groups.

JAMES P. KUTNEY, RODNEY A. BADGER, WILLIAM R. CULLEN, ROBERT GREENHOUSE, MASAKI NODA, VICENTE E. RIDAURA-SANZ, YING HUNG SO, ANTONIO ZANAROTTI et BRIAN R. WORTH. Can. J. Chem. **57**, 300 (1979).

La réduction contrôlée de l'iodure du *N*-méthyléthyl-3 pyridinium conduit à la dihydro-1,2 pyridine correspondante que l'on a stabilisée par complexation pour isoler les dihydro-1,2 (et -1,6) éthyl-3 *N*-méthylpyridines tricarbonylchrome(0). On a pu relier ces complexes stables et isomères par l'équilibration thermique. Des séries de réactions analogues avec des dérivés d'alcaloïdes plus complexes ont permis de former et de stabiliser par complexation des dihydro-1,2 (et -1,6) pyridines en présence d'autres fonctions comme des groupes indole et ester.

[Traduit par le journal]

The important role of 1,4-dihydropyridines in various biological systems is well known and the chemistry of such compounds has received considerable attention (2). On the other hand, although 1,2-dihydropyridines have been implicated in alkaloid biosynthesis with certain plant species (3), comparatively little is known in this area. Electron withdrawing substituents have been shown to stabilize dihydropyridine systems (2) and the relative stabilities of units lacking such stabilisation have been examined for a few simple cases (4, 5). These nonstabilised dihydropyridines are generally quite reactive and readily undergo Diels–Alder and enamine-type reactions. Our interest in intermediates such as dehydrosecodine (**1**) (1, 3) dictated that the 1,2-dihydro- and/or isomeric 1,6-dihydropyridines be formed, protected/stabilised, and regenerated under mild conditions.

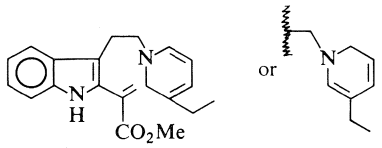

1

Metal carbonyls had found extensive application in the stabilisation of reactive π-electron systems (for extensive reviews see ref. 6) but, with the exception of one preliminary report (7), little information was available on such complexes in which a nitrogen hetero atom provided one of the chelating sites. Nevertheless a tricarbonylchromium(0) complex seemed a potential means of stabilising dihydropyridines. To develop the required methodology a simple model system was chosen. In this regard, inspection of dehydrosecodine (**1**) (1) suggested a 1,3-dialkylpyridine derivative, ideally 3-ethyl-*N*-methyldihydropyridine. This choice, through lack of symmetry in the molecule, also provided potential formation of isomeric 1,2- and 1,6-dihydropyridine derivatives.

Sodium borohydride reduction of pyridinium salts was known to yield the corresponding tetrahydro systems and as expected, reduction of 3-ethyl-*N*-methylpyridinium iodide (**2**) in this manner gave **3** in high yield. Consideration of the mechanism of this reduction suggested that suppression of the protonation of the initially formed dihydropyridine **4** (or its 1,6-dihydro isomer **5**) would prevent further reduction (8) to **3** and enable isolation of the target compound(s). In the event, sodium borohydride reduction of **2** in a vigorously stirred, two-phase

[1]For Part 1 see ref. 1.

[2]For a preliminary report on portions of this work see ref. 9.

0008-4042/79/030300-04$01.00/0

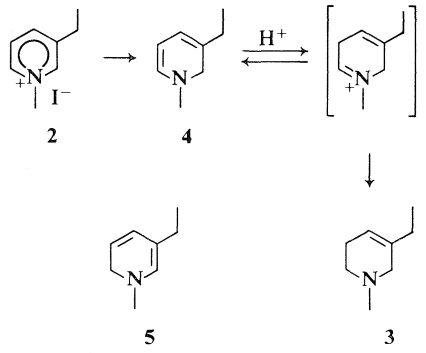

SCHEME 1

medium (ether, 2 *N* sodium hydroxide) gave the 1,2-dihydropyridine **4** in high yield. The product dimerised on standing at ambient temperature but the ^{1}Hmr spectrum of a freshly prepared sample indicated the structure **4** without observable contamination by the 1,6-dihydro isomer **5**. The ultraviolet spectrum showed the characteristic absorption maximum at 327 nm. Reaction of the crude product with trisacetonitriletricarbonylchromium(0) (9, 10) in ether solution at 0 to 20°C under an *oxygen free* atmosphere of dry nitrogen gave a deep red solution which was filtered through degassed Florisil to give a 67% yield of a mixture of two complexes together with ca. 8% yield of a complex of a dimeric unit (M^+ 382). This latter product was not identified unambiguously but was presumed formed by complexation of an already dimerised dihydropyridine. The major fraction was chromatographed on degassed silica gel, under a nitrogen atmosphere to give 1,2-dihydro-3-ethyl-*N*-methylpyridinetricarbonylchromium(0) (**6**) and 1,6-dihydro-3-ethyl-*N*-methylpyridinetricarbonylchromium(0) (**7**) in the ratio 65:35, respectively. Each complex exhibited the characteristic carbonyl absorption in the infrared region, and electron impact studies gave in each case a weak molecular ion at *m/e* 259, a fragment ion at 123 for the loss of the elements of $Cr(CO)_3$, a base peak at 122 ($C_8H_{12}N$), and significant ions at 107 (C_7H_9N) and 94 (C_6H_8N). The ^{1}Hmr spectra were sufficiently informative to characterise **6** and **7**. In deuteriobenzene, the 1,6-dihydro isomer (**7**) gave singlet absorbance at δ 4.58 for C(2)-*H* and a doublet (J = 7 Hz) at 4.83 for C(4)-*H*. The signal for C(5)-*H* appeared as an octet (J = 7, 5.5, and 1.5 Hz) centred at δ 3.09. Isomer **6** gave, also in deuteriobenzene, the following signals: δ 2.34 (2H, q, J_{AB} = 10 Hz, C(2)-H_2); 4.50 (2H, bd, $J \simeq$ 5 Hz, C(4)-*H* and C(6)-*H*); 5.00 (1H, dd, J = 5.5 and 4.5 Hz). The exact chemical shifts of all signals were significantly dependent on concentration and solvent. Unambiguous confirmation of these structural assignments was possible by X-ray crystal analysis (9).

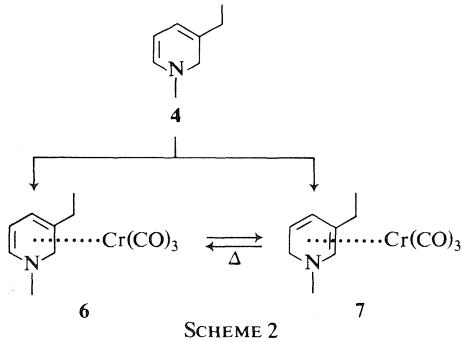

SCHEME 2

The curious formation of significant amounts of the 1,6-dihydro isomer **7** from **4** required some consideration. Careful ^{1}Hmr analysis of the borohydride reduction product indicated the presence of ca. 5% of the tetrahydro derivative **3** together with **4** (≥95%). Thus formation of **7** was presumed to occur via double bond isomerisation during complexation or by isomerisation of the formed 1,2-dihydropyridine complex **6**. That the latter explanation was unlikely was demonstrated by almost quantitative recovery of **6** after stirring in ether at ambient temperature for 18 h. Thermal isomerisation between **6** and **7** was, however, possible by heating in refluxing cyclohexane. At equilibrium, a 1:1 ratio of **6** and **7** was obtained. The pure complexes were stable in solid form if protected from oxygen and were stable in solution at or below ambient temperature provided that rigorous exclusion of oxygen was ensured.

Thus our initial objectives had been realised and attention turned to the stabilisation of alkaloid precursors bearing the dihydropyridine unit. The preceding report (1) described the preparation of several pyridinium salts, designed specifically for determining the generality of methodology outlined above.

TABLE 1. Thermal equilibration of the complexes **6** and **7**

Time (h)	Ratio **7**:**6** from **7***	Ratio **7**:**6** from **6***
1	76:24	31:69
2	66:34	—
3	63:37	45:55
4	57:43	—
5.5	55:45	50:50
8	50:50	50:50
14	50:50	50:50

*As determined by ^{1}Hmr ($CDCl_3$) integrals of the N—CH_3 signals at δ 2.42 for **6** and δ 2.39 for **7**.

Application of the procedure to the indole derivative **8** gave, after the usual work-up and chromatography, a red oil, assigned the structure **9** on the basis of spectral data. A small amount of a second complex was also isolated and identified as the 1,6-dihydropyridine derivative **10**. This simple experiment had demonstrated that the required complexes could be formed, although only in low yield, in the presence of the electron rich indole nucleus. To further test the method, the salt **11** was reduced and treated with trisacetonitriletricarbonylchromium(0) as before, to give the expected product **12** together with the descarbomethoxy derivative **13** and, surprisingly, **6**. These latter products were presumed formed via cleavages in the strongly basic medium during the reduction step. In each case spectral analysis indicated 1,2-dihydropyridinetricarbonylchromium(0) isomers and here the corresponding 1,6-dihydro products were not detected. The *N*-benzyl derivative **14** did not appear to undergo such fragmentation and here a single product **15** was isolated. The corresponding acrylic ester **16** also formed a single, stable complex but spectral analysis indicated that the reduction of the pyridinium system had occurred with concomitant conjugate reduction of the acrylic ester function leading to **17** in 35% yield.

These experiments indicated that the generally unstable dihydropyridine system could be generated and trapped to form stable complexes without interference from indole and ester functions. Specific

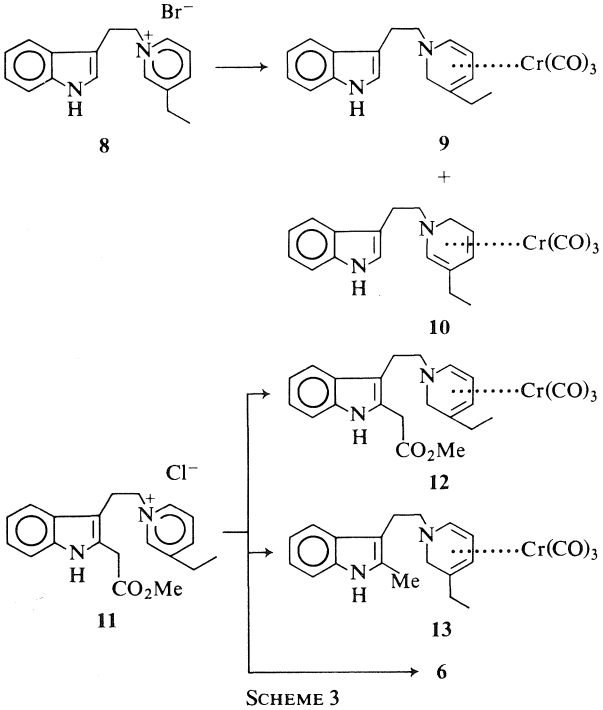

8 **9** **10** **11** **12** **13** **6**

SCHEME 3

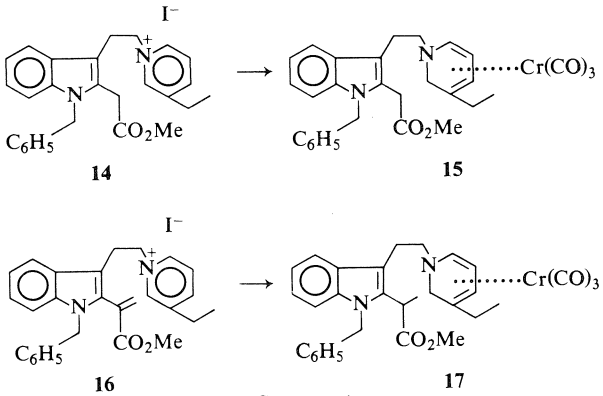

14 **15** **16** **17**

SCHEME 4

formation of the complex of a dehydrosecodine (**1**), regeneration of the diene and its reactions will be described at a later date. The complexes described here are interesting entities in themselves and investigations of their chemistry are presently underway in these laboratories.

Experimental

General experimental details are given in the accompanying report (1). *All* procedures involving the preparation, separation and purification of chromium complexes were carried out under a liberal flow of oxygen free, dry nitrogen.

3-Ethyl-N-*methyl-1,2,5,6-tetrahydropyridine (3)*

Sodium borohydride (100 mg) was added in portions to a solution of 3-ethyl-*N*-methylpyridinium iodide (250 mg) in methanol (15 mL). After 30 min, the solution was diluted with 3 *N* HCl and washed with ether. The aqueous layer was adjusted to pH 8 and extracted with dichloromethane. The extract was dried (Na_2SO_4) and carefully evaporated to give **3** (98 mg, 79%) as a colourless oil; ^{1}Hmr δ: 5.33 (1H, m, C(4)-H), 2.65 (2H, bs, C(2)-H_2), 2.20 (3H, s, —NCH_3), 0.95 (3H, t, J = 7 Hz, —CH_2CH_3); ms *m/e*: 125 (M^+), 124, 110, 96 (100%), 94, 82, 81, 67, 44, 43, 42, 39. High resolution molecular weight determination, calcd. for $C_8H_{15}N$: 125.1204; found: 125.1225.

1,2-Dihydro-3-ethyl-N-*methylpyridine (4)*

The salt **2** (3.0 g) was added, all at once, to a vigorously stirred mixture of 2.1 *N* NaOH (9 mL), methanol (9 mL), ether (36 mL), and sodium borohydride (547 mg), under a nitrogen atmosphere. The two-phase system was stirred at ambient temperature for exactly 5 min, the aqueous layer was removed, and the ether layer washed *briefly* with 2.1 *N* NaOH (9 mL), dried by passage through basic alumina (grade I), and evaporated to give **4** (1.294 g, 86%); uv λ_{max}: 327; ^{1}Hmr δ (C_6D_6): 5.73 (2H, m, superimposed doublets, one with J = 7 Hz, C(6)-*H* and C(4)-*H*), 4.74 (1H, dd, J = 7, ca. 7 Hz, C(5)-*H*), 3.58 (2H, s, C(2)-H_2), 2.27 (3H, s, —NCH_3), 1.88 (2H, q, J = 7 Hz, —CH_2CH_3), 1.00 (3H, t, J = 7 Hz, —CH_2CH_3); ms *m/e*: 123 (M^+), 122 (100%), 108, 107, 96, 94, 67. High resolution molecular weight determination, calcd. for $C_8H_{13}N$: 123.1047; found: 123.1041.

The Tricarbonylchromium(0) Complexes 6 and 7

The pyridinium salt **2** (10 g) was reduced as described above. The washed and dried ether solution of **4** was added under nitrogen to a solution of trisacetonitriletricarbonylchromium (1 equiv.) in dry ether at 0°C and the mixture stirred at

ambient temperature for ca. 20 h. The resulting red solution was filtered through previously degassed Florisil with degassed dichloromethane under a nitrogen atmosphere to afford a mixture of **6** and **7** (6.97 g, 67%; ratio ca. 65:35 by ^{1}Hmr spectroscopy). Elution with oxygen free tetrahydrofuran gave a third red complex (1.2 g, 8%; *m/e* 382). The major fraction was purified by chromatography on silica gel, again with rigorous exclusion of oxygen, to give the following.

*The complex (**6**)*—orange prisms, mp (benzene–hexane) 97–99°C; uv λ_{max}: 403 (3.64); ir ν_{max}: 1830, 1860, 1942; ^{1}Hmr (C_6D_6) δ: 5.00 (1H, dd, J = 5.5 and 4.5 Hz, C(5)-*H*), 4.50 (2H, bd, $J \simeq$ 5 Hz, C(4)-*H* and C(6)-*H*), 2.34 (2H, q, J_{AB} = 10 Hz, C(2)-H_2), 1.60 (2H, q, J = 7 Hz, —CH_2CH_3), 1.45 (3H, s, —NCH_3), 0.70 (3H, t, J = 7 Hz, —CH_2CH_3); ($CDCl_3$) δ: 5.66 (1H, dd, J = 5.5 and 4.5 Hz, C(5)-*H*), 5.41 (1H, d, J = 4.5 Hz, C(6)-*H*), 4.96 (1H, bd, J = 5.5 Hz, C(4)-*H*), 3.24 (2H, bs, C(2)-H_2), 2.42 (3H, s, —NCH_3), 2.10 (2H, bq, J = 7 Hz, —CH_2CH_3), 0.94 (3H, t, J = 7 Hz, —CH_2CH_3); ms *m/e*: 259 (M^+), 123, 122 (100%), 107, 94. *Anal.* calcd. for $C_{11}H_{13}NO_3Cr$: C 50.90, H 5.05, N 5.40; found: C 51.04, H 4.95, N 5.46.

*The complex (**7**)*—red prisms, mp (benzene–hexane) 68°C; uv λ_{max}: 399 (3.67); ir ν_{max}: 1825, 1860, 1942; ^{1}Hmr (C_6D_6) δ: 4.83 (1H, bd, J = 7 Hz, C(4)-*H*), 4.58 (1H, s, C(2)-*H*), 3.09 (1H, octet, J = 7, 5.5, 1.5 Hz, C(5)-*H*), 2.54 (1H, m, C(6)-*H*), 2.21 (1H, m, C(6)-*H*), 2.30 (2H, m, —CH_2CH_3), 1.45 (3H, s, —NCH_3), 1.12 (3H, t, J = 7 Hz, —CH_2CH_3); ($CDCl_3$) δ: 5.40 (1H, bs, C(2)-*H*), 5.29 (1H, bd, J = 7 Hz, C(4)-*H*), 3.69 (1H, octet, J = 7, 5.5, 1.5 Hz, C(5)-*H*), 3.42 (1H, m, C(6)-*H*), 3.15 (1H, m, C(6)-*H*), 2.73 (2H, m, —CH_2CH_3), 2.39 (3H, s, —NCH_3), 1.40 (3H, t, J = 7 Hz, —CH_2CH_3); ms *m/e*: 259 (M^+), 123, 122 (100%), 107, 94. *Anal.* calcd. for $C_{11}H_{13}NO_3Cr$: C 50.90, H 5.05, N 5.40; found: C 50.81, H 5.26, N 5.16.

*The Complexes **9** and **10***

Using the procedure described above, the salt **8** gave a 27% yield of the complex **9**; uv λ_{max}: 400 (3.60), 290 (4.02), 285 (4.11), 220 (4.96); ir ν_{max}: 1945, 1855, 1830; ^{1}Hmr (C_6D_6) δ: 7.0–7.6 (4H, m, aromatic-*H*) 6.29 (1H, bs, —indole C(2)-*H*), 4.97 (1H, dd, J = 5.5, 4.5 Hz, C(5)-*H*), 4.70 (1H, d, J = 4.5 Hz, C(6)-*H*), 4.65 (1H, bd, J = 5.5 Hz, C(4)-*H*), 2.69 (2H, bs, C(2)-H_2), 2.45 (4H, bs, —CH_2CH_2—), 1.90 (2H, q, J = 7 Hz, —CH_2CH_3), 0.84 (3H, t, J = 7 Hz, —CH_2CH_3); ms *m/e*: 388 (M^+), 304, 252, 144, 130, 122, 52.

A small amount (ca. 7%) of the isomeric complex **10** was also isolated; uv λ_{max}: 397, 288, 278, 272, 219; ir ν_{max}: 1950, 1870, 1835; ^{1}Hmr (C_6D_6) δ: 7.1–7.6 (4H, m, aromatic-*H*), 6.31 (1H, bs, —indole C(2)-*H*), 4.96 (1H, d, J = 7 Hz, C(4)-*H*), 4.80 (1H, bs, C(2)-*H*), 3.19 (1H, bdt, J = 7, 2 Hz, C(5)-*H*), 1.12 (3H, t, J = 7 Hz, —CH_2CH_3); ms *m/e*: 388 (M^+), 304, 252, 144, 130, 122, 52.

*The Complexes **12** and **13***

Reduction of the salt **11** and complexation of the intermediate dihydropyridines in the usual manner gave the following.

*The complex **6***—12% yield.

*The complex **12***—(15%); uv λ_{max}: 400 (3.3); ir ν_{max}: 1950, 1860, 1825, 1730; ^{1}Hmr δ: 8.50 (1H, bs, —N*H*), 7.0–7.6 (4H, m, aromatic-*H*), 5.65 (1H, dd, J = 5.5, 4.5 Hz, C(5)-*H*), 5.43 (1H, d, J = 4.5 Hz, C(6)-*H*), 5.03 (1H, d, J = 5.5 Hz, C(4)-*H*), 3.76 (3H, s, —OCH_3), 3.74 (2H, s, C(2)-H_2), 3.39 (2H, q, J_{AB} = 14 Hz, —CH_2CO_2Me), 2.82 (4H, m, —CH_2CH_2—), 2.19 (2H, q, J = 6 Hz, —CH_2CH_3), 1.02 (3H, t, J = 6 Hz, —CH_2CH_3); ms *m/e*: 460 (M^+), 376, 344, 324, 220, 202, 122, 52. High resolution molecular weight determination, calcd. for $C_{23}H_{24}N_2O_5Cr$: 460.1089; found: 460.1090.

*The complex **13***—(10%); uv λ_{max}: 400 (3.3); ir ν_{max}: 1930, 1840, 1815; ^{1}Hmr δ: 7.83 (1H, bs, —N*H*), 7.05–7.45 (4H, m, aromatic-*H*), 5.61 (1H, dd, J = 5.5, 4.5 Hz, C(5)-*H*), 5.39 (1H, d, J = 4.5 Hz, C(6)-*H*), 5.30 (1H, d, J = 5.5 Hz, C(4)-*H*), 3.38 (2H, s, —C(2)-H_2), 2.82 (4H, m, —CH_2CH_2—), 2.36 (3H, s, —indole C(2)-CH_3), 2.19 (2H, q, J = 6 Hz, —CH_2CH_3), 1.02 (3H, t, J = 6 Hz, —CH_2CH_3); ms *m/e*: 402 (M^+), 318, 266, 158, 144. High resolution molecular weight determination, calcd. for $C_{21}H_{22}N_2O_3Cr$: 402.1030; found: 402.1011.

*The Complex (**15**)*

Similarly, the benzyl derivative **14** gave, in 35% yield, the complex **15**; uv λ_{max}: 395 (3.10); ir ν_{max}: 1942, 1870, 1840, 1742; ^{1}Hmr δ: 6.8–7.5 (9H, m, aromatic-*H*), 5.54 (2H, m, C(6)-*H* and C(5)-*H*), 5.38 (2H, s, —$CH_2C_6H_5$), 4.99 (1H, d, J = 5.5 Hz, C(4)-*H*), 3.62 (2H, s, C(2)-H_2), 3.51 (3H, s, —OCH_3), 3.36 (2H, s, —$CH_2CO_2CH_3$), 2.85 (2H, m, —CH_2CH_2N—), 2.79 (2H, m, —CH_2CH_2N—), 2.15 (2H, q, J = 6 Hz, —CH_2CH_3), 1.00 (3H, t, J = 6 Hz, —CH_2CH_3); ms *m/e*: 550 (M^+), 466, 414, 306, 253, 122, 91. High resolution molecular weight determination, calcd. for $C_{30}H_{30}N_2O_5Cr$: 550.1548; found: 550.1533. *Anal.* calcd. for $C_{30}H_{30}N_2O_5Cr$: C 65.45, H 5.45, N 5.09; found: C 65.15, H 5.28, N 4.90.

*The Complex (**17**)*

Similarly, **16** gave a 35% yield of **17**; uv λ_{max}: 395 (2.6); ir ν_{max}: 1935, 1850, 1810, 1725; ^{1}Hmr δ: 6.8–3.55 (9H, m, aromatic-*H*), 5.50–5.70 (2H, m, C(6)-*H* and C(5)-*H*), 5.34 (2H, s, —$CH_2C_6H_5$), 5.00 (1H, d, J = 5 Hz, C(4)-*H*), 3.92 (1H, q, J = 7 Hz, —$CH(CH_3)CO_2CH_3$), 3.47 (3H, s, —OCH_3), 3.40 (2H, s, C(2)-H_2), 2.85 (4H, m, —CH_2CH_2—), 2.17 (2H, q, J = 6 Hz, —CH_2CH_3), 1.36 (3H, d, J = 7 Hz, —$CHCH_3$), 1.00 (3H, t, J = 6 Hz, —CH_2CH_3); ms *m/e*: 564 (M^+), 480, 428, 324, 306. High resolution molecular weight determination, calcd. for $C_{31}H_{32}N_2O_5Cr$: 564.1722; found: 564.1708.

Acknowledgements

This work was supported financially by the National Research Council of Canada. Invaluable discussions and advice from Dr. P. Legzdins and technical assistance from his research group is very gratefully acknowledged.

1. J. P. KUTNEY, R. A. BADGER, J. F. BECK, H. BOSSHARDT, F. S. MATOUGH, V. E. RIDAURA-SANZ, Y. H. SO, R. S. SOOD, and B. R. WORTH. Can. J. Chem. This issue.
2. U. EISNER and J. KUTHAN. Chem. Rev. **72**, 1 (1972).
3. J. P. KUTNEY. Heterocycles, **7**, 593 (1977).
4. F. W. FOWLER. J. Org. Chem. **37**, 1321 (1972).
5. F. W. FOWLER. J. Am. Chem. Soc. **94**, 5926 (1972).
6. I. WENDER and P. PINO (*Editors*). Organic synthesis via metal carbonyls. Vol. 1. Interscience, New York, NY. 1968; G. E. COATES, M. L. H. GREEN, and K. WADE. Organometallic compounds. Vol. II. Methuen and Co., London. 1968. Chapt. 3; R. B. KING. Acc. Chem. Res. **3**, 417 (1970).
7. E. O. FISCHER and K. ÖFELE. J. Organometal. Chem. **8**, P5 (1967); K. ÖFELE. Angew. Chem. Int. Ed. Engl. **6**, 988 (1967).
8. E. M. FRY and J. A. BEISLER. J. Org. Chem. **35**, 2809 (1970).
9. C. A. BEAR, W. R. CULLEN, J. P. KUTNEY, V. E. RIDAURA, J. TROTTER, and A. ZANAROTTI. J. Am. Chem. Soc. **95**, 3058 (1973).
10. D. P. TATE, W. R. KNIPPLE, and J. M. AUGL. Inorg. Chem. **1**, 433 (1962).

Stereochemical equilibration of the lithium derivatives of 1,2-diols

CLARKE E. SLEMON[1] AND PETER YATES

Lash Miller Chemical Laboratories, University of Toronto, Toronto, Ont., Canada M5S 1A1

Received August 9, 1978

CLARKE E. SLEMON and PETER YATES. Can. J. Chem. **57**, 304 (1979).

The dilithium derivatives of the ditertiary 1,2-diols, *cis*- and *trans*-1,2-dimethyl-1,2-cyclohexanediol, fail to undergo base-induced stereochemical equilibration under conditions that lead to such equilibration with the dilithium derivatives of the disecondary 1,2-diols, *cis*- and *trans*-1,2-cyclohexanediol. This casts doubt on the proposal that the latter equilibration proceeds by carbon–carbon bond cleavage of the dialkoxide to give a diketyl intermediate. It is highly probable that it involves oxidation–reduction as established by Doering in the case of monohydric alcohols. Examination of steroidal secondary-tertiary 1,2-diols under similar conditions shows that such systems can epimerize at both carbinol centres; this is interpreted in terms of sequential oxidation, α-ketol rearrangement, and reduction.

CLARKE E. SLEMON et PETER YATES. Can. J. Chem. **57**, 304 (1979).

Les dérivés dilithiés des diols-1,2 ditertiaires, *cis*- et *trans*-diméthyl-1,2 cyclohexanediols-1,2 ne subissent pas d'équilibrations stéréochimiques induites par les bases dans des conditions qui permettent de telles équilibrations avec les dérivés dilithiés des diols-1,2 disecondaires, *cis*- et *trans*-cyclohexanediols-1,2. Ces résultats jettent un doute sur la proposition à l'effet que la dernière équilibration se produit par l'intermédiaire de la rupture de la liaison carbone–carbone du dialcoolate conduisant à un intermédiaire dicétyle. Il est très probable que cette réaction implique une oxydo-réduction du type proposé par Doering dans le cas des monoalcools. Un examen de diols-1,2 stéroïdaux secondaire–tertiaire dans des conditions semblables montre que de tels systèmes s'épimérisent au niveau des deux centres carbinoliques; on interprète ces résultats en termes d'une oxydation séquentielle, d'une transposition α-cétolique et d'une réduction.

[Traduit par le journal]

Introduction

The mechanism by which secondary alkali metal alkoxides epimerize has been thoroughly examined (1, 2). The results are well accounted for by a reaction sequence (Scheme 1) wherein the substrate is

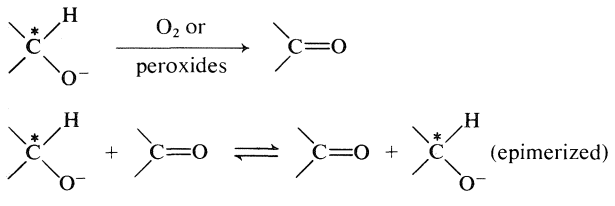

SCHEME 1

slowly oxidized by solvent impurities or atmospheric oxygen to form a catalytic quantity of the corresponding carbonyl compound. Small amounts of this hydride acceptor are sufficient to prime a chain of hydride transfers between substrate molecules that eventually results in complete stereochemical equilibration.

In agreement with this mechanism, the reaction shows a variable induction period depending upon the extent of exclusion of oxidizing impurities. Moreover, it has been observed that heating alkoxides racemizes asymmetric centres α to the carbinol carbon if they bear a hydrogen atom. Such data conform with the proposed mechanisms in which the alkoxide is converted to a carbonyl group thereby making the α-hydrogen exchangeable in the alkaline medium.

In a piece of elegant experimentation, Doering and Aschner (2) were able to demonstrate that by diligent exclusion of oxygen, alkali peroxides, and carbonyl compounds these epimerizations could be entirely arrested. Alternatively, by the addition of a mixture of fluorenone and fluorenol, one a facile hydride acceptor and the other a facile hydride donor, such stereochemically hindered substrates as α- and β-fenchol, which were inert under other conditions, could be epimerized.

In 1970 Schlosser and Weiss (3) reported the stereochemical equilibration of the dilithium derivatives of 1,2-diols in diglyme at 155°C. These derivatives were formed by treatment of the diols with butyllithium in diglyme, e.g., **1** or **2** gives an equilibrium mixture of **1** and **2** via their dilithium derivatives:

[1]Present address: Canada Packers Research Centre, 2211 St. Clair Ave. W., Toronto, Ont., Canada M6N 1K4.

0008-4042/79/030304-10$01.00/0

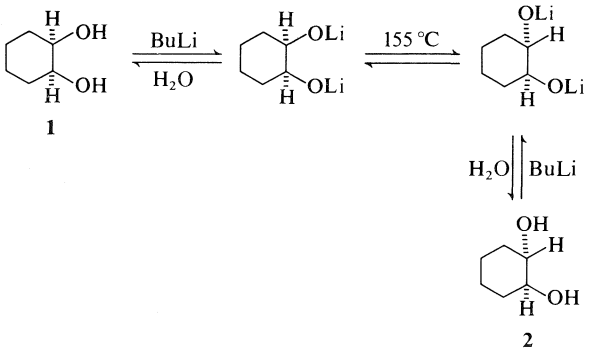

1 2

They proposed that the reaction proceeds by cleavage of the carbon–carbon bond to produce a diketyl **3** which subsequently rebonds[2] (Scheme 2).

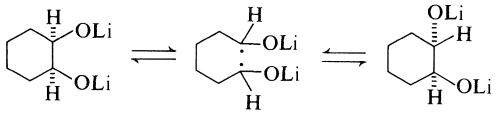

3

SCHEME 2

However, all of their substrates possessed the requisite hydrogen atoms for the operation of the transfer mechanism of Scheme 1.

Because of the intrinsic interest of the postulated carbon–carbon bond cleavage to give a diketyl, we have undertaken a further study of the reaction of 1,2-diols with butyllithium in diglyme followed by thermolysis. To avoid the mechanistic ambiguity of the earlier work we chose first to investigate a ditertiary 1,2-diol, where hydride transfer processes analogous to those of Scheme 1 could not be operative, whereas cleavage to a diketyl would be expected to be unimpeded and probably enhanced. This investigation has led us to conclude that the stereochemical equilibration of the dilithium derivatives of 1,2-diols is unlikely to proceed via diketyl intermediates. Furthermore, we have found that the diglyme solvent is extensively decomposed under the reaction conditions, giving rise to doubts as to whether the method actually produces the intermediate dialkoxide quantitatively. Nevertheless we have confirmed that the procedure is experimentally effective for secondary-secondary 1,2-diols and have extended it by showing that secondary-tertiary 1,2-diols can be converted to diastereoisomeric mixtures with epimerization at *both* carbinol centres.

Results and Discussion

cis- and *trans*-1,2-Dimethyl-1,2-cyclohexanediol (**4** and **5**) were treated with butyllithium in diglyme in the presence of a trace of triphenylmethane.[3] A large excess of butyllithium was used in an attempt to ensure that all the hydroxyl protons reacted. The resulting mixture was heated in a sealed tube at 200°C for 17 h. Neither **4** nor **5** showed any epimerization by gc and gc–ms analysis under conditions where 1% of either isomer could be detected in authentic mixtures of the two.

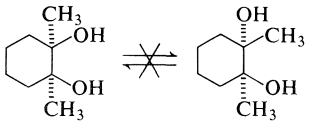

4 5

Since **1** and **2** and the other secondary-secondary 1,2-diols examined by Schlosser and Weiss (3), all undergo equilibration even at the lower temperature of 155°C, these experiments provide strong evidence that the equilibration requires at least one non-tertiary alcohol group. This is in complete accord with a route of the type of Scheme 1 but not readily explicable in terms of the diketyl intermediate **3** of Scheme 2. Furthermore, it cannot be argued that the methyl groups inhibit the reaction to give a diketyl, since it has been concluded that in aliphatic ketyls most of the radical character is associated with carbon and most of the anionic character with oxygen (4). Thus it would be expected that if **3** were an intermediate in the equilibration of **1** and **2**, the formation of the corresponding diketyl intermediate would probably be facilitated in the cases of **4** and **5**.[4]

To ensure that *cis*- and *trans*-1,2-cyclohexanediols (**1** and **2**) undergo equilibration under the exact conditions that we employed for **4** and **5** we subjected **1** and **2** to these conditions (200°C, 17 h, triphenylmethane present) and also to the conditions of Schlosser and Weiss (155°C, 17 h, no triphenylmethane). In the latter case we obtained from **1** a 3:97 mixture of **1** and **2** and from **2** a 2:98 mixture of **1** and **2**, in excellent accord with the results reported by the earlier workers. In the former case only the *trans* isomer **2** was detectable in the equilibrated system formed from either **1** or **2**. Although this is a

[2]In the single case examined involving an acyclic 1,2-diol, **3** would correspond to two ketyls.

[3]Triphenylmethane was added in the expectation that it would serve as an indicator of excess butyllithium and thus of complete conversion of the diol to its dilithium derivative. In fact we have found that butyllithium reacts with diglyme even at 0°C and no permanent colour ever develops.

[4]The possibility that such a diketyl is formed but does not undergo reclosure because of steric effects may be discounted because of the good recoveries of **4** and **5** after attempted equilibration.

noteworthy difference (and one for which we are currently unable to account) it in no way vitiates our conclusion above concerning the structural requirements for equilibration, since in the case of **4** and **5**, *neither* underwent conversion to the other.

We have observed that the epimerization reaction of **1** and **2** has a variable induction period as expected in terms of Scheme 1. This can be shortened with such additives as triphenylmethane, di-*tert*-butyl peroxide, fluorenone, and fluorenol or lengthened by the addition of lithium hydride. Unfortunately, in spite of considerable effort, it was not possible to bring all the factors affecting the induction period under experimental control and rate measurements were unreproducible.

If the equilibration of secondary-secondary 1,2-diols involves processes of the type of Scheme 1 there appears to be no reason why these epimerization conditions should not also be applicable to the lithium derivatives of simple secondary alcohols and we have in fact applied them successfully to *cis*- and *trans*-4-methylcyclohexanol (**6** and **7**).[5]

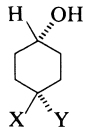

6 X = CH_3, Y = H
7 X = H, Y = CH_3

Having established the failure of tertiary-tertiary 1,2-diols to epimerize and confirmed the epimerization of secondary-secondary 1,2-diols we turned to the examination of secondary-tertiary 1,2-diols. To detect the stereochemical changes in the secondary-tertiary case it is necessary that the diol have at least one fixed chiral centre in relationship to which the retention or inversion of configuration of each carbinol carbon can be observed separately. The steroids 3β-methoxy-5α-cholestane-5,6β-diol (**8**) and 3β-methoxy-5α-cholestane-5,6α -diol (**9**) were selected as suitable for this purpose.

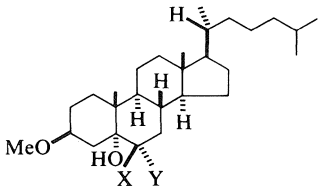

8 X = OH, Y = H
9 X = H, Y = OH

Treatment of **8** in diglyme with butyllithium in the presence and absence of triphenylmethane followed by heating at 200°C, for 17 h gave mixtures of compounds **10–13** in different relative amounts together with a little unconsumed **8** (see Table 1).[6] Similar treatment of **9** in the presence of triphenylmethane gave compounds **10** and **11** together with a considerable amount of unconsumed **9** (Table 1).

TABLE 1. Products from thermolysis of lithium derivatives of 3β-methoxy-5α-cholestane-5α,6β-diol (**8**) and -5α,6α-diol (**9**)[a]

Products	From 5α,6β-diol (**8**)		From 5α,6α-diol (**9**)
	No Ph_3CH	$+Ph_3CH$	$+Ph_3CH$
5α,6β-diol (**8**)	7	7	0
5α,6α-diol (**9**)	0	0	58
5β,6α-diol (**10**)	32	23	24
Δ^3-5,6-diols (**11**)	28	8	17
5α,6α-epoxide (**12**)	4	47	0
Δ^6-5α-ol (**13**)	29	15	0

[a]The figures given are percentage relative yields: the absolute yields were high in each case.

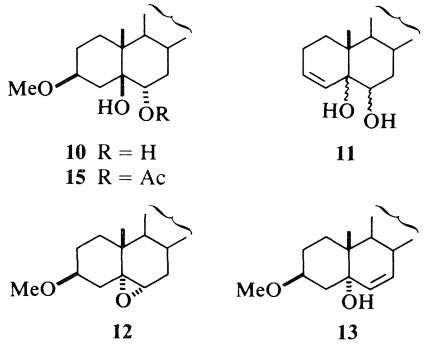

10 R = H
15 R = Ac

11

12

13

In each case the previously unknown 3β-methoxy-5β-cholestane-5,6α-diol (**10**) was a major component of the reaction mixture. The structure of this product was established as follows. It was shown to be stereoisomeric with **8** (and **9**) by oxidation with periodic acid to give the keto aldehyde **14**, which was

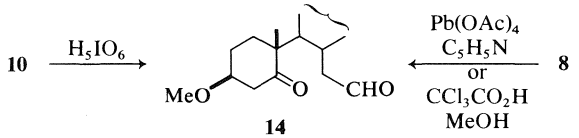

14

identical with the product formed on oxidation of **8** with lead tetraacetate in pyridine or trichloroacetic acid – methanol.[7] The ir spectrum (CS_2) of **10** shows two hydroxyl stretching bands: a weak but sharp

[5]Another, unidentified alcohol was also formed in the reaction.

[6]It cannot be assumed that the differences are due solely to the presence of triphenylmethane since, as we have already noted, there is some uncontrolled variation in the induction period for these reactions.

[7]Compare with refs. 5 and 6; the *trans*-diaxial diol **8** is inert to periodic acid and reacts only slowly with lead tetraacetate.

band at 3571 cm^{-1}, comparable with the single absorption band for free hydroxyl in the spectrum of *trans*-diaxial **8**, and a stronger and broader signal at 3497 cm^{-1}, characteristic of a hydrogen-bonded hydroxyl group. The most compelling evidence for the stereochemical assignment comes from the ^1H nmr spectrum of **10**. In the spectrum of **8** the C-19 methyl signal appears at δ 1.20, shifted downfield because of its rigid 1,3-diaxial orientation with respect to the C-6 hydroxyl group. In the spectrum of **10** no methyl signal appears at lower field than δ 0.93 and it can thus be concluded that the C-6 hydroxyl group is now equatorial. Corroboration comes from the coupling constants (J = 12, 5 Hz) for the C-6 proton in the ^1H nmr spectrum of **15**, the monoacetate of **10**, and from the single band at 1242 cm^{-1} in its ir spectrum (7, 8). Since **10** is stereoisomeric with **8** and **9** and has an equatorial secondary hydroxyl group it must have the 5β,6α-diol stereochemistry as assigned.[8]

The ^1H nmr spectrum of **10** shows two separate signals for the hydroxyl protons; these and the ir data (*vide supra*) are consistent with the existence of **10** in solution as a mixture of the hydrogen-bonded species **16***a–c* (9).

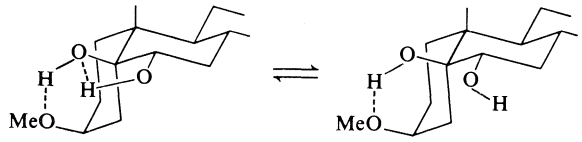

16*a* **16***b*

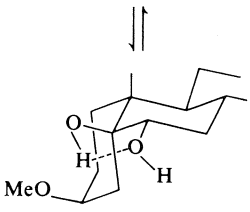

16*c*

The formation of **10** and **9** involves epimerization at the secondary carbinol carbon C-6 but its formation from **8** requires equilibration at both the tertiary and secondary carbinol carbons C-5 and C-6. At first sight this might appear to be explicable in terms of the C—C cleavage mechanism of Scheme 2 and not in terms of the oxidation–reduction mechanism of Scheme 1. However it is well documented (9, 10) that tertiary α-hydroxy ketones can be epimerized under basic conditions at the tertiary carbinol carbon via a reversible rearrangement of

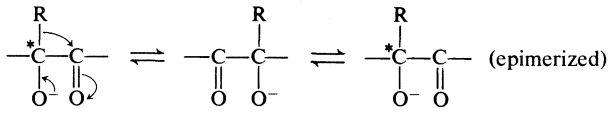

SCHEME 3

the type shown in Scheme 3. Such a process together with processes of the type of Scheme 1 can then account for the conversion of **8** to **10**. Because of our earlier discussed reservations regarding the diketyl mechanism of Scheme 2, we propose the reaction pathways for the conversion of **8** and **9** to **10** that are shown in Scheme 4.

The feasibility of the postulated equilibration of **18** and **19** in Scheme 4 was established by the demonstration that treatment of the hydroxy ketone **20** with methanolic potassium hydroxide gives a mixture of **20** and its C-5 epimer **21**.[9] The reaction mixture also contained a minor component that is tentatively assigned structure **22**.

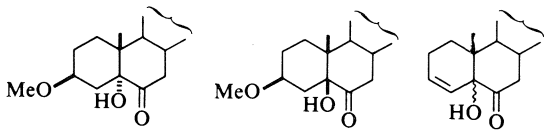

20 **21** **22**

It remains for us to discuss in terms of Scheme 4 the positions of the equilibria. Although we have not investigated these in detail our results indicate that the lithium derivative of **10** is greatly favoured over those of **8** and **9** and also over that of 3-methoxy-5β-cholestane-5,6β-diol (**23**), the fourth C-5,6 stereoisomer in the series. The preponderance of the lithium derivative of **10** is attributed to the relief of 1,3-diaxial interaction with the C-19 methyl group and the stabilization conferred by coordination of the methoxyl oxygen atom with the lithium cation associated with the C-5 oxygen atom (cf. **24**). It is considered that this stabilization, which is related to the hydrogen bonding equilibria in the case of **10** itself (*vide supra*), more than offsets the destabilization owing to the assumption of the *cis* A–B ring fusion.

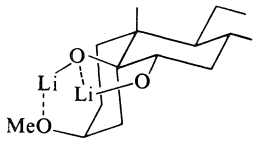

24

Next we discuss the other products formed together with **10** on the thermolysis of the lithium derivatives of **8** and **9** in diglyme (see Table 1). The

[8]Since the completion of this work, the preparation of **10** by reduction of 5-hydroxy-3β-methoxy-5β-cholestan-6-one (**20**) with sodium and ethanol has been reported (9).

[9]This epimerization has also been carried out recently by Campion *et al.* (9).

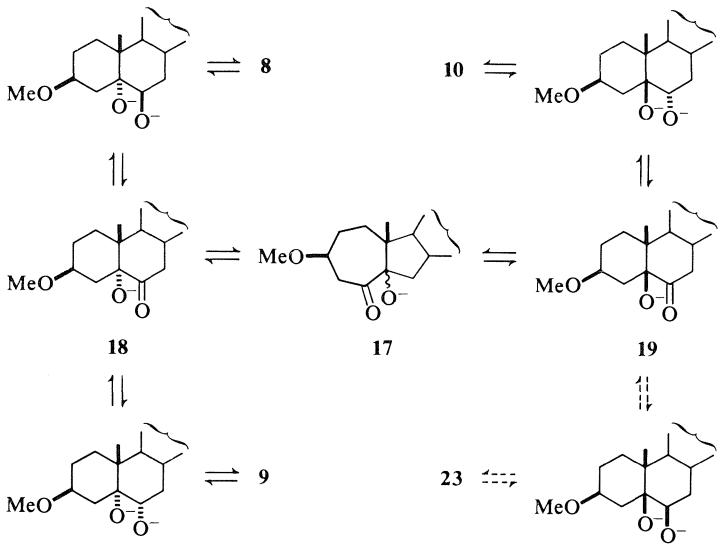

SCHEME 4

products were separated by preparative-layer chromatography and in the case of both **8** and **9** one band contained a mixture of similar compounds whose mass and ^{1}H nmr spectra showed that they had been formed by elimination of methanol. These fractions were not further investigated but are tentatively assigned structures of type **11**. These might arise by base-catalysed elimination of methanol from **8**–**10** but their formation is best interpreted in terms of elimination of methanol from the β-methoxy ketone **17** that is postulated as an intermediate in Scheme 4 (Scheme 5).

A major product from **8** was the epoxide **12**, which was not formed from **9**. This epoxide is a known compound (11, 12) and was identified on the basis of its elemental composition, physical constants, and spectra (see Experimental). A work-up of the reaction mixture after addition of butyllithium, but before heating, returned **8**, showing that **12** was formed by thermolysis. Variation in the procedure for quenching and working up the reaction

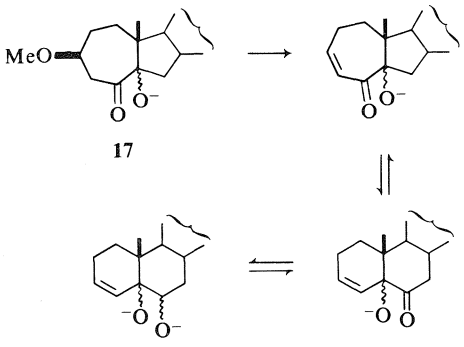

SCHEME 5

mixture after thermolysis did not appear to alter significantly the extent of its formation. The epoxide was also shown to be stable in the presence of lithium oxide under the conditions of the thermolysis, contraindicating its involvement as an intermediate in the interconversion of the stereoisomeric diols. It seemed most likely that the unexpected formation of this epoxide was associated with the decomposition of the solvent diglyme (*vide supra*) and in particular that **8** underwent conversion to an intermediate in which the C-6 oxygen function was converted to a better leaving group followed by *trans* diaxial displacement by the C-5 alkoxide to give **12**.

Evidence on this score was obtained by treatment of **8** in diglyme with 1.27 equiv. of butyllithium followed by thermolysis under the usual conditions. This gave a mixture containing 59% of **8** and 28% of a novel product **25**, a monoformate of **8**. This was identified by its spectral characteristics and by direct comparison with an authentic sample prepared by formylation of **8** with acetic formic anhydride. On hydrolysis it returned **8**. Treatment of **25** with lithium hydride in diglyme at reflux gave the epoxide **12** as the only product (Scheme 6).

These observations provide excellent support for the general pathway proposed for the formation of **12** on treatment of **8** with excess butyllithium in diglyme followed by thermolysis. They also confirm that decomposition of the solvent is involved in that considerations of mass balance alone in the reaction of **8** with 1 equiv. of butyllithium dictate that the formyl carbon of **25** is, at least in part, solvent derived. A possible route to the formate precursor is shown in Scheme 7. This involves lithiation of a terminal carbon atom of diglyme (facilitated by coordination

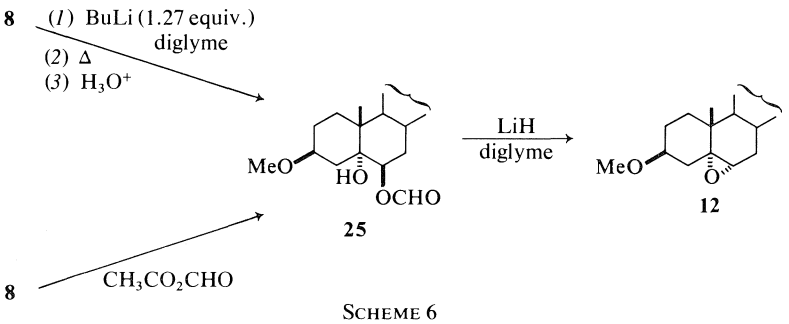

SCHEME 6

of the lithium with the two remote oxygen atoms) and autoxidation[10] of this to give **26**, which is converted by base to the formate **27**. The latter could then give rise to **25** via transesterification.[11]

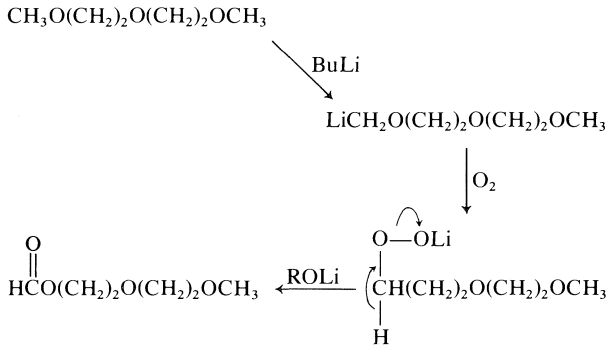

SCHEME 7

The remaining product from the thermolysis of the lithium derivative of **8** is the unsaturated alcohol **13**. Like **12**, this was not formed from **9**. The structural assignment was initially based on spectroscopic data (see Experimental) and the formation of **13** in association with that of **12**. In particular the ir spectrum shows a nonhydrogen-bonded hydroxyl group, favouring the 5α configuration since the hydroxyl group in the 5β isomer would be expected to hydrogen bond with the 3β-methoxyl group.[12]

An unusual feature in the ^{1}H nmr spectrum of **13** is the accidental equivalence of the two olefinic protons in deuteriochloroform, hexadeuterioacetone, and hexadeuteriobenzene solutions, This was unexpected and led us to consider the possibility that the double bond had migrated to the Δ^{11} position. This could be excluded, however, since an sp^3 C-11 signal is clearly evident at δ 21.1 (t) in the partially decoupled ^{13}C nmr spectrum of the product: in a 3-substituted cholestane derivative such a high-field methylene carbon signal can only be associated with a C-11 carbon.[13] Although the equivalence of the C-6 and C-7 protons in the ^{1}H nmr spectrum is unusual, it may be noted that a similar equivalence is observed in the spectrum of 1,5,5-trimethyl-2-cyclohexen-1-ol (15).

Corroboration for the structural assignment **13** and an indication of the origin of this product was provided by the observation that treatment of the epoxide **12** in diglyme with excess butyllithium and one molar equivalent of water followed by thermolysis gave **13** in high yield. Thus, it may be suggested that the formation of **13** in the thermolysis of the lithium derivative of **8** involved the intermediacy of **12**.[14] This interpretation accounts for the observation that although both **12** and **13** are formed from **8** neither type of product is formed from **9** or **10**. Neither **9** nor **10** has the favourable *trans*-diaxial orientation of the oxygen functions for epoxide formation, and in the absence of such an intermediate, formation of an unsaturated alcohol of type **13** does not occur.

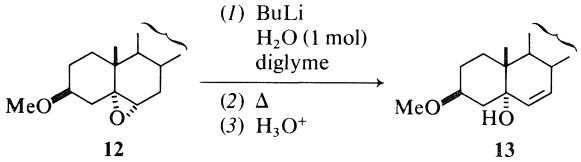

It may finally be noted that if, as proposed, the complexity of the reaction of **8** in diglyme with butyllithium stems from decomposition of the sol-

[10]Although the reaction with butyllithium was conducted under nitrogen, air could have been introduced during the transfer to the freeze–thaw degassing cycle.

[11]An alternative route involving fragmentation of the lithiation product to give formaldehyde, ethylene, and $LiO(CH_2)_2OCH_3$ followed by conversion of the formaldehyde to formate by a Cannizzaro reaction is considered to be less likely because of our failure to observe gas formation on treatment of diglyme with butyllithium in ether.

[12]*trans*-5-*tert*-Butyl-*cis*-1,3-cyclohexanediol which has both hydroxyl groups axial shows in its ir spectrum both free and intramolecularly hydrogen-bonded hydroxyl bands (13).

[13]The ^{13}C nmr spectra of compounds **8**–**10**, **13**, and **20** are given in Table 2; the signal assignments are based on comparison with the large body of literature data on the ^{13}C nmr spectra of steroids (14).

[14]An additional source of **13** could be the postulated precursor of **12**, the formate **25**.

TABLE 2. ^{13}C chemical shifts of compounds **8–10**, **13**, and **20**[a]

Assignment (Carbon No.)	$^{C}\delta$ ($CDCl_3$)				
	8	**9**	**10**	**13**	**20**
1	32.3	31.0	25.7	28.5	29.7
2	27.1	27.1	23.2	27.0	26.8
3	76.5*	76.3	71.4	75.9	75.9
4	37.5	35.0*	28.0†	37.6	32.8
5	76.2†	76.8	77.7	73.8	80.6
6	76.2*†	70.8	77.1	133.2*	212.1
7	34.7	35.3*	34.6	133.6*	41.9
8	30.3	33.7	33.9	38.5	37.4
9	46.1	44.7	43.5	45.2	44.7
10	38.7	39.5	41.2	38.4	43.2*
11	21.3	21.2	21.9	21.1	21.5
12	40.1	40.0	40.2	40.2	39.7
13	42.8	42.8	42.8	43.8	42.7*
14	56.1*	56.1*	56.4*	54.1	56.3*
15	24.2	24.2	24.3	23.9†	23.9†
16	28.3	28.3	28.2	28.3	28.0‡
17	56.5*	56.4*	56.6*	56.3	56.5*
18	12.2	12.1	12.1	12.2	12.1
19	16.8	15.5	17.2	14.6	14.0
20	35.9	35.9	35.8	35.9	35.8
21	18.8	18.7	18.7	18.8	18.7
22	36.3	36.3	36.2	36.3	36.2
23	24.0	24.0	23.9	23.9†	23.9†
24	39.6	39.6	39.6	39.6	39.6
25	28.0	28.0	28.0†	28.0	28.0‡
26	22.6	22.6	22.6	22.6	22.6
27	22.8	22.8	22.8	22.8	22.8
OCH_3	55.8	55.8	56.2	55.9	55.7

[a]Individual assignments cannot be made to pairs of close-lying signals marked with asterisks; signals considered to be superimposed are marked with a dagger or double dagger.

vent, cleaner and more efficient stereochemical equilibration should be achievable by the use of lithium hydride in diglyme or other high boiling solvents.[15]

Experimental

Melting points were determined on a Kofler block and are corrected. Infrared spectra were recorded in CS_2 solution on a Perkin Elmer model 327 or 237B spectrophotometer; the absorption maxima are reported in wavenumbers (cm^{-1}) calibrated with respect to the absorption band of polystyrene at 1602 cm^{-1}. Proton magnetic resonance (^1H nmr) spectra were recorded in deuteriochloroform solution at ambient temperature on a Varian T-60 instrument unless otherwise specified. The ^{13}C magnetic resonance (^{13}C nmr) spectra were recorded on a Bruker WP-80 instrument in deuteriochloroform solution unless otherwise specified. Chemical shift values are given on the δ scale downfield from tetramethylsilane as internal standard. Low resolution mass spectra were determined with a Bell and Howell CEC 21-490 spectrometer and high resolution mass spectra on an AEI MS-902 instrument.

Analytical thin-layer chromatography (tlc) was carried out on Brinkmann analytical silica gel plates with fluorescent indicator. Preparative-layer chromatography (plc) was carried out on 20 cm × 20 cm silica plates of 2-mm thickness from Brinkmann or Quantum Industries. Visualization was effected by spraying either the entire plate or a single edge of the plate with 0.5% vanillin in 80% v/v ethanol – sulfuric acid followed by heating the sprayed area.

Oxygen-free nitrogen was obtained by bubbling commercial nitrogen through one or two traps filled with a mixture of sodium and benzophenone in diglyme. The gas was then bubbled through concentrated sulfuric acid and passed up a drying tower filled with solid sodium hydroxide pellets. The rate of flow was monitored with a mercury bubbler.

Diglyme (BDH Chemicals) was purified by distillation at atmospheric pressure and dried just before use by refluxing over calcium hydride followed by redistillation under nitrogen. It was injected into the reaction vessel with a syringe.

Gas Chromatographic Analyses

The gc analyses were conducted either on an Aerograph A-170 instrument with a thermal conductivity detector and helium as the carrier gas or on a Perkin-Elmer F-11 instrument with a hydrogen flame detector and nitrogen as the carrier gas. The following columns were used: (*1*) 13 ft × $\frac{1}{4}$ in. aluminum, 5% UCON HB-2000 on 80–100 Chromosorb G-DMCS-AW; (*2*) 10 ft × $\frac{1}{8}$ in. stainless steel, 20% Carbowax 20M (SPA-64) on 80–100 Chromosorb W-HMDS-AW; (*3*) 10 ft × $\frac{1}{8}$ in. stainless steel, 10% DEGS on 80–100 Chromosorb P-DMCS-AW. Column *1* was used with the Aerograph instrument and columns *2* and *3* with the Perkin Elmer instrument.

Substrates

The following compounds were prepared by previously reported methods: *cis*-1,2-cyclohexanediol (**1**) (16), *trans*-1,2-cyclohexanediol (**2**) (17), *cis*-1,2-dimethyl-1,2-cyclohexanediol (**4**) (16), and *trans*-1,2-dimethyl-1,2-cyclohexanediol (**5**) (18). *cis*-4-Methylcyclohexanol (**6**) and *trans*-4-methylcyclohexanol (**7**) were obtained from Aldrich Chemical Co. It was determined by glc analysis that none of these substances was contaminated with a detectable amount of its epimer.

3β-Methoxy-5α-cholestane-5,6β-diol (**8**) was prepared by methylation of cholesterol to give cholesteryl methyl ether (19) and treatment of this with hydrogen peroxide and formic acid followed by hydrolysis with base (12).

3β-Methoxy-5α-cholestane-5,6α-diol (**9**) was prepared from cholesteryl methyl ether by an adaptation of the procedure for the *cis* hydroxylation of 5-cholestene (20). Cholesteryl methyl ether (794 mg, 1.25 mmol) was dissolved in dry ether (140 mL) containing dry pyridine (4 mL) with magnetic stirring. A capsule containing osmium tetroxide (0.5 g, 1.97 mmol) was broken and the two parts were dropped immediately into the solution. The flask walls were washed down with ether (5 mL), the flask was stoppered, and its contents were stirred for 123 h at ambient temperature. A stream of hydrogen sulfide was passed through the solution, and the precipitate was filtered. This was repeated until no more precipitate formed. The solution was extracted with saturated aqueous sodium bicarbonate and then with 3 *N* aqueous sodium hydroxide containing some mannitol. The organic layer was dried over sodium sulfate and filtered through a plug of Florisil. The solvent was evaporated and any pyridine still present was removed on the rotary evaporator by co-distillation several times with isopropyl alcohol. The crude solid product was chromatographed on a small column of silica gel. Elution with 4:1 v/v chloroform–ether gave cholesteryl methyl ether, and elution with ether gave **9**; yield 50% (75% based on unrecovered starting material). Compound **9** was recrystallized from acetonitrile (10 mL/100 mg) giving needles (87% recovery), mp 175–178°C, $[\alpha]_D^{28.5}$ +12° (*c* 1.0, $CHCl_3$) (lit. (7) mp 172°C (uncorrected), $[\alpha]_D$ +18°); λ_{max}: 3636, 3597 cm^{-1}; $^H\delta$: 0.66 (s, 3H, 18-Me), 0.90 (s, 3H, 19-Me), 3.32 (s,

[15]NOTE ADDED IN PROOF: For a related study that came to our attention after submission of this manuscript, see ref. 22.

3H, OMe) 3.6 (br m, 2H, 3-H and 5-H); *m/e*: 416 (49) ($M - H_2O$).

Thermolyses at Atmospheric Pressure

The following is a typical procedure for thermolyses at atmospheric pressure, which were carried out in the apparatus shown in Fig. 1. *cis*-1,2-Cyclohexanediol (237 mg) was dissolved with a few milligrams of triphenylmethane in distilled diglyme (15 mL). The solution was cooled under nitrogen to −21°C in a liquid nitrogen – carbon tetrachloride slush; ~2 *N* butyllithium in hexane (6.4 mL) was added until a transient red colour developed. The cold bath was removed and replaced with a heating mantle. A timer was started simultaneously with the heating. Hexane and solvent decomposition products distilled out, and then the diglyme was boiled under reflux for 3 h. The heating was stopped and the warm mixture was poured into saturated aqueous ammonium sulfate. The further work-up was identical with the procedure for thermolyses in sealed tubes below.

Thermolyses in Sealed Tubes

The following is a typical procedure. *cis*-1,2-Cyclohexanediol (233 mg, 2.01 mmol) was placed in a 60-cm Carius tube with triphenylmethane (10 mg). The tube was closed with a septum and purged with nitrogen, and purified diglyme (15.0 mL) was added by syringe. The solution was cooled to 0°C in ice and ~2 *N* butyllithium in hexane (6 mL, ~12 mmol) was added slowly by syringe with intermittent agitation of the tube. Towards the end of the addition the red colour of lithium triphenylmethide appeared in the upper part of the tube. The septum was quickly removed and replaced by the vacuum attachment shown in Fig. 2. The tube was cooled in dry ice and degassed at ~0.25 Torr to remove volatile substances. After two freeze–thaw cycles the tube was sealed and heated at ca. 200°C for 17 h in an electrically heated furnace. The tube was cooled, and the gelatinous contents were poured into a flask containing saturated aqueous ammonium sulfate (25 mL). The transfer was completed by washing the tube with 1:1 v/v benzene–ether, saturated aqueous ammonium sulfate, and distilled water. The organic layer was separated, and the aqueous phase was extracted with ether (2 × 25 mL). The total extracts were dried over sodium sulfate and evaporated. The diglyme was removed by short-path distillation at reduced pressure (0.25 Torr, ambient temperature) into a reservoir cooled with Dry Ice. The residue (222 mg) was analyzed by gc and gc–ms by means of the procedure below.

Analysis for cis- *and* trans-*1,2-Dimethyl-1,2-cyclohexanediol (**4**, **5**)*

Thermolysates were analyzed either on column *1* with injector 225°C, detector 208°C, column 124°C; or column *2* with injector setting 6, column 200°C, pressure 30 psi. Compounds **4** and **5** did not epimerize since in no case did the thermolysate from one isomer give rise to a peak of the correct retention time for the other. The identity of reisolated starting material was proven by gc–ms in each case on column *2* with injector 225°C, detector 230°C, column 200°C, carrier gas helium, solvent methanol, 13–18 mg/mL, 1.5 μL injection, 5 mV attenuation, giving a retention time for **4** of 9.75 min and for **5** of 11.75 min.

Analysis for cis- *and* trans-*1,2-Cyclohexanediols (**1**, **2**)*

Compounds **1** and **2** are separable on both columns *1* and *2*. Quantitative estimation of the ratio by integration of the peak areas from crude thermolysates was not justified in this case; however, because gc–ms of the mixtures showed that although the peak eluting with retention time corresponding to **2** was

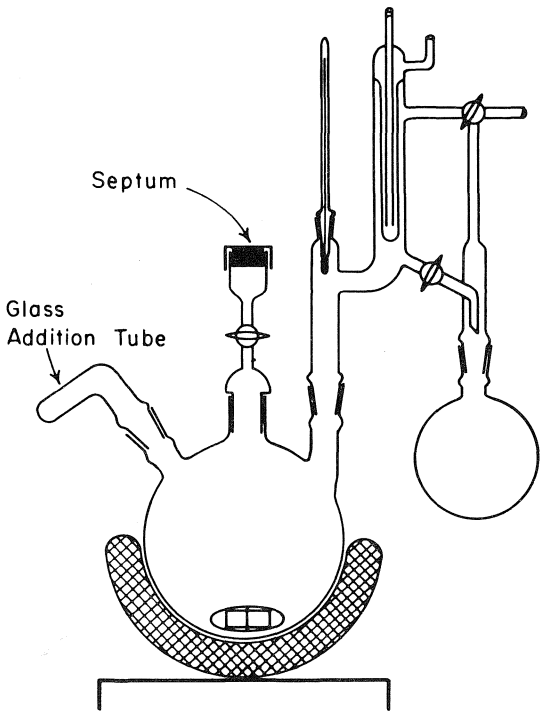

FIG. 1. Apparatus for atmospheric pressure reactions.

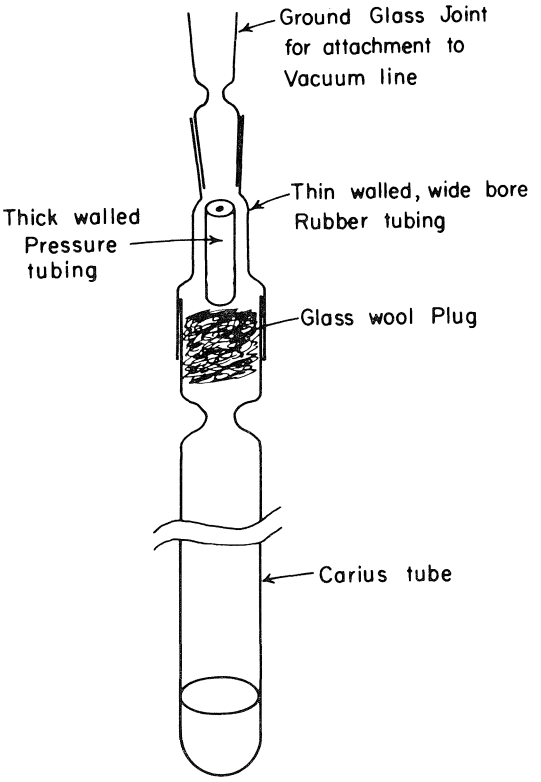

FIG. 2. Apparatus for sealed tube reactions.

pure **2**, the peak eluting with retention time corresponding to **1** was a mixture of **1** and an unknown impurity. Estimation of the ratio **1**:**2** was effected by first placing the crude thermolysate in 1% methanol–dichloromethane onto a short column of 80–200 mesh Brockmann neutral alumina and eluting with the same solvent mixture (fraction A) and then with methanol (fraction B). Fractions A and B both showed a gc peak with retention time corresponding to **1**, whereas only the latter showed a peak with retention time corresponding to **2**. Each of these fractions was acetylated (acetic anhydride, pyridine, ambient temperature, overnight) under conditions previously shown to give quantitative and complete derivatization of **1** and **2**. No peak in the gc on column *2* of acetylated fraction A had the same retention time as diacetylated **1** or **2**, showing that fraction A contains impurities only. The acetylated fraction B had only two peaks in its gc on column *2*, corresponding to diacetylated **1** and **2**. Acetylated fraction B also showed only two peaks, now better resolved, on column *3*. On this column with injection setting 5, column 170°C, pressure 30 psi, *cis*-1,2-diacetoxycyclohexane had a retention time of 21.05 ± 0.1 min and *trans*-1,2-diacetoxycyclohexane had 23.25 ± 0.1 min.

*Thermolysis of the Lithium Derivative of 3β-Methoxy-5α-cholestane-5,6β-diol (**8**)*

The thermolysis was conducted in a sealed tube for 17 h at 200°C according to the general procedure. The product mixture was separated by plc by multiple elution with 4:1 v/v chloroform–ether giving the following products in decreasing order of R_f.

*3β-Methoxy-5,6α-epoxy-5α-cholestane (**12**)*—mp 80–81°C; $[\alpha]_D^{28}$ −53.2° (*c* 1.2, $CHCl_3$) (lit. (11) mp 81°C, $[\alpha]_D^{20}$ −52.0 ± 1°; lit. (12) mp 81–81.5°C, $[\alpha]_D^{28}$ −51.5°); ν_{max}: no OH; $^H\delta$ (CCl_4): 0.60 (s, 3H, 18-Me), 1.03 (s, 3H, 19-Me), 2.72 (d, J = 4 Hz, 1H, 6-H), 3.25 (s, 3H, OMe), 3.25 (br m, 1H, 3-H); *m/e*: 416 (49). *Anal.* calcd. for $C_{28}H_{48}O_2$: C 80.71, H 11.61; found: C 80.43, H 11.46.

*3β-Methoxy-5α-cholest-6-en-5-ol (**13**)*—mp 133–134°C (from acetonitrile); $[\alpha]_D^{29}$ −44.5° (*c* 1.0, $CHCl_3$); ν_{max}: 3610 cm^{-1}; $^H\delta$: 0.68 (s, 3H, 18-Me), 0.92 (s, 3H, 19-Me), 3.36 (s, 3H, OMe), 3.6 (br m, 1H, 3-H), 5.60 (s, 2H, 6- and 7-H); $^H\delta$ (acetone-d_6, 80 MHz); 0.75 (s, 3H), 0.91 (s, 3H), 3.26 (s, 3H), 3.6 (br m, 1H), 5.53 (s, 2H); $^H\delta$ (benzene-d_6, 80 MHz): 0.62 (s, 3H), 0.87 (s, 3H), 3.28 (s, 3H), 3.9 (br m, 1H), 5.49 (s, 2H); *m/e*: 416 (1.5). *Anal.* calcd. for $C_{28}H_{48}O_2$: C 80.71, H 11.61; found: C 80.51, H 11.47.

*3β-Methoxy-5β-cholestane-5,6α-diol (**10**)*—mp 91–93°C; $[\alpha]_D^{28.5}$ +30.8° (*c* 1.0 $CHCl_3$) (lit. (9) mp 91–92°C, $[\alpha]_D$ +27.9°); ν_{max}: 3571, 3497 cm^{-1}; $^H\delta$: 0.67 (s, 3H, 18-Me), 0.93 (s, 3H, 19-Me), 2.54 (br s, 1H, exchangeable with D_2O, 6-OH), 3.37 (s, 3H, OMe), 3.70 (br m, 1H, 3-H), 3.78 (dd, J = 11, 4 Hz, 6-H), 4.35 (s, 1H, exchangeable with D_2O, 5-OH); *m/e*: 434 (18). *Anal.* calcd. for $C_{28}H_{50}O_3$: C 77.36, H 11.59; found: C 77.24, H 11.58. The *6-monoacetate **15*** was prepared by treatment of **10** with acetic anhydride in pyridine at room temperature overnight; mp 128–130°C (from acetonitrile); ν_{max}: 3484, 1736, 1242 cm^{-1}; $^H\delta$: 0.69 (s, 3H, 18-Me), 0.99 (s, 3H, 19-Me), 2.08 (s, 3H, OAc), 3.34 (s, 3H, OMe), 3.62 (br s, 1H, 3-H), 4.03 (br s, 1H, 5-OH), 4.95 (dd, J = 12, 5 Hz, 1H, 6-H); *m/e*: 476 (2).

*Cholest-3-ene-5,6-diols (**11**)*—gum; ν_{max}: 3590 cm^{-1}; $^H\delta$: 0.67 (s, 3H, 18-Me), 0.95 (s, 3H, 19-Me), 3.3–4.0 (m, 3H, 6-H and 5- and 6-OH), 5.95 (br s, 2H, 3- and 4-H); *m/e*: 402 (36).

*Cleavage of Diol **10** with Periodic Acid. Formation of Keto Aldehyde **14***

To a solution of diol **10** (24 mg, 0.054 mmol) in 95% ethanol (2.0 mL) was added all at once periodic acid (12 mg, 0.051 mmol) in water (0.5 mL). The solution was maintained at 40°C for 2.5 h. It was diluted with water (10 mL) and the resulting opaque suspension was extracted with ether (3 × 5 mL). Drying (Na_2SO_4) and evaporation of the solvent gave the keto aldehyde **14** as a gum that could not be crystallized; ν_{max}: 2775 (w), 1721, 1698 cm^{-1}. This was shown to be identical with the product obtained by oxidation of diol **8** with lead tetraacetate in either pyridine (5) or trichloroacetic acid – methanol (6) by ir spectral comparison and tlc with the following solvent systems: 4:1 v/v chloroform/ether (R_f 0.52), 9:1 v/v chloroform – ethyl acetate (R_f 0.41), and 5:7:1 v/v cyclohexane–benzene–methanol (R_f 0.58).

*Epimerization of 5α-Hydroxy-3β-methoxy-5α-cholestan-6-one **20**. Formation of **21** and **22***[9]

A 10% w/w solution of potassium hydroxide in anhydrous methanol (100 mL) was added to 5α-hydroxy-3β-methoxy-5α-cholestan-6-one (**20**; 334 mg) (12). The mixture was boiled at reflux under dry nitrogen for 48 h, added to ice water (500 mL) and extracted with ether (1 × 50, 2 × 100 mL). To the extract was added phenolphthalein solution (1 drop) in water (100 mL) and then 2 *N* sulfuric acid until the red colour was discharged. The ethereal solution was washed with saturated aqueous sodium bicarbonate (20 mL), dried ($MgSO_4$), and evaporated. The yield of crude product was 307 mg. Preparative-layer chromatography yielded in order of decreasing R_f a substance tentatively identified as **22**, the epimerized product **21**, and the starting material **20**, in the relative proportions 1:5:8.

*5-Hydroxy-5-cholest-3-en-6-one (**22**)*—gum; ν_{max}: 3436, 1706 cm^{-1}; $^H\delta$: 0.60 (s, 3H, 18-Me), 0.72 (s, 3H, 19-Me), 4.10 (s, 1H, exchangeable, OH), 5.32 (d, J = 10 Hz, 1H, 4-H), 5.95 (br d, 1H, J = 10 Hz, 3-H); *m/e*: 400 (92).

*5-Hydroxy-3β-methoxy-5β-cholestan-6-one (**21**)*—gum; ν_{max}: 3390, 1698 cm^{-1}: $^H\delta$: 0.68 (s, 3H, 18-Me), 0.80 (s, 3H, 19-Me), 3.35 (s, 3H, OMe), 3.60 (br s, $w_{1/2}$ = 8 Hz, 1H, 3H), 4.25 (s, 1H, exchangeable, OH); *m/e*: 432 (16).

*5-Hydroxy-3β-methoxy-5α-cholestan-6-one (**20**)*—mp 145–147°C; ν_{max}: 3571 (sh), 3401, 1712 cm^{-1}; $^H\delta$: 0.65 (s, 3H, 18-Me), 0.80 (s, 3H, 19-Me), 2.65 (s, 1H, exchangeable, OH), 3.37 (s, 3H, OMe), 3.6 (br m, $w_{1/2}$ = 20 Hz, 1H, 3-H); *m/e*: 432 (100).

*Thermolysis of the Monolithium Derivative of Diol **8**. Formation of 3β-Methoxy-5α-cholestane-5,6β-diol 6-Formate (**25**)*

Diol **8** (277 mg, 0.66 mmol) was placed into a dry, nitrogen-filled Carius tube and dissolved in diglyme (20 mL). The solution was cooled to 0°C and stirred by means of a small magnetic stirring bar within the tube and was treated with 2.11 *N* butyllithium in hexane (0.40 mL, 0.84 mmol, 1.27 equiv.). While the nitrogen atmosphere was retained the tube's inner walls were washed with additional solvent (10 mL) and the tube was quickly attached to a vacuum line and evacuated with stirring to remove hexane. It was then cooled in a liquid nitrogen – carbon tetrachloride slush and sealed under vacuum. The tube was heated in a furnace at 195–200°C for 18 h, cooled, and opened, and the contents were poured into saturated aqueous ammonium sulfate. The solution was extracted with ether, and the extract was washed with water, aqueous sodium bicarbonate, and brine, dried over sodium sulfate, and evaporated. The high boiling solvent was removed under high vacuum leaving a yellowish foam (312 mg). Preparative-layer chromatography with elution with 4:1 v/v chloroform–ether gave three fractions: recovered **8** (167 mg, 60%), an unidentified product (15 mg), and **25** (81 mg, 28%) as a gum that could not be crystallized; ν_{max}: 3636, 3610, 1730, 1175 cm^{-1}; $^H\delta$: 0.68 (s, 3H, 18-Me), 1.13 (s, 3H, 19-Me), 3.33 (s, 3H, OMe), 3.6 (br m, 1H, 3-H), 4.85 (m, $w_{1/2}$ = 6 Hz, 1H, 6-H), 8.10 (s, 1H, CHO); *m/e*: 462. *Mol. wt.* calcd. for

$C_{29}H_{48}O_3$ ($M - H_2O$): 444.3603; found (high resolution ms): 444.3597.

Hydrolysis of Monoformate ***25****. Formation of Diol* ***8***

The monoformate **25** (69 mg) was dissolved in benzene (4 mL) and 6 mL of a solution of potassium carbonate (317 mg) in water (5 mL) and methanol (80 mL) was added to give a homogeneous solution. After 21.5 h at room temperature tlc showed complete hydrolysis to a single product. The solution was diluted with brine and extracted once with chloroform and once with ether. The extract was dried ($MgSO_4$) and evaporated to give a solid (42 mg), which was recrystallized from benzene to give **8**, mp 153–154°C, with ir and ^1H nmr spectra identical with those of authentic material.

Monoformylation of Diol ***8****. Formation of Monoformate* ***25***

Acetic–formic anhydride was prepared by the method of Maramatsu *et al.* (21). The ^1H nmr spectrum of the product showed that it was 92% pure and contained 8% acetic anhydride. In a stoppered flask was placed diol **8** (104 mg), acetic–formic anhydride (92%; 60 drops from a disposable pipette) and benzene (40 drops). The stoppered flask was allowed to stand at room temperature with occasional agitation for 36 h. The contents were poured into saturated aqueous sodium bicarbonate and the mixture was extracted with ether. The extract was dried and evaporated to a foam (81 mg) whose ^1H nmr spectrum was identical with that of the product from **8** and butyllithium–diglyme except that the formate was accompanied by 8% of acetate. Attempted crystallization was unsuccessful but gave **25** as a gum that was free of acetate.

Treatment of Monoformate ***25*** *with Lithium Hydride. Formation of Epoxide* ***12***

The monoformate **25** (containing 8% monoacetate; 187 mg, 0.40 mmol) was dissolved in diglyme (7 mL) and lithium hydride (11.6 mg, 1.5 mmol) was added. The solution was stirred at reflux under nitrogen for 17 h and then worked up in the usual way. The ir and ^1H nmr spectra of the product were identical with those of the epoxide **12**. Crystallization gave **12** (99 mg), mp 80–81°C.

Conversion of Epoxide ***12*** *to Enol* ***13***

In a 60-cm Carius tube was placed triphenylmethane (8 mg). A septum was placed on the tube, which was purged with a slow stream of oxygen-free nitrogen. The length of the tube was heated to displace air and moisture. A 0.149 *M* solution of water in diglyme (5.0 mL, 0.745 mmol) was added by syringe and then butyllithium in hexane (7 mL, ~11 mmol) was added by syringe at 0°C. After ~3.5 mL of the latter solution had been added the mixture had become persistently red. A solution of the epoxide **12** (261 mg, 0.745 mmol) in diglyme (10.0 mL) was added by syringe all at once to the ice-cold solution of base. The red colour faded immediately to yellow but reappeared on standing. The tube was transferred to the vacuum line, given two freeze–thaw cycles, and then sealed. It was heated for 18 h at 200°C. The usual work-up gave a reddish oil that immediately showed signs of solidifying. This gave on tlc one predominant spot, which gave with sulfuric acid spray and heat the deep blue colour characteristic of the allylic alcohol **13**. The impure solid was triturated with cold methanol and then with cold acetonitrile to give an off-white solid. This was recrystallized from acetonitrile to give **13** (134 mg) as long white needles, mp 133–134°C, which was shown by ir and ^1H nmr spectroscopy to be identical with the enol obtained by thermolysis of the lithium derivative of **8**.

Acknowledgements

We gratefully acknowledge the help of Dr. Renuka Misra who performed the gc–ms measurements and Dr. J. E. McCloskey and Mr. J. D. Kronis for recording and discussing the ^{13}C nmr spectra. We thank the National Research Council of Canada for support of the work.

1. W. E. Doering, G. Cortes, and L. H. Knox. J. Am. Chem. Soc. **69**, 1700 (1947).
2. W. E. Doering and T. C. Aschner. J. Am. Chem. Soc. **71**, 838 (1949).
3. A. Schlosser and P. Weiss. Synthesis, 251 (1970).
4. N. Hirota and S. I. Weissman. J. Am. Chem. Soc. **82**, 4424 (1960).
5. H. R. Goldschmid and A. S. Perlin. Can. J. Chem. **38**, 2280 (1960).
6. C. A. Grob and P. W. Schiess. Helv. Chim. Acta, **43**, 1546 (1960).
7. C. R. Narayanan and K. N. Iyer. Tetrahedron Lett. 285 (1966).
8. R. N. Jones, P. Humphries, F. Herling, and K. H. Dobriner. J. Am. Chem. Soc. **73**, 3215 (1951); A. R. H. Cole. Festschr. Chem. Organ. Naturstoffe, **13**, 1 (1956).
9. T. H. Campion, G. A. Morrison, and J. R. Wilkinson. J. Chem. Soc. Perkin Trans. I, 2508 (1976).
10. Y. Mazur and M. Nussim. Tetrahedron Lett. 817 (1961).
11. G. Snatzke. Justus Liebigs Ann. Chem. **686**, 167 (1965).
12. Y. F. Shealy and R. M. Dodson. J. Org. Chem. **16**, 1427 (1951).
13. P. Chamberlain and G. H. Whitman. J. Chem. Soc. B, 1382 (1970).
14. J. B. Stothers. Carbon-13 nmr spectroscopy. Academic Press, New York, NY. 1972. pp. 439–443; H. J. Reich, M. Jautelat, M. T. Messe, F. J. Weigert, and J. D. Roberts. J. Am. Chem. Soc. **91**, 7445 (1969); D. Leibfritz and J. D. Roberts. J. Am. Chem. Soc. **95**, 4996 (1973); D. J. Chadwick and D. H. Williams. J. Chem. Soc. Perkin Trans. II, 1903 (1974); H. Eggert, C. L. Vanantwerp, N. S. Bhacca, and C. Djerassi. J. Org. Chem. **41**, 71 (1976); C. Konno and H. Hikino. Tetrahedron, **32**, 325 (1976); C. L. Vanantwerp, H. Eggert, C. D. Meakins, J. O. Miners, and C. Djerassi. J. Org. Chem. **42**, 789 (1977); J. W. Blunt and J. B. Stothers. Org. Magn. Reson. **9**, 439 (1977).
15. B. M. Trost. Problems in spectroscopy. W. A. Benjamin, Inc., New York, NY. 1967. Compound No. 119.
16. H. Meerwein. Justus Liebigs Ann. Chem. **396**, 264 (1912); K. B. Wiberg and K. A. Saegebarth. J. Am. Chem. Soc. **79**, 2822 (1957).
17. A. I. Vogel. A textbook of practical organic chemistry. 3rd ed. John Wiley, New York, NY. 1956. p. 894.
18. S. Nametkin and N. Delentorsky. Chem. Ber. **57**, 583 (1924).
19. M. Neeman, M. C. Caserio, J. D. Roberts, and W. S. Johnson. Tetrahedron, **6**, 36 (1959).
20. D. N. Jones, J. R. Lewis, C. W. Shoppee, and G. H. R. Summers. J. Chem. Soc. 2876 (1955).
21. I. Maramatsu, M. Mouratami, T. Yoneda, and A. Hagitoni. Bull. Chem. Soc. Jpn. **38**, 244 (1965).
22. J. E. McMurry and W. Choy. J. Org. Chem. **43**, 1800 (1978).

Reactions of *N*-3′-furylbenzamide with some dienophiles

JOHN N. BRIDSON

Department of Chemistry, Memorial University of Newfoundland, St. John's, Nfld., Canada A1B 3X7

Received July 11, 1978

JOHN N. BRIDSON. Can. J. Chem. **57**, 314 (1979).

N-3′-Furylbenzamide gives a conventional Diels–Alder adduct with maleic anhydride but with dimethyl maleate and methyl acrylate further reactions take place at the enamide grouping of the initially formed adducts. Compounds have been isolated in which molecules of an alcohol, used as solvent, or the starting furan have added to the double bond of the 1:1 adducts. In the first case unstable alkoxyamides are formed; in the second stable 2:1 adducts result from a novel uncatalysed addition to the double bond of the enamide. The stereochemistry of these and related compounds is discussed.

JOHN N. BRIDSON. Can. J. Chem. **57**, 314 (1979).

Avec l'anhydride maléique, le *N*-furyl-3′ benzamide fournit un adduit de Diels–Alder normal; toutefois le maléate ou l'acrylate d'éthyle conduisent à des réactions subséquentes au niveau du groupement ènamide des adduits qui se forment initialement. On a isolé des composés dans lesquels des molécules d'un alcool, utilisé comme solvant, ou le furanne de départ se sont additionnés à la double liaison des adduits 1:1. Dans le premier cas, il y a formation d'alkoxyamides instables; dans le deuxième cas, il en résulte des adduits 2:1 stables provenant d'une addition qui n'est pas catalysée à la double liaison de l'ènamide. On discute de la stéréochimie de ces composés et d'autres qui leur sont apparentés.

[Traduit par le journal]

Introduction

There has recently been considerable interest shown in the properties of derivatives of the 7-oxabicyclo[2.2.1]heptane system and the related alkene and diene. Papers and patents have been published referring to cytotoxic (1), antidiabetic (2), and the well known fungicidal and herbicidal activities of these compounds; structurally related molecules synthesized from these bicyclic systems have shown promise as analgesics and antiinflammatory drugs (3). Research into chemical and biological properties is however hampered by the difficulties encountered while constructing the bridged system by Diels–Alder reactions of furan and its derivatives. Such reactions are frequently easily reversible and in consequence lack endo selectivity, variable mixtures of *exo* and *endo* adducts resulting. The reactions often proceed slowly and in poor yield, e.g., furan and acrylonitrile are reported to form 7-oxabicyclo[2.2.1]hept-5-ene-2-nitrile in 39% yield after 5 weeks (4). Dauben and Krabbenhoft (5) have found that under extremely high pressure the reactions proceed more rapidly in satisfactory yield but nevertheless the synthetic utility of Diels–Alder reactions of furan and its more common derivatives seems to be limited.

In this laboratory a study of the diene reactivity of furan rings bonded to oxygen and nitrogen has been undertaken, anticipating that the enhanced availability of electrons in this group of compounds, to date relatively neglected by synthetic chemists, might facilitate their reactions with a variety of electron deficient dienophiles. This paper reports the results of experiments on *N*-3′-furylbenzamide (**1**), a particularly interesting potential diene, the adducts of which might easily be converted into muscarine analogs similar to those prepared by Nelson and Allen (6), in which the nitrogen atom was introduced *after* generation of the bicyclic ring system.

Results and Discussion

When maleic anhydride was added to a saturated ethereal solution of **1**, the colorless, analytically pure Diels–Alder adduct **2** separated in reasonable yield. In other solvents, no adduct crystallised and it seems that the equilibrium expressed in Scheme 1 is unfavourable with respect to product. A similar isolation taking advantage of the limited solubility of *endo,cis*-7-oxabicyclo[2.2.1]hept-5-ene-2,3-dicarboxylic acid is reported (7). The ^{1}Hmr spectrum of **2** indicated an *exo* configuration for the anhydride group, the bridgehead protons appearing as a singlet (1-H) and doublet (4-H), the latter coupled with the vinyl proton. Couplings with the 2-H and 3-H were undetectably small as observed in many similar compounds (see, for example, ref. 8). The amide proton resonance at δ 10.22 in DMSO-d_6 disappeared slowly after addition of D_2O, but the remaining absorptions were unchanged after several hours including the vinyl-H doublet at δ 6.03. Thus tautomerism to the *N*-benzoylimine **3** does not take place under these

0008-4042/79/030314-04$01.00/0

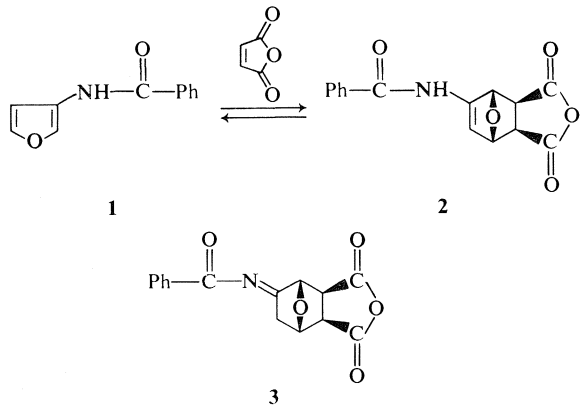

SCHEME 1

conditions and, despite their almost complete absence from the literature (see, however, ref. 9) enamides with a free N—H appear to be stable compounds, in contrast to the corresponding enamines (10).

Efforts to obtain Diels–Alder adducts with other dienophiles failed in a variety of solvents and under a variety of conditions, presumably because of reversion to starting materials. It is significant that **2** decomposed on attempted recrystallisation from hot solvents and that its mass spectrum showed no molecular ion but was simply a sum of the mass spectra of the component diene and dienophile. Similarly dimethyl maleate – furan adducts were not isolable directly from a Diels–Alder reaction (11) and when prepared by other means reverted to components very readily (7). In an effort to bypass the problem, advantage was taken of the ready addition of alcohols to enamides which, in the case of *N*-vinyl-2-pyrrolidinone in the presence of acid catalysts, proceeded in almost quantitative yield (12) giving **4**. At higher temperatures the reverse reaction of a closely related alkoxyamide has been observed (13). It was found that acidic catalysts caused extensive decomposition but that the reactions of dimethyl maleate and *N*-3′-furylbenzamide in alcoholic solvents gave the unstable alkoxyamides, in the absence of catalysts, quite cleanly, but reversibly. It proved impossible to isolate these sensitive compounds but their existence was clearly demonstrated by ^{1}Hmr spectra recorded on the crude reaction mixtures. Structures **5***a* and **5***b* have been assigned to the adducts formed in isopropanol and benzyl alcohol respectively. The bridgehead protons' resonances appear as doublets (1-H) and singlets (4-H) confirming the *exo* orientation of the ester groups. The 1-H couples with the *exo*-6-H but not the *endo* protons as anticipated from the respective dihedral angles. Stereochemistry at the 5-position is less certain but assuming that the *exo* position is less sterically hindered and that the reaction is reversible, it would seem that the bulky amide group should be *exo* when in competition with an isopropyloxy group, and possibly also in the benzyloxy case, particularly if the planar conformation of the amide group is dominant. This is supported by the 2-H and 3-H absorption appearing as an AB system in **5***b* but as a singlet in **5***a* and **2**. An *endo* benzyloxy group could cause selective shielding in certain conformations in which the aromatic group lies directly beneath the bicyclic system. The alkoxyamides were easily hydrolysed by traces of water in solvents and on silica columns and when sufficient water was deliberately added to the reaction mixture a quantitative yield of **6** mixed with an equimolar

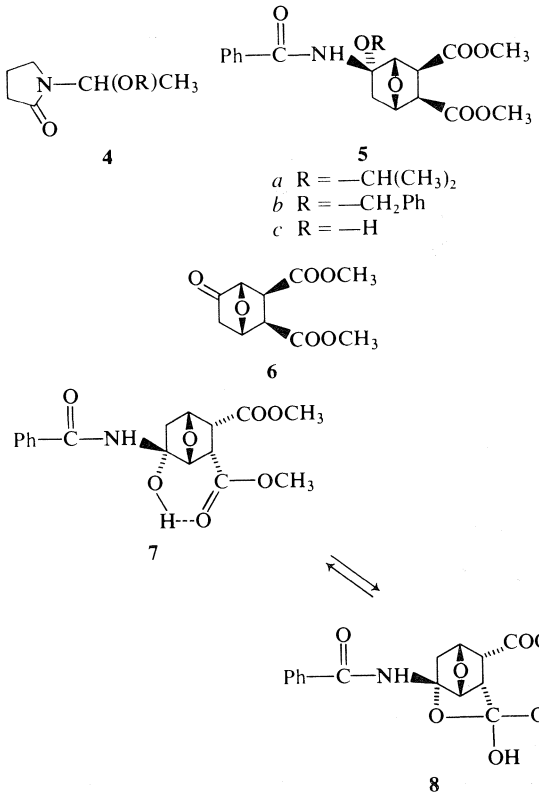

amount of benzamide was obtained after evaporation of excess alcohol. The keto diester **6** was identified by its ^{1}Hmr spectrum and by comparison of its melting point and that of its 2,4-dinitrophenylhydrazone with literature values. A possible intermediate in the formation of **6** is the hydroxyamide **5***c* and although this compound was never isolated, its stereoisomer **7** was obtained in very poor yield on one occasion when dimethyl maleate, furanamide, and methanol were heated together and subsequently chromatographed on silica. Surprisingly, **7** is reasonably stable and

could be recrystallised to give an analytically pure sample. The bridgehead protons appear in the ^{1}Hmr spectrum as partially overlapping multiplets suggesting the *endo* disposition of the two ester groups and the hydroxyl group is also tentatively assigned the *endo* configuration. The ir spectrum shows two clear C=O absorptions, a normal ester peak at 1738 cm^{-1} and a second peak at 1713 cm^{-1} which is assigned to the intramolecularly H-bonded 3-ester group. The —O—H stretching absorption appears, as expected, as a broad peak at 3400 cm^{-1}. The methyl group proton resonances appear at the normal position of δ 3.80 and at unexpectedly high field δ 3.33. It is possible that in solution **7** is rapidly equilibrating with **8** which might cause such an upfield shift. Attempts are being made to isolate more of this compound and further investigate its structure. The reluctance of **8** to lose methanol and form the lactone under the mild isolation conditions may be due to the increased strain in the tricyclic system which would result. Such lactones, although well known, are generally formed by internal quenching of a carbonium ion by a carboxylate group (14) rather than by an internal acyl substitution (transesterification). The difficulties associated with the latter route to the lactones are discussed in Zefirov's paper (15).

In refluxing toluene, 2:1 mixtures of *N*-3′-furylbenzamide and dimethyl maleate or methyl acrylate gave compounds **9***a* and **9***b*, respectively, presumably via the Diels–Alder adduct **10**. There is no precedent

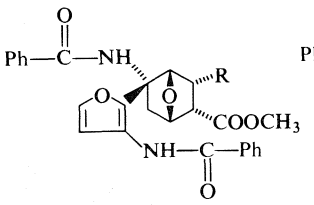

9

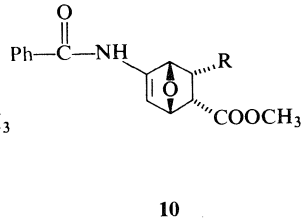

10

a R = —$COOCH_3$
b R = —H

for the uncatalysed addition of the second molecule of furanamide to the enamide and this interesting reaction is being further investigated. The ^{1}Hmr spectra of **9** again clearly demonstrate the geometry of the system, the bridgehead proton resonances showing couplings consistent with the *endo* configuration of the ester groups. The stability of these 2:1 adducts with respect to elimination and subsequent reverse Diels–Alder reaction would favor the isolation of *endo* isomers and would also lead one to suppose that the second furanamide molecule adds irreversibly from the least hindered *exo* side of the adduct **10**. The regioselectivity displayed in the acrylate reaction is the first indication of adherence to the '*para* rule' in a Diels–Alder reaction of a furanoid diene.

Experimental

Elemental analyses were performed by Atlantic Microlabs, GA, U.S.A. or by Memorial University Water Analysis Facility. ^{1}Hmr spectra were recorded on a Varian EM 360 instrument and ir spectra (Nujol mulls) on a Perkin-Elmer 237B grating spectrophotometer. Mass spectra showing the molecular ion and a base peak at *m/e* 105 (Ph—C≡O^+) were recorded for all new compounds, on an Hitachi-Perkin-Elmer RMU-6E spectrometer with direct inlet system. Melting points are uncorrected.

N-*3′-Furylbenzamide (**1**)*

3-Furoic acid was converted by standard methods into the hydrazide, mp 126–127.5°C, in 71% yield. 3-Furoylhydrazide (12.6 g, 0.1 mol) in water (300 mL) and 2 *N* H_2SO_4 (75 mL) was swirled at 0–5°C for 15 min whilst $NaNO_2$ (7 g in 30 mL H_2O) was added dropwise. After standing for 1 h at 0°C, the resulting white suspension was extracted with ether (2 × 250 mL), the ethereal solution of the azide separated, dried (Na_2SO_4 anhydrous), filtered, and cautiously distilled until approximately 300 mL of ether had been collected. Dry benzene (60 mL) was added and distillation continued until nitrogen evolution commenced (distillation temperature 75°C). The heating rate was adjusted until distillation almost ceased and continued for 5 h until nitrogen evolution was complete. The resulting solution was added dropwise to a cooled ethereal solution of phenylmagnesium bromide (0.1 mol) over 10 min. Aqueous acidic work up gave *N*-3′-furylbenzamide, mp 145–147°C (lit. (16) mp 142°C), 12.1 g, 64.7% from the hydrazide.

exo-N-*Benzoyl-5-amino-7-oxabicyclo[2.2.1]hept-5-ene-2,3-dicarboxylic Acid Anhydride (**2**)*

The furan (**1**) (0.25 g, 1.3 mmol) in dry ether (15 mL) was stirred with maleic anhydride (0.14 g, 1.4 mmol) at room temperature for 24 h. Filtration gave colorless crystals of **2**, 0.29 g, 75.9%; ir ν cm^{-1}: 3370, 1865, 1836 (shoulder), 1773, 1671, 1630; ^{1}Hmr (DMSO-d_6) δ: 3.24 (s, 2H), 5.07 (d, 1H), 5.21 (s, 1H), 6.03 (d, 1H), 7.1–7.7 (m, 5H), 10.22 (s, 1H), $J_{1,6}$ = 1.7 Hz. *Anal.* calcd. for $C_{15}H_{11}NO_5$: C 63.16, H 3.89, N 4.90; found: C 63.01, H 3.97, N 4.90.

Dimethyl endo,exo,exo,cis-N-*Benzoyl-5-isopropoxy-5-amino-7-oxabicyclo[2.2.1]heptane-2,3-dicarboxylate (**5**a)*

The furan (**1**) (0.28 g, 1.5 mmol) and dimethyl maleate (0.22 g, 1.53 mmol) were refluxed in isopropanol (5 mL) for 2 days. Evaporation gave a pale yellow oil estimated to contain ~85% of **5***a* plus unidentified by-products; ^{1}Hmr ($CDCl_3$) δ: 1.15 (d, 6H), 2.01 (d, 1H), 2.42 (dd, 1H), 3.5 (m, 2H), 3.61 (s, 3H), 3.63 (s, 3H), 3.93 (septet, 1H), 4.96 (d, 1H), 5.69 (s, 1H), 7.2–7.9 (m, 6H), $J_{(CH_3)_2CH}$ = 5.8, $J_{1,6}$ = 4.8, $J_{6,6}$ = 15.8 Hz.

Dimethyl exo-*5-Oxo-7-oxabicyclo[2.2.1]heptane-2,3-dicarboxylate (**6**)*

The furan (**1**) (0.56 g, 3.0 mmol) and dimethyl maleate (0.44 g, 3.1 mmol) were refluxed in isopropanol (7 mL) containing 0.5 mL water for 2 days. Evaporation gave in quantitative yield, pale yellow crystals of an equimolar mixture of benzamide and **6**, from which the latter could be separated by repeated recrystallisations from benzene or by preparative thin layer chromatography on silica; mp 128–129°C (lit. (17) mp 123–124°C); ir ν cm^{-1}: 1760, 1735, 1720 (shoulder); ^{1}Hmr ($CDCl_3$) δ: 2.07 (d, 1H), 2.60 (dd, 1H), 3.21 (s, 2H), 3.68 (s, 6H), 4.66 (s, 1H), 5.17 (d, 1H), $J_{1,6}$ = 5.6, $J_{6,6}$ = 17.8 Hz. *Anal.* calcd. for $C_{10}H_{12}O_6$: C 52.63, H 5.30; found: C 52.56,

H 5.30. 2,4-Dinitrophenylhydrazone mp 234–236 (lit. (17) mp 230°C).

Dimethyl endo,exo,exo,cis-N-*Benzoyl-5-benzyloxy-5-amino-7-oxabicyclo[2.2.1]heptane-2,3-dicarboxylate (5b)*

Prepared in crude form as for **5***a*, the unstable alkoxyamide **5***b* had mp 138–142°C; ^{1}Hmr ($CDCl_3$) δ: 1.91 (d, 1H), 2.38 (dd, 1H), 3.04 (d, 1H), 3.32 (d, 1H), 3.62 (s, 6H), 4.45 (d, 1H), 4.65 (d, 1H), 4.78 (d, 1H), 5.64 (s, 1H), 7.0–7.9 (m, 11 H), $J_{1,6}$ = 5.2, $J_{2,3}$ = 9.6, $J_{6,6}$ = 14.0, $J_{gem(benzyl)}$ = 16.4 Hz. Attempted purification by tlc failed, only benzamide and **6** being isolated.

Dimethyl endo,exo,endo,cis-N-*Benzoyl-5-hydroxy-5-amino-7-oxabicyclo[2.2.1]heptane-2,3-dicarboxylate (7)*

The furan (**1**) (0.28 g, 1.5 mmol) and dimethyl maleate (0.22 g, 1.53 mmol) were refluxed in absolute methanol (5 mL) for 4 days. Evaporation gave a yellow oil which was chromatographed on silica gel. Elution with toluene–ether (1:1) gave **7**, recrystallised from benzene as colorless needles (0.03 g, 5.7%), mp 142–144°C; ir ν cm^{-1}: 3380 (very broad), 1738, 1713, 1650; ^{1}Hmr ($CDCl_3$) δ: 2.35 (dd, 1H), 2.74 (d, 1H), 3.33 (s, 3H), 3.48 (narrow m, 2H), 3.80 (s, 3H), 5.0 (m, 1H), 5.1 (m, 1H), 7.3–7.9 (m, 5H), 8.60 (s, 1H), $J_{1,6}$ = 5.0, $J_{6,6}$ = 13.0 Hz. *Anal.* calcd. for $C_{17}H_{19}NO_7$: C 58.45, H 5.48, N 4.01; found: C 58.35, H 5.50, N 4.00.

Dimethyl exo,endo,endo,cis-N-*benzoyl-5-(N′-benzoyl-3′-aminofur-2′-yl)-5-amino-7-oxabicyclo[2.2.1]heptane-2,3-dicarboxylate (9a)*

The furan (**1**) (0.16 g, 0.86 mmol) and dimethyl maleate (0.06 g, 0.42 mmol) were refluxed in toluene (4 mL) for 10 h, cooled in an ice bath, and filtered to separate the tan crystals. Recrystallisation from toluene gave colorless plates (0.12 g, 55.1%), mp 214–216°C; ir ν cm^{-1}: 3270, 3200, 1735, 1725 (shoulder), 1658, 1622; ^{1}Hmr ($CDCl_3$) δ: 2.46 (d, 1H), 3.02 (dd, 1H), 3.5 (m, 2H), 3.57 (s, 3H), 3.71 (s, 3H), 4.84 (broad t, 1H), 5.65 (broad d, 1H), 6.96 (d, 1H), 7.27 (d, 1H), 7.2–8.2 (m, 10H), 9.28 (s, 1H), 10.47 (s, 1H), $J_{1,2} \approx$ 4.8, $J_{1,6}$ = 5.6, $J_{3,4}$ = 4.1, $J_{6,6}$ = 14.2, $J_{4',5'}$ = 1.9 Hz. *Anal.* calcd. for $C_{28}H_{26}N_2O_8$: C 64.86, H 5.05, N 5.40; found: C 64.92, H 5.09, N 5.35.

Methyl exo,endo,endo-N-*benzoyl-5-(N′-benzoyl-3′-aminofur-2′-yl)-5-amino-7-oxabicyclo[2.2.1]heptane-2-carboxylate (9b)*

In a manner similar to the preparation of **9***a*, the monoester (**9***b*) was isolated as colorless crystals (41%), mp 188–189°C; ir ν cm^{-1}: 3310 (shoulder), 3255, 1735, 1649, 1624; ^{1}Hmr ($CDCl_3$) δ: 2.10 (d, 1H), 2.0–3.3 (m, 4H), 3.64 (s, 3H), 4.72 (t, 1H), 5.58 (d, 1H), 7.0–8.1 (m, 13H), 10.44 (s, 1H), $J_{1,2} \approx J_{1,6} \approx$ 5.5, $J_{3,4}$ = 4.6, $J_{6,6}$ = 15.0 Hz. *Anal.* calcd. for $C_{26}H_{24}N_2O_6$: C 67.82, H 5.25, N 6.08; found: C 67.92, H 5.26, N 5.94.

Acknowledgements

The author thanks the National Research Council of Canada and Memorial University of Newfoundland for financial support.

1. W. K. Anderson and R. H. Dewey. J. Med. Chem. **20**, 306 (1977).
2. G. R. Evanega, D. E. Kuhla, and R. Sarges. U.S. Patent No. 3,914,426 (21st October 1975); Chem. Abstr. **84**, 43868r (1975).
3. R. Kubela and L. A. Hughes. U.S. Patent No. 3,957,795 (18th May 1976); Chem. Abstr. **85**, 159515y (1975).
4. F. Kienzle. Helv. Chim. Acta, **58**, 1180 (1975).
5. W. G. Dauben and H. O. Krabbenhoft. J. Am. Chem. Soc. **98**, 1992 (1976).
6. W. L. Nelson and D. R. Allen. J. Heterocycl. Chem. **9**, 561 (1972).
7. T. A. Eggelte, H. de Koning, and H. O. Huisman. Tetrahedron, **29**, 2491 (1973).
8. S. Iwase, T. Maeda, S. Hamanaka, and M. Ogawa. Nippon Kagaku Kaishi, **11**, 1934 (1975).
9. N. S. Crossley, C. Djerassi, and M. Kielczewski. J. Chem. Soc. 6253 (1965).
10. G. Wittig and H. Blumenthal. Ber. **60**, 1085 (1927).
11. J. Jolivet. Ann. Chim. **5**, 1165 (1960).
12. R. F. Smith. U.S. Patent No. 3,823,160 (9th July 1974); Chem. Abstr. **81**, 135943c (1974).
13. H. Böhme and G. Berg. Ber. **99**, 2127 (1966).
14. O. Diels and K. Alder. Justus Liebigs Ann. Chem. **490**, 243 (1931).
15. N. S. Zefirov, R. S. Filatova, and I. V. Yartseva. Zh. Obshch. Khim. **37**, 2630 (1967).
16. R. R. Burtner. J. Am. Chem. Soc. **56**, 666 (1934).
17. N. S. Zefirov, P. Kadziauskas, V. N. Bazanova, and Yu K. Yur'ev. Zh. Obshch. Khim. **36**, 614 (1966).

A correction in the published nuclear magnetic resonance spectra of *trans*-camphane-2,3-diols

MARK A. JOHNSON AND MICHAEL P. FLEMING
Thimann Laboratories, University of California, Santa Cruz, CA 95064, U.S.A.

Received April 12, 1978

MARK A. JOHNSON and MICHAEL P. FLEMING. Can. J. Chem. **57**, 318 (1979).

It is unequivocally shown that the published nmr spectra assigned to 2-*endo*,3-*exo*-camphanediol and 2-*exo*-3-*endo*-camphanediol should be reversed. The 2-*exo*,3-*endo* isomer is prepared unambiguously by hydroboration–oxidation of camphor enol silyl ether.

MARK A. JOHNSON et MICHAEL P. FLEMING. Can. J. Chem. **57**, 318 (1979).

On démontre sans équivoque que les spectres rmn publiés et attribués aux *endo*-2 *exo*-3 camphanediol et *exo*-2 *endo*-3 camphanediol devraient être inversés. On a préparé l'isomère *exo*-2 *endo*-3 sans ambiguité par hydroboration–oxydation de l'éther énolique silylé du camphre.

[Traduit par le journal]

During the course of our mechanistic investigations on the titanium-induced deoxygenation of 1,2-diols to olefins (1, 2), we found it necessary to prepare *cis* and *trans* (+)-camphane-2,3-diols. There are four possible (+)-camphane-2,3-diols, and all have been prepared, purified, and characterized (3, 4). In addition, the nmr spectra of the four have been recorded and analyzed in detail (5).

The 2-*exo*,3-*exo* isomer **1** is readily prepared by

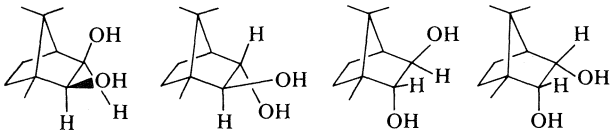

1 2-*exo*,3-*exo* **2** 2-*exo*,3-*endo* **3** 2-*endo*,3-*exo* **4** 2-*endo*,3-*endo*

$LiAlH_4$ reduction of camphorquinone (6). Hydride attack occurs almost exclusively from the less hindered *endo* face of the camphorquinone and we have verified the details of the synthesis as well as the reported (5) nmr spectrum (nmr (pyridine–D_2O) δ: 0.77 (s, 3 H), 1.03 (s, 3 H), 1.30 (s, 3 H), 3.70 (d, 1 H, J = 7 Hz), 3.95 (d, 1 H, J = 7 Hz)).

The *cis* diol **1** was thus readily available but we also needed a *trans* diol for our work. Rather than follow the rather tedious literature procedure, however, it occurred to us that 2-*exo*,3-*endo* diol **2** might be readily obtained by hydroboration–oxidation of (+)-camphor enol silyl ether. Hydroboration of the known (7) silyl ether **4** with BH_3 followed by basic hydrogen peroxide oxidation occurred without incident and yielded a 65:35 mixture of the two possible *trans*-camphane-2,3-diols. The major isomer had nmr (pyridine–D_2O) δ: 0.83 (s, 3 H), 0.99 (s, 3 H), 1.25 (s, 3 H), 3.90 (d, 1 H, J = 3 Hz), 4.29 (broad, 1 H) while the minor isomer had nmr (pyridine–D_2O) δ: 0.83 (s, 3 H), 0.99 (s, 3 H), 1.19 (s, 3 H), 3.70 (d, 1 H, J = 3 Hz), 4.66 (broad, 1 H). According to published spectral data (5), these results show that our major hydroboration product is the 2-*endo*,3-*exo* diol **3**, whereas the minor product is the 2-*exo*,3-*endo* diol **2**. This is most surprising since it indicates that hydroboration has occurred from the more hindered *exo* face of the enol silyl ether. We believe that this is unlikely and that there is in fact an error in the published spectral data (5) transposing the correct values for isomers **2** and **3**. Since nmr spectroscopy is the only convenient method for distinguishing between the isomers, we believe that this error should be corrected.

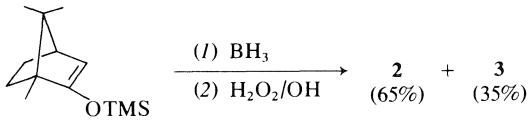

5

Confirmation of our structural assignments, and therefore of the literature error, was obtained by two further experiments. In the first of these, hydroboration with the hindered reagent thexylborane, followed by oxidation, gave a 90:10 mixture of **2** and **3**. One would expect this reaction to be quite selective for *endo* attack.

In the second experiment, we prepared a mixture of di-*p*-nitrobenzoates derived from the **2** + **3** mixture and measured the optical rotation. Angyal has reported (3) that the di-*p*-nitrobenzoate of **2** has $[\alpha]_D$ +134.5° whereas the di-*p*-nitrobenzoate of **3** has $[\alpha]_D$ −113°. The value of our **2** + **3** mixture was $[\alpha]_D$ +30°, corresponding to 60% **2** and 40% **3** (vs.

0008-4042/79/030318-02$01.00/0

65:35 by nmr integration). Both chemical and physical evidence is therefore in agreement that the published nmr data (5) for **2** and **3** should be reversed.

Experimental

A solution of (+)-camphor enol silyl ether (7) (11.220 g, 50.0 mmol) in 50 mL dry tetrahydrofuran (THF) was prepared and a solution of borane in THF (50 mL of 1 *M* solution) was slowly added over 30 min at room temperature. After stirring 2 h at room temperature and a further 2 h at 35°C, the solution was cooled to 0°C. Hydrogen peroxide (16 mL of 30% aqueous solution) and sodium hydroxide (16 mL of 3 *N* aqueous solution) were added and the mixture was heated to 35°C for 2 h. After cooling, the aqueous layer was separated and extracted with ether. The combined organic solutions were washed with 10% HCl and with brine, then dried ($MgSO_4$) and concentrated at the rotary evaporator. Recrystallization from benzene gave the 65:35 mixture of diols **2** and **3**; mp 251–252°C (lit. (3) **2** mp 250.5–252°C; **3** mp 254–256°C).

1. J. E. McMurry and M. P. Fleming. J. Org. Chem. **41**, 896 (1976).
2. J. E. McMurry, M. P. Fleming, K. L. Kees, and L. R. Krepski. J. Org. Chem. **43**, 3255 (1978).
3. S. J. Angyal and R. J. Young. J. Am. Chem. Soc. **81**, 5467 (1959).
4. T. Takeshita and M. Kitajima. Bull. Chem. Soc. Jpn. **32**, 985 (1959).
5. F. A. L. Anet. Can. J. Chem. **39**, 789 (1961).
6. L. W. Trevoy and W. G. Brown. J. Am. Chem. Soc. **71**, 1675 (1949).
7. G. C. Joshi and L. M. Pande. Synthesis, 450 (1975).

The carbon monoxide/nitrous oxide reaction. Kinetics of catalysis on TiO_2 (anatase) and ZnO and activity correlations for the first-row transition metal oxides

BORDAN WALTER KRUPAY[1] AND ROBERT ANDERSON ROSS

Department of Chemistry, Lakehead University, Thunder Bay, Ont., Canada P7B 5E1

Received June 23, 1978

BORDAN WALTER KRUPAY and ROBERT ANDERSON ROSS. Can. J. Chem. **57**, 320 (1979).

The catalytic reaction between carbon monoxide and nitrous oxide on titanium dioxide (anatase) and zinc oxide has been examined in a continuous flow reactor at atmospheric pressure. The experimental activation energy was 144 ± 4 kJ mol^{-1} from 723 to 793 K on TiO_2 and 121 ± 4 kJ mol^{-1} from 543 to 653 K on ZnO. Analyses of kinetic results indicated that a transient carbonate-like species may be involved in catalysis on both oxides. Relationships between the experimental activation energies for the CO/N_2O reaction on first-row transition metal oxides and (*i*) activation energies for isotopic oxygen exchange, (*ii*) heats of carbonate formation, and (*iii*) the charge/radius ratio of the cation are interpreted in terms of the influence on catalysis of the cohesive properties of the metal/oxygen bonds in the oxide surfaces.

BORDAN WALTER KRUPAY et ROBERT ANDERSON ROSS. Can. J. Chem. **57**, 320 (1979).

Opérant dans un réacteur à écoulement continue à pression atmosphérique, on a étudié la réaction catalytique du monoxyde de carbone et de l'oxyde nitreux sur le dioxyde de titane (anatase). L'énergie d'activation expérimentale est de 144 ± 4 kJ mol^{-1} de 723 à 793 K sur le TiO_2 et de 121 ± 4 kJ mol^{-1} de 543 à 653 K sur le ZnO. L'analyse des données cinétiques indique qu'une espèce transitoire ressemblant à un carbonate peut être impliquée dans la catalyse sur les deux oxydes. On a interprété les relations qui existent entre les énergies d'activations expérimentales pour la réaction du CO/N_2O sur des oxydes de métaux de transition de la première période et (*i*) les énergies d'activation des échanges isotopiques de l'oxygène, (*ii*) les chaleurs de formation du cabonate et (*iii*) le rapport charge/rayon du cation en termes de l'influence, sur la catalyse, des propriétés cohésives des liaisons métal/oxygène sur les surfaces des oxydes.

[Traduit par le journal]

Introduction

Kinetic results and mechanistic proposals for the catalytic reaction between carbon monoxide and nitrous oxide over several first-row transition metal oxides have been communicated recently (1–3). Although the oxides exhibited some differences in kinetic behaviour which could be ascribed to individual surface chemical factors, the overall course of catalysis could be generally related to (*i*) the reaction of carbon monoxide with surface oxygen via a cyclic transition state, (*ii*) the destabilization of an intermediate surface carbonate species, and (*iii*) the desorption of carbon dioxide which could occupy two surface sites.

The proposals have been further explored through kinetic measurements of the reaction on titanium dioxide, anatase, and zinc oxide and also by comparisons of catalytic activation energies for the 3*d* series of oxides with (*i*) oxygen isotope exchange energies, (*ii*) heats of carbonate formation, and (*iii*) charge/radius ratios of the oxide cations.

Experimental

The reaction was examined in a differential flow-reactor at atmospheric pressure with high-purity helium as the carrier gas. A thermal conductivity detector with stainless steel columns, 183 × 0.32 cm o.d., packed with 61 cm 'Carbosieve B' and the remainder with 'Poropak Q' at a column temperature of 353 K was sufficient to resolve nitrogen, carbon monoxide, carbon dioxide, and nitrous oxide in the Beckman GC-5 gas chromatograph.

The standard reacting gas mixture consisted of carbon monoxide and nitrous oxide each at a partial pressure of 5.33 kN m^{-2} (40 Torr). 'Blank' runs confirmed that reaction on the quartz wool and reactor walls reached 1% at 853 K which was 130 K above the highest temperature of catalysis. Preliminary experiments on titanium dioxide and zinc oxide established that diffusion phenomena (4, 5) did not influence the rate measurements at a total gas flow rate of 350 ml min^{-1} (NTP) for both catalysts.

Titanium dioxide (100% anatase), supplied by British Drug Houses Ltd., and zinc oxide, 99.99% pure, from Alfa Inorganics Inc., were heated at 873 K in air for 10 h and stored in desiccators over P_2O_5 prior to use. Carbon monoxide (C.P.; 99.5% minimum), carbon dioxide (Coleman; 99.99%), nitrogen (super-pure; 99.99%), nitrous oxide (99.9% minimum), and helium (high purity; 99.995%) were used as supplied.

Prior to the kinetic experiments, titanium dioxide was heated in helium for 5 h at 773 K and exposed to the standard gas mixture at 793 K. Catalyst activities reached steady levels after 1 h. The surface area (krypton; B.E.T.) and catalyst volume of

[1]Present address: Chemistry Division, National Research Council of Canada, Ottawa, Ont., Canada K1A 0R6.

0008-4042/79/030320-06$01.00/0

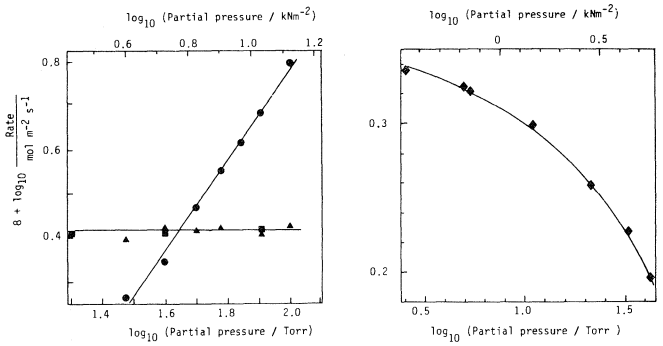

FIG. 1. Effects of variations in the partial pressures of carbon monoxide (●), nitrous oxide (▲), nitrogen (■), and carbon dioxide (◆) on the catalytic CO/N_2O reaction on titanium dioxide at 763 K.

the oxide after catalysis were 9.0 m^2 g^{-1} and 1.64 cm^3 g^{-1}, respectively. The largest conversion, 5.45%, was recorded at 793 K, the maximum temperature for the study. X-ray powder diffraction photographs revealed no structural changes in the oxide after catalysis.

The reaction was examined on zinc oxide from 653 to 543 K in the standard gas mixture. Steady catalyst activity, corresponding to a conversion level of 13.2%, was established at 653 K after 5 h and X-ray powder diffraction photographs of samples taken before and after catalysis were identical. The surface area (krypton; B.E.T.) of the oxide, 12.0 m^2 g^{-1}, and the catalyst volume, 1.36 cm^3 g^{-1}, were determined after the kinetic experiments were completed.

Results

Titanium Dioxide

With the nitrous oxide partial pressure fixed at 5.33 kN m^{-2}, the rate order with respect to carbon monoxide partial pressure was examined at 763 K from 4.00 to 13.3 kN m^{-2} (Fig. 1). This figure also shows the rate results for nitrous oxide in the partial pressure range 4.00 to 13.3 kN m^{-2} at 763 K with carbon monoxide maintained at 5.33 kN m^{-2}.

With both carbon monoxide and nitrous oxide fixed at 5.33 kN m^{-2}, the effect of variations in nitrogen partial pressure was examined from 2.67 to 10.7 kN m^{-2} at 763 K (Fig. 1). For the range of carbon dioxide partial pressures studied to determine kinetics, a rate order of -0.1 was approximated.

Thus for titanium dioxide, the experimental rate of reaction, r (mol m^{-2} s^{-1}), was expressed as:

$$[1] \qquad r = kP_{CO}{}^{0.9}/P_{CO_2}{}^{0.1}$$

Zinc Oxide

The partial pressure of carbon monoxide was varied from 1.33 to 16.0 kN m^{-2} at 593 K while nitrous oxide was maintained constant at 5.33 kN m^{-2} (Fig. 2). The rate order was 0.8 from 16.0 to 2.67 kN m^{-2} and 0.2 below this range. The effect of nitrous oxide partial pressure was examined at 593 K from 1.33 to 16.0 kN m^{-2} with carbon monoxide fixed at 5.33 kN m^{-2}. Between 1.33 and 4.00 kN m^{-2} the rate order of 0.2 changed to zero at higher partial pressures (Fig. 2).

With the carbon monoxide and nitrous oxide partial pressures both fixed at 5.33 kN m^{-2}, 1.45 kN m^{-2} carbon dioxide was continuously introduced to the gas stream. When the effluent was sampled 3 min later, the reaction rate with respect to nitrous oxide had increased to 15.5×10^{-8} mol m^{-2} s^{-1} which, when compared to an initial value of 1.51×10^{-8} mol m^{-2} s^{-1}, represented a 10-fold increase in the reaction rate. The reaction rate decreased continuously with time until a steady value of 0.30×10^{-8} mol m^{-2} s^{-1} was reached 2 h later. This rate did not change when the carbon dioxide partial pressure was subsequently increased step-wise to 5.79 kN m^{-2}. During the initial 2 h period, the measured carbon monoxide level in the gas stream remained constant while the nitrous oxide level gradually rose from zero to 5.31 kN m^{-2}. Thus, steady state conditions did not prevail and the surface reaction was

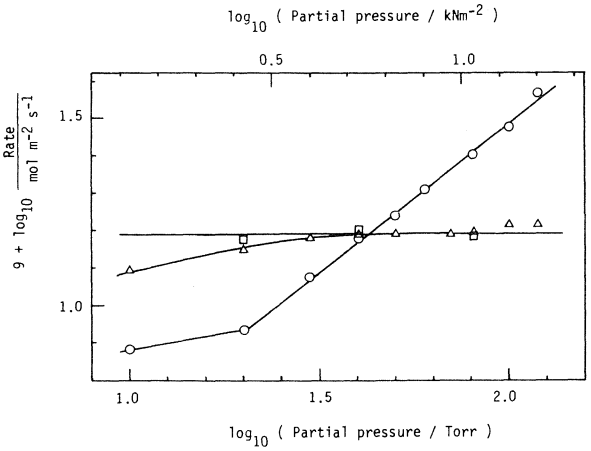

FIG. 2. Reaction rate order measurements for the CO/N_2O reaction on zinc oxide at 593 K with variations in the partial pressures of carbon monoxide (○), nitrous oxide (△), and nitrogen (□).

assumed to be proceeding mainly by reaction of nitrous oxide with carbon dioxide in a manner similar to that observed with cobalto-cobaltic oxide (3). Since a numerical value for the rate order with respect to carbon dioxide could not be established, subsequent determinations of rate constants were made on the assumption of zero order kinetics.

A reaction rate order of zero with respect to nitrogen in the partial pressure range 2.67 to 10.7 kN m^{-2} was determined.

The experimental reaction rate on zinc oxide, r (mol m^{-2} s^{-1}), at 593 K was expressed as:

$$[2] \qquad r = kP_{CO}{}^{0.8}$$

Temperature Effects

After pretreatment in the standard reaction mixture to establish steady catalytic activity at 793 K, the variation in the rate of catalysis with temperature on titanium dioxide was examined from 793 to 723 K at 6 K intervals. The Arrhenius plot was linear throughout the range and an experimental activation energy of 144 $\pm$ 4 kJ mol^{-1} was calculated using rate constants obtained by integrating eq. [1] (Fig. 3).

On zinc oxide, reaction rates were measured from 653 to 543 K at 10 K intervals once steady activity levels were established at 653 K using the standard reaction mixture. Rate constants calculated by integrating eq. [2] are shown in the Arrhenius plot (inset Fig. 3) from which an experimental activation energy of 121 $\pm$ 4 kJ mol^{-1} was calculated.

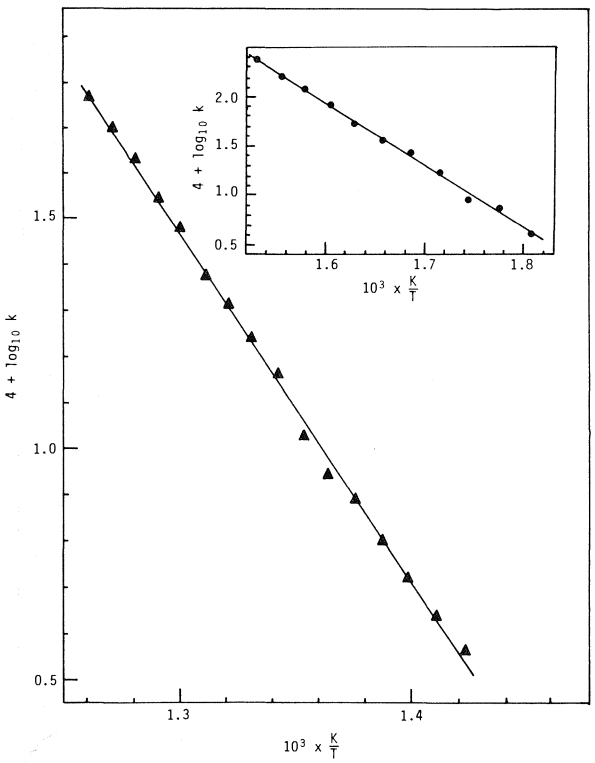

FIG. 3. Arrhenius plot of experimental reaction rate constants for the CO/N_2O reaction on titanium dioxide. Inset: Arrhenius plot for the CO/N_2O reaction on zinc oxide.

Discussion

Both stoichiometric zinc oxide and titanium dioxide may be regarded as semi-conductors with intrinsic energy gaps of 3.3 and 3.2 eV, respectively (6). Their surface properties may be influenced considerably by the presence of both adsorbed paramagnetic species and surface defects (7, 8) which can be related to the conditions of preparation. The defect structure of zinc oxide is associated with interstitial zinc ions (7) while that of anatase is explained by either the presence of oxygen vacancies or interstitial titanium ions (7).

The decomposition of nitrous oxide on TiO_2 has been shown to be insensitive to adsorbed oxygen (9), decomposition being restricted to special small areas of the surface where adjacent anion vacancies contain trapped electrons (type: R_2-centers). Their formation was attributed to O_2 desorption and rapid conversion to F-centers by surface migration making these inaccessible to gaseous oxygen. For ZnO prepared with different levels of interstitial zinc ions (10), the rate and extent of nitrous oxide decomposition did not substantially depend upon the zinc excess content of the oxide and rate control was associated with the diffusion of oxygen in the solid phase.

Titanium Dioxide

In the analysis of the present experimental results for anatase, a variety of kinetic expressions were examined with respect to the carbon monoxide and carbon dioxide rate order data and the best correlations were obtained with the equation:

$$[3] \qquad r = kP_{CO}\theta_{CO}$$

where

$$[4] \qquad \theta_{CO} = \frac{aP_{CO}}{1 + aP_{CO} + bP_{CO_2}{}^{1/2}}$$

The reduced plots are shown in Figs. 4 and 5. (The limitations inherent in the use of Langmuir–Hinshelwood type expressions in deriving mechanistic models have been documented (11, 12) and these equations are thus adopted as general guides to the nature of the surface reaction although, recently, further support regarding the specificity of such considerations has been presented (13) in the case of organic polymer ion-exchange catalysts.)

The zero order dependence of the catalytic reaction rate upon nitrous oxide partial pressure is indicative

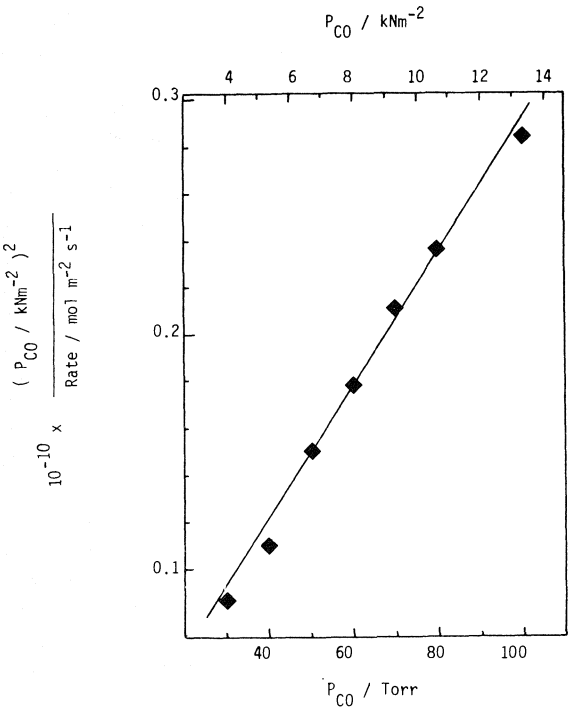

FIG. 4. Carbon monoxide rate order measurements plotted according to eq. [3] on titanium dioxide at 763 K.

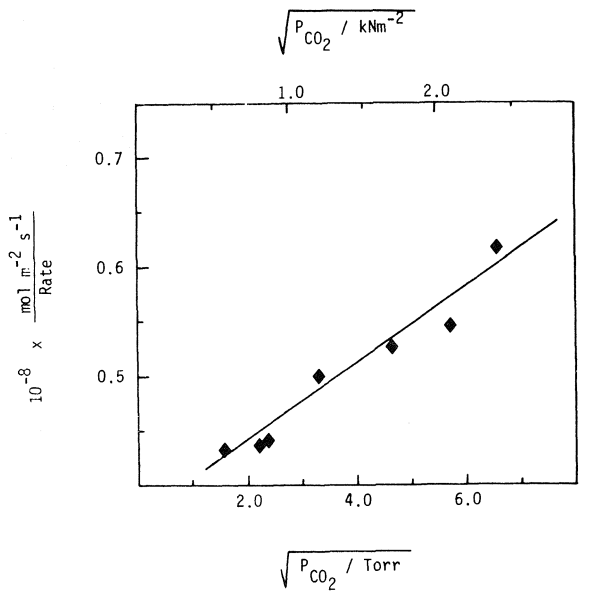

FIG. 5. Carbon dioxide rate order results plotted according to eq. [3] on titanium dioxide at 763 K.

of rapid chemisorption relative to that for carbon monoxide and thus the N_2O reaction may proceed at active defect regions of the oxide. There is some indication from the form of eq. [3] that a transient carbonate-like structure may be involved possibly arising from the reaction of CO with surface oxygen (from the rapid decomposition of N_2O) and a lattice oxygen in view of the high temperature range of catalysis (14).

Zinc Oxide

The apparent activation energy for the catalytic reaction between carbon monoxide and nitrous oxide was 121 ± 4 kJ mol^{-1} while the corresponding value of 172 kJ mol^{-1} for nitrous oxide decomposition (15) suggests that rate control of the CO/N_2O reaction is not exercised through N_2O decomposition. This is supported by the reaction rate order of 0.2 with respect to nitrous oxide at low partial pressures compared to 0.8 for carbon monoxide.

The carbon monoxide and nitrous oxide rate order results were analyzed in the same manner as that for anatase and the best fit was obtained with:

[5] $$r = kP_{CO}\theta_{CO}\theta_{N_2O}$$

where

[6] $$\theta_{CO} = \frac{aP_{CO}}{1 + aP_{CO}}$$

and

[7] $$\theta_{N_2O} = \frac{bP_{N_2O}}{1 + bP_{N_2O}}$$

The plots for these data are shown in Fig. 6. The expression accounts for only one N_2O molecule but two such molecules are necessary to preserve the stoichiometry of the reaction under steady-state catalysis and thus rapid adsorption and decomposition of a second N_2O molecule would be indicated. If the surface coverage for this molecule is given by $\theta = mP/(1 + mP)$, then relatively rapid chemisorption would result in $mP \gg 1$ and hence $\theta \simeq 1$ in accord with the form of eq. [5].

With the continuous addition of carbon dioxide

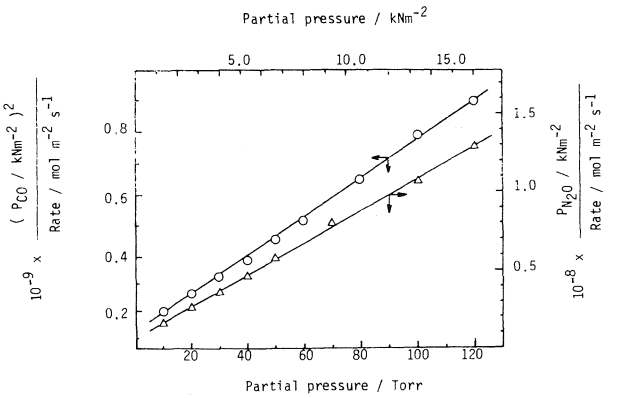

FIG. 6. Reduced plot of the carbon monoxide (○) and nitrous oxide (△) rate order results for the CO/N_2O reaction on zinc oxide at 593 K according to eq. [5].

to the reaction mixture an initial period of enhanced nitrogen production was noted while the level of unreacted carbon monoxide remained steady. Thus a precursor such as $CO_2^*(a)$, proposed for catalysis on Co_3O_4 (3), may be involved and if its formation was rate-controlling relative to the reaction involving the first N_2O molecule, and the reaction of the second N_2O was rapid, then this effect of carbon dioxide on catalysis may be rationalized. Thus, the adsorption of CO_2 would give rise to the $CO_2^*(a)$ species; the subsequent reaction of a second N_2O molecule to form the carbonate-like intermediate would be rapid and the enhanced production of nitrogen would be associated with a facile decomposition of nitrous oxide. Also, since the level of unreacted CO in the gas stream remained fixed, the formation of a surface carbonate-like intermediate is not likely to control the rate. Rather, the adsorption of the second CO involved in the reaction with the latter species may be rate-controlling.

This proposal is consistent with the form of eq. [5] where the P_{CO} term corresponds to low CO surface coverage, $1 \gg aP_{CO}$ such that $\theta_{CO} \simeq P_{CO}$. The eventual appearance of a retarding effect by carbon dioxide may arise after the most reactive sites with respect to $CO_2^*(a)$ formation are occupied with consequent inhibition on the adsorption of reactants.

Catalytic Activity Patterns

Some measure of independent support for the mechanistic proposals may be adduced from Fig. 7. The heats of carbonate formation from the corresponding oxide were calculated from available data (16) and revealed little variation for the oxides except for the formation of $Fe_2(CO_3)_3$. The basis for such a correlation would be that the metal cation and lattice oxygen participate in the formation of the carbonate. At high catalytic temperatures (>600 K) this proposal would be consistent for MgO and ZnO (14), however, lattice oxygen has not been implicated during the course of carbon monoxide oxidations below this temperature range (17–20). Generally, an associative mechanism involving the reactants has been proposed and, on this basis, the correlation between E_A and the heats of carbonate formation *from the elements* would seem more appropriate. The actual state may be intermediate to the two extremes.

All of the 'E_A' values have been calculated directly from experimental data with no a priori assumptions involved regarding the nature of the kinetics. A clear trend was also found in the variation of 'E_A' with the activation energy for isotopic oxygen exchange (21) determined on many of the same oxide samples (Fig. 8), thereby suggesting a dependence of catalysis on the strength of the labile metal/oxygen bond in the oxide surface.

A contribution of polarization effects to catalysis would be expected if carbon monoxide adsorption and reaction contributed significantly to the overall process. The simplest representation of bond polarization, the charge/radius ratio with respect to the cation (8, 21), can be refined but for the present purpose it does provide a useful indicator of the importance of polarization trends in the series of metal oxides (Fig. 9). The data indicate two series with only

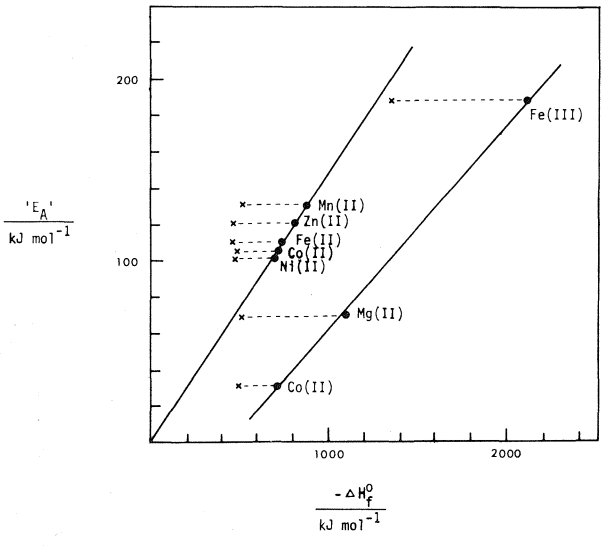

FIG. 7. Relationship between the experimental activation energy for the catalytic CO/N_2O reaction and the heats of carbonate formation from the corresponding 3*d* oxide (×) and from the elements (●).

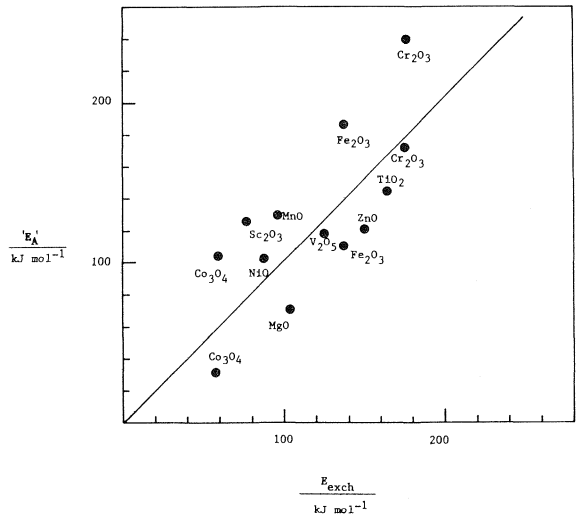

FIG. 8. Relationship between the experimental activation energy for catalysis, 'E_A', and isotopic oxygen exchange energy, E_{exch}.

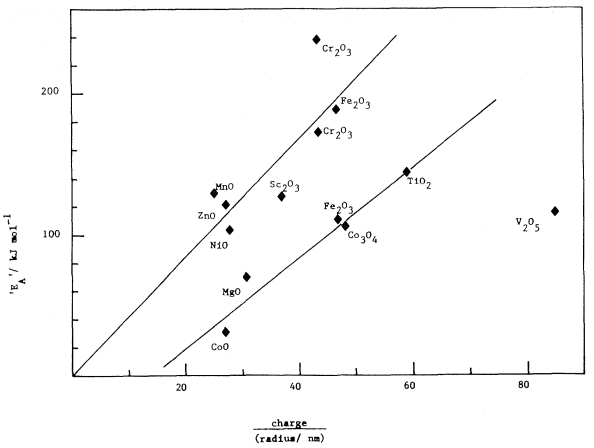

FIG. 9. Relationship between the experimental activation energy for catalysis, 'E_A', and the charge/radius ratio of the cation in the metal oxides.

V_2O_5 departing from linearity. The surface vanadium oxidation state during steady catalysis cannot be specified with certainty (8). The charge/radius ratios for the 4+ and 3+ states were 66.7 and 40.5 nm^{-1} respectively, but, for consistency, only the value corresponding to the 5+ oxidation state has been used.

Titanium dioxide possesses a larger metal/oxygen bond polarization than zinc oxide and this may, in part, account for the differences in the surface reactions on these oxides. In the case of anatase, the greater bond polarization would be expected to enhance the reactivity of adsorbed carbon monoxide with nitrous oxide. Thus, the zero order dependence of nitrous oxide partial pressure on anatase can be rationalized while the behaviour on zinc oxide would be associated with the lower polarization of the adsorbed carbon monoxide and a reduced reactivity with nitrous oxide. It is not clear whether this interaction proceeds through an associative surface complex or on adjacent sites through a redox type process, although in view of the high temperatures involved, the latter proposal seems more likely.

Acknowledgement

We are pleased to acknowledge financial assistance from Imperial Oil Ltd., Toronto, Canada.

1. B. W. KRUPAY and R. A. ROSS. J. Catal. **50**, 220 (1977).
2. B. W. KRUPAY and R. A. ROSS. Z. Phys. Chem. N.F. **106**, 83 (1977).
3. B. W. KRUPAY and R. A. ROSS. Can. J. Chem. **56**, 10 (1978).
4. D. A. DOWDEN and G. W. BRIDGER. Adv. Catal. **9**, 669 (1957).
5. O. LEVENSPIEL. Chemical reaction engineering. Wiley, New York. 1962. p. 453.
6. O. V. KRYLOV. Catalysis by non-metals. Academic Press, New York and London. 1970.
7. F. SOLYMOSI. *In* Contact catalysis. *Edited by* Z. G. Szabó. Elsevier Sci. Publ. Co., Amsterdam, Oxford, New York. 1976. Chapt. 6.
8. N. N. GREENWOOD. Ionic crystals, lattice defects and nonstoichiometry. Butterworths, London. 1968.
9. E. R. S. WINTER. J. Catal. **34**, 431 (1974).
10. N. DUPONT-PAVLOVSKY and F. CARALP. J. Catal. **46**, 426 (1977).
11. S. W. WELLER. *In* Chemical reaction engineering reviews. *Edited by* H. M. Hulburt. American Chemical Society, Washington, DC. 1975. p. 26.
12. M. BOUDART. AIChEJ. **2**, 62 (1956); **18**, 465 (1972).
13. L. BERÁNEK. Catal. Rev. **16**, 1 (1977).
14. W. E. GARNER (*Editor*). Chemistry of the solid state. Butterworths Scientific Publ. Co., London. 1955.
15. E. R. S. WINTER. J. Catal. **19**, 32 (1970).
16. M. KH. KARAPET'YANTS and M. L. KARAPET'YANTS. Thermodynamic constants of inorganic and organic compounds. Humphrey Sci. Publ., Ann Arbor. 1970; Handbook of chemistry and physics. 56th ed. C.R.C. Press. 1975–1976.
17. G. K. BORESKOV. Kinet. Catal. **14**, 2 (1973).
18. G. K. BORESKOV. Dokl. Akad. Nauk SSSR, **213**, 926 (1973).
19. G. K. BORESKOV, V. V. POPOVSKII, and E. A. MAMEDOV. Dokl. Akad. Nauk SSSR, **197**, 243 (1971).
20. G. K. BORESKOV, V. I. MARSHNEVA, and V. D. SOKOLOVSKII. Dokl. Akad. Nauk SSSR, **199**, 1091 (1971).
21. E. F. MCCAFFREY, D. G. KLISSURSKI, and R. A. ROSS. Proc. 5th Intern. Cong. Catalysis, Florida, 1972, **3**-151. North Holland Press, Amsterdam. 1973.

The synthesis and characterisation of the trifluoromethylsulfates of silver(II) and gold(III)

PATRICK C. LEUNG, KEITH C. LEE, AND FRIEDHELM AUBKE[1]

Department of Chemistry, The University of British Columbia, Vancouver, B.C., Canada V6T 1W5

Received August 23, 1978

PATRICK C. LEUNG, KEITH C. LEE, and FRIEDHELM AUBKE. Can. J. Chem. **57**, 326 (1979).

The new trifluoromethylsulfates $Ag(SO_3CF_3)_2$ and $Au(SO_3CF_3)_3$, as well as the compound $Cs[Au(SO_3CF_3)_4]$, are synthesised by the solvolysis of the corresponding fluorosulfates in an excess of trifluoromethyl sulfuric acid. The resulting compounds are characterised by their vibrational spectra and, in the case of $Ag(SO_3CF_3)_2$, also by esr.

PATRICK C. LEUNG, KEITH C. LEE et FRIEDHELM AUBKE. Can. J. Chem. **57**, 326 (1979).

On a synthétisé les nouveaux trifluorométhylsulfates, $Ag(SO_3CF_3)_2$, $Au(SO_3CF_3)_3$ ainsi que $Cs[Au(SO_3CF_3)_4]$, en procédant à la solvolyse des fluorosulfates correspondants dans un excès d'acide trifluorométhylsulfurique. On a caractérisé les composés obtenus à l'aide de leurs spectres vibrationnels et, dans le cas du $Ag(SO_3CF_3)_2$, grâce à la rpe.

[Traduit par le journal]

Introduction

Trifluoromethylsulfuric acid, CF_3SO_3H, has, since its discovery in 1954, attracted much attention (1). The acid is one of the strongest, simple protonic acids, exceeded only by fluorosulfuric acid in this respect (1–3). Many of its derivatives, both organic and inorganic in nature, have been reported (1). It is therefore somewhat surprising that only a rather small number of binary transition metal trifluoromethylsulfates seem to have been synthesized and characterized to date (1), whereas a relatively large number of corresponding fluorosulfates are known (4). This discrepancy is primarily due to the lack of suitable synthetic routes to transition metal trifluoromethylsulfates. The very limited thermal stabilities of oxidising agents such as bis(trifluoromethylsulfuryl)peroxide, $(CF_3SO_3)_2$ (5), and chlorine(I) trifluoromethylsulfate, CF_3SO_3Cl (6), restrict the available preparative methods to solvolysis reactions in CF_3SO_3H with metal-halides, -carboxylates, -oxides, and -carbonates as solutes. Hence the availability and the reactivity of these solutes become the limiting factors. The previously reported transition metal trifluoromethylsulfates $Cu^{I}(SO_3CF_3)$ (7), $Cu^{II}(SO_3CF_3)_2$ (7, 8), and $Co^{II}(SO_3CF_3)_2$ (8) have the metals in rather common oxidation states. $Mo_2(SO_3CF_3)_4$ (9) contains the quadruply bonded Mo_2^{4+} ion. All are prepared by solvolysis reactions.

The conversion of fluorosulfates into trifluoromethylsulfates, illustrated by the synthesis of $Ag(SO_3CF_3)_2$, $Au(SO_3CF_3)_3$, and $Cs[Au(SO_3CF_3)_4]$, widens the scope of the available routes to trifluoromethylsulfates and allows the synthesis of compounds with the metal in an unusual oxidation state.

[1]To whom all correspondence should be addressed.

Silver(II) fluorosulfate (10) is besides AgF_2 the only binary Ag^{2+} compound. Gold(III) fluorosulfate (11) was found recently (12) to act as a SO_3F^- ion acceptor and to behave as an acid in HSO_3F. It appears to be the only stable binary oxyacid derivative of tervalent gold.

Experimental Section

Chemicals

Gold powder, 100 mesh, 99.995% pure and silver powder, 100 mesh, 99.999% pure were obtained from the Ventron Corporation. Trifluoromethylsulfuric acid (Minnesota Mining and Manufacturing Co.) was distilled from concentrated H_2SO_4 under reduced pressure. Technical grade fluorosulfuric acid (Allied Chem. Corp.) was purified by double distillation. Bis(fluorosulfuryl)peroxide was prepared according to Cady and Shreeve (13). $Ag(SO_3F)_2$ (10) and $Au(SO_3F)_3$ (12) were obtained by the oxidation of Ag and Au, respectively, by a roughly equimolar mixture of HSO_3F and $S_2O_6F_2$. $Cs[Au(SO_3F)_4]$ (12) resulted from the reaction of 1:1 stoichiometric mixture of CsCl and Au with $HSO_3F/S_2O_6F_2$. All other chemicals were obtained from commercial sources in the highest grade of purity available.

Instrumentation

Infrared spectra were obtained on a Perkin-Elmer 457 grating spectrophotometer or on a Pye Unicam SP 1100 instrument. KRS-5, silver chloride, and bromide were used as window materials (all from Harshaw Chemicals). Due to the reactivity of the materials, no mulling agent was used. Spectra were obtained on thin films of solid materials pressed between the windows. Raman spectra were obtained with a Spex Ramalog 5 Spectrometer equipped with an argon ion laser using the line at 514.5 nm for excitation. The samples were contained in melting point capillaries. Electron spin resonance spectra were recorded on a Varian Associates E-3 spectrometer equipped with 100 kHz field modulation at room temperature and at liquid nitrogen temperature.

Magnetic susceptibilities were determined using a Gouy apparatus described before (14). Measurements were made at constant field strengths of approximately 4500 and 8000 G. All susceptibilities measured were found to be independant of field strength. Calibrations were carried out using $HgCo(CNS)_4$

0008-4042/79/030326-04$01.00/0

(15). Diamagnetic corrections were obtained from the literature (16).

All reactions were performed in Pyrex reaction vials of about 40 ml contents, fitted with Kontes Teflon stem valves. Volatile materials were handled using vacuum line techniques. Solids were handled in a Vacuum Atmosphere Corp. "Dri Lab" Model No. HE-43-2, filled with purified dry nitrogen and equipped with a "Dri-Train" Model No. HE-93-B circulating unit. Filtrations of moisture sensitive compounds outside the drybox were carried out in an apparatus described by Shriver (17).

Synthetic Reactions

$Ag(SO_3CF_3)_2$

An excess of distilled trifluoromethylsulfuric acid (~5 mL) was added to 1.012 g (3.31 mmol) of $Ag(SO_3F)_2$. The resulting suspension was magnetically stirred for 48 h at room temperature, subsequently filtered, and repeatedly washed with distilled HSO_3CF_3. Traces of volatile materials were removed in a dynamic vacuum. A dark brown solid (740 mg) was obtained. This extremely hygroscopic solid melted at 140°C under decomposition and analysed as $Ag(SO_3CF_3)_2$.

$Au(SO_3CF_3)_3$

$Au(SO_3F)_3$ (198 mg, 0.40 mmol) was dissolved in about 3 mL of HSO_3CF_3 by heating the mixture to 100°C. The red solution was kept at this temperature overnight. When allowed to cool to room temperature, yellow-brown crystals precipitated out, and removal of all volatiles yielded 250 mg (0.39 mmol) of $Au(SO_3CF_3)_3$. Gold(III) trifluoromethylsulfate is hygroscopic and thermally stable to +160°C.

$Cs[Au(SO_3CF_3)_4]$

$Cs[Au(SO_3F)_4]$ (478 mg, 0.66 mmol) was dissolved in ~3 mL of HSO_3CF_3 by heating the mixture to +50°C. The yellow-brown solution was kept at this temperature overnight. After all volatiles were removed *in vacuo*, 576 mg (0.63 mmol) of yellow $Cs[Au(SO_3CF_3)_4]$ were obtained. The compound is diamagnetic and melts at +190°C to a brown liquid.

Analysis

Chemical analysis was performed by Analytische Laboratorien (formerly A. Bernhardt), Gummersbach, West Germany. The carbon contents was determined by Mr. P. Borda of this department. The found and expected values for all three compounds are listed below.

Anal. calcd. for $Ag(SO_3CF_3)_2$: Ag 26.57, S 15.79, F 28.08, C 5.92; found: Ag 26.81, S 15.92, F 28.04, C 5.82.

Anal. calcd. for $Au(SO_3CF_3)_3$: Au 30.58, S 14.93, F 26.55, C 5.59; found: Au 30.83, S 15.11, F 26.32, C 5.90.

Anal. calcd. for $Cs[Au(SO_3CF_3)_4]$: Cs 14.35, Au 21.27, S 13.85, F 24.61; found: Cs 14.50, Au 21.40, S 14.04, F 24.57.

Results and Discussion

Synthesis

The successful quantitative conversion of a transition metal fluorosulfate into a trifluoromethylsulfate seems to follow the same general pattern of previously reported solvolysis reactions in HSO_3CF_3 with metal chlorides or carboxylates as reactants (7, 9). The general overall reaction may be formulated as:

$$[1] \qquad MX_n + n HSO_3CF_3 \rightarrow M(SO_3CF_3)_n + n HX$$

with X = Cl, O_2CR, or SO_3F. In order to achieve complete conversion and to avoid mixed products HX must be removed from the acid mixture, either as a volatile byproduct, like HCl in the solvolysis of metal chlorides, or as a soluble protonated species, as in the solvolysis of carboxylates. The solvolysis of a metal fluorosulfate in HSO_3CF_3 departs from these precedents in two important respects: (*a*) HSO_3F and HSO_3CF_3 have virtually identical boiling points at 760 Torr (162.7°C for HSO_3F (18) vs. 163°C for HSO_3CF_3 (19)), and similar volatilities in a vacuum of 10^{-2} Torr at room temperature; and (*b*) a stronger protonic acid (HSO_3F) appears to be generated by a weaker protonic acid (HSO_3CF_3) from its salts ($M(SO_3F)_n$). Hence, removal of HSO_3F by virtue of its volatility or by forming a protonated ion, such as $H_2SO_3F^+$, is rather improbable.

The possibility that HSO_3F is removed by a chemical reaction with HSO_3CF_3 appears to be more likely. Recently Olah and Ohyama (20) have obtained both the trifluoromethyl ester $CF_3OSO_2CF_3$, and trifluoromethylsulfuryl fluoride, CF_3SO_2F, in yields of 19 and 5.5%, respectively, when HSO_3CF_3 and HSO_3F at a molar ratio of 2:1 are refluxed. No other reaction products were reported and the overall reaction is not completely understood.

Because our solvolysis reactions are carried out with HSO_3CF_3 in excess, further involvement of HSO_3F in reactions is very likely. In all reactions described here a slight pressure increase is noted when the solvolysis is completed and a gas phase ininfrared spectrum, obtained on volatile byproducts from the reaction of $Cs[Au(SO_3F)_4]$ with HSO_3CF_3, shows bands attributable to CF_3SO_2F, CF_3OSO_2-CF_3, F_2CO, SO_2, and SiF_4 (21).

It must be concluded that HSO_3F, formed in the solvolysis according to [1], or the metal fluorosulfates directly, interact with trifluoromethylsulfuric acid to form volatile products, which do not interact with the metal trifluoromethylsulfates.

A number of alternative routes to the silver(II) and the gold(III) trifluoromethylsulfates were tried, but found to be either unsatisfactory or less useful: gold(III) chloride did not react with HSO_3CF_3 even at elevated temperatures. The attempted solvolysis of AgF_2 in HSO_3CF_3 (in a Kel-F reaction vessel) resulted in a rather impure product. The oxidation of silver or gold by $S_2O_6F_2$ in HSO_3CF_3 solution, a method previously used to synthesize $I(SO_3CF_3)_3$ (22), proceeded far too slowly to avoid the slow oxidative cleavage of the S—C bond in HSO_3CF_3 by $S_2O_6F_2$. This side reaction is rather exothermic and occasional explosions may result. A similar risk is encountered when $S_2O_6F_2$ is added to a solution of $AgSO_3CF_3$ in HSO_3CF_3, but if the resulting dark

TABLE 1. Vibrational spectra

$Ag(SO_3CF_3)_2$ (ir) $\nu(cm^{-1})$ Int.	$Cs[Au(SO_3CF_3)_4]$ (Raman) $\nu\Delta(cm^{-1})$ Int.	$Cs[Au(SO_3CF_3)_4]$ (ir) $\nu(cm^{-1})$ Int.	$Au(SO_3CF_3)_3$ (ir) $\nu(cm^{-1})$ Int.
1310 m, sh	1411 w	1420 m	1427 vw, sh
1274 vs	1380 ms	1388 s	1395 s
1222 s, sh	1370 w, sh	1374 s, sh	1380 ms
1202 vs		1285 vw	1362 s
~1140 ms, sh	1242 ms	1240 vs, b	1350 s
1122 vs	1213 m	1215 s	1338 ms
1035 s, b	1150 s, b	1148 s	1242 s, sh
775 w		1133 s	1224 vs, b
632 ms	980 s	985 mw	1208 s, b
610 m, sh	965 s	920 msh	1138 s
592 m	~880 vw	885 vs	1127 m, sh
580 msh			1085 s
522 vs	825 vw	828 s	1064 m
455 vw, b	775 m	776 ms	985 ms
365 ms		743 vw	972 ms
348 w, sh	662 s, sh	662 s, sh	960 ms
335 w	651 s, sh	650 s	~920 m, sh
325 vw	645 s	646 s, sh	895 vs, b
	620 vs	625 vs	824 m, sh
	574 w	582 s	774 ms
		575 s, sh	731 vw
	550 m	553 m	656 s
	520 mw	520 vs	635 s, sh
	514 w, sh		620 vs
	454 m	450 vw	570 mw
	393 s	390 w	515 ms
	331 m, b		
	293 w		
	268 vs		
	212 s		

brown solid is filtered immediately, reasonably pure $Ag(SO_3CF_3)_2$ is obtained. In summary it seems that none of the alternative methods tested has the same general applicability as the solvolysis of metal fluorosulfates in HSO_3CF_3.

Both $Ag(SO_3CF_3)_2$ and $Au(SO_3CF_3)_3$ are similar in colour to the corresponding fluorosulfates, but unlike these, they are virtually insoluble in the parent acid. The formation of $Cs[Au(SO_3CF_3)_4]$ indicates $Au(SO_3CF_3)_3$ may act as a trifluoromethylsulfate ion acceptor and may behave as an acid in HSO_3CF_3; however, the lack of any appreciable solubility precludes more detailed solution studies.

Like $Ag(SO_3F)_2$, silver(II) trifluoromethylsulfate is converted to the complex $[Ag(byp)_2](SO_3CF_3)_2$ by direct combination of α,α'-bipyridine (bpy) with $Ag(SO_3CF_3)_2$ in a manner described in detail (10) for $Ag(SO_3F)_2$. The resulting complex $[Ag(bpy)_2](SO_3CF_3)_2$ had been obtained previously via a different method (23), the oxidation of $[Ag(bpy)_2]SO_3CF_3$, and its vibrational spectrum and the esr parameter (10) are known.

Vibrational Spectra

Infrared spectra are obtained on all three compounds down to 300 cm^{-1}, while only the Raman spectrum of $Cs[Au(SO_3CF_3)_4]$ is reported. Gold(III) trifluoromethylsulfate shows strong fluorescence while the dark colour of $Ag(SO_3CF_3)_2$ prevents Raman scattering.

Tentative vibrational assignments for SO_3CF_3 derivatives have been reported for both a bidentate bridging group (9, 24) and for a monodentate group in an anionic complex (22), and will not be discussed here. In addition, the complexity of the molecules, the unavailability of Raman data for all compounds, and the coincidence and vibrational mixing of SO_3 and CF_3 vibrational modes prevent a more detailed assignment. The observed ir frequencies and Raman shifts are listed in Table 1 in order of decreasing frequencies. Except for occasional band splittings, good agreement between ir and Raman data for $Cs[Au(SO_3CF_3)_4]$ is observed.

The band positions for $Ag(SO_3CF_3)_2$ suggest strongly a bidentate SO_3CF_3 group when compared to the precedents (9, 24). A similar conclusion had been reached for $Ag(SO_3F)_2$ (10) and it is not surprising that both silver(II) compounds should show strong structural similarities. The lack of volatility and solubility in HSO_3CF_3 is also more consistent with the presence of bridging groups and hence a polymeric structure. The strong involvement of two

TABLE 2. g_0 and μ values of $Ag(SO_3F)_2$ and $Ag(SO_3CF_3)_2$

	T = 295 K		T = 80 K	
Compound	g_0	μ (BM)	g_0	μ (BM)
$Ag(SO_3F)_2$*	2.220	1.92	2.187	1.89
$Ag(SO_3CF_3)_2$	2.175	1.88	2.162	1.87

*Reference 10.

oxygens from the SO_3CF_3 groups would imply a square planar or a distorted (tetragonally elongated) environment for Ag^{2+}, not unreasonable for a metal ion with a d^9 electronic configuration.

For $Cs[Au(SO_3CF_3)_4]$, the presence of monodentate OSO_2CF_3 groups seems to be indicated. The observed band positions in particular in the stretching range are in reasonable agreement with reported data for $Rb[I(SO_3CF_3)_4]$ (22). Intense Raman bands at ~650, ~450, and ~270 cm^{-1} are also observed in the Raman spectrum of $Cs[Au(SO_3F)_4]$ (12). The corresponding vibrations seem to involve AuO_4 skeletal vibrations in a square planar environment. Such a structure for gold (consistent with the observed diamagnetism) is suggested for both the fluorosulfato and the trifluoromethylsulfato complexes.

Finally, the infrared data for $Au(SO_3CF_3)_3$ with numerous bands in the stretching frequency range (1500 to 800 cm^{-1}) suggest the presence of both mono and bidentate trifluoromethylsulfate groups. In addition, strong vibrational coupling (evident also for $Cs[Au(SO_3CF_3)_4]$) seems to cause further proliferation of bands. Even though a clear distinction between bands due to mono and bidentate SO_3CF_3 groups is not possible, a polymeric structure is indicated. Thus, the strong structural parallels between the corresponding fluorosulfates and trifluoromethylsulfates seem to extend to the gold(III) derivatives as well.

Electron Spin Resonance and Magnetic Susceptibilities of $Ag(SO_3CF_3)_2$

As for the silver(II) fluorosulfate (10), a broad, isotropic esr signal is obtained for solid $Ag(SO_3CF_3)_2$, both at room temperature and at liquid N_2 temperature. Comparable g_0 values for both compounds suggest similar magnetic properties as reflected in the magnetic moment values calculated by using the spin-only formula for one unpaired electron. The data are presented in Table 2.

Preliminary bulk magnetic susceptibilities on $Ag(SO_3CF_3)_2$ suggest a slightly lower μ_{eff} value of approximately 1.60 BM at room temperature. Further work is required, extending the measurements down to 80 K or even lower, to decide whether antiferromagnetic coupling is the cause for the low magnetic moment.

There is, however, no doubt that silver(II) trifluoromethylsulfate, like the corresponding bisfluorosulfate, is a true divalent silver compound with one unpaired electron.

Conclusions

The conversion of transition metal fluorosulfates into trifluoromethylsulfates by solvolysis in HSO_3CF_3, demonstrated here by the syntheses of $Ag(SO_3CF_3)_2$, $Au(SO_3CF_3)_3$, and the complex $Cs[Au(SO_3CF_3)_4]$, should have rather wide applications. Extension to other main group and transition metal fluorosulfates should be possible. Judging by the wide use other metal trifluoromethylsulfates have found in organic synthesis (1), the new compounds should find some use as reagents as well.

Acknowledgement

Financial support by the National Research Council of Canada is gratefully acknowledged.

1. R. D. HOWELLS and J. D. MCCOWN. Chem. Rev. **77**, 69 (1977).
2. D. G. RUSSELL and J. B. SENIOR. Can. J. Chem. **52**, 2975 (1974).
3. G. M. KRAMER. J. Org. Chem. **40**, 298 (1975); **40**, 302 (1975).
4. A. A. WOOLF. *In* New pathways in inorganic chemistry. Cambridge University Press, New York, NY. 1968. p. 327.
5. R. E. NOFTLE and G. H. CADY. Inorg. Chem. **4**, 1010 (1965).
6. D. D. DES MARTEAU. J. Am. Chem. Soc. **100**, 340 (1978).
7. C. L. JENKINS and J. K. KOCHI. J. Am. Chem. Soc. **94**, 843 (1972).
8. A. L. ARDUINI, M. GARNETT, R. C. THOMPSON, and T. C. T. WONG. Can. J. Chem. **53**, 3812 (1975).
9. E. H. ABBOTT, F. S. WOLF, and T. BACKSTROM. J. Coord. Chem. **3**, 255 (1974).
10. P. C. LEUNG and F. AUBKE. Inorg. Chem. **17**, 1765 (1978).
11. W. M. JOHNSON, R. DEV, and G. H. CADY. Inorg. Chem. **11**, 2260 (1972).
12. K. C. LEE and F. AUBKE. Inorg. Chem. To be published.
13. G. H. CADY and J. M. SHREEVE. Inorg. Synth. **7**, 124 (1963).
14. H. C. CLARK and R. J. O'BRIEN. Can. J. Chem. **39**, 1030 (1961).
15. B. N. FIGGIS and R. S. NYHOLM. J. Chem. Soc. 4190 (1958).
16. LANDOLT-BORNSTEIN. Numerical data and functional relationships in science and technology. Vol. 2 and Supplement II, 18 magnetic properties of coordination and organometallic transition metal compounds. Springer Verlag, Berlin. 1966 and 1976.
17. D. F. SHRIVER. The manipulation of air-sensitive compounds. McGraw-Hill, New York, NY. 1969.
18. J. BARR, R. J. GILLESPIE, and R. C. THOMPSON. Inorg. Chem. **3**, 1149 (1964).
19. R. N. HAZELDINE and J. M. KIDD. J. Chem. Soc. 4228 (1954).
20. G. A. OLAH and T. OHYAMA. Synthesis, 319 (1976).
21. K. O. CHRISTE and C. J. SCHACK. Adv. Inorg. Chem. Radiochem. **18**, 319 (1976).
22. J. R. DALZIEL and F. AUBKE. Inorg. Chem. **12**, 2707 (1973).
23. W. G. THORPE and J. K. KOCHI. J. Inorg. Nucl. Chem. **33**, 3958 (1971).
24. P. A. YEATS, J. R. SAMS, and F. AUBKE. Inorg. Chem. **10**, 1877 (1971).

Adsorption of Et_4NBr at the mercury/electrolyte interface from water and heavy water solutions

FRANK M. KIMMERLE AND HUGUES MENARD

Département de chimie, Faculté des sciences, Université de Sherbrooke, Sherbrooke (Qué.), Canada J1K 2R1

Received June 16, 1977[1]

FRANK M. KIMMERLE and HUGUES MENARD. Can. J. Chem. **57**, 330 (1979).

Droptime measurements of aqueous and deuterated Et_4NBr solutions indicate that the mercury/electrolyte interfacial tension differs by less than 1 mJ m^{-2} (dyn cm^{-1}). Et_4NBr is slightly more adsorbed from heavy water in dilute solutions, but the difference becomes relatively less important in concentrated electrolytes. This behaviour is interpreted in terms of interfacial transfer parameters and attributed to the nature of the solvent–solute interactions.

FRANK M. KIMMERLE et HUGUES MENARD. Can. J. Chem. **57**, 330 (1979).

Des mesures de temps de chute d'une goutte de mercure dans des solutions aqueuses et des solutions deuterées de Et_4NBr, indiquent un écart de la tension interfaciale de moins de 1 mJ m^{-2} (dyn cm^{-1}). Et_4NBr est adsorbé légèrement plus des solutions diluées d'eau lourde, mais les différences disparaissent en solution concentrée. Ce comportement est interprété à l'aide des fonctions de transfert à l'interface et peut être attribué à la nature des intéractions solvant–soluté.

Introduction

It has long been recognized (1) that water and deuterium oxide have very similar properties, but that small differences in the magnitude of several physical properties exist. Not the least important difference is the fact that more structural order exists in liquid D_2O than in H_2O. One way of detecting structural effects is to study the properties of solutions of the same solutes in two solvents (2). Another is to examine the electrode/electrolyte interface where it is now established that hydration entropy plays a predominant role in the case of the adsorption of the quaternary ammonium salts (3, 4).

The treatment follows directly from the general electrocapillary given by Mohilner (cf. eq. [52] of ref. 5) which can be simplified for a pure mercury electrode in contact with a three component aqueous solution containing one electrolyte $C_{\nu+}A_{\nu-}$ and one neutral organic compound H at constant temperature and pressure:

$$[1] \quad d\gamma = -\sigma^M dE^{\mp} - \Gamma_{H,S} d\mu_H - \frac{\Gamma_{\pm,S} d\mu_{C_{\nu+}A_{\nu-}}}{\nu\pm}$$

where γ is the interfacial tension of the mercury/electrolyte interface, σ^M is the excess charge density of the metal surface, $E^{\pm}$ is the potential of the polarized electrode with respect to an indicator electrode reversible to the anion (E^-) or (E^+), $\Gamma_{H,S}$ is the relative surface excess of neutral species H with respect to the solvent S, $\Gamma_{\pm,S}$, the relative excess of the anion or cation with respect to solvent S, μ_H and $\mu_{C\nu+C\nu-}$, the chemical potentials of the neutral and ionic solutes respectively, and $\nu\pm$ the stoichiometric coefficient of the cation or anion.

In order to compare bulk thermodynamic properties in two solvents, transfer parameters have been defined as the difference between observed quantities (e.g. the enthalpy, free energy, heat capacities, etc.) in the two solvents. Similarly, it is possible to define interfacial transfer properties. Thus we consider the interfacial energy of transfer, γ_{tr}, as the difference of the surface tensions of two interfacial regions: phase 0 (the electrode) in contact with phase 1 containing solvent 1 and phase 0 in contact with phase 2 containing solvent 2.

$$[2] \quad \gamma_{tr} = \gamma(\mu,E^{\pm},S_2) - \gamma(\mu,E^{\pm},S_1)$$

Transfer parameters involving the first and second derivatives are also readily defined, for example.

$$[3] \quad \sigma_{tr}{}^M = -\left\{\left(\frac{\partial\gamma}{\partial E^{\pm}}\right)_{T,p,\mu,S_2} - \left(\frac{\partial\gamma}{\partial E^{\pm}}\right)_{T,p,\mu,S_1}\right\}$$

Clearly the solution composition and thus μ_i must be held constant while performing the mathematical differentiation. However, some ambiguity exists as to the concentrations in solvents S_1 and S_2 that should be compared, since it is impossible to keep constant all of the chemical potentials including that of the solvent itself. Historically one might be inclined to keep the molality or the molarity constant and compare absorption in two solvents or solvent mixtures (6, 7). It may be more meaningful, however, to compare solutions at fixed mole fractions. Since $\sigma_{tr}{}^M$ refers to the variation in charge necessary to maintain a fixed electrode potential with respect to

[1]Revision received.

0008-4042/79/030330-05$01.00/0

an indicator electrode, it would furthermore be useful to employ a hypothetical indicator electrode whose response does not vary with the nature of the solvent. Alternately, it may be necessary to take into account the free energy of transfer of the solute, and thus compare the potential scale in one solvent to that in the other.

The subtraction and differentiation implicit in eq. [3] can be carried out in reverse order and we can write (at constant temperature and pressure):

$$[4] \qquad \sigma_{tr}{}^{M} = -\left(\frac{\partial \gamma_{tr}}{\partial E^{\pm}}\right)_{\mu'}$$

The relative surface excess of transfer for a neutral species can similarly be defined as:

$$[5] \quad \Gamma_{H,tr} = -\left\{\left(\frac{\partial \gamma}{\partial \mu_H}\right)_{\mu',E^{\pm},S_2} - \left(\frac{\partial \gamma}{\partial \mu_H}\right)_{\mu',E^{\pm},S_1}\right\}$$

where the subscript μ' indicates that the chemical potentials of all the components are held constant except that one with respect to which the differentiation is performed, and that of the solvent itself. For solvents having similar properties and hence where $\gamma(S_1) \sim \gamma(S_2)$ it is probably easier to calculate $\Gamma_{H,tr}$ according to:

$$[6] \qquad \Gamma_{H,tr} = -\left(\frac{\partial \gamma_{tr}}{\partial \mu_H}\right)_{\mu',E^{\pm}}$$

The relative surface excess may be expressed in terms of the absolute surface excess values and the mole fractions of solute X_H and solvent X_S in solution.

$$[7] \quad \Gamma_{H,tr} = \left\{\left(\Gamma_H{}^{S_2} - \frac{X_H}{X_{S_2}}\Gamma_{S_2}\right)_{S_2} - \left(\Gamma_H{}^{S_1} - \frac{X_H}{X_{S_1}}\Gamma_{S_1}\right)_{S_1}\right\}$$

If we compare solutions at fixed mole fraction ratio $X_H/X_{S_1} = X_H/X_{S_2}$, which can also be expressed as the molality divided by the number of moles of solvent/kg (m/55.5 for water), eq. [7] becomes

$$[8] \quad \Gamma_{H,tr} = (\Gamma_H{}^{S_2} - \Gamma_H{}^{S_1}) - \frac{m}{55.5}(\Gamma_{S_2} - \Gamma_{S_1})$$

A positive value, $\Gamma_{H,tr} > 0$, therefore implies that

$$[9] \qquad (\Gamma_H{}^{S_2} - \Gamma_H{}^{S_1}) > (m/55.5)(\Gamma_{S_2} - \Gamma_{S_1})$$

For dilute solutions, where $m/55.5 \ll 1$, it may be assumed that the neutral component H is more strongly adsorbed at the interface in solvent 2 than in solvent 1. In concentrated solutions a positive value, $\Gamma_{H,tr} > 0$ might conceivably imply that $\Gamma_{S_1} > \Gamma_{S_2}$ without necessarily dictating that $\Gamma_H{}^{S_2} > \Gamma_H{}^{S_1}$. Similarly a negative value, $\Gamma_{H,tr} < 0$, does not necessarily imply the desorption of the neutral component in solvent S_2, it could also reflect the fact that the interfacial region is relatively richer in solvent molecules S_1 than solvent molecules S_2 at equivalent concentration of the neutral component H.

In the case of electrolyte solutions, similar expressions arise. The ionic relative surface excess of transfer is given as

$$[10] \quad \Gamma_{\pm,tr} = (\Gamma_{\pm}{}^{S_2} - \Gamma_{\pm}{}^{S_1}) - \nu_{\pm}\frac{m}{55.5}(\Gamma_{S_2} - \Gamma_{S_1})$$

$\Gamma_{\pm,tr}$ can be calculated from the expressions analogous to eqs. [5] or [6] or again using Parson's function (8).

$$[11] \quad \Gamma_{\pm,tr} = -\nu_{\pm}\left\{\frac{\partial[\xi(\mu, S_2, \sigma_M) - \xi(\mu, S_1, \sigma_M)]}{RT\partial \ln a_{(C\nu_+ A\nu_-)}}\right\}_{\sigma^M}$$

The latter expression might prove particularly useful at the potential of zero charge, since the electrode potential with respect to a given reference electrode does not have to be known in order to calculate the relative surface excess nor the relative surface excess of transfer.

Because water and deuterium oxide have almost the same molar volumes (1) (18.069 and 18.134 cm^3/mol at 25°C) dilute solutions of equal molarity contain practically the same number of solvent molecules. Even for 1 *M* Et_4NBr the difference in concentration on a mole fraction basis is less than 3% so that either scale should prove satisfactory. The distinction becomes significant, however, when comparing solvents having significantly different volumes or higher solute concentrations in heavy water solutions.

Experimental

Surface tension data were calculated from droptime measurement recordings using the apparatus described previously (9). The time interval between successive drops was defined by the interruption of a light beam by the falling drop. The resulting signal from a Systron Donner frequency meter caused the time interval together with the drop potential controlled by a Tacussel PRT 30-0.1 potentiostat to be printed out by a HP 5150A printer. Although the electrode potential was actually recorded with respect to a saturated calomel electrode, conversion to a reversible indicator potential scale was later accomplished using the activity data of Lindenbaum and Boyd. All aqueous solutions were prepared from water distilled from alkaline-permanganate and twice recrystallized Et_4NBr (Baker reagent grade). D_2O (Stohler Isotope Chemicals) was used without further purification.

Results

The interfacial tension for tetraethylammonium bromide solution in contact with the mercury elec-

trode is plotted in Fig. 1 as a function of potential with respect to a reversible Br electrode in aqueous or deuterated solutions. Although γ_{D_2O} is consistently greater than γ_{H_2O}, the difference is usually less than 1 mJ m^{-2}, i.e. only ten times the experimental uncertainty near the E_{pzc} and about three times the experimental error at the extremities of the electrocapillary curves. Any interpretation of these results will therefore be limited by the experimental scatter of the data and could be distorted by even relatively minor systematic errors in the data treatment.

The interfacial energy of transfer, Fig. 2, decreases with increasing electrolyte concentration but seems to be relatively potential independent. Perhaps not unsurprisingly, in view of the reported negligible difference in dipole moments, dielectric constant, crystallographic parameters, and molar volumes of water and deuterium oxide (1), the electrode charge – potential relationship is also virtually identical in H_2O and D_2O Et_4NBr solutions, and any differences fall within the experimental uncertainty of the measurements.

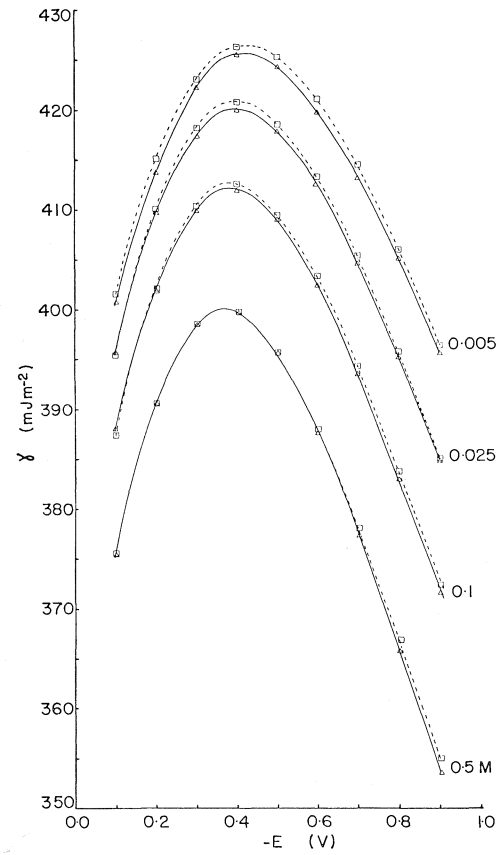

FIG. 1. Interfacial tension for tetraethylammonium bromide electrolytes: □, D_2O solutions; △, H_2O solutions. Electrode potentials refer to a reversible Br indicator electrode.

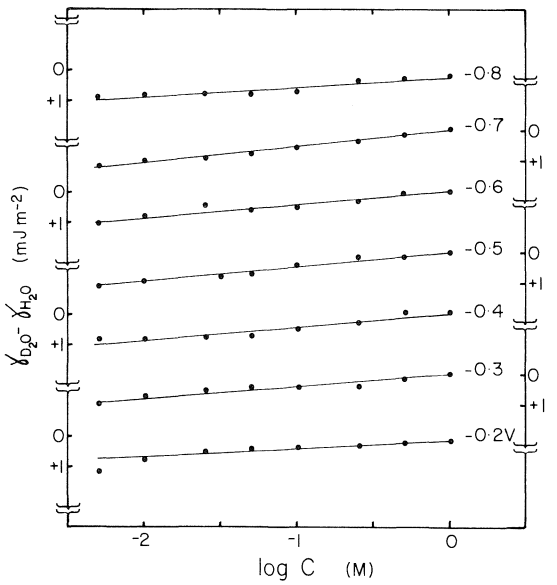

FIG. 2. Interfacial energy of transfer for Et_4NBr electrolytes. $\gamma_{tr} = \gamma_{D_2O} - \gamma_{H_2O}$.

The relative surface excess of transfer of the cation, $\Gamma_{+,tr}$ can be calculated according to eq. [6] from Fig. 2 provided that the activity coefficients are available. We have not found any measurements of Et_4NBr activity coefficients in the literature but have assumed that $\gamma^{\pm}(D_2O) = \gamma^{\pm}(H_2O)$. This assumption is justified by the fact that Wen and Chen reported (Tables III and V of ref. 10) ratios of activity coefficients $\gamma^{\pm}(D_2O)/\gamma^{\pm}(H_2O) > 1.0$ for $(CH_3)_4NBr$ and $\gamma^{\pm}(D_2O)/\gamma^{\pm}(H_2O) < 1.0$ for $(C_4H_9)_4NBr$ and $-15 < \Delta\bar{G}_{tr} < +15$ cal/mol. Levine and Wood (11) reported almost identical values of the excess enthalpy of dilution of Et_4NBr in H_2O and D_2O. Any differences in activity coefficients are probably less than 2% and approach the reliability $\gamma^{\pm}(H_2O)$ (12) itself.

The surface excess of transfer obtained by assuming that single ion activities can be replaced by mean ionic activities (and thus that the potential scale in D_2O is identical to that in H_2O) is found to be $\Gamma_{+,tr} = 8 \pm 1 \times 10^{-8}$ mol m^{-2}. This value does not depend on the electrode charge (+0.15 to −0.12 C m^{-2}), the electrolyte concentration (5×10^{-3} to 1.0 M), nor the relative surface excess ($\Gamma_{+,S} = 0.3$ to 3×10^{-6} mol m^{-2}) (13).

According to eq. [10] $\Gamma_{+,tr}$ could be explained by differences in the surface excess Γ_S, or in the surface excess of the solute Γ_+^S. In the former case we would expect $\Gamma_{+,tr}$ to vary with electrolyte concentration ($X_{\pm}/X_S$) and to become negligible at infinite dilution. The opposite behaviour is observed and we are forced to conclude that $\Gamma_{+,tr}$ must be attributed to

differences in the absolute amounts of Et_4NBr absorbed in the two solvents. Since the excess charge of transfer $\sigma_{M,tr} \simeq 0$, and

$$\sigma_{M,tr} = (\nu_+ F\Gamma_{+,tr} - \nu_- F\Gamma_{-,tr})$$

we must further conclude that $\Gamma_{Et_4N^+,tr} \sim \Gamma_{Br^-,tr}$ i.e. that the adsorption of the cation and anion are perturbed to approximately equal extent.

We can interpret $\Gamma_{\pm,tr}$ in view of the relationship between the hydration entropy and $\Gamma_{+,S}$ found by Ikeda *et al.* (3) and the relationship between the ion size and the free energy of adsorption of the tetraalkylammonium salts (15). When Et_4NBr is absorbed beyond the $\Gamma_{+,S}$ or $\Gamma_{-,S}$ values predicted from simple diffuse layer theory, the salt is said to be specifically or contact adsorbed. In deuterated solutions from 2 to 20% more Et_4NBr species are found in the interfacial region than in aqueous solutions. For aqueous and aqueous urea solutions we have previously found that contact adsorbed Et_4NBr seems to involve an equal number of anions and cations in the immediate neighbourhood of the electrode in a configuration not unlike Fig. 3. Such contact absorption can be described (14) by a general hangview isotherm:

$$[12] \qquad f(\theta) = \frac{X_H}{X_S} \exp -\frac{\Delta\bar{G}_H - n\Delta\bar{G}_S}{RT}$$

where $f(\theta) \simeq \theta/n(1-\theta)^n$ tends to θ at low surface coverages ($1 \gg \theta$). $\Delta\bar{G}_H$ and $\Delta\bar{G}_S$ are the standard free energies of adsorption of solute H and solvent S and n is the number of solvent molecules necessary to occupy the same surface area as the absorbed species H (here the anion–cation pair).

In aqueous Et_4NBr solutions we have already noted no significant charge dependence for the contact adsorbed anion or cation. It is therefore significant that in deuterated solutions the absorption of Br^- also is not favored over that of Et_4N^+ or vice versa. If only cations were contact adsorbed at $\sigma^M < 0$ and only anions contact adsorbed at $\sigma^M > 0$ then the solute–solvent interactions should show a strong charge dependence. As is obvious from Figs. 1 and 2 γ_{tr} varies in a monotone fashion. It thus follows, as indicated in Fig. 3*A* for intermediate positive σ^M values, that the number of anion–cation or solute–electrode interactions does not vary significantly from those found at intermediate negative σ^M values (Fig. 3*C*). We would further conclude that the interfacial properties of equimolar or constant mole fraction deuterated and aqueous solutions are very similar. With the possible exceptions of the quaternary ammonium salts of very hydrophillic anions they almost lie within the experimental limits (± 0.1 mJ m^{-2}) of present measuring techniques. The differential data acquisition via the transfer functions aids considerably in the interpretation but does not encourage us to undertake a major project on solvents as similar as H_2O and D_2O.

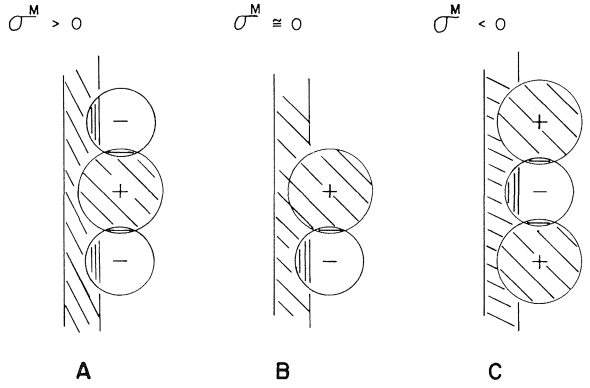

FIG. 3. Model of the structure of the electrode/electrolyte region for Et_4NBr electrolytes. (*A*) $\sigma^M > 0$, (*B*) $\sigma^M \sim 0$, (*C*) $\sigma^M < 0$.

According to eq. [12] or equivalent expressions it is to be expected that a difference in the free energy of adsorption of two solvents $\Delta\bar{G}_S$ results in difference of surface coverage or a $\Gamma_{H,tr}$ value proportional to the solute concentration. Such is not the case here. The concentration and charge independence of $\Gamma_{H,tr}$ could arise if $\Delta\bar{G}_H$ or $\Delta\bar{G}_S$ or both depend on the number of solute–solvent interactions and thus the surface coverage and solute concentration.

A part of the hydration structure, the electrode and a part of the hydration shell of the ions are detroyed or highly modified. In D_2O solutions for all values of σ^M (Fig. 3), a somewhat greater gain in free energy seems to result when water molecules in the interfacial region are returned to the bulk solution. As the solute concentration increases, the bulk structure differs less and less from that of the interfacial region and γ_{tr} and Γ_{tr} tend towards zero.

Acknowledgement

The support of this work by the National Research Council of Canada is gratefully acknowledged.

1. G. NÉMETHY and H. A. SCHERAGA. J. Chem . Phys. **41**, 680 (1964).
2. A. J. PARKER. Electrochim. Acta, **21**, 671 (1976).
3. O. IKEDA, Y. MATSUDA, H. YONEYAMA, and H. TAMURA. Electrochim. Acta, **21**, 519 (1976).
4. H. MÉNARD and F. M. KIMMERLE. Can. J. Chem. **55**, 3312 (1977).
5. D. M. MOHILNER. *In* Electroanalytical chemistry. Vol. 1. *Edited by* A. J. Bard. Marcel Dekker, New York, NY. 1966. pp. 241–409.
6. R. PARSONS and M. A. V. DEVANATHAN. Trans. Faraday Soc. **49**, 673 (1953).

7. J. KŮTA, L. POSPISIL, and I. SMOLER. J. Electroanal. Chem. **75**, 407 (1977).
8. R. PARSONS. Proc. R. Soc. **A261**, 79 (1961).
9. H. MÉNARD and F. M. KIMMERLE. J. Electroanal. Chem. **47**, 375 (1973).
10. W.-Y. WEN and C.-M. L. CHEN. J. Chem. Eng. Data, **20**, 384 (1975).
11. A. S. LEVINE and R. H. WOOD. J. Phys. Chem. **77**, 2390 (1973).
12. S. LINDENBAUM and G. G. BOYD. J. Phys. Chem. **68**, 911 (1964).
13. H. MÉNARD and F. M. KIMMERLE. Can. J. Chem. **54**, 2488 (1976); **54**, 3304 (1976).
14. F. M. KIMMERLE and H. MÉNARD. *In* Chemistry and physics of aqueous gas solutions. The Electrochemical Society, Princeton, New York. 1975. p. 337.
15. H. FRIEDMAN. *In* Water, a comprehensive treatise. Vol. 3. *Edited by* F. Franks. Plenum Press, New York, NY. 1973. p. 50.

Fragmentation and rearrangement processes in the mass spectra of perfluoroaromatic compounds. Part XI. Heterocyclic derivatives of phosphorus and some transition metals

TIMOTHY R. B. JONES AND JACK M. MILLER
Department of Chemistry, Brock University, St. Catharines, Ont., Canada L2S 3A1
AND
SYLVIA A. GARDNER AND MARVIN D. RAUSCH
Department of Chemistry, University of Massachusetts, Amherst, MA 01002, U.S.A.
Received August 10, 1978

TIMOTHY R. B. JONES, JACK M. MILLER, SYLVIA A. GARDNER, and MARVIN D. RAUSCH. Can. J. Chem. **57**, 335 (1979).

The mass spectra of a number of phospholes and metalloles of general structure **1** and **2** are

1 **2**

discussed with respect to their fragmentation and ion rearrangement processes. Of special interest is the migration of ring fluorines to the central atom during fragmentation. The bonding principles involved for the postulated intermediates are discussed.

TIMOTHY R. B. JONES, JACK M. MILLER, SYLVIA A. GARDNER et MARVIN D. RAUSCH. Can. J. Chem. **57**, 335 (1979).

On discute des spectres de masse d'un certain nombre de phospholes et de métalloles de structures générales I et II en rapport avec leurs processus de fragmentations et de trans-

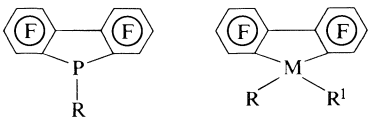

1 **2**

positions ioniques. Il est particulièrement intéressant de noter, au cours de la fragmentation, la migration des atomes de fluor des cycles, vers l'atome central. On discute des principes de liaisons impliquées dans les intermédiaires postulés.

[Traduit par le journal]

Introduction

Compounds of the general structure (**3**) are known for a variety of main group elements (1–10) and a number of transition metals (11–13).

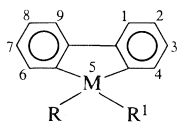

3

Nomenclature is based on the corresponding dibenzophospholes (M = P) or dibenzometalloles (M = metal, e.g., titanole for M = Ti). All the compounds referred to in this paper are of the perfluorinated moieties, i.e., 1,2,3,4,6,7,8,9-octafluorodibenzo species.

To the present time there has only been one detailed mass spectral study of these compounds. Hellwinkel *et al.* (14) reported the mass spectra of the Group VA derivatives with the structure **4**.

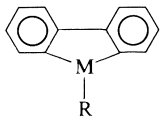

M = P, As, Sb, Bi
R = CH_3, C_6H_5, 2-$C_{12}H_9$

4

The basic trend was a decrease in molecular ion abundance as the size of the central atom increased. Along these same lines, an increase in the net abundance of hydrocarbon ions was noted. There was also evidence for proton abstraction by the

0008-4042/79/030335-07$01.00/0

TABLE 1. Elemental analysis of phospholes

Compound	Melting point (°C)	Analysis							
		Found				Calculated			
		C	F	P	H	C	F	P	H
$C_{12}F_8PC_6H_5$	123–4	53.22	37.90	7.66	1.12	53.49	37.60	7.66	1.25
$C_{12}F_8P^tC_4H_9$	121–23	50.00	39.77	7.80	2.40	50.02	39.56	8.06	2.36
$C_{12}F_8PC_6F_5$*	151–53								

*Insufficient quantity for elemental analysis.

central atom, a tendency which increased with atomic size.

Interest in the mass spectra of phospholes has been influenced by studies (15, 16) in the aromaticity of these compounds as compared to the related pyrroles and carbazoles. Mass spectral evidence is in support of at least partial aromatic character while other chemical and spectroscopic evidence is contradictory. It is therefore of interest to compare the behaviour of such phosphorus heterocycles to the triaryl phosphines with regard to the stability of related P-containing fragments.

Little data are currently available on the mass spectral fragmentation of perfluorinated metalloles, the only reported results being simple molecular weight determinations, except for our earlier work on perfluoroaromatic heterocyclic derivatives of Group IV (17*a*) of the type $(C_{12}F_8)_2M$. These heterocyclic complexes have provided some interesting additions to previous studies of perfluoroaromatics with regard to fluorine abstraction processes.

Experimental

The transition metal derivatives were prepared by Gardner *et al.* (13). The phospholes were prepared using the method of Chambers and Spring (7*b*). The 5-phenyl derivative has been prepared previously. 5-*tert*-Butyloctafluorodibenzophosphole and 5-pentafluorophenyloctafluorodibenzophosphole were synthesized in a similar manner, and isolated in yields of 68% and 5%, respectively. See Table 1 for elemental analysis.

Mass spectra were recorded on an AEI-MS30 double beam mass spectrometer at 70 eV with a 4 kV accelerating voltage, resolution 1000, and a source temperature of 180°C. Samples were admitted to beam I using the direct probe and concentric sample cups. High boiling PFK was admitted in beam II via a gas liquid probe to serve as a chemical mass marker, simultaneously recorded but not interfering with the spectrum under study. Metastable transitions were assigned with the aid of a Fortran computer program BMETAST, while isotopic patterns were calculated and overlapping species deconvoluted using the Fortran programs BMASROS and BMASABD, respectively.

All intensities are reported as a percentage of the total positive ion current and polyisotopic species have been summed over all isotopic contributions.

Transition Metal Derivatives

The partial mass spectra of these compounds are summarised in Table 2. A general metastable ion supported fragmentation scheme is given for the Group VIII complexes in Scheme 1 and for the titanole in Scheme 2 although metastable ions were not abundant for the titanole.

(*i*) The Group VIII metalloles all exhibit relatively strong parent ions, that of the rhodole being of lower abundance than either the cobaltole or iridole. A significant trend develops for the ion resulting from loss of carbonyl. As the size of the metal atom increases the abundance of this ion also increases. This pattern is probably a reflection of the increased polarizability and 'soft' character associated with the larger atoms.

When one considers the overall fragmentation, it is the rhodole which exhibits an inconsistent behaviour. The iridole gives rise to a large variety of iridium-containing ions resulting from sequential F and HF losses from the (M—CO) ion. A similar pattern is observed for the cobaltole although the abundance of the resulting ions is much lower. These ions are almost completely absent from the rhodole spectrum as one can see from the abundance of the species listed as $C_xF_yH_zM$ where Ir > Co > Rh.

This 'different' rhodole behaviour is consistent with other parameters determined for these com-

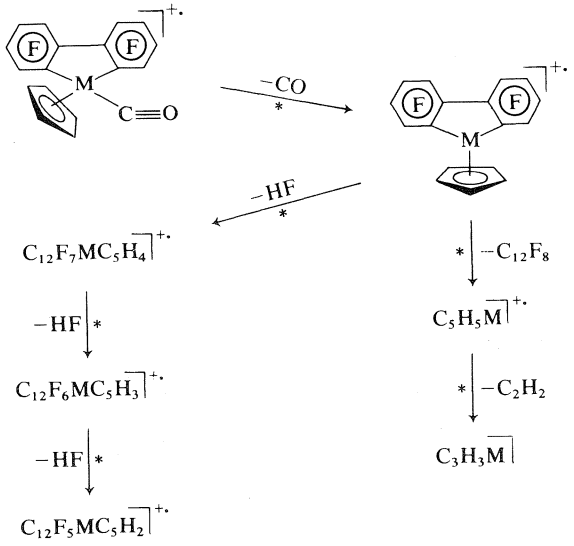

SCHEME 1

TABLE 2. Partial mass spectra of 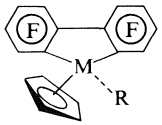

Ion	Abundance (% Σi)			
	M = Co R = C≡O	M = Rh R = C≡O	M = Ir R = C≡O	M = Ti R = η-C_5H_5
$C_{12}F_8M(\eta\text{-}C_5H_5)R$	7.1	4.5	8.1	5.3
$C_{12}F_7M(C_5H_4)R$	0.3	—	—	18.1
$C_{12}F_8M(C_5H_5)$	4.3	15.4	30.8	—
$[C_{12}F_8M(C_5H_5)]^{2+}$	0.6	0.7	7.0	—
$C_{12}F_8H_2$	3.8	1.6	2.0	0.4
$C_5H_5MF_2$	—	—	—	5.0
C_5H_5MF	—	—	—	32.2
C_5H_5M	36.3	46.5	0.3	2.5
C_3H_3M	2.4	4.0	1.8	—
C_3H_2M	0.5	—	0.9	3.6
C_5H_5	1.8	0.7	1.1	1.5
M	4.8	4.6	—	—
$C_xF_yH_zM^*$	9.6	1.0	21.0	3.4
$C_xF_yH_z$	28.5	21.0	27.0	28.0

*$12 \leq x \leq 17, y \leq 8, z \leq 5$ for M = Co, Rh, Ir; $12 \leq x \leq 22, y \leq 8, z \leq 10$ for M = Ti.

pounds by Rausch and co-workers (13). They found the rhodole exhibits a ν(CO) at higher frequency than either the cobalt or iridium derivative. The proton shifts for the cyclopentadienyl ring also indicated a decreased shielding in the rhodole with respect to either the cobaltole or iridole. This seems to suggest a preference for π-bonded ligands by rhodium with the cobalt and iridium showing progressively lower tendencies for such behaviour. Indeed, the abundance of the $C_5H_5M^+$ species adds further weight to this argument where M = Rh > Co ≫ Ir.

There is no metastable ion evidence for fluorine abstraction rearrangements by the central atom during fragmentation nor any MF^+ ions, and yet the formation of many of the coupled fragments such as $C_{17}F_7H_5^{+\cdot}$, $C_{17}F_6H_5^+$, etc. may have arisen by a neutral metal-fluoride elimination as has been observed in many other cases (17–30).

(*ii*) 5,5-Bis(η-cyclopentadienyl)-1,2,3,4,6,7,8,9-octafluorodibenzotitanole. The partial mass spectrum of this compound, shown in Table 2, reveals a significant difference in its fragmentation as compared to the Group VIII complexes. Most notable is the presence of the ions $C_5H_5TiF_2^+$ and $C_5H_5TiF^{+\cdot}$ which must arise by fluorine abstraction from the octafluorodibenzo substituent. Though no metastable ion sup-

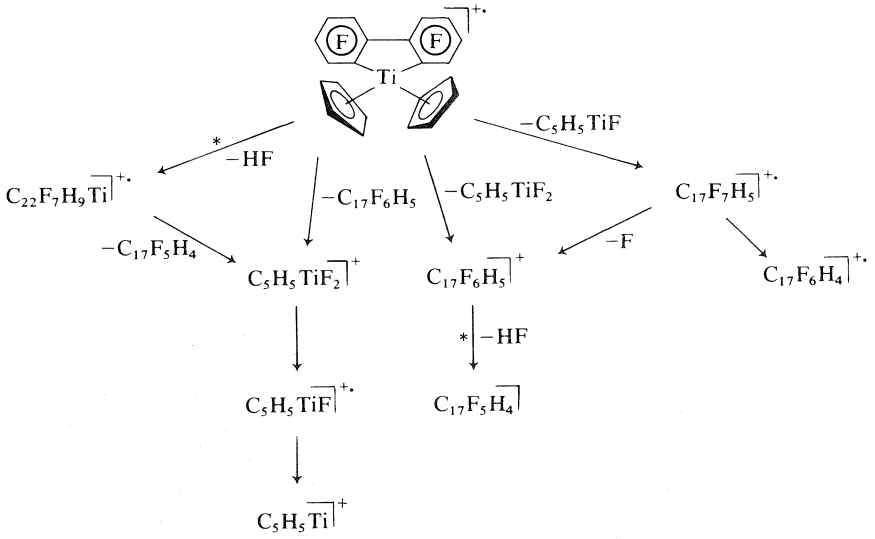

SCHEME 2

port is available, the formation of these ions should involve residues as were observed for the Group VIII compounds, i.e., $C_{17}F_7H_5^+$, $C_{17}F_6H_5^+$, etc.

The behaviour of the parent molecular ion for the titanole is quite different from the Group VIII complexes. The π-bonded cyclopentadienyl does not cleave readily to give a species similar to the (M—CO) fragment observed for the cobaltole, rhodole, and iridole. A $C_{12}F_8Ti(C_5H_5)$ fragment is detected in the spectrum, but at very low abundance. The titanole exhibits preferential loss of HF to give an intense ion formulated as $C_{22}F_7H_9Ti^{+\bullet}$. Such a species could have formed only via an interaction between the cyclopentadienyl and dibenzo substituents, which would seem to indicate the possibility of bond-forming rearrangements between the substituents, a fact which has been well-documented in many cases (17–23). Though somewhat speculative, this type of breakdown process helps to account for the formation of many of the fragments, especially $C_5H_5TiF_n$ (n = 1, 2) and $C_{19}F_xH_5$ (x = 6, 7), for which there is no metastable evidence.

There was little evidence for straightforward Ti—C cleavage of the heterocyclic system to form the titanocene ion. The latter was detected (*m/e* 178) in very low abundance (~0.08%). Alt and Rausch (31) reported the photochemical cleavage of dimethyl titanocene, zirconocene, and hafnocene. In all cases the methyl groups underwent homolytic cleavage giving rise to methane and a metallocene-type product. Since we do not observe an analogous Ti—C bond cleavage in the case of the titanole which would have resulted in the formation of either $(C_5H_5)_2Ti^+$ or $C_{12}F_8^+$ ions, there must be other stabilizing factors in this system. These may involve Ti-*d*-orbital interaction with the octafluorodibenzo π-system, an increase in ionic resonance energy of the fluorinated titanole, or other factors resulting in an enhanced stabilization (32, 33) (this is supported by the strong parent and parent–HF species observed in the spectrum).

Phosphole Derivatives

All of these compounds have the structure given below (**7**).

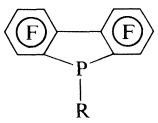

7, R = *t*-C_4H_9, C_6H_5, C_6F_5

The partial mass spectra of these phospholes is given in Table 3 and a general fragmentation scheme is also presented (Scheme 3).

The spectrum of the *tert*-butyl analogue is dominated largely by the stability of the *tert*-butyl cation. As a result, cleavage of the P—C alkyl bond is the major fragmentation mode leaving only a small number of ions of any interest. Despite this, there is still evidence for the operation of fluorine and proton abstraction processes. Proton abstraction from an alkyl substituent is a well-characterized process in the mass spectra of phosphorus compounds (34, 35) and it is seen in the expulsion of butene from the parent ion. The lone example of fluorine abstraction is also common to a number of perfluoroaromatic phosphorus compounds (18, 23).

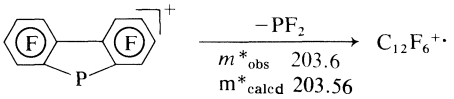

The 5-phenyl- and 5-pentafluorophenyloctafluorodibenzophospholes give rise to a large variety of fluoroaromatic fragments, many of which result from PF_n losses (n = 1, 2, 3). The most obvious of these species are the C_{18} fluoroaromatics which have been detected in a number of other systems including compounds of phosphorus (17–23). These probably have the triphenylene structure indicated below and are a good indication that PF, PF_2, and PF_3 or PHF_2 losses are being experienced by the parent ion. Such transitions can be rationalized in terms of intermediate species which may or may not involve higher coordination by phosphorus.

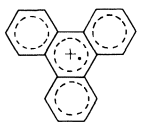

$C_{18}F_{12}$ or $C_{18}F_8H_4$ structure

The influence of the substituent R on parent ion stability is well illustrated in Table 3, reflecting the resonance stabilization for C_6H_5— and C_6F_5— versus the less effective inductive stabilization afforded by the *tert*-butyl group. There seems to be no indication of increased stabilization of the parent through participation of phosphorus in an aromatic π-system. If we compare the 5-phenyl and 5-pentafluorophenyl derivatives with their 'open' analogues, bis(pentafluorophenyl)phenylphosphine and tris(pentafluorophenyl)phosphine, one can see that any conclusions based on dibenzophosphole aromaticity (in particular, increased parent ion stability) are ambiguous (Table 4).

The mass spectrum of 5-phenyloctafluorodibenzophosphole-5-oxide is inconsistent with that of trispentafluorophenylphosphine oxide which only reluctantly shows loss of oxygen (17*b*). The partial mass spectrum, as given in Table 5, indicates a surprisingly large abundance for loss of oxygen, suggesting a

TABLE 3. Abundance of 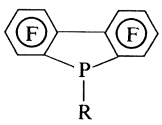

Ion	Abundance		
	R = *t*-C_4H_9	R = C_6H_5*	R = C_6F_5†
$C_{12}F_8PR$	0.6	28.4	22.7
$[C_{12}F_8PR]^{2+}$	—	0.7	2.1
$C_{12}F_8PR—H$	—	2.4	—
$C_{12}F_8PR—CH_3$	1.6	—	—
$C_{12}F_7PR$	—	2.8	3.3
$C_{12}F_8PF_2$	—	—	0.6
$C_{12}F_8PF$	—	—	—
$C_{12}F_8PH$	2.4	0.6	—
$C_{12}F_8P$	14.5	14.0	37.3
$C_{12}F_7PH$	0.9	—	—
$C_{12}F_7P$	—	—	0.5
PF_2	—	0.4	2.9
$C_{18}F_8X_5$	—	0.6	—
$C_{18}F_8X_4$	—	2.3	2.0
$C_{18}F_8X_3$	—	0.4	1.5
$C_{18}F_7X_5$	—	2.5	—
$C_{18}F_6X_4$	—	0.6	0.8
$C_{18}F_5X_5$	—	0.8	—
$C_{18}F_6X_3$	—	—	0.8
$C_{17}F_9$	—	—	0.4
$C_{12}F_8H_2$	0.6	—	—
$C_{12}F_8$	—	—	1.9
$C_{12}F_7H$	0.8	—	—
$C_{12}F_7$	—	—	—
$C_{12}F_6H$	0.6	0.3	—
$C_{12}F_6$	3.2	2.9	9.0
$C_{12}F_5$	—	0.4	1.4
$C_{11}F_5$	—	—	1.6
$C_{11}F_4$	—	0.4	1.7
$C_{11}F_3$	—	0.3	—
R	72.5	22.7	0.5
R − H	1.0	0.6	—
R − 2H	1.3	—	—
R − C_2H_2	—	9.8	—
$C_xF_yH_z$($x < 10$, $y < 6$, $z < 5$)	—	6.1	9.8

*X = H.
†X = F.

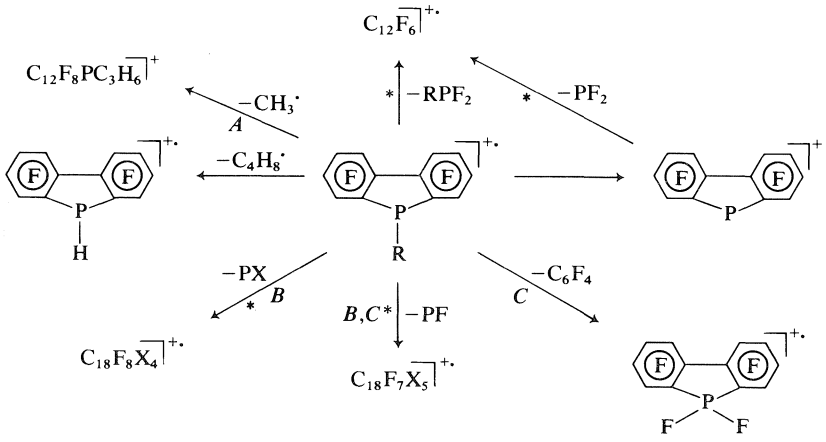

SCHEME 3. *A*, R = *t*C_4H_9; *B*, R = C_6H_5 (X = H); *C*, R = C_6F_5 (X = F); * metastable ions observed.

TABLE 4. Abundance of ions

Ion	Abundance	
	R = C_6H_5	R = C_6F_5
$(C_6F_5)_2PR$	15.7*	42.0*
$(C_6F_5)_2P$	0.3*	16.9*
$(C_{12}F_8)PR$	28.4	22.7
$(C_{12}F_8)P$	14.0	37.3

*Reference 18.

TABLE 5. Partial mass spectrum of $C_{12}F_8P(O)C_6H_5$

Ion	Abundance
$C_{12}F_8POC_6H_5$	11.7
$C_{12}F_8PC_6H_5$	7.3
$C_{12}F_8PO$	2.5
$C_{12}F_8P$	9.6
$C_{18}F_8H_5$*	10.8

*This ion is not observed in the spectrum of 5-phenyloctafluorodibenzophosphole.

strong resonance stability of phosphorus capable of compensating for cleavage of the normally strong phosphorus–oxygen bond. However, the second most abundant species in the spectrum is $C_{18}F_8H_5^+$ which results from expulsion of a PO fragment from the parent ion. This latter behaviour suggests that there could be little, if any, special stabilization of phosphorus in the ring system of the parent species. The fact that P—O cleavage is highly restricted in the fragmentation of many other phosphorus compounds (23, 34, 35) while easily lost in this case is not readily explained.

The anomalous behaviour of the phosphole oxide is not a result of thermal decomposition since it is quite volatile at source temperatures (180°C) below its melting point (189–190°C) (*7b*), using an unheated direct probe.

Summary

We have described previously a large number of cases of rearrangement involving fluorine transfer to the central atom in the mass spectra of perfluoroaromatic compounds, and have attributed this to the possibility of intermediate formation involving expanded co-ordination about a central atom with empty, available *p*- or *d*-orbitals capable of accepting fluorine *p*-electron density. Because the metalloles described in this report already had π-donor ligands (η-C_5H_5) it is highly unlikely that fluorine abstraction could proceed via π-bonded fluoroaromatic intermediates in consideration of the present concepts of bonding orbitals in these systems (36) and the resultant steric restrictions.

Though the mass spectra of the cobalt, rhodium, and iridium compounds give no direct evidence for fluorine transfer, many of the fragmentation products indicate possible neutral atom fluorine losses (see Scheme 1). The titanole, with its greater availability of empty frontier orbitals, shows ample evidence for the operation of fluorine abstraction processes. Since the titanium atom represents a d^0 configuration, one would predict a more favourable situation for overlap and subsequent rearrangement involving empty $(\eta\text{-}C_5H_5)_2Ti$ frontier orbitals than could be attained in the Group VIII complexes where cobalt, rhodium, and iridium have a d^6 configuration.

The obvious presence of suitable orbitals on phosphorus creates a situation where halogen transfer should be facile. This, combined with the fact that phosphorus can expand its co-ordination sphere to accommodate up to six ligands, can rationalize elimination of neutral PF, PF_2, and PF_3 species.

There is no convincing mass spectral evidence for delocalization of the phosphorus lone pair in the dibenzophosphole system, although some results can be explained only in terms of an increased stability of phosphorus in such heterocyclic systems.

The general behaviour for the phosphorus and titanium heterocycles is reminiscent of the Group IV compounds described earlier (*17a*). These all showed loss of MF_n (n = 1–4) species rather than expulsion of the metal atom and as a result gave rise to a variety of tetra-, tri-, and biphenylene species. A further example of comparable behaviour, which is common to the Group VIII metalloles as well, involves the consecutive losses of HF or F· from the basic heterocyclic species[1] to give a whole series of metal containing ions, again in preference to expulsion of the central atom.

In light of these considerations it is reasonable to suggest the operation of mechanisms involving expanded co-ordination about the central atom which is consistent with the rearrangement ions described previously for the Group IV compounds (*17a*).

Acknowledgements

We are most grateful to the Ontario Government for a scholarship (T.R.B.J.), the National Research Council of Canada (J.M.M.), and the National Science Foundation (M.D.R.) for financial support. We also wish to thank Dr. R. D. Chambers for a sample of 5-phenyloctafluorodibenzophosphole 5-oxide.

1. G. WITTIG and W. HERWIG. Chem. Ber. **88**, 962 (1955).
2. H. GILMAN and R. D. GORSICH. J. Am. Chem. Soc. **80**, 1883 (1958).
3. R. GELIUS. Chem. Ber. **93**, 1759 (1960).

[1]This refers to the parent ion in all cases except the Group VIII compounds where the $(M—CO)^+$ species is being considered.

4. J. GOUBEAU, T. KALMAR, and H. HOFMANN. Justus Liebigs Ann. Chem. **659**, 39 (1962).
5. R. KOSTER and G. BENEDIKT. Angew. Chem. Int. Ed. Engl. **2**, 323 (1963).
6. J. J. EISCH and W. C. KASKA. J. Am. Chem. Soc. (*a*) **84**, 1501 (1962); (*b*) **88**, 2976 (1966).
7. R. D. CHAMBERS and D. J. SPRING. J. Organomet. Chem. (*a*) **31**, 13 (1971); (*b*) **31**, 309 (1971).
8. G. WITTIG and A. MAERCKER. Chem. Ber. **97**, 747 (1964).
9. S. C. COHEN and A. G. MASSEY. J. Organomet. Chem. **10**, 471 (1967).
10. S. C. COHEN, M. L. N. REDDY, and A. G. MASSEY. J. Organomet. Chem. **11**, 563 (1968).
11. M. D. RAUSCH and L. P. KLEMANN. Chem. Commun. 354 (1971).
12. M. D. RAUSCH, H. B. GORDON, and E. SAMUEL. J. Coord. Chem. **1**, 354 (1971).
13. S. A. GARDNER, H. B. GORDON, and M. D. RAUSCH. J. Organomet. Chem. **60**, 179 (1973).
14. D. HELLWINKEL, C. WUNSCHE, and M. BACK. Phosphorus, **2**, 167 (1973).
15. L. D. QUIN, J. G. BRYSON, and C. G. MORELAND. J. Am. Chem. Soc. **91**, 3308 (1969).
16. A. N. HUGHES and D. KLEEMOLA. J. Heterocycl. Chem. **13**, 1 (1976).
17. (*a*) G. F. LANTHIER, J. M. MILLER, S. C. COHEN, and A. G. MASSEY. Org. Mass Spectrom. **8**, 235 (1974); (*b*) J. M. MILLER. J. Chem. Soc. A, 828 (1967).
18. A. T. RAKE and J. M. MILLER. J. Chem. Soc. A, 1881 (1970).
19. J. M. MILLER. Can. J. Chem. **47**, 1613 (1969).
20. T. CHIVERS, G. F. LANTHIER, and J. M. MILLER. J. Chem. Soc. A, 2556 (1971).
21. S. C. COHEN, A. G. MASSEY, G. F. LANTHIER, and J. M. MILLER. Org. Mass Spectrom. **6**, 373 (1972).
22. T. R. B. JONES, J. M. MILLER, J. L. PETERSEN, and D. W. MEEK. Can. J. Chem. **54**, 1478 (1976).
23. T. R. B. JONES, J. M. MILLER, and M. FILD. Org. Mass Spectrom. **12**, 317 (1977).
24. R. B. KING. J. Am. Chem. Soc. **89**, 6368 (1967).
25. R. B. KING and T. F. KORENOWSKI. Chem. Commun. 71 (1966).
26. M. I. BRUCE. J. Organomet. Chem. (*a*) **10**, 495 (1967); (*b*) **21**, 415 (1970).
27. M. I. BRUCE. Org. Mass Spectrom. **2**, 997 (1969).
28. D. M. ROE and A. G. MASSEY. J. Organomet. Chem. **17**, 429 (1969).
29. M. J. MAYS and R. N. F. SIMPSON. J. Chem. Soc. A, 1936 (1967).
30. M. D. RAUSCH, P. S. ANDREWS, and S. A. GARDNER. Organomet. Chem. Synth. **1**, 289 (1971).
31. H. ALT and M. D. RAUSCH. J.Am. Chem. Soc. **96**, 5936 (1974); J. Organomet. Chem. **141**, 299 (1977).
32. P. M. TREICHEL and F. G. A. STONE. Adv. Org. Chem. **1**, 178 (1964).
33. M. D. RAUSCH. Trans. N.Y. Acad. Sci. Ser. II, **28**, 611 (1966).
34. H. BUDZIKIEWICZ, C. D. JERASSI, and D. H. WILLIAMS. Mass spectrometry of organic compounds. Holden-Day, San Francisco. 1969. Chapt. 26.
35. R. G. GILLIS and J. L. OCCOCLOWITZ. Analytical chemistry of phosphorus compounds. *Edited by* M. Halmann. Interscience, New York. 1972. Chapt. 6.
36. J. W. LAUHER and R. HOFFMANN. J. Am. Chem. Soc. **98**, 1729 (1976).

The interaction between the excited triplet state of ketones and olefins: the role of triplet exciplexes[1]

RAFIK O. LOUTFY

Xerox Research Centre of Canada Ltd., 2480 Dunwin Drive, Mississauga, Ont., Canada L5L 1J9

AND

S. K. DOGRA[2] AND R. W. YIP

Division of Chemistry, National Research Council of Canada, Ottawa, Ont., Canada K1A 0R6

Received April 25, 1978

RAFIK O. LOUTFY, S. K. DOGRA, and R. W. YIP. Can. J. Chem. **57**, 342 (1979).

The quenching of triplet acetone in degassed acetonitrile solution by electron-rich and electron-deficient olefins has been measured by flash emission technique. With the exception of fumaronitrile, the efficiency of quenching of triplet ketones by olefins is not determined by the triplet energy of the ketone, but by the ability of the excited ketone to donate or accept electrons. The results are consistent with the assumption that back dissociation of the triplet exciplex is an important process in the overall reaction and accounts for quenching rate constants which are less than those for diffusion-controlled reactions. Lifetimes and binding energies of the triplet exciplexes have been estimated.

RAFIK O. LOUTFY, S. K. DOGRA et R. W. YIP. Can. J. Chem. **57**, 342 (1979).

Faisant appel à la technique de l'émission éclair, on a mesuré le piégeage de l'acétone à l'état triplet, en solution dans de l'acétone dégazée, par des oléfines riches et déficitaires en électrons. A l'exception du furamonitrile, l'efficacité du piégeage de cétones à l'état triplet par des oléfines n'est pas déterminée par l'énergie triplet de l'acétone mais plutôt par la capacité de la cétone excitée à donner ou à accepter des électrons. Les résultats sont en accord avec l'hypothèse que la redissociation de l'exciplex triplet est un processus important de la réaction globale et qu'il tient compte des constantes de vitesse de piégeage qui sont plus faibles que celles de réactions contrôlées par diffusion. On a évalué les temps de vie et les énergies de liaison des exciplex triplets.

[Traduit par le journal]

Introduction

The interaction of electronically excited ketone triplet states with ground state amines (1), olefins (2), aromatic and aliphatic hydrocarbons (3) in a process not involving electronic energy transfer has attracted considerable interest in the past decade. Consequences of such interaction are enhanced radiationless decay, chemical reactions, and electron transfer resulting in ion formation. These processes can be represented by the following general scheme.

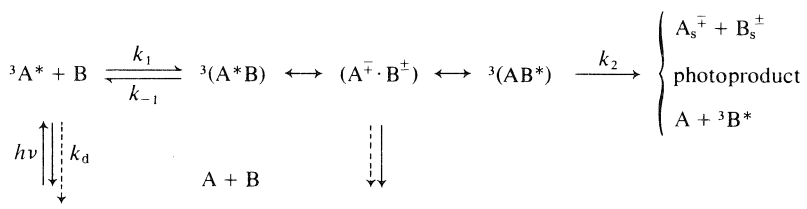

The interaction between triplet ketones and (electron-rich) olefins proceeds via a complex (exciplex) with weak charge-transfer character (2*a*, 2*c*) in which the ketone acts as an acceptor. In the case of triplet benzophenone interacting with 2-butene and isobutylene, isotopic and kinetic results suggest that the complexes are formed irreversibly (2*c*, 3*d*). Whether the conclusion applies to other or all triplet exciplexes has not yet been established. With electron-deficient olefins, such as chloroethylenes, the major quenching process has been suggested to be triplet energy transfer (2*a*, 2*c*) rather than charge transfer from ketone to the electron-deficient quencher, such as has been postulated to account for the quenching of ketones by substituted benzenes (3*b*). Thus, in terms of the above scheme, k_{-1} is considered to be negligible, as is the con-

[1]NRCC No. 17067.

[2]NRCC Postdoctorate Fellow.

0008-4042/79/030342-06$01.00/0

TABLE 1. Quenching rate constants of acetone, butyrophenone, and benzophenone triplet by substituted olefins

Quencher	IP[a] (eV)	k_q (M^{-1} s^{-1}) × 10^{-7} Acetone[b]	Butyrophenone[b]	Benzophenone[c]
Electron-rich olefins				
1-Ethoxy-1-butene	8.00	11.0	—	—
2,3-Dimethyl-2-butene	8.30	5.1	46.0	89.5
2-Methyl-2-butene	8.68	2.8	14.0	36.0
Cyclooctene	8.82	2.2	8.2	—
Cyclohexene	8.95	1.0	4.2	5.7
Norbornene	8.95	4.3	3.7	4.0
Cyclopentene	9.01	1.9	5.2	—
cis-2-Pentene	9.11	1.0	5.1	8.0
Electron-deficient olefins				
Fumaronitrile	11.0	650	580	120
Tetrachloroethylene	9.32	68.5	145	—
Trichloroethylene	9.45	42.0	72	—
trans-Dichloroethylene	9.66	18	40	1.3
Dienes				
cis-1,3-Pentadiene	8.68	400	500	500

[a]Photoionization values taken from ref. 12.
[b]This work, determined in acetonitrile using flash emission techniques.
[c]See ref. 2*b*, k_q's determined in benzene.

tribution of A^+B^- and the formation of $A + {}^3B^*$ via an exciplex. At present, owing to the absence of reported exciplex phosphorescence in solution, no information is available on the binding energy or lifetime of ketone–olefin triplet exciplexes.

We report here the results of the quenching of triplet acetone by olefins which are pertinent to the question of involvement of charge transfer complexation in the quenching of electron-deficient olefins, and the reversibility of ketone–olefin exciplex formation. In addition, we put forward calculations to provide a semi-quantitative estimation of the binding energies and lifetimes of ketone–olefin exciplexes.

Results and Discussion

The luminescent decay of triplet acetone in degassed acetonitrile solutions was measured by flash emission technique described earlier (4). The rate constants for quenching triplet acetone by a series of substituted olefins and the relevant values for quenching triplet butyrophenone (2*b*) and benzophenone (2*c*) are recorded in Table 1. Table 2 lists the dependence on temperature and the rate constants for quenching of triplet acetone by norbornene.

Quenching of triplet acetone by the formation of an intermediate π-type complex (exciplex) with partial charge transfer from electron-rich quenchers (1-ethoxy-1-butene and alkyl substituted olefins) is indicated by (*1*) the high rate constants, (*2*) the good correlation of log k_q with $IP_{quencher}$, and (*3*), the value of the slope of the plot of log k_q vs. $IP_{quencher}$ relative to that for a full electron-transfer reaction (5). The value of the slope, -0.072 kcal^{-1} mol (1.7 eV^{-1}), is ~10% of that for full electron transfer ($(2.303RT)^{-1} = 0.74$ kcal^{-1} mol (17 eV^{-1})) (5), and is in excellent agreement with the values reported by Schore and Turro (2*d*) for the quenching of singlet and triplet acetone by alkoxyethylenes.

TABLE 2. Quenching of acetone phosphorescence by norbornene in acetonitrile

Temperature (K)	k_q × 10^{-7a} (M^{-1} s^{-1})
273	3.63
291	3.87
297	4.16

[a]Determined from three points; errors estimated to be ±10%.

In a previous study on the quenching of triplet butyrophenone by chloroethylenes, Kochevar and Wagner (2*a*) observed that triplet butyrophenone (E_T 74.5 kcal mol^{-1}) was more rapidly quenched by *cis*-dichloroethylene than was triplet benzophenone (E_T 68.5 kcal mol^{-1}), and that the rate of triplet quenching by *cis*-dichloroethylene (IP 9.66 eV) was significantly higher than that by the alkylethylenes (IP ≤ 9.11 eV). On the basis of these results, it was concluded that energy transfer was the major quenching process, since both charge transfer complexing and radical addition would be slowed by

TABLE 3. Dependence of quenching rate constant on ($E_{1/2}^{ox} - E_T$) of ketone and $E_{1/2}^{red}$ of chloroethylenes

Ketone	E_T[a] (eV)	$E_{1/2}^{ox}$ (V)	$E_{1/2}^{ox} - E_T$ (eV)	$k_q \times 10^{-7}$ (M^{-1} s^{-1}) $Cl_2C{=}CCl_2$ (1.38)[b,c]	$Cl_2C{=}CHCl$ (1.64)[b,c]	*trans*-ClCH=CHCl (1.90)[b,c]
Acetone	3.36	2.59[a]	−0.77	68.5	42	18
Butyrophenone[e]	3.13	2.34[d]	−0.79	145	72	40
Benzophenone[e]	2.97	2.37[a]	−0.60			1.3

[a]Calculated values (ref. 13).
[b]$-E_{1/2}^{red}$ (V), ref. 14. The values given have been converted to acetonitrile as solvent.
[c]Values of $E_{1/2}^{ox}$ of the quenchers are: tetrachloroethylene 2.25 V, trichloroethylene 2.37 V, and dichloroethylene 2.55 V, calculated from their IP (ref. 15).
[d]Taken to be similar to the measured value for acetophenone (ref. 16).
[e]Rate constants, ref. 3*d*.

increasing chloro substitution (2*a*). A similar conclusion was reached for the quenching of triplet benzophenone by dichloroethylene (2*c*). In the present work, the rate constants obtained for the quenching of triplet acetone (E_T 76 kcal mol^{-1}) by the chloroethylenes (Table 1) are lower than that for butyrophenone. These results are clearly incompatible with a triplet energy transfer mechanism. We believe that the quenching of triplet ketones by the chloroethylenes is best explained by means of a complex with charge transfer character in which the direction of electron transfer is opposite that for the electron-rich olefins: i.e., in which the ketone is the donor and the chloroethylene is the acceptor.

The consideration of CT interaction obviously necessitates that the direction of transfer be determined. Based on arguments used previously to determine the relative energies of two possible donor–acceptor pairs (3*b*), we have as a condition for the pair with the lowest energy, in solution, the inequality,

$$(E^{ox} + E^{red})_{acceptor} > (E^{ox} + E^{red})_{donor}$$

Calculations based on the above inequality using the data recorded in Tables 1 and 3 show that the donor–acceptor pair with the lowest energy is that in which acetone is the donor and the chloroethylene is the acceptor. The conclusion that A^+B^- is important in the description of the exciplex formed between acetone (A) and the chloroethylene (B) provides a rationale for two features exhibited by the quenching results: (*1*) the absence of a correlation between log k_q and IP of the chloroethylenes, and (*2*) the correlation of log k_q with reduction potentials of the chloroethylenes (2*e*). The importance of 'reverse' electron transfer in the quenching of triplet ketones by the chloroethylenes is further emphasized by the correlation between log k_q and the excited ketone electron donating ability ($E^{ox} - E_T$) rather than with ketone triplet energy (see Table 2). For two triplet ketones, the relative magnitude of the rate constants for quenching by a given chloroethylene is

$$\frac{k_{q_1}}{k_{q_2}} = \frac{\exp -(E_{1/2}^{ox} - E_T)_1/RT}{\exp -(E_{1/2}^{ox} - E_T)_2/RT}$$

For example, the calculated value for acetone and butyrophenone is $k_{q(acetone)}/k_{q(butyrophenone)} = 0.46$ which falls within the experimental values of 0.45–0.58.

The rapid quenching of ketone triplets by fumaronitrile can be attributed to direct energy transfer. Consistent with this conclusion, k_q decreases from acetone to benzophenone, that is, with decreasing ketone triplet energy.

The quenching rate constants of triplet ketones by olefins are slower than those of diffusion-controlled processes. This could be due to the occurrence of reversible exciplex formation. In the case of α-cyanonaphthalene–olefin exciplexes, Ware *et al.* (6) have shown that reversible exciplex formation can lead to an observed quenching rate constant, k_q, significantly slower than the rate of exciplex formation, k_1.

In terms of the reaction scheme which we have put forward, the question is how important is k_{-1} relative to k_2. The experimental quenching rate constant k_q is given by

$$[1] \qquad k_q = \frac{k_1 k_2}{k_{-1} + k_2}$$

and therefore the experimental activation energy can be expressed in terms of the activation energies corresponding to k_{-1}, k_1, and k_2. In the event that $k_{-1} \geq k_2$, the presence of the term $-\Delta H_C$ (where ΔH_C is the binding energy of the complex) will tend to give a lower experimental activation energy than if it were absent. This is most readily seen in the case of $k_{-1} \gg k_2$, and $k_q = (k_1/k_{-1})k_2 = K_c k_2$ where $K_c = k_1/k_{-1}$. We have $E_q = -\Delta H_C + E_2$. In the extreme, where $\Delta H_C > E_2$, the observed activation energy, E_q, can even be negative (3*c*, 7, 8). There is one other case to be considered, that is the situation

TABLE 4. Slopes of log vs. IP or $E_{1/2}^{red}$ for quenching of ketone triplets by olefins

Triplet ketone	Quencher	Slope (kcal^{-1} mol)	Solvent	$b^{2\,c}$	Reference
Acetone(A)	alkylethylenes(D)	-0.072^a	CH_3CN	0.1	This work
Acetone(A)	alkoxyethylenes(D)	-0.065^a	CH_3CN	0.09	2*d*
Acetone(D)	chloroethylenes(A)	0.06^b	CH_3CN	0.08	This work
Butyrophenone(A)	olefins(D)	-0.047^a	Benzene	0.065	2*b*
Butyrophenone(D)	olefins(A)	0.045^b	Benzene	0.06	2*b*
Benzophenone(A)	olefins(D)	-0.036^a	Benzene	0.05	2*c*

[a] $\Delta \log k_q/\Delta IP$.
[b] $\Delta \log k_q/\Delta E_{1/2}^{red}$.
[c] b^2 = slope/0.74 kcal^{-1} mol, where 0.74 is the slope for full electron transfer.

TABLE 5. Data on exciplex formation between acetone[a] triplet state and electron-rich olefins (donor) in acetonitrile

Quencher	$E_{1/2}^{ox\,b}$ (V)	$E_{(A^-D^+)}{}^c$ (eV)	$E_{EX}{}^d$ (eV)	ΔG^{0e} (eV)	$k_q(10^7)$ (M^{-1} s^{-1})	K^f (M^{-1})	ΔH (eV)
1-Ethoxy-1-butene	0.78	2.985	3.32	−0.037	11.0	4.13	−0.27
2,3-Dimethyl-2-butene	1.16	3.365	3.36	0.00	5.1	0.98	−0.23
2-Methyl-2-butene	1.64	3.845	3.41	0.048	2.8	0.16	−0.186
Cyclooctene	1.81	4.025	3.43	0.066	2.2	0.08	−0.17
Cyclohexene	1.94	4.185	3.44	0.082	1.0	0.044	−0.15
Norbornene	1.82	4.025	3.43	0.066	4.3	0.08	−0.17
Cyclopentene	2.05	4.255	3.45	0.089	1.9	0.034	−0.14
cis-2-Pentene	2.18	4.385	3.46	0.102	1.0	0.021	−0.13

[a] $E_{1/2}^{red}$ = 2.3 V, ref. 13.
[b] Calculated from the correlation 1.27IP − 9.38 relating to IP of olefins to $E_{1/2}^{ox}$ (15).
[c] Calculated from eq. [2*a*].
[d] The triplet exciplex energy calculated according to $E_{EX} = b^2E_{CT}{}^0 + (1 - b^2)E_T$, where $b^2 = 0.1$.
[e] The free energy change for exciplex formation = $E_{EX} - E_T$.
[f] $K = \exp(-G^0/RT)$.

where $k_2 \gg k_{-1}$, and $k_q = k_1 < k_D$, where k_D is the diffusion-controlled rate constant. In this case, $E_q \geq E_D$ (~2–4 kcal mol^{-1} (9)) unless the Arrhenius factor associated with k_1 is low. The activation energy which we have obtained from the temperature-dependent quenching of triplet acetone by norbornene is 0.8 kcal mol^{-1}. In this instance, back dissociation of the exciplex is probably an important process.

For full charge transfer involving the reaction of an excited molecule, the free energy for the reaction is given by (5)

$$[2] \qquad \Delta G^0 = E_{CT}{}^0 - E^* \qquad \text{where}$$

$$[2a] \qquad E_{CT}{}^0 = E_D{}^{ox} - E_A{}^{red} - e^2/\varepsilon r$$

E^* is the excited (triplet) state energy, and ε is the dielectric constant of the solvent. The solvation energy of the CT complex is small compared with the terms in eq. [2*a*] (or implicit in eq. [2*a*]), and has been neglected. In acetonitrile (ε = 36), the term $e^2/\varepsilon r$ assumes a value of 0.1 eV for r = 3.4 Å. Although the value of $e^2/\varepsilon r$ changes with the ε of the solvent, this change is offset by an equal change in the values of E^{ox} and E^{red} with the ε of the solvent. In essence, this means that the total coulomb energy comprised of the 'mutual solvation energy' $e^2/\varepsilon r$ (that is, the coulomb energy arising from A^- and D^+ separated by a slab of dielectric, ε, at a distance r), and the solvation energies of D^+ and A^- (incorporated in E^{ox} and E^{red}) is constant. In a high dielectric solvent such as water, the coulomb energy between D^+ and A^- is negligibly small compared with the solvation energies of the ions D^+ and A^- in water. The converse applies in the case of a low dielectric constant solvent.

Similarly, the ΔG^0 for exciplex formation, in which partial charge transfer is involved, is given by

$$[3] \qquad \Delta G^0 = b^2(E_{CT}{}^0 - E^*)$$

where b^2 is the fraction of the electron transferred from donor to acceptor molecule, and can be obtained from the slope of log k_q vs. IP of the donor (2*d*, 3*d*). Values of b^2, ΔG^0, ΔH, and K are listed in Tables 4 and 5. The enthalpy of formation of the exciplex, ΔH ($\Delta H = \Delta G^0 + T\Delta S$) was calculated taking $\Delta S = -18.2$ eu (5*b*).

Triplet exciplex lifetimes and binding energies can be deduced from the quenching data if a number of assumptions are made. One of these is the assumption that exciplex reversal is important.

Since the values of ΔG^0 listed in Table 6 are all positive, with the exception of quenching with 1-ethoxy-1-butane, it is expected that the rate of exciplex reversal, k_{-1}, will be large. Assuming that $k_{-1} \gg k_2$, k_q reduces to

$$[4] \qquad k_q = (k_1/k_{-1})k_2 = Kk_2$$

The equilibrium constant K can be calculated from the free energy change for exciplex formation. Knowing K, we can calculate k_2 from the measured values of k_q using eq. [4].

To obtain the rate constant for exciplex reversal, k_{-1}, the rate constant for exciplex formation (k_1) is calculated and then substituted into the equation $k_1/k_{-1} = K$. The rate constant for exciplex formation can be written as

$$[5] \qquad k_1 = A_1 \exp(-\Delta G^{\ddagger}/RT)$$

where A_1 ($\sim 10^{11}\ M^{-1}\ s^{-1}$) (10) is the collision frequency between neutral molecules in solution. For reactions between unchanged species, the free energy of activation, $\Delta G^{\ddagger}$, for outer-sphere electron transfer can be expressed in terms of the standard free energy of the reaction, ΔG^0, according to (10)

$$[6] \qquad \Delta G^{\ddagger} = \frac{\lambda}{4}\left(1 + \frac{\Delta G^0}{\lambda}\right)^2$$

where λ is the solvent reorganization energy. For weak complexes with only partial charge transfer, the solvent reorganization parameter can be estimated to be 7.5 kcal/mol from the equation (11):

$$[7] \qquad \lambda = \frac{e^2}{2a}\left(\frac{1}{\varepsilon_o} - \frac{1}{\varepsilon_s}\right)$$

In eq. [7], e is the unit electron charge, $2a$ is the internuclear separation between the reactants, assumed to be 11 Å (11) for the acetone complexes, ε_o and ε_s are the optical and static dielectric constants of the solvent, respectively. The rates of exciplex formation, k_1, were calculated using eqs. [5] and [6], and found to approach the rate of diffusion-limited processes, while the rate of reversal, k_{-1}, were obtained from the ratio $k_1/k_{-1} = K$. Values of k_1, k_{-1}, and k_2 are recorded in Table 6. The values of k_{-1} are an order of magnitude greater than k_1 in most cases, in spite of the fact that ΔH is negative. This is due to the positive ΔS for the reversal. The values of k_1 and k_{-1} for the system are dependent on the accuracy of the term λ used in eq. [5], and A_1 used in eq. [6], and thus are by no means absolute. For example, in Fig. 1 plots of log k_1 against ΔG^0 correspond to (*a*), λ = 7.5 kcal/mol and (*b*), λ = 11.8 kcal/mol. A small change in λ had a significant effect on the calculated rate constant k_1. Nonetheless, the results allow us to estimate that the triplet exciplex lifetimes $\tau_{EX} = 1/(k_{-1} + k_2)$ is less than a nanosecond, in most cases. The extremely short exciplex lifetime is consistent with the lack of emission from these complexes. Similar analysis could be carried out for triplet ketones quenching by electron-deficient olefins.

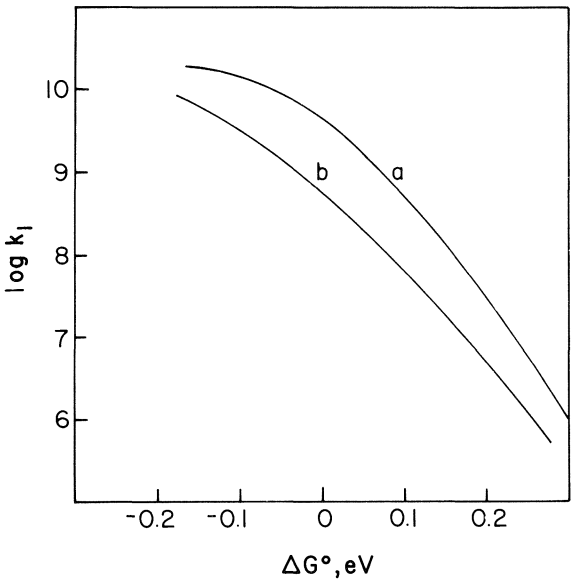

FIG. 1. Plot of log k_1 against ΔG^0; $Z = 10^{11}\ M^{-1}\ s^{-1}$. (*a*) λ = 7.5 kcal mol^{-1}, (*b*) λ = 11.8 kcal mol^{-1}.

TABLE 6. Calculated rate constants of: formation (k_1), reversal (k_{-1}), reaction (k_2), and lifetime for triplet acetone/olefin exciplexes

Quencher	$k_1(10^8)$ ($M^{-1}\ s^{-1}$)	$k_{-1}(10^9)$ (s^{-1})	$k_2(10^7)$ (s^{-1})	τ_{EX} (ns)
1-Ethoxy-1-butene	85.7	2.08	2.67	0.47
2,3-Dimethyl-2-butene	43.8	4.47	5.23	0.22
2-Methyl-2-butene	16.3	10.2	17.55	0.1
Cyclooctene	10.8	13.5	27.56	0.07
Cyclohexene	7.42	16.8	22.72	0.06
Norbornene	10.8	13.5	53.75	0.07
Cyclopentene	6.26	18.4	55.96	0.05
cis-2-Pentene	4.5	21.6	50.0	0.045

In summary, this study indicates that triplet acetone quenching by olefins involves the formation of a partial charge transfer complex or exciplex. With the exception of fumaronitrile, the efficiency of quenching of triplet ketones by olefins is not determined by the triplet energy of the ketone, but by the ability of the excited ketone to donate or accept electrons. The data are consistent with the assumption that back dissociation of the triplet exciplex is an important process in the overall reaction and accounts for quenching rate constants which are less than those for diffusion-controlled reactions. Life-

times and binding energies of the triplet exciplexes have been estimated.

Acknowledgements

The authors are grateful to Professor M. Winnik (University of Toronto), Dr. K. Zachariasse (Max-Planck Institute, Gottingen), Professor P. Wagner (Michigan State), and Dr. R. Menzel (Xerox Research of Canada) for their useful comments.

1. (*a*) S. G. COHEN, A. PAROLA, and G. H. PARSONS. Chem. Rev. **73**, 141 (1973) and references therein; (*b*) R. W. YIP, R. O. LOUTFY, Y. L. CHOW, and L. K. MAGDZINSKI. Can. J. Chem. **50**, 3426 (1972).
2. (*a*) I. E. KOCHEVAR and P. J. WAGNER. J. Am. Chem. Soc. **92**, 5742 (1970); (*b*) I. E. KOCHEVAR and P. J. WAGNER. J. Am. Chem. Soc. **94**, 3859 (1972); (*c*) R. A. CALDWELL, G. W. SOVOCOOL, and R. P. GAJEWSKI. J. Am. Chem. Soc. **95**, 2549 (1973); (*d*) N. E. SCHORE and N. J. TURRO. J. Am. Chem. Soc. **97**, 2482 (1975); (*e*) R. O. LOUTFY, R. W. YIP, and S. K. DOGRA. Tetrahedron Lett. 2843 (1977).
3. (*a*) D. I. SCHUSTER, T. M. WEIL, and A. M. HALPERN. J. Am. Chem. Soc. **94**, 8248 (1972); (*b*) R. O. LOUTFY and R. W. YIP. Can. J. Chem. **51**, 1881 (1973); (*c*) C. STEEL, L. GIERING, and M. BERGER. J. Am. Chem. Soc. **97**, 953 (1974); (*d*) P. J. WAGNER and R. A. LEAVITT. J. Am. Chem. Soc. 3669 (1973); (*e*) G. PORTER, S. K. DOGRA, R. O. LOUTFY, S. E. SUGAMORI, and R. W. YIP. J. Chem. Soc. Faraday Trans. I, **69**, 1462 (1973).
4. G. PORTER, R. W. YIP, J. M. DUNSTON, A. J. CESSNA, and S. E. SUGAMORI. Trans. Faraday Soc. **67**, 3149 (1971).
5. (*a*) D. REHM and A. WELLER. Ber. Bunsenges. Phys. Chem. **73**, 834 (1969); (*b*) H. KNIBBE, D. REHM, and A. WELLER. Ber. Bunsenges. Phys. Chem. **73**, 839 (1969).
6. W. R. WARE, D. WATT, and J. D. HOLMES. J. Am. Chem. Soc. **96**, 7853 (1974).
7. B. STEVENS and P. J. MCCARTIN. Mol. Phys. **3**, 425 (1960).
8. O. L. CHAPMAN and R. D. LURA. J. Am. Chem. Soc. **92**, 6352 (1970).
9. R. LIVINGSTON and W. R. WARE. J. Chem. Phys. **39**, 2593 (1963).
10. (*a*) R. H. MARCUS. J. Chem. Phys. **43**, 6761 (1975); (*b*) D. MEISEL. Chem. Phys. Lett. **34**, 263 (1975).
11. M. J. POWERS, D. J. SALMON, R. W. CALLAHAN, and T. J. MEYER. J. Am. Chem. Soc. **98**, 6731 (1976).
12. L. G. CHRISTOPHOROU. Atomic and molecular radiation physics. *Edited by* J. B. Birks and S. P. McGlynn. Wiley Interscience. 1971.
13. R. O. LOUTFY and R. O. LOUTFY. J. Phys. Chem. **77**, 336 (1973).
14. C. K. MANN and K. K. BARNES. Electrochemical reactions in non-aqueous systems. Marcel Dekker, New York. 1970.
15. L. L. MILLER, G. D. NORDBLOM, and E. A. MAYEDA. J. Org. Chem. **37**, 916 (1972).
16. D. R. ARNOLD and A. J. MARONTIS. J. Am. Chem. Soc. **98**, 5931 (1976).

Isomeric cyclic $[C_6H_{10}]^{+\cdot}$ ions. The energy barrier to ring opening

PEDER WOLKOFF AND JOHN L. HOLMES
Chemistry Department, University of Ottawa, Ottawa, Ont., Canada K1N 9B4

Received August 21, 1978

PEDER WOLKOFF and JOHN L. HOLMES. Can. J. Chem. **57**, 348 (1979).

Appearance energies and metastable peak shapes for methyl loss from the molecular ions of cyclohexene, methylcyclopentenes, methylenecyclopentane, bicyclo[3.1.0]hexane, and 2-methyl-1,4-pentadiene indicate that they have a common reaction pathway which produces [cyclopentenium]$^+$ as the daughter ion at threshold.

From measurements of appearance energies and from relative peak abundances and kinetic energy releases for the metastable losses of $CH_3^\cdot$ and labelled methyl from the deuterium labelled cyclic $[C_6H_{10}]^{+\cdot}$ molecular ions it was concluded that: (*a*) H/D mixing in [cyclohexene]$^{+\cdot}$ occurs in the intact ring prior to a concerted methyl extrusion; (*b*) [methylcyclopentenes]$^{+\cdot}$ loses methyl without *any* H/D mixing at or near to threshold by a straight C—C cleavage, possibly via the 3-isomer. Methyl losses involving H/D mixing are preceded by ring opening which has an activation energy of ca. 1 eV. However, [cyclopentenium]$^{+\cdot}$ is again the daughter ion; (*c*) methylenecyclopentane and bicyclo[3.1.0]hexane molecular ions isomerize to methylcyclopentenes prior to methyl loss.

H/D mixing (prior to methyl loss) in the molecular ion 1,1-$^2H_2$-2-methyl-1,4-pentadiene takes place before cyclisation to methylcyclopentene.

PEDER WOLKOFF et JOHN L. HOLMES. Can. J. Chem. **57**, 348 (1979).

Les énergies d'apparition et les formes des pics métastables dus à la perte de méthyles par les ions moléculaires du cyclohexène, de méthylcyclopentènes, du méthylènecyclopentane, du bicyclo[3.1.0]hexane et du méthyl-2 pentadiène-1,4 indiquent qu'elles procèdent par un chemin réactionnel commun qui fournit le [cyclopentènium]$^+$ comme ion-fille au seuil.

A partir des mesures des énergies d'apparition, des abondances relatives des pics et des énergies cinétiques émises lors des pertes de $CH_3^\cdot$ et de méthyles marqués provenant d'ions moléculaires $[C_6H_{10}]^{+\cdot}$ cycliques marqués au deutérium, on a conclu que: (*a*) le mélange H/D dans le [cyclohexène]$^{+\cdot}$ se produit dans le cycle intact avant l'expulsion concertée d'un groupe méthyle; (*b*) les [méthylcyclopentènes]$^{+\cdot}$ perdent un méthyle sans mélange H/D au niveau ou près du seuil par une rupture C—C simple possiblement par l'isomère-3. Des pertes de méthyles impliquant des mélanges H/D sont précédées par une ouverture de cycle accompagnée d'une énergie d'activation d'environ 1 eV. Toutefois le [cyclopenténium]$^{+\cdot}$ est à nouveau l'ion-fille; (*c*) les ions moléculaires du méthylène cyclopentane et du bicyclo[3.1.0]-hexane s'isomérisent en méthylcyclopentènes avant de perdre un méthyle.

Le mélange H/D (précédant une perte de méthyle) dans l'ion moléculaire $^2H_2$-1,1 méthyl-2 pentadiène-1,4 se produit avant la cyclisation en méthylcyclopentène.

[Traduit par le journal]

Introduction

Eight years ago (1) it was written that "the mass spectra of the alkenes is one of the most obscure chapters of mass spectrometry". Since then the picture has become less obscure, largely due to the development of experimental methods for studying ion fragmentations in well defined time frames (2) (e.g. metastable ion studies (3) and field ionisation kinetics (4) (F.I.K.)) and the introduction of collisional activation (C.A.) (5) as a method for inducing ion fragmentation. These techniques, combined with isotopic labelling (6), have led to the identification of reacting configurations of fragmenting ions, daughter ion structures, and, in some cases, where good thermochemical data are available, to the identification of the neutral fragment's structure as well (7).

Experiments on isomers of the hydrocarbons C_3H_6 (8), C_4H_8 (9–12), C_5H_8 (13), C_5H_{10} (11, 14, 15), and C_6H_{12} (11, 14, 15) have employed the above methods and although much has been learned concerning possible mechanisms for the interconversion of isomers prior to fragmentation and daughter ion structures, the complete loss of positional identity of C and H atoms among molecular ions of lifetimes greater than about 10^{-9} s often makes it difficult to draw unequivocal conclusions.

In a recent study of the isomeric octenes (16), it was concluded that the molecular ions had isomerised to a common structure (or structures) in less than 10^{-9} s. However, at times shorter than 10^{-10} s, the decomposing molecular ions retained their structural integrity and decomposed by specific mechanisms.

A F.I.K. study (17) of methylcyclopentane-α-^{13}C revealed that on the picosecond time scale, loss of

0008-4042/79/030348-07$01.00/0

methyl involved only the labelled group. At longer times (10^{-6} s) loss of $CH_3^{\bullet}$ and C_2H_4 was preceded by ring opening and randomisation of C atoms. Levsen *et al.* (18) have also investigated the behavior of cyclo-alkane molecular ions. 3-, 4-, and 5-membered rings were shown to open within 10^{-9} s to yield the corresponding 1-alkene molecular ions. 6-, 7-, and 8-membered rings were, however, found to remain intact prior to fragmentation from the pico- to micro-second time frames.

Comparatively little work has been reported on the isomeric C_6H_{10} hydrocarbons, with the exception of cyclohexene. The latter was thoroughly investigated by Derrick *et al.* in a F.I.K. study (19) of 3,3,6,6-$^2H_4$-cyclohexene. The methyl loss was envisaged as a ring contraction leading to a methylenecyclopentane-like ion which readily lost $CH_3^{\bullet}$ yielding [cyclopentenium]$^+$. Rapid 1,3-allylic H atom shifts were proposed to take place around the cyclohexene ring, leading to the loss of positional identity of H atoms; this was found to begin within 10^{-11} s and was complete by 10^{-9} s. Ausloos and co-workers (20) studied some ion–molecule reactions of molecular ions of cyclohexene, and 1-, 3-, and 4-methylcyclopentene produced by 10 eV photons and explained their results on the basis that these molecular ions of low internal energy content did not undergo appreciable rearrangement. However, Levsen and Hilt (21) concluded from their study of the C.A. mass spectra of cyclohexene, 1-methylcyclopentene, 3-methyl-1,2-pentadiene, 2-methyl-2,3-pentadiene, and 1-hexyne that the non-fragmenting molecular ions of these isomers have partially isomerised (but to different extents) in the first μs after ionisation.

The thermochemistry of C_6H_{10} isomers has been investigated by Winters and Collins (22) and more recently by Lossing and Traeger (14). The latter authors conclusively showed that at threshold, the $[C_5H_7]^+$ daughter ion from cyclohexene has the [cyclopentenium]$^+$ structure; this they showed to be the most stable $[C_5H_7]^+$ ion, (ΔH_f = 199 kcal mol^{-1}) with [dimethylcyclopropenium]$^+$ as the probable nearest $[C_5H_7]^+$ isomer (ΔH_f(estimated) = 217 kcal mol^{-1}). The very low ΔH_f for [cyclopentenium]$^+$ makes methyl loss the fragmentation of lowest activation energy, and so can account for m/z = 67 being the base peak in the compiled mass spectra of almost all C_6H_{10} isomers (23).

In this paper we report an investigation of the energetics and metastable ion characteristics of deuterium labelled cyclohexene, the methylcyclopentenes, methylenecyclopentane, and bicyclo[3.1.0]-hexane. The aim of the present work was to re-examine the behaviors of these cyclic C_6H_{10} isomers with respect to their fragmentation of lowest energy requirement, namely the loss of $CH_3^{\bullet}$, in order to understand better the earlier conclusions of Derrick *et al.* (19) and Levsen and Hilt (21).

Results

(1) Thermochemistry and Kinetic Energy Release for Metastable Fragmentations

The heats of formation, ΔH_f, of the molecular ions of cyclohexene, 1- and 3-methylcyclopentene, methylenecyclopentane, bicyclo[3.1.0]hexane, and 2-methyl-1,4-pentadiene and their corresponding $[C_5H_7]^+$ (methyl radical loss) daughter ions are presented in Table 1. Ionization (IE) and appearance energies (AE) were measured for us by Lossing using energy selected electrons (14, 24). The kinetic energy releases measured from the half-height widths of the metastable peaks, ($T_{0.5}$) for the fragmentations taking place in the first field-free region of a Kratos AEI MS 902S Mass Spectrometer, are also given in Table 1. The ΔH_f values for the molecular ions show that 1-methylcyclopentene is the most stable species. (This is to be expected, cf. $[CH_3—CH{=}CH—CH_2CH_3]^{+\bullet}$, ΔH_f = 198 kcal mol^{-1} and $[CH_3CH{=}C(CH_3)_2]^{+\bullet}$, ΔH_f = 190 kcal mol^{-1}) (25). The daughter ions $[C_5H_7]^+$ all have ΔH_f values corresponding to the cyclopentenium cation, the most stable $[C_5H_7]^+$ ion. The slightly higher value for bicyclo[3.1.0]hexane could be ascribed to a kinetic shift. Within experimental error, the $T_{0.5}$ values are considered to be essentially the same for all compounds and indeed the normalized metastable peaks (which are of Gaussian shape) are almost superimposable. From these data it is concluded that the six isomers fragment via a common transition state to yield [cyclopentenium]$^+$ as daughter ion.

(2) Deuterium Labelling Experiments

The metastable peak abundances and $T_{0.5}$ values for the losses of $CH_3^{\bullet}$ and deuterated methyl radicals from variously labelled cyclic C_6H_{10} molecular ions are shown in Table 2.

1-Deuterio and 1,3,3-Trideuterio Cyclohexenes

The metastable peak abundances for these deuterated cyclohexenes are close but not equal to those for random statistical positional mixing of H and D prior to fragmentation. It is, however, noteworthy that the relative daughter ion abundances (i.e. for ions generated at short times (<0.1 μs) in the ion source from high energy molecular ions) are in the exact random statistical ratio. These metastable peak observations are in agreement with those of Derrick *et al.* (19) on 3,3,6,6-$^2H_4$-cyclohexene. These authors found, in a field ionization kinetics experiment, that

TABLE 1. Heats of formation[a] of some $[C_6H_{10}]^{+\cdot}$ ions and $[C_5H_7]^+$ ions and the kinetic energy release ($T_{0.5}$) associated with the formation of the latter

Compound	$\Delta H_f(M^{+\cdot})$ (± 1.5 kcal mol^{-1})	$\Delta H_f[C_5H_7]^+$ (± 1.5 kcal mol^{-1})	$T_{0.5}$ (± 0.9 meV)
	205	201	17.5
	197	200	17.2
	208	199	17.1
	204	200[b]	17.9
	223	203[c]	16.0
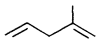	228	200[d]	18.1

[a]Reference 14.
[b]This work, IE = 8.70 eV, AE = 10.02 eV (± 0.05).
[c]This work, IE = 9.28 eV, AE = 9.88 eV (± 0.05).
[d]AE = 9.40 eV.

TABLE 2. Metastable peak abundance ratios (peak heights) and $T_{0.5}$ values (meV) for CH_xD_{3-x} loss from labelled C_6H_{10} molecular ions*

Compound		$CH_3^{\cdot}$	$T_{0.5}$	$CH_2D^{\cdot}$	$T_{0.5}$	$CHD_2^{\cdot}$	$T_{0.5}$	$CD_3^{\cdot}$	$T_{0.5}$
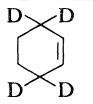	(19)	1.0 (1.0)		2.17 (2.18)		1.17 (1.36)			
		2.33 (2.33)	16.8	0.82 (1.0)	17.1				
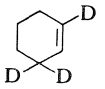		1.67 (1.67)	15.2	3.05 (3.00)	16.1	0.80 (1.0)	15.8	0.03 (0.05)	
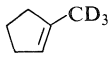		1.67 (1.67)	30	2.79 (3.00)	33	1.44 (1.0)	31	7.9 (0.05)	15.5
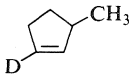		8.02 (2.33)	15.8	1.0 (1.0)	33.0				
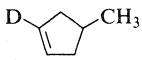		4.3 (2.33)	18.4	1.0 (1.0)	32.2				
		7.0 (7.00)	32±2	7.35 (7.00)	32±2	4.76 (1.0)	13±1.5		
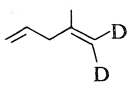		25 (7.00)	17.7	6 (7.00)	31.3	1.0 (1.0)	28.3		

*Values in parentheses are for random distribution of H and D. $T_{0.5}$ values ± 1.0 meV or less, except where indicated.

on the picosecond time scale the $^2H_4$ molecular ion predominantly lost CD_2H.

The $T_{0.5}$ values (Table 2) for the various methyl radical losses are, within experimental error, the same as that for the unlabelled molecule. Furthermore, the AE values for *m/z* 67 and 68 from the monodeuterio species were the same, 10.30 and 10.32 ± 0.05 eV, respectively.

1-Trideuteriomethylcyclopentene

The metastable peak abundance ratios for the various methyl losses from this compound are clearly far from statistical (Table 2).

The major loss is $CD_3^\cdot$, 57% (random statistical proportion 0.8%), but the metastable peaks for the losses of $CH_3^\cdot$, $CH_2D^\cdot$, and $CD_2H^\cdot$ have relative abundances quite close to the random ratios. At a nominal ionising electron energy of 20 eV the metastable peak for $CD_3^\cdot$ loss comprises 71% of the methyl loss and for the ion-source generated daughter ions (normal mass spectrum) this proportion rises to 80%.

The kinetic energy releases ($T_{0.5}$) for the metastable peaks are substantially different. For $CD_3^\cdot$ loss the $T_{0.5}$ value (15.5 meV) is slightly lower than that for the unlabelled compound (17.2 meV) while the other methyl loss peaks have $T_{0.5}$ values about twice as large (31 meV). The appearance energies of the daughter ions *m/z* 67, 69, and 70 (corresponding to losses of $CD_3^\cdot$, $CH_2D^\cdot$, and $CH_3^\cdot$) were measured using energy selected electrons (24) and were found to be 10.27, 11.18, and 11.18 eV (all ±0.05 eV), respectively. Thus the apparent heats of formation of the daughter ions were 200, 223, and 223 kcal mol^{-1}, respectively. A measurement of AE *m/z* 68 was not attempted because of interference from the ^{13}C contribution from *m/z* 67.

1-Deuterio-3-methylcyclopentene and 2-Deuterio-4-methylcyclopentene

The metastable peak abundances for losses of $CH_3^\cdot$ and $CH_2D^\cdot$ from these two labelled molecular ions are significantly different and neither is close to the ratio for random loss (Table 2). The 3-methyl compound (methyl at allylic position) shows a greater relative loss of $CH_3^\cdot$ than the 4-methyl isomer. Loss of $CH_3^\cdot$:$CH_2D^\cdot$ from the former increases from 8:1 (metastable peaks) to 12:1 (daughter ions, normal mass spectrum) and for the latter from 4.3:1 to 7:1, respectively. The kinetic energy releases for these two compounds show a behavior very similar to that of the trideuteriomethyl analogue. The difference in appearance energies (AE *m/z* 68 − AE *m/z* 67) was not accurately measured with energy selected electrons but was estimated to be not less than 1.0 eV from the AE values for the metastable peaks (semi-log plots, MS 902S Mass Spectrometer). This is essentially in agreement with the observations on the trideuteriomethyl compound.

α,α-*Dideuteriomethylenecyclopentane*

The metastable peak characteristics for this compound are similar to those for 3-trideuteriomethylcyclopentene, with loss of $CHD_2^\cdot$ predominant and having a low $T_{0.5}$, and with $CH_2D^\cdot$ and $CH_3^\cdot$ losses having larger $T_{0.5}$ values and relative abundances close to the random ratio.

1,1-Dideuterio-2-methyl-1,4-pentadiene

Metastable loss of $CH_3^\cdot$ is the major process here and the overall results ($T_{0.5}$ values and relative abundances) show similar trends to those of the 5-membered ring isomers.

Discussion

Cyclohexene

We propose that prior to fragmentation at or close to the thermochemical threshold for methyl loss, the cyclohexene molecular ion *irreversibly* isomerises to that of a methylcyclopentene (possibly the 3-isomer). (The intermediacy of alkadiene molecular ions can be ruled out on energetic grounds (26).) The above rearrangement is unlikely to be reversible for the following reasons: (*a*) whereas loss of C_2H_4 generates an important peak at *m/z* 54 and also gives rise to an intense metastable peak in the mass spectrum of cyclohexene (via a retro-Diels Alder reaction), it is of negligible intensity in the mass spectra of 1- or 3-methylcyclopentenes; (*b*) direct cleavage of the methyl group from methyl substituted cyclopentenes, *without loss of positional identity of labelled atoms*, is clearly the predominant threshold process (Table 2).

The atom mixing observed in labelled cyclohexene molecular ions must therefore take place in the six-membered ring prior to the loss of a methyl group. This H/D atom mixing in labelled cyclohexenes has adequately been explained by Derrick *et al.* (19) who proposed a series of 1,3-allylic hydrogen atom shifts. The same authors found that at the shortest times investigated ($\sim 10^{-11}$ s) the major methyl loss from —3,3,6,6-$^2H_4$-cyclohexene was $CHD_2^\cdot$. Ring *opening* by breaking a vinylic C—C bond is an energetically unfavourable process (27) and so a concerted extrusion similar to that proposed by Derrick *et al.* (19) is illustrated below.

[1]

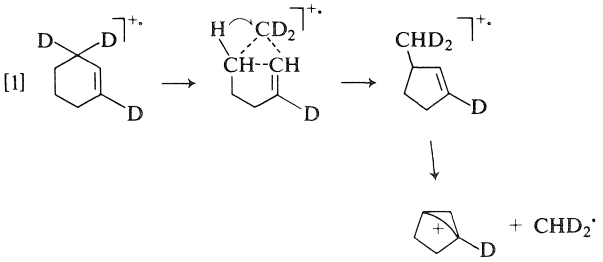

It is worthwhile to emphasize that neutral cyclohexene, under a variety of experimental conditions, readily isomerises to 1-methylcyclopentene (28).

Methylcyclopentenes

The AE and metastable peak measurements (Table 2) clearly demonstrate that at or near to threshold the methyl substituent is lost without any appreciable prior mixing of H/D between the ring and the methyl group. The results also indicate that 3-methylcyclopentene may well be the favoured reacting configuration, i.e. in which the methyl group occupies the allylic position.[1] This is seen by comparing the losses of $CH_3^{\cdot}$ from the monodeuterated 3- and 4-methylcyclopentenes with $CD_3^{\cdot}$ loss from the 1-trideuteriomethyl analogue (Table 2).

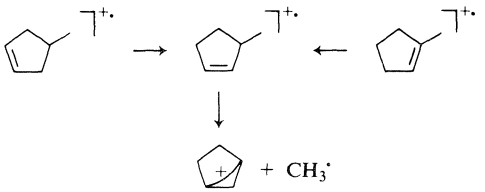

[2]

The methyl losses associated with the mixing of H/D have an AE 1.0 eV higher than that for the threshold methyl loss from the unlabelled molecule. However, these fragmentations are accompanied by a much larger kinetic energy release (31 meV) than that for the simple methyl cleavage reaction (15.5 meV). The apparent ΔH_f for the (labelled) $[C_5H_7]^+$ daughter ion, 223 kcal mol^{-1} is equal to that for the 3-vinylallyl cation (14), but the large kinetic energy release for that metastable decomposition leads us to suggest that this daughter ion is not being generated. We propose that the daughter ion is again [cyclopentenium]$^+$ and that the excess energy, 1.0 eV, represents that required to open the cyclopentene ring. The *acyclic* ion then undergoes rapid H/D randomisation and fragments to yield [cyclopentenium]$^+$ with the excess internal energy (required for ring opening) being partitioned into translational energy of the products. The only other feasible daughter ion (on thermochemical grounds) is the dimethylcyclopropenyl cation, whose ΔH_f has been estimated (14) to be $\sim$217 kcal mol^{-1}. We would argue that this is an improbable reaction product on the following grounds. We suggest that the partitioning of the excess internal energy of these various decomposing ions can adequately be evaluated for comparative purposes, by the semi-empirical equation of Haney and Franklin (29).

$$\varepsilon^{\ddagger} \simeq 0.44(3n - 6)T_{ave}$$

where $\varepsilon^{\ddagger}$ is the excess internal energy of a fragmenting ion available for partitioning among $(3n - 6)$ degrees of freedom (non-linear ion consisting of n atoms) and T_{ave} is the average translational energy acquired by the daughter ion. The average translational energies for the ions generated by the high and low AE methyl losses were evaluated from their respective kinetic energy release distributions obtained by analysis of the metastable peak shapes (30) and were 110 and 55 meV respectively. The difference in these values, 55 meV, substituted in the above equation yields the difference in average internal energies of the fragmenting metastable ions ($\Delta\varepsilon^{\ddagger} = 0.44 \times 42 \times 0.055 = 1.0$ eV) and is equal to the measured difference in AE values for the two processes. It is not possible specifically to identify the proposed ring-opened ion with any of the isomeric methylpentadiene or hexadiene molecular ions because (with the exception of 2-methyl-1,4-pentadiene) they all display different ΔH_f and $T_{0.5}$ values for $[C_5H_7]^+$ formation (26). The present results do not indicate whether the proposed ring closure takes place before or during the methyl radical loss.

Methylenecyclopentane and Bicyclo[3.1.0]hexane

The results shown in Table 2 indicate that the major loss of $CHD_2^{\cdot}$ from the molecular ion of the α,α-$^2H_2$ compound takes place from ionized (dideuteriomethyl)-cyclopentene, perhaps following a simple 1,3 hydrogen shift. This isomerisation also cannot be a reversible process, by analogy with the behavior of the methylcyclopentenes.

We propose that the bicyclic isomer also fragments via a methylcyclopentene molecular ion.[2]

2-Methyl-1,4-pentadiene

The daughter ion for loss of $CH_3^{\cdot}$ from the 1,1-$^2H_2$ compound clearly results in the main from the generation of [cyclopentenium]$^+$ (Tables 1 and 2). We propose that prior to this loss of methyl, ring closure to a methylcyclopentene molecular ion takes place rapidly (an exothermic reaction) without an activation energy. Molecular ions having greater than 1 eV excess internal energy (above the threshold for cyclopentenium plus methyl) do not ring close prior to methyl loss but yield cyclopentenium as daughter ion with positional randomisation of label atoms. These high energy ions decompose over the same potential surface as that for the ring opened cyclic molecular ions, hence the high T values for $CH_2D^{\cdot}$ and $CHD_2^{\cdot}$ losses. Nevertheless, there must be some positional mixing of H and D in the low energy process because the AE for m/z 67, 68, and 69 are the same (within experimental error) as that for $[C_5H_7]^+$ generated

[1]Methylenecyclopentane, 1-, 3-, and 4-methylcyclopentenes equilibrate in the presence of acidic alumina (250°C) to a mixture having proportions 1:80:13:6 respectively (37).

[2]Thermolysis of this compound yields 1-methylcyclopentene (38).

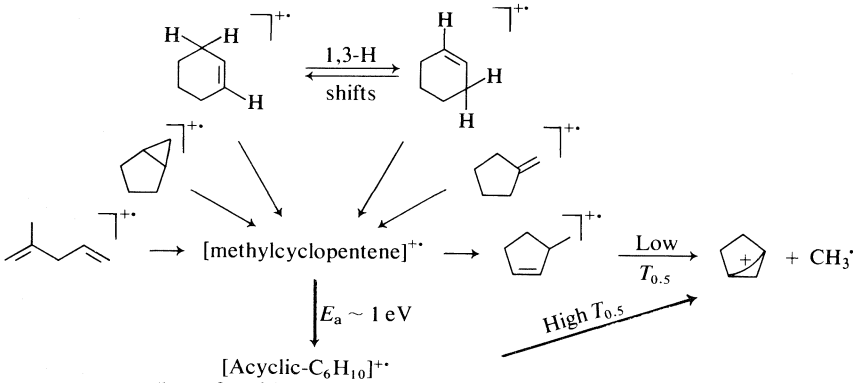

SCHEME 1

from the unlabelled molecule. A possible mechanism (which does not incorporate H/D mixing prior to ring closure) is shown below:

[3] 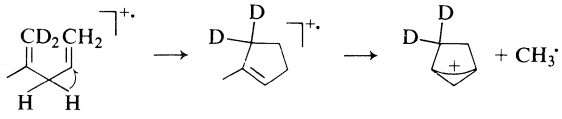

The general behavior of acyclic C_6H_{10} molecular ions will be discussed in detail elsewhere (26).

Summary

The mechanistic conclusions drawn from the above results are shown in Scheme 1 which illustrates the processes leading to loss of $CH_3^{\bullet}$ from various $[C_6H_{10}]^{+\bullet}$ isomers. All fragmenting cyclic molecular ions of low internal energy lose methyl without ring opening and yield the cyclopentenium cation; H/D mixing in labelled cyclohexenes occurs prior to the extrusion reaction [1]. Methylcyclopentenes lose methyl from low internal energy molecular ions by direct cleavage *without* prior mixing of H/D between the ring and the methyl group. A second methyl loss process, having an AE ~1 eV above the minimum energy for methyl loss, leads to almost complete loss of positional identity among H/D atoms prior to this higher energy fragmentation. For this process it is suggested that ring opening imposes the energy barrier but the $[C_5H_7]^+$ daughter ion is again proposed to be the cyclopentenium cation.

The above energy requirement for ring opening may usefully be compared with that for cycloalkanes. The energy required to open a cycloalkane ring has been estimated to be 0.1 eV or less (14, 31). Levsen *et al.*, from a recent collisional activation study of cycloalkanes, agreed that the energy barrier to ring opening was certainly below the lowest decomposition threshold and could not exceed 0.1 eV. It should also be noted that many of the isomeric acyclic $[C_6H_{12}]^{+\bullet}$ ions have lower heats of formation (14) than [cyclohexane]$^{+\bullet}$ or [methylcyclopentane]$^{+\bullet}$, ring opening and rearrangement for the latter are then exothermic processes. In contrast, the methylcyclopentenes and cyclohexene molecular ions have lower ΔH_f values than almost all their acyclic isomers (14, 26), and so analogous rearrangements would be endothermic.

Experimental Section

Metastable peak measurements were performed on a Kratos AEI MS 902S mass spectrometer operating under conditions of good energy resolution, as described previously (8). Sample pressures were 3–5 × 10^{-7} Torr. Energy releases ($T_{0.5}$) values were calculated in the usual way (3) with appropriate corrections for the width of the main beam and overlapping contributions from (natural abundance) ^{13}C processes.

Unlabelled compounds were purchased from Chem. Samples Co., isomeric purity better than 99%. Bicyclo[3.1.0]-hexane was prepared by a Simmon–Smith reaction (32), and purified by glc.

All labelled compounds were purified by pglc, columns were either silver nitrate – ethylene glycol on Chromosorb PAW (60–80 mesh) (33) or 20% carbowax 20M on Chromosorb WAW (60–80 mesh); structures and position of deuterium were confirmed by 100 MHz ^1H nmr.

Cyclohexene-1-$^2H_1$ was prepared by reduction of cyclohexanone with $LiAlD_4$, followed by dehydration of the alcohol in hexamethylphosphoric triamide (34) (98% $^2H_1$).

Cyclohexene-1,3,3-$^2H_3$ was made similarly starting with cyclohexanone-2,2,4,4-$^2H_4$ (97% $^2H_3$ and 3% $^2H_2$).

3-Methylcyclopentene-1-$^2H_1$ and 4-methylcyclopentene-2-$^2H_1$ were prepared by reduction of 3-methylcyclopentanone, followed by dehydration of the alcohol (34) (98% $^2H_1$).

1-Trideuteriomethylcyclopentene was prepared according to Bailey and Hale (35) using CD_3MgI (> 96% $^2H_3$).

Methylenecyclopentane-α,α-$^2H_2$ was made by a Wittig reaction using Ph_3PCD_3I and butyl lithium (~41% $^2H_2$, 43% $^2H_1$).

2-Methyl-1-4-pentadiene-1,1-$^2H_2$ (36) was a gift from Professor R. G. Miller (96% $^2H_2$).

Acknowledgements

This work was supported by the National Research Council of Canada. One of us (P.W.) acknowledges the receipt of a travel grant from the Danish National Science Research Council. We are

grateful to Professor R. G. Miller for a donation of 2-methyl-1,4-pentadiene-1,1-$^2H_2$. We also thank Dr. D. Tong for the preparations of cyclohexene-1-$^2H_1$ and cyclohexene-1,3,3-$^2H_3$. We thank Dr. J. Krause for assistance with the metastable peak measurements.

Finally, we especially wish to acknowledge our gratitude to Dr. F. P. Lossing for providing us with the thermochemical measurements which were so vital to the successful completion of this study, and for many stimulating discussions.

1. A. Maccoll and A. Loudon. *In* The chemistry of the alkenes. *Edited by* J. Zabicky. Wiley Interscience, New York. 1970. p. 356.
2. M. L. Gross (*Editor*). High performance mass spectrometry: chemical applications. Am. Chem. Soc. Symposium Series 70, Am. Chem. Soc. Washington, 1978. Chapts. 1–5.
3. R. G. Cooks, J. H. Beynon, R. M. Caprioli, and G. R. Lester. Metastable ions. Elsevier, Amsterdam. 1973.
4. P. J. Derrick. *In* International review of science, physical chemistry. Ser. 2, Vol. 5. *Edited by* A. Maccoll. Butterworths, London. 1975. Chapt. 1.
5. K. Levsen and H. Schwarz. Angew. Chem. Internat. Ed. **15**, 504 (1976).
6. J. L. Holmes. *In* International review of science, physical chemistry. Ser. 2, Vol. 5. *Edited by* A. Maccoll. Butterworths, London. 1975. Chapt. 6.
7. J. L. Holmes, J. K. Terlouw, and F. P. Lossing. J. Phys. Chem. **80**, 2860 (1976).
8. J. L. Holmes and J. K. Terlouw. Org. Mass Spectrom. **10**, 787 (1975).
9. R. P. Morgan and P. J. Derrick. Org. Mass Spectrom. **10**, 563 (1975).
10. T. Nishishita, F. M. Bockhoff, and F. W. McLafferty. Org. Mass Spectrom. **12**, 16 (1977).
11. K. Levsen and J. Heimbrecht. Org. Mass Spectrom. **12**, 131 (1977).
12. J. L. Holmes, G. M. Weese, A. S. Blair, and J. K. Terlouw. Org. Mass Spectrom. **12**, 424 (1977).
13. J. L. Holmes. Org. Mass Spectrom. **8**, 247 (1974).
14. F. P. Lossing and J. C. Traeger. Int. J. Mass Spectrom. Ion Phys. **19**, 9 (1976).
15. T. Nishishita and F. W. McLafferty. Org. Mass Spectrom. **12**, 75 (1977).
16. F. Borchers, K. Levsen, H. Schwarz, C. Wesdemiotis, and H. U. Winkler. J. Am. Chem. Soc. **99**, 6359 (1977).
17. A. M. Falick and A. L. Burlingame. J. Am. Chem. Soc. **97**, 1525 (1975).
18. F. Borchers, K. Levsen, H. Schwarz, C. Wesdemiotis, and R. Wolfshutz. J. Am. Chem. Soc. **99**, 1716 (1977).
19. P. J. Derrick, A. M. Falick, and A. L. Burlingame. J. Am. Chem. Soc. **94**, 6794 (1972).
20. R. Lescaux, S. Searles, L. Wayne Sieck, and P. Ausloos. J. Chem. Phys. **54**, 3411 (1971).
21. K. Levsen and E. Hilt. Liebigs Ann. Chem. 257 (1976).
22. R. E. Winters and J. H. Collins. Org. Mass Spectrom. **2**, 299 (1969).
23. A. Cornu and R. Massot. Compilation of mass spectral data. 2nd ed. Vol. 1. Heyden, London. 1975.
24. K. Maeda, G. P. Semeluk, and F. P. Lossing. Int. J. Mass Spectrom. Ion Phys. **1**, 395 (1968).
25. H. M. Rosenstock, K. Draxl, B. W. Steiner, and J. T. Herron. Energetics of gaseous ions. J. Phys. and Chem. Ref. Data, Vol. 6. Suppl. 1. 1977.
26. J. L. Holmes, P. Wolkoff, and F. P. Lossing. To be published.
27. F. W. McLafferty. Interpretation of mass spectra. 2nd ed. Benjamin, Reading. 1973.
28. H. Adkins and A. K. Roebuck. J. Am. Chem. **70**, 4041 (1948).
29. M. A. Haney and J. L. Franklin. J. Chem. Phys. **48**, 4093 (1968).
30. J. L. Holmes and A. D. Osborne. Int. J. Mass Spectrom. Ion Phys. **23**, 189 (1977).
31. R. F. Pottie, A. G. Harrison, and F. P. Lossing. J. Am. Chem. Soc. **83**, 3204 (1961).
32. R. J. Rawson and F. T. Harrison. J. Org. Chem. **35**, 2057 (1970).
33. J. Shabtai, J. Herling, and E. Gil-Av. J. Chromatog. **2**, 406 (1959).
34. R. T. Monson. Tetrahedron Lett. 567 (1971).
35. W. J. Bailey and W. F. Hale. J. Am. Chem Soc. **81**, 651 (1959).
36. H. J. Golden, D. J. Baker, and R. G. Miller. J. Am. Chem. Soc. **96**, 4235 (1974).
37. J. Herling, J. Shabtai, and E. Gil-Av. J. Am. Chem. Soc. **87**, 4107 (1965).
38. H. M. Frey and R. C. Smith. Trans. Faraday Soc. **58**, 697 (1962).

The conformational preference and barrier to internal rotation of an equatorial 3,5-dichlorophenyl group by the *J* method. Derivatives of cyclohexane, 1,3-dithiane, 1,3-dioxane, and 1,3-dioxolane

TED SCHAEFER, WALTER NIEMCZURA, AND WERNER DANCHURA
Department of Chemistry, University of Manitoba, Winnipeg, Man., Canada R3T 2N2

Received July 28, 1978

TED SCHAEFER, WALTER NIEMCZURA, and WERNER DANCHURA. Can. J. Chem. **57**, 355 (1979).

We report the preparation and the analysis of the phenyl ring proton magnetic resonance spectra of 3,5-dichlorophenylcyclohexane and of the 2-(3,5-dichlorophenyl) derivatives of 1,3-dioxane, 1,3-dithiane, and 1,3-dioxolane. With the exception of the dioxolanes these compounds exist predominantly as the equatorial isomers. The *J* method is used to show that the phenyl moiety prefers the conformation in which the α C—H bond lies in the phenyl plane. The predominantly twofold barriers to rotation about the carbon–carbon bond between the two ring systems are 2.0 ± 0.3, 0.4 ± 0.2, 2.2 ± 0.3, 0.85 ± 0.3 kcal/mol for these compounds, in the order given above. The low value for the barrier in the 1,3-dioxane derivative agrees reasonably well with molecular mechanics calculations and with the results of calorimetric and X-ray studies on equatorial 2-phenyl-1,3-dioxane.

TED SCHAEFER, WALTER NIEMCZURA et WERNER DANCHURA. Can. J. Chem. **57**, 355 (1979).

On rapporte la préparation et l'analyse des spectres de résonance magnétique nucléaire des protons des noyaux phényles du dichloro-3,5 phénylcyclohexane et des dérivés (dichloro-3,5 phényl)-2 du dioxanne-1,3 du dithianne-1,3 et du dioxolanne-1,3. A l'exception des dioxolannes, ces composés existent préférentiellement sous la forme d'isomères équatoriaux. On a utilisé la méthode *J* pour montrer que la portion phényle préfère la conformation dans laquelle la liaison C—H α se trouve dans le plan du phényle. Les barrières, principalement binaires, à la rotation autour de la liaison carbone–carbone entre les deux systèmes cycliques sont de 2.0 ± 0.3, 0.4 ± 0.2, 2.2 ± 0.3 et 0.85 ± 0.3 kcal/mol pour ces composés dans l'ordre cité. La faible valeur pour la barrière, dans le dérivé dioxanne-1,3, est en bon accord avec des calculs de mécanique moléculaire et avec les résultats d'études calorimétriques et de diffraction de rayons-X sur le phényl-2 dioxanne-1,3 équatorial.

[Traduit par le journal]

Introduction

The free energy difference between axial and equatorial conformers has been tabulated for many derivatives of cyclohexane, 1,3-dithiane, and of 1,3-dioxane (1, 2). Again, activation parameters for the inversion of the parent compounds, and some of their derivatives, have been measured by a variety of methods (2, 3). The classical nmr line-shape study of the inversion in cyclohexane (4) depended on the dephasing of magnetization as spin magnetic moments are transferred between sites of different Larmor frequencies (T_2 effects).

More recently, molecular mechanics calculations (5) and calorimetric techniques (6) have been used to tackle the determination of the stable conformers of, and of the barrier to internal rotation in, 2-phenyl-1,3-dioxane and lead to the conclusion that the rotation is essentially free in the equatorial isomer. Even if the barrier magnitude is not zero but comparable to kT, it is evident that the nmr line-shape methods will not be applicable. The lowest energy of activation ascertained by these methods stands at 4.2 kcal/mol (7).

However, another nmr technique may apply here. We have recently shown that reasonable values of small barriers to internal rotation can be derived from long-range spin–spin coupling constants over six formal bonds. This approach recognizes that ${}^6J_p^{H,CH}$, the coupling between a *para* proton in the benzene ring and a proton bound to the alpha carbon, varies as $\sin^2\theta$. The dihedral angle θ is defined by the $C_1C_2C_\alpha H$ fragment in **1**. One may write an equation

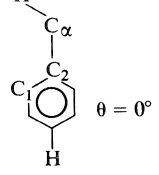

1

somewhat analogous to that of Heller and McConnell (8)

0008-4042/79/030355-05$01.00/0

[1] $$^6J_{obs} = {}^6J_o + {}^6J_{90}\langle\sin^2\theta\rangle$$

where $^6J_{90}$ is the value of ^6J at $\theta = 90°$ and $\langle\sin^2\theta\rangle$ is the expectation value of $\sin^2\theta$, an average over the populated rotational states. The maximum magnitude of ^6J occurs at $\theta = 90°$, as expected for a σ–π spin–spin coupling mechanism (sometimes called a hyperconjugative interaction) in which information about the unpaired electron density, induced in the σ C—H bond by the proton magnetic moment, is transmitted via the π electrons to the site of the *para* carbon atom and then to the *para* proton by spin polarization.

Such a mechanism implies $^6J < 0$. In toluene, $^6J_p^{H,CH}$ is -0.62 Hz (9) and, if the σ–π mechanism is operative, $^7J_p^{CH_3,CH_3}$ in *p*-xylene should equal $-{}^6J_p^{H,CH_3}$ in toluene, as it does (10, 11). The $\sin^2\theta$ dependence is supported by INDO MO FPT calculations (12). The barrier in toluene is only 0.014 kcal/mol (13), so that $\langle\sin^2\theta\rangle$ is 0.5 (essentially free rotation) and $^6J_{90}$ is therefore -1.24 Hz.

One test of the $\sin^2\theta$ dependence involves 2,6-dichloroethylbenzene where **2** is favored by at least 5 kcal/mol. Therefore $\langle\sin^2\theta\rangle$ must be close to 0.25 because θ lies near 30°. Hence $^6J_p^{H,CH_2}$ is predicted to be $-1.24/4$, or -0.31 Hz. Indeed, it is observed as -0.29 ± 0.02 Hz in benzene solution (14). The ring substituents and the methyl group apparently do not greatly perturb the $\sin^2\theta$ dependence of ^6J.

The rotation about the bond between the phenyl ring and the ethyl group can be treated as a hindered rotor problem in a manner similar to that employed by McClung and co-workers (15). Assuming a twofold hindering potential, e.g., in ethylbenzene V_2 is the energy difference between **2** and **3**, and an

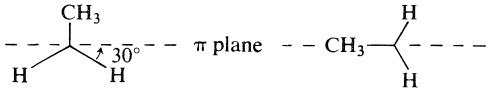

2 **3**

unperturbed basis set of 11 lowest free rotor functions eventually yields $\langle\sin^2\theta\rangle$ as a function of V_2 and of the reduced moment of inertia at a given temperature.

Application to 3,5-dibromoethylbenzene, chosen because a precise analysis of a very tightly coupled ring proton spectrum is unobtainable, gave $V_2 =$ 1.2 kcal/mol (16), in excellent agreement with a recent thermodynamic value of 1.16 kcal/mol (17). Conformer **2** is the most stable according to the ^6J method, in line with low resolution microwave data (18).

Some other examples, particularly appropriate to this paper, include isopropylbenzene, phenylcyclopropane, and styrene. The *J* method finds the 'bisected' conformation **4** as stable for the first two compounds (19, 20) and, assuming **5** as the high

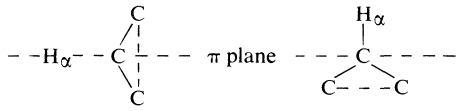

4 **5**

energy form and a twofold barrier, a V_2 of 2.0 kcal/mol for both. The *J* method yields 1.6 kcal/mol for V_2 in styrene (21), assuming a planar ground state, in reasonable agreement with a Raman value of 1.78 kcal/mol (22).

All these results assume a negligibly small ^6J_o in [1]. A test of this assumption for toluene is the result above, viz. $^6J_p^{H,CH_3} = -{}^7J_p^{CH_3,CH_3}$. Another test is that $^6J_p^{H,CH_2} = -{}^7J_p^{CH_2,CH_3}$ in 2,6-dichlorobenzyl bromide and its 4-methyl derivative.[1] Furthermore, the recent measurement of the internal barrier to rotation in benzyl cyanide derivatives (23) implies that $^6J_p^{H,CH}$ in 3,5-dibromoisopropylbenzene should be 0.03 Hz larger in magnitude than $^7J_p^{CH,CH_2}$ in *p*-isopropylbenzyl cyanide, as it is,[1] if the $\sin^2\theta$ mechanism is operative to the exclusion of a J_o component. These tests encompass a number of preferred θ values and strongly suggest that the J_o term in [1] is negligibly small.

In this paper, the *J* method is applied to the determination of the low energy conformations and of the barrier to internal rotation about the carbon–carbon bond between the two rings in R-cyclohexane, **6**; 2-R-1,3-dithiane, **7**; 2-R-1,3-dioxane, **8**; and 2-R-1,3-dioxolane, **9**; where R is the 3,5-dichlorophenyl substituent. The chlorine substituents at the *meta* positions allow an accurate determination of the relevant spectral parameters. There is no evidence that these substituents are significant perturbers of the ^6J values or of the conformational preferences to be discussed below.

Results and Discussion

Spectral Analysis

The ring proton spectra are the AB_2 subspectra of AB_2X spectra, where X is the proton on the carbon atom bonded to the aromatic group. The X proton in these compounds resonates at a frequency sufficiently different from the other alkyl protons, such that an AB_2X analysis represents an accurate approach. Figure 1 displays the observed *para* proton resonance of the dioxolane derivative, illustrating the spectral quality. Table 1 reports the results of the analyses,

[1]T. Schaefer, R. Sebastian, and L. Shengwai. Unpublished results.

TABLE 1. Chemical shifts and coupling constants for the 3,5-dichlorophenyl group in **6–9**

Parameter	Value			
	6[a]	**7**[b]	**8**[a]	**9**[a]
$\nu_2 = \nu_6$[c]	687.586(5)	729.792(3)	739.270(8)	729.053(4)
ν_4[c]	704.515(5)	719.423(3)	708.483(6)	709.202(4)
ν_a[c]	206.7	498.2	498.5	542.9
$^4J_m^{H,H}$	1.911(6)[d]	1.908(4)	1.98(7)	1.967(5)
$^4J_o^{H,CH\alpha}$	−0.576(11)	−0.481(6)	−0.727(16)	−0.572(8)
$^6J_p^{H,CH\alpha}$	−0.233(11)[e]	−0.218(7)	−0.399(11)	−0.329(5)
rms deviation	0.013	0.007	0.012	0.010

[a]10 mol% solution in benzene-d_6.
[b]10 mol% solution in CS_2.
[c]In Hz at 100.001 MHz to low field of internal tetramethylsilane.
[d]Coupling constants in Hz; numbers in parentheses give standard deviations in the last place.
[e]The coupling was the same in a CS_2 solution. In C_6D_6 solution the 10 other cyclohexyl protons resonated to high field of $\delta = 1.3$ ppm.

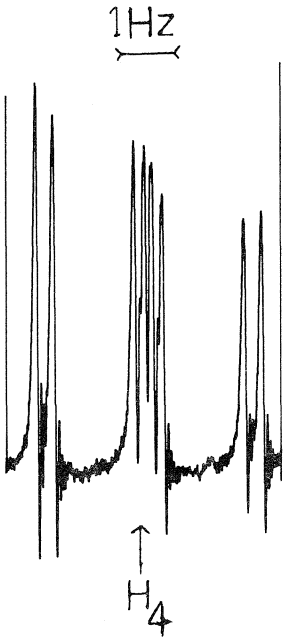

FIG. 1. The ^{1}H nmr spectrum at 100 MHz and 305 K of the *para* proton in a 10 mol% solution in benzene-d_6 of 2-(3,5-dichlorophenyl)-1,3-dioxolane. The spectrum was recorded at a sweep rate of 0.01 Hz/s and displays linewidths at half height of 0.10 ± 0.01 Hz. The outer doublets are split by 0.33 ± 0.01 Hz (repeated runs).

performed with the computer program LAME (24, 25).

Of course, it would have been preferable to analyze the spectra of compounds not containing chlorine substituents in the ring. Unlike phenylcyclopropane, however, in which the magnetic anisotropy of the cyclopropyl group causes dispersion of the phenyl proton resonances sufficient to allow an analysis (20), the phenyl derivatives of the alicyclic systems in this paper display very small internal shifts for the aromatic protons, vitiating attempts at a confident extraction of coupling constants below 0.5 Hz in magnitude.

Calculational Procedure

Plots of $\langle \sin^2 \theta \rangle$ were constructed as a function of temperature, reduced moments of inertia, and of V_2. Conformation **4** (bisected) was assumed to be of lowest energy for **6–9**, implying that $\langle \sin^2 \theta \rangle$ ranges from 0.5 for a vanishing twofold barrier to zero at an infinite barrier. The reduced moments of inertia of **6–9** were calculated for various conformations, including **4** and **5**. For these, the dithiane derivative, as an extreme example, had moments of 2.5 and 3.5×10^{-38} g cm^2, respectively. Fortunately, at 305 K the values of $\langle \sin^2 \theta \rangle$ are insensitive to differences of this magnitude, varying only in the third significant figure. This fact obviates the consideration of variations in the moments of inertia caused by changes in θ during the internal rotation and by the assumption of regular geometries. In the calculations, 11 basis functions were employed, quite sufficient for temperatures below 400 K.

3,5-Dichlorophenylcyclohexane (6)

The free energy of the equatorial isomer is 3.1 kcal/mol lower than that of the axial isomer in phenylcyclohexane, so that more than 99% of **6** likely exists in the equatorial form at 305 K, the temperature of the experiment. Inversion of the cyclohexyl moiety is many orders of magnitude slower than the rate of rotation about the bond between the two cyclic systems. The following discussion is couched in terms of the properties of a noninverting equatorial form. It is also assumed that the chlorine substituents do not materially alter the conclusions above.

A $^6J_{90}$ of −1.24 Hz, as for toluene, implies a $\langle \sin^2 \theta \rangle$ of 0.188 because the observed value of $^6J^{H,CH}$ for **6** is −0.233 Hz (Table 1). A reduced moment of inertia for conformation **4** of 1.72 ×

10^{-38} g cm^2 (it is 1.80×10^{-38} g cm^2 for **5**) then yields a V_2 of 2.1 kcal/mol.

However, $^6J_{90}$ in **6** need not be the same as in toluene. If the $C_{ring} \ldots C_\alpha \ldots H$ angle becomes greater than 109.5°, the overlap of the C_α—H bond with the π orbitals of the ring will decrease, leading to a lower magnitude of $^6J_{90}$. For example, when this angle in styrene is taken as 120°, the calculated $^6J_{90}$ is -1.05 Hz (21). In cyclohexane the H—C—H angle is $107.5 \pm 1.5°$ (26*a*) or perhaps 110.0° (26*b*) and the assumption will here be made that the $C_{ring} \ldots C_\alpha \ldots H$ angle is within 2° of tetrahedral, suggesting a possible difference of 0.04 Hz between $^6J_{90}$ in toluene and in **6**. If $^6J_{90}$ in **6** were as low in magnitude as -1.14 Hz, then V_2 would become 1.95 kcal/mol.

Allowing for an error of 0.02 Hz in the measured $^6J^{H,CH}$ and in $^6J_{90}$, it appears reasonable that V_2 in **6** is 2.0 ± 0.3 kcal/mol, with the bisected conformation **4** as the ground state. If **5** were the low energy conformer, $^6J^{H,CH}$ would have a magnitude of over 0.5 Hz for a finite V_2.

Conformation **4** minimizes steric hindrance between the C—H bonds and, if such interactions account for V_2, it appears possible that V_2 has similar values in **6**, in phenylcyclopropane, and in isopropylbenzene. As argued for phenylcyclopropane (20), V_2 should be the dominant component in the actual internal barrier for **6**.

Molecular mechanics calculations (26*c*) on phenylcyclohexane suggest that **4** is 3.9 kcal/mol more stable than **5**.

2-(3,5-Dichlorophenyl)-1,3-dithiane (7)

In the crystal (27*a*), 2-phenyl-1,3-dithiane exists in a conformation in which the phenyl plane is approximately perpendicular to the 'plane' of the 1,3-dithiane ring (bisected conformation, **4**). In gaseous 1,3-dithiane, nonchair forms have not been detected (27*b*). In CS_2 solution, the *p*-chlorophenyl derivative favours the equatorial form by a free energy of 1.7 ± 0.3 kcal/mol (28), suggesting that $94 \pm 3\%$ of **7** exists in this form at 305 K. The discussion below assumes an equatorial form.

If $^6J_{90}$ is -1.24 Hz, the usual procedure yields 2.25 kcal/mol for V_2, using the observed $^6J^{H,CH}$ in Table 1. Again, if $^6J_{90}$ is -1.14 Hz, V_2 becomes 2.1 kcal/mol. A V_2 of 2.2 ± 0.3 kcal/mol should easily encompass errors in measurement of ^6J and in $^6J_{90}$. If steric interactions between *ortho* C—H bonds of the phenyl group and bonds at the 1,3 positions in the saturated ring cause the barrier, then it seems that CH_2 moieties and sulfur atoms are very similar in their steric requirements in **6** and **7**.

2-(3,5-Dichlorophenyl)-1,3-dioxane (8)

Extensive X-ray (29) and calorimetric investigations (6), as well as molecular mechanics calculations (5), imply at most a very small barrier to internal rotation in equatorial 2-phenyl-1,3-dioxane, this isomer being favoured by a free energy of 3.1 kcal/mol (6).

In previous work (30), we have argued that highly electronegative substituents at the α carbon atom appreciably reduce $^6J_{90}$. Two fluorine substituents reduce the magnitude of $^6J_{90}$ to about -0.9 Hz (30). The reduction can be understood as a consequence of the polarization of the C—H bond, reducing the overlap of its orbitals with the neighbouring π electron system. A linear relationship between $^6J_{90}$ and the electronegativity of the substituents implies that $^6J_{90}$ is -0.96 Hz in **8**. Allowing for an error of 0.05 Hz in this number and for an error of 0.02 Hz in $^6J^{H,CH}$ in **8**, yields a V_2 of 0.4 ± 0.2 kcal/mol. We take this result as a confirmation of the conclusions (5, 6) described above. It is difficult to reconcile our observed couplings with entirely free rotation about the central carbon–carbon bond in **8**. Free rotation implies that $^6J_{90} = -0.89$ Hz (2×-0.40) in **8**, which we think is rather too low in magnitude.

2-(3,5-Dichlorophenyl)-1,3-dioxolane (9)

In the gas phase, 1,3-dioxolane is almost a free pseudorotor (31), whereas in solution the envelope form is apparently rather more stable (5, 32, 33). Detailed equilibration (34) and ^{13}C chemical shift (35) studies of various 1,3-dioxolane derivatives suggest to us that there exists very little preferred equatorial or axial character in **9**, the ring being highly flexible.

On the other hand, the observed $^6J^{H,CH}$ of -0.33 Hz means that the C—H_α bond prefers to lie in the plane of the benzene ring. Otherwise, its magnitude would be rather larger than 0.4 Hz (see discussion of **8** above). This conclusion is supported by the chemical shifts of the α proton in the isomers of 2,4,5-trimethyl-1,3-dioxolane and 2-phenyl-4,5-dimethyl-1,3-dioxolane (34). Substitution of methyl by phenyl causes a shift to low field of 0.8 ppm, best explained as arising from the magnetic anisotropy of the phenyl ring. The anisotropy causes marked downfield shifts for proton sites near the plane of the phenyl ring.

If, then, the small-amplitude ring puckering motion is rapid compared to rotation about the connecting carbon–carbon bond and the ground state conformation of the phenyl group is best represented by the bisected conformation, **4**, a treatment in terms of a twofold barrier is feasible. If $^6J_{90}$ is the same as for **8**, one has $\langle \sin^2 \theta \rangle$ as 0.33/0.96, or 0.34, then V_2 is 0.85 ± 0.3 kcal/mol; the quoted error allows for large errors in $^6J_{90}$. It

would be interesting if other methods were to confirm that the barrier in **9** is higher than in **8**.

Conclusions

The *J* method implies that the bisected conformations, **4**, are the most stable for **6**–**9**; further, that the twofold barrier to internal rotation in **6** and **7** is very similar in magnitude to those in phenylcyclopropane and isopropylbenzene; finally, that in **8** the barrier is finite but similar to kT at ambient temperatures, in rough agreement with other experimental and with theoretical approaches.

Experimental

Compounds **6**–**9** were prepared by standard procedures (34, 36–42) and gave satisfactory mass and ^{1}H nmr spectra (28, 43–47). These were repeatedly calibrated at 5-Hz intervals in the frequency sweep mode of an HA100 spectrometer at a probe temperature of 305 ± 1 K. The spectral dispersion was 1 Hz/cm and sweep rates were 0.02 and 0.01 Hz/s. The spectrum in Fig. 1 has linewidths at half height of 0.10 ± 0.01 Hz and illustrates that peaks separated by 0.3 Hz (outer doublets) were cleanly resolved.

Acknowledgments

We are grateful to the National Research Council of Canada for financial assistance.

1. E. L. Eliel, N. L. Allinger, S. J. Angyl, and G. A. Morrison. Conformational analysis. Interscience, John Wiley & Sons, New York, NY. 1965.
2. V. M. Gittens, E. Wyn-Jones, and R. F. M. White. *In* Internal rotations in molecules. *Edited by* W. J. Orville-Thomas. Interscience, John Wiley & Sons, New York, NY. 1974.
3. F. A. L. Anet and R. Anet. *In* Dynamic nuclear magnetic resonance spectroscopy. *Edited by* L. M. Jackman and F. A. Cotton. Academic Press, New York, NY. 1975.
4. F. A. L. Anet and A. J. R. Bourn. J. Am. Chem. Soc. **89**, 760 (1967).
5. N. L. Allinger and D. Y. Chung. J. Am. Chem. Soc. **98**, 6798 (1976).
6. W. F. Bailey, H. Connon, E. L. Eliel, and K. B. Wiberg. J. Am. Chem. Soc. **100**, 2202 (1978).
7. F. A. L. Anet and I. Yavari. J. Am. Chem. Soc. **99**, 6752 (1977).
8. C. Heller and H. M. McConnell. J. Chem. Phys. **32**, 1535 (1960).
9. M. P. Williamson, R. Kostelnik, and S. M. Castellano. J. Chem. Phys. **49**, 2218 (1968).
10. C. J. Macdonald and W. F. Reynolds. Can. J. Chem. **48**, 1002 (1970).
11. J. B. Rowbotham and T. Schaefer. Can. J. Chem. **52**, 489 (1974).
12. R. Wasylishen and T. Schaefer. Can. J. Chem. **50**, 1852 (1972).
13. H. Rudolph, H. Dreizler, A. Joeschke, and P. Wendling. Z. Naturforsch. Teil A, **22**, 940 (1967).
14. A. F. Janzen and T. Schaefer. Can. J. Chem. **49**, 1818 (1971).
15. P. B. Ayscough, M. C. Brice, and R. E. D. McClung. Mol. Phys. **20**, 41 (1971).
16. T. Schaefer, L. Kruczynski, and W. Niemczura. Chem. Phys. Lett. **38**, 498 (1976).
17. A. Miller and D. W. Scott. J. Chem. Phys. **68**, 1317 (1978).
18. M. S. Farag. Diss. Abstr. Int. B, **35**, 1594 (1974).
19. T. Schaefer, W. J. E. Parr, and W. Danchura. J. Magn. Reson. **25**, 167 (1977).
20. W. J. E. Parr and T. Schaefer. J. Am. Chem. Soc. **99**, 1033 (1977).
21. T. Schaefer and W. J. E. Parr. J. Mol. Spectrosc. **61**, 479 (1976).
22. L. A. Carreira and T. G. Townes. J. Chem. Phys. **63**, 5283 (1975).
23. T. Schaefer, W. Danchura, W. Niemczura, and J. Peeling. Can. J. Chem. **56**, 2442 (1978).
24. S. Castellano and A. A. Bothner-By. J. Chem. Phys. **41**, 3863 (1964).
25. C. W. Haigh and J. M. Williams. J. Mol. Spectrosc. **32**, 398 (1969).
26. (*a*) O. Bastiansen, L. Fernholt, H. M. Seip, H. Kambara, and K. Kuchitsu. J. Mol. Struct. **18**, 163 (1973); (*b*) R. A. Peters, W. J. Walker, and A. Weber. J. Raman Spectrosc. **1**, 159 (1973); (*c*) N. L. Allinger and M. L. Tribble. Tetrahedron Lett. 3259 (1971).
27. (*a*) H. T. Kalff and C. Romers. Acta Crystallogr. **20**, 490 (1966); (*b*) W. J. Adams and L. S. Bartell. J. Mol. Struct. **37**, 261 (1977).
28. H. T. Kalff and E. Havinga. Recl. Trav. Chim. Pays-Bas, **85**, 467 (1966).
29. E. L. Eliel, W. F. Bailey, H. Connon, K. B. Wiberg, and F. W. Nader. Justus Liebigs Ann. Chem. 2240 (1976).
30. T. Schaefer, W. Danchura, and W. Niemczura. Can. J. Chem. **56**, 36 (1978).
31. J. A. Greenhouse and H. L. Strauss. J. Chem. Phys. **50**, 124 (1969).
32. C. W. N. Cumper and A. I. Vogel. J. Chem. Soc. 3521 (1959).
33. R. U. Lemieux, J. D. Stevens, and R. R. Fraser. Can. J. Chem. **40**, 1955 (1962).
34. W. E. Willy, G. Binsch, and E. L. Eliel. J. Am. Chem. Soc. **92**, 5394 (1970).
35. K. Pihlaja and T. Nurmi. Finn. Chem. Lett. 141 (1971).
36. E. L. Eliel and M. Rerick. J. Am. Chem. Soc. **82**, 1367 (1960).
37. E. W. Garbisch and D. B. Patterson. J. Am. Chem. Soc. **85**, 3228 (1963).
38. E. L. Eliel and R. O. Hutchins. J. Am. Chem. Soc. **91**, 2703 (1969).
39. E. L. Eliel and F. W. Nader. J. Am. Chem. Soc. **92**, 584 (1970).
40. F. W. Nader and E. L. Eliel. J. Am. Chem. Soc. **92**, 3050 (1970).
41. R. Eidenschink, D. Erdmann, J. Krause, and L. Pohl. Angew. Chem. Int. Ed. Engl. **16**, 100 (1977).
42. D. Seebach, B. W. Erickson, and G. Singh. J. Org. Chem. **31**, 4303 (1966).
43. E. Caspi, T. A. Wittstruck, and D. M. Piatak. J. Org. Chem. **27**, 3183 (1962).
44. H. Booth. Prog. Nucl. Magn. Reson. Spectrosc. **5**, 149 (1969).
45. A. G. Abatjoglou, E. L. Eliel, and L. F. Kuyper. J. Am. Chem. Soc. **99**, 8262 (1977).
46. A. Anteunis, D. Tavernier, and F. Borremans. Bull. Soc. Chim. Belg. **75**, 396 (1966).
47. R. J. Abraham and W. Thomas. J. Chem. Soc. 335 (1965).

On the syntheses and the optical properties of optically active 2-pyrazoline compounds

MAKOTO MUKAI, TAKASHI MIURA, MASAHIRO NANBU, TOSHINOBU YONEDA, AND YOHJI SHINDO

Textile Research Institute, Faculty of Engineering, Fukui University, Fukui, Japan 910

Received June 7, 1978

MAKOTO MUKAI, TAKASHI MIURA, MASAHIRO NANBU, TOSHINOBU YONEDA, and YOHJI SHINDO. Can. J. Chem. **57**, 360 (1979).

Optically active 2-pyrazolines were synthesized and their optical properties were studied using various spectroscopic techniques to investigate the effects of substituents at the 3 and 5 positions of the 2-pyrazoline ring on their optical activity. It was found that in the case of 5-substituted-1,3-diphenyl-2-pyrazoline derivatives, the substituent at the 5 position has considerable influence on the optical activity, whereas in 3-substituted-1,5-diphenyl-2-pyrazoline derivatives, the substituent at the 3 position has no such influence.

MAKOTO MUKAI, TAKASHI MIURA, MASAHIRO NANBU, TOSHINOBU YONEDA et YOHJI SHINDO. Can. J. Chem. **57**, 360 (1979).

On a synthétisé certaines pyrazolines-2 optiquement actives et l'on en a étudié les propriétés optiques par différentes méthodes spectroscopiques, dans le but de déterminer l'influence qu'exerce sur l'activité optique les substituants aux positions 3 et 5 du noyau pyrazoline-2. Dans le cas des dérivés de la diphényl-1,3 pyrazoline-2 portant un substituant en position 5, on a observé que ce substituant exerce une influence importante sur l'activité optique; par contre, pour les diphényl-1,5 pyrazolines-2 possédant un substituant en position 3, ce substituant est sans effet.

[Traduit par le journal]

Introduction

A number of studies on 2-pyrazoline compounds have been carried out for the purpose of using them as optical brighteners (1, 2), scintillators (3–8), and photoconductive materials (9). As a result, some of their optical properties are well documented. However, no study on the optical activity of these compounds has been reported except that by Neunhoeffer and Ulrich (10) on sodium (+)-4-(3,5-diphenyl-2-pyrazolin-1-yl)benzenesulfonate, (+)-**1**. Furthermore, there are only a few studies (11, 12) on the optical activity of the pyrazoline derivatives. Thus, we decided to prepare some 2-pyrazolines in optically pure form and to investigate the effect of substituents at the 3 and 5 position of the 2-pyrazoline ring on their optical activity.

Results and Discussion

Among the many methods of synthesizing 2-pyrazolines (1, 8, 13–16) that outlined in Scheme 1 is most widely used owing to its ease and high efficiency (1). All our 2-pyrazoline compounds except sodium *dl*-4-(5-*tert*-butyl-3-phenyl-2-pyrazolin-1-yl)benzenesulfonate, *dl*-**6**, were readily obtained by this method, although *p*-hydrazinobenzenesulfonic acid, instead of phenylhydrazine, was used to resolve the compounds by the formation of separable diastereoisomers. An attempt to synthesize compound *dl*-**6** by the methods outlined in Scheme 2 (8, 14, 15) was unsuccessful. Thus, it was necessary to develop a completely new approach to synthesize compound *dl*-**6**.

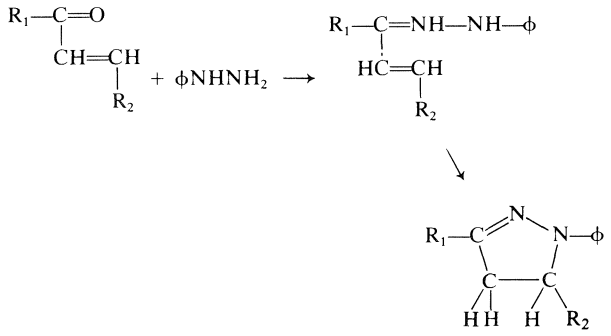

$R_1, R_2 = CH_3, C(CH_3)_3, C_6H_5$

SCHEME 1

Cinchonidine was found to be a good resolving agent for a series of 3- but not 5-substituted-1,5-diphenyl-2-pyrazoline derivatives and *dl*-**1** was successfully resolved using brucine. After several unsuccessful attempts to use alkaloids such as brucine, cinchonidine, strychnine, and quinine, the resolution of sodium *dl*-4-(5-methyl-3-phenyl-2-pyrazolin-1-yl)benzenesulfonate, *dl*-**2**, was achieved using (−)-α-methylbenzylamine. Our preliminary experiments also show that (−)-α-methylbenzylamine seems to be effective in the resolution of all the 2-pyrazoline compounds obtained, though its resolving power is not particularly good.

0008-4042/79/030360-07$01.00/0

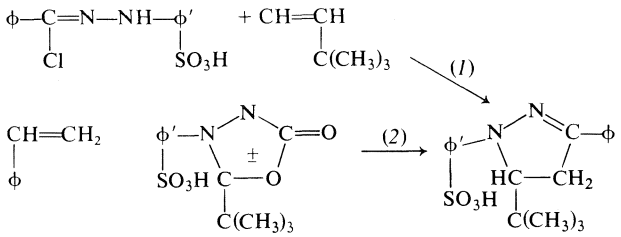

SCHEME 2

It is known from previous studies (17) on the uv spectra of 2-pyrazoline compounds that the spectrum has one maximum at about 240 nm when there is no substituent at the 1 position of the pyrazoline ring and that a second maximum at about 280 nm appears when the 1 position is substituted by a benzene ring. This long-wavelength band is not affected by a second substituent at the 3 position except when the substituent is a phenyl group. In such a case, the pyrazoline compounds exhibit a band shift to 354 nm and show a blue fluorescence whose maximum appears around 455 nm. The introduction of a third substituent at the 5 position of the pyrazoline ring causes no alteration in the established spectral pattern and such substituted pyrazoline compounds also show the same fluorescence as 1,3-diphenyl-2-pyrazoline (5). From an X-ray study of the crystal structure of 1,3-diphenyl-2-pyrazoline (18) it is evident that the N(1)—N(2), N(2)—C(3)—C(7), and N(1)—C(6) bonds are significantly shorter than a single bond. Those factors suggest that conjugation between the phenyl rings occurs via atom N(1), N(2), and C(3) (19) as shown in Scheme 3. This conjugated chromophore is common to a series of 1,3-diphenyl-2-pyrazoline derivatives and is responsible for the strong absorption and fluorescence bands at about 355 and 455 nm, respectively (20), which are due to the π–π^* transition (3).

As illustrated in Figs. 1 and 2, there is little difference in the uv and fluorescence spectra between compounds (+)-**1** and (−)-**2**. However, the ord and cd spectra, shown in Fig. 3, indicate that the two compounds are very different. In the case of compound (+)-**1**, the cd maximum peak, which corresponds to the uv maximum peak at 357 nm, appears at 349 nm, whereas in compound (−)-**2** both the cd and uv maximum peaks are observed at 358 nm. However, the molar ellipticity of the conjugated chromophore is about 3.0×10^4 in the both cases, indicating that the conjugated chromophores of those two have almost the same optical activity. Furthermore, in the 240–280 nm wavelength region there are more differences in the cd spectra between these two compounds. In (+)-**1**, two cd peaks at 275 and 250 nm, which have the same sign as the main cd peak at 349 nm, are found to appear at longer wavelengths than the two corresponding uv absorption peaks. On the other hand, in (−)-**2**, only one peak, whose sign is opposite to that of the strong

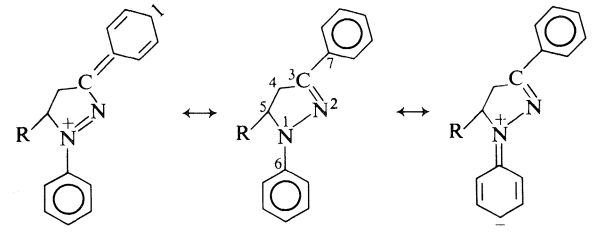

R = H, CH_3, C_6H_5

SCHEME 3

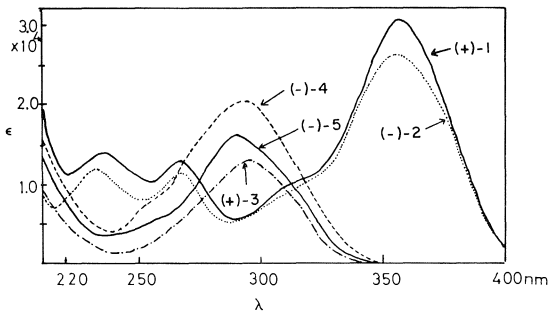

FIG. 1. The absorption spectra of sodium (+)-4-(3,5-diphenyl-2-pyrazolin-1-yl)benzenesulfonate, (+)-**1**, (——); sodium (−)-4-(5-methyl-3-phenyl-2-pyrazolin-1-yl)benzenesulfonate, (−)-**2** (---); sodium (+)-4-(5-phenyl-2-pyrazolin-1-yl)benzenesulfonate, (+)-**3** (—·—·—); sodium (−)-4-(3-methyl-5-phenyl-2-pyrazolin-1-ly)benzenesulfonate, (−)-**4** (— — —); sodium (−)-4-(3-*tert*-butyl-5-phenyl-2-pyrazolin-1-yl)benzenesulfonate, (−)-**5** (——); in methanol.

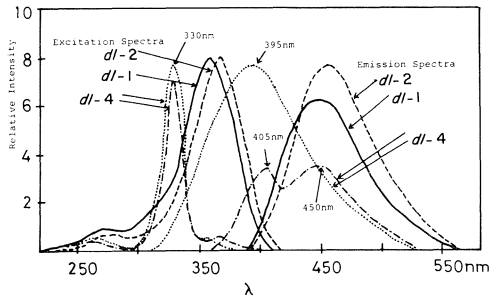

FIG. 2. The fluorescence excitation and emission spectra of sodium *dl*-4-(3,5-diphenyl-2-pyrazolin-1-yl)benzenesulfonate, *dl*-**1** (——), at 2.5×10^{-7} mol/L in methanol (excitation: 358 nm; emission: 450 nm); sodium *dl*-4-(5-methyl-3-phenyl-2-pyrazolin-1-yl)benzenesulfonate, *dl*-**2** (---), at 2.95×10^{-7} mol/L in methanol (excitation: 365 nm; emission: 450 nm); and sodium *dl*-4-(3-methyl-5-phenyl-2-pyrazolin-1-yl)benzenesulfonate, *dl*-**4**, at 2.95×10^{-4} mol/L in methanol: (---), excitation: 330 nm, emission: 395 nm; (—·—·—), excitation: 358 nm, emission: 450 nm.

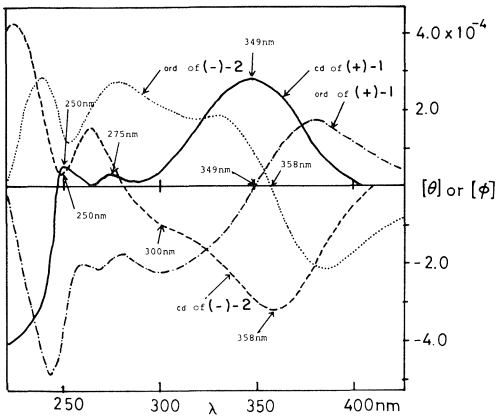

FIG. 3. The ord and cd spectra of sodium (+)-4-(3,5-diphenyl-2-pyrazolin-1-yl)benzenesulfonate, (+)-**1**, and sodium (−)-4-(5-methyl-3-phenyl-2-pyrazolin-1-yl)benzenesulfonate, (−)-**2**, in methanol.

cd peak at 358 nm, appears at 250 nm and a shoulder is observed at 300 nm in the main cd band. It is reported (6, 14) that the uv band at 265 nm arises from the phenyl ring whereas that at 234 nm is due to the pyrazoline ring. However, they are probably all strongly coupled and result, more or less, from the entire composite system. The same is also true for the cd and ord bands around 250 nm.

In the case of (+)-**1**, the phenyl group at the 5 position not only serves as a chromophore itself but also contributes greatly to the optical activity of the whole system by producing an asymmetric perturbation. On the other hand, the methyl group of (−)-**2** cannot act as a chromophore but it does induce an asymmetric environment such as to make other chromophores optically active. This factor certainly results in the considerable difference between the two compounds as seen in their cd and ord spectra. X-ray analysis (18) of 1,3-diphenyl-2-pyrazoline reveals that the two phenyl rings are not completely coplanar; that is, the dihedral angle between the planes of the phenyl rings is 11.0° and rotation about the C(6)—N(1) and C(3)—C(7) bonds gives the molecule a slight propeller shape. In other words, the conjugated chromophore is distorted slightly. The difference in the position of the maximum peaks between the cd and the uv spectra of (+)-**1** may, in some way, relate to the additional distortion (21, 22) of the conjugated chromophore due to the steric effect of the phenyl group at the 5 position of the pyrazoline ring or to the coupling between those two chromophores. On the other hand, the fact that both the uv and cd maxima occur at 358 nm in compound (−)-**2** may indicate that the methyl group at the 5 position causes almost no additional distortion to the conjugated chromophore.

It was considered worthwhile preparing compound *dl*-**6** to investigate more clearly the effect of a substituent at the 5 position on the optical properties of 1,3-diphenyl-2-pyrazoline derivatives.

Sodium (+)-4-(5-phenyl-2-pyrazolin-1-yl)benzenesulfonate, (+)-**3**, sodium (−)-4-(3-methyl-5-phenyl-2-pyrazolin-1-yl)benzenesulfonate, (−)-**4**, and sodium (−)-4-(3-*tert*-butyl-5-phenyl-2-pyrazolin-1-yl)benzenesulfonate, (−)-**5**, all exhibit similar patterns in their uv, cd and ord spectra. As shown in Fig. 1, only one maximum is observed at 290–294 nm for each of these compounds. The band at 290-294 nm is attributed to the chromophore through C(6), N(1), N(2), and C(3), —C=N—N—Ar, because, as mentioned earlier (5), this band is also observed in the uv spectrum of 1-phenyl-2-pyrazoline. This absorption band corresponds to the maximum peak in the cd curves and to the Cotton effect in the ord curves of the above three compounds as shown in Fig. 4. This means that the introduction of a methyl or a *tert*-butyl group at the 3 position of the pyrazoline ring has no effect on the optical activity of *dl*-**3**. As expected, the cd and ord spectra of compound (+)-**3** and (−)-**3** are mirror images as shown in Fig. 4.

There has been considerable discussion about the origin of the weak fluorescence observed in 3-methyl-1,5-diphenyl-2-pyrazoline (4, 7, 19). Neunhoeffer *et al.* (19) attribute it to the hyperconjugation of the methyl group and this is supported by Sandler and Tsuo (4). If the fluorescence is a consequence of such hyperconjugation, 3-methyl-1-phenyl-2-pyrazoline should show similar fluorescence because the presence and nature of a substituent at the 5 position is

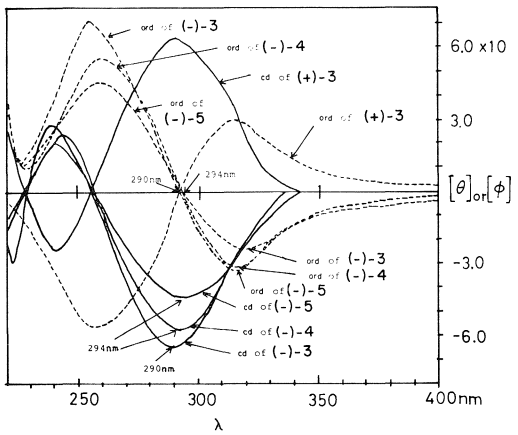

FIG. 4. The ord and cd spectra of sodium (+)-4-(5-phenyl-2-pyrazolin-1-yl)benzenesulfonate, (+)-**3**; sodium (−)-4-(5-phenyl-2-pyrazolin-1-yl)benzenesulfonate, (−)-**3**; sodium (−)-4-(3-methyl-5-phenyl-2-pyrazolin-1-yl)benzenesulfonate, (−)-**4**; sodium (−)-4-(3-*tert*-butyl-5-phenyl-2-pyrazolin-1-yl)benzenesulfonate, (−)-**5** in methanol.

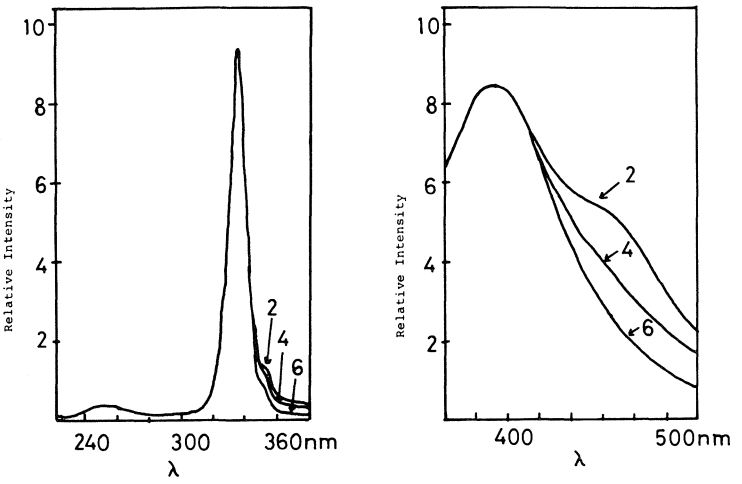

FIG. 5. The change in the fluorescence excitation and emission spectra of sodium *dl*-4-(3-methyl-5-phenyl-2-pyrazolin-1-yl)benzenesulfonate with purification: **2**, after two recrystallizations; **4**, after four recrystallizations; **6**, after six recrystallizations; (*a*) the excitation spectra at a concentration of 0.2 g/L in methanol (emission: 390 nm); (*b*) the emission spectra at a concentration of 0.29 g/L in methanol (excitation: 330 nm).

found to have little effect on the excitation process (20, 23). However, 3-methyl-1-phenyl-2-pyrazoline has been reported to be nonfluorescent (24). Furthermore, if hyperconjugation of the methyl group is related to the excited state of compound (−)-**4**, then the chromophore for compound (−)-**4**, CH_3—C=N—N—Ar, is different from that for compound (−)-**5**, $(CH_3)_3C$—C=N—N—Ar, and the ord and cd spectra of these two are expected to be different. However, as shown in Fig. 4, the optical properties of those two are almost identical. These facts indicate that the fluorescence of compound *dl*-**4** is not due to hyperconjugation of the methyl group. Owing to the possibility that the fluorescence was produced by trace impurities, compound *dl*-**4** was examined by thin-layer chromatography but no impurities were detected.

As seen in Fig. 2, the 330 nm excited emission spectrum has one peak at about 400 nm, whereas the one excited at 358 nm has two peaks, one at 400 and the other at 450 nm. The intensity of the fluorescence at 400 nm did not vary as the purity of *dl*-**4** was increased, whereas that at 450 nm gradually decreased as shown in Fig. 5. This fact indicates that the fluorescence at 400 nm is an inherent property of the compound and that the fluorescence observed at 450 nm is due to impurities. From a comparison of Figs. 1 and 2, it is noted that the excitation spectrum of compound *dl*-**4** is very different in shape from the absorption spectrum and that the wavelength of its excitation maximum is 40 nm longer than that of its absorption maximum. The other interesting observation is that fluorescence was hardly detected when compound *dl*-**4** was excited at 290 nm, i.e., at its absorption maximum. As shown in Fig. 6, the excitation spectrum of *dl*-**4** at a concentration of 0.1 g/L has two peaks, one at 330 and the other at 260 nm but at 0.005 g/L these two peaks disappear and one new peak appears at 310 nm. These facts indicate that the origin of the observed weak fluorescence may be due to the associated species.

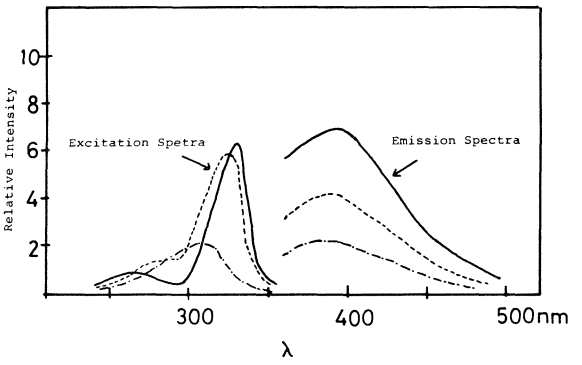

FIG. 6. The fluorescence excitation and emission spectra of sodium *dl*-4-(3-methyl-5-phenyl-2-pyrazolin-1-yl)benzenesulfonate at various concentrations in methanol; (——), 0.1 g/L; (---), 0.05 g/L; (—·—·—), 0.005 g/L (excitation: 330 nm; emission: 395 nm).

Experimental

Materials

Special grade benzylideneacetophenone (BDH Ltd.), benzylideneacetone (Wako Chemicals), pinacolone (Wako), cinnamaldehyde (Wako), brucine (Wako), cinchonidine

(Nakarai Chemical Ltd.), acetic anhydride (Wako), and tartaric acid (Kanto Chemical Ltd.) were used without further purification. Special grade 1-phenyl-2-buten-1-one (Tokyo Kasei Kogyo Ltd.) was purified by vacuum distillation before use. Crude *p*-hydrazinobenzenesulfonic acid (Wako) was recrystallized from water. Reagent grade benzaldehyde (Nakarai) was purified by steam distillation before use. Reagent grade *dl*-α-methylbenzylamine (Nakarai) was distilled under reduced pressure before use. Double distilled methanol, ethanol, and acetone were used throughout the experiments. For thin-layer chromatography, special grade Kieselgel nach Stahl (Merck), 1-butanol (Wako), and reagent grade soluble starch (Wako) were used without further treatment.

Instruments

A Shimadzu UV-20 spectrophotometer, a Shimadzu IR-27C spectrometer, an Hitachi 204 fluorescence spectrophotometer, and a JASCO J-20 spectropolarimeter were used for the measurement of uv, ir, fluorescence, cd, and ord, respectively. A JASCO DIPSL polarimeter was used for the determination of the optical purity of diastereomers.

Syntheses and Resolution of 2-Pyrazoline Compounds

Sodium dl-*4-(3,5-Diphenyl-2-pyrazolin-1-yl)benzenesulfonate (*dl-***1***)*

Preparation

A solution of benzylideneacetophenone (5 g) in 25 mL of ethanol and *p*-hydrazinobenzenesulfonic acid (4.5 g) in 8 mL of water was refluxed at 123–125°C for 7 h and then cooled. On the addition of 15 mL of 2 *N* sodium hydroxide, a yellow product precipitated immediately. The precipitate was filtered and recrystallized (seven times) from a mixture of methanol and water (2:1) to give 2.1 g of white plates, mp 198–201°C; uv and visible (100% CH_3OH, 23°C) λ_{max} (log ε): 234 (4.16), 276 (4.15), 357 (4.49) nm; ir (KBr pressed disc) ν_{max}: 1605 (s, C=N), 1505 (s, aromatic C=C), 1405 (s, CH_2), 1326 (m, Ar—N), 1200 (s, SO_3^-), 1130 (s, CH—N), 1040 (s, SO_3^-), 820 (m, aromatic CH *p*-substituted), 750 (s, aromatic CH 5-adjacent H atoms), 700 (s, aromatic CH) cm^{-1}. *Anal.* calcd. for $C_{21}H_{17}O_3SNa{\cdot}2.5H_2O$: C 56.62, H 4.98, N 6.29; found: C 56.59, H 4.96, N 6.18.

Resolution

A solution of the racemic compound (5 g) and brucine (5 g) in 50 mL of acetic anhydride was concentrated under reduced pressure giving an oily residue. To the residue, 50 mL of water was added under continuous stirring and the pale yellow brucine salt began to precipitate as a mixture of diastereoisomers. The precipitate was filtered and recrystallized (seven times) from a mixture of methanol and water (2:1). Ethanol (150 mL), water (50 mL), and 2 *N* sodium hydroxide (10 mL) were added sequentially to 2 g of the resolved brucine salt. After the addition of a large amount of water, the solution was kept cool overnight, and white crystals precipitated in the form of plates. The crystals were filtered and dried *in vacuo* to give compound (+)-**1**, mp 205–210°C, $[\alpha]_D^{25}$ +300° (*c* 0.06, CH_3OH); ord (*c* 0.0033(450–220 nm), *c* 0.06(700–400 nm), CH_3OH) 25°C: $[\phi]_{700}$ +760°, $[\phi]_{589}$ +1240°, $[\phi]_{380}$ +17 570° (peak), $[\phi]_{349}$ 0° (intersects), $[\phi]_{305}$ −23 030° (trough), $[\phi]_{282}$ −16 970° (peak), $[\phi]_{244}$ −50 300° (trough); cd (*c* 0.00011 *M*, CH_3OH) 25°C: $[\theta]_{410}$ 0, $[\theta]_{349}$ +28 000, $[\theta]_{285}$ 720, $[\theta]_{275}$ +2900, $[\theta]_{265}$ 0, $[\theta]_{250}$ +5440, $[\theta]_{246}$ 0, $[\theta]_{223}$ −41 800.

Sodium dl-*4-(5-Methyl-3-phenyl-2-pyrazolin-1-yl)benzenesulfonate (*dl-***2***)*

Preparation

A mixture of *p*-hydrazinobenzenesulfonic acid (3.7 g) in 30 mL of water and 1-phenyl-2-buten-1-one (3 g) in 15 mL of ethanol was refluxed at 130°C for 4 h and then concentrated to about one-third of its original volume. The concentrate was refluxed for an additional 3 h and then cooled. The yellow product began to precipitate on the addition of 2 mL of 10 *N* sodium hydroxide. The precipitate was filtered and washed with ethanol. Nine recrystallizations from a mixture of ethanol and water (16:1) gave 0.4 g of white needles, mp 257°C; uv and visible (100% CH_3OH, 23°C) λ_{max} (log ε): 234 (4.11), 267 (4.11), 358 (4.46) nm: ir (KBr pressed disc) ν_{max}: 1610 (s, C=N), 1515 (s, aromatic C=C), 1405 (s, CH_2), 1345 (m, Ar—N), 1190 (s, SO_3^-), 1140 (s, CH—N), 1055 (s, SO_3^-), 830 (m, aromatic CH *p*-substituted), 740 (s, aromatic CH 5-adjacent **H** atoms), 700 (s, aromatic CH) cm^{-1}. *Anal.* calcd. for $C_{16}H_{15}N_2O_3SNa{\cdot}0.5H_2O$: C 55.33, H 4.61, N 8.06; found: C 55.54, H 4.35, N 8.02.

Resolution

The racemic compound (4 g) and (−)-α-methylbenzylamine (1.8 g), prepared according to the procedure of Theilacker and Winkler (25), were added to 12 mL of 1 *N* hydrochloric acid under vigorous stirring. After the addition of 120 mL of water, the solution was heated until the product had dissolved completely. The solution was kept in a refrigerator overnight to precipitate yellow needles. The yellow crystals were filtered and dried *in vacuo* to give 5 g of the amine salt as diastereoisomers. The amine salt (5 g) dissolved in 40 mL of ethanol was carefully poured into 200 mL of ether and allowed to stand 60 min. Pale yellow crystals precipitated in the form of well developed plates. The precipitate was filtered and dried *in vacuo*. The amine salt was treated eight times in the above manner and was further recrystallized four times from ethanol to give 0.4 g of the resolved amine salt. The resolved amine salt (0.4 g) was treated with 0.9 mL of 1 *N* sodium hydroxide. The addition of a large amount of ether precipitated white crystals. After filtration, the crystals were recrystallized once more from a mixture of ethanol and water (30:4) to give 0.16 g of compound (−)-**2**, mp 254°C, $[\alpha]_D^{25}$ −360° (*c* 0.06, CH_3OH); ord (*c* 0.0021 (450–220 nm), *c* 0.06 (700–400 nm), CH_3OH) 25°C: $[\phi]_{700}$ −640°, $[\phi]_{589}$ −1280°, $[\phi]_{386}$ −21 870° (trough), $[\phi]_{356}$ 0° (intersects), $[\phi]_{330}$ +18 630° (shoulder), $[\phi]_{278}$ +27 540° (peak), $[\phi]_{253}$ +11 340° (trough), $[\phi]_{240}$ +28 350° (peak); cd (*c* 0.00003 *M*, CH_3OH) 25°C: $[\theta]_{410}$ 0, $[\theta]_{358}$ −25 270, $[\theta]_{315}$ −12 960 (shoulder), $[\theta]_{282}$ 0, $[\theta]_{265}$ +15 550, $[\theta]_{250}$ +3240, $[\theta]_{228}$ +40 820.

Sodium dl-*4-(5-Phenyl-2-pyrazolin-1-yl)benzenesulfonate (*dl-***3***)*

Preparation

A solution of *p*-hydrazinobenzenesulfonic acid (14 g) in 150 mL of water was stirred with 10 g of cinnamaldehyde for 7 h at 60°C. After the addition of 3.0 g of sodium hydroxide, the solvent was evaporated completely on a water bath. The yellow residue was recrystallized three times from water and twice from methanol to give 9.2 g of yellow needles, mp 244–245°C; uv and visible (100% CH_3OH, 23°C) λ_{max} (log ε): 290 (4.25) nm; ir (KBr pressed disc) ν_{max}: 1605 (s, C=N), 1510 (s, aromatic C=C), 1385 (s, CH_2), 1195 (s, SO_3^-), 1130 (s, CH—N), 1035 (s, SO_3^-), 830 (m, aromatic CH *p*-substituted), 750 (s, aromatic CH 5-adjacent H atoms), 705 (m, aromatic CH) cm^{-1}. *Anal.* calcd. for $C_{15}H_{14}N_2O_3Na{\cdot}2H_2O$: C 49.97, H 4.78, N 7.78; found: C 50.29, H 4.76, N 8.08.

Resolution

The racemic compound (10 g) and cinchonidine (9 g) were added to 30 mL of 1 *N* hydrochloric acid and warmed under continuous stirring. On filtration, 16.7 g of the crude cinchonidine salt was obtained as diastereoisomers. The cinchonidine salt was recrystallized once from methanol. The pure cinchonidine salt (10 g) dissolved in 300 mL of methanol was allowed to stand in a refrigerator for 90 min. White

crystals were filtered and dried *in vacuo*. The yield after the first recrystallization should be kept to about 30% to achieve good resolution. The same procedure was repeated five times.

The resolved cinchonidine salt (0.5 g) was treated with 1 mL of 1 *N* sodium hydroxide. After the addition of 10 mL of water, the reaction mixture was heated and insoluble cinchonidine was removed by filtration. The filtrate was evaporated to dryness on a water bath. The residue was recrystallized once from methanol to give 0.12 g of compound (+)-**3**, mp 244–245°C, $[\alpha]_D^{25}$ +320° (*c* 0.1, CH_3OH); ord (*c* 0.0045 (400–220 nm), *c* 0.1 (700–400 nm), CH_3OH) 25°C: $[\phi]_{700}$ +710°, $[\phi]_{589}$ +1040°, $[\phi]_{318}$ +31 100° (peak), $[\phi]_{292}$ 0° (intersects), $[\phi]_{255}$ −60 030° (trough), $[\phi]_{228}$ −12 290° (peak); cd (*c* 0.000028 *M*, CH_3OH) 25°C: $[\theta]_{340}$ 0, $[\theta]_{292}$ +63 640, $[\theta]_{254}$ 0, $[\theta]_{240}$ −26 030, $[\theta]_{228}$ 0, $[\theta]_{223}$ +33 990, $[\theta]_{217}$ 0.

Compound (−)-**3** is also obtained as follows; after the first filtrate of the 300 ml of methanol solution was allowed to stand in a refrigerator overnight, the precipitate was filtered and dissolved in warm methanol. The solution was then cooled in a refrigerator for 90 min and the resulting white crystals were filtered and dried *in vacuo*. The same procedure was repeated four times. The resolved cinchonidine salt was converted into the sodium salt by the above procedure, mp 244–245°C, $[\alpha]_D^{25}$ −320° (*c* 0.1, CH_3OH); ord (*c* 0.0044 (400–220 nm), *c* 0.1 (700–400 nm), CH_3OH) 25°C: $[\phi]_{700}$ −710°, $[\phi]_{589}$ −1040°, $[\phi]_{318}$ −32 030° (trough), $[\phi]_{292}$ 0° (intersects), $[\phi]_{255}$ +58 840° (peak), $[\phi]_{288}$ +14 150° (trough) cd (*c* 0.000027 *M*, CH_3OH) 25°C: $[\theta]_{340}$ 0, $[\theta]_{292}$ −66 290, $[\theta]_{254}$ 0, $[\theta]_{240}$ +26 810, $[\theta]_{228}$ 0, $[\theta]_{223}$ −29 040, $[\theta]_{218}$ 0.

Sodium dl-*4-(3-Methyl-5-phenyl-2-pyrazolin-1-yl)benzenesulfonate (*dl-***4***)*

Preparation

Benzylideneacetone (3 g) in 3 mL of ethanol and sodium *p*-hydrazinobenzenesulfonate (3.7 g) in 5 mL of water and 5 mL of acetic acid were mixed and heated at about 130°C for 4 h. The reaction mixture was concentrated to about one-third its original volume, refluxed for additional 3 h, and then cooled. On the addition of a large amount of ethanol, the product began to precipitate. The precipitate was filtered and washed with ethanol. Nine recrystallizations from ethanol containing a trace of water gave 0.7 g of pale yellow needles, mp 219–221 °C; uv and visible (100% CH_3OH, 23°C) λ_{max} (log ε): 294 (4.31) nm; ir (KBr pressed disc) ν_{max}: 2950 (m, CH_3), 1590 (s, C=N), 1500 (s, aromatic C=C), 1400 (m, CH_2), 1360 (m, CH_3), 1180 (s, SO_3^-), 1120 (s, CH—N), 1030 (s, SO_3^-), 830 (m, aromatic CH *p*-substituted), 740 (m, aromatic CH 5-adjacent H atoms), 700 (m, aromatic CH) cm^{-1}. *Anal.* calcd. for $C_{16}H_{15}N_2O_3SNa{\cdot}0.5H_2O$: C 55.33, H 4.61, N 8.08; found: C 55.48, H 4.60, N 7.99.

Resolution

The racemic compound (4 g) dissolved in 50 mL of glacial acetic acid and cinchonidine (3.5 g) in 50 mL of ethanol were mixed and the solvent was evaporated under reduced pressure. The residue was washed with water and dried *in vacuo*. The crude cinchonidine salt obtained as diastereoisomers was recrystallized once from a mixture of ethanol and water (2:1). The pure cinchonidine salt (5 g) dissolved in 100 mL of the above mixture of solvents was allowed to stand for 90 min in a refrigerator and the precipitate was filtered and dried *in vacuo*. This procedure was repeated four times. To the resolved cinchonidine salt (1.2 g) in 20 mL of water was added 1.2 mL of 2 *N* sodium hydroxide and the mixture was warmed slightly. White crystalline cinchonidine precipitated upon cooling. After filtration, the filtrate was concentrated to one-third of its original volume and cooled to precipitate any remaining cinchonidine. After the precipitate was removed, the filtrate was evaporated completely on an oil bath. The residue was recrystallized once from a mixture of ethanol and water (10:1) to give 0.7 g of compound (−)-**4**, mp 219°C, $[\alpha]_D^{25}$ −315° (*c* 0.1, CH_3OH); ord (*c* 0.0037 (400–220 nm), *c* 0.1 (700–400 nm), CH_3OH) 25°C: $[\phi]_{700}$ −940°, $[\phi]_{589}$ −1060°, $[\phi]_{316}$ −32 050° (trough), $[\phi]_{294}$ 0° (intersects), $[\theta]_{260}$ +55 860° (peak), $[\theta]_{227}$ +10 980° (trough); cd (*c* 0.000033 *M*, CH_3OH) 25°C: $[\theta]_{340}$ 0, $[\theta]_{294}$ −57 590, $[\theta]_{257}$ 0, $[\theta]_{245}$ +23 280, $[\theta]_{228}$ 0.

Sodium dl-*4-(3-*tert*-Butyl-5-phenyl-2-pyrazolin-1-yl)benzenesulfonate (*dl-***5***)*

Preparation

Sodium *p*-hydrazinobenzenesulfonate (3.8 g) in 10 mL of water, 4,4-dimethyl-1-phenyl-penten-3-one (3.8 g), synthesized according to the procedure of Bramen (26), in 5 mL of ethanol and 3 mL of acetic acid were mixed and refluxed at 123–125°C for 7 h. The reaction mixture was concentrated to one-third of its original volume, refluxed for additional 3 h, and then cooled. On the addition of a large amount of ethanol, the product began to precipitate as white needles. The crystalline precipitate was filtered, washed with ethanol, and then with acetone. Six recrystallizations from acetone containing a trace of water gave 3.2 g of white needles, mp 220–222°C; uv and visible (100% CH_3OH, 23°C) λ_{max} (log ε): 295 (4.10) nm; ir (KBr pressed disc) ν_{max}: 2900 (s, CH_3), 1590 (s, C=N), 1495 (s, aromatic C=C), 1360 (m, —$C(CH_3)_3$), 1260 (m —$C(CH_3)_3$), 1190 (s, SO_3^-), 1120 (s, CH—N), 1040 (s, SO_3^-), 830 (s, aromatic CH *p*-substituted), 750 (m, aromatic CH 5-adjacent H atoms), 700 (m, aromatic CH) cm^{-1}. *Anal.* calcd. for $C_{19}H_{21}N_2O_3SNa{\cdot}H_2O$: C 57.29, H 5.79, N 7.03; found: C 57.08, H 6.08, N 7.09.

Resolution

Cinchonidine (3 g) was added to the racemic mixture (4 g) and 10.2 mL of 1 *N* hydrochloric acid was added with continuous stirring. After the addition of 90 mL of water, the mixture was heated until the cinchonidine salt had dissolved completely. The solution was allowed to stand in a refrigerator overnight and white crystals precipitated as needles. On filtration, the crude cinchonidine salt was obtained as diastereoisomers. The cinchonidine salt was recrystallized once from a mixture of methanol and water (7:10). The pure cinchonidine salt (5 g) was dissolved in 300 mL of the above mixture of solvents and allowed to stand for 90 min in a refrigerator and the precipitate was filtered and dried *in vacuo*. The same procedure was repeated five times. The resolved cinchonidine salt was added to 14 mL of 0.1 *N* sodium hydroxide. To this solution a small amount of ethanol was added until the cinchonidine salt was completely dissolved. The solution was kept in a refrigerator overnight to precipitate white crystalline cinchonidine. After filtration, the filtrate was concentrated to one-third of its original volume and cooled to precipitate cinchonidine completely. After the removal of cinchonidine, the filtrate was evaporated to dryness on an oil bath. The residue was recrystallized once from a mixture of methanol and acetone to give 0.36 g of compound (−)-**5**, mp 222°C, $[\alpha]_D^{25}$ −275° (*c* 0.1, CH_3OH); ord (*c* 0.0028 (400–220 nm), *c* 0.1 (700–400 nm), CH_3OH) 25°C: $[\phi]_{700}$ −750°, $[\phi]_{589}$ −1080°, $[\phi]_{318}$ −48 500° (trough), $[\phi]_{294}$ 0° (intersects), $[\phi]_{260}$ +89 900° (peak), $[\phi]_{228}$ +22 800° (trough); cd (*c* 0.000014 *M*, CH_3OH) 25°C: $[\theta]_{340}$ 0, $[\theta]_{294}$ −85 960, $[\theta]_{258}$ 0, $[\theta]_{242}$ +40 110, $[\theta]_{228}$ 0.

Acknowledgement

The authors are indebted to Dr. Y. Ooshima for useful suggestions for the syntheses of 2-pyrazoline compounds.

1. A. WAGNER, C. W. SCHELLHAMMER, and S. PETERSEN. Angew. Chem. Int. Ed. Engl. **5**, 699 (1966).
2. H. GOLD. *In* The chemistry of synthetic dyes. Vol. 5. *Edited by* K. Venkataraman. Academic Press, New York, NY. 1971. p. 611.
3. R. N. NURMUKHAMETOV, N. A. LODYGIN, and G. I. GRISHINA. Opt. Spectrosc. **25**, 118 (1968).
4. S. R. SANDLER and K. C. TSUO. J. Chem. Phys. **39**, 1962 (1963).
5. S. R. SANDLER, S. LOSHAEK, E. BRODERICK, and K. C. TSUO. J. Phys. Chem. **66**, 404 (1962).
6. F. N. HAYES, D. G. OTT, V. N. KERR, and B. S. ROGERS. Nucleonics, **13**, 38 (1955).
7. R. H. WILEY, C. H. JARBOE, F. N. HAYES, E. HANSBURY, J. T. NIELSEN, P. X. CALLAHAN, and M. C. SELLARS. J. Org. Chem. **23**, 732 (1958).
8. R. HUISGEN, A. GOTTHARDT, and R. GRASHEY. Angew. Chem. **74**, 30 (1962).
9. F. BILLETTA and P. G. DIMARCO. Chim. Ind. **50**, 1191 (1968).
10. O. NEUNHOEFFER and H. ULRICH. Z. Electrochem. **59**, 122 (1955).
11. G. SNATZKE and J. HIMMERREICH. Tetrahedron, **23**, 4337 (1967).
12. W. HERZ, K. AOTA, M. HOLUB, and Z. ZAMEK. J. Org. Chem. **35**, 2611 (1970).
13. L. KNORR and K. DUDEN. Chem. Ber. **26**, 115 (1893).
14. C. F. DUFFIN and J. D. DENDALL. J. Chem. Soc. 408 (1954).
15. R. HUISGEN, M. SEIDEL, G. WALLBILLICH, and K. KNUPHER. Tetrahedron, **17**, 3 (1962).
16. I. G. KOLOKOL'TSEVA, U. N. CHISTOKLETOV, and A. A. PETROV. Zh. Obsch. Khim. **40**, 2612 (1970).
17. K. DIMROTH and O. LUDERITZ. Chem. Ber. **81**, 243 (1948).
18. B. DUFFIN. Acta Crystallogr. B, **24**, 1256 (1968).
19. O. NEUNHOEFFER, G. ALSDORF, and H. ULRICH. Chem. Ber. **92**, 252 (1959).
20. O. NEUNHOEFFER and D. ROSAHL. Z. Electrochem. **57**, 81 (1953).
21. K. L. WILLIAMSON and W. S. JOHNSON. J. Am. Chem. Soc. **83**, 4623 (1961).
22. P. CRABBÉ. Optical rotatory dispersion and circular dichroism in organic chemistry. Holden-Day, San Francisco. 1965. p. 107.
23. Z. RACISZEWSKI and J. F. STEPHEN. J. Am. Chem. Soc. **91**, 4338 (1969).
24. M. BLAISE. C. R. Acad. Sci. **142**, 216 (1906).
25. W. THEILACKER and H. G. WINKLER. Chem. Ber. **89**, 690 (1954).
26. H. BRAMEN. *In* Organic synthesis. Coll. Vol. I. *Edited by* H. Gilman. John Wiley and Sons Inc., New York, NY. 1932. p. 74.

Canadian Journal of Chemistry
Published by
THE NATIONAL RESEARCH COUNCIL OF CANADA

Journal canadien de chimie
Publié par
LE CONSEIL NATIONAL DE RECHERCHES DU CANADA

Volume 57 Number 4 February 15, 1979 Volume 57 numéro 4 15 février 1979

Alkanes with multiple asymmetric centers: synthesis, identification, and ^{13}C nuclear magnetic resonance spectra[1]

PIERRE LACHANCE, S. BROWNSTEIN, AND ARTHUR M. EASTHAM
Division of Chemistry, National Research Council of Canada, Ottawa, Ont., Canada K1A 0R9

Received January 16, 1978[2]

PIERRE LACHANCE, S. BROWNSTEIN, and ARTHUR M. EASTHAM. Can. J. Chem. **57**, 367 (1979).

The identification of aliphatic hydrocarbons containing multiple asymmetric centers can be difficult because of the complexity of the nmr spectra and because in capillary chromatography the diastereomers may be resolved to varying degrees. We suggest that the most effective method for identifying such hydrocarbons is through the pattern of retention times developed by the mixture of diastereomers on a suitable capillary glc column.

This paper presents the results of some studies of a series of alkanes having the general form C_2H_5—(CH—CH_3)$_n$—R, where n = 1 to 4, and includes the syntheses and ^{13}C nmr spectra of the compounds.

PIERRE LACHANCE, S. BROWNSTEIN et ARTHUR M. EASTHAM. Can. J. Chem. **57**, 367 (1979).

L'identification d'hydrocarbures aliphatiques possédant plusieurs centres asymétriques est parfois très difficile. La difficulté vient de la complexité de leur spectre rmn et du fait que la chromatographie en phase vapeur avec colonne capillaire peut résoudre, jusqu'à un certain point, les mélanges de diastéréoisomères. Nous proposons cependant que cette dernière méthode, grace aux temps de retention à motif obtenus par passage d'un mélange de diastéréoisomères sur une colonne capillaire appropriée, demeure la plus efficace pour l'identification de tels produits.

Dans cet article on décrit les résultats d'études portant sur une série d'alcanes de formule générale C_2H_5—(CH—CH_3)$_n$—R, où n = 1 à 4. On trouvera aussi les synthèses et les spectres de rmn du ^{13}C de ces composés.

We wish to report here the characterization of a series of alkanes of the general form,

$$CH_3CH_2-\left[\begin{array}{l}CH_3\\|\\-CH-\end{array}\right]_n-R \quad n = 1, 2, 3, \text{ or } 4;\ R = Me, Et, nPr$$

obtained from the oligomerization of 2-butene (1). Nuclear magnetic resonance spectroscopy can often be used to resolve such structural problems but is not effective for these compounds because the multiple asymmetric centers produce numerous diastereomers and consequently some very complex resonance spectra. (When n = 4, the ^{13}C spectrum shows more than 40 lines.) It thus becomes necessary to revert to traditional methods of identification which in practice means that the unknown is assigned tentative structures and is then compared with authentic samples, prepared when necessary by unequivocal synthesis.

Effective comparison of known with unknown is essential and major difficulties arise when, as in the present case, the unknown is a liquid yielding no solid derivative. In these circumstances a mixture melting point determination is not possible and various physical measurements such as infrared absorption, nmr spectra, glc retention time, etc., may not be sufficiently discriminatory.

For the alkanes under study the problem is especially acute. The presence of stereoisomers, which are resolved to varying degrees in capillary chromatography, makes it necessary to determine whether the compounds are 'pure,' i.e., whether the observed inhomogeneity is in fact due to stereoisomers, whether it arises from contamination of the

[1]NRCC No. 17064.
[2]Revision received October 2, 1978.

0008-4042/79/040367-10$01.00/0

sample by closely related structural isomers, or both. The simplest way to handle the problem is by careful synthesis of the alkane, followed by comparison of the synthetic product with the unknown in the same capillary chromatograph which revealed the composite character of the unknown in the first place. We are aware that glc identifications are not generally acceptable in the chemical journals but we wish to suggest that in the present circumstances capillary chromatography is not only the most suitable technique available for comparing two compounds but may even be definitive when, as here, a compound gives rise to a group of peaks having a well-defined pattern of retention times.

The basic procedure adopted for the synthesis was as follows: the 1,4-addition of an appropriate Grignard reagent to an α,β-unsaturated ketone yields a ketone which can then be treated with an organometallic reagent to give an alcohol corresponding to the desired alkane. The alcohol is dehydrated and the resulting olefin(s) hydrogenated. The chief concern with this series of reactions lies in the possibility that some unexpected product might arise, most probably by rearrangement during the dehydration step, and escape detection because of inadequate control methods. Most of the ketone intermediates in the syntheses did not yield solid derivatives suitable for analysis, presumably because of the presence of diastereomers (see below) but in any event, elemental analysis would not detect the presence of isomers. To minimize such dangers we have carried out the syntheses by at least two independent pathways on the assumption that if the two routes give mixtures of alkanes with identical retention times, then the products are most probably mixtures of stereoisomers and not mixtures of structurally different alkanes. The results seem to be consistent with this assumption.

Discussion

The alkanes to be identified were obtained from the oligomerization of 2-butene by careful fractional distillation of the olefin mixture followed by hydrogenation of the fractions. It was found that most of the lower molecular weight olefins (up to C_{10}) consisted of a single carbon skeleton with the double bond in various positions, giving rise to a single alkane on hydrogenation. These lower alkanes were readily identified since their nmr spectra were simple and good reference material was commercially available; from them it was therefore possible to make good predictions about the structures of the higher members, an important prerequisite to synthesis.

As a typical case of a higher alkane consider the dodecane obtained from the butene oligomers by hydrogenation of a close-boiling distillation fraction. The olefin, in ordinary chromatography (OV-101; 1/8 in. × 6 ft), appeared as a doublet which, when passed into the mass spectrometer, showed a parent mass of 168 only, corresponding to a butene trimer. Capillary glc (Squalane or OV-101; 0.01 in. × 150 ft) further resolved the doublet into about a dozen components which on hydrogenation took up roughly 1 mol equiv. of hydrogen and gave at least five new compounds (Fig. 1*C*). (Complete hydrogenation was difficult so a small amount of unchanged olefin is evident in the chromatogram.) Since from these results it seemed probable that the olefin consisted of a group of *cis–trans* pairs having the carbon skeleton of the normal butene trimer but with the double bond in various positions, it was decided to synthesize the corresponding alkane (**4**) in order to compare it with the group of alkanes obtained by hydrogenating the unknown.

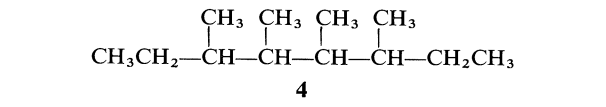

4

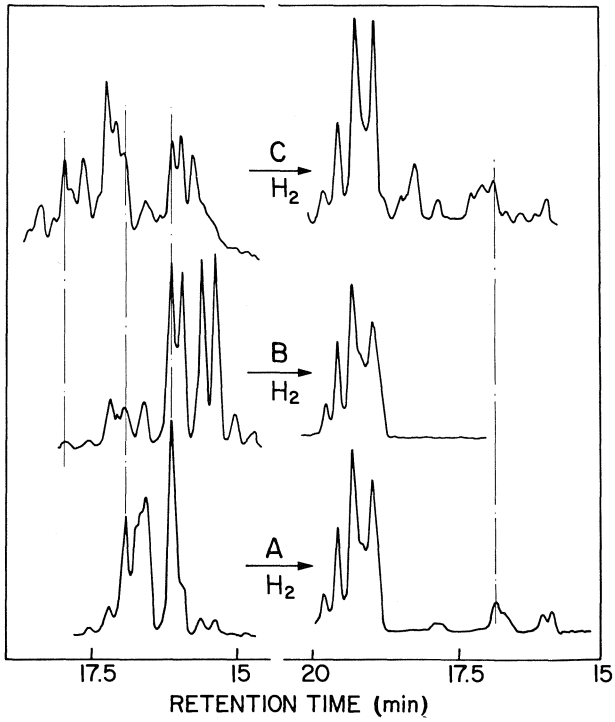

FIG. 1. Chromatograms for 3,4,5,6-tetramethyloctane (**4**) and the corresponding olefins: (*A*) olefins (**3**) prepared from 3,4-dimethylhexanone-2 and *sec*-butyl Li; (*B*) olefins (**8**) prepared from 4,5,6-trimethyloctanone-3 (**6**); (*C*) olefins obtained from the oligomerization of 2-butene. Hydrogenations over Pd/C; chromatograms WCOT squalane, 0.01 in. × 150 ft, 120°C.

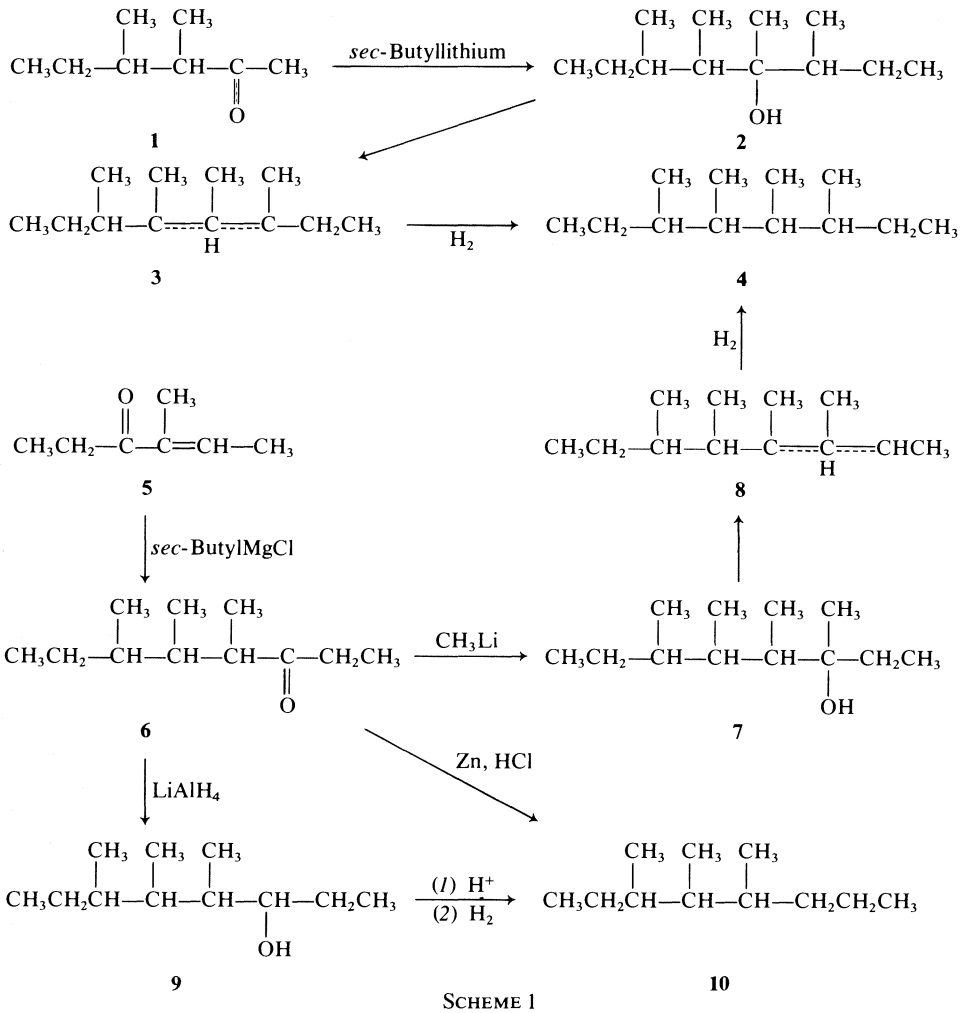

SCHEME 1

Two separate syntheses were carried out as shown in Scheme 1. In the first, 3,4-dimethyl-2-hexanone (**1**) was allowed to react with *sec*-butyllithium to give a dodecanol (**2**). In the other, 3-methyl-2-hexene-4-one (**5**) was treated with *sec*-butylmagnesium chloride to obtain, by 1,4-addition, the undecanone 4,5,6-trimethyl-3-octanone (**6**). Yield was good but the identity of the product could not be confirmed either by proton resonance or through preparation and analysis of a solid derivative. Capillary glc (UCON LB550X) showed the presence of two components of very similar retention times, assumed to be diastereomers. The presumed undecanone was treated with methyllithium to obtain the dodecanol **7**.

The two dodecanols **2** and **7** were dehydrated with acid and, as expected, gave different mixtures of olefins. However these, on hydrogenation, gave identical mixtures of alkanes (Fig. 1*A* and *B*) which in turn were identical with the major part of the product from hydrogenation of the unknown (Fig. 1*C*). We conclude therefore, perhaps somewhat tentatively, that the unknown alkanes and olefins have the carbon skeleton of 3,4,5,6-tetramethyloctane (4).

In the chromatogram of the unknown there is one peak (retention time about 18.5 min) which is not found in the synthetic product and which does not seem to correspond to unchanged olefin; we can only suppose that this material was an impurity, perhaps an isomeric dodecene, in the original olefin.

A comment should be made here about the use of the gas chromatograph – mass spectrometer combination (glc–ms). Throughout most of this work we have been restricted to the use of macro (1/8 in.) columns and electron impact ionization and have therefore used the instrument primarily for determining molecular weight and molecular weight homogeneity of olefin samples; olefins generally give easily observable parent ions. It would have been most helpful to have been able to make similar

measurements on the alkanes and alkanols but the former tend to fragment completely and the latter dehydrate in the electron beam to give the olefin spectra. Chemical ionization might get around this problem and permit better control over the syntheses. Very recently we have had access to capillary glc–ms and have used it to examine the groups of stereoisomers which make up some of the alkanes. By using a long (300 ft × 0.01 in.) squalane WCOT column it proved possible to obtain complete separation of five isomers of 3,4,5,6-tetramethyloctane[3] and of four isomers of 2,3,4,5-tetramethylheptane, and to obtain their individual cracking patterns. Within experimental error all of the stereoisomers for each compound had the same mass spectrum but we are unable to assess the usefulness of this observation in recognizing a group of stereoisomers. We have not found the mass spectrometer to be helpful in defining structures.

The undecane 2,3,4,5-tetramethylheptane (**14**) was prepared in much the same way as the 3,4,5,6-tetramethyloctane, by dehydration of two different undecanols and hydrogenation of the resulting olefins. The undecanols (**12** and **17**) were derived from the reaction of methyllithium with two different trimethylheptanones (**11** and **16**), one of which was obtained by 1,4-addition of isopropylmagnesium bromide to 3-methyl-2-hexene-4-one (**5**) and the other by addition of *sec*-butylmagnesium bromide to 3-methyl-3-hexene-1-one (**15**). A third quite independent synthesis of one of the undecanols (**17**) was based on the Favorskii rearrangement of the bromo ketone **21** and is outlined in Scheme 2.

The 2,3,4,5-tetramethylheptane system is particularly useful for studying these reactions because of the good isomer separation obtained in the capillary chromatogram. The undecanols were therefore dehydrated in different ways, naphthalenesulfonic acid, $SOCl_2$ in pyridine, $POCl_3$ in pyridine, to see if any rearrangement could be detected. Some of the results are shown in Fig. 2. As would be expected, the two alcohols give quite different mixtures of olefins but these can be equilibrated by acid catalysis to identical composition. However, irrespective of the olefin composition, the same group of four alkanes is obtained on hydrogenation. The ratio of the four isomers in the alkane mixture varies considerably with variations in the olefin mixture, presumably because the hydrogenation is stereospecific; also, because of differences in rates of hydrogenation it is sometimes possible to relate the disappearance of particular olefin peaks to the appearance of specific alkane peaks in the chromatogram. It seems clear from these results that no rearrangements are occurring during the reactions and that the mixture of alkanes obtained is a group of diastereomers having the desired skeletal structure.

One other point is perhaps worth noting. The synthetic trimethylheptanone **11** appears as a broad peak (unresolved doublet ?) in capillary chromatography but becomes a clear doublet on treatment with acid. If the synthetic product is allowed to react with methylmagnesium iodide to about 60% completion, the unreacted ketone then appears in the glc as a sharp singlet. The olefin mixture obtained from the ketone (via the alcohol) is essentially the same from either partial or complete reaction, and the unreacted ketone is converted back to a glc doublet by treatment with acid. The doublet has the same retention times as the unreacted ketone. We interpret these observations to mean that the ketone is 'pure' but a mixture of stereoisomers which react at different rates with the Grignard reagent.

The alkane 3,4,5-trimethyloctane (**10**) was prepared in two different ways but the diastereomers were unresolved in the capillary chromatograph. The single peak showed a slight shoulder near the apex, thus resembling the closely-related 3,4,5-trimethylheptane which is also largely unresolved. Since the starting materials, and the reactions used to synthesize this undecane, were the same as those used for the other syntheses we are confident of the preparation but the chromatogram is certainly not definitive.

^{13}C Nuclear Magnetic Resonance Results and Discussion

Chemical shifts and longitudinal relaxation times (T_1) for seven methyl branched hydrocarbons are listed in Table 1. Chemical shifts and assignments for the first two of these hydrocarbons have already been reported (2). They are included here to facilitate comparison with the other sets of data and because T_1 values were not previously measured. The assignment of lines to particular carbon atoms was done on the basis of calculated chemical shifts and the differences in relaxation time expected for primary, secondary, and tertiary carbon atoms. Chemical shifts were calculated for the different carbon atoms of the compounds listed in Table 1 by the methods given in refs. 2 and 3. An average deviation from the experimental results of 0.9 ppm was observed for the method of Lindeman and Adams and 1.2 ppm for the modified Grant and Paul approach.

[3]There was no sign of the sixth diastereomer for 3,4,5,6-tetramethyloctane; either it was not formed in the synthesis or was not resolved at all in the capillary chromatogram.

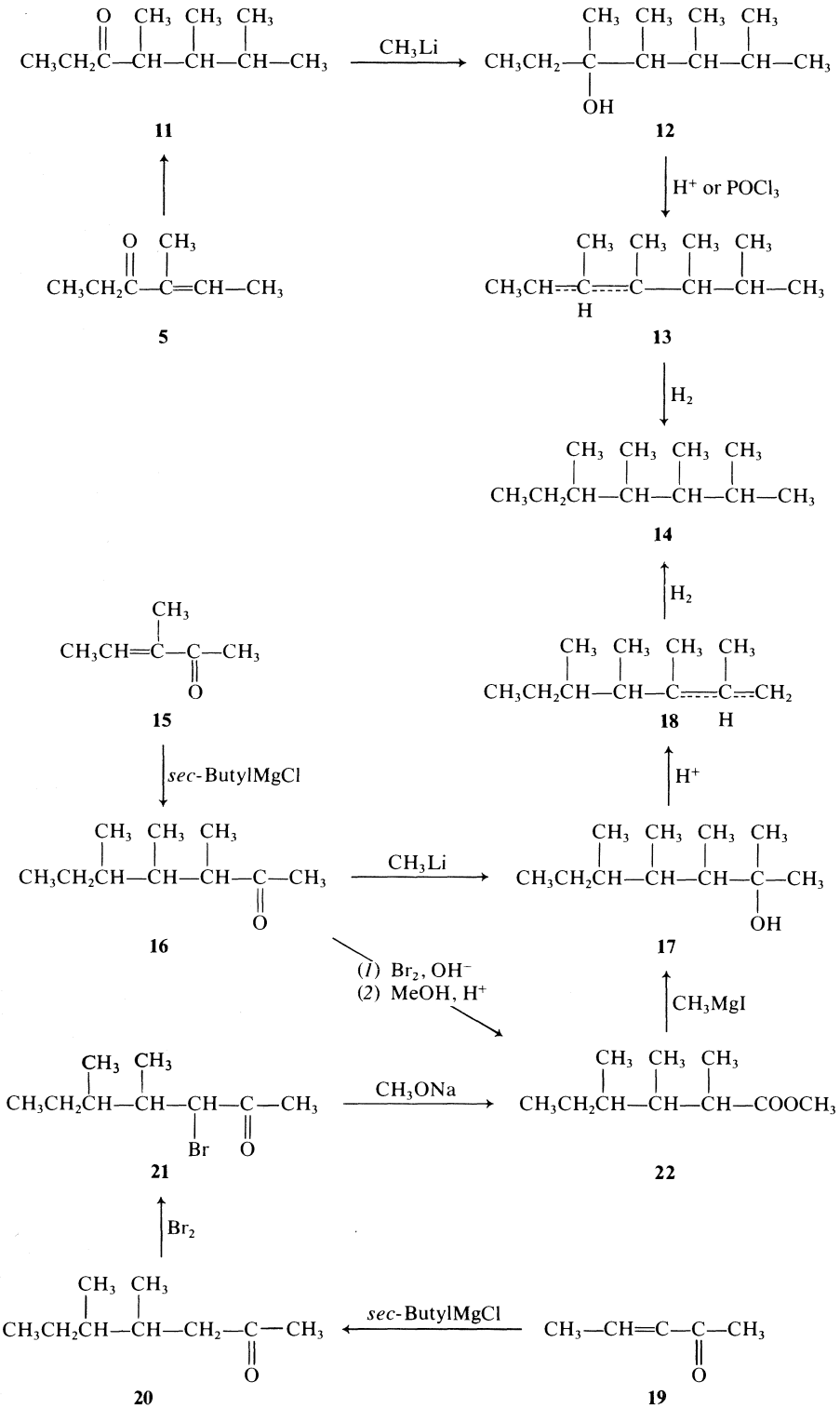

11 **12** **5** **13** **14** **15** **18** **16** **17** **21** **22** **20** **19**

SCHEME 2

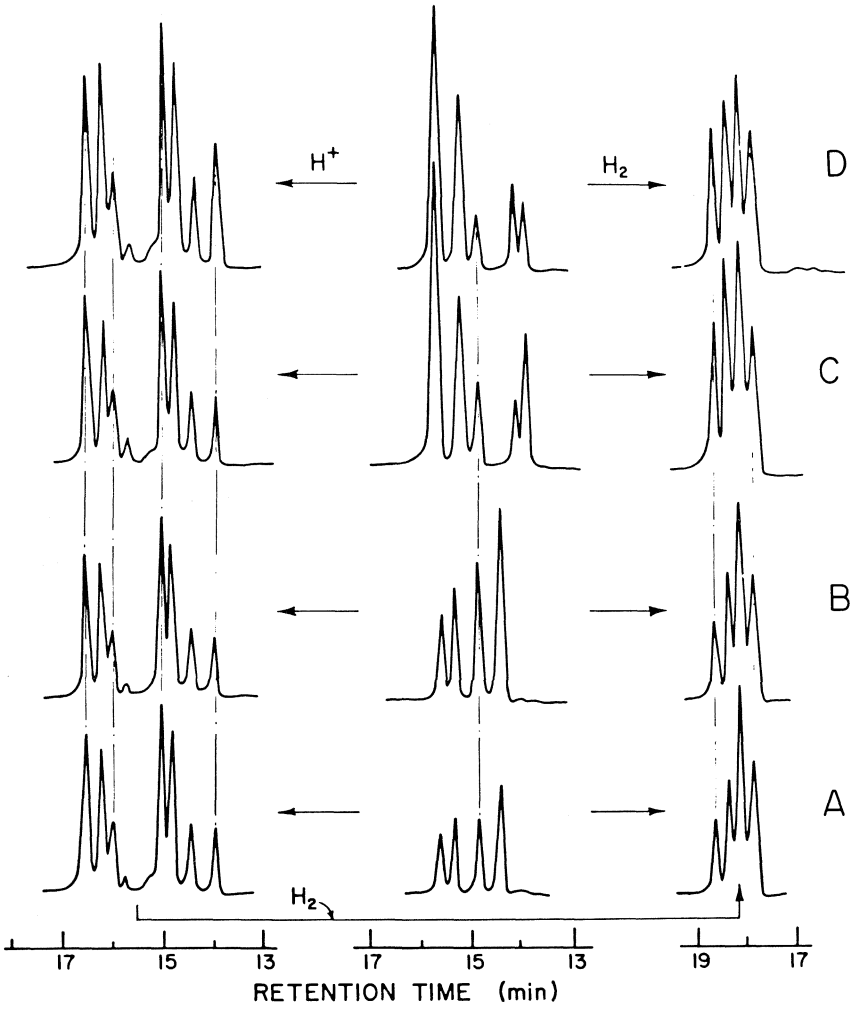

FIG. 2. 2,3,4,5-Tetramethylheptene (**13**) and (**18**) conversion to olefins and alkanes. The center column shows the chromatogram of the olefins as synthesized, the column on the left the olefins after isomerization by acid, and the column on the right the alkanes obtained by hydrogenation of the synthetic olefins or (*A*) of the equilibrium mixture. The synthetic products were obtained as follows: *A* and *B*, from undecanol **17** by dehydration with naphthalenesulfonic acid or with $POCl_3$ respectively; *C* and *D* from undecanol **12** with acid or $POCl_3$, respectively.

The assignment of peaks for 3,4-dimethylhexane and 3,5-dimethylheptane is that of Lindeman and Adams (2). The assignment of lines to particular carbon atoms in 2,3,4-trimethylhexane follows directly from the calculated values. There is excellent agreement between the number of lines observed and those theoretically expected for these compounds. 3,4,5-Trimethylheptane has three diastereomers. For the two *meso* forms there is magnetic equivalence about the center of the carbon chain, so that six lines from carbon atoms 1, 2, 3, 4, 8, and 9 are observed for each isomer. For the last, the *dl* diastereomer, there is a single line from each of the carbon atoms. This magnetic nonequivalence is similar to that observed for the isopropyl methyl carbons in 2,4,6-trimethylheptane and 2,5,8-trimethylnonane (2) and to that observed in triad and pentad sequences in isotactic polypropylene (4).

There are three chiral centers in 3,4,5-trimethyloctane (**10**) so four stereoisomeric pairs are possible. Since there are no equivalent carbon atoms in the molecule, 12 lines are expected from each of the methine and methylene carbons and 20 lines from the methyl carbons. The 24 lines of the secondary and tertiary carbons are clearly separated but because of extensive overlap not all the methyl lines are (separately) observed.

The compound 2,3,4,5-tetramethylheptane (**14**) has three chiral centers and therefore four pairs of optical isomers. All 11 carbon atoms will be mag-

netically nonequivalent in each of these four isomer pairs so a total of 44 lines should be found in the carbon resonance spectrum. At least 41 lines can be distinguished. The only ones which can be identified with any certainty are those from the CH_2 group in each of the four isomers. This was done by a combination of chemical shift, T_1 relaxation, and difference spectroscopy between samples with different isomeric composition (Fig. 2).

For 3,4,5,6-tetramethyloctane (**4**) there are six possible diastereomers, two of which have *meso* configurations. Two of the *dl* diastereomers have complete magnetic equivalence about the central 4–5 bond, the other two like 3,4,5-trimethylheptane have only nonequivalent carbons. From the glc data it is known that the compound contains at least five diastereomers, one of them in rather small concentration. If it is assumed that the least abundant isomer is one of those with no magnetic equivalence, it becomes possible to assign lines from the carbon resonance spectrum to C_2, C_3, and C_4 for five isomers (but see footnote 3).

Experimental

Melting points (evacuated capillaries) and boiling points are uncorrected. Reference alkanes were obtained when available, from Chemical Sample Co., Columbus, OH. Microanalyses were performed by C. Daesslé of Montreal or H. Seguin of these laboratories. Gas–liquid chromatographic comparisons were done by mixing the two components and examining the chromatogram for any sign of separation.

Reactions with organometallic reagents including Grignards were carried out under argon and were worked up by treating the reaction mixtures with NH_4Cl solution and extracting with ether. Olefin hydrogenations were accomplished at atmospheric pressure over 5% palladium-on-carbon as catalyst.

^{13}C resonance spectra with proton noise decoupling at ambient temperature were obtained with a Varian XL-100 spectrometer operating at 25.2 MHz and coupled to a Nicolet TT100A Fourier transform system. T_1 values were obtained by an inversion recovery sequence using the software of the manufacturer or by a saturation recovery sequence (5) using our own programme. Samples were prepared in CS_2 solvent without removal of oxygen, and referenced to internal tetramethylsilane. Chemical shifts are reported in ppm to low field of TMS and relaxation times are in seconds. Free induction decays of 16K were accumulated for spectral widths of 5000 Hz. This gives nominal resolution of 0.75 Hz which is broadened to 1.0 Hz by sensitivity enhancement.

*3,4,5,6-Tetramethyloctane (**4**)*

Method A

A 25.0 g sample of *3-methyl-2,4-pentanedione*, obtained by methylation of 2,4-pentanedione with methyl iodide and sodium *tert*-butylate, was refluxed for 2 h with a Grignard solution prepared from 13.0 g Mg and 40 mL ethyl bromide, to give 29.3 g of crude hydroxyketone. Distillation of the product with 2.0 g oxalic acid gave 20.7 g of unsaturated ketone, hydrogenated to 20.2 g of *3,4-dimethyl-2-hexanone* (**1**), bp 156–157°C (lit. (6) bp 153–154°C).

Compound **1** (5.0 g) was allowed to react at 0°C for 3 h with 50 mL of 11.6% *sec*-butyllithium (Foote Mineral Co.) in hexane to give 6.3 g of crude dodecanol (**2**). The alcohol dehydrates on heating so, without further purification, was treated with naphthalenesulfonic acid to give 1.7 g of olefin. The olefin was then hydrogenated to 1.5 g *3,4,5,6-tetramethyloctane* (**4**), bp 84°C/12 Torr; *n*, 1.4356.

Method B

A 15.0 g portion of *3-methyl-2-hexene-4-one* (**5**) (7) was added at 0°C to a Grignard reagent prepared from 4.0 g Mg and 18 mL *sec*-butyl chloride and the mixture then refluxed for 3 h to give 21.7 g of crude *4,5,6-octanone-3* (**6**). This ketone was fractionally distilled and the material distilling at 106°C/15–18 Torr collected. Yield, 9.2 g; *n*, 1.4342; ir ν_{max} 1710 cm^{-1} (carbonyl).

Ketone **6** (8.0 g) was added at 0°C to 75 mL of 3.5% methyllithium solution in ether and refluxed for 2 h, yielding 8.4 g of crude dodecanol (**7**). Dehydration with 2.0 g naphthalenesulfonic acid at 75°C gave 7.1 g of crude olefins which were fractionally distilled and the fraction passing over at 96–97°C/15–18 Torr retained (5.3 g). A small amount of residual starting ketone was removed by spinning band distillation. Hydrogenation then gave 3.1 g of *3,4,5,6-tetramethyloctane* (**4**), bp 85°C/12 Torr; *n*, 1.4353. The two alkanes prepared by methods *A* and *B* had identical infrared spectra and capillary chromatograms. *Anal.* calcd. for $C_{12}H_{26}$: C 84.60, H 15.39; found: C 84.79, H 15.09.

*3,4,5-Trimethyloctane (**10**)*

4,5,6-Trimethyl-3-octanone (**6**; 2.0 g) was refluxed in ether for 1 h with 0.25 g $LiAlH_4$ to give 1.3 g of undecanol **9**. The alcohol was then dehydrated with 0.5 g naphthalenesulfonic acid in ethanol to give 1.1 g of olefins which on hydrogenation gave 1.0 g *3,4,5-trimethyloctane* (**10**), bp 71°C/12 Torr; *n*, 1.4260; *Anal.* calcd. for $C_{11}H_{24}$: C 84.52, H 15.48; found: C 84.34, H 15.60.

Conversion of the ketone **6** to the alkane **10** can be accomplished by Clemmensen reduction; 1.0 g ketone in 15 mL 35% ethanol was refluxed 1 h with 35 g of zinc, 1.7 g of $HgCl_2$, and 25 mL concentrated HCl. More HCl (20 mL) was added over a further 2 h. A yellow oil (0.8 g) was recovered which, in capillary chromatography on squalane, showed only unchanged ketone and the 3,4,5-trimethyloctane described above. Yield, 30–40% with no indication of other products.

The undecanol **9** and alkane **10** were also prepared from the octanone **1** and *n*-propylmagnesium chloride.

*2,3,4,5-Tetramethylheptane (**14**)*

Method A

Aldol condensation (1% KOH) of 2-butanone with acetaldehyde yields a mixture of 2-hexene-4-one and 3-methyl-2-pentene-4-one (**15**). To obtain the latter in pure form the mixture was partially hydrogenated and then carefully distilled to remove the 2-hexene-4-one. The *3-methyl-2-pentene-4-one* thus obtained was allowed to react with *sec*-butylmagnesium chloride to give, in good yield, the ketone *3,4,5-trimethyl-2-heptanone* (**16**), bp 80–82°C/14 Torr; *n*, 1.4334; mol. wt. (ms) 156. A portion (5.0 g) of this ketone (**16**) was added at 0°C to 35 mL of 3.5% methyllithium solution, then refluxed for 2 h, to give 4.7 g of crude alcohol (**17**). The alcohol was dehydrated at 75°C with 1.0 g naphthalenesulfonic acid to give 2.3 g of olefins which were then hydrogenated to the alkane *2,3,4,5-tetramethylheptane* (**14**).

Method B

3-Methyl-2-hexene-4-one (**5**) (15.5 g; 8) was allowed to react with a Grignard reagent prepared from 4.0 g Mg and 13.8 g 2-chloropropane to give 20.4 g of crude ketone **11**. Fractionation of the product gave 16.8 g of *4,5,6-trimethyl-3-heptanone* (**11**), bp 81–82°C/14 Torr; *n*, 1.4301; mol. wt. (ms)

TABLE 1. Chemical shifts and spin lattice relaxation times for some branched alkanes*

Compound	Parameter	Carbon atom 1	2	3	4	5	6	7	8	9	10	11
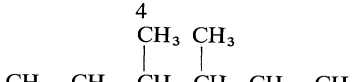 3,4-Dimethylhexane	δ	13.0 13.0	26.5 28.5	39.1 40.1	14.7 16.8							
	T_1	8.1 8.1	9.4 9.1	12.1 12.0	7.2 6.8							
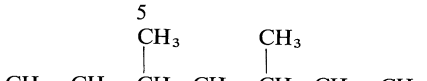 3,5-Dimethylheptane	δ	12.0 12.3	30.2 31.4	32.5 32.6	44.9 45.0	19.7 20.5						
	T_1	6.8 6.5	7.1 7.1	9.9 9.9	6.7 6.7	5.3 5.4						
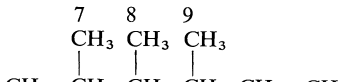 2,3,4-Trimethylhexane†	δ	22.2 22.6	30.2 31.1	43.4 44.9	36.6 37.4	25.6 29.2	12.5 12.7	19.2 20.6	11.6 12.0	14.8 18.4		
	T_1	5.6 5.6	10.2 10.2	10.5 10.0	10.1 10.1	7.3 7.3	6.8 6.7	5.9 5.7	6.2 6.1	5.9 5.6		
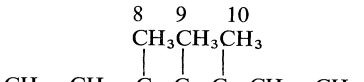 3,4,5-Trimethylheptane‡	δ	12.2 12.3 11.6	28.7 29.4 25.7	36.3 37.0 37.1	40.6 44.0 41.8	37.7	26.7	12.0	15.0 16.0 18.0	12.5 12.7 12.6	18.5	
	T_1	6.1 6.1 5.5	6.2 6.4 6.3	9.1 9.2 9.3	9.0 9.2 9.0	9.2	6.2	5.46	5.1 5.5 4.9	5.7 5.7 5.7	4.8	
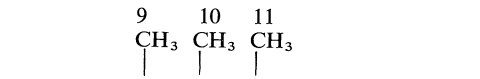 3,4,5-Trimethyloctane (**10**)	δ		25.1 26.0 27.8 28.5	35.7 36.3 36.5 37.1	40.4 41.3 41.5 43.6	33.5 34.3 34.4 35.2	34.6 35.7 37.9 38.5	20.4 20.4 20.6 20.7		14.6 14.6 15.4 15.6		17.3 17.8 17.9 18.5
	T_1		5.0 4.7 4.9 4.9	7.0 7.8 6.7 7.4	7.5 6.5 6.4 6.1	6.7 7.6 6.8 6.3	4.6 4.8 5.0 5.0	5.8 5.8 5.7 5.3		5.0 5.0 4.2 4.2		3.9 4.1 3.9 4.0

TABLE 1 (*Concluded*)

Compound	Parameter	Carbon atom 1	2	3	4	5	6	7	8	9	10	11
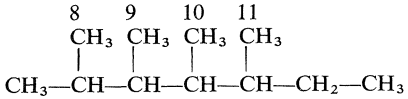 2,3,4,5-Tetramethylheptane (**14**)	δ						28.7 28.8 30.0 30.1					
	T_1						5.2 5.2 6.2 6.2					
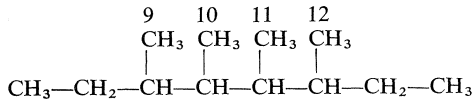 3,4,5,6-Tetramethyloctane (**4**)§	δ		25.0 26.0 28.6 29.8 23.1	35.7 37.8 38.2 36.0 36.9	38.7 39.7 40.7 42.3 39.2	39.2	36.9	23.2				
	T_1		3.8 3.6 3.7 3.8 3.6	5.0 5.2 5.2 5.3 5.3	5.2 5.2 5.2 4.8 5.1	5.1	5.3	3.6				

*Chemical shifts are reported in ppm to low field of TMS in CS_2 and relaxation times are in seconds.
†Particular lines assigned to carbons 1 and 7 could be reversed.
‡Four lines were observed for each carbon atom 1, 2, 3, and 8. Since there are three possible diastereomers, three lines were assigned arbitrarily to carbons 1, 2, 3, 8 and one to carbons 7, 6, 5, and 10 (see text).
§Six lines were found for each carbon atom 2, 3, and 4. Since the gas chromatograph shows five peaks, five lines were assigned arbitrarily to each of carbons 2, 3, and 4 and one to carbons 7, 6, and 5.

156; ir (carbonyl) ν_{max} 1705 cm^{-1}. On treatment with methyllithium, 16.8 g of ketone gave 18.1 g crude alcohol (**12**) which was dehydrated immediately with naphthalenesulfonic acid. The crude olefin product thus obtained was twice fractionally distilled to remove some unreacted ketone and yield a highly pure sample of olefin. Hydrogenation gave *2,3,4,5-tetramethylheptane* (**14**), bp 69°C/12 Torr; *n*, 1.4286. *Anal.* calcd. for $C_{11}H_{24}$: C 84.51, H 15.48; found: C 84.58, H 15.23.

Method C

A 15.0 g portion of *3-pentene-2-one* (**19**) (8) was added at 0°C to a Grignard solution prepared from 5.5 g Mg, 0.35 g CuCl, and 21.2 g 2-chlorobutane and the mixture was refluxed for 2 h and allowed to stand overnight. The 22.7 g of crude product on fractionation gave 12.7 g of *4,5-dimethyl-2-heptanone* (**20**), bp 107–108°C/23 Torr; *n*, 1.4279; ir ν_{max} (carbonyl) 1715 cm^{-1}, (CO—CH_3) 1165 cm^{-1} (lit. (9) 1720, 1162). The semicarbazone had mp 132–133°C (lit. (9) mp 121°C). *Anal.* calcd. for $C_{10}H_{21}N_3O$: C 60.26, H 10.53, N 21.08; found: C 59.76, H 10.78, N 21.22.

4,5-Dimethyl-2-heptanone (**20**; 13.0 g) was brominated with 14.7 g Br_2 in 50 mL dichloromethane and 10 drops acetic acid at 0°C. The crude bromo ketone **21** was added dropwise to 7.0 g sodium methoxide in ether and then refluxed for 3 h. Water was added and the product extracted with ether. Yield, 12.1 g crude, 10.9 g purified *methyl 2,3,4-trimethylhexanoate* (**22**), bp 92°C/15 Torr; *n*, 1.4293; ir ν_{max} ($COOCH_3$) 1735 cm^{-1}, (OCH_3) 1185 cm^{-1}.

An alternative synthesis of *2,3,4-trimethylhexanoic acid* was based on the haloform reaction (10). The methyl ester of the acid obtained in this way had the same pattern of retention times in the capillary glc as that prepared above.

When 5.0 g of the ester **22** was treated with 2 equiv. of methylmagnesium iodide, 5.3 g of oil having strong ir absorption at 3460 cm^{-1} was formed. Dehydration occurred on distillation under reduced pressure; spinning band distillation of the product gave 1.6 g of olefin which hydrogenated to *2,3,4,5-tetramethylheptane* (**14**).

Dehydration of the alcohols **12** and **17** by $POCl_3$ was accomplished by dissolving 1.5 g of alcohol in 12 mL dry pyridine and adding 3 mL $POCl_3$ dropwise at 0°C. The mixture was stirred at room temperature for 5 h, diluted with water, and extracted with ether to give about 1.2 g crude olefins. Hydrogenation then gave 2,3,4,5-tetramethylheptane.

1. P. LACHANCE and A. M. EASTHAM. J. Polym. Sci. Polym. Chem. Ed. **13**, 1843 (1975).
2. L. P. LINDEMAN and J. Q. ADAMS. Anal. Chem. **43**, 1245 (1971).
3. D. M. GRANT and E. G. PAUL. J. Am. Chem. Soc. **86**, 2984 (1964).
4. C. J. CARMAN, A. R. TARPLEY, and J. H. GOLDSTEIN. Macromolecules, **6**, 719 (1973).
5. G. G. MCDONALD and J. S. LEIGH. J. Magn. Reson. **9**, 358 (1973).
6. A. C. COPE, C. M. HOFMANN, and E. M. HARDY. J. Am. Chem. Soc. **63**, 1852 (1941).
7. J. E. DUBOIS and R. LUFT. Bull. Soc. Chim. Fr. 1153 (1954).
8. J. E. DUBOIS. Bull. Soc. Chim. Fr. 66 (1949).
9. J. ROYER and J. DREUX. Justus Liebigs Ann. Chem. **741**, 109 (1970).
10. C. DJERASSI and J. STAUNTON. J. Am. Chem. Soc. **83**, 736 (1961).

Violation of the '*para*' rule in the boron trifluoride catalyzed cycloaddition of 4,4-dimethyl-2,5-cyclohexadien-1-one to isoprene. Total synthesis of ionene

HSING-JANG LIU AND ERIC N. C. BROWNE

Department of Chemistry, University of Alberta, Edmonton, Alta., Canada T6G 2G2

Received August 18, 1978

HSING-JANG LIU and ERIC N. C. BROWNE. Can. J. Chem. **57**, 377 (1979).

In violation of the '*para*' rule, the boron trifluoride catalyzed addition of 4,4-dimethyl-2,5-cyclohexadien-1-one (**1**) to isoprene gave rise to the unexpected enone **3** as the only adduct. Under similar conditions, the addition of *trans*-piperylene proceeded as predicted by the '*ortho*' rule to give the single adduct **6**. Enone **3** was converted in three steps to the naturally occurring hydrocarbon ionene (**12**).

HSING-JANG LIU et ERIC N. C. BROWNE. Can. J. Chem. **57**, 377 (1979).

Contrairement à la "règle *para*", l'addition catalysée par le trifluorure de bore de la diméthyl-4,4 cyclohexadiène-2,5 one-1 (**1**) à l'isoprène conduit uniquement à la formation de l'énone **3** inattendue. Dans des conditions semblables, l'addition du *trans*-pipérylène conduit, tel que prévu par la "règle *ortho*", à un seul adduit, **6**. On peut transformer l'énone **3** en trois étapes à l'hydrocarbure ionène (**12**) que l'on retrouve dans la nature.

[Traduit par le journal]

In connection with a project directed towards the total synthesis of terpenoids, we have investigated the Diels–Alder reaction of 4,4-dimethyl-2,5-cyclohexadien-1-one (**1**) (1, 2) with isoprene. It has been well established both experimentally (3–6) and theoretically (7, 8, and references therein) that dienophiles in which the double bond is conjugated with an electron-withdrawing group undergo Diels–Alder reaction with 1- and 2-substituted dienes to give '*ortho*' and '*para*' adducts, respectively, as the predominant products. Equally well known is the pronounced enhancement of regioselectivity[1] when the reaction is carried out in the presence of a Lewis acid (8, 11–17). The production of adduct **2** is thus expected to predominate from the cycloaddition of dienone **1** to isoprene, particularly when catalyzed by a Lewis acid.

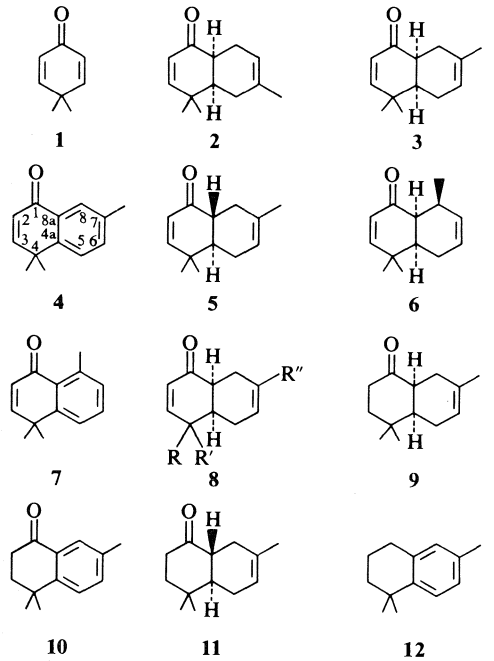

Treatment of dienone **1** with an excess of isoprene in ether at ambient temperature for 22 days using boron trifluoride as a catalyst resulted in the formation, in 61% yield, of a single 1:1 adduct as clearly indicated by examination of its spectral data.[2] To establish its orientation, the adduct was dehydrogenated with *N*-bromosuccinimide (18) in carbon tetrachloride. The principal product[3] so obtained was shown spectroscopically to possess structure **4**. In its nmr spectrum, the C-8 hydrogen atom, which lies within the deshielding zone of the carbonyl, appeared at a significantly lower field (δ 7.90) as a narrowly split multiplet (<1 Hz) whereas the two remaining aromatic protons appeared at δ 7.27 and 7.37 each with a large coupling constant of 8 Hz. These observations were in agreement only with the assigned structure **4**. It follows that the precursor of

[1]Except in the case of certain dienophiles of type XRC=CHY or XHC=CHY where X and Y are both conjugating and electron withdrawing. In such cases, the reversal of the orientation under thermal conditions could be achieved using the 'guidance-by-catalysis' approach illustrated by the elegant work of Valenta and co-workers (9, 10).

[2]See Experimental for details.

[3]The aromatic compound corresponding to structure **2** was not detected. The balance of the material consisted of bromo derivatives of **3** and **4** as shown by the nmr and mass spectra.

0008-4042/79/040377-04$01.00/0

4 must also possess a methyl group at C-7, as represented by structure **3**,[4] in violation of the '*para*' rule (3, 5, 6) for Diels–Alder addition.

The exclusive formation of such an '*anti-para*'[5] adduct from the addition of isoprene to dienone **1** is, to our knowledge, unprecedented. The unusual orientational effect could well be steric. The exclusion of the otherwise favoured formation of the '*para*' product could be attributed to the interference of the methyl groups of the two counterparts in development of the *endo* transition state (3, 5, 6) when approached in accordance with the '*para*' rule. In agreement with this postulate was the finding that the addition of *trans*-piperylene to dienone **1** under similar conditions proceeded normally to give enone **6**[6] as the only adduct.

From a synthetic viewpoint, the one-step formation of enone **3**, and possibly adducts of type **8** by suitable choice of the reactants, offers an efficient route for the construction of synthetically useful 1-decalone systems. To demonstrate the synthetic utility as well as to further confirm the structure of **3**, we have completed a simple total synthesis of ionene (**12**), a naturally occurring hydrocarbon (20, 21). Reduction of enone **3** with lithium in ammonia (22) afforded a 78% yield of *cis*-ketone **9** which, on treatment with *N*-bromosuccinimide, underwent dehydrogenation giving rise to aryl ketone **10** in 35% yield. The same compound could be prepared in a better yield of 45% from the *trans*-ketone **11** which was obtained in 91% yield by epimerization of **9** with aqueous sodium hydroxide in methanol. Wolff–Kishner reduction (23) of aryl ketone **10** resulted in the formation of ionene (**12**) in 64% yield. The ir, nmr, and mass spectra of the synthetic material were shown to be identical with those of an authentic sample prepared from β-ionone (24).

Experimental

General

Mass spectra were recorded on an AEI MS-50 spectrometer. Infrared spectra were obtained using a Perkin-Elmer Model 457 or a Nicolet 7-199 FT-IR spectrophotometer. Nuclear magnetic resonance spectra were recorded on an HR-100 spectrometer using tetramethylsilane as internal standard. Elemental analyses were performed by the microanalytical laboratory of this department.

cis-*4,4,7-Trimethyl-1,4,4a,5,8,8a-hexahydronaphthalen-1-one (3)*

To a solution of 4,4-dimethyl-2,5-cyclohexadien-1-one (**1**) (4.887 g, 40 mmol) in ether (100 mL) were added, 30 min apart, boron trifluoride etherate (2.46 mL, 20 mmol) and then freshly distilled isoprene (12 mL, 0.12 mol). The resulting solution was stirred at room temperature under a nitrogen atmosphere for 22 days during which time additional isoprene was added (12 mL after each 24-h period for 6 days and a further 40 mL each after 13 and 17 days). The reaction mixture was cooled to 0°C, made basic by dropwise addition of saturated aqueous sodium bicarbonate solution, and extracted with chloroform. The organic solution was washed with water, dried (Na_2SO_4), filtered, and concentrated. Column chromatography of the residue on silica gel, eluting with a solution of 80% ether in Skelly B, gave a mixture consisting of enone **3** and a small amount of polymer. This mixture was subjected to bulb-to-bulb distillation at 90°C/0.5 Torr. The pure enone **3** (4.624 g; 61% yield) thus obtained showed the following spectral data: ir (neat): 3010 (C=CH), 1685 (C=O), 1378, 1365 (CH_3), and 827 cm^{-1} (C=CH); nmr (CCl_4) δ: 1.09 (s, 3H, CH_3), 1.30 (s, 3H, CH_3), 1.66 (s, 3H, $=CCH_3$), 5.18 (br s, 1H, —CH=), 5.68 (d, 1H, J = 10 Hz, —CH=C*H*CO—), and 6.28 (dd, 1H, J = 10, $J' \simeq$ 1 Hz, —C*H*=CHCO—); ms M^+ 190.1354 (calcd. for $C_{13}H_{18}O$: 190.1358). *Anal.* calcd. for $C_{13}H_{18}O$: C 82.06, H 9.54; found: C 81.81, H 9.56.

4,4,7-Trimethyl-1,4-dihydronaphthalen-1-one (4)

Enone **3** (292 mg, 1.49 mmol) was dissolved in carbon tetrachloride (20 mL). *N*-Bromosuccinimide (530 mg, 2.98 mmol) and benzoyl peroxide (10 mg, 0.04 mmol) were added. The mixture was refluxed using a preheated oil bath for 45 min. After cooling to room temperature, it was filtered and concentrated to give an oil which was purified by column chromatography twice on silica gel eluting with a solution of 5–7% ether in petroleum ether. The aryl enone **4** (106 mg; 38% yield) thus obtained showed the following spectral data: ir (neat): 1665 (C=O), 1618, 1500 (C=C), 1383, 1374, 1364 (CH_3), 828, and 891 (aromatic CH); nmr (CCl_4) δ: 1.47 (s, 6H, 2 × CH_3), 2.43 (s, 3H, benzylic CH_3), 6.25 (d, J = 10 Hz, —CH=C*H*CO—), 6.78 (d, J = 10 Hz, —C*H*=CHCO—), 7.27 (md, 1H, J = 8, $J' <$ 1 Hz, C-6 H), 7.37 (d, 1H, J = 8 Hz, C-5 H), and 7.90 (m, 1H, $J <$ 1 Hz, C-8 H); ms M^+ 186.1053 (calcd. for $C_{13}H_{14}O$: 186.1044).

trans-*4,4,7-Trimethyl-1,4,4a,5,8,8a-hexahydronaphthalen-1-one (5)*

A solution of 1 *N* aqueous sodium hydroxide (10 mL) was added to a solution of *cis*-enone **3** (459 mg, 2.42 mmol) in 20 mL of methanol and stirred for 1 h. The mixture was then extracted with methylene chloride. The extracts were washed with water, dried ($MgSO_4$), filtered, and concentrated. Column chromatography on silica gel eluting with 3% ether in petroleum ether gave 400 mg (87% yield) of a mixture of enones **3** and **5** in a ratio of 30:70 as determined by glc analysis on a 8 ft × $\frac{1}{8}$ in. column of 10% diethyleneglycol succinate on 80–100 mesh Chromosorb W (DMCS treated, acid washed).

Recrystallization from ether gave 120 mg of pure **5**, mp 56–60°C, and 279 mg of recovered *cis–trans* mixture. The *trans*-enone **5** showed the following spectral data: ir ($CHCl_3$): 1673 (C=O), 1390, 1383 (CH_3), and 790 cm^{-1} (C=CH); nmr

[4]The stereochemistry of **3** follows from the *cis* principle (3, 5, 6) and its successful epimerization with aqueous sodium hydroxide in methanol to the *trans*-isomer **5**.

[5]This term is used to distinguish this effect from the '*meta*' addition observed by Fleming *et al.* (19), in cases where the substituents of both reactants are electron donating, an effect which was predicted by Houk (7). We wish to emphasize that, although the methyl substituent is '*meta*' to the directing group, the important feature is the violation of the rule which is expected to apply and not the application of a different rule.

[6]The structure of **6** was verified by dehydrogenation with *N*-bromosuccinimide to aryl ketone **7**. Its stereochemistry which is not of crucial importance for the present studies, was tentatively assigned on the basis of the *cis* principle and the *endo* rule (3, 5, 6).

(CCl_4) δ: 1.03, 1.13 (both s, 3H each, —$C(CH_3)_2$—), 1.67 (br s, 3H, =CCH_3), 5.31 (m, 1H, =CH—), 5.69 (d, 1H, J = 10 Hz, —COC*H*=CH—), and 6.55 (d, 1H, J = 10 Hz, —COCH=C*H*—); ms M^+ 190.1359 (calcd. for $C_{13}H_{18}O$: 190.1358). *Anal.* calcd. for $C_{13}H_{18}O$: C 82.06, H 9.54; found: C 81.94, H 9.78.

cis,syn-*4,4,8-Trimethyl-1,4,4a,5,8,8a-hexahydronaphthalen-1-one (**6**)*

To a solution of dienone (**1**) (116 mg, 0.935 mmol) in ether (10 mL), were added, 15 min apart, boron trifluoride etherate (66 mg, 0.468 mmol) and then *trans*-piperylene (1.87 mL, 18.7 mmol). The solution was stirred at room temperature under a nitrogen atmosphere for 6 days after which a solution of *trans*-piperylene (0.94 mL, 9.4 mmol) in ether (5 mL) was added. After further stirring for 3 days, the reaction mixture was made basic with saturated aqueous sodium bicarbonate and extracted with methylene chloride. The extracts were washed with water, dried over magnesium sulfate, and filtered. Concentration of the filtrate followed by column chromatography of residue on silica gel with ether – petroleum ether (1:50) elution gave enone **6** (123 mg; 69% yield); ir ($CHCl_3$): 1686 (C=O), 1397, 1386 (CH_3), and 716 cm^{-1} (HC=CH); nmr (CCl_4) δ: 1.10 (s, 3H, CH_3), 1.33 (s, 3H, CH_3), 1.38 (d, 3H, J = 8 Hz, CH_3), 5.46 (complex, 2H, —CH=CH—), 5.58 (d, 1H, J = 10 Hz, —CH=C*H*CO—), and 6.15 (dd, 1H, J = 10, J' = 1.5 Hz, —C*H*=CHCO—); ms M^+ 190.1359 (calcd. for $C_{13}H_{18}O$: 190.1358). *Anal.* calcd. for $C_{13}H_{18}O$: C 82.06, H 9.54; found: C 81.68, H 9.56.

*4,4,8-Trimethyl-1,4-dihydronaphthalen-1-one (**7**)*

To a solution of enone **6** (85 mg, 0.45 mmol) in carbon tetrachloride (10 mL), were added *N*-bromosuccinimide (159 mg, 0.89 mmol) and benzoyl peroxide (5 mg, 0.02 mmol). The mixture, after refluxing for 30 min, was cooled to room temperature and filtered. Concentration followed by column chromatography of the residue twice on silica gel using a solution of 1% ether in petroleum ether as eluent gave aryl enone **7** (10 mg; 12% yield); ir ($CHCl_3$): 1663 (C=O), 1592 (aromatic), 1395, 1377, and 1364 cm^{-1} (CH_3); nmr (CCl_4) δ: 1.45 (s, 6H, 2 × CH_3), 2.70 (s, 3H, benzylic CH_3), 6.15 (d, 1H, J = 10 Hz, —CH=C*H*CO—), 6.64 (d, 1H, J = 10 Hz, —C*H*=CHCO—), 7.05 (dd, 1H, $J = J'$ = 4 Hz, C-6 H), and 7.30 (d, 2H, J = 4 Hz, C-5 and C-7 H); ms M^+ 186.1039 (calcd. for $C_{13}H_{18}O$: 186.1044).

cis-*4,4,7-Trimethyl-1,2,3,4,4a,5,8,8a-octahydronaphthalen-1-one (**9**)*

Lithium ribbon (480 mg, 69 g-at.) was added over a 10-min period to 360 mL of liquid ammonia (freshly distilled from sodium) at −78°C under a nitrogen atmosphere. After 5 min, a solution of enone **3** (1 g, 5.26 mmol) in ether (60 mL) was added dropwise over 40 min and stirring was continued for an additional 90 min. Solid NH_4Cl was then added to discharge the blue color and ammonia was allowed to evaporate. Addition of water was followed by extraction with chloroform. After washing sequentially with water, 5% hydrochloric acid, and saturated aqueous sodium chloride, the chloroform solution was dried (Na_2SO_4), filtered, and concentrated. Column chromatography of the residue on silica gel eluting with ether – Skelly B (1:20) gave ketone **9** (791 mg; 78% yield); ir (neat): 3010 (C=CH), 1712 (C=O), 1390, 1379, 1366 (CH_3), and 808 cm^{-1} (C=CH); nmr (CCl_4) δ: 0.98 (s, 3H, CH_3), 1.32 (s, 3H, CH_3), 1.65 (br s, 3H, =CCH_3), and 5.17 (br s, 1H, —CH=); ms M^+ 192.1520 (calcd. for $C_{13}H_{20}O$: 192.1514). *Anal.* calcd. for $C_{13}H_{20}O$: C 81.20, H 10.48; found: C 81.44, H 10.59.

trans-*4,4,7-Trimethyl-1,2,3,4,4a,5,8,8a-octahydronaphthalen-1-one (**11**)*

To a solution of ketone **9** (91 mg, 0.47 mmol) in methanol (5 mL) was added 1 *N* aqueous NaOH (5 mL). After stirring at room temperature under a nitrogen atmosphere for 15 h, the reaction mixture was extracted with ether. The organic solution was washed with water and dried ($MgSO_4$). Filtration and concentration gave an oil which was purified by silica gel column chromatography. Elution with ether – petroleum ether (1:25) gave ketone **11** (83 mg; 93% yield); ir (neat): 3005 (C=CH), 1708 (C=O), 1372, 1392 (CH_3), and 793 cm^{-1} (C=CH); nmr (CCl_4) δ: 0.99 (s, 3H, CH_3), 1.07 (s, 3H, CH_3), 1.65 (br s, 3H, =CCH_3), and 5.24 (br s, 1H, —CH=); ms M^+ 192.1517 (calcd. for $C_{13}H_{20}O$: 192.1520). *Anal.* calcd. for $C_{13}H_{20}O$: C 81.20, H 10.48; found: C 81.06, H 10.31.

*4,4,7-Trimethyl-1,2,3,4-tetrahydronaphthalen-1-one (**10**)*

From trans-*Ketone **11***

Ketone **11** (63 mg, 0.32 mmol) was dissolved in carbon tetrachloride (10 mL) and *N*-bromosuccinimide (117 mg, 0.64 mmol) was added. The mixture was heated under reflux for 1 h. After cooling to room temperature, it was filtered. Concentration of the filtrate gave an oil which was purified by column chromatography on silica gel. Elution with a solution of 1.5% ether in petroleum ether gave aryl ketone **10** (28 mg; 45% yield); ir ($CHCl_3$): 1686 (C=O), 1611, 1498 (aromatic), 1390 and 1366 cm^{-1} (CH_3); nmr (CCl_4) δ: 1.34 (s, 6H, 2 × CH_3), 1.92 (complex, 2H, —C*H*$_2$CH$_2$CO—), 2.32 (s, 3H, benzylic CH_3), 2.57 (complex, 2H, —CH_2CO—), 7.18 (s, 1H, —C*H*=CH—) 7.19 (s, 1H, —CH=C*H*—), and 7.69 (s, 1H, C-8 H); ms M^+ 188.1195 (calcd. for $C_{13}H_{16}O$: 188.1201).

From cis-*Ketone **9***

Under similar conditions, oxidation of ketone **9** (99 mg, 0.52 mmol) with *N*-bromosuccinimide (148 mg, 1.04 mmol) in carbon tetrachloride (5 mL) gave aryl ketone **10** (34 mg; 35% yield).

*Ionene (**12**)*

Aryl ketone **10** (34 mg, 0.18 mmol) was dissolved in triethylene glycol (1.8 mL). Hydrazine hydrochloride (199 mg, 2.89 mmol) and anhydrous hydrazine (1.15 mL, 36.2 mmol) were added. The mixture was heated at 130°C (bath temperature) for 3 h. Powdered KOH (408 mg; 12.7 mmol based on 87% KOH) was added and the resulting mixture was heated at 190–200°C for 1 h and 230°C for 2 h; during that period condensers were exchanged and rinsed to remove volatile materials. The reaction mixture, after cooling to room temperature, was combined with rinsings and extracted with ether. The extracts were washed with 5% hydrochloric acid and water, dried ($MgSO_4$), filtered, and concentrated. Column chromatography of the residue on neutral alumina (Woelm II) with petroleum ether elution gave ionene (**12**) (20 mg; 64% yield); ir (neat; KBr window): 1885, 1745 (ArH), 1616, 1500 (C=C), 1386, 1365 (CH_3), 881 and 821 cm^{-1} (ArH); nmr (CCl_4) δ: 1.24 (s, 6H, 2 × CH_3), 1.66 (complex, 4H, —CH_2CH_2—), 2.21 (s, 3H, benzylic CH_3), 2.66 (t, 2H, J = 6 Hz, benzylic CH_2), 6.71 (s, 1H, CH_3—C=C*H*C=), 6.78 and 7.06 (both d, 1H each, J = 8 Hz, —CH=CH—); ms M^+ 174.1410 (calcd. for $C_{13}H_{18}$: 174.1408). The compound was found to be identical in spectral properties with an authentic sample prepared from β-ionone (24).

Acknowledgements

We are grateful to the National Research Council

of Canada and the University of Alberta for financial support.

1. H. E. ZIMMERMAN, P. HACKETT, D. F. JUERS, J. M. MCCALL, and B. SCHRÖDER. J. Am. Chem. Soc. **93**, 3653 (1971).
2. J. N. MARX and L. R. NORMAN. Tetrahedron Lett. 2867 (1973).
3. K. ALDER and G. STEIN. Angew. Chem. **50**, 510 (1937).
4. YU. A. TITOV. Russ. Chem. Rev. **31**, 267 (1962).
5. A. S. ONISHCHENKO. Diene synthesis. Israel Program of Scientific Translations, Jerusalem. 1964.
6. J. SAUER. Angew. Chem. Int. Ed. Engl. **6**, 16 (1967).
7. K. N. HOUK. J. Am. Chem. Soc. **95**, 4092 (1973).
8. K. N. HOUK. Acc. Chem. Res. **8**, 361 (1975).
9. Z. STOJANAC, R. A. DICKINSON, N. STOJANAC, R. J. WOZNOW, and Z. VALENTA. Can. J. Chem. **53**, 616 (1975).
10. M. KAKUSHIMA, J. ESPINOSA, and Z. VALENTA. Can. J. Chem. **54**, 3304 (1976).
11. P. YATES and P. EATON. J. Am. Chem. Soc. **82**, 4436 (1960).
12. G. I. FRAY and R. ROBINSON. J. Am. Chem. Soc. **83**, 249 (1961).
13. E. F. LUTZ and G. M. BAILEY. J. Am. Chem. Soc. **86**, 3899 (1964).
14. T. INUKAI and T. KOJIMA. J. Org. Chem. **31**, 1121 (1966); **32**, 869 (1967).
15. J.-C. SOULA, D. LUMBROSO, M. HELLIN, and F. COUSSEMANT. Bull. Soc. Chim. Fr. 2065 (1966).
16. A. W. MCCULLOCH and A. G. MCINNES. Can. J. Chem. **49**, 3153 (1971).
17. K. N. HOUK and R. W. STROZIER. J. Am. Chem. Soc. **95**, 4094 (1973).
18. R. A. BARNES. J. Am. Chem. Soc. **70**, 145 (1948).
19. I. FLEMING, F. L. GIANNI, and T. MAH. Tetrahedron Lett. 881 (1976).
20. G. V. PIGULEVSKII, V. I. KOVALEVA, and D. V. MOTUSKUS. Vopr. Khim. Terpenov Terpenoidov, Akad. Nauk Litovsk SSR Tr. Vses. Soveshchaniya Vil'nyus, 153 (1959); Chem. Abstr. **55**, 15842h (1961).
21. T. R. KEMP, L. P. STOLTZ, and L. V. PACKETT. Phytochemistry, **10**, 478 (1971).
22. E. PIERS and W. M. PHILLIPS-JOHNSON. Can. J. Chem. **53**, 1281 (1975).
23. W. NAGATA and H. ITAZAKI. Chem. Ind. 1194 (1964).
24. M. T. BOGERT and V. G. FOURMAN. J. Am. Chem. Soc. **55**, 4670 (1933).

Branched-chain sugars. Reaction of furanoses with formaldehyde: A simple synthesis of D- and L-apiose[1]

PAK-TSUN HO

Division of Biological Sciences, National Research Council of Canada, Ottawa, Ont., Canada K1A 0R6

Received July 20, 1978

PAK-TSUN HO. Can. J. Chem. **57**, 381 (1979).

A simple synthesis of D- and L-apiose using the aldol condensation of furanose with formaldehyde under alkaline conditions as a key reaction is described.

PAK-TSUN HO. Can. J. Chem. **57**, 381 (1979).

On décrit une synthèse simple du D- et du L-apiose faisant appel à une condensation aldolique du furannose avec le formaldéhyde en milieu alcalin comme étape clé.

[Traduit par le journal]

Introduction

D-Apiose which is a naturally occurring branched-chain sugar is widely distributed in the plant kingdom. The chemistry and biochemistry of apiose continue to be of interest. Several groups have reported the synthesis of D- or L-apiose (1).

In the previous paper (2), the author reported an efficient and stereospecific method for the preparation of 2-*C*-hydroxymethyl branched sugar by way of condensation of a furanose with formaldehyde under alkaline conditions. To demonstrate further the potential and generality of this type of condensation in the branched carbohydrate field, a simple synthesis of D- and L-apiose, using the aldol condensation as a key reaction, is described.

Results and Discussion

Treatment of 2,3:5,6-di-*O*-isopropylidene-D-mannofuranose (**1**) (3) with excess 37% aqueous solution of formaldehyde and potassium carbonate (at pH 10) in methanol at 80°C yielded exclusively the 2-*C*-hydroxymethyl derivative **2** in 86% yield (2). The product **2** was a chromatographically homogeneous syrup and exhibited a specific rotation of +11° (*c* 1.2, methanol). Its corresponding diacetate **3** was obtained under standard acetylation conditions in excellent yield, $[\alpha]_D$ +31.5° (*c* 1.4, chloroform). Interestingly, its ^{1}H nmr spectrum showed a sharp singlet at 6.30 ppm for the C-1 proton and suggested that one anomer was formed. Further, oxidation of **2** with bromine containing barium carbonate in water provided the lactone **4** in almost quantitative yield, mp 106°, $[\alpha]_D$ +34° (*c* 2.6, chloroform).

Now transformation of compound **2** to 2,3-*O*-isopropylidene-D-apiose (**6**) could be accomplished in a simple one-pot operation. Selective hydrolysis of compound **2** in aqueous methanol containing concentrated sulfuric acid at room temperature overnight resulted in removal of the 5,6-*O*-isopropylidene group and afforded exclusively 2-*C*-(hydroxymethyl)-2,3-*O*-isopropylidene-D-mannofuranose (**5**), which for the purpose of characterization could be isolated quantitatively as a homogeneous syrup, $[\alpha]_D$ +16.3° (*c* 3.2, acetone). In practice, however, the reaction mixture was neutralized to pH 7 and compound **5** was reduced readily with excess sodium borohydride at room temperature. After neutralization of the aqueous reaction mixture, oxidation of the resulting reduction product with sodium metaperiodate gave crystalline 2,3-*O*-isopropylidene-D-apiose (**6**), mp 72°C, $[\alpha]_D$ −40° (*c* 1.5, chloroform).[2] Using this one-pot reaction, crystalline compound **6** could be produced in 79% yield from compound **2**. Sharp singlets at 5.34 and 4.29 ppm for C-1 and C-2 protons in its ^{1}H nmr spectrum indicate that these protons have to be in *trans* configuration and that it is a β-D-anomer (5). Compound **6** after hydrolysis with Dowex 50W (H^+) in water at 70°C and removal of the 2,3-*O*-isopropylidene group yielded D-apiose (**7**) in almost quantitative yield, $[\alpha]_D$ +5.2° (*c* 1.1, water). Its *N*-benzyl-*N*-phenylhydrazone was identical with a sample prepared from natural apiose (4).

Treatment of 2,3-*O*-isopropylidene-D-hamamelose (**8**) (2) with excess sodium borohydride in water at room temperature afforded the corresponding reduction product, which, after neutralization of the aqueous reaction mixture with acetic acid, was oxidized subsequently with sodium metaperiodate to give crystalline 2,3-*O*-isopropylidene-L-apiose (**9**) in 82% yield, mp 74°C, $[\alpha]_D$ +39° (*c* 1.7, chloroform). Its ^{1}H nmr spectrum was completely identical with the spectrum of D-isomer **6**. On treatment of compound **9** under

[1]NRCC No. 17060.

[2]Williams and Jones (4) obtained compound **6** as a syrup, $[\alpha]_D$ −35° (*c* 0.87, methanol).

0008-4042/79/040381-03$01.00/0

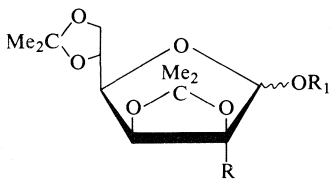

1 R = R_1 = H
2 R = CH_2OH, R_1 = H
3 R = CH_2OAc, R_1 = Ac

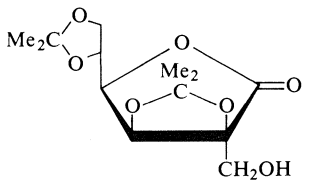

4

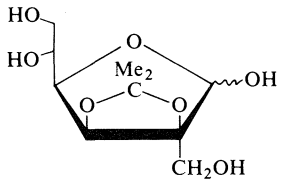

5

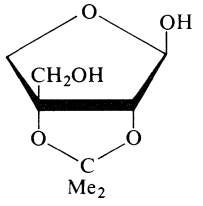

6

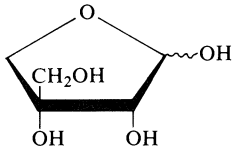

7

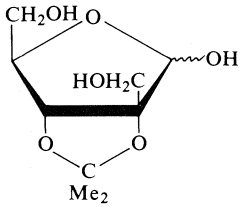

8

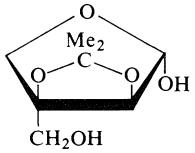

9

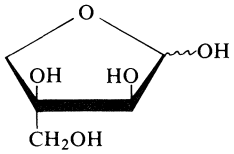

10

similar conditions described for the preparation of compound **6**, L-apiose (**10**) was obtained in excellent yield, $[\alpha]_D$ −5.0° (*c* 1.1, water), and was characterized as its *N*-benzyl-*N*-phenylhydrazone prepared by Schaffer's method, mp 136°C, $[\alpha]_D$ −76.5° (*c* 1.8, pyridine) (6).

Experimental

Melting points were determined on a Reichert hot stage apparatus and are uncorrected. Optical rotations were measured with a Perkin-Elmer Model 141 automatic polarimeter at room temperature. Infrared spectra were of chloroform solutions and ^{1}H nmr spectra were of deuteriochloroform solutions with TMS as internal reference. Thin-layer and preparative-layer chromatography was done using silica gel containing a fluorescent indicator (G_{254}).

2-C-(Hydroxymethyl)-2,3:5,6-di-O-isopropylidene-D-mannofuranose (2)

2,3:5,6-di-*O*-isopropylidene-D-mannofuranose (1) (4) (3.86 g) and potassium carbonate (2.8 g) were dissolved in methanol (50 mL) and 37% aqueous solution of formaldehyde (30 mL). The solution was heated at 85°C (oil bath temperature) under argon for 2 days, after which time it was neutralized with 10% aqueous sulfuric acid. Evaporation of the solvent to dryness gave a residue which was extracted with chloroform and the extracts were concentrated to a syrup. Chromatography of the crude product on silica gel using 4% methanol in chloroform as the eluant gave **2** as a chromatographically homogeneous syrup (3.84 g, 86%); $[\alpha]_D$ +11° (*c* 1.2, methanol); ir ($CHCl_3$): 3550 and 3380 cm^{-1} (hydroxyl); ^{1}H nmr ($CDCl_3$) δ: 5.43 (s, 1H, C-1 proton), 4.70 (d, 1H, C-3 proton), 3.92 (m, 2H, C-2′ protons), and 1.50 ppm (broad s, 12H, four methyls). *Anal.* calcd. for $C_{13}H_{22}O_7$: C 53.78, H 7.64; found: C 53.46, H 7.52.

1-O-Acetyl-2-C-(acetoxymethyl)-2,3:5,6-di-O-isopropylidene-D-mannofuranose (3)

2-*C*-(Hydroxymethyl)-2,3:5,6-di-*O*-isopropylidene-D-mannofuranose (**2**) (50 mg) was acetylated with acetic anhydride (10 drops) in dry pyridine (1 mL) at room temperature overnight. The reaction mixture was isolated in the usual manner and yielded compound **3** as a syrup (54 mg, 85%); $[\alpha]_D$ + 31.5° (*c* 1.4, chloroform); ir ($CHCl_3$): 1750 cm^{-1} (acetate); ^{1}H nmr ($CDCl_3$) δ: 6.30 (s, 1H, C-1 proton), 4.73 (d, 1H, C-3 proton), 4.46 (s, 2H, C-2′ protons), and 2.13 ppm (s, 6H, two acetoxyls). *Anal.* calcd. for $C_{17}H_{26}O_9$: C 54.54, H 7.00; found: C 54.68, H 7.12.

Oxidation of Compound 2 to the Corresponding Lactone 4

Barium carbonate (800 mg) was suspended in an aqueous solution of compound **2** (189 mg) in distilled water (10 mL). Bromine (0.6 mL) was added dropwise with stirring, after which time the reaction mixture was filtered and the filtrate was evaporated to dryness. The residue was extracted with chloroform. The extracts were concentrated to a syrup which was crystallized from ether–hexane to yield the pure lactone **4** (170 mg, 90%) and the product had melting point 106°C; $[\alpha]_D$ +34° (*c* 2.6, chloroform); ir ($CHCl_3$): 3500 (hydroxyl), 1785 cm^{-1} (lactone); ^{1}H nmr ($CDCl_3$) δ: 4.92 (d, 1H, C-3 proton), 4.58 (q, 1H, C-4 proton), 4.06 (q, 2H, C-2′ protons), and 1.50 ppm (broad s, 12H, four methyls). *Anal.* calcd. for $C_{13}H_{20}O_7$: C 54.16, H 6.99; found: C 54.21, H 6.97.

2-C-(Hydroxymethyl)-2,3-O-isopropylidene-D-mannofuranose (5)

A solution of compound **2** (280 mg) in 20% aqueous methanol (8 mL) containing small amount of concentrated

sulfuric acid (0.05 mL) was stirred at room temperature overnight and tlc showed the starting material had been completely consumed with the formation of a new component. The solution was neutralized with sodium bicarbonate and evaporated to dryness. The residue was then extracted with ethyl acetate. Evaporation of the solvent afforded the product **5** as a homogeneous syrup (237 mg, 98%). $[\alpha]_D$ +16.3° (*c* 3.2, acetone); ^{1}H nmr (acetone-d_6) δ: 5.29 (broad s, 1H, C-1 proton), 4.65 (d, 1H, C-3 proton), and 1.43 ppm (s, 6H, two methyls). *Mol. wt.* calcd. for $C_{10}H_{18}O_7$: 250; found (mass spectroscopy): 250.

*2,3-*O*-Isopropylidene-*β*-*D*-apiose (**6**)*

A solution of compound **2** (459 mg) in 20% aqueous methanol (12 mL) containing 1 drop of concentrated sulfuric acid was stirred at room temperature overnight, after which it was neutralized to pH 7 and an excess of sodium borohydride (180 mg) was added in portions with stirring. After 4 h at room temperature acetic acid was then added until the pH of the solution was at 7. To the stirred solution at 0°C, sodium metaperiodate (580 mg, 2 equiv.) was added in portions and the stirring was continued at room temperature for a further 1 h. Evaporation of the solvent to dryness gave a residue which was extracted with chloroform three times. Removal of the solvent yielded a solid material. Pure D-apiose derivative **6** (265 mg, 79%) was obtained by recrystallization from ether–hexane and melted at 72°C; $[\alpha]_D$ −40° (*c* 1.5, chloroform); ir ($CHCl_3$): 3500 cm^{-1} (hydroxyl); ^{1}H nmr ($CDCl_3$): δ 5.34 (d, J = 4 Hz, 1H, C-1 proton, singlet when D_2O added), 4.29 (s, 1H, C-2 proton), 4.10 (d, J = 4 Hz, OH, disappearing when D_2O added), 3.93 (s, 2H, C-4 protons) 3.74 (d, J = 5 Hz, 2H, C-3′ protons, singlet when D_2O added), 2.93 (t, J = 5 Hz, OH, disappearing when D_2O added), 1.40 and 1.30 ppm (25, 6H, two methyls). *Anal.* calcd. for $C_8H_{14}O_5$: C 50.52, H 7.42; found: C 50.58, H 7.56.

*D-Apiose (**7**) and its* N*-Benzyl-*N*-phenylhydrazone*

2,3-*O*-Isopropylidene-D-apiose **6** (250 mg) was hydrolyzed with Dowex 50W (H^+) resin (300 mg) at 70°C (oil bath temperature) for 5 h. The resin was removed by filtration and the filtrate was evaporated to dryness to afford D-apiose (**7**) as a syrup (198 mg, 96%), $[\alpha]_D$ +5.2° (*c* 1.1, water). D-Apiose (**7**) was treated with a solution of *N*-benzyl-*N*-phenylhydrazine (1.2 equiv.) in ethanol at room temperature for 3 h. Evaporation of the solvent gave a solid material. Recrystallization of the crude product from chloroform–methanol yielded pure *N*-benzyl-*N*-phenylhydrazone of **7**, $[\alpha]_D$ −75° (*c* 1.7, pyridine), mp 137°C. This was found to be identical in all respects (mp specific rotation, nmr) with a sample prepared from natural apiose. *Anal.* calcd. for $C_{18}H_{22}O_4N_2$: C 65.40, H 6.70, N 8.50; found: C 65.38, H 6.52, N 8.38.

*2,3-*O*-Isopropylidene-L-apiose (**9**)*

To a stirred solution of 2,3-*O*-isopropylidene-D-hamamelose (**8**) (3) (425 mg) in distilled water (20 mL) was added an excess of sodium borohydride (152 mg). The reaction mixture was stirred at room temperature for 1 h, after which time the reaction mixture was neutralized to pH 7 with acetic acid. Sodium metaperiodate (420 mg, 1 equiv.) was added with stirring. After 1 h at room temperature, the solution was taken to dryness and the residue was then extracted with chloroform. Evaporation of the solvent and recrystallization of the crude product from ether–hexane yielded the pure product **9** (302 mg, 82%), mp 74°C; $[\alpha]_D$ +39° (*c* 1.7, chloroform); its ^{1}H nmr spectrum was completely identical with the spectrum of compound **6**. *Anal.* calcd. for $C_8H_{14}O_5$: C 50.52, H 7.42; found: C 50.63, H 7.56.

*L-Apiose (**10**) and its* N*-Benzyl-*N*-phenylhydrazone*

2,3-*O*-Isopropylidene-L-apiose (**9**) (190 mg) was hydrolyzed under the same conditions used for the preparation of D-apiose (**7**), and L-apiose (**10**) (140 mg) was obtained as a syrup in 91% yield, $[\alpha]_D$ −5.0° (*c* 1.1, water). Its *N*-benzyl-*N*-phenylhydrazone was prepared by the same procedure described above for the *N*-benzyl-*N*-phenylhydrazone of **7**. It had melting point 136°C and $[\alpha]_D$ −76.5° (*c* 1.8, pyridine) and was identical in all respects with a sample prepared by Schaffer's method. *Anal.* calcd. for $C_{18}H_{22}O_4N_2$: C 65.40, H 6.70, N 8.50; found: C 65.41, H 6.65, N 8.42.

Acknowledgements

The author thanks Dr. O. E. Edwards for reading this manuscript and Mr. H. Seguin for the microanalyses and the mass spectra.

1. R. R. Watson and N. S. Orenstein. Adv. Carbohydr. Chem. Biochem. **31**, 135 (1975).
2. P.-T. Ho. Tetrahedron Lett. 1623 (1978).
3. R. S. Tipson, H. S. Isbell, and J. E. Stewart. J. Res. Natl. Bur. Stand. **62**, 257 (1959).
4. D. T. Williams and J. K. N. Jones. Can. J. Chem. **42**, 67 (1964).
5. D. H. Ball, F. H. Bissett, I. L. Klundt, and L. Long, Jr. Carbohydr. Res. **17**, 165 (1971).
6. (*a*) R. Schaffer. J. Am. Chem. Soc. **81**, 5452 (1959); (*b*) W. G. Overend, A. C. White, and N. R. Williams. Carbohydr. Res. **15**, 185 (1970).

Branched-chain sugars. Reaction of furanoses with formaldehyde: a stereospecific synthesis of L-dendroketose[1]

PAK-TSUN HO

Division of Biological Sciences, National Research Council of Canada, Ottawa, Ont., Canada K1A 0R6

Received July 20, 1978

PAK-TSUN HO. Can. J. Chem. **57**, 384 (1979).

A simple conversion of 2,3-*O*-isopropylidene-D-hamamelose, prepared by reaction of 2,3-*O*-isopropylidene-D-ribose with formaldehyde, into L-dendroketose is described.

PAK-TSUN HO. Can. J. Chem. **57**, 384 (1979).

On décrit une transformation simple du *O*-isopropylidène-2,3 D-hamamelose, obtenu par réaction du *O*-isopropylidène-2,3 D-ribose avec le formaldéhyde, en L-dendrocétose.

[Traduit par le journal]

Introduction

Reaction of 1,3-dihydroxy-2-propanone under alkaline conditions provided a biosynthetically interesting and unnatural branched-chain hexose, which was named dendroketose (1). It was also observed by the same investigator that the L-isomer is preferentially fermented by a mold and the D-isomer, 4-*C*-(hydroxymethyl)-D-*glycero*-pentulose, could then be isolated.

An effort to synthesize L-dendroketose from 2,3:4,5-di-*O*-isopropylidene-*aldehydo*-D-arabinose failed because the intermediate racemized when treated with base (2). However, very recently, the same group reported a successful synthesis of this sugar (3).

In the previous communication (4), a general and stereospecific method for the synthesis of branched sugar by way of condensation of furanoses with formaldehyde and the utilization of this facile technique in synthesis have been described. The present paper reports the further use of our method in a simple synthesis of L-dendroketose.

Results and Discussion

On treatment of 2,3-*O*-isopropylidene-D-hamamelose **1**, prepared by reaction of 2,3-*O*-isopropylidene-D-ribose with formaldehyde (4), with 2.2 equiv. of benzoyl chloride in pyridine and benzene at 0°C, the dibenzoate **2** after work-up and crystallization was obtained in 89% yield, mp 116°C, $[\alpha]_D$ −2.5° (*c* 2.2, chloroform). Compound **2** was reduced readily with excess sodium borohydride in aqueous tetrahydrofuran and yielded 5-*O*-benzoyl-2-*C*-(benzoyloxymethyl)-2,3-*O*-isopropylidene-D-*erythro*-pentitol **3** in 91% yield as a chromatographically homogeneous syrup $[\alpha]_D$ +24° (*c* 1.5, chloroform). Tritylation of compound **3** with 4,4′-dimethoxytrityl chloride in pyridine at room temperature provided quantitatively the 4,4′-dimethoxytrityl ether **4**, $[\alpha]_D$ −6.4° (*c* 1.1, chloroform).

It is noteworthy that compound **4** could be prepared by an alternative route with complete selectivity as follows. Reduction of compound **1** with sodium borohydride in water afforded the corresponding reduction product, which after work-up was treated carefully with 2.1 equiv. of benzoyl chloride in pyridine and benzene (1:1) at −5°C overnight and then treated subsequently with 4,4′-dimethoxytrityl chloride in the same reaction mixture at room temperature to give a homogeneous material in 60% yield from the starting compound **1**. This material was completely identical with compound **4** in all respects.

Now compound **4** could be oxidized to 1-*O*-benzoyl-4-*C*-(benzoyloxymethyl)-5-*O*-(4,4′-dimethoxytrityl)-3,4-*O*-isopropylidene-L-*glycero*-pentulose **5** in 80% yield by way of chromium trioxide–pyridine complex in anhydrous methylene dichloride, $[\alpha]_D$ −24° (*c* 1.5, chloroform). When the ketone **5** was treated with 80% aqueous acetic acid at room temperature overnight, crystalline 1-*O*-benzoyl-4-*C*-(benzoyloxymethyl)-3,4-*O*-isopropylidene-L-dendroketose **6** was obtained in 94% yield and exhibited a specific rotation of +47.2° (*c* 1.1, chloroform). It seemed unlikely that racemization at C-3 would take place under such mild acidic treatment. Finally alkaline hydrolysis of **6** in methanolic sodium hydroxide at room temperature gave crystalline 3,4-*O*-isopropylidene-L-dendroketose **7** in quantitative yield, mp 98°C, $[\alpha]_D$ +48.6° (*c* 1.4, chloroform). To establish the structure and configurational purity of our synthetic material, 1,2:3,4-di-*O*-isopropylidene-L-dendroketose **8** was prepared. When compound **7** was dissolved in anhydrous acetone containing a

[1]NRCC No. 17102.

0008-4042/79/040384-03$01.00/0

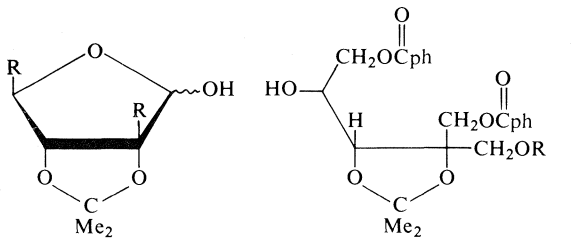

1 R = CH_2OH **3** R = H

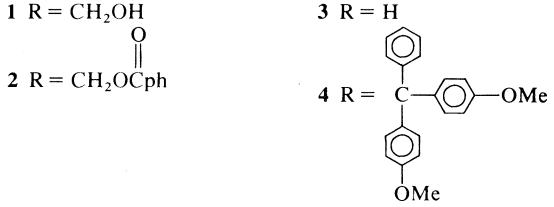

2 R = CH_2OCph **4** R =

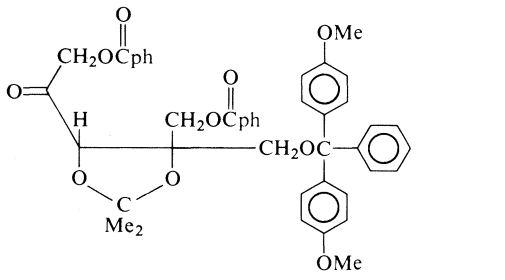

5

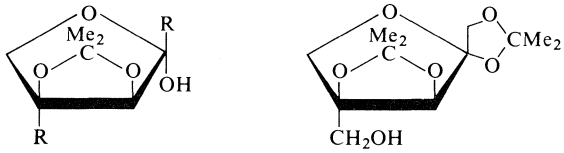

6 R = CH_2OCph
7 R = CH_2OH **8**

small amount of *p*-toluenesulfonic acid at room temperature, the desired compound **8** was obtained as the sole product, mp 87°C, $[\alpha]_D$ +122° (*c* 0.7, acetone), and it was identical with an authentic sample. The overall yield from **1** was 60%.

Experimental

Melting points were determined on a Reichert hot stage apparatus and are uncorrected. Optical rotations were measured with a Perkin–Elmer Model 141 automatic polarimeter at room temperature. ^{1}H nmr spectra were taken on a Varian E360 spectrometer using tetramethylsilane as an internal reference. Infrared spectra were of chloroform solutions. Thin-layer and preparative-layer chromatography was done using silica gel containing a fluorescent indicator (G_{254}).

*2-C-(Benzoyloxymethyl)-5-O-benzoyl-2,3-O-isopropylidene-*D*-hamamelose (2)*

To a stirred solution of 2,3-*O*-isopropylidene-D-hamamelose **1** (4) (764 mg) in dry pyridine (6 mL) and benzene (3 mL) was added dropwise a solution of benzoyl chloride (1.1 g, 2.2 equiv.) in benzene (6 mL) at 0°C and the reaction mixture was stirred at 0°C overnight. The reaction mixture was diluted with chloroform and washed with cold 10% aqueous sulfuric acid, then with aqueous sodium bicarbonate solution and finally with water. After drying over magnesium sulfate, evaporation of the solvent gave a syrup which crystallized on standing. Recrystallization from ether yielded compound **2** (1.3 g, 89%), mp 116°C; $[\alpha]_D$ −2.5° (*c* 2.2, chloroform); infrared ($CHCl_3$): 3500 (OH), 1720 cm^{-1} (benzoate); ^{1}H nmr ($CDCl_3$) δ: 5.55 (d, J = 4 Hz, 1H, C-1 proton, singlet when D_2O added), 4.83 (d, 2H, C-5 protons), 4.75 (s, 1H, C-3 proton), 4.60 (s, 2H, C-2′ protons), 4.33 (d, J = 4 Hz, OH, disappearing when D_2O added), 1.55 (s, 3H, methyl), and 1.46 ppm (s, 3H, methyl). *Anal.* calcd. for $C_{23}H_{24}O_8$: C 64.48, H 5.65; found: C 64.45, H 5.44.

*2-C-(Benzoyloxymethyl)-5-O-benzoyl-2,3-O-isopropylidene-*D*-erythro-pentitol (3)*

A solution of compound **2** (720 mg) in 10% aqueous tetrahydrofuran (40 mL) was cooled to 0°C and sodium borohydride (300 mg) was added with stirring. After 1 h, acetic acid was added dropwise until the solution became slightly acidic (pH 6). Sodium chloride was then added and the solution was extracted with chloroform several times. Drying over magnesium sulfate and evaporation of the chloroform solvent yielded the product **3** (660 mg) as a homogeneous syrup in 90% yield; $[\alpha]_D$ +24° (*c* 1.5, chloroform); infrared ($CHCl_3$): 3500 ~ 3400 (OH), 1720 cm^{-1} (benzoate); ^{1}H nmr ($CDCl_3$) δ: 4.70 (m, 2H, C-5 protons), 4.63 (s, 2H, C-2′ protons), 3.84 (s, 2H, C-1 protons), and 1.42 ppm (s, 6H, two methyls). *Mol. wt.* calcd. for $C_{23}H_{26}O_8$: 430; found (mass spectroscopy): 430.

Tritylation of Compound 3

Method A

A mixture of compound **3** (430 mg) and 4,4′-dimethoxytrityl chloride (410 mg, 1.2 equiv.) in pyridine (6 mL) was stirred at room temperature overnight. The solvent was evaporated *in vacuo* and the crude product was purified by preparative tlc on silica gel; 702 mg of the pure compound **4** was obtained as a foam and the yield was 95%; $[\alpha]_D$ −6.4° (*c* 1.1, chloroform); infrared ($CHCl_3$): 3470 (OH), 1720 cm^{-1} (benzoate); ^{1}H nmr ($CDCl_3$) δ: 4.87 (q, 2H, C-2′ protons), 4.34 (m, 2H, C-5 protons), 3.75 (s, 6H, two methoxyls), 3.50 (q, 2H, C-1 protons), 1.35 and 1.30 ppm (two s, 6H, two methyls). *Anal.* calcd. for $C_{45}H_{44}O_{10}$: C 72.56, H 5.95; found: C 72.62, H 6.01.

Method B

To a stirred solution of compound **1** (140 mg) in 90% aqueous tetrahydrofuran (6 mL) was added sodium borohydride (50 mg). The reaction mixture was stirred at room temperature for 2 h, neutralized with acetic acid, and then evaporated to complete dryness *in vacuo*. The crude product was treated with benzoyl chloride (196 mg, 2.1 equiv.) in pyridine (6 ml) at 0°C overnight, after which time 4,4′-dimethoxytrityl chloride (256 mg, 1.2 equiv.) was added and the reaction mixture was stirred at room temperature for 4 h. The yellow solution was then diluted with chloroform. The chloroform solution was washed with aqueous sulfuric acid and then with water, dried over anhydrous magnesium sulfate, and evaporated to dryness. The crude product **4** was purified by preparative tlc on silica gel. The pure **4** was obtained as a foamed material (156 mg, 60%) which was identical with the material prepared by method A.

1-O-*Benzoyl*-*4*-C-*(benzoyloxymethyl)*-*5*-O-*(4,4′-dimethoxytrityl)*-*3,4*-O-*isopropylidene*-L-glycero-*pentulose (**5**)*

A solution of the alcohol **4** (900 mg) in anhydrous methylene dichloride (10 mL) was added dropwise to a stirred solution of chromium trioxide – pyridine complex (3 g) in the same solvent (20 mL) and the mixture was stirred at room temperature for 5 h. The reaction mixture was diluted with ether (150 mL) and the dark precipitate was then removed by filtration. The filtrate was washed with water, dried over anhydrous magnesium sulfate, and concentrated to a syrup. Purification of the syrup by preparative tlc on silica gel yielded 720 mg (80%) of the ketone **5** as a homogeneous syrup; $[\alpha]_D$ −24° (*c* 1.5, chloroform); infrared ($CHCl_3$): 1720 cm^{-1} (benzoate and ketone); ^1H nmr ($CDCl_3$) δ: 5.16 (q, 2H, C-5 protons), 4.75 (s, 1H, C-3 protons), 4.60 (q, 2H, C-2′ protons), 3.75 (s, 6H, two methoxyls), 3.33 (q, 2H, C-1 protons), 1.73 and 1.45 ppm (two s, 2H, two methyls). *Anal.* calcd. for $C_{45}H_{42}O_{10}$: C 72.76, H 5.70; found: C 72.71, H 5.62.

1-O-*Benzoyl*-*4*-C-*(benzoyloxymethyl)*-*3,4*-O-*isopropylidene*-L-*dendroketose (**6**)*

A solution of the ketone **5** (440 mg) in 80% aqueous acetic acid (4 mL) was stirred at room temperature overnight, at which time the solution was evaporated to dryness *in vacuo*. Pure L-dendroketose derivative **6** was isolated by preparative tlc on silica gel and recrystallization from ether–hexane afforded 252 mg (94%) of **6**, mp 101°C; $[\alpha]_D$ +47.2° (*c* 1.1, chloroform); infrared ($CHCl_3$): 3560 and 3480 (OH), 1720 cm^{-1} (benzoate); ^1H nmr ($CDCl_3$) δ: 4.70 and 4.61 (2q, 4H, C-1 and C-4′ protons), 4.65 (s, 1H, C-3 proton), 4.19 (s, 2H, C-5 protons), 3.62 (s, OH, exchanged with D_2O), 1.56 and 1.47 ppm (two s, 6H, two methyls). *Anal.* calcd. for $C_{23}H_{24}O_8$: C 64.48, H 5.65; found: C 64.46, H 5.62.

3,4-O-*Isopropylidene*-L-*dendroketose (7)*

A solution of compound **6** (209 mg) and sodium hydroxide (40 mg) in methanol (7 mL) was stirred at room temperature for 1 h. The solution was neutralized with 5% aqueous sulfuric acid and evaporated to dryness. The residue was extracted several times with chloroform. Evaporation and crystallization from ether–hexane gave pure **7** (106 mg, 98%), mp 98°C; $[\alpha]_D$ +48.6° (*c* 1.4, chloroform); infrared ($CHCl_3$): 3500 and 3350 cm^{-1} (OH); ^1H nmr ($CDCl_3$ + D_2O) δ: 4.36 (s, 1H, C-3 protons), 4.04 (s, 2H, C-5 protons), 3.85 (broad s, 4H, C-1 and C-4′ protons), 1.52 and 1.43 ppm (two s, 6H, two methyls). *Anal.* calcd. for $C_9H_{16}O_6$: C 49.08, H 7.33; found: C 49.07, H 7.34.

1,2:*3,4*-*Di*-O-*isopropylidene*-L-*dendroketose (**8**)*

3,4-*O*-Isopropylidene-L-dendroketose **7** (100 mg) was stirred with anhydrous acetone (5 mL) containing a small amount of *p*-toluenesulfonic acid (1 mg) at room temperature for 1 h. The solution was neutralized with pyridine and compound **8** was isolated as crystalline material (102 mg). After recrystallization from hexane it melted at 87°C and was identical with an authentic sample in all respects, $[\alpha]_D$ +122° (*c* 0.7, acetone); infrared ($CHCl_3$): 3500 and 3350 cm^{-1} (OH); ^1H nmr ($CDCl_3$ + D_2O) δ: 4.33 (s, 1H, C-3 proton), 4.22 (q, 2H, C-1 protons), 3.90 (s, 2H, C-5 protons), 3.82 (broad s, 2H, C-4′ protons), 1.50 ppm (broad s, 12H, 4 methyls). *Anal.* calcd. for $C_{12}H_{20}O_6$: C 55.37, H 7.75; found: C 55.39, H 7.74.

Acknowledgements

The author wishes to thank Professor W. A. Szarek for a sample of 1,2:3,4-di-*O*-isopropylidene-L-dendroketose. The author also thanks Dr. O. E. Edwards for reading this manuscript and Mr. H. Seguin for the microanalyses and the mass spectra.

1. (*a*) L. M. Utkin. Dokl. Akad. Nauk SSSR, **67**, 301 (1949); (*b*) L. M. Utkin. Zh. Obshch. Khim. **25**, 530 (1955).
2. H. C. Jarnell, W. A. Szarek, J. K. N. Jones, A. Dmytraczenko, and E. B. Rathbone. Carbohydr. Res. **45**, 151 (1975).
3. W. A. Szarek, G. W. Schnarr, H. C. Jarnell, and J. K. N. Jones. Carbohydr. Res. **53**, 101 (1977).
4. P.-T. Ho. Tetrahedron Lett. 1623 (1978).

Thermodynamics of chloroform and methanol mixtures

PREM P. SINGH[1]
Department of Chemistry, Punjab Agricultural University, Ludhiana, India

BUTA R. SHARMA
Department of Chemistry, D.A.V. College, Jullundur, India

AND

KULJIT S. SIDHU
Department of Chemistry, Punjabi University, Patiala, India

Received May 3, 1978

PREM P. SINGH, BUTA R. SHARMA, and KULJIT S. SIDHU. Can. J. Chem. **57**, 387 (1979).

Heats of mixing and vapour pressures of chloroform (A)+ methanol (B_n) as a function of concentration have been determined at 303.15 K. The excess Gibbs free energy of mixing, G^E values, have been obtained from the measured vapour pressure data. The heats of mixing values are negative for solutions rich in methanol but they become positive for solutions rich in chloroform. On the other hand, G^E values are positive for all the methanol mole fractions and $G^E > H^E$. The results have been analysed in terms of Barker and ideal associated model theory of non-electrolyte solutions. The analysis has revealed that only the ideal associated model approach (which here assumes the presence of A_mB ($m = 1, 2$), AB_k ($k = 2$) and B_l ($l = 1$) molecular species) well describes the general behaviour of H^E with x_A over the entire chloroform concentration range for this mixture. The equilibrium constants for the various association reactions along with the enthalpy of formation of the various molecular species have also been calculated.

PREM P. SINGH, BUTA R. SHARMA et KULJIT S. SIDHU. Can. J. Chem. **57**, 387 (1979).

On a déterminé à 303.15 K la chaleur de mélange et la pression de vapeur de mélanges chloroforme (A) + méthanol (B_n) en fonction de la concentration. A l'aide des mesures de pression de vapeur, on a calculé les valeurs de l'énergie libre de Gibbs d'excès G^E pour le mélange. Les chaleurs de mélange sont négatives si les solutions sont riches en méthanol, mais elles deviennent positives si les solutions sont riches en chloroforme. D'autre part, la valeur de G^E est positive pour toutes les fractions molaires de méthanol et $G^E > H^E$. On a analysé les résultats en rapport avec la théorie de Barker et celle du modèle de l'association idéale pour les solutions de non-électrolytes. Cette analyse a révélé que seule le modèle de l'association idéale (en admettant l'existence des espèces moléculaires A_mB ($m = 1, 2$), AB_k ($k = 2$) et B_l ($l = 1$)) décrit bien la variation générale de H^E en fonction de x_A sur tout le domaine de concentrations de chloroforme. On a également calculé les constantes d'équilibre des réactions d'association, ainsi que l'enthalpie de formation des différentes espèces moléculaires.

[Traduit par le journal]

Introduction

Following Frank and Wen's model (1) of liquid water, it was believed that lower alcohols should also possess a similar type of cooperativity in the formation of hydrogen bonded polymers. However, there is considerable disagreement as to the identity of the predominant associated species (2–6). Again while the solution hetero-association data (7, 8) have been limited to calculation of equilibrium constants for 1:1 and 2:1 complexes only, Tucker and Christian (9) have interpreted the results of their distribution studies to indicate that methanol contains monomers, dimers, and higher *r*-mers. The present work describes interactions in methanol and chloroform mixtures.

Experimental

Materials

Reagent grade methanol (B.D.H.) was treated in the manner suggested by Vogel (10). Methanol (50–75 ml), 5 g Mg, and 0.5 g iodine were placed in a round bottomed flask. The mixture was warmed on a water bath until iodine disappeared and methoxide formed. Methanol (900 ml) was added, the mixture was boiled under reflux and then finally distilled. Chloroform B.D.H. (A.R.) was shaken as suggested by Vogel (10) several times with about half of its volume of water, dried over anhydrous calcium chloride, and finally distilled. The purity of the final samples was checked by density determinations at 295.15 ± 0.01 K which agreed to within 0.00005 g ml^{-1} with the literature values (11, 12).

Heats of mixing measurements at 303.15 ± 0.01 K were made in an adiabatic calorimeter similar in design to Fernandez-Garcia and Boissonas (13) and has been described

[1]To whom all correspondence should be addressed. Present address: Department of Chemistry, Maharshi Dayanand University, Rohtak, India.

0008-4042/79/040387-07$01.00/0

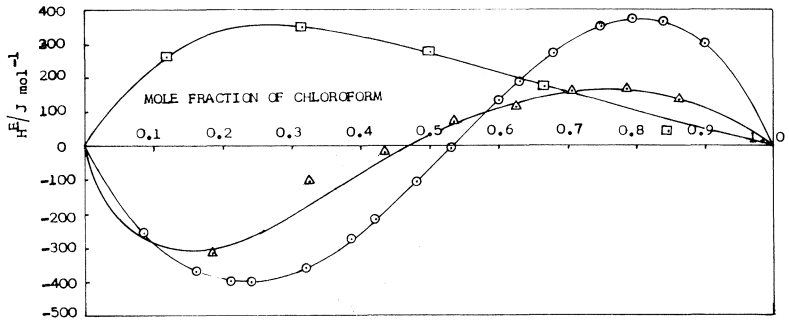

FIG. 1. Enthalpies of mixing H^E for chloroform (A) + methanol (B) at 303.15 K: ○, experimental H^E; △, calculated H^E according to ideal associated model that assumes the presence of AB, AB_2, A_2B, and B molecular species; □, calculated H^E according to ideal associated model that assumes the presence of AB, AB_2, AB_3, and B molecular species ($K_{1,0.5} = 0.4$, $\Delta H_{AB} = -1.0$ kJ mol^{-1}; $K_{0.5} = 0.04$, $\Delta H_B = 2.5$ kJ mol^{-1}; $K_{1.1} = 0.6$, $\Delta H_{AB_2} = -2.0$ kJ mol^{-1}; $K_{1,1.5} = 0.1$, $\Delta H_{AB_3} = -1.0$ kJ mol^{-1}).

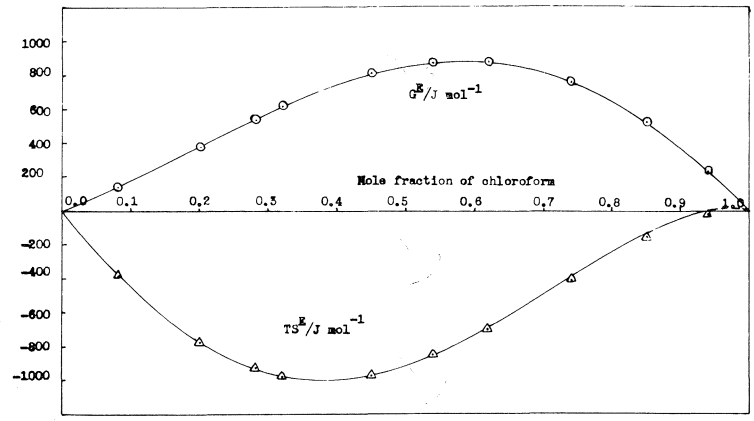

FIG. 2. Excess functions for chloroform (A) + methanol (B) at 303.15 K: ○, G^E and △, TS^E.

elsewhere (14). The performance of the calorimeter was tested by determining the heats of mixing of benzene and cyclohexane at 298.15 ± 0.01 K and these agreed to within 0.3% (over central range of concentration) with the corresponding literature values (15).

Vapour pressures of the methanol + chloroform mixtures were determined by a static method described previously (16). The apparatus (excluding the manometric part) was placed in a water thermostat which in turn was placed in another thermostat. The temperature of the outer thermostat was controlled to better than ±0.01 K and the temperature drift in the inner thermostat was of the order of ±0.002 K. The mercury heights in the manometer were read by a cathetometer which could read to ±0.001 cm. All vapour pressure measurements were reproducible to better than ±0.02 Torr.

The measured vapour pressure (155.49 Torr) of methanol at 303.15 K agreed within 0.3% with that (156.00 Torr) at 303.15 K obtained from the vapour pressure data (17, 18) reported for this compound at different temperatures. The measured vapour pressure of chloroform (241.15 Torr) also compares well with that (239.00 Torr) reported in the literature (19).

The H^E, G^E, and TS^E data are plotted in Figs. 1 and 2.

Results

The molar heats of mixing, H^E, and the measured vapour pressure data at 303.15 K for methanol and chloroform are recorded in Tables 1 and 2 respectively.[2]

The H^E data (Table 1) were fitted to the expression

$$[1] \quad H^E/x_A(1 - x_A) = h_0 + h_1(2x_A - 1) + h_2(2x_A - 1)^2$$

where x_A is the mole fraction of chloroform. The parameters h_0, h_1, and h_2 evaluated by fitting $H^E/x_A(1 - x_A)$ to expression [1] by the method of least-squares are given together with the standard deviation of the molar heats of mixing, $\sigma(H^E)$, in Table 1.

The vapour pressure data were used to evaluate the molar excess Gibbs free energy, G^E, by Barker's method (20). The form of the function used for G^E, following Redlich-Kister (21) is

$$[2] \quad G^E/RT = x_A(1 - x_A)[G_0 + G_1(2x_A - 1) + G_2(2x_A - 1)^2 + G_3(2x_A - 1)^3]$$

[2]Complete set of the actual experimental data is available, at a nominal charge, from the Depository of Unpublished Data, CISTI, National Research Council of Canada, Ottawa, Ont., Canada K1A 0S2.

TABLE 1. Parameters X_m ($X = h$ or G) of eqs. [1] and [2], standard deviation of pressure $\sigma(P)$ along with the standard deviation of H^E, $\sigma(H^E)$ for chloroform (A) + methanol (B) mixture at 303.15 K

	Value for m =					
Parameter	0	1	2	3	$\sigma(H^E)$/(J mol^{-1})	$\sigma(P)$/Torr
h_m	−264.30	4049.22	531.87	—	2.47	—
G_m	1.3559	0.5744	−0.2320	−0.0560	—	7.64

TABLE 2. Comparison of H^E values calculated according to Barker's theory with values interpolated from the measured values at three mole fractions of the component A and the interaction energies of chloroform (A) + methanol (B) at 303.15 K

Property	Values for mole fraction of the component A =			
(J mol^{-1})	0.3	0.5	0.7	Interaction energies/(J mol^{-1})
H^E_{exp}	−370.00	−67.0	302.00	
$H^{E(1)}$	65.40	41.62	39.26	$U_1^{(1)} = 25.53$, $U_2^{(1)} = -2099.35$, $U_3^{(1)} = -2408.72$
$H^{E(2)}$	−6.44	−19.02	−260.32	$U_1^{(2)} = 25.53$, $U_2^{(2)} = -2099.35$, $U_3^{(2)} = -2503.91$
$H^{E(3)}$	−76.45	−91.10	−63.92	$U_1^{(3)} = 25.53$, $U_2^{(3)} = -1618.18$, $U_3^{(3)} = -1618.18$, $U_4^{(3)} = -1481.81$

where G_0, G_1, G_2, and G_3 are adjustable parameters. These parameters are recorded in Table 1. The second virial coefficients of methanol and chloroform were evaluated from the Berthelot relation (22) using critical constant data (23, 24). The cross virial coefficients were taken as $(B_{11} + B_{22})/2$. The thermodynamic consistency of the data was tested (21) by plotting ln γ_A/γ_B vs. x_A. The positive and negative areas bounded by the curve ln γ_A/γ_B vs. x_A and the X-axis agreed to better than 0.2%.

Discussion

We are unaware of any H^E or G^E data for the chloroform and methanol system with which to compare our results.

Heats of mixing for chloroform (A) + methanol (B) are negative for solutions rich in methanol but they become positive for solutions rich in chloroform. The S-shaped H^E curve attains a maximum negative value of 400 J mol^{-1} at $x_{methanol} = 0.75$ and maximum positive value of 375 J mol^{-1} at $x_{methanol} = 0.19$. Further TS^E is negative at all the methanol mole fractions for which the experimental data are available and the curve of TS^E against $x_{methanol}$ is highly unsymmetrical about $x_{methanol}$.

At the simplest qualitative level the observed H^E data for this mixture may be accounted for if we assume that (*i*), methanol is self-associated and there is a change (decrease) in its self-association when it is mixed with chloroform, (*ii*), there is a hydrogen-bonded interaction between the hydroxyl oxygen of methanol and the chloroform hydrogen, and (*iii*), there is specific interaction between the hydroxyl hydrogen of methanol with the chlorine of chloroform. The negative values of H^E for high methanol concentrations are then due essentially to the factor (*ii*). This is because while interactions due to the factor (*ii*) can occur without breaking the alcohol–alcohol hydrogen bond, the same is not true of interactions due to factor (*iii*). Again the hydrogen-bonded interaction due to factor (*ii*) limits the orientational freedom of the chloroform molecules, thus making TS^E strongly negative so that G^E should be (as indeed is) positive. The positive values of H^E at high chloroform concentrations are due to the rupture of alcohol–alcohol hydrogen bonds followed by their subsequent hydrogen-bonded interaction with chloroform molecules. This in turn would require the TS^E at high chloroform concentrations to be considerably more positive than that at low chloroform concentrations and thus explains the unsymmetrical nature of TS^E vs. $x_{methanol}$ curve.

We examined our results using Barker's theory (25). It was assumed that chloroform (A) and methanol (B) have the following geometrical parameters:

Lattice

$$Z = 4$$

Chloroform molecules (A)

$$r_A = 4,\ Q_{H'}{}^A = 1,\ Q_{R'}{}^A = 9$$

Methanol molecules (B)

$$r_B = 2,\ Q_O{}^B = 2,\ Q_H{}^B = 1,\ Q_R{}^B = 3$$

where O, H, and R represent, respectively, hydroxyl oxygen, hydrogen, and hydrocarbon surface of methanol, and H′ and R′ represent the hydrogen and chlorine surface of chloroform. The interactions first considered were a specific (O...H′) interaction of

strength U_3 between the hydroxyl oxygen of methanol and the hydrogen of chloroform, a specific (O...H) interaction of strength U_2 between the hydroxyl oxygen and hydroxyl hydrogen of methanol, and a non-specific interaction for all the remaining contact points. For the sake of simplicity these non-specific interactions for all the remaining contact points were considered to have the same strength U_1. Excess energy of mixing at constant volume U_V^E, values at $x_A = 0.3$, 0.5, and 0.7 were then calculated (25) from this theory and they did not reproduce the corresponding experimental H^E values. (It is customary while testing a lattice theory to convert U_V^E values to measurements at constant pressure, H^E, using the relation $H_V^E = H^E - TV^E\alpha_m/(K_T)_m$ where α_m, $(K_T)_m$, and V^E are respectively the expansivity, isothermal compressibility, and excess volume of the mixture. However, since V^E is small (V^E for an equimolar mixture is -0.143 cm^3 mol^{-1}), contribution of the $TV^E\alpha_m/(K_T)_m$ term would be negligibly small and for the present analysis we have assumed $U_V^E \approx H^E$.) The best value of U_1, U_2, U_3 (designated as $U_i^{(1)}$ (i = 1 to 3)) and the corresponding H^E values designated as $H^{E(1)}$ are recorded in Table 2.

We next considered a slightly different model where, in addition to the above interactions, one of the chlorines of chloroform was assumed to be involved in a specific (H...Cl) interaction of strength U_4 with the hydroxyl of methanol. The chloroform was considered to have the following geometrical parameters

$$r_A = 4,\ Q_H{}^A = 1,\ Q_{Cl}{}^A = 1, \text{ and } Q_R{}^A = 8$$

The theoretical H^E values are now negative throughout the entire chloroform concentration range. The experimental H^E values for this mixture, on the other hand, are negative for $x_A \leq 0.53$ only. (The values of U_i (i = 1 to 4) and H^E are designated as $U_i^{(2)}$ and $H^{E(2)}$ in Table 2.) Models of chloroform molecules with two and higher hydrogen contact points were also considered but they failed to explain the overall behaviour of H^E with x_A for this mixture. The reason for the failure of the theory may be due to the simplicity of the models. Perhaps associated complexes of the general formula A_iB_j and B_n are present in these mixtures. H^E and G^E data for this mixture were next analysed in terms of the ideal associated model (26, 27).

TABLE 3. The equilibrium constants (mole fraction scale) for the various complexing reactions together with the enthalpies of formation of various molecular species and the variance of the fit $\sigma_D{}^2$ at 303.15 K

Equilibrium constant	Reaction of chloroform with methanol	Parameter	Mixtures of methanol (B_n) with chloroform (A)
$K_{1,0.5}$	0.40	ΔH_{AB}/(kJ mol^{-1})	−1.01
$K_{2,0.5}$	0.05	ΔH_{A_2B}/(kJ mol^{-1})	−1.00
$K_{1,1}$	0.80	ΔH_{AB} /(kJ mol^{-1})	−2.00
$K_{0.5}$	0.04	ΔH_B/(kJ mol^{-1})	2.50
		$\sigma_{D[10]}{}^2$	0.058
		$\sigma_{D[11]}{}^2$	0.060

It is assumed that in a binary solution of chloroform (A) and methanol (designated as B_n since methanol is self-associated) mutual equilibrium of the species A_mB, AB_k, and B_l (l = 1, 2, 3, ..., l; k = 1, 2, 3, ..., k; n = 1, 2, 3, ..., n; m = 2, 3, ..., m) exist according to the reactions

$$[3] \qquad (1+m)A + B_n \rightleftharpoons A_mB + AB_k + B_l$$

so that the equilibrium constants for the various association reactions represented by reaction [3] are

$$[4] \qquad K_{m,1/n} = a_{A_mB}/a_A{}^m a_{B_n}{}^{1/n}$$

$$[5] \qquad K_{1,k} = a_{AB_k}/a_A a_{B_n}{}^{k/n}$$

and

$$[6] \qquad K_{1/n} = a_{B_l}/a_{B_n}{}^{1/n}$$

where a denotes activities. If the activity coefficients of the various species represented in reaction [3] are assumed to be unity (26–29), the material balance equation for the system can be written as

$$[7] \qquad a_A + a_{B_n} + \sum_m K_{m,1/n} a_A{}^m a_{B_n}{}^{1/n} + \sum_k K_{1,k/n} a_A a_{B_n}{}^{k/n} + \sum_l K_{l/n} a_{B_n}{}^{1/n} = 1$$

Two simple cases were next considered.

Case (i), m = 1, 2, ..., m; n = 2; k = 2, 3, ..., k; l = 1, so that eq. [7] reduces to

$$[8] \qquad a_A + a_{B_2} + \sum_m K_{m,0.5} a_A{}^m a_{B_2}{}^{1/2} + \sum_k K_{1,k/2} a_A a_{B_2}{}^{k/2} + K_{0.5} a_{B_2}{}^{1/2} = 1$$

Case (ii), m = 1; n = 2; k = 2, 3, ..., k; l = 1, so that eq. [7] becomes

$$[9] \qquad a_A + a_{B_2} + K_{1,0.5} a_A a_{B_2}{}^{1/2} + \sum_k K_{1,k/2} a_A a_{B_2}{}^{k/2} + K_{0.5} a_{B_2}{}^{1/2} = 1$$

Algebraic manipulation of eqs. [8] and [9] yields

[10] $$\sum_m K_{m,0.5} a_A{}^m + \sum_k K_{1,k/2} a_A a_{B_2}{}^{(k-1)/2} + K_{0.5} = \frac{1 - a_A - a_{B_2}}{a_{B_2}{}^{1/2}}$$

and

[11] $$K_{1,0.5} a_A + \sum_k K_{1,k/2} a_A a_{B_2}{}^{(k-1)/2} + K_{0.5} = \frac{1 - a_A - a_{B_2}}{a_{B_2}{}^{1/2}}$$

respectively.

In order to evaluate the various K's in eqs. [10] and [11], the observed activities of the components of these binary mixtures were first corrected (30–32) for dispersion contributions by expressing

$$a_A = \gamma_A x_A / \gamma_A{}^*$$

$$a_{B_2} = \gamma_{B_2} x_{B_2} / \gamma_{B_2}{}^*$$

where $\gamma_A{}^*$ and $\gamma_{B_2}{}^*$ are the activity coefficients of a reference mixture. Since cyclohexane has nearly the same molar volume as chloroform, cyclohexane (A) + methanol (B_n) was taken as a reference system for the present analysis. Further, as the G^E data (33) for cyclohexane + methanol are available at 304.15 K, we assumed $G^E{}_{304.15K} \approx G^E{}_{303.15K}$ in order to evaluate the activity coefficient data for the components of this reference mixture at the various experimental mole fractions of methanol. A series of values were next assumed for the various K in eqs. [10] and [11] and the process was repeated till a set of K values was obtained which yielded

$$(1 - a_A - a_{B_2})/a_{B_2}{}^{1/2} = D$$

values that corresponded very closely to those obtained from the experimental a_A and a_{B_2} values. It was observed that eq. [10] with a set of K values ($K_{1,0.5}$, $K_{2,0.5}$, $K_{1,1}$, $K_{0.5}$) and eq. [11] with a set of K values ($K_{1,0.5}$, $K_{1,1}$, $K_{1,1.5}$, $K_{0.5}$) yield D values that reproduce equally well the corresponding values obtained from experimental values for this system.

The criterion of effectiveness was the variance of the fit $\sigma_D{}^2$ defined by

[12] $$\sigma_D{}^2 = \sum_i (D_{calcd} - D_{exp})^2/(q - p)$$

where q is the number of points used in the fit and p is the number of adjustable parameters. The various K and $\sigma_D{}^2$ for eqs. [10] and [11] are recorded in Table 3. $\sigma_{D[10]}{}^2$ and $\sigma_{D[11]}{}^2$ in Table 3 represent $\sigma_D{}^2$ for the activity data analysed in terms of eqs. [10] and [11], respectively. Since both eqs. [10] and [11] represent the corresponding D values obtained from experimental data equally well, the analysis of the activity coefficient data described above suggests that these mixtures may be assumed to have either AB, A_2B, AB_2, and B or AB, AB_2, AB_3, and B molecular species in solution. We next considered our H^E data.

Examination of the H^E data of this mixture involved consideration of (*i*), AB, A_2B, AB_2, and B and (*ii*), AB, AB_2, AB_3, and B molecular species. Consequently H^E was expressed as

[13] $$H^E = \left(\sum_{m=1}^{2} n_{AB_m} \Delta H_{AB_m} + n_{A_2B} \Delta H_{A_2B} + n_B \Delta H_B \right) \Big/ (N_A + N_{B_2})$$

and

[14] $$H^E = \left(\sum_{m=1}^{3} n_{AB_m} \Delta H_{AB_m} + n_B \Delta H_B \right) \Big/ (N_A + N_{B_2})$$

where n_{AB_m} represents the amount of species AB_m at equilibrium in the solution and N_A and N_{B_2} the stoichiometric amounts of A and B_2. If the equilibrium mole fractions of A, B_2, B, AB_m ($m = 1, 2$), and A_2B are represented by Z_A, Z_{B_2}, Z_B, Z_{AB_m}, and Z_{A_2B}, then for an ideal associated mixture A + B_2, containing AB, A_2B, AB_2, and B molecular species

[15] $$Z_A + Z_{B_2} + \sum_{m=1}^{2} Z_{A_mB} + Z_{AB_2} + Z_B = 1$$

where

$$Z_{A_mB} = K_{m,0.5} Z_A{}^m Z_{B_2}{}^{1/2}$$

$$Z_{AB_2} = K_{1,1} Z_A Z_{B_2}$$

$$Z_B = K_{0.5} Z_{B_2}{}^{1/2}$$

The experimental H^E values were again corrected for dispersion contributions by subtracting from H^E_{exp} the H^E values (34) at 298.15 K for cyclohexane + methanol. Consequently in eqs. [13] and [14]

$$H^E = H^E_{exp} - H^E_{cyclohexane+methanol} \quad [15a]$$

Algebraic manipulation of eqs. [13] and [14] and the material balance equations

$$N_A = n_A + \sum_{m=1}^{2} n_{AB_m} + 2n_{A_2B} \quad [16]$$

$$N_{B_2} = n_{B_2} + \tfrac{1}{2}\sum_{m=1}^{2} n_{A_mB} + n_{AB_2} + \tfrac{1}{2}n_B \quad [17]$$

leads to

$$jH^E = \sum_{m=1}^{2} K_{m,0.5} Z_{A_m}{}^m \Delta H_{A_mB} + Z_{B_2}{}^{1/2} K_{1,1} \Delta H_{AB_2} + K_{0.5}\Delta H_B \quad [18]$$

where

$$j = (Z_{B_2}{}^{1/2} + 0.5K_{1,0.5}Z_A + K_{1,1}Z_{B_2}{}^{1/2}Z_A + 0.5K_{2,0.5}Z_A{}^2 + 0.5K_{0.5})/x_{B_2}$$

Further combination of eqs. [15]–[17] gives

$$x_{B_2} = \frac{0.5K_{1,0.5}Z_AZ_{B_2}{}^{1/2} + K_{1,1}Z_AZ_{B_2} + 0.5K_{0.5}Z_{B_2}{}^{1/2} + 0.5K_{2,0.5}Z_A{}^2Z_{B_2}{}^{1/2} + Z_{B_2}}{Z_A + Z_{B_2} + 1.5K_{1,0.5}Z_AZ_{B_2}{}^{1/2} + 2K_{1,1}Z_AZ_{B_2} + 2.5K_{2,0.5}Z_A{}^2Z_{B_2}{}^{1/2} + 0.5K_{0.5}Z_{B_2}{}^{1/2}} \quad [19]$$

where

$$Z_{B_2}{}^{1/2} = \frac{-Y \pm \sqrt{Y^2 - 4(Z_A - 1)(1 + K_{1,1}Z_A)}}{2(1 + K_{1,1}Z_A)}$$

$$Y = (K_{1,0.5}Z_A + K_{2,0.5}Z_A{}^2 + K_{0.5})$$

Using the various K values described above for a solution containing AB, A_2B, AB_2, and B species, we calculated x_{B_2} from eq. [19] for various values of Z_A and assigned various values to ΔH_{A_mB}, ΔH_{AB_2}, and ΔH_B till they gave H^E values (from eqs. [15a] and [18]) that compared well with the corresponding experimental values. The various ΔH values are recorded in Table 3 and the calculated H^E values are plotted in Fig. 1. It is evident from Fig. 1 that the theoretical H^E values well describe the general behaviour of H^E with x_A for chloroform (A) + methanol (B) mixture.

A similar process was applied to the case when the mixture contain AB_m (m = 1 to 3) and B molecular species. The final expressions were

$$j'H^E = K_{1,0.5}Z_A\Delta H_{AB} + K_{1,1}Z_A\Delta H_{AB_2} + K_{1,1.5}Z_AZ_{B_2}{}^{3/2}\Delta H_{AB_3} + K_{0.5}\Delta H_B \quad [20]$$

where

$$j' = (Z_{B_2}{}^{1/2} + 0.5K_{1,0.5}Z_A + K_{1,1}Z_AZ_{B_2}{}^{1/2} + 1.5K_{1,1.5}Z_AZ_{B_2}{}^2 + K_{0.5}Z_{B_2}{}^{1/2})/x_{B_2}$$

$$x_{B_2} = \frac{Z_{B_2} + 0.5K_{0.5}Z_{B_2}{}^{1/2} + 0.5K_{1,0.5}Z_AZ_{B_2}{}^{1/2} + K_{1,1}Z_AZ_{B_2} + 1.5K_{1,1.5}Z_AZ_{B_2}{}^{3/2}}{Z_A + Z_{B_2} + 0.5K_{0.5}Z_{B_2}{}^{1/2} + 1.5K_{1,0.5}Z_AZ_{B_2}{}^{1/2} + 2K_{1,1}Z_AZ_{B_2} + 2.5K_{1,1.5}Z_AZ_{B_2}{}^{3/2}}$$

and

$$Z_A = (1 - K_{0.5}Z_{B_2}{}^{1/2} - Z_{B_2})/(1 + K_{1,0.5}Z_{B_2}{}^{1/2} + K_{1,1}Z_{B_2} + K_{1,1.5}Z_{B_2}{}^{3/2})$$

where

$$Z_{AB_m} = K_{1,m/2}Z_AZ_{B_2}{}^{m/2} \qquad m = 1, 2, 3$$

$$Z_B = K_{0.5}Z_{B_2}{}^{1/2}$$

However, no values of ΔH_{AB_m}(m = 1 to 3) and ΔH_B could yield H^E values that described the experimental behaviour of H^E with x_A for this mixture. The calculated H^E values are either positive or negative throughout the entire chloroform concentration range. Further the quantitative agreement is also not good (see Fig. 1 where only those ΔH_{AB_m} and ΔH_B values are considered that render H^E_{calcd} positive throughout the entire chloroform concentration range).

The analysis of H^E and activity coefficient data for chloroform + methanol mixtures thus suggests that this mixture is characterized by the presence of AB, AB_2, A_2B, and B molecular species in solution.

1. H. S. FRANK and W. Y. WEN. Discuss. Faraday Soc. **24**, 133 (1957).
2. K. B. WHETSEL and J. H. LADY. Spectroscopy of fuels. Plenum Press, New York, NY. 1970. pp. 259–279.
3. E. M. WOOLLEY, J. G. TRAVERS, B. P. ERNO, and L. G. HEPLER. J. Phys. Chem. **75**, 3591 (1971).
4. M. SAUNDERS and J. B. HYNE. J. Chem. Phys. **29**, 1319 (1958).
5. J. R. JOHNSON, S. D. CHRISTIAN, and H. E. AFFSPRUNG. J. Chem. Soc. A, 764 (1967).
6. D. CLOTMAN, D. VANDERBERGHE, and TH. Z. HUYSKENS. Spectrochim. Acta, A. **26**, 1621 (1970).
7. G. C. PIMENTAL and A. L. MCCLELLAN. The hydrogen bond. W. H. Freeman, San Francisco, CA. 1960.
8. H. L. LIAO and D. E. MARTIRE. J. Am. Chem. Soc. **96**, 2058 (1974).
9. E. E. TUCKER and S. D. CHRISTIAN. J. Am. Chem. Soc. **97**, 1269 (1975).
10. A. VOGEL. Practical organic chemistry. Longman Green and Co., London. 1968.
11. E. L. ECKFEDT and W. W. LUCASSE. J. Phys. Chem. **47**, 165 (1943).
12. B. E. TRAV. Bur. Int. Phys. Chim. Bruxelles J. Chem. Phys. **23**, 733 (1926).
13. J. G. FERNANDEZ-GARCIA and C. G. BOISSONAS. Helv. Chim. Acta, **50**, 1058 (1967).
14. R. K. NIGAM and B. S. MAHL. J. Chem. Soc. Faraday Trans. I, **8**, 1508 (1975).
15. K. N. MARSH. Int. Data Ser. A**2**, 110 (1973).
16. B. R. SHARMA and P. P. SINGH. J. Chem. Eng. Data, **20**, 360 (1975).
17. K. NAKANISHI, H. WADA, and H. TOUHARA. J. Chem. Thermodyn. **7**, 1125 (1975).
18. K. NAKANISHI, K. ASHITAMI, and H. TOUHARA. J. Chem. Thermodyn. **8**, 121 (1976).
19. E. BECKMAN and O. LIESCHE. Z. Phys. Chem. **88**, 23 (1914); **88**, 419 (1914).
20. J. A. BARKER. Aust. J. Chem. **6**, 207 (1953).
21. O. REDLICH and A. I. KISTER. Ind. Eng. Chem. **40**, 345 (1948).
22. A. SCATCHARD and L. B. TICKNOR. J. Am. Chem. Soc. **74**, 3724 (1952).
23. R. C. REID and T. K. SHERWOOD. The properties of gases and liquids. McGraw Hill Publ. Book Co., New York. 1958.
24. J. TIMMERMANS. Physico-chemical constants of pure organic compounds. Elsevier Publ. Co., Amsterdam. 1950.
25. J. A. BARKER. J. Chem. Phys. **20**, 1526 (1952).
26. M. L. MCGLASHAN and R. P. RASTOGI. Trans. Faraday Soc. **54**, 496 (1958).
27. D. V. FENBY and L. G. HEPLER. J. Chem. Thermodyn. **6**, 185 (1974).
28. L. SAROLEA-MATHOT. Trans. Faraday Soc. **8**, 99 (1953).
29. A. ALEXANDER. J. Phys. Chem. **74**, 2214 (1970).
30. W. J. GAW and F. L. SWINTON. Trans. Faraday Soc. **64**, 2023 (1968).
31. A. G. WILLIAMSON. Trans. Faraday Soc. **64**, 1763 (1968).
32. D. D. DESPANDE AND S. L. OSWAL. J. Chem. Soc. Faraday Trans. I, **68**, 1059 (1972).
33. S. E. WOOD. J. Am. Chem. Soc. **68**, 1963 (1946).
34. H. TOUHARA, M. IKEDA, K. NAKANISHI, and N. WATANABE. J. Chem. Thermodyn. **7**, 887 (1975).

Structural studies on di-μ-thiocyanato(*N*,*S*)-bis(ligand)diisothiocyanato metal(II)bis(triphenylphosphine)mercury(II) and selenocyanate analogs

P. P. SINGH AND S. P. YADAV

Chemistry Department, M. L. K. College, Balrampur, U.P., India

Received June 9, 1978

P. P. SINGH and S. P. YADAV. Can. J. Chem. **57**, 394 (1979).

Binuclear mixed-metal mixed-ligand monomeric bridged complexes of the type $(XCN)_2(L)_2M(NCX)_2Hg(PPh_3)_2$ (M = Co(II), Ni(II), Cu(II), Zn(II); L = pyridine, nicotinamide; PPh_3 = triphenylphosphine; X = S, Se) have been synthesized and characterized by elemental analysis, molar conductance, magnetic moment, and infrared and electronic spectral studies. In all the complexes, the most likely structure involves pyridine or nicotinamide linked to M and PPh_3 to Hg. Total softness calculations have also been made to extend support to the structure of the complexes.

P. P. SINGH et S. P. YADAV. Can. J. Chem. **57**, 394 (1979).

On a synthétisé les complexes pontés, monomères ligand-mixte, métal-mixte et binucléaires du type $(XCN)_2(L)_2M(NCX)_2Hg(PPh_3)_2$ (M = Co(II), Ni(II), Cu(II), Zn(II); L = pyridine, nicotinamide; PPh_3 = triphénylphosphine; X = S, Se); on les a caractérisés par analyse centésimale, conductivité molaire, moment magnétique et des études spectrales infrarouge et électronique. Dans tous les complexes, la structure la plus probable implique une pyridine ou une nicotinamide liée au M et une PPh_3 liée au Hg. On a effectué des calculs de mollesse totale afin d'étendre le support pour les structures des complexes.

[Traduit par le journal]

Introduction

Pyridine or its derivatives reacts with $MHg(XCN)_4$ (M = Co(II), Ni(II), Cu(II), Zn(II); X = S, Se), to yield polymeric bridged complexes (1–4) of the type $\rangle(XCN)_2(py)_2M(NCX)_2Hg\langle$ in which the ligand is coordinated to M. On account of this, the maximum coordination of M is achieved, but the coordination number of Hg(II) remains four against the maximum of six. This paves the way to further coordination at this site. It is at this site the triphenylphosphine has been introduced and an entirely new series of mixed-ligand complexes synthesized and studied.

Experimental

Materials and Manipulations

Nicotinamide (nia) (B.D.H.) was used after recrystallization from methanol. Pyridine (py) (B.D.H.) was purified by the known methods. Other materials were used as described earlier (5).

Preparation of the Complexes

These complexes were prepared by either of the following two methods.

First Method

$\rangle(XCN)_2(L)_2M(NCX)_2Hg\langle$ (M = Co, Ni, Cu, Zn; L = py, nia; X = S, Se) were first prepared by the methods described elsewhere (1–4). To the suspensions of these complexes in methanol, solutions of PPh_3 in the same solvent were added in 1:2 molar ratio and stirred for 30 h. In each case a solid was formed and was filtered off, washed with the solvent, and dried in vacuum at room temperature.

Second Method

$(L)_2M(NCX)_2$ was first prepared by stirring the solution of $M(NCX)_2$ in methanol with the excess of the solution of the ligand (py or nia) in the same solvent for 6 h. To the suspension of $Hg(XCN)_2$ in methanol, a solution of PPh_3 in the same solvent was added in 1:2 molar ratio and stirred for 10 h to get $(Ph_3P)_2Hg(XCN)_2$. In each reaction a solid mass was separated which was filtered, washed with the solvent, and dried *in vacuo*.

$(L)_2M(NCX)_2$ was dissolved in a mixture of methanol and pyridine or nicotinamide. This solution was added to the suspension of $(Ph_3P)_2Hg(XCN)_2$ in methanol in 1:1 molar ratio and the reaction mixture was stirred. After about 32 h a solid mass separated in each case which was isolated by filtration, washed with the solvent, and dried *in vacuo* at room temperature.

All the complexes are insoluble in most organic solvents, except for dimethylformamide.

Analysis and Physical Measurements

Analysis of the complexes and all other physical measurements were made as described earlier (5). Analytical data are included in Table 1.

Results and Discussion

On account of the insolubility of these complexes in suitable organic solvents, we could not find the molecular weight, and could not grow the single crystals. The structure of the complexes, therefore, have been proposed on the basis of analytical data, magnetic moments, chemical reactions, HSAB consideration, and ir and electronic spectral studies.

The analytical data as presented in Table 1 show that two molecules of PPh_3 react with one molecule of $\rangle(XCN)_2(L)_2M(NCX)_2Hg\langle$.

0008-4042/79/040394-06$01.00/0

The ligands show features of coordination. Pyridine and nicotinamide are coordinated through their ring nitrogen as is evidenced by the positive shift in the ring vibrations. Similarly, the X-sensitive *q*, *r*, *t*, and *y* (Whiffen's) bands of triphenylphosphine experience positive shift; this indicates that the ligand is coordinated (6, 7).

The incoming PPh_3 may either rupture the NCX bridge to form a cationic–anionic complex or may retain it to yield a bridging complex.

These complexes are only slightly soluble in dimethylformamide, and conductance values of the dilute solutions as presented in Table 1 show them to be nonconducting in nature. Thus the cationic–anionic structure may be set aside in favour of the bridge structure.

Bridged structure may be either polymeric or monomeric (2–4). In the absence of molecular weight data it is difficult to distinguish between the two. However, on the basis of the number and position of ir bands due to thio or selenocyanate fundamental vibrations and other qualitative considerations as presented below, the possibility for a monomeric bridged structure is more.

(*i*) The essential requirement of a monomeric bridged compex is the presence of both bridging and terminal thio or selenocyanate groups (2–5). The ir spectra of these complexes as presented in Tables 2 and 3 demonstrate the presence of three to four absorption bands in the CN stretching region. These bands possibly indicate the presence of both bridging and terminal NCX groups (8–12).

(*ii*) PPh_3 is a bulky ligand and obstructs the formation of a polymeric bridged complex, and it is on this account all the reported complexes of PPh_3 with $MM'(XCN)_4$ are monomeric bridged (1, 5, 13).

On the basis of the above considerations, the polymeric bridged structure is disclaimed. The monomeric bridged structure, which is the most likely species present, may have either of the following four structure **1**, **2**, **3**, and **4**.

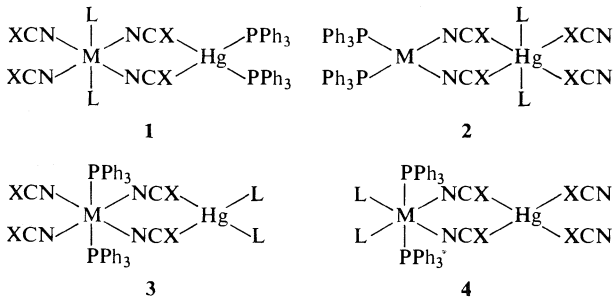

M = Co(II), Ni(II), Cu(II), Zn(II); L = pyridine, nicotinamide; X = S, Se

The electronic spectra and the magnetic moment

TABLE 1. Melting points, conductance values, and analytical results*

Complex	Colour	Melting point (°C)	M (%)		Hg (%)		S or Se (%)		N (%)		Λ_o ($S\,cm^2/mol$)
			Calcd	Obsd	Calcd	Obsd	Calcd	Obsd	Calcd	Obsd	
$(SCN)_2(py)_2Co(NCS)_2Hg(PPh_3)_2$	Pink	160d	5.0	4.8	17.1	17.0	10.9	10.8	7.1	6.8	8.3
$(SCN)_2(nia)_2Co(NCS)_2Hg(PPh_3)_2$	Pink	167d	4.7	4.6	15.9	15.7	10.1	10.0	8.9	8.6	7.6
$(SeCN)_2(py)_2Co(NCSe)_2Hg(PPh_3)_2$	Brown	198d	4.3	4.0	14.7	14.5	23.2	23.1	6.1	6.0	7.5
$(SeCN)_2(nia)_2Co(NCSe)_2Hg(PPh_3)_2$	Brown	205d	4.1	3.8	13.8	13.5	21.8	21.6	7.7	7.5	7.8
$(SCN)_2(py)_2Ni(NCS)_2Hg(PPh_3)_2$	Light blue	208d	5.0	4.9	17.1	16.8	10.9	10.8	7.1	7.0	7.8
$(SCN)_2(nia)_2Ni(NCS)_2Hg(PPh_3)_2$	Light blue	176d	4.6	4.4	15.9	15.8	10.1	9.8	8.9	8.7	8.0
$(SeCN)_2(py)_2Ni(NCSe)_2Hg(PPh_3)_2$	Violet	220d	4.3	4.2	14.7	14.5	23.2	23.0	6.1	5.9	7.2
$(SeCN)_2(nia)_2Ni(NCSe)_2Hg(PPh_3)_2$	Violet	216d	4.1	4.0	13.8	13.6	21.8	21.6	7.7	7.6	7.3
$(SCN)_2(py)_2Cu(NCS)_2Hg(PPh_3)_2$	Greenish yellow	128d	5.4	5.2	17.0	16.6	10.8	10.6	7.1	7.0	8.2
$(SCN)_2(nia)_2Cu(NCS)_2Hg(PPh_3)_2$	Greenish yellow	132d	5.0	4.7	15.8	15.6	10.1	10.0	8.8	8.6	7.9
$(SeCN)_2(py)_2Cu(NCSe)_2Hg(PPh_3)_2$	Light yellow	145d	4.6	4.4	14.7	14.6	23.1	22.8	6.1	6.0	6.9
$(SeCN)_2(nia)_2Cu(NCSe)_2Hg(PPh_3)_2$	Light yellow	160d	4.3	4.2	13.8	13.5	21.7	21.5	7.7	7.5	7.4
$(SCN)_2(py)_2Zn(NCS)_2Hg(PPh_3)_2$	White	178d	5.5	5.3	17.0	16.7	10.8	10.6	7.1	7.0	7.8
$(SCN)_2(nia)_2Zn(NCS)_2Hg(PPh_3)_2$	White	182d	5.1	5.0	15.8	15.5	10.1	10.0	8.8	8.4	8.1
$(SeCN)_2(py)_2Zn(NCSe)_2Hg(PPh_3)_2$	White	169d	4.7	4.4	14.6	14.4	23.1	23.0	6.1	5.8	7.7
$(SeCN)_2(nia)_2Zn(NCSe)_2Hg(PPh_3)_2$	White	180d	4.5	4.2	13.8	13.6	21.7	21.5	7.7	7.5	7.3

*M = Co, Ni, Cu, Zn; d = decomposition.

TABLE 2. Infrared spectral assignments for thiocyanate fundamental vibrations of $(SCN)_2(L)_2M(NCS)_2Hg(PPh_3)_2$*

Description	Symmetry species	L = py M = Co	L = nia M = Co	L = py M = Ni	L = nia M = Ni	L = py M = Cu	L = nia M = Cu	L = py M = Zn	L = nia M = Zn
NCS pa str	$A_1 + B_1$	2140(sh)	2135(sh)	2138(s)	2130(s)	2170(m)	2130(m)	2122(s)	2160(m)
$\nu(CN)_{br}$		2122(s)	2125(s)	2120(sh)	2122(sh)	2120(sh)	2110(sh)	2105(sh)	2108(sh)
NCS pa str	$A_1 + B_2$	2070(s)	2078(s)	2090(s)	2080(s)	2080(s)	2090(s)	2070(s)	2075(s)
$\nu(CN)_{te}$		2036(sh)	2030(sh)	2052(sh)	2040(sh)	2025(sh)	2050(sh)		2060(s)
NCS ps str	$A_1 + B_1$	740(s)	722(sh)	742(sh)	730(sh)	735(sh)	740(s)	748(s)	735(s)
$\nu(CS)_{br}$		755(sh)	750(s)	752(m)	740(s)	758(sh)	750(sh)	752(sh)	750(s)
NCS ps str	$A_1 + B_2$	800(s)	805(s)	800(s)	745(s)	805(m)	795(s)	802(s)	785(s)
$\nu(CS)_{te}$		835(s)	845(s)	830(s)	800(s)	746(s)	830(s)	845(s)	825(s)
M—NCS def	$A_1 + B_1$	440(sh)	438(s)	432(s)	440(s)	435(m)	445(sh)	430(sh)	446(sh)
$\delta(NCS)_{br}$		445(s)	455(m)	457(sh)				440(w)	460(s)
M—NCS def	$A_1 + B_2$	465(s)	478(m)	470(sh)	460(sh)	485(sh)	470(s)	460(s)	475(sh)
$\delta(NCS)_{te}$				480(s)	470(w)	490(s)	475(sh)		
M—N_4 str	$2A_1 + B_1 + B_2$	310(w)	312(m)	308(w)	300(sh)		310(m)	312(s)	310(m)
		275(sh)	280(sh)	290(m)	282(s)		292(w)	290(m)	280(m)
M—L_2 str	$A_1 + B_1$	260(s)	270(s)	272(sh)	255(sh)		272(sh)	270(s)	260(s)
		240(s)	255(sh)	260(s)	245(s)		260(s)	262(sh)	256(w)
Hg—S_2 str	$A_1 + B_2$	220(w)	218(s)	224(s)	215(sh)		220(sh)	222(m)	213(s)

*s = strong, m = medium, w = weak, sh = shoulder, pa = pseudo-antisymmetrical, ps = pseudo-symmetrical, str = stretching, br = bridging, te = terminal, def stands for the deformation M—N—C—S.

values as discussed later reveal that Co(II) or Ni(II) is in octahedral coordination geometry which disagrees with structure **2**, since in it M is tetracoordinated. On this ground the structure **2** is unacceptable. Since in all three other possible structures, the configuration of Co(II) or Ni(II) remains octahedral, the distinction cannot be made with the help of electronic spectra and magnetic moment values. The balance of evidence has, therefore, been derived on the other considerations which are as follows:

Triphenylphosphine never forms an octahedral complex with cobalt thiocyanate. In all the reported complexes of $CoM'(XCN)_4$ with PPh_3, the coordination number of Co(II) is four (1, 5, 13). Similarly, when PPh_3 is coordinated to $Ni(NCS)_2$ or $NiHg(XCN)_4$, Ni(II) acquires square planar configuration (5, 13, 14). It is, therefore, very unlikely that PPh_3 is linked to cobalt or nickel when they are in their octahedral coordination geometry. Furthermore, the blue complex $(Ph_3P)_2Co(NCX)_2Hg(XCN)_2$ does not become pink when reacted with pyridine (5) which indicates that pyridine cannot link to cobalt if the latter is already coordinated to PPh_3. On the basis of these observations, structures **3** and **4** can be disowned and structure **1** can be taken as the possible structure of these complexes. The evidences as mentioned below also lend support to the structure **1**.

(*i*) The formation of the complexes by the reaction between $(L)_4M(NCX)_2$ and $(Ph_3P)_2Hg(XCN)_2$ in methanol

$$(XCN)_2M(L)_4 + (NCX)_2Hg(PPh_3)_2 \rightarrow (XCN)_2(L)_2M(NCX)_2Hg(PPh_3)_2$$

also indirectly supports the structure **1**.

(*ii*) The difference in total softness values $[(\Delta TE_n{}^*(M—Hg)]$ of M and Hg is the highest in case of the structure **1**, hence it is the more probable out of the four. The description of total softness values and its application to the determination of the structure is discussed later.

(*iii*) The steric hindrance which plays an important role in the determination of the structure of PPh_3 complexes (5) is least in the case of the structure **1**.

(*iv*) Structure **1** possesses C_{2v} symmetry. Assuming this symmetry, we have calculated the number of ir active normal vibrations which are found to be in good agreement with the observed ones (see Tables 2 and 3).

Electronic Spectra of $(XCN)_2M(L)_2(NCX)_2Hg(PPh_3)_2$ (M = Co(II), Ni(II); X = S, Se)

In order to ascertain the coordination geometry around Co(II) or Ni(II) in these complexes, we have studied their electronic spectra. The assignment of the electronic spectral bands, their positions, and the spectral parameters are included in Table 4. The values of Dq and B' have been calculated from the values of ν_3 and ν_2 bands using the matrices of Tanabe and Sugano (15).

The positions of electronic spectral bands indicate that Co(II) and Ni(II) possess octahedral configuration in these complexes. Being formally a two electron transition the ν_2 band is weak in intensity

TABLE 3. Infrared spectral assignments for the selenocyanate fundamental vibrations of $(SeCN)_2(L)_2M(NCSe)_2Hg(PPh_3)_2$

Description	Symmetry species	L = py M = Co	L = nia M = Co	L = py M = Ni	L = nia M = Ni	L = py M = Cu	L = nia M = Cu	L = py M = Zn	L = nia M = Zn
NCSe pa str	$A_1 + B_1$	2170(sh)	2140(s)	2142(s)	2156(s)	2150(w)	2170(m)	2160(s)	2188(s)
$\nu(CN)_{br}$		2142(s)	2122(s)	2130(sh)	2118(sh)	2112(s)	2120(sh)	2100(s)	2150(s)
NCSe pa str	$A_1 + B_2$	2100(sh)	2102(s)	2100(s)	2035(s)	2080(s)	2102(s)	2080(w)	2100(sh)
$\nu(CN)_{te}$		2040(w)	2060(sh)	2080(sh)	2025(w)	2060(sh)	2065(sh)	2060(sh)	2040(s)
NCSe ps str	$A_1 + B_1$	572(s)	555(sh)	558(sh)	557(sh)	560(sh)	551(s)	540(sh)	535(sh)
$\nu(CSe)_{br}$		545(sh)	568(s)	575(s)	570(s)	572(s)	590(m)	570(s)	560(s)
NCSe ps str	$A_1 + B_2$	648(s)	590(sh)	592(w)	635(s)	630(s)	640(w)	595(w)	620(s)
$\nu(CSe)_{te}$			650(sh)	642(s)	658(s)	642(w)		635(s)	630(sh)
M—NCSe def	$A_1 + B_1$	385(w)	390(sh)	370(m)	380(sh)	370(w)	372(w)	370(sh)	380(m)
$\delta(NCSe)_{br}$		395(sh)			395(s)	380(sh)	395(m)	330(s)	398(s)
M—NCSe def	$A_1 + B_2$	455(s)	452(s)	450(s)	445(s)	455(s)	440(sh)	394(s)	430(s)
$\delta(NCSe)_{te}$				460(sh)		440(s)	460(s)	458(s)	420(sh)
M—N_4 str	$2A_1 + B_1 + B_2$	236(s)	230(s)	240(s)	249(s)	232(s)	230(s)	232(sh)	230(s)
		210(m)	208(w)	210(sh)	212(sh)	210(s)	210(s)	212(s)	214(s)
M—L_2 str	$A_1 + B_1$	252(sh)	250(s)	260(s)	278(s)	260(s)	265(w)	260(w)	260(m)
		282(w)	280(w)	283(s)			250(s)	270(m)	

TABLE 4. Selected electronic bands, spectral parameters and magnetic moments

Complex	$^4T_{1g}(F) \xrightarrow{\nu_3} {}^4T_{1g}(P)$ (cm^{-1})	$^4T_{1g}(F) \xrightarrow{\nu_2} {}^4A_{2g}$ (cm^{-1})	$^4T_{1g}(F) \xrightarrow{\nu_1} {}^4T_{2g}(F)$ (cm^{-1})	$10Dq$ (cm^{-1})	B' (cm^{-1})	β	μ_{eff} (BM)
$(SCN)_2(py)_2Co(NCS)_2Hg(PPh_3)_2$	21 060	18 750	9 950	9 980	900	0.92	5.04
$(SCN)_2(nia)_2Co(NCS)_2Hg(PPh_3)_2$	21 200	—	10 100	10 100	—	—	5.01
$(SeCN)_2(py)_2Co(NCSe)_2Hg(PPh_3)_2$	22 000	—	10 250	10 250	—	—	5.00
$(SeCN)_2(nia)_2Co(NCSe)_2Hg(PPh_3)_2$	21 590	19 000	10 200	10 220	950	0.97	4.98

Complex	$^3A_{2g} \rightarrow {}^4T_{1g}(P)$	$^3A_{2g} \rightarrow {}^3T_{1g}(F)$	$^3A_{2g} \rightarrow {}^3T_{2g}(F)$	$10Dq$ (cm^{-1})	B' (cm^{-1})	β	μ_{eff} (BM)
$(SCN)_2(py)_2Ni(NCS)_2Hg(PPh_3)_2$	27 300	16 800	10 480	10 500	840	0.81	3.22
$(SCN)_2(nia)_2Ni(NCS)_2Hg(PPh_3)_2$	27 260	16 770	10 540	10 480	839	0.81	3.21
$(SeCN)_2(py)_2Ni(NCSe)_2Hg(PPh_3)_2$	28 490	17 160	10 600	10 580	925	0.89	3.18
$(SeCN)_2(nia)_2Ni(NCSe)_2Hg(PPh_3)_2$	29 050	17 300	10 590	10 620	966	0.93	3.12

and in some cases not observed in the cobalt complexes. In these cases, the *Dq* values are derived from the position of ν_1 bands.

The *Dq* values of these complexes are in the range prescribed for the octahedral complexes of Co(II) and Ni(II), and are nearly the same as that of $\rangle(XCN)_2(L)_2M(NCX)_2Hg\langle$ (M = Co(II), Ni(II)) (1–4) which is, possibly, due to the presence of the same octahedron L_2MN_4 in the two. The *Dq* values of the selenocyanate complexes are higher than that of the corresponding thiocyanate complexes which reveals that the ligand field strength of the former is higher than that of the latter (16–18). The metal–ligand bond in selenocyanates is more covalent than in thiocyanates as is evidenced by the values of *B'*.

Magnetic moment values of these complexes as presented in Table 4 also suggest octahedral environment around cobalt and nickel. All the zinc complexes are diamagnetic and copper complexes possess the magnetic moment values in the range 1.8–2.0.

Description of Total Softness ($TE_n^{\ddagger}$) and its Application

The stability of thio and selenocyanate bridge in the complexes of mixed dithio-diselenocyanate complexes has recently been related (19) to the difference in total softness $[\Delta TE_n^{\ddagger}(M—M')]$ of M and M'. A higher value of $\Delta TE_n^{\ddagger}(M—M')$ suggests greater stability. In order to extend support to the proposed structure of the complexes of the present series, the total softness ($TE_n^{\ddagger}$) of M (Co, Ni, Cu, Zn) and Hg have been calculated in respect of the different structures of the complexes and the difference $\Delta TE_n^{\ddagger}(M—Hg)$ evaluated by adopting the pro-

TABLE 5. $\Delta TE_n^{\ddagger}$ values for probable and alternative structures of the complexes

Complex	Type	$TE_n^{\ddagger}$(M)	$TE_n^{\ddagger}$(Hg)	$\Delta TE_n^{\ddagger}$(M—Hg)
$(SCN)_2(py)_2Co(NCS)_2Hg(PPh_3)_2$	A	55.50	28.82	26.68
$(SCN)_2(Ph_3P)_2Co(NCS)_2Hg(py)_2$	B	46.18	38.14	8.04
$(SeCN)_2(nia)_2Co(NCSe)_2Hg(PPh_3)_2$	A	63.18	27.24	36.14
$(SeCN)_2(Ph_3P)_2Co(NCSe)_2Hg(nia)_2$	B	49.50	41.12	8.38
$(SCN)_2(nia)_2Ni(NCS)_2Hg(PPh_3)_2$	A	60.12	28.82	31.30
$(SCN)_2(Ph_3P)_2Ni(NCS)_2Hg(nia)_2$	B	46.24	42.70	3.54
$(SeCN)_2(py)_2Ni(NCSe)_2Hg(PPh_3)_2$	A	58.88	27.24	31.64
$(SeCN)_2(Ph_3P)_2Ni(NCSe)_2Hg(py)_2$	B	49.56	36.56	13.00
$(SCN)_2(py)_2Cu(NCS)_2Hg(PPh_3)_2$	A	56.00	28.82	27.18
$(SCN)_2(Ph_3P)_2Cu(NCS)_2Hg(py)_2$	B	46.68	38.14	8.54
$(SeCN)_2(nia)_2Cu(NCSe)_2Hg(PPh_3)_2$	A	63.88	27.24	36.64
$(SeCN)_2(Ph_3P)_2Cu(NCSe)_2Hg(nia)_2$	B	50.00	41.12	8.88
$(SCN)_2(nia)_2Zn(NCS)_2Hg(PPh_3)_2$	A	61.13	28.82	32.31
$(SCN)_2(Ph_3P)_2Zn(NCS)_2Hg(nia)_2$	B	47.25	42.70	4.55
$(SeCN)_2(py)_2Zn(NCSe)_2Hg(PPh_3)_2$	A	59.89	27.24	32.65
$(SeCN)_2(Ph_3P)_2Zn(NCSe)_2Hg(py)_2$	B	50.57	36.56	14.01

cedure as outlined below:

(i) $(SCN)_2(py)_2Co(NCS)_2Hg(PPh_3)_2$, *Structure* **1**

$$TE_n^{\ddagger}(Co) = E_n^{\ddagger}(Co) + 2E_m^{\ddagger}(py) + 4E_m^{\ddagger}(NCS)$$
$$= -0.22 + 2 \times (-11.44) + 4 \times (-8.10)$$
$$= -55.50$$

$$TE_n^{\ddagger}(Hg) = E_n^{\ddagger}(Hg) + 2E_m^{\ddagger}(SCN) + 2E_m^{\ddagger}(PPh_3)$$
$$= -4.86 + 2 \times (-5.20) + 2 \times (-6.78)$$
$$= -28.82$$

Here $E_n^{\ddagger}$ and $E_m^{\ddagger}$ are the softness values of the metal ions and the ligands, respectively. These values have been calculated by using the Klopman's equation (20).

Now

$$\Delta TE_n^{\ddagger}(Co—Hg) = TE_n^{\ddagger}(Hg) - TE_n^{\ddagger}(Co)$$
$$= -28.82 - \cdots -(-55.50)$$
$$= 26.68$$

(ii) $(SCN)_2(Ph_3P)_2Co(NCS)_2Hg(py)_2$, *Structure* **3**

$$TE_n^{\ddagger}(Co) = E_n^{\ddagger}(Co) + 2E_m^{\ddagger}(PPh_3) + 4E_m^{\ddagger}(NCS)$$
$$= -0.22 + 2 \times (-6.78) + 4 \times (-8.10)$$
$$= -46.18$$

$$TE_n^{\ddagger}(Hg) = E_n^{\ddagger}(Hg) + 2E_m^{\ddagger}(py) + 2E_m^{\ddagger}(SCN)$$
$$= -4.86 + 2 \times (-11.44) + 2 \times (-5.20)$$
$$= -38.14$$

So

$$\Delta TE_n^{\ddagger}(Co—Hg) = TE_n^{\ddagger}(Hg) - TE_n^{\ddagger}(Co)$$
$$= (-38.14) - (-46.18)$$
$$= 8.04$$

The above calculations show that the $\Delta TE_n^{\ddagger}$(Co—Hg) value is higher for structure **1**, hence it is the most likely structure. Since the other factors also favour the same structure, this should be adopted for the complexes of the present series. The total softness values of the metal ions and the difference derived from them in respect of all the complexes are presented in Table 5, along with the $\Delta TE_n^{\ddagger}$(M—Hg) values of the alternative structures. The possible structures are marked with A and the alternative ones with B. The $\Delta TE_n^{\ddagger}$(M—Hg) values for the adopted structures marked with A are higher than those marked with B.

Conclusions

(*i*) Most likely the triphenylphosphine coordinates to M (Co, Ni, Cu, Zn) in preference to Hg, when reacted with $MHg(SCN)_4$ or $MHg(SeCN)_4$ to yield monomeric bridged complexes of the type $(Ph_3P)_2M(NCX)_2Hg(XCN)_2$ (X = S, Se).

(*ii*) When pyridine or nicotinamide is already linked to M as in $>(XCN)_2(L)_2M(NCX)_2Hg<$, the incoming triphenylphosphine most likely coordinates to Hg, to yield monomeric bridged complexes of the type $(XCN)_2(L)_2M(NCX)_2Hg(PPh_3)_2$.

Acknowledgement

The authors gratefully acknowledge financial support from U.G.C. (New Delhi).

1. R. MAKHIJA, L. PAZDERNIK, and R. RIVEST. Can. J. Chem. **51**, 438 (1973); **51**, 2987 (1973).
2. P. P. SINGH and S. A. KHAN. Inorg. Chim. Acta, **14**, 143 (1975).
3. P. P. SINGH, A. K. SRIVASTAVA, and R. RIVEST. J. Inorg. Nucl. Chem. **38**, 439 (1976).
4. P. P. SINGH and S. B. SHARMA. J. Coord. Chem. **6**, 65 (1976).

5. P. P. SINGH, S. P. YADAV, and S. B. SHARMA. Aust. J. Chem. **30**, 1921 (1977).
6. G. B. DEACON and J. H. S. GREEN. Spectrochim. Acta, **24**A, 845 (1968).
7. G. B. DEACON and J. H. S. GREEN. Chem. Ind. 1031 (1965).
8. A. TURCO and C. PECILE. Nature, **191**, 66 (1961).
9. A. SABATINI and I. BERTINI. Inorg. Chem. **4**, 1665 (1965).
10. A. TURCO, C. PECILE, and M. NICOLINI. J. Chem. Soc. 3006 (1962).
11. Y. Y. KHARITONOV and G. V. TSINTSADZE. Zh. Neorg. Khim. **10**, 1191 (1965).
12. J. L. BURMEISTER. Coord. Chem. Rev. **1**, 205 (1966).
13. R. MAKHIJA and R. RIVEST. Spectrochim. Acta, **30**A, 977 (1974).
14. C. PECILE. Inorg. Chem. **5**, 210 (1966).
15. Y. TANABE and S. SUGANO. J. Phys. Soc. Jpn. **9**, 753 (1954).
16. O. BOSTRUP and C. K. JØRGENSON. Acta Chem. Scand. **11**, 1223 (1957).
17. S. M. NELSON and T. M. SHEPHERD. Inorg. Chem. **4**, 813 (1965).
18. H. C. A. KING, E. KÖRÖS, and S. M. NELSON. J. Chem. Soc. 4832 (1964).
19. P. P. SINGH and A. K. GUPTA. Inorg. Chem. **17**, 1 (1978).
20. G. KLOPMAN. J. Am. Chem. Soc. **90**, 223 (1968).

Etude par spectrométrie infrarouge de l'action de solvants aprotiques sur l'association ester–eau et ester–Ba^{2+}. Discussion du rôle catalytique du solvant et de l'ion Ba^{2+} dans l'hydrolyse alcaline du propionate de methyle

ANNE LE NARVOR ET PIERRE SAUMAGNE

Laboratoire de Spectrochimie Moléculaire, Faculté des Sciences et Techniques, 6, Avenue Le Gorgeu, 29283 Brest, Cedex, France

Reçu le 19 juillet 1978

ANNE LE NARVOR et PIERRE SAUMAGNE. Can. J. Chem. **57**, 400 (1979).

Les spectres ir de mélanges propionate de méthyle–eau et propionate de méthyle–Ba^{2+} dans le diméthylsulfoxyde et l'acétonitrile ont été enregistrés dans la région des vibrations νC═O de l'ester. On met en évidence la présence de différents types de complexes, et on suit l'évolution de leur concentration avec la composition du milieu. Les résultats spectroscopiques sont comparés à ceux de la cinétique d'hydrolyse alcaline obtenus dans les mêmes conditions. On montre que le contrôle orbitalaire rend mieux compte des résultats expérimentaux que la densité de charge portée par l'atome de carbone du carbonyle.

ANNE LE NARVOR and PIERRE SAUMAGNE. Can. J. Chem. **57**, 400 (1979).

The ir spectra of mixtures of methyl propionate/water and methyl propionate/Ba^{2+} in dimethylsulfoxide and in acetonitrile have been recorded in the region of the ν_{CO} mode of the ester. Evidence is presented to indicate the presence of different types of complexes; their concentration was determined as a function of the composition of the medium. The spectroscopic results are compared to those from the kinetics of the alkaline hydrolysis in the same conditions. It is demonstrated that the orbital control explains the experimental results better than does the charge density on the carbon of the carbonyl group.

[Journal translation]

Introduction

Une récente étude par spectrométrie infrarouge des interactions ester – solvant protique et ester–cation (1) a permis de montrer le rôle de la formation de complexes entre l'ester et le solvant ou le cation dans la cinétique de l'hydrolyse alcaline de l'ester. Nous avons entrepris l'analyse des spectres infrarouges montrant l'association propionate de méthyle–eau dans l'acétonitrile et le diméthylsulfoxyde (DMSO) en l'absence ou en présence d'un sel alcalino-terreux, afin de préciser l'influence de ces solvants basiques sur les associations ester–eau ou ester–cation.

Partie expérimentale

Le propionate de méthyle est un produit commercial qui a été purifié par distillation. Les solvants étudiés sont des produits pour spectroscopie et ont été desséchés sur tamis moléculaire 4 Å. L'eau lourde titre 99.7% en D_2O et provient du Commissariat à l'Energie Atomique.

Les spectres ont été enregistrés à la température ambiante sur un spectromètre Perkin-Elmer 225. La précision de lecture sur les fréquences et les demi-largeurs est de ± 1 cm^{-1}. Les cellules utilisées d'épaisseur 0.05 mm sont équipées de faces en CaF_2.

I. Interaction eau – propionate de méthyle – solvant basique

Résultats

On a représenté l'évolution du massif νC═O du propionate de méthyle en fonction des concentrations en eau et en acétonitrile sur la fig. 1, en eau et en DMSO sur la fig. 2.

La bande fine correspondant à la vibration νC═O de l'ester libre dans le solvant est située à 1739 cm^{-1} pour l'acétonitrile et à 1735 cm^{-1} pour le DMSO.

Aux faibles concentrations en eau dans l'acétonitrile, nous observons un léger déplacement du maximum à 1739 cm^{-1} vers les basses fréquences et surtout un élargissement très notable de la bande d'absorption dans le même sens. ($\Delta\nu_{\frac{1}{2}} = 15$ cm^{-1} pour $[D_2O] = 0$; $\Delta\nu_{\frac{1}{2}} = 21$ cm^{-1} pour $[D_2O] = 2.2\,M$.) Par contre, la bande νC═O située à 1735 cm^{-1} ne présente aucune évolution pour les faibles concentrations en eau dans le DMSO.

Quand $[D_2O] = 10\,M$, on note pour l'acétonitrile une bande au maximum aplati vers 1735 cm^{-1}; l'absorption dans le DMSO est plus fine et centrée à 1732 cm^{-1}.

Dans les solutions plus concentrées en eau (20 M), le profil du massif νCO centré à 1724 cm^{-1} est sensiblement le même avec les deux solvants.

Dans l'eau pure, la bande νCO vers 1709 cm^{-1} est dissymétrique et très élargie vers les hautes fréquences.

Interprétation

L'addition de quantités croissantes d'eau produit un déplacement accompagné d'un élargissement de la bande νCO avec apparition successive de deux maximums à 1724 puis 1709 cm^{-1}. On a montré (2) que ces deux maximums correspondent respectivement aux deux associations:

[1] $\mathrm{R{-}C(=O){-}OR'} + H_2O \rightleftarrows \mathrm{R{-}C(=O\cdots H{-}OH){-}OR'}$

1 ("complexe I-1")

0008-4042/79/040400-04$01.00/0

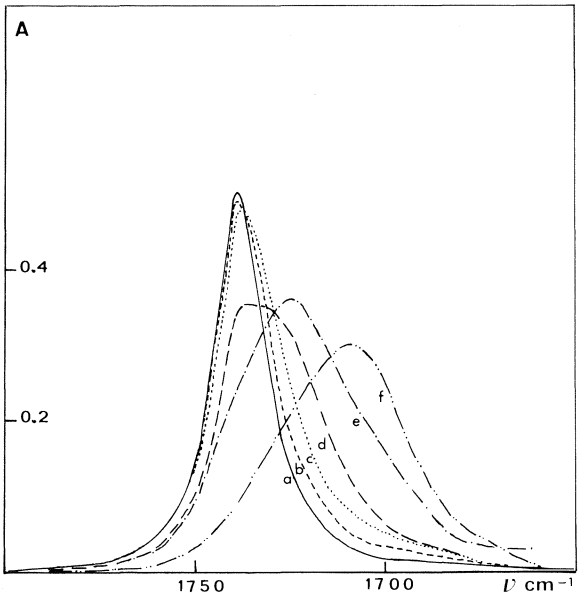

FIG. 1. Spectres d'absorption dans la région des vibrations νC=O du propionate de méthyle en solution dans des mélanges d'acétonitrile et d'eau (D_2O). Concentration en D_2O: a = 0, b = 0.5 M, c = 2.2 M, d = 10 M, e = 20 M, f = eau pure. Concentration en ester 0.2 M.

[2] 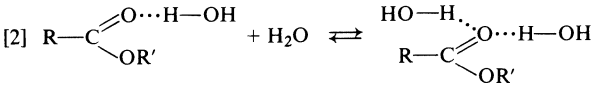

2 ("complexe 1-2")

Dans les solutions concentrées en eau (20 M et 10 M), le rôle du solvant organique est peu important, comme nous l'avons signalé dans un autre travail (3). N'existent donc en solution que les complexes 1-1 (**1**) et 1-2 (**2**).

Lorsque la concentration en eau est faible ($\leq$2.2 M), on peut attribuer l'absence de modification de la bande νC=O à 1735 cm^{-1} dans le DMSO au fait que l'eau s'associe préférentiellement au DMSO selon [3]:

[3] $$\text{Solv.} + \text{HOH} \rightleftarrows \text{Solv....HOH}$$

les complexes **1** et **2** sont vraisemblablement en concentration infime. En effet, les valeurs de la constante de complexation mesurée pour l'équilibre [3] établi dans le tétrachlorure de carbone sont:

$$K(\text{DMSO/eau}) = 200\ \text{L mol}^{-1}\ (4)$$

$$K(\text{propionate de méthyle/eau}) = 50\ \text{L mol}^{-1}$$

Au contraire, l'évolution de la bande νC=O du propionate dans l'acétonitrile à faible concentration en eau nous paraît traduire une compétition entre les trois équilibres [1], [2] et [3]. En effet, le pouvoir accepteur de proton de l'acétonitrile est inférieur à celui du propionate {K(acétonitrile/eau) = 25 L mol^{-1} (4)}.

II. Interaction propionate de méthyle – eau – solvant basique – perchlorate de baryum

Résultats

A l'addition de perchlorate de Ba à une solution de propionate de méthyle (0.2 M) et d'eau (2.2 M) dans l'acétonitrile, correspond l'apparition d'une nouvelle absorption à 1710 cm^{-1} et une diminution d'intensité de la bande à 1739 cm^{-1} (fig. 3).[1]

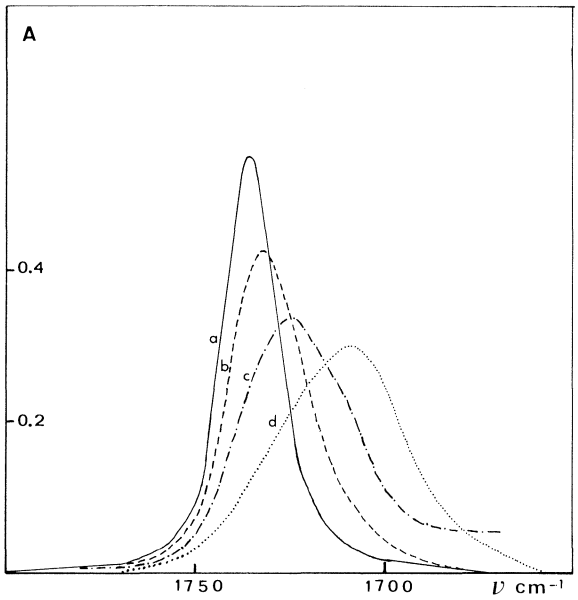

FIG. 2. Spectres d'absorption dans la région des vibrations νC=O du propionate de méthyle en solution dans des mélanges de DMSO et d'eau (D_2O). Concentration en D_2O: a = 0, b = 10 M, c = 20 M, d = eau pure. Concentration en ester 0.2 M.

Quand l'acétonitrile est remplacé par le DMSO, l'addition de perchlorate ne produit aucune modification de la bande νCO à 1735 cm^{-1} (fig. 2, courbe a).

Interprétation

On a montré (1) que la complexation du propionate de méthyle par l'ion Ba^{2+} s'établit par l'intermédiaire de l'oxygène du C=O de l'ester, plus basique que l'oxygène de l'eau, selon l'équilibre:

[4] 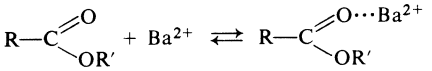

4

Le pouvoir donneur d'électrons de l'oxygène du carbonyle dépendra du solvant polaire par suite de compétition entre l'équilibre [4] et les équilibres [3] et [5]:

[5] 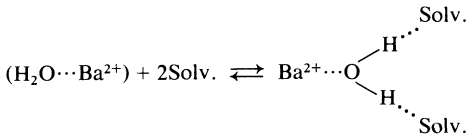

Dans l'équilibre [5] le caractère donneur d'électrons de l'oxygène de l'eau augmente avec l'interaction entre l'eau et le solvant.

Lorsque le solvant utilisé est l'acétonitrile, l'absorption à

[1]Il a été observé par ailleurs que l'abaissement de la fréquence CO par complexation de type **4** est plus grand avec l'ion Ba^{2+} qu'avec un ion alcalin M^+ (1).

1710 cm^{-1} correspond à la vibration νC=O perturbée par l'ion Ba^{2+} selon [4]. Avec le DMSO au contraire, l'absence de modification spectrale par addition de Ba^{2+} indique que, sans doute, l'équilibre [5] prédomine.

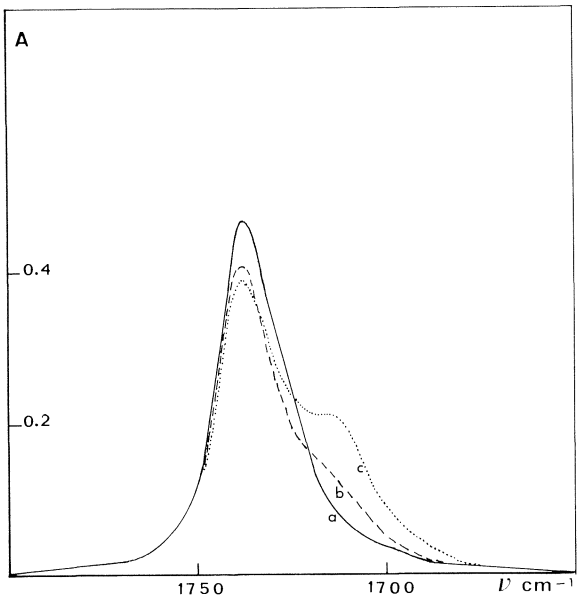

FIG. 3. Spectres d'absorption dans la région des vibrations νC=O du propionate de méthyle en solution dans un mélange eau–acétonitrile en l'absence (*a*) et en présence du perchlorate de baryum. Concentration en Ba^{2+}: $a = 0$, $b = 0.25$ *M*, $c = 0.50$ *M*. Concentration en eau: 2.2 *M*, concentration en ester: 0.2 *M*.

Discussion

Tommila et coll. (5, 6) ont étudié la vitesse d'hydrolyse alcaline de l'acétate d'éthyle dans divers mélanges eau–solvants. Ils ont montré que le rapport des constantes de vitesse k/k_{eau} en présence ou en absence de solvant, diminue habituellement quand la concentration en solvant augmente, mais qu'il augmente d'un facteur 4 à 5 dans le seul cas où le solvant est le DMSO. Pour ces auteurs, la réactivité de l'ion OH^- vis-à-vis de l'ester dépend de son degré d'hydratation ou de solvatation, qui est accru dans l'eau, le méthanol, l'acétone, le dioxanne mais au contraire, diminué dans le DMSO: ce dernier solvant accélère donc la réaction.

Nos résultats confirment ce point de vue. En effet, dans l'eau pure et jusqu'à des concentrations en eau de 10 à 20 *M*, seuls existent les complexes 1-1 et 1-2. Dans ce même domaine de concentration, le DMSO accélère la vitesse d'hydrolyse de 20% environ, alors que les autres solvants l'inhibent légèrement. Or l'évolution des spectres infrarouges est la même quel que soit le solvant. L'effet catalytique du DMSO s'exerce donc, non pas sur le carbone du carbonyle de l'ester, mais très vraisemblablement sur l'ion OH^-.

Cet ion OH^- est hydraté selon le schéma:

$$[6] \qquad OH^- + H_2O \rightleftarrows (H_2O...OH^-)$$

Le calcul de l'énergie de stabilisation de l'ion hydraté (7) donne la valeur $E = 1.265$ eV.

Dans le cas du DMSO, l'équilibre [3] est fortement déplacé vers la droite, ce qui a pour effet de faire rétrograder l'équilibre [6] dans le sens donnant des ions OH^- non hydratés. Cette action du DMSO, sensible dès les premières additions de ce solvant, est amplifiée avec la concentration. La dissociation de l'ion $(H_2O...OH^-)$ entraîne la remontée de l'orbitale haute occupée (HO) de l'ion OH^- qui tend à se rapprocher de l'orbitale basse vacante (BV) du carbonyle de l'ester, bien que cette dernière remonte également par destruction progressive et simultanée des complexes 1-1 et 1-2 (équilibres [1] et [2] (8)).

L'acétonitrile, au contraire, est un accepteur de proton trop faible pour perturber l'équilibre [6] autrement que par solvatation de l'ion $(H_2O...OH^-)$. Cette solvatation expliquerait l'effet inhibiteur de l'acétonitrile.[2]

Cette hypothèse semble confirmée si l'on se place dans le domaine des très fortes concentrations en solvant. L'addition des petites quantités d'eau à l'acétonitrile (jusqu'à 2 *M* en eau) provoque un déplacement visible de la bande νCO de l'ester par formation de complexe 1-1. On n'observe rien de semblable avec le DMSO.

On peut représenter schématiquement l'évolution des orbitales BV de l'ester et HO de l'ion OH^- sous l'action des solvants telle qu'elle vient d'être expliquée:

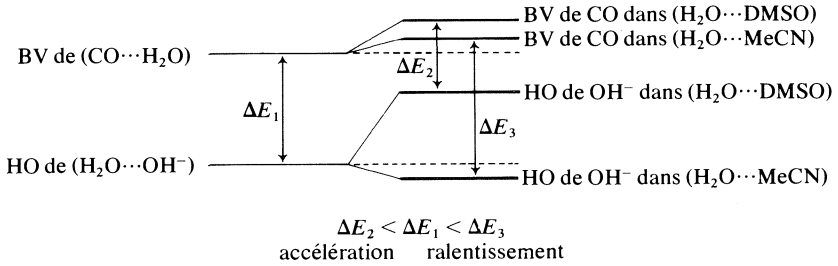

$\Delta E_2 < \Delta E_1 < \Delta E_3$
accélération ralentissement

[2]En fait les expériences de Tommila et coll. ont été réalisées avec l'acétone et le dioxanne. Mais nous avons montré que l'acétone, le dioxanne et l'acétonitrile ont un comportement semblable par rapport à l'eau (3, 4).

Le calcul théorique des énergies des orbitales et des valeurs des ΔE devrait permettre de confirmer ce schéma.

Quant à l'analyse de l'action de l'ion Ba^{2+}, faute de données cinétiques, nous sommes réduits à des hypothèses concernant l'effet catalytique du sel.

Lors d'études d'effet de sel, Corset et coll. (8) ont montré le rôle important de la formation du complexe $C{=}O...M^{+}$ dans le contrôle orbitalaire de la réaction d'hydrolyse de l'ester.

En nous inspirant de leurs conclusions, nous pouvons postuler que l'ion Ba^{2+} aura un effet accélérateur de la cinétique en abaissant le niveau d'énergie de l'orbitale BV du carbonyle dans l'acétonitrile à faible concentration en eau. Ceci est en accord avec l'apparition de l'absorption à 1710 cm^{-1} (fig. 3).

On a déjà signalé l'effet catalytique positif du DMSO. L'addition d'ions Ba^{2+} dans le milieu ne modifiant pas le spectre de vibration, on peut conclure, que vraisemblablement, les ions Ba^{2+} n'ont pas d'effet catalytique sur l'hydrolyse alcaline d'un ester dissous dans le DMSO.

Conclusion

Nos résultats expérimentaux font donc apparaître que l'effet du solvant ne s'exerce pas sur le carbonyle de l'ester mais plutôt sur le réactif OH^{-}. La charge portée par le carbone du carbonyle ne doit pas dépendre du solvant. La réaction d'hydrolyse d'un ester dans un solvant aprotique est donc sous contrôle orbitalaire.

Remerciements

Nous remercions Monsieur J. Corset, Maître de Recherches au Laboratoire de Spectrométrie Infrarouge et Raman du C.N.R.S. de THIAIS, pour l'intérêt qu'il a porté à ce travail et pour les discussions dont il nous a fait bénéficier.

1. R. M. Moravie, J. Corset, M. L. Josien, G. Nee, G. Leny et B. Tchoubar. Tetrahedron, **32**, 693 (1976).
2. J. Lascombe, Ch. Garrigou-Lagrange et Ph. Combelas. Ann. Chim. **5**, 315 (1970).
3. A. Le Narvor, E. Gentric et P. Saumagne. Can. J. Chem. **49**, 1933 (1971).
4. A. Le Narvor, E. Gentric, P. Saumagne et J. Lauransan. J. Chem. Soc. Faraday Trans. I, **72**, 1329 (1976).
5. E. Tommila, A. Koivisto, J. P. Lyyra, K. Antell et S. Heimo. Ann. Acad. Sci. Fenn. Ser. AII, No. 47 (1952).
6. E. Tommila et M. L. Murto. Acta Chem. Scand. **17**, 1947 (1963).
7. P. L. M. Plummer. *Dans* Intern. Conf. on Hydrogen Bonding, Ottawa, 21–22 août 1972.
8. J. Corset, E. Deschamps, F. Froment, G. Leny, A. Loupy, G. Nee et B. Tchoubar. Tetrahedron. Sous presse.

Infrared spectra of the ammonium ion in crystals. Part VI. Hydrogen bonding in simple and complex ammonium halides[1,2]

OSVALD KNOP AND IAN A. OXTON
Department of Chemistry, Dalhousie University, Halifax, N.S., Canada B3H 4J3
AND
MICHAEL FALK
Atlantic Regional Laboratory, National Research Council of Canada, Halifax, N.S., Canada B3H 3Z1

Received June 27, 1978

OSVALD KNOP, IAN A. OXTON, and MICHAEL FALK. Can. J. Chem. **57**, 404 (1979).

The ν_1 and ν_{4bc} infrared absorptions of the NH_3D^+ probe ion dispersed at low concentration in polycrystalline ammonium halides were used to investigate possible correlations between the frequencies of these absorptions and various structural and other parameters of the ammonium compounds. The most important among these parameters are the H...X distance, the acceptor strength of the halogen atom X for hydrogen bonding, and the coordination number C.N. and activation energy E_a for reorientation of the ammonium ion. It is found that the ν_1 and ν_{4bc} frequencies are affected by the acceptor strength and by the degree of 'compression' of the ammonium ion in the crystal, the volume effect. These two factors affect ν_{4bc} in the same direction but ν_1 in opposite directions. As a consequence, in a ν_{4bc} vs. ν_1 plot the halides are separated according to X, C.N., and certain other parameters. The effective radius of the ammonium ion in cubic $(NH_4)_2MX_6$ is shown to increase with the strength of hydrogen bonding.

The E_a vs. ν_1 plot contains two branches. The low-frequency branch is dominated principally by the strength of the hydrogen bonding and corresponds to C.N. 4 and 8 and to *normal* hydrogen bonds. The high-frequency branch is dominated principally by the volume effect and corresponds to C.N. 12 and to hydrogen bonds of highly dynamic character (*fluxional* hydrogen bonds). Ammonium ions with C.N. 6 may correspond to either branch, depending on the formal charge on X. Existence of the so-called symmetrically trifurcated hydrogen bond that has been proposed for the ammonium ion in certain coordinations is not supported by the present evidence.

The problem of the fundamental vibrational frequencies of the 'free' ammonium ion is discussed and values are proposed for the 'limiting' ν_1 and ν_{4bc} frequencies in ammonium halides. Criteria of hydrogen bonding in ammonium halides are reviewed and comment is offered on symmetry aspects of crystallographic transformations in cubic hexahalometallates(IV), A_2MX_6.

OSVALD KNOP, IAN A. OXTON et MICHAEL FALK. Can. J. Chem. **57**, 404 (1979).

Les absorptions infrarouge ν_1 et ν_{4bc} de l'ion sonde NH_3D^+ dispersé en faible concentration dans des halogénures d'ammonium polycristallins ont été utilisées afin d'établir d'éventuelles relations entre les fréquences de ces absorptions et des paramètres relatifs à la structure et à d'autres propriétés des composés de l'ammonium. Parmi ces paramètres, les plus importants sont la distance H...X, l'importance de l'affinité de l'atome halogène X pour la liaison hydrogène, la coordinence C.N. et l'énergie d'activation E_a nécessaire à la réorientation de l'ion ammonium. Il apparait que les facteurs qui ont une influence sur les fréquences ν_1 et ν_{4bc} sont l'importance de l'affinité pour la liaison hydrogène et le degré de "compression" de l'ion ammonium dans le cristal, c'est-à-dire l'effet de volume. Chacun de ces deux facteurs déplace la fréquence ν_{4bc} dans la même direction, mais leurs effets respectifs sur ν_1 ont lieu dans des directions opposées. Par conséquent, les halogénures sont différenciés selon X, C.N., et certains autres paramètres dans le graphique donnant ν_{4bc} en fonction de ν_1. On montre que le rayon effectif de l'ion ammonium dans les phases cubiques $(NH_4)_2MX_6$ s'accroît avec la force de la liaison hydrogène.

Le graphique donnant la variation de E_a avec ν_1 présente deux parties. La partie basse-fréquence est dominée principalement par la force de la liaison hydrogène et correspond à des coordinences 4 et 8 et à des liaisons hydrogène *normales*. La partie haute-fréquence est, elle, dominée principalement par l'effet de volume et correspond à une coordinence 12 et à des liaisons hydrogène de caractère dynamique très prononcé (liaisons hydrogène de type "*fluxional*"). Les ions ammonium en coordinence 6 peuvent correspondre à l'une ou l'autre des deux parties du graphique, selon la charge formelle sur X. Ces faits ne laissent pas supposer

[1]For Part V, see ref. 5.
[2]NRCC No. 17103.

0008-4042/79/040404-20$01.00/0

l'existence de la liaison hydrogène symétriquement trifurquée qui a été proposée pour l'ion ammonium dans certaines situations.

Le problème des fréquences vibrationnelles fondamentales de l'ion ammonium "libre" est traité, et des valeurs sont proposées pour les fréquences "limite" ν_1 et ν_{4bc} dans les halogénures d'ammonium. Les différents critères relatifs à la liaison hydrogène dans les halogénures d'ammonium sont présentés, ainsi qu'un apperçu sur les aspects de symétrie des transformations cristallographiques dans les hexahalométallates(IV) cubiques A_2MX_6.

Previous papers in this series (1–5) have dealt with the usefulness of the ir spectra of polycrystalline ammonium compounds at low deuteration for diagnosing the site symmetry and obtaining information on hydrogen bonding and motions of the ammonium ion. To avoid, or at least to reduce, spectroscopic complications encountered with the NH_4^+ and ND_4^+ ions (6), we studied the spectra of NH_3D^+ introduced into the crystals as an isotopic impurity by low-level (0.5–2%) deuteration. At these deuterium concentrations the frequencies of the $\nu_1(NH_3D^+)$ and $\nu_{4bc}(NH_3D^+)$ absorptions, which correspond essentially to the ND stretching and HND bending modes, respectively, of isotopically isolated NH_3D^+ ions, are not subject to vibrational coupling. Since they have also been shown (6) to be free from Fermi resonance, they are well suited for investigating the existence of correlations between vibrational frequency and crystallographic and other parameters. The NH_3D^+ probe is representative of the ammonium ion save for those properties that depend critically on the difference in the inertial character of NH_3D^+ (symmetric top) and NH_4^+ (spherical top).

In the present investigation we have attempted to see to what extent the use of the NH_3D^+ probe can contribute toward elucidation of certain poorly known aspects of the behaviour of the ammonium ion. By virtue of its charge and dimensional similarity to the Rb^+ ion, the ammonium ion occurs frequently in crystal environments in which formation of a hydrogen bond simultaneously involving more than one acceptor, typically a trifurcated hydrogen bond, appears possible. However, while the existence of a trifurcated bond has been suggested (7, 8), it has never been demonstrated. The fact that the ammonium ion cannot exist, under any practical conditions, as an isolated entity presents a further complication: it precludes the possibility of obtaining the fundamental vibration frequencies of the 'free' ion, i.e., convergence limits of the effect of hydrogen bonding on vibrational frequency and hence a standard for assessing the strength of individual hydrogen bonds. With these problems in mind we have studied the spectra of the NH_3D^+ probe ion in a number of additional ammonium compounds, most importantly in the cubic and trigonal hexahalometallates(IV), $(NH_4)_2MX_6$, and in ammonium halide and alkali halide matrices, both of the simple cubic (sc, CsCl) and face-centred cubic (fcc, NaCl) types.

To facilitate presentation of our results and conclusions, we deal with details of experimental evidence, and with matters outside the main line of argument, at the end of the paper. Consistent with the previous usage (cf. ref. 2), the term hydrogen bonding, as applied in the following to the ammonium ion, shall include all factors which restrict rotation of the ion to torsional oscillations.

Discussion

The isotopically isolated ND stretching frequencies $\nu_1(NH_3D^+)$ in simple and complex ammonium halides are plotted in Fig. 1 against the best estimates of the corresponding H...X distances. This figure summarizes all such frequencies available at this time. The positions of the H atoms have been determined only in NH_4F (9, 10), with some reservations in the other simple NH_4X halides and, approximately, in $(NH_4)_2SiF_6$ (11) and $(NH_4)_2SnCl_6$ (12) at room temperature. In all the other cases they had to be inferred from geometrical considerations; the estimated H...X distances refer to 'normal' (i.e., essentially straight) N—H...X bonds[3] and the H...X* distances to assumed symmetrically trifurcated bonds. The estimates are based on an assumed N—H distance of 1.03(2) Å and are probably no better than ±0.05 Å and in some cases much worse.

In the following, all the frequencies quoted are those of the NH_3D^+ probe ion at 77 K unless stated otherwise. The site symmetry of the ammonium N atom is denoted, as in ref. 6, by *S* and the effective symmetry of the NH_3D^+ probe ion by *E'*. The coordination number, C.N., is the number of atoms in the immediate environment of an ammonium ion.

NH_3D^+ in Ammonium and Alkali Halide Matrices: Expected Behaviour

NH_4F occupies a unique place in the plot of Fig. 1 in that it appears to be the only ammonium halide in which the immediate environment of the NH_4^+ ion consists of only four acceptors. Although the N atom is located on a polar axis, the axial and non-axial N—H...F distances have been found to be

[3]Where orientation of the NH_4^+ ion is unknown or indeterminate H...X represents the minimum N...X distance less 1.03 Å.

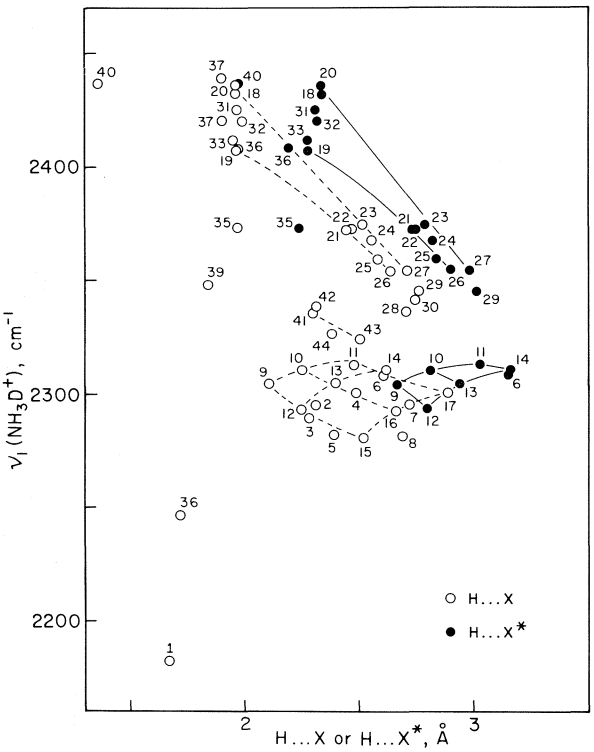

FIG. 1. Variation of $\nu_1(NH_3D^+)$ with H...X (or H...X*) distance in simple and complex ammonium halides. For key numbers refer to Tables 1–4 and text.

equal, within a small experimental error, and so the symmetry of the immediate environment of the N atom is effectively T_d. The single, narrow ν_1 band in the spectrum of NH_4F at 77 K is consistent with the crystallographic evidence. The frequency of this band is the lowest of all ND stretching frequencies reported to date.

The situation in the other simple ammonium halides is complicated by the occurrence of phase transitions. It is best exemplified by the iodide. In the ordered phase *III* each NH_4^+ ion is coordinated by eight I atoms at the corners of a tetragonally distorted cube ($S = D_{2d}$) and simultaneous formation of four normal N—H...I bonds is possible. All the iodine atoms are equivalent and only one type of hydrogen bond occurs. Hence a single, unbroadened ν_1 band is expected and found (Table 1). In the disordered sc phase *II* NH_4^+ is also surrounded by eight I atoms and the diffraction symmetry gives $S = O_h$. However, an iodine atom in this structure may be the recipient of zero to eight hydrogen bonds pointing at random in the eight possible directions, and so a distribution of acceptor strengths and I...H configurations will exist. As a result most of the coordination cubes will be slightly distorted, $S \neq O_h$, and the absorptions corresponding to the distribution of closely-spaced frequencies will appear as ν_1 and ν_{4bc} envelopes. Thus single ν_1 and ν_{4bc} bands will be expected, but this time broadened by the disorder as well as thermally. Single bands are in fact observed; for ν_1, $\Delta\nu_{1/2} \sim 50\ cm^{-1}$ at 250 K compared with $9\ cm^{-1}$ for $NH_4I(III)$ at 77 K. In phase *I*, the NH_4^+ ion is at the centre of an octahedron of iodine atoms and simultaneous formation of four normal N—H...I bonds is not possible. The *S* from diffraction evidence is O_h, and so one might again expect single ν_1 and ν_{4bc} bands but with additional broadening. The actual halfwidth of the single, symmetric ν_1 band was $\sim 65\ cm^{-1}$ at 290 K, and only one ν_{4bc} band was observed.

In the other NH_4X halides the situation is similar (Table 1). Phases *I* of NH_4Cl and NH_4Br occur at temperatures well above ambient and were not investigated, but there is no reason to suppose that the behaviour of the ammonium ion in $NH_4Cl(I)$ and $NH_4Br(I)$ is fundamentally different from that in $NH_4I(I)$. The sc $NH_4Br(IV)$ is the phase stable below 108 K but no spectral differences could be attributed in this work to the *III–IV* transition.

The range of ν_1 frequencies in the chloride, bromide, and iodide spans only about $30\ cm^{-1}$ (Fig. 2). The variation of the ν_1 frequencies between these halides is not clear-cut. While the ν_1 values of $NH_4Br(III)$ and $NH_4I(III)$ are practically the same, that of $NH_4Cl(III)$ is slightly higher. This is possibly related to the X...4H configuration, which is different in the cubic $NH_4Cl(III)$ and the tetragonal $NH_4Br(III)$ and $NH_4I(III)$: in the tetragonal phases each X atom is at the apex of a C_{4v} pyramid, with the four H atoms forming the base, while in $NH_4Cl(III)$ each Cl is *tetrahedrally* (T_d) coordinated by H atoms (7, 13). If the hydrogen bonding in the T_d configuration indeed *is* weaker than in the C_{4v} configuration, resulting in a higher ν_1 frequency in $NH_4Cl(III)$, a similar explanation could be applied to the observed increase in ν_1 associated with the $III \rightarrow II$ transition in the bromide and iodide: in a completely random phase *II* the C_{4v} configuration would account for only 6/70 ~ 8.5% of the X...4H and 6/256 ~ 2.3% of all the hydrogen-bonding geometries at the X atoms. It should be emphasized that the differences in ν_1 in the chloride, bromide, and iodide are very small compared to the difference of over $100\ cm^{-1}$ between ν_1 of NH_4F and NH_4Cl.

In the sc matrices **15–17** single narrow ν_1 bands are observed, consistent with $S = O_h$ and $E' = C_{3v}$ (6). Also observed is the anticipated increase in the ν_1 frequency from **15** to **17**. Single ν_1 and ν_{4bc} bands are also present in the spectra of the NH_3D^+ ion in

TABLE 1. ND stretching and bending frequencies (cm^{-1}) of the NH_3D^+ probe ion in ammonium and alkali halide matrices at 77 K

No.	MX	Phase	T, K	$\bar{a}$, Å[a]	H...X, Å[b]	NHX*, deg	ν_1	$\Delta\nu_{1/2}$	ν_{4bc}
1	NH_4F	*I*[c]	Room	3.939	1.67		2182.0	5 (5 K)	1326
2	NH_4Cl	*II* (sc)[c]	296	3.875	2.31		2295 (270 K)	~65	1265
3		*III* (sc)[d]	88	3.820	2.28		2289	7	1267
4	NH_4Br	*II* (sc)[c]	265	4.051	2.48		2300 (265 K)	~65	1244
5		*III*[c]	128	4.034	2.40		2281.5	6	1257
6	NH_4I	*I* (fcc)	Room	4.574	2.61 (3.15*)	110	2308 (290 K)	~65	1237
7		*II* (sc)[c]	248	4.333	2.72		2295 (250 K)	~50	
8		*III*[c]	100	4.324	2.69		2281	9	1247
9	KCl	fcc	80	3.938	2.11 (2.67*)	107	2304	18	1250
10	KBr	fcc	80	4.124	2.25 (2.81*)	108	2310	20	1243
11	KI	fcc	80	4.413	2.48 (3.03*)	109	2312	22	1236
12	RbCl	fcc	80	4.120	2.25 (2.80*)	108	2293	17	1253
13	RbBr	fcc	80	4.304	2.40 (2.94*)	109	2304	24	1246
14	RbI	fcc	80	4.584	2.62 (3.16*)	110	2310	28	1239
15	CsCl	sc	80	4.094	2.52		2280.4	5	1272
16	CsBr	sc	80	4.256	2.66		2292	3	1262
17	CsI	sc	80	4.526	2.89		2299.8	4	1245

[a] $\bar{a} = (V/Z)^{1/3}$.
[b] Values marked * refer to H...X* (symmetric trifurcation).
[c] See text.
[d] The possibility that the actual symmetry of NH_4Cl(*III*) is $P4_2/mcm$ (No. 132) (cf. ref. 64) does not affect the discussion of NH_4Cl(*III*) and NH_4Br(*III*) in the text, which is based on the distinction between the parallel (in the chloride) and the antiparallel (in the bromide and iodide) alignment of the ammonium ions.

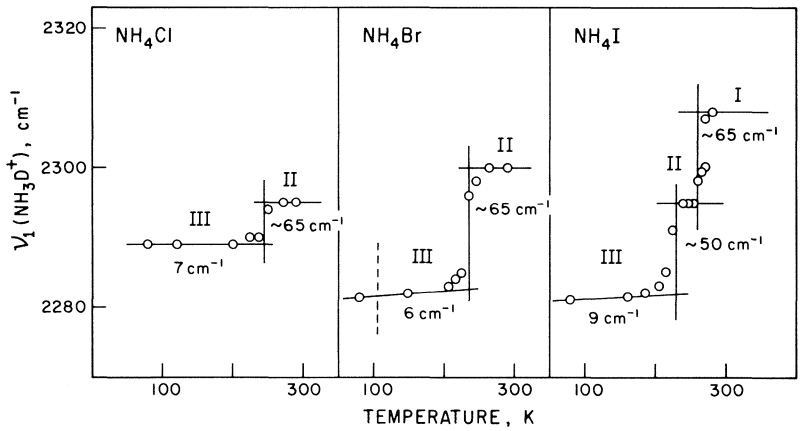

FIG. 2. Variation of $\nu_1(NH_3D^+)$ in simple ammonium halides with temperature. The halfwidths of the ν_1 absorptions are indicated.

the fcc matrices **9–14** ($S = O_h$) but the absorptions are significantly broader. The implications of these differences in bandwidth are discussed below.

Compared with the corresponding NH_4X halides, the acceptor strength of the X atoms in the CsX matrices is little affected by hydrogen bonding to neighbouring NH_4^+ ions because of the dilution, and an increase in hydrogen-bond strength and therefore lower ν_1 frequencies would be expected. This decrease is by no means evident. This means that it is masked by other effects of at least equal order of magnitude and possibly opposite direction (see below).

NH_3D^+ in Cubic and Trigonal $(NH_4)_2MX_6$: Unexpected Behaviour

In the cubic hexahalo compounds (Table 2) the ammonium ion is coordinated by 12 equidistant X atoms at the corners of four tetrahedrally disposed equilateral 3X triangles (= cuboctahedron of symmetry T_d) (Fig. 1 of ref. 1). A single ν_1 band is observed in the spectra of these crystals, consistent with $S = T_d$. The frequencies of this band show an unexpected trend: they *decrease* from F to Br and with increasing H...X (or H...X*) distance.

The trigonal $(NH_4)_2MX_6$ in this investigation are restricted to the fluorides (Table 3). Because of

TABLE 2. Cubic $(NH_4)_2MX_6$ halides: structural data at room temperature and frequencies (cm^{-1}) of the NH_3D^+ probe ion at 77 K

No.	MX	a, Å	x(X)	H...X, Å[a]	NHX*, deg	ν_1	ν_{4bc}	Reference[b]
18	SiF	8.396	0.205	1.96 (2.34*)	120	2432.0	1262.1	
19	PtF	8.455[c]	0.2297[c]	1.96 (2.28*)	125	2406.8	1261.8	
20	SnF	8.393(5)	0.205[d]	1.96 (2.34*)	120	2436.2	1264(5)	
21	PdCl	9.826	0.237[d]	2.45 (2.73*)	130	2372.0	1241.6	
22	PtCl	9.858	0.237[d]	2.46 (2.74*)	130	2372.0	1240.9	1
23	SnCl	10.041(5)	0.2412	2.52 (2.79*)	131	2374.5	1246.4	6
24	PbCl	10.161	0.242[d]	2.56 (2.82*)	132	2366.8	1245.4	
25	TeCl	10.202	0.245[d]	2.58 (2.84*)	132	2359	1243.9	1
26	PtBr	10.367	0.239[d]	2.64 (2.90*)	132	2354	1239.1	
27	SnBr	10.588(20)	0.243[d]	2.71 (2.98*)	131	2354 (200 K)	1243	
28				?		2336[e]	1248[e]	
29	TeBr	10.731(3)	0.2499(2)	2.76 (3.01*)	133	2345(4) (230 K)	1239	
30		[f]		?		2341[e] (100 K)	1242[e]	

[a]Values marked * refer to H...X* (symmetric trifurcation).
[b]Where no reference is given the frequencies were obtained in this work.
[c]Personal communication from Dr. J. H. Holloway.
[d]Estimated, see text.
[e]The ν_1 and ν_{4bc} values are the averages of the observed component frequencies; details will be published elsewhere.
[f]$P4/mnc$ (No. 128), $Z = 2$, $a = 7.501(5)$ Å, $c = 10.765(5)$ Å (< 214 K) (35).

TABLE 3. Trigonal $(NH_4)_2MF_6$: structural data at room temperature and frequencies (cm^{-1}) of the NH_3D^+ probe ion at 77 K

Parameter	Value			
	31 Si	**32** Ge	**33** Ti	**34** Sn
$\bar{a}$, Å	5.180	5.211	5.29	5.361
H...X, Å	1.97 (2.31*)	1.99 (2.32*)	1.95 (2.28*)	
NHF*, deg	123	124	124	
$\nu_1(a)$	2425	2419.5	2411.5	2408.0
$\nu_1(n)$	2413.5	2411.5	2399.0	2398.0
$\nu_{4bc}(a)$	1275.3 sh	1266.1	1259.5	1269.8
$\nu_{4b}(n)$	1278.2	1272.9	1268.0	1274.7
$\nu_{4c}(n)$	1256.8	1258.9	1263.2	1256.2

$S = C_{3v}$, $E' = C_{3v} + C_s$ (3), there are *two* ν_1 components, $\nu_1(a)$ and $\nu_1(n)$, in an intensity ratio of 1:3 (2). The $\nu_1(a)$ frequency is the higher of the two and corresponds to a symmetrically trifurcated situation. The values for the Si, Ge, Ti, and Sn fluorides fall between those of **18** and **19**.

The cubic $(NH_4)_2SnBr_6$ and $(NH_4)_2TeBr_6$ on cooling transform to phases of lower symmetry.[4] The symmetry reduction causes the ν_1 absorption in the cubic phases to split into four components at 77 K, but, more importantly, the frequency corresponding to the centroid of the composite absorption bands is lower than the ν_1 of the corresponding cubic phase. This implies that the strength of the hydrogen bonding has increased when the immediate environment of the ammonium ion has changed from one in which the 12 nearest Br atoms are distributed very uniformly (at the corners of an almost regular cuboctahedron) to a less symmetric (unknown) environment, presumably favouring formation of a preferred hydrogen bond.

[4]The spectra of NH_3D^+ in these low-symmetry phases are described more fully in the Experimental section. Certain symmetry aspects of transitions in A_2MX_6 are examined in the Appendix.

Acceptor Strength vs. Volume Effect

To account for the unexpected direction of variation of ν_1 with H...X let us first consider NH_3D^+ in the alkali halide matrices and in the cubic $(NH_4)_2MX_6$. In Fig. 1 the ν_1 vs. H...X points for the KX and RbX matrices form a net which joins smoothly with the corresponding points for CsX. Leaving aside for the moment the difference between the fcc and sc structures, we see that ν_1 increases, for a given cation, from Cl to I and decreases, for a given X, from K to Cs. The points for NH_4Cl, $NH_4Br(II)$, and $NH_4I(I)$ fall close to the corresponding points for RbX.

These trends demonstrate that ν_1 is affected by two factors acting in opposite directions: acceptor strength for hydrogen bonding and a volume effect.

The acceptor strength decreases from Cl to I, so that, for a given cation, the hydrogen bond weakens and ν_1 increases. On the other hand, for a given acceptor, decreasing the size of the matrix cation compresses the three-dimensional potential well of the H atoms in the probe and raises ν_1. Thus ν_1 in KI has the highest and in CsCl the lowest value of the nine. In NH_4F, in which the energy of the hydrogen bonds has been estimated to be about 3.5 kcal/mol (cf. ref. 9), the acceptor strength is clearly the dominant factor.

The cubic $(NH_4)_2MX_6$ set is not as complete. For some M,X combinations the chemistry or crystal chemistry are unfavourable, and spectra of NH_3D^+ in the iodides could not be obtained because of sample absorption. However, in the two series for which three points are available, Pt,X and Sn,X, ν_1 decreases with increasing H...X, i.e., from F to Br.

In the KX, RbX, and CsX series the ν_1 vs. H...X curves are concave while in the MCl, MBr, and MI series they are convex, tending to level off as H...X increases. In the $(NH_4)_2SnX_6$ series, however, the curve appears to be a straight line and in the $(NH_4)_2PtX_6$ series it is convex and tends to level off with *decreasing* H...X. This must mean that in the alkali halide matrices hydrogen bonding and the volume effect are almost equally significant and largely compensate each other as H...X increases,[5] while in the $(NH_4)_2MX_6$ compounds the volume effect dominates the variation of ν_1 with H...X. As H...X decreases, the hydrogen-bonding interaction, which is very weak for X = Br, becomes stronger and is significant in $(NH_4)_2SiF_6$. The progressive strengthening of the hydrogen bonding is sufficient to alter the concave curve expected for the pure volume effect to the observed straight line and moderately convex curve, respectively.

The presence of the volume effect in $(NH_4)_2MX_6$ would be demonstrated most directly if an increase in ν_1 of the NH_3D^+ probe was observed from Cs_2PtCl_6 to K_2PtCl_6. In these matrices the acceptor strength and geometry are practically the same, and replacing one alkali ion by another would be expected to affect NH_3D^+ (at a shortest distance of 5–5.2 Å from an alkali neighbour) merely through the changing volume of the matrix. Unfortunately, we did not succeed in our attempts to incorporate ammonium ion into A_2PtCl_6, A_2SnCl_6, or A_2SiF_6 in amounts sufficiently large to observe the NH_3D^+ spectrum. However, in the presence of significant hydrogen bonding the ND stretching frequency ν_1 would be expected to decrease, and the HND bending frequency ν_{4bc} to increase, with the strength of the bonding. This expectation is verified in the fcc alkali halide matrices, but in the $(NH_4)_2MX_6$ the trend is reversed (Fig. 3), showing that in these crystals the increase in ν_{4bc} is, but that in ν_1 is not, due to an increase in hydrogen-bonding strength. Figure 3 also shows that the positions of the points for the non-cubic low-temperature phases of $(NH_4)_2SnBr_6$ and $(NH_4)_2TeBr_6$ differ enough from those for the corresponding cubic phases (above T_{tr}) again to indicate that the strength of the hydrogen-bonding interaction has increased from the cubic to the less symmetric low-temperature phase.

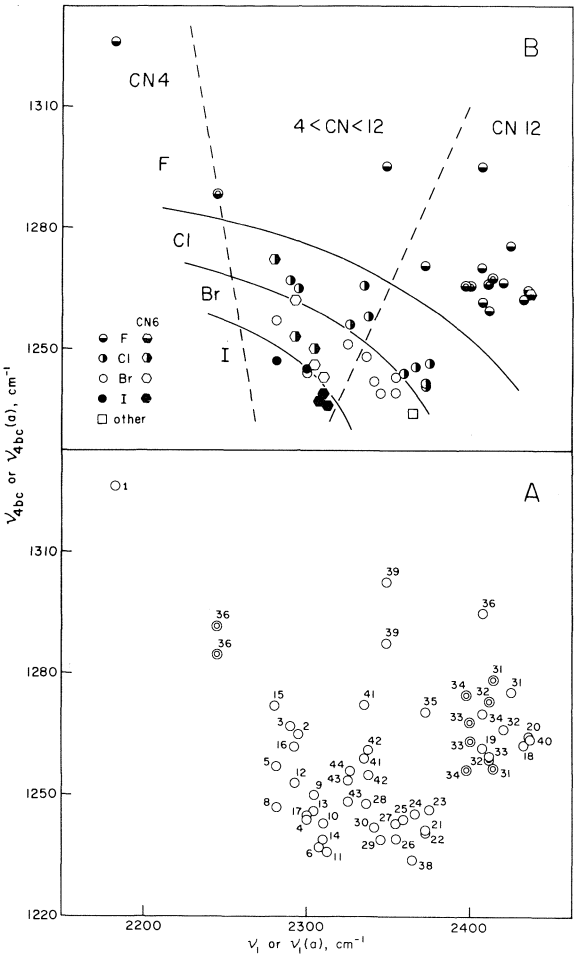

FIG. 3. Correlation of the ν_1 and ν_{4bc} frequencies of the NH_3D^+ probe ion in simple and complex ammonium halides. (*A*) All available values. The non-axial $\nu_{4b}(n)$ and $\nu_{4c}(n)$ values of **31–34** and **36** are shown as double circles. (*B*) Display of acceptor and C.N. For the alkali halide matrices (**9–17**), in which the NH_3D^+ ion is in a constrained situation, the separation by acceptor is not completely clean. Mean values are plotted where more than one component of the ND bending absorption occurs (**36, 39, 41–43**); $\nu_{4b}(n)$ and $\nu_{4c}(n)$ values of **31–34** have been averaged.

[5]The ν_1 for KCl, RbBr, and CsI are almost identical; so are the ν_1 for KBr and RbI and the ν_1 for RbCl and CsBr.

A clear demonstration of the existence of the volume effect as a general factor affecting the stretching frequency of a hydrogen bond is presented, for a *strong* bond, in Fig. 4: the antisymmetric stretching frequency ν_3 at room temperature, of the linear $(FHF)^-$ ion dispersed in alkali halide matrices increases with the decreasing linear dimension $\bar{a} = (V/Z)^{1/3}$ of the matrix (data taken from Fig. 1 of ref. 14). While each of the NaX, KX, and RbX series forms a separate correlation, Ketelaar and van der Elsken (14) showed that, on applying the Bauer–Magat correction, all the points in a ν_3(corr.) vs. $1/a$ plot fall on a smooth curve. In our presentation, $\nu_3(\text{corr.}) = c_1 + (c_2/\bar{a})^4$, with $r^2 = 0.999$ and $\sigma = 2.2\ \text{cm}^{-1}$.[6] The ν_3 values in pure $NaHF_2$ (at 5 and 35 kbar) and KHF_2 (at 1 atm and 40 kbar) (15) fall below the respective curves for NaX and KX, but their line segments have slopes comparable to those of the NaX and KX curves. When the $NaHF_2$(5 kbar) and KHF_2(1 atm) points are brought, by vertical displacement, in coincidence with the ν_3(corr.) vs. $\bar{a}$ curve, the points for $NaHF_2$(35 kbar) and KHF_2(40 kbar), on corresponding displacement, fall on its extension. Although the high-pressure compressibility data for the two acid fluorides are not available,[7] and leaving open the question of validity of the Bauer–Magat correction, it is clear that the effect on ν_3 of the variation of the dimensions of the potential field to which the *internally* hydrogen-bonded $(FHF)^-$ ion is subject in the matrix, is the same, be the variation of $\bar{a}$ produced by mechanical compression or by manipulating the volume of the host structure chemically. In $(FHF)^-$ a hydrogen bond of maximum strength already exists, and on compression the stretching frequency will be affected by a closer approach of ionic charges external to the $(FHF)^-$ ion, of atoms not participating in the hydrogen bonding, hence an essentially pure volume effect. By contrast, the strength of hydrogen bonding of the ammonium ion in $(NH_4)_2MX_6$ will depend on the extent of effective compression, and as the nearest-neighbour anions participate in the hydrogen bonding, further compression will tend to strengthen the hydrogen bond at the same time as it raises the stretching frequency through the stronger factor, the volume effect.

Another consequence of the volume effect in crystals in which it dominates is the direction of variation of the vibrational frequencies on cooling. In the absence of crystallographic transitions, cooling a crystal in which S is cubic[8] will raise all the internal frequencies because of the uniform, symmetry-preserving contraction of the charge field acting on the ammonium ion. The increase may be expected to be more pronounced in crystals containing less compressible (polarizable) counterions and, in general, when the contraction is imposed on a guest ion by the matrix. Taking the mean linear coefficient of thermal expansion α of KX and RbX to be, typically, $3.5 \times 10^{-5}\ \text{deg}^{-1}$ (16), and estimating from Fig. 1 the mean variation $\partial\nu_1/\partial(\text{H}\ldots\text{X})$ in the fcc matrices as $50\ \text{cm}^{-1}/\text{Å}$, leads to an expected increase in ν_1 of only about $3\ \text{cm}^{-1}$ on going from room temperature to 77 K.[9] The actual increase is no greater than $2\ \text{cm}^{-1}$ where the room-temperature frequency can be determined accurately. In **22** and **25** (1) the variation did not exceed $3\ \text{cm}^{-1}$, but the direction of the shift could not be determined because the ν_1 absorption in the room-temperature spectra was poorly defined (cf. Fig. 2 of ref. 1). The observed increases include the compensating effect of the strengthened hydrogen bonding attendant on the temperature reduction.

The conclusion that the strength of the hydrogen-bonding interaction in cubic $(NH_4)_2MX_6$ increases

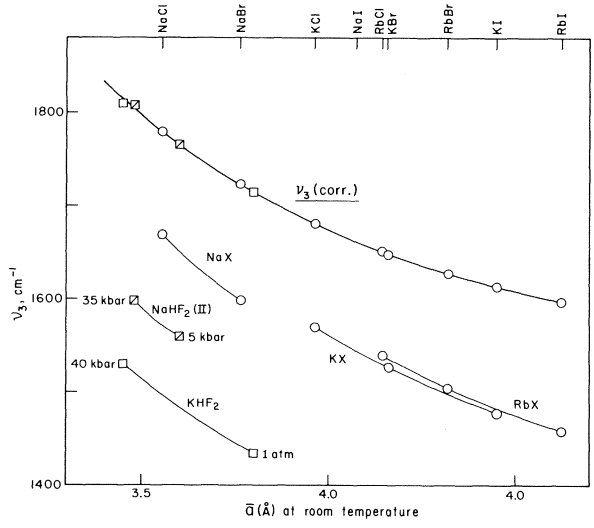

FIG. 4. Variation of the antisymmetric stretching frequency ν_3 of the $(FHF)^-$ ion with the linear dimension $\bar{a}$ of the host matrix.

[6]The coefficient of determination r^2 is the square of the correlation coefficient.

[7]The compressibilities of $NaHF_2$ and KHF_2 were assumed to be similar to those of NaBr and KBr, respectively.

[8]Sites of cubic symmetry occur in all 36 cubic space groups but nine: *Nos.* 198, 199, 205, 206, 212–214, 220, and 230.

[9]Similar considerations predict an increase of about 1.5 cm^{-1} for the ν_4 and about $4\ \text{cm}^{-1}$ for the $\nu_2 + \nu_4$ absorptions of the $^{11}BH_4^-$ ion in alkali halide matrices, with the expected increases in ν_3 and $2\nu_4$ intermediate and about equal. The observed increases on cooling, as estimated from Figs. 1 and 2 of ref. 17 (allowing for a misprint in the captions) and Fig. 11 of ref. 18, are of this order.

from Br to F is supported by the variation of the effective radius of the ammonium ion in these compounds, by consideration of the activation energies for reorientation of the ion and by the progressive increase in the temperature at which combination bands involving librations begin to appear in the spectra of the NH_4^+ ion. Some support comes also from diffraction experiments bearing on the whereabouts of the H atoms. This evidence, in turn, will be considered next.

Effective Radius of the Ammonium Ion

The existence of the large family of isostructural cubic A_2MX_6 halides affords an opportunity to examine in some detail the vexatious problem of the effective radius of the ammonium ion. Shannon (19), in his comprehensive compilation, remarks that "the nature of NH_4^+ made it impossible to define its ionic radius...Khan and Baur (8) derived an apparent radius of the NH_4^+ ion by analyzing the N—O distances in a large number of ammonium salts. They concluded that NH_4^+ has an octahedral radius of 1.61 Å, between that of Rb^+ (1.52 Å) and Cs^+ (1.67 Å). Alternatively, cell volumes of NH_4^+ and Rb^+ fluorides, chlorides, bromides, iodides, and oxides may be compared. This leads to the conclusion that

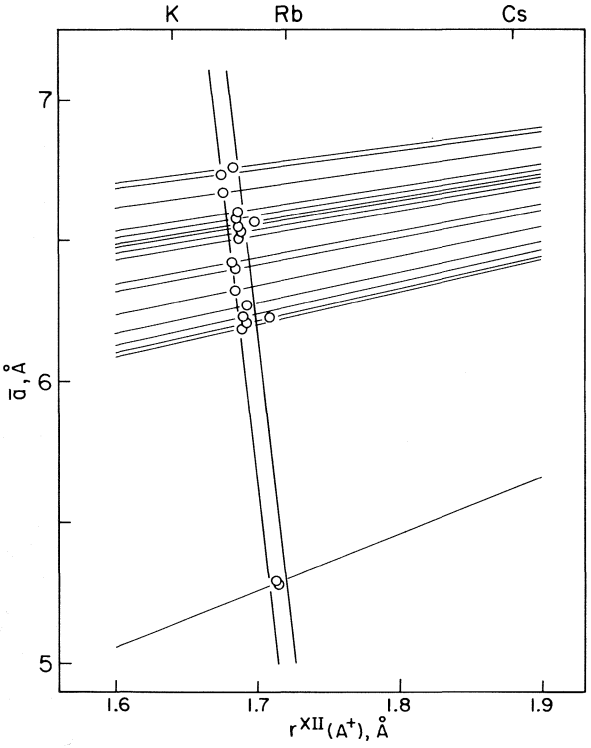

FIG. 5. Variation with $\bar{a}$ of the effective radius r^{xii} of the ammonium ion in cubic $(NH_4)_2MX_6$.

NH_4^+ is not significantly different in size from Rb^+. No explanation is offered for this inconsistency and therefore the radius of NH_4^+ is not included". Brown (20) used an empirical value of 1.56 Å for C.N. 12, compared with 1.60 Å for Rb^+. Agarwal and Shanker (21) attempted to estimate the 'crystal' radius of NH_4^+ (C.N. 8?) from a polarizability–radius relation; their value, 1.58 Å, is contrasted with Pauling's 1.48 Å and Slater's 1.90 Å.

When the room-temperature values of $\bar{a} = a/\sqrt[3]{4}$ for the cubic A_2MX_6 (A = K, Rb, Cs) are plotted against Shannon's ionic radii $r^{xii}(A^+)$ (K, 1.64; Rb, 1.72; Cs, 1.88 Å), the three points in each M,X series are linearly correlated, with $r^2 > 0.98$ and $\sigma < 0.04$ Å. In fact, for the chlorides of Ti, Pd, Pt, Mo, Sn, Pb, Te and bromides of Pd, Pt, Re, Sn, and Te, $r^2 \geq 0.998$ and $\sigma < 0.008$ Å. The fit was worse only for the fluorides, **18** ($r^2 = 0.993$, $\sigma = 0.029$ Å) and **20** ($r^2 = 0.988$, $\sigma = 0.037$ Å), probably owing to a genuine slight departure from linearity. Moreover, the $\bar{a}$ vs. $r^{xii}(A^+)$ straight lines are seen to converge with increasing values of the radius (Fig. 5). When they are treated as a pencil of lines, the point of intersection is at $r^{xii} = 2.805$ Å and $\bar{a} = 7.473$ Å. Constraining the correlation lines for the individual series by least squares to pass through this fictitious point[10] results in an overall σ of 0.010 Å (**18**, $\sigma = 0.021$ Å; **20**, $\sigma = 0.027$ Å). This is about twice the realistic estimate of a typical error on the reported a values. M,X series for which only two of the three points are available can now be included with some confidence.

When the observed room-temperature values of $\bar{a}$ for the NH_4^+ members of the series are used to calculate the respective $r^{xii}(NH_4^+)$ values from the smoothed correlation equations, $r^{xii}(NH_4^+)$ is seen to decrease with increasing $\bar{a}$, i.e. from F to Br (Fig. 5). A straight line fitted to the ammonium points, $r^{xii}(NH_4^+) = 1.836 - 0.023\bar{a}$, has $r^2 = 0.72$ and $\sigma = 0.006$ Å, while the total range of $r^{xii}(NH_4^+)$ is from about 1.714 to about 1.675 Å, *relative to the fixed* r^{xii} *values for* K^+, Rb^+, *and* Cs^+. This increase from Br to F is small but real and must be attributed to the increased hydrogen-bonding interaction in the hexafluoro compounds, which tends to expand the charge cloud of the ion. Thus the effective radius of the ammonium ion relative to Rb^+, which is similar in size, is not constant even in this one isostructural series of high crystallographic symmetry. In general, the radius will vary, for a given C.N., with the extent

[10]This procedure is merely an artificial smoothing device whose use is justified by the overall goodness of fit. It does not apply to composite cations like Me_4N^+; in $(Me_4N)_2SnCl_6$ a is determined by Cl...Me...Cl contacts (25).

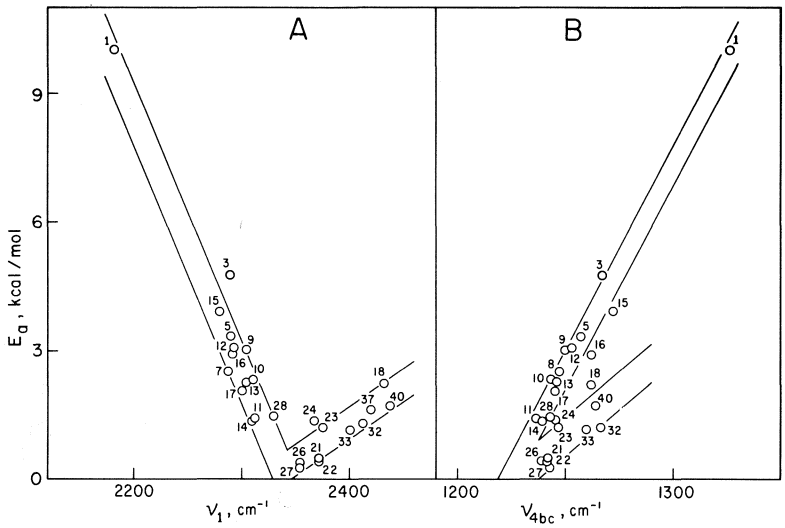

FIG. 6. Activation energy E_a for reorientation of the NH_4^+ ion plotted against $\nu_1(NH_3D^+)$ (*A*) and ν_{4bc} (*B*) frequencies. The vertical widths of the bands represent the $\pm 1\sigma$ limits of goodness of fit. The $\nu_1(n)$ frequencies have been used for **32**, **33**, and **37**, and weighted means of ν_4 for **32** and **33**.

of hydrogen bonding and no single fixed value can be given.

Activation Energy for Reorientation of the Ammonium Ion

This energy, E_a, would be expected to decrease with the strength of the hydrogen-bonding interaction, tending to zero as the barriers to reorientation are progressively reduced and the corresponding potential function becomes smoother, i.e., with increasing H...X and C.N. On the reasonable assumption that $E_a(NH_3D^+) \sim E_a(NH_4^+)$, for those compounds in which hydrogen bonding is significant the E_a value ought to correlate with ν_1. That this is the case can be seen in Fig. 6*A*. Although the functional nature of the E_a,ν_1 association is not known, for **1**–**17** and **28** a linear regression of E_a on ν_1 yields $r^2 = 0.90$ ($\sigma = 0.72$ kcal/mol), indicating that even a linear correlation is highly significant. On the other hand, the E_a,ν_1 points for cubic and trigonal[11] $(NH_4)_2MX_6$ (including **27**), NH_4BF_4, and NH_4PF_6 fall in a different correlation region: linear regression of E_a on ν_1 gives $r^2 = 0.69$ ($\sigma = 0.38$ kcal/mol), hence even this, separate, linear correlation is significant. This implies that as the volume effect, imposed on the ammonium ion by the electrostatic energy requirements of the matrix crystal (as compared with the corresponding Rb compound), becomes more significant the height of the barrier to reorientation increases and so does E_a. This increase in barrier height may be viewed as an increase in hydrogen-bonding interaction, in support of our above contention that this interaction increases from Br to F.[12] The strength of the hydrogen bonding therefore increases both to the left and to the right of the region of minimum E_a in Fig. 6*A*.

The E_a,ν_1 correlation would be represented more properly by a curve within the two $\pm 1\sigma$ bands of Fig. 6*A* and having a minimum corresponding to a very low E_a value in the vicinity of $\nu_1 = 2340$ cm^{-1}. Several such functions could be proposed, but the final choice will have to await the availability of further E_a data. No E_a values appear to exist for $(NH_4)_2MX_4$ or NH_4MF_3 salts but would clearly be of use; **41**, **36**, and the perovskite NH_4ZnF_3 (isostructural with **35**) would be obvious candidates for nmr studies.

A similar plot for ν_{4bc} (Fig. 6*B*) shows that E_a decreases with the frequency of the bending vibration. This is not unreasonable to expect, considering that the bending and librational modes involve motions perpendicular to the N—H...X bond and, if the reorientational motion is seen as a libration executed from one local minimum to another, across the hindering potential barrier. A linear regression of E_a on ν_{4bc} gave $r^2 = 0.75$ ($\sigma = 1.02$ kcal/mol) when all the available points were included; $r^2 = 0.48$ ($\sigma = 0.84$ kcal/mol) for all the points less

[11]The $\nu_1(n)$ values were used for **32** and **33**, and the lower of the two ν_1 values for **37**, on the view that at least three hydrogen bonds must be 'broken' in the reorientation, at least one of which being of necessity that corresponding to the stronger interaction and hence to lower stretching frequency.

[12]Bonori and Terenzi (22) remark that in some cubic $(NH_4)_2MX_6$ salts, E_a *increased* with decreasing lattice constant. This obviously corresponds to the high-frequency branch of our E_a vs. ν_1 plot of Fig. 6*A*.

NH_4F; $r^2 = 0.96$ ($\sigma = 0.44$ kcal/mol) for the points of the low-frequency branch of Fig. 6*A*; and $r^2 = 0.57$ ($\sigma = 0.45$ kcal/mol) for the high-frequency branch. All four regressions indicate that the correlation is significant. The regression lines intersect $E_a = 0$ at ν_{4bc} between 1225 and 1230 cm^{-1}; this range of values may be regarded as an upper-bound estimate of the 'limiting' ν_{4bc} frequency (= the 'free ion' value) in crystals of ammonium halogen compounds.

Combination Bands Involving the $\nu_6(NH_4^+)$ Librational Mode

In general, the $\nu_2 + \nu_6$ and $\nu_4 + \nu_6$ bands of NH_4^+ are observed in the room-temperature spectra of ammonium salts in which *normal* hydrogen bonds are present but not of those where the ammonium ion occurs in a trifurcated situation. However, in such cases they may appear when the temperature of the sample is lowered.

Gardner *et al.* (23), who studied the inelastic neutron scattering spectra of NH_4^+ in alkali halide matrices, found that in CsX peaks corresponding to the librational (torsional) fundamental ν_6 itself were quite well resolved even at room temperature. However, in the fcc matrices under comparable conditions, the corresponding peaks were so broad that for the iodides they could not be located with the instrument used; the torsional peaks remained much sharper in the CsX matrices down to liquid-helium temperature. Similar differences were observed, for the combination bands, in the ir spectra of NH_4^+ in such matrices. In the room-temperature ir spectra of $(NH_4)_2MX_6$ the combination bands occur only in **18–20** and in **31** and **32** (2). They were absent in the spectrum of **23** at 77 K, reflecting the weakness of the hydrogen bonding in the chloride **23** compared with the fluorides **18–20**, but the $\nu_4 + \nu_6$ band emerged on cooling the sample to 22 K (Fig. 7).[13] Its relative sharpness strongly suggests that a considerable change in the motions of the ammonium ion has occurred as a result of cooling.

Effect of Acceptor Atom on ν_1: Coordination Number, NHX Angle, and Formal Charge*

Returning to Fig. 1, we now can make certain observations concerning the effect of the acceptor atom X on ν_1. When the ν_1 values of a number of additional ammonium halides (Table 4) are introduced, trends associated with C.N., the NHX* angle, and the formal charge on X begin to emerge (Fig. 8).

NH_4F is the only ammonium halide in which C.N. equals the number of normal hydrogen bonds

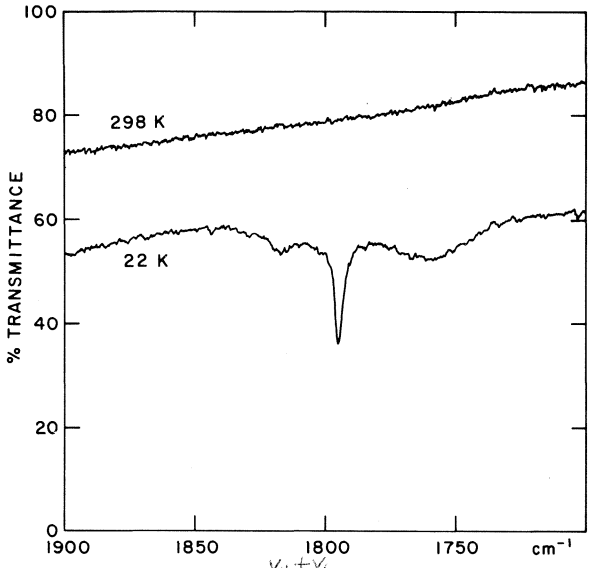

FIG. 7. The $\nu_2+\nu_6$ and $\nu_4+\nu_6$ region of the spectrum of NH_4^+ in $(NH_4)_2SnCl_6$ (**23**) at 298 and 22 K.

formed. NH_4SnF_3 is an intermediate case: C.N. is 6, but three of the ammonium hydrogens form normal N—H...F bonds with the three F atoms of an SnF_3^- ion (tetrahedral bonds similar to those in NH_4F) and the fourth point, along a C_3 axis, at the centre of a triangle of F atoms belonging to different SnF_3^- ions. This constitutes a symmetrically trifurcated situation and the C.N. is more properly 3 + 3. The $\nu_1 = 2246$ cm^{-1} frequency in **36** is the second lowest in Fig. 1. See errata, p. 423

The next compound encountered in the approximate direction of a straight line drawn through the **1** and **36** points in Fig. 2 is **39**, C.N. 8, followed by **35**, **37**, and $(NH_4)_2MF_6$, all of which have C.N. 12. In the perovskite NH_4MnF_3, which is cubic at 200 K and above, the coordination figure is an undistorted cuboctahedron ($S = O_h$), while in the cubic $(NH_4)_2MF_6$ the coordination cuboctahedron is of symmetry T_d.[14] In NH_4BF_4 the coordination figure is irregular, $S = C_s$. Since the H...X distance along this straight line does not vary greatly, the increase in ν_1 in the fluorides is attributed to the increase in C.N., even though C.N. is not the only factor (see below). A similar trend is observed for the chlorides and bromides.

The case of C.N. 6 is somewhat different in that there is no clear separation of the ν_1 frequencies for C.N. 6 from those for C.N. 8 (**2–5** and **7–17**). This point will be discussed in more detail later. NH_4PF_6 (C.N. 6) is close to **37** (C.N. 12), but here the low formal charge on the F atom is probably the domi-

[13]Although the possibility of a phase transition below 77 K has been raised (24) our NH_3D^+ spectra between 22 and 80 K showed no evidence of it.

[14]It approaches a metrically regular cuboctahedron as $x(X) \rightarrow \frac{1}{4}$, i.e. from F to Br.

TABLE 4. Complex ammonium halides: structural data at room temperature and frequencies (cm^{-1}) of the NH_3D^+ probe ion at 77 K

No.	Compound	S	C.N.	H...X, Å[a]	NHX*, deg	ν_1	ν_{4bc}	Reference[b]
35	NH_4MnF_3	O_h	12	1.97 (2.24*)	129	2373 (200 K)	1270.5	
36	NH_4SnF_3	C_3	3+3	1.97 (2.19*) (3×)	134	2408	1295.2	
				1.72 (3×)		2246	1291.5	
							1284.7	
37	NH_4BF_4	C_s	12	1.90[d]		2439 (3×)		4
						2420 (1×)		
38	NH_4BPh_4	D_{2d}[c]	4[c]			2364.0	1234.0	4
39	NH_4AlF_4	D_{4h}	8	1.84		2348.5	1302.2	
							1287.6	
40	NH_4PF_6	O_h[c]	6	1.35 (1.97*)[f]	100	2436.5	1263.8	4
41	$(NH_4)_2PdCl_4$	D_{2h}	8	2.30[e]		2335	1272.1	6
							1259.0	
42	$(NH_4)_2PtCl_4$	D_{2h}	8	2.31[f]		2338	1261.1	
							1255.0	
43	$(NH_4)_2PdBr_4$	D_{2h}[c]	8[c]	2.50[f]		2324.5	1253.8	
							1248.2	
44	$(NH_4)_2[CuCl_4(H_2O)_2]$	S_4	8	2.38		2326 (300 K)	1256	45

[a]Values marked * refer to H...X* (symmetric trifurcation).
[b]Where no reference is given the frequencies were obtained in this work.
[c]See text.
[d]This distance corresponds to the shortest N...F approach of twelve (varying from 2.93 to 3.44 Å). The H...F distances given in ref. 40 range from 2.16(7) to 2.50(5) Å, as determined by *X-ray* diffraction.
[e]D...Cl at 125 K; 2.34 Å at 295 K (43).
[f]Estimated.

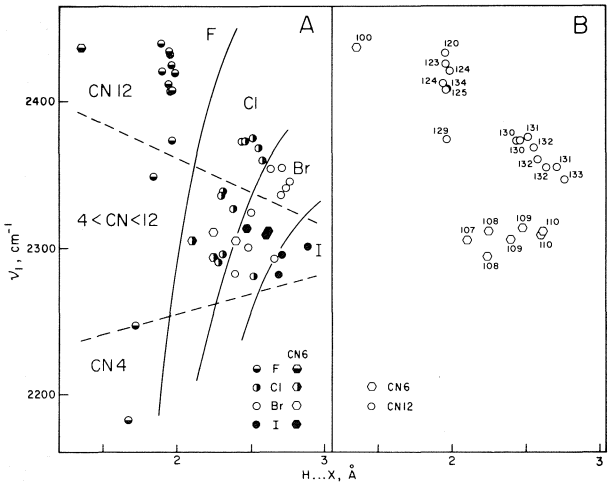

FIG. 8. Correlation of the coordination number (*A*) and NHX* angle (*B*) with $\nu_1(NH_3D^+)$ and H...X in simple and complex ammonium halides. For identification of the points see Fig. 1.

nant factor. With this exception, the periphery of the plot in Fig. 8, as seen from the NH_4F point, consists of points corresponding to C.N. 12.

The NHX* angle, in compounds where symmetric trifurcation (i.e. $S \supset C_3$) is obtained, is defined as the obtuse angle formed by the XH vector and the NH vector pointing at the centre of the equilateral triangle of X atoms. It cannot be divorced from C.N. In compounds with C.N. 6, NHX* = 100–110°; in those with C.N. 12, NHX* = 120–135°. For C.N. 12 a trend is discernible not only for ν_1 (Fig. 8) but also for ν_{4bc} (Fig. 9). In both cases the frequency decreases as NHX* increases, i.e., as the H atom moves away from the plane of the 3X triangle. There also appears to be a moderately strong ($r^2 = 0.54$) correlation between NHX* and E_a: the closer NHX* is to 90°, the higher is E_a.

In ammonium halides containing isolated or linked complex anions MX_n the acceptor strength does not depend only on the nature of the halogen atom but also on its formal charge. The latter is defined as $(pc/n) - 1$, where c is the formal charge on M and p is the C.N. of X relative to M. In addition, X may be a simultaneous recipient of a total of q hydrogen bonds from ammonium ions. These quantities are listed, for compounds of interest, in Table 5.

It is evident that the formal charge affects the variation of ν_1 but not independently of C.N. and NHX*; the effect of p and q is not clear. For example, the increase in ν_1 in the fluoride sequence **39**, **35**, **40** is associated with a decrease in the formal charge but also with a simultaneous increase in C.N. The ν_1 of **18** is about the same as that of **40**, in spite of the formal charge in **18** being $-1/3$ compared with $-1/6$ in **40**. However, q(**18**) = 4q(**40**) and this, together with the decrease in H...X and NHX* from **18** to **40**, appears to outweigh the doubling of the formal charge.

The 'Free Ion' ν_1 and ν_{4bc} Frequencies

The ν_1 frequencies of the several families of halides

TABLE 5. Formal charges on acceptor atoms in complex ammonium halides

	Compound	Structural arrangement	p	Formal charge	q
40	NH_4PF_6	NaCl, isolated [PF_6]	1	$-\frac{1}{6}$	1
18–20	$(NH_4)_2MF_6$	Anti-CaF_2, isolated [MF_6]	1	$-\frac{1}{3}$	4
45	$(NH_4)_3FeF_6$	Anti-'BiF_3', isolated [FeF_6]	1	$-\frac{1}{2}$	4+1
41	$(NH_4)_2PdCl_4$	Isolated planar [$PdCl_4$]	1	$-\frac{1}{2}$	4
35	NH_4MnF_3	CsCl, 3-dimensionally linked [MnF_6]	2	$-\frac{1}{4}$	4
39	NH_4AlF_4	CsCl, 2-dimensionally linked [AlF_6]	2	$-\frac{1}{2}$	4

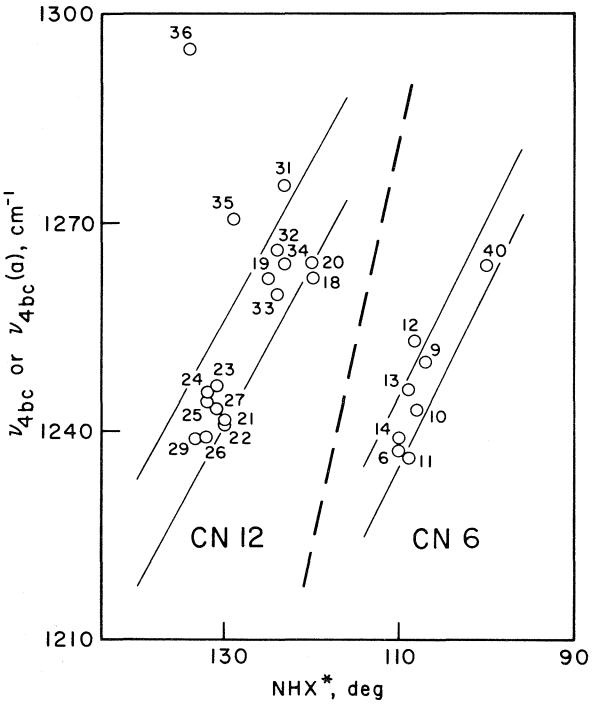

FIG. 9. Variation of $\nu_{4bc}(NH_3D^+)$ with the NHX* angle in simple and complex ammonium halides. The point for **36** was not included in the regression.

in the ν_1 vs. H...X plot of Fig. 1 are seen to converge, with increasing H...X, to a 'limiting' value somewhere in the region of 2320–2340 cm^{-1}. A similar convergence is observed in the ν_{4bc} vs. ν_1 plot of Fig. 3, to ν_{4bc} values in the vicinity of 1220 cm^{-1}, and also in Fig. 6. All these trends are manifestations of the same basic fact, viz. the division of the ammonium halides into two main groups, one in which ν_1 is dominated principally by hydrogen bonding and another, in which the dominant factor is the volume effect. The two frequencies, $\nu_{1,\infty}$ = 2330–2340 and $\nu_{4bc,\infty}$ = 1220–1230 cm^{-1}, may thus be regarded as corresponding to 'zero' hydrogen bonding and a minimum volume effect, i.e., to the 'free ion' state in halide crystals. The $\nu_{1,\infty}$ value is to be compared with that proposed recently (5) for the ν_1 vs. N...O correlation in the ammonium Tutton salts, 2450–2500 cm^{-1}. The cut-off H...X value corresponding to this hypothetical state of the ion is difficult to estimate but it would seem to be at least 3.4 Å.

In this connection it is of interest to observe that in NH_4BPh_4 (**38**), in which the ammonium ion has been regarded as non-hydrogen-bonded (26), the ν_1 is 2364 cm^{-1}, i.e., above the estimated $\nu_{1,\infty}$, but the ν_{4bc}, 1234 cm^{-1}, is the lowest in Tables 1–4 and Fig. 3. The only conceivable hydrogen bonding, to the π systems of the benzene rings, would be expected to lower ν_1, so we conclude that the ammonium ion in this crystal is in a state of compression imposed by electrostatic interactions similar to those existing in the presumably isostructural Rb salt. Thus the idea (27) that one should take the highest observed $\nu_3(NH_4^+)$ as representing the frequency of the 'free' ammonium ion must be considered dubious.

It should be noted that, as the volume effect cannot be evaluated *absolutely* but only along an isostructural series, the contribution of the 'compression' of the ammonium ion to ν_1 in an isolated compound can be estimated only with reference to the aggregate of available results for NH_3D^+, such as presented for the halides in Fig. 3.

Does a Symmetrically Trifurcated Hydrogen Bond Exist?

The answer to this question must be compatible with the evidence from the ir spectra of the NH_3D^+ probe ion: (*1*) Where favourable geometry for the possible existence of a trifurcated bond is obtained, only *one* ν_1 absorption is observed when *S* is cubic, and this absorption at 77 K is narrow. (*2*) The difference between the ν_1 value in $NH_4I(I)$ and those in $NH_4I(II)$ and $NH_4I(III)$ is small compared with the total ν_1 range of ca. 250 cm^{-1} in Fig. 1, about 13 cm^{-1} between phases *I* and *II* and about 27 cm^{-1} between *I* and *III*. (*3*) The difference between the ν_1 values in the fcc RbX and the corresponding sc CsX matrices amounts to only about 10 cm^{-1} if one allows for the volume effect (by comparison between the KX and RbX salts).

Comparison of the halfwidths of ν_1 at 77 K shows that $\Delta\nu_{1/2}$ is 3–9 cm^{-1} in cases where normal hydro-

gen bonds are expected (phases *III* of NH_4X and CsX matrices) but 17–28 cm^{-1} in the fcc matrices (Table 1). This striking difference is undoubtedly real and seems to be indicative of enhanced motions of the NH_3D^+ ion (and by implication the NH_4^+ ion) in the fcc environments. The extra breadth does not result from stronger hydrogen bonding, for the ν_1 frequencies are much the same in the sc and the fcc crystals. Its most likely origins are rapid reorientation and large librational amplitude. Gardner *et al.* (23) failed to observe, in their inelastic neutron scattering studies, any quasielastic broadening of the elastic peak and hence they ruled out the former. The origin of the extra breadth then appears to lie in large-amplitude librations of the ammonium ions.

The transition from the ordered phase *III* to the disordered phase *II* in simple ammonium halides is associated with a large increase in the halfwidth of ν_1 (Table 1): $\Delta\nu_{1/2}$ increases from 6–9 cm^{-1} to 50 cm^{-1} or more. A portion of the extra breadth must be due to the distribution of acceptor strengths attendant on disordering. When the already disordered sc $NH_4I(II)$ transforms to the fcc phase *I*, an additional increase in $\Delta\nu_{1/2}$ of about 15 cm^{-1} is observed. This is of the same order as the difference between the sc and fcc matrices at 77 K, though a fraction of this increase will come from the thermal broadening owing to the difference of about 40 deg between the temperatures of measurement. It thus seems that the change-over from the 'normal' to the 'trifurcated' regime is associated with an increase in $\Delta\nu_{1/2}$ of the order of 15 cm^{-1}, and that this increase corresponds to an enhanced librational motion of the ammonium ions.

Another kind of evidence which must be reconciled comes from diffraction studies. When the librational amplitude is large, interpretation of the results of such studies becomes difficult and ambiguous. Of the three available, room-temperature studies bearing on trifurcation in ammonium halides, one concerns **6**, another deals with **18**, and the third is an X-ray study of **23**. The conclusion from the detailed neutron-diffraction study of $NH_4I(I)$ is that there are six equivalent maxima in the proton-density distribution round the N atom; they are associated with the corners of the octahedron of iodine atoms (28). In $(NH_4)_2SiF_6$, according to the neutron-diffraction study of Schlemper and co-workers (7, 11), three local proton-density maxima are associated with each threefold axis of the ammonium ion in the directions pointing away from the Si atoms. In the view of those authors these maxima are to be looked upon as a manifestation of a dynamic rather than static disorder. The data of Schlemper *et al.* were re-analyzed, at our request, by Press using cubic harmonics (29) and the existence of the four triple maxima was confirmed.[15] The broad 0.9 e $Å^{-3}$ peaks at the 32(*f*) ($x = 0.30$) positions of *Fm*3*m* in a difference Fourier map of $(NH_4)_2SnCl_6$ (12), which were considered as probably corresponding to the H atoms, may be regarded as the (unresolved) electron-density counterparts of the local maxima in the proton-density distribution in $(NH_4)_2SiF_6$.

The picture that emerges is then as follows. In $NH_4I(I)$ (and we assume also in phases *I* of the chloride and bromide), the fcc matrices and cubic $(NH_4)_2MX_6$ the site symmetry at the ammonium ion is cubic and all conceivable orientations of the ion, consistent with *S*, are equivalent. Thus only one ν_1 absorption is observed. The ion undergoes librational motions of large amplitude, as witnessed by the breadth of the ν_1 absorption. The H atoms spend a considerable portion of their time near the acceptor atoms, away from the symmetrically 'trifurcated' equilibrium positions. This is evident from the positions of the local maxima in the electron and proton-density distributions and would be even clearer if low-temperature neutron diffraction studies of **18** and **23** were available. Hence the ν_1 values are not very different from the ν_1 values that would be expected for normal bonds of comparable length,[16] and similarly only small differences are observed on comparing the ν_{4bc} values. Analogous situations are likely to occur in **35**, **40**, and **45**, for which the relevant structural information does not exist.

In describing hydrogen bonding in such compounds, distinction must be made between symmetrically trifurcated *situations*, i.e. coordination geometry, and symmetrically trifurcated *bonds*. The hydrogen bond in these cases may be regarded as symmetrically trifurcated only in the sense that the coordination geometry of the acceptor atoms round each H atom of the ammonium ion provides positions of symmetry C_3 or C_{3v}, and these may be thought of as the equilibrium positions toward which the N—H vectors are directed. Because they are strongly influenced by the dynamics of the ammonium ion, the actual whereabouts of the H atoms cannot be specified beyond indicating diffuse regions between the equilibrium positions of the N atom and the acceptors, such as those suggested by the broad local maxima in the proton and electron-density distributions.

Hydrogen bonds encountered in symmetrically trifurcated situations are only a special case of hy-

[15]Personal communication.

[16]This accounts for the consistency of the trends in Fig. 1 when H...X rather than H...X* is used for the trifurcated situations.

drogen bonds lacking definite spatial relationship, between reorientations, to the acceptor atom(s). Such bonds may generally be expected to exist in crystals with C.N. > 8; the greatest librational freedom is likely to exist in situations where *S* is cubic. A more appropriate generic description of such bonds might be *fluxional* hydrogen bonds.

An exceptionally favourable situation for a study of the hydrogen bond in a symmetrically trifurcated but noncubic coordination appears to exist in **36**. Because three of the H atoms of the ammonium ion are engaged in strong normal hydrogen bonds to the F atoms of a single SnF_3^- ion, the fourth H atom can only point into a triangle of F atoms related by the unique threefold axis of the ammonium ion, and so an opportunity seems to exist for examining a single bond of this type in a relatively stationary ammonium ion. The trifurcated situation in this compound is, however, not quite similar to that in **18** or **6**. In **18** a hydrogen atom has three nearest H neighbours at 3.01 Å (laterally) and one next-nearest at 5.21 Å (along C_3); in **6** the nearest H neighbours of a hydrogen atom are at 3.45 Å (laterally), always assuming that the H atoms are at their equilibrium positions required by the space-group symmetry. In **36**, however, the nearest H neighbours, which occur in centrosymmetric pairs on C_3, are separated by only 1.66 Å. The H–H repulsion in **36** must thus be much more significant than in **18** and **6** and can be expected to raise the frequency of the axial ND stretching vibration over and above the increase due to the overall volume effect. This is indeed observed. The low $\nu_1(n)$ frequency, 2246 cm^{-1}, indicates that the three normal N—H...F bonds are strong, and the large values of the three components of the HND bending, 1284.7–1295.2 cm^{-1} (Table 4), and their small spread can be taken as evidence of the nonaxial bonds and the axial bond both being strong and of similar strength. However, the $\nu_1(a)$ value is 162 cm^{-1} above the $\nu_1(n)$, which is by far the largest difference between two ν_1 component frequencies of the NH_3D^+ probe observed to date in an ammonium compound. See errata, p. 423.

The strong H–H repulsion, which may also be regarded as an anisotropic volume effect, probably also accounts for the misfit of the NHF* angle of **36** in Figs. 8*B* and 9. A point corresponding to NHX* = 134° would be expected to fall appreciably below those of $(NH_4)_2MF_6$ in Fig. 8*B*. In Fig. 3*B* the point for the axial bond falls among the fluorides with C.N. 12, which is not in contradiction with the type of bond encountered here, although the region in which the point would have been expected to fall is 4 < C.N. < 12. Since the axial N—H bond in **36** probably comes closest to the notion of a symmetrically trifurcated *bond*, a neutron diffraction study of the crystal at two temperatures would be of considerable interest.

Criteria of Hydrogen Bonding of the Ammonium Ion in Crystals

Various criteria have been previously proposed in attempts to determine whether hydrogen bonding plays an important role in ammonium salts. They have been recently summarized by Hamann (30). Those pertinent to the present work are: (*i*) Hydrogen bonding is present if combination modes $\nu_i + \nu_6$ (i = 2 and 4) involving the librational mode ν_6 are observed in the ir spectra of NH_4^+, and (*ii*) if the frequency of the antisymmetric bending mode $\nu_4(NH_4^+)$ is higher than 1400 cm^{-1}.

Criterion *i* refers actually more to the *type* of the hydrogen-bonding interaction than to its strength. The most important single factor governing the presence of the NH_4^+ combination modes seems to be the C.N. and the attendant NHX* angle. We have seen that the hydrogen bonds in ammonium halides with C.N. 6 or 12 are most probably highly dynamic in nature and that motion of H atoms on a portion of a spherical surface in the regions between acceptor atoms is relatively free. In this situation, especially at room temperature (the temperature at which most studies have been conducted), there is reason to believe that no $\nu_i + \nu_6$ absorption would be observed because of the strong temperature dependence of the breadth of the $\nu_6(NH_4^+)$ fundamental (cf. ref. 23). Dunsmuir and Lane (31) only cite one salt of the cubic K_2PtCl_6 type, **18**, in which both combination modes were present. The sharp contrast between NH_4^+ in fcc alkali halide matrices (C.N. 6), in whose spectra $\nu_i + \nu_6$ are apparently absent, and the CsX matrices (C.N. 8), in whose spectra these bands were observed (18, 23), provides further support for this view, in that the *strength* of the hydrogen bonding, as measured by the ν_1 frequency of the NH_3D^+ probe, is much the same in both cases. It may be noted that the combination bands appear in the room-temperature spectra of the fluorides $(NH_4)_3MF_6$ (M = Fe, Al, Ga, In, Sc) (31, 32), which are structurally closely related to $(NH_4)_2MF_6$ and contain ammonium ions in both 6- and 12-coordination. It is likely that the increased formal charge on the F atoms in the triammonium compounds (Table 5) causes the combination bands in these salts to emerge more readily than in $(NH_4)_2MF_6$, even though direct evidence for this is lacking.

The suggestion that, for a hydrogen-bonded ammonium salt, $\nu_4(NH_4^+)$ will occur above 1400 cm^{-1}

(31) is not beyond doubt (cf. ref. 33). The volume effect applies equally to pure NH_4^+ spectra, and in those halides where it predominates over hydrogen-bonding effects it will tend to increase this frequency.

The commonly-held view that crystallographic dissimilarity of an ammonium salt and its K and Rb analogues should be attributed to the effects of hydrogen bonding also bears closer examination. It is undoubtedly correct in some cases, notably in NH_4F, but in many instances the stability of one phase relative to a second is only marginal, and the dissimilarity of the ammonium compound and the K and Rb compounds, *at a particular temperature*, may be the result of different lattice dynamics, without significant involvement of hydrogen-bonding interactions. Thus **18** is isostructural with K_2SiF_6 and Rb_2SiF_6 at room temperature, yet we have seen that hydrogen-bonding interactions are present in the ammonium compound. Similarly, $(NH_4)_2TeBr_6$ and Rb_2TeBr_6 are cubic at room temperature while K_2TeBr_6 is not; at 180 K the ammonium compound is noncubic while the Rb compound remains cubic, but below 77 K all three compounds are noncubic (24), even though the transformation in the Rb compound cannot be attributed to hydrogen bonding. As a *general* criterion, crystallographic comparisons of this kind must therefore be used with due caution.

A more reliable criterion than most, for ammonium halogen compounds, appears to be the position of the ν_1, ν_{4bc} point in Fig. 3. It is based entirely on internal, of necessity selfconsistent, evidence from the ir spectra, and it has the advantage of relating the *strength* of the hydrogen-bonding interaction to parameters associated with the *type* of hydrogen bonding. To what extent this criterion is applicable to ammonium salts of oxyacids cannot be determined at present because of the paucity of spectral data for the NH_3D^+ probe in such crystals.

Conclusions

This study is concerned with the problem of determining the extent of hydrogen bonding and the type of environment and motions of an ammonium ion in a crystal from ir spectra of polycrystalline simple and complex ammonium halides. Our results show that unambiguous information bearing on this problem can be obtained from spectra of the isotopically isolated NH_3D^+ probe ion but not from spectra of the NH_4^+ or ND_4^+ ions.

Contrary to what might be expected, the ν_1-(NH_3D^+) stretching frequency is not a monotonic indicator of the strength of the N—D...X bond. As Figs. 1, 3, 6, and 8 show, the frequency of the ν_1 vibration in a crystal is affected by two factors acting in opposite directions, the acceptor strength and a volume effect. The effect of each factor levels off with increasing D...X distance. As a result, the ν_1 frequencies converge to a value near 2330–2340 cm^{-1}; this value may be regarded as the 'free ion' value in ammonium halogen compounds. Observed ν_1 values significantly below this limit, say below 2310 cm^{-1}, correspond to C.N. between four and eight and to strong or moderately strong normal (i.e. 'straight') N—D...X bonds, while those significantly above, say 2350 cm^{-1} or higher, are most likely to correspond to C.N. 12 (possibly 8, rarely 6) and to weak or very weak hydrogen-bonding interactions (Fig. 8). However, formal charge on the acceptor atom also plays a part and must be considered when making an estimate of the hydrogen-bond strength.

When both the ν_1 stretching and ν_{4bc} bending frequencies of the NH_3D^+ probe are known, the situation in which the ammonium ion finds itself in the crystal can be determined with considerable confidence with reference to Fig. 3. This is possible because the acceptor strength and the volume effect act in the same direction on ν_{4bc} but in opposite directions on ν_1. Thus the ν_{4bc} frequency decreases steadily with the strength of hydrogen bonding, while the ν_1 frequencies separate into two limiting groups, a low-frequency, normal-hydrogen-bond one, dominated essentially by the acceptor strength, and a high-frequency one, dominated essentially by the volume effect and corresponding to hydrogen-bonding interactions pronouncedly dynamic in character. The points of the ν_{4bc} vs. ν_1 plot fall into well-separated regions according to the acceptor and C.N., which leads to assignment of NH_3D^+ spectra not studied previously to particular structural situations and makes predictions possible.

The factors that are responsible for the trends evident in the ν_{4bc} vs. ν_1 and ν_1 vs. H...X plots manifest themselves also in other ways. Thus when the activation energy E_a for reorientation of the ammonium ion in a crystal is plotted against ν_1 (Fig. 6), the correlation curve has a low-frequency and a high-frequency branch, the former corresponding to normal hydrogen bonds and C.N. < 12, the latter to hydrogen bonds of a highly dynamic character and C.N. 12. However, ammonium ions of C.N. 6 may fall on either branch, depending on the formal charge on the acceptor atom: on the low-frequency branch when the formal charge is high (e.g., $NH_4I(I)$), and on the high-frequency branch when the formal charge is low (e.g., NH_4PF_6). In either case the bonds for C.N. 6 are similar in character to those for C.N. 12.

The conclusions drawn from the combined evidence obtained from our ir spectra of the NH_3D^+ probe and from the results of published diffraction

studies do not support the view that in situations where C.N. is 6 or 12, e.g., in **6** or **18**, the ammonium ion is attached, between reorientations, by *normal* (i.e. essentially straight) hydrogen bonds to one or simultaneously to two or three acceptor atoms, for only *one*, symmetric ν_1 band is observed. The so-called 'trifurcated' hydrogen bond, which had been suggested to occur in such situations, is most likely a highly non-directional hydrogen-bonding interaction of a strength not much different from that of a normal hydrogen bond of comparable N...X length. For $\nu_1(NH_3D^+)$ in the alkali halide matrices the increase in $\Delta\nu_{1/2}$ on going from C.N. 8 to C.N. 6 is of the order of 15 cm^{-1}.

The desirability of comparing the vibrational frequencies of the isotopically isolated NH_3D^+ probe ion rather than those of NH_4^+ or ND_4^+ must be emphasized. Thus Dunsmuir and Lane (31), who obtained ir spectra of the NH_4^+ ion in a number of undeuterated complex ammonium halides, were not as successful as they might have been in establishing correlations between vibrational frequency and C.N. or what in our terms amounts to formal charge on the acceptor atom, even though their compounds were well selected for the purpose. This was in part due to the unreliable nature of the NH_4^+ frequencies, which becomes evident when the $\nu_4(NH_4^+)$ frequencies of Dunsmuir and Lane are plotted against their $\nu_3(NH_4^+)$ frequencies. The plot resembles in a general way the high-ν_1 region of our Fig. 3, but the separation of the points according to X and C.N. is much less obvious.

Experimental

Sample Preparation and Apparatus

The ammonium salts were either obtained commercially or prepared by literature methods. In most cases the salts were recrystallized from moderately concentrated solutions of the appropriate HX acid. A further recrystallization was then used to introduce a small proportion of deuterium into the samples, typically at a level of 0.5–2%. The sample of **19** was prepared at our request by Dr J. H. Holloway in a manner analogous to the K salt, followed by a cation exchange procedure. Ammonium fluoride containing 1% D was obtained by recrystallization from MeOH (1% D).

The spectra of NH_3D^+ in **18**, **22**, **23**, **25**, **31**–**33**, **37**, **38**, **40**, **41**, and **44** have been described elsewhere (1–4, 6). The spectra of the isotopically isolated NH_3D^+ ion in the rest of the salts are reported here for the first time. Details of the ir apparatus and technique will be found in previous papers of this series (1–5).

The KX, RbX, and CsX crystals containing low concentrations of ammonium ion were prepared by slow evaporation of aqueous solutions of the alkali halide and appropriate ammonium halide in the desired proportion; attempts to incorporate in this manner NH_3D^+ into NaX crystals were unsuccessful. Typically the alkali halide contained 5% NH_4^+ and the sample was crystallized hot from water containing 5% D. This rather high level was necessitated by the need to obtain a reasonable absorption in samples in these 'double-dilution' experiments. Samples suitable for our purposes were pressed into pellets which could be held in the low-temperature sample holder using indium gaskets.

Structural Information

In spite of our efforts we failed to find in the literature crystal-structure determinations for a few of the compounds, and in a number of cases we have had to accept determinations of inferior quality. A further difficulty was encountered where transitions occurred, or were suspected to occur, on cooling. Practically no detailed crystallography has been done on the low-temperature phases, so we had to assume that the H...X distances did not change drastically on lowering the temperature. Where no reference is given, particulars of the crystal structure will be found in ref. 13.

*Ammonium and Alkali Halides, **1–17** (Table 1)*

1, NH_4F (9, 10). $P6_3mc$ (No. 186), $Z = 2$, $S = C_{3v}$. Although *two* ν_1 bands, in a 3:1 intensity ratio, would be expected for $S = C_{3v}$, only a single band was observed. The band appeared to be symmetric when visual allowance was made for a slight distortion due to the Christiansen effect. The displacement between the N and F hcp sublattices is such that each ion is equidistant, at 2.708(3) Å, from its four nearest neighbours (9).

2, **3**, NH_4Cl. Phase *II* (242–457 K), $Pm3m$ (No. 221), $Z = 1$, S(diffraction) $= O_h$, S(local) $\neq O_h$ (see Discussion). Phase *III* (< 242 K), $P\bar{4}3m$ (No. 215), $Z = 1$, $S = T_d$.

4, **5**, NH_4Br (28, 34). Phase *II* (235–411 K), as in **2**. Phase *III* (< 235 K), $P4/nmm$ (No. 129), $Z = 2$, $S = D_{2d}$.

6, **7**, **8**, NH_4I (28). Phase *I* (> 259 K), $Fm3m$ (No. 225), $Z = 4$, $S = O_h$. Phases *II* (231–259 K) and *III* (< 231 K) as in NH_4Br.

Single ν_1 bands were observed for all three halides. In NH_4I the halfwidth was 9 cm^{-1} in phase *III* and increased to ~50 cm^{-1} in phase *II*. In $NH_4I(I)$ the band was very broad, ~65 cm^{-1} at 290 K. The variation of ν_1 with temperature is shown in Fig. 2.

In the KX and RbX matrices $S = O_h$, C.N. 6; in the CsX matrices, $S = O_h$, C.N. 8. The H...X values in Table 1 are those for the pure halides at 80 K; no account was taken of the size disparity of the guest and the host ions. The lattice parameters of the fcc alkali halides at 80 K were taken from ref. 16. Those of CsX were estimated on the assumption that the contraction percentage on cooling is the same as for the corresponding RbX.

*Cubic $(NH_4)_2MX_6$, **18–30** (Table 2)*

$Fm3m$ (No. 225), $Z = 4$, $S = T_d$, C.N. 12 (cf. Fig. 1 of ref. 1). The positional parameter x(X) has been determined accurately only for **18** (11), **19** (personal communication from J. H. Holloway), **23** (12, 25), and **29** (35). In all the other compounds in Table 2 it had to be estimated. To do this, the structures of all the cubic A_2MX_6 compounds in the NBS collection of X-ray powder diffractometer patterns (36) were refined by least-squares from the intensity data listed there, using X-ray scattering factors for neutral atoms and an overall temperature factor. Unfortunately many of the x(X), K, B refinements did not converge properly owing to the insufficient accuracy, and at times the small volume, of usable intensity data. Those of the refined x(X) values that were judged satisfactory were combined with the available literature values of x(X) (room temperature), and the entire set was regressed, separately for x(Cl) and x(Br), on the values of the effective radii $r^{xii}(A^+)$ and $r^{vi}(M^{4+})$. The x(F) values presented a problem because of their small range and poor accuracy; refinements from the NBS powder intensities gave 0.212 for K_2SiF_6, 0.208 for **18**, 0.217 for Rb_2SiF_6, and 0.211 for Cs_2GeF_6.

The radii used in the double regressions were those of ref. 19 except for Si, Ge, Pt, Hf, Zr, Pb, Pu, U, Th, and Po, for which the values from ref. 37 were employed. For Se and Te the values were 0.650 and 0.785 Å, respectively. The radius of NH_4^+ was calculated from the equation given in Discussion. The regressions are represented by the equations

$$x(\mathrm{Cl}) = 0.2493 - 0.0276r^{\mathrm{xii}}(\mathrm{A}^+) + 0.0548r^{\mathrm{vi}}(\mathrm{M}^{4+})$$

(28 compounds, $r^2 = 0.85$, $\sigma = 0.002$) and

$$x(\mathrm{Br}) = 0.2190 - 0.0158r^{\mathrm{xii}}(\mathrm{A}^+) + 0.0733r^{\mathrm{vi}}(\mathrm{M}^{4+})$$

(based on four compounds for which x(Br) had been determined accurately from single-crystal data; for a total of eight compounds, $r^2 = 0.87$, $\sigma = 0.002$).

The x(F) value of **20** was taken to be the same as that of **18**. No structural data are available for the low-temperature phases **28** and **30** except as noted in Table 2.

With the exception of **28** and **30**, single, sharp ($\Delta\nu_{1/2}$ = 5–9 cm^{-1}) ν_1 and ν_{4bc} absorptions were observed for all the compounds listed in Table 2. None of the bands was completely free from the Christiansen effect; the effect was very large in the spectra of **24**. No evidence of Fermi resonance between the $2\nu_{4bc}$ and ν_1 levels was found.

*Trigonal $(NH_4)_2MF_6$, **31–34** (Table 3)*

$P\bar{3}m1$ (No. 164), $Z = 1$, $S = C_{3v}$, C.N. 12 (cf. Fig. 1 of ref. 2). The three positional parameters, z(N), x(X), and z(X), have been determined only for **31** (38). The H...X values for **32–34** are estimates based on similarity to other compounds of this type (13, 36). The NH_3D^+ frequencies of **31** and **32** were reported in ref. 2; those of **33**, in ref. 6; those of **34** are new. Both the axial (a) and the non-axial (n) ν_1, in an intensity ratio of 1:3, correspond to H atoms in trifurcated situations: $\nu_1(a)$ to an equilateral and $\nu_1(n)$ to three isosceles triangles of fluorine atoms.

The $\nu_1(a)$ and $\nu_1(n)$ values for the four compounds show a strong correlation ($r^2 = 0.94$).

*Other Compounds, **35–45** (Table 4)*

35, NH_4MnF_3. Cubic perovskite. At ≥200 K, $Pm3m$ (No. 221), $Z = 1$. The spectrum of NH_3D^+ in the hitherto unreported low-temperature phase will be described elsewhere.

36, NH_4SnF_3 (39). $R\bar{3}$ (No. 148), $Z = 2$. The expectation for three normal N—H...F bonds and one in a trifurcated situation (on C_3, H...F* ~ 2.19 Å, NHF* ~ 134°) would be a 3:1 ν_1 doublet. Two components, with a separation of 162 cm^{-1}, are in fact observed. The 1295.2 cm^{-1} absorption is assigned to $\nu_{4bc}(a)$. No indication of transitions between room temperature and 77 K was found in the spectra. The strong hydrogen bonding inferred from the low $\nu_1(n)$ frequency is reflected in the very intense, sharp $\nu_2 + \nu_6$ and $\nu_4 + \nu_6$ combination bands of the NH_4^+ ion.

37, NH_4BF_4 (40). *Pnma* (No. 62), $Z = 4$.

38, NH_4BPh_4. The crystal structure does not appear to have been determined. For the corresponding K (41) and Rb (42) compounds, $I\bar{4}2m$ (No. 121), $Z = 2$, $S = D_{2d}$. If the ammonium compound is isostructural, which appears likely (4), the NH_4^+ ion is surrounded by four benzene rings belonging to two BPh_4^- ions.

39, NH_4AlF_4. $P4/mmm$ (No. 123), $Z = 1$.

40, NH_4PF_6. A structure determination is not available. While **40** has been presumed (46) isostructural with α-KPF_6 ($Pa3$ (No. 205), $Z = 4$, $S = C_{3i}$), the previously reported spectrum of NH_3D^+ in this compound (4) was consistent with *cubic* site symmetry down to 77 K. To estimate the H...X and NHF* values, **40** was assumed to be isostructural with $NaSbF_6$(*I*) ($Fm3m$ (No. 225), $Z = 4$) and P—F was taken as 1.58 Å.

41, $(NH_4)_2PdCl_4$. $P4/mmm$ (No. 123), $Z = 1$. At 125 K and above the ammonium ions are disordered between the two possible orientations at each N site. Krebs Larsen and Berg (43) could not see any evidence of phase change in the X-ray pattern of a crystal cooled to 90 K. The spectra of **42** $(NH_4)_2PtCl_4$ and **43** $(NH_4)_2PdBr_4$ were very similar and these compounds are presumed isostructural with **41**.

44, $(NH_4)_2[CuCl_4(H_2O)_2]$. At room temperature the space group is $P4_2/mnm$ (No. 136), $Z = 2$ (neutron diffraction, ref. 44), but on cooling transitions take place in the crystal; their nature has not yet been determined (45).

Transitions in Cubic $(NH_4)_2MX_6$

The existence of numerous thermally induced transitions in A_2MX_6 is well documented (cf. ref. 24). The transition temperature may be above (e.g., in K_2PbCl_6 (48) or K_2SnBr_6 (13)) or below room temperature. In the present study evidence of low-temperature transitions was detected in the spectra of $(NH_4)_2SnBr_6$ and $(NH_4)_2TeBr_6$, consistent with the DTA results on the stannate (T_{tr} = 124 and 145 K) and with nqr (49) and X-ray (35) results on the tellurate (T_{tr} = 194 and 214 K), but not in $(NH_4)_2SnCl_6$ and $(NH_4)_2PbCl_6$, for which T_{tr} of < 77 and 240 K, respectively, have been reported (24).

Above ~150 K a single broad ν_1 band and a single broad ν_{4bc} band were observed in the spectra of the stannate. These absorptions are consistent with $S = T_d$, but the breadth of the bands calls for caution in drawing definite conclusions about the site symmetry in this, the room-temperature, phase from the ir results alone. Between 124 and 145 K a multiple absorption was observed in the ν_1 region. Again the bands were broad and we are only able to say with any certainty that at least two components were present. Below 124 K *four* sharp bands were present in the ND stretching region.[17] Assuming that NH_4^+ in this phase occupies a single equipoint, the occurrence of four bands is consistent with $S = C_1$; the absence of diffraction data for the lowest-temperature phase precludes a more detailed conclusion.

The much greater breadth of the ν_1 components in the phase stable above 125 K is an indication that considerable reorientational motion of the ammonium ion occurs in this phase (cf. ref. 4). The halfwidth of each ν_1 component at 77 K was 6 cm^{-1}. It seems likely that a correlation time of less than about 10^{-11} s would be required to account for the broadening observed on passage through the 124 K transition point. This conclusion agrees well with the nmr results of Strange and Terenzi (50) which suggest a correlation time, for reorientation of the NH_4^+ ion at 130 K, of about 8×10^{-12} s. The activation energy of reorientation changes, at the 145 K transition, from 0.26 for the upper phase to 1.44 kcal/mol for the lower phase.

The quality of the $(NH_4)_2TeBr_6$ spectra was inferior by comparison. The ν_1 absorption of the room-temperature phase was again compatible with $S = T_d$. Below 214 K the NH_3D^+ absorptions were too broad to be of diagnostic value for S. At 77 K, in a third phase, the observed NH_3D^+ absorptions were very similar to those in the corresponding stannate phase, hence probably $S = C_1$.

The space group of the phase existing below 214 K was deduced by Das and Brown (35) from Weissenberg photographs as $P4/mnc$ (No. 128), $Z = 2$, hence $S = D_2$. An NH_3D^+ probe ion at such a site would be expected to give rise to a single ν_1 and two ν_{4bc} absorptions (6). In view of the implied rapid reorientational motion in this phase we were unable to verify the expected site symmetry from our spectra.

It is interesting to note that in both salts combination modes

[17]The NH_3D^+ frequencies of **28** and **30** and similar data for other low-temperature phases of ammonium halides will be published elsewhere.

involving librations are observed in the lowest phase. Their occurrence, together with an overall lowering of ν_1 by about 15 cm^{-1}, leaves little doubt that hydrogen bonding is implicated in the formation of this phase. One notes further that the observed combination modes $\nu_4 + \nu_6$ are broad ($\Delta\nu_{1/2} \sim 50\ cm^{-1}$), which is in agreement with the earlier discussion of the dependence of band breadth on C.N.

The hexabromostannate and tellurate provide an interesting illustration of the hydrogen-bonding behaviour of the ammonium ion in crystals. It is apparent that the ion itself is not responsible for the phase transitions, analogous transitions occur in the K and Rb salts, but whatever the specific cause of the transition, in the ammonium salts the consequence is stronger hydrogen bonding.

An observation concerning the crystallographic relationship of the lower-symmetry phases to the parent *Fm3m* phase will be found in the Appendix.

Estimation of the Activation Energies

Activation energies E_a for reorientation of the NH_4^+ ion have been estimated, mostly from nmr experiments, in a variety of ammonium halides. References for the compounds included in Fig. 6 are as follows: **1** (51), **2–8** (52), **18** (50), **21** (22), **22** (22, 53), **23** (50, 54, 55), **24** (cited in ref. 56), **26** (22, 53), **27** (50), **32** (57), **33** (58), **37** (59), **40** (60). In addition, estimates of E_a for **9–17** were obtained from the barrier heights (23) by subtracting the zero-point energies.

Acknowledgments

We are indebted to Dr. J. H. Holloway for supplying a sample and the structural data of **19**, and to Dr. W. Press for re-analyzing the neutron-diffraction intensities of **18** collected by Schlemper *et al.* (11). This investigation was supported by a research grant from the National Research Council of Canada to one of the authors (O.K.).

1. I. A. Oxton, O. Knop, and M. Falk. Can. J. Chem. **53**, 2675 (1975).
2. I. A. Oxton, O. Knop, and M. Falk. Can. J. Chem. **53**, 3394 (1975).
3. I. A. Oxton, O. Knop, and M. Falk. Can. J. Chem. **54**, 892 (1976).
4. I. A. Oxton, O. Knop, and M. Falk. J. Mol. Struct. **37**, 69 (1977).
5. I. A. Oxton and O. Knop. J. Mol. Struct. In press.
6. I. A. Oxton, O. Knop, and M. Falk. J. Phys. Chem. **80**, 1212 (1976).
7. W. C. Hamilton and J. A. Ibers. Hydrogen bonding in solids. W. A. Benjamin, New York. 1968.
8. A. A. Khan and W. H. Baur. Acta Crystallogr. B**28**, 683 (1972).
9. H. W. W. Adrian and D. Feil. Acta Crystallogr. A**25**, 438 (1969).
10. B. Morosin. Acta Crystallogr. B**26**, 1635 (1970).
11. E. O. Schlemper, W. C. Hamilton, and J. J. Rush. J. Chem. Phys. **44**, 2499 (1966).
12. J. A. Lerbscher and J. Trotter. Acta Crystallogr. B**32**, 2671 (1976).
13. R. W. G. Wyckoff. Crystal structures. 2nd ed. Vols. 1–3. Interscience Publishers, New York. 1963–1965.
14. J. A. A. Ketelaar and J. van der Elsken. J. Chem. Phys. **30**, 336 (1959).
15. S. D. Hamann and M. Linton. Aust. J. Chem. **29**, 479 (1976).
16. Y. Pautamo. Ann. Acad. Sci. Fenn. Ser. A, VI, 129 (1963).
17. J. A. A. Ketelaar and C. J. H. Schutte. Spectrochim. Acta, **17**, 1240 (1961).
18. W. C. Price, W. F. Sherman, and G. R. Wilkinson. Proc. R. Soc. London, A**255**, 5 (1960).
19. R. D. Shannon. Acta Crystallogr. A**32**, 751 (1976).
20. I. D. Brown. Can. J. Chem. **42**, 2758 (1964).
21. S. C. Agarwal and J. Shanker. Agra Univ. J. Res. Sci. **23**, 43 (1974).
22. M. Bonori and M. Terenzi. Chem. Phys. Lett. **27**, 281 (1974).
23. A. B. Gardner, T. C. Waddington, and J. Tomkinson. J. Chem. Soc. Faraday II, 1191 (1977).
24. K. Rössler and J. Winter. Chem. Phys. Lett. **46**, 566 (1977).
25. T. B. Brill, R. C. Gearhart, and W. A. Welsh. J. Magn. Reson. **13**, 27 (1974).
26. K. Nakamoto, M. Margoshes, and R. E. Rundle. J. Am. Chem. Soc. **77**, 2480 (1955).
27. J.-P. Mathieu and H. Poulet. Spectrochim. Acta, **16**, 696 (1960).
28. R. S. Seymour and A. W. Pryor. Acta Crystallogr. B**26**, 1487 (1970).
29. W. Press. Acta Crystallogr. A**29**, 257 (1973).
30. S. D. Hamann. Aust. J. Chem. **31**, 11 (1978).
31. J. T. R. Dunsmuir and A. P. Lane. Spectrochim. Acta, **28**A, 45 (1972).
32. R. A. Nyquist and R. O. Kagel. Infrared spectra of inorganic compounds. Academic Press, New York and London. 1971.
33. G. Mairesse, P. Barbier, J.-P. Wignacourt, A. Rubbens, and F. Wallart. Can. J. Chem. **56**, 764 (1978).
34. W. Press, J. Eckert, D. E. Cox, C. Rotter, and W. Kamitakahara. Phys. Rev. B**14**, 1983 (1976).
35. A. K. Das and I. D. Brown. Can. J. Chem. **47**, 4288 (1969).
36. M. C. Morris, H. F. McMurdie, E. H. Evans, B. Paretzkin, J. H. de Groot, R. J. Newberry, C. R. Hubbard, and S. J. Carmel. Natl. Bur. Stand. Monogr. 25, **14**, 122 (1977).
37. O. Knop and J. S. Carlow. Can. J. Chem. **52**, 2175 (1974).
38. E. O. Schlemper and W. C. Hamilton. J. Chem. Phys. **45**, 408 (1966).
39. G. Bergerhoff and H. Naumgung. Acta Crystallogr. B**34**, 699 (1978).
40. A. P. Caron and J. L. Ragle. Acta Crystallogr. B**27**, 1102 (1971).
41. K. Hoffmann and E. Weiss. J. Organomet. Chem. **67**, 221 (1974).
42. J. Ozols, S. Vimba, and A. Ieviņš. Latv. PSR Zinat. Akad. Vestis, No. 4, 93 (1961); Chem. Abstr. **56**, 8109*a* (1962).
43. F. Krebs Larsen and R. W. Berg. Acta Chem. Scand. A**31**, 375 (1977).
44. B. Matković, S. W. Peterson, and R. D. Willett. Croat. Chim. Acta, **41**, 65 (1969).
45. I. A. Oxton and O. Knop. Chem. Phys. Lett. **49**, 560 (1977).
46. H. Bode and H. Clausen. Z. Anorg. Allg. Chem. **265**, 224 (1951).
47. H. Bode and E. Voss. Z. Anorg. Allg. Chem. **290**, 1 (1957).
48. I. D. Brown and M. M. Lim. Can J. Chem. **45**, 678 (1967).
49. D. Nakamura, K. Ito, and M. Kubo. J. Am. Chem. Soc. **84**, 163 (1962).
50. J. H. Strange and M. Terenzi. J. Phys. Chem. Solids, **33**, 923 (1972).
51. L. E. Drain. Discuss. Faraday Soc. **19**, 200 (1955).
52. H. S. Gutowsky, G. E. Pake, and R. Bersohn. J. Chem. Phys. **22**, 643 (1954).
53. R. L. Armstrong, H. M. van Driel, and A. R. Sharp. Can. J. Phys. **52**, 369 (1974).

54. A. WATTON, A. R. SHARP, H. E. PETCH, and M. M. PINTAR. Phys. Rev. B, **5**, 4281 (1972).
55. D. SMITH. Chem. Phys. Lett. **25**, 348 (1974).
56. Z. T. LALOWICZ, C. A. MCDOWELL, and P. RAGHUNATHAN. J. Chem. Phys. **68**, 852 (1978).
57. E. E. YLINEN, J. E. TUOMI, and L. K. E. NIEMELÄ. Chem. Phys. Lett. **24**, 447 (1974).
58. L. K. E. NIEMELÄ and P. H. OKSMAN. Chem. Phys. Lett. **41**, 174 (1976).
59. J. W. HENNEL and Z. T. LALOWICZ. Proc. XVI Congr. Ampère, Bucharest, 637 (1971).
60. Z. T. LALOWICZ, C. A. MCDOWELL, and P. RAGHUNATHAN. Chem. Phys. Lett. **35**, 294 (1975).
61. H. BOYSEN and A. W. HEWAT. Acta Crystallogr. B, **34**, 1412 (1978).
62. S. SYOYAMA, K. OSAKI, and S. KUSANAGI. Inorg. Nucl. Chem. Lett. **8**, 181 (1972).
63. C. J. BRADLEY and A. P. CRACKNELL. The mathematical theory of symmetry in solids. Clarendon Press, Oxford. 1972.
64. J. F. SCOTT. Rev. Mod. Phys. **46**, 83 (1974).
65. R. L. ARMSTRONG, D. MINTZ, B. M. POWELL, and W. J. L. BUYERS. Phys. Rev. B**17**, 1260 (1978).
66. G. P. O'LEARY and R. G. WHEELER. Phys. Rev. B**1**, 4409 (1970).
67. H. G. SMITH and G. E. BACON. J. Appl. Phys. **37**, 979 (1966).

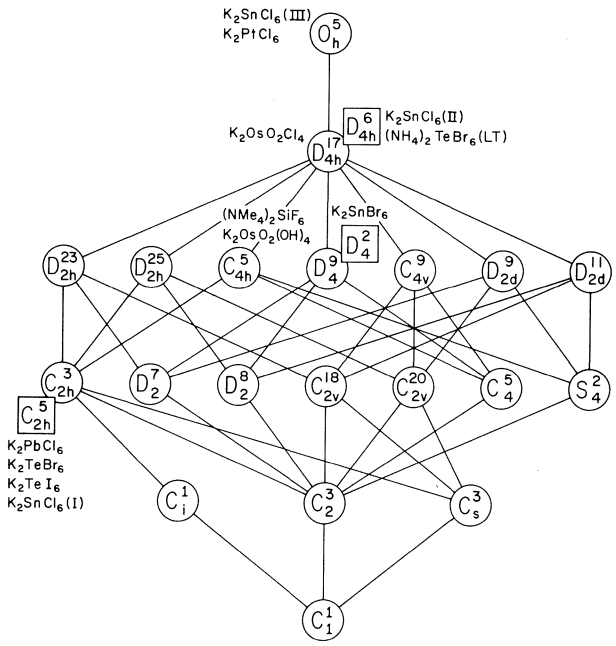

FIG. 10. Crystallographic transformations in A_2MX_6 via tetragonal distortions. The space groups framed in squares are not subgroups of O_h^5-$Fm3m$.

Appendix

A remark is in order concerning the crystallographic relationship of the lower-symmetry A_2MX_6 phases to the parent O_h^5 phase.[18] In none of the cases in which the space group H of the phase immediately below cubic has been reported — D_{4h}^6 in K_2SnCl_6 (61) and $(NH_4)_2TeBr_6$ (35) at low temperature, D_4^2 in K_2SnBr_6 at room temperature (13), and C_{2h}^5 in K_2TeBr_6 (20), K_2TeI_6 (62), and K_2PbCl_6 (48) at room temperature (and also in $K_2SnCl_6(I)$ (61), below the D_{4h}^6 phase II) — is H a subgroup of O_h^5, even though the structural similarity is evident (cf. ref. 20). However, each of the three space groups is a monochromatic subgroup of index two of a Shubnikov group Ш which corresponds to one of the subgroups G of O_h^5: $D_{4h}^6 \subset Ш_{128}^{410}(=P_I4/mnc)$, $D_4^2 \subset Ш_{90}^{102}$ $(=P_I42_12)$, $C_{2h}^5 \subset Ш_{14}^{83}$ $(=P_A2_1/b)$. When the colour-changing symmetry operations are retained but their chromatic nature is disregarded, $Ш_{128}^{410}$, $Ш_{90}^{102}$, and $Ш_{14}^{83}$ become, respectively, D_{4h}^{17}, D_4^9, and C_{2h}^3. The symmetry reduction *outside* the composition series of O_h^5 (cf. Fig. 10) can then be represented as $D_{4h}^{17}|D_{4h}^6$, $D_4^9|D_4^2$ and $C_{2h}^3|C_{2h}^5$, i.e. $(G \subset O_h^5)|(H \not\subset O_h^5)$: H is derived from O_h^5 by descent in symmetry along the composition series $O_h^5 \supset G_1 \supset G_2 \ldots \supset C_1^1$ to a subgroup G which generates a Ш having the requisite $G|H$ relationship. Omission of the chromatic symmetry operations from Ш then yields H. This loss of symmetry operations results in a reduction of symmetry-imposed restrictions in both the equilibrium positional parameters of the atoms affected and the dynamic freedom of the composite ions (e.g. with respect to 'rigid' rotation). For example, in K_2SnCl_6 the subgroup and chromatic-symmetry reductions produce the changes in positional coordinates and site symmetries shown in Table 6. The tetragonal (subgroup) distortion may manifest itself metrically but leaves the symmetry constraints on the individual atoms unchanged. The removal of reflections from the Sn site by the 'chromatic' distortion, however, not only makes possible rotation of the square of Cl atoms in the $z = 0$ plane from its $x,x,0$ etc. position, but also removes a symmetry restriction on the freedom of rotational and reorientation motions of the $SnCl_6$ octahedron in the 002 planes. The second transition, $II \rightarrow I$, corresponds to the subgroup symmetry reduction $D_{4h}^6 \supset D_{2h}^{12} \supset C_{2h}^5$ and carries a step further the distortion initiated by the 'chromatic' symmetry reduction $D_{4h}^{17}|D_{4h}^6$.

The above three Shubnikov groups are all of the so-called type IV (cf. for example, ref. 63), i.e. based on *dichromatic* Bravais lattices.[19] The 'chromatic' translation corresponds in this case to an *antiphase* rotation of the MX_6 octahedron, resulting in an

[18] To avoid explanations concerning changes in the setting of the unit cell, the Schönfliess symbols will be used for convenience.

[19] All $G \subset O_h^5$ are symmorphic; D_{4h}^6, D_4^2, and C_{2h}^5 are non-symmorphic.

TABLE 6. Changes produced in positional coordinates[a] and site symmetries on subgroup and chromatic symmetry reductions in a K_2SnCl_6 crystal

Phase[b]	S.G.[c]	Sn	K	Cl
III	$O_h^{5\,d}$	0,0,0 (O_h)	$0,\frac{1}{2},\frac{1}{4}$ (T_d)	$x,x,0$ (C_{4v})
	$D_{4h}^{17} \subset O_h^5$:			
	$[D_{4h}^{17}]^e$	0,0,0 (D_{4h})	$0,\frac{1}{2},\frac{1}{4}$ (D_{2d})	$x,x,0$ (C_{2v}); $0,0,z$ (C_{4v})
	$(D_{4h}^{17} \subset O_h^5) \mid (D_{4h}^6 \not\subset O_h^5)$:			
II	D_{4h}^6	0,0,0 (C_{4h})	$0,\frac{1}{2},\frac{1}{4}$ (D_2)	$x,y,0$ (C_s); $0,0,z$ (C_4)
	$D_{2h}^{12} \subset D_{4h}^6$:			
	$[D_{2h}^{12}]^e$	0,0,0 (C_{2h})	$0,\frac{1}{2},z$ (C_2)	$x,y,0$ (C_s); $x,y,0$ (C_s); $0,0,z$ (C_2)
	$C_{2h}^5 \subset D_{2h}^{12} \subset D_{4h}^6$:			
I	C_{2h}^5	0,0,0 (C_i)	x,y,z (C_1)	x,y,z (C_1); x,y,z (C_1); x,y,z (C_1)

[a]The coordinates of only one of the symmetry-related positions are given.
[b]Designation as in ref. 61.
[c]Space group.
[d]Change of setting from *F* to *I*.
[e]Formal step.

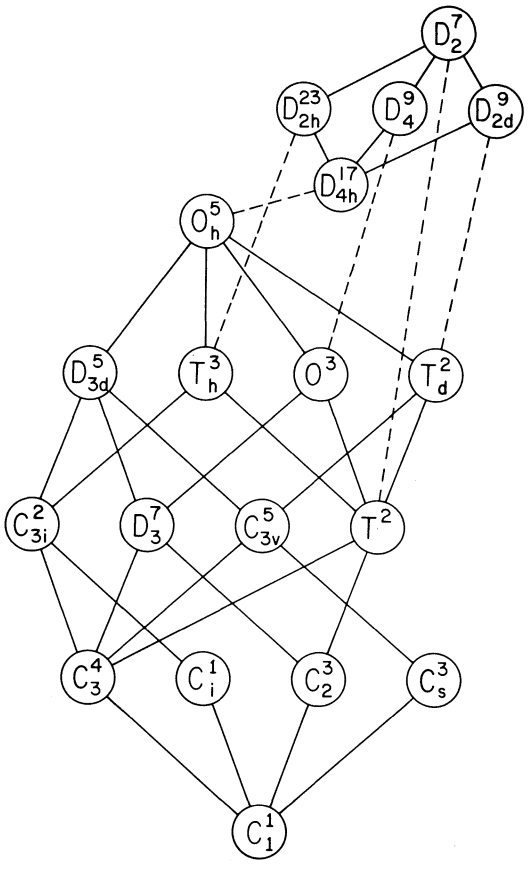

FIG. 11. Same as Fig. 10 but via cubic and trigonal distortions.

'antiferro' arrangement of the rotational displacements.

Symmetry changes similar to those in A_2MX_6 are also observed in the structurally closely related A_3MF_6 on cooling (47): $O_h^5 \rightarrow D_{4h}^6$ in $(NH_4)_3AlF_6$ and $(NH_4)_3FeF_6$, $O_h^5 \rightarrow C_{2h}^5$ in Na_3AlF_6, and $O_h^5 \rightarrow D_{4h}^{17}$ in K_3AlF_6. The involvement of soft modes (64) in these transitions remains to be determined.

Apparently the transitions in A_2MX_6 need not be of the 'antiferro' type. The space group of the low-temperature phase of K_2OsCl_6 has not been stated, but on evidence from limited neutron-diffraction data (65) the transition $K_2OsCl_6(O_h^5) \rightarrow K_2OsCl_6$-(LT) is continuous, showing no metric departures from cubic symmetry, and 'ferrorotative', characterized by a collective in-phase rotation of the $OsCl_6$ octahedra. In K_2ReCl_6 no fewer than four transitions have been detected (24, 66). The most probable chemical space group of the phase existing below 76 K, based on limited neutron-diffraction data, has been stated to be T_h^2, with the possibility of a disordered arrangement in O_h^4 (66, 67); an attempt has been made (66) to understand the nature of the transitions involving the other phases, using a combination of theory and experiment, of lattice dynamics and the Landau theory of second-order transitions. There is *no* $G|T_h^2$ pair. Here the only way to visualize the symmetry parentage of the phase would be via the common subgroup C_{3i}^2 (cf. Fig. 11): $O_h^5 \rightarrow (D_{3d}^5$ or $T_h^3) \rightarrow C_{3i}^2 \rightarrow T_h^2$. To what extent the various formal symmetry paths reflect actual transformation mechanisms remains to be seen.

In the first paragraph of the right-hand column on p. 413 and in the second paragraph of the left-hand column on p. 417 the discussion of NH_4SnF_3 is based, erroneously, on the assumption that the axial N—H vector points away from the Sn atom of the nearest SnF_3^- ion on the threefold axis and consequently, that the three equivalent nonaxial hydrogen bonds are to the F atoms of that SnF_3^- ion. In fact, even though the H atoms have not been located, the conclusion from the evidence presented in ref. 39 must be that the axial N—H vector points in the *opposite* direction, i.e., to the Sn atom. H–H repulsion cannot therefore be the cause of the high value of $\nu_1(a)$. This matter will be discussed more fully, together with additional ir results for NH_4SnF_3, in Part VIII of this series. The H...X and NHX* entries for **36** in Table 4 are correct.

Lone pair interactions in dimethoxymethane and anomeric effect

IGOR TVAROŠKA

Institute of Chemistry, Slovak Academy of Sciences, 809 33 Bratislava, Czechoslovakia

AND

TOMAŠ BLEHA

Polymer Institute, Slovak Academy of Sciences, 809 34 Bratislava, Czechoslovakia

Received January 12, 1977[1]

IGOR TVAROŠKA and TOMAŠ BLEHA. Can. J. Chem. **57**, 424 (1979).

Perturbation molecular orbital analysis has been used for a computation of the through-bond and through-space orbital interactions of oxygen lone pairs in dimethoxymethane (DMM). The analysis predicts the symmetrical combination of *p*-type lone pairs as a highest occupied orbital in an antiperiplanar conformation. The conformational dependence of through-bond orbital interactions has the character of the V_2 term in the Fourier expansion of the rotation potential function about the C—O bond. Contrary to the recent theoretical interpretation that the anomeric effect (preference of *gauche* conformation) is caused by superjacent orbital control, the orbital interactions in DMM are not dominant terms with respect to the anomeric or exoanomeric effect. The dipole–dipole interactions of the C—O bonds stabilizing the *gauche* conformation should thus be considered as the primary cause of the anomeric effect in DMM. The frontier orbital energies and geometric parameters in DMM are strongly influenced by a variation of orbital interaction with rotation. Results obtained for DMM are used to explain the conformational behaviour of other molecules containing the acetal moiety, such as pyrane heterocycles, sugars, and polyoxymethylene.

IGOR TVAROŠKA et TOMAŠ BLEHA. Can. J. Chem. **57**, 424 (1979).

On a utilisé une analyse de perturbation d'orbitale moléculaire pour calculer les interactions orbitalaires à travers les liaisons et à travers l'espace des paires libres d'oxygène du diméthoxyméthane (DMM). L'analyse prédit que la combinaison symétrique de la paire libre de type *p* sera l'orbitale haute occupée dans la conformation antipériplanaire. La dépendance sur la conformation des interactions orbitalaires à travers la liaison possède un caractère d'un terme V_2 dans une expansion de Fourier de la fonction de potentiel de rotation autour de la liaison C—O. Contrairement à l'interprétation récente de l'effet anomérique (préférence de la conformation gauche) par un contrôle orbitalaire superjacent, les interactions orbitalaires de DMM ne sont pas des termes dominants par rapport à l'effet anomérique ou exoanomérique. Les interactions dipôle–dipôle des liaisons C—O stabilisant la conformation gauche doivent donc être considérées comme la principale cause de l'effet anomérique dans le DMM. L'énergie des orbitales frontières et les paramètres géométriques du DMM sont fortement influencés par une variation de l'interaction orbitalaire avec la rotation. On a utilisé les résultats obtenus avec le DMM pour expliquer le comportement conformationnel d'autres molécules contenant une portion acétal, comme les hétérocycles du pyranne, les sucres et le polyoxyméthylène.

[Traduit par le journal]

Introduction

The influence of lone-pair electrons is often discussed in the explanation of conformational properties of molecules containing a segment of the type R—X—C—Y, where X denotes O, N, or S and Y denotes O, N, or another element having unshared electron pairs. The preference of the synclinal (*gauche*) position to the antiperiplanar one is characteristic of such a segment and has been called a generalized anomeric effect (1–3). This phenomenon, originally described in carbohydrate chemistry, also appears generally valid for a number of heterocyclic and acyclic compounds.

Probably the most familiar interpretation of the anomeric effect is that based on the dipole–dipole interaction between polar bonds (4). This type of interaction is frequently visualised as a repulsion of sp^3-hybridized lone pairs ('rabbit-ears effect'), especially if both X and Y are oxygen atoms (1–3, 5). However, other explanations for the anomeric effect have also been suggested. For example, an *ab initio* SCF calculation of fluoromethanol led Wolfe *et al.* (6) to conclude that the lone pairs are not oriented directionally and that their mutual interactions are consequently independent of molecular conformation. These authors interpret the generalized anomeric effect as being the result of the fine balance within the molecule between an electron–electron repulsion and a core–electron type attraction. On the other hand, Radom *et al.* (7) provide an explanation

[1]Revision received July 6, 1978.

0008-4042/79/040424-12$01.00/0

of the conformational properties of fluoromethanol calculated by the *ab initio* SCF method, based on the idea of directional orientation of lone pairs within the molecule. The 'rabbit-ears effect' concept has also been criticized by Zhdanov *et al.* (8, 9) who assume that the anomeric effect is not a consequence of steric, or lone-pair, or polar-bond interactions.

Apart from the 'rabbit-ears effect,' the delocalization of an unshared electron pair of oxygen (= X) into a suitably oriented antibonding σ^* orbital of the C—Y bond (3, 10–12) is frequently used to explain the anomeric effect. According to this latter idea, the highest delocalization occurs at a conformation which has unshared *p*-type electron pairs in an antiperiplanar arrangement with respect to the C—Y bond; the synclinal conformation in acyclic compounds and the axial one in heterocycles are therefore preferred. David *et al.* (13) have analyzed the nature of the synclinal stabilization in more detail and stress the significance of the two energetically nonequivalent oxygen lone pairs interacting with antibonding orbitals σ_{C-Y}^* and σ_{C-H}^*. The delocalization interaction has been used as a qualitative explanation of the geometrical changes in the simplest diols containing an H—O—C—O—H segment (14, 15) and for methoxymethanol (16). This interpretation of the anomeric effect has recently also been reconciled (17) with the apparently contradictory interpretation of Wolfe *et al.* (6) which effectively ignores lone pairs.

The aim of the present paper is to investigate to what extent the interactions between lone pairs are responsible for the anomeric effect in molecules containing a C—O—C—O—C segment and to estimate their significance in comparison with dipole–dipole interactions of polar bonds. Dimethoxymethane (DMM) represents the simplest model for this purpose, with the synclinal–synclinal conformation being the most stable in this compound (18). A similar conformational preference was found in some carbohydrates as well as in polyoxymethylene, a polymeric analogue of DMM. Both proposals to rationalize the anomeric effect in DMM are shown in Fig. 1. The electrostatic dipole–dipole repulsion of lone pairs in the conventional sp^3 hybridization (Fig. 1*b*) leads to the destabilization of the antiperiplanar conformation. According to the delocalization theory, donation from oxygen lone pairs to antibonding orbitals in DMM is most efficient in the coplanar arrangement of orbitals formed by a 90° rotation from the antiperiplanar conformation. This rotation simulates a *gauche* position and is shown in Fig. 1*c* on the left.

In this paper we present a theoretical analysis of

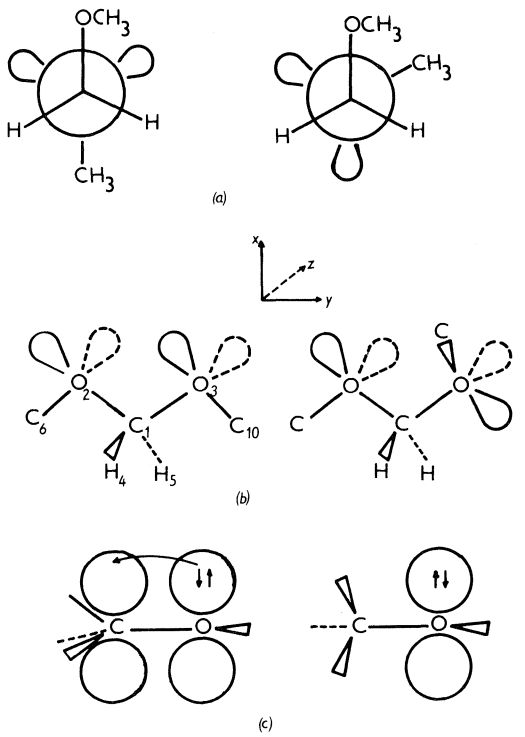

FIG. 1. (*a*) Newman projection of DMM in *ap* (left) and *sc* (right) conformations; (*b*) DMM with sp^3 hybridization of lone pairs on oxygens; (*c*) delocalization of *p*-type lone pair into antibonding orbital in *ap* and *og* conformation.

two distinct symmetry-controlled mechanisms for the interaction of oxygen lone pairs: (*i*) through-space overlap and (*ii*) through-bond or hyperconjugation interaction. We will show how a change in these interactions with rotation influences the geometric and conformational properties of the acetal segment. This procedure has been extensively used in the theoretical analysis of the interaction of nonbonding orbitals in different kinds of molecules along with EHT and CNDO/2 semiempirical methods (19, 20). Through-space and through-bond orbital interactions of lone pairs in an antiperiplanar conformation are analyzed using a simple perturbation molecular orbital (PMO) method (21) in the first part of the paper. The second part is devoted to a study of the conformational dependence of the above interactions and its significance in the anomeric effect in molecules with a C—O—C—O—C bond sequence is discussed.

Theory

Orbital Interaction Analysis

The antiperiplanar (*trans*) conformation (*ap*, $\varphi_1 = \varphi_2 = 180°$) of DMM is shown on the left-hand side of Fig. 1*b*. Conformations formed by rotation

about the O3—C1 bond are denoted as orthogonal (*og*) when $\varphi_1 = 90°$, synclinal (*sc*) when $\varphi_1 = 60°$ (*gauche*), and synperiplanar (*sp*) when $\varphi_1 = 0°$ (*cis*). Hydrogen atoms in methyl groups are assumed to be fixed in a staggered (*ap*) conformation with respect to the central C—O bonds.

An oxygen atom situated in an isolated —C—O—C— group is characterized by two lone pairs having different energies (22). According to the description of this group by means of molecular orbitals (MO), the lone pair having higher energy is of the *p* type, whereas that with lower energy is formed by a combination of *s* and *p* atomic orbitals (AO). A DMM molecule in the *ap* conformation contains two equivalent oxygen atoms. The individual lone pairs, degenerate in the absence of any interaction, may differ in energy as a result of through-bond and through-space interactions between the individual nonbonding orbitals. The energy splitting between these MO's is a prime operational measure of the extent of orbital interaction.

When the coordinate system for DMM in the *ap* conformation is oriented according to Fig. 1*b*, the *p*-type lone pair is in the direction of the p_z AO of oxygen and the *sp*-type lone pair is situated mainly in the p_x AO direction. The hyperconjugation of the p_z lone electron pair with the $\pi_z(CH_3)$ bonding and $\pi_z^*(CH_3)$ antibonding orbitals of the methyl groups (23) (Fig. 2) leads to the formation of the three doubly degenerate orbitals P_z, L_z, P_z^*. The P_z and P_z^* orbitals are predominantly localized at the methyl groups. The L_z orbital is, on the contrary,

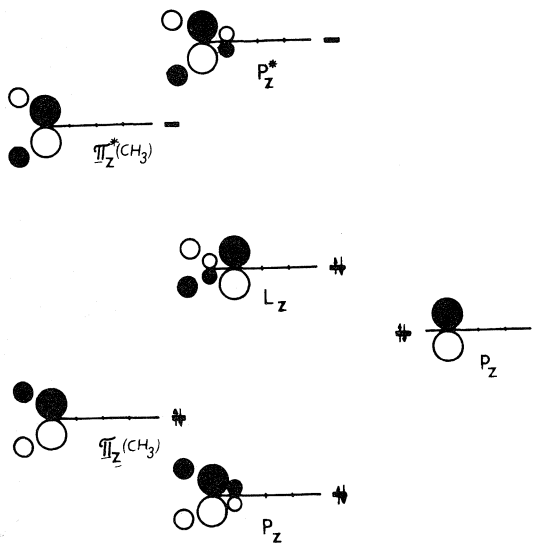

FIG. 2. Interaction of the *p*-type lone pair of oxygen with orbitals of the methyl group in *ap* conformation.

localized mainly at the p_z AO of the oxygen atoms and characterizes a *p*-type lone pair. The *sp* type lone pair interacts in an analogous way. In this case, however, $\pi_x(CH_3)$ and $\pi_x^*(CH_3)$ represent the symmetrically suitable orbitals and interaction leads to the creation of P_x, L_x, and P_x^* orbitals. For the through-bond and through-space interaction of oxygen atom lone pairs, the L_z and L_x will be mainly discussed in the present paper and the subscripts *z* and *x* will be omitted wherever possible.

Through-space and through-bond interactions of lone electron pairs can be expressed using the PMO theory (19, 21). Since we do not know the detailed form of the perturbational Hamiltonian *P*, we assume that the matrix element of $P_{\mu\nu}$ is proportional to the overlap integral as is customary in semiempirical MO theory (24) when expressing resonance integrals. The resulting expression for the orbital energy change (21) is

$$[1a] \quad E_i = E_i - E_i^0 = \sum_{j \neq i} \sum E(i,j) = \sum_{i \neq j} \sum_{\mu,\nu} c_{i\mu}^2 c_{j\nu}^2 \beta_{AB}^2 S_{\mu\nu}^2 / (E_i^0 - E_j^0)$$

$$[1b] \quad E(i,j) = E_i - E_i^0 = \pm \sum_{\mu,\nu} \sum c_{i\mu} c_{j\nu} \beta_{AB} S_{\mu\nu}$$

where E_i^0 and E_j^0 are the energies of the orbitals before interaction, $c_{i\mu}$, $c_{j\nu}$ are the coefficients of an LCAO expansion, and $S_{\mu\nu}$ refers to an overlap integral between μ and ν AO, and β_{AB} denotes a bonding parameter for the atom pair (24).

It should be pointed out that although these formulae do not contain the overlap explicitly, they possess an implicit dependence on overlap through the selected expression for the perturbational Hamiltonian. Obviously we could use the complete expression for the off-diagonal elements of the Hartree–Fock matrix for the perturbational Hamiltonian and, in this way, include the electron repulsion term in eq. [1]. However, in our approach this term depends only on the distance between two atoms and therefore does not change during rotation. These two equations allow for the expression of through-bond and through-space interactions, respectively, and for their dependence on conformation.

Through-space or direct interaction of lone pairs leads to the formation of a symmetrical combination, depicted as *L*(S), and an antisymmetrical one, *L*(A), of lone-pair orbitals. This process is illustrated schematically in the *xy* projection for an L_z-type of lone pair in the *ap*,*ap* conformation of DMM as shown in Fig. 3.

The order of the final MO levels also depends on whether *L*(S) and *L*(A) orbitals can interact with orbitals of the same symmetry. In the case of DMM,

hyperconjugating π_z,π_x, and π_z*,π_x* orbitals of the central methylene group may take part in this through-bond interaction but for symmetry reasons, only L(S) orbitals may interact, while the energy of the antisymmetric L(A) remains unchanged.

In Fig. 4 we again illustrate the through-bond interaction for L(A) and L(S) combinations of L_z lone pairs with π_z and π_z* orbitals of the central methylene group in the xy projection. The resulting orbitals are depicted as N(S) and N(A), respectively. In an analogous way we could describe through-bond and through-space interaction of the *sp* lone pairs.

Results and Discussion

Orbital Interaction in the Antiperiplanar Conformation

We have chosen MO's and energies of dimethyl ether (DME) calculated by the CNDO/2 method as unperturbed orbital values in calculating the through-bond and the through-space interactions in DMM according to eq. [1]. The LCAO expansion coefficients and the energies calculated for the most stable conformation of DME are listed in Table 1. For this purpose geometric parameters similar to DMM were used: 1.403 and 1.108 Å for the C—O and C—H lengths, 114.2 and 109.46° for the C—O—C and O—C—H angles, respectively, and a staggered position for the methyl group hydrogen atoms.

It is clear that the results of our analysis depend on the selection of the CNDO/2 method for a calculation of unperturbed orbitals. There have been several reports that the CNDO/2 method does not properly predict conformational properties of the rotation around the bond formed by two hetero atoms with lone pairs (25). However, there are only a few CNDO/2 calculations for molecules having atoms with lone pairs in the 1,3 position (26–30). The results of our calculations (26–28) on CH_3—O—CH_2—X, (where X = CH_3, OCH_3, F, Cl, NH_2, and NH_3^+) and those of Truax *et al.* (29) on fluoro alcohols and of Gorenstein *et al.* (30) on DMM and dimethylphosphate show that the CNDO/2 method describes fairly well the rotational barriers and conformational equilibria for molecules with hetero atoms in the 1,3 position. Moreover DME, which is the starting molecule for our PMO calculation, belongs to a group of molecules which does not suffer from the above problems (31, 32). On the basis of foregoing arguments we feel that the application of the CNDO/2 approach to the PMO analysis of the conformational dependence of lone-pair interactions in molecules of the DMM type is sound.

The through-space and through-bond interaction energies of lone pairs for DMM in an *ap* conformation, calculated from DME unperturbed values using eq. [1], are given in Table 2.

TABLE 1. CNDO/2 energy (au) and LCAO expansion coefficients of selected MO of oxygen and carbon for DME, in *ap* conformation

ψ_i^0	μ	E_i^0	$c_{i\mu}$(O)	$c_{i\mu}$(C)
Lp(*p*)	z	−0.5296	−0.7934	0.2212
Lp(*sp*)	s	−0.5791	0.2131	−0.0648
	x		0.5720	−0.3278
	y		0.3726	−0.1364
π_z		−0.6970		−0.4920
π_z*		0.3063		−0.4990
π_x	x	−0.7955	0.2907	−0.4634
	y		0.4720	0.1193
π_x*	s	0.2774		−0.4449
	x			0.1262
σ*	s	0.2606		−0.4191
	x			−0.2091
	y			−0.1087

It follows from the PMO analysis that the resulting order of the N(S) and N(A) levels, and also the difference in their energies, depends upon a mutual equilibrium between both kinds of interaction. As the distance between oxygen atoms in the DMM molecule is relatively large (ca. 2.35 Å), overlap between orbitals is low ($S = 0.0049$) and the through-space interaction comparatively weak. It is substantially less than a through-bond interaction (Table 2) and consequently, the highest occupied MO in DMM should be a symmetrical combination of lone electron pairs of the *p* type, i.e., N(S).

In applications of the simple PMO method (neglecting overlap), only interactions of occupied orbitals with unoccupied ones are relevant for the estimation of energy changes and electron density transfer in DMM. The mutual interaction of occupied orbitals is irrelevant in this respect, as its absolute value is much higher. The stabilization energy of DMM resulting from delocalization is given as a double sum of the interaction energy changes of the *p* and *sp* type lone pairs Lp(*p*) and Lp(*sp*) (in *ap* conformations this corresponds to L_z and L_x, respectively) with the π_{CH_2}* orbital. It follows from Table 2 that the value calculated by the PMO method for an *ap* conformation is $E_{stab} = -8.634$ kcal/mol. As evident from Fig. 4, two electrons originally localized in L(S) occupy, after interaction, an MO involving also a small contribution from the π_{CH_2}* orbital. The relative stabilization of DMM with respect to DME may be considered to be a consequence of delocalization of electrons originally localized on L(S).

The order of levels obtained by an analysis of the interaction between the lone pairs by means of the

TABLE 2. The values of the through-space and through-bond interaction energies of lone pairs (Lp) (in kcal/mol) calculated by means of the PMO method for DMM at *ap* and *og* conformations

MO	Lp(p)	Lp(sp)	π_z	π_z*	π_x	π_x*
Lp(p)	2.295[a]	0.073[b]	11.330[a]	−2.334[a]	4.537[b]	−1.738[b]
Lp(sp)	0.073[b]	1.095[a]	7.149[b]	−1.139[b]	6.585[a]	−1.983[a]

[a]*ap* conformation.
[b]*og* conformation.

TABLE 3. LCAO expansion coefficients of selected MO (Fig. 4) for DMM in the *ap* conformation calculated by means of the CNDO/2 method

MO atoms	$P_S(6)$	$P_A(9)$	$\pi'(11)$	$N_A(14)$	$N_S(16)$	$\pi'^*(21)$	$P_S(22)$	$P_A(24)$
Z_1	−0.490	—	−0.408	—	−0.259	0.521	—	−0.505
$Z_2 = Z_3$	−0.425	±0.408	−0.050	∓0.572	0.543	−0.029	∓0.085	0.144
$S_4 = S_5$	±0.274	—	∓0.291	—	±0.344	∓0.346	—	±0.320
$Z_6 = Z_{10}$	−0.276	±0.434	0.369	±0.234	−0.101	−0.353	±0.507	−0.364
$S_7 = S_{12}$ $S_8 = S_{10}$	±0.156	∓0.270	∓0.294	±0.244	±0.146	∓0.245	±0.343	∓0.241
$S_9 = S_{13}$	±0.156	∓0.270	±0.294	∓0.244	∓0.146	±0.245	∓0.344	±0.241

NOTE: Z denotes the $2p_z$ orbitals of oxygens and carbons; S, $1s$ orbital of hydrogens. The upper sign refers to an orbital introduced at first. Number of atoms is according to Fig. 1*b*, methyl group hydrogens on C6 are denoted as 8, 9, 10; those on C10 as 11, 12, 13.

PMO method may be compared with the order of DMM MO's calculated by the CNDO/2 method. In the CNDO/2 calculation, the DMM molecule consists of 32 valence electrons represented by 28 AO's leading to 28 MO's in the LCAO approximation. Sixteen of these are occupied by two electrons. Set B of geometrical parameters from ref. 26 was used in the calculation. All the LCAO expansion coefficients of the eight selected MO's which differ from the zero value for DMM in the *ap* conformation are summarized in Table 3. MO levels calculated by the CNDO/2 method may be assigned to PMO orbitals resulting from through-space and through-bond interactions of lone pairs by using LCAO expansion coefficients. Comparison of Table 3 with Figs. 3 and 4 confirms the results of the orbital interaction analysis obtained by the PMO theory. The symmetric combination of nonbonding orbitals N(S) is indeed the highest occupied orbital.

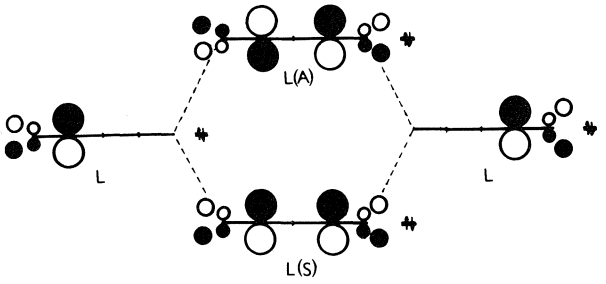

FIG. 3. Through-space interaction of the p-type lone pairs in *ap* conformation.

Conformational Dependence of Orbital Interactions

To estimate the role of the interaction between the lone pair orbitals for the anomeric effect in DMM we have investigated the conformational dependence of these interactions on the rotation about the C1—O3 bond. For the sake of simplicity we have fixed the torsional angle (φ) about the C1—O2 bond at $\varphi = 180°$, although it does not correspond to the value in the most stable conformation of DMM, (*sc*,*sc*). We believe that the effects responsible for the stabilization of the *sc*,*sc* conformation in comparison with the *ap*,*sc* one are the same as those for the stabilization of *sc*,*ap* over *ap*,*ap*, although the effects may not be additive. This choice of the φ_2 agrees at least with the model for rotation about a glycosidic bond in β-glycosides (so-called exoanomeric effect (2) i.e., preference of the *ap*,*sc* conformation in comparison with the *ap*,*ap* one). The variation of the interacting orbital orientation is described by θ, which is related to φ_1 by $\theta = 180° - \varphi_1$. To determine the conformational dependence of the interactions studied, it is necessary to evaluate the conformational dependence of the overlap integral on rotation about the C1—O3 bond. Since the axis of rotation does not lie in any of the coordinate axes (Fig. 1*b*) we have to express dependence of the overlap integral between the atomic orbitals on rotation. The usual means for solving this problem is to use an Euler transformation (33). Doing so, we get the overlap integrals as a function of θ (see Appendix). Substituting these functions in eq. [1] one obtains the dependence of the energy of orbital interactions on rotation about the C1—O3 bond (Appendix,

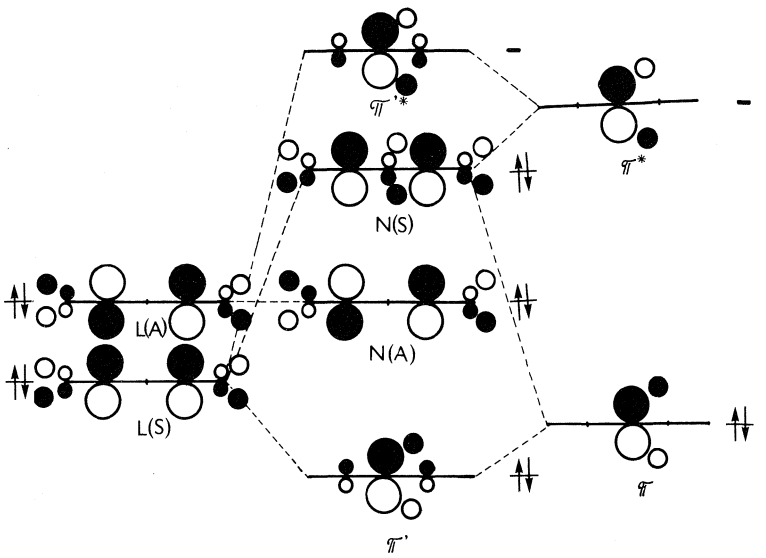

FIG. 4. Through-bond interaction of the *p*-type lone pairs in *ap* conformation.

eqs. [A1]–[A11]). Except for *sp* lone pair interaction with π_x orbitals, variation of the through-bond interactions with rotation may be described by the simple function $\cos^2\theta$.

Rotation about the C1—O3 bond causes the interactions of the *p* lone pair with π_z and π_z^* and of the *sp* lone pair with π_x and π_x^* to decrease, and the 'crossed' interactions of the *p* lone pair with π_x and π_x^* and the *sp* lone pair with π_z and π_z^* to increase. These interactions are demonstrated schematically for two extreme conformations, *ap* and *og*, in Fig. 5 and the values of the interactions for the *og* conformation are given in Table 2.

Conformational Dependence of HO

At first we shall study only the conformational dependence of orbital interactions for the highest occupied molecular orbital (HO) which is the most important MO from the viewpoint of the spectral behaviour and reactivity. The curve of the HO orbital energy may be expressed using the energy dependence of the *p* lone-pair interaction on rotation (see eq. [A1]–[A4], [A9], [A11] in the Appendix, and Fig. 5).

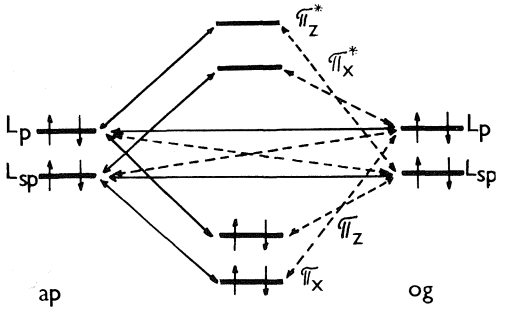

FIG. 5. Schematical representation of orbital interaction of the *p*- and *sp*-type lone pairs in *ap* and *og* conformations.

$$[2]\quad E_{HO}(\theta) = -E[Lp(p), Lp(p)]\cos\theta + \{E[Lp(p), \pi_z] - E[Lp(p), \pi_z^*]\}(1 + \cos 2\theta) + \{E[Lp(p), \pi_x] - E[Lp(p), \pi_x^*] - E[Lp(p), Lp(sp)]\}(1 - \cos 2\theta)$$

Substituting the values from Table 2 we get an expression for the variation of the HO energy with regard to the energy of the *ap* conformation:

$$[3]\quad E_{OH}(\theta) = 3.0620\cos 2\theta - 2.2949\cos\theta - 0.7671$$

Conformational dependences of individual interactions contributing to the energy of HO, calculated by the PMO method and listed in the Appendix, as well as their sum, which determines the resulting conformational dependence of HO (eq. [3]), are shown in Fig. 6. The variation of the HO energy with rotation, obtained by the usual CNDO/2 approach, is shown in the same figure for comparison. The HO energy profiles produced by both methods are similar; both show minima near 90° and maxima at 0° or 180°. The pronounced minimum at the *og* conformation is primarily due to the through-bond interaction of the Lp(*p*) orbital with π_z and π_x^*, (curves A1, A4) and by through-space interaction of Lp(*p*) orbitals (curve A9). The latter interaction is also responsible for the higher maximum of the HO energy at the *sp* conformation in comparison with the maximum at the *ap* conformation.

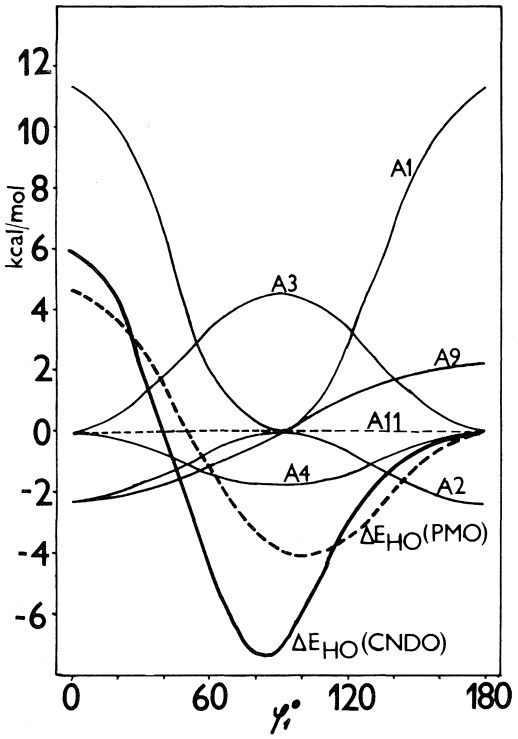

FIG. 6. Conformational dependence of orbital interactions at rotation about C1—O3 bond and the variation of HO energy calculated by PMO and CNDO/2 methods. Specification of orbital interaction curves according to the Appendix.

The close conformational dependence of the HO energy calculated by both PMO and CNDO/2 methods indicates that all important, conformationally dependent contributions to the energy of HO are included in our PMO treatment (eq. [2]).

According to the frontier orbital theory (34), the energy and symmetry of HO and the lowest unoccupied MO are the decisive factors in determining molecular reactivity. The torsional dependence of the HO level shown in Fig. 6 and given by eq. [3] may parallel the conformational dependence of the reactivity of DMM and the more complex molecules in which configuration of the segment —C—O—C—O—C— is fixed at various angles (φ_1). The acid-catalyzed hydrolysis of sugars, for which the first step involves the addition of a proton to oxygen, is an example.

It follows from Fig. 6 that the interaction of a proton with an acetal group in the *ap* position should be greater than the corresponding interaction in the *sc* position. This is in agreement with the higher rate of hydrolysis of β-D-glucopyranosides (corresponding to the *ap* conformation) in comparison with α-D-glucopyranosides (corresponding to the *sc* conformation) (35). Our preliminary results of the CNDO/2 study of the hypersurface of this proton transfer reaction support this explanation. The conformational dependence of the frontier orbitals may also be used to explain the stereoelectronic control mechanism in the cleavage of tetrahedral intermediate in the hydrolysis of esters and amides (36).

Stabilization Energy

From the conformational dependence of the interaction between lone pairs there follows the conformational dependence of the stabilization energy of DMM. Except for interactions of the Lp(*p*) orbital with π_{CH_2} orbitals (Fig. 6), inclusion of analogical interactions of the Lp(*sp*) orbital appears to be satisfactory for obtaining sufficiently representative conformational dependence of the DMM stabilization energy. The course of all through-bond orbital interactions is shown in Fig. 7 (curves A2, A4, A6, A8). In addition, combinations of these contributions are depicted in Fig. 7. The double value of an algebraic sum of curves A2 and A8 determines the total interaction of lone pairs with the π_z^* orbital (curve *a*) and similarly, with the π_x^* orbital (*b*, double sum of A4 and A6). Also shown is the con-

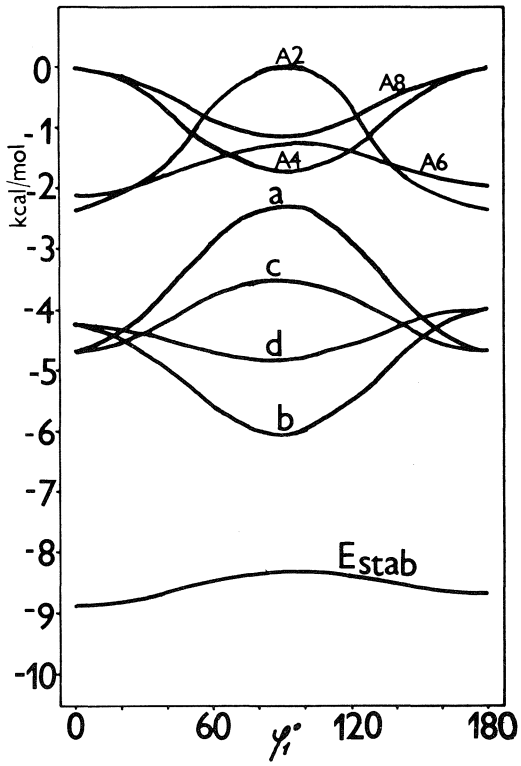

FIG. 7. Variation of orbital interactions, delocalization energies (*a–d*) and stabilization energy (E_{stab}) with rotation about C1—O3 bond in DMM.

formational dependence of interactions of the *p* lone pair (*c*, A2 + A6) and the *sp* lone pair (*d*, A4 + A8). An algebraic summation of the curves *a* and *b* or *c* and *d*, respectively, determines the total stabilization energy dependence (E_{stab}). It follows from Fig. 7 that orbital interactions have the form of the function cos 2θ. The stabilization energy of DMM resulting from the interaction of lone electron pairs is lowest in the *og* conformation and represents the net result of two conformationally opposite effects. For example, the stabilization energy obtained by delocalization into the π_z^* orbital exhibits maxima at *sp* and *ap* conformations and a minimum at *og*. In the case of interactions with π_x^*, the *og* conformation is the most stable. We suppose that the conformational dependence of the stabilization energy in Fig. 7 is negligibly influenced by consideration of the interactions with all remaining orbitals in DMM.

Geometrical Consequences

The energetic stabilization of DMM resulting from the interactions of occupied and unoccupied orbitals is accompanied by a transfer of charge. Owing to the interaction of lone pairs with the $\pi_{CH_2}^*$ orbital, transfer of electron density occurs from the oxygen atom to the methylene group and the electron density on the $\pi_{CH_2}^*$ orbital increases. The comparison of LCAO coefficients in Tables 1 and 3 for the *p*-type lone pair (−0.7934 and 0.543) and for the $2p_z$ orbital on carbon (−0.4990 and 0.521) confirms this transfer. The electron redistribution gives rise to several interesting structural consequences. Since the π_z^* orbital is antibonding along two methylene C—H bonds, we expect these bonds to lengthen. This orbital is also antibonding between the two C—H bonds so that the bond angle H—C—H should increase and the O—C—O angle should decrease.

The resulting geometry of an *ap* conformation should reflect a balance between the above influences. In the other conformations, electron transfer will decrease (increase) as a consequence of the conformational dependence of lone-pair interactions with the π_z^* (π_x^*) orbital. Therefore, more pronounced geometrical changes should occur. From the torsional dependence of orbital interactions in DMM (Fig. 7) one may obtain the following idea about the influence of through-bond interactions upon the geometry of the DMM molecule. Rotation about the C1—C3 bond should lead to its contraction as well as to an increase in the O2—C1—O3 bond angle and a decrease in the H4—C1—H5 angle.

The variation of bond lengths with rotation in simple diols and methoxymethanol has previously been rationalized in terms of qualitative PMO theory without quantitative estimation of various orbital interactions (14–16). That variation was also compared with the crystal structure data for carbohydrate systems and oligosaccharides (15, 16). The present more exact PMO treatment explains all changes, found previously by *ab initio* SCF computations, of bond lengths for simple model compounds (Table 4) including the shortening of bonds in *ap,ap* conformations. This effect is difficult to interpret with the simple concept of 'back donation' (15, 16) resulting in partial double-bond character of the C—O moiety. The experimental data for the C5—O5—C1—O1 bond sequence of α- and β-glycosides, for which DMM is a close model, are also listed in Table 4. This table shows that C—O bond lengths in the —O—C—O— moiety (37) are shorter than those for methanol. In agreement with the theoretical predictions in the foregoing paragraph it follows from the data in Table 4 that each rotation about the C—O bond produces its shortening and the elongation of the vicinal C—O bond. Similarly, the O—C—O bond angle is greater in an *sc,sc* conformation and lower in an *ap,ap* conformation than the tetrahedral angle. Recently several *ab initio* calculations of the geometry of DMM have been carried out (38, 39) within a 'restricted minimization frame.' The results of these calculations are shown in Table 4. We have carried out full optimization of the geometry of DMM in different conformations using the CNDO/2 method (28). The final geometries of the equilibrium conformers are shown in Table 4. Though the C—O bond lengths for the *ap,ap* and *sc,sc* conformers seem to be shorter in comparison with the results of *ab initio* restricted minimization (38, 39), the bond angle and bond lengths are in very good agreement with the experimental data (18) for the *sc,sc* conformation. The results show the great dependence of the O—C—O bond angle on conformation and confirm the PMO prediction of an increase in the O—C—O bond angle on going from the *ap,ap* to the *sc,sc* conformation. The results also show the ability of the CNDO/2 method to describe the conformational properties of molecules of this kind. A full account of these results together with a discussion of relaxational effects on conformational equilibrium will be published elsewhere (28). In conclusion, we wish to point out that contrary to stabilization energy there exists a strong conformational dependence of bond lengths and bond angles on torsional angles in DMM. Recently the similar strong coupling between polar methoxy rotors in

TABLE 4. Variation of geometrical parameters with torsional angles φ_1 and φ_2 in the bond-sequence $R_1—O—CH_2—Y$

Molecule R_1	Molecule Y	Conformation φ_1, φ_2	Bond length (Å) $r_{C—O}$	Bond length (Å) $r_{C—X}$	Bond angle O—C—O (deg)	Ref.
H	H		1.437			15
H	OH	(*ap*, *ap*)	1.409	1.409		15
		(*ap*, *sc*)	1.428	1.396		
		(*sc*, *sc*)	1.421	1.421		
CH_3	OH	(*sc*, *ap*)	1.424	1.398		16
		(*sc*, *sc*)	1.421	1.417		
		(*ap*, *sc*)	1.400	1.430		
CH_3	OCH_3	(*sc*, *sc*)			114.66	38
		(*sc*, *ap*)			109.35	
		(*ap*, *ap*)			103.72	
CH_3	OCH_3	(*sc*, *sc*)	1.423	1.423		39
		(*sc*, *ap*)	1.400	1.425		
		(*ap*, *ap*)	1.406	1.406		
		(*sc*, *sc*)			113.9	
		(*sc*, *ap*)			110.9	
CH_3	OCH_3	(*sc*, *sc*)	1.376	1.376	114.876	28
		(*sc*, *ap*)	1.377	1.378	110.047	
		(*ap*, *ap*)	1.378	1.378	104.633	
CH_3	OCH_3	(*sc*, *sc*)(exp.)	1.382	1.382	114.6	18
β-Glycoside		(*ap*, *sc*)	1.429	1.389	107.3	39
α-Glycoside		(*sc*, *sc*)	1.414	1.415	111.6	39

the acyclic phosphate ester has been demonstrated (38). Since the structure of this compound is very similar to DMM we may speculate that in this case the origin of the coupling can also be ascribed to lone-pair orbital interactions.

Orbital Interactions and Anomeric or Exoanomeric Effects

It follows from our analysis that the through-space and through-bond interactions of lone pairs are not responsible for the anomeric or exoanomeric effect in molecules with a C—O—C—O—C segment.

Delocalization of lone pairs into an antibonding $\sigma_{C—Y}$* orbital has often been invoked to explain the anomeric effect for molecules containing a segment of the —C—O—C—Y kind (where Y = O, N, Cl, F, etc.), though originally this conception was designed mainly for molecules with a —C—O—C—Cl segment (10, 11). The substantially greater interaction between a *p*-type lone pair and a $\sigma_{C—Cl}$* orbital in the *ap* conformation compared with the interaction in the *sc* conformation also confirms the C—Cl bonds lengths in α-chloroethers or heterocycles corresponding to them (11), as well as nuclear quadrupole resonance frequency values (40, 41). For this reason we have calculated in the same way the conformational dependence of the interaction between the oxygen lone pair with the antibonding orbital of the C—O bond (Table 1), which is situated in the *xy* plane. The conformational dependence of these interactions follows.

$$E[\mathrm{Lp}(p), \sigma^*] = -0.3376(1 - \cos^2\theta)$$

$$E[\mathrm{Lp}(sp), \sigma^*] = -3.6655 + 0.0656\cos\theta - 0.1218\cos^2\theta$$

and their sum

$$E(L, \sigma^*) = -3.7833 + 0.0656\cos\theta - 0.2158(1 - \cos^2\theta)$$

The last expression shows that the conformational dependence of the interaction of lone pairs with σ* in the case of DMM is not very important; for example, the change of their interaction energy in going from an *ap*,*ap* to an *ap*,*sc* conformation is only 0.2509 kcal/mol. Therefore, for both the through-space and through-bond interactions, more complete treatment including the interaction of lone pairs with σ* does not result in an appreciable stabilization of the *gauche* conformation in molecules with a C—O—C—O—C segment.

The total potential curve of the rotation about the C—O bond may be conveniently analyzed by means of the Fourier expansion

$$V(\varphi_1) = \sum_{i=1}^{3} 0.5V_i(1 - \cos i\varphi_1)$$

The coefficient V_1
action between di
The conformatior
bond orbital inter
$2\varphi_1$ function so tha
should determine t
sign for this term
From the Four
anomeric effect m
ference between t
(equatorial and a
for heterocycles)
$0.75(V_1 - V_2)$ (2
effect may therefo
result of the mutu
interaction of the
interactions of the
a potential energy
C1—O3 bond in
method we obtair
cients in kcal/mo
$V_3 = -0.899$ (27
It follows fron
that the $V_1 - V_2$
shifted toward e
tions. We suggest
the polar bonds is
effect in DMM ar
support this. The
interaction betwe
pairs is used to
represents an alte
(Fig. 1*b*). The dip
formation, where
and through-bon
sp and the *ap* cor
both these contri
the *sp* conformat
tween nonbondin
tributing to the va
considered in ou
the nearest stagg
all three contribu
corresponding to
energy ($\varphi_1 = 35$°
mines the rotatic
the *sp* conformat
Usually only
delocalization, e
C—O—C—Y se
literature regardl
stituent. Compar
for rotation in D
(CMM) led us r
either electrosta

The coefficient V_1 describes the dipole–dipole interaction between dipoles of both C—O—C groups. The conformational dependence of the through-bond orbital interactions has the shape of the cos $2\varphi_1$ function so that the lone-pair orbital interactions should determine the V_2 term. In DMM the positive sign for this term follows from Fig. 7 (curve E_{stab}).

From the Fourier expansion it follows that the anomeric effect may be expressed as an energy difference between the *ap* and the *sc* conformations (equatorial and axial conformations, respectively, for heterocycles): $E = V(180°) - V(60°) = 0.75(V_1 - V_2)$ (27). The anomeric or exoanomeric effect may therefore be generally interpreted as a result of the mutual balance between dipole–dipole interaction of the polar bonds and delocalization interactions of the lone pairs. Through an analysis of a potential energy curve of the rotation about the C1—O3 bond in DMM calculated by the CNDO/2 method we obtained the following values for coefficients in kcal/mol: $V_1 = 3.499$, $V_2 = 0.346$, and $V_3 = -0.899$ (27).

It follows from a comparison of these values, that the $V_1 - V_2$ balance in DMM is considerably shifted toward electrostatic dipole–dipole interactions. We suggest that dipole–dipole interaction of the polar bonds is the primary cause of the anomeric effect in DMM and the results of a previous analysis support this. The 'rabbit ears' scheme, in which an interaction between sp^3 hybridized oxygen atom lone pairs is used to depict electrostatic interactions, represents an alternative model for this interaction (Fig. 1*b*). The dipole interaction favours an *sp* conformation, whereas the net result of through-space and through-bond interactions is to favour both the *sp* and the *ap* conformations. The resulting effect of both these contributions leads to a stabilization of the *sp* conformation. Van der Waals' repulsion between nonbonding atoms and other interactions contributing to the value of the V_3 term, which were not considered in our analysis, shift the equilibrium to the nearest staggered conformation, *sc*. The sum of all three contributions determines the value of φ_1 corresponding to a rotational minimum in the total energy ($\varphi_1 = 35°$) (26, 42). That sum also determines the rotation barrier for a transition through the *sp* conformation.

Usually only one cause (either electrostatic, or delocalization, etc.) of the anomeric effect in the C—O—C—Y segment has been emphasized in the literature regardless of the character of the Y substituent. Comparison of the potential energy curves for rotation in DMM and chloromethoxymethylene (CMM) led us recently to the conclusion (27) that either electrostatic or delocalization effects can prevail according to the character of the Y substituent. For example, electronic delocalization effects (V_2 term) are more pronounced for molecules with Y = Cl than with Y = OCH_3 from the point of view of the anomeric effect. Thus, in contrast to molecules with a 1,3-dioxa group it indicates that, in the case of the C—O—C—Cl segment, the nature of the anomeric effect is determined by delocalization interactions between oxygen lone pairs and antibonding orbitals of the C—Cl and C—H bond, respectively, in agreement with the 'superjacent orbital control' proposal (13). The absolute value of the delocalization interaction leading to the stabilization in the C—O—C—Y bond sequence is probably higher for O—CH_3 than for Cl. However, from the point of view of the anomeric effect, only the conformational dependence of the delocalization interaction is important and that is more pronounced for Cl. The high stabilization energy of the C—O—C—O—C segment has been explained as a consequence of electron delocalization through double bond – no bond resonance (43). It follows from the experimental results that linear diethers containing two oxygen atoms separated by a methylene group are stabilized by about 4 kcal/mol, compared with aliphatic monoethers (44). The value of the stabilization owing to orbital interaction, which we have calculated by the PMO method for DMM, is in the range 8.2–8.9 kcal/mol (Fig. 7).

No account is taken of an electrostatic lone-electron pair repulsion in the simple PMO theory, which we used for the calculation of the through-space and through-bond interactions and their conformational dependences in DMM. Such repulsion of the lone pairs has not been considered in the present analysis because of the uncertainty in the distribution of the nuclear repulsion energy between the bonding and antibonding pairs (45). Van Catledge (46) attempted to express the conformational dependence of an electrostatic lone electron pair repulsion by means of the double-electron elements of the Hartree–Fock matrix. From the calculation of a repulsion between two lone pairs on neighbouring atoms there follows a conformational dependence of the cos φ type (46). Repulsion in the *sp* conformation prevails over the *ap* one.

Conclusions about the prevailing electrostatic interaction origin of the anomeric effect in DMM may be extended to other types of molecules containing an R—O—C—O—R segment. Alkoxysubstituted heterocycles of the pyrane type, and especially sugars, has been most frequently studied with respect to the anomeric effect. In fact, the dependence of the anomeric effect on solvent polarity, observed for 2-alkoxytetrahydropyrane (2, 3), has been used

as an argument favouring the electrostatic origin of the anomeric effect (1).

The preference of the *sc* (*gauche*) conformation to the *ap* (*trans*) one is also observed in the DMM polymer analogue polyoxymethane (POM) and is the cause of right- and left-handed helix formation in the polymer chain. This behaviour should be considered to be the result of the anomeric effect in polymer chemistry. This fact seems to have been omitted in the discussion of the anomalous conformational behaviour of POM (47). From the combustion heat measurement one obtains the constant stabilization energy of POM oligomers per CH_2O segment (44). This suggests that the nature of the anomeric effect is the same for both DMM and POM and so information obtained for DMM might be quantitatively transferred to POM.

Conclusions

The PMO calculation for DMM does not support the suggestion that the anomeric effect in a C—O—C—O—C bond sequence originates from lone pair interactions. The importance of dipole–dipole interactions in the conformational behaviour of this moiety is reconfirmed. On the other hand, through-bond orbital interactions are responsible for the relative stabilization of molecules with 1,3 dioxa groups compared with linear monoethers. Although lone pair interactions are not dominant with respect to conformational stability, they appear to be the most important factors in describing the strong coupling between the geometrical parameters and torsional angles in DMM and related molecules.

Acknowledgement

The authors are grateful to Drs. V. Klimo and V. Laurinc for discussion and critical reading of manuscript.

1. E. L. Eliel. Angew. Chem. Int. Ed. Engl. **11**, 739 (1972).
2. R. U. Lemieux. Pure Appl. Chem. **25**, 527 (1971).
3. A. J. De Hoog, H. R. Buys, C. Altona, and E. Havinga. Tetrahedron, **25**, 3365 (1969).
4. J. T. Edward. Chem. Ind. (London), 1102 (1955).
5. R. U. Lemieux. *In* Molecular rearrangements. Vol. II. *Edited by* P. de Mayo. Interscience, New York, NY. 1964. p. 713.
6. S. Wolfe, A. Rauk, L. M. Tel, and I. G. Csizmadia. J. Chem. Soc. B, 136 (1971).
7. L. Radom, W. J. Hehre, and J. A. Pople. J. Am. Chem. Soc. **93**, 289 (1971).
8. Yu. A. Zhdanov, R. M. Minyaev, and V. I. Minkin. J. Mol. Struct. **16**, 357 (1973).
9. Yu. A. Zhdanov, R. M. Minyaev, and V. I. Minkin. Dokl. Akad. Nauk USSR, Ser. Khim. **211**, 343 (1973).
10. E. A. C. Lucken. J. Chem. Soc. 2954 (1959).
11. C. Romers, A. Altona, H. R. Buys, and E. Havinga. Top. Stereochem. **4**, 39 (1969).
12. G. Baddeley. Tetrahedron Lett. 1645 (1973).
13. S. David, O. Eisenstein, W. J. Hehre, L. Salem, and R. Hoffmann. J. Am. Chem. Soc. **95**, 3806 (1973).
14. H. B. Bürgi, J. D. Dunitz, J. M. Lehn, and G. Wipff. Tetrahedron, **30**, 1563 (1974).
15. G. A. Jeffrey, J. A. Pople, and L. Radom. Carbohydr. Res. **25**, 117 (1972).
16. G. A. Jeffrey, J. A. Pople, and L. Radom. Carbohydr. Res. **38**, 81 (1974).
17. M. H. Whangbo and S. Wolfe. Can. J. Chem. **54**, 963 (1976).
18. E. E. Astrup. Acta Chem. Scand. **27**, 3271 (1973).
19. R. Hoffmann. Acc. Chem. Res. **4**, 1 (1971).
20. J. R. Swenson and R. Hoffmann. Helv. Chim. Acta, **53**, 2331 (1970).
21. M. J. S. Dewar. Molecular orbital theory of organic chemistry. McGraw-Hill, New York, NY. 1969.
22. S. Cradock and R. A. Whiteford. J. Chem. Soc. Faraday Trans. II, **68**, 281 (1972).
23. B. M. Gimarc. J. Am. Chem. Soc. **93**, 593 (1971).
24. J. A. Pople and D. Beveridge. Approximative molecular orbital theory. McGraw-Hill, New York, NY. 1970.
25. A. Veillard. Chem. Phys. Lett. **33**, 15 (1975).
26. I. Tvaroška and T. Bleha. J. Mol. Struct. **24**, 249 (1975).
27. I. Tvaroška and T. Bleha. Tetrahedron Lett. 249 (1975).
28. I. Tvaroška. In preparation.
29. D. R. Truax, H. Wieser, P. N. Lewis, and R. S. Roche. J. Am. Chem. Soc. **96**, 2327 (1974).
30. D. G. Gorenstein, D. Kar, B. A. Luxon, and R. K. Momii. J. Am. Chem. Soc. **98**, 1668 (1976).
31. H. Bock, P. Mollére, G. Becker, and G. Fritz. J. Organometal. Chem. **61**, 113 (1973).
32. C. Robinet, C. Leibovici, and J. F. Labarre. Chem. Phys. Lett. **15**, 90 (1972).
33. S. P. McGlynn, L. G. Vanquickenborne, M. Kinoshita, and D. G. Carroll. Introduction to applied quantum chemistry. Holt, Rinehart and Winston Inc., New York, NY. 1972.
34. K. Fukui. Fortschr. Chem. Forsch. **15**, 1 (1970).
35. E. H. Cordes. Progr. Phys. Org. Chem. **4**, 1 (1967).
36. P. Deslongchamps. Tetrahedron, **31**, 2463 (1976).
37. S. Arnott and W. E. Scott. J. Chem. Soc. Perkin II, 324 (1972).
38. D. G. Gorenstein and D. Kar. J. Am. Chem. Soc. **99**, 672 (1977).
39. G. A. Jeffrey, J. A. Pople, J. S. Binkley, and S. Vishveshwara. J. Am. Chem. Soc. **100**, 373 (1978).
40. L. Guibé, J. Augé, S. David, and O. Eisenstein. J. Chem. Phys. **58**, 5579 (1973).
41. Z. Ardalan and E. A. C. Lucken. Helv. Chim. Acta, **56**, 1715 (1973).
42. P. Bonnet, D. Rinaldi, and J. P. Marchal. J. Chim. Phys. **71**, 298 (1974).
43. J. Hine and A. W. Klueppel. J. Am. Chem. Soc. **96**, 2924 (1974).
44. M. Manson. Acta Chem. Scand. B, **28**, 895 (1974).
45. M. A. Robb, W. J. Haines, and I. G. Csizmadia. J. Am. Chem. Soc. **95**, 42 (1973).
46. F. A. Van Catledge. J. Am. Chem. Soc. **96**, 5693 (1974).
47. P. J. Flory. Statistical mechanics of chain molecules. Wiley, New York, NY. 1969.

Appendix

Calculation of the Conformational Dependence of the Energy of Orbital Interactions

We denoted cos α and sin α as A and B, respec-

tively, where α (56.
(bisector of the O-
system (Fig. 1*b*) a
and S_3 denote the
(5.172, 0.165), $S(2$
(10.074, 0.0), and
tively. The overla
overlapping AO's
a and *b* obtained
(33) are given by

$S(XC1,XC$
$S(YC1,XC$
$S(ZC1,XC$
$S(YC1,YC$
$S(ZC1,YC$
$S(ZC1,ZC$
$S(XO2,XC$
$S(YO2,XC$
$S(ZO2,XC$
$S(YO2,YC$
$S(ZO2,YC$
$S(ZO2,ZC$

tively, where α (56.3°) is the angle between the x axis (bisector of the O—C—O angle) of the coordinate system (Fig. 1*b*) and the C1—O3 bond. S_2, S_1, S_4, and S_3 denote the pure overlap integrals $S(2p_\pi,2p_\pi)$ (5.172, 0.165), $S(2p_\sigma,2p_\sigma)$ (5.172, 0.165), $S(2p_\pi,2p_\pi)$ (10.074, 0.0), and $S(2p_\sigma,2p_\sigma)$ (10.074, 0.0), respectively. The overlap integrals $S(\phi_a,\phi_b)$ for a pair of overlapping AO's ϕ_a and ϕ_b corresponding to atoms a and b obtained by applying Euler transformation (33) are given by

$$S(XC1,XO3) = A^2S_1 + B^2S_2\cos\theta$$
$$S(YC1,XO3) = ABS_1 - ABS_2\cos\theta$$
$$S(ZC1,XO3) = -BS_2\sin\theta$$
$$S(YC1,YO3) = B^2S_1 + A^2S_2\cos\theta$$
$$S(ZC1,YO3) = BS_2\sin\theta$$
$$S(ZC1,ZO_3) = S_2\cos\theta$$
$$S(XO2,XO3) = S_4(B^2\cos\theta + A^2)$$
$$S(YO2,XO3) = ABS_3(\cos\theta - 1)$$
$$S(ZO2,XO3) = BS_4\sin\theta$$
$$S(YO2,YO3) = S_3(A^2\cos\theta + B^2)$$
$$S(ZO2,YO3) = AS_4\sin\theta$$
$$S(ZO2,ZO3) = S_4\cos\theta$$

where X, Y, and Z are the $2p_x$, $2p_y$, and $2p_z$ AO's of the oxygen atoms 2 and 3 and carbon 1.

Substitution of $S(\phi_a, \phi_b)$ into eq. [1] provides the following expressions for the conformational dependence of the through-bond and through-space interactions of the lone pairs (in kcal/mol):

Through bond

[A1] $E[\mathrm{Lp}(p), \pi_z] = 11.3298\cos^2\theta$

[A2] $E[\mathrm{Lp}(p), \pi_z^*] = -2.3340\cos^2\theta$

[A3] $E[\mathrm{Lp}(p), \pi_x] = 4.5368(1 - \cos^2\theta)$

[A4] $E[\mathrm{Lp}(p), \pi_x^*] = -1.7377(1 - \cos^2\theta)$

[A5] $E[\mathrm{Lp}(sp), \pi_x] = 4.3722 - 0.1786\cos\theta + 2.3918\cos^2\theta$

[A6] $E[\mathrm{Lp}(sp), \pi_x^*] = -1.2790 + 0.0587\cos\theta - 0.7625\cos^2\theta$

[A7] $E[\mathrm{Lp}(sp), \pi_z] = 7.1488(1 - \cos^2\theta)$

[A8] $E[\mathrm{Lp}(sp), \pi_z^*] = -1.1368(1 - \cos^2\theta)$

Through space

[A9] $E[\mathrm{Lp}(p), \mathrm{Lp}(p)] = \pm 2.2949\cos\theta$

[A10] $E[\mathrm{Lp}(sp), \mathrm{Lp}(sp)] = \mp 0.1890 \mp 1.2839\cos\theta$

[A11] $E[\mathrm{Lp}(p), \mathrm{Lp}(sp)] = 0.0727(1 - \cos^2\theta)$

Microbial hydroxylation of steroids. 5. Metabolism of androst-5-ene-3,17-dione and related compounds by *Rhizopus arrhizus* ATCC 11145

HERBERT L. HOLLAND AND PETER R. P. DIAKOW

Department of Chemistry, Brock University, St. Catharines, Ont., Canada L2S 3A1

Received August 10, 1978

HERBERT L. HOLLAND and PETER R. P. DIAKOW. Can. J. Chem. **57**, 436 (1979).

The products of the incubation of androst-5-ene-3,17-dione (**2***a*), 3β-hydroxyandrost-5-ene-17-one (**2***b*), and androsta-3,5-diene-17-one (**3**) with *Rhizopus arrhizus* ATCC 11145 under a variety of conditions have been identified and the mechanisms of their formation discussed. In addition, several C-(4,5)- and C-(5,6)-epoxyandrostanes have been incubated with *R. arrhizus*, the products identified and possible pathways for their formation presented.

HERBERT L. HOLLAND et PETER R. P. DIAKOW. Can. J. Chem. **57**, 436 (1979).

On a identifié les produits obtenus par l'incubation de l'androstène-5 dione-3,17 (**2***a*), de l'hydroxy-3β androstène-5 one-17 (**2***b*) et de l'androstadiène-3,5 one-17 (**3**) avec le *Rhizopus arrhizus* ATCC 11145 sous diverses conditions; on discute de leurs mécanismes de formation. De plus, on a incubé plusieurs C-(4,5) et C-(5,6)-époxyandrostanes avec le *R. arrhizus*; on a identifié les produits et on présente des voies possibles pour leur formation.

[Traduit par le journal]

The C-6β hydroxylation of androst-4-ene-3,17-dione (**1***a*) by *R. arrhizus* ATCC 11145 proceeds via the $\Delta^{3,5}$-enol form of the ketone (1). In an attempt to gain further insight into this enzymic process, we have studied the metabolism of androst-5-ene-3,17-dione (**2***a*), the corresponding 3β-alcohol (**2***b*), and the $\Delta^{3,5}$-enol analogue **3**, by *R. arrhizus* under a variety of conditions. In addition we have incubated a series of epoxy steroids and related compounds, **4**–**9**.

Results

The results of the incubations of **2**–**9** are tabulated in the Experimental. The alcohol **2***b* gave predominantly the C-11α-hydroxy derivative **2***c*, while incubation of **2***a* involved changes in rings A and B. In the presence of oxygen, **2***a* gave the *C*-6β- and *C*-6α-Δ^4-3-keto alcohols, **1***b* and **1***c*, respectively, together with the Δ^4-3,6-dione, **1***e*; with live fungus C-11α hydroxylation was also observed. In the absence of oxygen, **2***b* was rearranged nonenzymically to the conjugated isomer **1***a*. The $\Delta^{3,5}$-diene **3** gave, along with some recovered starting material, small amounts of the isomeric 3α- and 3β-hydroxy-Δ^4-6β-alcohols **10***a* and **10***b*, respectively; no C-11α hydroxylation of **3** was observed. The structure of the major product, **10***a*, followed from an analysis of its ^{1}Hmr spectral data (2) (see Experimental) and oxidation to the known Δ^4-3,6-dione **1***e*. The structure of **10***b* was confirmed by a comparison of observed physical and spectral data with those published (3). For both **10***a* and **10***b*, the chemical shift of the C-19 hydrogens was diagnostic of the presence of a C-6β-hydroxyl function (2) and agreed well with that predicted from additivity parameters (2) (**10***a*, calcd.: 1.22; found: 1.20 δ; **10***b*, calcd.: 1.30; found: 1.28 δ).

The keto epoxide **4***a* gave, with both live and autoclaved fungus, the C-6α-alcohol **1***c*; some starting material was recovered under the latter conditions. In contrast, both the C-(5,6)α- and C-(5,6)β-epoxides, **4***b* and **5***a*, gave a complex mixture of products. The α-oxide **4***b* under normal incubation conditions gave the C-7α-hydroxy derivative **4***c* as the major product together with the 3β,5α-dihydroxy-6-ketone **9***b* and the triol **9***a*. The structure of **4***c* was deduced from its ^{1}Hmr spectrum (*q.v.*). The location of oxygen at C-7 was suggested by the downfield shift of the doublet assigned to the C-6β hydrogen (0.34 ppm with respect to starting material) (4) and confirmed by spin decoupling of the C-7β and C-6β hydrogens; irradiation at δ 4.15 (C-7βH) caused collapse of the doublet at δ 3.26. The chemical shift of the C-19 hydrogens of **4***c* (−0.01 ppm with respect to **4***b*) is also consistent with C-7α hydroxylation (2). The keto diol **9***b* was characterized by the upfield resonance of the C-19 hydrogens, a feature diagnostic of 6-keto-5α-steroids (2), and identified by comparison with authentic material. The triol **4***c* was formed in the presence of both live and autoclaved fungus.

An analogous series of products was obtained from the β-epoxide **5***a*. The structure of the 7α-hydroxy derivative **5***b* again followed from ^{1}Hmr data, the signal assigned to the C-6α hydrogen now appearing as a singlet at δ 3.20, and that of the C-7β hydrogen as a doublet (coupled only to the C-8 hydrogen) at δ 3.67. The absence of coupling between

0008-4042/79/040436-05$01.00/0

the C-6α and C-7β hydrogens is a consequence of the dihedral angle, estimated from models to be close to 90°. This interpretation is strengthened by the observation that the C-6α hydrogen of **5***a* appears as a well-resolved doublet (J = 3 Hz) at δ 3.10, coupled only to the C-7α hydrogen.

The (4,5)-epoxy steroids **6** and **7**, the 5α-hydroxy ketone **8**, the triol **9***a* and keto diol **9***b* were all recovered unchanged after incubation with *R. arrhizus*.

Discussion

The hydroxylation of **2***b* at 11α without extensive oxidation at C-3 is a feature of 11α-hydroxylating fungi such as *R. nigricans* (5) and *Aspergillus ochraceus* (6), a feature which is apparently shared by *R. arrhizus*.

The microbial oxidation of Δ^5-3-ketones has not been thoroughly examined but their nonenzymic oxidation, in the presence (7–9) or absence (10, 11) of fungus, to 6α- and 6β-oxygenated Δ^4-3-keto steroids is documented. The initial products are the 6α- and 6β-hydroperoxides, **1***f* and **1***g*. When produced nonenzymically in the presence of the fungus *Actinoplanes missouriensis*, these are reduced to the corresponding alcohols **1***c* and **1***b*, respectively (7–9).

The results obtained by incubation of **2***a* with *R. arrhizus* confirm that nonenzymic oxidation of **2***a* occurs. The 6α- and 6β-alcohols **1***c* and **1***b* are formed at both pH 5.3 and 6.8 in the presence of either living or autoclaved fungus. The formation of **1***b* and **1***c* with autoclaved fungus implies that, if the autoxidation follows the normal course and the hydroperoxides are the initial products (10, 11), then the alcohols **1***b* and **1***c* are formed in a secondary step. A mechanism has been proposed and discussed (11) for the autoxidation of cholest-5-ene-3-one to analogous products. The 6-ketone **1***e* also produced under a variety of incubation conditions may be readily formed by the dehydration of a peroxide intermediate.

The formation of the 6α-alcohol **1***c* and the 6-ketone **1***e* from **2***a* militates against the intermediacy of the Δ^5-3-ketone **2***a* in the normal C-6β hydroxylation of **1***a*: in our experience (1) neither C-6α-hydroxylated nor-C-6-keto steroids are produced during the C-6β-hydroxylation reaction. The possibility of a Δ^5-3-ketone is produced as a transient enzyme bound species, protected from aerial oxidation during the C-6β-hydroxylation process cannot be eliminated (12) but chemical analogies (1) indicate a direct conversion of $\Delta^{3,5}$-enol to 6β-hydroxy-Δ^4-3-ketone and thus support the present conclusions.

The isomerization of **2***a* to **1***a* during all the incubations performed indicates that, even at pH 6.8, **2***a* may be rapidly and nonenzymically isomerized in the presence of the incubation medium and either live or autoclaved fungus. The catalysis of the Δ^5-3-keto-Δ^4-3-keto steroid isomerization by amino acids has been reported (13) and may be operative under the conditions reported herein.

Further evidence for the direct oxidation of an enolic intermediate is provided by the products obtained from the $\Delta^{3,5}$-diene **3**. The formation of **10***a* and **10***b* may be rationalized by a mechanism involving electrophilic oxidation of the Δ^5 bond, with rearrangement and attack of water at C-3, as shown in Fig. 1. The stereochemistry of the products at C-6 is a result of stereoelectronic factors (1 and references therein) and a similar preference for axial attack at C-3 leads to the observed predominance of the C-3α-alcohol **10***a*.

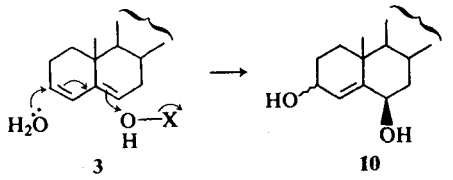

3 10

FIG. 1.

Microbial transformations of epoxy steroids have not been extensively studied, although dehydrogenation (14), C-11 hydroxylation (15, 16) and ring opening (17) have been reported. In analogy with earlier work (17), we found that **4***a* is opened nonenzymically to the 6α-hydroxy-Δ^4-3-ketone **1***c*. This facile conversion has been studied in the cholestane series (18) and demonstrates the possibility that an unstable (18) (5,6)β-epoxy-3-ketone (or its Δ^3-enol equivalent) may be an intermediate in the microbial C-6β hydroxylation, although no direct evidence for such an intermediate species exists.

The hydroxylation of **4***b* and **5***a* at C-7α is not a known reaction of the *Rhizopus* genus, although both C-7α and C-7β hydroxylation have been reported with its members (19). The production of the 3β,5α,6β-triol **9***a* from both **4***b* and **5***a* may be the result of nonenzymic hydrolysis, since both are produced with autoclaved fungus. The formation of the corresponding keto diol **9***b*, however, may be the result of enzymic oxidation of the epoxide; its formation by oxidation of **9***a* is precluded by the observation that **9***a* is recovered unchanged after incubation with *R. arrhizus* (*vide infra*) and its formation by autoxidation, although possible (20), unlikely in view of the fact that it is not formed in the absence of live fungus. Chemical analogy for the formation of **9***b* is

provided by the conversion of other 5,6α-oxides into 6-keto derivatives under oxidative conditions (21–23), although the mechanism of this reaction has not been defined.

Although *R. arrhizus* is an efficient C-11α hydroxylator (24), no C-11α hydroxylation of epoxides **4***a*, **4***b*, **5***a*, **6**, or **7** was observed, **6** and **7** being recovered unchanged from the incubation medium: the closely related fungus *R. nigricans* is reported to hydroxylate C-(4,5)-epoxides of the pregnane series at C-11α (16). Control incubations of compounds **8**, **9***a*, and **9***b* also failed to show detectable metabolism by *R. arrhizus*.

Experimental

Apparatus, Materials, and Methods

The apparatus and techniques used were as previously described (1). Incubations with *R. arrhizus* were performed as described (25); incubations under nitrogen were performed after the flasks were autoclaved, cooled, degassed, flushed with nitrogen, and sealed.

Preparation of Substrates

The following steroids were prepared by published procedures: Androst-5-ene-3,17-dione (**2***a*) (26), androsta-3,5-diene-17-one (**3**) (27, 28), (5,6α)-epoxy-5α-androstane-3,17-dione (**4***a*) (29), (5,6α)-epoxy-3β-hydroxy-5α-androstan-17-one (**4***b*) (1), (5,6β)-epoxy-3β-hydroxy-5β-androstan-17-one (**5***a*) (1), (4,5β)-epoxy-5β-androstane-3,17-dione (**6**) (16), (4,5α)-epoxy-5α-androstane-3,17-dione (**7**) (16), and 5-hydroxy-5α-androstane-3,17-dione (**8**) (1). 3β-Hydroxyandrost-5-ene-17-one (**2***b*) was a commercial sample.

3β,5,6β-Trihydroxy-5α-androstan-17-one (9a)

Perchloric acid (5.5 mL, 6.5% w/v) was added to a refluxing solution of (5,6α)-epoxy-3β-hydroxy-5α-androstan-17-one (2 g) in acetone (35 mL). After a further 10 min at reflux, the reaction mixture was cooled and the product collected by filtration, washed with ether, and dried, to give 1.9 g, mp 292–297°C (dec.). The product showed physical and spectral data identical with those published (3).

3β,5-Dihydroxy-5α-androstane-6,17-dione (9b)

This was prepared by a modification of the method of Fieser and Rajagopalan (30). 3β,5,6β-Trihydroxy-5α-androstan-17-one (3.2 g) was dissolved in a mixture of dioxan (50 mL) and water (5 mL). *N*-Bromosuccinimide (2 g) was then added and the resulting solution placed 2 ft from a G.E. sunlamp and maintained at 20–25°C by ice cooling. After 1 h, water (400 mL) was added and the solution extracted with chloroform. The chloroform extract was washed (water, 2 *N* sodium metabisulphite), dried, and evaporated. The residue was crystallized from ethyl acetate – hexane. Recrystallization from the same solvent gave the desired compound, 0.37 g, mp 281–283°C (dec.); ir (ν_{max}, KBr): 3450, 3300, 1740, 1700 cm^{-1}; nmr (δ, DMSO-d_6): 0.70 (3H, s, C-19H), 0.77 (3H, s, C-18H), 3.6–3.9 (1H, m, C-3αH), 4.47 (1H, d, J = 5 Hz, C-3βOH), 5.37 (1H, s, C-5αOH); ms (*m/e*, %): 320 (50), 302 (11), 287 (6), 220 (100). *Anal.* calcd. for $C_{19}H_{28}O_4$: C 71.22, H 8.81; found: C 71.02, H 8.87.

Incubations with Rhizopus arrhizus

The results of the incubations of **2** to **9** are presented in the table. In all cases, products were isolated following column chromatography on silica gel. The standard chromatographic procedure involved stepwise elution from benzene to ether (increments of 10% ether) followed by stepwise elution to 10% methanol (increments of 1% methanol). Physical and spectral data for hitherto unreported compounds are listed below. All other products were identified by comparison of physical and spectral data with those of authentic samples.

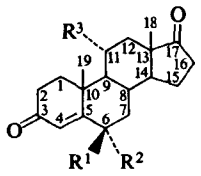

1

a $R^1 = R^2 = R^3 = H$
b $R^1 = OH, R^2 = R^3 = H$
c $R^2 = OH, R^1 = R^3 = H$
d $R^3 = OH, R^1 = R^2 = H$
e $R^1 + R^2 = O, R^3 = H$
f $R^1 = R^3 = H, R^2 = OOH$
g $R^2 = R^3 = H, R^1 = OOH$

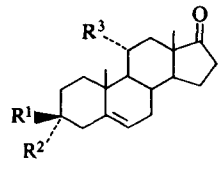

2

a $R^1 + R^2 = O, R^3 = H$
b $R^1 = OH, R^2 = R^3 = H$
c $R^1 = R^3 = OH, R^2 = H$

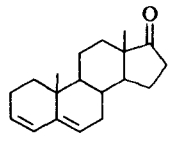

3

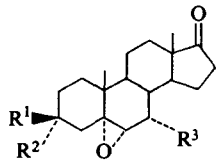

4

a $R^1 + R^2 = O, R^3 = H$
b $R^1 = OH, R^2 = R^3 = H$
c $R^1 = R^3 = OH, R^2 = H$

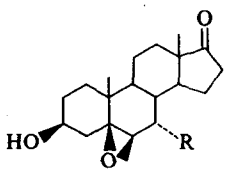

5

a R = H
b R = OH

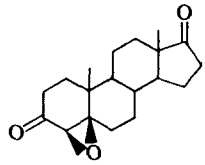

6

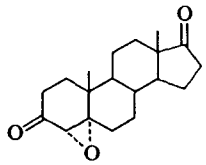

7

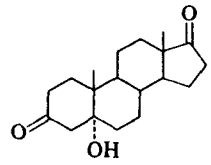

8

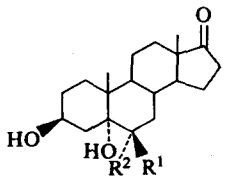

9

a $R^1 = OH, R^2 = H$
b $R^1 + R^2 = O$

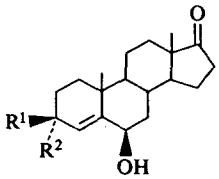

10

a $R^1 = H, R^2 = OH$
b $R^1 = OH, R^2 = H$

Substrate

2*b*
2*a*
2*a*
2*a*
2*a*
2*a*
2*a*
3
4*a*
4*b*
5*a*
6
7
8
9*a*
9*b*

*Unless

3α,6β-Dihydroxyan
(ethyl acetate – hexan
KBr), 3400, 1740 cm
1.20 (3H, s, C-19H),
(1H, d, J = 5 Hz, C-
(100), 271 (90). M^+
304.203. Oxidation w
androst-4-ene-3,6,17-
parisons of spectral
material.

3β,7α-Dihydroxy-(
mp 182–184°C (ethy
1735 cm^{-1}; nmr (δ,
C-19H), 3.26 (1H, c
C-3α,-7β H's); ms (*
(30), 286 (34), 284 (
H 8.81; found: C 71.

3β,7α-Dihydroxy-(
mp 177–179°C (ethy
ether), 0.35; ir (ν_{max},
0.86 (3H, s, C-18H),
3.5–4.1 (2H, m conta
ms (*m/e*, %): 320 (1
Anal. calcd. for C_{19}
found (M^+ 320.192)

We thank th
Canada for finan

1. H. L. Holland
694 (1978).
2. J. E. Bridgem
Evans, Sir Ew

Substrate	Incubation conditions*	Amount incubated (mg)	Amount isolated (mg)	Products (isolated %)
2*b*	Normal	1000	835	**2***c* (23) + **1***a* (2)
2*a*	Normal	1000	948	**1***a* (8), **1***b* (5), **1***c* (10), **1***d* (9), **1***e* (4)
2*a*	Normal, pH 6.8	1000	970	**1***a* (5), **1***b* (8), **1***c* (9), **1***d* (7), **1***e* (3)
2*a*	Autoclaved	480	504	**1***a* (9), **1***b* (10), **1***c* (5), **1***e* (3)
2*a*	Autoclaved, pH 6.8	480	462	**1***a* (7), **1***b* (7), **1***c* (6), **1***e* (2)
2*a*	Autoclaved, nitrogen	1000	810	**1***a* (62)
2*a*	Autoclaved, nitrogen, pH 6.8	1000	903	**1***a* (53)
3	Normal	1500	840	**3** (10), **10***a* (3), **10***b* (0.5)
4*a*	Normal	1000	965	**1***c* (35)
	Autoclaved	600	410	**4***a* (15), **1***c* (27)
4*b*	Normal	1500	1310	**4***c* (11), **9***a* (4), **9***b* (4)
	Autoclaved	1000	937	**4***b* (45), **9***a* (6)
5*a*	Normal	3000	1700	**5***b* (1), **9***a* (18), **9***b* (0.5)
	Autoclaved	200	134	**9***a* (48)
6	Normal	450	310	**6** (55)
7	Normal	450	342	**7** (62)
8	Normal	600	517	**8** (68)
9*a*	Normal	1200	630	**9***a* (42)
9*b*	Normal	100	72	**9***b* (51)

*Unless otherwise stated, incubations were performed unbuffered at pH 5.3.

*3α,6β-Dihydroxyandrost-4-ene-17-one (**10**a)*—mp 218–221°C (ethyl acetate – hexane); R_f (4% methanol–ether), 0.41; ir (ν_{max}; KBr), 3400, 1740 cm^{-1}; nmr (δ, $CDCl_3$): 0.92 (3H, s, C-18H), 1.20 (3H, s, C-19H), 4.0–4.3 (2H, m, C-3β, C-6α H's), 5.72 (1H, d, J = 5 Hz, C-4H); ms (*m/e*, %): 304 (24), 289 (40), 286 (100), 271 (90). M^+ calcd. for $C_{19}H_{28}O_3$: 304.204; found: 304.203. Oxidation with standard Jones' reagent (31) afforded androst-4-ene-3,6,17-trione in 72% yield, identical in comparisons of spectral and physical data with those of authentic material.

*3β,7α-Dihydroxy-(5,6α)-epoxy-5α-androstan-17-one (**4**c)*—mp 182–184°C (ethyl acetate – hexane); ir (ν_{max}, KBr): 3400, 1735 cm^{-1}; nmr (δ, $CDCl_3$): 0.82 (3H, s, C-18H), 1.09 (3H, s, C-19H), 3.26 (1H, d, J = 4.6 Hz, C-6βH), 3.7–4.3 (2H, m, C-3α,-7β H's); ms (*m/e*, %): 320 (100), 305 (10), 302 (35), 287 (30), 286 (34), 284 (35). *Anal.* calcd. for $C_{19}H_{28}O_4$: C 71.22, H 8.81; found: C 71.13, H 8.84.

*3β,7α-Dihydroxy-(5,6β)-epoxy-5β-androstan-17-one (**5**b)*—mp 177–179°C (ethyl acetate – hexane); R_f (4% methanol–ether), 0.35; ir (ν_{max}, KBr): 3400, 1740 cm^{-1}; nmr (δ, $CDCl_3$): 0.86 (3H, s, C-18H), 1.05 (3H, s, C-19H), 3.20 (1H, s, C-6αH), 3.5–4.1 (2H, m containing d, J = 8 Hz, at 3.67, C-3α,-7β H's); ms (*m/e*, %): 320 (100), 305 (9), 302 (45), 287 (35), 286 (70). *Anal.* calcd. for $C_{19}H_{28}O_4$ (M^+ 320.199): C 71.22, H 8.81; found (M^+ 320.192): C 70.63, H 8.69.

Acknowledgement

We thank the National Research Council of Canada for financial support.

1. H. L. Holland and P. R. P. Diakow. Can. J. Chem. **56**, 694 (1978).
2. J. E. Bridgeman, P. C. Cherry, A. S. Clegg, J. M. Evans, Sir Ewart R. H. Jones, A. Kasal, V. Kumar, G. D. Meakins, Y. Morisawa, E. E. Richards, and P. D. Woodgate. J. Chem. Soc. C, 250 (1970)
3. C. Amendolla, G. Rosenkranz, and F. Sondheimer. J. Chem. Soc. 1226 (1954).
4. P. Morand and A. Van Tongerloo. Steroids, **21**, 65 (1973).
5. G. Raspe and H. Richler. Ger. Patent No. 1,080,553 (April 28, 1960); Chem. Abstr. **55**, 13482b (1960).
6. A. M. Bell, J. W. Browne, W. A. Denny, E. R. H. Jones, A. Kasal, and G. D. Meakins. J. Chem. Soc. Perkin I, 2930 (1972).
7. G. E. Mallett, D. S. Fukuda, and G. J. Guynes. 150th Meeting Am. Chem. Soc., Atlantic City, NJ. 1965. p. 12Q.
8. G. E. Mallett. U.S. Patent No. 3,128,238 (April 7, 1964).
9. G. E. Mallett and D. S. Fukuda. Bacteriol. Proc. 26 (1962).
10. L. F. Fieser, T. W. Greene, F. Bischoff, G. Lopez, and J. J. Rupp. J. Am. Chem. Soc. **77**, 3928 (1955).
11. P. B. D. de la Mare and R. D. Wilson. J. Chem. Soc. Perkin II, 157 (1977).
12. P. H. Yu and L. Tan. J. Steroid Biochem. **8**, 825 (1977).
13. W. F. Benisek and A. Jacobson. Bioorg. Chem. **4**, 41 (1975); T. Okuyama, A. Kitada, and T. Fueno. Bull. Chem. Soc. Jpn. **50**, 2358 (1977).
14. K. Kieslich. Tetrahedron, **25**, 5863 (1969).
15. K. Kieslich and H. Wieglepp. Chem. Ber. **104**, 205 (1971).
16. R. H. Bible, C. Placek, and R. D. Muir. J. Org. Chem. **22**, 607 (1957).
17. S. S. Lee and C. J. Sih. Biochemistry, **3**, 1267 (1964).
18. P. B. D. de la Mare and R. D. Wilson. J. Chem. Soc. Perkin II, 975 (1977).
19. W. Charney and H. L. Herzog. Microbial transformations of steroids. A handbook. Academic Press, New York, NY. 1967.

20. S. BERGSTRÖM and B. SAMUELSSON. *In* Autoxidation and anti-oxidants. Vol. 1. *Edited by* W. O. Lundberg. Interscience, New York, NY. 1961.
21. J. R. HANSON and T. D. ORGAN. J. Chem. Soc. C, 2473 (1970).
22. J. A. CELLA, J. P. MCGRATH, J. A. KELLEY, O. EL SOUKKARY, and L. HILPERT. J. Org. Chem. **42**, 2077 (1977).
23. L. KNOF. Justus Liebigs Ann. Chem. **657**, 171 (1962).
24. S. H. EPPSTEIN, P. D. MEISTER, H. M. LEIGH, D. H. PETERSON, H. C. MURRAY, L. M. REINEKE, and A. WEINTRAUB. J. Am. Chem. Soc. **76**, 3174 (1954).
25. H. L. HOLLAND and B. J. AURET. Can. J. Chem. **53**, 2041 (1975).
26. J. B. JONES and D. C. WIGFIELD. Can. J. Chem. **47**, 4459 (1969).
27. G. ROSENKRANZ, S. KAUFMANN, and J. ROMO. J. Am. Chem. Soc. **71**, 3689 (1949).
28. F. C. CHANG and N. F. WOOD. Steroids, **4**, 55 (1964).
29. J. A. CAMPBELL, J. C. BABCOCK, and J. A. HOGG. J. Am. Chem. Soc. **80**, 4717 (1958).
30. L. F. FIESER and S. RAJAGOPALAN. J. Am. Chem. Soc. **71**, 3938 (1949).
31. C. DJERASSI, R. R. ENGLE, and A. BOWERS. J. Org. Chem. **21**, 1547 (1956).

^{13}C nuclear magnetic resonance spectral and conformational analysis of naturally occurring tetrahydrofuran lignans

SEBASTIÃO F. FONSECA, LAURO E. S. BARATA, AND EDMUNDO A. RÚVEDA
Instituto de Química, Universidade Estadual de Campinas, C.P. 1170 13100 Campinas, São Paulo, Brasil

AND

PAUL M. BAKER
Núcleo de Pesquisas de Produtos Naturais, Centro de Ciências da Saúde, Universidade Federal do Rio de Janeiro, Rio de Janeiro, Brasil

Received June 14, 1978

SEBASTIÃO F. FONSECA, LAURO E. S. BARATA, EDMUNDO A. RÚVEDA, and PAUL M. BAKER. Can. J. Chem. 57, 441 (1979).

The ^{13}C nmr spectra of the naturally occurring stereoisomers of the tetrahydrofuran lignans were recorded and the signals assigned. Based on these assignments, on the observed sensitivity of the benzylic carbon shifts to the orientation of the aryl groups, and on the comparison with previously reported ^{1}H nmr data, the most probable conformations for the mentioned stereoisomers are suggested.

SEBASTIÃO F. FONSECA, LAURO E. S. BARATA, EDMUNDO A. RÚVEDA et PAUL M. BAKER. Can. J. Chem. 57, 441 (1979).

On a enregistré les spectres rmn du ^{13}C de stéréoisomères naturels de lignanes tétrahydrofuranniques et on a attribué les signaux. En se basant sur ces attributions, sur la sensibilité observée pour les déplacements des carbones benzyliques sur l'orientation des groupes aryles et sur une comparaison avec les données de rmn de ^{1}H rapportées antérieurement, on fait des suggestions concernant les conformations les plus probables pour les stéréoisomères mentionnés.
[Traduit par le journal]

Of the six possible stereoisomers of the tetrahydrofuran lignans, **2**–**7**, only four, **2**–**5**, with a variety of oxygenated substituents in the aryl groups (1), have so far been isolated from plants.

By phenol oxidation, Sarkanen and Wallis (2) obtained four isomers of 2,5-bis-(3′,4′,5′-trimethoxyphenyl)-3,4-dimethyltetrahydrofuran, **2***a*, **3***a*, **5***a*, and **6**, which were analyzed by ^{1}H nmr spectroscopy to establish their most probable conformations. The availability of galbacin (**2***b*) and veraguensin (**5***b*), isolated from *V. surinamensis* (3) and di-*O*-methyltetrahydrofuroguaiacin B (**4**) and galgravin (**3***b*), obtained by simple synthetic procedures (4, 5), prompted us to study these stereoisomers by ^{13}C nmr spectroscopy, in order to extract as much conformational information as possible, and in continuation with our project on ^{13}C nmr spectral analysis of lignans and related families of natural products (6).

From ^{1}H nmr spectral analysis, it was shown that the segment of the cycle of pseudorotation (CYCLOPS) representing the most populated conformations of **2***a* are $^{2}T_{3}$–$^{4}T_{5}$, with torsion angles for $H_{2\beta}$–$H_{3\alpha}$ and $H_{4\beta}$–$H_{5\alpha}$ protons of approximately 150°, and with all the substituents pseudoequatorially oriented (2).[1] This is in agreement with the ^{13}C nmr spectrum of galbacin (**2***b*), which shows 10 signals readily assigned by standard chemical shift theory.

The similarity between the H_2–H_3 coupling constant of licarin B (**8**) and the corresponding ones of $H_{2\beta}$–$H_{3\alpha}$ and $H_{4\beta}$–$H_{5\alpha}$ of **2***b*, indicates that the dihedral angles for the methyl and piperonyl groups should be approximately the same in both compounds (7). Since the 3-Me group of **8** is considered to be free of steric interactions from the piperonyl group of C-2 (7), it can be suggested that the shielding of both methyls of **2***b*, at 13.7 ppm, is a consequence of a reciprocal γ effect, owing to the puckering of C-3 and C-4, confirming their pseudoequatorial orientation. The shift of C-1′ and C-1″ of **2***b* at 136.1 ppm, deshielded 2.1 ppm in comparison with C-1′ of **8** and with a δ value similar to the reported ones for C-1′ and C-1″ of the 'equatorially' oriented piperonyl units of the 2,6-diaryl-3,7-dioxabicyclo[3.3.0]octane lignans type (8), confirms the pseudoequatorial orientation of the piperonyl groups of **2***b* and also that the methyl groups are free of their steric interactions.

It was suggested, based on the *J* values of $H_{2\beta}$–$H_{3\alpha}$ and $H_{4\alpha}$–$H_{5\beta}$ protons, that the most probable conformations of **3***a* are the ones represented by the $^{3}T_{2}$–$^{5}T_{4}$ and $^{2}T_{3}$–$^{4}T_{5}$ segments of the CYCLOPS (2). The shift of C-1′ and C-1″ at 134.6 ppm, in the ^{13}C

[1]See **1** for numbering. The designations α and β are given to the substituents oriented below and above the plane of the paper, respectively.

0008-4042/79/040441-03$01.00/0

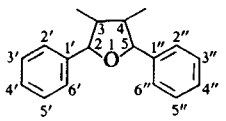

1

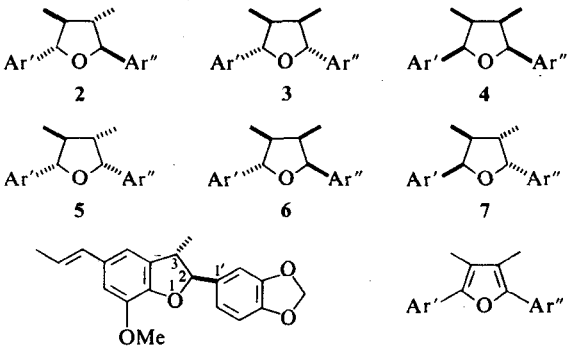

2 3 4

5 6 7

8

9

2*a*, **3***a*, **5***a*, **6**: Ar′ = 3′,4′,5′-trimethoxyphenyl; Ar″ = 3″,4″,5″-trimethoxyphenyl

2*b*: Ar′ = 3′,4′-methylenedioxyphenyl; Ar″ = 3″,4″-methylenedioxyphenyl

3*b*,**4**, **5***b*, **7**, **9**: Ar′ = 3′,4′-dimethoxyphenyl; Ar″ = 3″,4″-dimethoxyphenyl

nmr spectrum of galgravin **3***b*, similar to the ones for C-1′ and C-1″ of 'equatorial' veratryl groups of lignans of the 2,6-diaryl-3,7-dioxabicyclo[3.3.0]octane type (8), suggests that in **3***b*, both aryl groups are pseudoequatorially oriented and free of steric interactions. The signal at 12.9 ppm, assigned to the *cis*-methyl groups, shows that in **3***b* the reciprocal γ effect between them is stronger than in the all-*trans* isomer **2***b*. The forms V_4, $^5T_4$, $^2T_3$, and V_3 with torsion angles averaging 120° for $H_{2\beta}$–$H_{3\alpha}$ and $H_{4\alpha}$–$H_{5\beta}$ protons, allowing partial release of the *C*-methyl groups steric interactions and keeping the aryl groups pseudoequatorially oriented, probably represent the most populated conformations of galgravin **3***b*.

The reported $H_{2\alpha}$–$H_{3\alpha}$ and $H_{4\alpha}$–$H_{5\alpha}$ coupling constants of 6.5 Hz for the all-*cis* isomer di-*O*-methyltetrahydrofuroguaiacin B (**4**) (4), indicate a torsion angle for the mentioned protons of approximately 30°. Two groups of conformations ^3V,$^3T_4$,V_4 and V_3,$^4T_3$,^4V satisfy this requirement. Analysis of the ^{13}C nmr spectrum of **4**, shows that the methyl groups resonate at higher field, 11.6 ppm, compared with related groups of galgravin (**3***b*), 12.9 ppm. This difference can be attributed to the nonbonded interactions between the methyl groups and the pseudoaxially oriented veratryl groups of **4**, since the dihedral angles between the methyls are approximately the same in the proposed conformations of both stereoisomers and consequently, a similar γ effect could be expected. In view of the reciprocity of the γ effect, C-1′ and C-1″ of **4** are shielded by 1.8 ppm in comparison with similar sites of the stereoisomer **3***b*, confirming the above observations.

It has been observed that C-2,C-6; C-1,C-5; and C-4,C-8 shifts of the 2,6-diaryl-3,7-dioxabicyclo-[3.3.0]octane system are sensitive to the orientation of the aryl groups but not to the nature of their oxygenated substituents (8). The benzylic carbons, for example, show shifts at ca. 82 and 88 ppm, whereas the remaining methines resonate at ca. 50 and 54 ppm, according to the 'axial' or 'equatorial' orientation of the aryl groups, respectively. C-2,C-5 and C-3,C-4 of galbacin (**2***b*), with all pseudoequatorial substituents, show shifts at 88.1 and 50.9 ppm, respectively, whereas similar sites of di-*O*-methyltetrahydrofuroguaiacin B (**4**), with all pseudoaxial substituents, resonate at 82.4 and 41.2 ppm, respectively. In galgravin (**3***b*), the benzylic carbons have a shift of 87.1 ppm, in good agreement with the pseudoequatorial orientation of the veratryl groups, whereas C-3 and C-4 show shielding with an intermediate value, 44.3 ppm. These observations strongly suggest that in tetrahydrofuran lignans, the benzylic carbons are clearly sensitive to the orientation of the aryl groups and their chemical shifts could be of diagnostic importance for the conformational analysis of this system.

The ^1H nmr spectrum of **5***a*, very similar to that of veraguensin (**5***b*), suggested torsion angles for the $H_{2\beta}$–$H_{3\alpha}$ and $H_{4\beta}$–$H_{5\beta}$ protons of approximately 150 and 0°, respectively. All conformations of the ^5T_O–$^4T_5$ segment of the CYCLOPS satisfy these requirements but two of them, forms ^4V and $^4T_5$, were

TABLE 1. ^{13}C nucl
naturally

Position	2*b*
1′	136.1
2′	106.4
3′	147.5
4′	146.7
5′	107.7
6′	119.5
2	88.1
3	50.9
4	50.9
5	88.1
1″	136.1
2″	106.4
3″	147.5
4″	146.7
5″	107.7
6″	119.5
CMe	13.7
OMe	
OCH_2O	100.7

discarded owing
aryl groups. It
that the latter c
$^4T_3$, in spite of
axially oriented.
cis substituents
oxygen is one
spectrum analys
The shifts of C-
spectively, are i
equatorial and
corresponding
C-1″ are slight
respectively, co
gravin **3***b*, consi
shift of the meth
weaker steric
probably owing
all-*trans* isomer
tivity of carbon
^1H nmr spectru
hydrogens show
to C-3 and C-4

[2]In the series of
tropic shielding o
comparison with 1
reflected on the sh
are diagnostic of th

TABLE 1. ^{13}C nuclear magnetic resonance chemical shifts of naturally occurring tetrahydrofuran lignans

	Chemical shift (ppm)				
Position	**2***b*	**3***b*	**4**	**5***b*	**9**
1′	136.1	134.6	132.8	133.6	124.7
2′	106.4	109.6	109.5	110.5	108.7
3′	147.5	148.7	148.2	148.7	148.4
4′	146.7	148.2	147.4	148.3	147.5
5′	107.7	110.8	110.6	110.8	110.9
6′	119.5	118.4	118.2	119.1	117.9
2	88.1	87.1	82.4	87.1	146.4
3	50.9	44.3	41.2	45.9	117.4
4	50.9	44.3	41.2	47.8	117.4
5	88.1	87.1	82.4	82.8	146.4
1″	136.1	134.6	132.8	133.2	124.7
2″	106.4	109.6	109.5	109.7	108.7
3″	147.5	148.7	148.2	148.3	148.4
4″	146.7	148.2	147.4	147.8	147.5
5″	107.7	110.8	110.6	110.5	110.9
6″	119.5	118.4	118.2	118.4	117.9
CMe	13.7	12.9	11.6	14.9	9.6
OMe		55.8	55.6	55.7	55.5
OCH_2O	100.7				

discarded owing to steric interactions between both aryl groups. It is interesting to consider, however, that the latter conformations, together with the form $^4T_3$, in spite of having the aryl group on C-5 pseudoaxially oriented, minimize the eclipsing strain of the *cis* substituents carried by C-4 and C-5, while the oxygen is one of the in-plane atoms. The ^{13}C nmr spectrum analysis of **5***b* confirms these observations. The shifts of C-2 and C-5 at 87.1 and 82.8 ppm, respectively, are in good agreement with the pseudoequatorial and pseudoaxial orientations of their corresponding veratryl groups; further C-1′ and C-1″ are slightly shielded, 133.6 and 133.2 ppm, respectively, compared with related carbons of galgravin **3***b*, considered free of steric interactions. The shift of the methyl groups of **5***b* at 14.9 ppm suggests weaker steric interactions between both groups, probably owing to a larger torsion angle, than in the all-*trans* isomer **2***b* and further shows lower sensitivity of carbon shifts to anisotropic effects.[2] In the ^1H nmr spectrum of veraguensin (**5***b*) the methyl hydrogens show signals at δ 1.07 and 0.66, assigned to C-3 and C-4 methyl groups, respectively (2, 3).

[2]In the series of α-acylindole alkaloids however, the anisotropic shielding of the methoxy hydrogens of vobasine in comparison with 16-epivobasine, induced by the indole ring is reflected on the shifts of the CO and OMe carbons and they are diagnostic of the stereochemistry of C-16 (9).

Considering the δ value of C-3 (or C-4) of the all-*trans* isomer galbacin (**2***b*) at 50.9 ppm as standard for a pseudoequatorial orientation of its Me group, it can be concluded that the shift of C-4 of **5***b* at 47.8 ppm indicates that its Me group approximates this orientation, confirming the puckering on C-4 and C-5, while C-3 shows a shift similar to the one observed for related carbons of **3***b*.

The shifts of the fully aromatic di-*O*-methylfuroguaiacin (**9**), assigned by standard chemical shift theory and by analysis of its SFORD spectrum, together with the shifts of compounds **2***b*, **3***b*, **4**, and **5***b* are listed in Table 1.

Experimental

The ^{13}C nmr spectra were obtained in a 10-mm spinning tube from solutions of approximately 0.3 mmol in 1 mL of $CDCl_3$ at ambient temperature. The ^{13}C resonance of $CDCl_3$ was used as internal reference and converted to Me_4Si scale by the following correction: δ (Me_4Si) = δ ($CDCl_3$) + 76.9. The instrument employed was a Varian XL-100 nmr spectrometer operating at 25.2 MHz, interfaced with a Varian 620/L Fourier transform computer with 16K memory. The chemical shifts (±0.05 ppm) were measured at 5-kHz spectral width, with an acquisition time of 0.8 s, and a 15-μs pulse width, using an internal deuterium lock.

Acknowledgments

We thank FINEP (Financiadora de Estudos e Projetos) and FAPESP (Fundação de Amparo à Pesquisa do Estado de São Paulo) for financial support, and Professors F. de A.M. Reis and A. J. Marsaioli for helpful discussions.

1. O. R. GOTTLIEB. Fortschr. Chem. Org. Naturstoffe. In press.
2. K. V. SARKANEN and A. F. A. WALLIS. J. Heterocycl. Chem. **10**, 1025 (1973).
3. L. E. S. BARATA, P. M. BAKER, O. R. GOTTLIEB, and E. A. RÚVEDA. Phytochemistry, **17**, 783 (1978).
4. C. W. PERRY, M. V. KALNINS, and K. H. DEITCHER. J. Org. Chem. **37**, 4371 (1972).
5. J. G. BLEARS and R. D. HAWORTH. J. Chem. Soc. 1985 (1958).
6. S. F. FONSECA, J. P. CAMPELLO, L. E. S. BARATA, and E. A. RÚVEDA. Phytochemistry, **17**, 499 (1978).
7. E. WENKERT, H. E. GOTTLIEB, O. R. GOTTLIEB, M. O. DA S. PEREIRA, and M. D. FORMIGA. Phytochemistry, **15**, 1547 (1976).
8. A. PELTER, R. S. WARD, and C. NISHINO. Tetrahedron Lett. 4137 (1977).
9. A. AHOND, A. M. BUI, P. POTIER, E. W. HAGAMAN, and E. WENKERT. J. Org. Chem. **41**, 1878 (1976).

Reactions of phenyl(trichloromethyl)carbinol with substituted thioureas, thiobenzhydrazide, and amino thiols to form heterocyclic compounds[1]

WILKINS REEVE AND W. ROBERT COLEY III

Chemistry Department, University of Maryland, College Park, MD 20742, U.S.A.

Received March 10, 1978[2]

WILKINS REEVE and W. ROBERT COLEY III. Can. J. Chem. 57, 444 (1979).

Phenyl(trichloromethyl)carbinol reacts with bifunctional reagents containing nucleophilic sulfur such as thioureas, thiobenzhydrazide, *o*-aminothiophenol, etc., in a series of steps involving an initial attack of the sulfur anion on the intermediate epoxide **2** followed by ring closure to a heterocyclic compound. Thiazolidinones, thiadiazinones, benzothiazinones, and thiomorpholinones are easily obtained in yields ranging from 57–20%. Monosubstituted ureas react to give exclusively the 2-substituted iminothiazolidinones. Evidence is presented that these are actually in the aminothiazolone form with considerable zwitterionic character. 1,3-Disubstituted ureas do not give heterocyclic products. The reaction works particularly well with those nucleophiles which are stable to base, contain a sulfur nucleophilic center for the initial step of the reaction (**2** to **3**) and an amino or imino group properly positioned for the final ring closure to the heterocyclic compound.

Hydroxylamine forms α-oximinophenylacetohydroxamic acid, an oxidation–reduction reaction having occurred. Thiophenol forms phenyl(phenylthio)acetic acid in nearly quantitative yield.

WILKINS REEVE et W. ROBERT COLEY III. Can. J. Chem. 57, 444 (1979).

Le phényl (trichlorométhyl) carbinol réagit avec des réactifs bifonctionnels incorporant un soufre nucléophile, tels les thiourées, thiobenzhydrazide, *o*-aminothiophénol, etc. par une série d'étapes impliquant une attaque initiale de l'anion sulfuré sur l'époxyde intermédiaire **2** suivie d'une cyclisation en un composé hétérocyclique. On obtient facilement, avec des rendements de 57–20%, des thiazolidinones, des thiadiazinones, des benzothiazinones et des thiomorpholinones. Les urées monosubstituées réagissent pour fournir exclusivement des iminothiazolidinones substituées en position 2. On présente des données à l'effet que ces composés existent de fait sous la forme d'aminothiazolones avec un fort caractère zwitterionique. Les urées disubstituées en 1,3 ne fournissent pas de produits hétérocycliques. La réaction fonctionne particulièrement bien avec les nucléophiles stables en milieu basique qui contiennent un centre sulfuré nucléophile pour l'étape initiale de la réaction (**2** à **3**) et un groupe amino ou imino dans une position appropriée pour la cyclisation finale en composé hétérocyclique.

L'hydroxylamine forme un acide α-oximinophénylacétohydroxamique; il s'est produit une autre réaction d'oxydo–réduction. Le thiophénol forme de l'acide phényl(phénylthio) acétique avec un rendement pratiquement quantitatif.

[Traduit par le journal]

Introduction

It has previously been shown that nucleophiles with a thioamide function react readily with phenyl(trichloromethyl)carbinol to form heterocyclic compounds (1, 2; for a general review, see ref. 3). This new reaction sequence has provided a useful and novel synthesis of substituted thiazolidinones, thiadiazinones, and 4-hydroxythiazoles. The purpose of this research was to study the reaction of phenyl(trichloromethyl)carbinol with other bifunctional nucleophiles including mono- and disubstituted thioureas. Fifteen nucleophiles have been studied.

Substituted Thioureas

Methylthiourea was allowed to react with phenyl(trichloromethyl)carbinol under the same conditions as used before with thiourea (1), namely in a methanolic potassium hydroxide solution at 50°C for a few hours. The epoxide, **2**, forms *in situ* and reacts with the thioenolate anion of methylthiourea to form successively, **3** and **4**. Compound **4** (R = Me) was isolated in 20% yield. None of the isomeric 2-imino-3-methyl-5-phenyl-4-thiazolidinone could be isolated. Both isomers have been previously synthesized by other routes. The chemistry of **4** (R = Me) has been studied by Najer *et al.* (4–6) who assigned structure **4***c* to the material on the basis of its uv spectra and pK_a value. Proof of any of these structures by chemical means is difficult because of the

[1]Taken, in part, from the doctoral thesis of W. R. Coley, University of Maryland, 1972.

[2]Revision received September 28, 1978.

0008-4042/79/040444-06$01.00/0

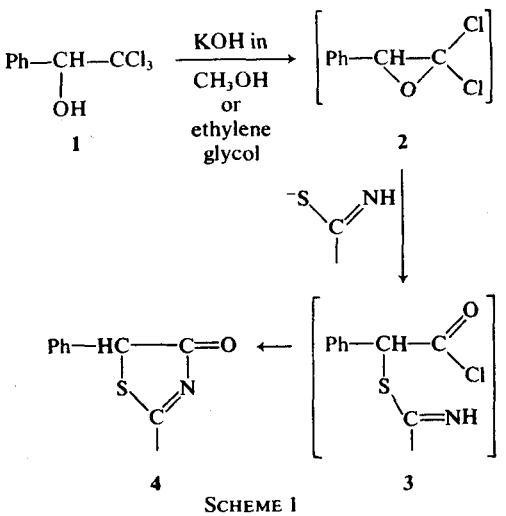

SCHEME 1

tendency of the heterocyclic ring to open at the amide linkage on treatment with acid or base. Thus, we found that refluxing **4** (R = Me) with 10% aqueous sulfuric acid gave a 20:1 mixture of 3-methyl-5-phenyl-2,4-thiazolidinedione and **5**, respectively. On refluxing with 3 *N* hydrochloric acid in ethanol, only the former is obtained (4). That **4** (R = Me), rather than 2-imino-3-methyl-5-phenyl-4-thiazolidinone, is the correct structure follows from the solubility of the material in 1 *N* sodium hydroxide and from its

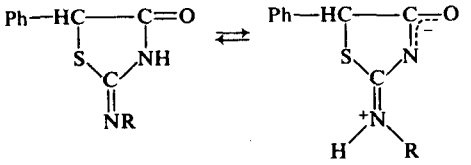

4*a* R = Me
4*d* R = Ph

4*b* R = Me
4*e* R = Ph
4*g* R = H

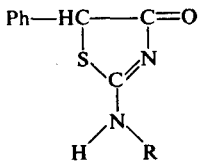

4*c* R = Me
4*f* R = Ph

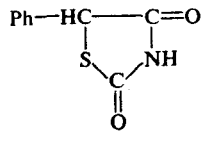

5

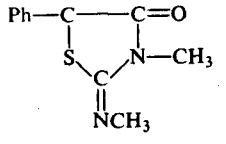

6

^{1}H nmr spectrum. This spectrum provided evidence that **4** (R = Me) is a mixture of **4***a* and the resonance hybrid **4***b* ↔ **4***c*. Compound **4***a* theoretically can exhibit *E* and *Z* isomerism but we have no evidence for the existence of such isomers. At δ 5.47, the customary benzylic proton signal showed a small shoulder on the upfield side which was reproducible in every spectrum. The methyl signal, instead of being a sharp singlet, consisted of a doublet at δ 3.07 with J = 4.6 Hz (due to **4***b* ↔ **4***c*) and a singlet with δ 2.95 (due to **4***a*). The N—H proton gave two signals, one a broad singlet at δ 9.75 (due to **4***a*) and the other a broad quartet at δ 9.32 (due to the resonance hybrid **4***b* ↔ **4***c*) with J = 4.6 Hz. The combined N—H signals integrated for one proton, the phenyl signal for five, the benzyl signal for one, and the combined methyl signals for three. The integration data suggest the ratio of **4***a* to the resonance hybrid **4***b* ↔ **4***c* to be 25:75. Decoupling experiments establish that the methyl group and the proton are both on the same nitrogen. Saturation of the N—H quartet at δ 9.32 caused the doublet at δ 3.07 to collapse to a singlet.

A high temperature nmr study established that **4** (R = Me) was composed only of **4***a* in equilibrium with the resonance hybrid **4***b* ↔ **4***c* and that the observed spectra could not be explained by the unsuspected presence of 2-imino-3-methyl-5-phenyl-4-thiazolidinone. Raising the temperature to 98°C caused the doublet and singlet of the methyl region to coalesce to a broad based singlet. Further heating to 138°C gave a sharp methyl singlet. Upon cooling to 35°C the spectrum was identical to the one obtained before heating, indicating no thermal isomerization had occurred. These changes in the observed spectra on heating would not have been observed if the 3-methyl isomer were one of the major components of the mixture.

Structures **4***b* and **4***c* are contributing forms to a resonance hybrid. The argument for the zwitterionic structure as the major contributing form to this resonance hybrid rests upon the high value of the chemical shift of the N—H resonance, by analogy to the unalkylated compound **4***g* for which nmr and crystal structure data support the zwitterionic structure in both solution (1) and the crystalline state (7), and the solubility behavior of compounds **4***b* and **4***g*, both of which have the same solubility characteristics as amino acids. The N—H resonance of the neutral structure **4***c* should be approximately the same as in methylaniline (δ in DMSO-d_6 = 5.4) whereas the resonance for the zwitterionic form should be more like that of the —NH_2— in methylaniline hydrochloride (δ in DMSO-d_6 = 10.5). The observed

chemical shift of δ = 9.32 for **4** (R = Me), and 8.85 and 9.18 (due to *cis–trans* isomerism of the iminonium ion) for **4***g* (1) argues strongly for the zwitterionic forms. Compound **4** (R = Me) is insoluble in water, easily soluble in 1 *M* sodium hydroxide (1 mequiv. in 50 mL), 1 *N* hydrochloric acid (1 mequiv. in 16 mL), insoluble in ether (1 part in 600), and of limited solubility in acetone (1 part in 160). In contrast, **5** is quite soluble in acetone and ether as is also 2-(methylimino)-3-methyl-5-phenyl-4(5*H*)-thiazolidinone (**6**). The latter cannot exist as a zwitterion like structure **4***b* and this accounts for the 60-fold increase in solubility in ether (1 part in 10) and acetone (1 part in 2). All of the above evidence suggest a structure consisting of around 25% **4***a* and 75% of the resonance hybrid **4***b* ↔ **4***c*, with the neutral structure **4***c* making less of a contribution to the resonance hybrid than the zwitterionic form **4***b*. Accordingly, 2-(methylamino)-5-phenyl-4(5*H*)-thiazolone is a better name for the product than 2-methylimino-5-phenyl-4-thiazolidinone.

Phenylthiourea was allowed to react with phenyl(trichloromethyl)carbinol under the same conditions as with methylthiourea and the known compound **4** (R = Ph) (4, 8–11) was isolated in 49% yield. It is soluble in 1 *N* sodium hydroxide and hydrolysis with 40% sulfuric acid gives mostly the dione **5** with only traces of the 3-phenyl-2,4-thiazolidinone being formed by rearrangement (8). There has been considerable discussion among previous investigators over the merits of **4***d* vs. **4***f* as possible structures for the product with **4***d* being favored by Najer *et al.* (5) and Ramsh *et al.* (12). Mornon *et al.* (13) carried out an X-ray crystallographic study which established the presence of a hydrogen on the exocyclic nitrogen but he did not consider the possible existence of the zwitterionic structure **4***e*. The zwitterionic form should be less likely in the case of **4***e* (vs. **4***b*) because the anilino function of **4** (R = Ph) would be expected to be 10^6 times less basic than the methylamino function of **4** (R = Me); on the other hand the zwitterionic form would be favored by delocalization of the positive charge by the adjacent phenyl ring. Our evidence strongly suggests that the zwitterionic structure (**4***e*) does make a contribution to the **4***e* ↔ **4***f* resonance hybrid; exactly how much is difficult to determine. In the ^{1}H nmr spectra, the sharp singlet for the CH resonance at δ 5.55 suggests that only one tautomeric form is present and Mornon's X-ray crystallographic data eliminate structure **4***d*. The NH resonance at δ 7.77 corresponds to the iminonium NH of **4***e* (vs. δ 9.32 for **4***b*). The NH signal for the neutral form **4***f* should occur near δ 5.4 (diphenylamine has δ ($CDCl_3$) of 5.4). Like diphenylamine the compound is insoluble in dilute hydrochloric acid. It is also insoluble in ether (approximately 1 part in 500) and this suggests some contribution by the zwitterionic form. Mornon's X-ray crystallographic data fit structure **4***e* as well as **4***f*. The bond distances between C-2 and N-3, and between C-2 and the exocyclic nitrogen were 1.32 and 1.34 Å, respectively, suggesting that the bond orders are more nearly alike than would be expected for either structure **4***d* or **4***f*. In summary, we believe **4***e* as well as **4***f* contributes to the structure of **4** (R = Ph).

The reaction of three disubstituted thioureas (1,3-dimethylthiourea, 1,3-diethylthiourea, and 1,3-diphenylthiourea) with phenyl(trichloromethyl)carbinol under the same conditions as before was studied but no heterocyclic compounds could be obtained. α-Mercaptophenylacetic acid (isolated as dithiobis-(phenylacetic acid)) appeared to be a major constituent of the complex mixture of acids formed. The expected heterocyclic compounds can be prepared by the sodium acetate catalyzed reaction of α-halo esters with 1,3-disubstituted ureas (5). Accordingly, 2-(methylimino)-3-methyl-5-phenyl-4(5*H*)-thiazolidinone (**6**) was prepared and treated with methanolic potassium hydroxide to see if the 3-substituted thiazolidinone was decomposed by potassium hydroxide under the conditions used in the reaction of the carbinol with the thioureas at 50°C. An immediate nitroprusside test for the thiol function was obtained. Titration of aliquots showed that no base was consumed; the thiobenzyloxy–carbon bond was cleaved. None of the thiazolidinone could be recovered after a reaction time of 1 h. It should be noted that **4***b* ↔ **4***c* is an imino thioester with resonance stabilization whereas **6** has no resonance stabilization.

Thiobenzhydrazide

This nucleophile reacted with phenyl(trichloromethyl)carbinol in an ethanolic potassium hydroxide solution at 55°C to form 2,6-diphenyl-4*H*-1,3,4-thiadiazin-5(6*H*)-one (**7**) in 57% yield (Scheme 2). Proof of the assigned structure follows from elemental analyses, the insolubility of **7** in dilute 6 *N* hydrochloric acid and its ir and nmr spectra. Absence of isomeric enolic forms is demonstrated by the presence of the carbon six proton signal at δ 5.2 as expected, a strong amide carbonyl band at 1660 cm^{-1} and a secondary amide NH stretching bond at 3220

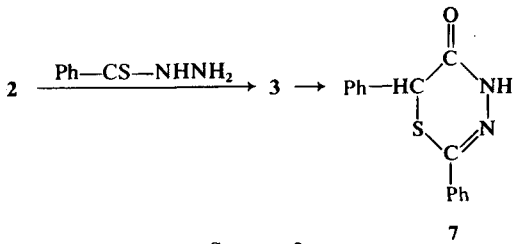

7

SCHEME 2

TABLE 1. Reaction of other nucleophiles with phenyl(trichloromethyl)carbinol

Nucleophile	Product*	Yield (%)
o-Aminothiophenol	2-Phenyl-2*H*-1,4-benzothiazin-3(4*H*)-one	50
2-Aminoethanethiol	2-Phenyl-3-thiomorpholinone	21
Ethylenediamine	3-Phenyl-2-piperazinone	2
Ammonium dithiocarbamate	5-Phenylrhodanine	6
Thiophenol	Phenyl(phenylthio)acetic acid	86

*All are known compounds.

cm^{-1}. The material is insoluble in 3 *N* sodium hydroxide solution. Methylation of **7** with dimethyl sulfate gave the 4-methyl derivative. Compound **7** was also prepared from methyl α-bromophenylacetate and thiobenzhydrazide and the two products found to be identical.

Hydroxylamine

Three moles of this nucleophile reacted with phenyl(trichloromethyl)carbinol in an oxidation–reduction sequence reminiscent of osazone formation with sugars. The known *Z* form of α-oximinophenylacetohydroxamic acid was formed in 23% yield. The other products of the reaction were a mixture of eight carboxylic acids; the methyl esters were prepared using diazomethane and the two major components shown by glpc and nmr to be methyl benzoate and methyl α-ethoxyphenylacetate.

Other Nucleophiles

Two nucleophiles, sulfamide and acetamidine, failed to give any heterocyclic products. Both hydrolyze easily in potassium hydroxide solution, and they may have been largely destroyed before they could react with the phenyl(trichloromethyl)carbinol. Ammonium dithiocarbamate (Table 1) also hydrolyzes easily.

General Conclusions

The condensation of phenyl(trichloromethyl)carbinol with bifunctional nucleophiles provides an excellent method for the formation of heterocyclic compounds provided that two conditions are met: first, the nucleophile, besides being a good nucleophile, must be stable in strongly alkaline solution. Nucleophiles which decompose before they can react with the phenyl(trichloromethyl)carbinol are obviously of little use. Second, the heterocyclics to be prepared should be at least somewhat stable to base. For these reasons the best bifunctional reagents for reaction with phenyl(trichloromethyl)carbinol are those with sulfur and nitrogen nucleophilic centers. The sulfur will attack the epoxide intermediate (**2**) to form an acid chloride intermediate (**3**) which then reacts with the nucleophilic nitrogen to close the heterocyclic ring. The heterocycle formed in this case is an amide which is relatively stable to base.

Experimental

Melting points and boiling points are corrected. The infrared spectra were determined with a Perkin-Elmer Model 337; the nmr spectra were obtained with a Varian A-60-A instrument. Chemical shift values are expressed as δ values (ppm) downfield from tetramethylsilane internal standard. ^{1}Hmr spectra obtained using hexadeuteriodimethyl sulfoxide as the solvent had as an internal standard the pentadeuteriodimethyl sulfoxide peak at δ 2.53. The mass spectrum was recorded on a Du Pont 492 double focusing, magnetic scanning mass spectrometer run at 70 eV. Elemental microanalyses were performed by Dr. Franz J. Kasler. The 100 MHz ^{1}Hmr spectrum of **4** (R = Me) was run by Mr. Mark Mattingly.

2-(Phenylamino)-5-phenyl-4(5H)-thiazolone (4, R = Ph)

The general procedure for the reaction for phenyl(trichloromethyl)carbinol with the substituted thioureas follows. To a solution of 11.2 g (0.05 mol) of phenyl(trichloromethyl)carbinol and 12.2 g (0.08 mol) of phenylthiourea in 75 mL of methanol at 50°C was added with stirring 19.8 g (0.3 mol) of 85% potassium hydroxide pellets in 50 mL of methanol over a 30 min period. The reaction mixture was heated to 50–60°C with an oil bath for 1 h, after which time it was allowed to cool to room temperature and was stirred for 24 h. The precipitated potassium chloride was filtered off, the filtrate diluted with an equal volume of water, and the alkaline solution extracted with three 75-mL portions of ether to remove neutral material. Acidification to pH 5 yielded 6.5 g of **4** (R = Ph) (49%), mp 180–185°C. The material was washed with water to remove inorganic impurities and recrystallized from absolute ethanol to give pure 2-(phenylamino)-5-phenyl-4(5*H*)-thiazolone: mp 188–189°C (lit. (4) mp 188–189°C, (10, 11) mp 191–191.5°C); ir (KBr): 3255, 3195, 3130, 3010, 1675, 1625, 1560, 1480, 1445, 1315, 1265, 1235, 1225, 1175, 740, 725, 680, and 645 cm^{-1}; ^{1}Hmr (DMSO-d_6) δ: 7.77 (broad s, 1, N*H*), 7.50–7.12, (m, 10, aromatic *H*), 5.55 (s, 1, Ph—C*H*<).

2-(Methylamino)-5-phenyl-4(5H)-thiazolone (4, R = Me)

This was prepared by the same procedure as above starting with a solution of 11.2 g (0.05 mol) of phenyl(trichloromethyl)-carbinol and 6.3 g (0.07 mol) of methylthiourea in 50 mL of methanol, and 19.8 g (0.3 mol) of potassium hydroxide pellets in 50 mL of methanol. After filtering off the potassium chloride the reaction mixture, acidified successively to pH values of 9, 7, and 1.2, was extracted with ether and the final aqueous layer was then adjusted to pH 7. From the second ether extract and from the final aqueous solution there was obtained on evaporation a total of 2.1 g of **4** (R = Me), mp 178–181°C. One recrystallization from acetone and five recrystallizations from absolute ethanol gave pure 2-(methylamino)-5-phenyl-4(5*H*)-

thiazolone (**4**, R = Me); mp 185–185.5°C (lit. (4) mp 181–182°C); ir (KBr): 3220–2950, 1680, 1605, 1395, 1280, 1250, 1150, 735, 690, 645, 625, and 520 cm^{-1}; ^{1}Hmr (DMSO-d_6 at 35°) δ: 9.75 (broad s, >N*H* of **4***a*) and 9.32 (broad q, J = 4.6 Hz, —N*H*CH_3 of **4***b*) with combined area 1, 7.35 (s, 5, Ph), 5.47 (s, 1, PhC*H*<), 3.07 (d, J = 4.6 Hz, CH_3NH— of **4***b*) and 2.95 (s, CH_3N= of **4***a*) with combined area 3. At 138°C the δ 0 to 8 spectrum was δ: 7.35 (s, 5, Ph), 5.37 (s, 1 Ph—C*H*<), 3.07 (s, 3, NC*H*$_3$). The ^{1}Hmr spectrum at 100 MHz was unchanged.

Refluxing 1 g (0.005 mol) of **4** (R = Me) with 10 mL of 10% sulfuric acid for 3 h gave a semisolid mass which crystallized to a white solid (0.8 g) after being leached with cyclohexane. After two recrystallizations from ethanol the mixture of 5-phenyl-2,4-thiazolidinedione and 3-methyl-5-phenyl-2,4-thiazolidinedione melted at 81–85°C. These were separated by stirring with 6 mL of ice-cold 1 *N* sodium hydroxide for 10 s and then filtering. The filtrate was acidified to give 0.03 g of 5-phenyl-2,4-thiazolidinedione, mp 124–126°C; a mixture mp with an authentic sample was 125–129°C (1). The solid which did not dissolve in the alkaline solution was 3-methyl-5-phenyl-2,4-thiazolidinedione, mp 92–94°C (lit. (4) mp 96°C).

Nuclear Magnetic Resonance Spectra of Methylaniline and its Hydrochloride

Methylaniline ^{1}Hmr (DMSO-d_6) δ: 7.4–6.5 (m, 5, Ph), 5.4 (broad s, 1, NH), and 2.65 (s, 3, CH_3).

The methylaniline hydrochloride was recrystallized twice from acetonitrile (14), mp 123.5–125°C (lit. (14) mp 124°C); ^{1}Hmr (DMSO-d_6) δ: 10.4 (s, 2, NH_2), 8.1–7.5 (m, 5, Ph), and 3.2 (s, 3, CH_3).

*2-(Methylimino)-3-methyl-5-phenyl-4-(5*H*)-thiazolidinone (6)*

This was prepared by Najer's method (5), mp 94–96°C (lit. (5) mp 93–94°C); ir (KBr): 2925, 1715, 1640, 1420, 1365, 1305, 1200, 1105, 1042, 1020, 898, 855, 767, 732, 695, and 640 cm^{-1}; ^{1}Hmr (DMSO-d_6) δ: 7.4 (s, 5, Ph), 5.74 (s, 1, CH), 3.1 (two singlets three cycles apart, 6, two N—CH_3).

*2,6-Diphenyl-4*H*-1,3,4-thiadiazin-5(6*H*)-one (7)*

Thiobenzhydrazide was prepared from thiobenzoylthioglycolic acid (from 50 g benzotrichloride, 126 g sodium sulfide nonahydrate, and 32 g chloroacetic acid) and excess hydrazine, all by the procedure of Holmberg (15) who gives no spectral data for the following compounds. The crude thiobenzoylthioglycolic acid (61% yield) was recrystallized twice from benzene and aqueous ethanol; mp 126°C (lit. (15) mp 127–128°C); ir (KBr): 3100–2500 (COOH), 1680 (CO), 1350, 1300, 1240, 1220, 1170, 1040, 885, 770, 680, and 670 cm^{-1}; ^{1}Hmr (DMSO-d_6) δ: 10.9–10.0 (broad s, 1, —COO*H*), 8.23–7.87 (m, 2, *o*-protons of Ph), 7.77–7.33 (m, 3, *m*- and *p*-protons of Ph), 4.37 (s, 2, —CH_2—). The thiobenzhydrazide (87% yield) was recrystallized twice from benzene; mp 70.5–71°C (lit. (15) mp 70–71°C); ir (KBr): 3250–3000, 1590, 1555, 1445, 1320, 1215, 1120, 960, 910, 765, and 690 cm^{-1}; ^{1}Hmr (DMSO-d_6) δ: 7.83–7.50 (m, 2, *o*-protons of Ph), 7.45–7.10 (m, 3, *m*- and *p*-protons of Ph), 6.65 (broad s, 3, —N*H*N*H*$_2$). A higher melting form, mp 81–82°C, is also sometimes obtained as noted by Holmberg (15); both work equally well in the following reaction.

2,6-Diphenyl-4*H*-1,3,4-thiadiazin-5(6*H*)-one (**7**) was prepared using the same procedure as in the preparation of **4**, starting with 11.2 g (0.05 mol) of phenyl(trichloromethyl)carbinol and 10.6 g (0.05 mol) of thiobenzhydrazide dissolved in 50 mL of absolute alcohol, and 19.8 g (0.3 mol) of potassium hydroxide pellets in 60 mL of absolute ethanol. The filtrate from the reaction mixture was acidified to pH 3 and 7.1 g of crude **7** precipitated. Another 0.5 g was obtained from an ether extraction of the initial alkaline, aqueous reaction mixture. Two recrystallizations from absolute ethanol gave white needles of **7**; mp 182–182.5°C; ir (KBr): 3220 (NH), 1670 (CO), 1320, 1235, 1145, 1070, 1030, 970, 860, 760, 740, 695, and 685 cm^{-1}; ^{1}Hmr (DMSO-d_6) δ: 11.7 (broad s, 1, NH), 8.0–7.7 (m, 2, *o*-protons of 2-Ph), 7.62–7.37 (m, 8, other Ph and *m*- and *p*-protons of 2-Ph), 5.20 (s, 1, Ph—CH<); ms (70 eV) *m/e* (relative intensity): 270(6.8), 269(18.2), 268(100), 122(19.7), 121(34.9), 119(16.5), 118(28.6). *Anal.* calcd. for $C_{15}H_{12}N_2OS$: C 67.14, H 4.51, N 10.44, S 11.95; found: C 66.95, H 4.63, N 10.48, S 11.74.

Compound **7** was also prepared in 90% yield by refluxing for 2 h a mixture of 1.5 g (0.0066 mol) of methyl α-bromophenylacetate, 1.0 g (0.0066 mol) of thiobenzhydrazide and 0.5 g of anhydrous sodium acetate. The material was identical with that prepared above.

*2,6-Diphenyl-4-methyl-4*H*-1,3,4-thiadiazin-5-(6*H*)-one*

This was prepared in 81% yield by heating at 62°C for 2 h, a mixture of 1.0 g (0.0037 mol) of **7**, 25 mL of 1.5 *N* sodium hydroxide solution, enough acetone to dissolve all of the solid, and 5 mL of freshly distilled dimethyl sulfate. Two recrystallizations from ethanol gave the pure material; mp 135–135.5°C (lit. (16) mp 137–138°C); ir (KBr): 1655 (CO), 1360, 1325, 1270, 1220, 1090, 1075, 1010, 840, 765, 740, 720, 710, and 690 cm^{-1}; ^{1}Hmr ($CDCl_3$) δ: 8.00–7.73 (m, 2, *o*-protons of 2-Ph), 7.57–7.17 (m, 8, 6-Ph and *m*- and *p*-protons of 2-Ph), 4.77 (s, 1, Ph—C*H*<), 3.63 (s, 3, N—CH_3). *Anal.* calcd. for $C_{16}H_{14}N_2OS$: C 68.06, H 5.00, N 9.92, S 11.36; found: C 67.94, H 5.07, N 10.20, S 11.40.

*2-Phenyl-2*H*-1,4-benzothiazin-3(4*H*)-one*

This was prepared, using the same procedure as in the preparation of **4** except the reaction mixture was not heated, starting with 11.2 g (0.05 mol) of phenyl(trichloromethyl)carbinol and 6.9 g (0.05 mol) of *o*-aminothiophenol dissolved in 50 mL of absolute methanol, and 19.8 g (0.3 mol) of potassium hydroxide pellets in 75 mL of absolute methanol. After filtering off the precipitated potassium chloride and diluting the reaction mixture with an equal volume of water, a light brown solid precipitated and was recrystallized from absolute ethanol to yield 3.8 g of **7**. Additional material was obtained on acidifying the reaction mixture to pH 2. The combined material (6 g after recrystallization (50% yield)) melted at 205–206°C (lit. (17) mp 205–206°C); ir (KBr): 3180, 3100, 3040, 2960, 2890, 1680 (C=O), 1480, 1370, 1235, 1160, 1075, 1025, 940, 820, 760, 740, and 695 cm^{-1}; ^{1}Hmr (DMSO-d_6) δ: 10.95 (broad s, 1, N*H*), 7.5–6.8 (m, 9, aromatic protons), 5.0 (s, 1, Ph—C*H*<).

2-Phenyl-3-thiomorpholinone

This was prepared by the general procedure, except the reaction mixture was not heated and the reaction period was reduced to 12 h, from 11.2 g (0.05 mol) of phenyl(trichloromethyl)carbinol and 6.7 g (0.06 mol) of 2-aminoethanethiol hydrochloride in 75 mL of absolute ethanol, and 23 g (0.35 mol) of potassium hydroxide pellets in 100 mL of absolute ethanol. The shorter reaction time was used because the amide linkage undergoes hydrolysis in the strongly alkaline reaction mixture. This has been previously observed with other thiomorpholinones (18). The hydrolysis product was also synthesized independently as described below. An ether extract of the alkaline mixture gave 3.5 g of gummy material. One recrystallization from 30 mL of benzene gave 2 g (21% yield)

of 2-phenyl-3-thion
recrystallization fror
to 159°C (lit. (19) m
2930, 1650 (C=O),
875, 830, 745, and 7(
s, 1, N*H*), 7.38 (s,
(m, 2, —NH—C*H*$_2$-

α-(2-Aminoethylthio

This was prepare
(0.01 mol) of α-bro
2-aminoethanethiol
anhydrous sodium
allowing the reactic
which formed was
dried. It weighed (
dissolved in an exce
evaporate to dryne
with a little 6 *N* hy
raised the melting
acetic acid hydroch
1715 (C=O), 1480
^{1}Hmr (DMSO-d_6)
7.70–7.27 (m, 5, Ph
—C*H*$_2$C*H*$_2$—). *An*
5.70, N 5.66, S 12.9

Z-α-Oximinophenyl

This was prepar
reaction mixture w
of phenyl(trichloro
hydroxylamine hyc
and a solution of
pellets in 100 mL
potassium chlorid
volume of water,
acid, and allowed t
of the residue was
tained a small am
stand for 18 h. T
leaving behind 2.2
One recrystallizati
yield) of *Z*-α-oxim
176.5°C dec. (lit. (
3400–2600, 1680–1
1095, 1020–1000, 8
that of ref. 21); ^{1}H
Anal. calcd. for C_8
C 53.40, H 4.17, N

Phenyl(phenylthio)

This was prepa
reaction mixture
mol) of phenyl(tric
thiophenol in 50 n
of potassium hydr

of 2-phenyl-3-thiomorpholinone, mp 155–156°C. Further recrystallization from benzene and acetonitrile raised the mp to 159°C (lit. (19) mp 160–162°C); ir (KBr): 3280, 3185, 3060, 2930, 1650 (C=O), 1490, 1415, 1335, 1205, 1150, 1115, 1070, 875, 830, 745, and 700 cm^{-1}; ^{1}Hmr (DMSO-d_6) δ: 8.03 (broad s, 1, N*H*), 7.38 (s, 5, Ph), 4.80 (s, 1, Ph—C*H*<), 3.73–3.30 (m, 2, —NH—C*H*$_2$—), 3.05–2.73 (m, 2, —S—C*H*$_2$—).

α-(2-Aminoethylthio)phenylacetic Acid Hydrochloride

This was prepared by refluxing for 1 h a solution of 2.1 g (0.01 mol) of α-bromophenylacetic acid, 1.1 g (0.01 mol) of 2-aminoethanethiol hydrochloride, and 1.6 g (0.02 mol) of anhydrous sodium acetate in 50 mL of absolute ethanol, and allowing the reaction mixture to stand for 2 days. The solid which formed was washed with 10 mL of water, filtered, and dried. It weighed 0.3 g, mp 207–208°C dec. The solid was dissolved in an excess of 6 *N* hydrochloric acid and allowed to evaporate to dryness. It then melted at 171–173°C. Washing with a little 6 *N* hydrochloric acid, in which it was insoluble, raised the melting point of the α-(2-aminoethylthio)phenylacetic acid hydrochloride to 175–177°C; ir (KBr): 3200–2500, 1715 (C=O), 1480, 1245, 1210, 1160, 720, and 635 cm^{-1}; ^{1}Hmr (DMSO-d_6) δ: 8.86 (broad s, 4, —N*H*$_3$ + COO*H*), 7.70–7.27 (m, 5, Ph), 4.95 (s, 1, Ph—C*H*<), 3.22–2.70 (m, 4, —C*H*$_2$C*H*$_2$—). *Anal.* calcd. for $C_{10}H_{14}NO_2SCl$: C 48.48, H 5.70, N 5.66, S 12.94; found: C 48.11, H 5.49, N 5.82, S 12.76.

Z-α-Oximinophenylacetohydroxamic Acid

This was prepared by the general procedure, except the reaction mixture was not heated, starting with 11.2 g (0.05 mol) of phenyl(trichloromethyl)carbinol and 10.4 g (0.15 mol) of hydroxylamine hydrochloride in 50 mL of absolute ethanol, and a solution of 26.4 g (0.4 mol) of potassium hydroxide pellets in 100 mL of absolute ethanol. After filtering off the potassium chloride, the filtrate was diluted with an equal volume of water, acidified to pH 4.5 with 6 *N* hydrochloric acid, and allowed to evaporate to dryness. An acetone extract of the residue was concentrated to an orange oil which contained a small amount of solid; the mixture was allowed to stand for 18 h. The oil was taken up in cold chloroform, leaving behind 2.2 g of cream-colored crystals, mp 164–166°C. One recrystallization from 30 ml of water gave 2.1 g (23% yield) of *Z*-α-oximinophenylacetohydroxamic acid; mp 176–176.5°C dec. (lit. (20, 21) mp 177°C, 173.5–175.5°C); ir (KBr): 3400–2600, 1680–1650 (C=O), 1610, 1500, 1430, 1300, 1230, 1095, 1020–1000, 850, 840, 760, 725, and 690 cm^{-1} (similar to that of ref. 21); ^{1}Hmr (DMSO-d_6) identical with that of ref. 21. *Anal.* calcd. for $C_8H_8N_2O_3$: C 53.33, H 4.48, N 15.55; found: C 53.40, H 4.17, N 15.75.

Phenyl(phenylthio)acetic Acid

This was prepared by the general procedure, except the reaction mixture was not heated, starting with 11.2 g (0.05 mol) of phenyl(trichloromethyl)carbinol and 5.5 g (0.05 mol) of thiophenol in 50 mL of absolute ethanol, and 19.8 g (0.3 mol) of potassium hydroxide pellets in 100 mL of absolute ethanol. After filtering off the potassium chloride, the neutral fraction was extracted with ether and 1.3 g of crude phenyl(trichloromethyl)carbinol was obtained. Acidification yielded 10.5 g (86% yield) of phenyl(phenylthio)acetic acid, mp 92–95°C. One recrystallization from a benzene–cyclohexane mixture gave crystals of pure phenyl(phenylthio)acetic acid; mp 101.5–102.5°C (lit. (22) mp 101–102°C, lit. (23) mp 102–103°C); ir (KBr): 3200–2400, 1690 (C=O), 1580, 1480, 1410, 1280, 950, 735, 725, 695, 690, and 675 cm^{-1}; ^{1}Hmr ($CDCl_3$) δ: 10.35 (broad s, 1, —COO*H*), 7.58–7.13 (m, 10, Ph), 4.90 (s, 1, Ph—C*H*<).

1. W. Reeve and M. Nees. J. Am. Chem. Soc. **89**, 647 (1967).
2. W. Reeve and E. Barron. J. Org. Chem. **34**, 1005 (1969); **40**, 1917 (1975).
3. W. Reeve. Synthesis, 131 (1971).
4. H. Najer, R. Giudicelli, C. Morel, and J. Menin. Bull. Soc. Chim. Fr. 1018 (1963).
5. H. Najer, R. Giudicelli, C. Morel, and J. Menin. Bull. Soc. Chim. Fr. 1022 (1963).
6. H. Najer, J. Armand, J. Menin, and N. Voronine. C. R. Acad. Sci. **260**, 4343 (1965).
7. L. A. Plastas and J. M. Stewart. Chem. Commun. 811 (1969).
8. F. A. Eberly and F. B. Dains. J. Am. Chem. Soc. **58**, 2544 (1936).
9. H. L. Wheeler. Am. Chem. J. **26**, 353 (1901).
10. E. C. Taylor, J. Wolinsky, and H. Lee. J. Am. Chem. Soc. **76**, 1866 (1954).
11. E. C. Taylor, J. Wolinsky, and H. Lee. J. Am. Chem. Soc. **76**, 1870 (1954).
12. S. M. Ramsh, K. A. V'yuonov, A. I. Ginak, and E. G. Sochiln. Zh. Org. Khim. **9**, 412 (1973); Chem. Abstr. **79**, 31323 (1973).
13. R. Bally and J.-P. Mornon. C. R. Acad. Sci. Ser. C, **274**, 609 (1972); Acta Crystallogr. Sect. B, **29**, 1157 (1973); G. Lepicard, J. Delettre, and J.-P. Mornon. C. R. Acad. Sci. Ser. C, **276**, 657 (1973).
14. W. H. Hunter and G. D. Byrkit. J. Am. Chem. Soc. **54**, 1948 (1932).
15. B. Holmberg. Ark. Kemi Mineral. Geol. A, **17**, No. 23 (1944); Chem. Abstr. **39**, 4065 (1945).
16. A. Takamizawa and H. Sato. Japanese Patent No. 27,896 (1969); Chem. Abstr. **72**, 55,523 (1970).
17. J. Krapcho, A. Szabo, and J. Williams. J. Med. Chem. **6**, 214 (1963).
18. K. Zahn. Chem. Ber. **56**, 578 (1923).
19. H. Lehr, S. Karlan, and M. W. Goldberg. J. Med. Chem. **6**, 136 (1963).
20. C. Gastaldi. Gazz. Chim. Ital. **54**, 220 (1924); Chem. Abstr. **18**, 3172 (1924).
21. J. V. Burakevich, R. S. Butler, and G. P. Volpp. J. Org. Chem. **37**, 593 (1972).
22. J. E. Banfield. J. Chem. Soc. 456 (1960).
23. E. A. Lehto and D. A. Shirley. J. Org. Chem. **22**, 989 (1957).

Comparison of the intramolecular hydrogen bonds and of the internal barrier to rotation of the hydroxyl and sulfhydryl groups in 2-methoxyphenol and 2-methoxythiophenol

TED SCHAEFER AND TIMOTHY A. WILDMAN

Department of Chemistry, University of Manitoba, Winnipeg, Man., Canada R3T 2N2

Received August 15, 1978

TED SCHAEFER and TIMOTHY A. WILDMAN. Can. J. Chem. **57**, 450 (1979).

The long-range spin–spin coupling constants involving the hydroxyl proton in 2-methoxyphenol are consistent with a potential function for rotation of the hydroxyl group derived from far infrared torsion data. The internally hydrogen bonded *cis* conformer is the only one detected by nmr. In contrast, the long-range couplings of the sulfhydryl group in 2-methoxythiophenol indicate that the *trans* conformer is favored over the *cis* conformer by a free energy difference of 0.2 ± 0.2 kcal/mol. Furthermore, the barrier to internal rotation of the sulfhydryl group is much smaller than that of the hydroxyl group in these two compounds. It is suggested that the barrier in the thiophenol derivative is 2.7 ± 0.6 kcal/mol, to be compared with a twofold component of 6 kcal/mol in the rotational potential function of the phenol analog.

TED SCHAEFER et TIMOTHY A. WILDMAN. Can. J. Chem. **57**, 450 (1979).

Les constantes de couplage spin–spin à longue distance impliquant le groupe hydroxyle du méthoxy-2 phénol sont en accord avec une fonction de potentiel établie, pour la rotation du groupe hydroxyle, à partir de données de torsion provenant de l'infrarouge lointoin. En rmn, on ne détecte que la présence du conformère *cis* impliqué dans une liaison hydrogène interne. Par ailleurs, les constantes de couplage à longue distance impliquant le groupe sulfhydryle de méthoxy-2 thiophénol indiquent que le conformère *trans* est plus favorisé que le conformère *cis*; la différence d'énergie libre est de 0.2 ± 2.0 kcal/mol. De plus, la barrière à la rotation interne du groupe sulfhydryle est beaucoup plus faible que celle du groupe hydroxyle dans ces deux composés. On suggère que la barrière dans le dérivé thiophénol est 2.7 ± 0.6 kcal/mol; on doit comparer cette valeur avec une composante binaire de 6 kcal/mol dans la fonction de potentiel de rotation de l'analogue oxygéné.

[Traduit par le journal]

Introduction

The intramolecular hydrogen bond in 2-methoxyphenol apparently is of intermediate strength. There occurs only one hydroxyl stretching band in the infrared. It is assigned to the intramolecularly hydrogen bonded *cis* conformer, **1** (1). In cyclo-

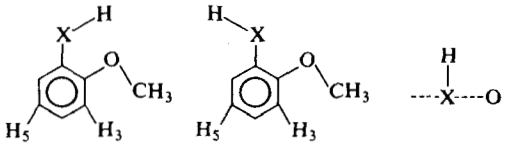

cis, θ = 0° (**1**) *trans*, θ = 180° (**2**) θ = 90° (**3**)

hexane solution, those far infrared bands assigned to the hydroxyl torsions are consistent with an equilibrium in which **1** is 2.00 kcal/mol more stable than **2** (1). Furthermore, conformation **3**, in which the OH bond is situated in a plane perpendicular to the benzene plane, lies 6.94 kcal/mol above **1**.

Carlson and Fateley (1) write:

$$[1] \quad V(\theta) = 2.00(1 - \cos\theta)/2 + 5.94(1 - \cos 2\theta)/2$$

in which $V_1 = 2.00$ kcal/mol is the onefold component (maximum at θ = 180°); whereas $V_2 = 5.94$ kcal/mol is the twofold component (maximum at θ = 90°) describing the torsional potential of the hydroxyl group about the C—O bond. In phenol, V_2 is 3.4 ± 0.2 kcal/mol (1–4).

If V_1 is identified as the enthalpy difference between **1** and **2** and if the entropy difference between **1** and **2** is small enough, then at 305 K the equilibrium constant is 0.036 (assuming equal activities for the isomers in a dilute solution). It follows that 3.5% exists as the *trans* conformer, **2**, at 305 K.

CNDO/2 MO calculations predict **1** as 1.32 kcal/mol more stable than **2** (5). Both conformers are reasonably assumed to have the CH_3 group staggered about the C—O bond. An empirical relationship (6) between hydroxyl torsional frequencies and the strength of the intramolecular hydrogen bond, suggests **1** as 1.7 ± 0.2 kcal/mol more stable than **2**. Apparently (5, 6) the intramolecular hydrogen bond is considerably weaker in 2-methoxyphenol than in 2-nitrophenol or in salicylaldehyde.

Infrared band intensities and dipole moment data were interpreted (7) as indicating preferred *cis* conformations, **1**, for 2-nitro- and 2-methoxythiophenol; although it was clear that intramolecular hydrogen bonding was less marked than in the corresponding

0008-4042/79/040450-04$01.00/0

phenol derivatives. A different set of dipole moment data (8) indicated roughly equal populations for **1** and **2** (X = S) for 2-methoxythiophenol in cyclohexane, benzene and dioxane solutions.

An extensive set of calculations, at the CNDO/2 and STO-3G levels of molecular orbital theory (5), on intramolecular hydrogen bonding in *ortho* substituted phenols and thiophenols successfully reproduces the stronger hydrogen bonds in the phenol derivatives. In particular, the *cis* form of 2-hydroxythiophenol, analogous to **1**, is calculated as more stable than the *trans* form, analogous to **2**. Furthermore, the lower values of V_2 in the thiophenol derivatives are also predicted (see below).

On the other hand, long-range spin–spin coupling constants over five bonds between the thiol proton and ring protons in 2-nitrothiophenol dissolved in chloroform or benzene imply that the conformer in which the SH bond lies *trans* to the nitro group is favoured over the *cis* conformer by a free energy difference of 0.5 ± 0.2 kcal/mol at 305 K (9). This implication depends on the stereospecificity of the five-bond coupling, $^5J_m^{H,XH}$ (X = O, S). References 9–14 give a discussion of this method of determining intramolecular equilibria in phenol and thiophenol derivatives.

In this paper, $^5J_m^{H,XH}$ measurements are used to compare strengths of the intramolecular hydrogen bonds in 2-methoxythiophenol and in 2-methoxyphenol. It turns out that a rough value for the barrier to rotation of the S—H group can also be deduced.

Experimental

2-Methoxyphenol, from Aldrich Chemical Co., was prepared as 5 mol% solutions in CCl_4 and in benzene-d_6. 2-Methoxythiophenol, from Tridom Chemical Inc., was made up as a 4.6 mol% solution in CCl_4. Degassed samples containing internal tetramethylsilane (TMS) as a reference material, were sealed under vacuum into 5-mm od nmr tubes. Intermolecular proton exchange was retarded as previously described (12).

The ^{1}H nmr spectra were recorded at a probe temperature of 305 K on an HA100 spectrometer. The spectra were repeatedly calibrated in the frequency sweep mode by placing markers at ca 5 Hz intervals. Interpolation between markers yielded peak positions whose rms deviations were typically less than 0.02 Hz. The spectral dispersion amounted to 1 Hz/cm and the spectra were swept at 0.02 and/or 0.01 Hz/s.

Results and Discussion

1. Spectral Analyses

The spectra were analyzed by means of the computer program LAME (15, 16). The spectral parameters appear in Table 1. The chemical shift between H-3 and H-4 in the CCl_4 solution of 2-methoxyphenol was only 2.0 Hz. In consequence, the analysis was not as precise as desired, even under conditions in which the methyl protons were decoupled from H-3. The benzene-d_6 solution yielded a more highly dispersed spectrum and proved amenable to a precise analysis (Table 1).

The spectral quality was similar to that recently portrayed for 2-methylphenol (14). The standard deviations in the spectral parameters in Table 1 should probably be multiplied by a factor of 3 to yield a measure of accuracy.

2. Intramolecular Equilibrium in 2-Methoxyphenol

In the following discussion it is assumed that $^5J_m^{XH,H_3} \equiv {}^5J_c$ in **1** and $^5J_m^{XH,H_5} \equiv {}^5J_c$ in **2**, vanish; i.e., that an observable $^5J_m^{H,XH}$ arises only from contributions over the all-*trans* path in **1** and **2**. Furthermore, it is assumed that ^5J_t in **1** and **2** are equal. These assumptions have led to self-consistent equilibrium measurements in a large variety of phenol derivatives (9–14) and to agreement with reliable data from other methods (17, 18). That ^5J_c is not observable under the conditions in this laboratory is known for a number of phenol derivatives (10–12).

In the benzene-d_6 solution (Table 1) $^5J_m^{OH,H_5}$ is 0.42 ± 0.01 Hz and $^5J_m^{OH,H_3}$ is −0.01 ± 0.01 Hz (not significantly different from zero). It follows that only the intramolecularly hydrogen bonded *cis* conformer, **1**, is detectably populated at 305 K under these conditions. If ΔG^0 is 2.00 kcal/mol, then the *trans* conformer would be populated to the extent of 3.5%. Hence, a $^5J_m^{OH,H_3}$ of 0.015 Hz (0.42 × 0.035) should be observed in principle. However, the spectral quality is not high enough to allow such an observation. Therefore, the present result is consistent with the far infrared conclusions above.

A substantial barrier to out-of-plane rotation of the hydroxyl group follows from the unobservably small coupling over six bonds, $^6J_p^{OH,H_4}$, between the hydroxyl proton and the *para* ring proton. Appreciable out-of-plane populations of the hydroxyl rotor, allowed by a V_2 of less than about 4 kcal/mol at 305 K, would lead to a detectable σ–π coupling (12).

Turning to the CCl_4 solution, it is plain that, because of tight coupling, the errors in the spectral parameters are much larger than in the benzene-d_6 solution. Within experimental error (three times the standard deviations), the $^5J_m^{OH,H}$ values are consistent with the conformational deductions based on the data for the benzene-d_6 solution.

The relative chemical shifts in the two solutions are of interest. In general, the magnetic anisotropy of benzene molecules causes marked shifts to high field of solute proton resonances, relative to those in CCl_4 solution. However, only the CH_3 and H-3 resonances in 2-methoxyphenol display a marked upfield shift

TABLE 1. Proton chemical shifts and spin–spin coupling constants for 2-methoxyphenol and 2-methoxythiophenol

Parameter[a,b]	2-Methoxyphenol		2-Methoxythiophenol
	CCl_4 (5 mol%)	C_6D_6 (5 mol%)	CCl_4 (4.6 mol%)
ν_{XH}	540.682 (5)	554.570 (2)	366.1
ν_{CH_3}	381.2	318.997 (1)	382.9
ν_3	671.859 (10)	646.906 (2)	672.427 (5)
ν_4	669.884 (8)	668.907 (2)	698.191 (4)
ν_5	675.644 (11)	675.233 (2)	674.990 (5)
ν_6	681.007 (10)	699.951 (1)	713.551 (4)
$^3J_{34}$	8.066 (12)	8.028 (3)	8.183 (7)
$^3J_{45}$	7.577 (12)	7.592 (2)	7.436 (6)
$^3J_{56}$	7.907 (11)	7.941 (2)	7.436 (6)
$^4J_{35}$	1.422 (8)	1.442 (4)	1.215 (5)
$^4J_{46}$	1.575 (10)	1.536 (4)	1.648 (5)
$^5J_{36}$	0.301 (13)	0.261 (2)	0.322 (6)
$^4J_o^{XH,H_6}$	−0.100 (11)	−0.098 (2)	0.0
$^5J_m^{XH,H_3}$	−0.041 (12)	−0.007 (2)	0.282 (8)
$^5J_m^{XH,H_5}$	0.376 (13)	0.420 (2)	0.211 (9)
$^6J_p^{XH,H_4}$	0.0	<0.03	−0.136 (8)
$^5J^{CH_3,H_3}$	—	(−)0.288 (1)	(−)0.28
Root-mean-square deviation	0.0139	0.0135	0.0122
Transitions calculated	85	704	90
Peaks observed	42	69	61
Transitions assigned	59	521	55

[a]The chemical shifts, ν, are given in Hz at 100 MHz to low field of internal tetramethylsilane at 305 K.
[b]Standard deviations in the last one or two significant figures are given in parentheses.

(Table 1). This observation can be rationalized as a preferential packing of the polarizable benzene solvent molecules about electron deficient sites in the solute molecule (19, 20). If the hydroxyl proton lies near the electron rich oxygen atom of the methoxyl group, as in conformer **1**, its *low-field* shift in benzene solution can be understood. When appreciable amounts of *trans* conformers, **2**, are present, the hydroxyl and H-6 protons display large upfield shifts (up to 1 ppm) in benzene solution (13).

The conformation of the methoxy group in 2-methoxyphenol is no doubt as indicated in **1** or **2**, as corroborated by the through-space coupling of −0.3 Hz between the CH_3 and H-3 protons (21, 22).

In summary, the ^1H nmr spectral parameters for 2-methoxyphenol are consistent with a conformation, **1**, whose energy relative to **2** has been calculated from the hydroxyl torsional modes.

3. Conformational Properties of 2-Methoxythiophenol

$^5J_m^{SH,H_3}$ is larger than $^5J_m^{SH,H_5}$. The *trans* conformer, **2**, is more stable (57% abundant) than the *cis* conformer, **1**, by a free energy difference of 180 ± 120 cal/mol. The quoted error assumes an accuracy in ^5J determined by three times the standard deviation. For reasons to be given in Section 4, we prefer to write $\Delta G^0 = 0.2 \pm 0.2$ kcal/mol. This result agrees with one set of dipole moment measurements (8), whose interpretation assumes the conformers **1** and **2** (including the specified orientation of the methoxy group). The *cis* conformer in 2-methoxythiophenol is relatively more stable than in 2-nitrothiophenol (9), very likely a consequence of less favourable steric interactions in the latter compound (7).

In contrast to the analogous coupling in phenol (12) and a variety of its derivatives (10–14), the six-bond coupling, $^6J_p^{SH,H}$, in thiophenol (23) and in 2-methoxythiophenol has a finite magnitude. If, as expected from a σ–π coupling mechanism, ^6J_p has a $\sin^2\theta$ dependence (θ being the angle by which the OH or SH bonds twist out of the aromatic plane), these coupling magnitudes are consistent with the known twofold barriers to internal rotation in phenol and thiophenol. Thus, the far infrared gas phase torsions for phenol imply a V_2 of 3.6 kcal/mol (*1*). This means that at 305 K the out-of-plane populations in phenol are small and, in terms of a hindered rotor model (23), $^6J_p^{H,OH}$ should be very small in magnitude. Again, torsion data on gaseous thiophenol yield a V_2 of 0.76 kcal/mol (24). In CCl_4 solution, $^6J_p^{SH,H}$ in thiophenol is −0.33 Hz (23) and was used to derive a V_2 of 1.1 ± 0.3 kcal/mol (23). This value of V_2 depended on an assumed value for $^6J_p^{SH,H}$ ($\theta = 90°$) of −1.06 Hz. If this number is changed to −0.97 Hz, V_2 becomes 0.76 kcal/mol. Of course, a small solvent effect on the barrier is a definite possibility.

The ^1H nmr data (25) on a series of *para* substituted thiophenol derivatives strongly suggested that π electron donors cause a decrease in V_2 and that π

electron accept
example, V_2 in
2 kcal/mol an
phenol. This t
change in conj
aromatic nucle
in V_2 are suppo
and are also fc
(26).

In 2-nitrothi
suggesting a b
than 3 kcal/mo

Now, in 2-n
ence between
than 0.2 kcal/
much smaller
hindered rotor
(25, 27, 28) be
0.02 Hz. If ^6J (
value of $\sin^2\theta$
2.7 ± 0.6 kcal,
than implied
indicate the ap

It appears t
so that one m
by analogy to

[2] V(kcal/m

Inclusion of V
principle, wou
that a theoreti
phenol deriva
V_{n+2} term am
term (5).

If this treat
barrier to int
considerably
derivatives.
decreases rela
1 kcal/mol (2
component ir
the parent
about the ori

4. The σ–π C

Because th
populations,
from the σ–
portional to
observed ^5J_m
used above.
$^5J_m^{SH,H}$ is av
bromo-3-me
compound i
phenol, so t

electron acceptors entailed an increase in V_2. For example, V_2 in 4-nitrothiophenol in solution was over 2 kcal/mol and was near zero in 4-methoxythiophenol. This trend was reasonably explained by a change in conjugation of the SH group with the aromatic nucleus. Such substituent induced changes in V_2 are supported by STO-3G MO calculations (25) and are also found in analogous phenol derivatives (26).

In 2-nitrothiophenol, ${}^6J_p^{SH,H}$ is -0.03 ± 0.02 Hz, suggesting a barrier to internal rotation of greater than 3 kcal/mol (9) for the SH group.

Now, in 2-methoxythiophenol, the energy difference between conformers **1** and **2** is apparently less than 0.2 kcal/mol and therefore V_1 may well be much smaller than V_2 (see eq. [1]). In that event a hindered rotor treatment based on a twofold barrier (25, 27, 28) becomes meaningful. ${}^6J_p^{SH,H}$ is -0.14 ± 0.02 Hz. If ${}^6J(\theta = 90°)$ is -0.97 Hz, the expectation value of $\sin^2\theta$ becomes 0.14 ± 0.02, yielding a V_2 of 2.7 ± 0.6 kcal/mol. The quoted error is rather larger than implied by the error in ${}^6J_p^{SH,H}$. It is meant to indicate the approximate nature of the model.

It appears that V_1 is indeed a small fraction of V_2, so that one may write for 2-methoxythiophenol (and by analogy to eq. [1])

$$[2] \quad V(\text{kcal/mol}) = (0.2 \pm 0.2)(1 - \cos\theta)/2 + (2.7 \pm 0.6)(1 - \cos 2\theta)/2$$

Inclusion of V_n terms with $n > 2$, although correct in principle, would not be suitable here. It may be noted that a theoretical analysis of the potential function in phenol derivatives indicates that the magnitude of a V_{n+2} term amounts to between 5 and 20% of the V_n term (5).

If this treatment of the SH motion is correct, the barrier to internal rotation in both compounds is considerably higher than in the corresponding *para* derivatives. In the *para* derivatives the barrier decreases relative to the parent compounds by about 1 kcal/mol (25, 26). In the *ortho* derivatives, the V_2 component increases by about 2 kcal/mol relative to the parent compounds. We hesitate to speculate about the origin of this phenomenon.

4. The σ–π Component of ${}^5J_m^{SH,H}$

Because the SH group has significant out-of-plane populations, ${}^5J_m^{SH,H}$ will contain a small contribution from the σ–π mechanism. This contribution is proportional to $\sin^2\theta$ and should be subtracted from the observed ${}^5J_m^{SH,H}$ to yield the stereospecific ${}^5J_t$ values used above. An estimate of the σ–π contribution to ${}^5J_m^{SH,H}$ is available from its value of 0.13 Hz in 4-bromo-3-methylthiophenol (25). The barrier in this compound is only about half that in 2-methoxythiophenol, so that a much larger out-of-plane population exists in the bromo compound; for which $\langle\sin^2\theta\rangle$ is about 0.3 (25). The ratio of $\langle\sin^2\theta\rangle$ in these two compounds is 0.14/0.3, or about 0.5. Then the σ–π contribution to ${}^5J_m^{SH,H_3}$ and ${}^5J_m^{SH,H_5}$ in 2-methoxythiophenol is roughly 0.5×0.13, or 0.06 Hz. ΔG^0 becomes $-RT \ln (0.21 - 0.06)/(0.28 - 0.06)$, or 0.23 kcal/mol at 305 K. In other words, the value of 0.2 ± 0.2 kcal/mol, quoted in [2], still stands.

Acknowledgments

We are grateful to the National Research Council of Canada for financial assistance.

1. G. L. Carlson and W. G. Fateley. J. Phys. Chem. **77**, 1157 (1973).
2. E. Mathier, D. Welti, A. Bauder, and Hs. H. Gunthard. J. Mol. Spectrosc. **37**, 63 (1971).
3. C. R. Quade. J. Chem. Phys. **48**, 5490 (1968).
4. H. D. Bist, J. C. D. Brand, and D. R. Williams. J. Mol. Spectrosc. **24**, 402 (1967).
5. S. W. Dietrich, E. C. Jorgensen, P. A. Kollman, and S. Rothenberg. J. Am. Chem. Soc. **98**, 3210 (1976).
6. T. Schaefer. J. Phys. Chem. **79**, 1888 (1975).
7. T. Kobayashi, A. Yamashita, Y. Furuya, R. Horie, and M. Hirota. Bull. Chem. Soc. Jpn. **45**, 1494 (1972).
8. H. Lumbroso, D. M. Bertin, and N. Marziano. Bull. Chem. Soc. Fr. 540 (1966).
9. T. Schaefer and W. J. E. Parr. Can. J. Chem. **55**, 3732 (1977).
10. J. B. Rowbotham and T. Schaefer. Can. J. Chem. **52**, 3037 (1974).
11. J. B. Rowbotham, M. Smith, and T. Schaefer. Can. J. Chem. **53**, 986 (1975).
12. T. Schaefer, J. B. Rowbotham, and K. Chum. Can. J. Chem. **54**, 3666 (1976).
13. T. Schaefer and J. B. Rowbotham. Can. J. Chem. **54**, 2243 (1976).
14. T. Schaefer and K. Chum. Can. J. Chem. **56**, 1788 (1978).
15. S. Castellano and A. A. Bothner-By. J. Chem. Phys. **41**, 3863 (1964).
16. C. W. Haigh and J. M. Williams. J. Mol. Spectrosc. **32**, 398 (1969).
17. A. W. Baker and A. T. Shulgin. Can. J. Chem. **43**, 650 (1965).
18. K. U. Ingold and D. R. Taylor. Can. J. Chem. **39**, 471 (1961); **39**, 481 (1961).
19. T. Schaefer. Can. J. Chem. **39**, 1864 (1961).
20. R. Wasylishen, T. Schaefer, and R. Schwenk. Can. J. Chem. **48**, 2885 (1970).
21. H. A. Gour, J. Vriend, and W. G. B. Huysmans. Tetrahedron Lett. 1999 (1969).
22. T. Schaefer, H. D. Gesser, and J. B. Rowbotham. Can. J. Chem. **54**, 2235 (1976).
23. W. J. E. Parr and T. Schaefer. J. Magn. Reson. **25**, 171 (1977).
24. N. W. Larsen and F. M. Nicolasien. J. Mol. Struct. **22**, 29 (1974).
25. T. Schaefer and W. J. E. Parr. Can. J. Chem. **55**, 552 (1977).
26. L. Radom, W. J. Hehre, J. A. Pople, G. L. Carlson, and W. G. Fateley. J. Chem. Soc. Chem. Commun. 308 (1972).
27. P. B. Ayscough, M. C. Brice, and R. E. D. McClung. Mol. Phys. **20**, 41 (1971).
28. T. Schaefer, J. B. Rowbotham, W. J. E. Parr, K. Marat, and A. F. Janzen. Can. J. Chem. **54**, 1322 (1976).

Tautomeric equilibria and pK_a values for 'sulfurous acid' in aqueous solution: a thermodynamic analysis

J. PETER GUTHRIE[1]

Department of Chemistry, University of Western Ontario, London, Ont., Canada N6A 5B7

Received June 2, 1978

J. PETER GUTHRIE, Can. J. Chem. 57, 454 (1979).

The free energy of formation of dimethyl sulfite in aqueous solution can be calculated as -91.45 ± 0.79 kcal/mol; this calculation required measurement of the solubility of dimethyl sulfite. From this value and the pK_a of $SO(OH)_2$, using previously reported methods, the free energy of formation of $SO(OH)_2$ can be calculated to be -129.26 ± 0.89 kcal/mol. Comparison of this value with the value obtained from the free energy of formation of 'sulfurous acid' solutions, calculated from the free energy of formation of sulfite ion and the apparent pK_a values, permits evaluation of the free energy of covalent hydration of SO_2 as 1.6 ± 1.0 kcal/mol, in agreement with earlier qualitative spectroscopic observations. From the apparent pK_a and the anticipated pK_a values for the tautomers ($SO(OH)_2$, p$K_1 = 2.3$; $HSO_2(OH)$, p$K_1 = -2.6$) it is possible to calculate the free energy change for tautomerization of $SO(OH)_2$ to H—SO_2-(OH) as $+4.5 \pm 1.2$ kcal/mol. All equilibrium constants required for Scheme 1, describing the species present in dilute aqueous solutions of SO_2, have been calculated. In agreement with previous Raman studies the major tautomer of 'bisulfite ion' is calculated to be H—SO_3^-.

J. PETER GUTHRIE. Can. J. Chem. 57, 454 (1979).

On peut calculer que l'énergie libre de formation du sulfite de diméthyle en solution aqueuse est égale à -91.45 ± 0.79 kcal/mol; afin d'effectuer ce calcul, il faut mesurer la solubilité du sulfite de diméthyle. En utilisant les méthodes rapportées antérieurement, on peut calculer que l'énergie libre de formation du $SO(OH)_2$ est égale à -129.26 ± 0.89 kcal/mol à partir de cette valeur et du pK_a de $SO(OH)_2$. Une comparaison de cette valeur avec celle obtenue à partir de l'énergie libre de formation de solutions "d'acide sulfureux," calculées à partir de l'énergie libre de formation de l'ion sulfite et des pK_a apparents, permet d'évaluer que l'énergie libre d'hydratation covalente du SO_2 est égale à 1.6 ± 1.0 kcal/mol, en accord avec des observations spectroscopiques qualitatives. En utilisant le pK_a apparent et les valeurs de pK_a attendues pour les tautomères ($SO(OH)_2$, p$K_1 = 2.3$; $HSO_2(OH)$, p$K_1 = 2.6$), on peut calculer que l'énergie libre du changement associée à la tautomérisation du $SO(OH)_2$ en $HSO_2(OH)$ est égale à $+4.5 \pm 1.2$ kcal/mol. On a calculé toutes les constantes d'équilibre impliquées dans le schéma 1 qui décrit les espèces en présence dans des solutions aqueuses diluées de SO_2. En accord avec les études Raman antérieures, on a calculé que le tautomère principal de l'ion "bisulfite" est le HSO_3^-.

[Traduit par le journal]

Introduction

It has been recognized for some time that 'sulfurous acid' does not exist as such in aqueous solution to any large extent (ref. 1, p. 878). Infrared spectra of concentrated aqueous solutions of sulfur dioxide show only bands due to sulfur dioxide and water (2) and it has been concluded that sulfurous acid ($SO(OH)_2$) is present to the extent of less than 1 part in 30 (2). Bell has pointed out (3) that there are two peculiar features about the behavior of these solutions: first that the pK_a for what are alleged to be solutions of sulfur dioxide in water has the value expected for $SO(OH)_2$; and second that the solubility of SO_2 is much greater than would be expected by comparison with CO_2. On this basis he suggested that hydration might be much more favorable than has been considered. The present work will show that the situation is in fact more complicated than has been considered in the past and that a satisfactory analysis, explaining both the infrared spectra and the pK_a behavior, is possible. A rationalization for the solubility can also be offered.

The present work builds upon recent work from this laboratory (4–6) which has shown that the free energies of hydrolysis of esters of inorganic oxy acids (for which resonance effects are not important) can be calculated with useful precision from the pK_a of the oxy acid, using a linear free energy relationship which appears to hold over the entire accessible range of pK_a values. This permits the free energy of formation of $SO(OH)_2$ to be calculated from the known heat of formation of $SO(OCH_3)_2$. From this fact, the known free energy of formation of sulfite ion, and the observed pK_a values, the entire system can be solved.

[1]Fellow of the Alfred P. Sloan Foundation, 1975–1979.

0008-4042/79/040454-04$01.00/0

Compound

SO_2
$(MeO)_2SO$

(*b*) Con

(*c*) Comp

[a]At 25°C, st
otherwise note
[b]In kcal mo
[c]In cal deg⁻
[d]Free energ
[e]Reference
[f]Calculated
[g]Calculated
[h]Reference
[i]Calculated
[j]This work.
[k]Standard s

Thermodyna
cussed in this p
in the literatur
measured in th
the free energ
aqueous soluti
of sulfurous a
methods whic
upon calculati
the ester. For
vided that res
X—OH, the f
corrected for

[1] X—

[2] $\Delta G'' = -$

by [2] (5). Thi
(5) and phosp

[2]In this pape
equilibrium mix
in water, sulfur
sulfonic acid wi
the monoanions
sulfite ion, and
nomenclature is
(8).

TABLE 1. Thermodynamic properties for compounds discussed in this paper[a]

(*a*) Compounds for which free energies of formation have not been reported previously

Compound	ΔH_f^0(g)[b]	S^0(g)[c]	ΔG_f^0(g)[b]	ΔG_t[b,d]	ΔG_f^0(aq)[b]
SO_2	−70.96[e]	50.40[e]	−71.79[e]	0.14[f]	−71.93[g]
$(MeO)_2SO$	−115.5(0.5)[h]	88.53(2.0)[i]	−88.98(0.78)[g]	−2.47(0.1)[j]	−91.45(0.79)[g]

(*b*) Compounds for which free energies of formation in aqueous solution have been reported previously

Compound	ΔG_f^0(aq)	Compound	ΔG_f^0(aq)
H_2O	−56.69[e,k]	SO_3^{2-}	−118.8[e]
CH_3OH	−41.88[e]		

(*c*) Compounds for which free energies of formation in aqueous solution have been calculated in this work

Compound	ΔG_f^0(aq)	Compound	ΔG_f^0(aq)
SO_2, free	−71.88(0.2)	CH_3OSO_3H	−110.65(0.84)
$SO(OH)_2$	−129.26(0.89)	$H—SO_3H$	−124.90(1.14)

[a]At 25°C, standard states are ideal gas at 1 atm, pure liquid, and 1 *M* aqueous solution with an infinitely dilute reference state, unless otherwise noted.
[b]In kcal mol^{-1}.
[c]In cal deg^{-1} mol^{-1}.
[d]Free energy of transfer, from gas at 1 atm to 1 *M* aqueous solution with an infinitely dilute reference state.
[e]Reference 13.
[f]Calculated from data in ref. 14.
[g]Calculated from other values in this table.
[h]Reference 15.
[i]Calculated by the method of atomic contributions; ref. 16.
[j]This work.
[k]Standard state is the pure liquid.

Results and Discussion

Thermodynamic properties for the compounds discussed in this paper are found in Table 1. From data in the literature, and the solubility of dimethyl sulfite measured in this work, it was possible to determine the free energy of formation of dimethyl sulfite in aqueous solution. Then the free energy of formation of sulfurous acid, $SO(OH)_2$[2] could be calculated by methods which we have reported previously, based upon calculation of the free energy of hydrolysis of the ester. For hydrolysis reactions of type [1], provided that resonance is not important for the acid X—OH, the free energy change for the hydrolysis, corrected for symmetry and steric effects is given

[1] $$X—OR + H_2O \rightleftharpoons X—OH + HOR$$

[2] $$\Delta G'' = -4.78(\pm 0.28) + 0.336(\pm 0.024)pK_a$$

by [2] (5). This equation has been used for phosphate (5) and phosphite esters (7), and has been tested for a wide range of species X—OH; it appears to hold for oxy acids over the pK_a range from −6 to 15 with X = Cl^{VII}, S^{VI}, P^{V}, As^{III}, Si^{IV}, and C (6). In this way were calculated the free energies of formation of sulfurous acid and monomethyl sulfite in Table 1. In these calculations, it is necessary to use the pK_a value for the acid corresponding to the ester but with OH replacing OR; in the present case the acid is sulfurous acid (or its monomethyl ester). For sulfurous acid the pK_a value calculated by Kossiakoff and Harker (10) was used; these authors used a simple electrostatic model which proved quite accurate for those acids where resonance is not important in either the acid or the anion. The estimated standard deviations are based upon the differences between observed and calculated values for all the acids which they studied where the model is appropriate and the structure and pK_a of the acid are known. For monomethyl sulfite the pK_a was estimated assuming that the effect of replacing OH by OMe was the same as the average value observed for phosphate esters (5) with suitable allowance for symmetry effects (6).

From the known and unambiguous free energy of formation of sulfite ion, SO_3^{2-}, in aqueous solution and the apparent pK_a values for 'sulfurous acid' the apparent free energy of formation of 'sulfurous acid' can be calculated. This value refers to the equilibrium

[2]In this paper 'sulfurous acid' will be used to mean the equilibrium mixture obtained when sulfur dioxide is dissolved in water, sulfurous acid will be used to refer to $SO(OH)_2$, sulfonic acid will be used to refer to $H—SO_2(OH)$; similarly the monoanions will be referred to as 'bisulfite ion,' hydrogen sulfite ion, and tetracoordinatesulfonate ion. This suggested nomenclature is analogous to that used for phosphorous acids (8).

mixture of SO_2 and $SO(OH)_2$; from the two free energies of formation, the equilibrium constant for hydration can be calculated, since it may be shown that

$$\Delta G_f^0(\text{'sulfurous acid'}) = \Delta G_f^0(SO(OH)_2) - RT \ln (1 + 1/K_h)$$

where K_h is the dimensionless equilibrium constant for hydration. This method leads to a free energy of hydration of $+1.6 \pm 1.0$ kcal/mol.

This value is in satisfactory agreement with the limit imposed by Giguere's infrared studies (2), which led to the conclusion that there was less than 1 part in 30 of sulfurous acid present. This would correspond to a free energy of hydration of $+2$. If the major species in solution is SO_2 then there is a problem explaining the pK_a which is observed, since the apparent pK_a is very close to that expected if the major species in solution were $SO(OH)_2$ but is much too acidic for a solution of SO_2 and a very minor fraction of $SO(OH)_2$. There is, however, another tautomer possible, i.e., $H—SO_2—OH$, which by analogy with the nomenclature of phosphorous compounds (8) should be called sulfonic acid. This is expected to be a strong acid and therefore could exert a marked influence on the apparent pK_a even if the equilibrium proportion is very small. The complete set of equilibria required to describe the monosulfur species present in aqueous solution is shown in Scheme 1.[3]

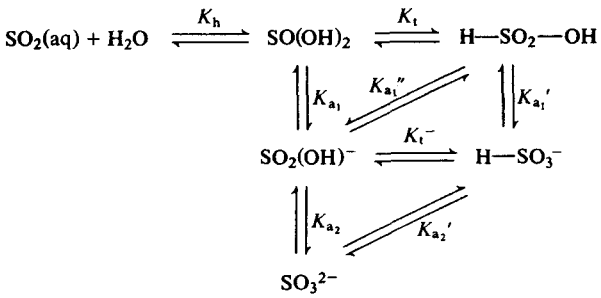

$$K_{a_1}^{app} = \frac{[H^+]\{[SO_2(OH)^-] + [H—SO_3]\}}{\{[SO_2] + [SO(OH)_2] + [H—SO_2—OH]\}}$$

$$K_{a_2}^{app} = \frac{[H^+][SO_3^{2-}]}{\{[SO_2(OH)^-] + [H—SO_3^-]\}}$$

SCHEME 1

From Scheme 1, the equilibrium constant K_t for tautomerization of $SO(OH)_2$ to $H—SO_2—OH$ can be expressed in terms of the other equilibrium constants as

$$[3]\quad K_t = (K_{a_1} - K_{a_1}^{app}(1 + 1/K_h))(K_{a_1}^{app} - K_{a_1}')$$

$K_{a_1}^{app}$ is of course known, being the observed apparent first pK_a of 'sulfurous acid;' pK_{a_1}, the true pK_a for $SO(OH)_2$, is not known experimentally; we will use the value calculated from an electrostatic model by Kossiakoff and Harker (10) of 2.3 ± 0.9 and also their value of 7.0 ± 0.9 for the second pK_a of $SO(OH)_2$. These values are imprecise but the results of the calculation are very insensitive to errors in them.

For sulfonic acid, the pK_a value was estimated by a Taft ρ^* correlation which was recently shown to give good predictions for sulfonic acids (6). The value so obtained is $pK_{a_1}' = 2.6 \pm 0.5$.

When these values were substituted in [3], the free energy of tautomerization was calculated as 4.36 ± 0.72 kcal/mol. All of the equilibrium constants required by Scheme 1 can now be calculated; the values are found in Table 2. These calculations simply involve calculating the one remaining equilibrium constant in a thermodynamic cycle.

Table 3 shows the concentrations of the species present in solutions of pH 1–10 for a total 'SO_2' concentration of 0.001 M. At high sulfite concentrations dimerization to 'metabisulfite' ions, $S_2O_5^{2-}$, can be important (1, p. 880; 9); this dimerization has been ignored in constructing Table 3 and is unimportant for concentrations less than 0.01 M (9).

The results of this analysis are in good agreement with earlier qualitative observations; the major monoanion is the sulfonate anion, as had been concluded from the Raman spectra of aqueous bisulfite solutions (11). There are obvious implications for the interpretation of studies of nucleophilic reactions of bisulfite ion if the reactive species (with a lone pair on sulfur) is not the major species of the monoanion but rather a minor tautomer. Fortunately the reinterpretation will not be enormous since the factor by which apparent rate constants will have to be corrected is less than 100-fold.

The contrast between the pK_a of $H—SO_3^-$, 8.6 ± 1.6, and that for $H—P(O)_2OH^-$, 28 ± 2 (7), is

TABLE 2. Equilibrium constants describing Scheme 1[a]

Parameter	Value	Parameter	Value
$\log K_{a_1}^{app}$	-1.89 ± 0.10[b]	$\log K_t$	-3.3 ± 0.9
$\log K_{a_2}^{app}$	-7.44[c]	$\log K_h$	-1.1 ± 0.7
		$\log K_t^-$	1.6 ± 1.4
$\log K_{a_1}$	-2.3 ± 0.9	$\log K_{a_2}$	-7.0 ± 0.9
$\log K_{a_1}'$	2.6 ± 0.5	$\log K_{a_2}'$	-8.6 ± 1.6
$\log K_{a_1}''$	1.0 ± 1.3		

[a]In aqueous solution at 25°C.
[b]Reference 14.
[c]Reference 17.

[3]Concentrated solutions of bisulfite ion dimerize to give pyrosulfite ion, $S_2O_5^{2-}$ (ref. 1, p. 880 and ref. 9). The present work deals only with the monomeric species.

TABLE 3. Co

pH
1.00
2.00
3.00
4.00
5.00
6.00
7.00
8.00
9.00
10.00

very striking
ing effect of
charge of th
bonded. The
There rem
attention (3)
in water. W
SO_2 in wate
formal posit
stronger dip
central S in S

The solubil
analysis of a
buffer, ionic st
to the solvent
M. The vapor
a plot of log
values lead to
1 atm to aque

I thank tl
and the Al
support of
technical as

TABLE 3. Concentrations of species present in aqueous solutions of SO_2 at various pH values, for a total concentration of 0.001 *M*

	$10^4 \times$ Concentration of species					
pH	SO_2	$SO(OH)_2$	$HSO_2(OH)$	$SO_2(OH)^-$	HSO_3^-	SO_3^{2-}
1.00	8.06	0.64	3×10^{-4}	0.03	1.27	3×10^{-8}
2.00	3.72	0.29	1×10^{-4}	0.15	5.84	1×10^{-6}
3.00	0.58	0.05	2×10^{-5}	0.23	9.14	2×10^{-5}
4.00	0.06	5×10^{-3}	2×10^{-6}	0.24	9.69	2×10^{-4}
5.00	6×10^{-3}	5×10^{-4}	2×10^{-7}	0.25	9.75	2×10^{-3}
6.00	6×10^{-4}	5×10^{-5}	2×10^{-8}	0.24	9.73	0.02
7.00	6×10^{-5}	5×10^{-6}	2×10^{-9}	0.24	9.52	0.24
8.00	5×10^{-6}	4×10^{-7}	2×10^{-10}	0.20	7.83	1.97
9.00	2×10^{-7}	1×10^{-8}	7×10^{-12}	0.07	7.83	7.10
10.00	2×10^{-9}	2×10^{-10}	1×10^{-13}	0.01	0.38	9.61

very striking and shows the very large acid strengthening effect of an increase by one unit of the formal charge of the atom to which hydrogen is directly bonded. The effect amounts to 19 ± 2.6.

There remains the problem, to which Bell called attention (3), of the high solubility of sulfur dioxide in water. We suggest that the greater solubility of SO_2 in water than of CO_2 in water is due to the formal positive charge on the sulfur, leading to much stronger dipole–charge interactions of water with the central S in SO_2 than with the central C in CO_2.

Experimental

The solubility of dimethylsulfite was determined by nmr analysis of a saturated aqueous solution (pH 7 phosphate buffer, ionic strength 0.1) integrating the methyl signals relative to the solvent signal. The solubility so obtained was 1.20 ± 0.02 *M*. The vapor pressure at 25°C (14.1 Torr) was calculated from a plot of log p vs. $1/T$, using data from Beilstein (12). These values lead to a free energy of transfer from the gas phase at 1 atm to aqueous solution at 1 *M* of −2.40 kcal/mol.

Acknowledgements

I thank the National Research Council of Canada and the Alfred P. Sloan Foundation for financial support of this work, and Patricia A. Cullimore for technical assistance.

1. M. SCHMIDT and W. SIEBERT. *In* Comprehensive inorganic chemistry. *Edited by* A. F. Trotman-Dickenson. Pergamon, Oxford. 1973.
2. M. FALK and P. A. GIGUERE. Can. J. Chem. **36**, 1121 (1958).
3. R. P. BELL. The proton in chemistry. 2nd ed. Cornell University Press, Ithaca, NY. 1973. p. 92.
4. J. P. GUTHRIE. Can. J. Chem. **53**, 898 (1975).
5. J. P. GUTHRIE. J. Am. Chem. Soc. **99**, 3991 (1977).
6. J. P. GUTHRIE. Can. J. Chem. **56**, 2342 (1978).
7. J. P. GUTHRIE. Can. J. Chem. **57**, 240 (1979).
8. J. H. FLETCHER, O. C. DERMER, and R. B. FOX. Nomenclature of organic compounds. American Chemical Society, Washington, DC. 1973. p. 279.
9. R. M. GOLDING. J. Chem. Soc. 3711 (1960).
10. A. KOSSIAKOFF and D. HARKER. J. Am. Chem. Soc. **60**, 2047 (1938).
11. A. SIMON and K. WALDEMAN. Z. Anorg. Allg. Chem. **281**, 113 (1955); **281**, 135 (1955).
12. BEILSTEIN. Handbuch der organischen Chemie. **1**, 282; **1**(2), 271; **1**(3), 1196; **1**(4), 1250.
13. F. D. ROSSINI, D. D. NAGMAN, W. H. EVANS, S. LEVINE, and J. JAFFE. Natl. Bur. Stand. (U.S.) Circ. 500 (1952).
14. H. F. JOHNSTONE and P. W. LEPPLA. J. Am. Chem. Soc. **56**, 2233 (1934).
15. J. D. COX and G. PILCHER. Thermochemistry of organic and organometallic compounds. Academic Press, New York, NY. 1970.
16. S. W. BENSON and J. H. BUSS. J. Chem. Phys. **29**, 546 (1958).
17. P. SALOMAA, R. HAKALA, S. VESALA, and T. AALTO. Acta Chem. Scand. **23**, 2116 (1969).

Structures and properties of mixtures of branched chain compounds and lecithin: phytol, α-tocopherol (vitamin E), and phytanic acid

ROBERT J. CUSHLEY, BRUCE J. FORREST, ANNE GILLIS, AND JENIFER TRIBE

Department of Chemistry, Simon Fraser University, Burnaby, B.C., Canada V5A 1S6

Received August 23, 1978

ROBERT J. CUSHLEY, BRUCE J. FORREST, ANNE GILLIS, and JENIFER TRIBE. Can. J. Chem. **57**, 458 (1979).

Phospholipid bilayers containing branched chain molecules, phytol (**1**), vitamin E (**2**), and phytanic acid (**3**), have been investigated by ^{31}P nmr, esr, and differential scanning calorimetry (dsc).

A ^{31}P lanthanide induced shift study indicated varying permeabilities to Pr^{3+} in the order phytanic acid > vitamin E > phytol > egg yolk lecithin alone; the half-lives (in days) were 0.002, 0.14, 0.83, and 6.5, respectively. The activation energy for Pr^{3+} permeation through the egg yolk lecithin – phytol membrane was found to be 84.9 ± 0.8 kJ.

The following esr order parameters, S_3, were obtained using the extrinsic spin label, 5-doxylpalmitic acid, in oriented mixed multibilayers: S_3 (**1**) = 0.29, S_3 (**2**) = 0.50, and S_3 (**3**) = 0.02.

Differential scanning calorimetry revealed a lowering of the gel–liquid crystalline phase transition temperature, T_c, as the concentration of incorporated isoprenoid compound increases, with eventual disappearance of the endotherm. Specific entropy, s, calculated for dipalmitoyl lecithin + 25 mol% **3** is 126 J kg^{-1} K^{-1} compared to s = 114.2 J kg^{-1} K^{-1} for **1** and s = 85 J kg^{-1} K^{-1} for **2**.

ROBERT J. CUSHLEY, BRUCE J. FORREST, ANNE GILLIS et JENIFER TRIBE. Can. J. Chem. **57**, 458 (1979).

Faisant appel à la rmn du ^{31}P, à la rpe et à l'analyse enthalpique différentiel (aed), on a étudié des doubles couches de phospholipides contenant des molécules à chaînes ramifiées comme le phytol (**1**), la vitamine E (**2**) et l'acide phytanique (**3**).

Une étude de déplacements induits par les lanthanides des spectres rmn du ^{31}P met en relief que les diverses perméabilités au Pr^{3+} sont dans l'ordre acide phytanique > vitamine E > phytol > EYL (seul); les demi-vies respectives (en jours) sont 0.002, 0.14, 0.83 et 6.5. L'énergie d'activation pour l'imprégnation du Pr^{3+} à travers une membrane de EYL–phytol est égale à 84.9 ± 0.8 kJ.

Dans des couches multiples mixtes orientées, les paramètres d'ordre S_3, mesurés en rpe en faisant appel à l'acide doxyl-5 palmitique, un marqueur de spin intrinsèque, sont les suivants: S_3 (**1**) = 0.29, S_3 (**2**) = 0.50 et S_3 (**3**) = 0.02.

La aed met en évidence un abaissement de la température, T_c, de transition de phase gel–cristal liquide au fur et à mesure de l'augmentation de la concentration du composé isoprénique incorporé; il se produit éventuellement une disparition de l'effet endothermique. L'entropie spécifique, s, calculée pour DPL + 25% de **3** est 126 J kg^{-1} K^{-1} comparée à une s = 114.2 J kg^{-1} K^{-1} pour **1** et une s = 85 J kg^{-1} K^{-1} pour **2**.

[Traduit par le journal]

Introduction

Isoprenoid compounds assume an important role in biological systems. We have studied the effects of three of the 'phytyl' family: phytol (3,7,11,15-tetramethylhexadecyl-*trans*-2-en-1-ol, compound **1**), α-tocopherol (2,5,7,8-tetramethyl-2-(4,8,12-trimethyltridecyl)-6-chromanol, compound **2**), and phytanic acid (3,7,11,15-tetramethylhexadecanoic acid, compound **3**), on the structure and function of lecithin model membranes.

The physiology of these isoprenoids is well known. The most important of the above three is vitamin E (α-tocopherol, **2**, is the most active of the chromanols making up the vitamin). The pathogenic consequence of vitamin E deficiency is the onset of sterility and/or nutritional muscular dystrophy in rats. Less clear, and still controvertible, is the biological function of tocopherol. The most widely held view is that vitamin E functions as an antioxidant, protecting unsaturated lipids from free radical attack (1). However it has also been proposed as a specific antioxidant for protection of protein bound Se or a cofactor in mitochondrial oxidation or oxidative phosphorylation (2).

The accumulation of phytanic acid (**3**) has been found to be a factor in the progression of Refsum's disease. Patients afflicted with this disorder are not able to α-oxidize and decarboxylate phytanic or similar branched chain fatty acids, and an accumulation of branched acids results. This build-up has been cited

0008-4042/79/040458-08$01.00/0

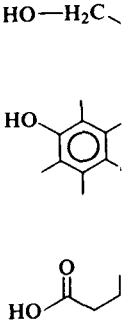

as a causative f
tion) of the ner
death (3).

Furthermore
made linking a
suggests these
in membranes.
have demonst
rabbit erythroc
vitro by α-toc
chain compou
squalene, ubiq
whereas *N,N'*-
are completely
tration of vita
cause extensiv
shown that cy
inactivated by
reactivated no
acetyl-α-tocop
It appears that
nol ring syste
activity but ra
branched natu

We wish to
dence garnere
vious ^{13}C rela
compounds **1**
affect the perr

Chemicals we
phytol, Nutriti
Chemical Co.;
lecithin (99%) (E
diaminetetraace
Co.; praseodym
acid (99.7%), Ar
and Dohme; pa
Elute (methanc
Aldrich Chemi
methyl-3-oxazol

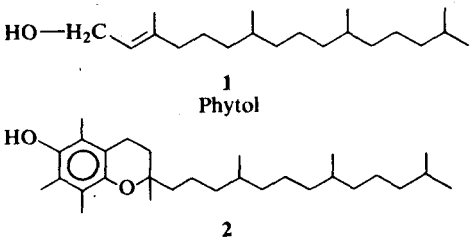

1
Phytol

2
Vitamin E

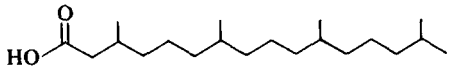

3
Phytanic acid

as a causative factor in the degeneration (demyelination) of the nervous system which eventually leads to death (3).

Furthermore, a number of observations have been made linking a common effect owing to **1–3** which suggests these compounds may play a structural role in membranes. For instance, Lucy and Dingle (4) have demonstrated that the rapid haemolysis of rabbit erythrocytes by added retinol is inhibited in vitro by α-tocopherol as well as other branched chain compounds, namely 6-*O*-acetyl-α-tocopherol, squalene, ubiquinone-30, vitamin K_1, and phytol, whereas *N,N'*-phenylenediamine and hydroquinone are completely ineffective. However, higher concentration of vitamin E and phytol were also found to cause extensive haemolysis (4). It has also been shown that cytochrome-c reductase which has been inactivated by its extraction from porcine liver is reactivated not only by vitamin E, but also by 6-*O*-acetyl-α-tocopherol, phytanic acid, and phytol (5). It appears that the effects are not due to the chromanol ring system in **2** which provides the antioxidant activity but rather that these effects are due to the branched nature of the phytyl side chain.

We wish to propose, based on the following evidence garnered at the molecular level and on previous ^{13}C relaxation studies (6, 7), that the phytyl compounds **1–3** act as *membrane destabilizers* and affect the permeability of model membranes.

Experimental

Chemicals were purchased from the following sources: phytol, Nutritional Biochemical Corporation or Aldrich Chemical Co.; vitamin E (*dl*-α-tocopherol) and dipalmitoyl lecithin (99%) (DPL), Sigma Chemical Co.; disodium ethylenediaminetetraacetate (EDTA) and cholesterol, Fisher Scientific Co.; praseodymium nitrate (99.9%), Alfa Inorganics; phytanic acid (99.7%), Analabs; deuterium oxide (99.7%), Merck, Sharp and Dohme; palmitic acid, J. T. Baker Chemical Co.; methElute (methanolic trimethylanilinium hydroxide, 0.2 *M*), Aldrich Chemical Co.; 2-(10-carboxydecyl)-2-butyl-4,4-dimethyl-3-oxazolidinyloxyl (5-doxylpalmitic acid) was a generous gift of Dr. A. C. Oehlschlager, Chemistry Department, Simon Fraser University.

Egg yolk lecithin was extracted from fresh yolks by the method of Singleton *et al.* (8). Thin-layer chromatographic analysis (0.25 mm silica gel G, developed with $CHCl_3$–MeOH–H_2O 65:35:4) showed a single spot when sprayed with 50% H_2SO_4 and heated or when exposed to I_2 vapour. The fatty acid composition of egg yolk lecithin was determined by means of glpc analysis of the corresponding methyl esters using the methylating agent, methElute (methanolic trimethylanilinium hydroxide, 0.2 *M*). Approximately 1 mg of purified egg yolk lecithin was added to 0.5 mL methElute and a 1 μL aliquot injected onto a 6 ft × 4 mm Silar 10C column. Settings were as follows: column temperature, 180°C; detector temperature, 250°C; injector temperature, 250°C. Peaks were identified by comparison with known standards.

Gas–liquid partition chromatography indicates an egg yolk lecithin composition of 42.7% palmitic acid, 16.9% stearic acid, 27.7% oleic acid, 11% linoleic acid, and 1.6% palmitoleic acid.

Vesicles

Lecithin dispersions (egg yolk lecithin or DPL, 10–20% w/v) were prepared by shaking the dry phospholipid with a suitable volume of an aqueous phase (3–4 mL of H_2O in the case of dsc and 0.05 *M* Tris pH 7.22, 0.05 *M* in KCl, in the case of ^{31}P spectra). The dispersions were then sonicated under nitrogen on a Biosonic III probe type sonicator above the phospholipid gel – liquid crystalline phase transition temperature until translucence. Sonication time was approximately 10 min, except in the case of egg yolk lecithin – phytol, 1:1 mol ratio, mixed vesicles which required more prolonged sonication (20 min–2 h). The temperature was maintained at approximately 10°C in the case of egg yolk lecithin preparations and at approximately 50°C in the case of DPL preparations by means of water flowing through a jacket surrounding the sample. The vesicle preparations were then centrifuged or passed through a 0.45 μm Millipore filter to remove titanium debris or any larger liposomes and subsequently transferred under nitrogen to sample tubes. The spectra were determined immediately.

Mixed vesicle preparations were prepared in a similar manner by first codissolving the components in chloroform, followed by solvent removal, and exhaustive pumping to obtain the dry lipid mixture.

Permeability Studies

^{31}P spectra were determined on a Varian XL-100-15 nmr spectrometer in the pulse Fourier transform mode at 40.5 MHz using an external ^{19}F field-frequency lock and a 2K dataset with external H_3PO_4 (85%), as a reference.

For permeability measurements of pure egg yolk lecithin and mixed vesicle systems to Pr^{3+} initial spectra were determined and a 150 μL portion of 0.1 *M* $Pr(NO_3)_3 \cdot 5H_2O$ in the aforementioned buffer solution was then added. The use of 3 mL of vesicle preparation resulted in a Pr^{3+} concentration of 0.005 *M*. Subsequent spectra were determined at intervals and the rate of disappearance of the sharp upfield ^{31}P resonance was monitored. After the disappearance of the upfield peak, 300 μL of 0.2 *M* EDTA which complexes with Pr^{3+} was routinely added, and the spectra redetermined.

Electron Spin Resonance Spectra

Electron spin resonance spectra were determined at 23°C on a Varian E-4 epr spectrometer operating in the X band at approximately 9.5 GHz. Typical spectrometer settings were: scan range, 100–400 G; receiver gain, 5×10^2; modulation amplitude, 0.5 G; time constant, 0.3 s; scan time, 4 min; microwave power, 10–100 mW.

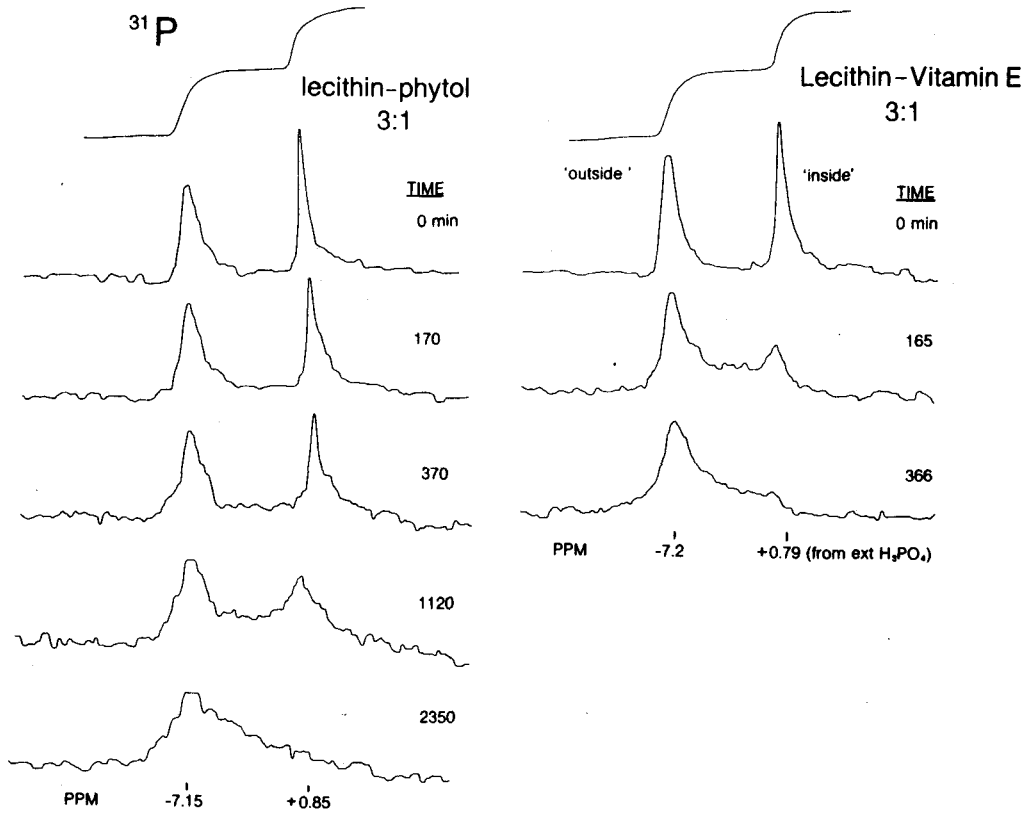

FIG. 1. ^{31}P nmr spectra of 10% w/v egg yolk lecithin vesicles containing 25 mol% phytol or 25 mol% vitamin E at the indicated times after the addition of 0.005 *M* Pr^{3+}.

Oriented lipid multilayers used in esr spectral determinations were prepared by slowly passing wet nitrogen through a quartz aqueous esr cell which contained approximately 0.10 mL of chloroform solution containing the multilayer components. This solution was prepared from stock solutions of 5×10^{-2} *M* lipid and 1×10^{-3} *M* spin label. The total lipid to spin label mol ratio was 100:1 unless otherwise specified. The lipid multilayers were then placed in the dark under vacuum for at least 3 h to remove residual chloroform and subsequently hydrated with 0.05 *M* Tris, pH 7.40. Each sample was used for at least two spectral determinations, one with the magnetic field parallel and another with the magnetic field perpendicular, to the flat cell surface.

Differential Scanning Calorimetry

Vesicle samples ($\simeq$10 wt% lecithin) were sealed in Perkin Elmer sample pans and examined on the differential scanning calorimeter (Perkin Elmer DSCI). A scan speed of 10 deg min^{-1} was used for heating and cooling runs over a temperature range of 275–350 K. Indium was used as a primary standard for power and temperature calibration. Values are accurate to ± 2 K.

Results

Lanthanide Induced Shift Studies

In a previous publication (7), preliminary results were presented which indicated that compounds **1**–**3** produced increases in the permeability of lecithin bilayers in the order **3** > **2** > **1** > lecithin alone. This work has been expanded to determine the effect of temperature and concentration on the rates.

When the lanthanide, Pr^{3+}, is added to preformed egg yolk lecithin vesicles, the phosphorus nuclei on the outside of the bilayer are shifted downfield (lis) as indicated in the top, left spectrum in Fig. 1 for egg yolk lecithin – phytol 3:1 and top, right for egg yolk lecithin – α-tocopherol 3:1. The technique used for the permeation studies is essentially that of Barsukov *et al.* (9) and Fernandez *et al.* (10) except ^{31}P nmr is substituted for ^{1}H nmr. The larger chemical shift differences of ^{31}P with added lanthanide and the simplicity of the ^{31}P spectra of phospholipid vesicles makes ^{31}P nmr more attractive for lis studies than ^{1}H nmr (11).

As Pr^{3+} crosses the bilayer phosphorus nuclei on the inside layer become shifted downfield to reside under the 'outside' resonance peak. The time lapse for the ^{31}P spectra are recorded in the rest of Fig. 1 and show the effects of Pr^{3+} on egg yolk lecithin vesicles containing both **1** and **2** (times are indicated on the spectra). The rate of disappearance of the upfield, 'inside' ^{31}P nmr signal is a zero-order process describing permeation of the bilayer by Pr^{3+}. The rate of leakage of Pr^{3+} through egg yolk lecithin

TABLE 1. Leak r

Mer
Egg yolk lecithi
Egg yolk lecithi
Egg yolk lecithi
Egg yolk lecithi

[a]800 transients;

bilayers for egg
vesicles at 33°C i

An examinatic
corporation of 2
for the vesicle le
vitamin E from
phytanic acid b
obtained for pur

After the dis
resonance due to
EDTA was rout
sible Pr^{3+} and
peaks were reso
phosphorus nucl
are directly exp
behaviour indic
pearance of the
initial addition
rupture. If the
sible for the dis
signal, the subs
result in a single
accessible for
vesicles are not
during the time
spectrum (3–10
indeed monitors

The ^{31}P nmr
studies which m
a time interval
observed half-li
is on the order
practical to cor
Therefore the o
subject to consi
rapid rates in tl
vesicle prepara
changes in peak
determinations
lecithin vesicles
each determin
mately $2 \times 10^{-}$
deviations as c
ment of the exp
order of 20–30

TABLE 1. Leak rates for lecithin and lecithin – phytyl compound vesicles at 33°C; lecithin–additive, 3:1 mol ratio (7)

Membrane	^{31}P chemical shift pre Pr^{3+} (ppm upfield[a] from 85% H_3PO_4)	'Inside' ^{31}P signal decay (% total/min)	Relative rate	Half-life (days)
Egg yolk lecithin	0.87	5.35×10^{-3}	1.00	6.5
Egg yolk lecithin + phytol	0.85	4.17×10^{-2}	7.79	0.83
Egg yolk lecithin + vitamin E	0.79	2.55×10^{-1}	47.66	0.14
Egg yolk lecithin + phytanic acid	0.91	15.50	2897	0.0022

[a]800 transients; pulse width = 10 μs (56° flip angle).

bilayers for egg yolk lecithin – phytyl compound vesicles at 33°C is shown in Table 1.

An examination of these rates shows that the incorporation of 25 mol% phytol decreases the half-life for the vesicle leak from 6.5 days to 20 h, 25 mol% vitamin E from 6.5 days to 3.4 h, and 25 mol% phytanic acid by nearly 2900 times over the rate obtained for pure egg lecithin vesicles to 3.2 min.

After the disappearance of the upfield 'inside' resonance due to Pr^{3+} entering the vesicles, sufficient EDTA was routinely added to complex with accessible Pr^{3+} and spectra redetermined. Again, two peaks were resolved, the upfield peak now due to phosphorus nuclei on the outside of the bilayer which are directly exposed to the added EDTA. Such behaviour indicates two things. First, the disappearance of the upfield resonance with time after the initial addition of Pr^{3+}, cannot be due to vesicle rupture. If the destruction of vesicles were responsible for the disappearance of the upfield protected signal, the subsequent addition of EDTA should result in a single upfield peak since all Pr^{3+} should be accessible for complexation. Second, the mixed vesicles are not appreciably permeable to EDTA during the time required for the determination of a spectrum (3–10 min). Thus, the ^{31}P lis procedure indeed monitors the permeability of lecithin vesicles.

The ^{31}P nmr method lends itself best to diffusion studies which may be followed to completion during a time interval of 0–4 days. As can be seen, the observed half-life for pure egg yolk lecithin vesicles is on the order of 1 week. It was understandably not practical to conduct experiments of such duration. Therefore the observed rate for egg yolk lecithin is subject to considerably more error than for the more rapid rates in the case of the aforementioned mixed vesicle preparations. This is due to the smaller changes in peak areas in the time available. Repeated determinations of the permeability of pure egg yolk lecithin vesicles, which were run as standards for each determination, yielded rates from approximately 2×10^{-3} to 5×10^{-3} %/min. The standard deviations as computed from a least-squares treatment of the experimental data were typically on the order of 20–30% of the calculated rate. The decay rates for the mixed vesicle systems are much more easily measured over a much wider change of spectral area and are considered to be accurate to ±10%. It is clear that the incorporation of phytol, vitamin E, and phytanic acid greatly increases the permeability of egg yolk lecithin bilayers. The effects of these compounds on permeability parallels their effect on the fluidity or, more correctly, the microviscosity, of the bilayer as shown by ^{13}C T_1 relaxation times (6, 7), i.e., phytanic acid > vitamin E > phytol > lecithin alone.

Experiments were also carried out to determine the effect of temperature on the permeability of lecithin–phytol (3:1 mol ratio) mixed vesicles. The results are shown in Table 2. Raising the temperature from 11 to 52°C results in a rate increase of almost two orders of magnitude. In Fig. 2 the logarithms of the rates were plotted against the inverse of the absolute temperature (Arrhenius plot). The plot is linear, yielding an activation energy of 84.9 ± 0.8 kJ. It is interesting that the activation energy for Pr^{3+} permeation is in quite close agreement not only with that reported for Na^+ permeation through lecithin – phosphatidic acid bilayers (12) but also with that reported for the transverse diffusion (flip-flop) of spin labelled lecithin molecules across phospholipid bilayers (80.8 kJ) (13).

The rates of Pr^{3+} permeation (relative to egg yolk lecithin, 1.00) for mixed vesicles containing various amounts of α-tocopherol (2) are given in Table 3 and show a linear relationship between vitamin E concentration and log (relative rate). The table shows that even the incorporation of a small amount of vitamin E (3 mol%) results in the increase of the inward diffusion of Pr^{3+} to approximately 300% of its

TABLE 2. Permeation rates of Pr^{3+} into egg yolk lecithin vesicles containing 25 mol% phytol at various temperatures

Temperature (K)	Permeability[a] (%/min)
325	$525 \times 10^{-3} \pm 25 \times 10^{-3}$
306	$42 \times 10^{-3} \pm 2 \times 10^{-3}$
284	$6.7 \times 10^{-3} \pm 3.8 \times 10^{-3}$

[a]The errors reflect the standard deviation in the individually determined rates.

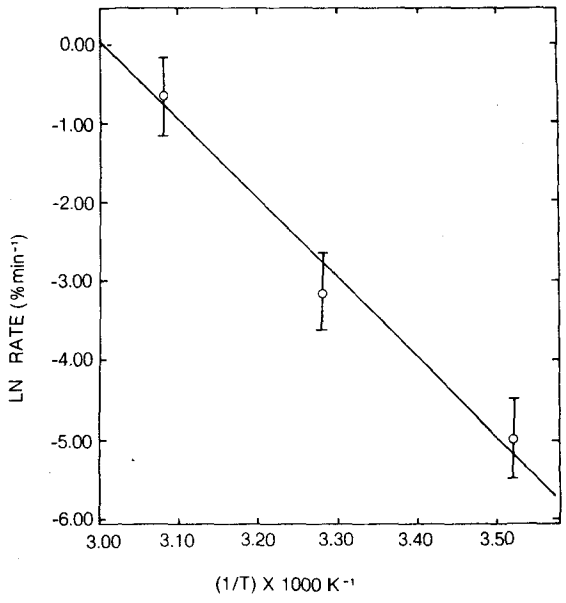

FIG. 2. Arrhenius plot of vesicle leak rate vs. the inverse of absolute temperature for 10% w/v egg yolk lecithin vesicles containing 25 mol% phytol.

original value. Thus, amounts of α-tocopherol, which approach the physiological ratios of α-tocopherol to phospholipid found in the human aorta (14, 15), exert a large effect on the permeability properties of the membrane.

Differential Scanning Calorimetry Measurements

Endotherms for the gel–liquid crystal phase transitions for bilayer membranes have been obtained using differential thermal analyses (dta) or differential scanning calorimetry (dsc). Figure 3 shows the dsc endotherms for phytol (**1**), α-tocopherol (**2**), and phytanic acid (**3**) incorporated into DPL at various mol percentages. As concentrations of **1**, **2**, and **3** are increased a lowering of the transition temperature, T_c, and a reduction in the heat of transition are observed. As concentrations approach 50 mol% the transition broadens out and eventually the endotherm disappears. This disappearance is no doubt due to the increased heterogeneity of the mixed DPL – phytyl compound system.

A plot of T_c vs. percentage composition for DPL–cholesterol, DPL–phytol, DPL–α-tocopherol, and DPL – phytanic acid mixtures is shown in Fig. 4. From the transition temperature lowering it is clear that phytanic acid causes the greatest destabilization of the membrane. Both phytol and α-tocopherol show similar thermal behaviour whereas **1**–**3** are all considerably lower than cholesterol.

The entropy associated with the melting of the fatty acyl chains of various DPL containing phytyl compounds can be calculated from the heat content at the transition temperature, T_c, since the Gibbs free energy for the order–disorder process is zero

$$[1] \qquad \Delta G = \Delta H - T_c \Delta S \simeq 0$$

hence $\Delta S = \Delta H/T_c$. The variation of ΔG with temperature is given by

$$[2] \qquad (\partial \Delta G/\partial T)_p = -\Delta S$$

A representative calculation of the entropy of gel – liquid crystal melt for identical mixtures (i.e., 25 mol% incorporated phytol, α-tocopherol, and phytanic acid) yields the specific entropy, s. For **1**, $s = 114.2\ \mathrm{J\ kg^{-1}\ K^{-1}}$; for **2**, $s = 85\ \mathrm{J\ kg^{-1}\ K^{-1}}$; and for **3**, $s = 126\ \mathrm{J\ kg^{-1}\ K^{-1}}$. This can be compared with the result for 25 mol% cholesterol incorporated into DPL which yields $s = 78\ \mathrm{J\ kg^{-1}\ K^{-1}}$ (specific enthalpy, $h = 24.27\ \mathrm{kJ\ kg^{-1}}$).

A significant increase in specific enthalpy is observed for the lecithin – phytanic acid – water system compared with lecithin–cholesterol–water. Lessened effects are observed for lecithin–phytol–water and lecithin – vitamin E – water mixtures show the smallest increase. As represented by the above values for s, the differences in enthalpy can be explained in terms of entropy differences. The significant difference in s values for α-tocopherol and phytol can be explained in terms of excluded volumes of **1** vs. **2** (see later).

Electron Spin Resonance

Nitroxide spin labels embedded in membranes, above T_c, undergo rapid anisotropic motion of limited amplitude. Jost *et al.* (16) used the following definition to describe the anisotropy about the molecular long axis:

$$[3] \qquad S_3 = \frac{T_{\parallel} - T_{\perp}}{T_{zz} - \frac{1}{2}(T_{xx} + T_{yy})}$$

Hubbell and McConnell (17) used a slightly modified form which takes into account the polarity of the bilayer;

$$[4] \qquad S_3 = \frac{T_{\parallel} - T_{\perp}}{T_{zz} - \frac{1}{2}(T_{xx} + T_{yy})} \frac{T_{xx} + T_{yy} + T_{zz}}{T_{\parallel} + 2T_{\perp}}$$

The order parameter, S_3, thus provides a good probe of local orientational mobility and order of lipid bilayers (18–20). In the present case relative order parameters for 5-doxylpalmitic acid in the mixed bilayers are presented, hence, the perturbing effect of the bulky nitroxide moiety is minimized. Order parameters have been determined for egg yolk lecithin multilayers containing 1% of the spin label 5-doxylpalmitic acid (2-(10-carboxydecyl)-2-butyl-4,4-dimethyl-3-oxazolidinyloxy) plus 25 mol% **1**, **2**, and **3**. 5-Doxylpalmitic acid is known to orient in egg yolk

ENDOTHERMIC

FIG. 3. Differ
The arrow indic

°K

TABLE 3. Per
lecithin vesic
of incorpora

Mol% vitami
25
15
8
3
0

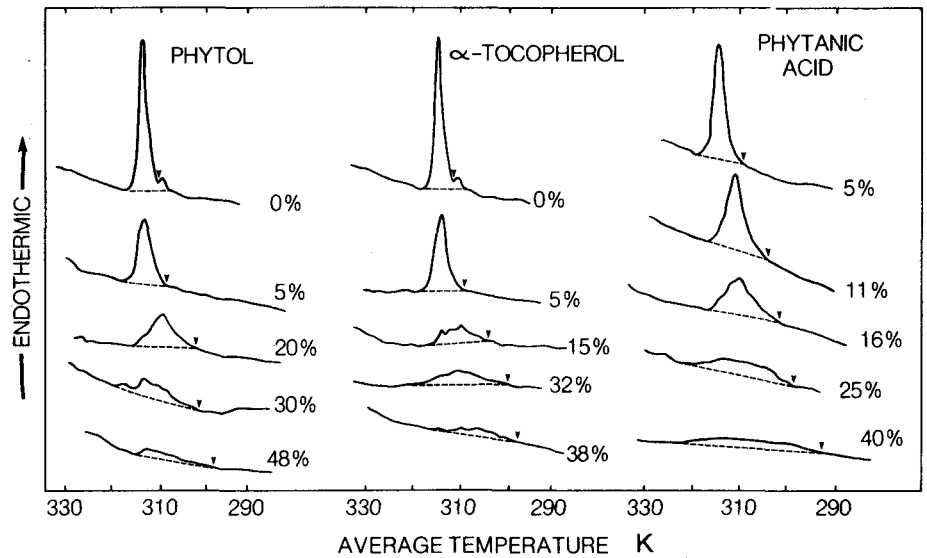

FIG. 3. Differential scanning calorimetry traces of DPL vesicles (10% w/v) plus varying amounts of compounds **1–3**. The arrow indicates the transition temperature, T_c.

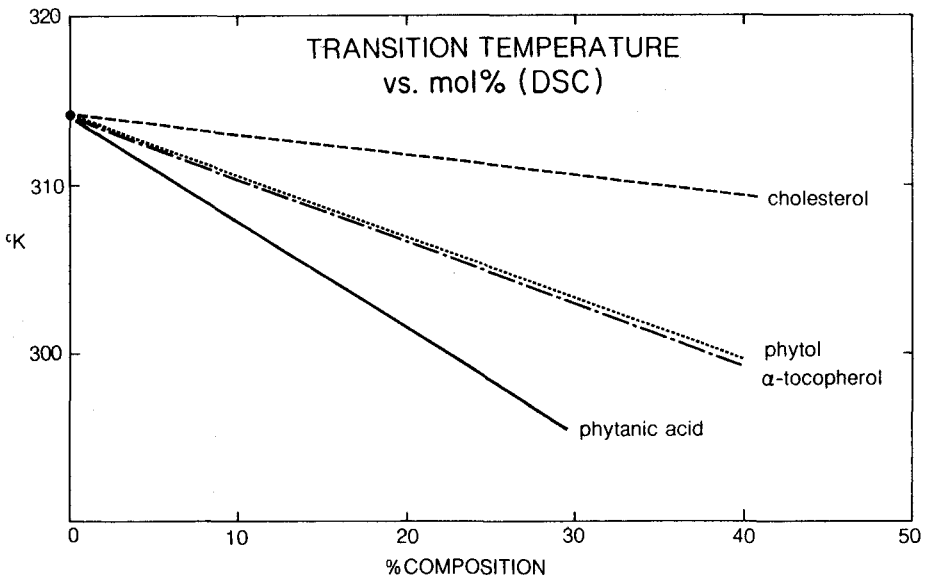

FIG. 4. Plot of transition temperature, T_c, vs. percentage **1**, **2**, or **3** or cholesterol.

TABLE 3. *Permeation rates of* Pr^{3+} *into egg yolk lecithin vesicles containing various concentrations of incorporated vitamin E at 33°C (relative to egg yolk lecithin = 1.00)*

Mol% vitamin E	Relative permeability
25	47.8
15	8.1
8	4.4
3	3.0
0	1.0

lecithin bilayers with the long axis of the fatty acid chain normal to the surface of the bilayer. Thus, $T_{\parallel}$ is the measured hyperfine tensor when B_0 is normal to the bilayer surface; $T_{\perp}$ when B_0 is parallel to the surface plane. S_3 for 5-doxylpalmitic acid in egg yolk lecithin containing 25 mol% phytol is 0.29, S_3 for egg yolk lecithin containing 25 mol% α-tocopherol is 0.50, and S_3 for egg yolk lecithin containing 20 mol% phytanic acid is 0.02, i.e., essentially isotropic. The value of S_3 for egg yolk lecithin alone is 0.54 in keeping with literature values (21–23). Thus, vitamin E, **2**,

has a small effect on the ordering of the phospholipids in the bilayer, phytol disorders the egg yolk lecithin bilayer more while phytanic acid completely disrupts the bilayer.

Discussion

The intercalation of phytol, vitamin E, or phytanic acid was previously shown to greatly increase the fluidity of the mixed membrane, as monitored by ^{13}C T_1 relaxation times (6, 7). The fluidizing effect was found to increase in the order phytol < vitamin E < phytanic acid. For example, the incorporation of 25 mol% vitamin E increased the ^{13}C T_1 relaxation times for the lecithin fatty acid carbons by 50–100%, whereas the largest increases, which were found upon the incorporation of 25 mol% phytanic acid, were on the order of 150–200%.

The perturbations caused by the incorporation of phytol, vitamin E, and phytanic acid as monitored by the ^{13}C T_1 values have been found to correlate with permeability increases of mixed phospholipid – phytyl compound vesicles to the Pr^{3+} cation using ^{31}P nmr spectroscopy. At 33°C, the permeability of egg yolk lecithin vesicles was increased by approximately 8 times upon the incorporation of 25 mol% phytol, by approximately 48 times upon the incorporation of 25 mol% vitamin E, and by approximately 2900 times upon the incorporation of 25 mol% phytanic acid. In other words, the permeability of the two component (lecithin – phytyl compound) vesicles increases in the order phytol < vitamin E < phytanic acid. This is the same order in which the ^{13}C T_1 relaxation times increase. From the ^{13}C T_1 values of the various lecithin carbons effective correlation times, τ_{eff}, can be obtained for the motion. These τ_{eff} reflect the relative change in 'fluidity' or, more precisely, microviscosity caused by the phytyl compounds at a particular position in the bilayer.

Incorporation of a smaller amount of vitamin E which approaches physiological concentrations (3 mol%) still results in a permeability increase to 300% of the rate for pure egg yolk lecithin vesicles (Table 3).

Monolayers of phytol, α-tocopherol, and phytanic acid occupy molecular areas of 55, 60, and 61 Å^2 per molecule at 0.5 dyn/cm, respectively (24), whereas cholesterol is known to form stable monolayers of area 40 Å^2 per molecule. Thus, the area requirements for the phytyl molecules is much higher. Such large monolayer areas must be due to the branched nature of the chains, since the unbranched C18 acid, stearic acid occupies monolayer areas of the order of 24 Å^2 per molecule (24).

Above the lecithin gel–liquid crystalline transition temperature, cholesterol is known to fit into cavities created by thermal motion of the fatty acyl chains causing an 'intermediate fluid' condition (25, 26). In addition, mixed monolayers of lecithin and cholesterol do not follow the additivity rule since cholesterol occupies pockets in the membrane and causes little proportional increase in the area/molecule of mixed monolayers. Such behaviour has been correlated with a decrease in permeability above T_c (12, 27). Very recently the monolayer behaviour of vitamin E in lecithin monolayers has been studied (28). It was found that in monolayers of distearoyl- or dioleoyllecithin the additivity rule was well followed, up to 50 mol% incorporated α-tocopherol. This indicates that, unlike cholesterol, α-tocopherol is not able to fit into the cavities between adjacent lecithin molecules and displaces its full area requirement in mixed lecithin–α-tocopherol systems. Such behaviour necessarily involves an increase in lipid–lipid separation due to intercalated vitamin E.

The total interaction energy owing to London – Van der Waals dispersion forces between the long hydrocarbon tails of phospholipids is proportional to the inverse fifth power of the intermolecular distance (29). Thus, even a small lateral expansion of the lipid bilayer would result in a large decrease in the interaction energies of adjacent lipid molecules. As an example, it has been found that the presence of a single methyl group in isostearic acid reduces the interaction energy from that of stearic acid by a factor of three (29). This decrease in intermolecular attraction would be expected to become even more severe for more highly branched molecules such as phytol, vitamin E, and phytanic acid.

Decreases in intermolecular attractions and increases in phospholipid–phospholipid packing distances due to the incorporation of phytol, vitamin E, and phytanic acid are consistent with the esr results. Vitamin E (**2**), with a monolayer area of 60 Å^2 per molecule, causes the least perturbation of the three. Although **2** has nearly the same area requirements as phytanic acid (60 vs. 61 Å^2/molecule) because of its extremely hydrophobic nature it is not expected to penetrate as far into the region of the lecithin headgroup. This is reflected in the order parameter for **2**, $S_3 = 0.50$, which is essentially unchanged from S_3 for egg yolk lecithin alone (0.54). Phytol, whose hydroxyl group we have shown previously (6) to penetrate to within hydrogen bonding distance of the head group phosphate, yields a smaller order parameter for the bilayer (S_3 (**1**) = 0.29) even though the surface area requirements for phytol are smaller than those for **2** and **3**. This becomes clear when it is remembered that, although the characteristic 'plateau' of S_3 vs. hydrocarbon chain position for phospholipid bilayers is constant from C1–C10 (30), the nitroxide moiety in 5-doxylpalmitic acid probes the

local region al
greatest disorc
addition to t
phytanic acid
philic region,
lecithin–lecithi
detergent effec
other hand, s
lecithin molec
distant, lecithi
action. The th
also consistent
deeply in the l

The very hig
parameter for
actions at the
portant with r
bilayer.

To confirm
fact due to the
the unbranche
in egg yolk lec
Pr^{3+} permeati
tion of 25 m
lecithin using
upfield ^{31}P sig
value, yielding
on the order
alone. Similar
palmitic acid
the 'fluidity' o
egg yolk leci
±10.7% from
error limit o
acid has a v
molecule), it
by thermal f
chains above
temperature a
little perturba
attractive forc
vitamin E, a
phospholipid
and reorienta
creased perm

Financial s
Research Cou
edged.

1. A. L. Tappi
2. I. Molenaa
45 (1975).

local region about C1 (31). Phytanic acid causes the greatest disorder in the bilayer ($S_3 = 0.02$) since in addition to the large surface area requirement, phytanic acid penetrates furthest into the hydrophilic region, further interfering with the normal lecithin–lecithin headgroup ionic interaction, the detergent effect. Phytol (**1**) and vitamin E (**2**), on the other hand, simply decrease the attraction of one lecithin molecule for an adjacent, but now more distant, lecithin molecule by nonbonded steric interaction. The thermodynamic calculations, above, are also consistent with the fact that **2** is embedded more deeply in the bilayer than **3** and **1**.

The very high permeation rates and very low order parameter for phytanic acid indicate that interactions at the lecithin headgroup are the most important with regard to the structural integrity of the bilayer.

To confirm that the effects on the bilayer are in fact due to the branched nature of the phytyl chains, the unbranched C16 acid, palmitic acid, was studied in egg yolk lecithin bilayers. No change in the rate of Pr^{3+} permeation was observed upon the incorporation of 25 mol% of palmitic acid into egg yolk lecithin using ^{31}P lis. Over a three day period, the upfield ^{31}P signal decayed to ~90% of its original value, yielding a rate of 2.4×10^{-3} %/min, which is on the order of that obtained for egg yolk lecithin alone. Similarly, the incorporation of 25 mol% of palmitic acid into egg yolk lecithin had no effect on the 'fluidity' of the bilayer since the ^{13}C T_1 values of egg yolk lecithin varied by only an average of ±10.7% from egg yolk lecithin alone (i.e., on the error limit of the measurements). Since palmitic acid has a very small area requirement (≃24 Å^2/molecule), it is able to fit into the cavities created by thermal fluctuations of the lecithin fatty acid chains above the gel–liquid crystalline transition temperature and, because it is unbranched, causes little perturbation of the London – Van der Waals attractive forces. In contrast, incorporation of phytol, vitamin E, and phytanic acid perturb the normal phospholipid packing, resulting in increased fluidity and reorientational disorder of the bilayer and increased permeability of the bilayer to ions.

Acknowledgement

Financial support of this work by the National Research Council of Canada is gratefully acknowledged.

1. A. L. TAPPEL. Vitam. Horm. **20**, 493 (1962).
2. I. MOLENAR, J. VOS, and F. A. HOMMES. Vitam. Horm. **30**, 45 (1975).
3. M. C. MACBRINN and J. S. O'BRIEN. J. Lipid Res. **9**, 552 (1968).
4. J. A. LUCY and J. T. DINGLE. Nature, **204**, 156 (1964).
5. F. WEBER, U. GLOOR, and O. WISS. Helv. Chim. Acta, **41**, 1038 (1958).
6. R. J. CUSHLEY and B. J. FORREST. Can. J. Chem. **54**, 2059 (1976).
7. R. J. CUSHLEY and B. J. FORREST. Can. J. Chem. **55**, 220 (1977).
8. W. S. SINGLETON, M. S. GRAY, M. L. BROWN, and J. L. WHITE. J. Am. Oil Chem. Soc. **42**, 53 (1965).
9. L. I. BARSUKOV, A. M. PARFEN'EVA, A. V. VIKTOROV, YU. E. SHAPIRO, V. F. BYSTROV, and L. D. BERGELSON. Biofizika, **19**, 456 (1974).
10. M. S. FERNANDEZ, H. CELIS, and M. MONTAL. Biochim. Biophys. Acta, **323**, 600 (1973).
11. V. F. BYSTROV, YU. E. SHAPIRO, A. V. VICTOROV, L. I. BARSUKOV, and L. D. BERGELSON. FEBS Lett. **25**, 337 (1972).
12. D. PAPAHADJOPOULOS, S. NIR, and S. OHKI. Biochim. Biophys. Acta, **266**, 561 (1972).
13. R. D. KORNBERG and H. M. MCCONNELL. *J. Am. Chem.* Soc. **94**, 4475 (1972).
14. E. C. MCCORMICK and R. H. MCCLUER. Circulation, **22**, 651 (1969).
15. T. ITO. Jpn. Circ. J. **33**, 25 (1969).
16. P. JOST, L. J. LIBERTINI, V. C. HEBERT, and O. H. GRIFFITH. J. Mol. Biol. **59**, 77 (1971).
17. W. L. HUBBELL and H. M. MCCONNELL. J. Am. Chem. Soc. **93**, 314 (1971).
18. J. SEELIG. *In* Spin labeling theory and applications. *Edited by* L. J. Berliner. Academic Press Inc., New York, NY. 1976. p. 373.
19. I. C. P. SMITH and K. W. BUTLER. *In* Spin labeling theory and applications. *Edited by* L. J. Berliner. Academic Press Inc., New York, NY. 1976. p. 411.
20. O. H. GRIFFITH and P. C. JOST. *In* Spin labeling theory and applications. *Edited by* L. J. Berliner. Academic Press Inc., New York, NY. 1976. p. 454.
21. S. SCHREIER-MUCCILLO, D. MARSH, H. DUGAS, H. SCHNEIDER, and I. C. P. SMITH. Chem. Phys. Lipids, **10**, 11 (1973).
22. J. SEELIG, H. LIMACHER, and P. BADER. J. Am. Chem. Soc. **94**, 6364 (1972).
23. B. G. MCFARLAND and H. M. MCCONNELL. Proc. Natl. Acad. Sci. U.S.A. **68**, 1274 (1971).
24. G. L. GAINES, JR. *In* Insoluble monolayers at liquid–gas interfaces. *Edited by* I. Prigogine. Wiley-Interscience, New York, NY. 1966. p. 1.
25. D. O. SHAH and J. H. SCHULMAN. J. Lipid Res. **8**, 215 (1967).
26. R. A. DEMEL, W. S. M. GEURTSVANKESSEL, and L. L. M. VANDEENEN. Biochem. Biophys. Acta, **226**, 26 (1972).
27. J. DEGIER, J. G. MANDERSLOOT, and L. L. M. VANDEENEN. Biochim. Biophys. Acta, **173**, 143 (1969).
28. B. MAGGIO, A. T. DIPLOCK, and J. A. LUCY. Biochem. J. **161**, 111 (1977).
29. L. SALEM. Can. J. Biochem. Physiol. **40**, 1287 (1962).
30. G. W. STOCKTON, C. F. POLNASZEK, A. P. TULLOCH, F. HAZAN, and I. C. P. SMITH. Biochemistry, **15**, 954 (1976).
31. P. E. GODICI and F. R. LANDSBERGER. Biochemistry, **13**, 362 (1974).

Application of the Osterberg–Sarkar–Kruck method for obtaining free ion concentrations in solutions of complex equilibria

ROGER GUEVREMONT AND DALLAS L. RABENSTEIN

Department of Chemistry, The University of Alberta, Edmonton, Alta., Canada T6G 2G2

Received September 1, 1978

ROGER GUEVREMONT and DALLAS L. RABENSTEIN. Can. J. Chem. 57, 466 (1979).

A titration system has been developed for collecting pH titration data of sufficient accuracy for use with the method developed by Osterberg, and Sarkar and Kruck, for extracting free metal and free ligand concentrations from pH titration data. Titrant is delivered from a gravimetric buret capable of part per ten thousand precision, and a concentrated metal or ligand solution is added from a second buret to satisfy the theoretical requirement that the total metal or ligand concentration remain constant. The entire system is computer controlled. Application of the titration system and procedures for extracting free ligand and free metal concentrations from pH titration data are demonstrated with a study of the complexation chemistry of zinc with aspartic acid.

ROGER GUEVREMONT et DALLAS L. RABENSTEIN. Can. J. Chem. 57, 466 (1979).

On a mis au point un système de titrage permettant de recueillir des données de dosage de pH assez précises pour être utilisées avec la méthode développée par Osterberg, et Sarkar et Kruck, pour déduire les concentrations de métal libre et de ligand libre à partir de données de titrages de pH. Le titrant est ajouté à l'aide d'une burette gravimétrique capable d'une précision d'une partie par dix milles; on ajoute une solution concentrée de métal ou de ligand à l'aide d'une deuxième burette afin de satisfaire aux exigences théoriques voulant que la concentration totale du métal ou du ligand soit constante. Le système global est contrôlé par un ordinateur. On a démontré la validité du système de titrage et des procédés nécessaires à l'extraction des concentrations de ligand libre et de métal libre à partir de titrages de pH à l'aide d'une étude de la chimie de complexation du zinc par l'acide aspartique.

[Traduit par le journal]

Introduction

In a previous paper (1), we reported on a study of the method developed by Osterberg (2) and Sarkar and Kruck (3) for estimating the concentrations of free ligand and free metal in solutions of complex equilibria. The results of that study indicate that successful application of this method, which we call the FICS method for *F*ree *I*on *C*oncentrations in *S*olution, requires a large quantity of highly accurate data and, as pointed out by Sarkar and Kruck (3) in their original publication on this method, careful design of the experimental system so as to satisfy the theoretical requirements of the method.

In this paper, we describe a titration system designed for the purpose of collecting potentiometric data suitable for the FICS method. The system has been designed to minimize those potential sources of error identified in previous publications (1, 3, 4). The heart of the system is a gravimetric buret (5), which is capable of part per ten thousand precision. To compensate for changes in metal or ligand concentration due to dilution by titrant, which can lead to large errors in the FICS method, a concentrated metal or ligand solution is added from a second buret. The entire system is computer controlled because of the large amount of data required. The titration system and the procedures described previously (1) for extracting formation constants from pH titration data by the FICS method are then tested with a study of the complexation chemistry of zinc with aspartic acid.

The FICS Method

The FICS method is based on the general relations (2, 3)

$$[1] \quad p[L] = p[L]_0 - \int_{pH_0}^{pH} \left(\frac{dC_H}{dC_L}\right)_{C_M,pH} dpH$$

$$[2] \quad p[M] = p[M]_0 - \int_{pH_0}^{pH} \left(\frac{dC_H}{dC_M}\right)_{C_L,pH} dpH$$

where C_H is the total concentration of titratable protons, C_L and C_M are the total analytical concentrations of ligand and metal, respectively, and [L] and [M] are their free concentrations. $p[L]_0$ is the negative logarithm of the concentration of free L at some initial pH_0. If possible, a pH_0 is usually chosen at which no complex is formed so that $[L]_0$ and $[M]_0$ are equal to (or can be calculated from) C_L and C_M. The integral of $(dC_H/dC_L)_{C_M,pH}$ or $(dC_H/dC_M)_{C_L,pH}$ is evaluated from pH_0 to the pH at which p[L] or p[M] are to be evaluated. This requires that $(dC_H/dC_L)_{C_M,pH}$ and $(dC_H/dC_M)_{C_L,pH}$ be determined experimentally

as a function o
given pH. One
$dC_L)_{C_M,pH}$ is to
C_L is varied w
components are
the C_H values fr
(3). The rate of
is equal to (d
titrations on s
provide $(dC_H/d$

As stated by
in our previou
remain constan
$dC_L)_{C_M,pH}$ and
this titration pr
as titrant is ad
evaluation of
systematic natu
cumulative, an
ence between p
tions in C_L cau
random errors
parts per thou
creased the err
[M] (1).

Apparatus

A schematic d
tiometric titratior
for the FICS meth
to the sample cell
capable of parts
sensing compone
balance with a ser
with a Corning
Na_2SO_4(satd)) el
sured with a sens
digital pH meter
of the pH meter
multiplexer circu
of six BCD digit
multiplexer. The
PDP11/10 minic
Laboratory Peri
digital input, 16
options. The dat
disc. To compen
ligand or metal
from an auxiliary

The program c
tiometric data wa
tions of this prog
the gravimetric b
to collect BCD d
to supply the ap
operations, and t
addition the pr
These include c
reached, estimat

0008-4042/79/040466-06$01.00/0

as a function of pH over the pH range pH_0 to the given pH. One way to accomplish this for $(dC_H/dC_L)_{C_M,pH}$ is to perform a series of titrations where C_L is varied while the concentrations of all other components are kept constant, and then to compare the C_H values from the series of C_L values at each pH (3). The rate of change in C_H with C_L at a given pH is equal to $(dC_H/dC_L)_{C_M,pH}$. Similarly, a series of titrations on solutions of varying C_M will serve to provide $(dC_H/dC_M)_{C_L,pH}$.

As stated by Sarkar and Kruck (3) and confirmed in our previous study (1), C_M and C_L must indeed remain constant to obtain correct values for $(dC_H/dC_L)_{C_M,pH}$ and $(dC_H/dC_M)_{C_L,pH}$, respectively, by this titration procedure. If C_M is allowed to decrease as titrant is added in the titrations designed for the evaluation of $(dC_H/dC_L)_{C_M,pH}$, serious error of a systematic nature results in p[L] (1). The error is cumulative, and increases in magnitude as the difference between pH_0 and pH increases. Similarly, variations in C_L cause errors in p[M]. We also found that random errors in C_H of a magnitude greater than 2 parts per thousand of the initial C_H significantly increased the errors in the final estimates of [L] and [M] (1).

Experimental

Apparatus

A schematic diagram of the computer controlled potentiometric titration system designed to collect data specifically for the FICS method is shown in Fig. 1. The titrant is delivered to the sample cell from an optically-coupled gravimetric buret capable of parts per ten thousand precision (5). The weight sensing component is a Sartorius 3015 electronic top loading balance with a sensitivity of 1 mg. The sample pH is monitored with a Corning glass electrode and a reference (Ag/AgCl, Na_2SO_4(satd)) electrode pair. The electrode potential is measured with a sensitivity of 0.1 mV with a Fisher Accumet 520 digital pH meter. The binary coded decimal (BCD) outputs of the pH meter and electronic balance are fed to a simple multiplexer circuit. Because output from the balance consists of six BCD digits, these are divided into two channels of the multiplexer. The data are collected from the multiplexer by a PDP11/10 minicomputer. The computer was equipped with a Laboratory Peripheral System (LPS) which included 16 bit digital input, 16 bit digital output, and programmable clock options. The data were stored on cassette tape or on floppy disc. To compensate for dilution by titrant, a concentrated ligand or metal solution was added to the sample solution from an auxiliary delivery system (Mettler DV11 piston buret).

The program controlling the automatic collection of potentiometric data was written in FORTRAN IV. The main functions of this program are to control the delivery of titrant from the gravimetric buret and from the Mettler DV11 piston buret, to collect BCD data from the pH meter and electronic balance, to supply the appropriate delay intervals and time the above operations, and to store the data for further manipulations. In addition the program performs several logical operations. These include deciding if electrode equilibrium has been reached, estimation of the quantity of titrant to be added before the next data point, and calculation of the quantity of concentrated ligand or metal solution to be added from the auxiliary delivery unit in order to compensate for dilution.[1]

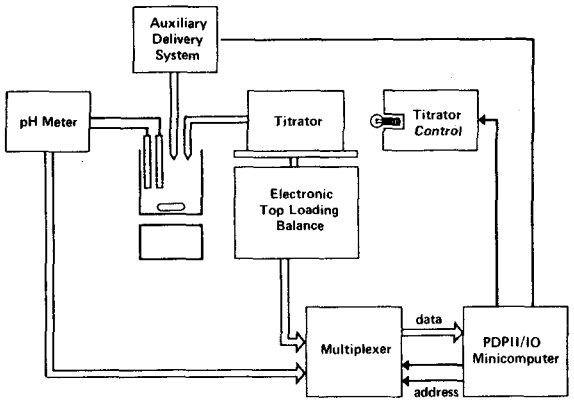

FIG. 1. Schematic diagram of the automatic titration system.

The most important logical processes are those involving electrode equilibrium and the delivery of titrant. The electrode potential is sampled over an interval of, for example, 6 s and the average, standard deviation (sd), and drift in those sampled values are calculated. Typically 5 values are taken over this time interval. Optimum values of allowable SD and drift are chosen to arrive at a working compromise between the selection of a reliable electrode potential and avoiding unnecessary repetition of sampling the electrode potential. The quantity of titrant to be added for the next data point is estimated on the basis of the effect of the previous addition on the electrode potential. If the electrode potential changes by less than some minimum value, perhaps 5 mV, then the previous addition is doubled. Within other appropriate limits the increment is increased or decreased by factors of two to five. The limits are chosen on the basis of the number of data points desired.

Procedure

The measured electrode potentials were converted to p_aH on the basis of standardization with NBS reference solutions of phthalate (pH 4.008), phosphate (pH 7.413), and carbonate (pH 10.012) (6). The role of the pH measurement in the FICS method (1) makes it unnecessary to convert hydrogen ion activity to hydrogen ion concentration.

All solutions were prepared or standardized on the basis of weight. Carbonate-free NaOH titrant was standardized by gravimetric titration of primary standard KHP. A standard zinc solution was prepared by dissolution of Zn metal in a small volume of HNO_3. The excess acid was neutralized with NaOH before dilution. $NaClO_4$ was added to bring the ionic strength to 0.3 mol/kg. Aspartic acid was recrystallized from cold ethanolic solution, washed thoroughly with ethanol, and dried in air. A stock solution prepared from the recrystallized aspartic acid and $NaClO_4$ (0.3 mol/kg) was standardized by gravimetric titration with NaOH. All of the sample solutions were prepared by combination of a weighed portion of a 0.3 mol/kg $NaClO_4$ stock diluent solution, a weighed portion of the zinc solution, and a weighed portion of the aspartic acid solution to bring the total to 200.00 ± 0.01 g. These solutions were titrated gravimetrically with NaOH at 25.0 ± 0.1°C and

[1]More details about the computer program can be obtained from the authors.

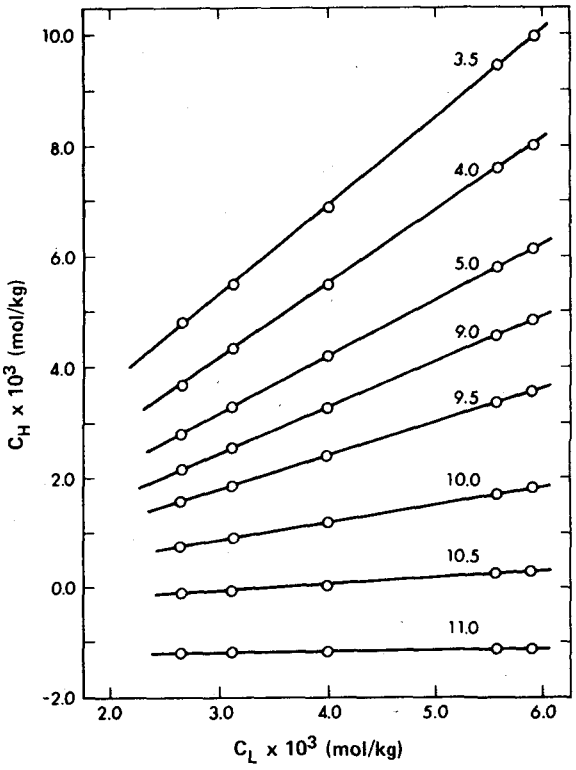

FIG. 2. C_H vs. C_L at selected pH values for aspartic acid.

under a CO_2-free nitrogen or argon atmosphere. The series of titrations in which each component was varied was carried out in the order C_3, C_2, C_4, C_1, and C_5 where $C_1 < C_2 < C_3 < C_4 < C_5$.

Results

The Protonation Constants of Aspartic Acid

A series of solutions of varying aspartic acid concentration (2.643×10^{-3} to 5.908×10^{-3} mol/kg) was titrated from pH 3.5 to pH 11.0. The concentration of titratable protons (C_H) was calculated, and the change in C_H with change in the total concentration of aspartic acid is shown in Fig. 2. The slopes of the lines are the experimental values of the term $(dC_H/dC_L)_{pH}$ of eq. [1]. The values of these derivatives are shown as a function of pH in Fig. 3. The overall formation constants of the protonated forms of aspartic acid were calculated from these data by the iterative procedure described previously (1). First, the concentration of completely deprotonated ligand, [L], was estimated to be equal to the total aspartic acid concentration at pH 11.0. The concentration of completely deprotonated ligand was then calculated as a function of pH with this estimated $p[L]_0$ and the data for (dC_H/dC_L) shown in Fig. 3. The overall formation constants of the protonated forms of aspartic acid were calculated from these values for [L] and the mass balance (C_L) for the aspartic acid,

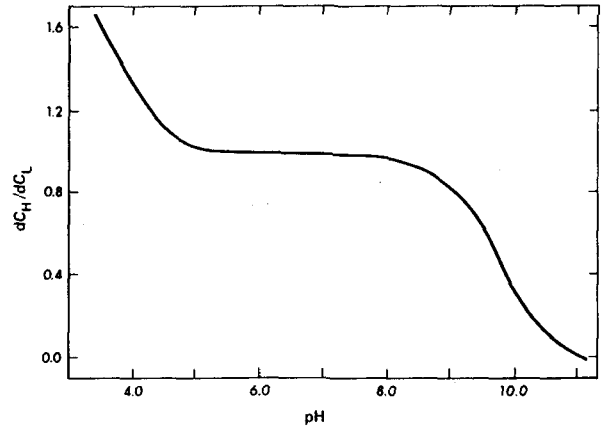

FIG. 3. (dC_H/dC_L) as a function of pH for aspartic acid.

and finally the value of [L] at pH 11 was calculated using these constants. As expected, the initial estimate that [L] equalled C_L was slightly incorrect and the calculated value of [L] was therefore taken as a next best estimate of $p[L]_0$ at pH 11.0. The above series of calculations was repeated to get a new estimate of $p[L]_0$ at pH 11.0. After three such iterations there was no change in the value of $p[L]_0$. The final values of the protonation constants are shown in Table 1. A summary of literature values (7–14) is also included in Table 1.

The Formation of Complexes Between Zinc and Aspartic Acid

Two series of titrations of mixtures of zinc and aspartic acid were carried out, the first designed to study the general nature of the changes in C_H with changes in the total aspartic acid concentration at a fixed zinc concentration, and the second designed to provide [L] and [M] data with which to calculate formation constants.

The first set of titrations was carried out at a constant zinc concentration of 9.370×10^{-4} mol/kg and total aspartic acid concentration varying from 1.1×10^{-3} to 5.6×10^{-3} mol/kg. The zinc concentration was maintained at a constant value by adding the appropriate amounts of a concentrated zinc solution after each addition of titrant. Plots of C_H as a function of the total aspartic acid concentration showed some curvature below a ligand-to-metal ratio of 2 to 1. Though the curvature was not severe, our previous studies (1) indicate that the most reliable results are obtained if the C_H vs. C_L plots are linear. To obtain linear C_H vs. C_L plots in the second set of titrations, ligand-to-metal ratios greater than 3 to 1 were used.

Ten titrations were performed, five at a constant zinc concentration of 9.370×10^{-4} mol/kg, and five at a constant aspartic acid concentration of $5.308 \times$

TABLE 1. Protonation constants of aspartic acid, and stability constants of zinc – aspartic acid complexes

log β[a]				Conditions		
H_2L	HL	ZnL	ZnL_2	Temperature	Ionic strength	Reference
13.36	9.68	5.66	10.14	25	0.3	This work
13.33	9.63			25	0.1	6
		5.73	10.20	25	0.2	7
13.4	9.46	5.84	10.15	30	0.1	8
12.87	9.27	6.01	10.10	37	0.15	9
13.34	9.63			25	0.1	10
13.34	9.87			25	0.1	11
13.32	9.62			25	0.1	12
13.31	9.61			25	1.0	13

[a]β is the overall protonation or stability constant; $\beta_{H_2L} = [H_2L]/[H]^2[L]$ and $\beta_{ZnL_2} = [ZnL]/[Zn][L]^2$.

10^{-3} mol/kg. The change in C_H with change in C_L at constant C_M is shown in Fig. 4 and the change in C_H with change in C_M at constant C_L is shown in Fig. 5. The slopes, $(dC_H/dC_L)_{C_M,pH}$ and $(dC_H/dC_M)_{C_L,pH}$, are plotted as a function of pH in Fig. 6. Data are shown in Figs. 4–6 for selected pH values; (dC_H/dC_L) and (dC_H/dC_M) were actually evaluated at 0.1 pH unit intervals. The curve for (dC_H/dC_L) is similar to, but not identical with, that shown in Fig. 3 for aspartic acid in the absence of zinc. The curve for (dC_H/dC_M) indicates that complexation begins in the pH range 4.0 to 5.0 where (dC_H/dC_M) first deviates significantly from zero.

The concentrations of free aspartic acid in the completely deprotonated form, [L], and free zinc, [M], were calculated using the (dC_H/dC_L) and (dC_H/dC_M) data and eqs. 1 and 2. It was assumed as a first approximation that [M] at pH 4.0 equalled C_M, and [L] was calculated from C_L and the protonation constants measured above. Using these as initial estimates for [L] and [M] over the pH range 5 to 8, formation constants were calculated by the procedure described previously (1). Since there is some complexation at pH 5.0, the iterative procedure was used to obtain final values for $p[L]_0$ and $p[M]_0$. The free ligand and free metal data were used as described previously (1) to determine the stoichiometries of the complexes. Over the pH range 5 to 8, the complexes ZnL and ZnL_2^{2-} account for nearly all the complexed zinc and aspartic acid, and the best estimates for $\log \beta_{ZnL}$ and $\log \beta_{ZnL_2}$ were 5.66 and 10.14, respectively. With a somewhat wider pH range, from 4.0 to 9.0, there appear to be complexes with the stoichiometries $HZnL^+$ and ZnL_3^{4-} forming at the extremes of the pH range. $\log \beta_{HZnL}$ and $\log \beta_{ZnL_3}$ were estimated to be 10.8 and 12.9, respectively. Other workers have reported the species $HZnL^+$ and $ZnL_2(OH)_2^{4-}$ (10).

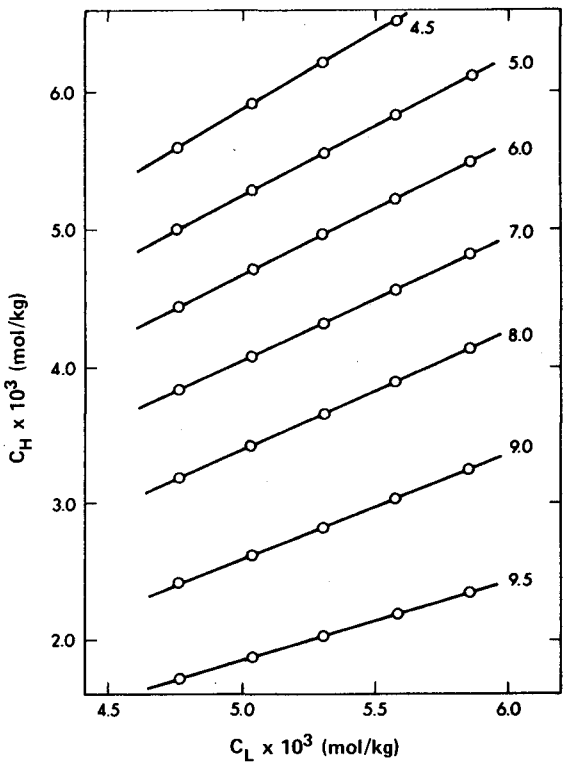

FIG. 4. C_H as a function of the total concentration of aspartic acid (C_L) for the zinc – aspartic acid system. The total zinc concentration was 9.370×10^{-4} mol/kg.

Discussion

A study of the complexation chemistry of zinc with aspartic acid was chosen to test the titration apparatus and the procedures described previously (1) for extracting free ion concentrations from titration data by the FICS method. A relatively simple system was chosen to avoid difficulty in assigning a model to the complexation equilibria. The fol-

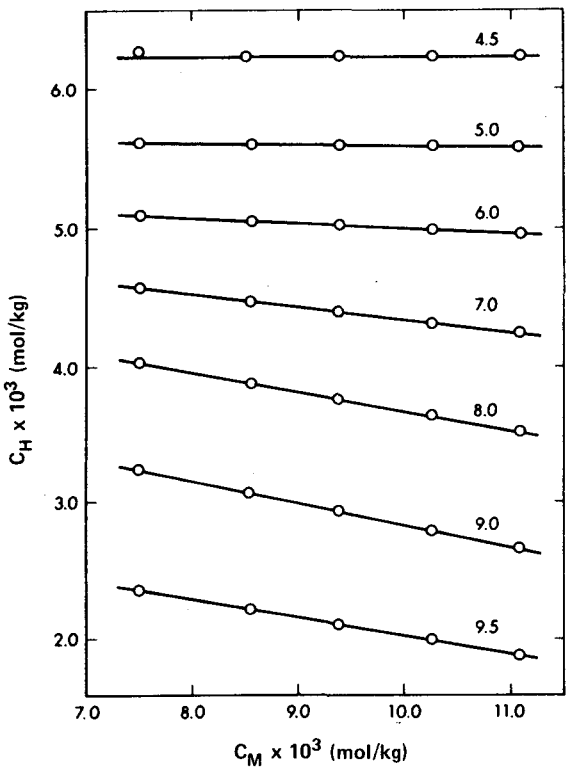

FIG. 5. C_H as a function of the total concentration of zinc (C_M) for the zinc – aspartic acid system. The total aspartic acid concentration was 5.308×10^{-3} mol/kg.

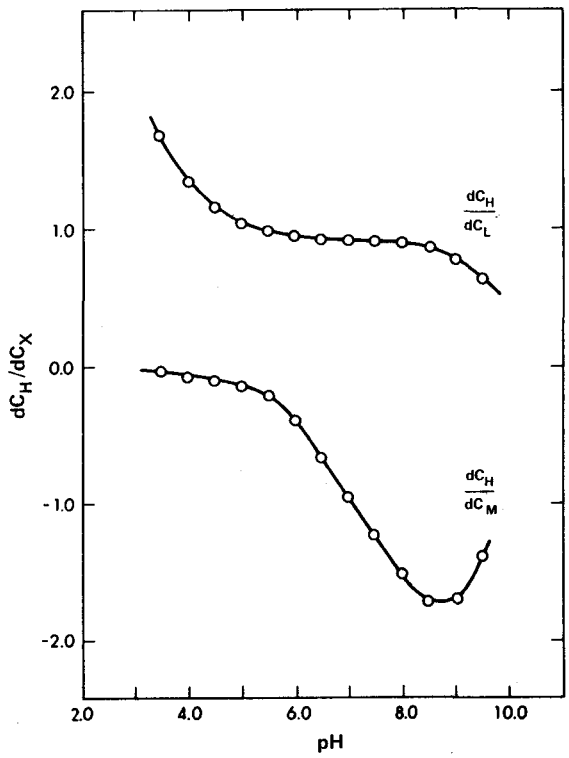

FIG. 6. (dC_H/dC_L) and (dC_H/dC_M) as a function of pH for the zinc – aspartic acid system. The derivatives were evaluated for a solution having a zinc concentration of 9.370×10^{-4} mol/kg and an aspartic acid concentration of 5.308×10^{-3} mol/kg.

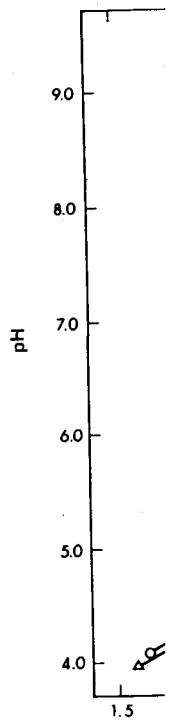

FIG. 7. Experim
for a solution co
5.308×10^{-3} mo
0.3925 mol NaOH

lowing discussion will deal first with details of the application of the FICS method, and then the results of the zinc – aspartic acid experiments.

Our earlier studies (1) based on simulated titration data revealed that the FICS method will provide accurate values of [L] and [M] only if the data are highly reliable and, as pointed out by Sarkar and Kruck (3), only if the theoretical requirements of the method are met. The experiments with the zinc – aspartic acid system have revealed several other difficulties which can be encountered in an application of the FICS method. The accuracy of the derivative terms, (dC_H/dC_L) and (dC_H/dC_M), is dependent on the accuracy of C_H, C_L, and C_M, and the changes in C_H, C_L, and C_M. The most severe problems are associated with obtaining data of sufficient accuracy below pH 4 and above pH 10. At these pH extremes, the pH is changing relatively slowly as titrant is added. The result is that the error in C_H due to an error of a fixed magnitude in pH, for example ± 0.1 mV which corresponds to ± 0.002 pH units, is larger than when the pH is changing more rapidly. However, it is necessary to start the titration at a low pH where the ligand is protonated and the metal ion free so that $p[L]_0$ and $p[M]_0$ can be estimated. In the study of the zinc – aspartic acid system, a pH of 5.0 was used for pH_0 even though some complex has formed at this pH. The correct values of $p[L]_0$ and $p[M]_0$ were then obtained by an iterative procedure (1). This is a workable solution to the problems associated with using a very low pH_0, unless a model cannot be found for the complexation at pH_0 or if a large portion of the metal and ligand is complexed at this pH.

The FICS method for extracting [L] and [M] as a function of pH from titration data has a considerable advantage over other calculation methods in that it provides free ligand and free metal concentrations without a priori assumptions about a model for complexation (3). Since the values of [L] and [M] obtained from the raw data do not reflect the effect of application of some arbitrary hypothetical model, a model may be systematically derived from the data. The method also has considerable advantage with respect to the role of the pH measurement (1). The calibration must be accurate and reproducible from titration to titration, but, as illustrated in this work, a conversion from hydrogen ion activity to hydrogen ion concentration is unnecessary if the C_M and C_L

mass balances
constants. Ho
used, the pH r
ion concentrat
The compar
and the forma
data is the fin
the FICS met
for the zinc –
from the form
for ZnL and Z

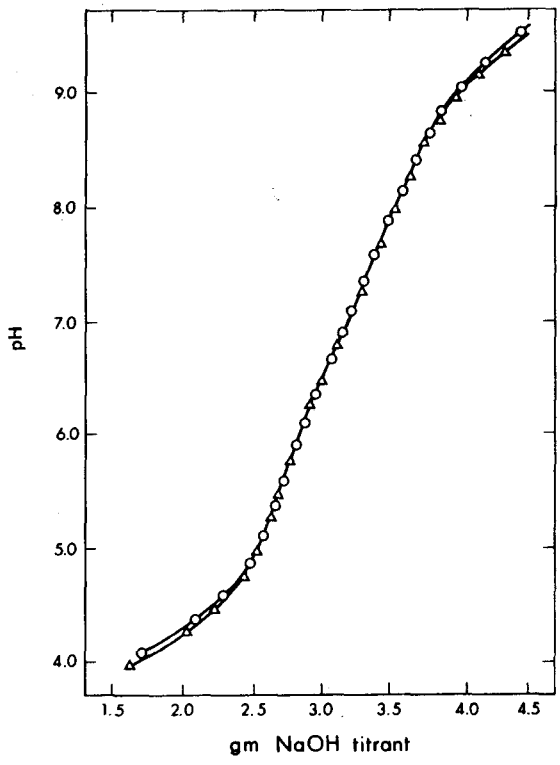

FIG. 7. Experimental (○) and simulated (△) titration curves for a solution containing 9.370×10^{-4} mol/kg of zinc and 5.308×10^{-3} mol/kg of aspartic acid. The titrant contained 0.3925 mol NaOH/kg titrant.

mass balances are used for extracting the formation constants. However, if the C_H mass balance is also used, the pH readings must be converted to hydrogen ion concentrations.

The comparison of data predicted by the model and the formation constants with the experimental data is the final important step in an application of the FICS method. The experimental titration curve for the zinc – aspartic acid system and that predicted from the formation constants obtained in this work for ZnL and ZnL_2^{2-} are shown in Fig. 7. The agreement is good over the pH region from which data were used for the evaluation of the formation constants. As discussed above, other complexes begin to form outside of the pH region 5 to 8.

The agreement between the acid dissociation constants and formation constants obtained in this work with those from other studies (Table 1) indicates that the FICS method can provide reliable equilibrium constants. It must be emphasized, however, that to obtain reliable results by the FICS method requires highly accurate data and careful design of the experiment to meet the theoretical requirements of the method (1, 3).

Acknowledgements

This research was supported in part by the National Research Council of Canada and the University of Alberta. Financial support to R.G. by a National Research Council of Canada Scholarship is gratefully acknowledged.

1. R. GUEVREMONT and D. L. RABENSTEIN. Can. J. Chem. **55**, 4211 (1977).
2. R. OSTERBERG. Acta Chem. Scand. **14**, 471 (1960).
3. B. SARKAR and T. P. A. KRUCK. Can. J. Chem. **51**, 3541 (1973).
4. B. SARKAR. J. Ind. Chem. Soc. **54**, 117 (1977).
5. R. GUEVREMONT and B. KRATOCHVIL. Anal. Chem. **50**, 1945 (1978).
6. R. G. BATES. Determination of pH. Theory and practice. Wiley-Interscience, New York, NY. 1973. p. 96.
7. A. E. MARTELL and R. M. SMITH. Stability constants. Vol. 1: Amino acids. Plenum Press, New York, NY. 1974.
8. A. GERGELY and E. FARKAS. Magy. Kem. Foly. **81**, 471 (1975).
9. S. CHABEREK and A. E. MARTELL. J. Am. Chem. Soc. **74**, 6021 (1952).
10. G. K. R. MAKAR, M. L. D. TOUCHE, and D. R. WILLIAMS. J. Chem. Soc. Dalton, 1016 (1976).
11. J. H. RITSMA, G. A. WIEGERS, and F. JELLINEK. Recl. Trav. Chim. **84**, 1577 (1965).
12. I. M. BATGAEU, S. V. LARINNOV, and V. M. SHULMAN. Russ. J. Inorg. Chem. **6**, 75 (1961).
13. R. F. LUMB and A. E. MARTELL. J. Phys. Chem. **57**, 690 (1953).
14. N. C. LI and E. DOODY. J. Am. Chem. Soc. **70**, 1891 (1950).

Canadian Journal of Chemistry
Published by
THE NATIONAL RESEARCH COUNCIL OF CANADA

Journal canadien de chimie
Publié par
LE CONSEIL NATIONAL DE RECHERCHES DU CANADA

Volume 57 Number 5 March 1, 1979

Volume 57 numéro 5 1 mars 1979

An ion cyclotron resonance study of competitive solvation of gas phase anions

R. L. CLAIR AND T. B. MCMAHON
Department of Chemistry, University of New Brunswick, Fredericton, N.B., Canada E3B 5A3

Received September 1, 1978

R. L. CLAIR and T. B. MCMAHON. Can. J. Chem. **57**, 473 (1979).

Reactions of trifluoromethoxide ion, CF_3O^-, with carboxylic acids have been examined. Facile fluoride transfer is observed to occur to the acids and a subsequent fluoride transfer equilibrium established in mixtures of carboxylic acids. From the equilibrium constant obtained for fluoride transfer acetic acid and propionic acid are found to have near identical fluoride binding energies. Further reaction between the acid solvated fluoride ions and the carboxylic acids is observed to occur resulting in HF displacement and formation of bicarboxylate anions. In mixtures of acetic and propionic acids acetate and propionate anion transfer equilibria are again established. An analysis of the energetics for these processes reveals that propionic acid binds the carboxylate anions more strongly than acetic acid by 0.1 to 0.2 kcal/mol.

R. L. CLAIR et T. B. MCMAHON. Can. J. Chem. **57**, 473 (1979).

On a étudié les réactions de l'ion trifluorométhylate, CF_3O^-, avec les acides carboxyliques. On a observé qu'un transfert facile de fluor vers les acides peut se produire et qu'il s'établit un équilibre de transfert de fluor subséquent dans des mélanges d'acides carboxyliques. En se basant sur des constantes d'équilibre obtenues pour les transferts de fluor, on a trouvé que les énergies de liaison des fluorures aux acides acétique et proprionique sont pratiquement identiques. On a observé que des réactions ultérieures se produisent entre les ions fluorés solvatés en milieu acide et les acides carboxyliques; il en résulte une élimination de HF et la formation d'anions bicarboxylates. Dans des mélanges d'acides acétique et proprionique, il se produit de nouveau des équilibres de transfert des anions acétate et proprionate. Une analyse des énergies impliquée pour ces processus révèle que l'acide proprionique lie les anions carboxylates plus fortement que l'acide acétique par environ 0.1 à 0.2 kcal/mol.

[Traduit par le journal]

Introduction

During the last decade the development of various techniques for the study of gas phase ion–molecule reactions has led to a detailed and quantitative understanding of the intrinsic stabilities of ionic species and the fundamental nature of electronic substituent effects (for excellent review of gas phase ion thermochemistry, see ref. 1). In many cases relative orderings of ionic stabilities are found to be in sharp contrast to those inferred from comparable solution data indicating that for ionic reactions in solution the solvent plays an important, if not dominant, role in determining relative reactivity and stability. In order to bridge the gap between gas phase and solution data Kebarle and co-workers have used a pulsed electron beam high pressure mass spectrometer to study the energetics of individual solvation steps for a wide variety of positive and negative ions (2–4). Such studies involve measurement of equilibria between ions $A^{\pm}$ in the presence of a typical solvent molecule, S, in the gas phase and the solvated species $AS^{\pm}$, eq. [1].

$$[1] \qquad A^{\pm} + S \underset{\leftarrow}{\overset{[M]}{\rightleftharpoons}} AS^{\pm}$$

In a number of cases solvation of ions by several molecules has been characterized by observation of the successive clustering equilibria given by eq. [2] (5–7).

$$[2] \qquad A^{\pm}(S)^{n-1} + S \underset{\leftarrow}{\overset{[M]}{\rightleftharpoons}} A^{\pm}(S)^{n}$$

0008-4042/79/050473-05$01.00/0

From the relative magnitudes of the enthalpy changes associated with individual solvation steps the relative total solvation energies may be inferred (5) and from these a correlation between gas phase and solution stabilities of ions deduced.

The study of equilibria involving solvated or cluster ions such as [1] or [2] is usually inaccessible to ion cyclotron resonance (ICR) experiments since thermalizing collisions with some bath gas M must occur within a time short compared to the lifetime of the initially formed cluster. This cluster ion will be produced with an amount of excess energy equal to the solvent binding energy and this energy must be dissipated by collision with the bath gas in order that the species be observable and in order that true thermodynamic equilibrium be established. This condition necessitates the use of pressures beyond those usually available to the ICR trapped-ion technique[1] and thus makes observation of termolecular clustering equilibria untenable.

In spite of the difficulties associated with observation of normal clustering equilibria by ICR *relative* solvation equilibrium processes may be readily obtained by use of appropriate bimolecular reactions leading to production of solvated ions. In the presence of two or more appropriate solvents cluster ions thus formed may undergo 'solvent switching' reactions and a bimolecular solvent transfer equilibrium thus established. This then allows the determination of accurate *relative* single molecule solvation energies. If an accurate absolute value for some individual single molecule solvation energy is known then all additional solvation energetics may be referenced to this species and an accurate scale of absolute solvation energies may therefore be established.

One such appropriate bimolecular reaction leading to the production of solvated species is fluoride transfer. As part of our continuing program of investigation of ion–molecule reactions of fluorinated organic and inorganic molecules it was found that the trifluoromethoxide ion, CF_3O^-, generated by dissociative electron attachment to trifluoromethylhypofluorite, CF_3OF, acts as an efficient fluoride donor in the gas phase to both protic and Lewis acids, eq. [3] (9).

$$[3] \qquad CF_3O^- + A \rightarrow AF^- + CF_2O$$

If two acidic species are present which have comparable fluoride affinities a fluoride transfer equilibrium may be established, eq. [4],

$$[4] \qquad AF^- + B \rightleftharpoons BF^- + A$$

and from the measured equilibrium constant accurate relative free energies of fluoride attachment obtained.

The equilibrium technique also offers the advantage of allowing study of systems where the fluoride affinity of the acidic molecule is very large. In the high pressure mass spectrometric experiment clustering equilibria cannot normally be studied where the free energy of binding is greater than about 35 kcal/mol since this would necessitate conditions of temperature and pressure beyond the normal range of the apparatus. Unfortunately most fluoride attachment free energies for even moderately acidic molecules lie above this upper limit (3, 9).

In addition to straightforward fluoride transfer processes protic acids, HX, of greater gas phase acidity than HF will initiate HF displacement reactions, eq. [5], where HF is preferentially replaced by HX as the more favorable solvent for a general anion, Y^- (10).

$$[5] \qquad YHF^- + HX \rightarrow YHX^- + HF$$

Further, if both HX and HY are present and have similar gas phase acidities another series of solvent exchange equilibria will be established, eq. [6].

$$[6a] \qquad XHX^- + HY \rightleftharpoons XHY^- + HX$$

$$[6b] \qquad XHY^- + HY \rightleftharpoons YHY^- + HX$$

In the present publication we wish to report equilibrium measurements for fluoride transfer between pairs of carboxylic acids and the subsequent displacement of HF to produce both symmetrical and mixed bicarboxylate ions. From equilibria involving these bicarboxylate ions relative solvation energies of carboxylate ions by carboxylic acids are obtained.

Experimental

All experiments were conducted at ambient temperature (25°C) using an ICR spectrometer of basic Varian V-5900 design but which had been extensively modified to permit trapped-ion experiments according to the method of McMahon and Beauchamp (11). Details of the design and operation of the trapped-ion ICR technique and conventional ICR single and double resonance experiments have been described in detail elsewhere (12, 13).

Trifluoromethylhypofluorite was obtained from PCR Inc. Acetic acid and propionic acid were analytical grade reagents obtained from Aldrich. All materials were used without further purification other than simple freeze–pump–thaw cycles to remove volatile impurities.

CF_3OF is an extremely toxic material that reacts vigorously with many organic and inorganic compounds (14). It is extremely moisture- and light-sensitive and it was found most desirous to use it in darkened, passivated vessels. Fresh samples were prepared for use daily.

Mixtures of acetic and propionic acids were prepared manometrically and ranged in ratios from 5:1 acetic:propionic acid to 2:1 propionic:acetic acid. Experiments were carried out over a pressure range of 10^{-6} Torr to 10^{-5} Torr and a range of trapping times up to 1 s. Where possible rate constants of equilibrium reactions were determined using the time-delayed

[1]At the pressures necessary to observe termolecular clustering reactions in trapped-ion ICR experiments ion loss effects become significant, see ref. 8.

ion ejection technique (15). Equilibrium constant values reported are an average of six separate experimental determinations.

Results

The variation of relative abundances for a 1:4:5 mixture of CF_3OF:$C_2H_5CO_2H$:CH_3CO_2H at a total pressure of 5×10^{-6} Torr is shown in Fig. 1. The reaction sequence initiated by the CF_3O^- ion confirmed by double resonance experiments is summarized by eqs. [7] to [15].

[7] $CF_3O^- + CH_3CO_2H \rightarrow CH_3CO_2HF^- + CF_2O$

[8] $CF_3O^- + C_2H_5CO_2H \rightarrow C_2H_5CO_2HF^- + CF_2O$

[9] $CH_3CO_2HF^- + C_2H_5CO_2H \rightleftharpoons C_2H_5CO_2HF^- + CH_3CO_2H$

[10] $CH_3CO_2HF^- + CH_3CO_2H \rightarrow (CH_3CO_2)_2H^- + HF$

[11] $CH_3CO_2HF^- + C_2H_5CO_2H \rightarrow (CH_3CO_2)(C_2H_5CO_2)H^- + HF$

[12] $C_2H_5CO_2HF^- + CH_3CO_2H \rightarrow (CH_3CO_2)(C_2H_5CO_2)H^- + HF$

[13] $C_2H_5CO_2HF^- + C_2H_5CO_2H \rightarrow (C_2H_5CO_2)_2H^- + HF$

[14] $(CH_3CO_2)_2H^- + C_2H_5CO_2H \rightleftharpoons (CH_3CO_2)(C_2H_5CO_2)H^- + CH_3CO_2H$

[15] $(CH_3CO_2)(C_2H_5CO_2)H^- + C_2H_5CO_2H \rightleftharpoons (C_2H_5CO_2)_2H^- + CH_3CO_2H$

In addition to the reactions of CF_3O^- a reaction sequence arising from F^- is also observed given by eqs. [16] to [18].

[16] $F^- + CH_3CO_2H \rightarrow CH_3CO_2^- + HF$

[17] $F^- + C_2H_5CO_2H \rightarrow C_2H_5CO_2^- + HF$

[18] $CH_3CO_2^- + C_2H_5CO_2H \rightleftharpoons C_2H_5CO_2^- + CH_3CO_2H$

The carboxylate ions are found to be unreactive toward either CF_3OF or the carboxylic acids permitting the proton transfer equilibrium, eq. [18], to be established. The known value of the equilibrium constant for eq. [18] of 7.6 (16) was reproducible, providing a confirmation of the ratio of pressures of the two carboxylic acids.

Equilibrium constants obtained from steady state ionic abundances and the known ratio of carboxylic acids for eqs. [9], [14], and [15] are summarized in Table 1. Also included are thermodynamic data derived from these equilibrium constants. Entropy changes have been estimated on the basis of symmetry changes in the equilibrium reactions.

Some care was taken to insure that true thermodynamic equilibrium rather than a steady state had been reached for the reactions studied. Within limits of normal experimental error all equilibrium constants were found to be in good agreement for the range of concentration ratios, pressures, and reaction

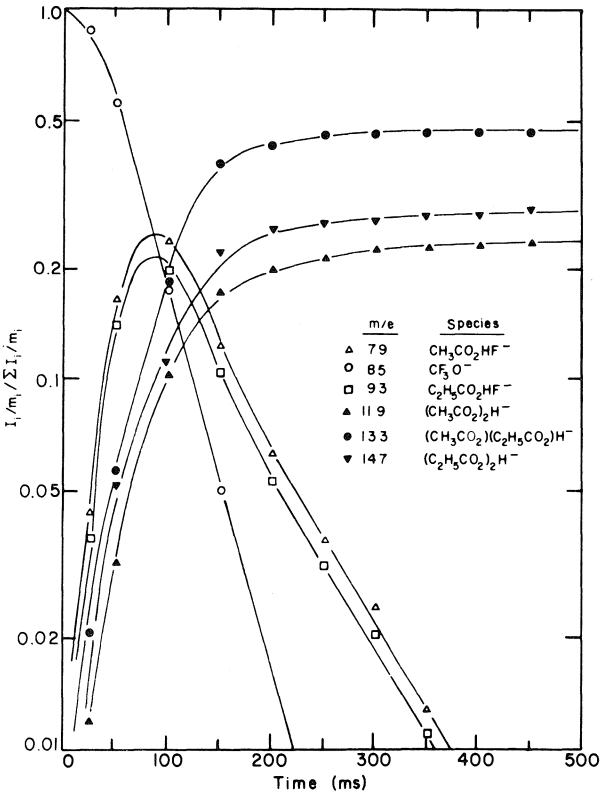

FIG. 1. Variation of relative ionic abundances with reaction time in a 1:4:5 mixture of CF_3OF:$C_2H_5CO_2H$:CH_3CO_2H at a total pressure of 5×10^{-6} Torr.

times studied. Cluster ions produced via exothermic bimolecular reactions become thermalized by a variety of processes analogous to those operative for proton transfer equilibria in low pressure ICR experiments. These are symmetric thermoneutral anion exchange reactions resulting in no observable reaction but diminishing any excess internal energy in the ionic species by a factor of one-half (17) and simple non-reactive collisional deactivation. In addition, although no quantitative data are available, radiative cooling may occur within the time scale of the trapped-ion ICR experiment.

For the fluoride exchange equilibrium, [9], the equilibrium constant was also determined from the ratio of forward and reverse rate constants obtained from time delayed ion ejection experiments (15). Within experimental error these rate constants are determined to be identical as $7.0 \pm 0.7 \times 10^{-10}$ cm^3 molecule^{-1} s^{-1}. The overall loss of *m/e* 79 and 93 via HF displacement proceeds with an average rate constant of $7.0 \pm 0.7 \times 10^{-11}$ cm^3 molecule^{-1} s^{-1}. According to the analysis of Davidson *et al.* (18) this permits fluoride transfer equilibrium to be established and observed since the fluoride exchange is ten times faster than HF displacement.

TABLE 1. Equilibrium constant and thermodynamic data for anion exchange equilibria

	Reaction	K	ΔG^0 (kcal/mol)	ΔS^0 (eu)	ΔH^0 (kcal/mol)
[9]	$CH_3CO_2HF^- + C_2H_5CO_2H \rightleftharpoons C_2H_5CO_2HF^- + CH_3CO_2H$	1.0 ±0.1	0.0±0.05	0	0.0±0.05
[14]	$(CH_3CO_2)_2H^- + C_2H_5CO_2H \rightleftharpoons (CH_3CO_2)(C_2H_5CO_2)H^- + CH_3CO_2H$	2.5 ±0.2	−0.5±0.1	1.4	−0.1±0.1
[15]	$(CH_3CO_2)(C_2H_5CO_2)H^- + C_2H_5CO_2H \rightleftharpoons (C_2H_5CO_2)_2H^- + CH_3CO_2H$	0.75±0.1	0.2±0.1	−1.4	−0.2±0.1

Due to the kinetic complexity of the sequence of carboxylate exchange equilibria all of the rate constants for the two equilibria [14] and [15] cannot be extracted from the time delayed ejection technique. However, both k_{14} and k_{-15} may be obtained and are found to be $2.4 \pm 0.2 \times 10^{-10}$ cm^3 molecule^{-1} s^{-1} and $1.3 \pm 0.1 \times 10^{-10}$ cm^3 molecule^{-1} s^{-1}, respectively. Using the A.D.O. theory (19) the collision rate constants for the bicarboxylate ions are estimated to be 1.4×10^{-9} cm^3 molecule^{-1} s^{-1}. Thus each ion will undergo between five and fifteen non-reactive collisions for every reactive carboxylate exchange reaction which occurs. During the time scale for the experiment for the pressures employed over 100 collisions will have occurred and given this ratio of non-reactive to reactive collisions thermalization of the ions is insured. Combining the measured values of K_{14} and K_{15} with the rate constants k_{14} and k_{-15} allows the determination of the remaining rate constants of the equilibria as $k_{-14} = 9.8 \times 10^{-11}$ cm^3 molecule^{-1} s^{-1} and $k_{15} = 9.7 \times 10^{-11}$ cm^3 molecule^{-1} s^{-1}.

Discussion

Previous experimental correlations (3) and recent *ab initio* calculations (20, 21) support the very small differences in observed anion binding energies of acetic and propionic acids. Yamdagni and Kebarle (3) have proposed a relationship, eq. [19], between anion binding energies and gas phase acidities of a number of protic solvents.

$$[19] \quad D(BH{-}X^-) = aD(H^+{-}X^-) - bD(H^+{-}B^-)$$

Based on values of $D(F^-{-}HCl)$ and $D(F^-{-}H_2O)$ of 50 and 23 kcal/mol, respectively, the constants a and b of eq. [19] for fluoride binding may be determined to be 0.56 and 0.47. Using gas phase acidity values of 348.5 and 347.3 kcal/mol for acetic and propionic acids fluoride binding energies of 42.6 and 43.7 kcal/mol, respectively, are calculated. Given the rather approximate nature of the relationship the difference in fluoride binding energies may be regarded as in excellent agreement with our experimental results. Applying eq. [19] to acetate and propionate ion binding energies leads to the values summarized in Table 2. Also included are the predicted binding energies of these anions to HF.

TABLE 2. Calculated bond dissociation energies $D(X^-{-}AH)$ in kcal/mol*

	D for AH =		
X^-	HF	CH_3CO_2H	$C_2H_5CO_2H$
F^-	—	42.6	43.1
$CH_3CO_2^-$	19.3	30.0	30.5
$C_2H_5CO_2^-$	18.6	29.3	29.9

*Calculated from eq. [19], by the empirical method outlined in ref. 3.

Ab initio calculations of fluoride binding energies to formic and acetic acids (20, 21) of 59.7 and 59.5 kcal/mol, respectively, also support the experimentally observed small difference in fluoride affinities of carboxylic acids. The magnitude of binding energies calculated is greater than that predicted experimentally from eq. [19]. This is known to be a common occurrence for Gaussian 70 calculations of fluoride affinities (22, 23).

The *ab initio* geometry optimization for fluoride – carboxylic acid adducts yields a structure with linear O...H...F$^-$ bonds and a coplanar arrangement of all heavy atoms (23). An examination of O—H and H—F bond distances in these adducts reveals a long O—H distance and a short H—F distance indicating that these species may be more correctly regarded as carboxylate ions solvated by HF rather than fluoride solvated by carboxylic acids. This is consistent with intuitive expectation based on the greater gas phase acidity of carboxylic acids than HF. Viewed in this manner eqs. [10] to [13] are readily seen to be solvent displacement reactions where the weakly acidic solvent HF is replaced by carboxylic acid solvents of greater acidity. From the data of Table 2, the HF displacement reactions are seen to each be roughly 11 kcal/mol exothermic.

Ab initio calculations have also been carried out for the energetics and structure of the biformate ion which may be regarded as a model for the bicarboxylate ions (24). These studies yield a planar *trans* configuration of C_{2v} symmetry with a linear O···H···O bond and a binding energy $D(HCO_2^-{-}HCO_2H)$ of 29 kcal/mol. This is in excellent agreement with the

values for other bicarboxylate ions obtained from empirical correlations given in Table 2. These values show transfer of acetate from acetic to propionic acid, eq. [14], to be 0.5 kcal/mol exothermic and transfer of propionate from acetic to propionic acid, eq. [15] to be 0.6 kcal/mol exothermic. The difference in exothermicity of 0.1 kcal/mol is again in excellent agreement with our experimentally determined difference.

Conclusions

The results presented above demonstrate that the ICR trapped ion technique may be extremely useful in the study of bimolecular solvent exchange equilibria and in the generation of accurate relative single molecule solvation energies. The experimental data have been shown to be in good agreement with *ab initio* calculations and empirical correlations from other solvation studies. In addition replacement of HF by carboxylic acids in fluoride – carboxylic acid adducts has been shown to be exothermic and to proceed facilely. Further studies of solvation energetics involving solvents of markedly weaker gas phase acidity are currently in progress.

Acknowledgements

The generous financial support of the National Research Council of Canada and the University of New Brunswick is gratefully acknowledged.

1. (*a*) P. KEBARLE. Ann. Rev. Phys. Chem. **28**, 445 (1977); (*b*) J. L. BEAUCHAMP. *In* Interactions between ions and molecules. *Edited by* P. Ausloos. Plenum, New York. 1975.
2. J. D. PAYZANT, R. YAMDAGNI, and P. KEBARLE. Can. J. Chem. **49**, 3309 (1971).
3. R. YAMDAGNI and P. KEBARLE. J. Am. Chem. Soc. **93**, 7139 (1971).
4. W. R. DAVIDSON and P. KEBARLE. J. Am. Chem. Soc. **98**, 6125 (1976).
5. M. ARSHADI, R. YAMDAGNI, and P. KEBARLE. J. Phys. Chem. **74**, 1475 (1970).
6. I. DZIDIC and P. KEBARLE. J. Phys. Chem. **74**, 1466 (1970).
7. A. J. CUNNINGHAM, J. D. PAYZANT, and P. KEBARLE. J. Am. Chem. Soc. **94**, 7627 (1972).
8. T. E. SHARP, J. R. EYLER, and E. LI. Int. J. Mass Spectrom. Ion Phys. **9**, 421 (1972).
9. T. B. MCMAHON and C. NORTHCOTT. Can. J. Chem. **56**, 1069 (1978).
10. M. S. FOSTER and J. L. BEAUCHAMP. Chem. Phys. Lett. **31**, 479 (1975).
11. T. B. MCMAHON and J. L. BEAUCHAMP. Rev. Sci. Instrum. **43**, 509 (1972).
12. J. L. BEAUCHAMP. Ann. Rev. Phys. Chem. **22**, 517 (1971).
13. J. M. S. HENIS. *In* Ion molecule reactions. *Edited by* J. L. Franklin. Plenum, New York. 1972.
14. R. S. PORTER and G. H. CADY. J. Am. Chem. Soc. **79**, 5625 (1957).
15. T. B. MCMAHON, R. J. BLINT, D. P. RIDGE, and J. L. BEAUCHAMP. J. Am. Chem. Soc. **94**, 8934 (1972).
16. R. YAMDAGNI and P. KEBARLE. J. Am. Chem. Soc. **95**, 4050 (1973).
17. T. B. MCMAHON and J. L. BEAUCHAMP. J. Phys. Chem. **81**, 593 (1977).
18. W. R. DAVIDSON, M. T. BOWERS, T. SU, and D. H. AUE. Int. J. Mass Spectrom. Ion Phys. **24**, 83 (1977).
19. T. SU and M. T. BOWERS. Int. J. Mass Spectrom. Ion Phys. **12**, 347 (1973).
20. J. EMSLEY, P. O. A. HOYTE, and R. E. OVERILL. J. Chem. Soc. Chem. Commun. 225 (1977).
21. J. EMSLEY, O. P. A. HOYTE, and R. E. OVERILL. J. Chem. Soc. Perkin Trans. **2**, 2079 (1977).
22. H. KISTENMACHER, H. POPKIE, and E. CLEMENTI. J. Chem. Phys. **58**, 5627 (1973).
23. P. KOLLMAN and I. KUNTZ. J. Am. Chem. Soc. **98**, 6820 (1976).
24. J. EMSLEY, O. P. A. HOYTE, and R. E. OVERILL. J. Am. Chem. Soc. **100**, 3303 (1978).

Structural changes at hydrophobic/hydrophilic interfaces induced by thermal changes and isotopic composition of the water

FRED Y. FUJIWARA[1] AND LEONARD W. REEVES[2]

Chemistry Department, University of Waterloo, Waterloo, Ont., Canada N2L 3G1

Received August 24, 1978

FRED Y. FUJIWARA and LEONARD W. REEVES. Can. J. Chem. **57**, 478 (1979).

A lyomesophase prepared from decylammorium tetrafluoroborate, ammonium tetrafluoroborate, and water, which orients in a magnetic field perpendicular to the directors (type II), has been investigated with respect to the isotopic composition, H_2O/D_2O of the aqueous compartment at constant overall chemical composition. An effect of the isotopic composition of the water has been discovered, which influences the packing of the water and tetrafluoroborate ions at the interface. An interface structure transition occurs at ~14 mol% D_2O in H_2O. The ammonium ions, which do not form part of the first bound layer at the interface, are affected to a much smaller degree and the sudden changes in the direction of variation of nmr parameters are not observed for this ion. The interface structure at > 14 mol% D_2O evidently does include more remote participation of NH_4^+ ions.

Recent low angle X-ray diffraction studies, available to us, indicate that the mesophases which orient in magnetic fields have two levels of structure, the packing of amphiphiles in discrete anisotropic micelles and the super-packing of the micelles themselves. These studies now enable us to reinterpret other similar thermally induced structural changes in the interface, from results previously encountered, in the decylammonium chloride system. It is possible to have changes in the packing of water, amphiphiles, and ions at the interface without changes in the superstructure. Such changes in interface packing might well go undetected in a measurement of bulk properties but are revealed by measurement of nmr parameters for the oriented mesophase of different species involved in the interface structure. The isotope effect on structural packing at the interface is absent in two other mesophases investigated.

FRED Y. FUJIWARA et LEONARD W. REEVES. Can. J. Chem. **57**, 478 (1979).

On a étudié une lyomésophase préparée à partir de tétrafluoroborate de décylammonium, de tétrafluoroborate d'ammonium et d'eau qui oriente dans un champ magnétique perpendiculaire aux directeurs (type II); ces études ont porté sur la composition isotopique, H_2O/D_2O du compartiment aqueux à des compositions chimiques globales qui étaient constantes. On a découvert un effet de composition isotopique de l'eau qui influence l'arrangement de l'eau et des ions tétrafluoroborates à l'interface. Il se produit une transition de structure d'interface à ~14 mol% de D_2O dans H_2O. Les ions ammonium qui ne font pas partie de la première couche liée à l'interface, sont moins affectés et il ne se produit pas de changement soudain dans la direction de la variation des paramètres rmn de cet ion. La structure interfaciale à > 14 mol% de D_2O contient évidemment plus de participation à distance des ions NH_4^+.

Des études récentes de diffraction de rayons-X à petits angles qui nous étaient disponibles indiquent que les mésophases qui orientent dans les champs magnétiques ont deux niveaux de structure: l'arrangement des amphiphiles dans des micelles anisotropes définies et des super-arrangements des micelles elles-mêmes. Ces études nous permettent maintenant de réinterpréter d'autres changements de structures semblables induits d'une façon thermique dans l'interface à partir de résultats obtenues antérieurement dans le système de chlorure de décylammonium. Il est possible d'obtenir des changements dans l'arrangement de l'eau des amphiphiles et des ions à l'interface sans changement dans la super-structure. De tels changements à l'interface pourraient passer inapercus lors de mesures de propriétés globales; on les décèle toutefois par des mesures de paramètres de rmn de la mésophase orientée de différentes espèces impliquées dans la structure de l'interface. Il n'y a pas d'effet isotopique sur l'arrangement de structure à l'interface dans les deux autres mésophases étudiées.

[Traduit par le journal]

We have recently been able to show that some effects of ions and water at a hydrophobic/hydrophilic interface can be detected and interpreted by the study of nmr spectra of oriented lyomesophases (1, 2). It is clear, for instance, that the hydration of carboxylate head groups is the principal reason for the higher ordering of water molecules in the interface for those systems in which this head group is mixed in different proportions with pyridinium and trimethylammonium (1). These last head groups are

[1]Present address: Instituto de Quimica, Universidade Estadual de Campinas, UNICAMP, Campinas, S.P., Brasil.

[2]To whom all correspondence should be addressed.

0008-4042/79/050478-05$01.00/0

not strongly hydrated and systems in which the interface is rich in these groups are characterised by a low degree of order for the water molecule O—D axis as measured from the partially averaged deuterium nuclear quadrupole splittings (1, 2). By preparing mesophases that are oriented by the magnetic field but with variations in the chemical nature of the amphiphiles which compose the basic bilayer structure, the subtle study of interface water becomes accessible.

It is now possible to ascert from these previous investigations by us (1, 2) and by others (3) that the order parameter measured by nmr studies is a very sensitive tool for studying the interface region from the aqueous side. Water and ions which reside remotely from the interface have low degrees of order, while ions or molecules at the interface near the highly ordered head groups have higher order parameters. The relationship between head group order and that of H_2O and Cl^- ions was discovered by Fujiwara and Reeves some time ago (4) in a decylammonium chloride mesophase system. The experimental work now accumulated indicates that, on the nmr time scale, rapid exchange between remote and low ordered water and ions and the more ordered interface water and ions occurs. The linear concentration average is the observable in the measured order parameter. Sodium ion in the mixed detergent mesophase systems dodecanoate/decyltrimethylammonium has three available specific sites, including strong association with the carboxylate, association between a shared carboxylate/trimethylammonium, and sodium remote from the interface. The bromide counter ion on the other hand achieves appreciable order only at interfaces rich in the $—N(CH_3)^+$ head group. The differential ordering of different ions at chemically varied interfaces is clearly observable (1, 4).

Since hydrogen bonding to polar and ionic head groups by water molecules is evidently a strong intermolecular force contributing to interface ordering of water molecules, we have searched for an isotope effect at the interface between H_2O and D_2O molecules, there being a difference in hydrogen bond strengths for these species. Such an observation, as reported here, has important bearing on this same type of interface in biological systems.

Experimental

The mesophase studied, in which evidence for isotope effects has been found, is similar to one reported earlier by us in a study of the distortion of the BF_4^- ion in unaxial media (5). Preparation and purification of the required compounds have been previously described (5). Mesophases of type II (6, 7), which orient with directors perpendicular to the applied field, were prepared from decylammonium tetrafluoroborate, ammonium tetrafluoroborate, deuteriated and normal water. The water used in the preparation of the mesophase was varied in deuterium content from 0 to 100%. The composition of mesophases was not varied in the mol% of detergent, electrolyte, and water. Table 1 gives these compositions. The water was always acidified to 0.1 *N* HCl in order to inhibit exchange of deuterium and/or protons between the ammonium ions and water. Proton, ^{19}F, ^{11}B, and ^2D nmr signals were detected using a Varian HR60 or a Varian HA 100 spectrometer. The frequency of the carrier was 7.95 MHz for deuterium, 15.1 MHz for ^{11}B, 94.1 MHz for fluorine, and 100 MHz for protons. The spectra of ^{11}B and deuterium were calibrated by the audio side band technique (8). The random error on peak position assignment was as indicated in the table of splittings observed.

As the H_2O/D_2O content of the aqueous compartment of the mesophase was varied; four nmr parameters were measured. The quadrupole splitting was investigated for the deuterium in the water signal and for the ^{11}B in the tetrafluoroborate ion. In the latter case the signal is a triplet from $I = 3/2$ and the measured splitting was between adjacent peaks. The magnitude of the scalar spin–spin coupling and dipole–dipole coupling between ^{11}B and ^{19}F, $|D_{BF} + J_{BF}|$, was measured between adjacent peaks in the ^{19}F spectrum. The ^{1}Hmr spectrum of NH_4^+, NDH_3^+, $ND_2H_2^+$, and ND_3H^+ were examined to determine the magnitude of the scalar plus dipolar coupling between ^{14}N and protons ($|J_{NN} + D_{NH}|$).

In a search for other interface isotope effects a decylammonium chloride mesophase (9) as well as a mesophase based on sodium decylsulphate, decanol, water, and sodium sulphate (10) were examined. The results were negative in both cases indicating that such detectable effects as will be described here are a special and not a general case.

Results

The investigation of the four nmr parameters listed in the Experimental section were necessarily, under the conditions available, measured on different days. Some small temperature differences were recorded for the different nuclei.

In the case of the deuterium doublet splittings from the water, the measurements were deliberately made at temperatures in separate series which were 3° apart to exaggerate any effect of temperature variation. Other than a small change in the absolute

TABLE 1. Compositions (mol%) of mesophases with varied isotopic content of water but mole fractions of components otherwise unchanged*

D_2O	H_2O	$D_2O + H_2O$	$DABF_4$	NH_4BF_4
90.47	0	90.47	8.03	1.50
67.76	22.77	90.53	7.97	1.50
45.42	45.08	90.50	8.02	1.49
22.70	67.78	90.48	8.02	1.50
9.75	80.72	90.47	8.03	1.50
5.02	85.45	90.47	8.03	1.50
0	90.46	90.46	8.03	1.51

*$DABF_4$ = decylammonium tetrafluoroborate.

TABLE 2. Nuclear magnetic resonance parameters measured for mesophases described in Table 1*

	$V_Q(D_2O)$ (Hz)		BF_4^-		NH_4^+	
$\frac{[D_2O] \times 100}{[D_2O] + [H_2O]}$	26.9°C	29.9°C	V_Q (kHz) at 26.9°C	$(D + J)$ (Hz) at 31.5°C	V_Q (Hz) at 29.9°C	$(D + J)$ (Hz) at 31.5°C
100	256±1	248±1	4.16±0.01	4.91±0.05	87±3	50.65±0.05
74.85	248±1	244±1	3.91±0.01	4.80±0.05	83±3	51.20±0.005
50.19	243±1	237±1	3.76±0.01	4.55±0.05		52.2 ±0.1
25.09	238±1	228±1	3.57±0.01	4.33±0.05		52.35±0.05
10.78	231±1	225±1	3.41±0.01	4.25±0.05		52.40±0.05
5.55	232±1	227±1	3.44±0.01	4.25±0.05		
0	?	?	3.52±0.01	4.28±0.05		52.40±0.05

*Mol% of D_2O in H_2O used to prepare the mesophase is given in the first column. The deuterium quadrupole splitting '$V_Q(D_2O)$' for water is given for 26.9°C and 29.9°C. The fourth and fifth columns list the quadrupole splitting of boron-11 and coupling $|D_{BF} + J_{BF}|$ for the BF_4^- ion. The last two columns list the deuterium quadrupole couplings for the ammonium ion and also the value $|D_{NH} + J_{NH}|$.

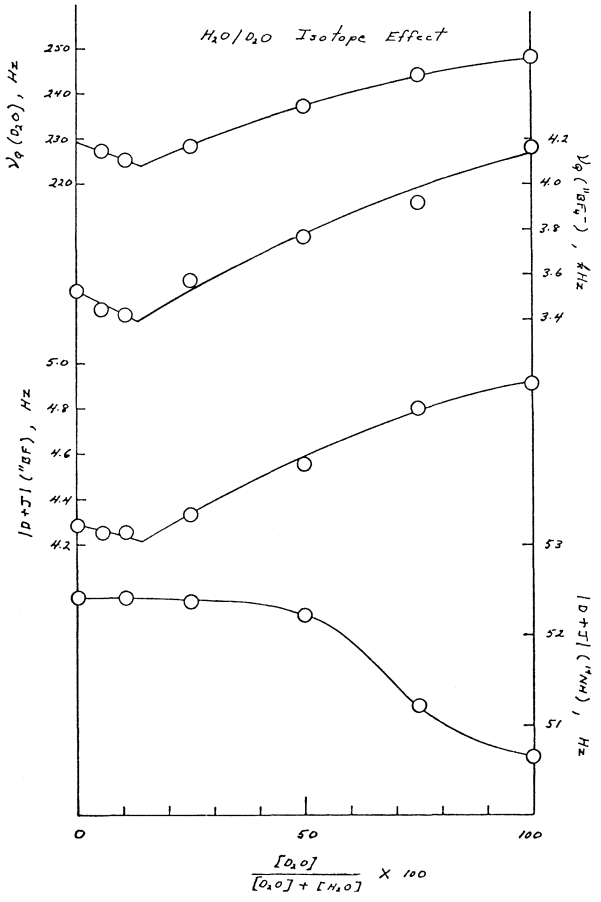

FIG. 1. Variations of the measured nmr parameters in mesophases of constant molar composition but varied fraction of deuterium content in the water compartment. The top curve shows the variation of the deuterium quadrupole splitting of the water against the left hand scale. The next curve down is the ^{11}B quadrupole splitting for the BF_4^- ion plotted against a scale on the right in kHz. The value of $|D_{BF} + J_{BF}|$ in Hz is the third curve from the top, against the scale in Hz at the left. The bottom curve was obtained from values of the proton ^{14}N coupling $|D_{NH} + J_{NH}|$ for the ammonium ion.

values of the quadrupole splittings measured, there was no change in the variation of nmr parameters with composition H_2O/D_2O of the water compartment, which variations clearly indicate an isotope effect at the interface. The sensitivity for detection of deuterium resonance in the ammonium ion was insufficient to measure the quadrupole splitting below 74% deuterium content in the water.

In Table 2 are listed the nmr parameters measured with the quoted error limits being the maximum obtained for random error over a typical set of repeated measurements. The results for all parameters measured are plotted in Fig. 1, selecting the deuterium quadrupole splittings for water at 29.9°C for display in the graph.

Discussion

The interface head groups in the system under study are cationic and the counter ions BF_4^- are of such a concentration that from the aqueous side a neutralising layer can be considered to be essentially complete at the interface. The ammonium ions, being positively charged, are not expected to be so closely bound at the interface sites. The number of water molecules per $-NH_3^+$ head group was 11.26 while the corresponding ratio for BF_4^- ions is 1.19 and for NH_4^+ ions 0.19. The effect of charge on an ion in determining its location at the charged interface or removed from it is an electrostatic consequence well known previously, but also illustrated in recent nmr measurements of parameter order by Lee *et al.* (1, 11).

The fact that the water and counter ion derive their order from the head group contact has been shown by Fujiwara and Reeves (4). In the case of similar mesophases of type II (6) formed using decylammonium chloride, ammonium chloride, with varied water content, the deuterium doublet splitting of the D_2O and the ^{35}Cl residual quadrupole coupling

vary linearly to a high degree of experimental precision with the deuterium quadrupole splitting measured for the $—ND_3^+$ head group of the decylammonium ion. Unlike the simple proportionality among the deuterium quadrupole splittings of the chain segments (4), there is a residual head group coupling constant of 500 Hz for the $—ND_3^+$ group when the water and ^{35}Cl splitting have become zero for the extrapolated state of very high water content (4). This intercept of residual order in the head group is the only difference in behaviour detected between hydrocarbon segments connected by chemical bonds to the head group and water or counter ions which are subject to the weaker hydrogen bonding, ion–dipole, and coulombic attraction at the interface.

The mesophases that have been the subject of study in this and our previous work (1, 2, 4, 6, 7, 9) have the significant property that they orient in an applied magnetic field normally used for nmr studies. It is now clear from recent low angle X-ray diffraction work that these lyotropic liquid crystals are not the classic superstructures reported for the middle (hexagonal) or neat (lamellar) mesophases (12, 13). Recent unpublished X-ray diffraction work[3] has shown that in the original type II mesophase reported by Lawson and Flautt (15) there are no repeated distances but the single diffraction spots are characteristic of two size factors in the colloid range. A distance of 38 Å is indicative of the bilayer thickness of an anisotropic micelle, while a diffuse diffraction has been associated with a water layer which has thicknesses distributed between 90 and 130 Å. The micelle sizes are evidently of finite dimensions and their shape and packing leads to the anisotropic properties of the uniaxial fluid. It is logical to associate at least one case of the type II (6) mesophase with disc-like micelles which orient with the plane of the disc in the magnetic field, and thus the director of the mesophase perpendicular to it. One case of the type I mesophase (6) can probably be associated with finite cylinders, which orient with their axes along the magnetic field, co-linear with the director of the mesophase. This is contrary to the speculations made before the X-ray work became available (4). In both type I and type II mesophases the extended hydrocarbon chains in the bilayer of the anisotropic micelles contrive to orient perpendicular to the magnetic field, that is, in the direction for minimum diamagnetic susceptibility. This is a rational driving force for the macroscopic orientation process in the magnetic field (16).

This recent understanding is a precursor to the consideration of isotope effects at the interface and it also serves to interpret more fully Fig. 4 of the work of Fujiwara and Reeves (4). A subtle change in slope of the dependence of $—CD_2$-segment quadrupole splittings with temperature is accompanied by an abrupt change in the deuterium quadrupole splitting of the D_2O in the same mesophase at the same temperature (32 ± 2°C). The dependence of the D_2O splitting on temperature changes slope from positive below 32°C to negative above 32°C. The fact that an anisotropic micelle could undergo an internal re-arrangement of amphiphile ion packing without affecting the superstructure packing of the micelles leaves us in principle with the possibility of a change in the structure of the interface without a phase change being strongly reflected in the superstructure or bulk liquid crystal properties. The liquid crystal depends for its anisotropic properties on the superstructure packing of micelles. The change in slope of the linear dependence of quadrupole splitting of deuterium in D_2O from positive below 32°C to negative above indicates a change in sign of the order parameter for the —O—D bonds. This must arise from a change in the hydration arrangement at the interface at which location the D_2O gains its order. This prior example of a subtle change in packing at the interface leads us to interpret the present results in a like manner.

The mesophase, used in this study, prepared from decylammonium tetrafluoroborate has some unusual features (4, 5). The ammonium ion ND_4^+ in a decylammonium chloride mesophase manifests a deuterium quadrupole splitting in the low range of ~7 Hz while in the mesophase containing tetrafluoroborate, the deuterium quadrupole splittings are found between 50 and 102 Hz (4, 5), being for the present mesophase ~85 Hz. This indicates that although the ND_4^+ ion is not in contact with the head $—NH_3^+$ groups, it is more distorted from tetrahedral shape in the tetrafluoroborate-containing mesophase (5). A reasonable conclusion would be that there is some association of the ammonium ions in the more remote part of a necessarily compact electrical double layer. It would be reasonable to assume that each $—NH_3^+$ head group is associated with about two water molecules in a strong hydrogen bonded association, while the BF_4^- ion must also enter into the interface structure. Using the fraction of the total water estimated at the interface and assuming non-interface water has zero degree of order a quadrupole coupling at the interface of ~1400 Hz can be computed assuming rapid exchange using the observed quadrupole couplings for water (Table 2). This is somewhat low, but the geometry of the interface association may involve

[3]L. Queiroz de Amaral, C. Pimentel, and M. Tavares. Private communication.

—OD axes being constrained to align near the magic angle of $\cos^{-1}(1/3)$ to the interface normal. The quadrupole coupling of —CD-groups adjacent to the ND_3^+ are indicative of the order parameter for rather rigid axes oriented in the plane of the interface (4) but with the freedom to take all orientations in this plane in very short time intervals.

The feature of the figure is the similarity in the position of a change in sign of the slope of the dependence of an nmr parameter on H_2O/D_2O content, close to 14% D_2O in the aqueous compartment, for the water and tetrafluoroborate ions. These parameters would be expected to have no dependence on isotropic content of the water or to have a very small but smooth variation without sudden changes or reversals in slope. These discontinuities can be interpreted as a change in the interface structure provoked by a change in the average hydrogen bond strengths and furthermore one which affects the arrangements of the water and the tetrafluoroborate ions. The ammonium ion has no direct involvement in this change in interface packing, but does show a small but smooth change in the parameter $|D_{NH} + J_{NH}|$. The value of J_{NH}, the scalar coupling between nitrogen-14 and protons, has been repeatedly measured in our previous work and is known to be $+52.24 \pm 0.05$ Hz. For mesophases which are rich in H_2O the figure shows that almost no distortion of the ammonium ion occurs. At high D_2O contents the value of D_{NH} is appreciable, reaching -1.59 ± 0.1 Hz at 100% D_2O in the aqueous compartment. The figure shows that the appearance of a dipole–dipole coupling between ^{14}N and protons in the ammonium ion is a smooth function of the D_2O content of the water and, furthermore, appreciable distortion of the ammonium ion occurs only after the subtle structural change at the interface, which involves the BF_4^- ions and water directly, has occurred. This is suggestive that although the NH_4^+ ion is not a species directly involved in the interface structure, it does play a secondary role in the Gouy or second hydration layer and thus is affected somewhat by a rather profound structural change associated with the BF_4^- and interface water arrangements. It would be premature at this stage of understanding of molecular and ionic packing at interfaces to venture specific models.

The bulk anisotropic properties of these liquid crystals, for example, diamagnetic anisotropy, are smaller than for thermotropic liquid crystals (14) and it is probable that with direct measurements of bulk physical properties parallel and perpendicular to the director, the changes in structural packing at the interface without changes in the superstructure packing of the large anisotropic micelles would pass undetected. This emphasizes the special and sensitive applicability of the nmr studies, which are appropriate for local microscopic studies of interface packing. These local structural changes must in their turn be of considerable importance in the chemical reactivity of ions, molecules, and amphiphiles at such interfaces. Such studies are being pursued.

Acknowledgement

This work was supported by operating funds made available to L.W.R. by the National Research Council of Canada.

1. Y. Lee, L. W. Reeves, and A. S. Tracey. To be published.
2. L. W. Reeves, A. S. Tracey, and M. M. Tracey. Can. J. Chem. In press.
3. G. J. T. Tiddy, G. Lindblom, and B. Lindman. Faraday Trans. I, 1290 (1978).
4. F. Y. Fujiwara and L. W. Reeves. J. Am. Chem. Soc. **98**, 6790 (1976).
5. D. Bailey, A. D. Buckingham, F. Fujiwara, and L. W. Reeves. J. Magn. Reson. **18**, 344 (1975).
6. K. Radley, L. W. Reeves, and A. S. Tracey. J. Phys. Chem. **80**, 174 (1976).
7. K. Radley and L. W. Reeves. Can. J. Chem. **53**, 2998 (1975).
8. H. J. Bernstein, W. J. Schneider, and J. A. Pople. High resolution nuclear magnetic resonance. McGraw Hill. 1959.
9. L. W. Reeves, A. S. Tracey, and M. M. Tracey. J. Am. Chem. Soc. **95**, 3799 (1973).
10. K. D. Lawson and T. J. Flautt. J. Am. Chem. Soc. **89**, 5491 (1967).
11. Y. Lee and L. W. Reeves. Can. J. Chem. **53**, 161 (1975).
12. V. Luzzati, H. Mustacchi, and A. Skoulios. Discuss. Faraday Soc. **25**, 43 (1958).
13. F. Husson, H. Mustacchi, and V. Luzzati. Acta Crystallogr. **13**, 660 (1969); **13**, 668 (1960).
14. F. Fujiwara and L. W. Reeves. Can. J. Chem. **56**, 2178 (1978).
15. K. D. Lawson and T. J. Flautt. J. Am. Chem. Soc. **89**, 3489 (1967).
16. L. W. Reeves and A. S. Tracey. J. Am. Chem. Soc. **96**, 5250 (1974).

New heteropolymetallic complexes of platinum(II) with palladium(II)-, gold(I)-, cadmium(II)-, or mercury(II)-chloride

FLAVIO BONATI[1] AND HOWARD C. CLARK

Guelph–Waterloo Centre for Graduate Work in Chemistry, Guelph Campus, University of Guelph, Guelph, Ont., Canada N1G 2W1

Received August 10, 1978

FLAVIO BONATI and HOWARD C. CLARK. Can. J. Chem. **57**, 483 (1979).

The platinum(II) complex *trans*-$PtCl(PEt_3)_2(CH{=}NC_6H_4\text{-}p\text{-}CH_3)$ gives 1:1 complexes with $CdCl_2$, $HgCl_2$, and AuCl and a 1:2 *trans*-adduct with $PdCl_2$, thus showing its character as a monodentate, *N*-ligand.

FLAVIO BONATI et HOWARD C. CLARK. Can. J. Chem. **57**, 483 (1979).

Le complexe de platine(II), *trans*-$PtCl(PEt_3)_2(CH{=}NC_6H_4\text{-}p\text{-}CH_3)$, donne des complexes 1:1 avec du $CdCl_2$, du $HgCl_2$, du AuCl et un adduit 1:2 *trans* avec $PdCl_2$; ces résultats démontrent son caractère de ligand azoté monodentate.

[Traduit par le journal]

Introduction

The problem of synthesizing mixed-metal chain oligomers with two or more different metals in specific ligand sites has been successfully tackled by the use of a metal-containing molecule in which the coordinatively saturated central atom is kinetically inert and where at least one basic function is available to serve as a donor group. Such a molecule, in reaction with a suitable acceptor, may then give a heteropolymetallic complex. Examples of this approach can be found in the adducts formed between various salts and $(ligand)_2Pt[C(OR){=}NR']_2$, or $(ligand)_2Pt(1\text{-pyrazolyl})_2$ complexes (1, 2) or the $[Cl(R_3P)Pt\{P(=O)(OMe)_2\}_2]^-$ anions (3); in the adducts, the platinum-containing compounds act as chelating ligands. Other metal complexes have been used as monodentate, or bidentate but not chelating ligands, e.g. $(Ph_3P)Au[C(OR){=}NR']$ (4), *trans*-$(Et_3P)_2PtH(CN)$ (5), or $Hg[C(OR){=}NR']_2$ (4), respectively.

A new family of such ligands has recently (6) been prepared by the insertion of isocyanide into platinum–hydrogen bonds to give compounds of the type *trans*-$PtCl(PEt_3)_2[CH{=}NAr]$ (Ar = substituted phenyl), L, and after further reaction (7) *trans*-$Pt(PEt_3)_2[C(OMe){=}NAr][CH{=}NAr]$, **1**, These compounds are potentially monodentate and bidentate *N*-ligands, respectively. In particular, L is known (6) from both chemical reactivity and nmr spectroscopic data to be weakly basic and hence, in view of its availability, stability, and solution behavior (6, 7), its characteristics as a ligand have now been investigated.

[1]On leave of absence from the University of Camerino, Italy. Author to whom correspondence should be addressed at Istituto di Chimica Generale, via Venezian 21, 20133 Milano, Italy.

Experimental

The starting material, *trans*-$Cl(PEt_3)_2PtCH{=}NC_6H_4\text{-}p\text{-}Me$, L, was prepared from *p*-tolyl isocyanide and [*trans*-$HPt(PEt_3)_2CNC_7H_7]Cl$, according to the literature (6, 7). Evaporation was always carried out under reduced pressure (water aspirator) unless otherwise stated. Infrared spectra were recorded on a Beckman-IR-5A (NaCl region) or Perkin-Elmer 457 (low frequency region) spectrometer. Nuclear magnetic resonance spectra were recorded on a Bruker instrument operating at 24.88 or 60 MHz for ^{31}P or ^1H, respectively. Analyses were carried out by MHW, Phoenix, Arizona.

*$L{\cdot}HgCl_2$, **2***

An ether solution (10 mL) of mercury(II) chloride (87.8 mg; 0.32 mmol) was added dropwise to a stirred solution of L (122.5 mg; 0.21 mmol) in the same solvent (15 mL). A white crystalline precipitate separated out, which was filtered 2 h later and washed with ether to afford compound **2** (161 mg; 89% on platinum); it was purified by dissolving in methylene chloride (2.5 mL) and precipitating with ether (20 mL) to give the analytical sample (56.8 mg) which, upon heating, softened at 114°C and melted at 116°C with subsequent decomposition. The compound is soluble in $CHCl_3$, CH_2Cl_2, and acetone, although the chloroform solution becomes turbid upon standing.

*$L{\cdot}CdCl_2$, **3***

Compound L (161.4 mg; 0.278 mmol) was dissolved in methanol (10 mL) and $CdCl_2{\cdot}2.5H_2O$ (170.1 mg; 0.245 mmol) added. The suspension was stirred for 4 days and then evaporated to dryness. The residue was extracted with dichloromethane (10 mL) and the extract concentrated to 1 mL; addition of diethyl ether (4–5 mL) gave a white crystalline precipitate, **3** (111 mg; 52% on platinum).

*L·AuCl, **4***

To a solution of L (202.9 mg; 0.347 mmol) in dichloromethane (1.7 mL) solid (dimethylsulphide)chlorogold (**1**) (105 mg; 0.357 mmol) was added. The solution became brownish-yellow and some insoluble, finely divided material was removed by filtration. After addition of more methylene chloride (0.5 mL), ether was added (2 mL) and the clear solution was concentrated to half volume; more ether was added to give a total volume of 5 mL and the analytical sample (174 mg; 60% on platinum) separated as a snow-white crystalline precipitate, which was washed with ether. The compound is light sensitive and may become bluish-gray during filtration.

0008-4042/79/050483-04$01.00/0

TABLE 1. Analytical and other data for the bimetallic complexes

Complex[a]	Colour	Analysis (%) C Found	C Calcd	H Found	H Calcd	N Found	N Calcd	Other Found	Other Calcd	Decomposition point (°C)
2, L·$HgCl_2$	White	27.89	28.0	4.48	4.44	1.55	1.63	23.1[b]	23.3[b]	116
3, L·$CdCl_2$	White	31.27	31.3	5.48	4.95	1.77	1.82	14.22[c]	13.88[c]	183
4, L·AuCl[d]	White	29.68	29.4	4.94	4.65	1.55	1.71			130
5, L_2PdCl_2	Yellow	35.33	35.70	5.75	5.65	1.81	2.08	10.59[c]	10.54[c]	168–169

[a]L is *trans*-$(Et_3P)_2ClPt$—CH=N-(*p*-tolyl).
[b]Mercury.
[c]Chlorine.
[d]The analytical sample was bluish-gray owing to the action of light.

*L_2·$PdCl_2$, **5***

A dichloromethane solution (1 mL) of L (162.5 mg; 0.278 mmol) was mixed with a solution of bis(acetonitrile)-dichloropalladium(II) (36 mg; 0.14 mmol) in the same solvent (6 mL). The solution was then concentrated to 1 mL, ether (6 mL) added, and the yellow, crystalline compound, **5** (114 mg; 61%), was filtered.

Miscellaneous Experiments

Only a dark, oily residue was left after solvent removal from an ether solution of L and $[(CO)_2RhCl]_2$. After evaporation of the reaction mixtures of L with zinc(II) chloride in ether, or with hydrated tin(II) chloride in methanol, compounds were obtained which cannot be adducts, because of the presence in the ir spectrum of the ν(NH) and δ(NH) bonds associated with the protonated form of L. A black precipitate was obtained on treatment of L with silver nitrate in methanol.

Results and Discussion

The reaction of L with suitable Lewis acids such as mercury(II) or cadmium(II) chloride, or the displacement by L of a volatile or labile ligand such as dimethylsulfide or acetonitrile from Me_2SAuCl or $(MeNC)_2PdCl_2$, gave readily the adducts **2**–**5** (Table 1).

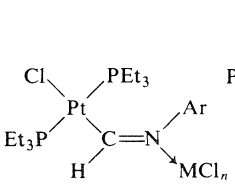

2, M = Hg, *n* = 2
3, M = Cd, *n* = 2
4, M = Au, *n* = 2

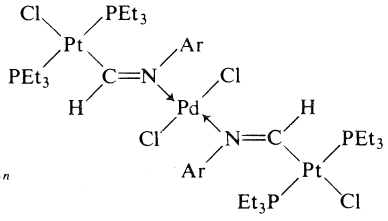

5

These adducts are white or yellow (**5**) crystalline solids which decompose on heating between 110 and 190°C, on exposure to laboratory light (**4**), or slowly in solutions in chlorinated solvents (**2** and **3**). As a consequence, a molecular weight determination could be carried out only on **5** which was found to be monomeric in chloroform solution. Similar measurements for the mercury and cadmium derivatives, **2** and **3**, gave ratios of 1.27 and 1.44, respectively, between the experimental and calculated molecular weights, in agreement with the partial formation of chlorine-bridged structures involving tetrahedrally coordinated M(II) species.

In the 5000–625 cm^{-1} region, the infrared spectra of the adducts **2**–**5** resemble that of the free ligand L. The most meaningful difference is the shift to lower frequency of ν(C=N) consequent upon the participation of the nitrogen atom in dative bonding. This shift is of the order 15–80 cm^{-1} (see Table 2) and is accompanied by a simplification of the band which in L is broad and flanked by a broad shoulder, perhaps connected with the presence of the *syn* and *anti* isomers, whose existence in solution can be established by nmr spectroscopy. In the far infrared region, bands due to both Pt—Cl and M—Cl (M = Cd, Hg, Pd, or Au) stretching frequencies are expected in the 300 cm^{-1} region. Two such bands are observed in all cases except for the cadmium derivative **3**, where only one broad band is observed. In the absence of additional data, it is not possible to make definite assignments to ν(Pt—Cl) and ν(M—Cl).

Both the ^1H and ^{31}P nmr spectra show the expected resonances. In particular, those due to the formylic hydrogen (Pt—C—*H*) are found at fields (−0.68 to −2.06τ) which are very low in comparison with that for L (−0.6τ). The assignment is supported by the presence of satellites due to coupling to ^{195}Pt and to two magnetically equivalent phosphorus nuclei with ^2J(PtCH) and ^3J(PPtCH) comparable, but different, to those in the starting ligand L. It should be noted that, both for the formylic and the aryl hydrogens, each of the two sets of signals corresponds to one of the two isomers (*syn* and *anti*) of L, a fact that shows how easily such protons are influenced by even a modest change of environment. Thus, substantial changes in position are observed for the resonances of the C_6H_4 protons of the adducts

TABLE 2. Selected ir data[a] for

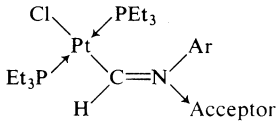

Compound	Acceptor	Infrared absorption frequencies: ν(C=N)	Infrared absorption frequencies: 400–250 cm^{-1} region
L[b]	—	1560s(br), 1582s(br)	402w, 375w, 322w, 255w
2	$HgCl_2$	1515s	412w, 376w, 328w, sh, 318m, 298m
3	$CdCl_2$	1545m	350m, br, 250
4	AuCl	1515s	390vw, 347m, 320w, sh, ca. 280m, br
5	$\frac{1}{2}(PdCl_2)$	1545s	376vw, 342w, 288s, br

[a]All data refer to Nujol mulls.
[b]Two isomers are possible and were detected by nmr in $CDCl_3$ solution (7).

TABLE 3. Nuclear magnetic resonance data[a] for

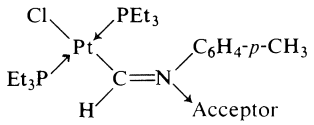

Compound No. acceptor	L *anti*[b] —	L *syn*[b] —	**2** $HgCl_2$	**3** $CdCl_2$	**4** AuCl	**5** $\frac{1}{2}PdCl_2$
			(^{1}H nmr)			
τ(PtCH)	−0.67[c]	−0.62[c]	−1.14	−2.06 broad	−1.15	−0.68
^2J(PtCH), Hz	93	117	57	20	95	46
^3J(PPtCH), Hz	5.5	5.8	3.5	[d]	3.5	3.8
τ(C_6H_4)	1.8–2.8pq	2–3.1pq	1.8–3.05	1.30–2.84	2.89s, br	1.6–3.1pq
τ(*p*-CH_3)	7.66s	7.66s	7.70s	7.77s	7.67s	7.73s
τ(Et_3P)	7.4–9.3c	7.4–9.3c	7.64–9.26c	7.47–9.27c	7.0–9.2c	7.4–9.4c
			(^{31}P nmr)			
δ	11.26[e]	12.86[e]	11.26	11.96	11.56	9.35
^1J(PtP), Hz	2864	2830	2590	2935	2582	2612

[a]The spectra were run in $CDCl_3$ at ca. 27°C using Me_4Si as internal reference or 85% phosphoric acid as external standard. Integration supports the assignments given in the table; s = singlet, c = complex, pq = pseudoquartet.
[b]Two isomers (*syn* and *anti* to the double bond) were found (6, 7).
[c]In the proton nmr the *anti*/*syn* ratio was found to be 2:1 (6, 7).
[d]The coupling was not observed probably owing to the broadness of the signal.
[e]In the ^{31}P nmr the intensity ratio of the signals due to the *anti* and to the *syn* form was found to be ca. 2:1.

2–**5**, while the *p*-methyl protons on the periphery of the molecules are scarcely affected. The phosphine–ethyl resonances are complex and spread over a wide range.

The ^{31}P spectrum (Table 3) of L shows two singlets, the more intense (ca. ×2) being assigned to the *anti* form in agreement with the results (5) of the proton nmr spectrum. Each singlet is flanked by satellites with ^1J(PtP) ~ 2.8 kHz. The adducts **2**–**5** give simple ^{31}P spectra, each showing only one singlet with satellites having ^1J(PtP) between 2.4 and 2.6 kHz. The two phosphorus nuclei are therefore magnetically equivalent, both in each isomer of the L and in the adducts **2**–**5**, in agreement with the requirements of a square planar arrangement about platinum and of a Pt—C=N plane perpendicular to it. In the case of the trinuclear compound **5**, the results are in agreement with a symmetric arrangement of the two platinum-containing ligands, L, around the palladium atom, an arrangement which also will minimize steric crowding around the innermost coordination centre. Hence, the ligand L coordinates only in one of the two possible forms in which it is capable of existing. It is highly likely that it coordinates in the *anti* form, since in this arrangement the metal atoms and their ligands will be kept on opposite sides of the C=N bond. Moreover, we previously found (4) by nmr studies that only this *anti* form interacts with lanthanide shift reagents. In any event, our results demonstrate the ability of the

compound L to act as an *N*-ligand which affords both binuclear and trinuclear complexes.

Acknowledgments

One of us (F.B.) thanks the Canada Council for a grant which enabled him to visit the University of Guelph. The continued financial support (to H.C.C.) of the National Research Council of Canada is gratefully acknowledged.

1. G. MINGHETTI, F. BONATI, and G. BANDITELLI. Inorg. Chem. **15**, 2649 (1976).
2. G. MINGHETTI, G. BANDITELLI, and F. BONATI. Chem. Ind. 123 (1977).
3. R. P. SPERLINE and D. M. ROUNDHILL. Inorg. Chem. **16**, 2612 (1977) and references therein.
4. F. BONATI and G. MINGHETTI. J. Organomet. Chem. **60**, C43 (1973); F. BONATI, G. MINGHETTI, and G. BANDITELLI. Synth. React. Inorg. Met.-Org. Chem. **6**, 383 (1976).
5. L. E. MANZER and P. Z. MEAKIN. Inorg. Chem. **15**, 3117 (1976).
6. D. F. CHRISTIAN, H. C. CLARK, and R. F. STEPANIAK. J. Organomet. Chem. **112**, 209 (1976).
7. D. F. CHRISTIAN, H. C. CLARK, and R. F. STEPANIAK. J. Organomet. Chem. **112**, 227 (1976).

Polarizable acid–acid and acid–water hydrogen bonds with H_3PO_2, H_3PO_3, H_3PO_4, and H_3AsO_4[1]

MARTIN LEUCHS AND GEORG ZUNDEL

Physikalisch-Chemisches Institut der Universität München, Theresienstraße 41, D-8000 München 2, West Germany

Received July 24, 1978

MARTIN LEUCHS and GEORG ZUNDEL. Can. J. Chem. **57**, 487 (1979).

Hypophosphorous, phosphorous, phosphoric, and arsenic acids, pure and their aqueous solutions were studied by ir spectroscopy. Strong continuous absorptions observed with the pure liquid acids and with solutions containing less than one water molecule per acid molecule demonstrate that acid–acid hydrogen bonds in these systems are easily polarizable. The discussion of the PO and AsO bands as well as the discussion of the structure of the continuum demonstrates, however, that the degree of asymmetry of the energy surfaces in these hydrogen bonds is relatively large. It is shown that extended networks of such bonds exist. Due to the polarizability of these bonds, the proton motion in these bonds is strongly correlated. With addition of water, easily polarizable acid–water hydrogen bonds (I) $AH\cdots OH_2 \rightleftharpoons A^-\cdots H^+\text{-}OH_2$ (II) are formed. The energy surfaces in these hydrogen bonds are similar to those in the acid–acid hydrogen bonds. With further addition of water, proton boundary structure II receives noticeable weight, i.e., the degree of asymmetry of the energy surfaces in these bonds decreases due to addition of water molecules. The degree of symmetry of the energy surfaces in the acid–water hydrogen bonds increases in the series arsenic, phosphoric, phosphorous, and hypophosphorous acid.

MARTIN LEUCHS et GEORG ZUNDEL. Can. J. Chem. **57**, 487 (1979).

Faisant appel à la spectroscopie ir, on a étudié les acides hypophosphoreux, phosphoreux, phosphorique et arsenique à l'état pur et en solutions aqueuses. Les absorptions continues intense observées dans les cas des acides liquides à l'état pur et dans des solutions contenant moins d'une molécule d'eau par molécule d'acide démontrent que les liaisons hydrogène acide–acide dans ces systèmes sont facilement polarisables. Une discussion des bandes PO et AsO de même qu'une discussion de la structure du continuum démontre toutefois que le degré d'asymétrie des surfaces d'énergie dans ces liaisons hydrogène est relativement large. On a montré qu'il existe un réseau étendu de telles liaisons. Due à la polarisabilité de ces liaisons, une forte corrélation existe avec le mouvement des protons dans ces liaisons. Par addition d'eau, il y a formation de liaisons hydrogènes eau–acide facilement polarisables, (I) $AH\cdots OH_2 \rightleftharpoons A^-\cdots H^+OH_2$ (II). Les surfaces d'énergie de ces liaisons hydrogènes sont semblables à celles des liaisons hydrogènes acide–acide. Par addition subséquente d'eau, le poids statistique de la structure limite (II) du proton augmente, c'est à dire que le degré d'asymétrie des surfaces d'énergie de ces liaisons diminue à cause de l'addition de molécules d'eau. Le degré de symétrie des surfaces d'énergie des liaisons hydrogènes acide–eau augmente dans la série des acides arsenique, phosphorique, phosphoreux et hypophosphoreux.

[Traduit par le journal]

Introduction

Hydrogen bonds with double minimum energy surface or with an energy surface having a very broad flat well are easily polarizable (1–3). All these energy surfaces are time-dependent. The absorption of a quantum proceeds, however, so rapidly that with strong hydrogen bonds, as considered in the following, it does not change considerably during the absorption process. These easily polarizable hydrogen bonds are indicated by continuous absorptions in the infrared spectra (4, 5). Easily polarizable are hydrogen bonds of the type

$$B^+H \cdots B \rightleftharpoons B \cdots H^+B$$

i.e., bonds with which the acceptor and the donor are the same. A large number of bonds of this type is summarized in Table 1 of ref. 5. Recently, it was shown that not only hydrogen bonds with symmetrical structure are easily polarizable but also bonds of type (6–10)

$$B_1H \cdots B_2 \rightleftharpoons B_1^- \cdots H^+B_2 \qquad B_1 \neq B_2$$

In the case of acids with $pK_a < 1$, easily polarizable acid–water hydrogen bonds

$$AH \cdots OH_2 \rightleftharpoons A^- \cdots H^+OH_2$$

are observed if these acids can be studied at very high concentrations (water:acid ratio, $n < 1$) (11–13).

Results and Discussion

In this paper, the following acids are studied with which the proton is not so easily removed from the

[1]Dedicated to Professor G.-M. Schwab on the occasion of his 80th birthday.

0008-4042/79/050487-07$01.00/0

anion: hypophosphorous acid H_2POOH, pK_a 1.1 (14); phosphorous acid $HPO(OH)_2$, pK_a of the first dissociation step 1.8 (14); phosphoric acid $PO(OH)_3$, pK_a of the first dissociation step 2.2 (14) (hydrogen bonding in aqueous solutions at pH values in the range of the second and the third dissociation step has been studied in ref. 15). For arsenic acid, $AsO(OH)_3$, the pK_a of the first dissociation step is 2.5 (14).

Figure 1 shows selected spectra of aqueous solutions of these acids at various concentrations. For comparison, spectra of aqueous solutions of primary sodium salts are given in the regions in which these groupings show characteristic vibrations. The most important bands and their assignment taken from refs. 15–17 are summarized in Table 1.

Degree of Dissociation

Hypophosphorous Acid (Fig. 1 a *and* b*)*

In the spectrum of the 5.7 *M* solution (*n*, number of water molecules per acid molecule = 7.3) $\nu_s PO_2$ of $H_2PO_2^-$ groupings is observed as a weak band. A quantitative estimation shows that the degree of dissociation is less than 0.25 in the 0.5 *M* solution.

Phosphorous Acid (Fig. 1 c *and* d*)*

In the spectrum of the 4.5 *M* solution ($n = 9.7$) $\nu_s PO_2$ of $(PO_2OH)^-$ groupings is found as a very weak shoulder which becomes stronger with increasing dilution. A quantitative estimation shows that the degree of dissociation at 0.5 *M*, however, is less than 0.15.

Phosphoric Acid (Fig. 1 e *and* f*)*

With dilution, in the spectrum of the 2.5 *M* solution ($n = 19.4$) the band of $\nu_s PO_2$ at 1065 cm^{-1} arises as a weak shoulder indicating $(PO_2(OH)_2)^-$ groupings, i.e., removal of the first protons from the phosphoric acid molecules. The degree of dissociation in the 0.5 *M* solution is also less than 0.15.

*Arsenic Acid (Fig. 1*g*)*

No bands of dissociated groupings can be found even in the 0.8 *M* ($n = 57$) solution.

Polarizable Hydrogen Bonds and Liquid Structure

In all spectra in this study, strong continuous absorption is found. The absorbance of these continua is plotted in Fig. 2 as a function of the mole fraction of water x_{H_2O} and as a function of *n*.

Pure Acids

Figure 2 shows that the continua do not vanish when the last water molecule is removed. Arsenic acid could not be studied pure. No decrease of the absorbance, however, is found with this acid in the region $n = 1$ to $n = 0.5$.

These continua demonstrate that in the water-free acids easily polarizable hydrogen bonds are present.

$$POH \cdots OP \rightleftharpoons PO^- \cdots H^+OP$$

or

$$AsOH \cdots OAs \rightleftharpoons AsO^- \cdots H^+OAs$$

I II

In the preceding section, however, it was shown that all protons are present at the anions. Thus the weight of proton boundary structure II in these bonds is very low.

From theory it is known (18) that with increasing degree of asymmetry of the double minimum energy surfaces the residence time in the higher well decreases much stronger than the fluctuation frequency of the proton. Even when the residence time of the proton in the higher well is very short, the polarizability is smaller but still appreciable. This theoretical result was confirmed by results with carboxylic acid – N-base systems. It was shown with these studies (see Fig. 2 of ref. 6) that when the proton is largely located at the N-base the absorbance of the continuum is weaker but can still be observed. These continua, however, no longer extend to the low wave number region. In the case of the acids studied in this paper in the region below 1400 cm^{-1}, the very intense νPO, νAsO, and δOH vibrations are observed. Therefore, the decrease of intensity of the continuum toward smaller wave numbers cannot be observed.

The absorbance of the continuum in the large wave number region shows three maxima, one very

TABLE 1. Assignment of bands of aqueous acid solutions

Compound	Wave number (cm^{-1})	Assignment
H_3PO_2	~2650	νOH
	2410	νPH_2
	1175	νP═O
	1160	$\nu_{as}PO_2^-(H_2PO_2^-)$
	1040	$\nu_s PO_2^-(H_2PO_2^-)$
	975	νP—OH
H_3PO_3	~2900	νOH
	2410	νP—H
	1175	νP═O
	1065	$\nu_s PO_2^-(H_2PO_3^-)$
	1025	$\nu_{as}P(OH)_2$
	935	$\nu_s P(OH)_2$
H_3PO_4	~3000	νOH
	1240	δPOH
	1170	νP═O
	1065	$\nu_s PO_2^-(H_2PO_4^-)$
	1008	$\nu_{as}P(OH)_3$
	885	$\nu_s P(OH)_3$
H_3AsO_4	~2900	νOH
	1230	δAsOH
	927	νAs═O
	808	$\nu_{as}As(OH)_3$
	760	$\nu_s As(OH)_3$

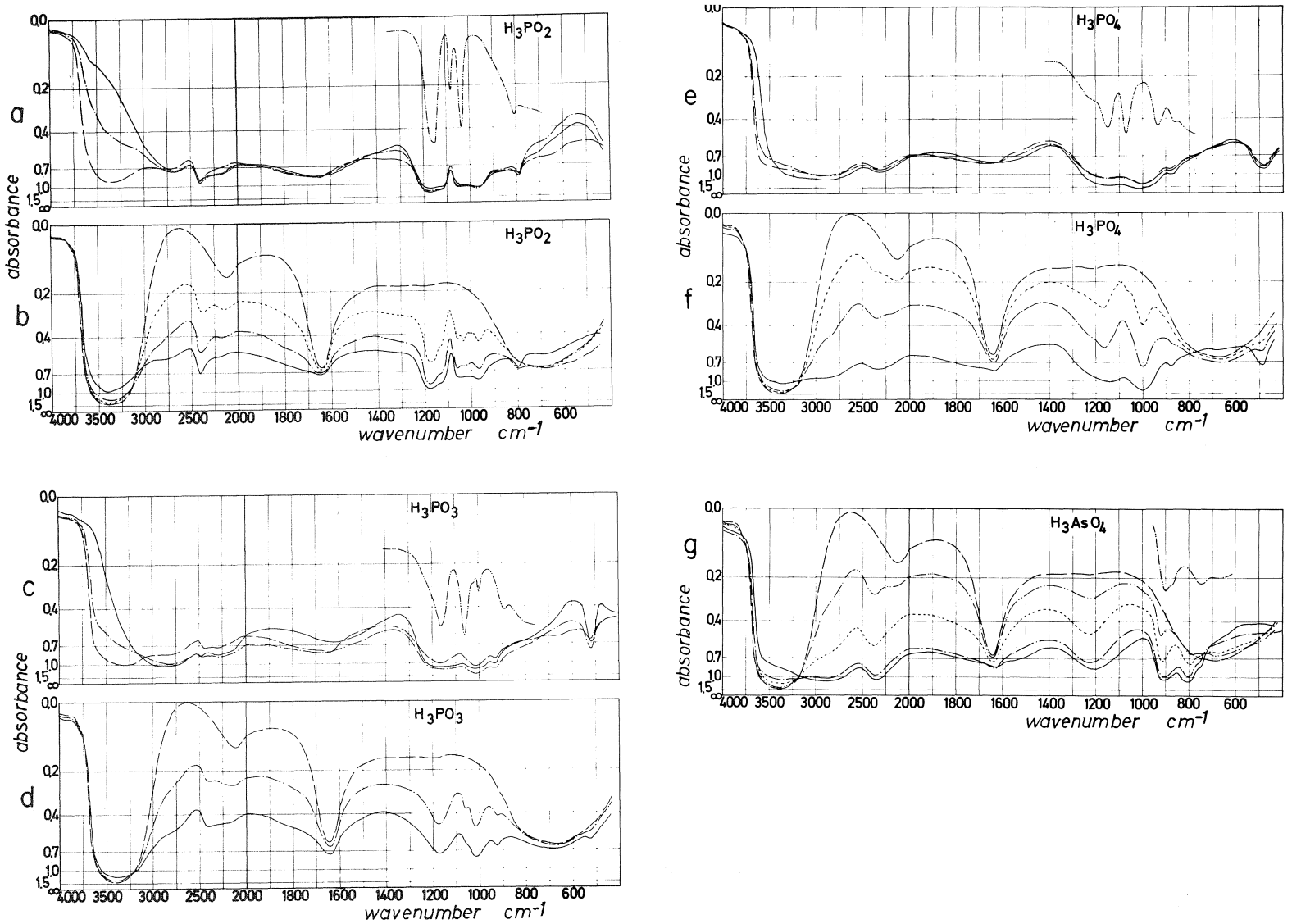

FIG. 1. Infrared spectra of aqueous acid solutions (layer thickness 9, 5 μm; temperature 293 K): (*a*) H_3PO_2, — 22.1 *M* (*n* = 0.0); ····· 19.7 *M* (*n* = 0.35); - - - 14.4 *M* (*n* = 1.4); ····· NaH_2PO_2 solution. (*b*) H_3PO_2, — 11.5 *M* (*n* = 2.4); ····· 5.7 *M* (*n* = 7.3); --- 2.9 *M* (*n* = 17.1); ---- H_2O. (*c*) H_3PO_3, — 19.6 *M* (*n* = 0.0); ····· 16.6 *M* (*n* = 0.7); --- 10.5 *M* (*n* = 2.5); ····· NaH_2PO_3 solution. (*d*) H_3PO_3, — 4.5 *M* (*n* = 9.7); ····· 1.9 *M* (*n* = 25.9); --- H_2O. (*e*) H_3PO_4, — 18.6 *M* (*n* = 0.1); ····· 14.7 *M* (*n* = 1.0); --- 12.2 *M* (*n* = 1.8); ····· NaH_2PO_4 solution. (*f*) H_3PO_4, — 9.1 *M* (*n* = 3.3); ····· 2.5 *M* (*n* = 19.4); --- 0.75 *M* (*n* = 7.1); ---- H_2O. (*g*) H_3AsO_4, — 14.8 *M* (*n* = 0.5); ····· 10.8 *M* (*n* = 1.9); --- 7.5 *M* (*n* = 9.5); ····· 1.4 *M* (*n* = 35.6); ---- H_2O; ····· NaH_2AsO_4 solution.

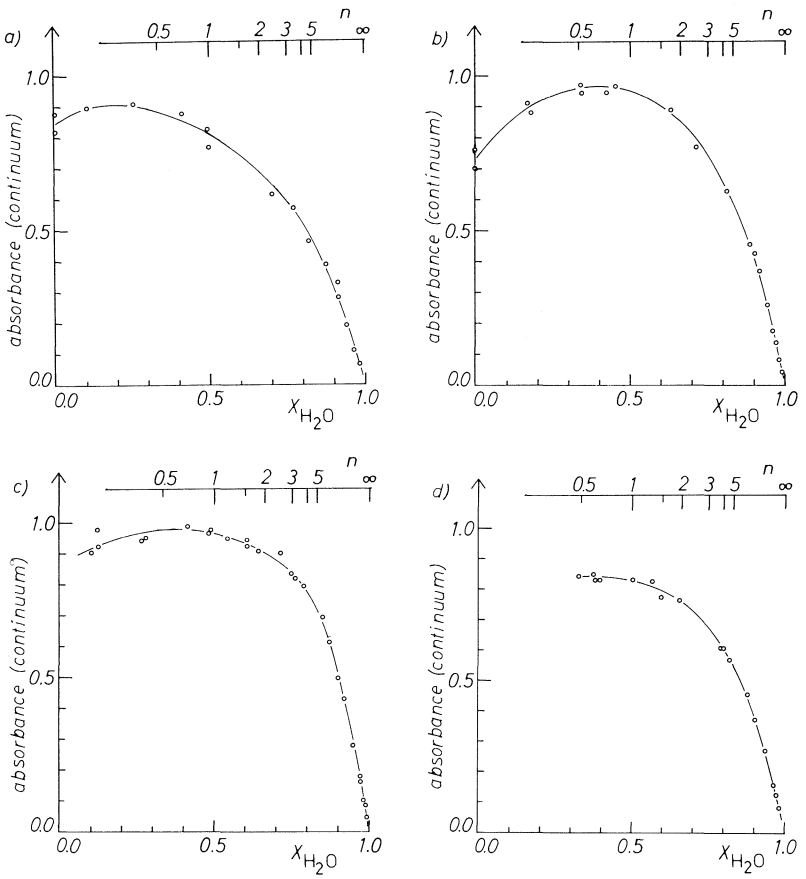

FIG. 2. Continuous absorption of acid solutions depending on the mole fraction of water x_{H_2O} and the mole ratio $n = M_{H_2O}/M_{acid}$. (*a*) H_3PO_2; (*b*) H_3PO_3; (*c*) H_3PO_4; (*d*) H_3AsO_4.

intense in the region 3000–2500 cm^{-1}, a less intense one in the region 2400–2200 cm^{-1} (the band at 2410 cm^{-1} with hypophosphorous acid and the band at 2410 cm^{-1} with phosphorous acid are caused by νPH vibrations), and finally a very broad maximum around 1600 cm^{-1}. This band-like structure is similar to the bands which are observed with asymmetrical acid–acid hydrogen bonds. Analogously, as with Hadži's ABC bands (19), with these acids, the broad band in the region 3000–2500 cm^{-1} is ascribed to νOH, and the band in the region 2400–2200 cm^{-1} to the 2δOH vibration which is intensified by Fermi resonance. With the acids studied in this paper, this band-like structure is most pronounced with arsenic acid. The above discussion of the dissociation behaviour shows that the proton is more strongly bound to the anion in the case of arsenic acid than in the case of the phosphorous-containing acids. Hence the energy surfaces in the acid–water hydrogen bond should be more asymmetrical with arsenic acid than with phosphoric acid. This is in good agreement with the result that the band-like structure is more pronounced with arsenic than with phosphoric acid.

All these results and considerations taken together show that the energy surfaces in these acid–acid hydrogen bonds are relatively asymmetrical but not so asymmetrical as to cause sharp bands instead of a continuum. Thus the polarizability of these bonds is much smaller than that of symmetrical hydrogen bonds with double minima, but much larger than the polarizability of asymmetrical hydrogen bonds.

Finally, it is important to consider the reasons why, in this pK_a region, hydrogen bonds between the acid molecules become so symmetrical that they are easily polarizable. The degree of asymmetry of the acid–acid bonds should decrease if the proton is less easily removed from the anions and if the hydrogen bond acceptor strength of the acceptor sites at the acid molecules increases. Hence, with increasing pK_a of the acids, a pK_a region should occur in which the

acid–acid hydrogen bonds are less asymmetrical. The prevailing results show that this is the case with the acids studied in this paper.

Liquid Structure of these Acids

Hypophosphorous Acid (Fig. 1a)

At 3570 cm^{-1}, a weak shoulder is found. This shoulder is caused by non-hydrogen bonded OH groups. The number of POH groups which cannot find an acceptor is very small. Thus extended chains of acid molecules are present

$$\begin{matrix} H & & H & & H \\ OPOH & \cdots & OPOH & \cdots & OPOH \cdots \\ H & & H & & H \end{matrix}$$

Because of the polarizability of these hydrogen bonds, the proton motion in these hydrogen bonds is strongly correlated (20).

Phosphorous Acid (Fig. 1c)

No band or shoulder of non-hydrogen bonded POH groups is found in the spectrum of the pure acid. Thus all POH groups are bound to PO groups of neighbouring acid molecules. Each PO group is an acceptor for two POH groups. Thus, an extended network of hydrogen bonds is present, because of the polarizability of these hydrogen bonds, the proton motion in these bonds is strongly correlated (20).

Phosphoric Acid (Fig. 1e)

In contrast to both other acids, a broad band occurs at the high wave number slope of the continuum. This band demonstrates that a large number of less strongly bound POH groups is present in the network of easily polarizable bonds between the phosphoric acid molecules. This occurs with phosphoric acid since the number of hydrogen bond donor groups is larger than the number of hydrogen bond acceptor sites.

Thus with all these water-free acids, chains or extended networks of easily polarizable bonds are present. Because of the polarizability of the hydrogen bonds, the proton motion in these bonds is strongly correlated (20).

Number of Water Molecules per Acid Molecule Less than One

When one water molecule per acid molecule is added the continua remain largely unchanged. This is true with regard to the structure of the continua as well as to its intensity. With H_3PO_4 and H_3PO_3, a small intensity increase is observed even though the molarity of the acid decreases.

These results show that the energy surfaces in the acid–water hydrogen bonds are very similar to those in the acid–acid hydrogen bonds. Although

$$POH \cdots OH_2 \rightleftharpoons PO^- \cdots H^+OH_2$$

or

$$AsOH \cdots OH_2 \rightleftharpoons AsO^- \cdots H^+OH_2$$

$$\text{I} \qquad\qquad \text{II}$$

are still easily polarizable, the weight of proton boundary structure II is so small that no anion bands are found in the spectra.

No scissor vibration band of the water molecules in this grouping is observed. Thus, this vibration couples with transitions of the proton of the easily polarizable hydrogen bond and merges in the continuum due to this coupling.

With hypophosphorous acid, the stretching vibration of the water molecules in these groupings is found as a broad band with maximum at 3370 cm^{-1}. Thus, the OH groups of these water molecules are bound via hydrogen bonds to acceptor sites of PO groups, and are in this way integrated in the network of hydrogen bonds of the liquid structure. With phosphorous acid, an intense shoulder is found at about 3600 cm^{-1}. This band is caused by the stretching vibration of non-hydrogen bonded OH groups of water molecules. Thus with this acid, a relatively large number of OH groups of water molecules is not, or only weakly, bound to their environment. With phosphoric acid, this number of non-hydrogen bonded OH groups of water molecules is even greater, as indicated by a very intense shoulder at about 3600 cm^{-1} (Fig. 1*a*). This series of increasing non-hydrogen bonded OH groups reflects the trend of the ratio of donor groups and acceptor sites with these acids.

Number of Water Molecules per Acid Molecule Greater Than One

With increasing n, the absorbance of the continuum decreases with all these acids since the concentration of easily polarizable acid–water hydrogen bonds decreases due to dilution.

As discussed in the section concerning the degree of dissociation, with increasing n, protons are removed from the anions. Before the protons transfer in the network of hydrogen bonds between water molecules, i.e., before $H_5O_2^+$ is formed, the weight of proton boundary structure II of the acid–water

$$POH \cdots OH_2 \rightleftharpoons PO^- \cdots H^+OH_2$$

$$\text{I} \qquad\qquad \text{II}$$

hydrogen bonds increases. As discussed with other systems (6, 8, 21–23) an increase of the weight of the polar proton boundary structure is caused by polar environments. Hence with these acid solutions, the additional water molecules cause the weight increase of proton boundary structure II. As shown by the

bands of the anions, removal of protons from the anions, i.e., a noticeable weight of proton boundary structure II, is observed, with hypophosphoric acid for $n = 7.3$ (Fig. 1*b*), with phosphorous acid for $n = 9.7$ (Fig. 1*d*), and with phosphorous acid for $n = 19.4$ (Fig. 1*f*). With arsenic acid, even in the 0.8 *M* solution, i.e., for $n = 57$, no removal of protons from the anions is found, within the limit of experimental error.

Conclusions

With the acids studied, the acid–acid hydrogen bonds

$$POH \cdots OP \rightleftharpoons PO^- \cdots H^+OP$$

or

$$AsOH \cdots OAs \rightleftharpoons AsO^- \cdots H^+OAs$$

I II

which are formed in water-free and highly concentrated solutions, cause very intense continuous absorbance, indicating polarizability of these hydrogen bonds. The weight of proton boundary structure II, however, is so small that no anion bands are found. Furthermore, the structure of the continuum indicates that the degree of asymmetry of the energy surfaces is relatively large. The energy surfaces in these bonds are, however, sufficiently symmetrical that these hydrogen bonds are still easily polarizable. The fact that the energy surfaces in these structurally asymmetrical hydrogen bonds become sufficiently symmetrical to be easily polarizable is explained as follows: with increasing pK_a, the protons are more strongly bound to the anions, and the hydrogen bond acceptor strength of the acceptor sites at the acid molecules becomes stronger. Both changes together cause a decrease of the degree of asymmetry of the acid–acid hydrogen bonds.

With hypophosphorous acid, extended chains of acid molecules, and with phosphorous, phosphoric acid, and arsenic acid, a network of hydrogen bonded acid molecules is present. The proton motion in these hydrogen bonds is correlated because of the polarizability of the hydrogen bonds. The number of less strongly bound OH groups increases from hypophosphorous to phosphoric acid, since the ratio of hydrogen bond donor groups to acceptor sites decreases in this series of molecules.

When one water molecule per acid molecule is added, easily polarizable acid–water hydrogen bonds

$$POH \cdots OH_2 \rightleftharpoons PO \cdots H^+OH_2$$

or

$$AsOH \cdots OH_2 \rightleftharpoons AsO \cdots H^+OH_2$$

I II

are formed. The energy surfaces of these bonds are very similar to those of the acid–acid hydrogen bonds. The OH groups of these water molecules are bound via moderately strong hydrogen bonds to acceptor sites at PO or AsO groups of acid molecules. The number of only weakly or non-hydrogen bonded OH groups increases, in the series from hypophosphorous to phosphoric acid, i.e., with increasing ratio of hydrogen bond donor groups to acceptor sites on the acid molecules.

With increasing number of water molecules per acid molecule, proton boundary structure II gains noticeable weight, and protons transfer in the network of hydrogen bonds formed between water molecules, i.e., they are present in $H_5O_2^+$ groupings. This removal of protons is indicated by anion bands, which become apparent in the spectra, for hypophosphorous acid at $n = 7.3$, for phosphorous acid at $n = 9.9$, and for phosphoric acid at $n = 19.4$. With arsenic acid no anion bands are found, even in the 0.8 *M* solution, i.e. at $n = 57$.

Materials and Methods

All phosphor acids, analytical grade, were purchased from Merck, Darmstadt, Germany. H_3PO_3 and H_3PO_2 were dried under vacuum and $P_2O_5 \cdot H_3AsO_4$ was prepared by mixing 3 mol As_2O_5 with 5 mol H_2O.

The ir spectra were recorded at 293 ± 1 K using a Perkin-Elmer double-beam spectrophotometer, model 325. The air in the spectrophotometer was dried and made CO_2-free by treatment with silica gel and sodium asbestos. The cells used had silicon windows and a wedge-shaped layer (mean thickness 9.5 μm) in order to avoid an interference pattern superimposed on the spectra. To take the wedge-shape into account, the absorbance was corrected as described in ref. 6. The absorbance of the continuum was determined as previously described (24) referring to the same background absorbance at 4700 cm^{-1}. Degree of dissociation was estimated comparing the spectra with bands of the respective anions in sodium salt solutions.

Acknowledgements

Our thanks are due to the Deutsche Forschungsgemeinschaft and to the Fonds der Deutschen Chemie for providing the facilities for this work.

1. E. G. Weidemann and G. Zundel. Z. Naturforsch. **25a**, 627 (1970).
2. R. Janoschek, E. G. Weidemann, H. Pfeiffer, and G. Zundel. J. Am. Chem. Soc. **94**, 2387 (1972).
3. R. Janoschek, E. G. Weidemann, and G. Zundel. J. Chem. Soc. Faraday II, **69**, 505 (1973).
4. G. Zundel. *In* The hydrogen bond—recent developments in theory and experiments. Vol. II. *Edited by* P. Schuster, G. Zundel, and C. Sandorfy. North Holland Publ. Co., Amsterdam. 1976.
5. G. Zundel. Hydration and intermolecular interaction. Academic Press, 1969, and Mir Moscow, 1972.
6. R. Lindemann and G. Zundel. J. Chem. Soc. Faraday II, **73**, 787 (1977).
7. M. Matthies and G. Zundel. Biochem. Biophys. Res. Commun. **74**, 831 (1977).

8. A. NAGYREVI and G. ZUNDEL. J. Phys. Chem. **82**, 687 (1978).
9. R. LINDEMANN and G. ZUNDEL. Biopolymers, **16**, 2407 (1977).
10. R. LINDEMANN and G. ZUNDEL. Biopolymers, **17**, 1285 (1978).
11. M. LEUCHS and G. ZUNDEL. J. Chem. Soc. Faraday II. In press.
12. M. LEUCHS and G. ZUNDEL. J. Phys. Chem. **82**, 1632 (1978).
13. M. LEUCHS and G. ZUNDEL. To be published.
14. A. ALBERT and E. P. SERJEANT. Ionization constants of acids and bases. Wiley, New York. 1962.
15. A. C. CHAPMAN and L. E. THIRLWELL. Spectrochim. Acta, **20**, 937 (1964).
16. R. W. LOVEJOY and E. L. WAGNER. J. Phys. Chem. **68**, 544 (1964).
17. H. SIEBERT. Anwendungen der Schwingungsspektroskopie in der Anorg. Chem. Springer, Berlin. 1966.
18. E. G. WEIDEMANN and G. ZUNDEL. Naturforsch. **28**a, 236 (1973).
19. D. HADŽI. Pure Appl. Chem. **11**, 435 (1965).
20. E. G. WEIDEMANN. *In* The hydrogen bond; recent developments in theory and experiments. Vol. I. *Edited by* P. Schuster, G. Zundel, and C. Sandorfy. North Holland Publ. Co., Amsterdam. 1976. Chapt. 5.
21. H. BABA, A. MARTSUYANA, and H. KOKOBUN. Spectrochim. Acta, **25**A, 1709 (1969).
22. J. JADŻYN and J. MAŁECKI. Acta Phys. Pol. A**41**, 599 (1972).
23. L. SOBCZYK. *In* The hydrogen bond—recent developments in theory and experiments. Vol. III. *Edited by* P. Schuster, G. Zundel, and C. Sandorfy. North Holland Publ. Co., Amsterdam. 1976.
24. D. SCHIÖBERG and G. ZUNDEL. Can. J. Chem. **54**, 2193 (1976).

σ complexes as biophysical and biochemical probes. Part III.[1] Competitive demethylation and σ-complex formation in reaction of 4,6-dinitro-7-methoxybenzofuroxan with nucleophiles

ERWIN BUNCEL,[2] NOEMI CHUAQUI-OFFERMANNS, ROBERT Y. MOIR, AND ALBERT R. NORRIS[2]

Department of Chemistry, Queen's University, Kingston, Ont., Canada K7L 3N6

Received July 11, 1978

ERWIN BUNCEL, NOEMI CHUAQUI-OFFERMANNS, ROBERT Y. MOIR, and ALBERT R. NORRIS. Can. J. Chem. **57**, 494 (1979).

4,6-Dinitro-7-methoxybenzofuroxan (**4**) reacts with MeONa–MeOH or with Et_2NH competitively by σ-complex formation and demethylation, by nucleophilic reaction at the aromatic and aliphatic carbon centers, respectively. Carbonate ion in $CHCl_3$ in the presence of 18-crown-6 polyether also results in rapid demethylation. The facile leaving group ability in these S_N2 displacements is consistent with the large acidity constant of 4,6-dinitro-7-hydroxybenzofuroxan (pK_a ca. -3.7), i.e., 4 pK units stronger than picric acid. Some unusual features exhibited in the nmr spectral characteristics of the σ-complexes are accounted for in terms of stereoelectronic effects.

ERWIN BUNCEL, NOEMI CHUAQUI-OFFERMANNS, ROBERT Y. MOIR et ALBERT R. NORRIS. Can. J. Chem. **57**, 494 (1979).

Le dinitro-4,6 méthoxy-7 benzofuroxanne (**4**) réagit avec le MeONa–MeOH ou avec le Et_2NH, en compétition avec la formation d'un composé σ et une diméthylation; les deux types de réactions proviennent respectivement de réactions nucléophiles au niveau des carbones aromatiques et aliphatiques. L'ion carbonate dans le $CHCl_3$ en présence de polyéther-6 couronne-18 conduit aussi à une diméthylation rapide. La facilité avec laquelle ces substitutions S_N2 se produisent est en accord avec la constante d'acidité élevée ($pK_a \approx -3.7$) du dinitro-4,6 hydroxy-7 benzofuroxanne qui est environ 4 unités de pK plus élevée que celle de l'acide picrique. On peut expliquer quelques caractéristiques inattendues des spectres rmn des complexes σ en termes d'effets stéréoélectroniques.

[Traduit par le journal]

In relation to our studies of σ complexes as biophysical and biochemical probes (1), we have been investigating σ-complex (2) formation in the nitro benzofuroxan and benzofurazan series, as this type of interaction has been implicated in explanation of the antileukemic activity of these compounds (3). We found (1*a*) that 7-methoxy-4-nitrobenzofuroxan (**1**) reacts with methoxide ion in dimethyl sulfoxide – methanol solution to yield the 5-methoxy adduct (**2**) in a kinetically preferred process and the 7-methoxy adduct (**3**) in a thermodynamically preferred process, Scheme 1; no other reactions were detected. Extension of the work to the 4,6-dinitro-7-methoxybenzofuroxan analog (**4**) has revealed a different type of behaviour which is the subject of the present report.

Results and Discussion

Reaction of 4 with Nucleophiles

The course of the reaction of **4** with methoxide ion was studied by nmr and uv–visible spectroscopy. When a solution of **4** in CD_3OD was treated with CD_3ONa–CD_3OD (final concentrations, [**4**] = 0.11 *M*, $[CD_3O^-]$ = 0.07 *M*), the solution color changed from pale yellow to orange. The nmr spectrum taken 5 min after mixing exhibited the H-5 signal at δ 8.80 characteristic of **4** and a signal at δ 9.03 which was assigned to H-5 of the σ-complex **5**.[3] In addition, a signal at δ 3.30 was present and could be assigned to CH_3OD resulting from methoxyl exchange between solvent and substrate. This exchange apparently also occurs via the σ-complex **5**. As the reaction progressed further the signals at δ 8.80 and 9.03 due to **4** and **5** decreased while a signal at δ 9.18 correspondingly increased in intensity. The latter could be assigned to H-5 of the anion of 4,6-dinitro-7-hydroxybenzofuroxan, i.e. **6**, by comparison with an authentic sample in this medium. After 12 h at ambient temperature only **6** could be detected. The above observations can be explained by the reaction scheme given in Scheme 2, i.e., a rapid reversible formation of σ-complex **5** occurring concurrently with a slower

[1]For Part II see ref. 1*b*.

[2]Authors to whom correspondence should be addressed.

[3]The conventional techniques used in this work allowed only the thermodynamically stable product **5** to be observed and it is presumed that a kinetically preferred σ adduct would be detected using fast reaction techniques, as has been found in related systems (4).

0008-4042/79/050494-06$01.00/0

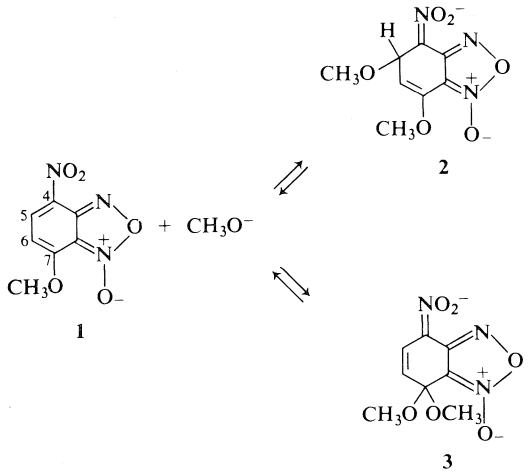

SCHEME 1

demethylation to yield **6**. Complete structural assignment for **5** was obtained by reacting **4** with CD_3O^- in CD_3OD–CD_3CN (6:94 v/v) which allowed the observation of H-5 as well as the methoxy signal of **5** occurring at δ 3.10, shifted from δ 4.23 in the substrate. The uv–visible spectral characteristics of **4**, **5**, and **6** are given in Table 1.

We sought to corroborate our results by investigating the reactivity of **4** with another common nucleophile, namely diethylamine. The reaction, in $CDCl_3$ solvent, was found by nmr to proceed as outlined in Scheme 2, i.e., initial rapid formation of a σ complex (H-5, δ 8.87) followed by slower formation of the demethylated product **6**. In contrast, reaction of **4** with triethylamine in $CDCl_3$ led to the rapid formation of **6**, with no indication of the formation of **5**, which is in agreement with the general finding that tertiary amines and nitroaromatic compounds do not normally give rise to stable σ complexes (2).

In view of the above results on demethylation it

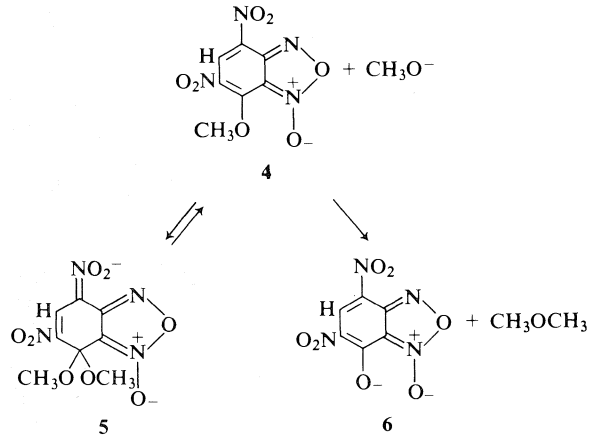

SCHEME 2

TABLE 1. Spectral characteristics of compounds **4**–**7**

Species	Solvent	λ_{max} (nm)	ε (M^{-1} cm^{-1})
4	$CHCl_3$	422	6 900
		352	3 000
		265	7 500
5	CH_3OH	452	26 700
		306	9 700
		266	7 900
6	H_2O	438	20 700
		400(sh)	14 200
		311	11 900
		265	10 500
7	65% H_2SO_4	424	8 300
		358	8 100
		275	13 000

appeared of interest to examine a weaker nucleophile and carbonate ion was chosen for this purpose using the nonpolar solvent chloroform in presence of 18-crown-6 ether to render solubilization. Immediate reaction was found to occur on mixing the reagents and the initially recorded nmr spectrum showed that complete conversion to **6** had occurred. A possible mechanism for this reaction would invoke attack by carbonate ion at the aromatic carbon to form a metastable σ-complex intermediate which would lose successively CO_2 and CH_3O^- to yield **6** as shown in [1]:

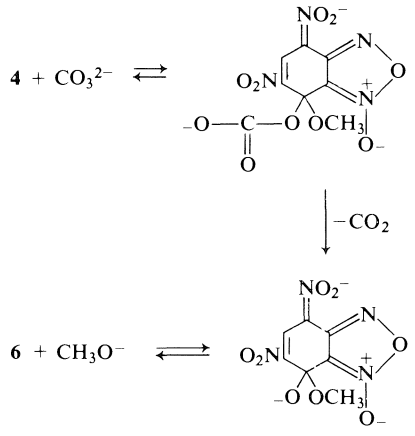

[1]

Although we cannot exclude this possibility on the basis of present evidence, we do not know of a precedent for CO_3^{2-} acting as an effective nucleophile at aromatic carbon (5). Demethylation by nucleophilic displacement at the methyl carbon would describe the observations fully and is in agreement also with the other results reported herein.

There are several cases recorded in the literature for competitive demethylation and σ-complex formation in attack by methoxide ion, notably 3,5-dinitro-

TABLE 2. Chemical shift data[a] in σ-complex formation for nitroaromatic and benzofuroxan series: origin of stereoelectronic effects

Reactant	σ complex	H_α Hz (ppm)	$H_{\alpha'}$ Hz (ppm)	ΔH_α Hz (ppm)
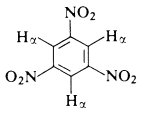 **12**	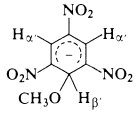 **13**	552 (9.20)	506 (8.43)	46 (0.77)
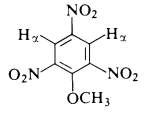 **10**	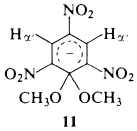 **11**	545 (9.08)	521 (8.68)	24 (0.40)
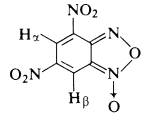 **8**	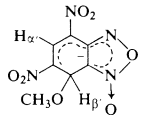 **9**	547 (9.12)	520 (8.67)	27 (0.45)
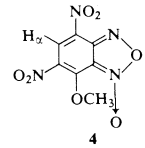 **4**	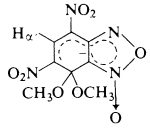 **5**	528 (8.80)	542 (9.03)	−14 (−0.23)

[a]Values of chemical shifts, in Hz, as obtained on a spectrometer operating at 60 MHz (see Experimental).

2-methoxypyridine (6) and 2,4-dinitroanisole (7). The latter was found to react with piperidine also by S_NAr attack at the ring carbon competitively with S_N2 displacement at the methyl carbon (8), which bears some analogy to the present observations with diethylamine. It is interesting that 2,4,6-trinitroanisole reacts with methoxide ion under corresponding conditions only by σ-complex formation. There is however no report of demethylation by carbonate in these or related nitroaromatic systems.

Stereoelectronic Effects in σ-complex Formation

An unusual feature of the nmr spectral characteristics of the σ-complex **5** is the downfield shift, by 14 Hz, of the H-5 resonance with respect to this signal in the reactant **4** (Table 2). Upfield shifts accompanying σ-complex formation have been uniformly observed hitherto (2) and have been explained on the basis of the increased charge density in the anionic σ complexes. For example, in the conversion of 1,3,5-trinitrobenzene (TNB) **12** to its methoxy adduct **13**, an upfield shift of 46 Hz is observed in the signal for H_α. The corresponding upfield shift in the conversion of 2,4,6-trinitroanisole **10** to the 1,1-dimethoxy σ-complex **11** is only 24 Hz and examination of Table 2 shows that the value has been lowered (with respect to that from **12** and **13**) in two ways. In the first place, H_α in the reactant **10** has been shielded (with respect to H_α in **12**) by the introduction of methoxyl, an effect conventionally attributed to the conjugative electron release of methoxyl having a small effect at a *meta* position. In the second place, H_α in the complex **11** is deshielded (with respect to H_α in **13**) by the introduction of the second methoxyl, an effect explicable by the inductive effect of the second tetrahedrally-bound methoxyl.

In the benzofuroxan series, σ-complex formation is expected to lead to a relatively smaller upfield shift in H_α as a result of the greater electron withdrawing capacity of the annelated furoxan ring relative to a nitro group (*vide infra*), which leaves a smaller net negative charge to be accommodated on the benzene ring in the σ complex. This effect is seen on comparing ΔH_α in the conversion **8** → **9** (27 Hz) with the analogous conversion **12** → **13** (46 Hz).

Another factor must however be operating to account for the reversed shift in H_α in the conversion **4** → **5**. Examination of the data in Table 2 shows that the reversed shift in **4** → **5** is due both to relative deshielding of H_α in the product **5** and to relative shielding of the same hydrogen in the reactant **4**. The deshielding of H_α in **5** (36 Hz with respect to **13**) is somewhat larger than the sum (29 Hz) expected for the combined effects of introduction of a second

methoxyl (15 Hz from **13** → **11**) and of replacement of nitro by the furoxan ring (14 Hz from **13** → **9**). It is proposed that the additional factor is steric compression between the methoxyl group and the *peri* *N*-oxide function in **4** and the relief of this interaction in formation of **5**. The magnitude of the effect of steric compression in **4** is manifested in the 19 Hz upfield shift between **8** and **4**, whereas the corresponding shift on going from **12** to **10** is only 7 Hz.

An approximate summation of the electronic and steric effects can be performed by means of the data in Table 2 and the above considerations regarding H_α shielding. The electronic effect of the furoxan ring in σ-complex formation can be taken from the differences of the H_α shifts in the pairs **12**,**13** and **8**,**9** which yields $\Delta\Delta H_\alpha = 46 - 27 = 19$ Hz. The steric decompression effect is taken from the pairs **8**,**4** and **12**,**10**, giving $\Delta\Delta H_\alpha = 19 - 7 = 12$ Hz. The sum of two $\Delta\Delta H_\alpha$ terms, 31 Hz, then represents the estimated overall downfield shift of the H-5 resonance in formation of **5**, relative to formation of **11**, from their respective precursors. The observed effect on the H_α shift (Table 2), i.e., 24 + 14 = 38 Hz, is of the same order of magnitude.

The deshielding of H_α as a result of the steric compression factor can be explained as arising from the magnetic anisotropy of the nearer oxygen in the nitro group situated above H_α in the figures (9). This effect will be larger the more nearly coplanar the nitro group is with its attached ring and the closer that the group is made to approach H_α. In both **10** and **4**, the adjacent methoxyl will have some effect in forcing the *ortho* nitro group out of coplanarity but the effect will be larger in **4** because of the presence of the *N*-oxide function in the fused furoxan structure. Thus in **4** it is to be expected that the nitro group will be tipped away from H_α, with a consequent decrease in its deshielding effect larger than that in **12**, **10**, or **8**. However the tetrahedrally disposed pair of methoxyls in **11** and **5** will tend both to return the nitro group to a more nearly coplanar position, and to press it backwards against H_α. As before, this effect should be greater in **5** than in the less rigid **11**, with a consequent increase in the relative deshielding of H_α in the former. Slight changes in geometrical alignments usually have large effects at the short distances present in the H_α–NO_2 systems, so that the local anisotropy effects would be expected to dominate any further secondary electronic effects that might be postulated for this group of compounds.

Acidity of 4,6-Dinitro-7-hydroxybenzofuroxan

The remarkably facile demethylation process undergone by **4** shows that this nucleophilic displacement is associated with an unusually good leaving group. Since leaving group ability is related to the pK_a of the conjugate acid, it was of interest to determine the acidity constant for the equilibrium in [2].

[2] 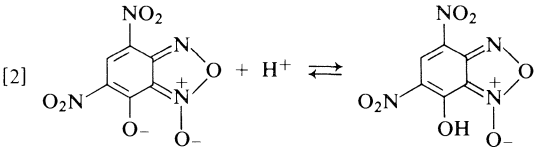

6 **7**

We have therefore studied the protonation of **6** in media of increasing acidity taking advantage of the different spectral characteristics of **6** and **7** in the uv–visible region. The resulting spectral changes are shown in Fig. 1 for sulfuric acid solutions of increasing concentrations. It is seen that the absorptions associated with the anionic species **6** (λ_{max} 438, 311 nm) decrease with acidity while the absorptions associated with the protonated species **7** (λ_{max} 358, 275 nm) correspondingly increase. Reasonably well defined isosbestic points occur at 372 and 328 nm. From the absorbance changes as a function of acid concentration one can estimate that 50% protonation occurs in a medium of ~45% H_2SO_4.

Since molarity (or % H_2SO_4) does not give a valid measure of the effective acidity of media in the moderately concentrated range, an operationally defined acidity function is used for this purpose. The acidity function appropriate to a protonation equilibrium of the charge type $A^- + H^+ \rightleftarrows AH$ is H_-, as given by (10) $H_- = -\log a_{H^+}(f_{A^-}/f_{AH})$. However it is now recognized that the protonation behaviour of anions of different structural types will not be subject to the same acidity function since the activity coefficient ratio will be structure dependent. Unfortunately literature data on H_- functions are available for only few structural types and over limited acidity ranges. An H_- acidity scale has been established (11) for the protonation of cyano substituted carbanions, eq. [3], covering the range up to 80% H_2SO_4. A more

[3] 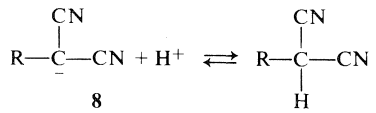

8 **9**

suitable acidity function for the process at hand would be given by the protonation of picrate anion or of the nitronate anion derived from the TNB–phenoxide σ complex (12) but these are limited to a lower acid concentration range corresponding to the smaller acidity constants of the conjugate acids (picric acid, $pK_a = 0.2$; nitronic acid, $pK_a = -1.2$). The anions **8**, are, however, charge delocalized

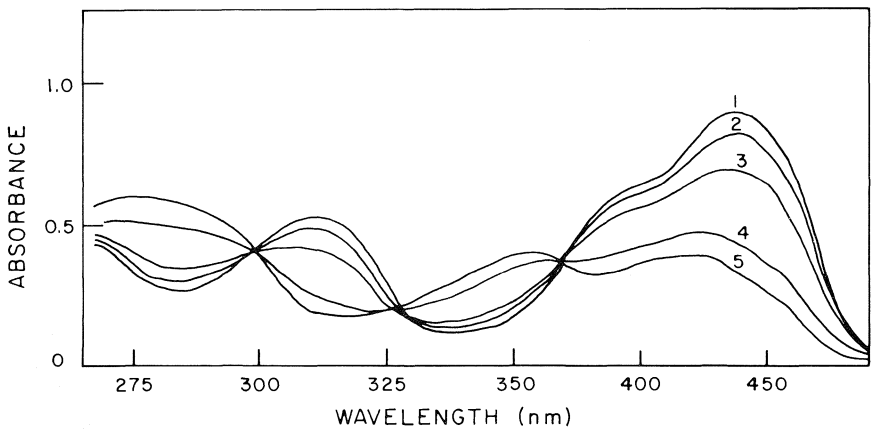

FIG. 1. Spectral curves illustrating the equilibrium protonation of **6** in aqueous H_2SO_4. Curve *1*, 0% H_2SO_4; *2*, 32.0% H_2SO_4; *3*, 45.0% H_2SO_4; *4*, 55.4% H_2SO_4; *5*, 64.6% H_2SO_4.

TABLE 3. Spectral data for equilibrium protonation of **6**

H_2SO_4 (wt.%)	H_-[a]	A_{438}[b]	I[c]
0	0	0.880	—
18.0	−0.82	0.835	12.1
32.0	−2.20	0.795	5.94
38.8	−2.80	0.750	3.54
45.0	−3.40	0.675	1.88
50.4	−4.00	0.485	0.494
55.4	−4.45	0.415	0.267
60.3	−5.00	0.330	0.073
64.6	−5.50	0.300	0.017

[a]Reference 11.
[b]Absorbance values of solutions with stoichiometric concentration of **4** = 4.24×10^{-5} *M* and cell path length of 1.00 cm.
[c]$I = [A^-]/[AH] = (A - A_{AH})/(A - A_{A^-})$ calculated at 438 nm using $A_{A^-} = 0.880$ and $A_{AH} = 0.290$.

species with negative charge essentially distributed on electronegative atoms and in this sense there is analogy with species **6**. Additionally, the degree of adherence to a given acidity function can be ascertained from the slope of the log I vs. H_- plot where I is the ionization ratio, i.e. $I = [A^-]/[AH]$. For a 'Hammett indicator' the slope should be unity.

The ionization ratios have been evaluated from the measured absorbance at each acid concentration. Thus $I = (A - A_{AH})/(A_{A^-} - A)$ where A is the measured absorbance whereas A_{AH} and A_{A^-} are the absorbance values due to the protonated and anionic species respectively at the given wavelength. The calculations were performed for absorbance values at 438 nm (λ_{max} for A^-) since this absorption undergoes the largest changes with acidity. The results for one set of determinations are given in Table 3. The plot of log I vs. H_- (11) while approximately linear showed appreciable deviation in the dilute acid range, suggesting that a differential medium effect is operating on the anionic species. Two such plots were constructed from two separate sets of determinations, yielding slope values of 0.75 and 0.80. The H_- values corresponding to log $I = 0$ were −3.7 and −3.8, respectively. A value for the pK_a could also be obtained by plotting A_{438} vs. H_- which yielded well defined sigmoid plots with H_- values at the inflexion point given by −3.8 and −3.6 for the two sets of experiments. In summary, a pK_a value of −3.7 is indicated by these results though it is apparent that the protonation behaviour is rather poorly represented by the given H_- function (11) of necessity employed.[4] Though the exact pK_a value may thus be somewhat in doubt, this does not affect appreciably our main conclusion.

The pK_a value of −3.7 for **7** when compared with the value 0.2 for picric acid shows that **7** is the stronger acid by ~4 pK_a units.[5] It follows from this result that the annelated furoxan ring has a powerful electron withdrawing capacity and that the anion **6** should be correctly written as

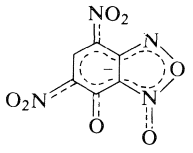

with negative charge delocalized over both rings. This conclusion is also in agreement with the results of quantitative studies on nucleophilic addition to benzofuroxan systems by Terrier and co-workers (13).

[4]It is recognized that the pK_a thus derived is not the thermodynamic pK_a and a more exact description of the experimental results should quote the H_- value (−3.7) at half-protonation.

[5]We note that the difference in the acidities of picric acid and **7** may not solely be ascribed to the difference in electron withdrawing power of the nitro and the furoxan moieties since picric acid is associated with an aromatic ring system whereas in **7** we have a diene type structure.

Concluding Remarks

In conclusion, it has been shown in this work that **4** is a methylating agent of unusually high reactivity (cf. ref. 14 for reactivity in alkylation by $ROSO_2Cl$ and $ROSO_2OAr$). As a corollary, **6** should be an exceedingly good leaving group and this is borne out by the observed pK_a value of -3.7 for the conjugate acid **7**. Also, the bifunctional reactivity of **4** in demethylation and σ-complex formation offers the possibility of evaluating selectivity in reactions of nucleophiles at aliphatic and aromatic carbon centers. Finally, the bifunctional reactivity of **4** could have implication in biological systems noting that the processes of methylation and σ-complex formation have both, separately, been considered of biological importance. The hypothesis that the observed antileukemic activity of nitrobenzofuroxan derivatives is the result of σ-complex formation by intracellular amino and thiol functions was discussed by us previously (1*b*) in light of the transformations undergone by the initially formed σ complex in the interaction of methoxide ion with 4-nitrobenzofuroxan.

Experimental

Materials

The purification of dimethyl sulfoxide and preparation of sodium methoxide solution have been described previously (1). Diethylamine was purified by conversion to the *p*-toluenesulfonamide which was recrystallized from dry ligroin (15*a*). Hydrolysis with aqueous HCl followed by treatment with NaOH and distillation three times under nitrogen yielded the purified diethylamine. Triethylamine was purified by treatment with acetic anhydride followed by distillation (15*b*).

4,6-Dinitro-7-methoxybenzofuroxan (4)

The preparation of **4** was effected by the nitration of **1**. To a solution of 1.2 g (5 mmol) of **1** (1*b*) in 25 mL 96% H_2SO_4 was added over 1 h 3 mL of nitrating mixture consisting of concentrated H_2SO_4 and fuming HNO_3 (3:1) while keeping the temperature at 0–5°C. Addition of the mixture to crushed ice gave a precipitate which was filtered, dried, and recrystallized from CCl_4 to give pale yellow crystals of product in 30% yield, mp 110°C; *m/e* 256. *Anal.* calcd. for $C_7H_4N_4O_7$: C 32.82, H 1.57, N 21.87; found: C 32.86, H 1.57, N 20.89.

4,6-Dinitro-7-hydroxybenzofuroxan (7)

This compound was obtained as the main product in the nitration of **1**, demethylation of **4** apparently occurring under the reaction conditions. The acidic aqueous solution obtained following the nitration and addition to ice was extracted with ether and the extracts were dried and evaporated to dryness. Recrystallization from benzene yielded orange crystals, mp 119°C; *m/e* 242. *Anal.* calcd. for $C_6H_2N_4O_5$: C 29.76, H 0.83, N 23.14; found: C 29.78, H 0.86, N 22.18.

The product obtained as above had identical physical properties to the product of demethylation obtained in the reaction of **4** with CH_3ONa–CH_3OH, CO_3^{2-}–18-crown-6–$CDCl_3$, or Et_2NH–$CDCl_3$.

Reaction of 4 with Nucleophiles

The course of the reactions was followed on a Bruker 60 MHz HFX-60 instrument using both the normal and the FT modes of operation. Tetramethylsilane was used as an internal standard. The species formed were also characterized by uv–visible absorption spectroscopy (Table 1).

pK_a Determination

Sulfuric acid solutions were prepared by dilution of Fisher reagent grade concentrated H_2SO_4 and standardized by titration with base. A stock solution of **7** was prepared in methanol and aliquots added to the H_2SO_4 solutions, the resulting solutions containing 0.2% CH_3OH by volume. The spectral measurements were performed using a Unicam SP800B and a Beckman 25 spectrophotometer.

Acknowledgments

We thank the National Research Council of Canada and the McLean Foundation (A.R.N.) for continuing financial support and Dr. R. Whitney for valuable discussions.

1. (*a*) E. Buncel, N. Chuaqui-Offermanns, and A. R. Norris. J. Chem. Soc. Perkin I, 415 (1977); (*b*) E. Buncel, N. Chuaqui-Offermanns, B. K. Hunter, and A. R. Norris. Can. J. Chem. **55**, 2852 (1977).
2. (*a*) R. Foster and C. A. Fyfe. Rev. Pure Appl. Chem. **16**, 16 (1966); (*b*) E. Buncel, A. R. Norris, and K. E. Russell. Q. Rev. Chem. Soc. **22**, 123 (1968); (*c*) M. R. Crampton. Adv. Phys. Org. Chem. **7**, 211 (1969); (*d*) M. J. Strauss. Chem. Rev. **70**, 667 (1970).
3. (*a*) P. B. Ghosh and M. W. Whitehouse. J. Med. Chem. **11**, 305 (1968); (*b*) P. B. Ghosh, B. Ternai, and M. W. Whitehouse. J. Med. Chem. **15**, 255 (1972).
4. (*a*) C. F. Bernasconi. MTP Int. Rev. Sci. Org. Chem. Ser. One, **3**, 33 (1973); (*b*) J. H. Fendler, W. H. Hinze, and L. J. Liu. J. Chem. Soc. Perkin II, 1768 (1975); (*c*) L. Di-Nunno, S. Florio, and P. E. Todesco. J. Chem. Soc. 1469 (1975); (*d*) F. Terrier, F. Millot, A. P. Chatrousse, M. J. Pouet, and M. P. Simonnin. Org. Magn. Reson. **8**, 56 (1976); (*e*) L. H. Gan and A. R. Norris. Can. J. Chem. **52**, 18 (1974).
5. (*a*) J. F. Bunnett. Ann. Rev. Phys. Chem. **14**, 271 (1963); (*b*) J. Miller. Nucleophilic aromatic substitution. Elsevier, Amsterdam. 1968.
6. C. Abbolito, C. Iavarone, G. Illuminati, F. Stegel, and A. Vazzoler. J. Am. Chem. Soc. **91**, 6746 (1969).
7. C. F. Bernasconi. J. Am. Chem. Soc. **90**, 4982 (1968).
8. J. F. Bunnett and R. H. Garst. J. Org. Chem. **33**, 2320 (1968).
9. (*a*) S. Safe and R. Y. Moir. Can. J. Chem. **43**, 437 (1965); (*b*) W. D. Chandler, W. MacF. Smith, and R. Y. Moir. Can. J. Chem. **42**, 2549 (1964).
10. (*a*) K. Bowden. Chem. Rev. **66**, 119 (1966); (*b*) L. P. Hammett. Physical organic chemistry. 2nd ed. McGraw Hill, New York. 1970; (*c*) C. H. Rochester. Acidity functions. Academic Press, London. 1970; (*d*) E. Buncel, E. A. Symons, D. Dolman, and R. Stewart. Can. J. Chem. **48**, 3354 (1970).
11. R. H. Boyd. J. Phys. Chem. **67**, 737 (1963).
12. E. Buncel and W. Eggimann. Can. J. Chem. **54**, 2436 (1976).
13. (*a*) F. Terrier, F. Millot, and W. P. Norris. J. Am. Chem. Soc. **98**, 5883 (1976); (*b*) A. P. Chatrousse and F. Terrier. C. R. Acad. Sci. Ser. C, **282**, 195 (1976).
14. (*a*) E. Buncel. Chem. Rev. **70**, 323 (1970); (*b*) E. Buncel, C. Chuaqui, and J. F. Wiltshire. J. Am. Chem. Soc. **95**, 799 (1973).
15. (*a*) A. I. Vogel. Practical organic chemistry. 3rd ed. Longman, London. p. 653; (*b*) E. Swift, Jr. J. Am. Chem. Soc. **64**, 115 (1942).

Thermodynamic studies in solution. Part IV.[1] Solvent effect on the solvolysis of *tert*-butyl chloride. A new treatment of the experimental data

JOAQUIM JOSE MOURA RAMOS AND JACQUES REISSE[2]

Chimie Organique E.P., Université Libre de Bruxelles, 50, avenue F.D. Roosevelt, B 1050 Bruxelles, Belgium

AND

M. H. ABRAHAM

University of Surrey, Guildford, Surrey, U.K.

Received February 9, 1978[3]

JOAQUIM JOSE MOURA RAMOS, JACQUES REISSE, and M. H. ABRAHAM. Can. J. Chem. **57**, 500 (1979).

A new treatment of the solvent effect on the solvolysis of *tert*-butyl chloride is proposed. This treatment is based on activation free energy measurements and on transfer free energy measurements of the reactant (R) on the one hand and of a model (M) of the activated complex (AC) on the other hand. Solute–solvent interaction free energies for the reactant, the activated complex and the model compound are estimated. This estimation involves the calculation of the free energy of cavity formation of these various solutes (R, AC, and M) in all the solvents. These cavity terms, which are a function of the cohesive properties of the solvent and of the surface of the cavity do not reflect the electronic structure of the solute whereas the interaction free energy term does. The method we propose can be described as a new 'experimental' approach for the study of the charge separation in an activated complex.

JOAQUIM JOSE MOURA RAMOS, JACQUES REISSE et M. H. ABRAHAM. Can. J. Chem. **57**, 500 (1979).

Un nouveau traitement de l'effet de solvant sur la vitesse de solvolyse du chlorure de tertiobutyle est proposé. La démarche suivie est basée sur des mesures d'énergie libre d'activation et aussi sur des mesures d'énergie libre de transfert pour le réactif d'une part, pour une molécule modèle du complexe activé d'autre part. Les termes d'énergies libres associées à l'interaction solvant–soluté sont estimés et ceci tant pour le réactif (R) que pour le complexe activé (AC) ou pour le dérivé modèle (M). Ces estimations nécessitent le calcul préalable de l'énergie libre associée à la formation de cavités dans les solvants et ceci pour les trois types de solutés étudiés (R, AC et M). Ces termes de cavité qui sont fonction des propriétés de cohésion du solvant et de la surface de la cavité ne reflètent pas la structure électronique du soluté alors que les termes d'interactions, eux, reflètent cette structure. La méthode que nous proposons peut être décrite comme une nouvelle approche "expérimentale" pour l'étude de la séparation de charge dans un complexe activé.

In the solvolysis of *tert*-butyl chloride, the reactant (R) is only slightly polar, whereas the activated complex (AC) is highly polar. There is therefore a large solvent effect on the rate of solvolysis of this compound (1) and Winstein and Grunwald (2) used the log k values to define a solvent scale (the Y scale). An interpretation of the solvent effect on the solvolysis[4] rate was given by one of us in 1972 (3, 4). This work was based on the determination of free energies of transfer of the reactant, the activated complex, and a model compound (M) that was chosen because of its similarity to the activated complex. The ion pair $Me_4N^+Cl^-$ was selected as the model because it is highly polar and is about the same size as the activated complex. From plots of free energy of transfer of AC against free energy of transfer of M, it was concluded that the charge separation in the activated complex is less in apolar solvents than in polar solvents (3).

We propose, in the present paper, a new method of treatment for the effect of solvents on the rate of solvolysis of *tert*-butyl chloride. The method has been discussed in detail by two of us in the case of enthalpies of transfer (5, 6) and the formal treatment is the same for free energies of transfer. In this method, the free energy of transfer of a solute (X) is considered as the sum of two contributions: (*i*) the free energy required to create a cavity in the solvent and (*ii*) the free energy term associated with the solute–solvent interactions. Since it is the latter term

[1]For Part III, see ref. 6.

[2]Author to whom all correspondence should be addressed.

[3]Revision received May 31, 1978.

[4]For *tert*-butyl chloride the term solvolysis is normally restricted to the reaction in hydroxylic solvents, leading mainly to *tert*-butyl alcohol and ethers together with some isobutene. In aprotic solvents, the product is only isobutene. For convenience, we use in this paper the term solvolysis to cover both of these types of reaction.

0008-4042/79/050500-03$01.00/0

only that is important in the deduction of the nature of the solute, we hope that by separating out this term for the solvolysis reaction, a better understanding of the nature of the activated complex will be obtained than was possible by the previous method used.

The free energy change associated with the transfer of a solute (X) from the gas phase (g) to a solvent (s) can be described as in [1], where $|\bar{G}_{cav}|_s$ is the free energy needed to create a cavity in the solvent and $|\bar{G}_{int}|_s$ is the free energy term corresponding to the solvent–solute interactions (7).

$$[1] \qquad |\bar{G}_t|_s^g = |\bar{G}_{cav}|_s + |\bar{G}_{int}|_s$$

$|\bar{G}_{cav}|_s$ is a function of the cohesive properties of the solvent (8) and is also a function of the surface of X if the surface tension is used to characterise the cohesion of s (7, 9). For reasons well discussed (10), the free energy of reorganisation of solvent molecules around the solute can be considered as negligible and thus no other terms are needed in [1]. The calculation of $|\bar{G}_{cav}|_s$ (cal mol^{-1}) is carried out through [2],

$$[2] \qquad |\bar{G}_{cav}|_s = 9.761 \times K(r) \times V_x^{2/3} \times \sigma_s$$

with

$$K(r) = 1 + (V_s/V_x)^{2/3}(K_s - 1)$$

where σ_s is the surface tension of s (dyn cm^{-1}), V_x and V_s are the molar volumes of X and s (cm^3 mol^{-1}), and K_s is a numerical factor characteristic of each solvent and introduced to take into account the microscopic dimensions of the cavity (9, 11). K_s can be derived from the solvent free energy of vaporization at 25°C. The derivation is similar but not identical to the one which has been used to calculate the corrective coefficient in the case of $\bar{H}_{cav}$ (6). In the particular case of $\bar{G}_{cav}$, the estimation of K_s also requires the knowledge of the gain of translational entropy which follows the transition liquid → gas. The details concerning the method we use to calculate K_s and the theoretical basis of [2] will be discussed elsewhere.[5]

We calculated the cavity term $|\bar{G}_{cav}|_s$ for R, M, and AC and then took methanol as the reference solvent to obtain the relative cavity terms $|\bar{G}_{cav}|_s^{s_1}$. Combination with the transfer free energies given in ref. 3 then enables the relative interaction terms, $|\bar{G}_{int}|_s^{s_1}$, to be obtained. Since the charge separation in a given solute will be reflected in $|\bar{G}_{int}|_s^{s_1}$ but not in $|\bar{G}_{cav}|_s^{s_1}$, it seems clear that the calculated $|\bar{G}_{int}|_s^{s_1}$ terms will provide a more sensitive probe for charge separation than the overall $|\bar{G}_t|_s^{s_1}$ terms used previously (3).

[5]J. J. Moura Ramos and J. Reisse. To be published.

TABLE 1. Relative interaction free energies at 25°C ($\S_1$ = CH_3OH)

Solvents	$\delta\|\bar{G}_{int}\|_s^{\S_1}$ (kcal mol^{-1})[a,b] AC	M	R
1 CH_3OH	0.0	0.0	0.0
2 Pentane	17.9	24.6	2.3
3 Ether	11.1	18.0	2.0
4 Benzene	8.2	14.0	0.0
5 C_6H_5Cl	6.5	11.7	−0.6
6 Acetone	5.7	7.9	0.5
7 CH_3CN	2.6	3.9	−1.0
8 1-Butanol	2.3	3.4	0.7
9 1-Propanol	1.3	1.9	−0.4
10 Ethanol	1.3	1.7	−0.1
11 CH_3NO_2	1.0	1.4	−2.0
12 Water	−11.7	−12.5	−5.2

[a]The signs are such that a positive value corresponds to a system less stable (on a free energy scale) in this solvent than in CH_3OH.

[b]The estimated errors of $\delta[\bar{G}_{int}]_s^{\S_1}$ for AC and M are of the order of ±1 kcal mol^{-1}, probably lower for R. The accuracy of the values obtained for C_6H_5Cl and CH_3NO_2 may be lower owing to the greater difficulty in estimating the entropy associated with the cavity formation in these solvents (because of lack of internal pressure values for these solvents).

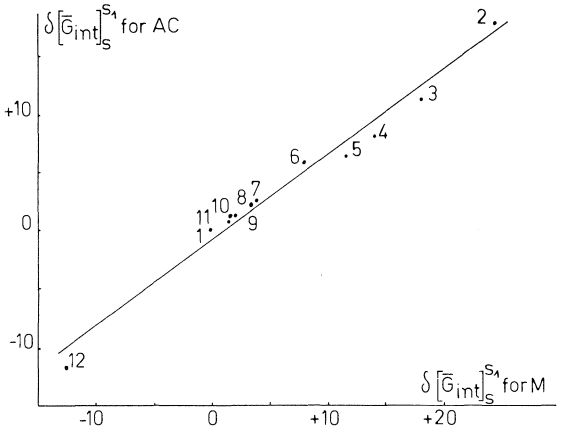

FIG. 1. The linear correlation between differential solvent–solute interaction enthalpy of AC and M ($\delta[\bar{G}_{int}]_s^{\S_1}$ in kcal mol^{-1}; numbers refer to Table 1).

In Table 1 are given the relative interaction free energies for R, M, and AC, and these interaction energies are compared directly for AC and M in Fig. 1. An excellent linear correlation exists between the $|\bar{G}_{int}|_s^{s_1}$ terms for AC and M over all the solvents studied (correlation coefficient: 0.99). The value of the slope (0.73) confirms again the highly polar nature (3) of the activated complex. The fact that the same straight line, Fig. 1, is obtained over all the solvents studied suggest that charge separation in the transition state must remain approximately constant.

Interestingly, this phenomenon does not seem to be unusual because in the Menschutkin reaction (3, 4) plots of the free energy of activation against various solvent parameters also yield straight lines over a wide range of solvents, so that, again the charge separation in the transition state seems to remain constant with change in the solvent.

The present method yields results that are quantitatively somewhat different from the previous results (3) although qualitatively similar. Futhermore, the present results are in excellent agreement with results of calculations, using the reaction field theory, that suggest in aprotic solvents the charge separation in the activated complex is 0.67 units (12).

Acknowledgments

We thank Doctors Marie-Louise Stien and Robert Ottinger for helpful discussions. This work was supported by a grant from the Fonds de la Recherche Fondamentale Collective (Belgium).

1. C. K. INGOLD. Structure and mechanism in organic chemistry. 2nd ed. Cornell University Press, Ithaca, NY. 1969. pp. 457–463.
2. E. WINSTEIN and S. GRUNWALD. J. Am. Chem. Soc. **70**, 846 (1948).
3. M. H. ABRAHAM. J. Chem. Soc. Perkin II, 1343 (1972).
4. M. H. ABRAHAM. Prog. Phys. Org. Chem. **11**, 1 (1974).
5. J. J. MOURA RAMOS, M. L. STIEN, and J. REISSE. Chem. Phys. Lett. **42**, 373 (1976).
6. J. J. MOURA RAMOS, M. LEMMERS, R. OTTINGER, M. L. STIEN, and J. REISSE. J. Chem. Res. (S), 56 (1977); J. Chem. Res. (M), 0658 (1977).
7. H. H. UHLIG. J. Phys. Chem. **41**, 1215 (1937).
8. D. D. ELEY. Trans. Faraday Soc. **35**, 1421 (1939).
9. T. HALICIOGLU and O. SINANOGLU. Ann. N.Y. Acad. Sci. **158**, 308 (1969).
10. (*a*) R. LUMRY and S. RAJENDER. Biopolymers, **9**, 1125 (1970); (*b*) A. BEN-NAIM. Biopolymers, **14**, 1337 (1975).
11. R. C. TOLMAN. J. Chem. Phys. **17**, 333 (1949).
12. M. H. ABRAHAM and R. J. ABRAHAM. J. Chem. Soc. Perkin II, 47 (1974).

Hydrogen–deuterium exchange in tetrahydroborate salts[1]

IAN A. OXTON

Department of Chemistry, Dalhousie University, Halifax, N.S., Canada B3H 4J3

AND

A. GAVIN MCINNES AND JOHN A. WALTER

Atlantic Regional Laboratory, National Research Council of Canada, Halifax, N.S., Canada B3H 3Z1

Received August 11, 1978

IAN A. OXTON, A. GAVIN MCINNES, and JOHN A. WALTER. Can. J. Chem. **57**, 503 (1979).

^{1}H nmr spectroscopy has been used to demonstrate hydrogen–deuterium exchange in solutions of $NaBH_4/NaB^2H_4$ in diglyme and KBH_4/KB^2H_4 in 18-crown-6 ether/chloroform. Earlier observations of such exchange with $LiBH_4/LiB^2H_4$ in an ethereal solvent were confirmed. Spectra were simplified by broadband decoupling of deuterium, facilitating quantitative measurement of the degree of exchange.

IAN A. OXTON, A. GAVIN MCINNES et JOHN A. WALTER. Can. J. Chem. **57**, 503 (1979).

On a fait appel à la rmn du ^{1}H pour mettre en évidence l'échange hydrogène–deutérium dans des solutions de $NaBH_4/NaB^2H_4$ dans le diglyme et de KBH_4/KB^2H_4 dans un mélange de couronne-18 éther-6/chloroforme. On a pu confirmer des résultats antérieurs relatifs à de tels échanges dans $LiBH_4/LiB^2H_4$ dans l'éther. On a simplifié les spectres par découplage de deutérium; ce procédé a rendu plus facile la détermination quantitative du degré d'échange.

[Traduit par le journal]

Introduction

Hydrogen–deuterium exchange in tetrahydroborate salts has been accomplished previously by rather inconvenient means (1, 2), usually involving hydrogen–deuterium gas mixtures at high temperatures and/or pressures. Recently it has been shown that this exchange could be performed readily with lithium tetrahydroborate merely by dissolving mixtures of $LiBH_4$ and LiB^2H_4 in an ethereal solvent (3, 4). This type of exchange would appear to provide an attractive way to incorporate low concentrations of the $BH_3{}^2H$ ion into tetrahydroborate salts for their study by the isotopic dilution technique (cf. refs. 5 and 6 for other tetrahedral species). We found that the exchange process could be extended to sodium tetrahydroborate in diglyme solution and potassium tetrahydroborate in 18-crown-6 ether/chloroform solution. Smith *et al.* (4) had previously reported that sodium tetrahydroborate did not exchange in diglyme. The isotopically-exchanged tetrahydroborate species were monitored by ^{1}H nmr spectroscopy, with ^{2}H-decoupling to facilitate the observation of peaks separated by deuterium isotope-induced differences in chemical shift and boron–hydrogen spin–spin coupling constant.

Experimental

Preparation of Samples

(*i*) Lithium tetrahydroborate. Approximately 20 mg each of $LiBH_4$ and LiB^2H_4 (both from ICN Pharmaceuticals Inc., Plainview, NY) were dissolved in ca. 1.0 mL tetrahydrofuran-$^2H_8$ containing 1/6 hexafluorobenzene by volume (for nmr lock) at room temperature.

(*ii*) Sodium tetrahydroborate. Approximately equal amounts (ca. 50 mg each) of $NaBH_4$ (BDH Chemicals, Montreal, P.Q.) and NaB^2H_4 (Merck, Sharp and Dohme Ltd., Montreal, P.Q.) were dissolved at room temperature in ca. 2.0 mL diglyme-$^2H_{14}$ (bis(2-methoxyethyl) ether-$^2H_{14}$), to which was added a small amount of hexafluorobenzene (ca. 1/6 of the solution volume).

(*iii*) Potassium tetrahydroborate. 18-Crown-6 ether (640 mg) (Aldrich Chemical Co., Milwaukee, WI) was warmed until just molten (ca. 40°C), then roughly equal amounts (ca. 61 mg) of KBH_4 (Anachemia Chemicals Ltd., Montreal, P.Q.) and KB^2H_4 (Merck, Sharp and Dohme Ltd., Montreal, P.Q.) were dissolved in it.

No special precautions to dry samples or solvents were taken and spectra were recorded after the usual small amount of hydrogen had been evolved.

Nuclear Magnetic Resonance Measurements

All ^{1}H nmr spectra were recorded with a Varian XL-100/15 Fourier-transform spectrometer equipped with a Varian 620L computer. Conditions were: frequency 100.06 MHz, spectral bandwidth 1000 Hz, acquisition time 8.0 s (16 000 data points), flip angle 90° (23 μs pulse length), delay between pulses 15 s, unweighted free induction decay used for Fourier transformation, broadband decoupling of ^{2}H at 15.36 MHz by 0 to 180° phase modulation (at 40 Hz) of decoupling field ($\gamma H_2/2\pi$ ca. 310 Hz), ^{19}F internal lock to C_6F_6, reference to internal $(CH_3)_4Si$, temperature ca. 30°C, 5 mm diameter sample tubes, sample compositions as above.

Results and Discussion

(*i*) $LiBH_4/LiB^2H_4$ in tetrahydrofuran-$^2H_8/C_6F_6$. The ^{1}H nmr results were consistent with those previously reported (3, 4), although chemical shifts

[1]NRCC No. 17117.

0008-4042/79/050503-03$01.00/0

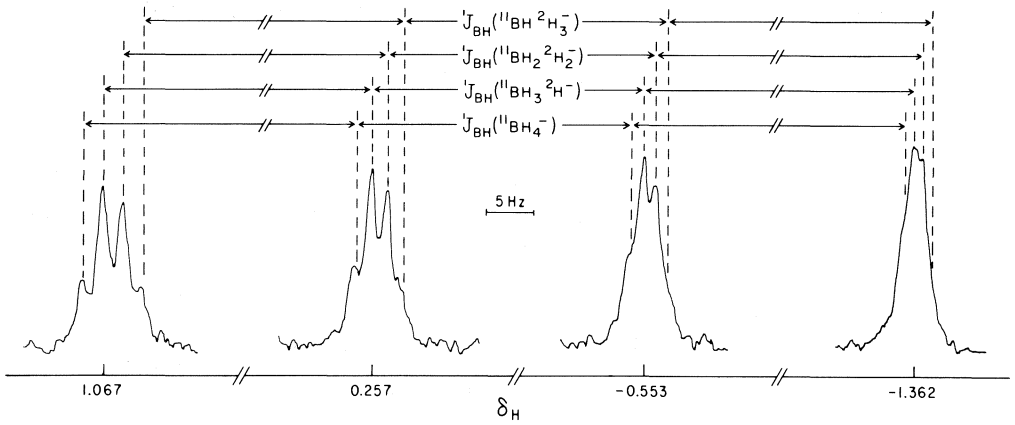

FIG. 1. ^1H nmr spectrum, ^2H-decoupled, of $K^{11}BH_4/K^{11}B^2H_4$ after complete $^1H \rightleftarrows {}^2H$ equilibration ($p = 0.62 \pm 0.02$). Individual components of the quartet due to ^{11}B–H coupling are shown on an expanded scale, with the distances between them truncated.

differed due to C_6F_6 in the solvent. The spectra were considerably simplified by decoupling ^2H. Hydrogens bonded to ^{11}B gave a quartet of quartets, very similar to that shown in Fig. 1 for $K^{11}BH_4/K^{11}B^2H_4$, due to ^{11}B–H spin–spin coupling and isotope effects on both the ^1H chemical shift and $^1J_{^{11}B-H}$ (4) for the species $^{11}BH_4^-$, $^{11}BH_3{}^2H^-$, $^{11}BH_2{}^2H_2^-$, $^{11}BH^2H_3^-$ (Table 1). Similar splittings of individual components of the septet due to ^{10}B–H spin–spin coupling were not resolved.

The ratios of intensities, e.g. $I(^{11}BH_4^-)$: $I(^{11}BH_3{}^2H^-)$ for each pair of peaks within the two well-resolved quartets at lowest field (as in Fig. 1) were in accord with the relation

$$I(^{11}BH_4^-):I(^{11}BH_3{}^2H^-):I(^{11}BH_2{}^2H_2^-):$$
$$I(^{11}BH^2H_3^-) = p^4:4p^3(1-p):6p^2(1-p)^2:4p(1-p)^3$$

where $p = 0.53 \pm 0.03$ is the probability of ^1H; $1 - p$ the probability of ^2H. This random distribution, which did not change with time or upon further heating, indicates a complete $^1H \rightleftarrows {}^2H$ exchange equilibration at (or below) probe temperature (30°C). Thus the degree of equilibration is readily monitored quantitatively using deuterium-decoupled ^1H spectra. Intensities should be unaffected, within error, by nuclear Overhauser enhancements due to irradiation of ^2H. The maximum theoretical enhancement is small ($\gamma(^2H)/2\gamma(^1H) = 0.077$) and would not be attained because of strongly competing dipolar spin–lattice relaxation via ^1H and/or ^{11}B. Saturation effects, due to differences in spin–lattice relaxation time in the tetrahydroborate species, were avoided by using a long delay time between radiofrequency pulses.

(*ii*) $NaBH_4/NaB^2H_4$ in diglyme-$^2H_{14}/C_6F_6$. The ^1H nmr spectrum was very similar to that of $LiBH_4/LiB^2H_4$ (Table 1) and, apart from chemical shift changes due to C_6F_6 in the solvent, agreed with previous results (4). In this case the peak intensities (see *i* above) showed only a slight degree of exchange after approximately 1 h at room temperature. It was necessary to warm the tetrahydroborate solution to ca. 60°C to attain exchange equilibration, indicated by peak intensities in agreement with the relation above (with $p = 0.64 \pm 0.02$) and unchanged after further heating at 75°C. This may explain why Smith *et al.* (4) observed $NaBH_4/NaB^2H_4$ exchange in a preliminary experiment, but were unable to reproduce this result.

(*iii*) KBH_4/KB^2H_4 in 18-crown-6 ether and chloroform-$^2H/C_6F_6$. The crown ether was chosen to test the premise that potassium tetrahydroborate would exchange, provided an ethereal solvent could be found. This salt is insoluble in simpler ethers but dissolves readily in molten 18-crown-6 ether, which is known to complex preferentially to K^+ (7). The resulting complex was heated at 175°C for 2 h and cooled to 20°C before being dissolved in 1.2 mL chloroform-^2H/0.1 mL C_6F_6. Nuclear magnetic resonance examination of this solution at 30°C showed no evidence of exchange, so it was heated at its boiling point (62°C) and periodically monitored by nmr, until $^1H \rightleftarrows {}^2H$ exchange equilibrium was attained (ca. 50 min). The peak intensities (see Fig. 1) were unchanged by further heating, the average value of p from four spectra being 0.62 ± 0.02.

TABLE 1. Deuterium isotope effects on δ_H* and $^1J_{^{11}B-H}$† from ^1H nmr spectra of $M^{11}BH_n{}^2H_{4-n}$ (M = Li, Na, K; n = 1 to 4)

M	Parameter	n = 4	3	2	1	Error
Li‡	δ_H(ppm)	−0.778	−0.791	−0.803	−0.816	±0.002
	$\Delta\delta_H$*(ppm)	0.0	0.013	0.025	0.038	±0.002
	$^1J_{^{11}B-H}$(Hz)	81.09	80.81	80.50	80.09	±0.06
	ΔJ†(Hz)	0.0	0.28	0.59	1.00	±0.10
Na‡	δ_H(ppm)	−0.598	−0.612	−0.626	−0.639	±0.002
	$\Delta\delta_H$*(ppm)	0.0	0.014	0.028	0.041	±0.002
	$^1J_{^{11}B-H}$(Hz)	81.00	80.63	80.23	79.84	±0.09
	ΔJ†(Hz)	0.0	0.37	0.77	1.16	±0.18
K‡	δ_H(ppm)	−0.132	−0.148	−0.162	−0.177	±0.002
	$\Delta\delta_H$*(ppm)	0.0	0.016	0.030	0.045	±0.002
	$^1J_{^{11}B-H}$(Hz)	81.49	81.03	80.63	80.35	±0.10
	ΔJ†(Hz)	0.0	0.46	0.86	1.14	±0.20

*δ_H referred to internal $(CH_3)_4$ Si. $\Delta\delta_H$ is isotope shift upfield of $^{11}BH_4^-$ peak.
†$\Delta J = {}^1J_{^{11}B-H}$ ($^{11}BH_4^-$) − $^1J_{^{11}B-H}$ ($^{11}BH_n{}^2H_{4-n}$).
‡Different solvents used for each compound; see text.

It is interesting to note the increasing difficulty of exchange on going from the lithium to the sodium and potassium salts, and the absence of exchange in the latter unless the crown ether complex is dissolved. The fact that each salt achieved a $^1H \rightleftarrows {}^2H$ exchange equilibrium corresponding to a constant p for all tetrahydroborate species, demonstrates that the free energies of the species in solution are indistinguishable. As regards the original intent of this study, to achieve isotopic exchange in the higher alkali tetrahydroborates, the most promising procedure would appear to be to secure isotopic equilibration in sodium tetrahydroborate, followed by metathetical reaction with a suitable salt of the desired cation in aqueous or alcoholic solution (8).

1. R. E. MESMER and W. L. JOLLY. J. Am. Chem. Soc. **84**, 2039 (1962).
2. E. H. COKER and D. E. HOFER. J. Chem. Phys. **53**, 1652 (1970).
3. B. D. JAMES, B. E. SMITH, and R. H. NEWMAN. J. Chem. Soc. Chem. Commun. 294 (1974).
4. B. E. SMITH, B. D. JAMES, and R. M. PEACHEY. Inorg. Chem. **16**, 2057 (1977).
5. I. A. OXTON, O. KNOP, and M. FALK. J. Phys. Chem. **80**, 1212 (1976).
6. I. A. OXTON. J. Mol. Struct. **41**, 195 (1977).
7. C. J. PEDERSEN and H. K. FRENSDORFF. Angew. Chem. Int. Ed. Engl. **11**, 16 (1972).
8. N. N. GREENWOOD. *In* Comprehensive inorganic chemistry. Vol. 1. *Edited by* A. F. Trotman-Dickenson. Pergamon, Oxford. 1973. Chapt. 11, p. 748.

The kinetics and equilibrium of the hydration of phthalaldehyde[1]

ROBERT S. MCDONALD AND EARL V. MARTIN
Department of Chemistry, Mount Saint Vincent University, Halifax, N.S., Canada B3M 2J6

Received August 1, 1978

ROBERT S. MCDONALD and EARL V. MARTIN. Can. J. Chem. **57**, 506 (1979).

The equilibrium position and the kinetics of the extensive hydration of the title compound **1** have been investigated by spectroscopic (uv and nmr) techniques. The hydrate exists exclusively as the geometrically isomeric 1,3-phthalandiols and the hydration equilibrium constant is 7.7 ± 0.5 at 25°C. From the temperature dependence of the equilibrium position, values of the enthalpy and entropy of hydration were calculated. The reaction is general acid – general base catalyzed; the Brønsted α and β coefficients are both near 0.5. Catalysis by Zn(II) is observed. The mechanism of the reaction (which probably proceeds via rate-determining formation of the normal *gem*-diol followed by rapid cyclization) is discussed.

An analysis of the thermodynamic data for the hydration of a variety of carbonyl compounds reveals that the degree of hydration is normally determined by both enthalpy and entropy contributions to the free energy. However, the extensive hydration of **1** is determined solely by the enthalpy term. No hydration could be detected for benzaldehyde or the other isomeric dialdehydes.

ROBERT S. MCDONALD et EARL V. MARTIN. Can. J. Chem. **57**, 506 (1979).

Faisant appel à des techniques spectroscopiques (uv et rmn), on a étudié la position de l'équilibre et la cinétique de l'hydratation du composé **1**. L'hydrate existe uniquement sous la forme des isomères géométriques du phtalanediol-1,3; la constante d'équilibre pour l'hydratation est égale à 7.7 ± 0.5 à 25°C. En se basant sur la variation de la position de l'équilibre avec la température, on a pu calculer les valeurs des enthalpie et entropie d'hydratation. La réaction subit une catalyse générale par les acides et par les bases; les valeurs des deux coefficients α et β de Brønsted sont près de 0.5. On a observé une catalyse par le Zn(II). On discute du mécanisme de la réaction qui procède probablement par la formation du *gem*-diol, comme étape déterminant la vitesse, suivie par une cyclisation rapide.

Une analyse des données thermodynamiques associées à l'hydratation d'un certain nombre de composés carbonylés révèle que le degré d'hydratation est généralement déterminé par des contributions à la fois de l'enthalpie et de l'entropie à l'énergie libre. Toutefois l'hydratation poussée de **1** résulte uniquement du terme enthalpique. On ne peut pas détecter d'hydratation dans le cas du benzaldéhyde ou d'autres dialdéhydes isomères.

[Traduit par le journal]

Reactions of phthalaldehyde (**1**) often involve chemical modification of both of the aldehyde groups. Thus, base-catalyzed condensations with active methylene compounds lead to 2-substituted-1-indanones (1) and reaction with amines yields a variety of compounds, most of which contain phthalimidine rings (2). Treatment with acidic methanol produces the cyclic bis-acetal, 1,3-dimethoxyphthalan (**3**) as one of the products (3).

During a recent study of the behavior of **1** in aqueous base, we observed anomalously low extinction coefficients (ε) in the 200–330 nm region of the uv spectrum. Other workers (4) have also observed this but interpreted these low ε values in terms of steric and electronic effects. However, these results, coupled with the recently reported proton nmr spectrum in D_2O (2) (which we had also observed independently), point towards extensive hydration of **1** in aqueous solutions [1] and, further, that the hydrate exists exclusively as the cyclic 1,3-phthalandiol **2**.

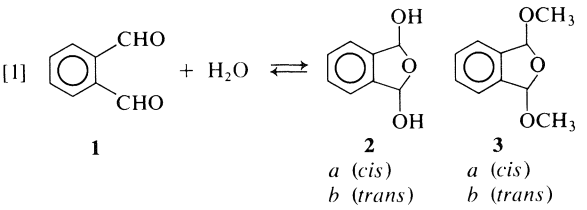

Seekles (5) reported the isolation of a compound proposed to be the monohydrate from concentrated aqueous solutions of **1**, although no structural information was given. Evaporation of aqueous solutions of **1** to dryness leads only to recovered starting material (2).

The position of equilibrium and the kinetics of the reversible hydration of carbonyl compounds have been studied extensively[2] but most of this work has

[1]Presented, in part, at the annual conference of the Chemical Institute of Canada, Winnipeg, Man., June, 1978.

[2]For an excellent review of much of the earlier work see ref. 6.

0008-4042/79/050506-11$01.00/0

been limited to aliphatic compounds since only these are normally significantly hydrated. Aromatic carbonyl compounds without strongly electron-withdrawing substituents are not significantly hydrated. Thus, although benzaldehyde itself has been estimated to have a hydration equilibrium constant (K_{H_2O}) of 1×10^{-2} (7, 8), values for the nitrobenzaldehydes are in the range 0.08–0.20 (7, 9, 10) whereas that for 4-pyridine carboxaldehyde is 1.5 (11).

Since **1** provides us with an example of an extensively hydrated aromatic aldehyde, we investigated in more detail the equilibrium position and the kinetics of the hydration reaction [1]. In the light of the unique cyclic structure of the hydrate, we were particularly interested in the thermodynamics of the equilibrium and the susceptibility of the reaction to catalysis by acids, bases, and a divalent metal ion. Hydration of aliphatic carbonyl compounds is known to be general acid and general base catalyzed (6). The uv and nmr spectra of benzaldehyde and the isomeric dialdehydes were recorded for comparison purposes.

Experimental

General

Melting points were taken on a Gallenkamp apparatus and are uncorrected. An Orion 601A pH meter equipped with a combination electrode was used to measure all pH values. The meter was standardized using Fisher certified buffer solutions at pH 1.00, 4.00, 7.00, and 10.00. Ultraviolet spectra were recorded on a Beckman model 24 spectrophotometer or on a Beckman DB-G instrument coupled to an Omniscribe recorder (Houston Instruments). Routine nuclear magnetic resonance spectra were taken on a Varian EM 360A 60MHz spectrometer. Those recorded at temperatures above ambient were taken on a Varian HA 100 instrument. Peak positions were measured in ppm (δ) relative to tetramethylsilane (TMS) as internal reference in $CDCl_3$ and relative to sodium 2,2-dimethyl-2-silapentane-5-sulfonate (DSS) in the aqueous solutions.

Materials

Benzaldehyde (Aldrich) was freshly distilled under vacuum (bp 43°C/2.5 Torr) immediately before use and stored under nitrogen until stock solutions were prepared. Isophthalaldehyde and terephthalaldehyde (Aldrich) were used as obtained. Phthalaldehyde (Aldrich) was twice recrystallized from ether – petroleum ether (30–50°C), the first time using decolorizing charcoal, to yield pale yellow needles, mp 56.5 58°C (lit. (12) mp 56–56.5°C, (13) mp 55.5–56°C).

Distilled water was used in the preparation of all solutions. Compounds used in the preparation of all buffer solutions were all reagent grade and used without further purification. Stock solutions of 1.0 and 0.10 *N* hydrochloric acid and sodium hydroxide were prepared by diluting the appropriate Fisher concentrate with freshly boiled, then cooled, distilled water.

The D_2O (Stohler Isotopes) was 99.8% enriched. 1,4-Dioxane (Fisher) used in the preparation of all stock solutions was purified before use by passage through a column of Super Grade I W-200 aluminum oxide (ICN Pharmaceuticals).

Kinetics

The rate of the hydration reaction [1] was measured by monitoring the decrease in intensity of the uv absorption bands which occurred when a few microlitres of a stock solution of **1** in dioxane were injected into water or buffered aqueous solution. The half-life for the disappearance of **1** in water was about 2 min. Identical (within experimental error) observed rate constants were obtained by monitoring the reaction at each of three λ_{max} values of **1** in water (i.e., at 222, 263 and 300 nm).

Buffer solutions were maintained at an ionic strength (μ) of 1.0 with KCl unless otherwise noted. All kinetic measurements were carried out at 28.0 ± 0.5°C in the cell compartment of the Beckman DB-G spectrophotometer described above. One-centimetre quartz cells with Teflon stoppers were used throughout.

Typically the kinetic run was initiated by injecting 5–25 μL of a 0.03 *M* stock solution of **1** in dioxane into 3.0 mL of buffer solution in a cuvette which had been preequilibrated in the cell compartment. After rapidly mixing the cell contents, the absorbance of the solution at the preselected wavelength was traced out on the recorder. The reaction was monitored over at least 4 half-lives and an 'infinity' absorbance was taken after at least 10 half-lives. Pseudo-first-order rate constants (k_{obs}) were then obtained from the slopes of the semi-logarithmic plots of ($A - A_\infty$) vs. time in the usual way. The kinetic plots were linear up to at least 80% reaction. Quoted rate constants are the average of at least duplicate determinations; agreement between replicate runs was normally within 5%. The pH of the kinetic solution was taken immediately after the run. Using this technique we were able to measure reliably the rates of reactions having half-lives as short as 4 s.

Varying the initial substrate concentration over the range $0.5–2.5 \times 10^{-4}$ *M* had no effect on the k_{obs} value. Similarly, the presence of up to 1% dioxane, introduced by injecting the substrate as a stock solution in dioxane, had no observable effect on the rate.

Runs were monitored at 263 nm in the carboxylate buffers and at 222 nm in the other buffer solutions. A steady A_∞ was obtained in all solutions except those in which tris(hydroxymethyl)aminomethane was a component of the buffer. In these cases, the absorbance continued to decrease very slowly even after 10 half-lives of the very rapid hydration reaction. This is presumably due to Schiff's base formation between the residual dialdehyde and the primary amine.[3] Choosing an A_∞ after 10 half-lives of the initial hydration reaction gave linear kinetic plots up to at least 2 half-lives for this reaction.

Results and Discussion

Hydration Equilibrium

As pointed out in the Experimental, fairly rapid decreases in intensity of the uv absorption bands of **1** were observed when a few microlitres of a stock

[3]We thank a referee for making the alternative suggestion that this absorbance decrease may be due to the formation of compound **7**. Compounds of this type have been detected (2) when **1** reacts with primary amines in ether and would be expected to absorb only weakly at these wavelengths.

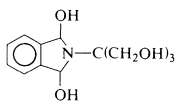

7

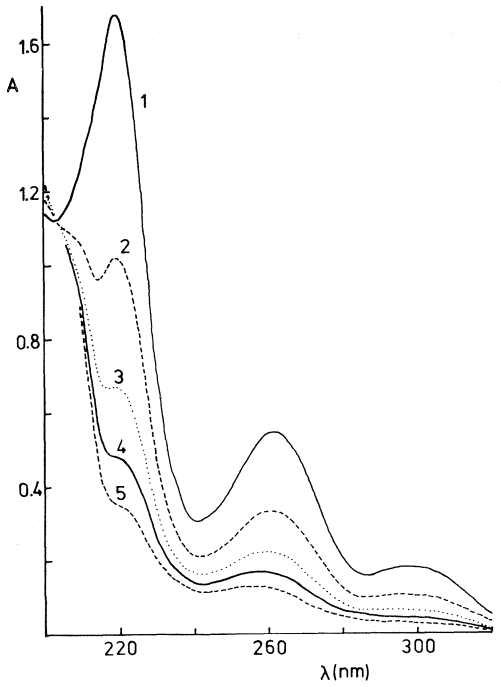

FIG. 1. Repetitive scans of the uv spectrum of **1** (1.0×10^{-4} *M*) in water, $\mu = 0$, 25°C. Scans (from 360 nm) were: *1*, 30 s; *2*, 170 s; *3*, 320 s; *4*, 500 s; *5*, 1100 s (times after mixing). The last scan represents the final spectrum in water.

solution of substrate were injected into water. The results of a series of repetitive scans are shown in Fig. 1. Extinction coefficients calculated from the residual (final) absorbances and those determined at the three λ_{max} values extrapolated back to the mixing time (initial) from kinetic runs are reported in Table 1. Also included in Table 1 are the spectral data for **1** in dioxane and methanol and that for benzaldehyde and the other isomeric dialdehydes in these three solvents.

It now seems clear that the very low absorbances of **1** in aqueous solution, rather than being due to steric inhibition of resonance (4), are indicative of extensive hydration. Correcting the final absorbance values at 263 and 300 nm for the small absorbance due to hydrate at these wavelengths,[4] we can calculate that there remains 10.5 ± 1% free dialdehyde at equilibrium in aqueous solution at 25°C. This compares remarkably well with results from nmr (below) which gives more direct and accurate information on the equilibrium position.

The 'initial' spectrum of **1** in water is similar to that in dioxane. For the other aromatic aldehydes, a change in solvent from dioxane to water causes only a small shift in λ_{max} and less than a 10% change in ε. However, owing to the uncertainty of comparing ε values in different solvents, we can only conclude that no spectral changes associated with appreciable (greater than 10%) hydration is occurring for any of these compounds. Spectra recorded immediately after mixing and after 30 min were superimposable.

The spectra in methanol were all recorded at least 30 min after mixing (corresponding to 'final' spectra). Absorptions associated with the carbonyl group have ε values significantly lower in methanol than those in dioxane or water. This is interpreted in terms of hemiacetal formation; the lowering of intensity of the $\pi \rightarrow \pi^*$ and the $n \rightarrow \pi^*$ bands of benzaldehyde by 10% is completely consistent with the equilibrium constant for hemiacetal formation in methanol of 0.09 (14). This value is expected to increase for benzaldehydes with electron-withdrawing substituents and the spectra for the *meta* and *para* dialdehydes in methanol are certainly in accord with more extensive hemiacetal formation. The spectrum of **1** in methanol shows even weaker absorptions than it does in water; nmr results indicate directly that less than 5% exists as the free dialdehyde and that the predominant products are the geometrical isomers of 3-methoxyphthalan-1-ol.

We have taken the residual absorbance (A_∞) at 222 or 263 nm of the aqueous solutions of **1** from the kinetic runs as a measure of the amount of free dialdehyde remaining in the solution. We find no significant or systematic shifts in the position of equilibrium with changes in ionic strength from 0 to 1, in HCl solution up to 0.01 *M*, or in the presence of any of the buffers (except Tris; see Experimental for an explanation) up to a concentration of 1.0 *M* and over the pH range 2.3–10.5 even where the rates were too rapid to be followed by our conventional techniques. In solutions of pH greater than 10.5, systematic absorbance decreases at 260 and 300 nm were observed up to 1.0 *M* NaOH. We interpret this behavior in terms of ionization of the hydrate [2] and have been able to assign a pK_a of 11.6 ± 0.2 to **2** at an ionic strength of 1.0 at 25°C. Further work is underway on the chemistry of **1** and **2** in more

[2] 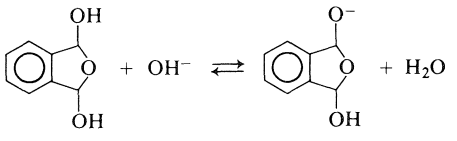

2

strongly basic solutions where we can also observe the much slower intramolecular Cannizzaro reaction leading to the *o*-hydroxymethylbenzoate ion.

Information on the structure of the hydrate comes

[4]The hydrate of structure **2** is assumed to have ε values in aqueous solution similar to those for *o*-xylene (i.e., $\varepsilon_{265} \approx 200$, $\varepsilon_{300} \approx 0$).

TABLE 1. Ultraviolet absorption data for benzaldehyde and the isomeric dialdehydes

Compound	Solvent[a]	λ_{max}[b] (nm) (ε)				
C_6H_5CHO	D			245(13700)		281(1340)
	M			247(12300)		281(1220)
	W	201(21500)		250(14000)		sh282(1600)
1,4-$C_6H_4(CHO)_2$	D			259(21200)	sh266(19000)	296(2120)
	M	202(18600)		253(16000)	sh266(9000)	290(1370)
	W	198(20000)		261(21600)	sh268(20000)	296(1950)
1,3-$C_6H_4(CHO)_2$	D		224(30000)	sh246(11500)		290(1010) 299(950)
	M	203(18700)	224(14400)	243(12010)		285(1070)
	W	196(16000)	228(28000)	sh248(13300)		292(1120)
1,2-$C_6H_4(CHO)_2$	D		222(26700)	256(8460)		297(2190)
	M			251(860)		sh281(150) sh292(115)
	W(i)[c]		222(28600)	263(8400)		300(2560)
	W(f)[d]		sh222(2530)	259(1060)		300(255)

[a]D = 1,4-dioxane, M = methanol, W = water.
[b]Errors are estimated to be ± 1 nm in λ_{max} and ± 5% in ε. The symbol sh denotes a shoulder.
[c]The initial (i) ε values for **1** in water were obtained from absorbance values in kinetic runs extrapolated back to the mixing time.
[d]The final (f) ε values were obtained from the spectrum after at least 10 half-lives of the hydration reaction.

from nmr spectral results. The spectrum of a saturated solution of **1** in D_2O is shown in Fig. 2. Clearly only residual peaks due to free dialdehyde are present (multiplet centred at δ 7.90, aromatic; δ 10.33, singlet, C*H*O). However, three new singlets have appeared at δ 6.27, 6.61, and 7.49 integrating in the ratio 1:1:4. These new signals are reasonably interpreted (2) in terms of extensive hydration where the hydrate exists exclusively as the geometrically isomeric 1,3-phthalandiols **2**. The spectrum cannot be interpreted in terms of 'normal' hydration at one or both of the aldehyde groups or a mixture of these forms with unreacted **1**. Furthermore such hydration would not be expected to occur to any significant extent from results of the other isomeric dialdehydes. As expected the aromatic protons of **2** resonate to higher field than those of **1** and are observed to be coincident at δ 7.49 for the *cis* and *trans* isomers. By analogy to assignments of the methine proton signals for the corresponding dimethyl acetals **3** (15), the δ 6.27 signal is assigned to the *cis* isomer and the δ 6.61 signal to the *trans* form. Multiple integrations over the two methine proton signals reveal a *cis* to *trans* ratio of 1.02 ± 0.06 (average of seven determinations).

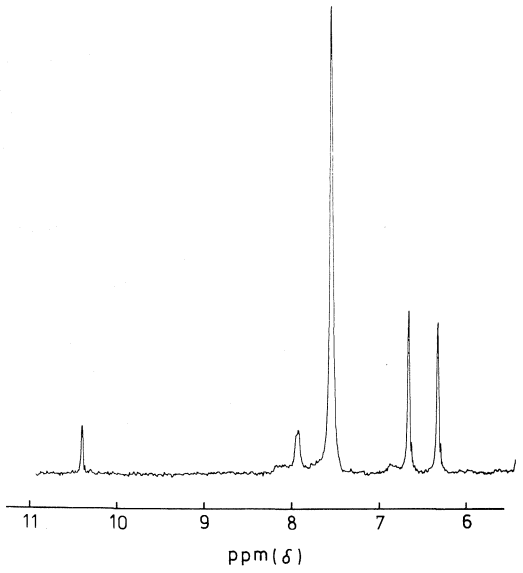

FIG. 2. The proton nmr spectrum of a saturated solution of **1** in D_2O at 25.5°C (relative to DSS at δ = 0.00).

The ratio of the integrals over the combined hydrate methine signals to that for the free dialdehyde at δ 10.33 reveal a hydrate to aldehyde ratio of 88.5:11.5 (±0.6%; average of seven determinations) at 25.5°C (EM 360A probe temperature). This corresponds to a hydration equilibrium constant in D_2O (K_{D_2O})[5] of 7.6 ± 0.5. These results agree well with those obtained from residual absorptions in the uv spectrum. Spectra recorded in D_2O solution in the presence of 0.01 *M* HCl or 0.001 *M* NaOH yielded the same value for K_{D_2O}. Spectra recorded in H_2O lead to a K_{H_2O} value of 7.6.

The methine proton signals of the hydrate at δ 6.27 and 6.61 appear as sharp singlets ($\nu_{1/2}$ = 1.2 Hz) in all of these solutions where the sulfonate salt, DSS, was used as internal reference. However, these peaks were very significantly broadened ($\nu_{1/2} \sim 8$ Hz) when the weakly basic internal reference, sodium 3-trimethylsilylpropionate-2,2,3,3-d_4 (TSP), was used. The position of equilibrium, however, remained unchanged. On warming the solution, the peaks broadened further, coalesced to a single very broad peak (at 40°C, $\nu_{1/2} \sim 16$ Hz) and finally to a fairly sharp resonance (at 70°C, $\nu_{1/2} \sim$ 4 Hz). Similar observations are made in NaOH solutions at concentrations above 0.01 *M* at room

[5]K_{D_2O} = [hydrate]/[aldehyde].

temperature. In 0.10 *M* NaOH, for example, a single fairly sharp resonance is observed at δ 6.49 due to these methine protons. We interpret this behavior in terms of the interconversion of the *cis* and *trans* hydrates (presumably via the free dialdehyde) which is slow on the nmr time scale in dilute HCl or NaOH. The equilibration is, however, catalyzed by either the high concentration (~10%) of the weakly basic carboxylate salt or by increasing concentration of NaOH and is more rapid at higher temperatures. The results in NaOH solution must be regarded with suspicion, however, since we know hydrate ionization [2] is significant under these conditions (see uv results above).

The position of the hydration equilibrium of **1** was investigated as a function of temperature in D_2O solution from the ratios of multiple integrations of the hydrate methine and free aldehyde signals. The K_{D_2O} values obtained over the temperature range 25.5–70°C are collected in Table 2. A plot of $\log_{10} K_{D_2O}$ vs. $1/T$ (Fig. 3) is reasonably linear and a short extrapolation yields a K_{D_2O} value of 7.7 ± 0.5 at 25.0°C (corresponding to a ΔG_{hyd} of −1.20 ± 0.04 kcal/mol). From the slope can be calculated $\Delta H_{hyd} = -8.90 \pm 0.34$ kcal/mol which leads to a value for $\Delta S_{hyd} = -25.8 \pm 1.1$ cal K^{-1} mol^{-1}.

The very limited solubility of the *meta* and *para* dialdehydes in D_2O precluded detection of any hydration for these compounds by nmr. However, spectra of concentrated solutions in 50 v/v% CH_3CN–D_2O revealed less than 2% hydrate could be present for either of these compounds under these conditions. Although solubility is considerably enhanced, hydration will be depressed in the mixed solvent. However, combined with the uv results, we conclude that an upper limit for K_{D_2O} for either of these compounds can be set at 0.05. This is in complete accord with the limited literature data (7–10) for the hydration of ring-substituted benzaldehydes. However, on the basis of polarographic measurements, Bover and Zuman (16) have concluded that although the *meta* isomer does not hydrate to any significant extent, *both* the *ortho* and the *para* isomers are significantly hydrated. This conclusion for the *para* isomer must be in error. Other reports of extensive hydration for *m*-chlorobenzaldehyde (17) and *o*-nitrobenzaldehyde (18), on the basis of polarographic measurements, have also required correction (9).

TABLE 2. Equilibrium constants for phthalaldehyde hydration in D_2O[a]

T (°C)	K_{D_2O} (n)[b]
25.5	7.66±0.44(7)
28	6.21±0.29(5)
40	3.99±0.16(4)
50	2.25±0.22(3)
55	1.99±0.07(4)
70	1.06±0.04(4)

[a]Determinations at 25.5°C were made on the EM 360A instrument. Those at 28°C and higher were made on the HA 100 instrument.
[b]K_{D_2O} = [hydrate]/[aldehyde]. The errors quoted are standard deviations of multiple integration ratios. n = number of separate determinations.

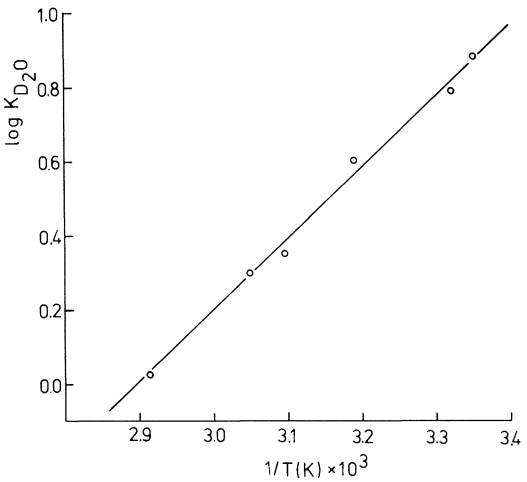

FIG. 3. A plot of $\log_{10} K_{D_2O}$ for **1** vs. the reciprocal of the absolute temperature.

Hydration Kinetics

Some preliminary kinetic results carried out in unbuffered H_2O solution at ionic strength 0.0 and 1.0 (with KCl) and in D_2O solution are collected in Table 3. The H_2O results include runs carried out with several different batches of distilled water, at each of the three λ_{max} values of **1**, and with several different substrate concentrations over the range 0.5–2.5 × 10^{-4} *M*. The k_{obs} value is independent of these effects and, further, is unaffected by a change in ionic strength from 0 to 1. However, the rate in D_2O is 30% lower than that in H_2O.

Kinetic runs were then carried out in aqueous (H_2O) solutions of dilute HCl and in a series of buffers over the pH range 2.6–7.8. The k_{obs} values

TABLE 3. Preliminary kinetic results for the hydration of **1** in unbuffered aqueous solutions at 28.0°C

Conditions	pH[a]	k_{obs} × 10^3 (s^{-1}) (n)[b]
H_2O (μ = 0.0)	6.7	6.3±0.2 (7)
H_2O (μ = 1.0)	6.6	6.2±0.1 (2)
D_2O (μ = 0.0)	7.3	4.5±0.1 (3)

[a]The pH values are only approximate in these unbuffered solutions. The value in D_2O is a pD value where pD = meter reading + 0.4.
[b]The k_{obs} values quoted are mean ± standard deviation. n = number of runs.

TABLE 4. Kinetic data for the hydration of **1** in aqueous solution, μ = 1.0, 28.0°C

Buffer ([HA]/[A⁻]; concentrations, *M*)	pH	*n*[a]	k_0[b] (s^{-1})	k_{B_t}[b] ($M^{-1}s^{-1}$)
Chloroacetate (1/1; 0.2–0.6)	2.66	6	0.170±0.006	0.125±0.014
HCl (2.0×10^{-3})	2.70	2	0.141±0.004	
Formate (3/1; 0.25–1.0)	2.99	8	0.084±0.003	0.099±0.004
HCl (1.0×10^{-3})	3.00	2	0.0784±0.0004	
Chloroacetate (1/3; 0.25–0.75)	3.18	6	0.069±0.002	0.076±0.003
HCl (5.0×10^{-4})	3.32	2	0.0420±0.0005	
Formate (1/1; 0.25–1.0)	3.52	8	0.038±0.002	0.070±0.003
Acetate (1/1; 0.25–0.75)	3.55	6	0.0354±0.0006	0.049±0.001
Chloroacetate (1/9; 0.25–0.75)	3.64	6	0.0254±0.0006	0.041±0.001
HCl (1.0×10^{-4})	4.00	2	0.0135±0.0003	
Formate (1/3; 0.25–1.0)	4.04	8	0.0161±0.0011	0.057±0.002
Acetate (1/1; 0.25–0.75)	4.56	6	0.0078±0.0012	0.060±0.002
Phosphate (9/1; 0.10–0.40)	5.36	8	0.0056±0.0031	0.203±0.010
Acetate (1/9; 0.10–0.50)	5.63	6	0.0060±0.0005	0.078±0.001
Phosphate (3/1; 0.10–0.30)	5.95	6	0.0066±0.0019	0.234±0.009
Phosphate (1/1; 0.10–0.30)	6.50	6	0.016±0.005	0.37±0.02
Phosphate (1/3; 0.09–0.36)	6.98	8	0.012±0.005	0.56±0.02
Tris (9/1; 0.05–0.20)	7.27	8	0.015±0.002	0.66±0.01
Phosphate (1/9; 0.10–0.30)	7.54	10	0.032±0.007	0.79±0.03
Tris (3/1; 0.02–0.08)	7.82	6	0.058±0.002	1.47±0.04

[a] *n* = number of runs.
[b] The errors quoted are standard deviations.

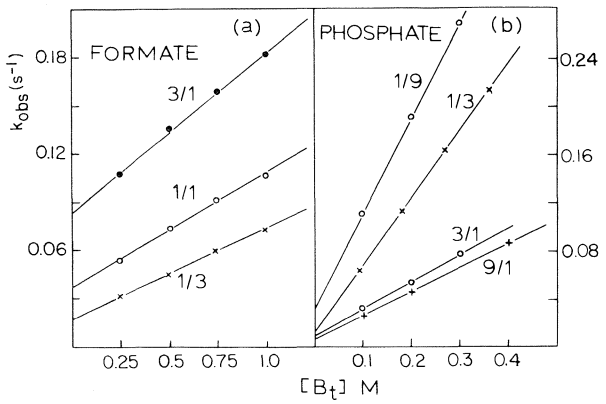

FIG. 4. Buffer plots for the hydration of **1** in aqueous solution, μ = 1.0, 28.0°C. The buffer ratios ([HA]/[A⁻]) are noted.

were found to be linear functions of the total buffer concentration, [B_t], for each buffer and buffer ratio employed [3]. At least duplicate runs were carried

$$[3] \qquad k_{obs} = k_0 + k_{B_t}[B_t]$$

out at each buffer concentration and normally three to four buffer concentrations were studied. The buffer plots for formate and phosphate (Fig. 4) are representative. The least-squares-calculated values of the intercepts of the buffer catalysis plots at zero buffer concentration, k_0, and the second-order buffer-catalyzed rate constants, k_{B_t}, are collected in Table 4.

The pH–rate profile (Fig. 5) illustrates the sensitivity of the k_0 values to pH. The k_0 values follow [4] where either the second or third terms can be

$$[4] \qquad k_0 = k_{H_2O} + k_H[H^+] + k_{OH}[OH^-]$$

neglected over certain ranges of pH. Thus, a plot of k_0 vs. [H^+] (calculated from the pH) for the data in Table 4 at pH values less than 4.6 (Fig. 6*a*), where the third term in [4] can be neglected, gave a linear correlation from which values of $k_H = 70.4 \pm 2.5\ M^{-1}\ s^{-1}$ and $k_{H_2O} = 0.010 \pm 0.003\ s^{-1}$ can be calculated from the slope and intercept, respectively. Similarly, a plot of k_0 vs. [OH^-] at pH values greater than 5.9 (Fig. 6*b*), where the second term in [4] can be neglected, also give a linear correlation from which values of $k_{OH} = (7.9 \pm 0.4) \times 10^4\ M^{-1}s^{-1}$ and

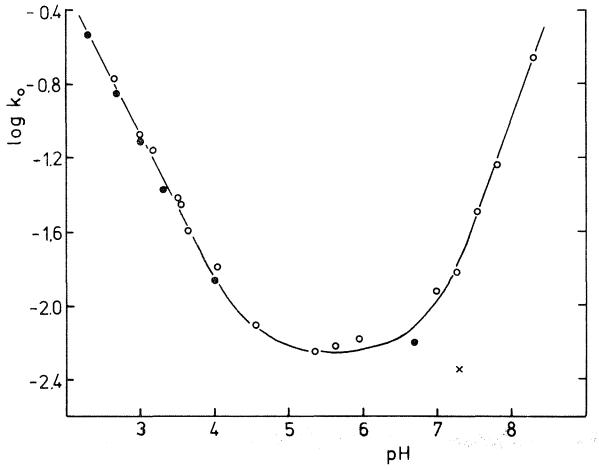

FIG. 5. The pH–rate profile for the hydration of **1** in aqueous solution at 28.0°C (●, HCl solutions and H_2O; ○, intercepts of buffer plots; ×, D_2O, pH = pD).

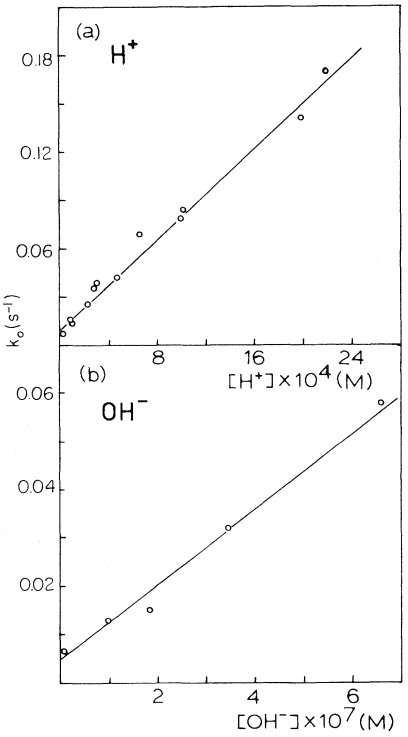

FIG. 6. Plots of k_0 vs. (*a*) [H^+] (at pH values less than 4.6), (*b*) [OH^-] (at pH values greater than 5.9) for the hydration of **1** at 28.0°C (μ = 1.0).

$k_{H_2O} = 0.005 \pm 0.001\ s^{-1}$ could be evaluated. The k_{H_2O} values from the intercepts of these plots are rather unreliable. We chose instead to correct the k_0 values obtained from the intercepts of the buffer plots in the plateau region (pH 4.5–6) for the contributions from the second and third terms in [4] which can now be calculated. This lead to a value for $k_{H_2O} = (5.6 \pm 0.4) \times 10^{-3} s^{-1}$. The solid curve in Fig. 5 follows [4] where k_H, k_{OH}, and k_{H_2O} have the values derived above. The minimum value of k_0 occurs at pH 5.5 where the last two terms in [4] contribute roughly 10% to its value.

The buffer-catalyzed rate constants, k_{B_t}, contain, in general, significant contributions from both the acidic and basic forms of the buffer. If k_{HA} and k_B are the second-order rate constants for catalysis by the acidic and basic forms of the buffer, respectively, then k_{B_t} is given by [5], where f_B is the fraction of the buffer in the basic form. Values of k_{HA} and k_B are

$$[5] \qquad k_{B_t} = k_{HA} + (k_B - k_{HA})f_B$$

then obtained from the intercepts at $f_B = 0$ and 1, respectively, of the plots of k_{B_t} vs. f_B (Fig. 7). The plots for the carboxylate buffers are reasonably linear and the extrapolations are straightforward. Only two buffer ratios (9:1 and 3:1) were employed

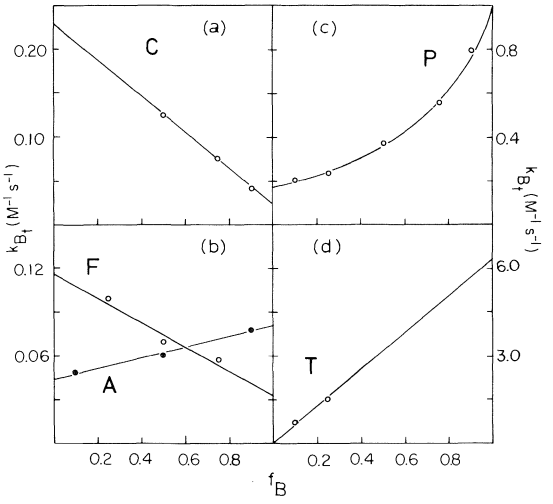

FIG. 7. Plots of the buffer-catalyzed rate constants vs. the fraction of base in the buffer. The buffer species are (*a*) chloroacetate; (*b*) formate (○), acetate (●); (*c*) phosphate; (*d*) Tris.

for Tris since lower ratios gave rates which were beyond the scope of our instrumentation. However, making the reasonable assumption that k_{HA} for Tris is zero,[6] a value for $k_B = 6.2 \pm 0.4\ M^{-1} s^{-1}$ can be calculated. The plot for the five phosphate buffers shows definite curvature. We have observed no systematic changes of pH with dilution which could account for such an effect. Curved plots of this type have been observed previously (19) but the interpretation (a change in rate-determining step with pH) has been questioned (20). We are not prepared to offer an explanation for this 'negative cooperativity' at this time and have simply made the rather short nonlinear extrapolations to $f_B = 0$ and 1 to obtain values for k_{HA} and k_B.

The acid–base catalysis data are collected in Table 5. Included are the values for k_H and k_{OH} and the value for k_{H_2O} which has been converted to a second-order rate constant and is included both as a potential general acid and a general base. The Brønsted plots for acid–base catalysis are illustrated in Fig. 8. The general acids H^+ and the carboxylic acids define a line of slope $\alpha = 0.52 \pm 0.03$. The point for water lies 3 powers of 10 above this line but it does fall nicely on the plot defined by the general bases. The point for $H_2PO_4^-$ lies above the line defined by the other buffer acids by 1.8 powers of 10. Such enhanced catalytic activity is commonly observed for phosphate (21, 22) since it can serve as a bifunctional acid–base catalyst in some proton transfer reac-

[6]This assumption would appear to be reasonable since, if k_{HA} for Tris falls on the Brønsted plot for the other acids, a value of $3 \times 10^{-4}\ M^{-1} s^{-1}$ can be calculated. Such weak catalysis would not be detectable.

TABLE 5. Rate constants for general acid – base catalysis of the hydration of **1** at 28.0°C

Catalyst (HA/B)	pK_{HA}[a]	k_{HA}[b] ($M^{-1}s^{-1}$)	k_B[b] ($M^{-1}s^{-1}$)
(*1*) H^+/H_2O	−1.74	70.4±2.5	(1.01±0.06)×10^{-4}
(*2*) $ClCH_2CO_2H/ClCH_2CO_2^-$	2.66	0.230±0.006	0.022±0.003
(*3*) HCO_2H/HCO_2^-	3.52	0.118±0.010	0.033±0.010
(*4*) $CH_3CO_2H/CH_3CO_2^-$	4.56	0.044±0.003	0.081±0.003
(*5*) $H_2PO_4^-/HPO_4^{2-}$	6.50	0.18±0.03	0.99±0.08
(*6*) Tris H^+/Tris	8.32	[c]	6.2±0.4
(*7*) H_2O/OH^-	15.74	(1.01±0.06)×10^{-4}	(7.9±0.4)×10^4

[a]For the buffer species (entries *2–6*), the pK_{HA} is taken to be the pH at half neutralization at μ = 1.0; pK_{H^+} = −log [H_2O]; pK_{H_2O} = pK_w + log [H_2O].
[b]The errors quoted are standard deviations.
[c]Assumed to be zero (see text).

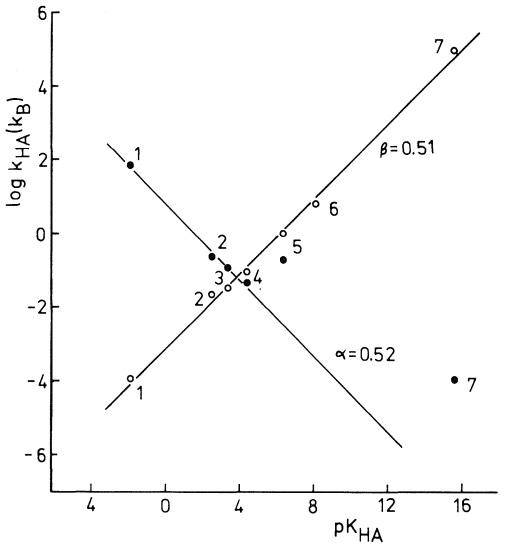

FIG. 8. Brønsted plots for general species catalysis of the hydration of **1** at 28.0°C (the numbers refer to the species in Table 5).

tions.[7] The points for $H_2PO_4^-$ and H_2O were omitted from the general acid correlation. Our series of buffer acids is limited by the dominance of the H^+- catalyzed pathway at pH values less than 2.5 and by the increasing importance of catalysis by the basic component of the buffer for acids having a pK_{HA} greater than 5.5.

The Brønsted plot for the general bases, however, is noteworthy. All species studied, representing a catalytic range of nearly 10^9 and several different base and charge types, fall on a single straight line with remarkably good correlation (β = 0.51 ± 0.01, correlation coefficient = 0.998). Water appears to be functioning as a general base in the spontaneous process. Hydroxide also falls on this line and there appears to be no need to invoke a nucleophilic pathway for this species. The statistically corrected plots (of $\log_{10} k_{HA}/p$ and $\log_{10} k_B/q$ vs. $\log_{10} qK_{HA}/p$) show no improvement in the correlations nor any significant changes in the slopes (α' = 0.50 ± 0.03; β' = 0.51 ± 0.02).

These rate constants refer to the overall rate of approach to equilibrium and thus are the sum of the hydration (k_{hyd}) and dehydration (k_{dehyd}) rate constants. However, since K_{H_2O} (= k_{hyd}/k_{dehyd}) is independent of pH, buffer type, and concentration over the range in which kinetic data were obtained, then k_{hyd} and k_{dehyd} must be proportional to one another and have α and β coefficients identical to those above.

Bell and co-workers (21, 23, 24) have reported Brønsted coefficients similar to those above for the hydration of several aliphatic aldehydes and ketones and for the dehydration of the hydrates. However, it is difficult to determine the sensitivity of the α and β values to the structure and reactivity of the carbonyl compound since some of Bell's earlier work was carried out at temperatures significantly different from 25°C and in mixed aqueous–organic solvents. Nevertheless, the observation of general species catalysis is indicative of proton transfer between substrate and catalyst occurring in the rate-determining step.

The mechanism of carbonyl hydration has been discussed in detail elsewhere (6, 25, 26). An analysis of the magnitude of the α values observed for the acid-catalyzed addition of a variety of nucleophiles to carbonyl compounds has lead Jencks (25, pp. 197–198) to conclude that the catalysis is true general acid catalysis in the forward direction (hydration) and that the reverse reaction (dehydration) is subject to specific acid – general base catalysis (kinetically indistinguishable from general acid). Possible pathways for the acid-catalyzed hydration equilibrium of **1** are outlined in Scheme 1. Mechanism [A1] involves general acid catalyzed water attack concerted with cyclization in the (slow) first step followed by rapid deprotonation of **5**. Alternatively, a stepwise pathway

[7]In fact, Bell and Evans (21) observed the k_{HA} values for chloroacetic acid and $H_2PO_4^-$ were identical although they differ by 4 units in pK_{HA} (also see our results).

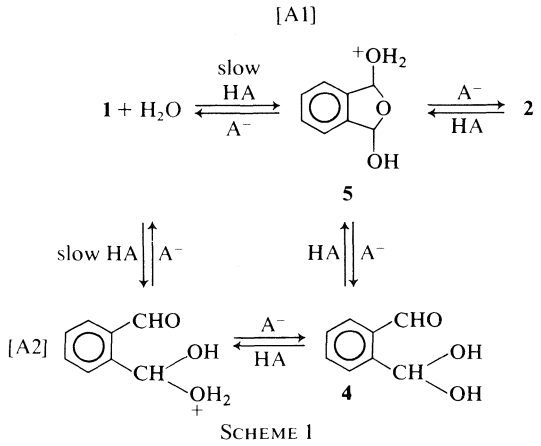

SCHEME 1

[A2] can be envisaged in which the slow general acid catalyzed water attack at one of the carbonyl groups is followed by rapid deprotonation to form the normal hydrate, the *gem*-diol **4**. Rapid (and presumably acid-catalyzed) cyclization of **4** followed by deprotonation of **5** leads to **2**. Two factors lead us to favor the stepwise pathway. Firstly, the Brønsted α coefficient for the hydration of **1** (0.52) is very similar to that measured by Bell *et al.* (23) for the hydration of acetaldehyde (0.54) under similar conditions. Secondly, our observed rates are similar to those measured by Sayer (10) for the hydration of *p*-nitrobenzaldehyde.[8] Since both of these latter cases involve formation of the *gem*-diol, we propose our mechanism also proceeds via formation of **4**. If the concerted pathway [A1] were preferred, one would expect some rate enhancement to be observed. Finally, Powell and Rexford (27) observed that when **1** was dissolved in ethanol, the disappearance of the uv carbonyl absorption band showed biphasic behavior; these authors proposed the intermediacy of the mono-hemiacetal which then went on to form the bis-hemiacetal although 3-ethoxyphthalan-1-ol might be the product of this reaction.

The analogous pathways for the base-catalyzed reaction are outlined in Scheme 2. Again Jencks (28) has proposed that catalysis of the forward reaction corresponds to true general base catalysis. Although our evidence is rather limited here, the similarity of the Brønsted β coefficients observed for the hydration of **1** (0.51) and acetaldehyde (0.45) (23), leads us to favor the stepwise pathway [B2] via the *gem*-diol **4** over the concerted pathway [B1].

The susceptibility of the hydration to catalysis by zinc(II) ions was investigated briefly. Carbonic anhydrase catalyzes the hydration of acetaldehyde (29) and the pyridine carboxaldehydes (30) as well as carbon dioxide, and is known to contain a hydrated zinc ion at the active site (31). Although the enzyme has been the subject of many investigations, the exact function of the zinc is not known. We find the hydration of **1** to be only weakly accelerated by Zn(II); a plot of k_{obs} vs. [$ZnSO_4$] (not shown) at pH 5.1 is linear from 0.10 to 1.0 *M* $ZnSO_4$ with a slope of $k_{Zn} = (2.30 \pm 0.12) \times 10^{-2}\ M^{-1}s^{-1}$. The reaction is only five-fold faster in 1.0 *M* $ZnSO_4$ than in water at this pH. This rate constant is not consistent with general acid catalysis by the hydrated ion ($pK_a = 9.6$ (32)) but rather suggests that the metal ion is providing some electrostatic polarization of the carbonyl group facilitating nucleophilic attack by water. Although weak catalysis of the hydration of aldehydes by zinc ions alone has been observed previously (33, 34), cooperative catalysis by zinc and acetate or pyridine is rather more pronounced (34). However, we did not investigate further such catalysis for **1**.

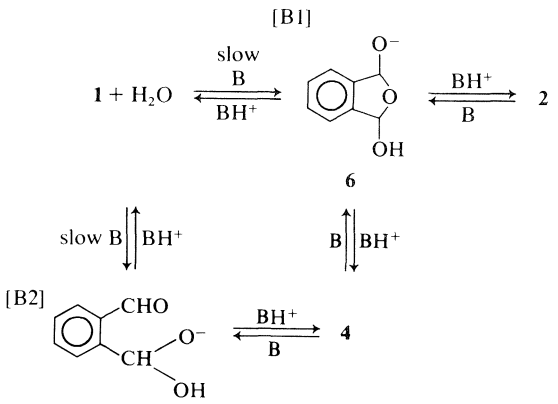

SCHEME 2

General Comments on Carbonyl Hydration

A modified Taft equation [6] has been proposed (35) to correlate the hydration equilibrium constants, K_{H_2O}, with the Taft σ^* substituent constants:

$$[6] \quad \log_{10} K_{H_2O} = 1.70 \sum\sigma^* + 2.03\,\Delta - 2.81$$

where Δ is a factor which distinguishes the behavior of aldehydes and ketones ($\Delta = 0$ for ketones, 1 for aldehydes, and 2 for formaldehyde). Thus, ketones are normally less hydrated than aldehydes owing to an electronic *and* an adjacent bond interaction (hyperconjugative) effect. Steric effects are concluded to be unimportant (35). This equation correlates the available K_{H_2O} data fairly well for aliphatic aldehydes and ketones of widely varying structure. Electron-withdrawing substituents favor hydration. However, aromatic carbonyl compounds have K_{H_2O} values 10^3-fold lower than this equation would predict.[9]

[8]We thank Dr. J. P. Guthrie for making this observation.

[9]Benzaldehyde is predicted by [6] to have a K_{H_2O} of 11.8 whereas the currently accepted value is near 1×10^{-2} (7, 8).

TABLE 6. Thermodynamic data for the hydration of some carbonyl compounds[a]

Compound	K_{H_2O}[b]	ΔG_{hyd}[c,d]	ΔH_{hyd}[d] (ΔH_{hyd}/(calcd.))[d,e]	ΔS_{hyd}[f]	Ref.
CH_2O	2.27×10^3	−4.58	−5.7		
			−8.0 (−8.0)	(−11)[g]	37
			−14.6		
CH_3CHO	1.06	−0.03	−5.6 (−5.6)	−19	38
CH_3COCH_3	1.4×10^{-3}	+3.89	[h] (−3.3)	(−24)	39
$(CH_3OCH_2)_2CO$	0.373	+0.58	−5.9 (−3.3)	−22	40
C_6H_5CHO	(1.1×10^{-2})[i]	(+2.7)	[h] (−3.7)	(−21)	7
4-C_5H_4NCHO[j]	1.53	−0.25	−3.8 (−3.7)	−12	11
1,2-$C_6H_4(CHO)_2$	7.7	−1.20	−8.9 (−6.9)	−26	This work

[a]All values refer to 25°C. Values in parentheses are estimated (see reference cited or text).
[b]K_{H_2O} = [hydrate]/[carbonyl].
[c]$\Delta G_{hyd} = -RT \ln K_{H_2O}$.
[d]In kcal/mol.
[e]Calculated by applying Benson's group additivity rules (36) to the normal hydration reaction or, for **1**, to the formation of **2**.
[f]In cal K^{-1} mol^{-1}.
[g]Calculated using the value of −8.0 kcal/mol for ΔH_{hyd}.
[h]Value not available.
[i]Value estimated by Greenzaid (7).
[j]4-Pyridine carboxaldehyde.

This must be due to the conjugative stabilization of the carbonyl group with the aromatic ring, a factor which this equation does not consider. This factor of 10^3 in K_{H_2O} corresponds to a stabilization free energy of 4.1 kcal/mol. Although the lack of solubility in water of aromatic carbonyl compounds hampers detection of the hydrate, it is clear that even moderately strong electron-withdrawing substituents do not favor hydration to any appreciable extent (see our results for the 1,3- and 1,4-dialdehydes). The K_{H_2O} value for *p*-nitrobenzaldehyde has been measured to be 0.15 (9) and 0.25 (10). Thus, the K_{H_2O} value of 7.7 for **1** is 10^2-fold larger than one would predict for normal hydration and the unique cyclic structure **2** of the hydrate is not totally unexpected.

In view of the results for **1**, we collected, for comparison purposes, thermodynamic data for the hydration of a variety of carbonyl compounds (Table 6). Much of the data is experimental but we have also included values for the enthalpy of hydration (ΔH_{hyd}) calculated by applying Benson's group additivity rules (36) to the normal hydration reaction or, for **1**, to the formation of **2**. Despite the fact that these calculated values refer to the gas phase, agreement with experimental values, where these are available, is good. Exceptions may occur where the carbonyl compound has remote electronic effects not considered in the calculation. Thus, the calculated ΔH_{hyd} value for both acetone and 1,3-dimethoxy acetone is −3.3 kcal/mol and that for the aromatic aldehydes (except **1**) is −3.7 kcal/mol. Where experimental ΔH_{hyd} data were not available, we have used the calculated value to evaluate ΔS_{hyd}.

Some general trends in the thermodynamic data may be noted. From the first three entries, it is clear that the increasingly unfavorable hydration observed as the hydrogens of formaldehyde are progressively replaced by methyl groups is reflected in both the ΔH_{hyd} and ΔS_{hyd} terms. The more extensive hydration of 1,3-dimethoxyacetone relative to acetone is determined mainly by the more exothermic (by 2.6 kcal/mol) ΔH_{hyd} term; the ΔS_{hyd} is similar to that estimated for acetone. Although the data for benzaldehyde are estimated, our calculations again reveal that much of the less favorable ΔG_{hyd} is reflected in the ΔH_{hyd} term while the ΔS_{hyd} is only 2 eu more negative than that for acetaldehyde. On the other hand, the appreciable hydration of 4-pyridine carboxaldehyde is determined by the much less negative ΔS_{hyd} relative to the other aldehydes while the ΔH_{hyd} is remarkably close to that estimated for an aromatic aldehyde. Obviously, there appears to be no correlation between the ΔH_{hyd} and ΔS_{hyd} terms (i.e., no isoequilibrium relationship exists) and the degree of hydration may be determined by either one or both of these terms. Finally, the extensive hydration of **1** is determined solely by the ΔH_{hyd} term which is some 5.2 kcal/mol more exothermic than that estimated for benzaldehyde. An inventory of bonds broken and made during hydration reveals that hydration of **1** to form **2** *should* be more than twice as exothermic as that to form the *gem*-diol **4**. The ΔS_{hyd} term is, in fact, 5–7 eu more negative than that observed or calculated for the other aldehydes, a result in accord with the loss of two rotational degrees of freedom accompanying ring formation.

Acknowledgements

We are pleased to acknowledge the technical assistance of Ms. Christine Sibley who processed much of the kinetic data and Mr. John Van Ingen of the Atlantic Regional Laboratory of the National Research Council of Canada who recorded the

variable temperature nmr spectra. We thank Dr. O. S. Tee and Dr. J. A. Pincock for valuable comments on parts of the work. The financial assistance of the National Research Council of Canada in the form of an operating grant (to R.S.M.) and a Negotiated Regional Development Grant is also gratefully acknowledged.

1. J. THIELE and K. G. FALK. Justus Liebigs Ann. Chem. **347**, 112 (1906); J. THIELE and J. SCHNEIDER. Justus Liebigs Ann. Chem. **369**, 287 (1909); Chem. Abstr. **4**, 1039[7] (1910); J. THIELE and E. WEITZ. Justus Liebigs Ann. Chem. **377**, 1 (1910); Chem. Abstr. **5**, 461[3] (1911).
2. T. DOMINH, A. L. JOHNSON, J. E. JONES, and P. P. SENISE, JR. J. Org. Chem. **42**, 4217 (1977).
3. F. WEYGAND, K. VOGELBACH, and K. ZIMMERMAN. Chem. Ber. **80**, 391 (1947); E. SCHMITZ. Chem. Ber. **91**, 410 (1958).
4. N. A. VALYASCKO and M. V. BOLTINA. J. Russ. Phys. Chem. Soc. **46**, 1741 (1914); Chem. Abstr. **9**, 2070[5] (1915); R.C. WEAST (*Editor*). Handbook of chemistry and physics. 50th edition. The Chemical Rubber Co., Cleveland, OH. 1969. p. C-430.
5. L. SEEKLES. Recl. Trav. Chim. Pays-Bas, **42**, 706 (1923); Chem. Abstr. **18**, 62 (1924).
6. R. P. BELL. Adv. Phys. Org. Chem. **4**, 1 (1966).
7. P. GREENZAID. J. Org. Chem. **38**, 3164 (1973).
8. J. P. GUTHRIE. Can. J. Chem. **56**, 962 (1978).
9. R. P. BELL and P. E. SØRENSEN. J. Chem. Soc. Perkin Trans. II, 1594 (1976).
10. J. M. SAYER. J. Org. Chem. **40**, 2545 (1975).
11. S. CABANI, G. CONTI, and P. GIANNI. J. Chem. Soc. A, 1363 (1969); S. CABANI, P. GIANNI, and E. MATTEOLI. J. Phys. Chem. **76**, 2959 (1972).
12. J. THIELE and O. GUNTHER. Justus Liebigs Ann. Chem. **347**, 106 (1906).
13. J. C. BILL and D. S. TARBELL. Org. Synth. **34**, 82 (1954).
14. M. R. CRAMPTON. J. Chem. Soc. Perkin Trans. II, 185 (1975).
15. C. ASO and S. TAGAMI. Macromolecules, **2**, 414 (1969).
16. W. J. BOVER and P. ZUMAN. J. Chem. Soc. Perkin Trans. II, 786 (1973).
17. R. G. BARRADAS, O. KUTOWY, and D. W. SHOESMITH. Can. J. Chem. **52**, 1635 (1974).
18. E. LAVIRON, H. TRONCIN, and J. TIROUFLET. Bull. Soc. Chim. Fr. 524 (1962).
19. C. J. BELKE, S. C. K. SU, and J. A. SHAFER. J. Am. Chem. Soc. **93**, 4552 (1971).
20. T. OKUYAMA and G. L. SCHMIR. J. Am. Chem. Soc. **94**, 8805 (1972).
21. R. P. BELL and P. G. EVANS. Proc. R. Soc. London A, **291**, 297 (1966).
22. M. F. ALDERSLEY, A. J. KIRBY, P. W. LANCASTER, R. S. MCDONALD, and C. R. SMITH. J. Chem. Soc. Perkin Trans. II, 1487 (1974).
23. R. P. BELL, M. H. RAND, and K. M. A. WYNNE-JONES. Trans. Faraday Soc. **52**, 1093 (1956).
24. R. P. BELL and W. C. E. HIGGINSON. Proc. R. Soc. London A, **197**, 141 (1949); R. P. BELL and M. B. JENSEN. Proc. R. Soc. London A, **261**, 38 (1961).
25. W. P. JENCKS. Catalysis in chemistry and enzymology. McGraw-Hill, New York, NY. 1969. pp. 211–215.
26. T. H. LOWRY and K. S. RICHARDSON. Mechanism and theory in organic chemistry. Harper and Row, New York, NY. 1976. Chapt. 8.
27. M. R. POWELL and D. R. REXFORD. J. Org. Chem. **18**, 810 (1953).
28. W. P. JENCKS. Prog. Phys. Org. Chem. **2**, 63 (1964).
29. Y. POCKER and J. E. MEANY. Biochemistry, **4**, 2535 (1965).
30. Y. POCKER and J. E. MEANY. Biochemistry, **6**, 239 (1967).
31. R. P. DAVIS. *In* The enzymes. Vol. 5. 2nd ed. *Edited by* P. D. Boyer, H. Lardy, and K. Myrback. Academic Press, New York, NY. 1961. p. 545; J. COLEMAN. J. Biol. Chem. **242**, 5212 (1967); J. COLEMAN. Biochemistry, **4**, 2644 (1965).
32. W. P. JENCKS and J. REGENSTEIN. *In* Handbook of biochemistry. *Edited by* H. A. Sober. The Chemical Rubber Company, Cleveland, OH. 1968. p. J-152.
33. Y. POCKER and J. E. MEANY. J. Am. Chem. Soc. **89**, 631 (1967); **89**, 1809 (1967).
34. R. H. PRINCE and R. P. WOOLLEY. J. Chem. Soc. Dalton Trans. 1548 (1972); P. R. WOOLLEY. J. Chem. Soc. Dalton Trans. 1570 (1975).
35. P. GREENZAID, Z. LUZ, and D. SAMUEL. J. Am. Chem. Soc. **89**, 749 (1967).
36. S. W. BENSON, F. R. CRUICKSHANK, D. M. GOLDEN, G. R. HAUGEN, H. E. O'NEAL, A. S. RODGERS, R. SHAW, and R. WALSH. Chem. Rev. **69**, 279 (1969).
37. P. VALENTA. Coll. Czech. Chem. Commun. **25**, 853 (1960); L. C. GRUEN and P .T. MCTIGUE. J. Chem. Soc. 5217 (1963); A. ILICETO. Gazz. Chim. Ital. **84**, 536 (1954); R. BIEBER and G. TRÜMPLER. Helv. Chim. Acta, **30**, 1860 (1947).
38. J. L. KURZ. J. Am. Chem. Soc. **89**, 3524 (1967).
39. J. HINE and R. W. REDDING. J. Org. Chem. **35**, 2769 (1970); J. HINE. J. Am. Chem. Soc. **93**, 3701 (1971).
40. J. HINE, L. R. GREEN, P. C. MENG, and V. THIAGARAJAN. J. Org. Chem. **41**, 3343 (1976).

Excess heats of tri-*n*-alkylamines and tetraalkyl tin compounds in linear and branched alkanes: correlations of molecular orientations and steric hindrance effect

R. PHILIPPE

Université de Lyon, Laboratoire de Chimie Analytique I, 43 Boulevard du 11 Novembre 1918, 69621 Villeurbanne, France

AND

G. DELMAS AND PHUONG NGUYEN HONG

Université du Québec à Montréal, Département de chimie, B.P. 8888, Montréal (Qué.), Canada H3C 3P8

Received March 17, 1978[1]

R. PHILIPPE, G. DELMAS, and PHUONG NGUYEN HONG. Can. J. Chem. **57**, 517 (1979).

Excess heats of the following mixtures of trialkylamines and tetraalkyl tin compounds with branched and linear alkanes have been measured at 25°C: five trialkylamines NR_3 (R = C_2H_5, C_3H_7, C_4H_9, $C_{10}H_{21}$, $C_{12}H_{25}$) with six linear alkanes, *n*-C_5, *n*-C_6, *n*-C_8, *n*-C_{10}, *n*-C_{12}, *n*-C_{16}, and three highly branched alkanes, 2,2,4-trimethylpentane, 2,2,4,6,6-pentamethylheptane, and 2,2,4,4,6,8,8-heptamethylnonane (br-C_{16}). Further measurements were carried out on tetrapropyl tin ($SnPr_4$) with *n*-C_8, *n*-C_{16}, and br-C_{16}.

Measurements were made to obtain more information on the heats of disordering of long chain compounds and on an exothermic contribution to the heats coming possibly from the sterically hindered character of one of the components of the mixture. The three short-chain trialkylamines have large heats with the linear long alkanes and small heats with the branched alkanes. On the other hand, the two long-chain trialkylamines have very small heats with linear alkanes and large heats with the branched alkanes. These results are interpreted as indicating no change of liquid or solution 'structure' when two ordered compounds (long alkanes and long-chain amines) are mixed but a change of 'structure' when an ordered compound (long alkane or long-chain amine) is mixed with a non-ordered one (branched alkane or short-chain amine). The heat of disordering of *n*-hexadecane is obtained with many order breakers and found to depend to some extent on the expansion coefficient of the order breaker. H^E values for the series of the shorter NR_3 do not vary regularly with molecular weight but are smaller for the propyl (and possibly the ethyl) derivative. Similarly, H^E of $SnPr_4$ in *n*-C_{16}, br-C_{16}, and *n*-C_8 are much lower than the corresponding heats with $SnEt_4$ and $SnBut_4$. This is attributed to the presence of the exothermic contribution to the heats, H^E(steric hindrance). The X_{12} parameter of the Flory theory has been calculated and is interpreted in terms of the disorder and steric hindrance contributions to the heats.

R. PHILIPPE, G. DELMAS et PHUONG NGUYEN HONG. Can. J. Chem. **57**, 517 (1979).

Nous avons mesuré les chaleurs de mélange d'amines trisubstituées et de composés d'étain tétrasubstitués avec des alcanes linéaires et ramifiés à 25°C. Les composés utilisés étaient les suivants: cinq amines NR_3 (R = C_2H_5, C_3H_7, C_4H_9, $C_{10}H_{21}$, $C_{12}H_{25}$) six alcanes linéaires *n*-C_5, *n*-C_6, *n*-C_8, *n*-C_{10}, *n*-C_{12}, *n*-C_{16} et trois alcanes très ramifiés 2,2,4-trimethylpentane, 2,2,4,6,6-pentamethylheptane et 2,2,4,4,6,8,8-heptamethylnonane (br-C_{16}). Les systèmes *n*-C_8, *n*-C_{16} et br-C_{16} avec le trétrapropylétain ($SnPr_4$) ont également été mesurés.

Les systèmes ont été choisis dans le but d'obtenir plus d'information (1) sur la chaleur de désordre des composés en chaine et (2) sur une contribution exothermique aux chaleurs associée à l'empêchement stérique présent dans un des constituants du mélange. Les amines globulaires à courtes chaines ont des chaleurs de mélange élevées avec les alcanes linéaires et faibles avec les alcanes ramifiés. Par ailleurs, les deux amines à longue chaine ont de très petites chaleurs avec les alcanes linéaires et de grandes chaleurs avec les alcanes branchés. L'interprétation de ce résultat est la suivante: la "structure" de la solution est semblable à celle des liquides purs quand deux composés ordonnés (alcanes ou amines à longue chaine) sont mélangés mais elle est différente si un composé ordonné est mélangé à un composé non-ordonné (alcane ramifié ou amine à courte chaine). La chaleur de désordre de l'hexadecane linéaire obtenue à partir de différents destructeurs d'ordre semble dépendre de l'état d'expansion du destructeur d'ordre. Les valeurs des chaleurs ne varient pas régulièrement avec le poids moléculaire du composé NR_3 dans la série mais sont plus faibles pour le dérivé propylé et peut-être éthylé. De la même façon, les chaleurs avec *n*-C_{16} et *n*-C_8 du composé $SnPr_4$ sont inférieures à celles obtenues avec $SnEt_4$ et $SnBut_4$. Cet effet est attribué à la présence d'une contribution exothermique H^E(empêchement stérique). Le paramètre X_{12} de la théorie de Flory a été calculé et interprété en termes de ces deux contributions.

[1]Revision received October 12, 1978.

0008-4042/79/050517-09$01.00/0

Introduction

In the case of the heats of mixing of non-polar mixtures, the importance of the difference in chemical nature of the two components has been recognized early and taken into account by several theories (1*a*). The difference of size and shape of the two components which influences the chemical positive contribution to the heats has been analysed and written in terms of surface fractions (1*b*, *d*). Contributions to the heats arising from non-zero volume of mixing have been calculated (1*c*). Theories, introduced in the last twenty years (Prigogine (2), Patterson (3*a*), Flory (4)), stress the importance of the difference of state of expansion (or free volume) of the two components mixed. In systems where this difference is large, negative contributions to H^E, V^E, and TS^E are found experimentally and can be calculated from equations of state for the liquids and the solution. Solution properties of mixtures (5–10) consisting of molecules of different shapes, such as globular and linear alkanes or multibranched compounds like MR_4 (M = C, Sn, or Si), have shown that another contribution depending on the shape of the molecule should be added. In the case of the heats of mixing, this contribution can be a positive term, related to the destruction of orientational order (5–8) or a negative one, namely, the condensation or steric hindrance term (5–10) or a combination of the two. In many instances, the total heat, either positive (3*b*, 5, 6) or negative (11), is constituted principally by these effects. Our aim is to obtain more information on the role of the shape of the molecules. Thermodynamic data (8–9) and depolarized Rayleigh scattering (12) on long-chain compounds, pure and in solution, are in agreement with the hypothesis that the 'structure' of the liquid is very sensitive to the molecular shape. Due to the anisotropy of the molecule, a long *n*-alkane keeps in the liquid state some of the order it had in the solid state. The chains are oriented one along the other in order to maximize the Van der Waals interaction along the chain. A branched alkane, being more isotropic, does not have such orientational order. The relatively large endothermic heats, obtained when a long alkane is mixed with a branched one, comes from the heat (H^E_{dis}) associated with the disordering of the chains of the long alkane, i.e. with the disappearance, in the solution, of the 'structure' which existed in the pure liquid. The much smaller heats evolved when two branched alkanes are mixed, are explained by the lack of correlations of orientations in a liquid consisting of globular molecules and consequent lack of the heat of disordering. This work presents the results of H^E of trialkylamines with linear and branched alkanes. The investigation is rather similar to those made on the SnR_4 compounds (5, 6). However, the use of the trialkylamines as probes of the alkanes has seemed to us worthwhile for other reasons: (*1*) the magnitude of the heats can give the balance of the polar and non-polar contributions in the case of the shorter members of the NR_3 series, (*2*) comparison of the heats of the trisubstituted compounds like NR_3 with those of the tetrasubstituted SnR_4 (this work and refs. 5 and 6) could show evidence of *intra*molecular correlations of orientations present in long-chain SnR_4 although less important in long-chain NR_3 compounds, (*3*) measurements of the thermal pressure coefficient on the pure compounds appear to show a correlation between high P^* values and steric hindrance within the molecule as seen by heats of mixing. Heats measured on another series could confirm the correlation.

Three important systems have been added, namely, $SnPr_4$ with *n*-C_8, *n*-C_{16}, and br-C_{16}. In the previous work on the SnR_4 + alkane systems (5), the SnR_4 molecules were used as order breakers of the alkanes due to their globular shape. Knowledge of the heats with every member was not expected to give supplementary information, so that heats were obtained with the methyl, ethyl, and butyl derivatives only. However, because of the unexpected values of the heats with $SnPr_4$ when mixed with $SnLaur_4$ and $SnOct_4$, it was decided that the heats of $SnPr_4$ with some alkanes should be measured, values of which are published here and compared to those obtained previously with $SnMe_4$, $SnPr_4$, and $SnBut_4$.

H^E results are given on the following 41 systems at 25°C: five trialkylamines NR_3 (R = C_2H_5, C_3H_7, C_4H_9, $C_{10}H_{21}$, $C_{12}H_{25}$) with six linear alkanes (C_5, C_6, C_8, C_{10}, C_{12}, C_{16}) and three highly branched alkanes in C_8 (2,2,4-trimethylpentane (br-C_8)) in C_{12} (2,2,4,6,6-pentamethylheptane (br-C_{12})), in C_{16} (2,2,4,4,6,8,8-heptamethylnonane (br-C_{16})); one SnR_4 ($SnPr_4$) with two linear alkanes, *n*-C_8 and *n*-C_{16}, and one branched alkane, (br-C_{16}). The abbreviated terms NEt_3, NPr_3, $NBut_3$, $NDec_3$, $NLaur_3$ are used in the text.

Experimental

Apparatus

The heats of mixing were measured using a tilting Tian-Calvet calorimeter. Details of the measurements, the cells, and the calibration can be found in refs. 5 and 14, and with the reference system (cyclohexane + hexane) our points agree within 2% of the published value (15). It was found useful to employ another reference system, benzene + CCl_4 (16), for which the heats seem to be less dependent on the purity of the compounds. Our results agree with the published value within 3%. The experimental heats of H^E are fitted to the following equation where x is the mole fraction:

$$[1] \qquad H^E\,(\text{J/mol}) = x_1x_2(ax_1^2 + bx_1 + c)$$

TABLE 1. Parameters for the pure compounds

Compounds	$d_{25°C}$	α (10^3 K^{-1})	γ (J cm^{-3} K^{-1})	P^* (J cm^{-3})	V^* (cm^3 mol^{-1})	s (Å^{-1})
NEt_3	0.7234	1.290	0.906	459.2	107.31	0.94
NPr_3	0.7523	1.064	0.865	409.6	151.06	0.90
$NBut_3$	0.7746	0.970	0.963	442.3	192.76	0.88
$NDec_3$	0.8151	0.808	1.072	465.3	445.10	0.835
$NLaur_3$	0.8211	0.787	1.104	475.5	528.7	0.830
$SnPr_4$	1.1013	0.890	1.071	478.9	215.79	0.84
n-C_5	0.6213	1.610	0.735	406	85.34	0.927
n-C_6	0.6548	1.385	0.814	423	99.58	1.04
n-C_8	0.6985	1.159	0.888	433	127.83	0.991
n-C_{10}	0.7260	1.05	0.930	439	155.60	0.959
n-C_{12}	0.7450	0.98	0.987	455	183.72	0.935
n-C_{14}	0.7592	0.94	1.007	458	198.39	0.917
n-C_{16}	0.7699	0.901	1.033	463	226.44	0.900
br-C_8	0.688	1.19	0.751	370	114.22	0.808
br-C_{12}	0.7414	0.969	0.855	393	170.34	0.820
br-C_{16}	0.7819	0.857	0.912	396.6	237.84	0.766

The curves are obtained from five to ten experimental points. In most cases, the difference between the experimental points and the calculated curve is less than 1%, but it could reach 5% for a few points with volatile components.

Chemicals

The alkanes and the lower amines were obtained from the same companies as in previous work (13).

Free Volume Theory

Parameters for the Pure Components

Densities, expansion coefficients, and thermal pressure coefficients have been found in the literature (17) for the alkanes and measured for the amines (13). Their values are listed in Table 1 together with the reduction parameters for the pressure P^*, for the volume V^* obtained from the experimental quantities, and from an equation of state for the liquid (3, 4). V^* can be construed as the core volume or the molar volume at 0 K.

Surface-to-volume Parameters

Models similar to those in general use for the alkanes (18) have been applied and are detailed in ref. 13 which also reports measurements on the pure components.

Calculation of the Free Volume Term

The free volume term depends only on the difference between the reduced volume of the pure components. We have chosen to apply an approximate (3) form of the Prigogine–Flory theory which separates the interactional and free volume contributions. The free volume contribution $H^E_{f.v.}$ is defined as

$$[2]\quad H^E_{f.v.}/(x_1U_1^* + x_2U_2^*) = \tilde{C}_p(\tilde{T}_U)(\psi_1\tilde{T}_1 + \psi_2\tilde{T}_2 - \tilde{T}_U)$$

Here $\tilde{T}_U$ is the average reduced temperature for the solution appropriate to the energy $\tilde{U}$ and is defined by:

$$\tilde{U}(\tilde{T}_U) = \psi_1\tilde{U}(\tilde{T}_1) + \psi_2\tilde{U}(\tilde{T}_2)$$

With the Van der Waals model, $\tilde{U} = -1/\tilde{v}$, so that the volume corresponding to $\tilde{T}_U$ is

$$1/\tilde{v}_U = \psi_1/\tilde{v}_1 + \psi_2/\tilde{v}_2$$

with

$$\psi_1 = x_1U_1^*/(x_1U_1^* + x_2U_2^*)$$

In this model, the reduced volume of the pure components is obtained from their expansion coefficients α and

$$\tilde{v}^{1/3} = (\tfrac{4}{3}\alpha T + 1)/(\alpha T + 1)$$

The reduced temperature is calculated from their reduced volume and

$$\tilde{T} = \tilde{v}^{-1}(1 - \tilde{v}^{-1/3})$$

with

$$\tilde{C}_p(\tilde{T}_U) = (\tfrac{4}{3}\tilde{v}_U^{-1/3} - 1)^{-1}$$

The energy reducing parameter is

$$U^* = P^*V^*$$

$$P^* = \gamma\tilde{v}^2T$$

where γ is the thermal pressure coefficient. Equation [2] does not depend on the surface-to-volume ratio. In the Flory terminology, the interactional contribution, which is the difference between the experimental value of the heat and the free volume contribution, is expressed through the X_{12} parameter. In the present form, X_{12} is obtained by eq. [3]:

$$[3]\quad (H^E_{exp} - H^E_{f.v.})/(x_1U_1^* + x_2U_2^*) = (X_{12}/P_1^*)\theta_2\psi_1 f(\tilde{v})$$

TABLE 2. Heats of mixing and experimental and calculated parameters for trialkylamines (1) with linear and branched alkanes (2) at 25°C

Systems (1)	(2)	H^E_{max} (J mol^{-1})	x_1	a	b	c	H^E_{max}/V^* (J cm^{-3})	$H^E_{f.v.}$ (J mol^{-1})	$X_{12}s_1^{-1}$ (J cm^{-3} Å)
NEt_3	+ n-C_5	60.0	0.615	309.79	−156.13	234.36	0.607	−11.6	2.97
	+ n-C_6	82.5	0.485	47.26	−97.33	366.33	0.798	−1.4	3.09
	+ n-C_8	105.9	0.500	47.10	−62.88	443.53	0.901	−3.4	3.69
	+ n-C_{10}	138.0	0.550	−374.22	647.45	314.44	1.068	−13.2	4.73
	+ n-C_{12}	200.0	0.540	198.53	−34.77	762.49	1.403	−24.1	6.64
	+ n-C_{14}	252.0	0.515	261.83	−176.71	1030.2	1.596	−33.4	8.17
	+ n-C_{16}	315.0	0.500	1306.5	−1330.5	1583.5	1.816	−42.6	9.98
	+ br-C_{12}	62.5	0.475	239.62	−285.58	406.86	0.422	−24.3	2.77
	+ br-C_{16}	57.0	0.540	−566.52	665.49	35.07	0.340	−52.8	3.19
NPr_3	+ n-C_5	−5.0	0.500	23	−21	−15.5	−0.042	−45.5	1.40
	+ n-C_8	38.0	0.425	45	−135	205	0.275	−2.3	1.20
	+ n-C_{12}	118.0	0.450	191	−378	611	0.697	−1.9	3.10
	+ n-C_{16}	238.0	0.375	1656	−2396	1685	1.153	−8.2	6.41
	+ br-C_8	23.5	0.450	13	−80	127	0.172	−3.8	0.89
	+ br-C_{12}	26.0	0.450	88	−165	161	0.153	−2.4	0.78
	+ br-C_{16}	26.0	0.375	253	−364	212	0.126	−12.8	1.07
$NBut_3$	+ n-C_5	−21.0	0.375	301.36	−127.82	−84.51	−0.167	−75.0	1.69
	+ n-C_6	−9.3	0.191	−212.78	301.52	−109.97	−0.79	−30.9	0.86
	+ n-C_8	35.6	0.360	119.94	−248.14	228.25	0.236	−10.4	1.26
	+ n-C_{10}	70.0	0.490	−306.25	268.22	220.83	0.402	−2.2	1.75
	+ n-C_{12}	119.0	0.490	117.70	−164.47	530.13	0.632	−0.03	2.68
	+ n-C_{14}	182.0	0.475	466.41	−639.52	926.91	0.898	−0.39	3.91
	+ n-C_{16}	232.0	0.400	2403.8	−2796.8	1704.1	1.050	−2.1	5.07
	+ br-C_{12}	15.0	0.400	37.17	−79.78	88.29	0.079	−0.00	0.38
	+ br-C_{16}	19.0	0.465	−71.72	41.07	71.94	0.087	−5.4	0.55
$NDec_3$	+ n-C_8	20.0	0.500	−155.4	99.60	73.41	0.069	−48.4	1.40
	+ n-C_{12}	4.0	0.500	12.0	−12.2	21.8	0.012	−17.3	0.35
	+ n-C_{16}	42.0	0.450	154.9	−260.9	257.1	0.126	−6.4	0.68
	+ br-C_8	198.0	0.375	488.63	−1307.1	1272.5	0.799	−57.6	5.54
	+ br-C_{12}	232.0	0.425	407.74	−952.47	1284.6	0.785	−15.3	4.24
	+ br-C_{16}	248.0	0.400	872.57	−1573.7	1523.9	0.773	−2.0	3.83
$NLaur_3$	+ n-C_7	90.0	0.425	−205.4	−30.15	421.9	0.310	−84.6	3.47
	+ n-C_8	86.0	0.450	−381.1	189.3	333.6	0.279	−60.3	2.76
	+ n-C_{12}	18.0	0.475	−4.664	−26.51	82.21	0.051	−23.6	0.64
	+ n-C_{16}	6.0	0.500	−90.6	104.4	−7.22	0.015	−10.1	0.22
	+ br-C_8	318.0	0.375	1092.6	−2133.9	1994.6	1.139	−67.8	8.00
	+ br-C_{12}	378.0	0.400	415.51	−1503.5	2096.2	1.172	−21.2	6.46
	+ br-C_{16}	388.0	0.375	−1613.5	−3021.9	2556.2	1.118	−4.3	5.66
$SnPr_4$	+ n-C_8	15.0	0.500	262.71	−242.27	107.84	0.087	−22.6	1.06
	+ n-C_{16}	266.0	0.420	497.38	100.94	867.22	1.161	−0.05	5.44
	+ br-C_{16}	−84.0	0.490	−204.86	−34.11	−328.38	−0.370	−0.1	−2.00[a]

[a]A negative X_{12} value is rare in non-polar systems. It is due to the absence of disordering and free volume contributions and to the negative heat due mainly to the steric hindrance effect.

$f(\tilde{v}) = (\tilde{v}^{-1} + \tilde{T}\tilde{C}_p)$ and is not very different from 1. ψ_1 and θ_2 ($= x_2V_2^*s_2/(x_1V_1^*s_1 + x_2V_2^*s_2)$) are used rather than the mole fractions, s_1 and s_2 are parameters calculated from a model characteristic of molecular shape. The units of X_{12} are energy per cm^3. The parameter $X_{12}s_1^{-1}$ tabulated in Table 2 for the concentration of the maximum is independent of the choice of 1 or 2 as a second component, i.e., $X_{12}s_1^{-1} = X_{21}s_2^{-1}$. The left side of eq. [3] does not depend on the s's while X_{12} and θ_2 do to some extent. $X_{12}s_1^{-1}$ also relies very little on the s's. For instance, a variation of 10% on s_1 will change $X_{12}s_1^{-1}$ by less than 2%. Because the $X_{12}s_1^{-1}$ values vary largely from one system to another, the discussion and interpretation of the results from these values are not sensitive to the exact choice of the s's.

Results and Discussion

Table 2 shows the experimental and calculated data for all the systems. The first columns give the maximum of the heats, H^E_{max}, the concentration of the maximum, and the three parameters of eq. [1]. The next column lists the experimental heats calculated per cm^3, $H^E_{max}/V^* = H^E_v$ (the core volume of the solution $V^* = x_1V_1^* + x_2V_2^*$ being used rather than the molar volume for the volume at maximum). The last two columns indicate the cal-

culated free volume terms and the parameter $X_{12}s_1^{-1}$ corresponding to H^E_{max}. Figure 1*a* shows H^E_v at the maximum for the three order-destroyer amines NEt_3, NPr_3, $NBut_3$, and Fig. 1*b* for the two ordered amines $NDec_3$ and $NLaur_3$ plotted against the number, *n*, of carbon atoms of the alkane. Comparison of Fig. 1 (H^E_v) with Fig. 2 ($X_{12}s_1^{-1}$) indicates that the trend of the experimental heats and that of the calculated parameter $X_{12}s_1^{-1}$, which corresponds to the heat minus the free volume term, are very similar. It has seemed worthwhile to present the two series of data since conclusions drawn from one or the other only may be misleading. On one hand, H^E_{exp} includes the free volume contribution which may represent a different proportion of H^E_{exp} from one system to another; on the other hand, $H^E_{f.v}$ and consequently X_{12} is calculated to be too large in systems with a large free volume difference (14) (see in Fig. 2 the rise of X_{12} for the long-chain amines from dodecane to octane while the corresponding H^E_{exp} hardly depends on the alkane chain length).

The characteristic features of the results are the

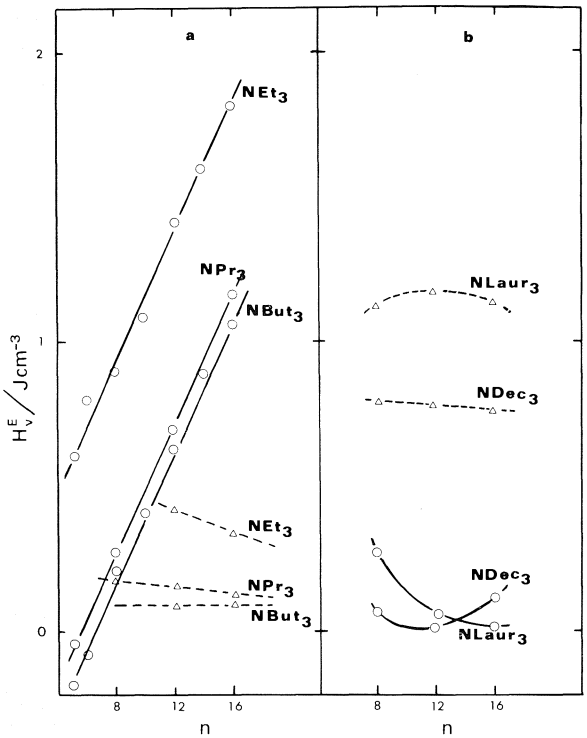

FIG. 1. Heats of mixing at the concentration of the maximum expressed in *J* per cm^3. H^E/V^* (V^* is the core volume of the solution) versus the carbon number of the alkane for: (*a*) order-destroyer amines with ○, the linear alkanes; △, the branched alkanes; (*b*) ordered amines with ○, the linear alkanes; △, the branched alkanes. The lines are drawn through the points corresponding to the same amine.

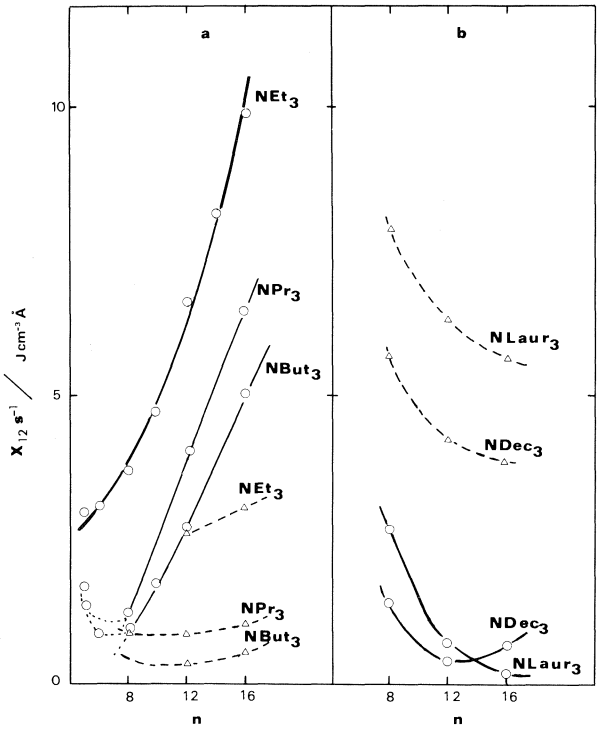

FIG. 2. $X_{12}s_1^{-1}$ in J cm^{-3} Å at the concentration of the maximum versus the carbon atom number of the alkane for: (*a*) the order-destroyer amines with ○, the linear alkanes; △, the branched alkanes; (*b*) the ordered amines with ○, the linear alkanes; △, the branched alkanes.

two following: (*1*) The magnitude of the heats for short- and long-chain amines confirms previous results on the SnR_4 and alkane systems: there is orientational order in long-chain compounds order which is destroyed by mixing with a globular molecule. H^E_{dis} is often the main contribution in these non-polar systems. (*2*) The negative steric hindrance contribution which lowers the experimental heats can be seen on the SnR_4 + alkane systems as well as on the SnR_4 + SnR_4 systems (10). The trialkyl amines (propyl or ethyl derivatives) appear to be also sterically hindered but the effect is much larger on the tin compounds (Fig. 3*b*) than on the NR_3 compounds (Fig. 3*a*).

The analysis of the data and the comparison of different systems raise other interesting points such as the concentration dependance of the heats (or of X_{12}), the value of the chemical term in similar compounds, the validity of the assumption that the different contributions are additive, the extent of the disordering of the ordered component in relation with the size and shape of the order breaker, the effect of the shape of the second component on the steric hindrance contribution. In the following discussion, some of the points come up but the con-

clusions are not as definitive as the two previously quoted. Furthermore, simplifying assumptions concerning these points have been put forward to make the conclusions less complex.

To obtain more information on the chemical contribution, we intend to study mixtures of homomorph compounds such as $NR_3 + HCR_3$ or $MR_4 + CR_4$. On the other hand, analysis of the concentration dependance of the heat (or of X_{12}) is likely to give physical insight and quantitative information about the balance of the different contributions at the extremes of the concentration range. This has not been reported in this paper but will be the subject of further work.

The experimental heats of mixing can be written formally as the sum of the different contributions:

$$[4] \quad H^E_{exp} = H^E_{chem} + H^E_{f.v.} + H^E_{dis} + H^E_{ster.hindr.}$$

In the present systems for which the contacts between unlike molecules is made of CH_2 and CH_3 groups, H^E_{chem} must be small enough. As the free volume contribution may be calculated (eq. [2]), the discussion of the experimental heats will be made in terms of the two other contributions, H^E_{dis} and $H^E_{ster.hindr.}$.

(A) Structure Effects

Order-destroyer Amines: NEt_3, NPr_3, $NBut_3$

The heats with the branched alkanes are small and almost independent of the branched alkane chain length, indicating that the four contributions in eq. [4] are small and that orientational order is absent in branched alkanes. The heats with the normal alkanes increase regularly with the chain length. This is in agreement with the existence of orientational order in the pure *n*-alkanes increasing regularly with chain length and then being destroyed by mixing with the globular NR_3 molecule. Values of the heats of disordering of the two chain alkanes *n*-C_{12} and *n*-C_{16} have been obtained in a manner similar to that described below for the long chain amines and are tabulated in the first two rows of Table 3. The extrapolation of H^E_{dis} found for *n*-C_{16} and *n*-C_{12} to short alkanes indicates as well as depolarized Rayleigh scattering (14) that *n*-C_7 has little orientational order at 25°C.

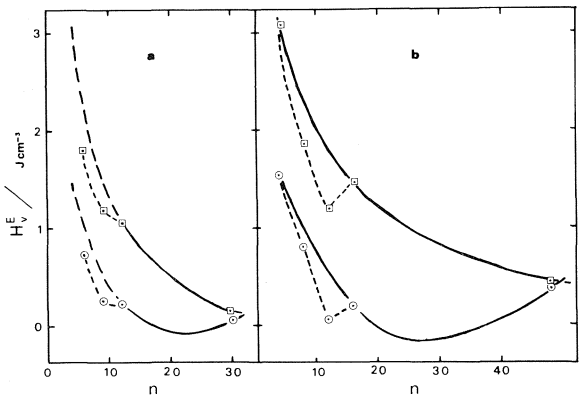

FIG. 3. H^E_v in J per cm^3 versus the atom carbon number of the non-alkane compound with □, *n*-C_{16}; and ○, *n*-C_8. (*a*) NR_3 series, (*b*) SnR_4 series. The lines are drawn through the points corresponding to the same alkane. In Fig. 2*b*, the propyl findings are from this work, the other SnR_4 results are from ref. 5.

Ordered Amines: $NDec_3$, $NLaur_3$

Quantitative evaluation of H^E_{dis}. Equation [4], which lists the contribution to the heats, can be written for two mixtures, one involving a linear alkane and the other a branched alkane of the same carbon atom number and with the same second component

$$[5] \quad H^E_{exp}(\text{linear}) = H^E_{chem} + H^E_{f.v.} + H^E_{dis} + H^E_{ster.hindr.}$$

$$H^E_{exp}(\text{branched}) = H^E_{chem} + H^E_{f.v.} + H^E_{ster.hindr.}$$

H^E_{dis} is assumed to be very small for a branched alkane mixture. Furthermore, if one assumes that the other contributions are either small (H^E_{chem}) and/or very similar for the linear and branched alkanes ($H^E_{f.v.}$ and $H^E_{ster.hindr.}$), one finds

$$[6] \quad H^E_{exp}(\text{linear}) - H^E_{exp}(\text{branched}) = H^E_{dis}$$

In other cases where there was no branched alkane available to give equations similar to [5] and [6], it was assumed that

$$[7] \quad H^E_{exp} = H^E_{dis}$$

which is a good approximation for mixtures of non-polar components whose expansion coefficients are not very different. Table 3 gives the values of H^E_{dis} for different order destroyers and different long-chain compounds obtained by either eq. [6] or [7]. These values are quite independent of any model or theory. Table 3 indicates that H^E_{dis} is relatively constant whatever order breaker is used for making the solution. For instance, H^E_{dis} for *n*-C_{16} obtained from eq. [6] varies between 1.14 and 1.37 J/cm^3 for five different order breakers. In the same way, H^E_{dis} derived from eq. [7] for $SnLaur_4$ varies between 1.22 and 1.28 J/cm^3 for five order breakers. This result justifies the simplified assumptions contained in eqs. [5] to [7]. Comparison of the orientational order of a linear alkane with *n* carbon atoms and that of an alkyl chain with the same length but attached to a large group (NR_2 or SnR_3) can be made. The dodecyl chains in $NLaur_3$ (1.1 J/cm$_3$) have orientational

TABLE 3. Comparison of H^E_{dis} of different ordered compounds obtained with several order breakers

Ordered compound	Order breaker									
	br-C_8	br-C_{12}	br-C_{16}	2,2-DMB	NEt_3	NPr_3	$NBut_3$	$SnEt_4$	$SnPr_4$	$SnBut_4$
n-C_{12}	0.83[a,h]	0.72[a,h]	0.66[a,h]	1.23[b,e]	0.98[b]	0.55[b]	0.56[b]	0.76[b,d,f]	—	1.0[b,f]
n-C_{16}	1.26[a,h]	1.32[a,h]	1.14[a,h]	1.83[b,e]	1.47[b]	1.03[b]	0.97[b]	1.29[b,f]	1.37[b]	1.55[b,f]
$NLaur_3$	1.14[a]	1.17[a]	1.12[a]	—	1.09[a,c]	0.74[a,c]	0.79[a,c]	—	—	—
$NDec_3$	0.80[a]	0.78[a]	0.77[a]	—	—	—	—	—	—	—
$SnLaur_4$	1.22[a,g]	1.25[a,g]	1.22[a,g]	—	—	—	—	1.28[a]	0.97[a]	1.24[a]

[a]According to eq. [7].
[b]According to eqs. [5] and [6].
[c]Reference 21.
[d]$H^E(SnEt_4 + \text{br-}C_{12})$ needed for the difference has been interpolated.
[e]Reference 3*b*.
[f]Reference 5.
[g]Reference 6.
[h]Unpublished work in this lab.

order of the same magnitude as those of $SnLaur_4$ (1.2 J/cm^3). On the other hand, dodecane (H^E_{dis} = 0.8 J/cm^3) appears to have only about two-thirds the orientational order of the attached dodecyl chain (1.15 J/cm^3). This may be due to more mobility of the smaller molecule. Values of H^E_{dis} are higher than the average if the order breaker is a volatile compound (2,2-DMB or NEt_3), or lower if it is a sterically hindered compound ($SnPr_4$). These cases will be discussed later in the context of the $X_{12}s_1^{-1}$ parameter.

(B) Steric Hindrance Effect

Comparison with the SnR_4 Series

Some unexpected exothermic heats have been found for non-polar systems where one of the components of the mixture appears to be sterically hindered. This effect has been called either condensasation effect or steric hindrance effect. The corresponding negative contribution is $H^E_{ster.hindr.}$. An example of such a system is 3,3-diethylpentane + *n*-C_8 measured by Mathot and Prigogine (11) whose negative heat (−80 J/mol) could not be explained by the difference in free volume. In the SnR_4 series, the system $SnBut_4$ + br-C_{16} (−41 J/mol) (5) was also much more negative than expected. In this work, $SnPr_4$ + br-C_{16} (−84 J/mol) is another striking example of negative heats in non-polar systems which cannot be explained by the usual contribution, and particularly not by the difference in free volume. This steric hindrance contribution is likely to occur as well in systems where the total heat has become positive due to other contributions. In such cases, the experimental heat will be less positive than expected by comparison with other systems. As seen in Table 1, the same $SnPr_4$ molecule gives a heat of mixing of 266 J/mol with *n*-hexadecane. This large value is due to the disordering of the alkane chains by $SnPr_4$. However, the magnitude of the heat is not that which could be expected from those obtained with the other members of the series such as 522 ($SnMe_4$), 333 ($SnEt_4$), and 354 ($SnBut_4$). The expected value intermediate between the ethyl and butyl derivative would be about 350 while an interpolated value between the butyl and methyl derivative would be approximately 400 J/mol.

The irregular trend of the heats can be better seen in Fig. 3*b* where the heats H^E_v of *n*-C_{16} and *n*-C_8 with the different members of the series have been plotted against *n* the carbon atom number of the SnR_4 compound. It is concluded then that these systems with a lower H^E_v involving $SnPr_4$ and $SnEt_4$ have a sizeable value for the negative contribution $H^E_{ster.hindr.}$ which is larger than for the systems involving the methyl and butyl derivatives. Similar results have been found (10) in mixtures where $SnLaur_4$ and $SnOct_4$ are the second components instead of *n*-C_{16} and *n*-C_{10}.

The Amines Series

In Fig. 3*a*, H^E_v for the amines have been plotted against *n*, the carbon atom number of the NR_3 compound. Comparison between Fig. 3 *a* and *b* indicates that the steric hindrance contribution occurs for NPr_3 and possibly NEt_3 but is less important than in the SnR_4 series. The lack of data on NMe_3 causes the conclusions to be less sure than in the case of the SnR_4 compounds.

The molecular origin of this steric hindrance contribution is not very clear. It is possible that the low mobility of the sterically hindered compound diminishes that of the second component. An alternative explanation is the better packing in solution than in the pure state of the sterically hindered compounds. However, excess volumes obtained on these systems[2] do not seem more negative than expected as would be the case if the solution was packed better than the pure components. The similarity of shape between the two molecules which appear the most sterically

[2]Bernard Rield and G. Delmas. To be published.

TABLE 4. $X_{12}s_1^{-1}$(disorder) of different ordered compounds obtained with several order breakers

Ordered compound	Order breaker									
	br-C_8	br-C_{12}	br-C_{16}	2,2-DMB	NEt_3	NPr_3	$NBut_3$	$SnEt_4$	$SnPr_4$	$SnBut_4$
n-C_{12}	3.1[a,h]	2.77[a,h]	2.65[a,c,d]	5.50[b,e]	3.87[b]	2.32[b]	2.30[b]	2.11[d,f]	—	4.40[b,f]
n-C_{16}	6.22[a,h]	5.43[a,h]	4.46[a,c]	7.54[b,e]	6.79[b]	5.34[b]	4.52[b]	5.53[b,f]	5.44[b,f]	7.33[b,f]
$NLaur_3$	8.0[a]	6.46[a]	5.66[a]	—	8.36[a,c]	4.63[a,c]	4.29[a,c]	—	—	—
$NDec_3$	5.54[a]	4.24[a]	3.83[a]	—	—	—	—	—	—	—
$SnLaur_4$	9.1[a]	7.1[a]	6.4[a]	—	—	—	—	5.8[a]	4.8[a]	5.7[a]

[a]Assuming a separation of X_{12} in different contributions as done on the H^E.
[b]Assuming that $X_{12}s_1^{-1}$(total) = $X_{12}s_1^{-1}$(disorder).
[c]Reference 21.
[d]H^E needed for the difference has been interpolated.
[e]Reference 3*b*.
[f]Reference 5.
[g]Reference 6.
[h]Unpublished work in this lab.

hindered, 3,3-diethylpentane (or CEt_4) and $SnEt_4$, is worth noting. A semiquantitative evaluation of $H^E_{ster.hindr.}$ for five sterically hindered compounds and second components of different size have been given (21).

Effects of the State of Expansion of the Order Breaker

Comparison of the heat of disordering alone for different order breakers cannot be done by using only H^E_{dis} since, for instance, from 2,2-dimethylbutane to br-C_{16} the free volume contribution in the *n*-C_{16} mixtures diminishes rapidly. Instead, comparison can be made on the $X_{12}s_1^{-1}$ parameter which corresponds to the experimental heats from which the free volume term has been subtracted. $X_{12}s_1^{-1}$ (disorder) can be obtained (Table 4) as H^E_{dis} in two ways: either by subtracting the values obtained for the branched alkane from that calculated for the linear alkane (Fig. 4*a*) or directly from the $X_{12}s_1^{-1}$ tabulated in Table 2 (Fig. 4*b*, *c*). The reasonably small scatter of H^E_{dis} as seen in Table 3 or of $X_{12}s_1^{-1}$ in Table 4 is an indication that eqs. [5] and [6] are good assumptions for most of the order breakers. However, as X_{12} seemed to depend on the state of expansion of the order breaker, it has been plotted in Fig. 4 against the expansion coefficients of the order breaker. It is to be noted that the two methods of calculating $X_{12}s_1^{-1}$ (respectively, Fig. 4 *a*, *b*, and *c*) give the same trend, although there are fewer points on the *b* and *c* curves. The smooth dependence of $X_{12}s_1^{-1}$ (disorder) on α as seen in Fig. 4 may have two origins: (*1*) Smaller molecules, i.e. molecules with a large α, are more efficient order breakers than larger molecules, hence the increase of $X_{12}s_1^{-1}$ or of H^E_{dis} for large α. (*2*) The negative steric hindrance contribution increases for large, more sterically hindered molecules, the effect of which would give the same trend for $X_{12}s_1^{-1}$ with α as in the preceding case. Several points have been added on Fig. 4 using oligomers and polymers as order-destroyers. These points are with the dimer, tetramer, and the polymer of dimethylsiloxane (19) and polyisobutylene (14). Their $X_{12}s_1^{-1}$ (disorder) follows undoubtedly the main curve because the shape of the polymer segment is not very different from that of the branched alkane or of the other non-polymeric order breakers shown on the graph.

The $X_{12}s_1$ obtained with cyclohexane (⌓), $SnMe_4$ (□), and dibromoethane (●) are quite outside the general curve. The assumption needed to go from eq. [5] to eq. [6] is undoubtedly not valid in the case of these three order breakers. Excess heat capacities may give more understanding of these heats. It has been found[2] that cyclohexane and $SnMe_4$ have in common the unusual feature to give in decahydronaphthalene solutions excess heat capacities which change sign with concentration. C_p^E is positive in solutions rich in the globular component and negative in the other region.

Heats of mixing of the trialkyl with the linear and branched alkanes have given an answer to two of the three questions detailed in the Introduction. Firstly, the magnitude of the heats seems to indicate that in alkane solution the trialkylamines behave as non-polar compounds. A compensation of larger negative and positive terms to give these small heats is possible but not very likely. Secondly, the very similar magnitude of H^E_{dis} with $NLaur_3$ and $SnLaur_4$ indicates no extensive contribution of *intra*molecular correlations of orientations. Had it been the case, H^E_{dis} for the tetraalkyl derivative would perhaps have been twice as large as that of trialkyl. On the third point, i.e. the correlation in pure compounds of high P^* and high steric hindrance, it is not possible to give a definite answer since the steric hindrance effect is relatively small in NPr_3 and its P^* value is not very different from that of the other members of the series.

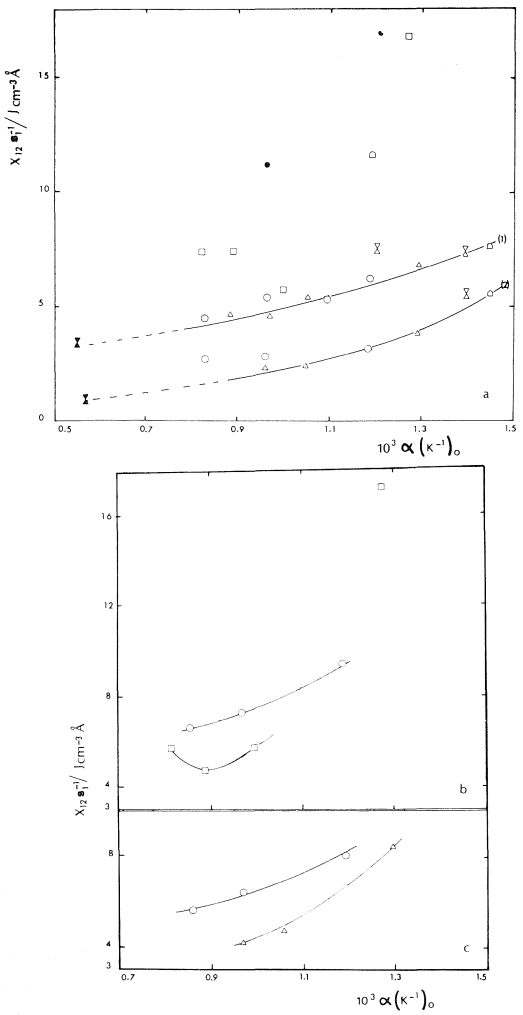

FIG. 4. $X_{12}s_1^{-1}$ (disorder) for long-chain compounds in J cm^{-3} Å versus α, the expansion coefficient of the order breaker. (*a*) Ordered compounds *n*-C_{16} (curve *1*) and *n*-C_{12} (curve *2*); (*b*) ordered compound, $SnLaur_4$; (*c*) ordered compound, $NLaur_3$. Symbols for the order breaker molecule: ⌓, 2,2-DMB; ○, br-C_n; △, NR_3; □, SnR_4; ⧖, dimer, tetramer, polymer of dimethylsiloxane (19); ⧗, polyisobutylene (14). The points outside curve (*1*) in Fig. 4*a* and *b* correspond to the solution in *n*-C_{16} compounds for which eq. [6] should not apply: □, $SnMe_4$; ⌓, cyclohexane ref. 3*b*; and ●, dibromoethane (20).

Acknowledgements

Collaboration between the Université de Lyon and the Université du Québec was supported by the France–Québec exchanges. Financial support was also received from the National Research Council of Canada and the Québec Ministère de l'Education.

1. (*a*) J. HILDEBRAND and R. SCOTT. The solubility of nonelectrolytes. Dover. 1964. Chapt. VII; (*b*) H. TOMPA. Polymer solutions. Butterworth. 1956; (*c*) E. GUGGENHEIM. Mixtures. Oxford University Press. 1953; (*d*) M. L. HUGGINS. J. Phys. Chem. **74**, 371 (1970).
2. I. PRIGOGINE. The molecular theory of solutions. North-Holland, Amsterdam. 1957.
3. (*a*) D. PATTERSON and G. DELMAS. Discuss. Faraday Soc. **49**, 98 (1970); (*b*) V. T. LAM, P. PICKER, D. PATTERSON, and P. TANCRÈDE. J. Chem. Soc. Faraday II, **70**, 1465 (1974).
4. P. J. FLORY, R. A. ORWOLL, and A. VRIJ. J. Am. Chem. Soc. **86**, 3507 (1964); **86**, 3515 (1964).
5. G. DELMAS and S. TURRELL. J. Chem. Soc. Faraday I, **70**, 572 (1974).
6. G. DELMAS and NG.T. THANH. J. Chem. Soc. Faraday I, **71**, 1172 (1975).
7. M. BARBE and D. PATTERSON. J. Phys. Chem. **80**, 2435 (1976); **82**, 30 (1978).
8. P. TANCRÈDE, P. BOTHOREL, and D. PATTERSON. J. Chem. Soc. Faraday II, **73**, 29 (1977).
9. P. TANCRÈDE, P. BOTHOREL, P. DE SAINT-ROMAIN, and D. PATTERSON. J. Chem. Soc. Faraday II, **73**, 15 (1977).
10. G. DELMAS and NG.T. THANH. J. Phys. Chem. **81**, 1730 (1977).
11. (*a*) V. MATHOT. Bull. Soc. Chim. Belg. **59**, 111 (1950); (*b*) I. PRIGOGINE and V. MATHOT. J. Chem. Phys. **18**, 765 (1950).
12. (*a*) P. BOTHOREL. J. Colloid Sci. **27**, 529 (1968); (*b*) P. BOTHOREL, C. CLÉMENT, and P. MARAVAL. C.R. Acad. Sci. **264**, 568 (1967); (*c*) P. BOTHOREL and G. FOURCHE. J. Chem. Soc. Faraday II, **69**, 411 (1973); (*d*) P. BOTHOREL, C. SUCH, and C. CLÉMENT. J. Chim. Phys. **70**, 516 (1972); (*e*) H. QUINONES and P. BOTHOREL. C. R. Acad. Sci. **277**, 133 (1973).
13. R. PHILIPPE, G. DELMAS, and M. COUCHON. Can. J. Chem. **56**, 370 (1978).
14. P. TANCRÈDE and G. DELMAS. Eur. Polym. J. **9**, 199 (1973).
15. G. C. BENSON. Int. Data Ser. Selected Data on Mixtures. Ser. A, **1**, 19 (1974).
16. K. N. MARSH. Int. Data Ser. Selected Data on Mixtures. Ser. A, **1**, 3 (1973).
17. (*a*) R. R. DREISBACH. Physical properties of chemical compounds. Adv. Chem. Ser. Am. Chem. Soc. Washington, DC. 1959; (*b*) Selected values of physical and thermodynamic properties of hydrocarbons and related compounds. API Research Project 44, Carnegie Press, Pittsburgh, PA. 1953.
18. R. A. ORWOLL and P. J. FLORY. J. Am. Chem. Soc. **89**, 6814 (1967).
19. P. TANCRÈDE. Ph.D. Thesis, McGill University, Montreal. 1976.
20. G. DELMAS and P. PURVES. J. Chem. Soc. Faraday II, **73**, Part 1, 1828 (1977); Part 2, 1838 (1977).
21. R. PHILIPPE, G. DELMAS, and PH.NG HONG. Can. J. Chem. **56**, 2856 (1978).

cis- and *trans*-Platinum compounds of substituted pyrimidines and their products from thiourea in Kurnakov's reaction

PI-CHANG KONG AND F. D. ROCHON

Département de chimie, Université du Québec à Montréal, C.P. 8888, Montréal (Qué.), Canada H3C 3P8

Received May 24, 1978

PI-CHANG KONG and F. D. ROCHON. Can. J. Chem. **57**, 526 (1979).

cis- and *trans*-$[Pt(pm)_2X_2]$ (where pm = 2-aminopyrimidine, 4-phenylpyrimidine, 4-methylpyrimidine and X = Cl, Br) were prepared and characterized. The *cis* compounds were isolated from the reaction of K_2PtCl_4 and pm in water, while *trans*-$[Pt(pm)_2X_2]$ was obtained by isomerization of *cis*-$[Pt(pm)_2X_2]$ in dimethylsulfoxide. The *cis*- and *trans*-isomers react with thiourea (tu) to give different products (Kurnakov's test).

$$cis\text{-}[Pt(pm)_2X_2] \xrightarrow{tu} [Pt(tu)_4]X_2$$

$$trans\text{-}[Pt(pm)_2X_2] \xrightarrow{tu} trans\text{-}[Pt(pm)_2(tu)_2]X_2$$

The complexes *trans*-$[Pt(pm)_2(tu)_2]X_2$ were isolated and characterized.

PI-CHANG KONG et F. D. ROCHON. Can. J. Chem. **57**, 526 (1979).

Les complexes *cis*- et *trans*-$[Pt(pm)_2X_2]$, où pm = amino-2 pyrimidine, phenyl-4 pyrimidine, méthyl-4 pyrimidine et X = Cl, Br, ont été préparés et caractérisés. Les composés *cis* ont été isolés de la réaction de K_2PtCl_4 avec pm dans l'eau, tandis que les composés *trans* ont été obtenus par l'isomérisation de *cis*-$[Pt(pm)_2Cl_2]$ dans le diméthylsulphoxyde. Les isomères *cis* et *trans* réagissent avec thiourée (tu) pour donner des produits différents (test de Kurnakov).

$$cis\text{-}[Pt(pm)_2X_2] \xrightarrow{tu} [Pt(tu)_4]X_2$$

$$trans\text{-}[Pt(pm)_2X_2] \xrightarrow{tu} trans\text{-}[Pt(pm)_2(tu)_2]X_2$$

Les complexes *trans*-$[Pt(pm)_2(tu)_2]X_2$ ont été isolés et caractérisés.

Introduction

The discovery that *cis*-$[Pt(NH_3)_2Cl_2]$ is an effective anti-tumor drug[1] has led a large research effort to synthesize complexes of the type *cis*-$[Pt(L)_2Cl_2]$ which would be active against a broad spectrum of tumor systems. Since *trans*-$[Pt(L)_2Cl_2]$ has no anti-tumor activity and *cis*-$[Pt(L)_2Cl_2]$ may isomerize in certain solvents to *trans*-isomers, the configuration assignments of the structures and the choice of solvents used for dissolving drugs are important. Recently, Stetsenko *et al.* (2) prepared two compounds from the reaction of K_2PtCl_4 with 2-aminopyrimidine and 2-amino-4-phenylpyrimidine in aqueous solution. The compounds have an experimental formula $[Pt(pm)_2Cl_2]$ (where pm = pyrimidine derivative). The compounds were assigned to have the *trans* configuration (2). This assignment suggests that the chemistry of pyrimidine with K_2PtCl_4 is not analogous to that of amines and pyridine which give the *cis*-isomers in the same conditions. However, the evidence used to assign the *trans* configuration to the pyrimidine complexes is not very conclusive. A more complete study of pyrimidine complexes was made in our laboratory in order to obtain more evidence for the assignment of the configuration. We have prepared the *cis*- and *trans*-isomers of $[Pt(pm)_2Cl_2]$ where pm = 2-aminopyrimidine (2AP), 4-phenylpyrimidine (4PhP), 4-methylpyrimidine (4MeP), and their bromo-analogs and we have found that the *cis*-isomer isomerizes to the *trans*-isomer in dimethylsulfoxide. The results of Kurnakov's test (3) on the isomers indicate that the previous assignment of the configuration was wrong.

[1]The most recent reports of the clinical status of the drug appear in a two-part issue of ref. 1.

Experimental

Microanalyses were performed by Chemalytics Inc., Tempe, AZ, U.S.A. Infrared spectra were measured as Nujol or hexachlorobutadiene mulls or KBr pellets on a Perkin-Elmer 621 grating spectrometer. Melting points were measured on a Fisher-Johns apparatus and are uncorrected.

The platinum salt was purchased from Johnson Matthey and Mallory and was recrystallised from water. 4-Phenylpyrimidine and 4-methylpyrimidine were obtained from Aldrich and used without further purification. 2-Aminopyrimidine (practical grade) from Eastman was purified twice from water by filtering its aqueous solution through charcoal.

0008-4042/79/050526-04$01.00/0

After recrystallization, the product was obtained as white crystals, mp 125°C (126°C (12)).

Solution of K_2PtBr_4

K_2PtCl_4 (0.83 g) and NaBr (0.5 g) were dissolved in 10 mL of water at room temperature. After 24 h the solution was ready to use.

cis-[*Pt(2AP)$_2$X$_2$*] (*X = Cl, Br*)

To an aqueous solution of K_2PtX_4 (0.83 g of K_2PtCl_4 in 10 mL of water or 10 mL solution of K_2PtBr_4) an aqueous solution of 2AP (0.6 g in 5 mL of water) was added. The resultant solution was left at room temperature for 5 h (X = Br, 3 h). The yellow precipitate was filtered off, washed with water, alcohol, and ether, and dried at 80°C under vacuum overnight. Yield 80% (65% X = Br).

cis-[*Pt(4PhP)$_2$Cl$_2$*]

4PhP (0.65 g) dissolved in 15 mL of alcohol was added to 0.415 g of K_2PtCl_4 dissolved in 15 mL of water. A yellow precipitate appeared after stirring the mixture at room temperature. After 2 h, the yellow precipitate was filtered off, washed with water and alcohol, and dried in a desiccator. When dried the product was dissolved in 5 mL dimethylformamide and filtered. Anhydrous ether (20 mL) was then added to the filtrate and a precipitate appeared immediately. The yellow precipitate was filtered, washed with ether, and dried at 100°C under vacuum overnight. Yield 50%.

cis-[*Pt(4PhP)$_2$Br$_2$*]

4PhP (1 g) dissolved in 15 mL of alcohol was added to 10 mL solution of K_2PtBr_4 at room temperature with stirring. Three hours later, the precipitate was filtered off, washed with water, alcohol, and ether, and dried at 80°C under vacuum overnight. Yield 60%.

cis-[*Pt(4MeP)$_2$Cl$_2$*]

4MeP (0.4 g) was added to a solution of 0.415 g of K_2PtCl_4 dissolved in 10 mL of H_2O at room temperature with stirring. One hour later, the precipitate was filtered off, washed with water, and dried at 80°C overnight. Yield 55%.

trans-[*Pt(pm)$_2$X$_2$*]

The *cis*-compound was dissolved in a minimum amount of dimethylsulfoxide (DMSO). The DMSO solution was heated at 65°C with stirring and 2 h later, the solution became cloudy. Three days later, the solution was cooled to room temperature. The precipitate was filtered off and washed with DMSO, alcohol, and ether. It was dried at 80°C under vacuum overnight. Yield 75%.

trans-[*Pt(pm)$_2$(tu)$_2$*]*Cl$_2$*

trans-[Pt(pm)$_2$Cl$_2$] (0.5 mmol) was suspended in 10 mL of dimethylformamide (DMF) with 0.38 g of thiourea (tu) and stirred overnight (pm = 2AP) or 10 h (pm = 4PhP). The yellow suspension became white. The compound was isolated by filtration and washed with DMF and ether. The compound was then dissolved in water and filtered in order to remove the small amount of starting material (water at room temperature for 2AP, at 80°C for 4PhP). The aqueous filtrate was evaporated to dryness with a rotatory evaporator and a water pump. The compound was dried at 80°C under vacuum overnight. Yield 65%.

trans-[*Pt(4PhP)$_2$(tu)$_2$*]*Br$_2$*

trans-[Pt(4PhP)$_2$Br$_2$] (0.5 mmol) was suspended in 10 mL of DMF with 0.38 g of thiourea and stirred overnight. The unreacted starting material was filtered off and a yellow-greenish filtrate was obtained. Ether (10 mL) was added to the filtrate and a white precipitate was obtained. The precipitate was isolated by filtration, washed with 20 mL of DMF–ether 1:1 mixture, in 4 portions. It was then washed with ether and dried at 80°C under vacuum overnight. Yield 70%.

Results and Discussion

K_2PtCl_4 mixed with nitrogen bases (L) such as pyridine and amine in aqueous solutions gives a yellow precipitate, *cis*-[Pt(L)$_2$Cl$_2$]. In similar conditions, pyrimidine with K_2PtCl_4 also gives a yellow precipitate with experimental formula [Pt(L)$_2$Cl$_2$]. By analogy to the chemistry of pyridine and amine, the pyrimidine complex should also have the *cis*-configuration. However, compounds of 2-aminopyrimidine and 2-amino-4-phenylpyrimidine prepared in aqueous solution were reported as having the *trans*-configuration (2). The configuration assignment was based on the following: (*a*) one Pt—Cl stretching band was observed in the infrared spectrum, (*b*) on heating the compounds with pyridine (py), pyrimidine was displaced and *trans*-[Pt(py)$_2$Cl$_2$] was obtained. Actually, these two evidences are not very conclusive: (*a*) we have repeated the reaction and noted that if the compound [Pt(2AP)$_2$Cl$_2$] is well dried, the Pt—Cl stretching is not a single band, but a doublet, (*b*) a final product, *trans*-[Pt(py)$_2$Cl$_2$], from the reaction between [Pt(pm)$_2$Cl$_2$] and pyridine was obtained, but it should not be used to justify the structure of the starting material, because isomerization can occur during the process of the reaction. For example, *cis*-[Pt(DMSO)$_2$Cl$_2$] (4) and *cis*-[M(py)$_2$Cl$_2$] (M = Pt (5) and Pd (6)) react with pyridine to give *trans*-[Pt(py)$_2$Cl$_2$]. To settle this controversy, both *cis*- and *trans*-isomers of [Pt(pm)$_2$Cl$_2$] are required. Usually, *trans*-isomers of pyridine and amine complexes are prepared as follows (7).

$$[Pt(L)_4]Cl_2 \xrightarrow[H_2O]{HCl} trans\text{-}[Pt(L)_2Cl_2]$$

[Pt(L)$_4$]Cl$_2$ can be obtained by refluxing *cis*- or *trans*-[Pt(L)$_2$Cl$_2$] with an excess of L. We tried this reaction to prepare [Pt(L)$_4$]Cl$_2$ from [Pt(L)$_2$Cl$_2$] (L = 2AP, 4PhP) without success.

A new method was found to prepare the *trans*-isomer. The compounds of pyrimidines, [Pt(pm)$_2$Cl$_2$], isolated from an aqueous solution according to ref. 2, were dissolved in DMSO at 65°C for 3 days. A lighter yellow precipitate was obtained. The results from the element analysis indicated that the experimental formula is the same as the starting material, [Pt(pm)$_2$Cl$_2$]. But there is a remarkable difference in their properties, especially their solubility in DMSO. The lighter yellow precipitate is, at least, 5 times less

TABLE 1. Element analysis, decomposing point of pyrimidine complexes*

Compounds	C	H	N	X	S	Melting point (°C)
cis-$[Pt(2AP)_2Cl_2]$	21.05	2.19	18.42	15.57		> 300
	20.37	2.10	17.83	15.73		
trans-$[Pt(2AP)_2Cl_2]$	21.05	2.19	18.42	15.57		> 300
	20.44	2.16	19.04	16.14		
	21.37	2.19				
cis-$[Pt(2AP)_2Br_2]$	17.61	1.83	15.41	29.36		> 300
	17.91	1.96	14.63	29.33		
trans-$[Pt(2AP)_2Br_2]$	17.61	1.83	15.41	29.36		> 300
	16.89	1.75	15.68	29.12		
cis-$[Pt(4PhP)_2Cl_2]$	41.52	2.77	9.69	12.28		270
	41.81	3.01	9.87	12.49		
trans-$[Pt(4PhP)_2Cl_2]$	41.52	2.77	9.69	12.28		280
	41.80	2.86	10.08	11.81		
cis-$[Pt(4PhP)_2Br_2]$	35.96	2.40	8.40	23.99		280
	35.90	2.66	9.10	23.51		
trans-$[Pt(4PhP)_2Br_2]$	35.96	2.40	8.40	23.99		290
	36.13	2.49	8.64	23.22		
cis-$[Pt(4MeP)_2Cl_2]$	26.43	2.64	12.33	15.64		> 300
	26.13	2.65	12.03	15.45		
trans-$[Pt(4MeP)_2Cl_2]$	26.43	2.64	12.33	15.64		238
	26.26	2.68	11.83	14.65		
trans-$[Pt(2AP)_2(tu)_2]Cl_2$	19.74	2.96	23.02	11.68	10.53	212
	19.75	3.23	22.71	11.56	11.45	
trans-$[Pt(4PhP)_2(tu)_2]Cl_2$	36.07	3.55	15.30	9.70	8.74	235
	35.70	3.37	14.98	9.24	9.36	
trans-$[Pt(4PhP)_2(tu)_2]Br_2$	32.23	2.93	13.68	19.54	7.81	225
	31.32	3.01	13.22	17.95	8.54	

*Calculated value in first row.

soluble than the starting material. The infrared spectra of the 4-methylpyrimidine complexes are shown in Fig. 1. The spectrum of the isomer from DMSO (*a*) showed one single sharp band at 345 cm^{-1} while the spectrum of the isomer from aqueous solution (*b*) showed two bands at 341 and 330 cm^{-1}. These bands are assigned as Pt—Cl stretching vibrations. The compounds of other pyrimidine derivatives showed the same Pt—Cl stretching as those of 4MeP. There are two single bands from 4MeP ligands at 390 and 510 cm^{-1} in Fig. 1*a*, while these two bands become doublets at 378, 390 and 500, 515 cm^{-1}, respectively, in Fig. 1*b*. Therefore the infrared spectra suggest that the isomer isolated from the DMSO solution is the *trans*-isomer while the starting material (isolated from K_2PtCl_4 and pm in aqueous solution) has the *cis* configuration. This method has been used to prepare pyridine and picoline compounds. *cis*-$[Pt(py)_2Cl_2]$ isolated from an aqueous solution was dissolved in DMSO and left at room temperature for 5 days. Water was then added to the DMSO solution and the precipitate formed proved to be *trans*-$[Pt(py)_2Cl_2]$ by infrared spectroscopy (8). From the infrared data and the isomerization of pyridine compounds in DMSO, the compounds with pyrimidine derivatives isolated from DMSO should be the *trans*-isomers.

Very fortunately, the two isomers respond to Kurnakov's test in dimethylformamide, i.e., *cis*- and *trans*-$[Pt(pm)_2X_2]$ react with thiourea (tu) to give different products (3).

$$[1] \qquad cis\text{-}[Pt(pm)_2X_2] \xrightarrow[DMF]{tu} [Pt(tu)_4]X_2$$

$$[2] \qquad trans\text{-}[Pt(pm)_2X_2] \xrightarrow[DMF]{tu} [Pt(pm)_2(tu)_2]X_2$$

The rate of the above reactions are quite different. Within 1 h, reaction [1] is complete and a clear yellow solution is obtained. However, 10 h is not enough for reaction [2].

The products from the above reactions can be distinguished by their elemental analyses and their infrared spectra. The configuration of the isomers can now be definitely assigned. The compound from the aqueous solution is the *cis*-isomer and the compound from DMSO is the *trans*-isomer.

Kurnakov's test was also tried in water and acetone at room temperature. Both reactions [1] and [2] were quite slow and only a small amount of product was obtained from the reactions. When the compounds were refluxed in water the test failed, both isomers gave $[Pt(tu)_4]Cl_2$. The test is reliable if the appropriate conditions and solvent are found and the compounds should be tested preferably in

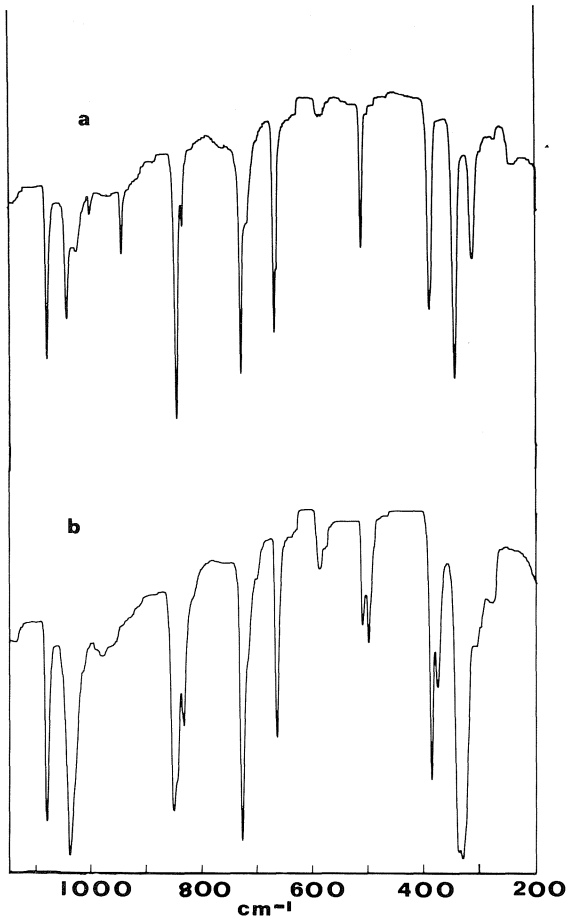

FIG. 1. Infrared spectra of (*a*) *cis*-[Pt(4MeP)$_2$Cl$_2$], (*b*) *trans*-[Pt(4MeP)$_2$Cl$_2$] in Nujol mull.

pairs. If the *trans*-isomer is refluxed in water without a parallel testing on the *cis*-isomer, it will be erroneously assigned as the *cis*-isomer based on reaction [1].

Because of the sterie hindrance of the phenyl group and the methyl group, the coordinating sites of 4PhP and 4MeP should be far from these groups, i.e. N_1. The binding site of 2-aminopyrimidine is N_1 (or N_3) rather than the amino group. Cytidine and cytosine derivatives coordinate to platinum through N_3 (9–11). The ν_{N-H} stretching of 2-aminopyrimidine is shifted to higher region upon complexation indicating that the amino group is not involved in the bonding.

In Fig. 1*a*, there is a band at 318 cm^{-1} which becomes a shoulder in *b* because of the broad Pt—Cl stretching very close to it. Free pyrimidine ligands do not have bands around this position. It is assigned as Pt—N stretching with comparison to the compounds of 4-methylpyridine having a Pt—N stretching band at 317 cm^{-1} (8).

In a previous work (5), we have found a method to prepare *trans*-[Pt(py)$_2$Cl$_2$] (py = pyridine and picoline) from DMF solution of *cis*-[Pt(py)$_2$Cl$_2$] and py. Pyrimidine compounds can also be made by this method. Crystals of *trans*-pyrimidine compounds were obtained from a DMF solution of *cis*-[Pt(pm)$_2$X$_2$] and pm at room temperature after 1 to 2 weeks.

Acknowledgments

The authors are grateful to the National Research Council of Canada and to the Cancer Research Society Inc. for financial support and to Johnson Matthey & Co. Limited for the loan of potassium chloroplatinate.

1. J. Clin. Hematol. Oncol. **7** (1977).
2. A. I. STETSENKO, E. S. DMITRIYEVA, and K. I. YAKOULEV. J. Clin. Hematol. Oncol. **7**, 522 (1977).
3. M. M. JONES. Elementary coordination chemistry. Prentice Hall, Inc., Englewood Cliffs, NJ. 1964. Chapt. 3. p. 58.
4. P. C. KONG, D. IYAMUREMYE, and F. D. ROCHON. Can. J. Chem. **54**, 3224 (1976).
5. P. C. KONG and F. D. ROCHON. Can. J. Chem. **56**, 441 (1978).
6. L. CATTALINI and M. MARTELLI. J. Am. Chem. Soc. **91**, 312 (1969) and references therein.
7. (*a*) G. B. KAUFFMAN and D. O. COWAN. Inorg. Synth. **7**, 239 (1963); (*b*) G. B. KAUFFMAN. Inorg. Chem. **7**, 249 (1963).
8. M. PFEFFER, P. BRAUNSTEIN, and J. DEHAND. Spectrochim. Acta, **30**, 331 (1974); **30**, 341 (1974).
9. P. C. KONG and T. THEOPHANIDES. Inorg. Chem. **13**, 1981 (1974).
10. R. MELANSON and F. D. ROCHON. Inorg. Chem. **17**, 679 (1978).
11. C. J. L. LOCK, R. A. SPERANZINI, and J. POWELL. Can. J. Chem. **54**, 53 (1976).
12. A. R. KATRITZKY, M. KINGSLAND, and O. S. TEE. J. Chem. Soc. B, 1484 (1968).

On the use of dilution calorimetry in the study of hydrogen-bonding self-association reactions: benzoic acid in benzene

TRICHUR KRISHNAN, WAYNE CARLTON DUER, AND SAUL GOLDMAN

Guelph–Waterloo Centre for Graduate Work in Chemistry, Guelph Campus, Department of Chemistry, University of Guelph, Guelph, Ont., Canada N1G 2W1

AND

JEAN-LUC FORTIER

Centre d'Application en Calorimétrie et Thermodynamique, Département de chimie, Université de Sherbrooke, Sherbrooke (Qué.), Canada J1K 2R1

Received July 20, 1978

TRICHUR KRISHNAN, WAYNE CARLTON DUER, SAUL GOLDMAN, and JEAN-LUC FORTIER. Can. J. Chem. **57**, 530 (1979).

A calorimetric dilution method was applied to the system benzoic acid in benzene at 25°C. Two different calorimeters, a batch calorimeter (at Guelph) and a flow microcalorimeter (at Sherbrooke), were used in this study. Our results were inconsistent with an ideal monomer–dimer model, which had been used in previous calorimetric studies on this and other similar systems. Our results were consistent with an ideal monomer–dimer–trimer model, for which we obtained: $K_2 = 625 \pm 100$ L/mol, $K_3 \simeq 10^4$ L^2/mol^2 for the dimerization and trimerization constants respectively, and $\Delta H_2^0 = -8.52 \pm 0.50$ kcal/mol, $\Delta H_3^0 = -13.48 \pm 2$ kcal/mol for the molar enthalpies of dimerization and trimerization, respectively.

TRICHUR KRISHNAN, WAYNE CARLTON DUER, SAUL GOLDMAN et JEAN-LUC FORTIER. Can. J. Chem. **57**, 530 (1979).

On a appliqué une méthode de dilution calorimétrique au système acide benzoïque/benzène à 25°C. Deux calorimètres différents — un calorimètre à masse (à Guelph) et un microcalorimètre à écoulement (à Sherbrooke) — ont été utilisés dans cette étude. Nos résultats ne concordent pas avec un modèle idéal monomère–dimère qui avait été utilisé dans des études calorimétriques antérieures sur ce système et d'autres semblables. Nos résultats sont en accord avec un modèle idéal monomère dimère–trimère pour lequel on a obtenu des valeurs respectives de $K_2 = 625 \pm 100$ L/mol, $K_3 = 10^4$ L^2/mol^2 pour les constantes de dimérisation et de trimérisation et des valeurs respectives de $\Delta H_2^0 = -8.52 \pm 0.50$ kcal/mol, $\Delta H_3^0 = -13.48 \pm 2$ kcal/mol pour les enthalpies molaires de dimérisation et de trimérisation.

[Traduit par le journal]

Introduction

Recently, a number of papers have appeared which describe a calorimetric dilution technique that enables one to determine the thermodynamic quantities ΔG^0, ΔH^0 (and ΔS^0) for self-association reactions that result from intermolecular hydrogen bonding (1–5). This technique is attractive because it is applicable to a wide variety of systems (5), and because it gives results rapidly. The method does, however, require the assumption that the heat evolved is due only to the change in the number of ideal molecular aggregates. When applied to carboxylic acids an ideal monomer–dimer model was invariably assumed (2, 3, 5).

Two fairly recent studies, however, cast doubt upon the validity of this model. In one (6) infrared data on the acetic acid – carbon tetrachloride system were investigated by the method of factor analysis. It was found that in all but the most dilute solutions species larger than dimers were present in appreciable concentrations. In a second article (7) it was found that monomers, dimers, and trimers were required to account for osmometric data on benzene solutions of long-chained carboxylic acids.

In view of these articles and the only fair agreement between the calorimetric results and those from others techniques for the benzoic acid in benzene system (5, 8–11), we considered it worthwhile to re-examine the calorimetric results. In the present work we used the results obtained from the heat of dilution values measured in two different laboratories. A batch calorimeter in Guelph and a Picker flow microcalorimeter in Sherbrooke were used.

Experimental

The benzene (Fisher, B-245 reagent grade) was purified and dried as described elsewhere (12), and stored over molecular sieves (Fisher, 4 Å). Traces of absorbed moisture in the benzoic acid (Analar, analytical reagent grade 99.9% assay) were removed by fusing in a platinum crucible at 135 ± 5°C. Two separate analyses on the final product by the sodium carbonate – sodium hydroxide method (13, 14) resulted in assay values of 99.97 and 100.00%.

At the University of Guelph, the heats of dilution (ΔH_{dil})

0008-4042/79/050530-08$01.00/0

were measured with a batch calorimeter, built by Dr. W. C. Duer, which is similar to one described in ref. 15. With this instrument, fragile glass ampoules (capacity of ~5 mL) fitted with capillary side-arms (designed to minimize solvent evaporation) were used for sample introduction. The heat of bulb breaking was found to be negligible. In all the experiments at Guelph the calorimeter vessel (volume of 200 mL) initially contained pure benzene and the ampoules contained a known weight of a benzoic acid – benzene stock solution. Different final concentrations of benzoic acid in benzene were achieved both by using different concentrations for the stock solutions, and by varying the quantity of stock solution in the ampoule.

The heats of dilution measured at the Université de Sherbrooke were obtained with the commercial version (Sodev Inc.) of the Picker flow microcalorimeter. The principle of this calorimeter is described in detail elsewhere (16, 17). The measurements were done at a dilution ratio $C_i/C_f \simeq 2$, where C_i and C_f are, respectively, the initial and final stoichiometric concentrations of benzoic acid in mol/L. Due to the strong concentration dependence of the relative apparent molar enthalpy ϕ_L in the low concentration region (Fig. 1) we measured most of the ΔH_{dil} on the flow system with $C_i \leq 0.1\ M$. The high sensitivity (1×10^{-6} °C) of the flow microcalorimeter allows such measurements with good precision, i.e., 0.5% or better.

The solutions were prepared by weight. Molality–molarity interconversions were made using solution densities, which were measured with a flow densimeter (18). The excess volume of mixing was found to be negligible.

The effect of the water content of the samples on the dilution data was checked and found to be appreciable, as already observed by Flitt and Jaycock and others (1, 19–21). Therefore special care was taken in both laboratories to minimize water contamination. This precaution was especially important in the flow experiments where the low concentration region was probed. The water content of all samples run on the flow system were therefore titrated before and after the dilution using an aquatest Karl Fischer titrimeter (Photovolt, model 702). We kept only the ΔH_{dil} values for samples with less than 25 ppm water, for reasons which are now explained.

A number of preliminary trial experiments were run with the flow calorimeter, in which water was deliberately added either to the solution, or to the solvent, or to both. Two concentrations of benzoic acid were used in these trials: 0.04 *m* and 0.40 *m*. With 450 ppm water in the solution, $\Delta\phi_L$ was found to increase (i.e. become more negative) with respect to the anhydrous situation by about 15%, for both the 0.04 *m* and the 0.40 *m* benzoic acid solutions. When 450 ppm water were present in both the solvent and the solution $\Delta\phi_L$ decreased by about 5% with the 0.04 *m* solution and it decreased by about 15% with the 0.40 *m* solution. In another experiment, where 120 ppm water were added to the 0.04 *m* solution, $\Delta\phi_L$ increased by about 2%. In still another set of preliminary experiments, two solutions of wet benzene containing 450 ppm and 120 ppm water (but no benzoic acid) were diluted with anhydrous benzene. The $\Delta\phi_L$ values observed in these trials were negligible with respect to our experimental uncertainty. These last experiments demonstrate that the effect of water on $\Delta\phi_L$ is due to changes in the extent of hydration of benzoic acid, rather than to the heat of dilution of water in benzene.

These observations made it imperative to reduce the water content of these solutions as far as possible. It was found, in practice, that by taking sufficient precautions it was possible in almost every run to reduce the total water content of our systems to 25 ppm or less. The water content of the solutions did not change significantly (the experimental uncertainty in the water analyses was 10 ppm) in the course of a dilution experiment. We found that when the water content of the solutions was within the range 0 to 25 ppm, the experimental $\Delta\phi_L$'s obtained from one run to the next were well within 0.50% of each other, which is our experimental uncertainty in $\Delta\phi_L$. Consequently we retained only those data obtained with the flow system where the water content was 0 to 25 ppm. The order of magnitude calculation given below provides a theoretical justification for the view that we can neglect the effect of water on our results provided the water content of our solutions is less than 25 ppm.

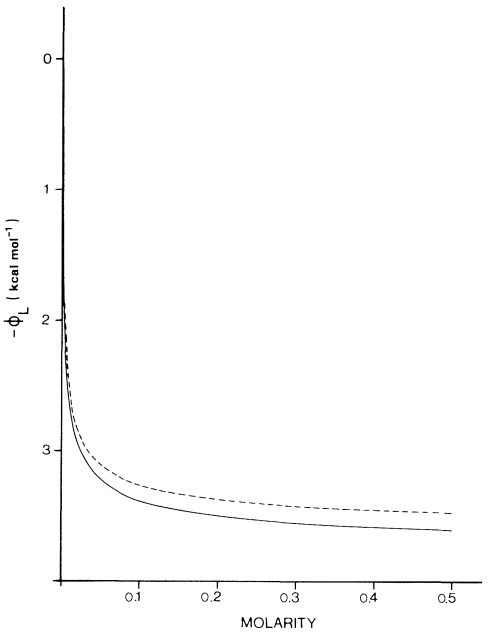

FIG. 1. Relative apparent molar enthalpy of benzoic acid in benzene at 25°C: solid line, this work; dashed line, calculated from K_2 and ΔH_2^0 of Woolley and Zaugg (5).

A previous study (which assumed a monomer–dimer model for the system benzoic acid in benzene) provides the following estimates for the hydration constants of benzoic acid in benzene at 25°C: $K_{11} = 12.4$ L/mol; $K_{12} = 248$ L^2/mol^2, $K_{21} = 582$ L^2/mol^2 where K_{11}, K_{12}, and K_{21} represent the hydration constants for the formation of the monomer-monohydrate, the monomer-dihydrate, and the dimer-monohydrate, respectively (22). In order to obtain an upper bound on the fractions of the benzoic acid species that were hydrated in our experiments with the flow calorimeter, we assume that all of the 25 ppm ($1.21 \times 10^{-3}\ M$) was in the form of free (i.e. nonbonded) water. Thus the maximum fraction of the benzoic acid monomer that can be hydrated in our solutions at 25°C is given by:

$$F = \frac{\text{Concentration of hydrated monomer}}{\text{Total monomer concentration}}$$

$$= \frac{\text{M}\cdot\text{H}_2\text{O} + \text{M}\cdot 2\text{H}_2\text{O}}{\text{M} + \text{M}\cdot\text{H}_2\text{O} + \text{M}\cdot 2\text{H}_2\text{O}}$$

$$= \frac{K_{11}[\text{H}_2\text{O}] + K_{12}[\text{H}_2\text{O}]^2}{1 + K_{11}[\text{H}_2\text{O}] + K_{12}[\text{H}_2\text{O}]^2}$$

TABLE 1. Experimental heat of dilution data at 25.0 ± 0.1°C using the batch solution calorimeter

Run 1			Run 2		
m_i[a] (molal)	m_f[a] × 10^2 (molal)	ΔH_{dil}[b] (cal/mol)	m_i[a] (molal)	m_f[a] × 10^2 (molal)	ΔH_{dil}[b] (cal/mol)
0.5464	0.1090	2195	0.5464	0.5608	1254
0.5464	0.1956	1758	0.7340	0.5844	1247
0.4754	0.2299	1844	0.7340	0.6918	1152
0.4792	0.2422	1768	0.5464	0.7135	1128
0.7340	0.2376	1787	0.5464	1.1306	888.9
0.5464	0.2823	1660	0.5464	1.4820	788.7
0.2407	0.3175	1606	0.7340	1.4283	814.4
0.5924	0.3232	1640	0.7330	1.4675	823.3
0.5464	0.3686	1490	0.5464	1.8947	680.2
0.5960	0.3493	1587	0.7340	1.9465	698.0
0.7340	0.3416	1579	0.7330	2.0196	683.2
0.5464	0.3686	1305	0.5464	2.3265	615.9
0.7340	0.4620	1384	0.7340	2.5158	606.7
0.3704	0.4985	1330	0.5464	2.6228	596.9
0.7325	0.4929	1386	0.7330	2.5152	623.1
			0.7340	3.5688	451.6
			0.7330	3.5614	504.9

[a] m_i, m_f = stoichiometric molality of benzoic acid in benzene in the ampoule, and in the calorimeter (after the ampoule is broken), respectively.
[b] ΔH_{dil} is the heat of dilution.

TABLE 2. Experimental heat of dilution data at 25.0 ± 0.1°C using the Picker flow microcalorimeter

Run 1			Run 2		
C_i[a] (molar)	C_f[a] (molar)	ΔH_{dil}[b] (cal/mol)	C_i[a] (molar)	C_f[a] (molar)	ΔH_{dil}[b] (cal/mol)
0.001627	0.000813	510.5	0.003734	0.001867	493.6
0.004097	0.002043	456.8	0.003734	0.001867	492.8
0.005684	0.002845	449.3	0.004667	0.002335	449.8
0.009890	0.004923	363.3	0.005665	0.002834	435.7
0.01870	0.009312	289.8	0.008911	0.004462	385.5
0.05695	0.02863	187.3	0.02066	0.01036	290.0
0.07216	0.03629	169.8	0.03685	0.01811	235.9
0.08472	0.04258	162.0	0.03685	0.01843	229.3
0.12705	0.06390	133.3	0.10577	0.05288	147.4
0.1880	0.09452	113.4	0.2632	0.1299	107.6
0.2660	0.1337	98.53	0.2632	0.1314	102.0
0.3276	0.1650	91.48	0.4430	0.2218	84.39
0.4778	0.2406	79.87			

[a] C_i and C_f are the initial and final concentrations.
[b] ΔH_{dil} is the heat of dilution.

or

$$F = 0.015$$

Similarly the maximum fraction of dimer that can be hydrated in our experiments is found to be 0.0011.

Thus by keeping the water content of the benzene solutions to 25 ppm or less we keep the extent of hydration very small indeed.

Results and Treatment of the Data

A total of 32 separate heat of dilution experiments were carried out in two runs with the batch calorimeter and 25 with the flow microcalorimeter. All the measurements were done at 25.0 ± 0.1°C. The raw data from both sets of experiments are entered in Tables 1 and 2.

It is conventional to report heat of dilution data in terms of ϕ_L. After several trial calculations, we found that the data obtained with the batch calorimeter did not extend sufficiently into the dilute concentration region (Fig. 1) to make such a reformulation either meaningful or useful. However, the data from the flow calorimeter did extend to low enough concentrations to make this re-formulation worthwhile. Therefore, the data in Table 2 were treated by a large-scale graphical interpolation procedure, similar to one that had been used previously in the Sher-

TABLE 3. Relative apparent molar enthalpy ($-\phi_L$) of benzoic acid in benzene at 25°C from a graphical interpolation procedure

M (molar)	$-\phi_L$ (cal/mol)	M (molar)	$-\phi_L$ (cal/mol)
0.002	1673	0.08	3337
0.004	2161	0.09	3362
0.006	2426	0.10	3382
0.008	2567	0.15	3451
0.01	2663	0.20	3497
0.02	2945	0.25	3525
0.03	3083	0.30	3549
0.04	3166	0.35	3568
0.05	3227	0.40	3583
0.06	3272	0.45	3595
0.07	3308	0.50	3604

brooke laboratory. The smoothed ϕ_L values so obtained are entered in Table 3. While a direct comparison of data in Tables 1 and 2 is not possible (because of the different concentration ranges involved and the difficulty of getting ϕ_L's from the data in Table 1) an indirect comparison (see text below and Table 4) indicated that the data from the two laboratories were consistent.

The principal source of error in the evaluation of ϕ_L stems from the required extrapolation to infinite dilution. While a large number of experiments on the flow system were run with $C_i < 0.1\ M$ in an attempt to minimize this uncertainty, a substantial residual error in the extrapolation remained. We estimate that the extrapolation led to an uncertainty of about ± 250 cal/mol in the absolute values of ϕ_L. The uncertainty in the values of $\Delta\phi_L$ was of course much less. We estimate that for $8 \times 10^{-4}\ M \leq C \leq 0.5\ M$, the values of $\Delta\phi_L$ are correct to $\pm 0.5\%$ or better.

Monomer–Dimer Model

Several methods can be used to obtain values for K_2 (the dimerization constant) and ΔH_2^0 (the enthalpy of dimerization) from heat of dilution data (1–3).

In this section we describe two methods that were applied to our data. For the dimerization equilibrium

$$2M \rightleftarrows D$$

wherein the monomers and dimers are each assumed to be ideal (see ref. 1 and below):

$$[1] \qquad K_2 = [D]/[M]^2$$

$$[2] \qquad [C] = [M] + 2[D]$$

where [C] is the stoichiometric concentration of the solute and [M] and [D] are the monomer and dimer concentrations, respectively (mol/L). Combining eqs. [1] and [2], one gets

$$[3] \qquad [D] = \{-1 + (1 + 8K_2[C])^{1/2}\}^2/16K_2$$

Method 1

ϕ_L can be related to the enthalpy of dimerization by the following equation

$$[4] \qquad [C]\phi_L = \Delta H_2^0[D]$$

Using eqs. [1] and [2], eq. [4] can be rearranged to give equation:

$$[5] \qquad \phi_L = \frac{\Delta H_2^0}{2} - \left(\frac{-\Delta H_2^0(-\phi_L)}{4K_2[C]}\right)^{1/2}$$

Thus a graph of ϕ_L vs. $(-\phi_L/[C])^{1/2}$ leads to the evaluation of ΔH_2^0 and K_2 from the intercept and the slope of the best linear fit. In fact, the plot of our ϕ_L results according to this equation shows a slight curve with values for $C < 0.1\ M$ as can be seen from Fig. 2. We will return to this point later. A linear least-squares fit gave $K_2 = 400$ L/mol and $\Delta H_2^0 = -7.6$ kcal/mol.

Method 2

It was found by experience that the values of ΔH_2^0 and K_2 that were obtained by method 1 were strongly dependent on the absolute values of ϕ_L which were used with eq. [5]. As explained previously, the absolute values of ϕ_L were subject to considerable

TABLE 4. K_2 and ΔH_2^0 for benzoic acid in benzene at 25°C calculated on the basis of an ideal monomer–dimer model

Data source	Method of data treatment[a]	K_2 (L/mol)	$-\Delta H_2^0$ (kcal/mol dimer)
This work, Table 1	Method 2	458	7.7
This work, Table 2	Method 2	500	8.4
This work, Table 2	Method 1	400	7.6
Reference 5	Method 1	400 ± 100[b]	7.3 ± 0.5[b]

[a]'Method 1' and 'method 2' are described in text.
[b]These standard deviations were obtained from Professor Earl Woolley in a private communication.

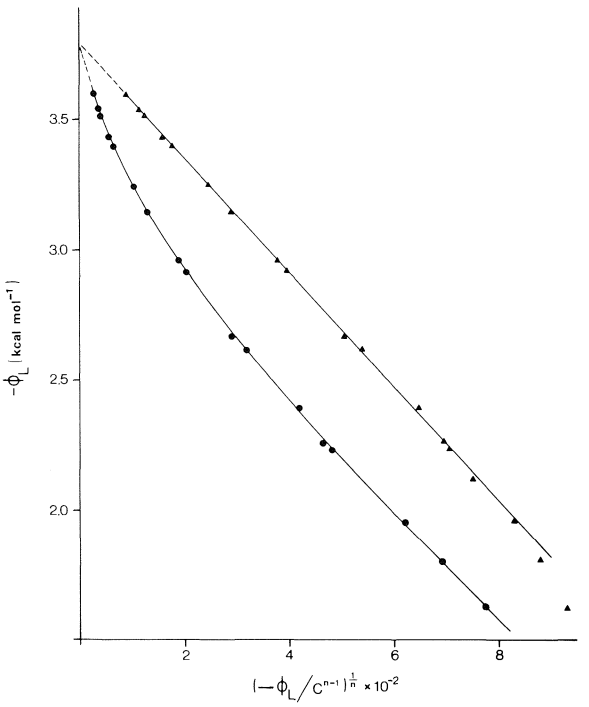

FIG. 2. Relative apparent molal enthalpy of benzoic acid in benzene at 25°C displayed as suggested by eq. [5] (monomer–dimer model, $n = 2$) and eq. [7] (monomer–trimer model, $n = 3$).

uncertainty due to the uncertainty in the extrapolation to infinite dilution. Therefore, it was desirable to treat our data by a second method. This method was applied to the data from both the batch and the flow calorimeters.

This method is an iterative procedure that can be summarized as follows: first an initial value for K_2 is chosen, and eq. [3] is used to calculate the change in the number of mole of dimers $\Delta n_D = n_f - n_i$ for each dilution experiment (the subscripts i and f refer to the initial and final states). Then the enthalpy of dimerization, ΔH_2^0, is computed by means of

$$[6]\ \Delta H_2^0 = \frac{q}{\Delta n_D} = \frac{\Delta H_{dil}}{n_f - n_i} = \frac{\Delta H_{dil}}{[D]_f V_f - [D]_i V_i}$$

where [D] means dimer concentration, V means volume, and q is the value of the measured heat change in the calorimeter.

The calculation is carried out for all the experimental values and subsequently an average and a standard deviation is obtained for ΔH_2^0. These calculations are repeated for a number of values of K_2. The 'best' values of K_2 and ΔH_2^0 were obtained from that pair of values for which the standard deviation of ΔH_2^0 was a minimum. When this procedure was applied to the data in Table 1 we obtained: $K_2 = 458$ L/mol; $\Delta H_2^0 = -7.7$ kcal/mol dimer. When applied to the data in Table 2 we found $K_2 = 500$ L/mol; $\Delta H_2^0 = -8.4$ kcal/mol dimer.

The values of K_2 and ΔH_2^0 from both methods are grouped together in Table 4, together with the values for these quantities reported previously by Woolley and Zaugg (5). These authors used the ϕ_L method on their calorimetric data which were obtained by a titrimetric procedure.

Several points are immediately apparent from the entries in Table 4. First the data obtained by the batch and the flow calorimeters in this work are mutually consistent, and they are both consistent with Woolley and Zaugg's data. Also, the uncertainties in this and in Woolley and Zaugg's work are of comparable magnitude. Thus the $\Delta\phi_L$'s obtained here and in Woolley's work are consistent. The discrepancy in the *absolute* ϕ_L values (apparent from Fig. 1) obtained in this and in Woolley's work is a consequence of the fact that accurate absolute ϕ_L values require very accurate data in the dilute solution regime. The titrimetric procedure used by Woolley and his collaborators inadequately probes this dilute solution region.

Of course, consistency of the above results really amounts to little more than a data check and certainly this consistency does not prove the validity of monomer–dimer model. Indeed we are prompted for several reasons to be suspicious of this model. First, other authors using methods as diverse as infrared spectroscopy (6) and osmometry (7) found that larger species in addition to dimers were required to account for their data on carboxylic acids in nonaqueous solvents. Second, the values listed in Table 4 for K_2 are somewhat lower than what is expected from previous studies involving other experimental techniques. This discrepancy is demonstrated by the point with the symbol ∇ in Fig. 3. We believe that the titrimetric calorimetric method employed by Woolley *et al.* gives more weight to the high concentration regime than do other experimental methods, so that the K_2 values extracted from the titrimetric data are too low. Third, we were bothered by the slight curvature, which we believe to be real, in the ϕ_L vs. $(-\phi_L/[C])^{1/2}$ plot (Fig. 2, upper graph). This curvature is apparent when a large scale graph is used. The scaling down and distortion that occurs on photographic reproduction makes this curvature unobservable in the upper graph of Fig. 2. We reasoned that if aggregates larger than dimers were present in our solutions, then the use of a monomer–dimer model should result in a concentration-dependent K_2. To test this idea we evaluated K_2 and ΔH_2^0 from ΔH_{dil} by applying method 2 to different concentration ranges. We split up our data from the batch

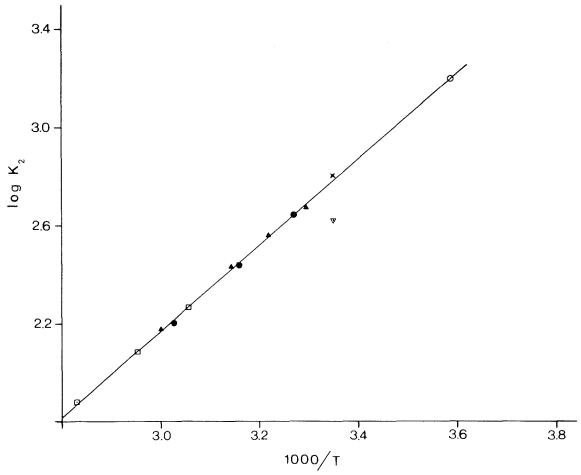

FIG. 3. Various values of K_2 (molar) for benzoic acid in benzene using the ideal monomer–dimer model: ▲, infrared (8); ●, isopiestic method (9); □, ebullioscopy (10); ○, cryoscopy (11); ▽, heat of dilution (5); ×, heat of dilution (this work with trimers included in the data treatment); solid line is linear least-squares line through all the values.

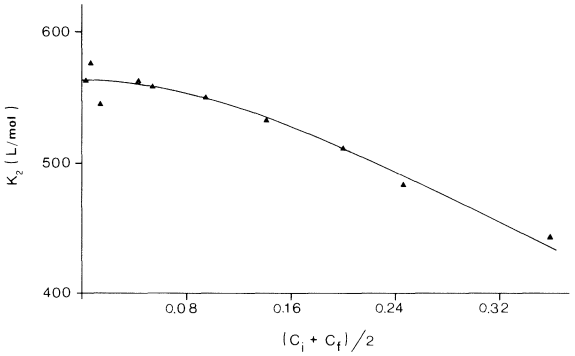

FIG. 4. The dimerization equilibrium constant (K_2) as a function of concentration.

calorimeter (Table 1) into two sets. In the first, the final solution concentration (i.e. the concentration of the solution in the calorimeter after the ampoule is broken) was always less than some selected value and in the second it was always greater than this value. The results of a number of such calculations clearly showed that K_2 dropped with increasing concentration. This concentration-dependence of K_2 is even more obvious with the data from the flow calorimeter (Table 2) since there the ΔH_{dil} were measured with solutions covering a wide range of initial concentrations, i.e., $0.0016\ M < C_i < 0.48\ M$. In Fig. 4, we plotted the value of K_2 calculated for each ΔH_{dil} (Table 2) using eqs. [6] and [3], assuming $\Delta H_2^0 = -8525$ cal/mol dimer (our 'best' value, details given below) and setting the concentration $C = (C_f + C_i)/2$. It is clear from Fig. 4 that when the ideal monomer–dimer is applied to our data, the values of K_2 that result are strongly concentration-dependent.

In view of these results, we considered it worthwhile to pursue other models, in an attempt to better account for our data.

Monomer–Trimer Model

This is an obvious alternative to the monomer–dimer model. Using the same approach as was taken in the monomer–dimer case (method 1) one can show that for the case of an ideal monomer–trimer equilibrium (1):

$$[7]\quad \phi_L = \frac{\Delta H_3^0}{3} - \tfrac{1}{3}(\Delta H_3^0)^{2/3}\left(\frac{1}{K_3}\right)^{1/3}\left(\frac{\phi_L}{[M]^2}\right)^{1/3}$$

where ΔH_3^0 is the molar enthalpy of trimerization and K_3 the trimerization constant. We applied eq. [7] to the data in Table 3; the results are plotted as the lower curve in Fig. 2. As is seen from Fig. 2, a very obvious curvature results. It was concluded that this model was clearly inconsistent with our data, and it was pursued no further.

Monomer–Dimer–Trimer Model

We next decided to fit our data to an ideal monomer–dimer–trimer model. This model is the simplest logical extension of the ideal monomer–dimer model and, as previously mentioned, it has been used to account for osmometric data on solutions of long-chained carboxylic acids in benzene (7). Of course in taking this approach we assume that the deviations we observed from the ideal monomer–dimer model are not due to non-ideality of the monomers and dimers themselves. While this is an unprovable assumption at present, it is consistent with much previous work in this area (e.g. see ref. 1 and references contained therein) and it is partially supported by the evidence that molecules that are geometrically similar to benzoic acid but do not have a carboxylic acid group (e.g. chlorobenzene) are very nearly ideal up to concentrations of $\sim 1\ M$ in non-aqueous solvents (1, 23). The approach described below is similar to one that has been previously described (4).

For the case where trimers are assumed to co-exist in equilibrium with monomers and dimers, the relevant equations (assuming all the species behave ideally) are:

$$[8]\quad [C] = [M] + 2K_2[M]^2 + 3K_3[M]^3$$

$$[9]\quad q = \Delta n_D \Delta H_2^0 + \Delta n_T \Delta H_3^0$$

$$[10]\quad [C]\phi_L = \Delta H_2^0[D] + \Delta H_3^0[T]$$

where the trimerization constant K_3 and the enthalpy of trimerization ΔH_3^0, refer to the process:

$$3M \rightleftarrows T$$

TABLE 5. Values of the dimerization constant (K_2), enthalpy of dimerization (ΔH_2^0), trimerization constant (K_3), and enthalpy of trimerization (ΔH_3^0) of benzoic acid in benzene at 25°C from heat of dilution measurements

Parameter	Value	
	Flow calorimeter	Batch calorimeter
K_2 (L/mol)	625[a]	—
ΔH_2^0 (cal/mol dimer)	−8 525[a]	—
K_3 (L²/mol²)	9 000[a]	—
ΔH_3^0 (cal/mol trimer)	−13 475 ± 100	−12 975 ± 435[b]

[a]See text for discussion of the uncertainties in these quantities.
[b]Calculated using $K_2 = 625$, $\Delta H_2^0 = -8525$, and $K_3 = 9000$.

In eq. [9], Δn_T is the change in the number of moles of trimers in a dilution experiment. To obtain unique values for the four constants K_2, K_3, ΔH_2^0, and ΔH_3^0 we proceeded in two steps. First, we divided the data in Table 2 into two sets, one with $C_i < 0.1$ M and the other with $C_i > 0.1$ M. Then we used an iterative procedure as follows. For the set $C_i < 0.1$ M we assume only monomers and dimers are present to get a first estimate of K_2 and ΔH_2^0. Then these values of K_2, ΔH_2^0 are used in the $C_i > 0.1$ M set to calculate a first estimate for K_3 and ΔH_3^0. These last values are now used to get an improved pair of values of K_2, ΔH_2^0, from the dilute range. The entire procedure is repeated until the values obtained for the four constants stabilize. As a final step, all the data in Table 2 are combined into one set and the iterative calculation is repeated, starting with the last values of the four constants, until the standard deviation (sd) for all the 25 points is minimum, where

$$\text{sd} \equiv \left[\frac{\sum_{i=1}^{25} (\Delta H_{dil}(\text{exp}) - \Delta H_{dil}(\text{calcd}))^2}{24}\right]^{1/2}$$

The values we thus obtained for the four constants are grouped in Table 5. Since it is not possible to obtain unique values for the four constants K_2, K_3, ΔH_2^0, ΔH_3^0 using the data from Table 1 alone, the stock solutions used being too concentrated, we utilized these newly obtained results ($K_2 = 625$ L/mol, $\Delta H_2^0 = -8525$ cal/mol dimer, $K_3 = 9000$ L²/mol²) to calculate a value for ΔH_3^0 using the batch calorimeter data. The value thus obtained for ΔH_3^0 is also entered in Table 5. As is seen from Table 5, both values of ΔH_3^0 agree to within their estimated standard deviations.

The entries in Table 5 provide a good fit to the data in Tables 1 to 3 in that the calculated values of ΔH_{dil} were found not to deviate in any systematic (i.e. concentration-dependent) way from the corresponding experimental values. In other words these values provide a good fit to sets of $\Delta\phi_L$ values that can be constructed from the ϕ_L values in Table 3.

The uncertainties in the values K_2 and ΔH_2^0 given in Table 5 are probably close to those that are deduced from the entries in Table 4 (i.e. sd $K_2 \sim \pm 100$; sd $\Delta H_2^0 \simeq 0.5$ kcal/mol dimer). It is much more difficult to assess, even roughly, the net uncertainties in K_3 and ΔH_3^0. (The values of ±100 and ±435 cal given in Table 5 for ΔH_3^0 are conditional uncertainties in that they depend on K_2, ΔH_2^0, and K_3 being perfectly correct.) This is because there is no concentration region in which trimers are the clearly predominant species. From unpublished trial calculations, however, we feel that ΔH_3^0 is probably correct to within 2 kcal, and that K_3 is of the right order of magnitude.

Discussion

Our values of K_2 and ΔH_2^0 calculated from the monomer–dimer–trimer model are in good agreement with those obtained from other work (Fig. 3). The slope ($d \log K_2/d(1/T)$) through all the points leads to $\Delta H_2^0 = -8.0$ kcal/mol dimer compared with −8.5 in the present work. Also our value for K_2 (625 L/mol) falls almost perfectly on the least-squares line.

It remains to account for the quasi-linearity of our ϕ_L vs. $(-\phi_L/C)^{1/2}$ plot (Fig. 2, upper graph). To get better insight into this type of plot, we evaluated ϕ_L and $(-\phi_L/C)^{1/2}$ using eq. [10] for different values of K_3, keeping K_2, ΔH_2^0, and ΔH_3^0 fixed at the values in Table 5. The results of these trial calculations showed that linearity of a ϕ_L vs. $(-\phi_L/C)^{1/2}$ plot is a poor criterion for the validity of the monomer–dimer model. For example, using $K_3 = 90\,000$ (i.e., 10 times our estimated value) which leads to an important relative contribution of trimers to the stoichiometric concentration (for $C = 0.10$, the fraction of acid in monomer:dimer:trimer form would be 0.06:0.42:0.52), the ϕ_L vs. $(-\phi_L/C)^{1/2}$ plot manifests only a slight curvature, which may, depending on the quality of the data, be considered almost negligible relative to experimental error.

Our value of ΔH_3^0 per mol ($\Delta H_3^0/3 = -4.49$ kcal/mol) is slightly more negative than ΔH_2^0 per

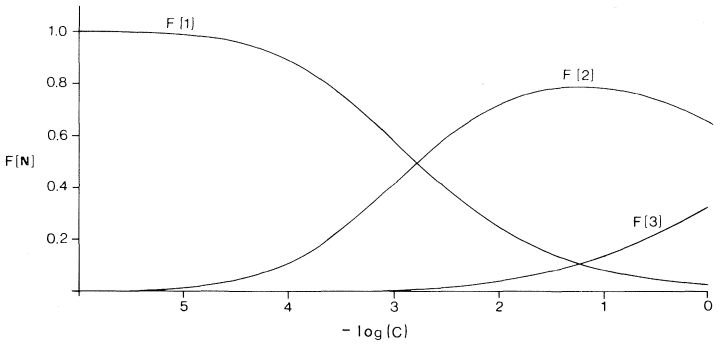

FIG. 5. $F(N)$ is the fraction of the stoichiometric benzoic acid concentration present as monomers, $F(1)$; dimers, $F(2)$; and trimers, $F(3)$. Curves obtained by eq. [8] with $K_2 = 625$ L/mol and $K_3 = 9000$ L^2/mol^2.

mol ($\Delta H_2^0/2 = -4.26$ kcal/mol). This trend in enthalpies has been noted for carboxylic acids in the gas phase (24), for long-chained carboxylic acid in benzene (7) and from quantum mechanical calculations (25). Also, our relative values of K_3 to K_2 are such that trimers make a significant contribution to the stoichiometric concentration for concentrations beyond 0.01 M. This is illustrated in Fig. 5, and is in line with what has been found for long-chained carboxylic acids in benzene (7) and for acetic acid in carbon tetrachloride (6).

We conclude, that except for very dilute solutions (i.e., less than 10^{-2} M), the ideal monomer–dimer model is of questionable value in the study of carboxylic acid self-association. For this reason, we believe that studies of H-bonding or self-association by the calorimetric dilution method have to be done in such a way that the dilute concentration region is well characterized, and this requires a highly sensitive microcalorimeter.

Acknowledgements

We are grateful to the National Research Council of Canada and Le Ministère de l'Education du Québec for financial support, to Dr. C. Jolicoeur who made possible this collaboration between the two laboratories, and to M. A. Simard for his technical assistance. We would also like to thank Dr. Loren Hepler for his helpful suggestions concerning the data treatment.

1. E. M. WOOLLEY, J. G. TRAVERS, B. P. ERNO, and L. G. HEPLER. J. Phys. Chem. **75**, 3591 (1971).
2. N. S. ZAUGG, S. P. STEED, and E. M. WOOLLEY. Thermochim. Acta, **3**, 349 (1972).
3. N. S. ZAUGG, L. E. TREJO, and E. M. WOOLLEY. Thermochim. Acta, **6**, 293 (1973).
4. E. M. WOOLLEY and D. S. RUSHFORTH. Can. J. Chem. **52**, 653 (1974).
5. E. M. WOOLLEY and N. S. ZAUGG. Anal. Calorim. **3**, 479 (1974).
6. J. T. BULMER and H. F. SHURVELL. J. Phys. Chem. **77**, 256 (1973).
7. O. LEVY, G. Y. MARKOVITS, and I. PERRY. J. Phys. Chem. **79**, 239 (1975).
8. G. ALLEN, J. G. WATKINSON, and K. H. WEBB. Spectrochim. Acta, **22**, 807 (1966).
9. F. T. WALL and F. W. BANES. J. Am. Chem. Soc. **67**, 898 (1945).
10. G. ALLEN and E. F. CALDIN. Trans. Faraday Soc. **49**, 895 (1953).
11. B. C. BARTON and C. A. KRAUS. J. Am. Chem. Soc. **73**, 4561 (1951).
12. S. GOLDMAN. Can. J. Chem. **52**, 1668 (1974).
13. R. H. STOKES. J. Am. Chem. Soc. **67**, 1968 (1945).
14. S. GOLDMAN, R. G. BATES, and R. A. ROBINSON. J. Solution Chem. **3**, 593 (1974).
15. G. L. BERTRAND, R. D. BEATY, and H. A. BURNS. J. Chem. Eng. Data, **13**, 436 (1968).
16. J.-L. FORTIER, P.-A. LEDUC, P. PICKER, and J.-E. DESNOYERS. J. Solution Chem. **2**, 467 (1973).
17. P. PICKER. Can. Res. Dev. **7**, 11 (1974).
18. P. PICKER, E. TREMBLAY, and C. JOLICOEUR. J. Solution Chem. **3**, 377 (1974).
19. D. S. FLITT and M. J. JAYCOCK. Ion exchange and solvent extraction. Vol. III. *Edited by* J. A. Marinsky and Y. Marcus. Marcel Dekker, NY. 1973.
20. S. D. CHRISTIAN, H. E. AFFSPRUNG, and S. A. TAYLOR. J. Phys. Chem. **67**, 187 (1963).
21. J. R. JOHNSON, S. D. CHRISTIAN, and H. E. AFFSPRUNG. J. Chem. Soc. A, 764 (1967).
22. R. VAN DUYNE, S. A. TAYLOR, S. D. CHRISTIAN, and H. E. AFFSPRUNG. J. Phys. Chem. **71**, 3427 (1967).
23. C. R. BURY and H. O. JENKINS. J. Chem. Soc. 688 (1934).
24. G. C. PIMENTAL and A. L. MCCLELLAN. The hydrogen bond. W. H. Freeman and Co., San Francisco. 1960; Ann. Rev. Phys. Chem. **22**, 347 (1971).
25. L. DEL BENE and J. A. POPLE. Chem. Phys. Lett. **4**, 426 (1969); J. Chem. Phys. **52**, 4858 (1970).

Modelling of interactions in solutions: alkali halides in DMSO

PEETER KRUUS AND BARBARA E. POPPE[1]

Department of Chemistry, Carleton University, Ottawa, Ont., Canada K1S 5B6

Received September 6, 1978

PEETER KRUUS and BARBARA E. POPPE. Can. J. Chem. **57**, 538 (1979).

A model of solutions of alkali halides in DMSO is developed. Each ion is described by a radius, a charge, a polarizability, and an exponential repulsion parameter. Each molecule is described by a polarizability, charges, 6-12 energy parameters, and 6-12 distance parameters centered on each of the 10 atoms in the molecule. The model is applied to calculate (*i*) the vaporization energy of solvent molecules, (*ii*) single ion solvation energies and configurations of the solvating molecules, and (*iii*) the energy as a function of reaction coordinate for the formation of an ion pair. The energies and configurations are obtained by allowing the systems to relax to minimum energy configurations by allowing motion of the molecules. The results of (*i*) give a vaporization energy 60% of the experimental. The results of (*ii*) give solvation energies in reasonable agreement with the experimental, and configurations which are reasonable from the point of view of mobilities of ions. The results of (*iii*) show the presence of a distinct solvent separated ion pair which actually has an energy lower than the contact ion pair. Advantages and problems involved in using this approach to model solutions are discussed.

PEETER KRUUS et BARBARA E. POPPE. Can. J. Chem. **57**, 538 (1979).

On a développé un modèle pour les solutions d'halogénures alcalins dans le DMSO. On décrit chaque ion grâce à son rayon, à sa charge, à sa polarisabilité et à un paramètre de répulsion exponentielle. On décrit chaque molécule grâce à sa polarisabilité, et à des charges et des paramètres d'énergie de distance 6-12 dont le centre coincide avec chacun des 10 atomes de la molécule. On a appliqué le modèle pour calculer (*i*) l'énergie de vaporisation des molécules de solvant; (*ii*) les énergies de solvatation des ions uniques et les configurations des molécules solvatantes; et (*iii*) l'énergie en fonction des coordonnées de la réaction conduisant à la formation d'une paire d'ions. On a obtenu les énergies et les configurations en permettant au systèmes d'atteindre des configurations d'énergie minimale grâce au mouvement des molécules. Les résultats de (*i*) conduisent à une énergie de vaporisation qui est égale à 60% de la valeur expérimentale. Les résultats de (*ii*) conduisent à des énergies de solvatation qui sont en bon accord avec les valeurs expérimentales et à des configurations qui sont raisonnables du point de vue des mobilités des ions. Les résultats de (*iii*) indiquent la présence d'une paire d'ions définie qui est séparée par le solvant et dont l'énergie est plus faible que celle d'une paire d'ions en contact. On discute des avantages et des problèmes impliquées dans l'utilisation de cette approche à des solutions modèles.

[Traduit par le journal]

Introduction

Modelling of solutions can be approached from two extremes: by consideration of a large number of necessarily simple particles, or by detailed, quantum mechanical consideration of a necessarily small number of particles. Realistic models of solutions containing geometrically more complicated molecules can be difficult to achieve via either of these approaches. The configurations present in solutions can be quite sensitive to the detailed geometry of the molecules, so that description by spheres, ellipsoids, quadrupoles, etc. is not satisfactory. At the same time, it may be necessary to include several molecules in any realistic model of a solvated species, so that reasonably accurate quantum mechanical calculations are prohibitively expensive.

An approach intermediate to the two limiting approaches was introduced for dimethyl sulfoxide solutions in ref. 1, where the geometry of the solvent molecules was described in detail. Similar approaches have been used for calculations involving interactions of very large molecules (2), conformations (3), liquids (4), crystals (5), and hydration of ions (6), nonelectrolytes (7), and even macromolecules (8). The intermolecular potentials used in these cases vary, but include primarily r^{-1} terms between point charges on atoms, r^{-6} attractive dispersion terms, and repulsive terms (r^{-12} or exponential). The intermolecular potentials used are in several cases calculated with the aid of quantum mechanics (e.g. refs. 2, 3, 5, 6, 7), but the subsequent calculations involve only sums of pair potentials, with no further allowance for charge transfer or three body effects (9, 10).

[1]Present address: Bell Canada, Ottawa K1G 3J4.

0008-4042/79/050538-14$01.00/0

Various molecular models of solvation of ions are summarized in ref. 11. Solvation of ions by organic solvents have been modelled by an approach similar to the above (12), but only one acetonitrile molecule was considered. There have been several complete quantum mechanical calculations involving methanol (13), formic acid (14), acetonitrile (15), and other solvents (16), all using the CNDO/2 approach. The absolute values obtained are in some cases in very poor agreement with experiment (13, 14), and the stabilization energies between Li^+ and acetonitrile predicted in refs. 15 and 16 differ by 320 kJ mol^{-1}.

Large numbers of quantum mechanical calculations involving water molecules have been made (e.g. ref. 17). Classical calculations involving dipoles, induced dipoles, quadrupoles, polarization, dispersion, and repulsion (18) give results for hydration of alkali metal ions which are essentially the same as the quantum mechanical SCF calculations (19). The repulsion parameters in the calculations in ref. 18 were empirically selected, however.

Different approaches to modelling of solutions are put in perspective in ref. 20 where three approaches are compared for simple solvents (H_2O and NH_3). The calculations presented here would fall under the discrete model, with contributions of the same type as those in ref. 20: electrostatic, dispersion, repulsion, and polarization. No allowance for any charge transfer (donor–acceptor) effects (21) is allowed for. This model is simple enough so that a system of up to 2 ions and 16 dimethylsulfoxide (DMSO) can be considered. However, as in ref. 20, a statistical mechanical (e.g., Monte Carlo) treatment is not feasible for such a complex system due to lack of computer resources. Thus thermal effects are neglected, and systems are simply allowed to relax to a minimum energy configuration.

The results of such calculations for DMSO are presented here in three stages: (*i*) pure solvent, (*ii*) ion solvation, and (*iii*) ion pairing. DMSO was chosen as the solvent model molecule because several aspects of DMSO had been investigated previously (1). It is also an important substance in its own right (22) and may be useful as a standard solvent for electrolytes (23). Only systems with univalent spherical ions were considered here. The approach can be readily extended to structurally more complicated charged species and to other solvent species, as well as to mixed solvents.

Computations

(a) Model

The model of the DMSO molecule chosen is an extension of that in ref. 1, with the geometry of the molecule and the charges on the atoms the same (Table 1). The charges were calculated in ref. 1 using experimental data on DMSO, dimethylsulfide, and methane. The geometry of the DMSO molecule was that obtained from X-ray data (24).

In ref. 1, the polarization was described by 9 bond polarizabilities, each with a transverse and a longitudinal component (25). Here each DMSO molecule was assumed to have a scalar polarizability $\alpha = 8.37 \times 10^{-24}$ cm^3 (26) close to the sulfur atom (1.22 Å from the O atom along the dipole axis). The position of the scalar polarizability was chosen so that energies obtained in calculations with the scalar polarizability were close to those obtained with polarizabilities on each of the 9 bonds. The value of the polarizability used (8.37×10^{-24} cm^3) is a calculated value (26); it is somewhat lower than the value 9.32×10^{-24} cm^3 obtained by summing over the bond polarizabilities used in ref. 1, but somewhat higher than 7.97×10^{-24} cm^3 calculated from molecular volume and dielectric constant (27). The use of a scalar polarizability instead of 9 matrices saves considerable computational time.

Repulsive and dispersion forces between DMSO molecules were described by 6-12 distance and energy parameters positioned on the centres of the 10 atoms in each molecule (Table 1). These parameters were calculated so that the atom–atom energy minima were the same as those used for calculations of lattice energies of crystals of organic molecules (5). The distance parameters were obtained by noting the O---H distance (2.34 Å) in DMSO crystals (24), and from Lennard-Jones distance parameters of O_2, CS_2, and COS (25). Attempts to use an r^{-6} attraction and an exponential repulsion as in ref. 2 were discontinued because of the difficulty of specifying a precise energy minimum for the interaction in that mathematical form.

The radii and the polarizabilities of the ions are the same as those used in ref. 1, i.e. from refs. 28 and 29, respectively. The repulsions are assumed exponential, with the power 2.94 (Table 2) and the

TABLE 1. Parameters describing a DMSO molecule*

Atom	Charge/10^{-10}esu	L-J energy parameter $\varepsilon/10^{-8}$ $erg^{1/2}$	L-J distance parameter σ/Å
O	−1.63	11.80	1.40
S	−0.474	5.47	1.56
C	+1.66	5.14	1.50
H	−0.202	5.09	0.94

*$v_{ij}(r) = 4\varepsilon[(\sigma/r)^{12} - (\sigma/r)^6]$, $\varepsilon = \varepsilon_i\varepsilon_j$, $\sigma = \sigma_i + \sigma_j$.

TABLE 2. Energy contributions considered in calculations (expressions for cgs esu units)

$E_{TOT} = E_{AC} + E_{CD} + E_{AD} + E_{DD}$

$E_{AC} = E_{ACP} + E_{ACI} + E_{IIR}$

$E_{ACP} = q_A q_C / r_{A,C}$

$E_{ACI} = q_A q_B(\alpha_C + \alpha_A)/(2r_{A,C}^4)$

$E_{IIR} = 0.243 \times 10^{-12} \exp[-2.94(r_{AC} - (\sigma_A + \sigma_C))]$ (in erg)

$E_{CD} = E_{CDP} + E_{CDI} + E_{DIR}$

$E_{CDP} = q_C \sum_{i,j} q_{i,j}/r_{C;i,j}$ for $i = 1, 16; j = 1, 10$

$E_{CDI} = -\frac{1}{2}\sum_i \boldsymbol{p}_i \cdot \boldsymbol{F}_{C,i}$ for $i = 1, 16$ with

$\boldsymbol{p}_i = \alpha_D(\boldsymbol{F}_{C,i} + \boldsymbol{F}_{A,i})$

$\boldsymbol{F}_{C,i} = q_C \boldsymbol{r}_{C,i}/r_{C,i}^3$

$E_{DIR} = \sum_{i,j} 0.082 \times 10^{-12} \exp[-3.98(r_{C;i,j} - (\sigma_{i,j} + \sigma_C))]$ (in erg) for $i = 1, 16; j = 1, 10$

$E_{AD} = E_{ADP} + E_{ADI} + E_{DIR}$

Expressions for E_{AD} contributions are analogous to those for E_{CD} contributions.

$E_{DD} = E_{PP} + E_{PI} + E_{II} + E_{LON} + E_{DDR}$

$E_{PP} = \frac{1}{2}\sum_{i,j}\sum_{k,l} q_{i,j}q_{k,l}/r_{i,j;k,l}$ $i = 1, 16; j = 1, 10; k = 1, 16; l = 1, 10; i \neq k$

$E_{PI} = -\sum_i \sum_{k,l} \boldsymbol{p}_i \cdot q_{k,l}\boldsymbol{r}_{i;k,l}/r_{i;k,l}^3$ $i = 1, 16; k = 1, 16; l = 1, 10; i \neq k$

$E_{II} = \sum_i \sum_k [\boldsymbol{p}_i \cdot \boldsymbol{p}_k/r_{i,k}^3 - 3(\boldsymbol{p}_i \cdot \boldsymbol{r}_{i,k})(\boldsymbol{p}_k \cdot \boldsymbol{r}_{i,k})/r_{i,k}^5]$ $i = 1, 16; k = 1, 16; i \neq k$

$E_{LON} = -\frac{1}{2}\sum_{i,j}\sum_{k,l} 4\varepsilon_{i,j}\varepsilon_{k,l}\left(\frac{\sigma_{i,j} + \sigma_{k,l}}{r_{i,j;k,l}}\right)^6$ $i = 1, 16; j = 1, 10; k = 1, 16; l = 1, 10; i \neq k$

$E_{DDR} = \frac{1}{2}\sum_{i,j}\sum_{k,l} 4\varepsilon_{i,j}\varepsilon_{k,l}\left(\frac{\sigma_{i,j} + \sigma_{k,l}}{r_{i,j;k,l}}\right)^{12}$ $i = 1, 16; j = 1, 10; k = 1, 16; l = 1, 10; i \neq k$

pre-exponential factor 0.243×10^{-12} erg chosen after ref. 28. Ion–atom repulsions are also assumed exponential with a power 3.98 (Table 2) taken following (30). A pre-exponential factor 0.082×10^{-12} erg $\simeq 2kT$ is chosen for ion–atom repulsion, as a repulsion of this order of magnitude would be expected when the ion and an atom are at their 'hard sphere' distance. A change in the pre-exponential factor is equivalent to a change in the ion and/or atom radii.

Table 2 lists the interactions which are included in the calculations. Induced dipoles p_i are assumed to be due to the ion fields only. Thus polarization of both the ions and other molecules due to fields of molecules are neglected. As pointed out in ref. 1, some additional terms are also neglected in dividing up the interaction between molecules in the field of ions into E_{PP}, E_{PI}, and E_{II}. A minimum distance of approach to the center of polarizability was specified to prevent an unrealistically large induced dipole moment for the case of small ions. The polarizability was assumed shielded by an amount equal to the distance (radius) parameter σ for sulfur.

The polarization of the molecules and ions is assumed linear, and any distortion of the geometry of DMSO molecules by the field is neglected. The DMSO are assumed rigid at all times, so that rotation of methyl groups is also not taken into account; the significance of this approximation is discussed in ref. 1. Other effects which are neglected are: (*i*) London dispersion forces between ions and molecules and (*ii*) any charge-transfer (21) or quantum mechanical effects.

The validity of the choice of the above model will be discussed following presentation of the results obtained using it. The parameters used were chosen

as far as possible from experimental data in the literature. There was no adjustment of these parameters during the calculations.

(b) Calculation Method

The strategy for the calculations is outlined in Fig. 1. Several different input files are used in the calculations to describe the initial positions of the DMSO molecules: (*i*) 16 DMSO's in the geometry of the crystal as determined by X-ray scattering; (*ii*) 16 DMSO's all at least 10 Å from the origin distributed approximately evenly around the origin; (*iii*) symmetrical configurations (trigonal, tetrahedral, trigonal bipyramid, octahedral) about the origin either 5 Å or 9 Å from the origin, and with dipoles pointing either into or out from the origin.

Since the energy contributions are calculated from atomic coordinates, then these must be specified. For a system of 16 molecules and 2 ions, the 3 dimensional coordinates of 162 particles must be given. However, when a new configuration is generated, the whole molecule must be moved; thus molecular coordinates are also necessary. The positions of individual atoms are described by cartesian coordinates, while the molecular configuration is described by the distance of the center of the molecule from the origin, the direction cosines of the vector from the origin to the molecule, the direction cosines of the permanent dipole of the molecule, and the direction cosines of the line between carbon atoms on a DMSO. These molecular coordinates make it easy to visualize the motion of molecules and to alter the position of molecules by editing input files.

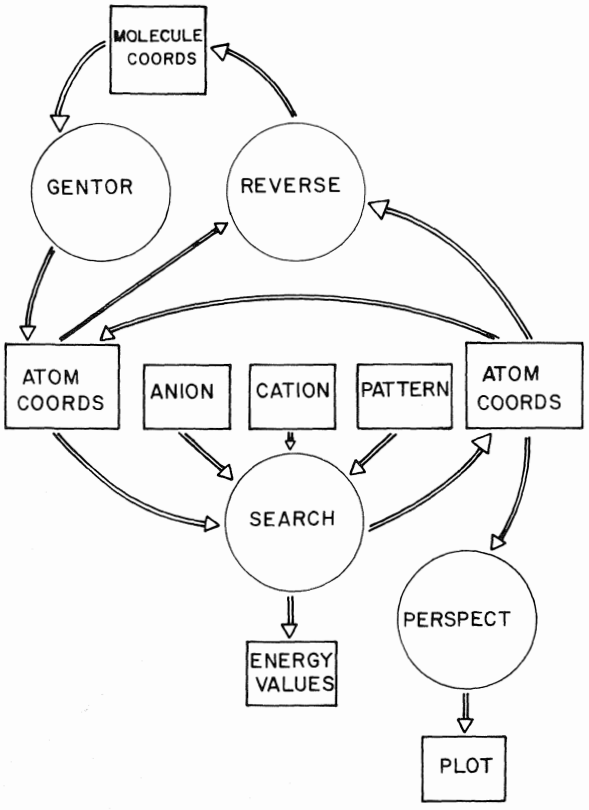

FIG. 1. Schematic diagram outlining the calculation strategy.

The relaxation of a configuration to an energy minimum is guided by a search pattern input file. This file specifies which molecule is to be moved, in which order the molecular coordinates of that DMSO are to be altered, the magnitude of a coordinate alteration, and the magnitude of the energy decrease to be considered significant enough to accept a new configuration. Temperature effects are thus neglected.

There is also an option in the search pattern to have the molecule interact with all other molecules, or only with those numbered less than itself. The latter routine is useful for building up an initial cluster of molecules containing fewer local minima. Since only one molecule at a time can be moved in this search pattern, configurations such as dimers removed from the main cluster are unlikely to break up if a molecule interacts with all its partners.

Achievement of an energy minimum for systems containing, e.g. an ion and 6 DMSO molecules, is fairly rapid, requiring at most 3 min CPU time to reach an equilibrium. The Xerox Sigma 9 computer has a CPU speed approximately 75% of the IBM/360-65. Several different minimizations with different initial coordinates and energy minimum search patterns are necessary to reasonably ensure that the configuration arrived at is not a subsidiary minimum.

When the system contains 16 molecules and 2 ions, at least 80 min CPU time is necessary to reach an energy minimum. This corresponds to the calculation of the energy of the order of 10 000 configurations at 0.42 s CPU time per configuration. Under the charge system used, the cost of obtaining the minimum energy configuration for a system of 2 ions and 16 molecules is of the order of $300. The core required for the calculations is not excessive, being only 32 000 bytes memory.

It was possible to view configurations on a screen in between steps, and to obtain hard copy plots of configurations (see Fig. 2). Figure 2 also gives the single molecules energies in units of -10^{-19} J. When a molecule is moved, it is sufficient to note the change in the energy contributions involving that molecule only, and not all molecules.

Results and Discussion

(a) Pure DMSO

Table 3 shows the results of calculations for systems of 2, 3, ..., 7, and 16DMSO molecules. In sys-

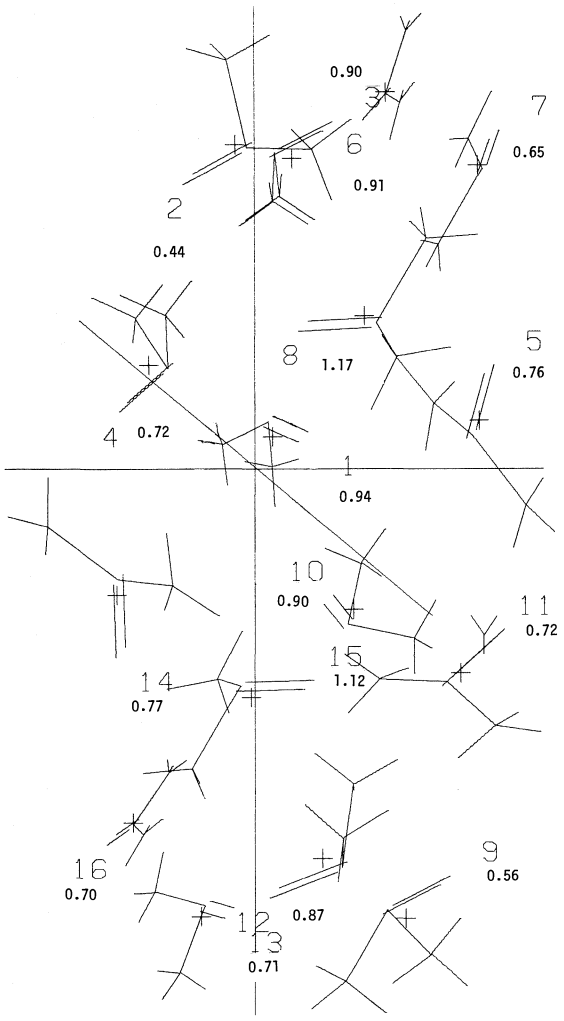

FIG. 2. The final (lowest energy) configuration of a system of 16DMSO molecules when the initial configuration consists of the experimentally determined crystal configuration. Energies of individual molecules in the configuration are given in units of -10^{-19} J.

tems with 2 to 7 molecules, the initial configuration consisted of molecule *1* near the origin and the others several Å away. A cluster of DMSO molecules was then formed by 'condensing' molecules one at a time onto the first. This cluster was then allowed to relax to its energy minimum.

For the system with 16 molecules, the initial configuration was the experimental crystal configuration (24). This was then allowed to relax to an energy minimum. The final minimum energy configuration achieved is shown in Fig. 2. The energies in -10^{-19} J of the individual molecules are shown beside the numbers labelling the molecules.

Table 3 indicates that contributions to the total energy from permanent charge distribution interactions (E_{PP}, Table 2) and London dispersion interactions (E_{LON}, Table 2) are of the same order of magnitude. Thus even in the case of quite polar molecules such as DMSO, dispersion forces are very significant. The repulsive (r^{-12}) term is separated out here from the 6-12 potential; often the sum of E_{LON} and E_{DDR} is considered as being the dispersion interaction. There are no further terms contributing to the total energy as there are no ions present and as the dipole moments p_i induced in the molecules are assumed to be due to ions only.

TABLE 3. Energy contribution in DMSO clusters (energies in 10^{-19} J)

Number of molecules	E_{TOT}	E_{PP}	E_{LON}	E_{DDR}
2	−0.23	−0.18	−0.13	+0.09
3	−0.42	−0.28	−0.31	+0.18
4	−0.94	−0.71	−0.65	+0.41
5	−1.41	−0.94	−1.11	+0.64
6	−1.79	−1.32	−1.30	+0.83
7	−2.34	−1.67	−1.63	+0.96
16	−6.38	−4.34	−4.66	+2.62
16*	−6.4	−4.5	−4.5	+2.6
16†	−2.51	−1.36	−1.69	+0.54

*Values extrapolated from values for clusters of 4, 5, 6, 7DMSO's ($\Delta E_{vap} \simeq 0.45 \times 10^{-19}$ J).
†Experimental crystal configuration.

The neglect of permanent-induced interactions for the systems in Table 3 will make the calculated energies less favourable. The mean nearest neighbour distance for the configuration in Fig. 2 is 4.18 Å. The energy of a DMSO molecule due to permanent charge and London interactions in such a case is of the order of -0.7×10^{-19} J. The greatest possible interaction energy between a dipole of 3.9 Debye and a polarizable entity of 8.4×10^{-24} cm^3 which are 4.18 Å apart is -0.10×10^{-19} J. Since the fields of nearest neighbours will have some cancellation effect, and since this most favourable orientation will not be achieved, the error due to neglect of permanent-induced interactions for the systems in Table 2 should be at most of the order of 10%.

The experimental energy of vapourization for DMSO is 50 kJ mol^{-1} (31). From the slope of E_{TOT} vs. number of DMSO (Table 2, Fig. 3), a value of 0.45×10^{-19} J molecule^{-1} = 27 kJ mol^{-1} is obtained for E_{vap} (really E for sublimation). Figure 2 indicates several surface molecules to have an energy of -0.7×10^{-19} J. Removal of such a molecule would mean an energy requirement of 42 kJ mol^{-1}. The 42 kJ mol^{-1} value is an activation energy for vapourization, so that when the cluster relaxes to fill the void, the net change is only 27 kJ mol^{-1}. Thus the calculations give an E_{vap} of the right order of magnitude but somewhat low. Calculation of such energies

TABLE 4. Ion solvation by DMSO molecules (energies in -10^{-19} J)

No. of DMSO	Energy for solvated species* = DMSO (α 8.37, σ ~2.8)	F^- (0.76, 1.19)	Cl^- (3.04, 1.65)	Br^- (4.28, 1.80)	I^- (6.54, 2.01)	H^+ (0.0, 0.10)	Li^+ (0.0, 0.90)	Na^+ (0.30, 1.21)	K^+ (1.23, 1.51)	Cs^+ (3.17, 1.80)
1	0.23	2.62	1.22	1.06	0.90	23.05	3.98	2.54	1.82	1.49
2	0.41	3.50	2.24	2.28	1.67	—	6.95	4.49	3.28	2.65
3	0.87	4.24	3.24	2.96	2.51	—	8.65	5.33	4.24	3.50
4	1.41	4.72	3.57	3.21	2.77	—	9.25	6.07	4.85	4.21
5	1.79	4.92	3.82	3.55	3.22	29.59	10.50	6.59	5.38	4.38
6	2.34	5.50	4.03	3.98	3.43	30.96	11.33	7.22	5.89	5.00

*Numbers in parentheses stand for ($\alpha/10^{-24}$ cm, σ/Å).

of vapourization or sublimation cannot be done very accurately given the limited amount of data used here (see, e.g., ref. 32). Detailed calculations of the lattice energy of benzene (10) also show how difficult it is to obtain agreement with experimental values in such cases. Thus the order of magnitude agreement with the experimental value should be considered satisfactory, and evidence that the model of the DMSO molecules used is likely to be quite realistic.

A cluster of 16DMSO molecules has a very large surface-to-volume ratio, and might therefore be considered as an inadequate model for a region of bulk liquid. However, the properties of a cluster of 16DMSO can already be reasonably well extrapolated from the properties of a cluster of 7DMSO as indicated by the data in Table 3.

The difference in the energy and configuration of the 'relaxed' cluster of 16DMSO and the DMSO in the regular crystal configuration is most likely primarily due to surface effects. The 16-molecule crystal used as an input configuration had no bulk molecules. When a very large number of DMSO are included in the calculation, then the regular crystal arrangement will be the lowest energy one. The computer resources available were, however, not sufficient to perform calculations involving more than 16 molecules, nor to allow for the repetitive units usually employed in Monte Carlo (MC) and molecular dynamics (MD) calculations to correct for surface effects.

The main emphasis in the calculations in part (*i*) is not to arrive at a definitive view of liquid DMSO, but simply to test the reasonableness of the model of the DMSO molecules chosen. A calculation such as this which neglects temperature effects cannot in any case describe a liquid properly. More sophisticated MC and MD calculations of liquids can include similar potentials, but then only of simpler molecules (2, 5), or else molecules where potentials are of a regular geometric shape (33, 34). The number of configurations used in these MC or MD calculations is at least an order of magnitude greater than the 10^4 feasible here.

(b) Ion Solvation

Table 4 and Fig. 3 summarize the results for ion solvation calculations. The DMSO column in Table 4 contains the same data as in Table 3, except that here a central DMSO is considered solvated by 1, 2, ..., 6 other DMSO's. All the energies in Table 4 are those for the lowest energy configuration of several configurations arrived at from different initial configurations and/or different patterns. At least 3 initial configurations were used for cases where there were 3 or more DMSO's: a symmetrical configuration close in, a symmetrical configuration 9 Å away, and an asymmetric configuration.

The configurations of the systems for which energies are available in Table 4 are not presented in detail here. To illustrate the type of information obtained, the plot of Cl^- with 5DMSO is shown in Fig. 4. The ion–DMSO distances and the orientations of the solvating DMSO's for this system are given in Table 5. Figure 5 summarizes the configurational data for the ions with 6DMSO's. The DMSO's are numbered in order of increasing distance from the ion and the distance–number relationship is plotted to indicate symmetry aspects of the solvating molecules.

Some examples of detailed energy contributions are listed in Table 6 in order to illustrate some aspects of the calculations.

The results in Table 4 and Fig. 3 are quite similar to the experimental results obtained for gas phase ion solvation by mass spectrometry (11, 12). Solvation of alkali metal ions by acetonitrile indicates that by the time the 5th solvent molecule is added, there is little dependence of the incremental enthalpy on the type of ion. In Fig. 3, this corresponds to the observation that the slopes of the curves of the energy vs. number of molecules are essentially the same from

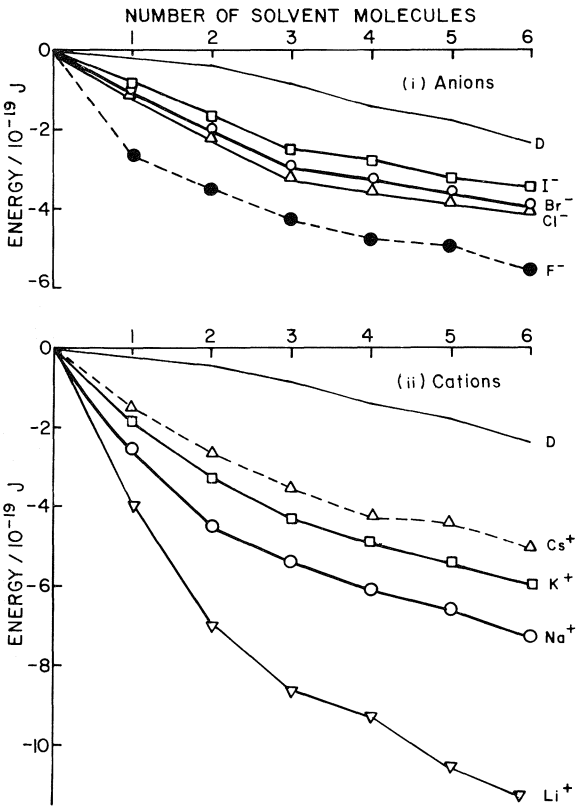

FIG. 3. Energies of DMSO clusters (data in Table 4).

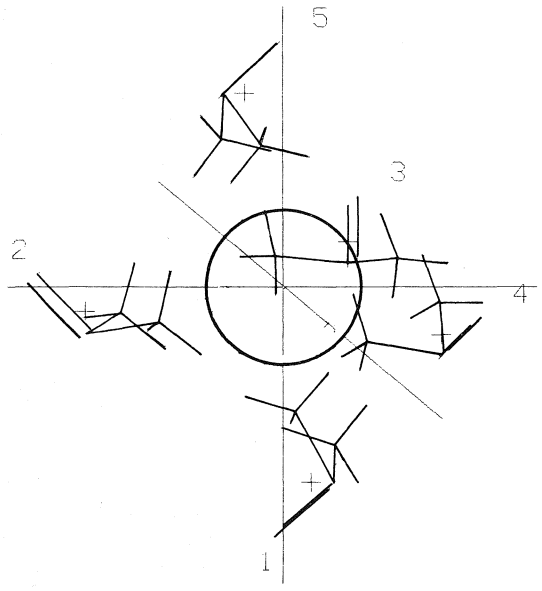

FIG. 4. Lowest energy configuration of Cl^- with 5DMSO (Table 5 and system 2 in Table 6).

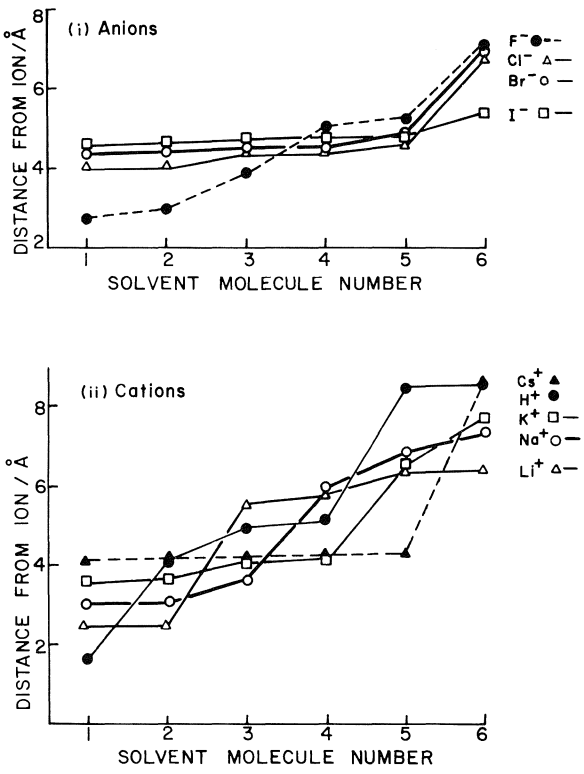

FIG. 5. Distribution of ion–DMSO distances for ions solvated by 6DMSO molecules.

4DMSO's onward for most ions. These slopes are also close to the slope of the energy vs. number of DMSO's curve for the case of a DMSO in the center instead of an ion. Thus from the point of view of energy, a relatively small number of solvent molecules are needed to describe a major proportion of the solvation of the ion.

Energies of solvation can be calculated for the ions from the data in Table 4. These are calculated by taking the values in the last row less the value of the energy of 6DMSO's (-1.79×10^{-19} J) and then adding a contribution from the Born energy of in-

TABLE 5. Positions and orientations of solvating molecules, Cl^- with 5DMSO (Fig. 4)

Molecule number	r	$\frac{\boldsymbol{r}\cdot\boldsymbol{p}}{r\cdot p}$
1	4.10	0.87
2	4.14	0.88
3	4.16	0.88
4	4.36	0.94
5	4.48	0.96

TABLE 6. Energy contribution in ion solvation by DMSO, energies in 10^{-19} J

System	E_{TOT}	E_{ion-D}	E_{iDP}	E_{iDI}	E_{DIR}	E_{DD}	E_{PP}	E_{PI}	E_{II}	E_{LON}	E_{DDR}
(1) Br^- (6D's)	−3.98	−4.99				1.01					
			−4.12	−1.19	0.33		0.48	0.58	0.17	−0.44	0.23
(2) Cl^- (5D's) (Plot in Fig. 4)	−3.82	−5.50				1.68					
			−4.49	−1.50	0.48		0.70	0.91	0.29	−0.28	0.06
(3) Na^+ (6D's)	−7.22	−8.01				0.80					
			−6.15	−2.88	1.01		0.04	0.44	0.49	−0.51	0.37
(4) Na^+ (4D's)	−6.07	−7.39				1.33					
			−5.72	−2.73	1.07		0.26	0.72	0.43	−0.23	0.14
(5) Na^+ (4D's, $\alpha_D = 0$)	−4.66	−5.04				0.40					
			−5.88	—	0.84		0.47	—	—	−0.17	0.10
(6) K^+ (4D's at 3.5, 3.6, 3.6, 8.1)	−4.85	−5.58				0.74					
			−4.65	−1.74	0.80		0.17	0.41	0.20	−0.13	0.09
(7) K^+ (4D's at 3.5, 3.7, 3.9, 4.1)	−4.78	−6.65				1.88					
			−5.35	−1.90	0.61		0.64	0.96	0.35	−0.07	0.01
(8) Li^+ (4D's)	−9.25	−9.52				0.28					
			−5.55	−5.33	1.35		−0.14	−0.22	0.54	−0.50	0.60

TABLE 7. Comparison of calculated and experimental ion solvation energies in DMSO (energies in −kJ mol^{-1})

Species	E'*	E_{solv}(calcd)†	E_{hyd}‡	E_{tr}§	E_{solv}(exp)‖	E_{class}¶
H^+	1756	1859	1103	25.5	1129	7200
Li^+	574	677	533	26.4	559	800
Na^+	327	430	417	27.7	445	595
K^+	247	350	333	34.9	368	478
Cs^+	179	307	289	30.0	319	400
F^-	211	339	502	—	(475)	606
Cl^-	145	273	366	−18.8	347	436
Br^-	129	257	335	−3.5	331	400
I^-	109	237	294	12.8	307	358

*Values from Table 4.
†$E' + 103$ for cations, $E' + 128$ for anions and Cs^+.
‡From ref. 35. These are up to ±50 kJ mol^{-1} depending on the convention used (36).
§From ref. 35. The Grünwald assumption is used, i.e. ΔH^θ_{tr} of Ph_4As^+ = that of BPh_4^-.
‖$E_{hyd} + E_{tr}$.
¶Values from the Born equation using radius values from Table 4.

teraction with the remainder of the solvent

$$[1] \quad E_{Born} = -\frac{q^2}{2r_B}\left(1 - \frac{1}{\varepsilon} - \frac{T}{\varepsilon}\left(\frac{\partial \ln \varepsilon}{\partial T}\right)_p\right)$$

where r_B is the radius of a sphere containing the ion solvated with 6DMSO's. From Fig. 5 this can be estimated as $\simeq 7$ Å giving $E_{Born} \simeq 103$ kJ mol^{-1}.

Figure 5 suggests that in the case of anions and Cs^+, a well-defined primary solvation shell containing 5DMSO is formed. Thus the anion calculations were done with the ion plus 5DMSO energies. The most reasonable radius for the Born energy calculations in this case is 5.6 Å.

There is considerable difficulty in making a precise assessment of the effective radius of the solvated ions. Thus the Born energy contributions could have an error of up to ±20 kJ mol^{-1}. In principle, the volume of the solvated ions can be obtained from the geometry of the configurations, e.g. Fig. 4, and partial molal volumes of ion could be obtained. However, the overall volume of a configuration such as that in Fig. 4 must be obtained to an accuracy of better than 7% for a Cl^- with 5DMSO if a molal volume of 25 cm^3 mol^{-1} (23) is to be detected, as the molar volume of DMSO is 71 cm^3 mol^{-1}.

Table 7 shows the resulting calculated solvation energies compared to the experimentally determined solvation enthalpies. The classical Born solvation energy (= solvation enthalpy) is also shown. The calculated solvation energies for Na^+, K^+, and Cs^+ are all about 20 kJ mol^{-1} less favourable than the experimental ones. This is good agreement, considering the latitude possible in the choice of the radius used for the Born contribution calculations and the uncertainty in the experimental solvation energy (really enthalpy) due to uncertainty in determining single ion values. Such uncertainties are removed when E_{solv} of pairs of ions are considered.

Data for some Li and K salts are available in ref. 37. A comparison of these data is given in Table 8.

As can be seen in Table 8, there is some uncertainty regarding the experimental solvation enthalpy values, but consideration of Tables 7 and 8 together indicate that the solvation energy calculated here for the Li^+ ion is too great. This is very possibly due to a break-down of the model for small ions where electric fields are high. As can be seen in Table 6, row 8, induced contributions to the Li^+–DMSO energy are of the same order of magnitude as permanent charge contributions. Calculations with data from ref. 38 give second order hyperpolarizability contributions an order of magnitude less than the linear contributions in a field 2 to 3 Å from an ion (see Fig. 5). Nevertheless, the assumption of a single scalar polarizability seems suspect at such small ion–molecule distances, and the induced interactions are far greater for Li^+ than for the other alkali metal and halide ions (except H^+). Representing induced interactions by E_{PI} and E_{II} terms alone has also a maximum error when ions and molecules are close.

Tables 7 and 8 also suggest that the solvation energies calculated for the other ions, but especially the large anions (Cl^-, Br^-, I^-) are too small. The three calculated values for Cl^-, Br^-, and I^- in Table 7 are within 5% of the experimental values if the Fajans convention ($K^+ = F^-$) (36) is used, but this extreme case is unlikely, and would mean larger errors for Na^+, K^+, and Cs^+.

The calculated energies would become considerably greater if radii recently calculated from compressibility data (39) are used. The suggested radii are 1.41 Å for Cl^- (1.65 in Table 4), 1.55 Å for Br^- (1.80 in Table 4), and 1.72 for I^- (2.01 in Table 4). This means that the E_{solv} calculated for I^- with the new radius from (39) would be close to that listed for Br^- in Table 7, in better agreement with the experimental value. Similarly, the new calculated value for Br^- would be close to the old for Cl^-, again in better agreement with the experiment. This indicates how sensitive the calculations are to the choice of input data for the model. Other aspects may, however, be responsible for the low calculated values in Table 7 for Cl^-, Br^-, and I^-.

TABLE 8. Comparison of calculated and experimental solvation energies in DMSO (energies in $-$kJ mol^{-1})

Salt	E_{solv}(calcd) (Table 7)	E_{solv}(exp) from Ref. 37	E_{solv}(exp) from Ref. 35
LiCl	950	896	906
LiBr	934	871	890
LiI	914	841	866
KBr	607	689	699
KI	587	659	675

One of the energy contributions not taken into account in the calculations is the London dispersion attraction between ions and atoms in the molecule. A calculation of this contribution is difficult, as when ion–atom distances are of the order of or less than the ion radius, it is invalid to assume the r^{-6} interaction to be between the centers of the moieties. This contribution could, however, be considerable when ions with a large polarizability such as Cl^-, Br^-, and I^- are involved. Table 3 indicates the London attraction between two DMSO 4.18 Å apart to be -0.13×10^{-19} J. The I^- is 4.6 Å from 5DMSO molecules according to Fig. 5. Thus dispersion interactions could contribute of the order of

$$0.13 \times 10^{-19} \times 5 \times (6.5/8.4) \times (4.18/4.6)^6 \simeq 0.3 \times 10^{-19} \text{ J}$$

or 20 kJ mol^{-1} to the solvation energy of I^-.

Nuclear magnetic resonance results (40) suggest that I^- is strongly solvated in DMSO. Experimental nmr data can also be interpreted to give an idea of the dipole orientation of the solvating molecules (40). As indicated in Table 5, the dipoles are oriented quite radially for all 5 molecules. Inclusion of ion–atom dispersion forces may alter such geometry, as well as the energy of solvation.

The calculations here are completely classical electrostatic. Thus any charge-transfer (donor–acceptor) effects are neglected. Such an approximation is common both for calculations of pure liquids (2, 5) and ion–solvent clusters (41). Parker (42) estimates that donor–acceptor effects may account for less than 10% of the solvation energy for such systems. *Ab initio* molecular orbital calculations (43) indicate that the net quantum mechanical contributions to the solvation of F^- by 4 waters is small (<7%). This is, however, due to fortuitous near-cancellation of an exchange and a charge-transfer term. Thus donor–acceptor considerations may be quite considerable in cases where species such as I^- are involved.

The calculations for H^+ are of a qualitative nature only with the H^+ taken as a charge with radius 0.1 Å and zero polarizability. An interesting effect can, however, be noted from the data in Table 4 and Fig. 5, namely that the H^+ essentially 'belongs' to a single DMSO molecule. This predicts that the mobility of H^+ in DMSO should be of the same magnitude as that of a DMSO molecule. The λ_0 for H^+ in DMSO is obtained at 16.0 Ω^{-1} cm^2 mol^{-1} in ref. 44. This predicts a mobility u for H^+ of $16.0 \times 10^{-4}/(96\,500)^2 = 1.72 \times 10^{-13}$ m s^{-1} N^{-1}. The self-

diffusion coefficient for DMSO is 0.8×10^{-5} cm^2 s^{-1} (40). This corresponds to a mobility for the DMSO molecule of $0.8 \times 10^{-5} \times 10^{-4}/(8.314 \times 298) = 3.2 \times 10^{-13}$ m s^{-1} N^{-1}, somewhat greater than that for the H^+ ion, as is reasonable.

Values of λ_0 for the other ions considered can be found in refs. 45 and 23, with the effective Stokes radii calculated in ref. 45. Li^+, Na^+, K^+ have λ_0 values of 13.3, 14.2, and 14.8 Ω^{-1} cm^2 mol^{-1} respectively, corresponding to Stokes radii of 3.2, 3.0, and 2.9 Å, respectively; well above their crystal radii. The mobilities of these ions would be of the same order as that of H^+, i.e. somewhat lower than that of a DMSO molecule. The Cl^-, Br^-, and I^- have λ_0 of 24.1, 23.7, and 23.5 corresponding to Stokes radii of 1.73, 1.76, and 1.75, of the order of, or less than the radii listed in Table 4. This is another indication of weak solvation of anions by DMSO, contrary to the nmr interpretations (40).

As can be seen from Fig. 5, the larger ions (Cl^-, Br^-, I^-) and Cs^+ have lowest energy configurations which are quite symmetrical, with 5DMSO's in a definable first solvation shell. However, the smaller ions have increasingly asymmetric configurations, although a primary solvation shell of 4DMSO can be identified for K^+, 3 for Na^+, 2 for Li^+ and F^-, and a single DMSO for H^+. Approaches which assume symmetrical solvation shells, e.g. ref. 1, cannot therefore arrive at the lowest energy ion–solvent configurations. At the same time, energy minimum search patterns which 'condense' one molecule after another into an ion–solvent cluster (see Calculation Method) cannot arrive at some symmetric configurations without excessive computation time.

Some other aspects of ion–solvent interactions can be noted by reference to Table 6. Systems 4 and 5 indicate the importance of including polarizability contributions in the calculations. There is a change of 23% in the total energy when α is neglected. Inclusion of the polarizability gives a looser solvent structure around the ion, as the induced dipoles in the first shell solvent molecules cause repulsion.

Systems 6 and 7 in Table 6 indicate the difficulty of defining a definite minimum energy configuration for systems. System 6 has 3 first shell solvent molecules and one second shell, while system 7 has essentially 4 first shell molecules. The energy of 6 is lower because the decrease in repulsion between molecules as compared to the more crowded configuration in system 7 is more than sufficient to overcome the less favourable ion–solvent interaction. Such a trade-off between ion–molecule attraction and molecule–molecule repulsion is present throughout Table 6. The only consistently attractive molecule–molecule term is the London contribution. When it is excluded, the lowest energy system becomes a loose structure with 'streamers' of solvent molecules with head–tail–head–tail orientation coming from the ion.

(c) Ion Pairing of Alkali Halides in DMSO

A series of calculations were made utilizing the model to examine ion pairing of Na^+ and Br^- in DMSO. Figure 6 summarizes the results by presenting the total energy and the various contributions to it as a function of anion–cation distance r_{AC}. These results were obtained by fixing the cation and anion at various positions and allowing 16 DMSO molecules to relax about them into a minimum energy configuration. At least 80 min CPU time were required to reach a final configuration for a particular value of r_{AC}. Figure 7 shows an example of the final configuration obtained.

Two runs were made with $r_{AC} = 4$ Å with different patterns of motion for the molecules. Although the total energy is in reasonable agreement, the final configurations for the two runs are quite different as indicated by the different E_{AD}, E_{CD}, and E_{DD} values. The possible error in E_{TOT} is probably of the order of 1×10^{-19} J, i.e. E_{TOT} values could be lower by up to that amount. This is already of the order of $25kT$ at 298 K. Several more runs under different condi-

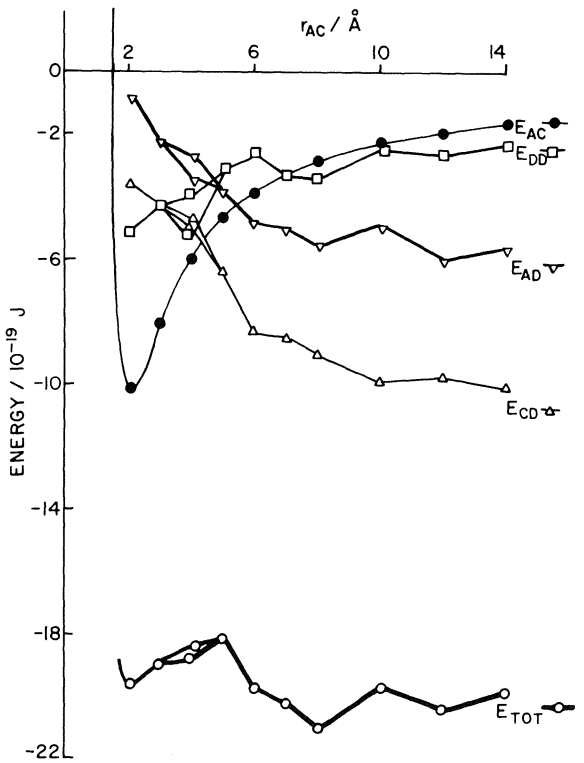

FIG. 6. Energies as a function of distance between Na^+ and Br^- with 16DMSO present.

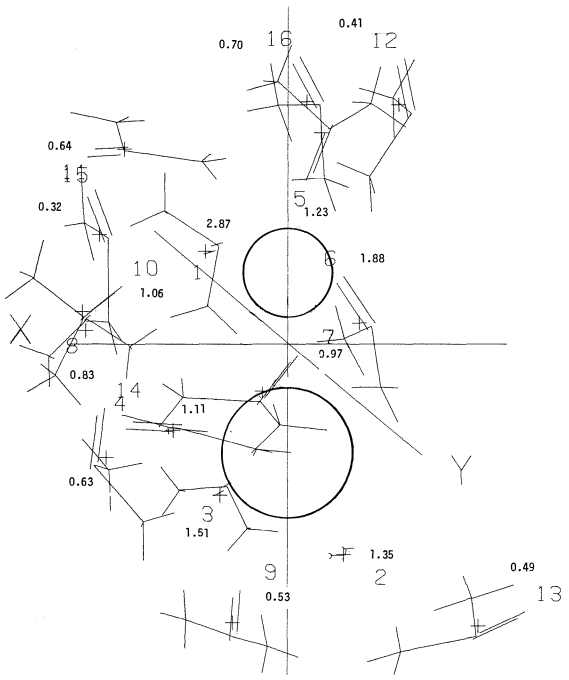

FIG. 7. Final (lowest energy) configuration of a system of 16DMSO and Na^+ and Br^- ions 5 Å apart. Energies of individual molecules in the configuration are given in units of -10^{-19} J.

tions would have to be necessary in order to test the reproducibility of the E_{TOT} values.

One source of error is the possibility of a molecule going into some subsidiary minimum. Some larger step sizes must be allowed for in the pattern governing the relaxation in order for a molecule to break out of a subsidiary energy minimum. It would be desirable to have a picture of the configuration appear at intervals during the relaxation (Fig. 1) so that molecules can be pulled out of obvious energy subminima.

The total energy indicates that the contact ion pair is not the lowest energy position, but instead a solvent separated ion pair with $r_{AC} \simeq 8$ Å. As can be seen from Fig. 7, it is not possible when $r_{AC} = 5$ Å for DMSO's to enter the space between the ions. At 8 Å, however, molecules can fit into this energetically favoured region. The anion and cation fields add constructively in this region, and give favourable ion–molecule energies.

The energy of a system with 16 molecules and the two ions at $r_{AC} = 14$ Å is considerably more favourable than that for two free ions. From Table 4, the energy of an Na^+ and a Br^-, each with 8DMSO molecules would be $(-8.12 - 4.88) \times 10^{-19}$ J $= -13 \times 10^{-19}$ J, considerably less favourable than the -20×10^{-19} J value. From systems 1 and 3 in Table 6 it can be seen that the E_{DD} terms are both repulsive. When $-2 \times 0.45 \times 10^{-19}$ J are added on to both terms to account for addition of two molecules, then the total E_{DD} is approximately zero. This is in agreement with the behaviour of E_{DD} in Fig. 6. As the ions approach, molecule–molecule interactions become more favourable. The value of E_{DD} with no ions present is -6.4×10^{-19} J, approximately where the E_{DD} curve extrapolates for completely overlapping ions ($r_{AC} = 0$).

The ion–molecule interactions terms become less favourable as r_{AC} decreases as there is greater cancellation of ion electric fields in regions other than the interior region. E_{AC} follows the curve postulated for two free gaseous ions in the model. Thus E_{TOT} is the sum of four major effects, two decreasing as r_{AC} decreases and two increasing.

It is likely that the calculations give unrealistically favourable energies for systems when ions have several molecules between them. Table 9 shows E_{CDI} and E_{ADI} contributions to be very large. This is because the fields of the ions add constructively in the interior region. Solvent molecules which would be aligned favourably in this field would give rise to fields opposing the ion fields. Since the induced dipoles are calculated using ion fields only, their magnitudes would be exaggerated giving rise to favourable E_{CDI}, E_{ADI} values.

The classical picture of such ion pairing involves generally smaller energy changes. The difference in energy $q^2/\varepsilon(1/r_1 - 1/r_2)$ in going from 8 Å to 2.1 Å is only 0.2×10^{-19} erg using the continuum value 46.7 for the dielectric constant ε. As indicated in Fig. 7, however, there are no molecules between the ions at $r_{AC} \leq 5$ Å.

Figure 6 indicates that the model predicts the existence of a solvent separated ion pair, and an activation energy for formation of a contact ion pair. This activation energy is from Fig. 6 of the order of 3×10^{-19} J $\simeq 180$ kJ mol^{-1}, an unrealistically high value. It is, however, arrived at by subtraction of two large somewhat uncertain numbers.

The existence of a solvent separated species was postulated in explaining ultrasonic absorption results (46). However, in ultrasonic studies of HCl in DMSO (47), it was not necessary to postulate a solvent separated species. This can be explained by referring to Fig. 5. As the H^+ is essentially solvated by only one molecule, there is greater freedom for the Cl^- to approach it without formation of a distinct solvent separated species. The Na^+ is better shielded by relatively strongly held first solvation shell molecules and cannot as readily be approached by anions.

TABLE 9. Energy contributions to ion pairing of Na^+ and Br^- (energies in 10^{-19} J)

Parameter	Value for $r_{Na^+—Br^-}$ = 2.1 Å	5.0 Å	8.0 Å	14.0 Å
E_{TOT}	−19.62	−18.02	−21.01	−19.77
E_{AC}	−10.17	− 4.70	− 2.90	− 1.65
E_{ACP}	−10.99	− 4.61	− 2.88	− 1.65
E_{ACI}	− 2.72	− 0.08	− 0.01	− 0.00
E_{IIR}	+ 3.53	+ 0.00	+ 0.00	+ 0.00
E_{CD}	− 3.64	− 6.34	− 9.04	−10.09
E_{CDP}	− 1.97	− 3.77	− 4.82	− 6.26
E_{CDI}	− 2.20	− 3.49	− 5.18	− 4.71
E_{DIR}	+ 0.53	+ 0.91	+ 0.97	+ 0.83
E_{AD}	− 0.74	− 3.83	− 5.67	− 5.69
E_{ADP}	− 1.35	− 2.65	− 3.94	− 3.89
E_{ADI}	+ 0.23	− 1.81	− 2.36	− 2.54
E_{DIR}	+ 0.38	+ 0.63	+ 0.63	+ 0.73
E_{DD}	− 5.07	− 3.16	− 3.41	− 2.34
E_{PP}	− 3.05	− 2.45	− 1.88	− 1.56
E_{PI}	− 0.96	− 0.59	− 0.97	− 0.10
E_{II}	+ 0.41	+ 1.00	+ 0.58	+ 0.97
E_{LON}	− 4.00	− 3.38	− 4.27	− 5.05
E_{DDR}	+ 2.53	+ 2.24	+ 3.13	+ 3.39

It was indicated that the choice of the radius for the ions was of great importance in arriving at ion solvation energies. It can be seen from Fig. 6 that the shape of the ion–ion potential (E_{AC}) is of crucial importance in determining the relative energies of the contact and solvent separated ion pairs, or even the existence of a distinct solvent separated ion pair.

The repulsive potential exponent used seems to be in agreement with later work (48), and the inclusion of an r^{-6} term seems not to be necessary (48). There is some question about the correct values to be used for the radii (39) and the polarizability (49, 50). The best comparison of the E_{AC} here would be with that of Woodcock (51) for gaseous alkali halides. The potential used in (51) also has an r^{-1} term, an r^{-4} term, and exponential term which is more complex. The Na^+Br^- potential has a minimum of -8.8×10^{-19} J at 2.5 Å, as compared with -10×10^{-19} J at 2.1 Å here. However, the more recent potential in ref. 52 shows differences from the potentials in ref. 51 which approach that used here (i.e. deeper, further in).

More accurate ion–atom potentials, including dispersion force contributions, would also be desirable, both in calculation of ion pairing and ion solvation phenomena. Such problems have been considered, e.g. ref. 53, but no reasonable simple mathematical forms are presented for the potential. Curves for the Cl^-—Ar potential (53) show, however, that the dispersion energy is approximately one quarter of the induced energy at the energy minimum, i.e. they are not negligible.

Individual contributions to the energy calculated here are listed in Table 9. None of the contributions considered are negligible, and different terms dominate at different values of r_{AC}. Thus it does not seem wise to simplify the calculations by excluding any contribution, and it seems desirable to add some.

Conclusions

The DMSO results discussed here indicate that valuable information regarding ion–solvent and ion pairing interaction can be obtained by this calculation method. Solvation energies, as well as configurations of likely ion–solvent and ion–ion structures, can be obtained with a reasonable amount of computer time. The results obtained are in good agreement with available experimental data, especially considering the fact that really no adjustable parameters were used in the calculations. The position of the scalar polarizability was chosen to reproduce results obtained using bond polarizabilities, but its value was not adjusted. This type of calculation procedure can be generalized to include solvents other than DMSO and more complex ions.

The point charges used to describe the molecule in the energy calculations can be obtained from quantum mechanical calculations, or from experimental data regarding that molecule and others containing common functional groups or bonds (1). The latter approach would seem advantageous for larger species where accurate quantum mechanical calculations are difficult to perform. It may be desirable to extend the point-charge model by also including point

charges in places other than atom centers, e.g. to describe lone pair electrons, or to give a directionality when hydrogen bonding should be included.

Dispersion and repulsion contributions are best described by 6-12 atom centered potentials. Parameters for these potentials are now quite readily available from calculations done on molecules of biological interest, e.g. refs. 3, 5. It seems desirable to extend consideration of dispersion interactions to include ion–atom contributions. A model of an r^{-6} interaction between the centers of an atom and a large ion will not be very accurate however.

Polarizability effects in the molecule cannot be neglected. For most purposes, it seems satisfactory to describe polarizability by one judiciously placed scalar polarizability for the whole molecule. For molecules larger than DMSO, it may, however, be necessary to distribute the polarizability in several places in the molecule, e.g. in the bond centers as in ref. 1. This results in a considerable increase in computation time.

Polarizability effects in the case of small ions seem to be overestimated. This could be alleviated by introducing a hyperpolarizability (i.e., setting $p_i = \alpha F - \beta F^2$). Hyperpolarizability would in any case have to be considered if multivalent ions are to be included. The addition of a second order term in the field may also be a method for compensating for terms left out by describing induced effects solely by E_{PI} and E_{II}. As pointed out in ref. 1, several higher order terms are left out, and these can achieve non-negligible values when ion–molecule distances are small.

It may be unsatisfactory to assume the induced dipoles in molecules to be due to ion fields only. If several aligned polar molecules are considered, then the contribution of the molecule fields may also be considerable. Inclusion of this in the calculations would increase the computation time considerably.

The choice of ion–ion and ion–molecule interactions can have considerable influence on the results. It seems feasible to describe ion–ion interactions reasonably by an r^{-1}, an r^{-4}, and an exponential repulsion term with the factor in the exponent being $\simeq 3$. An r^{-6} term can be added if dispersion interactions involving ions are to be considered. Ion–molecule (really ion–atom) interactions should be extended to include an r^{-6} term. The pre-exponential factor (i.e. the effective size) and the factor in the exponent (i.e. the effective compressibility of the interaction) are more doubtful for the ion–atom case.

The calculation method to arrive at the lowest energy configuration must be such that both symmetric and asymmetric configurations are possible. If only one molecule at a time is moved, this means that at least two patterns for the energy minimum search must be used: (*i*) where molecules are 'condensed' one by one into an ion–solvent cluster and (*ii*), where molecules begin in a symmetric configuration and relax to a minimum energy configuration.

In these calculations, the effect of temperature was neglected. The cut-off for meaningful configurational changes was set at 10^{-23} J $\simeq 5 \times 10^{-3} kT$, so that the precision of the energy of a configuration was $\pm 5 \times 10^{-3} kT$. However, in most cases, the uncertainty in the minimum energy which could be achieved was probably $\gtrsim kT$ (for $T = 298$ K) due to the possibility of subsidiary minima. Thus Monte Carlo calculations were not thought worthwhile, considering the order of magnitude or more of computer time which would have been required. In principle, either Monte Carlo or molecular dynamics simulations are possible for these systems, but with such a large increase in computation time that it would defeat the original intention of an inexpensive, generally usable calculation scheme. The minimum energy configurations obtained here would in MC and/or MD calculations be averaged with many other configurations. The configurations with higher energy would be averaged in with a probability $\exp(\Delta E/kT)$.

The calculations described here cannot readily take into account charge-transfer (donor–acceptor) effects. On any charge transfer, the charge distribution in the species involves changes, so that the complete description of the species must be altered. For systems where charge-transfer effects are minimal, the calculation system described seems quite useful. Copies of the programs used can be obtained from P.K.

Acknowledgements

The authors wish to thank the National Research Council of Canada for financial support through a post-doctoral fellowship to B.E.P. and Carleton University for a computing grant.

1. M. S. Goldenberg, P. Kruus, and S. K. F. Luk. Can. J. Chem. **53**, 1007 (1975).
2. F. H. Stillinger and Z. Wasserman. J. Phys. Chem. **82**, 929 (1978).
3. F. A. Momany, R. F. McGuire, A. W. Burgess, and H. A. Scheraga. J. Phys. Chem. **75**, 2361 (1975).
4. F. H. Stillinger and A. Rahman. J. Chem. Phys. **60**, 1545 (1974); **61**, 4973 (1974).
5. F. A. Momany, L. M. Carruthers, R. F. McGuire, and H. A. Scheraga. J. Phys. Chem. **78**, 1595 (1974).
6. F. F. Abraham, M. R. Mruzik, and G. M. Pound. J. Chem. Soc. Faraday Discuss. **61**, 34 (1976).
7. J. C. Owicki and H. A. Scheraga. J. Am. Chem. Soc. **99**, 7413 (1977).
8. A. T. Hagler and J. Moult. Nature, **272**, 222 (1978).

9. S. F. O'SHEA and W. J. MEATH. Mol. Phys. **28**, 1431 (1974).
10. D. J. EVANS and R. O. WATTS. Mol. Phys. **31**, 83 (1976).
11. P. SCHUSTER, W. JAKUBETZ, and W. MARIUS. Top. Curr. Chem. **60**, 1 (1975).
12. W. R. DAVIDSON and P. KEBARLE. J. Am. Chem. Soc. **98**, 6125 (1976).
13. M. SALOMON. Can. J. Chem. **53**, 3194 (1975).
14. B. M. RODE. Chem. Phys. Lett. **20**, 366 (1973).
15. P. P. S. SALUJA. Z. Phys. Chem. N.F. **94**, 187 (1975).
16. A. GUPTA and C. N. R. RAO. J. Phys. Chem. **77**, 2888 (1973).
17. E. CLEMENTI. Determinations of liquid water structure coordination numbers for ions and solvation for biological molecules. Springer, Berlin. 1976.
18. K. G. SPEARS and S. H. KIM. J. Phys. Chem. **80**, 673 (1976).
19. P. A. KOLLMAN and I. D. KUNTZ. J. Am. Chem. Soc. **96**, 4766 (1974).
20. P. CLAVERIE, J. P. DAUDEY, J. LANGLET, B. PULLMAN, D. PIAZZOLA, and M. J. HURON. J. Phys. Chem. **82**, 405 (1978).
21. V. GUTMANN. Electrochim. Acta, **21**, 661 (1976).
22. S. W. JACOB and R. HERSCHLER (*Editors*). Biological actions of dimethyl sulfoxide. Ann. N.Y. Acad. Sci. **243** (1975).
23. K. M. KALE and R. ZANA. J. Solution Chem. **6**, 733 (1977).
24. R. THOMAS, C. B. SHOEMAKER, and K. ERIKS. Acta Crystallogr. **21**, 12 (1966).
25. J. O. HIRSCHFELDER, C. F. CURTISS, and R. B. BIRD. Molecular theory of gases and liquids. Wiley, New York. 1954.
26. E. R. LIPPINCOTT, G. NAGARAJAN, and J. M. STUTMAN. J. Phys. Chem. **70**, 78 (1960).
27. A. J. PARKER. Chem. Rev. **69**, 1 (1969).
28. F. G. FUMI and M. P. TOSI. J. Phys. Chem. Solids, **25**, 31 (1964); **21**, 45 (1964).
29. A. J. MICHAEL. J. Chem. Phys. **51**, 5730 (1969).
30. S. KITA, K. NODA, and H. INOUYE. Chem. Phys. **7**, 156 (1975).
31. T. B. DOUGLAS. J. Am. Chem. Soc. **70**, 2001 (1948).
32. A. BONDI. *In* Condensation and evaporation of solids. *Edited by* E. Rutner, P. Goldfinger, and J. P. Hirth. Gordon and Breach, New York. 1964.
33. J. M. HAILE, D. LITCHINSKY, R. MCPHERSON, C. G. GRAY, and K. E. GUBBINS. J. Comput. Phys. **21**, 227 (1976).
34. J. KUSHICK and B. J. BERNE. J. Chem. Phys. **64**, 1362 (1976).
35. S. AHRLAND. *In* The chemistry of nonaqueous solvents. Vol. VA. *Edited by* J. J. Lagowski. Academic Press, New York. 1978.
36. E. A. MOELWYN-HUGHES. Physical chemistry. 2nd ed. Pergamon, New York. 1961. p. 875.
37. R. F. RODEWALD, K. MAHENDRAN, J. L. BEAR, and R. FUCHS. J. Am. Chem. Soc. **90**, 6698 (1968).
38. B. F. LEVINE and G. G. BETHEA. J. Chem. Phys. **63**, 2666 (1975); B. F. LEVINE. J. Chem. Phys. **63**, 115 (1975).
39. M. C. ABRAMS, C. CACCAMO, G. PIZZIMENTI, M. PARRINELLO, and M. P. TOSI. J. Chem. Phys. **68**, 2889 (1978).
40. H. WEINGARTNER and H. G. HERTZ. Ber. Bunsenges. Phys. Chem. **81**, 1204 (1977).
41. C. L. BRIANT and J. J. BURTON. J. Chem. Phys. **64**, 2888 (1976).
42. A. J. PARKER. Electrochim. Acta, **21**, 671 (1976).
43. J. O. NOELL and K. MOROKUMA. J. Phys. Chem. **80**, 2675 (1976).
44. C. MCCALLUM and A. D. PETHYBRIDGE. Electrochim. Acta, **20**, 815 (1975).
45. N. MATSUURA, K. UMEMOTO, and Y. TAKEDA. Bull. Chem. Soc. Jpn. **48**, 2253 (1975).
46. D. R. DICKSON and P. KRUUS. Can. J. Chem. **49**, 3107 (1971).
47. P. KRUUS and M. J. MCGUIRE. Can. J. Chem. **56**, 1881 (1978).
48. J. CORISH, B. M. C. PARKER, and P. W. M. JACOBS. Can. J. Chem. **54**, 3839 (1976).
49. K. FAJANS. J. Phys. Chem. **74**, 3407 (1970).
50. H. COKER. J. Phys. Chem. **80**, 2078 (1976); **80**, 2084 (1976).
51. L. V. WOODCOCK. J. Chem. Soc. Faraday II, **70**, 1405 (1974).
52. J. MICHIELSEN, P. WOERLEE, F. V. D. GRAAF, and J. A. A. KETCLAAR. J. Chem. Soc. Faraday II, **71**, 1730 (1975).
53. Y. S. KIM and R. G. GORDON. J. Chem. Phys. **61**, 1 (1974).

Ipso chlorination of 4-alkylphenols. Formation of 4-alkyl-4-chlorocyclohexa-2,5-dienones

ALFRED FISCHER AND GEORGE NARAYANAN HENDERSON

Department of Chemistry, University of Victoria, Victoria, B.C., Canada V8W 2Y2

Received September 5, 1978

ALFRED FISCHER and GEORGE NARAYANAN HENDERSON. Can. J. Chem. **57**, 552 (1979).

Chlorination of 4-methyl-, 4-ethyl-, 4-isopropyl-, and 4-*tert*-butylphenol, and of substituted 4-methylphenols, with chlorine in acetic anhydride gives 4-chloro-4-methyl-, 4-chloro-4-ethyl-, 4-chloro-4-isopropyl-, and 4-chloro-4-*tert*-butylcyclohexa-2,5-dien-1-one, and substituted 4-chloro-4-methylcyclohexa-2,5-dien-1-ones, respectively, in yields ranging from 19 to 100%.

ALFRED FISCHER et GEORGE NARAYANAN HENDERSON. Can. J. Chem. **57**, 552 (1979).

La chloration, par le chlore dans l'anhydride acétique, des méthyl-4 éthyl-4, isopropyl-4 et *tert*-butyl-4 phénols et de méthyl-4 phénols substitués conduit respectivement aux chloro-4 méthyl-4, chloro-4 éthyl-4, chloro-4 isopropyl-4 et chloro-4 *tert*-butyl-4 cyclohexadiène-2,5 ones-1 et aux chloro-4 méthyl-4 cyclohexadiène-2,5 ones-1 substituées avec des rendements allant de 19 à 100%.

[Traduit par le journal]

The formation of halo cyclohexadienones in the bromination and chlorination of cresols, xylenols, and trimethylphenol was recognized by Zincke over 80 years ago.[1] Although Auwers subsequently proposed nonketonic structures for these compounds, the dienone structures have long been accepted and modern spectroscopic methods have established them conclusively (2, 4). A very large number of halo cyclohexadienones are now known (e.g., 23 4-halocyclohexa-2,5-dienones are indexed in Vol. 86 of Chemical Abstracts). However, all but a very few of these are derived from phenols which are either fully substituted in the reactive *ortho* and *para* positions or, if the substrate phenol is not 2,4,6-trisubstituted, it becomes so through halogenation in the course of formation of the dienone (none of the 23 cyclohexa-2,5-dienones mentioned above is less than tetrasubstituted). Thus, it is not surprising that the view became current that the halo cyclohexadienones were only formed after prior nuclear halogenation of the phenol substrates (1) and that even in quite recent studies of the chlorination of phenols to form (poly)chlorocyclohexadienones the technique of exhaustive chlorination has been used without apparent consideration of the possibility of formation of the less substituted compounds (4, 5). Halocyclohexadienones occur in both the fully-conjugated *ortho* (i.e., 2,4-dienone) and cross-conjugated *para* (2,5-dienone) series, the 2,5-dienones being more stable than their 2,4-isomers (2).

In the present work we have synthesised a number of simple 4-chloro-2,5-dienones. These compounds are of interest as substrates for dienone–phenol rearrangement studies (cf. ref. 6) and also, in view of their functionalized nature, as potential intermediates for synthetic studies. The formation of the dienones is also of interest in relation to studies of 'abnormal' or 'non-conventional' pathways in reactions of aromatic substrates with electrophiles (7, 8). Of the compounds synthesised in the present work only 4-chloro-4-methylcyclohexa-2,5-dienone (9) and 4-chloro-3,4-dimethylcyclohexa-2,5-dienone (10, 11) have been reported previously. Bromocyclohexadienones were obtained by bromination of phenols with molecular bromine in solvents such as acetic acid, ether, hexane, and carbon tetrachloride, in the presence of a suitable basic species, which is required to accept the proton from the hydroxyl group (1, 2). Chlorocyclohexadienones were obtained by chlorination of phenols with chlorine in acetic acid or aqueous acetic acid (4, 11, 12–14), carbon tetrachloride (12), chloroform (15), ether (16), and in the solid state (17). Other chlorinating agents such as alkyl hypochlorites (13, 18, 19), sulfuryl chloride (15), hypochlorous acid (19), and antimony pentachloride (9) have been used. These reactions, with the exception of the last, were carried out at ambient or elevated temperatures and resulted in the formation of the mixtures of polychlorinated cyclohexadienones and cyclohexenones. Our objective was to prepare the 4-chlorocyclohexa-2,5-dienones under conditions such that

[1]Formation of halocyclohexadienones has been reviewed by Ershov *et al.* (1) and by Waring (2). References to the early literature may be found in ref. 1. Ershov and Volod'kin have themselves made extensive contributions to the study of the formation of halo dienones, e.g. ref. 3.

0008-4042/79/050552-06$01.00/0

the only other products were the chlorophenols obtained on normal substitution of the phenol substrates.

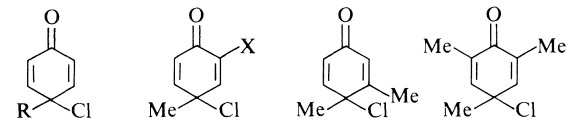

1 R = Me
2 R = Et
3 R = *i*Pr
4 R = *t*Bu

5 X = Cl
6 X = Me
7 X = *t*Bu
8 X = Br

9

10

Results and Discussion

Preliminary nmr studies of the chlorination of *p*-cresol with chlorine in a variety of solvents showed that the maximum yield (~33%) of 4-chloro-4-methylcyclohexa-2,5-dienone (**1**) was obtained in acetic anhydride. Good yields were also obtained in mixtures of acetic anhydride and acetic acid, chloroform, or ether, and also in aqueous acetic acid, chloroform, and pyridine–chloroform. Less dienone was obtained in neat ether and yields in methanol, dioxane, and acetonitrile were poor. Chlorination with sulfuryl chloride in acetic anhydride also gave a good yield of **1** and a similar yield of **1** was obtained when chlorine was used in the presence of a catalytic amount of iodine. In chlorination with molecular chlorine the yield of dienone measured at −40°C was not reduced when the temperature was subsequently raised, in one case to 35°C. When the ratio of the amount of chlorine to *p*-cresol was raised above 1:1 the total yield of dienones increased and 2,4-dichloro-4-methylcyclohexa-2,5-dienone (**5**) was obtained in addition to **1**. Preparative-scale (~0.1 mol) experiments confirmed these observations. Chlorination of *p*-cresol in acetic anhydride gave a 31% yield of dienone **1**. Chlorination in ether gave 20% of the dienone but chlorination in ether (1 dm^3 per mole of *p*-cresol) containing 16% acetic anhydride gave almost the same yield (29%) as in neat acetic anhydride and was more convenient for large scale preparations. Chlorination in aqueous acetic acid (1:3 v/v) gave a similar yield of dienone to that using ether – acetic anhydride. Chlorination using a mole ratio of chlorine to *p*-cresol of 1:1 gave a higher yield (34%) of dienone than did the normal 0.9:1 ratio but this included a small amount of 2,4-dichloro-4-methylcyclohexa-2,5-dienone. When the mole ratio of chlorine was increased to 1.5:1 the yield of dienones increased to 54% of which half was the dichloro compound. Separation of dienone **1** from accompanying phenols was more straightforward than the separation of the dienones **1** and **5**. For this reason we chose to use a chlorine to substrate ratio of 0.9:1 in the general preparative method, thus reducing the opportunity for dichlorination to occur. Apart from the preliminary reactions with *p*-cresol reactions were carried out by mixing the reactants at −78°C and then raising the temperature to −20°C. This was to minimize the possibility of dichlorination as a result of reaction occurring before complete mixing of the reactants. The low reaction temperature ruled out the use of acetic acid as solvent and the reactions were generally done in acetic anhydride. In a large-scale preparation (2 mol) use of the mixed solvent 16% acetic anhydride in ether made for a more convenient work-up.

Chlorination of the substituted phenols gave the corresponding 4-chlorocyclohexa-2,5-dienones in yields ranging from 19% (for **4**) to 100% (for **10**). In general the chlorophenol substitution products were also formed but these were removed by absorption on alumina in the process of isolating the dienones and were not themselves isolated and identified. 2,4-Dichloro-4-methylcyclohexa-2,5-dienone (**5**) was obtained, in addition to **1**, and was isolated and characterised from the chlorination of *p*-cresol using a chlorine to substrate ratio of 1.5:1.

The structures of the dienones are clearly established by their spectra. Infrared absorptions at 1675 (C=O) and 1640 cm^{-1} (C=C) in the spectrum of **1** confirm the presence of the conjugated enone system. The ^1H nmr shows that there are four vinylic protons (AB quartet) consisting of two pairs, the members of each pair being chemically identical. Thus the enone is a dienone and specifically a 2,5-dienone, with a plane of symmetry, rather than a less symmetrical 2,4-dienone. The ^{13}C nmr spectrum confirms the presence of two pairs of olefinic carbons, a quaternary carbon, and carbonyl carbon. These can only be accommodated by the 2,5-dienone structure. Similar arguments can be adduced to support the assigned structures for **2**, **3**, **4**, and **10**. The symmetry argument cannot be applied to distinguish between the *ortho*- and *para*-dienone structures in the cases of **5**, **6**, **7**, **8**, and **9**. However, it is apparent that the methyl group which appears at ~30 ppm in the ^{13}C nmr spectra must be attached to a quaternary carbon atom and thus **5**, **7**, **8**, and **9** must be 2,5-dienones. This is confirmed by the fact that this methyl group appears as a singlet in the ^1H nmr spectrum. In the *ortho*-dienone structure this methyl group would be attached to an unsaturated carbon and be split by a vinylic proton(s). Finally the close correspondence between the absorptions of groups in similar environments in both the ^1H and ^{13}C nmr spectra of **6** and **10** and more generally between **6** and the other 2,5-

dienones establishes that **6** must be a 2,5-dienone. Thus in the ^{13}C spectrum of **6** the methyl groups appear at almost exactly the same positions as those in **10**, indicative of the close structural similarity.

It is evident that in chlorination of phenols with molecular chlorine attack at a substituted *para* position is competitive with attack at an unsubstituted *ortho* position.[2] Furthermore it would appear that attack at a substituted *para* position is dominant over attack at a substituted *ortho* position: no *ortho* dienones were obtained from 2,4-disubstituted phenols and mesitol gave the 2,5-dienone as the sole product.[3] However since *para* dienones are known to be more stable than *ortho* dienones (2) it is possible that an initially formed *ortho* dienone is rapidly equilibrated to its more stable *para* isomer. A further illustration of the difficulty of forming *ortho* dienones in chlorination was provided by the failure of both 2,6-dimethylphenol and 2,5-dimethylphenol to form dienones (see below). The latter example is particularly significant since we have shown that this phenol gives a 90% yield of 2,5-dimethyl-2-nitrocyclohexadienone on nitration in acetic anhydride.[4]

Nilsson and co-workers (9) obtained **1** in close to quantitative yield on chlorination of *p*-cresol with a massive excess of antimony pentachloride in dichloromethane at $-60°C$. We were able to obtain a good yield of **1** following their procedure but the work-up proved troublesome and it was found necessary to centrifuge the mixture to separate the organic and aqueous phases. An added disadvantage of the method is the large amount of antimony pentachloride required. Hussain (10) obtained **9** as well as 4,6-dichloro- and 2,4,6-trichloro-3,4-dimethylcyclohexa-2,5-dienones on chlorination of 3,4-dimethylphenol with 3 mol of *tert*-butyl hypochlorite in 90% acetic acid. It was claimed that no dienones were formed when one and two moles of the chlorinating agent were used, but it seems more likely that **9** was formed under these conditions but was not noticed. de la Mare and co-workers (11) subsequently obtained **9** on chlorination of 3,4-dimethylphenol with molecular chlorine in acetic acid. They did not obtain the compound pure and stated that it is unstable and that it decomposes in acetic acid to a mixture of 3,4-dimethylphenol and 2-chloro-4,5-dimethyl phenol. We have found that the crystalline compound, like the other dienones, is quite stable in the pure state at ambient temperature and that a solution of the dienone in acetic acid did not react over a period of one week. de la Mare *et al.* (11) also observed a trichlorocyclohexenone in the products of chlorination of 3,4-dimethylphenol and they proposed that it is an intermediate in the formation of 2,4-dichloro-4,5-dimethylcyclohexa-2,5-dienone. Under our conditions we did not observe the formation of any trichlorocyclohexenones. A likely route to the dichlorocyclohexadienone is from the further chlorination at the substituted *para* position of the chlorophenol produced by *ortho* chlorination.

In addition to those for *p*-cresol preliminary nmr scale experiments were also carried out on the other phenol precursors to the dienones **2**–**4** and **6**–**10** to establish the conditions for the subsequent 0.1-mol scale dienone preparations. Yields of dienones were generally consistent with those obtained in the larger scale experiments. Nuclear magnetic resonance scale experiments were also carried out on 2,5-dimethyl-, 2,6-dimethyl-, 4-chloro-, 2,4-dichloro-, and 3-methyl-4-chlorophenol. In no case was any dienone detected. The dimethylphenols have been discussed above. In the cases of the chlorophenols it appears that substitution at the unsubstituted *ortho* position(s) occurs more readily than addition to the *para* position which is *ipso* to chlorine. Dienones have been formed from chlorophenols but only when the chlorophenols had no unsubstituted positions *ortho* or *para* to the hydroxyl group (4, 5, 12, 13, 19). For nitration, positions *ipso* and *meta* to chlorine are of comparable reactivity: $i_f^{Cl}:m_f^{Cl} = 1:1\text{–}2$ (20, 21). Chlorination, for which $\rho = -10$ (22), is more sensitive to small differences in substituent electronic effects than is nitration, for which $\rho = -6$ (22). Even so, some chlorination ($\sim 25\%$) should occur *ipso* to chlorine in *p*-chlorophenol and the fact that it does not suggests some specific *ipso* deactivation in chlorination. Even *p*-cresol is less susceptible to chlorination at the 4-position than expected. Phenol is chlorinated to about the same extent at the *ortho* and *para* positions (23) i.e., the *para* position is twice as reactive as an *ortho* position. For nitration $i_f^{Me}:m_f^{Me} = 2\text{–}4:1$ (24). Thus the methyl group is more activating at the *ipso* than the *meta* position and hence *p*-cresol should be chlorinated to a greater extent at the 4-position *ipso* to methyl than at the unsubstituted 2-position. In fact the 2- and 4- positions in *p*-cresol appear to be equally reactive towards chlorine with only one-third of the product arising from *ipso* attack. The lower than expected reactivity of *ipso* positions towards chlorination is also consistent with the behaviour of hydrocarbon substrates in chlorination. *p*-Xylene, 1,2,3,5-tetramethylbenzene (isodurene), and 5-*tert*-butyl-1,2,3-trimethylbenzene all give good

[2]It has been stated (9) that "chlorination of *p*-alkylated phenols with the traditional chlorinating agents usually gives *o*-chlorophenols..." with the intended and clearly incorrect implication that 4-chlorodienones are not formed.

[3]A 5% yield of *ortho* dienone would have been detected in the crude chlorination product from 2,4-dimethyl- and 2,4,6-trimethylphenol.

[4]Unpublished work.

yields of diene adducts in nitration (25). However, no adducts could be detected on chlorination nor were any side-chain products formed (which would point to the intermediate formation of an *ipso*-cyclohexadienyl cation intermediate (25)). It is of course also possible that an initially formed *ipso*-chlorocyclohexadienyl cation could revert to the reactants or rearrange to the non-*ipso* cation, precursor to the nuclear chlorination product, without forming adduct.

Nuclear magnetic resonance scale experiments were also carried out using *p*-cresyl acetate and *p*-methylanisole as substrates. These compounds were so much less reactive than the phenols that under conditions under which *p*-cresol reacted completely they were largely unreacted, although a small amount of dienone was formed in each case.

Experimental

4-Methyl, 4-ethyl-, 4-isopropyl-, 4-*tert*-butyl-, 2,4-dimethyl-, 2-*tert*-butyl-4-methyl-, 2-bromo-4-methyl-, 3,4-dimethyl-, and 2,4,6-trimethylphenol were from Aldrich. Alumina was Camag basic, activity I.

Infrared spectra were obtained on a Pye-Unicam SP1000 or a Perkin-Elmer 337 spectrophotometer. ^{1}H nuclear magnetic resonance spectra at 90 MHz were determined using a Perkin-Elmer R32 spectrometer. ^{13}C nmr spectra at 15.1 MHz were obtained with a Nicolet TT-14 spectrometer. Mass spectra were obtained on a Hitachi Perkin-Elmer RMU 7 spectrometer. High pressure liquid chromatography was carried out with a Waters Prep LC/System 500.

Nuclear Magnetic Resonance Scale Experiments

Chlorine (24 cm^3, 1 mmol) was injected from a hypodermic syringe into a solution of the substrate (1 mmol) in the appropriate solvent (400 mm^3) in an nmr tube at −78°C and the nmr spectra were recorded at −40°C and at successively higher temperatures until reaction was observed. Some experiments were carried out on a 0.5-mmol scale.

Chlorination of p-*Cresol: 4-Chloro-4-methylcyclohexa-2,5-dien-1-one (**1**) and 2,4-Dichloro-4-methylcyclohexa-2,5-dien-1-one (**5**)*

Chlorine (2.2 dm^3, 0.09 mol) was bubbled over 2 min, into a stirred solution of *p*-cresol (10.8 g, 0.1 mol) in acetic anhydride (200 cm^3) at −78°C. After 10 min the reaction mixture was warmed to −20°C for 15 min and then cooled to −78°C and poured into ether (1.5 dm^3) at −78°C. Ammonia was condensed into the vigorously stirred ether solution, which was cooled in solid carbon dioxide – acetone, at a rate such that the temperature did not rise above −65°C. Excess ammonia was aspirated and the mixture allowed to warm to 0°C. The solution was washed (×5) with ice water, dried ($MgSO_4$), and the solvent evaporated. The crude product (13.8 g) contained 28% of a single dienone (31% yield based on chlorine), 62% of chlorophenol(s), and 10% of *p*-cresol, by nmr. Filtration of a pentane solution of the mixture through 20 times its weight of basic alumina and elution with ether gave the pure dienone (when ether solutions of the residue were used two filtrations through alumina were required for purification). The 4-chloro-4-methylcyclohexa-2,5-dienone gave a positive Beilstein test (26)[5] and had ir: 1675 (C=O), 1640 (C=C), 708 cm^{-1} (C—Cl); ^{1}H nmr ($CDCl_3$) δ: 1.69 (s, 3, CH_3), 6.16(d, 2, J = 10 Hz, 2-*H* and 6-*H*), 6.95 ppm (d, 2, J = 10 Hz, 3-*H* and 5-*H*); ^{13}C nmr ($CDCl_3$) δ_C: 29.4 (*C*H$_3$), 59.9 (*C*-4), 126.5 (*C*-2 and *C*-6), 149.5 (*C*-3 and *C*-5), 184.1 ppm (*C*-1); ms (70 eV) *m/e* (relative intensity): 144 (20) and 142.022 (57, M_r ($^{12}C_7{}^1H_7{}^{35}Cl^{16}O$): 142.019), 108 (68), 107 (100, M − Cl), 79 (30), 77 (35).

Similar chlorinations were carried out in ether (18% dienone, 20% yield), 16% acetic anhydride in ether (26%, 29% yield) and, with a 1:1 mole ratio of chlorine to *p*-cresol, in acetic anhydride (34% dienone(s)) and, at −10°C, in aqueous acetic acid (1:3 v/v) (31% dienones).[6] Chlorination was also carried out with sulfuryl chloride by adding the chloride (7.3 cm^3, 0.09 mol) over 15 min to a solution of *p*-cresol (10.8 g, 0.1 mol) in acetic anhydride (200 cm^3), with stirring, at −78°C. After a further 15 min the mixture was warmed to −20°C, maintained at that temperature for 15 min and worked up in the usual manner to yield the mixture of the dienone (31%, 34% yield) and phenols. Chlorination with antimony pentachloride (9) was carried out by adding a solution of *p*-cresol (9.0 g, 0.083 mol) in dichloromethane (250 cm^3) at −50°C over 2 h to a solution of antimony pentachloride (60 cm^3, 0.47 mol) in dichloromethane (150 cm^3) at −70°C. The mixture was stirred for 10 min at −60°C, cooled to −78°C, and cold methanol (50 cm^3) was added dropwise keeping the temperature below −70°C. The mixture was poured into water (200 cm^3). The sticky mass produced could not be filtered (as called for in the literature procedure) and it was centrifuged to separate the organic layer, which was then washed with phosphate buffer (pH 6), diluted with ether, and washed (×3) with water. After drying and removal of the solvent the product (9.8 g) contained dienone (86%) and phenols (14%). Pure dienone (7.3 g) was obtained on passage of an ethereal solution of the crude dienone through alumina.

Chlorination of *p*-cresol in aqueous acetic acid with 1.5:1 mole ratio of chlorine to substrate gave a product containing both **1** (27%) and **5** (27%). High pressure liquid chromatography on silica using ether solvent afforded the mixed phenols, the mono- and the dichlorodienones. The 2,4-dichloro-4-methylcyclohexa-2,5-dienone (**5**) was further purified by filtration through basic alumina and had ir: 1680 (C=O) 1640 (C=C), 727 (C—Cl), 660 cm^{-1} (C—Cl); ^{1}H nmr ($CDCl_3$) δ: 1.86 (s, 3, CH_3), 6.27 (d, 1, J_{56} = 10 Hz, 6-*H*), 6.97 (dd, 1, J_{35} = 2.7 Hz, J_{56} = 10 Hz, 5-*H*), 7.12 ppm (d, 1, J_{35} = 2.7 Hz, 3-*H*); irradiation of the 6-*H* resonance at 6.27 collapsed the 5-H quartet to a doublet and irradiation of the 5-*H* resonance at 6.97 collapsed the 6-*H* doublet to a singlet; ^{13}C nmr ($CDCl_3$) δ_C: 29.5 (4-*C*H$_3$), 61.0 (*C*-4), 125.4 (*C*-6), 145.4 (*C*-3), 149.8 (*C*-5), 177.4 ppm (*C*-1); *C*-2 was not detected; ms (70 eV) *m/e* (relative intensity): 178 (20) and 175.981 (32, M_r ($^{12}C_7{}^1H_6{}^{35}Cl_2{}^{16}O$): 175.980), 144 (25), 143 (22), 142 (70), 141 (60), 113 (20), 108 (14), 107 (100), 78 (15), 77 (65).

*4-Chloro-4-ethylcyclohexa-2,5-dien-1-one (**2**)*

Chlorination of *p*-ethylphenol (12.2 g, 0.1 mol) in acetic anhydride gave crude product (14.9 g) containing 49% (54% yield) of dienone. Filtration of a solution in ether through basic alumina gave 4-chloro-4-ethylcyclohexa-2,5-dienone (**2**) as an oil; ir: 1672 (C=O), 1635 (C=C), 870 cm^{-1} (C—Cl); ^{1}H nmr ($CDCl_3$) δ: 0.96 (t, 3, J = 7.0 Hz, CH_2CH_3), 2.12 (q, 2, J = 7.0 Hz, CH_2CH_3), 6.25 (d, 2, J = 10 Hz, 2-*H* and 6-*H*), 6.88 ppm (d, 2, J = 10 Hz, 3-*H* and 5-*H*); ^{13}C nmr ($CDCl_3$) δ_C: 9.3 (CH_2CH_3), 35.3 (CH_2CH_3), 63.8 (*C*-4), 127.9 (*C*-2 and *C*-6), 148.6 (*C*-3 and *C*-5), 184.6 ppm (*C*-1); ms (70 eV) *m/e* (relative intensity): 156.035 (22, M_r($^{12}C_8{}^1H_9{}^{35}Cl^{16}O$):

[5]All of the chlorodienones gave a positive Beilstein test (26).

[6]Chlorinations in ether and aqueous acetic acid were worked up by washing with cold bicarbonate solution.

156.034), 141 (12), 130 (14), 128 (38), 122 (37), 121 (22), 113 (18), 107 (100), 93 (40), 91 (35), 78 (15), 77 (65).

*4-Chloro-4-isopropylcyclohexa-2,5-dien-1-one (**3**)*

Chlorination of *p*-isopropylphenol (13.6 g, 0.1 mol) in acetic anhydride gave crude product (16.4 g) containing 35% (39% yield) of dienone. Filtration of a solution in ether through basic alumina gave 4-chloro-4-isopropylcyclohexa-2,5-dienone (**3**) as an oil; ir: 1675 (C=O), 1635 (C=C), 870 cm^{-1} (C—Cl); ^1H nmr ($CDCl_3$) δ: 1.06 (d, 6, J = 7 Hz, $CH(CH_3)_2$), 2.23 (septet, 1, $CH(CH_3)_2$), 6.26 (d, 2, J = 10 Hz, 2-*H* and 6-*H*), 6.92 ppm (d, 2, J = 10 Hz, 3-*H* and 5-*H*); ^{13}C nmr ($CDCl_3$) δ_C: 17.7 ($CH(CH_3)_2$), 38.5 ($CH(CH_3)_2$), 67.4 (*C*-4), 128.2 (*C*-2 and *C*-6), 147.6 (*C*-3 and *C*-5), 184.7 ppm (*C*-1); ms (70 eV) *m/e* (relative intensity): 170.049 (6, $M_r(^{12}C_9{}^1H_{11}{}^{35}Cl{}^{16}O)$: 170.050), 155 (19, $M - CH_3$), 136 (35), 130 (32) and 128 (100, $M - C_3H_6$), 121 (94), 107 (13), 103 (12), 91 (42), 77 (16).

*4-*tert*-Butyl-4-chlorocyclohexa-2,5-dien-1-one (**4**)*

Chlorination of *p-tert*-butylphenol (15 g, 0.1 mol) in acetic anhydride gave crude product (17.2 g) containing 17% (19% yield) of dienone. Filtration of a solution in pentane through alumina and elution with ether gave 4-*tert*-butyl-4-chlorocyclohexa-2,5-dienone (**4**), which was recrystallized from pentane as colourless needles, mp 60°C; ir (Nujol): 1680 (C=O), 1660 (C=C), 872 cm^{-1} (C—Cl); ^1H nmr ($CDCl_3$) δ: 1.12 (s, 9, $C(CH_3)_3$), 6.24 (d, 2, J = 10 Hz, 2-*H* and 6-*H*), 7.05 ppm (d, 2, J = 10 Hz, 3-*H* and 5-*H*); ^{13}C nmr ($CDCl_3$) δ_C: 25.6 ($C(CH_3)_3$), 39.4 ($C(CH_3)_3$), 70.5 (*C*-4), 127.8 (*C*-2 and *C*-6), 147.7 (*C*-3 and *C*-5), 184.6 ppm (*C*-1); ms (70 eV) *m/e* (relative intensity): 184.068 (3, $M_r(^{12}C_{10}{}^1H_{13}{}^{35}Cl{}^{16}O)$: 184.065), 169 (14, $M - CH_3$), 150 (15), 135 (45), 128 (22), 107 (20), 91 (19), 77 (15), 57 (100, $C(CH_3)_3{}^+$). *Anal.* calcd. for $C_{10}H_{13}ClO$: C 65.04, H 7.10; found: C 65.40, H 7.28.

*4-Chloro-2,4-dimethylcyclohexa-2,5-dien-1-one (**6**)*

Chlorination of 2,4-dimethylphenol (12.2 g, 0.1 mol) in acetic anhydride gave crude product (14.4 g) containing 45% (50% yield) of dienone. Filtration of a solution in ether through alumina gave 4-chloro-2,4-dimethylcyclohexa-2,4-dienone (**6**) as an oil; ir: 1670 (C=O), 1647 (C=C), 890 cm^{-1} (C—Cl); ^1H nmr ($CDCl_3$) δ: 1.79 (s, 3, 4-CH_3), 1.88 (d, 3, J = 1.5 Hz, 2-CH_3), 6.15 (d, 1, J_{56} = 10 Hz, 6-*H*), 6.73 (m, 1, 3-*H*), 6.91 ppm (dd, 1, J_{35} = 3 Hz, J_{56} = 10 Hz, 5-*H*); ^{13}C nmr ($CDCl_3$) δ_C: 15.6 (2-CH_3), 29.7 (4-CH_3), 61.0 (*C*-4), 126.3 (*C*-6), 133.4 (*C*-2), 145.2 (*C*-3), 149.4 (*C*-5), 184.9 ppm (*C*-1); ms (70 eV) *m/e* (relative intensity): 158 (19) and 156.035 (58, $M_r(^{12}C_8{}^1H_9{}^{35}Cl{}^{16}O)$: 156.034), 141 (5, $M - CH_3$), 128 (25), 122 (75), 121 (100, M − Cl), 107 (57), 93 (30), 91 (55), 78 (15), 77 (45).

*2-*tert*-Butyl-4-chloro-4-methylcyclohexa-2,5-dien-1-one (**7**)*

Chlorination of 2-*tert*-butyl-4-methylphenol (16.4 g, 0.1 mol) in acetic anhydride gave crude product (18.3 g) containing 48% (53% yield) of the dienone. Filtration of a solution in pentane through alumina and elution with ether gave 2-*tert*-butyl-4-chloro-4-methylcyclohexa-2,5-dienone (**7**), obtained as pale yellow crystals after recrystallization from pentane, mp 39°C; ir (Nujol): 1667 (C=O), 1640 (C=C), 840 (cm^{-1}) (C—Cl); ^1H nmr ($CDCl_3$) δ: 1.22(s, 9, $C(CH_3)_3$), 1.79 (s, 3, 4-CH_3), 6.07 (d, 1, J_{56} = 10 Hz, 6-*H*), 6.69 (d, 1, J_{35} = 3 Hz, 3-*H*), 6.83 ppm (dd, 1, J_{35} = 3 Hz, J_{56} = 10 Hz, 5-*H*); ^{13}C nmr ($CDCl_3$) δ_C: 28.8 ($C(CH_3)_3$), 30.2 (4-CH_3), 34.4 ($C(CH_3)_3$), 61.5(*C*-4), 128.2 (*C*-6), 143.5 (*C*-2 and *C*-3) 147.2 (*C*-5), 184.4 ppm (*C*-1); ms (70 eV) *m/e* (relative intensity): 198.070 (3, $M_r(^{12}C_{11}{}^1H_{15}{}^{35}Cl{}^{16}O)$: 198.081), 183 (10, $M - CH_3$), 164 (36), 163 (41, M − Cl), 162 (24), 150 (86), 148 (22), 135 (16), 122 (20), 121 (100), 107 (18), 105 (20), 91 (24), 77 (26). *Anal.* calcd. for $C_{11}H_{15}ClO$: C 66.50, H 7.61; found: C 66.09, H 7.65.

*2-Bromo-4-chloro-4-methylcyclohexa-2,5-dien-1-one (**8**)*

Chlorination of 2-bromo-4-methylphenol (18.7 g, 0.1 mol) in acetic anhydride gave crude product (20.7 g) containing 44% (49% yield) of dienone. Filtration of a solution in ether through alumina followed by recrystallization from ether–pentane at −20°C gave 2-bromo-4-chloro-4-methylcyclohexa-2,5-dienone (**8**), mp 55°C; ir (Nujol): 1660 (C=O), 1600 (C=C), 915, 835 cm^{-1}; ^1H nmr ($CDCl_3$) δ: 1.83 (s, 3, 4-CH_3), 6.28 (d, 1, J_{56} = 10 Hz, 6-*H*), 6.96 (dd, 1, J_{35} = 2.5 Hz, J_{56} = 10 Hz, 5-*H*), 7.38 ppm (d, J_{35} = 2.5 Hz, 3-*H*); ^{13}C nmr ($CDCl_3$) δ_C: 29.2 (4-CH_3), 61.5 (*C*-4), 123.9 (*C*-2), 124.9 (*C*-6), 149.5 and 149.7 (*C*-3 and *C*-5), 177.1 ppm (*C*-1); ms (70 eV) *m/e* (relative intensity): 222 (3) and 219.934 (3, $M_r(^{12}C_7{}^1H_6{}^{79}Br{}^{35}Cl{}^{16}O)$: 219.929), 188 (70), 187 (40), 186 (74), 185 (37), 143 (27), 142 (11), 141 (73), 113 (15), 108 (12), 107 (100), 79 (15), 78 (60), 77 (75). *Anal.* calcd. for C_7H_6BrClO: C 37.96, H 2.73; found: C 37.93, H 2.77.

The presence of a significant amount of 2-bromo-*p*-cresol (*m/e*: 188 (62), 187 (23), 186 (62), 185 (20), 108 (20), 107 (100), 79 (13), 78 (24), 77 (42)) is evident in the mass spectrum. This must arise from thermolysis of the dienone within the mass spectrometer since no phenol could be detected by either ^1H nmr or ^{13}C nmr.

*4-Chloro-3,4-dimethylcyclohexa-2,5-dien-1-one (**9**)*

Chlorination of 3,4-dimethylphenol (12.2 g, 0.1 mol) in acetic anhydride gave crude product (15.0 g) which contained 41% (46% yield) of dienone. Filtration of a solution in ether through alumina followed by crystallization from ether gave 4-chloro-3,4-dimethylcyclohexa-2,5-dienone (**9**) as colourless crystals, mp 51°C; ir (Nujol): 1675 (C=O), 1630 (C=C), 887 cm^{-1} (C—Cl); ^1H nmr ($CDCl_3$) δ: 1.77 (s, 3, 4-CH_3), 2.17 (s, 3, 3-CH_3), 6.09 (broad s, 1, 2-*H*), 6.16 (dd 1, J_{26} = 1.5 Hz, J_{56} = 9 Hz, 6-*H*), 6.94 ppm (d, 1, J = 9 Hz, 5-*H*); ^{13}C nmr ($CDCl_3$) δ_C: 19.3 (3-CH_3), 28.3 (4-CH_3), 62.8 (*C*-4), 125.6 and 126.4 (*C*-2 and *C*-6), 150.3 (*C*-5), 157.7 (*C*-3), 185.1 ppm (*C*-1); ms (70 eV) *m/e* (relative intensity): 158 (14) and 156.034 (42, $M_r(^{12}C_8{}^1H_9{}^{35}Cl{}^{16}O)$: 156.034), 141 (7), 130 (24), 128 (69), 122 (71), 121 (100), 120 (19), 107 (72), 93 (70), 92 (19), 91 (93), 78 (18), 77 (95). *Anal.* calcd. for C_8H_9ClO: C 61.35, H 5.79; found: C 61.34, H 5.93.

*4-Chloro-2,4,6-trimethylcyclohexa-2,5-dien-1-one (**10**)*

Chlorination of 2,4,6-trimethylphenol (13.6 g, 0.1 mol) in acetic anhydride gave crude product containing 90% dienone (100% yield) and 10% of the unreacted phenol. Filtration of a solution in ether through alumina at 0°C, followed by crystallization from pentane at −20°C, gave 4-chloro-2,4,6-trimethylcyclohexa-2,5-dienone (**10**) as colourless crystals, mp 32°C; ir (Nujol): 1675 (C=O), 1647 (C=C), 900 cm^{-1} (C—Cl); ^1H nmr ($CDCl_3$) δ: 1.76 (s, 3, 4-CH_3), 1.88 (s, 6, 2-CH_3 and 6-CH_3), 6.73 ppm (s, 2, 3-*H* and 5-*H*); ^{13}C nmr ($CDCl_3$) δ_C: 15.7 (2-CH_3 and 6-CH_3), 30.1 (4-CH_3), 61.5 (*C*-4), 133.0 (*C*-2 and *C*-6), 145.1 (C-3 and C-5), 182.8 ppm (*C*-1); ms (70 eV) *m/e* (relative intensity): 172 (12) and 170.046 (34, $M_r(^{12}C_9{}^1H_{11}{}^{35}Cl{}^{16}O)$: 170.048), 169 (18), 136 (100), 135 (82), 121 (67), 107 (18), 105 (16), 91 (52), 79 (20), 77 (16). *Anal.* calcd. for $C_9H_{11}ClO$: C 63.35, H 6.50; found: C 63.65, H 6.55.

1. V. V. Ershov, A. A. Volod'kin, and G. N. Bogdanov. Russ. Chem. Rev. **32**, 75 (1963).
2. A. J. Waring. Adv. Alicyclic Chem. **1**, 172 (1966).
3. V. V. Ershov and A. A. Volod'kin. Izv. Akad. Nauk SSR, Otd. Fiz. Tekh. Khim. Nauk, 893 (1963).
4. E. Morita and M. W. Dietrich. Can. J. Chem. **47**, 1943 (1969).
5. L. Vollbracht, W. G. B. Huysmans, W. J. Mijs, and H. J. Hageman. Tetrahedron, **24**, 6265 (1968).

6. V. P. VITULLO and E. A. LOGUE. J. Org. Chem. **37**, 3339 (1972); V. P. VITULLO and N. GROSSMAN. J. Am. Chem. Soc. **94**, 3844 (1972); V. P. VITULLO and E. A. LOGUE. J. Org. Chem. **38**, 2265 (1973).
7. S. R. HARTSHORN. Chem. Soc. Rev. **3**, 167 (1974).
8. P. B. D. DE LA MARE. Acc. Chem. Res. **7**, 361 (1974).
9. A. NILSSON, A. RONLÁN, and V. D. PARKER. Tetrahedron Lett. 1110 (1975).
10. S. HUSAIN. Ind. J. Chem. **6**, 81 (1968).
11. P. B. D. DE LA MARE and B. N. B. HANNAN. Chem. Commun. 1324 (1971); P. B. D. DE LA MARE, B. N. B. HANNAN, and N. S. ISAACS. J. Chem. Soc. Perkin Trans. II, 1389 (1976).
12. E. MORITA and M. W. DIETRICH. J. Chem. Eng. Data, **17**, 260 (1972).
13. P. SEVEC and M. ZBIROVSKY. J. Chromatogr. **87**, 535 (1973).
14. P. SEVEC, A. M. SORENSEN, and M. ZBIROVSKY. Org. Prep. Proced. Int. **5**, 209 (1973).
15. H. SUZUKI, K. ISHIZAKI, and T. HANAFUSA. Nippon Kagaku Kaishi, 556 (1975).
16. R. F. CROZIER and D. G. HEWITT. Aust. J. Chem. **25**, 183 (1972).
17. R. LAMARTINE and R. PERRIN. J. Org. Chem. **39**, 1744 (1974).
18. L. DENIVELLE and M. HEDAYATULLAH. C.R. Acad. Sci. **253**, 2711 (1961).
19. R. FORT. Ann. Chim. (Paris), **4**, 203 (1959).
20. A. FISCHER and S. S. SEYAN. Can. J. Chem. **56**, 1348 (1978).
21. C. L. PERRIN and G. A. SKINNER. J. Am. Chem. Soc. **93**, 3389 (1971).
22. C. D. JOHNSON. The Hammett equation. Cambridge University Press, London. 1973. p. 43.
23. A. F. HOLLEMAN. Chem. Rev. **1**, 187 (1925).
24. A. FISCHER and G. J. WRIGHT. Aust. J. Chem. **27**, 217 (1974).
25. A. FISCHER and J. N. RAMSAY. Can. J. Chem. **52**, 3960 (1974); A. FISCHER and D. R. A. LEONARD. Can. J. Chem. **54**, 1795 (1976); A. FISCHER and K. C. TEO. Can. J. Chem. **56**, 1758 (1978).
26. A. I. VOGEL. Practical organic chemistry. 3rd ed. Longmans, Green and Co., London. 1956. p. 289.

The reactions of arenesulphonyl azides with tetrahydropyrido[1,2-*a*]indoles and the X-ray crystallographic structure determination of a resultant novel zwitterion, 1,2,3,4-tetrahydro-10-methyl-4*a*-*p*-tolylsulphonylaminopyrido[1,2-*a*] indole

T. Stanley Cameron, Ruth E. Cordes, and Aris Terzis

Department of Chemistry, Dalhousie University, Halifax, N.S., Canada B3H 4J3

AND

A. Sydney Bailey and Peter W. Scott

The Dyson Perrins Laboratory, South Parks Road, Oxford OX1 3QY, England

Received July 21, 1978

T. Stanley Cameron, Ruth E. Cordes, Aris Terzis, A. Sydney Bailey, and Peter W. Scott. Can. J. Chem. **57**, 558 (1979).

The reactions of arenesulphonyl azides with tetrahydropyrido[1,2-*a*]indoles have been examined. Compounds formed by elimination and by ring enlargement are obtained, including a compound with a novel zwitterion structure. The structure of this compound has been determined by X-ray crystallography.

T. Stanley Cameron, Ruth E. Cordes, Aris Terzis, A. Sydney Bailey et Peter W. Scott. Can. J. Chem. **57**, 558 (1979).

On a étudié les réactions des azotures d'arènesulfonyles avec les tétrahydropyrido[1,2-*a*]-indoles. On a obtenu des composés, résultant d'une élimination accompagnée d'une extension de cycle, parmi lesquels se trouve un composé comportant une nouvelle structure zwittérionique. On a déterminé la structure de ce composé par diffraction de rayons-X.

[Traduit par le journal]

We have described the reactions of arenesulphonyl azides with *N*-methyltetrahydrocarbazole (**1**) (1) and with the pyridocarbazole derivative (**2**) (2). It was of interest to extend this work by investigating the reactions of a tetrahydropyrido[1,2-*a*]indole and we chose the known (3) dimethyl derivative **3**; we also examined the reactions of the isomeric structure (**4**; R = H and R = Me) since the reactions of simple indolizines with azides have been reported (4). Compound **3** was prepared by the known route (3) via compound **5**; compounds **4**; R = H (5) and **4**; R = Me (6) were synthesised from 2-bromocyclohexanone.

Compound **3** was treated with *p*-chlorobenzenesulphonyl azide ($CbsN_3$) in chloroform solution and yielded two products (plus polymeric materials). The compounds were *p*-chlorobenzenesulphonamide and an unstable oil (50% yield) which darkened rapidly and could not be analysed. Structure **6** is supported by the nmr, mass, and uv spectra of the compound. The nmr spectral values are in good agreement with those reported (7) for compound **7**. We consider that compound **6** arises via the intermediates **8** and **9** although it is possible that **10** is formed as an intermediate (cf. the formation (1) of **11** from **1**) and the loss of $TsNH_2$ from **12** (8) to form **13**.

To determine if olefin formation occurred with simple alkylindoles containing a secondary alkyl group at position (2), the reactions of 1,3-dimethyl-2-isopropylindole (**15**) with tosyl azide was examined (**15** was obtained by hydrogenation of **14** (9)). The major product (yield 57%) was the 1:2 reaction product **16**. This structure was supported by its physical properties and by hydrolysis of **16** to form **18**. Compound **16** arises by addition of a second molecule of azide to **17** followed by ring enlargement (1, 10). Two other compounds were isolated from the reaction, *p*-toluenesulphonamide and the olefin **14** (yield 10%). The olefin arises from **17** by loss of $TsNH_2$ (cf. the formation of **6**). These observations suggest that the elimination of $TsNH_2$ from the cyclic intermediate **9** occurs faster than the attack of TsN_3 whilst for the acyclic compound **17** the converse occurs. It is impossible for compound **3** to give rise to ring-enlarged quinoline structures of type **16** by addition of second molecule of azide to **9** since such products would contain a '*meta*' bridge.

1,2,3,4-Tetrahydropyrido[1,2-*a*]indole (**4**; R = H) reacted smoothly with $CbsN_3$ giving a high yield of the azo compound (**20**) with its characteristic uv spectrum (4). The reaction of **4**; R = Me with $CbsN_3$ was more complex, tlc showing many products; only one compound was obtained crystalline (yield 23%). The ir spectrum of the compound showed the presence of a C=N—Cbs group (1620 cm^{-1}) and the absence of an NH group. We considered that the compound had structure **23** arising from **4** via **21** and **22**. With small quantities available it was decided to carry out an X-ray determination since crystals were suitable. It has been found that

0008-4042/79/050558-07$01.00/0

structure **23** originally considered is incorrect and the compound has the 'ionic' structure **25** and probably arises via **24**. The presence of the pyridinium ring explains the signals at very low field in the n.m.r. spectrum of the compound and the negatively charged NSO_2Ar group explains why the signals of the $SO_2C_6H_4$—Cl group have moved upfield from these 'normal' positions.

Crystal Structure of ***25***

Crystal data:

$C_{19}H_{19}ClN_2O_2S$ fw = 374.89

Monoclinic, $P2_1/c$, $a = 9.591(3)$, $b = 21.081(8)$, $c = 8.939(3)$ Å, $\beta = 90.75(3)$, $V = 1807.2$ Å^3, $Z = 4$, $\rho_c = 1.377$ g cm^{-3} (18 ± 2°C; $CuK_{\alpha 1}$, $\lambda = 1.54051$ Å (carbon monochromator) $\mu = 29.40$), $F(000) = 784$.

The cell dimensions (refined from 12 general reflections with 2θ between 70–76°) and intensities of 2786 independent reflections were measured on a Picker FACS-1 four circle diffractometer with an ω − 2θ scan and 2θ values between 4 and 120°. The minimum base-width was 2.2°. Three standard reflections were measured every 58 reflections. The intensity of these three reflections decreased steadily throughout the data collection but could be adjusted to a standard scale by a least-squares fit ($\sigma = 0.015$) to a first order decay; from the counting statistics the ratio of esd to reflection of these standards was 0.019. The data were reduced to $|F_o|$ by the routine procedure. No absorption or extinction corrections were applied. The scattering factors for neutral atoms were taken from ref. 11; they were corrected for the real part of the anomalous dispersion. Reflections with $|E| > 1.2$ were used to solve the structure by an application of the tangent formula that examined $4096 = 2^{12}$ sets of starting phases and successively eliminated all but the most likely. This program is part of an X-ray system written by Sheldrick (12). The position of all but the hydrogen atoms were found on the E map with the lowest Karle R factor (13).

The structure was refined by large-block least-squares ($\sum(\Delta|F|)^2 = \min$) initially with isotropic temperature factors using only the 2031 reflections with $I > 3\sigma(I)$. The atomic parameters for those hydrogen atoms with positions defined by the molecule were calculated and the remainder were located from a difference Fourier synthesis calculated when the conventional R was 0.13. The subsequent refinement with anisotropic temperature factors converged[1] with $R = 0.0518$. The hydrogens of the methyl group appeared to be disordered with at least two preferred locations. The methyl group was therefore refined as a rigid body (12) (see below). The least-squares weights were calculated from $w = 1/(\sigma^2|F_o| - 0.00043|F_o|^2)$, where σ is the weight for each reflection derived from the diffractometer counting statistics. The atomic coordinates are given in Table 1 and the interatomic distances and interbond angles are listed in Table 2. Figure 1 shows a single molecule and Fig. 2 gives its packing within the unit cell.

The crystal was found to be constructed from isolated molecules which contained a *p*-chlorophenylsulphone group bonded through a nitrogen atom to a hexahydropyrido[1,2-*a*]indole system (Fig. 1). The S—N(1), N(1)—C(3), C(3)—N(2), and N(2)—C(5) distances are 1.563(3), 1.432(4), 1.531(4), and 1.335(4) Å, respectively. A formal S=N double bond has been reported (14) at 1.52(2) and a S—NH— single bond at 1.635(8) in a tolylsulphenylamino group that has an sp^3 carbon atom bonded to the third valency at nitrogen (15). The N(1)—C(3) bond length is shorter than that normally quoted (16) (1.472(5)) for a bond between an sp^2 nitrogen and an sp^3 carbon, whereas the C(3)—N(2) length (1.531(4)) is very much longer. The N(2)—C(5) and N(2)—C(9) bonds of 1.335(4) and 1.362(4) are similar to those observed in pyridine derivatives (17). The two S—O bond lengths, 1.449(2) and 1.453(3), are slightly longer than those normally observed in this type of molecule (15). The nitrogen atom N(2) therefore formally forms four bonds and is positively charged, and the $-SO_2N$ group has a balancing negative charge which is situated predominantly upon the nitrogen atom. This can be written as the zwitterion **25**. A sulimido)pyridinium ylide has been observed (18) before and here too the negative charge is found on the sulphonyl nitrogen atoms. In this case though no X-ray structure has been determined.

The hexahydropyrido[1,2-*a*]indole fragment of the molecule has two six-membered rings separated by a five-membered ring. One six-membered ring, attached at C(2) and C(3), is largely saturated and has the chair conformation. The C(1)—C(2) bond, however, which is part of the adjoining five-membered ring has a length of 1.337(4) Å and is clearly a double bond. The angle C(3)—C(2)—C(14) is 115.6(3)° and compares with the mean internal angle of 110.8° for this ring. The C—C—C—C torsional angles around this ring (Table 3) have an absolute value which varies between 60.4° (C(14)—C(2)—C(3)—C(11)) and 52.5° (C(2)—C(14)—C(13)—C(12)), with a mean value of 56.6° so that the introduction of an sp^2 carbon at C(2) only slightly distorts the ring. The five-

[1]A list of structure factors (Table 4) and complete atomic parameters is available at a nominal charge from the Depository of Unpublished Data, CISTI, National Research Council of Canada, Ottawa, Ont., Canada K1A 0S2.

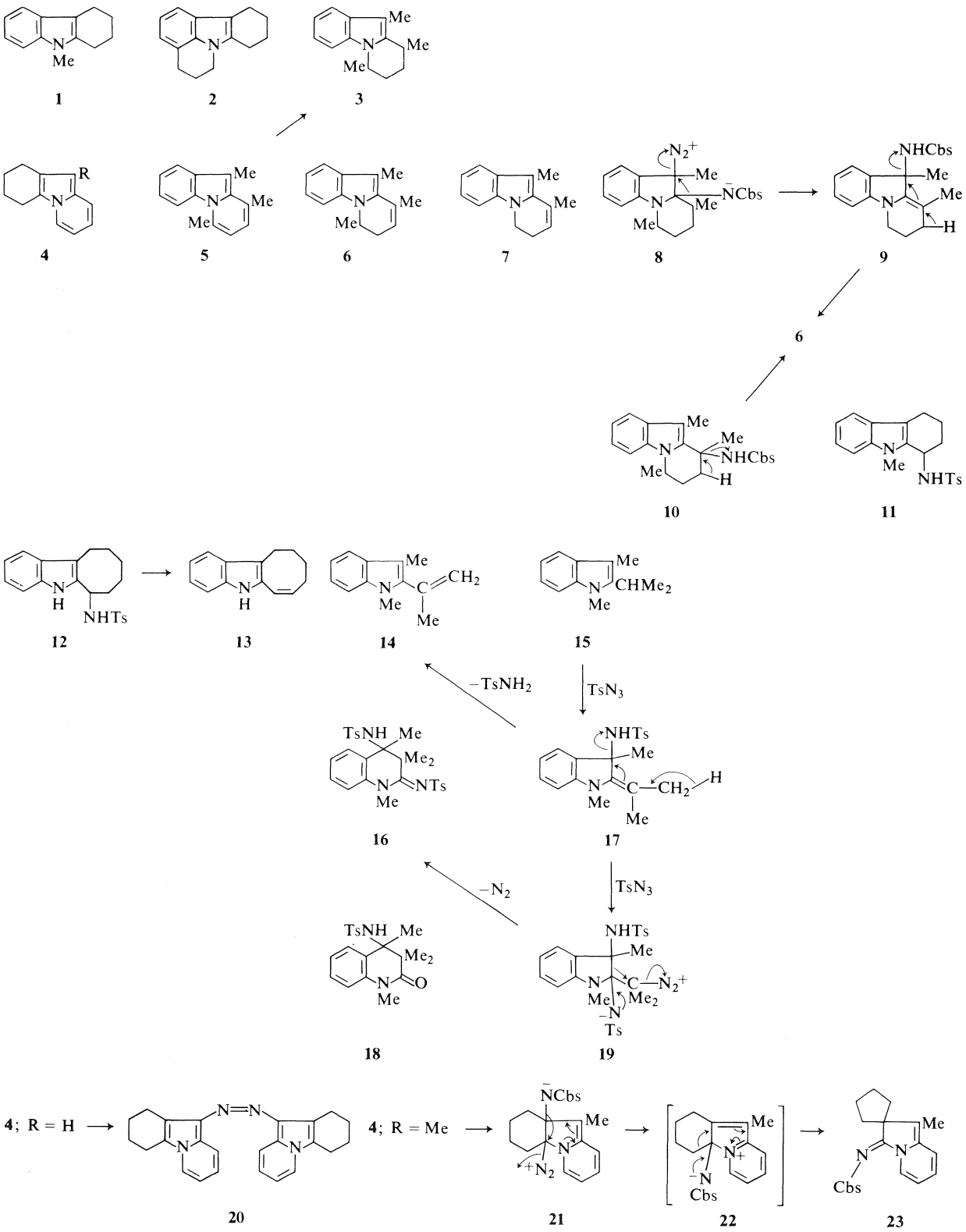

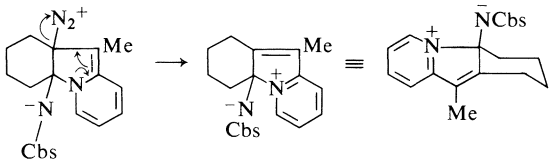

24 25

membered ring has a mean deviation from the least-squares best plane of 0.010 Å. As already noted, C(1)—C(2) is a double bond and is conjugated to the other six-membered ring, which is aromatic, through bond C(1)—C(9). This bond has a length of 1.459(4) Å which compares with 1.480 Å for the central bond in buta-1,3-diene (19). The hydrogen atoms of the methyl group at C(10) appeared in the difference map to have two alternative orientations, so in the refinement the whole CH_3 group was treated as a rigid body and was permitted to rotate about the C(1)—C(10) bond (12). These hydrogen atoms were constrained (20) to have equal temperature factors and to have a site occupation which summed to one for the two groups. The two possible methyl orientations refined with one rotated 38.6° about C(1)—C(10) with respect to the other. The six-membered ring attached at C(9) and N(2) is aromatic with a mean

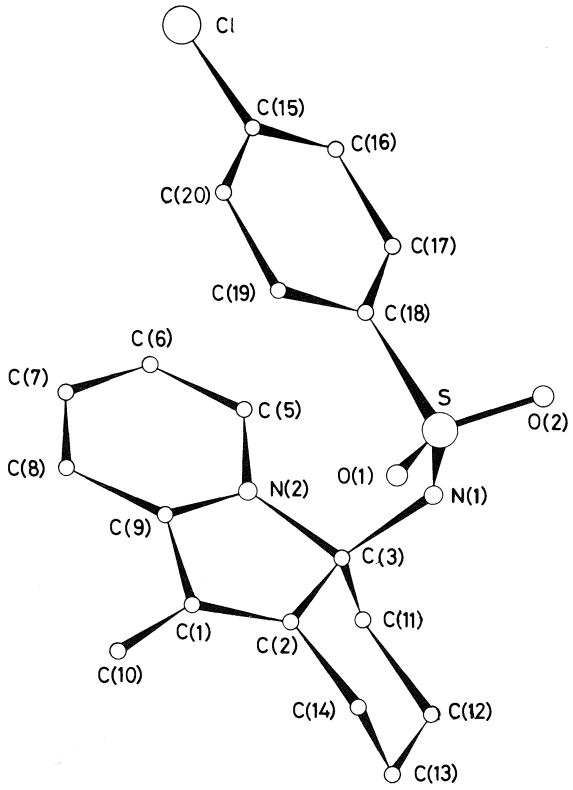

FIG. 1. The molecule **25**.

TABLE 1. Atomic parameters (× 10^4, except for hydrogen × 10^3)

Atom	*x*	*y*	*z*
Cl	5250(1)	1072(1)	195(1)
S	9699(1)	1445(1)	5368(1)
O(1)	10073(2)	814(1)	5878(3)
O(2)	8989(3)	1840(1)	6452(3)
N(1)	10917(3)	1850(1)	4724(3)
N(2)	11417(3)	1385(1)	2246(3)
C(1)	12539(3)	504(1)	3184(3)
C(2)	12622(3)	935(1)	4278(3)
C(3)	11957(3)	1564(1)	3809(3)
C(5)	10726(3)	1763(1)	1294(4)
C(6)	10359(4)	1529(2)	−95(4)
C(7)	10700(4)	912(2)	−47(4)
C(8)	11395(4)	533(2)	444(4)
C(9)	11769(3)	775(1)	1920(4)
C(10)	13146(4)	−149(2)	3127(5)
C(11)	13159(4)	2041(2)	3606(4)
C(12)	14018(4)	2087(2)	5053(4)
C(13)	14602(4)	1442(2)	5554(5)
C(14)	13442(4)	950(2)	5691(4)
C(15)	6518(4)	1172(2)	1595(4)
C(16)	6861(4)	1773(2)	2077(4)
C(17)	7824(4)	1853(2)	3228(4)
C(18)	8448(3)	1324(1)	3890(3)
C(19)	8134(4)	719(2)	3373(4)
C(20)	7151(4)	643(2)	2233(4)
H(5)	1055(4)	216(2)	166(4)
H(6)	993(4)	179(2)	−67(5)
H(7)	1039(4)	81(2)	−140(5)
H(8)	1154(4)	9(2)	33(5)
H(10A)	1246(8)	−44(4)	264(14)
H(10B)	1337(14)	−32(4)	414(5)
H(10C)	1401(7)	−15(4)	254(14)
H(10A′)	1245(8)	−48(2)	332(11)
H(10B′)	1357(9)	−23(3)	215(5)
H(10C′)	1388(5)	−17(3)	391(7)
H(11A)	274(3)	246(2)	332(4)
H(11B)	377(4)	187(2)	276(4)
H(12A)	483(4)	236(2)	489(5)
H(12B)	337(4)	228(2)	582(5)
H(13A)	537(5)	130(2)	474(6)
H(13B)	509(5)	151(2)	653(5)
H(14A)	283(4)	104(2)	644(4)
H(14B)	390(4)	54(2)	588(4)
H(16)	643(4)	213(2)	167(5)
H(17)	801(4)	228(2)	352(4)
H(19)	865(5)	36(2)	385(5)
H(20)	692(5)	20(2)	189(5)

deviation from the least squares best plane of 0.004 Å. The mean C—C bond length within the ring is 1.377(3) Å and the two distances to the nitrogen atom; C(9)—N(2), 1.362(4) and C(5)—N(2), 1.335 (4) Å are expected (17) to be noticeably shorter. There is no obvious reason why the bond C(9)—N(2), though short, is significantly longer than C(5)—N(2). The corresponding lengths (17) in 3-aminopyridine are 1.331(4) and 1.336(4) Å. However C(9)—N(2) is common to the five- and six-membered rings and as

TABLE 2. Interatomic distances and interbond angles

Bond	Length (Å)	Bond	Length (Å)
Cl—C(15)	1.747(4)	C(3)—C(11)	1.543(5)
S—O(1)	1.449(2)	C(5)—C(6)	1.378(5)
S—O(2)	1.453(3)	C(6)—C(7)	1.383(6)
S—N(1)	1.563(3)	C(7)—C(8)	1.374(6)
S—C(18)	1.792(3)	C(8)—C(9)	1.375(5)
N(1)—C(3)	1.432(4)	C(11)—C(12)	1.527(5)
N(2)—C(3)	1.531(4)	C(12)—C(13)	1.536(6)
N(2)—C(5)	1.335(4)	C(13)—C(14)	1.528(6)
N(2)—C(9)	1.362(4)	C(15)—C(16)	1.376(6)
C(1)—C(2)	1.337(4)	C(15)—C(20)	1.389(5)
C(1)—C(9)	1.459(4)	C(16)—C(17)	1.383(5)
C(1)—C(10)	1.495(5)	C(17)—C(18)	1.393(5)
C(2)—C(3)	1.526(4)	C(18)—C(19)	1.389(5)
C(2)—C(14)	1.479(5)	C(19)—C(20)	1.388(5)

Bond	Angle (deg)	Bond	Angle (deg)
O(1)—S—O(2)	115.6(1)	N(2)—C(5)—C(6)	118.7(3)
O(1)—S—N(1)	115.8(1)	C(5)—C(6)—C(7)	119.7(4)
O(1)—S—C(18)	105.2(1)	C(6)—C(7)—C(8)	120.1(4)
O(2)—S—N(1)	106.9(1)	C(7)—C(8)—C(9)	119.6(3)
O(2)—S—C(18)	104.9(1)	N(2)—C(9)—C(1)	109.2(3)
N(1)—S—C(18)	107.6(1)	N(2)—C(9)—C(18)	118.6(3)
S—N(1)—C(3)	120.6(2)	C(1)—C(9)—C(8)	132.2(3)
C(3)—N(2)—C(5)	126.4(3)	C(3)—C(11)—C(12)	109.7(3)
C(3)—N(2)—C(9)	110.3(2)	C(11)—C(12)—C(13)	112.4(3)
C(5)—N(2)—C(9)	123.3(3)	C(12)—C(13)—C(14)	111.2(3)
C(2)—C(1)—C(9)	108.9(3)	C(13)—C(14)—C(2)	109.0(3)
C(2)—C(1)—C(10)	129.2(3)	Cl—C(15)—C(16)	119.8(3)
C(9)—C(1)—C(10)	121.8(3)	Cl—C(15)—C(20)	119.5(3)
C(1)—C(2)—C(3)	111.7(3)	C(16)—C(15)—C(20)	120.6(3)
C(1)—C(2)—C(14)	131.6(3)	C(15)—C(16)—C(17)	120.0(4)
C(3)—C(2)—C(14)	115.6(3)	C(16)—C(17)—C(18)	119.8(3)
N(1)—C(3)—N(2)	113.3(2)	S—C(18)—C(17)	118.7(2)
N(1)—C(3)—C(2)	120.1(2)	S—C(18)—C(19)	121.1(2)
N(1)—C(3)—C(11)	108.6(2)	C(17)—C(18)—C(19)	120.2(3)
N(2)—C(3)—C(2)	99.9(2)	C(18)—C(19)—C(20)	119.5(3)
N(2)—C(3)—C(11)	107.3(2)	C(15)—C(20)—C(19)	119.8(3)
C(2)—C(3)—C(11)	106.8(2)		

the five-membered ring has a double bond in it (C(1)—C(2)) this probably introduces strain at the ring junction thus lengthening the common bond.

The distances in the *p*-chlorosulphonyl group are unexceptional. The sulphur–carbon distance of 1.792(3) compares with 1.776(4) in the *p*-toluenesulphonate ion (21) and the carbon chlorine bond length of 1.747(4) compares with 1.780(8) in 1-(2-chloro-4-dimethylaminophenyl)-2-nitroethylene (22).

Experimental

Infrared spectra were determined for Nujol mulls, uv spectra for solutions in ethanol, and nmr spectra for solutions in $CDCl_3$ unless otherwise stated. Chromatography (tlc and column) was carried out using silica–$CHCl_3$ unless otherwise stated. Solutions were dried using $MgSO_4$.

*6,7-Dihydro-6,9,10-trimethylpyrido[1,2-a]indole (**6**)*

6,9,10-Trimethylpyrido[1,2-*a*]indole **5** had mp 134–134.5°C (yield 70%) (lit. (3) mp 134°C); τ: 1.83 (1H, d, J = 8 Hz), 2.24 (1H, d, J = 8 Hz), 2.50–2.90 (2H, m), 3.54 (1H, q, J = 7 and 1 Hz C(8)H), 3.98 (1H, q, J = 7 and 1 Hz C(7)H), 7.12 (3H, sbr, C(6)CH_3), 7.25 (3H, s, C(10)CH_3), and 7.36 (3H, sbr, C(9)CH_3), these assignments were confirmed by decoupling experiments. Hydrogenation of **5** (3) afforded **1**, mp 75–79°C (lit. (3) mp 76–80°C); τ: 2.40–2.95 (4H, m), 5.3–5.65 (1H, m,

TABLE 3. Torsional angles in the six-membered ring attached at C(2) and C(3)

Bonds	Angles (deg)
C(2)—C(3)—C(11)—C(12)	−56.8
C(3)—C(11)—C(12)—C(13)	57.2
C(11)—C(12)—C(13)—C(14)	−54.6
C(12)—C(13)—C(14)—C(2)	52.5
C(13)—C(14)—C(2)—C(3)	−58.1
C(14)—C(2)—C(3)—C(11)	60.4

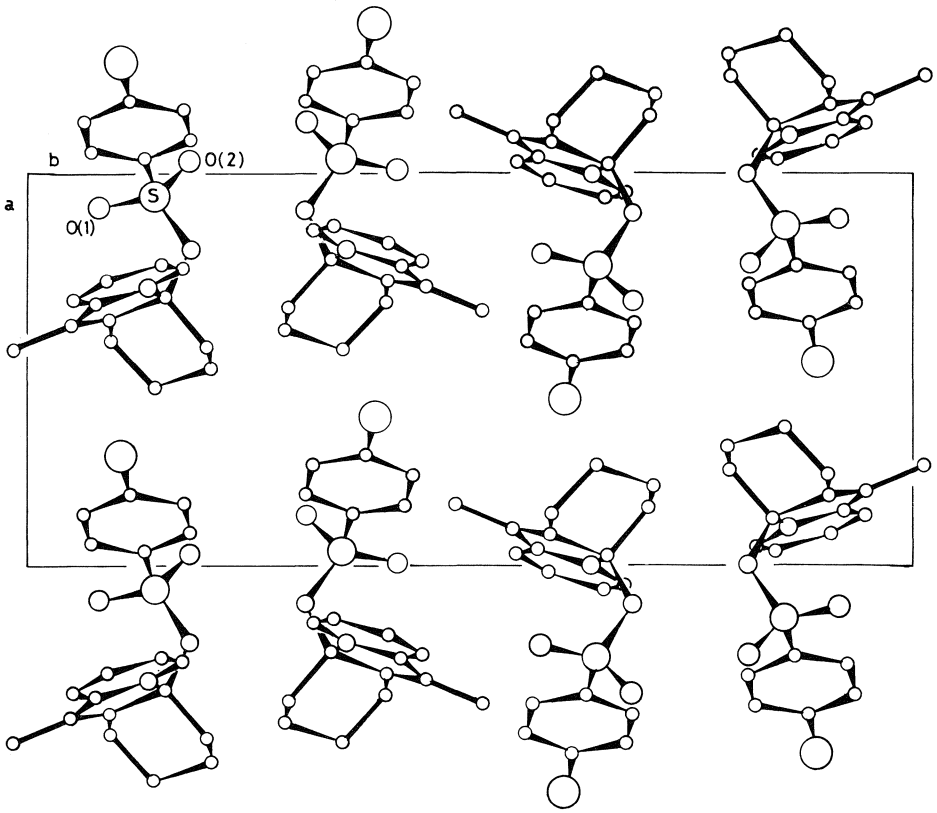

FIG. 2. The unit cell of **25**, viewed along *c*.

C(6)H), 6.65–6.95 (1 H, m, C(9)H), 7.70 (3H, s, C(10)CH_3), 7.85–8.35 (4H, m, C(7)H_2 + C(8)H_2), 8.50 (3H, d, J = 8 Hz, C(6)CH_3), and 8.62 (3H, d, J = 8 Hz, C(9)CH_3); assignment of C(6) and C(9) Me group signals was made by decoupling experiments on the corresponding methine signals; *m/e* (relative intensity): 213 (M^+, 100), 199 (30), 198 (95), and 182(15). A solution of this compound (1.1 g) in chloroform (20 mL) containing $CbsN_3$ (1.1 g) was kept in the dark for 4 weeks. Chromatography gave **6** (0.55 g), stable at 0°C; ν_{max}: 210, 235(sh), 254(sh), 263(infl), 307, 319(sh), 336(infl) nm (ε 21 500, 15 500, 9600, 6500, 15 500, 14 200, and 5050); ν_{max} (liquid film): 740 and 1465 cm^{-1}; τ: 2.4–2.6 (1H, m), 2.7–3.1 (3H, m), 4.35–4.6 (1H, m, C(8)H), 5.25–5.6 (1H, m, C(6)H), 7.0–8.0 (2H, m, C(7)H_2) 7.54 (3H, s, C(10)CH_3), 7.65–7.85 (3H, m, C(9)CH_3), and 8.86 (3H, d, J = 7 Hz, C(6)CH_3); irradiation of the signal at 8.86 showed that it was coupled to C(6)H; irradiation of the signal 7.75 showed that it was coupled to the vinyl proton, the complexity of the signals in **7** has been noted (7); *m/e* (relative intensity): 211 (M^+, 100), 196 (M − CH_3, 60, m* 182), 181 (196 − CH_3, 58, m* 167), and 196 (4). Further elution gave *p*-chlorobenzenesulphonamide (0.4 g) and a black tar (0.5 g).

The Reaction of 1,3-Dimethyl-2-isopropylindole with Azides

Hydrogenation (Pd/C, EtOH) of the olefin **14** afforded **15**, bp 130–140°C/0.2 Torr, mp 22–23°C; λ_{max}: 230, 281(infl), 286, and 293 nm (ε 41 100, 7900, 8900, and 8800); τ: 2.4–3.05 (4H, m), 6.33(3H, s, NCH_3), 6.68 (1H, heptet, J = 7 Hz, $CHMe_2$), 7.68 (3H, s, C—CH_3), and 8.62 (6H, d, J = 7 Hz, C(CH_3)$_2$); *m/e* (relative intensity): 187 (M^+, 55), 173 (16), 172 (M − CH_3, 100, m* 158), and 157 (172 − CH_3, 17, m* 143.3). *Anal.* calcd. for $C_{13}H_{17}N$: C 83.4, H 9.1, N 7.5; found: C 83.2, H 9.0, N 7.4. A mixture of this indole (1.0 g) and tosyl azide (2.1 g) was kept for 24 h at room temperature. Methanol (3 mL) was then added and 3 days later the solid was collected and recrystallised from methanol (yield 57%). 1,2,3,4-Tetrahydro 1,3,3,4-tetramethyl-4-*p*-tolylsulphonylamino-2-*p*-tolylsulphonyliminoquinoline **16** formed colourless rods, mp 230–232°C; λ_{max}: 222 and 282 nm (ε 26 900 and 18 000); ν_{max}: 1555 and 3230 cm^{-1}; τ: (DMSO) 2.24 (2H, d, J = 9 Hz), 2.35 (1H, s, NH, exchanged with D_2O), 2.65 (2H, d, J = 9 Hz), 2.50–3.10 (8H, m), 6.57 (3H, s, NCH_3), 7.58 and 7.63 (each 3H, s, 2 × $TsCH_3$), 8.40 (3H, s, CH_3), 8.72 (3H, s, CCH_3), and 9.28 (3H, s, CCH_3); *m/e* (relative intensity): 525 (M^+, 4), 461 (M − SO_2, 18, m* 405), 446 (13), 370 (25), 291 (60), 199 (63), and 147 (100). *Anal.* calcd. for $C_{27}H_{31}N_3O_4S_2$: C 61.7, H 5.9, N 8.0, S 12.2; found: C 61.6, H 5.9, N 8.0, S 12.0. Chromatography of the mother liquors afforded starting material (0.09 g), tosyl azide (0.1 g), and the olefin **14** (0.1 g) identical (tlc, ir, nmr) with an authentic sample. Hydrolysis of **16** (0.5 g) by boiling in EtOH (20 mL) with aqueous NaOH (10 mL, 2 M) for 1 h followed by dilution and extraction ($CHCl_3$) gave 1,2,3,4-tetrahydro-1,3,3,4-tetramethyl-4-*p*-tolylsulphonylaminoquinolin-2-one (**18**) (yield 75%) needles, from benzene–cyclohexane, mp 175–175°C; λ_{max}: 233 and 256 nm (ε 20 900 and 16 100); ν_{max}: 1660 and 3280 cm^{-1}; τ: 2.35–2.50 (1H, m), 2.70–3.15 (6H, m), 3.45–3.65 (1H, m), 5.17 (1H, s, NH, exchanged with D_2O), 7.12 (3H, s, NCH_3), 7.65 (3H, s, $TsCH_3$), 8.15 (3H, s, C—CH_3), 8.63 (3H, s, C—CH_3), and 9.16 (3H, s, C—CH_3); *m/e* (relative intensity): 372 (M^+, 23) 302 (M − (CH_3)$_2$CCO, 11, m* 245.2), 202 (M − TsNH, 17), 147 (302 − Ts, 100, m* at 71.5); and 132 (7). *Anal.* calcd. for $C_{20}H_{24}N_2O_3S$: C 64.5, H 6.5, N 7.5; found: C 64.6, H 6.5, N 7.3.

The Reactions of **4**; *R = H and* **4**; *R = Me with Azides*

1,2,3,4-Tetrahydropyrido[1,2-*a*]indole (**4**; *R = H*) had mp 54.5–55°C (lit. (5) mp 52°C); *m/e* (relative intensity): 171 (M^+, 57), 170 (26), 144 (13), and 143 (100, m* 119.6). Compound **4**; R = Me had mp 52–53°C (lit. (6) mp 41–43°C; *m/e* (relative intensity): 185 (M^+, 100), 184 (73), 158 (22), and 157 ($M - C_2H_4$, 100, m* 133). The indolizine **4**; R = H (0.85 g) was dissolved in chloroform (10 mL) and $CbsN_3$ (1.1 g) added. Seven days later the solid (yield 77%) was collected and recrystallised from chloroform. Blood-red needles mp > 340°C; λ_{max}: 260, 468(sh), and 504 nm (ε 16 600, 22 100, and 22 500); ν_{max}: 1503, 1528(w), and 1625(w) cm^{-1}; the compound was too insoluble to allow an nmr determination in $CHCl_3$ or DMSO; in TFA τ: 1.01 (1H, d, J = 7 Hz), 1.25–1.8 (4 H, m), 2.9–3.5 (3H, m), 4.45–4.8 (1H, m), and 6.5–8.7 (15H, m); *m/e* (relative intensity): 368 (M^+, 8), 186 (13), 171 (40), 157 (15), and 143 (100). *Anal.* calcd. for $C_{24}H_{24}N_4$: C 78.2, H 6.5, N 15.2; found: C 78.1, H 6.6, N 15.0. A solution of the indolizine **4**; R = Me (0.92 g) in chloroform (10 mL) containing $CbsN_3$ (1.1 g) was kept at room temperature for 15 weeks. The solvent was removed and methanol (5 mL) added. The solid (0.07 g) which separated was recrystallised (EtOAc–MeOH).

1,2,3,4-Tetrahydro-10-methyl-4a-*p*-tolylsulphonylaminopyridol[1,2-*a*]indole **25** formed colourless rods, EtOAc–MeOH, mp 199–200°C; λ_{max}: 213, 248, and 325 nm (ε 19 400, 17 400, and 4850); ν_{max}: 1620 cm^{-1}; τ: 1.14 (1H, d, J = 8 Hz), 1.75–1.95 (1H, m), and 2.35–2.9 (6H, m), 7.4–9.0 (8H, m), 7.88 (3H, s, CCH_3); *m/e* (relative intensity): 374 (M^+, 10), 200 (17), 199 (M – Cbs, 100, m* 106), 185 (15), 184 (28), and 183 (23). *Anal.* calcd. for $C_{19}H_{19}ClN_2O_2S$: C 60.9, H 5.1, N 7.5, Cl 9.3; found: C 60.7, H 5.3, N 7.5, Cl 9.0.

The mother liquors were concentrated and the residues chromatographed (SiO_2; MeOH), affording more compound **25** (0.35 g).

Acknowledgement

We thank the National Research Council of Canada for grants in aid of research for T.S.C. and A.T.

1. A. S. Bailey, R. Scattergood, and W. A. Warr. J. Chem. Soc. C, 2479 (1971); A. S. Bailey, A. J. Buckley, and J. F. Seager. J. Chem. Soc. Perkin I, 1809 (1973).
2. G. A. Bahadur, A. S. Bailey, and P. A. Baldry. J. Chem. Soc. Perkin I, 1619 (1977).
3. R. Robinson and J. E. Saxton. J. Chem. Soc. 3137 (1950).
4. A. S. Bailey, B. R. Brown, and M. C. Churn. J. Chem. Soc. C, 1590 (1971).
5. Y. Arata, T. Ohashi, and K. Uwai. J. Pharm. Soc. Jpn. **75**, 265 (1955).
6. J. Heer and K. Hoffman. Helv. Chim. Acta, **39**, 1820 (1956).
7. M. K. Eberle. J. Org. Chem. **41**, 633 (1976).
8. A. S. Bailey and J. F. Seager. J. Chem. Soc. Perkin I, 763 (1974).
9. G. A. Bahadur, A. S. Bailey, G. Costello, and P. W. Scott. J. Chem. Soc. Perkin I. In press.
10. A. S. Bailey, R. Scattergood, and W. A. Warr. J. Chem. Soc. C, 3769 (1971).
11. International Tables for X-ray Crystallography. Vol. IV. The Kynoch Press, Birmingham, England. 1974.
12. G. Sheldrick. X-ray system report. University Chemical Laboratory, Lensfield Rd., Cambridge, England. 1976.
13. J. Karle and I. L. Karle. Acta Crystallogr. **21**, 849 (1966).
14. E. M. Holt and S. M. Holt. J. Chem. Soc. Dalton, 1990 (1974).
15. T. S. Cameron, C. K. Prout, B. Denton, R. Spagna, and E. White. J. Chem. Soc. Perkin II, 176 (1975).
16. International Tables for X-ray Crystallography. Vol. III. The Kynoch Press, Birmingham, England. 1962.
17. M. Chao, E. Schempp, and R. D. Rosenstein. Acta Crystallogr. B, **31**, 2922 (1975); **31**, 2924 (1975).
18. R. A. Abramovitch and T. Takaya. J. Org. Chem. **37**, 2022 (1972).
19. B. P. Stoicheff. Adv. Spectrosc. 148 (1959).
20. J. Waser. Acta Crystallogr. **16**, 1091 (1963).
21. T. S. Cameron and J. W. Scheeren. J. Chem. Soc. Chem. Commun. 939 (1977).
22. T. S. Cameron and J. E. Thompson. Cryst. Struct. Commun. **3**, 503 (1973).

Anomalie de formation d'une goutte de mercure à une électrode polarographique

HUGUES MÉNARD
Département de Chimie, Université de Sherbrooke, Sherbrooke (Qué.), Canada J1K 2R1
ET
JACQUES DUBOIS
Département de Mathématiques, Université de Sherbrooke, Sherbrooke (Qué.), Canada J1K 2R1

Reçu le 5 juin 1978

HUGUES MÉNARD et JACQUES DUBOIS. Can. J. Chem. **57**, 565 (1979).

A l'aide d'un capillaire en polyéthylène comme électrode polarographique, il a été mis en évidence la formation d'une goutte de mercure ayant un col cylindrique anormal. Mathématiquement ce col est justifié mais chimiquement nous devons opérer en milieu NaOH afin d'avoir formation d'oxyde mercurique.

HUGUES MÉNARD and JACQUES DUBOIS. Can. J. Chem. **57**, 565 (1979).

Using a polyethylene capillary as polarographic electrode we could notice the formation of a mercury drop with an abnormal cylindric neck. This can be justified mathematically but chemically we must use NaOH so as to have the formation of mercuric oxide.

Introduction

La mise au point d'un capillaire en polyéthylène (1) pour l'application, comme électrode de travail en polarographie, dans des milieux extrêmements corrosifs au verre (tels le fluorure d'hydrogène et les solutions de soudes concentrées) a permis de mettre en évidence une formation d'une goutte de mercure ayant une géométrie complexe.

Partie expérimentale

Une solution de NaOH 1 *M* (A.C.S. Fischer Scientific Company) a été préparée avec de l'eau bidistillée. Une cellule en verre contenant un système à trois électrodes a été utilisée. L'électrode de référence est de calomel saturé avec double jonction et l'électrode auxiliaire est de platine. Un potentiostat tacussel type PRT 30-0.1 a permi d'y appliquer les différents potentiels d'oxydation.

Résultats

En effet dans une solution de NaOH 1 *M* et à des potentiels ≤ 0.0 V par rapport à une électrode de calomel saturé, c'est-à-dire à des potentiels d'oxydation, nous avons photographié (fig. 1), à des intervalles de temps de l'ordre de 3 s, la formation d'une goutte de mercure au bout d'un capillaire de polyéthylène. D'une goutte normale (fig. 1*a*) de mercure, nous avons après avoir atteint une masse critique, formation d'un col cylindrique qui devient extrêmement long par rapport à la goutte, (fig. 1 *b*, *c*, *d*, *e*). La longueur limite du col cylindrique de mercure dépend du potentiel appliqué à l'électrode et de la concentration de la soude.

Il est à remarquer qu'une diminution de la tête d'hydrostatique du mercure peut arrêter l'écoulement du liquide et fixer la goutte dans l'espace. De plus, un montage approprié assure l'élimination des vibrations mécaniques.

Discussion

Selon Armstrong et coll. (2), il y aurait formation à la surface de l'électrode d'une couche de HgO ayant une bonne conductivité électrique. De plus, selon Cotton et Wilkinson (3) l'oxyde de mercure possèderait une structure de chaîne en zigzag —Hg—O—Hg— avec une liaison de Hg—O = 2.03 Å et des angles de 109° pour HgOHg et 179° pour OHgO.

Il est en outre possible de fournir une justification mathématique pour ce phénomène. De façon précise nous allons, dans ce qui va suivre, présenter une équation mathématique devant être satisfaite par le profil de la goutte et nous allons vérifier comment cette équation nous permet de conclure que la présence d'un col est possible.

Fixons un temps t quelconque (après le début de formation de la goutte, mais avant sa chute). Désignons par h la hauteur de la goutte en ce temps et par r le rayon du capillaire.

Afin de concilier les faits qu'expérimentalement on observe une goutte suspendue et qu'il est habituel de dénoter par x (resp. z) les quantités mesurées horizontalement (resp. verticalement) avec le fait que mathématiquement une fonction n'est bien définie que si à chaque valeur de la variable indépendante on associe une et une seule valeur de la fonction, nous allons utiliser un système d'axes rectangulaires (z,x) ayant pour origine le point inférieur de la goutte et où cette fois z apparaît en abcisse et x en ordonnée. Utilisant cette convention tout à fait naturelle la

0008-4042/79/050565-03$01.00/0

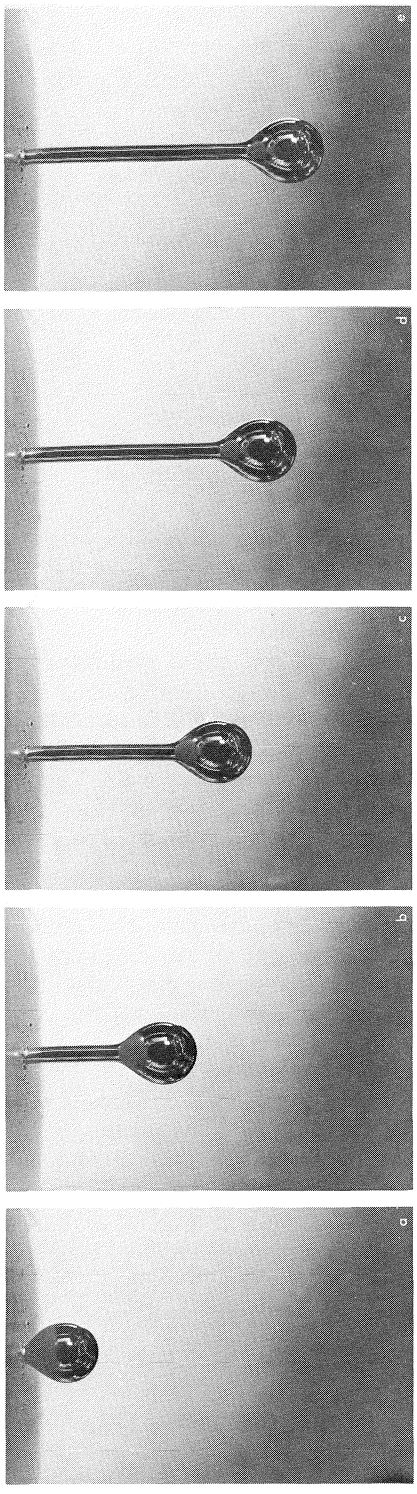

FIG. 1. Formation d'une goutte de mercure dans NaOH 1.0 *M*: (*a*) temps: 3 s; (*b*) temps: 6 s; (*c*) temps: 9 s; (*d*) temps: 12 s; (*e*) temps: 15 s.

goutte est alors délimitée par une surface de révolution engendrée par une fonction non négative, notée $X(z)$ at appelée la fonction profil, dont la valeur est nulle sur les intervalles $[-\infty, 0]$ et $[h, \infty]$ et qui est telle que $X(h) = r$ (voir fig. 2). Notons au passage que $X(z)$ dénote la valeur de la fonction profil au point z et que selon une coutume bien établie nous prendrons la liberté d'écrire tout simplement X à la place de $X(z)$ lorsque le contexte montrera clairement que X est une fonction de z.

Posons g = constante d'accélération due à la gravité; ρ_1 = masse spécifique du mercure; ρ_2 = masse spécifique de la solution de NaOH; σ = tension superficielle; R = rayon du cercle osculateur à la fonction profil au point (0,0); $V(z)$ = volume de révolution (dépendant de z) déterminé par la fonction profil restreinte à l'intervalle $[0,z]$; c'est-à-dire

$$[1] \qquad V(z) = \pi \int_0^z X^2(s)\mathrm{d}s$$

et $\theta(z)$ = angle (dépendant de z) formé au point $(z,X(z))$ par la normale (pointée extérieurement) à la fonction $X(z)$ et la verticale; c'est-à-dire

$$[2] \qquad \cos\theta(z) = [1 + (\dot{X}(z))^2]^{-1/2}$$

Dans ce travail, $\dot{X}$, $\ddot{X}$ désignent les dérivées (par rapport à z) première et seconde respectivement de la fonction $X(z)$. A nouveau lorsqu'il y a lieu de bien faire ressortir que ces dérivées dépendent de la variable z, on prendra le soin d'écrire $\dot{X}(z)$ et $\ddot{X}(z)$.

Une approche générale à la mise au point d'une méthode pour déterminer la tension superficielle à partir de la masse et du profil d'une goutte formée à l'extrémité d'un capillaire est présentée dans l'article de Badiali, Cachet, Cachet et Lestrade (4). Cette méthode est basée sur une relation rigoureuse qui doit exister entre la tension superficielle σ et la masse de la goutte. En supposant (ce que nous ferons nous aussi) que les pressions au sein des fluides ne varient qu'avec le champ de gravitation, les con-

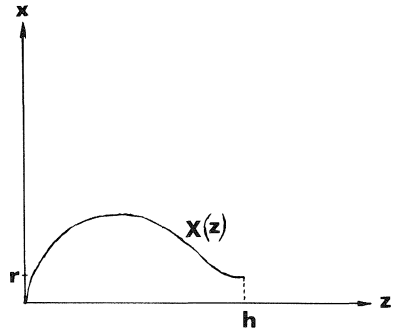

FIG. 2. Schéma de la goutte de mercure avant 3 s.

ditions d'équilibre mécanique de la goutte permettent d'établir que la fonction profil $X(z)$ doit satisfaire pour toute valeur de $z \in [0,h]$ l'équation de base suivante:

$$[3] \quad 2\pi\sigma X(z)\cos\theta(z) = g(\rho_1 - \rho_2)V(z) + \pi[X(z)]^2\,[(2\sigma/R) - g(\rho_1 - \rho_2)z]$$

Cette éq. [3] est précisément l'éq. [4] de la réf. 4 en page 744 et nous renvoyons le lecteur à cet article pour y trouver les détails conduisant à son établissement.

Maintenant si dans l'équation intégro-différentielle [3] on remplace $\cos\theta(z)$ et $V(z)$ par leurs expressions données en [2] et [1] respectivement et si on dérive par rapport à la variable z l'équation ainsi fournie, on obtient que la fonction profil satisfait l'équation différentielle:

$$[4] \quad X\dot{X}\ddot{X} = \dot{X}\left[1 + \dot{X}^2 - X\left[\frac{2}{R} - \frac{g}{\sigma}(\rho_1 - \rho_2)z\right] \times (1 + \dot{X}^2)^{3/2}\right]$$

ainsi que les conditions $X(0) = 0$, $X(h) = r$ et $\dot{X}(h) = 0$. Observons de plus que dans [3] et [4] R est relié à $X(z)$ par la formule:

$$[5] \qquad R^{-1} = \lim_{z\to 0^+} \frac{|\ddot{X}(z)|}{[1 + (\dot{X}(z))^2]^{3/2}}$$

Le point important pour nous consiste à observer que chacune des éqs [3] ou [4] fournit un modèle mathématique qui permet la formation d'une goutte avec un col. Afin de vérifier ceci, il nous faut montrer qu'étant donné h_1, $0 < h_1 < h$, et une fonction $X(z)$ satisfaisant [3] ou [4] sur l'intervalle $[0,h_1]$ et dont la valeur est constante et égale à r sur l'intervalle $[h_1,h]$ (voir fig. 3) il suit que $X(z)$ satisfait aussi [3] ou [4] sur l'intervalle $[0,h]$.

En effet, pour chaque valeur de $z \in [h_1,h]$ on a alors $\cos\theta(z) = 1$, $X(z) = r$, $V(z) = V(h_1) + \pi r^2(z - h_1)$. Utilisant maintenant le fait que [3] est vérifiée pour $z = h_1$ on obtient

$$[6] \quad 2\pi r\sigma = g(\rho_1 - \rho_2)V(h_1) + \pi r^2\,[(2\sigma/R) - g(\rho_1 - \rho_2)h_1]$$

ce qui peut être écrit sous la forme:

$$[7] \quad 2\pi r\sigma = g(\rho_1 - \rho_2)[V(h_1) + \pi r^2(z - h_1)] + \pi r^2[(2\sigma/R) - g(\rho_1 - \rho_2)z]$$

Or l'éq. [7] montre précisément que [3] est satisfaite également pour $z \in [h_1,h]$. D'autre part, l'éq. [4] indique bien que toute fonction $X(z)$ constante sur un intervalle satisfait cette équation sur cet intervalle car alors $\dot{X} \equiv 0$ sur l'intervalle en question.

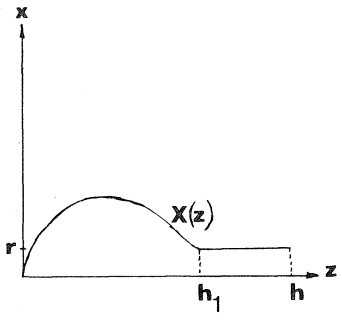

FIG. 3. Schéma de la goutte après 3 s.

Conclusions

En conclusion, nous pouvons faire remarquer qu'en milieux hallogénures ce phénomène de col n'est pas enregistré mais que, par contre, en milieu sulfure nous obtenons la formation d'une goutte similaire à celle présentée ici.

Devant la complexité de ce phénomène, l'identification par voie spectroscopique et la détermination de la tension interfaciale permettront d'identifier le film à la surface de l'électrode et de définir son importance.

Enfin le modèle mathématique présenté montre bien que la formation d'un col cylindrique est théoriquement possible et qu'il y a lieu de s'attendre à ce que le phénomène soit effectivement observé sous certaines conditions expérimentales. Malheureusement les équations fondamentales du modèle, les éqs [3] ou [4], sont trop complexes pour permettre la détermination d'une formule analytique pour la fonction profil $X(z)$ et ainsi arriver à prédire la forme d'une goutte. D'autre part nous n'avons pas réussi à déterminer la (les) relation(s) qui doit (doivent) exister entre les paramètres expérimentaux ρ_1, ρ_2 et σ pour que les éqs [3] ou [4] permettent de prédire la formation d'un col. Cette question importante reste ouverte pour le moment.

Remerciements

Les auteurs sont reconnaissants des octrois de recherche du CNRC et du M.E.Q. qui ont rendu ce travail possible.

1. H. MÉNARD et F. LEBLOND-ROUTHIER. Anal. Chem. **50**, 687 (1978).
2. R. D. ARMSTRONG, W. P. RACE et H. R. THIRSK. J. Electroanal. Chem. **19**, 233 (1968).
3. F. A. COTTON et G. WILKINSON. Advanced inorganic chemistry. Interscience Publishers, John Wiley & Sons, New York, London. 1967.
4. J. P. BADIALI, C. CACHET, H. CACHET et J. C. LESTRADE. J. Chim. Phys. 743 (1971).

Chemical reactions in glow discharges. IV. Production and removal of oxygen atoms in the dc glow discharge[1]

MOTILAL D. COSTA AND PRESTON A. ZULIANI

Lash Miller Chemical Laboratories, Department of Chemistry, University of Toronto, Toronto, Ont., Canada M5S 1A7

AND

JACQUES M. DECKERS

Lash Miller Chemical Laboratories, Department of Chemistry, University of Toronto, Toronto, Ont., Canada M5S 1A7 and Erindale College, University of Toronto, Mississauga, Ont., Canada L5L 1C6

Received May 15, 1978

MOTILAL D. COSTA, PRESTON A. ZULIANI, and JACQUES M. DECKERS. Can. J. Chem. **57**, 568 (1979).

An experimental technique for the measurement of the rate of formation and removal of atomic oxygen in an active glow discharge is described. The concentration of atomic oxygen was monitored with a mass spectrometer by sampling the gases flowing through the discharge. The rate of removal of oxygen atoms was found to be first order in atomic oxygen and 10 to 100 times faster than the corresponding recombination rate in the afterglow region. The measured rates of atom production are in agreement with those calculated by assuming electron impact dissociation of ground state molecular oxygen. The atoms are removed by a wall recombination process.

The ability of trace amounts of certain gases to enhance significantly the extent of dissociation in an electric discharge in oxygen has been studied. Only those added gases which contain a hydrogen or nitrogen atom are effective in enhancing the yield of atomic oxygen. For each hydrogen atom introduced into the oxygen stream about 300 extra oxygen atoms could be produced. This 'catalytic' effect is shown to be due to a marked decrease in the rate of recombination of O-atoms at the walls of the discharge tube. Whatever small change that occurs in the rate of O-atom production can be easily accounted for by a change in the energy distribution of the electrons in the discharge due to the effect of the additives.

MOTILAL D. COSTA, PRESTON A. ZULIANI et JACQUES M. DECKERS. Can. J. Chem. **57**, 568 (1979).

On décrit une technique expérimentale permettant de mesurer le taux de formation et d'enlèvement d'oxygène atomique actif dans une décharge électrique sous pression réduite. On a évalué la concentration de l'oxygène atomique par spectrométrie de masse en prélevant des échantillons de gaz s'écoulant à travers la décharge électrique. On a trouvé que le taux d'enlèvement des atomes d'oxygène est du premier ordre en oxygène atomique et est environ 10 à 100 fois plus rapide que le taux de recombinaison correspondant dans la région de la phosphorescence qui suit la décharge électrique. Les taux de production pour les atomes mesurés sont en accord avec ceux calculés en faisant l'hypothèse qu'il y a dissociation, sous impact électronique, de l'oxygène moléculaire dans son état fondamental. Les atomes sont enlevés par un processus de combinaison au niveau des parois.

On a étudié la propriété qu'ont certains gaz à l'état de trace d'augmenter d'une façon importante le taux de dissociation de l'oxygène sous l'influence d'une décharge électrique. Parmi les gaz additionnés, seuls ceux qui contiennent des atomes d'hydrogène ou d'azote sont efficaces pour rehausser le rendement en oxygène atomique. Pour chaque atome d'hydrogène introduit dans un courant d'oxygène, il se produit environ 300 atomes d'oxygène en supplément. On a montré que cet effet catalytique est dû à une diminution sensible du taux de recombinaison des atomes d'oxygène près des parois du tube de la décharge. Tout changement mineur dans le taux de production des atomes d'oxygène peut être expliqué par un changement dans la distribution d'énergie des électrons dans la décharge électrique dû à l'effet d'additifs.

[Traduit par le journal]

1. Introduction

There is much controversy concerning the mechanisms for atom production and removal in discharges in diatomic gases. It has been argued that the production of oxygen atoms occurs by a stepwise process involving some unspecified metastable species as an intermediate, a reaction sequence which has been postulated to occur in nitrogen discharges (Baker *et al.* (1), Young and St. John (2)). Others (Kaufman and Kelso (3, 4), Linnett and Marsden (5)) have felt that catalytic production schemes in-

[1]Abstracted, in part, from the Ph.D. theses of P. A. Z. and M. D. C. (see refs. 11, 12).

0008-4042/79/050568-12$01.00/0

volving trace impurities are responsible for the atom production. More recently, Kaufman (6) has proposed that the main atom production term in discharges in O_2, N_2, and H_2 involves the simple electron impact dissociation of the ground state molecules. While this proposal has not met with universal acceptance, at least for N_2, it seemed to us to be an attractive possibility for oxygen discharges. Kaufman (6) has also suggested that the wall recombination of atoms might be very much faster in the active discharge than in the afterglow and could be the dominant removal term.

In this paper we describe an experimental design which permits the sampling of an active discharge. The sampled products and intermediates are analysed continuously by mass-spectrometry. The measured profiles of atomic oxygen concentration versus time are then used for kinetic analysis in order to determine the dominant reaction mechanism.

Although discharges are commonly used to generate atoms for other studies, very little is known about parameters controlling the atom concentration in the discharge effluent. It has long been realized that addition of small amounts of other gases causes large increases in the extent of dissociation in diatomic gases. We report our studies of the effect of addition of small amounts of gases on the oxygen atom concentration in the discharge. Those effects have been extensively studied in the case of hydrogen and nitrogen (7, 8). However, surprisingly little is known in the case of oxygen. We will show that the dominant effect of these added gases is to inhibit the atom recombination process rather than to affect the atom production process.

2. Experimental

The experimental apparatus is illustrated schematically in Fig. 1. The gas or gas mixture which was to be studied was passed through a liquid nitrogen cold trap to remove traces of water vapor. The gas flow system was all glass and metal and the use of mercury was strictly avoided. The flow rates of the gases were measured with Hastings flow transducers. The average stream velocity of the gas $\bar{V}_s$ through the discharge was calculated from the total flow rate, the pressure in the discharge, and the tube diameter. The discharge was sustained in a U-shaped Pyrex glass tube with an inside diameter of 12.7 mm. A moveable anode was located in one of the arms of the U-tube. A small (0.07 mm radius) 'leak' was located in a thin glass membrane at the tip of a glass cone near the bottom of the U-tube in line with the anode. The gas entered the discharge tube upstream of the anode. A pressure transducer was used to record the pressure at a tap-off located 3 cm downstream of the leak. A small platinum wire probe was located about 1 cm downstream of the pinhole and was used to measure the floating potential in the discharge near the sampling orifice. A further side-arm in the anode region contained an additional electrode. When desired, a discharge could be struck between this electrode and the anode; in this case the mass spectrometer

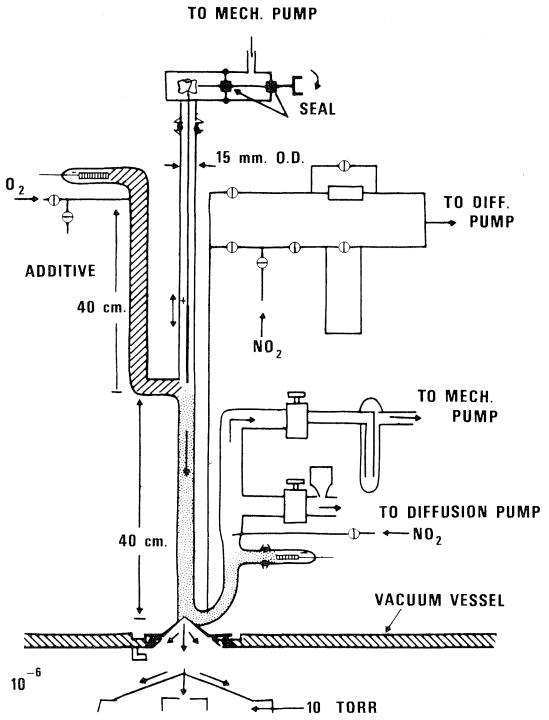

FIG. 1. Schematic of apparatus.

leak would be located in the afterglow region so that the afterglow atom concentrations could be measured directly. It was calculated that about 0.5% of the gas flowed through the sampling orifice.

The gas discharge was sustained by a regulated 5000 V power supply. The discharge was 'floated' in such a manner as to maintain the plasma in the vicinity of the pinhole very slightly negative with respect to the grounded mass spectrometer to prevent positive ions, formed in the discharge, from entering the mass spectrometer.

The electrodes were fashioned from copper. Care was taken that no detectable anode sputtering occurred in the positive column of the discharge during the reported runs. In particular, frequent cleaning of the discharge tube with nitric acid followed by copious rinsing with distilled water ensured that no complications occurred due to sputtering of electrode material on the walls. The cathode was a hollow cylinder located in a side-arm well downstream from the region in which measurements were taken.

The sample of discharged gas which had passed through the pinhole travelled about 6 cm in a 10^{-6} Torr environment before part of it flowed through a 2 mm diameter aperture at the apex of a second chamber which housed the mass spectrometer. The pressure in this chamber was maintained at less than 10^{-7} Torr by using differential pumping and liquid nitrogen cooling. An Extranuclear Laboratories high efficiency ionizer, quadrupole mass spectrometer, and 14 stage particle multiplier were used to analyze the gases.

The molecular beam emanating from the discharge was mechanically chopped at 400 Hz and the resulting ac signal was recovered by phase sensitive detection. By setting the

electron energy in the ionizer just below the threshold for the dissociative ionization of O_2, the relative concentration of O-atoms formed in the discharge could be measured as a function of experimental parameters. These concentrations were then converted to absolute O-atom concentrations by calibrating the mass spectrometer using the NO_2 titration technique. Titration experiments were always performed in the afterglow region of the discharge using the side-arm electrode, as it was found that, in the active discharge, the NO/NO_2 were also subjected to partial decomposition (see sections 3.6 and 4.4) which might affect the results of the titration.

3. Results and Interpretation

3.1 General

The fundamental measurement in this work involved the determination of the concentration of atomic oxygen as a function of distance between the pinhole and the anode location in either ultrapure oxygen or in oxygen to which measured trace amounts of another gas had been added. Simultaneously the potential at the floating probe was recorded. The mass spectrometric signal versus distance profile was then converted into atomic concentration versus time by taking into account the calibration factor of the mass spectrometer, the gas flow, the pressure, and the diameter of the discharge tube. A sample graph is shown in Fig. 2. The slope of the floating potential versus distance curve gave a measure of the electric field in the positive column of the discharge (9). After a discharge was struck, it was noticed that measured quantities such as the mass spectrometric signal, the potential at the electrodes, or the current through the discharge would drift, reaching a steady value after a couple of hours. All measurements reported are taken under the 'steady' conditions. Each time one or more of the discharge operating parameters were altered, it was necessary to wait from 5 min to as much as 1 h before a new steady measurement could be recorded.

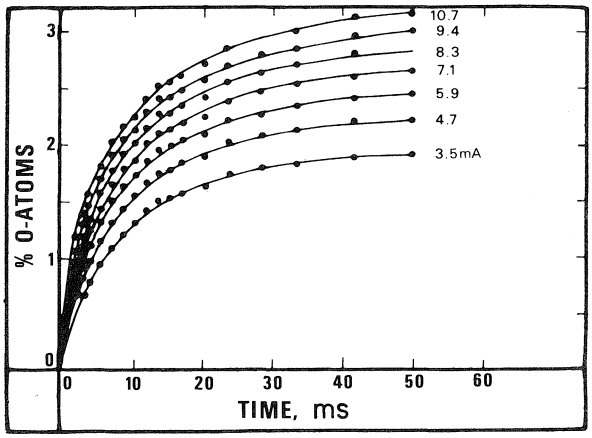

FIG. 2. Plot of % oxygen atoms produced versus time spent in the discharge for various currents (P = 0.798 Torr, $\bar{V}_s$ = 7.25 m s^{-1}).

3.2 Ultrapure Oxygen

The oxygen atom concentration was found to rise monotonically with the residence time of the gas in the discharge to achieve a final steady-state value $[O]_{ss}$. Plots of ln $([O]_{ss} - [O])/[O]_{ss}$ versus time were linear demonstrating that the rise was exponential and that the oxygen atom concentration at any time could be described by an equation of the type

$$[1] \qquad [O] = [O]_{ss}\{1 - \exp(-k_w t)\}$$

Here k_w is an arbitrary constant which is obtained from the slope of the logarithmic plot. A sample graph is shown in Fig. 3.

Let us now test the hypothesis that the O-atoms are being produced by simple electron impact dissociation with rate constant k_T and removed by a first order wall recombination process with rate constant k_w. Then

$$[2] \qquad O_2(X^3\Sigma_g^-) + e^* \xrightarrow{k_T} 2O(^3P) + e$$

$$[3] \qquad O(^3P) \xrightarrow{k_w} \tfrac{1}{2}O_2(X)$$

$$[4] \qquad d[O]/dt = 2k_T n_e[O_2] - k_w[O]$$

where n_e is the electron concentration. Integrating, one gets

$$[5] \qquad [O] = (2k_T n_e[O_2]/k_w)(1 - \exp -k_w t)$$

We can immediately see that this mechanism is consistent with the observed [O] versus t profiles where k_w is the first order removal rate constant and

$$[6] \qquad [O]_{ss} = 2k_T n_e[O]_2/k_w$$

We now attempt to test this mechanism further by calculating $[O]_{ss}$ from eq. [6] and comparing the calculated variation of $[O]_{ss}$ with discharge current and pressure with the experimentally determined profiles.

3.3 Variation of $[O]_{ss}$ versus Current and Pressure

Two of the parameters in eq. [6] necessary to calculate $[O]_{ss}$ are readily available. $[O_2]$ was determined by measuring the discharge pressure while k_w could be determined from the slope of the plots as shown in Fig. 3. In actual practice, k_w was determined by a least-squares fit to the [O] versus t data with corrections being made for back diffusion.[2]

Values for the electron concentration, n_e, were obtained using the equation

$$[7] \qquad I = n_e e v_e A$$

where I is the discharge current, A the tube cross section, e the electronic charge, and v_e the electron drift velocity. To obtain n_e as a function of discharge

[2]For details see Zuliani's Ph.D. thesis (11).

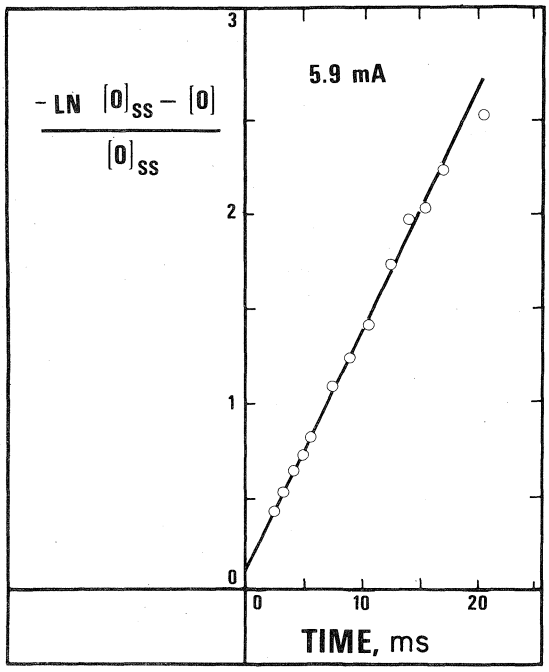

FIG. 3. Logarithmic plot of $([O_{ss}] - [O])/[O]_{ss}$ versus time spent in the discharge ($P = 0.798$ Torr, $\bar{V}_s = 7.25$ m s^{-1}).

current and pressure, it was necessary to measure the electric field as a function of these parameters. This was done using either the Langmuir probe and/or the moving anode technique (9). The electron concentration n_e could be calculated from $X_e = n_e v_e$ where the drift velocities were taken from Hake and Phelps (10) and X_e is the electric field.

Finally, k_T was calculated from the expression

$$[8] \qquad k_T = \int_0^\infty f(\varepsilon) Q(\varepsilon) \left(\frac{2}{m_e}\right)^{1/2} d\varepsilon$$

where $f(\varepsilon)$ is the electron energy distribution function, $Q(\varepsilon)$ the electron impact cross section for reaction [2], while ε and m_e are the energy and mass of the electron, respectively.

Actually, reaction [2] is a composite of three reactions:

$$[9] \qquad \begin{aligned} O_2(X^3\Sigma_g^-) + e^*(>4.5\text{ eV}) &\rightarrow O(^3P) + O(^3P) \\ O_2(X^3\Sigma_g^-) + e^*(>8.0\text{ eV}) &\rightarrow O(^3P) + O(^1D) \\ O_2(X^3\Sigma_g^-) + e^*(>9.7\text{ eV}) &\rightarrow O(^1D) + O(^1D) \end{aligned}$$

The cross sections for these three reactions are available as a function of the electron energy (10).

In this laboratory Rundle *et al.* (9) measured the electron energy distribution function over a limited range of discharge pressure. For extrapolating beyond this range, we assumed a Druyvesteyn energy distribution (16) since, where comparison was possible, this was a closer approximation to the measured distribution than was an equilibrium distribution.

The differences between values of k_T calculated by using a Druyvesteyn energy distribution versus those calculated using the functional form determined by Rundle *et al.* (9) were smaller than the experimental uncertainties.

In Fig. 4, we illustrate the effect of current on k_w and $[O]_{ss}$, while in Fig. 5 the effect of pressure on $[O]_{ss}$ is shown. The values of an expanded set of measurements of k_w obtained similarly (using a different oxygen supply) are tabulated as a function of pressure and current in Table 1. The magnitudes of the back diffusion correction, expressed as a percentage of k_w, are given in parentheses underneath the values of k_w. The effect of pressure on k_w is illustrated in Fig. 6.

In Fig. 7, the measured and calculated values for the % oxygen dissociation are presented for ultrapure oxygen. The agreement between calculated and experimental values is within a factor of 2 for the whole range of pressures investigated and provides further confirmation of the interpretation of the data.

3.4 Addition of Foreign Gases: General

Wherever hydrogen or nitrogen containing gas was added to the oxygen flow, the oxygen atom concentration in the discharge rose significantly and reached a new steady-state value after a certain time (usually a matter of a few minutes). When the flow of foreign gas was stopped, the atom yield started to decrease immediately, returning to its original 'steady' value after about an hour.

Results could be presented in two ways depending on the type of information desired. Recombination

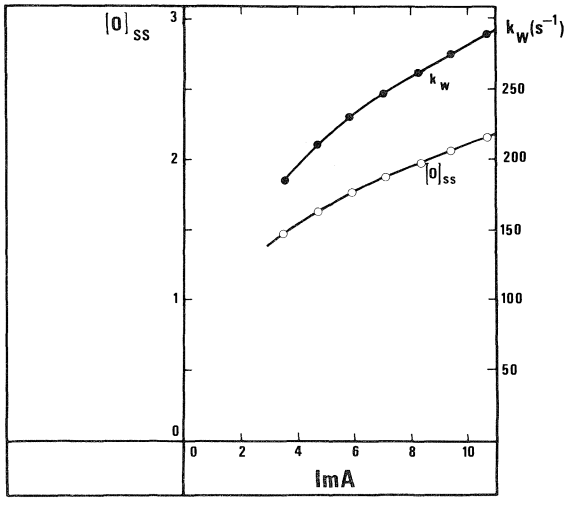

FIG. 4. Plot of % atomic oxygen in the steady state (○) and k_w (●) versus current ($P = 0.798$ Torr, $\bar{V}_s = 7.25$ m s^{-1}).

TABLE 1. Variation of k_w (s^{-1}) with current and pressure*

	k_w (s^{-1}) when pressure (Torr) =												
	0.430	0.492	0.588	0.675	0.798	0.945	0.990	1.02	1.13	1.23	1.58	2.08	2.35
I(mA) = 2	326 (24)	276 (25)	202 (11)	179 (11)	150 (9)	—	124 (7)	117 (7)	87 (5)	—	—	—	—
3	418 (26)	380 (31)	253 (13)	217 (12)	172 (10)	140 (9)	138 (8)	—	111 (5)	179 (6)	—	—	—
4	438 (28)	437 (32)	294 (15)	256 (14)	188 (10)	156 (10)	153 (8)	142 (7)	95 (5)	188 (6)	—	—	70 (4)
5	528 (31)	434 (33)	340 (16)	282 (15)	202 (10)	167 (10)	164 (9)	—	111 (6)	193 (6)	—	—	72 (4)
6	592 (34)	519 (35)	377 (18)	313 (16)	214 (10)	177 (11)	173 (9)	159 (8)	119 (6)	199 (7)	98 (8)	—	78 (4)
7	655 (35)	538 (37)	417 (20)	340 (17)	225 (11)	185 (11)	184 (10)	—	125 (6)	201 (7)	98 (8)	—	80 (4)
8	715 (36)	584 (38)	466 (21)	366 (18)	237 (12)	194 (11)	192 (11)	168 (8)	132 (7)	202 (7)	101 (8)	53 (3)	82 (4)
9	829 (38)	655 (40)	510 (22)	385 (19)	248 (12)	203 (12)	202 (12)	—	138 (7)	203 (7)	101 (9)	51 (3)	83 (4)
10	852 (40)	696 (41)	534 (23)	418 (20)	258 (12)	211 (12)	210 (12)	177 (9)	146 (8)	206 (7)	104 (9)	51 (3)	83 (4)
$\bar{V}_s$ (ms^{-1})	6.85	6.05	7.77	7.26	7.25	6.17	5.90	6.92	6.30	7.23	4.39	5.01	4.65
$\bar{P}$ (Torr)	0.452	0.512	0.614	0.699	0.822	0.965	1.01	1.04	1.15	1.25	1.59	2.10	2.37

*T = 340 K was used as the gas temperature in order to calculate $\bar{V}_s$ and k_w for all results, $\bar{V}_s$ is the average gas stream velocity in the discharge tube. The numbers in parentheses are the magnitudes of the back diffusion correction, expressed as a % of k_w.

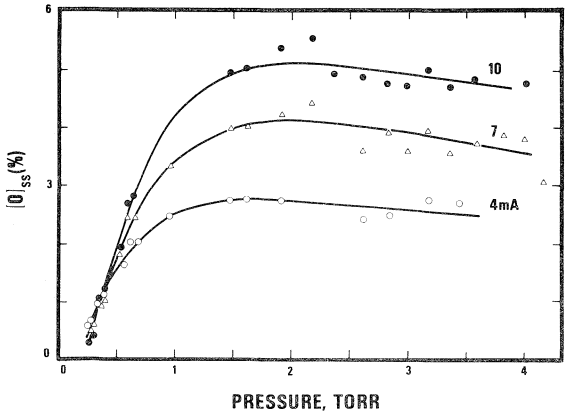

FIG. 5. Plot of % atomic oxygen in the steady state versus discharge pressure at various currents ($\bar{V}_s$ = ~3 m s^{-1}).

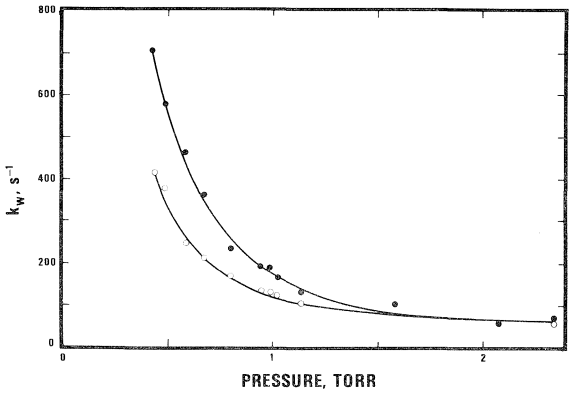

FIG. 6. Plot of k_w versus pressure at two values of the discharge current: ○, 3 mA, ●, 8 mA.

rate constants could be obtained for a given gas/additive ratio from the plotting procedure outlined in section 3.2. Alternately, the percent dissociation of O_2 could be plotted versus the percent of added gas, hence describing the effect of the additive on the overall oxygen atom concentration. In Fig. 8, we plot the percent dissociation versus the concentration of various additives in parts per million. In Fig. 9 the range of added gas is increased. It is immediately obvious from an examination of these curves that, even for very small amounts of gas added, several hundred additional oxygen atoms are produced per molecule of added gas. In fact, the slopes of the curves in Figs. 8 and 9 are equal to the number of oxygen atoms produced per added molecule; this slope is defined as the 'catalytic efficiency' of the additive gas. As can be seen from Figs. 8 and 9, the oxygen atom concentration rises sharply for small concentrations of the 'catalyst' (0–30 ppm) and less rapidly at larger concentrations. The catalytic efficiency is thus very large initially and decreases monotonically with increasing additive gas concentration. In Table 2 the

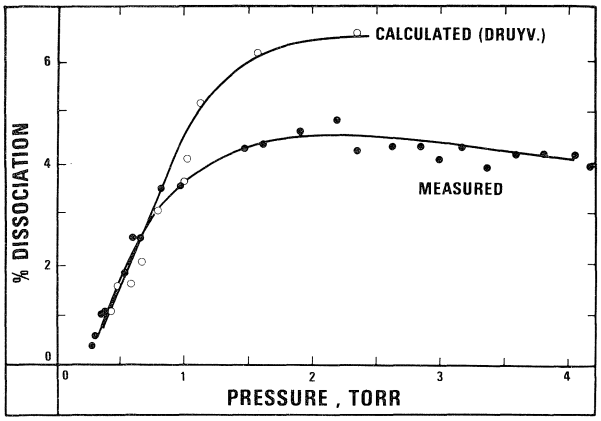

FIG. 7. Calculated and measured plots of extent of dissociation versus pressure at 8 mA in ultrapure oxygen (~10 ppm impurities). $\bar{V}_s = 6.8$ m s^{-1}.

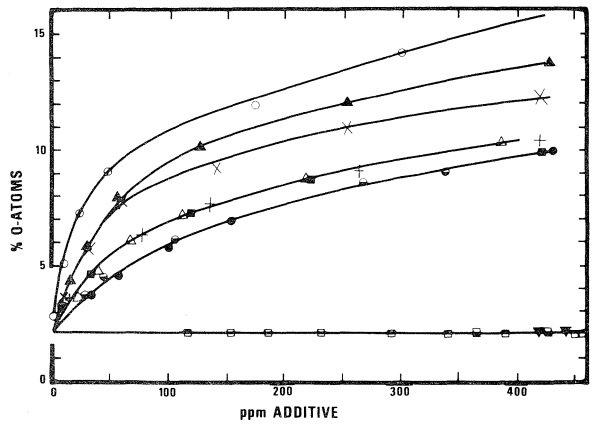

FIG. 8. Plot of % atomic oxygen produced versus concentration of additives in ppm. $P = 1.21$ Torr, $\bar{V}_s = 1.96$ m s^{-1} (at 8 mA), $T = 340$ K (at 8 mA). Symbols: NO, ◒; C_2H_4, +; H_2, ●; C_2H_2, △; CH_4, ■; C_4H_6 (1,2-butadiene), ▲; C_2H_6, ×; $(CH_3)_4C$, ○; CO, ▼; CO_2, ⬓; Ne, Kr, Xe, Ar, □.

initial slope has been tabulated in for a number of additive gases at various currents. In Table 3 the slope is plotted at the 0.1% additive level. A comparison of the values in these two tables illustrates the decrease in efficiency.

3.5 Hydrocarbon Additives

Plots of the percent of oxygen atoms produced versus the percent hydrocarbon added are characterized by very steep initial rises which gradually level off. For very large additions (~0.5%), the catalytic efficiencies assume negative values: the concentration of oxygen atoms in the discharge decreases upon further hydrocarbon additions. This decrease in the oxygen atom concentration is wholly accounted for by the consumption of the atoms by reaction with the hydrocarbons and their reaction

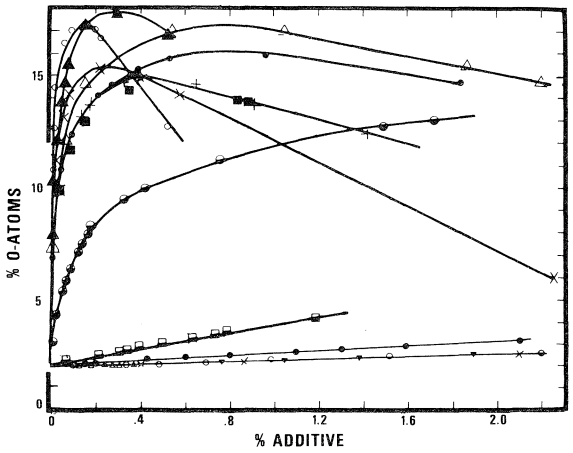

FIG. 9. Plot of % atomic oxygen produced versus concentration of additives in %. $P = 1.21$ Torr, $\bar{V}_s = 1.96$ m s^{-1} (at mA), $T = 340$ K (8 mA). Symbols: (upper range) NO, ◒; C_2H_4, +; H_2, ●; C_4H_6, ▲; CH_4, ■; $(CH_3)_4C$, ○; C_2H_6, ×; (lower range) He, △; CO, ●; Ne, ▼; CO_2, ⬓; Kr, ○; Ar, ×.

products. A plot of the catalytic efficiency of some gases is shown as function of current in Fig. 10.

3.6 Nitrogen Containing Additives

Plots of O atom concentration versus the concentration of nitrogen containing additives are shown in Figs. 11, 12.

3.7 Inert Gases, CO, CO_2

Plots of $[O]_{ss}$ versus percent of added inert gases are shown in Figs. 8, 9. Although these gases were quite ineffective in enhancing the atom yield, a finite slope was measured. For He, Ar, Kr, and Ne, this slope was <0.3 oxygen atom per inert gas atom. For CO the slope was ≤ 0.6, while for CO_2 it was ≤ 2 oxygen atom per impurity added. These low efficiencies are quite likely due to the small amounts of water present as an impurity in the gases.

4. Discussion

4.1 General

We wish to emphasize here that the sampling pinhole was located in the active discharge and not in the afterglow region. The only purpose of the additional electrode located in the side-arm was for establishing on an absolute scale the O atom concentration through the NO titration technique. Luminosity due to the discharge itself and the partial decomposition due to reactions interfered with the measurement when it was attempted in the active discharge.

Results in a given discharge tube were very reproducible, especially when trace amounts of catalytic gases were added. However, because of the extreme sensitivity of $[O]_{ss}$ to trace impurities in highly purified oxygen, it would be expected that

TABLE 2. The catalytic efficiency of added gases as a function of the discharge current

Added gas	Catalytic efficiency when discharge current (mA) = 2	4	6	8	10
He, Ar, Kr, Ne	≤0.3	≤0.3	≤0.3	≤0.3	≤0.3
CO	≤0.6	≤0.6	≤0.6	≤0.6	≤0.6
CO_2	≤0.2	≤0.2	≤0.2	≤0.2	≤0.2
SO_2	≤6	≤6	≤6	≤6	≤6
NO	464	406	420	378	380
N_2	34	49	54	84	84
N_2O	200	263	287	342	353
H_2	232	384	553	640	640
C_2H_2	354	455	519	519	568
CH_4	467	850	1100	1240	1460
C_2H_4	719	988	1080	1150	1310
C_2H_6	1080	1530	1870	1940	2040
C_4H_6	1030	1280	1540	1680	1780
C_5H_{12}	1510	2180	2570	2750	2850
NO_2	Comparable to NO				
$CHCl_2F$	300 ± 200 at 8 mA				

TABLE 3. Catalytic efficiency of added gases as a function of discharge current (0.1% additive)*

Catalyst	Catalytic efficiency when discharge current (mA) = 2	4	6	8	10
He, Ar, Kr, Ne	≤0.3	≤0.3	≤0.3	≤0.3	≤0.3
CO	≤0.6	≤0.6	≤0.6	≤0.6	≤0.6
CO_2	≤2	≤2	≤2	≤2	≤2
NO	77	100	108	112	117
N_2	10.4	16.2	22.1	26.8	31.3
N_2O	38	57	68	76	81.5
H_2	33.5	63	84.5	101	115
C_2H_2	41	69	89	105	123
CH_4	33	61	82	97	114
C_2H_4	38	68	87	102	118
C_2H_6	49	83	106	122	140
C_4H_6	54	95	124	147	167
C_5H_{12}	54	99.5	130	157	180

*P = 1.21 Torr, 8 mA, T = 340 K, V_s = 1.96 m s^{-1}, and residence time in the discharge = 163 ms.

different $[O]_{ss}$ values might be obtained in different laboratories, or indeed, with different oxygen cylinders, due to slightly different impurity levels. Hence, great care should be taken in lifting O-atom concentration to be used for other purposes.

In fact, at one time, after having run a discharge through oxygen – carbon monoxide mixtures for some time, it was no longer possible to obtain the very high values of k_w observed before this set of experiments was performed. Close examination of the discharge tube wall revealed that it was coated with a very thin brownish-black film. This film could not be removed by running the discharge for many hours through pure oxygen. Only after cleaning with concentrated HNO_3 mixed with HCl was the film removed and the original k_w values reproduced. Black particles (probably some form of polymeric carbon) were suspended in the solution. No further analysis of the phenomenon was attempted.

4.2 Pure Oxygen

The proposed mechanism predicts an [O] versus t profile which rises exponentially to a steady-state value in agreement with experiment. Moreover, calculations of the absolute value of $[O]_{ss}$ from eq. [6] agree to within a factor of 3 with the experimental values. This is within the uncertainty limits of the cross sections, the electron concentrations, and the energy distribution function used in the calculation.

Figure 13 shows that $[O]_{ss}$ increases strongly with current at high pressures, but decreases with current

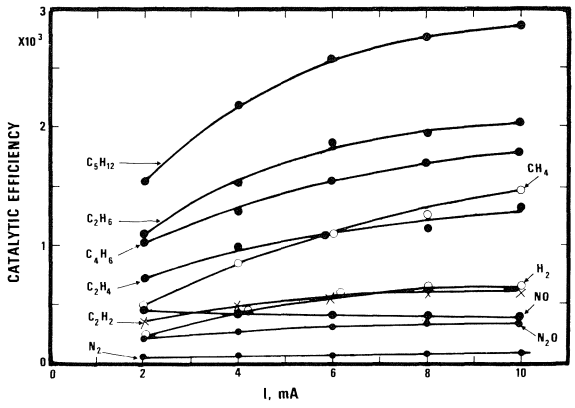

FIG. 10. Plot of the number of oxygen atoms produced for each foreign gas molecule added ('catalytic efficiency') versus the current for different gases (initial slope method). $P = 1.21$ Torr, $\bar{V}_s = 1.96$ m s^{-1}.

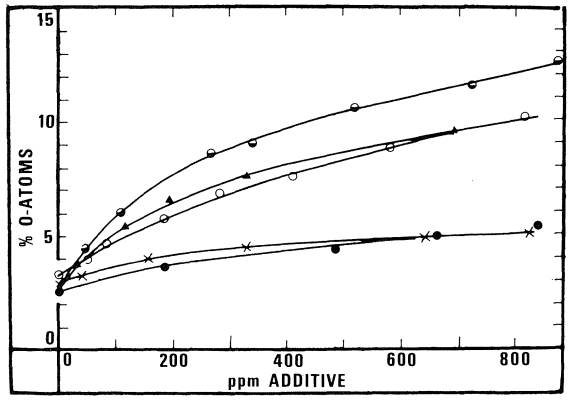

FIG. 11. Plot of % oxygen atoms produced versus the concentration of added catalyst for several gases which contain N atoms. $P = 1.21$ Torr, $\bar{V}_s = 1.96$ m s^{-1}. Symbols: NO_2, ○; NO, ◒; N_2, ×, ●; N_2O, ▲.

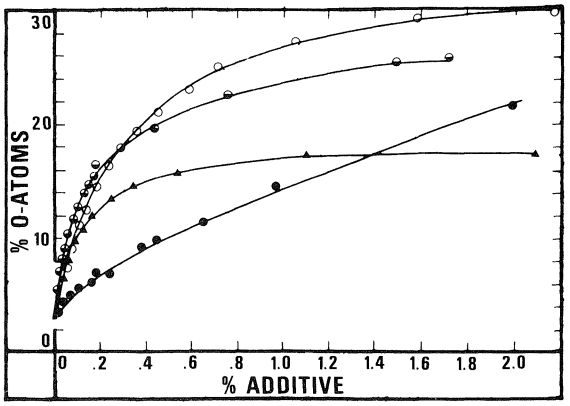

FIG. 12. Plot of % oxygen atoms produced versus the concentration (larger amounts) of added catalyst for several gases which contain N atoms. $P = 1.21$ Torr, $\bar{V}_s = 1.96$ m s^{-1}. Symbols as in Fig. 11.

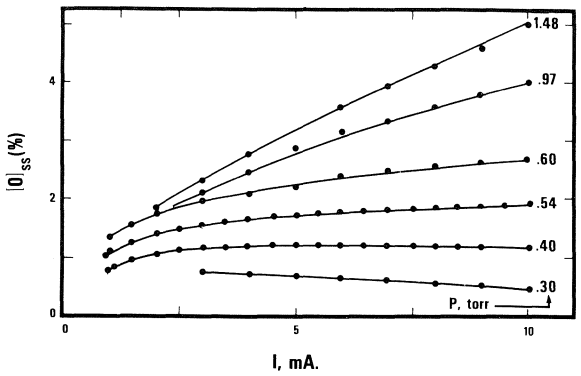

FIG. 13. Plot of $[O]_{ss}$ versus current at various pressures. $\bar{V}_s \sim 3$ m s^{-1}.

at low pressures. To determine whether the postulated mechanism is consistent with the observed trend, we may rearrange eq. [6] and use eq. [7]:

$$[10] \quad k_w[O]_{ss} = 2k_T[O_2]I/eV_eA = (\text{Constant}) \times I$$

Thus, this mechanism will explain the measured current dependence of $[O]_{ss}$ only if all plots of $k_w[O]_{ss}$ versus I are linear with zero intercept. Such behaviour was always observed, as can be seen in Fig. 14 where the product $k_w[O]_{ss} = \theta$ is shown at three pressures. The extrapolation to zero current intersects the origin within experimental uncertainty.

The calculations also predicted that the percent dissociation of O_2 should increase with increasing pressure, passing through a broad maximum from 2–4 Torr. As is shown in Fig. 7, this is in agreement with experiment. (The predicted curve was calculated using Hake and Phelps dissociation cross sections

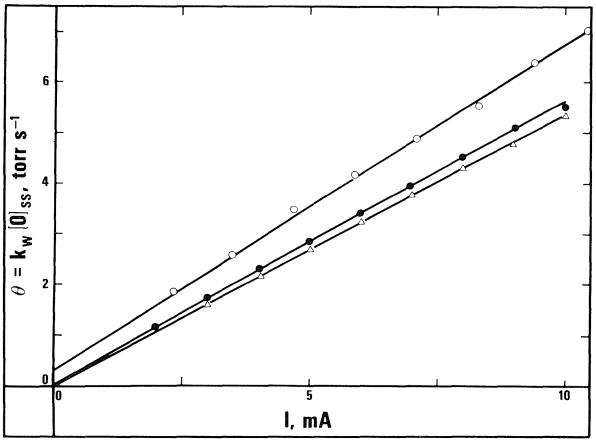

FIG. 14. Plot of $\theta = k_w[O]_{ss}$ versus current: $P = 0.59$ Torr, $\bar{V}_s = 7.8$ m s^{-1}; $P = 0.95$ Torr, $\bar{V}_s = 6.2$ m s^{-1}; $P = 1.2$ Torr, $\bar{V}_s = 5.2$ m s^{-1}.

(10) and drift velocities and assuming a Druyvesteyn energy distribution (16).)

Attempts have been made, without success, to correlate the value of k_w with known or suggested gas phase reactions to explain the observed first order removal of atomic oxygen. The fact that when the setting of an experimental parameter such as pressure, flow rate, or current was altered a significant lag time occurred for steady measurements is clear indication that wall effects play a dominant role in controlling the discharge.

The various observations related so far, especially those involving the observed inability to obtain very high k_w values when the walls of the discharge tube were coated with the brown-black deposit, establish quite unambiguously that the first order removal of O atoms is a wall process.

4.3 Hydrocarbon Additives

As the number of hydrogen atoms present in the additive gas molecule increases, the catalytic efficiency increases. Figure 15 shows a plot of the catalytic efficiency versus the number of hydrogen atoms in the additive molecule. The straight line obtained through the points has a slope of 300 oxygen atoms produced per hydrogen atom in the additive gas molecule. Since hydrocarbons added to the discharge decompose to form H_2 and CO as the dominant reaction products (13) this result is reasonable. As Figs. 8 and 9 show, H_2 is highly effective at increasing the atom yield in the discharge while CO and CO_2 are rather ineffective.

Winkler (7) has suggested that the catalytic efficiency of additives in enhancing the nitrogen atom yield in a N_2 discharge can be correlated with the molecular complexity of the additives. Such a plot is shown in Fig. 16. The correlation obtained with the number of hydrogen atoms is certainly better than the correlation obtained with the number of internal degrees of freedom. It is probable that for the much shorter residence times used by Winkler, the added hydrocarbons were only partially decomposed.

In Fig. 10, the catalytic efficiency, as calculated from the initial slope, is shown to increase with current in a non-linear fashion. For species containing the same number of hydrogen atoms (H_2, C_2H_2; CH_4, C_2H_4; C_2H_6, C_4H_6), the decrease at lower currents is greatest for those species which decompose most slowly in the discharge (H_2, CH_4, C_2H_6). The increased catalytic efficiencies at high currents may thus simply be the results of a greater conversion of the added hydrocarbon to hydrogen or its oxydation products.

4.4 Nitrogen Containing Impurities

Plots of the oxygen atom concentration versus the concentration of nitrogen containing additives are similar to those obtained when using hydrogen additives except that no maxima are observed for additions of up to 10%. Instead, the oxygen atom concentration increases monotonically with impurity concentration. Since oxygen atoms are not consumed by a reaction with nitrogen containing species, no maxima are expected.

From Figs. 11 and 12, it is apparent that the catalytic efficiency decreases less rapidly with increasing additive concentration in the case of nitrogen containing species than for hydrogen containing ones. It is also obvious that no correlation exists between the number of nitrogen atoms in the additive molecules and the catalytic efficiency. This is consis-

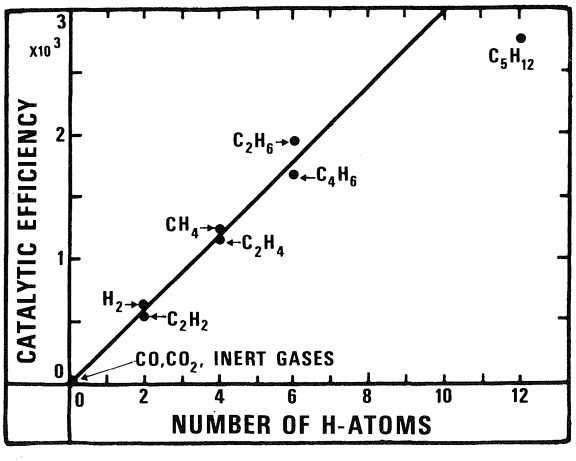

FIG. 15. Plot of the number of oxygen atoms produced for each foreign gas molecule added ('catalytic efficiency') versus the number of H-atoms in the additive. P = 1.21 Torr, $\bar{V}_s$ = 1.96 m s^{-1}; I = 8 mA.

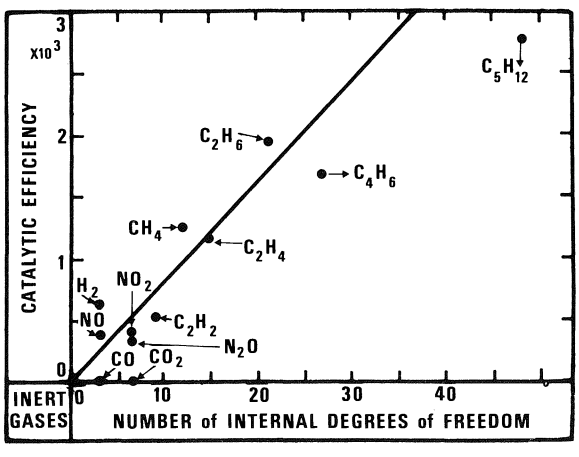

FIG. 16. Plot of the number of oxygen atoms produced for each foreign gas molecule added ('catalytic efficiency') versus the number of internal degrees of freedom in the additive. (Conditions as in Fig. 13.)

tent with the fact that interconversion between the nitrogen additives occurs: (*1*) NO addition: 50–60% remains intact; the remainder is converted to N_2. (*2*) N_2 addition: 95% remains intact; the remainder is converted to NO. (*3*) N_2O addition: 20% remains intact; 25% is converted to NO; 55% is converted to N_2. (*4*) NO_2 addition: 0% remains intact; 50% is converted to N_2; 50% is converted to NO.

Thus, if X% of NO, N_2, and N_2O were added to the discharges, then taking the stoichiometry into account, one would expect $X/2$%, $X/10$%, and $X/2$%, respectively, of NO to be present in the discharge. Thus the ratio of the percent NO present for each of these gases is approximately the same as the ratio of the catalytic efficiencies ($\sim$10:2:9 for NO, N_2, and N_2O, respectively). This suggests that either NO or some species proportional to the NO concentration (perhaps NO^+) is the active species.

5. Discussion

5.1

The remarkable enhancement in [O] when trace amounts of certain gases are added to an oxygen discharge must be ascribed either to the enhanced production or to the decreased removal of atoms (or a combination of these).

By measuring the time development of the oxygen atom concentration in the discharge, one can separate the effects due to the production and removal processes. When presenting the data, we have postulated that oxygen atoms in the discharge are produced by direct electron impact dissociation of ground state molecules while the atoms are removed by a first order process [2], [3].

Figure 17 illustrates the dependence of both $[O]_{ss}$ and k_w on concentration of added NO. Similar results were obtained with other catalytic gases. The marked enhancement in the atom concentration is seen to be accompanied by an equivalent decrease in the removal rate constant k_w. This established quite unequivocally that the production term $k_w[O]_{ss}$, from eq. [10], is independent of [NO] within the experimental error.

These results provide striking evidence that the catalytic effects are almost entirely the result of a decreased removal rate of atoms and not as a result of changes in electron energy distribution nor of catalytic production sequences. Indeed, measurements of the ratio of the electric field over gas density, E/N, which is a measure of the electron properties, were found to decrease by less than 2% for addition of hydrocarbons of up to 10% to the oxygen discharge. On this basis alone, one would have expected a decrease in the atomic oxygen production.

We have also attempted to account for the removal

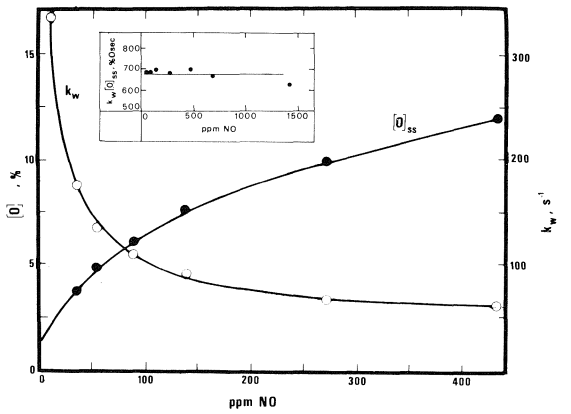

FIG. 17. Plots of $[O]_{ss}$ and k_w versus the concentration of added NO. P = 1.20 Torr, V_s = 5.64 m s^{-1}, I = 8 mA.

process via ion molecule processes. Although some of those processes have very large rate constants, the concentration of the various species, especially ions, are very small at the rather low current densities at which these experiments were carried out. Because of the low concentrations, none of the processes for which calculations were attempted had rates which were even within 1% of the measured rates, and almost all were many orders of magnitude lower.

Even when large amounts of nitrogen additives were present and that it was suspected that NO or NO^+ might play a significant role in the removal process, the results of calculated rates were too low to account for the k_w observed.

It is a well-known fact that because of the ambipolar diffusion which sustains the positive column of a glow discharge (17) the walls are coated with a layer of electrons while the core of the column contains a slightly positive charge. It is believed that when ultrapure oxygen is fed into the discharge, the walls are 'cleaned' from most impurities by this electron bombardment and many active sites are then formed on which oxygen atoms can condense. Because of the large number of electrons, these atoms should be fairly mobile and, hence, recombine efficiently. The catalytic efficiency of impurities is then explained by either accepting that the impurities (especially H, probably as OH) will preferentially be adsorbed at the active sites and thus poison them for oxygen recombination, or alternately, that the presence of those foreign molecules on the surface would inhibit significantly the diffusion of adsorbed O atoms, thus reducing the rate of recombination.

The rather long times elapsing before a new steady measurement could be taken after a change in either composition or some of the discharge parameter are consistent with this interpretation.

TABLE 4. Comparison of (O-atoms produced)/(catalyst molecules added) with results of other workers

Catalyst	Catalyst efficiency			
	Brown (ref. 8)	Kaufman (ref. 7)	Present study	
			0.01% addition	Initial slope
He, Ar	—	<0.2	<0.3	<0.3
CO_2	—	<0.2	<2	<2
NO	—	40–45	~300	~400
N_2	80–100	80–90	30–70	30–80
N_2O	—	80–90	150–300	200–350
H_2	150–200	160–200	130–400	200–650

5.2 Comparison With Other Results

In Table 4 the catalytic efficiencies in oxygen are compared with those found in the literature.

The studies of Kaufman and Kelso (3) and Brown (14) were conducted using nearly identical conditions in their microwave discharges and yielded similar results. Brown (14) also reports that the catalytic efficiency of H_2O is about 90 to 130 oxygen atoms produced per H_2O molecule added.

It is apparent that the catalytic efficiencies measured here are somewhat larger than those reported by Kaufman and Kelso. The difference is especially apparent in the case of NO.

The major difference between the experiments by Kaufman and Kelso and those reported here is that a microwave discharge was used in the former study while an electrode discharge was used in this study. Kaufman and Kelso used the NO_2 titration technique downstream of the discharge to measure O-atom concentrations and assumed that this was equivalent to the concentration in the discharge (i.e., they assumed that there was no large removal term at the end of the discharge as Kaufman (15) has more recently postulated).

Since the measurements in the present study were done at a slightly greater pressure (1.2 Torr compared to 0.8 Torr), higher catalytic efficiencies would be expected since both studies indicate that the efficiency increases with pressure. Also, Kaufman's catalytic efficiencies were reported for additions of 0.01% to 0.05% impurity. Since in the present study it was found that the catalytic efficiency decreases with impurity concentration the values from the present study for 0.01% impurity are best used for comparison.

6. Conclusions

We have been able to quantitatively measure the concentration of atomic oxygen in an active glow discharge. Concentration–time profiles have established that the atom production is a dissociative excitation of the oxygen molecule under electron impact. The recombination of atomic oxygen obeys first order kinetics and appears to occur at the walls of the discharge tube. This removal is more than two orders of magnitude faster than that occurring in the after-glow region. This observation was originally presented as a suggestion by Kaufman (15) and is thus confirmed experimentally. The variation of the recombination constant with pressure and current is in good agreement with calculations, taking into account the uncertainties with which these quantities are known.

We have further established that the rate of production of atomic oxygen is not significantly altered when a foreign gas is added to the oxygen stream, but that the rate of atom removal is decreased by up to two orders of magnitude (possibly more) leading to a very large increase in the atomic oxygen concentration. Most effective are hydrogen containing compounds while nitrogen containing species are less effective. Other compounds do not appear to have a significant influence. All evidence indicates that the removal step is a wall process. The increase in oxygen atom concentration is then the result of the deactivation of the recombination at the wall.

7. Acknowledgments

P.A.Z. acknowledges the award of a Centennial Science Scholarship and M.D.C. the award of a Graduate Fellowship from the National Research Council of Canada.

This work was supported by the National Research Council of Canada.

We wish to express our gratitude to Drs. D. R. Clarke, H. W. Rundle, J. N. Smith, and T. Svekis-Milman for helpful discussions.

F. Shaw was helpful in the design and construction of the equipment and W. Panning assisted in the building and testing of the electronic circuitry.

1. R. R. BAKER, A. JACOB, and C. A. WINKLER. Can. J. Chem. **49**, 1671 (1971).
2. R. A. YOUNG and G. A. ST. JOHN. J. Chem. Phys. **48**, 3505 (1968).
3. F. KAUFMAN and J. R. KELSO. 8th Symposium (International) on Combustion. The Combustion Institute – Williams and Wilkins, Baltimore, 1960. 1962. p. 230.
4. F. KAUFMAN and J. R. KELSO. J. Chem. Phys. **32**, 301 (1960).
5. J. W. LINNETT and D. G. H. MARSDEN. Proc. R. Soc. London, A**234**, 504 (1956).
6. F. KAUFMAN. Adv. Chem. Ser. **80**, 29 (1969).
7. A. N. WRIGHT and C. A. WINKLER. Active nitrogen. Academic Press, New York, NY. 1968.
8. P. R. RONY. Lawrence Radiation Laboratory Report. VC RL-16050.
9. H. W. RUNDLE, D. R. CLARKE, and J. M. DECKERS. Can. J. Phys. **51**, 144 (1973).
10. R. D. HAKE, JR. and A. V. PHELPS. Phys. Rev. **158**, A70 (1967).
11. P. A. ZULIANI. Ph.D. Thesis, University of Toronto, Toronto, Ont. 1972.
12. M. D. COSTA. Ph.D. Thesis, University of Toronto, Toronto, Ont. 1975.
13. J. N. SMITH, M. D. COSTA, and J. M. DECKERS. To be published.
14. R. L. BROWN. J. Phys. Chem. **71**, 2492 (1967).
15. F. KAUFMAN. Adv. Chem. Ser. **80**, 29 (1969).
16. M. J. DRUYVESTEYN. Physica, **10**, 69 (1930).
17. G. FRANCIS. Handbuch der Physik. Vol. 22. *Edited by* S. Flugge. Springer Verlag, Berlin. 1956. p. 53.

Self-adduct formation in the extraction of cobalt(II) chelates of certain 8-quinolinols

ARVIND T. RANE AND KASHINATH S. BHATKI[1]

Tata Institute of Fundamental Research, Colaba, Bombay 400005, India

Received January 31, 1978[2]

ARVIND T. RANE and KASHINATH S. BHATKI. Can. J. Chem. **57**, 580 (1979).

Equilibrium distribution ratios have been determined for the extraction of cobalt(II) with 8-quinolinol and its 2-methyl-, 4-methyl-, 5-chloro-, and 5-nitro- analogues into chloroform as a function of pH and reagent concentration at ambient temperature. Except in the case of 2-methyl-8-quinolinol, which formed a simple 1:2 chelate, the extractable complexes were mono-adducts, that is, 1:2 chelates to which a third molecule of the reagent was coordinated. The overall formation constants of the cobalt chelates in aqueous solution were determined. A linear correlationship was observed between the formation constants, adduct formation constants, and the basicity of the reagent. This dependence could be used to predict, based on known data, the stabilities of not yet studied complexes of cobalt with this family of ligands. The distribution coefficients of the chelates and the chelate adducts are discussed in terms of structural influences. A penta-coordinate, square pyramidal structure has been proposed for the self-adducts of cobalt(II) with 8-quinolinols (except 2-methyl analogue).

ARVIND T. RANE et KASHINATH S. BHATKI. Can. J. Chem. **57**, 580 (1979).

On a déterminé les rapports des équilibres de distribution pour l'extraction du cobalt(II) par le quinoléinol-2 et ses dérivés méthyl-2, méthyl-4, chloro-5 et nitro-5 dans le chloroforme, en fonction du pH et de la concentration du réactif, à température ambiante. A l'exception du cas du méthyl-2 quinoléinol-8 qui forme un chélate 1:2 simple, les complexes qui peuvent être extraits sont des mono-adduits, soit des chélates 1:2 auxquels une troisième molécule vient se coordonner. On a déterminé les constantes globales de formation des chélates de cobalt en solution aqueuse. On a remarqué une relation linéaire entre les constantes, les constantes de formation des adduits et la basicité du réactif; on pourrait utiliser cette relation pour prédire, à l'aide de données connues, les stabilités de complexes qui ne sont pas connus du cobalt avec ces familles de ligands. On discute des coefficients de distribution des chélates et des adduits de chélates en termes de facteurs structuraux. On propose la présence d'une structure penta-coordonnée à pyramide carrée pour les auto-adduits du cobalt(II) avec les quinoléinols-8 (à l'exception de l'analogue méthylé en 2).

[Traduit par le journal]

Introduction

In his review, Stary (1) reported the extraction and colorimetric determination of metals with 8-quinolinol (oxine). We reported recently (2) the extraction of the self-adduct of nickel(II) with oxine and its analogues from the aqueous phase with chloroform. Our successful attempts to determine the adduct formation constants spectrophotometrically in a single phase, chloroform, are also described (3). Both these studies (2, 3) confirmed the penta-coordinate square pyramidal structure for the self-adduct of nickel with oxines, except its 2-methyl analogue.

During his comprehensive study of several metal ions, Stary (4) recorded the extraction of Co(II) as a cobalt-oxinate adduct, $CoQ_2 \cdot 2H_2O$; whereas, Oki and others (5, 6) observed that the extraction of cobalt from perchlorate solutions occurred as $CoQ_2 \cdot HQ$. In order to resolve these controversies we attempted the extraction of cobalt with oxine and extended the study to know more about the influences of steric hindering groups present in the ligand on the formation of the adduct. This is described in the sequel.

Experimental

Apparatus

The shaking assembly, radioactive counting, and pH measurements have been described earlier (2).

Material

AR grade 8-quinolinol (E. Merck), 2-methyl-8-quinolinol (8-quinaldine, Fluka), 5-chloro-8-quinolinol (Aldrich), and 5-nitro-8-quinolinol (K and K) were recrystallised from absolute alcohol. This gave products having melting points 73, 74, 126, and 179°C, respectively, very close to the literature reported value. The 4-methyl-8-quinolinol was synthesized from *o*-aminophenol and methyl-vinyl ketone and purified as described previously (2).

Carrier-free cobalt-58 ($t_{1/2}$ = 72 days) activity was supplied by Isotope Division, B.A.R.C., Trombay as a solution of cobalt chloride. The activity was sufficiently diluted with distilled water to give 6×10^5 cts min^{-1} mL^{-1} and 0.2 mL aliquots were taken every time from this stock solution for the distribution study. A set of Clark and Lubs buffer solutions were prepared with pH varying successively by 0.2 units.

[1]To whom all the correspondence should be addressed.

[2]Revision received October 12, 1978.

0008-4042/79/050580-06$01.00/0

Requisite amounts of sodium perchlorate were added to the buffers to maintain a constant ionic strength at 0.25 *M*.

Procedure

Five millilitres of buffered cobalt-58 solution at a constant ionic strength ($\mu = 0.25$) at various pH (3.0–8.0), and 5 mL of the reagent solution of varying concentration (10^{-4} to 1.0 *M*) in chloroform, were equilibrated by shaking for 30 min. After the shaking was over, the mixtures were centrifuged and equal volumes of both phases were pipetted out in suitable counting tubes and counted for radioactivity separately at a constant and a reproducible geometry.

Results and Discussion

The extraction of a simple chelate is generally described by a plot of log *D* vs. pH, at a constant reagent concentration in the organic phase. These plots essentially consist of two linear portions; the log *D* increasing initially in the lower pH region with a slope *n*, the number of protons released on chelate formation and then eventually reaching a constant, pH-independent value, determined by K_{DC}, the distribution coefficient of the chelate. At a higher value of the reagent concentration, the entire curve shifts to the left, i.e. to a lower pH region, without alteration of either the slope or the value of the maximum log *D*, which remains equal to log K_{DC}. This situation changes when the extractable complex is not a simple chelate but an adduct. The adduct reagent concentration then influences the entire extraction curve. An increase in reagent concentration then causes the plateau region of the curve to shift to a higher log *D*, the initial linear portion of the curve shifting to a lower pH, without changing its slope. In Fig. 1 are shown the extraction curves (log *D* vs. pH) of cobalt(II) for the reagent 8-quinolinol (HQ) and its four substituted derivatives: 2-methyl-, 4-methyl-, 5-chloro-, and 5-nitro-. Various plots (drawn manually) in each part (Fig. 1*A*, 1*B* etc.) correspond to a different reagent concentration. The slopes of these plots are almost 2, indicating that in each of these extractions two protons are released on the formation of the extractable complex (7). In Fig. 1*A*, *C*, *D*, and *E*, the plateau region of each curve shifts to higher log *D*, indicating the formation of an adduct with the increase in adduct reagent concentration, whereas in the case of 2-methyl-8-quinolinol (Fig. 1*B*), all the curves in the higher pH region merge, indicating the absence of an adduct in the extraction system.

Plots of log *D* vs. the logarithm of the reagent concentration, log $[HQ]_0$, were constructed for the extraction of cobalt(II) with 8-quinolinols, and are shown in Fig. 2. The slopes of these plots show the number of reagent molecules incorporated in the extractable complex. The behaviour of the 2-methyl-8-quinolinol extraction indicates that the extractable

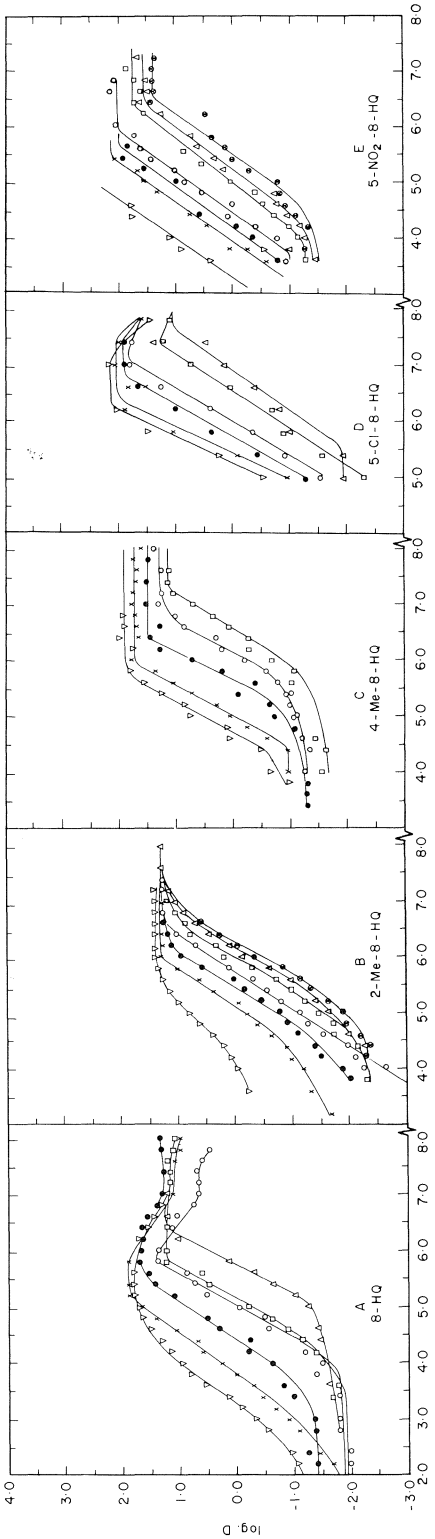

FIG. 1. Extraction of cobalt with 8-quinolinols, plot of log *D* vs. pH. (*A*) 8-Quinolinol: ▽, 6.022×10^{-2} *M*; ×, 4.048×10^{-2} *M*; ●, 2×10^{-2} *M*; ○, 10^{-2} *M*; □, 8.664×10^{-3} *M*; △, 4.044×10^{-3} *M*. (*B*) 2-Methyl-8-quinolinol: ▽, 4.0×10^{-1} *M*; ×, 2.0×10^{-1} *M*; ●, 1.5×10^{-1} *M*; ○, 10^{-1} *M*; □, 8.014×10^{-2} *M*; △, 7.343×10^{-2} *M*; ⊗, 5.019×10^{-2} *M*. (*C*) 4-Methyl-8-quinolinol: ▽, 8.366×10^{-3} *M*; ×, 6.47×10^{-3} *M*; ●, 2.237×10^{-3} *M*; ○, 9.795×10^{-4} *M*; □, 5.593×10^{-4} *M*. (*D*) 5-Chloro-8-quinolinol: ▽, 8.149×10^{-3} *M*; ×, 6.519×10^{-3} *M*; ●, 4.889×10^{-3} *M*; ○, 3.259×10^{-3} *M*; □, 1.629×10^{-3} *M*; △, 8.149×10^{-4} *M*. (*E*) 5-Nitro-8-quinolinol: ▽, 1.96×10^{-3} *M*; ×, 8.179×10^{-4} *M*; ●, 6.08×10^{-4} *M*; ○, 4.08×10^{-4} *M*; □, 1.96×10^{-4} *M*; △, 1.06×10^{-4} *M*; ⊗, 8.17×10^{-5} *M*.

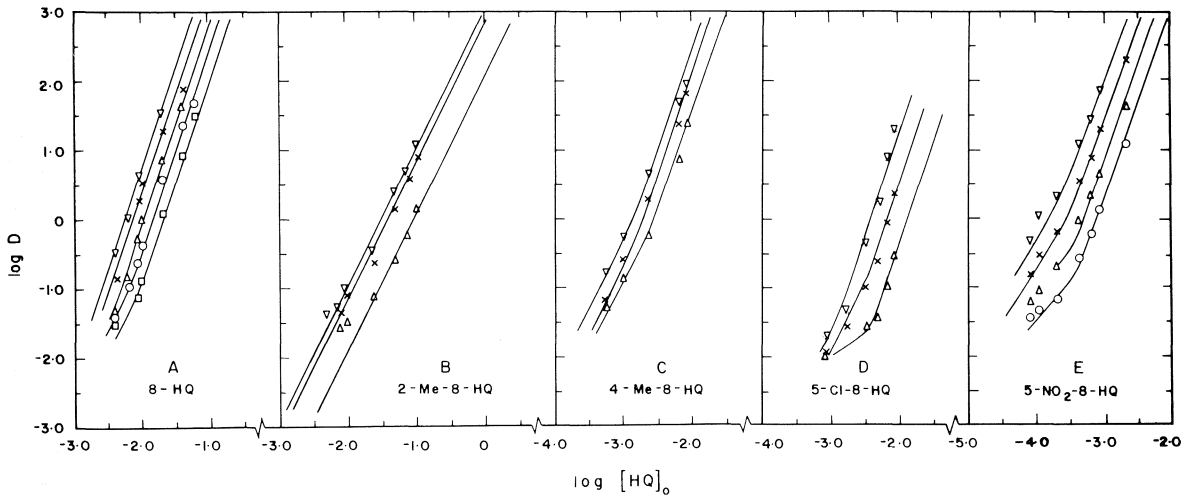

FIG. 2. Extraction of cobalt with 8-quinolinols, plot of log D vs. log $[HQ]_0$. (*A*) 8-Quinolinol: slope = 3.0; ▽, pH 5.5; ×, pH 5.3; △, pH 5.0; ○, pH 4.8; □, pH 4.4. (*B*) 2-Methyl-8-quinolinol: slope = 2.0; ▽, pH 6.4; ×, pH 6.0; △, pH 5.6. (*C*) 4-Methyl-8-quinolinol: slope = 3.0; ▽, pH 6.0; ×, pH 5.8; △, pH 5.5. (*D*) 5-Chloro-8-quinolinol: slope = 3.0; ▽, pH 5.8; ×, pH 5.4; △, pH 5.0. (*E*) 5-Nitro-8-quinolinol: slope = 3.0; ▽, pH 5.2; ×, pH 4.8; △, pH 4.4; ○, pH 4.0.

complex is a simple 1:2 chelate since two reagent molecules per cobalt ion are involved in the extraction. In other cases (Fig. 2*A*, *C*, *D*, and *E*), however, the slope of three of these plots indicates the additional reagent molecule utilised for the formation of a mono-adduct, e.g. $CoQ_2 \cdot HQ$.

These plots in Fig. 2 show a number of curves in each portion *A*, *B*, *C*, etc. These are drawn for various pH values from the data in plots of Fig. 1. It is interesting to note from these curves that at lower reagent concentration, the slopes (Fig. 2*A*, *C*, *D*, *E*) approach a value of 2 indicating the absence of the adduct. The slopes subsequently increase to 3 with the increase in reagent concentration showing that the adduct formation has taken place. In the case of 2-methyl-8-quinolinol (Fig. 2*B*), the slope remains 2 throughout, thus confirming the absence of any adduct in this system.

The distribution ratio D for the extraction of cobalt by oxine or its analogue is then given by (2, 7)

$$D = \frac{[Co]_0}{[Co]} = \frac{[CoQ_2]_0 + [CoQ_2 \cdot aHQ]_0}{[Co^{2+}] + [CoQ^+] + [CoQ_2] + [CoQ_2 \cdot aHQ]}$$

The equation can be modified when the adduct formation predominates over the simple CoQ_2 of the adduct complexes, $a = 1$ to $a = a$. The value of a can then be determined from the plot of log D vs. log $[HQ]_0$. Since two reagent molecules are involved in the formation of a simple 1:2 chelate, the slope of the resulting line should be $(2 + 0)$ as $a = 0$. It is seen from Fig. 2 that the value of a for 8-quinolinol, 4-methyl-, 5-chloro-, and 5-nitro-8-quinolinol systems is unity and for the 2-methyl-8-quinolinol system it is zero, i.e. no adduct formation is involved in the extraction of the cobalt chelate of 2-methyl-8-quinolinol, whereas a mono-adduct is involved in other chelates.

At lower concentrations of HQ when the formation of a simple 1:2 chelate cannot be ignored and at the lower pH range where Co^{2+} predominates in the aqueous phase, the distribution ratio D is then given by (2, 7)

$$D = \frac{K_{ex}[HQ]_0^2}{[H]^2}[1 + K_{AD_0}[HQ]_0^a]$$

where

$$K_{ex} = K_1 K_2 K_{DC} K_a / K_{DR}^2$$

K_{DC} and K_{DR} being the distribution coefficients of cobalt chelate and HQ, respectively; K_a being the dissociation constant of the reagent and K_{AD_0} the adduct formation constant.

The plot of log D vs. log $[HQ]_0$ gives two straight lines (2), the intersection of which gives the value for the adduct formation constant in the organic phase.

$$\log K_{AD_0} = -a \log [HQ]_0$$

at the intersection.

A plot of log $D[H]^2/[HQ]_0^2$ against log $[HQ]_0$ takes into account the variation both in pH and in the reagent concentrations simultaneously (8). Such a plot gives two straight lines. The horizontal line corresponds to log D = log K_{ex} and the line of slope a shows the number of neutral reagent molecules involved in the self-adduct formation. The intersection

of these lines gives the adduct formation constant, log K_{AD_0} (Fig. 3). Results for 2-methyl-8-quinolinol are also given in Fig. 3. The entire curve in the case of 2-methyl analogue is parallel to log $[HQ]_0$ axis indicating the absence of adduct formation in this case.

The overall formation constants, K_1K_2 or K_f, of the chelates may be evaluated from the extraction constant, K_{ex}, the K_{DR} and K_a values being obtained from the literature (9, 10).

Alternatively, a plot of log $D - a \log [HQ]_0$ vs. $-\log [Q^-]$ or pQ^-, where $[Q^-]$ represents the corresponding quinolinol anion concentration in the aqueous phase, takes into account the variations in the pH and the reagent concentration simultaneously giving two straight lines. The log K_f values may be obtained (7) from the intersection of the two lines, i.e. $pQ^- = \frac{1}{2} \log K_f$.

Such plots were constructed for 8-quinolinol, 4-methyl-, 5-chloro-, and 5-nitro-8-quinolinols and are shown in Fig. 4 while a plot for 2-methyl-8-quinolinol is given in Fig. 5. In these plots (except 2-methyl-), the value of $a = 1$ and the value of a, for a simple 1:2 chelate, such as that formed by cobalt(II) with 2-methyl-8-quinolinol, is zero. Figure 5 shows a plot of log D vs. pQ^- instead of

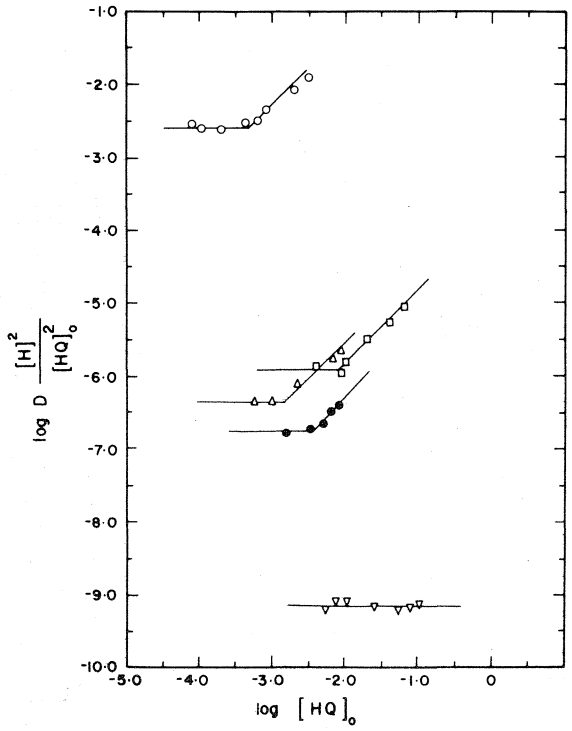

FIG. 3. log $D[H]^2/[HQ]_0^2$ vs. log $[HQ]_0$: ○, 5-NO_2-8-HQ; □, 8-HQ; △, 4-Me-8-HQ; ●, 5-Cl-8-HQ; ▽, 2Me-8-HQ.

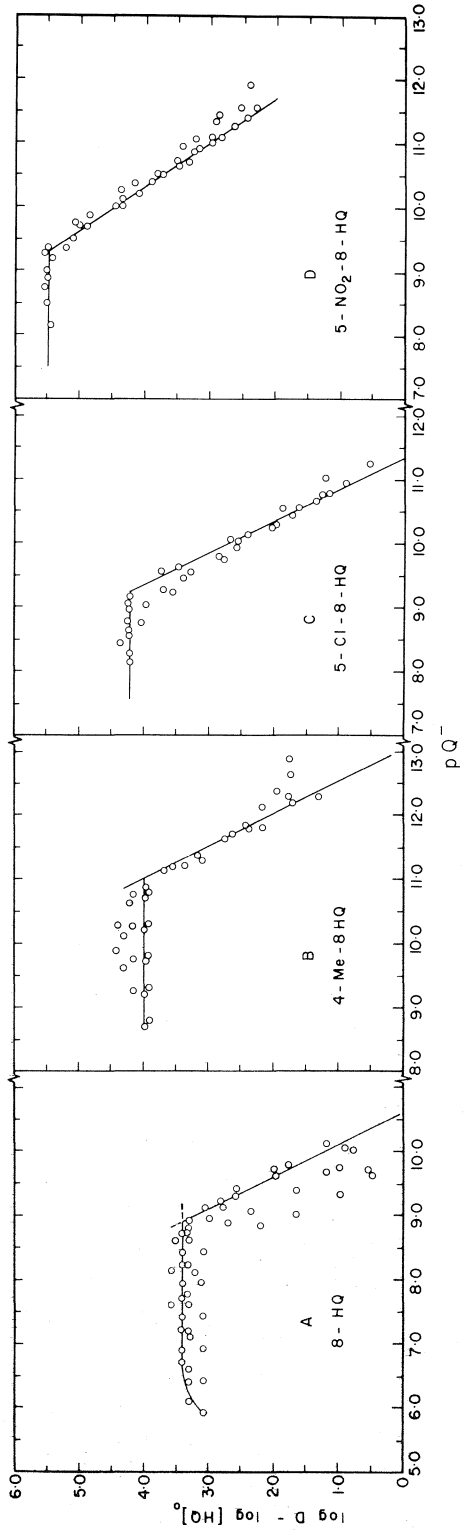

FIG. 4. log D − log $[HQ]_0$ vs. pQ^-: (*A*), 8-quinolinol; (*B*), 4-methyl-8-quinolinol; (*C*), 5-chloro-8-quinolinol; (*D*), 5-nitro-8-quinolinol.

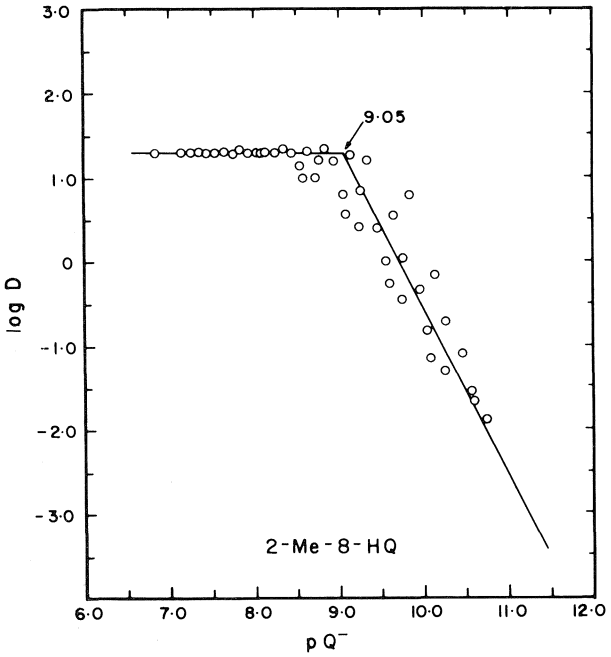

FIG. 5. log D vs. pQ^- for 2-methyl-8-quinolinol.

log D − log $[HQ]_0$ vs. pQ^-. All these curves were plotted manually.

Table 1 gives the summary of equilibrium constants for cobalt chelates of 8-quinolinol and its substituted products.

This study has also shown a similar difference between the behaviour of cobalt(II) with 2-methyl-8-quinolinol from other 8-quinolinols as in the case of nickel (2) and zinc (7). The reason for this difference is that the extraction of the simple chelate results from the steric hindrance to the adduct formation exerted by the substituent in the 2-position. Substitution at a particular position in the chelating molecule not only alters its basic strength, and the stability of the complex it forms as well, but also introduces steric effects. This is very well shown by the difference in the extraction behaviour of cobalt(II) by 2-methyl- and 4-methyl-8-quinolinols. The steric hindrance offered by the 2-methyl- group in the case of cobalt(II) is similar to the earlier findings observed in the extraction of nickel(II) (2).

In Fig. 2 a slope of 3 obtained in the plots of log D vs. log $[HQ]_0$ indicates that to each atom of cobalt are attached three molecules of the reagent, HQ. Whereas, only two protons are liberated in the course of extraction, as seen from the log D vs. pH plot (Fig. 1). It is obvious that 8-quinolinol is playing a dual role, firstly, by coordinating with cobalt as a bidentate ligand, forming a 1:2 chelate, and secondly, as an unidentate ligand in the adduct formation. The slope of 2 in the log D vs. pH plot indicates that cobalt is extracted as Co(II). It has been shown (6) that Co(III) complex can be extracted in the presence of 0.8 M hydrogen peroxide, and identified spectrophotometrically by the shift in the spectrum, presumably with respect to that of Co(II) complex. However, in the normal course oxidation of the Co(II) complex can readily be avoided if the extraction is carried out with a large excess of oxine solutions and in the absence of any oxidizing agents, such as hydrogen peroxide. Large excess of oxine prevents the oxidation of Co(II) to Co(III) in the complex. The possibility of formation of a self-adduct in Co(III) has not been reported so far.

When the logarithm of the chelate formation constants were plotted against pK_a values of the 8-quinolinols (where $pK_a = pK_{a_1} + pK_{a_2}$), the overall basicity of the donor atoms, a linear correlationship was observed (Fig. 6). In the same figure, a similar plot was constructed between the adduct formation constants and the pK_a values of the reagents. In this case also a linear dependence was observed. This dependence may be used to estimate, based on known data, the stabilities of not yet experimentally studied complexes in this series of ligands. It is seen from Fig. 6 that the chelate formation constants and the adduct formation constants are almost constant over

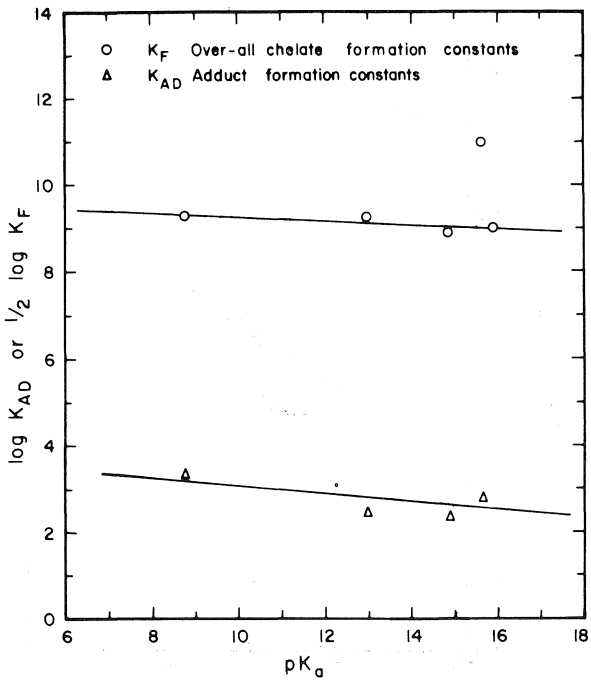

FIG. 6. Correlationship between adduct formation constants, chelate formation constants, and the basicities of the chelating agents: ○, log K_f; △, log K_{AD}.

TABLE 1. Summary of equilibrium constants for cobalt(II) chelates of 8-quinolinol and substituted 8-quinolinols at 28 ± 2°C

Substituted 8-quinolinol	log K_{ex}	log K_{AD_0}	log K_{DC}	$pK_{a_1} + pK_{a_2}$	log K_{DR}	log K_f
Parent	−5.93	2.10	1.28	14.9	2.64	17.8
2-Methyl-	−9.15	No adduct formation	1.30	15.9	3.22	18.1
4-Methyl-	−6.35	2.85	1.40	15.66	3.27	22.0
5-Chloro-	−6.75	2.45	1.73	13.00	3.32	18.55
5-Nitro-	−2.60	3.35	2.08	8.79	2.64	18.6

a wide range of pK_a values. This can be explained as follows: an adduct is formed between a Lewis base of the donor as well as the Lewis acid of the acceptor, the metal chelate. The Lewis acidity of the metal after chelation decreases with the increasing stability of the chelate. The overall effect would be a much smaller net decrease in the adduct formation constants for a relatively large increase in the reagent basicity. The 2-methyl- group in 8-quinaldine, however, does not produce any adverse effect on the linearity of the plot.

From the data obtained in the present study, it is presumed that cobalt(II) forms a penta-coordinate structure as observed in nickel (2) and zinc (7). During the extraction of Co(II) by oxine, the water molecules are pushed out of the coordination sphere and are replaced by the third molecule of the excess of the ligand present. The two molecules of 8-quinolinol form the square base of a pyramid and the unidentate ligand is in the axial position of the pyramid (point group C_{4v}) (11). The extracted species are presumably the anhydrous penta-coordinate adducts, except in the case of 8-quinaldine, where it forms a simple coplanar 1:2 complex, i.e. the base of the pyramid.

Presence of perchlorate ions, added to keep the ionic strength constant, does not produce any appreciable influence on the extraction of Co(II) by oxine. This was ascertained in a separate experiment, by varying the ClO_4^- concentration.

1. J. STARY. The solvent extraction of metal chelates. Pergamon Press, Oxford. 1964. pp. 80–100.
2. K. S. BHATKI, A. T. RANE, and H. FREISER. Indian J. Chem. **15**A, 983 (1977).
3. K. S. BHATKI and A. T. RANE. Indian J. Chem. In press.
4. J. STARY. Anal. Chim. Acta, **28**, 132 (1963).
5. S. OKI and I. TERADA. Anal. Chim. Acta, **61**, 49 (1972); **66**, 201 (1973).
6. S. OKI. Anal. Chim. Acta, **50**, 465 (1970).
7. F. C. CHOU, Q. FERNANDO, and H. FREISER. Anal. Chem. **37**, 361 (1965).
8. T. SEKINE and D. DYRSSEN. J. Inorg. Nucl. Chem. **26**, 1727 (1964).
9. F. C. CHOU and H. FREISER. Anal. Chem. **40**, 34 (1968).
10. A. J. FRESCO and H. FREISER. Anal. Chem. **36**, 631 (1964).
11. J. S. WOOD. *In* Progress in inorganic chemistry. Vol. 16. *Edited by* S. J. Lippard. Interscience Publishers, NY. 1972. pp. 227–486.

Synthesis and crystal and molecular structure of ethanolaminogallium dimethyl, $H_2NCH_2CH_2O \cdot GaMe_2$

KENNETH S. CHONG, STEVEN J. RETTIG, ALAN STORR, AND JAMES TROTTER

Department of Chemistry, University of British Columbia, Vancouver, B.C., Canada V6T 1W5

Received October 10, 1978

KENNETH S. CHONG, STEVEN J. RETTIG, ALAN STORR, and JAMES TROTTER. Can. J. Chem. **57**, 586 (1979).

Details of the synthesis and physical properties of $H_2NCH_2CH_2O \cdot GaMe_2$ are given. The compound crystallizes in the tetragonal space group $P4_3$, $a = 12.2771(2)$, $c = 9.7345(4)$ Å, $Z = 8$. The structure was solved by Patterson and Fourier syntheses and was refined by full-matrix least-squares procedures to a final R value of 0.028 and R_w of 0.036 for 1378 reflections with $I \geq 3\sigma(I)$. The structure consists of monomeric molecules containing tetrahedrally-coordinated gallium atoms. Molecules are linked by an extensive network of N—H...O hydrogen bonds. Bond lengths (corrected for libration) are: Ga—O, 1.916(5) and 1.917(4), Ga—N, 2.056(6) and 2.072(6), and Ga—C, 1.962–1.974(8–9) Å.

KENNETH S. CHONG, STEVEN J. RETTIG, ALAN STORR et JAMES TROTTER. Can. J. Chem. **57**, 586 (1979).

On rapporte les détails relatifs à la synthèse et aux propriétés physiques du $H_2NCH_2CH_2O \cdot GaMe_2$. Le composé cristallise dans le groupe d'espace tétragonal $P4_3$, $a = 12.2771(2)$, $c = 9.7345(4)$ Å, $Z = 8$. On a résolu la structure par des synthèses de Patterson et de Fourier et on l'a affinée par la méthode des moindres carrés (matrice complète) jusqu'à une valeur finale de R de 0.028 et de R_w de 0.036 pour 1378 réflexions avec $I \geq 3\sigma(I)$. La structure comprend des molécules monomères contenant des atomes de gallium tétracoordonnées. Les molécules sont liées entre-elles par de nombreuses liaisons hydrogène N—H...O. Les longueurs des liaisons (corrigées pour les librations) sont: Ga—O, 1.916(5) et 1.917(4), Ga—N, 2.056(6) et 2.072(6) et Ga—C, 1.962–1.974(8–9) Å.

[Traduit par le journal]

Introduction

A previous report (1) characterized the *N*,*N*-dimethylethanolaminogallium dimethyl dimer, $[Me_2NCH_2CH_2O \cdot GaMe_2]_2$, as a compound containing five-coordinate gallium atoms with distorted trigonal bipyramidal geometry. The present account details the synthesis and crystal structure determination of the ethanolaminogallium dimethyl compound, $H_2NCH_2CH_2O \cdot GaMe_2$, and compares the results with those previously obtained for similar boron complexes, $H_2NCH_2CH_2O \cdot BPh_2$ (2, 3) and $H_2NCH_2CH_2O \cdot B(p\text{-}RC_6H_4)_2$, where R = F (4) and R = Me (3), and for other similar gallium dimethyl complexes (1, 5).

Experimental

Starting Materials

Ethanolamine was refluxed over anhydrous $CaSO_4$ and distilled prior to use. Gallium trimethyl was prepared as described previously (6). Benzene solvent was dried by refluxing over molten potassium followed by distillation. All materials were handled in a glove-box filled with dry nitrogen or on a standard vacuum line.

Ethanolaminogallium Dimethyl, $H_2NCH_2CH_2O \cdot GaMe_2$

Ethanolamine (0.771 g, 12.64 mmol) was reacted with gallium trimethyl (1.451 g, 12.64 mmol) in refluxing benzene solvent until cessation of methane gas evolution.

$$H_2NCH_2CH_2OH + GaMe_3 \xrightarrow[\text{reflux}]{C_6H_6} H_2NCH_2CH_2O \cdot GaMe_2 + MeH$$

After removal of solvent from the clear product solution, the desired compound was isolated as an extremely air and moisture sensitive white solid. *Anal.* calcd. for $H_2NCH_2CH_2O \cdot GaMe_2$: C 30.1, H 7.5, N 8.8; found: C 29.9, H 7.0, N 8.5.

The ir spectrum in Nujol showed strong bands in the ν_{Ga-C} region of the spectrum at 573 and 533 cm^{-1}. A strong δ_{N-H} band at 1620 cm^{-1} was also a prominent feature but the ν_{N-H} region of the spectrum, ~3300 cm^{-1}, was not clearly resolved.

The ^1H nmr spectrum in C_6D_6 solution showed two well resolved triplets for the two CH_2 groups at $\tau = 6.66$ and 7.83 ppm ($J_{HCCH} \approx 5$ Hz), a broad NH_2 signal at $\tau = 9.09$ ppm, and a sharp singlet for the $GaMe_2$ group at $\tau = 10.13$ ppm. (All signals refer to $\tau_{C_6H_6} = 2.84$ ppm.) The sharp $GaMe_2$ signal indicates a fluxional ring in the C_6D_6 solution.

The mass spectrum of the compound, in addition to a strong signal corresponding to the monomer ion minus a methyl group, displayed strong signals at higher mass numbers corresponding to Ga_2- and Ga_3-containing moieties.

Crystalline samples suitable for X-ray study were obtained by slow sublimation in evacuated tubes. Selected crystals were positioned in capillaries under a nitrogen atmosphere to avoid atmospheric interference and to prevent sublimation within the capillary tube during the collection of X-ray data. The tubes were flame-sealed.

X-ray Crystallographic Analysis of Ethanolaminogallium Dimethyl

The crystal was mounted in a general orientation and had

0008-4042/79/050586-05$01.00/0

dimensions of ca. 0.20 × 0.32 × 0.50 mm. Unit-cell parameters were refined by least-squares on 2 sin θ/λ values for 25 reflections measured on a diffractometer with Cu K_α radiation (λ = 1.54184 Å). Crystal data (at 22°C) are:

$C_4H_{12}GaNO$ fw = 159.87
Tetragonal, a = 12.2771(2), c = 9.7345(4) Å, V = 1467.3(1) Å^3, Z = 8 (two molecules per asymmetric unit), ρ_c = 1.448 g cm^{-3}, $F(000)$ = 656, μ(Cu K_α) = 47.5 cm^{-1}. Absent reflections: $00l$, $l \neq 4n$. Space $P4_1$ (C_4^2, No. 76) or $P4_3$ (C_4^4, No. 78); the latter was confirmed by structure analysis for the particular crystal used.

Intensities were measured with nickel-filtered Cu K_α radiation on an Enraf-Nonius CAD4-F diffractometer. An ω scan at 0.91–6.71° min^{-1} over a range of (0.90 + 0.15 tan θ) degrees in ω (extended by 25% on both sides for background measurement) was employed. Data were measured to 2θ = 150°. The intensities of three check reflections, measured every 3600 s throughout the data collection, did not vary by more than 1%. After data reduction, an absorption correction was applied using the Gaussian integration method (7, 8). Transmission factors ranged from 0.265 to 0.444. Of the 1604 independent reflections measured, 1378 (86%) had intensities greater than $3\sigma(I)$ above background where $\sigma^2(I) = S + 2B + (0.04(S - B))^2$ with S = scan count and B = background count.

TABLE 1. Final positional parameters (fractional: O, N, and C × 10^4, Ga × 10^5, H × 10^3) with estimated standard deviations in parentheses

Atom	x	y	z
Ga(1)	90991(5)	26661(6)	39000
Ga(2)	23328(6)	58381(5)	36430(11)
O(1)	10601(3)	2662(3)	3413(5)
O(2)	2685(4)	6072(3)	5527(6)
N(1)	8773(4)	2281(4)	1878(6)
N(2)	2306(5)	4214(4)	4091(8)
C(1)	10714(6)	2658(7)	1945(11)
C(2)	9854(5)	1956(6)	1319(9)
C(3)	3085(7)	5084(5)	6088(10)
C(4)	2413(7)	4141(6)	5604(10)
C(5)	8729(7)	1422(7)	5064(10)
C(6)	8626(7)	4160(7)	4246(10)
C(7)	834(7)	6297(7)	3241(11)
C(8)	3579(7)	6198(8)	2461(10)
H(N1a)	839(5)	296(5)	163(8)
H(N1b)	824(6)	167(6)	165(9)
H(N2a)	266(5)	388(5)	391(8)
H(N2b)	162(6)	396(5)	397(9)
H(1a)	1143(6)	236(5)	170(9)
H(1b)	1057(7)	363(7)	144(12)
H(2a)	1002(6)	123(7)	166(10)
H(2b)	1006(7)	219(7)	39(11)
H(3a)	386(6)	488(6)	579(9)
H(3b)	276(10)	515(10)	709(18)
H(4a)	277(7)	354(8)	573(12)
H(4b)	158(10)	424(9)	592(15)
H(5a)	915	134	572
H(5b)	872	75	451
H(5c)	798	155	547
H(6a)	896	439	516
H(6b)	892	463	351
H(6c)	804	426	430
H(7a)	78	706	288
H(7b)	69	562	241
H(7c)	33	624	406
H(8a)	385	695	271
H(8b)	404	582	253
H(8c)	334	620	148

The positions of the two independent gallium atoms were determined from the Patterson function and those of O, N, and C atoms from a subsequent difference map. After full-matrix least-squares refinement of all non-hydrogen atoms with anisotropic thermal parameters to R = 0.041, a difference map gave positions for 18 of the 24 hydrogen atoms (all of those not located were methyl hydrogens, but at least one hydrogen on each methyl group was located). The remaining hydrogen positions were calculated by assuming ideal geometries. Attempts to refine the methyl hydrogen positions did not give satisfactory results and thus these atoms were left fixed in calculated positions during the final stages of refinement. The other 12 hydrogen atoms were included in the refinement with isotropic thermal parameters. The scattering factors of ref. 9 were used for non-hydrogen atoms and those of ref. 10 for hydrogen atoms. Anomalous scattering factors from ref. 11 were used for the non-hydrogen atoms. The weighting scheme, $w = 1/\sigma^2(F)$ where $\sigma^2(F)$ is derived from the previously defined $\sigma^2(I)$ gave uniform average values of $w(|F_o| - |F_c|)^2$ over ranges of $|F_o|$ and was employed in the final stages of refinement. An isotropic Type I extinction correction (Thornley–Nelmes definition of mosaic anisotropy with a Lorentzian distribution) was applied (12–14). The final value of g was 0.34(3) × 10^4. Convergence was reached at R = 0.028 and R_w = 0.036 for 1378 reflections with $I > 3\sigma(I)$. For all 1604 reflections R = 0.035 and R_w = 0.037.

Hamilton's test (15) was applied to the R factor ratios resulting from parallel refinements carried out in $P4_1$ and $P4_3$. For observed planes only, $R(P4_1)/R(P4_3) = 1.011$ and $R_w(P4_1)/R_w(P4_3) = 1.019$, indicating that $P4_3$ is the correct space group at a confidence level of > 99.5%.

On the final cycle of refinement the mean and maximum parameter shifts corresponded to 0.18 and 1.39σ, respectively. The mean error in an observation of unit weight was 1.0654. A final difference map showed maximum fluctuation of ±0.4 e Å^{-3}. The final positional and thermal parameters appear in Tables 1 and 2[1] respectively. Measured and calculated structure factors have been placed in the Depository of Unpublished Data.[1]

The ellipsoids of thermal motion for the non-hydrogen atoms are shown in Fig. 1. The thermal motion has been analysed in terms of the rigid-body modes of translation, libration, and screw motion (16) using the computer program MGTLS.[1] The rms standard error in the temperature factors σU_{ij} (derived from the least-squares analysis) is 0.0037 Å^2. Analyses were successful for each of the two independent molecules (rms ΔU_{ij} = 0.0034 and 0.0035 Å^2 for the molecules containing Ga(1) and Ga(2), respectively). The appropriate bond distances have been corrected for libration (17), using shape parameters q^2 of 0.08 for all atoms involved. Corrected bond lengths are shown in Fig. 1 and are listed in Table 3[1] along with uncorrected values (corrections were +0.007–0.014, mean 0.010 Å). Corrected bond angles do not differ by more than 1σ from the uncorrected values in Table 4. Intra-annular torsion angles are given in Table 5.

[1]The thermal motion analysis, structure factor table, and Tables 2 (thermal parameters) and 3 (bond lengths) are available, at a nominal charge, from the Depository of Unpublished Data, CISTI, National Research Council of Canada, Ottawa, Ont., Canada K1A 0S2.

TABLE 4. Bond angles (deg) with estimated standard deviations in parentheses

(*a*) Non-hydrogen atoms

Bonds	Angle (deg)	Bonds	Angle (deg)
O(1) —Ga(1)—N(1)	87.1(2)	O(2) —Ga(2)—N(2)	86.9(2)
O(1) —Ga(1)—C(5)	111.5(3)	O(2) —Ga(2)—C(7)	111.2(3)
O(1) —Ga(1)—C(6)	109.5(3)	O(2) —Ga(2)—C(8)	110.6(3)
N(1) —Ga(1)—C(5)	109.2(3)	N(2) —Ga(2)—C(7)	107.9(3)
N(1) —Ga(1)—C(6)	108.8(3)	N(2) —Ga(2)—C(8)	110.9(4)
C(5) —Ga(1)—C(6)	124.4(4)	C(7) —Ga(2)—C(8)	123.3(4)
Ga(1)—O(1) —C(1)	109.9(4)	Ga(2)—O(2) —C(3)	108.7(4)
Ga(1)—N(1) —C(2)	103.7(4)	Ga(2)—N(2) —C(4)	105.6(4)
O(1) —C(1) —C(2)	109.9(6)	O(2) —C(3) —C(4)	110.4(7)
N(1) —C(2) —C(1)	109.1(7)	N(2) —C(4) —C(3)	108.4(7)

(*b*) Angles involving hydrogen atoms

Bonds	Angle (deg)	Mean (deg)
R/H—C/N—H	92–129 (4–9)	106 (10)

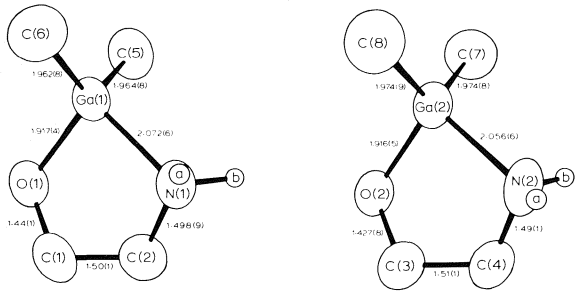

FIG. 1. The two independent molecules of ethanolaminogallium dimethyl. 50% probability thermal ellipsoids are shown for non-hydrogen atoms. Bond lengths are in Å (mean N—H = 0.89(18), C—H = 1.03(12) Å).

Results and Discussion

The reaction between ethanolamine and gallium trimethyl was investigated in connection with a series of anionic ethanolaminopyrazolylgallate ligands which were under study (18, 19). It was well known that gallium trimethyl would react with 'active hydrogen'-containing compounds to undergo methane elimination and produce associated gallium-containing species. The fact that enthanolamine bears 'active hydrogen' atoms on both the nitrogen and oxygen ends of the molecule prompted us to substantiate our prediction that the hydroxyl hydrogen would react preferentially in a 1:1 stoichiometric reaction leaving the amino group intact. Thus it is known that molecules with amino groups coordinated to gallium trimethyl require elevated temperatures for elimination of methane whereas molecules with hydroxyl groups coordinated to the gallium alkyls eliminate alkane much more readily at lower temperatures (20). The isolation of the title compound left no doubt that the preferential reaction was indeed occurring and this fact paved the way for the syntheses of the numerous complexes already reported incorporating the ethanolamino moiety in chelating anionic gallate ligands (19, 21).

The crystal structure of $H_2NCH_2CH_2O{\cdot}GaMe_2$ (Fig. 2) consists of discrete monomeric molecules (two per asymmetric unit) which display the gallium atoms in distorted tetrahedral environments. The individual monomer units are each linked to four others by an extensive network of N—H...O hydrogen bonds (see Table 6). Evidently this hydrogen bonding is quite strong since fragments containing two and three gallium atoms have been identified in the mass spectrum of the compound. Molecules of the related boron compounds $H_2NCH_2CH_2O{\cdot}BAr_2$ (Ar = C_6H_5, *p*-FC_6H_4, and *p*-$CH_3C_6H_4$) are also linked by N—H...O hydrogen bonds, but due to the bulky aromatic substituents attached to the boron atom only one of the protons bonded to nitrogen is involved in N—H...O hydrogen bonding. Apart from the hydrogen bonds, the packing is dominated by van der Waals contacts between hydrogen atoms with several H...H distances between 2.23 and 2.50 Å. The structure is quite different from those of the *N*,*N*-dimethylethanolamino derivatives $[Me_2NCH_2CH_2O{\cdot}GaR_2]_2$ (R = H or Me), which consist of well-separated dimeric units containing five-coordinate gallium atoms (1).

The two independent molecules (Fig. 1) are nearly identical; there are no significant differences between corresponding bond lengths but there are small but significant differences in some bond angles and torsion angles (see Tables 3–5). The gallium atoms are

TABLE 5. Intra-annular torsion angles (deg)

Bond	Angle (obs.)	Bond	Angle (obs.)
	Five-membered chelate rings		
Ga(1)—O(1)	13.1(4)	Ga(2)—O(2)	18.9(4)
O(1) —C(1)	−37.9(6)	O(2) —C(3)	−42.3(6)
C(1) —C(2)	50.8(7)	C(3) —C(4)	49.7(7)
C(2) —N(1)	−36.7(5)	C(4) —N(2)	−31.2(6)
N(1) —Ga(1)	13.5(4)	N(2) —Ga(2)	7.7(4)

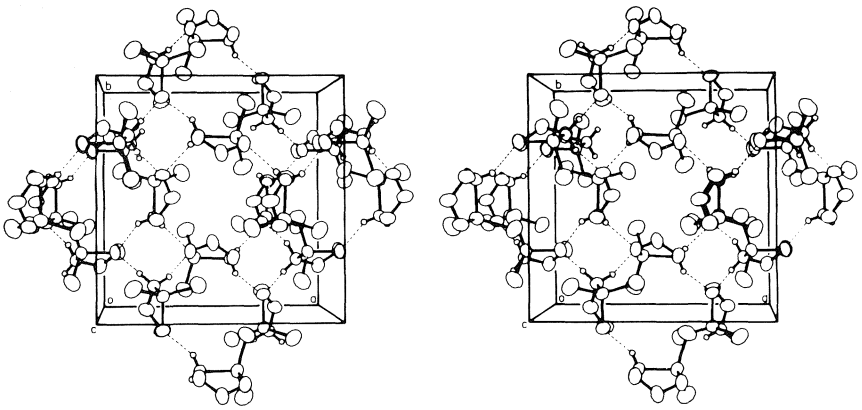

FIG. 2. Crystal structure of ethanolaminogallium dimethyl viewed normal to the *ab* plane.

TABLE 6. Hydrogen-bond data* (distances in Å and angles in deg)

D—H . . . A	H . . . A	D . . . A	∠DHA	∠XAH
N(1)—H(N1a) . . . O(2)[1]	2.08(7)	3.004(7)	155(6)	116(2), 121(2)
N(1)—H(N1b) . . . O(1)[2]	1.86(8)	2.871(6)	170(7)	126(2), 108(3)
N(2)—H(N2a) . . . O(2)[3]	2.31(6)	2.926(7)	175(9)	127(2), 102(2)
N(2)—H(N2b) . . . O(1)[4]	2.09(7)	2.907(6)	148(6)	121(2), 102(2)

*H...O(1)...H 86(3)°, H...O(2)...H 80(2)°. Superscripts refer to atoms at positions: [1] $1-x, 1-y, z-1/2$; [2] $1-y, x, z-1/4$; [3] $1-y, x-1, z-1/4$; [4] $x-1, y, z$.

four-coordinate with distorted tetrahedral coordination geometry; bond angles at gallium range from 86.9(2) (O—Ga—N) to 124.4(4)° (C—Ga—C). The Ga—O and Ga—C distances are normal for tetrahedral gallium (22–24) and very similar to equatorial Ga—O and Ga—C distances for trigonal bipyramidal gallium (1, 5). As in the boron compounds (2–4) the bonds to nitrogen are somewhat long, 2.056(6) and 2.072(6) Å, compared to values of 1.971–2.042 Å previously observed for tetrahedral Ga—N bonds (22–24 and references therein). The Ga—N bonds in the five-coordinate dimers $[Me_2NCH_2CH_2O{\cdot}GaR_2]_2$ (1) are axial with lengths of 2.279(3) Å for R = H and 2.479(4) Å for R = Me.

The geometry of the ethanolamino moiety is very similar to that observed for the boron compounds. The only significant difference is the O—C bond length which has a mean[2] value of 1.412(2) Å in the boron compounds and a mean value of 1.435(7) Å in the present structure. This may be due to the involvement of the oxygen in a second N—H...O hydrogen bond in the present study. The O—C distances in the dimers $[Me_2NCH_2CH_2O{\cdot}GaR_2]_2$ are significantly shorter at 1.369(5) and 1.384(7) Å, but the oxygen is trivalent, being bound to a carbon and two gallium atoms.

[2]Here and elsewhere in this report mean values are weighted means with rms deviations from the mean in parentheses.

Acknowledgements

We thank the National Research Council of Canada for financial support and the University of British Columbia Computing Centre for assistance. We are grateful to Mr. J. Nip for the mass spectrum, Mr. P. Borda for the C, H, N analyses, and Dr. S. O. Chan for the ^1H nmr spectrum.

1. S. J. RETTIG, A. STORR, and J. TROTTER. Can. J. Chem. **53**, 58 (1975).
2. S. J. RETTIG and J. TROTTER. Can. J. Chem. **51**, 1288 (1973).

3. S. J. RETTIG and J. TROTTER. Can. J. Chem. **54**, 3130 (1976).
4. S. J. RETTIG and J. TROTTER. Acta Crystallogr. Sect. B, **30**, 2139 (1974).
5. S. J. RETTIG, A. STORR, and J. TROTTER. Can. J. Chem. **52**, 2206 (1974).
6. A. STORR and B. S. THOMAS. Can. J. Chem. **48**, 3667 (1970).
7. P. COPPENS, L. LEISEROWITZ, and D. RABINOVICH. Acta Crystallogr. **18**, 1035 (1965).
8. W. R. BUSING and H. A. LEVY. Acta Crystallogr. **22**, 457 (1967).
9. D. T. CROMER and J. B. MANN. Acta Crystallogr. Sect. A, **24**, 321 (1968).
10. R. F. STEWART, E. R. DAVIDSON, and W. T. SIMPSON. J. Chem. Phys. **42**, 3175 (1965).
11. D. T. CROMER and D. LIBERMAN. J. Chem. Phys. **53**, 1891 (1970).
12. P. J. BECKER and P. COPPENS. Acta Crystallogr. Sect. A, **30**, 129 (1974); **30**, 148 (1974); **31**, 417 (1975).
13. P. COPPENS and W. C. HAMILTON. Acta Crystallogr. Sect. A, **26**, 71 (1970).
14. F. R. THORNLEY and R. J. NELMES. Acta Crystallogr. Sect. A, **30**, 748 (1974).
15. W. C. HAMILTON. Acta Crystallogr. **18**, 502 (1965).
16. V. SCHOMAKER and K. N. TRUEBLOOD. Acta Crystallogr. Sect. B, **24**, 63 (1969).
17. D. W. J. CRUICKSHANK. Acta Crystallogr. **9**, 747 (1956); **9**, 754 (1956); **14**, 896 (1961).
18. K. S. CHONG, S. J. RETTIG, A. STORR, and J. TROTTER. Can. J. Chem. **55**, 4166 (1977).
19. K. S. CHONG, S. J. RETTIG, A. STORR, and J. TROTTER. Can. J. Chem. **56**, 1212 (1978).
20. G. E. COATES and K. WADE. Organometallic compounds: the main group elements. Vol. 1. 3rd ed. Methuen, London. 1967.
21. K. S. CHONG and A. STORR. Can. J. Chem. **57**, 127 (1979).
22. R. T. BAKER, S. J. RETTIG, A. STORR, and J. TROTTER. Can. J. Chem. **54**, 343 (1976).
23. K. S. CHONG, S. J. RETTIG, A. STORR, and J. TROTTER. Can. J. Chem. **55**, 2540 (1977).
24. S. J. RETTIG, A. STORR, and J. TROTTER. Can. J. Chem. **53**, 753 (1975).

Band resolution of optical spectra of solvated electrons in water, alcohols, and tetrahydrofuran[1]

FANG-YUAN JOU AND GORDON R. FREEMAN

Chemistry Department, University of Alberta, Edmonton, Alta., Canada T6G 2G2

Received August 14, 1978

FANG-YUAN JOU and GORDON R. FREEMAN. Can. J. Chem. **57**, 591 (1979).

The optical absorption spectra of solvated electrons in water, alcohols, and tetrahydrofuran are empirically resolved into two Gaussian bands and a continuum tail. The first Gaussian band covers most of the low energy side of the spectrum. The second Gaussian band lies at an energy slightly above that of the absorption maximum of the total spectrum. With the exception of *tert*-butyl alcohol, in water and alcohols the following were observed: (*a*) the first Gaussian bands have the same half-width, but the oscillator strength in water is about double that in an alcohol; (*b*) the second Gaussian bands have similar half-widths and oscillator strengths; (*c*) the continuum tails have similar half-widths, yet that in water possesses only about one third as much oscillator strength as one in an alcohol. In *tert*-butyl alcohol and tetrahydrofuran the first Gaussian band and the continuum tail each carry nearly half of the total oscillator strength.

FANG-YUAN JOU et GORDON R. FREEMAN. Can. J. Chem. **57**, 591 (1979).

Les spectres d'absorbtion optique des électrons solvatés dans l'eau, les alcools et le tétrahydrofuranne peuvent être résolus empiriquement en deux courbes gaussiennes et en une queue continue. La première courbe gaussienne recouvre presque toute la partie de faible énergie du spectre. La deuxième courbe gaussienne se trouve à une énergie légèrement supérieure au maximum d'absorbtion du spectre global. A l'exception du *tert*-butanol, on observe généralement avec l'eau et les alcools, les faits suivants: (*a*) les largeurs à demi-hauteur des premières courbes gaussiennes sont approximativement les mêmes; la force de l'oscillateur dans l'eau est approximativement deux fois celle dans l'alcool; (*b*) les largeurs à demi-hauteur et les forces des oscillateurs des deuxièmes courbes gaussiennes sont semblables; (*c*) les largeurs à demi-qauteur des queues continues sont semblables; toutefois la force de l'oscillateur de celle de l'eau est environ trois fois moindre que celle d'un alcool. Dans le *tert*-butanol et le tétrahydrofuranne la force de l'oscillateur de la première courbe gaussienne est approximativement égal à cela de la queue continue.

[Traduit par le journal]

Introduction

Theoretical treatments of the optical absorption spectrum of solvated electrons in polar liquids have been moderately successful in rationalizing the transition energy at the absorption maximum, but have failed to explain the breadth and skewness of the band (1–3). Semi-empirical models for fitting the band shape help to provide a qualitative understanding of the spectrum (4, 5). Recent theoretical work (6) supports the suggestion (4) that the broad spectrum is comprised of overlapping bands for a small number of bound–bound transitions, with a tail towards high energies due to bound–continuum transitions.

In view of the Gaussian shape of the Franck–Condon factor (7) which governs the band shape of a bound–bound transition, the whole spectrum of solvated electrons was previously resolved into two Gaussian bands and a continuum tail (8). The empirical fitting requires extended measurement of the wings of the spectrum. Therefore, we have measured the spectra over wide ranges of wavelength in water, alcohols, and tetrahydrofuran. The results of the resolution are reported herein.

Experimental

The materials, purification, and optical system were described elsewhere (8–10). Ethanolamine (scintillation grade) was from Eastman Kodak Co. The purification was the same as for a normal alcohol but under reduced pressure.

The whole solvated electron spectrum in water and ethanolamine and the partial spectra at $\lambda > 900$ nm and $\lambda < 500$ nm in methanol, ethanol, 1-propanol, and 1-butanol, and that at $\lambda < 1000$ nm in tetrahydrofuran (THF) were measured in a 1.5 cm spectrosil cell. The ultraviolet and visible portions in water and alcohols were measured with 100 ns pulses (6×10^{16} eV/g) and those in THF with 1.0 μs pulses (30×10^{16} eV/g). The infrared portion in water and alcohols was measured with 1.0 μs pulses. Appropriate Corning glass filters were placed in front of the optical cell and the monochromator.

The operation of the 1P28 uv detector was limited to a light input of 1.0 ± 0.2 V, as the linearity was good only in this range (deviation ~2%). The high voltage was varied between 600–900 V, depending upon wavelength. The slits of the monochromator were kept at constant widths.

The irradiation temperature was 26 ± 1°C, except for THF which was − 99°C.

[1]Assisted financially by the National Research Council of Canada.

0008-4042/79/050591-07$01.00/0

TABLE 1. Parameters of optical absorption spectra of solvated electrons in ethanolamine, water, and alcohols at 26°C and tetrahydrofuran at −99°C[a]

Parameter	Value												
	EA	GL	EG	PD	W	M	E	1P	1B	1O	2P	*t*B	THF
E_{Amax}, eV	1.39	2.31	2.19	2.17	1.72	1.95	1.79	1.93	1.94	1.98	1.52	1.14	0.78
$W_{1/2}$, eV	1.16	1.41	1.41	1.51	0.85	1.37	1.51	1.62	1.60	1.55	1.35	0.96	0.52
W_b, eV	0.76	0.91	0.92	0.99	0.49	0.90	1.05	1.06	1.07	1.00	0.96	0.64	0.32
W_r, eV	0.40	0.50	0.49	0.52	0.36	0.47	0.46	0.56	0.53	0.55	0.40	0.32	0.20
W_b/W_r	1.9	1.8	1.9	1.9	1.4	1.9	2.3	1.9	2.0	1.8	2.4	2.0	1.6
$G_{fi}\varepsilon_{max}$[b]	3.0	2.2	1.8	1.4	5.0	1.8	1.5	1.4	1.3	1.0	1.4	1.5	1.5
I[c]	1.53	1.38	1.48	1.40	1.30	1.41	1.37	1.34	1.34	1.39	1.53	1.45	1.68

[a]EA = ethanolamine, GL = glycerol, EG = ethylene glycol, PD = 1,2-propanediol, W = water, M = methanol, E = ethanol, 1P = 1-propanol, 1B = 1-butanol, 1O = 1-octanol, 2P = 2-propanol, *t*B = *tert*-butyl alcohol, THF = tetrahydrofuran.

[b]In 10^4 (100 eV M cm)$^{-1}$.

[c]Integrated area of $\int_{-\infty}^{\infty} \frac{\varepsilon_E}{\varepsilon_{max}} d\left(\frac{E - E_{Amax}}{W_{1/2}}\right)$.

Results

The absorbance measured after a 0.1 μs pulse was not corrected for decay during the pulse, but that after a 1.0 μs pulse was corrected according to first-order decay kinetics and square pulse. The rate constant was taken from the first half-life of the observed maximum absorbance of individual pulse. At $\lambda < 400$ nm (700 nm in THF) correction was also made for radical absorption (9). The parameters of the optical absorption spectra of solvated electron in ethanolamine, water, alcohols, and THF are listed in Table 1 in which E_{Amax} (eV) is the energy at maximum absorption, $W_{1/2}$ (eV) is the width at half-peak height, i.e., half-width, and $G\varepsilon_{max}$ is the product of the free ion yield in (100 eV)$^{-1}$ and the decadic molar extinction coefficient in M^{-1} cm^{-1}. The half-width was separated to the blue, W_b, and red, W_r, sides of the absorption maximum. The ratio W_b/W_r shows the asymmetry of the spectrum.

Fitting the spectrum with a combined Gaussian–Lorentzian shape function (11) is satisfactory in water and aqueous solution (8, 11) for absorbances larger than 10% of the maximum absorbance, A_{max}, and in ethers (9, 12) for absorbances larger than one third of A_{max}. The fitting is, however, not satisfactory in alcohols (8). In general, all or most of the red side of a spectrum of solvated electrons follows the Gaussian shape function.

Lugo and Delahay (4) have previously resolved the solvated electron spectrum into several Gaussian bands, each having the same width, and a continuum tail. Since each band represents an ensemble of electronic and vibronic broadening, be it homogeneous or inhomogeneous, of many individual transition lines, they need not have the same width. Therefore, in the present spectrum fitting, the overlapping Gaussian bands are not restricted to having a same half-width.

The fitting starts from the low energy side of the spectrum. The Gaussian equation for the ith band is transformed to a linear form:

$$[1] \quad \ln A = \ln A_{max,i} - (\ln 2/g_i^2)(E_i - E)^2 \quad \text{for } E < E_i,\ i = 1, 2$$

where A is the absorbance at energy E (eV), E_i (eV) is the energy at maximum absorbance, $A_{max,i}$, and g_i is half of the width of the ith band at $0.5A_{max,i}$. E_i is varied and the correlation factor calculated. The final values of E_i, g_i, and $A_{max,i}$ are obtained from the equation that provides the largest correlation factor. Absorbances entering the least-squares fitting have in general at least 4% of the maximum. The first

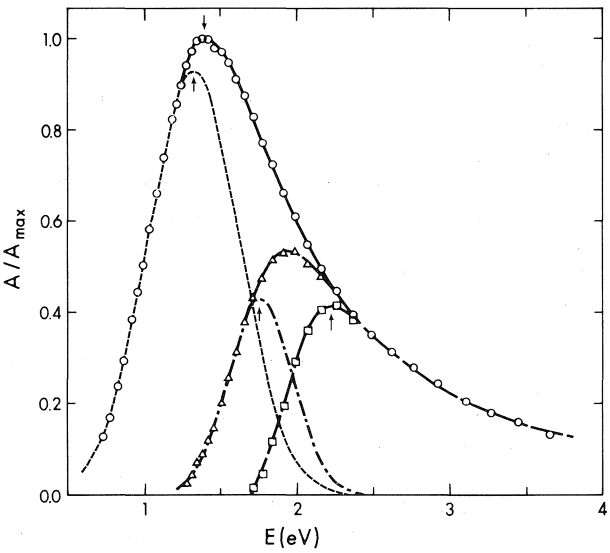

FIG. 1. The band resolution of the optical absorption spectrum of solvated electrons in ethanolamine at 26°C: ○, experimental; △, first remainder; □, second remainder; ---, first Gaussian; ·····, second Gaussian; – – –, continuum tail; ↓, spectrum maximum; ↑, band maximum.

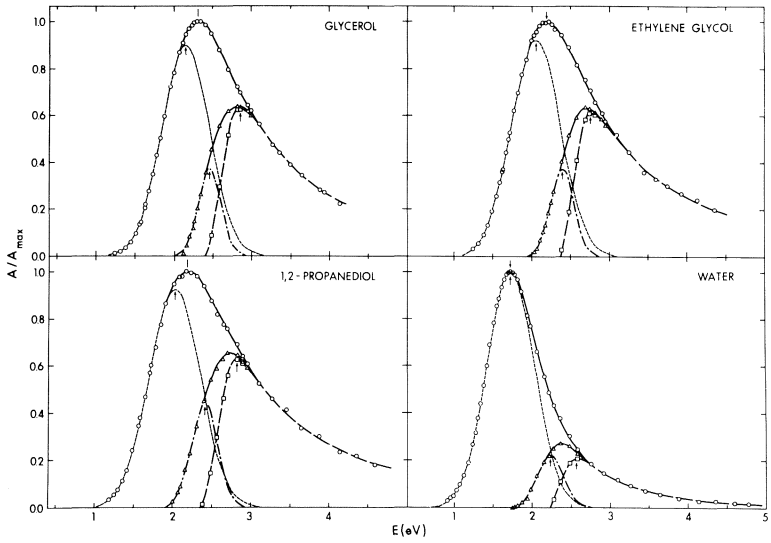

FIG. 2. Band resolution in glycerol, ethylene glycol, 1,2-propanediol, and water at 26°C. Symbols as in Fig. 1.

Gaussian is subtracted from the whole spectrum to obtain a remainder, which is then fitted with a second Gaussian. A third Gaussian, if it exists, would have a very narrow width. Therefore, the whole spectrum is resolved into only two Gaussians and a high energy tail. The resolution of the optical spectrum in ethanolamine at 26°C is shown in Fig. 1. The resolution was also done for spectra of solvated electrons in glycerol, ethylene glycol, 1,2-propanediol, water (Fig. 2), methanol, ethanol, 1-propanol, 1-butanol (Fig. 3), 1-octanol, 2-propanol, *tert*-butyl alcohol, and THF (Fig. 4). In *tert*-butyl alcohol and THF the experimental data on the low energy side are not extensive enough. The resolutions of these two spectra are tentative.

In water and all alcohols the widths at half-height of the first and second Gaussian bands are $2g_i = 0.71 \pm 0.07$ eV and 0.37 ± 0.08 eV, respectively, and the width at half-height of the high energy tail about 1.0 ± 0.2 eV.[2] If the optical excitation on the low energy side of the spectrum corresponds to a bound–bound transition, then the presently obtained Gaussian shape justifies the semi-classical Franck–Condon factor due to vibronic broadening (6, 7). The high energy tail has a rather steep rise on its low energy side. It is quite similar to the band shape of a theoretically calculated bound–continuum transition (13, 14). Therefore, the high energy tail is believed to be a bound–continuum transition. From the onset of the high energy tail, the threshold energy of photoionization of the solvated electrons (E_0) could be estimated. The threshold energy is 1.7 eV in ethanolamine, 2.4 eV in multihydric alcohols, 2.2 eV in water, 2.0–2.1 eV in normal monohydric alcohols, 1.8 eV in 2-propanol, and 1.5 eV in *tert*-butyl alcohol. These energies lie $\sim$0.1–0.3 eV above E_{Amax} of the overall spectrum in alcohols and 0.5 eV above in water. In THF the first Gaussian band has the same half-width as that of the second Gaussian band in alcohols. The second Gaussian band in THF is very small. The threshold energy of photoionization is 0.95 eV, which locates 0.18 eV higher than E_{Amax}. The parameters of the Gaussian bands and the continuum tail of each spectrum are listed in Table 2.

The high energy sides of the spectra were tested to see whether they follow a simple exponential law: $A/A_{\text{max}} \propto E^{-\alpha}$, where α is a constant and may be obtained from the slope of the plot $\ln(A/A_{\text{max}})$ vs. $\ln E$. Straight lines were obtained for $A/A_{\text{max}} \leq 0.6 \pm 0.1$. The value of α is 4.4 in water, $(8 \pm 1)/3$ in alcohols, and 2.2 in THF. The spectrum at the high energy side in ethanol at 77 K (15) and in 3-methyloctane at 127 K (16) were also examined. The fitting is $A/A_{\text{max}} = 41.26E^{-3.77}$ from 3.0 eV to 6.0 eV for the former and $0.54E^{-2.19}$ from 0.9 to 2.1 eV for the latter. The value of α is not 8/3 or 3 for electrons in

[2]The analysis includes the possibility that $g_1 = g_2$, but the best fit of the band shape always gave $g_2 < g_1$. The earlier assumption that $g_1 = g_2$ (4) was only tolerable if the measured band lacked most of the low energy side. When the present analysis was applied to spectra measured for the same solvent in different types of apparatus, such as a high pressure apparatus and a variable temperature apparatus, the values of g_1 at a given T and P were reproducible within 2–10%, while those of g_2 were reproducible within 20%.

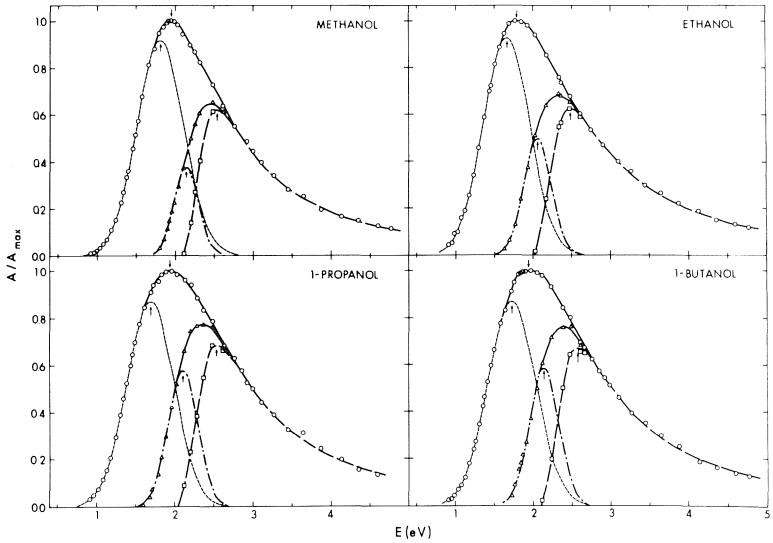

FIG. 3. Band resolution in methanol, ethanol, 1-propanol, and 1-butanol at 26°C. Symbols as in Fig. 1.

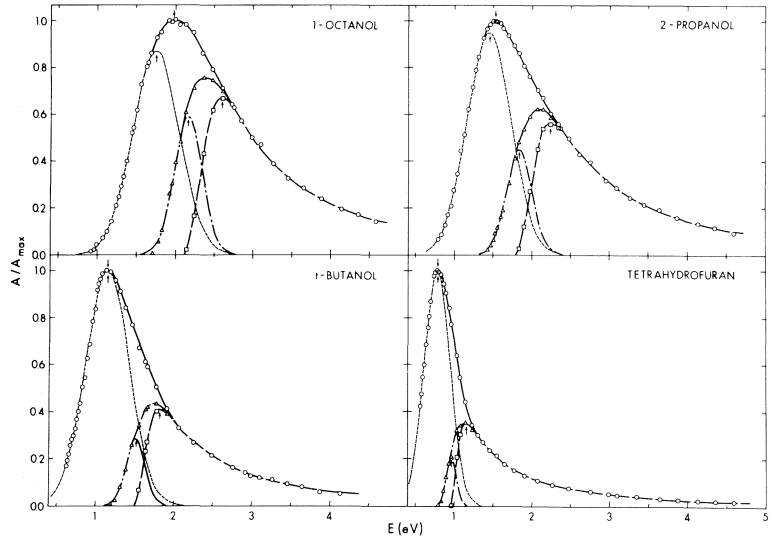

FIG. 4. Band resolution in 1-octanol, 2-propanol, *tert*-butyl alcohol at 26°C and THF at −99°C. Symbols as in Fig. 1.

all solvents, as suggested earlier (4); the variations from 2.2 to 4.4 mentioned above are well outside of the experimental uncertainty.

Discussion

The optical absorption spectra reported here cover a wide range of spectral region. Both sides of each spectrum maximum extend to the observation limit of our optical system. All the spectra have the well known broad, asymmetric shape and no noticeable fine structure. A cut-off energy, which is characteristic of bound–continuum transitions (ref. 13, sect. 74, refs. 14, 17), is not observed in the *ascending* part of the spectrum. The difference between Gaussian and (linear) cut-off shapes is most clearly visible at $A/A_{max} < 0.2$ on the low energy side (see Figs. 2 and 3). Theoretical studies of solvated electrons (1–6, 18) still do not conform with the experimental line shape. The studies of temperature dependence of the spectrum in ethers (9) and pressure dependence in alcohols (8) showed that the half-width of a spectrum is less informative about the nature of the transition than are the separate widths on the two sides of the band maximum.

The whole band was empirically resolved into two Gaussian bands and a continuum tail. The first

TABLE 2. Parameters of Gaussian bands and continuum tail[a]

Parameter	Value												
	EA	GL	EG	PD	W	M	E	1P	1B	1O	2P	*t*B	THF
E_1 (eV)	1.32	2.15	2.06	2.02	1.72	1.81	1.66	1.68	1.72	1.75	1.44	1.14	0.78
g_1 (eV)	0.35	0.36	0.37	0.39	0.36	0.36	0.36	0.35	0.36	0.36	0.34	0.33	0.20
A_1	0.93	0.90	0.93	0.93	1.00	0.92	0.93	0.87	0.87	0.87	0.95	1.00	1.00
f_1	0.39	0.35	0.35	0.36	0.69	0.36	0.33	0.30	0.31	0.31	0.33	0.50	0.48
E_2 (eV)	1.76	2.46	2.40	2.40	2.23	2.14	2.06	2.10	2.14	2.16	1.83	1.51	0.96
g_2 (eV)	0.25	0.18	0.18	0.20	0.20	0.19	0.21	0.23	0.22	0.22	0.20	0.15	0.08
A_2	0.43	0.37	0.38	0.44	0.22	0.38	0.50	0.58	0.55	0.59	0.45	0.29	0.21
f_2	0.13	0.07	0.07	0.09	0.08	0.08	0.10	0.13	0.13	0.13	0.09	0.06	0.04
E_c (eV)	2.22	2.85	2.76	2.81	2.58	2.54	2.48	2.53	2.58	2.60	2.23	1.81	1.16
g_c (eV)	0.59	0.58	0.60	0.60	0.43	0.54	0.60	0.58	0.58	0.56	0.57	0.46	0.32
A_c	0.41	0.62	0.61	0.62	0.21	0.62	0.63	0.68	0.67	0.67	0.56	0.41	0.35
f_c	0.48	0.58	0.58	0.55	0.23	0.56	0.57	0.57	0.56	0.56	0.58	0.44	0.48
E_0 (eV)	1.7	2.4	2.4	2.4	2.2	2.1	2.0	2.0	2.1	2.1	1.8	1.5	1.0
α	2.4	3.0	2.7	2.7	4.4	2.9	2.8	3.0	2.9	2.9	2.6	2.6	2.2

[a] E = band maximum, g = half of the width at half-height, A = relative absorbance, f = percentage of oscillator strength. Subscript 1 indicates first Gaussian band, 2 indicates second Gaussian band, c indicates continuum tail, E_0 = threshold energy of bound–continuum transition, α = descending power of A/A_{max} vs. E curve.

Gaussian band is a bound–bound transition. This proposition is based on the fact that in the photobleaching studies of trapped electrons in organic glasses (15, 19, 20), ice (21), and liquid methanol (22), the quantum yield is very low with photon energies at the red side of the absorption spectrum. This phenomenon was also observed by photoconductivity (23–26) and stimulated luminescence (27). It could be explained that the excited electron in the energy region of the first Gaussian band could still be bound by the same potential well. The small photoresponse that is observed in this energy region (15, 19–27) could arise from thermal agitation or tunnelling from the excited state to the continuum.

The second Gaussian band which lies slightly above E_{Amax} could be due to transition to higher excited states. This was speculated in theoretical studies but was concluded not to contribute significantly to the total width (1). Indeed, this band contributes only about 10% of the total oscillator strength (Table 2). Huang *et al.* (24, 25) postulated a possible second transition band of which the final state is in the continuum, on the basis that there was no temperature dependence of photobleaching yield and photocurrent in methyltetrahydrofuran and 3-methylhexane glasses. However, the latter work involved a double photon process, so the transition presumably passed through an intermediate state.

The continuum tail is characterized by a rapidly ascending and slowly descending A vs. E curve. The slope of both sides lies between those in neutral and negative hydrogen atoms (13). The overall band shape is very similar to the photoionization spectrum due to direct bound–continuum transition (28). The band maximum is higher than E_{Amax} by about 0.6 ± 0.1 eV in alcohols, 0.9 eV in water, and 0.4 eV in THF. This band resembles, in relative position, the detrapping curves of photobleaching yield (15, 19–21), photoconductivity (23–26), and stimulated luminescence intensity (27). The cut-off energy, i.e., threshold energy of the bound–continuum transition, was obtained by linear extrapolation of the low energy side of the continuum (Table 2).

By analogy with the hydrogen atom spectrum, the first Gaussian band is due to $1s \rightarrow 2p$ transition, the second Gaussian band to $1s \rightarrow 3p$ transition, and the high energy tail to $1s \rightarrow$ continuum. The widths come from the Franck–Condon factor (7). For hydrogen atoms the oscillator strength was calculated (ref. 13, sect. 63) to be $f_{1s\rightarrow 2p} = 42\%$, $f_{1s\rightarrow 3p} = 8\%$, and $f_{others} = 50\%$. In all alcohol liquids except *tert*-butyl alcohol the first Gaussian band carries ~33%, the second one ~10%, and the high energy tail ~55% of the total measured oscillator strength. In water the distribution of oscillator strength is 69, 8, and 23%, respectively. In *tert*-butyl alcohol and THF the first Gaussian band and the high energy tail each contribute nearly half of the total oscillator strength. It is to be noted that the first and second Gaussian bands both extend into the high energy tail due to phonon broadening effect (29). The overlapping portion between the two Gaussian bands and the high energy tail is about 2–4% each of the total strength. This may account for the 4% bound–continuum transition in aqueous glass with a photon energy on the red side of the first Gaussian band (30).

If a Slater type of $1S$ wave function, $\psi(1S) = (\beta^3/\pi)^{1/2} \exp(-\beta r)$, represents the ground state orbi-

tal of the solvated electron which is bound by a coulomb force $-\beta/r$, then the threshold energy for bound–continuum transition is $E_0 = \beta^2/2$ au. The unit of effective charge, β, is calculated to be 0.35 in ethanolamine, 0.42 in multihydric alcohols, 0.40 in water, 0.39 in normal alcohols, 0.36 in 2-propanol, 0.33 in *tert*-butyl alcohol, and 0.26 in THF. These values are, incidentally, very similar to the optimum ones calculated from the semi-continuum model with coordination number 4: 0.40 (31)[3] and 0.41 in water (2), 0.38 in methanol (2), and 0.36 in ethanol (2).[4] The effective charge obtained from the empirical resolution is always smaller than that which would arise from a long range polarization potential $\beta_p = 1/D_{op} - 1/D_{st}$, where D_{op} and D_{st} are the optical and static dielectric constants, respectively (32). According to the virial theorem and uncertainty principle, the uncertainty in position of the solvated electron should not be less than 1.3 Å in multihydric and normal alcohols and water, 1.4 Å in ethanolamine and 2-propanol, 1.5 Å in *tert*-butyl alcohol, and 1.9 Å in THF. The diameter of the void calculated in ref. 2 is 1.1 Å in water, 1.4 Å in methanol, and 1.5 Å in ethanol.

The length of the alkyl group in normal alcohols has been shown to have the effect of increasing the transition intensity on the high energy side, comparing with water (8). The empirical band resolution shows that the second Gaussian band has twice and the continuum tail three times the intensity in alcohols as in water, although the respective half-widths are similar in the different solvents (Figs. 2, 3, and 4). However, the overall half-width does not increase beyond 1-propanol (Table 1).

To compare the distribution of oscillator strength through the whole spectrum, the usual formula of oscillator strength f

$$[2] \qquad f = 3.49 \times 10^{-5} \int \varepsilon_E \, dE$$

was rearranged to

$$[3] \quad f = 3.49 \times 10^{-5} \varepsilon_{max} W_{1/2} \times \int_{-\infty}^{\infty} \left(\frac{\varepsilon_E}{\varepsilon_{max}}\right) d\left(\frac{E - E_{Amax}}{W_{1/2}}\right)$$

where ε_E (M^{-1} cm^{-1}) is the decadic molar absorbance at photon energy E (eV). The integral in [3] is shown in Fig. 5 for solvated electrons in water, 1-propanol, and 2-propanol at 26°C and THF at −99°C. It shows that water contributes more strength on the low energy side, and organic liquids more on the high energy side. The value of the integral is not constant, being 1.3 in water, 1.4 in normal and multihydric alcohols, 1.5 in ethanolamine and branched alcohols, and 1.7 in THF. These are to be compared with 1.06 for a Gaussian curve and 1.57 for a Lorentzian curve. The values of $\varepsilon_{max} W_{1/2}$ (see [3]) reported in the literature (8, 9, 33–36) range over a factor of two, partly due to the uncertainty in the value of ε_{max}. The most acceptable one is for water (35, 36), i.e.

$$\varepsilon_{max} W_{1/2} = 1.9 \times 10^4 \times 0.85 = 1.6 \times 10^4 \, M^{-1} \, \text{cm}^{-1} \, \text{eV}$$

which leads to $f = 0.73$. In normal alcohols (8, 36) ε_{max} was reported to be $1.0 \times 10^4 \, M^{-1} \, \text{cm}^{-1}$, giving $\varepsilon_{max} W_{1/2} = 1.4$ to $1.6 \times 10^4 \, M^{-1} \, \text{cm}^{-1}$ eV and $f = 0.67$ in methanol, 0.72 in ethanol, 0.76 in 1-propanol, and 0.75 in 1-butanol. If the same ε_{max} is applied to other alcohols then $f = 0.75$ in 1-octanol, 0.72 in 2-propanol, 0.68 in glycerol, 0.73 in ethylene glycol, and 0.74 in 1,2-propanediol. The most probable value of oscillator strength in water and alcohols is, therefore, $f = 0.72 \pm 0.05$.

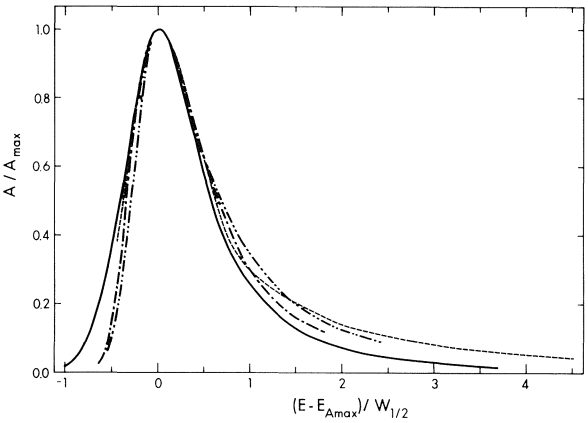

FIG. 5. Oscillator strength distribution of solvated electrons in water (—), 1-propanol (-·-·-·-), and 2-propanol (-···-) at 26°C and THF (---) at −99°C.

[3]Quasi-free energy $V_0 = 0.0$ eV.

[4]$V_0 = -1.0$ eV in water, −0.2 eV in methanol, and +0.2 eV in ethanol.

1. N. R. KESTNER and J. JORTNER. J. Phys. Chem. **77**, 1040 (1973).
2. K. FUEKI, D.-F. FENG, and L. KEVAN. J. Am. Chem. Soc. **95**, 1398 (1973).
3. M. D. NEWTON. J. Phys. Chem. **79**, 2795 (1975).
4. R. LUGO and P. DELAHAY. J. Chem. Phys. **57**, 2122 (1972).
5. T. SHIDA, S. IWATA, and T. WATANABE. J. Phys. Chem. **76**, 3683 (1972).
6. A. BANERJEE and J. SIMONS. J. Chem. Phys. **68**, 415 (1978).
7. M. LAX. J. Chem. Phys. **20**, 1752 (1952).
8. F.-Y. JOU and G. R. FREEMAN. J. Phys. Chem. **81**, 909 (1977).
9. F.-Y. JOU and G. R. FREEMAN. Can. J. Chem. **54**, 3693 (1976).

10. F.-Y. JOU and G. R. FREEMAN. J. Phys. Chem. **83**, Jan. (1979).
11. J. L. DYE, M. G. DEBACKER, and L. M. DORFMAN. J. Chem. Phys. **52**, 6231 (1970).
12. F.-Y. JOU and L. M. DORFMAN. J. Chem. Phys. **58**, 4715 (1973).
13. H. A. BETHE and E. E. SALTPETER. Quantum mechanics of one-and two-electron atoms. Academic Press, New York, NY. 1957.
14. J.-T. J. HUANG and F. O. ELLISON. Chem. Phys. Lett. **28**, 189 (1974).
15. A. BERNAS and D. GRAND. Chem. Commun. 1667 (1970).
16. H. A. GILLIS, N. V. KLASSEN, and R. J. WOODS. Can. J. Chem. **55**, 2022 (1977).
17. A. M. BRODSKII and A. V. TSAREVSKII. Dokl. Akad. Nauk SSSR, Engl. Transl. **217**, 773 (1975).
18. R. L. BUSH and K. FUNABASHI. J. Chem. Soc. Faraday Trans. II, **73**, 274 (1977).
19. A. HABERSBERGEROVA, L. JOSIMOVIC, and J. TEPLY. Trans. Faraday Soc. **66**, 656 (1970); **66**, 669 (1970).
20. H. B. STEEN and J. MOAN. J. Phys. Chem. **76**, 3366 (1972).
21. K. KAWABATA. J. Chem. Phys. **55**, 3672 (1971).
22. A. BROMBERG and J. K. THOMAS. J. Chem. Phys. **63**, 2124 (1975).
23. K. F. BAVERSTOCK and P. J. DYNE. Can. J. Chem. **48**, 2182 (1970).
24. T. HUANG, I. EISELE, D. P. LIN, and L. KEVAN. J. Chem. Phys. **56**, 4702 (1972).
25. T. HUANG and L. KEVAN. J. Am. Chem. Soc. **95**, 3122 (1973).
26. S. A. RICE and L. KEVAN. J. Phys. Chem. **80**, 847 (1977).
27. A. BERNAS, D. GRAND, and T. B. TRUONG. J. Chem. Soc. Chem. Commun. 759 (1972).
28. L. NEMEC, L. CHIA, and P. DELAHAY. J. Phys. Chem. **79**, 2935 (1975).
29. W. B. FOWLER. *In* Physics of color centers. *Edited by* W. B. Fowler. Academic Press, New York. 1968. p. 53.
30. T. Q. NGUYEN and D. C. WALKER. J. Chem. Phys. **67**, 2399 (1977).
31. D. A. COPELAND, N. R. KESTNER, and J. JORTNER. J. Chem. Phys. **53**, 1189 (1970).
32. J. JORTNER. J. Chem. Phys. **30**, 839 (1959).
33. R. K. QUINN and J. J. LAGOWSKI. J. Phys. Chem. **73**, 2326 (1969).
34. M. C. SAUER, JR., S. ARAI, and L. M. DORFMAN. J. Chem. Phys. **42**, 708 (1965).
35. B. D. MICHAEL, E. J. HART, and K. H. SCHMIDT. J. Phys. Chem. **75**, 2798 (1971).
36. K. N. JHA, G. L. BOLTON, and G. R. FREEMAN. J. Phys. Chem. **76**, 3876 (1972).

Dichotomous reactions of thioketones with tetracarbonylferrate

HOWARD ALPER, BERNARD MARCHAND, AND MASATO TANAKA
Department of Chemistry, University of Ottawa, Ottawa, Ont., Canada K1N 9B4

Received October 26, 1978

HOWARD ALPER, BERNARD MARCHAND, and MASATO TANAKA. Can. J. Chem. **57**, 598 (1979).

Treatment of nonenolizable and enolizable thioketones, first with disodium tetracarbonylferrate and then with an acid chloride, affords saturated and unsaturated thioesters, respectively. Mechanisms are proposed for these different reactions.

HOWARD ALPER, BERNARD MARCHAND et MASATO TANAKA. Can. J. Chem. **57**, 598 (1979).

Si l'on traite respectivement des thiocétones qui peuvent être énolisées et d'autres qui ne peuvent pas l'être par du tétracarbonylferrate de disodium puis par un chlorure d'acide, on obtient des thioesters saturés et insaturés. On propose des mécanismes pour ces diverses réactions.

[Traduit par le journal]

The reactions of thioketones with nucleophiles represent an intriguing aspect of the chemistry of these sulfur compounds. Thiophilic and carbophilic additions have been described in the literature (1). One of us has recently observed that the cyclopentadienylmetal carbonyl anions, $C_5H_5M(CO)_n^-$ (M = Mo, W, n = 3; M = Fe, n = 2), can effect desulfurization and coupling of thiobenzophenones to give fulvenes (2). We now wish to report on the dichotomous reactions of thioketones with disodium tetracarbonylferrate, a reagent of demonstrated (3) value in several areas of synthetic organic chemistry.

Disodium tetracarbonylferrate, generated from iron pentacarbonyl and sodium amalgam (4), was reacted with a nonenolizable thione such as 4,4′-dimethoxythiobenzophenone (**1**) in tetrahydrofuran (THF) at −50°C. Subsequent addition of an acid chloride (**2**) and work-up affords the thioesters **3** in

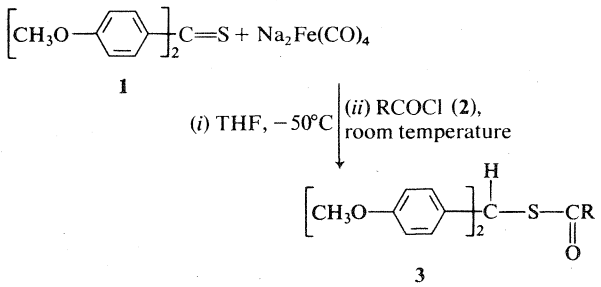

modest yields (R = CH_3, 20% yield, ir(ν_{CO}) 1690 cm^{-1}, nmr($CDCl_3$) δ 5.73 (s, 1H, CHS), ms (*m/e*) 302; R = Ph, 27% yield, ir(ν_{CO}) 1665 cm^{-1}, nmr($CDCl_3$) δ 6.01 (s, 1H, CHS), ms (*m/e*) 364). Adamantanethione, a nonenolizable cycloalkyl thione, reacted in a similar manner with tetracarbonylferrate and benzoyl chloride to give the analogous thioester in 40% yield (ir(ν_{CO}) 1665 cm^{-1}, ms (*m/e*) 272).

When an enolizable thione such as thiocamphor (**4**) was reacted under identical conditions as described for nonenolizable thioketones, unsaturated thioesters (**5**) were formed in 52–62% yields. Saturated thioesters were not detected in any of these reactions. The yields of **5**, together with pertinent spectral data for these new compounds, are listed in Table 1.

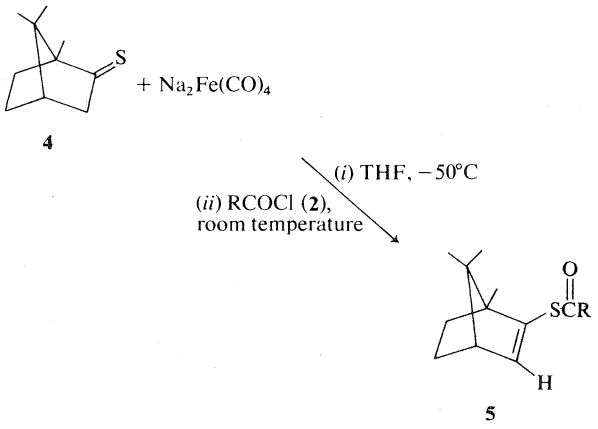

Saturated thioesters (**3**) may arise from initial thiophilic addition of the metal carbonyl dianion to a nonenolizable thione (e.g. **1**) to give the dianion **6**

0008-4042/79/050598-03$01.00/0

TABLE 1. Yields and analytical and pertinent spectral data for compound **5**

R	Yield (%)	Boiling point/ pressure (°C/Torr)	Analysis C Calcd.	C Found	H Calcd.	H Found	S Calcd.	S Found	ν_{CO}[a] (cm^{-1})	δ[b] (ppm)	*m/e*
CH_3	52	65(0.1)	68.52	68.90	8.63	8.61	15.24	15.27	1710	6.38	210
Ph	58	113(0.1)	74.96	74.45	7.40	7.60	11.77	11.87	1680	6.53	272
2-Furyl	62	112(0.15)	68.67	68.45	6.92	6.81	12.22	12.29	1670	6.51	262
p-$CH_3OC_6H_4$	60	150(0.15)	71.48	71.87	7.33	7.29	10.61	11.25	1670	6.47	302
Cyclopropyl	61	85(0.4)	71.13	70.92	8.53	8.49	13.56	13.71	1700	6.38	236

[a]Neat.
[b]The data cited are those for the vinylic proton which appears as a doublet (J = 3–4 Hz). The nmr spectra were recorded in $CDCl_3$, with TMS as an internal standard.

(Scheme 1). Acylation of the latter with an acid chloride (**2**), followed by reductive elimination to **8** (the $Fe(CO)_4$ formed trimerizes to $Fe_3(CO)_{12}$) and protonation would afford **3**. Some evidence for **7** comes from the reaction of **1** with $Fe(CO)_4^{2-}$ and **2**, followed by 1-bromo-2-methylpropane, which alkylates at the benzylic position.

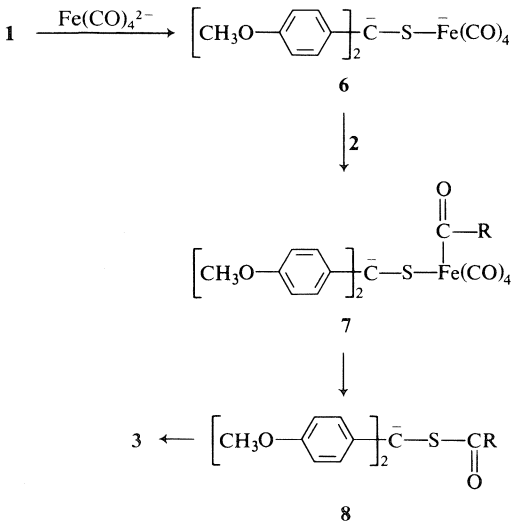

SCHEME 1

The results for thiocamphor clearly show that tetracarbonylferrate is a sufficiently strong base to effect proton removal from an enolizable thione, or its thioenol tautomer (**9**), to form the thioenolate anion **10** and the hydridotetracarbonylferrate anion **11** (3) (Scheme 2). The unsaturated thioester **5** would then result from reaction of **10** with the appropriate acid chloride **2**.

Related to the results for thiocamphor are some very recent findings by Werstiuk and Andrews (5). They showed that the *exo* and *endo* protons of thiocamphor (**4**) undergo NaOD catalyzed deuterium exchange at a considerably faster rate than the

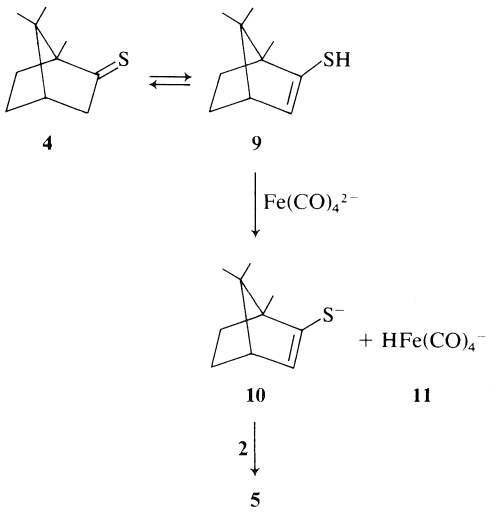

SCHEME 2

corresponding protons of camphor. We have observed that although, as noted above, $Fe(CO)_4^{2-}$ readily abstracts a proton from thiocamphor, camphor is inert to the metal carbonyl dianion.

The following general procedure was used. Iron pentacarbonyl (4.0 mL) in THF (7.5 mL) was added, over a 2-h period, at 0°C, to sodium amalgam (3.5 mL) in THF (10 mL). Excess amalgam was removed, the stirred solution was cooled to −50°C, and then the thioketone (9.9 mmol) in THF (5 mL) was added. The mixture was allowed to warm, with stirring, to room temperature. The acid chloride (**2**, 2.5 equiv.) was added and the reaction mixture was stirred for a short time, concentrated to approximately one-fifth its volume, and then treated with ether (60 mL). The solution was washed successively with water (15 mL), 10% sodium bicarbonate (10 mL), and water (15 mL). The dried organic phase was then chromatographed on silica gel (60–220 mesh, elution with benzene or 1:1 hexane–benzene) or fractionally distilled to give pure **3** or **5**.

Acknowledgement

We are grateful to the National Research Council of Canada for support of this work.

1. D. PAQUER. Bull. Soc. Chim. Fr. 1439 (1975).
2. H. ALPER and H. N. PAIK. J. Am. Chem. Soc. **100**, 508 (1978).
3. H. ALPER. Transition metal organometallics in organic synthesis. Vol. II. Academic Press, New York, NY. 1978.
4. T. MITSUDO, Y. WATANABE, M. YAMASHITA, and Y. TAKEGAMI. Tetrahedron Lett. 1385 (1974).
5. N. H. WERSTIUK and P. ANDREWS. Can. J. Chem. **56**, 2605 (1978).

Electron spin resonance observations of photochemically generated contact ammonium ion-pairs of fluoro-substituted ketones

K. S. CHEN, T. FOSTER, AND J. K. S. WAN

Department of Chemistry, Queen's University, Kingston, Ont., Canada K7L 3N6

Received November 10, 1978

K. S. CHEN, T. FOSTER, and J. K. S. WAN. Can. J. Chem. **57**, 600 (1979).

Contact radical ion-pairs of ammonium and fluoro-substituted ketones were generated in photochemical systems and their here-to-fore elusive esr spectra were characterized.

K. S. CHEN, T. FOSTER et J. K. S. WAN. Can. J. Chem. **57**, 600 (1979).

Des paires de contact d'ions ammonium et de radicaux de cétones substituées par fluor ont été généreés dans un systeme photochimique. On a pu caracterisé leur spectres rpe qui n'ont pas été observés auparavant.

[Traduit par le journal]

The mechanism involving electron transfer in the photoreductions of ketones by tertiary amines has remained controversial in recent years. Cohen and co-workers (1) initially suggested that amines react with excited carbonyl compounds via an electron transfer mechanism followed by a proton transfer from the amine radical cation. The earlier CIDEP results obtained in the photoreduction of quinones by amines were interpreted in terms of this electron transfer mechanism followed by a hydrogen transfer from the alcoholic solvent to the amine radical cation (see, for example, ref. 2). Subsequently, McLauchlan and Sealy (3) have demonstrated that in the CIDEP system involving the photoreduction of benzophenone by amine in the presence of biacetyl the primary process does not involve electron transfer. On the other hand, Wong (4) has recently concluded from his CIDEP experiments of the photoreduction of naphthoquinone by pyridine and by tertiary triethyl amine that the primary process is a hydrogen abstraction reaction in the first case and it becomes an electron transfer reaction in the latter case. Similarly, the early CIDNP results in the photoreduction of benzophenone by amines were interpreted based on an electron transfer mechanism (5). Further studies by Roth and co-workers (6) have revealed that the electron transfer mechanism is operative only when the amine used is the 1,4-diazobicyclo[2.2.2]octane. The CIDEP and CIDNP applications to photochemistry have been reviewed recently by Wan (7).

Flash photolysis with optical detection has also been applied to study the electron transfer mechanism in the ketone–amine systems (8). Arimitsu and co-workers (8) have reported that among a number of amines quenching the triplet benzophenone, only the *N*,*N*-dialkylanilines produce radical ions. Although esr spectroscopy is now commonly used to follow photochemical reactions in solution and to identify the transient intermediates, it has not been possible to confirm the presence and the fate of the counter amine radical cation in the ketone–amine photochemical systems.

We wish to report here the first high resolution esr observations of contact ammonium ion-pairs of hexafluoroacetone and the radical anion of α,α,α-trifluoroacetophenone.[1] While the results will shed some light on the controversial electron transfer

[1]A charged ion aggregate involving the ammonium cation and a ninhydrin anion radical, in rapid equilibrium with the free ninhydrin anion radical and the tetraalkylammonium salt, has been proposed to account for the variation of esr parameters as a function of the ammonium salt concentration (9).

0008-4042/79/050600-03$01.00/0

Acknowledgement

We are grateful to the National Research Council of Canada for support of this work.

1. D. PAQUER. Bull. Soc. Chim. Fr. 1439 (1975).
2. H. ALPER and H. N. PAIK. J. Am. Chem. Soc. **100**, 508 (1978).
3. H. ALPER. Transition metal organometallics in organic synthesis. Vol. II. Academic Press, New York, NY. 1978.
4. T. MITSUDO, Y. WATANABE, M. YAMASHITA, and Y. TAKEGAMI. Tetrahedron Lett. 1385 (1974).
5. N. H. WERSTIUK and P. ANDREWS. Can. J. Chem. **56**, 2605 (1978).

Electron spin resonance observations of photochemically generated contact ammonium ion-pairs of fluoro-substituted ketones

K. S. CHEN, T. FOSTER, AND J. K. S. WAN

Department of Chemistry, Queen's University, Kingston, Ont., Canada K7L 3N6

Received November 10, 1978

K. S. CHEN, T. FOSTER, and J. K. S. WAN. Can. J. Chem. **57**, 600 (1979).

Contact radical ion-pairs of ammonium and fluoro-substituted ketones were generated in photochemical systems and their here-to-fore elusive esr spectra were characterized.

K. S. CHEN, T. FOSTER et J. K. S. WAN. Can. J. Chem. **57**, 600 (1979).

Des paires de contact d'ions ammonium et de radicaux de cétones substituées par fluor ont été généreés dans un systeme photochimique. On a pu caracterisé leur spectres rpe qui n'ont pas été observés auparavant.

[Traduit par le journal]

The mechanism involving electron transfer in the photoreductions of ketones by tertiary amines has remained controversial in recent years. Cohen and co-workers (1) initially suggested that amines react with excited carbonyl compounds via an electron transfer mechanism followed by a proton transfer from the amine radical cation. The earlier CIDEP results obtained in the photoreduction of quinones by amines were interpreted in terms of this electron transfer mechanism followed by a hydrogen transfer from the alcoholic solvent to the amine radical cation (see, for example, ref. 2). Subsequently, McLauchlan and Sealy (3) have demonstrated that in the CIDEP system involving the photoreduction of benzophenone by amine in the presence of biacetyl the primary process does not involve electron transfer. On the other hand, Wong (4) has recently concluded from his CIDEP experiments of the photoreduction of naphthoquinone by pyridine and by tertiary triethyl amine that the primary process is a hydrogen abstraction reaction in the first case and it becomes an electron transfer reaction in the latter case. Similarly, the early CIDNP results in the photoreduction of benzophenone by amines were interpreted based on an electron transfer mechanism (5). Further studies by Roth and co-workers (6) have revealed that the electron transfer mechanism is operative only when the amine used is the 1,4-diazobicyclo[2.2.2]octane. The CIDEP and CIDNP applications to photochemistry have been reviewed recently by Wan (7).

Flash photolysis with optical detection has also been applied to study the electron transfer mechanism in the ketone–amine systems (8). Arimitsu and co-workers (8) have reported that among a number of amines quenching the triplet benzophenone, only the *N*,*N*-dialkylanilines produce radical ions. Although esr spectroscopy is now commonly used to follow photochemical reactions in solution and to identify the transient intermediates, it has not been possible to confirm the presence and the fate of the counter amine radical cation in the ketone–amine photochemical systems.

We wish to report here the first high resolution esr observations of contact ammonium ion-pairs of hexafluoroacetone and the radical anion of α,α,α-trifluoroacetophenone.[1] While the results will shed some light on the controversial electron transfer

[1]A charged ion aggregate involving the ammonium cation and a ninhydrin anion radical, in rapid equilibrium with the free ninhydrin anion radical and the tetraalkylammonium salt, has been proposed to account for the variation of esr parameters as a function of the ammonium salt concentration (9).

0008-4042/79/050600-03$01.00/0

mechanism in the ketone–amine photochemical reactions, the esr characterization of the here-to-fore elusive ammonium ion-pairs should be of wider interest to chemistry in general.

When a degassed cyclopropane solution of hexafluoroacetone and triethylamine was uv-irradiated within the esr cavity of a E-3 spectrometer at −78°C, a well resolved spectrum was observed (Fig. 1). The volume ratio of the sample solution was 1:1:5 for hexafluoroacetone, triethylamine, and cyclopropane, respectively. The experimental technique has been previously described (10). The spectrum in Fig. 1*a* represents a septet with only the major 5 group showing on scale. The septet can be unambiguously assigned to the six fluorines by comparison with the known fluorine splitting in the hexafluoroacetone ketyl generated electrochemically (11). The inserts with an expanded scale in Fig. 1*b* further resolve the triplet (1:1:1) splitting due to the nitrogen nucleus ^{14}N, $I = 1$. Additional but partially resolved second-order fluorine splittings are also observed which were predicted by Fessenden (12). The spectrum is therefore assigned to the contact ammonium ion-pair of the hexafluoroacetone. The esr parameters are listed in Table 1.

The contact ammonium ion-pair is produced probably via the following scheme:

$$[1]\quad (CF_3)_2C{=}O + h\nu \overset{ISC}{\rightsquigarrow} {}^3[(CF_3)_2C{=}O]$$

$$[2]\quad {}^3[(CF_3)_2C{=}O] + R_3N \rightarrow [R_3\dot{N}^{+}\,{}^{-}\dot{O}{-}C(CF_3)_2] \rightarrow R_2N\dot{C}HCH_3 + (CF_3)_2\dot{C}OH$$

$$[3]\quad (CF_3)_2\dot{C}OH + R_3N \rightarrow (CF_3)_2C\dot{O}^{-}\,{}^{+}NHR_3$$

(Ion-pair I)

Reactions [2] and [3] have been postulated for other ketone–amine systems by Davidson and co-workers (13) and recently by McLauchlan and Sealy (3). The ion-pair (I) formed in reaction [3] can be either a contact pair or a 'solvent separated' pair (14), depending upon the solvent involved. For example, contact ion-pairs of phenanthroquinone were normally observed in THF but the contact ion-pair would dissociate in a more polar solvent such as DMF. In the ammonium ion-pair case, a non-polar cyclopropane solvent had to be used because the ion-pair would dissociate even in the commonly used THF solvent. Thus, only the esr spectrum of the hexafluoroacetone radical anion was observed (Fig. 1*c* and Table 1) in THF. The choice of the proper solvent was probably the main reason why the contact ammonium ion-pairs had escaped esr observation until now.

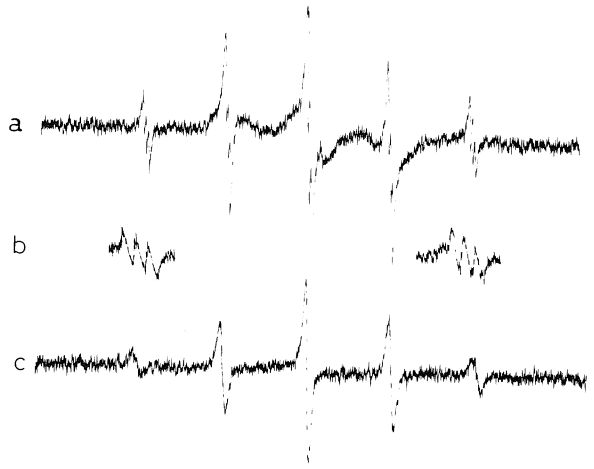

FIG. 1. Electron spin resonance spectra obtained during the photolyses of hexafluoroacetone and triethylamine in (*a*) cyclopropane at −78°C, (*b*) cyclopropane at −78°C but with an expanded scale (×4), (*c*) THF at −78°C.

Although the ketyl radical can be produced via an intermolecular hydrogen abstraction (15)

$$[4]\quad {}^3[(CF_3)_2C{=}O] + \text{cyclo-}C_3H_6 \rightarrow (CF_3)_2\dot{C}OH + \dot{C}_3H_5$$

this process is unlikely to compete favourably with the most efficient amine quenching reaction in [2]. Furthermore, the dissociation of the $(CF_3)_2\dot{C}OH$ radical into the radical anion $(CF_3)_2CO^{\dot{-}}$ and H^+ in the absence of amine was not observed even in the presence of added alkali metal salts such as the metal tetraphenylborate. In the presence of a tertiary amine, it is thought that the ionization in reaction [3] requires the formation of a complex in which the hydrogen bonding is essential between the ketyl radical and the nitrogen atom of the amine.

The effect of solvent on the observation of ammonium ion-pairs also depends upon the individual ketone used. When a THF solution of α,α,α-trifluoroacetophenone and triethylamine was photolyzed within an esr cavity, a contact ammonium ion-pair was readily observed. In addition to the well known pattern of the hyperfine splittings of the trifluoroacetophenone radical anion, the nitrogen triplet splitting was resolved (Table 1). However, if acetonitrile was used as the solvent such as in the CIDNP experiments, no contact ammonium ion-pair could be observed. If a THF solution of the unsubstituted acetophenone and triethylamine was irradiated, again no ammonium ion-pair was observed. It appears that a trifluoromethyl group next to a carbonyl is essential for the formation and observation of a 'stable' ammonium ion-pair, but this is not always sufficient. A series of compounds, CF_3-

TABLE 1. Electron spin resonance parameters of contact ammonium ion-pairs of $(CF_3)_2CO$ and trifluoroacetophenone

Ion-pair (or radicals)	Solvent	T (°C)	a_N (G)	a_F	a_H^o	a_H^m	a_H^p	a_H^{OH}
$(CF_3)_2\dot{C}\overset{+}{N}HEt_3$	Cyclopropane	−78	1.08	30.54±0.05				
$(CF_3)_2\dot{C}O/\overset{+}{N}HEt_3$	THF	−78	n.s.	31.65				
$(CF_3)_2\dot{C}O$ (ref. 11)	CH_3CN	25		34.7				
$(CF_3)_2\dot{C}OH$	Cyclopropane	−78		24.88				2.01
$(CF_3)(C_6H_5)\dot{C}\overset{+}{N}HEt_3$	THF	−65	1.04	27.32	4.01	1.04	5.08	
$(CF_3)(C_6H_5)\dot{C}O/\overset{+}{N}HMe_3$	THF	−65	n.s.	26.42	3.94	1.07	5.08	
$(CF_3)(C_6H_5)\dot{C}O$ (ref. 16)	DMF	25		24.2	3.3 3.9	1.2	4.8	
$(CF_3)(C_6H_5)\dot{C}OH$	IPA	−40		24.79	3.31 5.73	1.52	5.01	2.15

$COCH_2COX$, with X = CH_3, CF_3, and $\underset{S}{\square}$ have been systematically studied in their photoreduction by amines in THF and none led to the observation of the contact ammonium ion-pair. Perhaps an exceptionally electron-deficient carbonyl group such as that in the hexafluoroacetone and the trifluoroacetophenone is the prerequisite for the formation of a 'stable' ammonium ion-pair.

Finally, we point out that the type of amines used also plays an important role in the observation of the contact ammonium ion-pair. Thus, in the photoreduction of trifluoroacetophenone by amines in THF, triethylamine, tributylamine, and triamylamine all yield contact ammonium ion-pairs while trimethylamine does not lead to formation of the ion-pair.

Further investigation of these contact ammonium ion-pairs in photochemical systems including CIDEP experiments is in progress.

Acknowledgments

This research is supported by the NSERC of Canada.

1. S. G. COHEN, A. PAROLA, and G. H. PARSONS. Chem. Rev. **73**, 141 (1973).
2. A. J. DOBBS. Mol. Phys. **30**, 1073 (1975).
3. K. A. MCLAUCHLAN and R. C. SEALY. Chem. Phys. Lett. **39**, 310 (1976).
4. S. K. WONG. J. Am. Chem. Soc. **100**, 5488 (1978).
5. H. D. ROTH and A. A. LAMOLA. J. Am. Chem. Soc. **96**, 6270 (1974).
6. H. D. ROTH. *In* Chemically induced magnetic polarization. *Edited by* L. T. Muus, P. W. Atkins, K. A. McLauchlan, and J. B. Pedersen. Reidel Publishing Co., Holland. 1977. Chapt. IV.
7. J. K. S. WAN. *In* Advances in photochemistry. Vol. 12. *Edited by* J. N. Pitts, G. S. Hammond, and K. Gollnick. Wiley Interscience, New York. To be published.
8. S. ARIMITSU, H. MASUHARA, N. MATAGA, and H. SUBOMURA. J. Phys. Chem. **79**, 1255 (1975).
9. G. R. STEVENSON and W. MARTIR. J. Phys. Chem. **82**, 1171 (1978).
10. K. S. CHEN and J. K. S. WAN. J. Am. Chem. Soc. **100**, 6051 (1978).
11. E. G. JANZEN and J. L. GERLOCK. J. Phys. Chem. **71**, 4577 (1967).
12. R. W. FESSENDEN. J. Chem. Phys. **37**, 747 (1962).
13. R. S. DAVIDSON and R. WILSON. J. Chem. Soc. B, 71 (1970); R. S. DAVIDSON and M. SANTHANAM. J. Chem. Soc. Perkin II, 2355 (1972).
14. N. HIROTA and R. KREILICK. J. Am. Chem. Soc. **88**, 614 (1966); A. CROWLEY, N. HIROTA, and R. KREILICK. J. Chem. Phys. **46**, 4815 (1967).
15. P. J. KRUSIC, K. S. CHEN, P. MEALEIN, and J. K. KOCHI. J. Phys. Chem. **78**, 2036 (1974).
16. C. P. ANDRIEUX and J. M. SAVEANT. Bull. Soc. Chim. Fr. Part 2, 2090 (1973).

Canadian Journal of Chemistry
Published by
THE NATIONAL RESEARCH COUNCIL OF CANADA

Journal canadien de chimie
Publié par
LE CONSEIL NATIONAL DE RECHERCHES DU CANADA

Volume 57 Number 6 March 15, 1979 Volume 57 numéro 6 15 mars 1979

The crystal and molelcular structure of benzil bisthiosemicarbazonatocopper(II) and the antitumour mechanism of related compounds

GORDON W. BUSHNELL AND ANNIE Y. M. TSANG
Chemistry Department, University of Victoria, Victoria, B.C., Canada V8W 2Y2

Received September 1, 1978

GORDON W. BUSHNELL and ANNIE Y. M. TSANG. Can. J. Chem. **57**, 603 (1979).

The crystal structure of benzil bisthiosemicarbazonatocopper(II) has been solved and refined to an *R*-value of 0.082. The dark red triclinic crystal has cell dimensions a = 960.8(4), b = 1090.7(6), c = 895.8(4) pm, α = 106.23°(4), β = 92.36°(7), γ = 99.50°(7), and belongs to space group $P\bar{1}$ with two molecules per cell. The measured and calculated densities are 1.571 and 1.568 g cm^{-3}, respectively, using $C_{16}H_{14}CuN_6S_2$ (mol. wt. 417.99). The copper coordination is significantly non-planar. The five non-hydrogen atoms of each original thiosemicarbazide molecule lie close to planes set at a dihedral angle of 8.9°. The fold is away from the origin and the neighbouring molecule. Bond lengths to copper are: Cu—S(1) = 223.7(3), Cu—S(2) = 223.4(3), Cu—N(13) = 197.1(6), Cu—N(23) = 197.0(7) pm. The bond angles at the Cu atom are S(1)—Cu—S(2) = 108.62°(9), N(13)—Cu—N(23) = 81.1°(3), N(13)—Cu—S(1) = 85.1°(2), and N(23)—Cu—S(2) = 85.0°(2). The first and second phenyl rings are at 100.3° and 93.0° to the mean Cu coordination plane, which is at a perpendicular distance of 330 pm from a similar plane in the inverse molecule. Intermolecular double hydrogen bonding occurs at each side of the complex between the uncoordinated nitrogen atoms, thus linking the molecules into parallel ribbons.

GORDON W. BUSHNELL et ANNIE Y. M. TSANG. Can. J. Chem. **57**, 603 (1979).

On a résolu la structure cristalline du benzyl bisthiosemicarbonato cuivre(II) et on l'a affinée jusqu'à une valeur de R de 0.082. Les dimensions de la maille du cristal triclinique rouge foncé sont a = 960.8(4), b = 1090.7(6), c = 895.8(4) pm, α = 106.23°(4), β = 92.36°(7), γ = 99.50°(7); il appartient au groupe d'espace $P\bar{1}$ et compte deux molécules par maille. Se basant sur une formule moléculaire $C_{16}H_{14}CuN_6S_2$ (masse mol. 417.99), les densités mesurées et calculées sont respectivement 1.571 et 1.568 g cm^{-3}. La coordination du cuivre est loin d'être planaire. Les cinq atomes qui ne sont pas des hydrogènes de chacune des molécules de thiosemicarbazide originales se trouvent dans des plans formant un angle dièdre de 8.9°. Le plissement s'éloigne de l'origine et de la molécule voisine. Les longueurs des liaisons avec le cuivre sont: Cu—S(1) = 223.7(3), Cu—S(2) = 223.4(3), Cu—N(13) = 197.1(6), Cu—N(23) = 197.0(7) pm. Les angles de valence au niveau de l'atome du cuivre sont S(1)—Cu—S(2) = 108.62°(9), N(13)—Cu—N(23) = 81.1°(3), N(13)—Cu—S(1) = 85.1°(2) et N(23)—Cu—S(2) = 85.0°(2). Les premier et deuxième noyaux phényles sont respectivement à des angles de 100.3° et 93.0° par rapport au plan moyen de coordination du cuivre qui est lui même à une distance perpendiculaire de 330 pm d'un plan semblable dans la molécule inverse. Il se produit une liaison hydrogène intermoléculaire double de chaque côté du complexe entre les atomes d'azote qui ne sont pas coordonnées; il y a donc une liaison de molécules en rubans parallèles.
[Traduit par le journal]

Introduction

Thiosemicarbazide reacts with a wide variety of aldehydes and ketones to form thiosemicarbazones, which may be used as ligands. Compounds formed in this way are structurally interesting, since both sulfur and nitrogen atoms may be involved in the coordination, thus invoking the *a* or *b* character of the metallic centre. The chemistry of the transition metal complexes of thiosemicarbazide and thiosemicarbazones has been reviewed (1). Certain of the

0008-4042/79/060603-05$01.00/0

copper(II) compounds of this kind have significant antitumour activity, thus 3-ethoxy-2-oxobutyraldehyde bisthiosemicarbazonatocopper(II) (abbreviated CuKTS) is effective against the Walker 256 carcinosarcoma in rats (2, 3). Binding to DNA and RNA has been established for the *N*-methylisatin β-thiosemicarbazone copper complexes (4). Inhibition of the RNA directed DNA polymerase in the virion by thiosemicarbazone copper(II) complexes prevents malignant transformation by the Rous sarcoma virus (5).

While remarkable progress in understanding the antitumour activity of these copper complexes has been made by biological methods, the chemistry remains obscure in detail. The substances administered in animal tests have often been the free ligands, and one of the early postulated mechanisms was that of removal or translocation of essential metal ions involved in biological processes (6). The work of Petering and VanGiessen (7) has shown that in the case of CuKTS it is the complex which is active. It is recognised that the transport of the complex in the body depends on the balance between hydro- and lipophilic properties and on solubility, which are substituent dependent properties. Methylation of the terminal $-NH_2$ group in a thiosemicarbazone will affect the hydrogen bonding. Booth and Sartorelli suggest that CuKTS interferes with the incorporation of thymine into DNA (8). It has also been suggested that CuKTS interacts with cellular thiols, such as those in co-enzyme A and dihydrolipoate (9–11). Petering has suggested that reduction to the cuprous state may be involved (12). The crystal structures of CuKTS and the free ligand H_2KTS have been completed (12). In order to get more insight into the antitumour mechanism of these compounds, we decided to investigate benzil bisthiosemicarbazonatocopper(II) by chemical and crystallographic methods.

Experimental

Thiosemicarbazide was recrystallised from water. Preparation of benzil bisthiosemicarbazone has been described (13). The title compound was prepared by adding 1 mmol of $CuCl_2 \cdot 2H_2O$ in water to 1 mmol of benzil ditsc in 20 mL of dimethylformamide (dmf) slowly with stirring. The reddish brown powder precipitates on addition of water. Washed with dilute HCl, water, hot EtOH, and acetone. Yield 0.31 g. *Anal.* calcd. for $C_{16}H_{14}CuN_6S_2$: C 45.98, H 3.38, N 20.11; found: C 45.95, H 3.33, N 20.36, mp 250°C; uv/visible spectrum: $\lambda_{max} = 313$ nm, $\varepsilon = 2.2 \times 10^4$, shoulder at 360 nm, $\lambda_{max} = 510$ nm, $\varepsilon = 3.8 \times 10^3$, shoulder at 565 nm. Crystals were grown by diffusion of water from gelatin into a dmf solution of the complex. Preliminary photographic work on Weissenberg and precession cameras using CuK_α radiation gave a unit cell $a = 960$, $b = 1200$, $c = 895$ pm, $\alpha = 119°$, $\beta = 88°$, $\lambda = 100°$. Picker 4-circle diffractometer measurements of 16 pairs of reflections centered at $\pm 2\theta$, Delaunay reduction (transformation matrix: $-1,0,0$; $0,-1,-1$; $0,0,1$) and least-squares refinement of the cell gave $a = 960.8(4)$, $b = 1090.7(6)$, $c = 895.8(4)$ pm, $\alpha = 106.23°(4)$, $\beta = 92.36°(7)$, $\gamma = 99.50°(7)$. The cell volume is 0.8852(7) nm^3, density = 1.571 g cm^{-3} (flotation) and 1.568 g cm^{-3} (calcd.) with 2 molecules per cell. The linear absorption coefficient for MoK_α radiation, $\lambda = 71.069$ pm, was 15.19 cm^{-1}. The crystal shape is defined by perpendicular distances of six faces from a central origin: {1,0,0}, 0.0328; {0,1,−1}, 0.123; {0,1,0}, 0.458 mm. The goniometer head axis was parallel to the length of the crystal. Intensity measurements were done on the 4-circle diffractometer controlled by a PDP 11/10 minicomputer, scanning in 50 steps of 0.04° in 2θ, and counting for 1 s per step and for 25 s at each extremity. Three standards −900, 0–50, and 0–55 were measured at intervals of 50 reflections. The measurements (total scanned = 3583) were complete to $2\theta = 50°$. There was no visible or X-ray evidence of crystal decomposition. Analysis of the standards gave a mean instability constant of 0.023 which was used to get $\sigma(I)$. 2307 reflections and 210 standards for which $I/\sigma(I) > 3$ were retained. Lorentz, polarisation, and instrument variation factors were applied. Corrections for absorption used Gaussian quadrature (14) and a $4 \times 6 \times 4$ grid. The transmission range was 0.70 to 0.91. After sorting and merging, 2164 reflections remained in the data file.

Structure Determination

The structure was solved by the use of the Patterson function. The programs used were supplied by Penfold (15) and are based on ORFLS, FORDAP, ORTEP, and ORFFE. The atomic scattering factors were those of Cromer and Waber (16). All atoms were assumed to be uncharged, and the copper atom was treated as an anomalous scatterer (17). The *R* value was 0.46 with Cu only. The lighter atoms were found by difference syntheses. The full-matrix least-squares refinement, minimising $w(|F_o| - |F_c|)^2$, was uneventful. The weights derived from counting statistics were not completely satisfactory, so a weighting scheme was devised: $w = (A + Bx + Cx^2 + Dx^3)^{-1}$ where $x = |F_o|$, $A = 5.2830$, $B = -4.4944 \times 10^{-1}$, $C = 2.9134 \times 10^{-2}$, $D = -1.2204 \times 10^{-4}$. This gave approximate constancy of $\Sigma w \Delta^2$ in sets of reflections grouped according to $|F_o|$ or $\sin\theta/\lambda$. The refinement converged at $R = 0.082$, $R_w = 0.105$ with a maximum (change/error) ratio of 0.21. Most of the hydrogen atoms were located in the final difference map, including those involved in the hydrogen bonding. The maximum peak height was 1.38×10^{-6} electrons pm^{-3} near to the Cu atom. Tables containing the structure factors and the anisotropic temperature parameters are in the Depository of Unpublished Data.[1]

Results

Fractional atomic coordinates are given in Table 1.

Figure 1 shows the molecule with labels, bond lengths, and angles. The right and left halves of the figure are closely similar. The benzene rings are normal. The bonds C(12)—C(22), C(12)—C(13), and C(22)—C(23) are predominantly single (C—C = 154 pm, C=C = 134 pm). The lengths of the bonds running from N(11) to C(12) and from N(21) to C(22) suggest multiple bonding with partial delocalisation (C=N heterocyclic = 135 pm, C—N = 147 pm, N=N = 125 pm, N—N = 146 pm). Alternate bonds C(12)—N(13), N(12)—C(11) are shorter on the left hand side, but on the right of the diagram this alternation is a little less convincing. However,

[1]Copies may be obtained, at a nominal charge, from the Depository of Unpublished Data, CISTI, National Research Council of Canada, Ottawa, Ont., Canada K1A 0S2.

TABLE 1. Fractional atomic coordinates ($\times 10^4$)*

Atom	x	y	z
Cu	1009(1)	1696(1)	589(1)
S(1)	2051(2)	2180(2)	3014(3)
S(2)	2084(3)	251(3)	−1005(3)
N(11)	1357(8)	4003(8)	5335(8)
N(12)	−2(7)	3655(7)	3060(7)
N(13)	−169(7)	2981(6)	1516(7)
N(21)	1478(9)	−462(8)	−4059(9)
N(22)	100(7)	939(7)	−2778(7)
N(23)	−97(7)	1663(7)	−1329(7)
C(11)	1025(9)	3363(8)	3794(9)
C(12)	−1162(8)	3075(8)	552(8)
C(13)	−2248(8)	3899(8)	1001(8)
C(14)	−2098(10)	5131(9)	790(12)
C(15)	−3145(12)	5883(10)	1223(13)
C(16)	−4315(11)	5411(12)	1861(12)
C(17)	−4468(11)	4190(13)	2083(12)
C(18)	−3437(10)	3417(10)	1668(11)
C(21)	1132(9)	262(8)	−2708(9)
C(22)	−1132(8)	2303(7)	−1103(9)
C(23)	−2234(8)	2286(8)	−2304(8)
C(24)	−3533(11)	1451(10)	−2488(12)
C(25)	−4587(11)	1470(12)	−3636(15)
C(26)	−4307(12)	2265(12)	−4602(11)
C(27)	−3054(12)	3094(12)	−4380(12)
C(28)	−1987(10)	3116(10)	−3244(10)

*Estimated standard deviations are given in parentheses.

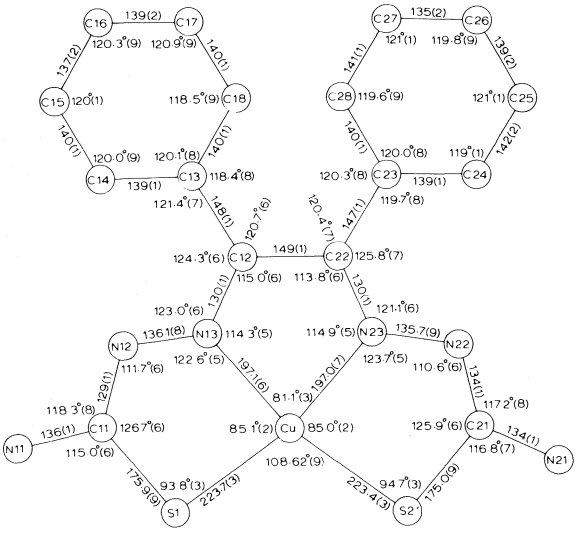

FIG. 1. Bond lengths and angles and the atom labelling scheme.

in the crystal structure of CuKTS (12) the bond lengths alternate in a similar way on both sides. The bonds to the terminal NH_2 groups are short in both compounds.

Table 2 gives comparative measurements for these two substances, emphasizing the copper coordination. There are slight differences where the sulfur atoms are concerned. Mean plane calculations show that both phenyl rings are close to planarity, the

TABLE 2. Comparison of bond lengths (pm) and angles

Bond	Length or angle: Title compound	CuKTS*
C(12)—C(22)	149(1)	145.4(5)
Cu—N	197.1(6), 197.0(7)	198.0(5), 195.9(2)
Cu—S	223.7(3), 223.4(3)	226.3(1), 226.7(1)
N—Cu—N	81.1°(3)	79.9°(1)
N—Cu—S	85.1°(2), 85.0°(2)	83.9°(6), 84.3°(1)
S—Cu—S	108.62°(9)	112.3°(5)

*Reference 12.

copper coordination group Cu, S(1), S(2), N(13), and N(23) is non-planar with deviations from the mean plane being −0.8, 1.3, 1.0, 4.5, and 10.5 pm, respectively. The angles between the first and second phenyl groups and the mean coordination plane were 100.3° and 93.0°, respectively. The mean coordination plane is 165 pm from the origin and hence 330 pm from its parallel and symmetrically related neighbour. All three five-membered rings containing Cu are non-planar. The five non-hydrogen atoms of each original thiosemicarbazide molecule are close to planarity (χ^2 = 29.4 and 12.6). These groups are set at a dihedral angle of 8.9°, with the coordination plane folded away from the origin and the neighbouring molecule, as can be seen in Fig. 2.

Table 3 gives the crystal packing results for the title compound. The copper atom has in addition to its distorted square coordination, an S(2)′ neighbour at a distance of 345.4(3) pm on one side only. Relevant bond angles are: S(1)—Cu—S(2)′ = 98.87°(8), S(2)—Cu—S(2)′ = 101.53°(9), N(13)—Cu—S(2)′ = 77.7°(2), N(23)—Cu—S(2)′ = 81.6°(2). Viewed perpendicular to the mean coordination planes, S(2)′ lies approximately over the centroid of the Cu, N(13), N(23) triangle. In Fig. 2, atom labels can be assigned using this information. In contrast the copper atom in CuKTS has neighbouring sulfur atoms on both sides of the coordination plane at distances of 310.1 and 331.2 pm (12).

Row 2 of Table 3 gives the hydrogen bonds present in the crystal structure. Use of Fig. 2 with mental c translations is recommended. Double hydrogen bonds link the molecules into polymeric ribbons. The hydrogen bonding in crystalline CuKTS involves the oxygen atom of the disordered ethoxy side chain. A sulfur atom also functions weakly as an H acceptor. The strongest hydrogen bond in CuKTS is a single one between a terminal NH_2 group and the central nitrogen of a thiosemicarbazonato moiety. There is therefore some resemblance between the two structures with respect to hydrogen bonding, and the differences can be ascribed to the side chain.

Comparison of the crystal structures of the title compound and CuKTS leads us to suggest that the

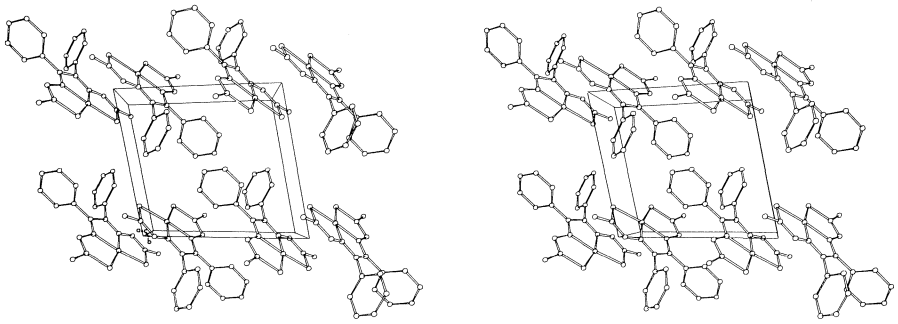

FIG. 2. The crystal structure of benzil bisthiosemicarbazonatocopper(II).

TABLE 3. Selected intermolecular distances (complete to 360 pm)

Bond	Symmetry position*	Distance	Bond	Symmetry position*	Distance
Cu—S(2)	I	345.4(3)	S(2)—N(13)	I	359.3(7)
N(11)—N(12)	II	308(1)	N(21)—N(22)	IV	303(1)
N(11)—C(13)	II	342(1)	N(21)—C(23)	IV	349(1)
N(11)—C(14)	II	335(1)	N(21)—C(27)	IV	344(1)
N(11)—C(15)	II	343(1)	N(21)—C(28)	IV	333(1)
N(11)—C(16)	II	357(1)	C(15)—C(16)	V	342(1)
N(11)—C(18)	II	355(1)	C(16)—C(16)	V	335(2)
N(11)—C(28)	III	359(1)	C(16)—C(26)	V	348(1)
S(1)—N(22)	I	362.3(8)	C(25)—C(25)	VI	339(2)

*Symmetry positions I, $-x,-y,-z$; II, $-x,1-y,1-z$; III, $x,y,1+z$; IV, $-x,-y,-1-z$; V, $-1-x,1-y,-z$; VI, $-1-x,-y,-1-z$.

bonding of sulfur to the axial copper sites is probably not totally dominant over the forces of double H-bonding. Hydrogen bonding may be an important factor in the antitumour mechanism. Adenine, guanine, and cytosine all have amine groups adjacent to unprotonated ring nitrogen atoms, and are thus well equipped to form double H-bonds with the bis(thiosemicarbazone)copper(II) complexes. We have also noticed a structural similarity between CuKTS and the nucleosides formed from guanine and ribose or deoxyribose:

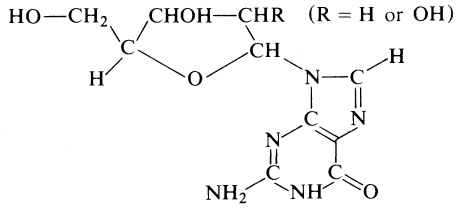

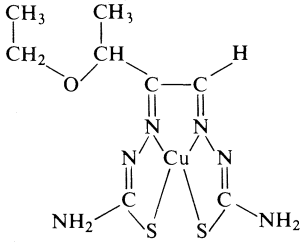

It seems from the literature that the particular effectiveness of CuKTS was discovered from animal testing studies, and that the above structural analogy has not been previously noticed. There are many thiosemicarbazone copper(II) complexes which have some antitumour activity, for which no such structural analogy can be drawn. Nevertheless, the relationship is a curious one, and warrants further investigation by crystallographic methods.

Acknowledgements

We thank the Provincial Government of British Columbia for supporting one of us (A.Y.M.T.) through its summer employment program. The National Research Council of Canada and the University of Victoria provided operating grants. The diagrams were produced with the technical assistance of K. Beveridge and B. Hawkins.

1. M. J. M. CAMPBELL. Coord. Chem. Rev. **15**, 279 (1975).
2. H. PETERING, H. BUSKIRK, and J. CRIM. Cancer Res. **27**, 1115 (1967).
3. J. CRIM and H. PETERING. Cancer Res. **27**, 1278 (1967).
4. P. MIKELENS, B. WOODSON, and W. LEVINSON. Biochem. Pharmacol. **25**, 821 (1976).
5. W. C. KASKA, C. CARRANO, J. MICHALOWSKI, J. JACKSON, and W. LEVINSON. Bioinorg. Chem. **8**, 225 (1978).
6. F. A. FRENCH and B. L. FREEDLANDER. Cancer Res. **18**, 1290 (1958).

7. H. G. PETERING and G. J. VANGIESSEN. The biochemistry of copper. Academic Press, New York. 1966. p. 197.
8. B. A. BOOTH and A. C. SARTORELLI. Mol. Pharmacol. **3**, 290 (1967).
9. G. J. VANGIESSEN, J. A. CRIM, D. H. PETERING, and H. G. PETERING. J. Natl. Cancer Inst. **51**, 139 (1973).
10. D. H. PETERING. Bioinorg. Chem. **1**, 255 (1972).
11. D. H. PETERING. Bioinorg. Chem. **1**, 273 (1972).
12. M. R. TAYLOR, J. P. GLUSKER, E. J. GABE, and J. A. MINKIN. Bioinorg. Chem. **3**, 189 (1974).
13. G. R. GUMMERUS. Soc. Sci. Fenn. Commentat. Phys.-Math. **32**, 43 (1966); Chem. Abstr. **67**, 63894*y* (1966).
14. P. COPPENS, L. LEISEROWITZ, and D. RABINOVICH. Absorption routines for the CDC 1604, Rehovoth, Israel.
15. B. R. PENFOLD. University of Canterbury crystallographic programs. Christchurch, New Zealand.
16. D. T. CROMER and J. T. WABER. Acta Crystallogr. **18**, 104 (1965).
17. D. T. CROMER. Acta Crystallogr. **18**, 17 (1965).

Thermodynamic and physical behaviour of some water + polyethyleneglycol mixtures. II. Dielectric properties

GÉRARD DOUHÉRET[1] AND MAURICE MORÉNAS

Laboratoire de Chimie Générale, Université de Clermont 2, B.P. 45, F-63170 Aubière, France

Received August 16, 1978

GÉRARD DOUHÉRET and MAURICE MORÉNAS. Can. J. Chem. **57**, 608 (1979).

Dielectric constants of water + glycol (mono-, di-, tri-, and tetraethyleneglycol) mixtures have been measured at 298.15 K over the entire composition range. The mixtures involving monoethyleneglycol have also been studied at temperatures from 308.15 to 288.15 K. Calculated deviations from ideality are always positive and show one maximum. Related properties have been computed: polarizability volume and excess polarizability volume, correlation factor of mixtures, and dipole moments of both components using the Mecke–Reuter treatment. Results support conclusions previously deduced from excess and partial molar volumes; they suggest that the addition of glycol molecules gives rise to a slight enhancement of the water-lattice in the water-rich region, followed by a progressive destructuring; the ether functions do not seem to play a prominent role.

GÉRARD DOUHÉRET et MAURICE MORÉNAS. Can. J. Chem. **57**, 608 (1979).

On a mesuré les constantes diélectriques de mélanges eau + glycol (mono-, di-, tri- et tétraéthylèneglycol), à 298.15 K, sur toute l'étendue de composition. Les mélanges eau + monoéthylèneglycol ont été également étudiés dans la gamme de température 288.15–308.15 K. Les écarts à la loi d'idéalité ont été calculés: ils sont toujours positifs et présentent un seul maximum. La polarisabilité et la polarisabilité d'excès, ainsi que le facteur de corrélation ont également été calculés, de même que le moment dipolaire de chacun des composés des mélanges binaires, ceci par le traitement de Mecke–Reuter. Tous ces résultats confirment les conclusions résultant des données précédemment obtenues relatives aux volumes d'excès et aux volumes molaires partiels: ils suggèrent que l'addition de molécules de glycol donne lieu à une augmentation modérée de la structuration du réseau de l'eau dans les régions riches en constituant aqueux, suivie d'une déstructuration progressive; les fonctions éther-oxyde ne paraissent pas jouer un rôle prédominant.

Introduction

In a previous systematic work on the physical and thermodynamic properties of mixtures of water + polyethyleneglycol [CH_2OH—(CH_2—CH_2O—)$_n$-CH_2OH]: n = 0, 1,2-ethanediol; n = 1, 2,2′-oxybis-ethanol; n = 2, 2,2′-[1,2-ethanediylbis(oxy)]bis-ethanol; n = 3, 2,2′-[oxybis-(2,1-ethanediyloxy)]bis-ethanol (more commonly known as mono-, di-, tri-, and tetraethyleneglycol, respectively), the acid–base properties of some of these mixtures were first investigated over the organic component mole fraction range x = 0 to 0.6 (1). Later, excess and partial molal volumes have been calculated over the whole composition range (2). These results suggest that a slight enhancement of the three-dimensional water-lattice may develop in the water-rich region, its magnitude increasing with the size of the hydrocarbon chain.

It seems worthwhile to support the foregoing conclusion by examining departures from ideality of other physical properties. The knowledge of the dielectric constant and of related excess properties appeared to us as an adequate approach to estimate the water–polyethyleneglycol interactions (3, 4). Therefore, the dielectric constants and the refractive indices were determined at 298.15 K for n = 0 to 3; the temperature effect was studied for n = 0 only. The dielectric constant deviations from ideality were computed using Decroocq's formula involving volume fractions (5). Using these results and the corresponding densities (2), the polarizability volumes, the excess polarizability volumes, the correlation factors, and the dipole moments have been calculated, following the Fröhlich theory (6) and the Mecke–Reuter treatment (7).

Experimental

Apparatus and Method

Dielectric constant measurements were carried out, at 1.8 MHz, by the heterodyne beat method with a Wissenschaftliche-Technische Werkstätten DK03 Dekameter.[2] The thermostated (±0.05 K) measuring cells (MFL-2 and MFL-3 type) were adequate to cover the dielectric-constant range (ε = 19 to 82) of water + glycol at relevant temperatures.[3] It

[1]Present address: Laboratoire de Thermodynamique et Cinétique Chimique, B.P. 45, F-63170, Aubière, France.

[2]Wissenchaftlich-Technische Werkstätten, Industriegebiet Trifthof, D-8120, Weilheim/Oberbayern, West Germany.

[3]Complete set of the actual experimental data is available, at a nominal charge, from the Depository of Unpublished Data, CISTI, National Research Council of Canada, Ottawa, Ont., Canada K1A 0S2.

0008-4042/79/060608-06$01.00/0

was checked that a good overlapping was obtained when passing from MFL-3 (ε_r = 20–90) to MFL-2 (ε_r = 7–24) measuring cells, the difference lying always within the experimental accuracy of the equipment. Reproducibility of measurements was approximately equal to ± 0.1 dielectric-constant unit. The cells were previously calibrated at 298.15 K with standard pure liquids: water, nitrobenzene, acetone, and ethylene chloride, in accordance with the manufacturer's specifications and with Natl. Bur. Stand. circular 514 (8). The results obtained for pure solvents are in very good agreement (within 0.1 unit) with the data published by Koizumi and Hanai (9); they are also in satisfactory agreement with results of Levin and Podlovchenko (10) although a systematic difference (~ 0.5 unit) is observed between the two sets of values, the difference being a little greater than the experimental accuracy of the equipment. Åkerlöf (11) published the first set of measurements on water + monoethyleneglycol covering the whole range of concentration. However, his data for the pure components show serious discrepancies with our results as well as with those of Koizumi and Hanai (9) and those of Levin and Podlovchenko (10). Furthermore, the discrepancy becomes larger as the concentration of glycol increases; it is thus likely that some systematic error has occurred in his measurements.

Refractive index measurements were carried out at 288.15, 298.15, and 308.15 K by means of a thermostated Abbé refractometer. Thermoregulation was the same as for dielectric constant measurements. Values were obtained for Na-D light (wave length: 589.3 nm). The reproductibility was as good as 0.0001. Comparison with literature data (12) for pure ethyleneglycol shows very good agreement.

Chemicals

Chemicals were used as follows.

Water was purified by means of a demineralizer. Its conductivity was always less than $1.0 \times 10^{-6}\ \Omega^{-1}\ cm^{-1}$. It was stored under previously purified dry nitrogen.

Ethyleneglycol and its derivatives were prepared from commercial best grade Fluka products. They were first dried over dehydrating agents and then fractionally distilled. The glycols were distilled under reduced pressure and the middle fraction was dried over anhydrous Na_2SO_4 for several days. The material was then redistilled and stored under nitrogen. The final products had a specific conductance less than $5 \times 10^{-7}\ \Omega^{-1}\ cm^{-1}$. The water content was measured, for all samples, by the Karl–Fischer method, and was always found to be less than 0.01%.

Mixtures were made up by weight using Mettler B5 and B6 balances, correcting for the vacuum. Samples of the mixtures have been thoroughly degassed so as to avoid air bubbles, the solubility of nitrogen in the mixtures being lower than that in the pure solvents.

Results

Dielectric Constants

Smoothing values for the dielectric constant on the whole organic component mole fraction range (x_2 = 0 to 1) are given by the following equation:

$$[1] \qquad \varepsilon_r = \sum_{i=0}^{6} a_i x_2^{\,i}$$

whose coefficients, obtained by a least-squares method, are summarized in Table 1.[3]

Deviations from ideality are determined by

$$[2] \qquad \varepsilon_r^{E} = \varepsilon_r - \varepsilon_r^{id}$$

where ε_r^{E} and ε_r^{id} are, respectively, the excess and the ideal dielectric constants. As shown by Fialkov (13), ε_r^{id} must be defined on the volume fraction scale (under certain conditions shown by Decroocq (5)). Thus we can write

$$[3] \qquad \varepsilon_r^{E} = \varepsilon_r - (1 - \phi)\varepsilon_r(1) - \phi\varepsilon_r(2)$$

where $\varepsilon_r(1)$ and $\varepsilon_r(2)$ are the dielectric constants of water and polyethyleneglycol, respectively, ϕ is the volume fraction defined on the partial molar volume basis (14)

$$[4] \qquad \phi = x_2 \overline{V}_2 / \{(1 - x_2)\overline{V}_1 + x_2 \overline{V}_2\}$$

$\overline{V}_2$ and $\overline{V}_1$ being the water and polyethyleneglycol partial molar volumes, respectively.

These excess dielectric constants characterize the water–polyethyleneglycol interactions; among them one can quote the dipole–dipole interactions and the H-bonded complexes. Figure 1 represents the changes of the excess dielectric constant when x_2 is allowed to vary over the entire composition range.

Polarizability Volumes

The static dielectric constant, $\varepsilon_r(\phi)$, of mixtures is used to calculate the polarizability volume $P(\phi)$ from the Kirkwood–Fröhlich equation:

$$[5] \qquad P(\phi) = [\varepsilon_r(\phi) - \{n(\phi)\}^2][2\varepsilon_r(\phi) + \{n(\phi)\}^2]V(\phi)/9\varepsilon_r(\phi)$$

where $V(\phi)$ is the molar volume of the mixture and $n(\phi)$ the refractive index. Some authors consider it sufficiently accurate to make a linear interpolation of $n(\phi)$ between the refractive index of the two pure liquids. However, to obtain higher accuracy we have measured refractive indices of all considered water–glycol systems at the relevant temperatures.[3] Smoothing values for the refractive index are given by

$$[6] \qquad n_D = \sum_{i=0}^{6} a_i' x_2^{\,i}$$

whose coefficients, also obtained by a least-squares method, are summarized in Table 2. Polarizability volume shows how the framework of a molecule (electrons and nuclei) is modified by an external electric field.

The variations of the excess polarizability volume in terms of x_2 are shown in Fig. 2. This excess function is calculated by an equation analogous to [2], where volume fractions have been substituted by mole fractions.

TABLE 1. Coefficients of eq. [1] applicable to the dielectric constant of mixtures: water + [CH_2OH—(CH_2—CH_2O)$_n$—CH_2OH] and standard deviation, σ_r

n	T/K	a_0	a_1	a_2	a_3	a_4	a_5	a_6	σ_r
0	308.15	74.8	−79.0	81.0	−27.5	−50.2	46.1	−8.0	0.1
0	298.15	78.3	−87.4	191.0	−620.7	134.2	−1414	551.3	0.1
0	288.15	82.0	−87.8	189.4	−624.4	1329	−1366	521.4	0.1
1	298.15	78.2	−193.2	625.9	−1627	2584	−2126	689.0	0.2
2	298.15	78.6	−276.5	921.3	−2077	2805	−2017	589.0	0.2
3	298.15	78.1	−395.4	1847	−5379	8709	−7121	2281	0.3

TABLE 2. Coefficients of eq. [6] applicable to the refractive index of mixtures: water + [CH_2OH—(CH_2—CH_2O)$_n$—CH_2OH] and standard deviation, σ_r

n	T/K	a_0'	a_1'	a_2'	a_3'	a_4'	a_5'	a_6'	$\sigma_r \times 10_4$
0	308.15	1.3318	0.3144	−0.5505	0.7778	−1.0802	1.0686	−0.4340	1
0	298.15	1.3329	0.3286	−0.7091	1.4298	−2.2456	2.0123	−0.7185	1
0	288.15	1.3337	0.3389	−0.7479	1.5438	−2.4826	2.2732	−0.8258	1
1	298.15	1.3330	0.6321	−2.1349	4.7921	−6.6022	4.9255	−1.4998	2
2	298.15	1.3327	0.9645	−4.6073	13.2536	−21.2157	17.1836	−5.4567	1
3	298.15	1.3332	1.2325	−6.7706	20.6836	−33.9333	27.8186	−8.9058	11

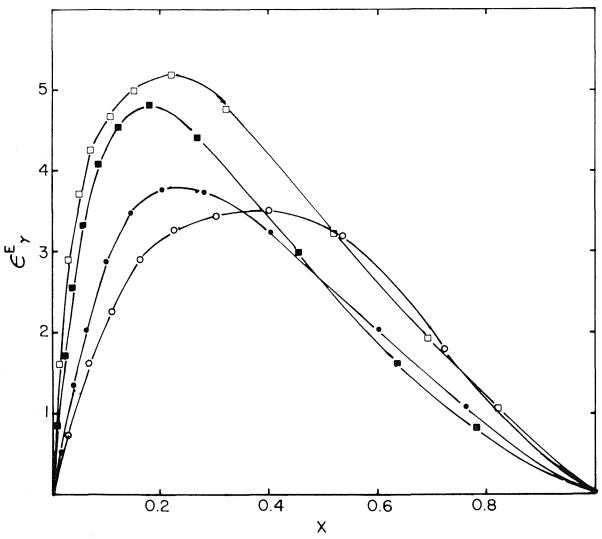

FIG. 1. The excess dielectric constant ε_r^E at 298.15 K, plotted against the mole fraction x_2 for the mixtures $(1 - x_2)$-H_2O + x_2[CH_2OH—(CH_2—CH_2O)$_n$—CH_2OH]. ○, $n = 0$; ●, $n = 1$; □, $n = 2$; ■, $n = 3$.

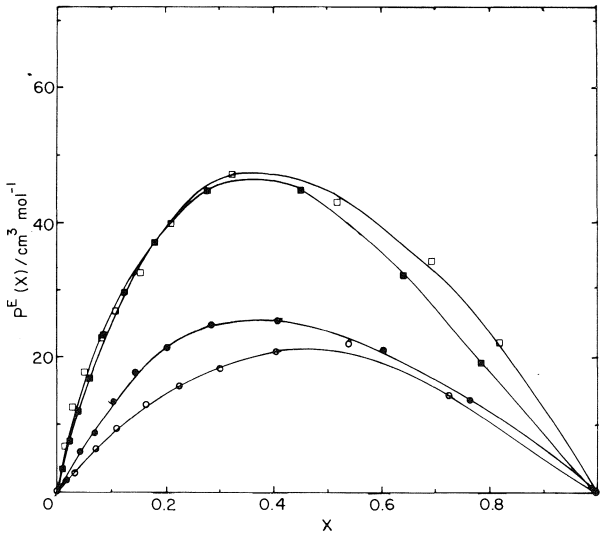

FIG. 2. The excess polarizability volume $P^E(x)$ at 298.15 K, plotted against the mole fraction x_2 for the mixtures $(1 - x_2)H_2O$ + x_2[CH_2OH—(CH_2—CH_2O)$_n$—CH_2OH]. ○, $n = 0$; ●, $n = 1$; □, $n = 2$; ■, $n = 3$.

Correlation Factors

Polarizability volumes lead further to the calculation of the correlation factor g, as pointed out by Kirkwood (15) in a general theory of the dielectric polarization of polar liquids (16). This factor tends to clarify the role of hindered molecular rotation; it shows how the contribution of the individual molecular dipoles to the dielectric constant of a liquid is modified in terms of the correlation in the orientation of the neighbouring molecules. The correlation factor g has been calculated from the Fröhlich theory (6), using the following equation:

$$[7]\quad g=\frac{[\varepsilon_r(\phi)-\{n(\phi)\}^2][2\varepsilon_r(\phi)+\{n(\phi)\}^2]9kTV(\phi)\varepsilon_0}{\varepsilon_r(\phi)[\{n(\phi)\}^2+2]^2 4\pi L[\mu^g(\phi)]^2}$$

where k and L are, respectively, Boltzmann's and Avogadro's constants, ε_0 is the permittivity of vacuum, while μ^g represents the gas-phase dipole moment of the considered solvent. The rule of additivity has been applied to get the gas-phase dipole moment $\mu^g(\phi)$ from the pure components gas-phase dipole moments $\mu^g(1)$ and $\mu^g(2)$.

TABLE 3. Coefficients of eq. [9] applicable up to the correlation factor g, the dipole moments μ_1 and μ_2, and standard deviations σ_r ($D \sim 3.3356 \times 10^{-30}$ C m)

n	T/K	A_0	A_1	A_2	A_3	A_4	$\sigma_r \times 10^3$
			Correlation factor g				
0	308.15	2.785	−0.164	0.470	−1.039	0.372	5
0	298.15	2.805	−0.101	0.417	−1.176	0.609	5
0	288.15	2.829	0.001	−0.075	−0.400	0.229	4
1	298.15	2.794	−0.088	0.171	−0.937	0.556	6
2	298.15	2.821	−0.587	0.297	−1.064	0.596	11
3	298.15	2.792	−1.023	1.546	−3.139	1.755	11
			Dipole moment: μ_1/D				
0	308.15	3.086	0.634	−0.091	0.356	−0.233	2
0	298.15	3.097	0.598	−0.250	−0.122	0.110	2
0	288.15	3.112	0.606	−0.179	0.074	−0.160	1
1	298.15	3.095	0.917	−0.160	−1.145	0.906	3
2	298.15	3.110	1.697	−1.916	1.659	−0.711	8
3	298.15	3.097	1.846	−1.434	−0.603	0.813	1
			Dipole moment: μ_2/D				
0	308.15	4.045	−0.777	1.208	−1.581	0.656	6
0	298.15	4.006	0.050	−1.664	2.165	−0.913	12
0	288.15	4.063	−0.071	−1.553	2.185	−0.959	9
1	298.15	4.472	1.348	−7.886	11.12	−4.991	21
2	298.15	5.611	−7.499	20.65	−25.77	11.13	60
3	298.15	5.348	−1.551	−0.621	2.268	−1.126	10

The $\mu^g(1)$ and $\mu^g(2)$ values relative to water and monoethyleneglycol were taken from the literature (17). For the higher homologs, an empirical equation given by Smyth (18) has been used to supply the lack of experimental data; it relates the dipole moment, μ^s, in the solvent S to that in the gas-phase, μ^g, through the following relationship:

$$[8] \qquad \mu^s = \mu^g\{1 + C[\varepsilon_r(S) - 1]\}$$

where $\varepsilon_r(S)$ is the dielectric constant of the solvent S and C is an empirical constant to which Müller (19) attributed the value 0.038. Smyth (18) has shown that this equation is valid for many substances. It should also be emphasized that gas-phase dipole moments are insensitive to temperature changes over a wide range. Consequently, the gas-phase dipole moments of the glycols were calculated from eq. [8], using the μ^s data determined for the glycols in dioxane solutions (20). Results relative to the different glycols are: $n = 0$, $\mu = 2.28$ D; $n = 1$, $\mu = 2.57$ D; $n = 2$, $\mu = 2.86$ D; $n = 3$, $\mu = 3.11$ D.

In comparison with the value given by ref. 17 for $n = 0$, 2.28 D, a very good agreement is observed.

The correlation factor for all systems continuously but slowly decreases as the mole fraction, x_2, goes from 0 to 1. Coefficients of the equation:

$$[9] \qquad g = \sum_{i=0}^{4} A_i x_2^{\,i}$$

are given in Table 3.

Dipole Moments

Finally, the dipole moments of both components of the mixtures were calculated from dielectric constant, refractive index, and density measurements. The Mecke–Reuter relationship [7], which takes into account the Onsager treatment of the reaction field of a molecule (16) allows the calculation of the dipole moment μ_2 by the following equation:

$$[10] \qquad \mu_2^{\,2} = [(\varepsilon_r, \text{app.})_2 - n_2^{\,2}]\left[2 + \frac{n_2^{\,2}}{\varepsilon_r(\phi)}\right] \times [9kTV_2\varepsilon_0/L]F/[n_2^{\,2} + 2]^2$$

If $(\varepsilon_r, \text{app.})_2$ is an apparent dielectric constant defined as

$$[11] \qquad (\varepsilon_r, \text{app.})_2 = [\varepsilon_r(\phi) - (1 - \phi)(\varepsilon_r)_1]/\phi$$

then, F, a correction factor is given as:

$$[12] \qquad F = 1 + XY$$

where

$$[13] \qquad X = \frac{[(\varepsilon_r, \text{app.})_2 - (\varepsilon_r)_1](1 - \phi_2)}{[2\varepsilon_r(\phi) + n_1^{\,2}][(\varepsilon_r, \text{app.})_2 - n_2^{\,2}]}$$

and

$$[14] \qquad Y = \frac{(n_2^{\,2} - n_1^{\,2})[2\varepsilon_r(\phi) + n_1^{\,4}/(\varepsilon_r)_1]}{2\varepsilon_r(\phi) + (\varepsilon_r)_1} - \frac{[(\varepsilon_r)_1 - n_1^{\,2}]n_1^{\,2}}{(\varepsilon_r)_1}$$

TABLE 4. Ordinates and abscissae (in parentheses) of the extrema in mixed systems H_2O–glycols

	Value for n =					
Parameter	0	0	0	1	2	3
T(K)	308.15	298.15	288.15	298.15	298.15	298.15
V^E	−0.38	−0.35	−0.32	−0.68	−0.81	−1.00
	(0.38)	(0.40)	(0.43)	(0.34)	(0.30)	(0.28)
$\overline{V}_1 - V_1^0$	~0.01	~0.01_5	~0.02	~0.02	~0.02	~0.02
	(0.02)	(0.05)	(0.08)	(0.04)	(0.03)	(0.02_5)
$\overline{V}_2 - V_2^0$	~−1.5	~−1.5	~−1.6	−3.9	−6.1	−8.7
	(0.02)	(0.05)	(0.08)	(0.04)	(0.02_8)	(0.01_2)
ε_r^E	+4.2	+3.5	+3.8_5	+3.8	+5.1	+4.8
	(0.36)	(0.38)	(0.36)	(0.23)	(0.22)	(0.18)
P^E	~+22	~+29	~+22.5	~+26	~+47.5	~+46.5
	(0.51)	(0.53)	(0.49)	(0.38)	(0.37)	(0.36)
μ_1	—	—	—	—	—	—
	(—)	(—)	(—)	(—)	(—)	(—)
μ_2	3.8	3.8	3.9	4.5_5	—	5.2_5
	(0.03)	(0.06)	(0.07)	(0.08)	—	(0.02)
g	2.7_9	2.8_0	2.8_1	2.8_0	2.8_3	—
	(0.03)	(0.05)	(0.08)	(0.04)	(0.03)	(—)

Parallel formulae can be written for the component 1.

Dipole moments are reported in Table 3, together with correlation factors; they too obey an equation of the type [9] whose coefficients A_0 to A_4 and standard deviation, σ_r, are given.

Discussion

Excess dielectric constants are positive for all the systems considered here. The magnitude of the extrema increases from mono- to triethyleneglycol (Fig. 1); at the same time, it is shifted towards water-rich region. No simple temperature dependence is observed for the water + monoethyleneglycol system: we observe a minimum at 298.15 K which is shifted towards the water-rich region when temperature is decreased.

The excess polarizability volumes are always positive too, showing the same trends as ε_r^E when the same variables, x_2 and T, are considered. It means that the strength of interactions between water and glycol is augmented when passing to higher homologs or when temperature is decreased. It appears therefore that the structure of separate components is somewhat distorted, because of the increasing disparity of the shapes of the neighbouring molecules in the different mixtures. This can be related to the phenomenon of hydrophobic hydration which is likely to occur at the same extent the hydrocarbon chains are able to counterbalance the dissociative power of polar groups, the ether oxygen atom developing a comparatively weak interaction with water (21–23).

If we now refer to the excess and partial molal volumes of these systems (2), the same remarks are valid relative to the deviations from ideality; one should nevertheless notice the slightly different concentration at which the extrema of V^E, ε_r^E, and P^E appear. The ordinates and abscissae of all extrema are summarized in Table 4.

If we consider now the variations of correlation factor, g, in terms of x_2, a slow decrease is generally observed over the whole range of concentration except for the water–monoethyleneglycol and water–diethyleneglycol systems, where a quasi-constancy of g occurs in the water-rich region ($x_2 < 0.3$–0.4), indicating that the number of neighbouring dipoles decreases, i.e. that the water molecules are progressively replaced by glycol molecules, whose correlation factor is lower. A flat maximum has also been postulated for water + monoethyleneglycol system by Hasted (24). The decrease of g suggests a progressive destructuring of the tetrahedral water-lattice. However, because of the initial slow decrease, or quasi-constancy, one cannot exclude a slight enhancement of the water-structure in the water-rich region. However, there is no point of comparison between such systems and the rapid decrease of g in water + acetonitrile mixtures (3), for which no enhancement of the aqueous structure was assumed to take place.

A supplementary argument to support this assumption lies in the variations of the dipole moments of glycols in the different systems. Except for the system water–triethyleneglycol, a maximum of μ_2 is observed, which was never the case for the above quoted water + acetonitrile solvents.

The above conclusions support a previous interpretation issued of the volumetric properties of these

binary solvents. Water–glycol systems may be classified in an intermediate position between systems like water + acetonitrile mixtures, where the role of the functional group is prominent compared to that of the hydrocarbon chain, and more structured systems, for example water + monohydric compounds, homologs of glycols; as a matter of fact, the hydrocarbon chain has to counterbalance to a far less extent the influence of polar hydroxy groups, due to the presence of ether functions.

Acknowledgment

We would like to express our best thanks to Dr. N. Morel-Desrosiers for her kind assistance in correcting the English text.

1. G. Douhéret. Bull. Soc. Chim. Fr. 517 (1968).
2. M. Morénas and G. Douhéret. Thermochim. Acta, **25**, 217 (1978).
3. C. Moreau and G. Douhéret. J. Chem. Thermodyn. **8**, 403 (1976).
4. G. Douhéret and H. Dégeilh. Adv. Mol. Rel. Int. Processes, **12**, 107 (1978).
5. D. Decroocq. Bull. Soc. Chim. Fr. 124 (1964).
6. H. Fröhlich. Theory of dielectrics. 2nd ed. Clarendon Press, Oxford. 1958.
7. R. Mecke and A. Reuter. Z. Naturforsch. **4**a, 368 (1949).
8. A. A. Maryott and E. R. Smyth. Table of dielectric constants of pure liquids. Natl. Bur. Stand. circular 514 (1951).
9. N. Koizumi and T. Hanai. J. Phys. Chem. **60**, 1496 (1956).
10. V. V. Levin and T. L. Podlovchenko. Zh. Strukt. Khim. **10**, 749 (1969).
11. G. Åkerlöf. J. Am. Chem. Soc. **54**, 4125 (1932).
12. J. Timmermans. Physico-chemical constants of pure organic compounds. Elsevier, New York. 1950. p. 337.
13. Yu. Ya. Fialkov. Russ. J. Phys. Chem. **41**, 398 (1967).
14. R. Reynaud. C. R. Acad. Sci. Paris, **266**C, 489 (1968).
15. J. G. Kirkwood. J. Chem. Phys. **7**, 911 (1939).
16. L. Onsager. J. Am. Chem. Soc. **58**, 1486 (1936).
17. C. D. Hodgman (*Editor*). Handbook of chemistry and physics. 45th ed. Chemical Rubber Publishing Co., Cleveland. 1964. p. E-37.
18. C. P. Smyth. Dielectric behaviour and structure. McGraw-Hill, New York. 1955. p. 19.
19. F. H. Müller. Phys. Z. **34**, 689 (1933).
20. T. Uchida, Y. Kurita, N. Koizumi, and M. Kubo. J. Polymer Sci. **21**, 313 (1956).
21. H. Nakayama and K. Shinoda. J. Chem. Thermodyn. **3**, 401 (1970).
22. K. Kusano, J. Suurkuusk, and I. Wadsö. J. Chem. Thermodyn. **5**, 757 (1973).
23. S. Harada, T. Nakajima, T. Komatsu, and T. Nakagawa. J. Sol. Chem. **7**, 463 (1978).
24. J. B. Hasted. *In* Water, a comprehensive treatise. *Edited by* F. Franks. Plenum Press, New York. 1973. p. 426.

Nuclear analogs of β-lactam antibiotics. XII. 2-Oxodesthiocephalosporins[1]

ALAIN MARTEL,[2] TERRENCE WILLIAM DOYLE,[3,4] AND BING-YU LUH

Bristol Laboratories of Canada, 100 Industrial Boulevard, Candiac, P.Q., Canada J5R 1J1

Received September 7, 1978

ALAIN MARTEL, TERRENCE WILLIAM DOYLE, and BING-YU LUH. Can. J. Chem. **57**, 614 (1979).

Epoxidation of Δ^2-1-carbacephems **2** followed by base treatment gave the allylic alcohols **4**. Oxidation of **4** gave the 2-keto-Δ^3-carbacephem **9** which could be reduced to the isomeric allylic alcohol **7**. Conversion of these intermediates to a series of biologically active cephalosporin analogs **13***g–l* and **14** is described.

ALAIN MARTEL, TERRENCE WILLIAM DOYLE et BING-YU LUH. Can. J. Chem. **57**, 614 (1979).

L'époxydation des Δ^2-carbacéphèmes-1 (**2**) suivie d'une réaction en milieu basique conduit aux alcools allyliques **4**. L'oxydation de **4** fournit les céto-2 Δ^3-carbacéphèmes **9** que l'on peut réduire en alcools allyliques isomères **7**. On décrit la transformation de ces intermédiaires en une série d'analogues (**13***g–l* et **14**) de céphalosporines biologiquement actifs.

[Traduit par le journal]

Previously, the syntheses of 1-carbacephalosporins carrying carboxylic acid, carboxylic acid ester, and bromo substituents at C(2) were described (1, 2). In view of the observation that increased antibacterial activity was seen in the 2-hetero-atom substituted analogs as the ability of the hetero atom to donate electrons to the chromophore was decreased, we were interested in the synthesis of an analog in which an electron withdrawing group would be placed at C(2).[5] For this purpose the carbonyl function was chosen as our target, e.g., **1** with X = C=O.

As we reported earlier, attempts to displace a 2-bromo function so as to give other 2-substituents, were disappointing (2). Consequently, an alternate approach departing from the Δ^2 ester **2***a* was devised. To provide a variety of ester functions which could be cleaved subsequently under mild conditions the conversion of the acid **2***b* (2) to the esters **2***c–e* was carried out.

Thus treatment of **2***b* with *tert*-butyl acetate in the presence of a catalytic amount of 60% perchloric acid gave **2***c* in 80% yield as well as recovered starting material in 18% yield (3). The conversion of **2***b* to **2***d* and **2***e* was carried out via treatment of the acid with the appropriate chloroformates so as to form the mixed anhydrides followed by thermal carbon dioxide extrusion. The yields of **2***d* and **2***e* were 89 and 62%, respectively.

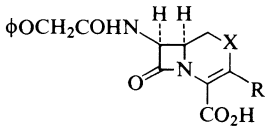

1

X = O, S, SO, SO_2, NCH_3, $NCO_2CH_2CH_3$, $C(CO_2R)_2$, $CH(CO_2R)$, CHBr

FIG. 1. Nuclear analogs of cephalosporins.

We reasoned that formation of the epoxide from compounds **2***a–e* followed by base treatment would yield the allylic alcohols **4** which by suitable manipulation could be converted to the desired target molecules (Scheme 1). Treatment of **2***a*, **2***c*, and **2***e* with *m*-chloroperbenzoic acid gave the desired epoxides **3***a–c* in good yield. In the case of **2***a* and **2***e* the only detectable products were the α-epoxides **3***a* and **3***c*, respectively. The epoxidation of **2***c* gave an excellent yield of the α-epoxide (91%) and an additional amount of material containing the β-epoxide **5** as a minor constituent (35–40% of the mixture). The assignment of the α configuration to the epoxides **3***a–c* is based upon the nmr spectra of these materials. An analysis of the coupling constants for **3***a–c* of the C(6) proton indicates that the most probable conformation for these molecules is that shown for **3***A* in Fig. 2. This, coupled with the fact that the proton at C(2) appears as a triplet (J = 2.3 Hz), establishes the configuration as α.

As expected, treatment of the α-epoxides **3***a–c* with DBN in methylene chloride gave the desired allylic alcohols **4***a–c* in 83, 93.5, and 100% yields, respectively. An examination of the proton nmr of the

[1]For Part X of this series see Ref. 1.

[2]Holder of an NRCC Industrial Postdoctoral Fellowship 1972–1974.

[3]To whom inquiries concerning this paper should be addressed.

[4]Present address: Bristol Laboratories, P.O. Box 657, Syracuse, NY 13201.

[5]For example, the activity in order of decreasing potency for the series previously reported is O > SO_2 > SO > S ≃ NCO_2Et > NMe.

0008-4042/79/060614-12$01.00/0

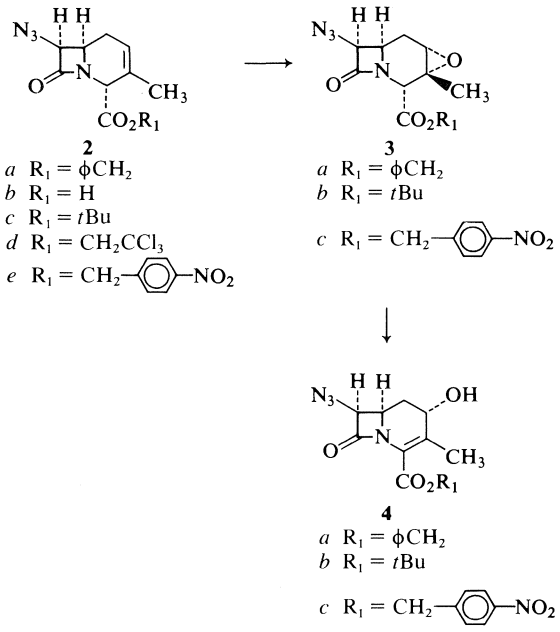

SCHEME 1

alcohols revealed that the C(2) proton appears at ~4.2 δ in **4***a*, **4***b*, and **4***c*. The coupling constants and coupling pattern are consistent with a pseudoaxial configuration for the alcohol as illustrated in Fig. 2. In an attempt to determine whether or not base-catalysed rearrangement of the β-epoxide would lead to the β-alcohol, the mixture of **3***b* and its isomer **5** was treated with DBN as for **3***b* alone. A quantitative yield of **4***b* was obtained based on the amount of **3***b* in the starting mixture. The only other detectable product was the pyridine derivative **6** obtained in 50% yield based on the amount of **5** estimated to have been present in the isomer mixture. No trace of the β-allylic alcohol **7** could be detected (Scheme 2). The

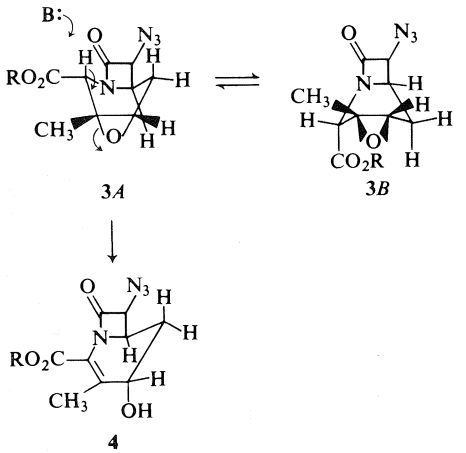

FIG. 2. Base elimination of d-epoxide.

structure of **6** is based on its ir and nmr spectra and its conversion to the carboxylic acid **8** a known compound (4). The formation of **6** rather than **7** on treatment of **5** with DBN may be due to the fact that the departing hydrogen and the epoxide are not transdiaxially oriented in the base catalysed abstraction of the C(4) proton in either of the two possible conformations of **5**. Proton abstraction would give the anion (**i**) which would have to either invert or become trigonal to give **ii** to effect rearrangement. A trigonal intermediate would have severe *gauche* interactions between the C(3)-methyl, C(4)-ester groups, and the β-lactam carbonyl, and the process of inversion would necessarily go through such a sterically hindered transition state. We propose that intermediate **i** instead undergoes a retro-cycloaddition to give **iii** which then rearranges to give **iv**. Dehydration of **iv** would give the observed product **6**. No attempt to trap the azidoketene which would be expected as a by-product in this reaction was made owing to the difficulty in obtaining **5**.

The preparation of the β-allylic alcohol **7** was carried out via oxidation of the α-alcohol to the

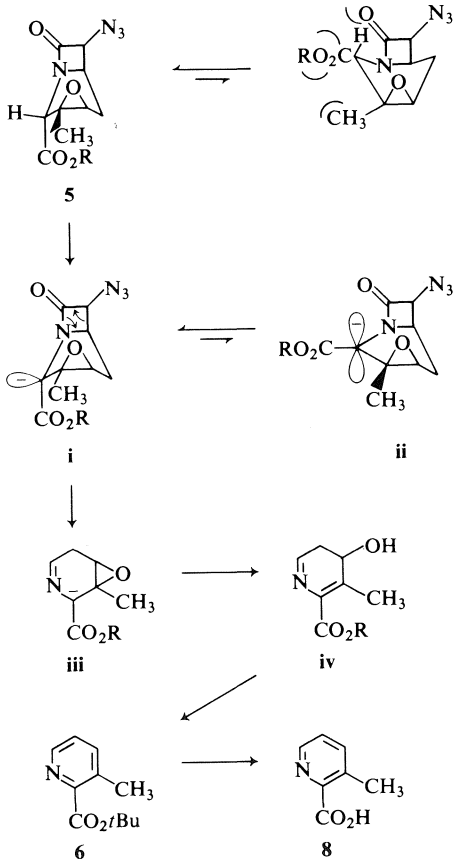

SCHEME 2

ketone followed by reduction. The oxidation of **4***a* to **9***a* was effected by the use of activated manganese dioxide in 41% yield. In view of the low yield of **9***a* obtained, an alternative oxidizing agent for the conversion of **4***b* to **9***b* was sought. Treatment of **4***b* with *N*-chlorosuccinimide – dimethyl sulfide in methylene chloride (5) gave, after work up, the desired ketone **9***b* in 75% yield. As a test of the stability of the 2-ketocarbacephalosporin system to acid, the removal of the *tert*-butyl ester of **9***b* was studied next. Treatment of **9***b* with trifluoroacetic acid gave the acid **9***c* in 98% yield, thus indicating the suitability of the *tert*-butyl ester protecting group in this series. Anticipating that protection of the ketone might well be desirable, the conversion of **9***a* and **9***b* to their respective ketals **10***a* and **10***b* was carried out. Treatment of **9***a* and **9***b* with ethylene glycol and a trace of *p*-toluenesulfonic acid at reflux in benzene, converted them to **10***a* and **10***b*, respectively, in moderate yields. Reduction of **9***b* with sodium borohydride gave the β-allylic alcohol **7** as the sole product of the reaction (97% yield). Conversion of **7** to its acetate **11***a* proceeded readily in 65% yield. The ester **11***a* was deblocked as the conversion of **9***b* to **9***c* to give **11***b* in good yield (Scheme 3). The structures of compounds **7**, **11***a*, and **11***b* were evident from their nmr spectra and are consistent with a β-allylic alcohol in the pseudoequatorial position.

The conversion of the azido esters to the appropriate 7-β-amido acids **13***g–l* was carried out in the usual fashion (1, 2). Reduction of **10***a* and **4***a* with hydrogen sulfide – triethylamine gave the amines **12***a* and **12***b*, respectively. These were coupled with phenoxyacetic acid using *N*-ethoxycarbonyl-2-ethoxy-1,2-dihydroquinoline (EEDQ) to give **13***a* and **13***b*, respectively, in 56 and 77% yields (6). Acetylation of **13***b* gave the acetate **13***c* (91.5%). Oxidation of **13***b* with manganese dioxide yielded **13***d* (63.5%) which was reduced to **13***e* using sodium borohydride (92%). Acetylation of **13***e* gave the acetate **13***f* (83%). With the esters **13***a–f* in hand, these were converted to the carboxylic acids **13***g–l* via hydrogenation using 10% palladium-on-carbon in ethyl acetate (Scheme 4).

As expected, **13***j* exhibited enhanced bioactivity in comparison to the parent 1-carbacephalosporin system whereas the alcohols **13***h* and **13***k* were less active and of approximately equal potency. The acetates exhibited quite different activity, **13***i* being inactive while **13***l* was close in potency to the ketone

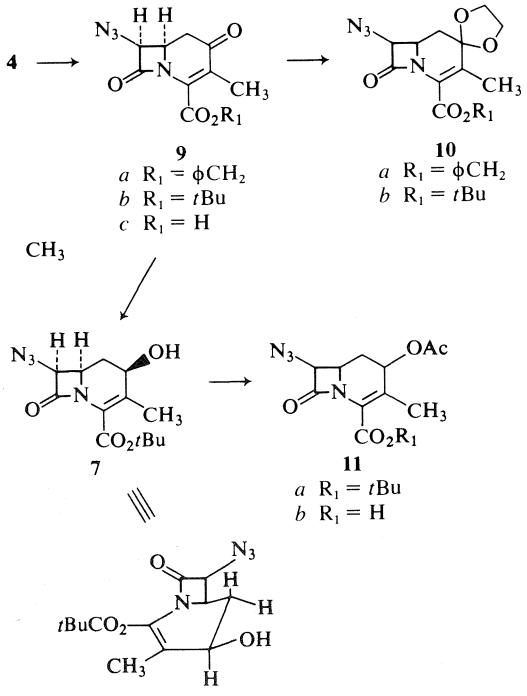

SCHEME 3

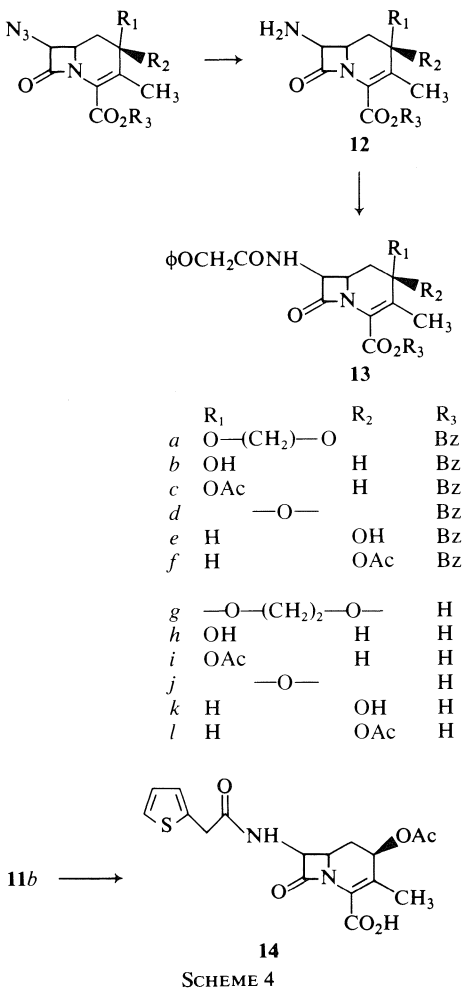

SCHEME 4

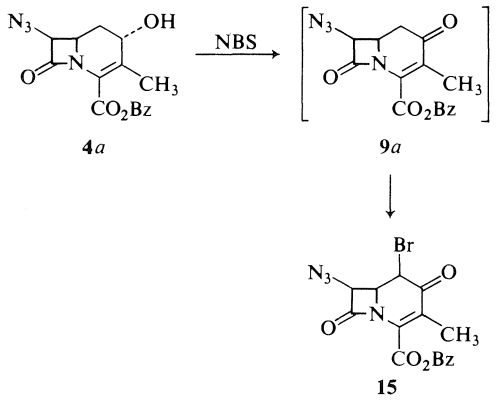

FIG. 3. NBS bromination of **4***a*.

13*j*. We speculate that the lack of activity for **13***i* may have been due to inactivation via solvolysis to a 4-hydroxy-Δ^2-desthiocephem by analogy with our results in the 2-bromo case (2).[6]

In view of the activity of **13***l*, the preparation of an analog having a side chain other than phenoxyacetamido was carried out. Thus **11***b* was treated with trimethylchlorosilane and triethylamine followed by hydrogen sulfide. The solution was evaporated to remove excess hydrogen sulfide and an equivalent of triethylamine added, followed by 2-thienylacetyl chloride. Work up gave the desired amide **14** in 70% yield from **11***b*.

The promising activity of **13***j*, **13***l*, and **14** encouraged us to attempt the preparation of a 3-acetoxymethyl analog of **13***j*. Attempts to brominate the C(3)-methyl function of **4***a* using *N*-bromosuccinimide (NBS) (Fig. 3) led to oxidation of the C(2) alcohol to the ketone followed by bromination at the C(1) position. Use of 1 equiv. of NBS gave a mixture of **4***a* and **15** in approximately equimolar amounts. Evidently oxidation of **4***a* to **9***a* occurs more slowly than the bromination of **9***a* to **15**. To avoid this side reaction, it was decided to protect the allylic alcohol in **4***b*. Treatment of **4***b* with 2,2,2-trichloroethyl chloroformate and 1,5-diazobicyclo[4.3.0]-5-nonene gave the carbonate **16** in 85% yield.

Treatment of **16** with NBS gave the crude bromomethyl compound **17** which was converted to the acetoxymethyl compound **18** by treatment with sodium acetate in dimethylformamide. The overall yield was 59.5% from **16**. The azido function was converted to the amine using hydrogen sulfide – triethylamine and the amine converted to the 2-thienylacetamide **20** in 53% yield from **18**. Cleavage of the 2,2,2-trichloroethyl carbonate with zinc dust in acetic acid proceeded smoothly (94% yield) to give the alcohol **21** (7). Oxidation of **21** with manganese dioxide gave two products. In addition to a low yield of the desired 2-keto compound **22** (25%) there was obtained traces of an overoxidation product **23** in which the methylene α to the thienyl group was oxidized to the ketone.

All attempts to remove the *tert*-butyl ester function of **22** led to decomposition of the material. In view of the publication of a more facile route to the 3-acetoxymethylcarbacephams by the Merck Laboratories, further work in this series was abandoned (8).

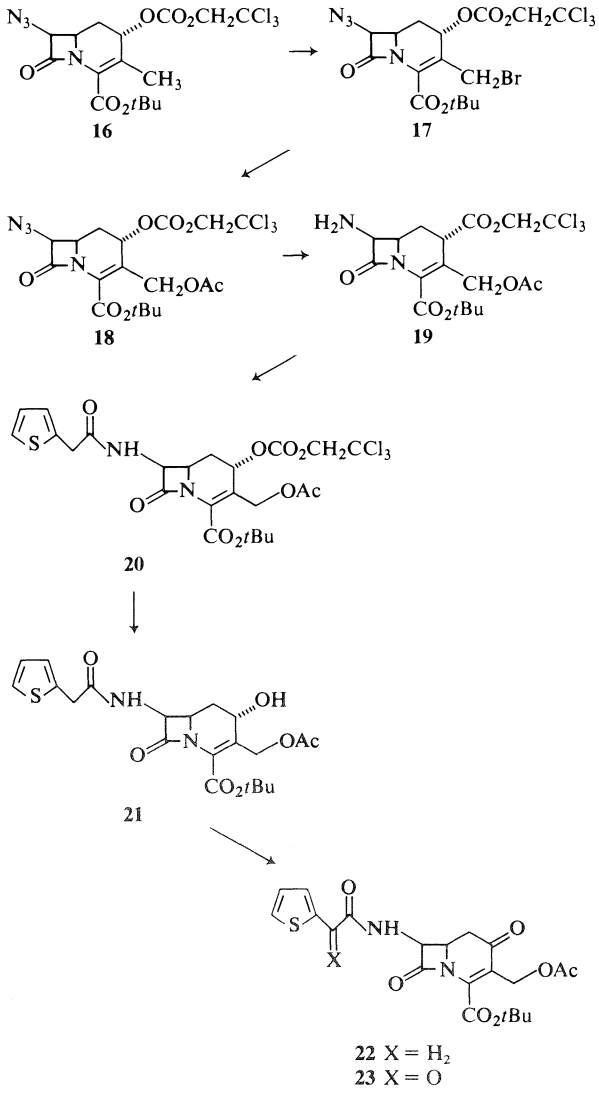

SCHEME 5

[6]The 2-bromo cephem **v** gave **vi** on silica gel chromatography.

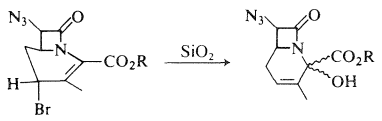

TABLE 1. Nuclear magnetic resonance spectra[a]

Compound	Aromatic and vinyl protons	C(1)-H_2	C(2)-H	C(6)-H	C(7)-H	ARCH_2—	CH_3	Other
2*c*	5.76(m, 1H)	2.41(m)		4.08(dt) $J_1 = 7.0$ $J_2 = 5.0$	4.96(d) $J = 5.0$		1.84(m, 3H) 1.53(s, 9H)	4.58(m, 1H, C(4)-H)
2*d*	5.74(m, 1H)	2.37(m)		4.04(dt) $J_1 = 7.0$ $J_2 = 5.0$	4.87(d) $J = 5.0$		1.82(m, 3H)	4.73(m, 1H, C(4)-H) 4.78(s, 2H, CH_2CCl_3)
2*e*	8.15(d, 2H, $J = 8.5$) 7.44(d, 2H, $J = 8.5$) 5.66(m, 1H)	2.35(m)		3.95(dt) $J_1 = 7.0$ $J_2 = 5.0$	4.80(d) $J = 5$	5.23(s)	1.72(m, 3H)	4.64(m, 1H, C(4)-H)
3*a*	7.37(s, 5H)	2.17(m)	3.18(t) $J = 2.3$	3.83(ddd) $J_1 = 4.50$ $J_2 = 6.50$ $J_3 = 9.5$	4.88(d) $J = 4.50$	5.23(s)	1.54(s, 3H)	4.64(s, 1H, C(4)-H)
3*b*		2.20(m)	3.20(t) $J = 2.3$	3.87(ddd) $J_1 = 4.5$ $J_2 = 6.3$ $J_3 = 9.5$	4.92(d) $J = 4.50$		1.59(s, 3H)	4.51(s, 1H, C(4)-H) 1.53(s, 9H, *t*Bu)
3*c*	8.16(d, 2H, $J = 8.5$) 7.50(d, 2H, $J = 8.5$)	2.20(m)	3.22(t) $J = 2.1$	3.84(ddd) $J_1 = 4.5$ $J_2 = 6.5$ $J_3 = 9.5$	4.9(d) $J = 4.50$	5.32(s)	1.60(s, 3H)	4.71(s, 1H, C(4)-H)
4*a*	7.37(s, 5H)	2.0(m)	4.22(t) $J = 2.5$	3.95(dt) $J_1 = 5.0$ $J_2 = 12.0$	4.94(d) $J = 5.0$	5.27(s)	2.13(s, 3H)	2.48(s, OH)
4*b*		2.0(m)	4.18(dd) $J_1 = 3.5$ $J_2 = 2.0$	3.94(dt) $J_1 = 5.0$ $J_2 = 12.0$	4.93(d) $J = 5.0$		2.08(s, 3H)	1.53(s, 9H, *t*Bu) 2.98(s, OH)
4*c*[b]	8.25(d, 2H, $J = 8.5$) 7.76(d, 2H, $J = 8.5$)	1.6–2.1(m)	4.26(m)	4.10(dt) $J_1 = 4.5$ $J_2 = 12$	5.33(d) $J = 4.5$	5.42(s)	2.12(s, 3H)	2.97(s, 1H, OH)
9*a*	7.38(s, 5H)	2.92(d)[i] 2.64(d)[i] $J = 16$ 2.66(bs)[i]		4.28(ddd) $J_1 = 5.0$ $J_2 = 7.5$ $J_3 = 11.0$	5.01(d) $J = 5.0$	5.31(s)	1.97(s)	
9*b*		2.98(d)[i] 2.62(d)[i] 2.80(d)[i] 2.50(d)[i] $J = 16.0$		4.31(ddd) $J_1 = 5.0$ $J_2 = 7.5$ $J_3 = 12.0$	5.02(d) $J = 5.0$		1.93(s)	1.57(s, 9H, *t*Bu)
9*c*[c]		3.05(d)[i] 2.66(d)[i] 2.85(d)[i] 2.54(d)[i] $J = 16$		4.55(ddd) $J_1 = 5.0$ $J_2 = 7.0$ $J_3 = 12.0$	5.40(d) $J = 5.0$		1.90(s, 3H)	8.45(s, 1H, OH)

TABLE 1 (*Continued*)

Compound	Aromatic and vinyl protons	C(1)-H_2	C(2)-H	C(6)-H	C(7)-H	ARCH_2—	CH_3	Other
10*a*	7.31(s, 5H)	1.90(m)[i,j]		4(m)	4.80(d) $J = 5.0$	5.25(s)	1.90(s, 3H)	4.25(m, 4H, OCH_2CH_2O)
10*b*		1.93(d)[i,j]		4(m)	5.86(d) $J = 5.0$		1.90(s, 3H)	1.30(s, 9H, *t*Bu) 4.08(m, 4H, OCH_2CH_2O)
1*b*		1.80–2.50(m)	5.22(t) $J = 2.5$	3.95(dt) $J_1 = 5.0$ $J_2 = 12.0$	4.99(d) $J = 5.0$		2.04(s, 3H)	1.54(s, 9H, *t*Bu) 1.78(s, 2H, OCH_2CCl_3)
7		1.80–2.63(m)	4.36(dd) $J_1 = 6.0$ $J_2 = 10.0$	3.96(ddd) $J_1 = 5.0$ $J_2 = 3.5$ $J_3 = 12.0$	4.85(d) $J = 5.0$		2.05(s, 3H)	1.54(s, 9H, *t*Bu) 3.60(s, 1H, OH)
11*a*		2.0–2.70(m)	5.58(dd) $J_1 = 6.5$ $J_2 = 10.0$	4.05(ddd) $J_1 = 5.0$ $J_2 = 3.5$ $J_3 = 12$	4.95(d) $J = 5.0$		2.13(s, 3H)	2.55(s, 9H, *t*Bu) 2.93(s, 3H, $OOCH_3$)
11*b*[d]		2.0–2.70(m)	5.70(dd) $J_1 = 7.0$ $J_2 = 9.5$	4.17(ddd) $J_1 = 5.0$ $J_2 = 4.0$ $J_3 = 12.0$	5.10(d) $J = 5.0$		2.08(s, 3H)	2.21(s, 3H, $COCH_3$)
5		2.00–2.20(m)	3.10(m)	3.55–4.05(m)	4.59(d) $J = 5.0$		1.37(s, 3H)	
6	7.13(dd) $J_1 = 4.2$ $J_2 = 8.0$ 7.47(dd) $J_1 = 1.5$ $J_2 = 8.0$ 8.46(dd) $J_1 = 1.5$ $J_2 = 4.2$						2.47(s, 3H)	1.62(s, 3H, *t*Bu)
13*a*	7.31(s, 5H)[f] 6.74–7.55(m)[g]	1.57–2.00(m)		3.83–4.27(m)	5.30(dd) $J_1 = 5.0$ $J_2 = 7.0$	5.22(s)	1.93(s, 3H)	4.00(s, 4H, OCH_2CH_2O) 4.47(s, 3H, ϕCCH_2CO)
13*b*[e]	7.35(s, 5H)[f] 6.75–7.35(m, 5H)[g]	1.60–2.10(m)	4.05(d) $J = 6.0$	4.16–3.70(m)	5.40(m)	5.22(s)	2.00(s, 3H)	4.56(s, 2H, ϕOCH_2CO) 8.80(d, 1H, NH) 5.40(1H, OH)
13*c*	7.30(s, 5H)[f] 6.70–7.40(m, 5H)[g]	1.40–2.10(m)	5.40(m)	4.92(dt) $J_1 = 4.5$ $J_2 = 12.5$	5.40(m)	5.22(s)	2.00(s, 3H)	2.07(s, 3H, —O$\overset{\overset{O}{\|}}{C}CH_3$) 4.97(s, 2H, ϕOCH_2) 7.79(d, 1H, NH) $J = 7.5$

TABLE 1 (*Continued*)

Compound	Aromatic and vinyl protons	C(1)-H_2	C(2)-H	C(6)-H	C(7)-H	ARCH_2—	CH_3	Other
13*d*	7.33(s, 5H)[f]	2.55(d)[i] $J = 9.0$		4.10–4.50(m)	5.35(dd) $J_1 = 5.0$ $J_2 = 7.0$	5.23(s)	1.95(s, 3H)	7.52(d, 1H, NH) $J = 7.0$ 4.50(s, 2H, φOCH_2—)
	6.70–7.40(m, 5H)[g]							
13*e*	7.42(m, 5H)[f]	1.73–2.18(m)	4.45(dd) $J_1 = 6.0$ $J_2 = 9.0$	4.05(dt) $J_1 = 5.0$ $J_2 = 10.0$	5.42(dd) $J_1 = 5.0$ $J_2 = 9.0$	5.25(s)	2.05(s, 3H)	3.0(bs, 1H, OH) 4.62(s, 2H, φOCH_2—) 8.24(d, 1H, NH) $J = 9.0$
	6.80–7.53(m, 5H)[g]							
13*f*	7.36(m, 5H)[f]	1.49–2.40(m)	5.51(m)	4.02(ddd) $J_1 = 5.0$ $J_2 = 4.0$ $J_3 = 12.0$	5.35(dd) $J_1 = 5.0$ $J_2 = 8.0$	5.26(s)	1.95(s, 3H)	2.05(s, 3H, CH_3CO_2) 4.52(s, 2H, φOCH_2—) 8.61(d, 1H, NH) $J = 8.0$
	6.76–7.40(m, 5H)[g]							
13*g*[c]	6.80–7.50(m, 5H)	1.86–2.15(m)		3.80–4.80(m)	5.46(dd) $J_1 = 5.0$ $J_2 = 9.0$		1.86(s, 3H)	4.05(s, 4H, —OCH_2CH_2O—) 4.56(s, 2H, φOCH_2—) 8.20(b, s, 1H, OH)
13*h*[f]	6.80–7.44(m, 5H)	1.56–2.20(m)	4.01(m)	3.68–4.20(m)	5.37(dd) $J_1 = 5.0$ $J_2 = 8.0$		1.98(s, 3H)	4.55(s, 2H, φOCH_2)
13*i*	6.80–7.42(m, 5H)	1.83–2.25(m)	5.44(t) $J = 2.5$	4.96(dt) $J_1 = 5.0$ $J_2 = 8.5$	5.56(dd) $J_1 = 5.0$ $J_2 = 8.5$		1.97(s, 3H)	2.07(s, 3H, CH_3CO_2) 8.30(d, 1H, NH) $J = 8.5$ 9.41(b, s, 1H, OH) 4.60(s, 2H, φOCH_2)
13*j*[c]	6.83–7.46(m, 5H)	2.46(dd) $J_1 = 5.5$ $J_2 = 16.0$ 3.08(dd) $J_1 = 14.0$ $J_2 = 16.0$		4.55(dt) $J_1 \simeq 5$ $J_2 = 14.0$	5.65(dd) $J_1 = 5.0$ $J_2 = 8.5$		1.90(s, 3H)	7.84(b, s, 1H, OH) 8.53(d, 1H, NH) $J = 8.5$ 4.67(s, 2H, φOCH_2)
13*k*[c]	6.85–7.47(m, 5H)	1.76–2.20(m)	4.46(dd) $J_1 = 6.5$ $J_2 = 9.0$	4.09(dt) $J_1 = 5.0$ $J_2 = 10.0$	5.43(dd) $J_1 = 5.0$ $J_2 = 9.5$		2.06(s, 3H)	6.87(b, s, 2H, OH) 8.20(b, s, 1H, NH) 4.62(s, 2H, φOCH_2)
13*l*[c]	6.84–7.50(m, 5H)	1.70–2.20(m)	5.33–5.76(m)	4.15(dt) $J_1 = 5.0$ $J_2 = 11.5$	5.33–5.76(m)		1.90(s, 3H)	2.09(s, 3H, CH_3CO_2—) 8.28(d, 1H, NH) $J = 9.5$ 6.84–7.50(1H, OH) 4.63(s, 2H, φOCH_2)
14[c]	6.99(m, 2H) 7.30(dd, 1H) $J_1 = 2.5$ $J_2 = 4.5$	1.78–2.20(m)	5.60(dd) $J_1 = 6.5$ $J_2 = 10.0$	4.15(ddd) $J_1 = 5.0$ $J_2 = 4.0$ $J_3 = 13.5$	5.35(dd) $J_1 = 5.0$ $J_2 = 8.5$	3.85(s)	1.92(s, 3H)	2.08(s, 3H, CH_3CO_2—) 6.33(b, s, 1H, OH) 7.97(d, 1H, NH) $J = 8.5$
17		1.90–2.80(m)	5.70(dd) $J_1 = 2.5$ $J_2 = 3.5$	3.80–4.17(m)	5.07(d) $J = 5.0$			1.56(s, 9H, *t*Bu) 4.47(d, 1H)[h] 4.08(d, 1H)[h]

TABLE 1 (*Concluded*)

Compound	Aromatic and vinyl protons	C(1)-H_2	C(2)-H	C(6)-H	C(7)-H	ARCH_2—	CH_3	Other
								$J = 10.0$ 4.80(s, 2H, —OCH_2CCl_3)
18		1.78–2.50(m)	5.51(dd) $J_1 = 2.5$ $J_2 = 3.0$	3.95(dt) $J_1 = 5.0$ $J_2 = 13.0$	4.97(d) $J = 5.0$			1.53(s, 9H, *t*Bu) 2.02(s, 3H, CH_3CO_2—) 4.73(s, 2H, —OCH_2CCl_3) 4.70(d, 1H)[h] 4.96(d, 1H)[h] $J = 13$
20	6.80(m, 2H) 7.10(dd, 1H) $J_1 = 2.0$ $J_2 = 4.5$	1.70–2.40(m)	5.45(b, s)	3.96(dt) $J_1 = 5.0$ $J_2 = 13.0$	5.37(dd) $J_1 = 5.0$ $J_2 = 8.0$	4.72(s)		1.52(s, 9H, *t*Bu) 2.00(s, 3H, CH_3CO_2—) 4.70(s, 2H, —OCH_2CCl_3) 5.05(d, 1H)[h] 4.63(d, 1H)[h] $J = 13$ 7.37(d, 1H, NH) $J = 8.0$
21[c]	6.80(m, 2H) 7.15(dd, 1H) $J_1 = 2.5$ $J_2 = 4.0$	1.74–2.10(m)	4.33(bs)	4.00(dt) $J_1 = 5.0$ $J_2 = 12.0$	5.36(dd) $J_1 = 5.0$ $J_2 = 7.5$	3.76(s)		1.49(s, 9H, *t*Bu) 1.98(s, 3H, CH_3CO_2—) 2.78(s, 1H, OH) 4.90(d, 1H)[h] 4.67(d, 1H)[h] $J = 12.5$ 7.70(d, 1H, NH) $J = 7.5$
22	7.82(m, 2H) 7.10(dd) $J_1 = 2.5$ $J_2 = 4.0$	2.53(d)[i] $J = 9.5$		4.32(dt) $J_1 = 5.0$ $J_2 = 9.5$	5.29(dd) $J_1 = 5.0$ $J_2 = 7.0$	3.75(s)		1.51(s, 9H, *t*Bu) 1.95(s, 3H, CH_3CO_2—) 4.93(d, 1H)[h] 4.64(d, 1H)[h] $J = 12.0$ 7.04(d, 1H, NH) $J = 7.0$
23	7.06(t, 1H) $J = 5.0$ 7.74(dd) $J_1 = 1.0$ $J_2 = 5.0$ 7.26(dd) $J_1 = 1.0$ $J_2 = 4.0$	3.90(d)[i] 2.60(d)[i] $J = 16$ 2.62(bs)[i]		4.46(ddd) $J_1 = 5.0$ $J_2 = 2.5$ $J_3 = 8.0$	5.36(dd) $J_1 = 5.0$ $J_2 = 7.0$			1.49(s, 9H, *t*Bu) 1.98(s, 3H, CH_3CO_2—) 4.84(ABq, 2H, —CH_2OAc) $J_{AB} = 12.0$ 8.08(d, 1H, NH) $J = 7.0$

[a]Recorded at 60 MHz in $CDCl_3$ unless otherwise noted. Coupling constants are recorded in Hz.
[b]$(CD_3)_2C{=}O$–DMSO-d_6.
[c]Acetone-d_6.
[d]Trifluoroacetic acid – $CDCl_3$.
[e]DMSO-d_6.
[f]C_6H_5—CH_2.
[g]C_6H_5—O.
[h]Arms of AB quartet.
[i]AB portion of ABX system.
[j]Obscured by C(3)-methyl signal.

TABLE 2. Ultraviolet spectra and elemental analyses

Compound	Ultraviolet[a] λ_{max}	Ultraviolet[a] ε	Analyses (%) Calculated C	Calculated H	Calculated N	Found C	Found H	Found N
2*c*			56.10	6.52	20.13	56.06	6.55	20.12
2*d*			37.36	3.14	15.85	37.23	3.23	15.95
2*e*			53.78	4.23	19.60	53.58	4.18	19.77
3*a*			58.53	4.91	17.06	58.46	5.03	17.00
3*b*			53.05	6.16	19.03	52.98	6.30	19.21
3*c*			51.47	4.05	18.76	51.44	4.03	18.93
4*a*	268	11 700	57.74	4.99	16.83	57.74	4.87	16.91
4*b*	267	9 500	53.05	6.16	19.04	53.02	6.22	19.03
4*c*	268	21 400	51.47	4.05	18.76	51.34	4.05	18.93
9*a*	317	8 600	58.89	4.32	17.17	59.15	4.40	17.12
9*b*	314	10 900	53.42	5.52	19.17	53.60	5.57	19.33
9*c*	312	12 100	45.76	3.41	23.72	45.75	3.46	23.72
10*a*	268.5	11 600	58.37	4.90	15.13	58.44	4.87	15.36
10*b*	268	11 050	53.56	5.99	16.66	52.93	6.00	16.68
15[b]	267	9 000	40.91	4.08	11.92	40.99	4.12	11.77
7	270	8 800	53.05	6.16	19.04	52.76	6.26	19.23
11*a*	270	12 000	53.50	5.96	16.65	53.11	6.03	16.63
11*b*	268	12 000	47.14	4.31	19.99	47.09	4.19	20.00
6			68.37	7.82	7.25	68.27	7.68	7.30
13*a*	268.5	12 250	65.25	5.47	5.85	65.15	5.53	5.87
13*b*	263	12 900	66.04	5.54	6.42	66.07	5.47	6.31
13*c*	268	14 200	65.26	5.48	5.85	65.43	5.60	5.69
13*d*	318	7 600	66.35	5.10	6.45	66.39	5.20	6.50
13*e*[c]	269	11 600	65.37	5.60	6.35	65.27	5.54	6.38
13*f*	269	12 600	65.26	5.48	5.85	65.31	5.62	5.78
13*g*			58.75	5.19	7.21	58.82	5.26	7.26
13*h*	263	11 000	58.95	5.24	8.09	58.72	5.29	8.02
13*i*	265	12 300	58.49	5.22	7.18	58.55	5.31	7.24
13*j*	315	7 200	59.29	4.68	8.14	59.08	4.82	8.08
13*k*[c]	269	8 750	58.20	5.32	7.98	58.56	5.58	7.66
13[d]	268.5	11 000	56.12	5.46	6.89	55.93	5.53	6.87
14[e,f]			53.36	5.32	6.72	53.62	5.29	6.70
18[g]	270	10 400	40.96	4.01	10.61	41.48	4.14	10.34
20[h]	238, 268	8 600, 7 400	46.05	4.34	4.47	46.07	4.36	4.61
21[i]	240, 268	14 200, 13 400	55.98	5.81	6.22	55.93	5.95	6.14
22[j]	232, 315	8 600, 8 600	56.24	5.39	6.24	56.00	5.43	6.21
23[k]	312	18 400	54.53	4.79	6.06	54.45	4.90	6.10

[a]Recorded in absolute ethanol. [b]Analysis for Cl: calcd.: 22.64; found: 22.66. [c]$\frac{1}{4}$ hydrate. [d]Hydrate. [e]$\frac{1}{2}$ hydrate, $\frac{1}{2}$ acetone. [f]Analysis for S: calcd.: 7.69; found: 7.65. [g]Analysis for Cl: calcd.: 20.15; found: 19.74. [h]Analysis for Cl: calcd.: 16.99; found: 17.04. Analysis for S: calcd.: 5.12; found: 5.34. [i]Analysis for S: calcd.: 7.12; found: 6.97. [j]Analysis for S: calcd.: 7.15; found: 7.10. [k]Analysis for S: calcd.: 6.93; found: 6.97.

An extensive discussion of the biological activities of the compounds discussed in this and earlier papers of the series will be forthcoming.

Experimental

The infrared spectra were recorded on a Unicam SP-200G grating ir spectrophotometer. The uv spectra were recorded on a Unicam SP-800 uv spectrophotometer. The nmr spectra were determined on a Varian A60-A spectrometer using tetramethyl silane as an internal standard. Melting points are uncorrected except where noted and were determined on a Gallenkamp melting point apparatus. The analyses were performed by Micro-Tech Laboratories, Skokie, IL.

tert-Butyl 3-Methyl-7-β-azido-Δ²-desthiocephem-4-carboxylate (2c)

To a solution of 2.50 g (11.25 mmol) of **2***b* in 75 mL of *tert*-butyl acetate was added 2 drops of 60% perchloric acid. The solution was let stand 6 days at ambient temperature (20–25°C). The solution was evaporated and the residue partitioned between ether and 10% sodium bicarbonate. The organic phase was washed twice with additional sodium bicarbonate solution, dried over sodium sulfate, and evaporated to yield 2.50 g (80%) of **2***c*, mp 69.5–70°C. The basic extracts were made acidic with 10% hydrochloric acid and extracted with methylene chloride. The extracts were dried over sodium sulfate and evaporated to yield 0.45 g of **2***b* (18%); ir ($CHCl_3$): 2110, 1765, 1730 cm^{-1}.

*2,2,2-Trichloroethyl 3-Methyl-7-β-azido-Δ^2-desthiocephem-4-carboxylate (**2**d)*

To a solution of 1.0 g (4.50 mmol) of **2***b* in 30 mL methylene chloride at −15°C (ice–methanol) was added 1 g (4.73 mmol) of 2,2,2-trichloroethyl chloroformate dropwise over 5 min. To this was added 0.366 mL pyridine in 15 mL methylene chloride over 10 min. The solution was stirred at −15°C for 1 h, then for 1 h at 25°C, and finally it was refluxed 1 h. The solution was poured into ice – 10% hydrochloric acid and the solution extracted with ether. The extracts were washed with 10% hydrochloric acid, water, sodium bicarbonate, and brine. The washed extracts were dried over sodium sulfate and evaporated to yield 1.41 g (89%) of **2***d*, mp 68.5°C (corrected) after recrystallization from petroleum ether (30–60°C).

p-*Nitrobenzyl 3-Methyl-7-β-azido-Δ^2-desthiocephem-4-carboxylate (**2**e)*

Treatment of 1.0 g (4.5 mmol) of **2***b* with 1.0 g (4.65 mmol) *p*-nitrobenzyl chloroformate and 0.366 mL pyridine as in the preparation of **2***d* gave 1.0 g of **2***e* (62%), mp 118–119°C. From the basic extracts there was recovered 0.36 g of **2***b* (36%); ir ($CHCl_3$): 2120, 1765, 1750 cm^{-1}.

*Preparation of **3**a–c*

*Compound **3**a*

To a solution of 2.4 g (7.3 mmol) of **2***a* in 30 mL CH_2Cl_2 was added 1.6 g (9.25 mmol, 85%) of *m*-chloroperbenzoic acid at 0–5°C (ice bath). The solution was left at 4°C for 24 h, after which it was diluted with 20 mL ether, washed with 10% aqueous $Na_2S_2O_3$ (2 × 20 mL), 10% $NaHCO_3$ (2 × 20 mL), and brine (2 × 20 mL). The organic layer was dried over Na_2SO_4 and evaporated to give an oily oxide which crystallized out on trituration with ether. Filtration gave 1.7 g (68%) of crystalline **3***a*, mp 108.5–109.5°C; ir ($CHCl_3$): 2110, 1765, 1753 cm^{-1}.

*Compound **3**b*

Treatment of 5.0 g (18.65 mmol) of **2***c* with 7.3 g of *m*-chloroperbenzoic acid as in the preparation of **3***a* gave an oil which on trituration with ether yielded 5.0 g (91%) of pure α-epoxide **3***b*, mp 121–121.5°C; ir ($CHCl_3$): 2110, 1762, 1740 cm^{-1}.

From the mother liquors an additional 400 mg of oil was obtained, the nmr spectrum of which indicated that the oil consisted of a mixture of the α- and β-epoxides plus a small amount of **2***c*. Chromatography of the oil on silica gel (15% water, w/w) using chloroform as an eluent gave 300 mg of a mixture of α- and β-isomers of the epoxide (5:3 ratio).

*Compound **3**c*

Treatment of 1 g (2.80 mmol) of **2***e* with 0.80 g (4 mmol) of *m*-chloroperbenzoic acid as in the preparation of **3***a* gave 800 mg (77%) of **3***c*, mp 117.5–118°C, recrystallized from chloroform–ether; ir ($CHCl_3$): 2110, 1770, 1750 cm^{-1}.

*Benzyl 2-α-Hydroxy-3-methyl-7-β-azido-Δ^3-desthiocephem-4-carboxylate (**4**a)*

To a cold (0–5°C) solution of 1.7 g (5.2 mmol) epoxide **3***a* in 30 mL CH_2Cl_2 was added dropwise 0.65 g DBN (5.2 mmol) in 10 mL CH_2Cl_2 over a 15-min period. Stirring was continued for 2 h at 0°C. The solution was diluted with 20 mL ether, washed with 10% HCl (1 × 50 mL), brine (3 × 20 mL), dried over Na_2SO_4, and evaporated. The oily residue upon trituration with ether crystallized. Filtration gave 1.4 g (83%) of crystalline **4***a*, mp 152–153°C; ir ($CHCl_3$): 3610, 3420, 2110, 1777, 1725, 1635(w) cm^{-1}.

tert-*Butyl 2-α-Hydroxy-3-methyl-7-β-azido-Δ^3-desthiocephem-4-carboxylate (**4**b)*

Treatment of 294 mg (1 mmol) of **3***b* (pure α-isomer) with 124 mg (1 mmol) DBN as in the above example gave 275 mg (93.5%) of **4***b*, mp 140.5–141°C, crystallized from ether; ir ($CHCl_3$): 3580(s), 3400, 2110, 1780, 1720, 1640(w) cm^{-1}.

p-*Nitrobenzyl 2-α-Hydroxy-3-methyl-7-β-azido-Δ^3-desthiocephem-4-carboxylate (**4**c)*

Treatment of 800 mg (2.14 mmol) of **3***c* with 100 mg (0.8 mmol) DBN as in the above example yielded 800 mg (100%) of **4***c*, mp 163.5–164°C, crystallized from ether; ir ($CHCl_3$): 3590(s), 3420(b), 2110, 1773, 1725, 1605 cm^{-1}.

*Benzyl 2-Keto-3-methyl-7-β-azido-Δ^3-desthiocephem-4-carboxylate (**9**a)*

To a solution of 500 mg (1.5 mmol) allylic alcohol **4***a* in 30 mL CH_2Cl_2 was added 2 g activated manganese dioxide. The mixture was stirred for 2 h at room temperature then checked by tlc. The reaction was brought to completion by further addition of 2 g activated MnO_2 and stirring 3 h more. The MnO_2 was filtered through Celite and the solvent evaporated. The residue crystallized upon trituration with ether. Filtration gave 200 mg (41%) crystalline **9***a*, mp 105.5–106.5°C; ir ($CHCl_3$): 2110, 1785, 1730, 1680, 1605(w) cm^{-1}.

tert-*Butyl 2-Keto-3-methyl-7-β-azido-Δ^3-desthiocephem-4-carboxylate (**9**b)*

To a suspension of 5.20 g (40 mmol) of *N*-chlorosuccinimide in 100 mL dry toluene was added 5 mL of dimethyl sulfide at −25°C. To this was added 1.60 g (5.45 mmol) of **4***b* in one portion and the solution was stirred 3 h at −15°C. To the solution was added 11 mL of triethylamine in 20 mL petroleum ether over 10 min. The cooling bath was removed and the solution stirred 10 min. To the solution was added 100 mL ether and it was washed with 5% hydrochloric acid, water, brine, dried over sodium sulfate, and evaporated to give an oil which crystallized on trituration with ether. Filtration yielded 1.20 g (74%), mp 117–118°C, of **9***b*; ir ($CHCl_3$): 2110, 1782, 1722, 1675, 1600 cm^{-1}.

*2-Keto-3-methyl-7-β-azido-Δ^3-desthiocephem-4-carboxylic Acid (**9**c)*

A solution of 200 mg (0.68 mmol) of **9***b* in 10 mL trifluoroacetic acid was evaporated to dryness at 40°C at reduced pressure. This procedure was repeated four times until the nmr spectrum of the residue indicated complete loss of the *tert*-butyl group. Trituration of the residue with chloroform induced crystallization. Filtration yielded 161 mg (98%) of **9***c*, mp 145–147°C (decomposition); ir (Nujol mull): 2110, 1780, 1725, 1640, 1595 cm^{-1}.

*Preparation of **10**a*

A solution of 300 mg (0.9 mmol) of **9***a* and 500 mg ethylene glycol in 50 mL benzene with ~25 mg *p*-toluenesulfonic acid added as a catalyst was refluxed for 48 h under a Dean–Stark trap. The solution was poured into water and extracted with ether. The combined extracts were washed with water, 5% sodium bicarbonate, and brine. After drying over sodium sulfate the extracts were evaporated. Trituration of the residual oil with ether and filtration gave 230 mg (67.5%) of **10***a*, mp 120–121°C; ir ($CHCl_3$): 2110, 1777, 1730, 1630(w) cm^{-1}.

*Preparation of **10**b*

Treatment of 100 mg (0.34 mmol) of **5***b* with 150 mg ethylene glycol as in the preparation of **6***a* gave 75 mg (65%) of **10***b*, mp 150–150.5°C; ir ($CHCl_3$): 2110, 1775, 1720 cm^{-1}.

*Preparation of **16***

To a solution of 5.56 g (18.9 mmol) of **4***b* in 100 mL methylene chloride at 0°C was added 4.14 g (19.5 mmol) 2,2,2-trichloroethyl chloroformate followed by 4.41 g (35.5 mmol)

DBN in 20 mL methylene chloride over 1 h. The solution was stirred 4 h at 25°C and washed with 10% hydrochloric acid, dried over sodium sulfate, and evaporated to give 7.4 g (84%) of **16** on trituration of the residual oil with ether, mp 145–145.5°C; ir ($CHCl_3$): 2110, 1775, 1765, 1755(s), 1720 cm^{-1}.

tert-*Butyl 2-β-Hydroxy-3-methyl-7-β-azido-Δ³-desthiocephem-4-carboxylate (**7**)*

To a solution of 1.20 g (4.12 mmol) of **9***b* in 40 mL tetrahydrofuran (~1% water added) at −15°C was added 81.5 mg (2.14 mmol) of sodium borohydride. The solution was stirred 30 min at −15°C and poured into 50 mL brine – 5 mL 10% hydrochloric acid. The organic phase was separated and the aqueous layer extracted with ether. The combined extracts were dried over sodium sulfate and evaporated to yield 1.15 g (97%) of **7** as an oil; ir (film): 3420(b), 2110, 1765, 1715, 1630(w) cm^{-1}.

tert-*Butyl 2-β-Acetoxy-3-methyl-7-β-azido-Δ³-desthiocephem-4-carboxylate (**11**a)*

A solution of 1.20 g (4.08 mmol) of **7** in 5 mL acetic anhydride and 7 mL pyridine was stirred 17 h at 25°C. The solution was poured into 50 mL of ice cold 10% hydrochloric acid and extracted four times with 50-mL portions of ether. The extracts were dried over sodium sulfate and evaporated. Trituration of the residual oil with ether gave 900 mg (65%) of **11***a*, mp 112–113.5°C; ir ($CHCl_3$): 2110, 1776, 1725 cm^{-1}.

*2-β-Acetoxy-3-methyl-7-β-azido-Δ³-desthiocephem-4-carboxylic acid (**11**b)*

Treatment of 500 mg (1.49 mmol) of **11***a* with trifluoroacetic acid according to the procedure given for the conversion of **9***b* to **9***c* gave 396 mg (95%) of **11***b*, mp 168–170°C (with decomposition) recrystallized from acetone; ir (Nujol mull): 2120, 2110, 1760, 1750(s), 1730, 1645 cm^{-1}.

*Preparation of **6***

To a solution of 294 mg (1 mmol) of a mixture of epoxides **3***b* and **5** (63% **3***b* and 37% **5**) in 10 mL methylene chloride at 0–5°C (ice bath) was added 124 mg (1 mmol) DBN in 5 mL methylene chloride over 5 min. The solution was stirred 1 h at 0–5°C followed by 1.5 h at 25°C. The solvent was evaporated and the residue was taken up in 25 mL ether. The ethereal layer was washed with 10 mL 5% hydrochloric acid, 5 mL water, and 25 mL brine. The organic phase was dried over magnesium sulfate and evaporated to give 275 mg of an oil. This oil was partitioned between 25 mL ether and 10 mL 10% hydrochloric acid. The acidic extract was made basic with sodium sulfate and extracted with methylene chloride (4 × 10 mL). The extracts were dried over sodium sulfate and evaporated to yield 36 mg of **6** (50.5% based on amount of β-epoxide **5** in starting material) as an oil; ir (neat): 1720, 1570 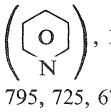 , 1370, 1310, 1260, 1235, 1175, 1140, 1105, 855, 815, 795, 725, 670 cm^{-1}.

The nonbasic ethereal layer was dried over sodium sulfate and evaporated to yield 229 mg of an oil which gave 151 mg of **4***b* on trituration with ether, identical with an authentic sample. From the mother liquors an additional 35 mg of **4***b* was isolated in slightly less pure form. The combined yield was 186 mg (100% based on the amount of α-epoxide in starting mixture).

*Hydrolysis of **6***

Treatment of 41 mg (0.212 mmol) of **6** with trifluoroacetic acid according to the procedure given for the conversion of **9***b* to **9***c* gave **7** as its trifluoroacetate salt. The salt was treated with 5 mL of a saturated methanolic solution of sodium bicarbonate at 25°C, and the solution was evaporated to dryness. The residue was extracted with chloroform to yield 7 mg of **7** which crystallized from chloroform, mp 100–106°C (lit. (4) mp 111°C).

*Preparation of **13**a*

Treatment of 220 mg (0.60 mmol) of **10***a* in 20 mL methylene chloride with hydrogen sulfide – triethylamine followed by coupling of the amine thus obtained with phenoxyacetic acid using EEDQ in the usual fashion (see preparation of **13***b*) gave 160 mg (56%) of **13***a*, mp 140–140.5°C; ir ($CHCl_3$): 3420, 1775, 1730, 1692, 1520, 1495 cm^{-1}.

*Benzyl 2-α-Hydroxy-3-methyl-7-β-(phenoxyacetamido)-Δ³-desthiocephem-4-carboxylate (**13**b)*

A solution of 1.40 g (4.27 mmol) of azide **4***a* in 30 mL CH_2Cl_2 was cooled to 0°C in an ice bath, then 1.8 mL TEA was added after which a stream of H_2S gas was bubbled through the solution for 15 min. The cooling bath was removed and the solution stirred 1 h. The solvent was evaporated and the residue pumped under high vacuum.

The crude amine was redissolved in 30 ml CH_2Cl_2 and cooled to 0°C. Then 1 g (6.66 mmol) phenoxyacetic acid and 1.5 g (6.08 mmol) EEDQ were added. The solution was let stand at 4°C for 17 h, washed with 10% HCl, saturated $NaHCO_3$ solution, brine, and dried over Na_2SO_4. Evaporation gave residue which crystallized out on trituration with CH_2Cl_2. Filtration gave 1.4 g (77%) of crystalline **13***b*, mp 176–176.5°C; ir ($CHCl_3$): 3600, 3420, 1770, 1725, 1690, 1530, 1495 cm^{-1}.

*Benzyl 2-α-Acetoxy-3-methyl-7-β-(phenoxyacetamido)-Δ³-desthiocephem-4-carboxylate (**13**c)*

Treatment of 100 mg (0.236 mmol) of **13***b* with acetic anhydride – pyridine (2 mL – 3 mL) as in the preparation of **11***a* gave 100 mg (91.5%) of pure **13***c*, mp 153.5–154°C, crystallized from ether; ir ($CHCl_3$): 3410, 1772, 1736 (1725 sh), 1690, 1520, 1495 cm^{-1}.

*Benzyl 2-Keto-3-methyl-7-β-(phenoxyacetamido)-Δ³-desthiocephem-4-carboxylate (**13**d)*

Treatment of 600 mg (1.43 mmol) of **13***b* in 80 mL methylene chloride with 5 g activated manganese dioxide for 5 h at 20°C gave 380 mg (63.5%) of **13***d*, mp 174.5–175°C; ir ($CHCl_3$): 3410, 1780, 1730, 1680 (1690s), 1520, 1495 cm^{-1}.

*Benzyl 2-β-Hydroxy-3-methyl-7-β-(phenoxyacetamido)-Δ³-desthiocephem-4-carboxylate (**13**e)*

Reduction of 380 mg (0.91 mmol) of **13***d* in 20 mL tetrahydrofuran (2% water) with 18.5 mg (0.475 mmol) sodium borohydride as in the preparation of **8** gave 350 mg (92%) of **13***e*, mp 152–153°C, on trituration of the reaction residue with ether; ir ($CHCl_3$): 3510, 3430, 3340, 1760, 1705, 1680, 1520, 1470 cm^{-1}.

*Benzyl 2-β-Acetoxy-3-methyl-7-β-(phenoxyacetamido)-Δ³-desthiocephem-4-carboxylate (**13**f)*

From 175 mg (0.415 mmol) of **13***e* was obtained 160 mg (83%) of **13***f*, mp 173–174°C, by the method previously described; ir ($CHCl_3$): 3410, 1775, 1730, 1685, 1520, 1495 cm^{-1}.

*Preparation of **13**g*

Hydrogenation of 130 mg (0.272 mmol) of **13***a* over 160 mg 10% Pd/C in 50 mL ethylacetate at 5 psi for 7 min gave 114 mg crude **13***g*. Recrystallization from methylene chloride gave 86 mg (81%) of pure **13***g*, mp 163–164°C (with decomposition); ir (Nujol mull): 2500–3600, 3340, 1775, 1685, 1670, 1520, 1495 cm^{-1}.

*2-α-Hydroxy-3-methyl-7-β-(phenoxyacetamido)-Δ³-desthiocephem-4-carboxylic Acid (**13**h)*

Reduction of 200 mg (0.472 mmol) of **13***b* as in the above example gave 120 mg (86%) of **13***h*, mp 151.5–152.5°C (with

decomposition), recrystallized from acetone; ir (Nujol mull): 3440, 3310, 2500–3600, 1763, 1730, 1710, 1645, 1545, 1495 cm^{-1}.

*2-α-Acetoxy-3-methyl-7-β-(phenoxyacetamido)-Δ^3-desthiocephem-4-carboxylic Acid (**13**i)*

Reduction of 200 mg (0.430 mmol) of **13***c* as in the previous examples gave 150 mg (90%) of **13***i*, mp 126.5–127.5°C (with decomposition), recrystallized from ether; ir (Nujol mull): 2500–3600, 3310, 1777, 1738, 1692, 1677 cm^{-1}.

*2-Keto-3-methyl-7-β-(phenoxyacetamido)-Δ^3-desthiocephem-4-carboxylic Acid (**13**j)*

Reduction of 150 mg (0.355 mmol) of **13***d* as in the previous example gave 89 mg (69%) of **13***j*, mp 162–162.5°C (with decomposition), recrystallized from acetone–ether; ir (Nujol mull): 2500–3600, 3340, 1760, 1725, 1683, 1655 cm^{-1}.

*2-β-Hydroxy-3-methyl-7-β-(phenoxyacetamido)-Δ^3-desthiocephem-4-carboxylic Acid (**13**k)*

Reduction of 175 mg (0.415 mmol) of **13***e* as in the previous examples gave 100 mg (70%) of **13***k*, mp 125.5–126.5°C (with decomposition), crystallized from ether; ir (Nujol mull): 2500–3600, 3480, 3300, 1765, 1695, 1655 cm^{-1}.

*2-β-Acetoxy-3-methyl-7-β-(phenoxyacetamido)-Δ^3-desthiocephem-4-carboxylic Acid (**13**l)*

Reduction of 140 mg (0.300 mmol) of **13***f* in the usual manner gave 80 mg (68%) of **13***l*, mp 133.5–135.5°C (with decomposition), crystallized from ether; ir (Nujol mull): 3600–2500, 3440(b), 3320, 1750, 1710, 1635 cm^{-1}.

*2-β-Acetoxy-3-methyl-7-β-(2′-thienylacetamido)-Δ^3-desthiocephem-4-carboxylic Acid (**14**)*

To a solution of 371 mg (1.325 mmol) of **11***b* in 10 mL methylene chloride at 0°C was added 0.146 g (1.34 mmol) trimethyl chlorosilane. To this was added 0.136 g (1.35 mmol) triethylamine in 2 mL methylene chloride and the solution was stirred for 10 min. To the stirred solution was added 0.5 mL triethylamine and hydrogen sulfide gas was passed through the solution for 10 min. The mixture was stirred at 0–5°C for 80 min after which the solvent was removed by evaporation. The semisolid residue was taken up in 10 mL methylene chloride to which 0.3 mL triethylamine had been added. The solution was cooled to 0–5°C and a solution of 270 mg (1.68 mmol) 2-thienylacetyl chloride in 4 mL of methylene chloride was added dropwise over 30 min. The solution was stirred 17 h at 25°C. To this was added 20 mL 5% hydrochloric acid and the solution was stirred for 15 min. The organic phase was removed, dried over sodium sulfate, and evaporated to give a residue which crystallized on trituration with ether. Filtration gave 351 mg (70%) of **14**, mp 169–170°C, recrystallized from acetone; ir (Nujol mull): 2500–3600, 3270, 1780, 1728, 1690, 1645, 1530 cm^{-1}.

tert-*Butyl 2-α-(2′,2′,2′-Trichloroethylcarbonate)-3-acetoxymethyl-7-β-azido-Δ^3-desthiocephem-4-carboxylate (**8**)*

A suspension of 1.79 g (3.82 mmol) of **16** and 1.0 g (5.6 mmol) of *N*-bromosuccinimide in 100 mL carbon tetrachloride was refluxed 25 min. The solution was washed with 5% sodium thiosulfate solution, water, and brine. The solution was then dried over sodium sulfate and evaporated to give 2.10 g of crude **17**.

The crude **17** was taken up in 20 mL of dry dimethylformamide at 0°C and 400 mg sodium acetate was added. The solution was stirred 4.5 h at 25°C and poured onto ice water. The aqueous solution was extracted with ether and the extracts were washed with water and brine then dried over sodium sulfate. Evaporation of the solution gave an oil which was chromatographed on 20 g of silica gel (15% water w/w) using benzene then benzene–ether (19:1) as eluent to yield 1.10 g (59.5%) of **18** as an oil; ir ($CHCl_3$): 2110, 1785, 1755, 1733 cm^{-1}.

tert-*Butyl 2-α-(2′,2′,2′-Trichloroethylcarbonate)-3-acetoxymethyl-7-β-(2′′-thienylacetamido)-Δ^3-desthiocephem-4-carboxylate (**20**)*

Reduction of 1.0 g (1.94 mmol) of **18** in methylene chloride using triethylamine – hydrogen sulfide in the usual manner gave the amine **19** which was taken up in 50 mL methylene chloride and cooled to 0°C. To this was added 350 mg (2.46 mmol) thienylacetic acid followed by 570 mg (2.30 mmol) EEDQ. The solution was let stand 18 h at 4°C and worked up as in the preparation of **13***b*. Trituration of the residual oil with benzene gave 650 mg (52.5%) of **20**, mp 131.5–132°C; ir ($CHCl_3$): 3320, 1780, 1755, 1730, 1680, 1510 cm^{-1}.

tert-*Butyl 2-α-Hydroxy-3-acetoxymethyl-7-β-(2′-thienylacetamido)-Δ^3-desthiocephem-4-carboxylate (**21**)*

To a solution of 920 mg (1.44 mmol) of **20** in 20 mL 90% acetic acid was added 7 g activated zinc powder. The suspension was stirred for 3 h, filtered through Celite, and the filtrate was diluted to 200 mL with ether. The solution was washed with water (3 × 50 mL), 10% sodium bicarbonate solution to neutrality, and finally with brine. The solution was dried over sodium sulfate and evaporated to give 620 mg (94%) of **21**, mp 145.5–147°C, crystallized from ether; ir ($CHCl_3$): 3400, 3320, 1780, 1725, 1680, 1515 cm^{-1}.

tert-*Butyl 2-Keto-3-acetoxymethyl-7-β-(2′-thienylacetamido)-Δ^3-desthiocephem-4-carboxylate (**22**)*

To a solution of 650 mg (1.35 mmol) of **20** in 25 mL methylene chloride under nitrogen was added 4 g manganese dioxide. The suspension was stirred for 36 h at 25°C and the MnO_2 removed by filtration and the filtrate was evaporated. The residual oil was chromatographed on 20 g silica gel (10% H_2O, w/w) using benzene as eluent. The solvent was slowly changed to benzene–ether then ether. The first compound which eluted from the column (benzene–ether, 19:1) was **23**. A total of 30 mg was obtained, mp 178–179°C.

Further elution of the column (benzene–ether, 9:1) gave 167 mg (25.5%) of the desired compound **22**, mp 155–156°C; ir ($CHCl_3$): 3400, 1777, 1720, 1685, 1598(w), 1500 cm^{-1}.

Acknowledgements

We wish to thank the National Research Council of Canada for partial financial support of this work through the Industrial Research Assistance Plan and Professor Bernard Belleau of McGill University for helpful discussions during the course of the work.

1. T. W. Doyle, T. T. Conway, G. Lim, and B.-Y. Luh. Can. J. Chem. **57**, 227 (1979).
2. T. W. Doyle, T. T. Conway, M. Casey, and G. Lim. Can. J. Chem. **57**, 222 (1979).
3. E. Taschner, C. Wasielewski, and J. S. Biernat. Justus Liebigs Ann. Chem. **646**, 119 (1961).
4. N. H. Cantwell and E. V. Brown. J. Am. Chem. Soc. **74**, 5967 (1952).
5. E. J. Corey, C. U. Kim, and M. Takeda. Tetrahedron Lett. 4339 (1972).
6. B. Belleau and G. Malek. J. Am. Chem. Soc. **90**, 1651 (1968).
7. R. B. Woodward, K. Heusler, J. Gosteli, P. Nargeli, W. Oppolzer, R. Ramage, S. Ranganathan, and H. Vorbruggen. J. Am. Chem. Soc. **88**, 852 (1966).
8. R. N. Guthikonda, C. D. Cama, and B. G. Christensen. J. Am. Chem. Soc. **96**, 7584 (1974).

Mechanisms of bromination of uracil derivatives. 4.[1] Formation of adducts in acidic aqueous solutions and their dehydration to 5-bromouracils

OSWALD S. TEE[2] AND SUJIT BANERJEE

Department of Chemistry, Concordia University, Montreal, P.Q., Canada H3G 1M8

Received July 31, 1978

OSWALD S. TEE and SUJIT BANERJEE. Can. J. Chem. **57**, 626 (1979).

The reactions of bromine with uracil, 1-methyluracil, 3-methyluracil, and with 1,3-dimethyluracil in 0.125–2.0 *M* aqueous sulfuric acid have been examined. Under these conditions *rapid* attack by bromine upon the uracil leads to the formation of an observable intermediate, a 5-bromo-5,6-dihydro-6-hydroxyuracil, which subsequently undergoes *slow* acid-catalyzed dehydration to the appropriate 5-bromouracil. The intermediates derived from uracil and 3-methyluracil also show acid independent dehydration. The dehydration of the adduct derived from 6-methyluracil proceeds much more rapidly and so precludes observation of that adduct. The dehydrations show significant primary isotope effects for the rupture of C(5)—H bonds of the intermediates. The mechanistic implications of these results are discussed.

OSWALD S. TEE et SUJIT BANERJEE. Can. J. Chem. **57**, 626 (1979).

On a étudié la réaction du brome avec l'uracil et les méthyl-1, méthyl-3 et diméthyl-1,3 uraciles en solution dans de l'acide sulfurique aqueux à 0.125–2.0 *M*. Dans ces conditions, il se produit une attaque *rapide* de l'uracile par le brome qui conduit à la formation d'un intermédiaire qui peut être mis en évidence, le bromo-5 dihydro-5,6 hydroxy-6 uracile, et qui subit une déshydratation acido-catalysée en bromo-5 uracile approprié. Les intermédiaires provenant de l'uracile et du méthyl-3 uracile se déshydratent aussi par un mécanisme n'impliquant pas d'acide. La déshydratation de l'adduit provenant du méthyl-6 uracile se produit beaucoup plus rapidement; on ne peut donc pas le mettre en évidence. Les déshydratations présentent des effets isotopiques primaires importants pour la scission de la liaison C(5)—H de ces intermédiaires. On discute des implications mécanistiques de ces résultats.

[Traduit par le journal]

Introduction

The occurrence of uracil (**1**, $R_1 = R_2 = H$) and thymine (5-methyluracil) in nucleic acids (4), and the biological activity of 5-halouracils (4) has stimulated much work on the chemistry of these pyrimidines (5). However, only recently have there been mechanistic studies of some of their reactions with electrophiles. Johnson *et al.* (6) studied the nitration of some simple uracils in sulfuric acid, and the hydrogen–deuterium exchange of various uracil derivatives in acidic and basic deuterium oxide has been studied by several workers (7, 8; 9 and references therein).

Prior to our bromination studies (1–3) there does not appear to have been any kinetic studies of the halogenation of uracils. Wang (10) proposed that uracil and 1,3-dimethyluracil (**1**, $R_1 = R_2 = H$ and Me) react rapidly with bromine in aqueous solution to yield intermediates (**2**) which subsequently undergo dehydration to the corresponding 5-bromouracil **3** (see eq. [1]). These products also react with aqueous bromine to give isolable 5,5,-dibromo-5,6-dihydro-6-hydroxyuracils **4** (5, 10, 11) which have structures very similar to those of the proposed intermediates **2**.

In strong acid the derivatives **4** revert to 5-bromouracils **3** by the loss of HOBr (10). In a recent paper we discussed the kinetics of this type of reaction for the 6-methyluracil analogue of **4** (2).

[1]

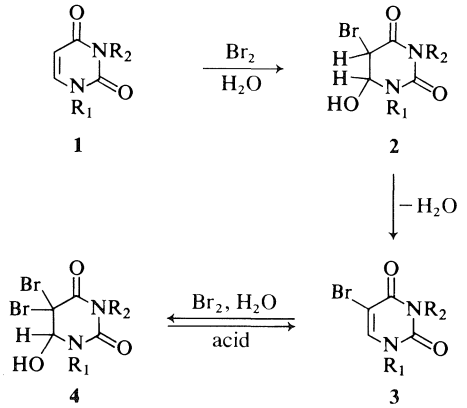

1 **2** **4** **3**

Moore and Anderson (11) made observations which are not totally explicable in terms of the sequence **1** → **2** → **3** → **4**. They carried out potentiometric and spectrophotometric titrations of uracils with bromine in an aqueous acetate buffer of pH 4.7. They found that 1,3-dimethyluracil (**1**, $R_1 = R_2 =$ Me) and uridine (**1**, R_1 = ribosyl, $R_2 = H$) react

[1]For Parts 1–3 see refs. 1–3.

[2]To whom correspondence should be addressed.

0008-4042/79/060626-09$01.00/0

with 1 mol equiv. of bromine to give, it was presumed, intermediates **2**. The conversion of **2** to 5-bromouracils **3** was then achieved by heating or by treatment with acid. In contrast, they found that uracil reacts with 2 mol equiv. of bromine and appears to give, in succession, 5-bromouracil (**3**, $R_1 = R_2 = H$) and its 5,5-dibromo derivative (**4**, $R_1 = R_2 = H$). Thus for two uracils possessing a substituent at N_1 the step **2** → **3** appeared to be quite slow, whereas for uracil the steps **1** → **3** → **4** all seem to occur fairly rapidly.

The literature now contains a fair amount of evidence which is supportive of the postulated intermediates **2**. As already mentioned, the related 5,5-dibromo derivatives **4** are isolable (5, 10, 11). More recently, Nofre and co-workers (12) have carried out ir and ^{1}Hmr spectral studies of a variety of dihydrouracils. Among these were the thymine adduct **5**, the

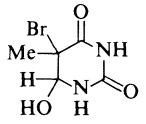

5

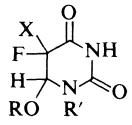

6

5,5-dibromo derivative **4** ($R_1 = R_2 = H$) and, more importantly, the adduct **2** ($R_1 = R_2 = Me$) (12*c*). Unfortunately they do not report (12*c*) how this adduct was made. Addition of various hypohalites to 5-fluorouracils gives adducts **6** (13). Likewise the 6-methoxy adduct **7** was prepared by addition of methyl hypobromite to 1-methyluracil (**1**, $R_1 = Me$, $R_2 = H$) and its ^{1}Hmr spectrum was reported (14).

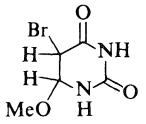

7

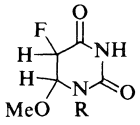

8

Quite recently Robins and co-workers (15) have accomplished synthetically useful fluorinations of uracil derivatives using trifluoromethyl hypofluorite in trichlorofluoromethane and methanol. Their initial products are the adducts **8**, which upon treatment with base undergo elimination of methanol to give good yields of 5-fluorouracils. It was shown (15) that the fluorine and methoxyl group of **8** have a *cis* relationship. On the other hand, in the adduct **6** (X = Br, R = Me, R′ = H), prepared from 5-fluorouracil, the bromine and the methoxyl are *trans* (15). Likewise, it appears that bromine and hydroxyl are *trans* in the thymine adduct **5** and in the 1,3-dimethyluracil adduct **2** ($R_1 = R_2 = Me$) (12).

We have undertaken kinetics studies of the bromination of uracils with a view to defining more precisely the mechanistic features. Previously published work concerned debrominations analogous to **4** → **3** (2) and the bromination of 6-azauracils (3). The main thrust of the present work was to establish the intermediacy of structures **2** and to study their conversion to the substitution products **3**. A preliminary account of this work has appeared (1).

Results and Discussion

We chose as substrates for our study uracil (**1**, $R_1 = R_2 = H$), 1-methyluracil (**1**, $R_1 = Me$, $R_2 = H$), 3-methyluracil (**1**, $R_1 = H$, $R_2 = Me$), and 1,3-dimethyluracil (**1**, $R_1 = R_2 = Me$). Some additional experiments were carried out using 6-methyluracil (**14**).

Titration Studies

We first carried out spectrophotometric titrations similar to those of Moore and Anderson (11) upon the four uracil substrates (**1**, R_1, R_2 = H, Me). In agreement with their observations (11) we found that at *low* acidity (<0.05 *M* sulfuric acid) uracils possessing a substituent on N_1 (**1**, $R_1 = Me$, $R_2 = H$ or Me) undergo a rapid 1:1 reaction with bromine, whereas uracils bearing hydrogen on N_1 (**1**, $R_1 = H$, $R_2 = H$ or Me) react with 2 mol equivs. In addition, however, we found that at *high* acidity (>0.05 *M* sulfuric acid) all four uracils **1** undergo a 1:1 reaction. The uv absorptions due to bromine and the uracil are extinguished rapidly but the appearance of absorptions appropriate to the 5-bromouracils **3** occurs relatively slowly. Thus at high acidity all four uracils **1** react rapidly with bromine to form intermediates which undergo subsequent slow conversion to the corresponding substitution products **3**. The intermediates could have structures **2**, as proposed by Wang (10), and be formed from **1** via **9** as shown in [2]. Confirmation of the intermediacy of **2** was provided by the following nmr studies.

[2] 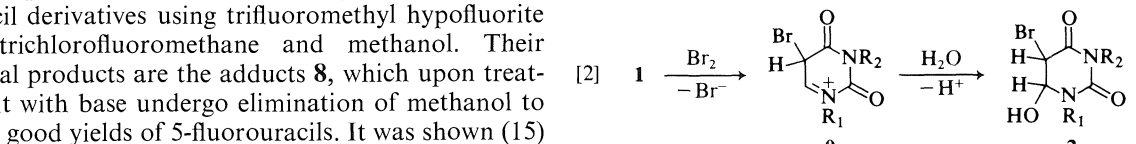

9 **2**

Proton Magnetic Resonance Spectra

The four uracil substrates **1** ($R_1 = H$ or Me, $R_2 = H$ or Me) show very simple spectra (Table 1) (5*b*). Upon addition of bromine to aqueous solutions of the substrates their absorptions are replaced by ones at higher field attributable to the proposed intermediates **2** (see Table 1). The 5- and 6-hydrogens

TABLE 1. Proton magnetic resonance spectral data for uracils **1** and adducts **2**

Structure	Solvent	Shifts (δ) 5-H	6-H	N(1)-Me	N(3)-Me	Other	$J_{5,6}$ (Hz)	Ref.
1 ($R_1 = R_2 = H$)	DMSO-d_6	5.47	7.40	—	—		7.6	This work
1 (R_1 = Me, R_2 = H)	D_2O	5.79	7.61	3.34	—		7.8	This work
1 (R_1 = H, R_2 = Me)	D_2O	5.85	7.50	—	3.26		7.4	This work
1 ($R_1 = R_2$ = Me)	0.1 *N* D_2SO_4/D_2O	5.83	7.59	3.40	3.25		7.5	This work
2 ($R_1 = R_2 = H$)	D_2O^a	4.37	5.10	—	—		2.2	This work
2 (R_1 = Me, R_2 = H)	D_2O^a	4.62	5.37	3.20	—		2.4	This work
2 (R_1 = H, R_2 = Me)	D_2O^a	4.58	5.32	—	3.17		2.4	This work
2 ($R_1 = R_2$ = Me)	D_2O^a	4.50	5.10	3.15	3.13		2.4	This work
	DMSO-d_6	4.55	4.98	3.08	3.03		2.2	12*c*
5 (from thymine)	D_2O^b	—	5.31	—	—	1.95 (C-Me)	—	This work
	DMSO-d_6	—	4.80	—	—	1.80 (C-Me)	—	12*c*
7	Acetone-d_6	4.66	4.92	3.18	—	3.55 (OMe)	2.1	14

[a]This medium was strongly acidic due to DBr formed during the bromination reaction.
[b]Plus 2 drops concentrated DCl/D_2O.

of **2** appear as doublets at δ ~ 4.5 and ~5.1, respectively. The coupling ($J_{5,6}$ ~ 2.3 Hz) between them was confirmed by spin–spin decoupling experiments. In addition, adducts **2** generated from 5-deuteriouracils lacked the signal at δ ~4.5 and the 6-hydrogen simply appeared as a singlet. Signals for *N*-methyl protons appear at δ 3.1–3.2.

These observations are very much what are to be expected for structures **2** when one considers the available literature (12–15) on similar compounds. For comparative purposes Table 1 contains literature data for three compounds: **2** ($R_1 = R_2$ = Me), **5**, and **7**. We also have observed the thymine adduct **5** but were unable to observe an adduct derived from 6-methyluracil which undergoes dehydration quite quickly (*vide infra*).

As mentioned earlier, Nofre and co-workers (12) have concluded that the bromine and hydroxyl are *trans* in the thymine adduct **5** and in the adduct **2** ($R_1 = R_2$ = Me). In view of the similarity of their chemical shifts and particularly of coupling constants ($J_{5,6}$ ~ 2.3 Hz) it appears that all of the adducts **2** have this stereochemical relationship.

In time the ^{1}Hmr signals due to the intermediates **2** decay and are replaced by signals of the 5-bromouracils (**3**). However, at the same time as **2** converts to **3** there are minor spectral changes which suggest that other processes are occurring. The intensity of the 5H doublet of **2** diminishes somewhat faster than that of the 6H doublet, even though the area of 6H resonances maintain a constant ratio to the area of appropriate *N*-methyl signals. These observations suggest that the 5-hydrogen of **2** undergoes slow exchange with the deuterated medium to produce **2** (5-*d*) [3]. Consistent with this interpretation the spectra show the appearance of a singlet in the centre

[3]

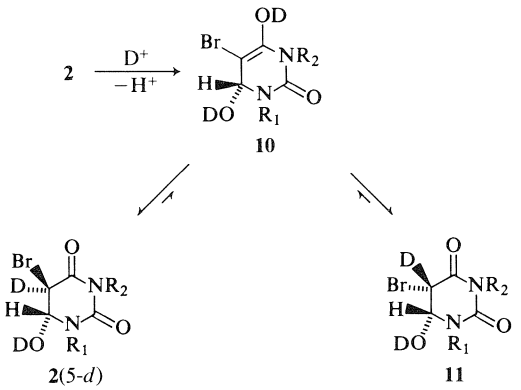

of the 6H doublet. More noticeable, however, is a singlet 3–4 Hz downfield of the 6H doublet which appears, reaches a maximum and then disappears with the appearance of the 5-bromouracil **3**. There is a similar growth and decay of an additional singlet in the *N*-methyl region. These last two observations we attribute to the formation of the diastereomer **11** with bromine and deuteroxyl *cis* to one another, and with deuterium at the 5-position (since no new peaks appear in the region of the 5H).

All of the above observations may be rationalized by enolization leading to concomitant exchange and diastereomerization as shown in [3]. In this acid-catalyzed loss of the 5-hydrogen of **2** (Br and OD *trans*) leads to the enol **10**. Ketonization of **10** can lead to either of the diastereomers **2** (5-*d*) or **11**.

We attempted to follow the kinetics of the ^{1}Hmr spectral changes to support the above rationalization and to find out the importance of the processes [3] relative to the conversion of **2** → **3**. Unfortunately the small differences in peak positions, and the ease with which the 5-bromo products **3** crystallize out of

solution prevented accurate measurements.[3] However, since we observed significant isotope effects for the conversion of **2** → **3** followed by uv spectrophotometry (next section), isotopic exchange of **2** must be slower than **2** → **3**.

As further evidence for the identity of the adducts **2**, addition of potassium iodide to the ^{1}Hmr solutions results in the regeneration of the starting uracil **1** and in the formation of iodine (eqs. [4] and [5]).

[4] $$\mathbf{2} + I^- + H^+ \rightarrow \mathbf{1} + IBr + H_2O$$

[5] $$IBr + I^- \rightarrow I_2 + Br^-$$

There are several precedents for this type of conversion in the literature. Iodide ion converts the 5,5-dibromo derivatives of barbituric acid, uracil, 6-methyluracil, and 4,6-dihydroxypyrimidine to their respective monobromo derivatives (2, 5). Also we have shown that the analogous bromide ion induced debrominations of the dibromo derivatives of 4,6-dihydroxypyrimidine and 6-methyluracil are acid catalyzed (eq. [6] and Scheme 1) (2).

[6] $$\mathbf{19} \underset{H_2O,\,-H^+}{\overset{H^+,\,-H_2O}{\rightleftharpoons}} \mathbf{18} \xrightarrow{Br^-} \mathbf{17} + Br_2$$

In summary, ^{1}Hmr studies fully support the intermediacy of the adducts **2** in the bromination of the uracils **1** in acidic media. There is some evidence of concomitant diastereomerization and isotopic exchange of **2** but in view of the observation of primary isotope effects these processes occur more slowly than the dehydration of **2** to **3**.

Kinetics

The titration studies described earlier established that in strongly acidic media (>0.05 *M* H_2SO_4) all four uracil substrates **1** react rapidly with bromine[4] in a 1:1 reaction but that the 5-bromouracils **3** appear only slowly. On the basis of the ^{1}Hmr studies the intermediates between **1** and **3** have structures **2**.

The slow appearance of the 5-bromouracils (**3**) follows first-order kinetics and the pseudo-first-order rate constants (k_{obs}) are independent of the initial concentrations of uracil **1** and of bromine. Thus the formation of the intermediates **2** is irreversible. The acidity dependence of k_{obs} values for various uracils are presented in Table 2.

For the intermediates **2** derived from 1-methyluracil (**1**, R_1 = Me, R_2 = H) and from 1,3-dimethyluracil (**1**, R_1 = R_3 = Me) the rates of appearance of the corresponding 5-bromouracils increase linearly with the acidity function H_0 (Fig. 1). The least-squares correlation lines are as follows.

For 1-methyluracil

[7] $$\log k_{obs} = -4.60 - 1.13H_0 \; (r = 0.9997)$$

For 1,3-dimethyluracil

[8] $$\log k_{obs} = -4.28 - 1.20H_0 \; (r = 0.9995)$$

Intermediates derived from 5-deuterio-1,3-dimethyluracil undergo dehydration more slowly, and give a primary kinetic isotope effect $k_H/k_D \simeq 3.4$ (see Table 2) for rupture of the C(5)—H bond.

The above results are compatible with the dehydration **2** → **3** having rate-determining deprotonation of the cation **9** (by water) formed in a pre-equilibrium from **2** (eq. [9]). Assuming [**2**] ≫ [**9**]

[9] 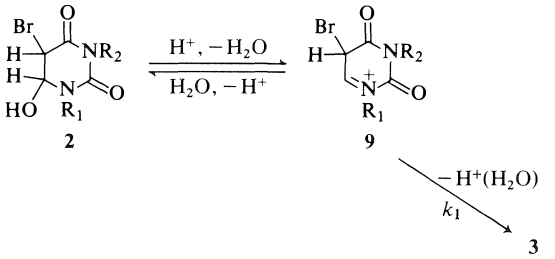

which is justified by the ^{1}Hmr studies, the mechanism shown in [9] requires that

[10] $$k_{obs} = k_1 h_x / K$$

and

[11] $$\log k_{obs} = \log k_1 + pK - H_x$$

where $K = [\mathbf{2}]h_x/[\mathbf{9}]$ and $H_x = -\log h_x$ is the acidity function governing the equilibrium. Clearly the correlation lines (eqs. [7] and [8]) are compatible with [11] in view of the known linear relationships between acidity functions (16).

The acidity dependences of the rates of appearance of 5-bromouracils from the intermediates **2** derived from uracil (**1**, R_1 = R_2 = H) and from 3-methyluracil (**1**, R_1 = H, R_2 = Me) are decidedly non-linear (see Fig. 2). At the highest acidities the slopes against H_0 approach −1, whereas at the lowest acidities they approach zero. Thus it appears that

[3]In general, observation of the adducts **2** in D_2O is not without its difficulties. Some of the uracils **1** are not particularly soluble; the 5-bromouracils **3** even less so. Thus as **2** converts to **3** the latter often crystallize out. Moreover, the acidity of the medium is difficult to control because of the large amount of hydrobromic acid produced in the initial reaction **1** + Br_2 → **2**. If one starts out with an acidic medium the total acidity becomes such as to make the conversion **2** → **3** fairly fast since this conversion is acid catalyzed (*vide infra*). Consequently we chose to start with essentially neutral D_2O which becomes acidic due to the production of DBr.

[4]Using the stopped-flow method we have recently shown that bromine attack upon uracil and upon 1,3-dimethyluracil has $k_2 = 5 \times 10^4$ and 10^5 M^{-1} s^{-1}, respectively. O. S. Tee and C. G. Berks. Unpublished results.

TABLE 2. Acidity dependence of pseudo-first-order rate constants for the appearance of 5-bromouracils (**3** and **17**)[a]

Substrate	$[H_2SO_4]$ (M)	H_0	$k_{obs} \times 10^5$ (s^{-1})
Uracil	0.125	0.76	1.09
(**1**, $R_1 = R_2 = H$)	0.15	0.68	1.13
	0.25	0.43	1.44
	0.375	0.26	1.65
	0.50	0.11	1.92
	0.60	0.01	2.17
	0.80	−0.15	2.90
	1.00	−0.30	3.52
	1.20	−0.43	4.30
	1.50	−0.61	6.27
	1.80	−0.78	8.05
	2.00	−0.89	9.80
5-Deuteriouracil	2.00	−0.89	2.27[b]
1-Methyluracil	0.25	0.43	0.83
(**1**, R_1 = Me, $R_2 = H$)	0.375	0.26	1.35
	0.425	0.19	1.51
	0.50	0.11	1.85
	0.60	0.01	2.38
	1.00	−0.30	5.48
	1.80	−0.78	19.0
	2.00	−0.89	25.7
3-Methyluracil	0.15	0.68	2.28
(**1**, $R_1 = H$, R_2 = Me)	0.25	0.43	2.80
	0.35	0.29	3.43
	0.50	0.11	4.40
	0.60	0.01	4.92
	1.00	−0.30	9.35
	1.80	−0.78	21.8
	2.00	−0.89	29.5
1,3-Dimethyluracil	0.125	0.76	0.675
(**1**, $R_1 = R_2$ = Me)	0.25	0.43	1.51
	0.375	0.26	2.57
	0.425	0.19	3.07
	0.50	0.11	3.63
	0.60	0.01	5.18
	0.80	−0.15	8.47
	1.00	−0.30	11.9
	1.20	−0.43	17.7
	1.50	−0.61	28.2
	2.00	−0.89	61.8
5-Deuterio-1,3-dimethyl uracil	1.00	−0.30	3.53[c]
	2.00	−0.89	17.7[d]
6-Methyluracil (**14**)	0.05	1.14	292
	0.10	0.86	556
	0.20	0.54	1060
	0.25	0.43	1340
	0.375	0.26	2120
	0.50	0.11	2880
5-Deuterio-6-methyl-uracil	0.50	0.11	1190[e]

[a]At 30°C. Each k_{obs} is the average of two or three determinations.
[b]Gives a primary kinetic isotope (k_H/k_D) of 4.32.
[c]Gives k_H/k_D = 3.37.
[d]Gives k_H/k_D = 3.49.
[e]Gives k_H/k_D = 2.42.

k_{obs} is made up of an acid dependent term and an acid independent term (k_0 say). For the appearance of 5-bromouracil we estimate $k_0 = 7.9 \times 10^{-6}\ s^{-1}$ and for the appearance of 5-bromo-3-methyluracil

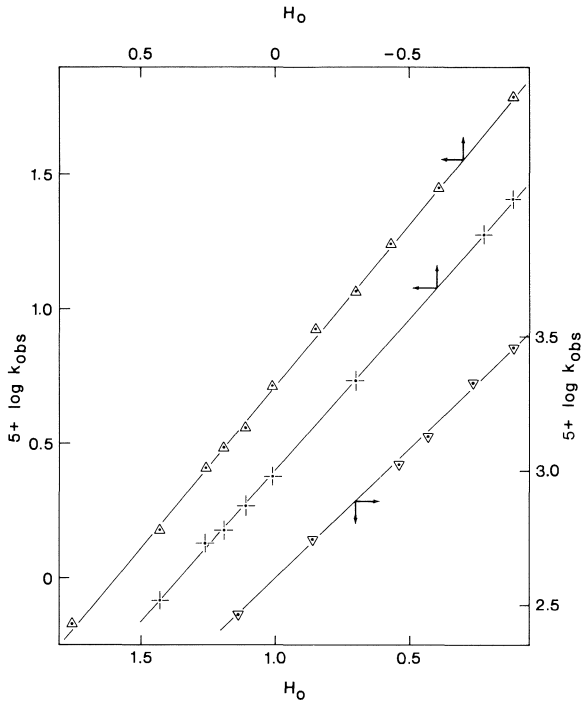

FIG. 1. Acidity dependence of k_{obs} for the formation of 5-bromouracils (**3** and **17**): △ for **3**($R_1 = R_2$ = Me) and + for **3**(R_1 = Me, $R_2 = H$), upper and lefthand scales; ▽ for **17**, lower and righthand scales.

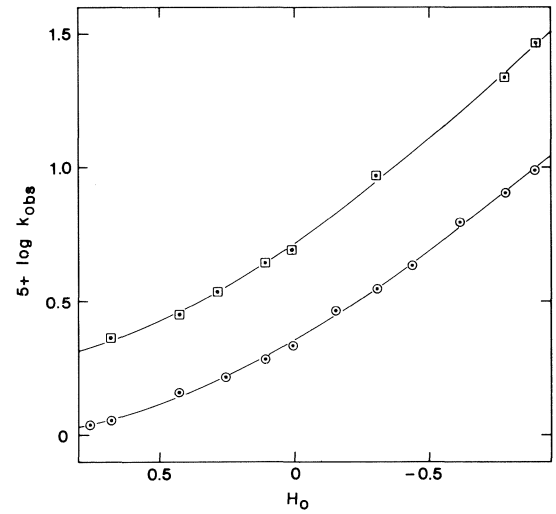

FIG. 2. Acidity dependence of k_{obs} for the formation of 5-bromouracils (**3**): □ for **3**($R_1 = H$, R_2 = Me) and ○ for **3**($R_1 = R_2 = H$).

$k_0 = 1.46 \times 10^{-5}\ s^{-1}$. Using these values the quantity $\log(k_{obs} - k_0)$ varies linearly with acidity as shown in [12] and [13].

For uracil

[12] $\log(k_{obs} - k_0) = -4.83 - 0.90H_0$ ($r = 0.9993$)

For 3-methyluracil

[13] $\log(k_{obs} - k_0) = -4.43 - 0.98H_0$ ($r = 0.9993$)

In 2 *M* sulfuric acid the intermediate derived from 5-deuteriouracil undergoes dehydration more slowly (see Table 2) and leads to $k_H/k_D = 4.32$.

In view of the similarity of the acidity dependences expressed by [12] and [13] to those of [7] and [8], and the observation of a primary isotope effect, it is reasonable to propose that the acid dependent components of the k_{obs} values for the formation of 5-bromouracil (**3**, $R_1 = R_2 = H$) and of 5-bromo-3-methyluracil (**3**, $R_1 = H$, $R_2 = Me$) are also due to the operation of mechanism [9]. The acid independent terms (k_0) may be due to either (or both) of two processes: (*a*) removal of the 5-hydrogen of cation **9** ($R_1 = H$) by hydroxide ion; (*b*) removal of the 5-hydrogen of the free base form of **9** (viz. structure

[14] 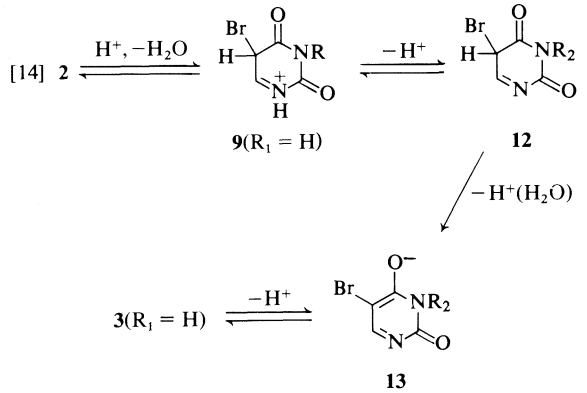

12) by water. The first of these seems unlikely. If process (*a*) operated on cations **9** ($R_1 = H$), one would expect it to operate on cations **9** ($R_1 = Me$) also but the data for **2** → → **3** ($R_1 = Me$) show no evidence of a k_0 term. Furthermore, under our reaction conditions $[OH^-] < 10^{-13}$ *M* and [**9**] < 10^{-4} *M*, and so even if attack by hydroxide on **9** ($R_1 = H$) were diffusion controlled ($\sim 10^{10}\ M^{-1}\ s^{-1}$) the pseudo-first-order rate constant for process (*a*) would be $<10^{-7}\ s^{-1}$, whereas the observed k_0 is about $10^{-5}\ s^{-1}$.

For these reasons we favour process (*b*) in which the unstable tautomer **12** is deprotonated by water to give the anion **13** of the product (see [14]). Since the pK_a of 5-bromouracil (**3**, $R_1 = R_2 = H$) is 8.0 (5*a*, *b*) the anions **13** are reasonably stable and the proposal of **12** → **13** is not unreasonable.

The bromination of 6-methyluracil (**14**) (Scheme 1) in sulfuric acid solutions appears to be considerably more complicated than that of the uracils **1**. The formation of 5-bromo-6-methyluracil (**17**) occurs in three distinct time frames. Immediately after mixing bromine with an equivalent amount of **14** in solution there is a rapid appearance of absorptions appropriate to **17**. This is followed by a slower ($t_{1/2}$ = 24 s in 0.5 *M* H_2SO_4) build-up of **17**. Finally, there is a much slower reaction, the rate of which is acid dependent and dependent upon bromide ion concentration ($t_{1/2}$ = 770 min, at $[Br^-] = 0.0036$ *M*, in 0.5 *M* H_2SO_4) which also yields 5-bromo-6-methyluracil **17**. This last step was dealt with in an earlier paper (2) and was shown to be due to the conversion of the 5,5-dibromo derivative **19** to **17** and bromine, the liberated bromine reacting with unreacted 6-methyluracil to produce more **17**.

The initial absorbance increase observed immediately after mixing bromine with an excess of **14** occurs too quickly to be followed by conventional means. However, the second process leading to the formation of 5-bromo-6-methyluracil **17** is easily monitored. Pseudo-first-order rate constants which were obtained are presented in Table 2 and plotted against H_0 in Fig. 1. They increase linearly with acidity according to [15].

For 6-methyluracil

[15] $\log k_{obs} = -1.44 - 0.96H_0$ ($r = 0.9992$)

This acidity dependence we ascribe to acid-catalyzed dehydration of the intermediate **16** by way of the

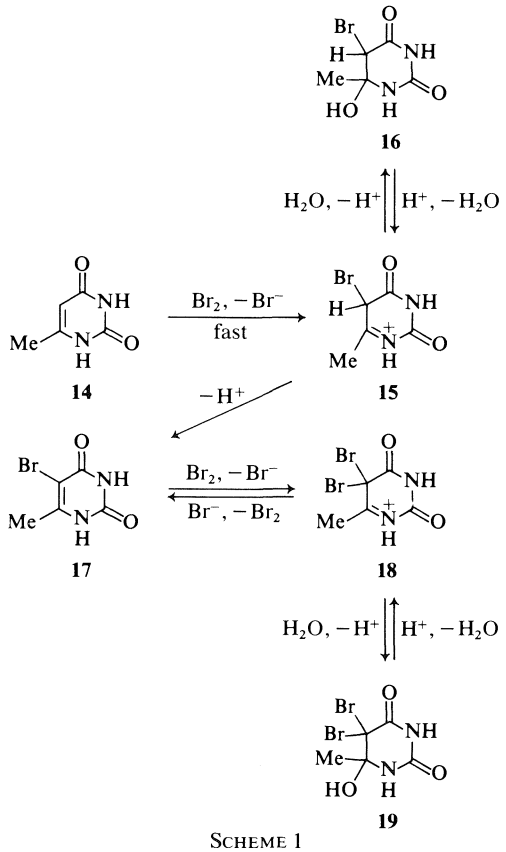

SCHEME 1

cation **15**. Partially or totally rate-determining deprotonation of **15** is supported by the observation of a primary kinetic isotope effect of 2.42 (see Table 2).

The steps **16** $\rightleftarrows$ **15** $\rightarrow$ **17** are in essence the same as those in mechanism [9] which was postulated earlier. However, the intermediate **16** derived from 6-methyluracil undergoes dehydration about 2500 times as fast as the intermediate (**2**, $R_1 = R_2 = H$) derived from uracil (**1**, $R_1 = R_2 = H$). This is perfectly reasonable in terms of the proposed mechanisms in that the formation of cation **15** from intermediate **16** should be more facile than the formation of **9** from **2** due to the electronic and steric effects of the 6-methyl group.

We presume that the adduct **16** arises by way of capture of water by the cation **15** formed initially by attack of bromine upon 6-methyluracil **14** (Scheme 1). This sequence is analogous to that proposed for the formation of the adducts **2** (eq. [2]). Moreover, the intermediacy of cation **15** can explain the rapid initial formation of 5-bromo-6-methyluracil (**17**) as well as the slower reaction we have measured and have ascribed to the dehydration of the adduct **16**.

The cation **15**, formed rapidly from bromine and 6-methyluracil **14**, may be partitioned between **16** and **17**. That is, it may be captured by water (k_{16}) to give the adduct **16** or it may be deprotonated by water (k_{17}) to give **17** (eq. [16]).[5] Clearly the kinetic

[16] $$\mathbf{14} + Br_2 \rightarrow \mathbf{15} \begin{matrix} \xrightarrow{k_{16}} \mathbf{16} \\ \xrightarrow{k_{17}} \mathbf{17} \end{matrix}$$

behaviour which is observed will depend upon the relative magnitudes of the first-order rate constants k_{16} and k_{17}. If they are of comparable magnitude there should be an initial relatively fast increase in absorbance due to **17** arising directly from **15** followed by a slower increase due to the slow acid-catalyzed dehydration of **16**. This is the sort of behaviour that we have observed.

The ratio k_{17}/k_{16} may be estimated from the ratio [**17**]/[**16**] before significant dehydration of **16**. At this stage the absorbance at the analytical wavelength[6] is due to **17**[5] and so [**17**] = $A_0/\varepsilon l$. The concentration of **16** may be estimated from the amount of **17** formed subsequently during the slow conversion of **16** to **17** and so [**16**] = $(A_\infty - A_0)\varepsilon l$. Accordingly the partition ratio may be obtained from

[17] $$k_{17}/k_{16} = [\mathbf{17}]/[\mathbf{16}] = A_0/(A_\infty - A_0)$$

Insertion of appropriate numerical values into [17] yields $k_{17}^{H}/k_{16} = 0.938$ (average of two values in 0.5 *M* H_2SO_4) for the 5-protio cation **15**.

For the cation **15** derived from 5-deuterio-6-methyluracil the rate constant k_{16} should be essentially unaffected, whereas k_{17} should be reduced due to a primary isotope effect. In agreement with this we find that $k_{17}^{D}/k_{16} = 0.219$ (averages of two values in 0.5 *M* H_2SO_4). From this ratio and that in the previous paragraph the isotope effect on k_{17} appears to be $k_{17}^{H}/k_{17}^{D} = 0.938/0.219 = 4.28$.

This value is similar to the kinetic isotope effect of 4.32 found for the dehydration of the adduct **2** ($R_1 = R_2 = H$) derived from uracil (Table 2) but higher than the value of 2.42 obtained directly from rate constants of the appearance of **17** (Table 2). This apparent discrepancy is removed when one takes account of the relative values of k_{16} and k_{17} (eq. [16]). Since these rate constants are of similar magnitude, the k_{17} step (**15** $\rightarrow$ **17**) is only partially rate determining in the overall dehydration of the adduct **16**, and consequently its isotope effect is attenuated.

Consider the proposed mechanism for the dehydration of **16** (eq. [18]).

[18] $$\mathbf{16} + H^+ \underset{k_{16}}{\overset{k_{15}}{\rightleftarrows}} \mathbf{15} \xrightarrow{k_{17}} \mathbf{17}$$

For a steady-state concentration of the reactive cation **15** this mechanism requires

$$k_{obs}^{H} = k_{15}k_{17}^{H}[H^+]/(k_{16} + k_{17}^{H})$$

for the 5-protio system and

$$k_{obs}^{D} = k_{15}k_{17}^{D}[H^+]/(k_{16} + k_{17}^{D})$$

for the 5-deuterio system. Division of these two equations leads to

[19] $$\frac{k_{obs}^{H}}{k_{obs}^{D}} = \frac{k_{17}^{H}}{k_{17}^{D}} \frac{(1 + k_{17}^{D}/k_{16})}{(1 + k_{17}^{H}/k_{16})}$$

Insertion of appropriate values from above into [19] gives

$$k_{obs}^{H}/k_{obs}^{D} = 4.28\,(1.219)/(1.938) = 2.69$$

which is in reasonable agreement with the value of 2.42 obtained directly from the measurement of rate constants.

Overall the observed spectral changes, rate con-

[5]Under the conditions of our kinetic experiments the formation of the 5,5-dibromo derivative **19** should be negligible since we used [**14**] > [Br_2] and **14** reacts more rapidly with bromine than **17** (2).

[6]The appearance of **17** was monitored at a wavelength where only it absorbs significantly and so ε is the extinction coefficient of **17** at the analytical wavelength. A_0 was estimated by least-squares analysis of ln $(A_\infty - A)$ vs. time, the same analysis providing the rate constant for the appearance of **17** (Table 2).

stants and the effects of isotopic substitution upon them are consistent with mechanism [18] and with $k_{16} \sim k_{17}$. Together with earlier results (2) they provide good evidence for the total mechanism set out in Scheme 1.

The acidity function behaviours exhibited by the rate data in Table 2 are similar to what we have observed in related systems. In the present work we have slopes against H_0 of −0.90, −0.96, −0.98, −1.13, and −1.20 (see [12], [15], [13], [7], and [8]). Analysis of the rate data (17) for the acid-catalyzed dehydration of the adducts **20** gives slopes of −0.93, −1.02, and −1.10. For the acid-catalyzed debromination of the 5,5-dibromo derivative **19** (eq. [6])

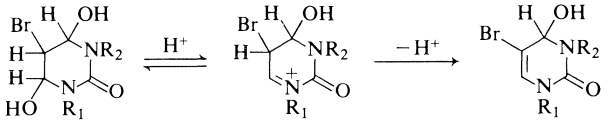

20 (R_1, R_2 = H or Me)

the slope is −1.20 (2). These similarities in behaviour add further support to our interpretation of the rate data in Table 2.

Conclusions

On the basis of the evidence presented above we propose that in strongly acidic aqueous media (>0.05 *M* sulfuric acid) simple uracils **1** undergo monobromination by the mechanism set out in Scheme 2. In this, initial *rapid* attack by bromine[4] leads to the formation of observable intermediates **2**, as originally proposed by Wang (10). These intermediates undergo slow acid-catalyzed dehydration **2** ⇄ **9** → **3**, with deprotonation of the cation **9** being rate determining. At low acidities intermediates **2** bearing hydrogen at N_1 (i.e. R_1 = H) also undergo dehydration by way of the neutral species **12**, that is, by the pathway **2** ⇄ **9** ⇄ **12** → **13** ⇄ **3**.

The reaction of 6-methyluracil **14** with bromine occurs via similar pathways as shown in Scheme 1. However, in this case it appears that deprotonation of the cation **15** and its capture by water (leading to **16**) are of comparable magnitude. As a consequence the deprotonation **15** → **16** is only partially rate determining and a reduced primary isotope effect is observed.

Experimental

The uracils used in this study were obtained from commercial sources and recrystallized before their use. The following compounds were prepared by literature methods: 5-deuteriouracil (8), 5-deuterio-1,3-dimethyluracil (8), 5-bromouracil (10), 5-bromo-1,3-dimethyluracil (10), 5-bromo-6-methyluracil (18), 5-bromo-6-hydroxy-5-methyldihydrouracil (19), and 5,5-dibromo-6-hydroxydihydrouracil (10).

5,5-Dibromo-6-hydroxy-6-methyldihydrouracil

Bromine (3.2 g, 20 mmol) was added to a suspension of 6-methyluracil (1.26 g, 10 mmol) in 15 mL of water. The mixture was stirred for 30 min, then refrigerated, and the solid was filtered off. Recrystallization from acetone–ligroin gave 2.28 g (88%) of the dibromo compound (20), mp 232–234°C (darkens above 200°C). *Anal.* calcd. for $C_5H_6N_2O_3Br_2$: C 19.89, H 2.00, N 9.28, Br 52.93; found: C 19.74, H 1.88, N 9.22, Br 52.85.

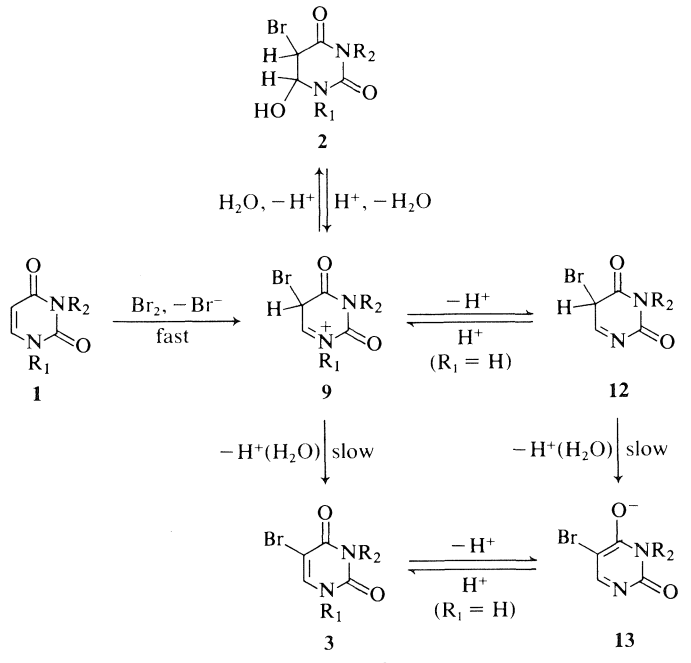

SCHEME 2

5-Deuterio-6-methyluracil

This was prepared from 6-methyluracil in 88% yield and with an isotopic purity above 95% using the literature method (8) reported for the deuteriation of uracil.

Kinetic Procedures

These were essentially the same as those used in earlier work (17), as were those used in the preparation of the sulfuric acid and the bromine solutions. The rate of appearance of the 5-bromouracils was monitored at wavelengths where only they absorb significantly (280–300 nm). Initial uracil concentrations were about 10^{-3} M; bromine concentrations slightly less. The cell holders of the Cary 14 spectrophotometer were thermostatted at 30°C as previously.

The higher values of the acidity function H_0 were interpolated from those given by Johnson *et al.* (21) as described before (17). To provide a continuous scale down into the 'pH' region H_0 values were calculated from the published log I values and the known pK_a of *p*-nitroaniline (21).

Proton Magnetic Resonance Spectra

Spectra of the uracils and their adducts were obtained in deuterated media using a Varian A-60 spectrometer (see Table 1 and footnote 3).

Acknowledgement

This work was made possible by an operating grant from the National Research Council of Canada.

1. S. Banerjee and O. S. Tee. Chem. Commun. 535 (1974).
2. S. Banerjee and O. S. Tee. J. Org. Chem. **39**, 3120 (1974).
3. S. Banerjee and O. S. Tee. J. Org. Chem. **41**, 4004 (1976).
4. T. L. V. Ulbricht. Purines, pyrimidines and nucleotides. Pergamon Press, London. 1964.
5. (*a*) D. J. Brown. The pyrimidines. *In* The chemistry of heterocyclic compounds. Vol. 16. *Edited by* A. Weissberger. Interscience, New York. 1962; (*b*) D. J. Brown. The pyrimidines. Suppl. I. Wiley-Interscience, New York. 1970; (*c*) E. Fahr. Angew. Chem. Int. Ed. Engl. **8**, 578 (1969).
6. C. D. Johnson, A. R. Katritzky, M. Kingsland, and E. F. V. Scriven. J. Chem. Soc. B, 1 (1971).
7. O. S. Tee. Ph.D. Thesis, University of East Anglia, Norwich, U.K. 1967.
8. D. V. Santi, C. F. Brewer, and D. Farber. J. Heterocyl. Chem. **7**, 903 (1970).
9. J. A. Rabi and J. J. Fox. J. Am. Chem. Soc. **95**, 1628 (1973).
10. S. Y. Wang. J. Org. Chem. **24**, 11 (1959).
11. A. M. Moore and S. M. Anderson. Can. J. Chem. **37**, 590 (1959).
12. (*a*) C. Nofre, M. Murat, and A. Cier. Bull. Soc. Chim. Fr. 1749 (1965); (*b*) M. Chabre, D. Gagnier, and C. Nofre. Bull. Soc. Chim. Fr. 108 (1966); (*c*) P. Rouillier, J. Delman, and C. Nofre. Bull. Soc. Chim. Fr. 3515 (1966); (*d*) P. Rouillier, J. Delman, J. Duplan, and C. Nofre. Tetrahedron Lett. 4189 (1966).
13. R. Duschinsky, T. Gabriel, W. Tautz, A. Nussbaum, M. Hoffer, E. Grunberg, J. H. Burchenal, and J. J. Fox. J. Med. Chem. **10**, 47 (1967).
14. L. Szabo, T. I. Kalman, and T. J. Bardos. J. Org. Chem. **35**, 1434 (1970).
15. M. J. Robins, M. MacCoss, S. R. Naik, and G. Ramani. J. Am. Chem. Soc. **98**, 7381 (1976).
16. K. Yates and R. A. McClelland. J. Am. Chem. Soc. **89**, 2686 (1967).
17. O. S. Tee and S. Banerjee. Can. J. Chem. **52**, 451 (1974).
18. R. C. Elderfield and R. N. Prasad. J. Org. Chem. **25**, 1583 (1961).
19. O. Baudisch and D. Davidson. J. Biol. Chem. **64**, 235 (1925).
20. R. Behrend. Justus Liebigs Ann. Chem. **229**, 18 (1885).
21. C. D. Johnson, A. R. Katritzky, and S. A. Shapiro. J. Am. Chem. Soc. **91**, 6654 (1969).

The conformation and reorientation of enclathrated 1,2-dichloroethane[1]

S. K. GARG, D. W. DAVIDSON, S. R. GOUGH, AND J. A. RIPMEESTER

Division of Chemistry, National Research Council of Canada, Ottawa, Ont., Canada K1A 0R9

Received July 20, 1978

S. K. GARG, D. W. DAVIDSON, S. R. GOUGH, and J. A. RIPMEESTER. Can. J. Chem. **57**, 635 (1979).

The rigid-lattice nmr line shape of the four-proton system in 1,2-dihaloethanes has been obtained by spectral simulation as a function of dihedral angle (ϕ) and used to show that 1,2-dichloroethane is encaged in the structure II hydrate in a *gauche* configuration with $\phi = 60 \pm 3°$. Very broad low-temperature dielectric absorption is associated with an average activation energy of 0.87 kcal/mol for guest-molecule reorientation.

S. K. GARG, D. W. DAVIDSON, S. R. GOUGH et J. A. RIPMEESTER. Can. J. Chem. **57**, 635 (1979).

On a déterminé l'allure des bandes rmn du système à quatre protons des dihalo-1,2 éthanes dans des réseaux solides; on a obtenu ces résultats en simulant les spectres en fonction des angles dièdres (ϕ) et on les a utilisés pour montrer que le dichloro-1,2 éthane est inséré dans l'hydrate de structure II dans une configuration *gauche* avec un $\phi = 60 \pm 3°$. Une absorbtion très large à basse température est associée à une énergie d'activation moyenne de 0.87 kcal/mol pour la réorientation de la molécule-hôte.

[Traduit par le journal]

Rotational isomerization of 1,2-dihaloethanes has long been a popular subject of study (see, for example, ref. 1). We show here that the shape of the rigid-lattice nmr spectrum of the four-proton system in these molecules is sensitive to the molecular configuration and may be used to determine the dihedral angle in the solid state.

A modified LAOCOON program (2) was used to simulate the four-proton spectrum of the polycrystalline powder as a function of dihedral angle. Figure 1 gives calculated derivative spectra for a number of dihedral angles (taken as zero for the *cis* or *syn* configuration) with the following molecular parameters assumed: $r_{CH} = 1.10$ Å, $r_{CC} = 1.51$ Å, all angles at C = 109.5°. These spectra have been subjected to Gaussian broadening, a relatively small value of β (0.5 G) being used to bring out clearly the spectral features. The shape is least perturbed from the doublet shape of the isolated proton pair for ϕ near 90° and most perturbed for the *cis* configuration. A pronounced central dip in the absorption occurs at all angles except those near 60°. It is clear that the angular dependence of the line shape may be used to determine the dihedral angle with considerable accuracy, provided that intermolecular broadening is sufficiently small and that the line shape is not appreciably perturbed (as it likely is for 1,2-difluoroethane) by magnetic interaction with the halogen atoms of the same molecule.

Rigid-lattice proton resonance line shapes have been recorded for 1,2-dichloroethane (*a*) in the solid solution with perdeuterated 1,2-dichloroethane and (*b*) in a D_2O clathrate hydrate lattice. Failure of 1,2-dichloroethane to form a clathrate hydrate by itself has been reported several times (3–5), although a hydrate of the doubtful (6) composition $C_2H_4Cl_2 \cdot 34H_2O$ has recently been reported to be formed in the presence of air (7). In the presence of H_2S a structure II double hydrate is readily formed (8), with 1,2-dichloroethane incorporated in the 16-hedral cages. Enclathration of this relatively large molecule may be expected to modify considerably the molecular conformation.

Figure 2 shows the proton spectrum of $C_2H_4Cl_2$ in solid solution in $C_2D_4Cl_2$ (99 at.% D) as recorded with a marginal oscillator and phase-sensitive detection. The narrow central line, whose relative amplitude decreases with increase in concentration of $C_2H_4Cl_2$, is attributed to $C_2D_3HCl_2$ impurity in the $C_2D_4Cl_2$. Otherwise the spectrum agrees well with that calculated for the *trans* (or *anti*) conformation ($\phi = 180°$) shown as the lowermost spectrum of Fig. 2. Solid 1,2-dichloroethane is well known to consist exclusively of the *trans* form (9).

The double hydrate of 1,2-dichloroethane and D_2S (98 at.% D) was prepared with D_2O (99.7 at.% D) by the procedure used to prepare neopentane–D_2S D_2O hydrate (10). Its spectrum (Fig. 3, lower curve) was recorded at very low temperatures to ensure the absence of motional narrowing. The well-defined central peak cannot be ascribed to $C_2H_4Cl_2$ and, in common with a similar feature in the spectra

[1]NRCC No. 17144.

0008-4042/79/060635-03$01.00/0

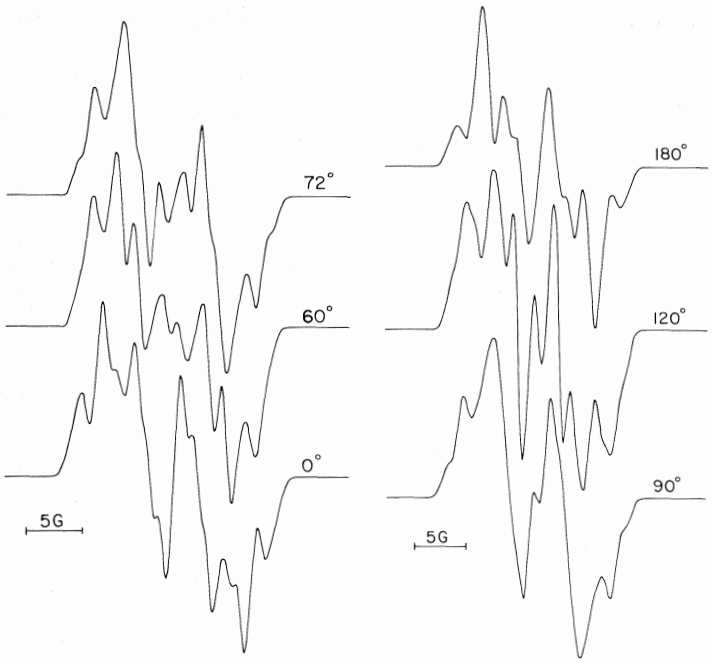

FIG. 1. Calculated derivative ^1H nmr spectrum of a 1,2-dihaloethane as a function of angle of rotation from the *cis* form.

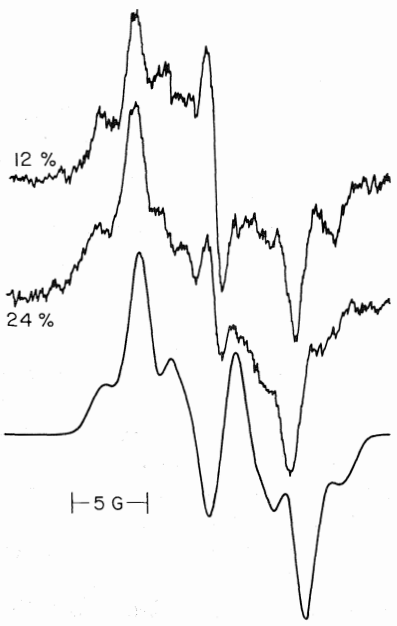

FIG. 2. Proton magnetic resonance spectra of 12 and 24% solutions of $C_2H_4Cl_2$ in $C_2D_4Cl_2$ recorded at ~57 MHz and 112 K. The bottom spectrum was calculated for the *trans* form and $\beta = 0.65$ G.

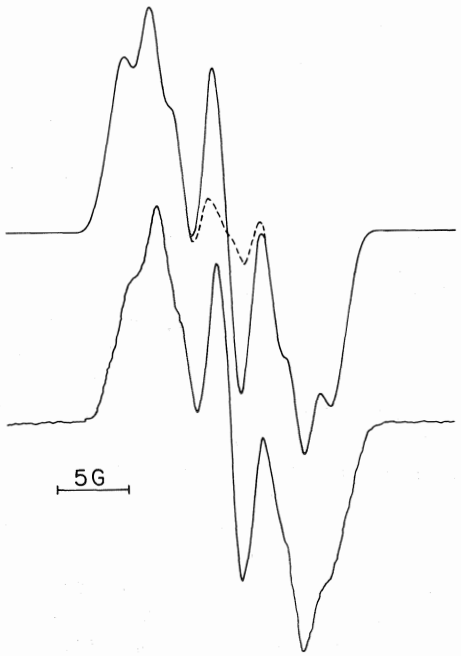

FIG. 3. Comparison of experimental ^1H nmr spectrum (below) of 1,2-dichloroethane–D_2S deuteriohydrate at ~20 MHz and 2.5 K and simulated rigid-lattice spectrum (above) with $\phi = 60°$ and HDO represented by an added central line.

of other deuteriohydrates (11), must be assigned to HDO. The remaining features may be satisfactorily assigned to 1,2-dichloroethane in which ϕ is close to 60°. The upper curve of Fig. 3 was calculated for this *gauche* conformation and $\beta = 0.65$ G, with the addition of a central (HDO) line of width $\beta = 0.75$ G and an integrated intensity 3.2% of that contributed by $C_2H_4Cl_2$. This magnitude corresponds to the presence of 0.36 at.% H in the D_2O.

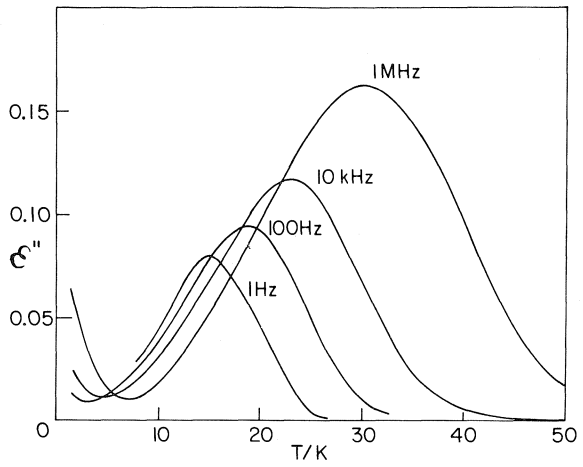

FIG. 4. Dielectric loss at low temperatures in 1,2-dichloroethane–H_2S hydrate.

The agreement between experimental and simulated spectra is decidedly poorer at angles only a few degrees removed from 60°. With due allowance for uncertainties in the assumptions made with respect to bond lengths and angles, Gaussian broadening, and neglect of conformation-dependent coupling of the protons to the chlorine nuclei, the average dihedral angle appears to be defined as $60 \pm 3°$. The configuration of the enclathrated molecule is thus not only entirely different from the *trans* form found in solid 1,2-dichloroethane but also differs from the *gauche* form which (together with the dominant *trans* form) occurs in the vapor (12). Electron diffraction studies have shown the dihedral angle of the vapor-phase *gauche* conformation to be $72 \pm 3°$ (13). Overlap repulsion of Cl atoms by water molecules in the cage walls undoubtedly plays the major role in modifying the conformation of the enclathrated molecule. The mean 'free diameter' of the 16-hedral cage is about 6.9 Å (14), whereas the van der Waals dimension of 1,2-dichloroethane through the Cl atoms is 8.1 Å for $\phi = 180°$, 7.2 Å for 72°, and 7.0 Å for 60°.

For the geometrically similar *n*-butane molecule, the *trans* form is also too large to be encaged: dielectric measurements have shown the presence of a dipolar *gauche* conformation for enclathrated *n*-butane (10). Results of low-temperature measurements of dielectric loss in the $C_2H_4Cl_2$–H_2S double hydrate are shown in Fig. 4. The rise in ε'' with decrease of temperature below 5 K arises from H_2S (10), the remaining frequency-dependent loss from 1,2-dichloroethane. From the variation of the temperature of maximum ε'' with frequency, an 'activation energy' of 0.87 kcal/mol for reorientation of 1,2-dichloroethane is obtained. The loss peak is exceptionally broad even for a hydrate-enclathrated molecule. It may be that the two loss peaks shown by *n*-butane (10), a dominant peak arising from molecular reorientation and a lower-temperature peak possibly associated with conformational interchange, are not distinguishable for 1,2-dichloroethane.

1. W. J. ORVILLE-THOMAS (*Editor*). Internal rotation in molecules. Wiley, New York, NY. 1974.
2. S. K. GARG, J. A. RIPMEESTER, and D. W. DAVIDSON. J. Magn. Reson. Submitted.
3. P. VILLARD. Ann. Chim. Phys. **11**, 289 (1897).
4. M. VON STACKELBERG. Naturwissenschaften, **36**, 327 (1949); **36**, 359 (1949).
5. M. VON STACKELBERG and M. MEINHOLD. Z. Elektrochem. **58**, 40 (1954).
6. D. W. DAVIDSON, S. R. GOUGH, F. LEE, and J. A. RIPMEESTER. Rev. Chim. Miner. **14**, 447 (1977).
7. J. C. ROSSO, R. FAVIER, and L. CARBONNEL. C. R. Acad. Sci. Ser. C, **286**, 9 (1978).
8. M. VON STACKELBERG and H. R. MÜLLER. Z. Elektrochem. **58**, 25 (1954).
9. W. N. LIPSCOMB and F. E. WANG. Acta Crystallogr. **14**, 1100 (1961).
10. D. W. DAVIDSON, S. K. GARG, S. R. GOUGH, R. E. HAWKINS, and J. A. RIPMEESTER. Can. J. Chem. **55**, 3641 (1977).
11. S. R. GOUGH, J. A. RIPMEESTER, and D. W. DAVIDSON. Can. J. Chem. **53**, 2215 (1975).
12. J. P. LOWE. Prog. Phys. Org. Chem. **6**, 1 (1969).
13. K. KEVSETH. Acta Chem. Scand. A, **28**, 482 (1974).
14. D. W. DAVIDSON. *In* Water: a comprehensive treatise. Vol. 2. *Edited by* F. Franks. Plenum Press, New York, NY. 1973. p. 115.

Correlation of the photoelectron and electronic spectra of thiochromones and thiochromanones with their electrochemical data

RAFIK O. LOUTFY

Xerox Research Centre of Canada Ltd., 2480 Dunwin Drive, Mississauga, Ont., Canada L5L 1J9

AND

IAN W. J. STILL, MICHAEL THOMPSON, AND TOONG S. LEONG

Department of Chemistry, University of Toronto, Toronto, Ont., Canada M5S 1A1

Received August 4, 1978

RAFIK O. LOUTFY, IAN W. J. STILL, MICHAEL THOMPSON, and TOONG S. LEONG. Can. J. Chem. **57**, 638 (1979).

The gas phase ionization potentials, electrochemical redox potentials and spectroscopic properties of a series of thiochroman-4-one and thiochromone derivatives have been studied. A dramatic shift in the energies of the lowest vacant and highest occupied molecular orbitals of the parent thiochromanone as a function of the addition of a double bond and/or oxidation of the sulphur atom was observed. This shift in energy of the molecular orbitals was reflected in their spectroscopic characteristics. The lowest singlet (and triplet) state of compounds **1–3** in solution is π,π^* in nature, while that of compounds **4–6** is n,π^*. These results are best explained in terms of substituent effects on the energetics of the acetophenone moiety. The change in the nature of the lowest excited state from π,π^* (**1–3**) to n,π^* (**4–6**) should result in quite different types of photochemistry for the two series.

A linear free-energy relationship between the singlet and triplet energies and the absolute difference between the oxidation and reduction potentials of the two series was found. These correlations have been utilized to estimate the half-wave oxidation potentials of compounds **3–6**. A correlation was found to exist between the gas phase ionization potential and the solution electrochemical oxidation potential.

RAFIK O. LOUTFY, IAN W. J. STILL, MICHAEL THOMPSON et TOONG S. LEONG. Can. J. Chem. **57**, 638 (1979).

On a étudié les potentiels d'ionisation en phase gazeuse, les potentiels d'oxydo-réduction électrochimiques et les propriétés spectroscopiques d'une série de dérivés de la thiochromanone-4 et de la thiochromone. On a observé des changements importants dans les énergies des orbitales moléculaires basse vacances (BV) et hautes occupées (HO) de la thiochromanone fondamentale lors de l'addition d'une double liaison et/ou lors de l'oxydation de l'atome de soufre. Ces déplacements dans les énergies des orbitales moléculaires se reflètent dans leurs caractéristiques spectroscopiques. La nature de l'état singulet (et triplet) le plus bas pour les composés **1** à **3** en solution est π,π^* alors que pour les composés **4** à **6**, elle est de n,π^*. On explique ces résultats en termes d'effets de substituants sur les niveaux énergétiques de la portion acétophénone. Le fait que la nature de l'état excité le plus faible passe de π,π^* (**1** à **3**) à n,π^* (**4** à **6**) doit être le résultat de types de photochimie assez différents pour chacune des séries.

On a noté une relation linéaire d'énergie libre entre les énergies singulet et triplet et la différence absolue entre les potentiels d'oxydation et de réduction des deux séries. On peut utiliser ces corrélations afin d'évaluer le potentiel d'oxydation à demi-vague des composés **3** à **6**. On a trouvé qu'il existe une corrélation entre le potentiel d'oxydation en phase gazeuse et le potentiel d'oxydation électrochimique en solution.

[Traduit par le journal]

Introduction

Recent years have seen the development of the use of electrochemical redox and gas phase ionization potential data to interpret photochemical reactions in which the excited states undergo electron or charge transfer processes (1). In order to understand these processes, it is necessary to know not only the excitation energy of the electrons, but also the oxidation and reduction potentials of the interacting molecules, which provide a convenient method for determining the absolute values of the energy levels of these molecules. A desire to develop the connection between spectroscopic and electrochemical data (2), coupled with our previous interest in the photochemical behavior of thiochroman-4-one derivatives (3, 4), prompted us to examine the gas phase ionization and electrochemical redox potentials, and the absorption and luminescence properties for a series of simple thiochromanones and thiochromones, **1–6** (Fig. 1).

0008-4042/79/060638-07$01.00/0

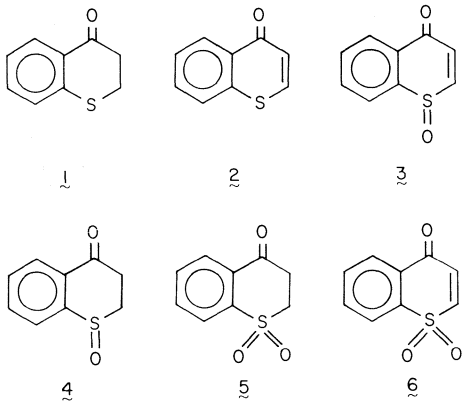

FIG. 1. The chemical structures of the thiochroman-4-one and thiochromone derivatives studied.

Interestingly, thiochromone 1-oxide (**3**), unlike other members of this series, had never been reported previously and proved to be inaccessible from thiochromone using standard oxidative procedures. Only recently did we successfully obtain thiochromone 1-oxide by a less direct route (5).

The objective of this study was, first, to carry out a molecular orbital assignment and to elucidate the nature of the singlet and triplet excited states in order to gain further insight into the photochemical behavior of this interesting series and, secondly, to establish the relationship between the lowest excited state energies and the electrochemical and gas phase parameters. These correlations were utilized (*a*) to predict the n,π* triplet energies of compounds **1**–**3**, which are undetectable by experimental spectroscopy, and (*b*) to estimate the oxidation potentials and gas phase ionization potentials of **4** and **5**, for which we were unable to obtain satisfactory photoelectron spectra because of their relative involatility.

Experimental

Thiochroman-4-one (97%) (**1**) is commercially available from Aldrich Chemical Co., Inc. and was further purified by column chromatography. Thiochromone (**2**) was prepared from **1** by dehydrogenation, as described previously (6). Thiochroman-4-one 1-oxide (**4**) and the two sulphones (**5**, **6**) were prepared by the respective oxidative procedures already described (3, 4). Thiochromone 1-oxide (**3**) was synthesized from thiochroman-4-one by a non-oxidative procedure which we have recently reported (5).

Electrochemistry

A Princeton Applied Research (PAR) model 174A polarographic analyzer, equipped with a drop mercury electrode or a Beckman 2 mm platinum button electrode model 39281, was employed for the polarographic reduction and voltammetric oxidation analysis.

The electrochemical cell assembly consisted of a PAR model 9301 and 9300, cell base and cover, with the mercury drop electrode as cathode and a platinum wire auxiliary electrode as anode. A Brinkmann model EA410 saturated calomel electrode, making contact via a PAR model 9361 non-aqueous liquid junction bridge, served as the reference electrode. For oxidation potential measurements a platinum disc electrode was employed as an anode and a Pt wire as auxiliary counter electrode.

The electrolyte, tetra-*n*-butylammonium perchlorate (TBAP), was polarographic grade and dried in a vacuum oven at 100°C for 6 h prior to use. Spectral grade methylene chloride was distilled from P_2O_5 before use. Methylene chloride was chosen as the solvent for a number of reasons. It is an excellent, yet relatively inert, solvent for a wide variety of organic compounds, it has an exceptionally wide potential window for the appropriate redox measurements, it is aprotic, and it has a low dielectric constant. Direct current (dc), normal pulse (np), and differential pulse polarograms were obtained from 0.05 m*M* solutions of compounds **1**–**6** in 0.1 *M* TBAP – methylene chloride. Measurements were performed at room temperature (22°C) under a dried argon atmosphere.

Absorption and Luminescence Spectroscopy

Ultraviolet absorption spectra were recorded on a Cary 17 spectrophotometer in spectral grade 2-methyltetrahydrofuran, methanol, methylene chloride, and acetonitrile.

Emission spectra were recorded on a Perkin-Elmer PMF4 spectrofluorimeter. Phosphorimetry was carried out using a conventional phosphorescence attachment at 77 K in 2-methyltetrahydrofuran. The luminescence excitation spectra were recorded in ratio mode. The quantum yield of luminescence was not determined.

Photoelectron Spectroscopy

The ultraviolet photoelectron spectra of compounds **1**, **2**, **3**, and **6** were recorded on the magnetic spectrometer described previously (7). The He(I) resonance line of 21.22 eV was used as the excitation source and spectra were calibrated against xenon lines at 12.13 and 13.44 eV, and the argon signal at 15.76 eV.

Results and Discussion

Gas Phase Ionization Potentials

The vertical ionization potentials obtained from the spectra of compounds **1**, **2**, **3**, and **6** shown in Fig. 2 are given in Table 1. The spectrum of **1** can be rationalized by consideration of previous analyses of the spectra of thioanisole (8) and substituted acetophenones (9). The spectrum of thioanisole in the lower IP region is discussed in terms of a 'p-model', i.e., delocalization of the sulphur lone-pair into the aromatic π-system. This results in the splitting of the parent benzene e_{1g} orbitals at 9.23 eV into three bands in thioanisole at 8.07 eV (significant sulphur character), 9.28 eV (largely unperturbed benzene π-antisymmetric orbital), and 10.14 eV (orbital of significant benzene π-symmetric character). The spectrum of *o*-methylacetophenone exhibits overlapping bands in the region 9.15–9.70 eV. The acetyl n-orbital IP occurs at 9.32 eV. The highest occupied orbital is given as the aromatic ring π-orbital at 9.15 eV. Thus we could expect for **1** four events at IP less than (approximately) 10.5 eV. The spectrum

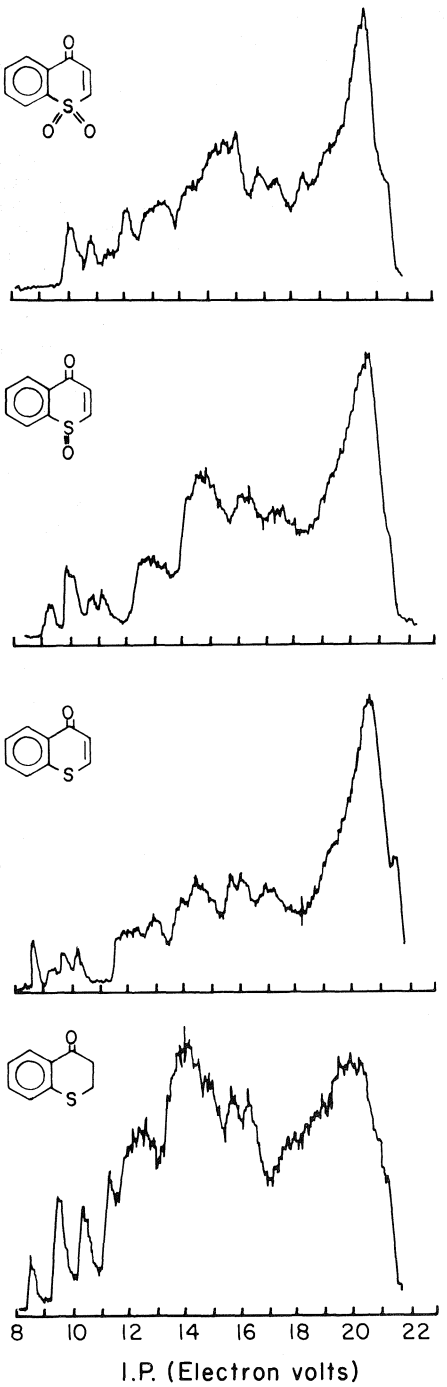

FIG. 2. Photoelectron spectra of compounds **1**, **2**, **3**, and **6**.

actually shows three bands in this region. However, the cross-section of the second peak suggests that this band contains two ionizations. Consideration of the above leads us to the conclusion that the band at 8.53 eV arises from a π-orbital with significant sulphur contribution. The composite band at 9.70 eV can be assigned to ionization of benzene-π and oxygen n-orbitals and the peak at 10.41 eV to the other of the split benzene e_{1g} orbitals. The appropriate π-IP's for **1** are greater than those for thioanisole, undoubtedly due to the presence of the electron-accepting carbonyl group. The oxygen n-ionization of 9.70 eV probably reflects the resultant effect of the sulphur atom and the increment in negative charge on the >C=O group due to electron migration from the benzene ring.

With regard to the spectrum of **2**, the addition of a further π-orbital to the situation described above for **1** will likely result in an additional ionization event in the region of 8.5–11.0 eV (10). The spectrum actually shows four peaks in this area. Therefore, the extra π-orbital is either overlapped in the lower IP region or is a component of the broad peak centred at 12.1 eV which has an adiabatic IP of about 11.4 eV. The peak at 8.68 eV can clearly be assigned to the π orbital with significant sulphur character.

As for the spectrum of **3**, the picture must now be modified to take account of a further factor expected to increase spectral complexity, the S=O bond. Previous results for alkyl-substituted sulphoxides (11) showed that the highest occupied orbital is the sulphur lone-pair (8.2–9.6 eV) followed by the S=O π-orbital (9.2–10.2 eV) and further oxygen lone-pair (11.2–12.9 eV). The spectrum of **3** shows four peaks in the range 9.0–11.5 eV. The intensity of the second peak (9.90 eV) clearly indicates that there is more than one ionization event associated with it. It seems reasonable, therefore, to assign the first band at 9.24 eV to a π-orbital of significant sulphur character and some oxygen character. As expected, the value is shifted to higher IP with the formation of the sulphur–oxygen bond. Furthermore, it is expected that the benzene e_{1g} orbitals will be shifted further to higher IP by the presence of the S=O bond. Clearly, the relatively intense peak at 9.90 eV arises in part from an ionization of one or both of these orbitals. The complexity of the spectrum prevents us from making further assignments.

Since the first ionization potential of methyl phenyl sulphone at 9.74 eV has been assigned to benzene πe_{1g} orbitals (12), it is tempting to assign the first peak in the spectrum of **6** (9.93 eV) to the related orbitals in that compound. However, the carbonyl lone-pair level is also expected to have a similar energy. Further evidence is thus required to make a positive assignment of this band. This was provided by an examination of the electrochemical and spectroscopic properties of the molecules studied in this work.

TABLE 1. Vertical ionization potentials measured by ultraviolet photoelectron spectroscopy (eV)

Compound	Ionization potential										
	1	2	3	4	5	6	7	8	9	10	11
1	8.53	9.70	10.41	11.52	12.2	14.0	14.9	15.7	16.1		
2	8.68	9.31	9.68	10.2	12.1	13.0	14.0	14.5	15.7	16.1	16.8
3	9.24	9.90	10.95	11.21	12.9	14.7	15.2	16.3			
6	9.93	10.74	12.04	13.1	14.2	15.5	16.7	17.3			

Polarographic Reduction and Voltammetric Oxidation

Figure 3 shows typical differential pulse and dc polarograms of compounds **1**, **4**, and **5** in methylene chloride, with TBAP as supporting electrolyte. The half-wave reduction potentials, $E_{1/2}^{red}$, for the first wave, are included in Table 2. (In all cases the limiting current was diffusion-limited, the number of electrons transferred was 1, and the electron transfer coefficient, α, was 0.5.) The $E_{1/2}^{red}$ values, which relate to the energy of the lowest vacant molecular orbital (π^*), become progressively anodic from the sulphides, through the sulphoxides to the sulphones. This anodic shift of the reduction potentials is typical of acetophenones substituted with electron-withdrawing groups (13).

A typical voltammogram, that of compound **2** in methylene chloride is shown in Fig. 4. No cathodic wave was observed, indicating an irreversible electron transfer process. The oxidation peak shifted by 60 mV (anodic) on increase of the scan rate by 10-fold. A plot of the anodic peak current versus the square root of the scan rate yields a straight line with a slope of 1. These results are in agreement with an irreversible one-electron transfer electrode process with a transfer coefficient of 0.5. The half-wave oxidation potentials for compounds **1** and **2** are included in Table 2.

Absorption and Luminescence Spectroscopy

The singlet energies, E_S, determined from the

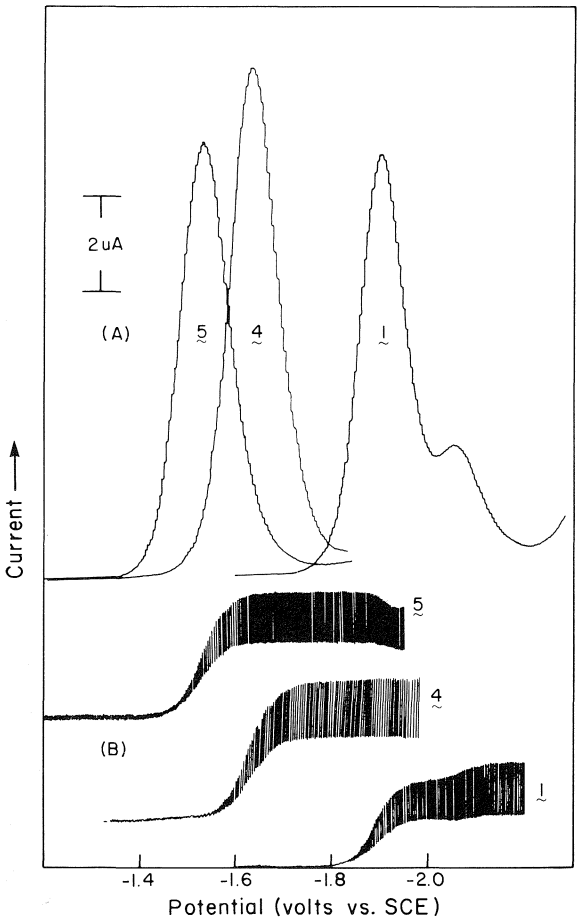

FIG. 3. Differential pulse (*A*) and dc (*B*) reduction polarograms of thiochroman-4-one **1**, its sulphoxide **4**, and sulphone **5** in CH_2Cl_2; 0.1 *M* TBAP at DME vs. sce.

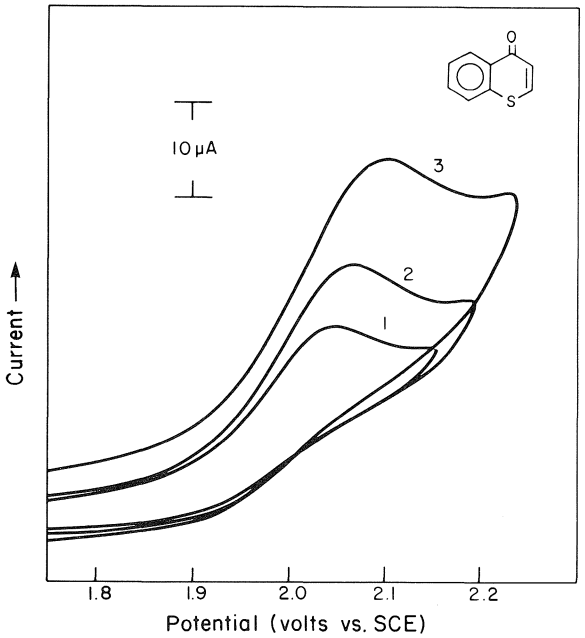

FIG. 4. Cyclic voltammogram of thiochromone **2** in CH_2Cl_2, 0.1 *M* TBAP at Pt disc electrode. Scan rate (*1*) 100, (*2*) 200, and (*3*) 500 mV/s.

TABLE 2. First vertical ionization potentials and solution redox potential data

Compound	IP from UPS (eV)	Electrochemical data (V vs. sce) $E_{1/2}^{ox}$	$E_{1/2}^{red}$	$(E_{1/2}^{ox} - E_{1/2}^{red})$
1	8.53	1.81	−1.90	3.71
2	8.68	1.96	−1.83	3.79
3	9.24	(2.52)[a]	−0.95	3.47
4	(9.43)[a]	(2.71)[b]	−1.64	(4.35)[b]
5	(9.53)[a]	(2.81)[b]	−1.53	(4.34)[b]
6	9.93	(3.21)[a] (3.17)[b]	−0.86	(4.07)[b]

[a]Estimated values according to $E_{1/2}^{ox} = IP - 6.72$.
[b]Calculated from eq. [5] using $J_{12} = 1.25$ eV.

TABLE 3. Absorption and luminescence data obtained in 2-methyltetrahydrofuran (eV)

Compound	Absorption $E_{S(\pi,\pi^*)}$[a]	Absorption $E_{S(n,\pi^*)}^{0-0}$	Luminescence $E_{T(\pi,\pi^*)}$	Luminescence $E_{T(n,\pi^*)}$	Luminescence $E_{T(n,\pi^*)}$[b]	ΔE_{S-T}	J_{12}
1	3.62 (342)		2.85 (435)		3.24	0.77	0.86
2	3.71 (334)		2.83 (438)		3.20	0.88	0.96
3	3.37 (368)		2.53 (490)		2.84	0.84	0.94
4	4.21 (294)	3.35 (370)		3.10 (399)	3.12	0.25	(1.25)[c]
5	4.23 (292.5)	3.33 (372)		3.09 (400)	3.08	0.24	(1.25)[c]
6	3.95 shoulder (313) 4.42 (282.5)	2.98 (415)		2.78 (445)	2.79	0.20	(1.29)[c]

[a]Wavelength (λ) in nm.
[b]Calculated by eq. [6].
[c]Predicted value, see ref. 2.

ultraviolet absorption spectra, recorded at ambient temperature in 2-methyltetrahydrofuran (2-MTHF), are given in Table 3 for compounds **1**–**6**. The spectra of all compounds in methanol, methylene chloride, or acetonitrile were identical to those obtained from the aforementioned solvent, with the single exception that **3** showed a shoulder at 368 nm in methanol.

Relatively strong fluorescence emission was observed for compound **1** in methylene chloride solution at ambient temperature (λ_{max}^{F}, 415 nm). Fluorescence from other members of the series was weak and difficult to determine. However, every compound exhibited relatively strong phosphorescence in 2-MTHF glass at 77 K. The phosphorescence emission from **1** and **2** is slightly structured (e.g., Fig. 5) and resembles luminescence from triplet π,π* states of aromatic ketones. Compounds **4**, **5**, and **6** show structured phosphorescence (e.g., Fig. 6) typical of n,π* triplet states of aromatic ketones. Compound **3** exhibited a unique low energy non-structured phosphorescence. The energies of the lowest excited triplet states of compounds **1**–**6** are included in Table 3.

Correlation between Gas-phase and Solution Ionization Energies

The effects of substituents on the redox potentials of molecules have been extensively studied during the past decade and several review articles and books have been written (14). Similarly, the effects of substituents on the gas phase ionization potential of molecules have also been reported (15, 16). On the other hand, few examinations of the interrelation between the gas phase ionization potential and the solution $E_{1/2}^{ox}$ are available (17–22). This is mainly due to the fact that reversible one-electron electrochemical oxidation potential data are scarce and also due to difficulties in allowing for the junction potential. Ionization potentials of some organic molecules are difficult to determine (e.g., **4** and **5**). Although ionization potentials have been calculated by

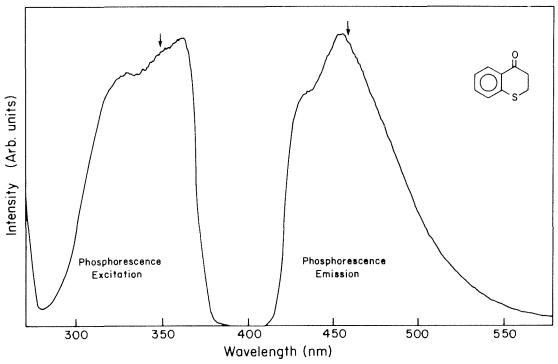

FIG. 5. Phosphorescence emission and excitation of thiochroman-4-one **1** in 2-MTHF at 77 K. The arrows indicate the wavelengths of excitation and monitoring.

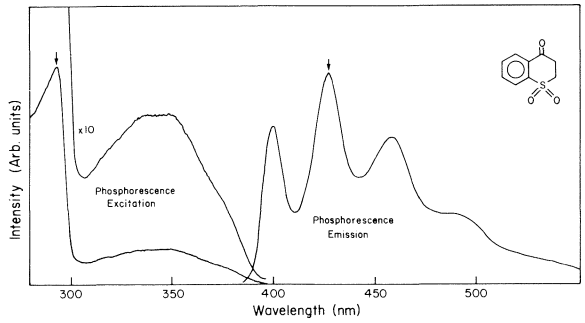

FIG. 6. Phosphorescence emission and excitation of thiochroman-4-one 1,1-dioxide **5** in 2-MTHF at 77 K. The emission is representative of the series **4**, **5**, and **6**.

studying charge transfer spectra, it would be useful to have another easily accessible experimental measure of relative ionization potentials.

It is well-known that half-wave oxidation potentials of organic compounds are closely related to the energy of their highest occupied molecular orbitals (23). This in turn is related to the gas-phase IP of a molecule by the expression

$$[1] \qquad E_{1/2}{}^{ox} = IP + \Delta F_S{}^{+} + E_{RE}{}^{0}$$

where $E_{RE}{}^{0}$ is a constant which includes the free energy of the electron in the reference electrode versus an electron *in vacuo* at infinity ($E^0 = -4.38$ V for the standard calomel electrode) (24), and $\Delta F_S{}^{+}$ is the differential real solvation energy of the radical cation (22). It is interesting to note that use of eq. [1] and the data of Table 2 results in a solvation energy of -2.34 eV for compounds **1** and **2**. This value is typical for molecules with relatively well-delocalized electron charge distribution and is consistent with the assignment of the first IP as being due to ionization of a π-orbital with significant sulphur character. The oxidation potentials of compounds **3** and **6** can be computed from their first IP's and eq. [1], assuming the same solvation energy found for compounds **1** and **2** applies. These values are shown in Table 2.

Correlation of Excited State Energies and Redox Potentials

The single configuration formula for the singlet and triplet excitation energies, E_S and E_T, respectively, can be given by the following equations (25):

$$[2] \qquad E_S = \varepsilon_1 - \varepsilon_2 - J_{12} + 2K_{12}$$

$$[3] \qquad E_T = \varepsilon_1 - \varepsilon_2 - J_{12}$$

where ε_1 and ε_2 are the energies of the highest occupied and lowest vacant molecular orbitals, respectively, J_{12} is the coulomb repulsion integral, and K_{12} is the exchange integral. A distinction must be made between the energy of the lowest vacant MO of a molecule when occupied by an electron after excitation and the energy of the empty orbital in a closed shell configuration. This difference, in the case of a singlet excited state, is $-J_{12} + 2K_{12}$ and for the triplet state is given by $-J_{12}$. Since the electrochemical half-wave oxidation and reduction potentials are related to the energies of the highest occupied (ε_1) and lowest vacant (ε_2) molecular orbitals, respectively, then the singlet and triplet excitation energies[1] can be given in terms of electrochemical redox potentials, as indicated below (2).

$$[4] \qquad E_S = a(E_{1/2}{}^{ox} - E_{1/2}{}^{red} - J_{12}{}^{s} + 2K_{12}{}^{s})$$

$$[5] \qquad E_T = b(E_{1/2}{}^{ox} - E_{1/2}{}^{red} - J_{12}{}^{s})$$

According to eq. [4], a linear relationship should exist between the absolute difference of the oxidation and reduction potentials and the energy of the singlet excited state for a series of closely related molecules, provided that the sum of the coulomb repulsion and the exchange integral is constant or varies in a regular manner within the series. Similarly, according to eq. [5], the existence of a linear free energy relationship between the redox properties of a series of molecules and their triplet energies is expected, provided that the coulomb repulsion integral is constant.

It was recently reported that a linear relationship exists between the n,π* triplet energies of a series of acetophenone derivatives and their half-wave reduction potentials (13). This correlation is only possible if both J_{12} and ε_1, or their difference, remain constant throughout the series. If we consider that the compounds **1**–**6** are simply derivatives of acetophenone, then it is possible to predict their n,π* triplet energies using the following equation (13):

$$[6] \qquad E_{T(n,\pi^*)} = -0.42(E_{1/2}\,(\text{V vs. sce}) - 0.33) + 2.3\ \text{eV}$$

The n,π* triplet energies of compounds **1**–**6**, calculated using eq. [6] from their experimental $E_{1/2}{}^{red}$ values, are shown in Table 3, along with the experimentally obtained triplet energies. It can be seen that the agreement between the calculated and experimental values is excellent for compounds **4**, **5**, and **6** which all possess a lowest n,π* triplet state. However, the triplet energies of compounds **1**, **2**, and **3** do not fit the above correlation. This strongly indicates that the lowest triplet transition of these compounds is a π → π* transition rather than a n → π* transition.

The singlet–triplet splitting energy (ΔE_{S-T}) is generally of the order of 1 eV for π,π* singlet–

[1]Where *a* and *b* are proportionality constants which, in most cases, were found to be near unity (1, 2).

triplet states and 0.2–0.5 eV for n,π* states. The mean value of ΔE_{S-T} for compounds **1**, **2**, and **3** is 0.83 eV, while that for compounds **4**, **5**, and **6** is 0.23 eV (Table 3). These results are in agreement with the assignment that **1**, **2**, and **3** possess π,π* lowest singlet and triplet states, while compounds **4**, **5**, and **6** have n,π* lowest singlet and triplet states.

According to eq. [5], the triplet energies of a series of structurally similar molecules should correlate with the absolute difference between their oxidation and reduction potentials. The data of Tables 2 and 3 show that such a correlation exists for compounds **1** **2**, and **3**. Although the oxidation potentials for compounds **4**, **5**, and **6** could not be measured experimentally, eq. [5] can be used to estimate the term $(E_{1/2}{}^{ox} - E_{1/2}{}^{red})$ and therefore the $E_{1/2}{}^{ox}$ values, through use of the experimentally determined $E_T(n,\pi^*)$ results and a value for $J_{1/2}{}^{s}$ of 1.25 eV (2). The $E_{1/2}{}^{ox}$ values are included in Table 2. It is interesting to note that, as expected, their values are beyond the experimentally attainable electrochemical potential limit.

The apparent difference between the lowest energy triplet states of compounds **3** and **6** (π,π* versus n,π*) is particularly interesting in the light of the observed differences in photochemical reactivity of these two compounds.[2] This, and related aspects of the photochemical behavior of these molecules, will be the subject of a forthcoming publication.

Conclusions

The gas phase ionization and the solution electrochemical oxidation–reduction potentials of a series of simple thiochromanones and thiochromones **1–6** have been determined. The highest occupied molecular orbital for compounds **1–3** was assigned as a π-orbital with significant sulphur character. This assignment was confirmed from the study of the ultraviolet absorption and phosphorescence spectra, where the lowest singlet and triplet states of **1–3** were found to involve π → π* transitions.

The photoelectron spectrum of compound **6** was too complex to make a definite assignment and those of **4** and **5** were experimentally unattainable. From the spectroscopic and electrochemical investigation of compounds **4–6**, the lowest singlets and triplets are clearly n,π* in nature. Therefore, the highest occupied molecular orbital in these cases is attributable to the n-orbital of the carbonyl group. A correlation between the n,π* triplet energies and the absolute difference between the oxidation and reduction potentials was utilized to estimate the half-wave oxidation potential of compounds **3–6**. Likewise, a correlation between IP and $E_{1/2}{}^{ox}$ was used to estimate the ionization potentials of compounds **4** and **5**.

[2]I. W. J. Still and T. S. Leong. Unpublished results.

Acknowledgements

We are indebted to Dr. Jack Betteridge of the University College of Swansea for assistance in obtaining the ultraviolet photoelectron spectra. In addition, we are grateful to the National Research Council of Canada for financial support (to I.W.J.S. and M.T.).

1. R. O. Loutfy and J. H. Sharp. J. Am. Chem. Soc. **99**, 4049 (1977); J. Photogr. Sci. Eng. **20**, 165 (1976).
2. R. O. Loutfy and R. O. Loutfy. Can. J. Chem. **54**, 1454 (1976).
3. I. W. J. Still, P. C. Arora, M. S. Chauhan, M-H. Kwan, and M. T. Thomas. Can. J. Chem. **54**, 455 (1976).
4. I. W. J. Still and M. T. Thomas. J. Org. Chem. **33**, 2730 (1968).
5. I. W. J. Still, P. C. Arora, and S. N. Sokolowsky. Org. Prep. Proced. Int. **7**, 159 (1975).
6. M. S. Chauhan and I. W. J. Still. Can. J. Chem. **53**, 2880 (1975).
7. D. Betteridge, A. D. Baker, P. Bye, S. K. Hasannudin, N. R. Kemp, and M. Thompson. J. Electron Spectrosc. Related Phenom. **4**, 165 (1974).
8. H. Bock, G. Wagner, and J. Kroner. Chem. Ber. **105**, 3850 (1972).
9. T. Kobayashi and S. Nagakura. Bull. Chem. Soc. Jpn. **47**, 2563 (1974).
10. D. Dougherty and S. P. McGlynn. J. Am. Chem. Soc. **99**, 3234 (1977).
11. H. Bock and B. Solouki. Chem. Ber. **107**, 2299 (1974).
12. B. Solouki, H. Bock, and R. Appel. Chem. Ber. **108**, 897 (1975).
13. R. O. Loutfy and R. O. Loutfy. Tetrahedron, **29**, 2251 (1973).
14. P. Zuman. Substituent effects in organic polarography. Plenum Press, New York. 1967.
15. B. W. Levitt and L. S. Levitt. J. Org. Chem. **37**, 332 (1972), and references therein.
16. H. W. Gibson. Can. J. Chem. **51**, 3065 (1973).
17. A. Streitwieser, Jr. Molecular orbital theory for organic chemists. J. Wiley and Sons, Inc., New York. 1961. Chapt. 7.
18. E. S. Pysh and N. C. Yang. J. Am. Chem. Soc. **85**, 2124 (1963).
19. W. C. Neikam, G. R. Dimeler, and M. M. Desmond. J. Electrochem. Soc. **111**, 1190 (1964).
20. M. E. Peover. Electroanal. Chem. **2**, 41 (1967).
21. L. L. Miller, G. D. Nordblom, and E. A. Mayeda. J. Org. Chem. **37**, 916 (1972).
22. R. O. Loutfy. J. Chem. Phys. **66**, 4781 (1977).
23. M. MacColl. Nature, **163**, 178 (1949).
24. R. E. Ballard. Chem. Phys. Lett. **42**, 97 (1976).
25. R. Ditchfield, J. E. Del Bene, and J. A. Pople. J. Am. Chem. Soc. **94**, 703 (1972).

A stereoselective synthesis of sucrose.[1] Part II.[2] Theoretical and chemical considerations

BERT FRASER-REID AND DAVID ERLE ILEY[3]

Guelph–Waterloo Centre for Graduate Work in Chemistry, Waterloo Campus, University of Waterloo, Waterloo, Ont., Canada N2L 3G1

Received June 29, 1978

BERT FRASER-REID and DAVID ERLE ILEY. Can. J. Chem. **57**, 645 (1979).

Under the agency of an iodonium ion, the tertiary anomeric hydroxyl of tetraacetyl fructofuranose adds stereoselectively in a 1,4 sense, to a pyranoid 4,6-*O*-benzylidenated conjugated diene receptor. The resulting disaccharide, isolated in 45% yield, is an hex-2-enopyranoside possessing an allylic primary iodide which can be oxidised to an aldehyde either directly or after hydrolysis to the allylic primary alcohol. The aldehyde is decarbonylated and the unsubstituted hex-2-enopyranoside formed undergoes hydroxylation giving exclusively the *manno*-diol. After protecting the equatorial hydroxyl as the benzoate ester, the axial 2-hydroxyl group is inverted via oxidation followed by borohydride reduction. Acetylation gives the known 4,6-*O*-benzylidene hexaacetyl derivative of sucrose, which is identified by mixture melting point.

BERT FRASER-REID et DAVID ERLE ILEY. Can. J. Chem. **57**, 645 (1979).

Sous l'influence d'un ion iodonium, le groupe hydroxyle anomère tertiaire du tétraacétyl du fructose s'additionne en 1,4 d'une façon stéréosélective, sur le récepteur diénique conjugué d'un pyrannoïde portant un groupe *O*-benzylidène en 4,6. On a isolé le disaccharide qui en résulte avec un rendement de 45%; il s'agit d'un hexèno-2 pyrannoside portant un iodure allylique primaire qui peut être oxydé en aldéhyde soit directement soit après hydrolyse en alcool allylique primaire. On peut décarbonylé l'aldéhyde; l'hexèno-2 pyrannoside non-substitué qui en résulte subit une hydroxylation conduisant uniquement au diol-*manno*. Après avoir protégé l'hydroxyle équatorial par un groupe benzoyle, on provoque une inversion du groupe hydroxyle axial en position 2 par une oxydation suivie d'une réduction au borohydrure de sodium. Une acétylation fournit le dérivé *O*-benzylidène-4,6 hexaacétylé connu que l'on identifie par son point de fusion.

[Traduit par le journal]

Introduction[4]

Sucrose (**1***a*) is the compound produced commercially in greatest quantity with the highest degree of purity.[5] In spite of this fact, the compound presented organic chemists with two challenges (*a*) determining its structure and (*b*) achieving its synthesis, both of which were met only a generation ago. For the majority of natural products, realization of the second objective would have concomitantly dispensed with the first. However, in the case of sucrose this was not the case. It had been known for decades that the components were glucose (**2***a*) and fructose (**3***a*) but

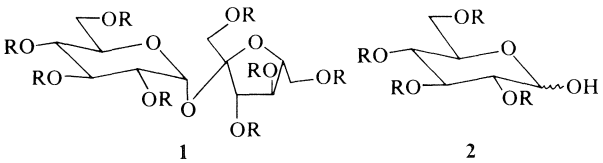

1
a R = H
b R = Ac
c R = Me

2
a R = H
b R = Ac
c R = Me

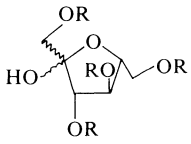

3
a R = H
b R = Ac
c R = Me
d R = $PhCH_2$

the nature of the anomeric linkages continually baffled organic chemists[6] and indeed was not promulgated (4) until five years *after* the first chemical synthesis had been announced by Lemieux and Huber (5).

[1]Dedicated to Professor Sir Derek Barton on the occasion of his 60th birthday.

[2]For Part I, see the preliminary account of this work (6).

[3]Holder of the NRCC Studentship 1973–1975. Taken from the M.Sc. Thesis of D.E.I., University of Waterloo, 1975. Present address: Ontario Hydro, W. P. Dobson Laboratories, 800 Kipling Ave., Toronto, Ont.

[4]In disaccharides such as **21**α, **21**β, **22**α, **32**β, etc., the 'α' or 'β' refers to the anomeric configuration of the *furanose* moiety, since the linkage of the pyranose anomeric centre is always 'α.' Use of **21**, **22**, **32**, etc., indicates a mixture of anomers at the furanose centre.

[5]Table sugar has a melting point of 183–185°C. The analytically pure material melts at 185–186°C. The annual production of sucrose is in excess of 60 million tons (1).

[6]Proof of the anomeric configurations by crystallographic methods had been obtained (2, 3).

0008-4042/79/060645-08$01.00/0

In 1975 we made a preliminary announcement of a new synthesis of sucrose in which all of the steps involved proceeded with complete stereoselectivity (6). In addition, the synthesis introduced a novel method for uniting two saccharides by a procedure which generated intermediates which were themselves interesting synthons for branched-chain and modified sugars.

Our synthesis (6) was predicated upon the stereoselective methoxybromination of the diene **8** (*vide infra*). However, we were cognisant of the fact that the stereochemical course of reactions at the anomeric centre of sugars frequently change when one goes from simpler to more complex alcohols (see, for example, ref. 7) (*vide infra*). The chemical manipulations were therefore undertaken with a high degree of faith and chemical vindication came only with the final isolation of a crystalline derivative of sucrose, **32**β.[4] However, while proceeding in this way, extensive spectroscopic studies were made on our intermediates which provide independent proof of structure. Thus in this paper we describe the chemical details of our synthesis and in the accompanying paper (8) the spectroscopic studies are considered.

Background

The simplest conception of a synthesis of sucrose involves the direct dehydrative union of appropriately protected glucosyl and fructosyl derivatives and this was indeed the approach in the earliest attempts. However, the acetates **2***b* and **3***b* could not be united to give octaacetyl sucrose **1***b* (9). Interestingly a more recent attempt using the methylated counterparts (**2***c* and **3***c*) and zinc chloride gave ~7% of **1***c* (10).

However, such direct condensations allow no control over the stereo- or regiochemistry of the process, so that myriad products were obtained (9*d*). This could be overcome by specifically activating the anomeric centre of one of the units. Traditionally such activation is achieved with glycosyl halides such as **4** which are usually stable, crystalline, well-characterised products. By contrast, the halide derived from **3** is, understandably, exceedingly unstable (9*b*). Thus most efforts have utilized glucosyl halides (**4**) and fructosyl alcohols (**3**). However, reaction of **4***a* with **3***b* gave the β-D-pyranoside **5** (isosucrose) (11) a result which reflects the participation of the C-2 acetoxy group of **4***a* in the reaction (12). Accordingly when nonparticipating benzyl groups were utilized (**4***b* + **3***d*) sucrose was obtained in 4.5% yield (13).

The above-described successful approaches to sucrose are in fact predated by Lemieux's historic breakthrough (5) in which the activated partner was the α-epoxy ether Brigl's anhydride (**6**). The synthesis

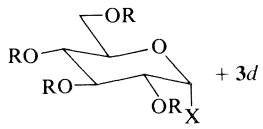

4

a R = Ac, X = Br
b R = $PhCH_2$, X = Cl

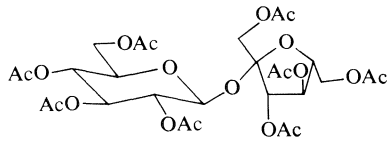

5

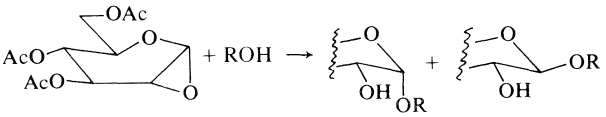

6 **7α** **7β**

was the climax of a series of studies in which it was observed that in the reactions of **6** with alcohols, the proportion of the anomers, **7**α and **7**β in the products increased as the residue R got more and more bulky. Thus use of the exceedingly bulky alcohol **3***b* led to an 8.8% yield of sucrose octaacetate (**1***b*) (5).

The three successful syntheses (5, 10, 13) above also give varying amounts of the β-linked isosucrose (e.g., **5**), a result which reflects the lack of stereoselectivity in the reaction at the glucosyl centre. Clearly, therefore, there are unfavourable stereoelectronic influences to be overcome in forging the link between the two saccharide units.

A method of some promise emanated from the observation (Scheme 1) that the novel diene **8** underwent methoxybromination to give α-product **11** quantitatively and exclusively (14). Predominant, although not exclusive, axial addition might have been anticipated since bromination of **8** would produce the highly delocalized allyl oxocarbonium ion **9***a*. Entry of the alcohol at the electron-deficient centre at C-1 could occur from above, leading to the β product **10**, or below, leading to the α product **11**. The latter allows for greater continuous overlap in going from the transition state to product and is therefore more favourable. This principle was originally enunciated by Corey in order to rationalize the initial formation of the axial halide as the kinetic product in the α-halogenation of ketones (15). However the first formed glycoside here, **11**, has the benefit of the anomeric effect (12, 16) and is therefore the preferred product.

To these favourable electronic considerations must be added the encouraging stereochemical circum-

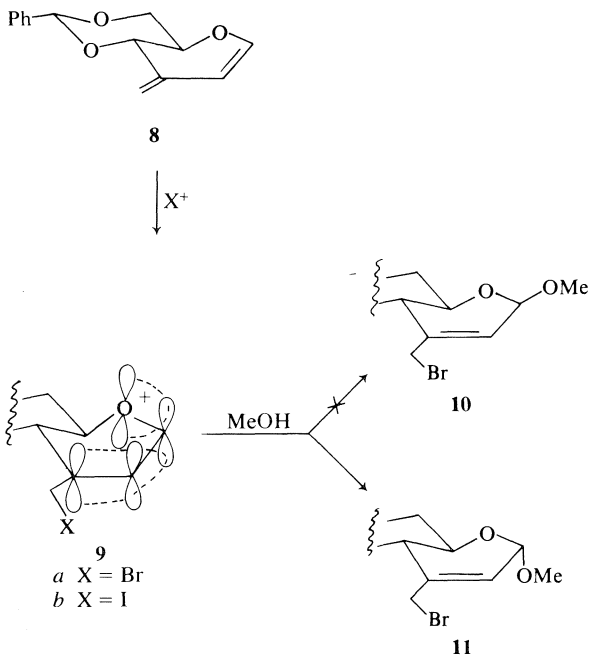

SCHEME 1

stance arising from the planar nature of the ion **9**, so that there are no obstacles in the path of the incoming nucleophile. The total prognosis, therefore, augured well for the addition of the troublesome tertiary alcohol of **3***b* to the α-face of **9**. With this secured the other functional groups would then be added subsequently.

We were mindful of the fact that a similar intermediate **13** can be invoked for the Ferrier reaction,[7] Scheme 2, which also gives a predominance of α-glycoside **14** (17). The use of this procedure for the proposed synthesis would be even more appropriate than our own (Scheme 1), since unlike **11**, compound **14** does not have the extra carbon at C-3 to be subsequently removed. However, our efforts to bring about the reaction of triacetyl glucal (**12**) (13)

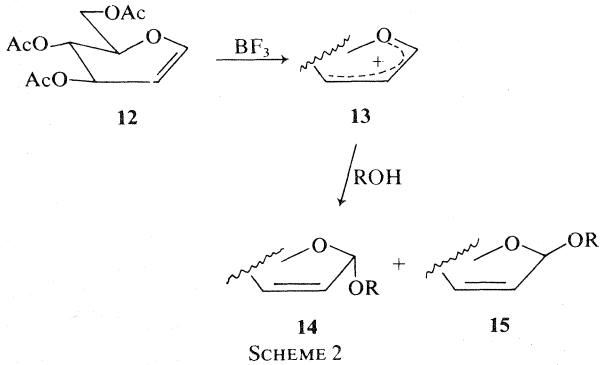

SCHEME 2

[7]However, see refs. 17 and 18 for further discussion.

and tetraacetyl fructose (**3***b*) under the standard Ferrier conditions went completely unrewarded. This was not entirely surprising since it had been reported that **12** undergoes self-condensation rather than glycosidation, when a sugar was used in Scheme 2 in the hope of forming a disaccharide (18).

The Lemieux–Nagabhushan reaction (Scheme 3) is currently widely used for the synthesis of α-glycosides, e.g., **7**α (ref. 19 and references cited therein). Interestingly, the intermediate in these reactions is the nitroso glycal **17**, a canonical form of which is the dipolar species **18** which bears a critical resemblance to **9** and **13**. However, attempts to glycosylate **16** with **3***d* were also unsuccessful in our hands.

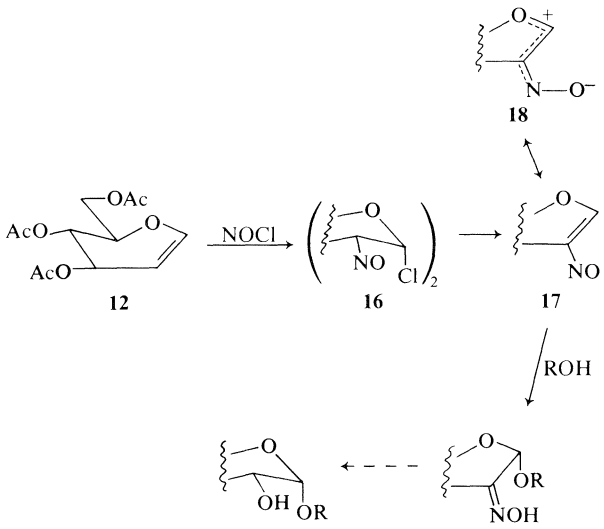

SCHEME 3

The Synthesis[4] (Schemes 4 and 5)

Although the halogen-promoted condensation of the diene **8** and methanol (Scheme 1) had proceeded so efficiently, it was found that with tetraacetyl fructose (**3***b*), the outcome was not encouraging. Reaction of equimolar amounts of **8**, **3***b*, and iodine in chloroform containing silver acetate or silver oxide, did afford a new product which according to tlc monitors had been formed immediately. However its concentration was low and attempts to increase its production either by use of excess iodine or by prolonged reaction times had the opposite effect. The reactive nature of the iodide in **20** was considered to be the cause of the extreme lability, but attempts to stabilize the product by solvolysis to the acetate ($Et_4N^+AcO^-$, benzene) led to decomposition.

The use of iodonium dicollidine perchlorate (**19**; $I^+(collidine)_2ClO_4^-$) as a ready source of iodonium

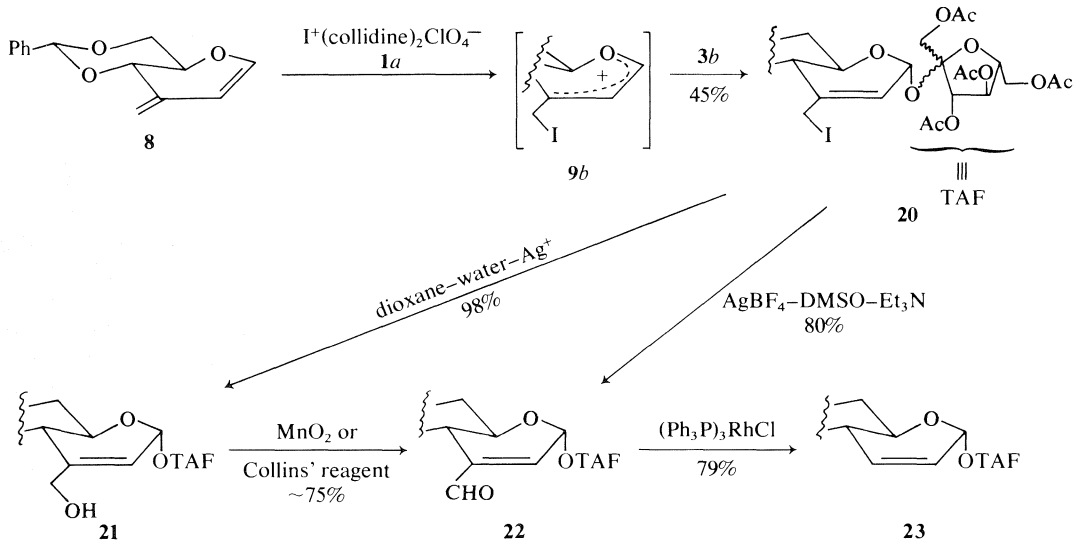

SCHEME 4

ions has been developed by Lemieux and Morgan (20) and it seemed ideal for our purposes particularly because of the nonnucleophilic counterion. With chloroform as solvent, the condensation product was formed but again it decomposed. However the condensation proceeded smoothly in benzene and the product (**20**) could be isolated in 45% yield (Scheme 4).

There were two other components in the product and one of these proved, upon isolation, to be unreacted tetraacetyl fructose (**3***b*). The other had the same R_f value as the diene **8** but it was different. Unfortunately it proved to be unstable and decomposed upon attempts to isolate it chromatographically, liberating molecular iodine.

The foregoing indicates that **20** was the only reaction product arising from the union of **8** and **3***b*. In view of its high reactivity, **20** was immediately solvolysed to the allylic alcohol **21**.

We had planned to remove the 'extra' carbon by decarbonylation (21) of the aldehyde **22** to give the alkene **23**. To this end, the alcohol was oxidised smoothly with either manganese dioxide or Collins' reagent (22). Alternatively, the iodide **20** could be oxidised directly to **22** by the procedure of Ganem and Boeckman (23).

It was our expectation based on the precedent in Scheme 1, that the orientation at C-1 of the pyranose residue of the condensation product **20** would be exclusively α, but since the tetraacetyl fructose (**3***b*) used was a mixture of α and β anomers, we expected to obtain two products differing in the anomeric configuration of the furanose portion. Indeed, patient, repeated silica column chromatography of the alcohol **21** and aldehyde **22** did afford the components **21**α, **21**β, **22**α, and **22**β which were all noncrystalline. Their identities were cross-checked by oxidation whereby **21**α gave **22**α, and **21**β gave **22**β, and their structures were confirmed spectroscopically (8).

The demands of these fractionations were so daunting that it was decided to use the mixtures (**21**–**23**) of furanose anomers in the hope that a more opportune stage for separation would arise subsequently.

The task was now to add equatorially oriented hydroxyl groups to the olefinic centres of **23**. A model study was carried out on the related monosaccharide **24** (Scheme 5) and it was advantageous that the transformation products **25** (24), **26** (25), and **27** (26) had already been reported in the literature. Thus the conversion of **24** into **28** was examined by us, and an overall yield of 45% was achieved.[8]

Accordingly, osmylation (24) of the alkene **23** gave the diol **29** in 75% yield. The problem of inverting the configuration at C-2 was solved by taking advantage of the greater reactivity of the equatorial hydroxyl group towards acylation (25). Thus benzoylation of **29** at −30°C in pyridine – methylene chloride solution (1:1) gave **30** (75%), which was oxidised with Collins' reagent (22) to **31** (80%). The latter was treated with excess sodium borohydride in methanol (27) and the product acetylated to give **32** (87%).

4,6-*O*-Benzylidenesucrose (**32**β) has recently been prepared by Khan by treating sucrose (**1***a*) with benzal bromide followed by acetic anhydride (28). Nucleation of our synthetic substance **32** with a

[8]This study was carried out by D. J. Balcarras as part of his year IV research project, University of Waterloo, Waterloo, Ont., 1974.

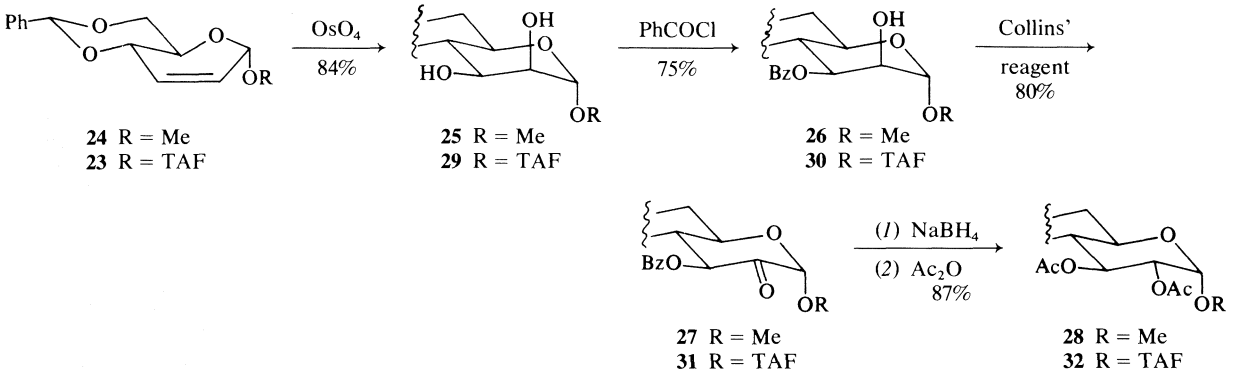

SCHEME 5

sample of the material obtained from Dr. Khan caused fractional crystallisation of the desired **32**β, identified as such by mixture melting point and microanalytical data.

Since **32**β can be debenzylidenated and converted to sucrose (**1***a*) or its octaacetate (**1***b*) the foregoing constitutes a total synthesis of sucrose.

In view of the fact that the intermediate (**13**) in the Ferrier reaction (17) (Scheme 2) and that (**9**) in our reaction (Scheme 1) are both allyl oxocarbonium ions, the complete failure of the former to react with the alcohol **3***b* is deserving of comment. The major difference between **9** and **13** is the C-3 substituent but the electron-withdrawing nature of the halomethyl group should make **9** *less stable* than **13** and concomitantly *less* prone to react with the hindered alcohol (**3***d*). A more probable reason might be sought in the differing conditions utilized in the two procedures. Thus the Lewis acid catalyst used in the Ferrier reaction undoubtedly complexes with the hydroxyl group of the alcohol thereby increasing its bulk and reducing its nucleophilicity.

In the light of the failure of the tertiary alcohol **3***b* to undergo the other α-glycosylation reactions summarized in Schemes 2 and 3 (*vide supra*), it appeared that the haloalkoxylation procedure would be even more efficient with less hindered alcohols.

An interesting alcohol for the test is cholesterol which undergoes both the Ferrier (Scheme 2) and Lemieux–Nagabhushan (Scheme 3) reactions. Accordingly, reaction of diene **8** with cholesterol as in Scheme 4 gave a product which was isolated chromatographically. The derived alcohol **33** (Scheme 6) was characterized as the benzoate. The α configuration was assigned on the basis of the H-1 absorption (5.21 ppm) which corresponds well with that (5.18 ppm) for the analogue **14** (R = cholesteryl). The yield of the latter from the Ferrier reaction (Scheme 2) was 50% (17); of **7**α (R = cholesteryl) in the Lemieux–Nagabhushan reaction (Scheme 3), 73.5% (29); and of **33** (Scheme 5), 84%.

The α-enone alcohol (cf. **34**) is a sensitive substance (30) and should therefore provide a test for the mildness of the condensation. In fact the iodinated disaccharide was obtained quantitatively as was the alcohol **34**. The latter was a crystalline material and its configuration was assigned on the basis of H-1 (5.12 ppm).

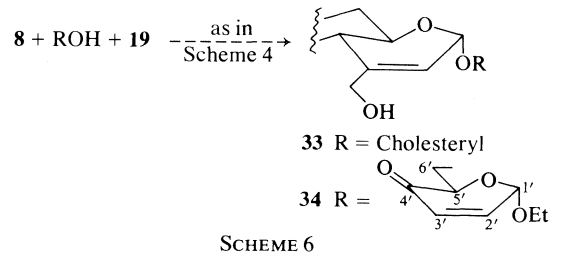

SCHEME 6

Experimental

General

The progress of all reactions was followed by thin-layer chromatography (tlc) which was performed on 5 cm × 20 cm and/or 20 cm × 20 cm glass plates coated with silica gel (HF-254, E. Merck) to a thickness of 0.3 mm. The chromatograms were first viewed under ultraviolet light, then sprayed with concentrated sulfuric acid, and finally heated in an oven at 110°C. Column chromatography was performed using silica gel 60 particle size 0.063–0.20 mm (70–230 mesh ASTM, E. Merck). Melting points were determined in capillary tubes in a Mel-Temp block and are uncorrected. Elemental analyses were performed by Microanalyses Laboratory, Toronto, Ont.

All solvents were removed on a rotary evaporator under reduced pressure at 40°C and the residues dried under high vacuum.

*Methyl 4,6-*O*-Benzylidene-1,2,3-trideoxy-3-*C*-methylene-*D*-erythro-hex-1-enopyranoside (**8**)*

The diene **8** was prepared by one of the six synthetic routes developed in our laboratory (31).

*1,3,4,6-Tetra-*O*-acetyl-*D*-fructofuranose (**3**b)*

The tetraacetate **3***b* was prepared from inulin by the method of Binkley and Wolfrom (**9***d*).

1′,3′,4′,6′-Tetra-O-*acetyl*-α *and* β-D-*fructofuranosyl 4,6*-O-*Benzylidene-2,3-dideoxy-3*-C-*(iodomethyl)*-α-D-erythro-*hex-2-enopyranoside (**20**)*

Freshly prepared (20) iodonium dicollidine perchlorate, **19** (1.40 g, 3.0 mmol) was added in small portions, over a 20-min period, to a solution of the diene **8** (460 mg, 2.0 mmol) and tetraacetyl fructofuranose (**3***b*) (3.48 g, 10.0 mmol) in anhydrous benzene (46 mL). During this time, the reaction mixture turned a light yellow colour as the powdery iodonium ion complex was consumed and replaced by microcrystalline collidinium perchlorate. The excess reagent was precipitated by the addition of diethyl ether (50 mL) to the reaction mixture. The solids formed were removed by filtration through a bed of Celite. The filter cake was washed with more diethyl ether and the filtrate extracted with saturated aqueous sodium thiosulfate, 5% hydrochloric acid, saturated aqueous sodium bicarbonate, and water. The organic layer was dried (Na_2SO_4) and concentrated to yield a syrupy residue which was immediately subjected to silica column chromatography. Elution with ethyl acetate – petroleum ether (30–60°C) (1:1) gave the material with R_f 0.48 in the same solvent system; yield 635 mg (45%). This compound which was judged by nmr to be the title compound, **20** (8), was unstable and decomposed at room temperature overnight or in the freezer (−15°C) within several days.

1′,3′,4′,6′-Tetra-O-*acetyl*-α *and* β-D-*fructofuranosyl 4,6*-O-*Benzylidene-2,3-dideoxy-3*-C-*(hydroxymethyl)*-α-D-erythro-*hex-2-enopyranoside (**21**)*

The iodide **20** (635 mg, 0.902 mmol) was dissolved in 25% aqueous dioxane (75 mL) and treated with silver carbonate (2.5 g, 9.0 mmol) and 1 *M* silver perchlorate (2.3 mL, 2.3 mmol). The mixture was stirred for 4 h at room temperature after which time tlc showed that an homogeneous product had formed (R_f 0.26, ethyl acetate – petroleum ether (30–60°C) (1:1)). The silver salts were removed by filtration through a bed of Celite and the filter cake was washed with chloroform (75 mL). The filtrate was extracted with water (50 mL). This aqueous extract was washed once with chloroform (75 mL). The combined organic layers were extracted with water, dried (Na_2SO_4), and concentrated to afford the title compound; yield 525 mg (98%). Compound **21** was resolved into its two anomers **21**α and **21**β by repeated silica column chromatography with diethyl ether – benzene (1:1) as eluant. These were converted into the aldehydes **22**α and **22**β, respectively, by oxidation with chromium trioxide – dipyridine complex in methylene chloride.

Spectroscopic data for **21**, **21**α, and **21**β are presented in the accompanying paper (8).

1′,3′,4′,6′-Tetra-O-*acetyl*-α- *and* β-D-*fructofuranosyl 4,6*-O-*Benzylidene-2,3-dideoxy-3*-C-*formyl*-α-D-erythro-*hex-2-enopyranoside (**22**)*

Method A

The allylic alcohol **21** (525 mg, 0.884 mmol) was dissolved in anhydrous methylene chloride (50 mL) and treated with chromium trioxide – dipyridine complex (22) (2.72 g, 10.6 mmol). Thin-layer chromatography showed that after 1 h, a faster running product had formed (R_f 0.34, ethyl acetate – petroleum ether (30–60°C) (1:1)). The reaction mixture was diluted with diethyl ether (50 mL) and the solid residue formed was removed by filtration through a bed of Celite. The filter cake was washed with diethyl ether and the filtrate was extracted with 5% hydrochloric acid, saturated aqueous sodium bicarbonate, and water. The dried (Na_2SO_4) organic layer after concentration afforded the title compound; yield 398 mg (76%). Compound **22** was resolved into **22**α and **22**β by silica column chromatography with diethyl ether – benzene (1:1) as eluant.

Method B

A solution of the allylic alcohol **21** (164 mg, 0.276 mmol) and manganese dioxide (1.4 g) in tetrahydrofuran (32 mL) was stirred at room temperature for 48 h. The manganese dioxide was removed by filtration through a bed of Celite and the filtrate evaporated to give the aldehyde **22**; yield 119 mg (73%). This material had physical properties identical to those of the material prepared by method A.

Method C (23)

The iodide **20** (95 mg, 0.135 mmol) was dissolved in anhydrous dimethyl sulfoxide (0.5 mL) and treated with silver tetrafluoroborate (39.5 mg, 0.203 mmol). The reaction mixture was stirred at room temperature for 10 min during which time a yellow precipitate formed. Anhydrous triethyl amine (0.05 mL) was added to the reaction mixture and stirring was continued for another 5 min. (*Caution*: Stirring with triethyl amine for periods longer than 5 min caused partial deacetylation of the product.) The aldehyde **22** was isolated by extraction with diethyl ether (3 × 20 mL). The combined extracts were washed with water (3 × 20 mL), dried (Na_2SO_4), and concentrated to afford **22**; yield 64 mg (80%).

For **22**: ir ν_{max}: 1670 (trisubstituted olefin), 1705 (α,β-unsaturated aldehyde), 1745 (OAc), 2860, 2920 (aldehyde) cm^{-1}.

Additional spectroscopic data for **22**, **22**α, and **22**β are presented in the accompanying paper (8).

1′,3′,4′,6′-Tetra-O-*acetyl*-α- *and* β-D-*fructofuranosyl 4,6*-O-*Benzylidene-2,3-dideoxy*-α-D-erythro-*hex-2-enopyranoside (**23**)*

A solution of the aldehyde **22** (398 mg, 0.672 mmol) in anhydrous benzene (40 mL) was stirred with tris(triphenylphosphine)chlororhodium (21) at 80°C for 1 h. Thin-layer chromatography then showed that an homogeneous product had formed (R_f 0.44, ethyl acetate – petroleum ether (30–60°C) 1:1)). During this time, the reaction mixture changed from the burgundy colour of the starting complex to the beige colour of the carbonylated complex. The reaction mixture was concentrated and treated with either diethyl ether or ethanol. The inorganic complex which precipitated was removed by filtration. The filtrate was concentrated and purified from some residual inorganic material by filtration down a short column of silica gel. Elution with ethyl acetate – petroleum ether (30–60°C) (1:1 gave syrupy **23**; yield 300 mg (79%)). The absence of the aldehyde group was readily apparent from nmr and ir spectra. Additional spectroscopic data for **23** are presented in the accompanying paper (8).

1′,3′,4′,6′-Tetra-O-*acetyl*-α- *and* β-D-*fructofuranosyl 4,6*-O-*Benzylidene*-α-D-*mannopyranoside (**29**)*

A 0.10 *M* solution of osmium tetroxide in pyridine and a solution of sodium bisulfite (1.8 g) in water (30 mL) and pyridine (20 mL) were prepared for use in the hydroxylation experiments. The olefin **23** (120 mg, 0.213 mmol) was allowed to react with the solution of osmium tetroxide (2.4 mL, 0.24 mmol) for 20 h at room temperature. As the reaction proceeded, the colour of the mixture turned from light yellow to dark brown or black. This colour change was accompanied by the precipitation of the pyridine-complexed osmate ester of the olefin. The latter was decomposed by the addition of a portion of the sodium bisulfite solution (3.4 mL) and stirring continued for another 4 h. The resulting orange solution was extracted with methylene chloride (6 × 10 mL) and the extract dried (Na_2SO_4) and concentrated to give syrupy

homogeneous **29**; yield 107 mg (84%) (R_f 0.12, ethyl acetate – petroleum ether (30–60°C) (1:1) or R_f 0.44, ethyl acetate).

The mass spectrum of **29** showed peaks at *m/e* 251 (hexopyranosyl cation), 331 (ketofuranosyl cation), and those characteristic of benzylidene acetals (see ref. 8). In the infrared: ν_{max}: 3300–3650 (OH) cm^{-1}.

*1′,3′,4′,6′-Tetra-*O*-acetyl-α and* β-D-*fructofuranosyl 2,3-di-*O*-Acetyl-4,6-*O*-benzylidene-*α-D-*glucopyranoside (**32**)—Synthetic 4,6-*O*-Benzylidenesucrose Hexaacetate (**32**β)*

A solution of benzoyl chloride (0.15 mL, 1.79 mmol) in anhydrous methylene chloride (20 mL) was prepared. The diol **29** (107 mg, 0.179 mmol) was dissolved in anhydrous pyridine (2 mL) and cooled to −30°C. To this solution was added a portion of the above benzoyl chloride solution (2 mL) representing one equivalent of that reagent. After stirring for 5 h, tlc showed that a trace unreacted starting material and that an homogeneous product (R_f 0.34, ethyl acetate – petroleum ether (30–60°C) (1:1)) had formed. A slight excess of the benzoyl chloride solution (0.05 mL) was added and stirring continued for another 5 h. The product (**30**) was isolated by conventional chloroform extraction procedures; yield 94 mg (75%).

A portion of this material (70 mg, 0.10 mmol) was oxidized with chromium trioxide – dipyridine complex (22) (1.5 g) in methylene chloride (15 mL). The product (**31**) was isolated in the usual manner; yield 56 mg (80%).

The latter was dissolved in methanol (30 mL) and treated with excess sodium borohydride (600 mg). The mixture was stirred for 4 h at room temperature and the excess reagent was then destroyed by dropwise addition of acetic acid. The mixture was concentrated to dryness and the resulting residue was dissolved in anhydrous pyridine (15 mL), cooled to 0°C, and allowed to react with acetic anhydride (15 mL) overnight. The reaction mixture was cooled in ice and the excess reagent destroyed by dropwise addition of methanol. The mixture was extracted several times with chloroform and the extracts were washed with dilute hydrochloric acid, aqueous sodium bicarbonate and then dried Na_2SO_4. The product (**32**) 44 mg (87%) was homogeneous on tlc and had an R_f value identical with that of an authentic sample of **32**β (28) (R_f 0.30, benzene – diethyl ether (1:1)). The mass spectrum of **32** showed peaks at *m/e*: 632 (M), 335 (hexopyranosyl cation), 331 (ketofuranosyl cation), and those characteristic of benzylidene acetals (see ref. 8).

Nucleation of a solution of **32** in diethyl ether – petroleum ether with an authentic sample of **32**β kindly supplied by Dr. Khan (28) afforded the desired material, mp 162–164°C; mixture mp 161.5–163°C; authentic sample mp 162.5–164°C. *Anal.* calcd. for $C_{31}H_{38}O_{17}$: C 54.55, H 5.61; found: C 54.71, H 5.64. Additional spectroscopic data for **32** and **32**β are presented in the accompanying paper (8).

*Cholesteryl 4,6-*O*-Benzylidene-2,3-dideoxy-3-*C*-(hydroxymethyl)-*α-D-*erythro-hex-2-enopyranoside (**33**) and its Benzoyl Derivative*

Iodonium dicollidine perchlorate (**19**) (20) (352 mg, 0.75 mmol) was added in portions over 20 min to a solution of the diene **8** (115 mg, 1.0 mmol) and cholesterol (387 mg, 1.0 mmol) in anhydrous benzene (10 mL). The reaction mixture was worked up as previously described above for **20**. The product (R_f 0.70, ethyl acetate – petroleum ether (30–60°C) (1:4)) was isolated by silica column chromatography (yield 310 mg, 84%) and was immediately dissolved in dioxane (37 mL) and water (5 mL) and treated with silver carbonate (1.38 g) and 1 *M* silver perchlorate (5 mL). The mixture was stirred at room temperature for 4 h after which time tlc showed that an homogeneous product had formed (R_f 0.25, ethyl acetate – petroleum ether (30–60°C) (1:4)). The product **33** was isolated as previously described for **21**; yield 249 mg (95%). This compound jelled on all attempts at crystallization and was therefore characterized as its benzoate ester, prepared in 90% yield via standard procedures.

In the mass spectrum of **33**, no molecular ion was observed but peaks at *m/e* 351 and 385 owing to cleavage of the glycosidic bond were readily apparent (8). Also present were the peaks characteristic of benzylidene acetals. In the infrared: ν_{max}: 1740 (aryl ester) cm^{-1}.

The ^{1}Hmr spectrum of **33** at 60 MHz showed ($CDCl_3$, TMS) δ: 0.5–2.6 (m, 44, cholesteryl protons), 3.6–4.6 (m, 4, H-4, H-5, H-6a, H-6e), 5.0 (m, 2, benzoxymethyl), 5.21 (m, 1, H-1), 5.36 (m, 1, cholesterylic olefin), 5.60 (s, 1, benzylidene methine), 5.80 (m, 1, H-2), 7.2–8.2 (m, 10, aromatic protons).

The benzoate of **33** was recrystallized from ethanol; mp 132–134°C. *Anal.* calcd. for $C_{48}H_{64}O_6$: C 78.22, H 8.75; found: C 78.39, H 8.59.

*Ethyl 2,3-Dideoxy-6-*O*-(4,6-*O*-benzylidene-2,3-dideoxy-3-*C*-(hydroxymethyl)-*α-D-*erythro-hex-2-enopyranosyl)-*α-D-glycero-*hex-2-enopyranosid-4-ulose (**34**)*

Iodonium dicollidine perchlorate (**19**) (20) (352 mg, 0.75 mmol) was added in portions over a period of 29 min to a solution of the diene **8** (115 mg, 0.50 mmol) the enone **97** (30) (172 mg, 1.0 mmol) in anhydrous benzene (10 mL). The reaction mixture was worked-up as previously described for **20** and the product (R_f 0.47, ethyl acetate – petroleum ether (30–60°C) (1:1)) was isolated by silica column chromatography; yield 264 mg (100%). The material was immediately dissolved in dioxane (26 mL) and water (5 mL) and treated with silver carbonate (1.38 g) and 1 *M* silver perchlorate (5 mL) at room temperature for 3 h after which time tlc showed that an homogeneous product had formed (R_f 0.26, ethyl acetate – petroleum ether (30–60°C) (1:1)). The product (**34**) was isolated as previously described; yield 210 mg (100%).

In the mass spectrum of **34**, peaks were observed at *m/e*: 419 (M + 1), 418 (M), 401 (M + 1 − H_2O), 400 (M − H_2O), 374 (M + 1 − OEt), 373 (M − OEt), and those characteristic of benzylidene acetals (8). Also prevalent were the peaks due to cleavage of the disaccharide linkage (i.e., *m/e* 247 and 171).

The ^{1}Hmr spectrum of **34** at 60 MHz showed ($CDCl_3$, TMS) δ: 1.25 (t, 3, OCH_2CH_3), 1.92 (bs, 1, exchangeable OH), 3.4–4.8 (m, 11, hydroxymethyl, H-4, H-5, H-6a, H-6e, OCH_2CH_3, H-5′, H-6a′, H-6e′), 5.12 (m, 1, H-1), 5.17 (d, 1, H-1′, $J_{1',2'}$ = 5.0 Hz), 5.60 (s, 1, benzylidene methine), 5.71 (m, 1, H-2′), 6.15 (d, 1, H-3′, $J_{2',3'}$ = 10.0 Hz), 6.92 (dd, 1, H-2′), 7.2–7.7 (m, 5, aromatic protons).

Compound **34** was recrystallized from diethyl ether – petroleum ether (30–60°C); mp 97–99°C. *Anal.* calcd. for $C_{22}H_{26}O_8$: C 63.15, H 6.26; found: C 63.12, H 6.37.

Acknowledgements

We are grateful to the National Research Council of Canada and Bristol Laboratories (Syracuse) for financial support of this work. We also express our thanks to Dr. Riaz Khan for a generous gift of compound **31**β (28).

1. J. Yudkin. *In* Sugar. *Edited by* J. Yudkin, J. Edelman, and L. Hough. Butterworths, London. 1971.
2. C. A. Beevers and W. Cochran. Proc. R. Soc. London Ser. A, **190**, 257 (1947).
3. G. M. Brown and H. A. Levy. Science, **141**, 921 (1963).

4. R. U. LEMIEUX and J. P. BARRETTE. J. Am. Chem. Soc. **80**, 2243 (1958).
5. R. U. LEMIEUX and G. HUBER. J. Am. Chem. Soc. **75**, 4118 (1953); **78**, 4117 (1956).
6. D. E. ILEY and B. FRASER-REID. J. Am. Chem. Soc. **97**, 2563 (1975).
7. C. SCHUERCH. Acc. Chem. Res. **6**, 184 (1973).
8. D. E. ILEY and B. FRASER-REID. Can. J. Chem. This issue.
9. (*a*) E. FISCHER and M. DELBRUCK. Ber. **42**, 2776 (1909); (*b*) J. C. IRVINE, J. W. H. OLDHAM, and A. F. SKINNER. J. Am. Chem. Soc. **51**, 1279 (1929); (*c*) A. PICTET and H. VOGEL. C. R. Acad. Sci. **186**, 724 (1928); (*d*) W. W. BINKLEY and M. L. WOLFROM. J. Am. Chem. Soc. **68**, 2171 (1946).
10. A. KLEMER and B. DIETZEL. Tetrahedron Lett. 275 (1970).
11. G. R. NEWKOME, J. D. SAUER, V. K. MAJESTIC, N. S. BHECIA, H. D. BRAYMER, and J. D. WANDER. Carbohydr. Res. **48**, 1 (1976).
12. R. U. LEMIEUX. *In* Molecular rearrangements. *Edited by* P. de Mayo. Interscience, New York, NY. 1964.
13. R. K. NESS and H. G. FLETCHER. Carbohydr. Res. **17**, 465 (1971).
14. B. FRASER-REID and B. RADATUS. Can. J. Chem. **50**, 2919 (1972).
15. E. J. COREY and R. A. SNEEN. J. Am. Chem. Soc. **78**, 6269 (1956).
16. B. CAPON. Chem. Rev. **69**, 407 (1969).
17. R. J. FERRIER and N. PRASAD. J. Chem. Soc. C, 570 (1969).
18. R. J. FERRIER. Adv. Carbohydr. Chem. **24**, 199 (1969).
19. R. U. LEMIEUX, T. L. NAGABHUSHAN, K. J. CLEMETSON, and L. C. N. TUCKER. Can. J. Chem. **51**, 53 (1973).
20. R. U. LEMIEUX and A. R. MORGAN. Can. J. Chem. **43**, 2190 (1965).
21. G. WILKINSON. J. Chem. Soc. A, 1711 (1966); J. TSUJI and K. OHNO. Synthesis, **1**, 157 (1969).
22. J. C. COLLINS, W. W. HESS, and F. FRANK. Tetrahedron Lett. 3363 (1968).
23. B. GANEM and R. K. BOECKMAN, JR. Tetrahedron Lett. 917 (1974).
24. C. L. STEVENS, J. B. FILIPPI, and K. G. TAYLOR. J. Org. Chem. **31**, 1292 (1966); S. MCNALLY and W. G. OVEREND. J. Chem. Soc. C, 1978 (1966).
25. A. C. RICHARDSON and J. M. WILLIAMS. Tetrahedron, **23**, 1641 (1967).
26. F. R. SEYMOUR. Carbohydr. Res. **34**, 65 (1974).
27. R. U. LEMIEUX, K. JAMES, and T. L. NAGABHUSHAN. Can. J. Chem. **51**, 27 (1973).
28. R. KHAN. Carbohydr. Res. **32**, 375 (1974).
29. R. U. LEMIEUX and T. L. NAGABHUSHAN. Methods Carbohydr. Chem. **6**, 487 (1972).
30. B. FRASER-REID, A. MCLEAN, and E. W. USHERWOOD. Can. J. Chem. **48**, 2977 (1970).
31. D. E. ILEY, S. Y-K. TAM, and B. FRASER-REID. Carbohydr. Res. **55**, 193 (1977).

A stereoselective synthesis of sucrose.[1] Part III.[2] Spectroscopic analyses of key intermediates

DAVID ERLE ILEY[3] AND BERT FRASER-REID

Guelph–Waterloo Centre for Graduate Work in Chemistry, Waterloo Campus, University of Waterloo, Waterloo, Ont., Canada N2L 3G1

Received June 29, 1978

DAVID ERLE ILEY and BERT FRASER-REID. Can. J. Chem. **57**, 653 (1979).

Condensation of the diene **1** with the α,β-anomeric mixture of tetraacetyl fructofuranose and processing of the resulting product gives rise to a series of disaccharides, **5**, **6**, and **7**, each of which is a mixture of two substances differing only in the anomeric configuration at the fructosyl centre, the linkage at the pyranosyl moiety being α in all cases. This conclusion is reached by careful comparison of the ^{1}Hmr and ^{13}Cmr spectra of these disaccharides with those of a number of fructofuranose derivatives. There are interesting correlations in configuration, conformation, and optical rotation.

DAVID ERLE ILEY et BERT FRASER-REID. Can. J. Chem. **57**, 653 1979).

La condensation du diène **1** avec le mélange des anomères α et β du tétraacétyl fructofurannose et la transformation du produit qui en résulte donne lieu à la série de disaccharides **5**, **6** et **7**; dans chaque cas, il s'agit d'un mélange de deux produits qui ne diffèrent que par la configuration du carbone anomère de la portion fructoyle puisque la liaison avec la moitié pyrannosyle est α dans tous les cas. On peut tirer cette conclusion en se basant sur une comparaison soignée des spectres rmn du ^{1}H et du ^{13}C de ces disaccharides avec ceux d'un certain nombre de dérivés fructofurannoses. On peut déduire des corrélations intéressantes concernant la configuration, la conformation et la rotation optique.

[Traduit par le journal]

In the accompanying paper (1) we gave details of a novel synthesis of sucrose. In spite of the theoretical considerations upon which the synthetic plan was devised, we were assured of the validity of our approach only at the final stages when a substance having the sucrosyl skeleton was finally isolated. Admittedly, the halogen-promoted addition of methanol to the diene **1** to give the α-glycoside **3** exclusively, was a promising precedent (2). However it is known that with glycosidation reactions, changing from simple to complex alcohols sometimes causes drastic variations not only in the stereochemistry (see, for example, ref. 3) but even in the pattern of the reaction (4). Thus unquestioning reliance upon our precedent seemed ill-advised and we therefore sought assurances by making detailed spectroscopic analyses of our key intermediates. Many of the latter are interesting in their own right, for being highly functionalised and amenable to diverse chemical manipulations they are promising synthons for the preparation of branched-chain and other modified sugars. In this paper we therefore describe various aspects of these spectroscopic studies.

Reaction of diene **1** with tetraacetyl fructose **2**, in the presence of iodonium dicollidine perchlorate gave the iodide **4** which was immediately solvolysed to the alcohol **5**. Oxidation of the latter gave the aldehyde **6**, decarbonylation of which gave the alkene **7** (1). The structures of these key intermediates were

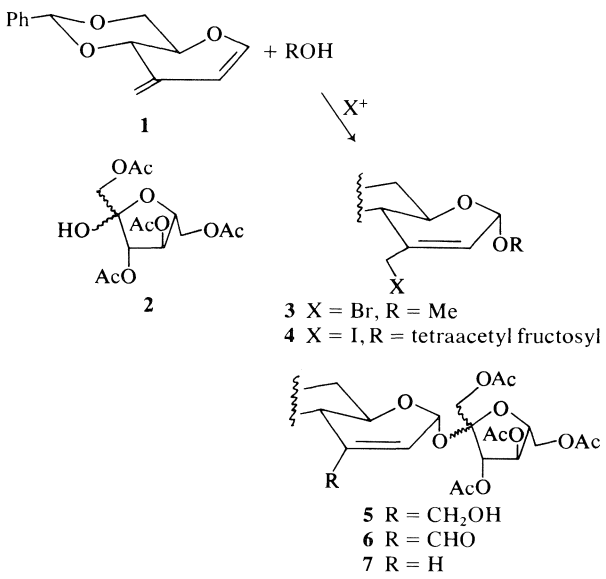

SCHEME 1

[1]Dedicated to Professor Sir Derek Barton on the occasion of his 60th birthday.

[2]For Part II, see the accompanying paper (1).

[3]Holder of the NRCC Studentship 1973–1975. Taken from the M.Sc. Thesis of D.E.I., University of Waterloo, 1975. Present address: Ontario Hydro, W. P. Dobson Laboratories, 800 Kipling Ave., Toronto, Ont.

0008-4042/79/060653-09$01.00/0

studied by mass spectroscopy, and proton and carbon-13 magnetic resonance.

Experimental

Proton magnetic resonance (^{1}Hmr) spectra were determined, unless otherwise stated, in deuteriochloroform containing 1% tetramethylsilane (TMS) as internal standard with either a Varian T-60 or Varian HR-220 spectrometer.[4] Coupling constants were obtained by measuring the spacings of spectra judged to be first order. Infrared (ir) spectra were determined on a Beckman model IR-10 spectrometer using 0.1-mm sodium chloride solution cells, chloroform being the solvent used. Mass spectra were determined on a Hitachi mass spectrometer model RMU-6E. Carbon-13 nuclear magnetic resonance (^{13}Cmr) spectra were recorded on a Bruker HX-90 spectrometer, operating at 22.63 MHz and equipped with a Nicolet 1083 instrument computer for Fourier transform spectroscopy.[5] The spectra were recorded in deuteriochloroform. The latter showed its characteristic absorptions at 78.5, 77.2, and 75.7 ppm downfield from tetramethylsilane.

Optical rotations were measured on a Carl Zeiss model LEP nür 370740 Lichtelektrisches Präzisionpolarimeter at 546 and 578 nm at 23°C.

Most of the compounds described in this paper are benzylidene acetals. The benzylidene group was detected by a five-proton multiplet at about 7.40 ppm (aromatic) and a one-proton singlet at about 5.60 ppm (H-7, benzylidene methine) in the ^{1}Hmr spectra. At 60 MHz the H_4, H_5, H_{6a}, and H_{6e} resonances formed a multiplet at about 3.7–4.6 ppm. The mass spectra of benzylidene acetals show, characteristically, peaks at *m/e*: 149 ($PhCHOCH_2CHO^+$), 106 ($PhCHO^+$), 105 ($PhCO^+$), 91 ($C_7H_7^+$), and 77 ($C_6H_5^+$). The compounds studied were obtained as described in the accompanying paper (1).

Results and Discussion

Mass Spectra

The mass spectra of **5** and **6** gave molecular ions

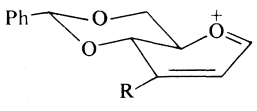

8 R = CH_2OH *m/e* 247
9 R = CHO *m/e* 245
10 R = H *m/e* 217

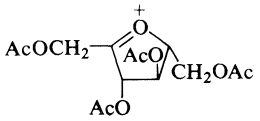

m/e 331
11

at *m/e* 594 and 592, respectively. Although the conventional electron impact mass spectrum of **7** failed to produce a molecular ion, field ionization mass spectroscopy showed a molecular ion at *m/e* 564 and chemical ionization mass spectroscopy gave a large peak at 582 representing the $M + NH_4^+$ ion corresponding to *m/e* 564.

The most readily observed fragmentation of these glycosides is cleavage of the glycosidic bond (5). Thus the mass spectra of **5**, **6**, and **7** showed peaks at *m/e*: 247, 245, and 217 attributed, respectively, to the hexopyranosyl cations **8**, **9**, and **10**, and all the spectra contained a relatively intense peak at *m/e* 331 for the ketofuranosyl cation **11**.

^{1}H Nuclear Magnetic Resonance Spectra

The Pyranosyl Moiety

It was anticipated that the chemical shift of H-1 of the simple hex-2-enopyranosides **12**α and **12**β (6) (Fig. 1) could be used as a probe for the determination of the configuration at the anomeric carbon of the pyranosyl residue of the olefinic disaccharides. Thus if the condensation reaction (Scheme 1) had proceeded stereoselectively to give only the α adduct, the H-1 resonance should appear around 4.9 ppm as against 5.3 ppm for the β adduct.

Unfortunately, the 60 MHz spectra of **5**, **6**, and **7** were not resolved well enough in the region of interest to allow such analyses and it was therefore necessary to study the model compounds **12**α, **12**β, **2**, **13**α, and **13**β at 220 MHz in an effort to sort out the complex disaccharide spectra.

The 220 MHz ^{1}Hmr data for **12**α and **12**β in deuterated chloroform, benzene, and pyridine solutions in Table 1 reveal that the different solvents caused only minor variations in chemical shift and that all the spectra were well resolved.

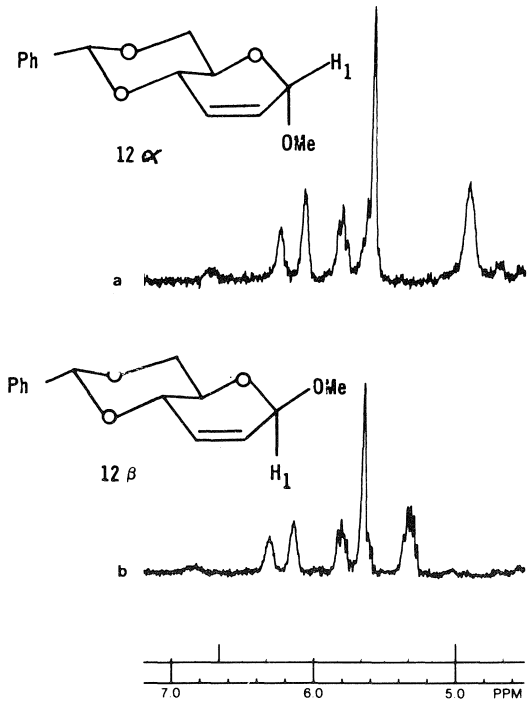

FIG. 1. The H-1 region of the ^{1}Hmr spectra (220 MHz) of compounds **12**α and **12**β.

[4]We are indebted to Dr. A. A. Grey of the Canadian 220 MHz NMR Centre for determining the 220 MHz spectra and for his help in their interpretation.

[5]We are indebted to Professor J. K. Saunders of the Université de Sherbrooke for determining the ^{13}Cmr spectra and for his help in their interpretation.

TABLE 1. ^{1}H nuclear magnetic resonance parameters for the anomeric hex-2-eno-pyranosides **12**α and **12**β

	Chemical shifts					
	12α			**12**β		
Proton	$CDCl_3$	C_6D_6	C_6D_5N	$CDCl_3$	C_6D_6	C_6D_5N
H-1	4.91	4.65	4.99	5.28	4.93	5.34
H-2	5.74	5.50	5.81	5.68	5.42	5.75
H-3	6.14	5.98	6.20	6.16	5.95	6.22
H-4	4.17	3.90	4.26	4.31	4.02	4.40
H-5	3.90	4.02	4.06	3.75	3.62	3.84
H-6a	3.82	3.58	3.90	3.88	3.62	3.95
H-6e	4.33	4.16	4.38	4.31	4.14	4.37
H-7	5.59	5.33	5.75	5.60	5.30	5.77
OMe	3.48	3.17	3.39	3.48	3.25	3.46
Ph	7.35	7.15	7.35	7.35	7.15	7.40
	7.50	7.60	7.70	7.50	7.57	7.70

Coupling constants (Hz)

Compound	$J_{1,2}$	$J_{1,3}$	$J_{1,4}$	$J_{2,3}$	$J_{2,4}$	$J_{3,4}$	$J_{4,5}$	$J_{5,6a}$	$J_{5,6e}$	$J_{6a,6e}$
12α	2.2	<0.2	1.5	10.0	|2.2|	1.0	9.0	9.5	4.5	|9.5|
12β	1.3	|1.2|	2.6	10.0	|2.5|	1.0	8.0	10.0	4.5	|10.0|

The 220 MHz ^{1}Hmr spectra of the methyl fructofuranoside derivatives **13**α and **13**β (7) were more difficult to analyze completely. Fortunately in both spectra the area of interest (4.8–6.0 ppm) was not obscured by the complex absorptions for H-1_a′, H-1_b′, H-5′, H-6_a′, and H-6_b′[6] occurring between 3.8 and 4.8 ppm. The results of the analysis of the area of interest are reported in Table 2 and the spectra in deuteriochloroform are displayed in Fig. 2.

These data can be used to determine the conformation of the furanose rings in **13**α and **13**β. Since $J_{4',5'}$ is the same (5.0 Hz) in both of these compounds but $J_{3',4'}$ is different, it seems probable, on the basis of Karplus considerations (8), that in the conformations of **13**α and **13**β, the dihedral angles must be the same for H-4′ and H-5′ but different for H-3′ and H-4′. The *E*-2 conformations shown for these substances accommodate these parameters. These conformational preferences can be rationalized by noting that because of the anomeric effect, the glycosidic oxygens will favour quasi-axial orientations (9) in both forms, and that the bulky acetoxymethyl groups should prefer to occupy quasi-equatorial orientations. It is noteworthy that in these conformations eclipsing interactions of large substituents are minimised.

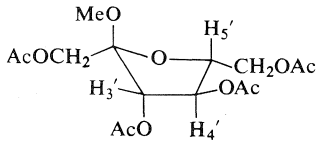

13α

$\phi_{3',4'} \simeq 100°$; $J_{3',4'} = 2.0$ Hz

$\phi_{4',5'} \simeq 120°$; $J_{4',5'} = 5.0$ Hz

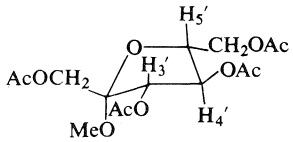

13β

$\phi_{3',4'} \simeq 140°$; $J_{3',4'} = 7.0$ Hz

$\phi_{4',5'} \simeq 120°$; $J_{4',5'} = 5.0$ Hz

The purpose of the foregoing model studies was to gain a better basis for analyzing the spectra of the disaccharides. It was hoped that the condensation of **1** and **2** would produce only two diastereomers arising from the presence of both the α and β anomeric forms of **5**. After prolonged efforts, it was found possible to resolve **5** into two components by chromatographic fractionation but the required procedure was so tedious that only small amounts of pure **5**α and **5**β could be accumulated. Unfortunately, these did not crystallize but their ^{1}Hmr spectra at 220 MHz were recorded.

Although the spectra were extremely complex, the 4.8–6.0 ppm regions displayed in Fig. 3 could be partially analyzed on a first-order basis. A visual comparison of the H-3′ and H-4′ resonances in Figs. 2 and 3 was undertaken to permit the assignment of configuration of the fructofuranosyl residues as shown in **5**α and **5**β. Thus, the slower running component **5**α was judged to possess the α-fructofuranosyl residue. The similar coupling constants, $J_{3',4'}$ and $J_{4',5'}$ (see Tables 2 and 3) in **5**α and **13**α imply that the furanose ring in the disaccharide **5**α is also in the *E*-2 conformation as was deduced above for **13**α. In contrast, the faster running component,

[6]The primed numbers will be used to refer to positions in the fructofuranose residue.

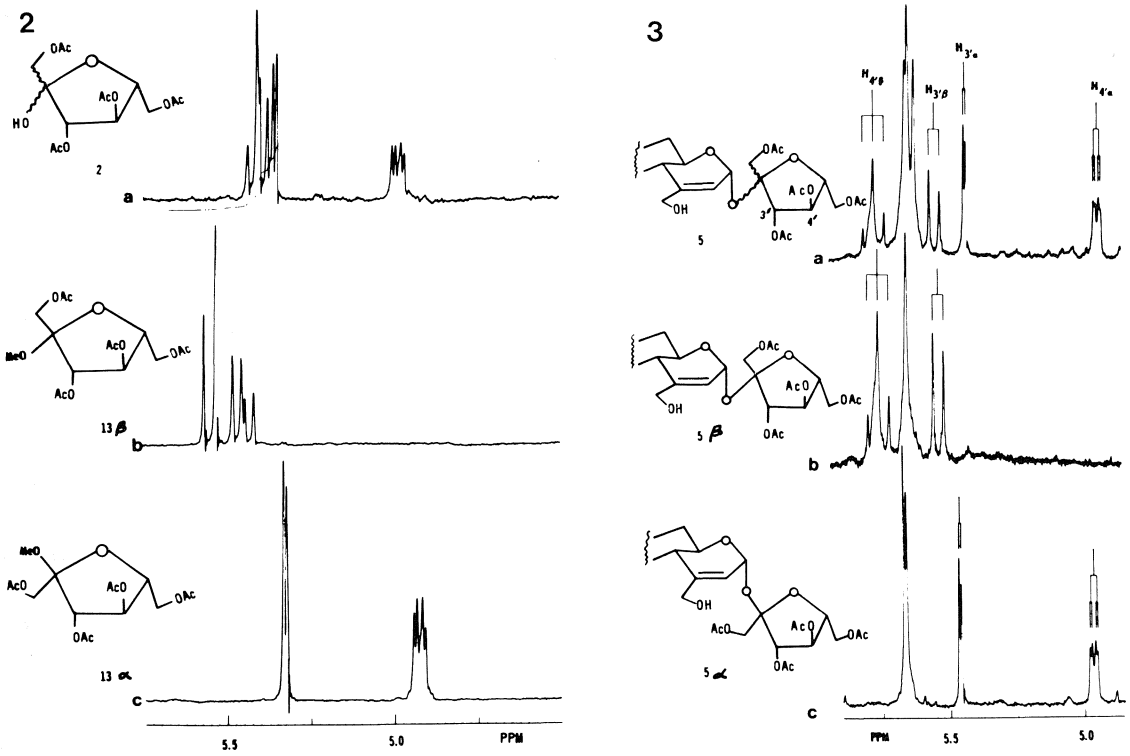

FIG. 2. The 220 MHz ^{1}Hmr spectra of fructofuranose derivatives.
FIG. 3. The 220 MHz ^{1}Hmr spectra of disaccharides **5**α and **5**β.

TABLE 2. Selected ^{1}H nuclear magnetic resonance parameters for the anomeric methyl fructofuranosides **13**α and **13**β

	Chemical shifts					
	13α			**13**β		
Proton	$CDCl_3$	C_6D_6	C_6D_5N	$CDCl_3$	C_6D_6	C_6D_5N
H-3′	5.30	5.65	5.74	5.50	5.76	5.94
H-4′	4.93	5.14	5.35	5.41	5.63	5.80

Coupling constants (Hz)		
Compound	$J_{3',4'}$	$J_{4',5'}$
13α	2.0	5.0
13β	7.0	5.0

5β, can be seen to have a different conformation than **13**β, since H-4′ appears as a triplet in the former compound. The *E*-4 conformation as expressed in **14**, for the furanose ring in the disaccharide **5**β may

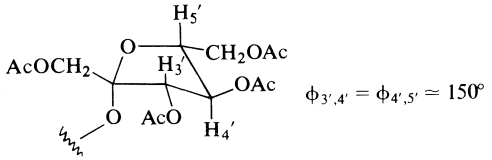

$\phi_{3',4'} = \phi_{4',5'} \simeq 150°$

14 (≡**5**β)

be assigned on the basis of the fact that the β-fructofuranosyl residue of sucrose exists in this form (10). This conformation accounts for the large coupling constants observed for $J_{3',4'}$ and $J_{4',5'}$ in **5**β. Hence the dihedral angle for H-3′ and H-4′ is the same as that for H-4′ and H-5′.

Attempts were made to obtain information about H-1 and H-2 of the pyranosyl moiety in **5**α and **5**β, and some relevant data are assembled in Table 3. It was assumed that the resonances for these protons were buried ~5.6 ppm (Fig. 3) but changing the solvent to benzene-d_6 proved to be ineffective.

Fortunately this problem was solved when it was found that the α,β-unsaturated aldehyde **6** was also resolvable (with considerable difficulty) into two components, namely **6**α and **6**β. These compounds also failed to crystallize but gave good ^{1}Hmr spectra. The region of interest, 4.8–6.0 ppm, is displayed in Fig. 4 and the results of the spectral analysis are reported in Table 3. Inspection of the H-3′ and H-4′ resonances clearly shows that **6**α and **6**β have the structures as shown with respect to the fructofuranose rings. Distinct absorptions for H-1 and H-2 of **6**α and **6**β can be seen, although their chemical shifts cannot be used to infer the anomeric configuration. In both compounds, H-1 appears as a broad signal but H-2 appears as a triplet. The coupling

TABLE 3. Selected ^{1}H nuclear magnetic resonance parameters for **5**α, **5**β, **6**α, and **6**β

	Chemical shifts			
Proton	**5**α	**6**α	**5**β	**6**β
H-1	—	5.75	—	5.90
H-2	—	6.48	—	6.53
H-3′	5.42	5.40	5.49	5.53
H-4′	4.97	4.97	5.69	5.70
H-6a	4.03	3.85	4.10	3.91
H-6e	—	—	4.67	4.60

Coupling constants (Hz)

Compound	$J_{1,2}$	$J_{2,4}$	$J_{3',4'}$	$J_{4',5'}$	$J_{5,6a}$	$J_{5,6e}$	$J_{6a,6e}$
5α	—	—	2.5	4.5	10.0	4.5	|10.0|
6α	2.5	|2.5|	2.0	4.0	10.0	4.5	|10.0|
5β	—	—	8.0	8.0	10.0	4.5	|10.0|
6β	2.5	|2.5|	8.0	8.0	10.0	4.5	|10.0|

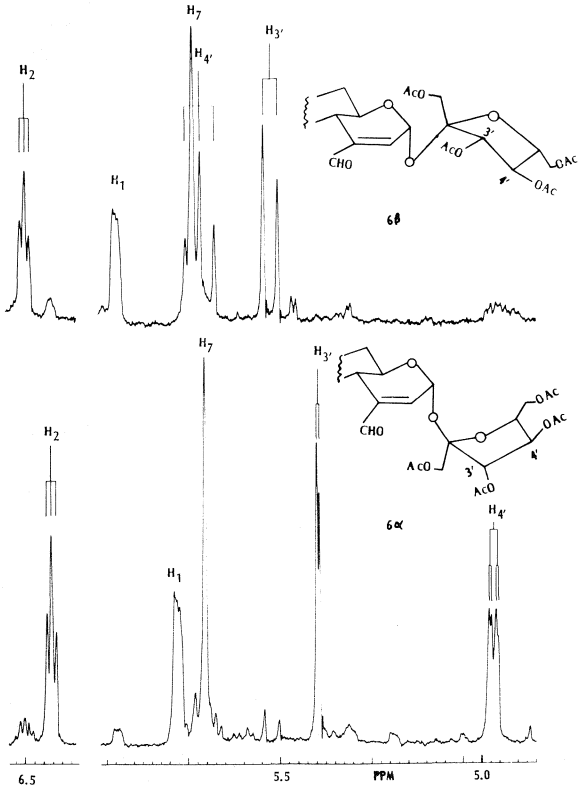

FIG. 4. The 220 MHz ^{1}Hmr spectra of disaccharides **6**α and **6**β.

constants $J_{1,2}$ and $J_{2,4}$ are the same as in the monomer **12**α (cf. Tables 1 and 2) and thus it can be concluded that in both of these compounds, the linkage at the pyranosyl residue is α. This result in turn confirmed the original supposition (1) that the alkoxy halogenation of the diene **1** proceeds stereoselectively giving α adducts exclusively.

Additional correlation of structure was obtained when the alcohols **5**α and **5**β were oxidized independently by chromium trioxidedipyridine complex in methylene chloride and gave products identical with **6**α and **6**β, respectively (1).

^{13}C *Nuclear Magnetic Resonance Spectra*

Added proof for the α configuration of the hex-2-enopyranosyl moiety of the disaccharides **5**, **6**, and **7** was sought from their ^{13}C nuclear magnetic resonance spectra. The correlation of the ^{13}C spectral peaks of a complex molecule with those of the constituent monomers has recently been utilised with great effectiveness by Wenkert and co-workers (11) in a study of tobramycin and related antibiotics of the kanamycin family.

The Pyranosyl Moiety

For the problem at hand, the monomeric derivatives **12**α, **12**β, **2**, **13**α and **13**β were subjected to ^{13}Cmr analysis. The natural abundance ^{13}C signals in the spectra of the compounds studied were assigned to specific carbons by means of the following procedures: (*a*) off-resonance decoupling techniques, (*b*) application of known chemical shift rules (12), and (*c*) comparison with the results of related studies from the literature (13).

A study of the ^{13}Cmr data for the olefins **12**α and **12**β (Table 4) reveals that there are very large chemical shift differences between the two anomers for C-5 ($\Delta\delta = -6.6$ ppm) and C-1 ($\Delta\delta = -3.1$ ppm). The former observation is by far the more important and is a direct consequence of the manifestation of the 'γ steric effect' (12*b*) also known as the 'steric compression shift' (12*a*). Interestingly, a similar trend is observed for the conformationally more labile derivatives **15** and **16** (see Table 4). This is

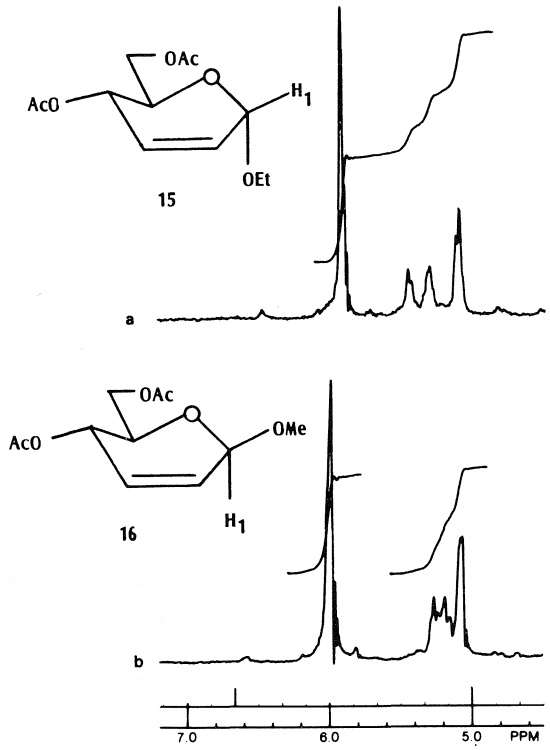

FIG. 5. The H-1 region of the ^{1}Hmr spectra (220 MHz) of compounds **15** and **16**.

TABLE 4. ^{13}C chemical shifts for the hex-2-enopyranosides **12α**, **12β**, **15**, and **16**

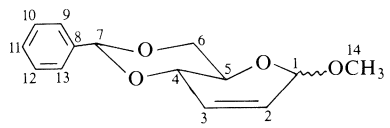

12

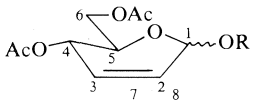

15 R = CH_2CH_3

16 R = CH_3

Carbon	12α	12β	Δδ	15	16	Δδ
1	96.1	99.2	−3.1	94.2	96.0	−1.8
2	126.6	128.1	−1.5	127.9	126.3	+1.6
3	130.7	131.6	−0.9	128.9	130.1	−1.2
4	75.2	75.0	+0.2	65.2	65.4	−0.2
5	63.9	70.5	−6.6	66.8	72.7	−5.9
6	69.4	69.1	+0.3	64.1	64.2	−0.1
7	102.1	102.1	0	63.0	55.2	—
8	137.4	137.4	0	15.2	—	—
9, 13	126.2	126.2	0	—	—	—
10, 12	128.2	128.3	−0.1	—	—	—
11	129.0	129.0	0	—	—	—
14	55.8	54.8	+1.0	—	—	—

noteworthy because the chemical shifts of H-1 in the proton spectra of **15** and **16** are so close that this data cannot be used to diagnose the anomeric configuration of these and structurally related compounds (see Fig. 5).

Thus the ^{13}C chemical shifts of C-1 and C-5 in the α anomers of hex-2-enopyranosides are shielded relative to the corresponding resonances in the β anomers. These observations lay the groundwork for the structural analysis of the related disaccharides with respect to the hex-2-enopyranosyl moiety.

The Furanosyl Moiety

The ^{13}Cmr spectrum of 1,3,4,6-tetra-*O*-acetyl-D-fructofuranose (**2**) was recorded as a model for the fructofuranosyl moiety of the structurally related disaccharides. The spectrum showed two distinct and clearly defined sets of resonances of different intensities. The two peaks at 103.9 and 101.5 ppm (see Table 5) were assigned to the anomeric carbons of the α and β anomers, respectively. This is in keeping with the recent assignment of the absolute anomeric configuration of the di-D-fructose anhydrides (13*d*) based on the observation that the ^{13}C chemical shift of the anomeric carbon of the α anomer of D-fructofuranosyl residues always resonates downfield from its β counterpart. Integration of these peaks revealed that the α to β ratio was 46:54. Thus, the predominant furanose anomer has the C-2′ hydroxymethyl group and the C-3′ hydroxyl group in a *trans* relationship as previously noted (13*a–c*).

The remaining 10 signals were readily assignable to the α or β anomer by their relative intensities. The signal at 63.3 ppm was assigned to C-1′ of **2α** because of the expected shielding effect of the C-3′ acetoxy group. C-6′ of **2α** was therefore the signal at 64.4 ppm. The signal at 64.8 ppm was assigned to C-6′ of **2β** because inversion at the anomeric centre would not greatly affect the chemical shift of C-6′. The only remaining methylene carbon at 65.3 ppm was therefore C-1′ of **2β**.

With regard to the three secondary carbons of **2α**, C-3′ and C-4′ should be the least and most shielded, respectively. Inversion of the anomeric centre should not affect C-4′ and C-5′ appreciably, and these carbons would therefore have similar chemical shifts in both **2α** and **2β**. On the other hand, C-3′ is greatly affected by inversion at the anomeric centre. Thus the large Δδ value of +4.3 ppm is immediately identified with C-3′.

To confirm these assignments the spectra of **13α** and **13β** were recorded and analyzed. The results (see Table 5) compare favourably and follow the expected trends. Also worthy of mention is the excel-

TABLE 5. ^{13}C chemical shifts for some fructofuranose derivatives

Carbon	17α[a]	17β[a]	Δδ	2α	2β	Δδ	13α[b]	13β[b]	Δδ
1′	63.1	62.9	+0.2	63.3	65.3	−2.0	58.2	62.1	−3.9
2′	104.8	101.9	+2.9	103.9	101.5	+2.4	106.9	103.0	+3.9
3′	82.2	74.7	+7.5	80.5	76.2	+4.3	80.3	75.8	+4.5
4′	76.3	75.7	+0.6	77.9	76.6	+1.3	78.1	76.4	+1.7
5′	81.5	80.9	+0.6	80.0	78.9	+1.1	79.6	78.1	+1.5
6′	61.2	62.5	−1.3	64.4	64.8	−0.4	63.1	64.4	−1.3

[a]See ref. 13*c*.
[b]The methoxy peaks in these compounds resonated at 48.7 (13α) and 49.8 (13β).

lent agreement of our assignments with those of Que and Gray (13*c*). Their assignments for α-D-fructofuranose (**17**α) and β-D-fructofuranose (**17**β) (see Table 5) were based on a study of the structurally related compound 2,5-anhydro-D-glucitol (**18**) and 2,5-anhydro-D-mannitol (**19**). It might also be noted

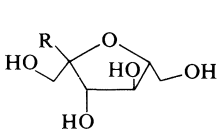

17α R = OH
18 R = H

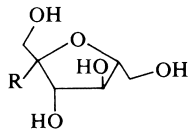

17β R = OH
19 R = H

that the resonances of **17**α assigned by Que and Gray (13*c*) have virtually the same chemical shifts as the β-D-fructofuranosyl resonances of sucrose recorded by Dorman and Roberts (14). The only discrepancy between our results and those of Que and Gray is in the assignment of the methylene carbons of **17**β. If their C-1′ and C-6′ assignments were reversed, then a more favourable comparison of Δδ values would result (i.e., for C-1′, Δδ = −1.7 vs. +0.2 cf. −2.0 and for C-6′, Δδ = −0.7 vs. −1.3 cf. −0.4).

Thus the ^{13}C chemical shifts of C-2′ and C-3′ in the β anomers of fructofuranoses are shielded relative to the corresponding resonances in the α anomers and this allows the ready assignment of the anomeric configuration of these derivatives.

^{13}C magnetic resonance analyses of **5**, **6**, and **7** revealed the presence of only two components arising from the presence of the α and β anomers in the furanose ring. The chemical shifts of C-5 in these compounds affirm the α linkages in the hex-2-enopyranosyl moieties. *As there are no other methine peaks in this region, the chemical shift of C-5 becomes totally diagnostic of the anomeric configuration of these compounds.* Accordingly, there are signals at 63.2 ppm in **5**, 64.4 ppm in **6**, and 63.5 ppm in **7** corresponding to the one at 63.9 ppm in the related monomer **12**α but none (ca. 70.5 ppm) corresponding to the β anomer, **12**β.

For C-1, signals were observed at 87.8 ppm in **5**, 87.5 ppm in **6**, and 87.9 ppm in **7**. These chemical shifts are shielded compared to that of C-1 in **12**α (cf. 96.1 ppm). This is attributable to the steric compression of C-1 caused by the attachment of the fructofuranosyl moiety.

TABLE 6. ^{13}C chemical shifts for the disaccharides **6**α and **6**β

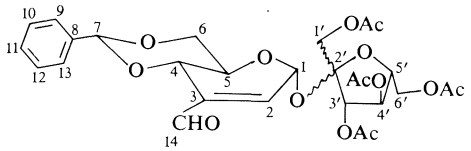

6

Carbon	6α	6β
1	87.5	87.5
2	139.6	139.2
3	153.0	146.3
4	73.9	73.7
5	64.3	64.5
6	69.1	68.8
7	102.2	102.0
8	137.2	137.1
9, 13	126.2	126.1
10, 12	128.3	128.3
11	129.2	129.1
14	NR	NR
1′	61.6	65.4
2′	107.9	102.7
3′	82.1	73.6
4′	77.9	75.6
5′	79.2	77.7
6′	63.0	63.1

A detailed analysis of the spectra of **5**, **6**, and **7** was not attempted, however; the two components of **6**, viz. **6**α and **6**β, were analyzed. The ^{13}C data for these two diastereomers are presented in Table 6. The resonances followed the expected trends observed in Tables 4 and 5. The anomeric configuration at C-1 was α as described above. The assignment of the anomeric configuration of the fructofuranose ring in **6**α and **6**β was readily made. The peaks at 102.7 and 73.6 ppm for C-2′ and C-3′ of **6**β were observed at higher field than the corresponding resonances, 107.9 and 82.1 ppm, for **6**α.

In conclusion, the ^{13}C spectral data proved unam-

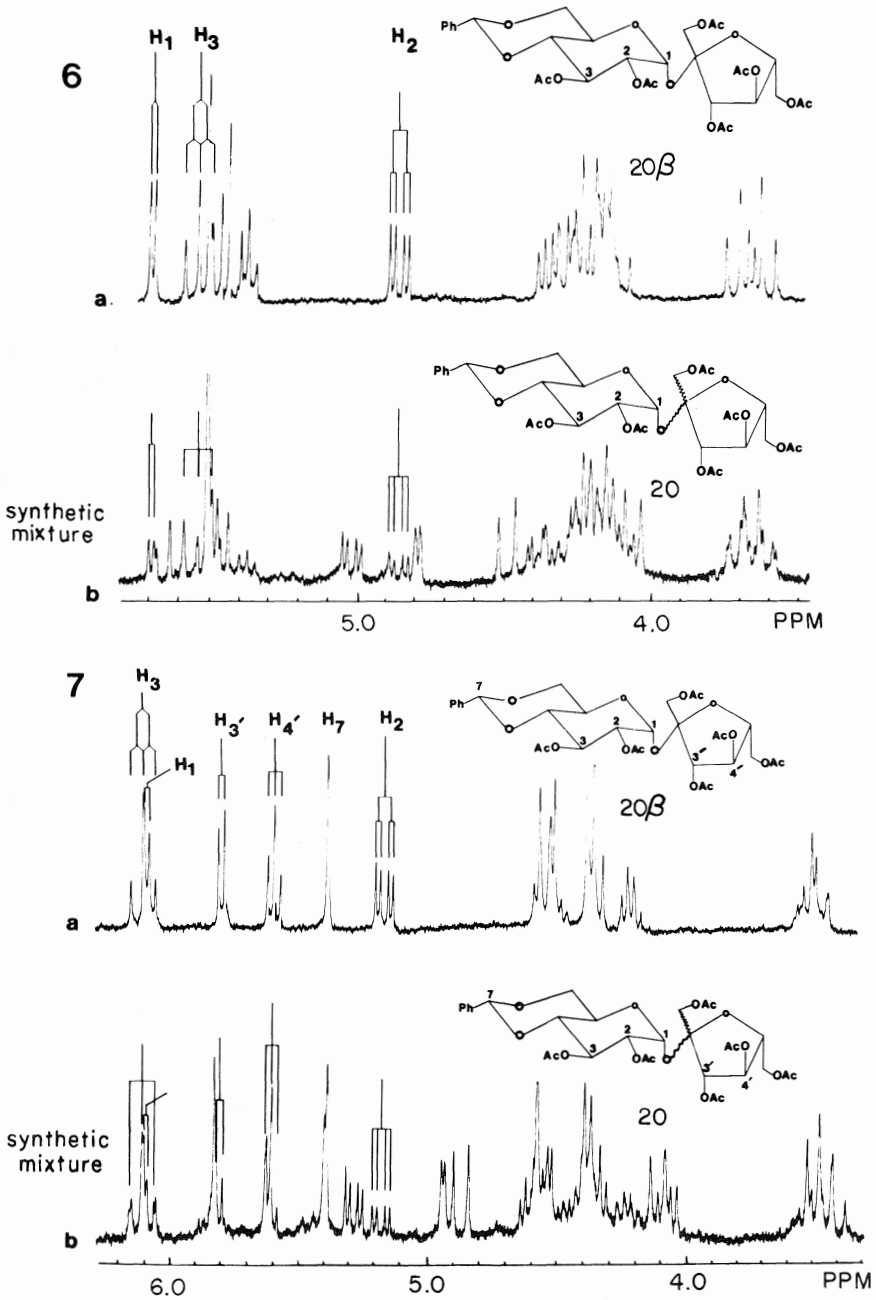

FIG. 6. The 220 MHz ^{1}Hmr spectrum ($CDCl_3$) of 4,6-*O*-benzylidenesucrose hexaacetate, **20**β: (*a*) authentic material; (*b*) admixed with α anomer (see footnote 4).

FIG. 7. The 220 MHz ^{1}Hmr spectrum (C_6D_6) of 4,6-*O*-benzylidenesucrose hexaacetate, **20**β: (*a*) authentic material, (*b*) admixed with α anomer (see footnote 4).

biguously, that **6**α was 1′,3′,4′,6′-tetra-*O*-acetyl-α-D-fructofuranosyl 4,6-*O*-benzylidene-2,3-dideoxy-3-*C*-formyl-α-D-*erythro*-hex-2-enopyranoside and that **6**β was 1′,3′,4′,6′-tetra-*O*-acetyl-β-D-fructofuranosyl 4,6-*O*-benzylidene-2,3-dideoxy-3-*C*-formyl-α-D-*erythro*-hex-2-enopyranoside.

Optical Rotation

Another interesting correlation between the disaccharides **6**α and **6**β and the fructofuranosides **13**α and **13**β is in their relative specific rotations. Inspection of Table 7 reveals that these compounds, and the known compounds listed, follow the trend that

TABLE 7. The specific rotation of some fructofuranose derivatives

Compound	Anomeric configuration[a]	$[\alpha]_D$	Reference
13α	α	+70.0° (*c* 1.0, $CHCl_3$)	This work
13β	β	−27.0° (*c* 1.05, $CHCl_3$)	This work
16α	α	+87° (*c* 1, H_2O)	7
16β	β	−49° (*c* 1, in H_2O)	7
6α	α	+48.4° (*c* 1.0, $CHCl_3$)	This work
6β	β	+21.7° (*c* 1.0, $CHCl_3$)	This work
21α	α	+83.5° (*c* 1.0, $CHCl_3$)	16*b*
21β (sucrose octaacetate)	β	+60° (*c* 1, $CHCl_3$)	17

[a]At the fructofuranose moiety.

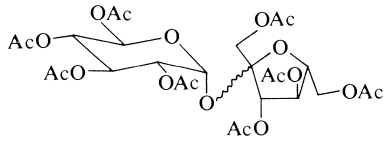

21

those derivatives possessing the α-fructofuranosyl residue all are more dextrorotatory than the corresponding β anomers.

Spectral Comparisons of Synthetic and Authentic Derivatives of Sucrose

Because of the extreme difficulty (*vide supra*) in separating the desired component (**5**β or **6**β) from the anomer (**5**α or **6**α), it was decided to test the feasibility of our planned route on the mixture **7**. If successful, the final product would contain sucrose in addition to one of its isomers, and spectroscopic verification of this fact would be extremely encouraging. Fortunately, 4,6-*O*-benzylidenesucrose hexaacetate (**20**β), a compound well correlated with our synthetic plan, was described by Khan (15). Compound **7** was therefore converted to **20** (1) and spectroscopic comparisons were undertaken.

The 3.0–6.0 ppm regions of the 220 MHz ^{1}Hmr spectra of authentic **20**β and the synthetic mixture **20** determined in deuteriochloroform and benzene-d_6 are shown in Figs. 6 and 7, respectively. In the case of the former, signals for H-1, H-2, and H-3 were assigned on a first-order basis for **20**β (Fig. 6*a*) and these signals were clearly recognisable in the synthetic mixture **20** (Fig. 6*b*).

With benzene-d_6 as solvent, the comparison was much more fulfilling, since discrete signals were observed for H-1, H-2, H-3, H-3′, H-4′, and H-7 of **20**β, the assignments being made on a first-order basis (Fig. 7*a*). Appropriately, these signals could all be identified in the synthetic mixture, **20** (Fig. 7*b*), thereby confirming that sucrose was present in the mixture.

It proved possible to obtain a crystalline sample of the synthetic material **20**β by nucleation with the authentic material (1).

Acknowledgements

We are grateful to the National Research Council of Canada and Bristol Laboratories (Syracuse) for financial assistance.

1. B. FRASER-REID and D. E. ILEY. Can. J. Chem. This issue.
2. B. FRASER-REID and B. RADATUS. Can. J. Chem. **50**, 2919 (1972).
3. C. SCHUERCH. Acc. Chem. Res. **6**, 184 (1973).
4. R. J. FERRIER. Adv. Carbohydr. Chem. **24**, 199 (1969).
5. R. J. FERRIER, N. VETHAVIYASAR, O. S. CHIZAV, V. J. KADANTSEV, and B. M. ZOLOTAREV. Carbohydr. Res. **13**, 269 (1970).
6. B. FRASER-REID and B. BOCTOR. Can. J. Chem. **47**, 393 (1969); R. U. LEMIEUX, E. FRAGA, and K. A. WATANABE. Can. J. Chem. **46**, 61 (1968).
7. I. AUGESTAD, E. BERNER, and E. WEIGNER. Chem. Ind. London, 376 (1953).
8. R. J. ABRAHAM, L. D. HALL, L. HOUGH, and K. A. MCLAUCHLAN. J. Chem. Soc. 3699 (1962).
9. R. U. LEMIEUX and R. NAGARAJAN. Can. J. Chem. **42**, 1270 (1964).
10. C. A. BEEVERS and W. COCHRAN. Proc. R. Soc. London Ser. A, **190**, 257 (1947).
11. K. F. KOCH, J. A. RHOADES, E. W. HAGAMAN, and E. WENKERT. J. Am. Chem. Soc. **96**, 3300 (1974).
12. (*a*) G. C. LEVY and G. L. NELSON. Carbon-13 nuclear magnetic resonance for organic chemists. Wiley-Interscience, Toronto, Ont. 1972. pp. 24, 162; (*b*) J. B. STOTHERS. Carbon-13 nmr spectroscopy. Academic Press, New York, NY. 1972. Chapt. 4.
13. (*a*) D. DODDRELL and A. ALLERHAND. J. Am. Chem. Soc. **93**, 2779 (1973); (*b*) A. S. PERLIN, N. CYR, H. J. KOCH, and B. KORSCH. Ann. N.Y. Acad. Sci. **222**, 935 (1973); (*c*) L. QUE, JR. and G. R. GRAY. Biochemistry, **13**, 146 (1974); (*d*) R. W. BINKLEY, W. W. BINKLEY, and B. WICKBERG. Carbohydr. Res. **36**, 196 (1974).
14. D. E. DORMAN and J. D. ROBERTS. J. Am. Chem. Soc. **93**, 4463 (1971).
15. R. KHAN. Carbohydr. Res. **32**, 375 (1974).
16. (*a*) G. S. BETHELL and R. J. FERRIER. Carbohydr. Res. **31**, 69 (1973); (*b*) A. KLEMER, K. GAUPP, and E. BUHE. Tetrahedron Lett. 4585 (1969); (*c*) R. P. LINSTEAD, A. RUTENBERG, W. G. DAUGEN, and W. L. EVANS. J. Am. Chem. Soc. **62**, 3260 (1940); E. J. COREY and R. A. SNEEN. J. Am. Chem. Soc. **78**, 6269 (1956); (*d*) D. E. DORMAN and J. D. ROBERTS. J. Am. Chem. Soc. **93**, 4463 (1971).
17. R. U. LEMIEUX and G. HUBER. J. Am. Chem. Soc. **78**, 4117 (1956).

Artificial carbohydrate antigens: synthesis of rhamnose disaccharides common to *Shigella flexneri O*-antigen determinants[1]

DAVID R. BUNDLE AND STAFFAN JOSEPHSON[2]

Division of Biological Sciences, National Research Council of Canada, Ottawa, Ont., Canada K1A 0R6

Received September 12, 1978

DAVID R. BUNDLE and STAFFAN JOSEPHSON. Can. J. Chem. **57**, 662 (1979).

Three disaccharides containing α-linked rhamnopyranoside units have been synthesised in a form suitable for covalent linkage to protein. The artificial antigens obtained in this manner represent structural elements similar to portions of the repeating unit of the *Shigella flexneri O*-antigen. The glycosylation reactions leading to the disaccharides utilised silver trifluoromethanesulphonate and *N,N*-tetramethylurea, or *sym*-collidine, conditions which generated the three 1,2-*trans*-linked glycosides in high yield and stereospecificity. The blocking groups used in these syntheses are consistent with further chain extension to tri- and tetrasaccharides. 2-Acetamido-3,4,6-tri-*O*-acetyl-2-deoxy-α-D-glucopyranosyl chloride and the 1,2-oxazoline derivative obtained from it were not effective in glycosylating the C-2 position of partially blocked rhamnopyranoside but 3,4,6-tri-*O*-acetyl-2-deoxy-2-phthalimido-D-glucosyl bromide gave the desired 1,2-*trans*-2-amino-2-deoxyglucoside in good yield. Selective conversion of the phthalimido group to an acetamido function in the presence of an ester function was achieved, thereby extending the utility of the phthalimido protecting group to sequential oligosaccharide synthesis, in which 2-acetamido-2-deoxy-β-D-glucosides are internal units. Proton nmr evidence in support of the *exo*-anomeric effect is presented.

DAVID R. BUNDLE et STAFFAN JOSEPHSON. Can. J. Chem. **57**, 662 (1979).

On a synthétisé trois disaccharides contenant des unités rhamnopyrannosides qui portent une liaison α et qui sont présents sous une forme appropriée à la formation d'une liaison covalente avec une protéine. Les antigènes artificiels obtenus de cette manière correspondent à des éléments de structures semblables à ceux de portions de l'unité de base du *O*-antigène du *Shigella flexneri*. Les réactions de glycosylation conduisant aux disaccharides font appel au trifluorométhanesulfonate et à la *N,N*-tétraméthylurée ou à la *sym*-collidine; ces conditions conduisent aux trois glycosides liés *trans*-1,2 avec de bons rendements et une haute stéréospécificité. Les groupes bloqueurs utilisés dans ces synthèses sont compatibles avec des extensions subséquentes des chaînes vers des tri- et des tétrasaccharides. Les chlorure de l'acétamido-2 tri-*O*-acétyl-3,4,6 désoxy-2 α-D-glycopyrannosyle et le dérivé oxazoline-1,2 qui en dérive ne sont pas des agents efficaces pour provoquer la glycosylation en position C-2 d'un rhamnopyrannoside partiellement bloqué; toutefois le bromure de tri-*O*-acétyl-3,4,6 désoxy-2 phtalimido-2 D-glycosyle conduit au glucoside *trans*-1,2 amino-2 désoxy-2 avec un bon rendement. La transformation sélective du groupe phtalimido en fonction acétamido en présence d'une fonction ester a pu être réalisée; ce résultat étend le champ d'application du groupe protecteur phtalimido à la synthèse séquencielle d'oligosaccharides dans lesquels les unités internes sont des acétamido-2 désoxy-2β D-glucosides. On présente des données de rmn du proton qui sont en accord avec un effet anomérique *exo*.

[Traduit par le journal]

Introduction

Structural studies of the lipopolysaccharides (LPS) from various strains of *Shigella flexneri* indicate a basic tetrasaccharide repeating unit common to all serogroups (1–5). The simplest structure is that of strain Y (3) which possesses the structure

$$\text{-}[\text{-}3)\text{-}\beta\text{-D-GlcNAc}p(1\rightarrow 2)\text{-}\alpha\text{-L-Rha}p(1\rightarrow 2)\text{-}\alpha\text{-L-Rha}p(1\rightarrow 3)\text{-}\alpha\text{-L-Rha}p(1\text{-}]_n$$

Other strains of *S. flexneri* possess LPS with different glycosyl or acyl substitution patterns upon this basic structure (4, 5). The serological classification of *S. flexneri* finds its basis in this variability of fine structure. The serogroup Y polysaccharide is a high molecular weight antigen containing approximately 40 repeating units (3). Since this polysaccharide has neither charged groups nor side chains which are known (6–8) to direct the synthesis of antibody complementary to these features, the structural units that constitute the immunodominant regions are not immediately obvious. It is known from published data (9, 10) that linear charged polysaccharides ellicit antibody populations with specificities for different portions of the polysaccharide structure. Extensive studies of the dextrans (11, 12) show that

[1]NRCC No. 17121.
[2]NRCC Research Associate.

0008-4042/79/060662-07$01.00/0

there is heterogeneity with respect to the specificity for α1,3 or α1,6 linkages and in the size of the combining site. Although the Y polysaccharide would be expected to exhibit similar immunogenic properties, the occurrence of several 1,2-glycosidic linkages (13) might be imagined to render a particular region of the repeating unit more 'accessible' to cell surface receptors responsible for initiating the process of antibody synthesis in vivo. Little is known of such immunodominant features of *S. flexneri.*

The objective of the work currently in progress in this laboratory and reported in part here is to investigate the immunodominant regions of *S. flexneri* by the use of artificial antigens. Advances in glycoside synthesis in conjunction with modern methods of artificial antigen synthesis (14, 15) and conformational analysis provide particularly attractive tools to probe this question. Oligosaccharides possessing 6-deoxyhexopyranosides were chosen for study in the expectation that high resolution nmr would provide important insights into the conformational basis of serological specificity (14). In addition synthetic oligosaccharides hold promise as diagnostic reagents either via artificial antigens (14) or immunoabsorbents. In this context we report the synthesis of three disaccharides in a form suitable for covalent linkage to proteins or solid supports. The blocking sequences employed are consistent with our ultimate goals, the syntheses of tri- and tetrasaccharide antigens which are currently in progress.

Results and Discussion

The three disaccharides, which are the object of this synthetic work are exclusively glycosides of the 1,2-*trans*-linked type. Each disaccharide has been synthesised as its 8-methoxycarbonyloctyl glycoside to allow subsequent covalent attachment to protein after removal of blocking groups. This necessitates the formation of two glycoside linkages both consistent with those portions of the LPS antigen to which the artificial antigen correspond. Consequently the three disaccharides required were of the following structure

α-L-Rha*p*(1 → 3)β-D-GlcNAc*p*(1 → R)

α-L-Rha*p*(1 → 2)α-L-Rha*p*(1 → R)

β-D-GlcNAc*p*(1 → 2)α-L-Rha*p*(1 → R)

where $R = O(CH_2)_8CO_2CH_3$ referred to here and elsewhere (15) as the 'bridging' or 'linking arm.'

The initial stage of the synthesis of 2-acetamido-2-deoxy-3-*O*-(α-L-rhamnopyranosyl)-β-D-glucopyranoside (**17**) required a 2-acetamido-2-deoxy-β-D-glucopyranoside selectively blocked at the 4 and 6 positions. The 4,6-*O*-benzylidene derivative **15** used in this work was previously synthesized by Lemieux *et al.* (14) as a precursor to Lewis-a blood-group antigens. The attachment of an α-linked rhamnopyranoside residue at the 3-position was a comparatively straight forward step. Although per-*O*-acetyl-α-rhamnopyranosyl and α-D-mannopyranosyl bromides are known to yield significant amounts of orthoester under Koenigs–Knorr conditions (16, 17), Helfrich conditions usually alleviate this problem (18) and indeed disaccharide **16** was synthesised in 52% yield by this procedure. Silver trifluoromethanesulphonate(triflate)tetramethylurea has been shown by Hanessian and Banoub (19) to be effective for 1,2-*trans*-glycoside synthesis. Related work utilising silver triflate – *sym*-collidine in conjunction with the phthalimido group as a limited participating group at C-2 establish these as conditions of choice for 2-amino-2-deoxyglycoside synthesis (20). The latter conditions lead to ortho ester formation when per-*O*-acetylated glycosyl bromides are used as the glycosylating species (Banoub and Bundle (28)) whereas glycosides result when the weaker base tetramethylurea is substituted for *sym*-collidine. When the protected glycoside **15** was reacted with **1** under these conditions (silver triflate – tetramethylurea) the yield of **16** was 67%, an increase from the 52% yield obtained with mercuric cyanide as the promotor. Since silver triflate – tetramethylurea effectively avoids the problem of ortho ester formation due to the acidic nature of these conditions, this procedure was used in all subsequent glycosylations leading to α-L-rhamnopyranosidic bonds.

The synthesis of 2-*O*-(α-L-rhamnopyranosyl)-α-L-rhamnopyranoside (**7**) resolved itself into the selective blocking of positions C-3 and C-4 of 8-methoxycarbonyloctyl-α-L-rhamnopyranoside. These protecting groups were required to be 'persistent' to allow the synthesis of a trisaccharide antigen, wherein, a β-linked 2-acetamido-2-deoxy-D-glucopyranose sugar could be linked to C-2 of the terminal rhamnose of disaccharide **7**.[3] This objective was most conveniently achieved by utilising the approach of Garegg and co-workers (21), in which a 1,2-ortho ester (**2**) is benzylated to give the derivative **3** which may be used directly to give the glycoside **4** using standard orthoester glycosylation procedures (22). Conversion of the acetate **4** to the alcohol **5** followed by reaction with **1** using silver triflate as promoter provided disaccharide **6** in 76% yield. Attempts to prepare the analogous 2-*O*-linked glucosamide (**12**) by

[3]Paper in preparation.

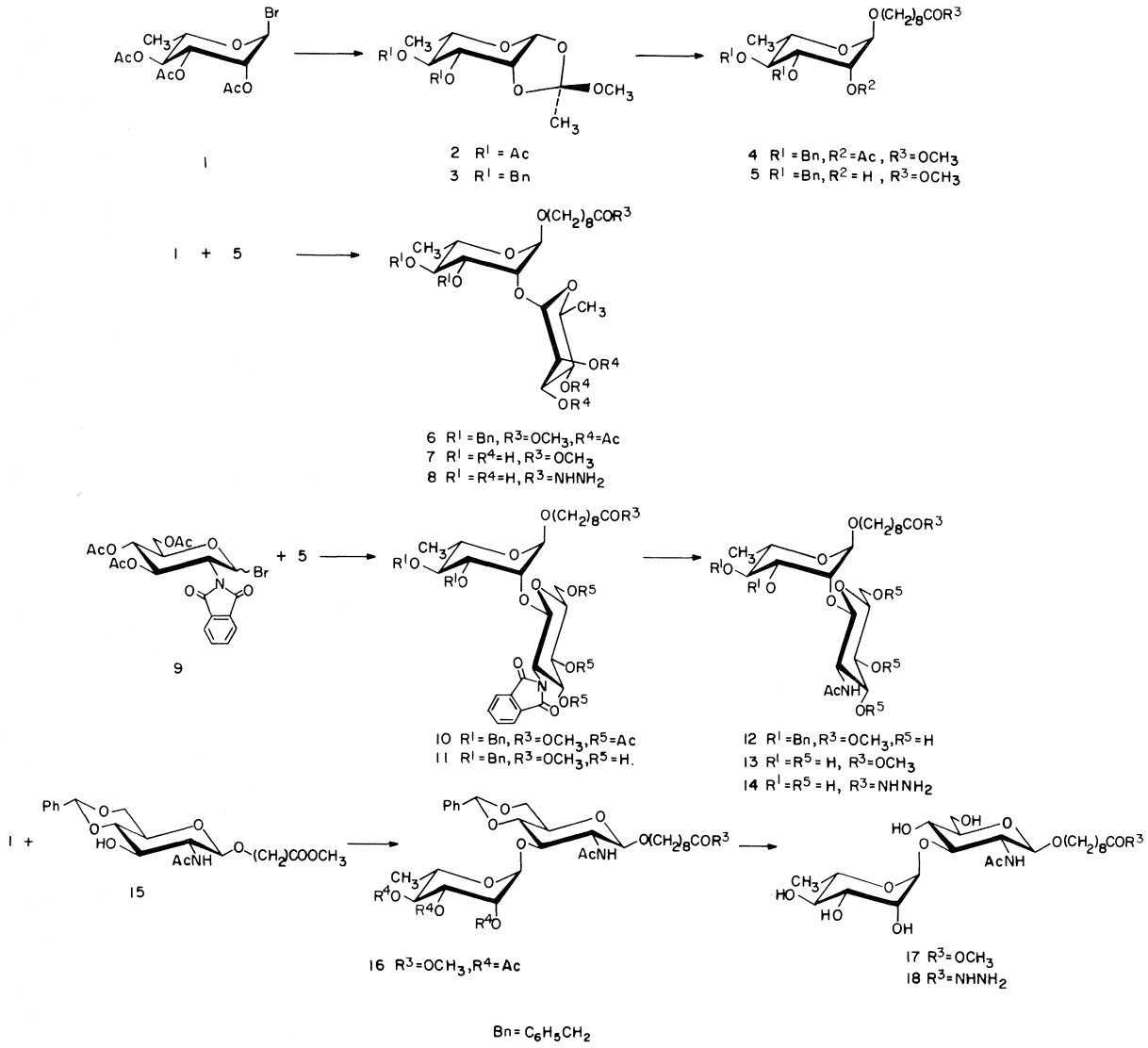

reaction of 2-acetamido-3,4,6-tri-*O*-acetyl-2-deoxy-α-D-glucopyranosyl chloride or the oxazoline derived from this compound with partially blocked rhamnoside **5** were not successful. However, using the conditions described by Lemieux and co-workers (20) the bromide **9** reacted with rhamnopyranoside **5** to give the expected glucosaminide **10** in 70% yield.

The deblocking of disaccharide **10** provided important findings which should allow the uses of the phthalimido protecting group in sequential oligosaccharide synthesis, where the glucosaminyl residue is not the terminal sugar. The approach to synthetic carbohydrate antigens developed by Lemieux *et al.* (14) and utilising the alcohol 8-methoxycarbonyloctanol has synthetic convenience in addition to the important biological effects associated with the choice of a nine carbon atom 'bridging arm' (15). However, the ester function of the bridging arm must be compatible with all reaction conditions, blocking, glycosylation and removal of protecting groups. In this connection it may be appreciated that strongly reducing conditions such as $LiAlH_4$, B_2H_6, or alkaline conditions, both of which destroy the ester function, must be avoided. The ester function is required to be converted to a hydrazide, e.g., **8**, **14**, or **18** in the final step preceding antigen preparation (cf. 13, 14). Conversion of the phthalimido function of **11** to a 2-amino-2-deoxy glucoside with hydrazine was anticipated to replace the 8-methoxy carbonyloctyl function by its hydrazide derivative, thereby necessitating selective *N*-acetylation to provide **14**. However, it was found that the phthalimido

group can be selectively converted by hydrazine without affecting the ester function. In addition it was found that catalytic de-*O*-acetylation of compound **10** by sodium in methanol proceeds smoothly without conversion of the phthalimido group to a 2′-carboxybenzamido function as reported by Baker *et al.* (23). When the disaccharide **11** was refluxed with hydrazine hydrate in ethanol, an 80% yield of the desired product **12** was obtained. Clearly the finding, that the phthalimido function is stable to conventional de-*O*-acetylation procedures and that the amino blocking group may be removed without destroying the essential ester function of the 'spacer' or 'bridging arm' permits manipulation of the glucosaminide residue such that another sugar may be attached at C-3, C-4, or C-6 positions with suitable ester or acetal blocking groups.

All compounds synthesised were characterised by both ^{1}H nmr and ^{13}C nmr. The results of the latter, particularly, establish the stereochemistry of the reaction products. The most striking feature of the ^{1}H nmr data was the 0.6 ppm upfield shift of the H-6′ protons of disaccharide **16**. That this is due to the influence of the aromatic ring of the benzylidene acetal and not to other conformational reasons was indicated by conversion of **16** to the 4,6-isopropylidene ketal. Both this ketal and the de-*O*-benzylidenated, tri-*O*-acetyl-rhamnopyranosyl-glucosaminide showed 'normal' shifts, $\delta \simeq 1.2$ ppm for the H-6′ protons. Consideration of the *exo*-anomeric effect with respect to orientation of the glucosamine residue about the C-1′ to glycosidic oxygen bond (torsional angle ϕ) indicates two possible staggered arrangements, one of which, with the C(1′)—C(2′) bond antiparallel to the O(1′)—C(3) bond, is predicted to be the more stable rotamer (24). The direction of chemical shift for the H-6′ protons indicates that they must lie close to the centre of the aromatic ring. Examination of molecular models shows that for the H-6′ protons to remain in this orientation it is necessary to restrict not only ϕ but also the second torsional angle, ψ, used to define disaccharide conformation at the glycosidic linkage. In fact the rotamer about O(1′)—C(3) that maintains the exocyclic methyl group in maximum overlap with the aromatic nucleus is that in which the C(3)—H(3) bond nearly eclipses the C(1′)—O(1′) bond. A similar conformation has been predicted from hard-sphere calculations based on the *exo*-anomeric effect for cyclohexyl-α-D-glucopyranosides (24). The ^{13}C nmr spectra for compound **16** show a related but opposite chemical shift for the C-6′ carbon. In other respects the ^{13}C nmr spectra of the compounds reported are consistent with the structures synthesised and do not warrant further comment at present.

Experimental

Thin-layer chromatography was performed with Merck precoated silica gel 60 F-254 plates and the detection of compounds was achieved by quenching of uv fluorescence and with 5% sulphuric acid in ethanol. Column chromatography utilised silica gel G60 (70–230 mesh) and redistilled solvents. The loading on all columns was 1:100 unless otherwise indicated. Skellysolve B refers to hexane supplied by Getty Refining and Marketing Company, Tulsa, OK. Palladium 10% on charcoal was purchased from Engelhard Industries, Newark, NJ. Solvents were purified and dried according to standard procedures (25). Processed solutions were dried over anhydrous sodium sulphate and solvent removal was achieved with bath temperatures 40°C or lower unless otherwise stated. Melting points were determined on a Fisher-Johns apparatus and are uncorrected. Optical rotations at the sodium-D-line were measured in a 1-dm cell at room temperature (20–23°C). Carbon-13 and ^{1}H nmr spectra were recorded at 20 and 79.9 MHz, respectively, in the pulsed Fourier transform mode on a Varian CFT-20 spectrometer. Proton chemical shifts are expressed relative to 1% tetramethylsilane (TMS) for deuteriochloroform, acetone-d_6 and methanol-d_4. Carbon-13 shifts are expressed relative to internal TMS in methanol-d_4 and assignments of ^{13}C resonances are tentative.

*3,4-Di-*O*-acetyl-1,2-*O*-(methoxyethylidene)*-β-L-*rhamnopyranose (2)*

Anhydrous methanol (19 mL, 469 mmol) was added to a stirred solution of 164.8 g (467 mmol) of 2,3,4-tri-*O*-acetyl-α-L-rhamnopyranosyl bromide (**1**) (26) in 235 mL of 2,6-lutidine. After 48 h at room temperature absolute chloroform (250 mL) was added and after 16 h **1** had been consumed. Filtration and quenching of the filtrate in cold water (1 L) followed by addition of 1 *M* hydrochloric acid to pH 8 produced an oil which was extracted with ethyl acetate (3 × 200 mL). The combined extracts were washed with water (3 × 300 mL), dried, concentrated, and the syrup taken up in ether – Skellysolve B. Crystallisation overnight at 4°C gave 53.6 g and a further 30.9 g on retreatment of the mother liquors. Both samples had mp 86–87°C, $[\alpha]_D$ 34.4° (*c* 1.0, $CHCl_3$) (mp 84–86°C, lit. (27) $[\alpha]_D$ 34.7° ($CHCl_3$)), and were pure by ^{1}H nmr (single isomer, *exo*-OCH_3) and by analysis; ^{1}H nmr ($CDCl_3$) δ: 1.19 (d, 3H, H-6), 1.68 (s, 3H, CH_3-C), 2.03 (s, 3H, CH_3CO), 2.07 (s, 3H, CH_3CO), 3.22 (s, 3H, CH_3O), 3.27–3.61 (m, 1H, H-5) 4.53 (dd, $J_{1,2} = 2.5$ Hz, $J_{2,3} = 4.0$ Hz, 1H, H-2), 4.99 (m, 2H, H-3, H-4), 5.26 (d, $J_{1,2} = 2.5$ Hz, 1H, H-1). *Anal.* calcd. for $C_{13}H_{20}O_8$: C 51.31, H 6.63; found: C 51.32, H 6.80.

The mother liquors contained 45 g of material which may be used directly as a syrup in the next step without significant decreases in yield. The purity of this material by ^{1}H nmr was approximately 90%.

*3,4-Di-*O*-benzyl-1,2-*O*-(methoxyethylidene)*-β-L-*rhamnopyranose (3)*

Crystalline **2** (50.9 g, 167 mmol) dissolved in dry methanol (200 mL) was treated with 100 mL of ammonia saturated methanol and left for 48 h at room temperature under anhydrous conditions. The crystalline residue obtained when this solution was evaporated could be recrystallised from ethyl acetate – Skellysolve B but was most conveniently dried as a solid mass and used directly. This solid (34.7 g), after drying under vacuum over phosphorous pentoxide, was dissolved in dry DMF (200 mL) and added slowly to a suspension of sodium hydride (16 g, 667 mmol) in 250 mL of DMF. Benzyl bromide (60 mL, 491 mmol) was added dropwise to the solid mixture formed by the addition of ortho ester to sodium hydride. The benzyl bromide was added over 30 min with

cooling to keep the reaction at approximately 20°C. The solution was then left stirring for 18 h and worked up by addition of methanol 50 mL. After 1 h the clear solution was poured into water (1 L) and brought to pH 8 with 1 *M* hydrochloric acid. Ethyl acetate (200 mL) was added and the aqueous phase extracted with ethyl acetate (2 × 200 mL). After washing with water (2 × 200 mL) the organic phase was dried, concentrated, and dissolved in ether – Skellysolve B. On standing at 4°C crystals (42.7 g, 64%) were deposited, mp 110–111°C, $[\alpha]_D$ 0.6° (*c* 1.0, $CHCl_3$). A further 3 g of material was obtained upon crystallisation of the mother liquors, mp 109–111°C, total yield 68%; ^{1}H nmr ($CDCl_3$) δ: 1.31 (d, 3H, H-6), 1.73 (s, 3H, CH_3-C), 3.27 (s, 3H, CH_3O), 3.27–3.79 (m, 3H, H-3, H-4, H-5) 4.38 (dd, $J_{2,3}$ = 4.0 Hz, $J_{1,2}$ = 2.5 Hz, 1H, H-2), 4.53–5.02 (m, 4H, $CH_2\phi$), 5.26 (d, $J_{1,2}$ = 2.5 Hz, 1H, H-1). *Anal.* calcd. for $C_{23}H_{28}O_6$: C 68.98, H 7.05; found: C 69.13, H 7.10.

*8-Methoxycarbonyloctyl 3,4-Di-*O*-benzyl-α-*L*-rhamnopyranoside (**5**)*

Ortho ester **3** (18.0 g) was refluxed for 30 min with 8-methoxycarbonyloctanol (9 g) in acetonitrile (200 mL) containing mercuric bromide (100 mg). The solvent was then distilled off leaving a light brown syrup to which dichloromethane (500 mL) was added. Following extraction with ice cold water (300 mL) the solution was dried, evaporated, and a small sample of the resulting syrup was chromatographed on silica gel using Skellysolve B – ethyl acetate (3:1) to provide pure **4** as a syrup, $[\alpha]_D$ −23.3° (*c* 1.1, $CHCl_3$); ^{1}H nmr ($CDCl_3$) δ: 0.9–1.7 (m, 15H, H-6 and —$(CH_2)_6$—), 2.12 (s, 3H, CH_3CO), 2.28 (t, 2H, CH_2CO—), 3.63 (s, 3H, —OCH_3), 3.20–4.25 (m, 4H, ring protons and OCH_2), 4.33–5.01 (m, 6H, —$CH_2\phi$ and ring protons), 5.32 (dd, $J_{1,2}$ = 1.8 Hz, $J_{2,3}$ = 3.4 Hz, 1H, H-2); ^{13}C nmr (CD_3OD) δ: 98.7 (Cl), 81.1, 80.9 ($OCH_2\phi$), 76.1 (C4), 72.7 (C2), 70.3 (C3), 68.8 (2C, C5 and OCH_2), 18.3 (C6).

The remaining portion of **4** was deacetylated directly in methanol (500 mL) containing a catalytic amount of sodium. Deionisation with Rexyn 101 (H^+) resin, concentration, and chromatography on a column of silica gel (1200 g) with Skellysolve B – ethyl acetate (1:1) gave pure **5** (14.5 g) and 3.0 g of methyl 3,4-di-*O*-benzyl-α-L-rhamnopyranoside. Pure, homogeneous syrup **5** had $[\alpha]_D$ −24.2° (*c* 1.0, $CHCl_3$); ^{1}H nmr ($CDCl_3$) δ: 0.90–1.75 (m, 15H, H-6 and —$(CH_2)_6$—), 2.30 (t, 2H, CH_2CO), 2.50 (d, 1H, OH), 3.62 (s, 3H, OCH_3), 3.23–4.18 (m, 7H, OCH_2 and ring protons), 4.43–5.01 (m, 4H, CH_2O), 7.23–7.27 (m, 10H, aromatic); ^{13}C nmr (CD_3OD) δ: 101.3 (C1), 81.1, 80.9 ($OCH_2\phi$), 76.0 (C4), 72.3 (C3), 69.1 (C2), 68.8 (OCH_2), 68.4 (C5), 18.3 (C6). *Anal.* calcd. for $C_{30}H_{42}O_7$: C 70.01, H 8.23; found: C 69.90, H 8.30.

*8-Methoxycarbonyloctyl 2-*O*-(2,3,4-Tri-*O*-acetyl-α-L-rhamnopyranosyl)-3,4-di-*O*-benzyl-α-L-rhamnopyranoside (**6**)*

The partially protected glycoside **5** (2.0 g, 3:9 mmol) was dissolved in dichloromethane (35 mL) containing silver triflate (1.9 g, 7.5 mmol) and tetramethylurea (3.6 mL, 30 mmol). This solution was cooled to −70°C and 2,3,4-tri-*O*-rhamnopyranosyl bromide (**1**) (2.4 g, 6.8 mmol) (26) dissolved in dichloromethane (15 mL) was added dropwise with stirring. The reaction was allowed to warm to room temperature overnight and then filtered. Following extraction with saturated sodium bicarbonate (20 mL), the concentrated syrup was purified on a silica gel column with Skellysolve B – ethyl acetate (2:1) as solvent. Pure disaccharide, **6** (2.0 g) was obtained in 73% yield $[\alpha]_D$ −42.7° (*c* 0.9, $CHCl_3$), R_f 0.48 (Skellysolve B – ethyl acetate, 2:1); ^{1}H nmr ($CDCl_3$) δ: 1.0–1.8 (m, 18H, H-6, H-6′, and —$(CH_2)_6$—), 1.95 (s, 3H, CH_3CO—), 2.02 (s, 3H, CH_3CO—), 2.06 (s, 3H, CH_3CO—), 2.28 (t, 2H, CH_2CO—), 3.56 (s, 3H, OCH_3), 3.10–4.16 (m, 7H, OCH_2 and ring protons), 4.45–5.51 (m, 7H, $OCH_2\phi$ and ring protons), 7.06–7.36 (m, 10H, aromatic); ^{13}C nmr (CD_3OD) δ: 100.3 (C1′), 99.8 (C1), 81.0, 80.7 ($CH_2\phi$), 77.3 (C2), 76.1 (C4), 73.1 (C3), 72.0 (C4′), 70.8 (C3′), 70.5 (C2′), 69.1 (OCH_2), 68.5 (C5), 68.0 (C5′), 18.2 (C6), 17.6 (C6′).

*8-Methoxycarbonyloctyl 2-*O*-(α-L-Rhamnopyranosyl)-α-L-rhamnopyranoside (**7**)*

Compound **6** (1.5 g) in methanol (200 mL) containing a catalytic amount of sodium was left for 16 h at room temperature. The syrup, obtained after removal of sodium ions with Rexyn 101 (H^+) resin, filtration, and evaporation, was dissolved in acetic acid (100 mL) and hydrogenated with palladium, 10% on charcoal (0.5 g), at 70 psi for 3 h. Filtration and co-evaporation with toluene (3 × 150 mL) followed by column chromatography on silica gel with the solvent, ethyl acetate – methanol – water (85:10:5) gave pure **7** (0.7 g, yield 74%), $[\alpha]_D$ −60.5° (*c* 1.0, methanol), R_f 0.40 (solvent 85:10:5 as above); ^{1}H nmr (acetone-d_6 δ: 1.19 (d, $J_{5,6}$ = 6 Hz, H-6), 1.22 (d, $J_{5,6}$ = 6 Hz, H-6′), 1.0–1.75 (m, 18 H, —$(CH_2)_6$—), 2.25 (t, 2H, CH_2CO), 3.60 (s, 3H, CH_3O), 3.10–4.16 (m, ring protons), 4.74 (bs, 1H, H-1′) 4.93 (bs, 1H, H-1); ^{13}C nmr (CD_3OD) δ: 103.9 (C1), 100.1 (C1′), 80.2 (C2), 74.1 (C4), 73.7 (C4′), 72.1 (C3), 72.0 (C3′), 71.8 (C2′), 70.0 (C5), 69.6 (OCH_2), 68.4 (C5′), 18.0 (C6), 17.8 (C6′).

*8-Hydrazinocarbonyloctyl 2-*O*-(α-L-Rhamnopyranosyl)-α-L-rhamnopyranoside (**8**)*

The fully deblocked disaccharide **7** (0.5 g) in ethanol solution (3 mL) was treated with hydrazine hydrate (0.5 g) at room temperature for 60 h. After evaporation and codistillation with ethanol, the solid residue was dried under vacuum. Purification on a column of silica gel with dichloromethane–methanol (1:1) gave pure **8** (0.45 g, 90% yield), $[\alpha]_D$ −53.6 (*c* 1.0, methanol), R_f 0.51 (1:1, as above); ^{1}H nmr (D_2O) δ: 1.1–1.9 (m, 18H, H-6, H-6′, —$(CH_2)_6$—), 2.20 (t, 2H, CH_2CO), 3.18–4.56 (m, 10H, ring protons, —CH_2O), 4.86 (bs, 1H, H-1′), 4.96 (bs, 1H, H-1). *Anal.* calcd. for $C_{21}H_{40}N_2O_{10}$: C 52.49, H 8.39, N 5.82; found: C 52.50, H 8.59, N 5.69.

*8-Methoxycarbonyloctyl 2-*O*-(3,4,6-Tri-*O*-acetyl-2-deoxy-2-pthalimido-β-D-glucopyranosyl)-3,4-di-*O*-benzyl-α-L-rhamnopyranoside (**10**)*

The partially benzylated rhamnopyranoside **5** (1.40 g, 2.7 mmol) was dissolved in dichloromethane (30 mL) together with collidine (0.37 g, 3.3 mmol) and silver triflate (0.85 g, 3.3 mmol). The solution was maintained under a dry nitrogen atmosphere and cooled to −40°C. The bromo sugar **9** (1.6 g, 3.2 mmol), prepared according to Lemieux and co-workers (20), dissolved in dichloromethane (20 mL) was added dropwise to the cooled solution of **5** and allowed to warm to room temperature overnight with constant stirring. After filtration, extraction of the filtrate with 3% hydrochloric acid, saturated sodium bicarbonate, and water, the solution was dried and evaporated. The product was purified on silica gel with Skellysolve B – ethyl acetate (1:1) as solvent to give pure **10** (1.75 g, 70% yield), $[\alpha]_D$ +8.0° (*c* 1.0, $CHCl_3$), R_f 0.58 (solvent as for column chromatography); ^{1}H nmr (CD_3OD) δ: 0.85–1.70 (m, 15H, H-6 and —$(CH_2)_6$—), 1.86 (s, 3H, CH_3CO), 2.02 (s, 3H, CH_3CO), 2.07 (s, 3H, CH_3CO), 2.25 (t, 2H, CH_2CO), 3.53 (s, 3H, CH_3O), 2.75–3.68 (m, 5H, ring protons, OCH_2), 3.68–4.57 (m, 9H, $OCH_2\phi$, ring protons), 4.67 (d, $J_{1,2}$ = 8 Hz, 1H, H-1′), 5.99 (t, $J_{2,3}$ = 9 Hz, 1H, H-3′), 6.85–7.86 (m, 14H, aromatic); ^{13}C nmr (CD_3OD) δ: 101.8 (Cl′), 100.1 (C1), 81.6, 79.6 ($OCH_2\phi$), 78.8 (C2), 75.8 (C5′),

73.2 (C4), 72.8 (C3′), 71.4 (C4′), 70.5 (C3), 69.0 (OCH_2), 68.3 (C5), 63.0 (C6′), 55.9 (C2′), 18.2 (C6).

*8-Methoxycarbonyloctyl 2-O-(2-Deoxy-2-phthalimido-β-D-glucopyranosyl)-3,4-di-O-benzyl-β-L-rhamnopyranoside (**11**)*

The fully protected disaccharide **10** (0.45 g, 0.48 mmol) was dissolved in methanol (70 mL) and a catalytic amount of freshly prepared sodium in methanol was added. The reaction was stirred overnight at room temperature, sodium ions were removed with Rexyn 101 (H^+) resin and the syrup was chromatographed using chloroform–methanol (7:1) with silica gel. Pure de-*O*-acetylated product **11** (0.35 g) was obtained in 90% yield, $[\alpha]_D$ −19.9° (*c* 1.1, methanol), R_f 0.54 (chloroform–methanol 7:1), mp 126–128°C (recrystallised from ether); ^{1}H nmr (CD_3OD) δ: 1.07 (d, 3H, H-6), 1.15–1.65 (m, 12H, —$(CH_2)_6$—), 2.23 (t, 2H, CH_2CO), 3.57 (s, 3H, CH_3O), 4.69 (d, $J_{1,2}$ = 2 Hz, 1H, H-1), 5.20 (d, $J_{1,2}$ = 8 Hz, 1H, H-1′), 6.80–7.90 (m, 14H, aromatic), 2.70–4.58 (remaining protons); ^{13}C nmr (CD_3OD) δ: 101.4 (C1′), 100.3 (C1), 81.8, 79.7 ($OCH_2\phi$), 78.6 (C2), 77.9 (C3′), 75.9 (C5′), 73.0 (C4), 72.5 (C3), 71.9 (C4′), 69.0 (OCH_2), 68.3 (C5), 62.6 (C6′), 58.6 (C2′), 18.1 (C6). *Anal.* calcd. for $C_{44}H_{55}NO_{13}$: C 65.58, H 6.88, N 1.74; found: C 65.46, H 6.89, N 1.88.

*8-Methoxycarbonyloctyl 2-O-(2-Acetamido-2-deoxy-β-D-glucopyranosyl)-3,4-di-O-benzyl-α-L-rhamnopyranoside (**12**)*

Compound **11** (0.35 g, 0.43 mmol) in ethanol (20 mL) was boiled with hydrazine hydrate (0.18 g of an 85% solution, 3 mmol) for 2 h. The reaction was monitored by tlc with chloroform–methanol (7:1) as solvent. In this system starting material possessed R_f 0.54 and the free amino derivative R_f 0.42. The solution was evaporated and thoroughly dried to remove traces of hydrazine. The product was then dissolved in methanol–water (1:1, 10 mL) and acetic anhydride (1 mL) was added. The solution was then stirred at room temperature overnight. Concentration followed by silica gel column chromatography with chloroform–methanol (7:1) gave pure **12** (0.25 g, 80% yield), $[\alpha]_D$ −8.8° (*c* 1.1, CH_3OH), R_f 0.52 (chloroform–methanol 7:1); ^{1}H nmr (CD_3OD) δ: 1.10–1.70 (m, 15H, H-6 and —$(CH_2)_6$—), 1.83 (s, 3H, CH_3CONH), 2.28 (t, 2H, CH_2CO), 3.52 (s, 3H, CH_3O), 7.00–7.80 (m, 10H, aromatic), 3.15–5.00 (remaining protons); ^{13}C nmr (CD_3OD) δ: 104.1 (C1′), 100.4 (C1), 81.7, 80.7 ($OCH_2\phi$) 77.8 (C2), 77.8 (C3′), 76.2 (C5′), 75.8 (C4), 73.1 (C3), 71.8 (C4′), 69.1 (OCH_2), 68.4 (C5), 62.6 (C6′), 57.9 (C2′), 18.3 (C6). *Anal.* calcd. for $C_{38}H_{55}NO_{12}$: C 63.58, H 7.72, N 1.95; found: C 63.46, H 7.63, N 1.85.

*8-Methoxycarbonyloctyl 2-O-(2-Acetamido-2-deoxy-β-D-glucopyranosyl)-α-L-rhamnopyranoside (**13**)*

Compound **12** (0.25 g, 0.35 mmol) was dissolved in acetic acid (50 mL) and palladium-on-charcoal (0.25 g) was added, the solution was hydrogenated at 70 psi for 3 h, filtered, and evaporated. The product was purified by column chromatography on silica gel with the solvent ethyl acetate – methanol – water (85:10:5) to give pure disaccharide **13** (0.17 g, 90% yield), $[\alpha]_D$ −25.4° (*c* 1.1, CH_3OH), R_f 0.18 (85:10:5); ^{1}H nmr (CD_3OD) δ: 1.10–1.75 (m, 15H, H-6 and —$(CH_2)_6$—), 1.99 (s, 3H, CH_3CONH), 2.29 (t, 2H, CH_2CO), 3.58 (s, 3H, CH_3O), 4.61 (d, $J_{1,2}$ = 8 Hz, 1H, H-1′), 4.84 (d, $J_{1,2}$ = 2 Hz, 1H, H-1), 3.15–4.35 (m, remaining protons); ^{13}C nmr (CD_3OD) δ: 104.3 (C1′), 100.3 (C1), 81.0 (C2), 77.8 (C3′), 76.2 (C5′), 74.1 (C4), 72.1 (C4′), 71.8 (C3), 69.6 (OCH_2), 68.5 (C5), 62.5 (C6′), 57.9 (C2′), 17.9 (C6). *Anal.* calcd. for $C_{24}H_{43}NO_{12}$: C 53.62, H 8.06, N 2.61; found: C 53.46, H 7.85, N 2.61.

*8-Hydrazinocarbonyloctyl 2-O-(2-Acetamido-2-deoxy-β-D-glucopyranosyl)-α-L-rhamnopyranoside (**14**)*

The fully deblocked disaccharide, **13** (0.3 g) in ethanol solution (3 mL) was treated with hydrazine hydrate (0.5 g) at room temperature for 60 h. After evaporation and codistillation with ethanol the residue was dried under vacuum. Purification on a column of silica gel with dichloromethane–methanol (1:1) gave pure **14** (0.27 g, 90% yield), $[\alpha]_D$ −21.5° (*c* 1.0, CH_3OH), R_f = 0.52 (dichloromethane–methanol 1:1); ^{1}H nmr (CD_3OD) δ: 1.23 (d, $J_{5,6}$ = 5.9 Hz, 3H, H-6), 1.0–1.75 (m, 12H, —$(CH_2)_6$—), 2.00 (s, 3H, CH_3CONH), 2.14 (t, 2H, CH_2CO), 4.63 (d, $J_{1,2}$ = 7.8 Hz, 1H, H-1′), 4.87 (d, $J_{1,2}$ = 1.5 Hz, 1H, H-1), 3.20–4.20 (m, remaining protons). *Anal.* calcd. for $C_{23}H_{43}N_3O_{11}$: C 51.39, H 8.06, N 7.82; found: C 51.25, H 8.21, N 7.63.

*8-Methoxycarbonyloctyl 2-Acetamido-3-O-(2,3,4-tri-O-acetyl-α-L-rhamnopyranosyl)-4,6-O-benzylidene-2-deoxy-β-D-glucopyranoside (**16**)*

(A) Mercuric Cyanide

The glucosaminide **15** (2.6 g, 5.4 mmol) was dissolved in dry acetonitrile (75 mL) containing mercuric cyanide (1.5 g, 5.9 mmol) and to this stirred solution maintained under an atmosphere of dry nitrogen was added dropwise a solution of a 2,3,4-tri-*O*-acetyl-α-L-rhamnopyranosyl bromide (**1**) (2.1 g, 6.0 mmol) (26) in acetonitrile (20 mL). After 16 h dichloromethane was added and the solution was extracted once with water, sodium bicarbonate, and again with water. Purification of the syrup obtained after solvent removal on a column of silica gel with the solvent ethyl acetate – Skellysolve B (3:1) gave pure **16** (2.1 g, 52% yield), $[\alpha]_D$ −41.8° (*c* 1.1, $CHCl_3$), R_f 0.62 (3:1), mp 149–151°C (recrystallised from ethyl acetate – Skellysolve B); ^{1}H nmr ($CDCl_3$) δ: 0.61 (d, $J_{5,6}$ = 6.5 Hz, 3H, H-6), 1.0–1.75 (m, 12H, —$(CH_2)_6$—), 1.90–1.95 (d, 9H, CH_3CO), 2.07 (s, 3H, CH_3CO), 2.20 (t, 2H, CH_2CO), 3.64 (s, 3H, CH_3O), 4.78 (d, $J_{1,2}$ = 2 Hz, 1H, H-1′), 4.93 (d, $J_{1,2}$ = 8 Hz, 1H, H-1), 5.46 (s, 1H, acetal H), 6.03 (bd, 1H, NH), 7.0–7.5 (m, 5H, aromatic), 2.85–5.35 (remaining protons); ^{13}C nmr (CD_3OD) δ: 103.2 (C1), 102.8 ($CH\phi$), 99.1 (C1′), 81.1 (C4), 78.3 (C3), 72.5 (C5), 71.7 (C4), 70.8 (C3′), 70.1 (C2′), 69.7 (OCH_2), 67.7 (C5′), 67.4 (C6), 57.5 (C2), 17.0 (C6′). *Anal.* calcd. for $C_{37}H_{53}NO_{15}$: C 59.11, H 7.11, N 1.86; found: C 58.89, H 7.15, N 1.98.

(B) Silver Triflate

Compound **15** (1.8 g, 3.8 mmol) was dissolved in dichloromethane (50 mL) together with silver triflate (1.6 g, 6.3 mmol) and tetramethylurea (3 mL, 25 mmol). The stirred solution was cooled to −40°C under a dry nitrogen atmosphere and the bromo sugar **1** (2.0 g, 5.7 mmol) in dichloromethane solution (20 mL) was added dropwise. The reaction mixture was allowed to warm to room temperature over 16 h. The reaction was worked up as described in A. After chromatography the yield of pure **16** was 1.9 g, 67%. The physical constants and ^{1}H nmr data were identical to those above.

*8-Methoxycarbonyloctyl 2-Acetamido-2-deoxy-3-O-(α-L-rhamnopyranosyl)-β-D-glucopyranoside (**17**)*

The disaccharide **16** (1.9 g, 2.5 mmol) was dissolved in methanol (200 mL) containing a catalytic amount of sodium. After 16 h the solution was deionised and concentrated. The residue was dissolved in 10 mL of 90% aqueous trifluoroacetic acid at 0°C and left for 45 min. Evaporation and codistillation with ethanol gave **17** which crystallized from ethanol – ethyl

acetate. Crystals of **17** (1.0 g, yield 77%) were collected, $[\alpha]_D$ −48.9° (*c* 1.2, CH_3OH), R_f 0.45 (dichloromethane–methanol 1:1), mp 175–177°C (recrystallized from ethanol–ethyl acetate 3:1); ^1H nmr (CD_3OD) δ: 1.10–1.75 (m, 15H, H-6′ and —$(CH_2)_6$—), 1.96 (s, 3H, CH_3CO), 2.28 (t, 2H, CH_2CO), 3.62 (s, 3H, CH_3O), 4.39 (d, $J_{1,2}$ = 8.0 Hz, 1H, H-1), 4.82 (d, $J_{1',2'}$ = 1.8 Hz, 1H, H-1′), 3.10–4.27 (remaining protons); ^{13}C nmr (CD_3OD) δ: 103.3 (C1), 102.3 (C1′), 83.8 (C3), 77.9 (C5), 73.8 (C4), 72.6 (C4′), 72.2 (C3′), 70.8 (C2′), 70.6 (C5′), 70.4 (OCH_2), 62.8 (C6), 56.9 (C2), 17.9 (C6′). *Anal.* calcd. for $C_{24}H_{43}NO_{12}$: C 53.62, H 8.06, N 2.61; found: C 53.33, H 8.10, N 2.80.

*8-Hydrazinocarbonyloctyl 2-Acetamido-2-deoxy-3-O-(α-L-rhamnopyranosyl)-β-D-glucopyranoside (**18**)*

The deblocked disaccharide **17** (0.50 g) was dissolved in ethanol (5 mL) containing hydrazine hydrate (0.5 g); the solution was stirred for 48 h, then evaporated and dried under high vacuum. Recrystallisation from ethanol gave pure **18** (0.45 g, 90% yield), $[\alpha]_D$ −48.3° (*c* 1.1, CH_3OH), R_f 0.54 (dichloromethane–methanol 1:1), mp 184–187°C (recrystallized from ethanol); ^1H nmr (CD_3OD) δ: 1.21 (d, $J_{5,6}$ = 6.3 Hz, H-6′), 1.05–1.70 (m, 15H, —$(CH_2)_6$— and H-6′), 1.95 (s, 3H, CH_3CONH), 2.12 (t, 2H, CH_2CO), 4.39 (d, $J_{1,2}$ = 8 Hz, 1H, H-1), 4.79 (d, 1H, H-1′), 3.15–4.27 (remaining protons). *Anal.* calcd. for $C_{23}H_{43}N_3O_{11}$: C 51.39, H 8.06, N 7.82; found: C 51.53, H 8.25, N 7.63.

Acknowledgements

We wish to thank Dr. J. Banoub for valuable discussions and Mr. J. Christ for technical assistance.

1. B. Lindberg, J. Lönngren, U. Rudén, and D. A. R. Simmons. Eur. J. Biochem. **32**, 15 (1973).
2. B. Lindberg, J. Lönngren, E. Romanowska, and U. Rudén. Acta Chem. Scand. **26**, 3808 (1972).
3. L. Kenne, B. Lindberg, K. Petersson, and E. Romanowska. Carbohydr. Res. **56**, 363 (1977).
4. L. Kenne, B. Lindberg, K. Petersson, E. Katzenellenbogen, and E. Romanowska. Eur. J. Biochem. **76**, 327 (1977).
5. E. Katzenellenbogen, L. Kenne, B. Lindberg, K. Petersson, and E. Romanowska. IXth Int. Symp. Carbohydr. Chem. London, England, April 10–14, 1978. Abstr. p. 503.
6. O. Lüderitz, A. M. Staub, and O. Westphal. Bacteriol. Rev. **30**, 192 (1966).
7. M. Katz and A. M. Pappenheimer. J. Immunol. **103**, 491 (1969).
8. Y. Karniely, E. Mozes, G. M. Shearer, and M. Sela. J. Exp. Med. **137**, 183 (1973).
9. M. Heidelberger, E. A. Kabat, and M. Mayer. J. Exp. Med. **75**, 35 (1942).
10. R. G. Mage and E. A. Kabat. Biochemistry, **2**, 1278 (1963).
11. E. A. Kabat and M. M. Mayer. Experimental immunochemistry. 2nd ed. Charles C. Thomas, Springfield, IL. 1961. Chapt. 5.
12. E. A. Kabat. Fed. Proc. **21**, 694 (1962).
13. D. A. Rees and W. E. Scott. J. Chem. Soc. B, 469 (1971).
14. R. U. Lemieux, D. R. Bundle, and D. A. Baker. J. Am. Chem. Soc. **97**, 4076 (1975).
15. R. U. Lemieux, D. A. Baker, and D. R. Bundle. Can. J. Biochem. **55**, 507 (1977).
16. P. A. J. Gorin and A. S. Perlin. Can. J. Chem. **37**, 1930 (1959).
17. H. R. Goldschmid and A. S. Perlin. Can. J. Chem. **39**, 2025 (1961).
18. D. M. van Niekerk and B. H. Koeppen. Experimentia, **15**, 123 (1972).
19. S. Hanessian and J. Banoub. Am. Chem. Soc. Symp. Ser. **39**, 36 (1976).
20. R. U. Lemieux, T. Takeda, and B. Y. Chung. Am. Chem. Soc. Symp. Ser. **39**, 90 (1976).
21. H. B. Boren, G. Ekborg, K. Eklind, P. J. Garegg, A. Pilotti, and C-G. Swahn. Acta Chem. Scand. **27**, 25 (1973).
22. N. K. Kochetkov, A. J. Khorlin, and A. F. Bochkov. Tetrahedron, **23**, 693 (1967).
23. B. R. Baker, J. P. Joseph, and R. E. Schaub. J. Am. Chem. Soc. **77**, 5905 (1955).
24. R. U. Lemieux and S. Koto. Tetrahedron, **30**, 1933 (1974).
25. D. D. Perrin, W. L. Armarego, and D. R. Perrin. Purification of laboratory compounds. Pergamon Press, London. 1966.
26. E. Fischer, M. Bergmann, and A. Rabe. Chem. Ber. **53**, 2362 (1920).
27. M. Mazurek and A. S. Perlin. Can. J. Chem. **43**, 1918 (1965).
28. J. Barnoub and D. R. Bundle. Submitted.

Kinetic isotope effect and tunnelling in the proton transfer reaction between 2,4,6-trinitrotoluene and 1,1′,3,3′-tetramethylguanidine in dimethylformamide solvent

ARNOLD JARCZEWSKI AND PRZEMYSLAW PRUSZYNSKI
Institute of Chemistry, Adam Mickiewicz University, Poznan, Poland
AND
KENNETH T. LEFFEK
Department of Chemistry, Dalhousie University, Halifax, N.S., Canada B3H 4H6

Received May 12, 1978

ARNOLD JARCZEWSKI, PRZEMYSLAW PRUSZYNSKI, and KENNETH T. LEFFEK. Can. J. Chem. **57**, 669 (1979).

The proton transfer reaction between 2,4,6-trinitrotoluene and 1,1′,3,3′-tetramethylguanidine in dimethylformamide solvent shows a large primary deuterium isotope effect, $k_H/k_D = 24.3$ at 0°C and 16.9 at 20°C. The enthalpy of activation difference $(\Delta H_D^{\ddagger} - \Delta H_H^{\ddagger}) = 2.6 \pm 0.4$ kcal mol^{-1} and the entropy of activation difference $(\Delta S_D^{\ddagger} - \Delta S_H^{\ddagger}) = 3.4 \pm 1.3$ cal mol^{-1} K^{-1}. This isotope effect, when fitted to Bell's equation, indicates that there is a considerable contribution to this reaction from tunnelling of the proton through the potential energy barrier.

ARNOLD JARCZEWSKI, PRZEMYSLAW PRUSZYNSKI et KENNETH T. LEFFEK. Can. J. Chem. **57**, 669 (1979).

La réaction de transfert de proton entre le trinitro-2,4,6 toluène et la tétraméthyl-1,1′,3,3′ guanidine dans le diméthylformamide comme solvant est accompagnée d'un effet isotopique primaire important, $k_H/k_D = 24.3$ à 0°C et 16.9 à 20°C. Les différences d'enthalpie d'activation $(\Delta H_D^{\ddagger} - \Delta H_H^{\ddagger})$ et d'entropie d'activation $(\Delta S_D^{\ddagger} - \Delta S_H^{\ddagger})$ sont respectivement 2.6 ± 0.4 kcal mol^{-1} et 3.4 ± 1.3 cal mol^{-1} K^{-1}. Lorsqu'on insère ces valeurs d'effets isotopiques dans l'équation de Bell, on en déduit que l'effet de tunnel du proton à travers la barrière à l'énergie potentielle contribue d'une façon importante à la réaction.

[Traduit par le journal]

Introduction

The reaction of 2,4,6-trinitrotoluene (TNT) with 1,1′,3,3′-tetramethylguanidine (TMG) gives, in polar aprotic solvents, the purple anion of TNT (1), the absorption maxima and molar absorptivities of which are very similar to those observed by Buncel *et al.* (2) for the reaction of TNT with ethoxide ion in ethanol. Despite some opposing views (3–6), it now appears established (1, 2, 7) that the proton transfer reaction takes place to form the anion under appropriate conditions, free of competing reactions such as nucleophilic attack on the benzene ring and radical anion formation.

The observation of a kinetic isotope effect, $k_H/k_D \simeq 7$ for the formation of the purple TNT anion upon treatment with ethoxide ion in ethanol (2), 8.4 for isopropoxide in isopropanol (9), and 8 for *tert*-butoxide in *tert*-butyl alcohol (10), have been reinforced by k_H/k_D values of 20.4 and 13.7 for the TMG reaction in acetonitrile and benzonitrile, respectively (1). Consistent with this primary kinetic isotope Buncel *et al.* (11) showed that TNT exchanged the hydrogens of the methyl group completely after 30 min at room temperature in alkaline 90% DMF – 10% D_2O.

This paper is a development of the previous work (1) on the reaction of TNT with tetramethylguanidine in polar aprotic solvents. Caldin *et al.* (12–16) have demonstrated large kinetic isotope effects in weakly polar solvents for reactions of this base and have suggested that in less polar solvents the lack of solvent reorganization accompanying the proton transfer allows proton tunnelling through the energy barrier which increases the isotope effect. In more polar solvents, some solvent reorganization takes place during proton transfer which increases the effective mass of the proton and thereby greatly reduces tunnelling. DMF was chosen as the solvent on the basis that it is a more bulky molecule than the nitriles already studied and therefore might reorganize to a lesser extent during the activation process of the proton transfer. Thus, even though DMF has the same dielectric constant as acetonitrile it should allow a greater contribution from the tunnel effect and therefore a larger isotopic rate ratio.

Results and Discussion

The reaction between TNT (1.5×10^{-5} *M*) and TMG ranging in concentration from 5×10^{-4} to 5×10^{-3} *M* in DMF gives the purple anion. No

0008-4042/79/060669-04$01.00/0

brown product, originally described by Caldin *et al.* (7), was observed. A careful examination of the possibility of side reactions has been made previously (1) for the reaction in acetonitrile and benzonitrile from which it was concluded that any competitive reactions to the proton transfer were negligible under these conditions. The absorption maxima for the product of the reaction in DMF are identical to those observed in acetonitrile (1) and the molar absorptivities differ by only about 5%. The maxima are 377 nm ($\varepsilon = 8500$ L mol^{-1} cm^{-1}), 526 nm ($\varepsilon = 13800$ L mol^{-1} cm^{-1}), and 645 nm ($\varepsilon = 6800$ L mol^{-1} cm^{-1}). The equilibrium constant K_{25} was calculated as 1800 L mol^{-1} from the slope of the plot [S]/OD vs. 1/[B] shown in Fig. 1 for the relationship shown in [1] where [S] is the initial

$$[1] \qquad [S]/\mathrm{OD} = \frac{1}{K\varepsilon}\frac{1}{[B]} + \frac{1}{\varepsilon}$$

concentration of TNT, [B] that of TMG, and OD is the optical density at 526 nm.

This equation was derived on the assumption that the anion and protonated base products exist in DMF solvent as an ion pair. If this assumption were not valid the plot in Fig. 1 would show a curvature.

Pseudo-first-order rate constants (k_1) were determined from runs carried out with excess base in which the change in optical density with time was monitored. A good fit to the first-order equation was found for both the proton and the deuteron transfer. The k_1 values were plotted against the base concentration and the slopes of these plots afforded the second-order rate constants. These are shown in Table 1 for both TNT and TNT-d_3. The error limits quoted are standard deviations. The second-order constants in DMF are greater than those observed in benzonitrile and acetonitrile (1) by factors of about 2 and 5, respectively. The activation parameters derived from the second-order rate constants are given in Table 2. For the proton transfer, $\Delta H^{\ddagger}$ in DMF is the same as that observed in benzonitrile and about 2.5 kcal mol^{-1} greater than that observed in acetonitrile. The rate differences are, therefore, due to an overriding entropy of activation effect. In acetonitrile ($\Delta S^{\ddagger} = -31.4$ cal mol^{-1} K^{-1}) the entropy of activation is about 12 cal mol^{-1} K^{-1} more negative than in DMF, from which it can be concluded that the DMF transition state solvation shell is less ordered than the acetonitrile solvation shell, i.e., that solvent reorganization is less complete in DMF.

The primary isotope effects in DMF are large, well in excess of the rate ratio of 7 at 300 K expected from the loss of zero-point energy associated with the C—H stretching vibration which is converted into a

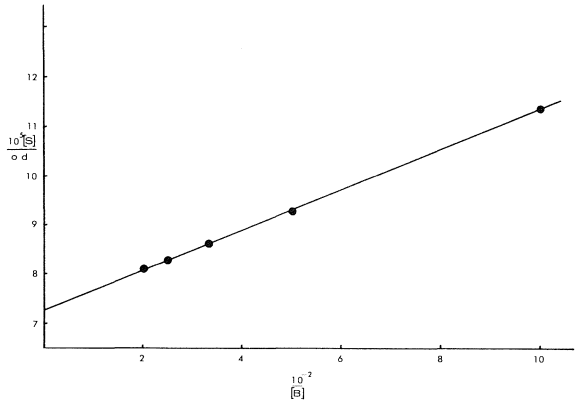

FIG. 1. Plot of 10^{-2}/[B] vs. 10^5[S]/OD for the reaction of 2,4,6-trinitrotoluene with 1,1′,3,3′-tetramethylguanidine in dimethylformamide solvent at 25°C.

translation during proton transfer. The value of $k_H/k_D = 16.9$ at 293 K falls between the 19.2 observed in acetonitrile and 13.1 in benzonitrile (1). Thus, we do not find a greater rate ratio as postulated from the solvent effect. However, from the isotope effects on the activation parameters, collated in Table 3, there does appear to be a larger tunnelling contribution in DMF, since the enthalpy of activation difference is much larger than the 1.1 kcal mol^{-1} arising from the loss of the stretching vibration.

These results confirm the general phenomenon of large isotope effects for TMG observed by Caldin and Mateo (5) with 4-nitrophenylnitromethane as substrate. Only acetonitrile is common to both sets of data and for this solvent the isotope effects on the activation parameters are very similar.

TABLE 1. Second-order rate constants for the reaction of normal and α-deuterated TNT with tetramethylguanidine in DMF

Temperature (°C)	k_{2H} (L mol^{-1} s^{-1})	k_{2D} (L mol^{-1} s^{-1})	k_{2H}/k_{2D}
0.0	4.75±0.08	0.19±0.01	24.3±0.8
5.0	6.30±0.01	—	—
10.0	—	0.42±0.01	—
12.5	10.85±0.22	—	—
20.0	15.84±0.63	0.94±0.02	16.9±0.4

TABLE 2. Activation parameters for the proton and deuteron transfer reactions from TNT and TNT-d_3 to tetramethylguanidine in DMF solvent at 25°C

Parameter	Proton transfer	Deuteron transfer
$\Delta H^{\ddagger}$(kcal mol^{-1})	9.8±0.3	12.4±0.3
$\Delta S^{\ddagger}$(cal mol^{-1} k^{-1})	−19.5±0.9	−16.1±0.9
$\Delta G^{\ddagger}$(kcal mol^{-1})	15.6±0.4	17.3±0.4
$\log_{10} A$	9.0±0.6	9.7±0.3

TABLE 3. Isotope effects on activation parameters for the proton transfer reaction from TNT to tetramethylguanidine in dipolar aprotic solvents

Parameter	DMF	Acetonitrile*	Benzonitrile*
$\Delta H_D^{\ddagger} - \Delta H_H^{\ddagger}$(kcal mol^{-1})	2.6±0.4	1.6±0.3	1.05±0.4
$\Delta S_D^{\ddagger} - \Delta S_H^{\ddagger}$(cal mol^{-1} K^{-1})	3.4±1.3	−0.6±1.0	−1.6±1.2
A_D/A_H	5.6	0.78	0.44

*From ref. 1.

In the extreme case of a complete loss of the C—H stretching frequency and two C–H bending frequencies during the activation process, the maximum isotope effect on the activation parameters is 2.1 kcal mol^{-1} for $\Delta H_D^{\ddagger} - \Delta H_H^{\ddagger}$, 1.4 cal mol^{-1} K^{-1} for $\Delta S_D^{\ddagger} - \Delta S_H^{\ddagger}$ and $A_D/A_H = 2.0$. Since our results in DMF solvent are in excess of these maximum values, it is assumed that there is a significant contribution from the tunnel effect. The results were fitted to Bell's equation (17–19) for a parabolic potential energy barrier, using the technique of Caldin and Mateo (13). For comparison, the tunnelling correction was also calculated for the isotope effects observed for the proton transfer reaction from 4-nitrophenylnitromethane to 1,8-bis(dimethylamino)naphthalene in *tert*-butyl alcohol solvent (20). For this reaction $k_H/k_D = 3.0$ at 30°C, $(\Delta H_D^{\ddagger} - \Delta H_H^{\ddagger}) = 1.1 \pm 0.7$ kcal mol^{-1} and $(\Delta S_D^{\ddagger} - \Delta S_H^{\ddagger}) = 1.5 \pm 2.3$ cal mol^{-1} K^{-1}, from which we concluded that there was probably no contribution from proton tunnelling (20). The tunnelling calculation is basically a trial and error fit of three parameters, E_H and E_D, the activation energies corrected for the tunnel effect for the protium and deuterated substrate, and $2b$, the width of the barrier at the base, to Bell's equation. The value of $E_D - E_H$ was limited to a maximum of 1.3 kcal mol^{-1}. The values of these parameters which give the best fit with the measured k_H/k_D over the temperature range are given in Table 4. The calculated parameters confirm the qualitative conclusion that the tunnelling contribution is important in the TNT reaction but insignificant in the reaction 4-NPNM with 1,8-bis(dimethyl)aminonaphthalene. In making these computations we have ignored the secondary isotope effect which arises from the fact that in the deuterated substrate only one of the three deuterium atoms is transferred. It is known that secondary effects of this type bring about a rate constant change of about 12 to 18% per D (21–23). However, they are difficult to measure in the presence of the primary effect and the uncertainties in the results are of the same magnitude as the secondary isotope effect itself, so it is impossible to measure the temperature dependence of the secondary effect in order to obtain the value of this effect on the activation parameters. Thus, although one can correct the rate ratio, using an estimated 15% per D atom for the secondary effect, this correction cannot be incorporated into the tunnel effect calculation which uses activation energies. Therefore, to make our computations directly comparable to those of Caldin and Mateo (13), we have followed the same method and ignored the secondary isotope effect, but we have allowed the activation energy difference to be as large as 1.3 kcal mol^{-1}, slightly larger than predicted by the loss of the C—H stretching frequency. For the TNT reaction, the values in Table 4 for the barrier width $2b$ and parameters C_t, ν_t, and $E_{H_{obs}}/E_H$ are very similar to those of a number of reactions, tabulated by Caldin (24), in which tunnelling is believed to be important. They are also very similar to those calculated by Caldin *et al.* (13) for 4-NPNM reacting with TMG in solvents such as tetrahydrofuran, dichloromethane and acetonitrile.

In contrast the reaction of 4-NPNM with 1,8-bis(dimethylamino)naphthalene yields a wide barrier of 3.3 Å and a correspondingly small curvature at the apex of the barrier C_t, with $E_{H_{obs}}/E_H$ close to unity. The different behaviour between the two bases may be correlated with the hybridization at the nitrogen atom to which the proton or deuteron is being transferred. As previously noted by Caldin *et al.* (14, 15) the larger isotope effects can be attributed to the smaller barrier widths with the more compact sp^2 hybridized orbitals at the nitrogen of TMG.

Experimental

Materials

2,4,6-Trinitrotoluene (TNT) was purified by repeated crystallization from ethanol with charcoal until a constant melting point of 81°C was reached. The purity of TNT was tested by ir and nmr methods (methyl protons δ 2.75 ppm, benzene ring protons δ 8.95 ppm in the ratio 3:2). The values obtained were in a good agreement with the literature.

Deuterated 2,4,6-trinitrotoluene (TNT-d_3) was obtained by reacting 0.1 *M* NaOD with 0.2 *M* TNT in a mixed solvent DMF–D_2O (90:10 v/v). Neutralization of this purple solution was effected after 2 h with a few drops of concentrated deuterium chloride in D_2O. The yellow solution was poured into an excess of D_2O, yellow crystals being obtained. This material was then recrystallized from deuterated ethanol and evaporated to dryness under vacuum. This procedure was carried out three times yielding deuterated material containing more than 96% D on the aliphatic carbon atom, as judged from the nmr spectrum. The peak at δ 2.75 ppm disappeared. The melting point of the TNT-d_3 was 80.5–81°C.

N,*N*-Dimethylformamide (DMF) was purified by the method of Zaugg and Schaefer (25).

TABLE 4. Tunnelling and barrier parameters*

Reaction	$E_{H_{obs}}$ (kcal mol^{-1})	$E_{D_{obs}}$ (kcal mol^{-1})	E_H (kcal mol^{-1})	E_D (kcal mol^{-1})	$2b$ (Å)	C_{tH} (kcal mol^{-1} Å^{-2})	ν_{tH} (cm^{-1})	$E_{H_{obs}}/E_H$	$E_{D_{obs}}/E_D$
TNT + TMG in DMF	10.4	13.0	11.8	13.1	1.18	67.8	887	0.88	0.99
4-NPNM + 1,8-bis(Me$_2$)amino naphthalene in *t*BuOH	13.5†	14.6†	14.0	14.6	3.30	10.3	345	0.96	1.00

*C_t is the curvature at the top of the barrier, ν_t is the frequency corresponding to the barrier dimensions.
†Reference 20.

1,1′,3,3′-Tetramethylguanidine (TMG) (Eastman) was dried over KOH, fractionally distilled over BaO under N_2, and collected at 161°C.

Kinetic Measurements

The kinetic measurements were carried with a Specord UV-VIS spectrophotometer equipped with a thermostating device to keep the cell temperature constant within 0.1°C.

The first-order rate constants (k_1) were obtained using considerable excess of the base. The values of k_1 were calculated according to the Guggenheim method (8). The following concentrations of the solutions were used: TNT, 1.5×10^{-5} *M* and TMG, 5×10^{-4} to 5×10^{-3} *M*. From the first-order rate constants (k_1), the k_2 values were calculated as a slope of the plot of k_1 against base concentration. The calculated second-order rate constants (k_2) were used for the Arrhenius relation of log $k_2 = f(1/T)$ from which, applying the transition state equation, the activation parameters ΔH^{+}, ΔS^{+}, and A were evaluated.

Both the second-order rate constants and the activation parameters were computed by the least-squares method.

1. P. PRUSZYNSKI and A. JARCZEWSKI. Rocz. Chem. **51**, 2171 (1977).
2. E. BUNCEL, A. R. NORRIS, K. E. RUSSELL, and R. TUCKER. J. Am. Chem. Soc. **94**, 1646 (1972).
3. R. FOSTER and C. A. FYFE. Rev. Pure Appl. Chem. **16**, 61 (1966).
4. E. BUNCEL, A. R. NORRIS, and K. E. RUSSELL. Q. Rev. Chem. Soc. **22**, 123 (1968).
5. M. R. CRAMPTON. Adv. Phys. Org. Chem. **7**, 211 (1969).
6. M. J. STRAUS. Chem. Rev. **70**, 667 (1970).
7. J. B. AINSCOUGH and E. F. CALDIN. J. Chem. Soc. 2528 (1956).
8. E. A. GUGGENHEIM. Philos. Mag. **2**, 538 (1926).
9. E. BUNCEL, A. R. NORRIS, K. E. RUSSELL, P. SHERIDAN, and H. WILSON. Can. J. Chem. **52**, 1750 (1974).
10. E. BUNCEL, A. R. NORRIS, K. E. RUSSELL, and H. WILSON. Can. J. Chem. **52**, 2306 (1974).
11. E. BUNCEL, K. E. RUSSELL, and J. WOOD. Chem. Commun. 252 (1968).
12. E. F. CALDIN and S. MATEO. Chem. Commun. 854 (1973).
13. E. F. CALDIN and S. MATEO. J. Chem. Soc. Faraday I, **71**, 1876 (1975).
14. E. F. CALDIN and C. J. WILSON. Faraday Symp. Chem. Soc. **10**, 121 (1975).
15. E. F. CALDIN and S. MATEO. J. Chem. Soc. Faraday I, **72**, 112 (1976).
16. E. F. CALDIN, D. M. PARBOO, F. A. WALKER, and C. J. WILSON. J. Chem. Soc. Faraday I, **72**, 1856 (1976).
17. R. P. BELL. Trans. Faraday Soc. **55**, 1 (1959).
18. R. P. BELL, W. H. SACHS, and R. L. TRANTER. Trans. Faraday Soc. **67**, 1995 (1971).
19. R. P. BELL. *In* The proton in chemistry. 2nd ed. Chapman and Hall, London. 1973. p. 275.
20. A. JARCZEWSKI, P. PRUSZYNSKI, and K. T. LEFFEK. J. Chem. Soc. Perkin II, 814 (1977).
21. K. T. LEFFEK. *In* Isotopes in organic chemistry. Vol. 2. *Edited by* E. Buncel and C. C. Lee. Elsevier, Armsterdam. 1976. Chapt. 3.
22. R. P. BELL and D. M. GOODALL. Proc. R. Soc. Sect. A, **294**, 273A (1966).
23. W. J. BOYLE, JR. Ph.D. Thesis, Northwestern University. 1971; Diss. Abstr. **32**, 3248B (1971).
24. E. F. CALDIN. *In* Reaction transition states. *Edited by* J. Dubois. Gordon & Breach, London. 1972. p. 247.
25. H. E. ZAUGG and A. D. SCHAEFER. Anal. Chem. **36**, 2121 (1964).

Volumes, expansivities, enthalpies of solution, and conductivities of K^+ and of Bu_4N^+ 1-adamantylcarboxylates in H_2O and in D_2O

NICOLE MOREL-DESROSIERS AND JEAN-PIERRE MOREL[1]

Laboratoire d'Etude des Interactions Solutés–Solvants, Université de Clermont, B.P. 45, 63170 Aubière, France

Received August 8, 1978

NICOLE MOREL-DESROSIERS and JEAN-PIERRE MOREL. Can. J. Chem. **57**, 673 (1979).

The standard molar volumes, the standard molar enthalpies of solution, and the limiting conductivities have been determined for potassium and tetrabutylammonium adamantylcarboxylates in water and heavy water, at 298.15 K. The temperature dependence of the volume and of the conductivity of the potassium salt has also been studied. The results are compared with those relative to potassium acetate. The change of the methyl group for the adamantyl one does not follow the behaviour normally expected for the transfer of hydrophobic solutes from water to heavy water.

NICOLE MOREL-DESROSIERS et JEAN-PIERRE MOREL. Can. J. Chem. **57**, 673 (1979).

Les volumes molaires standard, les enthalpies molaires standard de solution et les conductivités limites de l'adamantylcarboxylate de potassium et de l'adamantylcarboxylate de tétrabutylammonium ont été déterminés dans l'eau et dans l'eau lourde, à 298.15 K. Le volume et la conductivité du sel de potassium ont aussi été étudiés en fonction de la température. Les résultats ont été comparés à ceux relatifs à l'acétate de potassium. Le remplacement du groupe méthyle par le groupe adamantyle n'a pas l'effet normalement attendu lors du transfert de solutés hydrophobes de l'eau à l'eau lourde.

Introduction

During the last twenty years, much attention has been devoted to the study of hydrophobic phenomenon. Completely apolar molecules like the rare gases and the alkanes induce purely hydrophobic phenomenon when dissolved in water. Unfortunately, these solutes are so sparingly soluble in water that their solution properties are very difficult to measure and hence the paucity of such studies in the literature. This problem is usually circumvented by studying alkyl derivatives. As pointed out by Franks (1), alkyl derivatives that possess only one simple polar site are believed to behave like "soluble hydrocarbons", their functional group providing only a minor contribution to the thermodynamic properties of a homologous series (2). Carboxylates, however, seem to be an exception to this rule. On the other hand, these solutes are likely to represent closely what is encountered in proteins where the hydrophobic groups are usually in the neighbourhood of electrostatic entities. Therefore, despite the difficulty in interpreting their properties, the carboxylates should be interesting solutes.

Very few studies have been done on these systems. Snell and Greyson (3) have measured the heats of transfer and the free energies of transfer of the series sodium formate to sodium caproate from water to heavy water; the hydration properties of this particular transfer are believed "to be useful in reaching definite conclusions about hydrophobic interactions" (4). From the sign and magnitude of the transfer entropies they deduced that there was a transition from structure breaking to structure making in passing from sodium formate to sodium caproate. More recently, Lucas and Le Bail (5) measured the volumes and the heat capacities of transfer of sodium adamantylcarboxylate from water to heavy water and studied the ^1H nmr and Raman spectra of the potassium salt. The volumes of transfer did not give them significant structural information whereas the heat capacity results allowed them to consider sodium adamantylcarboxylate a structure former relative to sodium *tert*-butylcarboxylate. On the other hand, from their spectroscopic results potassium adamantylcarboxylate appeared to be a net structure breaker relative to smaller potassium *tert*-butylcarboxylate. Lucas and Bury (6) have also tried to measure the enthalpies of transfer of sodium adamantylcarboxylate from water to heavy water.

The adamantylcarboxylate anion (Fig. 1) is a very interesting solute and this has led us to precisely determine some of its properties in water and in heavy water. In order to have confidence in the ionic data, we have measured the properties of potassium and of tetrabutylammonium adamantylcarboxylates, the additivity rule serving as a check of the results. The standard volumes, expansivities (obtained for potassium adamantylcarboxylate only, from the temperature dependence of the volume), enthalpies of solution, and limiting conductivities were deter-

[1]To whom all correspondence should be addressed.

0008-4042/79/060673-05$01.00/0

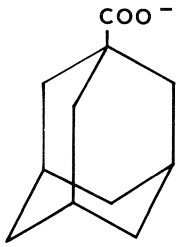

FIG. 1. The 1-adamantylcarboxylate anion.

mined at 298.15 K in water and in heavy water. As we intend to compare the adamantylcarboxylate to the acetate, we have also measured the conductivities of potassium acetate in water and in heavy water, at 298.15 K.

Experimental

The adamantylcarboxylates were prepared by stoichiometric neutralization of adamantylcarboxylic acid (Fluka, purum) with Bu_4NOH and KOH. The potassium salt (KAd) was recrystallized in water and dried under vacuum at 410 K during many days. The tetrabutylammonium salt (Bu_4NAd), obtained from the tetrabutylammonium methoxide in methanol (7), was recrystallized in ethyl acetate and dried under vacuum at 350 K during many days. The potassium acetate (KAc) (Prolabo) was recrystallized in anhydrous ethanol and dried under vacuum at 373 K. All solutions were prepared by weight with triply distilled water or with heavy water 99.8% minimum. For conductivity measurements, the solution concentration was varied by successively diluting the initial solution, using the Mettler DP11/DP101 weighing burette. Because of their hygroscopic nature, all manipulations of the salts were carried out under nitrogen atmosphere.

The conductivities, the densities, and the enthalpies of solution were measured with a Beckman RC-18-A conductivity bridge using a Tacussel CM 02 probe, a Picker flow differential densimeter, and a L.K.B. calorimeter, respectively, following the procedures described elsewhere (8–10). The conductivity cell was calibrated with aqueous KCl solutions on the concentration range suitable for our study (8). The solvent conductivity κ_0 is of the order of $2 \times 10^{-6}\ \Omega^{-1}\ cm^{-1}$. The uncertainty of our density measurements is about 3×10^{-6} g cm^{-3}. The densities of heavy water at 288.15, 298.15, and 308.15 K were determined relative to those of pure water; we have obtained 1.105728, 1.104278, and 1.101559 g cm^{-3}, respectively, using Kell's data for pure water (18). These results are in excellent agreement with the values of Millero *et al.* (15).

Results

The apparent molal volumes ϕ_v were derived from

$$[1] \qquad \phi_v = M_r/\rho + 1000(\rho_0 - \rho)/m\rho_0\rho$$

where M_r is the solute molecular weight, m is the molality, ρ and ρ_0 are the densities of the solution and the pure solvent, respectively. They were determined in the concentration range 0.02–0.08 m, at 298.15 K for KAc and for Bu_4NAd and at 288.15 K, 298.15 K, and 308.15 K for KAd in water and in heavy water.[2] The results are fitted to an equation of the type

$$[2] \qquad \phi_v = V^\theta + A_v(m\rho_0)^{0.5} + B_v m$$

where V^θ is the standard molar volume, A_v is the Debye–Hückel limiting slope, and B_v is an empirical constant determined from the experimental results. We have used for 1:1 electrolytes in H_2O and in D_2O the A_v parameters calculated by Perron *et al.* (11). We estimate the uncertainty in V^θ, including the error likely to arise from the extrapolation, to be less than 0.5 cm^3 mol^{-1}. From the temperature dependence of the standard molar volumes we have roughly estimated the standard molar expansivity $E^\theta = \partial V^\theta/\partial T$ of KAd in water and in heavy water, at 298.15 K.

The enthalpies of solution in H_2O and in D_2O were measured at concentrations around 0.015 m for KAd and 0.003 m for Bu_4NAd, at 298.15 K. The concentration dependence being generally similar in both solvents (11), we can assume the transfer functions at these concentrations to be approximately equal to the standard transfer enthalpies ΔH_{tr}^θ.

The conductivities were measured in the concentration range 0.001–0.01 m, at 298.15 K for KAc and Bu_4NAd and at 288.15 K, 298.15 K, and 308.15 K for KAd.[2] The limiting conductivities Λ^0 were obtained from the equation of Fuoss–Onsager, as described by Juillard *et al.* (8). The parameters of the equation were calculated at 288.15 K, 298.15 K, and 308.15 K using the dielectric constants of water and of heavy water as given by Malmberg and Maryott (12) and by Malmberg (13), respectively, and the viscosities as a function of temperature as given by Stokes and Mills (14) for water and by Millero *et al.* (15) for heavy water. The uncertainty in the limiting conductivities is of the order of 0.3 Ω^{-1} cm^2 mol^{-1}.

All these results are shown in Tables 1 and 2.

The additivity rule can be used as a check of some of our results. We have compared, for instance, the thermodynamic property differences between Bu_4NAd and KAd with that between Bu_4NBr and KBr. The differences of standard volumes in water and in heavy water agree to better than 0.5 cm^3 mol^{-1}, using the data of Perron *et al.* (11) for Bu_4NBr and that of Fortier *et al.* (16) for KBr. The differences of standard transfer enthalpies from water to heavy water agree to 0.3 kJ mol^{-1}, using Friedman and Krishnan's (4) compiled data. Using their ionic enthalpies of transfer, one would then predict an enthalpy of transfer of NaAd of 0.1 kJ mol^{-1} instead of the anomalously

[2]Complete set of the actual experimental data is available, at a nominal charge, from the Depository of Unpublished Data, CISTI, National Research Council of Canada, Ottawa, Ont., Canada K1A 0S2.

TABLE 1. Standard molar volumes and B_v parameters, expansivities, enthalpies of solution, and limiting conductivities of KAd, Bu_4NAd, and KAc in water and in heavy water, at 298.15 K

Property	Solvent	Value for KAd	Bu_4NAd	KAc
V^0 ($cm^3\ mol^{-1}$)	H_2O	143.9	410.6	49.5[a]
	D_2O	142.3	408.3	48.7
B_v ($cm^3\ mol^{-2}$)	H_2O	−1.9	−30.6	
	D_2O	−4.5	−15.0	−0.4
E^0 ($cm^3\ K^{-1}\ mol^{-1}$)	H_2O	0.2		
	D_2O	0.2		
ΔH_s^0 ($kJ\ mol^{-1}$)	H_2O	−21.7	−71.4	[b]
	D_2O	−21.4	−74.6	
Λ^0 ($\Omega^{-1}\ cm^2\ mol^{-1}$)	H_2O	98.1	43.4	114.0
	D_2O	81.9	36.0	93.5

[a]Reference 20.
[b]$\Delta H_{tr}^0(H_2O \rightarrow D_2O) = 0.4_5$ kJ mol^{-1} (obtained from a value for NaAc (3, 6) by using the ionic transfer enthalpies (4) of K^+ and Na^+).

TABLE 2. Temperature dependence of the standard molar volumes, of the B_v parameters, and of the limiting conductivities of KAd in water and in heavy water

Property	Solvent	Value at 288.15 K	298.15 K	308.15 K
V^0 ($cm^3\ mol^{-1}$)	H_2O	141.8	143.9	145.5
	D_2O	140.1	142.3	144.5
B_v ($cm^3\ mol^{-2}$)	H_2O	−2.4	−1.9	0.3
	D_2O	−9.6	−4.5	−1.9
Λ^0 ($\Omega^{-1}\ cm^2\ mol^{-1}$)	H_2O	78.6	98.1	119.0
	D_2O	63.6	81.9	100.7

large value of 4.6 kJ mol^{-1} given by Lucas and Bury (6).

Juillard *et al.* (8) give a value of 114.6 Ω^{-1} cm^2 mol^{-1} for the limiting conductivity of KAc. Their result is directly comparable with ours since both were extrapolated in the same way. The agreement is not perfect but this is not surprising with this type of electrolyte. However, we shall expect the comparison of our results in H_2O and D_2O to be relatively better as long as both sets of measurements are rigorously made under the same conditions.

Discussion

To gain a better understanding of anion–solvent interactions, it is desirable to evaluate the individual ionic contributions to the observed solvent isotope effect. This was done using the volume and the enthalpy of transfer for K^+ from water to heavy water (4) and the limiting ionic conductivity of K^+ in water and in heavy water (17). The transfer property data for acetate and adamantylcarboxylate anions are listed in Table 3.

TABLE 3. Ionic properties relative to the acetate and to the adamantylcarboxylate in water and in heavy water, at 298.15 K

Property	Value Ac^-	Ad^-
$\Delta V_{tr}^0(H_2O \rightarrow D_2O)$ ($cm^3\ mol^{-1}$)	−1.1	−1.9
$\Delta H_{tr}^0(H_2O \rightarrow D_2O)$ ($kJ\ mol^{-1}$)	−2.4	−2.4
λ^0 (H_2O) ($\Omega^{-1}\ cm^2\ mol^{-1}$)	40.5	24.6
λ^0 (D_2O) ($\Omega^{-1}\ cm^2\ mol^{-1}$)	32.1	20.5

The anionic volumes of transfer are negative and changing the methyl for the adamantyl group results in a more negative volume of transfer. The strong electrostriction associated with the $—COO^-$ group is probably responsible for the negative sign, as observed with the halides (4). The alkyl structural behaviour should attenuate this effect since the volumes of transfer of hydrophobic solutes are expected to be positive (4); furthermore, the cavity contribution to the volume of transfer ($H_2O \rightarrow D_2O$) of an alkyl group is positive and increases with the

TABLE 4. Ionic Walden products of the acetate and of the adamantylcarboxylate in H_2O and in D_2O

(*a*) Temperature dependence of the Walden product of adamantylcarboxylate in water

Walden product	Value at 288.15 K	Value at 298.15 K	Value at 308.15 K
$\lambda^o\eta_o$	0.217	0.219	0.219
$(\lambda^o\eta_o)_T/(\lambda^o\eta_o)_{288.15\,K}$	1	1.009	1.009

(*b*) Solvent-isotope effect on the Walden products of the acetate and of the adamantylcarboxylate, at 298.15 K

Walden product	Value Ac^-	Value Ad^-
$\lambda^o\eta_o(H_2O)$	0.360	0.219
$\lambda^o\eta_o(D_2O)$	0.352	0.225
$\lambda^o\eta_o(D_2O)/\lambda^o\eta_o(H_2O)$	0.978	1.027

alkyl size (19). Surprisingly, we observe the opposite effect when we increase the size of the alkyl group attached to the carboxylate.

The anionic enthalpies of transfer are negative; this was expected since, although for different reasons, both the strongly electrostatic anions and the hydrophobic groups give a negative enthalpy of transfer from water to heavy water (4). Amazingly, the ionic enthalpies of transfer seem independent of the spherical alkyl size, the large adamantyl group apparently perturbing the solvent as much as the small methyl group. Snell and Greyson (3), on the other hand, have observed a slight dependence with the increase of the linear alkyl chain, the ionic enthalpies of transfer varying from -2.2 to -2.9 kJ mol^{-1} by going from the methyl to the pentylcarboxylate.

In Table 4 we have listed the ionic limiting conductivity – solvent viscosity products (Walden products) of adamantylcarboxylate in water at 288.15 K, 298.15 K, and 308.15 K, calculated by using the viscosity of pure water as a function of temperature (14) and the ionic limiting conductivities of K^+ at 288.15 K (interpolated), 298.15 K, and 308.15 K (interpolated) of Kay and Evans (17). We have also listed the Walden products of the acetate and adamantylcarboxylate anions in H_2O and in D_2O, at 298.15 K. Structural information is usually obtained from the ratio of the Walden products at two temperatures or in two solvents. We have thus reported in Table 4 the ratio of the Walden product of adamantylcarboxylate in H_2O at temperature T over the Walden product at 288.15 K. We have also given the ratio of the Walden products in D_2O and in H_2O for the acetate and for the adamantylcarboxylate. The temperature dependence of the former is very slightly positive. This could be interpreted according to the classical models as reflecting the behaviour of a slightly hydrophobic solute. It could also mean that, of the two contributions involved, the carboxylate (electrostatic) one and the alkyl group (hydrophobic) one, the latter is more temperature dependent than the former. However, such small effects are hardly significant if we take into account the uncertainty in the limiting conductivities. Surprisingly, the ratio of the Walden products in D_2O and in H_2O is smaller than unity for the acetate and greater than unity for the adamantylcarboxylate. The classical interpretation of this ratio, which is based on the fact that there is more structural order in D_2O than in H_2O at the same temperature (17), implies the acetate is a structure former whereas the adamantylcarboxylate is a structure breaker, in apparent contradiction with what was just observed with the temperature effect. This unexpected conclusion and what was observed with the volumes and the enthalpies of transfer probably reflect the fact that the classical interpretations are not suitable for this type of solute. One reason for this could be that the 'structural' influences of both parts of the solute, the carboxylate one and the alkyl one, are not necessarily additive. This seems very important and should be kept in mind when studying biological systems since in proteins, for instance, alkyl groups are very often in the field of highly electrostatic entities. The comparison of the hydrophobic contribution of such alkyl groups with what is observed when we dissolve rare gases or hydrocarbons in pure water thus does not seem very helpful, the environment of these 'hydrophobic' entities being completely different.

Acknowledgments

We are indebted to Dr. M. Lucas for stimulating suggestions and helpful discussions. N. M.-D. thanks the National Research Council of Canada for the award of a post-doctoral fellowship.

1. F. Franks. *In* Water, a comprehensive treatise. Vol. 4. *Edited by* F. Franks. Plenum Press, New York. 1975. p. 1.
2. F. Franks. *In* Hydrogen-bonded solvent systems. *Edited by* A. K. Covington and P. Jones. Taylor and Francis, London. 1968. p. 31.
3. H. Snell and J. Greyson. J. Phys. Chem. **74**, 2148 (1970).
4. H. L. Friedman and C. V. Krishnan. *In* Water, a comprehensive treatise. Vol. 3. *Edited by* F. Franks. Plenum Press, New York. 1973. p. 1.
5. M. Lucas and H. Le Bail. J. Phys. Chem. **80**, 2620 (1976).
6. M. Lucas and R. Bury. J. Phys. Chem. **80**, 999 (1976).
7. R. M. Cundiff and P. C. Markunas. Anal. Chem. **34**, 512 (1962).
8. J. Juillard, J.-P. Morel, and L. Avédikian. J. Chim. Phys. **5**, 787 (1972).
9. P. Picker, E. Tremblay, and C. Jolicoeur. J. Solution Chem. **3**, 377 (1974).
10. L. Avédikian, J. Juillard, J.-P. Morel, and M. Ducros. Thermochim. Acta, **6**, 283 (1973).
11. G. Perron, N. Desrosiers, and J. E. Desnoyers. Can. J. Chem. **54**, 2163 (1976).
12. C. G. Malmberg and A. A. Maryott. J. Res. Natl. Bur. Stand. **56**, 1 (1956).
13. C. G. Malmberg. J. Res. Natl. Bur. Stand. **60**, 609 (1958).
14. R. H. Stokes and R. Mills. *In* Viscosity of electrolytes and related properties. Pergamon Press, Oxford. 1965. p. 74.
15. F. J. Millero, R. Dexter, and E. Hoff. J. Chem. Eng. Data, **16**, 85 (1971).
16. J.-L. Fortier, P. R. Philip, and J. E. Desnoyers. J. Solution Chem. **3**, 523 (1974).
17. R. L. Kay and D. F. Evans. J. Phys. Chem. **70**, 2325 (1966).
18. G. S. Kell. J. Chem. Eng. Data, **20**, 97 (1975).
19. P.R. Philip and C. Jolicoeur. J. Solution Chem. **4**, 105 (1975).
20. M. Palma and J.-P. Morel. J. Chim. Phys. **6**, 645 (1976).

Excess properties of cumene + *p*-dioxane system at 30°C

HORACIO N. SÓLIMO,[1] SILVIA DEL V. ALONSO, and MIGUEL KATZ

Cátedra de Físicoquímica, Facultad de Ciencias Exactas y Tecnología, Universidad Nacional de Tucumán, Tucumán, Argentina

Received December 16, 1977[2]

HORACIO N. SÓLIMO, SILVIA DEL V. ALONSO, and MIGUEL KATZ. Can. J. Chem. **57**, 678 (1979).

Densities, viscosities, enthalpies, and magnetic susceptibilities at 30°C were determined for the system cumene + *p*-dioxane. From the experimental results, the excess viscosity, excess enthalpy, excess volume, and excess molar magnetic susceptibility were calculated. The excess functions show deviations from the additivity law. An attempt has been made to explain the observed deviations on the basis of intermolecular interactions.

HORACIO N. SÓLIMO, SILVIA DEL V. ALONSO et MIGUEL KATZ. Can. J. Chem. **57**, 678 (1979).

On a déterminé les densités, les viscosités, les enthalpies et les susceptibilités magnétiques du système cumène/*p*-dioxanne, à 30°C. A l'aide de ces données expérimentales, on a calculé les viscosité, enthalpie, volume et susceptibilité magnétique molaires en excès. Les fonctions d'excès ne suivent pas la loi de l'additivité. On a essayé d'expliquer les déviations observées en se basant sur les interactions intermoléculaires.

[Traduit par le journal]

Introduction

The excess properties such as: η^E (excess viscosity), h^E (excess molar enthalpy), v^E (excess molar volume), and $\chi_M{}^E$ (excess molar diamagnetic susceptibility) have been studied to obtain information about the type and degree of interaction between molecules of the components. This is a continuation of our investigation of the thermodynamic properties of binary liquid mixtures (1, 2).

Densities, viscosities, enthalpies, and magnetic susceptibilities for the cumene + *p*-dioxane (C + D) system at different molar fraction were measured at 30°C, where one component (D) is non-polar and the other (C) weakly polar, without association in the pure state.

The diamagnetic molar susceptibility of the mixture is correlated with the molecular polarizability of the pure components by the Boyer–Donzelot equation (3).

Experimental

The methods used in our laboratory for the densities, viscosities, and enthalpies of binary liquid mixtures have been described previously (4).

Magnetic Susceptibility

The magnetic susceptibility was determined by a Gouy method using a Mettler H20T balance. Measurements have been made in a 9 kG magnetic field. The Gouy force ranged from 10 to 15 mg and the accuracy of its determination was estimated to be ±0.01 mg. Water twice distilled from alkaline permanganate ($\chi = -0.720 \times 10^{-6}$ cgs/g) and mercury tetrathiocyanate cobalt ($\chi = 16.49 \times 10^{-6}$ cgs/g) (5) were used as reference substances.

Materials and Solutions

Cumene and *p*-dioxane, Fluka p.a., were fractionally distilled over sodium under reduced pressure, and the middle colorless fraction was collected.

Mixtures were prepared by mixing weighed amounts of the pure liquids. Caution was taken to prevent evaporation.

Results

The experimental results for the pure liquids are reported in Table 1 along with the values from the literature for comparison.

The excess thermodynamic functions were calculated with the following equations:

$$[1] \qquad \eta^E = \eta - (x_1\eta_1 + x_2\eta_2)$$

$$[2] \qquad h^E = h_M - (x_1h_1 + x_2h_2)$$

$$[3] \qquad v^E = v - (x_1v_1 + x_2v_2)$$

$$[4] \qquad \chi^E = \chi_M - (x_1\chi_1 + x_2\chi_2)$$

where η, η_1, and η_2 = viscosity of the mixture and of the pure components; h_M, h_1, and h_2 = molar enthalpy of the mixture and of the pure components; v, v_1, and v_2 = molar volume of the mixture and of the pure components; χ_M, χ_1, and χ_2 = molar diamagnetic susceptibility of the mixture and of the pure components.

The molar volume of the mixture is defined by:

$$[5] \qquad v = (x_1M_1 + x_2M_2)/\rho$$

where M_1 and M_2 are the molecular weights of the components and ρ the density of the solution.

[1]Present address: Centro de Tecnología, Universidade Federal do Rio Grande do Norte, Natal, Brazil.

[2]Revision received October 12, 1978.

0008-4042/79/060678-04$01.00/0

TABLE 1. Properties characterizing the pure components at 30°C

Property*	Value					
	Cumene			*p*-Dioxane		
	Exp.	Lit.	Ref.	Exp.	Lit.	Ref.
Density	0.85330	0.85323	13	1.02297	1.02230	14
Viscosity	0.703	0.694	13	1.094	1.087	15
Refractive index	1.48628	1.48628	13	1.41906	1.41810	14
Molar magnetic susceptibility $\times 10^6$	−89.97	−89.53	16	−51.68	−52.16	16
Polarizability $\times 10^{24}$†	16.047	—		8.627	—	

*Units: ρ, g cm^{-3}; η, cP; χ_M, cgs mol^{-1}; α, cm^3 mol^{-1}.
†Calculated from the Lorentz–Lorenz equation.

TABLE 2. Values of coefficients for eq. [8] determined by the method of least squares*

Function	a_1	a_2	a_3	a_4	a_5	σ
η^E	−0.111	−1.675	3.934	−2.482	—	0.058
h^E	1371	11060	−45780	56320	−21190	32.7
v^E	2.424	−13.39	37.40	−44.87	18.76	0.011
$\chi_M{}^E$	−35.01	79.15	−8.586	—	—	0.47

*Units: η^E, cP; h^E, J mol^{-1}; v^E, cm^3 mol^{-1}; $\chi_M{}^E$, cgs mol^{-1}.

The experimental densities, viscosities, and molar enthalpies for the C + D systems were measured at different molar fractions, over a wide range of concentration.[3]

The diamagnetic susceptibility was related with the molecular polarizability by the Boyer–Donzelot equation (3), for organic pure compounds:

$$[6] \qquad \chi_i = f(n_i'\alpha_i)^{1/2}$$

For mixtures, we can assume to a first approximation that the additivity law for molar diamagnetic susceptibility is correct, then

$$[7] \qquad \chi_M = f\sum x_i(n_i'\alpha_i)^{1/2}$$

where f = constant = -3.46×10^6; n_i' = effective number of electrons, α_i = molecular polarizability of the component i. This effective number of electrons could be calculated by:

$$n_i' = n_i - n_0$$

where n_i = valence electrons of the component i and n_0 = characteristic constant for every family of substances (cumene = 10 and *p*-dioxane = 3.4).

The molar diamagnetic susceptibilities of the binary systems were measured over a wide range of concentration and compared with those calculated with eq. [7].[3]

The agreement between the observed and calculated values (e.g., for $x_C = 0.5059$: $\chi_M(\text{exp}) = -70.11 \times 10^{-6}$ cgs mol^{-1}; $\chi_M(\text{calcd}) = -71.90 \times 10^{-6}$ cgs mol^{-1}) points to the validity of the additivity law for this mixture.[3]

Each set of results was fitted with a Redlich–Kister (6) form of the type

$$[8] \qquad X^E = x_1(1 - x_1)\sum_{j=1}^{n} a_j x_1{}^{j-1}$$

where X^E represents the excess property under consideration; a_j = polynomial coefficients, and n = polynomial degree. The method of least-squares was used to determine the values of the coefficients a_j. In each case, the optimum number of coefficients was ascertained from an examination of the variation of the standard error of estimate with n:

$$[9] \qquad \sigma_x = [\sum(X^E{}_{obs} - X^E{}_{calcd}{}^2/(n_{obs} - n)]^{1/2}$$

where n_{obs} is the number of measurements.

The values adopted for the coefficients a_j (calculated with an IBM 1620 computer) and the standard error of the estimate associated with the use of [8] are summarized in Table 2.

Figures 1, 2, 3, and 4 show the experimental values obtained for the excess properties as a function of the molar fraction of cumene. The continuous curves were calculated from [8] using these values for the coefficients.

[3]Complete set of the actual experimental data is available, at a nominal charge, from the Depository of Unpublished Data, CISTI, National Research Council of Canada, Ottawa, Ont., Canada K1A 0S2.

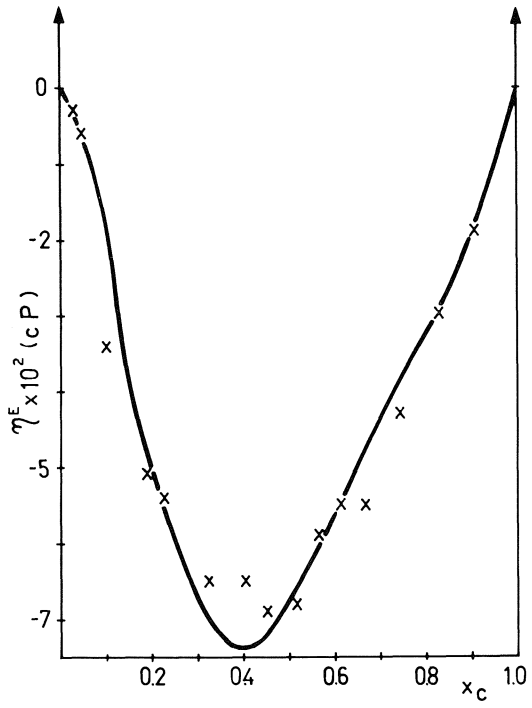

FIG. 1. Excess viscosity at 30°C for the C + D system. Experimental results: ×; continuous curve was calculated from eq. [8].

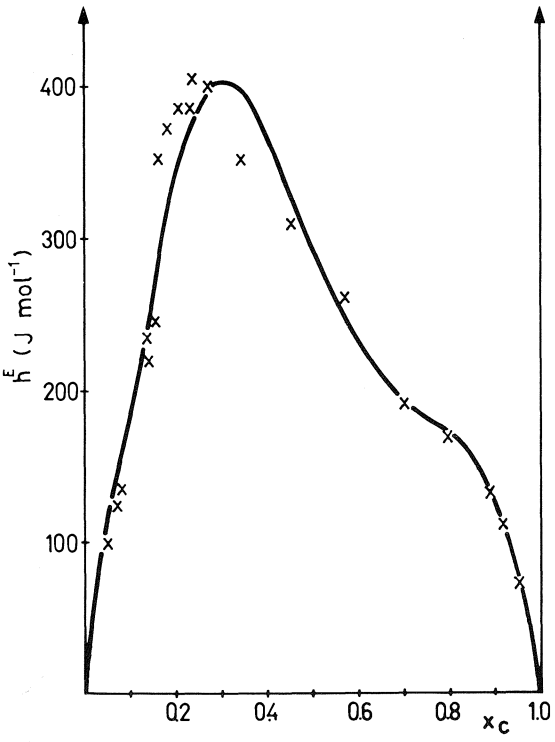

FIG. 2. Excess molar enthalpy at 30°C for the C + D system. Experimental results: ×; continuous curve was calculated from eq. [8].

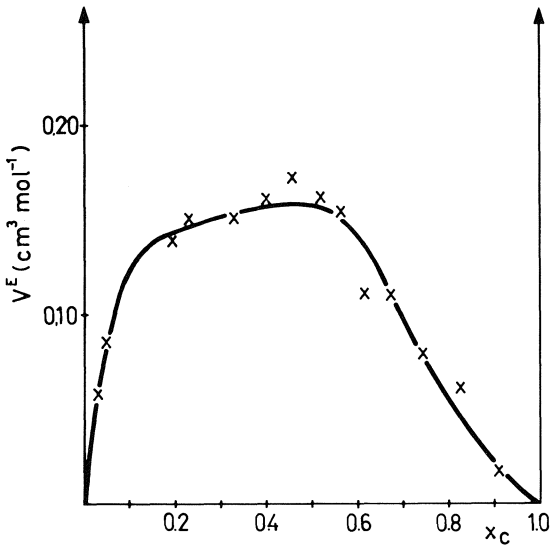

FIG. 3. Excess molar volume at 30°C for the C + D system. Experimental results: ×; continuous curve was calculated from eq. [8].

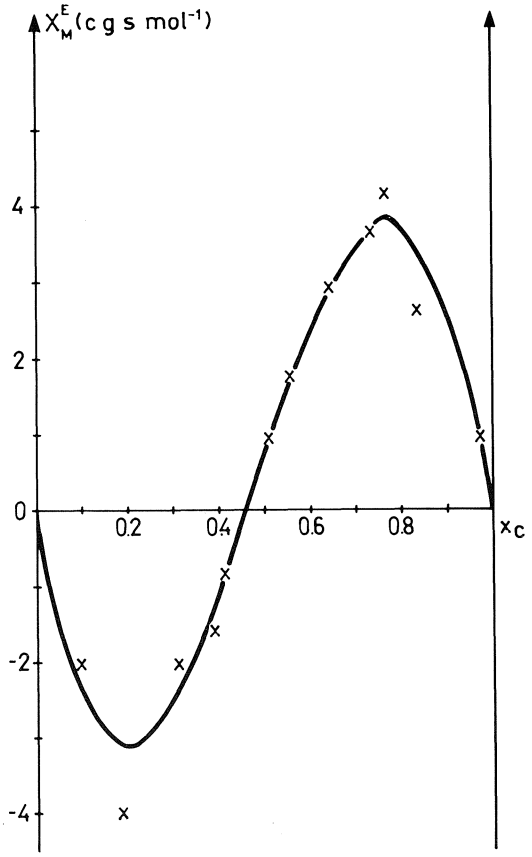

FIG. 4. Excess molar magnetic susceptibility for the C + D system. Experimental results: ×; continuous curve was calculated from eq. [8].

Discussion

Figure 1 shows negative excess viscosity for this system over the whole concentration range. Taking into account that neither of the components exhibits hydrogen bonding in the pure state, dispersion forces are dominant (7). However, since the minimum of the curve η^E vs. x_C is well marked, evidence of interaction between the molecules of different kinds is clear (8).

More quantitatively, evidence of this interaction is established taking into account h^E for C + *n*-heptane mixtures (h^E_{max}/J mol^{-1} (298 K) ~ 500) (9) and for D + cyclohexane mixtures (h^E_{max}/J mol^{-1} (298 K) ~ 1600) (10). The rather small h^E for C + D mixtures (h^E_{max}/J mol^{-1} (303 K) ~ 400) indicates that the interaction between C + D leads to a large decrease in h^E of about 1700 J mol^{-1} (1600 + 500 − 400 = 1700). This is not surprising since D gives rise to complex formation (n-π type or dipole-induced dipole type) with even non-polar molecules like benzene and CCl_4 with cumene, due to the inductive effect of the isopropyl group, the complex should be stronger.

Almost similar reasoning can be made for v^E: the contraction resulting in mixing C with D largely compensates the positive contribution observed ($v^E > 0$) in D and hydrocarbon mixtures (10).

In the case of mixtures in which one component is non-polar and the other weakly polar, the force field is envisaged as a superposition of a weak angular dependent field on a centrally spherical one (11). The cumene has a high polarizability and when it is mixed with *p*-dioxane there arises an induced dipole interaction because of the presence of these polarizable weakly polar molecules, and as expected gives rise to negative deviations in χ_M which produce a negative χ^E. As the concentration of cumene is increased there is an inversion at $x_C \sim 0.5$, which could be explained by the so-called "ring effect" (12) which causes an increase in the value of χ_M, that is, positive χ^E.

Acknowledgments

This work was supported by a SECYT research grant. We are indebted to Lic. Zulema N. Cardozo for help in computation programming.

1. H. N. SÓLIMO and M. KATZ. An. Quím. **72**, 322 (1976).
2. H. N. SÓLIMO, R. RIGGIO, J. A. ESPÍNDOLA, S. ALONSO, and M. KATZ. Can. J. Chem. **54**, 3125 (1976).
3. M. BOYER-DONZELOT. Thèse. Nancy. 1974.
4. H. N. SÓLIMO, R. RIGGIO, F. DAVOLIO, and M. KATZ. Can. J. Chem. **53**, 1258 (1975).
5. H. S. RADE. J. Phys. Chem. **77**, 424 (1973).
6. O. REDLICH and A. T. KISTER. Ind. Eng. Chem. **40**, 345 (1948).
7. R. J. FORT and W. R. MOORE. Trans. Faraday Soc. **62**, 1112 (1966).
8. YU YA FIALKOV. Russ. J. Phys. Chem. **37**, 1051 (1963).
9. E. PICQUENARD, H. KEHIAIAN, L. ABELLO, and G. PANNETIER. Bull. Soc. Chim. Fr. 120 (1972).
10. A. W. ANDREWS and K. W. MORCOM. J. Chem. Thermodyn. **3**, 513 (1971); **3**, 519 (1971).
11. R. G. GOPALAKRISHNAN. J. Prakt. Chem. **313**, 1178 (1971).
12. R. G. GOPALAKRISHNAN. Proc. Indian Acad. Sci. Sect. A, **58**, 229 (1963).
13. R. R. DREISBACH. Adv. Chem. Ser. 15 (1955).
14. J. TIMMERMANS. Physico-chemical constants of pure organic compounds. Elsevier Publishing Co., Inc., NY. 1950.
15. A. WEISSBERGER. Technique of organic chemistry. Vol. VII. Organic Solvents. 2nd ed. Interscience Publishing, NY. 1955.
16. R. C. WEST (*Editor*). Handbook of chemistry and physics. 49th ed. The Chemical Rubber Co. 1968.

Halogen-bridged complexes of platinum(II) and their reactions with dimethylformamide

PI-CHANG KONG AND F. D. ROCHON

Département de chimie, Université du Québec à Montréal, C.P. 8888, Montréal (Qué.), Canada H3C 3P8

Received June 14, 1978

PI-CHANG KONG and F. D. ROCHON. Can. J. Chem. **57**, 682 (1979).

Bridged compounds, $[Pt(L)Cl_2]_2$ (L = pyridine, picoline, and lutidine) have been prepared from the reactions between $K[Pt(L)Cl_3]$ and perchloric acid. The molecular weight measurements indicate that they are dimers in chloroform solutions. When $[Pt(L)Cl_2]_2$ is dissolved in dimethylformamide (DMF), $[Pt(L)(DMF)Cl_2]$ is formed and has been isolated. Infrared and nmr studies have shown that DMF is coordinated to platinum through the oxygen atom.

PI-CHANG KONG et F. D. ROCHON. Can. J. Chem. **57**, 682 (1979).

Des composés à ponts $[Pt(L)Cl_2]_2$ (L = pyridine, picoline et lutidine) ont été préparés par la réaction entre $K[Pt(L)Cl_3]$ et l'acide perchlorique. Les mesures de poids moléculaires indiquent que les composés sont des dimères en solution dans le chloroforme. Lorsque $[Pt(L)Cl_2]_2$ est dissout dans le diméthylformamide (DMF), $[Pt(DMF)(L)Cl_2]$ est formé et a été isolé. Des études de spectroscopie infrarouge et de rmn ont montré que le site de coordination du DMF est l'atome d'oxygène.

Introduction

General methods for the preparation of halogen-bridged complexes of platinum of the type $[Pt(L)Cl_2]_2$ were developed by Chatt and Venanzi (1). Two of these methods can be used to prepare amine or pyridine complexes. The first method is the thermal decomposition of olefin complexes:

$$2trans\text{-}[Pt(olefin)(L)Cl_2] \rightarrow [Pt(L)Cl_2]_2 + 2olefin$$

The reaction is very slow and requires a week to several months to obtain a reasonable yield of products. Complexes of piperidine, 4-*n*-pentylpyridine, 4-*n*-nonylpyridine, and toluidine were prepared by this method. The method was later modified. *trans*-$[Pt(acetylene)(L)Cl_2]$ was used and the rate of reaction was increased. However, only the bridged compound with pyridine has been prepared (2). The second method is the decomposition of acids:

$$2H[Pt(L)Cl_3] \rightarrow [Pt(L)Cl_2]_2 + 2HCl$$

The authors have pointed out that the method was strictly limited because the starting material is not very common. Only $[Pt(NH_3)Cl_2]_2$ has been prepared by this method.

Recently, we have developed a method to prepare salts, $K[Pt(L)Cl_3]$ (3), which can be readily converted to acid $H[Pt(L)Cl_3]$. Therefore the limitation of the second method no longer exists. A series of bridged complexes with various pyridine derivatives have been prepared and are described in this paper.

The bridged bonds can be easily cleaved even by weak nucleophiles which cannot displace chlorides from $PtCl_4^{2-}$. For example, when $[Pt(L)Cl_2]_2$ is dissolved in dimethylformamide (DMF), $[Pt(L)(DMF)Cl_2]$ is produced and can be isolated. These compounds are also discussed.

Experimental

Microanalyses were done by Chemalytics Inc., Tempe, AZ, U.S.A., and molecular weight measurements were done by Galbraith Laboratories, Inc., Knoxville, TN. Melting points were measured on a Fisher-Johns apparatus and are uncorrected. Nuclear magnetic resonance spectra were taken on a Perkin-Elmer R-12 spectrometer. Infrared spectra were measured on a Perkin-Elmer 621 grating spectrometer.

The platinum salt, K_2PtCl_4, was obtained from Johnson Matthey & Co. Limited. Pyridine (py), picoline (pic), and lutidine (lut) were purchased from Aldrich and Eastman and used without further purification. All the complexes were dried at 65°C under vacuum in the presence of P_2O_5.

Preparation of the Bridged Chloro Complexes

The freshly prepared salt, $K[Pt(L)Cl_3]$ (3) (0.4–0.5 g), was dissolved in a minimum amount of water and then 10 mL of $HClO_4$ (0.2 *M*) was added. The solution was allowed to stand at room temperature overnight and the $KClO_4$ was then filtered off. The filtrate was evaporated nearly to dryness and the red-yellow product was collected by filtration, washed with cold water, and dried. If the washings were still very yellow, more product was obtained by evaporating again to dryness.

Preparation of DMF Compounds

The bridged compound was dissolved in a minimum amount of DMF. The solution was allowed to stand 30 min and was then evaporated to dryness. The yellow product was washed with ether, collected by filtration, and dried. The yield is almost quantitative.

Results and Discussion

The Bridged Compounds

These compounds are reddish yellow. Their analytical data and melting points are listed in Table 1. They are soluble in most common organic solvents, such as chloroform, acetone, and tetra-

0008-4042/79/060682-03$01.00/0

TABLE 1. Analytical results, melting points, molecular weights, and vPt—Cl stretching frequencies of the bridged complexes

Compounds	C*	H	N	Cl	Melting point (°C)	Molecular weight in $CHCl_3$	Yield (%)	vPt—Cl (cm^{-1})
$[Pt(py)Cl_2]_2$	17.39	1.45	4.06	20.58				
	17.23	1.42	4.00	20.03	185		70	348 vs, 308 s
$[Pt(4\text{-pic})Cl_2]_2$	20.56	1.95	3.90	19.78		718		
	20.16	1.76	3.50	18.93	160	685	65	348 vs, 325 s, 311 sh
$[Pt(2\text{-pic})Cl_2]_2$	20.56	1.95	3.90	19.78				
	20.05	1.79	3.75	19.54	150		40	345 vs, 313 sh
$[Pt(2,4\text{-lut})Cl_2]_2$	22.52	2.43	3.75	19.03		746		
	22.42	2.34	3.80	18.31	150	690	55	345 vs, 311 m
$[Pt(2,6\text{-lut})Cl_2]_2$	22.52	2.43	3.75	19.03				
	21.97	2.35	3.63	19.30	225		70	346 vs, 318 s, 305 w

*The upper values represent the theoretical values.

hydrofuran. Compounds with substituted pyridine are soluble in benzene. All of them are insoluble in water. The measurements of molecular weight indicate that the compounds are dimers in chloroform solution (Table 1).

A crystallographic study of the 2,6-lutidine compound was done in our laboratory (4), and the results showed that it has the *trans*-configuration.

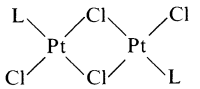

The dimers slowly form potassium salts $K[Pt(L)Cl_3]$ in the presence of potassium chloride in acidic solution. When the dimers are dissolved in DMF, solvated compounds characterized as $[Pt(L)(DMF)Cl_2]$ are obtained (see next section). When $[Pt(L)(DMF)Cl_2]$ is dissolved in chloroform, $[Pt(L)Cl_2]_2$ is partially formed. Crystals of $[Pt(2,6\text{-lutidine})Cl_2]_2$ were obtained from a dichloromethane solution of $[Pt(2,6\text{-lut})(DMF)Cl_2]$ at room temperature. Similarly Chatt and Venanzi found that [(4-*n*-pentylpyridine)(2,6-dibromo-4-*n*-dodecylaniline)dichloroplatinum] lost the aniline derivative in tetrachloromethane solution (5). It seems therefore that the bridged complexes are moderately favored in non-coordinating solvents, even in the presence of weak nucleophiles like DMF and aniline.

In acetone, the bridged complex of piperidine reacts with 4-*n*-pentylamine to give a mixture of *cis* and *trans* isomers, using stoichiometric proportions at room temperature or with an excess of ligand in boiling acetone (5). The mechanism of the reactions is uncertain. Using stoichiometric proportions at room temperature, we have found that the product of the reaction between $[Pt(py)Cl_2]_2$ and pyridine in DMF is *cis*-$[Pt(py)_2Cl_2]$.

In a previous work (3), we have found that *cis*-$[Pt(py)_2Cl_2]$ isomerized to *trans*-$[Pt(py)_2Cl_2]$ in the presence of pyridine at 80°C in DMF and that the reaction is not reversible. We may now conclude that in these cleavage reactions, the *cis*-compounds are first formed and the *trans*-compounds are formed from the subsequent isomerization of the *cis*-isomer.

DMF Compounds

DMF compounds can be obtained by the following two reactions:

$$[1]\quad [Pt(L)Cl_2]_2 + 2DMF \xrightarrow{DMF} 2[Pt(L)(DMF)Cl_2]$$

$$[2]\quad K[Pt(L)Cl_3] + AgNO_3 + DMF \rightarrow [Pt(L)(DMF)Cl_2] + AgCl\downarrow + KNO_3$$

The DMF compounds are soluble in many organic solvents. In chloroform a mixture of two compounds is in equilibrium.

$$2[Pt(L)(DMF)Cl_2] \rightleftharpoons [Pt(L)Cl_2]_2 + 2DMF$$

The nmr spectra showed that the complexed DMF and the free DMF are in equal amounts in chloroform solution. No free pyridine (L) was found. When the chloroform was evaporated the above reaction shifted to the left except for the 2,6-lutidine complex where both compounds were obtained.

The ir spectra of the DMF compounds in Nujol mull showed that the carbonyl stretching of DMF is lowered by 20–40 cm^{-1} (Table 2) indicating that the oxygen atom is the donor atom. The same conclusion was made for $[Pt(DMF)_2Cl_2]$ and $[Pt(DMA)_2Cl_2]$ (DMA = dimethylacetamide) by an infrared study (6). The nmr spectra of $[Pt(Py\text{-}d_5)(DMF)Cl_2]$ also indicated that the oxygen atom is the donor atom (Fig. 1). The aldehyde proton of DMF shifted from 8.15 to 8.35 ppm with a coupling constant of 40 Hz with ^{195}Pt while the methyl group on the nitrogen atom has no coupling. If nitrogen was the donor

TABLE 2. Analytical results, melting point, νC=O and νPt—Cl stretching frequencies of DMF complexes[a]

Compound	C	H	N	Cl	Melting point (°C)	νC=O (cm^{-1})	νPt—Cl (cm^{-1})
$Pt(py)(DMF)Cl_2$	22.97	2.87	6.70	16.99			
	22.97	2.75	6.92	18.00	125	1625 vs br	330 s, 315 sh
$Pt(4\text{-pic})(DMF)Cl_2$	25.00	3.26	6.48	16.40			
	24.26	3.02	6.24	16.38	122	1640 vs br	340 s, 308 m
$Pt(2\text{-pic})(DMF)Cl_2$	25.00	3.26	6.48	16.40			
	24.51	2.75	6.50	16.12	120	1628 vs br	337 s, 312 s
$Pt(2,4\text{-lut})(DMF)Cl_2$	26.94	3.40	6.28	15.92			
	26.66	3.55	5.90	15.30	122	1625 vs br	333 s
$Pt(2,6\text{-lut})(DMF)Cl_2$	26.94	3.40	6.28	15.92			
	26.92	3.66	5.83	16.00	160	1640 vs br	
DMF						1668 vs br	
$Pt(DMF)_2Cl_2$[b]						1625 vs br	
DMA						1631 vs br	
$Pt(DMA)_2Cl_2$[b]						1598 vs br	

[a]The upper values represent the theoretical values.
[b]From ref. 6.

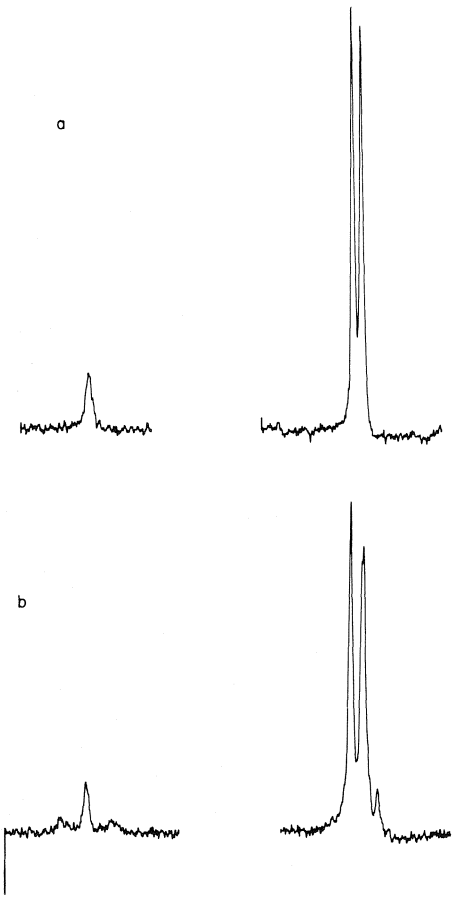

FIG. 1. Nuclear magnetic resonance spectra of (*a*) DMF and (*b*) $[Pt(Py\text{-}d_5)(DMF)Cl_2]$ in chloroform solution. Because C_5D_5N was used the signal of the aldehyde proton of DMF can be clearly observed, and shifted from 8.15 to 8.35 ppm with coupling of 40 Hz. The signals of the methyl groups shifted from 2.95 to 3.10 ppm. In (*b*) a small amount of dissociated DMF can be observed from the signals of the methyl group.

atom, the methyl group should have a coupling constant with ^{195}Pt of about 40 Hz like *N*-methyl-aminoacid in platinum compounds (7). The crystal structure of *trans*-$[Pt(2,6\text{-lutidine})(DMF)Cl_2]$ is presently being studied by X-ray diffraction in our laboratory. The results have confirmed that DMF is bonded to platinum through the oxygen atom (8).

Both *trans*- and *cis*-$[Pt(L)_2Cl_2]$ (L = py, 2-pic, or 4-pic) can be obtained from the reaction of $[Pt(L)(DMF)Cl_2]$ and L in DMF or $CHCl_3$ at room temperature (Pt:L = 1:1, conc. 0.05 *M* and time 1.5 h). The yield of *cis*-$[Pt(L)_2Cl_2]$ is quite low (20%). If an excess of L is used or if the time of the reaction is longer (5 h), only *trans*-$[Pt(L)_2Cl_2]$ is obtained. *trans*-$[Pt(2,6\text{-lut})(DMF)Cl_2]$ can be recovered from a DMF solution in the presence of an excess of 2,6-lut.

Acknowledgements

Grateful acknowledgements are made to the National Research Council of Canada and to the Cancer Research Society Inc. for financial support and to Johnson Matthey & Co. Limited for the loan of potassium chloroplatinite.

1. J. CHATT and L. M. VENANZI. J. Chem. Soc. 2787 (1955).
2. A. D. ALLEN and T. THEOPHANIDES. Can. J. Chem. **42**, 1551 (1964).
3. P.-C. KONG and F. D. ROCHON. Can. J. Chem. **56**, 441 (1978).
4. F. D. ROCHON and R. MELANSON. To be published.
5. J. CHATT and L. M. VENANZI. J. Chem. Soc. 3858 (1955).
6. J. M. GIORIA and B. P. SUSZ. Helv. Chim. Acta, **54**, 2251 (1971).
7. L. E. ERICKSON, M. D. ERICKSON, and B. L. SMITH. Inorg. Chem. **12**, 412 (1973).
8. R. MELANSON and F. D. ROCHON. To be published.

Determination of $\Delta H^0_{f298}(C_6F_{10},g)$ and $\Delta H^0_{f298}(C_6F_{12},g)$ from studies of the combustion of decafluorocyclohexene and dodecafluorocyclohexane in oxygen and calculation of the resonance energy of hexafluorobenzene

STANLEY JAMES W. PRICE[1] AND HENRY J. SAPIANO

Department of Chemistry, University of Windsor, Windsor, Ont., Canada N9B 3P4

Received September 7, 1978

STANLEY JAMES W. PRICE and HENRY J. SAPIANO. Can. J. Chem. **57**, 685 (1979).

The heats of formation of decafluorocyclohexene and dodecafluorocyclohexane have been determined by the direct combustion method previously developed and used for hexafluorobenzene and related compounds. The combustion of decafluorocyclohexene and dodecafluorocyclohexane formed the reaction products CO_2, CF_4, and F_2. In both cases a portion of the compound remained unburned. The unburned material was collected and quantitatively determined gravimetrically. A material balance was obtained for carbon and fluorine on the basis of CO_2, CF_4, and F_2 and the amount of unburned compound. With a ten-fold excess of oxygen, the average CO_2-to-CF_4 molar ratios for C_6F_{10} and C_6F_{12} are 2.03 ± 0.01 and 1.35 ± 0.01, respectively. The values obtained for the heats of formation are $\Delta H^0_{f298}(C_6F_{10},g) = -1906.6 \pm 7.2$ kJ mol^{-1} and $\Delta H^0_{f298}(C_6F_{12},g) = -2368.9 \pm 7.6$ kJ mol^{-1}. ΔH^0_{f298} for the reaction $C_6F_{10(g)} + F_{2(g)} \rightarrow C_6F_{12(g)}$ was calculated to be -462.3 ± 14.8 kJ mol^{-1} and the 'resonance energy' of C_6F_6 is estimated at -36.4 kJ mol^{-1}.

STANLEY JAMES W. PRICE et HENRY J. SAPIANO. Can. J. Chem. **57**, 685 (1979).

On a déterminé les chaleurs de formation du décafluorocyclohexène et du dodécafluorocyclohexane par la méthode de combustion directe développée antérieurement et utilisée pour l'hexafluorobenzène et des composés apparentés. La combustion du décafluorocyclohexène et du dodécafluorocyclohexane conduit au CO_2, au CF_4 et au F_2 comme produits de la réaction. Dans chacun des cas, une partie du produit est réfractaire à la combustion. On récupère le produit qui n'a pas réagi et on le détermine quantitativement par gravimétrie. On peut établir un bilan pour le carbone et le fluor en se basant sur les quantités de CO_2, de CF_4 et de F_2 obtenues et de produit récupéré. Lorsque l'excès d'oxygène est égal à 10 fois la quantité requise, les rapports molaires de CO_2 et de CF_4 pour le C_6F_{10} et le C_6F_{12} sont respectivement 2.03 ± 0.01 et 1.35 ± 0.01. Les valeurs obtenues pour les chaleurs de formation sont $\Delta H^0_{f298}(C_6F_{10},g) = -1906.6 \pm 7.2$ kJ mol^{-1} et $\Delta H^0_{f298}(C_6F_{12},g) = -2368.9 \pm 7.6$ kJ mol^{-1}. On a calculé que le ΔH^0_{f298} de la réaction $C_6F_{10(g)} + F_{2(g)} \rightarrow C_6F_{12(g)}$ est -462.3 ± 14.8 kJ mol^{-1} et on évalue à -36.4 kJ mol^{-1} l'énergie de résonance du C_6F_6.

[Traduit par le journal]

Introduction

To date no thermodynamic study for the heat of formation of C_6F_{12} has been reported. The combustion of C_6F_{10} in polyester bags has been reported by Cox and co-workers (1). To ensure complete combustion hydrogen-containing organic materials were added to the crucible. The approach taken in this study involves open dish combustion under anhydrous conditions and without auxiliary materials (2–5). This method has been adopted for the combustion of decafluorocyclohexene and of dodecafluorocyclohexane through the use of a steel crucible in a steel bomb. In each case some parent compound remained unburned but the only combustion products were CO_2, F_2, and CF_4. The quantity of unburned material was determined gravimetrically.

Experimental

Materials

(i) Decafluorocyclohexene

C_6F_{10} obtained from the Imperial Smelting Corporation was purified by preparative-scale gas chromatography. The final product had the following physical properties (the values in parentheses are those reported by the manufacturer) (6) bp = 53°C (53°C), $n_D^{25} = 1.29$ (1.29). Analysis by gas chromatography (6 ft. × 1/8 in. od Durapak *n*-octane/Porasil C, 100–200 mesh, N_2, 60 cm^3/min, column temperature 110°C, flame ionization detection) showed the presence of three impurities which represented a maximum of 0.02% of the sample. The impurities were collected and analyzed by mass spectrometry and nmr. They were identified to be $C_6F_{11}H$, C_6F_8, and $C_6F_{10}H_2$.

Vapour pressure measurements were made over the range of 4°C to 46°C. The data are adequately represented by

$$[1] \quad \log_{10} P\,(\text{cm}) = 10.474 - 1783.3/T - 1.236 \log_{10} T$$

[1]To whom all correspondence should be addressed.

0008-4042/79/060685-04$01.00/0

The resulting heat of vapourization and average heat capacity differences (vapour–liquid) are $\Delta H^0_{298} = 30.96$ kJ mol^{-1} and $\langle \Delta C_p, 4°C–46°C \rangle = -10.3$ J deg^{-1} mol^{-1}. The heat of vapourization is in good agreement with the value of 30.75 kJ mol^{-1} reported by Cox *et al.* (1).

(ii) Dodecafluorocyclohexane

C_6F_{12} obtained from the Imperial Smelting Corporation was used without further purification. Analysis by gas chromatography (same conditions as for C_6F_{10}) showed the presence of a minor impurity which represents a maximum of 0.01% of the sample. Vapour pressure measurements were made over the range 1°C to 49°C. The data can be adequately represented by:

$$[2] \quad \log_{10} P\,(\text{cm}) = 5.4180 - 1781.7/T + 0.7799 \log_{10} T$$

The resulting heat of sublimation and average heat capacity difference (vapour–solid) are $\Delta H^0_{298} = 35.98$ kJ mol^{-1} and $\langle \Delta C_p, 1°C–49°C \rangle = +6.49$ J deg^{-1} mol^{-1}.

(iii) CO_2, CF_4, F_2

CO_2, CF_4, and F_2 were obtained from the Matheson Chemical Company and were used without further purification.

Apparatus and Calorimetric Procedure

The apparatus and procedure used for the main combustion process were identical to those used for C_6F_5Br (5). A Parr model 1004C steel bomb and steel crucible were again used for the combustion process.

The rate of loss of C_6F_{10} and C_6F_{12} from the steel crucible in which they were weighed were 0.833 mg s^{-1} and 0.667 mg s^{-1}, respectively. The time between weighing the crucible containing the sample and closing the bomb was such that less than 1.7% of the total sample for C_6F_{10} and 1.3% for C_6F_{12} were lost by evaporation. The correction for the evaporation is estimated to be accurate to better than ±3%. The error generated by the correction procedure for C_6F_{10} and C_6F_{12} should therefore be less than ±0.05% and ±0.04%, respectively.

It must be remembered that the C_6F_{10} and C_6F_{12} samples are not contained in any way and that combustion occurs in a 320 cm^3 bomb with an initial temperature of 23.5°C and an initial pressure of 450 psi. The experimental procedure therefore involves the combustion of 1.23 g C_6F_{10} vapour and $(w - 1.23)$ g C_6F_{10} liquid where w = weight of C_6F_{10} sample in grams and the combustion of 1.18 g C_6F_{12} vapour and $(w - 1.18)$ g C_6F_{12} solid where w = weight of C_6F_{12} sample in grams. This means that on the average approximately 74% of the C_6F_{10} and 67% of the C_6F_{12} are in the vapour state before combustion.

Analysis of Reaction Products

The analytical procedures for CO_2, CF_4, and F_2 have been described elsewhere (2–5). The unburned material was collected in a glass U-trap which was immersed in an acetone – dry ice bath. The quantity of unburned material was determined gravimetrically. Mass spectra were obtained using a Varian MAT CH5-DF spectrometer controlled by an INCOS computer system. A Bausch and Lomb Spectronic 100 was used to determine iron with 1,10-phenanthroline (7).

Results and Discussion

In the combustion of C_6F_{10} and C_6F_{12} in the steel bomb it was observed that the formation of a green coloration was less extensive inside the bomb in both cases as compared with the amount observed in the study of C_6F_5Br (5). The amount of Fe(II) and Fe(III) fluorides after combustion of C_6F_{10} and C_6F_{12} was determined using a colorimetric procedure (7). In both cases the quantity found was 1.23 ± 0.01 mg. Approximately 80% of the iron fluoride was FeF_2. The correction to the heat of formation of C_6F_{10} and C_6F_{12} caused by the formation of FeF_2 and FeF_3 was less than 1.5 kJ mol^{-1} and 1.6 kJ mol^{-1}, respectively.

Apart from the small quantities of iron fluoride the products of combustion were CO_2, CF_4, and F_2. These products were identified and quantitatively determined in the same manner reported for the products of combustion of C_6F_6 (2), except that in the gas chromatographic procedure the silica gel column was replaced with a Porapak Q column.

The column used was a 6 ft. × 1/4 in. od Porapak Q column (25°C, He carrier, 48 cm^3/min). Calibrations were carried out using O_2–CF_4 and O_2–CO_2 mixtures. If pure CO_2 is used the CO_2 calibration is unaffected. If pure CF_4 is used the net result is that the relative response factor for CF_4 is increased by 3.5% resulting in values for $\Delta H^0_{f298}(C_6F_{10},g)$ and $\Delta H^0_{f298}(C_6F_{12},g)$ which are about 35.6 kJ mol^{-1} and 50.2 kJ mol^{-1} too high, respectively.

Gas chromatographic and mass spectrometric analyses indicate that observed unburned material in the study of both C_6F_{10} and C_6F_{12} is a portion of the original material. The mass spectrum of unburned C_6F_{12} was compared with that of an authentic sample and with API 0201 (8). No literature spectra could be found for C_6F_{10}. Table 1 presents the major peaks (R.A. > 4% base peak) for both an authentic sample and the recovered unburned material.

TABLE 1. Main peaks (R.A. > 4% base peak) for C_6F_{10} and for unburned material from the combustion of C_6F_{10} (isotope peaks omitted)

		Relative abundance	
m/e	Ion	C_6F_{10}	Unburned material
31	CF	6.5	6.2
69	CF_3	21.9	21.6
74	C_3F_2	4.2	4.2
93	C_3F_3	39.0	36.2
100	C_2F_4	5.4	4.9
112	C_3F_4	6.7	6.0
124	C_4F_4	7.4	7.7
131	C_3F_5	17.0	19.1
143	C_4F_5	24.0	25.4
155	C_5F_5	7.5	7.6
162	C_4F_6	100	100
193	C_5F_7	24.6	27.4
212	C_5F_8	5.1	5.4
243	C_6F_9	74.0	70.0
202	C_6F_{10}	26.0	30.9

TABLE 2. Combustion data and calculated enthalpy of formation for decafluorocyclohexene[e]

Mass C_6F_{10}[a] (g)	ΔT_{cor} (°C)	CO_2/CF_4[b] (by gc)	CO_2 collected (g)	F_2 collected (g)	% Theoretical yields[c] C	% Theoretical yields[c] F	Mass C_6F_{10}[d] (g)	% Theoretical yields[d] C	% Theoretical yields[d] F	$\Delta H^0_{f298}(C_6F_{10}, g)$ (kJ mol^{-1})
1.364	0.3437	2.03	0.709	0.158	77.0	77.0	1.050	100.0	100.0	−1905.8
1.671	0.3928	2.05	0.821	0.187	72.5	72.5	1.212	100.0	100.0	−1913.8
1.468	0.3541	2.04	0.731	0.167	73.6	74.1	1.083	100.0	100.5	−1905.8
1.501	0.4178	2.03	0.860	0.194	84.9	85.1	1.274	100.0	100.2	−1901.6
1.443	0.3954	2.03	0.817	0.184	83.9	84.0	1.211	100.0	100.1	−1906.2

[a]Mass of C_6F_{10} placed in the bomb.
[b]Molar ratio.
[c]Percent yield based on amount of C_6F_{10} placed in bomb.
[d]Based on recovery of carbon (from CO_2 and CF_4).
[e]Additional typical data (see ref. 14 for notation); ΔE, ign/J = 13.7, $\Delta E(J)(-t_c)$/J = −6778.0, ΔE^0_c/M(compound)/J g^{-1} = −5800.

TABLE 3. Combustion data and calculated enthalpy of formation for dodecafluorocyclohexane[e]

Mass C_6F_{12}[a] (g)	ΔT_{cor} (°C)	CO_2/CF_4[b] (by gc)	CO_2 collected (g)	F_2 collected (g)	% Theoretical yields[c] C	% Theoretical yields[c] F	Mass C_6F_{12}[d] (g)	% Theoretical yields[d] C	% Theoretical yields[d] F	$\Delta H^0_{f298}(C_6F_{12}, g)$ (kJ mol^{-1})
1.815	0.3485	1.37	0.696	0.160	75.4	75.2	1.369	100.0	100.0	−2365.2
1.696	0.3349	1.35	0.660	0.147	76.9	76.9	1.304	100.0	100.0	−2371.5
1.981	0.4082	1.36	0.806	0.183	80.2	80.1	1.589	100.0	99.5	−2361.4
1.741	0.3349	1.36	0.666	0.150	75.4	75.2	1.313	100.0	99.8	−2371.1
1.501	0.2653	1.35	0.521	0.113	68.7	68.3	1.031	100.0	99.5	−2362.3
1.945	0.3973	1.35	0.786	0.174	79.9	79.8	1.554	100.0	99.9	−2374.4
1.588	0.3065	1.35	0.607	0.133	75.6	75.4	1.200	100.0	99.7	−2376.5
1.790	0.3259	1.35	0.642	0.143	70.9	70.9	1.269	100.0	100.0	−2369.0

[a]Mass of C_6F_{12} placed in bomb.
[b]Molar ratio.
[c]Percent yield based on amount of C_6F_{12} placed in bomb.
[d]Based on recovery of carbon (from CO_2 and CF_4).
[e]Additional typical data (see ref. 14 for notation); ΔE, ign/J = 13.7, $\Delta E(J)(-t_c)$/J = −6055.3, ΔE^0_c/M(compound)/J g^{-1} = −4545.9.

The total material balance based on CO_2, CF_4, F_2, and unburned material was in general low by about 0.25%. This was shown to be due to small losses from the trapping systems used to recover the unburned material. Subsequent thermochemical calculations were therefore based on the CO_2–CF_4 recovery.

From the material balance shown in Table 2 along with the average CO_2/CF_4 molar ratio reaction [3] may be written to represent the combustion of decafluorocyclohexene

[3] $C_6F_{10} + 4.024O_2 \rightarrow 4.024CO_2 + 1.976CF_4 + 1.048F_2$

From the material balance shown in Table 3 along with the average CO_2/CF_4 molar ratio reaction [4] may be written to represent the combustion of dodecafluorocyclohexane

[4] $C_6F_{12} + 3.452O_2 \rightarrow 3.452CO_2 + 2.548CF_4 + 0.904F_2$

In treating a complex mixture of products possible interactions between the compounds must be taken into account. No detectable heat of mixing was observed when F_2, O_2, CF_4, and CO_2 were mixed under anhydrous conditions (4).

In carrying out the thermochemical calculations the following heats of formations have been used; CO_2(g), −393.512 kJ mol^{-1} (9); and CF_4(g), −933.0 kJ mol^{-1} (10).

Based on the preceding data and an estimated correction to standard state of 3.4 kJ mol^{-1}, $\Delta H^0_{f298}(C_6F_{10},g) = -1906.6 \pm 7.2$ kJ mol^{-1}. The previously reported values −1881.1 kJ mol^{-1} (1) and −1935.1 kJ mol^{-1} (11) were based on ΔH^0_{f298} (HF·20H_2O) = −316.44 and −322.00 kJ mol^{-1}, respectively. Hubbard's work (12) would seem to support the latter value which leaves a discrepancy of about 28 kJ mol^{-1} between the present result and that of Cox and Pilcher (11).

The value for $\Delta H^0_{f298}(C_6F_{12},g)$ based on the above data and an estimated correction to standard state of 2.9 kJ mol^{-1} is -2368.9 ± 7.6 kJ mol^{-1}.

It is possible from the present data and from the heat of formation of hexafluorobenzene to calculate the enthalpies of reactions [5] and [6]

[5] $C_6F_{10}(g) + F_2(g) \rightarrow C_6F_{12}(g)$

[6] $C_6F_6(g) + 3F_2(g) \rightarrow C_6F_{12}(g)$

and subsequently to calculate a value for the 'resonance energy' of hexafluorobenzene (defined as $\Delta H^0_{298}(Rx[6]) - 3\Delta H^0_{298}(Rx[5])$. Based on ΔH^0_{f298}-(C_6F_6,g) = −945.6 kJ mol^{-1} (4) this 'resonance energy' is found to be −36.4 kJ mol^{-1}, implying little difference in energy between hexafluorobenzene and the hypothetical triene. This conclusion

seems to be in agreement with 'destabilization' calculations by Cox *et al.* (13) which show that the destabilizing effects of the C—F dipoles do not seem to be significantly moderated by any 'resonance' effect.

It is interesting to note that if the values of Cox *et al.* for $\Delta H^0_{f298}(C_6F_{10},g)$ (11) and $\Delta H^0_{f298}(C_6F_6,g)$ (13) are used the calculated 'resonance energy' is -112.1 kJ mol^{-1}. However, if the enthalpies used here are recalculated using the older NBS selected value of $\Delta H^0_{f298}(HF{\cdot}20H_2O) = -319.16$ kJ mol^{-1} (9) rather than the more recent result of Hubbard, -322.1 kJ mol^{-1} (12), then the resonance energy is -44.7 kJ mol^{-1} and $\Delta H^0_{f298}(C_6F_{10},g) = -1908.1$ kJ mol^{-1}, both in good agreement with the present work. Although the implication here is far from conclusive it may indicate that further study of the heats of formation of aqueous HF solutions is needed.

Acknowledgements

The authors wish to thank Greg P. Johnson for very helpful discussions and suggestions. This work has been supported by an operating grant from the National Research Council of Canada, which the authors gratefully acknowledge.

1. J. D. Cox, H. A. Gundry, and A. J. Head. Trans. Faraday Soc. **60**, 653 (1964).
2. M. J. Krech, S. J. W. Price, and W. F. Yared. Can. J. Chem. **50**, 2935 (1972).
3. M. J. Krech, S. J. W. Price, and W. F. Yared. Can. J. Chem. **51**, 3662 (1973).
4. M. J. Krech, S. J. W. Price, and W. F. Yared. Can. J. Chem. **52**, 2673 (1974).
5. M. J. Krech, S. J. W. Price, and H. J. Sapiano. Can. J. Chem. **55**, 4222 (1977).
6. Highly fluorinated aromatic and alicyclic compounds. Imperial Smelting Company, St. Andrews Road, Avonmouth, Bristol BS119HP, England.
7. H. H. William, L. L. Merrit, and J. A. Dean. Instrumental methods of analysis. 4th ed. D. Van Nostrand Company Inc., New York, NY. 1969. p. 104.
8. E. Stenhagen, S. Abrahamsson, and F. W. McLafferty (*Editors*). Atlas of mass spectral data. Interscience, New York, NY. 1969.
9. F. D. Rossini *et al.* Selected values of chemical thermodynamic properties. Natl. Bur. Stand. (U.S.), Tech. Note No. 270-3. 1968.
10. E. Greenberg and W. H. Hubbard. J. Phys. Chem. **72**, 222 (1968).
11. J. D. Cox and G. Pilcher. Thermochemistry of organic and organometallic compounds. Academic Press, London and New York. 1970.
12. W. N. Hubbard *et al.* J. Chem. Thermodyn. **5**, 793 (1973).
13. Cox *et al.* J. Chem. Thermodyn. **1**, 77 (1969).
14. J. Coops, B. S. Jessup, and K. Van Nes. *In* Experimental thermochemistry. Vol. 1. *Edited by* F. D. Rossini. Interscience, New York, NY. 1956.

A shock-tube study of ammonia pyrolysis

JOHN E. DOVE AND WING S. NIP[1]

Department of Chemistry, Lash Miller Chemical Laboratories, University of Toronto, Toronto, Ont., Canada M5S 1A1

Received October 11, 1977[2]

JOHN E. DOVE and WING S. NIP. Can. J. Chem. **57**, 689 (1979).

The pyrolysis of NH_3 was studied behind reflected shock waves at temperatures 2500–3000 K, using mass spectrometric analysis of dynamically sampled gas. The initial mixtures contained 0.14% to 6% NH_3, with Kr as diluent, at total gas concentrations of about 2×10^{-6} mol cm^{-3}. Concentration profiles of NH_3, NH_2, NH, and N_2 were measured. It was found that the apparent rate coefficient for overall removal of NH_3 is increased by increasing the initial NH_3 concentration, but is decreased by addition of H_2. Addition of H_2 also suppressed NH, but left the NH_2 concentration relatively unchanged. A close correlation was found between NH_2 concentration and N_2 formation rate, indicating that NH_2 participates in the reaction which produces N_2.

The experimental results are consistent with a chain mechanism in which NH_3 is removed by unimolecular decomposition and by attack by H, NH, and NH_2. Computer analysis yields a rate constant of $1.2 \times 10^{16} \exp(-91\,000 \text{ cal mol}^{-1}/RT)$ cm^3 mol^{-1} s^{-1} for the unimolecular process.

JOHN E. DOVE et WING S. NIP. Can. J. Chem. **57**, 689 (1979).

Faisant appel à la spectrométrie de masse d'échantillons de gaz prélevés d'une façon dynamique, on a étudié la pyrolyse du NH_3, derrière des ondes de choc réfléchies, à des températures de 2500 à 3000 K. A des concentrations totales de gaz de 2×10^{-6} mol/cm^3, les mélanges initiaux contiennent de 0.14 à 6% de NH_3 lorsqu'on utilise du Kr pour diluer. On a mesuré les profils de concentration de NH_3, NH_2, NH et N_2. On a trouvé que le coefficient de vitesse apparent pour l'élimination globale de NH_3 augmente avec une augmentation de la concentration initiale du NH_3 mais qu'il diminue avec une addition de H_2. L'addition de H_2 supprime aussi la formation de NH mais influence peu la concentration de NH_2. On a trouvé une corrélation étroite entre la concentration de NH_2 et le taux de formation de N_2; ceci indique que le NH_2 participe à la réaction qui produit le N_2.

Les résultats expérimentaux sont en accord avec un mécanisme en chaîne dans lequel le NH_3 est éliminé par une décomposition unimoléculaire et par des attaques par H, NH et NH_2. Une analyse par ordinateur permet d'obtenir une constante de vitesse de $1.2 \times 10^{16} \times \exp(-91\,000 \text{ cal mol}^{-1}/RT)$ cm^3 mol^{-1} s^{-1} pour le processus unimoléculaire.

[Traduit par le journal]

Introduction

The thermal decomposition of gaseous ammonia provides a potentially interesting and important test case for the theory of unimolecular reactions. This decomposition has indeed already been the subject of a number of experimental studies (1–8), from which it is evident that the overall reaction is influenced by secondary processes. However, the reaction mechanism is by no means clear, and consequently it is difficult to deduce the unimolecular rate constant unambiguously from the observed kinetics.

Table 1 summarizes the literature values for the overall decomposition rate coefficient, k_D. There has been some doubt about the form of the overall rate equation. Jacobs (1) found orders of 1.5 and 0.5 with respect to NH_3 and diluent, respectively. Johnson (4), on the other hand, found that the rate was first order in NH_3 and zero order in diluent concentration. However, the variation in diluent concentration by these two workers was less than 50%, and hence their statements about the diluent concentration dependence should be viewed with caution. Most of the recent studies are in agreement that, at the total gas concentrations typical of shock-tube experiments, the overall rate is first order in NH_3 and first order in diluent, so that

$$-\mathrm{d}[NH_3]/\mathrm{d}t = k_D[NH_3][M]$$

The study by Michel and Wagner (2) over a 120-fold variation in NH_3 concentration, and an 8-fold variation in diluent concentration, is particularly convincing in this respect.

The values of k_D found by different workers vary substantially; e.g. at 2500 K, Takeyama and Miyama (5) report a value 6.3 times larger than that of Bradley *et al.* (6). However, the observed temperature dependences (Table 1) are all about 80 kcal mol^{-1}, which

[1]Present address: Division of Chemistry, National Research Council of Canada, Ottawa, Ont., Canada K1A 0R6.

[2]Revision received October 6, 1978.

0008-4042/79/060689-13$01.00/0

TABLE 1. Summary of literature rate coefficients for the overall decomposition rate of NH_3*

Temperature range (K)	$10^5 \times$ total gas concentration (mol cm^{-3})	Mol% NH_3 (in Ar)	k_D (cm^3 mol^{-1} s^{-1})	Reference
2000–3000	~0.6	1 and 8	2.5×10^{16} exp $(-77\,700/RT)$	1†
2100–2940	1.2 to 10	0.1 to 1.5	4.4×10^{15} exp $(-79\,500/RT)$	2
2300–3000	1 to 100		1×10^{16} exp $(-86\,500/RT)$	3
2400–3000	~3	6.8	1×10^{10} exp $(-83\,700/RT)$	4‡
2480–2970	~3	1	2.3×10^{15} exp $(-71\,100/RT)$	5
2000–3000	0.5 to 2.0	5, 10, and 20	4.0×10^{15} exp $(-83\,000/RT)$	6
2000–2750	1.5 to 6	4.25 and 8.5	4.2×10^{15} exp $(-83\,420/RT)$	7
2000–3000	0.15 to 1	1 to 3	5.8×10^{15} exp $(-77\,000/RT)$	8

*$k_D = -([NH_3]^{-1}[M]^{-1}(d[NH_3]/dt))$ except in refs. 1 and 4; units in cm^3 mol^{-1} s^{-1} with the activation energy in cal mol^{-1}. [M] = diluent gas concentration.
†In ref. 1, $k_D = -([NH_3]^{-1.5}[M]^{-0.5}(d[NH_3]/dt))$.
‡In ref. 4, $k_D = -([NH_3]^{-1}(d[NH_3]/dt))$ in s^{-1}.

is much lower than the N—H bond dissociation energy of 103 kcal mol^{-1}. There are several ways of explaining this difference between the activation energy and the exothermicity:

(*i*) If the unimolecular dissociation step

[1] $NH_3 + M \rightarrow NH_2 + H + M$ $\quad \Delta H_0^0 = 103$ kcal mol^{-1}

is rate-determining for the overall reaction, the lowering in activation energy could be ascribed to unimolecular fall-off. The lowering appears, however, to be rather large to be wholly explained in this way.

(*ii*) While it is usually assumed in the literature that the products of the unimolecular step are NH_2 and H, the formation of NH and H_2 is thermochemically somewhat more favourable:

[2] $NH_3 + M \rightarrow NH + H_2 + M$ $\quad \Delta H_0^0 \simeq 91$ kcal mol^{-1}

Allowing for some unimolecular fall-off, this endothermicity appears to fit the observed activation energy quite well.

(*iii*) An alternative is that the decomposition is a chain reaction, or at least that secondary reactions of lower activation energy also influence the rate of NH_3 removal. The occurrence of a chain reaction is supported by the results of Takeyama and Miyama (5), who observed an induction period in the pyrolysis process below 2400 K. The nature of the secondary reactions is by no means clear. Previously, it has usually been assumed (on the basis of low temperature rate data) that H atoms do not react with NH_3. This forced Bradley *et al.* (6) to conclude that the chain carrier must be NH_2. They proposed the following mechanism

[1] $NH_3 + M \rightarrow NH_2 + H + M$

[3] $NH_2 + NH_3 \rightarrow N_2H_3 + H_2$

[4] $N_2H_3 \xrightarrow{(M)} NH + NH_2$

[7′] $NH_2 + NH_2 \rightarrow$ products

However, it is now known (9) that H atoms do react with NH_3 at high temperatures. The mechanism of Bradley *et al.* therefore needs further examination.

Haluk (7) used a theoretical rate coefficient from the literature (10, 11) from a Johnston and Parr type of calculation, for the reaction of H with NH_3, and concluded that most of the secondary reactions must be carried out by H atoms. He proposed the following mechanism:

[1*a*] $NH_3 + Ar \rightarrow NH_2 + H + Ar$

[5] $H + NH_3 \rightarrow H_2 + NH_2$

[6] $H + NH_2 \rightarrow H_2 + NH$

[7] $NH_2 + NH_2 \rightarrow NH + NH_3$

[8*a*] $H + H + Ar \rightarrow H_2 + Ar$

[9] $NH + NH \rightarrow N_2 + H_2$

[10] $NH_2 + NH_2 \rightarrow N_2 + H_2 + H_2$

However, the theoretical value which he chose for k_5 is so much larger than all of the experimental values that it is almost certainly wrong. Hence he most probably overestimates the importance of H atoms. Johnson (4) also proposed that H atoms are important in ammonia pyrolysis, based on his finding that addition of H_2 increased the decomposition rate. However, his analyses were not conclusive.

NH has not been suggested as an important intermediate in the pyrolysis mechanism. Nevertheless, studies of its behaviour in NH_3 pyrolysis have been reported by three research groups (6, 8, 12) who agreed in proposing that NH was derived from NH_2, rather than from the direct decomposition of NH_3 into NH and H_2. However, there was no agreement about the observed kinetic behaviour. Bradley *et al.* (6) found that the NH concentration, measured by infrared emission, rose parabolically

$$[NH] = k[NH_3]^2[Ar]t^2$$

They proposed the following mechanism for formation of NH

[3] $$NH_2 + NH_3 \rightarrow N_2H_3 + H_2$$

[4] $$N_2H_3 \xrightarrow{(M)} NH + NH_2$$

which is consistent with their overall mechanism mentioned earlier. Cann and Kash (12) and Genich, Zhirnov, and Manelis (8) studied the ultraviolet emission of NH, and found an initial linear rather than parabolic rise:

$$d[NH]/dt = k'[NH_3]_0^2$$

However, this emission from electronically excited NH is apparently non-thermal, and it may well bear no direct relationship to the concentration of electronic ground state NH.

Evidently, there is still considerable uncertainty about the decomposition mechanism, and in particular about the possible role of radical intermediates. For this reason, we have made a shock-tube kinetic study using mass spectrometric detection. This method gives concentration versus time profiles of reactant, products, and some major intermediates, and therefore yields a very good overview of the processes taking place.

Experimental

Apparatus

The basic apparatus and detailed experimental procedure have been described previously (13) so that only a brief account will be given here. The equipment included a stainless steel shock tube coupled to a time-of-flight mass spectrometer. The hot reacting gas was sampled from the reflected shock region directly into the ion source of the mass spectrometer. A set of mass spectra, recorded sequentially from oscilloscopes at intervals of typically 15 to 25 μs, constituted the basic kinetic data from each experiment. The speed of the incident shock wave was measured by timing it over 4 successive intervals, using digital time interval meters of 0.1 μs resolution. The temperature, pressure, and density behind the reflected shock wave were then calculated from the shock speed (extrapolated to the end wall of the shock tube) using standard thermodynamic data (14) and computational methods.

Before commencing each experiment, the shock tube was pumped down to a pressure less than 10^{-5} Torr, measured by a hot filament ion gauge. Since NH_3 is polar and tends to adsorb on stainless steel, the shock tube was then flushed with ammonia, pumped down to about 1×10^{-3} Torr, and flushed with the reaction mixture before every experiment.

Before the present study, several significant changes were made to the original apparatus (13), as follows:

(*a*) A predynode gating circuit (15), designed in this laboratory, was added to the electron multiplier of the mass spectrometer. This allowed the very large mass peaks due to the diluent gas to be eliminated before amplification in the multiplier. The electron multiplier could then be operated at larger gain without danger of non-linearity due to saturation effects.

(*b*) The inlet cylinder to the differential pumping baffle in the flight tube of the mass spectrometer was replaced by a cylindrical grid. This change reduced the pressure build-up in front of the baffle which was the cause of a slight collision broadening of mass peaks found in earlier work with this instrument.

(*c*) The original glass manifold and gas handling system were replaced by a bakable all stainless steel system. Gas pressure measurements were made by a Texas Instruments quartz spiral gauge which was calibrated by the National Research Council of Canada.

Experimental Gases

Kinetic experiments were made with four mixtures: mixture 1: 6.2% NH_3, 5.0% Ar, 88.7% Kr; mixture 2: 6.0% NH_3, 1.2% H_2, 5.6% Ar, 87.2% Kr; mixture 3: 6.1% NH_3, 5.8% H_2, 6.4% Ar, 81.7% Kr; mixture 4: 0.14% NH_3, 0.16% Ar, 99.70% Kr. The mixtures were made up by manometric measurement of partial pressures. No further analysis was made of the mixture composition, but the purity was checked mass spectrometrically.

Unless otherwise stated, the gases used were obtained from Matheson of Canada: NH_3: "anhydrous" grade, 99.99% pure. The gas was further purified by fractional distillation from liquid nitrogen and from a dry ice – acetone bath at about −40°C. H_2: "ultra high purity" grade, 99.999%, used without further purification. Ar: "research purity" grade, 99.9999%, used without further purification. Kr: "research purity" grade, 99.99%, from Air Products and Chemicals Ltd., used without further purification. The only significant impurities were other inert gases. N_2: "high purity" grade, 99.99%, from Canadian Oxygen Ltd., used without further purification. (Used for calibration only.)

Mass Spectrometric Data

For measurements of the time-dependent NH_3 and N_2 concentration in the kinetic experiments, Ar was used as an internal standard, i.e. the mass peak heights were measured relative to the Ar^+ peak. Absolute concentrations could then be obtained using the appropriate relative sensitivity factors and the known Ar concentration. This procedure, rather than reliance on the measurement of absolute peak heights, was used to find concentrations because of its insensitivity to slight variations, from experiment to experiment, in the performance of the mass spectrometer and in the behaviour of the flow through the sampling orifice. The relative sensitivity factors were measured using known mixtures in shock wave experiments under conditions as close as possible to those of the kinetic experiments themselves; the gas temperature in the calibration experiments was, of course, kept low enough for the extent of reaction to be insignificant.

To follow the concentration profiles of NH_3, H_2, and NH, the electron beam energy was set at 25.0 eV. However, when NH_2 was being studied, the electron energy was lowered to 13.0 eV to avoid interference from the fragmentation of NH_3^+. (The appearance potential (16) of NH_2^+ from NH_3 is 16.0 eV.) With such a low energy, it is impossible to use Ar^+ as an internal standard, since the ionization potential of Ar is 15.8 eV. Therefore the NH_2^+ mass peaks were standardized to the NH_3^+ peak at time zero. (The height of NH_3^+ at time zero was obtained by extrapolation from the NH_3^+ peak in the first mass spectrum after arrival of the shock wave, knowing the decay rate of the ammonia peaks.) The question of mass spectrometer sensitivity to NH and NH_2 is discussed below.

Results

Kinetic experiments were carried out at temperatures of 2500 to 3000 K and total gas concentrations of about 1.7×10^{-6} mol cm^{-3}. The resulting mass spectrometric observations are summarized below.

Ammonia Analysis

In all of the mixtures studied, the NH_3 profile followed a pseudo-first order decay, to within experimental accuracy. Expressing the rate of de-

composition in the form

$$-\frac{d[NH_3]}{dt} = k_D[NH_3]([Kr] + [H_2]_0 + [Ar])$$

a second order decomposition rate coefficient k_D could be defined for each experiment. Arrhenius plots of k_D for the four mixtures are given in Figs. 1 and 2. The corresponding Arrhenius expressions are:

$$k_D(6\%\ NH_3) = 10^{15.78\pm0.59} \times \exp(-78\,400 \pm 7\,200/RT)$$

$$k_D(6\%\ NH_3, 1.2\%\ H_2) = 10^{13.80\pm0.25} \times \exp(-56\,800 \pm 6\,000/RT)$$

$$k_D(6\%\ NH_3, 6\%\ H_2) = 10^{13.96\pm0.63} \times \exp(-60\,300 \pm 8\,000/RT)$$

$$k_D(0.14\%\ NH_3) = 10^{16.08\pm0.67} \times \exp(-89\,500 \pm 8\,600/RT)$$

in $cm^3\ mol^{-1}\ s^{-1}$, with activation energies in cal mol^{-1}. The quoted uncertainties are standard deviations.

It will be seen from Fig. 1 that addition of NH_3 increases k_D. This implies that, over a large range of NH_3 concentrations, the reaction is not strictly first order with respect to $[NH_3]$. As shown by Fig. 2, addition of H_2 progressively decreases k_D.

NH_2 Analysis

As explained above, NH_2^+ mass peaks were standardized to NH_3^+. Because there appeared to be no reliable way of measuring a sensitivity factor for NH_2 relative to NH_3, the data presented in Fig. 3 assume a relative sensitivity of unity. Since the ionization potential (16) of NH_2 (11.4 eV) is higher than that of NH_3 (10.4 eV) and is fairly close to the electron energy used (13.0 eV), the NH_2 concentration deduced in this way is very probably an underestimate. Nevertheless the shapes of the NH_2 profiles are expected to be correct. Moreover, as shown later, a knowledge of the relative concentrations of NH_2 in different mixtures is useful in determining the reaction mechanism.

Because the concentration of NH_2 was small, the results from experiments with similar temperatures were grouped and averaged to reduce scatter. A typical NH_2 profile is shown in Fig. 3. Comparison of results from mixtures 1 and 3 showed that addition

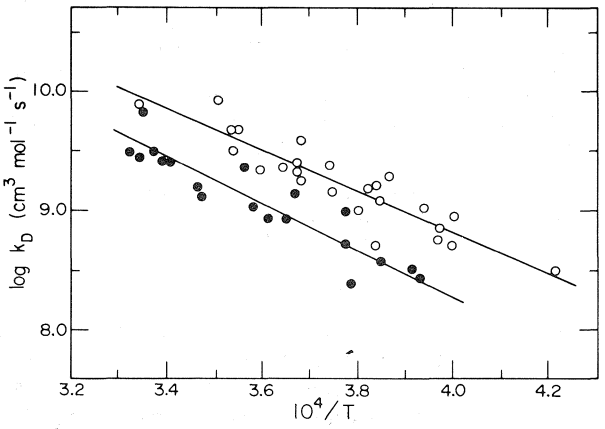

FIG. 1. Arrhenius plot of k_D, the rate constant for overall removal of NH_3, for NH_3/Kr mixtures: upper line and open points, 6.2% NH_3 in Kr; lower line and solid points, 0.14% NH_3 in Kr.

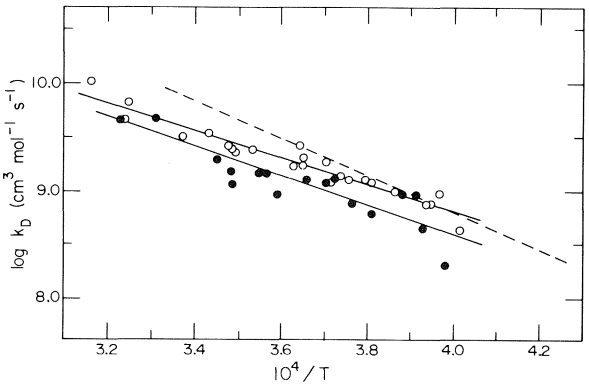

FIG. 2. Arrhenius plots showing how addition of H_2 progressively reduces k_D in ammonia pyrolysis: dashed line, k_D for 6.2% NH_3 in Kr (cf. Fig. 1); upper solid line and open points, k_D for 6.0% NH_3 + 1.2% H_2 in Kr; lower solid line and solid points, k_D for 6.1% NH_3 + 5.8% H_2 in Kr.

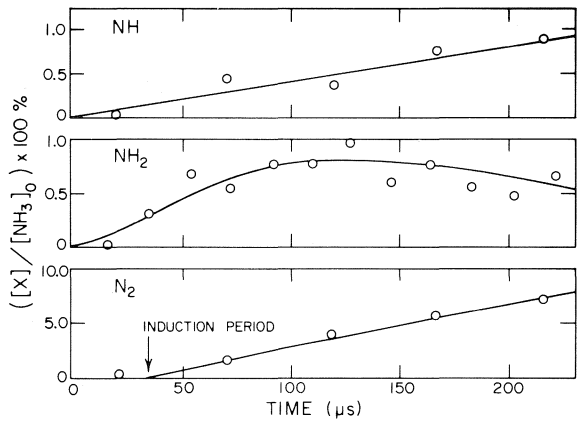

FIG. 3. Typical NH, NH_2, and N_2 concentration profiles in pyrolysis of mixture 1 (6.2% NH_3 in Kr). T = 2511 K. Total gas concentration = 1.7×10^{-6} mol cm^{-3}. The arrow on the lowest profile indicates the end of the induction period for N_2 formation. (The NH_2 and NH profiles use an arbitrary mass spectrometric sensitivity factor of unity, relative to NH_3; see the text for discussion of the actual sensitivity.)

of H_2 has very little effect on the NH_2 profiles over the present temperature range.

NH Analysis

The NH concentration profiles were deduced from the 25 eV experiments, corrected for NH_3^+ fragmentation. Fortunately this correction is found to be very small

$$([NH^+]_{fragment}/[NH_3^+]) = 0.03$$

No corrections were made for NH_2^+ fragmentation, because the mass 16 peak (NH_2^+) in these experiments could be accounted for almost entirely by NH_3^+ fragmentation; this implies that the contribution of NH_2 to mass 16 in the 25 eV experiments was very small and its contribution to mass 15 (NH^+) is probably even smaller. The data in Fig. 3 assume that the mass spectrometric sensitivity to NH is the same as to NH_3. This assumption under the present conditions is expected to be good to within a factor of two (17), since the electron beam energy is substantially higher than the ionization potentials of both species. Scatter of data again forced grouping of experiments under similar conditions.

In the 6% NH_3 mixture, the NH concentration shows a linear rise (Fig. 3) and falls slowly. This agrees with the observations of Cann and Kash rather than those of Bradley *et al.* Addition of hydrogen (1.2 mol%) reduced the concentration of NH; with an initial hydrogen concentration of 6 mol% the concentration of NH was below the detectability limit. This suppression of NH on addition of H_2 was also observed by Bradley *et al.* The fact that the NH concentration can be suppressed to below the detectability limit with the NH_2 concentration relatively unchanged confirms that the NH^+ from 6% NH_3 mixture was not formed from NH_2^+ by fragmentation.

N_2 Analysis

The N_2 profiles (Fig. 3) show an induction period before the N_2 concentration rises linearly. We define the induction period τ as the time between the shock arrival and the linear extrapolation of the N_2 concentration to the time axis. A plot of log τ vs. $1/T$ is shown in Fig. 4. Addition of hydrogen (6 mol%) decreases the induction period slightly, but has very little effect on the rate of linear rise (Fig. 5). Because of the limited number of mixtures, it is not possible to determine the dependence of the N_2 growth rate on $[NH_3]$ and [M].

Other Species

Masses 14, 29, 30, 31, and 32, corresponding to N, N_2H, N_2H_2, N_2H_3, and N_2H_4, were searched for but not found. The nitrogen mass balance was very good for the low temperature (<2700 K) experiments both

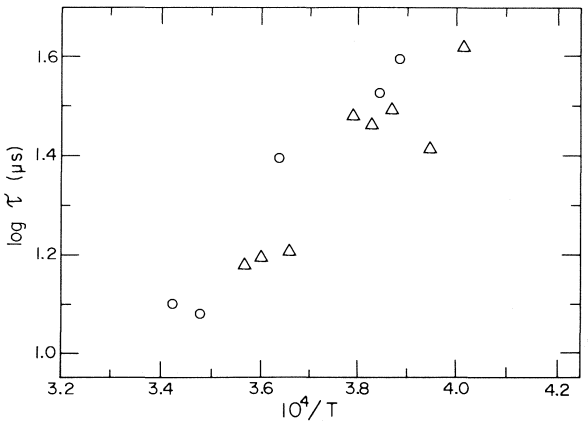

FIG. 4. Plot of the logarithm of τ, the induction period for N_2 formation, against $10^4/T$, in ammonia pyrolysis. ○, mixture 1 (6.2% NH_3 in Kr); △, mixture 3 (6.1% NH_3 + 5.8% H_2 in Kr).

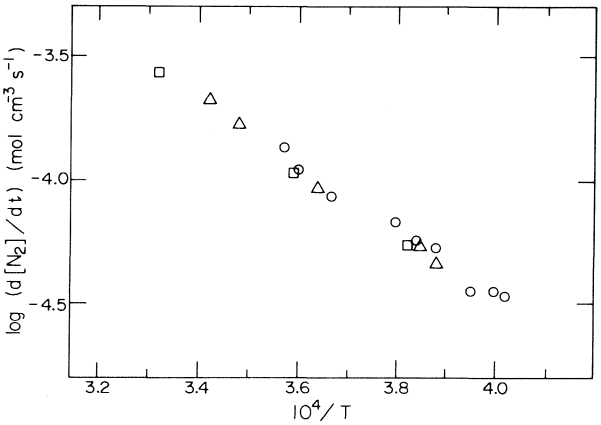

FIG. 5. Plot of log (rate of linear rise of $[N_2]$) against $10^4/T$ in NH_3 pyrolysis. Total gas concentration $\simeq 1.7 \times 10^{-6}$ mol cm^{-3}. ○, Mixture 1; □, mixture 2; △, mixture 3.

with and without H_2 in the initial mixture. At high temperatures the N balance was less satisfactory especially over long periods of time, although over 80% of the N was still recovered at times less than 100 μs. The cause of this discrepancy is not known. It is quite unlikely that there exist N-containing species other than those already mentioned. The relative sensitivity of N_2 to Ar has been found to be independent of temperature, and the mass peaks remained reasonably well shaped (i.e., there was no sign of pressure broadening of peaks). Because of this discrepancy, the results of high temperature experiments at times beyond 100 μs must be viewed with caution. Most of our kinetic analysis was done on the early part of the reaction, so that there should not be a serious effect on our conclusions.

Concentration profiles of H_2 and H atoms would be very useful in studying the reaction mechanism.

Unfortunately, the very low sensitivity of the mass spectrometer to these species made it impossible to obtain useful information about them.

Discussion

Values of k_D

Figure 6 shows that our second order decomposition rate coefficients k_D for mixtures 1 and 4 fall essentially in the range of previous observations. However, the present work is the first one using Kr as diluent, so that exact agreement with studies using Ar diluent is, in any case, not necessarily to be expected. The work of Michel and Wagner (2) and our own measurements with mixture 4 are the only two studies using very low NH_3 mole fractions. Comparison of these two studies implies that Ar is twice as efficient as Kr in decomposing NH_3 over the temperature range 2500–3000 K as far as the effect on k_D is concerned.

The factor of three difference in k_D obtained between our mixtures 1 and 4 is too large to be dismissed as probably due to experimental scatter. One possible explanation is the NH_3 has a much larger collision efficiency than Kr in decomposing ammonia.

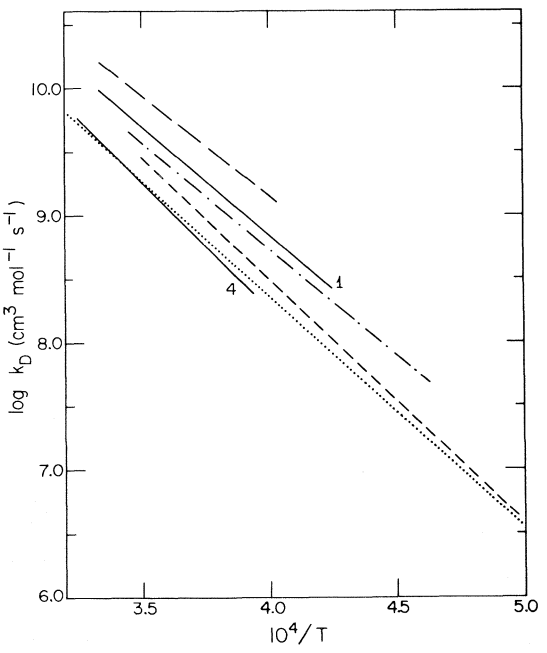

FIG. 6. Comparison of our results for k_D, the overall rate coefficient for NH_3 removal, with literature values. — *1*, this work, mixture 1 (6.2% NH_3 in Kr); — *4*, this work, mixture 4 (0.14% NH_3 in Kr; – – –, Takeyama and Miyama (5); ····· Michel and Wagner (2); - - -, Henrici (3); · · ·, Bradley *et al.* (6). For clarity, Haluk's line (7) has been omitted. It is essentially coincident with that of Bradley *et al.* in the range $10^4/T = 3.4$–5.0.

To explain the whole of the difference in this manner would require that NH_3 be about 40 times as efficient as Kr. An alternative is that secondary reactions become important at higher NH_3 concentrations; this explanation is supported by the slight decrease in activation energy when the NH_3 mole fraction is increased, implying the participation of other reactions of lower activation energy.

One possibility is that the reaction occurs by the following type of mechanism:

$$NH_3 + M \rightarrow A + P_1$$

$$A + NH_3 \rightarrow P_2 + P_3$$

where P_1, P_2, and P_3 are species which do not react with NH_3. Two mechanisms of this type are:

Mechanism 1

[1] $NH_3 + M \rightarrow H + NH_2 + M$

$\Delta H_0^0 \simeq 103$ kcal mol^{-1}

[5] $H + NH_3 \rightarrow NH_2 + H_2$

$\Delta H_0^0 \simeq 1$ kcal mol^{-1}

[10] $NH_2 + NH_2 \rightarrow N_2 + H_2 + H_2$

$\Delta H_0^0 \simeq -84$ kcal mol^{-1}

or

Mechanism 2

[2] $NH_3 + M \rightarrow NH + H_2 + M$

$\Delta H_0^0 \simeq 91$ kcal mol^{-1}

[−7] $NH + NH_3 \rightarrow NH_2 + NH_2$

$\Delta H_0^0 \simeq 15$ kcal mol^{-1}

[10] $NH_2 + NH_2 \rightarrow N_2 + H_2 + H_2$

$\Delta H_0^0 \simeq -84$ kcal mol^{-1}

However, this type of mechanism increases the rate of NH_3 removal by at most a factor of two. In order to explain entirely in terms of secondary reactions the finding that $k_D(6\%\ NH_3)/k_D(0.14\%\ NH_3) \simeq 3$, one must introduce also a reaction between NH_2 and NH_3. Of the two reactions

[3] $NH_2 + NH_3 \rightarrow N_2H_3 + H_2$

$\Delta H_0^0 \simeq 19$ kcal mol^{-1}

and

[11] $NH_2 + NH_3 \rightarrow N_2H_4 + H$

$\Delta H_0^0 \simeq 46$ kcal mol^{-1}

reaction [3] is favoured on thermochemical grounds.

N_2H_3 can break up by either of

[4] $N_2H_3 + M \rightarrow NH_2 + NH + M$

$\Delta H_0^0 \simeq 72$ kcal mol^{-1}

or

[12] $N_2H_3 + M \rightarrow N_2H_2 + H + M$

$\Delta H_0^0 \simeq 54$ kcal mol^{-1}

The products of either reaction (H or NH) can react with NH_3 to regenerate NH_2, thus constituting a chain.

The fact that successive additions of H_2 to the initial mixture decrease the overall decomposition rate (Fig. 2) also suggests a chain process. Mechanism 2 cannot be correct since it would predict no effect of addition of H_2, as long as the reverse of reaction [2] is slow, which is the case under the present conditions. Mechanism 1 predicts that under no conditions can the addition of H_2 decrease k_D by more than a factor of 2, whereas we find that, at high temperatures, the actual factor exceeds 3 (Fig. 2).

It thus appears that neither mechanism 1 nor mechanism 2 (and hence no combination of the two) can fully explain our values of k_D. We must therefore analyze the effects of introducing a reaction between NH_2 and NH_3, which will inevitably lead to a chain reaction. At this point we disagree with Haluk (7), who considered that such a reaction was not necessary in order to explain his results. However, we support the suggestion by Bradley *et al.* (6) of such a reaction, and the conclusion that the overall activation energy of about 80 kcal mol^{-1} does not represent exactly the activation energy of the primary step.

Reactions of NH

Our results for mixtures 1 and 2 show a linear rise in NH concentration followed by a drop, agreeing with the results of Cann and Kash but in conflict with the parabolic rise observed by Bradley *et al.* Cann and Kash found that the growth of NH follows a relationship

$$\frac{d[NH]}{dt} = k'[NH_3]_0^2$$

with

$$k' = 4.8 \times 10^{12} \exp\left(\frac{-23\,900}{T}\right) \text{cm}^3 \text{ mol}^{-1} \text{ s}^{-1}$$

Assuming the same dependence on ammonia concentration, Table 2 compares values of the rate coefficient k' computed from the present work and from the results of Cann and Kash. The scatter of experimental data forced grouping of a large number of experiments to obtain any reasonable estimate of the rates, hence the very few experimental points available for comparison. Agreement between the present work and Cann and Kash's data is very good, especially the two low temperature points.

TABLE 2. Apparent rate constant for NH formation. Comparison with results of Cann and Kash (12)

Temperature (K)	k' (cm^3 mol^{-1} s^{-1})	
	Cann and Kash	This work
2513	3.6×10^8	3.9×10^8
2563	4.4×10^8	4.3×10^8
2788	9.1×10^8	7.6×10^8

Addition of hydrogen to the reaction mixture suppresses the growth of NH. NH can only be formed from NH_2 or by splitting NH_3 into NH and H_2. In the NH_2 analysis, it was shown that addition of H_2 does not affect the NH_2 concentration profiles much; thus it is fairly safe to assume that the rate of formation of NH is not much affected by the addition of H_2. Presumably therefore the lowering of NH concentration is due to removal by reaction with H_2, probably by

[−6] $NH + H_2 \rightarrow NH_2 + H$

The other possible reaction with H_2, the combination reaction

[−2] $NH + H_2 + M \rightarrow NH_3 + M$

is probably a three body process and very slow. The formation and removal of NH can therefore be represented by

$$\xrightarrow{F} NH$$

[−6] $NH + H_2 \rightarrow NH_2 + H$

where F is the rate of production of NH. A value of F can be read from the early part of a profile of [NH] against time in the absence of added H_2. Then for mixture 2 (6% NH_3, 1.2% H_2), at a time in the very early part of the reaction, we can write

$$\frac{d[NH]}{dt} = F - k_{-6}[NH][H_2]_0$$

Using values of d[NH]/dt from mixture 2, we get

$$k_{-6} = 1.8 \times 10^{12} \text{ cm}^3 \text{ mol}^{-1} \text{ s}^{-1} \text{ at } 2601 \text{ K}$$

$$= 2.2 \times 10^{12} \text{ cm}^3 \text{ mol}^{-1} \text{ s}^{-1} \text{ at } 2788 \text{ K}$$

This simple analysis does not require a knowledge of the absolute sensitivity of the mass spectrometer to NH. k_{-6} deduced this way is expected to be accurate to within a factor of 3, the errors being mainly due to the uncertainty in determining the slope of the [NH] profile in the very early part of the reaction. This value of k_{-6} appears to be the first based on experimental measurements. There are theoretical calculations by Mayer and Schieler (10, 18) which agree well with the

present measurements; the closest agreement is with the results of (18*b*) which are 20% below our values at both 2601 and 2788 K. Calculations using k_{-6} indicate that in mixture 3, with 5.8% H_2, the concentration of NH should be too small to be observed, as was found in our experiments.

The above analysis predicts that addition of H_2 will convert NH to NH_2 through reaction [−6]. The resultant increase in $[NH_2]$ will be small, as observed experimentally, because even before adding H_2, the NH concentration is already substantially below that of NH_2, especially at short reaction times. Note that, as discussed above, our NH_2 profiles (cf. Fig. 3) should be multiplied by a factor which is almost certainly greater than unity; the computer analysis outlined later indicates that the factor is about 5.

Mechanism of N_2 Formation

A very interesting problem in ammonia pyrolysis is the mechanism of formation of molecular nitrogen. In principle, N_2 can be formed from mutual or cross combination of any of the species NH, NH_2, and NH_3. Comparison of the concentration profiles of these species with those for N_2 allows us to test which processes may be important.

In the previous section, we showed that addition of 6% H_2 to the initial reaction mixture drastically reduces the concentration of NH but has very little effect on N_2. This observation eliminates all reactions involving NH as the main source of N_2 in ammonia pyrolysis. The other possibilities are

[13] $$NH_2 + NH_2 \rightarrow \cdots \rightarrow N_2$$

[14] $$NH_2 + NH_3 \rightarrow \cdots \rightarrow N_2$$

[15] $$NH_3 + NH_3 \rightarrow \cdots \rightarrow N_2$$

Reaction [15] must be rejected as a major source of N_2 because it predicts a maximum rate of production of N_2 at the start of the reaction, contrary to our experimental observations. Reaction [13] predicts a very strong correlation between the induction period τ for the formation of N_2 and the build up of NH_2 radicals. Since only a small fraction of the NH_3 is decomposed during the induction period, reaction [14] also predicts a correlation between τ and the build up of NH_2 radicals. Figure 7 shows that, for either reaction [13] or [14], the correlation is very satisfactory.

The tests can be carried one step further. If most of the N_2 comes from the recombination of NH_2, reaction [13], then

$$(d[N_2])/dt = k_{13}[NH_2]^2$$

and

$$[N_2] = k_{13}\int_0^t [NH_2]^2\, dt$$

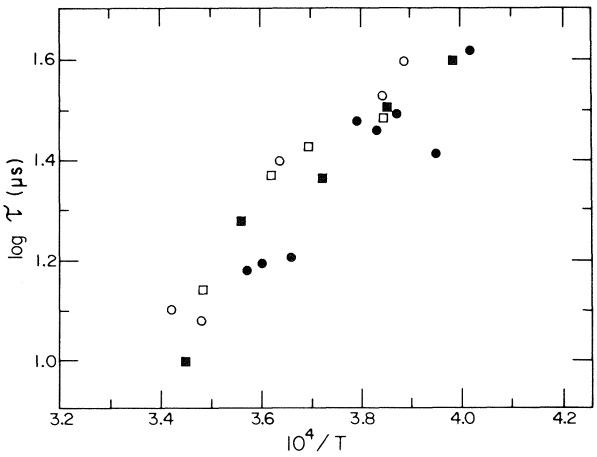

FIG. 7. Comparison of induction period τ for N_2 formation with time taken for $[NH_2]$ to reach 40% of its maximum value. Mixture 1 (6.2% NH_3 in Kr): ○, induction period τ; □, time t to reach 40% of maximum $[NH_2]$. Mixture 3 (6.1% NH_3 + 5.8% H_2 in Kr): ●, induction period τ; ■, time t to reach 40% of maximum $[NH_2]$.

Thus the concentration of N_2 at any time t should be proportional to the area under a $[NH_2]^2$ vs. time plot. Similarly, if one assumes that reaction [14] is the major producer of N_2, then

$$[N_2] = k_{14}\int_0^t [NH_2][NH_3]\, dt$$

and the concentration of N_2 at time t would be proportional to the area under a graph of $[NH_2] \times [NH_3]$ against t. The above two comparisons were made for mixtures 1 and 3. Satisfactory correlations were found assuming either reaction [13] or [14]. An example of the comparisons is shown in Fig. 8. We cannot decide at this stage whether reaction [13] or reaction [14] is responsible for the production of N_2 in the pyrolysis of ammonia.

It should be noted that our results do not rule out the possibility that NH contributes to the formation of N_2 in ammonia pyrolysis, but they do show that a major route to N_2 involves NH_2 and not NH.

The details of reactions [13] and [14] will now be considered. The reaction of two NH_2 radicals is often believed to lead to disproportionation to NH_3 and NH

[7] $$NH_2 + NH_2 \rightarrow NH_3 + NH$$

$$\Delta H_0^0 \simeq -11 \text{ kcal mol}^{-1}$$

However, if reaction [13] leads to N_2, then there must be a significant probability that a collision of two NH_2 radicals leads to products different from those of reaction [7], e.g.

[16] $$NH_2 + NH_2 \rightarrow N_2H_2 + H_2$$

$$\Delta H_0^0 \simeq -50 \text{ kcal mol}^{-1}$$

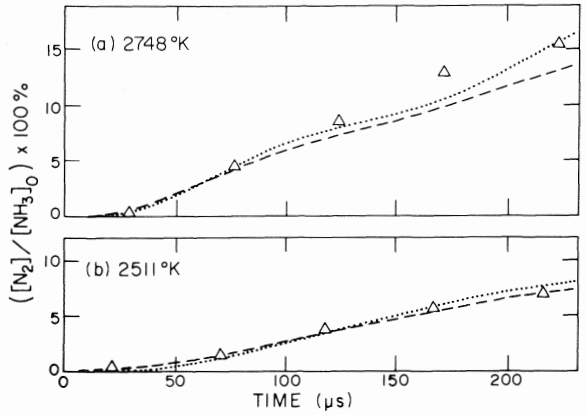

FIG. 8. An example of the comparison of the experimentally measured N_2 profiles with the time integrals of $[NH_2]^2$ and $[NH_2][NH_3]$. (*a*) Mixture 3 (6.1% NH_3 + 5.8% H_2 in Kr), $T = 2748$ K. (*b*) Mixture 1 (6.2% NH_3 in Kr), $T = 2511$ K. · · ·, $k\int[NH_2]^2\,dt$. - - -, $k'\int[NH_2][NH_3]\,dt$. k and k' were treated as adjustable parameters.

followed by

$$[17] \qquad N_2H_2 \xrightarrow{M} N_2 + H_2 \qquad \Delta H_0^0 \simeq -50 \text{ kcal mol}^{-1}$$

However, Michel and Wagner (2) suggested that N_2H_2 splits into N_2H and H. The sequence leading to N_2 formation would then be

$$[16] \qquad NH_2 + NH_2 \rightarrow N_2H_2 + H_2 \qquad \Delta H_0^0 \simeq -34 \text{ kcal mol}^{-1}$$

$$[18] \qquad N_2H_2 \rightarrow N_2H + H \qquad \Delta H_0^0 \simeq 82 \text{ kcal mol}^{-1}$$

$$[19] \qquad N_2H \rightarrow N_2 + H \qquad \Delta H_0^0 \simeq -28 \text{ kcal mol}^{-1}$$

Even though Michel and Wagner's suggestion does not alter the present argument about the source of the N_2, it will affect the overall kinetics of pyrolysis because it implies that the combination of NH_2 radicals is a chain propagation step rather than a termination reaction. One drawback of the above sequence is that it includes the highly endothermic reaction [18] which would be fairly slow. Possibly therefore reactions [18] and [19] occur in a single concerted process which would be much less endothermic. Azomethane, a close relative of N_2H_2, forms two radicals

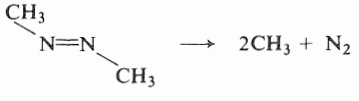

$$\longrightarrow 2CH_3 + N_2$$

apparently in a single step. However, Willis and Back (19) have studied the thermal decomposition of N_2H_2 at room temperature and found that free radical mechanisms are not important in the process. This tends to suggest that N_2H_2 does not split into N_2 and H atoms.

The most plausible reaction sequence for producing N_2 from NH_2 + NH_3 (reaction [14]) is

$$[3] \qquad NH_2 + NH_3 \rightarrow N_2H_3 + H_2 \qquad \Delta H_0^0 \simeq 17 \text{ kcal mol}^{-1}$$

$$[19] \qquad N_2H_3 + M \rightarrow N_2 + H_2 + H + M \qquad \Delta H_0^0 \simeq 4 \text{ kcal mol}^{-1}$$

Reaction [19] may not occur as written but may involve splitting off H and H_2 in two separate steps.

Computer Simulations

In order to study the kinetics of this system further, we have calculated concentration profiles by computer integration of the reaction rate equations, using different assumed mechanisms, and have compared these profiles with our experimental results. A serious handicap is that, not only are the rate coefficients of most of the elementary reactions quite unknown, but also there is considerable uncertainty about the thermochemistry of some of the chemical species (e.g. refs. 14, 20–25). Uncertainties in the thermochemistry, and hence in the equilibrium constants, introduce additional uncertainties into the kinetic analysis, since a standard procedure is to use the rate quotient law to calculate a reverse rate constant from the forward rate constant and the equilibrium constant.

Because it is not feasible to make a computer simulation analysis of every individual experiment, we represented our results by four sets of concentration profiles of NH_3, N_2, NH_2, and NH (each of which was the average of many experiments): (*a*) mixture 1 (6% NH_3, 94% diluent) at 2511 K, (*b*) mixture 1 at 2792 K, (*c*) mixture 3 (6% NH_3, 6% H_2, 88% diluent) at 2600 K, (*d*) mixture 3 at 2873 K, together with the following ratios of k_D for mixtures 1 and 4: (*e*) $k_D(6\%\,NH_3)/k_D(0.14\%\,NH_3) = 3.6$ at 2511 K, and (*f*) $k_D(6\%\,NH_3)/k_D(0.14\%\,NH_3) = 2.9$ at 2792 K. These data were chosen because their temperatures are fairly close to the middle of the experimental range, where the quality of the results is best, yet the temperature spread is large enough to allow the temperature dependence of the kinetics to be studied. Thermodynamic data from the JANAF Tables (14) were used in the computations.

Results

After a very large number of trials using various combinations of the elementary reactions discussed above, we found that a good fit to our chosen NH_3,

TABLE 3. Reaction rate coefficients and equilibrium constants used in computer fitting of experimental results*

(*a*) Set No. 1

Reaction number	Rate coefficient	Equilibrium constant	Reference for rate coefficient
[1]	$8.56\times10^{15}\exp(-92\,500/RT)$	$1.32\times10^{5}T^{-1.0}\exp(-105\,730/RT)$	†
[2]	$5.51\times10^{15}\exp(-91\,000/RT)$	$1.82\times10^{5}T^{-1.0}\exp(-94\,356/RT)$	†
[3]	$8.00\times10^{11}T^{0.5}\exp(-21\,567/RT)$	$2.61\times10^{-2}\exp(-14\,260/RT)$	†
[4]	$6.31\times10^{12}\exp(-10\,000/RT)$	$6.95\times10^{6}T^{-1.0}\exp(-80\,096/RT)$	†, ‡
[5]	$2.45\times10^{13}\exp(-17\,100/RT)$	$4.55\exp(3\,853/RT)$	9
[6]	$6.17\times10^{13}\exp(-5\,225/RT)$	$1.24\exp(12\,026/RT)$	This work
[7]	$6.30\times10^{12}\exp(-10\,000/RT)$	$0.267\exp(8\,287/RT)$	26
[8]	$9.00\times10^{17}T^{-1.0}$	$3.91\times10^{5}T^{-1.5}\exp(92\,600/RT)$	27
[9]	$3.60\times10^{11}T^{0.55}\exp(-1\,900/RT)$	$7.80\times10^{-3}\exp(162\,220/RT)$	28
[10]	$3.98\times10^{13}\exp(-12\,000/RT)$	$3.10\times10^{2}T^{-1.0}\exp(-94\,356/RT)$	26

*Rate coefficients are in cm^3 mol s units, with activation energies in cal mol^{-1}. Equilibrium constants for reactions [3] and [4] are estimates; others are taken from ref. 14.

†This work; obtained after numerous trials.

‡Thermochemical data suggest that the activation energy is too low; it can be increased to 20 kcal mol^{-1}, with corresponding reduction in A_4, without significantly worsening the fit.

(*b*) Set No. 2 is the same as No. 1 except for

$k_1 = 8.00\times10^{15}\exp(-89\,500/RT)$

$k_2 = 5.51\times10^{11}\exp(-91\,000/RT)$

$k_3 = 1.40\times10^{14}\exp(-28\,300/RT)$

(*c*) Set No. 3 is the same as No. 1 except for

$k_1 = 8.00\times10^{10}\exp(-89\,500/RT)$

$k_2 = 1.10\times10^{16}\exp(-89\,500/RT)$

$k_3 = 1.00\times10^{12}T^{0.5}\exp(-21\,567/RT)$

NH_2, and N_2 profiles, and to the k_D ratios of (*e*) and (*f*) above, could be obtained using the following mechanism with the rate data of Table 3:

[1] $NH_3 + M \rightleftarrows NH_2 + H + M$

[2] $NH_3 + M \rightleftarrows NH + H_2 + M$

[3] $NH_2 + NH_3 \rightleftarrows N_2H_3 + H_2$

[4] $N_2H_3 + M \rightleftarrows NH + NH_2 + M$

[5] $H + NH_3 \rightleftarrows H_2 + NH_2$

[6] $H + NH_2 \rightleftarrows H_2 + NH$

[7] $NH_2 + NH_2 \rightleftarrows NH + NH_3$

[8] $H + H + M \rightleftarrows H_2 + M$

[9] $NH + NH \rightleftarrows N_2 + H_2$

[10] $NH_2 + NH_2 \rightleftarrows N_2 + H_2 + H_2$

where, as discussed above, reaction [10] may take place in more than one stage. To get this agreement, the experimental NH_2 profiles had to be multiplied by 5, a factor which is very reasonable in view of the considerations about ionization potential discussed above. Two variations of this set of rate coefficients, which gave very similar fits, are also included in Table 3.

Discussion

The results in Table 3 must be viewed with caution for two reasons. Firstly, in a system with so many unknown parameters, there could well be other ways of fitting our rate data. Secondly, for one species, namely NH, the computed and measured profiles do not agree very well (Fig. 9). The discrepancies in shape of the NH profiles are more disturbing than the differences in magnitude, since the latter could be due to uncertainties in the sensitivity of the mass spectrometer to this unstable species. Therefore, there seems to be a real possibility that an important reaction involving NH has been omitted from our mechanism, or that one or more of the rate constants in Table 3 are wrong. However, a very substantial computer study of this problem did not give a better fit.

Because of the doubts expressed above, we will not discuss in detail the results in Table 3. However, we will briefly comment on two points of general importance which emerge from our calculations, namely, the predicted overall rate law and the rate of the unimolecular initiation step.

Kinetics of the Overall Reaction

An important question is why, if there is a chain mechanism as we suggest, most workers have found the rate equation to be

$$-d[NH_3]/dt = k_D[NH_3][M]$$

To test this, we ran computer simulations, using the first set of rate data from Table 3, for initial compositions in the range 0.08% to 20% NH_3. k_D was calculated from the time Δt for $[NH_3]$ to fall to 85%

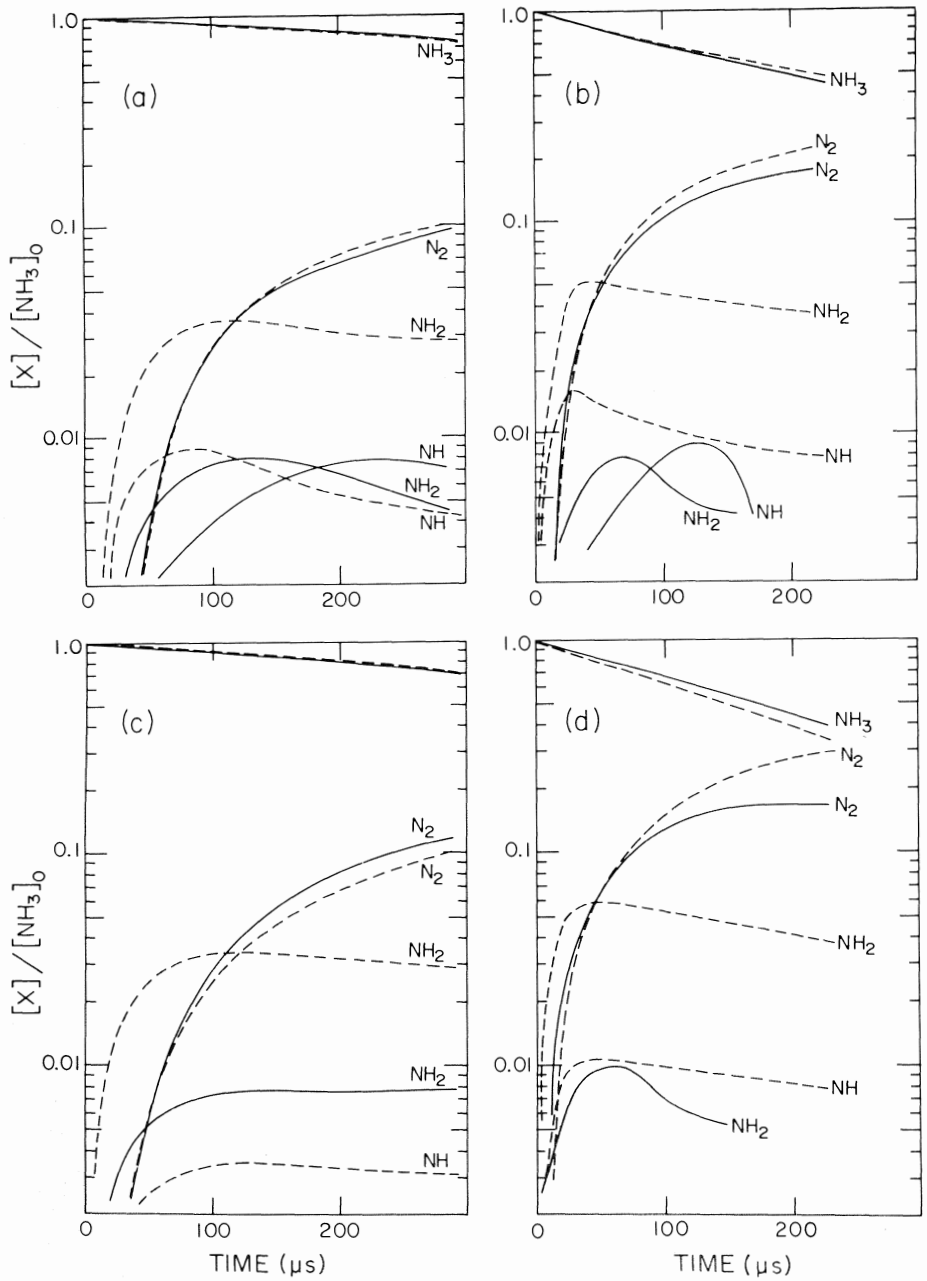

FIG. 9. Example of comparison of measured (solid lines) and computer simulated (dashed lines) concentration profiles in NH_3 pyrolysis. Computed profiles of species which were not measured have been omitted. All simulations showed $[N_2H_3]/[NH_3]_0 < 10^{-3}$. These simulations used the reaction scheme [1] to [10] in the text, including both forward and reverse processes, with the first set of rate coefficients of Table 3. In these diagrams, the experimental NH_2 profiles are those obtained using an arbitrary sensitivity factor of unity, relative to NH_3; as discussed in the text, these profiles should be multiplied by a factor of approximately 5, for comparison with the computed values. (*a*) Mixture 1 (6.2% NH_3) at 2511 K. [M] = 1.5×10^{-6} mol cm^{-3}. Note that the experimental and computed NH_3 profiles coincide. (*b*) Mixture 1 at 2792 K. [M] = 1.6×10^{-6} mol cm^{-3}. (*c*) Mixture 3 (6.1% NH_3 + 5.8% H_2) at 2600 K. [M] = 1.7×10^{-6} mol cm^{-3}. (*d*) Mixture 3 at 2873 K. [M] = 1.8×10^{-6} mol cm^{-3}.

of $[NH_3]_0$, i.e. $k_D = -(\ln 0.85)/[M]\Delta t$. The results (Fig. 10) agree with our observed variation in k_D between mixtures 1 and 4, and they suggest that the reason why most other workers did not see such a variation was either that they did not change $[NH_3]_0$ sufficiently, or that their NH_3 percentages fell in the range where k_D remains fairly constant. Thus Bradley *et al.* (6) used 5 to 20% NH_3; the resulting variation in k_D would be 40%, well within experimental scatter. Even though Michel and Wagner (2) varied the composition from 0.11% to 1.5% NH_3, we predict that k_D would only change by a factor of 2, again within experimental scatter. An exception to these comments seems to be the work of Jacobs, who used 1% and 8% NH_3. Assuming a rate law of the form

$$-d[NH_3]/dt = k[NH_3]^x[M]^y$$

our simulations predict that Jacobs would find $x = 1.36$, which is close to the value of 1.5 which he reported.

The Initiation Reaction

Our simulations could not distinguish between channels [1] and [2] for the initiation step. Irrespective of whether NH or NH_2 is produced initially, secondary reactions will rapidly shuffle these radicals.

The discussion in the previous section indicates that, while our mechanism may not reproduce all details of the secondary processes, it does adequately represent the way in which k_D increases with increasing $[NH_3]$. Therefore, it appears that we have succeeded in separating the effects of initiation and secondary reactions, so that our rate constant for the unimolecular initiation process should be fairly accurate. Our simulations, and comparison of results from mixtures 1 and 4, indicate an activation energy slightly larger than 89.5 kcal mol^{-1}. We propose

$$k_1 + k_2 = 1.2 \times 10^{16} \times \exp(-91\,000/RT)\ cm^3\ mol^{-1}\ s^{-1}$$

which we expect to be correct to within a factor of 2 under the conditions of our experiments. This expression is about 25% lower than k_D for mixture 4, 0.14% NH_3, at 2500–3000 K. Thus our analysis indicates that in this mixture, our measured k_D was not strongly influenced by secondary reactions.

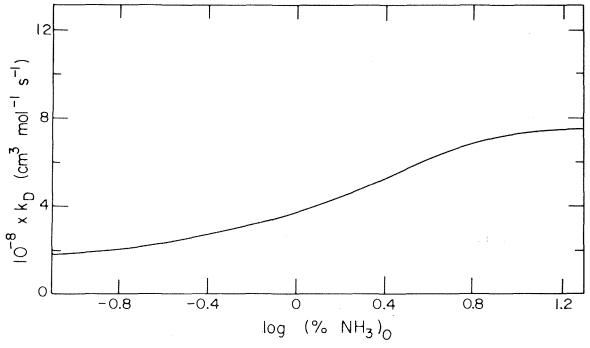

FIG. 10. Computed values of k_D, the second order rate coefficient for overall removal of NH_3, at 2511 K as a function of initial mole percentage of NH_3. The reaction mechanism used was reactions [1] to [10], with the first set of rate coefficients of Table 3.

Since the unimolecular reaction is almost certainly very close to its low pressure limit, it is interesting to compare our rate constant with the calculated strong collision value. We assume that $k_1 \gg k_2$ and that the minimum critical energy is the endothermicity of reaction [1], 101.7 kcal mol^{-1}. Using the recently published method of Troe (29), with molecular data from refs. 14 and 30, we calculate strong collision rate constants of 4.15×10^9 and 9.21×10^{10} cm^3 mol^{-1} s^{-1} at 2500 and 3000 K. Comparison with our experimentally derived values yields a collision efficiency β_c of 0.032 at 2500 K and 0.031 at 3000 K. These values of β_c are similar to those found (29) for the unimolecular dissociation of a number of other small polyatomic molecules in this temperature range, and they add further evidence that the strong collision assumption should not be used in the theoretical analysis of unimolecular rates at high temperatures.

Conclusions

Our experimental studies and analysis lead to the following main conclusions:

(*a*) The pyrolysis of ammonia is a chain reaction initiated by the unimolecular decomposition of NH_3. In the absence of added H_2, NH_3 is also removed by reaction with H, NH, and NH_2. Addition of H_2 markedly reduces the concentration of NH.

(*b*) Measurements of the effect of added H_2 show that the rate constant of the reaction

$$[-6] \qquad NH + H_2 \rightarrow NH_2 + H$$

is about 2×10^{12} cm^3 mol^{-1} s^{-1} in the temperature range 2600–2800 K.

(*c*) The principal reaction leading to N_2 is the recombination of NH_2 radicals or the reaction between NH_2 and NH_3. Our analysis slightly favours the first of these alternatives. Reactions involving NH are substantially less important in forming N_2.

(*d*) The rate constant of the unimolecular initiation step, at total gas concentrations of about 1.7×10^{-6} mol cm^{-3} is

$$k = 1.2 \times 10^{16} \exp(-91\,000/RT)\ cm^3\ mol^{-1}\ s^{-1}$$

with the activation energy in cal mol^{-1}. If this rate constant applies to the reaction

$$NH_3 + Kr \rightarrow NH_2 + H + Kr$$

then Kr has a collision efficiency of about 0.03 in the dissociation of NH_3 at 2500–3000 K.

Acknowledgments

We thank the National Research Council of Canada for a grant in aid of this research and for the award of a scholarship to W.S.N.

1. T. A. Jacobs. J. Phys. Chem. **67**, 665 (1963).
2. K. W. Michel and H. Gg. Wagner. 10th Symp. Int. Combust. The Combustion Institute, Pittsburgh. 1965. p. 353.
3. H. Henrici. Doctoral thesis. University of Göttingen, Germany. 1966.
4. D. L. Johnson. D.Sc. Thesis. Washington University, MO. 1966.
5. T. Takeyama and H. Miyama. Bull. Chem. Soc. Jpn. **39**, 2352 (1966).
6. J. N. Bradley, R. N. Butler, and D. Lewis. Trans. Faraday Soc. **63**, 1 (1967).
7. M. Haluk. Ph.D. Thesis. University of Toronto, Toronto, Ont. 1970.
8. A. P. Genich, A. A. Zhirnov, and G. B. Manelis. Kinet. Catal. **4**, 726 (1979); **4**, 729 (1975).
9. J. E. Dove and W. S. Nip. Can. J. Chem. **52**, 1171 (1974).
10. S. W. Mayer and L. Schieler. Aerospace Corp. Rept. TR-669 (9210-02)-3. 1966.
11. G. S. Bahn. Reaction rate compilation for the H—O—N system. Gordon and Breach, New York. 1968.
12. M. W. P. Cann and S. W. Cash. J. Chem. Phys. **41**, 3055 (1964).
13. S. C. Barton and J. E. Dove. Can. J. Chem. **47**, 521 (1969).
14. JANAF thermochemical tables. 2nd ed. NSRDS-NBS 37. National Bureau of Standards, Washington, DC. 1970.
15. M. A. Di Valentin. Ph.D. Thesis. University of Toronto, Toronto, Ont. 1969.
16. Ionization potentials, appearance potentials, and heats of formation of gaseous positive ions. NSRDS-NBS 26. National Bureau of Standards, Washington, DC. 1969.
17. D. Rapp and P. Englander-Golden. J. Chem. Phys. **43**, 1464 (1965).
18. (*a*) S. W. Mayer and L. Schieler. Aerospace Corp. Rept. TDR-669 (9210-02)-1. 1966; (*b*) Thermochemistry Res. Dept., Aerospace Corp. Aerospace Corp. Rept. TR-100 (9210-02)-1. 1966.
19. C. Willis and R. A. Back. Can. J. Chem. **51**, 3605 (1973).
20. D. M. Golden, R. K. Solly, N. A. Gac, and S. W. Benson. J. Am. Chem Soc. **94**, 363 (1972).
21. K. E. Seal and A. G. Gaydon. Proc. Leeds Philos. Lit. Soc. Sci. Sect. **89**, 459 (1966).
22. W. E. Kaskan and M. P. Nader. J. Chem. Phys. **56**, 2220 (1972).
23. W. J. Stevens. J. Chem. Phys. **57**, 2164 (1973).
24. S. N. Foner and R. L. Hudson. J. Chem. Phys. **29**, 442 (1958).
25. V. H. Dibeler, J. L. Franklin, and R. M. Reese. Advances mass spectrometry. Pergamon Press. 1959. p. 443.
26. K. W. Michel. 10th Symp. Int. Combust. The Combustion Institute, Pittsburgh. 1965. p. 351.
27. A. L. Myerson and W. S. Watt. J. Chem. Phys. **49**, 425 (1968).
28. S. W. Mayer, L. Schieler, and H. S. Johnston. 11th Symp. Int. Combust. The Combustion Institute, Pittsburgh. 1967. p. 837.
29. J. Troe. J. Chem. Phys. **66**, 4745 (1977); **66**, 4758 (1977).
30. J. O. Hirschfelder, C. F. Curtiss, and R. B. Bird. Molecular theory of gases and liquids. 2nd ed. Wiley, New York. 1963.

Evidence for the existence of complex ions in mixed solutions of indium trichloride and ammonium chloride

ALAN N. CAMPBELL

Department of Chemistry, University of Manitoba, Winnipeg, Man., Canada R3T 2N2

Received June 9, 1978

ALAN N. CAMPBELL. Can. J. Chem. **57**, 702 (1979).

The conductances, densities, and viscosities of concentrated solutions of ammonium chloride in water, at 25°C, have been determined with good agreement with existing conductance data. The same data have been obtained for mixed solutions of indium trichloride and ammonium chloride. The fact that the conductance is always much less than the sum of the individual conductances, in some cases less than that of indium chloride alone, points to the existence of a complex in solution.

ALAN N. CAMPBELL. Can. J. Chem. **57**, 702 (1979).

On a déterminé les conductivité, les densités et les viscosités de solutions concentrées de chlorure d'ammonium dans l'eau à 25°C; les valeurs obtenues sont en bon accord avec les données de conductivité existantes. On a aussi obtenu les mêmes données pour des solutions mixtes de chlorures d'indium et d'ammonium. Le fait que les conductivités des mélanges sont toujours plus faibles que la somme des conductivités individuelles et dans quelques cas plus faibles que celle du chlorure d'indium seul, suggère l'existence d'un complexe en solution.

[Traduit par le journal]

Introduction

It has been shown (1) that indium trichloride forms a double salt with ammonium chloride, whose formula is $2NH_4Cl{\cdot}InCl_3{\cdot}H_2O$. It is usually assumed that double salts, when dissolved in water, dissociate completely into their individual ions but so great is the tendency of indium chloride to form double salts with the chlorides of the metals of Groups 1 and 2 of the Periodic Table, that it is possible that when some of the indium chloride double salts dissolve to form concentrated solutions, a complex anion may exist in solution. In the case of the double salt quoted above the first result of solution could be

$$[1] \qquad 2NH_4Cl \cdot InCl_3 \rightarrow In^{3+} + ((NH_4Cl)_2{\cdot}Cl_3)^{3-}$$

followed on dilution by

$$[2] \qquad ((NH_4Cl)_2Cl_3)^{3-} \rightarrow 2NH_4^+ + 5Cl^-$$

Or, alternatively

$$[3] \qquad In(NH_4)_2Cl_5 \rightarrow (In(NH_4)_2Cl_4)^+ + Cl^-$$

followed on dilution by

$$[4] \qquad (In(NH_4)_2Cl_4)^+ \rightarrow 2NH_4^+ + In^{3+} + 4Cl^-$$

The method of investigation chosen by the author was that of conductance. If the double salt dissociates completely into its constituent single salts, then, apart from the inevitable effect on the activity due to the presence of the common ion, the measured conductance should be approximately equal to the sum of the individual conductances. A marked deviation from additivity should indicate complex ion formation. Such deviation was found; indeed, the conductance of a mixture of indium chloride and ammonium chloride is sometimes less than that of indium chloride alone.

Experimental

The methods of determining conductance are well known and have frequently been described by the author (2). Density was determined with a large pyknometer (capacity 50 cm^3) and therefore density figures are only good to four decimals but this is amply sufficient for the present purpose. Viscosity was determined with the viscometer of Cannon and Fenske. The product $\Lambda\eta$ (equivalent conductance multiplied by viscosity) offers a better comparison than the simple conductance.

The conductance of ammonium chloride in water at 25°C has been determined from 0.1 *N* to 0.01 *N* by Longsworth (3) and from 5.252 *N* to 0.1019 *N* by Wishaw and Stokes (4). Wishaw and Stokes have long been interested, in common with the present author, in the conductances of concentrated solutions, and have offered an equation for the expression of conductance as a function of concentration which, whatever its theoretical basis or lack of it, does in fact represent the conductance very well.

The author has repeated the work of Wishaw and Stokes on ammonium chloride and at the same time determined the density, viscosity, and apparent molal volume. The results are reproduced in Table 1. Equivalent conductance and conductance–viscosity products are shown in Fig. 1.

Although the conductances of indium trichloride solutions were determined previously (2), the measurements were now repeated with the same results. A weighed amount of ammonium chloride was then added and the conductance redetermined. The specific conductance of indium chloride was then subtracted from the specific conductance of the mixed solution and the apparent conductance of the ammonium chloride obtained, on the assumption that that of the indium

0008-4042/79/060702-03$01.00/0

TABLE 1. Densities, viscosities, specific and equivalent conductances, and apparent molar volumes of ammonium chloride in aqueous solution at 25°C*

N (equiv./L)	$\sqrt{N}$	$d_4^{25°C}$	$\eta(H_2O = 1)$ (relative viscosity)	κ (ohm^{-1} cm^{-1})	Λ	$\Lambda\eta$	ϕ_V (cm^3)
5.006	2.237	1.0681	1.110	0.4502	89.94	99.83	39.41
3.997	1.999	1.0548	1.069	0.3801	95.10	101.7	39.16
3.029	1.740	1.0427	1.029	0.3801	100.1	103.00	38.53
2.021	1.422	1.0278	1.021	0.2133	105.5	107.7	38.40
1.010	1.005	1.0147	1.019	0.1126	111.5	113.6	36.10

*N = equivalent molarity, d = density (with respect to water at 4°C), η = viscosity, κ = specific conductance, Λ = equivalent conductance, ϕ_V = apparent molal volume of NH_4Cl. Volume (solid NH_4Cl) = 35.03.

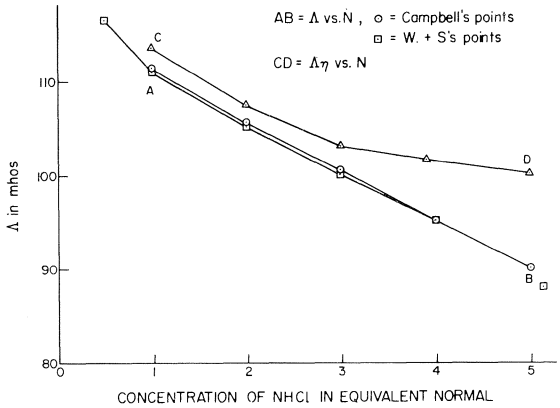

FIG. 1. Equivalent conductance and equivalent conductance × viscosity of NH_4Cl in water vs. $\sqrt{c}$.

chloride did not change. Actually, of course, it must change, the conductance measured being the sum of those of the ions In^{3+}, Cl^-, NH_4^+, and complex ions, but the assumption is only a basis of reference.

Discussion

Table 1, when compared with the results of Wishaw and Stokes (4), shows that the present results are in good agreement. If anything, the present results are a shade higher and this gives better agreement with the calculated results of Wishaw and Stokes. The apparent volumes are not of high accuracy since they rest on density determinations of only four decimal accuracy, but they show that the apparent volume decreases with dilution and approaches that of solid ammonium chloride. This is to be expected if ammonium chloride is completely ionized in the lattice.

Table 2 shows that with strong indium trichloride (13.73 N), addition of only 0.1 N ammonium chloride produces a conductance less than that of indium chloride alone. With 4.916 N indium chloride, the effect is similar. If Λ for 15.78 N indium chloride is multiplied by the viscosity of the mixed solution, containing 15.78 N indium chloride and

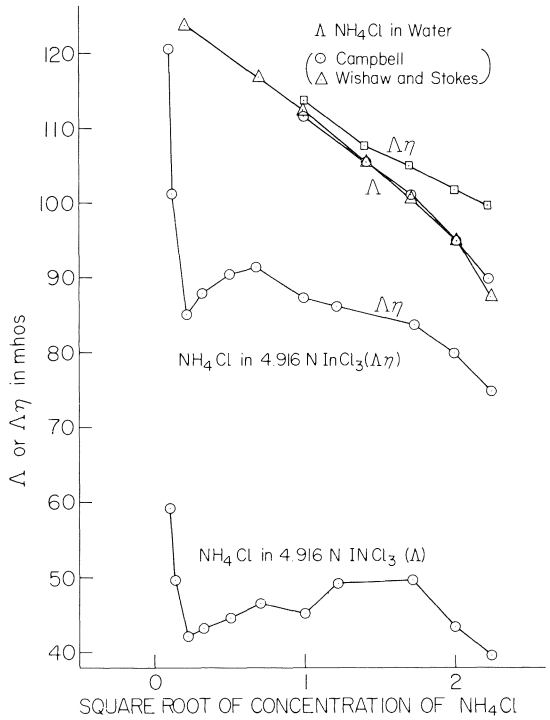

FIG. 2. Equivalent conductance and equivalent conductance × viscosity of NH_4Cl in $InCl_3$ solutions of fixed concentration vs. $\sqrt{c}$.

0.25 N ammonium chloride (1.406 × 21.3 = 29.95) the value of the product is much greater than the value (15.22) for the mixed solution, in other words, the presence of 0.25 N of NH_4Cl has greatly increased the viscosity without adding to the conductance. The value of the (apparent) equivalent conductance of ammonium chloride remains roughly constant over the concentration range 0.05 N to 0.5 N, and this is no doubt connected with an equilibrium of the form:

$$2NH_4^+ + In^{3+} + 4Cl^- \rightleftharpoons [In(NH_4)_2Cl_4]^+$$

With 13.73 N, the very great increase in viscosity

TABLE 2. Corresponding data for mixed solutions of indium trichloride and ammonium chloride, the indium trichloride being always 13.73 *N*, except for the last two concentrations where it was 15.78 *N*. The experiments could not be carried beyond 0.5 *N* NH_4Cl, as this represents the extent of solubility of NH_4Cl in such highly concentrated indium chloride

(*a*)

N_{InCl_3}	$N_{NH_4Cl_4}$	N_{Total}	$\sqrt{N_{Total}}$	d	η	κ_{Total}	κ_{NH_4Cl}	Λ_{NH_4Cl}	$\Lambda\eta$
13.73	—	13.73	3.705	1.7449	9.896	0.0130	—	—	—
13.73	0.01	13.74	3.707	—	—	0.01939	0.0000918	9.18	90.8
13.73	0.02	13.75	3.708	—	—	0.01947	0.0001694	8.47	83.82
13.73	0.05	13.78	3.712	—	—	0.01806*			
13.73	0.1	13.83	3.719	—	—	0.01576*			
15.78	0.25	16.03	4.004	1.8708	21.30	0.01145*			
15.78	0.5	16.28	4.035	1.8941	25.60	0.01062*			

*Conductance less than that of $InCl_3$ above.

(*b*)

N_{NH_4Cl}	N_{Total}	$\sqrt{N_{Total}}$	η	Λ_{Total}	$\Lambda\eta_{Total}$	Λ_{NH_4Cl}	$\Lambda\eta_{NH_4Cl}$
0.00	4.916	1.2704	2.038	11.48	23.41	—	—
0.01	4.926	—	—	11.58	23.60	59.10	120.2
0.02	4.936	—	—	11.64	23.72	49.50	100.9
0.05	4.966	—	—	11.79	24.03	42.00	85.60
0.10	5.016	—	—	12.11	24.69	43.10	87.84
0.25	5.166	—	—	13.08	26.66	44.36	90.41
0.50	5.416	—	—	14.61	29.77	45.30	91.64
1.00	5.916	1.2738	1.940	17.20	33.36	45.28	87.84
2.00	6.916	1.2755	1.910	21.21	40.50	49.12	86.18
3.00	7.916	1.2802	1.877	24.08	45.20	49.72	83.94
4.00	8.916	1.2851	1.846	25.76	47.56	43.31	79.95
5.00	9.916	1.2882	1.888	25.66	48.46	39.61	74.78

*The results of (*b*) are expressed graphically in Fig. 2.

(from 9.896 to 25.60) caused by the addition of only 0.5 *N* NH_4Cl (and where the apparent conductance has become negative) indicates that the added ammonium chloride exists largely as complex and that this complex is much bulkier than any of the component ions.

1. E. M. KARTZMARK. Can. J. Chem. **55**, 2792 (1977).
2. A. N. CAMPBELL. Can. J. Chem. **51**, 3007 (1973).
3. L. G. LONGSWORTH. J. Am. Chem. Soc. **57**, 1185 (1935).
4. B. F. WISHAW and R. H. STOKES. J. Am. Chem. Soc. **76**, 2065 (1954).

The density and vapour pressure of dimethylsulfoxide at various temperatures and the (hypothetical) critical density

ALAN N. CAMPBELL

Department of Chemistry, University of Manitoba, Winnipeg, Man., Canada R3T 2N2

Received June 14, 1978

ALAN N. CAMPBELL. Can. J. Chem. **57**, 705 (1979).

The density up to 257°C and the vapour pressure up to 189°C of dimethylsulfoxide have been determined directly. Dimethylsulfoxide decomposes below the critical temperature, but by indirect methods the (hypothetical) critical density is found to be

$$\rho_c = 0.366 \text{ g/cm}^3$$

or

$$V_c = 237.7 \text{ cm}^3$$

The vapour pressure measurements yield a molar heat of evaporation of 10.84 kcal/mol or 138.7 cal/g.

ALAN N. CAMPBELL. Can. J. Chem. **57**, 705 (1979).

On a déterminé, par des méthodes directes, la densité du diméthylsulfoxyde jusqu'à 257°C et sa tension de vapeur jusqu'à 189°C. Le diméthylsulfoxyde se décompose à une température inférieure à sa température critique; par des méthodes indirectes, on a toutefois pu calculer que la densité critique (hypothétique) est

$$\rho_c = 0.366 \text{ g/cm}^3$$

ou

$$V_c = 237.7 \text{ cm}^3$$

A partir des mesures de tension de vapeur, on peut évaluer une chaleur molaire d'évaporation de 10.84 kcal/mol ou 138.7 cal/g.

[Traduit par le journal]

Introduction

It should be said at the outset that it is not possible to determine directly the critical constants because of decomposition. It is, however, possible to arrive at an approximation to the critical density and in the attempt to do so good values of the vapour pressure and density have been obtained.

Experimental

The dimethylsulfoxide used was a Fisher product (certified A.C.S.). A small quantity was dried by standing over molecular sieves, as recommended by Perrin, Armarego, and Perrin (1), but this produced no change in the freezing point or density: for subsequent work, the product was used without further purification.

For the determination of density, all the customary precautions of the best pyknometry were used, viz. a large, but not too large, pyknometer (50 cm^3 capacity). The thermostat temperature was constant to ± 0.01°C, as determined with a Beckmann thermometer, which had been standardised against a standard platinum resistance thermometer. The pyknometer was left in the balance case for a fixed time before weighing. Conductance water was used for the calibration and buoyancy was eliminated by using an identical pyknometer as a counterpoise. Under these circumstances, it is usual to claim an accuracy of 0.0001 in the density, say 0.0003.

Above 92°C, density was obtained with a dilatometer, consisting of a bulb and graduated capillary: the apparatus was evacuated and sealed to prevent boiling of the liquid. The rise in the capillary was measured with a cathetometer reading to 0.01 cm. Measurements with the dilatometer are somewhat less accurate, since they depend on the accuracy of the cathetometer. An accuracy of 0.001 is claimed.

Vapour pressure was measured with a closed manometer up to a pressure of 78.1 cm of mercury and a temperature of 189°C. The DMSO in the manometer was repeatedly frozen, pumped down on a high vacuum line, melted, and the operation repeated. The manometer itself was flamed to remove occluded moisture from the glass. The accuracy is estimated as 0.1 cm. This means that for pressures less than 1.0 mm the error is high. Direct observation is not a good method for such low vapour pressures. Densities are given in Table 1 and vapour pressures in Table 2.

Results

Density has been determined by various investigators, at temperatures ranging from 20 to 80°C (2–4). The measurements of this paper extend to 257°C. Despite the wide range of temperature and the fact that density determinations above 92°C were made with a dilatometer, it was found that the results can be represented quite accurately by the equation:

$$d_t = d_{25}(1 - \alpha\Delta t - \beta(\Delta\tau)^2)$$

where

$$\Delta t = t - 25$$

When the experimental results were offered to the

0008-4042/79/060705-03$01.00/0

TABLE 1

(*a*) Density of dimethylsulfoxide at various temperatures

t (°C)	d_4
25.00	1.0961
48	1.0730
61	1.0623
72	1.0513
92	1.0323
116	1.004
172	0.945
188	0.925
195	0.910
250	0.855
257	0.845

(*b*) Results calculated and compared with those of previous workers*

t (°C)	Exp. value of *d*	Calcd.	Discrepancy
20	1.1014 (10)	1.0965	−0.0049
35	1.0855 (11)	1.0863	+0.0008
40	1.0825 (2)	1.0814	−0.0011
45	1.0745 (11)	1.0764	+0.0019
50	1.0721 (10)	1.0696	−0.0025
55	1.0637 (10)	1.0665	+0.0028
60	1.0637 (11)	1.0619	−0.0018
80	1.0472 (2)	1.0324	−0.0148

*Reference numbers in parentheses.

TABLE 2. Vapour pressures of dimethylsulfoxide

t	*T*	$1/T \times 10^3$	*p* in Torr	log *p*
44.1	317.3	3.152	0.095	−1.0223
65.0	338.2	2.957	0.710	−0.1487
76.5	349.7	2.860	1.233	0.2095
94.3	367.5	2.721	3.800	0.5798
113	386	2.591	7.943	0.9000
135	408	2.451	19.09	1.281
190	463	2.159	80.0	1.909
97	370	2.703	4.452	0.6486
139	412	2.427	18.84	1.275
155	428	2.336	32.24	1.508
163	436	2.294	39.585	1.598
172	445	2.247	51.3	1.710
178	451	2.217	61.1	1.786
180	453	2.208	65.7	1.818
182	455	2.198	68.1	1.833
185	458	2.183	72.3	1.859
186	459	2.179	74.3	1.871
187	460	2.174	74.3	1.871
188	461	2.169	76.1	1.881
189	462	2.164	78.1	1.893

computer, it obtained for the constants:

$$\alpha = 0.97514 \times 10^{-3}$$

$$\beta = 0.4400 \times 10^{-6}$$

The average discrepancy between calculated and observed results is 0.03966% and the maximum deviation is 0.8360% at 188°C. Table 1 gives the experimental results together with the densities calculated from the above equation for the temperatures of previous workers. Considering the conditions of experiment, the agreement is good, except that the previous figure for 20°C is obviously too high. The discrepancies between observed and calculated results are small and vary in algebraic sign.

It is surprising that so little work has been done on the vapour pressure of DMSO. The only work discovered by the author is that of Teichmann and Ziebarth (5), who give the vapour pressure as $p =$ 16 mm at 79.80°C and 12 mm at 72.50°C, and that of Douglas (6). Douglas determined the vapour pressure of DMSO over the temperature range 20 to 50°C. Comparing his results with those of this work, we have

Douglas	Campbell
3.07 Torr (t = 50°C)	7.10 Torr (t = 65°C)
2.27 Torr (t = 45°C)	0.95 Torr (t = 44°C)

Considering that the present method was the direct observation of a mercury column in a manometer and that of Douglas the more delicate one of the air-saturation method, the agreement is good enough. Perhaps Douglas' results may be low, since his method of saturating the air is hardly sufficient, according to modern technique. Douglas used the Kirchhoff equation to express his results:

$$\log p = A - B/T + C \log T \text{ (his } C \text{ is negative)}$$

Using Douglas' constants to calculate the vapour pressure at the experimental temperatures of this paper, very poor agreement results, e.g. at 189°C which is generally agreed to be the normal boiling temperature, the vapour pressure is calculated to be 1051 mm, instead of 760 mm. But this, of course, is not a criticism of Douglas, since his equation only purports to cover the range 20 to 50°C.

Discussion

The Kirchhoff equation assumes a constant ΔH_{vap} over the temperature range, but ΔH_{vap} is not constant. Nevertheless, the Kirchhoff equation satisfactorily describes the behaviour of many liquids over a wide range of temperature. For instance, mercury, ethanol, mesitylene, acetone, cyclohexane, and ether give very good straight line plots for log *p* vs. $1000/T$ over the temperature range 0 to 160°C, though ΔH_{vap} is not constant. The constant B of the Kirchhoff equation is proportional to ΔH_{vap}, but ΔH_{vap} is not constant. The slope of the log *p* vs. $1/T$ plot must therefore give a mean value of ΔH_{vap} over the temperature range. Compensating factors must account for the straightness of the plot. This criti-

cism applies to all ΔH values obtained from vapour pressure plots.

The results of Table 2 when plotted in the form of log p vs. $1/T$ give a good straight line. From the slope of the straight line, the heat of evaporation results as $\Delta H = 10.84 \pm 0.2$ kcal/mol (as a mean value over the range 25 to 189°C). Similar treatment of Douglas' (6) results gives 12.64 kcal over the range 20 to 50°C. A single and often quoted direct experimental determination for the heat of evaporation at the boiling point is that of Prückner (7) who gives 13.67 kcal. The application of Trouton's rule gives $\Delta H = 9.26$ kcal but Trouton's rule is only an approximation. The Nernst–Bingham rule: $\Delta S = 17 + 0.011T$ gives $\Delta S = 22.082$, and hence $\Delta H = 10.20$ kcal/mol.

TABLE 3. Data for the application of Hakala's rule*

t (°C)	$(r + \rho)/2$	$(r - \rho)^{10/3}$
25	0.5480	1.3578
48	0.5365	1.2647
61	0.5312	1.2231
72	0.5257	1.1815
92	0.5161	1.1106
116	0.5019	1.0112
172	0.4734	0.8248
188	0.4637	0.7662

*The above results are expressed graphically in Fig. 1. The intercept of the straight line = $\rho_c = 0.366$ g/cm³. From the slope, $k = 0.133$. V_c/mol = 237.7 cm³.

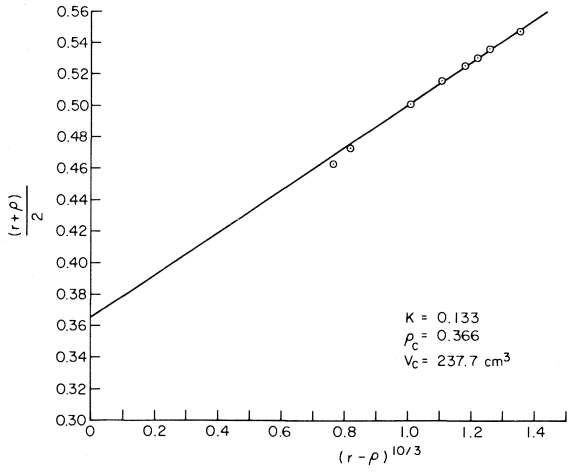

FIG. 1. Plot of $(r + \rho)/2$ vs. $(r - \rho)^{10/3}$.

The law of the rectilinear diameter while giving a straight line plot for the mean density of orthobaric liquid and vapour, for most of the temperature rise, is liable to bend in a distressing manner just before the critical temperature is reached. A modification of the rectilinear diameter rule by Hakala (8) has been found very successful. According to Sheehan (9) "In general, values of P_c found by this linear extrapolation agree with traditional methods; even when the densities are one hundred degrees from T_c, the values of P_c are correct within one percent." The rule takes the form:

$$(r + \rho)/2 = \rho_c + k(r - \rho)^{10/3}$$

where r = liquid density, ρ = density of saturated vapour, k = empirical constant, ρ_c = critical density.

In applying Hakala's rule to the present results, the density of the vapour up to 189°C and a vapour pressure of 1 atm was calculated from the observed vapour pressures and the ideal gas law: any deviations from ideal behaviour would not be significant, since the density of the vapour is so small in comparison with that of the liquid. The results are given in Table 3.

1. D. D. PERRIN, W. L. F. ARMAREGO, and D. R. PERRIN. Purification of laboratory chemicals. 1st ed. Pergamon Press, Oxford. 1966.
2. H. L. SCHLÄFER and W. SCHAFFERNICHT. Angew. Chem. **72**, 618 (1960).
3. W. S. MACGREGOR. Ann. N.Y. Acad. **141**, 3 (1967).
4. W. A. MILLEN and D. W. WATTS. J. Am. Chem. Soc. **89**, 6858 (1967).
5. B. TEICHMANN and D. ZIEBARTH. J. Prakt. Chem. (4), **32**, 230 (1966).
6. T. B. DOUGLAS. J. Am. Chem. Soc. **70**, 2001 (1948).
7. H. PRÜCKNER. Erdöl Kohle, **16**, 188 (1963).
8. R. W. HAKALA. Chem. Eng. News, March 16, 1959, p. 43 and May 4, 1959, p. 13.
9. W. F. SHEEHAN. Physical chemistry. 2nd ed. Allyn and Bacon, Inc., Boston. 1970. p. 48.
10. J. N. BUTLER. J. Electroanal. Chem. Interfacial Electrochem. **14**, 89 (1967).
11. N.-P. YAO and D. N. BENNION. UCLA Rep. 69-30 DA Contract No. Da-44-009-AMC-1661(T).

COMMUNICATION

A total synthesis of (−)-khusimone[1]

HSING-JANG LIU AND WING HONG CHAN

Department of Chemistry, University of Alberta, Edmonton, Alta., Canada T6G 2G2

Received November 24, 1978

HSING-JANG LIU and WING HONG CHAN. Can. J. Chem. **57**, 708 (1979).

A total synthesis of (−)-khusimone (**1**), an odoriferous norsesquiterpenoid ketone, has been achieved in 16 steps from the ammonium salt of *l*-10-camphorsulfonic acid.

HSING-JANG LIU et WING HONG CHAN. Can. J. Chem. **57**, 708 (1979).

On a réalisé la synthèse totale de la (−)-khusimone (**1**), une cétone norsesquiterpénique odoriférante, en 16 étapes à partir du sel d'ammonium de l'acide *l*-camphresulfonique-10.

[Traduit par le journal]

The norsesquiterpenoid (−)-khusimone, a highly odoriferous ketone found in vetiver oil (1, 2), has been shown to possess the tricyclic skeleton and absolute stereochemistry depicted in formula **1** (1) by spectroscopic and chemical evidence. Recently, Büchi and co-workers (3) reported an elegant total synthesis of its racemic modification using an intramolecular Diels–Alder approach. We wish to describe an efficient photochemical route leading to the naturally occurring ketone in optically active form.

(−)-α-Campholenic acid (**2**),[2] prepared in 50% yield from the commercially available *l*-10-camphorsulfonic acid ammonium salt by fusion with solid potassium hydroxide,[3] was esterified with methyl iodide and potassium carbonate in acetone (5). Ozonolysis of the resulting ester **3** followed by reductive work up using triphenylphosphine (6) gave keto aldehyde **4** which was smoothly cyclized by means of *p*-toluenesulfonic acid in refluxing benzene. The product **5** obtained in 70% yield from **2** was subsequently irradiated (450-W Hanovia high-pressure quartz mercury vapor lamp and Pyrex filter) with 1,1-diethoxyethene (7, 8) in benzene at room temperature for 3 h. The photocycloaddition proceeded with complete regioselectivity to give an inseparable mixture of at least two diastereomers (four sets of partially superimposed —OCH_2— quartets at δ 3.39 region in the nmr spectrum) of the head-to-tail adduct **6**.[4] When hydrolyzed with dilute hydrochloric acid in acetone, the mixture afforded, as the only products, two diastereomeric diketones **7** and **8**[5] (total 80% yield from **5**) in a ratio of 5:8. In the nmr spectra, the minor isomer showed two singlets at δ 1.21 and 0.97 for the *gem*-dimethyl group whereas the corresponding signals of the major isomer, which was obtained as a solid (mp 127–128°C), appeared at δ 1.12 and 1.06. The larger Δδ observed for the minor product suggested its structure was **7** (and thus that of the major isomer was **8**) as the most important contribution conformation could be represented by formula **7***a* in which the α-faced methyl is shielded and the β-methyl deshielded respectively by the cyclobutanone and the cyclohexanone carbonyl. These tentative structural assignments were substantiated by subsequent transformations. Direct conversion of diketone **8** to **7** was attempted without success using a variety of conditions which were expected to induce epimerization at both ring junction centers. However the desired isomerization could be achieved by a two-step sequence as follows. Treatment of diketone **8** with pyridinium bromide perbromide in acetic acid gave a 70% yield of unsaturated ketone **9** which was reduced to diketones **7** and **8** (3:2; 65% yield)[6] with zinc in acetic acid (9) at room temperature.

Before the incorporation of the required *exo*-

[1]Dedicated to Professor K. Wiesner on the occasion of his 60th birthday.

[2]All compounds were adequately characterized by spectroscopic methods (ir, nmr, and ms) and by exact mass measurement and/or elemental analysis.

[3]The published procedure (4) for the degradation of the sodium salt of *d,l*-10-camphorsulfonic acid to α-campholenic acid was used.

[4]The regioselectivity and the orientation of the photocycloaddition follow from the result obtained from the subsequent hydrolysis of the photoadduct.

[5]Regardless of the ring junction stereochemistry of the precursors, a *cis* ring juncture could be readily assigned to these compounds on the basis of reported observations (8).

[6]Our original plan was to introduce the desired stereochemistry more efficiently by the following intramolecular photochemical process:

0008-4042/79/060708-02$01.00/0

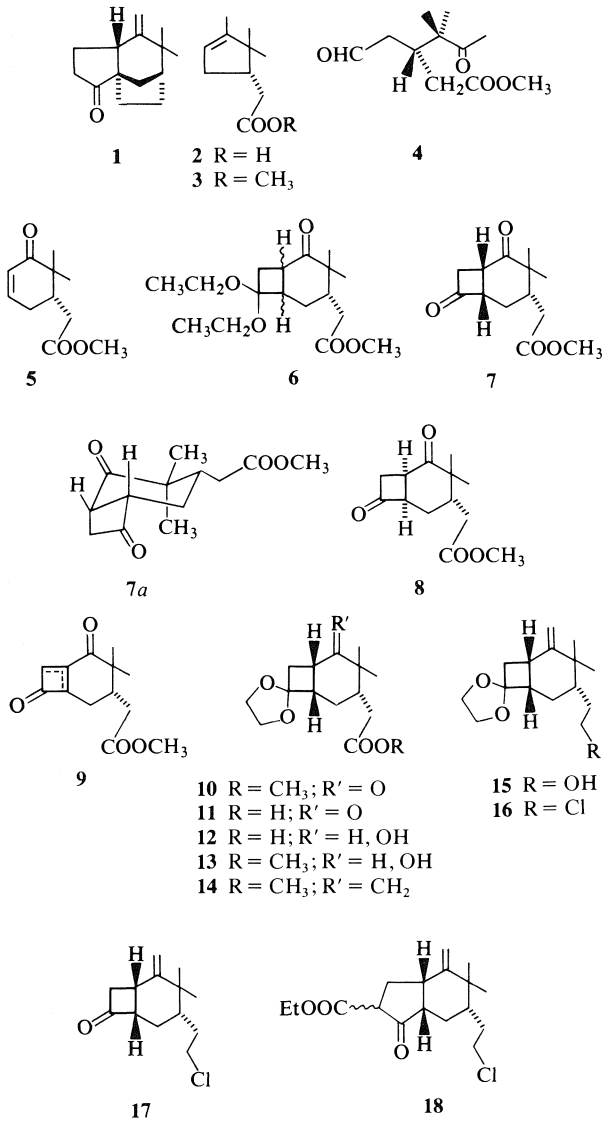

methylene group into diketone **7**, its cyclobutanone carbonyl was protected by means of selective transketalization with 2-ethyl-2-methyl-1,3-dioxolane at 95°C using *p*-toluenesulfonic acid as a catalyst. Hydrolysis of ester **10** with 2 *N* aqueous sodium hydroxide in refluxing methanol followed by treatment of the resulting acid **11** sequentially with 1 equiv. of sodium hydride and a fivefold excess of methyl magnesium bromide gave rise to hydroxy acid **12** which was esterified with diazomethane to afford hydroxy ester **13** (71% yield from **7**). On treatment with thionyl chloride and pyridine in benzene, hydroxy ester **13** underwent dehydration cleanly with exclusive formation of the exocyclic double bond as expected[7] and ester **14** was isolated in 89% yield. Ester **14** was reduced with lithium aluminum hydride and the resulting alcohol **15** converted by phosphorus oxychloride in pyridine to the corresponding chloride **16** in 70% yield over two steps. Hydrolysis of chloride **16** was effected by treatment with dilute hydrochloric acid to give quantitatively keto chloride **17**.

The transformation of keto chloride **17** to (−)-khusimone (**1**) requires two primary operations: one-carbon expansion of the cyclobutanone ring and cyclization. Each was accomplished by a single step. Boron trifluoride catalyzed ring expansion of keto chloride **17** with ethyl diazoacetate (10, 11) proceeded with high regioselectivity by the expected migration of the less substituted α-carbon (11, 12) to give keto ester **18** as the predominant product in 59% yield. When heated at reflux with 1 *N* sodium hydroxide in ethanol, keto ester **18** underwent concomitant decarbethoxylation and ring closure giving rise to (−)-khusimone (**1**) in 61% yield, which was shown to be identical in all respects with the natural material.

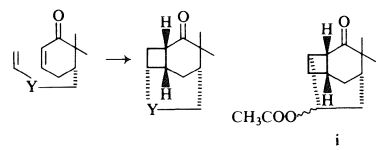

Of several suitable compounds studied, only one (Y = $CHOOCCH_3$) underwent intramolecular cycloaddition but in an undesirable head-to-head fashion to give keto acetate **i**.

Acknowledgements

We are grateful to the National Research Council of Canada and the University of Alberta for financial support and to Dr. G. Ohloff for a sample of natural (−)-khusimone.

1. D. C. Umrani, R. Seshadri, K. G. Gore, and K. K. Chakravarti. Flavour Ind. **1**, 623 (1970).
2. B. Maurer, M. Fracheboud, A. Grieder, and G. Ohloff. Helv. Chim. Acta, **55**, 2371 (1972).
3. G. Büchi, A. Hauser, and J. Limacher. J. Org. Chem. **42**, 3323 (1977).
4. R. R. Sauers. J. Am. Chem. Soc. **81**, 925 (1959).
5. H. J. Liu and P. C. L. Yao. Can. J. Chem. **55**, 822 (1977).
6. O. Lorenz and C. R. Parks. J. Org. Chem. **30**, 1976 (1965).
7. S. M. McElvain and D. Kundiger. Org. Synth. Coll. Vol. III, 123 (1955).
8. E. J. Corey, J. D. Bass, R. Le Mathieu, and R. B. Mitra. J. Am. Chem. Soc. **86**, 5570 (1964).
9. A. Windaus. Chem. Ber. **39**, 2249 (1906).
10. W. T. Tai and E. W. Warnhoff. Can. J. Chem. **42**, 1333 (1964).
11. H. J. Liu and T. Ogino. Tetrahedron Lett. 4937 (1973).
12. H. J. Liu and S. P. Majumdar. Synth. Commun. **5**, 125 (1975).

[7]The formation of an endocyclic double bond induces additional angular strain to the cyclobutane ring.

Canadian Journal of Chemistry

Published by
THE NATIONAL RESEARCH COUNCIL OF CANADA

Journal canadien de chimie

Publié par
LE CONSEIL NATIONAL DE RECHERCHES DU CANADA

Volume 57 Number 7 April 1, 1979

Volume 57 numéro 7 1 avril 1979

Raman spectra of single-crystal and liquid *s*-trioxane[1]

M. NAKAHARA,[2] P. T. T. WONG, AND E. WHALLEY

Division of Chemistry, National Research Council of Canada, Ottawa, Ont., Canada K1A 0R9

Received September 26, 1978

M. NAKAHARA, P. T. T. WONG, and E. WHALLEY. Can. J. Chem. **57**, 711 (1979).

The polarized Raman spectrum of *s*-trioxane has been measured in single-crystal phase I, the melt, and the chloroform-*d* solution and the measurements used to improve the assignments, particularly in the C—H stretching region.

M. NAKAHARA, P. T. T. WONG et E. WHALLEY. Can. J. Chem. **57**, 711 (1979).

On a mesuré le spectre Raman polarisé du *s*-trioxanne sous forme de cristal unique en phase I, de produit fondu et en solution dans le chloroforme-*d*; on a utilisé les mesures pour améliorer les attributions, en particulier dans la région de vibration de valence C—H.

[Traduit par le journal]

Introduction

It has recently been shown by a detailed analysis (1) of the infrared (2) and Raman (1) spectra under pressure that the puckered ring of trithiane, a six-membered ring compound $(CH_2S)_3$, is greatly flattened at 18 kbar, and by extrapolation appears to become flat at ~40 kbar. A few years ago, Brasch *et al.* (3) reported that when trioxane was squeezed between diamond anvils to pressures of the magnitude of 40 kbar its spectrum changed markedly at a change of phase that occurred (2) in a piston-cylinder apparatus at a nominal pressure of 27 kbar on increasing the load, and 8 kbar on decreasing, and several bands lost all or most of their intensity in the high-pressure phase. On releasing the pressure, the high-pressure spectrum persisted until at least 10 kbar, but was reported to revert to the low-pressure spectrum when the pressure was fully released. When a "single" crystal of trioxane was squeezed, the high-pressure phase was formed with considerable orientation, as shown by the strong polarization of the absorption spectrum of several bands. It was tentatively suggested, without a detailed analysis, that trioxane became flat under pressure.

As trithiane becomes flat under pressure (1), it is certainly expected that trioxane would become flat also, perhaps at a higher pressure than trithiane. However, a detailed analysis of the spectroscopic effects of flattening (4) suggested that the current assignment (5) of the spectrum and the observed effects of pressure were not consistent with flattening. This statement was also true (1) of the spectrum of trithiane as originally assigned, but several of the assignments could be changed in a reasonable manner to make the effect of pressure on the infrared spectrum agree with flattening.

It seemed that the assignment of trioxane could not be changed in a similar way, but nevertheless, there were some uncertainties in the assignment, and it seemed worth verifying by recording the polarized Raman spectra of a single crystal. In addition, the polarized spectra of the melt and of a solution in chloroform-*d* have been obtained. The spectra will also provide a basis for discussing the Raman spectrum of the high-pressure phase trioxane II, a phase which was first observed by Brasch *et al.* (3). As we shall see, the Raman spectrum of trioxane II (6) also helps to interpret that of trioxane I.

The vibrational spectra of trioxane have been investigated previously in the infrared for the gas (5, 7–10, 11), carbon tetrachloride solution (5, 7, 12), liquid (5, 11), and single crystal (5), and in the Raman

[1]NRCC No. 17171.

[2]NRCC Research Associate 1977–1978. Permanent address: Department of Chemistry, Faculty of Science, Kyoto University, Kyoto 606, Japan.

0008-4042/79/070711-07$01.00/0

using a mercury source for the liquid (9), carbon tetrachloride solution (13), and crystal (9).

Experimental Methods and Results

Experimental Methods

Practical grade *s*-trioxane was supplied by the Eastman Kodak Co. Single crystals were made by heating the solid to about 70°C in a bottle and storing at room temperature, 21.5°C. The vapor slowly condensed on the upper part of the wall to form clear long crystals. Single crystals were distinguished from polycrystals by the polarized Raman spectrum. The long axis of a crystal was assumed to coincide with the crystallographic *c* axis as has been observed by several workers (5, 14, 15), and the ends of the crystals were cut approximately perpendicular to the axis. The crystals were sealed in 3-mm-diameter glass tubes and mounted near the spectrometer slit, and were oriented to give the maximum intensity of the appropriate polarized components of several strong bands near 3000 cm^{-1}. Melt and solution samples were made by sealing trioxane either alone or with chloroform-*d* in a 3-mm-diameter glass tube. The melt was made by heating the tube to ~70°C with an air gun.

The Raman spectra were obtained using the 5145-Å argon line from a Coherent Radiation Laboratories model 52 argon-ion laser and a Jarrel–Ash model 25-300 spectrometer, using a 90° scattering angle. The polarization properties were measured using a half-wave plate for the exciting light and a polarization scrambler and an analyzer for the scattered light. They were checked by measuring the carbon tetrachloride bands (16). The intensity of the laser beam was ~1 W for the melt and solution spectra, and was reduced to ~300 mW for the single-crystal spectra to prevent sublimation. For the final spectra, the spectral slit width was 2.9 cm^{-1}, time constant 10 s, and scanning speed 10 cm^{-1} min^{-1}. The spectrum of a neon lamp (17) was recorded with several of the spectra, and the neon lines and the stronger plasma lines of the laser were used to calibrate the frequencies. Sharp bands were reproducible to ±0.2–0.3 cm^{-1}, and all are reported to ±1 cm^{-1}.

Results

Polarized spectra were run on 5 different single crystals. The polarized spectra of the crystal in the range 4000–200 cm^{-1} are shown in Fig. 1, in which the *a* and *a'* directions are perpendicular to the *c* axis of the crystal and to one another, and selected regions are shown on an expanded scale in Fig. 2. The polarized spectra in the region of the lattice vibrations are shown in Fig. 3. No laser Raman spectrum of liquid trioxane appears to have been published and so polarized spectra are shown in Fig. 4. The frequencies and peak intensities for the crystal are summarized in Table 1. The frequencies, qualitative relative intensities, and depolarization ratios for the liquid at ~70°C and the 0.3 *M* solution in chloroform-*d* are summarized in Table 2.

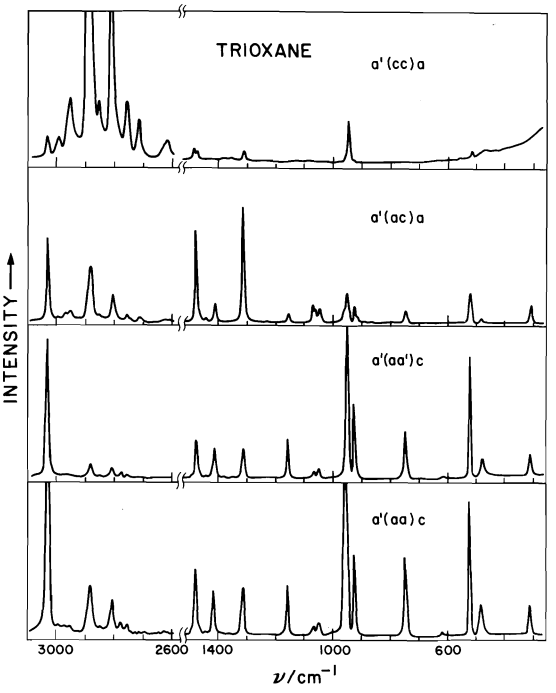

FIG. 1. Polarized Raman spectra of single-crystal trioxane in the range 4000–200 cm^{-1}. The polarizations are indicated in the frames. The scanning speed was 20 cm^{-1} min^{-1}, maximum counting rate 2000 s^{-1}, and time constant 2 s.

The Raman spectrum of polycrystalline trioxane has been reported by Stair and Nielsen (9) using mercury excitation, and their frequencies and assigned species are summarized in Table 1. The two measurements agree well, although Stair and Nielsen's experiments were not sensitive enough to detect some of the weaker bands.

The Raman spectrum of the lattice vibrations of the single crystal has recently been reported by Thomas (18). Our spectra agree with his except that the band he reported at 64 cm^{-1} was found at 69 cm^{-1} in this work, and he did not report the 54-cm^{-1} band although it seems to be present as a weak shoulder in his *cc* and *bc* spectra.

The infrared spectrum has been studied several times in the gas (5, 7–10), liquid (5, 12), and solution in carbon tetrachloride (5, 7, 11). Single crystals have been studied in the infrared by Kobayashi *et al.* (5), and a selection of their frequencies, particularly those assigned to the fundamentals, qualitative intensities, and polarizations are summarized in Table 1. Our frequencies agree reasonably well with

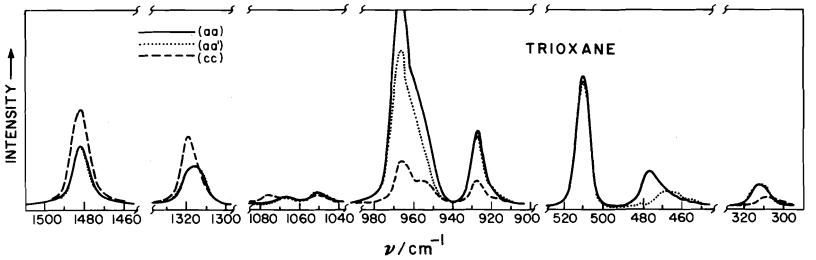

FIG. 2. Expanded polarized Raman spectra of single-crystal trioxane in selected frequency regions. The polarizations are indicated in the frames. The scanning speed was 10 cm^{-1} min^{-1}, maximum counting rate 2000 s^{-1}, and time constant 10 s.

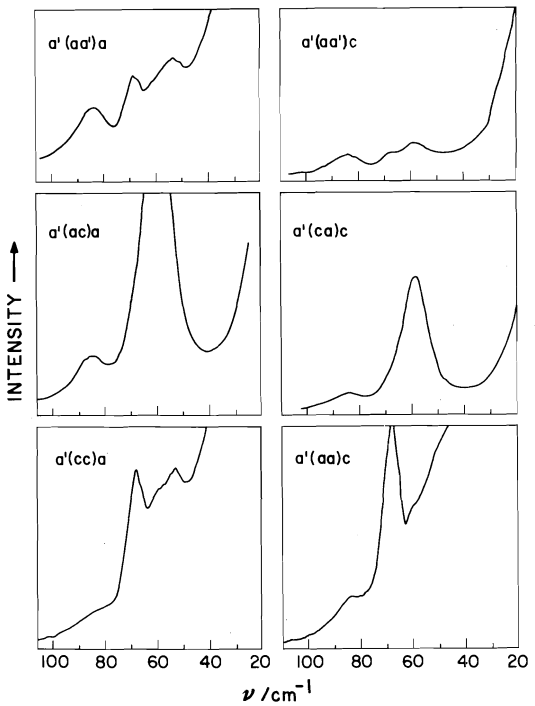

FIG. 3. Polarized Raman spectra of single-crystal trioxane in the region of the lattice vibrations. The polarizations are indicated in the frames. The scanning speed was 5 cm^{-1} min^{-1}, maximum counting rate 1000 s^{-1}, and time constant 40 s.

theirs except for the band that appears to be at 486 cm^{-1} in the Raman spectrum and 469 cm^{-1} in the infrared. It will be discussed in the following section.

Symmetry Assignment

The isolated trioxane molecule has symmetry C_{3v}. It has thirty fundamental vibrations which form the reducible representation $7A_1 + 3A_2 + 10E$. The A_1 and E vibrations are active in both the infrared and Raman spectra, and the A_2 vibrations are inactive in both. The crystal belongs to space group $R3c$, C_{3v}^6 with two molecules in the unit cell on sites of symmetry C_3 (14, 15). Under C_3 site symmetry, the distinction between A_1 and A_2 species disappears and both become A, and are active in both infrared and Raman. Under the unit-cell symmetry, each of the A vibrations splits by intermolecular coupling into an A_1 and an A_2 vibration, and only the A_1 vibrations are active. The E vibrations of the isolated molecule remain E under the site group, and each gives rise to two E vibrations which differ in frequency by the effects of intermolecular coupling. Thus, the A_1 vibrations of the isolated molecule remain active as A_1 vibrations in the crystal, the A_2 vibrations give A_1 vibrations and are presumably weakly active, and the E vibrations double. The intermolecular coupling is probably small, and the two coupled E vibrations probably differ little in frequency.

In the infrared, the A_1 vibrations are polarized parallel to the crystallographic c axis and the E vibrations parallel to a,b. In the Raman, the scattering matrix for the A_1 vibrations has the form

$$\begin{pmatrix} a & \cdot & \cdot \\ \cdot & a & \cdot \\ \cdot & \cdot & b \end{pmatrix}$$

and for the E vibrations the forms

$$\begin{pmatrix} c & \cdot & \cdot \\ \cdot & -c & d \\ \cdot & d & \cdot \end{pmatrix} \quad \text{and} \quad \begin{pmatrix} \cdot & -c & -d \\ -c & \cdot & \cdot \\ -d & \cdot & \cdot \end{pmatrix}$$

(19). The A_1 vibrations, therefore, occur in *aa* and *cc* polarizations only. The E vibrations occur in all polarizations except *cc*, and the *aa* and *ab* polarized spectra have the same intensity.

The Raman bands of the single crystal can therefore be assigned to their symmetry species as in Table 1. The assignment is straightforward for most bands. Several bands had strong *aa* and *aa'* components and a weak *cc* component. The *cc* component could be either an A_1 component or leakage, and an A_1 component was deduced only if the *aa* and *aa'* intensities were significantly different. There is no evidence that the coupled E vibrations derived from a particular E vibration of the isolated molecule differ significantly in frequency.

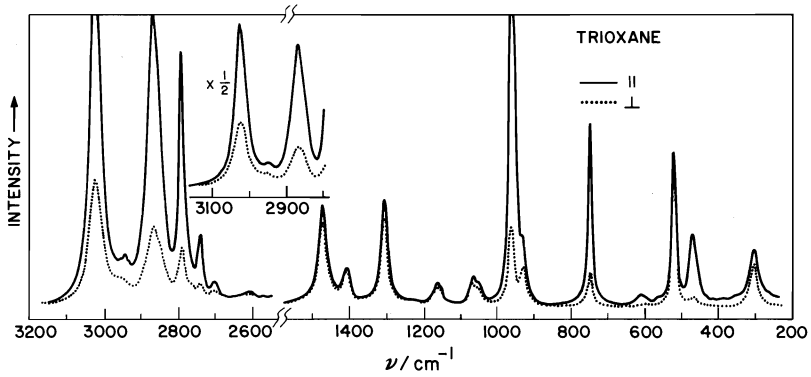

FIG. 4. Raman spectrum of liquid trioxane at ~70°C polarized parallel (∥), perpendicular (⊥) to the electric vector of the exciting light. The inset spectra are selected regions of the main spectra with the intensity scale reduced to one half. The scanning speed was 20 cm^{-1} min^{-1}, maximum counting rate 5000 s^{-1}, and time constant 2 s.

The species assigned by Kobayashi *et al.* (5) from their polarized infrared spectra of single crystals agree with ours, with a few exceptions which will be discussed below. The species assigned to the bands in the pure liquid and in solution based on the Raman polarization agree with the crystal assignments, again with a few apparent exceptions which will be discussed below.

The 3033-cm^{-1} Raman band of single-crystal trioxane has strong and nearly equal *aa* and *aa'* components. The *E* vibration, for which *aa* and *aa'* intensities are the same, dominates and the evidence for an A_1 vibration, i.e. that the *aa* and *aa'* components are not equal and there is a significant *cc* component, is not overwhelming. The Raman band of the liquid has a depolarization ratio of 0.29 and so has significant contribution from the A_1 band. The infrared spectrum is nearly all perpendicularly polarized, and so is due to the *E* vibration, and the A_1 is very weak at best. In the Raman spectrum (6) of trioxane II, a high-pressure phase which is produced at pressures about ~27 kbar at 22°C (2), most of the bands that are undoubtedly degenerate are split into two approximately equal components and none of the A_1 bands is split. No doubt the C_3 molecular axis is absent. The band at ~3033 cm^{-1} is split into two unequal parts, which can be interpreted as a strong doublet at 3037 and 3027 cm^{-1} derived from an *E* band and an A_1 component about 5 cm^{-1} lower than the mean *E* frequency of 3032 cm^{-1}, i.e., at ~3027 cm^{-1}. The spectrum of trioxane I is therefore probably due to a strong *E* vibration at 3033 cm^{-1} in both infrared and Raman and a weak A_1 vibration at ~3028 cm^{-1} in both infrared and Raman. In the polarized Raman spectrum the weak A_1 component seems to be dominated by leaked *E* spectra and the difference of frequencies is not evident.

The 2888-cm^{-1} Raman band of the single crystal is mainly the A_1 vibration, which agrees with the spectrum of the melt, and is largely *cc* polarized. In the infrared, there are clearly two bands, an A_1 at 2883 cm^{-1} and an *E* at 2877 cm^{-1}. In the Raman spectrum of trioxane II (6), there is a strong band and two weak sidebands. The sidebands are no doubt due to the split *E* vibration, and their mean frequency is ~6 cm^{-1} below that of the A_1. It seems likely, therefore, that the A_1 vibration of trioxane I is at 2888 cm^{-1} and the *E* components at ~2882 cm^{-1}. Apart from a frequency shift of 5 cm^{-1}, these agree with the infrared spectra.

Three of the combination bands, at 2855, 2630, and 1076 cm^{-1}, appear to have different species in the infrared and Raman spectra. Perhaps the two spectra see different combinations.

The 966- and 746-cm^{-1} bands appear to have significant A_1 and *E* contributions in the single-crystal Raman spectra, but to be only A_1 in the infrared. Their depolarization ratios in the liquid are 0.00 and 0.06 respectively. It seems likely that the apparently significant *E* component is due to leakage caused by imperfect alignment of the crystal and unwanted reflections and refractions.

The band at 480 cm^{-1} is clearly asymmetric in the Raman spectrum, and appears to consist of an A_1 band at 486 cm^{-1} and a weaker *E* band at 477 cm^{-1}. In the infrared (5), only a strong A_1 band at 469 cm^{-1} was reported.

The infrared spectrum has therefore been carefully recorded on a Perkin-Elmer model 521 infrared spectrometer. It is a broad asymmetric band, as is the Raman band, centered at about 475 cm^{-1}, and appears to be composed of two bands centered at ~484 and ~472 cm^{-1}, as does the Raman spectrum. However, according to Kobayashi *et al*'s. (5) Fig. 4, there is no perpendicularly polarized infrared band in this region, and the explanation of this discrepancy is not known.

TABLE 1. Polarized single-crystal Raman spectrum of trioxane at ~22°C. Polarized infrared spectra (5) of single-crystal and Raman spectra of polycrystal (9) trioxane are included for comparison

Single crystal									
Raman[a]						Infrared[b]			Polycrystal Raman[c]
ν/cm^{-1}	*aa*	*aa'*	*ac*	*cc*	Species[d]	ν/cm^{-1}	Polarization	Species	ν/cm^{-1}
3033	18.8	15.2	4.2	2.6	E, A_1[f]	3031s[e]	⊥	E	3032
2996	·	·	·	0.7	A_1	2991m	∥	A_1	—
2963	·	·	·	sh	A_1	2957sh	⊥	E	2960
2951	·	·	·	2.8	A_1	—	—	—	—
2888	2.0	1.8	2.8	27	A_1, E[f]	2883vs	∥	A_1	2887
—	—	—	—	—	—	2877s	⊥	E	—
2855	·	·	·	1.0	A_1	2853sh	⊥	E	—
2810	1.3	1.2	1.4	12.5	A_1	2807s	∥	A_1	2808
2780	0.8	0.8	·	·	E	2777m	⊥	E	—
2758	0.2	0.2	0.2	2.7	A_1	2757m	∥	A_1	2758
2717	·	·	·	2.0	A_1	2712w	∥	A_1	—
~2630	·	·	·	sh	A_1	2627vw	⊥	E	—
2615	·	·	·	0.8	A_1	—	—	—	—
1492	·	·	·	2.8	A_1	1494s	∥	A_1	—
1482	7.3	7.4	12.0	2.4	E	1483s	⊥	E	1479
1417	4.8	4.7	1.3	·	E	1419s	⊥	E	1418
1319	·	·	8.3	2.8	E	—	—	—	1319
1315	4.6	4.6	·	·	E	1313m	⊥	E	1314
—	—	—	—	—	—	1222vs	∥	A_1	
1160	5.7	5.8	0.3	·	E	1152vvs	⊥	E	1160
—	—	—	—	—	—	1087w	∥	A_1	—
1076	·	·	0.9	·	E	1074w	∥	A_1	1072
1067	0.9	0.9	sh	·	E	1067vvs	⊥	E	—
1051	1.4	1.4	0.9	·	E	—	—	—	1050
966	25.6	19.5	5.5	·	A_1[f]	951vvs	∥	A_1	959
951	sh	19.9	1.9	6.7	E	—	—	—	—
927	9.5	9.3	0.8	·	E	918vvs	⊥	E	927
746	11.5	6.5	·	·	A_1[f]	744vw	∥	A_1	747
620	0.4	·	·	·	A_1	624m	∥	A_1	—
520	16.6	16.1	2.6	·	E	521s	⊥	E	520
486	4.2	·	·	·	A_1	469s	∥	A_1	484
477	sh	2.1	·	·	E	—	—	—	—
312	2.8	2.7	·	·	E	305m	⊥	E	312
308	·	·	1.2	·	E	—	—	—	306
86	·	0.7	1.2	1.5	E	—	—	—	85[g]
69	6	·	0.5	12	A_1	—	—	—	64[g]
59	0.5	2.5	1.2	·	E	—	—	—	59[g]
54[h]	1.5	·	1.5	·	E	—	—	—	—

[a]This work.
[b]Reference 5. Most weak bands that do not coincide with Raman bands and appear to be combinations have been omitted.
[c]References 9 and 18.
[d]The stronger component is listed first.
[e]s = strong, m = medium, w = weak, v = very, sh = shoulder.
[f]See discussion in the text.
[g]Single crystal, ref. 18.
[h]This is a weak band and the polarizations are uncertain.

The Raman-active intermolecular rotational vibrations form the representation $A_1 + 2E$ and the only active translational vibration belongs to species E. They can be assigned as in Table 1. Thomas (18) assigned his 64-cm^{-1} band to the E species, but there seems little doubt that it is the A_1 band.

Discussion

Vibrational Assignment

The CH_2 stretching vibrations of the isolated molecule form the reducible representation $2A_1 + 2E$, of which $A_1 + E$ is caused by each of the symmetric and asymmetric stretches. When coupled in the crystal, each forms the reducible representation $A_1 + A_2 + 2E$, of which the A_2 vibration is inactive.

The coupling between the C—H stretches within a CH_2 group is expected to be much greater than the coupling between CH_2 groups, and so the designation symmetric and asymmetric should be a good approximation. The doubling of the E vibrations due to intermolecular coupling is probably

TABLE 2. Raman spectrum of trioxane in the liquid phase

Liquid, ~70°C		0.3 *M* solution in $CDCl_3$ at 22°C	
ν/cm^{-1}	ρ	ν/cm^{-1}	ρ
3024vs[a]	0.29	3021vs	0.20
2950w	—	2943w	—
2869vs	0.14	2866vs	0.10
~2852sh	—	2853sh	—
2794s	0.06	2789s	0.05
2742m	0.03	2738m	0.00
2704w	0.5	2700w	—
~2630vw	—	—	—
~2610vw	—	—	—
—	—	1419sh	—
1476m	0.70	1472m	0.72
1412m	0.71	1408m	0.73
1309m	0.70	1306m	0.73
1165w	0.67	1162m	0.66
—	—	1077sh	—
1071w	0.72	1068m	0.63
1052w	0.8	1053w	0.73
963vs	0.00	964vs	0.00
933m	—	930m	—
750s	0.06	750s	0.00
612w	0.00	Solvent	—
524s	0.62	524s	0.78
474m	0.01	475m	0.00
308m	0.76	309m	0.74

[a]Abbreviations are as for Table 1.

small, and so in a first approximation the symmetric and the asymmetric stretches each give an A_1 and two overlapping E Raman-active vibrations. The scattering matrices of the four CH_2 vibrations were calculated assuming that the polarizability of the C—H bond was cylindrically symmetrical. For simplicity, the C—H bonds were assumed to be parallel to or at the tetrahedral angle to the c axis, and the effective masses of the symmetric and asymmetric motions have been assumed equal. The predicted relative intensities of the Raman polarizations and the depolarization ratios are summarized in Table 3. The relative infrared intensities have been calculated assuming that the dipole-moment derivative for the stretching of the C—H bond is parallel to the bond direction. They are also summarized in Table 3.

Kobayashi *et al.* (5) assigned the E and A_1 asymmetric stretches to bands at 3031 and 2883 cm^{-1}, respectively, although their vibrational analysis predicted that their frequencies differed by only 4 cm^{-1}, which agrees with two other calculations (10, 20). Pickett and Strauss (10) assigned the 3025-cm^{-1} vapor band to the overlapping asymmetric stretches, and the 2850-cm^{-1} band to the symmetric stretches. Clark and Hewitt (20) assigned the asymmetric stretches to 3030 and 2852 cm^{-1} and the symmetric stretches to 2852 and 2790 cm^{-1}. Kobayashi *et al.* (5) also assigned the E and A_1 symmetric stretches to the widely spaced bands 2877 and 2807 cm^{-1} in spite of a calculated difference of only 1 cm^{-1}. The polarized infrared spectra shown in their Fig. 7 show that the 2883-cm^{-1} band has a strong A_1 component and a somewhat weaker E. The 3031-cm^{-1} band contains a very strong E component, and the A_1 component is so weak that it might be due to leakage. The Raman spectrum is, however, quite clear in requiring both A_1 and E components. The final assignment is summarized in Table 3.

The predicted polarizations agree qualitatively with experiment when the different experimental arrangements for the different polarizations are allowed for. For example, the ratio of *aa'* and *ca* intensities for the two E bands is predicted to be 4. It is about 4 for the asymmetric, and the symmetric is probably dominated by leakage of the A_1 band. The *cc* component of the A_1 symmetric band is predicted to be much stronger than the *aa*, as is observed. The *aa* component of both the symmetric and the asymmetric bands is predicted to be dominated by the E vibration, which is true for the

TABLE 3. Predicted relative intensities of the C—H stretching bands of single-crystal trioxane in the Raman and infrared spectra

		Raman[a,b]					Infrared[a,b]	
Band	Assigned frequency, cm^{-1}	*aa*	*aa'*	*ac*	*cc*	ρ[c]	*a*	*c*
A_1 (CH_2 symm. st.)	2888	$(2 + 7r)^2$	0	0	$(5 + 4r)^2$	3/49[d]	0	½
E (CH_2 symm. st.)	2882	$16(1 - r)^2$	$16(1 - r)^2$	$4(1 - r)^2$	0	¾	1	0
A_1 (CH_2 asymm. st.)	~3029	$4(1 - r)^2$	0	0	$16(1 - r)^2$	1/28	0	2
E (CH_2 asymm. st.)	3033	$16(1 - r)^2$	$16(1 - r)^2$	$3(1 - r)^2$	0	¾	1	0

[a]The factor $(4/3)\alpha_{\parallel}'^2$ multiplies the entries in the *aa*, *aa'*, *ac*, and *cc* columns for the Raman, and $24\mu'^2$ multiplies the columns *a* and *c* for the infrared.
[b]$r = \alpha_{\perp}'/\alpha_{\parallel}'$, $\alpha_{\perp}' = \partial\alpha_{\perp}/\partial r_{CH}$, $\alpha_{\parallel}' = \partial\alpha_{\parallel}/\partial r_{CH}$, $\alpha_{\perp}$ and $\alpha_{\parallel}$ are the components of the polarizability tensor perpendicular and parallel respectively to the bond axis, r_{CH} = C—H distance, $\mu' = \partial\mu/\partial r_{CH}$, μ = dipole moment.
[c]For the liquid.
[d]Approximately, assuming $r \ll 1$.

asymmetric; the E symmetric band is weak, and has unknown leakage from the strong cc of the A_1 band. The cc component of the A_1 symmetric band is predicted to be stronger than the A_1 asymmetric; it is about 10 times or more stronger.

The depolarization ratio of the combined asymmetric stretching vibrations was calculated as 0.38, independent of r. The experimental value for the pure liquid was 0.29, and for the solution in chloroform-d was 0.20. For the symmetric band the predicted values are $\frac{1}{3}$ for $r = 0$ and 0.13 for $r = 0.25$. The experimental values were 0.14 for the pure liquid and 0.10 for the solution. The agreement is reasonable.

In the infrared spectrum, the A_1 asymmetric stretch is predicted to be twice as strong as the E, and the E symmetric stretch to be twice as strong as the A_1. In fact, the relative intensities (5) are the inverse of the predicted, for reasons that are not understood.

All the other bands observed in the 3-μm region in the infrared and Raman spectra must be combinations. Several of them are quite strong in both the Raman and infrared, and are probably in Fermi resonance with the fundamentals. While assignments can be suggested for several combinations, there is no evidence that they are correct except the approximate coincidence of frequencies, and this is not reliable if several bands are in Fermi resonance, as seems to be so.

Kobayashi *et al.* (5) proposed a complete vibrational assignment of the molecule based on a normal coordinate analysis, and Pickett and Strauss (10, 21) have analyzed the ring vibrations that have significant internal rotation. Except in the C—H stretching region discussed above, our spectra do not require any revision of these assignments, except that the $A_1\nu_3$ internal rotation is at 484 cm^{-1} instead of 469 cm^{-1}. The companion E band at $\sim$477 cm^{-1} is presumably a combination, but there is no obvious candidate for it.

1. G. J. Lewis and E. Whalley. J. Chem. Phys. **68**, 1119 (1978).
2. S. D. Hamann, M. Linton, and C. W. F. T. Pistorius. High Temp. High Pressures, **5**, 575 (1973).
3. J. W. Brasch, A. J. Melveger, E. R. Lippincott, and S. D. Hamann. Appl. Spectrosc. **24**, 184 (1970).
4. G. J. Lewis and E. Whalley. Unpublished work.
5. M. Kobayashi, R. Iwamoto, and H. Tadokoro. J. Chem. Phys. **44**, 922 (1966).
6. M. Nakahara, P. T. T. Wong, and E. Whalley. To be published.
7. D. A. Ramsay. Trans. Faraday Soc. **44**, 289 (1948).
8. J. C. Decius, W. C. Steel, and R. G. Snyder. J. Chem. Phys. **19**, 806 (1951).
9. A. T. Stair and J. R. Nielsen. J. Chem. Phys. **27**, 402 (1957).
10. H. M. Pickett and H. L. Strauss. J. Chem. Phys. **53**, 376 (1970).
11. American Petroleum Institute Research Project 44, Catalog of Infrared Spectra, Serial Nos. 830-832, Naval Research Laboratory (1949).
12. W. R. Ward. Spectrochim. Acta, **21**, 1311 (1965).
13. L. Kahovec and K. W. F. Kohlrausch. Z. Phys. Chem. B**35**, 29 (1937).
14. V. Busetti, M. Mammi, and G. Carozzolo. Z. Kristallogr. **119**, 310 (1963).
15. V. Busetti, A. Del Pra, and M. Mammi. Acta Crystallogr. B**25**, 1191 (1969).
16. W. F. Murphy, M. V. Evans, and P. Bender. J. Chem. Phys. **47**, 1836 (1967).
17. J. Loader. Basic laser Raman spectroscopy. Heyden and Son Ltd., London. 1970. p. 23.
18. D. W. Thomas. J. Raman Spectrosc. **6**, 169 (1977).
19. R. Loudon. Adv. Phys. **13**, 423 (1964).
20. A. H. Clark and T. G. Hewitt. J. Mol. Struct. **9**, 33 (1971).
21. H. M. Pickett and H. L. Strauss. J. Am. Chem. Soc. **92**, 7281 (1970).

The catalytic reaction between carbon monoxide and nitrous oxide over chromium(III) oxide

BORDAN W. KRUPAY[1] AND ROBERT A. ROSS

Department of Chemistry, Lakehead University, Thunder Bay, Ont., Canada P7B 5E1

Received September 12, 1978

BORDAN W. KRUPAY and ROBERT A. ROSS. Can. J. Chem. **57**, 718 (1979).

The catalytic reaction between carbon monoxide and nitrous oxide over chromium(III) oxide has been investigated in a continuous flow system at atmospheric pressure from 525 to 583 K. Two kinetic regions with apparent activation energies of 172 ± 4 kJ mol^{-1} (525 to 559 K) and 239 ± 4 kJ mol^{-1} (565 to 583 K) were observed. The rate-controlling step in both regions was associated with the formation of an intermediate carbonate-like species during the consecutive decompositions of two nitrous oxide molecules. In the region of higher apparent activation energy, the presence of polymeric surface chromate groups may influence the reactivity of any carbonate-like intermediate and the subsequent desorption of carbon dioxide thereby leaving a vacant site for nitrous oxide decomposition.

BORDAN W. KRUPAY et ROBERT A. ROSS. Can. J. Chem. **57**, 718 (1979).

On a étudié la réaction catalytique du monoxyde de carbone avec l'oxyde nitreux sur de l'oxyde de chrome(III) dans un système à écoulement continu, à la pression atmosphérique, entre 525 et 583 K. On a observé deux régions cinétiques des énergies d'activation apparentes de 172 ± 4 kJ mol^{-1} (525 à 559 K) et 239 ± 4 kJ mol^{-1} (565 à 583 K). L'étape qui détermine la vitesse dans chaque région est associée à la formation d'une espèce intermédiaire ressemblant à un carbonate au cours des décomposition consécutives de deux molécules d'oxyde nitreux. Dans la région associée avec l'énergie d'activation apparente la plus élevée, la présence de groupes chromates polymères à la surface peut influencer la réactivité de tout intermédiaire ressemblant à un carbonate et la désorbtion subséquente du dioxyde de carbone qui laisse ainsi un site vacant pour la décomposition de l'oxyde nitreux.

[Traduit par le journal]

Introduction

The catalytic reduction of nitric oxide by carbon monoxide has received considerable attention (1). In regard to the relative activities of various transition metal oxides, the oxides of iron and chromium were more effective catalysts than those of nickel, cobalt, and manganese (2); a finding which differs from the usual pattern associated with oxidation reactions (3) although in later work (4, 5), the oxides of copper, cobalt, and manganese were reported to be most active. Further, it has been proposed that catalysis of the CO/NO reaction may proceed by an associative mechanism or if by a stepwise (regenerative) scheme oxide reduction would not be rate-determining (6).

Fewer studies have been reported on the catalytic reaction between carbon monoxide and nitrous oxide, a reaction which carries less immediate technological import. Reactivity patterns for the first row transition metal oxides (7) have suggested that three possible key contributory processes may explain catalysis: (*a*) the adsorption and reaction of carbon monoxide via a cyclic transition state involving the metal/oxygen bond, (*b*) the destabilization of a surface carbonate intermediate, and (*c*) the desorption of carbon dioxide which may be adsorbed on two surface sites.

The present study with chromium(III) oxide is a further contribution to kinetic work on the catalysis of the CO/N_2O reaction on transition metal oxides and also provides an opportunity to assess the general applicability of earlier hypotheses (7, 8).

Experimental

The catalytic reaction between carbon monoxide and nitrous oxide was examined in a differential-reactor flow system (9, 10) at atmospheric pressure. High-purity helium was used as the carrier gas in the flow system and Beckman GC-5 gas chromatograph. Nitrogen, carbon monoxide, carbon dioxide, and nitrous oxide were analyzed by a thermal conductivity bridge using stainless steel columns, 183 × 0.32 cm od, packed with 61 cm "Carbosieve B" and the remainder with "Poropak Q" at a column temperature of 353 K which was sufficient to resolve all components.

The standard reacting gas mixture consisted of carbon monoxide and nitrous oxide at a partial pressure of 5.33 kPa (40 Torr). "Blank" runs confirmed that reaction on the quartz wool and reactor walls reached 1% at 853 K which was 270 K above the highest temperature of catalysis. Preliminary experiments with the oxide catalysts established that diffusion phenomena (11, 12) did not influence the rate measurements at a total gas flow rate of 350 mL min^{-1} (NTP).

[1]Present address: Division of Chemistry, National Research Council of Canada, Ottawa, Ont., Canada K1A 0R9.

0008-4042/79/070718-05$01.00/0

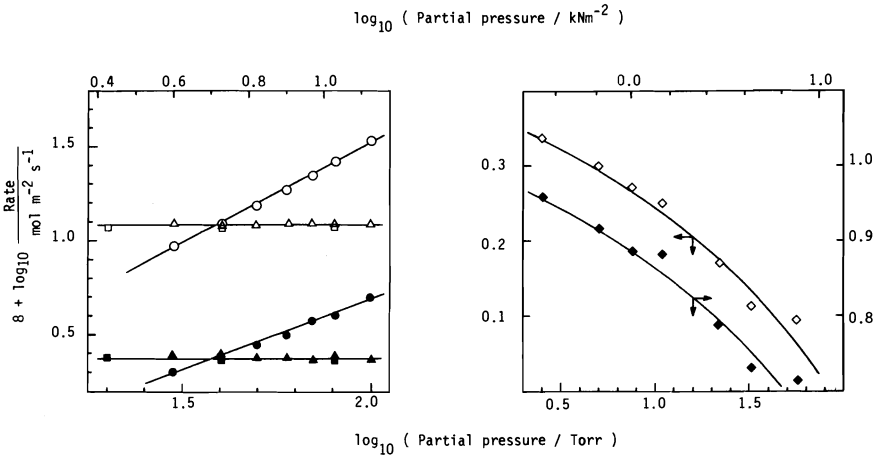

FIG. 1. The effects of variations in the partial pressures of carbon monoxide (△, ▲), nitrous oxide (○, ●), nitrogen (□, ■), and carbon dioxide (◇, ◆) on the catalytic CO/N_2O reaction on chromium(III) oxide at 567 and 545 K, respectively.

Chromium(III) oxide (99% w/w, Alfa Inorganics Inc.) was pelletized in a 1.27 cm die at 3 tons for 2 min and then calcined at 873 K for 10 h to increase tensile strength. After coarse crushing and sieving, particles with a 1–2 mm diameter were used for catalysis. The catalyst was heated in the reactor in flowing helium at 853 K for 30 min and then at 583 K for 3 h in the reacting gas mixture to establish steady catalyst activity. The conversion level at the highest temperature was 13.1%.

After the kinetic studies were completed, the surface area was 3 $m^2\ g^{-1}$ and bulk volume 0.65 $cm^3\ g^{-1}$. X-ray powder diffraction photographs before and after exposure to the standard gas mixture, consisting of 5.33 kPa each of carbon monoxide and nitrous oxide, did not reveal any changes in catalyst composition.

Carbon monoxide (C.P.; 99.5% minimum), carbon dioxide (Coleman; 99.99%), nitrogen (super-pure; 99.99%), nitrous oxide (99.9% minimum), and helium (high purity; 99.995%) were used as supplied.

Results

The reaction rate order with respect to carbon monoxide was determined at 545 and 567 K in the partial pressure range 4.00 to 13.3 kPa with nitrous oxide fixed at 5.33 kPa. At both temperatures, the reaction rate was independent of variations in the carbon monoxide partial pressure (Fig. 1).

The partial pressure of nitrous oxide was varied from 4.00 to 13.3 kPa with carbon monoxide maintained constant at 5.33 kPa. At 567 K, the reaction rate order with respect to nitrous oxide was 1.0 while at 545 K, a value of 0.8 was calculated (Fig. 1).

With the partial pressures of carbon monoxide and nitrous oxide each fixed at 5.33 kPa, the carbon dioxide partial pressure was varied from 0.33 to 5.79 kPa in individual experiments at 578 and 545 K. At both temperatures, the rate of reaction was retarded with increasing carbon dioxide partial pressure. The range of variation in the CO_2 partial pressure added to the reaction gas stream was much higher than the level of CO_2 produced from the CO/N_2O mixture. On this basis, the rate order for the gas was computed at the lowest CO_2 partial pressures and found to be -0.2 at both 578 and 545 K. The reaction rate was independent of variations in nitrogen partial pressure at both temperatures from 2.67 to 10.7 kPa. Thus, the rate of the reaction, r (mol $m^{-2}\ s^{-1}$), can be expressed as

$$[1] \qquad r = kP_{N_2O}{}^{1.0}/P_{CO_2}{}^{0.2} \quad \text{at 567 K}$$

and

$$[2] \qquad r = kP_{N_2O}{}^{0.8}/P_{CO_2}{}^{0.2} \quad \text{at 545 K}$$

Steady catalytic activity was attained at 583 K after 3 h with the standard gas mixture. Temperature was then progressively decreased from 583 to 525 K in 6 K intervals. Rate constants were calculated from the integrated forms of eq. [2] in the lower temperature region and eq. [1] at higher temperatures. The Arrhenius plot exhibited two apparent activation energies: 172 ± 4 kJ mol^{-1} from 525 to 559 K and 239 ± 4 kJ mol^{-1} from 565 to 583 K (Fig. 2).

Discussion

Infrared spectroscopic studies (13) indicate that α-Cr_2O_3 belongs to a class of oxidation catalysts that does not possess a metal/oxygen bond having double-bond character as evidenced by the absence of an infrared absorption band in the region near 1000–900 cm^{-1}. However, under oxidizing conditions, Cr_2O_3 can be oxidized to CrO_3 which does have some Cr—O double bond character. The catalytic properties are related to calcination tem-

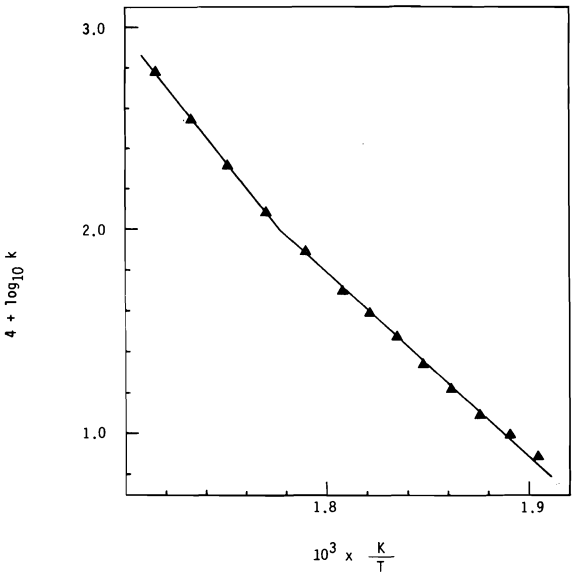

FIG. 2. Arrhenius plot of the rate constants for the CO/N_2O reaction on chromium(III) oxide.

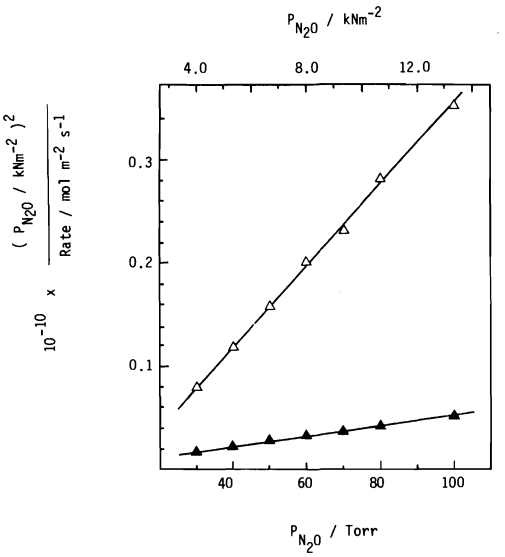

FIG. 3. Nitrous oxide rate order results plotted according to eq. [3] at 545 (△) and 567 K (▲) for the catalytic CO/N_2O reaction on chromium(III) oxide.

perature (14) while the extent of surface dehydration influences the sorption of carbon monoxide (15). Chromium(III) oxide exhibits intrinsic p-type semiconductivity (16) and lattice oxygen does not appear to be involved in catalytic oxidation (17, 18).

The rate order results were analyzed by testing various Langmuir–Hinshelwood kinetic expressions (19, 20). Correlations based on statistical fitting have been discussed (21, 22) and, in view of recent findings (23) regarding their interpretation, their use has been adopted as a general guide to the nature of the surface reaction. Only one kinetic expression accommodated both nitrous oxide and carbon dioxide rate order results:

$$[3] \qquad r = kP_{N_2O}\theta_{N_2O}$$

where

$$\theta_{N_2O} = aP_{N_2O}/(1 + aP_{N_2O} + b\sqrt{P_{CO_2}})$$

The relationship was valid for both components at 545 and 565 K (Figs. 3 and 4).

Since the experimental reaction rate was zero order with respect to carbon monoxide partial pressure, the adsorption and reaction of CO would necessarily be rapid relative to nitrous oxide. The form of eq. [3] may be interpreted to indicate that the rate-controlling step is associated with the formation of a surface carbonate-like intermediate which has been previously detected in calorimetric studies of carbon monoxide, carbon dioxide, and oxygen adsorption (24) on Cr_2O_3 and, more

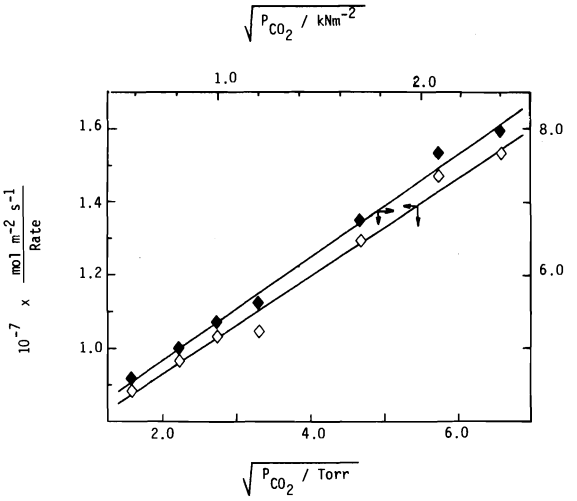

FIG. 4. Carbon dioxide rate order results for the CO/N_2O reaction on chromium(III) oxide at 545 K (◆) and 567 K (◇) plotted according to eq. [3].

specifically, could be the surface reaction involving nitrous oxide during the formation of this intermediate. In this respect, the value of the apparent activation energy, E_A, for the CO/N_2O reaction was 172 ± 4 kJ mol^{-1} (525 to 559 K) in good agreement with that reported for nitrous oxide decomposition (25) on Cr_2O_3, 167 kJ mol^{-1}, albeit in a 200 K higher temperature range when the decomposition of adsorbed nitrous oxide was proposed as the rate-determining step. The overall rate was associated

with the number of reaction sites available for N_2O decomposition determined by the inhibitory effect of adsorbed oxygen.

The formation of surface carbonates has been detected by infrared spectroscopy during the adsorption of carbon dioxide on α-Cr_2O_3 (26). The nature of the surface species depends on the degree of dehydration and the amount of CO_2 not removed at 473 K increases with activation time and temperature since bidentate carbonates formed on highly dehydrated surfaces are more strongly held than bicarbonates that predominate at low dehydration levels. Since the catalytic reaction rate is independent of CO partial pressure, the reactions involving N_2O may be proposed to intervene after the adsorption of carbon monoxide at a reactive site which has been identified as Cr^{3+} (15, 18). A surface scheme involving the simultaneous reaction between the reactants as adsorbed species does not seem likely since then the denominator of the kinetic expression should be squared (27). Further, the interaction between CO and N_2O yielding the intermediate carbonate-like species must proceed on specific sites since the introduction of CO_2 into the reacting gas mixture does not augment the catalytic reaction rate in the manner observed with Co_3O_4 (8).

The slight increase in rate order with respect to nitrous oxide partial pressure from 0.8 at 545 K to 1.0 at 567 K would not usually be regarded as significant but it did occur in step with the increase in apparent activation energy from 172 $\pm$ 4 kJ mol^{-1} (525 to 559 K) to 239 $\pm$ 4 kJ mol^{-1} (565 to 583 K) and hence may be associated with a variation in the surface reactivity of nitrous oxide. However, although the rate order was consistently zero with respect to carbon monoxide partial pressure at all temperatures, there remains the possibility that a change in the reactivity of this relatively strongly adsorbed reactant could occur within the two temperature zones. In this respect, correlations of E_A values obtained for the CO/N_2O reaction over 3*d* metal oxides with metal/oxygen bond polarization (7) and length (28) suggest that the adsorption of carbon monoxide via a cyclic intermediate does contribute to the catalytic reaction although the strengths of the metal/oxygen bonds may predominate in controlling the overall course of catalysis.

Oxygen desorption studies have revealed two surface oxygen states for Cr_2O_3 with desorption activation energies reported as 155 and 197 kJ mol^{-1} (29) and 146 and 230 kJ mol^{-1} (24). The non-uniformity of the surface oxygen of chromium(III) oxide has been examined by isotopic exchange (30) and samples annealed at 873 K exhibited parallel exchange with two types of surface oxygen species. The variation in non-uniformity and the amount of exchangeable oxygen on the surface was related to the presence of hexavalent chromium. Increase of temperature favoured the preponderance of polymeric surface chromate groups (14, 31) which possessed stronger metal/oxygen bonds resulting in higher activation energies for isotopic oxygen exchange and variations in the strength and form of the surface complex arising from CO_2 adsorption.

For the CO/N_2O reaction, the change in the apparent activation energy may be associated with a change in the bonding level of the catalyst metal/oxygen bond which could influence the reactivities of the reactants and also the ease of CO_2 desorption. Thus, the rate-determining step in the lower temperature region would be associated with the adsorption and decomposition of nitrous oxide and, at higher temperatures, the increase in activation energy would be related to a change in mechanism, similar to that observed in the catalytic oxidation of carbon monoxide (6), from an associative to a regenerative scheme. Finally, polymeric surface chromate groups would be expected to influence the decomposition of any carbonate-like intermediate as well as the desorption of carbon dioxide which relates in turn to the availability of vacant sites for nitrous oxide decomposition.

Acknowledgement

The authors are pleased to acknowledge financial assistance from Imperial Oil Enterprises Canada Ltd. (Toronto).

1. M. Shelef. Catal. Rev. Sci. Eng. **11**, 1 (1975).
2. M. Shelef, K. Otto, and H. Gandhi. J. Catal. **12**, 361 (1968).
3. O. V. Krylov. Catalysis by nonmetals. Academic Press, New York and London. 1970. Chapt. 7.
4. T. G. Alkhazov, G. Z. Gasan-Zade, M. O. Osmanov, and M. Yu. Sultanov. Kinet. Catal. **16**, 1061 (1975).
5. G. V. Glazneva, I. S. Sazonova, and N. P. Keier. Dokl. Akad. Nauk SSSR, **213**, 364 (1973).
6. G. K. Boreskov. Kinet. Catal. **14**, 7 (1973).
7. B. W. Krupay and R. A. Ross. Can. J. Chem. In press.
8. B. W. Krupay and R. A. Ross. Can. J. Chem. **56**, 10 (1978).
9. E. F. McCaffrey, D. G. Klissurski, and R. A. Ross. Can. J. Chem. **49**, 3778 (1971).
10. B. W. Krupay and R. A. Ross. J. Catal. **39**, 369 (1975).
11. C. N. Satterfield. Mass transfer in heterogeneous catalysis. M.I.T. Press. 1970.
12. P. Weisz and C. D. Prater. Adv. Catal. **3**, 143 (1951).
13. F. Trifiro and I. Pasquon. J. Catal. **12**, 412 (1968).
14. G. Eval'd, V. S. Muzykantov, and G. K. Boreskov. Kinet. Catal. **14**, 540 (1973).
15. A. Zecchina, S. Coluccia, E. Guglielminotti, and G. Ghiotti. J. Phys. Chem. **75**, 2274 (1971).

16. R. M. DELL, F. S. STONE, and P. F. TILEY. Trans. Faraday Soc. **49**, 201 (1953).
17. Y. Y. YAO. J. Catal. **28**, 139 (1973).
18. S. R. MORRISON. J. Catal. **47**, 69 (1977).
19. K. H. YANG and O. A. HOUGEN. Chem. Eng. Prog. **46**, 146 (1950).
20. O. A. HOUGEN and K. M. WATSON. Chemical process principles. Part III. Wiley, New York and London. 1966.
21. M. BOUDART. A.I. Ch.E. J. **2**, 62 (1956).
22. S. W. WELLER. Chemical reaction engineering reviews. *Edited by* H. M. Hulbert. Am. Chem. Soc., Washington, DC. 1975. p. 26.
23. L. BERÁNEK. Catal. Rev. Sci. Eng. **16**, 1 (1977).
24. F. S. STONE. Adv. Catal. **13**, 1 (1962).
25. E. R. S. WINTER. J. Catal. **19**, 32 (1970).
26. A. ZECCHINA, S. COLUCCIA, E. GUGLIELMINOTTI, and G. GHIOTTI. J. Phys. Chem. **75**, 2790 (1971).
27. A. CLARK. The theory of adsorption and catalysis. Academic Press, New York and London. 1970.
28. B. W. KRUPAY and R. A. ROSS. Unpublished work.
29. B. HALPERN and J. E. GERMAIN. J. Catal. **37**, 44 (1975).
30. V. S. MUZYKANTOV, G. E. WALD, and G. VON LEWIS. Kinet. Catal. **15**, 1335 (1974).
31. A. ZECCHINA, S. COLUCCIA, L. CERRUTI, and N. BORRELLO. J. Phys. Chem. **75**, 2783 (1971).

Passage des phosphorinènes aux hexadiényl-3,5-phosphines: un nouveau type de coordinat P(III)-diène pour les métaux de transition

FRANÇOIS MATHEY ET CATHERINE SANTINI

Equipe IRCHA-CNRS, 2-8 rue Henry Dunant, BP no 28, 94320 Thiais, France

Reçu le 19 juillet 1978

FRANÇOIS MATHEY et CATHERINE SANTINI. Can. J. Chem. **57**, 723 (1979).

La réaction du tertiobutyllithium sur la phényl-1-phosphorinanone-4 fournit un mélange d'alcools isomères qui sont partiellement séparés sous forme de sulfures. Ce mélange est déshydraté par P_4S_{10} pour fournir le sulfure de phényl-1-tertiobutyl-4-phosphorinène-3. Ce sulfure donne avec le nickélocène et l'iodure d'allyle un complexe P(III) → Ni(II) qui réagit avec $P(OMe)_3$ pour donner un sel de méthyl-phényl-phosphorinènium. Ce sel conduit par action du butyllithium et de la cyclohexanone à un produit à chaîne ouverte, l'oxyde d'hexadiényl-3,5-phosphine correspondant. Cet oxyde est réduit par $HSiCl_3$ et la phosphine obtenue est caractérisée sous forme de complexe avec $Fe(CO)_4$. Le sulfure de phosphorinène est métallé sur C(2) par le butyllithium dans le THF. Le dérivé lithié réagit avec l'acétone pour donner un mélange d'alcools "*cis*" et "*trans*" séparés et pleinement caractérisés. Des variations significatives des couplages ^2J(H–P), ^3J(H–P) et des fréquences ir ν(OH), ν(P═S) sont observées entre les deux isomères. Le mélange d'alcools "*cis*"–"*trans*" est déshydraté pour fournir un diène endo-exocyclique qui ne s'isomérise pas par réaction avec $Fe_3(CO)_{12}$. En fait, on observe une réduction-complexation du groupement P═S. Le lithio-2-phosphorinène réagit aussi avec l'iode pour donner un dimère ponté.

FRANÇOIS MATHEY and CATHERINE SANTINI. Can. J. Chem. **57**, 723 (1979).

The reaction of tertbutyllithium with 1-phenylphosphorinan-4-one yields a mixture of isomeric alcohols which are partly separated as their P-sulfides. This mixture is dehydrated by P_4S_{10} to afford 1-phenyl-4-tertbutylphosphorin-3-ene sulfide. This sulfide with nickelocene and allyl iodide gives a P(III) → Ni(II) complex which reacts with $P(OMe)_3$ to yield a methylphenylphosphorinenium salt. This salt with BuLi and cyclohexanone gives the corresponding open chain product, i.e. a hexa-3,5-dienylphosphine oxide. This oxide is reduced by $HSiCl_3$ to the corresponding phosphine which is characterized as its P → $Fe(CO)_4$ complex. The phosphorinene sulfide is metalated on C(2) by *n*-butyllithium in THF. The lithium derivative with acetone yields a mixture of '*cis*' and '*trans*' alcohols which are separated and fully characterized. Significant variations of ^2J(H–P), ^3J(H–P) coupling constants and ν(OH), ν(P═S) ir frequencies are observed between the two isomers. The mixture of '*cis*' and '*trans*' alcohols is dehydrated to give a endo-exocyclic diene which is not isomerized when reacted with $Fe_3(CO)_{12}$. A reduction-complexation of the P═S group is observed instead. The 2-lithiophosphorinene is also reacted with iodine to afford a bridged dimer.

Introduction

Les diènes conjugués comme les dérivés du phosphore trivalent font partie des quelques coordinats fondamentaux utilisés dans la chimie des métaux de transition. Cette constatation suffirait à expliquer l'intérêt que nous portons aux systèmes du type

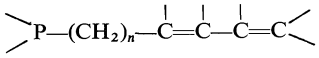

Avec un choix convenable de la valeur de *n*, ce genre de coordinat peut acquérir des propriétés chélatantes ou, du moins favoriser la création de liaisons métal–métal car le phosphore peut devenir suffisamment proche spatialement du système diénique. On peut alors espérer obtenir des complexes du type I dans lequel M désigne un centre mono- ou polymétallique:

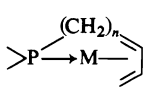

(I)

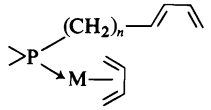

(II)

Des complexes d'un type apparenté ont d'ailleurs été décrits dans des cas particuliers (1, 2).

En présence d'un autre diène en excès, (I) pourrait évoluer pour donner réversiblement des complexes du type (II). Voir par exemple à ce sujet, les travaux de Caïs (3) sur les équilibres diène libre – diène complexé par $Fe(CO)_3$. Notons simplement que l'effet stabilisant de la chélation sur la liaison métal–diène dans (I) peut défavoriser la formation de (II). On conçoit néanmoins tout l'intérêt de tels systèmes pour catalyser certaines transformations des composés diéniques. L'étude des modèles de Dreiding mon-

0008-4042/79/070723-06$01.00/0

tre que l'obtention de complexes tels que (I) ne peut se produire que si $n \geq 2$. Dans le cas des hexadiényl-3,5-phosphines ($n = 2$) il faut en outre que le substituant $-(CH_2)_2PR_2$ et la double liaison $C_5{=}C_6$ soient en position "*cis*" (structure III) par rapport à la double liaison $C_3{=}C_4$ et non en position "*trans*" (structure IV).

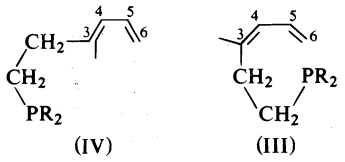

(dans III et IV les échelles ne sont pas respectées). Nous avons donc entrepris l'étude de quelques voies possibles d'accès aux hexadiényl-3,5-phosphines de structure "*cis*". Ce mémoire décrit nos premiers travaux synthétiques effectués dans cette optique.

Accès aux hexadiényl-3,5-phosphines

Pour respecter les conditions structurales imposées, nous avons fondé notre approche sur les travaux de Lednicer (4) qui a montré que les sels de phosphorinénium-3 possédant un substituant arylique R^1 en position 4 réagissaient sur les dérivés carbonylés en présence de base pour fournir des oxydes d'hexadiényl-3,5-phosphines dont la disposition "*cis*" était imposée par la nature cyclique du produit de départ:

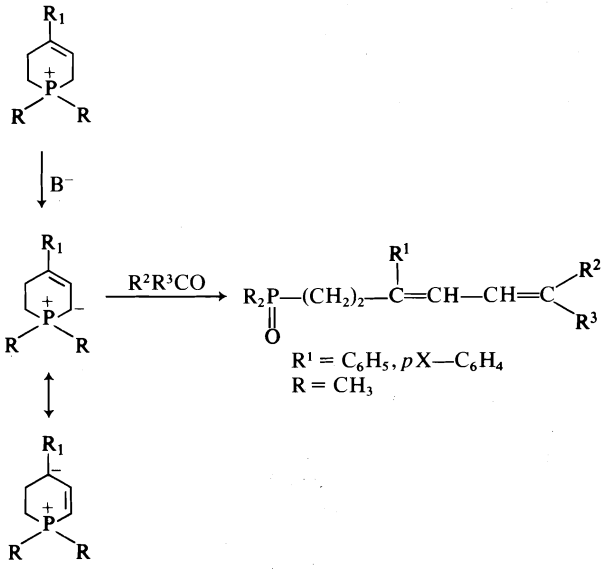

Le choix d'un substituant R^1 arylique est essentiel car, comme il se conjugue avec la double liaison du cycle, il facilite la synthèse du sel de phosphorinénium et permet un déroulement normal de la condensation de Wittig en diminuant le poids statistique de la forme mésomère de l'ylure. Cependant, nous nous sommes refusés à un tel choix car nous ne voulions pas désactiver le diène par des substituants électroattracteurs ni introduire des possibilités de coordination parasite faisant intervenir les doubles liaisons et le cycle benzénique de R^1. Pour éviter néanmoins une attaque du dérivé carbonylé sur la position 4 de l'ylure, nous avons choisi un substituant R^1 encombrant, le tertiobutyle. Ce choix nous a obligé en fait, à modifier de fond en comble le schéma réactionnel décrit par Lednicer. La séquence finalement retenue est décrite dans la fig. 1.

Nous avons fait réagir la phényl-1-phosphorinanone-4 (5) sur le tertiobutyllithium. Comme Quin dans un cas analogue (6), nous avons obtenu deux alcools isomères **1** + **2** avec un rendement quasi quantitatif.

Les deux isomères n'ont pas été séparés mais leur existence se manifeste par la présence de deux signaux *t*-Bu en rmn du proton situés respectivement à 0.75 et 0.95 ppm dans le rapport approximatif 2:1 ($CDCl_3$, TMS). On notera que la différence de déplacement chimique des protons des tertiobutyles est nettement plus importante dans ces alcools

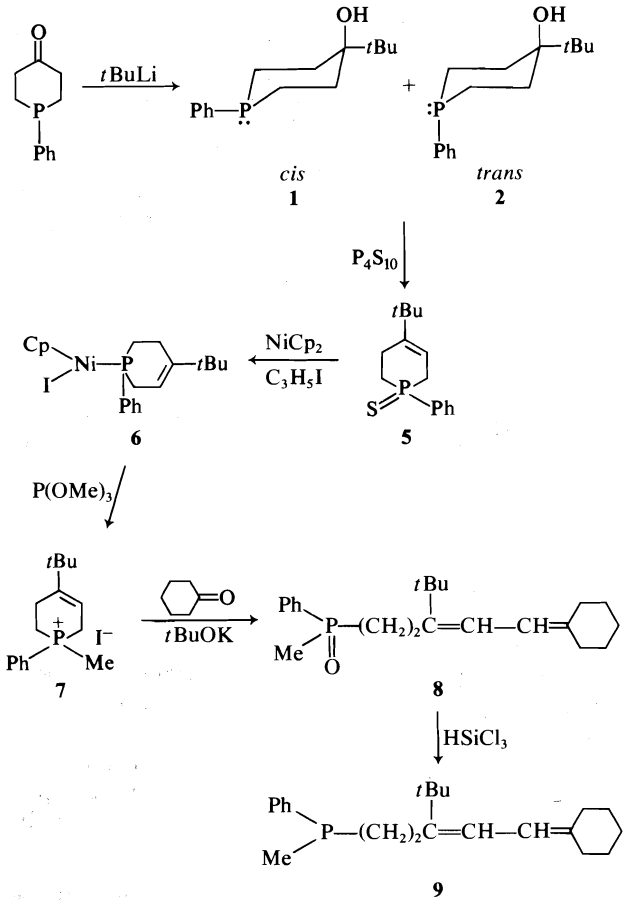

FIG. 1. La séquence finalement retenue.

P-phénylés que dans leurs homologues P-méthylés préparés par Quin. Après sulfuration dans le toluène à chaud, nous avons pu, par contre, séparer partiellement les isomères par chromatographie sur gel de silice (éluant: pentane–éther 1:3). Le produit passant en tête a été isolé à l'état pur et complètement caractérisé notamment par rmn ^1H, ^{13}C et ^{31}P.

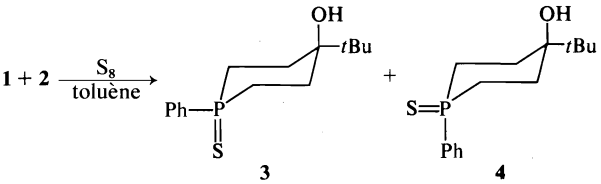

Nous lui attribuons la structure "*cis*" **3** (par rapport aux substituants phényle et hydroxy) par analogie avec les travaux de Quin sur des sulfures analogues (7) parce que son signal phosphore ($CDCl_3$, H_3PO_4 85%, δ positif à champ faible) est plus déblindé que celui du deuxième isomère auquel nous attribuons la structure "*trans*" **4** mais que nous n'avons pu isoler à l'état pur: $\delta^{31}P$ (**3**) = 34.4 ppm; $\delta^{31}P$ (**4**) = 31 ppm.

Pour déshydrater le mélange d'alcools **1** et **2**, nous avions à notre disposition trois techniques décrites dans la littérature. La première utilise l'acide chlorhydrique concentré dans le xylène au reflux (8), la deuxième l'acide *para*-toluènesulfonique dans les mêmes conditions (4) et la troisième l'alumine vers 400°C en phase vapeur (9). Les deux premières techniques ne nous ont donné aucun résultat; pour des raisons non éclaircies cette déshydratation s'avère en fait très difficile à effectuer. La troisième technique nécessite l'utilisation de quantités importantes d'alcool; nous n'avons pu l'employer malgré un essai préliminaire encourageant. Nous avons donc dû développer un nouveau procédé de déshydratation utilisant le pentasulfure de phosphore dans le toluène à reflux pendant 2 h. Evidemment, il n'est pas question dans ces conditions, de respecter la trivalence du phosphore et nous obtenons finalement le sulfure de phosphorinène-3 **5** avec un rendement de 45% (nous assurons la conversion complète du P(III) en P(IV)=S en ajoutant un peu de soufre dans le milieu réactionnel). Le spectre ir de **5** (KBr) comprend une bande d'absorption C=C faible à 1640 cm^{-1} et une bande P=S forte à 585 cm^{-1}. Le spectre rmn ^1H montre un singulet à 1.14 ppm correspondant au *t*Bu et un doublet de triplet correspondant au CH éthylénique centré à 5.91 ppm ^3J(H–H) = 6 Hz; ^3J(H–P) = 25.3 Hz. Le pic de résonance du phosphore apparaît à 31.9 ppm.

Pour convertir ce sulfure **5** en sel de phosphorinénium, la solution évidente consistait à le réduire en phosphine puis à quaternariser cette phosphine. Pour éviter toute migration ou destruction de la double liaison, nous avons préféré utiliser la technique très douce de la réduction-complexation des sulfures de phosphines par le nickelocène en présence d'iodure d'allyle (10). La réaction est conduite dans le benzène à 40°C, pendant 3 h. Le complexe **6** obtenu avec un rendement de 85% se présente sous la forme d'une huile rouge caractérisée par analyse élémentaire C, H, Ni et par rmn du proton ($CDCl_3$). Les résonances des protons du tertiobutyle et du cyclopentadiènyle apparaissent sous la forme de singulets fins respectivement à 0.99 et 5.27 ppm. Après découplage des CH_2, le proton éthylénique donne un doublet situé à 5.56 ppm (^3J(H–P) = 17.2 Hz). Enfin, après découplage du CH éthylénique, le CH_2P allylique se présente sous la forme d'un pseudo-doublet élargi à 3.03 ppm (^2J(H–P) = 9 Hz). Le complexe **6** a ensuite été détruit par le triméthylphosphite en excès pour donner directement l'iodure de phényl-1-méthyl-1-phosphorinénium correspondant: **7** avec un rendement de 83%. L'iodure de méthyle nécessaire à la quaternarisation provient de l'attaque par $P(OMe)_3$ du motif Ni—I du complexe intermédiaire $(C_5H_5)Ni(I)[P(OMe)_3]$ suivant un schéma qui rappelle celui de la réaction d'Arbuzov: voir réf. 11. Le spectre rmn de **7** ($CDCl_3$, TMS externe) comprend le pic de résonance des protons du tertiobutyle à 1.03 ppm, un doublet dû à CH_3P à 2.52 ppm (^2J(H–P) = 14 Hz) et un doublet de triplet centré à 5.64 ppm (^3J(H–P) = 22 Hz; ^3J(H–H) = 5 Hz) correspondant à la résonance du proton éthylénique.

L'iodure **7** réagit sur la cyclohexanone dans le THF en présence de *t*BuOK suivant la technique de Lednicer pour fournir l'oxyde diénique attendu **8** (rendement 61%). Son spectre de rmn ($CDCl_3$, TMS interne) montre un premier singulet à 1.03 ppm dû aux protons du tertiobutyle, un singulet élargi à 1.53 dû aux trois CH_2 cyclohexaniques non liés à la double liaison, un doublet dû au CH_3P à 1.72 ppm (^2J(H–P) = 12.8 Hz) et un système AB à 5.57 et 6.08 ppm ^3J(H–H) = 11.4 Hz dû aux deux protons éthyléniques. Le pic de résonance du phosphore apparaît à 37.2 ppm. Le spectre de masse (70 eV, 90°C) comprend le pic moléculaire de *m/e* 344. Enfin on observe dans le spectre ir (KBr) une bande moyenne d'absorption à 1600 cm^{-1}: ν(C=C) et une bande intense à 1180 cm^{-1}: ν(P=O).

La réduction de cet oxyde **8** par $HSiCl_3$ conduit à la phosphine correspondante **9** avec un rendement de 52% en produit distillé. Nous n'observons aucune hydrogénation détectable du système diénique contrairement à ce qui est constaté avec les oxydes de butadiénylphosphines (12).

Le spectre rmn de **9** est très semblable à celui de **8**. La principale différence est visible au niveau du

CH_3P qui se présente sous la forme d'un doublet à 1.31 ppm (^2J(H–P) = 2 Hz). Le phosphore apparaît à −33.5 ppm. L'unicité du signal phosphore suggère qu'il n'y a pas hydrogénation partielle du système diènique. Pour parfaire la caractérisation de **9**, nous avons préparé son complexe avec le fer-tétracarbonyle **10** par réaction avec $Fe(CO)_4(THF)$ (13):

9 + $Fe(CO)_4(THF)$

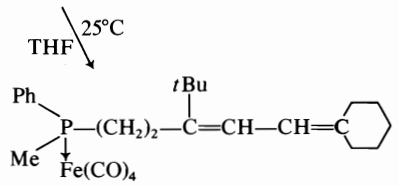

Rdt ~ 72%

10

La complexation se traduit par un déblindage très important du phosphore: $\delta^{31}P$ (**10**) = 51.3 ppm. Le spectre rmn ^1H ($CDCl_3$, TMS externe) ressemble beaucoup à celui de l'oxyde **8**: le tertiobutyle apparaît à 1.10 ppm, les CH_2 cyclohexaniques à 1.61 ppm, le doublet CH_3P à 1.95 ppm (^2J(H–P) = 9.9 Hz) et les protons éthyléniques à 5.73 et 6.17 ppm (^3J(H–H) = 11.4 Hz). A l'évidence donc le système diénique ne participe pas à la complexation du fer. Le spectre ir (cyclohexane) comprend 4 bandes d'absorption dûes aux CO à 2047, 1974, 1937 et 1933 cm^{-1}. Enfin le spectre de masse (70 eV, 80°C) comprend le pic moléculaire de *m/e* 496 et les différents pics correspondant à la perte des 4 CO, ce qui établit définitivement la formule.

Essais parallèles

A partir du sulfure **5**, nous avons également essayé de synthétiser le système diénique recherché à l'aide d'une réaction de Horner. Nous avons donc métallé **5** par le butyllithium dans le THF à −70°C puis condensé le dérivé métallé obtenu avec l'acétone. La condensation s'effectue uniquement sur la position 2 et conduit au mélange d'alcools diastéréoisomères: **11** + **12**:

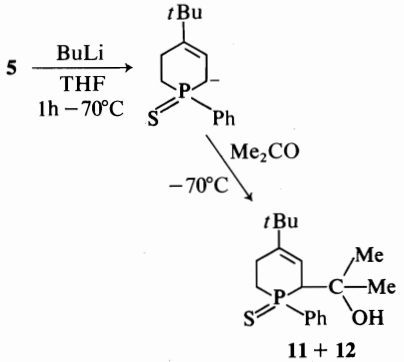

Rdt global 53%

11 + **12**

Les deux diastéréoisomères ont pu être séparés sur colonne de gel de silice. Ils sont présents en quantités sensiblement équivalentes. Les données rmn du proton sont les suivantes: **11**: δ = 1.13 (s, *t*Bu); 1.27 (s, Me); 1.35 (s, Me); 3.08 (dd, ^2J(H–P) 10.7, ^3J(H–H) 4.2, C_2*H); 4.58 (s, OH); 5.84 (dd, ^3J(H–P) 20.6, =CH) ppm. **12**: δ = 0.91 (s, Me); 1.19 (s, *t*Bu); 1.27 (s, Me); 3.11 (dd, ^2J(H–P) 20.5, ^3J(H–H) 4.5, C_2*H); 3.75 (s, OH); 5.62 (dd, ^3J(H–P) 9.7, =CH) ppm.

Lorsqu'on compare les données rmn de **11** et de **12**, on constate une forte variation des couplages ^2J(H–P) et ^3J(H–P) alors que le couplage ^3J(H–H) reste sensiblement constant. Compte tenu des données de la littérature (14) nous attribuons la structure "*cis*" (fonction carbinol en "*cis*" du P=S) à l'isomère possèdant le plus petit couplage ^2J(H–P) et le plus grand couplage ^3J(H–P) c'est à dire **11**.

Les spectres ir de **11** et **12** viennent à l'appui de cette interprétation: **11**: ν(OH) = 3400 cm^{-1} (pastille KBr ou solution CCl_4 à 2 concentrations); ν(P=S) = 596 cm^{-1}. **12**: ν(OH) = 3370 cm^{-1} (pastille KBr), 3410 cm^{-1} (solution CCl_4 à 2 concentrations); ν(P=S) = 638 cm^{-1}.

Dans **11**, l'abaissement de la fréquence de vibration ν(P=S) et la valeur constante de la fréquence de vibration ν(OH) en fonction de la concentration suggère la présence d'une liaison intramoléculaire OH...S=P.

La non sélectivité de la métallation permet de penser que le lithium n'est pas chélaté par le soufre dans l'organométallique intermédiaire.

Soumis à l'action de NaH à chaud, dans la diméthylformamide, **11** ne nous a pas fourni le produit diénique attendu:

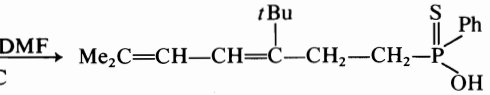

Nous avons donc abandonné cette voie. Auparavant, nous avons toutefois tenté la conversion de **5** en dihydrophosphorine en mettant à profit sa métallation aisée. Les dihydrophosphorines sont en effet des précurseurs des phosphorines elles-mêmes (15). Nous avons donc fait réagir l'anion dérivé de **5** sur l'iode. L'analyse C, H et la spectrométrie de masse (70 eV, 160°C: *m/e* 526, M, 30%; *m/e* 263, M/2, 100%) indiquent clairement que nous avons en fait obtenu le produit de pontage **13** et non le dérivé iodé dont la déshydrohalogénation nous aurait permis de préparer une dihydrophosphorine:

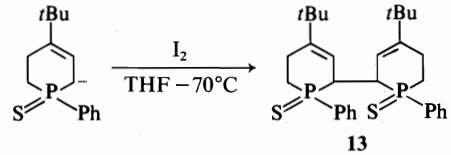

13

Nous avons effectué une deuxième approche plus indirecte. Par chauffage dans le toluène avec de l'acide paratoluène-sulfonique, les alcools **11** ou **12** se déshydratent sans difficulté:

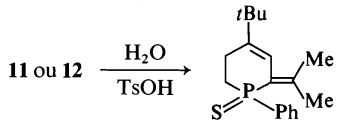

14

Le système diénique de **11**, compte tenu de sa géométrie, ne peut donner le complexe π avec $Fe(CO)_3$. Par contre, la dihydrophosphorine qui dérive de **14** par isomérisation peut fournir un tel complexe. Nous avons donc pensé que **11**, chauffé en présence de $Fe_3(CO)_{12}$, conduirait au complexe de cette dihydrophosphorine. En fait, nous avons observé non une isomérisation mais une simple réduction-complexation du P=S conduisant au complexe P → $Fe(CO)_4$ **15** selon un schéma déjà observé avec des sulfures de phosphines plus classiques (16):

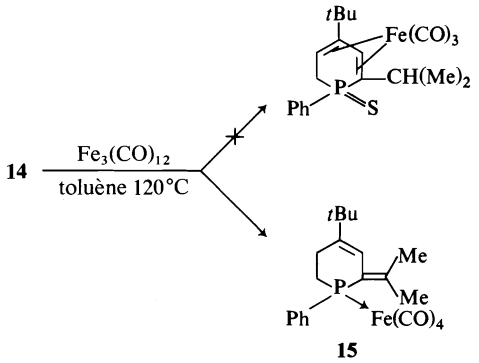

15

Conclusion

La préparation des hexadiènyl-3,5-phosphines de structure *cis* à partir des sels de phosphorinénium s'avère être un schéma viable. Cependant, pour exploiter pleinement cette voie, il nous faudra auparavant simplifier l'accès aux cycles phosphorinènes. A cette condition, nous pourrons probablement développer une intéressante chimie des complexes de métaux de transition avec ce type de coordinats.

Partie expérimentale

Toutes les réactions sont effectuées sous courant d'argon. Les points de fusion ont été déterminés au banc Kofler. Les spectres ir ont été enregistrés à l'aide d'un spectrophotomètre Perkin-Elmer 457 en pastille KBr, la position des bandes d'absorption est exprimée en cm^{-1}. Les spectres de masse ont été mesurés à l'aide d'un appareil MS 30 (AEI). Les analyses élémentaires ont été effectuées au service de Microanalyse de l'IRCHA (Vert le Petit). Les spectres de rmn (dans le deutério chloroforme) ont été enregistrés pour le proton sur appareils Perkin-Elmer R12 et R24 à 60 MHz et JEOL PS 100 FT à 100 MHz; pour le phosphore et le carbone sur JEOL PS 100 FT à respectivement 36.447 MHz et 22.63 MHz. Les déplacements chimiques sont comptés positivement à champ faible des références (TMS pour ^1H et ^{13}C, H_3PO_4 (85%, en capillaire) pour ^{31}P). Les chromatographies sont effectuées sur colonne de gel de silice (70–230 mesh).

La phényl-1-phosphorinanone-4 a été synthétisée comme décrit dans la littérature (5).

*Phényl-1-terbutyl-4-phosphorinanol-4 (**1** + **2**)*

A une suspension de 2.40 g (1.25×10^{-2} mol) de phényl-1-phosphorinanone-4 dans 50 cm^3 d'éther éthylique, refroidie à environ −50°C, sont ajoutés 20 cm^3 d'une solution 0.66 molaire de tertiobutyllithium. En fin d'addition, le milieu réactionnel est porté au reflux de l'éther pendant 3 h. Après hydrolyse acide, puis décantation, la phase organique est séchée sur Na_2SO_4 puis distillée, conduisant à 1.6 g (52%) du mélange d'isomères **1** + **2** (le rendement du produit brut est quantitatif) [Eb 130–135°C, *p*: 0.4 mm Hg] − *F* = 90°C. Analyse trouvé pour $C_{15}H_{23}OP$: C 71.68, H 9.27; calc.: C 71.97, H 9.26. ir: ν(OH) à 3400 cm^{-1}.

*Sulfure de phényl-1-terbutyl-4-phosphorinanol-4 (**3** + **4**)*

Dans 20 cm^3 de benzène, 1.4 g du mélange d'isomères (**1** + **2**) (cette étape peut être réalisée sur l'alcool (**1** + **2**) brut) et 1.5 g de soufre sont chauffés à reflux du solvant pendant 2 h. Le rendement est quantitatif. Par chromatographie sur colonne (silice 100 g, éluant éther éthylique 3 volumes; pentane 1 volume, fractions 20 cm^3) seuls 70 mg de l'isomère **3** ont pu être obtenus purs (fractions 15, 16, 17), les autres fractions étant des mélanges de **3** et **4** (*F*: 164°C (isomère pur)). Analyse trouvé pour $C_{15}H_{23}OPS$: C 63.78, H 8.14; calc.: C 63.82, H 8.15. ir ν(OH): 3430 F ν(P=S): 585 F. rmn: **3**: 1.08 [s, *t*Bu]; 1.55 [s, OH]; **4**: 0.9 [s, *t*Bu]; 1.82 [s, OH]. ^{13}C (isomère pur) δ_{COH}: 74.5 δ_{PCH_2}: 27.2 $^1J_{PC}$: 43.4 Hz $\delta C_{3,5}$: 26.2 ppm.

*Sulfure de phényl-1-terbutyl-4-phosphorinène-3 (**5**)*

Une suspension de 4.62 g (1.85×10^{-2} mol) de {**1** + **2**}, 13 g (2.9×10^{-2} mol) de pentasulfure de phosphore et 1 g (3.1×10^{-2} mol) de soufre dans 100 cm^3 de toluène est chauffée au reflux du solvant 3 h. Après filtration de l'excès de P_4S_{10}, le milieu réactionnel est agité vigoureusement (agitation mécanique) pendant 1 h avec une solution saturée en $NaHCO_3$. Après décantation, la phase organique est séchée sur Na_2SO_4, concentrée puis chromatographiée (silice 150 g, éluant: éther éthylique 1 volume, pentane 3 volumes) conduisant à 2.2 g (ρ = 45%) du produit attendu: ce rendement optimal a été obtenu pour des quantités de l'ordre de 4 g en alcool (**1** + **2**); pour des quantités supérieures (7 → 15 g) il a toujours été inférieur [≃30%]. F: 60°C. Analyse trouvé pour $C_{15}H_{21}PS$: C 68.28, H 8.05; calc.: C 68.15, H 7.95.

*Iodure de η⁵-cyclopentadiényl[phényl-1-terbutyl-4-phosphorinène-3] nickel(II) (**6**)*

Une solution de 1.6 g (6×10^{-3} mol) de **5**, 3.4 g de nickelocène (1.8×10^{-2} mol) et 0.85 cm^3 d'iodure d'allyle dans 100 cm^3 de benzène est chauffée à 40°C pendant 3 h. Après filtration de l'insoluble noir puis concentration, le résidu est chromatographié sur colonne de gel de silice (40 g éluant benzène). Passent en tête des impuretés organiques, puis le complexe dont la progression est aisément suivie grâce à sa coloration rouge sombre. Cette chromatographie est réalisée sous argon. Après évaporation du solvant 2.2 g (ρ: 85%) de complexe sont isolés. Analyse trouve: C 49.95, H 5.50, Ni 12.0; calc.: C 49.73, H 5.42, Ni 12.15.

*Iodure de phényl-1-méthyl-1-terbutyl-4-phosphorinen-3-ium (**7**)*

A une solution de 0.7 g (1.45×10^{-3} mol) de complexe **6** dans 50 cm^3 de benzène sont ajoutés, sous argon et avec une forte agitation, 0.6 g (4.85×10^{-3} mol) de triméthylphosphite. La solution est *agitée* 24 h à la température ambiante dans un

Erlenmeyer hermétiquement bouché. Les cristaux obtenus sont filtrés et lavés à l'éther −0.46 g (ρ: 83%) du sel de phosphonium sont obtenus. F: 153°C. Analyse trouvé pour $C_{16}H_{24}IP$: C 50.66, H 6.42; calc.: C 51.53, H 6.41. ir ν(C=C) 1635 et 1580 cm^{-1}.

*Oxyde de méthyl, phényl, (cyclohexylydène-5-terbutyl-3) pentèn-3-yl-phosphine (**8**)*

Un mélange de 1.6 g (4.27×10^{-3} mol) de **7**, 1 g de terbutylate de potassium et 1 cm^3 de cyclohexanone est chauffé à reflux du tétrahydrofuranne (fraîchement distillé sur Na/ϕ_2CO) pendant 20 h. Après évaporation du solvant le résidu marron est repris avec 100 cm^3 d'eau acidulée et 100 cm^3 de chlorure de méthylène. La phase organique après lavage à l'eau jusqu'à pH neutre, est séchée puis concentrée. Le résidu est chromatographié (45 g de silice éluant acétate d'éthyle 95 alcool méthylique 5) conduisant à 0.9 g (61%) de l'oxyde attendu. F: 92°C. Analyse trouvé pour $C_{22}H_{33}OP$: C 75.69, H 9.09; calc.: C 76.7, H 9.65. ir ν(C=C): 1590, 1600 ep, m. ν(P=O) = 1180 F.

*Méthyl, phényl, (cyclohexylydène-5-terbutyl-3) pentèn-3-yl-phosphine (**9**)*

0.4 g (1.16×10^{-3} mol) de **8** et 1 cm^3 de trichlorosilane dans 50 cm^3 de toluène sont chauffés à 120°C pendant 2 à 3 h. Après évaporation du toluène et de l'excès de $HSiCl_3$, le résidu est lavé au benzène puis avec une solution désoxygénée de carbonate de sodium afin d'éliminer les traces résiduelles de $HSiCl_3$. Après décantation, la phase organique est séchée puis concentrée; 0.2 g (53%) de phosphine sont obtenus après distillation à 160°C (p = 0.2 mm de Hg) dans un four tubulaire GKR.50 Bucchi.

*[Méthyl, phényl, (cyclohexylydène-5-terbutyl-3) pentèn-3-yl phosphine] tétracarbonyl fer (0) (**10**)*

Sous atmosphère d'oxyde de carbone, 0.6 g (1.65×10^{-3} mol) de fer nonacarbonyle et de phosphine brute **9** dans 80 cm^3 de tétrahydrofuranne (fraîchement distillé sur Na/ϕ_2CO) sont agités 3 h à 25°C. La solution orangée obtenue est concentrée puis chromatographiée (silice 40 g éluant hexane 90 benzène 10). 0.62 g (ρ = 72% par rapport à l'oxyde de phosphine **8**) du complexe 1:1 sont ainsi obtenus (huile jaune) spectre de masse (80°C, 70 eV) M 496, (M—CO) 468 et (M—2CO): 440. ir: ν(CO): 2047 F, 1971 F, 1930 TF.L, ν(C=C) 1600 f large rmn: 1.95 [d, ^2J(H–P): 9.9 Hz, Me] δ_A: 5.73, δ_B: 6.17 (système AB, =CH).

*Sulfure de phényl-1 (α-hydroxyisopropyl)-2-tertbutyl-4-phosphorinène-3 (**11** et **12**)*

A une solution (1.25 g, 4.73×10^{-3} mol) de **5** dans 50 cm^3 de tétrahydrofuranne (fraîchement distillé sur Na/ϕ_2CO)), refroidie à −78°C, sont ajoutés 3 cm^3 d'une solution hexanique de butyllithium (N = 1.75). La réaction de métallation se caractérisant par une coloration orange foncé du milieu, est spontanée. Cependant, le milieu réactionnel est lentement réchauffé à la température ambiante puis agité à cette température 30 min. Le milieu est, de nouveau refroidi à −78°C et 1 cm^3 d'acétone (fraîchement distillée sur P_2O_5) est ajouté, entraînant une décoloration quasi-spontanée du milieu. Après réchauffement à la température ambiante, le solvant est évaporé, le résidu repris avec 50 cm^3 d'eau acidulée puis 100 cm^3 de chlorure de méthylène. La phase organique, après lavage avec 3 × 20 cm^3 d'eau, est décantée, séchée sur Na_2SO_4 puis concentrée. Par chromatographie sur colonne (50 g silice éluant éther éthylique 1 volume: pentane 3 volumes), on obtient d'abord **11** (0.4 g), puis le mélange **11** + **12** (0.2 g), puis **12** (0.2 g), soit un rendement global de 53%, alors que 0.4 g de **5** sont recouvrés. F: **11**: 82°C; **12**: 118°C. Analyse (sur **11**) trouvé pour $C_{18}H_{27}OPS$: C 66.89, H 8.63; calc.: C 67.08, H 8.44. rmn: $\delta^{31}P$ (**11**) 33.56; $\delta^{31}P$ (**12**) 35.74/H_3PO_4).

*Bis[thio-1-phényl-1-terbutyl-4-phosphorinèn-3-yl-2] (**13**)*

La réaction de métallation est réalisée comme ci-dessus avec 2.2 g (8.3×10^{-3} mol) de **5** et 6 cm^3 d'une solution héxanique de butyllithium (2 N). Puis 2.5 g (9.8×10^{-3} mol) d'iode dans 20 cm^3 de tétrahydrofuranne sont ajoutés au milieu réactionnel qui est ensuite lentement réchauffé à la température ambiante. Après 1 h 30 min d'agitation, le milieu réactionnel est lavé avec une solution de bisulfite de sodium. Après évaporation du solvant, le résidu est repris au chlorure de méthylène (50 cm^3) et à l'eau (20 cm^3). La phase organique (après décantation) est séchée sur Na_2SO_4, concentrée puis chromatographiée (100 g silice, éluant: éther éthylique 1 volume, pentane 3 volumes). 0.43 g (20%) du produit ponté sont ainsi obtenus. F 210°C. Analyse trouvé pour $C_{30}H_{40}P_2S_2$: C 68.62, H 7.65; calc.: C 68.41, H 7.65. ir ν(C=C) 1635f, 1580, et 1560f ν(P=S) 600 cm^{-1}. rmn: δ = 6 ppm (dd, ^3J(H–P): 22 Hz, =CH).

*Sulfure de phényl-1-méthyléthylydène-2-terbutyl-4-phosphorinène-3 (**14**)*

En présence d'une quantité catalytique d'acide p-toluène sulfonique 0.25 g de **11** ou **12** sont chauffés à reflux du toluène pendant 2 h. Après évaporation du solvant, le résidu est chromatographié (40 g de silice éluant éther éthylique 1 volume, pentane 3 volumes) conduisant à 0.2 g (85%) du produit déshydraté F = 88°C. Analyse trouvé pour $C_{18}H_{25}SP$: C 70.61, H 8.29; calc.: C 71.07, H 8.27. ir ν(C=C): 1635f, 1575m large. rmn: 1.13 (s, tBu); 1.8 (d, ^5J(H–P): 1.5 Hz, Me); 1.93 (d, ^5J(H–P) = 1.5 Hz, Me); 6.45 (d, ^3J(H–P) = 24.3 Hz, =CH).

*[Phényl-1-méthyléthylydène-2-terbutyl-4-phosphorinène-3] tétracarbonyl fer (0) (**15**)*

0.2 g (0.65×10^{-3} mol) de **14** et 0.5 g (1×10^{-3} mol) de fer dodécacarbonyle dans 50 cm^3 de toluène sont chauffés à reflux du solvant pendant 2 h. Après filtration d'un précipité noir, la solution orangée obtenue est concentrée puis chromatographiée (silice 40 g éluant hexane 90 benzène 10) 0.240 g (ρ = 82%) du complexe sont isolés. ir (décaline) ν(CO): 2020F, 1955F, 1920FL (KBr) ν(C=C): 1570F. rmn: 1.1 (s, tBu); 1.66 (s, Me); 1.96 (s, Me); 6.29 [d, ^3J(H–P) = 20 Hz, =CH] $\delta^{31}P$: 41.34/H_3PO_4, spectre de masse [70°C, 70 eV]: m/e 440 (M); 412 (M—CO); 384 (M—2CO); 356 (M—3CO); 328 (M—4CO); pic de base à 257.

1. M. A. Bennett, R. N. Johnson et I. B. Tomkins. J. Am. Chem. Soc. **96**, 61 (1974).
2. W. Winter. Angew. Chem. **88**, 260 (1976).
3. M. Cais et N. Maoz. J. Chem. Soc. A, 1811 (1971).
4. D. Lednicer. J. Org. Chem. **35**, 2307 (1970).
5. R. P. Welcher, G. A. Johnson et V. P. Wystrach. J. Am. Chem. Soc. **82**, 4437 (1960).
6. L. D. Quin et J. H. Somers. J. Org. Chem. **37**, 1217 (1972).
7. S. I. Featherman, S. O. Lee et L. D. Quin. J. Org. Chem. **39**, 2899 (1974).
8. H. E. Shook, Jr. et L. D. Quin. J. Am. Chem. Soc. **89**, 1841 (1967).
9. F. Mathey et G. Muller. C. R. Acad. Sci. Paris, **269c**, 158 (1969).
10. F. Mathey. J. Organometal. Chem. **87**, 371 (1975).
11. V. Harder et H. Werner. Helv. Chim. Acta, **56**, 162 (1973).
12. F. Mathey et G. Muller. Can. J. Chem. **56**, 2486 (1978).
13. F. A. Cotton et J. M. Troup. J. Am. Chem. Soc. **96**, 3438 (1974).
14. A. Bond, M. Green et S. C. Pearson. J. Chem. Soc. B, 929 (1968).
15. G. Märkl. Phosphorus Sulfur, **3**, 77 (1977).
16. F. Mathey et G. Muller. J. Organometal. Chem. **136**, 241 (1977).

Molecular orbitals from group orbitals. IX. The problem of hybrid lone pairs

DANIEL KOST
Department of Chemistry, Ben Gurion University of the Negev, 84 120 Beersheva, Israel
H. BERNHARD SCHLEGEL
Department of Chemistry, Carnegie-Mellon University, Pittsburgh, PA 15213, U.S.A.
AND
DAVID JOHN MITCHELL AND SAUL WOLFE
Department of Chemistry, Queen's University, Kingston, Ont., Canada K7L 3N6

Received August 14, 1978

DANIEL KOST, H. BERNHARD SCHLEGEL, DAVID JOHN MITCHELL, and SAUL WOLFE. Can. J. Chem. **57**, 729 (1979).

The quantitative PMO analysis of the *ab initio* wavefunction of a molecule A—B is based upon a partitioning of the Fock matrix elements of this wavefunction to obtain the fragments A and B, followed by computation of the stabilizing and destabilizing orbital interactions between the orbitals of these fragments that contribute to the HOMO of A—B. However, when one or both of the fragments is NH_2 or a congeneric species, neither the $3a_1$ nor the $1b_1$ orbital of this fragment is appropriate for overlap with the second fragment, and the PMO analysis cannot be performed. A solution to this problem is proposed, and has been tested by application to various conformational properties of methylamine.

DANIEL KOST, H. BERNHARD SCHLEGEL, DAVID JOHN MITCHELL et SAUL WOLFE. Can. J. Chem. **57**, 729 (1979).

L'analyse quantitative PMO de la fonction d'onde *ab initio* de la molécule A—B est basée sur une partition des éléments de la matrice de Fock de cette fonction d'onde en vue d'obtenir les fragments A et B suivie par une évaluation des interactions orbitalaires stabilisantes et déstabilisantes entre les orbitales de ces fragments qui contribuent à la OM haute occupée de A—B. Toutefois si l'un ou les deux fragment est NH_2 ou une espèce congénère, ni l'orbitale $3a_1$ ni l'orbitale $1b_1$ de ce fragment n'est appropriée pour un recouvrement avec le deuxième fragment et l'on ne peut pas réaliser une analyse PMO. On propose une solution à ce problème et on l'a vérifié en l'appliquant à diverses propriétés conformationnelles de la méthylamine.
[Traduit par le journal]

The concept of the functional group has long been a part of the language of organic chemistry. In terms of this concept, 'chemical intuition' might be described as the ability to predict the properties of a molecule from a knowledge of the number, location, and different kinds of functional groups that are present.

Molecular orbital calculations also lead to predictions concerning molecular properties, but the notion of functional groups does not emerge naturally from such work. This has made it difficult to convey the results of theory in a manner compatible with chemical intuition.

Significant progress on this communication problem has been made recently, as a result of the observation that molecular orbitals can often be expressed qualitatively as a linear combination of a small number of canonical 'group orbitals' which recur from molecule to molecule (1). Using the language of perturbational molecular orbital (PMO) theory (2) to estimate the stabilizing and/or destabilizing effects associated with these linear combinations (orbital interactions) it has become possible, in principle (3), to treat the behaviour of every molecular orbital of a molecule in a manner that closely parallels the traditional conception of functional group interactions. For practical reasons, however, it has seemed desirable to focus attention upon the interactions that lead to certain specific molecular orbitals. In particular, it is of interest to consider the interactions in the highest occupied molecular orbital (HOMO), because trends in calculated total energies from one system to another are very often parallelled by trends in the energy of the HOMO (4).

The PMO interpretation of a molecular orbital calculation on the general system A—B, which contains the functional groups A and B, will, therefore, require the following information: (*i*) a knowledge of the nature, origin, and energies of the canonical orbitals of A and of B; (*ii*) a knowledge of the electron occupancies of these orbitals; (*iii*) a knowledge of which orbitals of A and of B contribute to the HOMO of A—B.

In several recent publications (5–9), we have de-

0008-4042/79/070729-04$01.00/0

scribed a quantitative PMO analysis of *ab initio* SCF-MO wavefunctions, in which the required information is obtained by a partitioning of the Fock matrix elements of these wavefunctions. The computer program for the analysis of A—B, with the fragmentation A···B, provides the orbitals of A and of B, their energies (e_i^0) and occupancies (i.e., gross populations), the interaction matrix elements, Δ_{ij}, the overlap integrals, S_{ij}, and an expansion of each of the molecular orbitals of A—B in terms of the fragment orbitals of A and of B. Equations [1] and [2] are then employed (5) to calculate, respectively, the stabilizing (i.e., doubly occupied with unoccupied) and destabilizing (i.e., doubly occupied with doubly occupied) interactions associated with the fragment orbitals that contribute to the HOMO of A—B.

$$[1]\quad \Delta e_{ij} = 2(\Delta_{ij} - S_{ij}e_i^0)^2/(e_i^0 - e_j^0)$$

$$[2]\quad \Delta e_{ij} = 2S_{ij}[-2\Delta_{ij} + (e_i^0 + e_j^0)S_{ij}]/(1 - S_{ij})^2$$

The molecules treated in this manner include ethane (5), propylene (5), $(CH_3)_2X$ (6), the dimethyl- (7) and difluoroethylenes (8), and XCH_2YH (X = CH_3, H_2N, HO, F, Cl; Y = O, S) (9). The results for these molecules have been characterized by the following general features: (*i*) the HOMO is comprised mainly of a linear combination of π-type and π*-type group orbitals and (where applicable) *p*-type lone pairs; (*ii*) the electron occupancies of these orbitals are either very close to 2 or very close to 0; (*iii*) the energy differences, from conformation to conformation or from molecule to molecule, that are calculated by application of eqs. [1] and [2], are close to the calculated total energy differences.

It has now been found that this quantitative procedure requires modification when the HOMO of the molecule contains a significant contribution from a hybrid lone pair orbital, as is the case in amines and their congeners. The purpose of this paper is to explain why the problem exists, and to provide a solution to it which otherwise retains the features of the general method.

Consider a molecule of ammonia, oriented as in Fig. 1, with one hydrogen on the *x*-axis of the coordinate system. If the fragmentation $H_2N\cdots H_x$ is performed, the amino group that results has the set of canonical orbitals shown in Fig. 1 as σ, π, n_σ, and n_π, and 7 valence electrons. The lower lying σ and π orbitals are each doubly occupied, leaving three electrons to populate n_σ and n_π. Our intuition suggests that one of these orbitals should be doubly occupied, and the other should be singly occupied. Moreover, the doubly occupied orbital should point in the direction of the lone pair of ammonia; and the singly occupied orbital should be directed along the *x*-axis, because it will form the bond to H_x. It is clear, however, that neither n_σ nor n_π meets these latter requirements. The quantitative PMO treatment of ammonia in the manner just described[1] leads to NH_2 orbitals corresponding to σ, π, n_σ, and n_π, and the electron occupancies of n_σ and n_π are found to be approximately 1.5 in each case. Equations [1] and [2] are, therefore, not applicable.

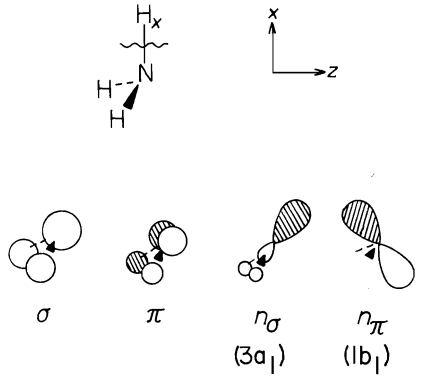

FIG. 1. The canonical orbitals of the NH_2 fragment of ammonia.

The problem arises because the C_{2v} axis of the NH_2 fragment does not coincide with the H_2N—H_x bond axis. This leads to significant overlap of H_x with both n_σ and n_π. As discussed in ref. 5, orbital occupancy depends upon the overlap between the fragment orbitals, because the gross population (Q_p) of an orbital ϕ_p^0 is defined as

$$[3]\quad Q_p = Q_{pp} + \sum_{i \neq p} Q_{pi}$$

where

$$[4]\quad Q_{pi} = 2\sum_n^{occ} S_{pi}T_{pn}T_{in}$$

with T the matrix that expresses the molecular orbitals in the fragment orbital basis. Fragment orbitals with populations close to 1.5 might be regarded as linear combinations of filled (population close to 2) and half-filled (population close to 1) orbitals. Therefore, one solution to the problem might consist of 'unmixing' these orbitals manually by taking a linear combination to form two new fragment orbitals with populations ca. 1 and ca. 2.

Alternatively, such a linear combination might be based upon the overlap properties of the two fragment orbitals. For any 2 × 2 rotation of a pair of orbitals ϕ_p^0 and ϕ_q^0 of one fragment, one has the

[1]All calculations were performed at the STO-3G level on a Burroughs B6700 computer, using a locally modified version of GAUSSIAN 70, and the optimized geometries reported in ref. 10.

result

$$[5] \qquad S'_{ip} = S_{ip} \cos\theta - S_{iq} \sin\theta$$

$$[6] \qquad S'_{iq} = S_{ip} \sin\theta + S_{iq} \cos\theta$$

where ϕ_i^0 is an orbital of the second fragment and S' is the overlap matrix after transformation. The sum of the squares of these overlap integrals with all n orbitals of the second fragment is invariant under the transformation, i.e.,

$$\sum_i^n (S'_{ip}{}^2 + S'_{iq}{}^2) = \sum_i^n \{(S_{ip} \cos\theta - S_{iq} \sin\theta)^2 + (S_{ip} \sin\theta + S_{iq} \cos\theta)^2\} = \sum_i^n (S_{ip}{}^2 + S_{iq}{}^2)$$

The angle θ should then be chosen so that $\sum_i^n S'_{ip}{}^2$ is maximized (while $\sum_i^n S'_{ip}{}^2$ is minimized), with the result that $\phi_p^{0'}$ more closely approximates the singly occupied σ-bonding orbital between the fragments, and $\phi_q^{0'}$ describes the lone pair orbital.

Application of this latter procedure to the $n_\sigma(3a_1)$ and $n_\pi(1b_1)$ orbitals of Fig. 1 leads to the hybrid fragment orbitals shown in Fig. 2. As can be seen, one of these is nearly aligned with the bond axis, and the other is nearly aligned with the C_{3v} symmetry axis of the molecule. In addition, the transformation has changed the electron occupancies, from 1.686 and 1.565 in n_σ and n_π, respectively, to 1.256 for the orbital on the bond axis and 1.996 for the orbital on the symmetry axis.

Methylamine

Figure 3 shows the effects of this transformation procedure upon the $3a_1$ and $1b_1$ fragment orbitals of the amino group of methylamine in its staggered conformation. As a result of the transformation, the computation of the destabilizing and stabilizing interactions between the nitrogen 'lone pair' ($4a'$) and the π_z and π_z^* methyl group orbitals becomes feasible. These are the only doubly occupied and unoccupied fragment orbitals that contribute to the HOMO. It is noteworthy that, since the axis of the methyl group coincides with the C—N bond axis, transformation of the orbitals of this fragment is not necessary, as is evident from the gross populations: π_z, 1.998; π_z^*, 0.019; π_x, 1.025.

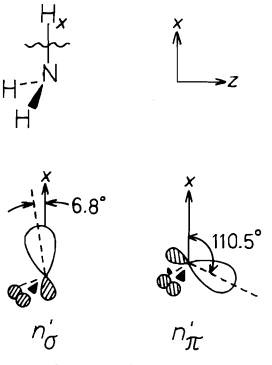

FIG. 2. Transformation of the n_σ and n_π canonical orbitals of the NH_2 fragment of ammonia based upon the criterion of maximization of the overlap of one of these orbitals with the fragmented H.

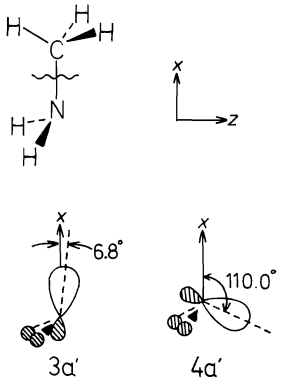

FIG. 3. The transformed n_σ and n_π orbitals of the NH_2 fragment of methylamine in its staggered conformation.

The quantitative PMO analysis of methylamine will, therefore, be based upon the interaction diagram shown in Fig. 4, which contains a destabilizing interaction between N_{lp} and π_z, and a stabilizing interaction between N_{lp} and π_z^*. The energies of these fragment orbitals, and the calculated interaction energies in the staggered and eclipsed conformations, are collected in Table 1. In terms of this analysis, the staggered conformation is found to be less destabilized by 0.20 kcal/mol, and more stabilized by 0.34 kcal/mol, than the eclipsed conformation.

The (N_{lp}–π_z^*) interaction is shown in Fig. 5. As a result of this interaction, antibonding CH regions become populated, and the CH bonds are weakened.

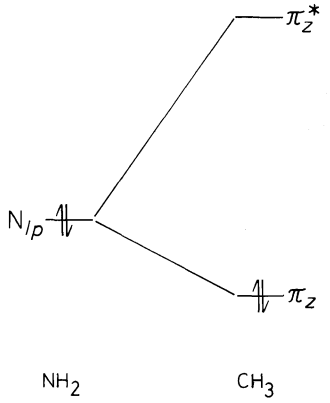

FIG. 4. Interaction diagram for the PMO analysis of methylamine.

TABLE 1. Quantitative PMO analysis of methylamine

Conformation	Fragment orbital	e_i^0 (au)	Interaction energy (kcal/mol) N_{lp}–π	Interaction energy (kcal/mol) N_{lp}–π^*
Staggered[a]	N_{lp}	−0.3592		
	π_{CH_3}	−0.5314	20.43	−4.95
	$\pi_{CH_3}^*$	0.6801		
Eclipsed[b]	N_{lp}	−0.3561		
	π_{CH_3}	−0.5274	20.63	−4.61
	$\pi_{CH_3}^*$	0.6780		

[a]Calculated total energy, −94.03286 au.
[b]Calculated total energy, −94.02838 au.

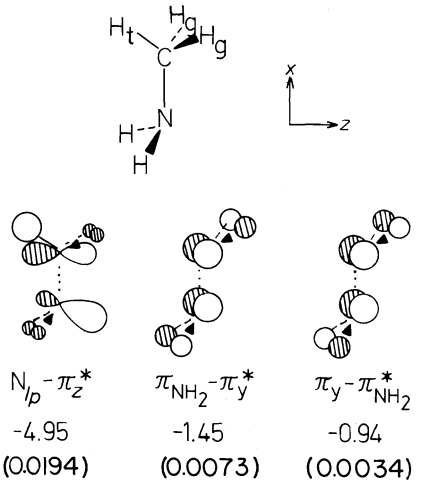

FIG. 5. The (N_{lp}–π_z^*), (π_{NH_2}–π_y^*), and (π_y–$\pi_{NH_2}^*$) orbital interactions in the staggered conformation of methylamine, and the values calculated for these interactions in kcal/mol. The numbers in parentheses are the gross populations of the π^* orbitals.

However, since H_t has a larger atomic orbital coefficient in π_z^* than does H_g, the C—H_t bond is weakened preferentially (11). An experimental manifestation of this effect is found in the Bohlmann bands (12), which appear in the infrared spectrum of methylamine (13).

Although they do not contribute to the HOMO, two other orbital interactions, shown in Fig. 5 as (π_{NH_2}–π_y^*) and (π_y–$\pi_{NH_2}^*$), also lead to weakening of CH bonds. In the (π_{NH_2}–π_y^*) interaction, the charge transfer is to antibonding C—H_g regions; this leads to preferential weakening of the C—H_g bonds. In the (π_y–$\pi_{NH_2}^*$) interaction, the charge transfer is from *bonding* C—H_g regions; this also weakens the C—H_g bonds preferentially. The values computed for the three orbital interactions are included in Fig. 5, together with the gross populations of the three π^* orbitals. These populations reflect the amount of charge transfer which occurs in each case. As can be seen, the (N_{lp}–π_z^*) interaction, which contributes to the HOMO, and weakens C—H_t preferentially, is significantly larger than the other two. This indicates that the Bohlmann band phenomenon has been predicted by a quantitative PMO analysis which is based upon examination of the interactions in the HOMO.

Acknowledgements

We thank the Advisory Research Committee of Queen's University and the National Research Council of Canada for financial support of this work.

1. W. L. JORGENSEN and L. SALEM. The organic chemist's book of orbitals. Academic Press, New York. 1973.
2. M. J. S. DEWAR and R. C. DOUGHERTY. The PMO theory of organic chemistry. Plenum Press, New York. 1975.
3. L. LIBIT and R. HOFFMANN. J. Am. Chem. Soc. **96**, 1370 (1974).
4. B. M. DEB. J. Am. Chem. Soc. **96**, 2030 (1974).
5. M.-H. WHANGBO, H. B. SCHLEGEL, and S. WOLFE. J. Am. Chem. Soc. **99**, 1296 (1977).
6. M.-H. WHANGBO and S. WOLFE. Can. J. Chem. **55**, 2778 (1977).
7. S. WOLFE, D. J. MITCHELL, and M.-H. WHANGBO. J. Am. Chem. Soc. **100**, 1936 (1978).
8. M.-H. WHANGBO, D. J. MITCHELL, and S. WOLFE. J. Am. Chem. Soc. **100**, 3698 (1978).
9. S. WOLFE, M.-H. WHANGBO, and D. J. MITCHELL. Carbohydr. Res. **69**, 1 (1979).
10. W. A. LATHAN, L. A. CURTISS, W. J. HEHRE, J. B. LISLE, and J. A. POPLE. Prog. Phys. Org. Chem. **11**, 175 (1974).
11. S. WOLFE, H. B. SCHLEGEL, M.-H. WHANGBO, and F. BERNARDI. Can. J. Chem. **52**, 3787 (1974).
12. F. BOHLMANN. Angew Chem. **69**, 641 (1957); Chem. Ber. **91**, 2157 (1958).
13. A. Y. HIRAKAWA, M. TSUBOI, and T. SHIMANOUCHI. J. Chem. Phys. **57**, 1236 (1972).

Chemical and microbiological remote functionalisation of (+)- and (−)-bornyl acetate[1]

MALCOLM S. ALLEN, NICHOLAS DARBY, PHILLIP SALISBURY, ELIN R. SIGURDSON, AND THOMAS MONEY

Chemistry Department, The University of British Columbia, Vancouver, B.C., Canada V6T 1W5

Received September 26, 1978

MALCOLM S. ALLEN, NICHOLAS DARBY, PHILLIP SALISBURY, ELIN R. SIGURDSON, and THOMAS MONEY. Can. J. Chem. **57**, 733 (1979).

Chemical oxidation of (−)-bornyl acetate provides a mixture of 3-, 5-, and 6-oxobornyl acetate, whereas microbiological hydroxylation with cultures of *Helminthosporium sativum* gives a mixture of 2,3-, 2,6-, and 2,5-bornanediols. In each case the reaction occurs preferentially at the C(5) position. Microbiological hydroxylation of (+)-bornyl acetate with *H. sativum* occurs almost exclusively at the C(5) position. Regiospecific hydroxylation of (+)- or (−)-bornyl acetate with cultures of *Fusarium culmorum* also occurs at the C(5) position but without concomitant hydrolysis of the acetoxy group.

MALCOLM S. ALLEN, NICHOLAS DARBY, PHILLIP SALISBURY, ELIN R. SIGURDSON et THOMAS MONEY. Can. J. Chem. **57**, 733 (1979).

L'oxydation chimique de l'acétate du (−)-bornyle conduit à un mélange des acétates des oxo-3, -5 et -6 bornyles; l'hydroxylation microbiologique par des cultures d'*Helminthosporium sativum* fournit un mélange des bornane-diols-2,3 -2,6 et -2,5. Dans chaque cas, la réaction se produit préférentiellement en position C(5). L'hydroxylation microbiologique de l'acétate du (+)-bornyle par le *H. sativum* se produit presqu'exclusivement en position C(5). L'hydroxylation régiospécifique des acétates des (+)- ou (−)-bornyles par des cultures de *Fusarium culmorum* se produit aussi en position C(5); elle n'est toutefois pas accompagnée d'une hydrolyse du groupe acétoxy.

[Traduit par le journal]

As part of our synthetic studies (2 and references cited therein) in the monoterpenoid and sesquiterpenoid area we have considered the possibility of using remote oxidation or hydroxylation reactions to convert commercially available or synthetically accessible mono- and sesquiterpenoids to more complex, oxygenated derivatives. Our interest in this approach to terpenoid synthesis was prompted by a consideration of biosynthetic evidence which demonstrates that the introduction of hydroxyl or carbonyl groups into unactivated positions (i.e., remote from activating functionality) is a characteristic feature of many biosynthetic sequences. In addition there are many reports in the literature which indicate that transformations of this type can be accomplished in the laboratory using microbiological (3) or chemical techniques (4). Since our immediate synthetic objectives were dependent on the synthesis of 2,5-disubstituted bornane (camphane) derivatives we directed our initial attention to the direct remote oxidation or hydroxylation of bornyl (**1**) and isobornyl acetate (**2**).[2]

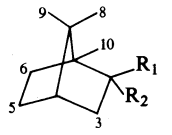

1 $R_1 = H, R_2 = OAc$
2 $R_1 = OAc, R_2 = H$

Remote Oxidation of (−)-Bornyl Acetate (1) with CrO_3/HOAc or CrO_3/HOAc/Ac_2O

Several reports in the literature have established that oxidation of bornyl acetate with CrO_3/HOAc (6) or CrO_3/Ac_2O/HOAc (7) provides 5-oxobornyl acetate (**3**) and its 6-oxo isomer (**8**) in ~15–35% yield. In our initial investigations we reexamined this remarkable transformation to assess its potential use in synthetic and biosynthetic studies.

Oxidation of (−)-bornyl acetate (**1**) with CrO_3/Ac_2O/HOAc (7) for 7 days at 0–25°C provided a mixture of products which was partially purified and separated into components by crystallisation, column chromatography, and/or preparative glc. The major product (~40% yield, see Table 1), readily isolated by crystallisation, was identified as 5-oxobornyl acetate (**3**) (7*c*) on the basis of its spectroscopic properties and conversion to 5-oxoborneol (**4**), 5-*exo*-hydroxyborneol (**5**) (7*c*), and bornan-2,5-dione (**6**) (7*c*). Minor components of the reaction mixture were identified as 5-*exo*-acetoxybornyl acetate (**7**), 6-

[1]The results described in this paper were previously reported in preliminary communications (1).

[2]Remote oxidation of isobornyl acetate (**2**) (5; M. S. Allen, D. H. Hunter, and T. Money. Unpublished observations) and its use in the synthesis of nojigiku alcohol and monoterpenoid analogs of *cis*-sativenediol, *trans*-sativenediol, and helminthosporal will be described in later papers (17).

0008-4042/79/070733-09$01.00/0

TABLE 1. Chemical oxidation of (−)-bornyl acetate (**1**)

Product	Yield (%)[a]	
	CrO_3/HOAc/Ac_2O	CrO_3/HOAc
(−)-Bornyl acetate (**1**)	2	5
Camphor	—	8
5-Oxobornyl acetate (**3**)	40	24
6-Oxobornyl acetate (**8**)	16	5
3-Oxobornyl acetate (**11**)	2	2
5-*exo*-Acetoxybornyl acetate (**7**)	6	1
Bornane-2,5-dione (**6**)	1	2
Bornane-2,6-dione (**10**)	5	—

[a]Estimated by glc analysis (prep. 30% SE-30 and QF-1) of total reaction product using samples of individual components as standards.

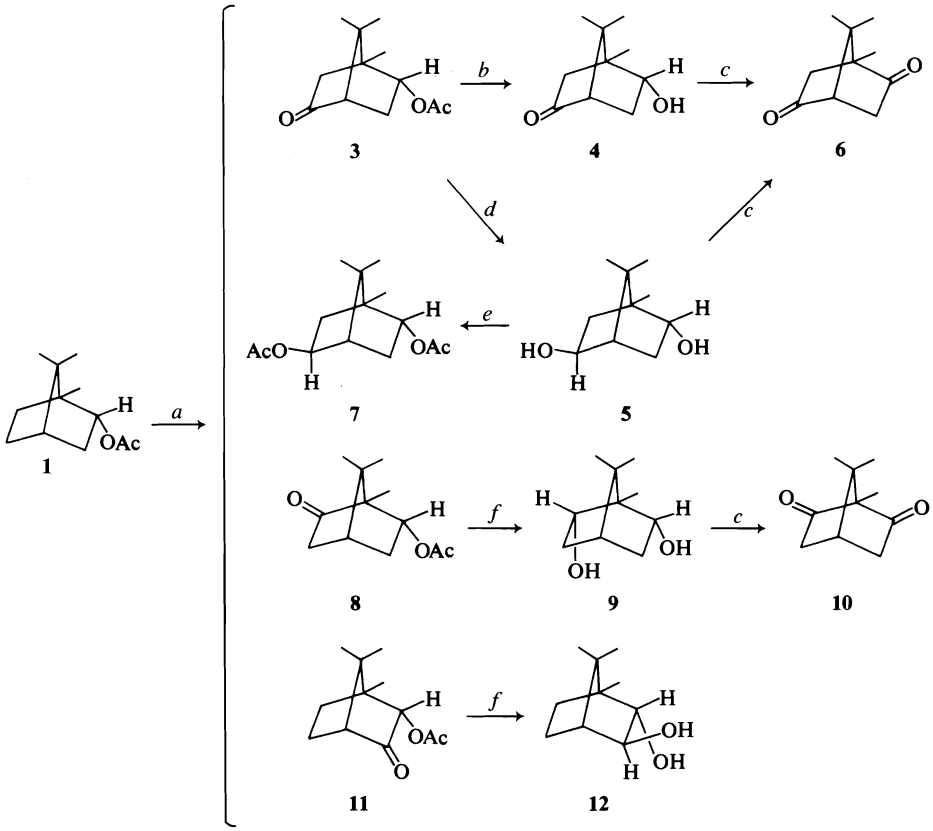

SCHEME 1. (*a*) CrO_3/Ac_2O/HOAc; (*b*) Na_2CO_3/H_2O/MeOH; (*c*) $C_5H_5N^+H\cdot CrO_3\cdot Cl^-$; (*d*) $LiAlH(OMe)_3$; (*e*) Ac_2O/C_5H_5N; (*f*) $LiAlH_4$.

oxobornyl acetate (**8**), and 3-oxobornyl acetate (**11**) by chemical correlation with bornan-2,6-dione (**10**),[3] 6-*endo*-hydroxyborneol (**9**), bornan-2,5-dione (**6**),[3] and 3-*exo*-hydroxyborneol (**12**) (8) (Scheme 1). The stereochemistry of the acetoxy group in **7** was established by its nmr spectrum and its synthesis from 5-*exo*-hydroxyborneol (**5**). Oxidation of (−)-bornyl acetate with CrO_3/HOAc (6) produced a similar mixture of products in lower yield (Table 1).

[3]Bornane-2,5-dione (6) and bornane-2,6-dione (10 and references cited therein) were also identified as minor components of the oxidation process.

Microbiological Hydroxylation of (−)- and (+)-Bornyl Acetate

The regiospecificity of the oxidative transformation described above led us to consider that a similar functionalisation of the C(5) position in more complex camphane systems could occur during the biosynthesis of several groups of sesquiterpenoids. For

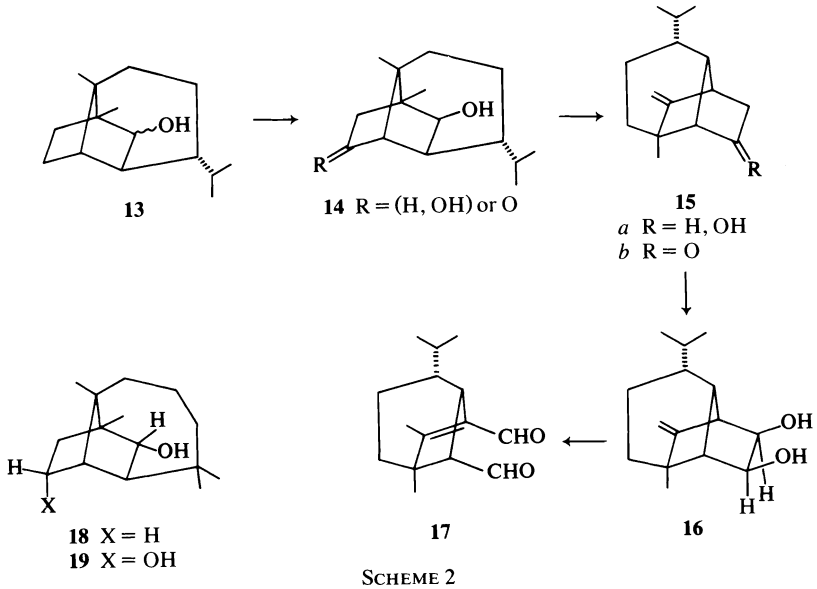

13 **14** R = (H, OH) or O **15** *a* R = H, OH *b* R = O **16** **17** **18** X = H **19** X = OH

SCHEME 2

TABLE 2. Hydroxylation of (−)-bornyl acetate (**5**) by *H. sativum*[4]

Product	Yield (%)[a]		
(−)-5-*exo*-Hydroxyborneol (**5**)	17	24	29
(−)-5-*endo*-Hydroxyborneol (**20**)	6	10	8
(−)-3-*exo*-Hydroxyborneol (**12**)	11	12	15
(−)-6-*exo*-Hydroxyborneol (**21**)	5	6	8

[a]For analytical procedure see Experimental.

example introduction of oxygen functionality into an ylangobornane derivative (**13**; OH *endo* or *exo*), followed by Wagner–Meerwein rearrangement of **14** to a 5-oxo- (**15***a*) or 5-hydroxysativene (**15***b*) could be involved in the biosynthesis of *cis*-sativenediol (**16**), helminthosporal (**17**), and related compounds produced by *Helminthosporium sativum* (cf. ref. 9) (Scheme 2).[4] Similarly we considered that the final step (?) in the biosynthesis of culmorin (**19**) (cf. ref. 10), a metabolite of *Fusarium culmorum*, could involve C(5)-hydroxylation of longiborneol (**18**) or a suitable derivative. A result of these biosynthetic considerations is the prediction that *H. sativum* and *F. culmorum* contain a C(5)-hydroxylase which may be capable of introducing oxygen functionality at the C(5) position in compounds such as borneol[5] or more complex compounds such as longiborneol, etc. Support for these predictions is described below.

Hydroxylation of (−)- and (+)-Bornyl Acetate with H. sativum[4]

(−)-Bornyl acetate (**1**) was added to 3-day-old cultures of *H. sativum* and, after 7–10 days, ether extraction of the broth provided (−)-borneol and a mixture of bornanediols which were separated by column chromatography. On the basis of their nmr spectra and chemical correlation with products obtained in the chemical oxidation of **1**, the various microbiological products were identified as (−)-5-*exo*-hydroxyborneol (**5**) (major), (−)-5-*endo*-hydroxyborneol (**20**), (−)-6-*exo*-hydroxyborneol (**21**), and (−)-3-*exo*-hydroxyborneol (**12**) (8). The overall yield of diols was ~50% and the relative proportions of 2,5-, 2,3-, and 2,6- isomers (~5:2:1) was calculated from glc analysis of their diacetates (Table 2).[6,7]

When (+)-bornyl acetate (**22**) was used as substrate with *H. sativum* the regiospecificity of hydroxylation increased considerably and the only major products were (+)-5-*exo*- (**23**) and (+)-*endo*-hydroxylborneol (**24**).[8] The yield of diols **23** and **24** was ~35–65% and their relative proportion, as

[4]Now classified as *Bipolaris sorokiniana*.

[5]Previous studies (3*a*, *b*) have shown that the methylene groups of camphor, fenchone, and isofenchone can be hydroxylated by microorganisms or animals.

[6]Other minor components of the reaction mixture have been tentatively identified as 6-ketoborneol and bornane-2,8-diol.

[7]We are unable to provide a satisfactory explanation for the variation in relative yields of products in successive microbiological experiments (see Tables 2 and 3).

[8]The only other reaction product, (+)-3-*exo*-hydroxyborneol (**25**) was formed in ~2% yield (see Table 3).

TABLE 3. Hydroxylation of (+)-bornyl acetate (**22**) by *H. sativum*

Product	Yield (%)[a]			
(+)-5-*exo*-Hydroxyborneol (**23**)	56	32	47	38
(+)-5-*endo*-Hydroxyborneol (**24**)	8	4	11	16
(+)-3-*exo*-Hydroxyborneol (**25**)	3.5	1	2	2

[a]For analytical procedure see Experimental.

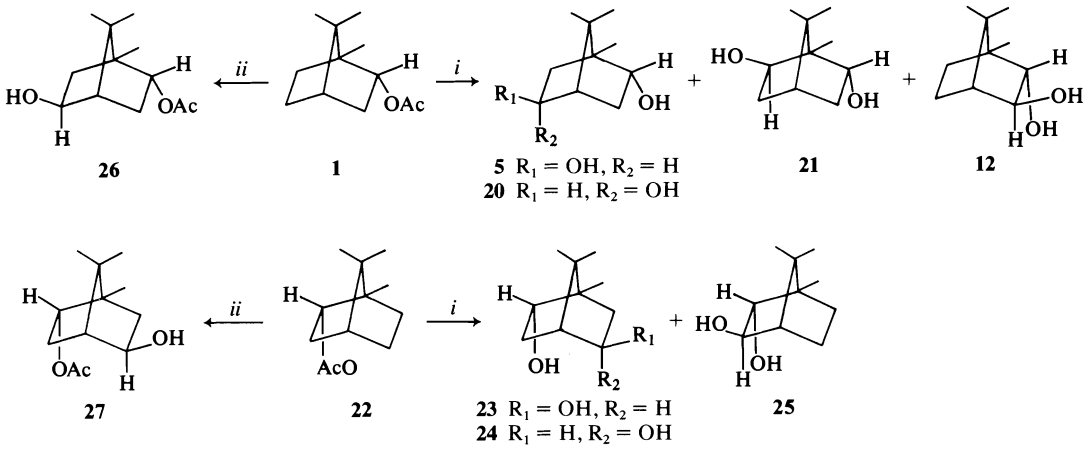

(*i*) *Helminthosporium sativum*; (*ii*) *Fusarium culmorum*.

SCHEME 3

determined by glc and nmr of the corresponding diacetates, varied from ~2.5:1 to ~7:1 (Table 3).[7]

Hydroxylation of (−)- and (+)-Bornyl Acetate with F. culmorum

Addition of (−)-bornyl acetate (**1**) to 7-day-old cultures of *F. culmorum* and work-up after 18 days provided 5-*exo*-hydroxybornyl acetate (**26**) as the only major product (~12% yield). The identity of this product was established by its spectroscopic properties and by its conversion to (−)-5-*exo*-acetoxybornyl acetate (**7**) and 5-oxobornyl acetate (**3**). An almost identical result was obtained when (+)-bornyl acetate (**22**) was used as substrate (Scheme 3).

The efficiency, regiospecificity, and stereoselectivity of the microbiological hydroxylations described above compare favourably with microbial transformations of other terpenoids (3*a–e*). In addition the regiospecificity of hydroxylation of (+)-bornyl acetate by *H. sativum* and the ability of *F. culmorum* to hydroxylate at C(5) while leaving the C(2)-acetoxy group intact[9] could be of value in subsequent synthetic studies.

[9]Preliminary observations (R. Zerr. Unpublished results) indicate that *F. culmorum* converts isobornyl acetate (2) to 5-hydroxyisobornyl acetate. Hence 5-oxo-isobornyl acetate is accessible by a microbiological route which complements the laboratory synthesis involving direct oxidation with CrO_3/HOAc/Ac_2O (5; M. S. Allen, D. H. Hunter, and T. Money. Unpublished results).

The remarkable correspondence in regiospecificity between the chemical and microbiological reactions described above probably reflects the greater accessibility of the C(5) position towards oxidising agents or enzymic systems. We have suggested a similar explanation for the partial regiospecificity of other direct remote oxidation reactions (11).

Experimental

Chromium trioxide (Mallinckrodt, Technical grade 99.75%), (−)-bornyl acetate (Aldrich Chemical Company), and (+)-camphor (Eastman Organic Chemicals) were used as received. (+)-Bornyl acetate, $[\alpha]_D$ +43.2° (*c* 2.47, $CHCl_3$), was prepared by calcium – liquid ammonia reduction (12) of (+)-camphor followed by column chromatography (alumina) and acetylation. Pyridine was dried over potassium hydroxide pellets before use and methylene chloride for pyridinium chlorochromate oxidations was dried by distillation from phosphorus pentoxide.

Nuclear magnetic resonance spectra were recorded at 100 MHz using either a Varian HA-100 or XL-100 machine, or the HA-100 magnet with Bruker TT23 console and Nicolet 16 K computer. Infrared spectra were recorded with Perkin Elmer 137 or 710A instruments.

Column chromatography was performed with aluminium oxide Woelm neutral, for column chromatography (ICN Pharmaceuticals) or with silicic acid, 100 mesh (Mallinckrodt). Alumina was deactivated to grade III before use. Thin-layer chromatography plates were made from silica gel GF-254 for tlc (E. Merck) and were visualised by spraying with a saturated solution of ceric sulphate in 12 *N* aqueous sulphuric acid followed by heating.

Gas–liquid chromatography was performed with either a Varian Aerograph model 90-P or Hewlett-Packard HP5831A

instrument, using thermal conductivity and flame ionisation detectors respectively. Analytical glc on the Varian instrument was conducted with 6 ft × 0.25 in. stainless steel columns using 3% SE-30, 10% OV-210, or 20% DEGS stationary phases on 60–80 or 80–100 mesh Chromosorb W. Preparative glc was performed with a 10 ft × 0.375 in. stainless steel column with 20% DEGS as the stationary phase on 60–80 mesh Chromosorb W. Mass spectra were recorded at 70 eV with a Varian/MAT CH4B spectrometer and high resolution mass measurements were determined with a Kratos-AEI MS50 instrument. Gas–liquid chromatography on the Hewlett-Packard instrument was performed with 6 ft × 0.125 in. stainless steel columns, using 3% OV-17, and 10% Carbowax stationary phases on 80–100 mesh Chromosorb W-HP support.

Optical rotations were measured with a Perkin-Elmer 141 or 241MC instrument and microanalyses were performed by Mr. P. Borda, Microanalytical Laboratory, University of British Columbia, Vancouver.

Oxidation of (−)-Bornyl Acetate with Chromium Trioxide in Acetic Anhydride – Acetic Acid

A solution of (−)-bornyl acetate (**1**) (60 g, 0.31 mol) in glacial acetic acid (260 mL) and acetic anhydride (115 mL) was cooled to 0°C. The solution was stirred and maintained at 0°C while a solution of chromium trioxide (85 g, 0.85 mol, 2.1 equiv.) in acetic anhydride (135 mL) was added in several portions over 24 h. After this time the mixture was allowed to warm to room temperature and stirring was continued at this temperature for a further 6 days. The green viscous reaction mixture was dissolved in water (2500 mL), extracted with ether (3 × 650 mL), using filtration through Celite 535 to aid phase separation, and the ether extracts washed successively with water, excess aqueous sodium bicarbonate, and saturated aqueous sodium chloride. Drying (Na_2SO_4) and evaporation provided a viscous yellow oil. Separation of the oxidation products (27.2 g; bp 90–96°C/0.85 Torr) from recovered starting material was achieved by fractional distillation *in vacuo*.

Typical Oxidation Procedure using Chromium Trioxide in Glacial Acetic Acid

A solution of (−)-bornyl acetate (**1**) (20 g, 0.10 mol) in glacial acetic acid (30 mL) was stirred and heated to reflux while a slurry of chromium trioxide (50 g, 0.50 mol, 3.75 equiv.) in glacial acetic acid (70 mL) was cautiously added in small portions over 40–80 min. A further portion of glacial acetic acid (70 mL) was used to wash the oxidising agent into the reaction vessel. Heating and stirring were continued for 30–80 min and the solution was cooled, diluted with water (600 mL), and extracted with ether (3 × 350 mL). The ether extracts were washed successively with excess aqueous sodium bicarbonate and saturated aqueous sodium chloride, dried (Na_2SO_4), and evaporated to give a pale yellow viscous oil. Separation of the oxidation products (7.3 g; bp 89–90°C/0.8 Torr) from unreacted starting material was achieved by fractional distillation *in vacuo*.

*Isolation of (−)-5-Oxobornyl Acetate (**3**)*

The fractionally distilled product from the oxidation of (−)-bornyl acetate with chromium trioxide in acetic acid readily crystallised upon standing at −20°C. Washing with ice-cold hexane followed by crystallisation from hexane gave (−)-*5-oxobornyl acetate* (**3**) as a colourless solid, mp 78°C (lit. (7*b*) mp 78°C, lit. (7*c*) mp 74–76°C); $[\alpha]_D^{25}$ −102.6° (*c* 1.96, $CHCl_3$) (lit. (7*c*) $[\alpha]_D$ −97° in $CHCl_3$)); ν_{max} (CCl_4): 1745, 1235, 1035 cm^{-1}; δ ($CDCl_3$): 0.94, 1.00, 1.01 (3H each, s, CH_3), 1.30 (1H, d of d, *J* = 3.5 and 14 Hz, 3-*endo*-H, collapses to d, *J* = 14 Hz, upon irradiation at 5.06 δ), 2.03 (3H, s, CH_3CO_2—), 2.16 (1H, d, *J* = 5 Hz, C(4)-H), 2.35–2.75 (2H, overlapping of d, *J* = 18 Hz (6 *endo*-H) and multiplet (3-*exo*-H), collapsing to d of d, *J* = 14 and 5 Hz, upon irradiation at 5.06 δ), 5.06 (1H, multiplet, collapsing to dd, *J* ~ 9 and 1–2 Hz, upon irradiation at 1.30 δ, 2-*exo*-H); *m/e* (relative intensity): 210(M^+, 24), 168(84), 124(36), 111(23), 109(32), 108(40), 107(34), 43(100), 41(24).

*(−)-5-Oxoborneol (**4**)*

A mixture of (−)-5-oxobornyl acetate (**3**) (1.00 g) and sodium carbonate decahydrate (1.37 g) in methanol (4 mL) and water (7 mL) was briefly heated to reflux and then allowed to stand for 48 h. The mixture was diluted with water, extracted with ether several times, and the ether extracts washed with water, dried (Na_2SO_4), and evaporated. Recrystallisation from cyclohexane gave (−)-*5-oxoborneol* (**4**) as a colourless solid (0.65 g, 81%), mp 239–241°C (sealed capillary) (lit. (7*c*) mp 247–248°C); $[\alpha]_D^{25}$ −87.0° (*c* 1.55, $CHCl_3$) (lit. (7*c*) $[\alpha]_D$ −74° in $CHCl_3$); ν_{max} ($CHCl_3$): 3630, 3480, 1745, 1035 cm^{-1}; δ ($CDCl_3$): 0.91, 0.95, 1.00 (3H each, s, CH_3), 1.27 (1H, d of d, *J* = 14 and 3.5 Hz, 3-*endo*-H), 1.86 (1H, d with fine coupling, *J* = 18 Hz, 6-*exo*-H), 2.13 (1H, d, *J* = 5 Hz, 4-H), 2.3–2.75 (2H, overlapping of doublet, *J* = 18 Hz, 6-*endo*-H, and of multiplet, 3-*exo*-H), 4.20 (1H, multiplet, 2-*exo*-H): d of d at 1.27 δ collapses to d (*J* = 14 Hz) upon irradiation of 4.20 δ; d with fine coupling at 1.86 δ collapses to d (*J* = 18 Hz) upon irradiation at 4.20 δ; *m/e* (relative intensity): 168(M^+, 49), 125(49), 124(100), 109(46), 71(30), 70(39), 55(32), 41(44).

*(−)-5-*exo-*Hydroxyborneol (**5**)*

To a freshly prepared solution of lithium trimethoxy aluminum hydride (13) (11.2 mmol) in tetrahydrofuran (25 mL), stirred under nitrogen at 0°C, was added a solution of 5-oxobornyl acetate (**3**) (250 mg, 1.2 mmol) in tetrahydrofuran (5 mL). Stirring was continued for 30 min at 0°C, then for 17 h at room temperature. Ether (25 mL) was added, followed by just sufficient water to decompose the excess reducing agent and produce a white, easily filtered precipitate. Filtration of the product followed by evaporation of the filtrate and crystallisation from benzene provided (−)-5-*exo*-hydroxyborneol (**5**) as a colourless solid (169 mg, 84%), mp 258–259°C (sealed capillary); $[\alpha]_D^{27}$ −16.3° (*c* 0.81, $CHCl_3$); ν_{max} ($CHCl_3$): 3650, 1040 cm^{-1}; δ ($CDCl_3$): 0.76, 0.81, 1.04 (3H each, s, CH_3), 1.25–1.50 (1H, multiplet), 1.73 (1H, d, *J* = 5 Hz, 4-H), 2.1–2.5 (2H, multiplet), 3.83 (2H, multiplet, 2-*exo*-H and 5-*endo*-H); *m/e* (relative intensity): 170(M^+, 4) 137(18), 126(29), 125(47), 111(100), 109(59), 83(17), 55(18), 43(22), 41(26). *Anal.* calcd. for $C_{10}H_{18}O_2$: C 70.55, H 10.66; found: C 70.50, H 10.76.

*(−)-5-*exo-*Acetoxybornyl Acetate (**7**)*

A solution of (−)-5-*exo*-hydroxyborneol (**6**) (50 mg) in pyridine (1.6 mL, dried by standing over potassium hydroxide pellets) and acetic anhydride (0.4 mL) was heated at 90°C with stirring while under nitrogen for 19 h. The mixture was diluted with water, extracted three times with ether, and the ether extracts washed successively with 1 *N* aqueous hydrochloric acid (excess), water, excess aqueous sodium bicarbonate, and saturated aqueous sodium chloride. The ether extracts were then dried (Na_2SO_4) and evaporated to give (−)-5-*exo*-acetoxybornyl acetate (**7**) as an almost colourless viscous oil (72 mg, 97%). Purification by preparative glc (30% SE-30) gave a colourless viscous oil; $[\alpha]_D^{27}$ −13.6° (*c* 1.49, $CHCl_3$); ν_{max} (CCl_4): 1740, 1230, 1030 cm^{-1}; δ ($CDCl_3$): 0.85, 0.90, 1.01 (3H each, s, CH_3), 1.49 (1H, multiplet), 1.88 (1H, d, *J* = 5 Hz, 4-H), 1.97 and 2.00 (3H each, s, CH_3CO_2—), 2.2–2.6 (2H, multiplet), 4.63 (1H, d of d, 5-*endo*-H), 4.78 (1H, multiplet, 2-*exo*-H); *m/e* (relative intensity): 254(M^+, 25), 195(30), 168(24), 152(27), 137(27), 135(27), 134(70), 126(30), 119(57),

109(73), 108(63), 93(37), 43(100). *Anal.* calcd. for $C_{14}H_{22}O_4$: C 66.12, H 8.72; found: C 66.16, H 8.67.

*Isolation of 6-Oxobornyl Acetate (**8**), 3-Oxobornyl Acetate (**11**), and 5-*exo*-Acetoxybornyl Acetate (**7**)*

The fractionally distilled oxidation product from the oxidation of bornyl acetate with chromium trioxide in acetic acid and acetic anhydride was cooled to −20°C for 7 days to promote crystallisation of 5-oxobornyl acetate (**3**). This was removed by filtration and the mother liquors subjected to column chromatography on silica gel (2.0 g of substrate, 200 g of silica gel deactivated to grade III; eluted with 15% ether in hexane). Two fractions were obtained, each of which was a mixture of two main components by glc (20% DEGS). Each component was isolated by preparative glc. Preparative glc (30% SE-30) of the more rapidly eluted fraction (0.42 g) provided 3-oxobornyl acetate (**11**) and 5-*exo*-acetoxybornyl acetate (**7**) in order of increasing retention time.

3-Oxobornyl acetate (**11**) was obtained as a colourless partially crystalline solid, a single component on tlc (silica gel, ether – petroleum ether 1:2) and glc (3% SE-30 and 5% QF-1); $[\alpha]_D^{25}$ −42.50° (*c* 1.0, $CHCl_3$); ν_{max} (CCl_4): 1755, 1250, 1060 cm^{-1}; δ ($CDCl_3$): 0.98 and 1.01 (6H and 3H respectively, s, CH_3), 2.11 (3H, s, CH_3CO_2—), 2.29 (1H, d, J = 5 Hz, 4-H) 5.19 (1 H, fine coupling, 2-*exo*-H); *m/e* (relative intensity): 210(M^+, 23), 168(39), 123(33), 122(18), 113(14), 81(14), 71(18), 69(12), 58(10), 55(13), 43(100); *Mol. Wt.* calcd. for $C_{12}H_{18}O_3$: 210.1256; found (mass spectrometry): 210.1237.

5-exo-*Acetoxybornyl acetate* (**7**) was obtained as a colourless viscous oil, identical with material from the acetylation of 5-*exo*-hydroxyborneol (**5**) by tlc (silica gel, ether – petroleum ether 1:1) and glc (3% SE-30 and 20% DEGS), as well as by nmr ($CDCl_3$) and ir (CCl_4) spectrometry.

Preparative glc (30% QF-1) of the less rapidly eluted fraction (1.31 g) provided 6-oxobornyl acetate (**8**) and 5-oxobornyl acetate (**3**) in order of increasing retention time.

6-Oxobornyl acetate (**8**) was isolated as a colourless partially crystalline solid, providing colourless crystals from hexane, mp 62–62.5°C; $[\alpha]_D^{25}$ +31.42° (*c* 1.13, $CHCl_3$); ν_{max} (CCl_4): 1750, 1245, 1075, 1050 cm^{-1}; δ ($CDCl_3$): 0.85, 0.94, 1.04 (3H each, s, CH_3), 1.27 (1H, d of d, J = 14 and 3 Hz, collapsing to d, J = 14 Hz, upon irradiation at 5.13 δ, 3-*endo*-H), 1.99 (3H, s, CH_3CO_2—), 5.13 (1H, d of d, J = 9 and 3 Hz, 2-*exo*-H); *m/e* (relative intensity): 210(M^+, 5), 168(46), 167(27), 153(100), 150(19), 121(21), 109(19), 108(58), 107(29), 43(39), 41(18). *Anal.* calcd. for $C_{12}H_{18}O_3$: C 68.55, H 8.63; found: C 68.49, H 8.55.

5-Oxobornyl acetate (**3**) was isolated as a colourless crystalline solid, identical with material previously isolated from the chromium trioxide – acetic acid oxidation of bornyl acetate by tlc (silica gel, ether – petroleum ether 1:2), glc (3% SE-30 and 5% QF-1), as well as by nmr ($CDCl_3$) and ir (CCl_4) spectrometry.

6-endo-*Hydroxyborneol* (**9**)

To a solution of 6-oxobornyl acetate (**8**) (81 mg) in dry ether (2 mL), stirred under nitrogen at −78°C, was added lithium aluminum hydride (37 mg, 3.4 equiv.) in three portions over 15 min. After stirring at −78°C for a further 3 h the mixture was allowed to warm to room temperature and the stirring continued for a further 19 h. Just sufficient water was added to decompose the aluminum salts to a readily filtered precipitate and the mixture was filtered and the filtrate evaporated. This provided a colourless viscous oil which was purified by column chromatography on silica gel (9 g, deactivated to grade III, and eluted with ether – petroleum ether 1:2). This gave 6-*endo*-hydroxyborneol (**9**) (53 mg, 81%), mp 258–260°C (from hexane) (sealed capillary); $[\alpha]_D^{25}$ −0.05 ± 0.06° (*c* 3.46, $CHCl_3$); ν_{max} (1% in $CHCl_3$): 3620, 3480, 1130, 1060 cm^{-1}; δ ($CDCl_3$): 0.84 (6H, s, C(8)- and C(9)-CH_3), 1.06 (3H, s, C(10)-CH_3), 1.34 (2H, d of d, J = 12.5 and 2.5 Hz; collapsing to d, J = 12.5 Hz, upon irradiation at 4.25 δ; collapsing to d, J = 2–3 Hz, upon irradiation at 2.47 δ; 3-*endo*- and 5-*endo*-H), 1.75 (1H, t, J = 5 Hz, collapsing to s upon irradiation at 2.47 δ, C(4)-H), 2.47 (2H, multiplet (d of d of d), J = 12.5, 9.5, and 5 Hz; collapsing to d of d, J = 12.5 and 5 Hz upon irradiation at 4.25 δ; collapsing to d of d, J = 12.5 and 9.5 Hz, upon irradiation at 1.75 δ; collapsing to d of d, J = 9.5 and 5 Hz upon irradiation at 1.34 δ; 3-*exo*- and 5-*exo*-H), 4.25 (2H, d, of d, J = 9.5 and 2.5 Hz, collapsing to doublet, J = 9.5 Hz, upon irradiation at 1.34 δ; collapsing to broad singlet upon irradiation at 2.47 δ; 2-*exo*- and 6-*exo*-H); δ (C_6D_6): 0.64 (6H, s, C(8)- and C(9)-CH_3), 1.08 (3H, s, C(10)-CH_3), 1.25–1.6 (3H, complex, 3-*endo*-, 5-*endo*-, and C(4)-H), 2.33 (2H, m, 3-*exo*- and 5-*exo*-H), 4.19 (2H, m, 2-*exo*- and 6-*exo*-H); δ (CCl_4): 0.82 (6H, s, C(8)- and C(9)-CH_3), 0.98 (3H, s, C(10)-CH_3), 1.30 (2H, poorly resolved d of d, J = 2–3 and 13 Hz, 3-*endo*- and 5-*endo*-H), 1.68 (1H, t, J = 4.5 Hz, C(4)-H), 2.39 (2H, m, 3-*exo*- and 5-*exo*-H), 4.12 (2H, poorly resolved d of d, J = 2–3 and 10 Hz, 2-*exo*- and 6-*exo*-H); *m/e* (relative intensity): 109(17), 108(100), 95(9), 93(18), 68(5), 55(5), 43(6), 41(112), no molecular ion visible. *Anal.* calcd. for $C_{10}H_{18}O_2$: C 70.55, H 10.66; found: C 70.56, H 10.74.

(−)-3-exo-*Hydroxyborneol* (**12**)

To a solution of 3-oxobornyl acetate (**11**) (approximately 10 mg) in dry ether (1 mL), stirred at −78°C under nitrogen, was added lithium aluminum hydride (22 mg). Stirring was continued at −78°C for 4 h then at 25°C for 18 h, and the mixture was worked up by adding just sufficient water to decompose the aluminum salts to a readily filterable precipitate. Filtration and evaporation of the ether followed by column chromatography (silica gel, 0.5 g, elution with ether – petroleum ether 1:2) provided (−)-3-*exo*-hydroxyborneol (**12**). The physical constants and spectroscopic and glc characteristics of this product were identical to those recorded for the sample of **12** isolated from *H. sativum* (*vide infra*).

*Oxidation of (−)-5-Oxoborneol (**4**) and (−)-5*-exo-*Hydroxyborneol (**5**)*

Treatment of (−)-5-oxoborneol (**4**) or (−)-5-*exo*-hydroxyborneol (**5**) with pyridinium chlorochromate (14) in methylene chloride at room temperature for 4–5 h provided (−)-bornane-2,5-dione (**6**) in ~80% yield; mp 207–209°C; $[\alpha]_D$ −113°. The product had the same ir (CCl_4), nmr (CCl_4 and C_6D_6), tlc (silica gel, petroleum ether – ether 1:1), and glc (3% SE-30, Carbowax C-20M, and 20% DEGS)[9] characteristics as authentic (+)-bornane-2,5-dione prepared from (+)-camphor.

Oxidation of 6-endo-*Hydroxyborneol (**9**)*

Treatment of 6-*endo*-hydroxyborneol (**9**) (11 mg) with pyridinium chlorochromate in CH_2Cl_2 (14) for 6 h gave, after preparative glc (20% DEGS), bornane-2,6-dione (**10**) as a colourless solid (31% yield) with the same spectroscopic and glc characteristics as authentic bornane-2,6-dione prepared from (+)-camphor (*vide infra*).

(+)-Bornane-2,5-dione and Bornane-2,6-dione

Oxidation of (+)-camphor with chromium trioxide in acetic acid – acetic anhydride according to the literature procedure (15) provided a mixture of bornanediones (~7% yield) which were separated by preparative glc (30% SE-30).[10]

Bornane-2,6-dione (**10**) of shorter retention time, crystallised

[10]10% Carbowax C-20M resolves 2,3-, 2,5-, and 2,6-bornanediones; 20% DEGS separates 2,6-dione from the 2,3- and 2,5-diones; and 3% SE-30 separates 2,5-dione from the 2,3- and 2,6-diones.

from hexane, mp 190–192°C (sealed capillary) (lit. (15) mp 194–195°C, lit. (16) mp 192–193°C); $[\alpha]_D$ +0.7° (*c* 2.59, $CHCl_3$); ν_{max} (CCl_4): 1770, 1735 cm^{-1}; δ ($CDCl_3$): 0.95 (3H, s), 0.99 (6H, s); δ (C_6D_6): 0.48 (6H, s), 0.97 (3H, s) 1.80 (1H, t, J = 5 Hz, C(4)-H); *m/e* (relative intensity): 166(M^+, 96), 123(38) 109(38), 97(61), 95(48), 83(40), 81(52), 69(65), 41(100), 39(52).

(+)-Bornane-2,5-dione (enantiomer of **6**) crystallised from hexane, mp 210–211°C (sealed capillary) (lit. (7*c*) mp 213–214°C); $[\alpha]_D^{26}$ +115° (*c* 1.71, $CHCl_3$); ν_{max} (CCl_4): 1755 cm^{-1}; δ ($CDCl_3$): 0.97 (3H, s), 1.05 (6H, s); *m/e* (relative intensity): 166(M^+, 93), 123(54), 95(37), 83(59), 81(31), 69(78), 67(23), 53(25), 41(100).

Fermentation with H. sativum

Helminthosporium sativum[11] was grown in 1-L Erlenmeyer flasks each containing modified Czapek-Dox medium (200 mL) (water (200 mL), sucrose (6 g), sodium nitrate (0.4 g), yeast extract (0.2 g), potassium dihydrogen phosphate (0.2 g), potassium chloride (0.1 g), magnesium sulphate heptahydrate (0.1 g), iron(III) (0.1 mg), zinc(II) (0.1 mg), manganese(II) (0.05 mg), and copper(II) (0.1 mg)) on a rotary shaker (106 rpm) at 26°C. After 3 days (+)- or (−)-bornyl acetate was added (0.2 g per flask). After a further 7–10 days the mycelium was separated by filtration and the culture filtrate extracted with ether, using a continuous extraction apparatus, for 3 days. The ether extract was dried (Na_2SO_4) and evaporated to provide the crude fermentation product.

Isolation of Hydroxyborneols ***5***, ***20***, ***21***, *and* ***12***

The crude fermentation product (2.0 g) from fermentation with (−)-bornyl acetate (~2 g) as substrate was purified by column chromatography on silicic acid (50 g). After elution of the less strongly absorbed material (0.4 g) with chloroform, the hydroxyborneols were removed as a mixture (1.2 g) with 3% methanol in chloroform. A portion of this mixture of hydroxyborneols (0.5 g) was purified further by several cycles of column chromatography (silica gel, deactivated to grade III, 100:1 ratio of adsorbant to substrate, eluted with ether – petroleum ether 1:1 then 2:1). This provided fractions that were sufficiently pure in each of the four hydroxyborneols for them to be purified by recrystallisation from benzene.

(−)-5-exo-*Hydroxyborneol* (**5**) (135 mg), mp 257–259°C (sealed capillary); $[\alpha]_D^{27}$ −15.9° (*c* 0.94, $CHCl_3$), identical to previously characterised 5-*exo*-hydroxyborneol (**5**) (*vide supra*) by nmr ($CDCl_3$), ir ($CHCl_3$ and Nujol mull), mass spectrometry as well as by tlc and mixture melting point.

(−)-5-endo-*Hydroxyborneol* (**20**) (37 mg), mp 244.5–245.5°C (sealed capillary); $[\alpha]_D^{25}$ −33.25° (*c* 0.8, $CHCl_3$); ν_{max} ($CHCl_3$): 3600, 3450, 1060 cm^{-1}; δ ($CDCl_3$): 0.82 (3H, s, CH_3), 0.91 (6H, s, CH_3), 1.6–1.85 (4H, complex), 1.9–2.4 (1H, complex), 4.06 (1H, d of d, J = 4 and 10 Hz, 2-*exo*-H), 4.44 (1H, complex, 5-*exo*-H); *m/e* (relative intensity): 170(M^+, 30), 152(30), 137(63), 111(50), 109(100), 108(84), 95(31), 41(27), 32(23). *Anal.* calcd. for $C_{10}H_{18}O_2$: C 70.55, H 10.66; found: C 70.73, H 10.60.

(−)-6-exo-*Hydroxyborneol* (**21**) (18 mg), mp 268–270.5°C (sealed capillary); $[\alpha]_D^{25}$ −56.4° (*c* 0.96, CH_3CN); ν_{max} ($CHCl_3$): 3600, 1070, 1050 cm^{-1}; δ ($CDCl_3$): 0.82, 0.95, 1.03 (3H each, s, CH_3), 1.6–1.95 (3H, complex), 2.0–2.4 (1H, complex), 4.04 (1H, d of d, J = 10 and 4 Hz, 2-*exo*-H) 4.33 (1H, m, 6-*endo*-H); *m/e* (relative intensity): 170(M^+, 1), 111(17), 109(41), 108(100), 95(16), 93(18), 55(13), 43(18), 41(23). *Anal.* calcd. for $C_{10}H_{18}O_2$: C 70.55, H 10.66; found: C 70.41, H 10.50.

[11]Subculture from single spore of culture isolated by Dr. Stanley Chinn (Canada Agricultural Research Station, Saskatoon, Sask.) from wheat (subculture sent to ATCC).

(−)-3-exo-*Hydroxyborneol* (**12**) (17 mg), mp 247–240°C (sealed capillary); $[\alpha]_D^{25}$ −19.4° (*c* 0.66, $CHCl_3$); ν_{max} ($CHCl_3$): 3650, 3470, 1060, 1050 cm^{-1} (cf. ref. 8*b*); δ ($CDCl_3$): 0.86, 0.89, and 1.09 (3H each, s, CH_3), 1.65–2.0 (3H, complex), 3.55 (1H, d, J = 2Hz, 3-*endo*-H), 3.97 (1H, m, 2-*exo*-H); the nmr spectrum in pyridine-d_5 with a trace of D_2O is identical to published spectrum (8*a*); *m/e* (relative intensity): 170(M^+, 3), 152(31), 123(18), 111(67), 109(32), 108(35), 95(100), 81(29), 69(25), 60(18), 55(18), 43(22), 41(28), 32(19), 31(18). *Anal.* calcd. for $C_{10}H_{18}O_2$: C 70.55, H 10.66; found: C 70.41, H 10.76.

5-exo-, 5-endo-, 6-exo-, *and* 3-exo-*Acetoxybornyl Acetates*

Hydroxyborneol **5**, **20**, **21**, or **12**, (5–15 mg) was stirred with pyridine – acetic anhydride (4:1, 2 mL) at 90°C under nitrogen for 18–21 h. After dilution with water (10 mL) and extraction with ether (3 × 5 mL), the ether extracts were washed successively with excess 1 *N* aqueous hydrochloric acid, water, excess saturated aqueous sodium bicarbonate, and saturated aqueous sodium chloride. Removal of solvent provided the appropriate acetoxybornyl acetate in almost quantitative yield.

5-exo-*Acetoxybornyl acetate* (**7**) was identical by tlc (silica gel, ether – petroleum ether 1:1) and glc (3% SE-30 and 20% DEGS) as well as nmr ($CDCl_3$), ir (CCl_4), and mass spectrometry to material isolated from chemical oxidation of bornyl acetate (*vide supra*).

5-endo-*Acetoxybornyl acetate* derived from **20**; ν_{max} (CCl_4): 1740, 1240 cm^{-1}; δ ($CDCl_3$): 0.83 (3H, s, CH_3), 0.97 (6H, s, CH_3), 2.07 and 2.10 (3H each, s, CH_3CO_2), 4.94 (1H, d of d, J = 9 and 3.5 Hz, 2-*exo*-H), 5.15 (1H, m, 5-*exo*-H); *m/e* (relative intensity): 254(M^+, 21), 195(73), 152(32), 137(27), 135(40), 134(27), 119(48), 109(53), 108(41), 93(43), 43(100), 32(25).

6-exo-*Acetoxybornyl acetate* derived from **21**; ν_{max} (CCl_4) 1740, 1235, 1060, 1040 cm^{-1}; δ ($CDCl_3$): 0.89, 0.93, and 1.03 (3H each, s, CH_3), 2.05 and 2.08 (3H each, s, CH_3CO_2—), 4.99 (1H, d of d, J = 10 and 3.5 Hz, 2-*exo*- or 6-*endo*-H), 5.31 (1H, d of d, J = 7.5 and 4 Hz, 2-*exo*- or 6-*endo*-H); *m/e* (relative intensity): 254(M^+, 15), 212(6), 197(6), 194(5), 152(14), 134(9), 119(12), 109(16), 108(100), 95(6), 93(9), 43(34), 41(7), 32(16).

3-exo-*Acetoxybornyl acetate* derived from **12**; ν_{max} (CCl_4): 1740, 1240, 1045 cm^{-1}; δ ($CDCl_3$): 0.87, 0.88, and 1.08 (3H each, s, CH_3) 2.06 and 2.10 (3H each, s, CH_3CO_2), 4.50 (1H, d, J = 3 Hz, 3-*endo*-H), 5.21 (1H, m, 2-*exo*-H); *m/e* (relative intensity): 254(M^+, 4), 152(51), 137(22), 135(28), 134(44), 124(10), 123(23), 119(29), 109(20), 108(13), 102(24), 96(10), 95(48), 83(14), 81(12), 80(22), 43(100), 41(14).

Oxidation of (−)-5-endo-*Hydroxyborneol (**20**)*

Treatment of 5-*endo*-hydroxyborneol (**20**) (8 mg) with pyridinium chlorochromate (14) for 6 h gave (−)-bornane-2,5-dione as a colourless solid (6 mg, 76% yield); nmr (in CCl_4 and C_6D_6), ir (CCl_4), tlc (silica gel, ether – petroleum ether 1:1), and glc (3% SE-30, 10% Carbowax C-20M, and 20% DEGS) characteristics identical to those of authentic bornane-2,5-dione (*vide supra*).

Oxidation of 6-exo-*Hydroxyborneol (**21**)*

Treatment of 6-*exo*-hydroxyborneol (**21**) (10 mg) with pyridinium chlorochromate (14) for 6 h gave bornane-2,6-dione (**10**) as a colourless solid after preparative glc purification (20% DEGS); nmr ($CDCl_3$ and C_6D_6), ir (CCl_4) spectra of this specimen of **10** were identical to those recorded for the authentic compound prepared from camphor (*vide supra*).

*Hydroxylation of (+)-Bornyl Acetate (**22**) by* H. sativum

The reaction product from fermentations using (+)-bornyl acetate (**22**) as substrate was acetylated and then analysed by comparing the nmr and glc characteristics with the diacetates derived from hydroxyborneols **5**, **20**, **21**, and **12** (*vide supra*).

The results obtained from four experiments indicated that the original microbiological product was a mixture of (+)-5-*exo*-hydroxyborneol (**23**), (+)-5-*endo*-hydroxyborneol (**24**), and (+)-3-*exo*-hydroxyborneol (**25**). The yields of diols from four separate fermentations are shown in Table 3.

Quantitative Gas–Liquid Chromatographic Analysis of H. sativum *Products*

Analysis of Fermentation Extracts Directly

This was performed on a Varian Aerograph model 90-P chromatograph fitted with TC detector and analytical 20% DEGS column, using 10–100 μL injections of solutions in ethyl acetate. With a column oven temperature of ~130°C the absolute quantity of hydroxyborneols was determined by injecting known quantities of the fermentation products and comparing the area of the peak corresponding to the hydroxyborneols with that arising from the injection of known quantities of pure 5-*exo*-hydroxyborneol as a standard. In the same way, using a column oven temperature of ~70°C and (−)-bornyl acetate as standard, it was possible to determine the absolute quantities of bornyl acetate and borneol. All injections were performed several times to ensure reproducibility of the results, and fermentation peak areas were only compared with those of standards that had been injected immediately beforehand.

Analysis of Acetylated Fermentation Extracts

Fermentation extracts were acetylated in the usual way and the acetylated products were analysed by glc (analytical 3% SE-30 column at ~100°C). The absolute quantities of acetoxybornyl acetates were determined by using 5-*exo*-acetoxybornyl acetate (**13**) as a standard, taking the same precautions that are described above. The identity of the peaks in the glc analysis was confirmed by isolation (preparative glc, 30% SE-30) and nmr analysis of the isolated components.

Fermentation with F. culmorum

Fusarium culmorum[12] was grown in 4-L Erlenmeyer flasks each containing Raulin–Thom medium (1 L) (water (1 L), glucose (50 g), tartaric acid (2.7 g), ammonium tartrate (2.7 g), ammonium phosphate $NH_4H_2PO_4$ (0.4 g), potassium carbonate (0.4 g), magnesium carbonate 0.27 g), ammonium sulphate (0.17 g), zinc sulphate heptahydrate (0.047 g), and ferrous sulphate heptahydrate (0.047 g)) on a rotary shaker (120 rpm) at 26°C. After 7 days, (+)- or (−)-bornyl acetate was added (1.0 g per flask). After a further 18 days the mycelium was separated by filtration and the culture filtrate extracted with ether using a continuous extraction apparatus for 3 days. The ether extract was dried (Na_2SO_4) and evaporated to provide the crude fermentation product.

*Isolation of 5-*exo*-Hydroxybornyl Acetate (**26**)*

The crude fermentation product (3.01 g) was purified by column chromatography (silicic acid, 180 g). Elution with $CHCl_3$ provided 5-*exo*-hydroxybornylacetate (**26**) (900 mg; 97% pure by glc); ν_{max} ($CHCl_3$): 3600, 1720, 1250, and 1040 cm^{-1}; δ ($CHCl_3$): 0.84, 0.86, 1.09 (3H each, s, CH_3), 1.99 (3H, s, CH_3CO_2—) 3.84 (1H, d of d, J = 7.5 and 3 Hz, 5-*endo*-H), 4.76 (1H, m, 2-*exo*-H).

*5-*exo*-Acetoxybornyl Acetate (**7**)*

5-*exo*-Hydroxybornyl acetate (**26**) (41 mg), isolated in 96% purity (glc, 10% Carbowax C-20M TPA) from silicic acid chromatography of the crude fermentation product, was stirred at 90°C under a nitrogen atmosphere with pyridine–acetic anhydride (4:1, 2 mL) for 22 h. The reaction mixture was diluted with water (10 mL), extracted with ether (3 × 5 mL), and the ether layers washed with excess aqueous 1 *N* hydrochloric acid, water, excess saturated aqueous sodium bicarbonate, and saturated aqueous sodium chloride. Removal of solvent provided 5-exo-*acetoxybornyl acetate* (**7**), identical by tlc (silica gel, ether – petroleum ether 1:2), glc (3% OV-17 and 10% Carbowax C-20M; HP-5831A), and by nmr ($CDCl_3$) and ir ($CHCl_3$) spectrometry to material prepared previously by lithium trimethoxy aluminum hydride reduction of 5-oxobornyl acetate (**3**) followed by acetylation (*vide supra*).

*Oxidation of 5-*exo*-Hydroxybornyl Acetate (**26**)*

Treatment of 5-*exo*-hydroxybornyl acetate (**26**) (46 mg) with pyridinium chlorochromate (14) for 7 h gave 5-oxobornyl acetate (**3**) (41 mg), identical by tlc (silica gel, ether – petroleum ether 1:2) and glc (3% OV-17 and 10% Carbowax C-20M TPA; HP-5831A) and by nmr ($CDCl_3$) and ir ($CHCl_3$) spectrometry with authentic material isolated from the oxidation of bornyl acetate with chromium trioxide – acetic acid (*vide supra*).

Quantitative Gas–Liquid Chromatographic analysis of F. Culmorum *Products*

Quantitative glc analysis of the fermentation products of (+)- and (−)-bornyl acetate was performed using (−)-camphorquinone as an added internal standard. The relative detector responses to borneol, bornyl acetate, 5-*exo*-hydroxybornyl acetate, and (−)-camphorquinone were determined by injection of a mixture of known quantities of the four substrates (10% Carbowax C-20M TPA; HP-5831A); an average of three determinations was taken. By injection of a mixture of a known quantity of the fermentation product and a known quantity of camphorquinone (10% Carbowax C-20M TPA; HP-5831A) the relative peak areas, after correction for the detector response, were used to determine the absolute quantities of borneol, bornyl acetate, and 5-*exo*-hydroxybornyl acetate; an average of two determinations was taken.

[12]Subculture of culture No. CBS 171.28 obtained from Centraal-bureau voor Schimmelcultures, Baarn, Holland.

Acknowledgements

We thank the National Research Council of Canada and the University of British Columbia for generous financial support.

1. M. S. Allen, N. Darby, P. Salisbury, and T. Money. J. Chem. Soc. Chem. Commun. 358 (1977); Tetrahedron Lett. 2255 (1978).
2. (*a*) P. Cachia, N. Darby, C. R. Eck, and T. Money. J. Chem. Soc. Perkin I, 359 (1976); (*b*) C. R. Eck, G. L. Hodgson, D. F. MacSweeney, R. W. Mills, and T. Money. J. Chem. Soc. Perkin I, 1938 (1974).
3. (*a*) G. Fonken and R. A. Johnson. Chemical oxidations with microorganisms. Marcel Dekker, New York, NY. 1972; (*b*) K. Kieslich. Microbial transformation of non-steroid cyclic compounds. Wiley-Thieme, Stuttgart, Germany. 1976; (*c*) A. S. Bailey, M. L. Gilpin, and Sir Ewart R. H. Jones. J. Chem. Soc. Perkin I, 265 (1977) and references cited; (*d*) A. B. Anderson, R. McCrindle, and J. K. Turnbull. J. Chem. Soc. Perkin I, 1202 (1975); Can. J. Chem. **53**, 1181 (1975); (*e*) J. R. Bearder, V. M. Frydman, P. Gaskin, I. K. Hatton, W. E. Harvey, and J. MacMillan. J. Chem. Soc. Perkin I, 178 (1976) and references cited; (*f*) G. Ellames and J. R. Hanson. J. Chem. Soc. Perkin I, 1666 (1976); (*g*) H. J. Vidic, G.-A. Hoyer, K. Kieslich, and D. Rosenberg. Chem. Ber. **109**, 3606 (1976).
4. (*a*) R. Breslow. Chem. Soc. Rev. **1**, 553 (1972); R. Breslow and L. M. Maresca. Tetrahedron Lett. 623 (1977);

887 (1978); R. BRESLOW, R. J. CORCORAN, B. B. SNIDER, R. J. DOLL, P. L. KHARMA, and R. KALEYA. J. Am. Chem. Soc. **99**, 905 (1977) and references cited; (*b*) J. ALLEN, R. B. BOAR, J. F. MCGHIE, and D. H. R. BARTON. J. Chem. Soc. Perkin I, 2402 (1973) and references cited; cf. A. NICKON, R. FERGUSON, A. BOSCH, and T. IWADARE. J. Am. Chem. Soc. **99**, 4518 (1977); (*c*) M. A. WINNIK. Acc. Chem. Res. **10**, 173 (1977) and references cited; (*d*) E. KEINAN and Y. MAZUR. Synthesis, 523 (1976); Z. COHEN, E. KEINAN, Y. MAZUR, and A. ULMAN. J. Org. Chem. **41**, 2651 (1976) and references cited; cf. A. L. J. BECKWITH and T. DUONG. J. Chem. Soc. Chem. Commun. 413 (1978); cf E. AKIYAMA, M. TADA, T. TSUYUKI, and T. TAKAHASHI. Chem. Lett. 305 (1978) and references cited; (*e*) J. T. GROVES and M. VAN DER PUY. J. Am. Chem. Soc. **97**, 7118 (1975); (*f*) N. C. DENO, E. JEDZINIAK, L. A. MESSER, M. D. MEYER, S. G. STROUD, and E. S. TOMEZSKO. Tetrahedron, **33**, 2503 (1977); (*g*) P. BRUN and B. WAEGELL. Tetrahedron, **32**, 518 (1976); (*h*) Z. CEKOVIC and T. SRNIC. Tetrahedron Lett. 561 (1976).

5. (*a*) N. J. TOIVONEN and A. HALONEN. Suom. Kemistil. B, **19**, 1 (1946); Chem. Abstr. **41**, 5487 (1947); (*b*) D. H. HUNTER. M.Sc. Thesis, University of British Columbia, Vancouver, B.C. 1974.
6. (*a*) J. BREDT and A. GOEB. J. Prakt. Chem. **101**, 273 (1921); Chem. Abstr. **16**, 250 (1922); (*b*) J. MEINWALD, J. C. SHELTON, G. L. BUCHANAN, and A. COURTIN. J. Org. Chem. **33**, 99 (1968).
7. (*a*) J. BREDT and P. PINTEN. J. Prakt. Chem. **119**, 104 (1928); (*b*) Y. ASAHINA, M. ISHIDATE, and T. TUKAMOTO. Chem. Ber. **69**, 349 (1936); Chem. Abstr. **30**, 3804 (1936); (*c*) D. E. BAYS, G. W. CANNON, and R. C. COOKSON. J. Chem. Soc. B, 890 (1966); (*d*) N. J. TOIVONEN, P. HIRSJARVI, A. MELAJA, A. KAINULAINEN, A. HALONEN, and E. PULKINNEN. Acta Chem. Scand. **3**, 991 (1949).
8. (*a*) F. A. L. ANET. Can. J. Chem. **39**, 789 (1961); (*b*) T. TAKESHITA and M. KITAJIMA. Bull. Chem. Soc. Jpn. **32**, 985 (1959); (*c*) S. J. ANGYAL and R. J. YOUNG. J. Am. Chem. Soc. **81**, 5467 (1959).
9. F. DORN, P. BERNASCONI, and D. ARIGONI. Chimia, **29**, 25 (1975).
10. J. R. HANSON and R. NYFELER. J. Chem. Soc. Perkin I, 2471 (1976).
11. G. EIGENDORF, C.-L. MA, and T. MONEY. J. Chem. Soc. Perkin I. In press.
12. (*a*) A. COULOMBEAU and A. RASSAT. Bull. Soc. Chem. Fr. 4399 (1970); (*b*) W. S. MURPHY and D. F. SULLIVAN. Tetrahedron Lett. 3707 (1971).
13. H. C. BROWN and P. M. WEISSMAN. J. Am. Chem. Soc. **87**, 5614 (1965); H. C. BROWN and H. R. DECK. J. Am. Chem. Soc. **87**, 5620 (1965).
14. E. J. COREY and J. W. SUGGS. Tetrahedron Lett. 2647 (1975).
15. (*a*) J. BREDT. J. Prakt. Chem. **106**, 336 (1923); Chem. Abstr. **18**, 826 (1924); (*b*) K. MIYAKE. Proc. Imp. Acad. (Tokyo), **11**, 106 (1935); **11**, 322 (1935); Chem. Abstr. **30**, 2949 (1936).
16. P. LIPP. Chem. Ber. **80**, 165 (1947).
17. (*a*) N. DARBY, N. LAMB, and T. MONEY. Can. J. Chem. This issue; (*b*) M. S. ALLEN, N. LAMB, T. MONEY, and P. SALISBURY. J. Chem. Soc. Chem. Commun. In press.

Synthesis and absolute configuration of nojigiku alcohol

NICHOLAS DARBY, NANCY LAMB, AND THOMAS MONEY
Chemistry Department, The University of British Columbia, Vancouver, B.C., Canada V6T 1W5

Received September 26, 1978

NICHOLAS DARBY, NANCY LAMB, and THOMAS MONEY. Can. J. Chem. **57**, 742 (1979).

The structure, absolute configuration and physical constants of nojigiku alcohol ((+)-6-*exo*-hydroxycamphene) and derivatives have been established by synthesis from (−)-isobornyl acetate.

NICHOLAS DARBY, NANCY LAMB et THOMAS MONEY. Can. J. Chem. **57**, 742 (1979).

On a déterminé la structure, la configuration absolue et les constantes physiques de l'alcool nojigiku ((+)-hydroxy-6 *exo*-camphène) et de ses dérivés grâce à une synthèse à partir de l'acétate du (−)-isobornyle.

[Traduit par le journal]

Nojigiku alcohol (**10**) (6-*exo*-hydroxycamphene), a metabolite of *Chrysanthemum japonense* (1), has previously been synthesised in low yield from camphene (2) and tricyclene (3). Our interest in applying remote oxidation techniques to the synthesis of various mono- and sesquiterpenoids has resulted in an alternative synthesis of this naturally occurring camphene derivative.

Remote oxidation of (−)-isobornyl acetate (**2**) with CrO_3/HOAc/Ac_2O provided a mixture (4:1) of 5-ketoisobornyl acetate (**3**) and its 6-keto isomer (**4**) in ~55% yield (4). Treatment of this mixture with SeO_2 gave 5,6-diketoisobornyl acetate (**5**) (50% yield) which underwent regiospecific and stereoselective reduction with Zn/HOAc (5–7) to provide 6-*endo*-hydroxy-5-ketoisobornyl acetate (**6**) (~82% yield).

The regiospecificity and stereoselectivity of the latter reaction was established by nmr and chemical evidence. For example the nmr of **6** showed absorption at 6.15 τ which is almost identical to that found in 2-*endo*-hydroxyepicamphor (**13**) (5–7) and differs markedly from the C(3)-*exo*-hydrogen absorption (5.78 τ) in 3-*endo*-hydroxycamphor (**14**) (5, 6). The presence of a C(6)-*endo*-hydroxy group in **6** is also supported by the fact that the C(2)-*endo*-hydrogen (4.75 τ) is shifted downfield from its expected position (cf. isobornyl acetate, C*H*OAc, 5.43 τ). This effect of a C(6)-*endo*-hydroxyl on the neighbouring C(2)-*endo*-hydrogen in bornane systems is also evident when the nmr of isoborneol (**15**) and 6-*endo*-hydroxyisoborneol (**16**) or isobornyl acetate (**2**) and 6-*endo*-hydroxyisobornyl acetate (**7**) are compared (8). Chemical evidence for the structure of **6** was obtained by an alternative synthesis involving low-yield α-hydroxylation (MoO_5/HMPA/C_5H_5N) (9) of 5-ketoisobornyl acetate (**3**). In addition reduction of the derived thioketal (*vide infra*) followed by hydrolysis provided 6-*endo*-hydroxyisoborneol (**16**), a compound whose structure has been confirmed by nmr evidence and oxidation to 2,6-bornanedione (8).

The regiospecificity of the Zn/HOAc reduction of 5,6-diketoisobornyl acetate (**5**) was totally unexpected since the analogous reaction involving camphorquinone provides a mixture (2:1) of 2-*endo*-hydroxyepicamphor (**13**) and 3-*endo*-hydroxycamphor (**14**) (5). We conclude, therefore, that the regiospecificity of the Zn/HOAc reduction of 5,6-diketoisobornyl acetate (**5**) is probably due to some unknown directing effect of the C(2)-acetate group.

Thioketalisation of **6** followed by reduction (Raney Ni) gave 6-*endo*-hydroxyisobornyl acetate (**7**) (14) which was converted to the *tert*-butyldimethylsilyl (TBDMS) (10) ether and subsequently hydrolysed (Na_2CO_3/MeOH) to hydroxyether **8** in 50% overall yield. Wagner–Meerwein rearrangement (MsCl/C_5H_5N) of **8** followed by removal of the TBDMS group with Bu_4NF/THF or HOAc/H_2O/THF (3:1:1) provided nojigiku alcohol (**10**) (1), mp 67.5–69.5°C (sealed tube), sublimation point 52°C (lit. (1) mp 52–53°C, lit. (2*c*) mp 59.5–60°C); $[\alpha]_D$ +58.6° (*c* 1.33, $CHCl_3$), +60.4° (*c* 1.16, $CHCl_3$) (lit. (1) $[\alpha]_D$ +12° (*c* 1.1, $CHCl_3$), lit. (2*c*) $[\alpha]_D$ +9°).

Although the nmr and ir spectra of our synthetic material are identical to those of the natural compound (12)[1] the specific rotation of **10** (measured at different concentrations and on two different instruments (Perkin Elmer 141 and 241MC)) was significantly different from the value quoted in the literature. Similar differences were noted for the corresponding acetate (**11**) (1), $[\alpha]_D$ +37.6° (*c* 1.11, $CHCl_3$) (lit. (1) $[\alpha]_D$ +20.9° (*c* 0.58, $CHCl_3$), +11.6° (*c* 1.20, $CHCl_3$)) and ketone (**12**) (1), mp 73.5–

[1]We are grateful to Dr. A. Matsuo and co-workers (Hiroshima University) for providing us with ir and nmr spectra of nojigiku alcohol.

0008-4042/79/070742-05$01.00/0

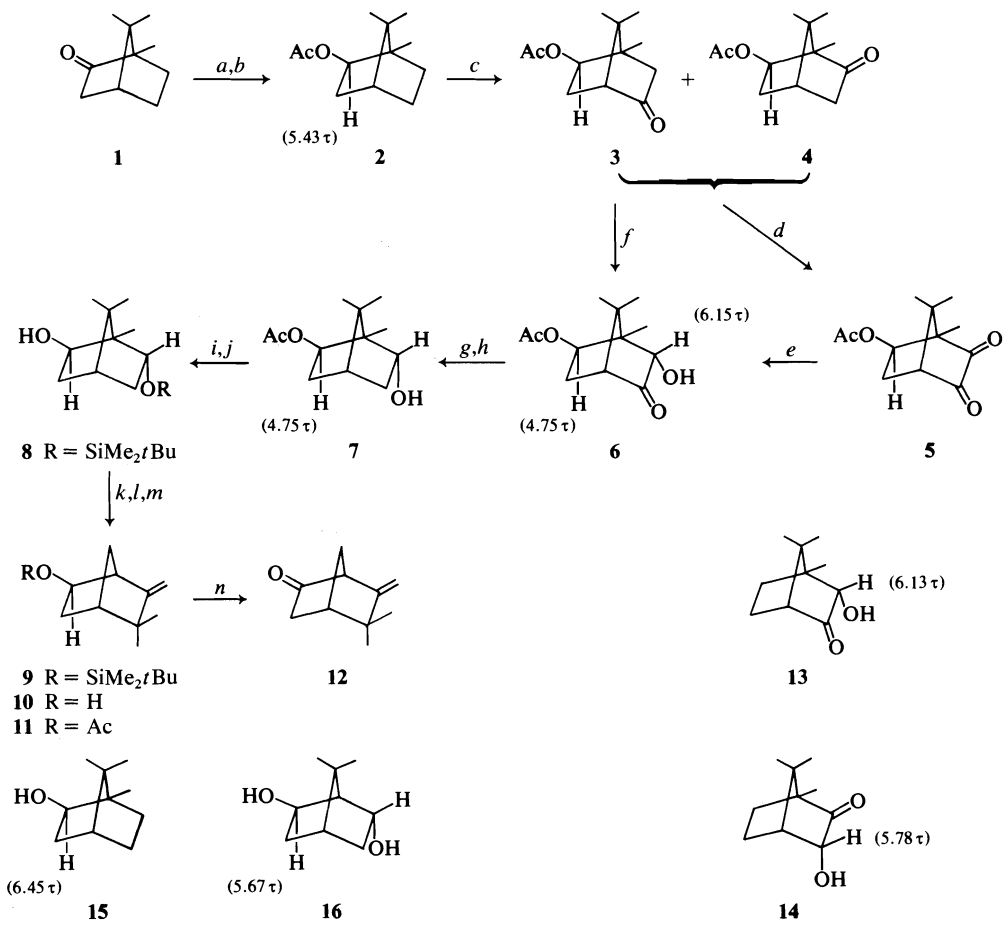

(*a*) $LiAlH_4$; (*b*) Ac_2O/C_5H_5N; (*c*) $CrO_3/Ac_2O/HOAc$; (*d*) SeO_2; (*e*) Zn/HOAc; (*f*) $MoO_5/HMPA/C_5H_5N$; (*g*) $(CH_2SH)_2/BF_3 \cdot Et_2O$; (*h*) Raney Ni; (*i*) $tBuMe_2SiCl$/imidazole; (*j*) KOH/EtOH; (*k*) $MsCl/C_5H_5N/\Delta$; (*l*) Bu_4NF/THF; (*m*) Ac_2O/C_5H_5N; (*n*) $CrO_3/C_5H_5N/HCl$

75.5°C (sealed tube), sublimation point 40°C; $[\alpha]_D$ +155.3° (*c* 0.91, $CHCl_3$) (lit. (1) mp 47–48°C; lit. (1) $[\alpha]_D$ +33.7° (*c* 0.86, $CHCl_3$)). Regeneration of 6-*exo*-hydroxycamphene (**10**), $[\alpha]_D$ +58.86° (*c* 0.88, $CHCl_3$), from acetate **11** and its subsequent oxidation to ketone **12**, $[\alpha]_D$ +158.2° (*c* 0.79, $CHCl_3$), provided further support for the authenticity of the physical constants we have recorded for these compounds.[2] Gas–liquid chromatographic evidence (see Experimental) demonstrated that the synthetic alcohol **10** was pure and the absence of common chemical shifts in the nmr spectra of **10** and its enantiomer, measured in the presence of a chiral shift reagent (TFMC-Eu) (13), indicated that our synthetic alcohol **10** was also optically pure. We conclude, therefore, that the specific rotation of (+)-6-*exo*-hydroxycamphene (nojigiku alcohol) (**10**) falls within the range, +55 to 61° (see Experimental). This conclusion is relevant to recent studies on the free radical benzoyloxylation of camphene (2*c*) since the mechanism proposed for that reaction was based, to some extent, on the assumption that the specific rotation of pure 6-*exo*-hydroxycamphene is approximately +12°.

Experimental

Unless otherwise stated the following are implied. Melting points (mp) were determined on a Kofler micro heating stage or a Thomas Hoover capillary melting point apparatus and are uncorrected. Gas chromatography was carried out on either a Hewlett-Packard model 5831A gas chromatograph using 6 ft × $\frac{1}{8}$ in. columns and nitrogen as carrier gas, or a Varian Aerograph model 90-P with 5 ft × $\frac{1}{4}$ in. columns and helium as carrier gas. The following columns were employed.

[2](−)-6-*exo*-hydroxycamphene, (−)-6-acetoxycamphene, and (−)-6-oxocamphene, synthesised from (−)-camphor by the route outlined above, have specific rotations numerically equivalent to those of the enantiomers (9–11).

Column	Dimensions	Stationary phase	Support	Mesh	
A	6 ft × ⅛ in.	3% OV17	Chromosorb W (HP)	80–100	Hewlett-Packard 5831A
B	6 ft × ⅛ in.	3% OV101	Chromosorb W (HP)	80–100	
C	6 ft × ⅛ in.	3% OV210	Chromosorb W (HP)	80–100	
D	6 ft × ⅛ in.	10% DEGS	Chromosorb W (HP)	80–100	
E	6 ft × ⅛ in.	10% Carbowax	Chromosorb W (HP)	80–100	
F	5 ft × ¼ in.	3% SE30	Varaport 30	100–120	Varian 90-P
G	5 ft × ¼ in.	20% DEGS	Chromosorb W	80–100	

Carrier gas flow rate for ¼ in. columns was about 60 mL/min and for ⅛ in. columns about 35 mL/min. The 60 MHz nmr spectra were recorded on a Varian Associates model T-60 whereas 100 MHz spectra were recorded on Varian Associates model HA-100 or XL-100. Signal positions are given in the Tiers tau scale (τ) with tetramethylsilane (TMS) as an internal reference. Signal multiplicity and integrated area are indicated in parentheses. Infrared spectra were recorded on a Perkin-Elmer 137 spectrophotometer and optical rotations were measured with either a Perkin-Elmer model 141 or 241 MC polarimeter. Low resolution mass spectra were recorded on a Varian/Mat model CH4B mass spectrometer and high resolution mass spectra were determined on the AEI model MS902 or model MS 50 instrument. Microanalyses were performed by Mr. P. Borda, Microanalytical Laboratory, University of British Columbia, Vancouver. All the solvents used for nmr, ir, and optical rotations were of Spectral grade. Zinc dust purchased from Fisher Scientific Company.

*(−)-Isoborneol (**15**)*

(+)-Camphor (**1**) (40.0 g, 0.26 mmol) (Eastman Kodak Co., $[\alpha]_D^{25}$ +41.2° (*c* 1.06, $CHCl_3$)) in dry THF (~100 mL) was added dropwise (1 h) to a stirred suspension of lithium aluminum hydride (10.0 g, 0.26 mmol) in dry tetrahydrofuran (100 mL) at 0–5°C. The reaction mixture was then stirred at 0°C for 4 h and excess lithium aluminum hydride hydrolysed by dropwise addition of water (10 mL), followed by 2 *N* sodium hydroxide (10 mL) and then water (40 mL). The white precipitate was filtered off, washed with ether and the combined filtrates dried with anhydrous magnesium sulphate. Removal of the solvent gave a colorless crystalline product (40 g) which was shown, by glc analysis (column *D*; carrier gas, nitrogen; flow rate 38 mL/min; 120°C), to be a mixture of (−)-isoborneol (retention time 3.49 min) (92%) and borneol (retention time 4.17 min) (8%). Recrystallization of the crude product from petroleum ether (30–60°C) provided isoborneol (98% pure by glc); τ (CCl_4): 6.49 (dd, 1H, J = 7.0 and 2.0 Hz), 9.02, 9.16, and 9.21 (three singlets, 9H); ν_{max} (CCl_4): 3790, 3500, 2850 and 2800, 1070 cm^{-1}.

*(−)-Isobornyl Acetate (**2**)*

A mixture of (−)-isoborneol (37.0 g, 0.24 mol), acetic anhydride (43.0 g, 0.42 mol), and dry pyridine (120 mL) was heated at 100°C under nitrogen for 11 h. The reaction mixture was cooled, diluted with water, and extracted with ether. The combined ether extract was washed with water, 2 *N* hydrochloric acid, water, saturated sodium bicarbonate, and dried over anhydrous magnesium sulphate. Removal of solvent followed by distillation (43–50°C/0.05 Torr) provided isobornyl acetate (**2**) as a colorless oil (45 g, 96% yield); τ (CCl_4): 5.44 (m, 1H), 8.10 (s, 3H), 9.06, 9.20 and 9.21 (3 singlets, 9H); ν_{max} (CCl_4): 2900, 2850, 1740, and 1245 cm^{-1}; *m/e*: 194(M^+), 154, 136; $[\alpha]_D$ −51.8° (*c* 1.29, $CHCl_3$) (lit. (11) $[\alpha]_D$ −50.2° (EtOH)).

*Oxidation of (−)-Isobornyl Acetate (**2**)*

Chromium trioxide (80.0 g, 0.80 mol) in acetic anhydride (140 mL) was slowly added (2 h) to a cooled (ice bath) and vigorously stirred solution of (−)-isobornyl acetate (**2**) (45.0 g, 0.23 mol) in glacial acetic acid (200 mL) and acetic anhydride (100 mL). The reaction mixture was then stirred for 8 days at room temperature, diluted with water, and extracted with ether. (The heavy emulsion formed during extraction was broken up by filtration through Celite.) The combined ether extract was neutralized with sodium carbonate and then washed successively with water, 3 *N* hydrochloric acid, water, saturated sodium bicarbonate, water, and dried over anhydrous magnesium sulphate. Removal of solvent and glc analysis of the crude oily product (36 g) showed that it was mainly a mixture of unreacted isobornyl acetate, 6-oxoisobornyl acetate (**4**) (retention time 7.19 min), and 5-oxoisobornyl acetate (**3**) (retention time 7.79 min) (column *A*, carrier gas, nitrogen; flow rate 41 mL/min; 110°C). Fractional distillation, using a 5-in. Vigreux column, gave a mixture of 5- and 6-oxoisobornyl acetate (about 4:1 by glc) (19.6 g, 40% yield); τ (CCl_4): 5.36 (dd, J = 7.5, 4.0 Hz), 5.14 (dd, J = 7.0, 4.5 Hz), 7.98 (s, 3H), 8.01 (s, 3H), 8.86, 8.89, 9.01, 9.05, 9.15, and 9.16 (six singlets, tertiary methyls); ν_{max} (CCl_4): 2900, 2750, 1750, 1235 cm^{-1}.

*(+)-5,6-Dioxoisobornyl Acetate (**5**)*

A mixture of 5- and 6-oxoisobornyl acetate (0.79 g, 3.75 mmol) was dissolved in acetic anhydride (1.0 mL, 10 mmol). Selenium dioxide (1.63 g, 14.6 mmol) was added and the stirred reaction mixture was refluxed for 18 h. After cooling to room temperature, the mixture was diluted with ether and the precipitate of selenium filtered and washed with ether. The filtrate was washed with water, saturated sodium bicarbonate, water, and dried over anhydrous magnesium sulphate. Removal of solvent gave an orange coloured product (0.72 g) which was chromatographed on silica gel (activity grade III). Elution with ether – petroleum ether (30–60°C) (30:70), followed by crystallisation from petroleum ether (30–60°C) gave (+)-5,6-dioxoisobornyl acetate (**5**) (0.36 g, 53% yield) as a yellow crystalline solid, mp 101–103°C, 97.5–99.5°C (sealed tube) (lit. (4) mp 95–96°C); $[\alpha]_D^{25}$ +37.3° (*c* 1.35, $CHCl_3$); τ (CCl_4): 5.26 (dd, 1H, J = 8.0 and 4.0 Hz), 7.31 (dd, 1H, J = 5.0 and 1.0 Hz), 8.00 (s, 3H), 8.80, 8.98, and 9.11 (three singlets, 9H); ν_{max} (CCl_4): 2900, 1825, 1780, 1760, 1230, 1200 cm^{-1}; *m/e* (relative intensity): 224(M^+, 9), 196(5), 154(5), 141(18), 136(50), 127(18), 121(45), 115(4), 111(9), 109(14), 108(18), 99(100). *Mol. Wt.* calcd. for $C_{12}H_{16}O_4$: 224.1049; found (high resolution mass spectrometry): 224.1050.

*(−)-5-Oxo-6-*endo*-hydroxyisobornyl Acetate (**6**)*

Zinc dust (0.40 g, 6.15 mmol) was added to a cooled solution of (+)-5,6-dioxoisobornyl acetate (**5**) (0.37 g, 1.65 mmol) in acetic acid (14 mL) and water (3 mL). The yellow color of the solution disappeared within 10 min and the reaction mixture was stirred at 0°C for 1 h. The filtrate obtained after removal of zinc dust was diluted with water, neutralized with sodium carbonate, and extracted with ether. Removal of solvent gave a pale yellow oil (0.4 g) which on short-path distillation (bulb-to-bulb, 120–160°C/0.05 Torr) afforded (**6**) as colorless crystals

(0.31 g, 82% yield), mp 120–122°C (from petroleum ether (30–60°C) – ether); $[\alpha]_D^{25}$ −68.0°(*c* 0.50, $CHCl_3$); τ (CCl_4): (dd, 1H, J = 7.0 and 4.5 Hz), 6.15 (d, 1H, J = 1.5 Hz), 6.75 (bs, 1H, exchanged with D_2O), 7.99 (s, 3H), 8.85, 8.91, and 9.03 (three singlets, 9H); ν_{max}: 3520, 2900, 1760, 1240 cm^{-1}; *m/e* (relative intensity): 226(M^+ 2), 198(18), 184(1), 167(3), 151(2), 138(100), 129(52), 123(55), 109(18). *Mol. Wt.* calcd. for $C_{12}H_{18}O_4$: 226.1204; found (high resolution mass spectrometry): 226.1204. *Anal.* calcd. for $C_{12}H_{18}O_4$: C 63.70, H 8.02; found: C 63.59, H 7.94.

(−)-6-endo-*Hydroxyisobornyl Acetate (7)*

To a solution of (−)-5-oxo-6-*endo*-hydroxyisobornyl acetate (**6**) (205 mg, 0.91 mmol) in 1,2-ethanedithiol (4 mL) was added freshly distilled boron trifluoride etherate (4 drops). A fine white precipitate was formed after 15 min and the reaction mixture was stirred at room temperature for 22 h. Water was added and the mixture was extracted with ether. Work-up in the usual way followed by removal of excess ethanedithiol by distillation (60–75°C/0.5 Torr) gave the ethylene thioketal as a colorless oil (233 mg, crude yield 85%). The crude product was distilled (bulb-to-bulb, 150–160°C/0.05 Torr) to give colorless crystals which on crystallization from petroleum ether (30–60°C) – ether, provided pure thioketal of (**6**), mp 102–104°C; τ (CCl_4): 5.22 (dd, 1H, J = 8.0 and 5.0 Hz) 6.14 (bs, 1H, $w_{1/2}$ = 10 Hz), 6.70–7.00 (m, 4H), 8.09 (s, 3H), 8.85, 9.00, and 9.16 (three singlets, 9H); ν_{max} (CCl_4): 3500, 2900, 1750, 1245 cm^{-1}; *m/e* (relative intensity): 302(M^+, 30), 274(20), 258(30), 242(5), 214(6), 186(100), 173(10), 168(30), 159(40), 134(20), 131(40), 126(20), 119(20), 111(20), 109(40). *Mol. Wt.* calcd. for $C_{14}H_{22}O_3S_2$: 302.1011; found (high resolution mass spectrometry): 302.1002. *Anal.* calcd. for $C_{14}H_{22}O_3S_2$: C 55.60, H 7.33, S 21.20; found: C 55.37, H 7.56, S 21.10.

In general the intermediate ethylene thioketal of **6** was desulfurized without purification. A slurry of Raney nickel (3 g) (Grace Davidson Chemical Co.) in ethanol was added to the ethylene thioketal of **6** (106 mg, 0.35 mmol) and the mixture refluxed for 1 h. Catalyst was removed from the cooled reaction mixture and the filtrate was concentrated by removal of most of the solvent. The residue was dissolved in ether and after washing (saturated sodium chloride) and drying (anhydrous magnesium sulphate) removal of solvent gave colorless solid (75 mg). Crystallization from petroleum ether (30–60°C) afforded 6-*endo*-hydroxyisobornyl acetate (**7**) (57 mg, 80% yield), $[\alpha]_D$ −70.7° (*c* 0.55, $CHCl_3$) (lit. (14) $[\alpha]_D$ −59.7° (*c* 1.5, $CHCl_3$)), mp 94.5°C (sublimation point ~80°C) (lit. (14) mp 94–94.5°C); τ (CCl_4): 4.72 (dd, 1H, J = 9.5 and 3.5 Hz), 8.06 (s, 3H), 9.05 and 9.18 (two singlets, 9H); ν_{max} (CCl_4): 3580, 2900, 1755, 1250 cm^{-1}; *m/e* (relative intensity): 212(M^+, 4), 194(1), 170(8), 155(18), 152(8), 137(6), 119(4), 108(100). *Mol. Wt.* calcd. for $C_{12}H_{20}O_3$: 212.1412; found (high resolution mass spectrometry): 212.1401. *Anal.* calcd. for $C_{12}H_{20}O_3$: C 67.89, H 9.50; found: C 68.07, H 9.53.

6-endo-tert-*Butyldimethylsilyloxyisoborneol (8)*

A mixture of (−)-6-*endo*-hydroxyisobornyl acetate (**7**) (400 mg, 1.88 mmol), *tert*-butyldimethylsilyl chloride (470 mg, 3.11 mmol) (Aldrich Chemical Co.), and imidazole (510 mg, 7.50 mmol) in dry dimethylformamide (10 mL) was heated at 85°C under nitrogen for 20 h. The reaction mixture was cooled, poured into water, and the solution extracted with a mixture (1:1) of ether and petroleum ether (30–60°C). Removal of solvent gave crude *tert*-butyldimethylsilyloxyisobornyl acetate (768 mg) which was hydrolysed without purification. A mixture of the acetate (730 mg) and potassium hydroxide (400 mg, 7.14 mmol) in 95% ethanol (15 mL) was refluxed for 1½ h. After cooling to room temperature part of the solvent was removed under reduced pressure and the residue dissolved in water and extracted with ether. The combined ether extract was washed thoroughly with water and dried over anhydrous magnesium sulphate. Removal of the solvent followed by column chromatography of the product on silica gel (activity grade III) yielded **8** as colorless solid (509 mg, 95% yield). Part of the product was sublimed (oil bath temperature 90°C, atmospheric pressure) to give **8** as colorless crystals, mp 77.0–78.0°C, sublimation point ~50°C; τ ($CDCl_3$, without TMS): 5.68 (dd, 1H, J = 7.0 and 4.0 Hz), 6.10 (dd, 1H, J = 10.0 and 3.5 Hz), 9.01, 9.12, 9.15, and 9.21 (four singlets, 18H, tertiary methyls), 10.02 and 10.04 (two singlets, 6H, $—SiCH_3$); ν_{max} (CCl_4): 3700, 3500, 3000, 1250 cm^{-1}; *m/e* (relative intensity): 284(M^+, 9), 269(23), 227(32), 151(100), 135(27), 123(18), 109(91). *Mol. Wt.* calcd. for $C_{16}H_{32}O_2Si$: 284.2171; found (high resolution mass spectrometry): 284.2184. *Anal.* calcd. for $C_{16}H_{32}O_2Si$: C 67.54, H 11.34; found: C 67.52, H 11.21.

6-exo-tert-*Butyldimethylsilyloxycamphene (9)*

6-*endo*-*tert*-Butyldimethylsilyloxyisoborneol (**8**) (509 mg; 1.79 mmol) in dry pyridine (15 mL) was treated with mesyl chloride (920 mg, 8.07 mmol) at room temperature under nitrogen for 15 min and then refluxed for 10 h. The resulting dark brown solution was cooled, diluted with water, and extracted with ether. The combined ether extract was washed with water and dried over anhydrous magnesium sulphate. Removal of solvent and chromatography of product (1.76 g) on silica gel (activity grade III) gave **9** as a colorless oil (192 mg, 40% yield); τ ($CDCl_3$, without TMS): 5.18 (bs, 1H), 5.40 (bs, 1H), 6.30 (dd, 1H, J = 7.0 and 3.0 Hz), 7.46 (bs, 1H), 9.00 (s, 3H), 9.05 (s, 3H), 9.15 (s, 9H), 10.00 (s, 6H); ν_{max} (CCl_4): 2950, 2900, 1650, 1460, 1360, 1260, 890 cm^{-1}; *m/e* (relative intensity): 266(M^+, 0.6), 251(4), 209(100), 191(6), 179(6), 165(6), 153(5), 135(13). *Mol. Wt.* calcd. for $C_{16}H_{30}OSi$: 266.2065; found (high resolution mass spectrometry): 266.2052.

Elution of the silica gel column with ether gave about 10 mg of colorless crystals with nmr, tlc, and glc characteristics of 6-*exo*-hydroxycamphene (nojigiku alcohol) (*vide infra*).

(+)-6-exo-*Hydroxycamphene (Nojigiku Alcohol) (10)*

Method A

6-*exo*-*tert*-Butyldimethylsilyloxycamphene (139 mg, 0.52 mmol) in dry tetrahydrofuran (10 mL) was stirred with tetra-*n*-butylammonium fluoride (10) (200 mg, 0.76 mmol) under helium in a dry box at room temperature for 15 min. Water was added, the solution extracted with ether, and the combined organic extracts washed with water and dried over anhydrous magnesium sulphate. Removal of solvent followed by column chromatography of product (165 mg) on silica gel (activity grade III) (4 g) provided compound **10** as colorless crystals (78 mg). Sublimation (oil bath temperature 70°C, atmospheric pressure) afforded **10** as colorless needles (62 mg, 78% yield), mp 67.5–69.5°C (sealed tube), sublimation point 52.0°C (lit. (1) mp 52–53°C, lit. (2*c*, 3*b*) mp 59.5–60°C, lit. (2*b*) mp 58–59°C, lit. (3*a*) mp 54–55°C); $[\alpha]_D^{25}$ +58.6° (*c* 1.33, $CHCl_3$), (lit. (1) $[\alpha]_D$ +12.0° (*c* 1.1, $CHCl_3$), lit. (2*c*) $[\alpha]_D^{20}$ +9°); τ (CCl_4): 5.21 (bs, 1H), 5.43 (bs, 1H), 6.29 (dd, 1H, J = 6.0 and 3.0 Hz), 7.48 (bs, $w_{1/2}$ = 4.0 Hz, 1H), 8.98 (s, 3H), and 9.30 (s, 3H); ν_{max} (CCl_4): 3700, 3400, 2900, 1670, 1060, 890 cm^{-1}; *m/e* (relative intensity): 152(M^+, 5), 137(7), 135(5), 134(2), 121(10), 119(12), 108(100). *Mol. Wt.* calcd. for $C_{10}H_{16}O$: 152.1201; found (high resolution mass spectrometry): 152.1209. *Anal.* calcd. for $C_{10}H_{16}O$: C 78.90, H 10.59; found: C 79.00, H 10.72.

The sublimed material was shown to be homogeneous on tlc (silica gel GF 254 with $CaSO_4$) and on various glc columns: 3% OV17 (90°C, from 120–200°C), 3% OV101 (90°C, from

120–200°C), 10% OV210 (from 120–200°C), 10% DEGS (from 120–170°C), and 10% Carbowax (from 90–200°C).

Method B

6-*exo*-*tert*-Butyldimethylsilyloxycamphene (**9**) (116.8 mg, 0.43 mmol) was dissolved in a mixture (10 mL) of acetic acid – water – THF (3:1:1). The solution was stirred at room temperature for 11 h then neutralized with sodium carbonate and extracted with ether. Work-up in the usual way afforded a colourless product (116.4 mg) which on column chromatography on silica gel (grade III) (4 g), elution with 10% ether–petroleum ether (30–60°C) provided (+)-6-*exo*-hydroxycamphene (62.0 mg, 94% yield) as colourless needles. Spectral data, glc retention time, tlc, R_f value, and specific rotation were identical to those of 6-*exo*-hydroxycamphene (**10**) prepared by method A.

*(+)-6-*exo*-Acetoxycamphene (**11**)*

A solution of (+)-6-*exo*-hydroxycamphene (**10**) (21.4 mg, 0.14 mmol) in acetic anhydride (100 mg, 0.99 mmol) and dry pyridine (10 mL) was heated at 100°C under nitrogen for 9 h. After cooling the reaction mixture was diluted with water and extracted with ether. Work-up in the usual way gave yellow oil (24 mg) which was chromatographed on silica gel (grade III) (2 g) to provide **11** as a colorless oil (19.6 mg, 72% yield); $[\alpha]_D^{25}$ +37.6° (*c* 1.11, $CHCl_3$) (lit. (1) $[\alpha]_D$ +20.9° (*c* 0.58, $CHCl_3$), +11.6° (*c* 1.20, $CHCl_3$)); τ (CCl_4): 5.08 (s, 1H), 5.35 (s, 1H), 5.56 (dd, 1H, J = 8.0 and 3.5 Hz), 7.30 (bs, $w_{1/2}$ = 4 Hz, 1H), 8.09 (s, 3H), 8.97 (s, 3H), 8.99 (s, 3H); ν_{max} (CCl_4): 2900, 1740, 1240, 1230, 895 cm^{-1}; *m/e* (relative intensity): 194(M^+, 21), 179(3), 150(100), 134(13), 119(13), 107(76). *Mol. Wt.* calcd. for $C_{12}H_{18}O_2$: 194.1306; found (high resolution mass spectrometry): 194.1320. *Anal.* calcd. for $C_{12}H_{18}O_2$: C 74.19, H 9.34; found: C 74.17, H 9.20.

*(+)-6-Oxocamphene (**12**)*

A solution of 6-*exo*-hydroxycamphene (**10**) (26.5 mg, 0.17 mmol) in methylene chloride (3 mL) was added to a suspension of pyridinium chlorochromate (12) (132 mg, 1.44 mmol) in methylene chloride (spectral grade) (3 mL). A dark brown precipitate was formed after 5 min and the reaction mixture was stirred at room temperature for 2 h. Filtration through a short Florisil column followed by removal of solvent from the filtrate gave a pale yellow oil (37 mg). Column chromatography of this oily product on silica gel (grade III) (3 g) afforded **12** as crystals (21 mg, 80% yield) which, on sublimation (bath temperature 50°C), provided colorless needles, mp 73.5–75.5°C (sealed tube), sublimation point 40°C (lit. (1) mp 47–49°C, lit. (2*b*) mp 65–70°C, lit. (3*a*) mp 75–76°C); $[\alpha]_D^{25}$ +158.2° (*c* 0.79, $CHCl_3$) (lit. (1) $[\alpha]_D$ +33.7° (*c* 0.86, $CHCl_3$); τ (CCl_4): 5.00 (bs, 1H), 5.25 (bs, 1H), 7.04 (bs, 1H), 8.81 (s, 3H), and 8.88 (s, 3H); ν_{max} (CCl_4): 2850, 1750, 1660, 895 cm^{-1}; *m/e* (relative intensity): 150(M^+, 100), 135(42), 121(25), 107(67), 106(83). *Mol. Wt.* calcd. for $C_{10}H_{14}O$: 150.1045; found (high resolution mass spectrometry): 150.1033. *Anal.* calcd. for $C_{10}H_{14}O$: C 79.95, H 9.39; found: C 79.72, H 9.25.

*(−)-6-*endo*-Hydroxyisoborneol (**16**)*

A mixture of (−)-6-*endo*-hydroxyisobornyl acetate (**7**) (74.5 mg, 0.35 mmol) and $Na_2CO_3 \cdot H_2O$ (100 mg, 0.8 mmol) in 5 mL methanol–water (1:1) was refluxed for 22 h. The reaction mixture was cooled and extracted with ether. Removal of solvent and crystallisation of the product from ether – petroleum ether (30–60°C) provided 6-*endo*-hydroxyisoborneol (**16**) (syn. 6-*exo*-hydroxyborneol) as colourless needles (see ref. 8 for physical constants).

Acknowledgements

We thank the National Research Council of Canada and the University of British Columbia for financial support.

1. (*a*) A. Matsuo, Y. Uchio, M. Nakayama, Y. Matsubara, and S. Hayashi. Tetrahedron Lett. 4219 (1974); (*b*) Y. Uchio. Bull. Chem. Soc. Jpn. **51**, 2342 (1978).
2. (*a*) B. H. Jennings and G. B. Herschbach. J. Org. Chem. **30**, 3902 (1965); (*b*) H. G. Richey, T. J. Garbacik, D. L. Dull, and J. E. Grant. J. Org. Chem. **29**, 3095 (1964); **30**, 3909 (1965); (*c*) M. Julia, D. Mansuy, and P. Detraz. Tetrahedron Lett. 2141 (1976).
3. (*a*) M. Gaitonde, P. A. Vatakencherry, and S. Dev. Tetrahedron Lett. 2007 (1964); (*b*) P. Lipp. Chem. Ber. **80**, 165 (1947).
4. N. J. Toivonen and A. Halonen. Suom. Kemistil. B, **19**, 1 (1946); Chem. Abstr. **41**, 5487 (1947); cf. D. H. Hunter. M.Sc. Thesis. University of British Columbia, Vancouver, B.C. 1974; M. S. Allen and T. Money. Unpublished observations.
5. B. Pfrunder and Ch. Tamm. Helv. Chim. Acta, **52**, 1630 (1969).
6. C. Coulombeau and A. Rassat. Bull. Soc. Chim. Fr. 505 (1971) and references cited.
7. I. Fleming and R. B. Woodward. J. Chem. Soc. C, 1389 (1968).
8. M. S. Allen, N. Darby, P. Salisbury, E. Sigurdson, and T. Money. Can. J. Chem. This issue.
9. E. Vedejs. J. Am. Chem. Soc. **96**, 5944 (1974); E. Vedejs, D. A. Engler, and J. E. Telschow. J. Org. Chem. **43**, 188 (1978).
10. E. J. Corey and A. Venkateswarlu. J. Am. Chem. Soc. **94**, 6190 (1972).
11. R. C. Weast (*Editor*). Handbook of chemistry and physics. 52nd ed. The Chemical Rubber Co., Cleveland, OH. 1971–1972.
12. E. J. Corey and J. W. Suggs. Tetrahedron Lett. 2647 (1975).
13. M. D. McCreary, D. W. Lewis, D. L. Wernick, and G. M. Whitesides. J. Am. Chem. Soc. **96**, 1030 (1974) and references cited; cf. K. A. Kime and R. E. Sievers. Aldrichimica Acta, **10**, 54 (1977).
14. J. de P. Teresa, I. S. Bellido, and J. F. S. Barrueco. An. Quim. **72**, 560 (1976).

Studies in membrane processes. VIII. A deuterium and sodium nuclear magnetic resonance investigation into the hexadecylpyridinium/hexadecyltrimethylammonium liquid crystalline system

LEONARD W. REEVES, ALAN S. TRACEY, AND MARCELLINE M. TRACEY
Department of Chemistry, University of Waterloo, Waterloo, Ont., Canada N2L 3G1
Received July 4, 1978

LEONARD W. REEVES, ALAN S. TRACEY, and MARCELLINE M. TRACEY. Can. J. Chem. **57**, 747 (1979).

Novel lyotropic mesophases that spontaneously orient in magnetic fields have been prepared using hexadecylpyridinium chloride and hexadecyltrimethylammonium bromide as well as, in limited regions, mixtures of the two detergents. These mesophases of type II provide the opportunity to study the behaviour of oriented water (DOH) at the hydrophobic interface, sodium ions, and the effect on hydrocarbon chain motions of variations in composition of the constituent bilayers formed by the mixed detergent systems. The pyridinium head group is especially accessible to definitive studies using deuterium magnetic resonance spectra of specifically deuteriated ring and adjacent hydrocarbon chain segments. Such investigations reveal the lack of cylindrical symmetry of motion about the extended chain axis near the pyridinium head group.

The deuterium resonance of the HOD species shows that both pyridinium and trimethylammonium head groups have a very small orienting effect on the adjacent water, which appears to be indifferent to the choice of these chemical identities. This is understandable in terms of the lack of hydrogen bonding to these moieties. Sodium ions also exhibit small quadrupole splittings in all systems studied here and thus probably play a passive role in the interface chemistry and structure.

LEONARD W. REEVES, ALAN S. TRACEY et MARCELLINE M. TRACEY. Can. J. Chem. **57**, 747 (1979).

On a préparé de nouvelles mésophases lyotropes qui s'orientent spontanément dans des champs magnétiques en utilisant du chlorure d'hexadécylpyridinium et du bromure d'hexadécyltriméthylammonium ainsi que, dans des régions limitées, des mélanges des deux détergents. Les mésophases de type II permettent d'étudier le comportement d'eau (DOH) orienté à l'interface hydrophobe, d'ions sodium et l'effet sur les mouvements de la chaîne hydrocarbonée de variations dans la composition des doubles couches constituantes formées par les systèmes de détergents mixtes. Le groupe pyridinium est particulièrement accessible pour des études définitives utilisant les spectres de résonance magnétique de cycles deutérés d'une façon spécifique et de segments de chaînes hydrocarbonées adjacentes. De telles études révèlent le manque de symétrie cylindrique dans le mouvement autour de l'axe prolongé de la chaîne près du groupe pyridinium.

La résonance du deutérium des espèces DOH montre que les groupes pyridinium ainsi que triméthylammonium ont un effet très faible sur l'orientation de l'eau adjacente qui semble être indifférente au choix de ces entités chimiques. On peut comprendre ce comportement en termes d'un manque de liaisons hydrogène vers ces moitiés. Les ions sodium présentent aussi de faibles couplages quadrupolaires dans tous les systèmes étudiées ici et jouent probablement un rôle insignifiant dans la chimie interfaciale et dans la structure.

[Traduit par le journal]

Introduction

The behaviour of water, alkali ions, halide ions, and hydrocarbon chains as a function of surfactant headgroup as well as the behaviour of the headgroups themselves are topics of considerable interest in various branches of chemistry, particularly those of colloid and interface chemistry, biochemistry of membranes, and the chemistry of lytropic liquid crystalline materials for which disciplines there are various broad areas of overlap.

One facet of lyotropic mesomorphic systems which has been of interest is how headgroups determine the motional behaviour of the hydrocarbon chains to which they are attached and also how they affect that of other alkyl chains with which they are associated in the bilayer. It has been found, for instance, that a carboxyl headgroup has a significantly greater restrictive effect on the hydrocarbon chain motions of neighbouring chains than does a trimethylammonium group (1). On the other hand, motions of individual chains are governed to a large extent by their respective headgroups (1, 2).

The headgroups of surfactants such as decyltrimethylammonium, decylsulfate, decylammonium,

0008-4042/79/070747-07$01.00/0

dodecanoate and others are all rather simple and as a result, using nuclear magnetic resonance techniques, it is often difficult to obtain information concerning the polar groups themselves. It has been found that liquid crystalline mesophases which spontaneously align in the magnetic field of an nmr spectrometer can be prepared from aqueous solutions of either hexadecylpyridinium chloride or hexadecyltrimethylammonium bromide (3). The pyridinium group is particularly useful since two order parameters may be measured for the pyridinium ring. None or only one such parameter may be obtained in most other cases. This headgroup is also of interest because of the inherently very large diamagnetic anisotropy of the aromatic ring compared to that of a hexadecyl chain. One question in this regard was whether the aromatic ring would cause a 90° rotation of the director from similar mesophases with the $-N(CH_3)_3$ headgroup since the diagmagnetic anisotropy of aromatic systems is opposite to that of hydrocarbon chains.

To investigate the behaviour of these two mesophases, the partially averaged deuterium quadrupole splittings from specifically and perdeuterated detergents and deuterated water as well as sodium quadrupole splittings from added sodium ions were utilized. Mixed detergent mesophases were also studied.

Results and Discussion

Lyotropic mesophases which are aligned by the magnetic fields of nmr spectrometers are readily prepared from both hexadecylpyridinium chloride and hexadecyltrimethylammonium bromide. Moreover, throughout a limited region the two mesophases can be prepared with the same molar proportions of all components, i.e., detergent, sodium chloride, decanol, and water. They may also be mixed in all proportions to give a mesophase with the same superstructure.

Preliminary experiments showed that both mesophases were of type II, that is, the directors are aligned perpendicular to the magnetic field (4, 5). This was established simply by observing the deuterium signal from a deuterated component of the mesophase and finding that spinning the sample tube in an iron core spectrometer had no effect on the deuterium doublet splitting. Type I mesophases align with their directors parallel to the magnetic field (4, 5) and spinning the sample provides a two dimensional powder spectrum immediately after cessation of spinning (6).

Several features of these mesophases were investigated. The anisotropic motions of the long hydrocarbon chains as determined from deuterium magnetic resonance of deuterated derivatives were of interest. Various properties of the pyridinium headgroup were investigated, particularly its alignment in these detergent systems. Some structural features of the pyridinium ring were determined.

Deuterium magnetic resonance studies of specifically or perdeuterated compounds in mesomorphic materials have proven to be of considerable value for obtaining degrees of order of micro-axes of such materials (1–11). This arises because the deuterium quadrupole splitting is generally not averaged to zero in liquid crystalline materials and the residual splitting is determined by the alignment of that material in the magnetic field. Quadrupole splittings arise from the presence of electric field gradients and the deuterium splitting, $\Delta\nu$, is given by the expression [1].

$$[1] \qquad \Delta\nu = \tfrac{3}{2}Q_D[S_{zz}^0 + (\eta/3)(S_{xx}^0 - S_{yy}^0)]$$

where Q_D is the deuterium quadrupole coupling constant, η given the asymmetry in the electric field gradients, and S_{zz}^0, S_{yy}^0, and S_{xx}^0 give the alignment of a coordinate system in which the Z^0 axis coincides with the major axis of the electric field gradient. For deuterated hydrocarbons the major axis of the field gradient is very close to the carbon–deuterium bond axis and is generally assumed to coincide with that axis. For saturated systems it is usually assumed that the asymmetry in the electric field gradient is negligibly small, the measured value for instance being less than 0.01 in deuterated cyclohexane (12). Assuming the two above conditions, eq. [1] reduces to [2]

$$[2] \qquad \Delta\nu = (3/2)Q_D S_{CD}$$

where S_{CD} gives the alignment of the carbon–deuterium bond in the magnetic field.

For aromatic systems the asymmetry parameter is not negligible, having values in the order of 0.04 to 0.06 (12, 13). In this particular case we are concerned with the alignment of the pyridinium group as a unit. If we adopt a pyridinium fixed coordinate system such as shown in Fig. 1, then by simple coordinate transformation we can obtain the expressions [3], [4], and [5] (14)

$$[3] \quad \Delta\nu_1 = \tfrac{3}{2}Q_{D_1}[S_{zz} - \cos^2\gamma_1(S_{zz} - S_{yy}) + (\eta_1/3)(2S_{yy} + S_{zz} + \cos^2\gamma_1(S_{zz} - S_{yy}))]$$

$$[4] \quad \Delta\nu_2 = \tfrac{3}{2}Q_{D_2}[S_{zz} - \cos^2\gamma_2(S_{zz} - S_{yy}) + (\eta_2/3)(2S_{yy} + S_{zz} + \cos^2\gamma_2(S_{zz} - S_{yy}))]$$

$$[5] \quad \Delta\nu_3 = \tfrac{3}{2}Q_{D_3}[S_{zz} + (\eta_3/3)(2S_{yy} + S_{zz})]$$

where S_{xx}, S_{yy}, and S_{zz} are the order parameters for a coordinate system fixed in the pyridinium ring. Since any differences between the quadrupole coupling constants, Q_{D_i}, and asymmetry parameters, η_i, will be unimportant, we can subtract [5] from [3] and [4]

TABLE 1. Deuterium quadrupole splittings from the perdeuterated pyridinium group in various concentrations in the mixed hexadecylpyridinium/hexadecyltrimethylammonium mesophase. Deuterium splitting from specifically labelled decanol are included as are the experimental ratios for cos γ_2/cos γ_1 (see Fig. 1) (HDPCl = hexadecylpyridinium chloride)

Composition		Quadrupole splittings (kHz)						
		Pyridinium*				Decanol-1,1,2,2-d_4†		Water*
Phase	Mol% HDPCl in total detergent	$\Delta\nu_{1,5}$	$\Delta\nu_{2,4}$	$\Delta\nu_3$	(cos γ_2/cos γ_1)	$\Delta\nu_1$	$\Delta\nu_2$	$\Delta\nu$
1	4.7	6.972	9.341	−8.911	1.0720	15.05	14.10	0.019
2	25.4	5.961	7.988	−7.680	1.0717	12.78	12.06	—
3	49.9	4.697	6.27	−6.27	1.069	9.64 (broad)		0.020
4	75.2	4.700	6.24	−6.24	1.068	9.62 (broad)		0.024
5	100.0	5.586	7.54	−7.54	1.072	11.41		0.029

*Errors in quadrupole splittings from non-overlapping transitions are estimated to be less than 5 Hz.
†Errors in quadrupole splittings are estimated to be less than 1%.

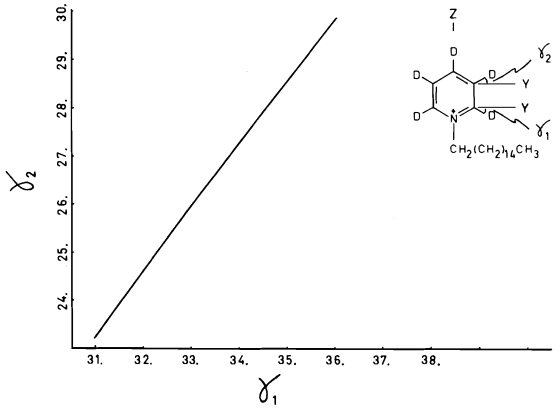

FIG. 1. The relationship between the angles γ_1 and γ_2 which are defined relative to a molecular fixed coordinate system is shown.

to obtain eqs. [6] and [7]

$$[6] \quad 2(\Delta\nu_1 - \Delta\nu_3) = Q_D \cos^2 \gamma_1 (S_{zz} - S_{yy})(\eta - 3)$$

$$[7] \quad 2(\Delta\nu_2 - \Delta\nu_3) = Q_D \cos^2 \gamma_2 (S_{zz} - S_{yy})(\eta - 3)$$

from which it is clear that

$$[8] \quad (\Delta\nu_1 - \Delta\nu_3)/(\Delta\nu_2 - \Delta\nu_3) = \cos^2 \gamma_1 / \cos^2 \gamma_2$$

Equations [3] to [7] by themselves are not particularly useful because of the large number of unknown parameters required. The quadrupole coupling constants may be estimated to be about 185 kHz (12, 13, 15) and the asymmetry parameter about 0.05 (12). The exact values are not critical but even so the above estimates are unlikely to be in error by more than 5.0 kHz and 0.01 in Q_D and η, respectively. The parameter S_{zz}, the alignment of the C_2 symmetry axis of the pyridinium, may be estimated reasonably well by neglecting η but from only deuterium quadrupole splittings no estimate of S_{yy} can be obtained without structural assumptions, i.e. either of the angles γ_1 or γ_2 which are related by eq. [8]. Equation [8] is a particularly useful expression since with even rather crude angle assumptions it will establish the relative signs of the quadrupole splittings. Specifically deuterated compounds were used to ascertain the proper assignments of quadrupole splittings.

Table 1 gives various deuterium splittings obtained from the pyridinium ring and as a reference, the deuterium splitting from decanol deuterated in the 1,2 positions. The ratio, cos γ_2/cos γ_1, is also given. In this case it should be noted that often transitions from deuteriums 2 and 3 overlap so that individual resonances were not observed and as a consequence the mean frequency was assigned to the splittings. Even so, the agreement between the various mesophases is extremely good. It is clear from the results that in order to obtain a constant ratio of cosines, the quadrupole splitting $\Delta\nu_3$ is of opposite sign to those of positions 1 and 2. The ratio obtained from only the completely resolved spectra (entries 1 and 2 from Table 1) is 1.0718 ± 0.0002 and the angles corresponding to this ratio are plotted in Fig. 1. The results shown in Fig. 1 demonstrate that the two angles must differ by 6 or 7°. Since the angular distortion from the 30° of a hexagon is caused mostly by the fact that the C—N bond is shorter than the C—C bond, it can be expected that γ_1 is greater than 30° while γ_2 is less than that value. If we make the following assumptions $\gamma_2 = 28°$, $\eta = 0.05$, and $Q_D = 185$ kHz we can determine from Fig. 1 that $\gamma_1 = 34.5°$ and from eqs. [5] and [7] and the specific quadrupole splittings $\Delta\nu_{1,5} = 7.208$ kHz and $\Delta\nu_3 = -9.731$ kHz that $S_{zz} = -0.0363$, $S_{yy} = 0.0552$, and finally $S_{xx} = -0.0189$. Note that relative signs of the order parameters are given, not absolute values. The value determined for S_{zz} is insensitive to the angle assumed for γ_2. S_{yy} depends on that value, increasing in magnitude about 3–4% for each 1° increment in angle assumed. For our purposes this effect is not important unless there is a very large error in the assumed angle.

We can now do a coordinate transformation from a coordinate system locked to the pyridinium headgroup to a new system fixed with respect to an axis located in the first methylene segment of the hexadecylpyridinium ion as depicted below.

The two coordinate systems are related by eq. [9]

$$[9] \quad S_{zz} = \cos^2 \phi_{zz} S_{zz}' + \cos^2 \phi_{yy} S_{yy}' + \cos^2 \phi_{xx} S_{xx}'$$

and similar expressions for S_{yy} and S_{xx} which combined with the trace relationship that $S_{xx} + S_{yy} + S_{zz} = 0$ give the following values for conformation A shown. $S_{xx}' = -0.0014$, $S_{yy}' = 0.0552$, and $S_{zz}' = -0.0538$. These values are extremely small, providing a calculated methylene quadrupole splitting about one-half that observed experimentally. Thus conformation A is probably not very important.

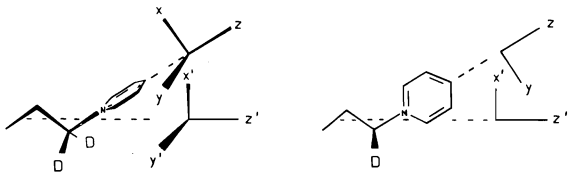

A B

Order parameters from conformation B give S_{xx}', S_{yy}', and S_{zz}' equal to $+0.1467$, -0.0189, and -0.1278, respectively. These are closer to experimental values.

The above transformation has been made in order to determine whether the pyridinium with its attached hydrocarbon chain behaves as an effectively cylindrically symmetric system at the headgroup. For this symmetry and an S_{zz}' of -0.1278, S_{xx}' and S_{yy}' should both equal $+0.0639$. Clearly this condition is not even approximately true at the pyridinium position. Different structural assumptions will change the calculated parameters, particularly because the pyridinium residue can rotate. However, if conformation B represents the dominant rotamer as is suggested by the values computed for S_{xx}', S_{yy}', and S_{zz}' the deuterium quadrupole splitting at the methylene group of position 1 can be calculated. The values are 16.3 kHz and 9.3 kHz using effective cylindrical symmetry from S_{zz}' and noncylindrical symmetry, respectively. The observed value is 11.71 kHz for the methylene splitting in the particular case corresponding to the pyridinium values previously used. The agreement is not particularly good. However, when we note the unusual and large increase in methylene quadrupole splitting by going from position 1 to 2, i.e., 11.71 kHz compared to 14.06 kHz, one sees that this latter value at the plateau of the order profile is in much better accord with an effective axial symmetry, a view which is supported by the fact that the 14 kHz splitting extends from methylene 2 to 9 inclusive. The lack of exact agreement in this latter case probably reflects the fact that the pyridinium is not fixed with respect to these methylenes but undergo hindered rotation about the C—N axis. Under the assumption that S_{zz}' is determined by the 14.06 kHz splitting, i.e. $S_{zz}' = -0.1103$, the parameters S_{xx}' and S_{yy}' may be determined for the α-methylene from the $\Delta\nu$ of 11.71 kHz and eq. [2] in conjunction with eq. [9]. The order parameters obtained are 0.0828, 0.0275, and -0.1103 for S_{xx}', S_{yy}', and S_{zz}', respectively. These calculations indicate strongly that there is a large deviation from axial symmetry at the α-methylene.

Referring again to Table 1, a comparison of the results from the specifically deuterated pyridinium ring in the various mixed mesophases shows that the mixing of the detergents has little effect on the alignment. The decanol specifically substituted in the 1 and 2 positions does show a small effect from the changing compositions. In the hexadecylpyridinium mesophase the two decanol resonances are well resolved. This contrasts with the results from the hexadecyltrimethylammonium phase where only one signal was observed for the two positions. Mixing of the detergents revealed a gradual collapse in separation between the splittings on going from the one extreme to the other. This gradual collapse coupled with the lack of significant change in the alignment of the pyridinium indicated that nothing extraordinary occurred to the micellar superstructure or the interface when mixing the two detergents, indeed the integrity of the mesophase is preserved.

Investigation of sodium ions and deuterated water showed that species in the aqueous region were also insensitive to changes in composition of the mesophase. Unfortunately deuterium resonance of deuterated water was not very helpful because of the very small water splittings, typically less than 30 Hz. This, however, does show that water associated with the cationic headgroups is essentially isotropic, particularly when one bears in mind the large differences in shape between pyridinium and trimethylammonium. Nuclear magnetic resonance spectra from the sodium ion showed that its behaviour was virtually unaffected by the replacement of one detergent with the other. The sodium quadrupole splittings changed very little on going from the extreme of one mesophase to the other (Table 2). Because of the similarity of the results from the various mixed mesophases it was decided to investigate the chain motion of the hexadecyl chains only at the two extremes of composition.

Methylene quadrupole splittings serve as a good indicator of the relative motion of the various methylene segments in the same chain. Figure 2

TABLE 2. Sodium quadrupole splittings for the various mixed mesophases indicated. The sodium splittings increase in magnitude as the sample warms from room temperature to magnet temperature (32°C) (HDTMABr = hexadecyltrimethylammonium bromide, HDPCl = hexadecylpyridinium chloride)

Phase composition (each component in mg)					Quadrupole splitting (Hz)*
HDTMABr	HDPCl	NaCl	H_2O	Decanol	^{23}Na
595	—	43	1052	114	1078
471	90	43	1050	114	966
446	139	43	1052	113	922
297	277	43	1050	116	897
149	416	43	1050	120	869
—	555	44	1054	114	759

*Errors in quadrupole splittings are estimated to be less than 1%.

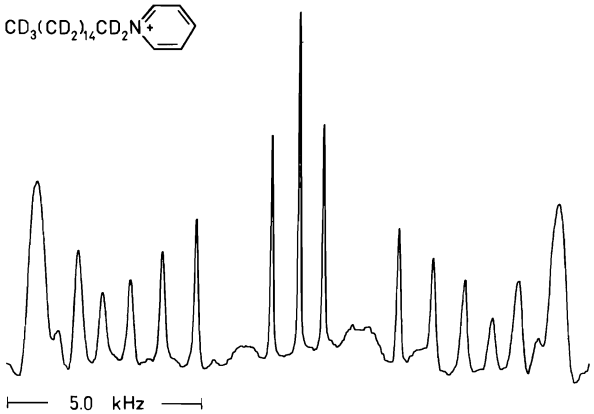

FIG. 2. A deuterium magnetic resonance spectrum from the perdeuterated chain of hexadecylpyridinium in a lyotropic mesophase.

shows a spectrum from a perdeuterated hexadecyl chain attached to the pyridinium headgroup. The relative linewidth of the intense outer transitions, which arise from superimposed methylene quadrupole splittings, compared to the other transitions show the small range of values over which those splittings are spread. Table 3 gives the measured deuterium quadrupole splittings from the various methylene groups for the hexadecylpyridinium mesophase. The values for the hexadecylpyridinium as a minor component in a hexadecyltrimethylammonium phase are included as are the corresponding results for the perdeuterated hexadecyl chain of the trimethylammonium derivative. The splittings for decanol, which is a minor component in the mesophases, are also given. Note that the values reported in Tables 1 and 3 are for a dilute ($\sim 10\%$ by weight) labelled component in total detergent.

The magnitudes of the splittings from the various components of the mesophases are all similar and provide minimal information concerning the relative chain motions. However, information can be extracted from these splittings by obtaining their ratios. Typically this is done by dividing all the methylene quadrupole splittings from a particular chain by the value obtained for the terminal methyl group. The advantage of these ratios is that the contributions to the deuterium quadrupole splittings which arise because of rigid body motions of the chain cancel. The resultant chain profiles provide information concerning the internal motion of the hydrocarbon chains and in particular allow comparisons to be drawn between different chains and between different mesophases (1). Figure 3 shows the chain motion profiles for the three components of the two mesophases investigated, 15.1 and 87.5 mol% hexadecylpyridinium chloride in total detergent, the second detergent of course being hexadecyltrimethylammonium bromide. A major feature of the hexadecyl chain profile from the pyridinium salt is the value for the ratio between the methyl and the plateau methylene quadrupole splittings. This ratio is 8.4 in the pyridinium mesophase and rises to 10.1 where hexadecylpyridinium is associated mainly with the trimethyl derivative. A ratio of three is expected for a rigid rapidly rotating chain. This value becomes larger with increase in chain flexibility which is related to the increased probability for random *gauche* rotamers to occur near the terminal positions of the hydrocarbon chains.

Figure 3 clearly shows that this ratio for the hexadecyl chain of hexadecylpyridinium increases as the pyridinium is diluted in trimethylammonium thus indicating more freedom for the formation of isolated *gauche* rotamers. A similar but opposite behaviour for the trimethylammonium's hexadecyl chain is also observed. The results indicate that in this latter case the hexadecyl chain is least restricted in its motion when in the pyridinium phase but becomes much more restricted with an increasing

TABLE 3. Deuterium quadrupole splitting from perdeuterated hexadecyl hydrocarbon chains and perdeuterated decanol. The mole fraction of hexadecylpyridinium chloride (HDPCl) in total detergent is also indicated for the various mesophases

Mol% HDPCl	Quadrupole splitting* (kHz) at positions															
	1	2	3	4	5	6	7	8	9	10	11	12	13	14	15	16
Hexadecyl-d_{33}-pyridinium																
100	12.24	14.54	14.54	14.54	14.54	14.54	14.54	14.54	14.54	13.48	12.56	11.49	10.16	8.47	6.50	1.73
14.1	11.44	13.44	13.44	13.44	13.44	13.44	13.44	13.44	13.44	12.44	11.44	10.14	8.67	7.03	5.26	1.34
Hexadecyl-d_{33}-trimethylammonium																
15.2	16.16	16.16	16.16	16.16	16.16	16.16	16.16	16.16	16.16	14.92	13.85	12.45	10.87	8.82	6.72	1.66
87.1	12.64	12.64	12.64	12.64	12.64	12.64	12.64	12.64	12.64	12.10	11.38	10.50	9.39	7.81	6.13	1.60
Decanol-d_{21}																
15.1	14.81	13.79	14.81	15.49	14.81	14.81	13.79	11.88	9.54	2.43						
84.9	11.47	11.47	11.47	12.02	11.47	11.47	10.74	9.51	7.75	2.06						

*Errors in quadrupole splittings are estimated to be less than 1%.

proportion of hexadecyltrimethylammonium. The relative motional freedom of the two chains have interchanged on going from the one extreme to the other. This type of behaviour has not been observed previously but since in both cases hexadecyl chains are being observed, this change in relative motion must be determined by the headgroup through both its own orienting influence and through its interaction with its neighbours. The very flat hexadecyl chain profile for the trimethylammonium derivative strongly suggests that only one order parameter is required for a description of its alignment, at least in the plateau region.

The chain profiles for deuterated decanol are relatively insensitive to the composition of the mesophase as is evident from Fig. 3. Of particular interest here is the fact that decanol, having a chain only ten carbons long, is significantly shorter than the other chains which are sixteen carbons long. As a consequence if the hydroxyl group is in the interface then effectively the whole decyl chain is confined to the highly aligned portion of the bilayer, i.e., the methylene quadrupole splittings from the hexadecyl chains begin dropping at carbon 10. This should have a substantial effect on the chain profile as compared to the profile from other mesophases prepared from shorter chain detergents such as decylammonium, decylsulfate, or dodecanoate, for example. In such mesophases the plateau to methyl splitting ratio varies from about 7 to 9 to compare with the value here of 6. Even this value is surprisingly large but probably results from the fact that the detergent headgroups are quite bulky and allow the chains to retain considerable motional freedom. In mesophases containing decyltrimethylammonium bromide, compared to hexadecyltrimethylammonium here, the ratios for decanol are the largest so far observed, being about 9 (1).

Recently the importance of pure components for the preparation of lyotropic liquid crystals was strongly stressed, the authors having difficulty in reproducing previously published results (19). Unfortunately those same authors used "commercially supplied detergents" without "purification". Commercial detergents simply are much too impure and generally three if not more recrystallizations from distilled solvents are required to obtain good reproducibility of results.

Experimental

Perdeuterated hexadecanoic acid was prepared using an adaption of the process of Stenhagen and Dinh-Nguyen (16). Adam's catalyst, PtO_2 (3.67 g in 50 mL D_2O), was reduced with D_2 gas under 1–2 atm pressure. The mixture was transferred with 100 mL D_2O to a stainless steel pressure vessel cooled in an ice/water bath, and Na_2O_2 (2.32 g) was added slowly. Potassium hexadecanoate (20 g) was added, followed by an

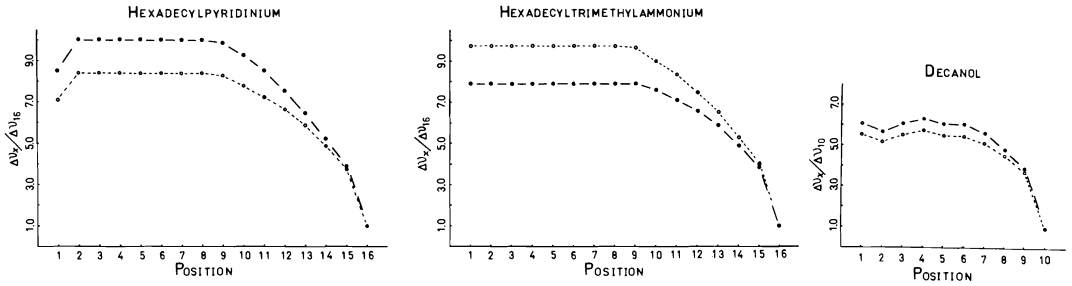

FIG. 3. Chain motion profiles for the three amphiphile components of the lyotropic mesophases. ○, 85 mol% hexadecylpyridinium chloride in total detergent; ●, 15 mol% hexadecylpyridinium chloride in total detergent. The second detergent is hexadecyltrimethylammonium bromide.

additional 75 mL D_2O. The vessel was equipped with a magnetic spin bar, then sealed, frozen in Dry Ice, and evacuated. The reaction mixture was heated, with stirring, using a salt bath (sodium nitrite:potassium nitrate 7:10 by weight) at 220°C for 10 days. The contents were acidified with HCl, and the acid extracted into $CHCl_3$. The chloroform layer was filtered to remove the spent platinum and the solvent removed under reduced pressure using a Buchi rotary evaporator. The acid was then distilled under reduced pressure. Approximately a 90% exchange of deuterium for hydrogen was obtained in 95% yield.

1-Hexadecyl-d_{33}-pyridinium Chloride

Perdeuterated hexadecanoic acid was converted to the acid chloride with thionyl chloride and the acid chloride reduced with $LiAlD_4$ to give the perdeuterated hexadecanol. The alcohol was converted to the bromide with constantly boiling HBr (17). Hexadecylpyridinium bromide was prepared by warming on a hot plate for $1\frac{1}{2}$ h equal molar proportions of hexadecylbromide and pyridine. The bromide was recrystallized from ethylacetate.

1-Hexadecylpyridinium bromide was dissolved in methanol and a slight molar excess of Ag_2O was added. (Water added at this point caused rapid decomposition of the pyridinium salt.) After the mixture was stirred for 1/2 h, the solution was filtered and the filtrate acidified with HCl. The methanol was removed under reduced pressure and the 1-hexadecylpyridinium chloride was crystallized from ethylacetate.

1-Hexadecyl-d_{33}-trimethylammonium Iodide

Perdeuterated hexadecanol was converted to the hexadecyliodide with red phosphorus and iodine using standard techniques (18). The iodide (3.6 g) was added to methanol (100 mL) and trimethyl amine (16 mL of a 25% solution in water) was added. The reaction mixture was stirred overnight at room temperature. Methanol and water were removed under reduced pressure and the resulting salt was crystallized from ethylacetate/ethanol. The corresponding chloride and bromide were prepared from the iodide by the Ag_2O method above. All salts were crystallized from ethylacetate.

Acknowledgements

We are thankful to the National Research Council of Canada for its financial support for this work and to Keith Radley for indicating to us that hexadecyltrimethylammonium bromide forms a liquid crystalline solution which spontaneously aligns in the magnetic field of an nmr spectrometer.

1. A. S. TRACEY, L. W. REEVES, and Y. LEE. To be published.
2. L. W. REEVES and A. S. TRACEY. J. Am. Chem. Soc. **97**, 5729 (1975).
3. F. FUJIWARA, L. W. REEVES, A. S. TRACEY, and M. M. TRACEY. Abstracts of Papers, 175th Am. Chem. Soc. Meeting, Anaheim, California, U.S.A. 1978.
4. C. L. KHETRAPAL, A. C. KUNWAR, A. S. TRACEY, and P. DIEHL. NMR Basic Principles and Progress, **9** (1975).
5. K. RADLEY, L. W. REEVES, and A. S. TRACEY. J. Phys. Chem. **80**, 174 (1976).
6. F. Y. FUJIWARA and L. W. REEVES. Can. J. Chem. **56**, 2178 (1978).
7. A. SEELIG and J. SEELIG. Biochemistry, **13**, 4839 (1974).
8. R. A. HABERKORN, R. G. GRIFFIN, M. D. MEADOWS, and E. OLDFIELD. J. Am. Chem. Soc. **99**, 7353 (1977).
9. G. W. STOCKTON, C. F. POLNASZEK, A. P. TULLOCH, F. HASAN, and I. C. P. SMITH, Biochemisty, **15**, 965 (1975).
10. N. O. PETERSEN and S. I. CHAN. Biochemistry, **16**, 2657 (1977).
11. J. H. DAVIS and K. R. JEFFREY. Chem. Phys. Lipids, **20**, 87 (1977).
12. R. G. BARNES and J. W. BLOOM. J. Chem. Phys. **57**, 3082 (1972).
13. F. S. MILLETT and B. P. DAILEY. J. Chem. Phys. **56**, 3249 (1972).
14. P. DIEHL and A. S. TRACEY. Can. J. Chem. **53**, 2755 (1975).
15. P. DIEHL and M. REINHOLD. Mol. Phys. **36**, 143 (1978).
16. E. A. STENHAGEN and N. DINH-NGUYEN. Chem. Abstr. **67**, 63814 (1971).
17. O. KAMM and C. S. MARVEL. Org. Synth. Coll. **I**, 25 (1941).
18. W. W. HARTMEN, J. R. BYERS, and J. B. DICKEY. Org. Synth. Coll. **II**, 322 (1943).
19. A. LOEWENSTEIN, M. BRENMAN, and R. SCHWARZMANN. J. Phys. Chem. **82**, 1744 (1978).

Nuclear magnetic resonance studies of the solvation of phosphorus(V) selenides, 1,2-bis(diphenylphosphino)ethane, and tris(dimethylamino)phosphine telluride by sulfur dioxide[1,2]

PHILIP A. W. DEAN

Department of Chemistry, University of Western Ontario, London, Ont., Canada N6A 5B7

Received September 12, 1978

PHILIP A. W. DEAN. Can. J. Chem. **57**, 754 (1979).

^{31}P and ^{77}Se nmr spectra have been measured for a range of phosphorus(V) selenides, diphosphorus(V) diselenides, and triphosphorus(V) triselenides in the inert solvent CH_2Cl_2 and in liquid SO_2. Significant roughly-correlated reductions in $|^1J(PSe)|$ and deshielding of the ^{77}Se resonance accompany change of solvent from CH_2Cl_2 to SO_2. These changes are shown to arise from 1:1 phosphorus(V) selenide:SO_2 donor:acceptor complex formation. Approximate thermodynamic constants for the formation of the complexes have been determined and possible structures for the 1:1 complexes with the diphosphorus(V) diselenides discussed. It is shown from ^1H and ^{31}P nmr spectral changes that $Ph_2P(CH_2)_2PPh_2$ forms a 1:1 complex with SO_2, and approximate thermodynamic data for the SO_2 complexation of the diphosphine have been established. Complexation is indicated by changes in both $|^1J(PTe)|$ and δ_P when $(Me_2N)_3PTe$ is dissolved in SO_2, but the chemical reactivity of this system precluded detailed study.

PHILIP A. W. DEAN. Can. J. Chem. **57**, 754 (1979).

On a déterminé les spectres rmn du ^{31}P et du ^{77}Se d'un certain nombre de sélénures de phosphore(V), de disélénures de diphosphore(V) et de trisélénures de triphosphore(V) dans le solvant inerte CH_2Cl_2 et dans le SO_2 liquide. Un changement de solvent de CH_2Cl_2 à SO_2 s'accompagne de réductions marquées qui présente une corrélation grossière des $|^1J(PSe)|$ et des déblindages de la résonance du ^{77}Se. On a montré que ces changements sont dus à la formation d'un complexe 1:1 donneur:accepteur sélénure de phosphore(V):SO_2. On a déterminé les constantes thermodynamiques approximatives pour la formation des complexes et on discute des structures possibles des complexes 1:1 avec les disélénures de diphosphore. On a montré, grâce aux changements dans les spectres rmn du ^1H et du ^{31}P, que le $PH_2P(CH_2)_2PPH_2$ forme un complexe 1:1 avec le SO_2 et on a déterminé les données thermodynamiques approximatives pour la complexation de la diphosphine par le SO_2. La complexation est révélée par des changements à la fois dans $|^1J(PTe)|$ et dans le δ_P lorsqu'on dissout du $(Me_2N)_3PTe$ dans le SO_2; la réactivité chimique de ce système ne permet par une étude plus détaillée.

[Traduit par le journal]

Introduction

Our studies of the complexation of phosphorus(V) selenides by metal ions in liquid sulfur dioxide (1–3) have, of necessity, required an nmr spectroscopic investigation of the ligands alone in this medium. Previously, this class of ligands has been studied in "inert" media by both ^{31}P (4–7) and ^{77}Se (7) nmr. Where there is overlap, our data are in agreement with earlier work, but we find that use of SO_2 as solvent leads to significantly different ^{31}P and ^{77}Se nmr parameters. Our results, and their interpretation in terms of specific SO_2-solvation of the phosphorus(V) selenides are presented here.

To further study the generality of SO_2-solvation of "soft" donors, we have also investigated the interaction of $Ph_2P(CH_2)_2PPh_2$ and $(Me_2N)_3PTe$ with SO_2. In an earlier ^{13}C nmr study, it was shown that SO_2 acts as an acceptor towards triphenylphosphine (1).

Results

In most cases, the ^{31}P and ^{77}Se nmr spectra of the compounds examined could be analyzed readily. The ^{77}Se satellites in the ^{31}P-{H} spectra, and the ^{77}Se-{H} spectra of monophosphorus(V) monoselenides, diphosphine monoselenides, and diphosphorus(V) diselenides are the appropriate parts of AX, AMX, and AA'X (ABX if the (experimentally unobserved) selenium isotope effect is included) spectra, X being ^{77}Se. Because of the zero values of $^4J(P–P)$ and $^5J(P–Se)$, $(Ph_2P(Se)CH_2)_3CMe$ gives rise to an AX spectrum. $Ph_2P(Se)(CH_2)_2(Se)PPh(CH_2)_2$-$P(Se)Ph_2$ gives rise to two sets of ^{77}Se satellites in the ^{31}P-{H} spectrum: the AB_2 part of an AB_2X spectrum from $Ph_2P(Se)(CH_2)_2(^{77}Se)PPh(CH_2)_2$-

[1]No reprints available.

[2]Presented, in part, at the 61st Annual Conference of the Chemical Institute of Canada, Winnipeg, Manitoba, Canada, June 1978, and the 6th International Conference on Non-aqueous Solvents, Waterloo, Ont., Canada, August, 1978.

0008-4042/79/070754-08$01.00/0

TABLE 1. Changes in $|^1J(PSe)|$ and δ_P of phosphorus(V) selenides caused by SO_2 solvation (308 K)

Phosphorus(V) selenide	$\|^1J(PSe)\|$(Hz)[a]		^{31}P chemical shift (ppm)[b]	
	CH_2Cl_2	SO_2	CH_2Cl_2	SO_2
$SeP(OMe)_3$[c]	957	934	75.9	73.2
$SeP(NMe_2)_3$	795	718	80.4	75.5
$SePPh_3$[d]	736	690	32.9	33.2
$SeP(p\text{-}C_6H_4Me)_3$	728	678	31.4	31.9
$SePMePh_2$[e]	725	670	21.0	23.4
$SeP(o\text{-}C_6H_4Me)_3$	711	664	25.8	26.8
$SePEt_3$	691	622	42.3	46.8
$SeP(C_6H_{11})_3$	683	618	56.3	60.1
$[Ph_2P(Se)]_2CH_2$[f]	753	719	23.1	23.8
$[Ph_2P(Se)]_2(CH_2)_2$[g]	736	696	33.6	34.7
$[Ph_2P(Se)]_2(CH_2)_3$	730	684	32.0	30.7
$[Ph_2P(Se)]_2(CH_2)_4$	730	679	31.6	33.2
$[Ph_2P(Se)]_2(CH_2)_5$	728	675	31.8	33.4
$[Ph_2P(Se)]_2(CH_2)_6$	728	675	31.5	33.4
$[Ph_2P(Se)CH_2]_3CMe$	722	691	20.9	22.0
$[Ph_2P(Se)(CH_2)_2]_2P(Se)Ph$	737[h]	700[i]	33.5	34.8
$[Ph_2P(Se)(CH_2)_2]_2P(Se)Ph$	734[h]	702[i]	39.8	41.6

[a]Reproducibility $\approx \pm 1$ Hz; $^1J(PSe)$ is known to be negative for phosphorus(V) selenides (7).
[b]Measured relative to external $OP(OMe)_3$ in $(CD_3)_2CO$ and corrected for susceptibility difference; downfield shifts positive.
[c]In pure $SeP(OMe)_3$, $|^1J(PSe)| = 961$ Hz.
[d]In $CHCl_3$, $|^1J(PSe)| = 731 \pm 2$; in acetone, $|^1J(PSe)| \sim 742$ Hz.
[e]In pure $SePMePh_2$, $|^1J(PSe)| = 728$ Hz.
[f]$|^2J(PP)| = 14.7$ Hz in CH_2Cl_2, 13.5 Hz in SO_2. $|^3J(PSe)| \sim 1.9$ Hz in both solvents.
[g]$^3J(PP) = \pm 64.9$ Hz in CH_2Cl_2, ± 66.2 Hz in SO_2. $^4J(PSe) = \mp 0.5$ Hz in both solvents.
[h]$^3J(PP) = \pm 62.6$ Hz; $^4J(P_{terminal}\text{–}Se) = \mp 4.1 \pm 1.0$ Hz; $^4J(P_{central}\text{–}Se) = \mp 1.4 \pm 0.8$ Hz.
[i]$^3J(PP) = \pm 63.9$ Hz; $^4J(P_{terminal}\text{–}Se) = 0.1 \pm 0.5$ Hz; $^4J(P_{central}\text{–}Se) = \mp 0.9 \pm 0.4$ Hz.

$P(Se)Ph_2$, and the AA′B (or ABC) part of an AA′BX spectrum (or ABCX spectrum with an isotope effect included) from $Ph_2P(^{77}Se)(CH_2)_2(Se)PPh(CH_2)_2P(Se)Ph_2$. In this case, the centreband obscured much of the satellite spectrum and only an approximate analysis was possible.

In Table 1 are presented ^{31}P nmr spectral parameters for the phosphorus(V) selenides in the inert solvent CH_2Cl_2 and in SO_2. Table 2 shows the analogous ^{77}Se nmr data for those compounds in Table 1 which were sufficiently soluble in the two solvents to make the measurement worthwhile.

The ^{31}P chemical shifts and one-bond phosphorus–selenium coupling constants of the selenides in SO_2 solution were independent of concentration, suggesting complete solute–solvent interaction in this medium. The stoichiometry of the interaction was determined for several representative selenides by measurement of the variation of δ_P and/or $^1J(PSe)$ as a function of SO_2/selenide in the systems selenide–SO_2–CH_2Cl_2 and computer-analysis of the titration curves. In all cases, even for the diphosphine diselenides, 1:1 complex formation is indicated; approximate stability constants and enthalpies and entropies of formation are given in Table 3.

To assess the extent of interaction between the two $Ph_2P(Se)$ groups of the diphosphorus(V) diselenides, the ^{31}P and ^{77}Se nmr spectra of $Ph_2P(CH_2)_nPPh_2$, $Ph_2P(Se)(CH_2)_nPPh_2$, and $Ph_2P(Se)(CH_2)_nP(Se)Ph_2$ ($n = 1$–6) have been obtained for CH_2Cl_2 solutions of equilibrium mixtures of the

TABLE 2. ^{77}Se nmr data for some phosphorus(V) selenides at 308 K

Selenide	δ_{Se}[a] (ppm)	
	CH_2Cl_2	SO_2
$SeP(NMe_2)_3$	33.2	432.0
$SeP(C_6H_{11})_3$	−72.3	258.6
$SePEt_3$	−22.5	297.6
$SePMePh_2$	113.9	342.0
$SeP(p\text{-}MeC_6H_4)_3$	125.8	342.1
$SeP(o\text{-}MeC_6H_4)_3$	188.3	[b]
$SePPh_3$	121.3	320.1
$SeP(OMe)_3$	−4.8	126.9
$[SePPh_2]_2CH_2$	139.3	294.8
$[SePPh_2]_2(CH_2)_2$	37.6	226.3
$[SePPh_2]_2(CH_2)_3$	46.5	251.7
$[SePPh_2]_2(CH_2)_4$	44.9	262.4
$[SePPh_2]_2(CH_2)_5$	44.6	267.3
$[SePPh_2CH_2]_3CMe$	94.0	232.7

[a]Relative to pure $SeP(OMe)_3$ ($\delta_{SeMe_2} = \delta_{SeP(OMe)_3} - 396.1$ ppm (7)); downfield shifts positive.
[b]$SeP(o\text{-}MeC_6H_4)_3$ has poor solubility in SO_2.

TABLE 3. Approximate thermodynamic constants for the formation of 1:1 complexes of phosphorus(V) selenides and diphosphorus(V) diselenides with SO_2

Selenide	Temperature (K)	K_1 [a] (M^{-1})	Data used for K_1 [a]	Error $\left(\frac{10^2\sigma}{\text{Total range}}\right)$	Approximate $-\Delta H^0$ (kJ mol^{-1})	Approximate $-\Delta S^0$ (J mol^{-1} K^{-1})
$SeP(OMe)_3$	308	0.10	Δ^1J(PSe)	2.3	3.9	31
	228	0.17	Δ^1J(PSe)	3.1		
$SePPh_3$	308	0.19	Δ^1J(PSe)	2.3		
$SeP(NMe_2)_3$	308	0.37	Δ^1J(PSe)	4.1		
	308	0.33	$\Delta\delta_P$	4.0	5.3 [b]	26 [b]
	228	0.77	Δ^1J(PSe)	5.9		
	228	0.97	$\Delta\delta_P$	6.1		
$SePEt_3$	308	0.35	Δ^1J(PSe)	2.0		
	308	0.27	$\Delta\delta_P$	2.2	7.5 [b]	33 [b]
	228	1.02	Δ^1J(PSe)	6.5		
	228	0.68	$\Delta\delta_P$	6.9		
$[(Se)PPh_2]_2CH_2$	308	0.19	Δ^1J(PSe)	0.4	6.3	34
	228	0.45	Δ^1J(PSe)	4.2		
$[(Se)PPh_2]_2(CH_2)_2$	308	0.18	Δ^1J(PSe)	0.2		
$[(Se)PPh_2]_2(CH_2)_4$	308	0.21	Δ^1J(PSe)	1.0	6.1	33
	228	0.48	Δ^1J(PSe)	1.0		
$[(Se)PPh_2]_2(CH_2)_6$	308	0.24	Δ^1J(PSe)	0.4		

[a]For method of calculation see Experimental section.
[b]Calculated from Δ^1J(PSe) for consistency.

three components. The comparison is made in Table 4. The data show the sensitivity of the nmr parameters to the proximity of a second phosphorus-containing group to be in the order δ_P, $\delta_{Se} < |^{1 \text{ or } (n+2)}J(PSe)| < |^{(n+1)}J(PP)|$, the least sensitive parameters suggesting virtually independent action of the two end groups at $n \geq 2$, the most sensitive at $n \geq 5$. On chemical evidence, the distribution of selenium when equimolar amounts of $Ph_2P(CH_2)_2PPh_2$ and Se react, it has been suggested that independent behaviour occurs when $n \sim 2$ (8).

The sensitivity of δ_{Se} and $|^1J(PSe)|$ but not δ_P to complexation of the selenides by SO_2 suggests that the selenium atom is the site of the interaction. The yellow colour of the phosphorus(V) selenide – SO_2 solutions is indicative of acceptor behaviour by sulfur dioxide (9). In addition, the solid, approximately 1:1, yellow adduct between $SeP(o\text{-}C_6H_4Me)_3$ and SO_2 shows $\nu(SO)_{sym}$ at 1134 ± 2 cm^{-1} in the Raman spectrum, in the range expected for

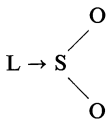

(pyramidal) coordination (10). (For comparison, the pyramidal ISO_2^- ion in $[PPh_3Bz](ISO_2)$ has $\nu(SO)_{sym}$ at 1123 cm^{-1} (10).) Clearly, the sulfur atom of SO_2 is acting as an acceptor in the selenide–SO_2 adducts.

The well-known (11) deceptively-simple, second-order, 'triplet' signal given by the aliphatic protons of $Ph_2P(CH_2)_2PPh_2$ dissolved in an inert solvent changes markedly when the compound is dissolved in liquid SO_2 (Fig. 1). The equivalence of the two phosphorus atoms is maintained, at least on a time-average, and the 'filling in' of the aliphatic triplet signal is consistent with either a reduction in $|^3J(PP)|$ or an increase in $|^2J(PH) - {}^3J(PH)|$, or both. Now oxidation or quaternization of phosphorus(III) is known to cause $^2J(PH)$ to become more negative and the positive $^3J(PH)$ to become more positive (12) while $|^3J(PP)|$ has been shown to increase on oxida-

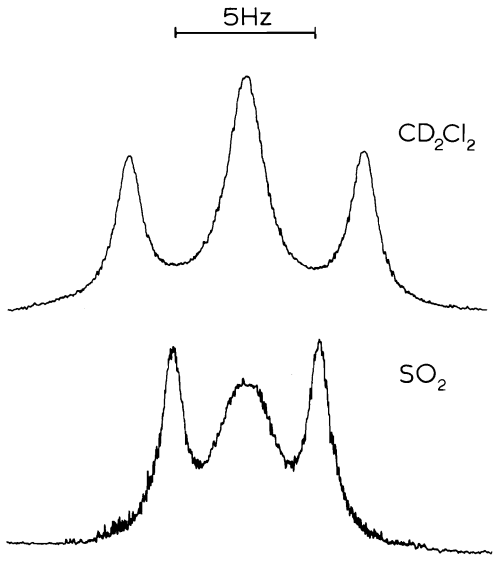

FIG. 1. Methylene region of the 100 MHz 308 K ^{1}H nmr spectrum of $Ph_2P(CH_2)_2PPh_2$ dissolved in CD_2Cl_2 (top) and in liquid SO_2 (bottom).

TABLE 4. A comparison of the ^{31}P and ^{77}Se nmr spectra of $[Ph_2P]_2(CH_2)_n$, $Ph_2P(CH_2)_nP(Se)Ph_2$, and $[Ph_2P(Se)]_2(CH_2)_n$ [a]

n	Compound	Phosphorus	δ_P [b] (ppm)	$\lvert^1J(PSe)\rvert$ (Hz)	$\lvert^{n+2}J(PSe)\rvert$ (Hz)	$\lvert^{n+1}J(PP)\rvert$ (Hz)	δ_{Se} [c] (ppm)
1	P_2		−24.4				
	P_2Se_2		22.9	754 [d]	~1.9 [d]	13.7	138.7
	P_2Se	P	−28.9			85.5	
		PSe	29.1	733	13.8		101.0
2	P_2		−14.6				
	P_2Se_2		34.2	737 [e]	~0.5 [e]	65.0	38.2
	P_2Se	P	−15.2			49.0	
		PSe	34.7	744	~0		37.3
3	P_2		−19.4				
	P_2Se_2		31.2	731	~0	~0	46.5
	P_2Se	P	−20.2			1.3	
		PSe	31.4	730	~0		46.3
4	P_2		−18.0				
	P_2Se_2		32.2	730	~0	1.3	44.8
	P_2Se	P	−18.0			1.5	
		PSe	32.3	728	~0		46.6
5	P_2		-18.2_6				
	P_2Se_2		32.3	730	~0	~0	45.0
	P_2Se_2	P	-18.3_4				
		PSe	32.2	730	~0	~0	43.7
6	P_2		−18.0				
	P_2Se_2		32.2_4 [f]	728	~0	~0	[g]
	P_2Se_2	P	-18.1_7				
		PSe	32.2_2 [f]	728	~0	~0	[g]

[a] Spectra of equilibrium mixtures from $Ph_2P(CH_2)_nPPh_2 + \frac{1}{8}Se_8$ in CH_2Cl_2 solution at 308 K.
[b] Relative to external $OP(OMe)_3$ in $(CD_3)_2CO$ ($\delta_{H_3PO_4} = \delta_{OP(OMe)_3} + 1.72$ ppm); downfield shifts positive.
[c] Relative to external neat $SeP(OMe)_3$ ($\delta_{SeMe_2} = \delta_{SeP(OMe)_3} - 396.1$ ppm (7)); downfield shifts positive.
[d] The relative signs of $^1J(PSe)$ and $^3J(PSe)$ could not be determined.
[e] $^1J(PSe)$ and $^4J(PSe)$ have opposite signs.
[f] These assignments may be interchanged.
[g] $Ph_2P(Se)(CH_2)_6P(Se)Ph_2$ has low solubility in CH_2Cl_2.

TABLE 5. Approximate thermodynamic constants for the formation of the 1:1 complex of $Ph_2P(CH_2)_2PPh_2$ with SO_2

Temperature (K)	K_1 (M^{-1}) [a]	$\frac{10^2\sigma}{\Delta\delta_{P,max}}$	Standard enthalpy and entropy of formation
308 [b]	0.09	3.8	$\Delta H^0 \approx -4.9$ kJ mol^{-1}
228	0.23	2.4	$\Delta S^0 \approx -42$ J mol^{-1} K^{-1}

[a] For method of calculation see Experimental section.
[b] Some oxidation of the diphosphine is evident at 308 K.

tion (13). The lower spectrum in Fig. 1 is thus consistent with complexation of the diphosphine at phosphorus, with the concomitant changes in the geminal and vicinal phosphorus–hydrogen coupling constants. Accordingly, the deshielding of the ^{31}P nmr signal of $Ph_2P(CH_2)_2PPh_2$ in SO_2 solution (3.89 ppm at 308 K, 17.99 ppm at 228 K relative to δ_P for CH_2Cl_2 solution) is assumed to result from complexation of the diphosphine. A ^{31}P chemical shift titration of $Ph_2P(CH_2)_2PPh_2$ with SO_2 in CH_2Cl_2 gives shifts consistent with the formation of a 1:1 complex; the stability and approximate enthalpy and entropy of formation are shown in Table 5. Some error in the value of K_1 at 308 K must be expected because SO_2-oxidation of the phosphine, an example of a well-studied general phenomenon (14), occurs at this temperature. On long standing at 308 K, the yellow colour of $Ph_2P(CH_2)_2PPh_2$—SO_2—CH_2Cl_2 solutions is discharged.

As indicated in Table 6, both $^1J(^{31}P–^{123}Te)$ and $^1J(^{31}P–^{125}Te)$ are visible in the ^{31}P nmr spectrum of colourless solutions of $(Me_2N)_3PTe$ in CH_2Cl_2. In the blood-red solutions of the telluride in SO_2, some decomposition occurs even at 228 K, giving broader lines, but a greatly reduced $^{31}P–^{125}Te$ satellite splitting is evident (Table 6). Attempts to ascertain the stoichiometry and stability of the $(Me_2N)_3PTe$—SO_2 adduct were thwarted by the evident decom-

TABLE 6. ^{31}P nmr spectral data for $(Me_2N)_3PTe$ in CH_2Cl_2 and in SO_2

Solvent	Temperature (K)	$\lvert^1J(P-^{125}Te)\rvert$ (Hz)	$\lvert^1J(P-^{123}Te)\rvert$ (Hz)	δ_P[a] (ppm)
CH_2Cl_2	308	2045	1709	54.3
	228	2003	1652	54.5
SO_2	228	~1544	[b]	39.2

[a]Relative to external $OP(OMe)_3$ in $(CD_3)_2CO$; downfield shifts positive.
[b]Not observed.

position occurring in CH_2Cl_2 solutions of $(Me_2N)_3PTe$ with SO_2 at 228 K. If, as expected by analogy with $(Me_2N)_3PSe$, a 1:1 complex is formed, K_1 appears to be of the order 0.1–1 M^{-1}, but the 1:1 stoichiometry could not be firmly established.

Discussion

Our results are consistent with all the phosphorus(V) selenides studied being completely complexed in liquid SO_2 to give 1:1 Lewis acid:Lewis base adducts containing a sulfur–selenium bond. To our knowledge, the only other example of SO_2 acting as an acceptor to a selenium-donor ligand is in the recently-reported $[NCSeSO_2]^-$ anion (10). It seems likely, however, that such behaviour by SO_2 is general. Thus it cannot safely be assumed that in SO_2 solution *direct* donation from a selenium-donor to an acceptor will always occur: *indirect* donation, e.g. via

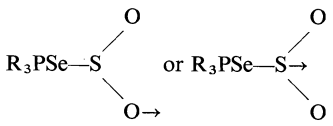

is a possibility needing consideration.

General medium effects on δ_P and $|^1J(PSe)|$ have been neglected, and only empirical allowance for changes in activity with system composition is made in calculation of the stability constants in Table 3. Nonetheless the degree of agreement between expected and found values, indicated by $10^2\sigma$/range, varies from reasonable to very good suggesting that the K_1's determined are good approximations. The SO_2 – phosphine selenide complexes are evidently weakly formed,[3] though their stability increases as expected with increasing electron-releasing ability of the substituents on phosphorus. The diphosphine diselenides $Ph_2P(Se)(CH_2)_nP(Se)Ph_2$ show insignificant change in K_1 for n = 1, 2, 4, or 6.

The SO_2 solutions provide an unusual opportunity to study the effects of complexation of a wide range of different phosphorus(V) selenides with a common acceptor, the solvent molecule. From the data in Table 1, it is clear that in the ^{31}P nmr spectrum a reduction in $|^1J(PSe)|$ from its value in an inert solvent is the most uniform indication of complexation: noticeable reductions in this coupling constant occur even when changes in δ_P are very small. In the ^{77}Se nmr spectrum, a large downfield shift from the free ligand (i.e. inert solvent) value accompanies complexation. Interestingly, there is a fair correlation between the changes in $|^1J(PSe)|$ and the changes in δ_{Se} accompanying complexation by SO_2, as shown in Fig. 1.[4] Such a correlation seems reasonable since both coupling constants involving ^{77}Se (16, 17) and ^{77}Se chemical shifts (18) are thought to depend on the nature and the number of the lone pairs of electrons on selenium.

In general, it seems that the more easily obtained ^{31}P spectra should provide a satisfactory indication of complexation of the phosphorus(V) selenides. However, when SO_2 or another acceptor solvent is used, the changes in $|^1J(PSe)|$ could be small, as the magnitude of this coupling will already have been reduced by complexation with the solvent.

The formation of only 1:1 complexes by all the diphosphine diselenides, $SePPh_2(CH_2)_nPh_2PSe$ (n = 1, 2, 4, 6) is perplexing. The $Ph_2P(Se)$ group is known to be electron-withdrawing (19), so that 1:1 complex formation at short aliphatic chain lengths is not surprising. However, as discussed above, the two $Ph_2P(Se)$ groups are certainly spectroscopically independent at n = 6 (see Table 4) and may act independently chemically at n = 2. It should be noted though that the two ends of

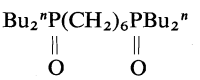

do not act independently upon protonation in nitromethane, the two pK_a's being 11.6 and 4.7 (20). In the present examples, the formation of a simple one-ended 1:1 complex (**1**) appears favoured by the

[3]For comparison, Zingaro and co-workers (15*a*) find K_1 to be 2.40 × 10^3 M^{-1} for $Ph_3PSe{\cdot}I_2$ in $CHCl_3$ at 308 K, while Bruno *et al.* (15*b*) find K_1 for $(Me_2N)_3PSe{\cdot}I_2$ to be 12 900 ± 650 M^{-1} under the same conditions.

[4]It should be noted that data for complexes of phosphorus(V) selenides with acceptors other than SO_2 do not correlate with the data for the SO_2 complexes, e.g., we find $\Delta|^1J(PSe)| = 306$ Hz and $\Delta\delta_{Se} \approx 387$ ppm at 308 K when $(MeSeP(NMe_2)_3)^+$ is formed from MeI and $SeP(NMe_2)_3$ in SO_2.

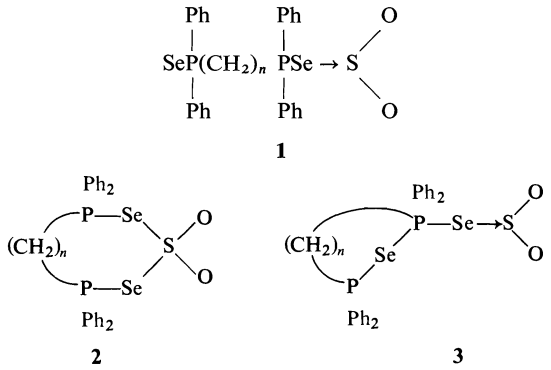

1 **2** **3**

thermodynamic data (Table 3) but from the spectroscopic results is most unlikely. The *exchange-averaged* values of $\Delta\delta_{Se}$ and $|^1J(PSe)|$ are in the ranges 155.5–222.7 ppm and 34–53 Hz, respectively, which means that complexation by SO_2 would have to produce changes in $\Delta\delta_{Se}$ of ca. 301–445 ppm and in $|^1J(PSe)|$ of ca. 68–106 Hz at the donor site: the largest of these changes, at least, would be anomalously high compared with the other data in Fig. 2. Thus ring-closure either by chelation as in **2**, or internally, perhaps as in **3**, must be occurring.[5] In either event, it is surprising that neither the thermodynamic data (Table 3) nor the spectroscopic data (Fig. 2) are anomalous. The nature of the 1:1 complexes of diphosphine diselenides and SO_2 must remain an open question.

The analogues of structures **1** and **2** are possibilities for the 1:1 complex of $Ph_2P(CH_2)_2PPh_2$ and SO_2, and the present data do not permit a choice. The stability of the diphosphine adduct is only a little less than those of the diphosphine diselenides, and like the selenides the diphosphine is apparently totally complexed in liquid SO_2. Earlier, it has been suggested on the basis of ^{13}C nmr data that PPh_3 is totally complexed in SO_2 (1). The earlier data for the system PPh_3—SO_2—CS_2 can be used to estimate that K_1 for $Ph_3P{\cdot}SO_2$ is ca. 0.03 M^{-1} at 305 K.[6] For both PPh_3 and $Ph_2P(CH_2)_2PPh_2$ adducts with SO_2, the formation of phosphorus–sulfur bond is indicated, supporting a previous suggestion (14*a*) that SO_2-oxidation of phosphines and related phosphorus(III) species proceeds through $R_3P \rightarrow SO_2$ adducts.

Both the blood-red colour of solutions of $TeP(NMe_2)_3$ in SO_2 or SO_2—CH_2Cl_2 and the remarkable changes in the ^{31}P spectral parameters which occur when the telluride is dissolved in an SO_2-containing medium (Table 6) are good evidence that an SO_2–$TeP(NMe_2)_3$ interaction occurs. Unfortunately the chemical instability of the system precluded more detailed characterization. However, the formation of a tellurium-to-SO_2 bond seems very likely from the large reduction in $^1J(PTe)$ occurring in SO_2 as solvent.

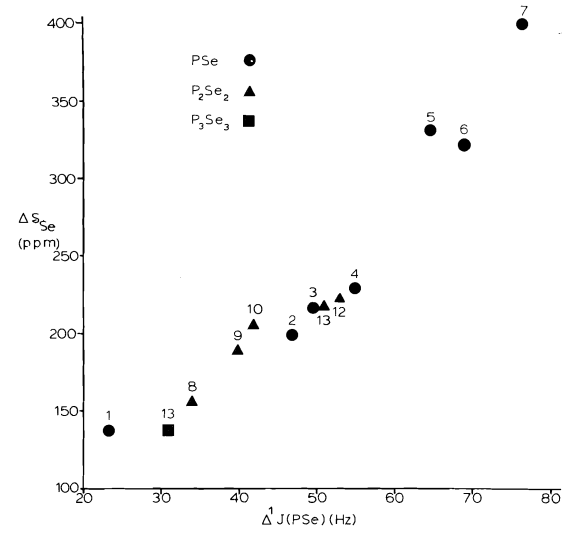

FIG. 2. Relationship between the downfield shift of the ^{77}Se resonance and the decrease in the magnitude of $^1J(PSe)$ occurring at 308 K when some phosphorus(V) selenides are dissolved in liquid SO_2 instead of CH_2Cl_2 (*1* = $SeP(OMe)_3$; *2* = $SePPh_3$; *3* = $SeP(p\text{-}C_6H_4Me)_3$; *4* = $SePMePh_2$; *5* = $SeP(C_6H_{11})_3$; *6* = $SePEt_3$; *7* = $SeP(NMe_2)_3$; *8–12* = $[SePPh_2]_2(CH_2)_n$, *n* = 1–5, respectively; *13* = $[SePPh_2CH_2]_3CMe$).

Experimental

Materials

Triethylphosphine (PCR, Inc.), tri-*o*-tolylphosphine (PCR, Inc.), tri-*p*-tolylphosphine (Eastman Chemicals), bis(diphenylphosphino)methane (PCR, Inc.), 1,3-bis(diphenylphosphino)propane (Strem Chemicals, Inc.), 1,5-bis(diphenylphosphino)pentane (Strem Chemicals, Inc.), 1,6-bis(diphenylphosphino)hexane (Strem Chemicals, Inc.), 1,1,1-tris(diphenylphosphinomethyl)ethane (Strem Chemicals, Inc.), bis(2-diphenylphosphinoethyl)phenylphosphine (Strem Chemicals, Inc.), and methyldiphenylphosphine (prepared by D. Stephan of this Department by Grignard synthesis) showed no significant impurities in their ^{31}P nmr spectra and were used as received, as was the CS_2 adduct of tricyclohexylphosphine (Strem Chemicals, Inc.). Triphenylphosphine (Eastman Kodak Co.) was recrystallized from ethanol, and both trimethylphosphite (Strem Chemicals, Inc.) and tris(dimethylamino)phosphine (Aldrich Chemical Co., Inc.) were purified by distillation under reduced pressure.

Literature methods were used in the synthesis and purification of 1,2-bis(diphenylphosphino)ethane (22) and 1,4-bis(diphenylphosphino)butane (23).

Trimethylselenophosphate, $(MeO)_3PSe$, was prepared by the direct reaction of a slight excess of finely-powdered selenium with freshly-distilled trimethylphosphite under a dry nitrogen atmosphere (24). The supernatant liquid showed no significant

[5]Intramolecular association similar to **3** has been suggested earlier to account for the anomalous vibrational spectra of tetrakis(diphenylphosphinoselenoyl and -thioyl)methanes (21).

[6]Such a calculation also shows that $^1J(P\text{–}C_1)$ must change sign on complexation of PPh_3 by SO_2.

impurity by either ^1H or ^{31}P nmr and was used without further purification. Crude tris(dimethylamino)phosphine selenide was prepared in a like manner (25). Purification was achieved by sublimation followed by dissolution in liquid SO_2, filtration, and removal of volatiles *in vacuo*. All of the other phosphorus(V) selenides were synthesized by refluxing a benzene solution of the phosphine with excess selenium shot under nitrogen (26). Methyldiphenylphosphine selenide was purified by reduced pressure distillation (27). The solid selenides were purified by recrystallization. (The solvents used were ethanol (for $SePEt_3$ and $SeP(C_6H_{11})_3$), benzene (for $SePPh_3$ and $(SePPh_2)_2(CH_2)_n$ (n = 3–6)), and *n*-butanol (for $SeP(o\text{-}C_6H_4Me)_3$, $SeP(p\text{-}C_6H_4Me)_3$, $(SePPh_2)_2(CH_2)_n$ (n = 1 or 2), $(SePPh_2CH_2)_3CMe$ and $[SePPh_2(CH_2)_2]P(SePh)$.) The two triselenides are new compounds; they are characterized by the spectral data reported in this paper and by their melting points (247–249 and 208–210°C(uncorr), for $(SePPh_2CH_2)_3CMe$ and $[SePPh_2(CH_2)_2]P(SePh)$ respectively).

Crude tris(dimethylamino)phosphine telluride was prepared by reaction of a slight excess of finely-powdered tellurium with freshly-distilled tris(dimethylamino)phosphine for 3 h in a sealed tube at 437 K (25, 28). Unreacted $P(NMe_2)_3$ was removed by pumping *in vacuo*. (This removal is crucial because rapid tellurium exchange between $P(NMe_2)_3$ and $TeP(NMe_2)_3$ is known to occur (29).) Excess tellurium was removed by filtration of a CH_2Cl_2 solution of the pumped product. Removal of the solvent *in vacuo* gave a straw-coloured product showing no significant impurities by either ^1H or ^{31}P nmr.

$(MeSeP(NMe_2)_3)I$ was prepared *in situ* in SO_2 by the direct reaction of MeI and $SeP(NMe_2)_3$ (30, 31). (^1H (30, 31) and partial ^{31}P (31) nmr spectra of this compound have been reported.) Methylene chloride (Fisher Scientific Co., Certified Grade) was dried by standing over 3A molecular sieves and used without additional purification. Sulfur dioxide (Matheson Anhydrous Grade) was dried by standing in the gas phase over 3A molecular sieves for 12–24 h.

Raman Spectrum

The Raman spectrum of solid $SeP(o\text{-}C_6H_4Me)_3$ 0.63 SO_2 in a melting point capillary was obtained using a Cary 82 Spectrometer and excitation by the 5145 Å line of an Ar^+ laser.

Nuclear Magnetic Resonance Spectra

All nmr spectra were obtained using a Varian XL-100-12 spectrometer system equipped with the Gyrocode Observe accessary.

^{31}P and ^{77}Se spectra were measured with samples in a 10 mm hand-made sample tube within a 12 mm precision nmr tube, the external lock material (and, for ^{31}P, the reference) being in the annulus. Generally a 32 K transform was used.

For ^{31}P, the lock/reference was a 2% solution of $OP(OMe)_3$ in $(CD_3)_2CO$ ($\delta_{OP(OMe)_3} = \delta_{H_3PO_4} - 1.72$ ppm). Typically, selenium satellites in the spectra of 0.1–0.2 *M* samples were clearly visible after 250–500 ca. 60° pulses at 8–10 min^{-1}. For ^{77}Se, the lock substance was either $(CD_3)_2CO$ or D_2O, and referencing to neat $SeP(OMe)_3$ was by sample interchange ($\delta_{SeP(OMe)_3} = \delta_{SeMe_2} + 396.1$ ppm (7)). For this nucleus, pulses of ca. 20° were used. The repetition rate was 10 min^{-1} for solutions in CH_2Cl_2; in these cases 1000–4000 transients gave acceptable spectra when the sample concentration was 0.1–0.2 *M*. In SO_2 solutions T_1, not unexpectedly, seems much longer: poorer spectra could be obtained in the same number of transients at 3 min^{-1}. The ^{77}Se nmr spectra of $Ph_2P(CH_2)_n$-PPh_2—Se_8 equilibrium mixtures (Table 4) were obtained from samples having a total phosphine concentration of ca. 0.5 *M*, as were the spectra of $SeP(C_6H_{11})_3$, $Ph_2P(Se)(CH_2)_n$—$P(Se)Ph_2$ (n = 4 or 5), and $(Ph_2P(Se)CH_2)_3CMe$ in SO_2.

Temperatures were measured using a Doric Trendicator Type 400 thermocouple thermometer, with a stationary probe. The temperature controller of the nmr spectrometer was able to hold 228 K to better than ±1 K.

Preparation of Nuclear Magnetic Resonance Samples

^1H nmr samples were made up in standard 5 mm od nmr tubes. ^{31}P and ^{77}Se samples were prepared in tubes made from 10 mm od standard wall Pyrex tubing. Those tubes which were to contain SO_2 had attached a length of 9 mm od special wall tubing to allow their connection to a vacuum system via 3/8 in. Ultratorr fittings. The solid components were added to the tubes by weight, and the CH_2Cl_2, if any, by volume. Samples without SO_2 were sealed with plastic pressure caps. For those which did contain SO_2, known amounts of the gas were condensed in from a calibrated conventional glass-and-Teflon vacuum line before flame-sealing at the special wall tubing.

The composition of each sample was determined from its total weight. Sample volumes at 308 and 228 K were found by measurement of the weight at room temperature of the same volume of CH_2Cl_2 (density 1.33 g cm^{-3}).

Analysis of Exchange-averaged Chemical Shift/Coupling Constant Titration Curves

The composition of each sample was corrected for the amount of SO_2 in the headspace, assuming ideal behaviour Incremental chemical shifts were corrected for changes in the magnetic susceptibility of the solutions with composition.

Titration curves of the exchange-averaged chemical shift and/or coupling constant versus SO_2/L were analyzed using the program LISA (32). The chemical shifts and coupling constants in SO_2 as solvent were independent of concentration, suggesting virtually complete complexation. Therefore SO_2/L for such solutions was arbitrarily set at 9999.99999 to ensure that the predicted curve passed close to these points and hence to obtain the best fit over the whole range of composition. The K_1's given in Table 3 were calculated in this way, and we take the reasonable to very good fits to justify the treatment. However, our conclusions regarding the formation of 1:1 complexes does not depend on inclusion of the point for neat SO_2.

It should be noted that in all cases examined $|^1J(PSe)|$ was temperature dependent, being smaller at lower temperatures. In the analysis of the data, the incremental changes for the appropriate temperature were used. At 228 K the values of $|^1J(PSe)|$(Hz) are: $SeP(OMe)_3$: 949 (CH_2Cl_2), 914 (SO_2); $SePEt_3$: 674 (CH_2Cl_2), 585 (SO_2); $SeP(NMe_2)_3$: 778 (CH_2Cl_2), 675 (SO_2); $Ph_2P(Se)CH_2P(Se)Ph_2$: 746 (CH_2Cl_2), 696 (SO_2); $Ph_2P(Se)(CH_2)_4P(Se)Ph_2$: 717 ($CH_2Cl_2$), 646 ($SO_2$).

Spectral Analysis

The ^{77}Se satellite spectra in the ^{31}P-{H} nmr spectrum of $Ph_2P(Se)(CH_2)_2(Se)PPh(CH_2)_2P(Se)Ph_2$ were analyzed iteratively using the program LAOCN3(33). The values of $^1J(PSe)$ (Table 1) were insensitive to small changes in $^4J(PSe)$.

Acknowledgements

The author is grateful to Eva E. Schlahetka for preliminary work on the $(Me_2N)_3PSe$ and $(Me_2N)_3$-PTe systems, and to Mary Hughes for the preparation of some of the selenides and for assistance with the computations. Dr. Bill Dawson (University of South Carolina) is thanked for helpful discussions on several aspects of ^{77}Se nmr, and Mrs. Heather Schroeder for expert technical assistance in obtaining some of the nmr spectra. The National Research Council of Canada kindly supported this research.

1. P. A. W. DEAN and D. G. IBBOTT. Can. J. Chem. **54**, 177 (1976).
2. P. A. W. DEAN and D. D. PHILLIPS. To be published.
3. P. A. W. DEAN and M. HUGHES. To be published.
4. I. A. NURETDINOV and E. I. LOGINOVA. Bull. Acad. Sci. USSR, Div. Chem. Sci. 2360 (1971).
5. W. J. STEC, A. OKRUSZEK, B. UZNANSKI, and J. MICHALSKI. Phosphorus, **2**, 97 (1972).
6. R. P. PINNELL, C. A. MEGERLE, S. L. MANNATT, and P. A. KROON. J. Am. Chem. Soc. **95**, 977 (1973).
7. W. MCFARLANE and D. S. RYCROFT. J. Chem. Soc. Dalton, 2162 (1973).
8. D. H. BROWN, R. J. CROSS, and R. KEAT. J. Chem. Soc. Chem. Commun. 708 (1977).
9. D. F. BUROW. *In* The chemistry of non-aqueous solvents. Vol. 3. *Edited by* J. J. Lagowski. Academic Press, New York. 1970. Chapt. 2.
10. P. G. ELLER and G. J. KUBAS. Inorg. Chem. **17**, 894 (1978).
11. A. J. CARTY and R. K. HARRIS. Chem. Commun. 234 (1967).
12. W. MCFARLANE. Proc. R. Soc. **306**A, 185 (1968).
13. S. O. GRIM, J. DEL GAUDIO, R. P. MOLENDA, C. A. TOLMAN, and J. P. JESSON. J. Am. Chem. Soc. **96**, 3416 (1974).
14. (*a*) B. C. SMITH and G. H. SMITH. J. Chem. Soc. 5516 (1965); (*b*) E. FLUCK and H. BINDER. Z. Anorg. Allg. Chem. **354**, 139 (1967).
15. (*a*) B. R. CONDRAY, R. A. ZINGARO, and M. V. KUDCHADKER. Inorg. Chim. Acta, **2**, 309 (1968); (*b*) P. BRUNO, M. CASELLI, C. FRAGALE, and S. MAGRINO. J. Inorg. Nucl. Chem. **39**, 1757 (1977).
16. W. MCFARLANE and D. S. RYCROFT. J. Chem. Soc. Chem. Commun. 10 (1973).
17. H. J. REICH and J. E. TREND. J. Chem. Soc. Chem. Commun. 310 (1976).
18. W. MCFARLANE and R. J. WOOD. J. Chem. Soc. Dalton, 1397 (1972).
19. R. F. DEKETELAERE and G. P. VAN DER KELEN. J. Mol. Struct. **27**, 33 (1975).
20. M. I. KABACHNIK, E. I. MATROSOV, T. YA. MEDVED', S. A. PISAREVA, and I. B. ROMANOVA. Teor. Eksp. Khim. Engl. Transl. **8**, 293 (1972); Chem. Abstr. **77**, 157148*s* (1972).
21. J. ELLERMAN and D. SCHIRMACHER. Chem. Ber. **100**, 2220 (1967).
22. W. HEWERTSON and H. R. WATSON. J. Chem. Soc. 1490 (1962).
23. T. YOSHIDA, M. IWAMOTO, and S. YUGUCHI. Japan Patent 11,934 (1967); Chem. Abstr. **68**, 105358*e* (1968); L. SACCONI and J. GELSOMINI. Inorg. Chem. **7**, 291 (1968).
24. P. CHABRIER and N. T. THUONG. C. R. **258**, 3738 (1967); I. A. NURETDINOV and N. P. GRECHKIN. Bull. Acad. Sci. USSR Div. Chem. Sci. 2685 (1968).
25. F. RÄUCHLE, W. POHL, B. BLAICH, and J. GOUBEAU. Ber. Bunsenges. Phys. Chem. **75**, 66 (1971).
26. L. MAIER. *In* Organic phosphorus compounds. Vol. 4. *Edited by* G. M. Kosolapoff and L. Maier. Wiley-Interscience, New York. 1972. Chapt. 7.
27. R. A. ZINGARO and R. E. MCGLOTHLIN. J. Chem. Eng. Data, **8**, 226 (1963).
28. N. P. GRECHKIN, I. A. NURETDINOV, and N. A. BUINA. Bull. Acad. Sci. USSR Div. Chem. Sci. 162 (1968).
29. W-W. DUMONT and H. J. KROTH. J. Organomet. Chem. **113**, C35 (1976).
30. I. A. NURETDINOV, N. A. BUINA, and N. P. GRECHKIN. Bull. Acad. Sci. USSR Div. Chem. Sci. 163 (1968).
31. A. SCHMIDPETER and H. BRECHT. Z. Naturforsch. **24**B, 179 (1969).
32. B. L. SHAPIRO and M. D. JOHNSTON, JR. J. Am. Chem. Soc. **94**, 8185 (1972).
33. A. A. BOTHNER-BY and S. M. CASTELLANO. LAOCN3. The Mellon Institute, Pittsburgh.

Mercury(II) cyanide complexes of bulky phosphines. Preparation, characterization, and spectral studies

RAM G. GOEL, WILLIAM P. HENRY, AND WILLIAM O. OGINI

Guelph–Waterloo Centre for Graduate Work in Chemistry, University of Guelph, Guelph, Ont., Canada N1G 2W1

Received September 12, 1978

RAM G. GOEL, WILLIAM P. HENRY, and WILLIAM O. OGINI. Can. J. Chem. **57**, 762 (1979).

Mercury(II) cyanide forms 1:2 complexes with triphenylphosphine and tri-*p*-tolylphosphine. Both 1:1 and 1:2 complexes are formed with tricyclohexylphosphine but only the 1:1 complex is obtained with tri-*tert*-butylphosphine, and no complex is formed with tri-*o*-tolylphosphine. The complexes have been characterized by elemental analyses and by infrared and Raman spectral measurements. Their behaviour in solution has been investigated by conductance, molecular weight, and ^{31}P nmr measurements. The infrared and Raman data for the 1:2 complexes are in accord with a pseudotetrahedral structure of C_{2v} skeletal symmetry. At least one of the 1:1 complexes is indicated to have a dimeric structure involving terminal and bridging CN ligands. The C≡N, Hg—CN, and Hg—P stretching frequencies and the ^{31}P—^{199}Hg spin–spin coupling for the complexes are discussed.

RAM G. GOEL, WILLIAM P. HENRY et WILLIAM O. OGINI. Can. J. Chem. **57**, 762 (1979).

Le cyanure de mercure(II) forme des complexes 1:2 avec la triphénylphosphine et la tri-*p*-tolylphosphine. Il se forme des complexes 1:1 ainsi que 1:2 avec la tricyclohexylphosphine alors que l'on n'obtient que des complexes 1:1 avec la tri-*tert*-butylphosphine; il ne se forme aucun complexe avec la tri-*o*-tolylphosphine. On a caractérisé les complexes grâces à leurs analyses centésimales et à leurs spectres infrarouges et Raman. On a étudié leur comportement en solution par des mesures de conductivité, de leurs poids moléculaires et de leurs spectres rmn ^{31}P. Les données infrarouge et Raman concernant les complexes 1:2 sont en accord avec une structure pseudotétraédrique de symétrie de squelette C_{2v}. Il semble qu'au moins un des complexes comporte une structure dimère impliquant des ligands CN terminaux servant de ponts. On discute des fréquences de vibration C≡N, Hg—CN et Hg—P ainsi que des couplages spin–spin ^{31}P—^{199}Hg des complexes.

[Traduit par le journal]

Introduction

Mercury(II) halides are known to form a variety of complexes(I) with tertiary phosphines (1) and a number of spectroscopic (2–10) as well as crystallographic studies (11, 12) on these complexes have been reported recently. An investigation on triphenylphosphine complexes of mercury(II) pseudohalides showed that, unlike mercury(II) halides, mercury(II) cyanide forms only a 1:2 complex (13). In another study (5), both 1:1 and 1:2 complexes of mercury(II) cyanide were obtained with trimethylphosphine. Apart from these studies no report has appeared on phosphine complexes of mercury(II) cyanide.

In continuation of our investigations on metal complexes of sterically hindered phosphines we have undertaken a systematic study of phosphine complexes of mercury(II) (7, 8, 14) and other d^{10} metals (15, 16). In the present work complexes of mercury(II) cyanide with tri-*tert*-butyl-, tricyclohexyl-, tri-*o*-tolyl-, and tri-*p*-tolylphosphines were investigated. In view of very limited information reported for the triphenylphosphine complex (13), it was also included in the study.

Results and Discussion

Like mercury(II) halides, mercury(II) cyanide forms only 1:1 complex with tri-*tert*-butylphosphine (7) and both 1:1 and 1:2 complexes with tricyclohexylphosphine (4). However, unlike mercury(II) halides, mercury(II) cyanide does not form any complex with tri-*o*-tolylphosphine (7). This is indeed due to the large steric requirement and relatively low basicity of tri-*o*-tolylphosphine. In agreement with the observation of previous workers (13), only 1:2 complexes could be isolated with triphenylphosphine as well as with tri-*p*-tolylphosphine.

The analytical, molecular weight, and conductance data for the complexes included in the present study are recorded in Table 1. All the complexes are white, air-stable solids, soluble in polar solvents such as dichloromethane, acetone, or acetonitrile. As shown by the conductance data, the complexes do not ionize to any significant extent in acetonitrile. The complexes $[(p\text{-tolyl})_3P]_2Hg(CN)_2$ and $(Cy_3P)_2Hg(CN)_2$ exist as undissociated molecular species in dichloromethane but significant dissociation is indicated for the complex $(Ph_3P)_2Hg(CN)_2$. The com-

0008-4042/79/070762-05$01.00/0

TABLE 1. Analytical, molecular weight, and conductance data

Compound	Melting point (°C)	%C		%H		Mol. wt.*		Λ_M†
		Calcd.	Found	Calcd.	Found	Calcd.	Found	
$(Ph_3P)_2Hg(CN)_2$	240	58.69	58.36	3.90	3.56	776	555	1.65
$[(p\text{-Tolyl})_3P]_2Hg(CN)_2$‡	204 (decom.)	61.32	60.68	4.88	4.85	860	860	1.00
$(Cy_3P)_2Hg(CN)_2$	77	56.20	56.21	8.10	8.72	812	788	5.77
$Cy_3PHg(CN)_2$	125	45.10	45.41	6.20	6.30	532	644 1000§	5.33
$(t\text{-Bu})_3PHg(CN)_2$	270	36.92	36.89	5.93	5.78	454	618	1.00

*In dichloromethane unless stated otherwise; concentration range 10^{-2} to 10^{-3} *M*.
†In ohm^{-1} cm^2 mol^{-1} for 10^{-3} *M* solutions in acetonitrile.
‡%N: calcd., 3.25; found, 3.03.
§In benzene.

plex $Cy_3PHg(CN)_2$ has a dimeric constitution in benzene. The molecular weight data for both $Cy_3PHg(CN)_2$ and $(t\text{-Bu})_3PHg(CN)_2$, in dichloromethane, are explicable in terms of partial dissociation of the dimeric species into monomers.

Vibrational Spectral Studies

Vibrational spectra for the complexes $(Ph_3P)_2HgX_2$ and $(Cy_3P)_2HgX_2$, X = Cl, Br, and I, are in accord with a pseudotetrahedral structure of C_{2v} skeletal symmetry (2, 10) and such a structure has been established for the complex $(Ph_3P)_2Hg(SCN)_2$ by a X-ray diffraction study (17). The infrared and Raman data for the dicyanobis(phosphine)mercury(II) complexes are also consistent with a pseudotetrahedral structure. The mercury–halogen stretching and bending frequencies (2, 10) for the dihalobis(phosphine)mercury(II) complexes are very similar to those for the corresponding HgX_4^{2-} complexes (18). The C≡N and Hg—CN stretching and the Hg—CN bending frequencies for the dicyanobis(phosphine)mercury(II) complexes are also found to be very similar to those for the cyano complex $Hg(CN)_4^{2-}$ (19).

The Raman spectrum of solid $[(p\text{-tolyl})_3P]_2Hg(CN)_2$, in the C≡N stretching region, showed a strong band at 2146 cm^{-1} and a weak band at 2141 cm^{-1}. A strong Raman band at 2143 cm^{-1} and a weak Raman band at 2130 cm^{-1} were observed for the complex $(Cy_3P)_2Hg(CN)_2$, and a very strong, broad Raman band at 2140 cm^{-1} was observed for $(Ph_3P)_2Hg(CN)_2$. The infrared bands due to the C≡N stretching frequencies for all three complexes were very weak. Two very weak infrared bands were observed at 2145 and 2130 cm^{-1} for $[(p\text{-tolyl})_3P]_2Hg(CN)_2$ but only a very weak band at ca. 2140 cm^{-1} was observed for the triphenylphosphine and tricyclohexylphosphine complexes. Therefore, the previously reported assignment (13) for the C≡N stretching frequency for the $(Ph_3P)_2Hg(CN)_2$ complex appears to be erroneous.

Previously reported assignments (13) for the Hg—P and Hg—CN stretching frequencies and the Hg—CN bending frequency for the $(Ph_3P)_2Hg(CN)_2$ complex are also indicated to be erroneous. The 432 and 395 cm^{-1} infrared bands assigned to the Hg—P and Hg—CN stretching frequencies, respectively, are in fact due to the internal vibrations of triphenylphosphine (20). Our infrared and Raman data show that the skeletal vibrations for the dicyanobis(phosphine)mercury(II) complexes occur in the region below 400 cm^{-1}. The observed infrared bands in the 400–130 cm^{-1} region and the Raman bands in the 400–100 cm^{-1} region for the three complexes, in the solid state, together with their assignment are listed in Table 2. The proposed assignments for the Hg—CN stretching and bending frequencies for the complexes follow from those for $Hg(CN)_4^{2-}$ (19). As discussed later, the ^{31}P—^{199}Hg spin–spin coupling constants for the mercury(II) cyanide complexes are of the same order of magnitude as those for the mercury(II) iodide complexes. Since the Hg—P stretching frequencies for the $(Ph_3P)_2HgI_2$ and $(Cy_3P)_2HgI_2$ complexes are indicated (2, 10) to occur in the 100–90 cm^{-1} region, the Hg—P stretching frequencies for the corresponding cyano complexes are expected to fall below 100 cm^{-1}.

For the complex $(Me_3P)_2Hg(CN)_2$ (5), an infrared band at 311 cm^{-1} has been assigned to the Hg—CN stretching frequency and a Raman band at 329 cm^{-1} has been assigned to the Hg—P stretching frequency. Our results suggest that the aforementioned bands are due to the antisymmetric and symmetric Hg—CN stretching frequencies, respectively. The CN stretching frequencies reported for the trimethylphosphine complex (5) are comparable to those observed in the present work.

A centrosymmetric dimeric structure of C_{2h}

TABLE 2. Infrared and Raman frequencies† for $(Ph_3P)_2Hg(CN)_2$, $[(p\text{-tolyl})_3P]_2Hg(CN)_2$, and $(Cy_3P)_2Hg(CN)_2$ in the region below 400 cm^{-1}

$(Ph_3P)_2Hg(CN)_2$		$[(p\text{-Tolyl})_3P]_2Hg(CN)_2$		$(Cy_3P)_2Hg(CN)_2$	
Infrared	Raman	Infrared	Raman	Infrared	Raman
395*	394*w	396*vw		390*w	393*w
			365*sh	383*w	
		260*w	357*m		
325m }	327s }	322s, b	321s	335s }	333m } νHg—CN
310s }	311m }			308mw }	310m }
	274*sh			288*sh	
268ms	268s	256ms	258ms	265ms	264ms δHg—CN
257*sh	257*w			242*w	
251*vw	250*vs			233*w	219*vs
222w	220s	222w	225m	216w	ρHg—$(CN)_2$
213*w	211*m				
196*w	198*m			198*w	
	194*m				178*s
186*w	184*w			162*w	
			144*sh		
	132sh				132sh ρHg$(CN)_2$

*Bands due to the internal vibrations of phosphine.
†In the solid state. Abbreviations: b, broad; m, medium; s, strong; sh, shoulder; v, very; w, weak; ν, stretching mode; δ, bending mode; ρ, rocking mode.

skeletal symmetry as shown below is indicated for the 1:1 triphenylphosphine[1] (2, 10) and tricyclohexylphosphine (10) complexes of mercury(II) halides.

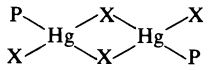

As shown by molecular weight measurement, the complex $Cy_3PHg(CN)_2$ is undoubtedly a dimer in benzene. The observed CN stretching frequencies for this complex in the solid state as well as in solution are in accord with the presence of terminal and bridging CN groups. Its infrared spectrum, in the solid state, showed weak bands at 2180 and 2146 cm^{-1}, and its Raman spectrum showed a strong band at 2149 cm^{-1} and a weak band at 2179 cm^{-1}. The higher frequency bands can be attributed to the bridging CN groups (21, 22) and the lower frequency bands to the terminal CN groups. Infrared measurements in chloroform showed that the CN stretching frequencies in solution are virtually identical to those observed in the solid state. Thus, the solid state structure of the complex appears to be maintained in solution. The infrared spectrum of $Cy_3PHg(CN)_2$, in the low frequency region (400–130 cm^{-1}), showed bands at 344 (m, b), 270 (m, b), and 230 (w, b) cm^{-1} which can be attributed to the vibrations involving Hg—CN bonds. The 344 cm^{-1} band can be assigned to the terminal Hg—CN stretching frequency but it is difficult to make clearcut assignments for the other two infrared bands. The Raman spectrum of $Cy_3PHg(CN)_2$ in the region below 400 cm^{-1} was not very informative.

In the C≡N stretching region, a medium infrared band at 2157 cm^{-1} and a strong Raman band at 2152 cm^{-1} were observed for the complex $(t\text{-Bu})_3PHg(CN)_2$, in the solid state. The infrared frequency was not altered when the complex was dissolved in dichloromethane. The observed frequencies attributable to the skeletal vibrations of the complex include infrared bands at 335 (m, b), 281 (mw), 273 (mw), and 170 (mw, b) cm^{-1} and the Raman bands at 336 (w) and 112 (s) cm^{-1}. The 335 cm^{-1} infrared band and the 336 cm^{-1} Raman bands can be assigned to the terminal Hg—CN stretching frequency. The 112 cm^{-1} Raman band is similar to that observed for the iodo complex $(t\text{-Bu})_3PHgI_2$ (7) and is assigned to the Hg—P stretching frequency.

Although definitive structural conclusions for the 1:1 complexes must await X-ray diffraction studies, the molecular weight and vibrational spectral data for the complex $Cy_3PHg(CN)_2$ are consistent with a dimeric structure involving bridging and terminal CN groups and tetrahedrally coordinated mercury atoms.

^{31}P *Nuclear Magnetic Resonance Studies*

The ^{31}P nmr data for the 1:2 as well as 1:1 complexes at ambient temperature and at 183 K are given in Table 3. As shown by the data in Table 3, the ^{31}P nmr spectra of the complexes of less basic and less bulky phosphines, i.e., triphenylphosphine and tri-*p*-tolylphosphine, consisted of a single peak at

[1]The structure of Ph_3PHgCl_2 has been established by a crystal structure determination (11).

TABLE 3. ^{31}P nmr data*

Compound	δ (ppm)		Δδ (ppm)		$J(^{31}P–^{199}Hg)$ (Hz)	
	Amb. temp.	183 K	Amb. temp.	183 K	Amb. temp.	183 K
$(Ph_3P)_2Hg(CN)_2$	12.6	18.7	18.4	27.7	—	2645
$[(p\text{-Tolyl})_3P]_2Hg(CN)_2$	5.0	16.2	13.5	28.2	—	2766
$(Cy_3P)_2Hg(CN)_2$	36.5	37.3	27.6	29.1	3416	3544
$Cy_3PHg(CN)_2$	50.4	50.4	41.8	42.2	4560	4998
$(t\text{-Bu})_3PHg(CN)_2$	87.0	82.6	26.3	21.6	4604	4858

*In dichloromethane at ambient temperature and at 183 K. Positive chemical shifts are downfield from external reference (85% H_3PO_4). $\Delta\delta$ = δ(complex) − δ(phosphine).

ambient temperature whereas the spectra for the tricyclohexylphosphine and tri-*tert*-butylphosphine complexes showed a main peak and two satellite peaks due to $^{31}P—^{199}Hg$ spin–spin coupling. The satellites due to $^{31}P—^{199}Hg$ spin–spin coupling for the $(Ph_3P)_2Hg(CN)_2$ and $(p\text{-tolyl})_3PHg(CN)_2$ complexes were observed when the spectra were recorded at 183 K. The solution behaviour of mercury(II) cyanide complexes is thus very similar to that of the corresponding halide complexes (8). The ^{31}P nmr spectra of the triphenylphosphine and tri-*p*-tolylphosphine complexes containing excess phosphine gave a single resonance peak even at 183 K, showing that the rate of phosphine exchange is increased markedly by the presence of free phosphine. The ^{31}P nmr spectrum of an equimolar mixture of the 1:1 complex, $Cy_3PHg(CN)_2$, and free phosphine, at ambient temperature, was identical to that of the 1:2 complex, $(Cy_3P)_2Hg(CN)_2$. Addition of another equivalent of phosphine, however, gave a spectrum showing only a single resonance peak. Upon cooling the solution to 183 K the spectrum showed characteristic peaks of the 1:2 complex and free phosphine. From these results we conclude that the phosphine exchange occurs via an associative mechanism.

The $J(^{31}P–^{199}Hg)$ values for the three non-labile complexes increase with a decrease in temperature and the largest increase is observed for the $Cy_3PHg(CN)_2$ complex. Increase in the $^{31}P—^{199}Hg$ spin–spin coupling with decreasing temperature is also observed for complexes of mercury(II) halides (9) and carboxylates (14). The increase in the $^{31}P—^{199}Hg$ spin–spin coupling for the mercury(II) halide complexes (9) has been explained in terms of decrease in the rate of phosphine exchange with decreasing temperatures. However, we believe that further investigations are required to explain the temperature dependence of the $^{31}P—^{199}Hg$ spin–spin coupling. Such studies are underway in our laboratory.

For the 1:2 complexes, the $^{31}P—^{199}Hg$ spin–spin coupling increases markedly with increasing basicity of the phosphine but the increase in the coordination chemical shift is not substantial. The $J(^{31}P–^{199}Hg)$ values for the 1:2 complexes $(Ph_3P)_2HgX_2$ and $(Cy_3P)_2HgX_2$, where X = Cl, Br, I, and CN, follow the order Cl > Br > I > CN. However, the coordination chemical shifts for the cyano complexes in both series are larger than those for the iodo complexes. These observations as well as our recent ^{31}P nmr data on mercury(II) carboxylates (14) show that the correlations between the $^{31}P—^{199}Hg$ spin–spin coupling and the coordination chemical shifts observed in previous studies (3, 8) are fortuitous.

In agreement with the ^{31}P nmr data for the complexes of mercury(II) halides (3, 8, 9) and carboxylates (14), the $J(^{31}P–^{199}Hg)$ value for the 1:1 complex, $Cy_3PHg(CN)_2$, is much higher than that for the 1:2 complex, $(Cy_3P)_2Hg(CN)_2$. The $J(^{31}P–^{199}Hg)$ values for the complexes in the series Cy_3PHgX_2, where X = Cl, Br, I, CN, follow the sequence Cl > Br > CN > I. The $J(^{31}P–^{199}Hg)$ values for the tri-*tert*-butylphosphine complexes also vary in the above order.

^{31}P nmr measurements on ethanol solutions containing mercury(II) cyanide and tri-*o*-tolylphosphine in 1:1, 1:2, and 1:10 mole ratios showed only the resonance signal due to free phosphine at ambient temperature as well as at 183 K indicating lack of any interaction between mercury(II) cyanide and the phosphine.

Experimental Section

Materials

Tri-*tert*-butylphosphine was prepared and purified as described previously (23). Triphenylphosphine (Eastman Kodak) was recrystallized twice from hot ethanol. Tricyclohexyl- and tri(*p*-tolyl)phosphines (Pressure Chemical) were used without further purification. The purity of phosphines was checked by their infrared and ^1H and ^{31}P nmr spectra. Mercury(II) cyanide was reagent grade. Ethanol was dried by refluxing over magnesium and subsequent distillation. Acetonitrile was treated with phosphorus pentoxide and distilled over potassium carbonate. Other solvents were reagent grade.

Physical Measurements

Elemental analyses were performed by M-H-W Laboratories, Garden City, MI. Molecular weights were determined by Galbraith Laboratories, Knoxville, TN. Conductances were determined at 25°C with a Yellow Springs Instrument con-

ductivity bridge using a cell with platinized platinum electrodes. The infrared spectra (4000–130 cm^{-1}) were recorded on a Perkin-Elmer 180 double beam spectrophotometer. Solid samples were prepared as mulls in Nujol, and KRS-5 and polyethylene discs were used for spectral measurements. Sealed sodium chloride cells were used for measuring the spectra in solution. Raman spectra were recorded on a Jarrel-Ash Raman spectrometer using the 5145 Å excitation of an argon ion laser (Spectra Physics). The samples were powdered and sealed in glass capillary tubes. ^{31}P nmr spectra were obtained with a Bruker WP-60 FT spectrometer at 24.3 MHz using 85% H_3PO_4 as external reference. The spectra were recorded at ambient temperature and at 183 K.

*Preparation of Complexes of Triphenylphosphine and Tri-*p*-tolylphosphine*

$Hg(CN)_2$ (0.100 mmol) was dissolved in 20 mL ethanol and this solution was added dropwise, with constant stirring, to an ethanol solution of the phosphine (2.00 mmol). The mixture was refluxed for 1 h. Upon cooling, a white precipitate was obtained which was filtered off and recrystallized from a mixture of dichloromethane and petroleum ether. Yields: over 80%. Reaction of mercury(II) cyanide and phosphine in 1:1 mole ratio afforded a mixture of 1:2 complex and mercury(II) cyanide.

*Preparation of Complexes of Tricyclohexylphosphine and Tri-*tert*-butylphosphine*

The phosphines were handled under an atmosphere of *oxygen-free* dry nitrogen in a controlled atmosphere glove-box. Stoichiometric amount of mercury(II) cyanide was added to the solution of phosphine in dichloromethane and the mixture was stirred to give a clear solution which was concentrated in vacuum. Upon adding hexane (in excess) to the above solution a white precipitate of the complex was formed which was filtered off. The complex $Cy_3PHg(CN)_2$ was recrystallized from benzene and the tri-*tert*-butylphosphine complex was recrystallized from a mixture of dichloromethane and hexane. The 1:2 complex $(Cy_3P)_2Hg(CN)_2$ was recrystallized from an ice-cold solution in ethanol. Reaction of $Hg(CN)_2$ and $(t\text{-}Bu)_3P$ in 1:2 mole ratio also gave 1:1 complex. Yields: ~80%.

*Attempted Preparation of Tri-*o*-tolylphosphine Complexes*

Mercury(II) cyanide and phosphine in 1:1 and 1:2 mole ratios were dissolved in alcohol, acetone, or dimethylacetamide and the solutions were refluxed for several hours. In each case, a mixture of mercury(II) cyanide and phosphine was recovered upon removal of the solvent.

Acknowledgements

Financial assistance of the National Research Council of Canada and the award of an Ontario Graduate Fellowship (to W.O.O.) are gratefully acknowledged.

1. R. C. Evans, F. G. Mann, H. S. Peiser, and D. Purdie. J. Chem. Soc. 1209 (1940).
2. G. B. Deacon, J. H. S. Green, and D. J. Harrison. Spectrochim. Acta, **24**A, 1921 (1968).
3. (*a*) R. L. Keiter and S. O. Grim. J. Chem. Soc. Chem. Commun. 521 (1968); (*b*) S. O. Grim, P. J. Lui, and R. L. Keiter. Inorg. Chem. **13**, 342 (1974).
4. F. G. Moers and J. P. Langhout. Recl. Trav. Chim. Pays-Bas, **92**, 996 (1973).
5. H. Schmidbaur and K. H. Rathlein. Chem. Ber. **106**, 249 (1973).
6. A. Yamasaki and E. Fluck. Z. Anorg. Allg. Chem. **396**, 297 (1973).
7. E. C. Alyea, S. A. Dias, R. G. Goel, and W. O. Ogini. Can. J. Chem. **55**, 4227 (1977).
8. E. C. Alyea, S. A. Dias, R. G. Goel, W. O. Ogini, P. Pilon, and D. W. Meek. Inorg. Chem. **17**, 1697 (1978).
9. S. O. Grim and D. P. Shah. Inorg. Nucl. Chem. Lett. **14**, 105 (1978).
10. R. G. Goel. Unpublished results.
11. N. A. Bell, M. Goldstein, T. Jones, and I. W. Nowell. J. Chem. Soc. Chem. Commun. 1036 (1976).
12. N. A. Bell, M. Goldstein, T. Jones, and I. W. Nowell. Inorg. Chim. Acta, **28**, 1169 (1978).
13. S. C. Jain and R. Rivest. Inorg. Chim. Acta, **4**, 291 (1970).
14. T. Allman, R. G. Goel, and P. Pilon. Can. J. Chem. **57**, 91 (1979).
15. R. G. Goel and W. O. Ogini. Inorg. Chem. **16**, 1968 (1977).
16. R. G. Goel and P. Pilon. Inorg. Chem. **17**, 2876 (1978).
17. R. C. Makhija, A. L. Beauchamp, and R. Rivest. J. Chem. Soc. Dalton Trans. 2447 (1973).
18. J. R. Ferraro. Low frequency vibrations of inorganic and coordination compounds. Plenum Press, New York. 1971. pp. 128, 129, and references therein.
19. L. H. Jones. Inorg. Chem. **13**, 2289 (1974), and references therein.
20. K. Shobatake, C. Postmus, J. R. Ferraro, and K. Nakamoto. Appl. Spectrosc. **23**, 12 (1969).
21. D. A. Dows, A. Haim, and W. K. Wilmarth. J. Inorg. Nucl. Chem. **21**, 33 (1961).
22. R. A. Decastello, C. P. MacCall, N. B. Egen, and A. Haim. Inorg. Chem. **8**, 699 (1969).
23. E. C. Alyea, G. T. Fey, and R. G. Goel. J. Coord. Chem. **5**, 143 (1976).

Syntheses and spectroscopic study of a new series of mixed-ligand complexes of As(III) and Sb(III) with dithio-ligands

FADEL M-N. KHEIRI, CONSTANTINOS A. TSIPIS, CHRISTOS L. TSIAMIS, AND GEORGE E. MANOUSSAKIS[1]

Laboratory of Inorganic Chemistry, University of Thessaloniki, Thessaloniki, Greece

Received September 12, 1978

FADEL M-N. KHEIRI, CONSTANTINOS A. TSIPIS, CHRISTOS L. TSIAMIS, and GEORGE E. MANOUSSAKIS. Can. J. Chem. **57**, 767 (1979).

Seventeen new mixed-ligand complexes of As(III) and Sb(III) with dithio-ligands have been prepared and studied. The preparation of the mixed-ligand complexes has been made by reacting the corresponding iodobis(dialkyldithiocarbamate) complexes with either CS_2 and HNR_2 or the sodium salt of the dithiocarbamate. Alteration of the second method facilitated the preparation of the mixed-ligand dithiocarbamate–xanthate complexes of Sb(III) whereas the analogous arsenic compounds have not been isolated. The study of these new compounds reveals that their stability depends on the nature of both ligand and central atom. The spectroscopic data of the compounds are discussed and compared with those of similar complexes of Bi(III).

FADEL M-N. KHEIRI, CONSTANTINOS A. TSIPIS, CHRISTOS L. TSIAMIS et GEORGE E. MANOUSSAKIS. Can. J. Chem. **57**, 767 (1979).

On a préparé et étudié dix-sept nouveaux complexes avec des ligands mixtes du As(III) et du Sb(III) avec des ligands disulfurés. On a préparé les complexes avec des ligands mixtes en faisant réagir les complexes iodobis(dialkyldithiocarbamate) correspondants soit avec du CS_2 et du HNR_2 ou le sel de sodium du dithiocarbamate. Une modification de la seconde méthode a facilité la préparation des complexes avec les ligands mixtes, dithiocarbamate–xanthate, du Sb(III) alors que l'on n'a pas pu isoler les composés analogues de l'arsenic. L'étude de ces nouveaux complexes révèle que leur stabilité dépend à la fois de la nature du ligand et de l'atome central. On discute des données spectroscopiques et on les compare avec celles de complexes semblables du Bi(III).

[Traduit par le journal]

Introduction

In previous papers (1, 2) we have reported the syntheses and study of some new mixed-ligand complexes of Fe(III) and Bi(III) with dithio-ligands. In the course of our studies on metal complexes with sulfur containing ligands, it seemed interesting to investigate the effect of the different size and electronegativity of the central atom on the stability and the electronic properties of the mixed-ligand dithio-complexes. In this paper we report the results concerning the preparation and study of some new mixed-ligand complexes of As(III) and Sb(III) with dithio-ligands and compare their properties with those of the Bi(III) analogues.

Experimental

Materials

The sodium dialkyldithiocarbamate salts, the potassium *O*-ethylxanthate, the iodobis(dialkyldithiocarbamate) complexes of As(III) and Sb(III) and the As(III) and Sb(III) *O*-ethylxanthates were prepared by previously reported methods (3–7).

Synthesis of the Mixed-ligand Complexes

The following two general methods were applied for the preparation of the mixed-ligand complexes of As(III) and Sb(III) of the general formula $M(R_2'dtc)(R_2dtc)_2$.

Method A

The preparation was carried out into a three-necked flask equipped with a magnetic stirrer, a reflux condenser, and a separatory funnel. Into the flask were charged 2.0 mmol of the iodobis(dialkyldithiocarbamato)arsine or -stibine, 2.0 mmol of CS_2 and 100 cm^3 of CCl_4 as a solvent.

To the resulting suspension 4.0 mmol of the amine ($R_2'NH$), dissolved in $\sim$30 cm^3 of CCl_4, were added slowly under continuous stirring in a period of 0.5 h.

The mixture was refluxed for 4–5 h and after cooling it was filtered. The filtrate was condensed up to a small volume ($\sim$30 cm^3) and upon addition of ethanol the mixed-ligand dithio-complex was precipitated as a crystalline solid. The products obtained were purified by dissolving them in a small volume of $CHCl_3$ or benzene and reprecipitating by adding methanol or petroleum ether.

Method B

The reaction was run into a conical flask. Into the flask were charged 3.0 mmol of the iodobis(dialkyldithiocarbamato)arsine (or -stibine) suspended into 60 cm^3 of chloroform. Then 3.0 mmol of sodium dialkyldithiocarbamate salt, dissolved in 15 cm^3 of ethanol, were added to the suspension slowly, under continuous magnetic stirring. The reaction mixture was left for 1 h at room temperature and then was filtered in order to remove the insoluble potassium iodide formed. The filtrate was condensed up to a small volume ($\sim$20 cm^3) and upon addition of ethanol or petroleum ether the mixed-ligand dithio-complex

[1]To whom all correspondence should be addressed.

0008-4042/79/070767-06$01.00/0

was precipitated. The crude product obtained was purified as described in method A.

The synthesis of the mixed-ligand dithiocarbamate–xanthate complexes of antimony has been done according to the following method. To a suspension of 2.5 mmol of iodobis(dialkyldithiocarbamato)stibine in 60 cm^3 of chloroform, 2.5 mmol of potassium *O*-ethylxanthate, dissolved in 10 cm^3 of ethanol, were added slowly under continuous stirring. The reaction mixture was left at room temperature for 1 h and then was filtered. The filtrate was condensed up to a small volume ($\sim$20 cm^3) and the mixed-ligand complex was precipitated by addition of petroleum ether. The crude product was purified by dissolving it in a small volume of benzene and reprecipitating by adding petroleum ether.

Measurements

Infrared spectra were recorded in the region of 4000–650 cm^{-1} with a Perkin-Elmer 257 spectrophotometer. Proton nmr spectra were obtained with a Varian A 60A (60 MHz) spectrometer in $CDCl_3$ and C_6H_6 solutions, using TMS as an internal standard. Electronic spectra in the region 200–1000 nm were measured at ca. 30°C using a Zeiss PMQII spectrophotometer. Solutions in chloroform were used in 1 cm "suprasil" cells fitted with Teflon stoppers, with pure solvent in the reference cell. Mass spectra were measured on an RMU-6L Hitachi Perkin-Elmer mass spectrometer with ionisation source of AT-2p type operating at $\sim$70 eV. Molecular weights in solution were determined using a Perkin-Elmer Model 115 molecular weight apparatus at a concentration ranging from 3×10^{-3} to 6×10^{-4} mol/kg in chloroform.

Results and Discussion

Seventeen new mixed-ligand complexes of arsenic and antimony with dithio-ligands have been prepared by reacting the iodobis(dialkyldithiocarbamate) complexes of As(III) and Sb(III) with sodium dialkyldithiocarbamate salts according to the following general equation

$$Na(R_2'dtc) + M(R_2dtc)_2I \rightarrow M(R_2'dtc)(R_2dtc)_2 + NaI$$

where M = As or Sb, $R_2'dtc$ = Et_2dtc, Pyrrdtc, Bz_2dtc, THPyrdtc, and R_2dtc = Et_2dtc, Pyrrdtc, Pipdtc (Et = C_2H_5, Pyrr = $(CH_2)_4N$, Bz = C_6H_5-CH_2, THPyr = 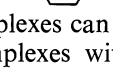 N, Pip = $(CH_2)_5N$).

These complexes can also be prepared by reacting the iodo-complexes with carbon disulfide and the amine (HNR_2') in one step according to the reaction:

$$2R_2'NH + CS_2 + M(R_2dtc)_2I \rightarrow M(R_2'dtc)(R_2dtc)_2 + R_2'NH{\cdot}HI$$

This method cannot be applied for the preparation of the mixed-ligand complexes, whenever the amine is the dibenzylamine.

The iodobis(dialkyldithiocarbamate) complexes of Sb(III) also react with potassium *O*-ethylxanthate to give the mixed-ligand dithiocarbamate–xanthate complexes according to the reaction:

$$Sb(R_2dtc)_2I + K(EtXanth) \rightarrow Sb(EtXanth)(R_2dtc)_2 + KI$$

where EtXanth = $EtOCSS^-$ and R_2dtc = Et_2dtc or Pyrrdtc.

However, in the case of the arsenic compounds, it was not possible to obtain mixed-ligand dithiocarbamate–xanthate complexes, as the products of the second reaction were the corresponding tris(dialkyldithiocarbamate) and tris(*O*-ethylxanthate) complexes of arsenic.

This may be due to a disproportionation reaction which undergoes the mixed-ligand dithiocarbamate–xanthate complexes of arsenic formed possibly as intermediates:

$$3As(EtXanth)(R_2dtc)_2 \rightleftharpoons 2As(R_2dtc)_3 + As(EtXanth)_3$$

In order to support the above idea, some ligand exchange experiments were performed. The tris(dialkyldithiocarbamate) and tris(*O*-ethylxanthate) complexes of arsenic were dissolved in $CHCl_3$ in a mole ratio 2:1 and the mixture was refluxed for several hours. From the reaction mixture only the starting materials were isolated.

The mixed-ligand dithio-complexes of arsenic and antimony are stable in air, in solid state as well as in solution. All the complexes are soluble in chloroform, methylene chloride, and benzene, and insoluble in methanol, ethanol, petroleum ether, and water. The analytical data and some physical properties of the complexes are given in Table 1.

Infrared Spectra

The thioureide band (1460–1500 cm^{-1}) of the complexes studied is a composite band, containing the frequencies of the C···N bonds of both types of the dithiocarbamato ligands. The maximum of these bands corresponds to the C···N stretching frequency of the dithiocarbamato ligand, which is in higher proportion in the molecule of the mixed-ligand complex. The stretching frequency of the C···N bond of the other ligand appears as a shoulder. Generally, there is no significant influence of the nature of the central atom on the position of the thioureide band.

There are some bands in the region 800–1000 cm^{-1} which are attributed (8) to the C···S stretching vibration of both types of the dithiocarbamato ligands. The position of these bands is about the same as those of the corresponding simple tris(dialkyldithiocarbamate) complexes. In the mixed-ligand dithiocarbamate–xanthate complexes of antimony, the C···S stretching frequencies of the xanthate moiety are higher than those of the dithiocarbamate group.

The asymmetric stretching vibration of the C···O bond of the xanthate group appears in the region of 1200–1300 cm^{-1} and depends heavily on the nature of the central atom (9–13). As the electronegativity of

TABLE 1. Elemental analysis results and some physical properties of the mixed-ligand complexes of As(III) and Sb(III) with dithio-ligands†

Compound	Yield (%)	Color	Melting point* (°C)	C (%)	H (%)	N (%)	S (%)	M (%)	Molecular weight
$As(Et_2dtc)(Pyrrdtc)_2$	64	white	220–223 d	35.00	5.18	7.88	37.10	14.62	518
				(34.94)	(5.08)	(8.14)	(37.30)	(14.83)	(515.7)
$Sb(Et_2dtc)(Pyrrdtc)_2$	82	yellow	191–193 d	31.84	4.50	7.14	34.06	21.18	567
				(32.30)	(4.66)	(7.47)	(34.20)	(21.64)	(562.6)
$As(Pyrrdtc)(Et_2dtc)_2$	69	white	226–228 d	35.01	5.32	8.07	37.23	14.34	524
				(34.90)	(5.45)	(8.11)	(37.16)	(14.48)	(517.7)
$Sb(Pyrrdtc)(Et_2dtc)_2$	86	yellow	165 d	31.81	4.85	7.25	33.82	21.26	561
				(31.91)	(5.00)	(7.44)	(34.08)	(21.57)	(564.5)
$As(Bz_2dtc)(Et_2dtc)_2$	70	white	50–52 d	46.50	5.44	6.46	29.78	11.27	587
				(46.64)	(5.32)	(6.52)	(29.88)	(11.64)	(643.8)
$Sb(Bz_2dtc)(Et_2dtc)_2$	62	pale-yellow	54 d	43.33	4.91	5.88	27.54	17.40	713
				(43.47)	(4.96)	(6.08)	(27.85)	(17.63)	(690.7)
$As(Bz_2dtc)(Pyrrdtc)_2$	82	white	100 d	47.11	4.36	6.08	30.04	11.57	654
				(46.93)	(4.73)	(6.56)	(30.07)	(11.71)	(639.8)
$Sb(Bz_2dtc)(Pyrrdtc)_2$	65	yellow	69 d	43.68	4.30	6.23	27.94	17.38	614
				(43.73)	(4.40)	(6.12)	(28.02)	(17.73)	(686.6)
$As(Et_2dtc)(Pipdtc)_2$	90	white	179	37.18	5.46	7.61	35.16	13.46	542
				(37.85)	(5.56)	(7.72)	(35.38)	(13.78)	(543.7)
$Sb(Et_2dtc)(Pipdtc)_2$	90	yellow	107–109	34.37	5.09	6.86	32.38	20.22	579
				(34.57)	(5.12)	(7.12)	(32.57)	(20.62)	(590.5)
$Sb(Bz_2dtc)(Pipdtc)_2$	73	yellow	82 d	44.94	4.49	5.64	26.43	16.97	728
				(45.37)	(4.79)	(5.88)	(26.92)	(17.03)	(714.7)
$As(THPyrdtc)(Pyrrdtc)_2$	78	pale-yellow	230–233	36.28	4.56	7.82	36.20	14.34	546
				(36.56)	(4.60)	(7.99)	(36.60)	(14.25)	(525.7)
$Sb(THPyrdtc)(Pyrrdtc)_2$	92	yellow	172 d	33.34	4.69	7.13	33.33	21.04	569
				(33.57)	(4.23)	(7.34)	(33.60)	(21.27)	(572.5)
$As(THPyrdtc)(Pipdtc)_2$	78	pale-yellow	214–215	39.16	4.84	7.68	34.52	13.21	519
				(39.04)	(5.10)	(7.59)	(34.74)	(13.53)	(535.7)
$Sb(THPyrdtc)(Pipdtc)_2$	92	yellow	196–198	35.65	4.33	6.61	31.84	20.64	584
				(36.00)	(4.70)	(7.00)	(32.03)	(20.27)	(600.6)
$Sb(EtXanth)(Et_2dtc)_2$	99	pale-yellow	116–117	29.12	4.60	5.03	35.26	22.32	517
				(28.94)	(4.67)	(5.19)	(35.66)	(22.57)	(539.5)
$Sb(EtXanth)(Pyrrdtc)_2$	88	yellow	221 d	29.40	3.95	5.57	35.62	22.46	504
				(29.16)	(3.93)	(5.23)	(35.93)	(22.74)	(535.4)

*d = decomposition.
†Figures in parentheses are the theoretical calculated values.

the central atom decreases, the band is shifted to lower frequencies. This dependence is more pronounced than that of the C⋯N bond of the dithiocarbamate ligand.

The C⋯O frequency for the mixed-ligand dithiocarbamate–xanthate complexes is lower than that for the corresponding tris(*O*-ethylxanthate) complexes. That would be expected for the dithiocarbamate group which, as a stronger electron donor, increases the electron density on the central atom. Thus the latter reduces the electron releasing ability of the xanthate group.

Proton Nuclear Magnetic Resonance Spectra

The ^1H nmr chemical shifts (τ, ppm) of the mixed-ligand complexes of As(III) and Sb(III) with dithio-ligands are given in Table 2.

There is a remarkable difference in the ^1H nmr spectra of the mixed-ligand complexes concerning the dithiocarbamate and xanthate ligands. In the xanthate ligand, as its electron releasing ability increases, the proton chemical shifts are moved to lower frequencies, while in the dithiocarbamate ligand only the protons, the most distant from the nitrogen atom, are deshielded. This can be explained on the basis of the different location of the protons in the shielding or deshielding cone, which is the consequence of the magnetic anisotropy of the C⋯O and C⋯N bonds in the xanthate and dithiocarbamate ligands, respectively. This explanation also holds true for the analogous behaviour observed (2) in the mixed-ligand Bi(III) dithio-complexes.

In benzene solution the usual Aromatic Solvent Induced Shift (ASIS) was observed. This is attributed to the formation of weak collision complexes between the solute and solvent molecules (14). In the mixed-

TABLE 2. ^{1}H nmr chemical shifts (τ, ppm) of the mixed-ligand complexes of As(III) and Sb(III) with dithio-ligands

Complex	Ligand	Chemical shift
$As(Et_2dtc)(Pyrrdtc)_2$	Et_2dtc	8.69(9.16)*(t, 6H, CH_3), 6.15(6.67)(m, 4H, —CH_2—)
	Pyrrdtc	7.96(8.97)(m, 8H, β—CH_2—), 6.15(6.67)(m, 8H, α—CH_2—)
$Sb(Et_2dtc)(Pyrrdtc)_2$	Et_2dtc	8.69(9.13)(t, 6H, —CH_3), 6.16(6.61)(m, 4H, —CH_2—)
	Pyrrdtc	7.96(8.95)(m, 8H, β—CH_2—), 6.16(6.61)(m, 8H, α—CH_2—)
$As(Pyrrdtc)(Et_2dtc)_2$	Pyrrdtc	7.69(8.97)(m, 4H, β—CH_2—), 6.16(6.66)(m, 4H, α—CH_2—)
	Et_2dtc	8.70(9.16)(t, 12H, —CH_3), 6.16(6.66)(m, 8H, —CH_2—)
$Sb(Pyrrdtc)(Et_2dtc)_2$	Pyrrdtc	7.96(8.95)(m, 4H, β—CH_2—), 6.15(6.62)(m, 4H, α—CH_2—)
	Et_2dtc	8.69(9.13)(t, 12H, —CH_3), 6.15(6.62)(m, 8H, —CH_2—)
$As(Bz_2dtc)(Et_2dtc)_2$	Bz_2dtc	2.65(—)(s, 10H, C_6H_5), 4.89(5.03)(s, 4H, —CH_2—)
	Et_2dtc	8.69(9.18)(t, 12H, —CH_3), 6.08(6.60)(q, 8H, —CH_2—)
$Sb(Bz_2dtc)(Et_2dtc)_2$	Bz_2dtc	2.62(—)(s, 10H, C_6H_5), 4.86(4.99)(s, 4H, —CH_2—)
	Et_2dtc	8.68(9.14)(t, 12H, —CH_3), 6.08(6.59)(q, 8H, —CH_2—)
$As(Bz_2dtc)(Pyrrdtc)_2$	Bz_2dtc	2.62(—)(s, 10H, C_6H_5), 4.87(4.99)(s, 4H, —CH_2—)
	Pyrrdtc	7.96(8.92)(m, 8H, β—CH_2—), 6.15(6.67)(m, 8H, α—CH_2—)
$Sb(Bz_2dtc)(Pyrrdtc)_2$	Bz_2dtc	2.62(—)(s, 10H, C_6H_5), 4.89(4.99)(s, 4H, —CH_2)
	Pyrrdtc	7.93(8.97)(m, 8H, β—CH_2—), 6.15(6.67)(m, 8H, α—CH_2—)
$As(Et_2dtc)(Pipdtc)_2$	Et_2dtc	8.70(9.16)(t, 6H, —CH_3), 6.09(6.56)(q, 4H, —CH_2—)
	Pipdtc	8.30(8.98)(Su, 12H, β, γ—CH_2—), 5.92(6.35)(su, 8H, α—CH_2—)
$Sb(Et_2dtc)(Pipdtc)_2$	Et_2dtc	8.69(9.10)(t, 6H, —CH_3), 6.08(6.60)(q, 4H, —CH_2—)
	Pipdtc	8.29(9.00)(su, 12H, β, γ—CH_2—), 5.90(6.40)(su, 8H, α—CH_2—)
$Sb(Bz_2dtc)(Pipdtc)_2$	Bz_2dtc	2.65(—)(s, 10H, C_6H_5), 4.89(5.00)(s, 4H, —CH_2—)
	Pipdtc	8.29(9.00)(su, 12H, β, γ—CH_2—), 5.94(6.40)(su, 8H, α—CH_2—)
$As(THPyrdtc)(Pyrrdtc)_2$†	THPyrdtc	7.53(8.36)(m, 2H, α—CH_2—), 5.79(6.27)(m, 2H, *b*—CH_2—), 5.43(5.82)(m, 2H, C—CH_2—), 4.07(—)(m, 1H, *d*=CH—), 4.20(—)(m, 1H, *e*=CH—)
	Pyrrdtc	7.96(8.94)(m, 8H, β—CH_2—), 6.04(6.63)(m, 8H, α—CH_2—)
$As(THPyrdtc)(Pipdtc)_2$	THPyrdtc	7.72(8.37)(m, 2H, α—CH_2—), 5.80(6.27)(m, 2H, *b*—CH_2—), 5.50(5.84)(m, 2H, C—CH_2—), 4.10(—)(m, 1H, *d*=CH—), 4.20(—)(m, 1H, *e*=CH—)
	Pipdtc	8.30(8.96)(su, 12H, β, γ—CH_2—), 6.15(6.66)(su, 8H, α—CH_2—)
$Sb(THPydtc)(Pipdtc)_2$	THPyrdtc	7.70(8.32)(m, 2H, α—CH_2—), 5.79(6.24)(m, 2H, *b*—CH_2—), 5.43(5.79)(m, 2H, *c*—CH_2—), 4.05(—)(m, 1H, *d*=CH—), 4.19(—)(m, 1H, *e*=CH—)
	Pipdtc	8.29(8.97)(su, 12H, β, γ—CH_2—), 5.89(6.33)(su, 8H, α—CH_2—)
$Sb(EtXanth)(Et_2dtc)_2$	EtXanth	8.56(9.09)(t, 3H, —CH_3), 5.34(5.69)(q, 2H, —CH_2—)
	Et_2dtc	8.68(9.18)(t, 12H, —CH_3), 6.11(6.66)(q, 8H, —CH_2—)
$Sb(EtXanth)(Pyrrdtc)_2$	EtXanth	8.56(8.99)(t, 3H, —CH_3), 5.30(5.70)(q, 2H, —CH_2—)
	Pyrrdtc	7.94(8.90)(m, 8H, β—CH_2—), 6.15(6.70)(m, 8H, α—CH_2—)

*Figures in parentheses are the τ values for the benzene solutions.

† 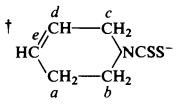

ligand dithiocarbamate complexes, the observed ASIS has approximately the same magnitude as that in the case of the tris-derivatives. This observation supports the notion that, in a complex, each dithiocarbamate ligand acts as an independent centre for electrophilic attack from the benzene molecules (14). The ASIS in the mixed-ligand dithiocarbamate–xanthate complexes is smaller than in the previous cases. The different ASIS between the xanthate and dithiocarbamate ligands is attributed to the different orientation of the attached benzene molecule as this orientation is dependent on the stereochemistry of the ligand and the magnitude of the positive charge on the oxygen or the nitrogen atom respectively.

Electronic Spectra

As shown in Table 3 the compounds gave, as expected (15), intense bands at approximately 255, 310, and 360 nm. Most authors (16–18) agree that the intense band near 255 nm, band I, should be assigned to intraligand $\pi^* \leftarrow \pi$ transition of the N⋯C⋯S group. In the mixed-ligand dithiocarbamate–xanthate complexes this band partly obscures the band at λ_{max} 245 nm due to an $\sigma^* \leftarrow \eta$ electronic transition of the xanthate moiety (19). Band II is attributed to a $\pi^* \leftarrow \pi$ transition of the S⋯C⋯S group. This band, which appears as a shoulder in dithiocarbamate and mixed dithiocarbamate complexes, exhibits a characteristic λ_{max} and a blue shift

TABLE 3. Electronic spectra of the mixed-ligand complexes of As(III) and Sb(III) with dithio-ligands

Compound	Band I		Band II		Band III	
	ν_{max}(kK)	log ε_{mol}	ν_{max}(kK)	log ε_{mol}	ν_{max}(kK)	log ε_{mol}
$As(Et_2dtc)(Pyrrdtc)_2$	39.8	4.77	32.3 sh*	4.19	28.1 sh	3.38
$Sb(Et_2dtc)(Pyrrdtc)_2$	39.1	4.76	31.8 sh	4.01	27.8 sh	3.45
$As(Pyrrdtc)(Et_2dtc)_2$	39.8	4.56	32.6 sh	4.02	28.6 sh	3.17
$Sb(Pyrrdtc)(Et_2dtc)_2$	38.9	4.86	32.4 sh	4.19	27.5 sh	3.49
$As(Bz_2dtc)(Et_2dtc)_2$	39.4	4.77	32.4 sh	4.22	28.2 sh	3.52
$Sb(Bz_2dtc)(Et_2dtc)_2$	39.1	4.78	32.3 sh	4.16	27.6 sh	3.52
$As(Bz_2dtc)(Pyrrdtc)_2$	39.5	4.60	32.3 sh	4.06	27.8 sh	3.21
$Sb(Bz_2dtc)(Pyrrdtc)_2$	39.1	4.61	31.5 sh	4.01	27.4 sh	3.42
$As(Et_2dtc)(Pipdtc)_2$	39.1	4.79	32.5 sh	4.37	27.9 sh	3.36
$Sb(Et_2dtc)(Pipdtc)_2$	38.8	4.73	32.3 sh	4.12	28.1 sh	3.84
$Sb(Bz_2dtc)(Pipdtc)_2$	38.5	4.69	—	—	28.1 sh	3.50
$As(THPyrdtc)(Pyrrdtc)_2$	39.2	4.76	32.6 sh	4.16	28.2 sh	3.42
$Sb(THPyrdtc)(Pyrrdtc)_2$	39.1	4.95	32.3 sh	4.34	27.4 sh	3.61
$As(THPyrdtc)(Pipdtc)_2$	39.2	4.74	32.6 sh	4.22	28.2 sh	3.42
$Sb(THPyrdtc)(Pipdtc)_2$	38.6	4.66	—	—	27.4 sh	3.35
$Sb(EtXanth)(Et_2dtc)_2$	41.0	4.77	35.1 sh	4.75	27.4 sh	3.35
$Sb(EtXanth)(Pyrrdtc)_2$	39.7	4.74	32.3 sh	4.24	27.4 sh	3.41

*sh = shoulder.

TABLE 4. Mass spectra of $As(Et_2dtc)_2(Bz_2dtc)$

m/e	I% (250°C)	I% (280°C)	Ion formulae	m/e	I% (250°C)	I% (280°C)	Ion formulae
42	18.0	46.1	$\|C_2H_4N\|^+$	117	10.5	25.6	$\|C_6H_5CH_2NC\|^{+\cdot}$
44	43.6	47.4	$\|CS\|^{+\cdot}$	118	6.0	15.3	$\|C_2H_4NCS_2\|^+$
			$\|C_2H_5NH\|^+$	149	40.6	56.4	$\|(C_2H_5)_2NCSSH\|^+$
55	8.2	37.1	$\|C_2H_5NC\|^{+\cdot}$				$\|C_6H_5CH_2NCS\|^+$
59	27.0	—	$\|HNCS\|^+$	150	6.7	12.8	$\|As_2\|^+$
60	33.8	12.8	$\|H_2NCS\|^+$	196	2.1	10.2	$\|(C_6H_5CH_2)_2N\|^+$
65	13.5	56.4	$\|C_5H_5\|^+$	240	4.5	3.5	$\|(C_6H_5CH_2)_2NCS\|^+$
72	16.5	—	$\|(C_2H_5)_2N\|^+$	255	21.0	2.8	$SAs\|(C_2H_5)_2NCS_2\|^+$
76	100.0	100.0	$\|CS_2\|^{+\cdot}$	264	1.8	—	$\|(C_2H_5)_2NCS\|_2S^{+\cdot}$
77	10.5	51.2	$\|C_6H_5\|^+$	300	0.7	1.0	$\|As_4\|^+$
87	39.0	—	$\|C_2H_5NCS\|^{+\cdot}$	321	1.5	1.6	$\|As_3S_3\|^+$
88	33.0	—	$\|C_2H_5NHCS\|^+$	371	1.5	—	$As\|(C_2H_5)_2NCS_2\|_2^+$
91	87.2	79.4	$\|C_6H_5CH_2\|^+$	380	0.7	0.5	$HSAs\|(C_6H_5CH_2)_2NCS_2\|^+$
105	12.0	51.2	$\|C_6H_5CH_2N\|^{+\cdot}$	396	5.2	3.5	$\|As_4S_3\|^+$
107	12.0	10.2	$\|AsS\|^+$	428	1.8	2.8	$\|As_4S_4\|^+$
116	51.1	20.5	$\|(C_2H_5)_2NCS\|^+$				

in the case of xanthate complexes. The same observations can be made for band III which is attributed to either an $\pi^* \leftarrow \eta$ transition located on the sulfur atom or a *d*-orbital ← ligand transition (5, 19, 20).

Mass Spectra

The mass spectra (ms) of the mixed-ligand dithiocarbamate and dithiocarbamate–xanthate complexes were obtained over a temperature range as these complexes might undergo a thermolytic decomposition at elevated temperatures (250–300°C). In common with dithiocarbamate and xanthate complexes, the molecular ion was not observed. Again, at the lower end of the temperature range, the base peak appeared at $(m/e) = 76$ attributed to the $|CS_2|^{+\cdot}$ ion. As the temperature was raised the fragmentation pattern changed and this was accompanied by a change in peak intensity. There was a sharp increase in the intensity of peaks attributed to ions $|CS|^{+\cdot}$, $|CO|^{+\cdot}$, $|R|^+$, $|R'|^+$. This and the appearance of sulfides of the general formula As_nS_m, Sb_nS_m, where $n, m = 1, 2, 3, 4$, are in support of a pyrolytic decomposition taking place (21). The mass spectra of a representative complex at different temperatures are given in Table 4.

The salient feature of the mass spectra of the dithiocarbamate–xanthate complexes is that no peak could be assigned to fragments containing the xan-

thate moiety bonded to the central ion. This is in support of the widely held opinion that the xanthate ligand is a weaker chelating agent than the dithiocarbamate.

1. C. A. TSIPIS, C. C. HADJIKOSTAS, and G. E. MANOUSSAKIS. Inorg. Chim. Acta, **23**, 163 (1977).
2. F. M-N. KHEIRI, C. A. TSIPIS, and G. E. MANOUSSAKIS. Inorg. Chim. Acta, **25**, 223 (1977).
3. L. M. COMPIN. Bull. Soc. Chim. Fr. **27**, 464 (1920).
4. I. S. SHUPE. J. Assoc. Off. Agric. Chem. **25**, 495 (1942); Chem. Abstr. **36**, 4670 (1942).
5. C. A. TSIPIS and G. E. MANOUSSAKIS. Inorg. Chim. Acta, **18**, 35 (1976).
6. L. MALATESTA. Gazz. Chim. Ital. **69**, 629 (1939).
7. T. DERENZINI and P. ROSSONI. Atti Soc. Toscana Sci. Nat. Pisa, P. V. **47**, 67 (1938).
8. G. DURGAPRASAD, D. N. SATHYANARAYANA, and C. C. PATEL. Can. J. Chem. **47**, 631 (1969).
9. G. W. WATT and B. J. MCCORMICK. Spectrochim. Acta, **21**, 753 (1965).
10. A. RAY, D. N. SATHYANARANAYANA, G. DURGAPRASAD, and C. C. PATEL. Spectrochim. Acta, **29**A, 1579 (1973).
11. M. G. MUMME and G. WINTER. Inorg. Nucl. Chem. Lett. **7**, 505 (1971).
12. B. F. HOSKINS and B. B. KELLY. Inorg. Nucl. Chem. Lett. **8**, 875 (1972).
13. V. AGARWALA, LAKSHMI, and P. B. RAO. Inorg. Chim. Acta, **2**, 337 (1968).
14. G. E. MANOUSSAKIS and C. A. TSIPIS. Z. Anorg. Allg. Chem. **398**, 88 (1973).
15. G. E. MANOUSSAKIS and C. A. TSIPIS. J. Inorg. Nucl. Chem. **35**, 743 (1973).
16. C. K. JØRGENSEN. J. Inorg. Nucl. Chem. **24**, 1571 (1962).
17. F. TAKAMI, S. WAKAHARA, and T. MAEDA. Tetrahedron Lett. **28**, 2645 (1971).
18. H. P. KOCH. J. Chem. Soc. 401 (1949).
19. M. L. SHANKARANARAYANA and C. C. PATEL. Acta Chem. Scand. **19**, 1113 (1965).
20. D. C. BRADLEY and M. H. GITLITZ. J. Chem. Soc. A, 1152 (1969).
21. G. E. MANOUSSAKIS, E. D. MIKROMASTORAS, and C. A. TSIPIS. Z. Anorg. Allg. Chem. **403**, 87 (1974).

Etude des complexes du tungsténe(VI) dans l'excès de acide malique

ANTONIO CERVILLA, AURELIO BELTRAN ET JOSÉ BELTRAN
Département de Chimie Inorganique, Faculté de Sciences, Université de Valencia, Espagne
Reçu le 10 août 1978

ANTONIO CERVILLA, AURELIO BELTRAN et JOSÉ BELTRAN. Can. J. Chem. **57**, 773 (1979).

L'étude polarimétrique des complexes de W(VI) avec l'acide malique montre, en présence d'un excès d'acide malique (H_2M), l'existance de trois complexes différents. La stoechiométrie et le degré de condensation de ces complexes sont fonction du pH. Les resultats obtenus indiquent que l'acide malique et l'acide tartrique montrent un comportement analogue. La constante de formation du complexe $[O_2W(OH)_2(M_2)]^{4-}$ a été determinée par deux méthodes différents.

ANTONIO CERVILLA, AURELIO BELTRAN, and JOSÉ BELTRAN. Can. J. Chem. **57**, 773 (1979).

The complex formation between W(VI) and malic acid (H_2M) has been investigated polarimetrically in excess malic acid. The formation of three different complexes is confirmed. The stoichiometry and the degree of condensation of these complexes can vary depending on the acidity. Furthermore, the results obtained show that both tartaric and malic acids behave similarly in forming complexes with W(VI). The formation constant of the complex $[O_2W(OH)_2(M_2)]^{4-}$ has been determined by two different methods.

Introduction

Le pouvoir rotatoire du tartrate ou malate neutre n'est pas modifié par l'addition de WO_4^{2-}, ce qui preuve qu'il ne se forme pas de complexe dans cettes conditions. Par contre, on a observé depuis longtemps (1) que l'acidification du mélange provoque une augmentation importante de son pouvoir rotatoire, ce qui indique la formation de complexes.

Desal (2) étudie les variations du pouvoir rotatoire en fonction de la neutralisation progressive des mélanges d'acide tungstique et d'acide 1(+)-tartrique ou 1(−)-malique. Avec l'acide tartrique, Desal ne reconnait qu'un seul complexe tungsto-tartrique (TWO_2Na_2), dextrogyre. Par contre, avec l'acide malique, les courbes polarimétriques de neutralisation misent en évidence deux groupes de complexes. Un complexe tungsto-dimalique levogyre ($M_2WO_2Na_2$) et un complexe ditungsto-malique destrogyre ($MWO_2(OH)Na_2WO_4H_2$). Il n'existe pas de complexes dans lesquels le rapport M/W = 1/1.

En 1961, Baillie et Brown (3) montrent, à partir des mesures polarimétriques de neutralisation des mélanges d'acide tungstique et d'acide 1(+)-tartrique ou 1(−)-malique, l'existence de trois espèces, avec un degré différent de protonation, donc le rapport M/W est toujours égale a 1/1.

Face à ces conclusions assez divergentes, dans un travail précedant (4), nous avons fait l'étude des complexes du W(VI) avec l'acide 1(+)-tartrique, en utilisant une méthode polarimétrique décrite par Viossat (5).

Les résultats obtenus sont partiellement en accord avec d'autres récemment parus dans la réf. 6.

Avec le propos de deduire l'influence des groupes alcooliques dans les complexes qui forme le W(VI) avec l'acide tartrique, dans ce travail nous allons étudier les complexes qui se forment avec l'acide malique.

Il faut remarquer, d'accord avec un travail publié en avance (7), que l'acide tartrique forme les espèces complexes antérieurement cités, indépendamment de la concentration de W(VI). Tout au contraire, il semble que l'acide malique forme des espèces complexes en l'excès de cet acide, différents a ceux qui se forment en présénce d'un excès de W(VI). Dans ce travail nous n'allons nous occuper que des complexes formés en excès d'acide malique.

Mise en évidence des différents complexes

Dans la fig. 1 (courbe *A*) on a porté le pouvoir rotatoire, face au pH pendant la neutralisation d'une disolution de H_2M 0.1 *M* avec NaOH.

Cette courbe *A* es très influenciée par la addition de Na_2WO_4 à la disolution initial de H_2M (courbe *B*, fig. 1). La concentration de Na_2WO_4 correspondant à la courbe *B* est de 4×10^{-3} *M*, c'est-à-dire $H_2M/WO_4^{2-} = 25$. Dans cette courbe *B* apparaisent superposées les rotations dues aux complexes existants et à l'excès d'acide malique.

Comme nous verrons après, la relation M/W dans les complexes formés ne sera pas plus grande de 2/1. Pourtant, l'excès d'acide malique ne sera jamais inferieur à 23 fois la concentration de WO_4^{2-} présente. Pour cela et etant donné que le pouvoir rotatoire de l'acide malique est très inférieur à celui des complexes formés, on peut déduir, avec une erreur négligeable, que la différence entre les courbes *A* et *B* (courbe *C*, fig. 1) répresente la

0008-4042/79/070773-04$01.00/0

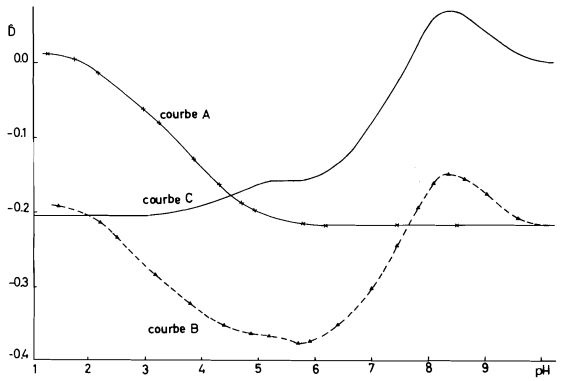

FIG. 1. $\hat{D} = f(\text{pH})$ à $\lambda = 436$ nm. Courbe A: H_2M seul 0.1 M. Courbe B: WO_4^{2-} 4×10^{-3} M + H_2M 0.1 M. Courbe C: courbe A − courbe B.

variation du pouvoir rotatoire avec le pH, dû aux complexes formés.

On peut deceler, à partir de la forme presentée par la courbe C, l'existance de trois zones distinctes. Ces trois zones correspondront à trois complexes différents.

Zone A: *pH compris entre 10 et 8.5*

Les courbes A et B (fig. 1) coincident à partir du pH égal à 10, ceci nous indiquerai l'absence de complexes pour les pH supérieurs à celui-ci. L'addition d'acide $HClO_4$ produit une montée brusque du pouvoir rotatoire, cela nous montre la formation d'un complexe que nous appellerons I. Au pH 8.5 on observe sur la courbe C un maximum, ceci indique que tout le W(VI) est complexé sous la forme I puisqu'il existe un excès de ions malate.

Les variations du pouvoir rotatoire dû aux complexes formés, courbe C, varient entre 0.000 et 0.072 pour des pH 10.0 et 8.5 respectivement. Cette variation servira à la détermination des ions H^+ necessaires au passage des ions WO_4^{2-} au complexe I, suivant la reaction:

$$WO_4^{2-} + nH^+ + zM^{2-} \rightleftarrows (1/a)I$$

où la valeur du paramètre a est lié au degré de condensation du complexe. En appelant α la fraction molaire de I formée, C la concentration total de W(VI), et en appliquant la loi d'action de masse à l'équilibre précédant, on obtient:

$$[1] \quad \log K + (1/a)\log a - \log C(1/a - 1) + z \log (M^{2-}) = \text{cte} = n\text{pH} + \log \alpha^{1/a}/(1 - \alpha)$$

Pour des valeurs de C et (M^{2-}) constants la connaissance des valeurs de α permet le calcul de la fonction $\log \alpha^{1/a}/(1 - \alpha)$ pour différents valeurs de a. Si on porte cette fonction envers le pH on obtient une série de courbes, la seule qui satisfait l'équation précédente est la droite, dont la pente détermine la valeur de n.

Les valeurs de α, pour un pH fixé, sont calculés à partir de la relation: $\hat{D} = \alpha \hat{D}_I = 0.072\alpha$; où $\hat{D}_I = \hat{D}(\text{pH} = 8.5)$ et $\alpha = 1$.

Sur la fig. 2 sont representées les courbes correspondant aux valeurs de a 1, 1/2 et 2. La seule droite correspond au valeur de $a = 1$, une pente de -1.98 et ordonnée à l'origine 19.83. On peut donc conclure que le complexe I est un monomère, dont la formation nécessite $2H^+/W$.

On peut calculer le rapport M/W present dans l'espèce I par la méthode de la droite d'Asmus (8).

Chaque échantillon a 1 mL de Na_2WO_4 0.2 M dans un volume total de 50 mL ($a_0 = 4 \times 10^{-3}$ M) et volumes croissants de H_2M ($b_0 = 2$ M). On ajoute à chaque échantillon la quantité necessaire de NaOH pour obtenir un pH de 8.5.

Dans la fig. 3 on represente $1/V^n$ face à $1/\hat{D}$, où $\hat{D}$ est le pouvoir rotatoire mesuré moins celui correspondant à l'acide malique qui èxiste. Dans cette graphique on peut voir que la ligne droite obtenue correspond à une valeur de $n = 2$, ce qu'indique que la rapport M/W dans l'espèce I est égal à 2/1. Ce resultat nous améne à la conclusion de que la formation du complexe I peut donc être représentée par l'equilibre suivant:

$$WO_4^{2-} + 2M^{2-} + 2H^+ \rightleftarrows [O_2W(OH)_2(M_2)]^{4-}$$

La droite obtenue quand on represente $1/V^n$ face à $1/\hat{D}$, a une ordonnée à l'origine de -0.0126. De ce valeur on déduit que la constante de formation du complexe $[O_2W(OH)_2(M_2)]^{4-}$ est de $K = 1.27 \times 10^{23}$.

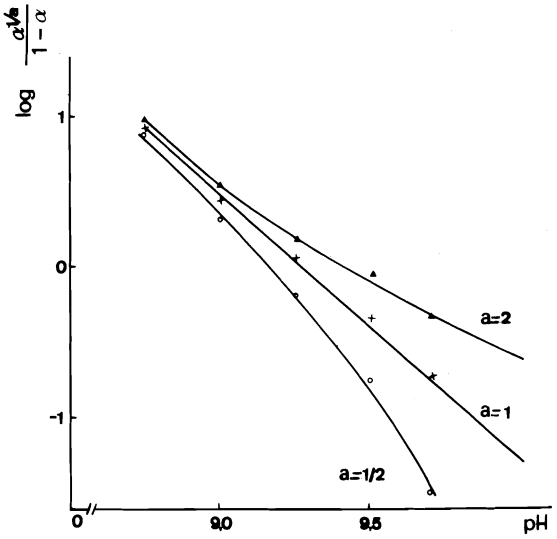

FIG. 2. $\log \alpha^{1/a}/(1 - \alpha) = f(\text{pH})$; pH compris entre 10 et 8.5.

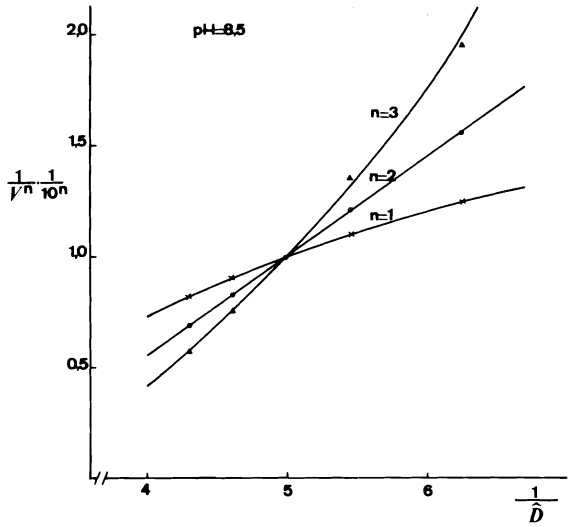

FIG. 3. Calcul de la relation M/W present à l'espèce I par la méthode de la droite d'Asmus. $V_t = 50$ mL, $a_0 = 4 \times 10^{-3}$ M, $b_0 = 2$ M, force ionique 1 M ($NaClO_4$). pH = 8.5, $\lambda = 365$ nm.

Également l'éq. [1] permet le calcul de K, puisqu'on connaît $(M^{2-}) = 0.1$ M, $C = 4 \times 10^{-3}$ M, $a = 1$, $z = 2$ et ordonnée à l'origine de la droite obtenue quand on represente $\log \alpha/(1 - \alpha) = f(\text{pH})$ égale à 20.63. On obtient la valeur de $K = 4.26 \times 10^{22}$. Cette valeur de K est comparable à celle obtenue avec la méthode d'Asmus.

Zone B: *pH compris entre 8.5 et 5.5*

Dans cette zone une diminution du pH entraîne une diminution du pouvoir rotatoire. Ceci indiquerai la formation d'une nouvelle espèce que nous apellerons II. Comme précédemment, l'équilibre:

$$[O_2W(OH)_2(M_2)]^{4-} + m\text{H}^+ \leftrightharpoons (1/b)\text{II}$$

a été suivi polarimétriquement. Il faut noter que la fraction molaire, β, de II est liée au pouvoir rotatoire du mélange $NaWO_4/25H_2M$ en fonction du pH, suivant l'équation: $\hat{D} = \hat{D}_I(1 - \beta) + D_{II}\beta$. La fig. 1 (courbe C) fournit, pour $\lambda = 436$ nm, les valeurs $\hat{D}_I = 0.072$ et $\hat{D}_{II} = 0.162$ degrés.

Avec le même raisonnement utilisé pour l'étude de la zone A il ressort, que la seule valeur de b satisfactoire est 2. La droite $\log \beta^{1/2}/(1 - \beta) = f(\text{pH})$ a une pente de -1.02.

Ces resultats montrent que l'espèce II est un dimère dont l'équilibre de formation peut s'exprimer:

$$[O_2W(OH)_2(M_2)]^{4-} + \text{H}^+ \leftrightharpoons (1/2)\text{II}$$

Pour le calcul de la relation M/W present à l'espèce II, nous avons appliqué, de façon similaire à celle de l'apartat A, la méthode de la droite d'Asmus, en excès d'acide malique et pH égal a 5.5.

En représentant $1/V^n$ face a $1/\hat{D}$ on obtient une droite pour $n = 1$, ce qu'indique que la espèce levogyre II presente un rapport M/W = 1/1 et son équilibre de formation, à partir de l'espèce I, on peut représenter par l'équation:

$$[O_2W(OH)_2(M_2)]^{4-} + \text{H}^+ \leftrightharpoons (1/2)[O_3W_2(OH)_4(M_2)]^{2-} + M^{2-} + (1/2)H_2O$$

Zone C: *pH compris entre 5.5 et 3.2*

Le pouvoir rotatoire dans cette zone diminue, apparaissant un minime au pH 3.2. L'espèce II doit se transformer dans une autre, III, suivant l'équilibre:

$$[O_3W_2(OH)_4(M_2)]^{2-} + p\text{H}^+ \leftrightharpoons (1/c)\text{III}$$

La constance des valeurs de $\hat{D}$, pour les pH inférieurs à 3.2, indique que l'espèce III est la seule stable dans cette zone.

L'étude de l'équilibre de formation de la espèce III a besoin des valeurs de γ, fraction de $[O_3W_2(OH)_4(M_2)]^{2-}$ transformée en III, calculées avec l'équation: $\hat{D} = \hat{D}_{II}(1 - \gamma) + \hat{D}_{III}\gamma = -0.162 \times (1 - \gamma) - 0.206\gamma$.

La fonction $\log \gamma^{1/c}/(1 - \gamma)$ face au pH donne une droite pour $c = 1$, dont la pente est de -0.96.

Ce résultat indique que les complexes II et III ont le même degré de condensation, c'est-à-dire il s'agit de deux espèces dimères.

La méthode d'Asmus, appliquée à pH 2.5, en excès d'acide malique nous indique aussi que le rapport M/W est égal à 1/1 pour l'espèce III.

Ainsi, l'équilibre de formation de cette espèce, à partir de $[O_3W_2(OH)_4(M_2)]^{2-}$, on peut écrire:

$$[O_3W_2(OH)_4(M_2)]^{2-} + \text{H}^+ \leftrightharpoons [HO_3W_2(OH)_4(M_2)]^-$$

Conclusion

En excès d'acide malique, le W(VI) forme un complexe tungsto-dimalique destrogyre et deux tungsto-malique levogyres. La formation de ces espèces, à partir de WO_4^{2-} et M^{2-}, necessite 2, 2, et 2.5 H^+/W respectivement.

Nous avons comprobé, aussi, que le degré de condensation de l'espèce $[O_2W(OH)_2(M_2)]^{4-}$ est 1, tandis que les autre deux, de stoechiométrie 1:1, son dimères.

De ce résultats on peut conclure que l'acide malique montre un comportement analogue à celui de l'acide tartrique (4).

La constant de formation de l'espèce $[O_2W(OH)_2(M_2)]^{4-}$ a été deduite par deux méthodes différents. De la valeur obtenue on déduit que cette complexe est plus stable que celle formée par l'acide tartrique ($K = 1.07 \times 10^{18}$) (4, 6).

Données expérimentales

Le pouvoir rotatoire des échantillons a été mesuré à l'aide d'un polarimétre photoélectrique Perkin-Elmer Mod. 141, à sortie digitale. La precision des mesures est de ± 0.002 degrés.

La cellule est thermostatée à 30 $\pm$ 0.05°C et a une longeur de 10 $\pm$ 0.002 cm. L'appareil permet effectuer les mesures à cinq longeurs d'onde différents (589, 578, 546, 436, 365 nm). Les résultats obtenus pour chacune de ces longeurs d'onde son comparables dans tous les cas.

Les pH sont mesurés à l'aide d'un pHmétre Radiometer 26, à 30°C. La force ionique des solutions est maintenue constante et égale à 1 à l'aide de $NaClO_4$.

1. D. GERNEZ. C. R. **104**, 783 (1887).
2. J. L. DELSAL. J. Chim. Phys. **35**, 356 (1938).
3. M. J. BAILLIE et D. H. BROWN. J. Chem. Soc. **3**, 3698 (1961).
4. J. BELTRAN, A. CERVILLA et A. BELTRAN. An. R. Soc. Esp. Fis. Quim. En cours de parution.
5. B. VIOSSAT. Rev. Chim. Min. **9**, 737 (1972).
6. F. CHAUVEAU, P. ROELENS et J. LEFEBVRE. Rev. Chem. Min. **13**, 564 (1976).
7. A. CERVILLA, A. BELTRAN et J. BELTRAN. Rev. Acad. Cienc. Zaragoza. En cours de parution.
8. E. ASMUS. Z. Anal. Chem. **178**, 104 (1960).

Determination of rates of hydrogen atom reactions with alkenes at 298 K by a double modulation technique[1]

K. OKA[2] AND R. J. CVETANOVIĆ

Division of Chemistry, National Research Council of Canada, Ottawa, Ont., Canada K1A 0R9

Received August 28, 1978

K. OKA and R. J. CVETANOVIĆ. Can. J. Chem. **57**, 777 (1979).

Hydrogen atoms and HgH radicals are the two precursors of the HNO($^1A''$) chemiluminescence in the mercury photosensitized reaction of gaseous mixtures of H_2, NO, and Hg and are responsible, respectively, for its slow and fast decaying component. The total intensity of the chemiluminescence is decreased when an olefin is added to the gaseous mixture and, with an excess of the olefin added, 85% of the luminescence is eliminated. This fraction corresponds to the slow component of the chemiluminescence, due to the reaction H + NO + M → HNO* + M, while the residual 15% is due to the reaction HgH + NO → HNO* + Hg. The magnitudes of the decrease of chemiluminescence intensity and of the increase of the rate of decay of its slow component at a given concentration of an added olefin provide information on the rate of H atom reaction with the olefin.

Relative values of the rate constants of H atom reactions with ethylene, propene, 1-butene, *cis*-2-butene, *trans*-2-butene, isobutene, and 1,3-butadiene have been determined in the present work from the observed dependence of the luminescence intensity on olefin concentration. At the same time, the absolute values of these rate constants have been determined from the relation between the decay rate of the slower component of the chemiluminescence and olefin concentration. The relative and the absolute values of the rate constants are compared with each other, to check their mutual consistency, and with the available relative and absolute values in the literature.

K. OKA et R. J. CVETANOVIĆ. Can. J. Chem. **57**, 777 (1979).

Les atomes de H et les radicaux HgH sont les deux précurseurs de la chemiluminescence HNO($^1A''$) dans la réaction photosensibilisée au mercure de mélanges gazeux de H_2, NO et Hg et ils sont les causes respectives des composantes lentes et rapides de la décroissance. L'addition d'un alcène aux mélanges gazeux produit une diminution de l'intensité totale de la chemiluminescence; si on ajoute un excès d'alcène, 85% de la luminescence est éliminée. Cette fraction correspond à la composante lente de la chemiluminescence due à la réaction H + NO + M → HNO* + M, alors que le 15% résiduel est dû à la réaction HgH + NO → HNO* + Hg. Les amplitudes des diminutions des intensités de la chemiluminescence et de l'augmentation du taux de décroissance de sa composante lente à une concentration donnée d'un alcène ajouté fournissent des renseignements concernant la vitesse de la réaction de l'atome de H avec l'oléfine.

Les valeurs relatives des constantes de vitesse des réactions des atomes H avec de l'éthylène, du propène, du butène-1, du butène-2 *cis*, du butène-2 *trans*, de l'isobutène et du butadiène-1,3 ont été evaluées dans ce travail en observant l'effet de la concentration en oléfine sur l'intensité de la luminescence. A la fois, on a évalué les valeurs absolues de ces constantes de vitesse en utilisant la relation qui existe entre le taux de décroissance de la composante plus lente de la chemiluminescence et la concentration en oléfine. On a comparé les valeurs relatives et absolues, soit les unes avec les autres pour vérifier leur accord mutuel, soit avec les valeurs relatives et absolues qui sont disponibles dans la littérature.

[Traduit par le journal]

Introduction

The chemiluminescence observed in the mercury photosensitized reaction of gaseous mixtures of H_2, NO, and Hg has been studied previously (1–3) and it has been established that it consists of two distinct components, decaying at very different rates. The two precursors of the chemiluminescence are H atoms and HgH radicals, which are both the primary products of the reaction of Hg6($^3P_1$) with H_2. The excited molecules which luminesce, HNO($^1A''$), are formed simultaneously by the following two reactions

[1] $$HgH + NO \rightarrow HNO + Hg$$

[2] $$H + NO + M \rightarrow HNO + M$$

and emit light in the 600–800 nm spectral region.

Since the decay rate of reaction [1] is 2–3 orders of magnitude faster than that of reaction [2], the individual decay rates can be evaluated by the

[1]NRCC No. 17168

[2]NRCC Research Associate.

0008-4042/79/070777-08$01.00/0

double modulation technique, in which the illuminating 253.7 nm radiation is modulated simultaneously at two different modulation frequencies.

In the experiments carried out, variation of the concentration of the olefin added to the gaseous mixture of H_2, NO, and Hg caused variations both in the intensity and in the decay rate of the chemiluminescence which were measured using the double modulation technique (1–3). The relative and the absolute values of the rate constants of reactions of H atoms with olefins were evaluated, respectively, from the observed variations in the intensity and in the decay rate of the slower component of the chemiluminescence as functions of the concentrations of the reactants. Although there is a considerable amount of information in the literature both on the relative and the absolute values of the rate constants of the reactions of H atoms with simple olefins, there are some substantial discrepancies between data from different sources. In view of these discrepancies, further determinations, especially when they can be done by entirely different techniques, are still necessary. The present results represent a new contribution of this kind.

Experimental

The experimental arrangement was the same as described previously (1–3).

The gases used were Matheson U.H.P. hydrogen, C.P. nitric oxide, propene, isobutene and *cis*-2-butene, and Phillips ethylene, *trans*-2-butene, 1-butene, and 1,3-butadiene. All the olefins used were research grade products. NO was passed through a column of freshly activated Linde Molecular Sieve 13× to remove any traces of NO_2. The range of H_2 flow rates (f.r.$_{H_2}$) was 3.0–6.5 × 10^{-4} mol s^{-1}.

The basic quantities measured have been the amplitudes of the modulated signals of the 253.7 nm incident radiation and of the chemiluminescence at the low frequency of 10 Hz and at higher frequencies in the kHz region. The three experimental parameters measured, x_0, x, and y, are, respectively, the relative values of the intensities of the total luminescence (x_0) and of the in-phase (x) and $-90°$ out-of-phase (y) components of the luminescence modulated in the kHz frequency region. The value of x_0 was measured at 10 Hz, since at this low modulation frequency the total luminescence intensity is to a good approximation confined to the in-phase component. The precise definitions and derivation of the relevant rate expressions are given in our earlier papers (1–3).

The luminescence measured is the sum of two processes, i.e., of a slow and a fast decaying component. The decay rate (m_{II}) of the slow luminescence is therefore given by the equation (1)

$$[I] \qquad m_{II} = 2\pi\nu_m C_{II} y/(x_0 - x)$$

where ν_m is the modulation frequency in the kHz region. The correction term C_{II} is a function of the ratio m_{II}/m_I of the decay rates of the slow (m_{II}) and the fast (m_I) luminescence (1). The latter corresponds to the decay rate of HgH, by reaction with NO or thermal decomposition, and is given by the equation

$$[II] \qquad m_I = k_{HgH+NO}[NO] + k_{HgH+M}[M]$$

where [M] is the total concentration. The rate constants k_{HgH+NO} and k_{HgH+M} have been measured before (3). Since the correction term C_{II} is close to unity (0.9–1) for the experimental conditions used and its dependence on m_{II}/m_I is very small, a simple procedure for evaluating m_{II} is to assume initially that $C_{II} = 1$ and calculate with it the first approximate value of m_{II}, which is then used to obtain an improved value of C_{II} and from it the final value of m_{II}.

Results

A. Luminescence Intensity in the Presence and Absence of Olefins

Luminescence intensity (x_0) in the absence of olefins is approximately proportional to the mole fraction of H_2 and inversely proportional to the total pressure (P). The inverse proportionality to P indicates that, at the pressures used, the quenching of $HNO(^1A'')$ is much faster than the light emitting process and a correction for this effect can be made simply by multiplying x_0 by P. The proportionality to the H_2 mole fraction is due to partial removal of Hg*, i.e., of $Hg6(^3P_1)$, by quenching with NO (and with the olefins, when added), a correction for which can be made by multiplying x_0 by F. This correction factor is given by

$$F = 1 + (k_{Hg^*+NO}[NO] + k_{Hg^*+Ol}[Ol])/k_{Hg^*+H_2}[H_2]$$

where Ol stands for the olefin and the relative values of the quenching rate constants ($k_{Hg^*+NO}/k_{Hg^*+H_2}$ and $k_{Hg^*+Ol}/k_{Hg^*+H_2}$) are taken from the literature (4). The product x_0PF represents therefore the luminescence intensity corrected for the above two quenching processes. x_0PF is to first approximation independent of P and [NO] in the absence of olefins.

Figure 1 shows the corrected luminescence intensity, x_0PF, plotted as a function of [NO][M′] for various experimental conditions. [M′] is the effective concentration of the third body for reaction [II], i.e.

$$[III] \qquad [M'] = [H_2] + (k_{2,NO}/k_{2,H_2})[NO] + (k_{2,Ol}/k_{2,H_2})[Ol]$$

where [Ol] is the concentration of the olefin added, k_{2,H_2}, $k_{2,NO}$, and $k_{2,Ol}$ are the rate constants of reaction [2] for H_2,NO and olefin, respectively, as the third body. The value of $k_{2,NO}/k_{2,H_2}$ has been obtained in previous work (2). The last term in eq. [III] is very small in the present study because $[H_2] > [NO] > [Ol]$.

Luminescence intensity decreases very strongly when 1,3-butadiene is added, as shown in Fig. 1 by half filled circles (◐). Since most of the H atoms are

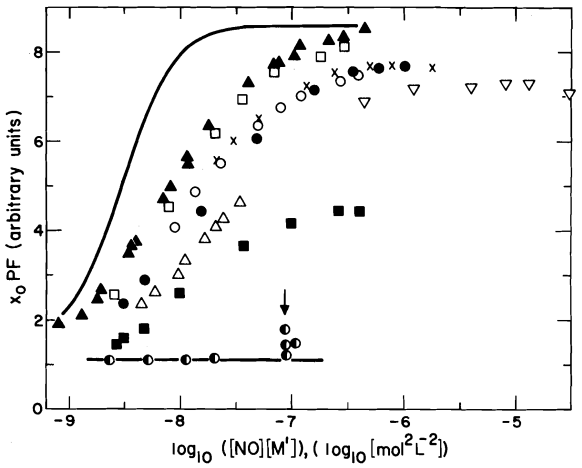

FIG. 1. Plots for several experimental conditions of the corrected luminescence intensity, x_0PF, as a function of [NO][M'] in the presence (◐) and absence (other symbols) of added 1,3-butadiene. The experimental conditions are: ○, P = 50 Torr, $I_{253.7\text{ nm}} = 8 \times 10^{13}$ photons s^{-1}, the flow rate of H_2 is f.r.$_{H_2} = 5 \times 10^{-4}$ mol s^{-1}, $P_{Hg} = 1.8 \times 10^{-13}$ Torr, T = 298 K; ▲, light intensity changed to $I_{253.7\text{ nm}} = 3 \times 10^{13}$ photons s^{-1}; □, $I_{253.7\text{ nm}} = 0.8 \times 10^{13}$ photons s^{-1}; ●, f.r.$_{H_2}$ changed to f.r.$_{H_2} = 1.6 \times 10^{-4}$ mol s^{-1}; ■, $P_{Hg} = 4.8 \times 10^{-4}$ Torr; △, P_{Total} = 20 Torr; ×, P_{Total} = 100 Torr; ▽, P_{Total} = 300 Torr; ◐, 1,3-butadiene is added, [1,3-C_4H_6] = 7×10^{-6} mol/L. The arrow indicates experimental points for [1,3-C_4H_6] varying from 2.7×10^{-5} to 16×10^{-5} mol/L, with the highest point corresponding to the lowest butadiene concentration. The horizontal line at x_0PF = 1.1 is the estimated net luminescence intensity of HNO* from reaction [1] (HgH + NO → HNO* + Hg). The solid line is the 'theoretical' curve, obtained assuming absence of any secondary consumption of H atoms.

then scavenged by the added olefin, the residual luminescence is due to the reaction of HgH with NO (reaction [1]). Removal of H atoms by olefins evidently competes efficiently with their termolecular combination with NO. Nevertheless, at large [NO], luminescence intensity increases slightly when the concentration of the 1,3-butadiene added is substantially smaller (as shown by the four experimental points in the region indicated by the arrow in Fig. 1) because of the less complete scavenging of H atoms by the olefin in this case.

The intensity of the chemiluminescence from HgH reaction with NO has been estimated by subtracting from the observed total intensity in the presence of 1,3-butadiene the small contribution of the luminescence from any residual (unscavenged) H + NO reaction. It is found to be independent of [NO][M'] under the experimental conditions used and is indicated by the horizontal line at x_0PF = 1.1 in Fig. 1.

In the absence of olefins the intensity of the luminescence increases with increasing [NO][M'] and reaches a plateau value at large [NO][M'], as shown in Fig. 1. The magnitude of the plateau value attained depends on the experimental conditions used. Since the transmittance of the 253.7 nm radiation increases with decreasing Hg vapor pressure, the small plateau value at small [Hg], as shown in Fig. 1 by filled squares (■), is due to the decreased light absorption in the cell.

At 50 and 100 Torr pressure, indicated, respectively, by open circles and crosses (○ and ×) in Fig. 1, the intensities fall approximately on the same curve. Under these conditions the intensity is independent of the flow rate of the gaseous mixture, except at small [NO][M'], as shown by filled circles (●).

The absorbance of the 253.7 nm line varies with the total pressure in the reaction cell and maximum absorption was found to occur between about 50 and 100 Torr. Both at 25 and 300 Torr the absorbance decreases slightly because of a mismatch between the lamp emission and the absorption contours of the 253.7 nm line. A slight reduction of the luminescence intensity at 25 and 300 Torr may therefore be partly due to the reduced absorbance of the 253.7 nm light. Since the luminescence intensity is small at 300 Torr, the errors in the measurements of the background luminescence also affect somewhat the values of x_0. At 25 Torr, the decrease of intensity is probably partly due to the loss of H atoms by diffusion to the cell wall and recombination on it.

As shown in Fig. 1 by filled triangles and open squares (▲ and □), the plateau value is slightly larger when the light intensity is decreased, although the curvature does not change. A potential cause for this slight increase is the secondary consumption of H atoms by reaction with some of the products (HNO, HgH, etc.). Another reason may be a slight change of the alignment of the optical path of the 253.7 nm radiation since a rough wire mesh was used to decrease its intensity.

The 'theoretical' curve (the solid curve in Fig. 1) was obtained in the following manner. The value of x_0 is defined as the ratio of the amplitudes of modulation at 10 Hz of the luminescence and of the 253.7 nm incident radiation and is proportional to $\cos \theta_{10}$, where θ_{10} is the phase shift at 10 Hz between the luminescence and the incident radiation. For the purpose of calculating the theoretical curve, it was assumed that the secondary consumption of H atoms is negligibly small so that their pseudo-first order decay rate is simply given by k_2[NO][M']. In view of this, the values of θ_{10} were obtained directly from the relation $\tan \theta_{10} = 2\pi \times 10/k_2$[NO][M']

and were used to calculate the values of x_0PF for the solid curve in Fig. 1. At larger values of [NO][M′], the modulation frequency of 10 Hz is much smaller than k_2[NO][M′] and θ_{10} is therefore negligibly small so that the theoretical curve is at a plateau value (since $\cos\theta_{10} \approx 1$). At smaller values of [NO][M′] this is no longer the case, the calculated value of θ_{10} begins to increase and the theoretical curve declines by a factor approximately equal to $\cos\theta_{10}$. (The value of this factor is actually slightly larger than $\cos\theta_{10}$ because of the contribution of the very fast decaying luminescence, due to the HgH + NO reaction.)

All the experimental points plotted in Fig. 1 are seen to be shifted to the right from the 'theoretical' curve, i.e., to the larger values of [NO][M′]. This shift indicates the occurrence of some secondary H atom consuming reactions, which are in fact responsible for the decrease in luminescence intensity at smaller values of [NO][M′]. It is actually found experimentally (1) that in this region θ_{10} remains small (and thus $\cos\theta_{10} \approx 1$). The reason for this is that θ_{10} is not determined by k_2[NO][M′] alone, as assumed above in the calculation of the 'theoretical' curve in Fig. 1, but by the substantially larger (at small [NO][M′]) sum k_2[NO][M′] + k', where k' is the pseudo-first order rate of consumption of H atoms in secondary reactions. Therefore, although the value of the $\cos\theta_{10}$ factor does not decline, the intensity nevertheless declines at smaller [NO][M′] because the secondary consumption of H atoms, i.e., the ratio k'/k_2[NO][M′], is relatively large. The intensity of luminescence is reduced by the factor equal to k_2[NO][M′]/(k_2[NO][M′] + k'). Assuming that k' is a constant, it is estimated from the trends in Fig. 1 that k' is about 1.5–2.0 × 10^2 s^{-1}.

B. Relative Rates of H Atom Reactions with Olefins

In the presence of olefins the intensity of the luminescence decreases with increasing olefin concentration. The ratios of the intensities in the presence of olefins and in their absence are plotted in Fig. 2 as functions of $\log_{10}$ ([Ol]/[NO][M′]). The x_0PF values used are corrected for the slight consumption of H atoms in secondary reactions, but this correction is very small in this case since large NO concentrations, in the range 0.6–6 × 10^{-4} mol/L, were used in the experiments. After this correction, the ratio of the intensities is given by

$$[\text{IV}]\quad \frac{x_0PF}{(x_0PF)_{[\text{Ol}]=0}} = a + (1-a)\left\{1 + \frac{k_{\text{H+Ol}}}{k_2}\frac{[\text{Ol}]}{[\text{NO}][\text{M}']}\right\}^{-1}$$

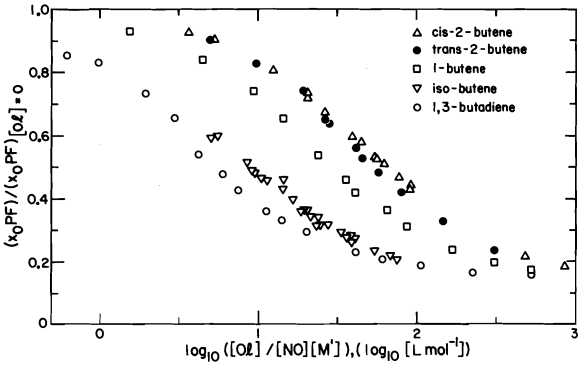

FIG. 2. Ratios of the corrected luminescence intensities in the presence and absence of olefin, $(x_0PF)/(x_0PF)_{[\text{Ol}]=0}$, plotted as a function of $\log_{10}$ [Ol]/[NO][M′] at 50 Torr total pressure for several C_4 olefins (△, *cis*-2-butene; ●, *trans*-2-butene; □, 1-butene; ▽, isobutene; ○, 1,3-butadiene. The luminescence intensities are corrected for the effect of the total pressure (P), the quenching of Hg6($^3P_1$) by NO and olefins (F), and the secondary consumption of H atoms).

where a is the ratio of the intensity of the chemiluminescence due to the HgH + NO reaction (reaction [1]) to the total intensity. As shown in Fig. 2, the ratios $(x_0PF)/(x_0PF)_{[\text{Ol}]=0}$ decrease with increasing [Ol]/[NO][M′] and level off at a lower plateau value of about 0.16, corresponding to the fraction of the luminescence intensity due to the HgH + NO reaction. A rough estimate of the value of $k_{\text{H+Ol}}/k_2$ is therefore given by the value of [NO][M′]/[Ol] in Fig. 2 at which $(x_0PF)/(x_0PF)_{[\text{Ol}]=0} = (a+1)/2$.

Better estimates of $k_{\text{H+Ol}}/k_2$ and of a can be obtained from the plots of the following rearranged linear form of eq. [IV].

$$[\text{V}]\quad \left\{1 - \frac{(x_0PF)}{(x_0PF)_{[\text{Ol}]=0}}\right\}\frac{[\text{NO}][\text{M}']}{[\text{Ol}]} = \frac{k_{\text{H+Ol}}}{k_2}\left\{\frac{(x_0PF)}{(x_0PF)_{[\text{Ol}]=0}} - a\right\}$$

In accordance with eq. [V], plots of $\{1 - (x_0PF)/(x_0PF)_{[\text{Ol}]=0}\}$[NO][M′]/[Ol] vs. $(x_0PF)/(x_0PF)_{[\text{Ol}]=0}$ are found to be linear. The x-intercepts give the values of a and the slopes of $k_{\text{H+Ol}}/k_2$. The values obtained are listed in Table 1 for several olefins. Since k_2 is constant, the values of $k_{\text{H+Ol}}/k_2$ provide the relative rate constants of the H atom reactions with olefins.

C. Absolute Rate Constants of the H Atom Reactions with Olefins

The rate of decay (m_{II}) of the slow decaying luminescence (due to the H atom reaction with NO), as defined by eq. [I], is close to the pseudo-first order

TABLE 1. Relative rate constants, k_{H+OI}/k_{H+NO+H_2}, of the reactions of H atoms with olefins and NO

Olefin	$\frac{k_{H+OI}}{k_{H+NO+H_2}}$ (mol/L)	$\frac{I_{HgH}}{I_{HgH}+I_H}$	Pressure (Torr)	No. of expts. (n)	Reactant concentrations[a] [NO] ($\times 10^{-4}$ mol/L)	[OI] ($\times 10^{-5}$ mol/L)
Ethylene	0.0251±0.0027	0.27	20	9	2.4–2.8	1.1–3.6
	0.0293±0.0008	0.16	50	12	1.2–2.1	1.3–4.1
	0.0341±0.0006	0.16	100	11	1.2–3.2	2.3–7.3
Propene	0.0481±0.0007	0.14	50	10	1.0–2.0	1.0–2.0
1-Butene	0.0494±0.0013	0.14	50	12	0.9–1.7	0.7–1.9
cis-2-Butene	0.0229±0.0005	0.15	50	17	0.7–1.9	1.7–2.0
trans-2-Butene	0.0265±0.0005	0.14	50	10	0.7–1.9	1.0–1.8
Isobutene	0.156±0.004	0.15	50	29	1.3–9.5	0.6–3.6
	0.147±0.006	0.16	100	22	1.2–7.8	0.4–5.5
1,3-Butadiene	0.250±0.010	0.16	20	19	1.3–2.9	0.1–0.3
	0.207±0.003	0.18	20[b]	9	0.6	0.03–0.13
	0.263±0.009	0.15	50	15	1.9–2.2	0.24–0.6
	0.276±0.005	0.15	100	11	3.3–4.0	0.5–1.0
	0.28±0.01	0.12	300	15	5.9–9.4	4.7–6.5

[a]The range of reactant concentrations providing points between $0.35 < (x_0PF)/(x_0PF)_{[OI]=0} < 0.65$.
[b]The intensity of the 253.7 nm incident radiation was reduced to 1/3.

rate of decay of H atoms under the conditions used, i.e.

[VI] $$m_{II} = k_2[NO][M'] + k_{H+OI}[OI] + k'$$

As will be discussed below, k', the rate of secondary consumption of H atoms, can be assumed to be negligibly small at larger [NO][M']. The slopes of the plots such as shown in Fig. 3 of $m_{II}/N[O][M']$ vs. [OI]/[NO][M'] provide then the absolute values of k_{H+OI}. The values obtained are listed in Table 2.

As discussed in our earlier paper (2), a slight experimental uncertainty may arise because of a probable small difference in the sensitivity of signal measurements at 10 Hz and in the kHz region of the modulation frequencies. However, since the exact magnitude of this sensitivity change is not known, the overall uncertainty in m_{II} is almost entirely due to it and much less to the random errors. In view of this, the uncertainties in k_{H+OI} shown in Table 2 have been evaluated as the differences between the observed values of the slopes of the plots in Fig. 3 and the corresponding values after allowing for a potential 1% error in x_0 due to the difference between the signal measurement sensitivities at 10 Hz and in the kHz region. From the analysis of x,y-semicircles in our previous work (2), we estimate approximately that the overall uncertainties in k_{H+OI} are probably within a factor of 3 of the uncertainties given in Table 2. It may be noticed that these uncertainties are 2–3 times larger than that for k_{H+NO+M} in the absence of olefins.

The experimental data for the plots of $m_{II}/[NO][M']$ vs. [OI]/[NO][M'] (such as shown in Fig. 3) were obtained in most cases (except at very large [OI]/[NO][M']) by varying olefin concentration without changing NO concentration. If k' is independent of [OI], its effect on the values of k_{H+OI} can be neglected. In any case, although the exact

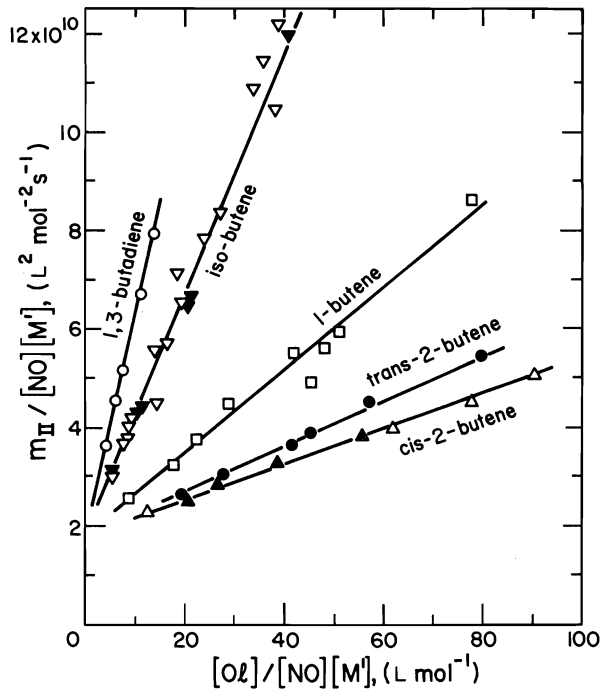

FIG. 3. The plots of $m_{II}/[NO][M']$ vs. [OI]/[NO][M'] at a total pressure of 50 Torr for several C_4 olefins. (The symbols are the same as in Fig. 2. The modulation frequencies are: ▽ and △, 15 kHz; remaining points 8 kHz.)

TABLE 2. The observed mean values of the rate constants, k_{H+OI}, for various olefins

Olefin	Pressure (Torr)	k_{H+OI}[a] ($\times 10^8$ L mol^{-1} s^{-1})	ν_m (kHz)	[NO] ($\times 10^{-4}$ mol/L)	[OI] ($\times 10^{-5}$ mol/L)	No. of expts.
Ethylene	20	4.09±0.11	8	2.4–2.8	0.28–2.1	5
	50	4.41±0.09	8	1.9–2.1	0.46–4.1	6
	100	4.69±0.15	8	1.6–3.2	1.8–7.3	5
Propene	50	8.33±0.16	8	1.9–2.1	0.31–2.0	6
1-Butene	50	8.36±0.16	8	0.88–1.9	0.43–2.7	9
cis-2-Butene	50	3.62±0.06	8, 15	0.69–1.9	0.44–2.0	8
trans-2-Butene	50	4.55±0.08	8	0.69–1.7	0.87–1.9	6
Isobutene	50[b]	24.3±0.9[b]	8, 15	1.2–9.5	0.6–4.2	23
	50	25.4±1.2	15	4.1–9.5	1.0–4.2	7
	50	23.9±0.7	15	1.9–2.8	0.6–2.9	9
	50	23.6±0.8	8	1.2–7.1	0.6–6.5	7
	100	25.2±1.2	8, 15	1.8–7.8	1.5–2.8	11
1,3-Butadiene	20[c]	36.1±1.3[c,d]	2, 8	1.7–3.2	0.04–0.21	6
	20[d]	47.9±1.7[d]	2, 8	1.2–2.9	0.07–0.33	10
	20	46.9±1.8	2	1.2–1.4	0.08–0.26	6
	20	50.8±0.8	8	2.8–2.9	0.07–0.33	4
	50	44.6±1.3	8	1.9–2.2	0.24–0.85	5
	100	42.7±2.6	8	2.4–4.0	0.28–1.0	6

[a]The indicated uncertainties are the differences between the observed values of the slopes of the plots of m_{II}/[NO][M'] vs. [OI]/[NO][M] and the corresponding values obtained after allowing for a potential 1% systematic error in x_0, as discussed in the text.
[b]Mean of all the values at 50 Torr and 8 and 15 kHz.
[c]The intensity of 253.7 nm radiation was reduced to 1/3 the value in the next experiment.
[d]Mean of all the values at 20 Torr and 2 and 8 kHz.

TABLE 3. Comparison of the absolute values of k_{H+OI} from Table 2 with the values obtained from the relative rate constants in Table 1[a]

		$10^{-9} \times k_{H+OI}$ (L mol^{-1} s^{-1})		
Olefin	Pressure (Torr)	*A*, absolute values from Table 2	*B*, derived from relative rates in Table 1	Ratio *B*/*A*
Ethylene	20	0.41	0.39	0.96
	50	0.44	0.46	1.04
	100	0.47	0.53	1.13
Propene	50	0.83	0.75	0.91
1-Butene	50	0.84	0.77	0.92
cis-2-Butene	50	0.36	0.36	0.99
trans-2-Butene	50	0.46	0.41	0.91
Isobutene	50	2.43	2.43	1.00
	100	2.52	2.29	0.91
1,3-Butadiene	20	4.79	3.90	0.81
	20[b]	3.61	3.23	0.89
	50	4.46	4.10	0.92
	100	4.27	4.31	1.01

[a]Calculated from k_{H+OI}/k_2 in Table 1 taking (1, 2) $k_2 = 1.56 \times 10^{10}$ L^2 mol^{-2} s^{-1}.
[b]The intensity of the 253.7 nm incident radiation reduced to 1/3 of the intensity in the preceding determination.

magnitude of the effect of k' is not certain, it is probably not as large as the uncertainty due to the potential sensitivity change discussed above.

Discussion

The relative rate constants listed in Table 1 can be compared with the absolute values in Table 2 by taking $k_2 = 1.56 \times 10^{10}$ L^2 mol^{-2} s^{-1}, the value determined in our earlier work. The comparison is made in Table 3, which lists the two sets of the k_{H+OI} values and, in the last column, their ratios. It is seen that in most cases the indirectly obtained values (set B) differ from the directly determined absolute values (set A) by less than about 10%, with only one difference of 13% and one of 19%. The two sets of values are therefore mutually consistent within the likely combined experimental uncertainties. Nevertheless, the set A values are somewhat preferable, because of their more direct method of determination, and will be used further below for comparison with the data in the literature.

The data in Tables 1–3 show that the value of the

TABLE 4. Comparison of the k_{H+O1} values obtained with the data in the literature

Compound	$10^{-9} \times k_{H+O1}$ (L mol^{-1} s^{-1})									
	AMR[a] 1953	JC[b,c] 1961	Y[c,d] 1962	BL[e] 1967	WC[f] 1969	CD[c,g] 1969	KPB[h,i] 1970/71	CKMY[j] 1971	DNW[k] 1971	Present[l] 1978
Ethylene	0.75	(0.44)[m]	0.54	0.60	0.52	0.50	0.82[h]	0.23[n]		0.47[o]
Propene	0.18	0.83[c]	0.83[c]		0.83	0.83[c]	0.97[i]	0.57	0.46[p](0.62)	0.83
1-Butene		0.93			0.83			0.78	0.83 (0.83)	0.84
cis-2-Butene	0.80	0.40	0.26					0.25	0.48 (0.41)	0.36
trans-2-Butene	0.63	0.52	0.29	0.60				0.33	0.54 (0.47)	0.46
Isobutene	0.57	2.0	7.9	2.3	2.0	2.0		2.1	(2.0)	2.4
1,3-Butadiene		4.0	10.8		3.9	4.2			5.0 (3.2)	4.3

[a]Allen, Melville, and Robb, ref. 11 (1953).
[b]Jennings and Cvetanović, ref. 12 (1961).
[c]Relative data converted to absolute values by taking $k_{H + propene} = 8.3 \times 10^9$ L mol^{-1} s^{-1}, the value of Woolley and Cvetanović in column 5 of this table.
[d]Yang, ref. 13 (1962).
[e]Braun and Lenzi, ref. 14 (1967).
[f]Woolley and Cvetanović, ref. 15 (1969); relative data converted to absolute values by taking $k_{H + H_2S} = 7.77 \times 10^9 \exp(-860/T)$ L mol^{-1} s^{-1}, as recommended by Natl. Bur. Stand.
[g]Cvetanović and Doyle, ref. 16 (1969).
[h]Kurylo, Peterson, and Braun, ref. 10*a* (1970).
[i]Kurylo, Peterson, and Braun, ref. 10*b* (1971).
[j]Cowfer, Keil, Michael, and Yeh, ref. 17 (1971).
[k]Daby, Niki, and Weinstock, ref. 18 (1971). The values in parentheses are for D atoms.
[l]Present results, the absolute values of $k_{H + O1}$ from Table 3 (set A).
[m]Less reliable value because of experimental difficulties (12).
[n]Pressure (10–15 Torr H_2) is lower than is required for the high pressure limiting value of k.
[o]Pressure (100 Torr H_2) is probably lower than is required for the high pressure limiting value of k.
[p]Pressure (2.4 Torr He) is probably lower than is required for the high pressure limiting value of k.

rate constant for H reaction with ethylene is pressure dependent. Initial formation of vibrationally excited ('hot') alkyl radicals in the exothermic addition of H atoms to olefins has been known for a long time (5) and it has been recognized that at low pressures they may undergo unimolecular decomposition (6) including back decomposition into H and the (original or isomerized) olefin (6–9). To what extent such back decomposition occurs in a particular system depends on the nature of the moderating gases present and their pressures. Kurylo, Peterson, and Braun (10*a*, *b*) have carried out detailed kinetic studies of the effect of pressure, using helium as the moderating gas, on the k_{H+O1} values for ethylene (10*a*) and propylene (10*b*). However, it is not possible to utilize their results directly to assess reaction systems with other moderating gases, which are expected to be more efficient deactivators of vibrational excitation than is helium. Since in the present work the uncertainties of the measurements become large at pressures greater than about 200 Torr, a detailed experimental study of the pressure dependence of k_{H+O1} was not feasible. It is probable that the value of the rate constant for ethylene obtained at the highest pressure of the moderating gas used (100 Torr H_2) may still be somewhat below the high pressure limiting value. It is possible that the value for propylene may also be slightly below the high pressure limiting value although the difference, if any, would be expected to be much smaller in this case because of the greater number of degrees of freedom and thus a longer life time of the 'hot' propyl radicals initially formed. Additional information on this point may be provided by the comparison with the literature values of the rate constants given further below.

The relative rate data for 1,3-butadiene in Table 1 may appear to suggest that there is a slight pressure dependence of the rate constant. However, the effect is very small and close to the experimental uncertainty. Furthermore, it is not confirmed by the absolute rate constants for 1,3-butadiene in Table 2, which seem to be pressure independent within the experimental scatter. The slight decrease in the value of the rate constant for 1,3-butadiene at 20 Torr after a three-fold decrease of light intensity is also uncertain because of the weaker luminescence signals and increased experimental errors at the reduced light intensity.

The present values of k_{H+O1} are compared in Table 4 with the corresponding values taken from some of the more comprehensive sets of data in the literature. The values of k_{H+O1} from different sources are listed in the chronological order of the year of publication. The three sets of relative rate constants obtained previously in this laboratory (12, 15, 16) and those of Yang (13) have been converted to absolute values in the following manner. Woolley and Cvetanović's (WC) values of k_{H+O1}, which have been measured relative to the rate constant of the reaction of H with H_2S at 25°C, have been converted to the absolute values in column 5 of Table 4 by taking the now available (and Natl. Bur. Stand. recommended (19)) value $k_{H+H_2S} = 7.77 \times 10^9$ exp

$(-860/T)$ L mol^{-1} s^{-1} of Kurylo, Peterson, and Braun (10*c*). Since this and the other three sets of relative rate constants in Table 4 (JC, Y, and CD, in columns 2, 3, and 6, respectively) have all been obtained in the presence of high pressures of relatively efficient moderating gases (CO_2, n-C_4H_{10}, C_3H_8, H_2), it is reasonable to assume that the $k_{H+propylene}$ values must all be very close to the high pressure limiting value. The WC value $k_{H+propylene} = 8.3 \times 10^8$ L mol^{-1} s^{-1} (column 5) was therefore used to convert the JC, Y, and CD relative data to absolute values. It is evident that the absolute rate constants in the JC and CD sets in Table 4 would remain unaltered if the conversions to absolute values were based on the WC rate constant for isobutene instead of for propylene. However, Yang's set of values (column 3) would be substantially altered, since, as has been pointed out before (15), it is not quantitatively consistent with the other sets of values in Table 4 although it clearly shows qualitatively similar trends. Similarly, the AMR values in column 1, obtained in the pioneering work of Allen, Melville, and Robb (11) by the ingeneous molybdenum trioxide technique, although very much of the right order of magnitude, show some quantitative disparities.

The absolute values of k_{H+OI} obtained in the present work, listed in the last column of Table 4, are, within the combined experimental uncertainties, consistent with the other data in the table (apart from some deviations of the AMR and Y data mentioned above and allowing for the fact that some of the values for ethylene and propylene are below the high pressure limiting values). The agreement with the previous three sets of relative determinations in this laboratory (JC, WC, and CD) is particularly good. The present value for propylene turns out to be identical with the WC value. Since the latter is believed to have been obtained under conditions required for the high pressure limiting value, the agreement suggests that the present value corresponds also to the high pressure limit. The difference of about 15% from the KPB high pressure extrapolated value for propylene (column 7) is probably not larger than the combined experimental error. The present value for ethylene is probably below the high pressure limit, as already mentioned. This may perhaps be also true for the JC, WC, and CD ethylene values and is no doubt so for the CKMY value (column 8). The KPB ethylene value of 8.2 $\times 10^8$ L mol^{-1} s^{-1} (column 7) provides a high pressure limit for this rate constant. However, Hikida, Eyre, and Dorfman (20) obtained a (seemingly) pressure independent value of 5.5×10^8, which could possibly be scaled up at most to 6.5×10^8 L mol^{-1} s^{-1} by applying KPB's empirical expression to extrapolate from 1500 Torr to infinite He pressure. KPB quote (10*c*) the results of Yokota (21) which seem to indicate a high pressure limit of 7.0×10^8 L mol^{-1} s^{-1}. Thus, there may still be an uncertainty of the order of about 10% in the high pressure limit of the H + C_2H_4 constant.

1. K. Oka, D. L. Singleton, and R. J. Cvetanović. J. Chem. Phys. **66**, 713 (1977).
2. K. Oka, D. L. Singleton, and R. J. Cvetanović. J. Chem. Phys. **67**, 4681 (1977).
3. K. Oka and R. J. Cvetanović. J. Chem. Phys. **68**, 4391 (1978).
4. (*a*) J. V. Michael and G. N. Suess. J. Phys. Chem. **78**, 482 (1974); (*b*) H. Horiguchi and S. Tsuchiya. Bull. Chem. Soc. Jpn. **44**, 3221 (1971); (*c*) B. deB. Darwent, M. K. Phibbs, and F. G. Hurtubise. J. Chem. Phys. **22**, 859 (1954); (*d*) S. D. Gleditsch and J. V. Michael. J. Phys. Chem. **79**, 409 (1975).
5. R. J. Cvetanović. Adv. Photochem. **1**, 115 (1963).
6. B. S. Rabinovitch, S. G. Davis, and C. A. Winkler. Can. J. Res. B**21**, 251 (1943).
7. A. H. Turner and R. J. Cvetanović. Can. J. Chem. **37**, 1075 (1959).
8. B. S. Rabinovitch, D. W. Setser, W. H. McLain, and J. H. Current. J. Chem. Phys. **32**, 493 (1960).
9. C. A. Heller and A. S. Gordon. J. Chem. Phys. **36**, 2648 (1962).
10. M. J. Kurylo, N. C. Peterson, and W. Braun. J. Chem. Phys. (*a*) **53**, 2776 (1970); (*b*) **54**, 4662 (1971); (*c*) **54**, 943 (1971).
11. P. E. M. Allen, H. W. Melville, and J. C. Robb. Proc. R. Soc. London, A**218**, 311 (1953).
12. K. R. Jennings and R. J. Cvetanović. J. Chem. Phys. **35**, 1233 (1961).
13. K. Yang. J. Am. Chem. Soc. **84**, 3795 (1962).
14. W. Braun and M. Lenzi. Discuss. Faraday Soc. **44**, 252 (1967).
15. G. R. Woolley and R. J. Cvetanović. J. Chem. Phys. **50**, 4697 (1969).
16. R. J. Cvetanović and L. C. Doyle. J. Chem. Phys. **50**, 4705 (1969).
17. J. A. Cowfer, D. G. Keil, J. V. Michael, and C. Yeh. J. Phys. Chem. **75**, 1584 (1971).
18. E. E. Daby, H. Niki, and B. Weinstock. J. Phys. Chem. **75**, 1601 (1971).
19. NBS Technical Note 866. U.S. Department of Commerce, Natl. Bur. Stand. Washington, DC. 1975. p. 51.
20. T. Hikida, J. A. Eyre, and L. M. Dorfman. J. Chem. Phys. **54**, 3422 (1971).
21. T. Yokota. Doctoral thesis, the Catholic University of America, Washington, DC. 1969.

Chemical reaction in electric discharge. V. Reaction kinetics in a low frequency modulated discharge[1]

JOHN N. SMITH AND MOTILAL D. COSTA
Department of Chemistry, University of Toronto, Toronto, Ont., Canada M5S 1A1
AND
JACQUES M. DECKERS
Department of Chemistry, University of Toronto, Toronto, Ont., Canada M5S 1A1 and Erindale College, University of Toronto, Mississauga, Ont., Canada L5L 1C6
Received May 15, 1978[2]

JOHN N. SMITH, MOTILAL D. COSTA, and JACQUES M. DECKERS. Can. J. Chem. **57**, 785 (1979).

A current modulation technique has been developed for the determination of kinetic information in glow discharges through flowing gases. A low frequency sinusoidal modulation superimposed on the dc discharge current produces modulations in the electron density and radical concentrations. Measurements of the amplitudes and phase shifts of radical concentrations can be used to elucidate reaction mechanisms and to determine rate constants for some reaction processes.

The kinetic response of discharge chemical phenomena to an applied current modulation is discussed for several general types of reaction mechanisms. Rates of O atom production and removal measured in a current modulated O_2 glow discharge are compared to rates measured in a dc glow discharge. The excellent agreement of these two sets of results provides an experimental foundation for the current modulation method.

JOHN N. SMITH, MOTILAL D. COSTA et JACQUES M. DECKERS. Can. J. Chem. **57**, 785 (1979).

On a développé une technique de modulation de courant afin de tirer des informations cinétiques des décharges électriques à travers des courants gazeux. Si on superpose une modulation sinusoidale de basse fréquence à un courant de décharge cd il se produit une modulation de la densité électronique et des concentrations radicalaires. On peut utiliser des mesures d'amplitudes et de déplacements de phase des concentrations radicalaires pour élucider les mécanismes réactionnels et pour déterminer les constantes de vitesse de quelques processus réactionnels.

On présente une discussion relative à la réponse cinétique du phénomène de décharge chimique à une modification de courant appliqué pour plusieurs types généraux de mécanismes réactionnels. On a comparé les vitesses de production et d'enlèvement d'atomes de O mesurées dans une décharge électrique de O_2 modulée par un courant avec celles mesurées dans une décharge électrique cd. Le bon accord entre ces deux séries de valeurs fournit une base expérimentale pour la méthode de modulation de courant.

[Traduit par le journal]

1. Introduction

For some time the kinetics of reactions occurring in glow discharges have been investigated in this laboratory (1). In order to determine additional information on the kinetics of reaction processes occurring in the glow discharge, a low frequency sinusoidal modulation has been superimposed on the dc current through the discharge. The rates of electron–molecule reactions are thereby modulated and the resulting response of the system to the applied modulation depends on the nature of the reaction mechanism. Observations of the perturbations thus produced in the concentrations of reactants, intermediates, or products can be used to elucidate the reaction mechanism and to determine the value of the rate constants.

Bair *et al.* (2) have previously employed a chemical modulation technique in their detection of free radical absorption spectra in a pulsed electrical discharge. Most other applications of chemical modulation techniques to gas phase systems have employed modulation of the intensity of the exciting light source in photolysis experiments. Burnnett and Melville (3) have discussed the theory of the rotating sector method as applied to the study of (free radical) chain reactions initiated in a photochemical system. Metcalfe (4) has measured the rates of consecutive and competing reactions in modulated fluorescence experiments. Johnston *et al.* (5) applied chemical modulation techniques to photolysis experiments in which the absorption spectrum of reactive interme-

[1]Taken in part from the Ph.D. theses of J.N.S. and M.D.C.
[2]Revision received November 15, 1978.

0008-4042/79/070785-11$01.00/0

diates was measured. Atkinson and Cvetanović obtained modulated concentrations of $O(^3P)$ atoms from the reaction $Hg(^3P) + N_2O \rightarrow O(^3P)$ and obtained kinetic information about the reactions of these O atoms with various substances (6), using phase shift techniques. For a review and further discussion of these techniques, see ref. 7.

In this paper we describe an experimental system designed to measure the amplitude and phase shift of radical concentrations in a current modulated oxygen glow discharge. We then discuss the equations which predict the kinetic response of a glow discharge to modulation of the current for several general types of reaction mechanisms. Finally, the experimental validity of the method is established for a two-step reaction mechanism.

2. Experimental

Most of the apparatus used in the experiments has been described previously (1, 8, 9). The modifications which have been made are in the electrical circuitry which controls the discharge current. Briefly, gas flows through a discharge tube which contains moveable electrodes. A pinhole located in the core of the tube allows us to sample the gas and analyze it mass-spectrometrically. The discharge power supply was operated to keep the location of the sampling hole near zero potential. The ac modulation was superimposed on the dc component through an especially designed unit. The frequency could be adjusted from 0 to 1000 Hz with less than 1% harmonic distortion.

The modulated output signal from the mass spectrometer was amplified and applied to the input of a 100 channel analog analyzer (PAR TDH-9 waveform educator). The amplitude of the observed signal and its phase relative to the applied current modulation could be measured graphically from a strip chart recording of the analyzer output or electronically, with a PAR lock-in phase detector. It was established that the phase angles between the signals measured by both methods did not differ by more than 1 deg.

To ensure that the amplification and detection system did not introduce a phase shift or distortion into the measured signal, a sinusoidal voltage was imposed on one of the focusing lenses of the mass spectrometer, with the discharge operating in the dc mode. It was verified by amplification and analysis of the resulting signal that no measureable phase shift or distortion was introduced into the mass spectrometer output signal.

3. Theory

3.1 General

The rates of electron molecule interactions in the positive column of the discharge can be described by the expression (10, 11)

$$[1] \quad dn_{ij}/dt = n_i n_e \int f(E) Q_{ij}(2E/m)^{1/2}\, dE = k_{ij} n_i n_e$$

where n_i is the concentration of molecules in state i, n_e is the electron concentration, j is the state populated in the collision, $Q_{ij}(E)$ is the cross section for the process, and $f(E)dE$ is the fraction of electrons having energy between E and $E + dE$. k_{ij} is the equivalent of a rate constant in chemical kinetics as applied to an inelastic collision between an electron and a molecule. It is shown below that, within experimental error, for discharges through oxygen, the electron energy distribution function, $f(E)$, remains invariant when a small modulation is superimposed on the dc current. If $f(E)$ remains constant, k_{ij} also remains constant while the current is modulated. Under some conditions, modulation of the current will produce both a modulation in the electron density and thus in the rates of electron–molecule interactions. From the analysis presented in this paper, it will become apparent that measurements of the phase shifts and amplitudes thus produced in radical concentrations can be used to characterize special features of the reaction mechanisms and to evaluate rate constants for specific steps in the mechanism.

3.2 Modulation of the Discharge Current, Experimental

We shall consider the case of a glow discharge with the electrodes positioned at each end of a cylindrical glass tube. The gas flows in the direction of the cathode with a stream velocity, v_s. For small stream velocities, we neglect the spatial pressure and temperature gradients and we assume the gas glow to be piston (plug) flow. The gas residence time, t_g, at a distance, d, in the discharge tube is then given by

$$[2] \quad t_g = d/v_s$$

A sinusoidal modulation, having a relative amplitude, α, and angular frequency, ω, is imposed on the dc current, i_0. The dependence of the current, i, on time, t, is given by

$$[3] \quad i = i_0(1 + \alpha \sin \omega t)$$

The total (integrated) current density to which a volume element of gas is exposed during its passage through the discharge tube is a function of both the gas residence time, t_g, associated with that volume element of gas and the phase angle, ωt, of the current density. Consequently, the rates of reactions occurring in each volume element of gas are also functions of t_g and ωt. In a steady state flow system, radical concentrations at a given point in the discharge corresponding to a given gas residence time, t_g, will be modulated and for some mechanisms, phase shifted with respect to the current modulation, as volume elements associated with different current phase angles pass the observation point.

3.3 Criteria for the Validity of the Method

The applicability of the current modulation technique to glow discharge systems depends on the following two criteria which will now be discussed.

Criterion 1: A sinusoidal modulation imposed on the dc current produces a modulation of identical phase and amplitude in the electron density through the discharge

Because no measurements of n_e have been made in the current modulated discharge, the validity of the above criterion must be judged indirectly. There is evidence from measurements conducted in a dc discharge that this criterion is valid under certain conditions.

Rundle *et al.* (12) employed a microwave absorption technique to measure the average electron concentration in the positive column of a dc oxygen glow discharge. They showed that n_e is directly proportional to the current density for $i = 2$–10 mA (at a pressure of 1 Torr) within the limits of the precision of their measurements.

The current density in the discharge, j, is equal to the flux of electrons through unit cross section of the discharge tube and is given by

$$[4] \qquad j = i/A_x = n_e e v_d$$

where v_d is the electron drift velocity, which itself depends on the electron energy distribution function, e is the electron charge, and A_x is the cross sectional area of the discharge tube. If v_d remains constant as i is varied then the electron density must vary directly with the current. The dependence of v_d on the ratio of the experimental parameters, E/N, where E is the electric field and N is the gas number density, has been measured for different gases by means of electron drift tube experiments (13, 14). Measurements of E/N in our laboratory show that this ratio varies by less than 2% in an oxygen discharge and by less than 5% in a nitrogen discharge as the current is varied from 2 mA to 10 mA in discharge tubes having a cross sectional area of 1.22 cm^2. It can be inferred from these results that, within the indicated limits, the drift velocity is nearly independent of the current at low pressures; thus n_e is directly proportional to the current to a good approximation.

At very low frequencies the current-modulated discharge can be considered as a dc discharge in which the current is slowly varied with time. Since the production and loss rates of electrons in the positive column are in balance, the ability of the electron concentration to follow the current modulation is determined both by the rate of loss of electrons through ambipolar diffusion to the walls of the discharge and by the local rate of production of electrons in the positive column. If these rates are large compared to the modulation frequency the electron density will follow the current modulation. Ambipolar diffusion leads to an apparent first order removal of the electrons with a time constant of the order of 10^{-5} s^{-1} (15) in discharges through gases such as oxygen and nitrogen. The pseudo first order rate of production of electrons by electron impact with ground state molecules is of the order of $10^6 n_e$ s^{-1} in oxygen and nitrogen discharges at the pressure of 1 Torr (14). For frequencies under 500 Hz, the phase shift induced in n_e by production and loss processes will then be less than 1 deg and, hence, negligible to a good approximation. Criterion 1 should be valid over the frequency range of 1–500 Hz.

It follows then that the electron density in the discharge is given by

$$[5] \qquad n_e = (i_0/A_x e v_d)(1 + \alpha \sin \omega t)$$
$$= n_e^0(1 + \alpha \sin \omega t)$$

where n_e^0 is the electron density in the dc discharge.

Criterion 2: The electron energy distribution and hence the average electron energy remain constant as the current density is varied through the range 1.8–10 mA/cm^2

Rundle and co-workers' (11) measurements of E and $f(E)$ in an oxygen glow discharge show that $f(E)$ does not depend on the current within the range of 2–10 mA. Therefore, the above criterion is valid for a dc discharge through oxygen.

The ability of the electrons to maintain the same E and $f(E)$ in a current modulated discharge depends on the electron relaxation time. The relaxation time can be considered to be the time taken for an ensemble of electrons to reestablish the original energy distribution after a perturbation in one or more of the parameters controlling it. We have estimated this to be of the order 10^{-5} s (or smaller) in the active discharge. Criterion 2 should, therefore, be valid for low frequencies (< 500 Hz) for discharges in which $f(E)$ is independent of the current.

Although criterion 2 is valid for the oxygen discharge, the same cannot be said for the nitrogen discharge and possibly other types of discharges. Chenery's (16) attempted measurements of $f(E)$ in the nitrogen discharge show that $f(E)$ depends more on the current than was the case in oxygen. Under these conditions, the applicability of the current modulation technique to the nitrogen discharge is limited by the possible failure of the system to conform to criterion 2.

It should be borne in mind that the drift velocity is mainly dependent on that part of the electron energy distribution which is most highly populated. Because the electron density at high energies is a small fraction of the total electron concentration, large variations in the high energy part of $f(E)$ correspond to relatively small changes in the drift velocity, and criterion 1 should remain valid.

4. Analysis of Some Reaction Mechanisms

In this section, eq. [6], for n_e in the current modulated discharge, is introduced into the rate equations for several simple reaction mechanisms which are typical of chemical processes in the discharge. Equations are determined for the phase shifts and amplitudes of radical concentrations as functions of the experimental parameters. It is shown by this analysis that phase shift measurements can be used not only to determine rate constants for some reaction processes but also to distinguish between various possible mechanisms.

4.1 Mechanism 1

A radical X_j is produced by electron impact with a reactant species X_i; X_j is then deactivated in a first order process

$$[6] \qquad X_i + e \xrightarrow{k_1} X_j + e$$

$$[7] \qquad X_j \xrightarrow{k_2} X_i$$

We shall assume that the depletion of X_i is small and its concentration, $[X_i]$, remains approximately equal to the initial concentration, $[X_i^0]$. The rate equation governing $[X_j]$ is

$$[8] \qquad d[X_j]/dt = k_1[X_i^0]n_e - k_2[X_j]$$

Substituting eq. [5] for n_e into the above equation, we obtain

$$[9] \quad d[X_j]/dt = k_1 n_e^0[X_i^0](1 + \alpha \sin \omega t) - k_2[X_j]$$

Integration of this equation gives

$$[10] \quad [X_j] = \frac{k_1 n_e^0}{k_2}[X_i]\left[1 + \frac{\alpha k_2}{\omega^2 + k_2^2} \times (k_2 \sin \omega t - \omega \cos \omega t)\right] + C \exp(-k_2 t)$$

where C is an integration constant. Integration over the gas residence time is accomplished by using the integration limits $t - t_g$ and t. C is evaluated and the resulting expression substituted in the above equation to give a complicated algebraic expression for $[X_j]$. Simplification of this expression for $[X_j]$ is accomplished by solving the following equation for a, A, and θ.

$$[11] \qquad [X_j] = a(1 + A \sin(\omega t - \theta))$$

to give

$$[12] \quad a = (k_1 n_e^0/k_2)[X_i^0][1 - \exp(-k_2 t_g)]$$

$$[13] \quad A = \frac{\alpha}{(1 + \omega^2/k_2^2)^{1/2}} \times \frac{[1 - 2\exp(-k_2 t_g)\cos \omega t_g + \exp(-2k_2 t_g)]^{1/2}}{1 - \exp(-2k_2 t_g)}$$

$$[14] \quad \theta = \arctan \omega/k_2 - \arctan \frac{\sin \omega t_g}{\exp k_2 t_g - \cos \omega t_g}$$

At each point in the discharge characterized by a given gas residence time, t_g, $[X_j]$ is a sinusoidal function of t, having an amplitude A and lagging n_e by a phase shift, θ.

For values of t_g which are large compared to k_2^{-1} (corresponding to large distances in the discharge tube), the terms in the above equations dependent on t_g become negligibly small and the above equations simplify to

$$[15] \qquad \theta = \arctan(\omega/k_2)$$

$$[16] \qquad A = \alpha/(1 + \omega^2/k_2^2)^{1/2}$$

Under this condition, $t_g \gg k_2^{-1}$, a pseudo steady state (PSS) is attained in the concentration of X_j. A measurement of either A or θ in this region of the discharge can be used to determine k_2 from the above equations. Empirically, it can be shown that the most accurate measurements of k_2 can be made in the frequency range $k_2 < \omega/2\pi < 10k_2$; the frequency should be of the same order of magnitude as the reciprocal lifetime of X_j. Because we are only concerned with low frequency modulation of the current, the most useful applications of this technique to glow discharge are the measurements of the lifetimes of long lived metastable species and to the elucidation of reaction mechanisms which involve metastable species.

The dependence of θ and the ratio A/α, on t_g and distance in the discharge (at a stream velocity, $v_s = 2.8\ ms^{-1}$) for values of k_2 ranging from $2\ s^{-1}$ to $200\ s^{-1}$ is illustrated in Figs. 1 and 2. The maxima and minimum which appear in both sets of curves become more pronounced for smaller values of k_2.

The dependence of θ and A/α on t_g is determined by the values of the experimental parameters, and k_2, and by the nature of the reaction mechanism. It can be shown that many different types of reaction mechanisms will give the pseudo steady state values of θ and A/α shown in Figs. 1 and 2, but these same mechanisms will give different profiles of θ and A/α as a function of t_g. Measurements made in the discharge region preceding the onset of a pseudo steady state (a region that has previously been neglected in chemical modulation experiments) provide a means of verifying the nature of the reaction mechanism

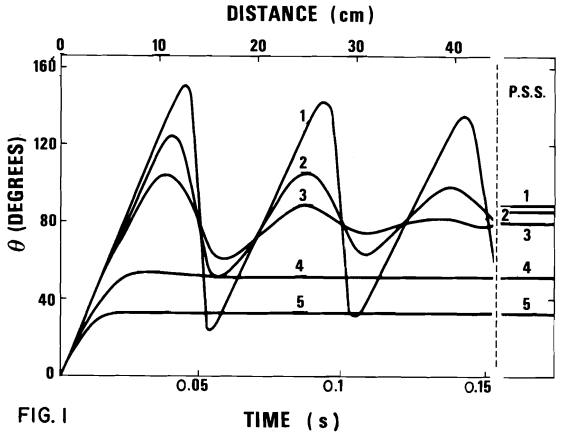

FIG. 1

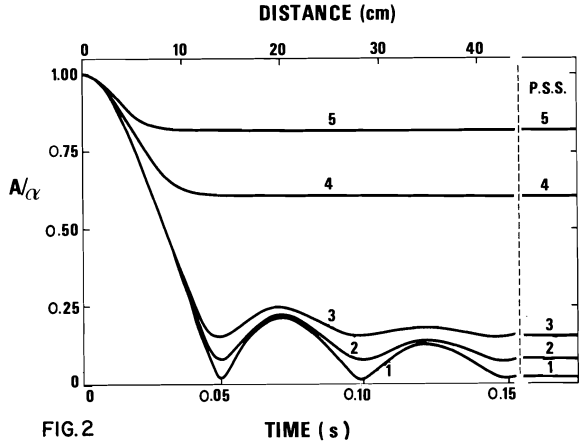

FIG. 2

FIG. 1. Phase shift, θ, of $[X_j]$ versus time and distance (mechanism 1): $v_s = 2.8$ m s^{-1}, $\nu = 20$ Hz, $n_e^0 = 3 \times 10^9$ cm^{-3}, $\alpha = 0.2$, $k_1 = 10^{-11}$ cm^3 s^{-1}, $k_2 = 2$ s^{-1} (curve 1), 10 s^{-1} (curve 2), 20 s^{-1} (curve 3), 100 s^{-1} (curve 4), 200 s^{-1} (curve 5).

FIG. 2. Ratio of amplitude A of $[X_j]$ to the amplitude α of n_e versus time and distance in the discharge (mechanism 1), conditions are the same as in Fig. 1.

and checking the values of rate constants measured in the pseudo steady state region.

4.2 Mechanism 2

If, in addition to the electron impact excitation and the first order removal of X_j, we also assume that de-excitation occurs via a superelastic collision with an electron, the phase shift and amplitude equations take a different form. This reaction sequence is described by

$$[17] \qquad X_i + e \xrightarrow{k_1} X_j + e$$

$$[18] \qquad X_j \xrightarrow{k_2} X_i$$

$$[19] \qquad X_j + e \xrightarrow{k_3} X_i + e$$

The concentration of X_j is governed by the rate equation:

$$[20] \quad d[X_j]/dt = k_1 n_e [X_i] - (k_2 + k_3 n_e)[X_j]$$

No restriction is placed on the concentration of X_j other than the conservation of mass:

$$[21] \qquad [X_i^0] = [X_i] + [X_j]$$

where $[X_i^0]$ is the total initial concentration. Substitution of $[X_i]$ in eq. [20] from the above equation allows us to eliminate $[X_i]$ from the former equation. Combining this equation with [6] then gives the rate equation for $[X_j]$ in the current modulated discharge. The integrated form of this rate equation simplifies considerably in the pseudo steady region of the discharge (large values of t_g) to give:

$$[22] \quad [X_j] = \frac{k_1 n_e^0 [X_i^0]}{k_2 + (k_1 + k_3) n_e^0} \times [1 + A \sin(\omega t - \theta)]$$

where $[X_j]$ is phase shifted (with respect to n_e) by an angle θ.

$$[23] \qquad \theta = \arctan \omega / [k_2 + (k_1 + k_3) n_e^0]$$

and has an amplitude A

$$[24] \quad A = \alpha k_2 / \{\omega^2 + [k_2 + (k_1 + k_3) n_e^0]^2\}^{1/2}$$

The rate equation for $[X_j]$ was integrated with the use of a series expansion. Higher order terms in α^n, where $n \geq 2$, are neglected in this calculation for the case in which the amplitude of the current, α, is small, $\alpha \ll 1$. This condition must be met experimentally to insure the applicability of the above equations to experimental results. The above equations can be solved simultaneously for measured values of θ and A in the pseudo steady state, and for a given frequency ω, to determine the value of k_2 and $(k_1 + k_3)n_e^0$. For the case in which $k_1 \ll k_3$ both the first order and electron impact removal rate constants, k_2 and $k_3 n_e^0$ can be measured by this method.

4.2.1 Phase Shift Dependence on Time

Phase shift and amplitude versus time curves should prove particularly useful for distinguishing between reaction mechanisms which generate similar results in the pseudo steady state. For example, phase shift versus time curves, determined by numerical integration of the rate equations for Mechanism 2, are shown in Fig. 3. The phase shift in the pseudo steady state (eq. [23]) of 78° is determined solely by the magnitude of $k_2 + k_3 n_e^0$ (for the case $k_1 \ll k_3$) which in this case is 50 s^{-1}. However, as the rate constant ratio, $k_3 n_e^0 / k_2$, is varied from 0

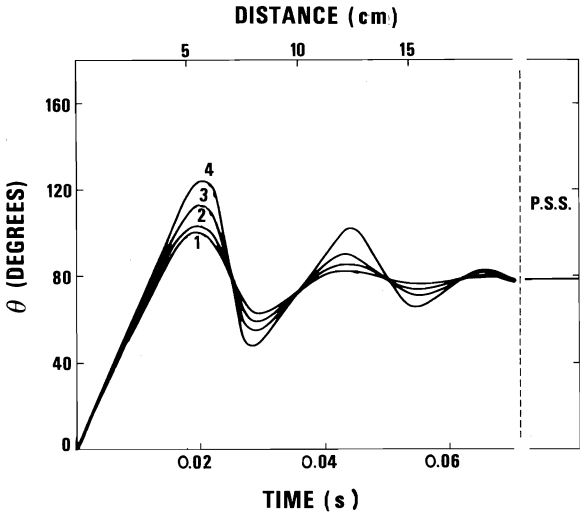

FIG. 3. Phase shift of $[X_j]$ versus distance in the discharge (mechanism 2): $v_s = 2.8$ m s^{-1}, $\nu = 40$ Hz, $n_e^0 = 5 \times 10^9$ cm^{-3}, $\alpha = 0.2$, $k_1 = 10^{-11}$ cm^3 s^{-1}; $k_2 = 50$ s^{-1}, $k_3 = 0$ (curve 1); $k_2 = 37.5$ s^{-1}, $k_3 = 2.5 \times 10^{-9}$ cm^3 s^{-1} (curve 2); $k_2 = 25$ s^{-1}, $k_3 = 5 \times 10^{-9}$ cm^3 s^{-1} (curve 3); $k_2 = 12.5$ s^{-1}, $k_3 = 7.5 \times 10^{-9}$ cm^3 s^{-1}.

to 3, the peak phase shift decreases from 125° to 90°. Measurements of the peak phase shift provide an additional experimental observable which in this case can be used to determine the relative values of $k_3 n_e^0$ and k_2.

4.2.2 Modulation of $[X_i]$: *Negative Phase Shifts*

Due to the conservation of mass (eq. [21]) $[X_i]$ is also modulated and phase shifted. The phase shift, θ, of $[X_i]$ in the pseudo steady state is given by

$$[25] \quad \theta = -180° + \arctan \omega/[k_2 + (k_1 + k_3)n_e^0]$$

for $\alpha \ll 1$ and has the amplitude A

[26]
$$A = \frac{\alpha k_1 n_e^0 k_2}{\{\omega^2 + [k_2 + (k_1 + k_3)n_e^0]^2\}^{1/2}(k_2 + k_3 n_e^0)}$$

The phase shift of $[X_i]$ is negative; the waveform of $[X_i]$ precedes that of n_e. Phase shifts in the first and second quadrants are defined as positive phase shifts while those in the third and fourth quadrants are defined as negative phase shifts. In general, the phase shifts of the concentrations of reaction intermediates and short lived states excited from reaction intermediates will be positive. On the other hand, the concentrations of reactants and short lived states excited directly from the reactant species will be negatively phase shifted.

Phase shifts of both types have been observed in this laboratory in the nitrogen glow discharge (7). A low frequency modulation superimposed on the discharge current resulted in modulations in the intensities of both the first positive system ($B^3\Pi_g$–$A^3\Sigma_u^+$) and the second positive system ($C^3\Pi_u$–$B^3\Pi_g$). The former intensities, proportional to the populations of the vibrational levels of the $B^3\Pi_g$ state, were positively phase shifted. It follows from these results that the $B^3\Pi_g$ state must be populated from a long lived intermediate. The intensities of the second positive system, proportional to the populations of the vibrational levels of the $C^3\Pi_u$ state, were negatively phase shifted. This result indicates that the $C^3\Pi_u$ state is excited mainly by electron impact from the ground electronic state which itself is depopulated by excitation processes.

4.3 Mechanism 3

Here, we consider the case of a short lived excited state, X_j^*, produced both by an electron impact reaction and by a first order (or pseudo first order) process from a long lived intermediate, X_j.

$$[27] \quad X_i + e \xrightarrow{k_1} X_j + e$$

$$[28] \quad X_j \xrightarrow{k_2} X_i$$

$$[29] \quad X_j + e \xrightarrow{k_3} X_j^* + e$$

$$[30] \quad X_j (+ M) \xrightarrow{k_4} X_j^* (+ M)$$

$$[31] \quad X_j^* \xrightarrow{k_5} X_j^{**} + h\nu$$

Because X_j^* is a short lived excited state, it radiates in the same region of the discharge in which it is produced, and its concentration, proportional to the emission intensity, I, is also proportional to the rate of production of X_j^* by reactions [29] and [30]

$$[32] \quad I = h\nu \sim [X_j^*] \sim (k_3 n_e + k_4)[X_j]$$

Hence, modulations in $[X_j]$ are reflected by modulations in the emission intensity I.

For the case $k_2 > k_3 n_e^0 + k_4$, $[X_j]$ is given by eq. [11], discussed for mechanism 1. If we substitute eq. [11] in the above expression for I and neglect higher order harmonic terms, for the case $\alpha \ll 1$, then we obtain an expression proportional to I in the pseudo steady state region.

The phase shift, θ, of I is

$$[33] \quad \theta = \arctan \left[\frac{k_2}{\omega} + \left(\frac{\omega}{k_2} + \frac{k_2}{\omega} \right) \times \left(1 + \frac{k_4}{k_3 n_e^0} \right)^{-1} \right]^{-1}$$

and the amplitude, A, is

$$[34] \quad A = \alpha\left(1 + \frac{\omega^2}{k_2{}^2}\right)^{-1/2} \times \left[1 + \left(3 + \frac{\omega^2}{k_2{}^2}\right)\left(1 + \frac{k_4}{k_3 n_e{}^0}\right)^{-1}\right]^{1/2}$$

The dependence of A and θ on the ratio, ω/k_2, for different ratios of the rate constants, $k_4/k_3n_e{}^0$, is shown in Figs. 4 and 5.

If $X_j{}^*$ is excited only by a first order or pseudo first order process, ($k_3n_e{}^0 = 0$), then the phase shift of both I and $X_j{}^*$ shows the same dependence on frequency as does the phase shift of X_j and approaches a value of 90° at high frequencies. On the other hand, if any of the production of $X_j{}^*$ occurs by electron impact with X_j, then the phase shift must approach 0° at high frequencies.

For large values of ω/k_2, the amplitude (eq. [34]) attains a constant value

$$[35] \quad A = \left(1 + \frac{k_4}{k_3 n_e{}^0}\right)^{-1/2}$$

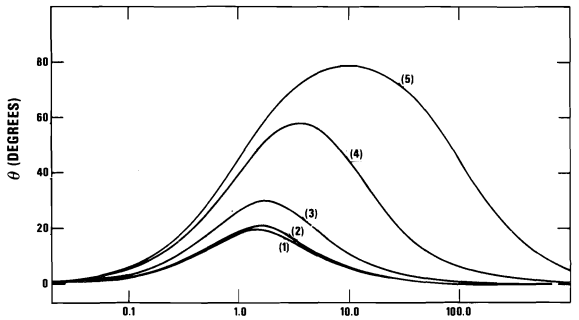

FIG. 4

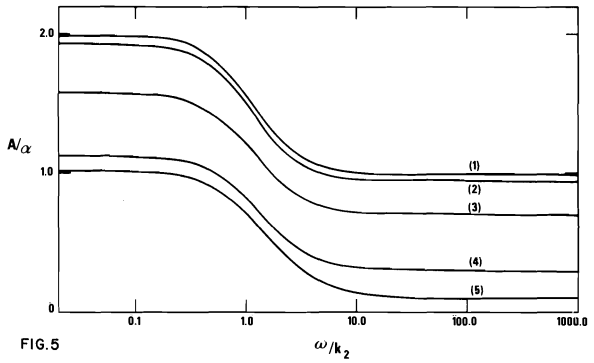

FIG. 5

FIG. 4. Phase shift, θ, of $[X_j{}^*]$ versus ω/k_2 (mechanism 3): $k_4/k_3n_e{}^0 = 0.01$ (curve 1), 0.1 (curve 2), 1 (curve 3), 10 (curve 4), 100 (curve 5).

FIG. 5. Ratio of amplitude A of $X_j{}^*$ to the amplitude α of n_e versus ω/k (mechanism 3), conditions are the same as in Fig. 4.

which is independent of the value of k_2. A measurement of the amplitude of $X_j{}^*$ at high frequencies provides a direct measurement of the rate constant ratio, $k_4/k_3n_e{}^0$.

This result illustrates an important application of chemical modulation techniques. At frequencies which are large compared to the removal rate constants for intermediate species (in this case, X_j; the amplitude of X_j approaches a value of 0 (see eqs. [16] and [34])). But eq. [35] shows that A attains a constant value different from 0 for ω going to infinity. Measurements of the amplitude of the concentration of short lived excited states at high frequencies provide a direct measurement of the relative rates of excitation of these states by first order and electron impact processes, regardless of how many intermediate states are involved in the reaction mechanism. It would be impossible to determine this type of kinetic information from measurements performed in a dc discharge unless the reaction mechanism was simple and well defined. Clearly, kinetic information can be obtained by measurements of the limiting high frequency phase shift and amplitude of modulated radical concentrations.

The phase shift, θ_{max}, at the maximum of the curves in Fig. 4 is given by

$$[36] \quad \theta_{max} = \arctan\left[\frac{1 + k_4/k_3n_e{}^0}{2(2 + k_4/k_3n_e{}^0)}\right]^{1/2}$$

A measurement of this quantity, for this specific mechanism, is sufficient to determine the rate constant ratio, $k_4/k_3n_e{}^0$.

The frequency, ω_{max}, at which this maximum occurs is given by

$$[37] \quad \omega_{max} = k_2(2 + k_4/k_3n_e{}^0)^{1/2}$$

The value of k_2 can be determined from a measurement of ω_{max}, and the ratio $k_4/k_3n_e{}^0$.

An interesting case is that for which $k_3n_e{}^0 \gg k_4$ (curve 1 in Figs. 4 and 5). Here, ω_{max} is given by

$$[38] \quad \omega_{max} = 2^{1/2}k_2$$

and the phase shift at the maximum is

$$[39] \quad \theta_{max} = \arctan 1/2\sqrt{2} = 19.5°$$

The position of the maximum is determined solely by the value of k_2; the largest possible phase shift in the pseudo steady state becomes 19.5°. Measurements of θ and A as a function of the frequency can be used to both identify this particular mechanism and also to determine values of the rate constants k_2 and the ratio $k_4/k_3n_e{}^0$.

Other reaction mechanisms can be treated in a

similar manner to those discussed above. In most cases approximate solutions for θ and A in the pseudo steady state can be readily obtained. However, when extremely complex mechanisms are considered, it becomes more convenient to use computer methods to determine the phase shift and amplitude by integrating numerically the rate equations corresponding to an assumed mechanism.

4.4 Conclusions

For a limited number of reaction mechanisms, rate constants can be deduced from measurements of radical concentrations as a function of the gas residence time in the dc current discharge. The analogous experiment in the current modulated discharge is the measurement of the phase shift of a radical concentration as a function of the frequency in the pseudo steady state region. This shift in emphasis from gas residence time (a calculated parameter which is poorly defined under many experimental conditions in flow tubes) to the frequency (an experimental parameter which can be accurately determined) allows for greater flexibility and accuracy in the measurement of rate constants in glow discharges.

Measurements performed in the dc current discharge are only useful for the case in which the reaction mechanism is simple and well established. Phase shifts and amplitudes are dimensionless parameters which have physical significance, regardless of the complexity of the reaction mechanism. Consequently, measurements performed in a current modulated discharge can be used to elucidate complex mechanisms for cases in which dc current techniques can provide only marginal kinetic information.

Another advantage of current modulation techniques is that phase shift and amplitude measurements in the pseudo steady state region are independent of the gas stream velocity. Although there are spatial concentration gradients in this region of the discharge, as there are along the entire length of the discharge, the phase shift and amplitude of radical concentrations will be identical in each volume element of gas in the pseudo steady state. This follows from the definition of PSS as being the discharge region in which the radical amplitude and θ attain constant values. Although there may be spatial concentration gradients in this region as there are in the dc discharge, the phase and amplitude of the modulated concentrations are identical in each volume element of gas. Hence, it is unnecessary to make any assumption regarding the nature of the gas flow (such as the commonly employed assumption of plug flow) to determine accurate rate constants. Since phase shifts and amplitudes in the pseudo steady state are unaffected by radial or axial gradients in the stream velocity, corrections for these gradients, which must be applied to measurements performed in a dc current discharge, need not be considered for experiments in a current modulated discharge.

The application of chemical modulation techniques to a gas flow discharge system provides an additional experimental observable, the peak phase shift (defined as the maximum phase shift measured along the length of the discharge). For many mechanisms, this quantity exhibits an entirely different dependence on frequency compared to the phase shift measured in the pseudo steady state region. In contrast to the pseudo steady state parameters, transient phenomena such as the peak phase shift are dependent on the gas flow profile. The phase shift peaks predicted theoretically may be distorted as a consequence of stream velocity gradients and diffusion of metastable species. Measurements of the peak phase shift can provide kinetic information in a manner which has not been considered in previous applications of chemical modulation techniques.

5. Experimental Testing of the Current Modulated Technique

5.1 General

The mechanism for the production and removal of O atoms in a flowing oxygen glow discharge was determined in this laboratory. Mass spectrometric measurements (1) of the atom concentration profile in the active discharge have established that the atoms are produced by direct electron impact dissociation of the molecule and removed by a process first order in the atom concentration

$$[40] \qquad O_2 + e \xrightarrow{k_1} O + O + e$$

$$[41] \qquad O \xrightarrow{k_w} \tfrac{1}{2}O_2$$

The magnitude of the removal rate constant, k_w, was found to be from 10 to 100 times larger than the corresponding value in the afterglow. In the present study measurements obtained in a dc glow discharge have been compared by investigating the kinetics of O-atom formation using the current modulated technique, under otherwise identical experimental conditions. This mechanism is of the type discussed in section 4.1 where X_i is O_2 and X_j the O atom. The response of the important measured quantities are given by eqs. [13]–[16], where $k_2 = k_w$.

The concentration of oxygen atoms thus can be visualized as consisting of two parts: a dc component which is identical to that in a dc current discharge and a modulated component with a relative amplitude, A, which is phase-shifted with respect to n_e by a phase angle θ. Both θ and A are functions of the

residence time t, and rate constant k_2 in addition to the modulation parameters. By flowing ultrapure oxygen through the discharge tube and adjusting the energy of the ionizing electron beam of the mass spectrometer so as to ionize O atoms (but not O_2), one can obtain a measure of X_j as a function of the resident time in the discharge (1) and hence determine k_w. Alternately, phase angles and amplitudes of the modulated atom concentration could be obtained experimentally at various values of the gas residence time as a function of the applied frequency and amplitude of modulation.

Within the limits of detection, the modulation induced in the oxygen atom concentration was found to be sinusoidal and consequently could be described by a phase shift and an amplitude of the fundamental frequency only. Any phase shift introduced by the flight time of the atoms in the molecular beam between the sampling orifice and the mass spectrometer could be determined by operating the discharge in the dc mode and chopping the molecular beam at the appropriate frequency.

5.2 Results

The dependence of the phase shift and relative amplitude of the modulation in the oxygen atom concentration is plotted against time in the discharge in Figs. 6 and 7. As the applied frequency was increased, the relative amplitude was found to decrease while the phase shift increased. At large values of time both the phase shift and relative amplitude assumed a constant value.

The theoretical phase shifts and amplitude of the oxygen atom concentration for the postulated mechanism were fitted to the experimental points. The only nonexperimental parameter available for this fitting procedure is the value of k_w. The best fit of the experimental and calculated points was obtained for a value of k_w of 280 s^{-1} for any value of the gas residence time t.

At large values of t_g the equations for the calculated phase shift and relative amplitude simplify to [15] and [16]. Note that both θ and A for this special case are independent of t in the pseudo steady state region of the discharge.

Figures 8 and 9 show the dependence of both the phase shift and relative amplitude as a function of the applied frequency. As the frequency is increased the phase shift asymptotically approaches a value of 90° while the relative amplitude decreases to a value of 0°. Excellent agreement is thus obtained between the calculated and experimental values for the entire experimental frequency range (10–500 Hz).

A value of the first order recombination rate constant was also determined in the dc discharge. The technique consisted of monitoring the [O] as a function of gas residence time. A plot of $\ln([O]_{ss} - [O]_t)/[O]_{ss}$ versus t yielded a straight line with a sloped (k_w) of 330 s^{-1} (Fig. 10). This value is in good agreement with that determined using the current modulated technique.

In Fig. 11 the value of k_w determined at various frequencies from a reading in the PSS is plotted. This shows that the value of k_w thus obtained is independent of frequency.

The excellent fit obtained for both the θ and A over the entire range of experimental parameters and the good agreement obtained between the rate constant determined using both methods is taken as evidence for the correctness of the postulated mechanism and hence the soundness of the current modulated tech-

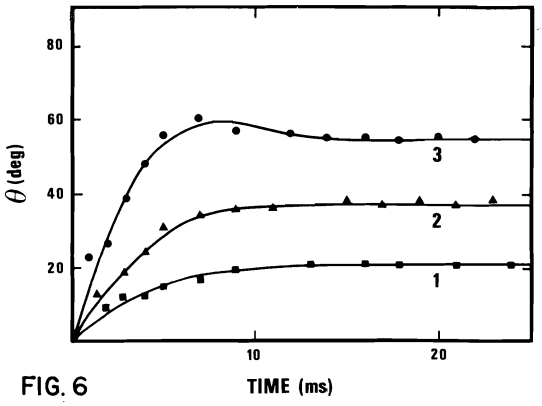

FIG. 6

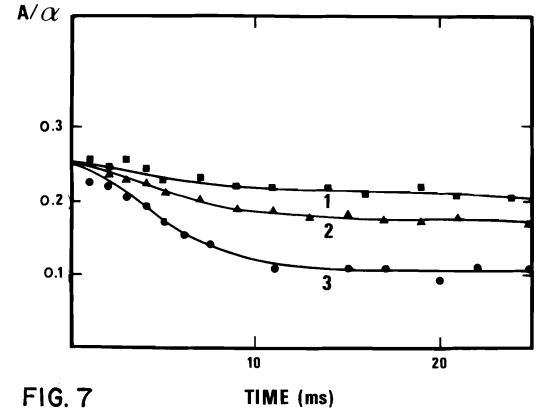

FIG. 7

FIG. 6. Phase shift, θ, of the oxygen atom concentration versus residence time in the discharge: p = 1.0 Torr, v_s = 9.0 m s^{-1}, α = 0.25, I_0 = 8 mA. Experimental points: ■, ν = 20 $h\nu$; ▼, ν = 40 $h\nu$; ●, ν = 80 $h\nu$. Solid lines: calculated values for k_w, 280 s^{-1}, curve 1 = 20 $h\nu$; curve 2 = 40 $h\nu$; curve 3 = 80 $h\nu$.

FIG. 7. Relative amplitude, A/α, of the oxygen atom concentration versus residence time in the discharge, conditions are the same as in Fig. 6.

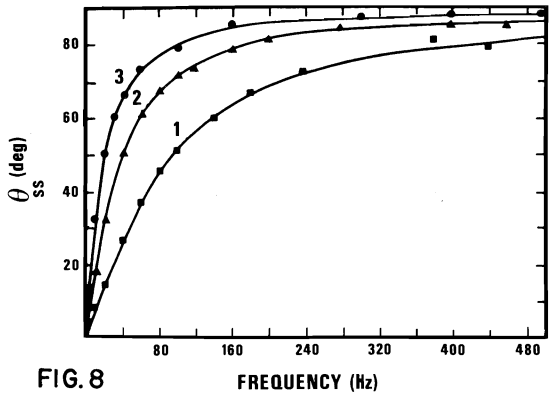

FIG. 8

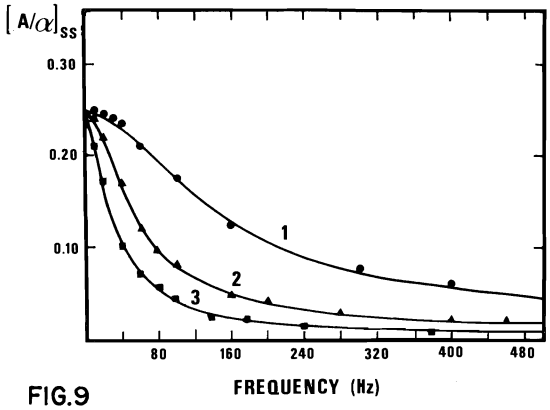

FIG. 9

FIG. 8. Steady state phase shift, θ_{ss}, of the oxygen atom concentration versus applied frequency in the discharge. v_s = 6.0 m s^{-1}, I_0 = 8 mA, α = 0.25. Experimental points: ●, p = 0.55 Torr; ▲, p = 0.80 Torr; ■, p = 1.5 Torr. Solid lines: calculated values, curve 1, k_w = 500 s^{-1}; curve 2, k_w = 210 s^{-1}; curve 3, k_w = 110 s^{-1}.

FIG. 9. Steady state relative amplitude, A_{ss}/α, of the oxygen atom concentration versus applied frequency in the discharge, conditions are the same as in Fig. 8.

nique. It should be noted that the suggested mechanism was the only one among the many tested which predicted the correct variations of the phase shift and relative amplitude with the experimental parameters.

These results illustrate convincingly several advantages of using the current modulated technique over the DC technique in the determination of k_w. Since both the phase shift and relative amplitude in the pseudo steady state are exclusive functions of k_w and modulation parameters (α,ν) the value of k_w can be determined from either of these measurements in this region of the discharge. The experimental errors associated with the determination of k_2 from measurements associated with short residence times of a dc current discharge are thus eliminated.

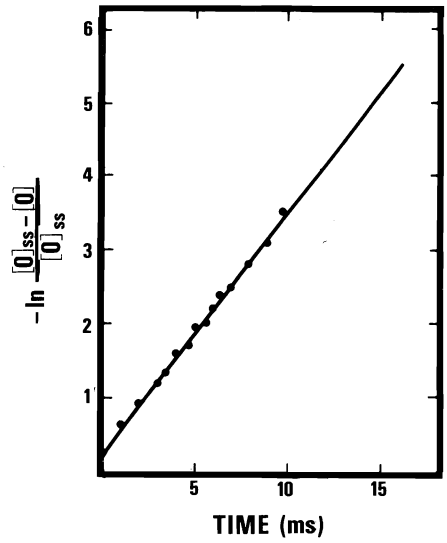

FIG. 10. Logarithm of $([O]_{ss} - [O]_t)/[O]_{ss}$ versus residence time in the discharge, v_s = 9.5 m s^{-1}, p = 1.00 Torr, I_0 = 8 mA.

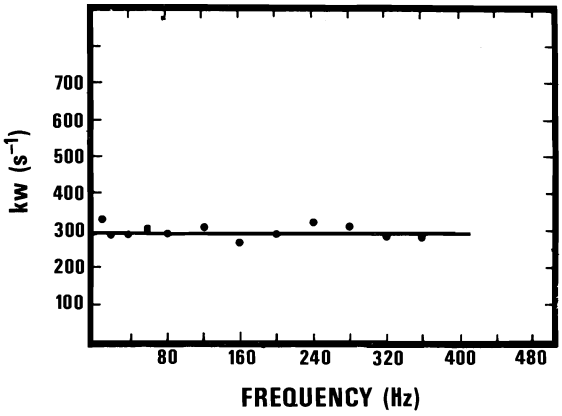

FIG. 11. Tangent of the steady state phase shift (tan θ_{ss}) of the oxygen atom concentration versus applied frequency in the discharge, p = 1.00 Torr, v_s = 9.0 m s^{-1}, α = 2.5, I_0 = 8 mA.

Acknowledgements

M.D.C. acknowledges the award of a Graduate Fellowship from the National Research Council of Canada. This work was supported by the National Research Council of Canada.

We wish to express our gratitude to Drs. D. R. Clark, H. W. Rundle, S. A. G. Chenery, and T. Svekis-Milman for helpful discussions.

F. Shaw was helpful in the design and construction of the equipment and W. Panning assisted in the building and the testing of the electronic circuitry.

1. M. D. COSTA, P. A. ZULIANI, and J. M. DECKERS. Can. J. Chem. **57**, 568 (1979).

2. E. J. BAIR, J. T. LUND, and P. C. CROSS. J. Chem. Phys. **24**, 961 (1956).
3. G. M. BURNETT and H. W. MELVILLE. Technique of organic chemistry. Vol. VIII. Part II. *Edited by* S. L. Friesse, E. S. Lewis, and A. Weissberger. Interscience Publishers, New York. 1963. p. 1107.
4. W. S. METCALFE. J. Chem. Soc. London, 3726 (1960).
5. H. S. JOHNSTON, G. E. MCCRAW, T. T. PAUDERT, L. W. RICHARDS, and J. VAN DEN BOEGAERDE. Proc. Natl. Acad. Sci. **57**, 1146 (1967).
6. R. ATKINSON and R. J. CVETANOVIĆ. J. Chem. Phys. **55**, 659 (1971); **56**, 432 (1972); D. L. SINGLETON, S. FURUYAMA, R. C. CVETANOVIĆ, and R. S. IRWIN. J. Chem. Phys. **63**, 1003 (1975); S. FURUYAMA, R. ATKINSON, A. COLUSSI, and R. J. CVETANOVIĆ. Int. J. Chem. Kinet. **6**, 741 (1974).
7. L. F. PHILLIPS. Prog. React. Kinet. **7**, Part 2, 83 (1973).
8. J. N. SMITH. Ph.D. Thesis. University of Toronto, Toronto, Ont. 1974.
9. M. D. COSTA. Ph.D. Thesis. University of Toronto, Toronto, Ont. 1975.
10. R. W. LUNT and A. H. GREGG. Trans. Faraday Soc. **36**, 1062 (1940).
11. J. L. PEETERS, H. W. RUNDLE, and J. M. DECKERS. Can. J. Chem. **44**, 2981 (1966).
12. H. W. RUNDLE, D. R. CLARKE, and J. M. DECKERS. Can. J. Phys. **51**, 144 (1973).
13. R. D. HAKE and A. V. PHELPS. Phys. Rev. **158**, A70 (1967).
14. R. M. CROMPTON and D. J. SUTTON. Proc. R. Soc. London, A**215**, 467 (1952).
15. G. FRANCIS. Handbuch der Physik. Vol. 22. *Edited by* S. Flügge. Springer Verlag, Berlin. 1958. p. 53.
16. S. A. G. CHENERY. Ph.D. Thesis. University of Toronto, Toronto, Ont. 1970.

Erratum: Enrichment of nitrogen-15 by the direct laser photolysis of ammonia-d_3 in the $\tilde{A}$–$\tilde{X}$ transition

P. A. HACKETT, R. A. BACK, AND S. KODA
PIE Group, Division of Chemistry, National Research Council of Canada, Ottawa, Ont., Canada K1A 0R6
Received December 14, 1978
(Ref.: Can. J. Chem. **56**, 2981 (1978))

The diagrams for Figs. 1 and 2 have been interchanged so that Fig. 1 appears above the caption for Fig. 2 and vice versa.

Erratum: Pyrazolato bridged binuclear complexes of palladium and platinum

FLAVIO BONATI[1] AND HOWARD C. CLARK
Guelph–Waterloo Centre for Graduate Work in Chemistry, Guelph Campus, University of Guelph, Guelph, Ont., Canada N1G 2W1
Received December 12, 1978
(Ref.: Can. J. Chem. **56**, 2513 (1978))

In the abstract "1-monosubstituted" should be "1-unsubstituted".

Dans le résumé on devrait lire "nonsubstitué" au lieu de "monosubstitué".

[1]Present address: Instituto di Chimica Generale, via Venezian 21, 20133 Milano, Italy.

The enol content of simple carbonyl compounds: a kinetic approach

J. PETER GUTHRIE[1]

Department of Chemistry, University of Western Ontario, London, Ont., Canada N6A 5B7

Received June 16, 1978

J. PETER GUTHRIE. Can. J. Chem. **57**, 797 (1979).

Following a suggestion of Lienhard and Wang, we demonstrate that the enol content of simple carbonyl compounds can be estimated as the ratio of the rate constants for acid-catalyzed enolization of the carbonyl compound and acid-catalyzed hydrolysis of the corresponding methyl enol ether. Values so estimated are in excellent agreement with those determined by our thermochemical method. Sufficient data are available for the following; compound, pK_{Enol}: acetaldehyde, 4.7; propionaldehyde, 4.2; isobutyraldehyde, 2.7; acetone, 7.0; cyclopentanone, 6.7; cyclohexanone, 5.3; cycloheptanone, 7.2; cyclooctanone, 6.6; *p*-nitroacetophenone, 4.9; *p*-bromoacetophenone, 6.2; acetophenone, 6.6; *p*-methylacetophenone, 7.0; *p*-methoxyacetophenone, 7.3; and by estimating the rate constants for enolization, the following; indanone, 7; 2-phenyl-2-propanone, 4; cyclopropyl methyl ketone, 8; chloroacetaldehyde, 2 (corrected for hydration); phenylacetaldehyde, 2.

J. PETER GUTHRIE. Can. J. Chem. **57**, 797 (1979).

A la suite de la suggestion de Lienhard et Wang, on démontre que l'on peut évaluer le taux d'énol dans des composés carbonylés simples en faisant le rapport des constantes de vitesse de l'énolisation acido-catalysée du composé carbonylé et de l'hydrolyse acido-catalysée de l'éther énolique méthylique correspondant. Les valeurs évaluées de cette manière sont en excellent accord avec celles déterminées par notre méthode thermochimique. Des données suffisantes sont disponibles dans les cas suivants; composé, pK_{enol}; acétaldéhyde, 4.7; propionaldéhyde 4.2; isobutyraldéhyde, 2.7; acétone, 7.0; cyclopentanone, 6.7; cyclohexanone, 5.3; cycloheptanone, 7.2; cyclooctanone, 6.6; *p*-nitroacétophénone, 4.9; *p*-bromoacétophénone, 6.2; acétophénone, 6.6; *p*-méthylacétophénone, 7.0; *p*-méthoxyacétophénone, 7.3; et si l'on fait une évaluation des constantes de vitesse de l'énolisation, les données seraient aussi disponibles pour les cas suivants; indanone, 7; phényl-2 propanone-2, 4; cyclopropylméthylcétone, 8; chloroacétaldéhyde, 2 (corrigé pour l'hydratation); phénylacétaldéhyde, 2.

[Traduit par le journal]

Introduction

Although the question of the enol content of simple carbonyl compounds has been addressed at intervals for a long time (1–5), the problems involved in obtaining an unambiguous answer have remained formidable (3, 6). Recently (7) we reported a thermochemical method which appeared to offer a general and unambiguous answer to this problem. In the course of the investigations leading to the thermochemical method, we found that a quite independent method of comparable generality exists but has not been exploited. This method is based upon the work of Lienhard and Wang (8), who pointed out, in an investigation of the mechanism of hydrolysis of enol ethers, that the accepted mechanism for general-acid-catalyzed enolization of a ketone (and therefore for the ketonization of an enol) requires that the rate constants for general-acid-catalyzed hydrolysis of an enol ether must be approximately equal to the rate constant for the general-acid-catalyzed ketonization of the corresponding enol, if protonation of the enol ether on carbon is the rate-determining step. Lienhard and Wang demonstrated that this identity obtains for cyclohexanone and drew the appropriate mechanistic conclusions.

It is obvious that if this approximate identity is generally valid, then from the rate of acid-catalyzed hydrolysis of an enol ether (equal to the rate of ketonization of the enol) and the rate of acid-catalyzed enolization of the corresponding keto tautomer one can determine the enol content of the carbonyl compound. It is curious that although this has been recognized (9, 10) there seems to have been no real attempt to utilize this potentially very powerful method. One serious difficulty hindering the acceptance of this method is the dearth of simple compounds, for which the enol content is known, which could be used to test the method. With a set of equilibrium constants for enolization determined by our thermochemical method (7) now in hand, it is possible to demonstrate that the kinetic method implicit in the work of Lienhard and Wang (8) is indeed quite general and has the potential for great

[1]Alfred P. Sloan Fellow, 1975–1979.

0008-4042/79/070797-06$01.00/0

utility.[2] The available data are already sufficient to show that the method can not be exactly correct (which was hardly to be expected), since the rate constant for acid-catalyzed hydrolysis of an alkyl enol ether depends upon the nature of the alkyl group (11). The rate factors are fairly small for simple alkyl groups, so that these facts do not invalidate the method but simply demonstrate an inherent imprecision.

Results and Discussion

In Table 1 are summarized the available data for acid-catalyzed enolizations of carbonyl compounds and hydrolysis of the corresponding enol ethers. The list is believed to be essentially complete for hydrolyses of methyl enol ethers (some other compounds which differ only in the alkyl or substituted aryl substituent and are closely similar to related compounds in Table 1 have been studied; these other compounds are referred to in the table) but is less complete for acid-catalyzed enolization, for which there are numerous compounds for which the enol ether has not been studied.

Table 1 reports only rate constants for methyl enol ethers (some of which are estimated from the corresponding ethyl enol ethers); although in a few thoroughly studied enol ether systems a variety of other alkyl or aryl groups have been present in place of methyl (or ethyl), this restriction does not reduce the number of carbonyl compounds considered.

Assuming that the rate constant for acid-catalyzed hydrolysis of an enol ether is the same as the rate constant for ketonization of the corresponding enol, the equilibrium constant for enolization can be calculated as the ratio of the rate constant for enolization to the rate constant for hydrolysis. It is convenient to use $pK_{Enol} = -\log K_{Enol}$ as a measure of the tendency of a carbonyl compound to enolize. These values are also found in Table 1. This method for estimating K_{Enol} as the ratio of rate constants will be referred to as the 'kinetic method' in this paper.

For 1-methoxypropene both the methyl and ethyl ethers of both *E* and *Z* isomers have been studied (11). As is generally the case the ethyl ethers are about twice as reactive as the corresponding methyl ethers. The *Z* isomers are about three times as reactive as the corresponding *E* isomers. This difference in reactivity is not a reflection of differences in stability of the two isomers because the equilibrium constant for geometrical isomerization is 1.2 (12). Assuming that the proton transfer to (or from) carbon is the rate-determining step for ketonization (or enolization), the observed rate constant for enolization is the sum of the rate constants for formation of the *E* and the *Z* enol, and the corresponding overall rate of ketonization is given by:

$$k_{ketonization} = (k^{E\text{-Enol}}_{ketonization} + k^{Z\text{-Enol}}_{ketonization} \cdot K_{Z/E})/(1 + K_{Z/E})$$

$$K_{Z/E} = [Z\text{-Enol}]/[E\text{-Enol}]$$

For all cases except the alkyl isopropenyl ethers where both ethyl and methyl ethers have been studied the methyl ether is the less reactive by a factor of about twofold. The average value for the five cases excluding alkyl isopropenyl ethers is $k_{OMe}:k_{OEt} = 0.48 \pm 0.05$. In contrast to this pattern, the value for k_{H^+} reported for methyl isopropenyl ether (13) is larger than the value for ethyl isopropenyl ether (11, 14). The experiments were done in different laboratories, under slightly different conditions (0.04 as opposed to 0.08 *M* ionic strength); the most likely source of the discrepancy is that the rate constant for the methyl ether is based upon experiments done in phosphate buffers where the hydronium ion catalyzed reaction makes only a small contribution to the observed rate, although the errors are claimed to be only 1.3%. For methyl isopropenyl ether and for 1-methoxycyclopentene rate constants for acid-catalyzed hydrolysis were estimated from the observed rate constants for the ethyl ethers (11) and the average value of 0.48 for the methyl to ethyl rate ratio. In the case of methyl isopropenyl ether we consider that this estimated value is probably the better one to use.

The data supporting the value of the methyl to ethyl rate ratio are collected in Table S-I, which has been placed in the Depository for Unpublished Data.[3]

Rate constants for enolization of the aldehydes were taken from the work of Talvik and Hiidmaa (15) and are observed rate constants for the equilibrium mixture of aldehyde and hydrate, not corrected for number of enolizable hydrogens. There appear to have been no studies of the enolization of cycloalkanones in water except for the studies of cyclohexanone by Lienhard and Wang (8). Schechter *et al.*

[2]A referee has pointed out that on *a priori* grounds one might have expected that the method would not work since hydroxy and alkoxy should differ in their ability to stabilize a developing positive charge. However since the rate constants for acid-catalyzed hydrolysis of an enol ether or ketonization of the corresponding enol are in fact approximately equal (8) it seems clear that this difference is really quite small.

[3]Copies of material on deposit may be obtained, at a nominal charge, from the Depository of Unpublished Data, CISTI, National Research Council of Canada, Ottawa, Ont., Canada K1A 0S2.

TABLE 1. Kinetic data permitting calculation of enolization constants[a]

Enol ether	Rate constant[b] for hydrolysis (M^{-1} s^{-1})	Carbonyl compound	Rate constant[b] for enolization (M^{-1} s^{-1})	pK_{Enol}[c]
CH_2=CH—OMe	0.760[d]	CH_3—CHO	1.65×10^{-5}[e]	4.66
(*Z*)-CH_3—CH=CH—OMe	0.255[d] } 0.154	CH_3CH_2CHO	1.88×10^{-5}[e]	3.91
(*E*)-CH_3—CH=CH—OMe	0.072[d] }			
$(CH_3)_2C$=CH—OMe	0.0252[d]	$(CH_3)_2CH$—CHO	4.95×10^{-5}[e]	2.71
CH_2=$C(CH_3)$—OMe	278[d,f]	$(CH_3)_2CO$	2.76×10^{-5}[g]	7.02
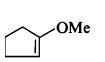	218[d,f]		4.4×10^{-5}[h]	6.70
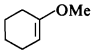	42.3[d]		2.3×10^{-4}[i]	5.26
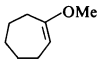	209[d,f]		3.0×10^{-5}[h]	6.84
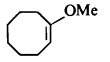	299[d,f]		1.7×10^{-4}[h]	6.25
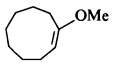	130[d,f]			
		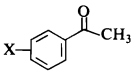		
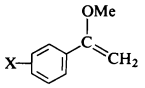				
$X = p$-NO_2	0.96[f,l]	$X = p$-NO_2	1.12×10^{-5}[m]	4.93
$X = p$-Br	17.3[f,l]	$X = p$-Br	1.20×10^{-5}[m,n]	6.16
X = H	53.3[l]	X = H	1.26×10^{-5}[o]	6.63
$X = p$-CH_3	133[f,l]	$X = p$-CH_3	1.49×10^{-5}[m]	6.95
$X = p$-OCH_3	310[f,l]	$X = p$-OCH_3	1.52×10^{-5}[m]	7.31
	57.9[l]		$\sim10^{-5}$[j,u]	(7)
(*E*)-Ph—CH=$C(CH_3)$—OMe	1.67[d]	Ph—CH_2—CO—CH_3	$\sim10^{-4}$[j,u]	(4)
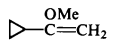	7.49×10^{3}[p]		$\sim10^{-5}$[j,u]	(8)
Cl~CH=CH—OMe	2×10^{-4}[f,q,r]	Cl—CH_2—CHO	$\sim10^{-6}$[j,u,v]	(2)
			$\sim10^{-7}$[j,u,w]	(3)
(*Z*)-Ph—CH=CH—OMe	1.58×10^{-2}[f,r–t]			
(*E*)-Ph—CH=CH—OMe	8.48×10^{-3}[f,r–t]	Ph—CH_2—CHO	$\sim10^{-4}$[j,u]	(2)

[a]In water at 25°C.
[b]Acid catalyzed; for 1 methoxypropene a weighted average rate constant for hydrolysis was calculated: see text.
[c]K_{Enol} = [Enol]/[Keto]; pK_{Enol} = log K_{Enol}; values in parentheses are approximate, based on estimated rate constants for enolization.
[d]Reference 11.
[e]Reference 15.
[f]Calculated from the rate constant for the ethyl ether, using a ratio k_{OMe}/k_{OEt} = 0.48.
[g]Reference 25.
[h]Calculated from the results in ref. 16 measured in 90% acetic acid with HCl as catalyst assuming that relative rates would be the same as in water. Cyclohexanone was used as the standard (ref. 8).
[i]Reference 8.
[j]Not available.
[k]For other substituted α-methoxy styrenes, bearing COOMe, COOH or COO^-, see ref. 32.
[l]Reference 33.
[m]Calculated from the rate constant for acetophenone measured at 25°C (ref. 17) using relative rates from ref. 18, measured at 30°C in 1.4 *M* $HClO_4$.
[n]Assumed to be the same as *p*-Cl.
[o]Reference 17.
[p]Reference 34.
[q]Reference 19.
[r]Calculated from rate constants determined in 80:20 dioxane–water, using a linear free energy relationship, see text.
[s]Reference 20.
[t]For further examples of styryl ethers see ref. 20; for β-alkyl substituted vinyl ethers see ref. 21.
[u]Estimated as described in the text.
[v]For the keto tautomer.
[w]Apparent value for the equilibrium mixture of keto and hydrate.

TABLE 2. Comparison of enolization constants obtained by various methods[a]

Carbonyl compound	pK_{Enol}[b] Kinetic[c] method	pK_{Enol}[b] thermochemical[d] method	Direct measurement
CH_3CHO	4.7	5.3(0.6)	
CH_3CH_2CHO	3.9	3.9(1.0)	
$(CH_3)_2CH—CHO$	2.7	2.8(1.1)	
$CH_3—CO—CH_3$	7.0	7.2(0.9)	8.8(0.9)[e] >6.0[f] 5.8[g,h] 5.6[i]
	6.7	7.2(1.2)	4.9[f] 4.5[j,k] 3.0[h,l]
	5.3	5.7(1.1)	4.3[i] 5.4[f] 2.1[h,l] 3.6[i]
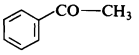	6.6	6.7(1.0)	4.7[j,k] 3.5[g,h]

[a]All referring to dilute aqueous solutions at 25°C unless otherwise noted, quantities in parentheses are estimated uncertainties.
[b]$pK_{Enol} = -\log K_{Enol}$; K_{Enol} = [Enol]/[Keto].
[c]This work.
[d]Reference 7.
[e]References 5, 6, 7*b*.
[f]Reference 3.
[g]Reference 2.
[h]Extrapolated to neat liquid.
[i]Reference 1.
[j]Reference 28.
[k]In 40% *tert*-butyl alcohol – water.
[l]Reference 35.

(16) studied a series of cycloalkanones in 90% acetic acid with HCl as catalyst. We have estimated the rate constants for the other cycloalkanones in water from these data assuming that the relative rates in water at 25°C will be the same as in 90% acetic acid at 20°C.

The rate constant for the acid catalyzed enolization of acetophenone was taken from studies at 25°C using 0.053 or 0.109 *M* H_2SO_4 as catalyst (1). Rate constants for ring-substituted acetophenones were calculated from this value assuming that relative rates will be approximately the same as those for a study at 30°C in 1.39 *M* $HClO_4$ (18).

A number of enol ethers have been studied in 80:20 dioxane–water (19–21); these rate constants have been corrected to pure water as solvent by taking advantage of the linear free energy relation between rate constants in dioxane–water and water. This relation can be expressed as

$$\log k_{water} = 1.244 + 0.971 \log k_{dioxane-water}$$

with a correlation coefficient of 0.992. The rate constants upon which the correlation is based, as well as the corrected rate constants for all compounds studied in dioxane–water are found in Table S-II, which has been placed in the Depository for Unpublished Data.[3]

It is of interest to attempt to estimate the enol content for the final group of compounds in Table 1, for which only the rate of hydrolysis for the enol ether is available. For indanone, the observation that acetone and cyclopentanone have very similar rates of enolization suggests that indanone will be very similar to acetophenone, with a rate constant of ca. 10^{-5} M^{-1} s^{-1}. Although there has been no investigation of the enolization of phenylpropanone under conditions where the reaction is unambiguously acid catalyzed reaction of the ketone, an investigation of exchange in acetic acid (22) showed that the methylene position in 1-phenyl-2-propanone exchanged faster than either position in butanone; comparison with rates of acid-catalyzed enolization for butanone in water (23) suggests that the rate constant for phenyl propanone is about 10^{-4} M^{-1} s^{-1}. The rate constant for enolization of the keto tautomer of chloroacetaldehyde can be estimated from the rate constant for acetaldehyde by using the rate ratio for chloroacetone to acetone. The rate constants for acid-catalyzed enolization (in the case of chloroacetone, expressed in terms of the keto form, corrected for hydration) have been measured at 15°C (24, 25). Taking the observed values at $H_0 = 0.0$ as the desired second-order rate constants (in both cases plots of log k_{obs} vs. H_0 are linear with unit slope in this H_0 region), one finds that the rate constants are 1.4×10^{-6} M^{-1} s^{-1} for chloroacetone (24) and

$5.0 \times 10^{-6}\ M^{-1}\ s^{-1}$ for acetone (25). Thus one estimates that the rate constant for enolization of the keto tautomer of chloroacetaldehyde will be ca. $10^{-6}\ M^{-1}\ s^{-1}$; the apparent rate constant would be slower because of the extensive formation of hydrate to be expected: $K_{hydration} = 10$, estimated from ref. 26. The apparent rate constant for enolization of an equilibrium mixture of chloroacetaldehyde and its hydrate would be about $10^{-7}\ M^{-1}\ s^{-1}$.

These estimated rate constants lead to predicted values of pK_{Enol} shown in Table 1; of particular interest are the predictions for 1-phenyl-2-propanone, for which $pK_{Enol} = 4$; chloroacetaldehyde, for which $pK_{Enol} = 2$, although hydration would lead to an apparent value (for K^{app}_{Enol} = [Enol]/([Aldehyde] + [Hydrate])) of $pK^{app}_{Enol} = 3$; and phenylacetaldehyde, for which $pK_{Enol} = 2$. For the closely related 2-phenylpropanal, the enol content in DMSO at 60°C is about 10% (27). Since one expects that the extra methyl group might well favor the enol, this result is not inconsistent with our prediction.

Table 2 compares the results from the application of the 'kinetic method' with those from our thermochemical method and also with the various values reported by other laboratories, using more direct methods. It must be borne in mind that the earlier attempts to use halogen titrations were probably subject to systematic errors (3, 6); furthermore the latest attempts to use halogen titration (3, 28) lead to values which are sometimes in disagreement with expectations based upon the overall chemical behaviour of the systems concerned (9, 10).

For cyclohexanone the agreement with Bell's measured value is good, but for cyclopentanone the agreement is very poor; the discrepancy amounts to two orders of magnitude. Hine and Arata (9, 10) have pointed out that Bell's result for cyclopentanone is inconsistent with a considerable body of information concerning relative behaviour of five- and six-membered ring compounds; one is reluctantly driven to consider the possibility that Bell's result is in error. This is extremely serious since if one of the values reported is in error, the other cannot be trusted entirely and there remains *no* firmly established and directly measured equilibrium constant for enolization of a simple carbonyl compound. For acetone the value which we obtain is consistent with the limit placed by Bell's work. The other recent investigation of the enol content of acetone was by Toullec and Dubois (4, 5), who measured the rate of halogenation of acetone under acidic conditions where tautomerization was rapid and the rate-determining step was reaction of enol with halogen. They concluded that the reaction occurred at the diffusion controlled limit from the identity of the rate constants for chlorine, bromine and iodine. Using a rate constant for diffusion controlled reaction of $1 \times 10^{10}\ M^{-1}\ s^{-1}$ (29) one obtains an equilibrium constant for enolization of 1.5×10^{-9} (7*b*).

This corresponds to a pK_{Enol} of 8.8, which is disturbingly far from the values estimated by our methods. As Dubois and Toullec (5) point out, their value is only approximate, because of uncertainties concerning the appropriate values of the parameters used to estimate the rate of diffusion. It is difficult to estimate the uncertainty in the pK_{Enol} values calculated by the 'kinetic method' but it should be less than 1 pK unit. (Although the reasons for choosing the estimated value for k_{OMe} for 2-methoxypropene continue to seem convincing it should be noted that the value from ref. 13 would give a $pK_{Enol} = 7.5$, in closer agreement with the value of Dubois and Toullec (6).)

Novack and Loudon (28) have reported measurements, in 40% *tert*-butyl alcohol – water, of the enol content of cyclopentanone and acetophenone (28). It is most disturbing that they obtain the same value for cyclopentanone as was reported by Bell and Smith (3), in view of the arguments mentioned above for thinking that this value is out of line with other chemistry of cyclopentanone. For acetophenone the value which Novack and Loudon report is not consistent with the pK_a^{Enol} which they report (28) on the basis of independent experiments studying the aminolysis of enol esters and the value of pK_a^{Keto} which can be derived (7*b*) from Bartlett and Vincent's (30, 31) studies of the rate of chlorination. Consequently we are led to propose that there is some systematic error in the halogenation titration used by Bell and Smith (3) and also by Novack and Loudon (28), which is not associated with trace impurities, although it may be associated with products of reactions induced under the experimental conditions.

The agreement between the 'kinetic method' and the thermochemical method is clearly excellent. Since the two approaches are entirely independent, this agreement tends to increase confidence in both methods.

Conclusions

The 'kinetic method' leads to reliable values of pK_{Enol}, is quite general, and for many simple carbonyl compounds may be the method of choice. It would be exceedingly valuable to have rate constants for the hydrolysis of a greater range of enol ethers, incorporating more of the structural features (halogen, alkyl, aryl, alkoxy, etc., substituents) important in synthetic applications of enolization.

Acknowledgments

I wish to thank the National Research Council of Canada, the Alfred P. Sloan Foundation and the

Academic Development Fund of the University of Western Ontario for financial support of this research.

1. G. SCHWARTZENBACH and C. WITTWER. Helv. Chim. Acta, **30**, 689 (1947).
2. A. GERO. J. Org. Chem. **19**, 1960 (1954).
3. R. P. BELL and P. W. SMITH. J. Chem. Soc. B, 241 (1966).
4. J. TOULLEC and J. E. DUBOIS. Tetrahedron, **29**, 2851 (1973).
5. J. E. DUBOIS and J. TOULLEC. Tetrahedron, **29**, 2859 (1973).
6. J. E. DUBOIS and G. BARBIER. Bull. Soc. Chim. Fr. 682 (1965).
7. (*a*) J. P. GUTHRIE. Can. J. Chem. **57**, 236 (1979); (*b*) J. P. GUTHRIE. Can. J. Chem. In press.
8. G. E. LIENHARD and T. C. WANG. J. Am. Chem. Soc. **91**, 1146 (1969).
9. J. HINE and K. ARATA. Bull. Chem. Soc. Jpn. **49**, 3085 (1976).
10. J. HINE and K. ARATA. Bull. Chem. Soc. Jpn. **49**, 3089 (1976).
11. A. J. KRESGE, D. S. SAGATYS, and H. L. CHEN. J. Am. Chem. Soc. **99**, 7228 (1977).
12. J. HINE. Structural effects on equilibrium in organic chemistry. Wiley, New York, NY. 1975. p. 124.
13. P. SALOMAA, A. KANKAANPERA, and M. LAJUNEN. Acta Chem. Scand. **20**, 1790 (1966).
14. A. J. KRESGE, H. L. CHEN, Y. CHIANG, E. MURRIL, M. A. PAYNE, and D. S. SAGATYS. J. Am. Chem. Soc. **93**, 413 (1971).
15. A. J. TALVIK and S. O. HIIDMAA. Org. React. (Tartu), **5**, 121 (1968).
16. H. SCHECHTER, M. J. COLLIS, R. DESSY, Y. OKUZUMI, and A. CHEN. J. Am. Chem. Soc. **84**, 2905 (1962).
17. L. ZUCKER and L. P. HAMMETT. J. Am. Chem. Soc. **61**, 2791 (1939).
18. S. MISHRA, P. L. NAYALE, and M. K. ROUT. J. Indian Chem. Soc. **46**, 645 (1969).
19. D. M. JONES and N. F. WOOD. J. Chem. Soc. 5400 (1964).
20. T. OKUYAMA, T. FUENO, and J. FURAKAWA. Bull. Chem. Soc. Jpn. **43**, 3256 (1970).
21. T. OKUYAMA, T. FUENO, H. NAKATSUJI, and J. FURUKAWA. J. Am. Chem. Soc. **89**, 5826 (1967).
22. S. MOON and H. BOHM. J. Org. Chem. **37**, 4338 (1972).
23. P. T. MCTIGUE and J. M. SIME. Aust. J. Chem. **20**, 905 (1967).
24. U. L. HALDNA, L. E. J. ERRELINE, and H. J. KUURA. Org. React. (Tartu), **5**, 86 (1968).
25. U. L. HALDNA and H. J. KUURA. Org. React. (Tartu), **4**, 84 (1967).
26. P. GREENZAID, Z. LUZ, and D. SAMUEL. J. Am. Chem. Soc. **89**, 749 (1967).
27. H. ALLBRECHT, W. FUNK, and M. TH. REINER. Tetrahedron, **32**, 479 (1976).
28. M. NOVAK and G. M. LOUDON. J. Org. Chem. **42**, 2494 (1977).
29. M. EIGEN. Angew. Chem. Int. Ed. Engl. **3**, 1 (1964).
30. P. D. BARTLETT and J. R. VINCENT. J. Am. Chem. Soc. **57**, 1596 (1935).
31. P. D. BARTLETT. J. Am. Chem. Soc. **56**, 967 (1934).
32. G. M. LOUDON, C. K. SMITH, and S. E. ZIMMERMAN. J. Am. Chem. Soc. **96**, 465 (1974).
33. Y. CHIANG, W. K. CHWANG, A. J. KRESGE, L. H. ROBINSON, D. S. SAGATYS, and C. I. YOUNG. Can. J. Chem. **56**, 456 (1978).
34. A. J. KRESGE and A. K. CHWANG. J. Am. Chem. Soc. **100**, 1249 (1978).
35. A. GERO. J. Org. Chem. **26**, 3156 (1961).

^{13}C nuclear magnetic resonance studies. 81.[1] Conformational inversion barriers of some *cis*-decalins determined by ^{13}C nuclear magnetic resonance

LOIS M. BROWNE

Department of Chemistry, University of Alberta, Edmonton, Alta., Canada T6G 2N8

AND

R. E. KLINCK[2] AND J. B. STOTHERS

Department of Chemistry, University of Western Ontario, London, Ont., Canada N6A 5B7

Received September 29, 1978

LOIS M. BROWNE, R. E. KLINCK, and J. B. STOTHERS. Can. J. Chem. **57**, 803 (1979).

The ^{13}Cmr spectra of 5β,10β-dimethyldecalin, 10β-decal-5β-ol, and 10β-methyldecal-5β-ol have been examined as a function of temperature to determine the barriers to conformational inversion. Lineshape fitting was employed to extract rate data from which the thermodynamic parameters governing the inversion processes were extracted. Comparison of these results with those obtained by molecular mechanics calculations indicates that the barrier for chair-twist to twist-twist interconversion dominates the conformational inversion profile.

LOIS M. BROWNE, R. E. KLINCK et J. B. STOTHERS. Can. J. Chem. **57**, 803 (1979).

On a déterminé les spectres rmn ^{13}C des diméthyl-5β,10β décaline, 10β-décalol-5β et méthyl-10β décalol-5β en fonction de la température dans le but d'évaluer les barrières à l'inversion conformationnelle. On a utilisé la technique de la superposition des formes des pics pour en tirer les données à partir desquelles on a pu évaluer les paramètres thermodynamiques qui gouvernent les processus d'inversion. Une comparaison de ces résultats avec ceux obtenus grâce à des calculs de mécanique moléculaire indique que la barrière à l'interconversion chaise-croisée à croisée-croisée domine le profil de l'inversion conformationnelle.

[Traduit par le journal]

Introduction

Conformational inversion of the *cis*-decalin ring system [1] has been the subject of several nmr investigations (1–5). Gerig and Roberts (1) used ^{19}Fmr spectra to measure the inversion barriers for a series of 2,2-difluoro substituted *cis*-decalins whereas Altman *et al.* (2) analyzed the ^{1}Hmr spectra of *cis*-decalins bearing $-CH_2R$ substituents at the ring junction to estimate the barriers. More recently, the utility of ^{13}Cmr for such determinations has been demonstrated (3–5). In addition to their barrier determinations Gerig and Roberts (1) carried out potential energy calculations to obtain an energy profile for the inversion process. Their calculations showed the chair-chair (*CC*) conformation to be the preferred ground state, as expected, with the major barrier involving a half-chair-twist ($\frac{1}{2}CT$) form (see Fig. 1). The symmetrical boat-boat (*BB*) conformation was found not to represent a significant barrier to inversion, i.e., $A > B$ in Fig. 1. Because inversion from one *CC* form to the other requires passage through two equivalent $\frac{1}{2}CT$ forms a transmission coefficient (κ) of 0.5 has been used in the Eyring treatment of the rate constants in the more recent studies (3–5).

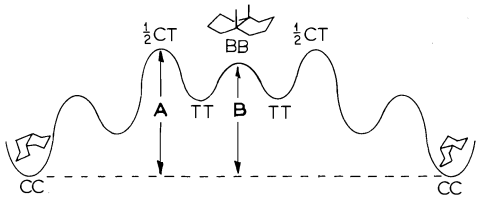

FIG. 1. Energy profile for the conformational inversion of the *cis*-decalin skeleton.

During the study of ^{13}C shieldings in a series of *cis*-decalins, we decided to investigate the inversion barriers for examples with substituents at the ring junction. It was felt that such substitution should increase the energy of the symmetrical *BB* form and in disubstituted derivatives perhaps alter the profile for inversion such that this form constitutes the highest point, i.e., $A < B$ in Fig. 1. If this were the case, a κ value of 0.5 would be inappropriate in the Eyring analysis. To provide a comparison with the observed energy barriers and to obtain an energy profile for the inversion process, molecular mechanics calculations have been examined.

Three substituted *cis*-decalins, 10β-decal-5β-ol (**1***a*), 10β-methyldecal-5β-ol (**1***b*), and 5β,10β-dimethyl-

[1]For Part 80, see ref. 14; Part 79, see ref. 15.

[2]Present address: Adirondack Community College, Glens Falls, New York, NY.

0008-4042/79/070803-04$01.00/0

[1] 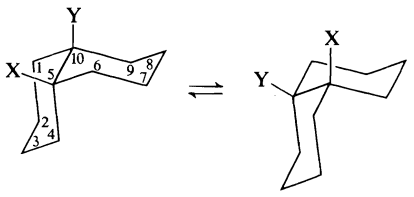

	X	Y
1*a*	OH	H
1*b*	OH	Me
1*c*	Me	Me
1*d*	H	H
1*e*	Me	H

decalin (**1***c*) were chosen for study. Molecular mechanics calculations were also carried out for *cis*-decalin (**1***d*) and its 5β-methyl analog (**1***e*), experimental barriers for which had been determined previously by ^{13}Cmr (4, 5). During the course of this work, inversion parameters were published for **1***b* (5) and these provide an independent check for the present experimental results.

Experimental

Materials

*10β-Decal-5β-ol (**1**a)*

This alcohol, mp 52–56°C, was prepared as described by Huckel *et al.* (6).

*10β-Methyldecal-5β-ol (**1**b)*

A mixture of 4β,5β-epoxy-10β-methyldecal-3-one (0.108 g), prepared by the method of Kuehne and Nelson (7), hydrazine hydrate (0.25 mL), glacial acetic acid (2 drops), and methanol (2 mL) was stirred at room temperature for 2 h. After dilution with water (5 mL), the mixture was extracted with pentane. The pentane extract was washed successively with buffer pH 5, $NaHCO_3$ solution, brine, and dried over $MgSO_4$. The solvent was removed by distillation at atmospheric pressure to give Δ^3-10β-methyldecal-5β-ol (0.086 g, 87% yield). This alcohol had the following properties: ir (neat): 3460, 1655, 940, 910 cm^{-1}; ^{1}Hmr ($CDCl_3$)δ: 1.00 (s, 3H, 10-CH_3), 5.49 (d of t, 1H, J = 1, 5 Hz, 4-H), 5.74 (d of t, 1H, $J \sim 2$, 5 Hz, 3-H); (C_5D_5N)δ: 1.20 (s, 3H, 10-CH_3); *Exact mass* calcd. for $C_{11}H_{18}O$: 166.1358; found (high resolution ms): 166.1354.

This octalol (0.050 g), triethylamine (1 drop), and ether was hydrogenated over 5% Pd/C in a Parr hydrogenator at 40 psi for 1 h. The solution was filtered through a small plug of silica gel and the solvent removed to give **1***b* (0.050 g). Its spectral data agree with those reported (8): ir (neat): 3470 cm^{-1}; ^{1}Hmr ($CDCl_3$)δ: 0.98 (s, 3H, 10-CH_3); (C_5D_5N)δ: 1.11 (s, 3H, 10-CH_3). *Exact mass* calcd. for $C_{11}H_{20}O$: 168.1514; found (high resolution ms): 168.1509.

*5β,10β-Dimethyldecalin (**1**c)*

Methyllithium (0.55 g, 30 mL, 0.7 *M*) was added to a cooled, stirred solution of cuprous iodide (2.48 g) in ether (50 mL). After stirring at 0°C for 10 min, Δ^4-10β-methyldecal-3-one (1.25 g) in ether (20 mL) was added over 30 min. Stirring was continued for 1 h and then the reaction was quenched with saturated NH_4Cl solution. The two-phase system was stirred rapidly for 10 min, filtered *in vacuo*, and the layers separated. The aqueous fraction was extracted with ether (3 × 20 mL) and the combined extracts dried over $MgSO_4$. Removal of the ether afforded 1.0 g of product from which 5β,10β-dimethyldecal-3-one (0.74 g, 54% yield) was isolated by chromatography over silica gel. This material had the following properties: mp 108–120°C (lit. (9) mp 108–118°C); ir (CCl_4): 1715 cm^{-1}; ^{1}Hmr (CCl_4)δ: 0.89 (s, 3H), 1.02 (s, 3H); *Exact mass* calcd. for $C_{12}H_{20}O$: 180.1515; found (high resolution ms): 180.1510.

Reduction of the carbonyl group of this ketone was accomplished using the Huang–Minlon modification of the Wolff–Kishner reaction as described by Ireland *et al.* (10) to yield **1***c* in 54% yield. This hydrocarbon exhibited essentially the same properties as those reported for **1***c* by Ireland *et al.* (10). The observed mp of 55–70°C, however, indicated contamination with a small amount of the *trans* isomer since the melting range is the same as that reported for a similar mixture (10). The ^{13}C spectra of **1***c* confirmed that the compound was >95% pure and the requisite data were readily obtained.

Spectra

Methylene-d_2 chloride employed as the solvent for this study was obtained from Merck, Sharp and Dohme, Canada and used without further purification. Solution concentrations ranged from 5–8 mol%.

The spectra were obtained with a Varian XL 100-15 system equipped with variable temperature accessories and operated in the FT mode using the solvent signal for a lock. Probe temperatures were monitored before and after the collection of each spectrum with a thermocouple placed in a sample tube containing toluene. Temperature measurements should be reliable to ±1°C. Initially spectral widths of 2500 Hz were used to follow the temperature dependence of the spectra from −60 to +100°C, to obtain zero exchange separations and approximate coalescence temperatures and to identify the optimum temperature ranges for the spectra required for complete lineshape analysis. Subsequent spectra were recorded from 0 to 100°C at 10° intervals with smaller steps in the region of coalescences. Spectral widths of 800 Hz (8 K transforms) spanned the signals for exchanging carbons. For lineshape fitting, 100 Hz portions of these spectra were used in conjunction with the EXCHG program to obtain the best fits (11).

The ^{13}C shielding data for these derivatives will be presented and discussed with the results for several other *cis*-decalins in a forthcoming paper.

Molecular Mechanics Calculations

The Allinger MM1 program with the 1973 force field parameters (12) was used to investigate the energy profile for the inversion process. Input coordinates were generated with COORD 4 (13) using 109.5°C for the tetrahedral angle and the following bond lengths: C—C, 1.54 Å; C—H, 1.10 Å; C—O, 1.44 Å; O—H, 0.94 and 0.5 Å for an oxygen lone pair. The energies of the *BB*, *TT*, and ½*CT* forms (see Fig. 1) relative to that of the *CC* conformation were computed. A symmetrical *BB* conformation requires a X—C—C—Y dihedral angle of 0°C. It was necessary to restrict the motion of these atoms to maintain this condition. For **1***c* and **1***d*, this restriction resulted in eclipsing the 2-hydrogens with those on C-3 as well as the 7-hydrogens with those on C-8. For the other, less symmetrical cases, however, eclipsing interactions did not occur about the C-2,-3 and C-7,-8 bonds. Without these restrictions energy

minimization led to structures consistent with twist-twist (*TT*) conformations. A symmetrical *BB* arrangement constitutes an energy maximum between the *TT* forms and less symmetric species of lower energy are probably involved in the actual interconversion between *TT* forms. Thus, the values calculated for barrier *B* represent upper limits. For the $\frac{1}{2}CT$ forms, there are three possible conformers which represent six different cases for **1**, X ≠ Y; each was investigated using input coordinates obtained from the aforementioned bond lengths and typical dihedral angles available from calculations for cyclohexane. Since these forms represent energy maxima, restriction of the motions of certain atoms was necessary to fix the conformation. Initially, the motion of the carbons in the half-chair (C-1,-2,-3,-4,-5 and -10 in $\frac{1}{2}CT$-**1**) were constrained to obtain a first approximation of the energy for each form. Removal of the constraint for C-5 or -10 maintained the $\frac{1}{2}CT$ form but, in most cases, removal of the restrictions on both C-5 and -10 led, after minimization, to inappropriate conformations of much lower energy, for example, to a *TT* form. Although, in principle, all possible $\frac{1}{2}CT$ forms could be attained, the $\frac{1}{2}CT$-**1** conformation is

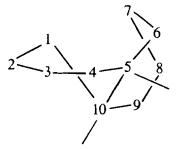

$\frac{1}{2}CT$-**1**

required to proceed to a symmetrical *BB* form and, in general, it was found that this form has the lower calculated energy. The values computed for the $\frac{1}{2}CT$-**1** forms were used in each case for the estimates of barrier *A* in Fig. 1.

Results and Discussion

Rate constants for the inversion process were obtained for all pairs of exchanging carbons in each of **1***a–c*. Because there are significant differences in the coalescence temperatures for the various exchanging nuclei it was possible to cover a wide temperature range without resorting to the use of data only from very fast or very slow exchange rates (4). For each case, from 15 to 27 rate constants were utilized in the Eyring and Arrhenius treatments (see Fig. 2). The results are summarized in Table 1 which includes published data for **1***d* and *e* for comparison. Agreement with recently reported parameters for **1***c* (5) is excellent indicating a negligible solvent effect since the latter data were obtained for the neat liquid. Although the experimental $\Delta H^{\ddagger}$ values for the disubstituted derivatives are greater than those for *cis*-decalin and the mono-

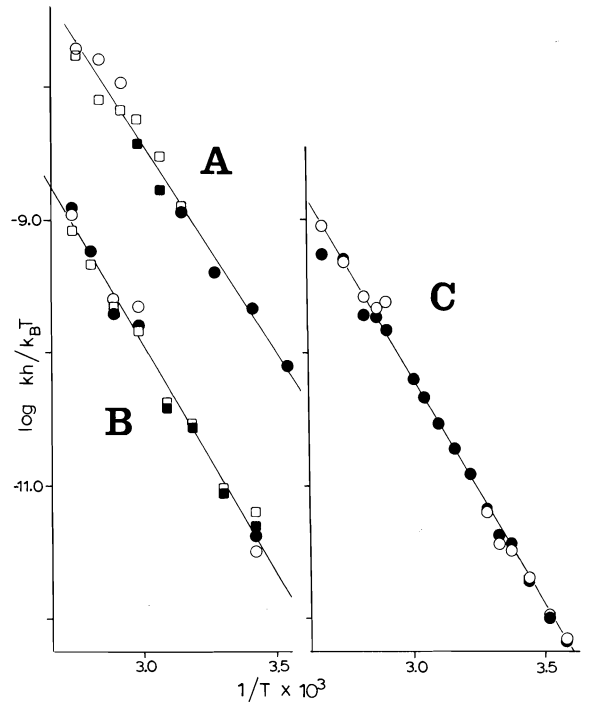

FIG. 2. Eyring plots from the data for the exchanging sites is **1***a* (*A*), **1***b* (*B*), and **1***c* (*C*).

substituted derivatives, no conclusion regarding the relative magnitudes of the barriers *A* and *B* for these cases can be drawn from these results alone. It may be noted that the observed $\Delta S^{\ddagger}$ values do not exhibit a regular variation as had been reported previously (2) for the change from symmetrical to unsymmetrical substitution at the ring junction. The activation energies, E_{act}, for inversion of **1***a–d* are listed for comparison with the results of the molecular mechanics calculations, which are included in Table 1 in terms of the barriers *A* and *B*. For all cases, it was found that $A > B$ indicating that passage through the $\frac{1}{2}CT$ conformation represents the dominant barrier to inversion, in agreement with the original conclusion of Gerig and Roberts (1) for *cis*-decalin itself. It had been suggested (5) that the presence of bulky substituents at both ring junction positions could render $B > A$ because of a greater destabilization of the *BB* form through the eclipsing interaction of these substituents. However, the present results indicate that this is not the case for two methyl groups. For the disubstituted derivatives there is a significant increase in the calculated value for barrier *B* but there is a concomitant increase for barrier *A* involving the $\frac{1}{2}CT$ form. Clearly, destabilizing interactions of the substituents with the ring skeleton are comparable to the eclipsing interactions. For the hydrocarbons reasonable agreement

TABLE 1. Experimental and calculated activation parameters for inversion of *cis*-decalins

Compound No.	X	Y	Experimental results						Calculated barriers (kcal/mol) (see Fig. 1)	
			Ref.	Solvent	$\Delta H^{\ddagger}$ (kcal/mol)	$\Delta S^{\ddagger}$ (eu)	$\Delta G^{\ddagger}_{298}$ (kcal/mol)	E_{act} (kcal/mol)	*A*	*B*
1*d*	H	H	3	Nil	13.6±0.7	3.5±3	12.6	[b]		
			4	CD_2Cl_2	12.4±0.1	0.2±0.4	12.3	12.9±0.1	14.8	8.5
1*e*	Me	H	3	Nil	12.4±0.7	−0.7±3	12.6	[b]	13.1	7.3
1*c*	Me	Me	[a]	CD_2Cl_2	15.6±0.3	1.4±0.8	15.2	16.2±0.3	16.9	10.1
1*a*	OH	H	[a]	CD_2Cl_2	14.1±0.6	4.9±1.8	12.6	14.7±0.6	14.0	7.4
1*b*	OH	Me	5	Nil	15.9±0.3	2.9±1.2	15.0	16.7±0.2		
			[a]	CD_2Cl_2	15.7±0.4	3.0±1.3	14.8	16.4±0.4	12.1	6.9

NOTE: Errors shown are standard deviations obtained from the least-squares analysis.
[a]Present study.
[b]Not reported.

is observed between the calculated values for barrier *A* and the experimental E_{act} values with the calculated results tending to be somewhat greater. A comparison of the energies for the same conformation for the three hydrocarbons indicates that the major effect of methyl substitution is to alter the bending and compression contributions to the total strain energy. This is consistent with the finding that skeletal changes in the ring system resulting from methyl substitution dominate the energy profile rather than the eclipsing interactions in the *BB* forms.

Since the force field parameters for hetero atoms are not so well refined as those for carbon and hydrogen, agreement between calculated and experimental inversion barriers cannot be expected to be as good for the decalols as found for the hydrocarbons. The strain energies for the various decalol conformers seem to differ but slightly from those for the hydrocarbons indicating that the parameters for oxygen are inadequate. In contrast to the findings for the hydrocarbons, the major differences for the decalols appear to arise from contributions calculated for the van der Waals interactions. In any event, the general tendency is the same, namely, $A > B$ for the two decalols.

Since, in each case, the difference between the calculated values for the two barriers is at least 5 kcal/mol, one can conclude that passage through the $\frac{1}{2}CT$ conformation represents the dominant barrier to conformational inversion in each of these systems. Thus, a transmission coefficient of 0.5 is required for the Eyring treatment of the rate data. It remains to be established whether bulkier substituents can render the *BB* form dominant in the energy profile.

Acknowledgements

We are grateful to the National Research Council of Canada for financial support of this work and to Ms. Marlene Brown and Ms. Cheryl DuCharme for technical assistance.

1. J. T. GERIG and J. D. ROBERTS. J. Am. Chem. Soc. **88**, 2791 (1966).
2. J. ALTMAN, H. GILBOA, D. GINSBURG, and A. LOEWENSTEIN. Tetrahedron Lett. 1329 (1967).
3. D. K. DALLING, D. M. GRANT, and L. F. JOHNSON. J. Am. Chem. Soc. **93**, 3678 (1971).
4. B. E. MANN. J. Magn. Reson. **21**, 17 (1976).
5. J. W. BLUNT, J. M. COXON, N. B. LINDLEY, and G. A. LANE. Aust. J. Chem. **29**, 967 (1976).
6. W. HUCKEL, D. MAUCHER, O. FECHTIG, J. KURZ, M. HEINZEL, and A. HUBELE. Justus Liebigs Ann. Chem. **645**, 115 (1961).
7. M. E. KUEHNE and J. A. NELSON. J. Org. Chem. **35**, 161 (1970).
8. J. A. MARSHALL and A. R. HOCHSTETTER. J. Org. Chem. **31**, 1020 (1966).
9. J. A. MARSHALL, W. I. FANTA, and H. ROEBKE. J. Org. Chem. **31**, 1016 (1966).
10. R. E. IRELAND, M. I. DAWSON, C. J. KOWALSKI, C. A. LIPINSKI, D. A. MARSHALL, J. W. TILLEY, J. BORDNER, and B. L. TRUS. J. Org. Chem. **40**, 973 (1975).
11. R. E. KLINCK and J. B. STOTHERS. Can. J. Chem. **54**, 3267 (1976).
12. N. L. ALLINGER, M. T. TRIBBLE, M. A. MILLER, and D. H. WERTZ. J. Am. Chem. Soc. **93**, 1637 (1971); D. H. WERTZ and N. L. ALLINGER. Tetrahedron, **30**, 1579 (1974).
13. M. J. S. DEWAR and N. C. BAIRD. COORD program 136, QCPE Indiana University, Bloomington, IN.
14. R. B. KELLY, S. J. ALWARD, K. S. MURTY, and J. B. STOTHERS. Can. J. Chem. **56**, 2508 (1978).
15. A. STOESSL and J. B. STOTHERS. Can. J. Bot. **56**, 2589 (1978).

Spin–spin coupling constants between side-chain and ring fluorine nuclei in some benzotrifluoride, benzal fluoride, and benzyl fluoride derivatives: coupling mechanisms

TED SCHAEFER, WALTER NIEMCZURA, CHIU-MING WONG, AND KIRK MARAT

Department of Chemistry, University of Manitoba, Winnipeg, Man., Canada R3T 2N2

Received September 27, 1978

TED SCHAEFER, WALTER NIEMCZURA, CHIU-MING WONG, and KIRK MARAT. Can. J. Chem. **57**, 807 (1979).

A complete analysis of the ^1H and ^{19}F nmr spectra of 2,5- and 3,4-difluorobenzotrifluoride, together with multiple resonance experiments, yields the signs and magnitudes of the long-range $^{19}F,^{19}F$ and $^1H,^{19}F$ spin–spin coupling constants. The coupling mechanisms are discussed. In particular, the coupling over six bonds, $^6J_p^{F,CF_3}$, whose sign is interpretable in terms of a σ–π mechanism, is too large in magnitude when compared to $^6J_p^{H,CH_3}$, $^6J_p^{F,CH_3}$, and $^6J_p^{H,CF_3}$ in the analogous compounds. These latter three couplings are consistent in sign and magnitude with what is known about hyperfine interaction constants. The magnitudes of $^6J_p^{F,CF_3}$ are reported for 4-fluorobenzotrifluoride, 3-amino-4-fluorobenzotrifluoride, 3-nitro-4-fluorobenzotrifluoride, as are $^6J_p^{F,F}$ values for *p*-fluorobenzal fluoride and *p*-fluorobenzyl fluoride. In contrast to $^6J_p^{H,CH}$ and $^6J_p^{F,CH}$, it seems unlikely that, unless its coupling mechanism becomes more precisely understood, $^6J_p^{F,CF}$ will be a reliable indicator of conformational preferences.

TED SCHAEFER, WALTER NIEMCZURA, CHIU-MING WONG et KIRK MARAT. Can. J. Chem. **57**, 807 (1979).

Une analyse complète des spectres rmn du ^1H et du ^{19}F des difluoro-2,5 (et 3,4) benzotrifluorures, de concert avec des expériences de résonance multiple, permet de déterminer les signes et les amplitudes des constantes de couplage spin–spin $^{19}F,^{19}F$ et $^1H,^{19}F$ à longue distance. En particulier l'amplitude du couplage à travers six liaisons, $^6J_p^{F,CF_3}$, dont on peut interpréter le signe en termes d'un mécanisme σ–π, est trop grande comparée aux $^6J_p^{H,CH_3}$, $^6J_p^{F,CH_3}$ et $^6J_p^{H,CF_3}$ observées dans les composés semblables. Les trois derniers couplages sont en accord, tant en ce qui a trait au signe qu'à l'amplitude, avec ce qui est connu concernant les constantes d'interactions hyperfines. On rapporte les amplitudes des $^6J_p^{F,CF_3}$ des fluoro-4, amino-3 fluoro-4 et nitro-3 fluoro-4 benzotrifluorures de même que les $^6J_p^{F,F}$ des fluorures de *p*-fluorobenzal et de *p*-fluorobenzyle. Par opposition aux $^6J_p^{H,CH}$ et $^6J_p^{F,CH}$, il est peu probable, que les $^6J_p^{F,CF}$ puissent êtres utilisés comme indicateurs surs des préférences conformationnelles à moins qu'on arrive à une meilleure compréhension de leur mécanisme de couplage.

[Traduit par le journal]

Introduction

The σ–π electron contributions to the long-range spin–spin coupling constants over four, five, and six bonds, $J_{o,m,p}^{H,CH_3}$ and $J_{o,m,p}^{F,CH_3}$, in toluene derivatives have been discussed in some detail (1–12). In addition to their intrinsic interest as indicators of electronic structure, some of these couplings are useful in the determination of conformational preferences and, indeed, of internal barriers to rotation in benzene derivatives (13–16).

On the other hand, the signs and magnitudes of $J_{o,m,p}^{F,CF_3}$ in benzotrifluoride derivatives have been less thoroughly investigated (17–23). This paper briefly reports on these parameters for 2,5-difluorobenzotrifluoride, (**1**) and for 3,4-difluorobenzotrifluoride (**2**).

In addition some spectral parameters, useful in the discussion of **1** and **2**, are given for *p*-trifluoromethylbenzotrifluoride and 3-nitro-4-methylbenzotrifluoride; for *p*-fluorobenzotrifluoride and its

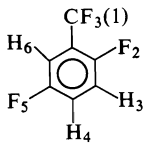

1

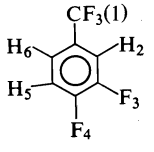

2

3-amino and 3-nitro derivatives; and for *p*-fluorobenzal fluoride and *p*-fluorobenzyl fluoride.

Experimental

The preparation of **1** involved repeated nitration and diazotization of benzotrifluoride whereas that of **2** necessitated a diazotization of 3-amino-4-fluorobenzotrifluoride (Pierce Chemical Co.). The details of the syntheses are in ref. 24*a*.

The preparation of 3-nitro-4-methylbenzotrifluoride involved 10 g of the benzoic acid (Aldrich Chemical Co.) and 26.7 g of SF_4, heated to 150°C/12 h in a 150 mL steel cylinder. The product, 6 g, 29% yield, distilled at 178°C/100 Torr.

The *p*-fluorobenzal fluoride was prepared from 1.1 g of the aldehyde (Pierce Chemical Co.) and 3.8 g of SF_4 by heating in a 75 mL steel cylinder, 125°C/17 h. The product was trap-to-trap distilled. No boiling point was determined but the ^1H nmr

0008-4042/79/070807-06$01.00/0

TABLE 1. ^1H and ^{19}F spectral parameters for 2,5- and 3,4-difluorobenzotrifluoride

	2,5-Difluorobenzotrifluoride[a]		3,4-Difluorobenzotrifluoride[b]	
Parameter[c,d]	100.001 MHz[e]	56.443 MHz[f]	100.001 MHz[e]	56.443 MHz[f]
ν_1	—	1108.5 (2)	—	1072.8 (2)
ν_2		−2176.52 (15)	719.39 (2)	—
ν_3	681.68 (4)[g]	—	—	−3019.57 (2)
ν_4	688.13 (4)	—	—	−2852.42 (2)
ν_5	—	−1991.34 (2)	686.51 (2)	—
ν_6	710.11 (4)	—	707.89 (2)	—
$^4J_{12}$	—	13.10 (2)	−0.61 (3)	—
$^5J_{13}$	0.74 (3)	—	—	0.82 (1)
$^6J_{14}$	−0.62 (3)	—	—	1.89 (2)
$^5J_{15}$	—	0.56 (2)	0.86 (3)	—
$^4J_{16}$	−0.59 (2)	—	−0.76 (3)	—
$^3J_{23}$	9.49 (7)	9.53 (6)	10.13 (5)	10.13 (3)
$^4J_{24}$	3.70 (7)	3.67 (6)	7.22 (5)	7.20 (3)
$^5J_{25}$	—	17.91 (2)	0.33 (4)	—
$^4J_{26}$	5.46 (3)	5.41 (3)	2.27 (3)	—
$^3J_{34}$	9.09 (4)	—	—	−20.30 (2)
$^4J_{35}$	4.11 (6)	4.13 (5)	7.63 (4)	7.64 (3)
$^5J_{36}$	0.36 (4)	—	−1.59 (5)	−1.59 (4)
$^3J_{45}$	7.48 (7)	7.44 (5)	9.80 (4)	9.83 (4)
$^4J_{46}$	3.21 (4)	—	4.04 (5)	4.03 (3)
$^3J_{56}$	7.94 (3)	7.92 (3)	8.65 (4)	—
Root-mean-square error	0.031	0.031	0.038	0.030
Peaks assigned	202	184	220	191
Peaks calculated[h]	278	239	302	255

[a]50 vol% in benzene-d_6 and 5 vol% TMS and 5 vol% CF_3CCl_3.
[b]30 vol% in benzene-d_6 and others as in footnote *a*.
[c]The proton shifts are given in Hz relative to internal TMS at 305 K for 100 MHz spectra.
[d]The ^{19}F shifts are given in Hz relative to internal CF_3CCl_3 at 301 K for 56.4 MHz spectra. Negative values are to high field of reference.
[e]Analysis of 100 MHz ^1H nmr spectra.
[f]Analysis of 56.4 MHz ^{19}F nmr spectra.
[g]Numbers in parentheses are equal to 5× standard deviation in the last significant figure.
[h]Counting those transitions whose relative intensities were greater than 0.05.

spectrum gave the characteristic triplet components for the side-chain proton ($^2J^{H,F} = 56.4$ Hz).

The *p*-fluorobenzyl fluoride was prepared in a similar way from *p*-fluorobenzyl alcohol (Aldrich Chemical Co.) and gave the characteristic doublet components for the side-chain protons in the ^1H nmr spectrum. The physical properties of a series of benzyl fluoride derivatives, including the *p*-fluoro compound, have been described (24*b*).

Degassed samples of **1** and **2** in benzene-d_6 (details in footnotes to Table 1) had their ^1H nmr and ^{19}F nmr spectra calibrated on HA100 and DA60I spectrometers, respectively. Calibration markers, obtained by reading sweep and manual oscillator frequencies, were placed at 2 to 5 Hz intervals. Repeated calibrations were performed in the *frequency sweep mode* at spectral dispersions of 1 and/or 2 Hz/cm and at sweep rates of 0.02 and 0.01 Hz/s. Probe temperatures were determined by means of a thermocouple.

Weak irradiation experiments (25) on the ^{19}F nmr spectra were performed in the usual manner.

The ^1H nmr spectrum at 100 MHz of a 20 vol% solution of 3-nitro-4-methylbenzotrifluoride was also recorded and calibrated in the manner described above; 50 vol% solutions in C_6D_6 of all other compounds contained internal CF_3CCl_3 and TMS. Degassed samples were used to record and calibrate ^1H nmr and ^{19}F nmr spectra as described for **1** and **2**. An exception was *p*-trifluoromethylbenzotrifluoride (Chemical Procurements Co.) which was used as 95 vol% solution in CF_3CCl_3.

INDO MO FPT calculations (26) were performed on an IBM 370/158 system, using standard geometries (27).

Results and Discussions

Spectral Analysis of 1 and 2

These were performed with the computer program LAME (28, 29). The ^1H nmr spectra at 100 MHz were analyzed first. The parameters obtained in this way were used in an iterative analysis of the ^{19}F spectra at 56.4 MHz. The spectral parameters from the latter analysis were again used in an iterative analysis of the ^1H spectra. The final parameters satisfactorily reproduced the 60 MHz ^1H nmr spectra of **1**.

The spectral parameters are found in Table 1. Good agreement between the parameter sets is evident; the numbers in parentheses are *five* times the standard deviations. Iterations were not performed on the peaks from the CF_3 groups, severe overlap of peaks yielding ambiguities in their

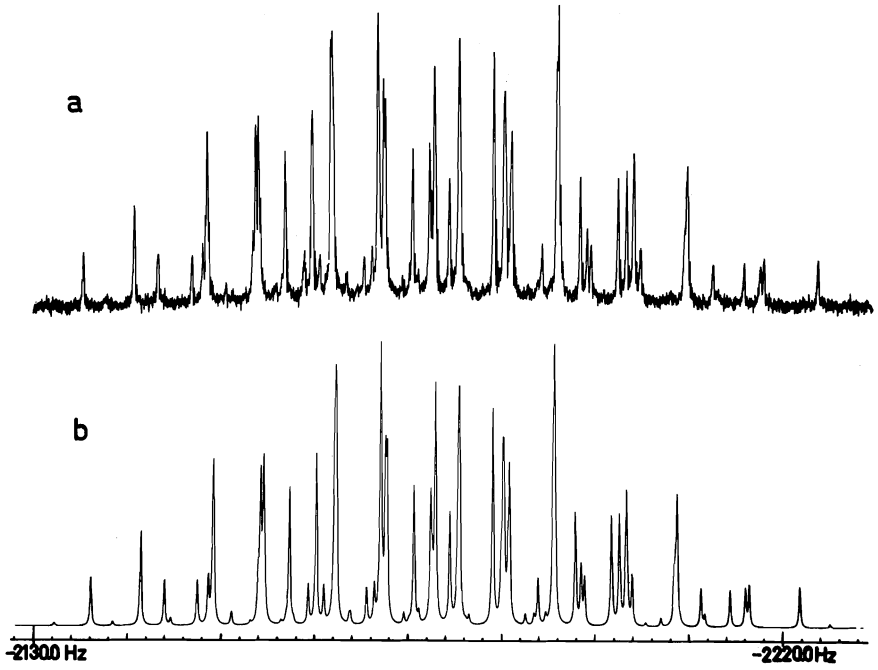

FIG. 1. The ^{19}F nmr spectrum of F-2 in 2,5-difluorobenzotrifluoride, **1**, observed at 56.44 MHz at 30 K for a 50 vol% solution in benzene-d_6 is shown in *a*. In *b* the calculated spectrum is displayed, employing the parameters in Table 1. The scale refers to frequencies to high field of the internal lock, CF_3CCl_3.

frequencies. However, the calculated spectra for these groups bore every resemblance to the observed spectra.

Figure 1 gives an example of observed and calculated ^{19}F nmr spectra, those of F-2 in **1**. Figure 2 displays the ^{19}F spectrum of the CF_3 group of **1**.

Relative Sign Determinations in 1 and 2

Sutcliffe and co-workers (20, 23) have given a series of detailed descriptions of double resonance experiments designed to determine the signs of $^{19}F,^{19}F$ coupling constants in fluoroaromatic compounds. Our experiments are very similar and will not be described in detail; complete descriptions can be found in ref. 24*a*. In particular, the present series of double irradiations showed that $^4J_o^{F,CF_3}/^5J_p^{F,F} > 0$, $^4J_o^{F,CF_3}/^5J_m^{F,CF_3} > 0$, $^6J_p^{F,CF_3}/^3J_o^{F,F} < 0$, $^5J_m^{F,CF_3}/J_o^{F,F} < 0$, $^5J_m^{F,CF_3}/^6J_p^{F,CF_3} > 0$, $^4J_m^{H,F}/^5J_p^{H,F} < 0$. As, invariably (30), $^5J_p^{F,F} > 0$, $^3J_o^{F,F} < 0$, $^4J_m^{H,F} > 0$, the signs in Table 1 follow.

A number of the double resonance spectra were calculated by the computer program DOR (31), modified to accommodate eight nuclei. Good agreement with experimental spectra was found.

The Spectral Analysis of p-*Fluorobenzal Fluoride*

In the ^1H nmr spectrum at 100 MHz, 288 transitions were assigned, leading to a root-mean-square

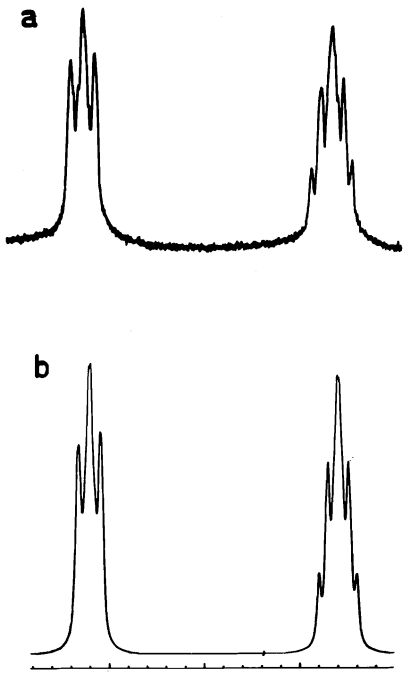

FIG. 2. The observed, *a*, and calculated, *b*, ^{19}F nmr spectrum of the CF_3 group in **1** (see Fig. 1). Each small division on the scale represents 1 Hz. The midpoint of the spectrum falls at 1108.5 Hz to low field of internal CF_3CCl_3.

deviation of 0.02 Hz between calculated and observed peaks. However, there exist three correlation coefficients greater than 0.5 in this analysis. There were also some curious intensity anomalies, which could not be removed despite considerable effort, suggesting unknown errors in at least some of the parameters. Consequently, the spectral parameters are not tabulated here.

However, the ^{19}F nmr spectrum did yield $^{6}J_{p}^{F,CF_2}$ as $\pm 3.45 \pm 0.05$ Hz, certain, even though the ring ^{19}F peaks overlapped one of the two bands ($^{2}J^{H,F} = 56.4$ Hz) from the CF_2H group. Because benzal fluoride itself has been satisfactorily analyzed (32), the analysis of *p*-fluorobenzal fluoride was terminated at this stage.

The ^{19}F spectrum of *p*-fluorobenzyl fluoride yielded $^{6}J_{p}^{F,F}$ as $\pm 5.8 \pm 0.2$ Hz.

$^{7}J_{p}^{CH_3,CF_3}$ *in 3-Nitro-4-methylbenzotrifluoride*

A full analysis was not made and attempts to determine the sign of $^{7}J^{CH_3,CF_3}$ were unsuccessful. However, a partial analysis indicates that this coupling is $\pm 0.76 \pm 0.05$ Hz, assumed positive.

$^{6}J_{p}^{F,CF_3}$ *in* p-*Fluorobenzotrifluoride and its 3-Amino and 3-Nitro Derivatives*

Again, the spectra were not fully analyzed. However, it was clear that $^{6}J_{p}^{F,CF_3}$ had the values given in Table 2, where the ^{19}F chemical shifts are also found.

$^{7}J^{CF_3,CF_3}$ *in* p-*Trifluoromethylbenzotrifluoride*

Because $^{4}J_{o}^{H,CF_3}$ and $^{5}J_{m}^{H,CF_3}$ are nearly of the same magnitude but of opposite sign (33), the ^{13}C side bands in the ^{19}F nmr spectrum at 56.4 MHz are (somewhat distorted) quartets arising from long-range $^{19}F,^{19}F$ coupling. $^{7}J_{p}^{CF_3,CF_3}$ is 0.85 ± 0.05 Hz, very likely positive. $^{1}J^{^{13}C,\,^{19}F}$ is 271.9 ± 0.4 Hz in magnitude, close to the literature value (34). The ^{19}F chemical shift is 1012 Hz (17.93 ppm) to low field of CF_3CCl_3.

The ^{19}F *Chemical Shifts*

If the ^{19}F shift in fluorobenzene is taken as 31.0 ppm to high field of CF_3CCl_3 and that in $C_6H_5CF_3$ is 18.4 ppm to low field of CF_3CCl_3(35), then the observed shifts in Table 2 are compatible with known substituent perturbations (35). The ring ^{19}F shifts in **1** agree closely with earlier observations (36). Although the chemical shifts in the ring follow the common substituent effects, in that electron donating substituents cause increased shielding, the ^{19}F shifts of the CF_3 group display the opposite trend (36, 37). A similar but more marked substituent dependence for the CH_2F group has been discussed periodically, if not explained (38–40).

The CF_2H group displays a shift similar to that of ring fluorine nuclei (Table 2) and this can lead to overlapping bands.

TABLE 2. Fluorine chemical shifts[a] in ppm relative to internal CF_3CCl_3 and $^{19}F,^{19}F$ coupling constants over six or seven bonds

Compound[b]	Ring F	CF_3	$^{6,7}J$
4-F, 1-CF_3	−26.13	19.45	1.97 (2)
4-F, 3-NO_2, 1-CF_3	−30.63	18.84	1.67 (4)
4-F, 3-NH_2, 1-CF_3	−49.63	19.53	1.96 (2)
2,5-diF, 1-CF_3	−38.56 (F-2) −35.28 (F-5)	19.64	—
3,4-diF, 1-CF_3	−53.50 (F-3) −50.54 (F-4)	19.01	+1.89 (2)
1,4-diCF_3[c]	—	17.93	0.80 (5)
4-F, 1-CF_2H	−28.22	−27.72[d]	3.45 (5)
4-F, 1-CFH_2	—	−126.3[d]	5.8 (2)[e]

[a]A negative sign indicates a shift to high field of CF_3CCl_3.
[b]50 vol% in benzene-d_6, containing also 5 vol% TMS and 5 vol% CF_3CCl_3.
[c]95 vol% in CF_3CCl_3.
[d]Shift of the CF_2H group or of the CFH_2 group.
[e]Coupling constants are in Hz, the uncertainty in the last place being given in parentheses.

The Coupling Constants Within the Ring

There are no exceptional magnitudes of these couplings and the reader is referred to refs. 41–43 for full discussions.

Long-range $^{19}F,C^{19}F_3$ *Couplings*

Over Six Bonds, $^{6}J_{p}^{F,CF_3}$

$^{6}J_{p}^{F,CF_3}$ is +1.89 Hz in **2**; tentatively, and now very likely, +1.33 Hz in perfluorotoluene (23). This coupling equals ± 1.97 Hz in 4-fluorobenzotrifluoride, ± 1.96 Hz in the 3-amino derivative, and sinks to ± 1.67 Hz in the 3-nitro derivative. In view of the known sign for **1**, these couplings are very likely positive. The following observations are pertinent.

In contrast to $^{6}J_{p}^{H,CH_3} = -0.62$ Hz and $^{6}J_{p}^{F,CH_3} = 1.12$ Hz in toluene (8) and *p*-fluorotoluene (15), respectively, it seems unlikely that $^{6}J_{p}^{F,CF_3}$ can be interpreted in terms of a *simple* σ–π mechanism (2). For such a mechanism, $J_{p}^{H,CH_3} \propto Q_{CF}Q_{CCH}$, where the Q parameters are hyperfine interaction constants between an electron in an aromatic π orbital and the proton or fluorine nucleus. $Q_{CF} > 0$ (44) and an appropriate value is 41.1 G, derived from nickel(II) aminotroponeimineate derivatives in which a small spin density is delocalized into the *p*-fluorophenyl groups (45). Q_{CH} is −22.5 G, so that $^{6}J_{p}^{H,CH_3}/^{6}J_{p}^{F,CH_3} = -0.62/1.12 = -0.55 = -22.5/41.1$, as expected for a σ–π coupling mechanism.

However, $^{6}J_{p}^{H,CF_3}$ in benzotrifluoride is −0.64 Hz (32) and, if this coupling is also dominated by a σ–π mechanism, it follows that $^{6}J_{p}^{F,CF_3}$ in *p*-fluorobenzotrifluoride should equal $-0.64(41.1/-22.5)$ or 1.17 Hz. Yet its value is 1.97 Hz. It is tempting to attribute this result to a large increase in Q_{CF} relative to

p-fluorotoluene and to argue that the reduction to 1.67 Hz in 3-nitro-4-fluorobenzotrifluoride is caused by a polarization of the C—F bond by the *ortho* nitro group. Because Q_{CF} is a composite term, dependent on the extension of the π-electron system to the fluorine atom (44), such an interpretation has its attraction.

It is then difficult to account for the very small changes (10% or less) in $^6J_p^{F,CH_3}$ observed in *p*-fluorotoluene (2, 15), 2-fluoro-5-methylpyridine (3), 5-fluoro-2-methylpyridine (3), and in some *p*-fluorotoluene derivatives (2), these results being consistent with very minor changes in Q_{CF} (Q_{CH} is also largely substituent independent, $^6J_p^{H,CH_3}$ being invariant in toluene (8), tetrachlorotoluene (11), and some polynitrotoluenes (12)).

On the other hand, $^6J_p^{F,CF_3}$ is rather insensitive to amino or fluoro substituents placed *ortho* to the C—F bond (Table 2).

INDO MO FPT calculations of the type previously described for toluene (5) and benzotrifluoride (46) gave a $\sin^2\theta$ dependence for $^6J_p^{F,CF_3}$ (θ is the angle by which the exocyclic C—H or C—F bond twists out of the benzene plane), thereby implying a σ–π mechanism. Because the barrier to internal rotation in benzotrifluoride is only 0.010 kcal/mol (47), the average value of $\sin^2\theta$ is 0.5. The calculations yield $^6J_p^{F,CF_3}$ as 2.8 Hz, an overestimate probably attributable to the parameters employed for the CF_3 group (46).

That a σ–π mechanism is at least partially operative, is supported by our observations of $^6J_p^{F,CF}$ as $\pm 3.45 \pm 0.05$ and $\pm 5.8 \pm 0.2$ Hz, respectively, in *p*-fluorobenzal fluoride and *p*-fluorobenzyl fluoride. The decrease in magnitude of $^6J_p^{F,CF}$ on successive substitution to CH_2F, CHF_2, and CF_3 groups is expected if the group orbitals become successively lower in energy and interact to a lesser degree with the π electron system (48, 49).

Returning to Q_{CCF}, it is interesting that $^6J_p^{H,CF_3}$ is −0.62 Hz in **1** and is −0.64 Hz in benzotrifluoride, i.e., the same as $^6J_p^{H,CH_3}$ in toluene; suggesting that $Q_{CCF} \sim Q_{CCH}$ if $^6J_p^{H,CF_3}$ is due solely to a σ–π mechanism. One test of this mechanism involves the very reasonable assumption that coupling constants over seven bonds arise from a σ–π mechanism. $^7J_p^{CH_3,CF_3}$ is 0.76 ± 0.05 Hz in 3-nitro-4-methylbenzotrifluoride, implying a positive σ electron contribution[1] of +0.1 to +0.2 Hz to $^6J_p^{H,CF_3}$.

A further test involves the 0.85 ± 0.05 Hz measured for $^7J^{CF_3,CF_3}$ in 4-trifluoromethylbenzotrifluoride. These results indicate $Q_{CCF}/Q_{CCH} \sim 0.85/0.76 = 1.1 \pm 0.1$, close to the ratio of unity derived for the neutral $CF_3CH_2\cdot$ and $CH_3CH_2\cdot$ radicals (51, 52). It appears that $^6J_p^{H,CF_3}$ contains a σ electron component of 0.15 ± 0.05 Hz.

In consequence, it seems that the large value of $^6J_p^{F,CF_3}$ in *p*-fluorobenzotrifluoride could be attributed to a large σ electron component of $+0.7 \pm 0.1$ Hz present only in the F,CF_3 combination; a rather unsatisfactory situation.

In summary, whereas $^6J_p^{H,CH_3}$ and $^6J_p^{F,CH_3}$ are interpretable in terms of a simple σ–π electron coupling mechanism, which is rather insensitive to ring substitution, $^6J_p^{F,CF_3}$ is larger than expected in *p*-fluorobenzotrifluoride on this basis and displays a peculiar substituent dependence. The successful use of $^6J_p^{F,CF}$ in aromatic compounds in the derivation of preferred conformations and of internal rotation barriers (50) is therefore unlikely.

Over Five Bonds, $^5J_m^{F,CF_3}$

In toluene (5) and 3-fluorotoluene (10), $^5J_m^{H,CH_3}$ and $^5J_m^{F,CH_3}$ can be interpreted as composites of σ and σ–π electron coupling mechanisms. The σ contributions are positive. The σ–π contribution to $^5J_m^{H,CH_3}$ is also positive because, although Q_{CH} and Q_{CCH} are of opposite sign, the induced π electron spin density at C-3 is negative (a result of electron correlation, the spin densities at C-2 and C-4 being positive), as discussed previously (10). On the other hand, the σ–π contribution to $^5J_m^{F,CH_3}$ is negative because Q_{CF} and Q_{CCH} have the same sign, positive, and this contribution outweighs the σ electron component, resulting in a negative $^5J_m^{F,CH_3}$.

In **1** and **2**, respectively, $^5J_m^{F,CF_3}$ is 0.56 and 0.86 Hz. By analogy to $^5J_m^{F,CH_3}$ and noting that Q_{CF} and Q_{CCF} are both positive, it follows that the negative σ–π electron component is outweighed by a positive σ contribution. INDO MO FPT calculations on $^5J_m^{F,CH_3}$ in 3-fluorotoluene reproduce the model behaviour very well (10), predicting substantial negative values at $\theta = 90°$ and large positive values as θ approaches 180° (all-*trans* conformation). Similar calculations on **1** and **2** show the same qualitative behaviour[2] (the plots are entirely similar to that in Fig. 3 of ref. 10) and suggest that the two-component model is adequate.

In perfluorotoluene (23), $^5J_m^{F,CF_3}$ is +0.62 Hz, implying that substituent perturbations will not change the sign of this coupling constant.

Over Four Bonds, $^4J_o^{F,CF_3}$

This coupling of 13.1 Hz in **1** is an example of a 'through-space' coupling, discussed in detail by Sutcliffe and co-workers (21, 23). They point out that its attribution to a predominant Fermi contact mechanism (53) is unsatisfactory. We note here that

[1]A σ electron contribution of +0.3 Hz to $^6J_p^{H,CF_2}$ in benzal fluoride is indicated (50) by this methyl group replacement technique (4).

[2]Details are given in ref. (24*a*), where calculations on $^6J_p^{F,CF_3}$ and $^4J_o^{F,CF_3}$ are also tabulated.

our INDO MO FPT calculations confirm their criticism, the calculated average coupling being of the same magnitude as ${}^6J_p^{F,CF_3}$ with a maximum at $\theta = 90°$. In other words, the Fermi contact contribution is calculated by INDO MO FPT to have a large σ–π component.

Conclusions

The long-range coupling constants over six bonds between methyl protons and *para* ring protons or fluorine nuclei in toluene and *p*-fluorotoluene, and perhaps between fluorine nuclei and ring protons in benzotrifluoride, are satisfactorily interpreted in terms of a σ–π electron coupling mechanism in which $Q_{CH} > 0$, $Q_{CCH} \sim Q_{CCF} > 0$, and $Q_{CF} > 0$. By way of contrast, the corresponding six-bond coupling between fluorine nuclei in *p*-fluorobenzotrifluoride, although of the sign expected for a σ–π mechanism, is much too large to be consistent with the other six-bond couplings. The six-bond fluorine–fluorine coupling constants involving CR_2F and CRF_2 groups are unlikely to be very reliable conformational indicators.

Acknowledgments

We are grateful to the National Research Council of Canada for financial assistance.

1. (*a*) D. J. Blears, S. S. Danyluk, and T. Schaefer. J. Chem. Phys. **47**, 5037 (1967); (*b*) K. D. Bartle, D. W. Jones, and R. S. Matthews. Rev. Pure Appl. Chem. **19**, 191 (1969).
2. R. Wasylishen and T. Schaefer. Can. J. Chem. **49**, 94 (1971).
3. J. B. Rowbotham and T. Schaefer. Can. J. Chem. **50**, 2344 (1972).
4. R. Hoffman and S. Gronowitz. Ark. Kemi, **16**, 471 (1960).
5. R. Wasylishen and T. Schaefer. Can. J. Chem. **50**, 1852 (1972).
6. J. B. Rowbotham and T. Schaefer. Can. J. Chem. **52**, 489 (1974).
7. C. J. Macdonald and W. F. Reynolds. Can. J. Chem. **48**, 1002 (1970).
8. M. P. Williamson, R. Kostelnik, and S. M. Castellano. J. Chem. Phys. **49**, 2218 (1968).
9. (*a*) M. Barfield and B. Chakrabarti. Chem. Rev. **69**, 757 (1969); (*b*) M. Barfield, R. J. Spear, and S. Sternhell. Chem. Rev. **76**, 593 (1976).
10. T. Schaefer, W. Danchura, and W. Niemczura. Can. J. Chem. **56**, 2233 (1978).
11. H. Rottendorf and S. Sternhell. Aust. J. Chem. **17**, 1315 (1964).
12. D. G. Gehring and G. S. Reddy. Anal. Chem. **40**, 792 (1968).
13. T. Schaefer, W. J. E. Parr, and W. Danchura. J. Magn. Reson. **25**, 167 (1977).
14. W. J. E. Parr and T. Schaefer. J. Am. Chem.Soc. **99**, 1033 (1977).
15. T. Schaefer, W. Danchura, and W. Niemczura. Can. J. Chem. **56**, 2229 (1978).
16. T. Schaefer, W. Danchura, W. Niemczura, and J. Peeling. Can. J. Chem. **56**, 2442 (1978).
17. R. E. Richards and T. Schaefer. Trans. Faraday Soc. **54**, 1447 (1958).
18. J. Jonas and H. S. Gutowsky. J. Chem. Phys. **42**, 140 (1965).
19. J. Jonas. J. Chem. Phys. **47**, 4884 (1967).
20. R. D. Chambers, L. H. Sutcliffe, and G. J. T. Tiddy. Trans. Faraday Soc. **66**, 1025 (1970).
21. J. Hilton and L. H. Sutcliffe. J. Magn. Reson. **14**, 241 (1974).
22. J. Jonas, L. Borowski, and H. S. Gutowsky. J. Chem. Phys. **47**, 2441 (1967).
23. C. W. Haigh, J. Hilton, L. H. Sutcliffe, and G. J. T. Tiddy. J. Magn. Reson. **18**, 241 (1975).
24. (*a*) W. Niemczura. M.Sc. Thesis. University of Manitoba, Winnipeg, Man. 1976; (*b*) C. Béguin and A. Meary-Tertian. Bull. Soc. Chim. Fr. 795 (1967).
25. R. Freeman and W. A. Anderson. J. Chem. Phys. **37**, 2053 (1962).
26. J. A. Pople, J. W. McIver, Jr., and N. S. Ostlund. J. Chem. Phys. **49**, 2960 (1968); **49**, 2965 (1968).
27. J. A. Pople and M. S. Gordon. J. Am. Chem. Soc. **89**, 4253 (1967).
28. S. Castellano and A. A. Bothner-By. J. Chem. Phys. **41**, 3863 (1964).
29. C. W. Haigh and J. M. Williams. J. Mol. Spectrosc. **32**, 398 (1969).
30. W. B. Moniz and E. Lustig. J. Chem. Phys. **50**, 1905 (1969).
31. G. Govil and D. H. Whiffen. Mol. Phys. **12**, 449 (1967).
32. J. B. Rowbotham, A. F. Janzen, J. Peeling, and T. Schaefer. Can. J. Chem. **52**, 481 (1974).
33. R. J. Kostelnik, M. P. Williamson, I. E. Wisnosky, and S. M. Castellano. Can. J. Chem. **47**, 3313 (1969).
34. I. I. M. Schuster. J. Magn. Reson. **17**, 104 (1975).
35. J. W. Emsley and L. Phillips. Prog. Nucl. Magn. Reson. Spectrosc. **7**, 1 (1971).
36. H. S. Gutowsky, D. W. McCall, B. R. McGarvey, and L. H. Meyer. J. Am. Chem. Soc. **74**, 4809 (1952).
37. C. L. Bumgardner. J. Org. Chem. **28**, 3225 (1963).
38. C. Béguin. Bull. Soc. Chim. Fr. 4214 (1967).
39. W. Adcock, M. J. S. Dewar, R. Golden, and M. A. Zeb. J. Am. Chem. Soc. **97**, 2198 (1975).
40. J. Bromilow, R. T. C. Brownlee, and A. V. Page. Tetrahedron Lett. 3055 (1976).
41. R. J. Abraham, D. B. Macdonald, and E. S. Pepper. J. Am. Chem. Soc. **90**, 147 (1968).
42. S. L. Manatt and M. A. Cooper. J. Am. Chem. Soc. **99**, 4561 (1977).
43. J. E. Loemker, K. M. Pryse, J. M. Read, Jr., and J. H. Goldstein. Can. J. Chem. **47**, 209 (1969).
44. P. H. H. Fischer and J. P. Colpa. Z. Naturforsch. Teil A, **24**, 1980 (1969).
45. D. R. Eaton, A. D. Josey, W. D. Phillips, and R. E. Benson. Mol. Phys. **5**, 407 (1962).
46. R. E. Wasylishen and M. Barfield. J. Am. Chem. Soc. **97**, 4545 (1975).
47. T. Ogata and A. P. Cox. J. Mol. Spectrosc. **61**, 265 (1976).
48. I. Biddles, J. Cooper, A. Hudson, R. A. Jackson, and J. T. Wiffen. Mol. Phys. **25**, 225 (1973).
49. M. B. Yim and D. E. Wood. J. Am. Chem. Soc. **98**, 3457 (1976).
50. T. Schaefer, W. Danchura, and W. Niemczura. Can. J. Chem. **56**, 36 (1978).
51. M. Jinguchi, K. C. Lin, C. A. McDowell, and P. Raghunathan. J. Chem. Phys. **65**, 3910 (1976).
52. R. W. Fessenden and R. H. Schuler. J. Chem. Phys. **39**, 2147 (1963).
53. K. Hirao, H. Nakatsuji, and H. Kato. J. Am. Chem. Soc. **95**, 31 (1973).

Synthèse et étude du rearrangement SR ⇋ NR des diazoles-1,3 : alkyl-1 alkylthio-2 (allylthio, arylthio, cycloalkylthio) imidazoles. Partie I. Synthèse et études physicochimiques

JACKY KISTER,[1] GEORGES ASSEF,[1] GILBERT MILLE[2] ET JACQUES METZGER[1]

Faculté des Sciences et Techniques, Aix-Marseille III, Rue Henri Poincaré – Saint Jérôme, 13397, Marseille, France

Reçu le 2 octobre 1978

JACKY KISTER, GEORGES ASSEF, GILBERT MILLE et JACQUES METZGER. Can. J. Chem. **57**, 813 (1979).

Nous avons étudié la synthèse et le réarrangement SR ⇋ NR de thioéthers des séries imidazoliques *N*- et *S*-substituées (60 composés). Les études physicochimiques complètes des thioéthers, thiones, catalyseurs de réarrangement et des éventuels produits d'hydrolyse ont été effectuées, ainsi que l'étude des cinétiques de réarrangement SR ⇋ NR à diverses températures. Ces résultats de réarrangement et d'hydrolyse ont été comparés à ceux des alkyl-1 méthylthio-2 Δ-2-imidazolines et alkyl-1 méthylthio-2 Δ-2-tétrahydropyrimidines. Les effets électroniques et stériques sont discutés. Dans cette première partie nous présentons uniquement l'aspect synthétique et les résultats des études physicochimiques.

JACKY KISTER, GEORGES ASSEF, GILBERT MILLE, and JACQUES METZGER. Can. J. Chem. **57**, 813 (1979).

The synthesis and the SR ⇋ NR rearrangement of thioethers in the *N*- and *S*-substituted imidazolic series have been studied (60 compounds). The physicochemical studies of the thioethers and mercapto compounds, catalysts of the rearrangement, and of the eventual hydrolysis products have been carried out and the kinetics of rearrangement have been examined at several temperatures. The rearrangement and hydrolysis results are compared with those of 1-alkyl-2-methylthio-Δ-2-imidazolines and 1-alkyl-2-methylthio-Δ-2-tetrahydropyrimidines and the electronic and steric effects are discussed. In this first part the synthetic aspect and physicochemicals results are presented.

Introduction

Dans le cadre d'une étude générale sur un procédé photographique non argentique à haute résolution (1–3), nous avons récemment rapporté la préparation et l'étude du réarrangement SR ⇋ NR des méthyl-1 méthylthio-2 imidazole, imidazoline et tétrahydropyrimidine et des réactions secondaires s'y rattachant (2–5).

Plusieurs études concernant des thioéthers de séries azahétérocycliques montrent que le taux de réarrangement SR ⇋ NR (comme la quaternisation des thioéthers) est notablement influencé par la nature de l'hétérocycle et sa substitution (6–13). Dans cette optique nous nous sommes intéressés dans un premier temps à l'influence de la *N*-substitution sur le réarrangement de composés des séries apparues comme les plus réactives dès 1974 (2): les séries imidazolinique et tétrahydropyrimidinique (3, 7, 14) (fig. 1)

Cependant l'existence de réactions parasites gênantes pour le procédé photographique (2) et provoquant soit un réarrangement parallèle, soit une dégradation du cycle, a orienté nos travaux vers des séries moins rapides *a priori*, mais présentant l'avantage de ne pas être le siège de réactions secondaires importantes (2).

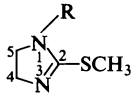

Alkyl-1 méthylthio-2 Δ-2-imidazoline (C_2)

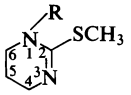

Alkyl-1 méthylthio-2 Δ-2-tétrahydropyrimidine (C_3)

FIG. 1. Les séries imidazolinique et tétrahydropyrimidinique.

Ainsi il nous a semblé intéressant d'entreprendre la synthèse et l'étude du réarrangement de thioéthers imidazoliques *N*- et *S*-substitués, ainsi que de divers composés substitués en position 4 et 5 (3, 7). Les composés **5**, **6** et **7** (fig. 2) sont donc susceptibles de présenter des différences intéressantes avec leurs homologues méthylés en position 1 et 2 et leurs homologues des séries saturées à cinq ou six chaînons.

L'analyse des résultats des réactions de réarrange-

[1]Laboratoire de Chimie Moléculaire et de Pétroléochimie; Contrat DRME 77/003.

[2]Centre de Spectroscopie Moléculaire.

0008-4042/79/070813-09$01.00/0

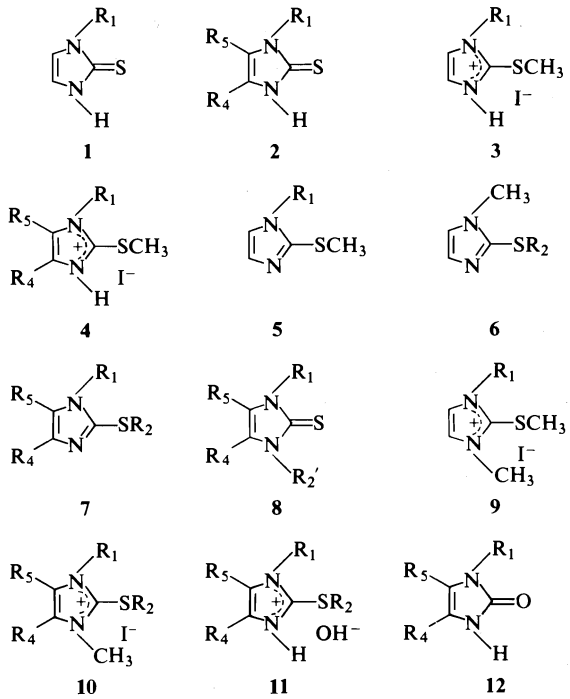

R_1 = H, Me, Et, *i*Pr, *t*Bu, C_6H_5, *n*Bu
R_2 = H, Me, Et, *i*Pr, *n*Pr, *n*Bu, Benzyl, Cyclopentyl, Allyl, Acétonyl, Dodécyl
$R_4 = R_5$ = H, Me

FIG. 2. Les composés imidazoliques *N*- et *S*-substitués et les divers composés substitués en position 4 et 5.

ment SR ⇋ NR nous a permis de comparer les effets de cycle et de substitution pour ces séries hétérocycliques de type diazole-1,3 et diazine-1,3 (14*b*). Une étude plus générale des relations qui existent entre le taux de réarrangement et le pK_a des thioéthers est menée sur des composés hétérocycliques benzocondensés, aromatiques ou saturés à cinq ou six chaînons (fig. 3) et permet une analyse cohérente des effets structuraux, effets de cycle, de champ, de substitution (3). Cette généralisation fera l'objet d'un mémoire indépendant (15).

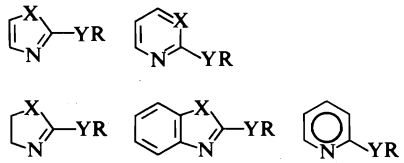

X = N, S, O
Y = S, O
R = Alkyl, Aryl, Allyl, Acétonyl, Dodécyl

FIG. 3. Les composés hétérocycliques benzocondensés, aromatique ou saturés.

Partie théorique

Synthèse des thioéthers ***5***, ***6*** *et* ***7***

La synthèse de ces thioéthers procède soit par alkylation des thiones **1** et **2** suivie d'une neutralisation de l'iodhydrate **3** et **4** (schéma 1), soit par une réaction de catalyse polyphasique menée sur ces thiones (schéma 2). Nous avons donc été amenés à synthétiser initialement des thiones de type **1** et **2**.

Synthèse des thiones de type ***1*** *et* ***2***

La synthèse des alkyl-1 Δ-4-imidazolinethiones-2 substituées ou non en position 4 et 5 est beaucoup plus complexe que celle de leurs homologues en séries imidazolinique et tétrahydropyrimidinique (14).

(*a*) Ces composés sont accessibles par chauffage d'α-hydroxycétones ou α-hydroxyaldéhydes et de thiourées convenablement substituées (16–21) (schéma 3). Cette méthode a été appliquée pour la thione **2** ($R_1 = R_4 = R_5$ = Me) conduisant au triméthyl-1,4,5 méthylthio-2 imidazole et triméthyl-1,4,5 isopropylthio-2 imidazole. Récemment Lespagnol *et al.* (22) a préparé les alkyl-4 (5) Δ-4-imidazolinethiones-2, par la méthode de synthèse qui consiste à faire réagir, comme l'avaient fait Posner et coll. (23), des α-aminocétones ou α-aminoaldéhydes sur des dérivés de l'acide thiocyanique.

(*b*) Les composés de type alkyl-1 Δ-4-imidazolinethiones-2 non substituées en position 4 et 5 peuvent être obtenus par réaction d'un isothiocyanate d'alkyle (éthyle, phényle) sur l'aminoacétaldéhyde

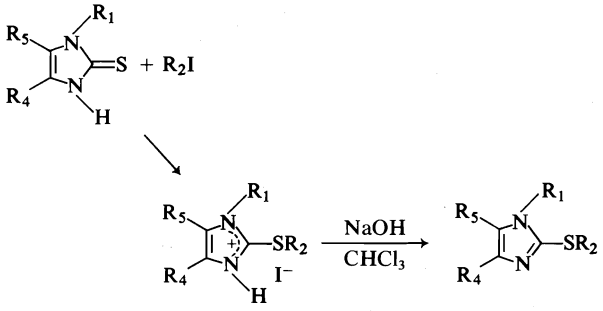

SCHÉMA 1

diéthylacétal, selon la méthode de Wohl et Marckwald (24–26) (schéma 4), ou par la méthode de Jones et Kovtunovskaya (27, 28) par action du thiocyanate de potassium et de l'acide chlorhydrique sur les

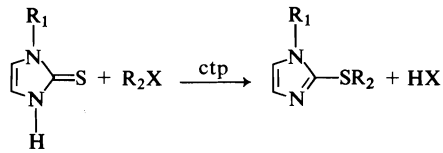

SCHÉMA 2

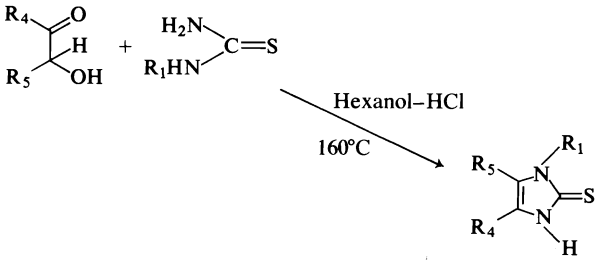

SCHÉMA 3

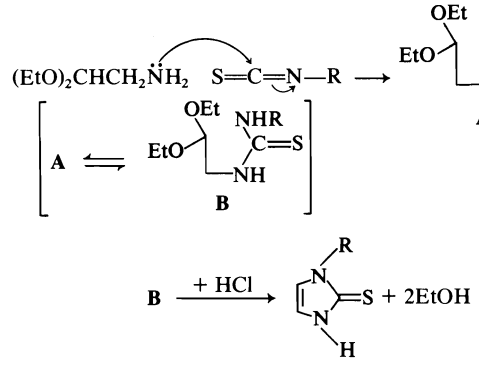

SCHÉMA 4

N-alkylaminoacétaldéhyde diéthylacétals (éthyle, isopropyle, tertiobutyle) précédemment synthétisés par action d'amines primaires sur les bromoacétaldéhyde diéthylacétals (27, 29–32) (schéma 5 et synthèse des intermédiaires). La méthode de Wohl et Marckwald est directement utilisable pour les seuls isothiocyanates commerciaux substitués par un groupement éthyle ou phényle. La synthèse du phénylaminoacétaldéhyde diéthylacétal ayant échouée nous avons synthétisé directement la phényl-1 Δ-4-imidazolinethione-2 par cette méthode.

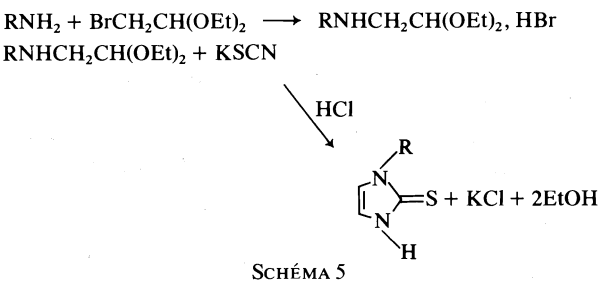

SCHÉMA 5

En 1932, Easson et Pyman (33) ont utilisé une variante de la réaction précédente, comportant une étape supplémentaire. Ils préparaient d'abord un acétylcarbamide qui réagissait ensuite sur une alkylamine pour donner un diéthylacétal d'aldéhyde α-isothiocyanate.

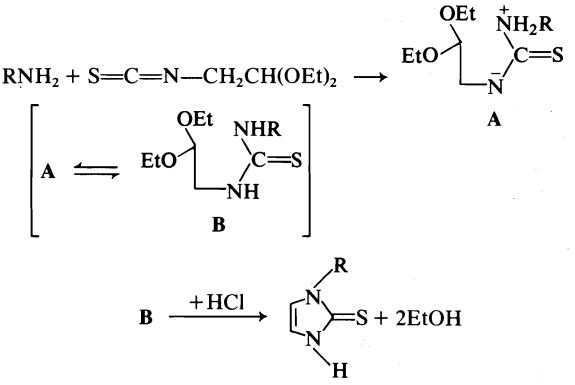

SCHÉMA 6

D'autres auteurs (34) ont utilisé la méthode de Easson et Pyman (33) en préparant d'abord l'acétal de l'aldéhyde α-isothiocyanate par action de l'aminoacétaldéhyde diéthylacétal sur le sulfure de carbone, suivant le schéma 7.

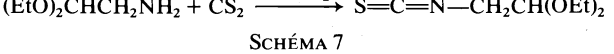

SCHÉMA 7

Nous citerons à titre d'exemple la méthode utilisant des intermédiaires ayant un groupe carboxylate en position 5, méthode surtout développée par Jones (35). Le mécanisme de cette réaction est donné par le schéma 8. Il existe encore diverses autres méthodes moins utilisées (21, 36–39).

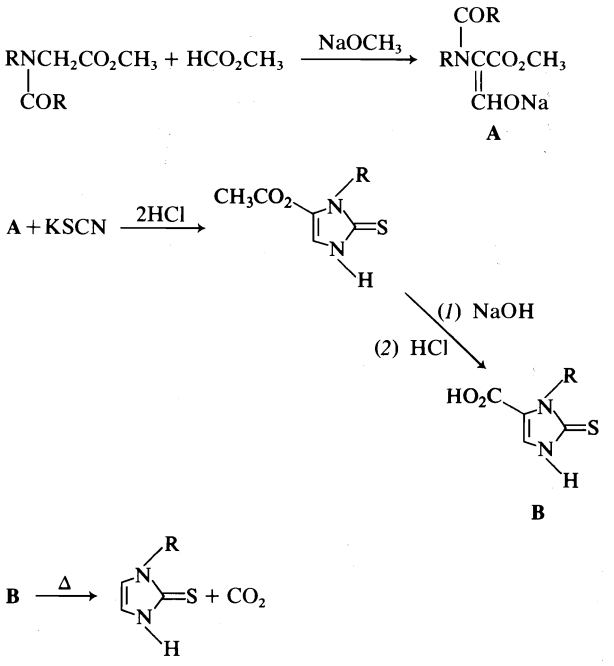

SCHÉMA 8

Synthèse des thioéthers ***5***, ***6*** *et* ***7***

(*a*) Par quaternisation à froid avec l'iodure de méthyle dans l'acétone anhydre, nous isolons les iodhydrates **3** et **4** qui conduisent aux thioéthers par déprotonation basique dans des conditions analogues à celles décrites pour les alkyl-1 méthylthio-2 Δ-2-imidazolines et Δ-2-tétrahydropyrimidines (14). Seuls les iodhydrates **3** ont été isolés et étudiés. Les iodhydrates **4** n'ont pas été isolés, la réaction en deux étapes ayant lieu dans le même ballon.

(*b*) *Malgré une optimisation poussée* des synthèses intermédiaires, nous préférons à ce schéma en deux étapes (rendement global >70%), la technique de catalyse interfaciale (ctp) (40). Outre le gain de temps puisque la synthèse est réalisée en une étape, s'ajoute aussi un gain de pureté puisque le produit *S*-alkylé est obtenu de manière univoque sans réactivité de l'atome d'azote (schéma 2). Ce point de vue doit cependant être complété, par le fait que la réaction de *S*-alkylation est univoque en série aromatique, tandis qu'en série saturée, la *S*-alkylation est accompagnée d'environ 5% de *N*-alkylation. Cette réactivité particulière de l'anion ambident NCS a été vérifiée sur les Δ-4-thiazolinethiones-2 et Δ-4-imidazolinethiones-2 (41–42). Les rendements obtenus sont plus faibles quand on utilise des halogénures d'alkyle à longue chaîne (40). La méthode peut utiliser des bromures ou chlorures d'alkyle, les iodures conduisant à une inhibition du catalyseur.

Indiquons schématiquement le principe de la catalyse par transfert de phase qui est appliquée ici: un système biphasique, contenant une solution aqueuse d'un hydroxyde d'ammonium quaternaire (obtenu *in situ* par réaction d'un sel d'ammonium quaternaire avec une solution de soude concentrée) et une solution organique d'agent alkylant (halogénure d'alkyle) et de substrat (), est mis en réaction par agitation et chauffage (40–45). En fin de réaction, le mélange réactionnel est refroidi et laissé au repos. La phase organique contenant le produit attendu est alors séparée puis traitée de manière conventionnelle.

Le choix du solvant de la réaction et du sel quaternaire catalyseur a été effectué lors d'études antérieures menées sur la *N*-alkylation des imidazoles et pyrazoles (43). Le solvant doit favoriser au maximum l'extraction de l'espèce $NR_4^+ OH^-$, ne pas être réactif et permettre les conditions de température et de solubilité des réactifs. Le benzène est le plus souvent utilisé. Le système biphasique étant fixé, le catalyseur utilisé est le bromure de tétrabutylammonium (commercial) à la concentration de 4% en mole par mole de substrat.

La catalyse interfaciale apparaît donc dans notre cas comme une méthode de choix pour l'obtention de dérivés *N*,*S*-alkylés, à partir de thiones ayant un ou plusieurs hydrogènes mobiles, permettant la formation d'anions ambidents N—C—O ou N—C—S. Dans le cas de la Δ-4-imidazolinethione-2 non substituée, deux protons mobiles sont présents dans la molécule et l'on peut obtenir des *N*,*S*-alkylations.[3] La Δ-4-imidazolinethione-2 étant commerciale, l'on juge bien de l'intérêt de ces *N*,*S*-alkylations qui font éviter les synthèses délicates des alkyl-1 Δ-4-imidazolinethiones-2. Cette technique a été appliquée à la synthèse du triméthyl-1,4,5 méthylthio-2 imidazole à partir de la triméthyl-1,4,5 Δ-4-imidazolinethione-2.

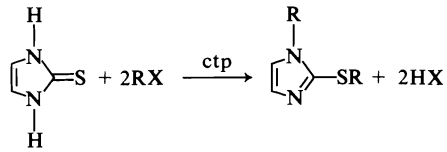

SCHÉMA 9

Par contre la catalyse par transfert de phase n'est pas utilisable quand on veut fixer en position 2 un groupe acétonyle. En présence de soude, la réaction de Darzens avec la chloroacétone devient prépondérante (46, 47); nous avons synthétisé le méthyl-1 acétonylthio-2 imidazole en deux étapes par le mode de synthèse classique (48). Cependant ces substrats intéressants par le gain de réarrangement en phase liquide ne seront pas utilisables en phase adsorbée (support solide du procédé photographique) du fait d'une complexation parasite du groupement acétonyle provoquant une diminution notable du taux de réarrangement.

Les conditions de réaction et caractéristiques physiques et physicochimiques des composés **1**–**7** sont rassemblées dans les tableaux 1–3. La synthèse des intermédiaires est donnée dans la partie expérimentale.

Synthèse des catalyseurs et thiones de réarrangement

La réaction de réarrangement que nous étudions est une réaction autocatalytique ionique contrôlable thermiquement et dont le schéma général (schéma 10) est le suivant.

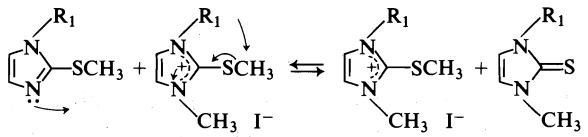

SCHÉMA 10

Nous avons donc synthétisé et purifié les catalyseurs utilisés: les sels quaternaires **9**. La synthèse correspond toujours à une alkylation par l'iodure de

[3]J. Kister. Travaux non publiés.

TABLEAU 1. Caractéristiques physiques et physicochimiques des composés **1** et **2**

Composés				rdt		R_f (ccm, SiO_2, $CHCl_3$–MeOH	uv (EtOH)	rmn ^1H (acétone-d_6)				ir (solide)† ν (cm^{-1})		
No	R_1	R_2	R_4R_5	(%)	pf (°C)	90:10)	λ_{max}(nm)	δ (ppm) (nombre de protons)				ν(NH)	δ(NH)	ν(C=C)
1	H	H	H	92	225	0.39	259	6.85(2)*				3130F	1467F	1580F
	Me	H	H	100	143	0.64	260	6.90(1)	6.80(1)	3.50(3)		3115F	1462F	1572F
	Et	H	H	71	77	0.69	261.5	6.94(1)	6.80(1)	4.05(2)	1.28(3)	3090F	1477F	1572F
	*i*Pr	H	H	65	170	0.74	260	6.97(1)	6.80(1)	4.91(1)	1.30(6)	3103F	1480F	1575F
	*t*Bu	H	H	65	189	0.76	267	6.90(1)	6.65(1)	1.70(9)		3080F	1478F	1575F
	Ph	H	H	66	181	0.75	283	7.60–7.30(5)		6.82(1)	6.77(1)	3090F	1500F	1572m
2	Me	H	Me	40	214–217	0.73	267	3.50(3)	2.06(6)			3085F	1495F	1658m

*Spectre enregistré dans $CDCl_3$.
†Les intensités des bandes infrarouges sont indiquées par les lettres m, moyenne; F, forte.

TABLEAU 2. Caractéristiques physiques et physicochimiques des composés **3** et **4**

Composés				rdt	pf	uv (EtOH)	rmn ($CDCl_3$) δ (ppm) (nombre de protons)					ir (solide)* ν(cm^{-1})			
No	R_1	R_2	R_4R_5	(%)	(°C)	λ_{max} (nm)						+ ν(NH)	+ δ(NH)	ν(C=C)	+ ν(C=N)
3	H	Me	H	75	167	218–253	8.85(2)	7.62(2)	2.99(3)†			2950F	1451m	1584F	1483m
	Me	Me	H	99	150	220–253	6.78(2)	3.81(3)	2.71(3)			2985F	1465e	1575F	1486F
	Et	Me	H	92	170	220–253	7.39(2)	4.20(2)	3.02(3)	1.50(3)		2990F	1463f	1572m	1480F
	*i*Pr	Me	H	93	190	219–252	7.50(1)	7.40(1)	4.55(1)	3.05(3)	1.55(6)	2998F	1468m	1575m	1457F
	*t*Bu	Me	H	93	210	220–253	7.45(1)	7.30(1)	3.10(3)	1.72(9)		3048F	1462e	1570F	1469F
	Ph	Me	H	52	162	219–261	7.70–7.45(7)		3.02(3)			2960F	1454e	1573m	1472m
4	Me	At‡	H	90	178	220–278	7.60(2)	5.0(2)	4.0(1)	2.50(3)	1.60(3)	—	—	—	—

*Les intensités des bandes infrarouges sont indiquées par les lettres F, forte; m, moyenne; f, faible; e, épaulement.
†Spectre enregistré dans acetone-d_6.
‡At = acétonyl.

TABLEAU 3. Caractéristiques physiques et physicochimiques des composés **5**, **6** et **7**

Composés				rdt	pf ou pé	R_f (ccm, SiO_2)		uv (EtOH)	rmn ^1H ($CDCl_3$) δ (ppm) (nombre de protons)*	ir (solide)† ν(cm^{-1})			
No	R_1	R_2	R_4R_5	(%)	(°C)	$CHCl_3$–MeOH 90:10	C_6H_6–AcEt 80:20	λ_{max} (nm)		ν(=CH)		ν(C=N) et ν(C=C)	
5	H	Me	H	78	137	0.40		220–250.5	8.30(1) 7.02(2) 2.58[3]	3132f	~3100f	1528m	~1440e§
	Me	Me	H	70	48/0.5 Torr	0.81	0.12	223–250.5	6.95(1) 6.85(1) 3.56(3) 2.52[3]	3130f	3104f	1507m	1462F
	Et	Me	H	90	62/1.3 Torr	0.84		224–250.5	6.95(1) 6.85(1) 3.85(2) 2.53[3] 1.30(3)	~3128e	3102f	1506m	1434F
	*i*Pr	Me	H	80	70/0.7 Torr	0.88		224–250	7.02(1) 6.97(1) 4.43(1) 2.53[3] 1.40(6)	~3130e	3104f	1502f	1442F
	*t*Bu	Me	H	86	60	0.90		225–253.5	7.01(1) 6.90(1) 2.53[3] 1.60(9)	3158f	3108f	1507f	1423m§
	Ph	Me	H	81	95/0.15 Torr	0.92		260	7.50–7.20(5) 7.09(1) 7.01(1) 2.50[3]	3120f	3105f	1497F	1438m
6	Me	Et	H	93	90/0.05 Torr		0.13	223–250	7.0(1) 6.90(1) 3.56(3) 3.02[2] 1.28[3]	3130f	3108m	1509m	1456F
	Me	*i*Pr	H	64	63/0.05 Torr		0.14	225–249.5	7(1) 6.91(1) 3.58(3) 3.46[1] 1.28[6]	3129f	3107m	1508m	1456F
	Me	Pr	H	68	68/1.5 Torr		0.18	222.4–250	6.88(1) 6.76(1) 3.50(3) 2.98[2] 1.60[2] 0.99[3]	3135f	3110m	1510m	1457F
	Me	Bu	H	82	80/1.5 Torr		0.23	222.3–250	6.84(1) 6.72(1) 3.48(3) 2.98[2] 1.50[4] 0.80[3]	3130f	3108m	1510m	1460F
	Me	Bz	H	54	110/0.1 Torr		0.20	215–257	7.12[5] 7.04(1) 6.80(1) 4.08(2) 3.16(3)	3129f	3103m	1507m	1452F
	Me	Cp	H	55	85/0.08 Torr		0.22	225.6–250	7.0(1) 6.90(1) 3.58(3) 3.60[1] 2.20–1.40[8]	3128f	3104m	1507m	1454F
	Me	Al	H	65	87/0.08 Torr		0.18	225.5–252.6	7.1(1) 6.88(1) 5.86[1] 5.05[2] 3.60[2] 3.57(3)	3131f	3108m	1507m	1456F
	Me	At	H	35	104/2 Torr	—		240–278	7.02(1) 6.98(1) 3.97[2] 3.67(3) 2.28[3]	—	—	—	—
	Me	Dd	H	15	Non distillé	—		222–250	7.10(1) 6.90(1) 3.60[3] 3.10[2] 1.30[20] 0.95[3]	—	—	—	—
7	Bu	Bu	H	80	Non distillé	—		224–250.5	6.75 (2) 3.80(2) 3.0[2] 0.72–0.70[7×2]	—	—	—	—
	Me	Me	Me	40	75/0.6 Torr	0.86	0.17	234–250.5	3.60(3) 2.54[3] 2.08(6)‡	—	—	—	—

NOTE: Ph, phényl; Bz, benzyl; Cp, cyclopentyl; Al, allyl; At, acétonyl; Dd, dodécyl.
*Les nombres entre crochets indiquent les protons du substituant lié à l'atome de soufre.
†Les intensités des bandes infrarouges sont indiquées par les lettres: f, faible; m, moyenne; F, forte; e, épaulement.
‡Spectre enregistré dans DMSO-d_6.
§Spectre enregistré à l'état liquide.

TABLEAU 4. Caractéristiques physiques et physicochimiques des composés **8**

Composés				rdt	pf	uv (EtOH)	^1Hmr ($CDCl_3$) δ (ppm)	ir (solide)* ν(cm^{-1})			
No	R_1	R'_2	R_4R_5	(%)	(°C)	λ_{max} (nm)	(nombre de protons)	ν(=CH)		ν(C=C)	ν(C—N)
8	H	Me	H	100	143	260	6.80(2) 3.68(3)†	3160f	3128m	1572F	1335m
	Me	Me	H	100	181	260	6.81(2) 3.60(6)†	3153m	3113m	1573m	1387FF
	Et	Me	H	100	51	262	6.47(2) 3.90(2) 3.43(3) 1.30(3)	3155m	3090m	1567f	1413FF
	*i*Pr	Me	H	100	87	262	6.43(2) 4.83(1) 3.44(3) 1.30(6)	3158m	3090m	1566f	1407FF
	*t*Bu	Me	H	100	53	265	6.92(1) 6.80(1) 3.55(3) 1.82(9)	3170f	3100f	1572f	1373FF
	Ph	Me	H	100	188	260	7.6–7.2(5) 6.70(1) 6.65(1) 3.52(3)	3158m	3122m	1568f	1375FF‡
	Me	Me	Me	100	148	267.5	3.48(6) 2.06(6)†	—	—	1659m	1382FF
	Me	At	H	100	—	260–320–350§	7.24(2) 4.17(2) 3.60(3) 2.28(3)†	—	—	—	—

*Les intensités des bandes infrarouges sont indiquées par les lettres: f, faible; m, moyenne; F, forte; FF, très forte.
†Spectre enregistré dans DMSO-d_6.
‡Spectre enregistré à l'état liquide.
§Spectre enregistré dans CH_2Cl_2.

méthyle, la quaternisation se faisant sur l'azote N_3 et non sur le soufre exocyclique. Lorsque la quaternisation est trop lente à température ambiante, les catalyseurs sont obtenus par fusion du thioéther et d'un net excès d'iodure de méthyle sans solvant, puis recristallisés dans l'éthanol et parfaitement séchés. Les caractéristiques physiques et physicochimiques des sels **9** et **10** sont rassamblées dans le tableau 5.

De la même façon certaines thiones de type **8** ont été isolées directement par réaction de réarrangement des thioéthers. Les caractéristiques physiques et physicochimiques sont rassemblées dans le tableau 4.

D'une façon générale, les études de spectrométrie ultraviolette (49), infrarouge (50) et de résonance magnétique nucléaire du carbone-13 (51) ont fait l'objet de mémoires indépendants. L'étude des réactions de réarrangement SR ⇋ NR et l'analyse des effets structuraux fera l'objet de la seconde partie de ce mémoire (14*b*). Les effets de substitution sur l'azote N_1, le soufre S_2 et en position 4 et 5 seront discutés ainsi que les effets de température et de catalyseur.

Dans l'analyse des résultats nous étudierons les relations pK_a/réarrangement pour les thioéthers de la série C_1 imidazolique et nous les comparerons à ceux déjà exposés des séries C_2 imidazolinique et C_3 tétrahydropyrimidinique. Les diverses réactions parasites, issues de l'hydrolyse des thioéthers (réarrangement parasite et réactions de dégradations) seront étudiées.

Partie expérimentale

Les points de fusion ont été déterminés au banc Kofler. Les spectres rmn du ^1H ont été enregistrés sur des appareils du type Varian HA 100 et JEOL C 60 H. Sauf indications contraires, les spectres ont été enregistrés dans le chloroforme deutérié à une concentration de 10% avec le tétraméthylsilane comme référence interne. Les déplacements chimiques sont donnés en ppm par rapport au TMS (s, singulet; d, doublet; t, triplet; q, quadruplet; qd, quadruplet dedoublé; m, multiplet). Les spectres infrarouges ont été enregistrés à l'état solide entre 4000 et 400 cm^{-1} sous forme de pastille KBr ou KI à l'aide d'un spectrographe Perkin-Elmer modèle 225. Les échantillons liquides ont été étudiés sous une épaisseur de 15 μ dans des cellules scellées à lame de bromure de potassium. Les spectres ultraviolets ont été enregistrés dans l'éthanol sur un spectrophotomètre Cary 14.

Synthèse des intermediaires

Synthèse d'alkyl-1 aminoacétaldéhyde diéthylacétal

Les aminoacétaldéhydes *N*-substitués sont obtenus en chauffant en ampoule scellée à haute température pendant 24 h un chloro- ou un bromoacétaldéhyde diéthylacétal avec un excès d'amine primaire. Comme l'ont décrit déjà Knorr (29) et Paal et Gember (30), ainsi que d'autres auteurs (27, 31, 32), il se forme d'abord un bromhydrate qui sera libéré par une solution de potasse à 50%. Les aminoacétaldéhyde diéthylacétals sont ensuite distillés avant leur utilisation ultérieure en vue de l'obtention des alkyl-1 Δ-4-imidazolinethiones-2 (C_1). Le mécanisme est décrit par le schéma 11.

TABLEAU 5. Caractéristiques physiques et physicochimiques des composés **9** et **10**

Composés																
												ir (solide)† ν(cm^{-1})				
No	R_1	R_2	R_4R_5	rdt (%)	pf (°C)	uv (EtOH) λ_{max} (nm)	rmn ^1H ($CDCl_3$) δ (ppm) (nombre de protons)*					ν(=CH)		ν(C=C)	ν(C⋯N)$^+$	
9	H	Me	H	99	150	220–253	6.78(2)	3.81(3)	2.71[3]			3098F	3042m	1575F	1486F	
	Me	Me	H	96	189	221–261	7.65(2)	3.80(6)	2.48[3]			3067F	3050F	1568m	1501F	
	Et	Me	H	91	182	222–260	7.90(2)	4.45(2)	4.10(3)	2.65[3]	1.75(3)	3075F	3040m	1564m	1494F	
	*i*Pr	Me	H	98	165	222–262	8.0(1)	7.82(1)	5.50(1)	4.0(3)	2.65[3] 1.60(6)	3090F	3080F	1558m	1484F	
	*t*Bu	Me	H	50	176	221–265	7.95(1)	7.55(1)	4.15(3)	2.67[3]	1.82(9)	3092F	3085e	1559m	1473F	
	Ph	Me	H	61	180	221–266	8.19(1)	7.80(1)	7.9–7.5(5)		4.20(3) 2.43[3]	—	—	—	—	
10	Me	Me	Me	85	191	220–260	4.10(6)	2.63[3]	2.10(6)			—	—	—	—	
	Me	Et	H	80	‡	221–260.5	8.10(2)	4.16(6)	3.13[3]	1.33[2]		3065F	3042m	1568m	1497F	
	Me	*i*Pr	H	90	‡	228–258.6	8.16(2)	4.16(6)	3.70[1]	1.36[6]		3081F	3063F	1568m	1501F	
	Me	Pr	H	95	‡	221.4–260	8.10(2)	4.16(6)	3.06[2]	1.7[2]	1.06[3]	3076F	3045F	1568m	1500F	
	Me	Bu	H	90	‡	221.1–260.5	8.10(2)	4.13(6)	3.06[2]	1.86–1.2[4]	0.93[3]	3080F	3050F	1568m	1500F	
	Me	Bz	H	60	‡	219–265	7.90(2)	7.26[5]	4.30[2]	3.63[6]		3100F	?	1564m	1497F	
	Me	Cp	H	55	‡	221.7–264	8.10(2)	4.16(6)	1.76[8]			3072F	3058F	1569m	1504F	
	Me	Al	H	40	‡	220.5–260	8.06(2)	6.2–5.7[1]		5.36–5.03[2]	3.71[2]	3090m	3077F	1562m	1498F	
	Me	Dd	H	25	‡	221–261	8.10(2)	4.16(6)	3.0[2]	1.30[20]	0.95[3]	—	—	—	—	
	Me	At	H	40	‡	220–266	8.12(2)	4.16(6)	4.0[3]	2.30[2]		—	—	—	—	

*Les nombres entre crochets indiquent les protons du substituant lié à l'atome de soufre.
†Les intensités des bandes infrarouges sont indiquées par les lettres: f, faible; m, moyenne; F, forte; FF, très forte.
‡Non recristallisé.

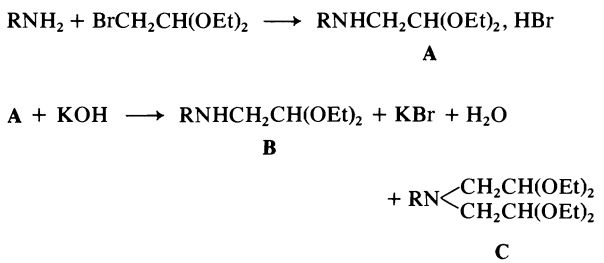

SCHÉMA 11

Préparation du N-*éthylaminoacétaldéhyde diéthylacétal (27, 29, 30, 32, 36)*

L'éthylamine ayant une température d'ébullition de 16°C on prendra soin de tremper les ampoules dans une solution d'acétone–carboglace. Dans une ampoule préalablement refroidie, on place 0.2 mol (40 g) de bromoacétaldéhyde diéthylacétal et très rapidement à l'aide d'une seringue on ajoute 0.6 mol (27 g) d'éthylamine. L'ampoule est rapidement scellée et placée ensuite dans une gaine métallique que l'on met dans une étuve thermostatée à 140°C pendant 24 h. Souvent le produit cristallise sur les parois de l'ampoule. On ajoute ensuite 70 cm^3 d'une solution de potasse à 50%. On filtre le bromure de potassium formé, décante et récupère la phase organique. L'excès d'amine dans le cas de la tertiobutyl et isopropylamine est distillé sous pression réduite puis on distille l'alkyl aminoacétaldéhyde diéthylacétal. Par une voie analogue nous avons synthétisé les substrats suivants.

Composé **1** $\left(\begin{smallmatrix} a & b & c & d & e & f & g \\ CH_3CH_2NHCH_2CH(OCH_2CH_3)_2 \end{smallmatrix}\right)$—Rendement 50%; pé 90°C/20 Torr; rmn ^1H: a 1.10 (t), b 2.60 (q), d 2.65 (d), e 4.55 (t), f 3.60 (qd), g 1.20 (t).

Composé **2** $\left(\begin{smallmatrix} a & b & c & d & e & f \\ CH_3CH_2N(CH_2CH(OCH_2CH_3)_2)_2 \end{smallmatrix}\right)$—Rendement 10%; pé 160°C/20 Torr; rmn ^1H ($CDCl_3$/TMS): a 1.05 (t), b 2.60 (q), d 4.50 (t), c 2.63 (d), e 2.60 (qd), f 1.19 (t).

Composé **3** $\left(\begin{smallmatrix} a & b & c & d & e & f & g \\ (CH_3)_2CHNHCH_2CH(OCH_2CH_3)_2 \end{smallmatrix}\right)$—Rendement 80%, pé 88°C/21 Torr; rmn ^1H ($CDCl_3$/TMS): a 1.03 (d), b 2.72 (s), d 2.65 (d), e 4.52 (t), f 3.60 (qd), g 1.20 (t).

Composé **4** $\left(\begin{smallmatrix} a & b & c & d & e & f \\ (CH_3)_3NHCH_2CH(OCH_2CH_3)_2 \end{smallmatrix}\right)$—Rendement 80%; pé 193°C/760 Torr; rmn ^1H ($CDCl_3$/TMS): a 1.10 (s), d 4.55 (t), c 2.65 (d), e 3.60 (qd), f 1.20 (t).

Remarques

Contrairement aux auteurs précédents (26–32), lors de la distillation du *N*-éthylaminoacétaldéhyde diéthylacétal, nous avons isolé un sous produit (**2**) ayant une température d'ébullition de 160°C/20 Torr, 25% à côté du produit attendu qui bout à 90°C/20 Torr (**1**).

La spectrométrie de masse et la résonance magnétique nucléaire du proton nous ont permis de déterminer la structure de ce sous produit:

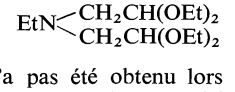

Ce sous produit n'a pas été obtenu lors de la synthèse de l'isopropyl et du *tert*-butylaminoacétaldéhyde diéthylacétal à cause de la gêne stérique qui interdit la double condensation.

Une expérience supplémentaire d'optimisation de cette étape de synthèse a été effectuée en utilisant un rapport 5:1 d'amine – bromoacétaldéhyde diéthylacétal au lieu du rapport 3:1 de l'expérience précédente. Ainsi nous avons obtenu le produit **B** (schéma 11) avec quelques traces de **C**.

Par la même méthode, nous avons tenté de synthétiser le phénylaminoacétaldéhyde diéthylacétal. A plusieurs reprises les ampoules scellées ont explosé. Etant moins nucléophile que ses homologues aliphatiques, l'aniline réagit moins bien sur le bromoacétaldéhyde. Ce dernier (pé 50°C/760 Torr) se trouve très rapidement à 140°C dans l'ampoule avant même de réagir sur l'amine, il se crée une forte surpression suivie d'explosion. Par contre les amines aliphatiques étant très réactives, le bromoacétaldéhyde a déjà réagi sur l'amine avant même que l'ampoule ait atteint 140°C.

Nous avons enfin effectué la réaction en autoclave sous pression à diverses températures: nous n'avons recueilli que des goudrons dont l'analyse par chromatographie en couche mince a décelé quelques traces du produit **B** (schéma 11). Ce mode expérimental, inexploitable dans ce cas, nous a obligé à rechercher une autre voie de synthèse. Nous avons donc effectué la synthèse directe de la phényl-1 Δ-4-imidazolinethione-2 par la méthode de Wohl et Marckwald, l'éthyl et le phényl isothiocyanate étant commerciaux (Fluka A.6).

Synthèse de la phényl-1 Δ-4-imidazolinethione-2

Dans un réacteur mini d'un vibreur et d'un réfrigérant on place 0.75 mol (100 g) d'aminoacétaldéhyde diéthylacétal, on ajoute goutte à goutte 0.83 (100 cm^3) de phényl isothiocyanate en 20 min. Un précipité blanc se forme et la température du réacteur passe de 50 à 80°C en fin d'addition. On ajoute 300 cm^3 d'éthanol et on laisse 2 H à reflux. Le rendement brut après filtration et séchage est de 80%.

Synthèse de la tert-*butyl-1 Δ-4-imidazolinethione-2*

Dans un réacteur de 1 L muni d'un vibreur et d'un réfrigérant ascendant, on place 0.40 mol (75.6 g) de *N-tert*-butylaminoacétaldéhyde diéthylacétal en solution dans 400 cm^3 d'alcool absolu. On ajoute 0.48 mol (48 g) de thiocyanate de potassium et 200 cm^3 d'acide chlorhydrique 2 *N*. Le mélange réactionnel est mis à reflux pendant une nuit. On évapore ensuite le solvant et récupère le résidu solide. On le solubilise dans une solution de soude diluée, le traite avec du charbon actif pendant 30 min à reflux. On filtre le charbon, reprécipite le solide avec une solution diluée d'acide chlorhydrique. Le produit obtenu par filtration est recristallisé dans un mélange acétone–éther 50:50.

Synthèse de l'iodure de tert-*butyl-1 méthylthio-2 imidazolium*

Dans un bicol de 1 L surmonté d'un réfrigérant ascendant et d'une ampoule à brome, muni d'un agitateur mécanique, on place 0.40 mol (72.4 g) de *tert*-butyl-1 Δ-4-imidazolinethione-2 dans 700 cm^3 d'acétone anhydre. On ajoute lentement 0.42 mol (59.64 g) d'iodure de méthyle. On laisse sous agitation à température ambiante pendant 3 h. Le solide obtenu est filtré, puis recristallisé dans de l'éthanol absolu.

Synthèse de la tert-*butyl-1 méthylthio-2 imidazole*

Dans un réacteur de 2 L muni d'un vibreur et d'un réfrigérant ascendant, on place 0.30 mol (89.4 g) d'iodure de *tert*-butyl-1 méthylthio-2 imidazolium en suspension dans 1 L d'éther anhydre. On ajoute une quantité stoéchiométrique de soude pulvérisée. On chauffe à reflux pendant 4 h. On filtre ensuite l'iodure de sodium formé, évapore le solvant et distille sous pression réduite.

Synthèse de la tert-*butyl-1 méthyl-3 Δ-4-imidazolinethione-2*

On place dans une ampoule 0.05 mol de *tert*-butyl-1 méthylthio-2 imidazole et on ajoute 3% mol d'iode pulvérisée. L'ampoule scellée est placée dans une gaine métallique à l'étuve à 140°C pendant 24 h. La thione obtenue est purifiée par chromatographie préparative. On peut isoler directement la thione lors des expériences de réarrangement classique catalysées par le sel quaternaire correspondant.

Synthèse de l'iodure de tert-*butyl-1 méthylthio-2 méthyl-3 imidazolium*

On place 0.05 mol de *tert*-butyl-1 méthylthio-2 imidazole dans un microballon avec 0.09 mol d'iodure de méthyle dans l'acétone anhydre et on laisse sous agitation à température

ambiante pendant 3 h. Le sel obtenu est ensuite recristallisé dans l'éthanol absolu.

Synthèse par catalyse polyphasique (ctp)

S-*Alkylation de la méthyl-1 Δ-4-imidazolinethione-2*

Procédure générale (40)—0.05 mol (5.71 g) de méthyl-1 Δ-4-imidazolinethione-2, 0.05 mol de bromure d'alkyle et 0.97 g (0.003 mol, 6% mol par rapport au thioéther) de bromure de tétrabutylammonium sont placés dans 150 mL de benzène et 15 mL de soude (40%). Le mélange est agité pendant 6 h au minimum à 60°C. La phase organique est séparée, séchée et concentrée et le résidu est distillé ou recristallisé (40).

NS-*Dialkylation*

NS-*Dibutylation de la Δ-4-imidazolinethione-2*—5.01 g (0.05 mol) de Δ-4-imidazolinethione-2, 13.7 g (0.1 mol) de bromo-1 butane et 1.95 g (0.006 mol) de bromure de tétrabutylammonium sont placés dans 150 mL de benzène et 15 mL de soude (40%). Le mélange est agité 6 h à 60°C, puis la phase organique est séparée, séchée et le solvant est évaporé. Le produit brut est obtenu avec un rendement de 80% (8.51 g) et analysé par rmn ^{1}H (40).

N,S-*Diéthylation de la Δ-4-imidazolinethione-2*—Dans les mêmes conditions avec 2.5 équiv. de bromure d'éthyle on recueille après 12 h à température ambiante, 67% de composé *N,S*-diéthylé (5.5 g) et 2% de composé *N,N'*-diéthylé. L'analyse a été effectuée par spectrométrie de masse (40).

Synthèse du méthyl-1 acétonylthio-2 imidazole

Une mixture de 7.5 de méthyl-1 Δ-4-imidazolinethione-2 et 6.8 g de chloracétone est placée dans 400 cm^3 de butanone-2. Après 3 h de reflux et évaporation partielle du solvant, refroidissement et filtration, on obtient le chlorhydrate que l'on reprend par l'eau et que l'on neutralise par une solution de carbonate saturé. On extrait au chloroforme et on sèche sur sulfate de sodium. Après évaporation du solvant de distillation, on recueille le thioéther (pé 104°C/2 Torr; rendement 25%) (3, 48).

Synthèse de la triméthyl-1,4,5 Δ-4-imidazolinethione-2

Une mixture de 0.2 mol de *N*-méthylthiourée et 0.2 mol d'acétoïne est mis à reflux 12 h dans 100 mL de pentanol-1[4] ou hexanol-1 (16). Après distillation azéotropique, le mélange est refroidi. Le solide formé est recristallisé dans l'éthanol. Le rendement est de 25% (pf 216°C). La purification est effectuée par chromatographie préparative (C_6H_6–AcEt 80:20) sur silice.

Synthèse de la tétraméthyl-1,3,4,5 Δ-4-imidazolinethione-2

La thione est obtenue par chauffage à reflux d'un mélange équimoléculaire de *N,N'*-diméthylthiourée et d'acétoïne dans l'hexanol-1 (16).

1. J. METZGER. Brevet Fr. no 7,328,538 (novembre 1973).
2. J. KISTER. Thèse Spécialité, Marseille. 1974.
3. J. KISTER. Thèse Sciences, Marseille. 1977.
4. J. KISTER, G. ASSEF, H. J. M. DOU et J. METZGER. Tetrahedron, **32**, 1395 (1976).
5. G. ASSEF, J. KISTER, G. MILLE et J. METZGER. C. R. Acad. Sci. Ser.C, **284**, 273 (1977).
6. A. CHAMBONNET. Thèse Dr. Ing., Marseille. 1962.
7. G. ASSEF. Thèse Spécialité, Marseille. 1976.
8. M. CHANON. Bull. Soc. Chim. Fr. **7**, 2968 (1968); **7**, 2981 (1968).
9. M. CHANON, M. CONTE, J. MICOZZI et J. METZGER, Int. J. Sulfur Chem. Part C, **6**, 85 (1971).
10. F. P. REED, A. ROBERTSON et W. A. SEXTON. J. Chem. Soc. 473 (1938).
11. B. BEILENSON et F. M. HAMER. J. Chem. Soc. 143 (1939).
12. C. G. MORE et E. S. WAIGHT. J. Org. Chem. **17**, 4237 (1952).
13. J. J. D'AMICO, R. H. CAMPBELL, S. T. WEBSTER et CH. E. TWINE. J. Org. Chem. **30**, 3625 (1965).
14. (*a*) G. ASSEF, J. KISTER et J. METZGER. Bull. Soc. Chim. Fr. Sous presse; (*b*) J. KISTER, G. ASSEF, G. MILLE et J. METZGER. Can. J. Chem. Ce numéro.
15. J. KISTER et J. METZGER. Communication Société Chimique de France, Palaiseau, 1978, et Phosphorus and Sulfur (en cours).
16. G. KJELLIN et J. SANDSTRÖM. Acta Chem. Scand. **23**, 2879 (1969).
17. H. B. KÜNNE. Chem. Ber. **28**, 2036 (1895).
18. R. ANSCHUTZ et K. SCHWIEKERATH. Justus Liebigs Ann. Chem. 284 (1895).
19. A. BASE et H. KLINGER. Chem. Ber. **31**, 1217 (1898).
20. P. M. KOCHERGIN. J. Gen. Chem. USSR, **31**, 1010 (1961).
21. P. M. KOCHERGIN, V. E. BOGACHEV et M. G. FOMENKO. Brevet USSR no 137,517 (1960).
22. A. LESPAGNOL, C. LESPAGNOL et P. MARCINAL. Chim. Ther. **5/6**, 292 (1966).
23. S. GABRIEL et T. POSNER. Chem. Ber. **27**, 1038 (1894).
24. A. WOHL et W. MARCKWALD. Chem. Ber. **22**, 1352 (1889).
25. W. MARCKWALD. Chem. Ber. **25**, 2354 (1892).
26. A. WOHL et W. MARCKWALD. Chem. Ber. **22**, 568 (1889).
27. R. G. JONES et E. C. KORNFELD. J. Am. Chem. Soc. **71**, 4000 (1949).
28. I. B. SIMON et I. I. KOVTUNOVSKAYA. Zh. Obshch. Khim. **25**, 1226 (1955).
29. L. KNORR. Chem. Ber. **32**, 729 (1899).
30. V. C. PAAL et L. V. GEMBER. Arch. Pharm. **T246**, 306 (1905).
31. A. WOHL et M. LANGE. Chem. Ber. **41**, 17 (1908).
32. L. RUGHEIMER et P. SHON. Chem. Ber. **41**, 17 (1908).
33. A. P. T. EASSON et F. L. PYMAN. J. Chem. Soc. 1806 (1932).
34. I. B. SIMON et I. I. KOVTUNOVSKAYA-LEVSHINA. Tr. Ukr. Inst. Eksp. Endokrinol. **18**, 345 (1901).
35. R. G. JONES. J. Am. Chem. Soc. **71**, 644 (1949).
36. A. WOHL et M. LANGE. Chem. Ber. **40**, 4727 (1907).
37. A. A. BITE. Khim. Geterotsikl. Soedin. **2**, 329 (1968).
38. S. CARBONI, E. GROTHE et M. F. SAETTONE. J. Pharm. Sci. **57**, 1063 (1968).
39. H. ZELLER. Brevet Autrichien no 176,560 (1953).
40. P. HASSANALY, H. J. M. DOU, J. METZGER, G. ASSEF et J. KISTER. Synthesis, **4**, 253 (1977).
41. H. J. M. DOU, P. HASSANALY, J. KISTER et J. METZGER. Phosphorus Sulfur, **3**, 355 (1977).
42. H. J. M. DOU, P. HASSANALY, J. KISTER, G. VERNIN et J. METZGER. Helv. Chim. Acta, **61**, 3143 (1978).
43. H. J. M. DOU et J. METZGER. Bull. Soc. Chim. Fr. **11/12**, 1801 (1976).
44. H. J. M. DOU. Actual. Chim. 41 (1976).
45. H. KOMEILI-ZADEH, H. J. M. DOU et J. METZGER. C.R. Acad. Sci. Ser C, **283**, 41 (1976).
46. A. JONCZYK, K. BANKO et M. MAKOSZA. J. Org. Chem. **40**, 266 (1975).
47. A. JONCZYK, M. FEDROYNSKI et M. MAKOSZA. Tetrahedron Lett. **23**, 2395 (1972).
48. D. L. GARMAISE et A. P. GAUNCE. J. Org. Chem. **33**, 4422 (1968).
49. (*a*) G. ASSEF, D. BOUIN-ROUBAUD, J. KISTER et J. METZGER. C.R. Acad. Sci. Ser. C, **283**, 143 (1976); (*b*) J. KISTER, D. BOUIN-ROUBAUD, H. J. M. DOU, P. HASSANALY et J. METZGER. C.R. Acad. Sci. Ser. C, **287**, 201 (1978).
50. G. MILLE, J. KISTER, G. ASSEF et J. CHOUTEAU. C.R. Acad. Sci. Ser. C, **286**, 477 (1978).
51. (*a*) G. ASSEF, J. KISTER, J. METZGER, R. FAURE et E. J. VINCENT. Tetrahedron Lett. **37**, 3313 (1976); (*b*) R. FAURE, E. J. VINCENT, G. ASSEF, J. KISTER et J. METZGER. Org. Magn. Reson. **9**, 688 (1977).

[4]C. Roussel. Communication personelle.

Synthèse et étude du réarrangement SR ⇋ NR des diazoles-1,3 : alkyl-1 alkylthio-2 (allylthio, arylthio, cycloalkylthio) imidazoles. Partie II. Réarrangement et réactions parasites

JACKY KISTER,[1] GEORGES ASSEF,[1] GILBERT MILLE[2] ET JACQUES METZGER[1]

Faculté des Sciences et Techniques, Aix-Marseille III, Rue Henri Poincaré – Saint Jérôme, 13397, Marseille, France

Reçu le 2 octobre 1978

JACKY KISTER, GEORGES ASSEF, GILBERT MILLE et JACQUES METZGER. Can. J. Chem. **57**, 822 (1979).

Les études cinétiques de la réaction de réarrangement SR ⇋ NR ont été réalisées à diverses températures sur les composés de type alkyl-1 alkylthio (ou allylthio, arylthio, cycloalkylthio)-2 imidazoles. Ces études de réarrangement et d'hydrolyse ont été comparées à celles menées sur les alkyl-1 méthylthio-2 Δ-2-imidazolines et Δ-2-tétrahydropyrimidines. Les effets électroniques et stériques sont discutés et un parallèle pK_a–réarrangement est proposé. La limite de ce parallèle est d'ordre structural, due à des interactions stériques directes (effet *ortho*) ou indirectes (déformation de cycle) ou à des modifications géométriques des hétérocycles étudiés (cycles à cinq ou six chaînons). L'ensemble de ces résultats a permis le choix cohérent du substrat d'amplification d'un procédé photographique non conventionnel.

JACKY KISTER, GEORGES ASSEF, GILBERT MILLE, and JACQUES METZGER. Can. J. Chem. **57**, 822 (1979).

The kinetics of the SR ⇋ NR rearrangement reaction for a series of 1-alkyl-2-alkylthio (or allylthio, arylthio, cycloalkylthio) imidazoles has been studied at various temperatures. The rearrangement and hydrolysis results have been compared with those of 1-alkyl-2-methylthio-Δ-2-imidazolines and 1-alkyl-2-methylthio-Δ-2-tetrahydropyrimidines. Electronic and steric effects are discussed and a parallel between pK_a and rearrangement is proposed. The limit of this parallel is either a structural effect such as direct (*ortho* effect) or indirect (cycle deformation) steric interactions or geometric modifications of the heterocycles studied (five- or six-membered cycles). All these results permitted the coherent choice of the amplification compound of a nonconventional photographic process.

Introduction

Dans un premier mémoire nous avons décrit la synthèse et les études physicochimiques des alkyl-1 alkylthio-2 (ou allylthio, arylthio, cycloalkylthio) imidazoles (1).

Récemment nous avons rapporté l'étude du réarrangement SR ⇋ NR des méthyl-1 méthylthio-2 imidazole, Δ-2-imidazoline et Δ-2-tétrahydropyrimidine, ainsi que les réactions secondaires s'y rattachant (2–5). Ces études sont liées au développement d'un procédé photographique non argentique dans lequel la réaction de réarrangement SR ⇋ NR constitue l'étape d'amplification du signal photochimique primaire (2, 3, 6).

Plusieurs travaux concernant des thioéthers de séries azahétérocycliques montrent l'influence de la nature de l'hétérocycle et de sa substitution sur le taux de réarrangement (7–13). Recherchant des conditions d'amplification du signal photographique assez douces, nous nous sommes intéressés dans un premier temps à l'influence de la *N*-substitution sur le réarrangement de composés des séries apparues comme les plus réactives dès 1974 (2): les séries imidazolinique et tétrahydropyrimidine (3, 14, 15).

L'existence de réactions secondaires parasites provoquant, soit un réarrangement parasite, soit une suite de réactions de dégradation, a orienté nos travaux vers des séries moins réactives *a priori*, mais présentant l'avantage de ne pas être le siège de réactions secondaires importantes (2, 5). Ainsi nous avons synthétisé les thioéthers de la série imidazolique, en faisant varier la substitution de l'azote N_1, du soufre S_2 et éventuellement des positions 4 et 5 de l'hétérocycle (fig. 1) (13, 14). Les thioéthers **5**, **6** et **7** sont donc susceptibles de présenter des différences intéressantes avec leurs homologues méthylés en position 1 et 2 et leurs homologues des séries saturés à cinq ou six chaînons. L'analyse des résultats de cinétique du réarrangement SR ⇋ NR nous permet de comparer les effets de substitution pour les divers hétérocycles à cinq ou six chaînons et par là même, d'analyser l'effet du cycle.

Une étude plus générale des relations qui existent entre le taux de réarrangement et le pK_a des thioéthers menée sur des composés hétérocycliques ben-

[1]Laboratoire de Chimie Moléculaire et de Pétroléochimie. Contrat DRME 77/003.

[2]Centre de Spectroscopie Moléculaire.

0008-4042/79/070822-09$01.00/0

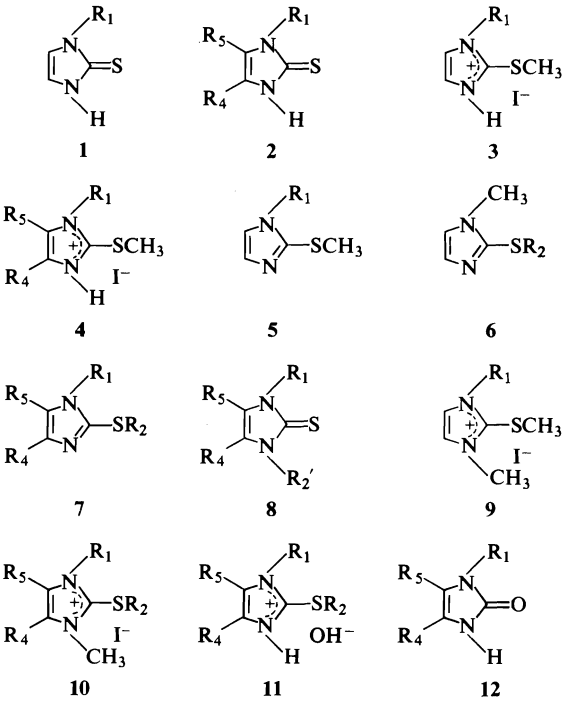

FIG. 1. Composés imidazoliques *N*- et *S*-substitués et composés substitués en position 4 et 5.

zocondensés, aromatiques ou saturés à cinq ou six chaînons rend possible une analyse cohérente des effets structuraux (effet de cycle, de champ, de substitution) (3). Cette généralisation fera l'objet d'un mémoire indépendant (16).

Etude du réarrangement autocatalytique ionique SR⇋NR des thioéthers 5, 6 et 7

Généralités

Le mécanisme de cette réaction est identique à celui décrit pour les alkyl-1 méthylthio-2 Δ-2-imidazolines et Δ-2-tétrahydropyrimidines (2–4, 14 et 15). Bien que plusieurs mécanismes aient été discutés (2–5, 7–15), c'est celui de type Chambonnet et d'Amico qui a été adopté (2, 7). Le réarrangement SR ⇋ NR est donc un réarrangement autocatalytique ionique contrôlable thermiquement pouvant être schématisé de la façon répresentée dans le schéma 1. Cette réaction correspond à un mécanisme de substitution nucléophile bimoléculaire (S_N2). Le caractère intermoléculaire et la réversibilité du réarrangement ont été étudiés (9) en série thiazolique. Dans le cas des diazoles et diazines-1,3, nous avons vérifié ce

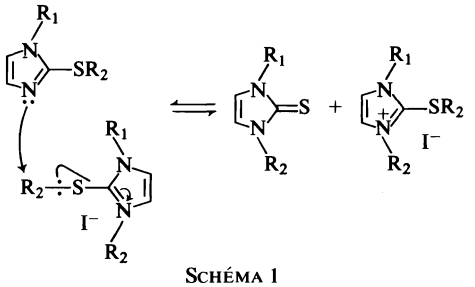

SCHÉMA 1

caractère intermoléculaire de la réaction. Celle-ci est bien réversible, mais pratiquement déplacée vers la forme thione. Nous avons vérifié la non élimination du groupe migrant en étudiant la réaction de réarrangement du méthyl-1 isopropylthio-2 imidazole en présence de 3% mol d'iodure de méthyl-1 isopropylthio-2 isopropyl-3 imidazolium. Nous n'avons observé que du produit résultant de la S_N2, sans aucune trace de produit d'élimination (12, 14).

Les thioéthers **5**, **6** et **7** examinés sont généralement purifiés par distillation sur potasse et conservés sur potasse afin d'éviter les réactions parasites dues à l'eau résiduelle (2–5, 14, 15). Pour chaque substrat nous contrôlons la stabilité thermique en vérifiant ainsi l'existence et l'importance des réactions parasites. Rappelons que le méthyl-1 acétonylthio-2 imidazole ne peut être purifié et conservé sur potasse du fait de la possibilité de réaction de Darzens (17–18). Cette même réaction ne permet pas la synthèse de ce thioéther par catalyse par transfert de phase (1). Nous effectuerons donc à diverses températures la cinétique de réarrangement des substrats d'amplification suivants: alkyl-1 (aryl-1) méthylthio-2 imidazoles, **5**; méthyl-1 alkylthio-2 (benzylthio...) imidazoles, **6**; et triméthyl-1,4,5 méthylthio-2 imidazole, **7**.

Conditions d'étude du réarrangement SR ⇋ NR

Elles sont du même type que celles retenues pour l'étude des thioéthers des séries imidazolinique et tétrahydropyrimidinique (2–5, 14–15). Les études sur les thiazolines étaient réalisées en ampoules scellées à l'étuve, en présence d'iodure de méthyle formant *in situ* le sel quaternaire, véritable catalyseur de la réaction (8, 9).

Ici, nous étudions la cinétique de migration S → N d'une façon différente: les transpositions sont réalisées dans un microballon ouvert, la phase liquide étant continuellement agitée et maintenue à une température régulée (2–4). Le catalyseur utilisé sera toujours le véritable catalyseur correspondant au sel quaternaire issu de la quaternisation par l'iodure de méthyle du thioéther étudié (1). Ces catalyseurs (**9** et **10**) qui sont donc les sels quater-

TABLEAU 1. Pourcentage de thione en fonction du temps, de la température et du substituant R_1 sur N_1: cas des alkyl-1 (phényl-1) méthylthio-2 imidazoles

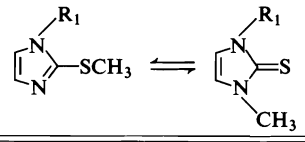

		Temps (min)							
R_1	°C	0	5	15	30	45	60	120	160*
Me	140	0	20.0	28.96	42.22		47.73	53.84	1.5
	120	0	6.66	12.50	16.30	21.38	23.57	32.14	1.0
Et	140	0	23.4	30.5	46.9		52.8	58.4	2.9
	120	0	8.5	20.7	29.3		37.5	40.8	2.3
*i*Pr	140	0	28.57	42.71	55.04		66.38	67.0	3.20
	120	0	17.85	32.25	40.29		48.38	53.73	1.56
*t*Bu	140	0	23.0	40.0	45.80	49.37	52.79	60.0	3.05
	120	0	6.97	23.40	30.43		40.91	50.0	2.50
Phényle	140	0	15.69	23.85	29.25		35.25	40.0	<1
	120	0	9.45	14.81	20.0		22.33	26.5	<1

*Stabilité.

TABLEAU 2. Pourcentage de thione en fonction du temps et du substituant R_2 sur le soufre (T = 140°C): cas des méthyl-1 alkylthio (allylthio, benzylthio, acétonylthio)-2 imidazoles

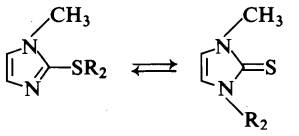

	Temps (min)							
R_2	5	15	30	60	90	120	150	160*
Me	20.0	28.96	42.22	47.78			53.84	1.5
Et			32.69	41.66	50.98		60.0	5.0
*i*Pr			8.69	13.04	16.66		28.26	4.6
Allyle		29.27	44.44	54.17		78.13	80.77	35.90
Benzyle		79.41	88.23	93.0		94.74	96.0	30.0
Acétonyle	23.0	37.0	47.0	67.0			74.0	7.5

*Stabilité.

naires iodés des thioéthers sont les plus efficaces (9, 14), ils sont synthétisés, isolés et purifiés par double recristallisation dans l'éthanol anhydre (1). L'influence de l'anion associé du catalyseur sera étudiée pour le méthyl-1 méthylthio-2 imidazole. Le taux de catalyseur retenu pour l'étude cinétique est de 3% mol.

Nous avons recherché différents modes de dosage. Le dosage par spectrométrie ultraviolette s'est avéré inutilisable par suite de la grande analogie entre les spectres ultraviolets des formes thioéthers **5**, **6** et **7** et thiones de transposition **8** dans le cas des diazoles et diazines-1,3 (1, 19). Nous avons envisagé un mode de dosage par spectrographie de masse utilisable en phase adsorbée en présence de semi-conducteur et de liant (conditions technologiques liées au procédé photographique). L'étude en phase liquide a montré la possibilité théorique de réarrangement, mais le manque de précision, dû au mélange hétérogène entre thioéther (le plus souvent liquide) et thione (solide) nous a obligé à revenir au mode classique de dosage par résonance magnétique nucléaire du proton mis au point en 1974 (2, 4).

Lors de la transposition, des prélèvements sont effectués à intervalles de temps réguliers et la réaction est subitement arrêtée après chaque prélèvement par refroidissement. La précision de ce dosage est de l'ordre de 3%. Les quantités de thioéther utilisées par étude cinétique sont de 1 g, permettant ainsi six prélèvements.

Le calcul du taux de réarrangement s'effectue par l'étude en rmn du ^1H de la disparition de la bande du groupe SMe ou SR du thioéther en faveur de l'apparition de la bande NMe ou NR de la thione (2–4).[3] Les tableaux 1 et 2 et la fig. 2 donnent les taux

[3]Toutes les caractéristiques de synthèse et caractéristiques physico-chimiques nécessaires à l'étude et au dosage du réarrangement des thioéthers en thiones sont indiquées dans la réf. 1.

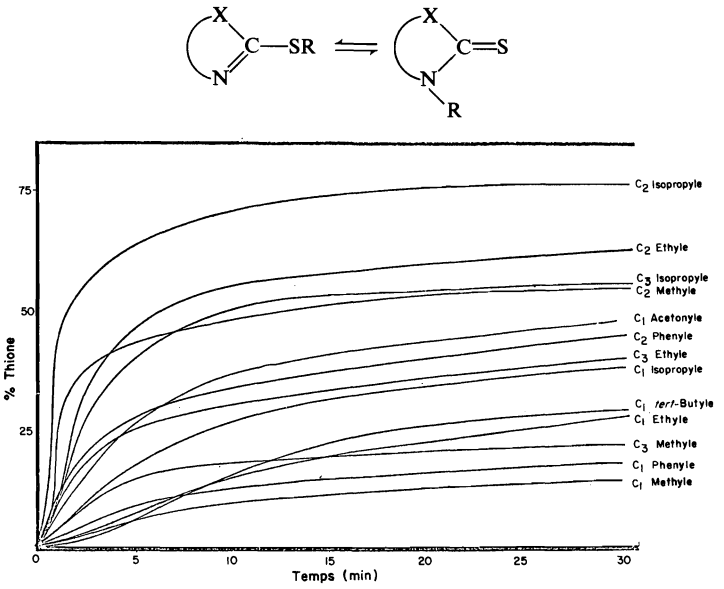

FIG. 2. Pourcentage de thione en fonction du temps, du substituant R_1 sur N_1 et du cycle ($T = 120°C$): cas des alkyl-1 methylthio-2 imidazoles, des alkyl-1 methylthio Δ-2-imidazolines et des alkyl-1 methylthio-2 Δ-2-tétrahydropyrimidines.

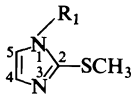
Alkyl-1 méthylthio-2 imidazole (C_1)

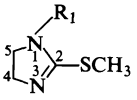
Alkyl-1 méthylthio-2 Δ-2-imidazoline (C_2)

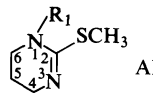
Alkyl-1 méthylthio-2 Δ-2-tétrahydropyrimidine (C_3)

$R_1 = CH_3, C_2H_5, iC_3H_7, tC_4H_9$ et C_6H_5

de réarrangement en thione en fonction du temps, de la température et de la structure du thioéther.

Phénomènes secondaires

Quand les thioéthers ne sont pas purifiés et conservés sur potasse ou quand ces substrats sont en présence d'eau, deux types de réactions parasites sont mises en évidence: *le réarrangement parasite* et les *réactions de dégradation* (2–5, 14–16). L'existence d'un intermédiaire tétraêdrique en équilibre avec un hydroxyde d'ammonium quaternaire **11** formé par hydrolyse des thioéthers a été démontrée en 1974 (2, 4) et généralisée aux composés des séries diazolique et diazinique-1,3 *N*-substituées (3, 5, 14, 15). La structure du sel **11** est proche de celle des sels **3** et **4**, intermédiaires de synthèse des thioéthers **5**, **6** et **7** obtenus à partir des thiones **1** et **2** (1). Nous ne rappelerons donc que les conclusions intéressant les composés diazoliques-1,3.

L'étude de la stabilité thermique (sans catalyseur) de ces substrats nous a permis de montrer que les réactions "*sans catalyseur*" sont en réalité des réactions autocatalytiques ioniques de type Chambonnet (7) catalysées par un sel parasite formé *in situ* par hydrolyse lente du thioéther. Le mécanisme a déjà été décrit (2–5, 14–15). Alors qu'un thioéther distillé sur potasse reste stable à 140°C (cf. tableau 1), l'adjonction de traces de sel formé par hydrolyse et préalablement isolé et identifié, provoque un *réarrangement parasite* qui conduit aux thiones de transposition classique **8** (2, 4).

L'étude des thioéthers imidazoliniques et tétrahydropyrimidiniques, nous a permis de proposer un mécanisme général de compétition entre cette voie de catalyse parasite et des voies de dégradations passant par un intermédiaire tétraêdrique (2–5, 14–15) (schéma 2).

Nous avons déjà montré que la prépondérance de l'une ou de l'autre voie dépend de la structure et de la substitution de l'hétérocycle (2, 3, 14). Dans le cas des composés imidazoliques, seule la voie *1* → *2* a pu être mise en évidence. Aucun composé de dégrada-

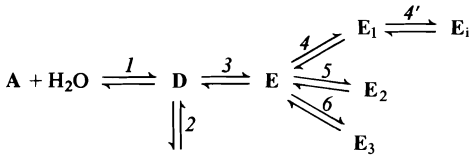

Réarrangement parasite

A Thioéther
D Hydroxyde d'ammonium quaternaire
E Intermédiaire tétraédrique
E_i Composés de dégradation

SCHÉMA 2. Réactions parasites: la voie *1* → *2* correspond à la catalyse parasite; les voies *1* → *3* → *4*, *1* → *3* → *5*, *1* → *3* → *6*, ... correspondent aux voies de dégradation.

tion n'a été identifié et les intermédiaires **D** et **E** n'ont pas été isolés. Contrairement aux composés imidazoliniques et tétrahydropyrimidiniques (2–4, 14–15), ces réactions parasites sont de faibles importances et la purification par simple distillation sur potasse permet d'obtenir une très bonne stabilité par chauffage (tableaux 1 et 2). Nous verrons que la substitution peut intervenir directement sur l'importance et l'existence de cette catalyse parasite

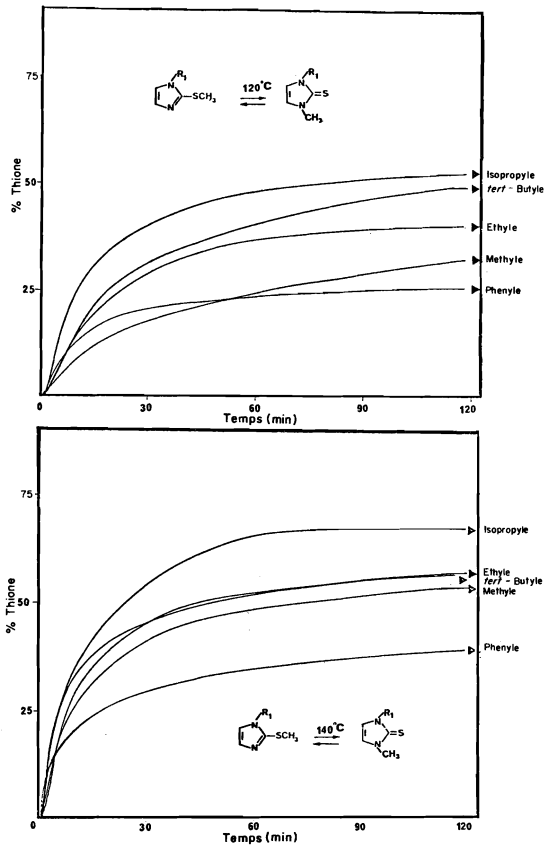

FIG. 3. Pourcentage de thione en fonction du temps et du substituant sur N_1 à 120 et 140°C: cas des alkyl (aryl)-1 méthylthio-2 imidazoles.

comme nous l'avons déjà démontré pour les alkyl-1 méthylthio-2 Δ-2-imidazolines et Δ-2-tétrahydropyrimidines (14–15).

Interprétation des résultats

Etude du réarrangement SR ⇋ NR: modifications structurales

Une analyse des tableaux 1 et 2 et des courbes *1–4* montre bien la variation du taux de réarrangement SR ⇋ NR en fonction de la substitution en position N_1 et S_2 et en fonction de la grandeur ou de l'aromaticité du cycle.

Influence du substituant R_1 fixé sur l'azote N_1 (fig. 3)

Au sein d'une même famille, nous notons une augmentation du taux de réarrangement en thione allant du méthyle à l'isopropyle, puis une décroissance pour les groupements *tert*-butyle et phényle en position 1.

La croissance du taux de réarrangement des groupements méthyle, éthyle et isopropyle s'explique par un effet électronique dû au groupement alkyle R_1. Cet effet inductif donneur du groupement R_1 tend à augmenter la densité électronique sur l'azote N_3 et ainsi renforce la nucléophilie de cet azote N_3. *A une augmentation du pK_a correspond une augmentation du taux de réarrangement.* L'abaissement du taux de thione transposée dans le cas du *tert*-butyle est dû à une gêne stérique qui l'emporte sur l'effet inductif. L'étude de rmn du ^{13}C confirme bien cette déformation du cycle diazolique (20).

Comme le montre le schéma 3, on peut penser que les substituants méthylthio sont repoussés par les groupements *tert*-butyle et ainsi les méthylthio du substrat et du catalyseur entrent en interaction. L'abaissement dans le cas du composé porteur du phényle en position N_1 est dû à un effet électronique. Ce groupement a tendance à attirer les électrons de l'azote N_3 pour se conjuguer avec l'ensemble du cycle. *Ainsi à un abaissement de pK_a correspond un abaissement du taux de réarrangement.* L'augmenta-

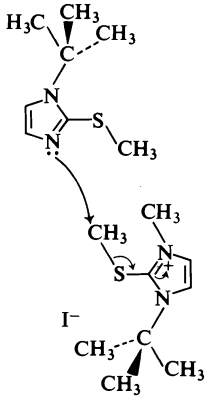

SCHÉMA 3

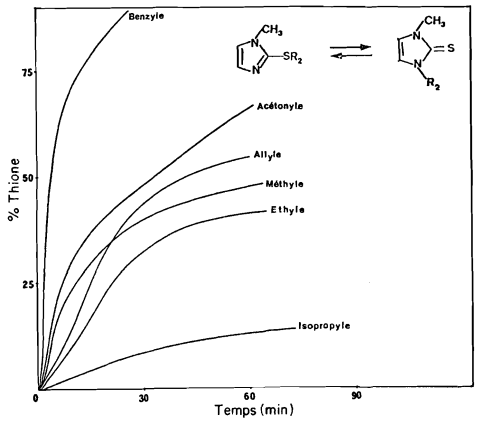

FIG. 4. Pourcentage de thione en fonction du temps et du substituant R_2 sur le soufre (T = 140°C): cas des méthyl-1 alkylthio (allylthio, acétonylthio et benzylthio)-2 imidazoles.

tion du taux de réarrangement pour R_1 = isopropyle est due à l'augmentation de l'effet inductif, la gêne stérique étant atténuée du fait d'une configuration privilégiée.

Influence du substituant R_2 fixé sur le soufre (fig. 4)

Dans le cas où R_2 = éthyle et isopropyle, nous observons une baisse du taux de réarrangement, baisse beaucoup plus significative pour l'isopropyle. Le réarrangement SR ⇌ NR se faisant par mécanisme S_N2, l'attaque du substrat se fera d'autant plus difficilement que le groupement R_2 est encombrant.

Dans le cas d'un groupement benzyle, nous constatons un accroissement du taux de réarrangement. La réaction S_N2 passe par un état de transition de type Y --- C --- X. Toute insaturation sur le carbone en α du carbone central augmente la stabilité de l'intermédiaire par une possibilité de conjugaison et par là même, influe sur la réactivité du substrat.

Pour le substrat substitué par un groupement allylthio, comme précédemment, l'intermédiaire réactionnel est stabilisé par conjugaison, la stabilisation étant inférieure à celle du méthyl-1 benzylthio-2 imidazole. Remarquons que le substrat chauffé seul sans catalyseur, donne un taux de réarrangement important. En accord avec Hayami et coll. (21) nous pouvons admettre qu'un mécanisme concerté se superpose à la réaction S_N2.

Le cas de la substitution par un groupement acétonyle est un peu plus délicat. En phase liquide ce substituant provoque un accroissement du taux de réarrangement. Ainsi le méthyl-1 méthylthio-2 imidazole donne 42% de thione à 140°C en 30 min et le méthyl-1 acétonylthio-2 imidazole donne 47% dans les mêmes conditions. Cet effet est classique et vérifié aussi pour les séries imidazolinique et tétrahydropyrimidinique. Cependant en phase adsorbée sur semi-conducteur (oxyde de titane type anastase AT_1 (Thann et Mulhouse)), le taux de réarrangement devient inférieur à celui du méthyl-1 méthylthio-2 imidazole par stabilisation du groupe migrant par complexation (3).

Influence des substituants fixés en position 4 et 5

Indépendamment des variations de substituants en position 1 et 2, nous pouvons étudier l'influence des substituants en position 4 et 5. L'analyse qui en résulte diffère fondamentalement des effets de pK_a. Ainsi, lors d'une étude afférente au doublet de l'azote dans la série du thiazole, conduite simultanément par une étude cinétique d'alcoylation et une étude d'équilibre de protonation, Chanon *et al.* (22) dégage deux effets de substitution.

Les premiers sont les effets électroniques transmis par le squelette, qui peuvent augmenter la réactivité au niveau du doublet de l'azote (cas du méthylthio-2 méthyl-5 thiazole), ou la diminuer (cas du méthylthio-2 thiazole). Ces effets sont additifs et sont traduits directement par le pK_a (3).

Le second effet est transmis à travers l'espace et il est de nature stérique. Dans le cas d'encombrement *ortho/ortho*, les effets sont exaltés par rapport à ce qu'on aurait pu attendre par simple additivité. Ainsi en position 4, l'influence d'un méthyle est remarquable: par son effet électronique, il devrait augmenter la constante de vitesse de quaternisation et le taux de réarrangement comme il augmente le pK_a. Au contraire, l'effet stérique provoque une diminution de la constante de vitesse et du taux de réarrangement.

On retrouve alors l'ordre de quaternisation et de réarrangement suivant (les deux réactions étant de type S_N2):

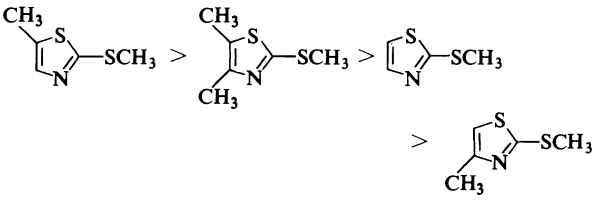

De tels effets de substitution seront particulièrement intéressants au niveau du choix de substrat de réarrangement dans la *série imidazolique*. Nous avons vérifié cet aspect prévisionnel en étudiant les composés **b** et **c**. Ainsi le méthyl-1 méthylthio-2 imidazole (pK_a = 5.5) donne 48% de thione à 140°C en 60 min et le triméthyl-1,4,5 méthylthio-2 imidazole (pK_a = 6.68) donne 57% dans les mêmes conditions (**b** > **c**).[4]

[4]La détermination des pK_a des divers hétérocycles étudiés a été réalisée par corrélations ou approximation à partir des composés étudiés par Perrin (23), Katritzky et Lagowski (24), Chanon *et al.* (22), Kjellin et Sandström (25), Deady (26) et Gonzalez (27). On retrouvera une étude complète des pK_a dans les références (3, 16, 28).

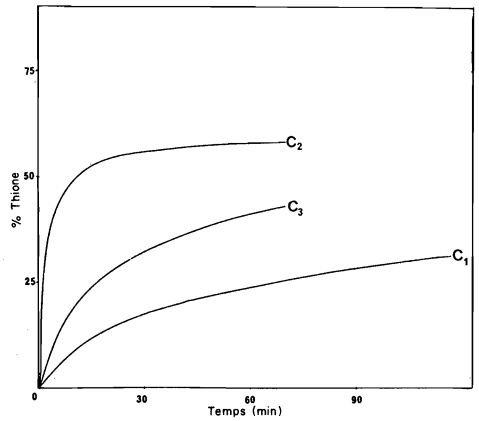

FIG. 5. Pourcentage de thione en fonction du temps et du cycle: cas des méthyl-1 méthylthio-2 imidazole (C_1), des méthyl-1 méthylthio-2 Δ-2-imidazoline (C_2) et des méthyl-1 méthylthio-2 Δ-2-tétrahydropyrimidine (C_3).

L'effet accélérateur (pK_a) est nuancé par l'effet ralentisseur de l'*ortho*-substitution (effet stérique):

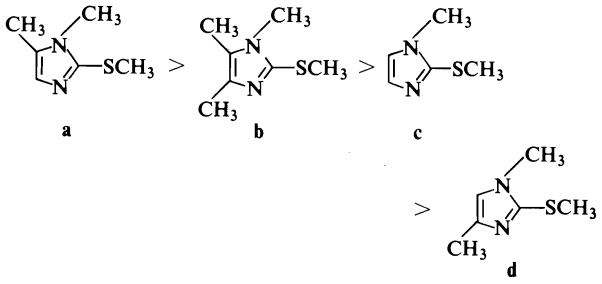

Effet de cycle (*figs. 2 et 5*)

On peut raisonner de la même façon pour les cycles saturés à cinq et six chaînons et les effets de substitution 44′/55′ en série imidazolinique. Toujours dans le même esprit, regardons le passage d'un cycle à cinq à un cycle à six chaînons:

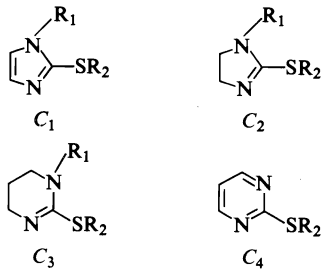

L'échelle des pK_a de ces composés (3, 16, 28) correspond à $C_3 > C_2 \gg C_1 > C_4$. L'ordre expérimental de réarrangement (3) correspond à $C_2 > C_3 \gg C_1$. Si nous observons ces échelles, nous constatons un fort accroissement du taux de réarrangement par passage des séries C_1 à C_2. Cet accroissement correspond à une augmentation importante du pK_a. Par contre l'étude des composés de la série des tétrahydropyrimidines (C_3) fait intervenir un facteur stérique supplémentaire, qui est le passage du cycle à cinq au cycle à six chaînons. La principale différence observée dans ces séries est donc une modification structurale. Il semble donc que le parallèle pK_a–réarrangement ne puisse être appliqué qu'à des structures comparables. Cette remarque avait déjà été faite par Deady (26) et Chanon *et al.* (9) lors de la comparaison de thiazoles et pyridines. La série pyrimidinique (C_4) présente pour le réarrangement des effets de pK_a et des effets stériques (six chaînons) défavorables. Synthétisés par catalyse par transfert de phase (29) ces composés ont un taux de migration S → N pratiquement nul en 1 h à 140°C (3).

Le parallèle pK_a–réarrangement est évident. Comme la quaternisation, le réarrangement est une réaction de type S_N2. Toute corrélation établie pour la quaternisation sera donc applicable à l'optimisation du substrat d'amplification. Nous venons de voir que l'effet de substitution en N_1 répond aussi au parallèle pK_a–réarrangement. Les limites à ce parallèle sont des limites stériques qui peuvent être indirectes ($R_1 = t$Bu) ou directes (*ortho*-substitution). Cependant à partir des figs 1 et 4, on constate que les séries C_2 et C_3 (15) sont plus sensibles à la *N*-substitution que la série C_1. Dans la série aromatique les effets électroniques sont beaucoup plus dilués que dans les séries imidazolinique et tétrahydropyrimidinique, où la délocalisation électronique se limite aux azotes N_1 et N_3. Cette observation est vérifiée en particulier par les études de rmn du carbone-13 (20) au niveau de l'effet de la *N*-substitution sur les carbones 2 et 5 ou 2 et 6 dans les séries à cinq ou six chaînons, et principalement, dans le cas particulier du groupement *tert*-butyle.

En réaction de réarrangement comme en rmn du ^{13}C, ou en spectroscopie ultraviolette (19), l'écart observé entre les thioéthers **5** ou thiones **1** et **8** substitués par les groupements éthyle, isopropyle et *tert*-butyle est maximum pour les séries imidazolinique et tétrahydropyrimidinique.

Effets de température sur le taux de réarrangement (*fig. 6*)

La fig. 6 et le tableau 1 traduisent ces effets. Les thioéthers de la série imidazolinique (C_1) étant moins réactifs que ceux des séries imidazolinique (C_2) et tétrahydropyrimidinique (C_3), les études sont le plus souvent menées à 140°C (15).

Effets des catalyseurs (*influence de l'anion associé*)

Ces effets ont déjà été discutés en série thiazolique (9); c'est d'ailleurs ce qui avait orienté le choix *de nos sels quaternaires* ***9*** *et* ***10****, comme catalyseurs optimum: "les iodures de méthyl-3 azolium."*

Nous avons étudié le réarrangement SR ⇌ NR du méthyl-1 méthylthio-2 imidazole à 140°C catalysé

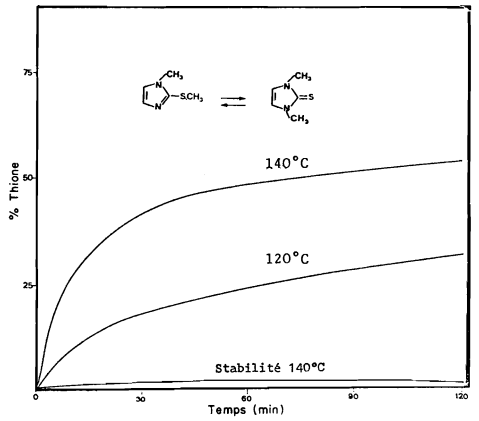

FIG. 6. Pourcentage de thione en fonction du temps et de la température: cas du méthyl-1 méthylthio-2 imidazole.

par les sels de type iodure, tosylate, chlorure de diméthyl-1,3 méthylthio-2 imidazolium (3% mol).

La réaction de réarrangement étant une réaction de type S_N2, nous retrouvons l'échelle établie pour la quaternisation ..... $I^- > TSO^- > Cl^-$ ..... Expérimentalement nous obtenons un taux de 50% en 1 h pour l'iodure, 37% en 1 h pour le tosylate et 10% en 1 h pour le chlorure.

Ces mêmes expériences effectuées en présence d'iode ou de tosylate de méthyle (3% mol) en ampoule scellée à 140°C donnent les résultats suivants: 80% de réarrangement en 2 h pour l'iode et 25% de réarrangement en 2 h pour le tosylate de méthyle.

Ces résultats sont proches de ceux obtenus par Chanon *et al.* en série thiazolique (9). L'explication de ces résultats est purement mécanistique et suggère la présence de légère quantité d'iodure de méthyle libre dans le milieu (9).

Réactions parasites

Contrairement aux thioéthers des séries imidazolinique et tétrahydropyrimidinique (4, 5, 15) aucun intermédiaire de type **11** ou composés de dégradation de type **12** n'a été isolé ou identifié en phase liquide.

Seule la voie de catalyse parasite *1,2* (schéma 2) a pu être mise en évidence (tableau 1). Cependant, d'une façon générale cette réaction parasite est trés faible et une simple distillation sur potasse limite le "back-ground" à 3%. Le taux de réarrangement sans catalyseur pour les benzylthio-2 et allylthio-2 imidazoles, traduit un mécanisme de migration différent de la réaction de réarrangement du type Chambonnet mécanisme concerté (21), réaction de Claisen ou Chapman. Il semble que cette hydrolyse parasite soit favorisée par les mêmes conditions que celles qui favorisent le réarrangement, cependant les variations de réactivité des thioéthers vis-à-vis de l'eau sont beaucoup plus importantes pour les séries imidazolinique et tétrahydropyrimidinique. Ces réactions parasites peuvent devenir très importantes sur support semi-conducteur selon la nature et la variété cristalline du support (TiO_2AT ou RL, ZnO, Al_2O_3, SiO_2, etc.).

Ainsi les composés de dégradation $\mathbf{E}_i$ (schéma 2) ont été identifiés sur support TiO_2AT (oxyde de titane anastase, Thann et Mulhouse). Le choix du support est donc un critère important pour la réalisation des expériences photographiques utilisant la réaction de réarrangement SR ⇋ NR comme réaction d'amplification (réf. 3 et renvoi 5).

Généralisation et conclusion

Les divers effets de cycle, de substitution, de champ (hétéroatome en position 1) etc., ont été étudiés systématiquement pour des thioéthers aromatiques, saturés ou benzocondensés à cinq ou six chaînons (3, 16).

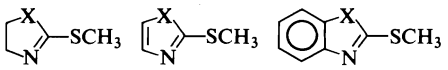

X = O, S, NR

Le parallèle pK_a–réarrangement est alors vérifié pour l'ensemble des substrats hétérocycliques.

Ainsi pour les diazoles-1,3 (X = NR), on observe que l'échelle de pK_a (3, 16, 28) est:

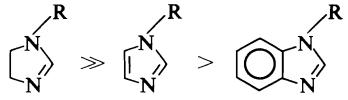

l'échelle de réarrangement observée (3, 16) est:

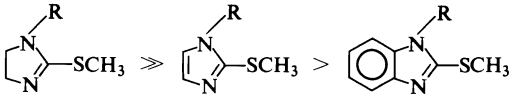

L'ensemble des résultats présentés dans ce mémoire pour les séries imidazolique et pyrimidinique, ainsi que ceux des séries imidazolinique et tétrahydropyrimidinique (15) permet le choix cohérent du substrat de réarrangement qui sera le substrat d'amplification du procédé photographique (2, 3, 6). La limite du parallèle pK_a–réarrangement permettant cette optimisation du substrat d'amplification du procédé photographique est bien d'ordre structural. Elle peut être due à des interactions stériques directes (effet *ortho*) ou indirectes (déformation de cycle) ou à des modifications géométriques des hétérocycles étudiés (cycles à six ou cinq chaînons).

1. J. KISTER, G. ASSEF, G. MILLE et J. METZGER. Can. J. Chem. Ce numéro.
2. J. KISTER. Thèse spécialité, Marseille. 1974.
3. J. KISTER. Thèse Sciences, Marseille. 1977.

[5]J. Kister. Travaux non publiés.

4. J. KISTER, G. ASSEF, H. J. M. DOU et J. METZGER. Tétrahedron, **32**, 1395 (1976).
5. G. ASSEF, J. KISTER, G. MILLE et J. METZGER. C.R. Acad. Sci. Ser. C, **284**, 273 (1977).
6. J. METZGER. Brevet Fr. no 7,328,538 (novembre 1973).
7. A. CHAMBONNET. Thèse Dr. Ing., Marseille. 1962.
8. M. CHANON. Bull. Soc. Chim. Fr. **7**, 2968 (1968); **7**, 2981 (1968).
9. M. CHANON, M. CONTE, J. MICOZZI et J. METZGER. Int. J. Sulfur Chem. Ser. C, **6**, 85 (1971).
10. F. P. REED, A. ROBERTSON et W. A. SEXTON. J. Chem. Soc. 473 (1938).
11. B. BEILENSON et F. M. HAMER. J. Chem. Soc. 143 (1939).
12. C. G. MOORE et E. S. WAIGHT. J. Org. Chem. **17**, 4237 (1952).
13. J. J. D'AMICO, R. H. CAMPBELL, S. T. WEHATER et CH. E. TWINE. J. Org. Chem. **30**, 3625 (1965).
14. G. ASSEF. Thèse spécialité, Marseille. 1976.
15. G. ASSEF, J. KISTER et J. METZGER. Bull. Soc. Chim. Fr. 1978. Sous presse.
16. J. KISTER et J. METZGER. Communication Société Chimique de France, Palaiseau, 1978, et Phosphorus and Sulfur (en cours).
17. J. JONCZYK, K. BANKO et M. MAKOSZA. J. Org. Chem. **40**, 266 (1975).
18. J. JONCZYK, M. FEDROYNSKI et M. MAKOSZA. Tetrahedron Lett. **23**, 2395 (1972).
19. (*a*) G. ASSEF, D. BOUIN-ROUBAUD, J. KISTER et J. METZGER. C.R. Acad. Sci., Ser. C, **283**, 143 (1976); (*b*) J. KISTER, D. BOUIN-ROUBAUD, H. J. M. DOU, P. HASSANALY et J. METZGER. C.R. Acad. Sci. Ser. C, **287**, 201 (1978).
20. (*a*) G. ASSEF, J. KISTER, J. METZGER, R. FAURE et E. J. VINCENT. Tetrahedron Lett. **37**, 3313 (1976); (*b*) R. FAURE, E. J. VINCENT, G. ASSEF, J. KISTER et J. METZGER. Org. Magn. Reson. **9**, 12 (1977); **9**, 688 (1977).
21. T. TAKAHASHI, A. KAJI et J. I. HAYAMI. Bull. Inst. Chem. Res. Kyoto Univ. **51**, 163 (1973).
22. M. CHANON, R. GALLO, J. M. SURZUR et J. METZGER. Bull. Soc. Chim. Fr. **7**, 2885 (1968).
23. D. PERRIN. Dissociation constants of organic bases in aqueous solution. Butterworths, London. 1965.
24. A. R. KATRITZKY et J. M. LAGOWSKI. Adv. Heterocycl. Chem. **1**, 311 (1963); **1**, 341 (1963); **2**, 1 (1963); **2**, 28 (1963).
25. G. KJELLIN et J. SANDSTRÖM. Acta Chem. Scand. **23**, 2888 (1969).
26. L. W. DEADY. Aust J. Chem. **26**, 1949 (1973).
27. E. GONZALEZ. Thèse Sciences, Montpellier. 1965.
28. J. KISTER, U. BERG, R. GALLO et J. METZGER. Bull. Soc. Chim. Sous presse.
29. H. J. M. DOU, P. HASSANALY, J. KISTER et J. METZGER. Phosphorus Sulfur, **3**, 355 (1977).

Cyclization of the 4-cyanobutyl radical[1]

DAVID GRILLER, PETER SCHMID,[2] AND KEITH U. INGOLD
Division of Chemistry, National Research Council of Canada, Ottawa, Ont., Canada K1A 0R6

Received October 13, 1978

DAVID GRILLER, PETER SCHMID, and KEITH U. INGOLD. Can. J. Chem. **57**, 831 (1979).

The rate constant for the irreversible cyclization of the 4-cyanobutyl radical to the cyclopentiminyl radical, $k_c^{C\equiv N}$, has been measured from −52 to 12°C by kinetic epr spectroscopy. The temperature dependence of this rate constant can be represented by,

$$\log (k_c^{C\equiv N}/s^{-1}) = (9.9 \pm 1.0) - (8.6 \pm 1.0)/\theta$$

where $\theta = 2.3RT$ kcal/mol. This rearrangement is somewhat slower than the analogous cyclizations of the 5-hexenyl and 5-hexynyl radicals.

DAVID GRILLER, PETER SCHMID et KEITH U. INGOLD. Can. J. Chem. **57**, 831 (1979).

On a mesuré les constantes de vitesse de la cyclisation irréversible du radical cyano-4 butyle en radical cyclopentiminyle, $k_c^{C\equiv N}$, à des températures allant de −52 à 12°C en faisant appel à la spectroscopie rpe. On peut représenter la relation entre la constante de vitesse et la température grâce à l'équation

$$\log (k_c^{C\equiv N}/s^{-1}) = (9.9 \pm 1.0) - (8.6 \pm 1.0)/\theta$$

où $\theta = 2.3RT$ kcal/mol. Cette transposition est un peu plus lente que les cyclisations analogues des radicaux hexényle-5 et hexynyle-5.

[Traduit par le journal]

Introduction

Free-radical ring closure reactions occur when a suitably constituted radical undergoes intramolecular addition to an unsaturated function. Many such reactions are known, the most thoroughly studied being the cyclization of 5-hexenyl, **1**, to form cyclopentylmethyl, **2** (for recent reviews of ring closure

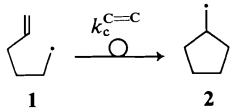

1 **2**

reactions see ref. 1). This rearrangement first achieved prominence as a quantitative probe for the presence of primary alkyl radicals in reaction systems (1). Subsequently, the rate constant for this cyclization, $k_c^{C=C}$, was determined by a 'classical' procedure at 25°C (2) and later by kinetic epr spectroscopy over a range of temperatures (3, 4). This reaction is frequently employed to determine the rates at which primary alkyls react with suitable molecules (4, 5).

Many analogs of the 5-hexenyl cyclization have been reported (1) but the rate constants for these reactions have, at best, been determined only by competitive methods and generally at a single temperature (see for example ref. 6). A particularly interesting rearrangement belonging to this general class of radical cyclization was first described in 1975 by Ogibin *et al.* (7) who found that cyclopentanone was produced in high yield when 4-cyanobutyl, **3**, was generated in an aqueous medium. Clearly, the cyclopentylketiminyl radical, **4**, must be an intermediate

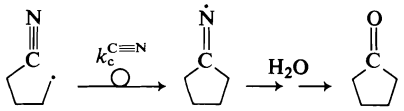

3 **4**

in this reaction (7, 8). Trapping experiments with Cu^{II} indicated that cyclization was rapid (7, 8).

Although there are some examples of intermolecular (9) and of intramolecular (10, 11) addition of alkyl radicals to alkyl nitriles there do not appear to have been any measurements of the rates of such processes. We wished, therefore, to measure $k_c^{C\equiv N}$ and compare its magnitude with that of $k_c^{C=C}$ which we had previously determined (2–4). However, the kinetic epr technique (3, 4) can be applied *only* if rearrangement is irreversible, i.e., only if **4** ⇌ **3**. To check this point it was necessary to generate **4** in some direct manner from a cyclopentyl precursor. The usual route to ketiminyls, which involves hydrogen abstraction from ketimines (12), was inapplicable since cyclopentylketimine appears to be unknown. Other routes to ketiminyl radicals are known (13, 14) but none of those we investigated proved suitable.

In 1977 Cooper *et al.* (15) reported that photochemically generated *tert*-butoxy radicals reacted

[1]Issued as NRCC No. 17204.
[2]NRCC Research Associate, 1975–1977.

0008-4042/79/070831-04$01.00/0

with alkyl azides to produce iminyl radicals 'cleanly' and at concentrations suitable for epr spectroscopic study. This procedure worked well with cyclopentyl azide and, over the temperature range (−10 to 40°C, *vide infra*), the epr spectrum of the cyclopentylketiminyl was entirely free of the 4-cyanobutyl spectrum. Thus, conditions can be found where the **3** ⟶ **4** cyclization is irreversible.[3]

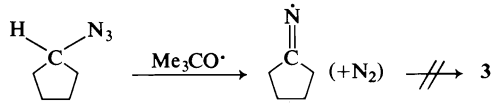

In the present paper we report measurements of $k_c^{C\equiv N}$ and derive Arrhenius parameters for this cyclization.[4]

Experimental

The kinetic epr method which is used to measure the rates of unimolecular radical reactions has been described previously (3, 4, 17). Radicals **3** and **4** were generated photochemically in solution in isooctane directly in the cavity of a Varian E-4 epr spectrometer under conditions of slow flow (0.2 mL/min). Radical **4** was generated as described above. Radical **3** was generated by bromine abstraction from 5-bromovaleronitrile using tri-*n*-butyltin radicals generated by photolysis of hexa-*n*-butylditin.

$$BrCH_2(CH_2)_3CN \xrightarrow{n Bu_3Sn\cdot} {\cdot}CH_2(CH_2)_3CN$$

Materials

5-Bromovaleronitrile was prepared from tetramethylene bromide and potassium cyanide according to the procedure of Leonard and Wildman (18). Distillation yielded a colorless liquid (bp 111°C/15 Torr (lit. (18) bp 114–115°C/12 Torr)) which was purified by preparative vpc before use. This compound was rather immiscible with isooctane and it was therefore used at concentrations ≤0.05 *M*. Cyclopentyl azide was prepared from cyclopentyl bromide and sodium azide in diethyleneglycolmonomethyl ether according to the procedure of Lieber *et al.* (19) and was purified by distillation (bp 62°C/50 Torr (lit. (19), bp 72°C/77 Torr)). This compound was used at a concentration of 0.01 *M*.

All other compounds were commercial materials that were purified by standard methods before use.

Results

Electron Paramagnetic Resonance Spectra

Bromine abstraction from 5-bromovaleronitrile at temperatures ≤ −70°C gave only **3**. This radical showed a spectrum typical of a primary alkyl, viz., $g = 2.00237 \pm 5 \times 10^{-5}$, $a^{H_\alpha}(2H) = 21.75 \pm 0.05$, $a^{H_\beta}(2H) = 27.50 \pm 0.05$, $a^{H_\gamma}(2H) = 0.55 \pm 0.05$ G at −10°C. At higher temperatures the spectrum of **4** appeared and this was the only radical observable at temperatures ≥17°C. The epr parameters for **4** generated from cyclopentyl azide at −7°C are: $g = 2.00300 \pm 1 \times 10^{-5}$, $a^N = 9.40 \pm 0.05$, $a^{H_\alpha}(4H) = 4.43 \pm 0.05$, $a^{H_\beta}(4H) = 1.94 \pm 0.05$ G. It is noteworthy that the epr signal due to **4** has much sharper lines than that due to **3**. In the kinetic experiments **3** was monitored at a modulation amplitude of 1.6 G and **4** at 0.16 G.

Steady-state Kinetic Measurements

Absolute concentrations of **3** and **4** were measured under conditions of steady photolysis in the temperature range (−57 to 12°C) where both radicals could be detected when **3** was generated from 5-bromovaleronitrile. From these concentrations the rate constant ratio, $k_c^{C\equiv N}/2k_t^4$ can be determined from the expression (3, 4)

$$k_c^{C\equiv N}/2k_t^4 = [\mathbf{4}](1 + [\mathbf{4}]/[\mathbf{3}])$$

where $2k_t^4$ is the rate constant for the bimolecular self-reaction of **4**, provided this reaction is diffusion controlled.[5] The results of these experiments are summarized in Table 1.

Measurement of $2k_t^4$

This rate constant was determined in the usual way (22) by monitoring the decay of **4** when the light was chopped by a rapidly rotating sectored disc. At 18.5°C this radical was found to decay with 'clean' second-order kinetics. The measured rate constant for decay, $2k_t^4 = 5.9 \times 10^9\ M^{-1}\ s^{-1}$, indicates that this reaction is diffusion controlled, just as we would expect for this sterically unhindered ketiminyl (12). The variation of $2k_t^4$ with temperature was computed from the temperature coefficient of viscosity of the solvent (21). It can be represented by

$$\log [2k_t^4(M^{-1}\ s^{-1})] = 11.56 - 2.42/\theta$$

where $\theta = 2.303\ RT$ kcal/mol. Values of $2k_t^4$ calculated from this relation have been used to calculate the values of $k_c^{C\equiv N}$ which have been listed in Table 1.

Discussion

The rate constant for cyclization of 4-cyanobutyl can be represented[6] by

$$\log (k_c^{C\equiv N}/s^{-1}) = (9.9 \pm 1.0) - (8.6 \pm 1.0)/\theta$$

[3]The ring opening reaction **4** ⟶ **3** does occur in the gas phase at temperatures >250°C (16).

[4]The rate constant for this reaction has also been determined at −10°C by Dr. B. P. Roberts (private communication) using the kinetic epr method.

[5]The actual requirement is that $2k_t^4$ be equal to the rate constant for the bimolecular reaction between **3** and **4** (3, 4, 17). Since the latter reaction involves unhindered radicals it will certainly be diffusion controlled (see e.g., refs. 2–4, 20, 21).

[6]The error limits given for the *A* factor and activation energy reflect the uncertainty introduced when extrapolating beyond the experimental temperature range to determine the activation energy and *A* factor. Within the experimental range the error in $k_c^{C\equiv N}$ is reasonably small and is probably not greater than a factor of 2 or 3.

TABLE 1. Values of radical concentrations and $k_c^{C\equiv N}/2k_t$[4] at various temperatures

T (K)[a]	[3] $\times 10^7$ (M^{-1})	[4] $\times 10^7$ (M^{-1})	$k_c^{C\equiv N}/2k_t$[4] $\times 10^7$ (M^{-1})
221	1.202	0.121	0.133
222	1.689	0.139	0.150
227	1.440	0.196	0.223
227	1.280	0.242	0.288
234	0.982	0.277	0.355
234	1.296	0.277	0.336
244	0.881	0.423	0.626
244	1.155	0.436	0.601
253	1.150	0.611	0.936
254	0.973	0.586	0.939
264	0.698	0.941	2.210
265	0.831	0.734	1.382
276	0.863	1.063	2.372
278	0.653	1.012	2.580
285	0.374	0.982	3.560

[a]Held to within ±0.5K during the course of each measurement.

which yields $k_c^{C\equiv N} = 4.0 \times 10^3\ s^{-1}$ at 25°C and $4.0 \times 10^4\ s^{-1}$ at 80°C. For comparison, the rate constant for the 5-hexenyl cyclization can be represented by (4)

$$\log (k_c^{C=C}/s^{-1}) = (9.5 \pm 1.1) - (6.1 \pm 1.1)/\theta$$

which yields, $k_c^{C=C} = 1.1 \times 10^5\ s^{-1}$ at 25°C and $5.3 \times 10^5\ s^{-1}$ at 80°C. The rate constant for cyclization of the 5-hexynyl radical, i.e., **5**⟶**6**, has been

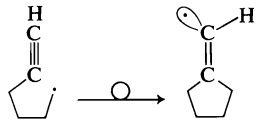

5 **6**

estimated to be $1.2 \times 10^5\ s^{-1}$ at 80°C.[7] The cyclizations of **1**, **3**, and **5**, therefore proceed at rates which are not grossly dissimilar and the differences in rate can probably *primarily* be attributed to differences in activation energy. The Arrhenius preexponential factors are smaller than might have been anticipated for such simple cyclizations (4).

It is not unreasonable that **1**, **3**, and **5**, should cyclize at similar rates since the reactants are structurally related and even their thermochemistry must be very similar. The latter point can be illustrated by considering the estimated thermochemistry of three model reactions, viz., hydrogen atom addition to ethylene, acetonitrile,[8] and acetylene. The following heats of formation, ΔH_f^0 (in kcal/mol), have been measured or estimated for the species involved in these three reactions: C_2H_4, 12.5 (23); $C_2H_5^{\bullet}$, 26.0 (24);[9] CH_3CN, 19.0 (25); $CH_3CH{=}N^{\bullet}$, 34.4 (26); C_2H_2, 54.2 (23); $H_2C{=}\dot{C}H$, 69.0 (26); $H^{\bullet}$, 52.1 (26). The three model reactions and their calculated exothermicities are:

$$H^{\bullet} + H_2C{=}CH_2 \rightarrow H_3C{-}\dot{C}H_2 \qquad -38.6\ \text{kcal/mol}$$

$$H^{\bullet} + CH_3C{\equiv}N \rightarrow CH_3CH{=}\dot{N} \qquad -36.7\ \text{kcal/mol}$$

$$H^{\bullet} + HC{\equiv}CH \rightarrow H_2C{=}\dot{C}H \qquad -37.3\ \text{kcal/mol}$$

Rates of cyclization of other analogs of 5-hexenyl are currently under investigation.

1. A. L. J. BECKWITH. Chem. Soc. Spec. Publ. No. 24, 239 (1970); M. JULIA. Acc. Chem. Res. **4**, 386 (1971); Pure Appl. Chem. **40**, 553 (1974); J. W. WILT. *In* Free radicals. Vol. 1. *Edited by* J. K. Kochi. Wiley, New York, NY. 1973. Chapt. 8; J. F. GARST, J. A. PACIFICI, C. C. FELIX, and A. NIGAM. J. Am. Chem. Soc. **100**, 5974 (1978).
2. D. J. CARLSSON and K. U. INGOLD. J. Am. Chem. Soc. **90**, 7074 (1968).
3. D. LAL, D. GRILLER, S. HUSBAND, and K. U. INGOLD. J. Am. Chem. Soc. **96**, 6355 (1974).
4. P. SCHMID, D. GRILLER, and K. U. INGOLD. Int. J. Chem. Kinet. In press.
5. P. SCHMID and K. U. INGOLD. J. Am. Chem. Soc. **100**, 2493 (1978).
6. A. L. J. BECKWITH, G. E. GREAM, and D. L. STRUBLE. Aust. J. Chem. **25**, 1081 (1972); A. L. J. BECKWITH, I. A. BLAIR, and G. PHILLIPOU. Tetrahedron Lett. 2251 (1974); J. Am. Chem. Soc. **96**, 1613 (1974); A. L. J. BECKWITH and G. MOAD. J. Chem. Soc. Perkin Trans. II, 1726 (1975); M. JULIA, C. DESCOINS, M. BAILLARGE, B. JACQUET, D. UGUEN, and F. A. GROEGER. Tetrahedron, **31**, 1737 (1975); T. W. SMITH and G. B. BUTLER. J. Org. Chem. **43**, 6 (1978).
7. YU. N. OGIBIN, E. I. TROYANSKII, and G. I. NIKISHIN. Izv. Akad. Nauk SSSR Ser. Khim. 1461 (1975).
8. YU. N. OGIBIN, E. I. TROYANSKII, and G. I. NIKISHIN. Izv. Akad. Nauk SSSR Ser. Khim. 843 (1977).

[7]A. L. J. Beckwith and A. G. Lawrence. Private communication.

[8]Chosen in place of HCN (which would have been more appropriate) because ΔH_f^0 for $H_2C{=}N^{\bullet}$ appears to be unknown.

[9]A value of 28.4 has been proposed recently (25).

9. R. A. KABA, D. GRILLER, and K. U. INGOLD. J. Am. Chem. Soc. **96**, 6202 (1974).
10. J. KALVODA, C. MEYSTRE, and G. ANNER. Helv. Chim. Acta, **49**, 424 (1966); J. KALVODA. Helv. Chim. Acta, **51**, 267 (1968).
11. D. G. HAWTHORNE and D. H. SOLOMON. J. Macromol. Sci. Chem. **9**, 149 (1975); D. G. HAWTHORNE, S. R. JOHNS, and R. L. WILLING. Aust. J. Chem. **29**, 315 (1976).
12. D. GRILLER, G. D. MENDENHALL, W. VAN HOOF, and K. U. INGOLD. J. Am. Chem. Soc. **96**, 6068 (1974).
13. J. F. OGILVIE. Chem. Commun. 359 (1965); R. W. BINKLEY. J. Org. Chem. **33**, 2311 (1968); R. F. HUDSON, A. J. LAWSON, and E. A. C. LUCKEN. Chem. Commun. 807 (1971); R. F. HUDSON, A. J. LAWSON, and K. A. F. RECORD. J. Chem. Soc. Perkin Trans. II, 869 (1974); Chem. Commun. 488 (1974); S. ISHIKAWA, H. SAKURAGI, M. YOSHIDA, N. INAMOTO, and K. TOKUMARU. Chem. Lett. 819 (1975); H. OHTA and K. TOKUMARU. Bull. Chem. Soc. Jpn. **48**, 2393 (1975); H. SAKURAGI, S. ISHIKAWA, T. NISHIMURA, M. YOSHIDA, N. INAMOTO, and K. TOKUMARU. Bull. Chem. Soc. Jpn. **49**, 1949 (1976).
14. A. R. FORRESTER, M. GILL, E. M. JOHANSSON, C. J. MEYER, and R. H. THOMSON. Tetrahedron Lett. 3601 (1977).
15. J. W. COOPER, B. P. ROBERTS, and J. N. WINTER. Chem. Commun. 320 (1977).
16. W. D. CROW and A. N. KHAN. Aust. J. Chem. **29**, 2289 (1976); W. D. CROW, H. MCNAB, and J. M. PHILIP. Aust. J. Chem. **29**, 2299 (1976).
17. D. GRILLER and B. P. ROBERTS. Chem. Commun. 1035 (1971); J. Chem. Soc. Perkin Trans. II, 747 (1972); A. G. DAVIES, D. GRILLER, and B. P. ROBERTS. J. Chem. Soc. Perkin Trans. II, 993 (1972); G. B. WATTS, D. GRILLER, and K. U. INGOLD. J. Am. Chem. Soc. **94**, 8784 (1972); B. MAILLARD and K. U. INGOLD. J. Am. Chem. Soc. **98**, 1224 (1976); B. MAILLARD, D. FORREST, and K. U. INGOLD. J. Am. Chem. Soc. **98**, 7024 (1976).
18. N. J. LEONARD and W. C. WILDMAN. J. Am. Chem. Soc. **71**, 3101 (1949).
19. E. LIEBER, T. S. CHAO, and C. N. R. RAO. J. Org. Chem. **22**, 238 (1957).
20. K. U. INGOLD. *In* Free radicals. Vol. 1. *Edited by* J. K. Kochi. Wiley, New York, NY. 1973. Chapt. 2.
21. H. SCHUH and H. FISCHER. Helv. Chim. Acta, **61**, 2130 (1978).
22. K. ADAMIC, D. F. BOWMAN, T. GILLAN, and K. U. INGOLD. J. Am. Chem. Soc. **93**, 903 (1971).
23. S. W. BENSON, F. R. CRUICKSHANK, D. M. GOLDEN, G. R. HAUGEN, H. E. O'NEAL, A. S. RODGERS, R. SHAW, and R. WALSH. Chem. Rev. **69**, 279 (1969).
24. H. E. O'NEAL and S. W. BENSON. *In* Free radicals. Vol. 2. *Edited by* J. K. Kochi. Wiley, New York, NY. 1973. Chapt. 17.
25. W. TSANG. Int. J. Chem. Kinet. **10**, 821 (1978).
26. S. W. BENSON. Thermochemical kinetics. Wiley, New York, NY. 1968.

The effect of tetra-*n*-butylammonium bromide on the proton magnetic resonance of 1-X-2,4-dinitrobenzenes

D. R. McLaughlin and J. D. Reinheimer[1]

Department of Chemistry, The College of Wooster, Wooster, OH 44691, U.S.A.

Received September 5, 1978

D. R. McLaughlin and J. D. Reinheimer. Can. J. Chem. **57**, 835 (1979).

The chemical shifts of the ring protons of 1-X-2,4-dinitrobenzenes are changed with the addition of tetrabutylammonium bromide. In general, the chemical shift of proton 3 decreases with salt addition, that of proton 5 may increase or decrease, while that of proton 6 increases. Where X is an oxygen containing group, the changes are somewhat more pronounced.

D. R. McLaughlin et J. D. Reinheimer. Can. J. Chem. **57**, 835 (1979).

Les déplacements chimiques des protons aromatiques des dinitro-2,4 X-1 benzènes varient lors de l'addition de bromure de tétrabutylammonium. En général, le déplacement chimique du proton en 3 diminue par addition du sel; celui du proton en 6 augmente alors que celui du proton en 5 peut augmenter ou diminuer. Lorsque X est un groupement contenant un oxygène, les changements sont quelque peu plus prononcés.

[Traduit par le journal]

Introduction

In connection with our studies of salt effects on the rate of aromatic nucleophilic substitution reactions (1–3), we found the study of Hyne and Fabris (4). Hyne and Fabris suggested that tetrabutylammonium bromide and iodide associated with both the aryl ring and the nitro group of nitrobenzene as an ion pair. The anion was placed over the *meta* and *para* positions of the benzene ring. If it were a nucleophile, the anion would be well positioned to attack the ring and form a σ anionic complex (5). This study was an extension of Hyne and Fabris' work to a series of dinitro compounds.

Experimental

All spectra were taken in the solvent methylene chloride. The Varian T-60 was locked on the solvent peak and peak positions were determined by a frequency counter.

The samples were commercial chemicals which were recrystallized until the melting point range was 1°C and agreed with the literature melting point. The tetra-*n*-butylammonium bromide was recrystallized twice from benzene and then dried in an Abderhalden drying pistol for 24 h. Samples were sealed and stored in a desiccator over $CaSO_4$; mp 117–119°C, lit. (6) mp 118°C. The solvent was dried over $CaSO_4$ and distilled before use. Sample solutions were prepared by weighing the compound and diluting to volume in a 1-mL volumetric flask.

The effect of water was investigated as follows: a control sample of dried tetra-*n*-butylammonium bromide in CH_2Cl_2 was prepared by performing all manipulations in a plastic glove bag filled with dry nitrogen. The second sample was prepared from purified tetra-*n*-butylammonium bromide that had been on the laboratory bench for several days. The third sample was taken from the commercial tetra-*n*-butylammonium bromide sample. The spectra of 1-chloro-2,4-dinitrobenzene with each salt solution were identical within experimental error. Next, 2 drops of water were added to the dried sample in the nmr tube. After vigorous shaking, no change in nmr spectrum was noted.

[1]To whom correspondence should be sent.

Discussion

The chemical shift changes are more complex with

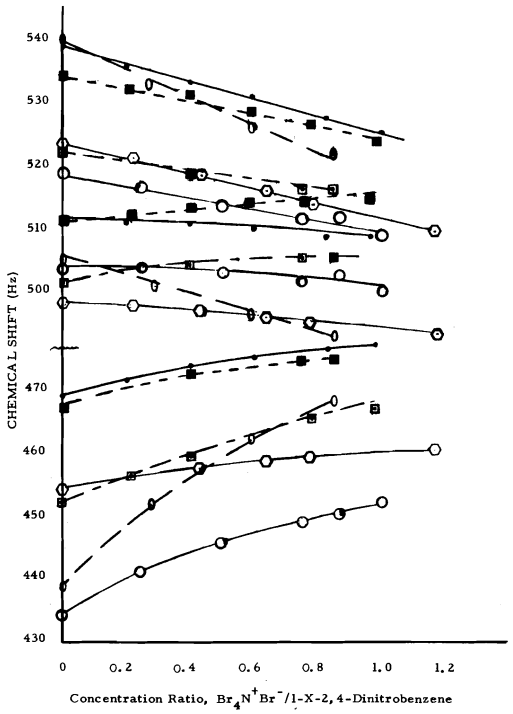

FIG. 1. Chemical shift vs. concentration ratio. H, •——•; Cl, ⊡—⊡; F, ■---■; OH, ○---○; OCH_3, ○—○; CH_3, ⬡—⬡. At zero salt concentration, proton 3 is found at 517–540 Hz, proton 5 at 495–515 Hz, and proton 6 at 430–470 Hz.

0008-4042/79/070835-03$01.00/0

TABLE 1. Variation of chemical shifts for 1-X-2,4-dinitrobenzenes in CH_2Cl_2 with added tetra-*n*-butylammonium bromide

Substituent X	[Salt]/[X]	Chemical shifts[a] Proton 3	Proton 5	Proton 6
H	0	538.3	511.9	468.4
	0.200	535.5	511.5	471.1
	0.402	532.8	510.7	473.0
	0.595	530.4	509.9	474.5
	0.827	527.1	508.7	475.8
	0.978	525.1	507.8	476.5
Cl	0	521.9	501.4	466.7
	0.398	518.2	504.3	471.9
	0.749	516.1	505.2	474.2
	0.854	515.9	505.1	474.3
OH	0	539.7	505.1	438.5
	0.290	532.6	500.6	451.6
	0.590	526.0	495.7	461.7
	0.850	521.7	492.8	467.9
OCH_3	0	518.5	503.5	434.0
	0.246	516.3	503.9	441.0
	0.494	513.6	502.8	445.3
	0.750	511.1	501.6	448.9
	0.870	511.8	502.4	450.1
	1.01	508.0	500.0	452.4
F	0	534.0	511.2	452.3
	0.210	531.8	512.4	456.4
	0.400	530.7	513.5	459.4
	0.590	528.1	514.1	462.3
	0.780	525.8	514.1	464.8
	0.980	523.7	514.3	466.6
CH_3	0	523.2	498.3	454.1
	0.222	520.7	497.8	455.8
	0.430	518.0	496.9	457.2
	0.640	515.8	496.1	457.9
	0.780	513.8	495.3	458.6
	1.17	509.4	493.4	459.9

[a]Chemical shifts were measured in Hz from TMS.

the dinitro series. In nitrobenzene, Hyne and Fabris (4) found that the change for the *ortho* position was very small, whereas the downfield changes for the *meta* and *para* protons were greater. Our data (Fig. 1 and Table 1) reveal an upfield change of chemical shift for proton 3 (*ortho* to both NO_2 and *meta* to X) with all X. The magnitude of this change is largest for X = OH, smallest for X = Cl and similar for all other X. For proton 5, (*ortho,para* to the NO_2 groups and *meta* to X), a small upfield change is observed for all X except the halogens. Again, the greatest change is found for the OH group. The halogens give rise to a slight downfield change. For proton 6 (*meta* to both NO_2 and *ortho* to X), the change is downfield for all X. The magnitude of this change is greatest for OH and OCH, large for F, and about the same for Cl, CH_3, and H. The chemical shift vs. concentration ratio plot is not linear in all cases; this is in contrast to Hyne and Fabris' data.

The chemical shift changes were attributed to an association of the tetrabutylammonium ion with a nitro group and the halide ion with the benzene ring. The fact that the dinitro compounds dissolved much more rapidly in tetrabutylammonium bromide solution than in pure solvent provides weak evidence for association.[2]

[2]A referee has suggested that the solubility rate statement does not clearly delineate between thermodynamic and kinetic data. A better experiment would have been the investigation of the change in solubility of dinitro compounds with added tetrabutylammonium bromide. We did not make this study; our qualitative observation was that the dinitro compound dissolved in salt solution after one or two inversions of the volumetric flask but a period of minutes and many inversions for solution in the pure solvent. The unstated assumption was that the rate of solution would depend on the relative unsaturation of the solution with respect to the dinitro compound. If the species that is in solution is a salt – dinitro compound complex, the concentration of dinitro compound would be low and its rate of solution correspondingly fast.

The crucial question is where the ions are positioned with respect to the aromatic ring. If the tetrabutylammonium salt were complexed to X, the 3 and 5 positions are symmetrically placed and their change in chemical shift should be quite similar. A survey of Fig. 1 shows that this is not the case. Association of the cation of potassium *tert*-butoxide with the nitro group of *o*- and *p*-fluoronitrobenzene was postulated by Del Cina *et al.* (7). Ehrlich and Popov (8) have demonstrated that a downfield shift of the Na^+ resonance occurs in an ion pair (Na^+, I^-). These data are indicative of an association of the Br^- with the aryl ring and the tetrabutylammonium cation with the nitro group. In short, they support the Hyne–Fabris model. Additional support may be found in the following result. If the cation were above the benzene ring, the ring current should affect the butyl protons. This chemical shift should move upfield with added salt. To eliminate any NO_2 group effect, the nmr spectra of tetrabutylammonium bromide with nitromethane (A), with 2,4-dinitrochlorobenzene (B), and with no added solute (C) were taken. The aliphatic spectra of A and C were identical, but B was slightly different. The chemical shifts of B were downfield. If this is a ring current effect, the cation must not be above the benzene ring; a reasonable position is at the NO_2 group. This experiment is not a definitive result, but it provides more support for the Hyne–Fabris model.

In summary, the tetrabutylammonium bromide is associated with the nitro group or groups and the benzene ring. We postulate, with Hyne and Fabris, the association of the cation with the nitro group and the anion with the electron deficient benzene ring.

1. J. D. Reinheimer and W. Hostetler. J. Org. Chem. **33**, 510 (1968).
2. J. D. Reinheimer and W. Hostetler. Ohio J. Sci. **68**, 304 (1968).
3. J. D. Reinheimer, W. F. Kieffer, S. W. Frey, J. C. Cochran, and E. W. Barr. J. Am. Chem. Soc. **79**, 1263 (1957).
4. J. B. Hyne and A. R. Fabris. Can. J. Chem. **46**, 73 (1968).
5. M. J. Strauss. Chem. Rev. **70**, 667 (1970).
6. Beilstein. Handbuch der organischen Chemie. Vol. IV. 4th ed. Springer-Verlag, Berlin. 1964. p. 157.
7. F. Del Cima, C. Biggi, and F. Pietra. J. Chem. Soc. Perkin Trans. II, 55 (1971).
8. R. H. Ehrlich and A. I. Popov. J. Am. Chem. Soc. **93**, 5522 (1971).

Canadian Journal of Chemistry

Published by
THE NATIONAL RESEARCH COUNCIL OF CANADA

Volume 57 Number 8 April 15, 1979

Journal canadien de chimie

Publié par
LE CONSEIL NATIONAL DE RECHERCHES DU CANADA

Volume 57 numéro 8 15 avril 1979

The reactivity of allyl and propargyl alcohols with solvated electrons: temperature and solvent effects[1]

ALEXEI M. AFANASSIEV,[2] KIYOSHI OKAZAKI, AND GORDON R. FREEMAN

Chemistry Department, University of Alberta, Edmonton, Alta., Canada T6G 2G2

Received September14, 1978

ALEXEI M. AFANASSIEV, KIYOSHI OKAZAKI, and GORDON R. FREEMAN. Can. J. Chem. **57**, 839 (1979).

The rate constants k_1 for the reaction of solvated electrons with allyl alcohol in a number of hydroxylic solvents differ by up to two orders of magnitude and decrease in the order *tert*-butyl alcohol > 2-propanol > 1-propanol ≈ ethanol > methanol ≈ ethylene glycol > water. In methanol and ethylene glycol the rate constants ($7 \times 10^7\ M^{-1}\ s^{-1}$ at 298 K) and activation energies (16 kJ/mol) are equal, in spite of a 32-fold difference in solvent viscosity (0.54 and 17.3 cP, respectively) and 3-fold difference in its activation energy (11 and 32 kJ/mol, respectively). The reaction in *tert*-butyl alcohol is nearly diffusion controlled and has a high activation energy that is characteristic of transport in that liquid ($E_1 = 31$ kJ/mol, $E_\eta = 39$ kJ/mol). The activation energies in the other alcohols are all 16 kJ/mol, and it is 14 kJ/mol in water. They do not correlate with transport properties. The solvent effect is connected primarily with the entropy of activation. The rate constants correlate with the solvated electron trap depth. When the electron affinity of the scavenger is small, a favorable configuration of solvent molecules about the electron/scavenger encounter pair is required for the electron jump to take place. The behavior of the rate parameters for propargyl alcohol is similar to that for allyl alcohol, but k_1, A_1, and E_1 are larger for the former. The ratio k(propargyl)/k(allyl) at 298 K equals 10.5 in water and decreases through the series, reaching 1.3 in *tert*-butyl alcohol. Rate parameters for several other scavengers are also reported.

ALEXEI M. AFANASSIEV, KIYOSHI OKAZAKI et GORDON R. FREEMAN. Can. J. Chem. **57**, 839 (1979).

Les constantes de vitesse k_1, pour la réaction d'électrons solvatés par le l'alcool allylique dans un certain nombre de solvants hydroxylés diffèrent par des facteurs allant jusqu'à 100 et diminuent dans l'ordre *tert*-butanol > propanol-2 > propanol-1 ≈ éthanol > méthanol ≈ éthylène glycol > eau. Dans le méthanol et l'éthylene glycol, les constantes de vitesse ($7 \times 10^7\ M^{-1}\ s^{-1}$ à 298 K) et les énergies d'activation (16 kJ/mol) sont égales mêmes s'il existe un rapport de 32 dans les viscosités des solvants (0.54 et 17.3 cP) et un rapport de 3 dans les énergies d'activation de viscosité (respectivement 11 et 32 kJ/mol). La réaction dans le *tert*-butanol est pratiquement contrôlée par la diffusion et possède une énergie d'activation élevée qui est caractéristique du transport dans ce liquide ($E_1 = 31$ kJ/mol, $E_\eta = 39$ kJ/mol). Dans tous les autres alcools, les énergies d'activation sont toutes égales à 16 kJ/mol; dans l'eau E_a est égale à 14 kJ/mol. Ces valeurs ne peuvent pas être reliées avec les propriétés de transport. L'effet de solvant est principalement lié à l'entropie d'activation. Il y a un corrélation entre les constantes de vitesse et les profondeurs des pièges des électron solvatés. Lorsque l'affinité électronique pour le soluté est faible, il faut une configuration favorable des molécules de solvant autour de la paire électron-soluté qui se rencontre pour que le saut électronique puisse s'effecteur. Le comportement des paramètres de vitesse pour l'alcool propargylique est semblable à celui de l'alcool allylique; les valeurs de k_1, A_1 et E_1 sont toutefois plus élevées

[1]Assisted financially by the National Research Council of Canada.

[2]Exchange scientist, assisted by the Social Sciences and Humanities Research Council of Canada. Permanent address: Chemistry Department, Moscow State University, Moscow, USSR.

0008-4042/79/080839-07$01.00/0

dans le premier cas. Le rapport k(propargyl)/k(allyl) à 298 K est égal à 10.5 dans l'eau et diminue pour toute la série pour atteindre une valeur de 1.3 dans le *tert*-butanol. On rapporte des paramètres de vitesse pour plusieurs autres solutés.

[Traduit par le journal]

Introduction

The temperature dependence of solvated electron reaction rates has not been extensively studied (1–9), in spite of the importance of the subject. Perhaps one reason for that was the near constance of the observed activation energies for rate constants that varied by several orders of magnitude (1–3). These results indicated that there were greater variations in the entropy than in the enthalpy effects, and kinetics models are usually more suited to considerations of the latter.

Recent measurements have turned up systems in which the differences between the reaction activation energies E_a are greater than the experimental uncertainty (2*d*, 3*b*). For efficient scavengers in a series of alcohols and glycerol/water mixtures, the activation energy for solvated electron reaction was related to that, E_η, of viscous flow: $E_a = \alpha E_\eta + \beta$, where $\alpha = 0.44$–0.65 and $\beta = 3$–12 kJ/mol (3*b*). In another study, E_a for the inefficient scavenger benzene was found to be nearly double that for more efficient scavengers (2*d*). However, the values of E_a for benzene and toluene in C_1–C_4 alcohols are all 25–33 kJ/mol, and do not reflect the two-fold variations in E_η and the activation energies of dipolar rotational relaxation (2*e*).

The present work is devoted to the study of the effect of temperature on the reactivity of solvated electrons with two inefficient scavengers, allyl and propargyl alcohols, in a series of hydroxylic solvents that have different molecular structures.

Experimental

Materials

Allyl alcohol (2-propen-1-ol, 99%) and propargyl alcohol (2-propyn-1-ol, 97%) were Analyzed grade from Aldrich Chemical Co. The solvents were water (triply distilled), methanol (Spectroanalyzed, Fisher Scientific Co.), ethanol (U.S.P. anhydrous 200 proof, U.S. Industrial Chemical Co.), 1- and 2-propanol (Analyzed or Spectral grade, 99+%, Aldrich Chemical Co.), *tert*-butyl alcohol (99.5%, Aldrich Chemical Co.), and ethylene glycol (99%, Fisher Scientific Co.).

Methanol, 1- and 2-propanol, *tert*-butyl alcohol, and allyl and propargyl alcohols were treated for 1 day under argon with sodium borohydride (1 g/L) at 40, 60, 50, 50, 65, and 40°C, respectively. The alcohol was then fractionated through an 80 × 2.3 cm column packed with glass helices. The middle 50% was collected and kept under argon. Allyl and propargyl alcohols were treated twice in this manner. An argon (UHP, Matheson Co.) pressure and syphon system was used to transfer the alcohol without contacting air.

Ethylene glycol was distilled under reduced pressure at ~100°C. The first 15% and last 35% fractions were discarded and the middle 50% kept under an atmosphere of UHP argon.

Ethanol was used as received (10), but was kept under argon.

Techniques

The methods of sample preparation (11), temperature control, irradiation, and optical measurement (12–14) were essentially the same as described in the indicated references. In brief, a 0.1 μs pulse of 1.8 MeV electrons delivered 1–2 × 10^{16} eV/g to the sample. The dosimeter was oxygen saturated 5 mM potassium thiocyanate, using $G\varepsilon(478\text{ nm}) = 2.1 \times 10^4$ (100 eV M cm)$^{-1}$ for $(SCN)_2^-$.

The temperature during an experiment at a given temperature was constant to within 1°C. The absorbed dose/cm^3 and solute concentration were adjusted for the change of solvent density with temperature (15).

In water, methanol, and ethanol optical measurements were made at the absorption maximum, λ_{emax}, of the solvated electron band at each temperature. In 1- and 2-propanol and in ethylene glycol the wavelength was held constant at the λ_{emax} for 298 K, respectively 645, 815, and 566 nm. For *tert*-butyl alcohol the use of the fast response detector prevented measurements being made at λ_{emax} (298 K) = 1220 nm, so 950 nm was used.

Results and Discussion

The Solvents

The quality of each alcohol solvent was assessed by measuring the first order decay constant of solvated electrons in the absence of added solute, at several temperatures over an ~80 deg range. Temperatures from 298 K downwards were used for the propanols, from 298 K upwards were used for ethylene glycol and *tert*-butyl alcohol, while those for methanol and ethanol straddled 298 K. When a decay curve displayed an initial faster decay portion (geminate reaction), only the first order tail was measured. For example, geminate reaction was observable for 3 μs in *tert*-butyl alcohol at 300 K, so the rate constant was then taken from the decay between 6 and 16 μs. The values of the rate constants at 298 K and of the Arrhenius parameters are listed for the different alcohols in Table 1. The alcohols compare favorably with the purest used earlier (2*d*, 16–18).

The activation energy for *tert*-butyl alcohol is double that for the other alcohols (Table 1).

The electron half life in the purified water was 20 μs at 298 K.

Reaction of e^-_{solv} with Allyl and Propargyl Alcohols

Pseudo first order decay constants of e^-_{solv} were measured for several different concentrations of a solute S at a given temperature. The value of the rate constant of reaction [1] was obtained from the slope

[1] $$e^-_{solv} + S \rightarrow \text{product}$$

of a plot of the first order constants against the solute concentration. The nature and quality of the results are illustrated by the decay constants obtained for the

TABLE 1. Rate parameters for first order decomposition of e^-_{solv} in purified alcohols[a]

Alcohol	k/s^{-1} (298 K)	log (A/s^{-1})	E_a/kJ mol^{-1}	Comment
Methanol	2.2×10^5	8.56	18	
	$\leq 1.4\times10^5$ [b,c]	8.70[b], 8.15[c]	20[b], 17[c]	1 m*M* base
Ethanol	9×10^4	9.58	26	
	$\leq 8\times10^4$ [b,c]	8.45[b], 9.15[c]	20[b], 24[c]	1 m*M* base
1-Propanol	5×10^5	8.95	18	
	1.7×10^7 [d]	10.6[d]	20[d]	1×10^{17} eV/g
2-Propanol	1.1×10^5	7.61	15	
	3×10^4 [b]	7.6[b]	17[b]	1 m*M* base
tert-Butyl alcohol	7×10^4	11.5	38	
	2.6×10^5 [e]			
Ethylene glycol	1.1×10^6	9.26	18	
	4.5×10^5 [f]			

[a] $k = A \exp(-E_a/RT)$.
[b] Reference 16.
[c] Reference 8.
[d] Reference 17.
[e] Reference 18.
[f] Reference 32.

methanolic solutions at different temperatures (Figs. 1 and 2).

Arrhenius plots of k_1 for allyl alcohol in the different solvents are shown in Fig. 3. The rate constant and activation energy are largest in *tert*-butyl alcohol. The activation energies in the other alcohols are all equal to about half that in *tert*-butyl alcohol. The rate constants at a given temperature decrease in the order 2-propanol > 1-propanol ≈ ethanol > methanol ≈ ethylene glycol. The rate constant and activation energy are smallest in water. Numerical values of k_1 at 298 K and of the Arrhenius parameters A_1 and E_1 are listed in Table 2.

The behavior of the rate constants for propargyl alcohol is similar to that for allyl alcohol (compare Figs. 4 and 3). The values of k_1 for the former are larger and tend to be grouped into two clusters. One cluster includes the solvents *tert*-butyl alcohol, 2-propanol, 1-propanol, and ethanol, while the other includes methanol, ethylene glycol, and water (Fig. 4). Values of k_1 at 298 K and of the Arrhenius parameters are listed in Table 2. The values of A_1 and E_1 are all larger for propargyl than for allyl alcohol.

There is no correlation between the activation energies of the reactions and those of transport in the liquids. The latter are related to those of dielectric relaxation (Table 2 and refs. 19–21) and shear viscosity (Table 2 and ref. 15). Consider, for example, the activation energies in ethylene glycol and methanol: E_1 differs by 10% or less in these two solvents, whereas E_η differs by a factor of 2.9 and E_τ by a factor of 1.8 (Table 2).

There is also no correlation between the values of the rate constants in the different solvents and their activation energies (Table 2). The solvent effect is

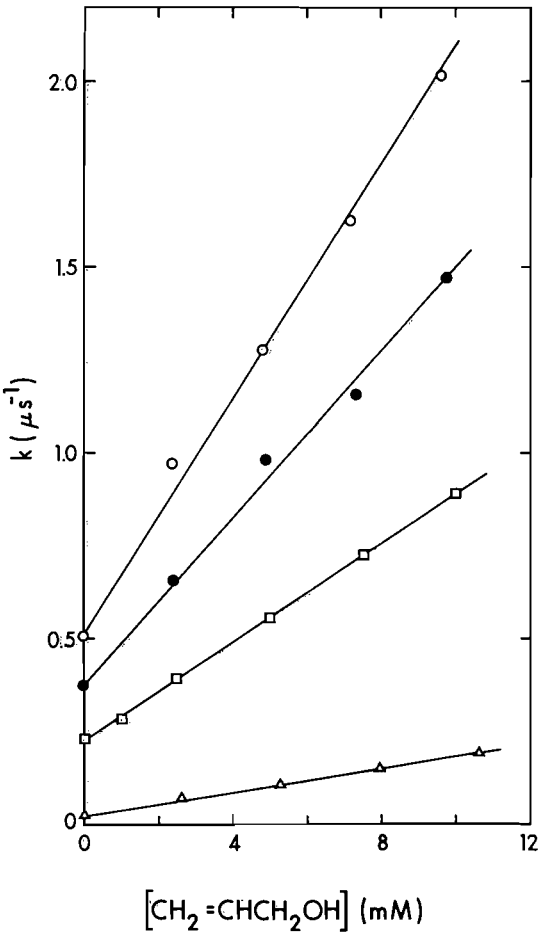

FIG. 1. Pseudo first order rate constants for the reaction of solvated electrons in methanolic solutions of allyl alcohol at 243 K (△), 298 K (□), 320 K (●), and 336 K (○).

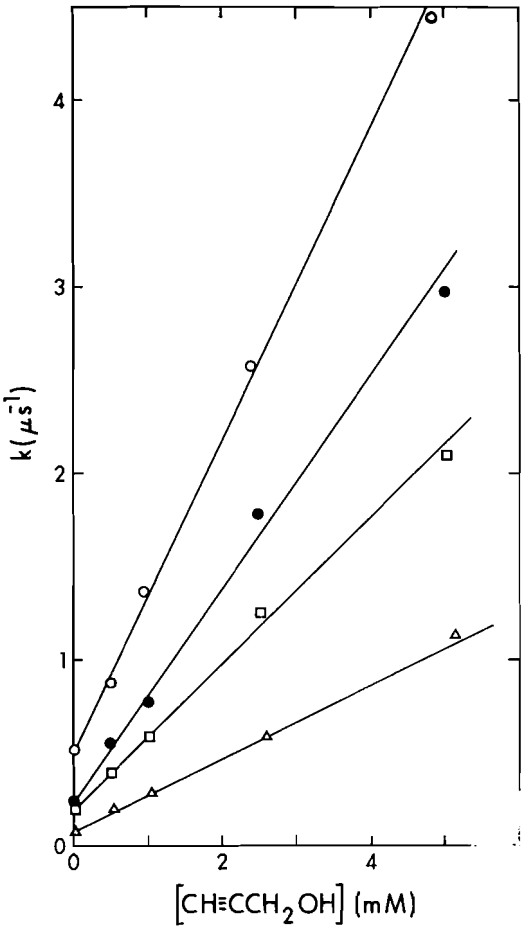

FIG. 2. Pseudo first order rate constants for the reaction of solvated electrons in methanolic solutions of propargyl alcohol at 273 K (△), 299 K (□), 310 K (●), and 333 K (○).

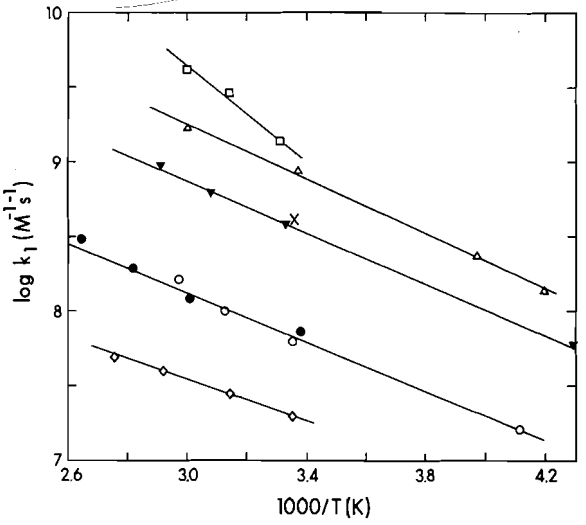

FIG. 3. Arrhenius plots of k_1 (M^{-1} s^{-1}) for allyl alcohol in water (◇), methanol (○), ethanol (▼), 1-propanol (×), 2-propanol (△), *tert*-butyl alcohol (□), and ethylene glycol (●).

therefore connected primarily with the entropy of activation.

The rate constant for propargyl alcohol is designated k_P and that for allyl alcohol k_A. The ratio k_P/k_A at 298 K equals 10 in water, in which the rate constants are smallest. As the values of k_A and k_P increase, their ratio tends to decrease. A plot of k_P/k_A against log k_A is shown in Fig. 5. The ratio extrapolates to unity at $k_A = 3 \times 10^9$ M^{-1} s^{-1}, which is the value one calculates for the diffusion controlled reaction using a reaction radius of 4 Å, a molecular diffusion coefficient of 3×10^{-6} cm^2/s (22) and an electron diffusion coefficient of 7×10^{-6} cm^2/s. This estimate for the diffusion coefficient of e^-_{solv} in *tert*-butyl alcohol at 298 K is consistent with earlier estimates of $2–8 \times 10^{-5}$ cm^2/s in methanol and $1–4 \times 10^{-5}$ cm^2/s in ethanol (23*a*, 24).[3]

The rate constants for these scavengers are largest in the alcohol in which the electron trap depth is the smallest, *tert*-butyl alcohol. Provided that the number of bound levels is similar for electrons solvated in different alcohols, the trap depth is related to the optical absorption energy (25). When the electron affinity of the scavenger is small, it is more difficult for an electron to jump from a deeper trap than from a shallower trap onto the scavenger molecule. The great breadth of the optical absorption band indicates that all the electrons are not in traps of the same depth in a given liquid. Electrons in the shallower traps have a greater probability of reacting per unit time than do those in deeper traps. We therefore choose as an indicator of the trap depth for kinetics purposes the quantity $E_r = (E_{\epsilon max} - W_r)$, where $E_{\epsilon max}$ is the energy at absorption maximum and W_r is the portion of the width at half height that is on the red side of $E_{\epsilon max}$ (13, 26). E_r is therefore the energy half way up the red side of the band. There is a significant correlation between log k_A and E_r in the alcohols (Fig. 6). Water lies well off the curve.

A plot of log k_A against $E_{\epsilon max}$ shows a poorer correlation than that in Fig. 6. The fact that E_r works better than $E_{\epsilon max}$ supports the heterogeneous broadening interpretation of the optical band in alcohols (27).

With the exception of the *tert*-butyl alcohol system, the activation energy of the reaction is nearly independent of E_r (Table 2). The solvent effect acts through the entropy of activation. A favorable configuration of solvent molecules about the electron/scavenger encounter pair is required for the electron jump to take place (28). The desired configuration would tend to stabilize the molecular anion and to

[3]Mobilities estimated from refs. 23 *b* and *c*.

TABLE 2. Rate parameters for reaction of e^-_{solv} with unsaturated alcohols in different solvents

Solvent	Allyl alcohol			Propargyl alcohol					
	k_1,[a] 298 K	log A_1[a]	E_1[b]	k_1,[a] 298 K	log A_1[a]	E_1[b]	E_τ[b,c]	E_η[b,d]	E_r[b,e]
Water	2.0×10^7	9.7	14	2.1×10^8	11.4	18	21[f]	18	131
Ethylene glycol	7×10^7	10.6	16	3.2×10^8	12.1	21	28[g]	32	164
Methanol	7×10^7	10.6	16	3.9×18^8	12.0	19	16[f,g]	11	144
Ethanol	3.8×10^8	11.5	17	1.6×10^9	12.0	16	18[f]	14	129
1-Propanol	4.2×10^8	—	—	1.2×10^9	—	—	24[f,h]	17	132
2-Propanol	9.1×10^8	11.9	17	1.9×10^9	12.7	19	27[f]	21	108
tert-Butyl alcohol	1.4×10^9	14.5	31	1.8×10^9	15.6	36	—	39	80

[a] In M^{-1} s^{-1}. k_1 at 298 K.
[b] In kJ/mol.
[c] Activation energy of solvent dielectric relaxation near 298 K, calculated from data in the indicated reference. The values of τ_1 were used when more than one relaxation mode was observed.
[d] Activation energy of solvent shear viscosity near 298 K. Calculated from data in ref. 15.
[e] $E_r = (E_{\epsilon max} - W_r)$ is the energy on the red side of the optical absorption band at half the maximum absorbance, for e^-_{solv}. References 13 and 26.
[f] Reference 19.
[g] Reference 20.
[h] Reference 21.

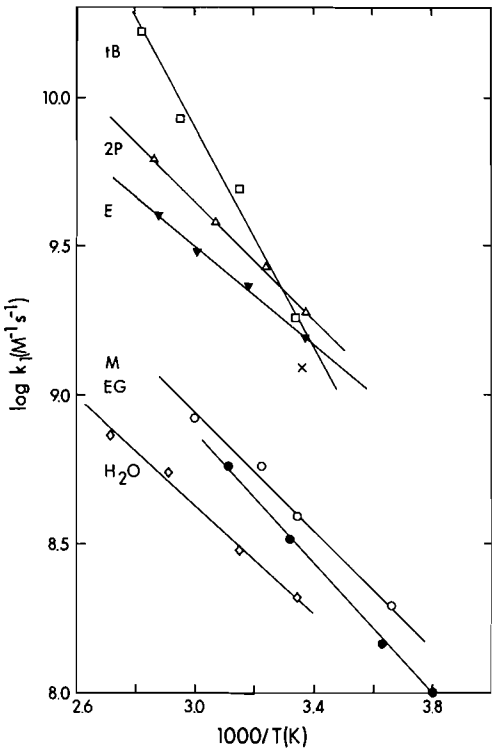

FIG. 4. Arrhenius plots of k_1 (M^{-1} s^{-1}) for propargyl alcohol in water (◇), methanol (○), ethanol (▼), 1-propanol (×), 2-propanol (△), *tert*-butyl alcohol (□), and ethylene glycol (●).

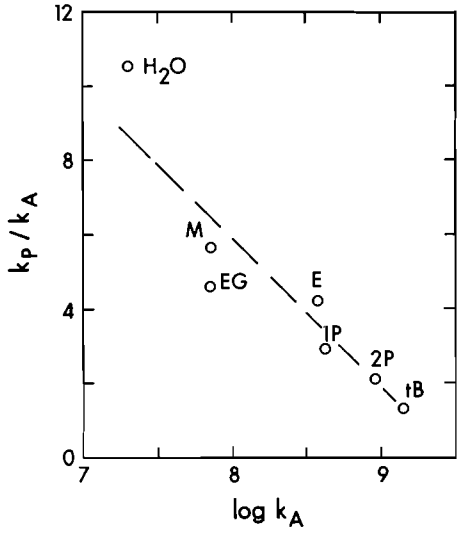

FIG. 5. Plot of k_P/k_A against log k_A, where k_P and k_A designate k_1 for propargyl and allyl alcohol, respectively, in a given solvent. T = 298 K.

make a less stable site for the electron in the solvent. The anion is probably finally stabilized by protonation (29).

[2] $$e^-_{solv} + S \rightleftharpoons S^-_{solv}$$

[3] $$S^-_{solv} + ROH \rightarrow SH + RO^-_{solv}$$

One may therefore write

[4] $$k_1 = k_2k_3/k_{-2}$$

Based upon earlier results in methanol and ethanol (29), one may predict that the overall volume of activation of process [1], $\Delta V_1^{\neq}$, is +3 cm^3/mol for allyl alcohol in methanol and +7 cm^3/mol in ethanol. For propargyl alcohol $\Delta V_1^{\neq}$ should be near 7 cm^3/mol in both solvents if the reaction mechanism is [2, 3].

The rate constants for propargyl alcohol are greater than those for allyl alcohol, which implies a greater electron affinity for the former. The values of k_P are therefore less sensitive to E_r than are those of k_A, so the ratio k_P/k_A increases with E_r (Fig. 6).

The value of k_1 in *tert*-butyl alcohol is near the diffusion controlled limit (Figs. 5 and 6). The large values of E_1 are caused mainly by the activation energy of diffusion in this solvent (compare E_1 with

TABLE 3. Energies and entropies of activation

Solvent	Allyl alcohol E_1 (kJ/mol)	Allyl alcohol $\Delta S_1^{\ddagger}$ (J/mol K)	Propargyl alcohol E_1 (kJ/mol)	Propargyl alcohol $\Delta S_1^{\ddagger}$ (J/mol K)
Water	14	−60	18	−27
Ethylene glycol	16	−42	21	−13
Methanol	16	−42	19	−15
Ethanol	17	−25	16	−15
2-Propanol	17	−17	19	−2
tert-Butyl alcohol	31	+33	36	+54

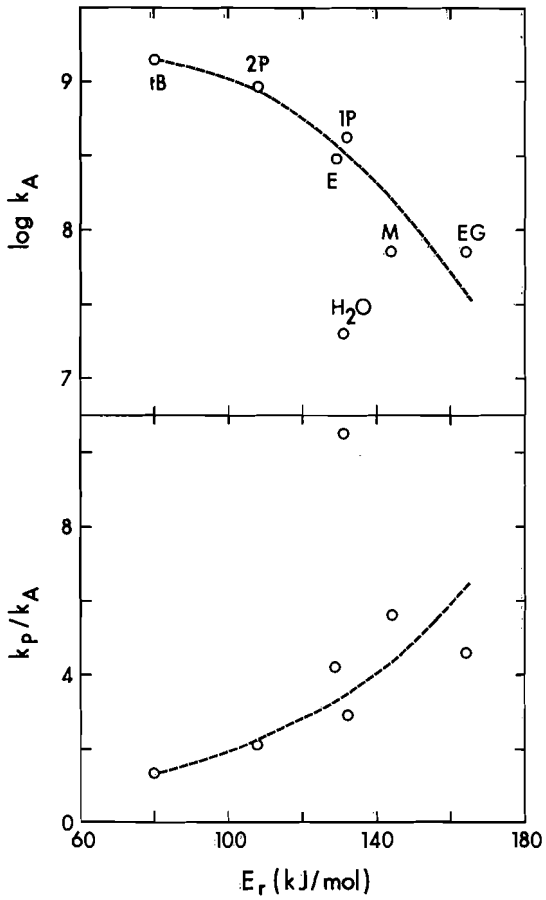

FIG. 6. Plots of log k_A and k_P/k_A against E_r (see Table 1).

E_η in Table 2). Transport has a higher activation energy in liquid branched chain compounds than in their straight chain counterparts (22, 30). The branched structure is more rigid and probably requires a greater amount of rearrangement of neighboring molecules to undergo a diffusion step.

Entropies of Activation

To estimate relative values of $\Delta S_1^{\ddagger}$ one may write

[5] $$\exp(-E_1/RT) \approx \exp(-\Delta H_1^{\ddagger}/RT)$$

and

[6] $$\log A_1 \approx \log(kT/h) + (\Delta S_1^{\ddagger}/2.3R)$$

At 298 K one has

[7] $$\log A_1 \approx 12.8 + (\Delta S_1^{\ddagger}/19)$$

where $\Delta S_1^{\ddagger}$ is in units of J/mol K. Values of $\Delta S_1^{\ddagger}$ so calculated are compared with E_1 in Table 3. The entropies vary relatively much more than do the energies of activation.

The capture of a solvated electron by a scavenger that has a low electron affinity is dependent upon the occurrence of a favorable configuration of solvent dipoles about the reaction site. A favorable configuration would increase the solvation energy of the molecular anion and decrease that of the electron. A more negative entropy of activation signifies the smaller probability of occurrence of a sufficiently favorable configuration.

Further interpretation of the positive and less negative values of ΔS_1 (less negative than, say, −20 J/mol K) requires knowledge of the parameter values for diffusion of e^-_{solv} and S. The value of k_1 can be divided into two components,

[8] $$k_1^{-1} = k_d^{-1} + k_r^{-1}$$

or

[9] $$\exp(\Delta G_1^{\ddagger}/RT) = \exp(\Delta G_d^{\ddagger}/RT) + \exp(\Delta G_r^{\ddagger}/RT)$$

where k_d and $\Delta G_d^{\ddagger}$ refer to the diffusion together of the reactants, while k_r and $\Delta G_r^{\ddagger}$ refer to the reaction of an encounter pair. Electron diffusion coefficients in alcohols are difficult to measure, but there is now great need of the information.

Other Scavengers

Rate parameters for a number of other scavengers in water, methanol, and ethanol are listed in Table 4. The smaller values of k_1 are limited by a large negative entropy of activation. However, acetonitrile has a high enthalpy of activation, which indicates that

TABLE 4. Rate parameters for other scavengers

S	Solvent = H_2O				Solvent = CH_3OH				Solvent = C_2H_5OH			
	log k_1 [a]	log A_1 [a]	E_1 [b]	$\Delta S_1^{\neq}$ [c]	log k_1 [a]	log A_1 [a]	E_1 [b]	$\Delta S_1^{\neq}$ [c]	log k_1 [a]	log A_1 [a]	E_1 [b]	$\Delta S_1^{\neq}$ [c]
Perchloric acid					10.73	13.1	13	+6	10.52	13.4	17	+11
Nitrobenzene	10.62	13.26	15	+9	10.36	12.5	12	−6	10.18	12.4	13	−8
Acetone	9.83	11.95	12	−16	9.63	11.7	11	−21	9.67	11.8	12	−19
Naphthalene					9.48	11.9	13	−17	9.63	12.0	13	−15
Acetonitrile	7.64	11.66	23	−22	8.11	12.50	25	−6				
Ethyl acetate	7.66	10.51	16	−44								
Phenol	7.20	9.84	15	−57	7.0	10.3	19	−48	7.70	10.9	18	−36

[a] In M^{-1} s^{-1}. k_1 at 299 K.
[b] In kJ/mol.
[c] In J/mol K.

its reaction is in the border region between dependence on and independence of reaction [3] to stabilize the anion (27, 31).

Acknowledgement

We would like to thank the staff of the Radiation Research Center for help with the electronics.

1. (*a*) M. ANBAR, Z. B. ALFASSI, and H. BREGMAN-REISLER. J. Am. Chem. Soc. **89**, 1263 (1967); (*b*) M. ANBAR, M. BAMBENEK, and A. B. ROSS. NSRDS-NBS 43, U.S. Dept. of Commerce, Washington, DC. 1973. p. 3.
2. (*a*) K. N. JHA and G. R. FREEMAN. J. Chem. Phys. **48**, 5480 (1968); (*b*) **51**, 2839 (1969); (*c*) **51**, 2846 (1969); (*d*) G. L. BOLTON, K. N. JHA, and G. R. FREEMAN. Can. J. Chem. **54**, 1497 (1976); (*e*) K. OKAZAKI and G. R. FREEMAN. Can. J. Chem. **56**, 2313 (1978).
3. (*a*) B. ČERČEK. Nature, **223**, 491 (1969); (*b*) Int. J. Radiat. Phys. Chem. 7, 223 (1975).
4. B. BOCKRATH and L. M. DORFMAN. J. Phys. Chem. **77**, 1002 (1973).
5. G. BAKALE, U. SOWADA, and W..F. SCHMIDT. J. Phys. Chem. **79**, 3041 (1975).
6. J. H. BAXENDALE, B. P. H. M. GEELEN, and P. H. G. SHARPE. Int. J. Radiat. Phys. Chem. **8**, 371 (1976).
7. H. BOLL, P. S. CHILDS, R. R. DEWALD, and R. L. JONES. J. Chem. Phys. **65**, 2916 (1976).
8. FARHATAZIZ and L. M. PERKEY. J. Phys. Chem. **80**, 122 (1976).
9. E. J. RASBURN and H. B. MICHAELS. Rad. Phys. Chem. **10**, 289 (1977).
10. S. M. S. AKHTAR and G. R. FREEMAN. J. Phys. Chem. **75**, 3756 (1971).
11. K. N. JHA, G. L. BOLTON, and G. R. FREEMAN. J. Phys. Chem. **76**, 3876 (1972).
12. F.-Y. JOU and G. R. FREEMAN. Can. J. Chem. **54**, 3693 (1976).
13. F.-Y. JOU and G. R. FREEMAN. J. Phys. Chem. **81**, 909 (1977).
14. K. OKAZAKI and G. R. FREEMAN. Can. J. Chem. **56**, 2305 (1978).
15. R. W. GALLANT. Physical properties of hydrocarbons. Vols. 1 and 2. Gulf Publishing Co., Houston, TX. 1968.
16. J. H. BAXENDALE and P. WARDMAN. Chem. Commun. 429 (1971).
17. R. S. DIXON, V. J. LOPATA, and C. R. ROY. Int. J. Radiat. Phys. Chem. **8**, 707 (1976).
18. G. G. TEATHER and N. V. KLASSEN. Int. J. Radiat. Phys. Chem. **7**, 475 (1975).
19. F. BUCKLEY and A. A. MARYOTT. Natl. Bur. Stand. Circular 589, U.S. Dept. of Commerce, Washington, DC. 1958.
20. B. P. JORDAN, R. J. SHEPPARD, and S. SZWARNOWSKI. J. Phys. D**11**, 695 (1978).
21. S. K. GARG and C. P. SMYTH. J. Phys. Chem. **69**, 1294 (1965).
22. J. R. PARTINGTON, R. F. HUDSON, and K. W. BAGNALL. J. Chim. Phys. **55**, 77 (1958).
23. (*a*) J.-P. DODELET, K. SHINSAKA, and G. R. FREEMAN. J. Chem. Phys. **59**, 1293 (1973); (*b*) P. FOWLES. Trans. Faraday Soc. **67**, 428 (1971); (*c*) B. CONWAY. Electrochemical data. Elsevier, Amsterdam. 1952. p. 162.
24. R. A. VERMEER and G. R. FREEMAN. Can. J. Chem. **52**, 1181 (1974).
25. J. JORTNER and R. M. NOYES. J. Phys. Chem. **70**, 770 (1966).
26. F.-Y. JOU and G. R. FREEMAN. J. Phys. Chem. In press.
27. F.-Y. JOU and G. R. FREEMAN. Can. J. Chem. **57**, 591 (1979).
28. R. A. MARCUS. J. Chem. Phys. **24**, 966 (1956), and references therein.
29. G. L. BOLTON, M. G. ROBINSON, and G. R. FREEMAN. Can. J. Chem. **54**, 1177 (1976).
30. D. W. MCCALL, D. C. DOUGLASS, and E. W. ANDERSON. J. Chem. Phys. **31**, 1555 (1959).
31. G. L. BOLTON and G. R. FREEMAN. J. Am. Chem. Soc. **98**, 6825 (1976).
32. A. V. RUDNEV, A. V. VANNIKOV, and N. A. BAKH. High Energy Chem. **6**, 416 (1972).

Polymorphism of crystalline *tert*-butyl chloride-d_0 and *tert*-butyl chloride-d_9: a Raman spectroscopic study[1]

S. SUNDER[2]

Arorganisch-Chemisches Institut der Universität, 6900 Heidelberg, W. Germany
and
Division of Chemistry, National Research Council of Canada, Ottawa, Ont., Canada K1A 0R9

Received August 14, 1978

S. SUNDER. Can. J. Chem. **57**, 846 (1979).

Raman spectra of the three solid phases of *tert*-butyl chloride-d_0 and -d_9 have been recorded for the regions of the intramolecular vibrations. The spectra of solid I are typical of those seen for plastic crystals and those of solid II of solids with partial orientational order. The transition from solid I to solid II results in the ordering of the three-fold molecular symmetry axes but the axes perpendicular to the molecular symmetry axes remain randomly oriented. The transition from solid II to III results in a more-or-less ordered structure. The spectra of phase III at 90 K suggest an ordered solid with the molecules on sites of symmetry C_s or C_1.

S. SUNDER. Can. J. Chem. **57**, 846 (1979).

On a enregistré les spectres Raman de trois phases solides du chlorure de *tert*-butyle-d_0 et -d_9 dans les régions des vibrations intramoléculaires. Les spectres du solide I sont typiques de ceux observés avec des cristaux plastiques alors que ceux du solide II se comparent à ceux de solides comportant un ordre partiel d'orientation. La transition d'un solide I en solide II provoque une orientation des axes tertiaires de symétrie moléculaire alors que les axes perpendiculaires aux axes de symétrie moléculaire restent orientés au hasard. La transition d'un solide II en III conduit à une structure plus ou moins orientée. Le spectre de la phase III à 90 K indique la présence d'un solide orienté comportant des molécules sur les sites de symétrie C_s ou C_1.

[Traduit par le journal]

Introduction

tert-Butyl chloride (TBC), $(CH_3)_3CCl$, is a globular molecule and shows two phase transitions in its solid state, with the I–II and II–III phase transitions occurring at 219.6 K and 183 K, respectively, under 1 atm pressure and its freezing point being 247.5 K (1). The three solid phases of TBC have been investigated using several physical techniques, e.g., heat capacity measurements (2–6), dielectric measurements (2, 3, 6, 7), nmr (8–10), nqr (11), ir (6), far-ir (12–14), X-ray diffraction (15–17), and more recently by inelastic neutron scattering (18). Their Raman spectra, however, have been reported only for the region below 100 cm^{-1}, i.e., only for the lattice modes (intermolecular vibrations) according to the information available to us (14). There seems to be general agreement about the nature of phase I (the high temperature phase), that it is plastic crystalline in nature and that molecules undergo hindered reorientations around all possible axes. Also, there seems to be agreement that at or below 90 K solid III has a fixed lattice. But there appears to be differences in opinion about the nature of solid II, and about that of solid III at temperatures above liquid air temperature. The nmr (10) and X-ray (17) data have been interpreted to indicate that the CCl bonds of the TBC molecules are fixed in solid II and the molecules can reorient about the molecular symmetry axis (CCl bond). Neutron scattering data, on the other hand, has been interpreted to suggest that the molecules can reorient both about the molecular symmetry axis and the axes perpendicular to it (18). Neutron scattering data did not suggest any molecular reorientations in phase III at temperatures around 173 K while the nmr data indicated the presence of molecular reorientations about the CCl bonds as well as the rotations of the methyl groups around the CC bonds at these temperatures in phase III. In light of the above interest in the solid phases of TBC we report here the Raman spectra of *tert*-butyl chloride-d_0 (TBC-d_0) and *tert*-butyl chloride-d_9 (TBC-d_9) in the regions of the intramolecular vibrations for their three solid phases, and discuss and compare the evidence obtained from Raman spectra regarding the structure, disorder, and molecular motions in the three solid phases with that derived from the other techniques. Earlier we presented a similar study of the three solid phases of *tert*-butyl bromide, a very closely related system (19–21).

[1]NRCC No. 17123.

[2]Present address: Anorganisch Chemisches Institut der Universität, 6900 Heidelberg, W. Germany.

0008-4042/79/080846-07$01.00/0

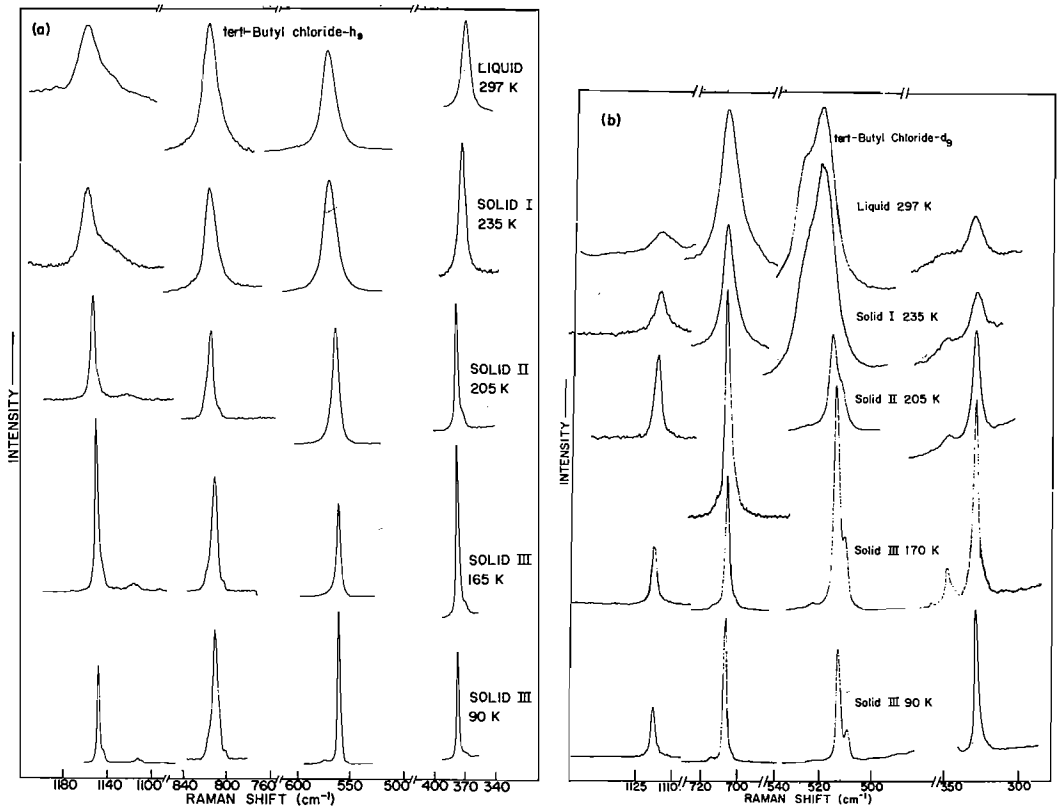

FIG. 1. Laser Raman spectra of the 'well-separated' A_1 modes of *tert*-butyl chloride in the liquid and the three solid phases using 4880 Å excitation: (*a*) *tert*-butyl chloride-d_0; (*b*) *tert*-butyl chloride-d_9.

Experimental

TBC-d_0 was obtained from B.D.H. Co. of England and was purified following the procedure of Baker and Smyth (2). TBC-d_9 was obtained from Merck, Sharp and Dohme of Canada and used without further purification. Its isotopic purity was better than 99% as indicated by its Raman spectra in the CH and CD stretching regions. The liquid samples were sealed in melting-point Pyrex capillaries (id 1 mm) and placed in an unsilvered vacuum jacketed transfer tube (22). Temperature control was achieved using a cold nitrogen gas stream flowing over a heater-sensor system in the transfer tube. The sample temperature was measured with a separate thermocouple placed near the sample and the reported temperatures are accurate to ± 3 K. The two transitions from phase I to II and from II to III were found to be spectroscopically complete when the solid samples were held for ~ 30 min at 205 K and 170 K, respectively (19, 21). Therefore all the spectra of phase II were recorded after the samples had been kept at 205 K for at least 40 min and the samples were held at 170 K for at least 40 min before recording any spectra of phase III.

The Raman scattering excited by the 4880 Å line from a Coherent Radiation 52 GA argon ion laser was recorded with a 90° scattering geometry using a Spex model 1400 dual monochromator, a photomultiplier tube (EMI 6256), and photon counting electronics. The laser output was filtered to remove extraneous emission lines and the power at the sample was about 250 mW. The frequency scale was calibrated using a neon lamp. No correction was applied to the observed intensities for the frequency-dependence of the instrument response.

Results

tert-Butyl chloride has $8A_1$ and $12E$ Raman active modes under C_{3v} molecular point group symmetry (19, 23–25). Assignment of the Raman bands of liquid TBC-d_0 and TBC-d_9 has been discussed in the literature (23–24). Here we have collected the bands due to the 'well-separated' and 'unambiguous' A_1 and E modes in Figs. 1 and 2, respectively, for the purpose of comparison. The assignment of the features in the CH_3 (CD_3) stretching and deformation regions are less certain due to the occurrence of several fundamentals and overtone/combination vibrations in these regions and the Fermi-resonance between them (19, 23–26). The spectra for these regions are shown in Fig. 3. The spectra of solid III are shown at two temperatures, at ~ 170 K, just below the II–III transition temperature, and at ~ 90 K, the lowest temperature used in this work. The spectra of phase III shown

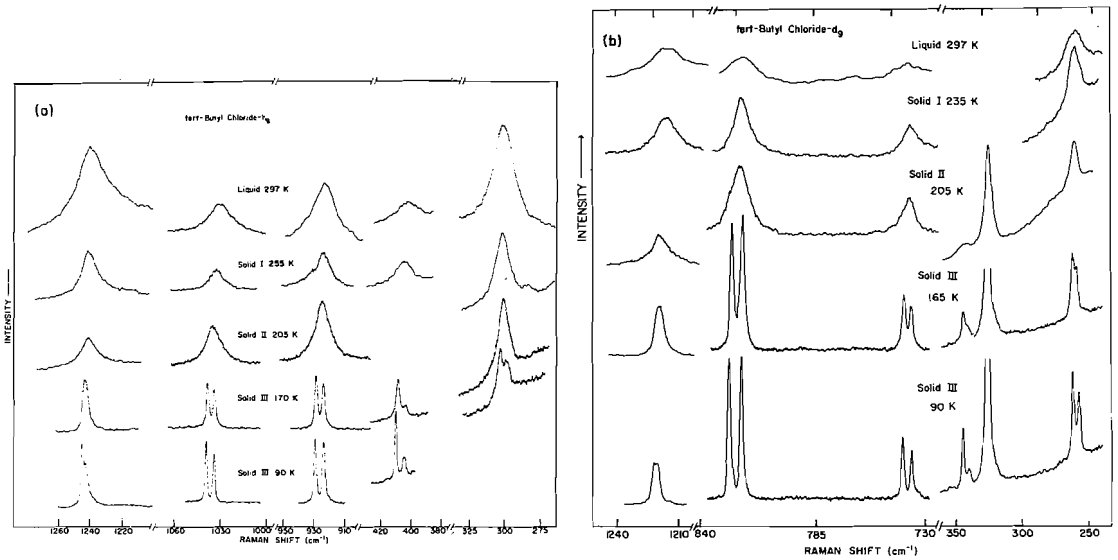

FIG. 2. Laser Raman spectra of the 'well-separated' E modes of *tert*-butyl chloride in the liquid and the three solid phases using 4880 Å excitation: (*a*) *tert*-butyl chloride-d_0; (*b*) *tert*-butyl chloride-d_9.

here are recorded at $\sim 1.5\ cm^{-1}$ spectral slitwidth, while those of the high temperature phases were recorded at $\sim 2.5\ cm^{-1}$ spectral slitwidth for better signal-to-noise ratio. The spectra of the high temperature phases were also studied at $\sim 1.5\ cm^{-1}$ resolution, but no additional features were observed. Here it may be mentioned that the spectra shown in Figs. 1–3 are photocopies of the original spectra and that the monochromator used was linear in wavelength. The Raman shifts of the observed features in the regions of the intramolecular fundamental vibrations are listed in Tables 1 and 2 for TBC-d_0 and TBC-d_9, respectively, for their three solid phases as well as the liquid phase. The frequency accuracy is believed to be $\pm 2\ cm^{-1}$ for the sharp features. These tables also contain the qualitative relative intensities of the observed features. The intensities are relative within the same phase. The spectra shown in Figs. 1–3 were recorded under different vertical expansions for the purpose of clearer presentation.

The spectra of solid I are very similar to those of the liquid (Figs. 1–3). The main exception to the above is that the shoulder on the high frequency side of the ν_7 band of TBC-d_9, at around $527\ cm^{-1}$, shows a marked decrease in its intensity in solid phase I. The feature was assigned to an H-impurity in ref. 24 but the progressive decrease in its intensity with the lowering of the temperature suggests that this feature probably arises from a 'difference transition' of TBC-d_9 itself and not from any impurity. The transition from solid I to solid II does not produce any marked change in the bands due to the E modes (Fig. 2) but it does cause a sharp decrease in the halfwidths of the bands due to the A_1 modes (Fig. 1). Each of the A_1 modes shows a single band in the solid II phase. Additional very weak features seen near some of the A_1 bands are believed to be due to the combinations and/or overtones. The features assigned to ν_1 in TBC-d_0 and to ν_1 and ν_2 in TBC-d_9 also show considerable sharpening in going from solid phase I to phase II (Fig. 3) which thus supports their assignment to A_1 modes. Transition from solid II to III is accompanied by the splitting of the bands due to the well separated E modes into two sharp bands (Fig. 2) while the bands due to the A_1 modes show no such splitting. Further cooling to 90 K does not produce any new splitting, but it does sharpen the features. The sharpening of the bands due to cooling in the phase III is maximum for the bands due to the methyl (methyl-d_3) torsion vibrations. A similar behaviour was seen for the corresponding bands in the far-ir (14).

Discussion

All three phases of TBC are isotopically grossly disordered due to the occurrence of chlorine as two isotopes, ^{35}Cl and ^{37}Cl, in a ratio of about 3:1. The isotopic splitting due to the two chlorine isotopes can be of significance mainly for the bands due to ν_7, ν_8, and ν_{23} according to the isotopic studies on TBC (27). However, no splitting or broadening is seen in the spectra, even in the bands due to these modes at ~ 90 K, which can be associated with the presence of two chlorine isotopes (Figs. 1 and 2).

TABLE 1. Raman spectra of the three solid phases of *tert*-butyl chloride-d_0[a]

Solid III		Solid II	Solid I		
90 K	170 K	205 K	235 K	Liquid[b]	Assignment
2987vs	2987	2984ms	2984ms	2985ms	$\nu_{13}(E)$
2975vs	2976	2975s	2974ms	2973ms	$\nu_1(A_1),\nu_{14}(E)$
2968sh	2969				
2950br	2950	2950m	2947mw	2945w	$2\nu_{16}$
2933s	2933	2931s	2929s	2922s	$\nu_2(A_1),\nu_{15}(E)$
2921br	2921	2921sh	2922sh		
2907ms	2907	2905ms	2901m	2897m	$\nu_{16}+\nu_{17}$
2863br	2864	2865mw	2863br	2863mw	$\nu_4+\nu_{17}$
		2845w	2845br		
1484vw	1484	1480vw,br			$\nu_{16}(E)$
1478vvw	1479				
1466m	1465	1460m	1460sh	1460sh	$\nu_{17}(E)$
1457m	1456				
1450m	1449	1446m	1446ms	1448s	$\nu_3(A_1)$
1445w	1445	1443vw,sh			$\nu_5+\nu_{23}$
1436mw	1436	1437m	1437sh	1437w,sh	$\nu_{20}+\nu_{22}$
1420vvw					$\nu_5+\nu_{24}$
1399vw	1399	1399vw	1397vw	1392vw	$\nu_4(A_1)$
1371w	1371	1372w	1371w	1366w	$\nu_{18}(E)$
1368vw	1369				
1245m	1243	1241mw	1240mw	1236m	$\nu_{19}(E)$
1241w	1241				
1144s	1145	1147s	1155ms	1156ms	$\nu_5(A_1)$
1141sh,vw	1141	1141	1143sh	1130w	$\nu_3-\nu_{23}$
1109vw	1109	1113w			$\nu_6+\nu_{23}$
1105w					
1041w	1040	1037w	1036w	1030w	$\nu_{20}(E)$
1035w	1035				
930w	930	929w	928mw	927mw	$\nu_{21}(E)$
925w	925				
816w,sh	816				$\nu_7+\nu_{12}$
808s	808	809s	810s	810s	$\nu_6(A_1)$
801vw,sh	801	804vw,sh			$2\nu_{22}$
571vw					$2\nu_{24}$
557vs	558	560vs	566vs	569vs	$\nu_7(A_1)$
409w	408	407w	407w	404	$\nu_{22}(E)$
403vw	403				
374vs	374	374vs	372vs	369s	$\nu_8(A_1)$
370vvw	370	370vvw,sh			$\nu_{23}+L$[c]
305m	305	303m	303ms	302s	$\nu_{23}(E)$
300w	301				
295vw	294				$\nu_{24}(E)$
290vw	290				

[a]Raman shifts ($\Delta\nu$) are in wave numbers (cm^{-1}) and are listed only for the spectral region of intramolecular fundamental vibrations. s, m, w, v, sh, and br stand for strong, medium, weak, very, shoulder, and broad, respectively.
[b]Liquid data are from ref. 24.
[c]Possible combinations with a lattice mode, see ref. 14 for lattice vibrations in TBC.

Therefore we have assumed that the system is within the 'amalgamation limit' (28), and that the spectra due to the intramolecular vibrations can be qualitatively treated as though the disorder in the masses of chlorine atoms was not present (21, 29).

Solid phase I of TBC has been shown to be plastic crystalline, and its X-ray diffraction data indicated that the molecules occupy sites of cubic symmetry even though the molecular symmetry is only C_{3v} (15). Nuclear magnetic resonance (11),

TABLE 2. Raman spectra of the three solid phases of *tert*-butyl chloride-d_9[a]

Solid III		Solid II	Solid I		
90 K	170 K	205 K	235 K	Liquid	Assignment
2239vs	2238	2239s	2240s	2240s	$\nu_{13}(E)$
2222vs	2221	2222vs	2223s	2221s	$\nu_1(A_1),\nu_{14}(E)$
2208w,br	2208				
			2187w	2183w	$\nu_3 + \nu_{17}$
2139ms,br	2139	2138ms,br	2138s	2136s	
2121vs	2120	2119vs	2117vs	2116vs	$\nu_2(A_1), \nu_{15}(E)$
2116sh		2110br			
2105br					
2083br	2083	2083br	2083m,br	2082m	$2\nu_4$
2048vs	2048	2048vs	2048s	2048s	$\nu_4 + \nu_5$
2040w					
1222mw	1221	1218mw	1217mw	1216m	$\nu_{16}(E)$
1220mw	1219				
1119mw	1119	1118mw	1117mw	1117mw	$\nu_3(A_1)$
1085vw,br	1085	1083br			
1070w	1070	1069w	1067w	1067w	$2\nu_7$
1059m	1059	1055sh			
1055w					
1050ms	1049	1047s	1046s	1045s	$\nu_4(A_1),\nu_{17}(E),$
1037w	1037	1036sh	1037sh		$\nu_{18}(E)$
1031w	1031				
1021br	1022				
984s	984	988s	1006s	1005s	$\nu_5(A_1),\nu_{19}(E)$
979vw	978				
829m	828	825mw	824mw	824mw	$\nu_{20}(E)$
823m	823				
742w	742	740w	740w	740w	$\nu_{21}(E)$
737w	738				
712vvw	710	710vvw			$\nu_7 + \nu_{24}$
706s	706	708s	708s	708s	$\nu_6(A_1)$
523vw,br	523	523vw	526sh	527sh	$\nu_{21} - \nu_{24}, 2\nu_{23}$
511vs	511	514vs	520vs	520vs	$\nu_7(A_1)$
507w	507	508w,sh			$\nu_{22} + \nu_{12}$
345m	345	345w,br	345wbr	343w,br	$\nu_{22}(E)$
340w	341				
330vs	329	328vs	326s	324s	$\nu_8(A_1)$
266ms	266	265s	265s	265s	$\nu_{23}(E)$
262m	263				
222vw	222				$\nu_{24}(E)$
219vw	220				

[a]Raman shifts ($\Delta\nu$) are in wave numbers (cm^{-1}) and are listed only for the spectral region of intramolecular fundamental vibrations.

dielectric (6, 7), and more recently neutron scattering studies (18) have shown that the molecules can undergo hindered reorientations about all possible axes at rates greater than $10^9\ s^{-1}$ in solid I. The similarity between the spectra of the liquid and solid phase I is in agreement with the above conclusions that there is no loss of reorientational freedom in going from the liquid to solid I. Similar conclusions have been drawn from the vibrational spectra of other plastic crystals (19, 20, 22, 30–34). The 'large' halfwidth of the vibrational bands of the plastic crystals has been attributed to the disorder in their structure as well as to the reorientational motions of the molecules (19, 20, 22, 34). Both the molecular reorientations and the disorder in the orientations of the molecules contribute to the observed breadth of Raman bands in solid I of TBC, as was shown also for the plastic crystal phase of *tert*-butyl bromide (19, 20), a very similar system. Although all Raman bands are quite broad in the liquid and plastic crystal phase, it can be seen from Figs. 1–3 that the bands due to the A_1 modes are less broad than the bands due to the E modes at the same temperature. This is consistent with the facts that

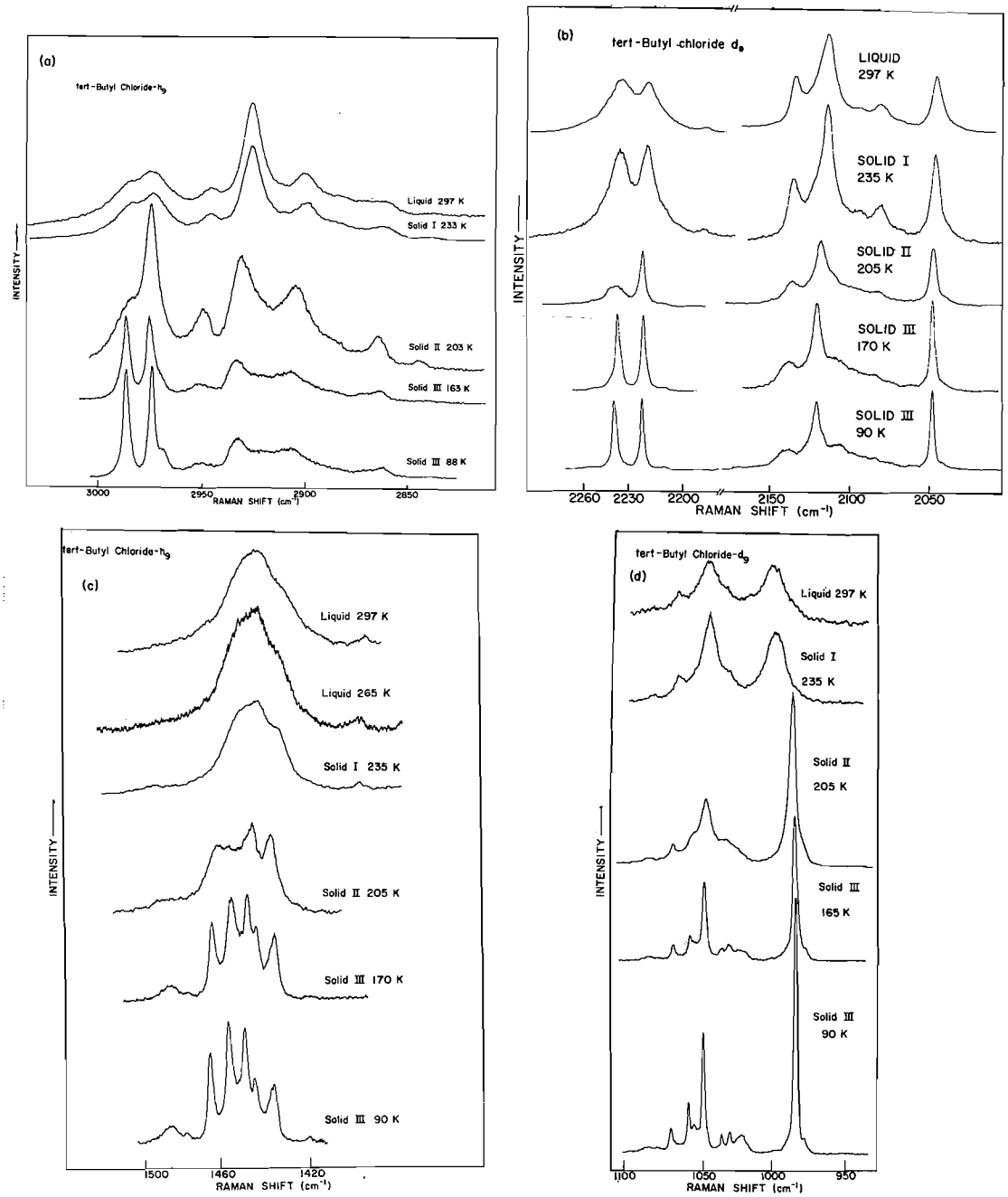

FIG. 3. Laser Raman spectra of the liquid and the three solid phases of *tert*-butyl chloride for the methyl (methyl-d_3) stretching and deformation regions using 4880 Å excitation: (*a*) CH_3 stretching vibrations in TBC-d_0; (*b*) CD_3 stretching vibrations in TBC-d_9; (*c*) CH_3 deformations in TBC-d_0; (*d*) CD_3 deformations in TBC-d_9.

(*a*) the reorientational motions of the molecules affect only the anisotropic part of Raman scattering, (*b*) the E mode bands are sensitive to both the tumbling motions of molecules (reorientations about the directions perpendicular to the molecular symmetry axis), and to the motions about the C_3 axis while the A_1 bands are sensitive only to the tumbling motions (34), and (*c*) the A_1 bands are polarized or partially polarized (24) and therefore the major contribution to their intensities is from the isotropic Raman scattering rather than the anisotropic Raman scattering.

The X-ray studies indicated that in solid phase II of TBC the dipolar axes of the molecules are ordered, but there is 'orientational disorder' about this axis (17). Sharp features seen for the A_1 modes (Fig. 1), and broad features seen for the E modes (Fig. 2) in the Raman spectra are consistent with these X-ray results. Similar spectral results have been obtained for other systems with similar partial orientational disorder, e.g. methyl ammonium halides (35) and *tert*-butyl bromide (19, 21). The sharpness of the features due to the A_1 modes suggests that the tumbling motion of the molecules in phase II indicated by the neutron scattering study, if present, is not able to affect the halfwidth of the A_1 bands to a significant extent.

The splitting of the bands due to the E modes into two sharp features in solid phase III (Fig. 2) suggests that the transition from phase II to III is accompanied by the ordering of the molecules in the directions perpendicular to the molecular symmetry (C_3) axes as well. The appearance of the bands due to the methyl torsion vibrations in the far-ir (14) and the Raman spectra at temperatures below the II–III transition temperature indicate that the methyl groups do not undergo 'free-rotation' in the solid phase III. At about 90 K, most of the observed features are quite sharp, indicating thereby that at this temperature the TBC lattice is not only fixed (10) but also *ordered*. The splitting of all the well-separated bands due to the E-modes into two sharp features while all the A_1 modes are showing only one feature indicates that the splitting of the E-modes is probably due to 'site-group-splitting'. This is possible only if the molecules are on sites of symmetry C_s or C_1 in solid III (19, 21). The 'absence' of 'factor-group-splitting' suggests that either there is only one molecule per 'unit-primitive-cell' or that the factor-group-splitting is less than the observed halfwidth of the bands, which at about 90 K is less than 3 cm^{-1} for most of the bands shown in Figs. 1 and 2. At present there are no published X-ray data about the structure of solid III to check the above conclusions (16).

Acknowledgements

The author is grateful to Professor H. H. Eysel for making helpful comments on the manuscript and to Dr. H. J. Bernstein for his encouragement during this work.

Assistance of Mr. B. Francis in recording and measuring some of the spectra reported here is acknowledged.

1. J. G. Aston. Physics and chemistry of organic solid state. Vol. I. *Edited by* D. Fox, M. M. Labes, and A. Weissberger. Interscience, New York. 1963. p. 543.
2. W. O. Baker and C. P. Smyth. J. Am. Chem. Soc. **61**, 2798 (1939).
3. L. M. Kushner, R. W. Crow, and C. P. Smyth. J. Am. Chem. Soc. **72**, 1091 (1950).
4. A. Dworkin and M. Guillamin. J. Chim. Phys. **63**, 53 (1966).
5. L. Silver and R. Rudman. J. Phys. Chem. **74**, 3134 (1970).
6. S. Urban, J. A. Janik, J. Lenik, J. Mayer, T. Waluga, and S. Wróbel. Phys. Status Solidi, **10**, 271 (1972).
7. J. G. Powles, D. E. Williams, and C. P. Smyth. J. Chem. Phys. **21**, 136 (1953).
8. J. G. Powles and H. S. Gutowsky. J. Chem. Phys. **21**, 1695 (1953).
9. E. O. Stejskal, D. E. Woessner, T. C. Farrar, and H. S. Gutowsky. J. Chem. Phys. **31**, 55 (1959).
10. D. E. O'Reilly, E. M. Peterson, C. E. Scheie, and E. Seyfarth. J. Chem. Phys. **59**, 3576 (1973).
11. H. S. Gutowsky and D. W. McCall. J. Chem. Phys. **32**, 548 (1960).
12. B. Lassier and C. Brot. J. Chim. Phys. **65**, 1723 (1968).
13. C. Brot, B. Lassier, G. W. Chantry, and H. A. Gebbie. Spectrochim. Acta, **24A**, 295 (1968).
14. J. R. Durig, S. M. Craven, and J. Bragin. J. Chem. Phys. **51**, 5663 (1969).
15. R. S. Schwartz, B. Post, and I. Fankuchen. J. Am. Chem. Soc. **73**, 4490 (1951).
16. R. Rudman. J. Chem. Educ. **44**, 331 (1967).
17. R. Rudman and B. Post. Mol. Cryst. **5**, 95 (1968).
18. L. Månsson and K. E. Larsson. J. Chem. Phys. **67**, 4996 (1977).
19. S. Sunder. Ph.D. Thesis, University of Alberta, Edmonton, Alta. 1972.
20. J. E. Bertie and S. Sunder. J. Chem. Phys. **59**, 3853 (1973).
21. J. E. Bertie and S. Sunder. Spectrochim. Acta, **30A**, 1373 (1974).
22. S. Sunder and R. E. D. McClung. Chem. Phys. **2**, 467 (1973).
23. H. Hutter and W. Zeil. Spectrochim. Acta, **22**, 1007 (1966).
24. J. C. Evans and G. Y. S. Lo. J. Am. Chem. Soc. **88**, 218 (1966).
25. J. E. Bertie and S. Sunder. Can. J. Chem. **51**, 3344 (1973).
26. S. Sunder, R. Mendelsohn, and H. J. Bernstein. Chem. Phys. Lipids, **17**, 456 (1976).
27. R. C. Williams and J. W. Taylor. J. Am. Chem. Soc. **95**, 1710 (1973).
28. P. N. Prasad and R. Kopelman. J. Chem. Phys. **57**, 863 (1972); **58**, 126 (1973).
29. S. Sunder and R. E. D. McClung. Can. J. Phys. **52**, 2299 (1974).
30. A. Anderson and R. Savoie. J. Chem. Phys. **43**, 3468 (1965).
31. R. P. Fournier, R. Savoie, F. Bessette, and A. Cabana. J. Chem. Phys. **49**, 1159 (1968).
32. R. J. Obremski, C. W. Brown, and E. R. Lippincot. J. Chem. Phys. **52**, 2253 (1970).
33. R. P. Fournier, R. Savoie, N. D. The, R. Belzile, and A. Cabana. Can. J. Chem. **50**, 35 (1972).
34. F. J. Bartoli and T. A. Litovitz. J. Chem. Phys. **56**, 404 (1972); **56**, 413 (1972).
35. E. Whalley. J. Chem. Phys. **51**, 4040 (1969).

Free energy relationship of the equilibrium ionization constants of disulfonyl carbon acids in 80% (w/w) dimethyl sulfoxide – water solvent at 25°C

THOMAS W. S. LEE AND KOK-PENG ANG

Department of Chemistry, University of Singapore, Bukit Timah Road, Singapore 10

Received September 27, 1978

THOMAS W. S. LEE and KOK-PENG ANG. Can. J. Chem. **57**, 853 (1979).

A series of eight carbon acids, α,α-bis(benzylsulfonyl)toluene and 7 substituted α,α-bis-(benzylsulfonyl)toluenes, was synthesized and their equilibrium ionization constants were determined by spectrophotometric measurement in 80% (w/w) dimethyl sulfoxide – water solvent at 25°C. From a plot of $-\log K$ versus σ for the 'well-behaved' substituents and σ^- for *para*-cyano and *para*-nitro substituents, a ρ value of 2.53 is obtained. The correlation coefficient is 0.99. Comparing this ρ value with the reported ρ value of 12 for the substituted toluenes in dimethyl sulfoxide, it shows that the acidities of the disulfonyl toluenes are at least 8 to 9 orders of magnitude less sensitive to substituent effects than are the acidities of substituted toluenes implying that, for disulfonyl toluenes, the negative charge on the benzylic carbon is extensively delocalised into the two adjacent sulfonyl groups.

THOMAS W. S. LEE et KOK-PENG ANG. Can. J. Chem. **57**, 853 (1979).

On a synthétisé une série d'acides comportant huit atomes de carbone, le α,α-bis-(benzylsulfonyl) toluène et 7 α,α-bis-(benzylsulfonyl) toluènes substitués et on a déterminé les constantes d'ionisation à l'équilibre par des mesures spectrophotométriques dans des solutions à 80% (p/p) de diméthylsulfoxyde dans l'eau à 25°C. A l'aide de la courbe de $-\log K$ versus σ dans le cas des substituants "se comportant bien" et σ^- pour les substituants *p*-cyano et *p*-nitro, on a pu obtenir une valeur de ρ de 2.53. Le coefficient de corrélation est 0.99. Une comparaison de cette valeur de ρ avec la valeur de ρ de 12 toluènes substitués en solution dans le diméthylsulfoxyde montre que les acidités des disulfonyltoluènes sont au moins 8 à 9 ordres de grandeur moins sensibles aux effets de substituants que les acidités des toluènes substitués; cette observation suggère que, dans les disulfonyltoluènes, la charge négative du carbone benzylique est fortement délocalisée par les deux groupes sulfonyles adjacents.

[Traduit par le journal]

Introduction

Evidence for the acid-strengthening effect of sulfonyl group on the hydrogens attached to the α-carbon atom is compelling (1–6) but interpretation of the nature of this effect is not always unanimous. Some authors (1, 2, 5) have attributed the acidifying effect on the C—H to conjugative interaction between sulfur and the carbon atom presumably involving the sulfur *d*-orbitals while others (7, 8) have been skeptical of such an interaction.

The recent finding of Bordwell *et al.* (9) on the acidities of substituted toluenes has prompted us to report our results on the p*K* values and the Hammett plot of a series of substituted α,α-bis(benzylsulfonyl)-toluenes.

Experimental

Melting points were determined on a Thomas-Hoover capillary melting point apparatus. Microanalyses were performed by the Microanalytical Laboratory of the University. Infrared spectra were recorded on a Perkin-Elmer Model 337 spectrometer. Ultraviolet spectra were obtained on a Beckman DU-2 spectrophotometer coupled to a Hewlett-Packard 3465A multimeter for digital readout of the percentage transmission. Routine ^{1}H nmr spectra were recorded on a Perkin-Elmer R12B spectrometer with tetramethylsilane as internal standard.

Materials

Spectrophotometric grade dimethyl sulfoxide (Aldrich Chemical Co.) was used for preparing the solvent mixture. Buffer solutions were prepared from carbonate-free sodium hydroxide solution. Cresol red was purified according to the method of Baughman and Kreevoy (10).

Syntheses of bis(benzylsulfonyl)methane, **1**; α,α-bis(benzylsulfonyl)-*p*-xylene, **2**; α,α-bis(benzylsulfonyl)-*p*-fluorotoluene, **3**; α,α-bis(benzylsulfonyl)-*p*-chlorotoluene, **4**; α,α-bis(benzylsulfonyl)-*p*-bromotoluene, **5**; 4-[bis(benzylsulfonyl)-methyl]-benzonitrile, **7**; and α,α-bis(benzylsulfonyl)-*p*-nitrotoluene, **8** had been reported previously (6, 11).

α,α-Bis(benzylsulfonyl)-*m*-nitrotoluene, **6**, prepared by the same method as the *para* isomer: mp 214–215°C; ir ν_{max} (Nujol): 1320, 1150 cm^{-1} (SO_2); ^{1}H nmr (C_2D_6SO) δ 4.72, 4.88 (q, J = 13.8 Hz, 4H, benzylic H), 6.90 (s, 1H, CH), 7.40 (s, 10H, aromatic H), 7.68–8.50 (m, 4H, nitrophenyl H). *Anal.* calcd. for $C_{21}H_{19}NO_6S_2$: C 56.6, H 4.3, N 3.1, S 14.4; found: C 56.8, H 4.4, N 2.9, S 14.4.

Spectrophotometric Measurements

All spectrophotometric measurements were made on triplicate solutions at 25°C using matched 1-cm silica cells. The temperature of the thermostated cell compartment was maintained at 25 ± 0.1°C and the temperature of the air-conditioned room was kept close to 25°C. The experimental details and methods of calculation of the p*K* values are given in ref. 6.

Results and Discussion

These disulfonyl carbon acids are all high-melting crystalline products with very low solubility in water. As a result, spectrophotometric measurements for uv

0008-4042/79/080853-03$01.00/0

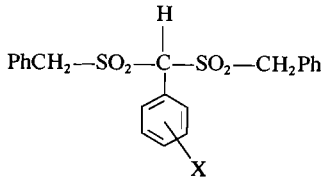

1 X = H	**5** X = *p*-Br
2 = *p*-CH_3	**6** = *m*-NO_2
3 = *p*-F	**7** = *p*-CN
4 = *p*-Cl	**8** = *p*-NO_2

chromophores and p*K* values were all carried out in 80% (w/w) dimethyl sulfoxide – water solvent at 25°C.

Results of uv measurements of these compounds, in both acidic and anionic forms, are shown in Table 1. The equilibrium ionization constants of compounds **1** to **5** were determined by using the spectrophotometric indicator method (10, 12). Their p*K* values were calculated from the spectral data of cresol red indicator in buffer solutions containing a carbon acid and its salt. For compounds **6**, **7**, and **8**, their p*K* values were calculated from their spectral absorption data in acetate buffers (6). Each of these p*K* values, with a precision of ±0.02 p*K* unit, is an average of triplicate measurements at seven wavelengths near the λ_{max} of a chromophore; Table 2 gives a typical sample of the experimental data for compound **5**. The p*K* values of all the compounds studied are shown in Table 3.

A plot of these p*K* values against σ for the 'well-behaved' substituents and σ^- for *p*-cyano and *p*-nitro substituents yields a ρ value of 2.53 (Fig. 1). The correlation coefficient for the plot is 0.99 and the standard error is ±0.16. The need to use exalted substituent constants (σ^-) for *p*-cyano and *p*-nitro groups supports the expected effect of through conjugation between the benzylic carbanions and the two strongly electron-withdrawing substituents.

The ρ value of 2.53 for this plot is highly significant. It is remarkably low compared to the recently reported ρ value of 12 for the ionization of substituted toluenes in dimethyl sulfoxide at 25°C (9). Although it is reasonable to assume that our ρ value could have been slightly larger had it been determined in pure dimethyl sulfoxide (ρ value generally increases with less polar solvent because of decreasing degree of charge stabilization by solvation of the acid anion relative to the undissociated acid) (13), still the difference in the ρ values of the two systems would not likely be less than 8 or 9 units. The high sensitivity of the acidity of toluene to substituent effects was, in fact, long predicted by Dolman and Stewart (14) based on the argument that the equal electronegativity of the carbon atom at the reaction site and the carbon atoms of the aromatic ring permits extensive charge delocalization into the aryl ring of the benzylic anion. In view of this, it is apparent that the smaller charge density in the aryl ring of the disulfonyl benzylic anion, as evidenced by the much lower sensitivity of the acidity of disulfonyl toluene to substituent effects, must have been due to extensive electron withdrawal from the carbanion site by the two sulfonyl groups.

Although polarization and conformational con-

TABLE 1. Ultraviolet spectral data of α,α-bis(benzylsulfonyl)-toluenes in 80% (w/w) DMSO–H_2O at 25°C

	In HCl (0.01 *M*)		In NaOH (0.1 *M*)	
Compound	λ_{max} (nm)	$10^{-3}\varepsilon$	λ_{max} (nm)	$10^{-3}\varepsilon$
1*	266	1.26	274	8.41
2	254	1.32	263	8.81
3	261	0.98	267	8.24
4	257	1.26	289	8.30
5	255	2.28	294	8.68
6	273	5.15	285	12.67
7*	255	13.20	254	6.50
			341	21.90
8*	270	24.90	257	10.00
			453	17.40

*Reference 6.

TABLE 2. p*K* of α,α-bis(benzylsulphonyl)-*p*-bromotoluene (HA) in 80% (w/w) DMSO–H_2O at 25°C*

	α,α-Bis(benzylsulphonyl)-*p*-bromotoluene		
λ (nm)	D_2 (in 0.1 *M* NaOH)	*D*	p*K*
570	0.635	0.251	10.017
575	0.733	0.294	10.028
580	0.842	0.337	10.026
585	0.936	0.371	10.019
590	0.971	0.380	10.010
595	0.914	0.360	10.015
600	0.764	0.303	10.020
	Average p*K* = 10.019 ± 0.006		

*HA, 2.50 × 10^{-3} *M*; sodium salt, 7.51 × 10^{-3} *M*; log ([salt]/[acid]) = 0.478; cresol red, 1.22 × 10^{-5} *M*; 1-cm cells; D_1 (in 0.01 *M* HCl) is 0 for λ570–600 nm. p*K* = 10.68 for cresol red (ref. 10). D_1, D_2, and *D* are the optical densities of the same concentration of indicator in acid solution, alkaline solution, and the disulphonyl carbon acid buffer solution, respectively.

TABLE 3. p*K* values of α,α-bis(benzylsulfonyl)-toluenes in 80% (w/w) DMSO–H_2O at 25°C*

Substituent	p*K*	σ	σ^-
p-CH_3	11.31	−0.17	
H	*11.13*	0.00	
p-F	10.52	0.06	
p-Cl	10.22	0.23	
p-Br	10.02	0.23	
m-NO_2	8.88	0.71	
p-CN	*8.55*		0.88
p-NO_2	*7.75*		1.27

*σ values from ref. 15; σ^- values from ref. 16; italic values from ref. 6.

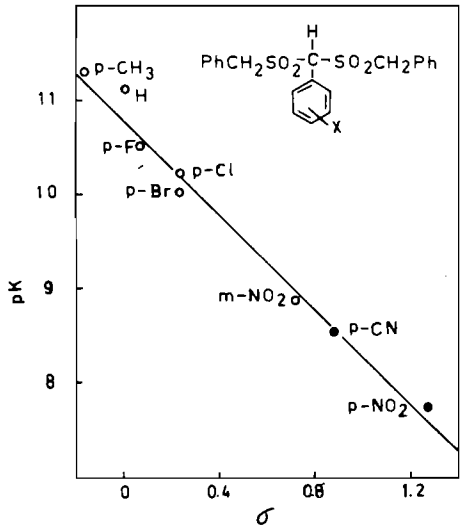

FIG. 1. pK values of disulfonyl toluenes vs. substituent constants: ○, σ values; ●, σ^- values.

straint may affect the charge distribution on the carbanion site, yet, without considering the conjugative effect it would be very difficult to justify the huge difference of over 28 pK units between the acidity of α,α-bis(benzylsulfonyl)toluene, **1** (pK = 11.1), and that of toluene (pK = 42) (9), assuming that the solvent effect is not likely to change the pK by more than 3 units (6).

In conclusion we believe that our results on the equilibrium ionizations of these disulfonyl carbon acids have quantitatively provided a strong evidence for the conjugative effect of sulfonyl group and this evidence is certainly in line with that of Bordwell *et al.* (5) who, based on the polar effect of trimethylammonio group $N(CH_3)_3^+$, suggested that the acidifying effect of sulfonyl group caused by polarization was small compared to that caused by conjugative interaction.

1. E. A. TEHNEL and M. CARMACK. J. Am. Chem. Soc. **71**, 231 (1949).
2. E. VON DOERING and L. K. LEVY. J. Am. Chem. Soc. **77**, 509 (1955).
3. E. J. COREY, H. KONIG, and T. H. LOWRY. Tetrahedron Lett. 515 (1962).
4. F. G. BORDWELL, N. R. VANIER, W. S. MATTHEWS, J. B. HENDRICKSON, and P. C. SKIPPER. J. Am. Chem. Soc. **97**, 7160 (1975).
5. F. G. BORDWELL, M. VAN DER PUY, and N. R. VANIER. J. Org. Chem. **41**, 1883 (1976).
6. K. P. ANG and T. W. S. LEE. Aust. J. Chem. **30**, 521 (1977).
7. A. RAUK, S. WOLFE, and I. G. CSIZMADIA. Can. J. Chem. **47**, 113 (1969).
8. S. WOLFE, A. RAUK, and I. G. CSIZMADIA. J. Am. Chem. Soc. **91**, 1567 (1969).
9. F. G. BORDWELL, D. ALGRIM, and N. R. VANIER. J. Org. Chem. **42**, 1817 (1977).
10. E. H. BAUGHMAN and M. M. KREEVOY. J. Phys. Chem. **78**, 421 (1974).
11. K. P. ANG, S. F. TAN, and T. W. S. LEE. Aust. J. Chem. **30**, 2473 (1977).
12. K. P. ANG. J. Chem. Soc. 3822 (1959).
13. C. D. JOHNSON. The Hammett equation. Cambridge University Press, London. 1973. p. 8.
14. D. DOLMAN and R. STEWART. Can. J. Chem. **45**, 911 (1967).
15. D. H. MCDANIEL and H. C. BROWN. J. Org. Chem. **23**, 420 (1958).
16. A. I. BIGGS and R. A. ROBINSON. J. Chem. Soc. 388 (1961).

Salt desorption from surfaces of non-aqueous solvents

ROBERT AVEYARD AND YVONNE THOMPSON

Department of Chemistry, The University of Hull, Hull, England HU6 7RX

Received August 8, 1978

ROBERT AVEYARD and YVONNE THOMPSON. Can. J. Chem. **57**, 856 (1979).

Following previous studies of the desorption of salts from the surface of water, the desorption of several salts from various non-aqueous solvents has been investigated. Three protic and 3 dipolar-aprotic liquids were used. The surface properties of the solvents in the absence of electrolytes are discussed and it is observed that the molar excess surface entropies of the aprotic solvents are more positive than those of the protic solvents. Salt desorption, determined from measurements of surface tension, is discussed in terms of purely electrostatic models, and also ion solvation. The extent of salt desorption in systems where strong ion solvation exists is related to the thickness of the primary solvation sheath around the ions. In the present context water does not behave as an anomalous solvent but in a way similar to the other protic solvents.

ROBERT AVEYARD et YVONNE THOMPSON. Can. J. Chem. **57**, 856 (1979).

Suite à des études antérieures concernant la désorbtion de sels de la surface de l'eau, on a étudié la désorbtion de plusieurs sels de divers solvants non aqueux. On a utilisé trois liquides protiques et 3 liquides dipolaires aprotiques. On discute des propriétés superficielles des solvants en l'absence d'électrolytes et on observe que les entropies molaires de surface en excès dans le cas des solvants aprotiques sont plus positives que celles des solvants protiques. On discute de la désorbtion des sels, déterminée à partir de mesures de tensions superficielles, ainsi que de la solvation des ions, en termes de modèles strictement électrostatiques. Le taux de désorbtion des sels dans des systèmes où il existe une forte solvatation ionique est relié à l'épaisseur de la première couche de solvatation autour de ces ions. Dans le contexte actuel, l'eau ne se comporte pas d'une façon anormale mais plutôt d'une façon semblable à celle des autres solvants protiques.

[Traduit par le journal]

Introduction

We have previously investigated the desorption of simple inorganic salts in aqueous solutions from both air–water and organic liquid – water interfaces in connection with a study of salt effects on non-ionic materials at interfaces (1–3). The present investigation is concerned with desorption of electrolytes from the surfaces of the organic solvents methanol, formamide, *N*-methylformamide, *N*,*N*-dimethylformamide, dimethylsulphoxide, and propylene carbonate. The salts studied are LiCl, LiBr, LiI, NaI, and KI. The choice of these systems has allowed us to consider the effects on desorption of ion solvation, and of changing the dielectric constant of the solvent from less than half to more than double that of water. A considerable interest in the physical chemistry of non-aqueous electrolyte solutions has grown up in recent years (4). Apart from providing a general insight, this has furnished some of the thermodynamic data necessary for a useful surface-chemical study of the solutions. The present work points the way to future investigations, which should prove to be an interesting facet of the study of non-aqueous solvents in general.

We note that a fair amount of work has previously been reported on non-aqueous electrolyte solutions in contact with liquid mercury (5, 6).

Experimental

Materials

Dimethylsulphoxide (DMSO), dimethylformamide (DMF), *N*-methylformamide (NMF), and propylene carbonate (PC) were all Aldrich (England) samples of greater than 99% purity, and the formamide (F), a BDH (England) sample, also had a minimum purity of 99%. DMSO, which had a water content as determined by nmr of 0.07 wt% (0.3 mol%) was used untreated. The DMF, which as supplied contained 0.58 wt% water, was stored over P_2O_5 for 3 days and distilled under a reduced pressure of N_2, and the final water content was 0.2 mol%. As bought, PC had a water content of 0.42 wt% which was reduced to undetectable levels by distillation at 76°C under a low pressure of N_2. NMF was allowed to stand over P_2O_5 for 48 h and then distilled at 94°C under N_2; no water was detectable in the final product. Molecular sieve 5A was used to dry F, which was subsequently distilled under N_2 at 116°C, and the distillate contained no detectable water. Finally, a pure sample of methanol (M) was prepared from "puriss" grade material by refluxing with I_2 and Mg and distilling at atmospheric pressure. The surface tension and density of each of the samples are listed in Table 1 together with reliable literature values, where available.

Lithium chloride, NaI, and KI, all AnalaR samples, were heated for 48 h in silica containers at 450°C and stored in a desiccator. Anhydrous LiBr and LiI (both 99+% pure) were from Alfa Products (U.S.A.) and were used without further treatment.

Measurement of Surface Tension

The drop-volume technique was used as described elsewhere (1), with the exception that the thermostatted tube housing the barrel of the drop-volume apparatus was initially purged with

0008-4042/79/080856-07$01.00/0

TABLE 1. Surface tension, γ_0, and density, ρ, of solvents at 25°C*

Solvent	γ_0	γ_0 (literature)	Reference	ρ This work	ρ Literature
M	22.30	22.28	7	0.7867	0.7866
DMSO	42.94	42.93	8	1.0964	1.0958
DMF	36.42	—		0.9453	0.9443
PC	41.39	—		1.1998	1.198
F	58.15	57.91 58.5	9 10	1.1295	1.1292
NMF	39.46	—		0.9987	0.9976

*γ_0 in mN m^{-1}, ρ in g cm^{-3}; literature values of ρ taken from the compilation on p. 5 of ref. 4. Of the literature values of γ_0 for F, that given in ref. 10 is probably the more nearly correct since the sample was highly purified.

dry N_2 and then during measurements a steady stream of dry N_2 was passed. All solutions were prepared in a polythene glove bag (I2R, U.S.A.) filled with dry N_2. Surface tensions were reproducible to better than 0.1%.

The necessary densities, ρ, were determined to within $\pm 2 \times 10^{-4}$ g cm^{-3} using a 25 cm^3 density bottle. Densities of salt solutions were in all cases linear functions of salt molality, m_2, and densities were frequently interpolated from plots of ρ against m_2.

Results and Discussion

Surfaces of Pure Solvents

One of several factors which can influence the desorption of salts at liquid surfaces is the surface 'structuring' of the solvent. The solvents employed here all have high dielectric constants (>30) and can be classified as either protic or dipolar aprotic liquids. The surface tension, γ_0, of a solvent tells us little about the nature of that solvent in that both protic and aprotic solvents can have high or low surface tensions. Since we are concerned with the ordering of surface solvent molecules, 'surface entropies' are of more potential interest than γ_0. The excess surface entropy per unit area, s^σ, of a solvent is given by

$$[1] \qquad s^\sigma = -\mathrm{d}\gamma_0/\mathrm{d}T = s^s - \Gamma S_m$$

where s^s is the total entropy of the material (Γ moles) in unit area of surface, and S_m is the molar entropy of solvent in bulk. We have, where necessary, determined γ_0 as a function of T, the absolute temperature in the range 293 to 303 K (Table 2) and the (constant) values of s^σ are given in Table 3, together with s^σ for sulpholane (S), acetone (A), and ethylene glycol (EG) obtained from literature values of γ_0. As with γ_0, there is no obvious correlation between s^σ and solvent type. However, as a result of the different molecular sizes Γ varies from solvent to solvent. Assuming that the surface layer of solvent is monomolecular, we can calculate from the molar volume V_m of the liquid an approximate partial molar surface area, σ_m, and hence a *molar* surface excess entropy S_m^σ using

$$\sigma_m \simeq N_A^{1/3} V_m^{2/3}; \; S_m^\sigma = s^\sigma \sigma_m$$

where N_A is the Avogadro constant.

The quantity S_m^σ, which is the difference between the molar entropies of solvent in bulk and surface,

TABLE 2. Surface tension, γ_0, as a function of temperature

T (°C)	γ_0 (mN m^{-1}) DMF	DMSO	PC	NMF
20	37.00	43.51	41.93	39.98
22	36.74	43.26	41.66	39.79
24	36.49	43.04	41.42	39.65
25	36.44	42.95	41.39	39.46
26	36.32	42.85	41.27	39.42
28	36.11	42.62	40.98	39.23
30	35.93	42.36	40.83	39.07

TABLE 3. Excess surface entropies per unit area, s^σ, and molar excess surface entropies, S_m^σ, for protic and aprotic solvents*

(*a*) Protic solvents

Parameter	Value when solvent = M	EG	W	F	NMF
s^σ/(mJ m^{-2} K^{-1})	0.088	0.060	0.155	0.097	0.092
S_m^σ/(J mol^{-1} K^{-1})	8.8	7.4	9.0	9.6	11.9

(*b*) Aprotic solvents

Parameter	Value when solvent = S	A	DMF	DMSO	PC
s^σ/(mJ m^{-2} K^{-1})	0.091	0.123	0.106	0.117	0.110
S_m^σ/(J mol^{-1} K^{-1})	16.0	18.3	16.2	16.9	17.9

*Entropies obtained in the range 20 to 30°C except for sulpholane which is for 30 to 60°C, and methanol which is for 20 to 50°C. Values for M, EG, W, F, S, and A were obtained from γ_0 values reported in, respectively, refs. 11, 1, 12 ,10, 13, and 8.

is seen to be positive in all cases (Table 3). It is more positive for aprotic solvents as a group (between 16 and 18 J mol^{-1} K^{-1}) than for protic solvents (between 7 and 12 J mol^{-1} K^{-1}). Since protic solvents are probably more "structured" in bulk than are aprotic liquids (14) it seems likely that the surfaces of the protic solvents are more "structured" in an absolute sense than those of aprotic solvents.

The above arguments are not rigorous since, *inter alia*, we have assumed that the surface region is confined to a monolayer of solvent. More importantly we cannot deduce from thermodynamic data alone what form a "structured" surface will take. The most widely studied interface is that between air and water, and there now appears to be a consensus of opinion that the H-atoms of surface water molecules on average face the liquid phase, although the extent of orientation is not agreed. Surface potentials, $\Delta\chi$, of aqueous 1,1-electrolytes suggest that often, solvated anions approach the surface more closely than do cations, as might be expected from the direction of orientation of surface water. In the case of water then, information concerning the state of interfacial solvent, ion solvation in bulk, and surface potentials taken together furnishes a reasonable picture of the observed salt desorption (1). It will not be possible at present to use information regarding surface structure in non-aqueous solvents in this way since $\Delta\chi$ values for the relevant salt solutions are not available. As well as aiding in the understanding of salt desorption, however, surface potentials could be used in conjunction with desorption data to throw light upon the orientation of surface solvent. This remains an interesting possibility for the future.

General Observations of Salt Effects on Surface Tension

In all the systems investigated surface tension, γ, is, within experimental error, a linear function of salt molality, m_2.[1] Results have been fitted by the method of least-squares to

$$[2] \qquad \gamma = A + Bm_2$$

and the values of B (with rms errors) and of A are recorded in Table 4. Experimental points fall within ± 0.04 mN m^{-1} of the fitted lines except for γ_0 for the system LiCl/DMSO; in this case A differs from γ_0 by 0.06 mN m^{-1} which could mean that the initial slope of γ versus m_2 (below $m_2 \simeq 0.025$ mol kg^{-1}) is greater than the recorded value of B. The results for KI in PC are the least reliable since these were confined to $m_2 < 0.15$ mol kg^{-1} as a result of the low salt solubility. The most extensive results are those for LiCl in DMSO and in DMF.

The extent of salt desorption from concentrated solutions, and hence the increase in γ, depends on various factors in a complicated way. The solvation of ions and degree of ion association, which together are reflected in the electrolyte activity coefficients, are of obvious importance. One might also expect the solvent dielectric constant, and surface structure to play a role in the desorption. These factors will be discussed later, but in view of all this it is surprising that γ should be an apparently linear function of m_2. As might be expected, however, B values for a given salt (LiCl) in a series of solvents are not simply related to solvent type or to solvent properties such as dielectric constant, dipole moment, molecular size, or surface tension.

Application of Electrostatic Theory for Low Salt Concentrations

Theories based on the Coulombic repulsion of ions from the interface between two dielectrics give the limiting law for the variation of γ with concentration at high dilution. Our present results are for concentrated solutions but since γ varies linearly with m_2 for $m_2 \simeq 0.02$ mol kg^{-1} upwards, it is worthwhile to compare the predicted increments in γ with our experimental results. It should be remembered, however, that for a strictly valid comparison, experimental results for very low concentrations would be required.

Consider the interface between dielectrics α and β with dielectric constants ε_α and ε_β. A particle, carrying a charge e, in phase α and at a normal distance x from the interface, is repelled from that interface as if by a charge e' (the image charge) at a distance $2x$ in a medium of uniform dielectric constant ε_α. The image charge is given by $e' = e\lambda$ where

$$\lambda = (\varepsilon_\alpha - \varepsilon_\beta)/(\varepsilon_\alpha + \varepsilon_\beta)$$

In purely electrostatic theories of salt desorption (15) the electrolyte is supposed to consist of point charges, and each of the dielectrics is treated as a continuum. On this basis Bellemans (16) obtained the equation, written here for a 1,1-electrolyte,

$$[3] \quad \Delta\gamma = -\frac{69.38c_2}{\varepsilon_\alpha}\left\{\lambda \ln\left[\frac{4.20 \times 10^6 \lambda c_2^{1/2}}{(\varepsilon_\alpha T)^{3/2}}\right] - 0.35\lambda - (1+\lambda)\left[\ln 2 - \frac{1+\lambda}{2\lambda}\ln(1+\lambda)\right]\right\}$$

in which $\Delta\gamma = \gamma - \gamma_0$, and c_2 is the molarity (mol dm^{-3}) of salt and γ is in mN m^{-1}. For the case where $\varepsilon_\beta \simeq 1$ and $\varepsilon_\alpha \gg 1$ (i.e. $\lambda \simeq 1$), [3] reduces to the limiting form, given previously by Onsager and

[1]Data on surface tension are available, at a nominal charge, from the Depository of Unpublished Data, CISTI, National Research Council of Canada, Ottawa, Ont., Canada K1A 0S2.

TABLE 4. Constants of eq. [2] for various systems at 25°C

(*a*) Constants for LiCl in various solvents

Parameter	Value when solvent = M	DMF	DMSO	F	NMF
A/(mN m^{-1})	22.20	36.41	43.00	58.15	39.46
B/(mN m^{-1} m^{-1})	1.22±0.02	1.42±0.01	2.02±0.02	1.60±0.01	1.10±0.02
Data points	7	17	18	7	6
Maximum m_2	1	1	1	1	0.5

(*b*) Constants for salts other than LiCl

Parameter	Value when system = LiI/PC	NaI/PC	KI/PC	LiBr/DMSO	LiI/DMSO
A/(mN m^{-1})	41.38	41.38	41.37	42.91	42.97
B/(mN m^{-1} m^{-1})	1.04±0.07	1.47±0.09	1.20±0.14	2.81±0.08	2.38±0.07
Data points	7	6	7	6	8
Maximum m_2	0.3	0.25	0.15	0.5	0.5

Samaras (17),

$$[4]\quad \Delta\gamma = \frac{79.9}{\varepsilon_\alpha} c_2 \log \left\{ \frac{1.141 \times 10^{-13} (\varepsilon_\alpha T)^3}{c_2} \right\}$$

Equations [3] and [4] give differing values of $\Delta\gamma$ for the liquid/vapour interface ($\varepsilon_\beta = 1$), at higher concentrations ($c_2 > 10^{-2}$ mol dm^{-3}) and lower ε_α (<50). For $c_2 \gtrsim 0.01$ mol dm^{-3}, however, the predicted $\Delta\gamma$ are essentially equal for all ε_α relevant to the present study.

The comparisons between the theoretical $\Delta\gamma$ and $\Delta\gamma$ computed from values of B (Table 4) are shown in Fig. 1 for DMSO, F, NMF, and water (W). The agreement is surprisingly good for NMF, which has the highest ε_α (182) of the solvents studied, and quite reasonable, i.e. well within a factor of 2, for F ($\varepsilon_\alpha = 110$), W ($\varepsilon_\alpha = 78$), and DMSO ($\varepsilon_\alpha = 47$). For M ($\varepsilon_\alpha = 33$) and DMF ($\varepsilon_\alpha = 37$) the agreement, although less satisfactory, is still within a factor of 2 for $c_2 = 0.05$ mol dm^{-3}.

The equations, however, cannot be expected to hold for the more concentrated systems which have been the main concern in this work, and we now consider the results for solutions up to concentrations of 1 mol kg^{-1}.

The Surface Excess of Salts in Concentrated Solutions

The extent of salt desorption can be expressed in terms of the surface excess of salt Γ_2^σ. For a 1,1-electrolyte, A^+B^-, the Gibbs equation may be expressed (17) as

$$[5]\quad \Gamma_{A^+}{}^\sigma = \Gamma_{B^-}{}^\sigma = \Gamma_2{}^\sigma = -\frac{1}{2RT}\left(\frac{d\gamma}{d \ln a_\pm}\right)$$

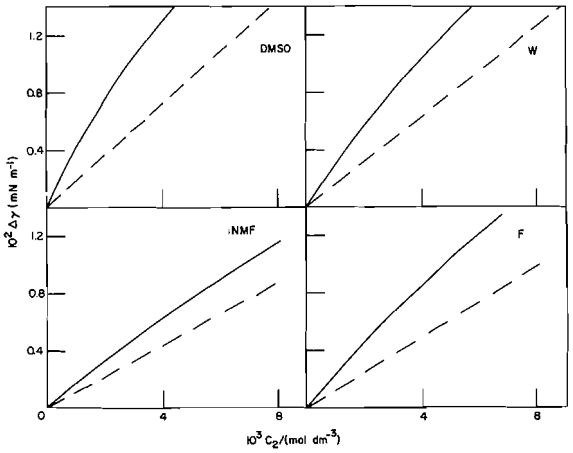

FIG. 1. Theoretical (full lines) and experimental (interpolated, see text) $\Delta\gamma$.

where the Γ^σ are surface excesses relative to a Gibbs dividing surface for which the excess of solvent is zero, and $a_\pm$ is the mean ionic activity of the salt. The availability of (molal) activity coefficients in the literature (4) was one of the main constraints on the choice of systems for study.

In Fig. 2 we have plotted surface tension increments, $\Delta\gamma$, against $-\ln a_\pm$ for LiCl in various solvents, including W (from ref. 1) for comparison. It is apparent that the $\Gamma_2{}^\sigma$ values are all negative, and vary with concentration. To compare behaviour it is necessary to choose a fixed (arbitrary) concentration, and we list in Table 5 values of $\Gamma_2{}^\sigma$ for $m_2 = 0.25$ mol kg^{-1}.

The most striking observation is that for LiCl, the desorption is stronger for the aprotic solvents (DMF

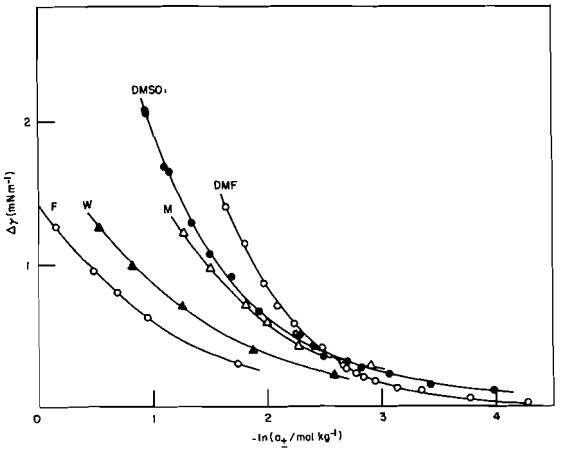

FIG. 2. Surface tension increments as a function of $-\ln a_{\pm}$ at 25°C for LiCl in various solvents.

and DMSO) than for the 3 protic solvents. In a simple picture it might be expected that the more strongly solvated an ion the more strongly it will be desorbed. However, it is known (14) that although Li^+ is similarly strongly solvated in all 5 solvents, Cl^- is much more strongly solvated in the protic solvents, where the desorption is small, than in the aprotic solvents.

A further observation is that the desorption of LiX (X = Cl^-, Br^-, I^-) from DMSO is similarly strong for all three halides although the halide ions are all weakly solvated in this solvent. It is possible that this arises from a preferential orientation of DMSO at the surface with the negative poles (O atoms) on average pointing into the bulk liquid and thus repelling anions from the surface. This however is purely speculative. We do not have at present any explanation of the order of desorption from PC of LiI and NaI; Li^+ is very much more strongly solvated by PC than is Na^+.

TABLE 5. Surface excess of salt at 25°C for m_2 = 0.25 mol kg^{-1}*

System	$-10^7\Gamma_2^{\sigma}$/(mol m^{-2})
LiCl/DMSO	1.2
LiCl/DMF	1.2
LiCl/M	0.6
LiCl/W†	0.8
LiCl/F‡	0.7
LiBr/DMSO	1.4
LiI/DMSO	1.1
LiI/PC	0.5
NaI/PC	1.4

*Result not given for LiCl/NMF since activity coefficients not available.
†Obtained using results in ref. 1.
‡Obtained using activity coefficients for freezing point (≃2.5°C).

In order to gain a clearer insight into some of the above findings we now consider a more specific model for the desorption process.

The Ion-free Layer Approach to Desorption

Strongly solvated ions will approach a surface with their primary solvation layers intact. To a first approximation, therefore, we may assume in such cases that the ions meet an infinite potential barrier close to the surface, and that there is an ion-free layer of solvent, thickness δ, at the surface. For univalent ions δ is expected to be of the order of the diameter of a solvent molecule. This model, which is discussed elsewhere, leads to the form of the Gibbs equation (1, 18, 19),

$$[6] \qquad -d\gamma = c_1\delta d\mu_1$$

where c_1 is the concentration in mol vol^{-1}, subscript 1 refers to solvent, and μ is the chemical potential. The molal osmotic coefficient, φ, of a solution of 1,1-electrolyte is defined by (20)

$$[7] \qquad \ln a_1 = -2m_2M_1\phi$$

where M_1 is the molar mass (kg mol^{-1}) of solvent. Combination of eqs. [6] and [7] gives

$$[8] \qquad d\gamma = (2c_1\delta RTM_1)d(m_2\phi)$$

Noting that $c_1M_1 \simeq \rho_0$, the density of the solvent, δ is given to a reasonable approximation by

$$[9] \qquad \delta \simeq [d\gamma/d(m_2\phi)]/[2\rho_0RT]$$

Osmotic coefficients are not directly available for the systems of present interest and so have been obtained by graphical integration using the expression (20)

$$[10] \qquad \phi = 1 + m_2^{-1}\int_{m_2=0}^{m_2} m_2\, d\ln\gamma_{\pm}$$

and the mean molal activity coefficients, $\gamma_{\pm}$, given in the compilations of ref. 4. In the case of LiCl in DMF it was necessary to interpolate values of $\gamma_{\pm}$ for intermediate m_2 by the use of the equation (21)

$$[11] \qquad \ln\gamma_{\pm} + Am_2^{1/2}/(1 + m_2^{1/2}) = 2\beta m_2$$

where A = 3.572 for DMF at 25°C, and β is a constant. For LiI in PC the data were not available for the above analysis but over the concentration range of present interest ($0.05 < m_2 < 0.3$) $\gamma_{\pm}$ in this system is fairly constant (0.75 ± 0.02). For constant $\gamma_{\pm}$ it is readily shown from eq. [6] that

$$[12] \qquad \delta = (2\rho_0RT)^{-1}(d\gamma/dm_2)$$

Equation [12] has also been used to obtain a rough estimate of δ for LiCl in F where $\gamma_{\pm}$ is only available at the freezing point (≃ 2.5°C). It must be remarked

TABLE 6. Ion-free layer thickness δ and related parameters*

	Value							
	LiCl					LiI		LiBr
Parameter	DMSO	DMF	M	W	F	DMSO	PC	DMSO
δ	0.46	0.45	0.31	0.32	0.3	0.42	0.18	0.53
σ_{L-J}	0.51	0.52	0.37	0.28	0.38	0.51	0.52	0.51
r^+	0.43	0.42	0.38	0.28	0.35	0.43	(0.35)†	0.43
r^-	0.18	0.14	0.26	—	0.15	0.14	—	0.16

*All values in nm.
†The value listed is the uncorrected Stokes radius, which will be less than r^+.

in this case that for m_2 between 0.2 and 1 mol kg^{-1}, $\gamma_\pm$ varies between 0.94 and 1.11 and so the value of δ can only be taken as a very rough guide. Activity coefficients are not available at the required concentrations for LiCl in NMF, and our results for KI in PC extend only up to $m_2 \simeq 0.15$ mol kg^{-1} and are unsuitable for use in the above analysis.

Plots of $\Delta\gamma$ against $m_2\phi$ are shown for some of the systems investigated in Fig. 3 and good linearity is observed indicating the constancy of δ, values of which are given in Table 6. In some cases, the plots do not pass through the origin (e.g., LiCl in DMSO and in M as seen in Fig. 3) and it likely that δ values for low m_2 (<0.05 mol kg^{-1}) are somewhat larger than those given in Table 6. A similar situation is known to exist for various aqueous electrolytes (22).

Values of δ are now compared with quantities related to the size of solvent molecules. A reasonable measure of solvent molecule diameter is the Lennard-Jones σ parameter, σ_{L-J}, values of which (23) are given in Table 6. There is a very reasonable correspondence between δ and σ_{L-J} except in the case of LiI in PC, where it is known that I^- is only very weakly solvated and (relative to Li^+ in W) Li^+ is also weakly solvated (14).

The comparison of δ and σ_{L-J} makes no direct reference to any differences which exist between anions and cations. Perhaps a more informative approach is to compare δ with the solvodynamic radii of the ions. For all the systems represented in Table 6, except Li^+ and I^- in PC, and Cl^- in W, corrected Stokes radii, $r_s^\pm$, for anions and cations are available. If the crystallographic radius, $r_c^\pm$, is subtracted from $r_s^\pm$, an estimate is obtained for the thickness of the solvation sheath immediately surrounding an ion. The quantity $r_s^\pm - r_c^\pm$ is written in $r^\pm$ in Table 6; the values of Gourary and Adrian (24) were used for $r_c^\pm$, and the corrected Stokes radii were taken from refs. 20, 25, and 26.

The similarity between δ and r^+ is obvious; r^- is always considerably smaller than r^+. It appears then that for both the protic and the aprotic solvents it is the cation that is largely responsible for the extent

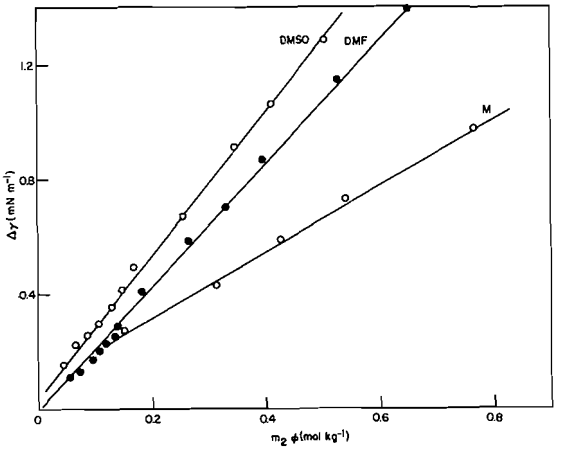

FIG. 3. Plots according to eq. [8] for LiCl in three solvents.

of salt desorption. The high Γ_2^σ (Table 5) for aprotic solvents is seen to result from the large molecular diameter of these liquids. Judging from the δ values the anions (with the exception of I in PC), though relatively weakly solvated, do not approach the surface significantly more closely than the cations. We have suggested earlier the possibility of a surface orientation of DMSO with the negative poles to the liquid phase; DMF is similar to DMSO in that the positive pole is shielded by 2 methyl groups, and it may also be oriented with the negative poles on average pointing into the liquid. There is evidence (27) that this is the orientation assumed by surface molecules of M. Water, however, is known to have the opposite orientation and so would not have the tendency to repel anions from the surface. Surface potentials indicate that halide ions do in fact approach the water surface more closely than do alkali metal cations, but in the case of LiCl, for which δ = 0.32 nm, we do not expect the segregation of anions and cations normal to the surface to be very great.

Conclusions

(*1*) The molar excess surface entropies of the protic solvents investigated are less positive than those of

the aprotic solvents. The results are consistent with the presence of a more highly structured surface layer in the protic solvents.

(*2*) There is no obvious correlation between the (constant) values of $d\gamma/dm_2$ for LiCl in various solvents, and the physical properties of these solvents.

(*3*) The electrostatic theories of Onsager and Samaras, and Bellemans, give reasonably good agreement with the (assumed) low concentration surface tension increments caused by the 1,1-electrolytes. The agreement is better for the solvents with the higher dielectric constants.

(*4*) The desorption of LiCl is smaller from the protic than from the aprotic solvents. This appears to result from the smaller molecular size of the former solvents as a group. The ion free layer thicknesses are comparable in most cases to the thickness of the cation primary solvation sheath and to the solvent molecular diameters.

(*5*) A very useful further insight into salt desorption in non-aqueous systems could be gained from surface potential measurements.

1. R. AVEYARD and S. M. SALEEM. J. Chem. Soc. Faraday Trans. I, **72**, 1609 (1976); **73**, 896 (1977).
2. R. AVEYARD, S. M. SALEEM, and R. HESELDEN. J. Chem. Soc. Faraday Trans. I, **73**, 84 (1977).
3. R. AVEYARD and S. M. SALEEM. Can. J. Chem. **55**, 4018 (1977).
4. A. K. COVINGTON and T. DICKINSON (*Editors*). Physical chemistry of organic solvent systems. Plenum Press, London. 1973.
5. D. J. SCHIFFRIN. Electrochemistry. Vol. 3. *Edited by* G. J. Hills (Specialist Periodical Reports). The Chemical Society, London. 1973. Chapt. 4.
6. P. PAYNE. *In* Advance electrochemistry electrochemical engineering. Vol. 7. *Edited by* P. Delahay and C. W. Tobias. Interscience. 1970. p. 1.
7. J. KOEFOED and J. V. VILLADSEN. Acta Chem. Scand. **12**, 1124 (1958).
8. E. TOMMILA and R. YRJOVUORI. Suom. Kemistil. **B42**, 90 (1969).
9. C. SMITH. J. Chem. Soc. 802 (1931).
10. A. COUPER, G. P. GLADDEN, and B. T. INGRAM. Faraday Discuss. Chem. Soc. No. 59, 63 (1975).
11. E. TOMMILA and T. AUTIO. Suom. Kemistil. **B42**, 107 (1969).
12. International critical tables. Vol. IV. McGraw-Hill, New York. 1928.
13. E. TOMMILA, E. LINDELL, M. L. VIRTALAINE, and R. LAAKSO. Suom. Kemistil. **B42**, 95 (1969).
14. B. G. COX, G. R. HEDWIG, A. J. PARKER, and D. W. WATTS. Aust. J. Chem. **27**, 477 (1974).
15. J. E. B. RANDLES. *In* Advance electrochemistry electrochemical engineering. Vol. 3. *Edited by* P. Delahay and D. W. Tobias. Interscience. 1963. p. 1.
16. A. BELLEMANS. Physica, **30**, 924 (1964).
17. R. AVEYARD and D. A. HAYDON. Introduction to the principles of surface chemistry. Cambridge University Press. 1973.
18. E. SCHMUTZER. Z. Phys. Chem. Leipzig, **204**, 131 (1955).
19. K. JOHANSSON and J. C. ERIKSSON. J. Colloid Interface Sci. **49**, 469 (1974).
20. R. A. ROBINSON and R. H. STOKES. Electrolyte solutions. Butterworth, London. 1955.
21. J. N. BUTLER and J. C. SYNNOTT. J. Am. Chem. Soc. **92**, 2602 (1970).
22. B. CASE. Reactions of molecules at electrodes. *Edited by* N. S. Hush. Interscience. 1971. p. 45.
23. J. I. KIM. J. Phys. Chem. **82**, 191 (1978).
24. B. S. GOURARY and F. J. ADRIAN. Solid State Phys. **10**, 127 (1960).
25. R. GOPAL and J. S. JHA. J. Phys. Chem. **78**, 2405 (1974).
26. M. DELLA MONICA and L. SENATORE. J. Phys. Chem. **74**, 205 (1970).
27. S. MINC, I. ZAGORSKA, and Z. KOCZOROWSKI. Rocz. Chem. Ann. Soc. Chim. Polonorum, **41**, 1983 (1967).

Photolyse du méthyl-2-butène-1, du méthyl-3-butène-1 et du *cis*-pentène-2 à 174, 163 et 147 nm

GUY J. COLLIN,[1] HÉLÈNE DESLAURIERS ET SYLVAIN AUCLAIR
Département des Sciences Pures, Université du Québec à Chicoutimi, Chicoutimi (Qué.), Canada G7H 2B1

Reçu le 30 octobre 1978

GUY J. COLLIN, HÉLÈNE DESLAURIERS et SYLVAIN AUCLAIR. Can. J. Chem. **57**, 863 (1979).

L'étude de la photolyse du méthyl-2-butène-1 (M2B1), du *cis*-pentène-2 (CP2) et du méthyl-3-butène-1 (M3B1) a été faite systématiquement à 163 nm, et l'effet de pression a été mesuré à la fois à 147, 163 et 174 nm. On observe que le processus majeur de fragmentation de ces trois oléfines est la rupture de la liaison C—C située en position β par rapport à la double liaison: $\Phi \simeq 0.9 \pm 0.1$. Le radical α-méthallyle obtenu dans le cas du M3B1 et du CP2 se fragmente partiellement à basse pression en butadiène-1,3 et en atome d'hydrogène. Le radical β-méthallyle produit lors de la photolyse du M2B1 se fragmente en allène et en un radical méthyle. Les rendements en butadiène-1,3 et en allène suivent la relation linéaire de type Stern–Volmer. Cela permet de déduire le rapport des constantes de dissociation et de stabilisation par collision, k_d/k_s, des radicaux α-méthallyles et β-méthallyles. On en conclut que la distribution de l'excès d'énergie du photon dans les fragments suit une (des) loi(s) particulière(s), cette loi n'étant pas statistique.

GUY J. COLLIN, HÉLÈNE DESLAURIERS, and SYLVAIN AUCLAIR. Can. J. Chem. **57**, 863 (1979).

Photolysis of 2-methyl-1-butene (M2B1), *cis*-2-pentene (CP2), and 3-methyl-1-butene (M3B1) has been systematically studied at 163 nm. Pressure effect has been measured at 147, 163, and 174 nm. The main fragmentation process of the photoexcited olefine is the C—C split of the bond located in position β relative to the double bond: $\Phi \simeq 0.9 \pm 0.1$. α-Methallyl radicals obtained in the M3B1 and CP2 photolysis decompose partly at low pressure, giving rise to the formation of 1,3-butadiene and hydrogen atoms. β-Methallyl radicals decompose also at low pressure into allene and methyl radicals. Butadiene and allene quantum yields follow the Stern–Volmer law, and this allows us to determine the ratio of the rate constant of dissociation relative to the rate constant of stabilization, k_d/k_s, through collision of the α- and β-methallyl radicals. From these values, we conclude that the excess of photon energy is not statistically distributed into the fragments, and that the decomposition process follows one (or several) particular law(s).

Introduction

Nous avons récemment étudié la photolyse des différents butènes vers 174 et vers 163 nm (1). La diversité des molécules étudiées n'a pas permis d'extraire le comportement général des oléfines photoexcitées dans ce domaine, bien que les travaux obtenus en photolyse éclair par d'autres laboratoires montrent l'importance quantitative de la scission des liaisons situées en position β par rapport à la double liaison (2, 3). Nous avons étendu nos précédentes études au méthyl-3-butène-1 (M3B1), *cis*-pentène-2 (CP2) et méthyl-2-butène-1 (M2B1), hydrocarbures qui possèdent chacun une liaison C—C en position β par rapport à la double liaison. En outre, nous sommes évidemment intéressés à connaître le comportement chimique des radicaux allyliques provenant de la scission de cette liaison. L'existence de certains radicaux a été éliminée lors de la photolyse des butènes (1). Nous présenterons ici des arguments définitifs qui justifient cette élimination.

[1]Auteur auquel toute correspondance devrait être envoyée.

Méthode expérimentale

Les méthodes expérimentales ont été largement décrites dans la littérature (1). C'est le cas des lampes d'irradiation au xénon (8.4 eV, 147 nm) (4), au brome (7.6 eV, 163 nm) (1*d*) ainsi que celle à l'azote (7.1 eV, 174 nm) (1*b*). L'origine et la préparation des échantillons a elle aussi été rapportée. Nous y avons apporté une modification quant à l'usage de l'iodure d'hydrogène et du sulfure d'hydrogène en utilisant les produits perdeutériés (Merck, Sharp and Dohme of Canada) car ils présentent une pureté moléculaire beaucoup plus grande que les produits commerciaux perhydrogénés correspondants. Etant donnée l'importance de la précision quant à la mesure des rendements quantiques dans l'établissement des courbes de type Stern–Volmer (voir plus loin), l'actinométrie dans ces cas a été faite de la façon suivante: dans chacun des cas, et ce chaque jour où ont été faites ces mesures, une irradiation du *cis*-butène-2 pur (133 N m^{-2}) a été faite au début et à la fin de la journée. Les photolyses des oléfines en C_5 faites en cours de journée ont été comparées à ces deux photolyses témoins (1*b*, *c*). En règle générale, la stabilité des lampes, ainsi que le positionnement de la lampe dans la cavité microonde maintient une fluctuation du débit de lampe inférieure à 5%.

Résultats

Les résultats sont indiqués dans les tableaux et les

0008-4042/79/080863-07$01.00/0

figures qui accompagnent le texte. Ils sont indiqués sous forme de rendements quantiques.

Cas du méthyl-2-butène-1 (M2B1) à 163.3 nm

Les produits majeurs obtenus dans la photolyse du produit pur sont l'éthane ($\Phi \geq 0.27$), l'allène ($\Phi \leq 0.16$), le méthane ($\Phi \leq 0.14$) ainsi qu'un certain nombre de produits qui apparaissent en quantités mineures ($\Phi \leq 0.05$) (tableau 1). En présence d'oxygène (10%), les rendements s'amenuisent: l'éthane, l'isobutane et le diméthyl-2,2-butane disparaissent. On a également indiqué dans le tableau 1 l'effet du D_2S ou de DI sur certains produits. Il faut ajouter en outre qu'en présence d'oxygène le rendement en méthane est constant entre 60 et 6600 N m^{-2}: $\Phi(CH_4) = 0.012 \pm 0.003$. L'addition de D_2S montre un rendement en isopentane de 0.18 ± 0.05 et en méthane de 1.5 ± 0.1. Finalement l'addition de DI ne donne pas de valeurs reproductibles. On note cependant une augmentation du rendement en méthane: $0.2 \leq \Phi_{DI}(CH_4) \leq 0.9$, en butène-2: $0.06 \leq \Phi_{DI}(C_4H_8\text{-}2) \leq 0.76$, dépendant de la pression totale du réacteur (133–7050 N m^{-2}) et du pourcentage moléculaire de DI. L'habileté qu'ont les atomes d'iode de réagir avec les oléfines (5) semble responsable de la disparition (?) du DI avant la fin de l'irradiation. On a noté en effet une isomérisation importante du M2B1 (6). A la fin de la photolyse de ces mélanges 40% de l'oléfine pouvait être isomérisée en méthyl-2-butène-2.

Finalement l'effet de pression observé est surtout important sur l'allène (fig. 1). Le tableau 1 montre un effet de pression qui semble présent sur plusieurs produits d'origine radicalaire. C'est le cas du méthane, de l'éthane, etc. Par contre les rendements en éthylène, propène et propyne ne sont pas ou peu affectés par l'augmentation de pression.

TABLEAU 1. Photolyse du méthyl-2-butène-1 pur à 163 nm[a]: rendements quantiques

Pression (N m^{-2})	12	133	1330	10 600
CH_4	0.040	0.058	0.095	0.14
C_2H_2[c,f]	n.m.[e]	0.001	<0.001	n.m.[e]
C_2H_4[c,f]	0.017	0.021	0.013	0.006
C_2H_6[b]	0.27	0.46	0.50	0.28
Propyne[c]	0.013	0.020	0.019	0.011
C_3H_6[c]	0.005	0.012	0.011	0.007
Allène[c,f]	0.16	0.14	0.065	0.013
Iso-C_4H_8[c]	0.053	0.044	0.029	0.024
Iso-C_5H_{12}[b]	n.m.[e]	0.022	0.012	0.016
C_6H_{14}[b,d]	n.m.[e]	0.043	0.035	0.031

[a]22 expériences faites entre 12 et 10 600 N m^{-2}; incertitude relative: $\Delta\Phi/\Phi \simeq 5\%$ et 10% si Φ supérieur ou inférieur à 0.1 respectivement.
[b]Produits dont les rendements sont inférieurs à 0.005 en présence de 10% d'oxygène.
[c]Produits peu ou pas affectés par la présence de 10% d'oxygène.
[d]Diméthyl-2,2-butane.
[e]n.m. = non mesuré.
[f]Produits peu ou pas affectés par la présence de DI ou de D_2S.

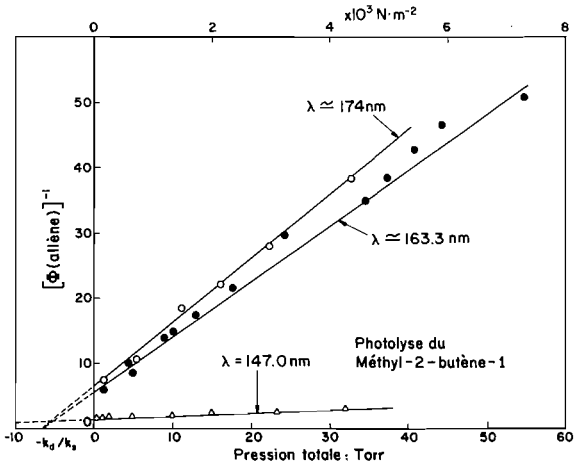

FIG. 1. Photolyse du méthyl-2-butène-1. Inverse du rendement quantique de l'allène en fonction de la pression à diverses longueurs d'onde.

Cas du méthyl-3-butène-1 (M3B1) à 163.3 nm

Les tableaux 2 et 3 résument les rendements quantiques des produits obtenus. Le comportement de ces rendements en présence d'additifs est similaire à celui déjà rapporté pour le M2B1. Par contre, on a eu ici aucune difficulté dans l'usage de DI comme intercepteur radicalaire. Tout au plus a-t-on observé une isomérisation marginale de l'oléfine. De l'accroissement des rendements en méthane et en isopentane, on a déduit facilement le rendement des radicaux CH_3 et C_5H_{11} en tenant compte de la réaction (7):

[1] $\quad R + XD \rightarrow RD + X \quad$ (où X = DS ou I)

Donc $\Phi(CH_3) \simeq 1.4$ et $\Phi(C_5H_{11}) \simeq 0.4$ à 133 N m^{-2}. De la même façon on peut déduire le rendement

TABLEAU 2. Photolyse du méthyl-3-butène-1 pur à 163 nm[a]: rendements quantiques

Pression (N m^{-2})	26	133	2660	6400	Note
CH_4	0.06	0.08	0.14	0.16	f
C_2H_2	0.014	0.012	0.007	0.006	e
C_2H_4	0.07	0.05	0.035	0.02	e
C_2H_6	0.37	0.34	0.34	0.28	d
C_3H_6	0.017	0.013	0.009	0.006	e
Propyne	0.015	0.009	0.007	0.005	e
Iso-C_4H_{10}	0.015	0.010	0.007	0.005	d
C_4H_6-1,3	0.52	0.48	0.19	0.10	e
C_4H_8-2[b]	0.20	0.075	0.020	0.015	e
Iso-C_5H_{10}	0.03	0.035	0.035	n.m.[g]	d
C_5H_{10}-2[c]	0.106	0.18	0.29	0.26	d
C_6H_{14}	n.m.[g]	n.m.[g]	0.08	0.04	d

[a]14 expériences faites entre 26 et 6400 N m^{-2}. Incertitude relative: voir tableau 1, note [e].
[b]Le rapport *trans*-butène-2/*cis*-butène-2 est de 2.0.
[c]Le rapport *trans*-pentène-2/*cis*-pentène-2 est de 1.3.
[d]Produits qui disparaissent par addition de 10% d'oxyde nitrique.
[e]Produits pas ou peu affectés par l'addition de 10% d'oxyde nitrique.
[f]$\Phi(CH_4) = 0.018 \pm 0.004$ entre 133 et 6400 N m^{-2} en présence de 10% de O_2.
[g]n.m. = non mesuré.

TABLEAU 3. Photolyse du méthyl-3-butène-1 à 163 nm en présence d'additifs[a]: rendements quantiques

Additif (%) pression C_5H_{10} ($N\ m^{-2}$)	H_2S (24–32) 133	DI (5–15) 133	1330	6600
CH_4	1.3	1.30	1.50	1.65
C_2H_2	0.01	0.02	0.013	0.01
C_2H_4	0.11	0.11	0.085	0.08
C_2H_6	0.04	0.008	0.005	0.005
C_3H_6	n.m.[e]	0.017	0.012	n.m.[e]
C_3H_8	n.m.[e]	0.03	0.05	n.m.[e]
C_4H_8-1 + C_4H_6-1,3	n.m.[e]	0.64	0.52	0.35
C_4H_8-1	0.00	0.15	n.m.[e]	n.m.[e]
C_4H_8-2	0.17[b]	0.17[c]	0.40[c]	0.60[c]
Iso-C_5H_{10}	0.41	0.27[d]	0.20[d]	0.10[d]

[a]Incertitude relative: ± 10%.
[b]Rapport *trans*-butène-2/*cis*-butène-2 ≃ 2.0.
[c]Rapport *trans*-butène-2/*cis*-butène-2 ≃ 1.45.
[d]Rendements qui décroissent quand le pourcent de DI croît; les valeurs indiquées ont été mesurées à 10% de DI.
[e]n.m. = non mesuré.

en radicaux α-méthallyles:

[2*a*] $CH_3—\dot{C}H—\dot{C}H—CH_2 + XD \rightarrow C_4H_8\text{-}2 + X$

[2*b*] $CH_3—\dot{C}H—\dot{C}H—\dot{C}H_2 + XD \rightarrow C_4H_8\text{-}1 + X$

Ici la mesure exacte du rendement $\Phi(C_4H_7)$ est plus laborieuse. Tout d'abord, il faut noter que les *cis*- et *trans*-butène-2 sont formés en présence de 10% d'oxyde nitrique, via l'addition des atomes d'hydrogène libres sur le M3B1, suivis de la fragmentation du radical C_5H_{11} excité (8, 9)

[3] $H + M3B1 \rightarrow C_5H_{11}^*$

[4] $C_5H_{11}^* \rightarrow CH_3 + cis\text{-}$ ou $trans\text{-}C_4H_8\text{-}2$

[5] $C_5H_{11}^* + M \rightarrow M + C_5H_{11}$

La formation du butène par cette voie dépend de la pression et n'est appréciable qu'aux faibles pressions: $P \leq 133\ N\ m^{-2}$. En outre, pour des raisons analytiques, la séparation du butadiène-1,3 du butène-1 n'a pas été faite à toutes pressions. Cependant en soustrayant du total $\Phi(C_4H_6\text{-}1,3 + C_4H_8\text{-}1)$ la valeur $\Phi(C_4H_6\text{-}1,3)$ obtenue en présence d'oxyde nitrique, on peut tirer la valeur du rendement $\Phi(C_4H_7)$:

$$\Phi(C_4H_7) = \Phi_{DI}(C_4H_6\text{-}1,3 + C_4H_8\text{-}1) + \Phi_{DI}(C_4H_8\text{-}2) - \Phi_{NO}(C_4H_6\text{-}1,3) - \Phi_{NO}(C_4H_8\text{-}2)$$

D'où $\Phi(C_4H_7) = 0.26$, 0.61 et 0.83 à 133, 1330 et 6600 $N\ m^{-2}$. L'isomérisation du M3B1 en M2B2 n'a pas été observée à 133 $N\ m^{-2}$ ($\Phi(M2B2) \leq 0.02$). Par contre elle devient importante à 1330 ($\Phi \simeq 0.3$–0.8) et à 6600 $N\ m^{-2}$ ($\Phi \simeq 6$).

Finalement, l'effet de pression sur le rendement en butadiène-1,3 est indiqué à la fig. 2.

Cas du cis-*pentène-2 (CP2) à 163.3 nm*

Le tableau 4 indique les rendements des produits

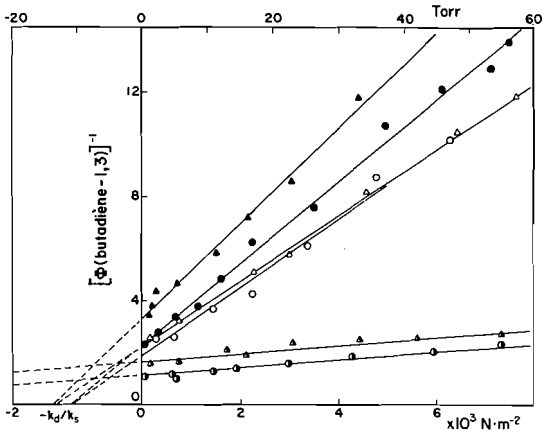

FIG. 2. Photolyse du M3B1 (●, ○, ◑) et du CP2 (▲, △, ◭). Inverse du rendement quantique en butadiène-1,3 en fonction de la pression à 174 (▲, ●), 163 (△, ○) et 147 nm (◭, ◑). Note: L'actinométrie n'a pas été rigoureusement faite dans le cas de la photolyse du CP2 à 174 nm (▲).

obtenus dans l'oléfine pure ou photolysée en présence d'additifs. Les résultats sont très semblables à ceux obtenus dans le cas du M3B1. On retrouve ici comme produit majeur, l'éthane qui disparaît en présence d'oxygène et le butadiène-1,3 qui a un rendement fortement sensible à l'augmentation de pression (fig. 2). DI augmente de façon importante les rendements en méthane, et en C_4H_8, avec une légère augmentation de l'éthylène et du propène.

Discussion

Réactions radicalaires

Dans ces systèmes, l'éthane dont la formation est perturbée de façon importante par la présence d'oxygène, d'oxyde nitrique ou d'iodure d'hydrogène, provient par voie radicalaire. Comme le butane normal n'apparaît jamais, et qu'en outre l'addition de DI ou de D_2S fait apparaître une quantité importante de méthane, la formation de l'éthane ne peut être attribuée qu'à la combinaison de radicaux méthyles. En outre, les autres produits majeurs mesurés en présence de DI sont les radicaux C_4H_7. Dans les systèmes sans additif on retrouve aussi les produits de combinaison des radicaux méthyles et C_4H_7. Ainsi dans le M3B1, le radical C_4H_7 a la structure α-méthallyle et les réactions de combinaison envisagée conduisent au M3B1, et aux *cis*- et *trans*-pentène-2. Il est intéressant de noter que le rapport *cis*-/*trans*-pentène-2 qui est voisin de 1.3 (tableau 2) est en accord avec celui connu dans la littérature (10, 11). Inversement, dans la photolyse du CP2, le M3B1 est un produit aussi attribuable aux mêmes réactions de combinaison. Comme on n'a pas mesuré le produit de la combinaison des radicaux C_4H_7 (les C_8H_{14}) il est difficile d'évaluer le rendement absolu en radicaux

TABLEAU 4. Photolyse du *cis*-pentène-2 à 163.3 nm (pur ou en présence d'additifs)[a]: rendements quantiques

CP2 ($N\ m^{-2}$)	133	650	2800	133	1330	6600	133–6600
					+5–15% DI		+10% O_2
CH_4[b]	0.05	0.08	0.10	1.3	1.4	1.5	0.017
C_2H_2	0.008	0.01	0.006	0.02	0.01	0.01	0.006
C_2H_4[b]	0.050	0.055	0.035	0.10	0.06	0.04	0.026
C_2H_6[b]	0.54	0.44	0.47	0.10	0.09	0.09	0.006
C_3H_6	0.046	0.035	0.030	0.06	0.05	0.06	0.015
Propyne + C_3H_8	0.04	0.04	0.03	0.007	0.006	0.006	<0.001
Allène	0.005	0.005	0.053	0.012	0.005	0.002	n.m.[d]
C_4H_6-1,3	0.37	0.35	0.21	0.64	0.43	0.33	—[c]
C_4H_8-1	0.00	0.00	0.00				0.00
C_4H_8-2	0.00	0.00	0.00	0.12	0.34	0.44	n.m.[d]
M3B1	0.10	0.175	0.19	0.00	0.00	0.00	<0.005

[a]$\Delta\Phi/\Phi \simeq 5\%$ dans les systèmes purs ou en présence de O_2; $\Delta\Phi/\Phi \simeq 10\%$ dans les systèmes contenant du DI.
[b]Effet de D_2S similaire à celui de DI.
[c]Voir fig. 2.
[d]n.m. = non mesuré.

TABLEAU 5. Rendements radicalaires obtenus dans la photolyse d'oléfines à 163 nm[a]

$\Phi(R)$	M2B1	M3B1			CP2		
	133	133	1330	6600	133	1330	6600
CH_3	1.5	1.3	1.2	1.0	1.4	1.4	1.4
CH_3—$\dot{C}H$—$\dot{C}H$—$\dot{C}H_2$	0.00	0.30	0.61	0.83	0.4	0.5	0.73
$\dot{C}H_2$—$\dot{C}(CH_3)$—$\dot{C}H_2$	≥0.4	0.00	0.00	0.00	0.00	0.00	0.00
C_2H_5	0.10	0.00	0.00	0.00	0.10	0.09	0.09
C_2H_3	0.00	0.08	0.05	0.06	0.06	0.03	0.02
C_3H_7	0.00	0.03	0.03	n.m.[b]	0.00	0.00	0.00
H	0.18	0.40	0.28	0.16	n.m.[b]	n.m.[b]	n.m.[b]

[a]L'évaluation du rendement de chacun des radicaux est faite en tenant compte du rendement des produits sensibles à la présence de O_2 ou de NO, de l'effet de DI ou de D_2S (voir texte). L'incertitude relative est au moins 10%.
[b]n.m. = non mesuré.

α-méthallyles. Cependant, une estimation grossière à travers la loi statistique simple

$$R(A + B)^2/[R(A + A)\cdot R(B + B)] \simeq 4$$

où $R(A + A)$ est le rendement de la réaction de combinaison des radicaux méthyles, et $R(A + B)$ est celui de la réaction entre les radicaux méthyles et α-méthallyles, permet d'évaluer le rendement $\Phi(C_4H_7)$. Ce rendement, avec d'autres, est indiqué dans le tableau 5. Les autres radicaux observés sont aussi indiqués et proviennent essentiellement de la mesure de l'effet de DI. L'évaluation du rendement en radicaux méthyles est aussi faite en faisant la somme suivante (cas du M3B1)

$$\Phi(CH_3) = 2\Phi(C_2H_6) + \Phi(C_6H_{14}) \times 1.2 + \Phi(C_5H_{10}\text{-}2) \times 1.2 \quad (8\text{–}11)$$

En outre, l'évaluation du rendement en atomes d'hydrogène, à travers la mesure de l'isopentane (cas du M3B1 en présence de DI) est corrigée pour l'interception directe des atomes d'hydrogène par le DI (12).

Il reste un point d'intérêt qu'il faut soulever ici, c'est l'augmentation du rendement en méthane "radicalaire" avec l'augmentation de la pression de l'oléfine pure. A basse pression, où une part importante des radicaux C_4H_7 se fragmente (voir plus loin), la réaction majeure de disparition des radicaux méthyles est celle de combinaison $CH_3 + CH_3$. La réaction de combinaison $CH_3 + C_4H_7$ croît en importance au fur et à mesure que la pression croît. Par conséquent, la dismutation correspondante croît en importance, et explique qualitativement la croissance du rendement en méthane "radicalaire". Il existe une valeur du rapport k_{dismut}/k_{comb} pour la paire $CH_3 + \alpha\text{-}C_4H_7$: $\Delta(CH_3,\alpha\text{-}C_4H_7) = 0.02$ (11). Etant donnée la valeur du rendement en méthane "radicalaire" obtenue dans le cas du M3B1 et du CP2, cette valeur est insuffisante pour expliquer l'augmentation du rendement en méthane. Une valeur $\Delta(CH_3,\alpha\text{-}C_4H_7)$ de l'ordre de 0.2 serait plus convenable à moins que d'autres processus interfèrent comme par exemple la dismutation des radicaux méthyles et C_5H_{11}: $\Delta(CH_3,(CH_3)_2CH\text{—}\dot{C}H\text{—}CH_3) = 0.2$ ou 0.4 (8, 9) qui croît aussi en importance avec l'augmentation de pression.

Fragmentation des molécules photoexcitées

Le bilan complet qui vient d'être fait (tableau 5) montre sans ambiguités, l'importance des intermédiaires radicalaires que sont les radicaux méthyles et C_4H_7. Dans le cas du M3B1 et du CP2, le produit "moléculaire" formé en quantités majeures est le butadiène-1,3 suggérant le mécanisme suivant:

[6] $\text{M3B1 ou CP2} + h\nu \rightarrow C_5H_{10}^{**}$

[7] $C_5H_{10}^{**} \rightarrow CH_3 + \alpha\text{-}C_4H_7^*$

[8] $\alpha\text{-}C_4H_7^* \xrightarrow{k_d} H + C_4H_6\text{-}1,3$

[9] $\alpha\text{-}C_4H_7^* + M \xrightarrow{k_s} M + \alpha\text{-}C_4H_7$

Ainsi, si l'on ajoute au rendement du butadiène-1,3 celui des radicaux allyles mesuré à travers l'effet de DI on trouve que ces réactions, donc que la scission de la liaison C—C en position β de la molécule photoexcitée, comptent pour au moins 85% du total. Cette valeur est par défaut car il n'est pas exclu qu'une part mineure des radicaux allyles disparaît dans d'autres voies réactionnelles.

Dans le cas du M2B1, le bilan est plus difficile à réaliser, étant données les réactions secondaires déjà mentionnées des atomes d'iode. Néanmoins si l'on ajoute, le rendement de l'allène, à celui des radicaux β-méthallyles, on obtient une valeur au moins égale à 0.55 et pouvant être aussi élevée que 0.90: la scission de la liaison C—C en position β est encore prépondérante.

[10] $\text{M2B1} + h\nu \rightarrow C_5H_{10}^{**}$

[11] $C_5H_{10}^{**} \rightarrow CH_3 + \beta\text{-}C_4H_7^*$

[12] $\beta\text{-}C_4H_7^* \xrightarrow{k_d} CH_3 + C_3H_4 \text{ (allène)}$

[13] $\beta\text{-}C_4H_7^* + M \xrightarrow{k_s} M + \beta\text{-}C_4H_7$

Parmi les autres scissions possibles notables, il y a la scission de la liaison C—C en position α par rapport à la double liaison. La formation de radicaux propyles et du propène dans le cas du M3B1 en est un indice, de même que la formation de l'acétylène et des radicaux vinyles.

[14] $\text{M3B1}^{**} \rightarrow \text{s-}C_3H_7^* + C_2H_3^*$

[15] $\text{s-}C_3H_7^* \rightarrow C_3H_6 + H$

[16] $C_2H_3^* \rightarrow C_2H_2 + H$

Les deux dernières réactions sont, bien entendu, en compétition avec les réactions de stabilisation par collision de sorte que les sommes $\Phi(C_3H_7) + \Phi(C_3H_6)$ et $\Phi(C_2H_3) + \Phi(C_2H_2)$ donnent une valeur maximum au rendement de la scission de la liaison α(C—C). Ces deux valeurs sont 0.05 et 0.07 respectivement. Dans le cas du CP2, la mesure est un peu plus délicate, car il y a deux liaisons α(C—C). La somme $\Phi(C_2H_5) + \Phi(C_2H_4) \simeq 0.14$ correspond à la rupture d'une de ces liaisons. L'autre scission est difficilement appréciable car ses produits disparaissent dans la formation de produits par d'autres voies. Le fait que la chaleur de liaison α(C—CH_3) soit environ 3 kcal mol^{-1} plus énergétique que celle de la liaison α(C—C_2H_5) ne permet pas de dire si la rupture α(C—CH_3) se produit ou pas, bien qu'elle soit thermodynamiquement moins probable. Dans le cas du M2B1, on retrouve le même problème. La somme des rendements $\Phi(C_2H_5) + \Phi(C_2H_4) \simeq 0.12$ donne à nouveau une valeur maximum à la rupture de la liaison α(C—C_2H_5). Par contre, on n'a pas de moyen d'évaluer la rupture de la liaison α(C—CH_3). Disons seulement qu'un écart de 3 kcal mol^{-1} dans les énergies de liaisons, ΔH(C—CH_3) − ΔH(C—C_2H_5), donne une valeur $e^{-3000/RT}$ inférieure à 0.01. Cet argument tendrait à éliminer la scission de la liaison C—CH_3.

Il est intéressant de noter, cas du M3B1, que le rapport de la probabilité, *P*, de rupture de la liaison α(C—C_3H_7) par rapport à celle de la rupture de deux liaisons β(C—CH_3) est tel que

$$P[\alpha(\text{C—C})]/2P[\beta(\text{C—C})] = 0.06/2(0.90) = 1/7.5$$

Dans le cas du CP2, on obtient le rapport suivant:

$$P[\alpha(\text{C—C})]/P[\beta(\text{C—C})] \simeq 0.13/0.84 \simeq 1/6.5$$

Un rapport similaire peut être déduit dans le cas du M2B1, bien que la mesure exacte ne puisse être facilement obtenue à partir des résultats présentés ici. Lors de leur étude par photolyse éclair, Bayrakceken *et al.* (3) ont observé un rapport $P[\alpha(\text{C—C})]/P[\beta(\text{C—C})]$ de l'ordre de 1/13. Bien qu'il soit difficile de savoir comment cette valeur a été calculée, on peut penser à la possibilité d'un effet notable de la longueur d'onde: une énergie plus faible favorisant la rupture de la liaison β(?).

Les autres processus possibles, scission des liaisons C—H, ne sont pas directement visibles à la lumière des résultats. Les liaisons C—H en position β devraient être aussi plus fragiles que les autres liaisons C—H étant donnée l'énergie de résonance du radical allylique. Dans le cas du M3B1 ou du M2B1 on devrait trouver l'isoprène. En effet, les radicaux allyliques résultant conduisent à la formation de ce produit (13). Les techniques utilisées n'ont pas permis d'éclaircir ce point: le rendement en isoprène étant toujours non mesurable. Quand bien même il y aurait-il eu quelques traces d'isoprène, qu'il aurait aussi fallu compter avec les réactions possibles d'abstraction des radicaux chauds, tels que

[17] $CH_3^* + C_5H_{10} \rightarrow CH_4 + C_5H_9$

Les radicaux méthyles chauds sont probablement

produits dans la scission de la molécule photoexcitée (réaction [7]), les deux fragments emportant l'excès de l'énergie du photon.

On note cependant (cas du M3B1), qu'en présence de DI, on forme à 133 N m^{-2} une faible quantité de M2B2: $\Phi \simeq 0.02$. Cela peut indiquer une valeur maximum du rendement en radicaux α,α-diméthallyles, compte tenu des remarques faites à propos de l'isomérisation des oléfines catalysée par les atomes d'iode, et de l'attaque possible du M3B1 par des radicaux chauds. Donc, la scission de la liaison C—H en position β est un processus mineur: $\Phi \leq 0.02$.

Cette remarque a déjà été observée dans la photolyse directe du butène-1 (une autre oléfine ayant une liaison C—C en position β) à 185 nm (14), ainsi qu'à 174 nm (1*c*). On a cependant noté un accroissement de l'importance de cette scission avec l'augmentation de l'énergie du photon (1*c*).

Effet de longueur d'onde

L'analyse du rendement de l'allène (cas du M2B1) et du butadiène (cas du M3B1 et du CP2) en fonction de la pression, montre que les rendements de ces produits suivent une loi de type Stern–Volmer (15):

$$\frac{1}{\Phi(X)} = \frac{1}{\Phi_0(X)} + \frac{1}{\Phi_0(X)}\frac{k_s}{k_d}[M]$$

où $\Phi(X)$ et $\Phi_0(X)$ sont les rendements de l'allène ou du butadiène-1,3 à pression quelconque ou nulle respectivement; [M] tient lieu de pression. k_s et k_d sont les constantes de vitesse d'ordre 2 de stabilisation par collision et d'ordre 1 de fragmentation respectivement du radical précurseur du produit X: figs 1 et 2.

L'interception de ces droites avec l'axe des pressions donne la valeur du rapport $-k_d/k_s$ en unités de pression (tableau 6). On note que les rapports obtenus à 7.1 et 7.6 eV sont les mêmes pour chaque oléfine (à l'intérieur de l'incertitude expérimentale). Par contre, les valeurs obtenues à 8.4 eV sont nettement différentes. Les états électroniques impliqués dans la photoactivation des molécules sont peut-être différents. En fait on sait que l'émission obtenue avec les lampes à azote (7.1 eV) et à brome (7.6 eV) correspond à une bande d'absorption $\pi^* \leftarrow \pi$ tandis que celle de la lampe à xénon (8.4 eV) correspondrait plutôt à l'excitation d'électrons σ.

TABLEAU 6. Valeurs des rapports k_d/k_s (Torr) obtenus dans différents systèmes pour les radicaux α- et β-méthallyles

Radical	α-Méthallyle		β-Méthallyle
Activation photochimique indirecte du	M3B1	CP2	M2B1
7.1 eV	11.1	13.0	7.0
7.6	10.9	13.5	7.0
8.4	48	63	34.5
Activation chimique (réf. 16) ($H + CH_3—CH=C=CH_2$)		≃0.6	—

Une deuxième remarque concerne les valeurs identiques observées à 7.1 et à 7.6 eV. Malgré la différence d'énergie des photons incidents (≃11.5 kcal mol^{-1}), la constante de vitesse de dissociation du radical intermédiaire n'est pas affectée. En terme de la théorie RRK, cela implique que les intermédiaires ont la même énergie interne. Autrement dit, qu'ils soient formés à 7.1 ou à 7.6 eV, ils véhiculent la même quantité d'énergie interne. Cela va à l'encontre d'une distribution statistique de l'excès de l'énergie du photon dans les fragments (la statistique étant faite sur les degrés de liberté de vibration).

Finalement, la variation des valeurs obtenues pour une même énergie avec la structure du monomère traduit probablement entre autres (*a*) les variations des diamètres moléculaires des intermédiaires et des oléfines, (*b*) la différence dans la distribution de l'énergie dans les fragments qui obéit à d'autres lois que celle de la distribution statistique rapportée plus haut.

En outre, il faut ici rappeler que lors de la photolyse du butadiène-1,2 à 8.4 eV, Diaz et Doepker ont montré que le butadiène-1,3 provient de la fragmentation du radical α-méthallyle produit lors de l'addition des atomes d'hydrogène sur le butadiène-1,2 (16). En admettant que les atomes d'hydrogène sont thermiques;

[18] $H + C_4H_6\text{-}1,2 \rightarrow CH_3\dot{C}H—\dot{C}H—\dot{C}H_2{}^*$

$\Delta H = 250$ kJ mol^{-1}

La fragmentation de ces radicaux chimiquement activés suit une loi linéaire de type Stern–Volmer et le rapport k_d/k_s obtenu est voisin de 0.6 Torr. Hormis la différence mineure dans les diamètres de collision, il apparaît que la vitesse de décomposition des radicaux α-méthallyles obtenus lors de la photolyse du M3B1 et du CP2 est plus rapide en admettant, bien sûr, une constante de vitesse k_s identique dans chacun des cas.

Remerciements

Nous voulons spécialement remercier le ministère de l'Environnement du Canada, ainsi que l'Université du Québec pour l'aide généreuse accordée à ce projet.

1. (*a*) A. WIĘCKOWSKI et G. J. COLLIN. Can. J. Chem. **55**, 3636 (1977); (*b*) J. Phys. Chem. **81**, 2592 (1977); (*c*) G. J. COLLIN et A. WIĘCKOWSKI. J. Photochem. **8**, 103 (1978); (*d*) A. WIĘCKOWSKI et G. J. COLLIN. Can. J. Chem. **56**, 1435 (1978).
2. A. B. CALLEAR et H. K. LEE. (*a*) Nature, 693 (1967); (*b*) Trans. Faraday Soc. **64**, 308 (1968); **64**, 2017 (1968).

3. F. BAYRAKCEKEN, J. H. BROPHY, R. D. FINK et J. E. NICHOLAS. J. Chem. Soc. Faraday Trans. **169**, 228 (1973).
4. R. GORDEN, JR., R. E. REBBERT et P. AUSLOOS. NBS Technical Note, 496 (1969).
5. P. J. GORTON et R. WALSH. J. Chem. Soc. Commun. 783 (1972).
6. Z. B. ALFASSI, D. M. GOLDEN et S. W. BENSON. Int. J. Chem. Kinet. **6**, 155 (1973) et les références citées.
7. P. AUSLOOS, R. E. REBBERT et S. G. LIAS. J. Photochem. **2**, 267 (1974).
8. J. H. GEORGAKAKOS, B. S. RABINOVITCH et C. W. LARSON. Int. J. Chem. Kinet. **3**, 535 (1971).
9. G. J. COLLIN et C. BERTRAND. J. Photochem. **3**, 123 (1974).
10. N. YOKOYAMA. Bull. Chem. Soc. Jpn. **43**, 2975 (1970).
11. D. C. MONTAGUE. Int. J. Chem. Kinet. **5**, 513 (1973).
12. G. J. COLLIN et K. BUKKA. J. Photochem. **6**, 381 (1976/77).
13. G. J. COLLIN, H. DESLAURIERS et J. DESCHÊNES. Can. J. Chem. Ce numéro.
14. P. BORRELL et P. CASHMORE. Ber. Bunsenges. Phys. Chem. **72**, 182 (1968).
15. W. FORST. *In* Theory of unimolecular reaction. Academic Press. New York, NY. 1973.
16. Z. DIAZ et R. DOEPKER. J. Phys. Chem. **81**, 1442 (1977).

Photolyse du propène et du méthyl-2-butène-2 vers 174 et à 163 nm

GUY J. COLLIN,[1] HÉLÈNE DESLAURIERS ET JOVETTE DESCHÊNES

Département des Sciences Pures, Université du Québec à Chicoutimi, Chicoutimi (Qué.), Canada G7H 2B1

Reçu le 30 octobre 1978

GUY J. COLLIN, HÉLÈNE DESLAURIERS et JOVETTE DESCHÊNES. Can. J. Chem. **57**, 870 (1979).

On a étudié la photolyse du propène à 163 nm et vers 174 nm, ainsi que celle du méthyl-2-butène-2 à 163 nm. A cette dernière longueur d'onde (7.6 eV), la molécule de propène photoexcitée se décompose principalement par rupture de la liaison β(C—H): $\Phi = 0.565$ et α(C—C): $\Phi = 0.335$. Le rapport β(C—H)/α(C—C) est donc voisin de 1.69. Dans le cas du méthyl-2-butène-2, les deux ruptures précédentes constituent encore la majorité des réactions de fragmentation de la molécule photoexcitée. Cependant le rapport est inversé: β(C—H)/α(C—C) $\simeq 0.58$. Ce rapport a également été mesuré pour le butène-2 dans un autre travail et il est voisin de l'unité. En outre, afin d'expliquer la formation de l'allène et du butadiène-1,3 dans la photolyse du méthyl-2-butène-2, on propose l'isomérisation des radicaux vinyliques intermédiaires en conformité avec les observations de Callear et Lee.

GUY J. COLLIN, HÉLÈNE DESLAURIERS, and JOVETTE DESCHÊNES. Can. J. Chem. **57**, 870 (1979).

We have studied the 163 nm photolysis of propene and of 2-methyl-2-butene and a few results on the 174 nm photolysis of propene are also included. At 163 nm (7.6 eV), the main decomposition processes of the photoexcited propene molecule are β(C—H) split ($\Phi = 0.565$) and α(C—C) split ($\Phi = 0.335$). Thus, the β(C—H)/α(C—C) ratio is close to 1.69. In the case of the photolysis of 2-methyl-2-butene, the same ratio is reversed: β(C—H)/α(C—C) $\simeq 0.58$. In another work, the ratio obtained in the photolysis of 2-butene was close to unity. Finally, in order to explain the allene and 1,3-butadiene formation in the photolysis of 2-methyl-2-butene, isomerisation of vinylic radical intermediates is proposed, in agreement with observations made by Callear and Lee.

Introduction

Dans la publication précédente (1), nous avons montré que la décomposition des molécules oléfiniques, photoexcitées dans la région de l'uv sous vide (vers 160 ± 15 nm), se fait principalement par le bris de la liaison C—C située en position β par rapport à la double liaison: $\Phi \simeq 0.9$. Cette scission libère un radical allylique et un radical alkyle. Dans ce présent rapport nous avons concentré notre attention sur la photodécomposition des oléfines qui n'ont pas de telle liaison β(C—C). Déjà, un certain nombre de rapports existent sur la photolyse du propène (2–4), du butène-2 (5, 6) et de l'isobutène (7–9). Cependant les observations qui y sont rapportées sont incomplètes: soit qu'il manque les rendements quantiques, soit que les mécanismes de fragmentation n'aient pu être clairement mis en évidence pour toutes sortes de raisons. En plus de l'étude systématique du propène et du méthyl-2-butène-2 à 7.1 et surtout à 7.6 eV, nous rediscuterons rapidement de certaines valeurs obtenues pour le butène-2.

Partie expérimentale

Les techniques expérimentales ont toutes été rapportées dans la littérature. Le propène est un produit de Matheson of Canada, "Research Grade" dont les impuretés principales sont: le propane: 105 ± 5 ppm, l'éthane: 4.48 ppm et l'éthylène: 2.67 ppm. Le méthyl-2-butène-2 est un produit "A.P.I." de pureté moléculaire affichée 99.4 ± 0.4%. Les impuretés observées sont: le méthyl-3-butène-1: 40.0 ppm, le méthyl-2-butène-1: 50.6 ppm, l'isoprène: 11.4 ppm et l'isopentane: 18.7 ppm. Les concentrations des impuretés varient légèrement d'un échantillon à l'autre (≤10%), ainsi que pour un échantillon entre le début et la fin de son utilisation. Les autres produits, les techniques ont été décrites ailleurs (1, 6, 9), de même que les lampes d'irradiation et l'actinométrie (6, 10). Il faut mentionner les précautions particulières prises pour l'actinométrie (1).

Les analyses ont été faites par chromatographie en phase gazeuse à l'aide d'un détecteur à double flammes ionisantes. La majorité des produits ont été analysés sur une colonne de squalane (6*c*). On a en outre utilisé une colonne d'alumine en programmation de température pour séparer le propane du propène, une colonne de *n*-octane/porasil C pour séparer le butène-1 de l'isobutène et du butadiène-1,3 (6*c*) et enfin une colonne de UCON LB 550 × 20% pour séparer l'allène du propène (11).

Résultats

Les résultats sont indiqués sous la forme de rendements quantiques dans les figures et les tableaux qui accompagnent le texte.

Cas du propène

La photolyse du propène est relativement simple, elle donne lieu, lorsque 5 à 10% d'oxyde nitrique sont ajoutés, à la formation de méthane ($\Phi(CH_4) = 0.05 \pm 0.01$ entre 66 et 26 600 N m^{-2}),[2] d'acétylène et

[1]Auteur auquel toute correspondance devrait être envoyée.

[2]133 N m^{-2} = 1 Torr.

0008-4042/79/080870-06$01.00/0

d'allène (fig. 1). Pour des raisons analytiques on n'a pas cherché à mesurer le propyne. Par contre, la photolyse du monomère pur (dégasé à la température de l'azote liquide) montre une variété de produits allant du méthane aux C_6. Parmi les produits principaux, on trouve ceux cités plus haut ainsi que l'isobutane, le méthyl-4-pentène-1 et le diméthyl-2,3-butane (tableau 1). L'addition de D_2S ou de DI (10 à 20%) au propène augmente de façon marquée les rendements en propane, méthane, éthylène et acétylène (tableau 2). Dans aucun de ces systèmes on a trouvé de quantités appréciables ($\Phi \leq 0.002$) de cyclopropane, méthylcyclopropane, vinylacétylène et de méthyl-3-butyne-1 quelle que soit la pression entre 66 et 26 600 N m^{-2}. Il faut en outre noter un effet de pression marqué sur le rendement en acétylène, éthylène et allène (fig. 1) ainsi que sur d'autres produits (tableau 1). Enfin, la photolyse à 174 nm, donne des résultats en tout point similaires à ceux rapportés ici. On n'a montré ici que les rendements en acétylène et en allène (fig. 1).

Cas du méthyl-2-butène-2 à 163 nm

La photolyse du méthyl-2-butène-2 donne aussi lieu à une variété importante de produits. En présence de 10% d'oxygène un certain nombre de produits ont des rendements indépendants de la pression entre 20 et 2600 N m^{-2}. Ce sont: le méthane: 0.033 ± 0.01, l'acétylène: 0.005 ± 0.002, l'éthylène: 0.015 ± 0.010 et le propène: 0.005 ± 0.002. Par contre les rendements en propyne, allène, butadiène-1,3 et isoprène ont des rendements qui décroissent avec la pression (fig. 2). Les rendements de ces produits extrapolés à pression nulle sont: Φ_0(propyne) $= 0.065 \pm 0.005$, Φ_0(allène) $= 0.022 \pm 0.002$, Φ_0(butadiène-1,3) $= 0.105 \pm 0.01$ et Φ_0(isoprène) $= 0.27 \pm 0.03$. L'addition de D_2S ou DI (10 à 20%) au méthyl-2-butène-2 n'a pas ou peu d'effet sur les rendements en acétylène, éthylène, propène, propyne et allène. Il augmente cependant de façon importante le rendement en méthane (tableau 3). On y observe aussi un rendement important en isopentane. L'effet avec DI est similaire à celui du D_2S bien que la reproductibilité expérimentale laisse à désirer ($\pm 25\%$). En particulier, dans ce cas on a observé une formation importante d'un composé dont le rendement croît très vite avec le pourcentage de DI ($0.2 \leq \Phi \leq 2.0$) et attribué à des réactions secondaires. On n'a pas poursuivi plus à fond l'étude de ce produit qui a le même temps de passage que l'isobutène ou le butadiène-1,3 sur la colonne de squalane.

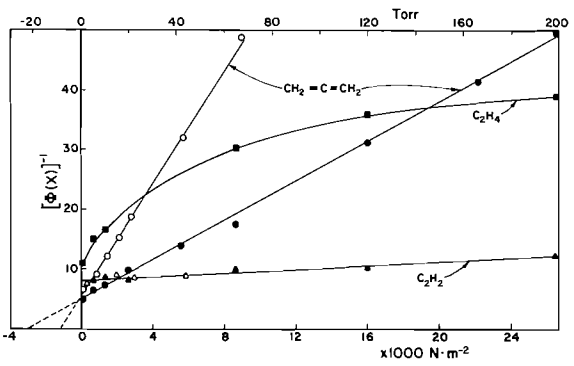

FIG. 1. Photolyse du propène à 163 nm (■, ●, ▲) et vers 174 nm (○, △). Inverse du rendement quantique en fonction de la pression totale du système: propène:oxyde nitrique (1.0:0.10).

TABLEAU 1. Photolyse du propène pur à 163 nm: rendements quantiques

Pression (N m^{-2})	133[b]	1330	6650	13 300
Méthane	0.096	0.041	0.085	0.098
Acétylène	0.235	0.21	0.19	0.20
Ethylène	0.152	0.099	0.079	0.076
Ethane	0.083	0.063	0.062	0.064
Allène	0.219	0.130	0.060	0.035
Propane	0.095	0.09	n.m.	n.m.
Isobutane	0.169	0.130	0.112	0.114
Butène-1	0.10	0.12	0.13	0.13
Butadiène-1,3	≃0.00	0.01	0.00	
n-Butane	0.005	0.010	0.017	0.017
Butène-2[a]	0.002	0.005	0.006	0.006
Méthyl-3-butène-1	0.002	0.026	0.017	0.012
Pentadiène-1,4	0.024	0.019	0.031	0.028
Isopentane	0.011	0.016	0.021	0.22
Méthyl-4-pentène-1	0.185	0.219	0.254	0.236
Hexadiène-1,5	≃0.00	0.040	0.045	0.30
Diméthyl-2,3-butane	0.165	0.128	0.116	0.110
Méthyl-2-pentane	≃0.00	0.024	0.023	0.014
Hexène-1	≃0.00	0.009	0.017	0.019

[a] *trans*/*cis* ≃ 2.0.
[b] Taux de conversion 2% à 133 N m^{-2} (1 Torr) et inférieur à 0.4% à 1330 N m^{-2} (10 Torr).

TABLEAU 2. Photolyse du propène en présence de D_2S ou de DI (10 à 20%) à 163 nm: rendements quantiques

Pression totale[b]	133	1330	6650
Méthane	0.43[a]	0.42	0.40
Acétylène	0.22	0.16	0.15
Ethylène	0.32	0.25	0.25
Propane	0.80	0.85	0.72

[a] $\Delta\Phi/\Phi \simeq 0.10$.
[b] N m^{-2}.

Discussion

Cas du propène

L'analyse des résultats montre que la majorité des produits disparaît lorsque la photolyse est faite en présence d'oxyde nitrique, suggérant ainsi la nature

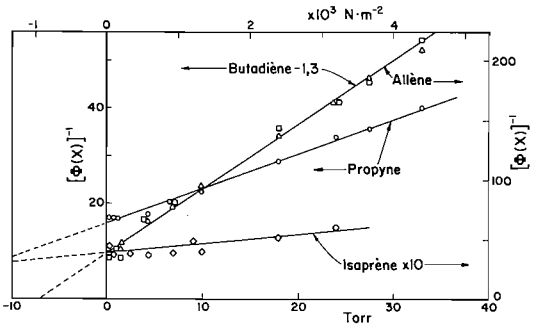

FIG. 2. Photolyse du méthyl-2-butène-2 à 163 nm. Inverse du rendement quantique en fonction de la pression totale du système: méthyl-2-butène-2:oxygène ou oxyde nitrique (1.0:0.10). Attention: les rendements en allène et en butadiène sont représentés par la même droite, mais non par le même axe des ordonnées.

radicalaire du mécanisme de leur formation. Les principaux produits en C_6 étant le diméthyl-2,3-butane et le méthyl-4-pentène-1, les intermédiaires radicalaires les plus probables sont les radicaux propyles secondaires et allyles. Il faut mentionner deux produits en C_4 issus des radicaux méthyles et allyles d'une part et méthyles et iso-propyles d'autre part et qui sont le butène-1 et l'isobutane respectivement. Compte tenu des rapports des constantes des réactions de dismutation et combinaison, k_d/k_c, donnés dans la littérature, on peut estimer à chaque pression le rendement quantique des radicaux.

$$\Phi(\text{iso-}C_3H_7) \geq 2\Phi(\text{diméthyl-2,3-butane}) \times 1.66 + \Phi(\text{méthyl-2-pentane}) + \Phi(\text{méthyl-4-pentène-1}) + \Phi(\text{isopentane}) \times 1.30 + \Phi(\text{isobutane}) \times 1.16 + \Phi(\text{méthyl-3-butène-1})$$

$$\Phi(n\text{-}C_3H_7) \simeq \Phi(\text{hexène-1}) + \Phi(\text{méthyl-2-pentane}) \times 1.41 + \Phi(n\text{-butane}) \times 1.05$$

$$\Phi(\text{allyl}) \geq \Phi(\text{hexène-1}) + 2\Phi(\text{hexadiène-1,5}) \times 1.01 + \Phi(\text{méthyl-4-pentène-1}) + \Phi(\text{pentadiène-1,4}) + \Phi(\text{butène-1})$$

$$\Phi(CH_3) \geq \Phi(n\text{-butane}) \times 1.06 + \Phi(\text{isobutane}) \times 1.16 + 2\Phi(\text{ethane}) + \Phi(\text{butène-1})$$

et

$$\Phi(C_2H_3) \simeq \Phi(\text{pentadiène-1,4}) + \Phi(\text{méthyl-3-butène-1})$$

Ces cinq relations sont discutables, puisque un bon nombre de rapports k_d/k_c sont inconnus (12). On peut estimer que les réactions de dismutation sont peu importantes bien que ce soit pas nécessairement le cas. Compte tenu des rendements des produits de combinaison, parmi ceux qui manquent, deux sont importants: celui se rapportant au couple méthyl + allyl et celui se rapportant au couple iso-propyl + allyl. Le premier couple produit la paire $CH_4 + C_3H_4$. La valeur du rendement en méthane radicalaire impose un rendement maximum de 0.03 à cette dismutation, c'est-à-dire le rendement en méthane radicalaire, diminué de celui provenant de la dismutation méthyl + iso-propyl calculable à partir de la formation de l'isobutane. L'autre couple est moins facilement accessible. La dismutation de ce couple conduit soit à la paire $C_3H_8 + C_3H_4$ soit à la paire $C_3H_6 + C_3H_6$. La première paire est de peu d'importance, car tout le propane formé est explicable par la dismutation des radicaux iso-propyles. Quant à l'autre paire, elle n'est pas accessible ici. Enfin ces relations n'expliquent pas le rendement important en ethylène et en acétylène qui sont inhibés par la présence d'oxyde nitrique et qui peuvent provenir via l'abstraction d'un atome d'hydrogène sur le monomère par le radical convenable.

TABLEAU 3. Effet de D_2S (20–30%)[a] dans la photolyse du méthyl-2-butène-2 à 163 nm: rendements quantiques

Pression totale[f]	150	700	1500
Méthane[b]	0.76	0.66	0.65
Isopentane[c]	0.60	0.56	0.60
Butène-2[d,b]	0.06	0.09	0.11
Méthylbutène[b,e]	0.07	0.08	0.10

[a]10% de D_2S sont insuffisants pour intercepter tous les radicaux méthyles: $\Phi(C_2H_6) = 0.11$ et $\Phi(CH_4) = 0.65$ à 150 N m^{-2}. Avec 20% et plus, $\Phi(C_2H_6) \leq 0.04$.
[b]Résultats similaires dans les mélanges C_5H_{10}:DI.
[c]En présence de DI, les valeurs Φ(iso-C_5H_{12}) sont plus faibles.
[d]Le rapport *trans*/*cis* $\simeq$ 2.0.
[e]Le rapport méthyl-2-butène-1/méthyl-3-butène-1 $\simeq$ 4.
[f]N m^{-2}.

Pour résoudre ce problème, DI et D_2S ont été utilisés pour intercepter les radicaux libres (tableau 2). Le rendement du produit XD obtenu en présence de DI ou de D_2S diminué de celui obtenu en présence de NO est attribué à la réaction.

[1] $$X + DI(D_2S) \rightarrow XD + I(DS)$$

Cette différence est donc égal au rendement du radical X. On trouve une bonne concordance entre les valeurs obtenues par cette méthode et ceux obtenus à l'aide des précédentes relations (tableau 4). Tout d'abord, les valeurs $\Phi(C_3H_7)$ obtenues par la méthode d'interception, sont un peu plus faibles que la somme Φ(iso-C_3H_7) + $\Phi(n\text{-}C_3H_7)$. Les atomes d'hydrogène sont les précurseurs de ces radicaux (voir plus loin) et sont partiellement interceptés par l'additif (13). Quant aux autres radicaux l'accord est acceptable. La formation des radicaux méthyles, vinyles et allyles est facilement compréhensible. Les radicaux propyles sont formés par addition des

TABLEAU 4. Photolyse du propène à 163 nm: rendements quantiques[a]

Pression ($N\ m^{-2}$)		Rendements des radicaux 133	1330	6650	13 300
$\Phi(iso\text{-}C_3H_7)$	A	0.90	0.85	0.82	0.82
$\Phi(n\text{-}C_3H_7)$	A	0.03	0.05	0.07	0.05
$\Phi(C_3H_7)$	DX	0.80	0.85	0.72	n.m.
Φ(allyl)	A	0.34	0.45	0.51	0.51
$\Phi(C_2H_3)$	A	0.064	0.084	0.079	0.071
	B	0.21	0.215	0.20	0.25
	DX	0.21	0.24	0.21	n.m.
$\Phi(CH_3)$	A	0.47	0.48	0.40	0.43
	DX	0.43	0.42	0.40	n.m.

[a]A: déduit des 5 relations, photolyse du propène pur; DX: déduit de l'effet de D_2S ou de DI; B: valeurs obtenues en A augmentées du rendement en acétylène et en éthylène radicalaire (voir texte).

atomes d'hydrogène sur le monomère.

[2a] $H + C_3H_6 \rightleftarrows iso\text{-}C_3H_7^*$

[2b] $H + C_3H_6 \rightarrow n\text{-}C_3H_7$

$\Delta H = -143\ kJ\ mol^{-1}$

[2c] $H + C_3H_6 \rightarrow H_2 + C_3H_5$

où $k_{2b}/k_{2a} \simeq 0.06$ (13) et $k_{2c}/k_2 \simeq 0.04$ (12). Les radicaux iso- et n-C_3H_7 sont chimiquement excités et se décomposent à basse pression: la réaction [2a] est réversible et le radical n-$C_3H_7^*$ se décompose en radical méthyle et en éthylène (14).

[3] $n\text{-}C_3H_7^* \rightarrow CH_3 + C_2H_4$

$\Delta H = +96\ kJ\ mol^{-1}$

En admettant que les atomes d'hydrogène sont thermiques, la majorité (>99%) des radicaux isopropyles sont stabilisés par collision à une pression de 133 $N\ m^{-2}$. Par contre, il faut au moins une pression de 800–1000 $N\ m^{-2}$ pour stabiliser la moitié des radicaux n-propyles (14). A basse pression une part importante de l'éthylène est donc formé via la réaction [3]. Une autre possibilité de formation de l'éthylène est l'éjection d'un groupe méthylène par la molécule photoexcitée. On n'a pu mesurer de formation de méthyl-cyclopropane (addition d'un groupe méthylène sur le monomère) malgré qu'à 13 300 N m^{-2} une part importante de ce produit soit stabilisé par collision (15). A basse pression où le méthylcyclopropane s'isomérise en butènes linéaires (15), on n'observe que de faibles rendements en C_4H_8. En admettant qu'à 13 300 N m^{-2}, les radicaux n-propyles ne se fragmentent plus, la mesure du rendement en éthylène à cette pression donne une valeur limite à cette réaction

[4] $C_3H_6 + h\nu \rightarrow C_3H_6^{**}$

[5] $C_3H_6^{**} \rightarrow CH_2 + C_2H_4$

$\Phi \simeq 0.02$

Enfin le rendement en acétylène augmente ($\Delta\Phi \simeq 0.05$) lors de l'addition de D_2S ou de DI. Sur la base de la réaction [1], cette augmentation est attribuable au radical C_2H bien que dans ce cas l'efficacité puisse être douteuse (16). En l'absence, ou en présence de NO, ce radical réagit très rapidement avec le propène (17). Il se forme le vinylacétylène et un polymère. Cela explique pourquoi on n'observe pas le produit de combinaison entre les radicaux C_2H et iso-C_3H_7: le méthyl-3-butyne-1. Seule, la valeur obtenue en utilisant D_2S ou DI, donne une valeur fiable et suggère la réaction suivante

[6a ou b] $C_3H_6^{**} \rightarrow C_2H + (CH_4 + H)$ ou $(CH_3 + H_2)$

$\Phi \simeq 0.05$

L'allène est formé, même en présence d'oxyde nitrique. A basse pression, c'est le produit majeur et son rendement dépend fortement de la pression et suit une loi de type Stern–Volmer (18):

$$\Phi^{-1} = \Phi_0^{-1} + \Phi_0^{-1}(k_s/k_d)[M]$$

où Φ_0 et Φ sont les rendements quantiques à pression nulle et à pression P, k_s et k_d les constantes de vitesse de stabilisation par collision (d'ordre 2) et de décomposition (d'ordre 1) de l'intermédiaire qui précéde la formation de l'allène, et [M] est ici la pression du propène. L'intermédiaire probable de l'allène est le radical allyle. En effet, la somme Φ(allyle) + Φ(allène) = 0.565 ± 0.02 entre 133 et 13 300 N m^{-2}. La décomposition du monomère photoexcitée est quantitative dans ce domaine de pression; il n'est donc pas l'intermédiaire recherché.

[7] $C_3H_6^{**} \rightarrow H + \dot{C}H_2\text{—}\dot{C}H\text{—}\dot{C}H_2^*$

$\Phi = 0.565$

[8] $\dot{C}H_2\text{—}\dot{C}H\text{—}\dot{C}H_2^* \rightarrow H + CH_2{=}C{=}CH_2\ (k_d)$

[9] $\dot{C}H_2\text{—}\dot{C}H\text{—}\dot{C}H_2^* + M \rightarrow M + \dot{C}H_2\text{—}\dot{C}H\text{—}\dot{C}H_2\ (k_s)$

L'acétylène est aussi formé en présence d'oxyde nitrique, et son rendement suit aussi une loi de type Stern–Volmer et la somme $\Phi(C_2H_3) + \Phi(C_2H_2)$ est aussi constante dans le même domaine de pression: $\Phi(C_2H_3) + \Phi(C_2H_2) = 0.335 \pm 0.02$.

[10] $C_3H_6^{**} \rightarrow CH_3 + C_2H_3^*$

$\Phi = 0.335$

[11] $C_2H_3^* \rightarrow C_2H_2 + H$

[12] $C_2H_3^* + M \rightarrow M + C_2H_3$

Il reste finalement un produit formé en présence d'oxyde nitrique: le méthane. La réaction [6] a déjà été envisagée comme source de méthane. Cependant, une alternative est possible. Une émission simultanée de méthane et d'acétylène n'est pas

exclue.

[13] $C_3H_6^{**} \rightarrow CH_4 + C_2H_2$

Il est tentant de se baser sur les rendements en atomes hydrogène et en radicaux méthyles pour tenter de justifier ou d'éliminer l'une ou l'autre des réactions [6] et [13]. Cependant ces mesures ne permettent pas une précision expérimentale pour ce faire, bien qu'elles favorisent la réaction [6*a*], au détriment de [6*b*] et donc au détriment de [13] (tableau 5).

Il est intéressant de noter que le changement de longueur d'onde n'a pas d'effet sur le rendement en acétylène. Par contre, la formation d'allène est fortement influencée par ce changement (fig. 1). Alors que le rapport $k_d/k_s = 9.0$ Torr à 174 nm, il devient égal à 21.5 Torr à 163 nm. L'effet de l'énergie interne est évidemment visible sur la fragmentation du radical allyle.

Enfin, il faut noter que pour cette molécule qui n'a pas de liaison β(C—C), la scission principale est celle de la liaison β(C—H) suivie par celle de la liaison α(C—C) dans le rapport β(C—H)/α(C—C) = 1.69 ± 0.15. A 185 nm, ce rapport a été mesuré: 1.2 (4). A 147 nm, le mécanisme proposé est plus complexe et il n'est pas facile d'extraire ce rapport de résultats (2, 3) bien que la scission α(C—C) semble favorisée.

Cas du méthyl-2-butène-2

En présence de D_2S (tableau 3) les produits majeurs sont le méthane et l'isopentane. De façon similaire à ce qui a été dit pour la photolyse du propène, ces produits, via la réaction [1], proviennent des radicaux méthyles et C_5H_{11}

[14*a*] $H + (CH_3)_2C{=}CHCH_3 \rightarrow (CH_3)_2CCH_2CH_3^*$

[14*b*] $H + (CH_3)_2C{=}CHCH_3 \rightarrow (CH_3)_2CHCHCH_3^*$

Si les radicaux secondaires se fragmentent à très basse pression, à une pression supérieure à 133 N m^{-2} ils sont stabilisés par collision. Quant au radicaux tertiaires ils ne se décomposent pas dans les conditions présentes sauf si les atomes d'hydrogène véhiculent une part importante d'énergie cinétique. La quantité importante d'isopentane permet d'ignorer ces réactions de décomposition. En outre, même à 22 N m^{-2} le rendement $\Phi(C_4H_8\text{-}2)$ est inférieur à 0.015, confirmant le peu d'importance de cette fragmentation (19).

[15] $(CH_3)_2CHCHCH_3^* \rightarrow CH_3 + C_4H_8\text{-}2$

L'addition de D_2S augmente aussi les rendements du butène-2 et du méthyl-2-butène-1 et méthyl-3-butène-1 mais dans de moindres proportions. La réaction [1] suggère la présence de radicaux C_4H_7 et C_5H_9. Ausloos et coll. ont montré que l'hydrogène sulfuré n'intercepte pas les radicaux allyliques (20). Par conséquent, les radicaux C_4H_7 doivent avoir une structure vinylique: $CH_3C{=}CHCH_3$. Dans le cas de la formation du méthyl-2-butène-1 et méthyl-3-butène-1 les structures des radicaux C_5H_9 devraient être $CH{=}C(CH_3)C_2H_5$ et $(CH_3)_2CHC{=}CH_2$ ou $(CH_3)_2CHCH{=}CH$. Il n'est pas facile d'établir l'origine de ces radicaux (voir plus loin).

TABLEAU 5. Photodécomposition du propène à 163 nm

Réaction	$C_3H_6^{**} \rightarrow$	Φ
[7]	$C_3H_5^* + H \hookrightarrow CH_2{=}C{=}CH_2 + H$	0.565
[10]	$C_2H_3^* + CH_3 \hookrightarrow C_2H_2 + H$	0.335
[6*a*]	$C_2H + (CH_4 + H)$	≃0.05
[5]	$CH_2 + C_2H_4$	0.02
	Total	0.97

Parmi les produits "moléculaires", l'isoprène est le plus important, et demande la formation concurrente de deux atomes ou d'une molécule d'hydrogène. Le bilan global (voir plus loin) favorise sa scission en deux étapes, avec formation d'un intermédiaire allylique.

[16] $(CH_3)_2C{=}CHCH_3 + h\nu \rightarrow (CH_3)_2C{=}CHCH_3^{**}$

[17*a*] $(CH_3)_2C{=}CHCH_3^{**} \rightarrow (CH_3)_2\dot{C}\dot{C}H\dot{C}H^* + H$ (A)

[17*b*] $(CH_3)_2C{=}CHCH_3^{**} \rightarrow \dot{C}H_2\dot{C}(CH_3)\dot{C}HCH_3^* + H$ (B)

[18] A* ou B* → $CH_2{=}C(CH_3)CH{=}CH_2 + H$

[19] A* ou B* + M → M + A ou B

Ce mécanisme est basé sur le fait que le rendement en isoprène suit une loi de type Stern–Volmer (fig. 2). Les autres produits "moléculaires" importants que sont le propyne, l'allène et le butadiène-1,3 peuvent s'expliquer sur la base de rupture primaire d'une liaison α(C—C):

[20] $(CH_3)_2C{=}CHCH_3^{**} \rightarrow CH_3 + CH_3C{=}CHCH_3^*$

[21*a*] $CH_3C{=}C{-}CH_3^* \rightarrow CH_3C{\equiv}CH + CH_3$

[21*b*] $CH_3C{=}CHCH_3^* \rightarrow CH_3\dot{C}H\dot{C}H\dot{C}H_2^*$

[22] $CH_3\dot{C}H\dot{C}H\dot{C}H_2^* \rightarrow CH_2{=}CHCH{=}CH_2 + H$

et

[23] $(CH_3)_2C{=}CHCH_3^{**} \rightarrow (CH_3)_2C{=}CH^* + CH_3$

[24*a*] $(CH_3)_2C{=}CH^* \rightarrow CH_3C{\equiv}CH + CH_3$

[24*b*] $(CH_3)_2C{=}CH^* \rightarrow \dot{C}H_2\dot{C}(CH_3)\dot{C}H_2^*$

[25] $\dot{C}H_2\dot{C}(CH_3)\dot{C}H_2^* \rightarrow CH_2{=}C{=}CH_2 + CH_3$

Les réactions [21], [22], [24] et [25] sont bien sûr en compétition avec les réactions de stabilisation par collision. Il s'ensuit que les rendements en propyne, allène et butadiène-1,3 suivent la loi "Stern–Volmer" (fig. 2).

Les réactions d'isomérisation [21*b*] et [24*b*] ont été observées dans d'autres systèmes (21). Elles demandent la formation d'un complexe cyclique à quatre côtés, donc possédant une forte énergie interne. En particulier les radicaux β-méthallyles ont été observés dans la photolyse éclair de ce monomère (22). L'énergie disponible après la rupture primaire de la liaison α(C—C) est suffisante pour permettre à la réaction de passer par dessus la barrière de potentielle (23), bien que tous les radicaux C_4H_7 issus des réactions [20] et [23] peuvent ne pas avoir suffisemment d'énergie pour ce faire. En particulier, la présence de radicaux vinyliques C_4H_7 est l'indice qu'au moins une part des radicaux $CH_3C{=}CHCH_3$* ne s'isomérisent pas en structure allylique. Quant aux réactions [22] et [25] elles ont été proposées dans la publication précédente (1).

Finalement, il est intéressant d'essayer de mesurer l'importance relative de la scission β(C—H) par rapport à celle de la liaison α(C—C). Il n'est facile d'extraire le rapport β(C—H)/α(C—C) car tous les produits radicalaires n'ont pu être mesurés convenablement. Néanmoins, le rendement en atomes d'hydrogène -Φ(isopentane) obtenu en présence de D_2S- diminué du rendement des réactions (18) -Φ(isoprène)- et [22] -Φ(butadiène-1,3)- et en ajoutant le rendement des atomes d'hydrogène qui réagissent directement avec D_2S plutôt qu'avec le monomère, permet d'évaluer le rendement de la réaction [17]: Φ_{cal}(réaction [17]) $\simeq 0.35 \pm 0.05$. De la même manière, les réactions [20] et [23] peuvent être évaluées à partir de la mesure du rendement en radicaux méthyles en présence de D_2S, diminué du rendement en méthane "moléculaire", ainsi que de ceux des réactions [21*a*], [24*a*] et [25]. On trouve alors $\Phi([20]) + \Phi([23]) \simeq 0.60 \pm 0.05$. Le rapport β(C—H)/α(C—C) est donc égal à 0.58 ± 0.16. Ce rapport est l'inverse de celui obtenu avec le propène. Dans le cas du *cis*-butène-2, le même rapport était voisin de l'unité (1*c*). L'effet de substitution sur le groupe éthylénique, ou la grosseur de la molécule, a donc un rôle dans la scission de la molécule. Le remplacement successif d'un atome d'hydrogène par un radical méthyle semble affaiblir la liaison α(C—C) par rapport à la stabilité de la liaison β(C—H). On a également montré un effet de longueur d'onde dans le cas du *cis*-butène-2 (1*c*).

Remerciements

Nous aimerions remercier spécialement le Conseil de Recherches en Sciences Naturelles et en Génie du Canada, ainsi que le ministère de l'Education du Québec (programme FCAC) pour l'aide substantielle accordée à la réalisation de ce projet.

1. G. J. COLLIN, H. DESLAURIERS et S. AUCLAIR. Can. J. Chem. Ce numéro.
2. D. A. BECKER, H. OKABE et J. R. MCNESBY. J. Phys. Chem. **69**, 538 (1965).
3. E. TSCHUIKOW-ROUX. J. Phys. Chem. **71**, 2355 (1967).
4. P. BORRELL, A. CERVENKA et J. W. TURNER. J. Chem. Soc. B, 2293 (1971).
5. P. BORRELL et F. C. JAMES. Trans Faraday Soc. **62**, 2452 (1966); P. BORRELL et A. CERVENKA. J. Chem. Soc. Faraday Trans. I, **68**, 345 (1972).
6. (*a*) G. J. COLLIN et P. M. PERRIN. Can. J. Chem. **50**, 2823 (1972); (*b*) G. J. COLLIN et K. BUKKA. J. Photochem. **6**, 381 (1976/77); A. WIĘCKOWSKI et G. J. COLLIN. (*c*) J. Phys. Chem. **81**, 2592 (1977); (*d*) Can. J. Chem. **55**, 3636 (1977).
7. P. BORRELL et P. CASHMORE. Trans. Faraday Soc. **65**, 1595 (1969).
8. J. A. HERMAN, K. HERMAN et P. AUSLOOS. J. Chem. Phys. **52**, 28 (1970).
9. G. J. COLLIN et A. WIĘCKOWSKI. J. Photochem. **8**, 103 (1978).
10. A. WIĘCKOWSKI et G. J. COLLIN. Can. J. Chem. **56**, 1435 (1978).
11. J. GAWLOWSKI, J. NIEDZIELSKI et A. BIERZYŃSKI. Chem. Anal. **15**, 721 (1970).
12. A. F. TROTMAN-DICKENSON et G. S. MILNE. NSRDS-NBS 9 (1967); E. RATAJCZAK et A. F. TROTMAN-DICKENSON. OSTI, UWIST (1970) et les références qui y sont citées.
13. J. A. KERR et M. J. PARSONAJE. *Dans* Evaluated kinetic data on gas phase addition reactions. CRC Press, Cleveland, Ohio. 1972, et les références qui y sont citées.
14. W. E. FALCONER, B. S. RABINOVITCH et R. J. CVETANOVIĆ. J. Chem. Phys. **39**, 40 (1963).
15. F. H. DORER et B. S. RABINOVITCH. J. Phys. Chem. **69**, 1952 (1965); **69**, 1964 (1965).
16. K. L. HILL et R. D. DOEPKER. J. Phys. Chem. **76**, 1112 (1972).
17. A. M. TARR, O. P. STRAUSZ et H. E. GUNNING. Trans. Faraday Soc. **62**, 1221 (1966).
18. W. FORST. *Dans* Theory of unimolecular reactions. Academic Press, New York, NY. 1973. p. 235.
19. C. W. LARSON, B. S. RABINOVITCH et D. C. TARDY. J. Chem. Phys. **47**, 4570 (1967).
20. P. AUSLOOS, R. E. REBBERT et S. G. LIAS. J. Photochem. **2**, 267 (1973/74).
21. T. IBUKI, A. TSAJI et Y. TAKEZKI. J. Phys. Chem. **80**, 8 (1976).
22. A. B. CALLEAR et H. K. LEE. Trans. Faraday Soc. **64**, 2017 (1968).
23. G. J. COLLIN. Rev. Chem. Intermediates, sous presse.

Etude de l'ion $HC_2O_4^-$ en solution aqueuse par spectrométrie infrarouge et Raman

M. JABER[1] ET F. BERTIN

Laboratoire de Chimie Analytique II, 43 boulevard du 11 Novembre 1918, Université de Lyon I, Villeurbanne, France

ET

M. T. FOREL

Laboratoire de Spectroscopie Infrarouge associé au C.N.R.S., Université de Bordeaux I, 351 Cours de la Libération, 33405 Talence, France

Reçu le 6 septembre 1978

M. JABER, F. BERTIN et M. T. FOREL. Can. J. Chem. **57**, 876 (1979).

Les auteurs ont examiné les solutions aqueuses de l'ion hydrogénooxalate par spectroscopie infrarouge et Raman. Ils montrent l'existence de l'équilibre entre une structure monomère plane liée par liaison hydrogène aux molécules d'eau du solvant et une forme associée. Un tel équilibre peut fournir une explication satisfaisante des spectres obtenus et de leur modification avec la température et la concentration. Un calcul de champ de forces de valence utilisant les coordonnées normales de l'ion $HC_2O_4^-$ supposé plan, permet de vérifier les attributions proposées pour la forme monomère de cet ion.

M. JABER, F. BERTIN, and M. T. FOREL. Can. J. Chem. **57**, 876 (1979).

The authors have investigated aqueous solution of the hydrogenooxalate ion by infrared and Raman spectroscopy. They show the existence of an equilibrium between a planar monomer structure linked by hydrogen bond to solvent molecules and an associated form. Such an equilibrium can provide a satisfactory explanation for the experimental spectra and their dependence upon temperature and concentration. The assignments for the monomeric form are supported by a normal coordinate analysis and by a calculation of the valence force field.

Introduction

L'étude structurale de l'ion $HC_2O_4^-$ à l'état cristallisé a déjà fait l'objet de plusieurs publications; nous ne résumerons que les plus importantes. Tellgren et Olovsson (1) montrent à partir des spectres de diffraction X du composé $NaHC_2O_4$, H_2O et de son dérivé deutérié que la maille cristalline est triclinique et que les ions $HC_2O_4^-$ s'associent en chaînes définies par l'intermédiaire d'une liaison hydrogène OH---O très courte (2.571 Å). Les molécules d'eau forment des ponts entre ces chaînes constituant ainsi des liaisons hydrogène longues (2.808 et 2.826 Å).

De Villepin et Novak (2–4) analysent les spectres infrarouges et Raman des hydrogénooxalates cristallisés de Li, Na et K, hydratés et anhydres, obtenus à deux températures différentes (température ambiante et $-180°C$). Ces auteurs proposent une attribution des bandes observées aussi bien pour les groupements oxalates que pour les molécules d'eau liées à ces groupements; pour justifier leurs attributions, les auteurs s'appuient sur les données cristallographiques de Tellgren et sur les modifications spectrales dues à la deutériation.

Nous avons étudié par spectrométrie Raman la dissociation de l'acide oxalique en solution aqueuse en fonction du pH, et identifié les bandes caractéristiques des trois espèces en équilibre: $H_2C_2O_4$, $HC_2O_4^-$ et $C_2O_4^{2-}$ (5). Dans ce mémoire nous discutons essentiellement les résultats obtenus pour $HC_2O_4^-$ en utilisant chaque fois que cela est possible les données de l'infrarouge. Nous comparerons les spectres de vibration de cet ion à ceux de l'ion $DC_2O_4^-$ en solution dans D_2O. Après avoir discuté les différents types d'association possibles pour ces ions en solution nous proposons une interprétation de leurs spectres et nous tentons de justifier nos hypothèses à l'aide d'un calcul de vibration.

Conditions expérimentales

Les solutions de $HC_2O_4^-$ 0.25 *M* sont préparées en neutralisant une seule acidité de l'acide oxalique par la potasse suivant un procédé déjà décrit (5).

Pour obtenir une concentration plus élevée en $HC_2O_4^-$ nous avons utilisé l'hydrogénooxalate de césium car il est soluble jusqu'à une concentration proche de 0.7 *M*. Ce sel est préparé par action, dans l'eau bouillante de l'acide oxalique sur le carbonate de césium introduits en quantités équimoléculaires; après dégagement du gaz carbonique il faut recristalliser le produit plusieurs fois pour obtenir des cristaux blancs de $CsHC_2O_4$. On redissout alors ces cristaux dans de l'eau distillée; la solution ainsi obtenue doit être assez rapidement utilisée car elle noircit après plusieurs jours.

[1]Boursier du C.N.R.S. Libanais.

0008-4042/79/080876-07$01.00/0

TABLEAU 1. Fréquences infrarouge et Raman des ions $HC_2O_4^-$ et $DC_2O_4^-$ en solution aqueuse*

IR	H_2O					1240	1305?		1400?						1725
						F									F
	D_2O			855		1270			1415				1640	1700	1720
				f		e_p			m				TF	e_p	F
R	H_2O	453	725	868		1240	1305	1380	1410	1444					1725
		F	f	TF		tf	tf	m	m	m					F
	D_2O	450	685	853	950	1060	1270			1421		1560	1640	1700	1720
		F	f	TF	tf	tf	e_p			TF		tf	f	e_p	F

*TF: très forte; F: forte; m: moyenne; f: faible; tf: très faible; e_p: épaule.

Quelles que soient les solutions préparées, il est impossible d'isoler un domaine de pH dans lequel la concentration en ions $HC_2O_4^-$ représente plus que 91% de la concentration analytique totale; les 9% restants sont constitués d'ions $C_2O_4^{2-}$ ou de molécules $H_2C_2O_4$ non dissociées.

Les solutions de $DC_2O_4^-$ dans D_2O sont obtenues en dissolvant $Na_2C_2O_4$ anhydre, produit Merck pour analyse, dans D_2O (99.75%) et en acidifiant progressivement cette solution de départ par une solution de DCl, 7.8 *N* environ, dont la teneur en D_2O est de 99.5%. Les produits deutériés sont fournis par le C.E.A. Les manipulations sont réalisées dans une boite à gants. Les spectres infrarouges et Raman sont ceux de solutions 0.20 *M* de $NaDC_2O_4$.

Les spectres infrarouges sont enregistrés à la température ordinaire avec un spectromètre P.E. 457, en utilisant des cellules à liquide munies de fenêtres en Irtran II séparées par un joint de Téflon d'épaisseur 27 μm. Une cellule identique contenant le solvant (H_2O ou D_2O) est disposée sur le faisceau référence du spectromètre. Les domaines observables sont alors les suivants: 2000–1700 cm^{-1}, 1500–900 cm^{-1} dans H_2O et 2000–1300 cm^{-1} et 1100–800 cm^{-1} dans D_2O.

Les spectres Raman sont obtenus à l'aide d'un spectromètre CODERG PHO équipé d'un laser à argon ionisé; la raie excitatrice, 488 nm, fournit une puissance de 1 à 1.2 W. Les conditions moyennes d'enregistrement sont les suivantes: tension d'alimentation du photomultiplicateur 950 V, fentes 6 cm^{-1}, vitesse de défilement des réseaux 25 cm^{-1}/mn. Pour les spectres enregistrés à température ambiante, les solutions sont placées dans des cuves parallélepipédiques de 0.3 ou 1 mL. Pour enregistrer les spectres à différentes températures comprises entre 4 et 90°C on dispose l'une d'elles dans une jaquette cylindrique en verre dans laquelle circule de l'eau dont la température est maintenue constante par un thermostat.

Analyse des spectres

Le tableau 1 rassemble les fréquences ir et Raman caractéristiques des espèces $HC_2O_4^-$ et $DC_2O_4^-$ en solution.

Les spectres des solutions dont le pH est compris entre 2.1 et 2.4, domaine dans lequel ces espèces sont prépondérantes, présentent des bandes faibles dues aux molécules $H_2C_2O_4$ ou $D_2C_2O_4$ non dissociées ou à l'ion $C_2O_4^{2-}$ (5). Pour éviter toute confusion, ces bandes parasites sont identifiées en enregistrant les spectres de solutions très acides où $H_2C_2O_4$ et $D_2C_2O_4$ sont seuls et de solutions neutres où $C_2O_4^{2-}$ est totalement formé.

L'examen des spectres montre qu'il existe un grand nombre de coïncidences entre les fréquences infrarouges et Raman aussi bien pour $HC_2O_4^-$ que pour $DC_2O_4^-$. Toutes les bandes Raman sont polarisées donc si l'on admet que la molécule est plane, seuls les modes de vibration symétriques situés dans le plan sont observés. La modification fondamentale, en passant du composé hydrogéné ou deutérié, est le remplacement du quadruplet 1305–1380–1410–1444 cm^{-1} par trois bandes à 950, 1060 et 1421 cm^{-1}, cette dernière étant très intense.

Etude vibrationnelle du modèle monomère

Nous avons montré que la position des bandes Raman de $HC_2O_4^-$ reste fixe en fréquence malgré leur changement d'intensité corrélatif à la variation d'acidité du milieu. De plus nous avons vérifié que la hauteur de certaines bandes Raman est rigoureusement proportionnelle à la concentration de l'espèce $HC_2O_4^-$ en solution, calculée d'après les constantes de formation de l'acide oxalique. Ceci accrédite l'hypothèse de la formation d'une espèce de structure bien définie, au moins à température constante.

Si l'espèce qui se forme en solution est un ion monomère, plan, plus ou moins solvaté par les molécules d'eau, elle appartient au groupe de symétrie C_s et possède 11 vibrations de type A'.

Par analogie avec les attributions proposées par De Villepin et Novak (2, 3) pour l'hydrogénooxalate cristallisé, nous pouvons proposer une première interprétation des spectres Raman (tableau 2). Pour les spectres infrarouges la comparaison avec l'état solide est plus difficile par suite de l'étroitesse du domaine observable en solution aqueuse et des im-

précisions sur les maxima de certaines bandes, dues à la forte absorption du solvant.

Région 1800–1500 cm^{-1}

Dans H_2O la mise en évidence des bandes caractéristiques est difficile en raison de la large bande de diffusion à 1640 cm^{-1} due au solvant; on observe toutefois un maximum à 1725 cm^{-1}, déplacé par deutériation à 1720 cm^{-1} et attribuable à ν(C=O).

Dans D_2O une autre bande, affirmée par l'absence de celles caractéristiques de HOD (1450 cm^{-1}) et H_2O (1640 cm^{-1}) en milieu très acide et neutre, apparait à 1640 cm^{-1}; elle correspond au mode ν_a(COO) en accord avec les conclusions de De Villepin et Novak (2). Dans ce solvant on constate en outre la présence d'une bande faible à 1560 cm^{-1} et d'une épaule à 1700 cm^{-1}, difficilement attribuable à des vibrations du modèle monomère.

Région 1500–1000 cm^{-1}

Dans ce domaine de fréquences on attend trois bandes correspondant aux modes ν_s(COO), ν(C—O) et δ(OH) ou δ(OD), or le spectre du composé hydrogéné comporte cinq bandes dont l'une, située à 1240 cm^{-1} est probablement due à ν(C—O). Dans le cas du dérivé deutérié cette région perturbée par la bande intense de D_2O à 1204 cm^{-1}, présente quatre bandes (tableau 1). La vibration δ(OD) doit correspondre à l'une des fréquences observées à 1060 ou 950 cm^{-1}.

Région 1000–250 cm^{-1}

La raie Raman intense située à 868 cm^{-1} dans H_2O et à 853 cm^{-1} dans D_2O est attribuée à la vibration ν(C—C). Les bandes à 725 et 453 cm^{-1}, déplacées respectivement à 685 et 450 cm^{-1} par deutériation, correspondent respectivement à des déformations des groupements COOH et COO^-; on ne peut cependant préciser leurs modes.

Il apparait donc entre 1750 et 900 cm^{-1} un certain nombre de raies qui ne peuvent pas être attribuées aux vibrations du monomère plan. Il est très peu probable qu'elles proviennent de combinaisons car celles-ci sont généralement peu intenses en Raman. L'hypothèse d'une seule forme monoprotonée est donc insuffisante pour interpréter la totalité des fréquences expérimentales. Nous sommes donc amenés à supposer l'existence d'au moins deux formes en équilibre entre-elles. L'une est très probablement la forme monomère, l'autre serait alors associée, pour laquelle diverses structures seront envisagées.

Mise en évidence d'un équilibre d'association pour $HC_2O_4^-$ en solution

Afin de vérifier l'existence d'un équilibre, nous avons étudié l'influence de différents facteurs physiques et chimiques sur le spectre Raman de la solution. Celle-ci est maintenue à un pH voisin de 2.4 car l'espèce $HC_2O_4^-$ est alors majoritaire.

Influence de la température

Nous avons suivi de façon systématique l'évolution du spectre Raman de $HC_2O_4^-$ et $DC_2O_4^-$ en fonction de la température. Dans H_2O cet effet porte principalement sur les bandes du quadruplet 1305–1380–1410–1444 cm^{-1}. L'intensité des bandes à 1305 et 1410 cm^{-1} croît régulièrement avec la température (fig. 1). Comme cet effet doit être relié à la rupture des associations entre les groupements $HC_2O_4^-$ nous attribuons ces deux bandes à la forme monomère et celles à 1380 et 1444 cm^{-1} à une forme plus ou moins associée (tableau 2). Notons qu'il se produit simultanément des diminutions de fréquences de l'ordre de 5 cm^{-1}.

Aucune variation importante de l'intensité des bandes n'est observée pour les solutions deutériées. A 60°C on constate seulement que la raie intense à 1421 cm^{-1} s'est déplacée jusqu'à 1415 cm^{-1} et qu'elle semble présenter une épaule vers 1400 cm^{-1}.

Influence de la concentration

Nous avons enregistré le spectre d'une solution d'hydrogénooxalate de césium trois fois plus concentrée que la solution utilisée jusqu'à présent (0.7 *M*). On relève la présence d'une nouvelle bande très faible vers 600 cm^{-1} et on constate une légère diminution relative des intensités des bandes à 1305 et 1410 cm^{-1} par rapport à 1380 et 1444 cm^{-1} sans changement appréciable de fréquences. L'augmentation de concentration doit en effet conduire à un renforcement des associations au détriment de la forme monomère; ceci est donc compatible avec l'effet de température.

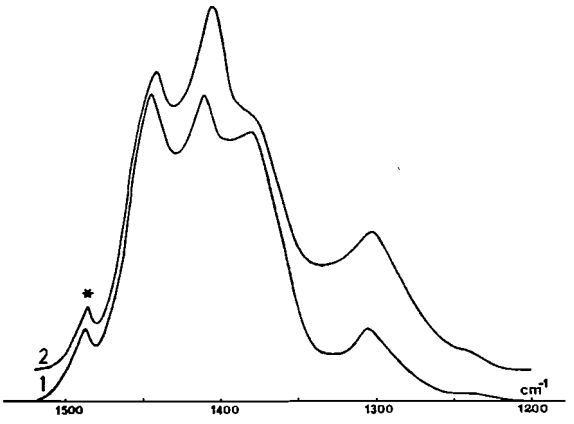

FIG. 1. Spectre Raman du composé $HC_2O_4^-$ en solution aqueuse, à deux températures différentes, dans la région 1200–1500 cm^{-1}. *1*: $T = 4°C$; *2*: $T = 90°C$. *Bande de $C_2O_4^{2-}$ à 1486 cm^{-1}.

Influence de la nature du solvant

Nous avons suivi l'évolution du quadruplet Raman 1305–1380–1410–1444 cm^{-1} de l'ion $HC_2O_4^-$ en solution, en ajoutant à l'eau différents composés donneurs ou accepteurs de protons tels que $CHCl_3$, HCN, CD_3CN afin de modifier l'équilibre entre les formes. Ces solvants ne doivent pas posséder de bandes Raman intenses dans le domaine de fréquence étudié. Ainsi CH_3CN n'a pu être utilisé et a dû être remplacé par CD_3CN après avoir vérifié que l'échange deutérium–hydrogène était inexistant; CD_3CN possède cependant trois bandes entre 1250 et 1450 cm^{-1} dont deux à 1393 et 1451 cm^{-1} sont de très faible intensité, la troisième à 1281 cm^{-1} étant plus gênante.

L'addition de $CHCl_3$ ou de HCN n'apporte aucune information car le premier est très peu miscible à l'eau et le second ne parait pas interagir avec $HC_2O_4^-$. Par contre l'addition progressive, jusqu'à 28% en volume de CD_3CN à une solution d'hydrogénooxalate, 0.25 *M* provoque une augmentation régulière de l'intensité de la bande à 1410 cm^{-1}, qui s'abaisse à 1404 cm^{-1}, tandis que la bande à 1444 cm^{-1} se déplace à 1440 cm^{-1}. Il n'y a pas de modification mesurable des intensités des bandes à 1380 et 1444 cm^{-1}. L'évolution de la bande à 1305 cm^{-1} ne peut pas être chiffrée en raison de la présence à 1281 cm^{-1} de la raie plus intense de CD_3CN.

L'influence du CD_3CN peut s'interpréter par une compétition entre les formes associées de l'ion $HC_2O_4^-$ et une entité du type:

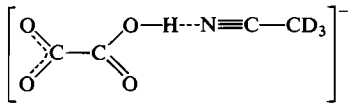

Les mêmes mesures effectuées pour les solutions de $NaDC_2O_4$ dans D_2O ne permettent pas de déceler des modifications significatives.

L'ensemble des résultats obtenus nous conduit à proposer une répartition des fréquences entre formes monomères et formes associées (tableau 2).

Proposition de structure pour l'espèce $HC_2O_4^-$ en solution aqueuse

Pour la forme monomère, les interprétations de structures de Davies et Sutherland (11), Lascombe et coll. (12) et De Villepin et coll. (13, 14) concernant des monoacides carboxyliques en solution dans des mélanges H_2O–CCl_4 ou dans des solvants donneurs ou accepteurs de protons, nous conduisent à supposer la formation d'un hydrogénooxalate monomère, lié par liaison hydrogène aux molécules d'eau du solvant suivant les enchaînements (A), (B), (C) ou (D) envisagés par De Villepin et Lascombe:

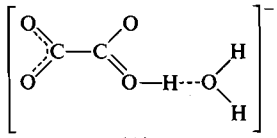

(A)

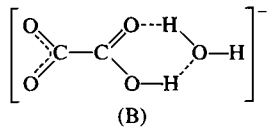

(B)

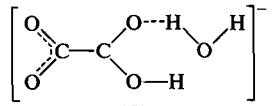

(C)

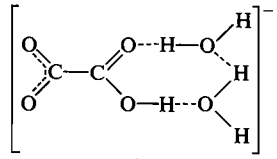

(D)

Pour la forme associée, à l'état cristallisé, De Villepin et Novak (2) admettent que l'association en chaînes longues, mises en évidence par Tellgren et Olovsson (1), permet d'expliquer leurs résultats spectroscopiques. En solution, la longueur des chaînes dépend du pH et on peut admettre que leur rupture entraîne des variations de fréquences ce qui est contraire aux observations expérimentales. La présence de telles chaînes est donc peu probable, ceci est confirmé par l'absence de certaines bandes observées sur les cristaux.

D'autre part une structure dimère fermée du type:

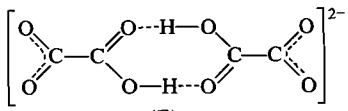

(E)

parait peu compatible avec les données spectroscopiques. En effet, d'après les travaux de plusieurs auteurs (6–10) si une telle structure dimère existe, elle présente un centre de symétrie et doit conduire à deux modes (C=O), l'un asymétrique actif en infrarouge et situé vers 1750 cm^{-1}, l'autre symétrique actif en Raman et vibrant entre 1650 et 1700 cm^{-1}. La coïncidence infrarouge Raman observée pour l'hydrogénooxalate à 1725 cm^{-1} (H_2O) et 1720 cm^{-1} (D_2O) rejette donc l'hypothèse du modèle (E).

L'existence d'une structure de dimères ouverts associés à des molécules d'eau suivant le schéma:

TABLEAU 2. Attribution des bandes Raman

Type de vibration	Monomère (A), (B) ou (D)		Associé (F) ou (G)		Résultats de De Villepin et Novak à l'état cristallisé (2)	
	H_2O	D_2O	H_2O	D_2O	$NaHC_2O_4.H_2O$	$NaDC_2O_4.D_2O$
ν(OH) ou ν(OD)	?	?	?	?		
ν(C═O)	1725	1720			1719	1720
$\nu_a(COO^-)$		1560 ou 1640		1640	1600	1632
$\nu_s(COO^-)$	1410	1400 ?	1444	1421	1416	1436
δ(OH)	1305		1380		1458	
δ(OD)		950		1060		1074
ν(C—O)	1240	1270	1240	1270	1219	1263
ν(C—C)	868	853	868	853	888	882
δ(OCOH)	725		725		719	
δ(OCOD)		685		685		673
$\delta(OCO^-)$					597	592
$\delta(OCO^-)$					502	492
ou	453	450	453	450		
$\delta(OCO^-)$					479	481

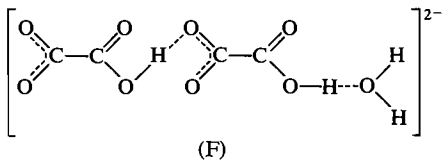

(F)

ne peut être totalement exclue, mais la concentration d'une telle association doit être assez faible car le pouvoir solvatant de l'eau est tel que cette autoassociation ne devrait apparaître qu'à concentration élevée.

Il reste donc la possibilité d'association dipolaire entre les formes monomères liées par les molécules du solvant tel que:

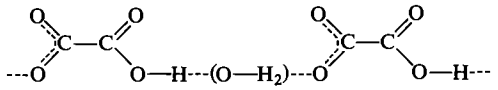

(G)

L'hypothèse d'un équilibre entre la forme monomère de type (A), (B) ou (D) et une association de type (F) et (G) peut expliquer les phénomènes observés par spectrométrie Raman.

Nous avons effectué un calcul des modes normaux des vibrations planes de l'ion $HC_2O_4^-$ monomère afin de préciser l'interprétation des spectres et d'expliquer les modifications de fréquence et d'intensité entrainées par la deutériation.

Calcul de vibration de l'ion $HC_2O_4^-$ pour la forme monomère

Le calcul a été réalisé par la méthode de Wilson et coll. (15) et les paramètres de structure utilisés pour calculer la matrice **G** sont ceux donnés par Tellgren et Olovsson (1). Nous les rappelons ci-dessous:

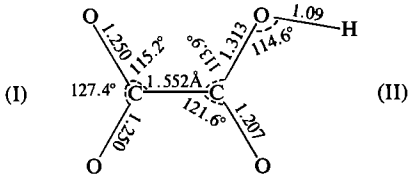

(I) (II)

Nous utilisons dans notre discussion la notation (I) et (II) pour désigner respectivement les groupes COO^- et COOH.

Choix du champ de force

Pour obtenir la matrice **F** de l'ion $HC_2O_4^-$ nous transférons 19 constantes de force provenant soit du champ de forces de valence du groupe —C—COO^- déduit des données spectrales de l'ion $^+NH_3$—CH_2—COO^- à l'état solide et en solution (16), soit du champ de force du groupement —COOH de l'acide formique à l'état gazeux (17). Les coordonnées utilisées pour le calcul sont les mêmes que celles des ions de référence. Nous disposons également des champs de forces proposés par Murata et Kawai (18, 19) pour l'ion $C_2O_4^{2-}$ et la molécule $H_2C_2O_4$; les constantes de force principales données par cet auteur et utilisées plus récemment par Bardet et Fleury (20) pour le même type de calcul sont du même ordre de grandeur de celles de Caillet et Destrade, excepté pour la liaison C—C.

Ce champ de force initial a été ajusté. Ainsi, la constante de force de la liaison C—C a été posée égale à 4.9 mdyn $Å^{-1}$. Nous avons augmenté les constantes de force de déformation δ(OH) et $\delta(OCO)_{II}$ et diminué celles des vibrateurs ν(C═O) et ν(C—O) du groupe COOH afin de tenir compte du changement d'état physique. Nous admettons que la constante de force du rocking du groupement COOH dont nous ne connaissons pas la fréquence de vibra-

TABLEAU 3. Constantes de forces pour l'hydrogénooxalate monomère plan. Les constantes de force de valence sont exprimées en mdyn $Å^{-1}$, celle de déformation en mdyn Å rad^{-2} et les interactions angles-liaison en mdyn rad^{-1}

Constantes de force principales			Constantes de force d'interaction		
1	$F(\nu C—C)$	4.90‡	11	$F(\nu C—O, \nu C—O)_I$	1.10†
2	$F(\nu C—O)_I$	9.40†	12	$F(\nu C=O, \nu C—O)_{II}$	0.186*
3	$F(\nu C—O)_{II}$	4.55‡	13	$F(\nu C—O, \nu C—C)_I$	1.10†
4	$F(\nu C=O)_{II}$	10.00‡	14	$F(\nu C—O, \delta OH)_{II}$	−0.235‡
5	$F(\nu OH)_{II}$	7.20*	15	$F(\nu C—C, \delta OCO)_I$	−0.400†
6	$F(\delta OCO)_I$	1.45†	16	$F(\nu C—O, r OCO)_I$	1.100†
7	$F(\delta OCO)_{II}$	1.80‡	17	$F(\delta OCO, \delta OH)_{II}$	−0.106*
8	$F(r OCO)_I$	1.59†	18	$F(\nu C—O, \delta OCO)_I$	0.200†
9	$F(r OCO)_{II}$	1.59§	19	$F(\nu C=O, r OCO)_{II}$	−0.500§
10	$F(\delta OH)_{II}$	0.900‡	20	$F(\nu C=O, \delta OH)_{II}$	−0.094*
			21	$F(\nu C—O, \delta OCO)_{II}$	0.300*
			22	$F(\nu C—C, \delta OCO)_{II}$	−0.500§

*Constantes de forces données par Caillet (17).
†Constantes de forces données par Destrade (16).
‡Constantes de forces modifiées.
§Constantes de forces nouvellement introduites.

tion est du même ordre de grandeur que celle du groupement COO^-. De plus, nous avons introduit deux constantes d'interactions supplémentaires numérotées 19 et 22 dont les valeurs sont ajustées par approximations successives. L'interaction 19, analogue à l'interaction ($\nu_{C=O}$, $\delta_{C—H}$) de l'acide formique, a pour effet de diminuer la fréquence $\nu(C=O)$ trop élevée avec le champ de forces initial. Il n'est pas possible de modifier davantage le champ de forces présenté dans le tableau 3 en raison de l'insuffisance des données expérimentales.

Résultats

Le tableau 4 regroupe les fréquences calculées et observées pour la forme monomère des ions $HC_2O_4^-$ et $DC_2O_4^-$. Il permet de comparer l'attribution initialement proposée à la répartition de l'énergie potentielle de chaque mode.

Fréquences calculées

La fréquence de l'élongation $\nu(C=O)$ de l'ion $HC_2O_4^-$ est supérieure de 3% à la valeur expérimentale. Seule l'introduction et l'ajustement des constantes d'interaction entre ce vibrateur et les déformations $r(OCO)_I$ et $r(OCO)_{II}$ permettraient d'améliorer l'accord entre le calcul et l'expérimental, mais les modes mettant surtout en jeu $r(OCO)_I$ et $r(OCO)_{II}$ sont inobservés pour l'ion $HC_2O_4^-$ en solution. Le problème est donc indéterminé.

Les modes situés à 1240 et 1305 cm^{-1} ($HC_2O_4^-$) et à 1270 cm^{-1} ($DC_2O_4^-$) sont calculés à des fréquences de 2 à 4% supérieures aux fréquences observées, mais le petit nombre de données expérimentales ne permet pas un affinement; quant au mode calculé à 1108 cm^{-1} pour $DC_2O_4^-$, il peut correspondre soit à la bande observée à 1060 cm^{-1}, primitivement attribuée aux formes associées, soit à une fréquence masquée par la très large bande de D_2O à 1204 cm^{-1}; les écarts sur $\delta(OH)$ et $\delta(OD)$ peuvent s'expliquer en partie par le fait que ces vibrations doivent être anharmoniques en raison des liaisons hydrogène.

Le calcul reproduit bien l'influence de la deutériation sur l'évolution des fréquences. En particulier $\nu_s(COO)_I$ s'abaisse alors que $\nu(C—O)$ augmente; ces variations sont dues aux couplages entre ces élongations et les déformations $\delta(OH)$ ou $\delta(OD)$.

Modes de vibrations

Dans l'ion $HC_2O_4^-$ le mode attribué à $\nu_s(COO)_I$ met également en jeu $\delta(OH)$ et $\nu(C—C)$; dans le composé deutérié la contribution de $\delta(OD)$ devient nulle alors que celles de $\nu(C—C)$ et $\nu_s(COO)_I$ augmentent. Ceci est cohérent avec l'exaltation de l'intensité diffusée à 1400–1421 cm^{-1}.

Les différences spectrales observées dans le domaine 1450–1300 cm^{-1} sont dues principalement aux modifications de couplage entre la vibration $\delta(OH)$ ou $\delta(OD)$ d'une part et les mouvements $\nu_s(COO)_I$, $\nu(C=O)$, $\delta(OCO)_I$, ... d'autre part.

Le mode de vibration calculé à 1360 cm^{-1} contient seulement 22% du $\delta(OH)$ tandis que la déformation $\delta(OD)$ participe pour 56% au mode situé à 1108 cm^{-1}.

La polarisation de la bande attribuée à $\nu_a(COO)_I$ s'explique par des élongations d'amplitudes différentes des deux liaisons C—O et par une mise en jeu de la liaison C—C.

Les modes situés vers 870 $\pm$ 10 cm^{-1} et attribués à $\nu(C—C)$ correspondent en fait à une élongation en phase de toutes les liaisons.

Enfin le mode observé vers 450 cm^{-1} correspond à une ouverture en phase des angles:

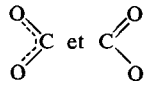

TABLEAU 4. Fréquences de vibration et répartition de l'énergie potentielle pour les deux ions $HC_2O_4^-$ et $DC_2O_4^-$ en solution

	$HC_2O_4^-$		
Attribution	ν_{exp}	ν_{calcd}	Distribution d'énergie potentielle $100L_{ik}^2F_{ii}/\lambda_k$
ν(OH)	?	3593	100 ν(OH)
ν(C═O)	1725	1764	59ν(C═O) + 13δ(OH) + 13r(OCO)$_{II}$ + 11ν(C—O) + 10r(OCO)$_I$
ν_a(COO)$_I$	?	1638	104ν_a(COO)$_I$ + 10r(OCO)$_I$
ν_s(COO)$_I$	1410	1423	37δ(OH) + 25ν(CC) + 21ν_s(COO)$_I$ + 13δ(OCO)$_{II}$ + 10δ(OCO)$_I$
δ(OH)	1305	1360	50ν_s(COO)$_I$ + 22δ(OH) + 18δ(OCO)$_I$ + 14ν(CC) + 10ν(C═O)
ν(C—O)	1240	1274	28δ(OCO)$_{II}$ + 26ν(C—O) + 17ν(CC) + 13δ(OH) + 11ν(C═O) + 10ν_s(COO)$_I$
ν(C—C)	868	883	38δ(OCO)$_I$ + 21ν_s(COO)$_I$ + 17ν(CC)
δ(OCO)$_{II}$	725	720	33δ(OCO)$_{II}$ + 13ν(C—O) + 11ν(C═O) + 10δ(OH) + 10δ(OCO)$_I$ + 10r(OCO)$_I$
r(OCO)$_{II}$	?	608	38ν(C—O) + 27r(OCO)$_I$ + 21r(OCO)$_{II}$
δ(OCO)$_I$	453	485	33ν(CC) + 28δ(OCO)$_I$ + 18δ(OCO)$_{II}$
r(OCO)$_I$	?	338	52r(OCO)$_I$ + 50r(OCO)$_{II}$

	$DC_2O_4^-$		
Attribution	ν_{exp}	ν_{calcd}	Distribution d'énergie potentielle $100L_{ik}^2F_{ii}/\lambda_k$
ν(OD)	?	2621	100 ν(OD)
ν(C═O)	1720	1743	64ν(C═O) + 14r(OCO)$_{II}$ + 12ν(C—O) + 10r(OCO)$_I$ + 10ν_s(COO)$_I$
ν_a(COO)$_I$	1640	1634	102ν_a(COO)$_I$ + 10ν(C═O)
ν_s(COO)$_I$	1400?	1391	55ν_s(COO)$_I$ + 47ν(CC) + 23δ(OCO)$_I$ + 10δ(OCO)$_{II}$
ν(C—O)	1270	1304	36δ(OCO)$_I$ + 25ν_s(COO)$_I$ + 21ν(C—O)
δ(OD)	?	1108	56δ(OD) + 20ν(C═O) + 13ν(C—O)
ν(C—C)	853	879	41δ(OCO)$_I$ + 21ν_s(COO)$_I$ + 16ν(C—O)
δ(OCO)$_{II}$	685	673	23r(OCO)$_I$ + 20δ(OCO)$_{II}$ + 16δ(OD) + 13r(OCO)$_{II}$ + 10δ(OCO)$_I$
r(OCO)$_{II}$	?	585	46ν(C—O) + 16δ(OD) + 15r(OCO)$_I$ + 14r(OCO)$_{II}$ + 12δ(OCO)$_{II}$
δ(OCO)$_I$	450	482	32ν(C—O) + 27δ(OCO)$_I$ + 19δ(OCO)$_{II}$
r(OCO)$_I$	?	332	51r(OCO)$_I$ + 50r(OCO)$_{II}$

qui entraîne une contraction de la liaison C—C. La participation de ν(CC) explique la polarisation de la bande.

Conclusion

L'étude de la structure de l'ion $HC_2O_4^-$ en solution aqueuse par spectrométrie moléculaire, nous permet de mettre en évidence l'existence d'un équilibre d'association entre deux formes au moins; l'une d'entre elles, prépondérante à température élevée, est probablement de type monomère.

Le calcul de vibration, effectué en transférant les constantes de forces déjà connues pour les molécules voisines, confirme nos attributions. En effet les valeurs calculées sont en assez bon accord avec les résultats expérimentaux et reproduisent bien les variations spectroscopiques observées quand on passe de $HC_2O_4^-$ à $DC_2O_4^-$.

1. R. TELLGREN et I. OLOVSSON. J. Chem. Phys. **54**, 127 (1971).
2. J. DE VILLEPIN et A. NOVAK. Spectrochim. Acta, **27A**, 1259 (1971).
3. J. DE VILLEPIN et A. NOVAK. Spectrosc. Lett. **1**, 391 (1971).
4. J. DE VILLEPIN et A. NOVAK. J. Mol. Struct. 225 (1976).
5. M. JABER. Thèse, Lyon. no 475. 1975.
6. E. J. AMBROSE, A. ELLIOT et R. B. TEMPLE. Proc. R. Soc. A, **206**, 192 (1951).
7. D. HADZI et N. SHEPPARD. Proc. R. Soc. (London), **216**, 247 (1953).
8. A. B. F. DUNCAN et F. A. MATSEN. Chemical application of spectroscopy. *Edité par* W. West. Interscience Publishers, New York. 1956. p. 497.
9. J. LECOMTE. Handbuch der physik band XXVI. Gottingen. 1958. pp. 527–531.
10. S. K. FREEMAN. Applications of laser Raman spectroscopy. *Edité par* John Wiley and Sons, New York. 1974. p. 99.
11. M. DAVIES et G. SUTHERLAND. J. Chem. Phys. **6**, 755 (1938).
12. J. LASCOMBE, M. HAURIE et M. JOSIEN. J. Chem. Phys. **59**, 1233 (1962).
13. J. DE VILLEPIN, M. SAUMAGNE et M. JOSIEN. C.R. Acad. Sci. Paris, **259**, 365 (1964).
14. J. DE VILLEPIN, A. LAUTIE et M. JOSIEN. Ann. Chim. Fr. 365 (1966).
15. E. WILSON, J. DECIUS et P. CROSS. Molecular vibrations. McGraw-Hill, London. 1955.
16. C. DESTRADE, C. GARRIGOU-LAGRANGE et M. T. FOREL. J. Mol. Struct. **10**, 203 (1971).
17. P. CAILLET et M. T. FOREL. Ann. Chim. Fr. **10**, 311 (1975).
18. H. MURATA et K. KAWAI. J. Chem. Phys. **25**, 589 (1956).
19. H. MURATA et K. KAWAI. J. Chem. Phys. **25**, 796 (1956).
20. L. BARDET et G. FLEURY. C.R. Acad. Sci. Paris, **265**, 983 (1967).

Stereoselective interaction of a tridentate Schiff base complex of nickel(II) and amino acids

B. ERNO AND R. B. JORDAN

Department of Chemistry, University of Alberta, Edmonton, Alta., Canada T6G 2G2

Received September 12, 1978

B. ERNO and R. B. JORDAN. Can. J. Chem. **57**, 883 (1979).

It has been observed that a tridentate Schiff base complex of nickel(II), triaquotribenzo-[*b*,*f*,*j*][1.5.9]-triazacyclodecinenickel(II), commonly called (TRI)Ni$(OH_2)_3^{2+}$, shows substantial stereoselectivity on complexing with several amino acids. This provides a convenient way to resolve (TRI)Ni$(OH_2)_3^{2+}$ using histidine as a resolving agent, and either ion exchange or perchlorate salt crystallization techniques.

The resolved (TRI)Ni$(OH_2)_3^{2+}$ may then be used to resolve other amino acids or as a sensitive test of the stereochemistry of an amino acid. The test can be done on milligram quantities because of the insolubility of the complex perchlorate salt and because of the relatively large molecular rotation (2×10^5 deg at 283 nm) of (TRI)Ni$(OH_2)_3^{2+}$. The amino acid is easily released by treatment of the complex with dilute acid (pH $\approx$ 2). The procedure has been tested with histidine, tyrosine, methionine, and phenylglycine.

B. ERNO et R. B. JORDAN. Can. J. Chem. **57**, 883 (1979).

On a noté qu'un complexe entre du nickel(II) et une base de Schiff tridentate, triaquotribenzo[*b*,*f*,*j*][1.5.9]-triazacyclodécine nickel(II) généralement connue sous le nom de(TRI)Ni-$(OH_2)_3^{2+}$, présente une stéréosélectivité importante lors de sa complexation avec plusieurs acides aminés. Cette réaction fournit une méthode utile pour résoudre le (TRI)Ni$(OH_2)_3^{2+}$ faisant appel à l'histidine comme agent de résolution et des techniques d'échange d'ions ou de cristallisation du sel de perchlorate.

Le (TRI)Ni$(OH_2)_3^{2+}$ résolu peut alors être utilisé soit pour résoudre d'autres acides aminés soit comme une sonde sensible à la stéréochimie d'un acide aminé. Les essais peuvent être effectués sur des quantités de l'ordre du milligramme à cause de la faible solubilité du perchlorate du complexe et à cause de la rotation moléculaire relativement élevée (2×10^5 deg à 283 nm) du (TRI)Ni$(OH_2)_3^{2+}$. On peut regénérer facilement l'acide aminé en traitant le complexe avec de l'acide dilué (pH 2). On a évalué la méthode avec l'histidine, la tyrosine, la méthionine et la phénylglycine.

[Traduit par le journal]

Introduction

The observation of a stereoselective interaction of one optical isomer of a ligand by a metal ion generally requires the presence of a second ligand of specific stereochemistry on the metal ion. This second ligand should be stable, both stereochemically, and with respect to displacement from the metal ion. This ligand should also have sufficient steric bulk so that there is some interaction between the two ligands when complexed to the metal ion.

The tridentate Schiff base complex of nickel(II), triaquotribenzo[*b*,*f*,*j*][1.5.9]-triazacyclodecinenickel-(II), commonly, and hereinafter, referred to as (TRI)Ni$(OH_2)_3^{2+}$ (Fig. 1), seems to satisfy these requirements. The complex has been resolved (1) and is stable in aqueous solution at pH < 7. Observations are reported here on the interaction of this complex with histidine and several other amino acids.

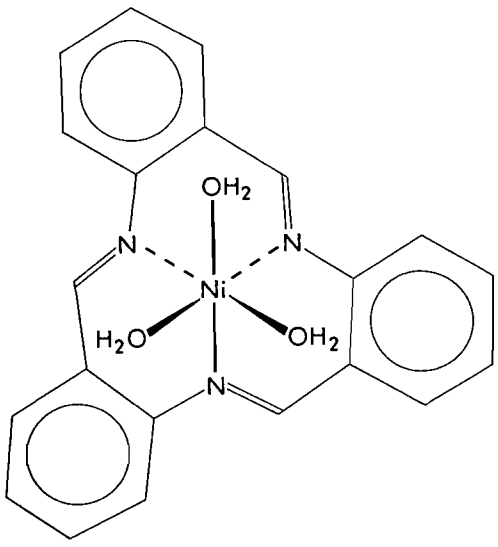

FIG. 1. Structure of (TRI)Ni$(OH_2)_3^{2+}$.

Experimental

Materials

The complex (TRI)Ni$(OH_2)_3(NO_3)_2$ was prepared by the method suggested by Taylor *et al.* (2). The method of Smith and Opie (3) was used to prepare *ortho*-aminobenzaldehyde, and this product was allowed to trimerize in dilute HCl as described by McGeachin (4). The trimer (1 g) was heated with an equimolar amount of Ni$(OH_2)_6(NO_3)_2$ in 40 mL of ethanol

0008-4042/79/080883-03$01.00/0

for 1 h. The initially green solution turned yellow-orange, and on cooling in ice yielded (TRI)Ni$(OH_2)_3(NO_3)_2$ (1.5 g).

The perchlorate salt was prepared by adding 10 mL of 3 *M* $NaClO_4$ to 1.5 g of the nitrate salt in 100 mL of warm (~50°C) water. The perchlorate salt was recrystallized twice from aqueous sodium perchlorate and dried under vacuum over calcium sulfate. *Anal.* calcd. for (TRI)Ni$(OH_2)_3(ClO_4)_2$: C 40.62, H 3.41, N 6.78; found: C 40.75, H 2.79, N 6.85. The electronic spectrum of the complex showed maxima at 315 nm and 275 nm, with molar absorbtivity coefficients of 1.18×10^4 dm^3 mol^{-1} cm^{-1} and 4.10×10^4 dm^3 mol^{-1} cm^{-1}, respectively, in agreement with previous results (1).

The histidine complex of $(TRI)Ni^{2+}$ was prepared as described in the Results section and characterized by the fact it could be converted to (TRI)Ni$(OH_2)_3^{2+}$ with aqueous acid, and by analysis. *Anal.* calcd. for (TRI)Ni(histidine)$(OH_2)(ClO_4)$: C 50.7, H 3.94, N 13.1; found: C 50.7, H 3.98, N 12.5.

The L-(+)-histidine (Nutritional Biochemicals) was recrystallized twice from 50% aqueous ethanol and dried over calcium sulfate. *Anal.* calcd. for $C_6H_9N_3O_2$: C 46.5, H 5.81, N 27.1; found: C 46.9, H 5.83, N 27.5. D-(−)-Histidine and D(−)-*d*-aminophenylacetic acid (D-(−)-*C*-phenylglycine) (Sigma Chemical Co.) were used as supplied, as were L-(−)-tyrosine (Eastman Organic Chemicals) and L-(+)-methionine (Aldrich Chemical Co.).

Instrumentation

Electronic spectra were recorded on a Cary 14 spectrophotometer. A Jasco Model ORD/UC-5 was used to measure ORD spectra, while routine optical rotations in the visible region were measured on a Perkin-Elmer 241 polarimeter.

Solvent proton transverse relaxation times were measured on a Bruker SXP 4-100 spectrometer at 61 MHz. The standard 180°–τ–90° pulse sequence was used and the temperature was controlled at 25 ± 0.5°C with a standard Bruker temperature controller.

Results and Discussion

Preliminary examination of models indicated that there might be a steric interaction between histidine and the phenyl rings of (TRI) in a (TRI)Ni(histidine)$^+$ complex. As a resolving agent histidine also has the attraction of a cheap, widely available optical isomer. Subsequent studies have shown that (TRI)Ni$(OH_2)_3^{2+}$ can be resolved with L-(+)-histidine by either an ion exchange or a fractional crystallization method. The details are described below, but it is useful to bear in mind that the (TRI)Ni(histidine)$^+$ complex is rapidly dissociated in acidic solution (pH $\lesssim$ 2) to (TRI)Ni$(OH_2)_3^{2+}$, and that the perchlorate salt of the latter cation is almost quantitatively insoluble in solutions containing 3–4 *M* perchlorate ion.

In the ion exchange method a column (2 cm × 20 cm) of weak acid cation resin (Baker CGC-271) in the sodium ion form was charged with 50 mL of a solution containing 0.062 g (0.1 mmol) of (TRI)Ni$(OH_2)_3(ClO_4)_2$, and 0.077 g (0.5 mmol) of L-(+)-histidine free base in 0.04 *M* sodium acetate at pH 6. The column was eluted with increasing concentrations of sodium acetate (pH 6) always containing 10^{-2} *M* L-(+)-histidine. The complex moved down the column with 0.08 *M* sodium acetate, and was collected in six, 20 mL fractions. Each fraction was acidified (pH 1–2) with 6 *M* perchloric acid to convert the (TRI)Ni–histidine complex (yellow-orange) to (TRI)Ni$(OH_2)_3^{2+}$ (yellow). The ORD spectra of the acidic solutions showed that the first two fractions contained $(+)_{546}$(TRI)Ni$(OH_2)_3^{2+}$ and the last two contained $(-)_{546}$(TRI)Ni$(OH_2)_3^{2+}$. The product was recovered by adding 4 *M* sodium perchlorate to the acidic solutions to precipitate 12 mg of the $(+)_{546}$ isomer from the first two fractions and 9 mg of $(-)_{546}$ isomer from the last two fractions. The ORD spectrum of the $(+)_{546}$ isomer was essentially the same as that reported by Taylor and Busch. The maximum and minimum in the ORD spectrum of the $(+)_{546}$ isomer occurred at 254 nm and 283 nm, with molecular rotations of $+7.0 \times 10^4$ deg and -1.9×10^5 deg, respectively. The $(-)_{546}$ isomer gave corresponding molecular rotations of -6.8×10^4 deg and $+2.1 \times 10^5$ deg.

The precipitation method is shown in the following reaction scheme

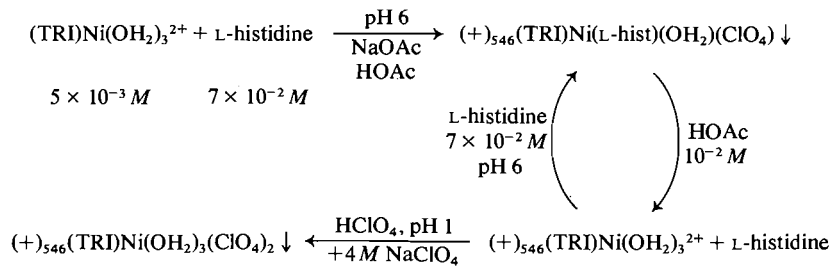

The precipitate of (TRI)Ni(L-hist)$(OH_2)(ClO_4)$ was redissolved in 10^{-2} *M* HOAc (100 mL per mmol) and reprecipitated with an equal volume of L-(+)-histidine. A total of three precipitations was sufficient to produce no further change in optical activity of the product. The $(+)_{546}$(TRI)Ni$(OH_2)_3^{2+}$ product gave molecular rotations of $+6.5 \times 10^4$ deg and -2.0×10^5 deg at 254 nm and 283 nm, respectively, in good agreement with results from the ion exchange method. The $(-)_{546}$ isomer may be re-

covered by adding D-histidine to the filtrate from the first step with L-histidine.

Clearly the success of the precipitation method depends on the low solubility of the perchlorate salt of the (TRI)Ni^{2+}–histidine complex. The tetrafluoroborate salt is similarly insoluble, but the nitrate and chloride salts are too soluble to be used efficiently in the precipitation method.

On the other hand, the success of the ion exchange method implies that complex formation is stereoselective. An attempt has been made to measure the formation constants of the histidine complexes. Because (TRI)$Ni(OH_2)_3^{2+}$ is not stable in alkaline solution, the usual potentiometric titration method could not be used. A spectrophotometric method was investigated but the $\sim 10\%$ decrease in absorbance at 275 nm on complexing was too small to yield accurate measurements.

It was found that measurements of the solvent proton longitudinal relaxation rates (T_1^{-1}) as a function of ligand concentration could be used to calculate the formation constants. This method relies on the fact that histidine replaces rapidly exchanging water molecules (5) from (TRI)$Ni(OH_2)_3^{2+}$, and as these are replaced the effect of the paramagnetic complex on the solvent proton T_1^{-1} decreases proportionately. For example, at pH 6.2 and 25°C, the value of $(T_1^{-1})/[(TRI)Ni]_{total}$ decreases from ~ 550 s^{-1} M^{-1} to ~ 130 s^{-1} M^{-1} as the [histidine]/[(TRI)Ni] ratio increases from 0 to 2. The data analysis is directly analogous to that used in a spectrophotometric method. The results for the titration of racemic (TRI)$Ni(OH_2)_3^{2+}$ and L-(+)-histidine gave the logarithm of the formation constant as 7.26 ± 0.1, while $(-)_{546}$(TRI)$Ni(OH_2)_3^{2+}$ and D-(−)-histidine gave 7.42 ± 0.1. The differences are too small relative to the experimental uncertainty to show any definite difference in formation constants.

Since the stereoselectivity observed with histidine did not seem to be due to any dramatic formation constant differences it seemed possible that other amino acids might also demonstrate this effect. If this is the case (TRI)$Ni(OH_2)_3^{2+}$ could be a useful resolving agent for amino acids, or, because of its high molecular rotation, could be used to test for the presence of a particular stereoisomer. In fact stereoselectivity was shown by the amino acids tested.

As a general procedure a solution of 5×10^{-3} M (TRI)$Ni(OH_2)_3(ClO_4)_2$ and 3×10^{-3} M amino acid in dilute acid (e.g., 10^{-2} M acetic acid) was treated with sodium carbonate to a final pH of 6.2–6.5. Precipitate formation begins after a few minutes of stirring or a few drops of 4 M $NaClO_4$ may be added until precipitation begins. After cooling in ice for 2 h the precipitate may be collected by filtration or centrifugation depending on the scale of the experiment. For ORD measurements a 4×10^{-5} M solution of the product in 10^{-2} M $HClO_4$ in a 1 cm cell gave an easily measured rotation of $3–5 \times 10^{-2}$ deg at 283 nm. In the cases tested L-(+)-histidine, L-(−)-tyrosine, L-(+)-methionine, and D-(−)-*C*-phenylglycine the $(+)_{546}$ isomer of (TRI)Ni^{2+} was precipitated preferentially.

In summary it appears that the (TRI)$Ni(OH_2)_3^{2+}$–amino acid system shows a degree of stereoselectivity which can be useful in studies involving optical isomers of amino acids.

Acknowledgement

The authors wish to acknowledge the financial support of this work by the National Research Council of Canada.

1. L. T. TAYLOR and D. H. BUSCH. J. Am. Chem. Soc. **89**, 5372 (1967).
2. L. T. TAYLOR, S. C. VERGEZ, and D. H. BUSCH. J. Am. Chem. Soc. **88**, 3170 (1966).
3. L. I. SMITH and J. W. OPIE. Org. Synth. **28**, 11 (1948).
4. S. G. MCGEACHIN. Can. J. Chem. **44**, 2324 (1966).
5. J. E. LETTER, JR. and R. B. JORDAN. J. Am. Chem. Soc. **93**, 864 (1971).

Etude structurale du monofluorophosphate de potassium K_2PO_3F

JEAN-LUC PAYEN, JEAN DURAND ET LOUIS COT

Laboratoire de Chimie Minérale Appliquée, Chimie des Matériaux, ERA 314, Ecole Nationale Supérieure de Chimie, 8 rue de l'Ecole Normale, 34075 Montpellier, France

ET

JEAN-LOUIS GALIGNE

Laboratoire de Minéralogie et Cristallographie, groupe de Dynamique des Phases Condensées, LA 233, Université des Sciences et Techniques du Languedoc, place Eugène Bataillon, 34060 Montpellier, France

Reçu le 10 août 1978

JEAN-LUC PAYEN, JEAN DURAND, LOUIS COT et JEAN-LOUIS GALIGNE. Can. J. Chem. **57**, 886 (1979).

Le K_2PO_3F est orthorhombique, groupe d'espace *Pnma*, avec $a = 7.554(4)$, $b = 5.954(5)$, $c = 10.171(6)$ Å et $Z = 4$. On a mesuré les données d'intensité à l'aide d'un diffractomètre automatique muni d'une source de radiations CuK_α. On a déterminé la structure cristalline par analogie avec celle du K_2SO_4 et on a mis en évidence une interaction "F---K" importante. La valeur finale de R est de 0.065 pour 353 réflexions observées.

JEAN-LUC PAYEN, JEAN DURAND, LOUIS COT, and JEAN-LOUIS GALIGNE. Can. J. Chem. **57**, 886 (1979).

K_2PO_3F is orthorhombic, space group *Pnma*, with $a = 7.554(4)$, $b = 5.954(5)$, $c = 10.171(6)$ Å, and $Z = 4$. Intensity data have been measured on an automatic diffractometer with CuK_α radiation. The crystal structure was determined by analogy with that of K_2SO_4 and shows an important interaction 'F---K'. The final R index is 0.065 for 353 observed reflections.

Ce travail s'inscrit dans le cadre de l'étude systématique des composés oxyfluorés du phosphore V (1–9). Les résultats obtenus ont permis de montrer l'isostructuralité de certains composés sulfites et monofluorophosphates (anions à symétrie $3m$) d'une part puis de certains composés sulfates et fluoroberylattes (anions à symétrie $43m$) d'autre part (6). Il n'y a isotypie entre sulfates et monofluorophosphates que lors d'intéractions fortes "cation---fluor". Il était intéressant de déterminer la structure de K_2PO_3F, isotype de K_2SO_4, pour vérifier cette remarque sur un nouvel exemple.

Par ailleurs, K_2PO_3F est utilisé industriellement dans le cadre de la passivation des surfaces métalliques après phosphatation et avant peinture (7).

La résolution de la structure de K_2PO_3F avait été réalisée en 1958 par Robinson (10) mais, par suite du clivage des monocristaux utilisés, les résultats obtenus sont trop peu précis pour être utilisables ($R = 0.185$).

Partie expérimentale

Par cristallisation à 30°C d'une solution saturée de K_2PO_3F, nous avons obtenu des monocristaux en forme de bâtonnets. Ils sont stables à la température du laboratoire. Les constantes cristallographiques et le groupe d'espace ont été déterminés par les méthodes du monocristal. Les paramètres ont été affinés à partir des diffractogrammes de poudre enregistrés avec une précision de $\pm 1/100$ de degré θ. La masse volumique observée ρ_m a été mesurée par pycnométrie dans le benzène à 20.0 ± 0.1°C.

	Robinson	Ce travail
Système de groupe d'espace	orthorhombique *Pnma* ou	*Pn2₁a*
a (Å)	7.543(4)	7.554(4)
b (Å)	5.943(5)	5.954(5)
c (Å)	10.16 (1)	10.171(6)
V (Å³)	455.45 (1)	457 (1)
ρ_m (g/cm³)	2.55 (2)	2.57 (1)
ρ_x (g/cm³)	2.576(5)	2.579(6)
Z	4	4

L'étude structurale a été réalisée à partir d'un monocristal en forme de bâtonnet de $0.42 \times 0.18 \times 0.18$ mm³. Les mesures d'intensité ont été effectuées sur diffractomètre automatique Enraf–Nonius type CAD 3 avec la radiation CuK_α monochromatisée. 435 réflexions ont été mesurées jusqu'à un angle de Bragg θ égal à 60°.

Les réflexions de référence 013 et $01\bar{3}$ étaient repérées à intervalle régulier de 50 réflexions.

Les intensités ont été corrigées des effets de Lorentz polarisation. Les corrections d'absorption ont été effectuées en assimilant le bâtonnet à un cylindre et en utilisant les programmes permettant de traiter les cristaux cylindriques. Les 353 réflexions indépendantes pour lesquelles $\sigma(I)/I$ est inférieur à 0.3 ont été conservées.

Affinement de la structure

La structure a été résolue par isotypie avec le sulfate de potassium K_2SO_4 β forme basse température.

En début d'affinement les positions des atomes K,

0008-4042/79/080886-04$01.00/0

TABLEAU 1. Paramètres de position et coefficient d'agitation thermique anisotrope ($10^4\beta_{ij}$)*

	x/a	y/b	z/c
K(1)	0.1735(3)	1/4	0.0755(2)
K(2)	0.0093(3)	1/4	0.7209(2)
P	0.2359(3)	1/4	0.4131(2)
O(1)	0.3158(10)	1/4	0.5459(8)
O(2)	0.2655(7)	0.0404(9)	0.3368(6)
F	0.0263(8)	1/4	0.4414(7)

	β_{11}	β_{22}	β_{33}	β_{12}	β_{13}	β_{23}
K(1)	44(4)	74(8)	64(3)	0	2(2)	0
K(2)	42(4)	150(8)	46(3)	0		0
P	19(4)	106(8)	43(3)	0		0
O(1)	98(14)	242(27)	60(8)	0		0
O(2)	143(11)	125(17)	86(6)	2(11)	13(7)	−42(8)
F	39(11)	383(31)	98(8)	0	15(7)	0

*Expression du facteur de température: $T = \exp\ [-(\beta_{11}h^2 + \beta_{22}k^2 + \beta_{33}l^2 + 2\beta_{12}hk + 2\beta_{13}hl + 2\beta_{23}kl)]$.

P, O et F sont respectivement celles des atomes K, S et O de la molécule K_2SO_4.

Le groupement PO_3F^{2-} est symétrique par rapport au miroir *m* du groupe d'espace *Pnma* situé à $y = 1/4$ ou $y = 3/4$. Afin de pouvoir identifier l'atome de fluor, nous avons assimilé celui-ci à un atome d'oxygène. Dans le calcul d'affinement avec agitation thermique isotrope, un des 2 atomes d'oxygène en position 4*c* (c'est-à-dire dans le miroir *m*), voit son agitation thermique prendre une valeur nettement inférieure à celle de l'autre: il s'agit de l'atome de fluor ($Z = 9$). De plus un calcul de distances montre que la distance de cet atome au phosphore auquel il est lié est nettement supérieure à celle des trois autres atomes à ce phosphore.

A ce niveau le facteur de reliabilité se stabilise à $R = 0.112$. L'affinement s'est poursuivi avec agitation thermique anisotrope; R converge alors vers la valeur de 0.065 pour les 353 réflexions utilisées.

Les facteurs de diffusion atomique utilisés sont ceux donnés par Doyle et Turner pour K^+, P, O et F (11).

En fin d'affinement les positions atomiques ainsi que les coefficients d'agitation thermique anisotrope sont rassemblés dans le tableau 1.[1]

Description de la structure

La fig. 1 représente la projection de la structure sur le plan $y0z$. Les atomes K(1), K(2), P, O(1) et F sont dans les miroirs *m* situés à $y = 1/4$ et $y = 3/4$. Cet arrangement peut être décrit à partir de tétraèdres PO_3F^{2-} isolés et de cations K^+. Le tableau 2 rassemble les distances et angles interatomiques dans le tétraèdre PO_3F^{2-}.

L'atome de potassium K(1)—possède un environnement constitué par 9 atomes d'oxygène et un atome de fluor (fig. 2*a*): d'une part, 4 atomes d'oxygène O(2) et 2 atomes O(1) situés à des côtes voisines de $x = 0.173$; d'autre part, 3 atomes d'oxygène d'un tétraèdre PO_3F situés aux côtes x voisines de -0.200; enfin, l'atome de fluor d'un tétraèdre PO_3F situé à $x = 0.526$.

L'environnement de l'atome K(2)—est assuré par (fig. 2*b*): 6 atomes d'oxygène disposés en antiprisme déformés. Ces antiprismes se développent selon l'axe $0x$ en mettant une face en commun; 1 atome de fluor situé dans le plan *m*, à une distance F---K de 2.845 Å.

Les atomes d'oxygène O(1) et O(2)—possèdent un environnement octaédrique déformé constitué par un atome de phosphore auquel ils sont liés et à 5 atomes de potassium. (Les distances sont rassemblées dans les tableaux 2 et 3.)

Le fluor est environné—par 4 atomes de potassium et l'atome de phosphore auquel il est lié, avec cependant des interactions nettement différentes (fig. 3). Cet environnement est du type bipyramide trigonale: K(1) à 2.671(7) Å: distance voisine de la somme des rayons ioniques $K^+ + F^- = 2.69$ Å; K(2) à 2.845(8) Å: interaction moyenne; 2K(2) à 3.415(4) Å: interaction très faible.

Discussion

Il apparait que ce type d'arrangement se déduit directement de la structure K_2SO_4 β (12).

[1]On peut obtenir la liste des facteurs de structure observés et calculés, à un prix nominal, en s'adressant au Dépôt de données non publiées, ICIST, Conseil national de recherches du Canada, Ottawa (Ont.), Canada K1A 0S2.

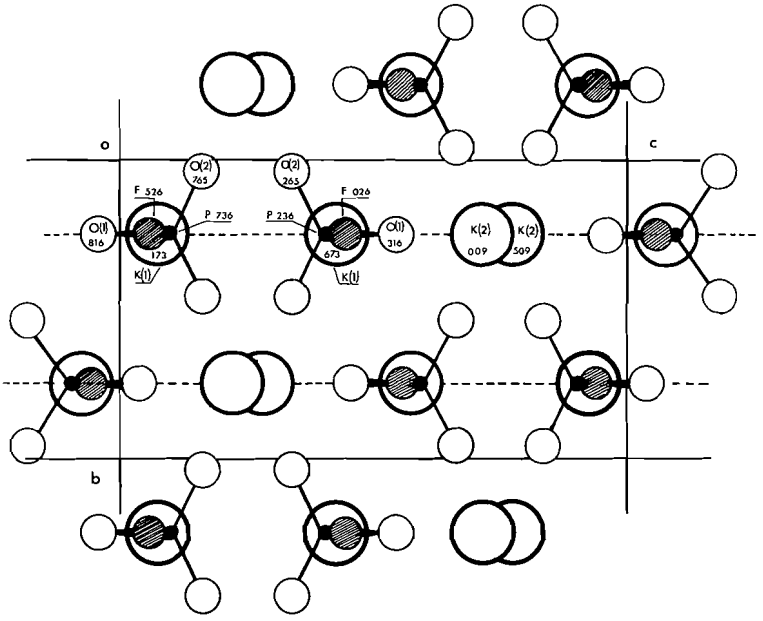

FIG. 1. Projection de la structure de K_2PO_3F sur le plan $y0z$.

TABLEAU 2. Distances et angles interatomiques*

P—O(1)	1.479(8)
P—O(2)	1.486(6)
P—O(2′)	1.486(6)
P—F	1.609(7)
O(1)—P—O(2)	114.5(3)
O(1)—P—O(2′)	114.5(3)
O(2)—P—O(2′)	114.2(5)
O(1)—P—F	103.8(4)
O(2)—P—F	104.0(3)
O(2′)—P—F	104.0(3)

* ′ désigne la position équivalente x; $1/2 - y$; z.

TABLEAU 3. Distances potassium–oxygene (ou fluor) pour les deux types d'environnement du potassium

	x/a	y/b	z/c	Distances
		Environnement K(1)		
K(1)	0.1735	1/4	0.0755	
O(1)	−0.1842	1/4	−0.0459	2.971(8)
O(1)	0.1842	−1/4	0.0459	2.993(2)
O(1)	0.1842	3/4	0.0459	2.993(2)
O(2)	0.2655	0.0404	0.3368	3.017(6)
O(2)	−0.2345	0.4596	0.1632	3.442(6)
O(2)	0.2345	−0.0404	−0.1632	3.016(6)
O(2)	0.2345	0.5404	−0.1632	3.016(6)
O(2)	0.2655	0.4596	0.3363	3.017(6)
O(2)	−0.2345	0.0404	0.1632	3.442(6)
F	0.5263	1/4	0.0586	2.671(7)
		Environnement K(2)		
K(2)	0.0093	1/4	0.7209	
O(1)	0.3158	1/4	0.5459	2.920(8)
O(1)	−0.1842	1/4	0.9541	2.786(8)
O(2)	−0.2655	0.5404	0.6632	2.765(6)
O(2)	0.2345	−0.0404	0.8368	2.697(6)
O(2)	−0.2655	−0.0404	0.6632	2.765(6)
O(2)	0.2345	0.5404	0.8368	2.697(6)
F	0.0263	1/4	0.4414	2.845(8)

En effet, les atomes K(2) ont des projections sur le plan $y0z$ différentes quoique plus proches que dans K_2SO_4 β. Leur environnement est identique.

De plus K(1), P et F ont également des projections très voisines. L'axe ternaire du groupement PO_3F situé dans le miroir m fait un angle voisin de 10° avec l'axe $0x$.

Du fait de la distance K(1)---F = 2.671(7) Å (légèrement inférieure à la somme des rayons ioniques K^+ et F^- égale à 2.69 Å) la structure de K_2PO_3F est un exemple où l'atome de fluor de PO_3F^{2-} subit, de la part du cation voisin, une interaction forte.

Cet exemple montre l'isostructuralité entre monofluorophosphate et sulfate correspondant. Cette isostructuralité se retrouve pour l'ensemble des sels simples alcalins anhydres ainsi que pour les sels de formule $NaM_3(PO_3F)_2$ de structure glasérite. On constate alors que l'interaction métal alcalin---fluor est forte:

$$r_{K^+} + r_{F^-} = 2.671 \text{ Å pour } K_2PO_3F$$

$$r_{K^+} + r_{F^-} = 2.584 \text{ Å pour } NaK_3(PO_3F)_2$$

Par contre, lorsque la distance M^+---F^- est

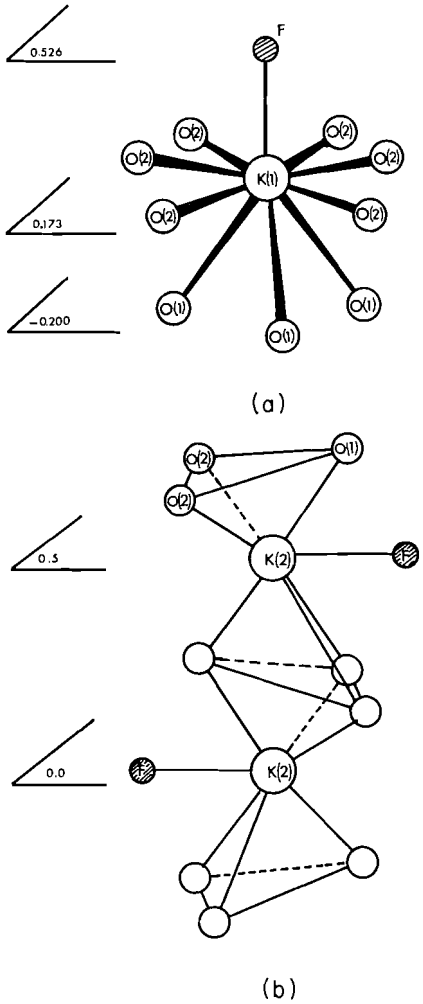

FIG. 2. (*a*) Environnement de l'atome de potassium K(1). (*b*) Environnement de l'atome de potassium K(2).

supérieure à la somme des rayons ioniques, cette intéraction est faible et les monofluorophosphates ne sont plus isostructuraux des sulfates correspondants. C'est en particulier le cas des sels doubles anhydres de la série lithium soit $LiMPO_3F$ (6). Dans ce dernier cas, les monofluorophosphates présentent des

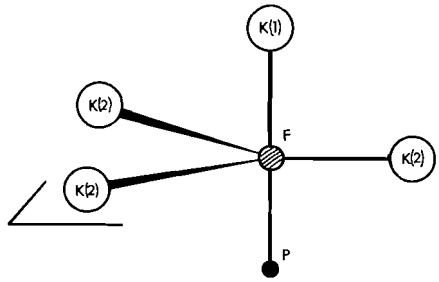

FIG. 3. Environnement de l'atome de fluor.

arrangements en couches tandis que les sulfates sont caractérisés par des structures en canaux.

La géométrie de l'anion PO_3F^{2-} (tableau 2) est de type C_{3v}; elle est comparable à celle trouvée dans la bibliographie (1–6 et 9), avec une distance P—F supérieure d'environ 0.1 Å par rapport à P—O. Il a été trouvé (13) un résultat identique pour l'anion SO_3F^-: S—O = 1.45 Å et S—F = 1.55 Å.

1. J. L. GALIGNE, J. DURAND et L. COT. Acta Crystallogr. B**30**, 697 (1974).
2. J. DURAND, J. L. GALIGNE et L. COT. Acta Crystallogr. B**30**, 1565 (1974).
3. J. DURAND, W. GRANIER, J. L. GALIGNE et L. COT. Acta Crystallogr. B**31**, 1533 (1976).
4. W. GRANIER, J. DURAND, J. L. GALIGNE et L. COT. Acta Crystallogr. B**31**, 2506 (1975).
5. J. DURAND, J. L. GALIGNE et L. COT. Acta Crystallogr. B**33**, 1414 (1977).
6. J. DURAND, J. L. GALIGNE et L. COT. Acta Crystallogr. B**34**, 388 (1977).
7. J. L. PAYEN, J. DURAND, W. GRANIER, B. PARANT et L. COT. Revue Imphos, 1977. Actes du 1° Congrès International des Composés Phosphorés. 17–21 octobre 1977. Rabat, Maroc.
8. J. DURAND, H. FALIUS, J. L. GALIGNE et L. COT. J. Solid State Chem. **24**, 345 (1978).
9. A. SERAFINI, J. F. LABARRE, W. GRANIER et L. COT. J. Chim. Phys. **73**, 13 (1976).
10. M. T. ROBINSON. J. Phys. Chem. **62**, 925 (1958).
11. P. A. DOYLE et P. S. TURNER. Acta Crystallogr. A**24**, 390 (1968).
12. M. GAULTIER et G. PANNETIER. Bull. Soc. Chim. Fr. **1**, 105 (1968).
13. K. O'SULLIVAN, R. C. THOMPSON et J. TROTTER. J. Chem. Soc. A**10**, 1814 (1970).

Chemistry of phenoxo complexes. VI. Reactions of phenoxocopper(I) complexes with carbon tetrachloride

JOHN F. HARROD AND PATRICK VAN GHELUWE
Chemistry Department, McGill University, Montreal, P.Q., Canada H3A 2K6

Received August 28, 1978

JOHN F. HARROD and PATRICK VAN GHELUWE. Can. J. Chem. **57**, 890 (1979).

The reactions of several substituted cuprous phenoxides with CCl_4 in acetonitrile were examined. Phenoxides without *ortho*-substituents usually gave high yields of tetraarylorthocarbonates. It is shown that the latter are also produced catalytically from sodium phenoxides and CCl_4 in the presence of small amounts of cuprous chloride. Cuprous phenoxides with *ortho*-chloro substituents, in the absence of facile hydrogen transfer agents, gave stable mixed oxidation state complexes of approximate composition: $Cu_2{}^{I}Cu^{II}Cl_2(OAr)_2$. In the presence of facile hydrogen atom transfer agents, such as free phenol or ascorbic acid, both the phenoxides without *ortho*-substituents and the *ortho*-chlorinated phenoxides gave moderate yields of triarylorthoformates. Some reactions of tritertbutylphenol and tritertbutylphenoxyl with copper complexes are described. The mechanisms of the various reactions are interpreted in terms of homo- and cross-coupling between phenoxyl and $\cdot CCl_3$ radicals.

JOHN F. HARROD et PATRICK VAN GHELUWE. Can. J. Chem. **57**, 890 (1979).

On a étudié les réactions de plusieurs phénolates cuivreux substitués avec le CCl_4 dans l'acétonitrile. Les phénolates qui ne portent pas de substituants en *ortho* conduisent généralement à de bons rendements d'orthocarbonates de tétraaryles. On a montré que l'on peut aussi obtenir ces derniers par une réaction catalytique des phénolates de sodium et du CCl_4 en présence de faibles quantités de chlorures cuivreux. Les phénolates cuivreux portant un chlore en *ortho*, en l'absence d'agents permettant des transferts faciles d'hydrogènes, conduisent à des complexes stables comportant des états d'oxydation mixtes et de composition approximative $Cu_2{}^{I}Cu^{II}Cl_2(OAr)_2$. En présence d'agents permettant des transferts faciles d'atomes d'hydrogène, tels du phénol libre ou de l'acide ascorbique, les phénolates sans substituants en *ortho* de même que les phénolates portant des chlores en *ortho* conduisent à des rendements moyens d'orthoformates de triaryles. On décrit quelques réactions du tri-*tert*-butylphenol et du radical tri-*tert*-butylphenoxyle avec des complexes de cuivre. On interprète les mécanismes des diverses réactions en termes de couplages homolytiques et croisés entre les radicaux phénoxyle et $\cdot CCl_3$.

[Traduit par le journal]

Introduction

An earlier paper (1) described a mechanistic study of reaction [1], first reported by Blanshard *et al.* (2).

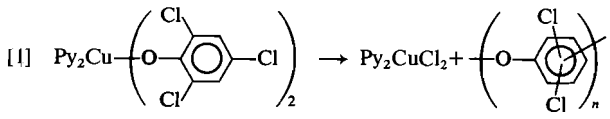

1 **2**

One conclusion of this study was that the initial step in reaction [1] is the homolytic ligand transfer from **1** to an initiator radical as depicted in [2] (1).

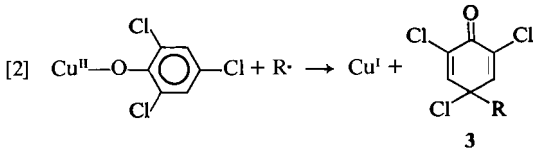

3

It was further suggested that one of the modes of participation of carbon tetrahalides in reaction [1] involved the formation and reaction of trihalomethyl radicals according to [2], to produce unstable trihalomethylcyclohexadienones, **3***a*, as intermediates (1).

Although a number of substituted trichloromethylcyclohexadienones have been synthesized, it is evident that their formation is favoured by alkyl substitution and strongly disfavoured by halogen substitution (3, 4). It is possible, however, that the latter empirical observation is the result of mechanistic rather than thermodynamic effects. To our knowledge there is a single reported example of a cyclohexadienone bearing both a chlorine and a trichloromethyl substituent on the same ring carbon.

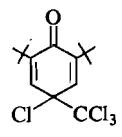

4

This compound, **4**, was prepared by Pirkle and Koser and although no specific reference to its ther-

0008-4042/79/080890-09$01.00/0

mal stability was made, it is certainly of relatively long-term stability under ambient conditions (5). Thus, the plausibility of **3***a* as an unstable intermediate in reaction [1], catalyzed by carbon tetrachloride, remained open to question.

In order to further test the plausibility of **3***a* as an intermediate it was decided to take advantage of the well known tendency of copper(I) complexes to undergo reaction with carbon tetrachloride according to reaction [3] (6, 7).

[3] $$Cu^{I} + CCl_4 \rightarrow Cu^{II}Cl + {}^{\bullet}CCl_3$$

By using a phenoxocopper(I) complex in reaction [3] the possibility existed that both phenoxocopper(II) species and trichloromethyl radicals could be generated simultaneously in high concentration, thereby fulfilling all of the requirements for testing reaction [2]. The results of such a study are reported in the present paper.

Results

The results of the reactions studied may be classified in terms of the principal products obtained. These products are (*i*) aryl orthocarbonates, (*ii*) aryl orthoformates, (*iii*) cyclohexadienone derivatives. Only in the case of cuprous tritertbutylphenoxide was the anticipated trichloromethylcyclohexadienone obtained as the major product.

All of the reactions described below were carried out in acetonitrile except where otherwise stated. Acetonitrile is particularly appropriate for the *in situ* preparation of cuprous phenoxides by reaction of cuprous chloride with the appropriate sodium phenoxide.

Orthocarbonate-forming Reactions

As previously reported (8), certain cuprous phenoxides undergo smooth reaction with CCl_4 under ambient conditions to produce the corresponding tetraarylorthocarbonate as the principal product. The most important criteria for success in this reaction are the requirements that there be no *ortho*-substituents on the phenoxo group and that the substituents not be exceptionally reactive towards radical attack.

The operation of the first criterion is illustrated by the high yields of orthocarbonate from reaction of 3-methyl and 4-methylphenoxocopper(I), but very low yields from 2-methylphenoxocopper(I).[1] A similar result was obtained with the monochlorophenoxo analogues.

The operation of the second criterion is illustrated by the failure of any methoxy-substituted phenoxide to yield orthocarbonate. This failure seemed to be due to the extreme ease of hydrogen atom abstraction from the methyl group. The mixtures of products obtained in such reactions were not characterised.

Reactions of *ortho*-methylated phenoxide gave products typical of phenoxyl radical coupling. The usual complex mixture, typical of oxidative coupling (9), was obtained from 2-methylphenoxocopper(I). The 2,6-dimethylphenoxo complex reacted rapidly and cleanly according to reaction [4]:

[4] 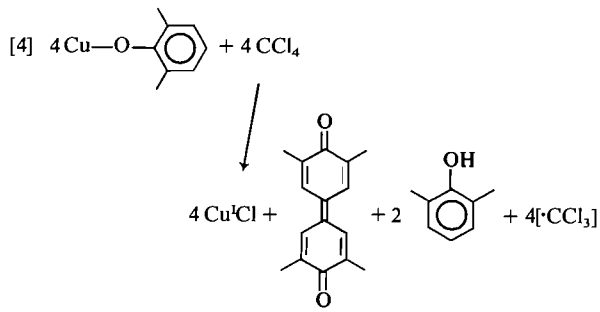

The precise fate of the $^{\bullet}CCl_3$ in reaction [4] was not determined. None of the reactions described herein was ever found to produce perchloroethane. A number of analyses by vpc all showed the presence of chloroform in solvent removed by distillation at the end of the reaction. It therefore seems reasonable to assume that $^{\bullet}CCl_3$ radicals are removed by hydrogen abstraction rather than coupling.

A reaction of dicopper(I) catecholate with CCl_4 produced the previously prepared bisphenylene orthocarbonate in good yield (10).

Since cuprous chloride is both a reactant and a product in the orthocarbonate forming reaction, it was anticipated that cuprous chloride would catalyse the reaction of a sodium phenoxide with CCl_4. A reaction in which an equimolar mixture of sodium 4-methylphenoxide and CCl_4 was reacted in the presence of 0.05 molar equivalents of cuprous chloride gave a high yield of orthocarbonate, thus confirming the expected catalysis.

Orthoformate-forming Reactions

The production of orthocarbonates described above only occurs in high yield under scrupulously anhydrous conditions. The use of undried acetonitrile as solvent led to the formation of triarylorthoformate as a major reaction product. Such reactions were also accompanied by precipitation of yellow cuprous oxide due to hydrolysis of the cuprous phenoxide.

An especially interesting case of orthoformate

[1]Although small amounts of orthoesters were detected in the reaction product by ir they were not successfully separated.

TABLE 1. Some properties of aryl ortho esters

Compound	Mass spectrum *m/e* (abundance)			^{1}H nmr ($CDCl_3$)[c]	Melting point (°C)
Phenyl[a]	291(4)	228(1)	214(62)	7.75(m)	95 (lit. 96–98)
	170(28)	154(2)	77(100)		
3-Methyl phenyl[a]	333(100)	256(2)	242(3)	7.5(m); 2.55(s)(4:3)	84–85
	198(6)	182(16)	91(70)		
4-Methylphenyl[a]	333(100)	256(1)	242(2)	7.2(s); 2.35(s)(4:3)	101
	198(4)	182(5)	91(23)		
4-Chlorophenyl[a]	393(28)	282(2)	238(3)	7.98(d); 7.80(d)(1:1)	129–130
	222(3)	111(100)			
1,2-Phenylene[a]	228(100)	120(34)	92(68)	7.2(s)	109 (lit. 109)
	64(60)				
4-Methylphenyl[b]	333(1)	242(3)	227(76)	7.1(s); 6.5(s); 2.4(s)(12:1:9)	104
	198(4)	107(100)	91(73)		
2-Chlorophenyl[b]	393(100)	282(4)	266(4)	7.75(m)[d]	177
	247(3)	222(2)	111(44)		
2,4,6-Trichlorophenyl[b]	439(9)	404(100)	196(36)	7.6(3); 7.2(s)(6:1)	165–167
	179(27)				
Pentachlorophenyl[b]	555(1)	539(1)	291(1)	7.3(s)	224–226
	263(1)	247(1)	78(100)		

[a]Orthocarbonate.
[b]Orthoformate.
[c]Chemical shifts in δ units (s = singlet, d = doublet, m = multiplet). The figures in parentheses are the ratios of protons in the order of cited chemical shifts.
[d]The methine proton was coincident with the aromatic multiplet in this compound and was not assigned.

production was observed with cuprous 2,4,6-trichlorophenoxide. Under conditions normally used for the formation of orthocarbonate, the latter compound reacts to give a stable product of approximate composition $[Cu_2{}^{I}Cu^{II}Cl_2(OAr)_2]$. This reaction always leads to the production of a small amount of tris(trichlorophenyl)orthoformate and, by implication, cuprous chloride, thus rendering exact analysis of the Cu^{I}/Cu^{II} complex impossible. Equivalent results were obtained using cuprous pentachlorophenoxide.

When the products of reactions of excess CCl_4 with either cuprous pentachloro- or trichlorophenoxide were treated with a facile hydrogen atom transfer agent such as ascorbic acid, or a reducing phenol such as 2,6-xylenol, the intense reddish-brown colour was rapidly bleached and workup of the reaction mixture gave the polyhalophenyl orthoformate in substantial yield (see Table 1). Reduction of the reddish-brown mixed oxidation state complex with stannous chloride also resulted in rapid bleaching, but no orthoformate could be detected in the product.

When the ascorbic acid reduction of the reddish-brown material was carried out in the presence of carbene scavengers such as cyclohexene or norbornene, no dichlorocarbene adducts were detected and the formation of orthoformate proceeded normally.

Reactions Involving Tritertbutylphenoxyl Species

The reaction of cuprous 2,4,6-tritertbutylphenoxide with CCl_4 was quite different from those of relatively unhindered phenoxides. The reaction shown in [5] occurred rapidly and cleanly:

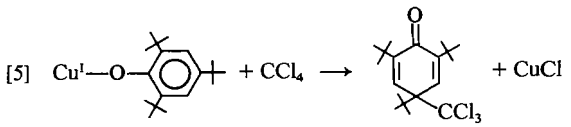

5

Since CuCl is generated in [5] and the cuprous phenoxide is easily formed from CuCl and sodium phenoxide, the cyclohexadienone can be synthesised in good yield from the reaction of CCl_4 and the sodium phenoxide in the presence of a catalytic amount of CuCl.

A reaction of equimolar amounts of 2,4,6-tritertbutylphenoxyl radical and cuprous trichlorophenoxide in the presence of CCl_4 also yielded **5** as the major product (ca. 50%). The remainder of the tertbutylphenoxyl radical was recovered as the peroxide, **6** (ca. 25%), and the quinol ether, **7** (ca. 25%). The product **6** resulted from oxygenation of unreacted radical during workup.

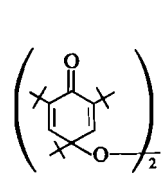

6

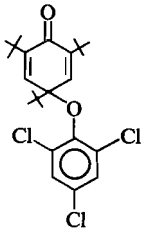

7

A similar reaction in which the tertbutylphenoxyl radical was replaced by 2,4,6-tritertbutylphenol resulted in a substantial increase in the yield of **7** at the expense of **5**.

No reaction occurred between tritertbutylphenoxyl and either bis(pyridine)bis(trichlorophenoxo)copper(II) or the mixed oxidation state product of the cuprous trichlorophenoxide/CCl_4 reaction.

Reaction [6] was found to proceed readily for X = Cl, but did not occur for X = CH_3COO, SCN, or OCH_3.

[6] $CuX_2 +$ 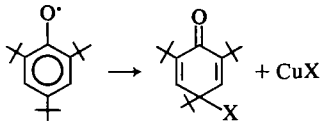 $+ CuX$

8

Discussion

Ortho Ester-forming Reactions

All of the experimental results described above can be accommodated by mechanisms involving free radicals. The production of ortho esters evidently occurs by an analogy of reaction [3] in which a copper(I)phenoxide generates a CCl_3 radical by chlorine atom abstraction from CCl_4 (see Scheme 1). If the phenoxide ligand is easily oxidised to the radical, such radical production should take place following oxidation of the Cu(I) by CCl_4. The simultaneously produced CCl_3 and phenoxyl radicals may undergo a number of different reactions, of which cross-coupling to produce an aryl trichloromethyl ether is presumably the precursor to ortho ester production. The fact that no mixed aryloxychloromethanes are observed in the ortho ester-producing reactions, even in the presence of a large excess of CCl_4, indicates that further substitutions into the trichloromethyl ethers are rapid compared to the initial substitution into CCl_4. The further substitutions could conceivably occur by simple nucleophilic attack by phenoxide (11) but the formation of orthoformates, as discussed below, is best explained on the assumption that they occur by a sequence of radical processes involving chlorine abstraction by copper(I).

In the case of phenoxyl radicals that are unencumbered in the *ortho* positions the cross-coupling reaction to give ortho esters seems to occur with high efficiency. Alkyl substitution in the *ortho*-positions seems to favour homo-coupling of phenoxyl radicals relative to the cross-coupling reaction. This is probably a result of the reduced effectiveness of the bulky CCl_3 radical when it is competing with phenoxyl radical for a ring carbon position rather than for an unencumbered oxygen. Only in the case of the tritertbutylphenoxyl radical, where phenoxyl radical homocoupling is precluded, is carbon–carbon cross-coupling to CCl_3 observed.

The extreme rapidity of reaction [4] (complete

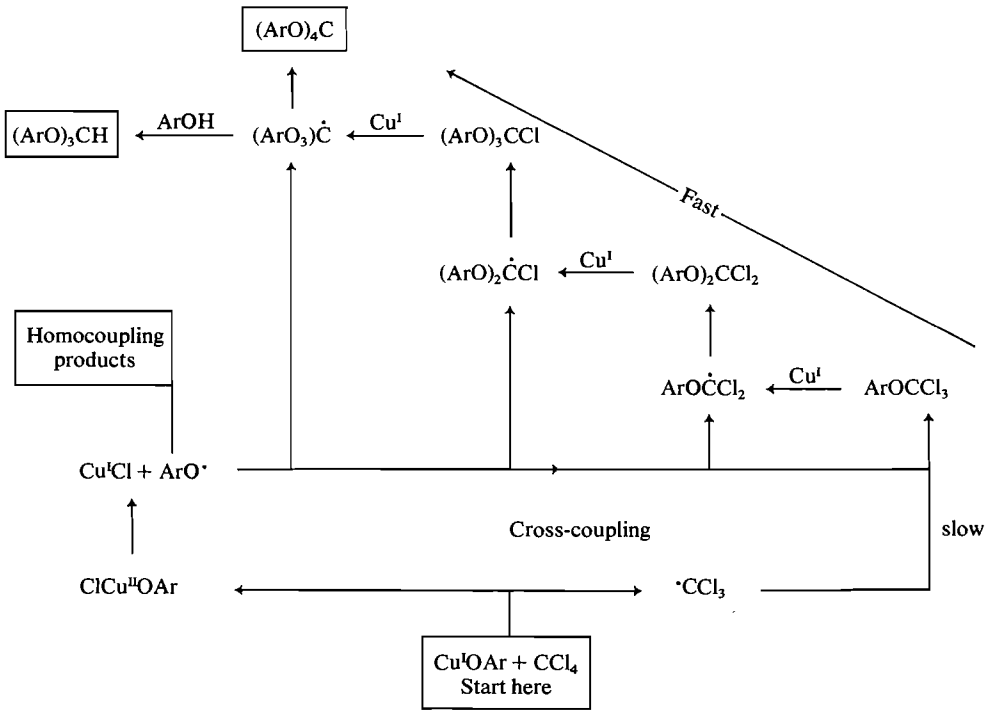

SCHEME 1. Production of ortho esters.

within a few minutes) suggests that phenoxyl radicals are generated in high concentration but that their rate of homo-coupling is much faster than either C—C, or C—O, coupling to trichloromethyl radicals. The stoichiometry of phenol production in the reaction also suggests that hydrogen abstraction from the primary coupling product, **9**, or its enol isomer, by phenoxyl radicals is fast compared to radical coupling, or to abstraction of hydrogen from solvent.

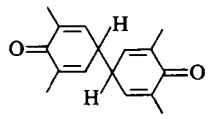

9

The formation of diphenoquinone rather than C—O coupled phenolic oligomers conforms to the generally accepted view that the diphenoquinone is the normal product of the coupling of 2,6-dimethylphenoxyl *free* radicals.

The observed formation of 2,4,6-trichlorophenyl orthoformate under certain reaction conditions proves that the steric impediment to cross-coupling at oxygen is not overly severe when both *ortho* positions are substituted with chlorine (in view of the similar steric size the same is surely true of methyl substituents). There is no doubt that the low stability of the homo-coupled phenoxyl dimers (either C—O or C—C) of the trichlorophenoxyl radical also directs the reaction towards orthoformate production. An examination of molecular models makes clear that orthocarbonate formation is sterically impossible in this case and it is expected that the triaryloxymethyl radicals will terminate by hydrogen atom abstraction. Even in the cases where there are no *ortho*-substituents the formation of orthoformate is observed when a facile hydrogen atom transfer agent, such as hydrolytically produced free phenol, is present. Since the mixed oxidation state products resulting from partial oxidation of cuprous penta- or trichlorophenoxides by CCl_4 are stable at room temperature, the generation of phenoxyl radicals in these systems most probably occurs via hydrogen atom abstraction from free phenol by other radicals in the system, and in particular by trichloromethyl radicals. Thus, in the absence of added hydrogen donor, a small amount of adventitious free phenol could yield phenoxyl radicals by hydrogen transfer to CCl_3 radicals generated by reaction [3].

The resulting phenoxyl radicals are then scavenged by cross-coupling with $CCl_3^{\cdot}$. The low yield of orthoformate results from the limited amount of $CCl_3^{\cdot}$ available and the inability of the phenoxide to recycle the Cu^{II} to Cu^{I} by reduction. These limiting factors are obviated by the addition of a protic reducing agent which can both recycle the Cu^{II} to Cu^{I} (thus ensuring a continuous supply of $CCl_3^{\cdot}$) and generate free phenol by protolysis of the phenoxide complexes (see Scheme 2).

The alternative possibility that orthoformate might be generated via insertion of dichlorocarbene into the O—H bond of free phenol is considered unlikely since no carbene derived products could be detected when the reactions were carried out in the presence of the carbene scavenger norbornene. It is not unlikely that dichlorocarbene might be extruded from an unstable trichloromethylcopper intermediate if it were formed. The present evidence provides little support for such a mechanism. The further possibility that orthoformate may arise from reaction of chloroform, resulting from hydrogen atom transfer to CCl_3 radicals, may be excluded on the grounds that chloroform was found to react only very slowly with cuprous phenoxides.

Reactions of Tritertbutylphenoxide and Tritertbutylphenol

All of the reactions of cuprous tritertbutylphenoxide and of tritertbutylphenol investigated in the present study gave products consistent with free radical mechanisms. The trichloromethylcyclohexadienone produced by reaction of cuprous tritertbutylphenoxide with CCl_4 is the expected product of cross-coupling between the phenoxyl radical and CCl_3 when steric hindrance precludes coupling at oxygen. The fact that only the 4-trichloromethyl derivative was isolated probably gives no clear indication of the stereoselectivity of the primary coupling process. The ^1H nmr spectrum of the crude reaction product indicated the presence of appreciable amounts of a 2-substituted cyclohexadienone. The failure to isolate such a compound may have been due to its spontaneous isomerisation to the more stable 4-isomer. The general failure to observe 2-substituted products from tritertbutylphenoxyl coupling reactions has previously been attributed to spontaneous isomerisation (12). The production of the quinol ether, **7**, in reactions of tritertbutylphenoxyl and tritertbutylphenol with cuprous trichlorophenoxide and CCl_4 is very likely due to protolysis of the cuprous trichlorophenoxide, followed by hydrogen abstraction from the free phenol to yield trichlorophenoxyl radicals. The reaction of tritertbutylphenoxyl with trichlorophenol is known to produce **7** in high yield (13). Since tritertbutylphenol introduces more protons into the system than the phenoxyl radical (where the protons come from hydroxylic impurities), it favours the formation of larger amounts of **7**.

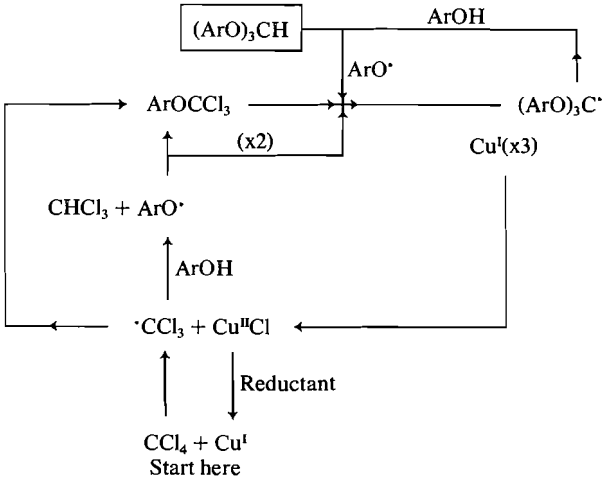

SCHEME 2. Production of orthoformates from trichlorophenoxide.

The ligand abstraction reaction shown in [6], where X = Cl, is quite typical of ligand transfer reactions from cupric compounds to organic radicals (14); it is, we believe, the first such example involving an aryloxy radical. As such it raises some interesting speculation regarding the mechanisms of phenol substitution reactions mediated by metal complexes. For example, the well-known chlorination of phenols by cupric chloride is most simply explained by assuming the generation of a phenoxyl radical, followed by chlorine atom abstraction from $CuCl_2$ (15). Chlorine attachment at an unsubstituted *ortho-* or *para*-carbon would be followed by rapid enolisation to the phenol. In our study of reaction [6] it was also observed that use of $CuCl_2 \cdot 4H_2O$, rather than anhydrous $CuCl_2$, did not result in any decrease in the yield of **8**. Such behaviour parallels that of the reactions of alkyl radicals with copper(II) compounds, where the rates of transfer of chlorine or bromine atoms are very fast compared to reactions of ligands bonding through oxygen. The much higher reactivity of phenoxyl radicals towards chlorine ligand, rather than water or hydroxyl, also explains the relatively clean generation of monochlorophenol product in the copper catalyzed oxychlorination reaction [7] (16).

[7] 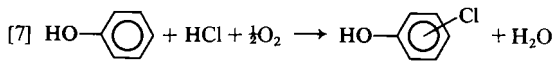

Given the fact that chlorination can occur by ligand transfer it is reasonable to ask whether there is any condition under which hydroxylation can occur by a similar process, particularly in view of the important role played by metalloenzymes in biological hydroxylation (17). In a number of preliminary experiments we were unable to effect reaction [6] where X = CH_3O, CH_3COO, or CNS. Although the compound **7** was isolated from reactions of tritertbutylphenoxyl and tritertbutylphenol with cuprous trichlorophenoxide, its formation was more likely due to the known reaction of tritertbutylphenoxyl with free trichlorophenol (13) than to ligand transfer. An unequivocal resolution of the latter uncertainty is very difficult since solutions of tritertbutylphenoxyl radical are difficult to free of hydroxylic impurities. Since the lowering of oxidation potential of the metal by ligation to oxygen, rather than chloride, impairs transfer of oxygen bonded ligands, the problem may be solved by design of a more suitable non-reacting ligand environment about the copper (e.g., more polarisable ligands such as those found in copper-containing oxidases (17)).

Experimental

Solvents were generally of reagent grade. Hydrocarbons were freshly distilled from sodium benzophenone dianion before use. Acetonitrile was distilled from calcium hydride and stored over molecular sieves. Ethanol was dried with sodium and distilled under dry nitrogen prior to use. Phenols were obtained as reagent grade materials and subject to either a single recrystallisation or distillation prior to use. Cuprous chloride was prepared according to a standard procedure (18) and stored under vacuum.

Preparation of Cuprous Phenoxides

A sample of the appropriate sodium phenoxide was prepared by dissolution of sodium (2.3 g) in dry ethanol (150 mL) under nitrogen. Following dissolution of the sodium the phenol was added in slight excess (1.05 equivalent) and solvent was removed by distillation until solid began to appear. The remaining solvent and excess phenol were removed by heating at 90°C and 0.001 Torr for 16 h. The resulting sodium phenoxide was ground to a fine powder under dry nitrogen and used immediately.

Sodium phenoxide (100 mmol) in deoxygenated, dry acetonitrile (200 mL) was stirred to achieve a fine suspension and then cuprous chloride (100 mmol) was added. After stirring for 1 h the white precipitate was sometimes filtered off under nitrogen and identified as sodium chloride (ca. 5.8 g), but normally the NaCl was not removed and further reactions were carried out directly on the solution of cuprous phenoxide.

Preparation of Orthocarbonates

A solution of cuprous phenoxide, prepared as above, was treated with CCl_4 (9 mL; 100 mmol). On contact with the solution the CCl_4 initially generated an intense blue colour which almost instantly turned dark brown. After stirring for 12 h the brown colour was usually either completely discharged or considerably faded. Sodium chloride was removed by filtration and the filtrate was evaporated to dryness on a rotary evaporator to yield a white, sticky solid. Extraction of the solid with CCl_4 yielded insoluble CuCl (~100 mmol). The remaining solution contained essentially pure orthocarbonate in the cases of phenyl, 4-methylphenyl, 3-methylphenyl, and 4-chlorophenyl (by ^1H nmr). Evaporation of CCl_4 and recrystallisation from absolute ethanol gave the pure orthocarbonates in ca. 50% yield. The product from the reaction of cuprous 2-chlorophenoxide contained a considerable amount of phenol and some ortho ester (by ir). Removal of the phenol by vacuum sublimation and recrystallisation of the residue from ethanol gave a small amount of tris(2-chlorophenyl)

orthoformate (14% based on reactant phenol). Although the product of the cuprous 2-methylphenoxide reaction contained some ortho ester (by ir), neither orthocarbonate nor orthoformate was successfully isolated from the mixture of products.

A reaction of dicopper(I) catecholate (50 mmol) with CCl_4 (200 mmol) gave a dark green/black suspension with considerable evolution of heat. After stirring for 12 h the mixture was added to an excess of water, extracted with CH_2Cl_2, dried and evaporated to a dark brown viscous oil. The oil was deposited on a Florisil column and eluted with CH_2Cl_2 to yield pure bisphenylene orthocarbonate (50% yield).

Some properties of the orthocarbonates are summarised in Table 1.

Catalytic Synthesis of 4-Methylphenyl Orthocarbonate

To a stirred suspension of sodium 4-methylphenoxide (100 mmol) in acetonitrile (200 mL) was added cuprous chloride (5 mmol) and CCl_4 (100 mmol). After stirring for 12 h at room temperature the product was worked up as in the stoichiometric reaction and the yield of orthocarbonate was essentially the same.

Synthesis of 4-Methylphenyl Orthocarbonate in Wet Acetonitrile

The stoichiometric synthesis of 4-methylphenyl orthocarbonate was carried out using exactly the procedure described above, except for the use of reagent grade acetonitrile containing 0.2 to 0.3% water. Removal of a small amount of free phenol from the crude organic product by vacuum sublimation left a mixture of orthocarbonate and orthoformate in the ratio of 10:1 (by ^1H nmr).

Reaction of Cuprous 2,6-Dimethylphenoxide with CCl_4

Cuprous chloride (9.9 g) was added to a stirred suspension of sodium 2,6-dimethylphenoxide (14.4 g) in acetonitrile (100 mL). After 1 h CCl_4 (10 mL) was added. The mixture immediately turned dark brown, but after a few minutes the dark brown colour had completely faded to be replaced by the dark orange suspension of 2,2′,6,6′-tetramethyldiphenoquinone. The latter was filtered and washed with water to remove sodium chloride (yield: 5.8 g). The filtrate was evaporated to dryness and the resulting sludge was slurried with CCl_4 (100 mL). The precipitated CuCl was filtered off and the solution was evaporated to a brown oil. Sublimation of the oil under vacuum yielded xylenol (4.5 g) and left a dark brown tar (1.0 g) which contained a small amount of diphenoquinone together with other unidentified products.

Reactions of Cuprous 2,4,6-Trichlorophenoxide and Pentachlorophenoxide

Reactions of the title compounds with CCl_4 under the conditions described for orthocarbonate synthesis led to dark red-brown solutions of more or less indefinite stability at room temperature. The colour changes were much slower for the pentachlorophenoxide than for other phenoxides. Evaporation of the acetonitrile on a rotary evaporator gave an amorphous dark brown solid whose infrared spectrum was identical to that of the uncomplexed copper(II) trichloro- or pentachlorophenoxide (19).

Extraction of the solid derived from the trichlorophenoxide with ether yielded trichlorophenyl orthoformate in ca. 10% yield. Extraction of the solid derived from the pentachlorophenoxide with toluene yielded pentachlorophenyl orthoformate in ca. 10% yield.

Reactions in the Presence of Hydrogen Transfer Agents

A reaction of cuprous 4-methylphenoxide was carried out under the same conditions as the orthocarbonate synthesis but in the presence of one equivalent of 4-methylphenol. The crude organic product yielded cresol (77% based on total 4-methylphenoxyl) on vacuum sublimation and a residue containing only orthocarbonate and orthoformate in 2:1 molar ratio (by ^1H nmr) (50% based on sodium phenoxide).

A similar reaction with cuprous trichlorophenoxide and free trichlorophenol, using the same workup as that used in the stoichiometric orthocarbonate synthesis, yielded a crude organic product from which free phenol was sublimed (75% based on total trichlorophenoxyl) to leave essentially pure trichlorophenyl orthoformate (45% based on sodium phenoxide).

A solution of cuprous trichlorophenoxide, prepared from the sodium phenoxide (1.0 g) and cuprous chloride (0.46 g) in acetonitrile was reacted with CCl_4 (3 mL). 2,6-Dimethylphenol (0.58 g) was added and the solution was stirred until the dark brown colour was discharged. The precipitate was recovered and washed with water to yield 2,2′,6,6′-tetramethyldiphenoquinone (0.3 g). Evaporation of the filtrate to dryness and extraction with CCl_4 gave a crude organic fraction (1.1 g) containing mainly trichlorophenyl orthoformate, trichlorophenol, and xylenol. Removal of the phenols by vacuum sublimation left a residue consisting almost entirely of orthoformate (0.49 g; 44% yield).

Repetition of the latter reaction, but using ascorbic acid (0.88 g) in place of xylenol, resulted in a similar bleaching of the dark brown solution. The initial precipitate contained sodium chloride and unreacted ascorbic acid (only slightly soluble in CH_3CN). The CCl_4 extraction left a residue of CuCl mixed with dehydroascorbic acid. The CCl_4 soluble material was a mixture of trichlorophenol and trichlorophenyl orthoformate (0.91 g total weight). Removal of the phenol and recrystallisation of the residue from ethanol yield the pure orthoformate (0.36 g; 40%).

Synthesis of 2,4,6-Tritertbutyl-4-trichloromethylcyclohexa-2,5-dienone

Sodium tritertbutylphenoxide (1.29 g) was suspended in acetonitrile under nitrogen. Cuprous chloride (0.45 g) was added and the mixture was stirred for 1 h before addition of CCl_4 (5 mL). The mixture turned slowly from yellow, to green, to blue, and was left at room temperature several hours. The product was evaporated to dryness and the resulting green mass was extracted with CCl_4. Slow evaporation of the CCl_4 solution yields the product **5** as a pale yellow crystalline powder (1.38 g; 80%; mp 71–72°C, lit. 68–71°C (20)). *Anal.* calcd. for $C_{19}H_{29}OCl_3$: C 60.1, H 7.64, Cl 28.04; found: C 59.16, H 8.05, Cl 26.93. ^1H nmr (CCl_4): $\delta = 1.9$ (S, 27H); $\delta = 7.35$ (S, 2H); ir: $\nu_{C=O} = 1660$ and 1640 cm^{-1} (KBr pellet).

A small amount of the peroxide **6** was isolated by concentration of the mother liquor. This product had properties identical to those previously reported (12).

A catalytic reaction was carried out using the sodium phenoxide (0.7 g; 2.5 mmol) and CuCl (0.025 g; 0.25 mmol) in acetonitrile (40 mL) and an excess of CCl_4. After stirring at room temperature for 5 h a conversion of phenoxide to **5** of 65% was estimated by ^1H nmr.

Reaction of the Cuprous Trichlorophenoxide/CCl_4 Reaction Product with 2,4,6-Tritertbutylphenoxyl

A solution of cuprous trichlorophenoxide was prepared by reaction of the sodium phenoxide (1.1 g) and cuprous chloride (0.5 g) in acetonitrile (15 mL). Following a standard procedure (21), the phenoxyl radical was prepared under N_2 by stirring tritertbutylphenyl (2.0 g) with MnO_2 (6 g) in benzene (100 mL). The radical solution was introduced into the cuprous phenoxide by filtration through a Schlenk filter under pressure of N_2. Carbon tetrachloride (3 mL) was injected and the mixture was stirred for 1 h. The product was evaporated to dry-

TABLE 2. Results of analyses of two complexes obtained from cuprous polyhalophenoxides*

	Cu(I)TCP/CCl_4	Cu(I)PCP/CCl_4
Approximate stoichiometry	[CuTCP][CuCl][CuClTCP]	[CuPCP][CuCl][CuClPCP]
Cu(I): calcd.	19.40	16.04
found	19.78	11.18
Cu(total): calcd.	29.11	24.05
found	26.68	23.83
Phenoxide: calcd.	60.04	66.99
found	59.6	68.5
Cl^-: calcd.	10.85	8.96
found	8.98	
C: calcd.	22.00	18.18
found	17.37	17.46
H: calcd.	0.61	0.00
found	1.01	0.55
Cl: calcd.	43.39	53.79
found	43.85	53.50

*TCP = trichlorophenoxide; PCP = pentachlorophenoxide.

ness and extracted with hexane. Slow evaporation of the hexane solution yielded the trichloromethylcyclohexadienone, **5** (1.5 g, 51% based on tritertbutylphenol). The residual mother liquor was shown by ^1H nmr to contain the peroxide **6** and the quinol ether **7** in roughly equal amounts. The compound **7** was crystallised by concentration of the mother liquor and its identity confirmed by comparison of its properties with those cited in the literature (22).

A similar reaction in which the tritertbutylphenol was used directly, without preoxidation to the radical, yielded a crude product which was shown by ^1H nmr to contain **5** and **7** in roughly equal proportions and only a small amount of **6**.

Reaction of 2,4,6-Tritertbutylphenoxyl with $CuCl_2$

The radical was prepared by oxidation of the phenol (2.62 g) with MnO_2 (12 g) in benzene (100 mL). The radical solution was filtered into a solution of anhydrous $CuCl_2$ (2.0 g) in acetonitrile (50 mL). The blue colour of the radical was discharged on contact with the $CuCl_2$ solution and on completion of the addition the solution was dark green/brown. Filtration, to remove precipitated CuCl, and evaporation yielded a sticky, black solid which was extracted with hexane. Evaporation of the hexane extract yielded an oil (2.2 g) which was shown by nmr to be a mixture of 4-chloro-2,4,6-tritertbutylcyclohexa-2,5-dienone, **8** (70%), and 4-hydroxy-2,4,6-tritertbutylcyclohexa-2,5-dienone, **10** (30%). The compound **8** was recovered by recrystallisation of the mixture from absolute ethanol (mp: 89–90°C, lit.: 94–96°C (23)), ir (thin film) 1665, 1645, 1370, 920 cm^{-1}; ^1H nmr (CCl_4): $\delta = 1.6$ (S, 9H); $\delta = 1.79$ (S, 18H); $\delta = 7.1$ (S, 2H).

Examination of a sample of the reagent radical solution showed it to be contaminated with **10** before reaction with the $CuCl_2$.

Treatment of a solution of **8** with CuCl in acetonitrile led to the rapid appearance of a dark blue colour, indicating the reversibility of reaction [6].

Similar reactions of the phenoxyl radical were carried out with bis(pyridine)bis(trichlorophenoxo)copper(II) and a number of other simple copper compounds. In each case the peroxide **6** was isolated in high (>75%) yield following aerobic workup of the reaction mixture. No ligand transfer products were identified.

Analysis of the Cuprous Polyhalophenoxides/CCl_4 Reaction Products

Samples of cuprous trichloro- or pentachlorophenoxide were prepared in acetonitrile as described above. Following removal of acetonitrile the orthoformate was removed from the product by washing with either ether (trichlorophenoxide) or toluene (pentachlorophenoxide). The resulting dark brown, amorphous powders were then dried under vacuum.

An accurately weighed sample was hydrolyzed in dilute nitric acid and carefully extracted with ether to remove phenol. The ether solution was evaporated and the phenol residue was weighed. The ionic chloride content of the aqueous hydrolysate was determined by both a gravimetric AgCl determination (23*a*) and by the Fajans method (23*b*).

The total copper and the relative amounts of Cu(I) and Cu(II) were determined using a procedure described by Kochi (24). Elemental analyses for C, H, and Cl were performed by Schwartzkopf Microanalytical Ltd. The results of these analyses are shown in Table 2.

Acknowledgements

Financial support for this work and a scholarship (P.v.G.) from the National Research Council of Canada are gratefully acknowledged.

1. B. G. CARR and J. F. HARROD. J. Am. Chem. Soc. **95**, 5707 (1973).
2. H. S. BLANSHARD, H. FINKBEINER, and G. RUSSELL. J. Polym. Sci. **58**, 469 (1962).
3. T. ZINCKE and R. SUHL. Chem. Ber. **39**, 4148 (1906).
4. M. S. NEWMAN and A. G. PINKUS. J. Org. Chem. **19**, 978 (1954).
5. W. H. PIRKLE and G. F. KOSER. J. Am. Chem. Soc. **90**, 3598 (1968).
6. M. ASSHER, A. OR, and D. VOFSI. J. Chem. Soc. Perkin, **2**, 1000 (1973).
7. J. K. KOCHI (*Editor*). Free radicals. Wiley Interscience. 1973. Chapt. 11.
8. T. H. CHAN, J. F. HARROD, and P. VAN GHELUWE. Tetrahedron Lett. **49**, 4409 (1974).
9. W. I. TAYLOR and A. R. BATTERSBY (*Editors*). Oxidative coupling of phenols. Marcel Decker, New York. 1967.
10. H. GROSS, A. RIEKE, and E. HOFT. Chem. Ber. **94**, 544 (1961).
11. T. TAKEKOSHI. J. Polym. Sci. **10**, 3509 (1972).
12. E. MULLER and K. LEY. Z. Naturforsch. **8**b, 694 (1953).

13. L. R. MAHONEY and M. A. DAROOGE. J. Am. Chem. Soc. **97**, 4722 (1975).
14. J. K. KOCHI. Science, **155**, 415 (1967).
15. E. M. KOSOWER, W. J. COLE, G. S. WU, D. E. CARDY, and G. MEISTER. J. Org. Chem. **28**, 630 (1963); E. M. KOSOWER and G. S. WU. J. Org. Chem. **28**, 633 (1963).
16. R. M. CRAWFORD. Chem. Eng. Prog. **46**, 483 (1950).
17. R. MALKIN. The copper containing oxidases. *In* Inorganic biochemistry. *Edited by* G. Eichorn. Elsevier, Amsterdam and New York. 1973. Chapt. 21.
18. W. C. FERNELIUS. Inorganic syntheses. Vol. II. New York and London. 1946. p. 1.
19. J. F. HARROD. Can. J. Chem. **47**, 637 (1969).
20. R. H. S. WANG. J. Org. Chem. **37**, 2776 (1972).
21. E. MULLER and K. LEY. Chem. Ber. **87**, 922 (1954).
22. H. D. BECKER. J. Org. Chem. **29**, 3068 (1964).
23. R. B. FISHER and D. G. PETERS. Quantitative chemical analysis. W. B. Saunders. 1969. (*a*) p. 153; (*b*) p. 257.
24. J. K. KOCHI. J. Am. Chem. Soc. **77**, 5274 (1955).

Sur quelques sulfites de cations monovalents; étude structurale de $LiCsSO_3 \cdot 2H_2O$

CHRISTIAN ARCHER, JEAN DURAND ET LOUIS COT

Laboratoire de Chimie Minérale, Chimie des Matériaux, E.R.A 314, Ecole Nationale Supérieure de Chimie, 8, rue de l'Ecole Normale, 34075 Montpellier, France

ET

JEAN LOUIS GALIGNE

Laboratoire de Minéralogie et Cristallographie, groupe de Dynamique des Phases Condensées, LA 233, Université des Sciences et Techniques du Languedoc, Place Eugène Bataillon, 34060 Montpellier, France

Reçu le 10 août 1978

CHRISTIAN ARCHER, JEAN DURAND, LOUIS COT et JEAN LOUIS GALIGNE. Can. J. Chem. **57**, 899 (1979).

L'étude cristallographique des sulfites de cations monovalents permet de mettre en évidence un plus grand nombre de composés isotypes des sels à anions C_{3v} (PO_3F^{2-}), que des sels à anions T_d (SO_4^{2-} ou BeF_4^{2-}): F de PO_3F^{2-} ou la paire libre de S^{IV} ne sont pas liés avec les atomes voisins.

$LiCsSO_3 \cdot 2H_2O$ cristallise dans le système monoclinique, $a = 11.927(7)$, $b = 5.670(3)$, $c = 4.828(2)$ Å, $\beta = 109.26(4)°$, $V = 308.2(9)$ Å^3, $\rho_o = 2.758(9)$ g/cm^3, $Z = 2$, $\rho_x = 2.771(6)$ g/cm^3 (20°C; MoKα, $d = 0.7107$ Å).

La structure est caractérisée par des chaînes de groupements de SO_3 et LiO_4 parallèles à l'axe *b*. Ces chaînes sont liées entre elles par un système de liaison hydrogène. L'anion SO_3^{2-} est pyramidal, le doublet libre de S^{4+} se localise sur l'axe ternaire. Les dimensions moyennes de l'ion sulfite sont: S—O = 1.526 Å et O—S—O = 105.4°. La valeur finale de *R* est 0.046.

CHRISTIAN ARCHER, JEAN DURAND, LOUIS COT, and JEAN LOUIS GALIGNE. Can. J. Chem. **57**, 899 (1979).

A crystallographic study of some monovalent cation sulfites allows us to propose a larger number of salt anions with C_{3v} symmetry (e.g., PO_3F^{2-}) than with T_d symmetry (SO_4^{2-} or BeF_4^{2-}). In PO_3F^{2-} the F atom and the lone pair of S^{IV} in SO_3^{2-} are not bonded to neighbouring atoms.

$LiCsSO_3 \cdot 2H_2O$ crystallises in the monoclinic system, $a = 11.927(7)$, $b = 5.670(3)$, $c = 4.828(2)$ Å, $\beta = 109.26(4)°$, $V = 308.2(9)$ Å^3, $\rho_o = 2.758(9)$ g/cm^3, $Z = 2$, $\rho_x = 2.771(6)$ g/cm^3 (20°C; MoKα, $d = 0.7107$ Å).

The structure is characterised by chains of SO_3 and LiO_4 groups parallel to the *b* axis. These chains are connected by a system of hydrogen bonds. The SO_3^{2-} anion is pyramidal with the sulphur lone pair on the ternary axis. The average dimensions of the sulfite ion are S—O = 1.526 Å and O—S—O = 105.4°. The final *R* value is 0.046.

[Journal translation]

Analogie avec les sels à anions tétraèdriques de symétrie T_d ou C_{3v}

Il existe une identité structurale très étroite entre $(NH_4)_2SO_3$, H_2O et $(NH_4)_2PO_3F \cdot H_2O$. Le doublet de S^{IV} de l'ion SO_3^{2-} occupe exactement la place de F^- de l'ion PO_3F^{2-} et a un volume sensiblement égal (1). L'atome de fluor excepté, tous les autres éléments occupent des positions identiques.

A côté de cet exemple particulièrement net où le doublet de S^{IV} a une activité stéréochimique analogue à celle de F^-, il était intéressant de préciser la cristallochimie des sulfites de cations monovalents, afin de définir leur isotypie avec les sels correspondants d'anions de symétrie C_{3v} (PO_3F^{2-}) ou T_d (SO_4^{2-} ou BeF_4^{2-}) et de mettre en évidence de nouveaux exemples où l'activité stéréochimique du S^{IV} soit comparable à celle de F^- ou de O^{2-}.

Nous avons pu préparer, puis identifier cristallographiquement plusieurs familles de sels simples et doubles, pour la plupart totalement inédits:

$M_2SO_3 \cdot xH_2O$ avec $x = 1$ si M = Li et NH_4
$x = 0$ si M = Li, Na, K, Rb, Cs

$LiMSO_3 \cdot xH_2O$ avec $x = 2$ si M = Rb ou Cs
$x = 1$ si M = K
$x = 0$ si M = K, Rb, Cs, NH_4

$NaM_3(SO_3)_2$ avec M = Rb et Tl

$Na_xK_{2-x}SO_3$ avec $0 \leq x \leq 2$

il s'agit d'une solution solide continue. Le principe de préparation des sulfites alcalins est le suivant (2). Pour les sels simples (*i*) formation du pyrosulfite $M_2S_2O_5$ par action du SO_2 sur la base correspon-

0008-4042/79/080899-05$01.00/0

TABLEAU 1. Constantes cristallographiques des sels simples $M_2^1SO_3 \cdot (x)H_2O$

	Système				
	Monoclinique (*C*2, *Cm* ou *C*2/*m*)	Hexagonal ($p\bar{3}$)		Orthorhombique (*Pnma*)	
Groupe d'espace	Li ($x = 1$)	Na ($x = 0$)	K ($x = 0$)	Rb ($x = 0$)	Cs ($x = 0$)
a (Å)	18.544(9)	5.467(5)	5.919(5)	7.430(6)	7.953(6)
b (Å)	4.804(5)			6.116(5)	6.287(5)
c (Å)	8.172(6)	6.176(6)	6.945(6)	10.550(9)	11.019(9)
β (deg)	97.86(5)				
V (Å^3)	721.1(6)	159.8(6)	210.7(6)	479.6(9)	551.0(9)
ρ_x(g/cm^3)	2.063(6)	2.619(6)	2.494(6)	3.477(6)	4.170(6)
ρ_m(g/cm^3)	2.054(9)	2.608(9)	2.495(9)	3.465(9)	4.158(9)
Z	8	2	2	4	4

TABLEAU 2. Constantes cristallographiques des sels doubles $LiMSO_3 \cdot (x)H_2O$

	Système				
	Monoclinique ($P2_1/c$)			Monoclinique (*Cm*)	
Groupe d'espace	LiK ($x = 1$)	LiK ($x = 0$)	$LiNH_4$ ($x = 0$)	LiRb ($x = 2$)	LiCs ($x = 2$)
a (Å)	5.251(5)	5.349(6)	5.414(6)	11.489(9)	11.927(7)
b (Å)	7.053(6)	4.861(5)	4.903(5)	5.589(6)	5.670(3)
c (Å)	12.490(10)	13.224(10)	14.089(9)	4.807(5)	4.828(2)
β (deg)	108.52(5)	91.56(5)	91.38(5)	108.45(5)	109.26(4)
V (Å^3)	438.7(9)	343.8(9)	373.9(9)	292.8(9)	308.2(9)
ρ_x(g/cm^3)	2.181(6)	2.435(6)	1.866(6)	2.364(6)	2.771(6)
ρ_m(g/cm^3)	2.175(9)	2.418(10)	1.847(9)		2.758(9)
Z	4	4	4	2	2

dante:

$$2MOH + 2SO_2 \rightarrow M_2S_2O_5 + H_2O$$

(*ii*) formation du sulfite M_2SO_3 par action de la base MOH sur le pyrosulfite:

$$M_2S_2O_5 + 2MOH \rightarrow 2M_2SO_3 + H_2O$$

Pour les sels doubles (*i*) action du SO_2 sur la base MOH:

$$2MOH + 2SO_2 \rightarrow M_2S_2O_5 + H_2O$$

(*ii*) action de la base MOH sur la pyrosulfite $M_2S_2O_5$:

$$M_2S_2O_5 + 2M'OH \rightarrow 2MM'SO_3 + H_2O$$

La solution est alors concentrée à chaud (60°C) puis portée à température inférieure à l'ambiante, entre 5 et 15°C. La cristallisation fait apparaître des monocristaux sous forme d'aiguille. Le contrôle de la pureté des produits se fait par dosage du groupement sulfite et caractérisation de l'ion SO_3^{2-} par spectroscopie d'absorption infrarouge.

Les déterminations cristallographiques (système cristallin et paramètres de maille) ont été conduites par les techniques du monocristal et sont rassemblées dans les tableaux 1–3. Certains composés n'ont pu être isolés sous forme de monocristaux. Il s'agit de $Li_2SO_3\beta$ (forme haute température), $LiRbSO_3$ et $LiCsSO_3$. Ils ont été caractérisés par leur diagramme de poudre.[1]

D'après la connaissance des paramètres cristallographiques, l'*isostructuralité des sulfites avec les sels d'anions tétraèdriques de symétrie T_d est très limitée*: seuls Rb_2SO_3 et Cs_2SO_3 d'une part, et $NaRb_3(SO_3)_2$ d'autre part sont respectivement de types structuraux $K_2SO_4\beta$ et glasérite (3): composé de formule $CaBa_3(SiO_4)_2$. Par contre l'*isostructuralité avec les composés à anion tétraèdrique de symétrie C_{3v} est plus riche*; ainsi nous avons respectivement les isostructuralités suivantes. Sels simples (*a*) Rb_2SO_3 et Cs_2SO_3 avec M_2PO_3F pour M = K, Rb, Cs; (*b*) $(NH_4)_2SO_3 \cdot H_2O$ et $(NH_4)_2PO_3F \cdot H_2O$ (1). Sels doubles: (*a*) $LiKSO_3 \cdot H_2O$ avec $LiKPO_3F \cdot H_2O$ (4); (*b*) $LiKSO_3\alpha$ et $LiNH_4SO_3$ avec $LiMPO_3F$ (5) pour

[1]On peut obtenir les listes des distances interreticulaires, les intensités relatives, les facteurs de température anisotrope ainsi que la liste des facteurs de structure observés et calculés, à un prix nominal, en s'adressant au Dépôt de données non publiées, ICIST, Conseil national de recherches du Canada, Ottawa (Ont.), Canada K1A 0S2.

TABLEAU 3. Constantes cristallographiques des sulfites doubles $NaM_3(SO_3)_2$

	Système	
	Hexagonal ($P\bar{3}ml$)	
Groupe d'espace	$NaRb_3(SO_3)_2$	$NaTl_3(SO_3)_2$ (7)
a (Å)	5.936(4)	5.74(1)
c (Å)	7.269(5)	7.18(1)
V (Å^3)	221.8(5)	204.8 (9)
ρ_x(g/cm^3)	3.119(10)	6.48(5)
ρ_m(g/cm^3)	3.106(12)	
Z	1	1

M = K, Rb, Cs et NH_4; (*c*) $NaRb_3(SO_3)_2$ et $NaTl_3(SO_3)_2$ avec $NaM_3(PO_3F)_2$ (6) pour M = K et Rb.

Enfin les sels $LiKSO_3\beta$ (forme haute température), $LiRbSO_3$ et $LiCsSO_3$ (isotypes entre eux) ne sont pas isotypes des composés à anions tétraèdriques de symétrie T_d (SO_4^{2-} et BeF_4^{2-}) et de symétrie C_{3v} (PO_3F^{2-}).

Les températures de deshydratation de $Li_2SO_3\cdot H_2O$, $LiKSO_3\cdot H_2O$, $LiRbSO_3\cdot 2H_2O$ et $LiCsSO_3\cdot 2H_2O$ sont respectivement de 78, 53, 5 et 55°C. L'oxydation des sulfites alcalins se produit vers 330, 435, 475, 720 et 740°C respectivement pour Li_2SO_3, Na_2SO_3, K_2SO_3, Rb_2SO_3 et Cs_2SO_3; puis vers 260, 290 et 330°C pour $LiKSO_3$, $LiRbSO_3$ et $LiCsSO_3$. Les sels d'ammonium, $(NH_4)_2SO_3\cdot H_2O$ et $LiNH_4SO_3$ se décomposent dès 30°C.

Le sulfite double $LiKSO_3$ obtenu par déshydratation de $LiKSO_3\cdot H_2O$ à 53°C est isotype des monofluorophosphates $LiMPO_3F$ anhydres; il possède une deuxième variété allotropique: dès 212°C, il passe à la forme $LiKSO_3\beta$ (appelée forme haute température) isotype des sels doubles anhydres $LiRbSO_3$ et $LiCsSO_3$.

En conclusion, les anions SO_3^{2-} et PO_3F^{2-}, à symétrie C_{3v} induisent autour de leur environnement une assymétrie de charge responsable d'une plus grande isostructuralité entre les sels de ces anions qu'entre les sels d'anions à symétrie T_d. En effet dans la grande majorité des structures réalisées sur les monofluorophosphates (1, 4–6) le F n'est pas lié avec ses voisins; il en est de même de la paire libre du S dans les composés sulfites isotypes correspondants.

Etude structurale de $LiCsSO_3\cdot 2H_2O$

Après avoir montré les isostructuralités entre certaines de ces phases et les monofluorophosphates correspondants, il était intéressant de connaître l'arrangement structural dans l'une de ces phases non isotypes; notre choix s'est porté sur $LiCsSO_3\cdot 2H_2O$ isostructural de $LiRbSO_3\cdot 2H_2O$.

L'étude sur monocristal en chambre de Weissenberg indique que $LiCsSO_3\ 2H_2O$ cristallise dans le système monoclinique groupe spatial $C2/m$, $C2$ ou Cm avec les paramètres indiqués dans le tableau 2.

Un test sur poudre montre que $LiCsSO_3\cdot 2H_2O$ a une réponse en optique non linéaire de l'ordre de 30 fois le quartz ce qui permet de ne retenir que les groupes non centro-symétriques, soit Cm ou $C2$.

Les mesures d'intensités ont été réalisées à température ambiante sur un monocristal de dimensions $0.34 \times 0.20 \times 0.15$ mm^3 à l'aide d'un diffractomètre Enraf-Nonius type CAD 3 utilisant la radiation MoKα monochromatisée. Un balayage $\theta/2\theta$ a été utilisé et 776 réflections ont été mesurées jusqu'à un angle de Bragg $\theta = 35°$. Nous avons éliminé toutes les réflections pour lesquelles $\sigma(I)/I$ était supérieure à 0.30. Les 729 réflections indépendantes restantes ont été corrigées des effets de Lorentz polarisation mais non d'absorption (μMoKα = 6.39 cm^{-1}).

Résolution de la structure

La structure a été résolue à partir d'une synthèse de Patterson tridimentionnelle qui a permis de localiser l'atome de césium en position particulière 2(*a*) pour le groupe d'espace *Cm*. Cette synthèse de Patterson n'est pas exploitable dans le groupe *C*2. Une synthèse de Fourier tridimentionnelle utilisant la contribution de cet atome de césium, dont les coordonnées ont été bloquées afin de fixer l'origine, a permis de localiser l'atome de S également en position particulière 2(*a*). Après affinement, une nouvelle synthèse de Fourier nous a permis de localiser les atomes d'oxygène des groupements SO_3 ainsi que ceux des deux molécules d'eau. L'affinement des coordonées de ces atomes ainsi que de leurs facteurs de température isotrope converge vers une valeur du coefficient de reliabilité:

$$R = \sum|F_o - |F_c||/\sum F_o = 0.108$$

A ce niveau une synthèse différence de Fourier permet de localiser l'atome de lithium en site tétraèdrique, mais non les atomes d'hydrogène des molécules d'eau. Les liaisons hydrogène possibles permettent de déterminer les positions des atomes d'hydrogène H_{11} et H_{12} de la molécule d'eau W(1), mais ceux de W(2) ne peuvent pas être positionnés. Le problème a été résolu par un calcul de minimisation de l'énergie électrostatique du réseau à l'aide d'un programme écrit par Tordjman.[2] Les positions déterminées alors ont été introduites pour un calcul

[2]G. Tordjman. Communication privée.

TABLEAU 4. Paramètres de positions atomiques (les écarts types mis entre parenthèses portent sur la dernière décimale)

	x/a	*y/b*	3/*c*
Li	0.174(3)	1/2	0.622(7)
Cs	0	0	0
S	0.2582(5)	0	0.719(1)
O(1)	0.3927(10)	0	0.833(3)
O(2)	0.2211(8)	0.215(1)	0.860(2)
W(1)	0.504(2)	0	0.426(3)
W(2)	0.271(2)	1/2	0.352(5)
H(11)	0.465	0	0.573
H(12)	0.465	0	0.215
H(20)	0.268	0.348	0.257

d'affinement et après trois cycles d'affinement avec agitation thermique anisotrope pour les atomes de Li, Cs, S et O et isotrope pour les atomes H, le coefficient de reliabilité non pondéré se stabilise à $R = 0.046$. Ce résultat confirme le choix du groupe *Cm* choisi pour la structure. Les facteurs de diffusion utilisés sont ceux donnés par Doyle et Turner (8) pour Li^+, Cs, S, O et ceux donnés par Stewart *et al.* (9) pour les atomes d'hydrogène. Le tableau 4 rassemble les positions atomiques finales.

Description de la structure

La fig. 1 donne la projection de la structure sur le plan *xOz*. L'arrangement structural peut être décrit à partir de chaines parallèles à l'axe *Oy*. Ces chaines sont formées de pyramides SO_3 et de tétraèdres LiO_4 ayant un sommet commun O(2). Li et S sont situés au niveaux $y = 0$ et $y = \frac{1}{2}$. Les différentes chaines SO_3—LiO_4 sont reliées entre elles par deux réseaux de liaison hydrogène, d'une part un réseau parallèle au plan *xOz* (niveau $y = 0$ ou $y = \frac{1}{2}$) à partir de W(1), d'autre part un second réseau perpendiculaire à ce plan à partir de la molécule W(2) (fig. 2).

La pyramide SO_3 a une symétrie proche de la symétrie C_{3v} (3*m*). Les valeurs des distances S—O dans l'ion sulfite (tableau 5), correspondent bien à la valeur théorique suggérée par Gillespie et Robinson (10): 1.54 Å. Ces distances sont en accord avec les valeurs trouvées pour plusieurs sulfites (11–19). Dans ce type de composés les oxygènes sont liés soit à des hydrogènes, soit à des métaux. Ces valeurs sont nettement plus élevées que celles rencontrées dans le cas où les atomes d'oxygène du motif SO_3^{2-} sont peu liés aux proches voisins (20, 21).

Le lithium est environné par quatre atomes d'oxygène, deux atomes d'oxygène O(2) de deux groupements SO_3 différents appartenant à une même chaine et deux atomes d'oxygène de deux molécules d'eau W(1) et W(2) situés au même niveau que l'atome de lithium soit $y = 0$ ou $y = \frac{1}{2}$, tableau 5.

Le césium se dispose dans des canaux perpendiculaires au plan *xOz*. Son environnement est contsitué par six proches voisins: deux oxygènes O(1) à $y = 0$ et 1 pour Cs($\frac{1}{2}$, $\frac{1}{2}$, 1); deux oxygènes O(2) à $y = 0.715$ et 0.285 pour Cs($\frac{1}{2}$, $\frac{1}{2}$, 1); deux oxygènes de W(1) à $y = 0$ et 1 et $z = 1.426$ pour Cs($\frac{1}{2}$, $\frac{1}{2}$, 1); et quatre autres voisins à des distances supérieures à 3.5 Å: 2W(1) ($y = 0$ et 1, et $z = 0.426$) et 2W(2) ($y = 0$ et 1, et $z = 1.352$) pour Cs($\frac{1}{2}$, $\frac{1}{2}$, 1).

Le doublet du S^{IV} est sur l'axe ternaire du groupement SO_3^{2-}. Cet axe fait un angle de 27° avec la direction S...Cs (fig. 3). La distance S...Cs de 3.80 Å est de 18% inférieure à la distance S—O...Cs linéaire de 4.64 Å rencontrée dans la bibliographie pour Cs_2SO_4 (20).

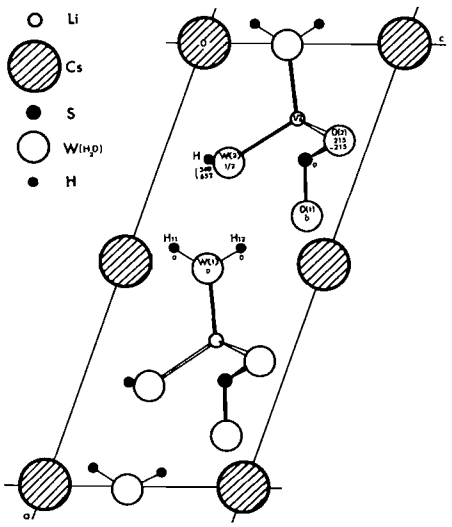

FIG. 1. Projection sur le plan *xOz* de la structure $LiCsSO_3 \cdot 2H_2O$.

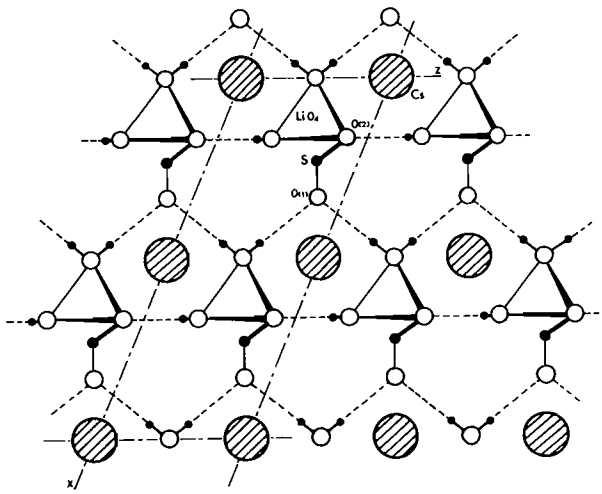

FIG. 2. Représentation du réseau de liaisons hydrogène reliant les chaines LiO_4—SO_3 dans le plan *xOz*.

TABLEAU 5. Distances et angles interatomiques (entre parenthèses sont notés les écarts types portant sur la dernière décimale)

(*a*) Ion SO_3^{2-}

Distances (Å)	Angles (deg)
S—O(1) 1.514(14)	O(1)—S—O(2) 105.3(5)
S—O(2) 1.532(8)	O(1)—S—O(2′) 105.3(5)
S—O(2′) 1.532(8)	O(2)—S—O(2′) 105.6(7)

(*b*) Tétraèdre LiO_4

Distances (Å)	Angles(deg)
Li—O(2) 1.95(2)	O(2)—Li—O(2′) 111.5(1.5)
Li—O(2′) 1.95(2)	O(2)—Li—W(1) 109.9(1.1)
Li—W(1) 1.93(3)	O(2)—Li—W(2) 105.4(1.0)
Li—W(2) 2.01(4)	O(2′)—Li—W(1) 109.9(1.1)
	O(2′)—Li—W(2) 105.4(1.0)
	W(1)—Li—W(2) 114.6(1.8)

(*c*) Molécules d'eau

W (1)		W (2)	
Paramètre	Valeur	Paramètre	Valeur
W(1)—H(11)	0.97 Å	W(2)—H(20)	0.97 Å
W(1)—H(12)	0.97 Å	W(2)—H(20′)	0.97 Å
H(11)—W(1)—H(12)	126 (7)°	H(20)—W(2)—H(20′)	125 (8)°

(*d*) Environnement du césium

Paramètre	Valeur
Cs—O(1)	3.105(5) (×2)
Cs—O(2)	3.175(9) (×2)
Cs—W(1)	3.493(9) (×2)

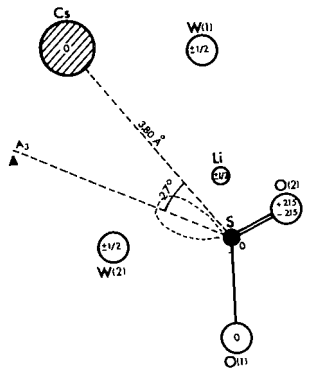

FIG. 3. Représentation du proche environnement du soufre dans la structure $LiCsSO_3 \cdot 2H_2O$.

Il a été signalé (1) une semblable diminution pour $(NH_4)_2PO_3F \cdot H_2O$ par rapport à $(NH_4)_2SO_3 \cdot H_2O$ puis Na_2PO_3F par rapport à Na_2SO_3. Il semble donc que l'activité stéréochimique de la paire électronique de S^{IV} (traduite par son encombrement) soit légèrement inférieure à celle du fluor.

$LiCsSO_3 \cdot 2H_2O$ présente un pouvoir de doublage de fréquence optique remarquablement élevé. L'étude de cette propriété sur monocristal est en cours de réalisation.

1. J. DURAND, J. L. GALIGNE et L. COT. Acta Crystallogr. B, **33**, 1414 (1977).
2. FOERSTER, BRUSCHE et NORBERG-SCHULTZ. Z. Phys. Chem. **110**, 1924, 435.
3. R. WYCKOFF. Crystal structures. Vol. III. Wiley-Interscience, New York, NY. 1965.
4. J. L. GALIGNE, J. DURAND et L. COT. Acta Crystallogr. B, **30**, 697 (1974).
5. J. DURAND, J. L. GALIGNE et L. COT. Acta Crystallogr. B, **34**, 388 (1978).
6. J. DURAND, W. GRANIER, L. COT et J. L. GALIGNE. Acta Crystallogr. B, **31**, 1533 (1975).
7. Y. ODDON, C. CARANONI et A. TRANQUARD. C.R. Acad. Sci. Paris Ser. C, **276**, 61 (1973).
8. P. DOYLE et P. TURNER. Acta Crystallogr. A, **24**, 390 (1968).
9. R. STEWART, E. DAVIDSON et W. SIMPSON. J. Chem. Phys. **42**, 3175 (1965).
10. J. R. GILLESPIE et E. A. ROBINSON. Can. J. Chem. **41**, 2074 (1963).
11. L. F. BATELLE et K. N. TRUEBLOOD. Acta Crystallogr. **19**, 531 (1965).
12. S. BAGGIO et L. N. BECKA. Acta Crystallogr. B, **25**, 1150 (1969).
13. B. NYBERG. Acta Chem. Scand. **26**, 857 (1972).
14. L. O. LARSON. Acta Chem. Scand. **23**, 2261 (1969).
15. B. NYBERG et P. KIERKEGAAND. Acta Chem. Scand. **23**, 581 (1968).
16. L. NIINISTO et L. O. LARSON. Acta Crystallogr. B, **29**, 623 (1973).
17. P. KIERKEGAAND et B. NYBERG. Acta Chem. Scand. **19**, 2189 (1965).
18. L. HUERTEIN et B. NYBERG. Acta Chem. Scand. **27**, 345 (1973).
19. L. O. LARSON et P. KIERKEGAAND. Acta Chem. Scand. **23**, 2253 (1969).
20. S. BAGGIO et L. N. BECKA. Acta Crystallogr. B, **25**, 946 (1969).
21. M. A. SPINULER et L. N. BECKA. J. Chem. Soc. 1199 (1967).
22. H. F. FISCHMEISTER. Monatsh. Chem. **93**, 420 (1962).

Cycloadditions and other chemistry of 4-oxygenated pyrazoles

PAUL J. FAGAN, ELI E. NEIDERT, MARTIN J. NYE,[1] MICHAEL J. O'HARE, AND WAH-PIU TANG

Guelph–Waterloo Centre for Graduate Work in Chemistry (Guelph Campus), Department of Chemistry, University of Guelph, Guelph, Ont., Canada N1G 2W1

Received August 11, 1978

PAUL J. FAGAN, ELI E. NEIDERT, MARTIN J. NYE, MICHAEL J. O'HARE, and WAH-PIU TANG. Can. J. Chem. **57**, 904 (1979).

Several synthetic routes to some new substituted pyrazol-4-ols and the reactions: methylation, acetylation, Michael addition, and oxidation are reported. Synthesis and cycloaddition reactions of the systems pyrazolium-4-olate and 3,4-diazacyclopentadienone are also reported. The former does not cycloadd, whereas the latter behaves as both a diene and a dienophile in various cycloadditions.

PAUL J. FAGAN, ELI E. NEIDERT, MARTIN J. NYE, MICHAEL J. O'HARE et WAH-PIU TANG. Can. J. Chem. **57**, 904 (1979).

On rapporte de nouvelles méthodes de synthèse de nouveaux pyrazolols-4 substitués et leurs réactions de méthylation, d'acétylation, d'additions de Michael et d'oxydation. On rapporte aussi la synthèse et des réactions de cycloaddition des systèmes pyrazolium-olate-4 et diaza-3,4 cyclopentadiènones. Les premières ne donnent pas de réaction de cycloaddition alors que les dernières se comportent à la fois comme des diènes et des diénophiles lors de diverses réactions de cycloaddition.

[Traduit par le journal]

Pyrazoles bearing an oxygen atom in the 4 position are of interest since one would expect some of the chemical reactions particularly cycloaddition to differ markedly from the 3- and 5-oxygenated analogues (1). Another point of interest is that the 4-oxygenated pyrazoles are in general less accessible synthetically and hence have received much less attention. This work was initiated from an interest in the possible cycloaddition reactions of the systems **1** and **2**. Compound **1** was found to cycloadd but compound **2** did not. This paper[2] includes these results and reports a number of new compounds synthesized incidently.

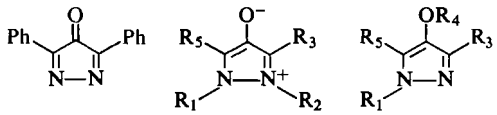

1 **2** **6**

(for key to $R_1R_2R_3R_4R_5$ see Tables 1 and 2)

Results and Discussion

Ring Synthesis

Four general ways of synthesizing pyrazol-4-ols have already been reported (4). Of these the preferred route (route *2*) is shown in Scheme 1. The fifth and sixth methods first used by Bertho and Nüssel (5) and Freeman *et al.* (6), respectively, and used in this laboratory are also shown in Scheme 1.

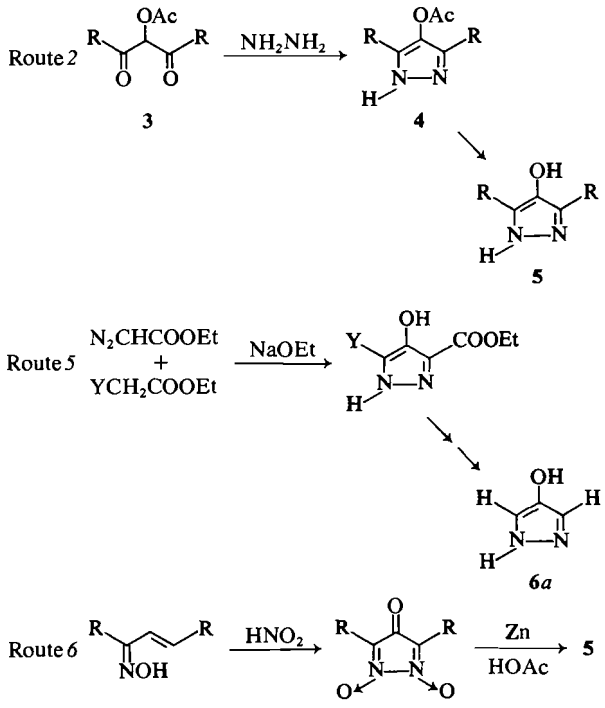

(Y = COOEt or CN. When Y = COOEt, ***6a*** can be produced by hydrolysis and decarboxylation)

SCHEME 1

In the case of the fifth method for preparation of

[1]To whom correspondence should be addressed.

[2]The results in this paper are in part found in the Ph.D. and M.Sc. theses of W. P. Tang (2) and P. J. Fagan (3), respectively, and have been partly reported in preliminary form (4).

0008-4042/79/080904-09$01.00/0

TABLE 1. Synthesis of substituted pyrazol-4-ols (6)

R_1	R_3	R_4	R_5	Compound	Route	% yield	Melting point (°C) (lit. mp (ref.))
H	H	H	H	6*a*	*5*	15	116–118 (118(5))
H	Me	H	Me	6*b*	*2*	87	177–179 (173.5(7))
Me	Me	H	Me	6*c*	*2*‡	89	187–189
Ph	Me	H	Me	6*d*	*2*§	89	138–140
H	Me	H	Ph	6*e*	*6*	39	192–194 (194–196(7))
Me	Me*	H	Ph*	6*f*	*2*‡	70	126–140
Ph	Me†	H	Ph†	6*g*	*2*§		172–173 (175(8))
H	Ph	H	Ph	6*h*	*2*	97	235–237
Me	Ph	H	Ph	6*i*	*2*‡	92	175–177
Ph	Ph	H	Ph	6*j*	*2*§		252(dec.)
H	COOEt	H	COOEt	6*k*	*5*		149–151 (128–130(5))
H	COOEt	H	CN	6*l*	*5*	5	228–229
H	COOMe	H	COOMe	6*m*	‖	80	240–242 (232(9))
H	COOEt	H	$CONH_2$	6*n*	‖	41	261–263
H	Ph	Ac	Ph	6*o*	*2*	85	162–168
Me	Ph	Ac	Ph	6*p*	*2*‡	85	109–111
Ph	Ph	Ac	Ph	6*q*	*2*§	62	138–140

*The product is a mixture of 70% of this compound with 30% of the compound with the methyl and phenyl reversed.
†The 3-methyl and 5-phenyl might be reversed.
‡Using methylhydrazine instead of hydrazine.
§Using phenylhydrazine instead of hydrazine.
‖See Experimental.

6*l* several by-products were obtained and identified (Scheme 2). Under conditions of aqueous work-up the main products were the hydrazones **7**, **8**, and **9**, whereas under anhydrous conditions **6***l*, **10**, and **11** were the isolated products. Compound **10** was shown to be the precursor to **6***l* and **11**.

Synthesis of **6***m* and **6***n* from **6***k* by action of methanolic potassium hydroxide at room temperature and ammonium acetate at 130°C, respectively, are reported. It is curious in the latter case that none of the 3,5-dicarbamyl product could be isolated even when the temperature and duration of the reaction were increased.

Methylation

O-Methylated pyrazol-4-ols (**6***r* and **6***s*) may be synthesized in 60–70% yields by shaking a solution of the pyrazole in aqueous sodium hydroxide with dimethyl sulfate (presumably via an anion intermediate), whereas *N*-methyl derivatives (**6***i*, **6***s*, and

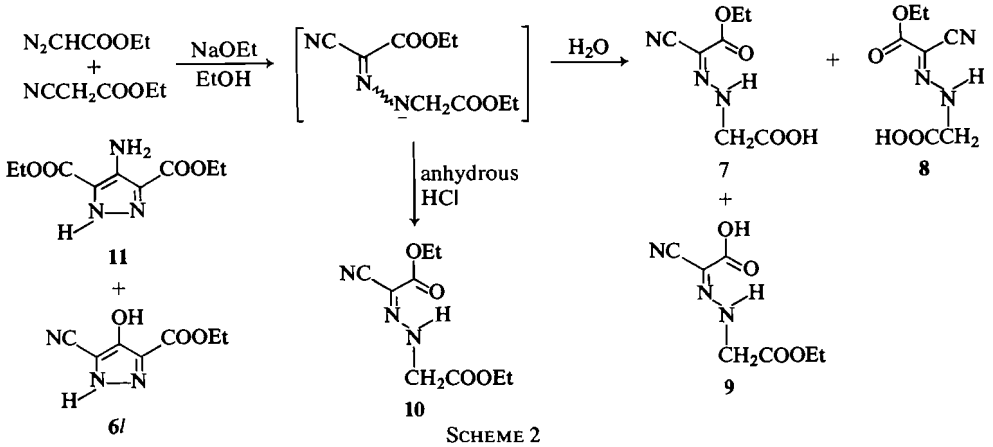

SCHEME 2

TABLE 2. Methylation and acylation of pyrazol-4-ols to give **2** or **6** (route *7*: DMS + alkali; route *8*: DMS; route *9*: via *N,N'*-dimethylhydrazine; route *10*: acetyl chloride; route *11*: DMAD, Y = MeOOCCH=CCOOMe)

R_1	R_2	R_3	R_4	R_5	Compound	Route	% yield	Melting point (°C)
H	—	Ph	Me	Ph	**6***r*	*7*	80	161–163
Me	—	Ph	Me	Ph	**6***s*	*7*	72	89–90
Me	—	Ph	H	Ph	**6***i*	*8*	78	175–177
Me	—	COOEt	H	COOEt	**6***t*	MeI	65	90–95
Me	Me	H	—	H	**2***a*†	MeI	72	160–165
Me	Me	Me	—	Me	**2***b*†	*8*	64	158–161
						9	50	
Me	Me	Me	—	Ph	**2***c*†	*8*	81	110–112
Me	Ph	Me	—	Me	**2***d*†	*8*	40	Oil
Me	Ph	Me*	—	Ph*	**2***e*†	*8*	62	138–142
Me	Me	Ph	—	Ph	**2***f*	*8*	91	201–203
						9	42	(dec.)
Me	Ph	Ph	—	Ph	**2***g*	*8*	40	139–141
Me	Me	COOEt	—	COOEt	**2***h*‡	*8*	71	234–235
Ac	—	Ph	H	Ph	**6***u*	*10*	91	155–157
Ac	—	Ph	Ac	Ph	**6***v*	*10*	94	146–148
Ac	—	Ph	Me	Ph	**6***w*	*10*	95	79–80
PhCO	—	Ph	H	Ph	**6***x*	PhCOCl	73	163–165
Y	—	Ph	H	Ph	**6***y*	*11*	30	118–120
Y	—	Ph	Y	Ph	**6***z*	*11*	26	143–144

*The positions of Me and Ph might be reversed.
†As monohydrates.
‡As hemihydrate.

6*t*) may be prepared by direct heating with dimethyl sulfate (DMS) or methyl iodide. Similarly, *N,N'*-disubstituted pyrazolium compounds may be made directly from either an *N*-substituted or from an *N*-unsubstituted pyrazol-4-ol by heating it with excess dimethyl sulfate or methyl iodide to give the methosulfate or iodide salt which is then treated with alkali or passed down an ion exchange column to generate the zwitterion (**2***a–h*). The zwitterions **2***b* and **2***f* have also been prepared by treating 2-acetoxy-1,3-diphenyl-1,3-propanedione and 3-acetoxy-2,4-pentanedione (**12**) with *N,N'*-dimethylhydrazine. The analogous reactions of **12** with *N,N'*-diphenylhydrazine and *N*-methylhydroxylamine were unsuccessful. Table 2 summarizes the yields and melting points.

Acetylation

Acetylation of pyrazol-4-ols by refluxing with acetic anhydride occurs at both the N_1 and O positions but the rate of *N*-acetylation is faster. Hence depending on the time of reaction one can isolate either *N*-acetyl- or *N,O*-diacetylpyrazol-4-ols as the main products (see Scheme 3). Conveniently the *O*-acetylpyrazol-4-ols can be prepared by monodeacetylation of the diacetyl compounds by passing them down a column of neutral alumina. For example **6***o* is formed by deacetylation of **6***v* in 93% yield. The site of acetyl substituent is readily revealed by the carbonyl band in the ir spectrum

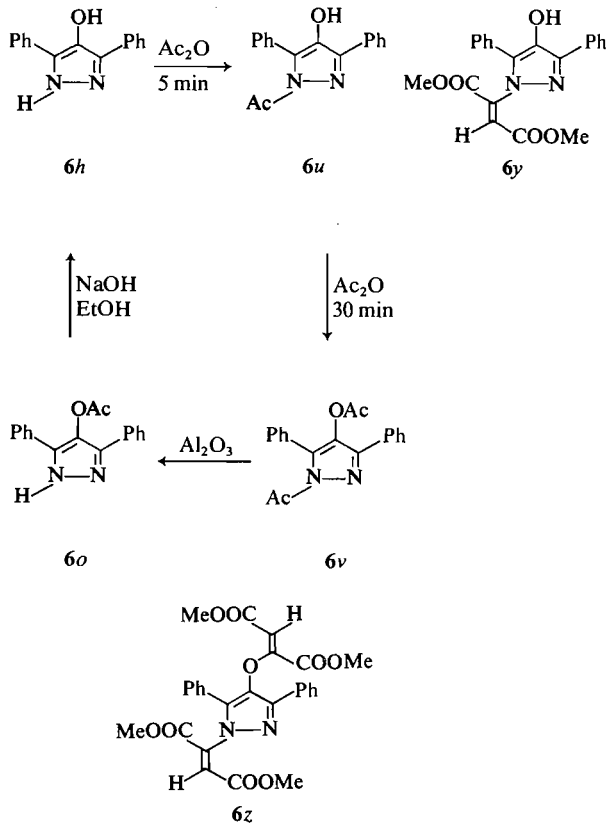

6*h* **6***u* **6***y*

6*o* **6***v*

6*z*

SCHEME 3

(*O*-acetyl ~ 1760 cm^{-1}, *N*-acetyl ~ 1740 cm^{-1}). An alternative route to *O*-acetyl compounds is via route *2* in Scheme 1.

N-Benzoylation is effected on pyrazol-4-ols by heating them at 100°C with benzoyl chloride. Table 2 reports yields and melting points.

Michael Additions

Attempts at cycloadditions between 1,3-diphenylpyrazol-4-ol and dimethylacetylene dicarboxylate (DMAD) yielded the 1:1 and 1:2 Michael adducts **6***y* and **6***z* instead (Table 2).

Oxidation

1,3-Diphenylpyrazol-4-ol (**6***h*) is oxidized to 1,3-diphenyl-3,4-diazacyclopentadienone (**1**) by lead

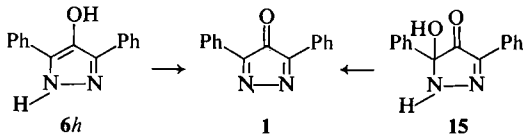

dioxide in dry ether. It is a purple solid, deep red in acetonitrile solution and purple in concentrated sulfuric acid – acetonitrile mixtures, like tetraphenylcyclopentadienone (**13**) in all these respects. However, unlike **13**, **1** has a barely detectable ir carbonyl band (at 1740 cm^{-1}) in the solid state. Weak ir bands are known (10) to occur when the change in dipole moment during transition is close to zero and this could conceivably be the case for **1** as the polarity of the CO bond would be greatly reduced compared to normal ketones by the contribution from the five resonance structures represented by **14** which are stabilized by virtue of the aromatic sextet and also the presence of the electronegative nitrogen atoms. The charges calculated for **1** and cyclopentadienone by the HMO method, although imprecise, clearly show the expected trend (Fig. 1).

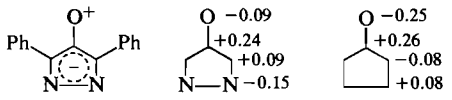

FIG. 1. Charges calculated for **1** and cyclopentadienone.

Conversion of **6***h* to **1**, observed by visible spectrophotometry, can also be effected in solution by thionyl chloride or by butyl nitrite both of which have been used for analogous reactions by Büchi and Lukas (11). Further confirmation of the structure of **1** is gained by its observed formation in solution from 5-hydroxy-3,5-diphenylpyrazolin-4-one (**15**) (prepared by reaction of diphenyltriketone with hydrazine (4)), by treatment with concentrated sulfuric acid.

Solutions of **1** are very unstable at room temperature even in the dark and within 30 min are practically completely decomposed. A crystalline product may be isolated from the solution and had previously been tentatively assigned (3) structure **16** from elemental analysis, uv, ir, and ^{1}Hmr spectra. This structure was later confirmed by Trost and Whitman (12) by mass and ^{13}C spectra.

Cycloadditions of the Diazacyclopentadienone (1)

Two questions were of great interest in connection with the cycloadditions of **1**. Firstly, does it react as a diene (13–15), as a dienophile (13, 16), or as a 1,3 dipole (13, 16)? Secondly, if **1** behaves as a diene, is it an example of the rare class of electron deficient dienes described by Sauer and Weist (17) which are highly reactive towards unactivated (electron rich) alkenes?

When **1** was treated with a wide variety of cycloaddition reagents with various conditions of solvent and temperature, it behaved either as a diene or a dienophile but not as a 1,3 dipole. As a dienophile it reacted with 2,3-dimethyl-1,3-butadiene to give **17** and with cyclopentadiene to give an analogous product. As a diene it reacted with [2.2.1]bicycloheptene to give **18**, presumably via **19** by loss of carbon monoxide and hydrogen. The latter steps have plenty of analogies (18). No products were isolated when **1** was treated with maleic anhydride, dimethylacetylene dicarboxylate, diphenylacetylene, dimethyl fumarate, carbon disulfide, isobutyl vinyl ether, cyclohexene, and cyclopentene.

Although the diene and dienophile reactivities of **1** were anticipated, the self condensation to give **16** is unusual. The first step, a simple Diels–Alder dimerization to give **20**, is presumed but one would then anticipate formation of **21** by loss of carbon monoxide as normally observed for cyclopentadiene dimers (18) and as occurs when **18** is formed from **19**. Instead nitrogen is lost. A possible explanation is that although carbon monoxide is lost by concerted reverse cycloaddition, nitrogen may be eliminated by a two-step free radical process (**10** → **22** → **23**). There is a precedent (15) for this mechanism in that **24** on heating (120°C) is converted to **25** and a diradical intermediate analogous to **23** was proposed. The factor which encourages the free radical mechanism for both **20** and **24** could be the presence of a stabilizing nitrogen substituent attached directly to the carbon radical generated in the initial bond breaking step. Note that this substituent is absent in **19** and hence the radical mechanism would be discouraged in favour of a concerted reverse cycloaddition. The final product **16** could then arise by two-step cycloaddition of **23** to another mole of **1**.

The above suggested mechanism has the advantage of avoiding symmetry problems associated with the simpler mechanism (**20** → **26** → **16**). If the latter mechanism is concerted, according to the Frontier Molecular Orbital (FMO) theory (19, 20), the overlapping lobes of the HOMO orbital of one reactant and the LUMO orbital of the other reactant should have the same phase. Figure 2 shows the eigenvector coefficients of the HOMO's and LUMO's of **1** and **26** as calculated by the Huckel π method and reveals a mismatch for suprafacial attack and therefore the reaction is disallowed. Similarly suprafacial extrusion of N_2 from **20** is disallowed. Hence a four-step radical mechanism for conversion of **20** to **16** is probable but a four-step heterolytic mechanism or a combination of both cannot be ruled out. Trost *et al.* (12) observed the formation of **16** from the bis-diazoketone **27** and proposed a mechanism in which **27** is converted to **1** and further **27** reacts with 2 moles of **1** with elimination of 2 moles of N_2. This mechanism may still be correct provided **27** is present but this current work reveals an alternative route which does not require reaction of **27** with **1**. The ability of **1** to react with [2.2.1]bicycloheptene but not maleic anhydride is intimately connected with its strong electron affinity and this property is further emphasized by the observation that it can oxidize hydrochloric acid to chlorine. When dry hydrogen chloride is passed through a solution of **1** in dry ether, chlorine gas is readily detected and a quantitative yield of 1,3-diphenylpyrazol-4-ol hydrochloride is produced. The low intensity carbonyl ir band of **1** is a manifestation of the comparable electron affinity of the heterocyclic ring relative to the exocyclic oxygen atom and this situation might also give rise to susceptibility of the oxygen of the carbonyl group towards nucleophilic attack. Indeed **1** reacts immediately with triphenylphosphine as does also the similarly electron-deficient 2,5-diphenyl-3,4-dicyanocyclopentadienone. In the latter case a crystalline adduct was obtained and characterized (21) but in the case of **1**, triphenylphosphine oxide and **6***h* were isolated which implies formation of **28** followed by hydrolysis in work-up.

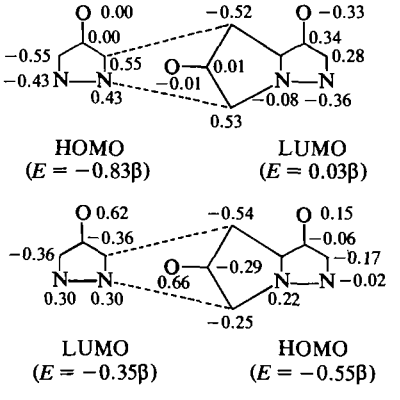

FIG. 2. Eigenvector coefficients and orbital energies of the HOMO's and LUMO's of **1** and **26**.

Cycloadditions of 4-Oxidopyrazolium (2)

In a previous paper (22) a first example of a heterocyclic zwitterion cycloadding to a diene was reported (**29** → **30**) and using FMO theory it was predicted that the 4-oxidopyrazolium system (**2**) should behave in a similar way (**2** → **31**). Figure 3 shows the eigenvector coefficients of the interacting lobes of the frontier orbitals. Since then exhaustive attempts to cycloadd **2** bearing methyls at the 1 and 2 positions and either H (**2***a*), phenyl (**2***f*), or ethoxycarbonyl (**2***h*) at the 3 and 5 positions with numerous dienes and activated alkenes and alkynes have failed. The most likely compound to succeed was thought to be **2***h* as it bears electron withdrawing activating groups but it suffered from instability problems. For example it is completely destroyed by heating it for 15 h at 100°C in bromoform. The nmr spectrum indicated conversion to 1-methyl-3,5-diphenyl-4-methoxypyrazole. This type of behaviour had been observed previously for derivatives of **2** bearing phenyl or methyl substituents (2, 23). In the presence of moisture the decomposition accelerates and 1-methylpyrazol-4-ol arises by hydrolysis and decarboxylation. For example acetonitrile containing 0.02% water decomposes **2***h* in 12 h at room temperature. So in the case of **2***h* any cycloaddition activity was masked by the highly competitive side reactions. For **2***a* and **2***f* the explanation of inactivity must be the fact that neither the HOMO nor LUMO lies close to zero and rates of cycloaddition are roughly inversely proportional to the energy difference between the interaction frontier orbitals (20).

Experimental

Infrared spectra were recorded on a Beckmann IR5A spectrophotometer as Nujol mulls unless otherwise stated and major peaks are reported in reciprocal centimeters. Nuclear magnetic resonance spectra were recorded on a Varian A-60A spectrometer using the internal standards DSS (sodium 2,2-dimethyl-2-silapentane-5-sulfonate) and TMS in $CDCl_3$ unless otherwise stated, and the data are presented in the order; chemical shift in ppm relative to the standard, multiplicity, number of protons, and assignment. Ultraviolet spectra were recorded on a Unicam SP-800 spectrophotometer in 95% ethanol unless otherwise stated and the data are presented in the following order: λ_{max} in nm, molar extinction coefficient (in parentheses). Mass spectra were run on a Varian MAT CH7 spectrometer. Symbols have the following meanings: b, broad; i, inflection; sh, shoulder; s, singlet; m, multiplet; d, doublet; t, triplet; q, quartet. Melting points were determined on a Mel-Temp apparatus and are uncorrected. Most of the

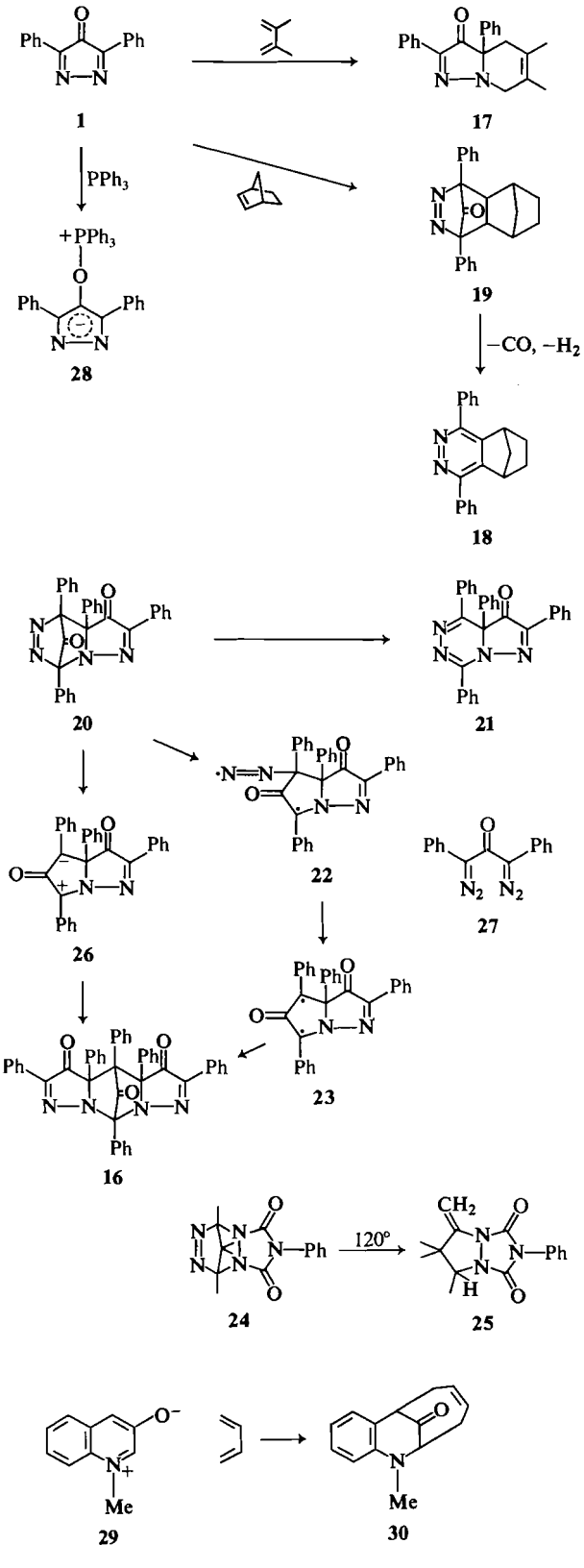

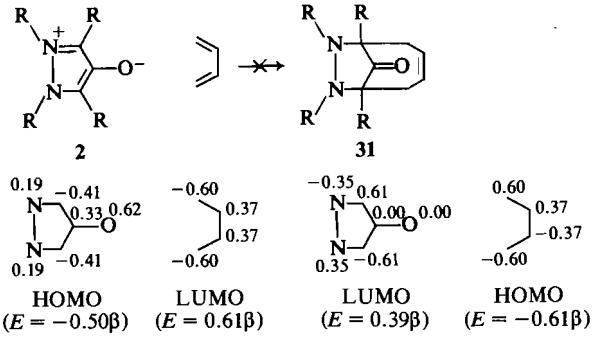

FIG. 3. Eigen-vector coefficients and orbital energies of the HOMO's and LUMO's of **2** and 1,3-butadiene.

elemental analyses (performed by A. B. Gygli, Microanalysis Laboratories Ltd., Toronto; C. Daesslé, Organic Microanalyses, Montreal; and H. S. McKinnon, Chemistry Department, University of Guelph) and ir spectra have been omitted for brevity and are available from the Depository of Unpublished Data.[3] All new compounds had satisfactory elemental analysis.

Route 2 (3 → 4 → 5)

The starting materials, 1,3-diphenyl-2-acetoxy-1,3-propanedione, 3-acetoxybenzoylacetone, and 3-acetoxypentane-2,4-dione, were prepared according to the methods of Neufville and Pechmann (24), Böhme and Schneider (8), and Auwers and Auffenberg (25), respectively. Typical procedures are given below for **6***j* and **6***q*, together with ^{1}Hmr and uv spectra for the products.

*3,5-Dimethylpyrazol-4-ol (**6**b)*—uv: 232 (5270); ^{1}Hmr (acetic-d_3 acid-d_1) 2.23 (s, 6H, CH_3).

*1,3,5-Trimethylpyrazol-4-ol (**6**c)*—^{1}Hmr: 2.13 (s, 6H, CH_3), 3.65 (s, 3H, N—CH_3).

*1-Phenyl-3,5-dimethylpyrazol-4-ol (**6**d)*—uv: 225(i) (7890), 263 (11 550); ^{1}Hmr; 1.99 (s, 3H, CH_3), 2.04 (s, 3H, CH_3), ca. 6.80 (b, 1H, OH), 7.18 (s, 5H, aromatic).

*1,3-Dimethyl-5-phenylpyrazol-4-ol (70%) mixed with 1,5-dimethyl-3-phenylpyrazol-4-ol (30%) (**6**f)*—^{1}Hmr: 208 (s, 3H, CCH_3), 3.54 (s, 3 × 70% H, NCH_3), 3.59 (s, 3 × 30% H, NCH_3), 7.17–7.95 (m, 5H, aromatic).

*3-Methyl-1,5-diphenylpyrazol-4-ol or 5-methyl-1,3-diphenylpyrazol-4-ol (**6**g)*—^{1}Hmr: 2.13 (s, 3H, CH_3), 7.2 (m, 10H, aromatic).

*3,5-Diphenylpyrazol-4-ol (**6**h)*—uv: 252 (22 700), 276(sh) (17 100), 295(sh) (10 000); ^{1}Hmr (DMSO-d_6): 7.32–7.67 (m, 7H, aromatic + OH), 7.94–8.11 (m, 4H, aromatic), 8.40 (b, 1H, NH).

*1-Methyl-3,5-diphenylpyrazol-4-ol (**6**i)*—uv: 245 (21 500), 276(sh) (10 600); ^{1}Hmr: 3.80 (s, 3H, CH_3), 7.35–7.62 (m, 9H, aromatic + OH), 7.98–8.14 (m, 2H, aromatic).

*1,3,5-Triphenylpyrazol-4-ol (**6**j)*—phenylhydrazine (0.5 mL, 0.005 mol) was added to a warm solution of 1,3-diphenyl-2-acetoxy-1,3-propanedione (1.13 g, 0.004 mol) in 95% ethanol (10 mL). After refluxing the solution for 1.5 h orange crystals separated and were collected by filtration.

*4-Acetoxy-3,5-diphenylpyrazole (**6**o)*—uv: 251 (29 900); ^{1}Hmr: 2.26 (s, 3H, CH_3), 7.30–7.50 (m, 6H, aromatic), 7.60–7.77 (m, aromatic), 10.68 (bs, 1H, NH).

[3]Photocopies may be obtained, at a nominal charge, upon request from the Depository of Unpublished Data, CISTI, National Research Council of Canada, Ottawa, Ont., Canada K1A 0S2.

1-Methyl-4-acetoxy-3,5-diphenylpyrazole (6p)—uv: 247 (27 800); ^{1}Hmr: 2.13 (s, 3H, CH_3), 3.83 (s, 3H, NCH_3), 7.32–7.55 (m, 8H, aromatic), 7.75–7.92 (m, 2H, aromatic).

4-Acetoxy-1,3,5-triphenylpyrazole (6q)—phenylhydrazine (0.42 mL, 0.0042 mol) was added with stirring to a solution of 1,3-diphenyl-2-acetoxy-1,3-propanedione (1.13 g, 0.004 mol) in acetic acid (10 mL). The mixture was stirred for 1 h, left for 18 h, evaporated at reduced pressure, and the crude mass triturated with ether (5 mL) to yield 1.03 g (72%) crude product; uv: 248 (27 300), 271(i) (21 500), 283(i) (14 800); ^{1}Hmr: 2.15 (s, 3H, CH_3), 7.08–7.38 (m, 13H, aromatic), 7.66–7.83 (m, 2H, aromatic).

Route 5 (Preparation of 3-Carbethoxy-5-cyanopyrazol-4-ol (6l) and By-products 7–11)

A solution of 2.2 g (0.02 mol) of ethyl cyanoacetate, 2.2 g (0.02 mol) ethyl diazoacetate, and 20 mL of absolute ethanol was added to a solution of 1 g (0.04 mol) sodium in absolute ethanol. The solution was maintained at 0–5°C during the addition and for 3 h thereafter. After stirring at room temperature for an additional 14 h the solution was divided into two equal portions which were worked up, individually, as follows.

Anhydrous Work-up

Dry hydrogen chloride was bubbled into the solution followed by evaporation to dryness. The crude grey residue was triturated with 5 × 50 mL anhydrous ether. The ether was removed under reduced pressure leaving a viscous brown oil. Thin-layer chromatographic analysis showed that this oil consisted of one major component and several minor components. Purification by preparative tlc yielded 730 mg (33%) of a clear yellow oil identified as (*Z*)-ethyl ethoxycarbonylmethylhydrazonocyanoacetate (**10**) on the basis of the following spectral properties; ir (neat): 3210, 2980, 2230, 1740, 1720 (sh), 1690, 1220–1150, 1022, 785; ^{1}Hmr (CD_3CN): 1150 (b t), $J \simeq 5$ Hz, 1H, NH), 3.39 (d, $J = 5$ Hz, 2H, NCH_2), 4.30 (q, $J = 7$ Hz, 2H, CH_2CH_3), 4.20 (q, $J = 7$ Hz, 2H, CH_2CH_3), 1.34 (t, $J = 7$ Hz, 3H, CH_2CH_3), 1.25 (t, $J = 7$ Hz, 3H, CH_2CH_3), addition of D_2O causes NH to exchange and the NCH_2 peak to collapse to a singlet; ms: molecular ion at *m/e* 227; uv: 295.5 (1.5–1.8 × 10^4).

Aqueous Work-up

The remaining half of the solution was diluted with 4 volumes of water and extracted with 2 × 125 mL of ether. These ether layers were discarded. The remainder of the aqueous phase was acidified to pH 4–5 with dilute hydrochloric acid and extracted with 4 × 125 mL ether. The combined ether layers were washed with saturated sodium chloride solution and dried over anhydrous sodium sulfate. Upon removal of the ether under reduced pressure a viscous yellow oil consisting of two major components at R_f 5.1 and 4.2 (tlc) and several minor components was isolated. Purification by two successive collections from preparative tlc enabled the isolation of the two major components as white crystalline solids. The product having R_f 5.1 (360 mg, 19%) was identified as (*Z*)-ethoxycarbonylmethylhydrazonocyanoacetic acid (**9**), mp 104–106°C, on the basis of the following spectral properties; ir (KBr): 3500–2500(b, several bands), 2230, 1735, 1695, 1530, 1220–1170(strong), 1020, 776; ^{1}Hmr (CD_3CN): 8.80 (bs, 1H, NH), 7.32 (bs, 1H, COOH), 4.38 (d, $J = 5$ Hz, 2H, NCH_2), 4.32 (q, $J = 7$ Hz, 2H, CH_2CH_3), 1.32 (t, $J = 7$ Hz, 3H, CH_2CH_3), addition of D_2O causes NH and COOH to exchange and the NCH_2 peak to collapse to a singlet; ms: molecular ion at *m/e* 199; uv: 302.5 (1.48 × 10^4). *Anal.* calcd. for $C_7H_9N_3O_4$: C 42.21, H 4.56, N 21.09; found: C 42.37, H 4.66, N 21.16.

The material having R_f 4.2 (380 mg, 20%) was identified as a 2:1 mixture of (*Z*)-ethyl carboxymethylhydrazonocyanoacetate (**7**) and its (*E*)-isomer (**8**), respectively. It was not possible to separate these isomers by any simple techniques, thus the spectral data following is a superimposition of the spectral properties of **7** and **8**. From the ^{1}Hmr spectrum of the mixture it was possible to derive the spectra of **7** and **8** individually. These spectral properties were as follows; ir (KBr): 3500–2500(broad, several bands), 2200, 1730, 1690, 1235, 1180, 1160(sh), 767; ^{1}Hmr (**7**) (CD_3CN): 8.77 (bs, 1H, NH), 7.83 (bs, 1H, COOH), 4.46 (d, $J = 5$ Hz, 2H, NCH_2), 4.38 (q, $J = 7$ Hz, 2H, CH_2CH_3), 1.38 (t, $J = 7$ Hz, 3H, CH_2CH_3); ^{1}Hmr (**8**) (CD_3CN): 7.01 (bs, 1H, COOH), 4.29 (q, $J = 7$ Hz, 2H, CH_2CH_3), 3.29 (s, 2H, NCH_2), 1.27 (t, $J = 7$ Hz, 3H, CH_2CH_3); addition of D_2O causes NH and COOH protons to exchange immediately and the NCH_2 protons of **8** to exchange slowly (half-life 0.5 h), and the NCH_2 protons of **7** to collapse to a singlet; ms: molecular ion at *m/e* 199; uv: 298 (1.73 × 10^4). *Anal.* calcd. for $C_7H_9N_3O_4$: C 42.21, H 4.56, N 21.09; found: C 42.26, H 4.60, N 21.00.

A solution of 500 mg (2.2 mmol) of diester **10** was heated at reflux in 20 mL absolute ethanol containing 100 mg (4.35 mmol) of sodium for a period of 8 h. The solution became a very dark clear brown at the end of this time. Water (80 mL) was added to the solution followed by the addition of 6 *N* HCl until pH 8 was reached. The aqueous layer was extracted with 6 × 50 mL ether. The combined ether layers were washed with saturated sodium chloride solution and dried over anhydrous sodium sulfate. Removal of the ether under reduced pressure gave a viscous brown oil which crystallized slowly. Recrystallization from acetonitrile–chloroform yielded 40 mg (8%) of a white crystalline solid, mp 143–145°C (lit. (5) mp 144°C), identified as 3,5-dicarbethoxy-4-aminopyrazole (**11**) on the basis of the following spectral properties; ir (KBr): 3450, 3340, 3180(b), 2980, 1710, 1615, 1285, 1250, 1130, 788, 770; ^{1}Hmr (CD_3CN): ~12.9 (very broad elevation in base line, NH), 5.25 (bs, 2H, NH_2), 4.38 (q, $J = 7$ Hz, 4H, CH_2CH_3), 1.39 (t, $J = 7$ Hz, 6H, CH_2CH_3); ms: molecular ion at *m/e* 227; uv: 312 (8.27 × 10^3), (+0.1 *N* NaOH) 296 (6.24 × 10^3). *Anal.* calcd. for $C_9H_{12}N_3O_4$: C 47.57, H 5.77, N 18.49; found: C 47.50, H 5.52, N 18.75.

The remainder of the aqueous layer was acidified further to pH 5–6 and again extracted with 6 × 50 mL ether. After washing with saturated sodium chloride solution, the combined ether layers were dried over anhydrous sodium sulfate. The ether was removed under reduced pressure leaving a viscous brown oil consisting (tlc) of several components. The major component R_f 0.22 was collected by preparative tlc. Recrystallization from acetonitrile–chloroform yielded 20 mg (5%) of **6***l*, mp 228–229°C; ir (KBr): 3200(b), 2225, 1730, 1595, 1295, 1255, 1198, 1034, 782, 717; ^{1}Hmr (DMSO-d_6): ~5.1 (broad elevation in base line NH, OH), 4.19 (q, $J = 7$ Hz, 2H, CH_2CH_3), 1.26 (t, $J = 7$ Hz, 3H, CH_2CH_3); ms: molecular ion at *m/e* 181; uv: 283 (7.5 × 10^3), 329 (1.5 × 10^3), (+0.1 *N* NaOH) 329 (8.5 × 10^3).

3,5-Dicarbomethoxypyrazol-4-ol (6m)

A solution of 100 mg 3,5-dicarbethoxypyrazol-4-ol (**6***k*), 100 mg potassium hydroxide, and 10 mL methanol was stirred at room temperature for 12 h, 40 mL water was added, and the solution acidified with dilute hydrochloric acid to pH 6–7. This aqueous solution was extracted with 4 × 25 mL ether. The ether was removed under reduced pressure leaving a gray solid which was readily recrystallized from chloroform–hexane. Pure 3,5-dicarbomethoxypyrazol-4-ol (**6***m*) was isolated as a white solid, mp 240–242°C; ir (KBr): 3400, 3210, 1705, 1675, 1535, 1310, 1295, 1210, 1075, 1012, 887; ^{1}Hmr

(DMSO-d_6): 3.83 (s, 6H, OCH_3); uv: 275 (8×10^3), (+0.1 *N* NaOH) 319 ($7–8 \times 10^3$).

3-Carbamyl-5-carbethoxyl-5-carbethoxypyrazol-4-ol (6n)

A mixture of 100 mg (0.44 mmol) 3,5-dicarbethoxypyrazol-4-ol (**6***l*) and 4 g (0.05 mol) ammonium acetate was heated at 130°C (mixture melts at 100–120°C) for 2 h and the crude fusion products completely dissolved by addition of water followed by dilute HCl to pH 5–6. The combined ether extract (3×50 mL portions) was dried over anhydrous sodium sulfate and concentrated. Thin-layer chromatographic analysis revealed the presence of three components one of which was starting material. The major component (bottom spot) was readily purified by recrystallization leaving 35 mg (41%) of 3-carbamyl-5-carbethoxypyrazole-4-ol (**6***n*) as a white crystalline solid, mp 261–263°C; ir (KBr): 3460, 3315, 3200, 1685, 1678, 1655, 1325, 1173, 1023, 820, 784, 750; ^{1}Hmr (DMSO-d_6): 4.28 (q, $J = 7$ Hz, 2H, CH_2CH_3), 1.27 (t, $J = 7$ Hz, 3H, CH_2CH_3); uv: 271 ($10–12 \times 10^3$).

Route 7 *(O-Methylation of Pyrazol-4-ols)*

Typical *O*-methylations are illustrated below.

4-Methoxy-3,5-diphenylpyrazole (6r)—A solution of **6***h* (1.18 g, 5 mmol) in 10% NaOH (60 mL) was heated to 60°C to dissolve and diluted to a volume of 90 mL with water; 2.5 mL of dimethyl sulfate was added and the two phases vigorously shaken. Solids were filtered and more methyl sulfate (2.5 mL) added to the filtrate to give a second crop of solid. The combined products were washed with water and dried; uv: 255 (28, 100), 291(sh) (6000); ^{1}Hmr: 3.63 (s, 3H, CH_3), 7.28–7.53 (m, 6H, aromatic), 7.83–8.00 (m, 4H, aromatic), 10.87 (s, 1H, NH).

1-Methyl-4-methoxy-3,5-diphenylpyrazole (6s)—uv: 251 (24 100); ^{1}Hmr: 3.55 (s, 3H, OCH_3), 3.83 (s, 3H, NCH_3), 7.33–7.86 (m, 8H, aromatic), 8.02–8.18 (m, 2H, aromatic).

Route 8 *(N-Methylation of pyrazol-4-ols)*

Typical examples are given below.

1,2-Dimethylpyrazolium-4-olate monohydrate (2a)—^{1}Hmr (DMSO-d_6): 7.02 (s, 2H, aromatic), 3.79 (s, 6H, CH_3); uv (H_2O): 285 (4000).

1,2,3,4-Tetramethylpyrazolium-4-olate monohydrate (2b)—uv (H_2O): 289 (7900); ^{1}Hmr (D_2O): 3.77 (s, 6H, NCH_3), 2.21 (s, 6H, CCH_3).

1,2,3-Trimethyl-5-phenylpyrazolium-4-olate monohydrate (2c)—uv (H_2O): 311 (9200); ^{1}Hmr (D_2O): 7.55 (s, 5H, aromatic), 3.87 (s, 3H, NCH_3), 3.69 (s, 3H, NCH_3), 2.32 (s, 3H, CCH_3).

1,3,5-Trimethyl-2-phenylpyrazolium-4-olate monohydrate (2d)— uv (H_2O): 297 (7500); ^{1}Hmr (D_2O): 7.84–7.38 (m, 5H, aromatic), 3.56 (s, 3H, NCH_3), 2.35 (s, 3H, CCH_3), 2.05 (s, 3H, CCH_3).

1,3-Dimethyl-2,5-diphenylpyrazolium-4-olate monohydrate or 1,5-dimethyl-2,3-diphenylpyrazolium-4-olate monohydrate (2e)—uv (H_2O): 322 (10 200); ^{1}Hmr (D_2O): 7.69–7.18 (m, 10H, aromatic), 3.55 (s, 3H, NCH_3), 2.45 (s, 3H, CCH_3).

1,2-Dimethyl-3,5-diphenylpyrazolium-4-olate (2f)—uv: 226 (14 200), 248(i) (6700), 325 (9700); ^{1}Hmr (D_2O): 8.61 (s, 10H, aromatic), 3.75 (s, 6H, CH_3).

1-Methyl-2,3,5-triphenylpyrazolium-4-olate (2g)—uv (H_2O): 341 (11 500); ^{1}Hmr: 8.02–7.16 (m, 15H, aromatic), 3.58 (s, 3H, aromatic).

1,2-Dimethyl-3,5-dicarbethoxypyrazolium-4-olate (2h)—A solution of 500 mg (2.2 mmol) 3,5-dicarbethoxypyrazol-4-ol (**6***k*) in 6 mL dimethyl sulfate was heated at 100°C for 2 h. After cooling to room temperature, dry ether was added dropwise until crystallization was initiated. The product was filtered and recrystallized from acetonitrile–ether to yield 600 mg (60%) of 3,5-dicarbethoxy-1,2-dimethylpyrazolium-4-ol methosulfate, mp 133–134°C; ^{1}Hmr (CD_3CN): 4.54 (q, $J = 7$ Hz, 4H, CH_2CH_3), 4.35 (s, 6H, N—CH_3), 3.48 (s, 3H, $MeSO_4$), 1.42 (t, $J = 7$ Hz, 6H, CH_2CH_3). A 100 mg (0.27 mmol) sample of the methosulfate was dissolved in a minimum amount of acetonitrile at room temperature. To this solution was added 1 equiv. of triethylamine and an immediate appearance of precipitate was noted (**2***h*). Maximum crystallization was achieved by adding carbon tetrachloride and cooling; uv: 278 (10 000 est.); ^{1}Hmr (D_2O): 4.28 (q, $J = 7$ Hz, 4H, CH_2CH_3), 4.08 (s, 6H, NCH_3), 1.22 (t, $J = 7$ Hz, 6H, CH_2CH_3), internal standard: acetone taken as 2.07.

1-Methyl-3,5-diphenylpyrazol-4-ol (6i)—A mixture of **6***h* (2.36 g, 0.01 mol) and dimethyl sulfate (4.8 mL, 0.05 mol) was heated in an oil bath (100–130°C) until dissolution and then for 10 min more. After cooling, 150 mL of water was added with stirring to dissolve excess dimethyl sulfate. A precipitate of **6***i* formed, and was filtered and washed with water.

Route 9

A typical example is given below.

1,2,3,5-Tetramethylpyrazolium-4-olate (2b)—A mixture of 1,2-dimethylhydrazine hydrochloride (1.40 g 10.5 mmol), 3-acetoxy-2,4-pentanedione (1.40 g, 10.4 mmol) and 80% aqueous ethanol (25 mL) was heated at reflux for 3 h. The solution was concentrated under vacuum to 20 mL and extracted with 3×20 mL of ether and the combined layers were washed with 2×10 mL portions of water. The water layers were concentrated to a viscous oil which crystallized on standing. Recrystallization was effected with acetone–acetonitrile mixture. This product, the hydrochloride of **2***b* was converted to **2***b* by ion exchange over Amberlite IR45 resin.

Route 10

Typical mono- and diacetylations are given below.

1-Acetyl-3,5-diphenylpyrazol-4-ol (6u)—A mixture of **6***h* (0.94 g, 4 mmol) and acetic anhydride (1.6 mL, 17 mmol) was heated at reflux for 5 min. After cooling, 15 mL of water was added and the precipitate (**6***u*) filtered; uv: 233(i) (20 500), 298 (18 900), 376 (784); ^{1}Hmr: 8.12–8.28 (m, 2H, aromatic), 7.42–7.65 (m, 8H, aromatic), 4.90 (s, 1H, OH), 2.70 (s, 3H, CH_3).

4-Acetoxy-1-acetyl-3,5-diphenylpyrazole (6v)—A mixture of **6***h* (0.94 g, 4 mmol) and acetic anhydride (5 mL, 52 mmol) was heated at reflux for 30 min. Cooling and addition of water caused **6***v* to precipitate; uv: 232 (20 400), 273 (20 300); ^{1}Hmr: 7.87–8.03 (m, 2H, aromatic), 7.42–7.65 (m, 8H, aromatic), 2.77 (s, 3H, $NCOCH_3$), 2.11 (s, 3H, $OCOCH_3$).

1-Acetyl-4-methoxy-3,5-diphenylpyrazole (6w)—uv: 233 (19 600), 287 (19 800); ^{1}Hmr: 8.14–8.31 (m, 2H, aromatic), 7.44–7.66 (m, 8H, aromatic), 3.55 (s, 3H, OCH_3), 2.73 (s, 3H, $OCOCH_3$).

1-Benzoyl-3,5-diphenylpyrazole (6x)—^{1}Hmr: 7.20–7.65 (m, 11H, aromatic), 7.93–8.20 (m, 4H, aromatic).

Deacetylation

A typical selective deacetylation was the conversion of **6***v* to **6***o* which was effected by passing a warm solution of **6***v* (640 mg) in minimum benzene through a column packed with neutral alumina (200 mesh) (20 g); **6***o* was eluted with benzene–acetone mixture (6:1).

Route 11

1:1 and 1:2 Adducts (6y and 6z)

A mixture of **6***h* (1.18 g, 5 mmol) and dimethylacetylene dicarboxylate (DMAD) (2.13 g, 15 mmol) in 60 mL of acetonitrile was heated at reflux for 3 h. The solvent was removed under vacuum, the residue dissolved in benzene, and chroma-

tographed on a neutral alumina column. Using benzene, acetone, and methanol as eluting solvents, the order of elution was DMAD, **6***z*, and **6***y*; **6***y*: uv: 239 (23 000), 275(sh) (13 500), 335 (4200); ^{1}Hmr: 8.07–8.23 (m, 2H, aromatic), 7.38–7.63 (m, 9H, aromatic + OH exchangeable with D_2O), 6.93 (s, 1H, C═CH), 3.63 (s, 3H, CH_3), 3.55 (s, 3H, CH_3); **6***z*: uv: 238 (24 100), 323 (17 000); ^{1}Hmr: 7.93–8.10 (m, 2H, aromatic), 7.37–7.55 (m, 8H, aromatic), 6.05 (s, 1H, C═CH), 5.90 (s, 1H, C═CH), 3.68 (s, 3H, CH_3), 3.67 (s, 3H, CH_3), 3.58 (s, 3H, CH_3), 3.57 (s, 3H, CH_3).

2,5-Diphenyl-3,4-diazacyclopentadienone (1)

Compound **6***h* (1.0 g, 4.3 mmol), lead dioxide powder (20 g, 84 mmol), and 1500 mL of anhydrous ether were stirred vigorously for 10 min. The lead dioxide was filtered and the red solution evaporated under vacuum as quickly as possible. The purple solid was washed with carbon tetrachloride; yield: 0.9 g (85%), mp 110°C (dec.); ir: 3150, 1565, 1535, 1255, 982, 885; uv (ether): 253 (13 000), 433 (900). *Anal.* calcd. for $C_{13}H_{10}N_2O$: C 77.95, H 5.12, N 7.91; found: C 77.71, H 5.47, N 8.02.

1,4,6,7,8,10-Hexaphenyl-2,3,11,12-tetraazatetracyclo-[5.5.1.0^{2,6}0^{8,12}]trideca-3,10-diene-5,9,13-trione (16)

Compound **6***h* (1.0 g, 4.3 mmol), lead dioxide powder (20 g, 84 mmol), and 1500 mL of anhydrous ether were stirred vigorously for 1 h. The lead dioxide was filtered and the yellow solution reduced to 20 mL by vacuum distillation; yield 0.5 g (50%), mp 205–207°C (dec.) (lit. (12) mp 206–208°C).

1,9-Diaza-3,4-dimethyl-6,8-diphenylbicyclo[4.3.0]-3,8-nonadien-7-one (17)

An ether solution of **1** was prepared as above and immediately after filtering the lead dioxide, 2,3-dimethyl-1,3-butadiene (1.0 g, 0.012 mol) was added. The red solution turned yellow after 10 min and the ether was removed under vacuum. The gummy residue was extracted with chloroform leaving the by-product **6***h* behind. Petroleum ether (bp 80–100°C) was added to the extract to give a slightly cloudy solution which was allowed to crystallize open to the air to yield 500 mg (37%) of **17**, which was recrystallized three times from carbon tetrachloride, mp 159–160°C; ir: 3040, 1680, 1188, 990, 830; uv: 270 (17 500), 392 (8200); ^{1}Hmr: 8.20 (m, 2H, aromatic), 7.40 (m, 8H, aromatic), 4.36 (m, 2H, NCH_2), 2.70 (q, J = 17 Hz, 2H, CH_2), 1.63 (m, 6H, CH_3). *Anal.* calcd. for $C_{21}H_{20}N_2O$: C 79.75, H 6.33, N 8.86; found: C 79.05, H 6.44, N 8.77.

4,5-Diaza-3,6-diphenyltricyclo[6.2.1.0^{2,7}]-2,4,6-undecatriene (18)

An ether solution of **1** was prepared as above and immediately after filtering the lead dioxide, [2.2.1]bicycloheptene (1.0 g, 0.011 mol) was added. After 4 h the red solution had turned yellow and the ether was evaporated under vacuum. The product (**18**) was crystallized twice from carbon tetrachloride to give 150 mg (13%) of flaky crystals, mp 230.5–231.5°C; ir: 3070, 1550, 1370, 1132, 767, 694, 667; uv: 265 (22 500); ^{1}Hmr: 8.20–7.45 (m, 10H, aromatic), 3.73 (m, 2H, CH), 2.14 (m, 2H, bridge CH_2), 1.63 (m, 4H, CH_2CH_2). *Anal.* calcd. for $C_{21}H_{20}N_2$: C 84.60, H 6.04, N 9.39; found: C 84.66, H 6.22, N 8.83.

1. R. H. Wiley and R. Wiley. Pyrazolones, pyrazolidones, and derivatives. John Wiley and Sons, New York, NY. 1964. p. 11.
2. W. P. Tang. Ph.D. Thesis. University of Guelph, Guelph, Ont. 1971.
3. P. J. Fagan. M.Sc. Thesis. University of Guelph, Guelph, Ont. 1971.
4. (*a*) M. J. Nye and W. P. Tang. Can. J. Chem. **48**, 3563 (1970); (*b*) P. J. Fagan and M. J. Nye. J. Chem. Soc. Chem. Commun. 537 (1971).
5. A. Bertho and H. Nüssel. Justus Liebigs Ann. Chem. **457**, 278 (1927).
6. J. P. Freeman, J. J. Gannon, and D. L. Surbey. J. Org. Chem. **34**, 187 (1969).
7. F. Sachs and A. Rohmer. Chem. Ber. **35**, 3307 (1902).
8. H. Böhme and H. Schneider. Chem. Ber. **91**, 1100 (1958).
9. O. Dimroth and E. Eberhardt. Justus Liebigs Ann. Chem. **355**, 107 (1904).
10. H. W. Thompson. *In* Molecular spectroscopy. *Edited by* E. Thornton and N. H. Thompson. Pergamon Press, New York, NY. 1959. p. 165.
11. G. Büchi and G. Lukas. J. Am. Chem. Soc. **86**, 5654 (1964).
12. B. M. Trost and P. J. Whitman. J. Am. Chem. Soc. **96**, 7421 (1974).
13. J. Hamer (*Editor*). 1,4-Cycloaddition reactions. Academic Press, New York, NY. 1967. p. 182.
14. L. A. Paquette and L. M. Leichter. J. Am. Chem. Soc. **92**, 1765 (1970).
15. A. B. Evnin and D. R. Arnold. J. Am. Chem. Soc. **90**, 5330 (1968).
16. M. B. Hocking. J. Heterocycl. Chem. **14**, 829 (1977).
17. J. Sauer and H. Weist. Angew. Chem. Int. Ed. Engl. **1**, 269 (1962).
18. C. F. H. Allen. Chem. Rev. **37**, 209 (1945).
19. R. B. Woodward and R. Hoffmann. The conservation of orbital symmetry. Verlag Chemie, Academic Press, Weinheim, Germany. 1970.
20. K-L. Mok and M. J. Nye. J. Chem. Soc. Perkin Trans. I, 1810 (1975).
21. R. C. Cookson and M. J. Nye. J. Chem. Soc. C, 2009 (1965).
22. K-L. Mok and M. J. Nye. J. Chem. Soc. Chem. Commun. 608 (1974).
23. T. Norris. Ph.D. Thesis. Chelsea College, University of London, London. 1974.
24. R. de Neufville and H. v. Pechmann. Chem. Ber. **23**, 3375 (1890).
25. K. V. Auwers and E. Auffenberg. Chem. Ber. **50**, 929 (1917).

Etude structurale des chlorure et sulfate de béryllium hydratés par spectrométrie infrarouge et Raman

FRANÇOIS BERTIN

Laboratoire de Chimie Analytique II, Université de Lyon I, 43 boulevard du 11 Novembre 1918, 69621 Villeurbanne, France

ET

JEAN DEROUAULT

Laboratoire de Spectroscopie Infrarouge, Université de Bordeaux I, 351 cours de la Libération, 33405 Talence, France

Reçu le 13 juin 1978

FRANÇOIS BERTIN et JEAN DEROUAULT. Can. J. Chem. **57**, 913 (1979).

Les auteurs ont étudié, la nature du composé qui se forme lors de l'hydratation directe du chlorure de béryllium. On a analysé le composé par voie chimique, par spectroscopie infrarouge et Raman et par comparaison de ses spectres avec ceux du sulfate tétrahydraté. Les résultats sont en accord avec la formule $[Be(OH)(H_2O)_2{}^+Cl^-]_n$.

On fait l'hypothèse que le composé est un trimère cyclique et on a effectué une analyse simplifiée des coordonnées en vue de trouver un appui pour ces attributions.

FRANÇOIS BERTIN and JEAN DEROUAULT. Can. J. Chem. **57**, 913 (1979).

The authors have investigated the nature of the compound which is formed by direct hydration of beryllium chloride. The compound is analysed by chemical means, by infrared and Raman spectroscopy, and by comparison with the spectra of tetrahydrated sulphate. The results are consistent with the formula $(Be(OH)(H_2O)_2{}^+ Cl^-)_n$.

A cyclic trimeric compound is assumed and a simplified coordinate analysis is performed in order to support these assignments.

[Journal translation]

L'affinité particulière du béryllium pour les groupements oxygénés donneurs d'électrons permet d'obtenir de nombreux complexes stables (1). Cette stabilité est d'ailleurs renforcée lorsque des composés de coordination formés sont du type chélate comportant des liaisons Π plus ou moins conjuguées.

Certains de ces complexes sont dits polynucléaires hydroxydés lorsqu'ils renferment plusieurs ions métalliques séparés par des ponts hydroxo; par exemple, l'anion bicoordinateur (2) pyridine carboxylate-2 conduit au composé neutre dont la structure, établie par radiocristallographie (3), est schématisée ci-dessous.

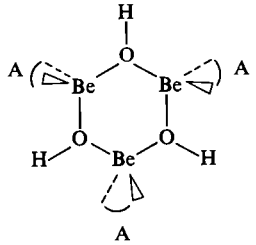

A

En solution, les techniques basées sur les lois de la thermodynamique: potentiométrie, cryométrie, permettent de déterminer le degré de condensation des complexes du béryllium; ainsi on a pu mettre en évidence en milieu aqueux l'espèce trinucléaire hydroxydée $(Be_3(OH)_3(H_2O)_6)^{3+}$ (4, 5). De même, on peut suivre la substitution progressive des molécules d'eau de cette espèce par des bicoordinats tels que l'acide pyridine-carboxylique-2, les diacides carboxyliques, le sulfosalicylaldéhyde et certains amino-acides (1, 6). Il est à noter que peu de coordinats donnent des complexes contenant un seul atome de béryllium. Toutefois les techniques précédentes ne permettent pas une observation directe des espèces formées ce qui limite la validité des modèles proposés; par contre l'utilisation de la spectrométrie moléculaire (ir, Raman, rmn) peut donner des informations sur la structure des composés obtenus.

Lors d'un travail préliminaire (7) nous avons discuté les spectres ir et Raman des solutions aqueuses de chlorure de béryllium à concentration et pH variables; cette étude nous a permis de confirmer les résultats antérieurs obtenus par potentiométrie (5) à savoir l'existence de l'équilibre:

$$3Be(H_2O)_4{}^{2+} + 3OH^- \rightleftarrows (Be_3(OH)_3(H_2O)_6)^{3+} + 6H_2O$$

Dans une série d'articles concernant divers sels de béryllium, Grigor'ev et coll. (8) indiquent quelques fréquences infrarouges et Raman d'un composé solide présenté comme étant $BeCl_2 \cdot 4H_2O$ et les interprètent par la formation du cation $(Be(H_2O)_4)^{2+}$.

Nous avons cherché à compléter l'étude entreprise

0008-4042/79/080913-07$01.00/0

par Grigor'ev et à déterminer s'il est possible d'isoler une espèce autre que le complexe $(Be(H_2O)_4)^{2+}\cdot 2Cl^-$.

Nous avons cristallisé, par différentes méthodes, un hydrate solide du chlorure de béryllium et son homologue deutérié et nous avons enregistré leurs spectres ir et Raman; il apparaît que cette espèce est différente de celle étudiée par Grigor'ev. Afin de disposer d'éléments de comparaison, nous avons analysé les spectres du sulfate de béryllium tétrahydraté également étudié par cet auteur. Par un calcul de vibration simplifié, nous vérifions que la structure proposée pour le composé hydraté, que nous avons isolé à partir du chlorure de béryllium, est plausible.

Etude expérimentale

Préparation des produits solides

Sulfate

Le sulfate de béryllium tétrahydraté est un produit Prolabo. On le recristallise plusieurs fois dans l'eau pour disposer d'échantillons convenables pour les mesures Raman. L'analyse thermogravimétrique est compatible avec la formule $BeSO_4\cdot 4H_2O$: à 200°C le produit de départ a perdu quatre molécules d'eau et la calcination complète à 1000°C laisse l'oxyde BeO comme résidu.

Le composé $BeSO_4\cdot 4D_2O$ est obtenu directement en dissolvant le sulfate anhydre dans un grand excès d'eau lourde. Le produit obtenu par évaporation est redissous et précipité deux fois dans D_2O; sa cristallisation est difficile. Après séchage par P_2O_5 l'analyse thermogravimétrique confirme que le composé obtenu contient bien quatre molécules de D_2O par molécule de $BeSO_4$. Toutes les manipulations sont effectuées dans une boîte à gants.

Chlorures

Différents modes de préparation ont été essayés. Dans tous les cas, on part de $BeCl_2$ anhydre Merck. L'hydratation et la deutériohydratation sont réalisées façon identique.

(*a*) *L'hydratation lente*: elle est effectuée dans une boîte à gants en introduisant dans un récipient hermétiquement fermé, quelques cristaux de $BeCl_2$ anhydre d'une part, et d'autre part, un excès d'eau légère ou d'eau lourde. On s'arrange pour qu'il n'y ait pas de contact direct entre les cristaux et le liquide. Après quelques heures, les cristaux sont devenus pâteux puis sirupeux.

(*b*) *La dissolution brutale en milieu neutre*: la dissolution directe dans l'eau est une réaction violemment exothermique qui rompt les ponts Be—Cl et s'accompagne d'un dégagement de gaz chlorhydrique. On parvient à faire cristalliser un produit évidemment différent du composé $BeCl_2\cdot 4H_2O$ mentionné par Grigor'ev et coll. (8).

(*c*) *La dissolution brutale en milieu acide chlorhydrique*: $BeCl_2$ anhydre est mélangé à une solution plus ou moins concentrée de HCl (jusqu'à 10 *N*) dans un récipient totalement clos.

Les préparations obtenues suivant les modes *a*, *b* ou *c* sont désséchées par P_2O_5. Dans tous les cas il apparaît après quelques jours, une masse blanche que l'on broie, à l'abri de l'air, avant de terminer le séchage sous vide. Le départ de l'eau excédentaire est contrôlé périodiquement par l'enregistrement du spectre infrarouge de prises d'essais de ces composés. Comme les spectres des produits finaux sont tous identiques, il semble que, quel que soit le mode de préparation, on parvienne à un composé unique.

L'analyse élémentaire de ce composé a été effectuée (tableau 1): dosage de la teneur en chlore: précipitation de AgCl par addition de nitrate d'argent en excès; dosage de la teneur en métal: calcination à 1000°C pour transformer le produit en BeO.

Les pourcentages obtenus ne correspondent pas du tout au composé $BeCl_2\cdot 4H_2O$; ils se rapprochent davantage d'une composition du type $(BeCl(OH)(H_2O)_2)_n$: la teneur un peu élevée en chlore peut provenir d'une élimination incomplète de HCl, mais il est à noter que le rapport stoechiométrique en métal/chlore est très voisin de l'unité.

Enregistrement des spectres

Les spectres infrarouges sont obtenus au moyen d'un spectromètre Perkin-Elmer PE 457, à partir de pastilles dans KBr et avec des conditions normales d'enregistrement.

Les spectres Raman sont enregistrés sur un spectromètre Coderg PH ϕ avec la raie excitatrice à 488 nm d'un laser Spectra-Physics SP 165. Les conditions moyennes d'enregistrement des spectres sont les suivantes: puissance du laser 400 mW, tension d'alimentation du photomultiplicateur 850 V, largeur spectrale de fente 3 cm^{-1}, vitesse d'enregistrement 50 cm^{-1} par minute. Pour $BeSO_4\cdot 4H_2O$ on dispose un cristal sur un support; pour le dérivé deutérié on enferme les cristaux dans un tube conique en verre, scellé afin d'éviter l'échange entre D_2O et H_2O de l'atmosphère. Nous avons enregistré les spectres des chlorures en tube scellé également, mais les bandes observées ont une intensité très faible.

Description des spectres et interprétation

Sulfates

La fig. 1 présente les spectres ir et Raman de $BeSO_4,4H_2O$ et de son homologue deutérié enregistrés dans un domaine de fréquence inférieur à 1700 cm^{-1}.

En accord avec la littérature (9), nous retenons comme hypothèse de structure la juxtaposition d'ions tétraèdriques $Be(H_2O)_4^{2+}$ et SO_4^{2-} plus ou moins déformés. Nous présentons donc (tableau 2) une répartition des bandes observées par ir et Raman, entre les groupes BeO_4 et SO_4 et les molécules d'eau de coordination et une attribution de ces bandes aux modes normaux des groupes de symétrie respectifs. La présence de certaines bandes Raman peut s'expliquer par l'existence d'effets de corrélation qui entraînent des éclatements ou rendent actifs des modes interdits dans un motif isolé.

Nous comparons ces résultats à ceux de Grigor'ev et coll. (8) et nous soulignons les principaux points de désaccord. Par exemple, il ne nous paraît pas possible d'attribuer la bande ir à 975 cm^{-1} au mode $\nu_1(A_1)$ de SO_4^{2-}, en raison de l'écart de fréquence avec la bande Raman correspondante (17 cm^{-1}) et de l'intensité qui paraît trop importante pour un mode normalement interdit en ir, même si l'on admet une distorsion importante de l'ion SO_4^{2-} dans le cristal de l'hydrate, qui se traduit par des éclatements des modes fondamentaux de cet ion (à l'exception de ν_1). D'ailleurs cette bande disparaît complètement par deutériation pour être remplacée par une bande intense à 860 cm^{-1}. Grigor'ev observe,

TABLEAU 1. Analyse élémentaire du chlorure de béryllium hydraté

% pondéraux	Résultats expérimentaux	Hypothèse $BeCl_2 \cdot 4H_2O$	Hypothèse $(BeCl(OH)(H_2O)_2)_n$
Cl	39.7	46.7	36.4
Be	9.6	5.9	9.3

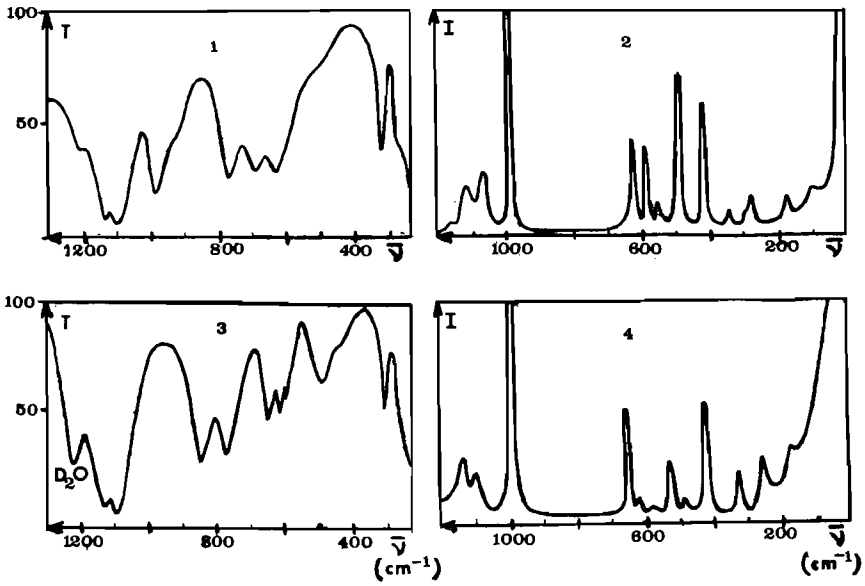

FIG. 1. Spectres infrarouges et Raman des sulfates de béryllium cristallisés. $BeSO_4 \cdot 4H_2O$: *1*, infrarouge; *2*, Raman. $BeSO_4 \cdot 4D_2O$: *3*, infrarouge; *4*, Raman.

lui aussi, une bande à 859 cm^{-1} sur $BeSO_4 \cdot 4H_2O$ et à 850 cm^{-1} sur $BeSO_4 \cdot 4D_2O$; il l'attribue à une composante du mode $\nu_3(F_2)$ de BeO_4. Cependant nous n'avons jamais observé de bande dans cette région pour l'hydrate, de plus l'éclatement proposé par Grigor'ev pour le mode $\nu_3(F_2)$: 690–859 cm^{-1} pour $Be(H_2O)_4^{2+}$ et 660–850 cm^{-1} pour $Be(D_2O)_4^{2+}$ nous paraît trop important; en conséquence, nous attribuons les bandes à 980 cm^{-1} (H_2O) et 860 cm^{-1} (D_2O) à un mouvement de rocking ou de wagging des molécules d'eau de coordination des ions Be^{2+}, en accord avec le rapport isotopique observé: 1.14.

Ces résultats concordent avec ceux obtenus par Gardiner et coll. (10) et Chang (11) sur le nitrate $Be(NO_3)_2 \cdot 4H_2O$ et avec nos propres résultats concernant les solutions acides de $BeCl_2$ (7) ou l'espèce $Be(H_2O)_4^{2+}$ est prépondérante (tableau 2).

Chlorures solides

Bien que l'enregistrement des spectres Raman soit très délicat, nous avons observé une bande vers 510 cm^{-1} déplacée par deutériation à 490 cm^{-1}, et il semble qu'il existe une bande à 415 cm^{-1}.

Les spectres infrarouges (fig. 2) présentent les caractéristiques communes suivantes: Une bande étroite, intense, située à 1120 cm^{-1} déplacée à 920 cm^{-1} par deutériation. Sa fréquence augmente lorsque le séchage est insuffisant et tend à rejoindre la fréquence observée sur les solutions (7). Un massif avec deux maxima à 860 et 890 cm^{-1} (H_2O) ou à 820 et 880 cm^{-1} (D_2O); l'observation est souvent rendue difficile par la présence d'une bande large, intense, à 950 cm^{-1} (H_2O) ou à 780 cm^{-1} (D_2O) due à l'eau d'hygroscopie de composés insuffisamment desséchés. Une bande à 690 cm^{-1}, déplacée à 550 cm^{-1} par deutériation; de plus il apparaît une bande de faible intensité située vers 540 cm^{-1} sur les spectres des produits hydratés et vers 400 cm^{-1} sur ceux des produits deutériés.

Ces résultats n'ont aucun point commun ni avec ceux de Grigor'ev qui suppose la formation d'une espèce $BeCl_2 \cdot 4H_2O$ à l'état solide, ni avec nos propres observations concernant les solutions acides de $BeCl_2$ (tableau 2). En particulier, l'absence d'une bande intense dans la région 300–350 cm^{-1}, observée sur tous les tétrahydrates cristallisés: sulfate, nitrate, perchlorate, ..., aussi bien en infrarouge qu'en

TABLEAU 2. Proposition d'attribution des bandes ir et Raman observées sur $BeSO_4 \cdot 4H_2O$ et son homologue deutérié; comparaison avec les attributions de Grigor'ev et coll (8); rappel des attributions proposées pour $BeCl_2 \cdot 4H_2O$ en solution aqueuse (7) (fréquences données en cm^{-1})

(*a*) $BeSO_4 \cdot 4H_2O$

	Ce travail											Résultats de Grigor'ev (8)										Solution acide de $BeCl_2$ (7)					
	BeO_4[a]				SO_4[a]				H_2O[b]			BeO_4				SO_4				H_2O		BeO_4[f]				H_2O[b]	
	ν_1	ν_2	ν_3	ν_4	ν_1	ν_2	ν_3	ν_4	δ	ρ	w	ν_1	ν_2	ν_3	ν_4	ν_1	ν_2	ν_3	ν_4	δ	ρ	ν_1	ν_2	ν_3	ν_4	δ	ρ,w
	[e]	[e]	780	325	[e]	[e]	1080	625				—	—	690						1651	520						
Infrarouge							1130		1640	*980*	550			771	312	*975*	—	1058	—	1667	à	[e]	[e]	[d]	[d]	1640	990
							1200	690[c]			750			859				1121		1678	660						
				(280)		415	1080	588						697			412	1081	593								
Raman	542	190	[d]		992		1110		[d]	[d]	[d]	563	—		335	1000	505	1120	638	—	—	534	[d]	[d]	357	1640	[d]
				340		495		628						781								P			DP		
							1120																				

(*b*) $BeSO_4 \cdot 4D_2O$

	Ce travail											Résultats de Grigor'ev (8)										Solution acide de $BeCl_2$ (7)					
	BeO_4[a]				SO_4[a]				D_2O[b]			BeO_4				SO_4				D_2O		BeO_4[f]				D_2O[b]	
	ν_1	ν_2	ν_3	ν_4	ν_1	ν_2	ν_3	ν_4	δ	ρ	w	ν_1	ν_2	ν_3	ν_4	ν_1	ν_2	ν_3	ν_4	δ	ρ	ν_1	ν_2	ν_3	ν_4	δ	ρ,w
	[e]	[e]	770	307	[e]	[e]	1090	613	1240		*420*	—	—	660			*412*	1078	589		440						
Infrarouge							1120	660[c]		*860*	*490*			767	302	*962*				1240	à	[e]	[e]	[d]	[d]	1210	840
														850			*507*	1142	613		490						
				(255)		410	1091	570														512	[d]	[d]	330	1210	[d]
Raman	516	180	[d]		992	488	1120	610	[d]	[d]	[d]	—	—	—	—	—	—	—	—	—	—	P			DP		
				315				652																			

[a]La notation correspondant à la symétrie T_d est conservée pour le groupe BeO_4 malgré la symétrie différente dans $Be(H_2O)_4^{2+}$; dans l'hypothèse de la symétrie T_d, le dénombrement est $\Gamma = 1A_1(\nu_1), 1E(\nu_2), 2F_2(\nu_3,\nu_4)$.

[b]Mouvements de déformation des molécules d'eau de coordination de l'ion Be^{2+}, δ: scissoring, ρ: rocking, w: wagging.

[c]Attribution incertaine (attribuable aussi au mode ν_3 de BeO_4).

[d]Vibration active non observée sur nos spectres.

[e]Vibration inactive.

[f]P: bande polarisée; DP dépolarisée.

REMARQUES: Les fréquences en italiques correspondent aux principaux points de désaccord entre nos résultats et ceux de Grigor'ev (le signe — représente les valeurs non indiquées par cet auteur; aucun résultat n'est reporté pour $BeSO_4$, $4D_2O$). Le doublet 412–507, attribué par Grigor'ev à la $\nu_2(E)$ de SO_4^{2-} pour le spectre ir de $BeSO_4 \cdot 4D_2O$, nous a paru plutôt correspondre aux mouvements des molécules d'eau, par analogie avec le spectre de $BeSO_4,4H_2O$ pour lequel ce même doublet n'est pas repéré en ir; cependant les spectres Raman de ces deux composés (fig. 1) présentent des différences importantes qui suggèrent qu'un changement de symétrie s'est produit dans le cristal au cours de la deutériation.

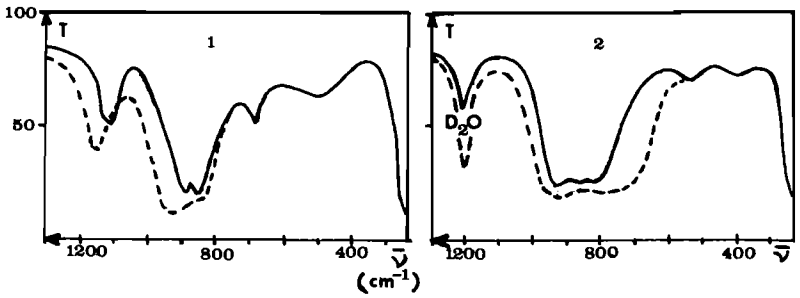

FIG. 2. Spectres infrarouges des chlorures de béryllium cristallisés. *1*, A l'état hydraté; *2*, à l'état deutériohydraté; *en pointillé*: l'allure du spectre lorsque le produit est insuffisamment sec.

Raman, exclut la présence de tétraèdres $Be(H_2O)_4^{2+}$. Par contre ces résultats correspondent assez bien à ceux que nous avons reportés pour les solutions neutres de $BeCl_2$ (7). Ainsi, l'existence d'une bande intense à 1100–1150 cm^{-1} voisine de celle que nous observons en solution nous conduit à admettre la formation d'un composé possédant des ponts hydroxo-, probablement polynucléaires, du type $((H_2O)_2Be(OH))_n^{n+} \cdot nCl^-$. Dans cette région en effet, une bande infrarouge a été observée par Scargill (12) sur les composés hydroxydés de l'étain et attribuée par cet auteur à la vibration de déformation du groupement SnOH. Les autres bandes que nous avons observées sont dues, soit à des vibrations symétriques ou asymétriques des liaisons métal–oxygène (515 cm^{-1} et 860–890 cm^{-1}), soit à des mouvements γ, hors du plan, des enchaînements Be—O—H (690 cm^{-1}) si l'on suppose que l'espèce formée est cyclique, ce que l'on ne peut affirmer avec certitude.

Nous remarquons que l'hypothèse de la formation de cette espèce est en bon accord avec les résultats de l'analyse élémentaire (tableau 1).

Le caractère hygroscopique particulièrement marqué de ce composé ne nous a pas permis de faire une étude radiocristallographique et d'établir avec certitude sa structure, mais l'hypothèse d'un trimère cyclique, déjà observé avec de nombreux composés du béryllium (1, 3 à 6) peut être envisagée.

Calcul des modes de vibrations de modèles simplifiés pour les cations $Be(H_2O)_4^{2+}$ et $(BeOH(H_2O)_2)_3^{3+}$

Le but de ce calcul de vibration n'est pas de déterminer des champs de forces précis, mais seulement de vérifier si les propriétés mécaniques d'un composé cyclique sont compatibles avec l'analyse des spectres proposée ci-dessus. Afin de disposer de constantes de forces de valeur raisonnable, nous avons déterminé en premier lieu le champ de forces d'un tétraèdre régulier BeO_4, comme modèle du cation $Be(H_2O)_4^{2+}$. Ensuite nous avons transféré les résultats au modèle cyclique $(BeOH(H_2O)_2)_3$. Nous tiendrons compte de l'existence des groupes hydroxo- mais nous négligerons les atomes d'hydrogène des molécules d'eau coordinées.

Ces calculs ont été effectués selon la méthode de Wilson et coll. (13), à l'aide de programmes écrits au laboratoire (14).

Tétraèdres BeO_4

Les paramètres géométriques du groupe BeO_4 sont ceux d'un tétraèdre régulier, avec distance BeO prise égale à 1.58 Å, en accord avec la littérature (3, 8). Pour tenir compte approximativement de la deutériation, nous avons affecté l'oxygène de masses égales à 18 ou 20. La détermination des constantes de forces des modes de symétrie A et E est sans ambiguité car il n'y a qu'un seul mode par espèce de symétrie, et donc pas de constante d'interaction. Les modes de symétrie F_2 étant au nombre de deux, il existe une constante d'interaction et le système est indéterminé. Selon la méthode de Torkington (15), la résolution de l'équation séculaire conduit à deux fonctions reliant une constante principale et la constante d'interaction dont les termes dépendent de la géométrie, des masses et des fréquences de vibration de la molécule. Les courbes obtenues $F_{11}^{F_2} = f_1(F_{12})$ et $F_{22}^{F_2} = f_2(F_{12})$ sont des ellipses. On trouve ainsi une infinité de champs de forces conduisant aux fréquences exactes, mais correspondant à des séparations d'énergie potentielle différentes. En l'absence des fréquences de dérivés isotopiques, le choix d'une solution est arbitraire; celle qui correspond à la constante de force de déformation minimum est souvent préférée (16) car les valeurs de la constante de force de valence obtenues ainsi sont en général les plus satisfaisantes. Les résultats que nous avons obtenus en appliquant la méthode ci-dessus aux tétraèdres BeO_4 (O = 18 et O = 20) conduisent aux valeurs moyennes mentionnées dans le tableau 3. Bien que la précision des effets isotopiques calculés paraisse bonne, cela ne signifie pas forcément que dans le cation réel $Be(H_2O)_4^{2+}$ les interactions entre les modes du groupe BeO_4 et les mouvements de l'eau soient négligeables, mais que celles-ci demeurent presque inchangées après deutériation.

TABLEAU 3. Champ de forces et fréquences calculées pour les modèles BeO_4

Constantes de forces		Modes	BeO_4 O = 18 ν_{calc} (cm^{-1})	BeO_4 O = 18 ν_{exp} (cm^{-1})	BeO_4 O = 20 ν_{calc} (cm^{-1})	BeO_4 O = 20 ν_{exp} (cm^{-1})
F BeO	2.47	ν_{F_2} BeO_4	780	780	770	770
f BeO BeO	0.218	ν_{A_1} BeO_4	543	545	515	515
F^E δBeO_4	0.318	δ_{F_2} BeO_4	323	325	309	307
$F^{F_2}\delta BeO_4$	0.562	δ_E BeO_4	190	190	180	180
$f\nu^{F_2}$ δ^{F_2}	$0.371\cdot\sqrt{2}$					

REMARQUES: Les constantes de forces de liaison sont exprimées en mdyn $Å^{-1}$, celles de déformation en mdyn rad^{-2} Å et celles d'interaction liaison–angle en mdyn rad^{-1}.

TABLEAU 4. Champs de forces et fréquences calculées pour les modèles $(BeOH(O_2))_3$

F	CF_1	CF_2	ν_{exp} (cm^{-1}) H	ν_{exp} (cm^{-1}) D	ν_{calcd} (CF_1) (cm^{-1}) H	ν_{calcd} (CF_1) (cm^{-1}) D	ν_{calcd} (CF_2) (cm^{-1}) H	ν_{calcd} (CF_2) (cm^{-1}) D	Modes
F_i(BeO)	2.47	3							
F_e(BeO)	2.47	2.47	3300_S	2400_S	3302	2405	3302	2405	νOH E'
f_{ii}(BeO,BeO)	0.218	0.218	1120_S à 1170_L	920_S à 940_L	1138	977	1169	922	δOH E'
f_{ie}(BeOBe)	0	0.3	890_S	880_S	827	774	890	888	$\nu(BeO)_i$ E'
F_α^E(OBeO)	0.318	0.318	855_S	820_S	732	683	820	770	$\nu(BeO)_{i,e}$ E'
$F_\alpha^{F_2}$(OBeO)	0.562	0.562	690_S	550_S	697	607	685	572	γOH A_2''
$f_{d\alpha} - f_{d\alpha'}$	0.371	0.371	*$\sim 510_S$*	*$\sim 490_S$*	596	548	615	588	νBeO_e E'
FνOH	6.04	6.04	*515_L*	*505_L*	508	493	531	515	$\nu BeO_i,\alpha,\beta A_1'$
Fβ(BeOBe)	0.3	0.3	*415_L*	*395_L*	423	404	437	418	$\nu BeO_{i,e},\alpha,\beta A_1'$
FδOH	0.29	0.35							
FγOH	0.21	0.14							
f(BeO$_i$,δOH)	0	0.115							
f(BeO$_e$,γOH)	0	−0.04							
FτBeO	0.1	0.1							

REMARQUES: i: interne au cycle; e: externe au cycle; fréquence en italique: Raman; unités voir tableau 3; S: solide; L: solution.

Cycle $(BeOH(O_2))_3$

D'après l'équilibre de cyclisation vu précédemment, il nous a paru logique de prendre comme modèle pour ce dérivé cyclique l'édifice atomique obtenu en joignant trois tétraèdres BeO_4 par leurs sommets, avec mise en commun des atomes d'oxygène.

La distance BeO a été gardée égale à 1.58 Å et les angles autour du béryllium ont été maintenus à 109° 28′. Nous avons fait l'hypothèse d'un cycle plan, ce qui conduit à un angle Be—O—Be égal à 130° 31′.

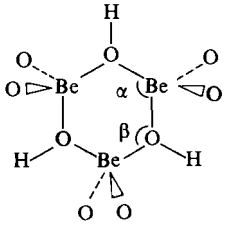

Comme ci-dessus, l'effet isotopique dû aux molécules d'eau a été simulé en affectant des masses de 18 ou 20 aux atomes d'oxygène correspondants. Cependant en raison de l'importance de la bande attribuée aux mouvements δOH au cours de l'analyse des spectres, nous avons tenu compte des hydroxydes OH réels et non des masses ponctuelles. La distance OH a été posée égale à 0.97 Å et les angles BeOH pris tous égaux.

Pour un tel modèle, de symétrie D_{3h}, les 39 modes se répartissent comme suit: $\Gamma = 5A_1' + 3A_2' + 8E' + 1A_1'' + 4A_2'' + 5E''$. Seuls les modes de type A_1', E' et E'' sont actifs en Raman alors qu'en infrarouge on ne peut observer que les modes A_2'' et E'.

Les coordonnées de vibration ont été écrites à partir de celles des tétraèdres, en distinguant toutefois les liaisons du cycle et les liaisons hors du cycle. Les déformations des angles Be—O—Be et Be—OH, ainsi que les déformations hors du plan γOH et τBeO ont été prises en compte. Les coordonnées surabondantes propres au cycle ont été éliminées au cours du calcul numérique, tandis que celles qui correspondent aux angles entourant les atomes de béryllium

ou d'oxygène (OH) ont été éliminées directement afin de pouvoir transférer les constantes de forces provenant du calcul précédent de BeO_4.

Un premier calcul a été effectué avec le champ de forces CF_1 (tableau 4). Dans ce champ de forces, les constantes transférées depuis BeO_4 ont conservé leur valeur d'origine et seules les constantes principales indispensables ont été définies pour le cycle (δBe—O—Be, τBeO) et les groupements hydroxydes (νOH, δOH et γOH). Le tableau 4 présente également les fréquences calculées pour les modes susceptibles de correspondre aux bandes observées. On voit que les fréquences de cycle sont trop faibles et l'effet isotopique sur δOH est trop transmis aux valences; de même le mouvement γOH a un effet isotopique trop faible. Le champ de forces CF_2, dans lequel la constante de force des liaisons BeO du cycle a été augmentée et quelques interactions introduites pour remédier aux défauts ci-dessus, conduit à des résultats assez satisfaisants (tableau 4).

Le nombre de constantes de forces calculées paraît élevé mais un grand nombre d'entre elles ont été transférées directement de BeO_4 sans modification.

En conclusion, ces calculs montrent que les propriétés mécaniques du modèle cyclique sont compatibles avec notre interprétation des résultats spectroscopiques. De plus, avec les réserves nécessaires dues aux approximations, il est possible de préciser l'attribution des bandes observées.

1. F. BERTIN et G. THOMAS. Bull. Soc. Chim. Fr. 3467 (1971).
2. P. SOUCHAY. Ions minéraux condensés. Masson Ed., Paris, France. 1969.
3. R. FAURE, F. BERTIN, H. LOISELEUR et G. THOMAS-DAVID. Acta Crystallogr. B**30**, 462, (1974).
4. H. KAKIHANA et L. G. SILLEN. Acta Chem. Scand. **10**, 985 (1956).
5. F. BERTIN, G. THOMAS et J. C. MERLIN. Bull. Soc. Chim. Fr. 2393 (1967).
6. G. DUC, F. BERTIN et G. THOMAS-DAVID. Bull. Soc. Chim. Fr. 793 (1974); 495 (1975); 414 (1976); 196 (1977); 645 (1977).
7. F. BERTIN et J. DEROUAULT. C.R. Acad. Sci. C973 (1975).
8. A. I. GRIGOR'EV, V. A. SIPACHEV et A. V. NOVOSELOVA. Dokl. Akad. Nauk SSSR, **160**, 383 (1965); Zh. Strukt. Khim. **10**, 820 (1969); **11**, 458 (1970).
9. D. A. EVEREST. The chemistry of beryllium. Elsevier, Amsterdam, London, New York. 1964; R. E. CONNICK et D. FIAT. J. Chem. Phys. **39**, 1349 (1963); A. FRATIELLO, R. E. LEE, V. M. NISHIDA et R. E. SCHUSTER. J. Chem. Phys. **48**, 3705 (1968).
10. D. J. GARDINER, R. E. HESTER et E. MAYER. J. Mol. Struct. **22**, 327 (1974).
11. T. G. CHANG. Ph.D. Thesis, University of Waterloo, Waterloo, Ontario, Canada; *cité par* D. E. IRISH *dans* Structure of water and aqueous solution. *Edité par* W. A. P. Luck. Verlag Chemie, Weinheim, Germany. 1974. p. 338.
12. D. SCARGILL. J. Chem. Soc. 4440 (1961).
13. E. B. WILSON, J. C. DECIUS et P. C. CROSS. Molecular vibrations. McGraw Hill Book Company Inc., New York. 1955.
14. J. DEROUAULT, M. T. FOREL et P. MARAVAL. Can. J. Spectrosc. **23**, 67 (1978).
15. P. TORKINGTON. J. Chem. Phys. **17**, 357 (1949).
16. J. DEROUAULT et M. T. FOREL. Ann. Chim. 131 (1971).

The kinetics of the reactions of boric acid with 5-substituted salicylate ions

ALAN QUEEN, LORNE DAVIES, AND ANDREW CON

Parker Chemical Laboratory, University of Manitoba, Winnipeg, Man., Canada R3T 2N2

Received August 24, 1978

ALAN QUEEN, LORNE DAVIES, and ANDREW CON. Can. J. Chem. **57**, 920 (1979).

Salicylate ions form 1:1 complexes with boric acid. The kinetics of these reactions have been studied by the stopped-flow method and stability constants have been calculated from absorption measurements on the solutions at equilibrium. Temperature studies of the rates of reaction of boric acid and unsubstituted salicylate ions at pH 5.29 have been carried out. The data correlate well with the Arrhenius equation.

ALAN QUEEN, LORNE DAVIES et ANDREW CON. Can. J. Chem. **57**, 920 (1979).

Les ions salicylates forment des complexes 1:1 avec l'acide borique. On a étudié la cinétique de ces réactions par la technique des flux stoppés et on a calculé les constantes de stabilité à partir de mesures d'absorption de solution à l'équilibre. On a effectué des études sur la variation des vitesses de réaction de l'acide borique avec des ions salicylates non-substitués à un pH de 5.29 en fonction de la température. Les données sont en bon accord avec l'équation d'Arrhénius.
[Traduit par le journal]

Introduction

α-Hydroxyacids form 1:1 and 1:2 complexes with boric acid. At low hydroxy acid concentrations only the 1:1 complexes are important (1–5). Although the 1:1 complexes have not been isolated, the 1:2 complex formed from salicylate ions and boric acid has been shown (5) to have the spiro structure **1**. These results suggest that the 1:1 complex has the cyclic structure **2**. Further support for this view is provided by the observation (6) that borate ions specifically catalyse the hydrolysis of phenyl salicylate but not the corresponding reaction of phenyl *o*-methoxybenzoate. Moreover, we have found that boric acid causes large changes in the uv spectra of 5-substituted salicylate ions and *o*-hydroxybenzyl alcohol but has no effect on the spectra of methyl salicylate, *o*-methoxybenzoate ions, *p*-hydroxybenzoate ions, or *p*-hydroxybenzyl alcohol.

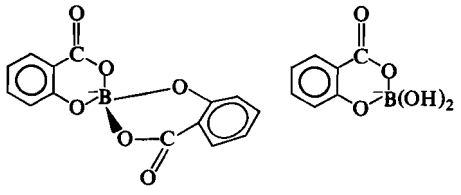

1 **2**

The rates of complexation of boric acid with salicylate ions may be readily measured by the stopped-flow method. A previous study (7) has shown that, at pH 5.29, the first-order rate constants are independent of the wavelength used to monitor the reaction. However, at pH 3.45, wavelength-dependent rate constants are observed. These results suggest that the reactions proceed through the intermediates **4** and **6** (Scheme 1).

It was thought that further information about the mechanism of the reaction might be obtained by studying the effects of temperature on the rate constants and by measuring the effects of substituents on the rate and equilibrium constants for complex formation. The results of these studies are reported.

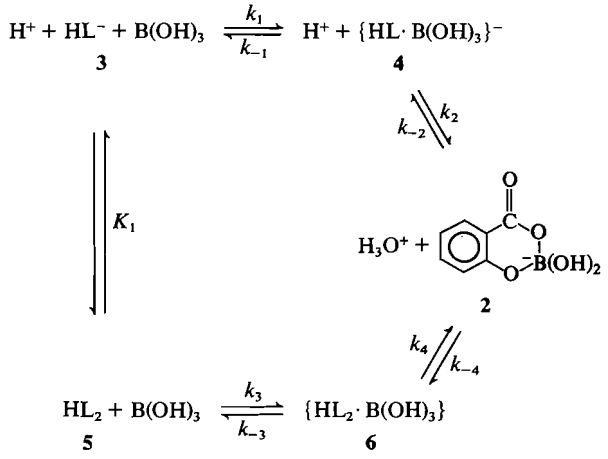

SCHEME 1

Experimental

The 5-substituted salicylic acids were commercial samples which were recrystallised from water or aqueous ethanol to constant melting point. Boric acid was Fisher Certified Reagent. All materials were dried *in vacuo* over phosphorus pentoxide.

Temperatures were measured with a platinum resistance thermometer and were constant to within ±0.01°C. The kinetic data were obtained from measurements of the changes in transmitted light at 320 nm using a standard Canterbury

0008-4042/79/080920-04$01.00/0

stopped-flow apparatus (8). Rate constants were calculated by an on-line method that has been described (9) and were accurately first order over at least three half-lives. Each rate constant was measured 10 times in separate kinetic runs.

The equilibrium constants were calculated from spectroscopic data recorded at 320 nm, using the method of Rose and Drago (10) as previously described (7).

pH measurements were carried out at 25°C using a Radiometer pH meter calibrated at pH 4.00 ± 0.02 and pH 6.00 ± 0.02.

Results

Under the conditions used in the stopped-flow experiments, concentration changes are too small to be measured at low pH values where the salicylic acids are undissociated (7). For this reason, the present studies have been carried out at pH > 5, where the only reactants present in significant amounts are boric acid and salicylate ions.

The pseudo-first-order rate constants fit eq. [2], in all cases. Rate data for the salicylate ion reaction at pH 5.29 are listed in Table 1 for five different temperatures.

$$[2] \qquad k_{obs} = k_b + k_f[H_3BO_3]$$

The results at 24.76°C are only in fair agreement with our previous values for this reaction at 25°C and pH 5.29. These earlier data were obtained by fluorescence stopped-flow experiments using exciting light at 335 nm. However, measurements were also made at other wavelengths and with transmission measurements and no dependence of the rate constants on wavelength was observed. We are unable to explain the differences in the two sets of results but it is possible that an error was made in recording the pH value. The differences would be explained by a lower pH value for the earlier experiments. In any case, the conclusions drawn in the earlier paper are not changed and, importantly, the value of the ratio k_f/k_b is not greatly altered.

Plots of ln k_b and ln k_f against T^{-1} are shown in Fig. 1. Both plots are linear within the experimental error. The enthalpies and entropies of activation for the forward and backward reactions are given at the bottom of the table. The values of the ratio k_f/k_b are compared with those of the formation constant, K_{HL^-}, at 5, 15, and 25°C.

The rate constants for the reactions of 5-substituted salicylate ions with boric acid at pH 5.48 are summarised in Table 2. The equilibrium constants for complex formation, K_{HL^-}, are also shown in the same table together with the first dissociation constants, K_1, of the substituted salicylic acids (11).

Discussion

If the reaction between the salicylate ions and

TABLE 1. The effect of temperature on the rate of reaction of salicylate ions with boric acid at pH 5.29

	k_{obs} (s^{-1})								
	$[H_3BO_3]$ (M)								
T (K)	0.03252	0.05943	0.07415	0.09410	0.1139	k_b (s^{-1})	k_f (s^{-1} M^{-1})	k_s/k_b (M^{-1})	K_{HL^-} (M^{-1})
277.98	1.10±0.01	1.51±0.01	1.73±0.02	2.02±0.02	2.29±0.02	0.63±0.02	14.7±0.2	23.3±0.2	23.4±1.2
283.24	1.64±0.02	2.14±0.02	2.41±0.03	2.80±0.03	3.20±0.02	1.01±0.02	19.1±0.2	18.9±0.2	
288.11	2.28±0.02	2.89±0.03	3.27±0.02	3.69±0.03	4.21±0.04	1.50±0.03	23.6±0.4	15.7±0.4	15.4±0.4
293.13	3.23±0.03	4.02±0.03	4.43±0.04	5.01±0.05	5.54±0.06	2.32±0.02	28.4±0.3	12.2±0.3	
297.92	4.32±0.04	5.38±0.05	5.69±0.06	6.54±0.06	7.27±0.08	3.16±0.12	35.9±1.5	11.4±1.7	11.0±0.2

NOTE: $\Delta H_f^* = 6.65 \pm 0.19$ kcal mol^{-1}; $\Delta S_f^* = -29.1 \pm 0.6$ cal mol^{-1} deg^{-1}; $\Delta H_b^* = 12.86 \pm 0.28$ kcal mol^{-1}; $\Delta S_b^* = -13.0 \pm 1.0$ cal mol^{-1} deg^{-1}.

TABLE 2. Rate and equilibrium constants for the reaction of 5-substituted salicylate ions with boric acid at 25°C and pH 5.48

Substituent	λ (nm)	k_b (s^{-1})	k_f ($s^{-1} M^{-1}$)	k_f/k_b (M^{-1})	K_{HL^-} (M^{-1})	$10^3 K_1$[c]
SO_3^-	320	2.69±0.05	31.1±1.5	11.6±1.6	7.1±0.1	—
CH_3	320	4.57±0.28	50.2±1.8	11.0±2.1	11.3±0.2	0.931
H[a,b]	320	3.16±0.12	35.9±1.5	11.4±1.6	11.0±0.2	1.02
CH_3O	320	7.90±0.07	82.3±1.1	10.4±1.2	10.7±0.3	1.15
Cl	320	5.53±0.06	49.3±0.9	8.3±1.0	7.1±0.3	1.99
Br	320	5.03±0.04	44.3±0.6	8.8±0.6	7.4±0.3	2.43
NO_2	320	2.38±0.11	13.3±0.7	5.6±0.8	3.0±0.1	4.81

[a]pH 5.29.
[b]Previous results (7) obtained from fluorescence stopped-flow studies: $k_b = 3.55\ (s^{-1})$; $k_f = 39.4\ (s^{-1} M^{-1})$; $K_{HL^-} = 10.6\ (M^{-1})$.
[c]Reference 11.

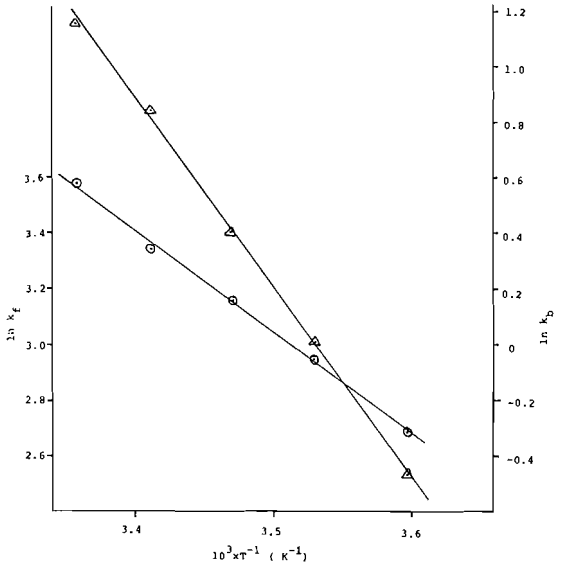

FIG. 1. Arrhenius plots for the reaction of salicylate ions with boric acid at pH 5.29: ⊙ forward reaction; △ backward reaction.

boric acid proceeds through the intermediate **4**, k_b and k_f will be complex functions of the rate constants k_1, k_{-1}, k_2, and k_{-2}. Hence, the Arrhenius plots for k_b and k_f might be appreciably curved. Figure 1 shows that this is not the case, so that any intermediate formed in the reaction must rapidly reach steady-state concentrations. If this is so, k_{obs} is given by [3]

$$[3] \quad k_{obs} = \frac{k_{-1}k_{-2}}{k_{-1} + k_2} + \frac{k_1 k_2}{k_{-1} + k_2}\,[H_3BO_3]$$

Hence, the equilibrium constant for the reaction is given by [4]

$$[4] \quad k_f/k_b = k_1k_2/k_{-1}k_{-2} = K_1K_2 = K_{HL^-}$$

This is consistent with the closely similar values of the rate ratios and equilibrium constants for most of the reactions summarised in Tables 1 and 2. The same correspondence of the kinetic and thermodynamic equilibrium constants would be observed if the reactions were one step processes. However, the k_f/k_b ratios and the values of K_{HL^-} are not the same for the reactions involving 5-sulfo- and 5-nitrosalicylate ions. Moreover, the values of k_{obs} vary slightly in the case of the sulfo compound (Table 3). These results suggest that, at least in some cases, kinetically significant intermediates such as **4** are formed during the course of the complexations.

The values of log k_b, log k_f, and log K_{HL^-} do not linearly correlate with any of the standard σ values. Since the carboxylate group is *meta* and the hydroxyl group is *para* to the substituent, this is perhaps not surprising. However, linear free energy correlations such as [5] were not significantly more successful in

TABLE 3. Rates of reaction of 5-substituted salicylate ions with boric acid at 25°C and pH = 5.48: the effects of wavelength changes

Substituent	$[H_3BO_3]$ (M)	λ (nm)	k (s^{-1})
SO_3^-	0.0517	280	4.06±0.06
		300	4.31±0.05
		320	4.29±0.06
		340	4.48±0.06
CH_3	0.0349	300	6.14±0.08
		320	6.04±0.05
		340	5.96±0.06
CH_3O	0.0517	300	12.3±0.1
		320	12.3±0.2
		340	12.2±0.2
Cl	0.0517	300	8.03±0.10
		320	8.07±0.06
		340	7.98±0.06
Br	0.0517	300	7.63±0.06
		320	7.52±0.06
		340	7.55±0.08
NO_2	0.1877	300	4.77±0.06
		320	4.83±0.06
		340	4.98±0.06

correlating the data than the Hammett equation. It is interesting that the dissociation constants of the salicylic acids do not correlate particularly well with any combination of the various σ values (11). Not surprisingly, the best linear free energy relationship was obtained by plotting log K_{HL^-} or log k_f/k_b against pK_1. However, the separate values of log k_b and log k_f do not linearly correlate with pK_1. We interpret this to indicate that the rate constants are complex quantities, as required by Scheme 1.

$$[5] \qquad \log k = \sigma_m \rho_m + \sigma_p \rho_p$$

The activation parameters for the reaction of the unsubstituted salicylate ions with boric acid do not show any unusual features that would require the presence of an intermediate in the reaction. However, the results do not exclude the formation of such an intermediate but if one is formed it must reach steady-state concentration during the early stages of the reaction.

It was not expected that the entropy term would play such a large role in limiting the ease of complex formation. The transition state and the intermediate, if formed, must be very ordered compared to the reactants. This suggests strong solvation effects and the possibility of steric hindrance to the free rotation of the $B(OH)_3$ group.

Acknowledgements

The authors gratefully acknowledge financial support by the National Research Council of Canada and the Research Board of the University of Manitoba.

1. K. KUSTIN and R. PIZER. J. Am. Chem. Soc. **91**, 317 (1969).
2. G. LORBER and R. PIZER. Inorg. Chem. **15**, 978 (1976).
3. J. MEULENHOFF. Z. Anorg. Allg. Chem. **142**, 373 (1925).
4. N. VERMAAS. Recl. Trav. Chim. Pays-Bas, **51**, 67 (1932).
5. J. BOESCHEN. Adv. Carbohydr. Chem. **4**, 189 (1949).
6. B. CAPON and B. C. GHOSH. J. Chem. Soc. B, 472 (1966).
7. A. QUEEN. Can. J. Chem. **55**, 3035 (1977).
8. E. F. CALDIN, J. E. CROOKS, and A. QUEEN. J. Phys. E, **6**, 930 (1973).
9. A. QUEEN, J. L. CHARLTON, E. DAWSON, and W. BUCHANNON. Chem. Instrum. **6**, 153 (1975).
10. N. J. ROSE and R. S. DRAGO. J. Am. Chem. Soc. **81**, 6138 (1959).
11. G. E. DUNN and FEI-LIN KUNG. Can. J. Chem. **44**, 1261 (1966).

Synthesis related to the octodiose in apramycin. Part III

HAROLD C. JARRELL AND WALTER A. SZAREK

Department of Chemistry, Queen's University, Kingston, Ont., Canada K7L 3N6

Received July 31, 1978

HAROLD C. JARRELL and WALTER A. SZAREK. Can. J. Chem. **57**, 924 (1979).

A synthesis of methyl 2,3-di-*O*-benzyl-7,8-dideoxy-4-*O*-methylthiomethyl-D-*glycero*- and L-*glycero*-α-D-*gluco*-oct-7-enopyranoside (**11** and **12**) has been achieved by the reaction of methyl 2,3-di-*O*-benzyl-4-*O*-methylthiomethyl-α-D-*gluco*-hexodialdo-1,5-pyranoside (**9**) with vinylmagnesium bromide; the stereochemistry at C-6 was established by degradation of **12** to the enantiomer of a known heptose derivative. Olefin **12** was converted, in six steps, into a mixture of dialdose derivatives **18** and **19** from which methyl glycosides **21** and **20**, respectively, were prepared and shown to have the desired *trans*-decalin structure. The stereochemistry at C-7 in glycosides **20** and **21** was established by nmr spectroscopy.

An intramolecular reaction involving the methylthiomethyl function has been observed and shown to give rise to *O*-methylene derivatives.

HAROLD C. JARRELL et WALTER A. SZAREK. Can. J. Chem. **57**, 924 (1979).

On a réussi une synthèse des di-*O*-benzyl-2,3 didéoxy-7,8 *O*-méthylthiométhyl-4 D-glycéro- et L-glycéro-α-D-*gluco* octène-7 pyrannosides de méthyle (**11** et **12**) grâce à la réaction du di-*O*-benzyl-2,3 *O*-méthylthiométhyl-4 α-D-glucohexodialdo-1,5 pyrannoside de méthyle (**9**) avec le bromure de vinylmagnésium; on a déterminé la stéréochimie en C-6 par une déshydratation de **12** vers l'énantiomère de dérivé heptose connu. L'alcène **12** a pu être transformé, en six étapes, en un mélange de dérivés dialdoses **18** et **19** à partir desquels on a pu préparer les glycosides de méthyle **21** et **20** respectivement; ceci démontre qu'ils possèdent la structure décalinique *trans* désirée. On a démontré la stéréochimie en C-7 des glycosides **20** et **21** grâce à la spectroscopie rmn.

On a noté une réaction intramoléculaire impliquant le groupe méthylthiométhyle qui donne lieu à des dérivés *O*-méthylène.

[Traduit par le journal]

Introduction

Antibiotics have proven to be a rich source of higher-carbon amino sugars (1) which include the aminooctose in lincomycin (2) and in the ezomycins (3) as well as an 11-carbon amino sugar, namely, hikosamine, which is a component of the nucleoside antibiotic hikizomycin (4). Recently, apramycin (**1**) (5) and oxyapramycin (**2**) (6) have been shown to be components of the aminocyclitol antibiotic complex nebramycin (7). Structural studies have revealed that apramycin contains the unusual aminooctodiose **3** (8) whereas oxyapramycin contains **4** (6). In addition to its unique structural features, apramycin is of interest because it has been found to be a potent antibiotic relative to neamine (9*a*) and has been reported (10) to be inactivated by only one aminoglycoside-inactivating enzyme. Replacement of the terminal 4-amino-4-deoxy-D-glucose moiety in apramycin with a methyl group yields a cyclitol derivative which exhibits an antimicrobial spectrum similar to that of apramycin (9). In view of the latter result, this laboratory has been investigating the preparation of octodioses which are related to structures **3** and **4** and which may be useful in the synthesis of pseudodisaccharides containing these structures. An earlier report (11) from this laboratory described the synthesis of two octodioses which were not successfully converted into the desired *trans*-decalin structure. The present article describes in detail results, which have been outlined (12), of a synthesis of derivatives of two octodioses having a *trans*-decalin structure.

Results and Discussion

The synthesis utilizing a chain extension of the readily available derivative **9** is shown in Scheme 1. Methyl 2,3-di-*O*-benzyl-α-D-glucopyranoside (**5**) was selectively benzoylated with benzoyl chloride in pyridine to give methyl 6-*O*-benzoyl-2,3-di-*O*-benzyl-α-D-glucopyranoside (**6**) in good yield. In the ^{1}Hmr spectrum of **6** in dimethyl-d_6 sulfoxide, the hydroxyl proton gave a doublet at τ 4.48 ($J_{H,OH}$ = 6 Hz); this result established that acylation had occurred at O-6. Methylthiomethyl ether **7** was prepared by a modification of a procedure reported by Pojer and Angyal (13); **7** could not be isolated in a pure form. Crude **7** was *O*-debenzoylated to give crystalline **8** in 66% yield from **6**. Oxidation of **8** gave aldehyde **9** which was characterized by conversion into the crystalline 1,3-diphenylimidazolidine derivative **10**. Treatment

0008-4042/79/080924-09$01.00/0

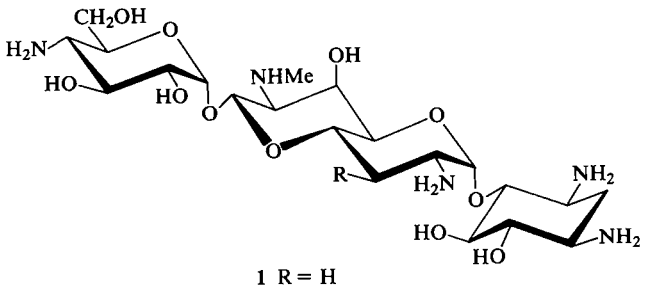

1 R = H
2 R = OH

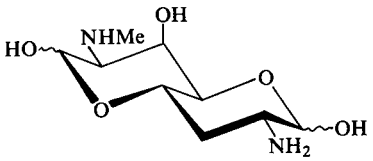

3

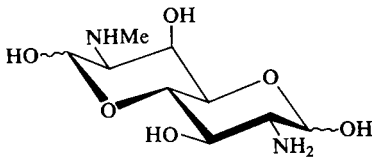

4

of compound **9** with vinylmagnesium bromide afforded the epimeric, dideoxy derivatives **11** and **12** in an approximately 1:5 ratio, respectively.

The stereochemistry at C-6 in compounds **11** and **12** was established by the route outlined in Scheme 2 (see below). Attempted removal of the methylthiomethyl group in **12** with methyl iodide (13) gave methyl 2,3-di-*O*-benzyl-7,8-dideoxy-L-*glycero*-α-D-*gluco*-oct-7-enopyranoside (**13**) and an equal quantity of a second product, namely, methyl 2,3-di-*O*-benzyl 7,8-dideoxy-4,6-*O*-methylene-L-*glycero*-α-D-*gluco*-oct-7-enopyranoside (**23**). Compound **23** presumably arises from attack of O-6 on the intermediate sulfonium ion resulting from *S*-methylation of the thioether function. The facility with which cyclization occurs is evidenced by the formation of **23** when an excess of water was present in the reaction mixture. Attempted removal of the methylthiomethyl function with silver nitrate and 2,6-lutidine (14) in aqueous tetrahydrofuran gave **13** and **23**. When the epimeric olefin **11** was treated with methyl iodide, methyl 2,3-di-*O*-benzyl-7,8-dideoxy-4,6-*O*-methylene-D-*glycero*-α-D-*gluco*-oct-7-enopyranoside (**24**) was formed as the major product. These results indicate that the intramolecular reaction occurred more readily in the case of compound **11** than in that of **12** and, therefore, reflect the stereochemistry of these derivatives at C-6. Structure **25** represents the projection along the C-5—C-6 bond of the rotamer of **12** which would be required for the cyclization of **12** to give **23**. Similarly, structure **26** represents the steric situation for the formation of compound **24** from **11**. Rotamer **26** might be expected to be more favored than rotamer **25**, and hence formation of **24** from **11** might be expected to be more facile than formation of **23** from **12**. In view of the preceding considerations, the major product from the Grignard reaction, namely **12**, may be assigned the L configuration and the minor product the D configuration at C-6, a conclusion which is supported by other results (see below). The problem experienced with the methylthiomethyl group may prove to be a general limitation on its usefulness in compounds in which an hydroxyl group is situated such that it can react at the methylthiomethyl group's methylene carbon during deprotection procedures.

To establish unambiguously the configuration at C-6 in compounds **11** and **12**, compound **12** was degraded by the sequence of reactions shown in Scheme 2. Acetylation of **12** afforded **14** which reacted smoothly with methyl iodide to give **15** in 80% yield. Treatment of compound **15** with osmium tetroxide in the presence of sodium metaperiodate, followed by reduction of the resulting aldehyde with sodium borohydride, afforded methyl 2,3-di-*O*-benzyl-L-*glycero*-α-D-*gluco*-heptopyranoside (**27**). Re-

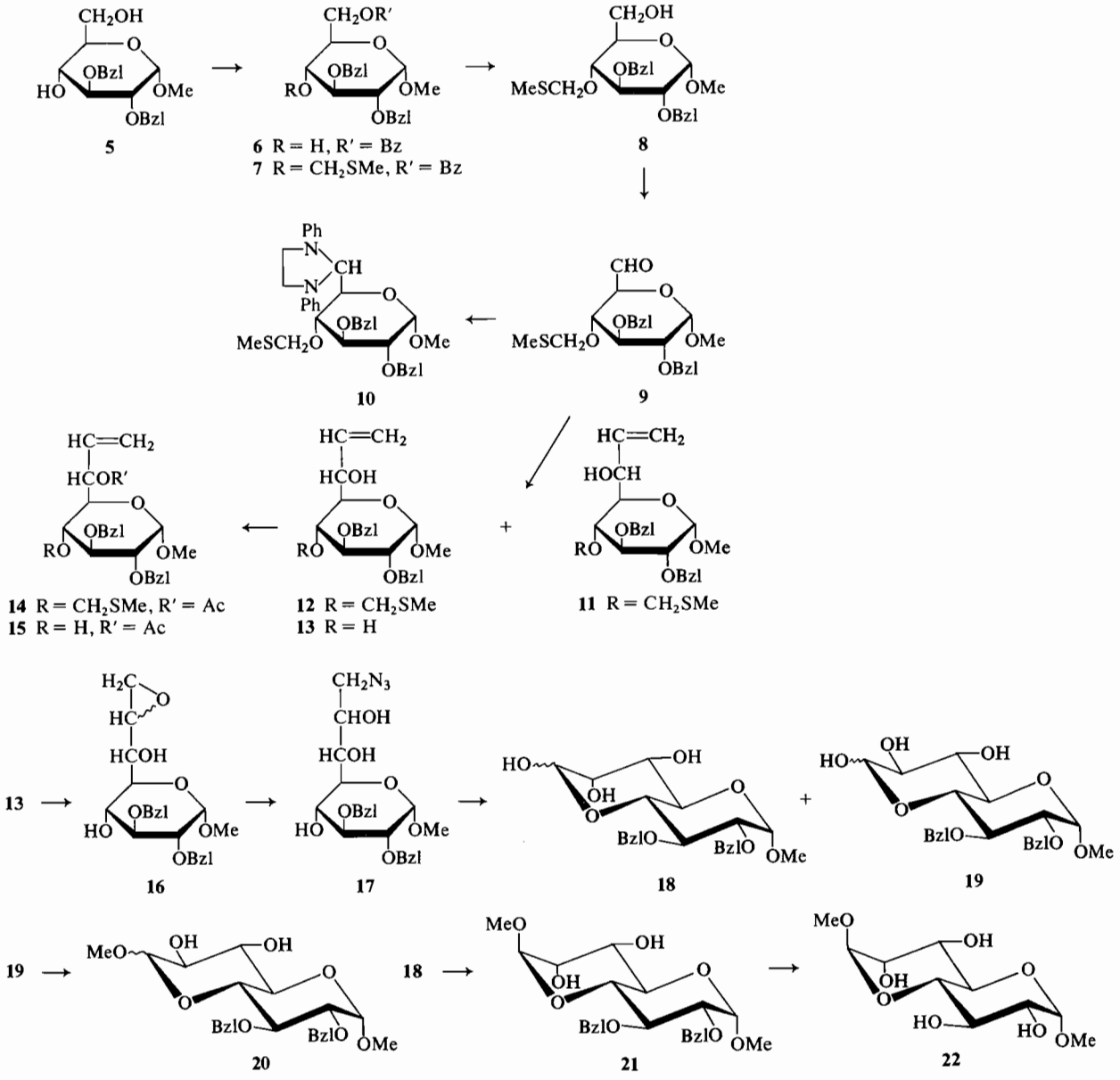

SCHEME 1

moval of the benzyl groups by hydrogenolysis over palladium-on-charcoal afforded methyl L-*glycero*-α-D-*gluco*-heptopyranoside (**28**) which had mp 163–165°C and $[\alpha]_D$ +137.8°. For methyl D-*glycero*-α-L-*gluco*-heptopyranoside, mp 167.5–169°C and $[\alpha]_D$ −142° have been reported (15). Thus, the major product of the Grignard reaction, namely **12**, has the L configuration and compound **11**, the minor product, has the D configuration at C-6.

Treatment of compound **15** with aqueous methanol containing triethylamine afforded **13** in 80% yield. It was felt that an aldehyde function could be introduced most readily by the photolysis (16) of an azido derivative which was only partially protected; in this way the necessity of selectively protecting hydroxyl groups might be avoided. Epoxidation of compound **13** with *m*-chloroperbenzoic acid afforded the diastereomeric 7,8-anhydro derivatives **16** which migrated as a single spot in tlc. Treatment of the anhydro derivatives **16** with sodium azide in the presence of ammonium chloride (17) gave the epimeric, 8-azidooctose compounds **17** which were not separable by column chromatography on silica gel. Irradiation with uv light of azides **17** in benzene–

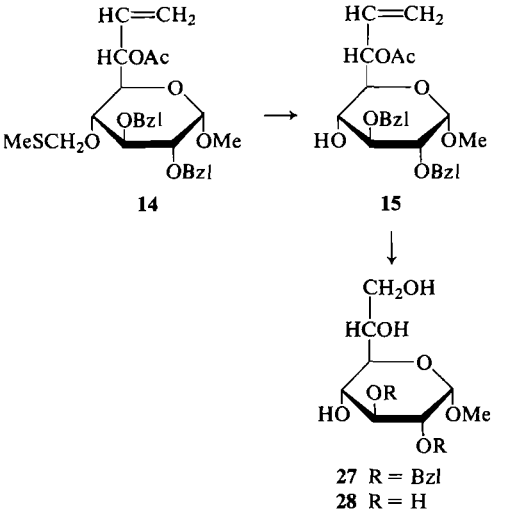

SCHEME 2

2-methoxyethanol afforded a mixture of dialdose derivatives **19** and **18** from which the former was isolated as a solid foam while the latter was obtained as crystals which showed no ir absorption attributable to an aldehyde group. ^{1}Hmr spectroscopy suggested that the products exist primarily as cyclic structures (*trans*-decalin) as evidenced by the absence of an aldehydic proton signal.

The reducing dialdose derivative **18** was treated with methanol in the presence of acidic, ion-exchange resin to give crystalline **21** in 49% yield. In the ^{1}Hmr spectrum (220 MHz) of compound **21** H-1 gives rise to a doublet at τ 5.42 ($J_{1,2}$ = 3.8 Hz) and H-8 appears as a doublet at 5.21 ($J_{7,8}$ = 1.8 Hz). Coxon (18) has reported that the H-1's of methyl 4,6-*O*-benzylidene-α-D-gluco- and -mannopyranoside resonate at τ 5.35 ($J_{1,2}$ = 3.5 Hz) and 5.35 ($J_{1,2}$ = 0.6 Hz), respectively. The values of the coupling constants $J_{1,2}$ and $J_{7,8}$ observed for H-1 and H-8, respectively, are also consistent with those observed for $J_{1,2}$ in the spectra of methyl α-D-gluco- and -mannopyranoside (19) as well as their derivatives

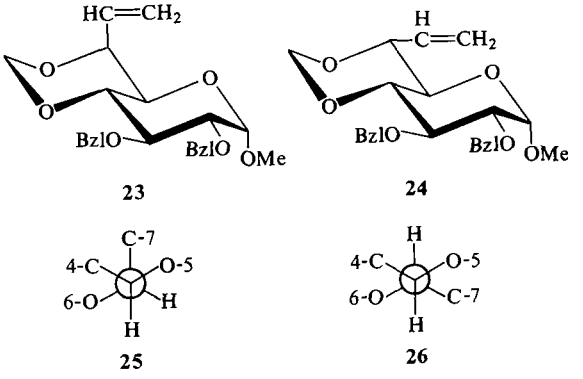

(18). Therefore, the product is assigned the L-*erythro*-D-*gluco* configuration as shown in structure **21**. Interestingly, the protons of the hydroxyl groups at C-6 and C-7 give rise to doublets; irradiation of the hydroxyl protons resulted in the partial collapsing of the multiplets arising from H-7 and H-6 at τ 6.01 and 6.11, respectively. Irradiation of H-6 and H-7 allowed the resonances at τ 7.31 ($J_{H,OH}$ = 3 Hz) and 7.34 ($J_{H,OH}$ = 4.5 Hz) to be assigned to HO-7 and HO-6, respectively.

Support for the stereochemical assignment of C-7 in compound **21** was obtained from ^{13}Cmr spectroscopy. In the ^{13}Cmr spectrum of **21** resonances at δ 101.0 and 99.0 can be assigned to C-8 and C-1, respectively. Gorin and Mazurek (20) have reported that for methyl α-D-gluco- and -mannopyranoside the anomeric carbons resonate at δ 100.3 and 101.9, respectively, whereas the corresponding 4,6-*O*-benzylidene derivatives have anomeric carbon resonances δ 99.9 and 101.7, respectively (21). The close agreement of the chemical shift observed for C-8 with the reported chemical shifts of C-1 of mannopyranosides supports the above assignment of the stereochemistry at C-7. Finally, only two resonances attributable to methyl groups were observed in both the ^{1}Hmr and ^{13}Cmr spectra of compound **21**, a result which establishes that in **21** there exists only one anomeric form at each of C-1 and C-8.

Removal of the benzyl groups in **21** by hydrogenolysis over palladium-on-charcoal afforded **22** which had mp 192–196°C (dec.) and $[\alpha]_D$ +56.3°. The ^{1}Hmr spectrum (220 MHz) of **22** showed doublets at τ 5.13 (J = 4.0 Hz) and 5.18 (J = 1.8 Hz) for H-1 and H-8, respectively. Irradiation of H-1 resulted in the H-2 signal's appearing as a doublet at τ 6.37 (J = 10 Hz). The observed splitting of H-8 (J = 1.8 Hz) is in agreement with the value (1.5 Hz) observed for $J_{1,2}$ in the spectrum of methyl α-D-mannopyranoside (19).

^{13}Cmr data for compound **22**, and for methyl α-D-gluco- and -mannopyranoside and their 4,6-*O*-benzylidene derivatives, are given in Table 1. The C-1 and C-2 resonances observed for **22** are in close agreement with the corresponding resonances reported for the D-glucose derivatives. The chemical shifts observed for C-8 and C-7 are in good agreement with those reported for C-1 and C-2, respectively, of the D-mannose derivatives. Thus, the ^{1}Hmr and ^{13}Cmr data establish that the product has the stereochemistry assigned in **22** and, therefore, corroborate the stereochemical conclusion which was reached for compound **21**.

Compound **19** was treated with methanol in a manner similar to that used for the preparation of **21**. Crystalline **20** was obtained, which was more dex-

TABLE 1. Carbon-13 chemical-shift data[a] for compound **22** and some related aldopyranosides

Compound	C-1	C-2	C-3	C-4	C-5	C-6	C-7	C-8	OMe
22	99.8	72.4	70.9[e]	68.3	67.4	70.1	70.5[e]	101.7	55.2 54.7
Methyl α-D-glucopyranoside[b]	100.3	72.5	74.2	70.6	72.7	61.7			56.2
Methyl 4,6-*O*-benzylidene-α-D-glucopyranoside[c]	99.9	72.4	70.5	80.8	62.0	68.5			54.9
Methyl α-D-mannopyranoside[b]	101.9	71.2	71.8	68.0	73.7	62.1			55.9
Methyl 4,6-*O*-benzylidene-α-D-mannopyranoside[c]	101.7	70.6	68.0	78.5	62.9	68.4			54.4
Methyl β-D-glucopyranoside[b]	104.3	74.2	76.9	70.8	76.9	61.9			58.3
Methyl β-D-mannopyranoside[d]	101.0	70.3	73.0	66.8	76.3	61.1			56.6

[a]In ppm from tetramethylsilane in deuterium oxide for compound **22**.
[b]Data are those reported in ref. 20.
[c]Data are those reported in ref. 21.
[d]Data are those reported in ref. 22.
[e]Assignments may be reversed.

trorotatory than **21** and was shown to be a mixture of glycosides. In the ^{1}Hmr spectrum of the methanolysis product three signals attributable to methoxyl groups were observed at τ 6.42, 6.55, and 6.58, results which establish that the product was a mixture of anomers **29** and **30**. The stereochemistry of the octodiose derivatives **29** and **30** was assigned using the follow-

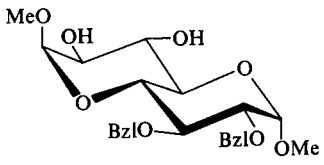

29

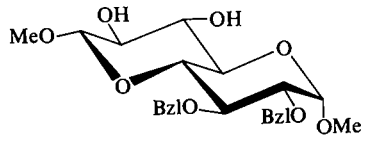

30

ing considerations. In the product's ^{1}Hmr spectrum (220 MHz) in chloroform-*d*, doublets at τ 5.19 (J = 3.3 Hz), 5.39 (J = 3.8 Hz), 5.41 (J = 3.8 Hz), and 5.75 (J = 7.5 Hz) have been assigned to H-8, H-1, H-1′, and H-8′, respectively, the nonprimed numbers referring to **29** and the primed numbers to **30**. The observed spacings of 3.8 Hz are consistent with that observed for H-1 (α anomer) in compound **21** and with the value of 3.6 Hz observed for $J_{1,2}$ in methyl α-D-glucopyranoside (19) and its derivatives (18). The assignment of the resonances at τ 5.39 and 5.41 to H-1 and H-1′ (assignments may be reversed) was based upon the observation that H-1 in **21** resonates at τ 5.42. The doublet for H-8′ has a spacing of 7.5 Hz, a value which is indicative of a *trans*-diaxial orientation of H-8′ and H-7′ and, therefore, of the β configuration in **30**.

The assignment of the signals for H-1, H-1′, H-8, and H-8′ were confirmed in the following way. The spectrum of the product mixture **20** in a mixture of chloroform-*d* and acetone-d_6 exhibited signals which were shifted relative to the corresponding signals observed in chloroform-*d*. Signals in the region of τ 6.20–6.60 were sequentially irradiated and positions were noted of signals which on irradiation caused the anomeric proton signals to collapse. This procedure

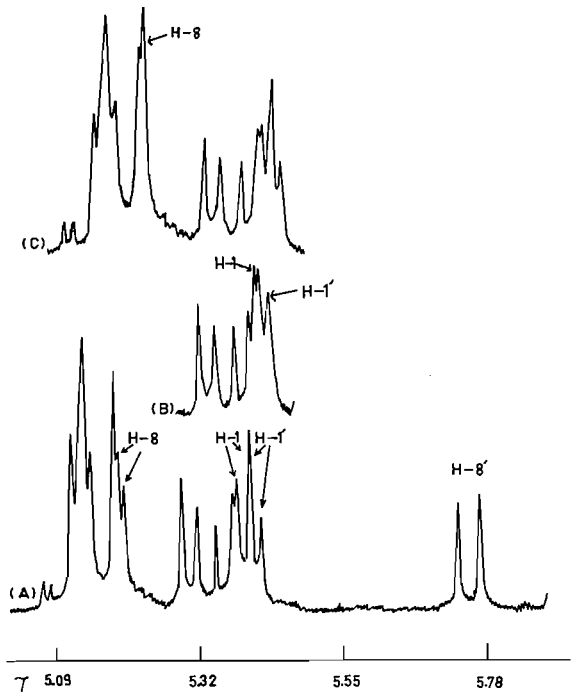

FIG. 1. (*A*) Partial ^{1}Hmr spectrum (chloroform-*d*) at 220 MHz of compounds **29** and **30**; (*B*) partial ^{1}Hmr spectrum (chloroform-*d*) at 220 MHz of compounds **29** and **30** with irradiation of H-2 and H-2′; (*C*) partial ^{1}Hmr spectrum (chloroform-*d*) at 220 MHz of compounds **29** and **30** with irradiation of H-7.

permitted the signals for H-2, H-2′, H-7 and H-7′ to be located. The corresponding signals in the spectrum in chloroform-*d* were then irradiated (see Fig. 1), a procedure which resulted in the signals for H-1, H-1′, and H-8 to be identified. Irradiation of the H-1's resulted in the multiplets, observed for H-2 and H-2′, to collapse to doublets with a spacing of 10 Hz, a value which is in agreement with that observed (18) for the coupling between *trans*-diaxial protons. The assignments of the signals for H-1, H-1′, H-8, and H-8′ were thus confirmed.

The observed values of 3.5 Hz and 7.5 Hz for the coupling constants $J_{7,8}$ and $J_{7',8'}$, respectively, are in agreement with the values of 3.0 and 7.5 Hz which have been reported (19) for $J_{1,2}$ in methyl α- and β-D-glucopyranoside, respectively. The ^{1}Hmr data establish that the product from the methanolysis of **19** is composed of a 1:1 mixture of anomeric glycosides (**29** and **30**) of D-*threo*-D-*gluco*-octodiose.

The present approach provides access to structures which are analogs of those found in **1** and **2**. To the authors' knowledge compounds **21**, **22**, **29**, and **30** represent the first synthetic examples of dialdoses which have the *trans*-decalin structure. Investigations into improvements in the synthesis of octodioses and the preparation of pseudodisaccharides containing these moieties are currently underway.

Experimental

Melting points were determined on a Fisher-Johns apparatus and are uncorrected. Optical rotations were measured with a Perkin-Elmer model 141 automatic polarimeter at 26 ± 3°C. Infrared spectra were recorded with a Unicam SP 1000 or a Perkin-Elmer 180 spectrophotometer. The ^{1}Hmr spectra were recorded at 60 MHz or with a Varian HR-220 spectrometer at 220 MHz in chloroform-*d* with tetramethylsilane (TMS) as the internal standard, unless otherwise stated. The ^{13}Cmr spectra were determined at 15.09 MHz on a Bruker HX-60 spectrometer equipped with an FT60M Fourier transform accessory; chemical shifts are given in parts per million downfield from TMS. Thin-layer chromatography (tlc) was performed with silica gel G, containing 1–3% of the indicator Lumilux Green ZS (Brinkmann), as the adsorbent in the following solvent systems (v/v): (*A*) 4:1 benzene – ethyl acetate; (*B*) 5:2 petroleum ether – ethyl acetate; (*C*) 1:1 benzene – ethyl acetate; (*D*) ethyl acetate; (*E*) 1:1 ethyl acetate – methanol. The term 'petroleum ether' refers to the fraction of bp 60–110°C. The developed plates were air dried and compounds located by heating the plates at 150°C after they had been sprayed with 10% aqueous sulfuric acid containing 1% cerium sulfate and 1.5% molybdic acid; benzyl ethers were detected by irradiation of the developed plates with short-wavelength uv light from a 2537 Å 'Mineralight.' Column chromatography was performed on Brinkmann silica gel (70–230 mesh).

Ultraviolet irradiations were performed with a 450-W Hanovia medium-pressure mercury-arc lamp (Cat. No. 679A-36) contained in a water-cooled, quartz immersion well. The whole assembly was mounted in a borosilicate glass reaction vessel.

Methyl 6-O-Benzoyl-2,3-di-O-benzyl-α-D-glucopyranoside (6)

To a cooled (0°C) solution of **5** (23) (3.7 g) in pyridine (50 mL), benzoyl chloride (1.25 mL) in pyridine (10 mL) was added dropwise with stirring. Thin-layer chromatography (solvent *A*) revealed that after 3 h compound **5** (trace), a major component (R_f 0.46), and a trace of a minor component (R_f 0.73) were present. The reaction mixture was poured into ice water and the resulting mixture was extracted with chloroform; the chloroform extract was washed successively with cold 2 *N* sulfuric acid, saturated aqueous sodium hydrogen carbonate, and water. Concentration of the dried ($MgSO_4$) chloroform solution afforded a syrup which was adsorbed onto silica gel and the column eluted (solvent *A*). Compound **6** was obtained as a colorless syrup (3.6 g, 76%) which solidified on standing. Recrystallization from petroleum ether afforded **6** as white needles having mp 75–77°C, $[\alpha]_D$ +22 ± 1° (*c* 1.4, $CHCl_3$); ν_{max} (KBr): ~3485 (OH) and 1695 cm^{-1} (OBz); ^{1}Hmr τ: 1.80–2.00 (2H, aromatic H's), 2.37–2.95 (12H, aromatic H's), 4.88–5.60 (7H, H-1—H-3, 2 CH_2—C_6H_5's), 5.90–6.65 (7H, H-4, H-5, H-6's, OMe), 3.30 (1H, OH, exchanged in D_2O); ^{1}Hmr (dimethyl-d_6 sulfoxide) τ: 4.48 (1H, d, $J_{H,OH}$ = 6 Hz, OH). *Anal.* calcd. for $C_{28}H_{30}O_7$: C 70.3, H 6.3; found: C 69.7, H 6.4.

Methyl 2,3-Di-O-benzyl-4-O-methylthiomethyl-α-D-glucopyranoside (8)

Glacial acetic acid (4 mL) and acetic anhydride (6.6 mL) were added to a solution of compound **6** (1.43 g) in dry dimethyl sulfoxide (10 mL), and the mixture was stirred at room temperature for 24 h. The reaction mixture was poured into cold, saturated sodium hydrogen carbonate. The neutral mixture was extracted with chloroform (3 × 20 mL); the extract was washed with water, dried ($MgSO_4$), and concentrated to a syrup (1.3 g) which was shown by tlc (solvent *B*) to be composed of two compounds having R_f 0.59 (major) and R_f 0.53 (minor). Column chromatography and an attempted distillation of the crude product failed to provide pure **7**.

Crude **7** (1.3 g) in methanol (30 mL) was treated for 4 h at 5°C with methanolic sodium methoxide (5 mL, ~1 *M*). Neutralization of the reaction mixture with Dry Ice followed by evaporation of the resulting mixture afforded a residue which was dissolved in chloroform. The chloroform extract was washed with water, dried ($MgSO_4$), and concentrated to a syrup. Crystallization from petroleum ether afforded **8** as white needles (690 mg, 53%) having mp 88.5–89.5°C, $[\alpha]_D$ +153.2 ± 2° (*c* 2.2, $CHCl_3$); ^{1}Hmr τ: 2.70 (10H, aromatic H's), 4.60–6.60 (14H, H-1—H-5, H-6's, 2 CH_2—C_6H_5's, SCH_2O, OH), 6.53 (3H, OMe), 7.85 (3H, s, SMe). *Anal.* calcd. for $C_{23}H_{30}O_6S$: C 63.6, H 7.0, S 7.4; found: C 63.3, H 6.8, S 7.5.

Methyl 2,3-Di-O-benzyl-4-O-methylthiomethyl-α-D-gluco-hexodialdo-1,5-pyranoside (9)

Methyl 2,3-di-*O*-benzyl-4-*O*-methylthiomethyl-α-D-glucopyranoside (**8**, 4.35 g) in dry dimethyl sulfoxide (75 mL) was treated with *N*,*N*′-dicyclohexylcarbodiimide (8.0 g), pyridine (0.4 mL), and trifluoroacetic acid (0.4 mL) for 18 h at room temperature to give a single product having R_f 0.7 (solvent *C*). The reaction mixture was diluted with ethyl acetate (50 mL) and a solution of oxalic acid dihydrate (3.75 g) in methanol (10 mL) was added to the mixture. After 30 min the mixture was poured into ice cold, saturated aqueous sodium chloride and the resulting mixture was filtered. The organic phase was separated and the aqueous solution was extracted with ethyl acetate (2 × 20 mL). The combined phase was washed with saturated aqueous sodium hydrogen carbonate and then with water. The aqueous washings were extracted with ethyl

acetate and the organic phases were combined, dried ($MgSO_4$), and concentrated to dryness. The syrupy residue was dissolved in warm acetone (20 mL) and the remaining *N,N'*-dicyclohexylurea was removed by filtration. The filtrate was concentrated to give **9** as an orange syrup which had ν_{max}(film) 1730 cm^{-1} (C=O) and which was used without further purification.

*1,3-Diphenyl-2-(methyl 2',3'-di-*O*-benzyl-4'-O-methylthiomethyl-α-*D*-gluco-pentopyranosid-5'-yl)imidazolidine (**10**)*

Compound **8** (870 mg) was oxidized as described above. After oxalic acid dihydrate (0.75 g) in methanol (5 mL) had been added to the reaction mixture, the mixture was filtered and *N,N'*-diphenylethylenediamine (400 mg) was added to the filtrate. After 24 h at room temperature the mixture was refrigerated to give **10** as colorless needles (800 mg). Recrystallization from ethanol gave **10** as colorless needles having mp 113–115.5°C, $[\alpha]_D$ −32.0 ± 0.9° (*c* 1.09, $CHCl_3$); ^{1}Hmr τ: 2.53–3.47 (20H, aromatic H's), 4.30 (1H, s, H-2), 4.85–5.67 (7H, H-1', OCH_2S, 2 CH_2—C_6H_5's), 5.75–6.77 (8H, H-4's, H-5's, H-2'—H-5'), 6.90 (3H, s, OMe), 7.83 (3H, s, SMe). *Anal.* calcd. for $C_{37}H_{42}N_2O_5S$: C 70.9, H 6.8, S 4.5; found: C 70.9, H 6.7, S 4.0.

*Methyl 2,3-Di-*O*-benzyl-7,8-dideoxy-4-*O*-methylthiomethyl-*D*-glycero- and -*L*-glycero-α-*D*-gluco-oct-7-enopyranoside (**11** and **12**)*

A solution of crude **9** (~4.35 g) in dry tetrahydrofuran (15 mL) was added dropwise with vigorous stirring to a tetrahydrofuran (10 mL) solution of vinylmagnesium bromide (prepared from vinyl bromide (3.9 mL) and magnesium turnings (1.37 g)). The reaction mixture was stirred at room temperature for 4 h after which time tlc (solvent *A*) revealed that all of the starting material had disappeared. Aqueous ammonium chloride (30 mL) was added dropwise to the cooled (0°C) reaction mixture. Ethyl acetate (30 mL) was added and the organic phase separated; the aqueous phase was extracted with ethyl acetate (2 × 30 mL). The combined organic solution was washed with saturated aqueous sodium chloride, dried ($MgSO_4$), and concentrated to a syrup. Column chromatography on silica gel (solvent *A*) gave methyl 2,3-di-*O*-benzyl-7,8-dideoxy-4-*O*-methylthiomethyl-*L*-*glycero*-α-*D*-*gluco*-oct-7-enopyranoside (**12**) as a colorless syrup (2.9 g, 62.9%) having R_f 0.67, $[\alpha]_D$ +109.7 ± 0.8° (*c* 1.29, $CHCl_3$); ν_{max} (film): 3500 (OH) and 1455 cm^{-1} (C=C); ^{1}Hmr τ: 2.65 (10H, aromatic H's), 3.65–4.30 (1H, m, vinyl H), 6.40–5.75 (10H, 2 vinyl H's, 2 CH_2—C_6H_5's, SCH_2O, H-1, H-2), 5.80–6.75 (7H, H-3—H-6, OMe), 7.03 and 7.15 (1H, OH, exchanged in D_2O), 7.80 (3H, SMe). *Anal.* calcd. for $C_{25}H_{32}O_6S$: C 65.2, H 7.0, S 7.0; found: C 65.4, H 6.9, S 6.8.

Methyl 2,3-di-*O*-benzyl-7,8-dideoxy-4-*O*-methylthiomethyl-*D*-*glycero*-α-*D*-*gluco*-oct-7-enopyranoside (**11**) was isolated as a homogeneous syrup (560 mg, 12.1%) which crystallized on standing. Recrystallization from hexane afforded **11** as white needles having R_f 0.39, mp 93–94°C, $[\alpha]_D$ +115.5 ± 0.5° (*c* 2.1, $CHCl_3$); ν_{max} (KBr): 3450 (OH) and 1450 cm^{-1} (C=C); ^{1}Hmr τ: 2.73 (10H, aromatic H's), 3.65–6.75 (18H, H-1—H-7, H-8's, 2 CH_2—C_6H_5's, SCH_2O, OMe), 7.05 (1H, bs, OH, exchanged in D_2O), 7.90 (3H, s, SMe). *Anal.* found: C 64.9, H 6.8, S 6.9.

*Treatment of Compound **12** with Methyl Iodide*

A mixture of **12** (660 mg), methyl iodide (0.75 mL) and sodium hydrogen carbonate (0.6 g) was refluxed for 12 h. Thin-layer chromatography (solvent *A*) revealed that all of **12** had reacted to give a mixture (1:1) of two components having R_f 0.70 and 0.16. Water (2.5 mL) was added to the reaction mixture and then the mixture was concentrated to dryness. The residue was partitioned between chloroform and water; the chloroform solution was washed with water, dried ($MgSO_4$), and evaporated to an orange syrup. The syrup was adsorbed onto a column of silica gel and fractions were eluted (solvent *A*). Methyl 2,3-di-*O*-benzyl-7,8-dideoxy-4,6-*O*-methylene-*L*-*glycero*-α-*D*-*gluco*-oct-7-enopyranoside (**23**) was isolated as a homogeneous syrup having R_f 0.70, $[\alpha]_D$ −25.1 ± 1° (*c* 0.88, $CHCl_3$); ν_{max} (film): 1460 cm^{-1} (C=C); no ir absorption attributable to OH; ^{1}Hmr τ: 2.67 (10H, aromatic H's), 3.45–5.60 (12H, 3 vinyl H's, H-1, H-2, H-6, OCH_2O, 2 CH_2—C_6H_5's), 5.70–6.80 (6H, H-3—H-5, OMe). *Anal.* calcd. for $C_{24}H_{28}O_6$: C 69.9, H 6.8; found: C 70.4, H 6.9.

Methyl 2,3-di-*O*-benzyl-7,8-dideoxy-*L*-*glycero*-α-*D*-*gluco*-oct-7-enopyranoside (**13**) was isolated as crystals which upon recrystallization from petroleum ether gave white needles having R_f 0.16, mp 109–110°C, $[\alpha]_D$ −1.6 ± 0.8°, $[\alpha]_{365}$ −29.4 ± 0.8° (*c* 1.2, $CHCl_3$); ^{1}Hmr τ: 2.65 (10H, aromatic H's), 3.70–4.35 (1H, m, vinyl H), 4.45–5.75 (8H, 2 vinyl H's, H-1, H-2, 2 CH_2—C_6H_5's), 6.00–6.70 (7H, H-3—H-6, OMe), 6.90–7.60 (2H, 2 OH's). *Anal.* calcd. for $C_{23}H_{28}O_6$: C 69.0, H 7.1; found: C 68.8, H 7.1.

The reaction was repeated using the same procedure as outlined above except that acetone was replaced by water–acetone (1:1 (v/v)) as the solvent. Thin-layer chromatography revealed that compounds **13** and **23** were produced in approximately equal proportions.

*Treatment of **12** with Silver Nitrate and 2,6-Lutidine*

Silver nitrate (288 mg) was added to **12** (157 mg) and 2,6-lutidine (107 mg) in tetrahydrofuran–water (0.8 mL, 4:1 (v/v)) and the mixture was stirred for 16 h at room temperature. Thin-layer chromatography (solvent *A*) showed that **12**, **13**, and **23** were present with **23** being the preponderant component.

*Treatment of Methyl 2,3-Di-*O*-benzyl-7,8-dideoxy-4-*O*-methylthiomethyl-*D*-glycero-α-*D*-gluco-oct-7-enopyranoside (**11**) with Methyl Iodide*

Compound **11** (560 mg) in acetone (5 mL) was treated with methyl iodide (0.75 mL) and sodium hydrogen carbonate (600 mg) as described for **12** (see above). Thin-layer chromatography (solvent *A*) showed that after 12 h the reaction mixture contained a major component (R_f 0.84) and a trace of a minor component (R_f 0.12) but no starting material. The major product was isolated by the procedure described for **23** to give, after column chromatography on silica gel (solvent *A*), methyl 2,3-di-*O*-benzyl-7,8-dideoxy-4,6-*O*-methylene-*D*-*glycero*-α-*D*-*gluco*-oct-7-enopyranoside (**24**) as an amorphous solid (70 mg) which could not be crystallized. The product had $[\alpha]_D$ +30.9 ± 0.8° (*c* 1.2, $CHCl_3$); ν_{max} (film): 1450 cm^{-1} (C=C); no ir absorption attributable to OH; ^{1}Hmr τ: 2.67 (10H, aromatic H's), 3.73–5.47 (10H, 3 vinyl H's, OCH_2O, 2 CH_2—C_6H_5, H-1), 5.65–6.75 (8H, H-2—H-6, OMe). *Anal.* calcd. for $C_{24}H_{28}O_6$: C 69.9, H 6.8; found: C 69.6, H 7.1.

*Methyl 6-O-Acetyl-2,3-di-O-benzyl-7,8-dideoxy-4-O-methylthiomethyl-L-glycero-α-D-gluco-oct-7-enopyranoside (**14**)*

Compound **12** (2.9 g) in pyridine (30 mL) was treated with acetic anhydride (3 mL) for 48 h at room temperature and then the mixture was poured with vigorous stirring into ice water (300 mL). The aqueous mixture was extracted with chloroform; the chloroform extract was washed successively with cold 2 *N* sulfuric acid, saturated aqueous sodium hydrogen carbonate, and water. Concentration of the dried ($MgSO_4$) chloroform solution afforded a syrupy residue which was fractionated on silica gel (solvent *A*) to give **14** as a homogeneous syrup (2.9 g, 92.7%) having R_f 0.78, $[\alpha]_D$ +82.3 ± 1.2° (*c* 0.85, $CHCl_3$); ν_{max} (film): 1745 cm^{-1} (OAc); no ir

absorption attributable to OH; ^{1}Hmr τ: 2.70 (10H, aromatic H's), 3.85–6.70 (15H, 3 vinyl H's, H-1—H-6, OCH_2S, 2 CH_2—C_6H_5's, OMe), 7.87 (6H, SMe, OAc). *Anal.* calcd. for $C_{27}H_{34}O_7S$: C 64.5, H 6.8, S 6.4; found: C 65.1, H 7.0, S 6.3.

*Methyl 6-*O*-Acetyl-2,3-di-*O*-benzyl-7,8-dideoxy-*L*-glycero-α-*D*-gluco-oct-7-enopyranoside (15)*

A mixture of compound **14** (2.9 g), methyl iodide (4.2 mL), and sodium hydrogen carbonate (3.6 g) in acetone (60 mL) was refluxed overnight to give a single component having R_f 0.44 (solvent *A*). The reaction mixture was processed in the usual way (see above) to give, after column chromatography on silica gel (solvent *A*), compound **15** as a colorless syrup (2.3 g, 80%) having $[\alpha]_D$ +2.9 ± 0.4°, $[\alpha]_{365}$ −17.2 ± 0.9° (*c* 1.05, $CHCl_3$); ν_{max} (film): 3520 (OH) and 1730 cm^{-1} (OAc); ^{1}Hmr τ: 2.65 (10H, aromatic H's), 3.70–5.40 (9H, 3 vinyl H's, H-1, H-2, 2 CH_2—C_6H_5), 5.70–6.70 (7H, H-3—H-6, OMe), 6.97–7.10 (1H, OH, exchanged in D_2O), 7.90 (3H, s, OAc). *Anal.* calcd. for $C_{25}H_{30}O_7$: C 67.9, H 6.8; found: C 67.9, H 6.8.

*Methyl 2,3-Di-*O*-benzyl-*L*-glycero-α-*D*-gluco-heptopyranoside (27)*

A mixture of compound **15** (2.3 g) and osmium tetroxide (10 mL of a 1% solution of osmium tetroxide in *tert*-butyl alcohol) in ethyl ether – water (50 mL, 1:1 (v/v)) was treated with sodium metaperiodate (5.5 g) and the mixture was vigorously stirred overnight at room temperature. Thin-layer chromatography (solvent *A*) revealed the absence of **15** (R_f 0.44) and the presence of one product (R_f 0.23). The ether solution was separated, and the aqueous phase was extracted with ethyl ether (2 × 50 mL); the combined ether solution was concentrated to a small volume to which methanol (100 mL) was added. Sodium borohydride (900 mg) was added to the methanol solution and the mixture was stirred overnight at room temperature. The reaction mixture was neutralized (pH 7) with concentrated hydrochloric acid and the neutral mixture was evaporated to a residue which was concentrated several times with methanol. Thin-layer chromatography (solvent *D*) showed that the syrupy residue contained a major component (R_f 0.25) and a trace of material which did not migrate. The residue was extracted with hot ethyl acetate (3 × 50 mL) and the extract was concentrated to a syrup which was fractionated on a column of silica gel (solvent *D*) to give **27** as a homogeneous syrup (1.4 g, 64%) having $[\alpha]_D$ +15.6 ± 0.5° (*c* 1.0, $CHCl_3$); ν_{max} (film): 3450 cm^{-1} (OH); no ir absorption attributable to acetyl or aldehyde functions; ^{1}Hmr τ: 2.69 (10H, aromatic H's), 4.90–5.60 (5H, H-1, 2 CH_2—C_6H_5), 5.70–6.85 (13H, H-2—H-6, H-7's, OMe, 3 OH's, 3 exchanged in D_2O). *Anal.* calcd. for $C_{22}H_{28}O_7$: C 65.3, H 7.0; found: C 64.9, H 7.4.

Methyl L-glycero-α-D-gluco-Heptopyranoside (28)

Compound **27** (500 mg) in ethanol (75 mL) was hydrogenated (60 psig) over 10% palladium-on-charcoal for 6 h to give one product (R_f 0.51, solvent *E*). The reaction mixture was filtered and the filtrate was concentrated to a solid residue which was recrystallized from ethanol to give **28** as white needles (220 mg, 80%) having mp 163–165°C and $[\alpha]_D$ +137.8 ± 0.5° (*c* 1.5, H_2O). For methyl D-*glycero*-α-L-*gluco*-heptopyranoside mp 167.5–169°C and $[\alpha]_D$ −142° have been reported (16). *Anal.* calcd. for $C_8H_{16}O_7$: C 42.9, H 7.2; found: C 43.2, H 7.5.

*Methyl 2,3-Di-*O*-benzyl-7,8-dideoxy-*L*-glycero-α-*D*-gluco-oct-7-enopyranoside (13)*

Methyl 6-*O*-acetyl-2,3-di-*O*-benzyl-L-*glycero*-α-D-*gluco*-oct-7-enopyranoside (**15**) (3.2 g) in a mixture of triethylamine (5 mL), water (5 mL), and methanol (10 mL) was left overnight at room temperature. The reaction mixture was concentrated to a residue which was partitioned between chloroform and water. The dried ($MgSO_4$) chloroform extract was concentrated to a solid which was recrystallized from petroleum ether to give **13** as needles (2.3 g, 80%) having mp 106–107°C; for another sample of **13** mp 109–110°C had been observed (see above). The product had the same mobility (tlc) as the other sample of **13** and the ^{1}Hmr spectra of the two samples were indistinguishable.

*Methyl 7,8-Anhydro-2,3-di-*O*-benzyl-*D*-threo- and -*L*-erythro-α-*D*-gluco-octopyranoside (16)*

m-Chloroperbenzoic acid (1.03 g) was added to a stirred solution of **13** (1.9 g) in dry dichloromethane (50 mL). After 48 h the reaction mixture was filtered and the filtrate was washed with aqueous sodium hydrogen carbonate. Concentration of the dried ($MgSO_4$) dichloromethane solution afforded a residue which was fractionated on a column of silica gel (solvent *C*). Compounds **16** were isolated as a mixture which was a white solid (1.55 g, 78.7%) having R_f 0.24, mp 118.5–120.5°C (softened at 111.5°C), $[\alpha]_D$ +9.0 ± 0.9° (*c* 1.22, $CHCl_3$); ^{1}Hmr τ: 2.67 (10H, aromatic H's), 4.90–5.55 (5H, H-1, 2 CH_2—C_6H_5's), 5.90–7.35 (13H, H-2—H-7, H-8's, 2 OH's, OMe). *Anal.* calcd. for $C_{23}H_{28}O_7$: C 66.3, H 6.8; found: C 66.0, H 7.1.

*Methyl 8-Azido-2,3-di-*O*-benzyl-8-deoxy-*D*-threo- and -*L*-erythro-α-*D*-gluco-octopyranoside (17)*

A mixture of sodium azide (1 g), ammonium chloride (500 mg), and anhydro derivatives **16** (1.55 g) in 2-methoxyethanol (25 mL) – water (2.5 mL) was refluxed for 1 h. The reaction mixture was partitioned between chloroform and water; the dried ($MgSO_4$) chloroform extract was concentrated to a solid which was purified by column chromatography on silica gel (solvent *C*). Azides **17** were obtained as an amorphous solid mixture (1.39 g, 82%) which had R_f 0.34 (solvent *C*), mp 122–128°C (softened at 110°C), $[\alpha]_D$ +9.9 ± 1° (*c* 1.01, $CHCl_3$); ν_{max} (KBr): 2095 (N_3) and 3380 cm^{-1} (OH); ^{1}Hmr τ: 2.65 (10H, aromatic H's), 4.90–5.60 (5H, H-1, 2 CH_2—C_6H_5's), 5.87–7.53 (14H, H-2—H-7, H-8's, OMe, 3 OH's, 3 exchanged in D_2O). *Anal.* calcd. for $C_{23}H_{29}N_3O_7$: C 60.1, H 6.4, N 9.1; found: C 59.7, H 6.3, N 9.0.

Photolysis of Compounds 17

A solution of azides **17** (1.6 g in benzene–2-methoxyethanol (100 mL, 9:1 (v/v)) under nitrogen was irradiated with uv light for 6 h after which time tlc (solvent *D*) showed that all of the starting material had reacted. The reaction mixture was concentrated to a syrup which was adsorbed onto silica gel; the column was eluted with solvent *D*. A mixture of two components (560 mg, 36.7%) having R_f 0.44 and 0.35 was obtained as a syrup which solidified on standing and which reduced Fehling's solution. Recrystallization from hexane – ethyl acetate gave compound **18** as a white powder (210 mg) having R_f 0.45 (solvent *D*), mp 88–89°C, $[\alpha]_D$ +20.6 ± 0.5° (*c* 2.13, $CHCl_3$); ν_{max} (KBr): 3400 cm^{-1} (OH); no ir absorption attributable to an aldehyde group; ^{1}Hmr τ: 2.50–2.90 (10H, aromatic H's), 4.87–5.65 (6H, H-1, H-8, 2 CH_2—C_6H_5), 5.70–7.45 (12H, H-2—H-7, OMe, 3 OH's, 3 exchanged in D_2O). Compound **18** reduced Fehling's solution. *Anal.* calcd. for $C_{23}H_{28}O_8$: C 63.9, H 6.5; found: C 63.9, H 6.5.

In a second experiment azides **17** (1.4 g) afforded **18** and **19** as a mixture (755 mg, 57.3%) from which **19** (R_f 0.35) was isolated as a solid foam (140 mg); the sample of **19** was revealed by tlc (solvent *D*) to be contaminated with compound **18** (≤10%). This material had $[\alpha]_D$ +14.8 ± 0.5°, $[\alpha]_{365}$ +27.3 ± 0.5° (*c* 1.76, $CHCl_3$); ^{1}Hmr τ: 2.40–2.91 (10H,

aromatic H's), 4.70–6.93 (18H, H-1—H-8, 2 CH_2—C_6H_5's, OMe, 3 OH's).

Methanolysis of Compound ***18***

Compound **18** (100 mg) in dry methanol (30 mL) was refluxed for 16 h in the presence of Dowex 50 ion-exchange resin (H^+) with the exclusion of moisture. The reaction mixture was filtered and the filtrate was concentrated to a crude product which was purified by column chromatography on silica gel (solvent *D*) to give **21** as white crystals (50 mg, 48.5%). Recrystallization from hexane – ethyl acetate gave **21** as white needles having R_f 0.59 (solvent *D*), mp 148.5–150°C, $[\alpha]_D$ $-11.6 \pm 0.9°$, $[\alpha]_{365}$ $-53.1 \pm 0.9°$ (*c* 1.20, $CHCl_3$); ^{1}Hmr (220 MHz) τ: 2.61–2.82 (10H, aromatic H's), 5.06, 5.15, 5.16, and 5.37 (4 1H d's, J_{vic} = 10.5 Hz, 2 CH_2—C_6H_5's), 5.21 (1H, d, $J_{7,8}$ = 1.8 Hz, H-8), 5.42 (1H, d, $J_{1,2}$ = 3.8 Hz, H-1), 6.01 (1H, m, H-6), 6.00, 6.20, and 6.49 (3 1H t's, J = 9.5 Hz, H-3, H-4, H-5), 6.52 (1H, m, $J_{2,3}$ = 10 Hz, H-2), 6.60 and 6.61 (2 3H s's, 2 OMe's), 7.31 (1H, d, $J_{7,OH}$ = 3.0 Hz, HO-7), 7.34 (1H, d, $J_{6,OH}$ = 4.5 Hz, HO-6); ^{13}Cmr data ($CDCl_3$) δ: 128.4, 128.3, 128.1, 127.9, and 127.5 (aromatic), 101.0 (C-8), 99.0 (C-1), 55.3 and 54.8 (2 OMe's). *Anal.* calcd. for $C_{24}H_{30}O_8$: C 64.6, H 6.8; found: C 64.5, H 6.7.

Methanolysis of Compound ***19***

Compound **19** (140 mg) was treated with dry methanol (30 mL) in a manner similar to that used with **18**. After a reaction time of 48 h, tlc (solvent *D*) revealed that the reaction mixture contained a trace of **19** (R_f 0.35) and a component having R_f 0.50. The product was isolated by the procedure which was used for **21** to give compound **20** as a white solid (70 mg). Recrystallization from hexane – ethyl acetate gave white crystals having mp 120–122°C, $[\alpha]_D$ $+15.2 \pm 0.6°$, $[\alpha]_{365}$ $+25.4 \pm 0.6°$ (*c* 1.58, $CHCl_3$); ^{1}Hmr (220 MHz) τ: 2.91–2.84 (10H, aromatic H's), 5.11–5.37 (4H, 2 CH_2—C_6H_5's), 5.19 (0.5H, d, $J_{7,8}$ = 3.5 Hz), 5.39 (0.5H, d, J = 3.8 Hz, H-1 or H-1′), 5.41 (0.5H, d, J = 3.8 Hz, H-1 or H-1′), 5.75 (0.5H, d, $J_{7',8'}$ = 7.5 Hz, H-8′), 5.98–7.48 (14H, H-2—H-7, 2 OH's, 2 OMe's). The protons of the methoxyl groups gave three singlets having chemical shift values of τ 6.42, 6.55, and 6.58. Double-resonance experiments are described in Results and Discussion. *Anal.* calcd. for $C_{24}H_{30}O_8$: C 64.6, H 6.8; found: C 64.7, H 6.9.

Preparation of Compound ***22***

Compound **21** (200 mg) in ethanol (50 mL) was hydrogenated (50 psig) over 10% palladium-on-charcoal to give a single product having R_f 0.60 (solvent *E*). The reaction mixture was concentrated to give **22** as a white solid (100 mg, 84%) having mp 192–196°C (dec.), $[\alpha]_D$ $+56.3 \pm 0.5°$, $[\alpha]_{365}$ $+168° \pm 1°$ (*c* 1.07, $CHCl_3$); ^{1}Hmr data (220 MHz, D_2O with sodium 2,2-dimethyl-2-silapentane-5-sulfonate as the internal standard) τ: 5.13 (1H, d, $J_{1,2}$ = 4.0 Hz, H-1), 5.18 (1H, d, $J_{7,8}$ = 1.8 Hz, H-8), 6.01 (1H, m, $J_{7,6}$ = 3.2 Hz, H-7), 6.05–6.11 (1H, m, H-6), 6.16 and 6.20 (2 1H t's, J = 10 Hz, 4-H, H-5), 6.37 (1H, $J_{2,3}$ = 10 Hz, H-2), 6.43–6.52 (1H, m, H-3), 6.55 and 6.57 (2 3H s's, 2 OMe's); ^{13}Cmr (D_2O) δ: 101.7 (C-8), 99.8 (C-1), 72.0, 70.9, 70.5, and 70.1 (C-2, C-3, C-6, C-7), 68.3 and 67.4 (C-4, C-5), 55.2 (OMe, α-*manno*), and 54.7 (OMe, α-*gluco*). *Anal.* calcd. for $C_{10}H_{18}O_8$: C 45.1, H 6.8; found: C 44.7, H 7.2.

Acknowledgements

The authors are grateful to the National Research Council of Canada for its generous financial support of this work in the form of a scholarship (to H.C.J.) and a grant (to W.A.S.). They also wish to acknowledge the encouragement and interest of the late Professor J.K.N. Jones, and to thank Dr. Arthur Grey for obtaining the 220-MHz ^{1}Hmr spectra.

1. S. Hanessian and T. H. Haskell. *In* The carbohydrates. Vol. 2A. *Edited by* W. Pigman and D. Horton. Academic Press, New York, NY. 1970. Chapt. 31; S. Umezawa. M.T.P. Int. Rev. Sci. Org. Chem. Ser. Two. Vol. 7 (Carbohydrates). *Edited by* G. O. Aspinall. Butterworths, London. 1976. Chapt. 5.
2. R. R. Herr and G. Slomp. J. Am. Chem. Soc. **89**, 2444 (1967); W. Schroeder, B. Bannister, and H. Hoeksema. J. Am. Chem. Soc. **89**, 2448 (1967); G. Slomp and F. A. Mackella. J. Am. Chem. Soc. **89**, 2454 (1967); B. J. Magerlein, R. D. Birkenmeyer, R. R. Herr, and F. Kagan. J. Am. Chem. Soc. **89**, 2459 (1967).
3. K. Sakata, A. Sakuria, and S. Tamura. Tetrahedron Lett. 3191 (1975).
4. B. C. Das, J. Defaye, and K. Uchida. Carbohydr. Res. **22**, 293 (1973); S. Ennifar and B. C. Das. Chem. Commun. 41 (1977).
5. S. O'Connor and L. K. T. Lam. Am. Chem. Soc. Meeting, April 8–13, 1973, Dallas, TX. Abstr. Pap. **165**, MED 16 (1973).
6. D. E. Dorman, J. W. Paschal, and K. E. Merkel. J. Am. Chem. Soc. **98**, 6885 (1976).
7. W. M. Stark, M. M. Hoehn, and N. G. Knox. Antimicrob. Agents Chemother. 314 (1968).
8. S. O'Connor, L. K. T. Lam, N. D. Jones, and M. O. Chaney. J. Org. Chem. **41**, 2087 (1976).
9. (*a*) K. E. Price and J. C. Godfrey. Adv. Appl. Microbiol. **18**, 191 (1974); (*b*) H. Umezawa. Adv. Carbohydr. Chem. Biochem. **30**, 183 (1974).
10. J. Davies and S. O'Connor. Antimicrob. Agents Chemother. **14**, 69 (1978).
11. H. C. Jarrell and W. A. Szarek. Carbohydr. Res. **67**, 43 (1978).
12. H. C. Jarrell and W. A. Szarek. Can. J. Chem. **56**, 144 (1978).
13. P. M. Pojer and S. J. Angyal. Tetrahedron Lett. 3067 (1976).
14. E. J. Corey and M. J. Bock. Tetrahedron Lett. 3269 (1975).
15. B. Pettersson and O. Theander. Acta Chem. Scand. B, **28**, 29 (1974).
16. D. Horton, A. E. Luetzow, and J. C. Wease. Carbohydr. Res. **8**, 366 (1968); D. M. Clode and D. Horton. Carbohydr. Res. **14**, 405 (1970).
17. R. D. Guthrie and D. Murphy. J. Chem. Soc. 5288 (1963).
18. B. Coxon. Tetrahedron, **21**, 3481 (1965).
19. E. Gros, J. O. Mastronardi, and A. R. Frasca. Carbohydr. Res. **16**, 232 (1971).
20. P. A. Gorin and M. Mazurek. Can. J. Chem. **53**, 1212 (1975).
21. E. Conway, R. D. Guthrie, S. D. Gero, G. Lukacs, A. M. Sepulchre, E. W. Hagaman, and E. Wenkert. Tetrahedron Lett. 4879 (1972).
22. W. Voelter and E. Breitmaier. Org. Magn. Reson. **5**, 311 (1973).
23. J. Bell and J. Lorber. J. Chem. Soc. 453 (1940).

Hydrogenation during ligand exchange reactions between ferrocene and pyrene

CHOI CHUCK LEE, KEN J. DEMCHUK, AND RONALD G. SUTHERLAND

Department of Chemistry and Chemical Engineering, University of Saskatchewan, Saskatoon, Sask. Canada S7N 0W0

Received November 1, 1978

CHOI CHUCK LEE, KEN J. DEMCHUK, and RONALD G. SUTHERLAND. Can. J. Chem. **57**, 933 (1979).

From ligand exchange reactions between ferrocene and pyrene, carried out in the presence of $AlCl_3$–Al, the η^6-pyrene-η^5-cyclopentadienyliron, η^6-4,5-dihydropyrene-η^5-cyclopentadienyliron, and η^6-4,5,9,10-tetrahydropyrene-η^5-cyclopentadienyliron monocations (**2**, **3**, and **4**, respectively) as well as the η^6-pyrene-*trans*-bis-η^5-cyclopentadienyliron and η^6-4,5,9,10-tetrahydropyrene-*trans*-bis-η^5-cyclopentadienyliron dications (**5** and **7**, respectively) were isolated and identified. A possible mechanism for the partial hydrogenation of the pyrene ligand is discussed.

CHOI CHUCK LEE, KEN J. DEMCHUK et RONALD G. SUTHERLAND. Can. J. Chem. **57**, 933 (1979).

A partir de réactions d'échange de ligands entre le ferrocène et le pyrène effectuées en présence de Al–$AlCl_3$ on a pu identifier et caractériser les monocations η^6-pyrène η^5-cyclopentadiénylfer, η^6-dihydro-4,5 pyrène η^5-cyclopentadiénylfer et η^6-tétrahydro-4,5,9,10 pyrène η^5-cyclopentadiénylfer (respectivement **2**, **3** et **4**) ainsi que les dications η^6-pyrène *trans*-bis-η^5-cyclopentadiénylfer et η^6-tétrahydro-4,5,9,10 pyrène *trans*-bis-η^5-cyclopentadiénylfer (respectivement **5** et **7**). On discute d'un mécanisme possible pour l'hydrogénation partielle du ligand pyrène.

[Traduit par le journal]

In 1975, the first observation of a partial hydrogenation of the aromatic ligand during the ligand exchange reaction between ferrocene and naphthalene or anthracene, carried out in the presence of $AlCl_3$-Al, was reported from this laboratory (1). Other polycyclic aromatic ligands have also been found to give similar hydrogenations (2), and it is of interest to note that in a recent communication on the synthesis of bis(η^6-naphthalene)chromium(0) (3), it was stated in a footnote that control experiments with naphthalene–$AlCl_3$–Al–$CrCl_3$ in C_6H_5Cl as solvent gave bis(η^6-tetralin)chromium(0) as the main product. On the basis of the observation of a stereospecific hydrogenation when 9,10-dimethylanthracene was the aromatic ligand, a mechanism for the hydrogenation process has also been proposed recently (4). As an extension of these studies, the present work was undertaken on the ligand exchange reaction between ferrocene and pyrene in order to ascertain the extent of hydrogenation that might occur during ligand exchange with this tetracyclic aromatic system.

In ligand exchange reactions between ferrocene and phenanthrene, effected in the presence of $AlCl_3$–Al, hydrogenation could take place at the C-9,10 positions giving rise to η^6-phenanthrene-η^5-cyclopentadienyliron and η^6-9,10-dihydrophenanthrene-η^5-cyclopentadienyliron monocations and η^6-phenanthrene-*trans*-bis-η^5-cyclopentadienyliron and η^6-9,10-dihydrophenanthrene-*trans*-bis-η^5-cyclopentadienyliron dications (5). In similar reactions with pyrene (**1**), if analogous partial hydrogenations occur at C-4,5 and C-9,10, monocations **2**, **3**, and **4**, and dications **5**, **6**, and **7**, might be obtained. In the present work, attempts were made to isolate and characterize these cations.

The extent of hydrogenation in ligand exchange reactions between ferrocene (FcH) and polycyclic arenes has been found to be highly dependent on reaction conditions such as the molar ratio of the reactants, the reaction temperature and the nature

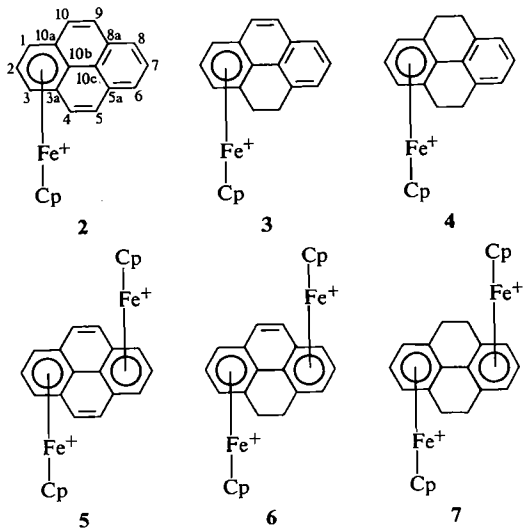

0008-4042/79/080933-04$01.00/0

TABLE 1. ^{1}H nmr data from monocations **2**, **3**, and **4** and from dications **5** and **7**

Ion*	Solvent	δ (ppm from TMS)			
		CH_2	Cp	Complexed aromatic	Uncomplexed aromatic
2	CD_3CN		4.20(s, 5H)	6.37(m, C-2, 1H) 6.97(d, C-1,3, 2H)	7.98(d, C-4,10, 2H) 8.17(m, C-6,8, 3H) 8.26(d, C-5,9, 2H)
3	CD_3NO_2	3.60(m, C-4,5, 4H)	4.76(s, 5H)	6.52(d, C-1,3, 2H) 7.20(m, C-2, 1H)	7.79(d, C-10, 1H) 7.82(m, C-6,8, 3H) 8.09(d, C-9, 1H)
4	CD_3CN	3.07(m, C-4,5,9,10, 8H)	4.82(s, 5H)	6.20(m, C-1,2,3, 3H)	7.30(m, C-6,7,8, 3H)
5	CD_3CN		4.58(s, 10H)	6.63(m, C-2,7, 3H) 7.09(m, C-1,3,6,8, 4H)	8.18(s, C-4,5,9,10, 4H)
7	CD_3NO_2	3.27(bs, C-4,5,9,10, 8H)	4.90(s, 10H)	6.43(m, C-1,2,3,6,7,8, 6H)	

*As the mono- or dihexafluorophosphate salt.

of the solvent. For example, in the formation of the tetralin complex from naphthalene, an increase in the relative amount of $AlCl_3$ or a decrease in the relative amount of FcH tended to increase the proportion of the hydrogenated product (2). Moreover, the use of *n*-alkanes as solvent instead of alicyclic hydrocarbons such as decalin tended to decrease the extent of hydrogenation (2, 5). Utilizing the usually employed molar ratio of 1:1:2:1 for arene–FcH–$AlCl_3$–Al, and an *n*-alkane as solvent to minimize hydrogenation, attempts were made to prepare nonhydrogenated products such as ion **2**. However, often mixtures of products were obtained. Thus reaction with a molar ratio of 1:1:2:1 for **1**–FcH–$AlCl_3$–Al in refluxing *n*-hexane (69°C) for 20 h or in refluxing *n*-heptane (98°C) for 16 h gave about 16% yields of a 3:1 mixture of the η^6-pyrene-η^5-cyclopentadienyliron cation (**2**) and the η^6-4,5-dihydropyrene-η^5-cyclopentadienyliron cation (**3**), and these products, as their hexafluorophosphate salts, were separated by passage through an alumina column. When the same reaction was carried out in refluxing *n*-decane (174°C) for 16 h, a 24% yield of **2** was obtained directly without chromatographic separation. At this higher temperature, besides a greater yield of **2**, any hydrogenated product such as **3** has apparently been decomposed. Using a molar ratio of 1:1:10:1 for **1**–FcH–$AlCl_3$–Al, reaction in decalin at 115°C for 16 h gave a 9% yield of the η^6-4,5,9,10-tetrahydropyrene-η^5-cyclopentadienyliron cation (**4**). When **2**, **3**, and **4**, as their hexafluorophosphate salts, were subjected to pyrolytic sublimation under reduced pressure (4), pyrene, 4,5-dihydropyrene, and 4,5,9,10-tetrahydropyrene, respectively, were recovered, thus confirming the nature of the arene ligands in ions **2**, **3**, and **4**.

From the work with naphthalene on the effect of varying the amount of $AlCl_3$ on the extent of hydrogenation, interpolation of the data suggested that a reaction carried out with a molar ratio of 1:1:5.6:1 for naphthalene–FcH–$AlCl_3$–Al at 140°C for 4 h in decalin would give a 1:1 mixture of the nonhydrogenated and hydrogenated naphthalene and tetralin complexes (2). Using these conditions with **1** instead of naphthalene, only a 6% yield of the η^6-4,5,9,10-tetrahydropyrene-*trans*-bis-η^5-cyclopentadienyliron dication (**7**) was obtained. Morrison *et al.* (6) have previously reported the preparation, from ligand exchange reactions, of a number of dications including the nonhydrogenated η^6-pyrene-*trans*-bis-η^5-cyclopentadienyliron dication (**5**). Using the conditions of Morrison *et al.* (molar ratio of 1:20:100:33 for **1**–FcH–$AlCl_3$–Al in refluxing cyclohexane (81°C) for 16 h), we have obtained, in 35% yield, only the tetrahydro dicationic product **7**. With a molar ratio of 1:2:2:1 for **1**–FcH–$AlCl_3$–Al, a reaction carried out in refluxing *n*-decane (174°C) for 16 h gave a mixture of products from which a 5% yield of the nonhydrogenated dication **5**, as its hexafluorophosphate salt, was recovered. In the present work, however, it has not been possible to obtain the η^6-4,5-dihydropyrene-*trans*-bis-η^5-cyclopentadienyliron dication (**6**).

The identification of the structures of ions **2**, **3**, **4**, **5**, and **7** was greatly facilitated by their ^{1}H and ^{13}C nmr spectra. These spectral data are summarized in Tables 1 and 2. When hydrogenation occurs at C-4,5 or at C-4,5, and C-9,10, these carbon positions become methylene groups and only in the hydrogenated ions **3**, **4**, and **7** do methylene absorptions in the aliphatic region appear in both the ^{1}H and ^{13}C spectra (Tables 1 and 2). For dications **5** and **7**, the symmetry of the structures greatly simplified both their ^{1}H and ^{13}C spectra. The two CpFe groups are assigned a *trans* geometry by analogy with similar assignments in dications formed from other poly-

TABLE 2. ^{13}C nmr data from monocations **2**, **3**, and **4** and from dications **5** and **7**

		δ (ppm from TMS)			
Ion*	Solvent	CH_2	Cp	Complexed aromatic	Uncomplexed aromatic
2	CD_3CN		75.7	82.4(C-1,3) 84.7(C-2) 88.4(C-10b) 93.0(C-3a,10a)	126.5, 128.6, 129.6, 131.4, 132.9 (C-4-10,5a,8a,10c)
3	CD_3NO_2	25.5(C-4,5)	75.8	83.2, 84.2, 84.4 (C-1,2,3) 88.4, 92.9, 99.5 (C-3a,10a,10b)	124.3, 125.7, 126.5, 127.3, 129.4, 131.4, 133.0, 135.4 (C-6-10,5a,8a,10c)
4	CD_3CN	26.2, 26.3 (C-4,5,9,10)	76.9	84.3(C-2) 85.9(C-1,3) 93.5(C-10b) 99.1(C-3a,10a)	125.4, 126.5 130.0, 136.7 (C-6-8,5a,8a,10c)
5	CD_3NO_2		77.8	85.5(C-1,3,6,8) 86.7(C-2,7) 93.6(C-3a,5a,8a,10a)	131.8(C-4,5,9,10)
7	CD_3CN	25.1(C-4,5,9,10)	77.9	86.3(C-2,7) 86.6(C-1,3,6,8) 89.2(C-10b,10c) 100.2(C-3a,5a,8a,10a)	

*As the mono- or dihexafluorophosphate salt.

cyclic arenes (1, 4–7). Moreover, if the two CpFe groups were *cis*, in dication **7**, four of the C-4,5,9,10 protons would be on the same side (*endo*) and the other four would be on the opposite side (*exo*) relative to the two CpFe groups, and it would be unlikely for these protons to appear as a broad singlet in the ^1H spectrum as was observed (Table 1).

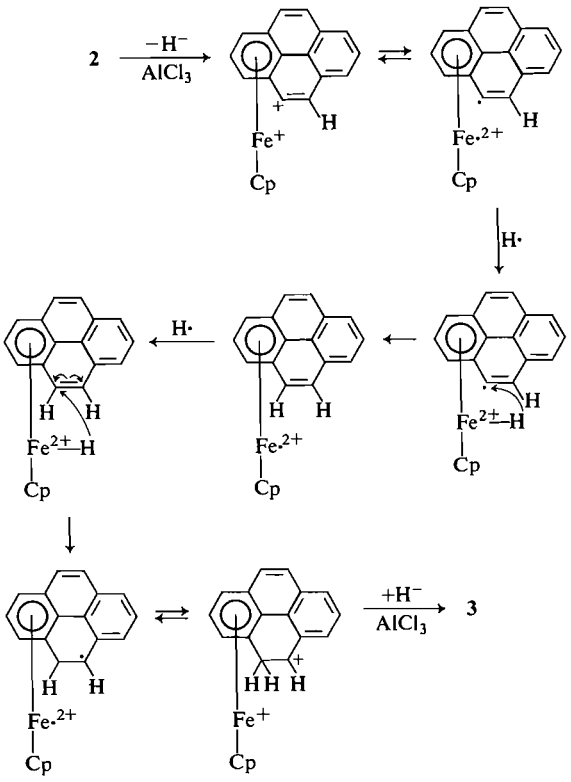

SCHEME 1

The partial hydrogenation of the pyrene ligand observed in the present work may be formulated via the ion–radical mechanism which has been proposed and discussed earlier (4). The formation of ion **3** from **2** is illustrated in Scheme 1. The hydrogenation is initiated by the hydride abstraction from C-4 of **2** by $AlCl_3$ to give a carbonium ion. An intramolecular oxidation–reduction would then take place through the transfer of an electron from Fe(II) to give Fe(III), while the carbonium ion center is reduced to a radical, and this is followed by reactions with H atoms as previously described (4). The process may be repeated starting with hydride abstraction from C-10 of **3**, eventually giving rise to the tetrahydro cation **4**. It may be noted that the carbonium ions derived from hydride abstraction from C-4 of **2** and C-10 of **3** should be of high stability and could be formed quite readily since they are structurally analogous to α-ferrocenyl substituted carbocations which have extraordinarily high stability (8, 9). Further hydrogenation of the uncomplexed aromatic ring of **4** is not feasible since hydride abstraction from this ring would not give a stable carbonium ion analogous to an α-ferrocenyl substituted carbocation.

Experimental

Ligand Exchange Reactions

Ligand exchange reactions between pyrene (**1**) and ferrocene (FcH), effected in the presence of $AlCl_3$–Al, were carried out using a general procedure as previously described (1), but with

TABLE 3. Reaction conditions for the preparation of and analytical data from ions **2**, **3**, **4**, **5**, and **7**

Ion*	Molar ratio (1–FcH–$AlCl_3$–Al)	Solvent	Temp. (°C)	Reaction time (h)	Yield (%)	Analysis for	Calcd. (%) C	Calcd. (%) H	Found (%) C	Found (%) H
2	1:1:2:1	Decane	174	16	24	$C_{21}H_{15}FePF_6$	53.87	3.23	53.95	3.20
3	1:1:2:1	Hexane	69	20	4†	$C_{21}H_{17}FePF_6$	53.64	3.64	53.45	3.70
	1:1:2:1	Heptane	98	16	4†					
4	1:1:10:1	Decalin	115	16	9	$C_{21}H_{19}FePF_6$	53.42	4.06	53.03	3.97
5	1:2:2:1	Decane	174	16	5‡	$C_{26}H_{20}Fe_2P_2F_{12}$	42.53	2.75	42.38	2.81
7	1:1:5.6:1	Decalin	140	4	6	$C_{26}H_{24}Fe_2P_2F_{12}$	42.31	3.28	42.29	3.46
	1:20:100:33	Cyclohexane	81	16	35					

*Isolated as the mono- or dihexafluorophosphate salt.
†Separated from a 3:1 mixture of **2** and **3** through an alumina column by elution with acetone.
‡Separated by passage through an alumina column with elution by nitromethane after all monocations were removed by elution with acetone.

the experimental conditions varied as summarized in Table 3 to give cations **2**, **3**, **4**, **5**, and **7**. The following is an illustration of a typical experiment.

A mixture of 5.1 g (25 mmol) of pyrene, 4.7 g (25 mmol) of ferrocene, 6.7 g (50 mmol) of $AlCl_3$, and 0.65 g (25 mmol) of Al powder in 50 mL of *n*-heptane was heated under N_2 and under reflux (98°C) for 16 h. After cooling to room temperature, 50 mL of H_2O was added and the mixture was filtered to remove all solid material. The aqueous layer was separated, washed with hexane, and then filtered into a concentrated solution of ammonium hexafluorophosphate (4.0 g, 25 mmol, in 10 mL of H_2O). The hexafluorophosphate salts that precipitated were collected by filtration, redissolved in acetone and passed through an alumina column (chromatographic activated alumina F-20, Sargent-Welch Scientific Co.). Elution with acetone gave 1.4 g (12%) of the hexafluorophosphate salt of η^6-pyrene-η^5-cyclopentadienyliron cation (**2**) and 0.5 g (4%) of the hexafluorophosphate salt of η^6-4,5-dihydropyrene-η^5-cyclopentadienyliron cation (**3**). These products, as well as the hexafluorophosphate salts of **4**, **5**, and **7**, were identified by their ^1H and ^{13}C nmr spectra (Tables 1 and 2). The data from the C and H analyses are given in Table 3.

Pyrolytic Sublimation of 2, 3, and 4

The hexafluorophosphate salt of monocation **2**, **3** or **4** was pyrolytically sublimed at 0.1 Torr and at 180°C in an oil bath as previously described (4) to give, respectively, pyrene, 4,5-dihydropyrene, or 4,5,9,10-tetrahydropyrene in yields of 85–90%. The pyrene so obtained, mp 150°C, was identical to a commercial sample. The 4,5-dihydropyrene and 4,5,9,10-tetrahydropyrene melted, respectively, at 132°C (lit. (10) mp 132°C) and 136°C (lit. (11) mp 134–136°C), and their mass spectra show parent ions at *m/e* 204 and 206, respectively, as expected.

Acknowledgement

Financial support in the form of grants given by the National Research Council of Canada to C.C.L. and R.G.S. are gratefully acknowledged.

1. R. G. SUTHERLAND, S. C. CHEN, J. PANNEKOEK, and C. C. LEE. J. Organomet. Chem. **101**, 221 (1975).
2. R. G. SUTHERLAND, W. J. PANNEKOEK, and C. C. LEE. Ann. N.Y. Acad. Sci. **295**, 192 (1977).
3. C. ELSCHENBROICH and R. MÖCKEL. Angew. Chem. Int. Ed. Engl. **16**, 870 (1977).
4. R. G. SUTHERLAND, W. J. PANNEKOEK, and C. C. LEE. Can. J. Chem. **56**, 1782 (1978).
5. C. C. LEE, K. J. DEMCHUK, W. J. PANNEKOEK, and R. G. SUTHERLAND. J. Organomet. Chem. **162**, 253 (1978).
6. W. H. MORRISON, E. Y. HO, and D. N. HENDRICKSON. J. Am. Chem. Soc. **96**, 3603 (1974).
7. C. C. LEE, R. G. SUTHERLAND, and B. J. THOMSON. J. Chem. Soc. Chem. Commun. 907 (1972).
8. J. W. LARSEN and P. ASHKENAZI. J. Am. Chem. Soc. **97**, 2140 (1975).
9. C. C. LEE, S. C. CHEN, W. J. PANNEKOEK, and R. G. SUTHERLAND. Can. J. Chem. **55**, 1024 (1977).
10. C. S. MARVEL and B. D. WILSON. J. Org. Chem. **23**, 1483 (1958).
11. A. PADWA and A. MAZZU. Tetrahedron Lett. 4471 (1974).

Structure et réactivité des benzoxazoles : étude par résonance magnétique nucléaire du carbone-13

JEANINE LLINARES, JEAN-PIERRE GALY, ROBERT FAURE[1] ET EMILE-JEAN VINCENT

Laboratoire de Chimie Organique Physique, Université d'Aix-Marseille III, Rue Henri Poincaré, 13397, Marseille, France

ET

JOSÉ ELGUERO[1]

Laboratoire de Chimie Moléculaire, Université d'Aix-Marseille III, Rue Henri Poincaré, 13397, Marseille, France

Reçu le 1 août 1978

JEANINE LLINARES, JEAN-PIERRE GALY, ROBERT FAURE, EMILE-JEAN VINCENT et JOSÉ ELGUERO. Can. J. Chem. **57**, 937 (1979).

Les spectres de rmn du ^{13}C de 34 benzoxazoles, de l'oxazole et de 10 *o*-aminophénols ont été enregistrés. Tous les déplacements chimiques ont été attribués à partir des effets de substituant. Les structures des produits obtenus par nitration du benzoxazole ont été déterminées par rmn du ^{13}C. Les perturbations induites par une substitution en position 2 sont discutées en fonction d'un modèle empirique qui fait intervenir les paramètres structuraux *F*, *R* et *Q**. Nous discutons également de la tautomèrie azido–tétrazole (position 2 substituée par un groupement N_3) et de la tautomèrie prototropique (position 2 substituée par des groupements NH_2, OH et SH). Enfin, nous avons comparé les déplacements chimiques et les constantes de couplage de l'oxazole et du benzoxazole.

JEANINE LLINARES, JEAN-PIERRE GALY, ROBERT FAURE, EMILE-JEAN VINCENT, and JOSÉ ELGUERO. Can. J. Chem. **57**, 937 (1979).

Thirty-four benzoxazoles, oxazole, and 10 *o*-aminophenols have been studied by ^{13}C nmr spectroscopy. All the signals have been attributed from substituent effects. The structure of products obtained by nitration of benzoxazole have been determined by ^{13}C nmr. The shifts induced by substitution at the 2 position have been discussed as a function of an empirical model using the structural parameters *F*, *R*, and *Q**. Azido–tetrazole equilibria (N_3 in position 2) and prototropic tautomerism (NH_2, OH, and SH in position 2) have been also discussed. The chemical shifts and coupling constants of oxazole and unsubstituted benzoxazole have been compared.

Introduction

Dans le cadre d'études physicochimiques entreprises depuis plusieurs années sur les benzazoles (benzimidazole (1, 3, 8), indazole (1, 4, 5, 7, 8), benzotriazole (1, 8) et benzothiazole (2, 6, 9)), nous présentons dans ce mémoire les résultats de la résonance magnétique nucléaire du carbone-13 des dérivés benzoxazoliques du type **I**. Notre travail portera principalement sur les effets de la substitution en position 2, effets que nous comparerons avec ceux de la série benzothiazolique (9). Lors de la synthèse de dérivés nitrés, nécessaires pour attribuer les déplacements chimiques, certains problèmes nous ont conduits à étudier le mécanisme de la nitration en série benzoxazolique.

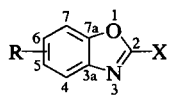

I

Partie expérimentale

Les spectres de carbone-13 ont été enregistrés sur un spectromètre Varian CFT-20. Les composés ont été étudiés à la température de 28 ± 2°C, en solution dans le diméthyl sulfoxyde hexadeutérié. Les déplacements chimiques, mesurés sur les spectres découplés par bruit par rapport à la raie centrale du solvant, sont rapportés au signal du TMS par la relation [1] (10), et sont donnés avec une précision supérieure à 0.1 ppm.

$$[1] \quad \delta_{TMS} = \delta_{DMSO\text{-}d_6} + 39.6 \text{ ppm } (\delta \text{ en ppm})$$

Les constantes de couplage sont mesurées sur les spectres couplés, avec une erreur absolue de 0.5 Hz.

La plupart des composés étudiés ont déjà été décrits dans la littérature (la première référence renvoie au mode de synthèse utilisé, la seconde à l'article où sont données les principales caractéristiques du produit; dans certains cas, ces deux références peuvent coincider): **1** (11, 12), **1***a* (13, 14), **1***b*,[2] **2** (11, 15), **3**,[2] **4** (16), **5** (11, 17), **6** (11), **7** (18), **8** (19), **9**,[2] **9***a* (20), **9***b*,[2] **10** (21, 22), **11**,[2] **11***a* (23, 24), **11***b* (23, 25), **12** (26), **13** (26, 27), **14** (28), **15** (22, 29), **16** (30), **17** (31), **18** (32), **19** (33), **20** (32, 33), **21** (33), **22** (34), **23**,[2] **24**,[2] **25**,[2] **26**,[2] **27** (23), **33** (35, 36), **34** (37), **35**,[2] **36** (38), **37** (39, 40), **38**[2], **39** (41, 42).

Par contre, les produits suivants n'étaient pas connus (tous les produits ont été recristallisés dans l'éthanol).

[1]Auteurs auxquels la correspondance doit être adressée.

[2]Ces produits sont commerciaux.

0008-4042/79/080937-09$01.00/0

Le chloro-5 benzoxazole **11***c* est obtenu en chauffant le chloro-4 formamido-2 phénol vers 160–180°C sous une pression de 10^{-2} Torr, selon le procédé de Bamberger (23). Ce composé est un solide de couleur beige qui cristallise en paillettes, pf 36–37°C.

L'azido-2 benzoxazole **14** traité par l'acide nitrique fumant en présence d'acide sulfurique, selon la méthode décrite par Newberry et Phillips (20), donne l'azido-2 nitro-6 benzoxazole **14***a*. Ce dernier est un solide jaune-orangé, pf 207°C (déc.).

Les formanilides **28, 29** et **30** sont préparés par action de l'acide formique sur les aminophénols correspondants (43): (*i*) le formamido-2 nitro-4 phénol **28** a été étudié en uv par Passerini (25), mais n'a pas été décrit. C'est un solide rouge brique, pf 245°C (déc.); (*ii*) le formamido-2 nitro-5 phénol **29** est un solide jaune-vert, pf 235°C (déc.); (*iii*) le chloro-4 formamido-2 phénol **30** cristallise en paillettes marron foncé, pf 165°C.

Par action de l'acide nitrique fumant sur les dérivés mononitrés **28** et **29** (20), on obtient les dérivés dinitrés: (*i*) le dinitro-4,6 formamido-2 phénol **31**, solide jaune clair, pf 196°C (déc.); (*ii*) le dinitro-3,5 formamido-2 phénol **32**, solide jaune, pf 165°C (déc.).

Résultats

Attribution des déplacements chimiques

Lors de précédents travaux dans la série du benzothiazole (6, 9), nous avons présenté une méthode d'attribution des déplacements chimiques des carbones protonés de l'homocycle. Ce procédé, basé sur l'hypothèse que les perturbations sur le cycle hexagonal sont similaires en grandeur et en direction à celles observées en série benzénique (44), conduit à d'excellents résultats, même lorsque le domaine de résonance de ces atomes est peu étendu, comme dans le cas du benzothiazole (6, 9).

A notre avis, le substituant le plus adapté pour l'étude de ce genre de problème est le groupement nitro; les raisons de ce choix sont les suivantes: (*i*) d'une part les effets de ce substituant sont nettement différenciés selon la position considérée; ainsi, en série benzénique (44), les perturbations sont les suivantes: *ipso* = 19.6, *ortho* = −5.3, *meta* = 0.8 et *para* = 6.0 ppm; (*ii*) d'autre part, du moins en ce qui concerne la série benzothiazolique, la nitration est une réaction facile à mettre en oeuvre. Toutefois, un des aspects négatifs de ce choix est la faible solubilité des dérivés nitrés, ce qui nécessite un temps d'accumulation plus élevé.

En série benzoxazolique, l'utilisation du substituant nitro entraine des complications supplémentaires. Comme nous le montrerons dans le cas du benzoxazole lui-même **11**, certains dérivés nitrés, moins stables que leurs homologues soufrés, s'ouvrent en milieu acide. En conséquence, l'obtention, dans cette série, de substrats nitrés est plus aléatoire. Par ailleurs, ces composés nitrés peuvent également s'hydrolyser durant l'étude spectroscopique; ainsi, dans le spectre rmn du ^{13}C du méthyl-2 nitro-6 benzoxazole **9***a* (solvant: DMSO-d_6), on note l'apparition progressive de nouvelles raies de résonance attribuables à un produit d'hydrolyse (il est bien connu que les solvants polaires aprotiques, comme le DMSO, accélérent l'attaque nucléophile de l'eau).

Néanmoins, comme le domaine de résonance des carbones protonés de l'homocycle des dérivés benzoxazoliques est relativement large, les effets d'autres substituants que le groupe nitro permettent également de réaliser une attribution complète des déplacements chimiques. La seule ambiguïté concerne les signaux des carbones C-5 et C-6, lorsque l'écart entre les déplacements de ces deux carbones est inférieur ou égal à 0.5 ppm; dans ces conditions, certaines des attributions du tableau 2 peuvent être inversées.

Dans le tableau 1 sont rassemblées les perturbations dues à une substitution sur l'homocycle (valeurs entre parenthèses), pour quelques dérivés benzoxazoliques substitués en position 2. Au cours de notre étude en série benzothiazolique (9), nous avons observé une légère dépendance entre la grandeur de la perturbation et la nature du substituant en position 2; cependant ceci ne rend pas notre approche inopérante. Les valeurs du tableau 1 montrent qu'il en est de même en série benzoxazolique, du moins dans le cas des substituants nitro et chloro, et que, de plus, cette dépendance semble plus importante qu'en série soufrée. Le manque de données ne nous permet pas d'effectuer une étude quantitative de ce phénomène.

Dans le tableau 2 sont présentées les valeurs des déplacements chimiques des divers benzoxazoles substitués en position 2. La plupart des attributions ont été faites par analogie avec les résultats précédents ou par analyse des spectres couplés (cas des chloro-2 et bromo-2 benzoxazoles, **16** et **17**). En ce qui concerne les benzoxazoles substitués par un groupement électron attracteur, nous avons considéré que le signal du carbone C-6 résonnait à une fréquence plus élevée que celui relatif à C-5, et ce pour les raisons suivantes: (*i*) d'une part on observe un comportement similaire en série benzothiazolique; (*ii*) d'autre part, une permutation des attributions conduit à de plus mauvaises corrélations avec les paramètres structuraux.

Enfin, signalons que l'azido-2 benzoxazole **14** peut présenter un phénomène de tautomèrie azido–tétrazole (A ⇄ T):

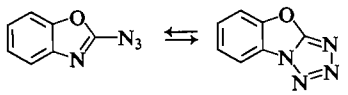

14A **14T**

Les résultats de la rmn du ^{13}C indiquent que seule

TABLEAU 1. Déplacements chimiques du ^{13}C.* Effets de substituant sur l'homocycle

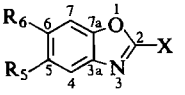

Composé	X	R_5	R_6	C-2	C-3a	C-4	C-5	C-6	C-7	C-7a	Autres
1	NH_2	H	H	163.0	143.8	115.5	123.7	120.2	108.6	148.2	
1*a*	NH_2	H	NO_2	166.4	151.0	114.1	121.0	140.4	104.5	147.2	
				(3.4)	(7.2)	(−1.4)	(−2.7)	(20.2)	(−4.1)	(−1.0)	
1*b*	NH_2	Cl	H	164.3	145.4_5	115.3	128.2	119.8	109.4	147.1	
				(1.3)	(1.6_5)	(−0.2)	(4.5)	(−0.4)	(0.8)	(−1.1)	
9	CH_3	H	H	163.5	141.4	119.0	124.1†	123.8†	110.0	150.5	CH_3:13.7
9*a*	CH_3	H	NO_2	169.3	146.6_5	119.3	120.3	144.4	107.1	149.3	CH_3:14.5
				(5.8)	(5.2_5)	(0.3)	(−3.8)	(20.6)	(−2.9)	(−1.2)	
9*b*	CH_3	CH_3	H	163.4	141.8	119.1	133.2	125.1	109.3_5	148.9	CH_3(2):13.8;
				(−0.1)	(0.4)	(0.1)	(9.1)	(1.3)	(-0.6_5)	(−1.6)	CH_3(5):20.7
11	H	H	H	153.7	140.0	120.1	124.3	125.3	110.8	149.6	
11*a*	H	H	NO_2	158.8	144.9	120.5	120.5	145.2	107.9	148.7	
				(5.1)	(4.9)	(0.4)	(−3.8)	(19.9)	(−2.9)	(−0.9)	
11*b*	H	NO_2	H	157.4	‡	116.4	‡	121.7	112.1	‡	
				(3.7)		(−4.1)		(−3.6)	(1.3)		
11*c*	H	Cl	H	155.7	141.0	119.9	128.9_5	125.7	112.3_5	148.2	
				(2.0)	(1.0)	(−0.2)	(4.6_5)	(0.4)	(1.5_5)	(−1.4)	
14	N_3	H	H	156.9	141.0	118.4	125.1	124.4	110.5	149.5	
14*a*	N_3	H	NO_2	161.7	146.8	118.5	121.5	144.0	107.2	148.7	
				(4.8)	(5.8)	(0.1)	(−3.6)	(19.6)	(−3.3)	(−0.8)	

*Les déplacements chimiques sont exprimés en ppm par rapport au TMS; les valeurs entre parenthèses représentent les effets de substituant.
†Déplacements dont l'attribution peut être inversée.
‡Ces raies ne sont pas observables (voir texte).

la forme azide est présente en solution dans le DMSO-d_6, en accord avec nos résultats antérieurs sur ce type d'équilibre (45).

Etude de la réaction de nitration du benzoxazole

Certaines structures benzoxazoliques peuvent s'hydrolyser, plus ou moins rapidement, en milieu acide. Ainsi, dans le cas du benzoxazole **11**, l'hydrolyse acide conduit à l'*o*-formylamino phénol **27**.

Cette hydrolyse intervient durant la nitration de **11**, puisqu'au lieu des dérivés normalement attendus, **11***a* et **11***b*, on obtient les formylamino phénols mononitrés, **28** et **29** (25% de **28** et 75% de **29**); par chauffage sous pression réduite, le mélange conduit aux nitro-5 et nitro-6 benzoxazoles, **11***a* et **11***b* (schéma 1). En aucune façon, la réaction ayant été répétée plusieurs fois, nous n'avons observé de dérivés benzéniques dinitrés.

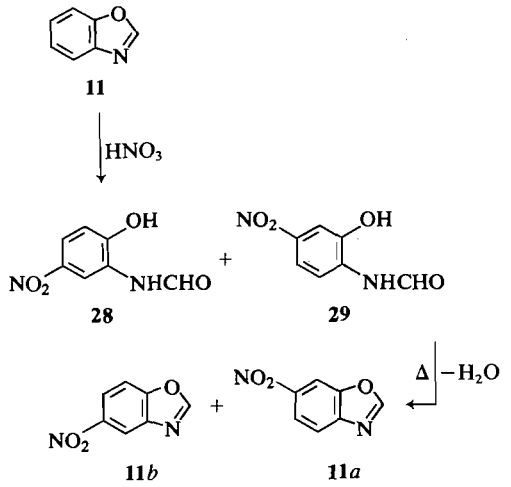

SCHÉMA 1.

Les structures des différents produits de la réaction de nitration du benzoxazole ont été déterminées par une étude comparative des déplacements chimiques du ^{13}C; à cet effet, nous avons synthétisé, et ce de façon univoque, chacun des produits représentés dans le schéma 1, selon la voie réactionnelle du schéma 2.

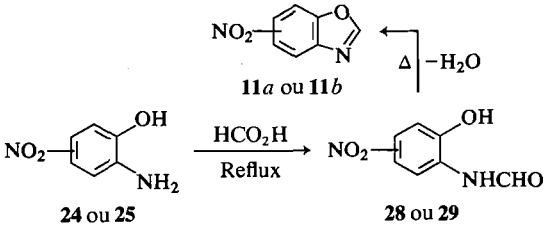

SCHÉMA 2.

L'hydrolyse du benzoxazole est donc une réaction parasite intervenant lors de la nitration de celui-ci. Le problème que l'on veut résoudre est la connaissance de l'ordre dans lequel ces deux réactions vont se réaliser. Dans cette intention, nous avons nitré l'*o*-formylamino phénol (produit d'hydrolyse du benzoxazole) **27**. Par une étude comparative des déplacements chimiques du ^{13}C et par des synthèses

TABLEAU 2. Déplacements chimiques du ^{13}C des benzoxazoles substitués en position 2*

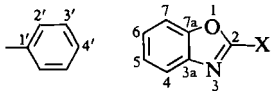

Composés	X	C-2	C-3a	C-4	C-5	C-6	C-7	C-7a	Autres
1	NH_2	163.0	143.8	115.5	123.7	120.2	108.6	148.2	
2	$NHCH_3$	163.3	143.6	115.6	123.7	120.2	108.6	148.5	CH_3: 29.0
3	NHC_2H_5	162.4	143.5_5	115.5	123.6	120.0	108.5	148.2	CH_2: 37.2_5; CH_3: 14.7
4	$N(C_2H_5)_2$	161.6	143.6	115.3	123.5	119.6	108.4	148.4	CH_2: 42.4; CH_3: 13.0
5	$NHNH_2$	165.2	143.1	115.9	123.9	120.6	108.9	148.6	
6	NHC_6H_5	158.2	142.7	116.8	124.1	121.7†	109.0	147.2_5	C-1′: 139.0; C-2′: 117.9 C-3′: 129.1; C-4′: 122.2_5†
7		161.8	142.9	116.0	124.1	120.6	108.9	148.4	$CH_2(\alpha)$: 45.4; $CH_2(\beta)$: 65.4
8	OCH_3	163.8	140.9	117.6	124.1	122.6	109.6	148.2	CH_3: 58.7
9	CH_3	163.5	141.4	119.0	124.1†	123.8†	110.0	150.5	CH_3: 13.7
10	C_2H_5	167.5	141.3	119.1	124.1†	123.8†	110.0	150.4_5	CH_2: 21.4; CH_3: 10.3
11	H	153.7	140.0	120.1	124.3	125.3	110.8	149.6	
12	SCH_3	165.0	141.5	117.9	124.0	123.5	109.6	151.4	CH_3: 14.1
13	SC_2H_5	164.2	141.5	117.9	123.9	123.5	109.5	151.2	CH_2: 26.1; CH_3: 14.4
14	N_3	156.9	141.0	118.4	125.1	124.4	110.5	149.5	
15	C_6H_5	162.1	141.5	119.6	125.1	124.4	110.5	150.1	C-1′: 130.6; C-2′: 127.0 C-3′: 128.8; C-4′: 131.4
16	Br	138.7	141.0	118.9	125.2	124.7	110.1	151.9	
17	Cl	150.0	140.5	119.1	125.4	124.9	110.2_5	151.0	
18	$C{=}NH(OCH_3)$	153.5	140.1_5	120.9	125.5	127.3	111.7	150.1	CN: 156.2; CH_3: 53.6_5
19	$CONH_2$	157.1	140.1	121.1	125.6	127.4	111.8	150.4	CO: 156.0
20	$CO_2C_2H_5$	152.7	140.0_5	121.7	125.8	128.3	111.9	152.7	CO: 155.8; CH_2: 62.7 CH_3: 13.9
21	CN	137.0	138.7_5	121.5	126.6	129.3	111.8	149.8	CN: 109.6
22	SO_3K	162.1	139.8_5	120.9	125.2	126.6	111.5	150.0	

*Les déplacements chimiques sont exprimés en ppm par rapport au signal du TMS.
†Déplacements dont l'attribution peut être inversée.

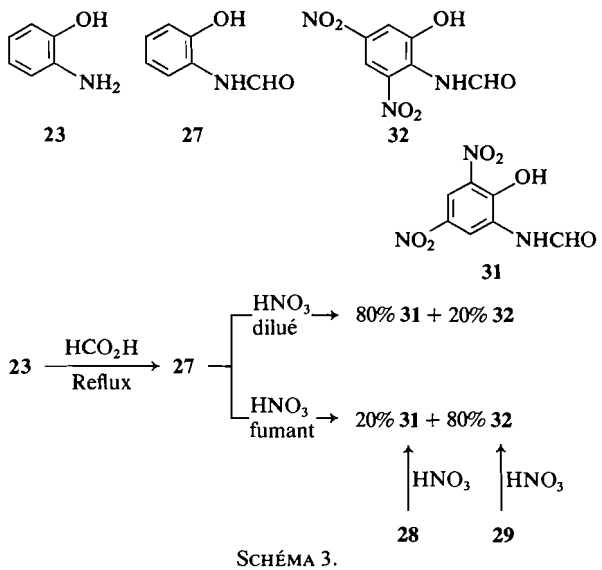

SCHÉMA 3.

univoques (nitration de **28** et **29**), nous avons pu identifier les différents composés obtenus (schéma 3).

On obtient toujours deux dérivés dinitrés dont la proportion dépend de l'acidité du milieu réactionnel. Compte tenu du site de nitration, on peut admettre qu'en milieu fortement acide le substrat est une espèce protonée sur le groupe formamido.

Ces expériences (obtention des dérivés mononitrés **28** et **29** à partir du benzoxazole **11**, et obtention des dérivés dinitrés **31** et **32** à partir de l'*o*-formylamino phénol **27**) démontrent avec certitude que la nitration (formation de **11***a* et **11***b*) précède l'hydrolyse.

Les déplacements chimiques des différents phénols sont rassemblés dans le tableau 3; l'étude des dérivés **26** et **30** sert à confirmer les attributions.

Discussion

Corrélations empiriques entre déplacements chimiques du ^{13}C et paramètres structuraux

En série hétéroaromatique, la déficience des calculs de mécanique quantique à prédire correctement les valeurs des déplacements chimiques a conduit de nombreux auteurs à relier les résultats expérimentaux avec certains paramètres structuraux, caractéristiques de la nature du substituant (46, 47).

Comme dans le cas des dérivés benzothiazoliques (9), et dans l'intention de réaliser des corrélations avec les effets de substituant observés en série benzoxazolique, nous avons utilisé l'équation triparamétrique [2] proposée par Smith et Proulx (48, 49).

$$[2] \qquad \Delta\delta^{13}C = aF + bR + cQ^* + d$$

Dans cette équation, F et R sont les paramètres structuraux de Swain et Lupton (50); F représente une mesure des effets de champ et R une mesure des effets de résonance. Q^* est un paramètre semi-

TABLEAU 3. Déplacements chimiques du ^{13}C des dérivés benzéniques*

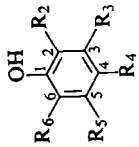

Composé	R_2	R_3	R_4	R_5	R_6	C-1	C-2	C-3	C-4	C-5	C-6	Autres
23	NH_2	H	H	H	H	144.8	136.7	115.6†	120.4	117.8	115.3†	
24	NH_2	H	NO_2	H	H	150.9	137.7	108.1	140.5	113.4	113.4	
25	NH_2	H	H	NO_2	H	145.8	143.2	119.0	112.1	136.8	109.7	
26	NH_2	H	Cl	H	H	143.3	138.6	114.0	123.6	115.7†	116.0_5†	
27	NHCHO	H	H	H	H	147.0	126.2	121.2	119.3	124.5	115.5	CO:160.3
28	NHCHO	H	NO_2	H	H	153.2	126.5	115.6	139.5	120.7	114.6	CO:161.0
29	NHCHO	H	H	NO_2	H	146.6	133.0	119.1	115.5	142.7	109.2_5	CO:161.0
30	NHCHO	H	Cl	H	H	145.8	127.6	120.4	122.8_5	123.8	116.3	CO:160.7
31	NHCHO	H	NO_2	H	NO_2	150.0	131.2	117.8†	137.3	116.1†	134.8	CO:161.7
32	NHCHO	NO_2	H	NO_2	H	147.3	134.5_5	138.5_5	108.8	140.4	111.3_5	CO:163.5

*Les déplacements chimiques sont exprimés en ppm par rapport au TMS.
†Déplacements dont l'attribution peut être inversée.

TABLEAU 4. Coefficients de l'équation $\Delta\delta^{13}C = aF + bR + cQ^* + d$

Coefficients	Composés	C-2	C-3a	C-4	C-5	C-6	C-7	C-7a
a	BZT*	−2.58±3.02	−5.35±1.96	1.79±0.59	2.21±0.47	2.24±0.27	0.63±0.17	0.69±1.34
	BZO	−9.86±7.44	−2.11±1.38	0.90±0.63	2.54±0.61	3.48±0.56	1.07±0.33	−2.53±1.04
b	BZT	17.32±7.04	0.96±4.57	7.61±1.36	4.01±1.09	5.97±0.63	3.92±0.41	2.22±3.32
	BZO	4.76±1.88	−7.21±3.49	7.68±1.59	3.38±1.54	13.05±1.43	5.17±0.84	−8.60±2.64
c	BZT	−15.48±1.59	0.81±0.97	−0.52±0.29	−0.72±0.23	−0.21±0.13	−0.68±0.09	0.72±0.71
	BZO	−8.90±4.69	0.80±0.83	−0.39±0.38	−0.49±0.37	−1.28±0.34	−0.54±0.20	2.71±0.63
d	BZT	2.43±2.83	0.77±1.79	−0.55±0.53	0.20±0.42	−0.04±0.24	0.09±0.16	1.09±1.30
	BZO	2.61±4.32	0.49±0.74	−0.15±0.33	−0.09±0.32	0.10±0.30	−0.16±0.18	0.49±0.56
r	BZT	0.9852	0.7797	0.9746	0.9542	0.9945	0.9815	0.8204
	BZO	0.9745	0.9366	0.9914	0.9742	0.9967	0.9913	0.9552

*BZT: benzothiazole (9 points, substituants: NH_2, OCH_3, CH_3, H, F, Cl, Br, CN, NO_2); BZO: benzoxazole (mêmes substituants sauf: F et NO_2).

TABLEAU 5. Déplacements chimiques des substituants. Comparaison benzoxazole–benzothiazole

	Y	
X	S*	O
$CONH_2$	165.0	156.0
CO_2R	160.3‡†	155.8
CN	113.3	109.6
CH_3	19.5	13.7
CH_2CH_3	27.0	21.4

*Valeurs de la réf. 9.
†Cette publication, produit 33.

empirique défini par Schaefer et coll. (51) comme étant égal à P/Ir^3 (P représentant la polarisabilité de la liaison C—X, I le premier potentiel d'ionisation de l'élément X et r la distance C—X). Les auteurs de la référence (51) ont également suggéré que Q^* pouvait être une mesure empirique du terme paramagnétique σ_p^A de l'équation de Ramsey (52).

Dans le tableau 4 sont réunis les résultats de ces corrélations: coefficients de régréssion, écart type et coefficients de corrélation (r). Pour comparaison, dans le même tableau, nous donnons les résultats obtenus précédemment en série benzothiazolique (9).

Un premier examen des résultats du tableau 4 montre qu'à l'exception du carbone C-2 les corrélations sont bien meilleures en série benzoxazolique, plus particulièrement en ce qui concerne les carbones de jonction. On peut critiquer, à juste titre, cette dernière affirmation, étant donné la non-similitude du nombre et de la nature des substituants dans les deux séries. Cependant, nous avons vérifié que l'omission des valeurs relatives aux groupements fluoro et nitro n'améliorent pas les corrélations en série benzothiazolique.

Dans la corrélation relative au carbone C-2, et comme en série benzothiazolique (9), nous avons exclu la valeur du groupement amino, car, pour ce substituant, l'écart entre la valeur expérimentale et la valeur calculée est trop élevé (~10 ppm). Cette déviation, qui ne semble pas due à la présence d'une certaine quantité de tautomère imino-2 benzoxazoline, pourrait plutôt être attribuée à l'existence d'importantes associations avec le solvant (53); en effet, les paramètres structuraux du groupement amino (et Q^* en particulier) ont été déterminés à partir d'études portant sur des dérivés de l'aniline (54), substrat dans lequel de telles associations n'interviennent pas.

Par ailleurs, contrairement à ce que l'on observe en série benzothiazolique (9), le déplacement du carbone C-2 dépend peu du paramètre Q^*. Si on

considère que ce paramètre structural représente une mesure grossière de l'effet stérique, on peut expliquer cette absence de relation par des interactions plus faibles entre le substituant et l'hétéroatome lorsque ce dernier est un oxygène. Par contre, l'effet inductif de cet atome se traduit par d'importantes modifications des valeurs des déplacements chimiques du substituant en position 2; on observe un effet de blindage par rapport au dérivé soufré. Ces résultats sont rassemblés dans le tableau 5.

Les déplacements des carbones, C-4 et C-6 sont surtout fonction des effets de résonance, ce que l'on peut expliquer par la prépondérance des structures canoniques dipolaires suivantes:

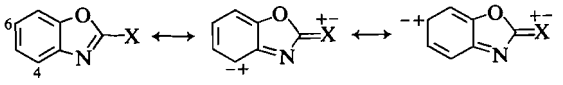

Le déplacement du carbone C-6 dépend également des effets de champ (paramètre F) et de Q^*. Il est intéressant de remarquer que les déplacements de C-6 sont les seuls à être fonction des trois paramètres F, R et Q^*, et que la position 6 de l'homocycle est la plus réactive vis-à-vis des réactions de substitution électrophile.

Dans le cas de C-4, C-5 et C-7 les coefficients de régréssion sont peu dépendants de la nature de l'hétéroatome (S ou O). Par contre, dans le cas de C-6, les coefficients, bien que de même signe, ont une valeur plus grande pour le dérivé oxygéné, ce qui traduit une relation plus importante avec le substituant en position 2.

Enfin, le fait que les carbones C-5 et C-6 dépendent également de Q, confirme que ce paramètre ne représente pas seulement la mesure des effets stériques.

Etude de la tautomérie prototropique

Certains benzoxazoles substitués en position 2 présentent un phénomène de tautomérie prototropique:

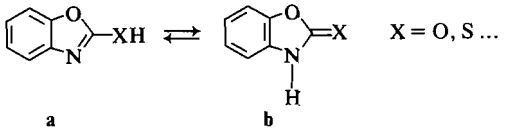

a **b**

Ce type d'équilibre a fait l'objet de nombreux travaux en série hétérocyclique aromatique (55). Au cours de précédentes études, nous avons montré les avantages et les inconvénients de l'utilisation de la rmn du ^{13}C pour de possibles analyses qualitatives et quantitatives de ce problème (9, 56). Sans revenir sur ces résultats, précisons néanmoins que, lorsque l'hétéroatome X représente un atome de soufre ou d'oxygène, l'équilibre est très fortement déplacé vers la forme **b**, et que l'influence de l'état physique (solide, solution ou phase vapeur) est très importante (57).[3]

Les déplacements chimiques des composés pouvant présenter ce phénomène de prototropie, ainsi que les valeurs de certains produits modèles (dans lesquels le proton pyrrolique a été remplacé par un groupement méthyle), sont rassemblés dans le tableau 6. Les effets du groupement nitro (composé **36**) permettent, comme nous l'avons précédemment expliqué, de réaliser une attribution complète des déplacements chimiques des carbones de l'homocycle du dérivé **35**. Compte tenu de la similitude des spectres, nous garderons la même attribution pour le composé **38**. En toute rigueur, l'utilisation des effets de substituant pour attribuer les signaux de structures prototropes est critiquable. En pratique, comme l'équilibre est fortement déplacé vers l'une des formes tautomères, l'introduction d'un substituant sur le noyau benzénique ne modifie pas, d'une manière appréciable par la méthode spectroscopique, la position de l'équilibre.

La comparaison des déplacements chimiques des carbones du cycle oxazolique des différents composés du tableau 5 montre que l'équilibre est très déplacé vers les structures de type **b**. De plus, comme nous l'avons signalé en série benzothiazolique (9), le carbone C-4 est plus blindé dans **b**. Cet effet est attribué à la variation de l'électronégativité de l'atome d'azote N_3. Les autres carbones de l'homocycle sont, quant à eux, peu influencés par le phénomène de tautomérie.

Récemment (58), dans le cas de la phényl-4 Δ-4-thiazolinethione-2 **40** et de son homologue oxygéné **41**, nous avons mis en évidence des couplages entre le proton pyrrolique et les carbones du cycle (en particulier avec C-2).

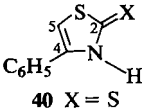

40 X = S
41 X = O

On n'observe pas ce type de couplage dans le cas du dérivé non substitué; on explique ce phénomène par un ralentissement de l'échange du proton pyrrolique avec le milieu environnant, lorsque le cycle est substitué par un groupement phényle.

La benzocondensation ne conduit pas à une observation similaire: dans le spectre couplé de **35**, le signal du carbone 2 représente un singulet; quant aux figures de couplage des carbones de jonction,

[3]L'existence en solution de structures associées (dimérisation ou association avec le solvant) a été mise en évidence pour ce type de composés (53). De plus, dans le cas du diméthylsulfoxyde, les constantes d'association sont relativement importantes.

TABLEAU 6. Déplacements chimiques du ^{13}C.* Etude de la tautomérie prototropique

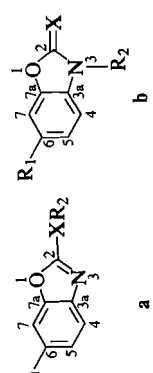

a

b

Composés	X	R_1	R_2	Forme	C-2	C-3a	C-4	C-5	C-6	C-7	C-7a	Autres
35	O	H	H	ou	154.9	130.7	109.6†	123.8	121.9	109.9†	143.7	
36	O	NO_2	H	ou	154.5	137.0	109.7	121.1	142.3	105.5	144.0	
8	O	H	CH_3		163.8	140.9	117.6	124.1	122.6	109.6	148.2	CH_3: 58.7
37	O	H	CH_3		154.0	131.7	108.9†	123.7	122.0	109.3†	141.9_5	CH_3: 27.9
38	S	H	H	ou	180.2	131.2_5	109.9†	125.0_5	123.6	110.4†	148.2	
12	S	H	CH_3		165.0	141.5	117.9	124.0	123.5	109.6	151.4	CH_3: 14.1
39	S	H	CH_3		179.8	132.1	109.9†	124.9	124.2	110.4†	146.3	CH_3: 31.9

*Les déplacements chimiques sont exprimés en ppm par rapport au TMS.
†Déplacements dont l'attribution peut être inversée.

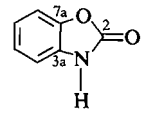

35

C-3a et C-7a, elles ne peuvent être analysées à cause de leur mauvaise résolution.

Effets de la benzocondensation et analyse des couplages $^nJ(C,H)$

Les perturbations créées par la condensation d'un noyau benzénique sur des hétérocycles pentagonaux-1,3 sont présentées dans le tableau 7.

Comme pour la série monohétéroatomique (59), l'effet de la benzocondensation sur le carbone en position 2 dépend, non pas de l'électronégativité de l'hétéroatome adjacent, mais de sa taille. En effet, on observe, pour ce carbone, l'ordre de variation suivant:

TABLEAU 7. Effets de la benzocondensation en série pentagonale-1,3

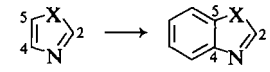

A *B*

X	ΔC-2*	ΔC-4*	ΔC-5*
O†	1.8	13.5_5	10.3
S‡	1.6	9.9	14.1
NCH_3§	5.5	13.9	14.4

*$\Delta C = \delta C_B - \delta C_A$.
†Les déplacements chimiques de l'oxazole 34, mesurés dans le DMSO-d_6 à la température de 28°C, sont les suivants: $\delta C_2 = 151.9$ ppm; $\delta C_4 = 126.4_5$ ppm et $\delta C_5 = 139.3$ ppm.
‡Valeurs de la réf. 9.
§Valeurs de la réf. 8.

TABLEAU 8. Constantes de couplage $^nJ(C,H)$

Oxazole†

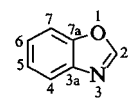

Benzoxazole‡

Paramètre	Valeur	Paramètre	Valeur
$^1J(C_2,H_2)$	231.1	$^1J(C_2,H_2)$	233.1
$^3J(C_2,H_4)$	10.6	$^3J(C_{3a},H_2)$	5.2
$^3J(C_2,H_5)$	8.1	$^3J(C_{3a},H_5) = {}^3J(C_{3a},H_7)$	8.5
$^1J(C_4,H_4)$	195.2	$^1J(C_4,H_4)$	164.3
$^2J(C_4,H_5)$	16.4	$^3J(C_4,H_6)$	8.1
$^3J(C_4,H_2)$	8.8	$^1J(C_5,H_5)$	161.7
$^1J(C_5,H_5)$	209.0	$^3J(C_5,H_7)$	7.4
$^2J(C_5,H_4)$	18.8	$^1J(C_6,H_6)$	162.6
$^3J(C_5,H_2)$	3.9	$^3J(C_6,H_4)$	7.9
		$^1J(C_7,H_7)$	166.5
		$^3J(C_7,H_5)$	8.5

*Les constantes de couplage sont exprimés en Hz; les spectres ont été analysés au premier ordre.
†Les couplages à longue distance, ^2J et ^3J, des carbones C-4 et C-5 ont été attribués par comparaison avec les résultats du (pyridyl-4′)-2 oxazole (M. N. Dinia et C. Marzin. Résultats non publiés.
‡La figure de couplage du carbone C-7a est mal résolue.

$S < O < NCH_3$. En ce qui concerne les effets sur les atomes de jonction, comme nous l'avons déjà montré (9), la perturbation est plus importante sur le carbone adjacent à l'hétéroatome le moins électronégatif. Dans le cas du couple oxazole-benzoxazole, nous avons $\Delta C\text{-}4 > \Delta C\text{-}5$.

Les constantes de couplage $^nJ(C,H)$ du benzoxazole et de l'oxazole sont données dans le tableau 8.

1. A. Escande, J. Lapasset, R. Faure, E. J. Vincent et J. Elguero. Tetrahedron, **30**, 2903 (1974).
2. M. Calafell, J. Elguero et A. Fruchier. Org. Magn. Reson. **7**, 84 (1975).
3. A. Maquestiau, Y. Van Haverbeke, R. Flammang, M. C. Pardo et J. Elguero. Org. Mass Spectrom. **10**, 313 (1975).
4. A. Maquestiau, Y. Van Haverbeke, R. Flammang, M. C. Pardo et J. Elguero. Org. Mass Spectrom. **10**, 558 (1975).
5. J. Elguero, A. Fruchier et M. C. Pardo. Can. J. Chem. **54**, 1329 (1976).
6. J. Elguero, R. Faure, R. Lazaro et E. J. Vincent. Bull. Soc. Chim. Belg. **86**, 95 (1977).
7. P. Bouchet, A. Fruchier, G. Joncheray et J. Elguero. Org. Magn. Reson. **9**, 716 (1977).
8. M. Begtrup, R. M. Claramunt et J. Elguero. J. Chem. Soc. Perkin II, 99 (1978).
9. R. Faure, J. Elguero, R. Lazaro et E. J. Vincent. Org. Magn. Reson. Sous presse.
10. G. C. Levy et G. L. Nelson. ^{13}C nmr for organic chemists. Wiley-Interscience, New York, NY. 1972.
11. Brevet français no 773,944 (28 novembre 1934); Chem. Abstr. **29**, 2177 (1935).
12. S. Skraup. Justus Liebigs Ann. Chem. **419**, 68 (1919).
13. T. P. Sycheva, I. D. Kiseleva et M. N. Shchukina. Khim. Geterotsikl. Soedin. 205 (1966).
14. S. Palazzo et B. Tornetta. Ann. Chim. (Rome), **48**, 657 (1958).
15. H. Ogura, S. Sugimoto et K. Shimura. Yakugaku Zasshi, **90**, 796 (1970).
16. S. B. Advani et J. Sam. J. Pharm. Sci. **57**, 1963 (1968).
17. T. P. Sycheva, I. D. Kiseleva et M. N. Shchukina. Khim. Geterotsikl. Soedin. 43 (1967).
18. K. Davidkov et D. Simov. Dokl. Bolg. Akad. Nauk, **21**, 1193 (1968). Chem. Abstr. **70**, 57714 (1969).
19. L. J. Darlage, T. H. Kinstel et C. L. McIntosh. J. Org. Chem. **36**, 1088 (1971).
20. G. Newbery et M. A. Phillips. J. Chem. Soc. 116 (1928).
21. D. A. Drapkina, V. G. Brudz, V. A. Inshakova et N. I. Badaikova. Metody Poluch. Khim. Restinov, **15**, 184 (1967). Chem. Abstr. **68**, 105062 (1968).
22. S. Skraup et M. Moser. Chem. Ber. **55**, 1080 (1922).
23. E. Bamberger. Chem. Ber. **36**, 2051 (1903).
24. Brevet allemand no 1,124,499 (1 Mars 1962). Chem. Abstr. **52**, 9858 (1962).
25. R. Passerini. J. Chem. Soc. 2256 (1954).
26. B. Belenson et F. M. Hamer. J. Chem. Soc. 143 (1939).
27. B. A. Arbuzov et V. M. Zoroastrova. Izv. Akad. Nauk SSSR Odt. Khim. Nauk. 1037 (1959); Chem. Abstr. **54**, 1498 (1960).
28. G. A. Reynolds, J. A. Van Allan et J. F. Tinker. J. Org. Chem. **24**, 1205 (1959).
29. E. L. Holljes et E. C. Wagner. J. Org. Chem. **9**, 31 (1944).
30. H. N. McCoy. Am. Chem. J. **21**, 111 (1899).
31. D. S. Jones, G. W. Kenner et R. C. Sheppard. J. Chem. Soc. 4393 (1965).
32. H. Moller. Justus Liebigs Ann. Chem. **749**, 1 (1971).
33. K. Dickore, K. Sasse et K. D. Bode. Justus Liebigs Ann. Chem. **733**, 70 (1970).
34. Brevet français no 772,968 (9 novembre 1934); Chem. Abstr. **29**, 1658 (1935).
35. H. Gilman et J. A. Beel. J. Am. Chem. Soc. **71**, 2338 (1949).
36. K. Zahn. Chem. Ber. **56**, 584 (1923).
37. J. W. Conforth et R. H. Conforth. J. Chem. Soc. 96 (1947).
38. G. Bender. Chem. Ber. **19**, 2271 (1886).
39. J. Sam, J. L. Valentine et C. W. Richmond. J. Pharm. Sci. **57**, 1763 (1968).
40. W. J. Close, B. D. Tiffany et M. A. Spielman. J. Am. Chem. Soc. **71**, 1265 (1949).
41. M. Chanon, M. Conte, J. Micozzi et J. Metzger. Int. J. Sulfur Chem. **6**, 85 (1971).
42. J. Seidel. J. Prakt. Chem. (2) **42**, 448 (1890).
43. A. I. Vogel. Practical organic chemistry. Longmans, London. 1972 p. 655.
44. J. B. Stothers. ^{13}C nmr spectroscopy. Academic Press, New York, NY. 1972. p. 197.
45. R. Faure, J. P. Galy, E. J. Vincent et J. Elguero. J. Heterocycl. Chem. **14**, 1299 (1977).
46. J. W. Emsley et L. Phillips. Progress in nmr spectroscopy. Vol. 7. Pergamon Press, Oxford. 1971.
47. G. J. Martin, M. L. Martin et S. Odiot. Org. Magn. Reson. **7**, 2 (1975).
48. W. B. Smith et T. W. Proulx. Org. Magn. Reson. **8**, 205 (1976).
49. W. B. Smith et T. W. Proulx. Org. Magn. Reson. **8**, 567 (1976).
50. C. G. Swain et E. C. Lupton. J. Am. Chem. Soc. **90**, 4328 (1968).
51. F. Hruska, H. M. Hutton et T. Schaefer. Can. J. Chem. **43**, 2392 (1965).
52. N. F. Ramsey. Phys. Rev. **78**, 699 (1950).
53. E. Gentric, J. Lauransan, C. Roussel et J. Metzger. J. Chem. Soc. Perkin II, 1015 (1977).
54. W. B. Smith, A. M. Ihrig et J. L. Roark. J. Phys. Chem. **74**, 812 (1970).
55. J. Elguero, C. Marzin, A. R. Katritzky et P. Linda. The tautomerism of heterocycles. Academic Press. New York, NY. 1976.
56. R. Faure, E. J. Vincent, G. Assef, J. Kister et J. Metzger. Org. Magn. Reson. **9**, 688 (1977).
57. P. Beak. Acc. Chem. Res. **10**, 186 (1977).
58. R. Faure, A. Assaf, E. J. Vincent et J. P. Aune. J. Chim. Phys. Sous presse.
59. R. Faure. Thèse d'état, Marseille, France. 1978.

COMMUNICATION

Nucleophilic reactions of zwitterionic species from deprotonation of η^6-arene-η^5-cyclopentadienyliron cations

CHOI CHUCK LEE, BARRY R. STEELE, KEN J. DEMCHUK, AND RONALD G. SUTHERLAND

Department of Chemistry and Chemical Engineering, University of Saskatchewan, Saskatoon, Sask., Canada S7N 0W0

Received December 18, 1978

CHOI CHUCK LEE, BARRY R. STEELE, KEN J. DEMCHUK, and RONALD G. SUTHERLAND. Can. J. Chem. **57**, 946 (1979).

A variety of η^6-arene-η^5-cyclopentadienyliron cations in which the arene ligand has an α-carbon substituent containing one or more hydrogens can be deprotonated with base to give the corresponding neutral zwitterionic species. These zwitterions can react *in situ* as nucleophiles with different substrates, such as CH_3I, CO_2, and CS_2, to give a wide range of synthetic applications.

CHOI CHUCK LEE, BARRY R. STEELE, KEN J. DEMCHUK et RONALD G. SUTHERLAND. Can. J. Chem. **57**, 946 (1979).

Un grand nombre de cations η^6-arène η^5-cyclopentadiénylfer dans lesquels le ligand arène possède un carbone en α portant un ou plusieurs hydrogènes peuvent être déprotonés à l'aide de bases et donnent naissance aux espèces zwittérioniques neutres correspondantes. Ces zwittérions peuvent réagir *in situ* comme nucléophiles avec divers substrats, tels CH_3I, CO_2 et CS_2, donnant lieu à un large éventail d'applications en synthèse.

[Traduit par le journal]

Recently, Johnson and Treichel (1) reported that the deprotonation of the η^6-fluorene-η^5-cyclopentadienyliron cation (**1**) with *tert*-BuOK in C_6H_6 gave the neutral, zwitterionic η^6-fluorenyl-η^5-cyclopentadienyliron (**2**) which subsequently can react as a nucleophile with alkyl halides such as CH_3I. Similarly, Helling and Hendrickson (2) also obtained **2** from the reaction of **1** with sodium bis(trimethylsilyl)amide in benzene, as well as the analogous neutral complexes from the treatment, with $NaNH_2$ in NH_3, of η^6-arene-η^5-cyclopentadienyliron cations in which the aromatic ligands were triphenylmethane, diphenylamine, and carbazole. While the crystallographic studies of Johnson and Treichel (1) indicated that **2** may be formulated with the zwitterionic structure **2***a*, Helling and Hendrickson (2) also stressed the contribution from a π-cyclohexadienyliron complex with an exocyclic double bond (e.g., **2***b*), especially in the case where the original arene ligand was triphenylmethane.

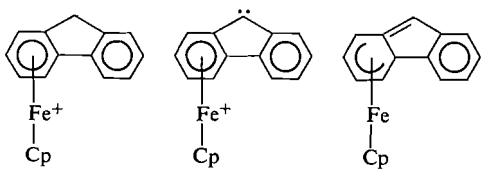

1 **2***a* **2***b*

In conjunction with our studies on ligand exchange reactions between arene and ferrocene (3–5), we have also observed the formation of **2** from **1**, even under the relatively mild, basic conditions of K_2CO_3 in dimethylformamide (DMF). We wish to report that the deprotonation to give zwitterionic species is not restricted to systems such as **1** but can occur in a variety of η^6-arene-η^5-cyclopentadienyliron cations (**3**) in which the arene ligand possesses one or more saturated α-hydrogens. The zwitterion can then react *in situ* as a nucleophile to provide a wide range of synthetic possibilities.

The η^6-arene-η^5-cyclopentadienyliron cations (**3**) were prepared from ligand exchange reactions between the arene and ferrocene in the presence of $AlCl_3$–Al (4, 5). In a typical experiment, 2.0 mmol of **3**, as the hexafluorophosphate salt, was stirred in tetrahydrofuran (THF) at a given temperature. Upon addition of an equivalent or an excess of *tert*-BuOK, there was an immediate change in color to deep red or dark blue, indicative of the formation of the zwitterionic species.[1] The substrate such as CH_3I was added and the mixture was stirred for 30 min and then allowed to warm to room temperature.

[1]As sample cases, from cation **3** with mesitylene or triphenylmethane as the arene ligand, after the THF solution was concentrated, the zwitterion was isolated by chromatographic separation on silica gel and identified by mass spectroscopy.

0008-4042/79/080946-03$01.00/0

TABLE 1. Data from nucleophilic substitution reactions of zwitterionic species from deprotonation of η^6-arene-η^5-cyclopentadienyliron cations (3)

Aromatic ligand in 3	Reaction	Aromatic ligand in product	Yield (%)
CH_3Ph	I[a]	EtPh	20
		i-PrPh	10
CH_3Ph	I, −60°C	EtPh	60
EtPh	I	*i*-PrPh	10
o-$(CH_3)_2Ph$	I	*o*-CH_3(Et)Ph	60
o-$Cl(CH_3)Ph$	I	*o*-Cl(Et)Ph	55
1,3,5-$(CH_3)_3Ph$	I	1-Et-3,5-$(CH_3)_2Ph$	70
Ph_2CH_2	I	Ph_2CHCH_3	70
		$Ph_2C(CH_3)_2$	10
Ph_3CH	I	Ph_3CCH_3	95
Tetralin	I, −20°C	α-Methyltetralin	80
9,10-Dihydroanthracene	I, −20°C	9,10-Dihydro-9-methylanthracene	7
		cis-9,10-Dihydro-9,10-dimethylanthracene	20
Xanthene	I	9-Methylxanthene	65
CH_3Ph	IIA[b]	$PhCH(CH_3)COOCH_3$	60
CH_3Ph	IIA, −50°C	$PhCH_2COOCH_3$	70
CH_3Ph	IIB[b]	$PhCH{=}C(SCH_3)_2$	80
EtPh	IIA	$PhCH(CH_3)COOCH_3$	50
EtPh	IIB	$Ph(CH_3)C{=}C(SCH_3)_2$	40
i-PrPh	IIA	$PhC(CH_3)_2COOCH_3$	85
i-PrPh	IIB	$PhC(CH_3)_2CSSCH_3$	65
Fluorene	III,[c] EtI	9-Ethylfluorene	60
		9,9-Diethylfluorene	30
Fluorene	III, 1-Cl-2,4-$(NO_2)_2Ph$	9-(2,4-Dinitrophenyl)fluorene[d]	65
Fluorene	III [ClPhFeCp][PF_6]	PhFeCp[PF_6] 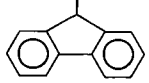	70

[a]Reaction I involves deprotonation of 3 with 1 equiv. of *tert*-BuOK in THF followed by treatment with CH_3I, the whole process being carried out at room temperature or at the temperature indicated.
[b]Reaction II involves deprotonation of 3 with an excess of *tert*-BuOK in THF followed by treatment with CO_2 (IIA) or CS_2 (IIB) and then with $(CH_3)_2SO_4$, the whole process being carried out at room temperature or at the temperature indicated.
[c]Reaction III involves deprotonation of 3 with an excess of K_2CO_3 in DMF followed by treatment with the indicated RX, the whole process being carried out at room temperature.
[d]The initial product was the blue zwitterionic η^6-9-(2,4-dinitrophenyl)-9-fluorenyl-η^5-cyclopentadienyliron which upon treatment with HCl gave the 65% yield of the η^6-9-(2,4-dinitrophenyl)fluorene-η^5-cyclopentadienyliron cation.

During the reaction, the color also changed to yellow or orange. Upon quenching the reaction with H_2O containing NH_4PF_6, the product, η^6-substituted arene-η^5-cyclopentadienyliron cation (**4**), as the hexafluorophosphate salt, was extracted with CH_2Cl_2 and then precipitated from the dried extract by the addition of ether. When necessary, purification and separation of mixed products were effected by chromatography through an alumina column (4, 5). All the product ions (**4**) were identified by their ^1H and ^{13}C nmr spectra. The results are summarized in Table 1.

The variety of reactions given in Table 1 serves only to illustrate the wide range of synthetic applications. The ready formation of the zwitterions apparently arises from complexing the arene with the highly electron withdrawing $CpFe^+$ group. Similar activations of the α-carbon in nucleophilic reactions by carbonylchromium groups in systems such as methyl arylacetate – chromium tricarbonyl and related compounds have also been reported (6, 7).

We wish to communicate the present results in preliminary form since the method used is apparently of general applicability. It is likely that a variety of zwitterions besides those given in Table 1 may also be utilized in nucleophilic substitution reactions with many other substrates, thus providing a wide ranging possibility for the alkylation and functionalization of η^6-arene-η^5-cyclopentadienyliron cations. Since we have already shown that the aromatic ligand in cations such as **4** may be regenerated as the substituted arene itself either photolytically (4), or in better yields by pyrolytic sublimation under reduced pressure (5), the synthetic applications may be extended to include the preparation of substituted arenes. As an example, 9-methylxanthene was recovered in

85–90% yield from vacuum sublimation of the η^6-9-methylxanthene-η^5-cyclopentadienyliron cation (Table 1). Currently, we are extending our studies to include similar reactions with other heterocyclic ligands. Cations **3** with heterocyclic ligands other than xanthene (thioxanthene, 9,10-dihydroacridine, and phenothiazine) have been prepared and their deprotonation and subsequent nucleophilic substitution reactions are under investigation.

Acknowledgments

Financial support from the President's Fund and from grants to C.C.L. and R.G.S. given by the National Research Council of Canada are gratefully acknowledged.

1. J. W. JOHNSON and P. M. TREICHEL. J. Am. Chem. Soc. **99**, 1427 (1977).
2. J. F. HELLING and W. A. HENDRICKSON. J. Organomet. Chem. **141**, 99 (1977).
3. C. C. LEE, R. G. SUTHERLAND, and B. J. THOMSON. J. Chem. Soc. Chem. Commun. 907 (1972).
4. R. G. SUTHERLAND, S. C. CHEN, W. J. PANNEKOEK, and C. C. LEE. J. Organomet. Chem. **101**, 221 (1975); **117**, 61 (1976).
5. R. G. SUTHERLAND, W. J. PANNEKOEK, and C. C. LEE. Can. J. Chem. **56**, 1782 (1978).
6. G. JAOUN, A. MEYER, and G. SIMOUNEAUX. J. Chem. Soc. Chem. Commun. 813 (1975).
7. H. DES ABBAYES and M.-A. BOUDEVILLE. J. Org. Chem. **42**, 4104 (1977).

Canadian Journal of Chemistry
Published by
THE NATIONAL RESEARCH COUNCIL OF CANADA

Journal canadien de chimie
Publié par
LE CONSEIL NATIONAL DE RECHERCHES DU CANADA

Volume 57 Number 9 May 1, 1979

Volume 57 numéro 9 1 mai 1979

Temperature dependence of rate constants for reaction of oxygen atoms, O(^3P), with allene and 1,3-butadiene[1]

W. S. NIP,[2] D. L. SINGLETON, AND R. J. CVETANOVIĆ
Division of Chemistry, National Research Council of Canada, Ottawa, Ont., Canada K1A 0R9

Received December 11, 1978

W. S. NIP, D. L. SINGLETON, and R. J. CVETANOVIĆ. Can. J. Chem. **57**, 949 (1979).

Rate constants were determined for the reactions of O(^3P) atoms with allene and with 1,3-butadiene by a phase shift technique in which oxygen atoms were generated by modulated mercury photosensitized decomposition of nitrous oxide and monitored by the chemiluminescence from their reaction with NO. Over the temperature interval 297–574 K, the Arrhenius equation for the O(^3P) + allene reaction is $k_{1A} = (2.99 \pm 0.41) \times 10^{-11} \exp[(-941 \pm 54)/T]$ cm^3 molecule^{-1} s^{-1}, where the indicated uncertainties are 95% confidence limits. At 299 and 488 K, the rate constant for O(^3P) + 1,3-butadiene is essentially the same, within 10%, with an average value of 2.07×10^{-11} cm^3 molecule^{-1} s^{-1}.

W. S. NIP, D. L. SINGLETON et R. J. CVETANOVIĆ. Can. J. Chem. **57**, 949 (1979).

On a déterminé les constantes de vitesse des réactions des atomes O(^3P) avec l'allène et le butadiène-1,3 en faisant appel à la technique du déplacement de phase dans laquelle les atomes d'oxygène sont générés par une décomposition modulée photosensibilisée par le mercure de l'oxyde nitreux et contrôlée par la chimiluminescence de leur réaction avec NO. A des températures allant de 297 à 574 K, l'équation d'Arrhénius pour la réaction O(^3P) + allène est $k_{1A} = (2.99 \pm 0.41) \times 10^{-11} \exp[(-941 \pm 54)/T]$ cm^3 molécule^{-1} s^{-1} où les incertitudes indiquées sont à l'intérieur de limites de confiance de 95%. A 299 et 488 les constantes de vitesse pour la réaction de O(^3P) + butadiène-1,3 sont pratiquement les mêmes à ±10%, et la valeur moyenne est 2.07×10^{-11} cm^3 molécule^{-1} s^{-1}.

[Traduit par le journal]

Introduction

The reactions of ground state oxygen atoms with diolefins have not been studied as extensively as the reactions with olefins. Analyses of products at high (1–7) and low (8) pressures suggest that the general mechanism of the diolefin reactions is similar to that of the olefins, i.e. electrophilic addition of O(^3P) to the double bond.

The only determinations of absolute rate constants for reactions of atomic oxygen with diolefins have been for allene and 1,3-butadiene,

[1*A*] O(^3P) + allene → products

[1*B*] O(^3P) + 1,3-butadiene → products

The two absolute values at room temperature for k_{1A} (9, 10) differ from the relative values of Havel (4) by more than a factor of two. The relative (1, 11) and absolute (9) results for k_{1B} agree well at room temperature, but there is only one reported determination of the temperature dependence (9). In the present work the phase-shift technique is used to determine absolute values of k_{1A} and k_{1B}, and their temperature dependence.

Experimental

The apparatus has been described in detail elsewhere (12–14) and will be described only briefly here. O(^3P) atoms were produced by mercury photosensitized decomposition of nitrous oxide using a sinusoidally modulated low pressure mercury lamp. The concentration of O(^3P) was monitored by the chemiluminescence from NO_2* when NO was introduced into the flowing reaction mixture. The reaction sequence is

[1] NRCC No. 17258.
[2] NRCC Research Associate.

0008-4042/79/090949-04$01.00/0

$$Hg6(^1S_0) + h\nu(253.7\,nm) \rightarrow Hg6(^3P_1) \quad \text{(fast)}$$

$$Hg6(^3P_1) + N_2O \rightarrow Hg6(^1S_0) + N_2 + O(^3P) \quad \text{(fast)}$$

[1] $$O(^3P) + \text{diolefin} \rightarrow \text{products}$$

[2] $$O(^3P) + NO + M \rightarrow NO_2^* + M$$

$$NO_2^* \rightarrow NO_2 + h\nu \quad \text{(fast)}$$

$$NO_2^* + M \rightarrow NO_2 + M \quad \text{(fast)}$$

The phase-shift, ϕ, between the incident 253.7 nm light and the NO_2^* chemiluminescence was measured with photomultipliers and a lock-in amplifier. The 253.7 nm light was isolated with an interference filter between the lamp and the reaction cell, and at the entrance to the photomultiplier tube which viewed the incident light. A Corning 3-70 filter was used with the photomultiplier viewing the chemiluminescence. Since the reactions labeled 'fast' do not contribute significantly to the phase shift, ϕ is related to the reaction rates according to

[3] $$2\pi\nu/\tan\phi = k_1[\text{diolefin}] + k_2[NO][M]$$

where ν is the modulation frequency (1600 or 5970 Hz). For constant [NO] and [M], a plot of $2\pi\nu/\tan\phi$ vs. [diolefin] gives a straight line with slope equal to k_1 and intercept, k_2[NO][M].

Reagents flowed into the reaction cell via calibrated flow meters. The temperature of the reaction cell was measured by a thermocouple and controlled to better than 1 K. Oxygen atoms were generated at the rate of 7×10^{12} s^{-1}. The flow rates were such that the maximum consumption of diolefin was less than 0.04%.

The purities of the gases were, according to the manufacturers: allene, $\geq$ 97%; 1,3-butadiene, 99.9%; N_2O, 98%; NO, 99.0%. The NO was passed through a molecular sieve trap to remove NO_2 and H_2O. The other gases were used without further purification.

Results

Typical plots of $2\pi\nu/\tan\phi$ vs. [diolefin] for allene and 1,3-butadiene are shown in Figs. 1 and 2. The linearity of these plots indicates the validity of eq. [3]. The rate constants determined from the slopes of these plots using a linear least-squares analysis are shown in Table 1. The rate constants for allene can be represented by the Arrhenius equation

$$k_{1A} = (2.99 \pm 0.41) \times 10^{-11} \times \exp[(-941 \pm 54)/T]\ \text{cm}^3\ \text{molecule}^{-1}\ \text{s}^{-1}$$

which is plotted in logarithmic form in Fig. 3. The indicated uncertainties are 95% confidence limits based on 5 degrees of freedom and a Student's t value of 2.571. The rate constants for the reaction with 1,3-butadiene are plotted also in Fig. 3. Although a slight negative Arrhenius activation energy is evident in the case of 1,3-butadiene, it is probably better, because data were obtained at only two temperatures, to consider the rate constants to be, within the experimental error, independent of temperature in this interval. The average of the two values of k_{1B} is 2.07×10^{-11} cm^3 molecule^{-1} s^{-1}.

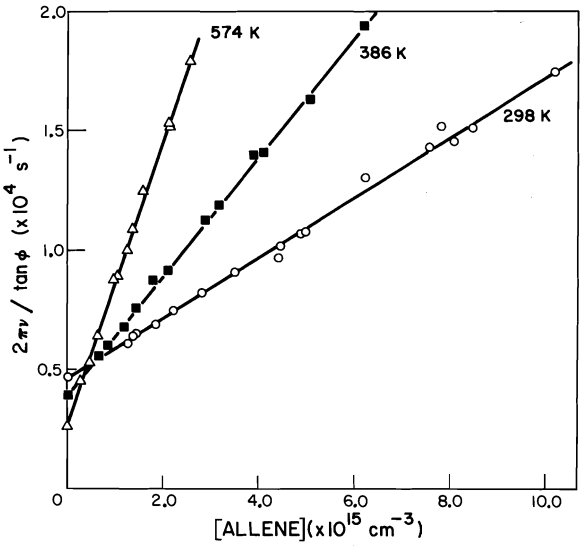

FIG. 1. Plots of $2\pi\nu/\tan\phi$ vs. concentration of allene at three different temperatures. The concentration of NO and the total pressure were constant at each temperature.

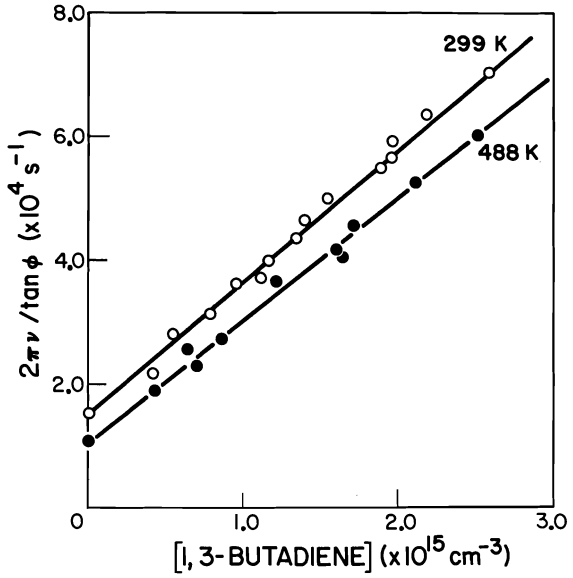

FIG. 2. Plots of $2\pi\nu/\tan\phi$ vs. concentration of 1,3-butadiene at two temperatures. The concentration of NO and the total pressure were constant at each temperature.

Any systematic error in k_{1A} and k_{1B} is probably less than 20%, based on estimated potential systematic errors in phase shift (14), flow rate, and pressure measurements.

Values of k_2 obtained from the intercepts of plots of $2\pi\nu/\tan\phi$ vs. [diolefin] are given in Table 1. They are slightly higher than the literature values (14–16). A possible explanation could be the presence of a small amount of NO_2 in the N_2O used in the present

TABLE 1. Rate constants for reaction of $O(^3P)$ atoms with allene and with 1,3-butadiene[a]

T (K)	Total concentration (10^{17} molecules cm^{-3})	[NO] (10^{16} molecules cm^{-3})	Number of points	k_1 (10^{-12} cm^3 molecule^{-1} s^{-1})	k_2 (10^{-32} cm^6 molecule^{-2} s^{-1})
		$O(^3P)$ + Allene			
298	9.38	2.95	19	1.28±0.02	16.9 ±0.2
298	19.1	1.53	12	1.32±0.04	17.8 ±0.3
336	8.72	5.60	13	1.86±0.03	7.97±0.12
386	7.54	3.84	13	2.54±0.03	13.3 ±0.2
434	6.81	3.36	12	3.34±0.04	12.0 ±0.2
491	6.33	3.98	14	4.50±0.12	10.4 ±0.5
574	5.81	4.74	12	5.97±0.09	9.19±0.25
		$O(^3P)$ + 1,3-Butadiene			
299	9.54	10.3	15	21.7 ±0.7	14.7 ±0.6
488	7.08	12.6	11	19.7 ±0.8	11.7 ±0.7

[a]The indicated uncertainties are one standard deviation.

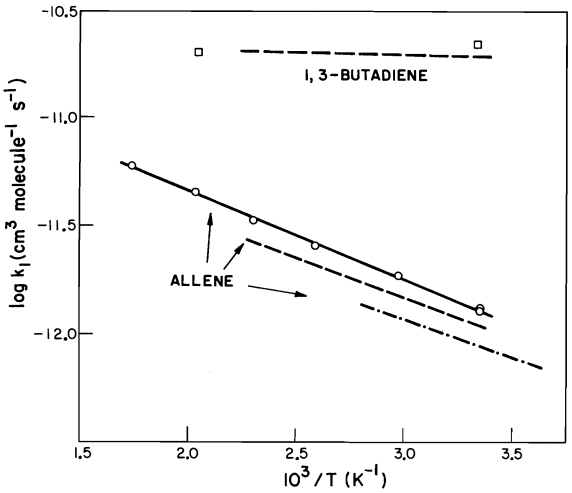

FIG. 3. Arrhenius plots of the rate constants of reaction of $O(^3P)$ with allene and with 1,3-butadiene. $k_{O+allene}$: ○ and solid line, this work; --- ref. 9, ·-·-· ref. 10. $k_{O+1,3\text{-butadiene}}$: □, this work; ---, ref. 9.

work. About 150 ppm of NO_2 would be required to account for the difference. The NO_2 content was found to vary dramatically among three different cylinders of N_2O that were analyzed. Concentrations of NO_2 between 2.6 and 0.01 ppm were found. Unfortunately, the cylinder of N_2O which was used for the rate constant determinations was depleted before the decision to analyze for NO_2 was made, so that it is uncertain whether the NO_2 content could have been as high as 150 ppm. It should be noted that this amount of NO_2 would not affect the values of k_1 obtained from the slopes of plots of $2\pi\nu/\tan\phi$ vs. [diolefin].

Discussion

The concentration of oxygen atoms in the present work is sufficiently small that secondary reactions of $O(^3P)$ with products of reaction [1*A*] or [1*B*] are negligible. Less than 0.9% and 0.2% of the oxygen atoms in reactions [1*A*] and [1*B*], respectively, are consumed by secondary reactions at room temperature, according to calculations based on a generalized mechanism previously outlined (13). The phase shift measurements showed no significant effect due to a factor of 10 reduction in the intensity of the incident 253.7 nm light (hence a factor of 10 change in the rate of production of $O(^3P)$).

The rate constants for $O(^3P)$ + allene, k_{1A}, obtained in the present work agree well (<20% difference) with the flash photolysis results of Atkinson and Pitts (9), who determined k_{1A} over a slightly smaller temperature range. The agreement with the discharge–flow results of Herbrechtsmeier and Wagner (10) is not as good, as seen in Fig. 3, but the difference is no more than 35%. Havel (4) determined k_{1A} relative to $k_{O+1\text{-butene}}$ and $k_{O+isobutene}$ at a total pressure of 610 Torr. With our recent values of $k_{O+1\text{-butene}}$ and $k_{O+isobutene}$ (17), Havel's value of k_{1A} is $\sim 3 \times 10^{-12}$ cm^3 molecule^{-1} s^{-1}, which is more than a factor of two higher than that from the present work. The reason for the discrepancy is not clear. Although it is possible that secondary reactions may have occurred in Havel's experiments because of the high conversions (~30%), the same results, within 6%, were obtained from relative disappearance of reactants and from relative appearance of products (4).

The trend in the values of k_{1A} reported in the literature may appear to suggest increasing values of the rate constant with increasing pressure. The reported values at room temperature vary from 0.87×10^{-12} at 5 Torr (10), to $\sim 1.2 \times 10^{-12}$ at 26–50 Torr (ref. 9, present work), to $\sim 3 \times 10^{-12}$ cm^3 molecule^{-1} s^{-1} at 610 Torr (4). However, in the present work there was no significant difference

between the rate constants determined at 29 and at 59 Torr. Also, the rate constants of the reactions of $O(^3P)$ with olefins are independent of pressure (17, 18). It would be desirable to have values of k_{1A} obtained by one technique over an extended range of pressures.

The present results for O + 1,3-butadiene are in excellent agreement with those reported by Atkinson and Pitts (9), and confirm that k_{1B} is essentially independent of temperature over the range 297–500 K, as seen in Fig. 3. Furthermore, the activation energy reported by Cvetanović (1) for O + 1,3-butadiene relative to O + 1-butene, when combined with our results for O + 1-butene (17), is 0.06 kcal mol^{-1}, consistent with the present results. The relative rate constants at 298 K of Cvetanović (2) and McClenny (11), taken relative to 1-butene, are 4.2 (1) and 5.4 (11), respectively, which can be put on an absolute scale using our value of $k_{O+1\text{-butene}}$ (17). The relative values of k_{1B} become 1.7×10^{-11} and 2.2×10^{-11}, respectively, again in good agreement with the present average value of 2.07×10^{-11} cm^3 $molecule^{-1}$ s^{-1}.

The low activation energies for the diolefin reactions are consistent with an addition mechanism proposed on the basis of product analyses (1–8), i.e., addition of the oxygen atom to the double bond followed by stabilization, rearrangement, or fragmentation of the adduct, as occurs for olefins. The room temperature rate constants for O + allene and O + 1,3-butadiene have been shown (9) to fit adequately into the correlation of $k_{O+olefin}$ vs. the ionization potential of the olefin. Also, the activation energies for reactions [1*A*] and [1*B*] are consistent with the correlation between activation energies for O + olefin reactions vs. ionization potential of the olefin (19). On the other hand, the pre-exponential factors for O + allene and O + 1,3-butadiene are somewhat larger ($2–3 \times 10^{-11}$) than those for most of the O + olefin reactions ($1–1.5 \times 10^{-11}$, except for tetramethylethylene, for which it is 2.1×10^{-11} cm^3 $molecule^{-1}$ s^{-1}) (17), reflecting, perhaps, the number of double bonds. However, because there is evidence of curvature in the Arrhenius plots for some O + olefin reactions (17, 18), trends in pre-exponential factors should be interpreted with caution.

Acknowledgement

The authors are grateful to R. Ironside for the analysis of nitrogen dioxide in nitrous oxide samples.

1. R. J. Cvetanović. Adv. Photochem. **1**, 115 (1963).
2. R. J. Cvetanović and L. C. Doyle. Can. J. Chem. **38**, 2187 (1960).
3. R. J. Cvetanović. J. Chem. Phys. **33**, 1063 (1960).
4. J. J. Havel. J. Am. Chem. Soc. **96**, 530 (1974).
5. J. J. Havel and K. H. Chan. J. Org. Chem. **39**, 2439 (1974).
6. J. J. Havel and K. H. Chan. J. Am. Chem. Soc. **97**, 5800 (1975).
7. K. Nakamura and S. Koda. Int. J. Chem. Kinet. **9**, 67 (1977).
8. M. C. Lin, R. G. Shortridge, and M. E. Umstead. Chem. Phys. Lett. **37**, 279 (1976).
9. R. Atkinson and J. N. Pitts, Jr. J. Chem. Phys. **67**, 2492 (1977).
10. P. Herbrechtsmeier and H. Gg. Wagner. Ber. Bunsenges. Phys. Chem. **76**, 517 (1972).
11. W. A. McClenny. J. Chem. Phys. **60**, 793 (1974).
12. R. Atkinson and R. J. Cvetanović. J. Chem. Phys. **55**, 659 (1971).
13. S. Furuyama, R. Atkinson, A. Colussi, and R. J. Cvetanović. Int. J. Chem. Kinet. **6**, 741 (1974).
14. D. L. Singleton, S. Furuyama, R. J. Cvetanović, and R. S. Irwin. J. Chem. Phys. **63**, 1003 (1975).
15. R. Atkinson and J. N. Pitts, Jr. Chem. Phys. Lett. **27**, 467 (1974).
16. F. Kaufman. Ann. Rev. Phys. Chem. **20**, 45 (1969).
17. D. L. Singleton and R. J. Cvetanović. J. Am. Chem. Soc. **98**, 6812 (1976).
18. J. T. Herron and R. E. Huie. J. Phys. Chem. Ref. Data, **2**, 467 (1974).
19. I. R. Slagle, F. Baiocchi, and D. Gutman. J. Phys. Chem. **82**, 1333 (1978).

Decomposition of vinyl chloride induced by multiphoton absorption of infrared radiation. I. Decomposition yields[1]

A. GANDINI, C. WILLIS, R. A. BACK, AND J. M. PARSONS

Division of Chemistry, National Research Council of Canada, Ottawa, Ont., Canada K1A 0R6

Received September 11, 1978

A. GANDINI, C. WILLIS, R. A. BACK, and J. M. PARSONS. Can. J. Chem. **57**, 953 (1979).

The infrared induced decomposition of vinyl chloride has been studied as a function of pressure and as a function of exciting wavelength with a pulsed CO_2 laser. The main reaction gives C_2H_2 and HCl

$$C_2H_3Cl \rightarrow C_2H_2 + HCl$$

but smaller amounts of C_2H_4 are observed. At pressures below 0.5 Torr, the yield of C_2H_4 shows apparent enhancement relative to C_2H_2. In an earlier publication it had been speculated that this was due to dissociation from higher vibrational levels attained in the multiphoton absorption process. Present data indicate this is not the case and suggest rather strongly that the enhanced C_2H_4 yield is derived from infrared induced decomposition of C_2H_3Cl on cell windows and walls.

The effective quantum yield of C_2H_2 increases approximately linearly with pressure in the range 0–2.5 Torr and C_2H_3Cl, H_2, and O_2 produce similar behaviour. This is interpreted in terms of collisional enhancement of photon absorption associated with depletion of specific rotational states by the laser radiation.

A. GANDINI, C. WILLIS, R. A. BACK et J. M. PARSONS. Can. J. Chem. **57**, 953 (1979).

Utilisant un laser à CO_2 on a étudié la décomposition, induite par l'infrarouge, du chlorure de vinyle en fonction de la pression et en fonction de la longueur d'onde servant à exciter. La réaction principale fournit du C_2H_2 et du HCl,

$$C_2H_3Cl \rightarrow C_2H_2 + HCl$$

mais on a observé la formation de quantités plus faibles de C_2H_4. A des pressions inférieures à 0.5 Torr, le rendement en C_2H_4 subit une augmentation par rapport à C_2H_2. Dans une publication antérieure, il avait été suggéré que ceci est dû à une dissociation provenant de niveaux vibrationnels supérieures obtenues dans un processus d'absorption multiphoton. Les données rapportées ici indiquent que ce n'est pas le cas et suggèrent plutôt fortement que l'augmentation du rendement en C_2H_4 provient de la décomposition induite par l'infrarouge du C_2H_3Cl sur les fenêtres et les parois de la cellule.

Le rendement quantique effectif de C_2H_2 augmente d'une façon approximativement linéaire avec la pression entre 0 et 2.5 Torr. Le C_2H_3Cl, H_2 et O_2 provoquent des comportements semblables. On interprète ces résultats en termes d'une augmentation collisionnelle de l'absorption des photons qui est associée avec une diminution des états rotationels spécifiques provoquée par la radiation laser.

[Traduit par le journal]

Introduction

In a recent communication (1) on the isotopically selective infrared photolysis of vinyl chloride, C_2H_3Cl, we reported preliminary results which showed that below 1 Torr the isotopic selectivity of the decomposition decreased with decreasing pressure. It was suggested that this behaviour was due to enhanced amounts of C_2H_4 being produced at low pressures which led to non-selective disappearance of the substrate. On the basis of a few results we speculated that the ratio of molecular elimination (2), reaction [1], to bond scission (3), reaction [2],

[1] $C_2H_3Cl \rightarrow C_2H_2 + HCl \qquad E_A = 69$ kcal/mol

[2] $C_2H_3Cl \rightarrow C_2H_3 + Cl \qquad \Delta H = 90$ kcal/mol

$\downarrow$

C_2H_4 + products

was varying with pressure. This implied that a competition between multiphoton absorption, collisional deactivation, and decomposition determined the energy content of the decomposing molecules and thereby their mode of decomposition. If true, this interpretation is important to the understanding of the physical processes involved in multiphoton dissociation, and therefore we have investigated the phenomenon in greater detail. The present results suggest that the processes at low pressures leading

[1]NRCC No. 17262. Presented, in part, at International Quantum Electronics Conference held at Atlanta, May 1978.

0008-4042/79/090953-05$01.00/0

predominantly to ethylene are unrelated to the gas-phase multiphoton decomposition, and that in the latter the ratio of molecular elimination to bond scission is pressure independent.

During the progress of the present studies a paper by Lussier and Steinfeld (4) covering some aspects of the infrared induced decomposition of vinyl chloride was published. Using 0.1–1.0 J pulses from a CO_2 TEA-laser focussed with a relatively long focal length lens into 10 Torr of C_2H_3Cl they report production of only C_2H_2 and HCl. In a few experiments using a much shorter focal length lens they observed break-down and report a new product absorption in the ir analysis which was tentatively assigned to diacetylene.

Experimental

Radiation from a line-tunable CO_2 TEA-laser (Lumonics Model 103: pulse duration ~250 ns, pulse energy 5–6 J, beam intensity ~1.3 J cm^{-2}) was focussed into a cylindrical Pyrex cell (40 mm id, 60 mm long) fitted with NaCl windows (Harshaw laser-grade) by a germanium lens ($f = 40$ mm) placed approximately 1 cm from the front window. The focal point coincided roughly with the centre of the cell. Samples were irradiated (normally for 15 min at 36 pulse/min) and the entire cell contents were transferred to an inlet tube of a gas chromatograph where the amounts of C_2H_2 and C_2H_4 formed were determined. Mass spectrometric analysis was used to identify other minor products. Experiments with vinyl chloride alone were restricted to pressures below ~2.5 Torr, above which break-down was observed. With added H_2 total pressures up to 20 Torr were possible without break-down.

Results

The absorption spectrum of vinyl chloride contains two main bands in the region accessible to CO_2-laser radiation, the CH_2 rocking mode (ν_7) centred around 1040 cm^{-1} and the twist mode (ν_{10}) around 950 cm^{-1}. We have investigated laser-induced decomposition in both regions. The yield per pulse is reported as an *effective reaction volume*, the amount of reagent decomposed expressed as a volume at the ambient reagent pressure and temperature. If in the focal region there is a sharp fluence threshold beyond which decomposition is virtually complete, the volume defined by this threshold will in fact equal the effective reaction volume. It is in any case a convenient way to present the data, whether or not such threshold behaviour pertains. It should be noted that this usage tacitly includes a first-order reagent pressure term, so that the effective reaction volume is proportional to a percent decomposition or a decomposition probability.

Effect of Pressure

Figure 1 shows the observed yields of products as a function of vinyl chloride pressure the P_{18} line of the 10.6 μm band. Figure 2 shows similar data for

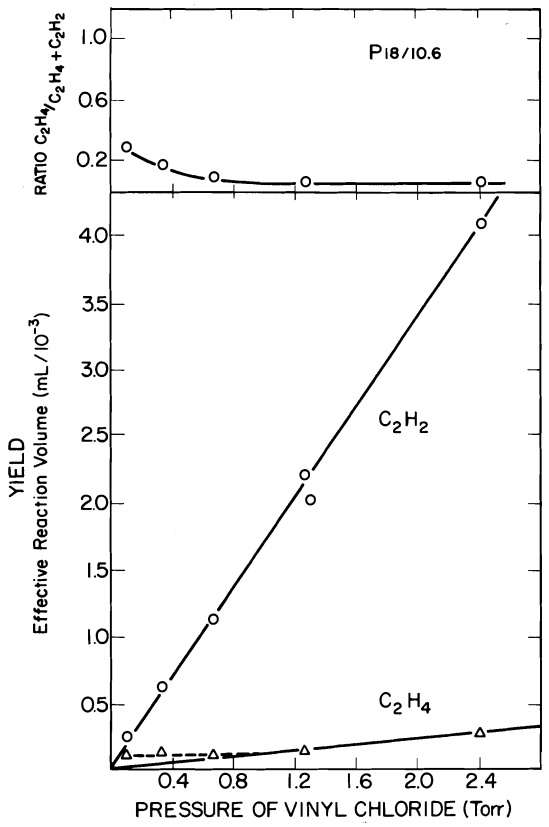

FIG. 1. Observed yields of C_2H_2 and C_2H_4 as a function of pressure of vinyl chloride for irradiation with P_{18} line of 10.6 μm band of CO_2 laser (6.7 J/pulse).

the P_{20} line of the 9.6 μm band. These data are typical of the experiments carried out in the two regions. The yield of C_2H_2 decreases linearly towards zero with decreasing pressure, whereas that of C_2H_4 is enhanced at low pressure. Irradiation in the ν_{10} band shows only a slight enhancement in the fraction of C_2H_4 in the products; irradiation in the ν_7 bands shows a much larger increase with C_2H_4 becoming the dominant product below 0.4 Torr.

Starting with 0.1 Torr vinyl chloride, addition of H_2 leads to a decrease in C_2H_4 yield but an increase in C_2H_2. Data for the variation of yields with pressure for irradiation with the P_{20}/10.6 μm line are collected in Table 1.

Effect of Irradiation Time

The amounts of C_2H_2 and C_2H_4 formed were linear with time for low conversions, shown for a series of experiments in Fig. 3. The invariance of yields per pulse suggests that both are primary products of photolysis, although secondary decomposition within a single pulse cannot be ruled out.

Effect of Wavelength

The yields of C_2H_4 and C_2H_2 for irradiation with

TABLE 1. Effect of pressure on yields (P_{20}/9.6 μm line; 6.2 J/pulse; 15 min irradiation at 36 pulse/min)

Pressure of vinyl chloride (Torr)	Pressure of additive (Torr)	Amount of product (mol/10^{-9})		Effective reaction volume (mL/10^{-3})	
		C_2H_4	C_2H_2	C_2H_4	C_2H_2
0.08	—	7.45	0.65	3.22	0.28
0.10	—	4.70	0.54	1.63	0.19
0.17	—	6.37	1.76	1.29	0.36
0.29	—	5.14	2.81	0.61	0.33
0.56	—	4.22	10.00	0.26	0.62
1.12	—	7.53	35.3	0.23	1.08
2.63	—	39.7	199	0.52	2.60
0.10	0.14 (H_2)	1.32	0.75	0.45	0.26
0.10	0.32 (H_2)	1.87	1.25	0.64	0.43
0.10	1.00 (H_2)	1.16	3.01	0.40	1.04
0.10	1.00 (O_2)	1.05	2.46	0.36	0.85
0.10	3.90 (H_2)	0.89	4.01	0.31	1.38
0.10	20.00 (H_2)	0.64	5.28	0.22	1.82

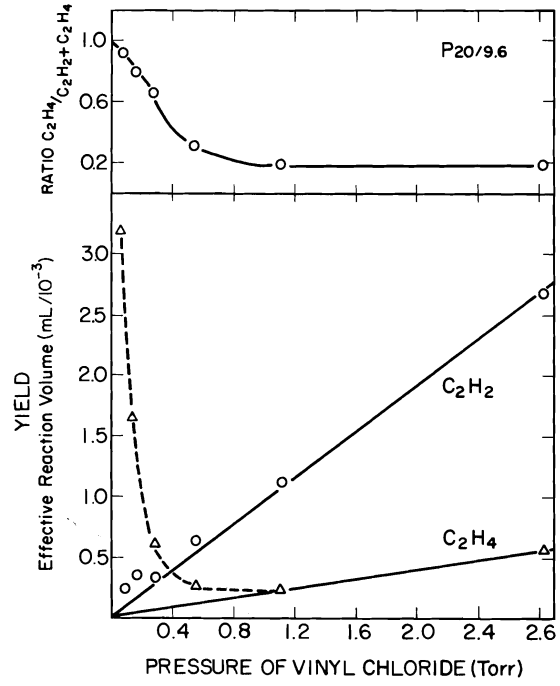

FIG. 2. Observed yields of C_2H_2 and C_2H_4 as a function of pressure of vinyl chloride for irradiation with P_{20} line of 9.6 μm band of CO_2 laser (6.2 J/pulse).

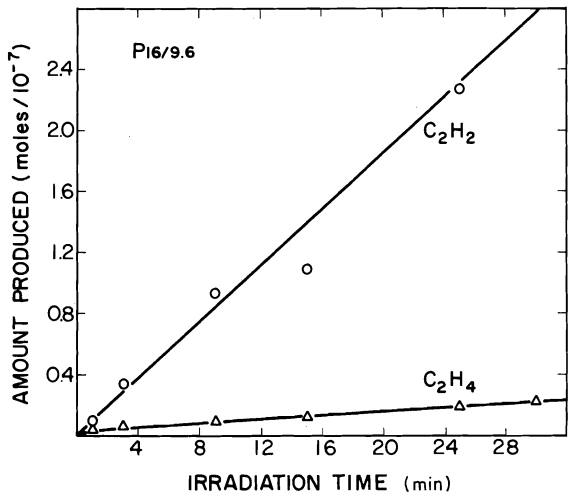

FIG. 3. Formation of C_2H_2 and C_2H_4 as a function of irradiation time: pulse rate, 36 pulses/min of P_{16} line of 9.6 μm band, 1.0 Torr C_2H_3Cl.

various laser lines are given in Table 2. All yields are normalized to the same pulse energy using the dependence to the power 2.3 (below) and were measured with 1.0 Torr vinyl chloride plus 5.0 Torr H_2. The H_2 was added in an attempt to minimize variations with pressure.

Effect of Varying Energy per Pulse

The yields of decomposition were measured at 2, 4, and 6 J/pulse with the P_{20} line at 9.6 μm. The amount of product formed for two pressures of vinyl chloride, 0.36 Torr and 2.00 Torr, fitted a simple expression giving a dependence of yield on pulse energy to the 2.3 ± 0.2 power.

Discussion

The main results to be discussed are the increase in C_2H_4 yield observed at low pressure and the variation of C_2H_2 yields with pressure. Only brief mention will be made of the variation of yields with wavelength of the laser radiation. As will be seen, such a spectral dependence will be a complex function of pressure, fluence, and probably flux. Moreover, recent work by Steinfeld and co-workers (5) has examined this aspect in some detail making further comment here redundant.

TABLE 2. Yields from irradiation with various CO_2 laser lines (15 min irradiation at 36 pulse/min; 1.0 Torr C_2H_3Cl, 5.0 Torr H_2)

Line	Energy per pulse (J)	Amount of product ($mol/10^{-9}$)		Effective reaction volume ($mL/10^{-3}$) (normalized to 6 J/pulse incident)	
		C_2H_4	C_2H_2	C_2H_4	C_2H_2
P_{16}/9.6 μm	6.2	13.8	44.3	0.44	1.41
P_{20}/9.6 μm	6.2	12.6	91.6	0.40	2.92
P_{26}/9.6 μm	5.9	55.2	125	1.97	4.47
P_{18}/10.6 μm	6.7	9.5	192	0.26	5.13
P_{20}/10.6 μm	7.0	27.3	228	0.66	5.51
P_{22}/10.6 μm	6.9	12.1	224	0.31	5.59
P_{32}/10.6 μm	5.4	9.1	195	0.40	8.55

TABLE 3. "Empty-cell" experiments[a]

Pressure in cell (Torr)	Amount produced ($mol/10^{-6}$)		Comparison[b] ($mol/10^{-6}$)	
	C_2H_4	C_2H_2	C_2H_4	C_2H_2
0.0[c]	1.91×10^{-3}	3.42×10^{-4}	2.98×10^{-2}	2.61×10^{-3}
0.0[d]	4.60×10^{-4}	3.35×10^{-5}	2.98×10^{-2}	2.61×10^{-3}
0.0[e]	1.88×10^{-2}	Not detected	2.98×10^{-2}	2.61×10^{-3}
0.11	3.06×10^{-3}	4.35×10^{-4}	2.98×10^{-2}	2.61×10^{-3}
1.00	1.76×10^{-3}	8.14×10^{-4}	3.01×10^{-2}	1.41×10^{-1}

[a]All experiments involve the same irradiation time (15 min) and were carried out with unfocussed output of laser with P_{20} line of 9.6 μm band unless otherwise stated.
[b]Nearest equivalent data points for focussed output. Zero pressure data are compared to yields from 0.1 Torr C_2H_3Cl.
[c]Flushed with 2 Torr C_2H_3Cl and pumped for 15 min before irradiation.
[d]Flushed with 2 Torr C_2H_3Cl and pumped for 18 h before irradiation.
[e]Flushed with 2 Torr C_2H_3Cl and pumped for 60 min before irradiation with *focussed* output.

Formation of Ethylene at Low Pressure

A probable mechanism for formation of C_2H_4 in the multiphoton decomposition of C_2H_3Cl is through the vinyl radical,

$$[2] \qquad C_2H_3Cl \xrightarrow{nh\nu} C_2H_3 + Cl$$

$$[3] \qquad C_2H_3 + C_2H_3Cl \rightarrow C_2H_4 + \text{products}$$

This hypothesis was tested by photolysing C_2H_3Cl with added DBr or I_2 which should give characteristic products in reactions with vinyl radicals,

$$[4] \qquad C_2H_3D + Br \rightarrow C_2H_3D + Br$$

$$[5] \qquad C_2H_3 + I_2 \rightarrow C_2H_3I + I$$

Photolysis of 0.1 Torr C_2H_3Cl with the P_{20} line at 9.6 μm with either 1.0 Torr DBr or 0.3 Torr I_2 followed by mass spectrometric analysis showed no detectable C_2H_3D or C_2H_3I. Limits of detection corresponded to the interception of less than 1% of the vinyl radicals required to produce the observed yield of C_2H_4, a strong indication that C_2H_3 radicals were not involved in its formation.

In a series of experiments where photolysis of C_2H_3Cl was interspersed with experiments involving other compounds, it was noted that the 'enhanced' C_2H_4 yield was much less reproducible than the C_2H_2 yields and showed dependence on cell history. This led to the suspicion that adsorption of C_2H_3Cl on cell walls and windows was involved and further that C_2H_4 was being formed outside the focal region. The data given in Table 3 were taken to test this hypothesis. The three experiments at nominally zero pressure involved flushing the cell with vinyl chloride at a relatively high pressure and then pumping. As can be seen, significant yields of C_2H_4 were formed in all three cases: pumping overnight reduced the yield compared to that obtained with only 15 min pumping and focussing the beam in the 'empty' cell led to yields of C_2H_4 very similar to those obtained with 0.1 Torr C_2H_3Cl in the cell. The yields of C_2H_2 were very much smaller than those observed for the low-pressure photolysis of C_2H_3Cl. The other experiments for increasing pressures of C_2H_3Cl photolysed with the unfocussed beam all gave similar yields of C_2H_4, comparable to those obtained in the focussed beam experiments, but C_2H_2 yields which again were very much smaller.

Taken together, this evidence argues against significant formation of C_2H_4 in the collisionless multiphoton decomposition of C_2H_3Cl. Although

there is a distinct wavelength dependence and the behaviour is not observed to the same extent in other vinyl compounds we have studied (6), C_2H_4 formation is most likely associated with decomposition of C_2H_3Cl adsorbed on the cell walls and windows. The detailed mechanism of the induced decomposition on the cell walls is probably complex and more extensive study does not seem warranted at present.

Variation of Yields with Pressure

If small corrections are made for the amount of C_2H_2 apparently formed on the cell walls or windows, the C_2H_2 yield increases linearly both with pressure of vinyl chloride and with pressure of added gas up to about 2 Torr (Figs. 1 and 2, Table 1). This behaviour was not expected. Elsewhere (7) it has been shown that the product yields in some multiphoton decompositions with focussed beams follow the general expression

$$[6] \qquad \text{Yield} = a + bP$$

The first team corresponds to the yield arising from essentially collisionless decomposition. The second term, linear in substrate pressure, represents the product formed by a collisional energy pooling mechanism. It is not reasonable to explain the observed behaviour of C_2H_3Cl in this way. The pressure dependent term usually tends to become dominant only at much higher pressures than found with vinyl chloride (8) and more importantly, when collisional energy pooling makes a significant contribution, addition of a non-absorbing inert gas decreases rather than increases the yield (7, 9).

A much more reasonable explanation of the observed pressure dependence is that pressure affects the photon absorption process. The rotational envelopes of the absorption bands in vinyl compounds are very broad compared to the effective bandwidth of the exciting radiation, even when power broadening is taken into account. In the absence of rotational repopulation, only a small fraction of the molecules is accessible to the laser radiation.[2] The most obvious effects of pressure are simple pressure broadening, and an increase in the rate of rotational repopulation during the laser pulse, so that the effect of line bleaching is reduced and a larger fraction of molecules becomes accessible to excitation. Absorption studies on C_2H_3Cl strongly support this explanation (5).

The observed dependence of the amount of product formed on (pulse energy) 2.3 is larger than the 3/2-power dependence usually found with focussed beams. One could speculate that power broadening of the exciting radiation could lead to spectral overlap with more rotational levels as the energy per pulse is increased, resulting in higher-order dependence on pulse energy than would otherwise be expected. However, uncertainties in the variations of power density in the reaction zone make a quantitative assessment of this effect difficult.

Variation of Yields with Wavelength

The variation in the acetylene yields with wavelength shown in Table 2 follows approximately the low-intensity low-resolution absorption spectrum of vinyl chloride (4), except for the yield with the P_{32} line at 933 cm^{-1}, which lies in a more structured region of the absorption spectrum, and showed the highest yield both in the present and previous studies (4). In view of the probably complex effects of pressure, dynamic Stark modulation, and line bleaching on the absorption, already discussed in some detail by Steinfeld *et al.* (4, 5), and in view of the uncertain power gradients in the focussed beam, further discussion of the wavelength dependence is unwarranted here.

Conclusions

The enhanced yield of C_2H_4 observed in the low pressure decomposition of vinyl chloride is probably not formed in the gas phase multiphoton process, but rather on the vessel surface. The observed linear pressure dependence of the C_2H_4 yields is more significant. We have attributed this behaviour to collisional repopulation of J-states depleted by absorption, without which only a small fraction of the molecules are accessible to excitation. This type of behaviour may be general, especially in hydrogen-containing species, which tend to have broad rotational envelopes.

[2]This should not be true for irradiation on the Q-head ($\Delta J = 0$) which will allow a much higher fraction of molecules to be excited. In the bands involved in the present study there is not a well developed Q-head and the suggestion cannot be tested.

1. A. GANDINI, C. WILLIS, and R. A. BACK. Can. J. Chem. **55**, 4156 (1977).
2. F. ZABEL. Int. J. Chem. Kinet. **IX**, 651 (1977).
3. S. W. BENSON. Thermochemical kinetics. J. Wiley and Sons, New York. 1976.
4. F. M. LUSSIER and J. I. STEINFELD. Chem. Phys. Lett. **50**, 175 (1977).
5. F. M. LUSSIER, J. I. STEINFELD, and T. F. DEUTSCH. Chem. Phys. Lett. **58**, 277 (1978).
6. A. GANDINI, C. WILLIS, R. A. BACK, and J. M. PARSONS. Unpublished data.
7. P. A. HACKETT, M. GAUTHIER, and C. WILLIS. J. Chem. Phys. **69**, 2924 (1978).
8. L. SELWYN, R. A. BACK, and C. WILLIS. Chem. Phys. **32**, 323 (1978).
9. R. CORKUM, C. WILLIS, and R. A. BACK. Chem. Phys. **24**, 13 (1977).

Phosphorus-31 nuclear magnetic resonance spectra of methylplatinum(II) and methylpalladium(II) cations containing 4-substituted pyridine ligands

HOWARD C. CLARK[1] AND CHARLES R. MILNE

Department of Chemistry, University of Western Ontario, London, Ont., Canada N6A 3K7

Received September 12, 1978

HOWARD C. CLARK and CHARLES R. MILNE. Can. J. Chem. **57**, 958 (1979).

The ^{31}P nmr spectra of the compounds *cis*-[$M(CH_3)(L)$diphos]PF_6, where M = Pd, Pt; L = 4-C_5H_4NX; X = CH_3, H, NMe_2, COOMe, COMe, CN; diphos = 1,2-bisdiphenylphosphino ethane, have been recorded. The ^{31}P chemical shifts and ^{31}P–^{195}Pt coupling constants decrease regularly as the ρ values of the substituent on pyridine decrease. These trends are attributed to decreasing lone pair donation from phosphorus as the electron donating ability of the other ligands on the metal increases. The *trans* influence of the coordinated pyridine molecule, as measured by $J(^{195}Pt$–$^{31}P)$, is greater than its *cis* influence on the phosphorus atoms.

HOWARD C. CLARK et CHARLES R. MILNE. Can. J. Chem. **57**, 958 (1979).

On a déterminé les spectres rmn ^{31}P des composés *cis*-[$M(CH_3)(L)$diphos]PF_6 où M = Pd, Pt; L = X-4C_5H_4N; X = CH_3, H, NMe_2, CO_2Me, COMe, CN; diphos = bisdiphényl-phosphino-1,2 éthane. Les déplacements chimiques du ^{31}P et les constantes de couplage ^{31}P–^{195}Pt diminuent régulièrement avec une diminution des valeurs ρ des substituants de la pyridine. On attribue ces tendances à une diminution de la disponibilité de la paire libre du phosphore lorsque le caractère électrodonneur des autres ligands sur le métal augmente. L'influence *trans* de la molécule de pyridine coordonnée, telle que mesurée par $J(^{195}Pt$–$^{31}P)$, est plus grande que son influence *cis* sur les atomes de phosphores.

[Traduit par le journal]

Introduction

The factors contributing to the nature of ^{31}P chemical shifts and coupling constants are not particularly well defined. It has been suggested that the electronic and steric properties of the substituents on phosphorus determine ^{31}P chemical shifts and coupling constants by varying the amount of *s* character associated with the phosphorus lone pair (1–4). In addition, ^{31}P chemical shifts and coupling constants of coordinated tertiary phosphines are also affected by the properties of the other ligands at the metal centre. We are particularly interested in the latter contribution to ^{31}P chemical shifts and coupling constants.

Accordingly we have prepared and have obtained the ^{31}P nmr spectra of complexes of the type [$M(CH_3)$diphos(L)]PF_6 where L is a pyridine substituted in the 4 position, M = Pd or Pt and diphos = 1,2 bisdiphenylphosphino ethane. We hoped to be able to correlate ^{31}P chemical shifts, $J(^{31}P$–$^{31}P)$ and $J(^{31}P$–$^{195}Pt)$ values with the electronic properties of the substituted pyridines as measured by the Hammett substituent constant ρ (5). The use of the chelating diphosphine, diphos, allows the measurement and comparison of both *trans* and *cis* influences with the same molecule, while the study of analogous Pd and Pt complexes allows comparisons of trends between second and third row transition metals.

Results and Discussion

The ^{31}P chemical shifts and coupling constants of the new compounds are summarized in Table 1. We have not determined the relative signs of the coupling constants; thus their absolute values are presented.

The ^{1}H decoupled ^{31}P nmr spectra of the cations where M = Pd consist of two doublets with chemical shifts of about 60 and 40 ppm, having a mutual coupling constant of about 23 Hz. The ^{1}H decoupled spectra where M = Pt consist of two signals at around 57 and 37 ppm. Each signal is flanked by ^{195}Pt satellites of ca. one-fourth intensity. No ^{31}P–^{31}P coupling is observed.

The low field signals have a $J(^{31}P$–$^{195}Pt)$ of about 1720 Hz while the high field signals have a $J(^{31}P$–$^{195}Pt)$ of about 3700 Hz. Thus, the low field signal in each spectrum is assigned to the phosphorus atom *trans* to the methyl group, P^c, and the high field signal to the phosphorus atom *trans* to the substituted pyridine (6, 7) P^t.

The assignment of the resonances of the palladium cations is based on the argument that the chemical shifts of the phosphorus nuclei should be similar to those in a similar environment in the platinum compounds.

The ^{31}P resonances of P^t, the phosphorus atom *trans* to the pyridine, for both M = Pd and Pt, occur

[1]To whom all correspondence should be addressed. Present address: Department of Chemistry, University of Guelph, Guelph, Ont., Canada N1G 2W1.

0008-4042/79/090958-03$01.00/0

TABLE 1. ^{31}P nmr data for compounds of the type $[M(CH_3)(py\text{-}X)diphos]PF_6$

M	X	δP^c (ppm)	δP^t (ppm)	$\lvert J(P^t\text{–}P^c)\rvert$ (Hz)	$\lvert J(Pt\text{–}P^c)\rvert$ (Hz)	$\lvert J(Pt\text{–}P^t)\rvert$ (Hz)
Pt	NMe_2	49.12	38.26		1712.9	3654.8
Pt	Me	50.35	37.72		1719.1	3723.9
Pt	H	50.70	37.36		1720.4	3736.8
Pt	COOMe	51.04	37.47		1725.2	3766.1
Pt	COMe	51.08	37.40		1725.7	3770.4
Pt	CN	51.74	37.40		1728.2	3822.2
Pd	NMe_2	59.04	37.50	22.59		
Pd	Me	59.52	38.66	23.00		
Pd	H	59.57	39.02	23.20		
Pd	COOMe	59.75	39.51	23.55		
Pd	COMe	59.89	39.64	23.71		
Pd	CN	60.10	39.84	23.81		

around 37 ppm while those for P^c, the phosphorus atom *cis* to the pyridine, occur at around 59 for M = Pd and 50 ppm for M = Pt. The chemical shift values for P^t are obviously influenced by changing the pyridine 4-substituent but for M = Pt, unexpectedly, the changes show no relationship to ρ values. For M = Pd, the ^{31}P chemical shifts of P^t decrease in a regular way with decreasing σ values of the substituent (Fig. 1).

The values of the ^{31}P chemical shift for P^c, on changing the substituent on pyridine, decrease in an essentially linear fashion, for both M = Pd and Pt, with decreasing ρ value of the *para* substituent (Fig. 1), although the changes are smaller than for P^t.

These trends can be understood by considering the relation between the electron density at the metal and the amount of electron density on the phosphorus lone pair. On coordination to a transition metal, the ^{31}P chemical shift of a tertiary phosphine invariably moves to lower field from its free value (3). This downfield shift is due to removal of electron density from the phosphorus lone pair *via* donation to suitable metal orbitals. It would seem reasonable, therefore, that an increase in the electron density on the metal would lessen the availability of metal orbitals to accept electron density from the phosphorus. Thus, in this case increasing the electron density at the metal by increasing the donating ability of the pyri-

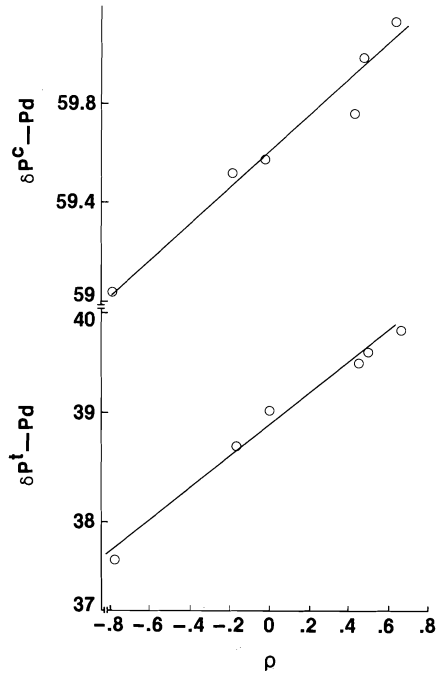

FIG. 1. Plot of $\delta(P^t\text{–}Pd)$ and $\delta(P^c\text{–}Pd)$ vs. ρ.

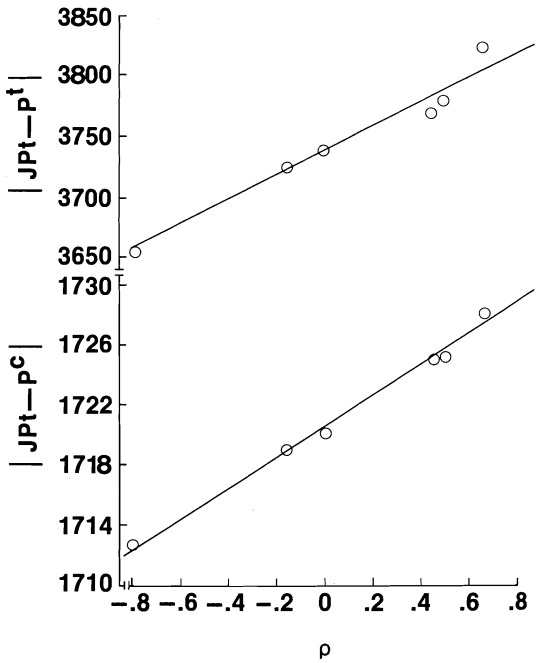

FIG. 2. Plot of $|J(Pt\text{–}P^c)|$ and $|J(Pt\text{–}P^t)|$ vs. ρ.

dine causes the observed decrease in ^{31}P chemical shifts for both the *trans* and *cis* phosphorus atoms.

The ^{31}P–^{195}Pt coupling constants for P^t increase in an essentially linear fashion from 3654 Hz ($X = NMe_2$, $\rho = -0.79$) to 3822 Hz ($X = CN$, $\rho = +0.66$) as ρ increases. The ^{31}P–^{195}Pt coupling constant for P^c also increases, although not so dramatically, in a steady manner from 1713 Hz to 1728 Hz as ρ increases from -0.79 to $+0.66$ (Fig. 2). Note that, in Fig. 2, different scales are used for P^c and P^t and that the effect on $J(Pt–P^t)$ is about 10 times greater than for $J(Pt–P^c)$.

The larger ranges for P^t than for P^c are a result of *trans* influence being larger than *cis* influence. It is widely believed that the Fermi contact term makes the major contribution to the magnitude of platinum–phosphorus coupling constants (8). Therefore, factors which allow the platinum 6*s* orbital to participate more fully in bonding to a phosphorus atom will increase the platinum–phosphorus coupling constant. In this case, decreasing the electron donation of the other ligands on the metal by increasing the ρ value of the 4-substituent on pyridine increases the availability of the Pt 6*s* orbital to the phosphorus atoms resulting in larger values for both $|J(P^c–Pt)|$ and $|J(P^t–Pt)|$.

Conclusions

It has been shown that ^{31}P chemical shifts and ^{31}P–^{195}Pt coupling constants of tertiary phosphine atoms bonded to Pd and Pt are sensitive to small changes in the electronic properties of the other ligands on the metal. Increasing the electron donating ability of these other ligands leads to regular decreases in both ^{31}P chemical shifts and ^{31}P–^{195}Pt coupling constants. Although both *cis* and *trans* phosphorus atoms are affected, the changes in $J(^{31}P–^{195}Pt)$ are greater for the *trans* phosphorus atom.

Experimental

Phosphorus-31 nmr spectra of the cations in dichloromethane solution were measured in 5 mm tubes with a 12 mm reference tube of 1% H_3PO_4. Chemical shifts *downfield* from this reference are in *positive* ppm. A Varian XL-100 spectrometer at 40.5 MHz was employed along with Fourier transform techniques.

The compounds Pd(Me)(Cl)diphos and Pt(Me)(Cl)diphos were prepared as described previously (9, 10). The cationic compounds [M(Me)(Py-X)diphos]PF_6 were all prepared in a similar manner; thus, only a representative preparation is described.

To a suspension of Pd(Me)(Cl)diphos (0.200 g) in tetrahydrofuran (10 mL) was added one equivalent of pyridine followed by a tetrahydrofuran solution of $AgPF_6$ (0.095 g). After an hour the solution was stripped to dryness and extracted with dichloromethane (10 mL). Passage of the dichloromethane solution through a 1/2 in. column of Florosil, concentration and subsequent addition of diethylether gave white crystals of Pd(Me)(py)diphosPF_6 in 80% yield. All of the compounds listed in Table 1 are analysed for the correct C, H, and N content.

1. C. A. TOLMAN. Chem. Rev. **77**, 313 (1977).
2. M. M. CRUTCHFIELD, C. H. DUNGAN, J. H. LETCHER, V. MARK, and J. R. VAN WAZEN. ^{31}P nuclear magnetic resonance. Top. Phosphorus Chem. **5** (1967).
3. J. F. NIXON and A. PIDCOCK. Ann. Rev. NMR Spectrosc. **2**, 345 (1969).
4. G. MAVEL. Ann. Rev. NMR Spectrosc. **5B**, 1 (1973).
5. C. D. RITCHIE and W. F. SAGER. Prog. Phys. Org. Chem. **2**, 323 (1964).
6. F. H. ALLEN and S. N. SZE. J. Chem. Soc. A, 2054 (1971).
7. T. G. APPLETON, M. A. BENNETT, and I. B. TOMPKINS. J. Chem. Soc. Dalton Trans. 439 (1976).
8. T. G. APPLETON, H. C. CLARK, and L. E. MANZER. Coord. Chem. Rev. **10**, 335 (1973).
9. H. C. CLARK, C. R. C. MILNE, and C. S. WONG. J. Organomet. Chem. **136**, 265 (1977).
10. L. E. MANZER. Ph.D. Thesis, University of Western Ontario, London, Ont. 1973.

Thermodynamics of transfer of hydrogen halides from water to glycerol–water mixtures and the structuredness of the solvents

INDRA NARAYAN BASUMALLICK[1] AND KIRON K. KUNDU[2]

Physical Chemistry Laboratories, Jadavpur University, Calcutta 700032, India

Received June 5, 1978[3]

INDRA NARAYAN BASUMALLICK and KIRON K. KUNDU. Can. J. Chem. **57**, 961 (1979).

Standard free energies (ΔG_t^0) and entropies (ΔS_t^0) of transfer of HX (X = Br and I) from water to glycerol–water mixtures containing 10, 30, 50, and 70 wt.% glycerol have been determined from emf measurements on the cell: Pt, H_2(g, 1 atm)/HX(*m*), solvent/AgX–Ag at seven equidistant temperatures ranging from 10–40°C. The observed ΔG_t^0–composition profiles of HBr, HI, and also of HCl obtained from the relevant literature data are essentially similar to those in aquo-alcoholic and aquo-glycolic systems. But the observed short maxima in $T\Delta S_t^0$(HX)–composition profiles with their relative order: HI > HBr > HCl in water-rich compositions and the reverse order at higher proportions of glycerol are indicative of the effect of small structure promoting propensity of glycerol. Comparison of $T\Delta S_t^0$(HI)–composition profiles of methanol, isopropanol, and *tert*-butyl alcohol on the one hand and that of methanol, ethylene glycol, and glycerol on the other, leads us to suggest that the structure promoting ability of hydrophobic —CH_3 group is significantly reduced due to 'specific site hydration' effect when its one H-atom is being replaced by one hydrophilic —OH group. Also, the compositions at which the characteristic maxima appear, either in the former cases or in the latter, are, as expected, the size effect of the co-solvents.

INDRA NARAYAN BASUMALLICK et KIRON K. KUNDU. Can. J. Chem. **57**, 961 (1979).

Les énergies libres (ΔG_t^0) et entropies (ΔS_t^0) standard de transfert de HX (X = Br et I) de l'eau vers des mélanges de glycérol–eau contenant 10, 30, 50 et 70% en poids de glycérol ont pu être déterminées à partir de mesures de fem sur la cellule: Pt, H_2(g, 1 atm)/HX(*m*), solvant AgX–Ag à sept températures équidistantes allant de 10 à 40°C. Les profils observés pour ΔG_t^0–composition pour HBr, HI et aussi pour HCl, obtenus à partir de données appropriées provenant de la littérature, sont presque semblables à ceux obtenus dans des systèmes aquo-alcoolique et aquo-glycolique. Toutefois les légers maxima observés dans les profils de $T\Delta S_t^0$(HX)–composition avec leur ordre relatif: HI > HBr > HCl à des compositions riches en eau et les ordres inverses à des proportions plus élevées de glycérol indiquent qu'il existe un léger effet favorisant la formation de structures dans le glycérol. Les profils de $T\Delta S_t^0$(HI)–composition du méthanol, de l'isopropanol et du *tert*-butanol d'une part et ceux du méthanol de l'éthylèneglycol et du glycérol d'autre part permettent de suggérer que la facilité avec laquelle le groupe hydrophobe —CH_3 favorise la formation de structures diminue d'une façon importante, à cause d'un effet "d'hydratation d'un site spécifique" lorsqu'on remplace un de ses hydrogènes par un groupe-OH hydrophile. De plus, les "compositions magiques" auxquelles les maxima caractéristiques apparaissent soit dans les premiers ou les derniers cas, sont, tels que prévus, dû à l'effet de grosseur des co-solvants.

[Traduit par le journal]

Introduction

Denaturation of aqueous solutions of proteins by urea and their stabilization by glycerol and their possible genesis from the alteration of water structure are a subject of wide biochemical interest (1–4). Whilst the numerous studies made so far (1–3) have helped reveal the structuredness of urea–water mixtures to a large extent, the corresponding studies in glycerol–water mixtures are remarkably few and hence the effect of glycerol on water structures is yet a conflicting issue (4–9).

It is now increasingly recognized (10–16) that, like various direct and indirect techniques, the thermodynamic quantities, specifically the standard enthalpies and entropies of transfer, of various solutes serve as fairly useful probes for gaining structural information of aquo-organic solvents. Previously, as part of the studies of ion–solvent interactions as well as the structuredness of aquo-organic solvents, Kundu and co-workers (3) reported the free energies (ΔG_t^0) and entropies (ΔS_t^0) of transfer of hydrogen halides in urea–water mixtures and drew important reflections on the structuredness of the solvents. So, it should be of particular interest to extend such studies to glycerol–water mixtures as well. Moreover, glycerol being intermediate between mono-ols and mono-

[1]Holder of a Teacher Fellowship of the University Grants Commission, New Delhi.

[2]Author to whom all correspondence should be addressed.

[3]Revision received December 15, 1978.

0008-4042/79/090961-07$01.00/0

saccharides, such studies are also expected to be amply useful in correlating structural effects of simple alcohols and simple sugars.

In glycerol–water mixtures transfer free energies of HCl or the related standard potentials (E^0) of the Ag–AgCl electrode are known at different temperatures (17–19) and those of HBr and HI or the E^0 values of Ag–AgBr and Ag–AgI electrodes are known (5*a*) at one temperature only. A recent study (15) has, however, emphasized that studies of transfer entropies of HCl, HBr, and HI side by side rather than any of the solutes alone provide an additional support to the effectiveness of ΔS_t^0(HX) as a probe for solvent structures. So, the chief object of the present paper is to report the ΔS_t^0 of HBr and HI in this solvent system as obtained by determining the E^0 values of the Ag–AgBr and Ag–AgI electrodes at seven equidistant temperatures ranging from 10–40°C and to examine the structuredness of the solvents. Cell [A]

[A] Pt, H_2(g, 1 atm)/HX(*m*), glycerol (Y) + water/AgX–Ag

where X = Br or I and Y = 10, 30, 50, and 70 wt.% glycerol, has been used for the determination of E^0 values.

Experimental

Glycerol (G.R., Merck) was purified by vacuum distillation with considerable rejection of head and tail fractions. Deionized water was distilled from alkaline $KMnO_4$ and redistilled before use. Purification of HBr and HI (Riedal de Haenag), preparation of solutions and electrodes, cell design, and the general experimental procedure were essentially the same as described before (3, 20). Electromotive force measurements were made with a precision potentiometer and a moving coil galvanometer (Cambridge Instrument Co.). The time taken to reach equilibrium was 3–4 h and the constancy ±0.1 mV for 1 h was taken to be the criterion of equilibrium. Final readings were occasionally checked with a freshly platinized Pt-electrode and were found to agree to within ±0.2 mV. Equilibrium values were recorded first at lowest temperature and then at successively higher temperatures. The equilibrium emf values when checked at a lower temperature were found to be reproducible to within ±0.2 mV.

Solvent densities (21), vapour pressure data (21) computed at each temperature as before (15) using Rault's law, and the dielectric constant values (ε_s) taken from Akerlof's data (22) are given elsewhere.[4]

Results

The standard potential E_m^0 (on the molal scale) of the Ag–AgX electrode at any temperature for any solvent was obtained by use of an extrapolation function $E^{0\prime}$ defined by [1] (20*a*)

[1] $$E^{0\prime} = E + 2k' \ln m - 2k'A_0B_0m^{1/2} \times (1 + a_0Bm^{1/2})^{-1} - 2k' \ln (1 + 0.002M_sm) = E_m^0 - 2k'\beta m$$

where the parameters have their usual significance (20*a*). The emf values (E) corrected to a hydrogen pressure of 1 atm against the molalities (m) of HX have been tabulated elsewhere.[4] The relevant parameters including Debye–Hückel constants A_0B_0 ($= 2.303 \times 1.824 \times 10^6 d_s^{1/2}(\varepsilon_s T)^{-3/2}$) and B_0 ($= 50.29 d_s^{1/2}(\varepsilon_s T)^{-1/2}$) are given in Table 1. Computed $E^{0\prime}$ values were fitted to a linear plot against m by a least-squares procedure, from which E_m^0 and the slope $2k'\beta$ values were determined. As earlier (20), the value of a_0 was taken as zero, since this gave a good linear plot in each case and reasonable variation of a_0 had no significant influence on E_m^0. Table 1 gives the values of E_m^0 and $2k'\beta$ for the Ag–AgX electrodes for the solvent mixtures at different temperatures. The average standard deviation in E_m^0 values is ±0.3 mV and average uncertainty in $2k'\beta$ values is ±0.004 V mol^{-1} kg.

As shown in Table 1, E_m^0 values for the Ag–AgBr electrode at 25°C compare fairly well with those of Khoo (5*a*); but the values for the Ag–AgI electrode increasingly differ and the divergence is as large as 4 mV at 50 wt.% glycerol. It should be noted that Khoo's data for the Ag–AgI electrode are based on cells comprising borate buffer and KI instead of pure HI as in cell [A]. But it is well known that boric acid forms borospiranic acid complex [B] with glycerol (23) imparting enchanced acidity to the solution.

[B] 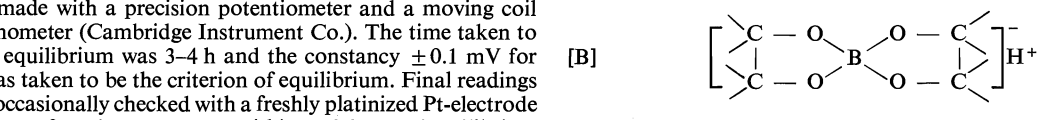

This is also evident from the pK_a data reported by Khoo (5*a*), which are found to decrease from 7.308 at 10 wt.% glycerol to 5.947 at 50 wt.% glycerol, in contrast to what are expected from the decreased dielectric constant of the solvents. Moreover, Khoo's values impart a hump in the related ΔG_t^0–composition profile, which seems rather unusual, as no such hump is exhibited either by the present set of data or by those for HCl and HBr reported by Khoo (5*a*) and others (17, 19) as obtained by use of cell [A] comprising of pure HX instead of borate buffers.

The E_m^0 values of the Ag–AgX electrodes at different temperatures for each solvent were fitted by the method of least-squares to [2]

[2] $$E_m^0 = a + b(t - 25) + c(t - 25)^2$$

where t is the temperature in deg Celsius. The co-efficients a, b, and c for the electrodes in different

[4]Complete set of the actual experimental data and the solvent constants required for computing $E^{0\prime}$ (eq. [1]) are available, at a nominal charge, from the Depository of Unpublished Data, CISTI, National Research Council of Canada, Ottawa, Ont., Canada K1A 0S2.

TABLE 1. The values of E_m^0 of the Ag–AgX electrode and constant $2k'\beta$ of [1] at different temperatures in different glycerol + water mixtures*

Wt.% glycerol	Parameter	Value at 10°C	15°C	20°C	25°C	30°C	35°C	40°C
				X = Br				
10	E_m^0/V	0.0719	0.0699	0.0678	0.0656 (0.0662)	0.0631	0.0602	0.0569
	$2k'\beta$/(V mol^{-1} kg)	0.086	0.090	0.091	0.091	0.094	0.102	0.104
30	E_m^0/V	0.0599	0.0579	0.0558	0.0534 (0.0539)	0.0508	0.0479	0.0447
	$2k'\beta$/(V mol^{-1} kg)	0.100	0.101	0.109	0.114	0.121	0.123	0.125
50	E_m^0/V	0.0482	0.0452	0.0422	0.0392 (0.0389)	0.0362	0.0332	0.0301
	$2k'\beta$/(V mol^{-1} kg)	0.161	0.165	0.173	0.179	0.185	0.192	0.203
70	E_m^0/V	0.0250	0.0214	0.0177	0.0137 (0.0138)	0.0097	0.0057	0.0017
	$2k'\beta$/(V mol^{-1} kg)	0.140	0.147	0.150	0.154	0.155	0.154	0.163
				X = I				
10	E_m^0/V	−0.1509	−0.1520	−0.1533	−0.1548 (−0.1541)	0.1565	−0.1584	−0.1606
	$2k'\beta$/(V mol^{-1} kg)	0.210	0.230	0.218	0.217	0.230	0.235	0.230
30	E_m^0/V	−0.1599	−0.1610	−0.1623	−0.1638 (−0.1617)	−0.1655	−0.1675	−0.1698
	$2k'\beta$/(V mol^{-1} kg)	0.092	0.102	0.103	0.101	0.101	0.112	0.119
50	E_m^0/V	−0.1657	−0.1681	−0.1705	−0.1729 (−0.1686)	−0.1753	−0.1777	−0.1801
	$2k'\beta$/(V mol^{-1} kg)	0.216	0.229	0.234	0.230	0.238	0.230	0.238
70	E_m^0/V	−0.1796	−0.1830	−0.1865	−0.1900	−0.1935	−0.1970	−0.2007
	$2k'\beta$/(V mol^{-1} kg)	0.233	0.230	0.231	0.232	0.229	0.234	0.242

*Values in parentheses are reported by Khoo (*5a*).

TABLE 2. The constants a in V, b in V °C^{-1}, and c in V °C^{-2}, of eq. [2] for Ag–AgX electrodes in glycerol + water mixtures

Wt.% glycerol	X = I			X = Br			X = Cl*		
	a	$-b \times 10^4$	$-c \times 10^6$	a	$-b \times 10^4$	$-c \times 10^6$	a	$-b \times 10^4$	$-c \times 10^6$
0†	−0.15242	3.19	2.84	0.07109	4.87	3.08	0.2224	6.396	3.18
10	−0.1548	3.22	4.20	0.0656	4.93	5.20	0.2165	6.53	3.10
30	−0.1638	3.28	4.70	0.0534	5.04	4.90	0.2022	6.66	3.60
50	−0.1729	4.82	0.20	0.0392	6.02	0.20	0.1840	7.45	3.30
70	−0.1900	7.02	0.70	0.0137	7.80	1.60	—	—	—

*These values were obtained using E_m^0 values of the Ag–AgCl electrode from 10 to 40°C reported by Knight *et al.* (18) and Harned and Nestler (17).
†Reference 3.

solvent mixtures are presented in Table 2. Those for the Ag–AgCl electrode computed from Knight *et al.*'s relevant data (18) for 10 and 30 wt.% glycerol and from Harned *et al.*'s data (17) for 50 wt.% glycerol are also included in Table 2.

The free energy changes (ΔG_t^0) accompanying the transfer of 1 mol of HX from the standard state in water to the standard state in each of the mixed solvents were evaluated on the mole fraction scale at 25°C using [3]

$$[3]\quad \Delta G_t^0(\mathrm{HX}) = -F\,[(E_m^0)_s^{\,25°C} - (E_m^0)_w^{\,25°C}] - 2 \times 298.15R \ln M_s/M_w$$

and the corresponding entropy changes (ΔS_t^0) by [4]

$$[4]\quad \Delta S_t^0(\mathrm{HX}) = F(b_s - b_w) + 2R \ln M_s/M_w$$

where the subscripts s and w refer to the solvent and water, respectively. As before (20), probable uncertainties in ΔG_t^0 and ΔS_t^0 are 21 J mol^{-1} and ±1 J K^{-1} mol^{-1} respectively, ΔG_t^0, ΔS_t^0, and $T\Delta S_t^0$ (T = 298.15 K) values for HBr, HI, and HCl are presented in Table 3.

Discussion

Free Energies of Transfer

ΔG_t^0(HX)–composition profiles for this solvent system (Fig. 1) resemble closely those in aqueous alcohols (15, 20), glycol (24), etc. and typical of systems having decreasing dielectric constant and

TABLE 3. Standard free energies (ΔG_t^0), entropies (ΔS_t^0), and related quantities $\Delta Y = T\Delta S_t^0(H^+) + T\Delta S_{t,ch}^0(X^-)$ of transfer of HX (X = Cl, Br, or I) from water to glycerol + water mixtures at 25°C

Wt.% glycerol	Mol% glycerol	ΔG_t^0/(kJ mol^{-1})			ΔS_t^0/(J K^{-1} mol^{-1})			$\Delta Y = T\Delta S_t^0(H^+) + T\Delta S_{t,ch}^0(X^-)$/(kJ mol^{-1})		
		HCl	HBr	HI	HCl	HBr	HI	HCl	HBr	HI
10	2.10	0.16*	0.12	−0.18	0.1	0.8	1.1	0.47	0.61	0.70
30	7.73	0.55*	0.34	−0.27	2.0	3.0	3.7	1.95	2.13	2.24
50	16.46	1.21*	0.52	−0.58	−1.6	−2.6	−7.0	1.88	1.39	−0.05
70	31.30	2.40†	1.47	−0.48	—	−14.5	−23.2	—	−0.79	−3.73

*Computed from the data given in ref. 18.
†Reference 5*a*.

more or less similar variation of chemical nature, including acidity, basicity, hydrogen-bonding capacity, and structural features. Thus, as the proportion of the co-solvent increases, the transfer of both HCl and HBr is found to be increasingly unfavourable and that of HI, though favourable at water-rich compositions, has a tendency to become unfavourable at co-solvent-rich compositions. Moreover, at any given composition, ΔG_t^0(HX) decreases in the order HCl, HBr, HI, as is expected if, as in aqueous alcohols, the effects of decreased dielectric constant and the acidity of the mixed solvents destabilize the anions (5, 15, 25).

When the electrostatic effects (26), $\Delta G_{t,el}^0$(HX), which arise from the difference in the dielectric constant of the solvents, are tentatively computed by the simple Born equation (27) using $r_{H_3O^+} = 2.76$ (28) and Pauling's crystallographic radius for X^- (29) and are subtracted from the respective ΔG_t^0(HX) values, the resulting 'non-electrostatic' or 'chemical' contributions, $\Delta G_{t,ch}^0$(HX), become increasingly negative, as shown in Fig. 1. As has been found to be the case in aqueous alcohols (15), if the solvation of these ions be assumed to be dictated chiefly by 'acid–base' type ion–solvent interactions (25), and the acid–base nature of the solvents be essentially similar (5*a*) to those of aqueous alcohols (15), the results would apparently suggest that in this solvent system as well H^+ is solvophilic and halide ions hydrophilic and that the solvophilicity of H^+ exceeds the hydrophilicity of the halide ions at least in the range of composition studied. This would then imply that these mixed solvents are more 'basic' but less 'acidic' than water. This 'basicity' and 'acidity' of course mean electron-pair donicity and acceptibility of the solvents respectively (25).

However, for a better understanding of the ion–solvent interactions the splitting of ΔG_t^0(HX) to individual ion contributions is in order. Till recently two sets (5*a*, 30) of $\Delta G_t^0(i)$ values have been reported for these ions. The data obtained by Khoo (5*a*) using Feakins-type extrapolation procedure (25), however,

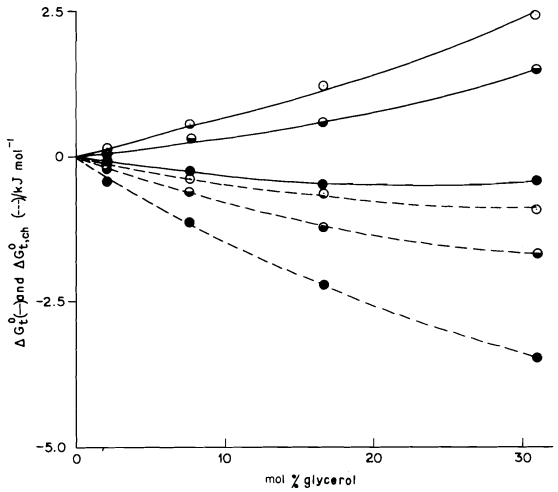

FIG. 1. Variation of ΔG_t^0(HX) and $\Delta G_{t,ch}^0$(HX) (broken lines) at 25°C with mol% glycerol: ○, HCl; ◒, HBr; ●, HI.

differ from those obtained by Wells' method (30) not only in magnitude but even in sign, as in the cases of H^+ and I^-. Consequently, the interpretation of the results and the nature of the ion–solvent interactions derived thereof are also different in the two cases. Under the circumstances, the attempt for elucidating the true picture of the solvation of these ions in these solvents should await till individual ion contributions are obtained by other suitable methods (31), particularly by reference electrolyte Ph_4AsBPh_4 (Ph = phenyl) method which has been very recently demonstrated (32) to be theoretically sound and hence more useful than others.

Entropies of Transfer

As in aquo-alcoholic systems (15), $T\Delta S_t^0$(HX)–composition profiles for this system (Fig. 2) exhibit 'characteristic' maxima at water-rich compositions followed by downward trends at higher co-solvent compositions. Also, the relative order of $T\Delta S_t^0$(HX) values in the region of maxima is a regular one: HI > HBr > HCl; but a reverse one at higher composition of glycerol. Moreover, when ΔS_t^0(HX)

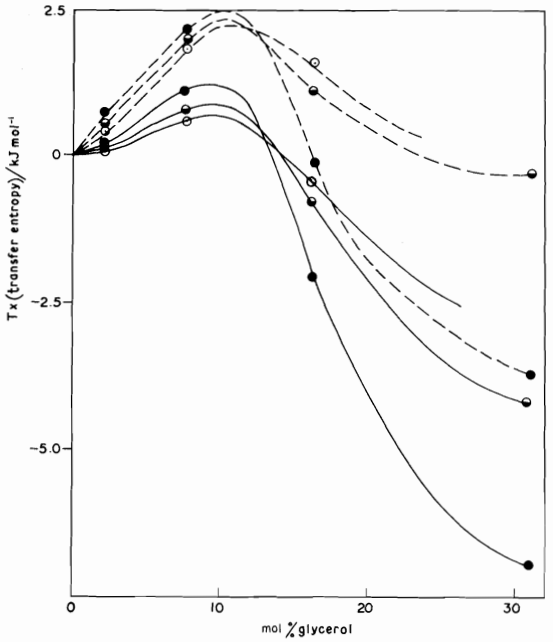

FIG. 2. Variation of $T\Delta S_t^0(HX)$ and $\Delta Y = T\Delta S_t^0(H^+) + T\Delta S_{t,ch}^0(X^-)$ (broken lines) with mol% glycerol: ○, HCl; ◒, HBr; ●, HI.

values are tentatively rationalized by subtracting the Born-type electrostatic contributions of the halide ions computed in a manner described earlier (27), one finds that as in aquo-alcoholic solvents (15) the quantities $\Delta Y = T\Delta S_t^0(H^+) + T\Delta S_{t,ch}^0(X^-)$ (Fig. 2) are shifted upwards, retaining the essential features of $T\Delta S_t^0(HX)$–composition profiles all the same.

The implications of the observed $T\Delta S_t^0(HX)$, or more preferably, ΔY–composition profiles for this system can be visualized in the light of our previously proposed semi-quantitative theory (15). This was essentially based on the Frank and Wen (33) model of ion-solvation and on our earlier views (3, 15, 20, 34) that the transfer of any of these ions from water to a mixed solvent consists of four successive steps: (*i*) dismantling of the hydration zones to give the bare ion and infinitely dilute gas of water molecules, (*ii*) condensation of the gas to give normally structured liquid water, (*iii*) evaporation of solvent molecules required for step (*iv*) from the bulk solvent to give dilute gas of solvent molecules, and (*iv*) solvation of the bare ion and its introduction into the solvent.

Taking into account the detailed entropy changes for the composite transfer process and assuming that for the solvents containing up to at least 50 wt.% co-solvent the primary solvation zone is composed wholly of water (31), it has been concluded (15) that

(*a*) when solvent structure > pure water structure

$$\Delta S_{t,ch}^0(HX) > 0 \text{ and } \Delta S_{t,ch}^0(HI) > \Delta S_{t,ch}^0(HBr) > \Delta S_{t,ch}^0(HCl)$$

(*b*) when solvent structure < pure water structure

$$\Delta S_{t,ch}^0(HX) < 0 \text{ and } \Delta S_{t,ch}^0(HI) < \Delta S_{t,ch}^0(HBr) < \Delta S_{t,ch}^0(HCl)$$

Moreover, since small amounts of monohydric alcohols by virtue of their hydrophobic moieties promote three-dimensional (3D) ice-like structures while larger amounts break up the same due to increased packing imbalance (35) and also the observed $\Delta S_{t,ch}^0(HX)$–composition profiles for these aqueous alcohols are in accord with the dictates of the above theory, it has been concluded that ΔY–composition profile should serve as a useful probe for the structuredness of other aquo-organic solvents.

In the light of the above observations the results of the present study could be taken to suggest that like the monodrydic alcohols small addition of glycerol also promotes water structure but larger amounts break up the same and that the maximum structure promotion occurs at about 9 mol% glycerol. Moreover, it may be observed from Fig. 3, where ΔY–composition profiles for a number of co-solvents are illustrated, that while the characteristic maxima of isopropanol and *tert*-butyl alcohol are significantly sharper, narrower, and higher compared to that of methanol, those of ethylene glycol and glycerol are somewhat flat and short as that of methanol. Since the monohydric alcohol containing larger hydrophobic group causes a more rapid and more extensive promotion followed by an equally rapid and complete collapse due to packing imbalance, the compositions at which the maximum in $T\Delta S_t^0$ or ΔY appears will be smaller for the larger hydrophobic moiety of the alcohol. Consequently, the flat maxima of nearly similar heights for methanol, ethylene glycol, and glycerol suggest that the structure promoting propensities of these co-solvents are more or less similar and much smaller compared to higher monohydric alcohols and that their observed compositions of maxima are also in accord with their respective sizes.

Again, the significant difference between the maxima in isopropanol + water and glycerol + water systems indicates that the effect of structure promoting propensities of hydrophobic $—CH_3$ groups in isopropanol is appreciably reduced when replaced by $—CH_2OH$ groups in glycerol. This is possibly due to the fact that the monomeric 'dense' water in equilibrium with 'bulky' 3D structure of water instead of being repelled due to hydrophobicity

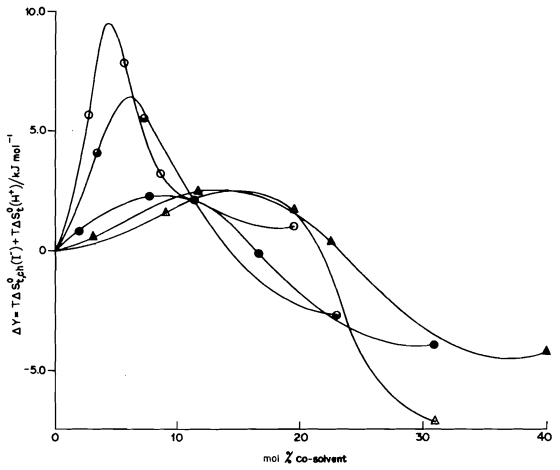

FIG. 3. Variation of $\Delta Y = T\Delta S_{t,ch}^{0}(I^-) + T\Delta S_t^0(H^+)$ with mol% co-solvents: ○, *tert*-butyl alcohol (20*a*); ◒, isopropanol (15); ●, glycerol (present work); ▲, ethylene glycol (24); and △, methanol (estimated from the data of ref. 41).

of $-CH_3$ groups and inducing 'ice-berg' formation (36) or 'hydrophobic hydration' (36) are likely to induce 'specific site hydration' (37) forming hydrogen bonds with hydrophilic —OH sites of $-CH_2OH$ groups and thus causes an appreciable reduction in structure promotion. This further explains why there is little difference in the heights and extensiveness of characteristic maxima in the cases of ethylene glycol and glycerol compared to that of methanol, as two of its H-atoms in methyl group are successively substituted by less hydrophobic and less structure-promoting $-CH_2OH$ groups. The observed shifting of maximum towards lower co-solvent compositions is also indicative of the result of an increased number of $-CH_2OH$ groups of the co-solvents. This seemingly suggests that the characteristic maxima of higher polyols would be shifted to so low co-solvent compositions that those polyols are likely to behave as effective structure breakers, as are evidenced from various studies (38) and also expected from the effect of 'specific site hydration' as well as the compatibility of polyol conformation with the solvent structure (37). In the cases of lower polyols like glycerol, however, the structure-promoting effects of hydrocarbon skeletons seem hardly augmented by the structure-breaking effects of 'specific site hydration' as these polyols are likely to assume conformations which are completely compatible (4, 39) with the water structure at least in water-rich compositions.

Notably, close similarity of the variations of Washburn number in glycerol–water mixtures with that in methanol–water mixtures also led Khoo (5*b*) to invoke the same type of structural variation as contended from the results of the present study. Moreover, the observed maxima in the β (cf. [1])–composition profiles for HCl and HBr in glycerol–water mixtures have also been attributed by Khoo (5*a*) to similar structural changes of the solvents. Variations of some physical properties such as water activities (6), viscosities (7), sound absorption (7, 8), and partial molar volumes (9), however, indirectly suggest that the incremental addition of glycerol simply affects a gradual breakdown of 3D structure of water. Moreover, a comparison (4) of apparent volumes and heat capacities of transfer of several ionic solutes from water to glycerol–water mixtures and literature data for the said transfer quantities to D_2O and to 3 *m* urea solutions suggests that as in urea–water mixtures there is less structural order in glycerol–water mixtures than in water. But present observations when compared with our earlier findings in urea–water mixtures (3) reflect some apparent differences in the structural behaviour of the two co-solvents. Thus, while increasing addition of urea (up to 3 *m*) shifts the equilibrium: water (dense) ↔ water (bulky) to the left glycerol like the simple mono-ols shifts the same to the right at least up to the composition of its characteristic maxima. As the conformation of urea (40) and glycerol (4, 39) are compatible with the water structure, the effect of 'specific site hydration' presumably induces urea to shift the equilibrium towards the left while the predominant effect of hydrophobic character over 'specific site hydration' induces glycerol to shift the same towards the right.

Acknowledgement

Thanks are due to the University Grants Commission, New Delhi, for granting a Teacher Fellowship to I.N.B.

1. (*a*) P. R. PHILIP, J. E. DESNOYERS, and A. HADE. Can. J. Chem. **51**, 187 (1973); P. R. PHILIP, G. PERRON, and J. E. DESNOYERS. Can. J. Chem. **52**, 1709 (1974); (*b*) N. DESROSIERS, G. PERRON, J. G. MATHIESON, B. E. CONWAY, and J. E. DESNOYERS. J. Soln. Chem. **3**, 789 (1974) and relevant references therein.
2. T. S. SARMA and J. C. AHLUWALIA. Chem. Soc. Rev. **2**, 203 (1973) and relevant references therein.
3. K. K. KUNDU and K. MAZUMDAR. J. Chem. Soc. Faraday Trans. I, (*a*) **69**, 806 (1973); (*b*) **71**, 1422 (1975).
4. G. DIPAOLA and B. BELLEAU. Can. J. Chem. **53**, 3452 (1975) and relevant references therein for earlier work.
5. K. H. KHOO. J. Chem. Soc. Faraday Trans. I, (*a*) **68**, 554 (1972); (*b*) **69**, 1313 (1973).
6. G. SCATCHARD, W. HAMER, and S. WOOD. J. Am. Chem. Soc. **60**, 3061 (1938).
7. M. L. SHEELY. Ind. Eng. Chem. **24**, 1060 (1932).
8. (*a*) F. H. WILLIS. J. Am. Chem. Soc. **19**, 242 (1947); (*b*) R. KUHNKIS and W. SCHAAFS. Akust. Beit. **12**, 254 (1962); Chem. Abstr. **58**, 3918*a* (1963).
9. K. N. NAKANISHI. Bull. Chem. Soc. Jpn. **33**, 793 (1960).

10. R. LUMRY and S. RAJENDER. Biopolymers, **93**, 1125 (1970).
11. (*a*) E. M. ARNETT, W. G. BENTRUDE, J. J. BURKE, and P. MC. DUGGLEBY. J. Am. Chem. Soc. **87**, 1541 (1965); (*b*) E. M. ARNETT. *In* Physico-chemical processes in mixed aqueous solvents. *Edited by* F. Franks. Heinemann, London. 1967. p. 105.
12. G. L. BERTRAND, F. J. MILLERO, C. H. HU, and L. S. HEPLER. J. Phys. Chem. **70**, 699 (1966).
13. (*a*) A. BEN-NAIM and S. BAER. Trans. Faraday Soc. **60**, 1731 (1964); (*b*) A. BEN-NAIM. J. Phys. Chem. **71**, 4002 (1967); (*c*) A. BEN-NAIM. *In* Water and aqueous solutions. *Edited by* R. A. Horne. Wiley-Interscience, New York, NY. 1972 . p. 425.
14. K. BOSE and K. K. KUNDU. Can. J. Chem. **55**, 3961 (1977).
15. K. BOSE, K. DAS, A. K. DAS, and K. K. KUNDU. J. Chem. Soc. Faraday Trans. I, **74**, 1051 (1978).
16. K. BOSE, K. DAS, A. K. DAS, and K. K. KUNDU. J. Phys. Chem. **82**, 1242 (1978).
17. H. S. HARNED and F. H. M. NESTLER. J. Am. Chem. Soc. **68**, 665 (1946).
18. S. B. KNIGHT, H. D. CROCKFORD, and F. W. JAMES. J. Phys. Chem. **57**, 463 (1953).
19. R. N. ROY, W. VERNON, and A. L. M. BOTHWELL. J. Electrochem. Soc. **118**, 1302 (1971).
20. (*a*) K. BOSE, A. K. DAS, and K. K. KUNDU. J. Chem. Soc. Faraday Trans. I, **71**, 1838 (1975); (*b*) K. DAS, K. BOSE, and K. K. KUNDU. J. Chem. Soc. Faraday Trans. I, **73**, 655 (1977); (*c*) K. DAS, K. BOSE, A. K. DAS, and K. K. KUNDU. Electrochim. Acta, **23**, 159 (1978).
21. E. W. WASHBURN (*Editor*). International critical tables of numerical data. Physics, chemistry and technical tables. Vol. III. McGraw-Hill. 1928.
22. G. AKERLOF. J. Am. Chem. Soc. **54**, 4125 (1932).
23. I. L. FINAR. Organic chemistry. Vol. I. 5th ed. Longman Group Ltd., London. 1967. p. 286.
24. K. K. KUNDU, D. JANA, and M. N. DAS. Electrochim. Acta, **18**, 95 (1973).
25. (*a*) D. FEAKINS. *In* Physico-chemical processes in mixed aqueous solvents. *Edited by* F. Franks. Heinemann, London. 1967. p. 71; (*b*) D. FEAKINS and P. WATSON. J. Chem. Soc. 4734 (1963).
26. R. G. BATES. *In* Hydrogen-bonded solvent systems. *Edited by* A. K. Covington and P. Jones. Taylor and Francis, London. 1968. p. 49.
27. U. SEN, K. K. KUNDU, and M. N. DAS. J. Phys. Chem. **71**, 3665 (1967).
28. M. PAABO, R. G. BATES, and R. A. ROBINSON. J. Phys. Chem. **70**, 247 (1966).
29. H. S. HARNED and B. B. OWEN. Physical chemistry of electrolytic solutions. 3rd ed. Reinhold, New York. 1958. p. 164.
30. C. F. WELLS. J. Chem. Soc. Faraday Trans. I, **70**, 695 (1974).
31. O. POPOVYCH. Crit. Rev. Anal. Chem. **1**, 73 (1970).
32. J. I. KIM. J. Phys. Chem. **82**, 191 (1978).
33. H. S. FRANK and W. Y. WEN. Discuss. Faraday Soc. **24**, 133 (1957).
34. K. K. KUNDU. Indian J. Chem. **10**, 548 (1972).
35. F. FRANKS and D. J. IVES. Q. Rev. **20**, 1 (1966).
36. H. S. FRANK and M. W. EVANS. J. Chem. Phys. **13**, 507 (1945).
37. M. J. TAIT, A. SUGGETT, F. FRANKS, S. ABLETT, and P. A. QUICKENDEN. J. Solution Chem. **1**, 131 (1972).
38. G. DIPAOLA and B. BELLEAU. Can. J. Chem. **55**, 3825 (1977) and relevant references therein.
39. D. T. WARNER. Nature, **196**, 1055 (1962).
40. H. S. FRANK and F. FRANKS. J. Chem. Phys. **48**, 4746 (1968).
41. J. M. MCINTYRE and E. S. AMIS. J. Chem. Eng. Data, **13**, 371 (1968).

The preparation and crystal structure of pentaiodinium hexafluoroantimonate(V) containing I_{15}^{3+}

JACK PASSMORE, PETER TAYLOR, TOM WHIDDEN, AND PETER S. WHITE

Department of Chemistry, University of New Brunswick, P.O. Box 4400, Fredericton, N.B., Canada E3B 5A3

Received October 12, 1978

JACK PASSMORE, PETER TAYLOR, TOM WHIDDEN, and PETER S. WHITE. Can. J. Chem. **57**, 968 (1979).

Crystalline pentaiodinium hexafluoroantimonate was prepared by the reaction of I_2 and SbF_5 in AsF_3. The crystals were triclinic, $a = 8.295(4)$ Å, $b = 15.61(1)$ Å, $c = 8.390(4)$ Å, $\alpha = 81.49(4)°$, $\beta = 110.02(4)°$, $\gamma = 85.06(4)°$, $Z = 3$, space group $P\bar{1}$. The structure was solved by multiple-solution direct methods and Fourier syntheses and refined by full-matrix and blocked-matrix least-squares procedures to a final R of 0.062 and R_w of 0.090 for 2229 reflections with $I \geq 3\sigma(I)$. The two crystallographically independent planar, bent I_5^+ chains (one centrosymmetric, the other essentially centrosymmetric), each have two collinear central bonds of 2.899(2) Å (×2); 2.896(2), and 2.920(2) Å, bond angles 180° and 178.7(6)°, respectively, and two shorter terminal bonds of 2.680(3) Å (×2); 2.666(3) and 2.698(2) Å, with bond angles between central and terminal bonds of 94.53(6)° (×2); 93.86(7) and 93.17(7)°, respectively. Three I_5^+ units are joined by a weak (3.416(3) Å) interaction to form what may be regarded as an I_{15}^{3+} unit. The SbF_6^- anions are approximately octahedral.

JACK PASSMORE, PETER TAYLOR, TOM WHIDDEN et PETER S. WHITE. Can. J. Chem. **57**, 968 (1979).

On a préparé l'hexafluoroantimonate de pentaiodinium cristallin en faisant réagir du I_2 avec du SbF_5 dans le AsF_3. Les cristaux sont tricliniques, $a = 8.295(4)$ Å, $b = 15.61(1)$ Å, $c = 8.390(4)$ Å, $\alpha = 81.49(4)°$, $\beta = 110.02(4)°$, $\gamma = 85.06(4)°$, $Z = 3$, groupe d'espace $P\bar{1}$. On a résolu la structure par des méthodes directes de solutions multiples et des synthèses de Fourier et on l'a affinée par la méthode des moindres carrés (matrices complète et diagonale) jusqu'à une valeur finale de R de 0.062 et R_w de 0.090 pour 2229 réflexions avec $I \geq 3\sigma(I)$. Les deux chaînes de I_5^+ sont planes, recourbées et indépendantes du point de vue cristallographique; l'une est centrosymétrique et l'autre est essentiellement centrosymétrique et chacune possède des liaisons centrales mesurants 2.899(2) Å; 2.896(2) et 2.920(2) Å avec des angles de liaisons respectifs de 180° et 178.7(6)° et deux liaisons terminales plus courtes de 2.680(3) Å (×2); 2.666(3) et 2.698(2) Å avec des angles entre les liaisons centrales et terminales qui sont respectivement de 94.53(6)° (×2); 93.86(7) et 93.17(7)°. Il y a trois unités de I_5^+ qui sont réunies par une interaction faible (3.416(3) Å) formant ce qu'on peut considérer comme une unité de I_{15}^{3+}. Les anions de SbF_6^- sont approximativement octaédriques.

[Traduit par le journal]

Introduction

A wide variety of halogen homopolyatomic anions have been well characterized for some time (1–3). More recently, polyatomic halogen cations have been prepared and identified (1, 4). The structure of Br_2^+ and I_2^+ in $Br_2Sb_3F_{16}$ (5) and $I_2Sb_2F_{11}$ (6) have been determined by X-ray crystallographic methods. Vibrational evidence (4) has been given in support of the bent Cl_3^+, Br_3^+, and I_3^+ cations. Evidence has recently been presented for salts of Br_5^+ (7) and Cl_2^+ (8). Of the iodine cations, I_3^+, I_5^+, and possibly I_7^+ have been observed in fluorosulphuric acid and 100% sulphuric acid solutions (4) but no structural data for the latter two ions were obtained. The following salts of polyatomic iodine cations have been prepared as solid compounds: $I_2M_2F_{11}$ (M = Sb, Ta) (9), I_3SO_3F and I_7SO_3F (10), I_3AsF_6 (11) and I_3SbF_6 (12), and I_3AlCl_4 and I_5AlCl_4 (13). Nuclear quadrupole resonance measurements (13) indicated that I_3^+ in I_3AlCl_4 has a bent structure with an angle of 97.1°. The compound I_5AlCl_4 was prepared in the same study but no structural data were reported.

In this work we have prepared I_5SbF_6 by the oxidation of I_2 with SbF_5 and have determined its structure by X-ray diffraction methods.

Experimental

Preparation of Pentaiodinium Hexafluoroantimonate(V)

Preparative techniques are described in ref. 11. In the reaction from which single crystals were obtained, iodine (5.89 g, 23.2 mmol) and SbF_5 (3.08 g, 14.2 mmol) were reacted in AsF_3 (7.09 g, 53.7 mmol) for 1 h at room temperature. The resulting dark brown solution was filtered through a sintered disk and the washing repeated until only a white solid remained. The AsF_3 and excess I_2 were condensed back onto this solid and allowed to stand overnight. Further reaction was found to occur, the solution becoming coloured. The entire

0008-4042/79/090968-06$01.00/0

process was repeated three times after which no further reaction was evident. Slow removal of the solvent produced a black, highly crystalline solid which was pumped to constant weight in order to remove trace amounts of iodine. The weight of soluble product (7.72 g) was not inconsistent with the formation of I_5SbF_6. Elemental analysis of the white insoluble solid (0.82 g) agrees with the stoichiometry SbF_3; however, the Raman spectrum is very different from that of SbF_3 but similar to $(SbF_3)_x{\cdot}(SbF_5)$, where x very approximately equals 5, this is the subject of further investigation.[1]

X-ray Crystallography of Pentaiodinium Hexafluoroantimonate(V)

The crystal chosen for study approximated to a right parallel-piped of dimensions ca. 0.033 × 0.027 × 0.014 cm, and included angle of approximately 125° between the two long edges. This was mounted in a rigorously dried glass capillary. Preliminary Weissenberg and precession photographs showed the crystal to be triclinic and yielded initial unit cell dimensions. Accurate cell parameters were obtained using a least-squares fit of cell dimensions and an orientation matrix to the diffractometer settings for 11 well-centered reflections ($30° \leq 2\theta \leq 40°$) distributed through the hemisphere in which data were collected. Crystal data for I_5SbF_6 are:

I_5SbF_6 fw = 870.3
Triclinic, $P\bar{1}$, a = 8.295(4) Å, b = 15.61(1) Å, c = 8.390(4) Å, α = 81.49(4)°, β = 110.02(4)°, γ = 85.06(4)°, V = 999 Å^3, Z = 3, ρ_c = 4.34 g cm^{-3}, $F(000)$ = 1110, $\mu(MoK_\alpha)$ = 138.4 cm^{-1} (λ = 0.71069 Å, 20(±2)°C).

The reduced cell is obtained by the transformation (100)/(00$\bar{1}$)/(010) and has parameters a = 8.295 Å, b = 8.390 Å, c = 15.612 Å; α = 81.489°, β = 85.055°, γ = 69.98°. This cell satisfies the conditions for the reduced cell stated by Buerger (14, 15).

Intensities were collected on a Picker FACS-I four-circle diffractometer using graphite crystal monochromated MoK_α radiation. An ω–2θ scan with a base width of 2° (2θ) corrected for dispersion of the K_α doublet, and a scan rate of 1° per min was employed. Background counts (20 s) were measured at each end of the scan. Data were collected for $2\theta \leq 45°$. Two reflections were measured as standards every thirty reflections. These varied less than 1.5σ from their mean throughout the data collection.

A total of 2593 independent reflections were measured in four octants. Of these, 2229 (86%) were initially classified as observed, being greater than 3$\sigma(I)$ where $\sigma(I)$ is estimated from counter statistics (16). Corrections for Lorentz and polarization factors were applied to the data. Application of an absorption correction (17) to the data was purposefully delayed until a reasonably low R value was obtained. This method was used to make certain that crystal definition was correct and the application of the correction improved the model. When applied, the correction reduced R from 0.126 to 0.090. Maximum and minimum transmission factors were 0.22 and 0.07, respectively.

Structure Determination

Data reduction and structure refinement utilized the X-RAY 76 program package (18). Atomic scattering factors for the neutral atoms were taken from Cromer and Mann (19) and the iodine and antimony scattering factors were corrected for anomalous dispersion (20). Statistical treatment of the normalized structure factors indicated a centric crystal system and the structure determination was therefore carried out in the space group $P\bar{1}$. Initial positional parameters were determined using the MULTAN system of direct methods programs (21). A total of 243 reflections with $E \geq 1.70$ were used as input to MULTAN. An E-map phased by the best solution from MULTAN gave the positions of 9 out of the 10 iodine and antimony atoms. An F_o synthesis using these parameters determined the position of the remaining heavier atom and two of the fluorines. With these atomic positions included in the calculation, two cycles of least-squares refinement reduced the R value to 0.134. The function minimized by the procedure was $\Sigma w(|F_o| - |F_c|)^2$ with $w = 1$. Another F_o synthesis at this point allowed the determination of the remaining fluorine positions. Including all atoms in the calculation with isotropic thermal parameters, refinement converged at R = 0.126. The absorption correction was then applied as noted above. When the thermal parameters of the iodine and antimony atoms were varied anisotropically R dropped to 0.081.

Weighting factors for the procedure were changed to $w = 1/\sigma(F)^2$ where $\sigma(F)$ is directly derived from $\sigma(I)$ (15). With the inclusion of the new weighting scheme the refinement converged to R = 0.062, R_w = 0.090 for 2229 reflections. Average shift/error for the final cycle was 0.049 with a maximum value of 0.294 associated with a fluorine atom. A ΔF synthesis at this point showed a maximum electron density of 2.13 e$^-$/Å^3 at (0.0908, 0.0410, −0.0113), 1.04 Å from Sb1, indicating essentially no misplaced or uncounted atoms. The high noise level due to the fluorescence in the sample may be the cause of this. A number of other peaks approaching this height are distributed throughout the unit cell. Final positional parameters appear in Table 1.[2]

An attempt was made to refine the structure in the space group $P1$. The atoms were displaced from their centric posi-

TABLE 1. Final atomic positional parameters (fractional × 10^4) with estimated standard deviations in parentheses

Atom	x/a	y/b	z/c
Sb1	0	0	0
Sb2	4854(2)	6574(1)	1427(2)
F1	193(20)	702(10)	1694(18)
F2	914(18)	823(10)	−1192(18)
F3	2218(16)	−591(10)	1279(18)
F4	4055(23)	5684(12)	2525(23)
F5	5688(20)	7436(11)	342(23)
F6	4338(24)	6026(15)	−508(20)
F7	5298(23)	7090(11)	3339(17)
F8	2613(19)	7205(13)	473(22)
F9	7085(17)	5945(10)	2324(23)
I1	3477(2)	838(1)	6024(2)
I2	4535(2)	−720(1)	8221(2)
I3	2419(2)	−1658(1)	5745(2)
I4	336(2)	−2639(1)	3289(2)
I5	1670(2)	−4174(1)	5432(2)
I6	0	1/2	0
I7	2924(2)	3906(1)	2746(2)
I8	1532(2)	2426(1)	2412(2)

[1]Peter Taylor, Jack Passmore, and Shantha Nandana. Unpublished results.

[2]Photocopies of tables of the structure factors and thermal parameters may be obtained, at a nominal charge, from the Depository of Unpublished Data, CISTI, National Research Council of Canada, Ottawa, Ont., Canada K1A 0S2.

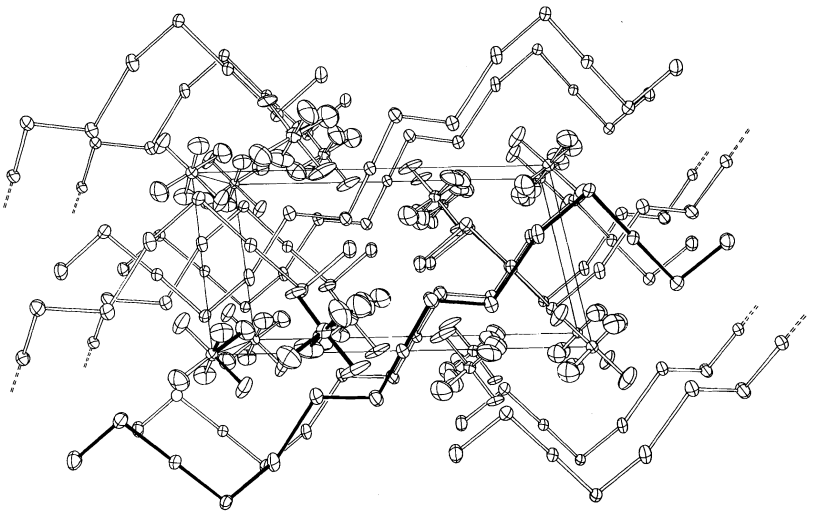

FIG. 1. The crystal packing in $I_5^+SbF_6^-$ as viewed down a vector perpendicular to the *bc* plane.

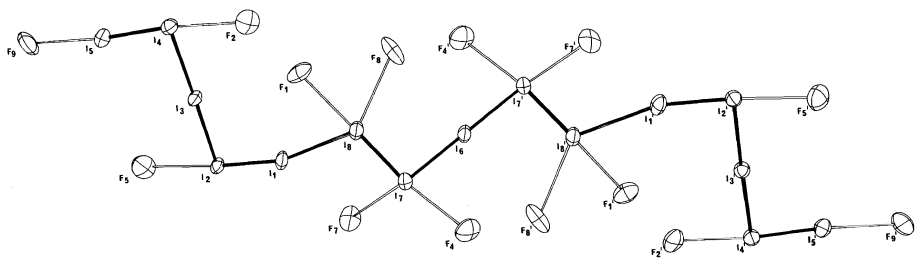

FIG. 2. The configuration of I_{15}^{3+} showing interionic contacts. Crystallographic centre of symmetry at I_6 (0, 1/2, 0).

tions and then refined by least-squares methods. It was found that the shifts generated by the least-squares refinement tended to return the atoms to the centric configuration. No improvement in the *R* value occurred with refinement converging at the significantly poorer *R* value of 0.111. This indicates that the space group had been correctly chosen as $P\bar{1}$.

Results and Discussion

The crystal packing is shown in Fig. 1 and the structure of the iodine cations and the interionic contacts are illustrated in Fig. 2. Appropriate bond lengths and angles are presented in Tables 2 and 3. There are no anion–cation contacts less than 2.98(1) Å (Table 2) suggesting that $I_5^+SbF_6^-$ is predominantly an ionic species. Shorter contacts (2.89(2) Å) have been observed (6) in $I_2^+Sb_2F_{11}^-$ for the more electrophilic I_2^+ ion.

The distance between I(1) and I(8) (3.416(3) Å, Table 2, Fig. 2) is comparable to bonds found between atoms in elemental I_2 (in-plane intermolecular I_2–I_2 distance = 3.496(6) Å, ref. 22) and in some iodine anions (central I—I bond in I_{16}^{4-} = 3.450(3) Å, ref. 23). These are significantly less than the sum of Van der Waals radii for iodine (3.92 Å, ref. 24) and have been considered as weak bonding interactions (22). The next closest iodine–iodine contact is between iodine cations and is essentially at Van der Waals distance (I(5)–I(5′) = 3.906(3) Å, Table 2). Therefore, the centrosymmetric I_{15}^{3+} grouping can be identified (Fig. 2) giving rise to an overall formulation of I_{15}^{3+}-$(SbF_6^-)_3$. This species may gain an extra measure of stability by delocalization of electrons over the larger chain. The two independent I_5^+ units are planar[3] and the angle between each plane and the next is 22.7°, small enough that the I_{15}^{3+} unit itself may be considered very roughly planar. The configuration of the I_5^+ units (and the I_{15}^{3+} as a whole) may reflect some type of π-bond delocalization and/or may minimize electrostatic repulsions.

The two crystallographically independent I_5^+ units, one required by crystal symmetry to be centrosymmetric, contain bond distances and angles that are similar (see Tables 2 and 3). The terminal I—I bonds are comparable with those found in I_2 (22, 25). They have bond distances of 2.666(3)–2.698(2) Å. The central collinear bonds have dis-

[3]Photocopies of table giving least-squares plane through I_5^+ cations may also be obtained, at a nominal charge, from the Depository of Unpublished Data, CISTI, National Research Council of Canada, Ottawa, Ont., Canada K1A 0S2.

TABLE 2. Bond lengths (Å) with estimated standard deviations in parentheses

(*a*) Intramolecular		(*b*) Intermolecular[a]	
Bond	Distance	Bond	Distance
I(1) · · · I(5)		Inter-ionic	
I(5)—I(4)	2.666(3)	I(1)—I(8)	3.416(3)
I(4)—I(3)	2.920(2)	I(2)—I(2′)	3.907(3)
I(3)—I(2)	2.896(2)	I(5)—I(5′)	3.906(3)
I(2)—I(1)	2.698(2)	I(1) · · · I(5)	
I(8) · · · I(8′)		I(5)—F(9)	2.98(1)
I(8)—I(7)	2.680(3)	I(4)—F(2)	2.99(1)
I(7)—I(6)	2.899(2)	I(2)—F(5)	3.03(2)
SbF_6^-		I(8) · · · I(8′)	
Sb(1)—F(1)	1.89(2)	I(8)—F(1)	3.06(2)
—F(2)	1.88(2)	—F(8)	3.40(1)
—F(3)	1.86(1)	I(7)—F(4)	3.01(2)
Sb(2)—F(4)	1.85(2)	—F(7)	3.19(1)
—F(5)	1.83(2)		
—F(6)	1.88(2)		
—F(7)	1.84(2)		
—F(8)	1.87(2)		
—F(9)	1.86(1)		

[a]Included are I—I distances ≤ 4.00 Å, and all I—F distances ≤ 3.40 Å.

tances 2.896(2)–2.920(2) Å and are comparable with bond lengths observed for the symmetric linear I_3^- ion in $(C_6H_5)_4AsI_3$ (26) (2.920(2) Å). We note that the average I—I distance in various symmetric and asymmetric I_3^- ions remains very close to the same value (1). This appears to be true also of $I_5^+SbF_6^-$ (average central bond length I(1) · · · I(5) = 2.908(3) Å, I(8) · · · I(8′) = 2.899(2) Å; average terminal bond length I(1) · · · I(5) = 2.682(3) Å, I(8) · · · I(8′) = 2.680(3) Å). The variation in bond lengths in I_5^+ suggests that it may be described by valence bond structures **I** and **II**

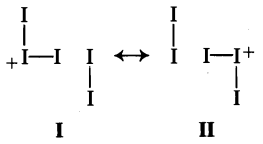

I **II**

giving formal bond orders of 1.0 and 0.5 for terminal and central bonds, respectively. The observed bond angles, similar in both I_5^+ units (Table 3, Fig. 2) are consistent with this model. The angle at I(2), I(4), and I(7) (94 ± 1°) is somewhat smaller than that calculated for I_3^+ from nqr measurements (97.1°, ref. 13) and that observed in the isoelectronic Te_3^{2-} (113.1(2)°, ref. 27) presumably in part because of reduced bond–bond repulsions.

There is weak interaction between the iodines containing the formal positive charge and the fluorines in the anions (Table 2, Fig. 2), whereas the central bridging iodines in both crystallographically different I_5^+ units show no such interaction. However, there are other interactions which involve I_5^+ terminal atoms. (N.B. Resonance structures **III** and **IV** place some positive charge on I(8), see below.) The geometry about I(1) and I(8) would suggest that I(8) donates an electron pair to I(1) (angles of 90° have been found with halogens acting as donors in various adducts and 180° with acceptors (29)). This would lead to some positive charge on I(8). The stereochemistries about all iodine atoms (including I–F contacts less than 3.39 Å and I–I contacts less than 3.90 Å) are consistent with VSEPR theory (28).

Further support for an interpretation of the species as I_{15}^{3+} is found in the minor variations observed in formally similar bond lengths. The terminal I(4)—I(5) bond (2.666(3) Å) of the I_{15}^{3+} unit is significantly shorter than the related I(1)—I(2) and I(7)—I(8) bonds (Table 2). This may be a consequence of the interaction between I(1) and I(8) linking the I_5^+ units and subsequently lengthening the I(1)—I(2) (2.698(2) Å) and I(7)—I(8) (2.680(3) Å) bonds, thus causing them to approach the distance observed in solid I_2 (2.715(6) Å, ref. 22). The I(4)—I(5) bond, being more isolated, is closer to the length found for gaseous I_2 (2.666 Å, ref. 25). Subsequent polarisation may lead to the observed lengthening of I(4)—I(3) and shortening of I(3)—I(2) relative to I(7)—I(6). Perhaps valence bond structures such as **III** and **IV** make a small contribution to the bonding in I_{15}^{3+}.

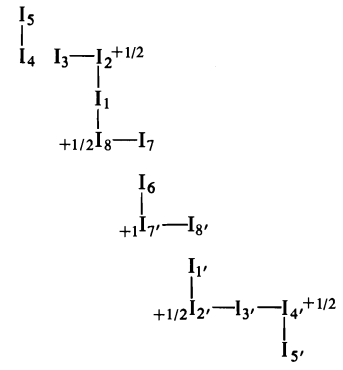

III

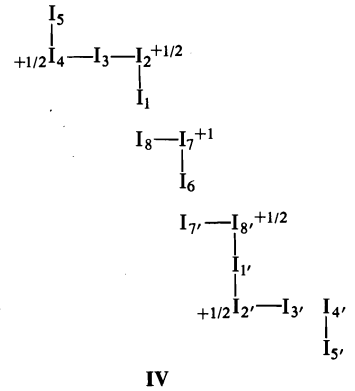

IV

TABLE 3. Bond angles (deg) with estimated standard deviations in parentheses

Bond	Angle	Bond	Angle
SbF_6^-		$I(1)\cdots I(5)$	
F(1)—Sb(1)—F(2)	89.9(7)	I(1)—I(2)—I(3)	93.86(7)
—F(3)	89.9(7)	I(2)—I(3)—I(4)	178.7(6)
F(2)—Sb(1)—F(3)	90.5(7)	I(3)—I(4)—I(5)	93.17(7)
F(4)—Sb(2)—F(5)	178.6(8)	$I(8)\cdots I(8')$	
—F(6)	89.0(9)	I(8)—I(7)—I(6)	94.53(6)
—F(7)	89.1(9)	I(7)—I(6)—I(7′)	180
—F(8)	90.0(8)	Inter-ionic	
—F(9)	90.6(7)	I(2)—I(1)—I(8)	162.88(8)
F(5)—Sb(2)—F(6)	90.4(9)	I(7)—I(8)—I(1)	111.54(7)
—F(7)	91.4(8)	I(1)—I(2)—F(5)	173.5(4)
—F(8)	91.2(8)	I(3)—I(2)—F(5)	80.8(3)
—F(9)	88.1(7)	I(5)—I(4)—F(2)	173.6(4)
F(6)—Sb(2)—F(7)	177.9(9)	I(3)—I(4)—F(2)	80.5(3)
—F(8)	88.9(8)	I(4)—I(5)—F(9)	175.5(4)
—F(9)	89.9(8)	I(6)—I(7)—F(4)	76.4(3)
F(7)—Sb(2)—F(8)	90.2(8)	—F(7)	150.1(4)
—F(9)	91.0(8)	I(8)—I(7)—F(4)	170.4(3)
F(8)—Sb(2)—F(9)	178.6(1.0)	—F(7)	81.8(3)
		F(4)—I(7)—F(7)	107.5(5)
		I(7)—I(8)—F(1)	172.3(3)
		—F(8)	112.3(3)
		I(1)—I(8)—F(1)	70.9(2)
		—F(8)	129.9(3)
		F(1)—I(8)—F(8)	68.9(4)

These would lead to some bonding between I_5^+ units and provide an explanation of the slight lengthening of I(3)—I(4) and I(1)—I(2) and the small shortening of I(2)—I(3) and I(4)—I(5) with respect to the average bond lengths at their respective positions in the I_5^+ cation (see Table 2). Thus the bond distances in the central centrosymmetric I_5^+ unit are 'average', and the asymmetric bond distances are to be found in the outer I_5^+ cations.

We note that, from observation of the number and strength of the I–F contacts (Table 2), the more numerous cation–anion interactions present in the central I_5^+ unit suggest that it possesses more positive character than the terminal units. This would be in keeping with some contribution from valence bond structures **III** and **IV** which place a positive charge of 1.5 on the central I_5^+ cation and 0.75 on each terminal I_5^+ unit.

Both SbF_6^- anions are regular octahedra (average Sb—F distance 1.86 ± 0.02 Å, average F—Sb—F angle 90 ± 1°, Tables 2 and 3). Some variation in Sb—F distance is to be expected as a consequence of varying involvement in cation–anion interactions; however, within the limits of error, no obvious differences were detected.

Acknowledgement

We thank the National Research Council of Canada for financial assistance.

1. K. F. TEBBE. *In* Homatomic rings, chains, and macromolecules of main group elements. *Edited by* A. L. Rheingold. Elsevier Scientific Publishing Co., New York. 1977. p. 551 and references therein.
2. E. H. WIEBENGA, E. E. HAVINGA, and K. H. BOSEWIJK. *In* Advances in inorganic chemistry and radiochemistry. Vol. 3. *Edited by* H. J. Emeléus and A. G. Sharpe. Academic Press, New York. 1961. p. 133 and references therein.
3. A. I. POPOV. Halogen chemistry. Vol. 1. *Edited by* V. Gutmann. Academic Press, New York. 1967. p. 255.
4. R. J. GILLESPIE and J. PASSMORE. *In* Advances in inorganic chemistry and radiochemistry. Vol. 17. *Edited by* H. J. Emeléus and A. G. Sharpe. Academic Press, New York. 1975. p. 49 and references therein.
5. A. J. EDWARDS and G. R. JONES. J. Chem. Soc. A, 2318 (1971).
6. C. G. DAVIES, R. J. GILLESPIE, P. R. IRELAND, and J. M. SOWA. Can. J. Chem. **52**, 2048 (1974).
7. W. W. WILSON, K. C. LEE, P. C. LEUNG, H. IMOTO, and F. AUBKE. American Chemical Society Division of Fluorine Chemistry, 175th ACS National Meeting, Anaheim, California, Abs. 4, March 14, 1978.
8. W. E. FALCONER, N. BARTLETT, L. GRAHAM, A. J. EDWARDS, J. E. GRIFFITHS, and W. A. SUNDER. 6th European Symposium on Fluorine Chemistry, Abs. 17, March 28 – April 1, 1977, Dortmund, Germany.
9. R. D. W. KEMMITT, M. MURRAY, V. M. MCRAE, R. D. PEACOCK, M. C. R. SYMONS, and T. A. O'DONNELL. J. Chem. Soc. A, 862 (1968).
10. C. CHUNG and G. H. CADY. Inorg. Chem. **11**, 2528 (1972).
11. J. PASSMORE and P. TAYLOR. J. Chem. Soc. Dalton, 804 (1976).
12. R. J. GILLESPIE, M. J. MORTON, and J. M. SOWA. *In* Advances in Raman spectroscopy. Vol. 1. *Edited by* J. P. Mathieu. Heyden and Son Ltd., London. 1973. p. 539.
13. D. J. MERRYMAN, J. D. CORBETT, and P. A. EDWARDS. Inorg. Chem. **14**, 428 (1975).

14. M. J. BUERGER. Z. Kristallogr. **109**, 42 (1957).
15. M. J. BUERGER. Z. Kristallogr. **113**, 52 (1960).
16. P. W. R. CORFIELD, R. J. DOEDENS, and J. A. IBERS. Inorg. Chem. **6**, 197 (1967).
17. W. R. BUSING and H. A. LEVY. Acta Crystallogr. **10**, 180 (1957).
18. J. M. STEWART (*Editor*). The X-ray system-version of 1976. Technical Report TR-446 of the Computer Science Centre, University of Maryland, College Park, Maryland.
19. D. T. CROMER and J. B. MANN. Acta Crystallogr. A**24**, 321 (1968).
20. C. H. DAUBEN and D. H. TEMPLETON. International tables for X-ray crystallography. Vol. III. Kynoch Press, Birmingham. 1962. p. 213, Table 3.3.2A.
21. P. MAIN, M. M. WOOLFSON, and G. GERMAIN. Acta Crystallogr. A**27**, 368 (1971).
22. F. VAN BOLHUIS, P. B. KOSTER, and T. MIGCHELSEN. Acta Crystallogr. **23**, 90 (1967).
23. F. H. HERBSTEIN and M. KAPON. J. Chem. Soc. Chem. Commun. 677 (1975).
24. A. BONDI. J. Phys. Chem. **68**, 441 (1964).
25. I. L. KARLE. J. Chem. Phys. **23**, 1739 (1955).
26. J. RUNSINK, S. SWEN-WALSTRA, and T. MIGCHELSEN. Acta Crystallogr. B**28**, 1331 (1972).
27. A. CISAR and J. D. CORBETT. Inorg. Chem. **16**, 632 (1977).
28. R. J. GILLESPIE. Molecular geometry. Van Nostrand, Rheinhold, London. 1972.
29. H. A. BENT. Chem. Rev. **68**, 587 (1968).

The application of DPASV to the determination of the low temperature solubility of lead sulphate in sulphuric acid solutions[1,2]

EUGENE M. L. VALERIOTE[3] AND LLOYD D. GALLOP

Energy Conversion Division, Defence Research Establishment Ottawa, Ottawa, Ont., Canada

AND

PEDRO J. ARAGON[4]

Cominco Product Research Centre, Sheridan Park, Mississauga, Ont., Canada L5K 1B4

Received October 12, 1978

EUGENE M. L. VALERIOTE, LLOYD D. GALLOP, and PEDRO J. ARAGON. Can. J. Chem. **57**, 974 (1979).

Measurements of the solubility of lead sulphate in 35% by weight sulphuric acid, pure water, and at two intermediate acid concentrations have been made over the temperature range 25°C to −50°C using differential pulse anodic stripping voltammetry.

Values of the standard enthalpy of solution, derived from the data and from that of other workers, have been found to be higher than those obtained from emf measurements. The extent of lead sulphate ion pairing is analyzed at 25°C and discussed. The slowness of equilibration of acid solutions supersaturated with lead sulphate was judged of importance in deciding the relevance of the use of thermodynamically calculated lead ion concentrations with respect to lead acid battery mechanisms.

EUGENE M. L. VALERIOTE, LLOYD D. GALLOP et PEDRO J. ARAGON. Can. J. Chem. **57**, 974 (1979).

Nous avons mesuré la solubilité du sulfate de plomb, à des températures variant de −50°C à 25°C, dans une solution d'acide sulfurique à 35%, dans de l'eau pure, et dans deux solutions intermédiaires par la méthode de voltammétrie de décapage anodique à pulsation différentielle.

Des valeurs de l'enthalpie standard de solution, derivées de nos données et de celles d'autres chercheurs, étaient plus hautes que celles obtenues par la mesure de forces électromotrices. Nous avons analysé et étudié le degré de formations de paires d'ions de sulfate de plomb à 25°C. On a jugé que la lenteur de mise à l'équilibre des solutions acides, sursaturées en sulfate de plomb, était importante pour décider de la pertinence de l'usage des concentrations de l'ion de plomb, calculées thermodynamiquement en regard du mécanisme de l'accumulateur de type plomb-acide.

Introduction

Information on the low temperature solubility of lead sulphate is of importance to the understanding of the reaction processes involved in the operation of lead acid batteries under conditions of severe cold. For reasons that are not yet established, the lead acid battery, at very low temperatures (≤ -30°C), is incapable of accepting recharge at acceptably rapid practical rates. It has been suggested that the electrochemical reactions of both the $PbSO_4/PbO_2$ positive electrode (1) and the $Pb/PbSO_4$ negative electrode (2) are related to the solution rate of lead sulphate and that the precipitation or dissolution of $PbSO_4$ is controlled by its solubility. Although the evidence is stronger for a dissolution–precipitation mechanism at the negative than at the positive electrode, both mechanisms appear to be very complicated (3–6), giving rise to a need for low temperature lead sulphate solubility and dissolution rate data.

Measurements of lead sulphate solubility do not appear to have been made at temperatures below 0°C, and particularly not at temperatures near the freezing points of concentrated H_2SO_4 solutions, although the need for such data is clear (7). Lead sulphate solubilities have been determined as a function of sulphuric acid concentrations in the temperature range of 0 to +50°C (8–14).

A method based on the reaction of dissolved lead with dithizone to form a coloured complex which could be detected photometrically (8, 9) gave good agreement with iodometric determination of lead, following evaporative concentration of dissolved lead chromate (10). Other methods (11–13) also agreed well, except for the lead chromate-colorimetric method of Crockford and Brawley (14), where

[1]Prepared for presentation at International Conference on Modern Electrometric Techniques for Investigating Chemical Systems, at Carleton University, July 13–16, 1976.

[2]DREO Report No. 802.

[3]To whom all correspondence should be addressed. Present address: Cominco Product Research Centre, Sheridan Park, Mississauga, Ont., Canada L5K 1B4.

[4]Present address: Instituto de Investigaciones Petroleras, Edificio Los Chaguaros, Avda, 5 de Julio Con 9B, Appartado 98, Maracaibo, Venezuela.

0008-4042/79/090974-08$01.00/0

competition between chromate and sulphate ion pairing may be the cause of the low values in the range of 0.5–50% acid.

In order to understand the role of dissolved lead at very low temperatures, a knowledge of its concentration is required. This may be estimated by application of the van't Hoff equation, using values of ΔH obtained from solubility measurements at higher temperatures, as has been done in order to interpret the low temperature charging kinetics of anodic films on lead in sulphuric acid solutions (5). However, the validity of such an extrapolation remains to be demonstrated experimentally.

The previous methods cited were not sufficiently sensitive to determine lead quantitatively at concentrations much less than 1 ppm, whereas at −50°C, concentrations of the order of 40 ppb might be expected on the basis of extrapolation of the van't Hoff expression, using the Craig and Vinal data (8). However, measurement of such low concentrations of lead are well within the capability of modern analytical techniques such as atomic absorption spectroscopy (AA) and stripping voltammetry and both methods were assessed for the present work. Although AA was a suitably sensitive method for analysis of lead in pure (acidified) water, strong interference by sulphuric acid was observed at the two strongest lead absorption wavelengths (283.2 nm and 217.0 nm) and this technique was abandoned. However, it has been used successfully recently in a study (15) in which micro-aliquots of sulphuric acid were evaporated to dryness prior to atomization of the residual lead.

Of the various stripping voltammetry methods, differential pulse anodic stripping voltammetry with deposition at a hanging mercury drop electrode (HMDE) was chosen for reasons of required accuracy, minimal deposition time, and availability of equipment.

Experimental

The concentrations of lead sulphate in water and in aqueous sulphuric acid solutions, equilibrated at various temperatures, were determined using differential pulse anodic stripping voltammetry (DPASV) at a hanging mercury drop electrode, calibrated by determination of standard solutions containing known quantities of lead (16). The work was carried out cooperatively at the Defence Research Establishment Ottawa (DREO) and at the Cominco Product Research Centre (CPRC), using essentially the same methods but with some differences of detail as discussed below. At CPRC lead sulphate solubilities were determined in pure water and in three concentrations of sulphuric acid: 0.1, 1.0, and 4.4 *M* at temperatures from 25°C to near the freezing point of the solutions, or to −40°C for 4.4 *M* acid. At DREO measurements were also made for pure water and a more extensive study of 35% sulphuric acid was carried out covering a temperature range from +25°C to −50°C.

Apparatus and Instrumentation

A Princeton Applied Research Corporation polarograph (PARC Model 174A), with HMDE and polarographic cell, was used. At DREO the reference electrode was $Hg/Hg_2SO_4/35\%\ H_2SO_4$ and at CPRC a PARC saturated calomel electrode was used. The pulse (25 mV pp) was superimposed on a 2 mV/s potential scan. The current was sampled at the end of, and immediately before, the application of each pulse and the difference was recorded on a suitable *x–y* or *x–t* recorder.

Thermostatted ethanol–water baths (FTS Multicool, FTS Systems Inc., Stone Ridge, NY) were used to equilibrate solutions (±0.3°C). A magnetic stirrer, built into the bath, was used to stir the solution by means of a magnetic bar in the 1 L glass (DREO) or 500 mL polyethylene (CPRC) bottle. In later experimental work at DREO, this stirrer failed and periodic manual agitation was required during the lengthy equilibration periods. The same magnetic stirrer stirred both the solution and the bath fluid at CPRC, but at DREO, a paddle stirrer was used for the bath so that stirring of the solution and the bath fluid were independent.

Chemicals and Purity

Standard solutions of acidified lead nitrate were made up using high purity (<1 ppb Pb) nitric acid (Baker Ultrex®) and water which was prepared by multiple distillation, pyrodistillation (17), deionization, pre-electrolysis, or a combination of these. The standard solutions and the solvent were periodically checked by comparison of new standard solutions with older ones or by blank runs on solutions containing no added lead, using AA or DPASV. The lead concentrations of the solvent water were generally less than 2 ppb. Reagent or analytical grades of $PbSO_4$, $PbNO_3$, and sulphuric acid were normally used. For runs with added chloride or for blank determinations in sulphuric acid, Baker ULTREX® acids (<1 ppb Pb) were used. Care was taken to ensure that all solutions containing lead were acidic (pH < 2) at all times, whether they were in glass or polyethylene containers, to prevent significant lead adsorption on container surfaces (18).

At DREO, the polarographic cell and all glassware were soaked in 30% nitric acid for several hours and rinsed in lead-free (<1 ppb) distilled water before each use and the cell was dried in a vacuum oven following the final rinse. At CPRC, blank determinations were repeated for dilute nitric acid solutions following the rinse step until the DPASV lead peak reached a steady value characteristic of less than 3 to 4 ppb Pb before proceeding to the analysis of the unknown samples.

Mercury was triply distilled, with further prior purification steps at DREO such as passage through a pin-hole filter, agitation with an air stream under dilute nitric acid and a Hulett distillation procedure (19). Nitrogen for deoxygenation was scrubbed, by passage through vanadous chloride solutions (20) and water, before admission to the cell. Disposable Eppendorf pipettes were used for transfer (spiking) of standard solutions.

Analytical Procedures

At each temperature of the study, sulphuric acid solutions containing excess solid lead sulphate were equilibrated with continuous and intermittent stirring. From time to time, samples were withdrawn for analysis following a settling period during which the solutions were not stirred. At DREO 1 mL samples were withdrawn through a medium-porosity fritted disc after an overnight stand without stirring. At CPRC, to avoid excessive temperature excursions, due to the ganging of the two

stirring systems, settling times of only 5 to 10 min were allowed. For 35% acid, a relatively inefficient glass wool – filter paper – glass wool filtration system was used at CPRC but this was changed to a medium-porosity fritted disc and filter paper for the lower acid concentrations. For the 35% H_2SO_4 solutions it was found necessary to dilute the sample 10- to 20-fold in order to eliminate background noise and loss of reproducibility. Accordingly at DREO, the 1 mL samples were added to 20 mL of water in the polarographic cell. At CPRC for the lower concentrations of acid, 12 mL samples were withdrawn, the first being used to rinse the sampling system and the second being added to the cell or transferred to a polyethylene storage bottle containing 4 drops of concentrated ULTREX® nitric acid.

Dilution of the sample of 35% acid carried with it the disadvantage of necessitating a correction for the lead contributed by the dilution water, which was done in three ways. Firstly, in most of the early determinations, this correction (~1 ppb) was obtained for the dilution water, acidified with ULTREX® nitric acid directly. In the second method, two 1 mL aliquots of the unknown were added to the solution and determinations made after each addition. The difference in currents between the second and first aliquot could then be taken as due to the second aliquot only. The results using both methods agreed within experimental error.

Finally a third method of eliminating background and other dilution water contributions to the measured current was used for the last analyses of 35% H_2SO_4 at 25°C, 0°C, −20°C, and −40°C. This emerged as the method of preference. Twenty mL of 0.5 *M* ULTREX® hydrochloric acid solution was added to the polarographic cell and degassed for at least 45 min by nitrogen bubbling through the cell. The HCl was added to desorb organic contaminants which may have been adsorbing on the mercury drop and causing spurious results, due to variations of electroactive area, from run to run. It has been shown (21) that many organic molecules which are adsorbed from sulphate solutions at the potential of the lead peak are desorbed in chloride solutions.

One or two aliquots of standard solution were added to the supporting electrolyte before addition of 1 mL of the unknown, followed by at least three more standard additions. Without such prior additions of lead, sensitivity often appeared to change subsequent to addition of the unknown. After each addition, lead was deposited on the mercury drop at a uniform stirring rate and for a fixed selected potential and time. The differential pulse polarograms were then run at room temperature. Some typical results obtained for samples from solutions of 35% sulphuric acid equilibrated at −40°C are shown in Fig. 1. The differences between the peak current in the solutions containing the unknown plus the standard additions and the peak current immediately prior to the addition of the unknown are plotted against the lead added to the unknown as standard additions. The intercept at zero then gives the concentration of lead in the unknown, which must then be corrected for the dilution factor. Thus the concentrations shown are those in the polarographic cell; the concentration in the 1 mL sample of unknown before dilution was approximately 20 times larger than shown by the intercept.

The third procedure (described above) appeared to give the best reproducibility and most constant detection sensitivity during a series of lead additions (such as in Fig. 1). Furthermore it automatically corrected for any residual lead contributed by the dilution water. For these reasons it was found to be the preferred method, although it was only used for a limited part of the work (see Fig. 2).

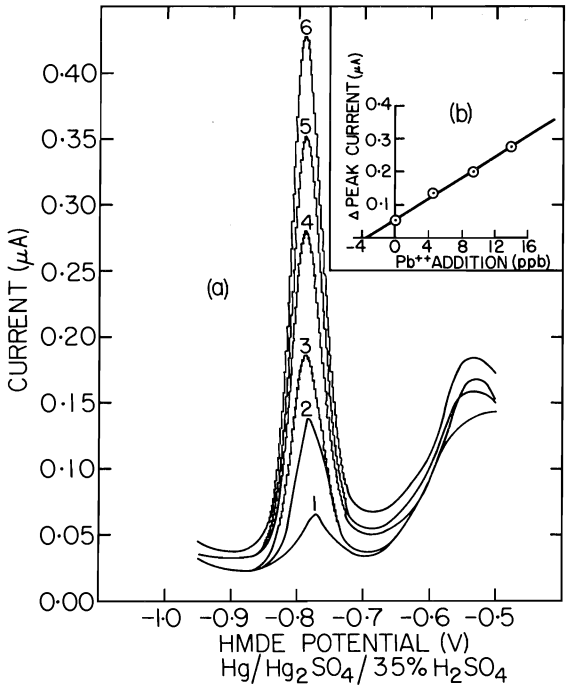

FIG. 1. (*a*) Plots of experimentally observed pulsed anodic stripping scans for 20 mL solutions of 0.5 *M* HCl supporting electrolyte, degassed for 45 min using N_2 passed through a vanadous chloride scrubber with no addition (*1*) and with additions of 10 μL of a $PbNO_3$ standard solution (0.0100 g/L lead), i.e. 1.00×10^{-7} g of lead (*2*); plus 1 mL of 35% sulphuric acid, saturated with $PbSO_4$ at −40°C (*3*); plus three more 10 μL additions of the standard lead nitrate solution (*4*, *5*, and *6*). (*b*) Plot of current peak heights for peaks *3* to *6* minus the peak height of peak *2*, from (*a*) vs. the increment by standard addition of concentration of lead to the 20 mL solution containing the unknown lead sulphate aliquot (i.e. peak *3* is plotted as zero added lead).

Results and Discussion

Treatment of Data

For the equilibrium

[1] $$PbSO_4(s) \rightleftharpoons Pb^{2+}(aq) + SO_4^{2-}(aq)$$

the solubility product at constant pressure can be shown (22) to vary with temperature according to a form of the van't Hoff isochore:

[2] $$[\mathrm{d} \ln K_{sp}/\mathrm{d}(1/T)]_P = -\Delta H^0/R$$

for ideal solutions where ΔH^0 is the standard enthalpy of solution.

This equation can be rewritten as:

[3] $$\left(\frac{\mathrm{d} \ln C_{Pb^{2+}(satn)}}{\mathrm{d}(1/T)}\right)_P + \left(\frac{\mathrm{d} \ln C_{SO_4^{2-}(satn)}}{\mathrm{d}(1/T)}\right)_P + \left(\frac{\mathrm{d} \ln \gamma_\pm^{\,2}}{\mathrm{d}(1/T)}\right)_P = -\frac{\Delta H^0}{R}$$

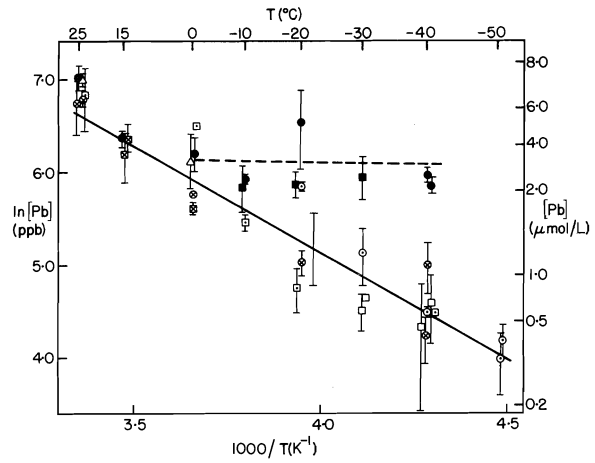

FIG. 2. Logarithm of experimentally determined values of saturation lead concentration in 35% sulphuric acid as a function of reciprocal equilibration temperature: data of Craig and Vinal (8), △; CPRC data for solutions previously equilibrated at a higher temperature, ●, or a lower temperature, ■; DREO data for solutions previously equilibrated at a higher temperature, ⊙, or at a lower temperature, ⊡, and containing no chloride; DREO data for solutions previously equilibrated at a higher temperature, ⊗ or at a lower temperature, ⊠, determined in 0.5 *M* HCl solutions. Right hand ordinate scale refers to volume at 25°C.

where $\gamma_{\pm}$ is the stoichiometric mean molal activity coefficient of $PbSO_4$.

If concentrations are expressed as molal quantities (or on any other weight basis) the analytical concentration of sulphate will be negligibly dependent on temperature in sulphuric acid which is sufficiently concentrated that the contribution to the total sulphate concentration due to lead sulphate dissociation is negligible. Then if the temperature coefficient of $\gamma_{\pm}$ can be neglected, the following approximation is obtained

$$[4] \qquad \left(\frac{\mathrm{d} \ln C_{Pb^{2+}(satn)}}{\mathrm{d}(1/T)}\right)_P \simeq -\frac{\Delta H^0}{R}$$

In pure water, the first two terms of eq. [3] contribute equally to ΔH^0 and the third term represents the variation of interionic forces with temperature, including ion-pairing effects. In sulphuric acid solutions, where the main source of sulphate ion is the acid, the third term will also include acid association effects.

From a plot of $\ln C_{Pb^{2+}(satn)}$ vs. $1/T$, ΔH^0 can be estimated from the slope according to eq. [4]. The value of the slope will be $-\Delta H^0/R$ in moderately concentrated acid solutions and $-\Delta H^0/2R$ (by comparison with eq. [3]) in pure water.

The analytical results obtained for 35% sulphuric acid solutions saturated with lead sulphate are given in Fig. 2. The points represent sets of experimental results grouped according to the supporting electrolyte (presence of chloride or quantity of sulphuric acid added), and modifications of experimental technique or chronology. The solid straight line was obtained from a linear regression analysis of 81 concentrations, experimentally determined at DREO. A correlation coefficient of -0.91 was obtained with a slope of $2.29 \pm 0.23R$ at the 95% confidence level, corresponding to a value of $\Delta H^0 = 4.56 \pm 0.46$ kcal mol^{-1}.[5] The standard error about the central point is indicated by the vertical bars. Where the point plotted represents an average of at least three experimental determinations, the standard deviation is indicated by vertical bars. Where no bars appear the point represents only two determinations.

Results obtained at CPRC and by Craig and Vinal, using a dithizone method (8), are also shown for comparison. At temperatures of 0 to -40°C (broken line) there is very little correlation (correlation coefficient $= -0.26$) between the solubilities (determined at CPRC) and temperature. The correlation improves but remains poor (-0.47) if the 15°C data are included. This is probably due to inadequate settling time (5–10 min) and inadequate filtration, resulting in the inclusion of suspended lead sulphate in the sample. As noted previously, the filtration system was changed for later CPRC work, for which $PbSO_4$ concentrations were much higher; inclusion of suspended lead did not appear to be a problem at the lower H_2SO_4 concentrations and at high temperatures. Reasonably close agreement with the dithizone method (8) was obtained at 0 and 25°C.

When the linear regression analysis was repeated, including the Craig and Vinal (8) and the CPRC data for 0–25°C, along with the 24 DREO points plotted in Fig. 2, a correlation coefficient of -0.95 was obtained giving a value of $\Delta H^0 = 4.74 \pm 0.61$ (95% confidence). Even at the 75% confidence level, where the estimated error term is one-half that given, these two samples are insignificantly different.

Results obtained for the three sulphuric acid concentrations and for pure water, in the temperature range of 0 to 25°C, are similarly plotted and compared with literature values in Fig. 3. Because of the limited number of points, the uncertainties in ΔH^0 given are at the 75% confidence level. There is no statistically significant dependence of ΔH^0 on concentration within the limits of experimental uncertainty. Thus a reasonable estimate of lead sulphate solubility at a sulphuric acid concentration in the

[5] 1 kcal = 4.1840 kJ.

range of 0 to 4.5 M and 0 to 25°C would be obtained by application of the van't Hoff isochore using $\Delta H^0 = 5.6 \pm 0.5$ kcal mol^{-1} and an experimental value of solubility for the same acid concentration at only one temperature. A somewhat more accurate estimate to include temperatures below 0°C, and for acids of battery strength, would be obtained from a value of $\Delta H^0 = 4.7 \pm 0.3$ kcal mol^{-1} (75% confidence).

Although the larger errors in the higher temperature data of Fig. 3 make it impossible to determine a concentration dependence of ΔH^0, the more precise data of Fig. 2 may correspond to a genuinely lower value of ΔH^0 in 4.5 M acid, compared to 1.0 M acid or less.

All of these values of ΔH^0 are appreciably higher than the value of 3.0 kcal mol^{-1} derived from emf (23) measurements or from standard heats of formation (24). Even for the case of lead sulphate in pure water, which one might expect to most closely obey the Debye–Hückel theory, and therefore give values of ΔH^0 most comparable to those from emf data, measurements of the temperature dependence of solubility in the range 0 to 25°C consistently yield values of ΔH^0 greater than those derived from emf measurements. From solubility determinations by five groups of workers, using gravimetric and conductivity methods, over the range 0 to 25°C (11), a value of $\Delta H^0 = 5.9$ kcal mol^{-1} can be calculated. Determinations by other groups using a lead chromate-iodometric method (10, 11, 14) yield values of $\Delta H^0 = 4.0$ kcal mol^{-1} over the range 0 to 35°C but 3.6 kcal mol^{-1} for 25 to 50°C.

This discrepancy cannot be explained as due to increasing non-ideality of solution as temperature decreases, which might have made neglect of the third term of eq. [3] unjustified. If $\gamma_\pm$ becomes smaller as the temperature decreases, due to increased ion pairing for example, or as predicted by Debye–Hückel theory, neglect of this term would yield values of ΔH^0 smaller than the true values, since the third term of eq. [3] would be negative. Nor can the discrepancy be explained as due to insufficient equilibration of solutions or uptake of suspended lead sulphate in the samples, since both these experimental problems would cause a reduced dependence of measured lead content on temperature and (again) a smaller derived value of ΔH^0 than the true value. Thus the discrepancy would become even larger if the temperature coefficient of $\gamma_\pm$ could not be neglected.

One possible reason for the discrepancy may be related to some unreliability of the temperature coefficient of the standard emf of the lead – lead sulphate electrode, on which the value of $\Delta H^0 = 3.0$ kcal mol^{-1} appears to be based. Harned and Hamer (25), whose work yields a value of 2.9 kcal mol^{-1}, formed an adverse opinion of the reliability of this electrode in acid solutions (26). This may be related to the formation of oxides or basic sulphates beneath the oxide layer (4, 6). Other emf measurements on the lead – lead sulphate electrode and the lead amalgam – lead sulphate electrode (26) yield values of ΔH^0 of 3.7 and 3.8 kcal mol^{-1}, respectively.

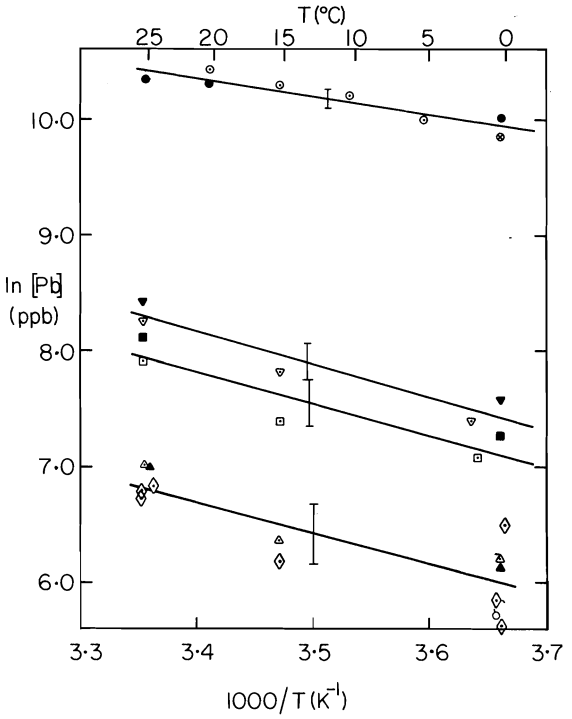

FIG. 3. Logarithm of lead concentration in water and in sulphuric acid solutions saturated with lead sulphate at various temperatures. Water: ●, from refs. 10, 14; ⊗, from ref. 12; ⊙, CPRC data; – slope × $2R = \Delta H^0 = 6.2 \pm 1.4$ kcal mol^{-1} for fitted least-squares line (75% confidence level). 0.1 M H_2SO_4: ■, from ref. 8; ⊡, CPRC data; – slope × $R = \Delta H^0 = 5.4 \pm 1.9$ kcal mol^{-1}. 1.0 M H_2SO_4: ▼, from ref. 8; ▽, CPRC data; – slope × $R = \Delta H^0 = 5.6 \pm 1.5$ kcal mol^{-1}. 35% (4.5 M) H_2SO_4: ▲, from ref. 8; △, CPRC data; ◇, DREO data; – slope × $R = \Delta H^0 = 5.2 \pm 1.2$ kcal mol^{-1}.

Since there appears to be good reason to believe that the value of $\Delta H^0 = 4.7 \pm 0.6$ kcal mol^{-1} (95% confidence level) obtained from Fig. 3 is not too high, some re-examination of the E^0 values may be in order to resolve the discrepancy.

Ion Pairing Effects

The probable effect of change of degree of ion pairing with temperature on the calculated values of ΔH^0 has already been indicated. In the experimental work described, the concentration of free unpaired

TABLE 1. Lead sulphate solubility as a function of sulphuric acid concentration

$[H_2SO_4]$ (mol L^{-1})	Experimental $PbSO_4$ solubility (mol L^{-1})	$(f_\pm)_a$	$[SO_4^{2-}]$ $([SO_4^{2-}]_a + \alpha C_{Pb})$ (mol L^{-1})	Calculated assuming (33): log $K_{assn} = 2.4$		
				$f_\pm$	α	$[Pb^{2+}]$ αC_{Pb} (mol L^{-1})
0.000	1.46×10^{-4}	0.860	1.42×10^{-4}	0.886	0.973	1.42×10^{-4}
0.001	3.46×10^{-5}	0.716	8.96×10^{-4}	0.760	0.885	3.06×10^{-5}
0.005	2.18×10^{-5}	0.484	3.10×10^{-3}	0.536	0.817	1.78×10^{-5}
0.010	1.70×10^{-5}	0.432	5.01×10^{-3}	0.493	0.766	1.30×10^{-5}
0.050	1.52×10^{-5}	0.263	0.015	0.307	0.738	1.12×10^{-5}
0.100	1.62×10^{-5}	0.178	0.030	0.208	0.754	1.22×10^{-5}
0.500	2.01×10^{-5}	0.074	0.142	0.0832	0.802	1.61×10^{-5}
1.00	2.20×10^{-5}	0.051	0.275	0.0566	0.819	1.80×10^{-5}
3.0	1.28×10^{-5}	0.036	0.98	0.0428	0.689	8.82×10^{-6}
4.5	6.65×10^{-6}	0.041	1.40	0.0651	0.401	2.67×10^{-6}
7.11	3.56×10^{-6}	0.049	1.90	$\rightarrow \infty$	$\rightarrow 0$	$\rightarrow 0$

ions in the sulphuric acid solutions was measured using DPASV by means of calibration using lead nitrate standard additions for which the degree of ion pairing would be expected to be small. The 35% acid was diluted by a factor of at least 10 and normally 20 for DPASV analyses in order to reduce the concentration of ion pairs as much as possible, yet retain a sufficiently concentrated total lead content to permit precise analyses. Other researchers cited, complexed the lead as dithizone (8, 9), or precipitated the lead and determined it as lead chromate (10, 13, 14). In spite of the different methods used, generally good agreement between this work and that of other workers was obtained with the exception of the gravimetric study of Crockford and Brawley (14) for sulphuric acid solutions. (Their results for pure water, however, were obtained by iodometric titration of the chromate and were in good agreement with other determinations.)

In order to assess the extent and importance of ion pairing at 25°C, the overlapping and consistent experimental data of Craig and Vinal (8) and Purdum and Rutherford (10) for lead sulphate solubility as a function of sulphuric acid concentration were used. The latter data, obtained at 20°C, were corrected to 25°C using an equation of the form of eq. [4] for the correction. The values are given in Table 1 as a function of sulphuric acid concentration. These are also shown in Fig. 4, as a plot similar to that given by Craig and Vinal (8) although their temperature correction to the Purdum and Rutherford data was somewhat less theoretically based than that used here.

From the experimentally determined lead solubility, it is possible to calculate the apparent mean ionic activity coefficient $(f_\pm)_a$ from the solubility product,

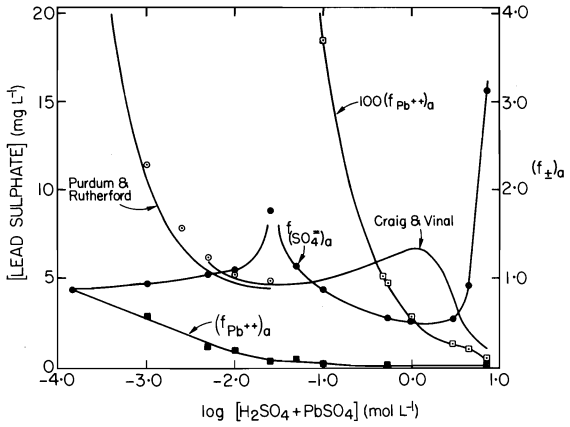

FIG. 4. Values of lead sulphate solubility as determined by Craig and Vinal (8) at 25°C (solid curve) and Purdum and Rutherford (10) at 20°C corrected to 25°C using a van't Hoff isochore for extrapolation (solid curve) or a linear extrapolation (8) (open circles). Values of calculated apparent ionic activity coefficients (see text) for sulphate ion (●), lead ion (■), and lead ion expanded 100 times (⊡).

using values of the sulphate ion concentration (27) determined by Raman spectroscopy (28–30).

$$[5]\quad K_{sp} = a_{Pb^{2+}}a_{SO_4^{2-}} = (f_\pm)_a^2 C_{Pb}[SO_4^{2-}] = 1.585 \times 10^{-8}\ \text{mol}^{-2}\ \text{L}^{-2}$$

The term $(f_\pm)_a$ is an apparent value as is the apparent concentration of lead ion C_{Pb}, which is the sum of the concentrations of free lead ions and of ion pairs in solution:

$$[6]\quad C_{Pb} = [Pb^{2+}] + [PbSO_4]_{aq}$$

Thus $(f_\pm)_a$ absorbs any errors due to a lack of knowledge of ion pairing by treating the electrolyte as if only unpaired ions existed. The values of $(f_\pm)_a$

so calculated are given in the third column of Table 1. From the stoichiometric mean molal activity coefficients for sulphuric acid solutions (31), a formal sulphate ion activity can be calculated, which can be combined with the solubility product to give a value of lead ion activity. From the spectroscopically determined sulphate ion concentrations and the measured lead solubilities, formal values of the apparent lead and sulphate mean ionic activity coefficients, respectively, can be calculated. These have been plotted in Fig. 4.

Ion pairing can be taken into account explicitly, and values of $f_\pm$ (for free ions) can be calculated, given a value for the association constant of lead sulphate

$$[7] \quad K_{assn} = [PbSO_4]_{aq}/(f_\pm)^2[Pb^{2+}][SO_4^{2-}]$$

for the equilibrium

$$\begin{matrix} & (1-\alpha)C_{Pb} & \alpha C_{Pb} & [SO_4^{2-}] \\ [8] & PbSO_4(aq) & \rightleftharpoons Pb^{2+}(aq) & + SO_4^{2-}(aq) \end{matrix}$$

where, for an ionization constant of the ion pair, α, the concentrations of each species are indicated above the equation. Then

$$[9] \quad K_{assn} = (1-\alpha)/\alpha(f_\pm)^2[SO_4^{2-}]$$

where

$$[10] \quad [SO_4^{2-}] = [SO_4^{2-}]_a + \alpha C_{Pb}$$

i.e. the sum of sulphate ion contributed from the sulphuric acid solution and that contributed by the dissociation of lead sulphate, and

$$[11] \quad K_{sp} = \alpha (f_\pm)^2 C_{Pb} [SO_4^{2-}]$$

Equations [9] to [11] can be solved directly to obtain values of $f_\pm$ and α:

$$[12] \quad \alpha = 1 - [K_{sp}K_{assn}/C_{Pb}]$$

$$[13] \quad f_\pm = (K_{sp}/\alpha C_{Pb}[SO_4^{2-}])^{1/2}$$

although at concentrations of H_2SO_4 between 0.000 and 0.001 M, where the terms on the right hand side of eq. [10] would be comparable to one another, an iterative process might be necessary to obtain values of $f_\pm$ and $[SO_4^{2-}]$. A value of the association constant, given by $\log K_{assn} = 2.4$ (32), is independently available from conductivity and radiochemical solubility measurements of $PbSO_4$ in water and Na_2SO_4 solutions (29). The values for $[SO_4^{2-}]$, $f_\pm$, and α, so obtained, are given in columns 4 to 6 of Table 1. In column 7, the concentration of unpaired lead is also given.

It is apparent from Table 1 that at concentrations of sulphuric acid greater than 0.1 M, more than 25% of the lead in solution is bound up in ion pairs and that in battery strength acid, more than half is so bound. The formation of these neutral complexes in solution has been found to be slow (29) in agreement with our observations that several days of continuous stirring or several weeks of intermittent stirring were necessary before obtaining time-invariant solubilities. For example the lowest solubility point at -40°C in Fig. 2 was an average for solutions previously at 25°C and equilibrated for 3 to 7 weeks at -40°C; during this time the measured solubilities decreased from 82 ppb after 22 days of equilibration to 56 ppb at 33 days and 51 ppb at 47 days. This would suggest that if the values of measured solubility at very low temperatures are in error, they are too high for solutions previously at higher temperatures and in such a case the value of ΔH^0 estimated is too low. The time required for equilibration following an increase in temperature or dilution of the sample seemed to be less. There was no apparent increase of the peak current with time for successive scans, following dilution of the 1 mL unknown sulphuric acid aliquot by the 20 mL of acidified water in the polarographic cell which one might expect if ion pair dissociation was a slow process.

The values of apparent ionic activity coefficient for sulphate ion, given in Fig. 4, are not altered if $f_\pm$ values are used instead of $(f_\pm)_a$. However, the values of $f_{Pb^{2+}}$ will be greater than those of $(f_{Pb^{2+}})_a$ according to the equation

$$[14] \quad f_{Pb^{2+}} = (f_{Pb^{2+}})_a/\alpha$$

The curve for the lead ionic activity coefficient in Fig. 4 would be increased somewhat at high concentrations of acid if $(f_{Pb^{2+}})_a$ were replaced by $f_{Pb^{2+}}$. However, this will not substantially alter the basic interpretation of the relationship between solubility and activity coefficients which can be drawn from the graph.

Thus the solubility minimum, near 0.025 M H_2SO_4, is due to a strong maximum in the sulphate ion activity, prior to which the common ion effect determines lead solubility. The lead solubility then increases up to an acid concentration of about 1 M because the decreasing sulphate ionic activity coefficient causes a decrease in sulphate activity despite its increasing concentration. There is a minimim in the sulphuric acid activity coefficient at about 1.7 M (30) however, so that sulphate activity increases once again at higher concentrations leading to a further decrease of lead solubility after the maximum.

Summary and Conclusions

The temperature dependence of lead sulphate solubility in 35% sulphuric acid has been determined down to -50°C and confirmed for other acid concentrations and for pure water. Solubility data deter-

mined using DPASV, as well as for those using other analytical methods, appear to give larger positive values of the standard enthalpy of solution, as obtained by application of the van't Hoff equation, than have been obtained from emf data. Values of saturation lead ion and lead sulphate ion pair concentrations at 25°C have been calculated. The data for 35% sulphuric acid are not sufficiently precise to state that ΔH^0 is completely independent of temperature over the temperature range of 25°C to −50°C studied. If subsequent work confirms the linearity of Fig. 4 with greater accuracy, however, the temperature-independent ΔH^0 value may suggest that the degree of ion pairing is independent of temperature since, due to the experimental technique, the measured lead is the sum of paired and unpaired lead in solution. Alternatively, increased ion pairing at lower temperatures may be compensated for by other factors such as shifts of hydration or bisulphate dissociation equilibria.

The lengthy equilibration time required to attain constant concentrations raises a question of the significance of using thermodynamic values of lead sulphate solubilities in trying to interpret lead acid battery behaviour. Based on the present observations, solutions in a battery might exist for days or weeks in a state of supersaturation with respect to lead sulphate, following a discharge or a reduction of temperature. However, the higher surface area (per unit electrolyte volume) of lead sulphate crystals in battery plates might provide more effective equilibration than observed in the solutions studied here. Only accurate measurements of lead sulphate solubility at various temperatures, and with samples from actual batteries, can resolve this question. In the meantime it must be assumed that the kinetics of lead sulphate dissolution and precipitation are of at least as much importance in discussing battery reactions as are the thermodynamics and that assumptions of thermodynamically calculated lead concentrations must be made with caution.

Acknowledgements

The AA analyses done by Dr. E. Samuels, Bureau of Chemical Hazards, Health and Welfare Canada are gratefully acknowledged, as is the advice of Professor H. W. Nürnberg, Institute of Applied Physical Chemistry, Nuclear Research Centre (KFA), Juelich, Federal Republic Germany, who suggested the addition of chloride to the supporting electrolyte.

1. E. Willihnganz. Power sources 5. Proc. 9th Int. Symp. Brighton, 1974. *Edited by* D. H. Collins. Academic Press, London. 1975. p. 43.
2. D. Berndt. Power sources 2. Proc. 6th Int. Symp. Brighton, 1968. *Edited by* D. H. Collins. Pergamon Press, London. 1970.
3. E. M. L. Valeriote and L. D. Gallop. Power sources 5. Proc. 9th Int. Symp. Brighton, 1974. *Edited by* D. H. Collins. Academic Press, London. 1975. p. 55.
4. E. M. L. Valeriote and L. D. Gallop. J. Electrochem. Soc. **124**, 370 (1977).
5. E. M. L. Valeriote and L. D. Gallop. J. Electrochem. Soc. **124**, 380 (1977).
6. T. G. Chang, M. M. Wright, and E. M. L. Valeriote. Power sources 6. Proc. 10th Int. Symp. Brighton, 1976. *Edited by* D. H. Collins. Academic Press, London. 1977; DREO Report No. 753, February 1977.
7. P. Ruetschi. Power sources 5. Proc. 9th Int. Symp. Brighton, 1974. *Edited by* D. H. Collins. Academic Press, London. 1975. p. 71.
8. D. N. Craig and G. W. Vinal. J. Res. Natl. Bur. Stand. **22**, 55 (1939).
9. I. M. Kolthoff, R. W. Perlich, and D. Weiblen. J. Phys. Chem. **46**, 561 (1942).
10. R. B. Purdum and H. A. Rutherford. J. Am. Chem. Soc. **55**, 3221 (1933).
11. A. Seidell. Solubilities of inorganic and metal organic compounds. Vol. 1. 3rd ed. D. Van Nostrand Co. Inc., New York. 1940. p. 1409.
12. A. Seidell and W. F. Linke. Solubilities of inorganic and organic compounds. Supp. to 3rd ed. D. Van Nostrand Co. Inc., New York. 1952. p. 509.
13. M. Huybrechts and H. Ramelot. Bull. Soc. Chim. Belg. **36**, 239 (1927).
14. H. D. Crockford and D. J. Brawley. J. Am. Chem. Soc. **56**, 2600 (1934).
15. F. J. Langmyhr and J. T. Håkedal. Anal. Chim. Acta, **83**, 127 (1976).
16. H. Siegerman and G. O'Dom. American Laboratory, June (1972); Princeton Applied Research Corporation Application Note AN-107; J. B. Flato. Anal. Chem. **44**, 75A (1972).
17. E. E. Criddle. Proc. Symp. Oxide-Electrolyte Interfaces. *Edited by* R. S. Alwitt. Electrochem. Soc. Princeton, NJ. 1973. p. 200.
18. A. W. Struempler. Anal. Chem. **45**, 2251 (1973).
19. G. J. Hills and D. J. G. Ives. Reference electrodes. *Edited by* D. J. G. Ives and G. J. Janz. Academic Press, NY. 1961. p. 133.
20. L. Meites. Polarographic techniques. Interscience Publishers Inc., New York. 1955. p. 34.
21. E. M. L. Valeriote. Ph. D. Thesis, University of Toronto, Toronto, Ont. 1968.
22. S. Glasstone. Textbook of physical chemistry. 2nd ed. MacMillan and Co. Ltd., London. 1946. p. 829.
23. A. J. de Bethune and N. A. Swendeman Loud. Standard aqueous electrode potentials and temperature coefficients at 25°C. *Edited by* C. A. Hampel, Skokie, IL.
24. R. C. Weast (*Editor*). Handbook of chemistry and physics. 45th ed. The Chemical Rubber Co., Cleveland, OH. 1964. p. D-38.
25. H. S. Harned and W. J. Hamer. J. Am. Chem. Soc. **57**, 33 (1935).
26. D. J. G. Ives and F. R. Smith. Reference electrodes. Theory and practice. *Edited by* D. J. G. Ives and G. J. Janz. Academic Press, New York. 1961. Chapt. 8.
27. C. H. Brubaker, Jr. J. Chem. Ed. **34**, 325 (1957).
28. T. F. Young and L. A. Blatz. Chem. Rev. **44**, 93 (1949).
29. H. M. Smith. Ph.D. Thesis, University of Chicago, Chicago, IL. 1949.
30. T. F. Young. Rec. Chem. Prog. **12**, 81 (1951).
31. R. Parsons. Handbook of electrochemical constants. Butterworths, London. 1959.
32. K. H. Lieser, G. Beyer, and E. Lakatos. Z. Anorg. Chem. **339**, 208 (1965).

π-Complex equilibria between ethylene and $PdCl_4^{2-}$ in aqueous solution

RAJ N. PANDEY[1] AND PATRICK M. HENRY

Guelph–Waterloo Centre for Graduate Work in Chemistry, Guelph Campus, Department of Chemistry, University of Guelph, Guelph, Ont., Canada N1G 2W1

Received October 3, 1978

RAJ N. PANDEY and PATRICK M. HENRY. Can. J. Chem. **57**, 982 (1979).

The interaction of aqueous $PdCl_4^{2-}$ with ethylene to form π-complexes has been reinvestigated using a reactor with high efficiency gas–liquid mixing. This reactor permitted study of the equilibria at low $[H^+]$ and $[Cl^-]$, the conditions under which the oxidation of ethylene to acetaldehyde proceeds rapidly.

$$C_2H_4 + PdCl_4^{2-} + H_2O \rightarrow CH_3CHO + 2HCl + Pd(0) + 2Cl^-$$

Previously the π-complex formation had been determined at high $[H^+]$ and $[Cl^-]$ to retard the oxidation reaction which interfered with study of the non-oxidative equilibria.

Two equilibria reactions were reported where K_1 and K_2 have appreciable values.

$$PdCl_4^{2-} + C_2H_4 \underset{}{\overset{K_1}{\rightleftharpoons}} PdCl_3(C_2H_4)^- + Cl^-$$

$$H_2O + PdCl_3(C_2H_4)^- \overset{K_2}{\rightleftharpoons} PdCl_2(H_2O)(C_2H_4) + Cl^-$$

The present measurements give K_1 values close to those previously reported: $K_1 = 19.6$ at $\mu = 2\ M$ (adjusted with $NaClO_4$); 11.0 at $\mu = 3\ M$ (adjusted with $NaClO_4$); and 14.7 at $\mu = 3\ M$ (adjusted with $LiClO_4$). However, the K_2 values are much less than those reported earlier. Thus the maximum possible value of K_2 at $\mu = 3\ M$ ($LiClO_4$) consistent with the present data is less than 0.01 while the previously reported value was 0.22. Possible reasons for the differences between the two studies are discussed.

The values of the aquation constant K_h needed for treating the gas uptake data were determined spectrally

$$PdCl_4^{2-} + H_2O \overset{K_h}{\rightleftharpoons} PdCl_3(H_2O)^- + Cl^-$$

and found to be 0.012 at $\mu = 2\ M$ and 0.0060 at $\mu = 3\ M$ ($NaClO_4$). Spectra taken at high [Pd(II)] indicate dimeric species are *not* formed under these conditions.

RAJ N. PANDEY et PATRICK M. HENRY. Can. J. Chem. **57**, 982 (1979).

Faisant appel à un réacteur permettant un mélange gaz/liquide très rapide, on a réétudié l'interaction entre le $PdCl_4^{2-}$ aqueux avec l'éthylène formant des complexes π. Ce réacteur a permis d'étudier l'équilibre à de basses concentrations de H^+ et de Cl^-, les conditions permettant une oxydation rapide de l'éthylène en acétaldéhyde.

$$C_2H_4 + PdCl_4^{2-} + H_2O \rightarrow CH_3CHO + 2HCl + Pd(0) + 2Cl^-$$

Antérieurement, on avait déterminé la formation du complexe π à des concentrations élevées de H^+ et de Cl^- afin de retarder la réaction d'oxydation qui interfère avec l'étude de l'équilibre non-oxydant.

On avait rapporté l'existence de deux réactions d'équilibre possédant des valeurs de K_1 et de K_2 importantes.

$$PdCl_4^{2-} + C_2H_4 \underset{}{\overset{K_1}{\rightleftharpoons}} PdCl_3(C_2H_4)^- + Cl^-$$

$$H_2O + PdCl_3(C_2H_4)^- \overset{K_2}{\rightleftharpoons} PdCl_2(H_2O)(C_2H_4) + Cl^-$$

Les mesures effectuées dans le présent travail donnent des valeurs de K_1 semblables à celles rapportées antérieurement: $K_1 = 19.6$ à $\mu = 2\ M$ (ajusté avec du $NaClO_4$); 11.0 à $\mu = 3\ M$ (ajusté avec du $NaClO_4$); et 14.7 à $\mu = 3\ M$ (ajusté avec du $LiClO_4$). Toutefois les valeurs de K_2 sont beaucoup plus faibles que celles rapportées antérieurement. Ainsi la valeur maximale possible pour K_2 à $\mu = 3\ M$ ($LiClO_4$) et en accord avec les données actuelles est moins que 0.01 alors que la valeur rapportée antérieurement est 0.22. On discute des raisons qui permettraient d'expliquer les différences entre les deux études.

On a déterminé spectrométriquement les valeurs pour la constante, K_h, d'aquation nécessaire

---

[1]Present address: Guelph Chemical Laboratories, 500 York Road, Guelph, Ont., Canada N1E 3J4.

0008-4042/79/090982-08$01.00/0

pour le traitement des données d'assimilation des gaz et on a trouvé que cette constante est égale à 0.012 à $\mu = 2\ M$ et 0.0060 à $\mu = 3\ M$ ($NaClO_4$).

$$PdCl_4^{2-} + H_2O \underset{}{\overset{K_h}{\rightleftharpoons}} PdCl_3(H_2O)^- + Cl^-$$

Des spectres déterminés à des concentrations élevées de Pd(II) indiquent qu'il n'y a *pas* de formation d'espèces dimères dans ces conditions.

[Traduit par le journal]

Introduction

The basic reaction of the Wacker Process for acetaldehyde manufacture is the oxidation of ethylene by $PdCl_4^{2-}$ in aqueous solution to give acetaldehyde (1). The kinetics and mechanism of [2]

$$[1] \quad C_2H_4 + (1/2)O_2 \xrightarrow[\text{aq.HCl}]{\overset{PdCl_2}{CuCl_2}} CH_3CHO$$

$$[2] \quad PdCl_4^{2-} + C_2H_4 + H_2O \rightarrow CH_3CHO + Pd(0) + 2HCl + 2Cl^-$$

have been studied by several groups of researchers (1–10). There is general agreement that under a range of reaction conditions ($[Pd(II)] = 0.005$–$0.04\ M$; $[Cl^-] = 0.1$–$1.0\ M$; $[H^+] = 0.04$–$1.0\ M$), the rate expression is given by [3]. Analogous rate expressions have been found for other acyclic olefins (8, 11).

$$[3] \quad \frac{-d[C_2H_4]}{dt} = \frac{k_1[PdCl_4^{2-}][C_2H_4]}{[H^+][Cl^-]^2}$$

On the basis of the kinetic studies plus other evidence, the following general reaction sequence is accepted by most workers in the field.

$$[4] \quad PdCl_4^{2-} + C_2H_4 \underset{}{\overset{K_1}{\rightleftharpoons}} \underset{\mathbf{1}}{PdCl_3(C_2H_4)^-} + Cl^-$$

$$[5] \quad \mathbf{1} + H_2O \underset{}{\overset{K_2}{\rightleftharpoons}} \underset{\mathbf{2}}{PdCl_2(H_2O)(C_2H_4)} + Cl^-$$

$$[6] \quad \mathbf{2} + H_2O \xrightarrow{-H^+} \underset{\mathbf{3}}{PdCH_2CH_2OH}$$

$$[7] \quad \mathbf{3} \rightarrow CH_3CHO + Pd(0)$$

In spite of the effort expended in studying this oxidation there is still controversy concerning several aspects of the reaction pathway. For instance the form of the rate expression at low $[H^+]$ and $[Cl^-]$ (2), the mode of transformation of **2** to **3** (12) as well as the mode of decomposition of **3** to final products (2) have all been topics of discussion. Two controversial points, which are experimentally related, involve the form of the rate expression at high [Pd(II)] and the value of K_2 in [5].

Moiseev and co-workers, using a reactor which did not contain a gas phase, were able to fit their data to a two term rate expression (6–8):

$$[8] \quad \frac{-d[olefin]}{dt} = k_I \frac{[PdCl_4^{2-}][olefin]}{[H^+][Cl^-]^2} + k_{II} \frac{[PdCl_4^{2-}]^2[olefin]}{[H^+][Cl^-]^2}$$

One characteristic of the experimental technique of these workers is that the calculation of the rate constant from the experimental data is very sensitive to the values of K_1 and K_2 in [4] and [5], respectively. Unfortunately these values were not measured under conditions the oxidation kinetics were determined but rather at high $[Cl^-]$ and $[H^+]$ to prevent the oxidation reactions, [6] and [7], from interfering with the equilibrium measurements (13–16). Furthermore, although constant ionic strength was maintained with ClO_4^- as $[Cl^-]$ was varied, the variation in $[Cl^-]$ was in some cases as much as 75% of the total ionic strength. The principle of constant ionic strength would not be expected to hold with such changes in solution composition.

One of the authors used a high efficiency gas–liquid mixing reactor to measure the kinetics of the oxidation of ethylene and other acyclic olefins (9). This reactor, which contained a gas phase, was suitable for measuring values of K_1 and K_2 under the actual reaction conditions the kinetics were determined. At an ionic strength of 2, adjusted with ClO_4^-, the value of K_2 was found to be less than 10^{-2} from a rather limited set of data. At the same ionic strength Moiseev reported that a value of 0.14 for K_2 is most consistent with his experimental results (7, 16).

Later one of the authors measured the kinetics of the oxidation at high Pd(II) at $\mu = 2\ M$ and found no evidence for the second term (10). It was suggested that the second term may be an artifact arising from using inaccurate values of K_1 and K_2 in treating the kinetic data for the one phase reactor system. However, the very high efficiency gas–liquid reactor was not available for this study and it was later claimed that the second term was not detected because of diffusion limitations (7) of the reactor used.

Since the presence of a second term in the rate expression could have very interesting mechanistic implications in Pd(II) chemistry, it is worthwhile to examine both the π-complex equilibria under the reaction conditions as well as the kinetics at high Pd(II) using a high efficiency gas–liquid mixing reactor. This paper will describe a study of the first, the equilibria between $PdCl_4^{2-}$ and ethylene under the reaction conditions.

Finally it has been suggested (7) that one reason that equilibrium [5] was not detected in earlier studies (9) is that the aquation of $PdCl_4^{2-}$ under the reaction conditions was not taken into account.

$$[9] \qquad PdCl_4^{2-} + H_2O \underset{}{\overset{K_h}{\rightleftharpoons}} PdCl_3(H_2O)^- + Cl^-$$

Thermodynamic values of K_h range from 2–4 × 10^{-2} (17–22). The value of K_h at higher ionic strength might be expected to be lower since $PdCl_4^{2-}$ would be stabilised more than the simply charged ions. One determination of K_h at $\mu = 2\ M$ gave a value of 2.56×10^{-2} (22). This value of K_h would indicate aquation is only important at low $[Cl^-]$. In any case it seems worthwhile to check this value since it is higher than expected from the thermodynamic values. Another point that deserves checking is the possibility that monomer–dimer equilibrium exists at high [Pd(II)].

$$[10] \qquad 2PdCl_4^{2-} \underset{}{\overset{K_D}{\rightleftharpoons}} 2Pd_2Cl_6^{2-} + 2Cl^-$$

The presence of such an equilibrium could seriously affect the interpretation of kinetic data. A potentiometric study suggested that dimeric Pd(II) complexes do not exist under the conditions the oxidation reaction was studied (23). Confirmation of this important point by spectral studies is desirable.

Experimental

Materials

The palladous chloride was purchased from Engelhardt, Inc. All other chemicals were of reagent grade. Preparation of reaction mixtures has been described (10).

Spectral Studies

The spectra were recorded on a Cary 118 spectrophotometer at 25°C. The cells were of 10 mm or 0.5 mm pathlength depending on the palladium(II) concentration.

Ethylene Uptake Studies

The reactor, shown in Fig. 1, has a volume of ca. 500 mL. Near the bottom it has a sintered glass base, sealed to the sides of the reactor. During the course of a reaction the ethylene is continuously circulated through the reactor by means of a varistaltic pump (VP). As the gas passes through the glass frit it is broken into small bubbles. The reaction mixture is also stirred by means of a magnetic stirring bar. The amount of ethylene absorbed is measured using a gas buret. The mercury in the leveling bulb is constantly raised so the levels in the bulb and the gas buret are at the same height, thus maintaining atmospheric pressure. To minimize escape of gas by diffusion through vinyl tubing, glass tubing was used as much as possible to connect the varistaltic pump and gas buret to the reactor. Where flexible tubing was required thick walled vinyl tubing was used. The temperature was maintained by circulating thermostated water at 25.0 ± 0.1°C through the outer jackets of the reactor and gas buret.

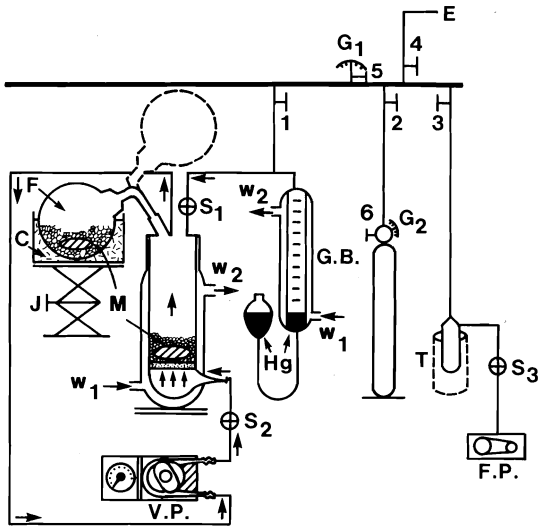

FIG. 1. Schematic diagram of reactor: C, constant temperature bath; J, adjustable jack; E, fume hood; 1–6, metal valves (vacuum tight); S_1–S_3, glass stopcocks; G_1, G_2, gauges; W_1, W_2, inlets and outlets of thermostated water; VP, varistaltic pump; FP, forepump; R, glass reactor; F, delivery flask; M, stirring magnets; G.B., gas buret.

To start a run 25 mL of the reaction solution is placed in the flask (F) which is placed in a constant temperature bath (C) at 25 ± 0.1°C. The bath is held on an adjustable jack (J). After the reaction mixture came to temperature the tube between the Hg leveling bulb and the gas buret was clamped to prevent Hg from flowing into the pump. The valves 1, 2, 3, and 5 and glass stopcocks S_1, S_2, and S_3 were opened and the forepump (FP) turned on to evacuate the system up to the ethylene cylinder. While the pump was on the magnetic stirrer in the flask F was turned on to aid in removing dissolved gases. After a couple of minutes the stirring bar was turned off and ethylene was added until slightly over 1 atm was attained. Then the clamp was removed from the tubing on the gas buret and gas was allowed to escape by means of the valve No. 4 to a fume hood (E). When 1 atm of gas was in the reactor as indicated by the equal mercury levels in leveling bulb and buret, valve No. 4 was closed and the varistaltic pump and magnetic stirring bar in the reactor activated. The reaction solution was then added to the reactor by revolving the flask F to the position indicated by the dotted line.

As it has been suggested that ethylene uptake prior to start of a run could be a source of error (7), the amount of gas uptake was measured by the solution in flask F before transfer to the reactor. For several minutes there is no appreciable gas uptake. Since in an actual run there is only a delay of seconds between charging with ethylene and start of a run, this cannot be a source of error.

Results

All equilibrium studies were carried out at 25°C. The π-complex equilibria studies were made at 1 atm ethylene pressure.

TABLE 1. Calculation of aquation constants, K_h, at 25°C[a]

$[MCl]_0$ ($M \times 10^2$)	$[Cl^-]^2$ ($M^2 \times 10^4$)	D_i λ278	ΔD_i λ278	$P_0/\Delta D \times 10^4$	$[PdCl_4^{2-}]$ ($M \times 10^5$)	$[PdCl_3(H_2O)^-]$ ($M \times 10^5$)	K_h ($M \times 10^2$)
			M = Na; μ = 2 M (adjusted with $NaClO_4$)				
1.10	1.21	0.175	0.633	1.26	4.07[b]	3.92[b]	1.06
1.90	3.61	0.265	0.545	1.47	4.63[b]	3.36[b]	1.38
3.00	9.00	0.430	0.360	2.17	5.57	2.22	1.20
5.00	25.0	0.544	0.246	3.17	6.28	1.52	1.20
7.00	49.0	0.605	0.185	4.21	6.65	1.14	1.20
9.00	81.0	0.635	0.155	5.03	6.84	0.956	1.26
12.0	144.0	0.675	0.115	6.78	7.09	0.709	1.20
15.0	225.0	0.680	0.110	7.09	7.12	0.679	1.43
						Average	1.21[c]
			M = Li; μ = 3 M (adjusted with $LiClO_4$)				
1.20	1.44	0.300	0.533	1.50	5.70[b]	2.29[b]	0.48
2.00	4.00	0.435	0.395	2.02	6.29[b]	1.70[b]	0.54
3.00	9.00	0.519	0.294	2.65	6.53	1.26	0.58
5.00	25.0	0.602	0.211	3.69	6.89	0.91	0.66
7.00	49.0	0.660	0.153	5.10	7.14	0.66	0.64
9.00	81.0	0.700	0.113	6.90	7.31	0.48	0.59
12.0	144.0	0.728	0.085	9.17	7.43	0.36	0.58
15.0	225.0	0.739	0.074	10.5	7.48	0.32	0.64
20.0	400.0	0.762	0.051	15.3	7.58	0.22	0.58
						Average	0.60[d]

[a] K_h is for equilibrium given by [9]; $[HClO_4] = 0.31$ M for all runs.
[b] Total [Pd(II)] = 7.99×10^{-5} for these runs and 7.79×10^{-5} for the remainder.
[c] Value of K_h calculated from plot of [11] is 1.2×10^{-2} M with $\Delta\varepsilon = 1.62 \times 10^4$.
[d] Value of K_h calculated from plot of [11] is 0.60×10^{-2} M with $\Delta\varepsilon = 2.33 \times 10^4$.

Tetrachloropalladate(II) Aquation Equilibrium

The equilibrium given by [9] was studied at μ = 2 M adjusted with $NaClO_4$ and μ = 3 M adjusted with $LiClO_4$.

Ultraviolet spectra in the range 400–200 nm of solutions at fixed Pd(II) and with $[Cl^-]$ varying from 0.01 to 0.6 M give isosbestic points at 260 and 310 nm, suggesting that the two species are in equilibrium in this range. The changes in spectra indicate that one species is gradually being converted to a second species. At $[Cl^-] = 0.6$ M the conversion is complete and further increase in $[Cl^-]$ causes no change in spectra.

Assuming the equilibrium given by [9] is operative, a relationship between change in optical density and K_h can be derived. This relationship, which has been derived previously (24), is given by [11]

$$\frac{P_0}{\Delta D} = \frac{1}{\Delta\varepsilon l} + \frac{[Cl^-]}{\Delta\varepsilon l} \qquad [11]$$

where P_0 = total [Pd(II)]; $\Delta\varepsilon$ is the difference in extinction coefficients between the two species at a given wavelength, l = pathlength, and $\Delta D = D_\infty - D_i$ where D_i are the optical densities at various $[Cl^-]$ and D_∞ is obtained from the final spectrum above 0.6 M $[Cl^-]$. Plots of $P_0/\Delta D$ vs. $[Cl^-]$ at several [Pd(II)] and different wavelengths give straight lines from which $\Delta\varepsilon$ and K_h can be calculated. Some typical data are shown in Table 1. If the data are treated in a similar fashion assuming [10] is operative, the values of K_D do not remain constant but vary over a factor of about 4. Thus [10] cannot be the correct equilibrium at low [Pd(II)].

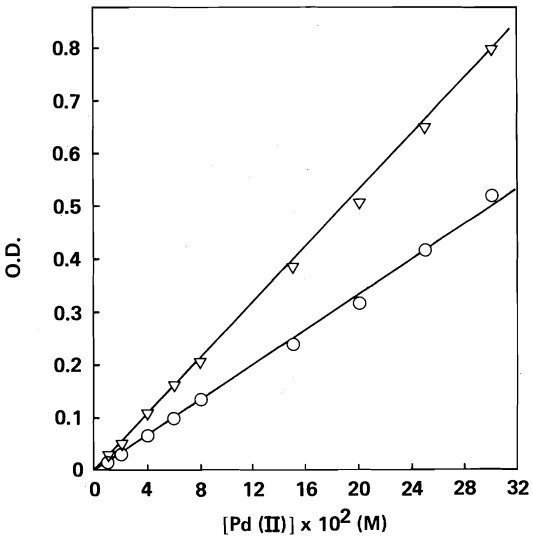

FIG. 2. Plots of O.D. vs. [Pd(II)] at μ = 2 M (adjusted with $NaClO_4$) and 25°C. $[HClO_4] = 0.20$ M, $[Cl^-] = 0.20$ M.

Spectra were also taken at high [Pd(II)] concentration to see if there was any evidence of equilibria such as [10] becoming important in this range. As shown in Fig. 2 there is a linear relationship between optical density and [Pd(II)] indicating that there is no polymeric species formed at high [Pd(II)].

π-Complex Formation

π-Complex formation was determined from initial ethylene uptake using the rapid gas–liquid mixing reactor shown in Fig. 1. The rate of gas absorption this reactor can achieve was determined by the measuring of CO_2 uptake by 0.2 *M* NaOH. The measured rate was 600 mL CO_2/min/25 mL. Since the maximum rate of ethylene uptake due to the oxidation was 10 mL/min/25 mL, the initial fast uptake of ethylene due to ethylene solution and π-complex formation would be complete before any appreciable oxidation occurs. In all runs this was the observed result and if a small correction for uptake due to oxidation was required, it was made by extrapolation to zero time. The amount of uptake due to solubility was determined by blank runs in which all reagents but the palladium(II) chloride were present.

In addition to the equilibrium given in [4] and [5] there is the possibility of the following two equilibria being operative:

$$[12] \quad PdCl_4^{2-} + 2C_2H_4 \overset{K'}{\rightleftharpoons} PdCl_2(C_2H_4)_2 + 2Cl^-$$

$$[13] \quad PdCl_2(C_2H_4)(H_2O) + H_2O \overset{K_3}{\rightleftharpoons} PdCl_2(C_2H_4)(OH)^- + H_3O^+$$

Moiseev found that [12] and [13] were inconsistent with his experimental results (8) and the present study confirms the fact they are not present. Thus values of K_1' calculated at various $[Cl^-]$ varied over a wide range and the amount of π-complex formed was independent of $[H^+]$ thus eliminating [13].

Assuming that the true equilibria are given by [4] and [5] the following equality can be written

$$[14] \quad [C_2H_4]_\varepsilon = [C_2H_4] + [PdCl_3(C_2H_4)^-] + [PdCl_2(C_2H_4)(H_2O)]$$

where $[C_2H_4]_\varepsilon$ represents the total ethylene absorbed and $[C_2H_4]$ is the ethylene solubility.

Dividing [14] by $[C_2H_4]$ and expressing the concentration ratios in terms of K_1, K_2, $[PdCl_4^{2-}]$, and $[Cl^-]$, [15] is readily derived where $\phi = [C_2H_4]_\varepsilon / [C_2H_4]$.

$$[15] \quad \frac{[\phi - 1][Cl^-]^2}{[PdCl_4^{2-}]} = K_1[Cl^-] + K_1K_2$$

Thus a plot of the left hand side of [15] vs. $[Cl^-]$ should give a plot with slope equal to K_1 and intercept equal to K_1K_2. In Fig. 3 is shown the plot of the data at $\mu = 2$ *M* adjusted with $NaClO_4$. Both the original data (9) as well as the present results are included. The data are corrected for the aquation reaction [9], using the value of 0.012 for K_h.

All points but the highest $[Cl^-]$ of the older data fall on a straight line. The least-squares fit excluding this point gives a value of K_1 of 19.6 ± 1.3 from the slope. The intercept is 0.063 which gives a value of 3.2×10^{-3} for K_2. The value calculated using the maximum positive variation of the intercept at the 95% confidence level is 0.33 which gives a maximum K_2 of 0.016. The arrow shows the intercept required to give a K_2 of 0.14, the previously reported value (16). The data used for the plot are listed in Table 2.

A similar plot for $\mu = 3$ *M* adjusted with $NaClO_4$ is shown in Fig. 4. In this case the data were corrected for [9] using $K_h = 0.0060$, the value found for the $LiClO_4$ system at the same ionic strength (see Table

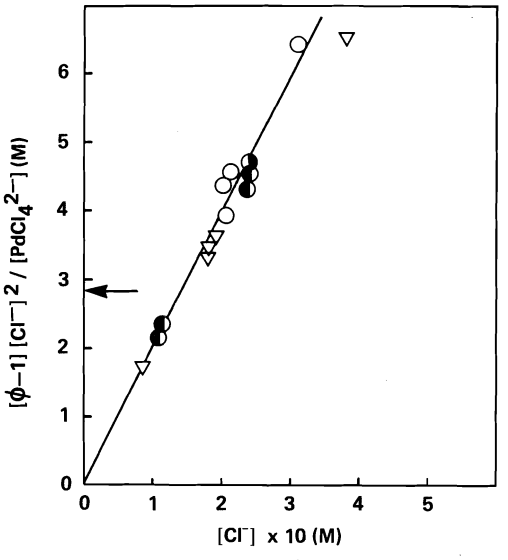

FIG. 3. Plots of $[\phi - 1][Cl^-]^2/[PdCl_4^{2-}]$ vs. $[Cl^-]$ at $\mu = 2$ *M* (adjusted with $NaClO_4$). Data from Table 2. Arrow indicates intercept of Levanda and Moiseev (ref. 16). $[HClO_4]$ = ○, 0.2 *M*; ◐, 0.8, 0.6 *M*; ◑, 0.25 *M*; ▽, corrected data of Henry (ref. 9).

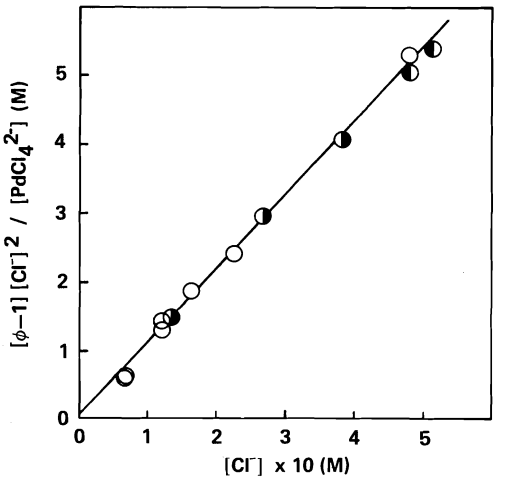

FIG. 4. Plots of $[\phi - 1][Cl^{-2}]/[PdCl_4^{2-}]$ vs. $[Cl^-]$ at $\mu = 3$ *M* (adjusted with $NaClO_4$). Data from Table 3; an average value has been plotted for identical runs. $[HClO_4]$ = ◑, 0.2 *M*; ○, 0.4 *M*; ◐, 0.8 *M*.

TABLE 2. Ethylene uptake data used for calculation of K_1 and K_2 at $\mu = 2\ M$ ($NaClO_4$)[a]

$[HClO_4]$ (M)	Total [Pd(II)] ($M \times 10^2$)	$[PdCl_4^{2-}]$ ($M \times 10^2$)	$[Cl^-]$[b] ($M \times 10$)	$[PdCl_3(H_2O)^-]$[c] ($M \times 10^4$)	$[C_2H_4]_\epsilon$[d] ($M \times 10^3$)	$[\phi - 1][Cl^-]^2/[PdCl_4^{2-}]$[d] ($M$)
			Present results			
0.800	1.25	0.71	1.05	8	4.6	2.25
0.800	2.50	1.45	1.09	16	8.8	2.29
0.200	0.20	0.14	2.01	1.0	0.50	4.42
0.200	2.40	1.77	2.05	10	5.2	3.96
0.200	5.0	3.62	2.12	21	11.6	4.56
0.600	20.0	15.5	2.37	79	36.9	4.26
0.800	20.0	15.4	2.38	78	38.4	4.53
0.250	20.0	15.3	2.39	77	39.4	4.71
0.200	5.0	3.99	3.09	16	8.5	6.46
			Previous results recalculated for hydrolysis[e]			
0.200	0.90	0.49	0.82	7.0	33.0	1.72
0.200	0.97	0.72	1.82	5.0	2.0	3.44
0.200	0.90	0.68	1.84	4.5	1.8	3.26
1.000	0.72	0.53	1.87	3.0	1.6	3.60
0.200	0.89	0.78	3.83	25.0	0.90	6.52

[a] K_1 and K_2 defined by [4] and [5], respectively. Ethylene solubility $= 3.14 \times 10^{-3}\ M$.
[b] Cl^- added as NaCl.
[c] Calculated using $K_h = 0.012$.
[d] These quantities defined by [14] and [15].
[e] From ref. 9.

TABLE 3. Ethylene uptake data used for calculation of K_1 and K_2 at $\mu = 3\ M$ ($NaClO_4$)[a]

$[HClO_4]$ (M)	Total [Pd(II)] ($M \times 10^2$)	$[PdCl_4^{2-}]$ ($M \times 10^2$)	$[Cl^-]$[b] ($M \times 10$)	$[PdCl_3(H_2O)^-]$[c] ($M \times 10^4$)	$[C_2H_4]_\epsilon$[d] ($M \times 10^3$)	$\frac{[\phi - 1][Cl^-]^2}{[PdCl_4^{2-}]}$[d] ($M$)
0.200	5.00	3.80	1.35	17	10.3	1.52
	8.00	6.77	2.10	20	10.3	2.06
	10.0	8.59	2.62	20	12.1	2.96
	15.0	13.6	3.87	21	12.1	4.09
0.400	2.26	1.43	6.26	14	6.9	0.576
	2.26	1.39	6.31	13	7.3	0.647
	5.64	4.16	12.0	20	12.8	1.35
	5.64	4.21	11.9	21	12.1	1.25
	5.64	4.19	11.9	21	12.4	1.30
	4.51	3.30	12.2	16	10.5	1.45
	6.80	5.29	15.7	20	13.1	1.87
	18.8	16.1	22.3	43	22.9	2.16
	18.8	15.8	22.6	41	26.2	2.60
	15.0	13.5	38.8	21	12.8	4.34
	15.0	13.6	38.7	21	12.3	4.15
	18.8	17.4	48.2	22	12.2	5.03
	18.8	17.2	48.4	21	13.6	5.63
0.800	5.64	4.25	11.9	21	11.8	1.20
	18.8	17.4	48.2	21	12.3	5.03
	15.0	13.9	50.9	17	9.5	5.42
1.000	15.0	13.4	38.9	20	13.9	4.80

[a] K_1 and K_2 defined by [4] and [5], respectively. Ethylene solubility $= 3.27 \times 10^{-3}\ M$.
[b] Cl^- added as NaCl.
[c] Calculated using $K_h = 6.0 \times 10^{-3}$.
[d] These quantities defined by [14] and [15].

1). A value of 11.0 ± 0.3 is calculated from the slope with the intercept being -0.015. The maximum value of the intercept at the 95% confidence level is 0.076 which gives a value of 0.007 for K_2. Data are listed in Table 3. The plot for the $LiClO_4$ at $\mu = 3\ M$ is shown in Fig. 5. The value of 0.0060 for K_h is used to correct the data. The slope is 14.7 ± 1.7 and the intercept is 0.10 which gives a value of 0.007 for K_2. The arrow indicates the intercept which would give a K_2 of 0.22, the previously reported value (16).

Discussion

The most important result of this study is the demonstration that values of K_2 for the equilibrium

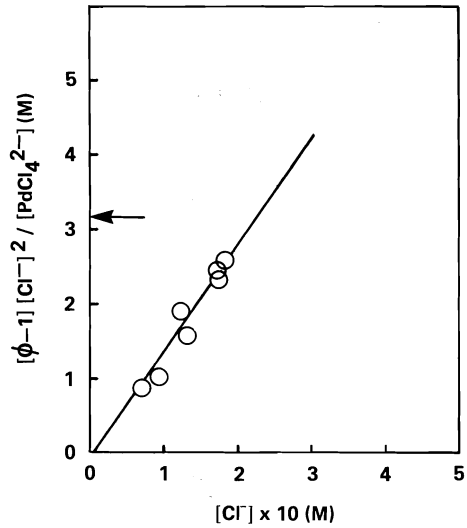

FIG. 5. Plots of $[\phi - 1][Cl^-]^2/[PdCl_4^{2-}]$ vs. $[Cl^-]$ at $\mu = 3\ M$ (adjusted with $LiClO_4$). Data from Table 4. Arrow indicates intercept of Levanda and Moiseev (ref. 16).

given by [5] are actually much less than those reported previously (7, 16) and, in fact, are too small to be accurately measured by the present techniques. Thus in both the $NaClO_4$ systems the intercept of the least-squares treatment of the data is actually negative while the corresponding intercept at $\mu = 2\ M$ gives a K_2 of 3.2×10^{-3} which is approximately 1/40 of the previously reported value of 0.14 ± 0.16. Even the maximum possible intercepts from the data are much below the previous values. This value is 0.016 for the $\mu = 2\ M$ systems and <0.01 for the $\mu = 3.0\ M$ systems with $LiClO_4$ as supporting electrolyte, the previous value was 0.22 (16).

The variation in values of K_2 obtained in the two studies must result from the difference in experimental techniques. In the earlier study the gas uptakes were measured at high $[Cl^-]$ and $[H^+]$ to prevent interference from the oxidation. It is true that a constant ionic strength was maintained with perchlorate ion but the fluctuations in solution composition were quite large. Thus chloride concentration was as high as 75% of the total ionic strength. Errors in this study could arise from two sources. First the extrapolation from the lowest $[Cl^-]$ used to $[Cl^-] = 0$ is quite large. Thus the lowest $[Cl^-]$ used was usually $>0.7\ M$. Extrapolation from this concentration to $[Cl^-] = 0$ must be considerably less accurate than extrapolations from $[Cl^-] \approx 0.1\ M$ as in the present study. Secondly, over the wide range of solution composition used the principle of constant ionic strength would not be expected to hold. A systematic variation in activity coefficients would give an erroneous slope. With such a large extrapolation even small errors in slope would cause large errors in the intercept. In the present study the highest $[Cl^-]$ is less than 20% of the total ionic strength so there should be little or no change in activity coefficients over the range of $[Cl^-]$ used.

As might be expected the differences in K_1 values in the two studies are much less than the K_2 values. This results from the fact that the slope is much less sensitive to the factors discussed above than is the intercept. The value of K_1 of 19.6 at $\mu = 2\ M$ is just a little higher than the average value of 17.4 previously found by one of the writers and the value of 15.0 reported by Levanda and Moiseev (16). At $\mu = 3\ M$ adjusted with $LiClO_4$ the present value of K_1 is 14.8 (16). The $NaClO_4$ system at $\mu = 3\ M$ has a little lower value of 11.0. This difference between the $LiClO_4$ and $NaClO_4$ systems might be expected since anionic species are mainly involved in the equilibrium given in [4] (Table 4).

The absolute values of K_1 and K_2 are of little direct importance to the mechanism of the oxidation of ethylene by aqueous $PdCl_4^{2-}$. It is true that a quantitative knowledge of the concentrations of **1** and **2** in [4] and [5], respectively, under various reaction conditions would allow the more accurate estimation of subsequent rate constants but this is only of basic importance in the demonstration that certain routes, such as [16], are impossible because of diffusion control (9).

$$[16] \qquad PdCl_2(C_2H_4)(H_2O) + OH^- \xrightarrow{\text{slow}} \mathbf{3}$$

However, this last calculation is valid even if K_2 has a value as high as 1.0.

Of more importance is the use of correct values of K_1 and K_2 in calculation of rate constants from experimental data. Errors of the order of those in the previous reported values would not affect the calculated values of the rate constants in the reactions with a gas phase but in the reactions without a gas phase the use of these incorrect values of K_1 and K_2 would cause considerable error in rate constants. Furthermore these errors in K_1 and K_2 will give systematic errors in the calculated rate constants which vary as $[Cl^-]$ and $[PdCl_4^{2-}]$ vary (10). The form of the rate expression at high $[PdCl_4^{2-}]$ as well as a discussion of the errors in K_1 and K_2 on the interpretation of the kinetic data of Moiseev and co-workers will be the topic of a later paper (25).

A few minor points deserve comment. First, the present work confirmed the conclusion of Levanda *et al.* (23) that dimeric species are not present in the reaction system and thus their involvement cannot be responsible for the two term rate expression given by [8].

The previous calculation of equilibrium constants by one of the authors (9) has been criticized because the aquation equilibrium, [9], was not taken into

TABLE 4. Ethylene uptake data used for calculation of K_1 and K_2 at $\mu = 3\ M$ ($LiClO_4$)[a]

Total [Pd(II)] ($M \times 10^2$)	$[PdCl_4^{2-}]$ ($M \times 10^2$)	$[Cl^-]$[b] ($M \times 10$)	$[PdCl_3(H_2O)^-]$[c] ($M \times 10^4$)	$[C_2H_4]_e$[d] ($M \times 10^3$)	$\frac{[\phi - 1][Cl^-]^2}{[PdCl_4^{2-}]}$[d] ($M$)
2.25	1.26	0.646	12	8.8	0.899
3.38	2.24	0.872	15	9.8	1.02
4.51	3.09	1.25	15	12.8	1.96
15.0	11.3	1.32	51	32.1	1.51
10.0	7.72	1.73	26	20.0	2.38
10.0	7.69	1.74	26	20.4[e]	2.46
15.0	11.6	1.80	39	29.8	2.54

[a] K_1 and K_2 defined by [4] and [5], respectively. Ethylene solubility = $3.27 \times 10^{-3}\ M$. $[HClO_4] = 0.40\ M$ for all runs.
[b] Cl^- added as LiCl.
[c] Calculated using $K_h = 6.0 \times 10^{-3}$.
[d] These quantities defined by [14] and [15].
[e] All but this run are the average of at least two determinations.

account (7). This criticism is valid although at the time of the initial measurements the reported values of K_h (26) indicated the correction would be insignificant. In any case the correction is small and the recalculation of the original data (using a K_h of 0.0256) to give a K_2 of 0.05 (7) does not result from this correction but rather the fact the point of highest $[Cl^-]$ is inaccurate. This is obvious from Fig. 3.

The values of K_h determined in this work (0.012 M at $\mu = 3\ M$) are lower than Levanda's values of 0.0256 at $\mu = 2\ M$ and 0.017 at $\mu = 3\ M$ (22) but, as mentioned in the Introduction, his values seem high for the thermodynamic constants reported by a number of other workers.

Finally, several arguments advanced by Moiseev to justify his extrapolation over such a range of Cl^- and ClO_4^- solution compositions at constant μ rebut the suggestions of one of the authors (9) that his values of K_2 were in error because of changes in activity coefficients (8). The main thrust of these arguments is that a change in anion composition over the range used would change the activity coefficients relatively little (<10%). However a *systematic* error of this magnitude over the range of conditions used followed by a long extrapolation from the lowest chloride ion concentration would give a considerable error in the intercept. In actual practice the error would seem to be larger. Thus at $\mu = 2\ M$ the correct slope was found to be 19.6 while the value of Moiseev was 15.0.

Acknowledgements

The authors thank the National Research Council of Canada for support of this research. We also thank Ms. Anne Hostetter for making the glass portions of the reactor and Mrs. Sushma Kohli for technical assistance.

1. J. SMIDT, W. HAFNER, R. JIRA, R. SIEBER, J. SEDLMEIER, and A. SABEL. Angew. Chem. **71**, 176 (1959); Angew. Chem. Intern. Ed. **1**, 80 (1962); Chem. Ind. London, 54 (1962).
2. R. JIRA, J. SEDLMEIER, and J. SMIDT. Justus Liebigs Ann. Chem. **693**, 99 (1966).
3. I. I. MOISEEV, M. N. VARGAFTIK, and Y. K. SIRKIN. Dokl. Akad. Nauk SSSR, **153**, 140 (1963).
4. M. N. VARGAFTIK, I. I. MOISEEV, and Y. K. SIRKIN. Dokl. Akad. Nauk SSSR, **139**, 1396 (1961); **147**, 399 (1962); Izv. Akad. Nauk Otd. Khim. Nauk, 1144 (1963); 1147 (1963).
5. I. I. MOISEEV, M. N. VARGAFTIK, S. V. PESTRIKOV, O. G. LEVANDA, T. N. ROMANOVA, and Y. K. SIRKIN. Dokl. Akad. Nauk SSSR, **171**, 1365 (1966).
6. O. G. LEVANDA and I. I. MOISEEV. Kinet. Katal. **12**, 567 (1971).
7. I. I. MOISEEV, O. G. LEVANDA, and M. N. VARGAFTIK. J. Am. Chem. Soc. **96**, 1003 (1974).
8. I. I. MOISEEV. Am. Chem. Soc. Div. Pet. Chem. Prepr. **14**, B49 (1969).
9. P. M. HENRY. J. Am. Chem. Soc. **86**, 3246 (1964).
10. P. M. HENRY. J. Am. Chem. Soc. **94**, 4437 (1972).
11. P. M. HENRY. J. Am. Chem. Soc. **88**, 1595 (1966).
12. J. K. STILLE and R. DIVAKARUNI. J. Am. Chem. Soc. **100**, 1303 (1978).
13. I. I. MOISEEV, M. N. VARGAFTAK, and Y. K. SIRKIN. Dokl. Akad. Nauk SSSR, **152**, 147 (1963).
14. S. V. PESTRIKOV, I. I. MOISEEV, and T. N. ROMANOVA. Zh. Neorg. Khim. **10**, 2203 (1965).
15. S. V. PESTRIKOV, I. I. MOISEEV, and L. M. SVERZH. Zh. Neorg. Khim. **11**, 2081 (1966).
16. O. G. LEVANDA and I. I. MOISEEV. Kinet. Katal. **12**, 354 (1971).
17. L. I. ELDING. Inorg. Chim. Acta, **6**, 647 (1972).
18. A. A. GRINBERG, N. V. KISELEVA, and M. I. GEL'FMAN. Dokl. Akad. Nauk SSSR, **153**, 1327 (1963).
19. K. BURGER and D. DYRSSEN. Acta Chem. Scand. 1489 (1963).
20. K. BURGER. Acta Chem. Akad. Sci. Hung. **40**, 261 (1964).
21. V. I. SCHLENSKAYA and A. A. BIRYUKOV. Vestn. Mosk. Univ. Ser. Khim. **3**, 65 (1964).
22. O. G. LEVANDA. Zh. Neorg. Khim. **13**, 3311 (1968).
23. O. G. LEVANDA, I. I. MOISEEV, and M. N. VARGAFTIK. Izv. Akad. Nauk SSSR, Ser. Khim. 2368 (1968).
24. H.-B. LEE and P. M. HENRY. Can. J. Chem. **54**, 1726 (1976).
25. R. N. PANDEY and P. M. HENRY. To be published.
26. H. A. DROLL, B. P. BLOCK, and W. C. FERNELIUS. J. Phys. Chem. **61**, 1000 (1957).

Electrochemical synthesis of some 1,2-dimethyl 1,2-disubstituted ethylenes[1]

ROGER N. RENAUD AND PHILIPPE J. CHAMPAGNE

Division of Chemistry, National Research Council of Canada, Ottawa, Ont., Canada K1A 0R6

Received August 8, 1978

ROGER N. RENAUD and PHILIPPE J. CHAMPAGNE. Can. J. Chem. **57**, 990 (1979).

The anodic oxidation of sodium acetate in the presence of a series of 1,2-disubstituted ethylenes was performed in acetonitrile–water solution. Under low concentration of substrates, very good yields of the monomeric 1,2-dimethylated products were obtained. In the case of diethyl fumarate, an increase in concentration caused a decrease in the ratio of monomer to polymer when all other parameters were held constant.

The stereoisomers of the products were separated and their physical properties are reported.

ROGER N. RENAUD et PHILIPPE J. CHAMPAGNE. Can. J. Chem. **57**, 990 (1979).

L'oxydation de l'acétate de sodium en présence de molécules d'éthylène substituées en position 1 et 2 dans un mélange acétonitrile–eau fut étudiée. A basse concentration du substrat, de bons rendements en produits diméthylés furent obtenus. Il a été constaté dans le cas du fumarate d'éthyle que le rapport monomère/polymère diminue avec une augmentation de la concentration de l'ester.

Les stéréoisomères des produits furent séparés et leurs propriétés physiques sont rapportées.

The electrochemical oxidation of acetate anions in the presence of unsaturated substrates has been widely studied. Isolated double bonds usually give low yields of a mixture consisting of more than twelve compounds (1, 2). Important quantities of acetoxy and methoxy derivatives were obtained when the reaction was done in methanol. These results can be explained by a mechanism involving cationic intermediates which react with nucleophiles present in the medium. Ethylene has been reported to undergo either additive dimerization (3) or dimethylation (4) depending on the reaction conditions used. Butadiene as substrate also gave very low yields of adducts. The main products isolated in this case were dimers (5). Stilbene gave mainly diacetoxy derivatives which can be explained by a direct oxidation of the substrate (6). When the double bond is activated by one electron withdrawing group such as COMe, CHO, CO_2R, or CN, the radical formed by the addition of the methyl radical at the β-carbon is resonance-stabilized and, therefore, dimerizes in good yields (7). The reaction was represented as follows:

$$CH_3COO^- \xrightarrow{-e} CH_3^\bullet + CO_2$$

$$CH_3^\bullet + H_2C{=}CH{-}Y \longrightarrow CH_3CH_2{-}\dot{C}HY$$

$$2CH_3CH_2{-}\dot{C}HY \longrightarrow \begin{matrix} CH_3{-}CH_2{-}CHY \\ | \\ CH_3{-}CH_2{-}CHY \end{matrix}$$

The objectives of this present study were to determine the effect of two electron withdrawing groups on the methylation of double bonds and to develop a general synthetic procedure for the alkylation of activated double bonds. While our work was in progress a short communication appeared in the literature (8) concerning the methylation of dimethyl fumarate and dimethyl maleate. The authors claimed that the yields of dimethyl 1,2-dimethylsuccinate were nearly quantitative and that the maleate reacted faster than the fumarate. However, their results did not agree with our observations. Therefore, it was decided to complete our systematic study on a series of disubstituted ethylenic molecules.

Experimental

All starting materials were commercially available except for compound **4** which was prepared according to a method described in the literature (9). All melting points are uncorrected. The cell used in this study is illustrated in Fig. 1. Gas–liquid chromatographic analyses and separations were performed respectively on a Fisher/Victoreen Series 4400 and an Aerograph Autoprep model A-700 using a 20 ft × 3/8 in. column, 30% SE 30 on 45/60 chromosorb P. Proton magnetic resonance spectra were taken in deuteriochloroform on a Varian Associates spectrometer model E. M. 360 and are reported in the δ scale. The molecular weight determinations were carried out on a Hitachi Perkin-Elmer RMU-6D mass spectrometer.

Electrolysis of Sodium Acetate in the Presence of an Ethylenic Substrate (General Procedure)

The anodic solution consisted of a solution of the ethylenic substrate (Table 1) in a mixture of acetonitrile (170 mL) and water (70 mL). To this solution was added a solution of NaOH (6 g) in acetic acid (60 mL). The electrolysis was carried out at a current of 1.8 A (140 mA/cm²) at 20–25°C for 6 h or until 0.4 mol of electrons had been transferred. The anodic solution was then concentrated on a rotary vacuum evaporator and the low vapor pressure residue was poured into water (600 mL). The aqueous solution was extracted three to six times with 100

[1]NRCC No. 17256.

0008-4042/79/090990-04$01.00/0

TABLE 1. Electrochemical oxidation of sodium acetate in the presence of 1,2-disubstituted ethylenes

Substrate	Molarity	Product	Yield%[a]	Ratio of monomer to polymer
1, Diethyl fumarate	0.03	**6**, Diethyl 2,3-dimethylsuccinate	80(84)	>15:1
	0.30		53(64)	2.5:1
	1.00		30(41)	1:1
2, Diethyl maleate	0.03	**6**, Diethyl 2,3-dimethylsuccinate	21(65)	
3, Fumaronitrile	0.03	**7**, 2,3-Dimethylsuccinonitrile	55[b]	
4, *N*-Phenylmaleimide	0.03	**8**, 2,3-Dimethyl *N*-phenylsuccinimide	80	
5, *N*-Ethylmaleimide	0.03	**9**, 2,3-Dimethyl *N*-ethylsuccinimide	88	

[a]Numbers in parentheses refer to yield based on amount of substrate consumed.
[b]Yield not optimized.

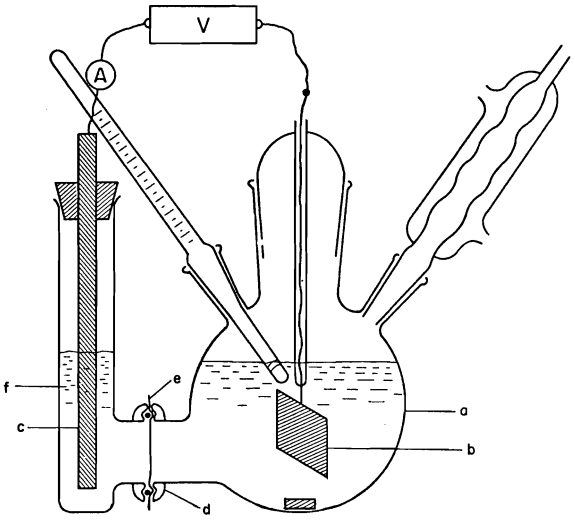

FIG. 1. Schematic diagram of the electrochemical cell assembly: *a*, 300 mL flask; *b*, Pt electrode 3.8 cm × 3.2 cm; *c*, carbon rod electrode; *d*, O-ring joint 25 mm; *e*, cellulose membrane; *f*, 2.0 *M* aqueous NaOH.

mL methylene chloride and the combined extracts were concentrated on an evaporator.

Purification and Physical Properties of the Products

(A) Diethyl 2,3-Dimethylsuccinate **6**

(*i*) From diethyl fumarate (**1**)

Distillation of the extracted oil at 75°C under a pressure of 0.01 Torr gave a colourless liquid which by vpc was mostly **6**, along with a small amount of starting material and traces of side reaction products. The monomeric product was further purified by preparative glc to give a colourless oil in 80% yield. This product, on vpc, showed two approximately equal peaks partly superimposed. This was taken to be a 1:1 mixture of the *meso* and *dl* isomers of **6**: nmr 4.2 (4H, q, J = 6.6 Hz, methylenes), 2.85 (2H, m, methines), 1.28 (6H, t, J = 6.6 Hz, methyls of ester groups), 1.24 (6H, d, J = 7.0 Hz, methyls at C-2 and C-3). *Anal.* calcd. for $C_{10}H_{18}O_4$: C 59.41, H 8.91; found: C 59.57, H 8.80.

Careful collection by preparative glc of the first of the superimposed peaks and the tailings of the second peak gave colourless oils with slightly different retention times on the analytical vpc and whose nmr's and elemental analyses were identical to that given above for the mixture. The slower moving fraction was hydrolyzed under acidic conditions to a diacid which melted at 124–127°C (literature (10) value for the *dl*-diacid is 127°C). The faster moving peak then corresponds to the *meso*-diester.

(*ii*) From diethyl maleate (**2**)

Distillation of the extracted oil as above gave a colourless oil which, by analytical vpc, contained **2** (70% of initial amount) and the same mixture of *meso*:*dl*-dimethylated monomer **6** as obtained above but in only 21% yield. No further attempts were made to separate these compounds.

(B) 2,3-Dimethylsuccinonitrile (7) from Fumaronitrile (3)

Distillation of the extracted solid and oil mixture at 140°C under a pressure of 0.01 Torr gave a colourless solid oil mixture which on repeated centrifuging in a 'Craig Tube' gave a dry, white solid melting at 45–46°C, and which showed two equal but well separated peaks on the vpc. These were shown to be the *meso*- and *dl*-isomers of **7**. The residual oil, by vpc analysis, also consisted mainly of the same two products plus a small amount of a slower moving product. This mixture was separated by column chromatography (silica gel column with 4:1 hexane/ethyl acetate as eluent). The column chromatography resulted in separation of the two solid products such that each showed only one peak on vpc. A sample of the solid which moved slower on the vpc, when treated with sodium methoxide in methanol, was converted to the same mixture of solids as obtained above.

Meso:*dl* isomeric mixture of **7**: mp 45–46°C (55% yield), nmr 2.73 (2H, m, methines), 1.29 (6H, d, J = 7.0 Hz, methyls); ms *m*/*e* 107 $(M - 1)^+$, 93 $(M - CH_3)^+$, 82 $(M - CN)^+$, 54 $(M/2)^+$. *Anal.* calcd. for $C_6H_8N_2$: C 66.64, H 7.46, N 25.91; found: C 66.34, H 7.42, N 25.79.

dl-Isomer of **7**: mp 57–59°C (assigned as the *dl*-isomer in ref. 10), nmr and ms as above. *Anal.* found for $C_6H_8N_2$: C 66.21, H 7.51, N 25.48.

Meso-isomer of **7**: mp 73.5–75°C (lit. (10) 46°C); nmr and ms as above. *Anal.* found for $C_6H_8N_2$: C 66.40, H 7.31, N 26.02.

(C) 2,3-Dimethyl-N-phenylsuccinimide **8** *from N-Phenylmaleimide* **4**

Extraction of the reaction mixture with CH_2Cl_2 yielded an oily solid product. Repeated extraction of the oil from this mixture with diethyl ether, in which the solid was relatively insoluble, gave a white solid which showed two separate and equal peaks on vpc analysis. This product was shown to be a 1:1 mixture of *cis*- and *trans*-isomers of **8** and corresponded to a yield of 80%. Melting point 124–126°C, nmr 7.40 (5H, m,

aromatic), 3.15 (1H, m, methine), 2.65 (1H, m, methine), 1.4 (6H, d of d's, methyls).

The chromatographic separation on silica gel column gave two different solids each of which had the same retention time on vpc as one or the other of the compounds in the original mixture of solids. These were shown, by comparison of melting points and nmr spectra with the literature values, to be the *cis*-**8** (melting at 127–129.5°C, lit. (11) 126°C) and *trans*-**8** (melting at 144–146°C, lit. 146°C). Treatment of the solid which moved slower on the vpc (*cis*-**8** or *meso*) with sodium methoxide in methanol resulted in its conversion to *trans*-**8** (*dl*) to the extent of about 95% conversion by vpc analysis.

*(D) 2,3-Dimethyl-*N*-ethylsuccinimide* **9** *from* N*-Ethylmaleimide* **5**

The mixture obtained from the extraction was fractionally distilled on a vacuum line. The low vapor pressure oil was collected in a stock trap and consisted of nearly pure *cis*- and *trans*-**9** (88% yield of 1:1 mixture). Pure **9** was obtained by a careful distillation in a Späth bulb at 0.01 Torr: nmr 1.28 (9H, m, methyls), 2.45 and 3.00 (2H, 2m, *cis*- and *trans*-methines), 3.58 (2H, q, methylene), ms *m/e* 155 $(M)^+$, 140 $(M - CH_3)^+$. *Anal.* calcd. for $C_8H_{13}NO_2$: C 61.94, H 8.39, N 9.03; found: C 61.76, H 8.27, N 9.08.

The *cis*- and *trans*-isomers were separated by preparative glc. The product corresponding to the second peak was converted to the product corresponding to the first peak in the presence of a methanolic solution of sodium methoxide. Therefore, assuming that the *trans*-isomer is thermodynamically more stable than the *cis*-isomer, as was found for **8**, the first peak should correspond to the *trans*-isomer and the second peak to the *cis*-isomer.

cis-**9**: nmr 3.56 (2H, q, $J = 7.4$ Hz, methylene), 2.95 (2H, m, methines), 1.2 (6H, d, $J = 7.0$ Hz, methyls at C-2 and C-3), 1.18 (3H, t, $J = 7.4$ Hz, methyl of the *N*-ethyl group). *Anal.* found: C 62.07, H 8.27, N 9.18.

trans-**9**: nmr 3.58 (2H, q, $J = 7.4$ Hz, methylene), 2.41 (2H, m, methines), 1.35 (6H, d, $J = 7.0$ Hz, methyls at C-2 and C-3), 1.18 (3H, t, $J = 7.4$ Hz, methyl of *N*-ethyl group). *Anal.* found: C 61.88, H 8.28, N, 8.99.

Results and Discussion

The electrochemical oxidation of sodium acetate in aqueous acetonitrile solution was carried out in the presence of five substrates (Table 1). Diethyl fumarate (**1**) and diethyl maleate (**2**) in 0.03 *M* solution gave diethyl 2,3-dimethylsuccinate (**6**) in 80% and 21% yields respectively. The use of methanol as solvent as described in ref. 8 did not improve the yields. The quantitative yields reported in ref. 8 were not obtained. Increasing the concentration of diethyl fumarate from 0.03 *M* to 1.00 *M* solution under the same experimental conditions caused a significant decrease in the monomer/polymer ratio. The amount of unreacted material also increased. Furthermore, a run was tried at a current density of 20 mA/cm^2 as reported in ref. 8 and no addition products were obtained. It was also mentioned in this reference that dimethyl maleate reacts faster with methyl radicals than dimethyl fumarate. It was observed by us that the fumarate reacted faster when equivalent amounts of dimethyl fumarate and diethyl maleate were used as substrates. The same observation was obtained for a mixture of diethyl fumarate and dimethyl maleate. Also, under the same experimental conditions, the diethyl fumarate was greater than 90% consumed during electrolysis while the diethyl maleate was only about 30% consumed.

The fumaronitrile (**3**) was methylated in acceptable yields. The melting point of the product was 46°C. Linstead and Whalley (10) reported melting points of 46 and 58°C for the *meso*- and the *dl*-2,3-dimethylsuccinonitrile respectively. Therefore, it seemed that the electrochemical dimethylation of fumaronitrile was stereospecific. However, we found by glc that the product melting at 46°C was an equal mixture of *meso*- and *dl*-stereoisomers. They were separated by column chromatography and one isomer melted at 58°C, corresponding to the *dl*-isomer found by Linstead, and the other at 73.5–76°C, corresponding to the *meso*-isomer. Linstead did not obtain a "clearcut" inversion of the isomers simply because the *meso*-isomer was in reality the *meso*:*dl* mixture. Each isomer could be converted into the same mixture of *meso*- and *dl*-isomers melting at 46°C in the presence of a base.

The methylation of *N*-ethylmaleimide **5** and *N*-phenylmaleimide **4** gave very good yields of dimethylated products, **9** and **8** respectively. The synthesis of *cis*- and *trans*-2,3-dimethyl *N*-phenylsuccinimide has been reported in the literature starting from the corresponding *erythro*- and *threo*-2,3-dimethylsuccinic acids (11). The products obtained by the electrolytic method was a mixture containing equal amounts of *cis*- and *trans*-stereoisomers. The *cis*-isomer was easily converted to the more stable *trans*-isomer in the presence of methoxide ion in methanol. The melting points, the mass spectra, and the nmr spectra agree well with the reported data for the *trans*- and the *cis*-isomers (11).

The unknown 2,3-dimethyl-*N*-ethylmaleimide was also obtained as a mixture of equal amounts of *cis*- and *trans*-stereoisomers. The more stable isomer was taken as the *trans*-isomer based on the fact that in the case of the *N*-phenyl derivative the *trans* is the more stable isomer.

It can be concluded that the methylation of ethylenic compounds substituted in the 1 and 2 positions with electron withdrawing groups, utilizing the electrochemical oxidation of acetate anion, results in high yields of the monomeric 1,2-dimethylated products. Practically no dimers or polymers were found under the described conditions. These products are readily isolated and purified and, except in the case of the fumarate and maleate, the stereoisomers are easily separated and characterized.

One observation which remains to be discussed is the great difference between the rates of methylation

of the fumarate and the maleate esters. The low reactivity of the maleate ester relative to the fumarate ester (and also the *N*-substituted maleimides) seems to indicate an effect of absorption and orientation of the substrate near the electrode. The orientation of the radical and the double bond relative to each other and to the electrode must be such that the rate of addition is fast compared to the rate of Kolbe product formation. The absorption of the maleate ester might be expected to be the same as that of the fumarate ester but the orientation of the double bonds may differ between the two. Such an effect is supported by another observation obtained in our laboratory[2]. Butadiene sulfone is absolutely inert toward methylation under the conditions of electrolysis described in the present work, even though other examples of methylation have been shown for unactivated double bonds such as ethylene (3, 4), butene-1 (2), and butene-2 (1). Therefore, the SO_2 group of the sulfone molecule may orient the double bond in such a way that the methylation is extremely slow relative to formation of the Kolbe product. Further studies on this subject are in progress.

[2]R. N. Renaud and P. J. Champagne, unpublished results.

Acknowledgements

We wish to acknowledge Mr. C. Stevens for his technical help and Mr. H. Séguin for the elemental analyses and the mass spectral determinations.

1. P. Courbis and A. Guillemonat. C.R. Acad. Sci. Paris, **t262**, 1435 (1966).
2. W. B. Smith and Y. H. Yuh. Tetrahedron, **24**, 1163 (1968).
3. K. G. Karapetyan, L. A. Kanevskii, A. M. Skundin, and Yu. B. Vasilev. Elektrokhimiya, **12**, 662 (1976).
4. K. G. Karapetyan, I. V. Proskurovskaya, A. A. Bezzubov, L. S. Kanevskii, A. M. Skudin, and Y. B. Vasilev. Sov. Electrochem. **13**, 465 (1977).
5. R. V. Lindsey, Jr. and M. L. Peterson. J. Am. Chem. Soc. **81**, 2073 (1959).
6. F. D. Mango and W. A. Bonner. J. Org. Chem. **29**, 1367 (1964).
7. M. Chkir and D. Lelandais. Chem. Commun. 1369 (1971).
8. K. G. Karapetyan, A. A. Bezzubov, L. S. Kanevskii, A. M. Skundin, and Y. B. Vasilev. Elektrokhimiya, **12**, 1623 (1976).
9. N. E. Searle. Chem. Abstr. **42**, 7340 (1939); Patent U.S. 2,444,536.
10. R. P. Linstead and M. Whalley. J. Chem. Soc. 3722 (1954).
11. J. Bode and H. Brockmann, Jr. Chem. Ber. **105**, 34 (1972).

Reactions of silicon fluorides with some non-metal hydrides

JAMES CHARLTON THOMPSON AND ARTHUR PAUL GERALD WRIGHT

Lash Miller Chemical Laboratories, University of Toronto, Toronto, Ont., Canada M5S 1A1

Received August 23, 1978

JAMES CHARLTON THOMPSON and ARTHUR PAUL GERALD WRIGHT. Can. J. Chem. **57**, 994 (1979).

The reactions of SiF_4, Si_2F_6, and SiF_2 with PH_3, CH_3PH_2, $(CH_3)_2PH$, $(CH_3)_4P_2$, $HSCH_3$, and $HSi(CH_3)_3$ have been studied. Several new compounds resulting from insertion of Si—F containing units into P—H, S—H, or Si—H bonds have been identified.

JAMES CHARLTON THOMPSON et ARTHUR PAUL GERALD WRIGHT. Can. J. Chem. **57**, 994 (1979).

On a étudié les réactions de SiF_4, Si_2F_6 et SiF_2 avec PH_3, CH_3PH_2, $(CH_3)_2PH$, $(CH_3)_4P_2$, $HSCH_3$ et $HSi(CH_3)_3$. On a identifié plusieurs nouveaux composés provenant de l'insertion d'unités contenant des Si—F dans des liaisons P—H, S—H ou Si—H.

[Traduit par le journal]

Introduction

The chemistry of the divalent silicon species, silicon difluoride (SiF_2), has been extensively studied in recent years (1). Reactions with over seventy target molecules have been reported, and many of these reactions produce novel products. These commonly contain monomeric, dimeric, or trimeric SiF_2 units and result from addition and/or insertion on the reagent molecule. Relatively few reactions in which SiF_2 reacts with a non-metal hydride have been described, though it is likely that a variety of compounds could be formed by SiF_2 insertion with the non-metal hydride bond.

SiF_2 reacts with GeH_4 to form $H(SiF_2)_nGeH_3$ where $n = 1$–3 (2). There have been no reported reactions of SiF_2 with compounds containing Si—H bonds, though it is well known that other divalent silicon species such as $(CH_3)_2Si$ will react, for example, with $HSi(CH_3)_3$ (3).

The reaction with H_2S (4) produced the 1:1 insertion product $HSiF_2SH$ as well as rearrangement products $HSiF_2SSH$ and SiF_3SiF_2SSH. Reactions with H_2O (5), B_2H_6 (6), and NH_3 (7) have also been described. More recently PH_3 (8) was found to produce $HSiF_2PH_2$, SiF_3PH_2, $HSiF_2SiF_3$, and a number of other compounds which were too unstable thermally to characterize.

Our continuing investigations into the chemistry of silicon fluorides (9) have also led us to study the PH_3 reaction and the reaction of a number of other phosphorus derivatives including CH_3PH_2, $(CH_3)_2$-PH, and $(CH_3)_4P_2$. In addition, we report here the reactions of SiF_2 with $HSCH_3$ and $HSi(CH_3)_3$. Since our method of preparation of SiF_2 always results in a mixture of SiF_2 and SiF_4, we have studied separately the interaction of SiF_4 with these compounds. The polymerization of SiF_2, which always occurs during the reactions, presumably involves the formation of Si—Si bonds, which thus may offer further possible sites for reaction. We have therefore studied the interactions of Si_2F_6 as the simplest example of a silicon fluoride with a Si—Si bond, with this series of molecules.

Experimental

(*i*) SiF_2 was prepared by the method of Timms *et al.* (10). PH_3 (11), CH_3PH_2 (12), $(CH_3)_2PH$ (13), and $(CH_3)_4P_2$ (14) were prepared by standard methods. Si_2F_6 was prepared by fluorination of Si_2Cl_6 (15). $HSCH_3$ was obtained from Matheson and $HSi(CH_3)_3$ was obtained from Peninsular Chem. Research Inc.

(*ii*) Reactions with SiF_4 or Si_2F_6 were studied initially in sealed nmr tubes employing variable temperature ^1H and ^{19}F spectra from a Varian A56/60D spectrometer. Any reactions which seemed to offer some hope of isolation of useful products were then run on a larger scale on the vacuum line.

(*iii*) The hydrides were condensed with SiF_2 at −196°C. After warm-up the products were manipulated by conventional vacuum line techniques. In some cases a low temperature fractional distillation apparatus (16) was employed in an attempt to obtain purer compounds.

(*iv*) ^1H nmr spectra were obtained on Varian T60, A56/60D, and HA100 spectrometers. ^{19}F spectra were obtained on the Varian A56/60D machine while ^{31}P spectra were run in the FT mode on a Varian XL100 spectrometer. Mass spectra were obtained on a Dupont 21-490 mass spectrometer.

Results

(*i*) *Reactions with SiF_4 and Si_2F_6*

No reaction was observed between either SiF_4 or Si_2F_6 and PH_3 at low temperatures or on warm-up to room temperature. Si_2F_6 reacted with $(CH_3)_4P_2$ at −40°C in a complicated way. Si_2Cl_6 reacts with $(CH_3)_4P_2$ to give $SiCl_3P(CH_3)_2$ (17). Si_2F_6 has been reported to react with $(CH_3)_4P_2$ to produce $SiF_3P(CH_3)_2$ in 9% yield (18). In our reaction the

0008-4042/79/090994-05$01.00/0

TABLE 1. Products of the reactions of silicon fluorides with non-metal hydrides*

Hydride	Reaction products with SiF_4	Si_2F_6	SiF_2
PH_3	NR	NR	$HSiF_3$, $HSiF_2SiF_3$, $HSiF_2PH_2$, SiF_3PH_2, $HSiF_2SiF_2PH_2$, Si_3F_8, involatile solid
CH_3PH_2	Yellow solid	Yellow solid	Si_2F_6, Si_3F_8, $HSiF_3$, $HSiF_2SiF_3$, involatile solid, no volatile Si—P compounds
$(CH_3)_2PH$	Yellow solid	Yellow solid	Si_2F_6, involatile solid, no volatile Si—P compounds
$(CH_3)_4P_2$	Yellow solid	$SiF_3P(CH_3)_2$ Yellow solid	$SiF_3P(CH_3)_2$, involatile solid
$HSCH_3$	NR	$HSiF_3$ SiF_3SCH_3	$HSiF_2SCH_3$, $HSiF_2SiF_2SCH_3$, SiF_3SCH_3, Si_2F_6, Si_3F_8, $HSiF_3$, $HSiF_2SiF_3$, $HSi(SiF_3)_2SCH_3$, $FSi(SiF_3)_2SCH_3$, $HSi(SiF_3)(SCH_3)_2$, $SiF_3Si(SCH_3)_3$, $HSiF_2Si(SCH_3)_3$, involatile solid
$HSi(CH_3)_3$	NR	NR	$FSi(CH_3)_3$, $SiF_3Si(CH_3)_3$, Si_3F_8, $HSiF_2Si(CH_3)_3$, $HSiF_2SiF_2Si(CH_3)_3$, involatile liquid

*NR = no reaction.

major product was an involatile yellow solid. A very small yield of $SiF_3P(CH_3)_2$ was produced. The compound was identified by nmr (data in Table 2).

CH_3PH_2 and $(CH_3)_2PH$ also produced unidentified yellow solids when reacted with Si_2F_6. Considerable broadening of both proton and fluorine nmr spectra was observed at −40°C when CH_3PH_2, $(CH_3)_2PH$, or $(CH_3)_4P_2$ were sealed with SiF_4 although only uncharacterized yellow solids were formed on warm-up. SiF_4 forms a 1:1 and a 2:1 adduct with $(CH_3)_3P$ at −78°C (19).

A 1:1 mixture of $HSCH_3$ and Si_2F_6 underwent little reaction at −40°C but after 1 h at room temperature only traces of starting materials remained and approximately equal quantities of $HSiF_3$ and SiF_3SCH_3 were produced. No reaction occurred between SiF_4 and $HSCH_3$.

$HSi(CH_3)_3$ did not react with Si_2F_6 or SiF_4.

(ii) Reactions with SiF_2

(a) General

Equal quantities of SiF_4 and hydride (0.07 mol) were taken for each reaction. Based on recovered SiF_4, the conversion to SiF_2 was around 50% for all reactions. The yield of total volatiles from the PH_3, $HSi(CH_3)_3$, and $HSCH_3$ reactions was about 10% based on condensed hydride. The relative yields of volatile products containing hydride moieties were similar in the three reactions. Yields from the other reactions were less than 1%. The ratio of hydride to SiF_2 in the involatile residues was not determined. These residues burn readily in air and are insoluble in organic solvents. All the residues were solid except that from $HSi(CH_3)_3$ which was a dense liquid. Nothing is yet known of the composition or structures of these residues.

When mixed in the gas phase SiF_4, SiF_2, and either $(CH_3)_2PH$ or $(CH_3)_4P_2$ reacted and deposited brown or purple solids on the walls of the apparatus prior to the co-condensation trap cooled to −196°C. No volatile products were obtained. However, by condensing alternate layers of reactants at −196°C, thereby avoiding mixing in the gas phase, small quantities of volatile product could be obtained, at least in the case of $(CH_3)_4P_2$.

Most of the volatile products from the PH_3, $HSCH_3$, and $HSi(CH_3)_3$ reactions which contained more than one SiF_2 or SiF_3 unit were thermally unstable, leaving solid residues in the vacuum line. This instability made attempts at purification by distillation or chromatography extremely difficult. Most of the identification is thus based on the low temperature nmr spectra of samples which had been subjected to minimum warming and which in many cases contained mixtures of compounds. The products identified from each reaction are shown in Table 1.

(b) PH_3 Reaction

We have identified the compounds (also found by Odom (8)) $HSiF_2PH_2$, SiF_3PH_2, and $HSiF_2SiF_3$. $HSiF_3$ was also recovered as a decomposition

TABLE 2. Summary of nmr data from the products of the reactions of SiF_2 with PH_3, CH_3PH_2, $(CH_3)_2PH$, $(CH_3)_4P_2$, $HSCH_3$, and $HSi(CH_3)_3$*

	Chemical shifts							Coupling constants												
Compound	δH Si	δH X	δF SiF_3—X	δF H—SiF_2—X	δF X—SiF_2—X	δF F—Si—X_3	δP	$^1J_{PH}$	$^2J_{HF}$	$^2J_{PF}$	$^2J_{PH}$	$^3J_{HF}$	$^3J_{FF}$	$^3J_{HH}$	$^3J_{FP}$	$^3J_{HP}$	$^4J_{HH}$	$^4J_{FF}$	$^4J_{HF}$	$^5J_{HF}$
SiF_4			164.8 s																	
Si_2F_6			124.9 s																	
Si_3F_8			136.1 t		140.1 sep								9.0							
$HSiF_3$	4.53 q		136.1 d						96.5											
$HSiF_2SiF_3$	5.02 d of q		127.7 d of t	143.4 d of q					54.8			13.0	11.1							
SiF_3PH_2		1.58 d of q	115.8 d of t				291.5 t of q	187.8		22.6		4.1								
$HSiF_2PH_2$	5.62 t of d of t	1.44 d of t of d		126.2 d of d of t			263.2 t of d of t	184.9	63.0	15.0	25.0	8.5		0.6						
$HSiF_2SiF_2PH_2$	5.02 t of t of d	1.55 d of m		146.1 d of t of d	142.5 m		251.6 tof t of q	188.0	52.4	26.2		5.8	11.0		3.0	3.0				
$SiF_3P(CH_3)_2$		1.24 d of q	130.2 d of sep							18.7	3.1								1.0	
SiF_3SCH_3		2.24 q	132.7 q																0.9	
$HSiF_2SCH_3$	5.30 t	2.02 t		131.5 d of q					76.3											1.0
$HSiF_2SiF_2SCH_3$	5.28 t of t	2.08 t of t		145.1 d of t	128.8 q of q				53.6			9.2	9.4						1.1	0.6
$HSi(SiF_3)_2SCH_3$	4.71 sep	2.33 d of sep	118.6 d of q									6.2					1.5	3.0		0.5
$FSi(SiF_3)_2SCH_3$		2.43 m	123.8 d of q			Not observed							8.2							0.4
$HSi(SiF_3)(SCH_3)_2$	5.59 q of sep	Not observed	119.1 d of sep									7.0								0.5
$SiF_3Si(SCH_3)_3$		Not observed	120.7 decet																	0.4
$HSiF_2Si(SCH_3)_3$	Not observed	Not observed		147.0 d of decets					55.0											2.0
$FSi(CH_3)_3$		0.31 d				152.6 decet						7.2								
$SiF_3Si(CH_3)_3$		0.40 q	122.6 decet																0.8	
$HSiF_2Si(CH_3)_3$	5.17 t	0.31 t		144.9 d of decets					50.5										0.6	
$HSiF_2SiF_2Si(CH_3)_3$	5.45 t	Not observed		135.4 d of t	Not observed				54.0			8.0								

*Positive δ values are chemical shifts in ppm downfield relative to internal TMS for proton resonances, upfield relative to internal CCl_3F for fluorine resonances, and upfield relative to external H_3PO_4 for phosphorus resonances. All coupling constants are in Hz. s = singlet, d = doublet, t = triplet, q = quartet, sep = septet, m = multiplet.

product from the less volatile fractions but was not trapped out immediately after warm-up of the reaction mixture. The ^{19}F chemical shift of $HSiF_3$, which we have consistently found to be around 136 ppm (upfield relative to internal CCl_3F) from this and a number of other reactions, differs from the literature value of 109.5 ppm (20). We can find no reason for this discrepancy but suspect the literature value may be in error. The remaining chemical shifts and coupling constants agree with published values. SiF_3PH_2 has been prepared by a variety of routes not involving SiF_2 (21).

In addition to these compounds we have also been able to identify a new 2:1 compound $HSiF_2SiF_2PH_2$ which could be obtained by trap-to-trap distillation but which did not survive distillation in the low temperature column. This compound was fairly stable once dissolved in a TMS/CCl_3F solution. It was volatile at $-45°C$ and was trapped out at $-63°C$ together with some Si_2F_6, some unidentified compounds, and a large amount of Si_3F_8. The relatively high yield of Si_3F_8 prevented the isolation of a pure sample of $HSiF_2SiF_2PH_2$ since these compounds could not be separated on our distillation apparatus. Both ^{19}F resonances of Si_3F_8 are to low field of and are well separated from those of $HSiF_2SiF_2PH_2$. A large amount of yellow solid appeared in the nmr tube containing this mixture after 1 day at room temperature. The nmr data are given in Table 2, and the spectra of $HSiF_2SiF_2PH_2$ are shown in Fig. 1. No full analysis of the second order ^1H and ^{19}F spectra has yet been attempted.

Mass spectral evidence in the form of molecular ion peaks and reasonable fragment ions was also obtained. There was also evidence for $Si_2F_5PH_2$ and $Si_3F_7PH_2$ from the mass spectra of the unseparated reaction products.

(c) $(CH_3)_4P_2$ Reaction

By careful low temperature operation of the vacuum system $SiF_3P(CH_3)_2$ was recovered. This compound is also formed in the reaction with Si_2F_6 (18). Our nmr spectral parameters agree with the published values except for δF which we found at 130.2 ppm (literature value 109 ppm).

(d) CH_3PH_2 and $(CH_3)_2PH$ Reactions

No volatile Si—P compounds have been found that were sufficiently stable to permit identification. Si_2F_6, Si_3F_8, $HSiF_3$, and $HSiF_2SiF_3$ were recovered from the CH_3PH_2 reaction while only Si_2F_6 was found in the $(CH_3)_2PH$ reaction.

(e) $HSCH_3$ Reaction

A number of unexpected compounds were produced in this reaction in addition to the 1:1 product $HSiF_2SCH_3$ (largest yield), 2:1 product $HSiF_2SiF_2SCH_3$, SiF_3SCH_3, Si_2F_6, Si_3F_8, $HSiF_3$, and

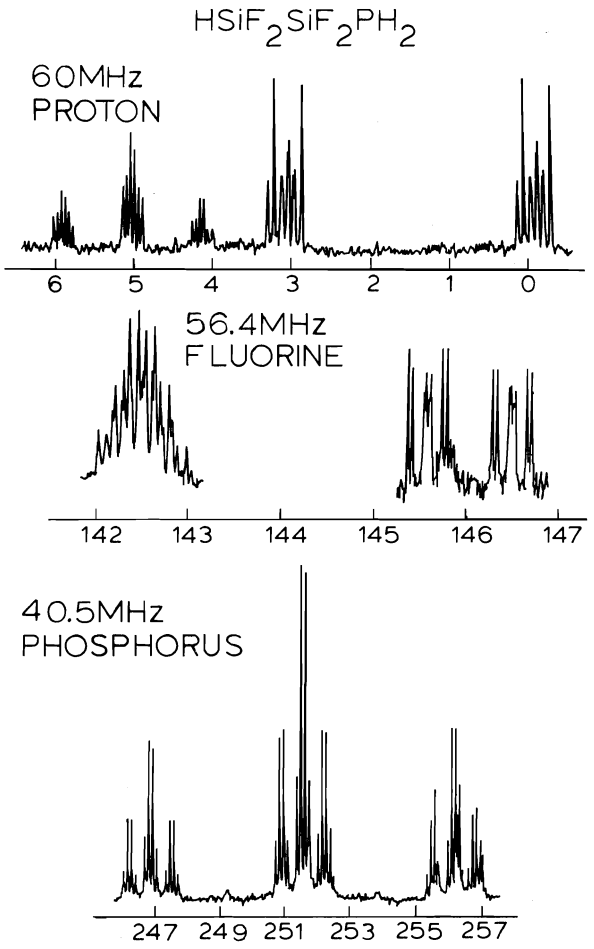

FIG. 1. Nuclear magnetic resonance spectra of $HSiF_2SiF_2PH_2$. Positive δ values are downfield from internal TMS for proton, upfield from internal CCl_3F for fluorine, and upfield from external H_3PO_4 for phosphorus.

$HSiF_2SiF_3$. The unexpected compounds contained varying numbers of SiF_3 and SCH_3 groups and included $HSi(SiF_3)_2SCH_3$, $FSi(SiF_3)_2SCH_3$, $HSi(SiF_3)(SCH_3)_2$, $SiF_3Si(SCH_3)_3$, and $HSiF_2Si(SCH_3)_3$. The nmr data which led to the identification of these compounds are given in Table 2. In some cases some of the ^{19}F and ^1H resonances were not observed. This was because the compounds were identified as mixtures in nmr tubes. Fractionation frequently changed the relative amounts of each compound but never separated them cleanly. The distribution of recovered products also varied from reaction to reaction. Thus these compounds were identified from a large number of nmr samples containing differing quantities of products. The diversity of the products in each tube resulted in a low concentration for each and frequent overlap of peaks in the ^1H spectra. These factors coupled with the low sensitivity of the available A56/60D spectrometer

relative to modern FT machines leave some doubt as to the identity of some of these compounds.

(f) $HSi(CH_3)_3$ Reaction

The product formed in highest yield was $FSi(CH_3)_3$. $SiF_3Si(CH_3)_3$ and Si_3F_8 were also produced. The 1:1 product $HSiF_2Si(CH_3)_3$ was formed in larger amounts than the 2:1 product $HSiF_2SiF_2Si(CH_3)_3$. Some unidentified volatile compounds were also produced. The involatile polymer was a clear viscous liquid. The nmr data are summarized in Table 2.

Discussion

The non-metal hydrides PH_3, $HSCH_3$, and $HSi(CH_3)_3$ all produced the 1:1 and 2:1 insertion product. Addition of methyl groups to P resulted in a loss of Si—P containing volatile products. It may be that the products were too unstable to isolate even though $SiF_3P(CH_3)_2$ was recovered from the $(CH_3)_4P_2$ reaction with SiF_2 and Si_2F_6. As mentioned above $(CH_3)_2PH$ reacts with SiF_2 at room temperature so that facile reaction occurs; but these products are not volatile, perhaps indicating that radical reactions and not simple insertion are dominant.

In the case of $HSCH_3$ more varied volatile products are produced than in the H_2S reaction. The 1:1 and 2:1 insertion products are formed as well as products from possible radical reactions. The sulphur radicals may be stabilized by the methyl group.

Similarly $HSi(CH_3)_3$ produces 1:1 and 2:1 insertion products as well as $FSi(CH_3)_3$ and $SiF_3Si(CH_3)_3$ and some unidentified unstable products.

The large amounts of $HSiF_3$, $HSiF_2SiF_3$, Si_2F_6, and Si_3F_8 might be products of the decomposition of thermally unstable products or might be formed by combination of radicals.

Acknowledgements

We wish to thank the National Research Council of Canada for financial support and Professor E. A. V. Ebsworth of the University of Edinburgh for the ^{31}P nmr spectra.

1. D. L. Perry and J. L. Margave. J. Chem. Educ. **53**, 696 (1976).
2. D. Solan and P. L. Timms. Inorg. Chem. **7**, 2157 (1968).
3. P. S. Skell and E. J. Goldstein. J. Am. Chem. Soc. **86**, 1442 (1964).
4. K. G. Sharp and J. L. Margrave. Inorg. Chem. **8**, 2655 (1969).
5. J. L. Margrave, K. G. Sharp, and P. W. Wilson. J. Am. Chem. Soc. **92**, 1530 (1970).
6. D. Solan and A. B. Burg. U.S. Natl. Tech. Inform. Serv., A.D. Rep. No. 730752. 1971.
7. J. L. Margrave and P. W. Wilson. Acc. Chem. Res. **4**, 145 (1971).
8. G. R. Langford, D. R. Moody, and J. D. Odom. Inorg. Chem. **14**, 134 (1975).
9. A. P. G. Wright. M.Sc. Thesis. University of Toronto, Toronto, Ont. 1975.
10. P. L. Timms, R. A. Kent, T. C. Ehlert, and J. L. Margrave. J. Am. Chem. Soc. **87**, 2824 (1965).
11. S. D. Gokhale and W. L. Jolly. Inorg. Synth. **9**, 56 (1967).
12. K. D. Crosbie and G. M. Sheldrick. J. Inorg. Nucl. Chem. **31**, 3684 (1969).
13. G. W. Parshall. Inorg. Synth. **11**, 157 (1968).
14. G. Kordosky, B. R. Cook, J. Gloyd, Jr., and D. W. Meek. Inorg. Synth. **14**, 14 (1973).
15. R. B. Johannesen, T. C. Farrar, F. E. Brinckman, and T. D. Coyle. J. Chem. Phys. **44**, 962 (1966).
16. J. Dobson and R. Schaeffer. Inorg. Chem. **9**, 2183 (1970).
17. T. A. Banford and A. G. MacDiarmid. Inorg. Nucl. Chem. Lett. **8**, 733 (1972).
18. R. Demuth. Z. Anorg. Allg. Chem. **427**, 221 (1976).
19. J. R. Beatie and G. A. Ozin. J. Chem. Soc. A, 2267 (1969).
20. E. A. V. Ebsworth and J. J. Turner. J. Phys. Chem. **67**, 805 (1963).
21. R. Demuth. Z. Naturforsch. **29**b, 42 (1974); G. Fritz, H. Schäfer, R. Demuth, and J. Grobe. Z. Anorg. Allg. Chem. **407**, 287 (1974); G. Fritz and H. Schäfer. Z. Anorg. Allg. Chem. **407**, 295 (1974).

Spectrophotometric study of ion pairing in diphenylmethyl alkali metals salts[1]

E. BUNCEL, B. C. MENON, AND J. P. COLPA
Department of Chemistry, Queen's University, Kingston, Ont., Canada K7L 3N6

Received October 12, 1978

E. BUNCEL, B. C. MENON, and J. P. COLPA. Can. J. Chem. **57**, 999 (1979).

A spectrophotometric study of diphenylmethyllithium (DPM^-Li^+) and diphenylmethylpotassium (DPM^-K^+) in ethereal solvents has yielded information on ion pairing and solvation phenomena in these carbanion systems. Different spectral absorptions are observed, characteristic of two types of contact ion pairs (unsolvated and partially solvated) as well as the solvent separated ion pair species, on varying the cation and solvent. This contrasts with our previous observations with triphenylmethyl alkali metal salts where only contact and solvent separated ion pairs were observed. The effect of 18-crown-6 polyether and the effect of temperature changes on the ion pairing equilibria are evaluated. Thermodynamic parameters are obtained for equilibria pertaining to the DPM^-Li^+/THF and DPM^-Li^+/DME systems. The results are discussed in relation to literature reports on ion pairing in these systems as derived from nmr studies. Comparison with triphenylmethyl alkali metal salts yields information relating to delocalization and steric effects on ion pairing.

E. BUNCEL, B. C. MENON et J. P. COLPA. Can. J. Chem. **57**, 999 (1979).

Une étude spectrophotométrique du diphénylméthyllithium (DPM^-Li^+) et du diphénylméthylpotassium (DPM^-K^+) dans des solvants éthérés a fournit des informations concernant les paires d'ions et la solvatation dans ces systèmes carbanioniques. Lorsqu'on a fait varier le cation et le solvant, on a observé diverses absorbtions spectrales qui sont caractéristiques de deux types de paires d'ions de contact (non-solvaté et partiellement solvaté) de même que des paires d'ions séparés par le solvant. Ces résultats diffèrent de ceux obtenus au cours de nos travaux antérieurs avec les sels triphénylméthyles de métaux alcalins alors qu'on avait observé uniquement la présence de paires d'ions de contact ou séparés par le solvant. On a évalué l'effet de polyéther-6 couronne-18 et de changements de température sur les équilibres des paires d'ion. On a obtenu des paramètres thermodynamiques pour l'équilibre relatif aux systèmes DMP^-Li^+/THF et DMP^-Li^+/DME. On discute des résultats en fonction de rapports, parus dans la littérature, concernant les paires d'ions présentes dans ces systèmes qui sont basés sur des études rmn. Une comparaison avec des sels triphénylméthyles de métaux alcalins fournit des informations concernant les effets stériques et la délocalisation sur le pairage des ions.

[Traduit par le journal]

In our study of triphenylmethyllithium (TPM^-Li^+) and triphenylmethylpotassium (TPM^-K^+) in ethereal solvents by uv–visible spectroscopy, it was found that these carbanion alkali metal salts showed spectral behaviour characteristic of contact or solvent-separated ion pairs, depending on the nature of the solvent, cation, temperature, and complexing agents (1). The results could be compared with a parallel study of these carbanion systems by ^1H nmr spectroscopy (2).

In this paper we have extended the systematic study to investigation of diphenylmethyl carbanion alkali metal salts (3). It was anticipated that comparison with the triphenylmethide system would be informative regarding delocalization and steric effects on ion pairing. In addition, a recent ^{13}C nmr study (4) of diphenylmethyl carbanion alkali metal salts has given evidence on ion pairing and solvation effects, providing an independent measure for comparison of our results. The necessity of investigating ion-pairing phenomena by different experimental techniques has been emphasized (5). An earlier spectrophotometric study (6) of 1,1-diphenylhexyllithium in THF or di-*n*-propyl ether and benzene or hexane mixtures was interpreted in terms of formation of specific complexed species such as RLi·2THF and RLi·4THF. Study (7) of the 1,1,4,4-tetraphenylbutane dianion, $Ph_2\bar{C}CH_2CH_2\bar{C}Ph_2$, in THF at various temperatures gave evidence of formation of more than one type of ion pair, though overlap of the absorption bands did not permit the separate observation of each ion pair. Some related spectrophotometric studies of carbanions, including the fluorenyl (8, 9) and phenylallyl (10, 11) systems have been described. We have now found that, in contrast to our previous study with triphenylmethyl alkali metal salts, the results with the diphenylmethyl system point to the presence of three types of ion pair species differing in solvation state. Whereas contact and solvent separated ion pairs have been

[1]Carbanion mechanisms. Part 10. For Part 9, see ref. 1.

0008-4042/79/090999-07$01.00/0

well characterized spectrally, there have been only scant reports in the past of partially solvated contact ion pairs in the carbanion series.

Results and Discussion

Diphenylmethyllithium (DPM^-Li^+) in THF solution was readily prepared by reaction of diphenylmethane (DPM) with *n*-butyllithium (12). The reactions in DME and Et_2O, however, proceeded only to partial completion and solutions of DPM^-Li^+ in these solvents were obtained from the THF solution by removal of THF under vacuo and replacement by the desired solvent. Diphenylmethylpotassium (DPM^-K^+) was obtained by reaction of DPM with potassium amide in THF or DME (13). The Et_2O solution of DPM^-K^+ was prepared from the THF solution as in the case of DPM^-Li^+/Et_2O above.

Effect of Solvent on Spectral Characteristics and the Nature of Ion Pairing

The spectrum of DPM^-Li^+ in Et_2O and DME at room temperature exhibits a single absorption maximum at 407 and 448 nm, respectively, while in THF two broad peaks at ca. 418 and 448 are present (Fig. 1). By analogy with reasoning detailed previously (1), these observations would suggest that DPM^-Li^+ exists in Et_2O predominantly as the contact ion pair, in DME predominantly as the solvent separated ion pair, and in THF as a mixture of both species in comparable concentrations. The bathochromic shift on passing from contact to solvent separated ion pairs is a characteristic feature of carbanion alkali metal systems studied hitherto (14). The greater effective solvating capability of DME relative to THF is evident by the fact that in the former case an appreciably larger proportion of solvent separated ion pairs are present. As these two solvents have virtually identical dielectric constants, it is probable that the possibility of bidentate coordination towards the cation of DPM^-Li^+ by DME is responsible for this effect.

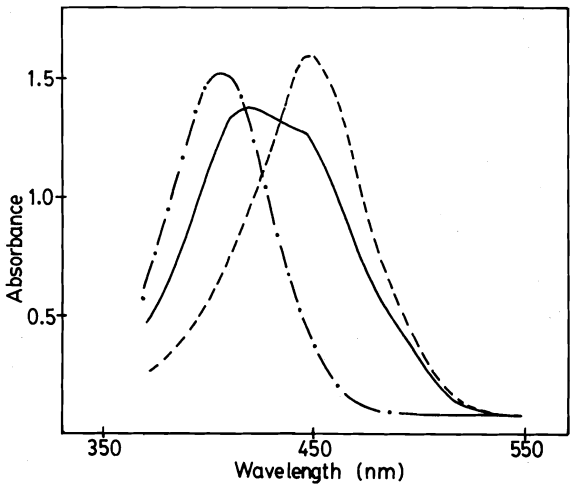

FIG. 1. Visible absorption spectra of diphenylmethyllithium in ether (·····), tetrahydrofuran (—), and dimethoxyethane (---) at room temperature.

However, the current results with diphenylmethyl carbanions (Table 1) differ from those obtained in our study of the triphenylmethyl system (Table 2). In the TPM^-Li^+ case the contact ion pair species, associated with the shorter wavelength absorption, were only observed in ether so that the results did not allow evaluation of the effect of solvent on the contact ion pair absorption. In the DPM^-Li^+ case, on the other hand, as is apparent from Fig. 1, the shorter wavelength absorption in THF is appreciably shifted with respect to Et_2O. By comparison, in studies of the fluorenyl anion system by uv–visible spectroscopy, from which we derive most of our current knowledge of the spectral characteristics of the different types of ion pairs, the F^-,Li^+ contact ion pair exhibited negligible shift (2 nm) in λ_{max} with change in solvent (9).

The present results bring forth the question whether in the DPM^-Li^+ system more than one type of contact ion pair is present, differing in solvation state. Corresponding evidence was presented (10) in the case of the 1,3-diphenylbutene anion (DPB^-) for formation of an externally solvated contact ion pair (DPB^-,M^+,S_n), in addition to the conventional (virtually unsolvated) contact ion pair (DPB^-,M^+), and the solvent separated ion pair ($DPB^-||M^+$) species. Thus the equilibria [1]–[3] were invoked on the basis of the following observations

$$[1] \qquad DPB^-,M^+ + nS \rightleftharpoons DPB^-,M^+,S_n$$

$$[2] \qquad DPB^-,M^+ + mS \rightleftharpoons DPB^-||M^+$$

$$[3] \qquad DPB^-,M^+,S_n + xS \rightleftharpoons DPB^-||M^+$$

and reasoning. (*a*) Equilibrium [1] involving formation of the externally solvated ion pair was indicated by the continuing shift in λ_{max} (467 → 502 nm) for DPB^-Li^+ in weakly solvating ethereal solvents such as Et_2O. (*b*) In media of intermediate solvating power such as tetrahydropyran absorption maxima were found to be present at 530 and 565 nm, in accord with equilibrium [3] being operative. (*c*) In dioxolane and *m*-dimethoxybenzene the two bands occurred at 500 and 565 nm, indicating that three species were present, apparently formed through combination of [1] and [2] or [1] and [3]. (*d*) In more powerful solvating media such as DME only the long wavelength (565 nm) absorption was found, characteristic of the solvent separated ion pair species.

TABLE 1. Contact (R^-,M^+), externally solvated contact (R^-,M^+,S_p), solvent separated ($R^-\|M^+$), and crown-ether complexed (R^-,X,M^+) ion pairs of diphenylmethyl carbanions

		λ_{max} (ε)[a,b]				
R^-M^+	Solvent	R^-M^+	R^-,M^+,S_p	$R^-\|M^+$	Fraction[c] of $R^-\|M^+$ at 25°C	λ_{max} R^-,X,M^+
DPM^-Li^+	Et_2O	407 (30 800)			0.0	445
	THF		418	448	0.4[d]	452
	DME			448 (37 000)	0.8[d]	448
DPM^-K^+	Et_2O	432 (40 000)			0.0	444
	THF		440 (43 000)		0.0	448
	DME		441 (43 800)		0.0	445

[a]Extinction coefficient (L mol^{-1} cm^{-1}) at absorption maximum.
[b]The λ_{max} value refers to the predominant species in the given solvent.
[c]Reckoned as $[R^-\|M^+]/([R^-,M^+] + [R^-,M^+,S_n] + [R^-\|M^+])$.
[d]This fraction is estimated from $K = [SS]/[C_2]$ at 25°C, as calculated from absorbance changes at a single wavelength, i.e. λ_{max} for the solvent separated species (see text). The results are in qualitative agreement with a procedure based on the construction of the absorption spectra by means of the component curves due to the respective ion pairs.

TABLE 2. Contact (R^-,M^+) and solvent separated ($R^-\|M^+$) ion pairs of triphenylmethyl carbanions in ethereal solvents at room temperature: effect of solvent and counterion

		λ_{max}		
R^-M^+	Solvent	R^-,M^+	$R^-\|M^+$	Fraction of $R^-\|M^+$ at 25°C
TPM^-Li^+	Et_2O	446, 390 sh		0.15
	THF		500, 435 sh	0.95
	DME		496, 432 sh	1.00
TPM^-K^+	Et_2O	476, 414 sh		0.00
	THF		486, 420 sh	0.65
	DME		494, 430 sh	0.85

The results of our work can similarly be interpreted. Thus we propose that in the DPM^-Li^+ system the 407 nm absorption is associated with the unsolvated contact ion pair $DPM^-,Li^+(C_1)$, the 418 nm absorption with the externally solvated contact ion pair $DPM^-,Li^+,S_p(C_2)$, and the 448 nm absorption with the solvent separated ion pair $DPM^-\|Li^+(SS)$. Hence in Et_2O we have present predominantly C_1, possibly in equilibrium with a small proportion of C_2 (eq. [4]). In THF the equilibrium would involve mainly C_2 and SS (eq. [5]), the two species being present in comparable amounts. In DME equilibrium [5] would be substantially on the right hand side.

$$[4] \qquad DPM^-,Li^+ + pS \rightleftharpoons DPM^-,Li^+,S_p$$

$$[5] \qquad DPM^-,Li^+,S_p + qS \rightleftharpoons DPM^-\|Li^+$$

The ambient spectrum of DPM^-K^+ in Et_2O, THF, and DME exhibits single absorption maxima at 432, 440, and 441 nm, respectively (Fig. 2). By analogy with TPM^-K^+ in Et_2O (1) as well as other potassium salts of carbanions (11) one would expect DPM^-K^+ in Et_2O to exist as the contact ion pair (C_1). The bathochromic shift of 25 nm on going from DPM^-Li^+ to DPM^-K^+ in Et_2O would then correspond to the 30 nm shift observed for $TPM^-Li^+ \rightarrow TPM^-K^+$ (1). Bathochromic shifts of this order of magnitude are generally associated with increase in cationic radius for contact ion pairs and have been attributed (15) to a greater destabilization of the

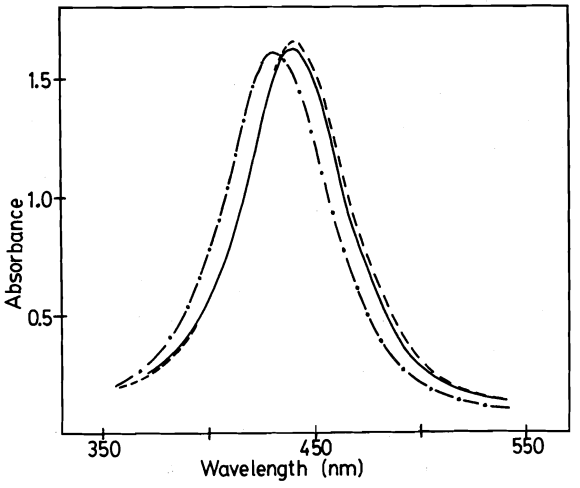

FIG. 2. Visible absorption spectra of diphenylmethylpotassium in ether (-·····-), tetrahydrofuran (—), and dimethoxyethane (---) at room temperature.

ground state than of the excited state with the larger cation. In the ground state the dipole is minimized by locating the cation close to the center of negative charge but on excitation there is a re-distribution of charge density, and hence an increased dipole, since the position of the cation is unaffected according to the Franck–Condon principle. This leads to a lower energy transition with the larger cation.

The λ_{max} value of DPM^-K^+ in THF or DME shows that in these media solvent separated ion pair species are present in negligible extent. The shift in λ_{max} from 432 nm in Et_2O to 440/441 nm in THF/DME can be ascribed to formation of the C_2 species by analogy with the above argument. We thus conclude that DPM^-K^+ in Et_2O exists predominantly as the C_1 species and in THF or DME predominantly as the C_2 species. In going from DPM^-Li^+ to DPM^-K^+ one would expect the degree of solvent separated ion pair formation to decrease, while contact/externally solvated contact ion pairs should increase, in a given solvent, in accord with the lesser solvation requirements of K^+ relative to Li^+. The results for THF and DME solvents (Table 1) bear out this expectation.

Externally solvated contact ion pairs are probably more commonly found than hitherto believed, though they may not always be spectrally resolvable. One can consider the solvent molecules in this type of ion pair to be peripherally coordinated to the cation, whereas in the solvent separated ion pair the cation is totally enveloped by the solvent molecules. Thus in the externally solvated contact ion pair charge delocalization takes place to a much lesser extent than in the solvent separated ion pair. This will be reflected in a smaller bathochromic shift for the former than for the latter, relative to the absorption maximum of the unsolvated contact ion pair.

Effect of 18-Crown-6 Ether

The addition of 18-crown-6 ether to DPM^-Li^+ in Et_2O or THF causes a shift in λ_{max} to 445 and 452 nm, respectively (Table 1), but for DME there is no noticeable change in the spectral absorption. Since crown ether complexed ion pairs have absorptions alike to the solvent separated ion pairs (1), this is further evidence that in the absence of crown DPM^-Li^+ in DME is present predominantly as the solvent separated ion pair. The shifts observed in the case of THF or Et_2O are in accord with our earlier conclusions that in the absence of crown DPM^-Li^+ exists in THF as a mixture of mainly the C_2 and SS species while in Et_2O predominantly C_1 is present. One would expect that crown ether should convert both types of contact ion pairs to the crown complexed species, as observed.

When 18-crown-6 ether was added to DPM^-K^+ in Et_2O, THF, and DME, there resulted in each case a shift in the absorption maxima, the final λ_{max} values being 444, 448, and 445 nm, respectively. These spectral characteristics correspond closely to crown ether complexed diphenylmethyllithium. Since change in cation generally has little effect on λ_{max} of solvent separated or complexed ion pairs (8–11), this corroborates our earlier conclusion that in the absence of crown ether DPM^-K^+ is present in these solvents as the two types of contact ion pairs. The small variation in λ_{max} of the crown ether complexed DPM^-K^+ ion pair with solvent change is quite comparable to corresponding observations with TPM^-K^+ (1).

Effect of Temperature

The absorption spectrum of solutions of DPM^-K^+ in Et_2O, THF, and DME remained unchanged over the temperature range 25 to −50°C. Thus there is no change in the type of ion pair present over this range.

Solutions of DPM^-Li^+ exhibited different spectral behaviour with change in temperature depending on the solvent. The effect of lowering the temperature below ambient was explored first. For DME or Et_2O the absorption spectrum remained unchanged on cooling to −50°C. In the former case this result is to be expected on the basis of the evidence that DPM^-Li^+ exists in DME predominantly as the solvent separated ion pair already at room temperature. Conversely it follows that in the latter case the contact ion pair is the predominant species present over the entire temperature range investigated.

The DPM^-Li^+/THF system has been found to exhibit large spectral changes on cooling to −60°C. Thus the absorption at 418 nm decreases while that at 448 nm increases in peak height (Fig. 3). The spectral changes are reversible, indicating that an equilibrium between two species is established. Since the DPM^-Li^+/THF system has been shown to contain the C_2 and SS species (see above), the spectral changes as a function of temperature correspond to a shift in the equilibrium [5] towards the right hand side, i.e. increased formation of solvent separated ion pairs at low temperatures.

Since in the DPM^-Li^+/DME system the ambient temperature spectrum suggested the predominance of SS species in the equilibrium [5], the effect of raising the temperature was examined on the expectation that a shift in position of the equilibrium would occur towards the C_2 species. A small effect was observed as anticipated on increasing the temperature 0 → 40°C, beyond which decomposition of the carbanion became important as shown by irreversibility of the spectral changes.

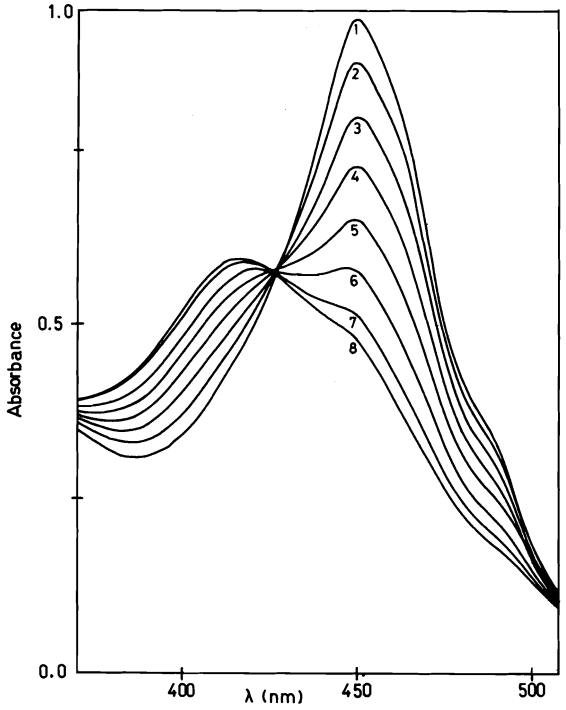

FIG. 3. Temperature variation of absorption spectra of diphenylmethyllithium in THF. Spectrum *1*, −58.0°C; *3*, −38.0°C; *5*, −14.5°C; *8*, +23°C.

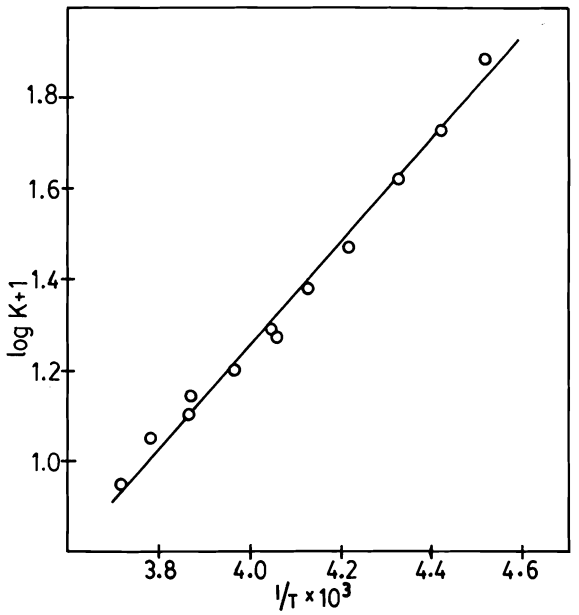

FIG. 4. log K vs. $1/T$ plot for diphenylmethyllithium in THF.

The spectral study as a function of temperature for the DPM^-Li^+/THF and DPM^-Li^+/DME systems allowed evaluation of the ΔH and ΔS parameters pertaining to equilibria [5]. The equilibrium constant at a given temperature was calculated from the expression

$$[6] \qquad K = [S]/[C] = (A - A_c)/(A_s - A)$$

where A is the observed (density corrected) absorbance value at 448 nm (λ_{max} corresponding to the SS species), while A_c, A_s are the absorbance values at 448 nm due to 100% C_2 and SS species, respectively. Since the spectrum of the C_2 species is not available, the absorption value at 448 nm due to 100% C_2 has been estimated from (*a*) the spectrum of DPM^-Li^+ in Et_2O (C_1), or (*b*) the spectrum of DPM^-Li^+ in THF at −64°C (SS), assuming that the extinction coefficients and shapes of the spectra of the C_1, C_2, and SS species are similar. From plots of log K vs. $1/T$ (e.g. Fig. 4 for DPM^-Li^+/THF) values of ΔH and ΔS were calculated. For DPM^-Li^+/THF one obtains $\Delta H = -5.4$ or -6.1 kcal/mol, $\Delta S = -20.2$ or -24.4 eu, respectively, when methods (*a*) or (*b*) were used to calculate the absorbance for 100% C_2 species at 448 nm. For DPM^-Li^+/DME, $\Delta H = -13.2$ kcal/mol, $\Delta S = -41$ eu. The error limit associated with these values is believed to be in the range 10–20%. Negative enthalpies and entropies have been characteristic of contact ⇌ solvent separated ion pair equilibria (14), and evidently the same principles apply in the formation of solvent separated ion pairs from the externally solvated contact ion pair species.

Comparison of Ultraviolet–Visible and Nuclear Magnetic Resonance Studies

Ion pairing in diphenylmethyl alkali metal salts was recently investigated by ^{13}C nmr spectroscopy (4) and the results are of interest in relation to the present work. The chemical shift changes observed for the α and *para* carbons as a function of solvent and temperature were interpreted in terms of contact and solvent separated ion pair formation. DPM^-Li^+ in DME at 25°C was found to be present almost exclusively as the solvent separated ion pair and in THF predominantly so, while DPM^-K^+ showed nmr evidence of only contact ion pairs in THF or DME.

The conclusions of the present work are in qualitative agreement with those derived from the ^{13}C nmr study, with the exception that the uv–visible study has allowed us to discern two types of contact ion pairs. Otherwise the degree of formation of solvent separated ion pairs is found to be of the same order of magnitude in both studies when the cation and solvent are varied. An important aspect of the nmr studies concerning which uv–visible spectroscopy yields no information is the sp^2 hybridized state of the central carbon in arylmethyl carbanions (16, 17), as expected on theoretical grounds (18).

Concluding Remarks

A significant finding of the present study is that the uv–visible spectral observations in the diphenylmethide system have allowed us to discern two types of contact ion pairs in addition to the solvent separated ion pairs, whereas the triphenylmethide system gave evidence of only one type of contact ion pair and the solvent separated ion pair (1).

Apart from the above finding, there is overall agreement between the conclusions of the present work and those derived from a ^{13}C nmr study of diphenylmethyl alkali metal salts (4). Previously substantial agreement had been found between our uv–visible study of triphenylmethyl alkali metal salts (1) and a corresponding ^{1}H nmr study (2) regarding the dependence of contact and solvent separated ion pair equilibria on the nature of the cation, solvent, and temperature.

A remarkable parallel of the TPM^- and DPM^- systems is the magnitude of the transition energy difference for the contact and the solvent separated (or crown ether complexed) ion pair absorptions. Thus for TPM^-Li^+, in Et_2O solvent, the transition energy difference on going from contact to complexed ion pairs is 6.3 kcal/mol, while for DPM^-Li^+ this takes the value 6.0 kcal/mol. The corresponding values for TPM^-K^+ and DPM^-K^+ are 1.9 and 1.8 kcal/mol, respectively. These parallel results are noteworthy in view of the different steric and delocalization characteristics of the two carbanions, a factor considered further below.

The tendency for solvent separated ion pair formation is greater for the Li^+ salt of both carbanions, in agreement with the greater solvation requirement of Li^+ versus K^+. However, on going from TPM^-Li^+ to DPM^-Li^+, or TPM^-K^+ to DPM^-K^+, the tendency for contact ion pair formation increases. This appears to arise in part due to delocalizability and in part to steric effects. The greater charge delocalization in TPM^- results in decreased electrostatic attraction for the cation, compared to DPM^- and its counterion. Concomitantly, the increased steric interaction between the cation and the anionic center in the "propeller" shaped trityl anion (18) will make contact ion pair formation more difficult, with the result that the solvent separated ion pair will be energetically preferred.

Finally we wish to draw attention to the conceptual difficulties involved in the clear definition of the various types of ion pairs. Thus in passing from contact to solvent separated ion pairs an intermediate state could be encountered with respect to the interaction between the charge separated solute species and the solvent molecules. This intermediate state has been termed as peripheral or external solvation, which should be of increased importance compared to the situation in contact ion pairs. Alternatively one could visualize the intermediate state as one in which the distance between the ions is larger than in the contact ion pair but not yet so large that a solvent molecule can be entirely placed between the two ions. The perturbation of the energy levels of the carbanion by the electric field of the cation will be influenced by this incipient solvation, with consequent effect on the spectral absorption. The present results have shown further that such intermediate states can have sufficient stability so as to be observable as separate species.

Experimental

Diphenylmethane (Eastman) was distilled under vacuo, bp 125°C (10 mm). *n*-Butyllithium in hexane (Aldrich or Ventron) was standardized by titration. The solvents employed were purified and dried as given previously (19). The reaction vessel used in the spectrophotometric method has been described (20). DPM^-Li^+ solutions in THF were prepared from DPM and *n*-BuLi as described previously for the case of TPM^-Li^+/THF (1). Solutions of DPM^-Li^+ in Et_2O or DME were prepared from the THF solution by removal of this solvent under vacuo and distillation of the desired solvent from a reservoir, under vacuo. This solvent replacement was performed at least twice in each case. The spectrophotometric measurements were performed as previously (1).

The spectra shown in Figs. 1 and 2 were taken in a 1 mm cell on a Unicam SP800B spectrophotometer. The carbanion concentrations were calculated from the weights of DPM and solvent employed. In Fig. 1 we have the $[DPM^-Li^+]$ values: Et_2O, 4.65×10^{-4} *M*; THF, 4.67×10^{-4} *M*; DME, 4.34×10^{-4} *M*. In Fig. 2 the $[DPM^-K^+]$ values are: Et_2O, 3.84×10^{-4} *M*; THF, 3.54×10^{-4} *M*; DME, 3.44×10^{-4} *M*.

The spectra given in Fig. 3 were taken on a Beckman Acta IV spectrophotometer using a 10 mm cuvette with $[DPM^-Li^+] = 3.18 \times 10^{-5}$ *M*.

Acknowledgment

We thank the National Research Council of Canada for continuing financial support of this research.

1. E. Buncel and B. C. Menon. J. Org. Chem. **44**, 317 (1979).
2. J. B. Grutzner, J. M. Lawlor, and L. M. Jackman. J. Am. Chem. Soc. **94**, 2306 (1972).
3. E. Buncel and B. C. Menon. Chem. Commun. 758 (1978).
4. D. H. O'Brien, C. R. Russell, and A. J. Hart. J. Am. Chem. Soc. **98**, 7427 (1976).
5. P. Chang, R. V. Slates, and M. Szwarc. J. Phys. Chem. **70**, 3180 (1966).
6. R. Waack, M. A. Doran, and P. E. Stevenson. J. Am. Chem. Soc. **88**, 2109 (1966).
7. R. Waack and M. A. Doran. J. Phys. Chem. **67**, 148 (1963).
8. J.-P. Pascault and J. Golé. Bull. Soc. Chim. Fr. 362 (1974).
9. T. E. Hogen-Esch and J. Smid. J. Am. Chem. Soc. **88**, 307 (1966).
10. J. W. Burley and R. N. Young. J. Chem. Soc. B, 1018 (1971); J. Chem. Soc. Perkin Trans. II, 835 (1972).

11. R. J. BUSHBY and G. J. FERBER. J. Chem. Soc. Perkin Trans. II, 1688 (1976).
12. B. C. MENON and E. BUNCEL. J. Organomet. Chem. **159**, 357 (1978).
13. E. BUNCEL and B. C. MENON. J. Organomet. Chem. **141**, 1 (1977).
14. J. SMID. *In* Ions and ion pairs in organic reactions. Vol. 1. *Edited by* M. Szwarc. Wiley-Interscience, NY. 1972.
15. H. V. CARTER, B. J. MCCLELLAND, and E. WARHURST. Trans. Faraday Soc. **56**, 455 (1960).
16. H. O. HOUSE, A. V. PRABHU, and W. V. PHILLIPS. J. Org. Chem. **41**, 1209 (1976).
17. D. H. O'BRIEN, A. J. HART, and C. R. RUSSELL. J. Am. Chem. Soc. **97**, 4410 (1975).
18. E. BUNCEL. Carbanions. Mechanistic and isotopic aspects. Elsevier, Amsterdam. 1975.
19. E. BUNCEL and B. C. MENON. J. Am. Chem. Soc. **99**, 4457 (1977).
20. E. BUNCEL and B. C. MENON. Can. J. Chem. **54**, 3949 (1976).

Erratum: A Mössbauer study of organotellurium compounds. Part III. Tellurium heterocycles and related compounds

NIGEL S. DANCE AND COLIN H. W. JONES
Department of Chemistry, Simon Fraser University, Burnaby, B.C., Canada V5A 1S6

Received January 9, 1979
(Ref.: Can. J. Chem. **56**, 1746 (1978))

Reference 12 on page 1751 should read
D. D. TITUS, J.-S. LEE, and R. F. ZIOLO. J. Organomet. Chem. **120**, 381 (1976).

Ultrasonic velocities, compressibilities, and heat capacities of water + tetrahydrofuran mixtures at 298.15 K[1]

OSAMU KIYOHARA,[2] PATRICK J. D'ARCY, AND GEORGE C. BENSON

Division of Chemistry, National Research Council of Canada, Ottawa, Ont., Canada K1A 0R6

Received October 12, 1978

OSAMU KIYOHARA, PATRICK J. D'ARCY, and GEORGE C. BENSON. Can. J. Chem. **57**, 1006 (1979).

Ultrasonic velocities and volumetric heat capacities at constant pressure were measured at 298.15 K for water + tetrahydrofuran mixtures over the whole concentration range using pulse–echo-overlap equipment and a flow microcalorimeter respectively. Isentropic and isothermal compressibilities and heat capacities at constant pressure and at constant volume were derived from the results in combination with the results of previous studies of thermal expansivities and excess volumes. The significance of the excess compressibilities and excess heat capacities is discussed in terms of molecular interactions.

OSAMU KIYOHARA, PATRICK J. D'ARCY et GEORGE C. BENSON. Can. J. Chem. **57**, 1006 (1979).

On a mesuré les vitesses ultrasoniques et les capacités calorifiques volumétriques à pression constante et à 298.15 K à toutes les concentrations de mélanges d'eau et de tétrahydrofuranne en faisant appel respectivement à un appareil de superposition d'écho pulsé et d'un microcalorimètre continu. On a déduit les compressibilités isentropes et isothermes ainsi que les capacités calorifiques à pression constante et à volume constant à partir des résultats examinés de concert avec des résultats d'études antérieures d'expansivités thermiques et de volumes en excès. On discute de la signification des compressibilités en excès et des capacités calorifiques en excès en termes d'interactions moléculaires.

[Traduit par le journal]

Introduction

Excess enthalpies, excess volumes, and thermal expansivities of water + tetrahydrofuran (THF) mixtures at 298.15 K have been reported previously (1, 2). The present paper describes the extension of our investigation of the thermodynamic properties of water + THF mixtures to include isobaric and isochoric heat capacities, and isentropic and isothermal compressibilities.

Experimental

Purification and handling of the THF and water were the same as in our previous work (1). The density of the THF used for the present measurements was 0.88197 g cm^{-3} at 298.15 K.

Ultrasonic velocities in water + THF mixtures were determined in a successive dilution mixing cell using a pulse–echo-overlap method (3, 4) with the rf generator operating at 3 MHz. The error of the velocities measured relative to water (1496.687 m s^{-1} at 298.15 K (5)) is believed to be less than 0.2 m s^{-1}; the error of the compositions of the mixtures is less than 0.02%.

The heat capacities of water + THF mixtures were studied in a Picker flow microcalorimeter. Details of this apparatus and its operation have been described previously (6, 7). A single reference procedure was used, in which the difference of the volumetric heat capacity $\Delta(C_p/V)$ of the mixture from that of water was determined. A value of 75.292 J K^{-1} mol^{-1} was adopted for the heat capacity of water at 298.15 K (8). The error of the molar heat capacity is estimated to be less than 0.1 J K^{-1} mol^{-1}. Mixtures were prepared by mass and the error in the mole fraction is less than 5×10^{-5}.

Results

Experimental values of the velocity of ultrasound u in water + THF mixtures are listed in Table 1, where x_1 is the mole fraction of water. The result for pure THF (1277.44 m s^{-1}) is somewhat lower than the value 1284.1 m s^{-1} interpolated from the measurements by Deshpande *et al.* (9) at 293 K and 308 K. There is a fairly sharp maximum of u at $x_1 = 0.938$. Our results are qualitatively similar to those of Baumgartner and Atkinson (10) which are available only in graphical form.

Isentropic compressibilities κ_S were calculated from the equation

$$[1] \qquad \kappa_S = (\rho u^2)^{-1}$$

where values of the density ρ were estimated from the densities of the pure components and the smoothing function for the excess volume of water + THF mixtures (1). The values obtained for κ_S are reported in Table 1.

Although absorption of ultrasound in the frequency range 10–60 MHz has been reported by Werblan *et al.* (11) for water + THF mixtures at 298 K, it appears that such absorption will not

[1]NRCC No. 17257. This work was presented in part at the 33rd Annual Calorimetry Conference, Utah State University, Logan, Utah, U.S.A., July 25–29, 1978.

[2]NRCC Research Associate from 1975.

0008-4042/79/091006-05$01.00/0

TABLE 1. Ultrasonic velocities u, isentropic compressibilities κ_S, and excess isentropic compressibilities κ_S^E, for water (1) + THF (2) mixtures at 298.15 K

x_1	u (m s^{-1})	κ_S (TPa^{-1})	κ_S^E (TPa^{-1})	x_1	u (m s^{-1})	κ_S (TPa^{-1})	κ_S^E (TPa^{-1})
0.0	1277.44	694.81	0.0	0.93019	1587.59	402.59	−166.63
0.01312	1278.74	692.97	−3.21	0.93516	1588.17	401.93	−160.71
0.03789	1281.38	689.26	−9.47	0.93772	1588.29	401.69	−157.46
0.04003	1281.56	688.98	−9.97	0.94299	1587.53	401.71	−150.04
0.08670	1286.40	682.04	−21.65	0.94697	1586.28	402.08	−143.88
0.10110	1287.98	679.79	−25.34	0.95399	1582.12	403.74	−131.54
0.20245	1299.42	663.35	−51.40	0.96256	1574.18	407.29	−114.10
0.35090	1319.53	635.53	−90.62	0.97424	1556.77	415.74	−85.10
0.46863	1340.40	608.84	−121.94	0.98351	1538.22	425.27	−57.78
0.56534	1363.85	581.58	−147.60	0.99098	1520.59	434.69	−32.99
0.65170	1393.31	550.74	−170.05	0.99265	1516.35	436.99	−27.11
0.65388	1394.26	549.81	−170.65	0.99424	1512.22	439.25	−21.40
0.71661	1424.75	521.29	−186.37	0.99485	1510.62	440.12	−19.19
0.78193	1468.21	485.08	−200.28	0.99558	1508.70	441.17	−16.53
0.80570	1487.26	470.52	−203.61	0.99676	1505.56	442.90	−12.18
0.83266	1511.25	453.20	−205.58	0.99779	1502.77	444.43	−8.34
0.88734	1561.73	419.55	−197.06	0.99835	1501.25	445.26	−6.24
0.90434	1575.13	411.02	−188.61	0.99860	1500.55	445.65	−5.29
0.91730	1582.97	405.92	−179.21	0.99931	1498.57	446.72	−2.60
0.92468	1585.99	403.81	−172.40	0.99973	1497.43	447.34	−1.02
0.92729	1586.87	403.17	−169.76	1.0	1496.687*	447.74	0.0

*Reference 5.

TABLE 2. Changes of volumetric heat capacity $\Delta(C_p/V)$, heat capacities C_p, and excess heat capacities C_p^E for water (1) + THF (2) mixtures at 298.15 K

x_1	$\Delta(C_p/V)$ (J K^{-1} cm^{-3})	C_p (J K^{-1} mol^{-1})	C_p^E (J K^{-1} mol^{-1})	x_1	$\Delta(C_p/V)$ (J K^{-1} cm^{-3})	C_p (J K^{-1} mol^{-1})	C_p^E (J K^{-1} mol^{-1})
0.0	−2.6556	123.56	0.0	0.73142	−1.2380	100.61	12.35
0.03587	−2.6237	122.57	0.73	0.75216	−1.1450	99.85	12.59
0.05212	−2.6027	122.57	1.52	0.76980	−1.0624	99.14	12.73
0.07748	−2.5733	122.23	2.41	0.79673	−0.9387	97.65	12.54
0.10118	−2.5408	122.20	3.52	0.80382	−0.9096	97.09	12.33
0.15000	−2.4793	121.41	5.09	0.81227	−0.8607	96.81	12.45
0.17571	−2.4436	121.07	5.99	0.85132	−0.6378	94.81	12.35
0.20002	−2.4073	120.82	6.91	0.88972	−0.4281	91.70	11.09
0.22479	−2.3748	120.14	7.43	0.90467	−0.3438	90.33	10.44
0.25105	−2.3353	119.64	8.19	0.92957	−0.1954	87.96	9.27
0.30514	−2.2585	117.90	9.06	0.95491	−0.0874	84.32	6.85
0.35692	−2.1793	116.07	9.74	0.95972	−0.0727	83.48	6.25
0.40332	−2.1042	114.23	10.14	0.96557	−0.0571	82.42	5.46
0.41744	−2.0782	113.76	10.34	0.96963	−0.0477	81.64	4.89
0.45347	−2.0147	112.19	10.52	0.97493	−0.0373	80.60	4.09
0.50073	−1.9219	110.18	10.79	0.97969	−0.0291	79.63	3.36
0.51052	−1.8976	109.95	11.03	0.98511	−0.0206	78.51	2.50
0.55386	−1.8005	108.05	11.23	0.98932	−0.0140	77.63	1.82
0.60481	−1.6578	106.38	12.01	0.99414	−0.0074	76.60	1.02
0.67315	−1.4533	103.23	12.16	1.0	0.0	75.292*	0.0
0.69837	−1.3602	102.28	12.43				

*Reference 8.

significantly vitiate the interpretation of κ_S as the thermodynamic isentropic compressibility.

The results of the calorimetric measurements are summarized in Table 2, where the values of $\Delta(C_p/V)$ denote the deviation of the volumetric heat capacity of the mixture from that of pure water. Molar heat capacities C_p were derived from these values using densities estimated in the manner already described. The result for pure THF (123.56 J K^{-1} mol^{-1}) is in reasonable agreement with values in the recent literature (C_p/J K^{-1} mol^{-1} = 120 (12) and 123.9 (13)).

Isothermal compressibilities κ_T and isochoric heat

capacities C_V were calculated from the equations

$$[2] \qquad \kappa_T = \kappa_S + TV\alpha^2/C_p$$

and

$$[3] \qquad C_V = C_p\kappa_S/\kappa_T$$

where α is the thermal expansion coefficient and V is the volume at temperature T. Values of α for pure THF and water + THF mixtures at 298.15 K were taken from our previous work (2); $\alpha = 0.2572\ \mathrm{kK}^{-1}$ was used for water at 298.15 K (8).

Excess compressibilities and heat capacities of the mixtures were obtained from the general relation

$$[4] \qquad X^{\mathrm{E}} = X - X^{\mathrm{id}}$$

where X and X^{id} are the values of the particular property for the real mixture and the corresponding ideal mixture, respectively. The following formulas were used for the properties of the ideal mixture:

$$[5] \qquad \bar{V}^{\mathrm{id}} = \sum x_i \bar{V}_i^0$$

$$[6] \qquad \bar{C}_p^{\mathrm{id}} = \sum x_i \bar{C}_{pi}^0$$

$$[7] \qquad \kappa_T^{\mathrm{id}} = \sum \phi_i \kappa_{Ti}^0$$

$$[8] \qquad \alpha^{\mathrm{id}} = \sum \phi_i \alpha_i^0$$

and

$$[9] \qquad \kappa_S^{\mathrm{id}} = \kappa_T^{\mathrm{id}} - T\bar{V}^{\mathrm{id}}(\alpha^{\mathrm{id}})^2/\bar{C}_p^{\mathrm{id}}$$

where the superbar denotes a molar quantity and the superscript zero indicates a value for a pure component. In eqs. [7] and [8]

$$[10] \qquad \phi_i = x_i \bar{V}_i^0/\bar{V}^{\mathrm{id}}$$

is the volume fraction of component i. Results for κ_S^{E} and C_p^{E} are listed in Tables 1 and 2, respectively.

We were unable to find smoothing functions to represent the experimental results for κ_S^{E} and C_p^{E} accurately over the entire mole fraction range. Similar difficulties were experienced in our previous studies of other excess thermodynamic properties of water + THF mixtures (1, 2). The best representations were obtained with the functional form

$$[11] \qquad X^{\mathrm{E}} = z(1-z)\sum_{j=1}^{n} a_j(1-2z)^{j-1}$$

with z equal to the volume fraction in the case of κ_S^{E} and z equal to the mole fraction in the case of C_p^{E}. Values of the coefficients determined by the method of least squares with all points weighted equally are listed in Table 3, along with the standard deviations of the representations. These functions are suitable for interpolation over most of the mole fraction range, but are less reliable near the ends of the range, particularly for evaluating slopes near $x_1 = 1$.

TABLE 3. Coefficients a_j and standard deviations σ for representations of κ_S^{E} and C_p^{E} by eq. [11]*

Parameter	Value for κ_S^{E} (TPa^{-1})	Value for C_p^{E} ($\mathrm{J\,K^{-1}\,mol^{-1}}$)
a_1	−818.88	43.82
a_2	97.24	−15.44
a_3	−164.41	39.02
a_4	−217.77	−20.03
a_5		22.36
a_6		−56.48
σ	0.29	0.14

*For κ_S^{E}, $z = \phi_1$; for C_p^{E}, $z = x_1$.

Plots of the experimental results for κ_S^{E} and C_p^{E} and of their representations by [11] are shown in Figs. 1 and 2. Also included in these figures are curves for κ_T^{E} and C_V^{E} calculated from the smoothed values of κ_S^{E} and C_p^{E}, and of $V^{\mathrm{E}}(1)$ and $\alpha^{\mathrm{E}}(2)$. Glew and Watts (14) reported excess enthalpies H^{E} for water + THF mixtures at 283 K and 298 K. Assuming that H^{E} varies linearly with temperature (i.e. C_p^{E} is independent of temperature) we estimated the values of $\partial H^{\mathrm{E}}/\partial T$ which are shown in Fig. 2. These

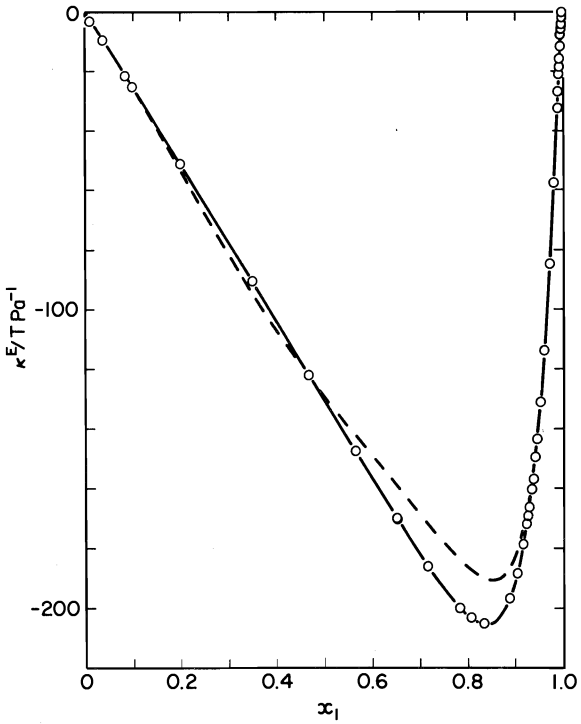

FIG. 1. Excess compressibilities of water (1) + THF (2) mixtures at 298.15 K. Points: ○, experimental results for κ_S^{E}. Curves: ——, κ_S^{E}; ---, κ_T^{E}.

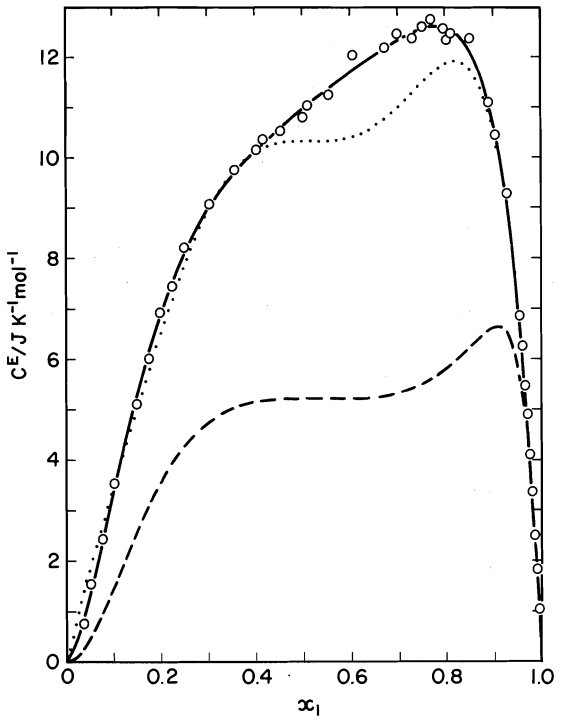

FIG. 2. Excess heat capacities of water (1) + THF (2) mixtures at 298.15 K. Points: ○, experimental results for C_p^E. Curves: ——, C_p^E; ---, C_V^E; · · ·, $\partial H^E/\partial T$ estimated from Glew and Watts (14).

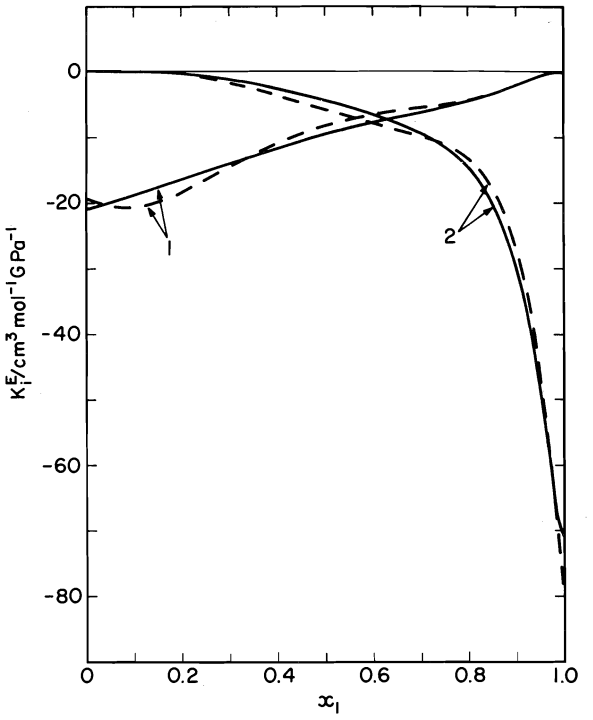

FIG. 3. Partial molar excess compressibilities of water (1) + THF (2) mixtures at 298.15 K. Curves: ——, $K_{S,i}^E$; ---, $K_{T,i}^E$. Labels denote component i.

agree reasonably well with the results of our more direct calorimetric determinations.

Discussion

Previous studies of excess volumes, enthalpies, and thermal expansivities (1, 2) suggest that the THF molecule enhances water structure in dilute water + THF mixtures. Over the central mole fraction range, the mixture behaves like a pseudo two-phase system, and in THF-rich mixtures hydrogen bonding is the predominant interaction between water and THF molecules.

The excess isentropic and isothermal compressibilities in Fig. 1 are both negative over the whole mole fraction range with deep minima near $x_1 = 0.85$. The curves cross several times and the differences between them are relatively small. In Fig. 2 the excess heat capacities at constant pressure and at constant volume are positive. The maximum of C_p^E occurs at $x_1 = 0.78$, that of C_V^E at $x_1 = 0.91$. The C_V^E curve is relatively flat over the central mole fraction range.

The behavior of the excess compressibilities and of the excess heat capacities qualitatively support the view that strong hydrophobic hydration occurs in water + THF mixtures. To investigate this aspect further, partial molar excess compressibilities $K_{S,i}^E$ and $K_{T,i}^E$ and partial molar excess heat capacities $C_{p,i}^E$ and $C_{V,i}^E$ were calculated.[3] Over most of the mole fraction range, the smoothing equations for the excess properties κ_S^E, C_p^E, V^E, and α^E were used for this calculation. However, values for dilute THF mixtures were obtained by smoothing the experimental results with cubic splines. Curves of the partial molar excess compressibilities and heat capacities are plotted in Figs. 3 and 4. Values of $C_{p,2}^E$ from the literature (12) are included in Fig. 4 for comparison. At infinite dilution, the limiting value of $K_{S,2}^E$ is -71 cm^3 mol^{-1} GPa^{-1} and of C_p^E is 172 J K^{-1} mol^{-1}. These agree fairly well with values derived from the literature ($K_{S,2}^E$/cm^3 mol^{-1} GPa^{-1} $= -70.4$ (15); $C_{p,2}^E$/J K^{-1} mol^{-1} $= 160 \pm 11$ (16), 171 (17), 172 (12)).

The most interesting feature of the curves in Figs. 3 and 4 is the rapid change of the partial molar excess values for THF in the dilute THF region. Differences between the partial molar excess compressibilities at constant entropy and at constant temperature are relatively insignificant, and the variation of $K_{S,1}^E$ (and $K_{T,1}^E$) is nearly linear in x_1. The partial molar excess heat capacities for water are approximately

[3]By definition, $K_{S,i}^E$ and $K_{T,i}^E$ are the partial derivatives of the quantities $(V\kappa_S)^E$ and $(V\kappa_T)^E$ with respect to the moles of component i.

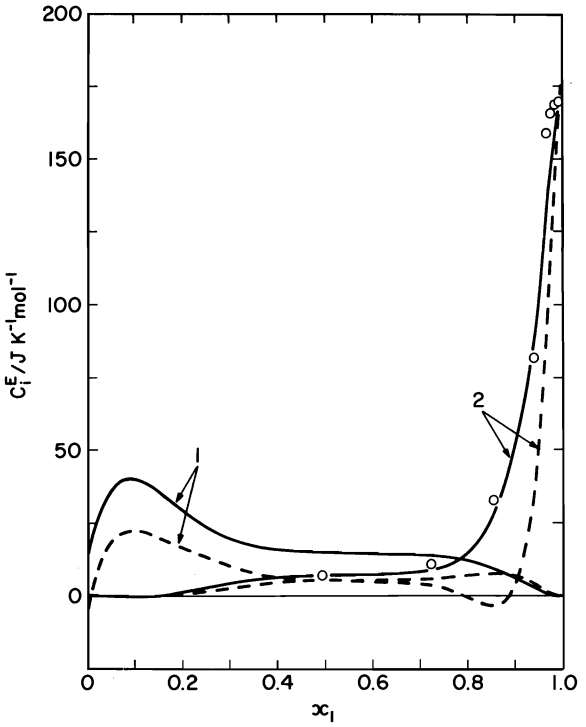

FIG. 4. Partial molar excess heat capacities of water (1) + THF (2) mixtures at 298.15 K. Curves: ——, $C_{p,i}{}^E$; ---, $C_{V,i}{}^E$. Labels denote component *i*. Points: ○, $C_{p,2}{}^E$ from ref. 12.

constant over the central mole fraction range and have small broad maxima near $x_1 = 0.1$. The general pattern of the curves in Fig. 4 is quite similar to that of the partial molar excess expansivities, apart from the sharp peak observed for the partial molar excess expansivity of THF at $x_1 = 0.94$ (2).

The positive slopes of $C_{p,1}{}^E$ and $C_{V,1}{}^E$ for $x_1 < 0.1$ are subject to rather large uncertainties because of the paucity of our measurements of C_p in this region. However, we believe that the elevated values of $C_{p,1}{}^E$ and $C_{V,1}{}^E$ for THF-rich mixtures are real and that they may be due to interactions between unlike species which promote association of water molecules. The subsequent flat behavior of these properties over the central mole fraction range supports the suggestion of a pseudo two-phase region consisting of clusters of water molecules and a random phase comprising water and THF molecules. Stabilization of the water clusters in the random molecular environment is reflected in the negative excess compressibilities and positive excess heat capacities. This picture is in accord with infrared studies (18) which show that the hydrogen bonding of water molecules is stronger in the range $x_1 = 0.15$–0.82 than in pure water, and also with nmr relaxation time measurements (19) which show an increase of water reorientation times in the water-rich region. However it should be noted that Dawber (20) has recently concluded from magneto-optical rotation studies that THF breaks the water structure over the whole mole fraction range. This contradiction appears to be largely semantic since the magneto-optical measurement is based on a comparison with pure water and formation of a clathrate cage is regarded as a disruption of the normal water structure (21).

Acknowledgements

We are indebted to J. D. Hazlett for carrying out some of the heat capacity measurements and to C. J. Halpin for purifying the THF.

1. O. KIYOHARA and G. C. BENSON. Can. J. Chem. **55**, 1354 (1977).
2. O. KIYOHARA, P. J. D'ARCY, and G. C. BENSON. Can. J. Chem. **56**, 2803 (1978).
3. O. KIYOHARA, J.-P. E. GROLIER, and G. C. BENSON. Can. J. Chem. **52**, 2287 (1974).
4. O. KIYOHARA, C. J. HALPIN, and G. C. BENSON. Can. J. Chem. **55**, 3544 (1977).
5. V. A. DEL GROSSO and C. W. MADER. J. Acoust. Soc. Am. **52**, 1442 (1972).
6. J.-L. FORTIER, G. C. BENSON, and P. PICKER. J. Chem. Thermodyn. **8**, 289 (1976).
7. J.-L. FORTIER and G. C. BENSON. J. Chem. Thermodyn. **8**, 411 (1976).
8. G. S. KELL. J. Chem. Eng. Data, **20**, 97 (1975).
9. D. D. DESHPANDE, L. G. BHATGADDE, S. OSWAL, and C. S. PRABHU. J. Chem. Eng. Data, **16**, 469 (1971).
10. E. K. BAUMGARTNER and G. ATKINSON. J. Phys. Chem. **75**, 2336 (1971).
11. L. WERBLAN, J. LESIŃSKI, and L. SKUBISZAK. Rocz. Chem. **49**, 221 (1975).
12. O. D. BONNER and P. J. CERUTTI. J. Chem. Thermodyn. **8**, 105 (1976).
13. B. V. LEBEDEV, I. B. RABINOVICH, V. I. MILOV, and V. YA. LITYAGOV. J. Chem. Thermodyn. **10**, 321 (1978).
14. D. N. GLEW and H. WATTS. Can. J. Chem. **51**, 1933 (1973).
15. F. FRANKS, J. R. RAVENHILL, and D. S. REID. J. Solution Chem. **1**, 3 (1972).
16. F. FRANKS, M. A. J. QUICKENDEN, D. S. REID, and B. WATSON. Trans. Faraday Soc. **66**, 582 (1970).
17. S. CABANI, G. CONTI, A. MARTINELLI, and E. MATTEOLI. J. Chem. Soc. Faraday Trans. I, **69**, 2112 (1973).
18. O. D. BONNER and Y. S. CHOI. J. Phys. Chem. **78**, 1727 (1974).
19. E. V. GOLDAMMER and M. D. ZEIDLER. Ber. Bunsenges. **73**, 4 (1969).
20. J. G. DAWBER. J. Chem. Soc. Faraday I, **74**, 1702 (1978).
21. J. G. DAWBER. J. Chem. Soc. Faraday I, **74**, 960 (1978).

Nucleophilic substitution in tris(pentafluorophenyl)phosphine

HANNA R. HANNA AND JACK M. MILLER[1]

Department of Chemistry, Brock University, St. Catharines, Ont., Canada L2S 3A1

Received September 28, 1978

HANNA R. HANNA and JACK M. MILLER. Can. J. Chem. **57**, 1011 (1979).

Reaction of tris(pentafluorophenyl)phosphine with various nucleophiles (DMF, HMPA, HEPA, diethylformamide, hydrazine, UDMH, phenylhydrazine, formamide, and aniline) gave exclusively the replacement of all three *para* fluorines with the exception of aniline, phenylhydrazine, and formamide which gave mixtures of the mono- and bis-4-substituted phosphines. Sodium bisulphide and various alkoxides led mainly to C—P bond rupture though some alkoxides did under certain conditions give some of the expected substitution product. ^{19}F, ^{31}P, and ^{1}H nmr and mass spectral data are presented.

HANNA R. HANNA et JACK M. MILLER. Can. J. Chem. **57**, 1011 (1979).

La réaction de la tris(pentaphényl)phosphine avec divers nucléophiles (DMF, HMPA, HEPA, diéthylformamide, hydrazine, UDMH, phénylhydrazine, formamide et aniline) conduit uniquement à la substitution des trois fluors en *para* à l'exception de l'aniline, de la phénylhydrazine et de la formamide qui conduisent à des mélanges de phosphines mono- et bis-substituées. Le bisulfure et divers alcoolates de sodium conduisent à la rupture de la liaison C—P même si quelques alcoolates ont conduits, dans certains cas, à un peu du produit de substitution attendu. On présente des données de spectroscopie de masse et de rmn du ^{19}F, du ^{31}P et du ^{1}H.

[Traduit par le journal]

Introduction

As part of our continuing study of rearrangements in the mass spectra of perhaloaromatic compounds (1, 2) we wish to look at a series of substituted tetrafluorophenyl derivatives of phosphorus. Rather than preparing these by reaction of the corresponding fluoroaromatic lithium reagent with PX_3, etc., we investigated the possibility of their preparation by nucleophilic displacement of fluorine from tris(pentafluorophenyl)phosphine (**1**).

Reaction of hexafluorobenzene with nucleophiles such as NH_3 (3, 4), *N*-methylacetamide (5), amines (6–8), alkoxides (9–13), etc., is a well-known route for the production of pentafluorophenyl compounds. Studies of nucleophilic attack on pentafluorobenzene and its derivatives C_6F_5X (14–19) show that the fluorine *para* to the hydrogen or other substituent X is most readily substituted (e.g., X = H, Me, SMe, NMe_2) but *meta* substitution is possible (X = NH^-, O^-). Burdon (20) and Epiotis and Cherry (21) have explained these observations on both qualitative and on a MO basis.

There have been two previous reports of nucleophilic displacement of fluorine for pentafluorophenyl phosphorus compounds. Burdon *et al.* (22) have studied reactions of nucleophiles with pentafluorophenyldiphenylphosphine (**2**), its oxide (**3**), and sulphide (**4**). With NaOMe in MeOH, **2** gave the 4-methoxytetrafluorophenyl derivative, whereas with $MeNH_2$ in MeOH the 4-*N*-methylaminotetrafluorophenyl derivative was produced. In the case of **3** and in part **4**, methoxide resulted in cleavage of the C_6F_5 group from the phosphorus, though for **4** the 4-methoxy derivative was the main product (59%) along with some 21% of the 2,4-dimethoxytrifluorophenyl derivative. Methylamine with **3** or **4** resulted in mixtures of the *ortho*- and *para*-substituted tetrafluorophenyl compound when benzene was the solvent but exclusive *para* replacement was observed in ethanol as solvent. Magnelli *et al.* (11) report that the reactions of Me_2NH with $(C_6F_5)_2PCl$ gave a mixture of $(4\text{-}NMe_2C_6F_4)_2$ $PNMe_2$ or $[C_6F_3(NMe_2)_2]P(C_6F_5)(NMe_2)$.

In this work we have reacted **1** with a wide variety of nucleophiles with the results as noted below.

Results and Discussion

Tris[4-(N,N-dimethylamino)-2,3,5,6-tetrafluorophenyl]phosphine (5)

Pedersen *et al.* (24) showed that hexamethylphosphoric triamide (HMPA) is an excellent nucleophilic reagent for the introduction of a dimethylamino group into *para*-substituted nitrobenzenes, whereas high pressures were required for corresponding reactions of dimethylamine. The reaction was surprisingly fast, giving, after only 10 min, the trisubstituted *para* product (**5**) which was isolated in good yield. A small amount of the corresponding

[1]Author to whom correspondence should be addressed.

0008-4042/79/091011-07$01.00/0

phosphine oxide was also detected as a by-product, presumably formed by air oxidation while the reaction mix was refluxing.

An analogous reaction using dimethylformamide (DMF) also yielded product **5** but in a very much slower reaction (51 h). This slow reaction permits the preparation of the mono- and bissubstituted derivatives as well as **5** since after 3 h only 14% of the starting material is consumed and the product at that point shows substitution in one of the rings. Substitution on the second ring begins after 7 h and substitution on all three rings begins to be detected after about 12 h. The yield in the DMF preparation is lower than when HMPA is used and more phosphine oxide impurity is produced by the longer reflux times.

The diethylamino derivatives (**6**) corresponding to **5** could be similarly prepared from diethylformamide (DEF) or hexaethylphosphoric triamide (HEPA); the latter reaction is much faster than the former, but requires 30 min for incomplete reaction compared with 10 min for the complete reaction with HMPA. This is consistent with the lower nucleophilicity of HEPA vs. HMPA (25, 26). The DEF route is preferred here on the basis of cost.

Another simple amine derivative was obtained from the reaction of aniline in ethanol with **1**, yielding the bis derivative after 71 h. With aniline as the solvent the same results were seen after only 6 h. Addition of KF to the aniline gave similar results in only 3 h, an example of enhanced nucleophilicity due to hydrogen bonding (27–32).

Reactions of $(C_6F_5)_3P$ with Hydrazines

Aqueous hydrazine in ethanol gave a good yield of tris(4-hydrazine-2,3,5,6-tetrafluorophenyl)phosphine (**7**). No oxidation of the phosphine was observed, possibly as a result of competing oxidation of the hydrazine. The reactions were solvent dependent, a good yield being obtained with a large excess of ethanol. Tetrafluorophenylhydrazine was the major product obtained at ethanol–water mixtures on the order of 2:1 or if aqueous hydrazine alone was used. In dioxane an exothermic reaction rapidly produced the phosphine oxide, $(C_6F_5)_3PO$.

N,N-Dimethylhydrazine reacted slowly with **1** under reflux conditions (40% after 7 h) but in the presence of finely divided anhydrous potassium fluoride a 71% yield was obtained in a shorter time (1½ h). This is due to the formation of a strongly hydrogen bonded solvate, with electron density donated by the fluoride ion via the hydrogen bond being able to improve the nucleophilicity of the $—NH_2$ group of the hydrazine. In addition the KF can convert HF produced to KHF_2. This improvement in yield is another example of strong hydrogen-bond-assisted reactions studied by Clark and Miller in a recent series of papers (27–32). Theoretical calculations of Emsley *et al.* (33) showed that the Mulliken charges on the hydroxy oxygen are greater in the acetic acid – fluoride system than in free acetate ion itself, consistent with the observed results.

Although the mass spectrum showed the expected molecular ion (*m/e* 652), proton and fluorine nmr spectra revealed a mixture of two isomeric compounds. Upon recrystallization, the major product obtained was tris[4-(*N,N*-dimethylhydrazine)-2,3,5,6-tetrafluorophenyl]phosphine (**8**) as shown by the nmr (^1H δ 2.6 ppm, sharp singlet, $(CH_3)_2N—$; δ 4.5 ppm, triplet due to coupling to 2 ring fluorines, —NH—: ^{19}F δ −156.9 ppm, multiplet 2 fluorines *ortho* to —NH— and δ −134.3 ppm, 2 fluorines *ortho* to phosphorus). The second product obtained from the mother liquor was the isomer with the hydrazine isomerized from unsymmetrical to symmetrical dimethylhydrazine, i.e., tris[4-(*N,N'*-dimethylhydrazine)-2,3,5,6-tetrafluorophenyl]phosphine (**9**), contaminated by a small amount of **8**. The ^1H nmr spectra show one methyl resonance at δ 2.6 and a second at 3.0 split into a triplet by the *ortho*-ring fluorines, the chemical shift being similar to that in compound **5**. Similarly, the ^{19}F nmr spectra has a new multiplet at δ −152.5 very similar to that observed for the two fluorines *ortho* to the $—NMe_2$ group in **5**. The other two fluorine resonances overlap those of **8**, such that their integrated intensity is equal to the two sets of fluorines *ortho* to nitrogen at δ −152.5 and −156.9. We are unable to account for this isomerization. On refluxing **1** with phenylhydrazine in THF a monosubstituted derivative was isolated, this being bispentafluorophenyl-(4-β-phenylhydrazine-2,3,5,6-tetrafluorophenyl)phosphine, ^1H and ^{19}F nmr confirming the structure.

Substitution by NH_2 Groups

Reaction of ammonium hydroxide with **1** in refluxing ethanol or THF with or without the presence of KF was unsuccessful but at elevated pressure in ethanol, mono- (**10**), di- (**11**), and tri- (**12**) substituted species were observed along with mixed species involving attack of both NH_2^- and ethoxide ion. In isopropanol the major product was the trisamino derivative (**12**). In hexane, a mixture of **11** and **12** was obtained. Ammonium hydroxide with no ethanol gave a mixture of **10**, **11**, and **12**, though anhydrous ammonia in ethanol did not react after 24 h. However, in THF at 130°C in the presence of anhydrous KF, anhydrous ammonia gave **11** as the sole product after 24 h or a mixture at a shorter time. This is another example of a hydrogen-bond-assisted reaction.

Refluxing **1** with commercial formamide gave a

mixture of **10**, **11**, and **12** plus a side product identified as $(NH_2C_6F_4)_2PC_6F_4NHCHO$ (**13**).

Other Nucleophiles

The reactions of **1** with different alkoxides in the corresponding alcohols lead mainly to C—P bond cleavage giving pentafluorobenzene and alkoxytetrafluorobenzene as the main products. When triphenylphosphine itself was subjected to similar conditions it was recovered unchanged. In pentafluorophenyldiphenylphosphine C—P bond cleavage did not occur but rather the fluorinated ring was substituted in the 4 position (22). It thus appears that on increasing fluorine substitution in the rings, the C—P bond becomes more susceptible to nucleophilic attack. However, with some of the higher alkoxides such as *tert*-butoxide, reaction at room temperature slowly gave a mono-substituted derivative. When methanol was replaced by ether as the solvent in the reaction of **1** with sodium methoxide, a 20% yield of tris(4-methoxy-2,3,5,6-tetrafluorophenyl)phosphine (**14**) was obtained as well as the usual cleavage products.

Somewhat similar behaviour was observed for tris(pentafluorophenyl)phosphine oxide (**15**), i.e.,

$$(C_6F_5)_3PO \xrightarrow[CH_3OH \text{ or hexane}]{NaOCH_3} (CH_3O)_2C_6F_3{-}\overset{\overset{O}{\parallel}}{P}{-}(OCH_3)_2$$

15 **16**

SH^- nucleophiles resulted only in cleavage products.

Nuclear Magnetic Resonance Studies

The ^1H, ^{19}F, and ^{31}P nmr spectra of the *para*-trissubstituted derivatives are summarized in Table 1. The proton nmr data are similar to that observed for the corresponding substituted benzene or pentafluorophenyl derivative, a fact which aided appreciably in the determination of substitution and isomerization in the case of the hydrazine derivatives.

In the ^{19}F spectra, $\delta_{2,6}$, the chemical shift of the fluorines *ortho* to phosphorus are only slightly affected, the range of shifts being from a low of -130.6 ppm for X = F to a maximum of -135.2 ppm for X = NH_2. Crudely, there is an electronegativity effect, on changing the substituting atom from F to O to N. All five nitrogen derivatives fall into the narrow range of -134.1 to -135.2 ppm. The range is only 0.7 ppm if —NH_2 is not considered.

The second ^{19}F shift, $\delta_{3,5}$, that of the fluorines *ortho* to the nucleophile and *meta* to the phosphorus show a much wider variation. The shift now ranges from -150.8 to -162.5 ppm in the following order of shifts upfield of $CFCl_3$: $NEt_2 < NMe_2 < NHNH_2 < NHNMe_2 < OCH_2 < F < NH_2$.

The F—F coupling constants show little variation, what there is usually being characteristic of the nucleophile X. For example, $J_{2,3}$ is in the narrow range of 19–21 Hz for nitrogen nucleophile vs. 16.7 for —OMe and 24.2 for F. None of the other F–F couplings of the AA′BB′X system show any systematic variation. Similarly, the P–F couplings show little variation on substitution of the fluorine at position 1 by various species, J_{P-F} falling into a narrow range of 35.8–37.8 Hz.

There was also very little variation in the ^{31}P chemical shifts. By far the greatest variation was noted when deuterioacetone rather than the $CDCl_3$ had to be used as the solvent.

Mass Spectra

The mass spectra of these compounds did not exhibit the dominant losses of PF_3, PF_2, and PF neutral species previously reported for **1** and related compounds (34, 35). Rather, the spectra appear to be dominated by fragmentation of the substituent. Only one compound, the amino derivative **12** showed metastable ion supported loss of PF_2 from the R_2P^+ ion (Scheme 1). This is contrasted with the fragmentation of the dimethylamine compound **5** shown in Scheme 2. Here the metastable ions show either loss of entire ligands or fragmentation of the ring substituent. The loss of HF is a common mode of fragmentation. The concentration of fragmentation modes involving the nitrogen or oxygen based nucleophiles suggests that the lone pairs on these atoms are the site of ionization, rather than the phosphorus lone pair suggested in the case of **1**.

For all the derivatives studied, the parent ions were of high intensity, being the base peak for compounds **1**, **5**, **12**, and **14**. For the remaining compounds the base peak is derived from losses of simple moieties from the nucleophile. All compounds showed loss of a first C_6F_4X group followed by a second, consistent with the behaviour of the parent compound $(C_6F_5)_3P$. Similar fragmentation of substituents is observed from the parent ion, R_3P^+, and the two products of the above cleavages, the R_2P^+ and RP^+ ions. For example, NMe_2 is lost from each in the case of **5**, C_2H_5 or CH_3 lost from each in the spectra of **6**, NH in the case of **7**, CH_3 from **8**, and OCH_3 or CH_3 in fragmentation of **14**. For almost all the derivatives studied, high mass ions carried the bulk of the positive ionization.

Experimental

Infrared spectra were recorded on PE 225 or 237B spectrometers using KBr disks. Nuclear magnetic resonance spectra were obtained on a Bruker WP-60 FT nmr spectrometer operating at 60 MHz (^1H, 90° pulse = 3.8 μs), 56.45 MHz (^{19}F, 90° pulse = 4.0 μs), and 24.288 MHz (^{31}P, 90° pulse = 11 μs). Spectra were normally run in $CDCl_3$ solution using deuterium lock, internal TMS reference (^1H), internal C_6F_6 reference (^{19}F reported relative to $CFCl_3$, negative numbers being upfield shifts) and external 85% H_3PO_4 (^{31}P). Some of

TABLE 1. Nuclear magnetic resonance parameters

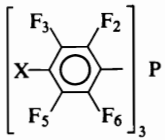

Compound No.	X	^{1}H nmr δ (ppm)	^{1}H nmr J (Hz)	^{1}H nmr Multiplicity	^{19}F Shifts (ppm) from $CFCl_3$* δ $F_{2,6}$	^{19}F Shifts (ppm) from $CFCl_3$* δ $F_{3,5}$	^{19}F J (Hz) $J_{X,3}$	$J_{2,3}$	$J_{3,5}$	$J_{3,6}$	$J_{2,6}$	$J_{F_{2,6}-P}$	^{31}P δ† (ppm)	^{31}P $J_{P-F_{2,6}}$ (Hz)	Solvent
5	$-N(CH_3)_2$	3.0	J_{H-F} 2.5	t	−134.8	−152.7	2.4	19.0	—	6.8	3.2	36.0	−76.86	36.1	$CDCl_3$
6	$-N(CH_2-CH_3)_2$	1.1 3.3	J_{H-H} 7.0	t q	−134.7	150.8	0	20.0	0.6–2.5	6.0	3.2	36.3	−76.52	36.3	$CDCl_3$
7	$-NH-NH_2$	2.9 7.8	— —	s m	−134.1	−155.6	0	19.6	3.2	6.5	3.4	37.2	−71.84	37.3	$(CD_3)_2CO$
8	$-NH-N(CH_3)_2$	2.6 4.5	 3.7	s m	−134.3	−156.9	0	21.0	3.2	7.0	3.5	36.6	−76.26	36.6	$CDCl_3$
8	$-NH-N(CH_3)_2$	2.6 6.2	 2.7	s m	—	—	—	—	—	—	—	—	—	—	$(CD_3)_2CO$
12	$-NH_2$	4.2		s	−135.2	−162.5	0	20.1	—	6.85	3.43	37.8	−77.24	37.8	$CDCl_3$
14	$-OCH_3$	4.1	J_{H-F} 1.8	t	−133.3	−157.9	1.72	16.7	—	6.7	3.45	35.8	−75.46	35.8	$CDCl_3$
1	F	—	—	—	−130.6	−159.8	20.0	24.2	4.6	8.8	—	36.5	−74.22	36.2	$CDCl_3$

NOTE: abbreviations: s, singlet; t, triplet; q, quartet; m, multiplet.
*δ ^{19}F in ppm reported as being negative shifts upfield of $CFCl_3$ (referenced to C_6F_6; δ −163.0 ppm as internal reference).
†^{31}P spectra show septets from coupling to three sets of two fluorines in positions 2 and 6. Referenced to external 85% phosphoric acid, negative shifts indicate the upfield direction.

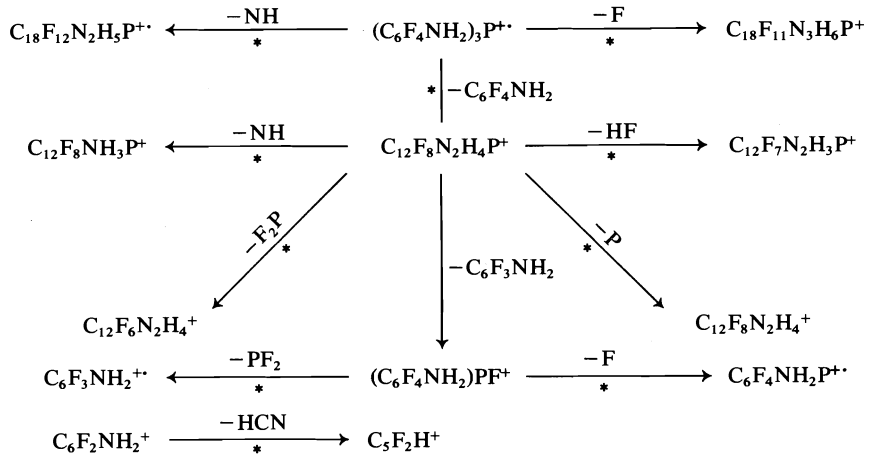

SCHEME 1. Mass spectral fragmentation of $(C_6F_4NH_2)_3P$.

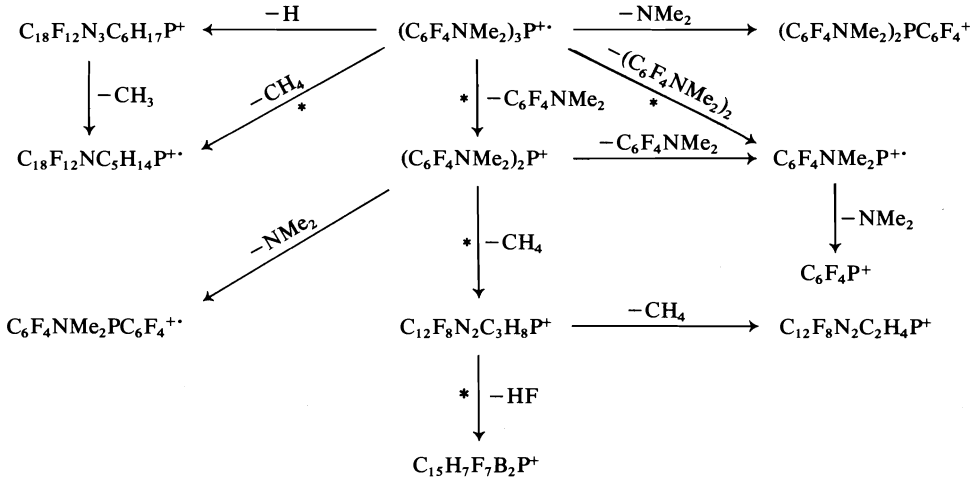

SCHEME 2. Mass spectral fragmentation of $(C_6F_4NMe_2)_3P$.

the spectra were obtained using quadrature detection after retrofit of this facility. Spectra were normally accumulated using a 30° flip angle in PAPS modes. Spectrometer operation was under the control of the Bruker FT nmr programs both disk and nondisk versions; 8K data blocks were collected giving 4K spectral blocks. Computed spectra and interactive fits of coupling constants were calculated on the WP-60 using the program NMRCAL + ITRCAL. The nmr data are summarized in Table 1.

Mass spectra were obtained on an AEI MS-30 double beam, double focussing mass spectrometer, operating at 70 eV ionizing energy, 4 kV acceleration voltage, 100 μA trap current, 1000 resolution, and a source temperature of 180°C. Solids were introduced into beam I via a solid probe and referenced to PFK in beam II inserted via a gas probe. Gas chromatographic – mass spectral analyses were carried out on a Pye 104 chromatograph interfaced to the MS-30 via both a glass frit and membrane separator, the former being preferable for these compounds. A 6 ft × ¼ in. glass column packed with 3% SE30 on Chromosorb W was used for all separations. Spectra are reported relative to the base peak equalling 100%.

Starting materials were prepared by literature methods for **1** (36) and **15** (23) with slight modifications to improve yields. Representative synthetic reactions are described below.

Reactions of 1 with HMPA and DMF

To a two-necked 100-mL flask fitted with a condenser and N_2 inlet, **1** (2.2 g, 4.0 mmol) was added along with hexamethylphosphoric triamide (15 mL) and stirred under reflux for 10 min at 230°C. On cooling, a pale yellow solid (2.2 g, 92%) was precipitated with 75 mL of sodium bicarbonate solution. The crude material recrystallized from ethanol and gave short white needles of tris[4-(*N*,*N*-dimethylamino)-2,3,5,-6-tetrafluorophenyl]phosphine (**5**) (1.8 g, 75% yield), melting at 110°C; ms *m/e* (relative intensity): 608(27), 607(M^+, 100), 606(11), 416(8), 415(32), 399(10), 223(22), 222(8), etc., ir ν_{max}: 2925(m), 2875(m), 2800(m), 1625(s), 1520(s), 1460(s), 1430(s), 1380(m), 1230(s), 1065(s), 960(m), 815(w) cm^{-1}; nmr, see Table 1. *Anal.* calcd. for $C_{24}H_{18}F_{12}N_3P$: C 47.45, H 2.97, N 6.92, F 37.56, P 5.11; found: C 47.0, H 2.85, N 7.14, F 37.43, P 5.09.

In an analogous reaction, **1** (1.5 g, 2.8 mmol) and DMF

(50 mL) were refluxed 51 h at 150°C. Work up as above gave **5** after recrystallization (1.2 g, 71% yield, mp 110°C), confirmed by spectral data and microanalysis. A similar reaction was monitored over a period of 23 h and the variations in the products are summarized below.

	Composition of product mix (%)*				
Product	3 h	7 h	9 h	13 h	23 h
$(C_6F_5)_2PC_6F_4NMe_2$	14	24	40	45	50
$C_6F_5P(C_6F_4NMe_2)_2$	0	2	4	25	25
$(C_6F_4NMe_2)_3P$	0	0	0	0.1	10
$(C_6F_5)_3P$	86	74	56	30	15

*Determined by ^1H and ^{19}F nmr.

*Reactions of **1** with DEF, HEPA, and Aniline*

Compound **1** (4 g, 7.6 mmol) was reacted for 71 h under reflux at 170°C with diethylformamide (50 mL). After cooling, the mixture was stirred for 1 h with a dilute solution of sodium bicarbonate. If no precipitate is obtained at this point, the mixture may be extracted with ether and the ethereal layer dried over $MgSO_4$ and evaporated to yield a brown liquid. This material, when chromatographed with toluene on a 60 cm silica gel column (50–200 mesh), gave a white solid, which, when recrystallized from ethanol, yielded white crystals of tris(4-*N*,*N*-diethylamino-2,3,5,6-tetrafluorophenyl)phosphine (**6**) (2.6 g, 50% yield), mp 135°C; ms *m/e* (relative intensity): 691(M^+ 81), 676(100), 662(5), 648(5), 632(16), 604(6), 574(5), 560(6), etc.; ir ν_{max}: 2965(m), 2925(w), 2865(w), 1625(s), 1455(s), 1367(d), 1340(w), 1195(s), 1085(s), 965(m), 815(m); nmr; see Table 1. *Anal.* calcd. for $C_{30}H_{30}N_3F_{12}P$: C 52.1, H 4.34, N 6.08, F 33.00, P 4.49; found: C 52.31, H 4.31, N 6.01, F 33.03, P 4.33.

In an analogous reaction, compound **1** (1 g, 2 mmol) was stirred under reflux with 10 mL of HEPA for 30 min. Reaction was not complete, with the disubstituted derivatives being observed. On the basis of cost this reaction was not pursued.

Reactions of **1** with aniline were tried under various conditions and the product identified spectroscopically. The mixture of mono-, di-, and trisubstituted product was not separated. A summary of these reactions is given below.

$(C_6F_5)_3P$ (g)	Aniline (mL)	C_2H_5OH (mL)	Reflux time (h), (temperature °C)	Substitution product (%) Mono	Di	Tri
1.1	35	35	2(86)	80	20	—
1.1	20	35	41(86)	70	25	5
1.1	20	35	48(86)	30	60	10
1.1	30	35	71(86)	10	80	10
1.1	30	—	6(180)	10	88	2
1.1	20	0.74 g KF added	3(180)	?	90	?

*Reactions of **1** with Hydrazine*

Compound **1** (3.2 g, 6.0 mmol) in absolute ethanol (105 mL) and 6.0 g of 64% aqueous hydrazine were stirred under reflux for 16.5 h. After cooling, the mixture was poured into 250 mL of water and a white solid (2.8 g) was collected by filtration. Recrystallization from aqueous ethanol gave white crystals of tris(4-hydrazino-2,3,5,6-tetrafluorophenyl)phosphine (**7**) (2.7 g, 79% yield), mp 145°C; ms *m/e* (relative intensity): 568(M^+, 93), 523(100), 508(95), 359(57), 344(45), 343(41), 342(48), 210(55), etc.; ir ν_{max}: 3300(s, br), 2580(w), 1640(s), 1464(s), 1376(m), 1296(m), 1272(s), 1184(m), 1152(s), 1112(m), 1088(m), 1048(w), 972(s), 916(m), 856(w), 832(w), 800(m) cm^{-1}; nmr, see Table 1. *Anal.* calcd. for $C_{18}H_9F_{12}N_6P$: C 38.03, H 1.58, N 14.79, F 40.14, P 5.46; found: C 37.95, H 1.55, N 14.90, F 40.23, P 5.46.

Compound **1** (2.1 g 4 mmol), *N*,*N*-dimethylhydrazine (UDMH, 99%, 6.0 g, 100 mmol), and potassium fluoride (2 g, 35 mmol) were stirred under reflux for 90 min and, after cooling, treated with a dilute sodium bicarbonate solution. The precipitate gave a white solid (2.1 g, 80.5%), mp 110°C. The nmr showed two isomers present (see Discussion). Recrystallization from ligroin (30–60°C) produced a white crystalline solid of tris(4-*N*,*N*-dimethylhydrazino-2,3,5,6-tetrafluorophenyl)phosphine (**8**) (1.8 g, 71% yield), mp 117°C; ms *m/e* (relative intensity): 652(M^+, 65), 608(43), 607(100), 565(35), 564(97), 238(85), 195(48), 69(41); ir ν_{max}: 3250(s), 2950(m), 2850(m), 2825(m), 2775(m), 2550(w), 1635(s), 1455 (s,br), 1375(s), 1270(s), 1625(w), 1210(w), 1110(s), 1015(w), 965(w), 875(m), 815(w), 725(s) cm^{-1}; nmr, see Table 1. *Anal.* calcd. for $C_{24}H_{21}N_6F_{12}P$: C 44.17, H 3.22, N 12.88, F 34.97, P 4.75; found: C 43.9, H 3.55, N 13.0, F 34.79, P 4.76.

The mother liquid yielded a material which showed the same mass spectra and an nmr spectrum indicative of a mixture of **8** and its SDMH isomer.

Compound **1** (1 g, 2 mmol), tetrahydrofuran (35 mL), and phenylhydrazine (2.0 g, 97.5%) were stirred under reflux for 8 h. After cooling and adding water, the product was extracted into ether, the ethereal extracts dried over $MgSO_4$, and evaporated giving a yellow solid. Recrystallization from aqueous ethanol gave yellow crystals of bispentafluorophenyl-(4-β-phenylhydrazino-2,3,5,6-tetrafluorophenyl)phosphine (0.4 g, 32%), mp 110°C; ms *m/e* (relative intensity): 620(M^+, 46), 529(46), 528(27), 362(35), 198(22), 105(27), 92(100), 77(81), 69(39), etc.; ^1H nmr δ: 5.87 (m, 1H), 613 (m, 1H), 6.99 ppm (m, 5H); ^{19}F nmr δ: −131.50 (m, 4F), −132.78 (m, 2F), −149.92 (m, 2F), −158.78 (m, 2F), −161.06 (m, 4F).

*Reactions of **1** with NH_4OH*

Compound **1** (1 g, 2 mmol), ammonium hydroxide (5 mL, 28–30% NH_3), potassium fluoride (3 g, 52 mmol), and THF (5 mL) were placed in a large glass test tube (16 × 3.6 cm) and placed in a 3000 psi Parr bomb (198-mL capacity). The bomb was cooled in liquid N_2 and the air evacuated. The sealed bomb was heated for 22 h at 130°C. On cooling the bomb was opened and its contents treated with dilute sodium bicarbonate solution, followed by extraction with ether. The ethereal extract gave a pale yellow solid (0.6 g) which was recrystallized from ligroin (30–60°) to give white crystals of tris(4-amino-2,3,5,6-tetrafluorophenyl)phosphine (0.5 g, 50%), mp 159°C; ms *m/e* (relative intensity): 541(21), 523(M^+, 100), 508(7.3), 360(8.3), 359(48), 290(9.6), 195(14.6), 79(33), etc.; ir ν_{max}: 3500(m), 3400(s), 2600(w), 1650(s), 1510(s), 1475(s), 1375(s), 1300(w), 1270(s), 1175(m), 1115(s), 290(m), 825(w), 750(w), 735 cm^{-1}; nmr, see Table 1. *Anal.* calcd. for $C_{18}H_6F_{12}N_3P$: C 41.30, H 1.15, F 43.59, N 8.03, P 5.93; found: C 41.31, H 1.03, N 8.18, F 43.52, P 5.80.

*Reaction of **1** with Sodium Methoxide*

To a solution of **1** (2.2 g, 4.0 mmol) in ether (200 mL) a solution made by dissolving sodium (0.276 g, 13 mmol) in dry methanol (15 mL) was added dropwise over 1 h. After 2 h at room temperature, the solution was treated with water and extracted with ether. Gas-chromatography – mass spectrometry showed the ethereal extract to contain four compounds with molecular ions of 168, 180, 140, and 568 corresponding to pentafluorobenzene, tetrafluoroanisole, trimethylphosphite, and tris(methoxytetrafluorophenyl)phosphine. Chromatography on silica using benzene as eluant gave a 20% yield of

a yellow liquid, tris(4-methoxy-2,3,5,6-tetrafluorophenyl)-phosphine; ms *m/e* (relative intensity): 569(30), 568(M^+, 100), 469(9), 389(38), 229(26), 210(50), 193(10), 167(10), etc.; ir ν_{max}: 2910(m), 2820(m), 1640(s), 1525(w), 1475(s), 1435(s), 1375(s), 1275(w), 1190(s), 1110(s), 980(m), 910(m), 813(m), 725(s) cm^{-1}; nmr, see Table 1.

Acknowledgement

The authors thank the National Research Council of Canada for financial support.

1. T. R. B. Jones, J. M. Miller, and M. Fild. Org. Mass. Spectrom. **12**, 317 (1977).
2. J. M. Miller and G. L. Wilson. *In* Advances in inorganic chemistry and radiochemistry. Vol. 18. *Edited by* H. J. Emeléus and A. G. Sharpe. Academic Press, New York, NY. 1976. pp. 229–285.
3. L. A. Wall, W. J. Plummer, J. E. Fearn, and J. M. Antonucci. J. Res. Natl. Bur. Stand. Sect. A, **67**, 481 (1963).
4. G. M. Brooke, J. Burdon, M. Stacey, and J. C. Tatlow. J. Chem. Soc. 1768 (1960).
5. F. I. Abezgauz, S. V. Sokolov, and I. Ya. Postovskii. Zh. Vses. Khim. Ova. **11**, 116 (1966).
6. M. Bellas, D. Price, and H. Suschitzky. J. Chem. Soc. C, 1249 (1967).
7. J. Burdon, V. A. Damodaran, and J. C. Tatlow. J. Chem. Soc. 763 (1964).
8. J. M. Birchall, R. N. Haszeldine, and A. R. Parkinson. J. Chem. Soc. 4966 (1962).
9. D. P. Craig and G. Doggett. Mol. Phys. **8**, 485 (1964).
10. M. Fild. Angew. Chem. Int. Ed. Engl. **3**, 801 (1964).
11. D. D. Magnelli, G. Tesi, J. U. Lowe, Jr., and W. McQuistion. Inorg. Chem. **5**, 457 (1966).
12. J. Dodonov and H. Medox. Chem. Ber. **61**, 907 (1928).
13. J. M. Antonucci and L. A. Wall. J. Res. Natl. Bur. Stand. Sect. A, **71**, 33 (1967).
14. L. S. Kobrina. Fluorine Chem. Rev. **7**, 1 (1974).
15. J. Burdon, W. B. Hollyhead, and J. C. Tatlow. J. Chem. Soc. 6336 (1965).
16. E. Nield, R. Stephens, and J. C. Tatlow. J. Chem. Soc. 166 (1959).
17. R. Stephens and J. C. Tatlow. Chem. Ind. (London), 821 (1957).
18. G. M. Brooke, J. Burdon, and J. C. Tatlow. J. Chem. Soc. 3253 (1962).
19. J. Burdon, P. L. Coe, C. R. Marsh, and J. C. Tatlow. Tetrahedron, **22**, 1183 (1966).
20. J. Burdon. Tetrahedron, **21**, 3373 (1965).
21. N. D. Epiotis and W. Cherry. J. Am. Chem. Soc. **98**, 5432 (1978).
22. J. Burdon, I. N. Rozhkov, and G. M. Perry. J. Chem. Soc. C, 2615 (1969).
23. B. R. Ezzell and L. D. Freedman. J. Org. Chem. **34**, 1777 (1969).
24. E. B. Pedersen, J. Perregard, and S. O. Lawesson. Tetrahedron, **29**, 4211 (1973).
25. H. Normant. Angew. Chem. Int. Ed. Engl. **6**, 1046 (1967).
26. M. W. Hanson and J. B. Bouck. J. Am. Chem. Soc. **79**, 5631 (1957).
27. J. H. Clark and J. M. Miller. J. Am. Chem. Soc. **99**, 498 (1975).
28. J. H. Clark, H. L. Holland, and J. M. Miller. Tetrahedron Lett. 3361 (1976).
29. J. H. Clark and J. M. Miller. Tetrahedron Lett. 599 (1977).
30. J. H. Clark and J. M. Miller. J. Chem. Soc. Perkin Trans. I, 1743 (1977).
31. J. H. Clark and J. M. Miller. J. Chem. Soc. Perkin Trans. I, 2043 (1977).
32. J. H. Clark and J. M. Miller. Chem. Commun. 466 (1978).
33. J. Emsley, O. P. A. Hoyte, and R. E. Overill. J. Chem. Soc. Perkin Trans. II, 2079 (1977).
34. J. M. Miller. J. Chem. Soc. A, 828 (1967).
35. J. M. Miller and A. T. Rake. J. Chem. Soc. A, 1881 (1970).
36. L. A. Wall, R. E. Donadio, and W. J. Plummer. J. Am. Chem. Soc. **82**, 4846 (1960).

Hydrolysis and ammonolysis of EDTA in aqueous solution[1]

RAMUNAS J. MOTEKAITIS, DAVID HAYES, AND ARTHUR E. MARTELL
Coordination Chemistry Consultants, Bryan, TX 77801, U.S.A.
AND
WAYNE W. FRENIER
Dowell Division, Dow Chemical USA, Tulsa, OK 74102, U.S.A.

Received October 11, 1978

RAMUNAS J. MOTEKAITIS, DAVID HAYES, ARTHUR E. MARTELL, and WAYNE W. FRENIER. Can. J. Chem. **57**, 1018 (1979).

The hydrolysis and ammonolysis of EDTA were studied in aqueous solution over a range of temperatures and at various pH values with the aid of nmr, gc, and gc – mass spectroscopic techniques. At high pH in the presence of ammonia, both ammonolysis and hydrolysis occur with the production of *N*-(2-aminoethyl)iminodiacetic acid (UEDDA), *N*-(2-hydroxyethyl)-iminodiacetic acid (HEIDA), and iminodiacetic acid (IDA) in molar ratios such that [IDA] = [UEDDA] + [HEIDA]. The first-order rate constant for the disappearance of EDTA at 175°C in dilute aqueous ammonia is 8.6×10^{-5} s^{-1} whereas in the absence of ammonia its hydrolysis constant is 4.2×10^{-5} s^{-1}. The value of ΔH^0 for this reaction is approximately 35 kcal/mol. When methylamine replaces ammonia, the UEDDA is replaced by *N*-(2-methyl-aminoethyl)iminodiacetic acid. The rate of hydrolysis is increased by the presence of a tertiary amine but the latter does not become incorporated into the reaction products. A reaction mechanism is proposed involving bimolecular S_N2 attack by base on a carbon atom of the ethylene bridge adjacent to a protonated nitrogen atom of EDTA with concomitant displacement of iminodiacetic acid.

RAMUNAS J. MOTEKAITIS, DAVID HAYES, ARTHUR E. MARTELL et WAYNE W. FRENIER. Can. J. Chem. **57**, 1018 (1979).

On a étudié l'hydrolyse et l'ammonolyse de l'AEDT dans des solutions aqueuses à diverses températures et divers pH en faisant appel à des techniques de rmn, de cpg et de spectroscopie de masse couplée à la cpg. A des pH élevés, en présence d'ammoniaque, il se produit une ammonolyse ainsi qu'une hydrolyse avec formation d'acides *N*-(amino-2 éthyl)iminodiacétique (AAEID), *N*-(hydroxy-2 éthyl)iminodiacétique (AHEID) et iminodiacétique (AID) dans les rapports molaires tels que [AID] = [AAEID] + [AHEID]. La constante de vitesse du premier ordre pour la disparition de l'AEDT à 175°C en solution dans l'ammoniaque dilué est égale à 8.6×10^{-5} s^{-1} alors qu'en l'absence d'ammoniac, la constante d'hydrolyse est égale à 4.2×10^{-5} s^{-1}. La valeur du ΔH^0 pour cette réaction est approximativement 35 kcal/mol. Si l'on remplace l'ammoniaque par de la méthylamine, il se forme de l'acide *N*-(méthylamino-2 éthyl)iminodiacétique au lieu de AAEID. La vitesse d'hydrolyse est accélérée par la présence d'une amine tertiaire; celle-ci n'est toutefois pas incorporée dans les produits de la réaction. On propose un mécanisme réactionnel impliquant une attaque S_N2 bimoléculaire par la base sur un atome de carbone du pont éthylène voisin de l'atome d'azote de ARDT protoné avec une substitution simultanée de l'acide iminodiacétique.

[Traduit par le journal]

Introduction

Since important applications of EDTA involve its use in aqueous solution at high temperature and pressure and possibly in the presence of ammonia or other basic compounds, it seemed that a study of the kinetics and mechanism of such reactions would be of importance. Earlier studies of EDTA hydrolysis at elevated temperatures (1–6) resulted in conflicting reports. These experiments were carried out at relatively high temperatures, which precluded accurate determination of reaction rates. The present work describes hydrolytic measurements at more moderately elevated temperatures that allow the measurement of the rates of appearance of reaction products and the rates of disappearance of EDTA. The influence on reaction rate and product distribution resulting from the addition of basic substances such as ammonia and methylamine was also studied and was found to have mechanistic implications.

The pH was generally maintained at or near 9.3 by the addition of ammonia as a buffer as well as a reactant. The temperature range employed in this investigation, 145–175°C, was selected to provide a

[1]This work was carried out in the course of a contract between Dow Chemical Company and Coordination Chemistry Consultants.

0008-4042/79/091018-07$01.00/0

convenient range of reaction rates for experimental measurements.

Experimental

Materials

EDTA, methylamine, and triethylamine were obtained from Eastman Chemical Company. Hydroxyethyliminodiacetic acid (HEIDA) and iminodiacetic acid (IDA) were obtained from Aldrich Chemical Company. Reagent grade ammonia and gaseous hydrogen chloride for esterification were obtained from Matheson, Coleman and Bell. Methanol and potassium carbonate were obtained from Baker Chemical Company. The water employed was distilled from glass and the methanol was dried over Linde Molecular Sieves. The 50% NaOD/D_2O solution and 99.7% D_2O were obtained from Merck, Sharp and Dohme. Ethylenediamine-*N*,*N*-diacetic acid was synthesized by alkaline alkylation of *N*-acetylethylenediamine with bromoacetic acid, followed by alkaline hydrolysis of the amido group. *N*-Acetylethylenediamine was prepared by refluxing excess ethylenediamine with ethyl acetate for a 12-h period.

Instrumentation

The nmr spectra were recorded with a Varian T-60 nmr spectrometer which was found to be sufficiently accurate for quantitative determinations with the use of the sample preparation procedure described below. The gas chromatograms were obtained at 200°C on a Hewlett-Packard Model HP 5834a gas chromatograph equipped with a 12-ft, 3% OV-1 column and both FID and TC detectors. The gc mass spectrograms were measured with a Hewlett-Packard Model HP-5982-59-33, housed and operated by the Texas A&M Center for Trace Characterization, with the same chromatographic column but with linear temperature programming to shorten data collection time.

pH was measured at room temperature with a Beckman Research Model pH meter equipped with extension glass and calomel electrodes and was calibrated with standard strong acid and base to measure hydrogen ion concentration directly. The pH values cited in this paper were those measured at room temperature although the pH values at the high temperatures of the experimental runs may be estimated with known values of the heats of dissociation of water and heats of dissociation of the various bases used as buffers.

Procedure

Typical experimental runs were carried out as follows: a 2-L titanium glass-lined autoclave equipped with a titanium stirrer was charged with 1.50 L of 0.015–0.695 *M* EDTA, previously adjusted to the desired pH in the range 5.5–11, and was heated rapidly to the desired temperature in the range 145–175°C. Samples of the reaction solution were withdrawn at timed intervals and were analyzed either by nmr, gc, or gc – mass spectrometry. The nmr samples were prepared and measured in alkaline D_2O relative to TMS as an internal standard. The solvent was replaced by D_2O several times, followed by evaporation, and finally the solution was made up to 0.50 ml with 5% NaOD in D_2O. Precision nmr tubes were employed and calibrated by integration of a standard EDTA solution. Samples for gas chromatography were prepared through the use of a quantitative Fischer (7) methyl esterification procedure. Excess HCl was removed by vacuum evaporation followed by dilution to the desired concentration with dry methanol. Solid potassium carbonate was used to liberate the free esters from their hydrochloride salts immediately before injection in the gas chromatograph. Samples for gc – mass spectrometer analysis were prepared in the same manner.

Results and Discussion

Product Identification

EDTA (**1**) was found to decompose in dilute aqueous ammonia solution at 145–175°C by the nucleophilic attack of ammonia (eq. [1]) on **1** to produce *N*-(2-aminoethyl)iminodiacetic acid (**2**) and iminodiacetic acid (**3**) and by a similar hydroxyl attack (eq. [2]) to give *N*-(2-hydroxyethyl)iminodiacetic acid (**4**) in addition to **3**. The aminolysis reaction (eq. [1]) is new and had not been described previously, while the hydrolysis reaction (eq. [2]) is consistent with previous studies (1, 4, 5, 8) which had been made at much higher temperatures in ammonia-free systems.

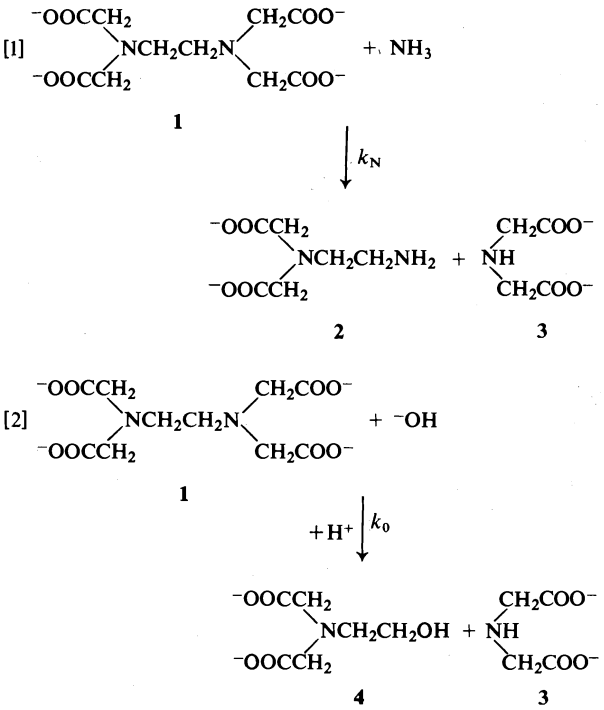

Originally, tentative product identification was made through nmr spectral analysis. Although it had been reported earlier that the hydrolytic cleavage of EDTA produces **4** and **3**, the similarity in the values of the chemical shifts between the respective protons in acetate groups of compounds **2**, **3**, **4**, and even **1** precluded an unequivocal determination by the nmr method that **2** had indeed been formed. As is also shown in Table 1, a similar ambiguity arose which was caused by the proximity of the ethylene proton chemical shifts in the starting material **1** and the ammonia cleaved product **2**.

TABLE 1. Nuclear magnetic resonance spectra (60 MHz) of reference compounds measured in 0.15 *M* D_2O solutions containing 5% NaOD; chemical shifts are reported in Hz relative to trimethylsilylpropanesulfonate (TMS*)

Compound	Chemical shifts[a] Acetate	Ethylene
Ethylenediaminetetraacetic acid (**1**)	190(2)	160(1)
Ethylenediamine-*N*,*N*-diacetic acid (**2**)	185(1)	154(1)
Iminodiacetic acid (**3**)	186	
N-Hydroxyethyliminodiacetic acid (**4**)	191(2)	214(1)[b] 160(1)[b]
Glycine($NH_2CH_2COO^-$)	186	

[a]Relative integrated intensities in parentheses.
[b]Triplet.

A more direct confirmation of the new reaction product **2** was obtained through comparisons of the retention times shown in Table 2 from gas–liquid chromatograms of the methyl ester derivatives of the standard compounds with those obtained from the methyl esterified reaction mixture shown in Table 3. The gc technique also helped confirm the presence of the normal hydrolysis products, **3** and **4**, which had already been shown to form under the conditions of higher temperature even in the absence of ammonia. Table 2 contains a summary of the gc analytical data which were not only indispensable in fixing the reaction products but also provided evidence for the absence of any significant quantities of other side products. Thus, the reaction cleanly led only to the three products shown in [1] and [2].

To help appreciate the mechanism and the scope of these reactions, other reagents were substituted for dilute ammonia for adjusting pH, and representative samples of the results obtained are also presented in Table 3. All these reactions appear clean under a variety of reagent conditions as evidenced by the absence of gc peaks corresponding to the appearance of side products.

In the absence of ammonia, only the normal water-cleaved EDTA hydrolysis products were found. These experiments were carried out using NaOH, or TEA (triethylamine), or borax buffers. By contrast, ammonia was found to become incorporated into EDTA through the formation of UEDDA (**2**) and in an analogous way methylamine was found to react with EDTA according to [3] to give *N*-(2-methylaminoethyl)iminodiacetic acid (**5**) and the usual IDA (**3**). These assignments were made through the comparison of retention times listed in Table 3. In particular, the evidence for **5** was the appearance of a new single gc peak at 4.04 min replacing the 4.88 peak for UEDDA. The nmr spectrum (Fig. 1) of the product showed additional resonances at 2.26 and 2.92 ppm relative to TMS* (trimethylsilylpropionate), which are ascribable to

TABLE 2. Retention times and relative intensities/unit concentration of gas chromatographic peaks representing the methyl ester derivatives of compounds encountered in this study of EDTA in dilute ammonia solutions at 145–175°C and pH 5.5–11.0

No.	Compound	Retention time (min)	Relative sensitivity[a]
1	EDTA	21.05	1.00
2	UEDDA	4.88	0.39
3	IDA	1.05	0.55
4	HEIDA	2.73	0.34

[a]Values depend on both yield of derivative and on detector (FID) response.

TABLE 3. The gas chromatographic determinations of the esterified reaction products formed in the employment of various buffers to achieve an initial pH of 9.3 on EDTA solutions which were subsequently heated at 175°C[a]

Original composition	Derivative retention time (min)	Product assignment
EDTA + NaOH	1.03	IDA
	2.67	HEIDA
	21.53	EDTA
EDTA + NH_3	1.04	IDA
	2.69	HEIDA
	4.85	UEDDA
	21.55	EDTA
EDTA + NH_3 + 7.2 atm O_2 at 145°C	1.16	IDA
	2.57	HEIDA
	20.86	EDTA
EDTA + TEA[b]	1.03	IDA
	2.62	HEIDA
	21.03	EDTA
EDTA + CH_3NH_2	1.03	IDA
	2.65	HEIDA
	4.04	*N*-CH_3-*N*′,*N*′-EDDA
	20.47	EDTA
EDTA + borax	1.07	IDA
	2.85	HEIDA
	21.15	EDTA

[a]Unless stated otherwise.
[b]TEA = triethylamine.

[3] 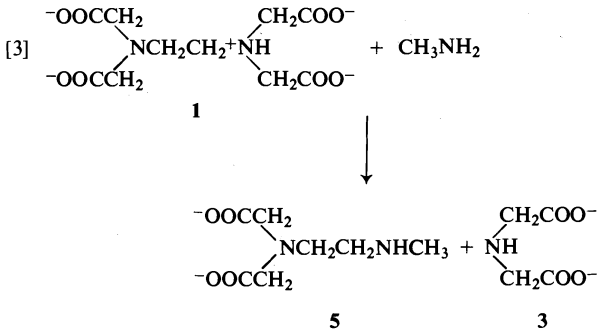

1 5 3

$N—CH_3$ and $N—CH_2CH_2—N$ type proton groupings. The 2.26/2.92 peak ratio is ~3:4.

The chemical shift assignments were confirmed by comparison with the chemical shifts observed for an 'analogous' N-methyl compound measured under identical conditions. Thus for *N,N'*-dimethylethylenediamine the resonance for $N—CH_3$ appears at 2.28 ppm and the remaining resonance for the dimethylene bridge protons is at 2.63 ppm from TMS*.

The degradation experiment under added oxygen was performed at 145°C and confirms that EDTA is stable toward oxidation by molecular oxygen. However, the presence of UEDDA was not detected at this temperature indicating a higher temperature reaction coefficient for ammonolysis as compared with the hydrolysis. For safety reasons, the reaction was not investigated under pressurized oxygen at higher temperatures.

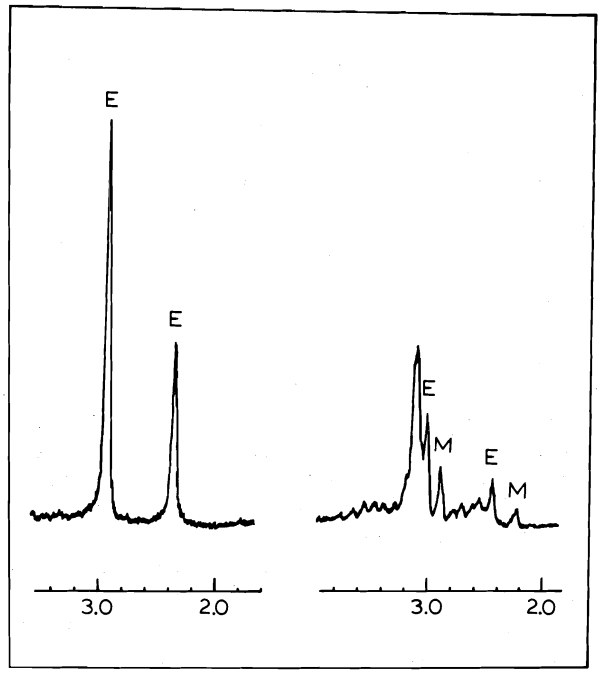

FIG. 1. Nuclear magnetic resonance spectra of two samples from the hydrolysis of EDTA at 175°C pH (25°C) 9.3 buffered with methylamine. Scale is in ppm relative to internal trimethylsilylpropionate: left, before heating; right, after 4.0 h of heating. Peaks marked M (see text) indicate the incorporation of methylamine through the formation of *N*-methylethylenediamine-*N'*,*N'*-diacetic acid; E represents EDTA peaks.

Ultimate identification of the reaction products shown in [1] and [2] was obtained through the comparison of gc – mass spectrometric data measured on the methyl esterified hydrolysis reaction products with those obtained on a set of methyl esterified known reference compounds. The mass patterns were identical in peak position, ratio, and number for corresponding pairs of compounds. The last four peaks and the strongest peaks are tabulated in Table 4.

An examination of the mass spectra indicates that EDTA and IDA esterify normally to yield the tetramethyl ester, 348 u, and the diester, 161 u, respectively, whereas UEDDA cyclizes during the acidic treatment with methanol to produce the monomethyl lactam, 172 u, while HEIDA forms a cyclic monomethyl lactone, 173 u. However, it is believed that under the experimental basic aqueous solution conditions, the actual products **2**, **3**, and **4** exist in their respective open forms.

Kinetics of EDTA Decomposition

For the chemical changes specified by [1] and [2], the overall rate of disappearance of EDTA through parallel solvolytic and ammonolysis paths was found to be proportional to the concentration of unreacted EDTA. Since the pH of the medium remained constant and a large excess of NH_3 was generally employed, first-order reaction conditions prevailed over a significant portion of the reaction time. Although the overlap in the nmr peak positions precluded the routine determination of the rates of formation of the three individual reaction products, the nmr method provided a very convenient means for following the rate of disappearance of EDTA itself.

The kinetic data listed in Table 5 were obtained from the slopes of plots of $\log_e I$ vs. t (I = integrated intensity of the $—CH_2CH_2—$ resonance) reflecting the observed first-order kinetic expression shown in [4]. These rate constants were measured at two

$$[4] \qquad -\mathrm{d[EDTA]}/\mathrm{d}t = k_{obs}\,[\mathrm{EDTA}]$$

concentrations and three temperatures as shown, yet appeared to be concentration independent within the scatter of the data. From a plot of $\log_e k_{obs}$ against reciprocal absolute temperature, the activation parameter $\Delta H_a^{\ddagger}$ was found to be 34.6 ($\sigma = 0.7$) kcal/mol.

With the fundamental rate law established for aqueous ammonia at pH 9.30 and 175°C and a firm

TABLE 4. Gas chromatographic – mass spectrometric data for EDTA-tetramethyl ester and esterified reaction products formed in ammoniacal solutions of EDTA at 145–175°C

No.	Compound	Mass (u)	Form	Last four peaks				Strongest peak
1	EDTA	348	Tetraester	317.1	348.2	349.2	350.2	174.1
2	UEDDA	172	Monoester lactam	157.1	163.0	172.1	173.0	113.1
3	IDA	161	Diester	130.0	146.1	161.1	162.0	102.0
4	HEIDA	173	Monoester lactam	171.0	173.1	174.1	175.1	114.0

TABLE 5. The pseudo-first-order rate constants for the disappearance of EDTA measured in aqueous NH_3 at pH 9.3 as a function of temperature and concentration

$[EDTA]_0$ (mol/L)	Time-averaged temperature	σ (°C)	k_{obs} (s^{-1})	σ (s^{-1})
0.015	174	4	7.8×10^{-5}	0.5×10^{-5}
0.065	175	1	8.8×10^{-5}	0.5×10^{-5}
0.015	162	1	2.5×10^{-5}	0.2×10^{-5}
0.065	163	1	2.8×10^{-5}	0.3×10^{-5}
0.015	149	1	7.5×10^{-6}	0.8×10^{-6}
0.065	149	1	8.1×10^{-6}	1.4×10^{-6}

proof of the reaction products formed, other reaction conditions were tried and the results of the variation in temperature, reagents, and pH are listed in Table 6. Thus, when ammonia is not present and NaOH is used to adjust the pH to 9.4, the value of the observed rate constant k_{obs} is reduced to about one-half of the original magnitude observed when NH_3 is present. Likewise, when pyridine was employed to effect 'neutralization' and just enough NH_3 was added to raise the pH, the value of the rate constant exceeded that of the NH_3-free run but was much lower than the NH_3-buffered solutions. Triethylamine in place of ammonia showed definite catalytic activity with a k_{obs} of $6.4\times10^{-5}\ s^{-1}$, yet only hydrolytic products were formed. Methylamine approached the reactivity of ammonia with a resulting k_{obs} of $7.8\times10^{-5}\ s^{-1}$ with the reaction progressing according to [4].

Variation in pH on the ammonia system showed that at pH 6.01, which corresponds to about half neutralization of EDTA, the rate constant was about the same as in the absence of ammonia at pH 9.3, with $k_{obs} = 3.6\times10^{-5}\ s^{-1}$. On the other hand, a very large excess of ammonia, pH 11.08, led to a pronounced increase of the rate with $k_{obs} = 1.1\times10^{-4}\ s^{-1}$.

The variation in k_{obs} measured under a variety of conditions indicates that the rate law may be a composite of both hydrolytic and ammonolysis terms with each term in turn depending on the degree of protonation of the EDTA anion itself. Therefore, in the most general case, the rate law may be expanded, as shown in [5], to include all the individual EDTA species present in the pH range over which the measurements have been made. The pseudo-first-order kinetic expression shown in [4] becomes identical with [5] only under three conditions: (*i*) the reactive species of EDTA predominates to the virtual exclusion of the other species in equilibrium with it; (*ii*) only one form of EDTA is reactive, irrespective of its concentration, while the remaining species are sufficiently less reactive to be neglected; (*iii*) the very remote possibility that the rate constants of the various forms are equivalent for reaction with NH_3, OH, OH_2 (i.e., $k_{NH_3}^{(1)} = k_{NH_3}^{(2)} = k_{NH_3}^{(3)}$, $k_{OH}^{(1)} = k_{OH}^{(2)} = k_{OH}^{(3)}$, and $k_{H_2O}^{(1)} = k_{H_2O}^{(2)} = k_{H_2O}^{(3)}$. This possibility may be discarded since reactivities of differently charged species cannot possibly be equivalent. The fact that first-order kinetics have indeed been observed under a variety of conditions provides preliminary evidence that mechanism *ii* is most likely.

$$[5]\quad -d[EDTA]/dt = \{k_{NH_3}^{(1)}[L^{4-}] + k_{NH_3}^{(2)}[HL^{3-}] + k_{NH_3}^{(3)}[H_2L^{2-}]\}[NH_3] + \{k_{OH}^{(1)}[L^{4-}] + k_{OH}^{(2)}[HL^{3-}] + k_{OH}^{(3)}[H_2L^{2-}]\}[OH^-] + \{k_{H_2O}^{(1)}[L^{4-}] + k_{H_2O}^{(2)}[HL^{3-}] + k_{H_2O}^{(3)}[H_2L^{2-}]\}$$

At this point, it is necessary to consider the detailed solution equilibria at 175°C, the temperature of the reaction. To accomplish this, the pK_a values for EDTA and NH_4^+ and K_W for water are needed at this elevated temperature. Although a direct measurement was not possible, an inverse temperature extrapolation technique was utilized to determine the ion product concentration constant for water and the proton association constants of EDTA at $\mu \simeq 0.100$ and $T = 175$°C. The values of $-\log K_W$ for water and $\log K_L^H$ for EDTA were measured at several elevated temperatures up to the boiling point of water and were then extrapolated to 175°C; $-\log K_W$ was found to be 10.72 while the successive log protonation constants for EDTA were determined to be 8.79, 5.62, 3.61, and 2.6. The pK_a for

TABLE 6. Smoothed values[a] of k_{obs} from Table 5 and k_{obs} values determined under other reaction conditions

System	Temperature (°C)	σ (°C)	pH	k_{obs} (s^{-1})	σ (s^{-1})
$EDTA/NH_3$	175		9.30	8.6×10^{-5}	0.6×10^{-5}
$EDTA/NH_3$	163		9.30	2.8×10^{-5}	0.3×10^{-5}
$EDTA/NH_3$	149		9.30	7.5×10^{-6}	0.3×10^{-6}
$EDTA/NH_3$	175	1.2	11.08	1.1×10^{-4}	0.1×10^{-4}
$EDTA/NH_3$	175	0.8	6.01	3.6×10^{-5}	0.3×10^{-5}
EDTA/NaOH	175	1.5	9.40	4.28×10^{-5}	0.08×10^{-5}
$EDTA/Py/NH_3$	175	2.0	9.39	5.0×10^{-5}	0.3×10^{-5}
$EDTA/CH_3NH_2$	175	0.9	9.45	7.8×10^{-5}	0.3×10^{-5}
$EDTA/(C_2H_5)_3N$	175	1.9	9.35	6.4×10^{-5}	0.3×10^{-5}

[a]First three entries; subsequent entries are results of individual experiments.

NH_4^+ was taken from the literature (9, 10) and corrected for ionic strength while that for boric acid was calculated from the work of Mesmer *et al.* (11). The final values of log K^H used in the calculation of the initial species concentration at 175°C shown in Table 7 were 6.19 for NH_4^+ and 8.26 for H_3BO_3.

Table 7 illustrates some very important observations concerning the changes in species distributions upon elevating the temperature from 25 to 175°C. In all cases, the pH at 175°C is lower than the original to different extents, depending mainly on the principal buffer present. For example, Table 6 contains an entry which shows that the rate of hydrolysis promoted by NaOH at pH 9.4 and 25°C is characterized by a $k_{obs} = 4.28 \times 10^{-5}\ s^{-1}$. The use of material and electrobalance equations shows, in Table 7, that at 175°C, and pH 7.62, the hydroxide ion concentration rises some 20 times, while the predominating EDTA species, HL^{3-}, remains at ~93% of the total EDTA. Also the low pH solution dropped only ~0.8 pH units on heating while the free NH_3 concentration approached 10% of the total NH_3 added. The pK_a for NH_4^+ drops 2.94 log units in this temperature interval. In contrast, the borate buffered solution remained relatively alkaline, yet demonstrated a remarkably small k_{obs}. The remarkable catalytic effect of ammonia and the lack of catalysis by borate suggest an important role for low pH EDTA species in the hydrolysis reaction.

After calculation of high temperature initial distributions of the species under a variety of reaction conditions, the predominating species (*vide supra*, case *i*) model was tried both with and without k_{H_2O}. No satisfactory fit of the data could be obtained and the calculated results were inconsistent.

It was then assumed that only one protonated form of the EDTA was reactive while the remaining two were relatively unreactive. H_2L^{2-} was chosen as the reactive species because such a choice would be in conformity with several important observations. When HEIDA, or IDA, or NTA were subjected to the hydrolytic conditions described in this paper, no decomposition was observed over several half-lives of EDTA hydrolysis. The property which sets EDTA apart is that its structure possesses two basic nitrogen atoms on adjacent carbon atoms capable of facile protonation. The increased localization of positive charge resulting from diprotonation contributes to the affinity for negatively charged nucleophiles and lone pairs on amine bases, thus greatly increasing the reactivity and rate of initial nucleophilic attack. Presumably, the other EDTA species (i.e., HL^{3-} and L^{4-}) can also react with the same nucleophiles but require higher temperatures (i.e., their reaction rates are much lower).

With H_2Y^{2-} as the reactive species, [5] may be simplified considerably to give [6]. Since $[H_2L^{2-}]$ is

$$[6] \quad -d[EDTA]/dt = \{k^{(3)}[NH_3] + k^{(3)}[OH^-] + k^{(3)}\}[H_2L^{2-}]$$

only a part of the EDTA present in solution, at each pH (175°C) a concentration correction is necessary to equate terms in [4] to corresponding terms of [6]. Thus

$$[7] \quad k_{obs} = \frac{K_1^H K_2^H [H]^2 k_{obs}'}{1 + K_1^H[H^+] + K_1^H K_2^H [H^+]^2}$$

and

$$[8] \quad k_{obs}' = k_{NH_3}^{(3)}[NH_3] + k_{OH}^{(3)}[OH^-] + k_{H_2O}^{(3)}$$

Equation [8] was analyzed in two ways. First, a regression analysis was performed which in addition to giving a very poor overall fit, provided a very large $k_{H_2O}^{(3)}$ which rendered the contributions from hydroxide attack and ammonia attack relatively unimportant. The actual values obtained in this way also do not make chemical sense ($k_{OH}^{(3)} = 3.2 \times 10^{-3}\ M^{-1}\ s^{-1}$, $k_{NH_3}^{(3)} = 1.0 \times 10^{-2}\ M^{-1}\ s^{-1}$, and $k_{H_2O}^{(3)} = 3.9 \times 10^{-3}\ M^{-1}\ s^{-1}$ or $7.0 \times 10^{-5}\ M^{-1}\ s^{-1}$ for 55.5 *M* H_2O).

Another analysis of [8] was made assuming that $k_{H_2O}^{(3)}$ is relatively unimportant and as such can be

TABLE 7. Initial concentrations of reactants and initial distribution of species calculated for 175°C from high temperature equilibrium constants[a,b,i]

$[EDTA]_T$	$[NH_3]_T$	pH (25°C)[c]	pH (175°C)[d]	$[OH^-]$	$[NH_3]_0$[d,e]	$[H_2Y^{2-}]$[d,f]	$[HY^{3-}]$[d,f]	$[Y^{4-}]$[d,f]	k_{obs} (s^{-1})	k_{obs}' (s^{-1})
0.0150	0.0366	6.01	5.18	2.87×10^{-6}	2.62×10^{-3}	1.10×10^{-2} (73.3%)	3.98×10^{-3} (26.5%)	9.71×10^{-7} (<0.1%)	3.6×10^{-5}	4.9×10^{-5}
0.0150	0.120	9.30	6.53	6.53×10^{-5}	7.65×10^{-2}	1.62×10^{-3} (10.8%)	1.33×10^{-2} (88.7%)	7.40×10^{-5} (0.5%)	8.6×10^{-5}	7.9×10^{-4}
0.0150	2.20	11.08	7.94	1.65×10^{-3}	2.10	6.30×10^{-5} (0.4%)	1.31×10^{-2} (87.3%)	1.84×10^{-3} (12.3%)	11.0×10^{-5}	2.6×10^{-2}
0.0150[g]	[g]	9.40	7.62	7.97×10^{-4}	0	1.39×10^{-4} (0.9%)	1.39×10^{-2} (92.7%)	9.43×10^{-4} (6.3%)	4.28×10^{-5}	4.6×10^{-3}
0.0150[h]	[h]	9.20	8.24	3.28×10^{-3}	0	2.83×10^{-5} (0.2%)	1.17×10^{-2} (78.8%)	3.27×10^{-3} (21.8%)	2.0×10^{-5}	1.1×10^{-2}

[a]Corrections were not made for solution density.
[b]$-\log K_w = 10.72$; for EDTA, $\log K_1^H = 8.79$, $\log K_2^H = 5.62$, $\log K_3^H = 3.61$, and $\log K_4^H = 2.6$; for NH_3, $\log K^H = 6.19$; for H_3BO_3, $\log K^H = 8.26$; all at $\mu \approx 0.1$ and $T = 175°C$.
[c]Did not vary more than ~0.05 units during the course of any given kinetic run.
[d]175°C values.
[e]As free ammonia, the remainder is NH_4^+.
[f]$Y = EDTA^{4-}$ anion.
[g]Solution made up with NaOH instead of NH_3.
[h]Solution made up using borax buffer.
[i]Concentrations in mol/L.

eliminated from [8]. A linear least-squares regression computation was made which gave $k_{NH_3}^{(3)} = 8.5 \times 10^{-3}\,M^{-1}\,s^{-1}$ and $k_{OH}^{(3)} = 5.1\,M^{-1}\,s^{-1}$ ($\sigma = 18\%$). This is a remarkable fit, which suggests that the kinetic model chosen is probably the correct one.

It appears then that the reaction pathways indicated by [1] and [2] may proceed by the attack of the respective nucleophiles (NH_3 or OH^-) on the diprotonated form of EDTA as shown in [9] and [10].

[9]

[10]

1. A. E. MARTELL, R. J. MOTEKAITIS, A. R. FRIED, J. S. WILSON, and D. T. MACMILLAN. Can. J. Chem. **53**, 3471 (1975).
2. D. L. VENEZKY and W. B. MONIZ. NRL Report 6747, Naval Research Laboratory, Washington, DC, August, 1968.
3. D. L. VENEZKY and W. B. MONIZ. Anal. Chem. **41**, 11 (1969).
4. D. OSBORN, J. S. WILSON, A. R. FRIED, and W. M. PRYOR. Final Report of Contract G-9-2-D, American Society of Mechanical Engineers, 1973.
5. J. S. WILSON and A. R. FRIED. Proc. Am. Power Conf., 35th Annual Meeting, Chicago, IL, 1973.
6. D. L. VENEZKY. 32nd Ann. International Water Conference, Engineers' Society of Western Pennsylvania, Pittsburg, PA, Nov. 1977.
7. E. FISCHER and A. SPEIR. Chem. Ber. **28**, 3252 (1895).
8. P. J. SNIEGOWSKI and D. L. VENEZKY. J. Chromatogr. Sci. **12**, 359 (1974).
9. L. G. SILLEN and A. E. MARTELL. Stability constants of metal–ion complexes. The Chemical Society, London. 1971.
10. H. C. HELGESON. J. Phys. Chem. **71**, 3121 (1967).
11. R. E. MESMER, C. F. BAES, and F. H. SWEETON. Inorg. Chem. **11**, 537 (1972).

Enzymes in organic synthesis. 14.[1] Stereoselective horse liver alcohol dehydrogenase catalyzed oxidations of diols containing a prochiral centre and of related hemiacetals

J. Bryan Jones and Kar P. Lok

Department of Chemistry, University of Toronto, Toronto, Ont., Canada M5S 1A1

Received November 7, 1978

J. Bryan Jones and Kar P. Lok. Can. J. Chem. **57**, 1025 (1979).

The asymmetric synthetic potential of horse liver alcohol dehydrogenase catalyzed oxidations of variously 3-substituted pentane-1,5-diols has been further delineated. The oxidations proceed with enantiotopic selectivity to give the corresponding (3*S*)-3-substituted valerolactones of up to 78% ee. The reactions occur via initial oxidation of the pro-*S* hydroxyethyl group, with the initially-formed hydroxyaldehydes undergoing further *in situ* enzyme-catalyzed oxidation in their hemiacetal forms to give the (3*S*)-lactones directly. The hemiacetal oxidation step is also stereoselective, with oxidation of the (4*S*)-enantiomer being much preferred. The size of the substituent at C-3 in the diols (C-4 in the hemiacetals) affects both the enantiotopic and enantiomeric specificity of the enzyme. Both types of stereospecificity are highest when the substituents are smallest, such as methyl or ethyl, and diminish progressively for diol or hemiacetal substrates bearing large aliphatic or aromatic substituents. All reactions were carried out on a preparative (up to 2 g) scale.

J. Bryan Jones et Kar P. Lok. Can. J. Chem. **57**, 1025 (1979).

On a délimité d'une façon plus précise les possibilités en synthèse asymétrique d'oxydations catalysées par l'alcool déshydrogénase du foie de cheval de pentane-diols-1,5 varies. Les oxydations se produisent avec sélectivité énantiopique pour donner les 3*S* valérolactones correspondantes avec des èe allant jusqu'à 78%. Les réactions se produisent par l'intermédiaire d'une oxydation initiale du groupe hydroxyéthyle pro-*S*, avec une oxydation *in situ* catalysée par les enzymes, des hydroxyaldéhydes formés initialement et présents sous forme d'hémiacétals conduisant directement aux 3*S*-lactones. L'étape de l'oxydation de l'hémiacétal est aussi stéréosélective; l'oxydation de l'énantiomère 4*S* est de beaucoup favorisée. La taille des substituants en C-3 des diols (C-4 des hémiacétals) affecte la spécificité énantiotope et énantiomère de l'enzyme. La stéréospécificité de chaque type est à son maximum avec les substituants les moins volumineux tels un méthyle ou un éthyle et elle diminue progressivement lorsque les diols ou les hémiacétals portent des substituants aliphatiques ou aromatiques plus volumineux. On a effectué toutes les réactions au niveau préparatif (jusqu'à 2 g).

[Traduit par le journal]

Exploitation of the chiral catalytic properties of enzymes for asymmetric synthesis purposes is attracting increasing attention (2). HLADH,[2] a commercially available NAD^+-dependent alcohol dehydrogenase which catalyzes $CH(OH) \rightleftharpoons C{=}O$ oxidoreductions for a broad spectrum of substrates of organic chemical interest, is one of the most versatile of the enzymes of proven practical value (2). Of particular asymmetric synthesis value is its ability to effect enantiotopically selective transformations on substrates containing a prochiral centre. This was demonstrated previously (1*b*) with the diol substrates **1***a*, *d*, and *f*. The overall reactions observed are summarized in Scheme 1. For each of **1***a*, *d*, and *f*, enantiotopically selective oxidation of the pro-*S* hydroxyethyl group was the predominant reaction, with the initially-formed hydroxy aldehydes **2** undergoing subsequent HLADH-catalyzed oxidation in their hemiacetal forms **3** to give the lactones **4***a*, *d*, and *f* directly.

It is clear that two types of HLADH stereospecificity can influence the degree of enantiomeric enrichment observed in the product lactones **4**. These are enantiotopic selectivity in the **1** → **2** step and stereoselectivity during oxidation of the hemiacetal diastereomers **3**. The original study (1*b*) indicated that both types of stereospecificity could be important and that the extent of asymmetric synthesis was also affected by the nature of the R-group at C-3. However, no firm conclusions could be drawn from the limited data available.

We have now examined these important questions in more detail using the broadened structural range of diol substrates **1***a–h*. The stereospecificity of hemiacetal oxidation reaction has also been evaluated. The results show that the enantiotopic selectivity of HLADH in the **1** → **2** oxidation step

[1]For previous papers in this series, see ref. 1, and references therein.

[2]Abbreviations used: HLADH, horse liver alcohol dehydrogenase; NAD^+, nicotinamide adenine dinucleotide; FMN, flavin mononucleotide; ee, enantiomeric excess.

0008-4042/79/091025-08$01.00/0

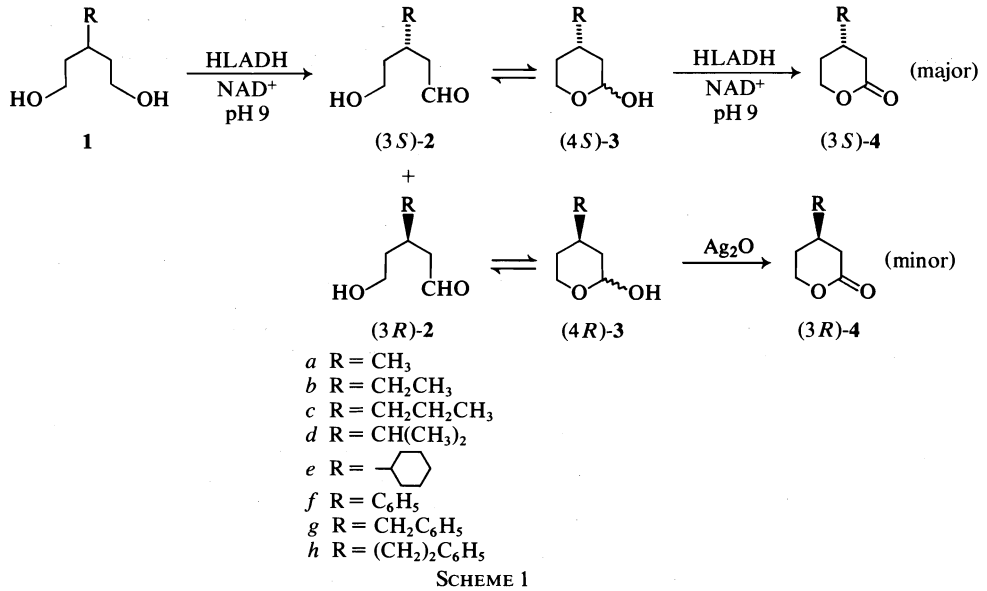

SCHEME 1

is the most important factor in determining the enantiomeric excess of the final lactone product **4** from diols **1** and that the stereospecificity of the enzyme diminishes for both **1** → **2** and **3** → **4** oxidations as the substituent R becomes larger.

Results

The diols **1***a–h* and the racemic lactones **4***a–h* were prepared by the methods used previously (1*a*, *b*) and diastereomeric mixtures of the hemiacetals **3***a–h* by reduction of (±)-**4***a–h* with diisobutylaluminum hydride (3).

Preparative-scale HLADH-catalyzed oxidations of the diols **1***a–h* and of the hemiacetals **3***a–h* were carried out at pH 9 using FMN recycling of catalytic amounts of the expensive NAD^+ coenzyme (1*d*). The reaction products contained the lactones (3*S*)-**4***a–h* and the hemiacetals (4*R*)-**3***a–h* of varying degrees of optical purity. The (4*R*)-enriched hemiacetals were oxidized to the corresponding (3*R*)-lactones with silver oxide, and the enantiomeric excesses and absolute configurations of each pair of lactones then determined. All enantiomeric excesses were determined directly (4). Absolute configurations were correlated by comparison with previously assigned (1*b*) lactones (**4***a*, *d*, and *f*) or by conversion to a 2-substituted succinic acid **7** or 3-substituted valeric acid **8** of known configuration using one of the Scheme 2 degradations. The results are summarized in Tables 1 and 2. A kinetic analysis of the hemiacetal substrate oxidations was also carried out. The data are recorded in Table 3.

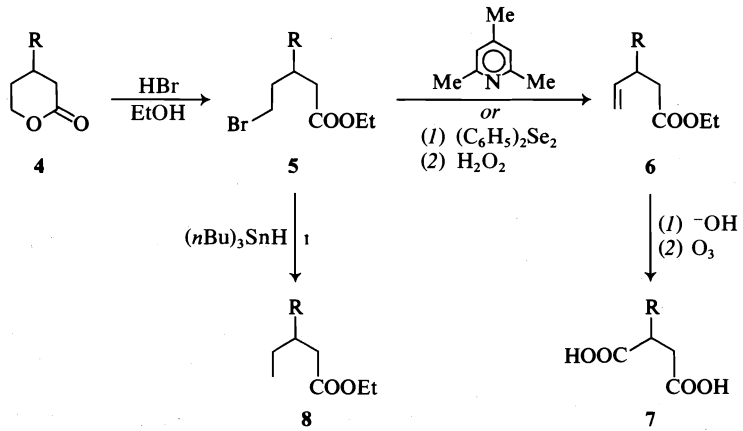

SCHEME 2

TABLE 1. Enantiomeric excesses and absolute configurations of lactones **4***a–h* obtained via HLADH-catalyzed oxidations of diols **1***a–h*[a]

Substrate	Products[b]	% yield	% ee
1*a*	(3*S*)-**4***a*	53	78
	(3*R*)-**4***a*	3	15
1*b*	(3*S*)-**4***b*	56	74
	(3*R*)-**4***b*	6	21
1*c*	(3*S*)-**4***c*	48	68
	(3*R*)-**4***c*	3	11
1*d*	(3*S*)-**4***d*	44	46
	(3*R*)-**4***d*	2	36
1*e*	(3*S*)-**4***e*	67	18
	(3*R*)-**4***e*	2	26
1*f*	(3*S*)-**4***f*	44	16
	(3*R*)-**4***f*	2	6
1*g*	(3*S*)-**4***g*	72	20
	(3*R*)-**4***g*	2	68[c]
1*h*	(3*S*)-**4***h*	60	18
	(3*R*)-**4***h*	2	36

[a]Reactions allowed to go to completion at pH 9.
[b]3*R*-Lactones obtained by silver oxide oxidation of the 4*R*-hemiacetals isolated from the individual reaction mixtures.
[c]Anomalously high, see Discussion.

TABLE 2. Enantiomeric excesses and absolute configurations of lactones **4***a–h* obtained via HLADH-catalyzed oxidations of hemiacetals **3***a–h*[a]

Substrate	Products[b]	% yield[c]	% ee
3*a*	(3*S*)-**4***a*	70	73
	(3*R*)-**4***a*	30	66
3*b*	(3*S*)-**4***b*	68	44
	(3*R*)-**4***b*	24	53
3*c*	(3*S*)-**4***c*	80	29
	(3*R*)-**4***c*	16	24
3*d*	(3*S*)-**4***d*	64	20
	(3*R*)-**4***d*	24	22
3*e*	(3*S*)-**4***e*	96	12
	(3*R*)-**4***e*	12	10
3*f*	(3*S*)-**4***f*	58	13
	(3*R*)-**4***f*	18	11
3*g*	(3*S*)-**4***g*	78	12
	(3*R*)-**4***g*	16	8
3*h*	(3*S*)-**4***h*	84	14
	(3*R*)-**4***h*	8	8

[a]Reactions terminated at 50% oxidation stage at pH 9.
[b]3*R*-Lactones obtained by silver oxide oxidation of the recovered 4*R*-hemiacetals.
[c]Based on 50% reaction.

Discussion

All of the enzyme-catalyzed reactions were carried out on synthetically significant (up to 2 g) amounts of the substrates. The hemiacetal oxidations were stopped after ~50% of reaction. (Enzyme-catalyzed resolutions of chiral substrates are traditionally terminated at this point since this is the stage at which optically pure products are obtained if the enzyme's stereospecificity is absolute). In contrast, with the symmetrical diol substrates **1**, the reactions were allowed to proceed to completion since enantiotopically selective transformations are true asymmetric inductions. Operating on symmetrical substrates thus has the great advantage that it avoids the inevitably lower (50% maximum) yields of a desired stereoisomer obtained when the substrate is a racemate. In the latter cases the unwanted enantiomers are generally wasted.

The experimental techniques used to carry out the enzyme-catalyzed oxidations were quite straightforward. The work-up procedure was also simple, consisting of continuous chloroform extraction, first at pH 3 to isolate the 3*S*-enriched lactones **4***a–h*, followed by a second continuous extraction at pH 12 to recover the 4*R*-enriched hemiacetals **3***a–h* present. The latter were all smoothly oxidized to the corresponding 3*R*-lactones with silver oxide. Good yields of the 3*S*-lactones were isolated in all cases. However, the amounts of 3*R*-enriched lactones obtained were somewhat reduced by mechanical losses during the hemiacetal extraction and subsequent oxidation stages. No attempt was made to optimize the yields in any reaction. The percentages listed in the Tables 1 and 2 can undoubtedly be improved significantly.

The optical purities of the 3*S*-lactones **4***a*, *g*, and *h* obtained previously (1*b*) were estimated from optical rotation data. Optical methods are, however, well recognized to be unreliable at times and all enantiomeric excesses reported in the present work were determined directly by gas chromatographic analysis of their (2*R*,3*R*)-butanediol orthoester derivatives (4). Care was taken during the absolute configuration correlations of Scheme 2 to ensure that no epimerization occurred at any stage.[3] Dehydrohalogenation of **5** to **6** using the diphenyldiselenide procedure (7) proved much superior to the 2,4,6-trimethylpyridine-mediated elimination used initially (1*b*).

The kinetic data (Table 3) on the hemiacetals **3***a–g* showed that each was a very good substrate of the enzyme, thereby confirming the earlier supposition (1*b*) that they were intermediates in the overall oxidation of **1** → **4**. With the exception of the

[3]The apparent discrepancies (1*b*, 6*a*) in the optical purity and absolute configuration assignments of the phenyl lactone **4***f* has now been resolved (6*b*). The (+)-enantiomer has the 3*S* absolute configuration (1*b*). A detailed investigation (6*b*) of the properties of **4***f* has shown that the erroneous 3*R* assignment (6*a*) was due to the unsuspected sensitivity of (+)-**4***f* to distillation. The other 3-substituted lactones are stable. The ee values for **4***f* based on optical rotation (1*b*, 6*b*) and the orthoester glc data of this paper are now in total agreement.

TABLE 3. Kinetic parameters for HLADH-catalyzed oxidations of the hemiacetals **3***a–h*[a]

Substrate	K_m(app) (mM)	V_{max}(s^{-1})
3*a*	2.9	1.67
3*b*	2.4	1.85
3*c*	0.9	1.56
3*d*	5.3	0.75
3*f*	0.6	1.28
3*g*	2.2	1.49
Ethanol[b]	0.70	2.38
Cyclohexanol[c]	0.90	3.30

[a]Determined at 25°C in 0.05 M glycine–NaOH buffer, pH 9 with [NAD^+] 5.0×10^{-4} M and [hemiacetal] $10^{-4} - 10^{-2}$ M.
[b]From ref. 5.
[c]From ref. 1*a*.

isopropyl compound **3***d*, each hemiacetal is oxidized at effectively the same maximum velocity. Furthermore, the V_{max} values are not significantly different from those of ethanol and cyclohexanol, for which NADH dissociation from the enzyme–NADH complex in the final step is rate determining (5, 8). NADH dissociation is thus the predominant rate determining step in the oxidation of the hemiacetals **3***a–c*, *e–f* also, just as it is for the diols **1***a–f* (1*a*). The much lower V_{max} value for **3***d* indicates that the hydride transfer step has become slow enough to be at least partly rate determining.

The results of the preparative-scale experiments summarized in Tables 1 and 2 are of considerable asymmetric synthesis interest. As Table 1 shows, HLADH always exhibits pro-*S* selectivity in its catalysis of the oxidation of the enantiotopic hydroxyethyl groups of the diols **1***a–h*. The degree of enantiotopic selectivity is strongly influenced by the size of the substituent at C-3. When it is small, e.g., methyl (**1***a*), the 3*S*-lactone isolated has a very high optical purity. The enantiomeric excess diminishes as the size of the R group is increased through ethyl (1*b*) to propyl (1*c*) but remains high as long as the steric bulk of the C-3 substituent remains below a critical threshold level. The isopropyl function has clearly begun to exceed the tolerance of the enzyme in this regard with the optical purity of (3*S*)-**4***d* being only 46%. Further increases in the size of the C-3 substituent lead to progressively diminishing enantiomeric excesses; for oxidation of the diols **1***e–h*, the optical purities of the lactone products are too low to be of asymmetric synthesis interest. The 3*S*-enriched lactones **4***a–h* are obtained in good yield and are the only major products. The amounts of the 3*R*-lactones obtained by chemical oxidation of the residual 3*R*-hemiacetals in the reaction mixtures were very low. Furthermore, their enantiomeric excess levels were unexciting, except for (3*R*)-**4***g*. In this case, the anomalously high optical purity of 68% is probably the result of an unusually powerful effect of substrate concentration on the relative rates of enzymic oxidation of the diastereomeric hemiacetal intermediates (1*a*).

From Table 2, it is seen that HLADH-mediated oxidation of the racemic hemiacetals (+)-**3***a–h* is routinely enantiomerically selective for the 4*S*-enantiomer.[4] The chemical yields of (3*S*)-**3***a–h* are very respectable, those of (3*R*)-**3***a–h* are low owing to the losses incurred during purification following chemical oxidation of their 4*R*-hemiacetal precursors. Again the enantiomeric excesses of the lactones are high when the C-4 group is small and diminish progressively as this substituent becomes larger. However, for the hemiacetal substrates, the stereoselectivity of the enzyme is far more sensitive to the size of the C-4 substituent than with the corresponding diol substrates. With the exception of **3***a*, the enantiomeric excesses of the lactones of Table 2 are not of practical asymmetric synthesis value.

As is usual in enzymic resolutions of racemates, the optical purities of the enantiomeric pairs of lactones **4***a–h* are effectively equal. This contrasts the situation in Table 1 where the optical purities of the enantiomeric lactones derived from the better diol substrates **1***a–c* are dramatically different. This fact, together with the disparities between the hemiacetal yields of the diol-derived 3*R*- and 3*S*-lactone pairs, proves conclusively that the enzyme is exhibiting true pro-*S* enantiotopic selectivity in its catalysis of the oxidation of the diols **1***a*, *b* to the initial hydroxyaldehyde products (3*S*)-**2***a–h*. Fortuitously, the second oxidation, **3** → **4**, also occurs with *S* stereoselectivity.

The enantiomeric excess levels of the 3*S*-lactones isolated from the diol precursors therefore reflect the combined effects of these enzyme specificity properties. From the data of Tables 1 and 2, it is seen that the enantiotopic selectivity factor is most important when the R substituent is smallest. Its influence diminishes as its bulk increases and becomes inconsequential when R is larger than isopropyl.

The results summarized in Tables 1 and 2 are all rationalizable in terms of the system of coordinates, termed the diamond lattice (2), whereby the preferred and allowed orientations of a substrate at the active site of the HLADH can be identified. The diol and hemiacetal analyses described previously (1*b*) apply without qualification.

[4]Oxidation of the hemiacetals is considered to take place with the C-2-hydroxyl group axially oriented in the ES complex (1*b*). Enantiomeric selectivity has also been observed in the HLADH-catalyzed oxidation of five-membered ring hemiacetals (1*c*).

The benzyl (**1***g*, **3***g*) and phenethyl (**1***h*, **3***h*) substrates were included in this study in order to ascertain whether or not the adverse interactions of the phenyl group of **1***f* and **3***f* with forbidden regions of the active site (1*b*) could be alleviated by progressive insertion of methylene groups. This is clearly not the case. Any large group in this region of the active site is evidently undesirable.

Experimental

Melting points were determined on a Fisher-Johns apparatus and are uncorrected. Infrared and nmr spectra were recorded for all compounds; in each case the spectra were unexceptional and selected spectral data only are reported. Optical rotations all refer to $CHCl_3$ (*c*, 1) solutions unless specified otherwise. Gas–liquid chromatographic analyses were performed using 1 m × 3 mm columns of 2% QF-1 on Chromosorb G with flame ionization detection. NAD^+ and FMN were purchased from Sigma. HLADH (EC 1.1.1.1) may be purchased from Worthington or Boehringer. It was assayed (8*c*) before use; the amounts of HLADH quoted represent milligrams of active enzyme.

Preparation of the 3-Substituted Pentanediols **1**a–h

The diols **1***a–d*, *f*, *g* were prepared as described previously (1*a*, *b*).

*3-Cyclohexylpentane-1,5-diol (***1***e)*

Diethyl cyclohexylmalonate (34 g, 0.14 mol, prepared as described by Hope and Perkin (9)) in dry tetrahydrofuran (200 mL) was added dropwise with stirring at 20°C to a suspension of lithium aluminum hydride (7.6 g, 0.2 mol) in dry tetrahydrofuran (400 mL). The mixture was heated on an oil bath at 60°C for 1 day and then cooled to 0°C. The reaction was quenched carefully with 3% aqueous sodium hydroxide (40 mL), filtered, and the dried ($MgSO_4$) filtrate evaporated. The residue was recrystallized from acetone to give *2-cyclohexylpropane-1,3-diol*, (16.5 g) mp 90–91°C.

Methanesulfonyl chloride (16.2 mL, 0.21 mol) was added dropwise to a solution of the above diol (15.8 g, 0.1 mol) in dry benzene (100 mL) and dry pyridine (50 mL) cooled to 5°C. The mixture was then stirred overnight at 20°C. The solid present was filtered off and washed with benzene and the combined organic filtrates washed with saturated aqueous sodium bicarbonate followed by saturated brine. The dried (Na_2SO_4) organic layer was evaporated to give *2-cyclohexylpropane-1,3-diol bismethanesulfonate* (30 g, 0.097 mol). This was dissolved in ethanol (150 mL) and potassium cyanide (13.7 g, 0.21 mol) in water (50 mL) added. The mixture was refluxed for 6 h, then 10 *N* aqueous sodium hydroxide (50 mL) was added and refluxing continued for a further 20 h. The resulting solution was concentrated to ~150 mL and washed with ether. The aqueous layer was decolourised with Norite, filtered, and the filtrate cooled in an ice bath and acidified with 6 *N* hydrochloric acid. The resulting solid was filtered off, dissolved in saturated aqueous sodium bicarbonate and then reprecipitated with 6 *N* hydrochloric acid to give, after drying, *3-cyclohexylglutaric acid* (8.28 g, 0.04 mol).

The cyclohexylglutaric acid (5.0 g, 24 mmol) in dry tetrahydrofuran (50 mL) was added dropwise with stirring at 20°C to lithium aluminum hydride (1.9 g, 50 mmol) in dry tetrahydrofuran (100 mL). The resulting suspension was refluxed for 8 h, then cooled to 0°C, and the reaction quenched by the careful addition of 2% aqueous sodium hydroxide (10 mL). The solid produced was filtered off, washed with tetrahydrofuran, and the combined filtrate and washings dried (Na_2SO_4) and concentrated. The residual oil was distilled to give 3-cyclohexylpentane-1,5-diol (**1***e*, 3.5 g) bp 131°C/0.05 Torr; ^1H nmr (C^2HCl_3) δ: 0.8–2.2 (16H, m) and 3.3–3.9 (6H, m) ppm. *Anal.* calcd. for $C_{11}H_{22}O_2$: C 70.92, H 11.90; found: C 70.77, H 11.78.

*3-Phenethylpentane-1,5-diol (***1***h)*

Sodium (11.5 g, 0.5 mol) was dissolved in ethanol (200 mL) and ethyl malonate (80 g, 0.5 mol) added. The mixture was maintained at 60°C during the slow addition of phenethyl bromide (92.5 g, 0.5 mol) and then refluxed for 20 h. The cooled (20°C) mixture was diluted with water (300 mL), the organic solution separated, and the aqueous layer extracted with ether. The combined organic solutions were dried ($MgSO_4$), evaporated, and the residue distilled to give diethyl phenethylmalonate (75 g), bp 168–170°C/2.5 Torr; ir (film): 1725 cm^{-1}; ^1H nmr (C^2HCl_3) δ: 1.3 (6H, t, J = 6 Hz), 2.0–2.9 (4H, m), 3.3 (1H, t, J = 7 Hz), 4.2 (4H, q, J = 6 Hz), and 7.2 (5H, s) ppm. *Anal.* calcd. for $C_{15}H_{15}O_4$: C 68.16, H 7.62; found: C 68.04, H 7.50.

The subsequent procedures were as described above for **1***e*. Reduction of the phenethylmalonate (74.5 g, 0.34 mol) gave *2-phenethylpropane-1,3-diol* as a crystalline product (40.3 g), mp 57°C; ^1H nmr (C^2HCl_3) δ: 1.3–2.0 (2H, m), 2.4–2.8 (3H, broad t), 3.4–4.0 (4H, m), and 7.2 (5H, s) ppm. *Anal.* calcd. for $C_{11}H_{16}O_2$: C 73.30, H 8.95; found: C 73.33, H 9.14. This diol (9 g, 50 mmol) was converted to *2-phenethylpropane-1,3-diol bismethanesulfonate* (16.7 g, 50 mmol) which was transformed directly into *3-phenethylglutaric acid* (3.6 g after recrystallization from water), mp 99–100°C; ^1H nmr (($C^2H_3)_2SO$) δ: 1.4–2.0 (2H, m), 2.1–2.9 (7H, m), and 7.1 (5H, s) ppm. Reduction of 3-phenethylglutaric acid[5] (11.8 g, 50 mmol) yielded *3-phenethylpropane-1,3-diol* (**1***h*, 8.53 g), bp 152–154°C/0.5 Torr; ^1H nmr (C^2HCl_3) δ: 1.3–1.9 (7H, m), 2.4–2.8 (2H, m), 3.3–4.1 (6H, m), and 7.2 (5H, s) ppm. *Anal.* calcd. for $C_{13}H_{20}O_2$: C 74.96, H 9.68; found: C 74.88, H 9.76.

Preparation of Hemiacetals **3**a–h

The 4-methylhemiacetal **3***a* was synthesized by the literature method (11). The remaining hemiacetals **3***b–h* were prepared by reduction of the corresponding lactone **4***b–h* with diisobutylaluminum hydride according to the procedure of Schmidlin and Wettstein (3). All of the hemiacetals were relatively unstable. These were used immediately following chromatographic purification.

*2-Hydroxy-4-ethyltetrahydropyran ((±)-***3***b)*

Diisobutylaluminum hydride (10 g, 70 mmol, 20% solution in *n*-hexane) was added dropwise with stirring under nitrogen at −78°C to 3-ethylvalerolactone ((±)-**4***b*, (1*a*), 3.9 g, 30 mmol) in dry toluene (300 mL). Stirring at −78°C was continued for a further 3 h and the reaction was then quenched by the slow addition of methanol until gas evolution ceased. The mixture was stirred for 30 min at 20°C, then diluted with ether (100 mL). Saturated brine (100 mL), followed by 6 *N* hydrochloric acid (50 mL) to destroy the resulting emulsion, were added and the organic layer separated. The aqueous solution was reextracted with ether and the combined ether solutions washed with saturated brine and then dried ($MgSO_4$). The solvent was rotary evaporated carefully at 20°C and the oil obtained chromatographed quickly on silica gel (50 cm × 2 cm column, ether – petroleum ether, bp 40–60°C (30:70) elution). Evaporation of the desired eluant fractions yielded 2-hydroxy-4-ethyltetrahydropyran ((±)-**3***b*, 2.9 g); ^1H nmr δ: 0.7–2.2 (10H, m) and 3.2–5.4 (4H, m) ppm.

[5]Subsequently prepared by the method of Koppang *et al.* (10).

This basic procedure was used to prepare each of the following hemiacetals (±)-**3***c–h*.

*2-Hydroxy-4-*n*-propyltetrahydropyran ((±)-**3***c*)*

This was obtained in 64% yield from 3-*n*-propylvalerolactone ((±)-**4***c* (1*a*), 5 g, 35 mmol); ^{1}H nmr (C^2HCl_3) δ: 0.8–2.2 (12H, m) and 3.2–5.4 (4H, m).

*2-Hydroxy-4-isopropyltetrahydropyran ((±)-**3**d)*

This was obtained in 76% yield from 3-isopropylvalerolactone ((±)-**4***d* (1*b*), 5 g, 35 mmol); ^{1}H nmr (C^2HCl_3) δ: 0.9 (6H, d, J = 6.4 Hz), 1.1–2.1 (6H, m), and 3.2–5.4 (4H, m) ppm.

*4-Cyclohexyl-2-hydroxytetrahydropyran ((±)-**3**e)*

3-Cyclohexylglutaric acid (8.28 g, 40 mmol, see preparation of **1***e*) was refluxed with acetic anhydride (50 mL) for 10 h. Excess acetic anhydride and acetic acid were removed by rotary evaporation and the residue distilled to give *3-cyclohexylglutaric anhydride* (6.3 g), bp 158°C/0.75 Torr; ir (film): 1750, 1820 cm^{-1}; ^{1}H nmr (C^2HCl_3) δ: 0.6–2.2 (12H, m) and 0.6–2.2 (4H, m) ppm. *Anal.* calcd. for $C_{11}H_{16}O_3$: C 67.32, H 8.22; found: C 67.21, H 8.18.

The anhydride (4.9 g, 25 mmol) in dry tetrahydrofuran (40 mL) was added at 0°C to sodium borohydride (0.95 g, 25 mmol) in dry tetrahydrofuran (10 mL). Stirring was continued for 10 h at 20°C, then 6 *N* hydrochloric acid (10 mL) was added cautiously and the mixture concentrated. Water (100 mL) was added and the solution extracted with ether (3 × 50 mL). The ether extract was dried (Na_2SO_4) and evaporated to give *3-cyclohexylvalerolactone* ((±)-**4***e*, 3.3 g), bp 120–121°C/0.2 Torr; ^{1}H nmr (C^2HCl_3) δ: 0.6–2.2 (14H, m), 2.2–2.7 (2H, m), and 4.0–4.6 (2H, m) ppm. *Anal.* calcd. for $C_{11}H_{18}O_2$: C 72.49, H 9.95; found: C 72.64, H 9.89.

Reduction of (±)-**4***e* by the Schmidlin and Wettstein (3) method gave 4-cyclohexyl-2-hydroxytetrahydropyran ((±)-**3***e*, 60% yield, acetone–hexane (1:3) elution) as a more-than-usually unstable hemiacetal.

*2-Hydroxy-4-phenyltetrahydropyran ((±)-**3**f)*

This was prepared from 3-phenylvalerolactone ((±)-**4***f* (12), 6.06 g, 35 mmol) in 55% yield (methanol – methylene chloride (1:20) elution); ^{1}H nmr (C^2HCl_3) δ: 0.8–4.2 (9H, m) and 7.2 (5H, s) ppm.

*4-Benzyl-2-hydroxytetrahydropyran ((±)-**3**g)*

This was obtained by reduction of 3-benzylvalerolactone ((±)-**4***g* (1*a*), 6.72 g, 35 mmol) in 61% yield; ^{1}H nmr (C^2HCl_3) δ: 0.9–4.3 (11H, m) and 7.3 (5H, s) ppm.

*2-Hydroxy-4-phenethyltetrahydropyran ((±)-**3**h)*

3-Phenethylglutaric acid (4.7 g, 20 mmol, see preparation of **1***h*) was converted to the anhydride as described above for (±)-**3***e*. *3-Phenethylglutaric anhydride* (2.78 g after recrystallization from ether – petroleum ether (bp 40–60°C)) had mp 69.5–70°C; ^{1}H nmr (C^2HCl_3) δ: 1.5–3.3 (9H, m) and 7.2 (5H, m). *Anal.* calcd. for $C_{13}H_{14}O_3$: C 71.54, H 6.47; found: C 71.47, H 6.54.

The above anhydride (10.9 g, 0.05 mol) in dry tetrahydrofuran (50 mL) was added at 0°C with stirring to sodium borohydride (2.0 g, 0.05 mol) in dry tetrahydrofuran (10 mL). Stirring was continued for 10 h at 20°C and 6 *N* hydrochloric acid (20 mL) then added cautiously. After concentrating, water (100 mL) was added to the mixture and it was extracted with ether (3 × 50 mL). The ether extract was dried (Na_2SO_4), evaporated, and the residual oil distilled to yield *3-phenethylvalerolactone* ((±)-**4***h*, 6.3 g) bp 153–154°C/0.25 Torr which subsequently solidified, mp 43–43.5°C; ^{1}H nmr (C^2HCl_3) δ: 1.3–3.0 (9H, m), 4.0–4.7 (2H, m), and 7.2 (5H, s) ppm. *Anal.* calcd. for $C_{13}H_{16}O_2$: C 76.44, H 7.89; found: C 76.52, H 7.84.

The lactone (±)-**4***h* (4.08 g, 0.02 mol) was reduced in the usual way to give 2-hydroxy-4-phenethyltetrahydropyran ((±)-**3***h*) in 75% yield (*n*-hexane–acetone (7:3) elution) as a colourless solid, mp 60–64°C; ^{1}H nmr (C^2HCl_3) δ: 0.8–2.8 (10H, m), 3.2–4.8 (3H, m), and 7.2 (5H, s) ppm.

*HLADH-Catalyzed Oxidation of the Diols **1**a–h*

The oxidations were effected on a 10 mmol of substrate scale using the previously described procedure (1*b*).[6] The enantiomeric excess of the product lactones (3*S*)- and (3*R*)-**4***a–h* were measured directly by glc examination of their orthoesters with (2*R*,3*R*)-butane-2,3-diol (4). The results are summarized in Table 1.

The physical properties of the lactones were as described previously (1*a*, *b*) or as given above for the racemates. The optical rotations observed are given below.

Compound	$[\alpha]_D^{25}$	% ee	Compound	$[\alpha]_D^{25}$	% ee
(3*S*)-**4***a*	−23.6°	78	(3*R*)-**4***a*	+4.7°	15
(3*S*)-**4***b*	−20.4°	74	(3*R*)-**4***b*	+5.8°	21
(3*S*)-**4***c*	−13.5°	67	(3*R*)-**4***c*	+2.0°	11
(3*S*)-**4***d*	−14.4°	46	(3*R*)-**4***d*	+11.5°	36
(3*S*)-**4***e*	+4.3°	18	(3*R*)-**4***e*	(−3.9°)[a]	26
(3*S*)-**4***f*	+0.8°	16	(3*R*)-**4***f*	−0.4°	6
(3*S*)-**4***g*	−19.1°	20	(3*R*)-**4***g*	(+24.2°)[a]	68
(3*S*)-**4***h*	−14.3°	18	(3*R*)-**4***h*	(+17.1°)[a]	36

[a]These compounds were obtained in very low yields (Table 1) and the quantities isolated were insufficient for accurate specific rotation measurements.

*HLADH-Catalyzed Oxidations of the Hemiacetals (±)-**3**a–h*

The enzyme-catalyzed oxidations of the hemiacetals (±)-**3***a–h* were each carried out on a 10 mmol of substrate scale. The physical properties of the product lactones **4***a–h* were as detailed previously (1*a*, *b*) or as given above for the racemates. Their ee's were determined directly by the orthoester glc analytical method (4). The overall results are summarized in Table 2.

The procedure for oxidation of the 4-methyl hemiacetal (±)-**3***a* is representative.

2-Hydroxy-4-methyltetrahydropyran (1.2 g, 10 mmol), NAD^+ (0.65 g, 1 mmol) and FMN (9.6 g, 20 mmol) were dissolved in 0.05 *M* pH 9 glycine – sodium hydroxide buffer (900 mL). The pH of the resulting solution was then readjusted to 9 with 10 *N* aqueous sodium hydroxide and HLADH (35 mg) added. The reaction mixture was kept in a stoppered flask for 12 h and the pH readjusted to 9 once again. After a further 7 h, glc analyses indicated the desired 50%-of-reaction point had been reached. The pH was then raised to 12 with 10 *N* aqueous sodium hydroxide and the mixture continuously extracted with chloroform for 2 days. (The aqueous solution was retained for further work-up, *vide infra*.) The dried ($MgSO_4$) chloroform extract was evaporated and the residual (4*R*)-hemiacetal **3***a* (514 mg) was oxidized with silver oxide (prepared by adding sodium hydroxide (2.4 g, 60 mmol) in water (10 mL) to silver nitrate (5 g, 30 mmol) in 60% aqueous ethanol (30 mL)). The mixture was stirred overnight and was then filtered and continuously extracted with chloroform for 1 day. The chloroform extract was discarded. The aqueous solution was acidified to pH 3 with 6 *N* aqueous hydrochloric acid and continuously extracted with chloroform for 36 h. After evaporation of the dried ($MgSO_4$) chloroform extract and molecular distillation of the residue, (3*R*)-3-methylvalerolactone ((3*R*)-**4***a*, 180 mg); $[\alpha]_D^{25}$ +20.0° (66% ee) was obtained.

The aqueous solution retained from the initial extraction

[6]Reactions were monitored by glc. The longest reaction period required was 6 days.

was brought to pH 3 with 6 *N* aqueous hydrochloric acid and then continuously extracted with chloroform for 2 days. Evaporation of the dried ($MgSO_4$) chloroform solution yielded, after molecular distillation, (3*S*)-3-methylvalerolactone ((3*S*)-**4***a*, 425 mg); $[\alpha]_D^{25}$ −21.5° (73% ee).

Oxidation of the remaining hemiacetals (±)-**4***b–h* in an exactly similar manner yielded lactones **4***b–h*, respectively.[6] The optical rotations observed are given below.

Compound	$[\alpha]_D^{25}$	% ee	Compound	$[\alpha]_D^{25}$	% ee
(3*S*)-**4***b*	−12.3°	44	(3*R*)-**4***b*	+12.9°	53
(3*S*)-**4***c*	−6.4°	29	(3*R*)-**4***c*	+5.2°	24
(3*S*)-**4***d*	−6.1°	20	(3*R*)-**4***d*	+7.0°	22
(3*S*)-**4***e*	+3.6°	12	(3*R*)-**4***e*	−1.5°	10
(3*S*)-**4***f*	+0.8°	13	(3*R*)-**4***f*	−0.7°	11
(3*S*)-**4***g*	−12.8°	12	(3*R*)-**4***g*	+6.8°	8
(3*S*)-**4***h*	−8.6°	14	(3*R*)-**4***h*	+4.2°	8

*Determination of Absolute Configurations of Lactones (3S)- and (3R)-**4**a–h*

The absolute configurations of (3*S*)- and (3*R*)-**4***a*, *d*, and *f* were known (1*b*).

*Correlation of (−)-(3S)-**4**b*

(−)-(3*S*)-Ethylvalerolactone (**4***b*, 1.28 g, 0.01 mol, $[\alpha]_D^{25}$ −20.4°) in absolute ethanol (20 mL) was treated with excess dry hydrogen bromide at 0°C. After being stirred overnight at 20°C, the solution was diluted with water (120 mL) and extracted with ether (3 × 50 mL). The ether extract was washed with saturated aqueous sodium bicarbonate, then with brine, dried ($MgSO_4$) and evaporated. Distillation of the residual oil gave (−)-*ethyl* (3R)-*5-bromo-3-ethylpentanoate* (2.16 g) bp 98–99°C/5 Torr, $[\alpha]_D^{25}$ −8.2°; ^{1}H nmr (C^2HCl_3) δ: 0.95 (3H, t, *J* = 6.0 Hz), 1.3 (3H, t, *J* = 7.0 Hz), 0.9–2.4 (7H, m), 3.45 (2H, t, *J* = 7.0 Hz), and 4.15 (2H, q, *J* = 7.0 Hz) ppm. *Anal.* calcd. (on racemate) for $C_9H_{17}O_2Br$: C 45.59, H 7.23; found: C 45.44, H 7.18.

The above ester (2.16 g, 9 mmol) was refluxed in 2,4,6-trimethylpyridine (10 mL) for 3 h. The cooled mixture was poured into saturated aqueous copper sulfate solution (200 mL) and extracted with ether. Evaporation of the dried ($MgSO_4$) ether solution followed by distillation yielded (−)-*ethyl* (3R)-*3-ethylpent-4-enoate* (280 mg), bp 70–71°C/15 Torr, $[\alpha]_D^{25}$ −4.6°; ^{1}H nmr (C^2HCl_3) δ: 0.9 (3H, t, *J* = 7.0 Hz), 1.2 (3H, t, *J* = 7.0 Hz), 1.4–1.9 (3H, m), 2.2–2.5 (2H, m), 4.1 (2H, q, *J* = 7.0 Hz), 4.8–5.0 (1H, m), 5.1 (1H, broad s), and 5.5–6.0 (1H, m) ppm. *Anal.* calcd. (on racemate) for $C_9H_{16}O$: C 69.20, H 10.32; found: C 68.61, H 10.69.

Hydrolysis of this olefinic ester (280 mg) was effected by refluxing in 5% ethanolic potassium hydroxide (20 mL) for 2 h. The cooled solution was then diluted with water (80 mL), acidified with 6 *N* hydrochloric acid, and continuously extracted with ether for 24 h. Evaporation of the dried ($MgSO_4$) ether extract afforded the free acid; this was dissolved immediately in methylene chloride and ozonized at −78°C for 45 min. After purging excess ozone with oxygen, the solution was concentrated to 15 mL and heated on a steam bath with formic acid (6 mL) in 30% hydrogen peroxide (60 mL) for 2 h.

The excess peroxide was decomposed with 10% Pd–C, and the mixture filtered and evaporated. Recrystallization of the solid obtained from ethyl acetate – petroleum ether (bp 40–60°C) gave (−)-(2*R*)-2-ethylsuccinic acid (65 mg) mp 93–94°C, $[\alpha]_D^{25}$ −8.7° (*c* 1, $(CH_3)_2CO$) (lit. (13) mp 96°C, $[\alpha]_D^{25}$ −15.4° ($(CH_3)_2CO$)).

*Correlation of (−)-(3S)-**4**c*

This was effected in an identical manner. (−)-(3*S*)-3-*n*-Propylvalerolactone (**4***c*, 1.14 g, 8 mmol) was treated with hydrogen bromide to give (−)-*ethyl-(3R)-5-bromo-3-n-propylpentanoate* (1.92 g), bp 107–109°C/4 Torr, $[\alpha]_D^{25}$ −5.8°, ^{1}H nmr (C^2HCl_3) δ: 0.95 (3H, t, *J* = 7.0 Hz), 1.25 (3H, t, *J* = 7.0 Hz), 0.9–2.4 (9H, m), 3.45 (2H, t, *J* = 7.0 Hz), and 4.5 (2H, q, *J* = 7.0 Hz). *Anal.* calcd. (on racemate) for $C_{10}H_{19}O_2Br$: C 47.82, H 7.63; found: C 47.90, H 7.53. On refluxing with 2,4,6-trimethyl pyridine, this ester (1.92 g) yielded (−)-*ethyl* (3R)-*3*-n-*propylpent-4-enoate* (153 mg), bp 77–78°C/15 Torr, $[\alpha]_D^{25}$ −3.6°; ^{1}H nmr (C^2HCl_3) δ: 0.9 (3H, t, *J* = 7.0 Hz), 1.2 (3H, t, *J* = 7.0 Hz), 1.4–1.9 (5H, m), 2.2–2.5 (2H, m), 4.1 (2H, q, *J* = 7.0 Hz), 4.8–5.0 (1H, m), 5.15 (1H, m), and 5.4–6.0 (1H, m) ppm. *Anal.* calcd. (on racemate) for $C_{10}H_{18}O_2$: C 70.55, H 10.66; found: C 70.42, H 10.54.

Subsequent hydrolysis followed by ozonolysis afforded (−)-(2*R*)-2-*n*-propylsuccinic acid (21 mg), mp 98–100°C (from benzene – petroleum ether (bp 40–60°C)), $[\alpha]_D^{25}$ −6.2° (*c* 1, $(CH_3)_2CO$) (lit. (13) mp 103–104°C, $[\alpha]_D$ −18°).

*Correlation of (−)-(3S)-**4**h*

Treatment of (−)-(3*S*)-3-phenethylvalerolactone (**4***h*, 1.3 g, 63 mmol, $[\alpha]_D^{25}$ −14.3°) with hydrogen bromide gave (−)-*ethyl* (3R-*5-bromo-3-phenethylpentanoate* (1.52 g), $[\alpha]_D^{25}$ −2.3°; ^{1}H nmr δ: 1.2 (3H, t, *J* = 6.0 Hz), 1.4–2.8 (9H, m), 3.4 (2H, t, *J* = 7.0 Hz), 4.1 (2H, q, *J* = 6.0 Hz), and 7.2 (5H, s) ppm. *Anal.* calcd. (on racemate) for $C_{15}H_{21}O_2Br$: C 57.51, H 6.75; found: C 57.32, H 6.88.

Sodium borohydride (0.104 g, 3 mmol) was added slowly with stirring at 0°C under nitrogen to a solution of diphenyl diselenide (0.78 g, 2.5 mmol) in dry ethanol (10 mL) until the yellow colour disappeared (7). The bromo ester (1.5 g, 4.5 mmol) was then added and the mixture refluxed overnight. The solution was cooled to 0°C and tetrahydrofuran (60 mL) added, followed by 30% hydrogen peroxide (7.6 mL, 8.4 mmol). $MgSO_4$ (2g) was added and the resulting slurry stirred at 20°C for 1 day. The mixture was then diluted with water and extracted with ether. The ether extract was washed with saturated aqueous sodium bicarbonate, dried (Na_2SO_4) and evaporated. Molecular distillation of the residual oil yielded (+)-*ethyl* (3R)-*3-phenethylpent-4-enoate* (372 mg), $[\alpha]_D^{25}$ +7.9° (*c* 1, C_6H_6); ^{1}H nmr δ: 1.3 (3H, t, *J* = 6.0 Hz), 1.5–2.0 (2H, m), 2.2–2.8 (5H, m), 4.1 (2H, q, *J* = 6.0 Hz), 4.8–6.1 (3H, m), and 7.2 (5H, s) ppm. *Anal.* calcd. (on racemate) for $C_{15}H_{20}O_2$: C 77.55, H 8.68; found: C 77.69, H 8.92. Hydrolysis of this olefinic ester (360 mg, 1.5 mmol) followed by ozonolysis gave (2*R*)-2-phenethylsuccinic acid (131 mg after recrystallization from ether – petroleum ether (bp 40–60°C)), mp 124–126°C, $[\alpha]_D^{25}$ +7.3° (*c* 0.5, EtOH) (lit. (14) mp 136–137°C, $[\alpha]_D^{25}$ +38.1°, EtOH).

*Correlation of (−)-(3S)-**4**g*

This was effected using the same procedures.[7] (−)-3*S*-3-Benzylvalerolactone (**4***g*, 1.5 g, 7.9 mmol, $[\alpha]_D^{25}$ −19.1°) was converted to (−)-ethyl (3*R*)-benzyl-5-bromopentanoate (1.7 g), bp 130°C/0.25 Torr, $[\alpha]_D^{25}$ −0.01° (*c* 1.8, EtOH), ^{1}H nmr δ: 1.2 (3H, t, *J* = 7.0 Hz), 1.7–2.8 (7H, m), 3.4 (2H, t, *J* = 7.0 Hz), 4.15 (2H, q, *J* = 7.0 Hz), and 7.2 (5H, m) ppm. The bromo ester (1.49 g, 5.2 mmol) was dehydrobrominated by the diphenyldiselenide – peroxide method to give (+)-*ethyl* (3R)-*3-benzylpent-4-enoate* (870 mg), $[\alpha]_D^{25}$ +6.6° (*c* 0.8, C_6H_6): ^{1}H nmr δ: 1.2 (3H, t, *J* = 7.0 Hz), 2.2–3.2 (5H, m), 4.1 (2H, q, *J* = 7.0 Hz), 4.85 (1H, m), 5.1 (1H, m), 5.5–6.05 (1H, m), and 7.25 (5H, m) ppm. *Anal.* calcd. (on racemate) for $C_{14}H_{18}O_2$: C 77.04, H 8.30; found: C 76.89, H 7.95. This

[7]Part of this work was done by Dr. H. B. Goodbrand.

unsaturated ester (870 mg, 4 mmol) was hydrolyzed and then ozonized to give, after chromatography on silica gel (ethyl acetate elution), (2*R*)-2-benzylsuccinic acid (620 mg), mp 159.5–160.5°C, $[\alpha]_D^{25}$ +5.4° (*c* 0.4, EtOAc) (lit. (15) for 2*S*-enantiomer, mp 160.5°C, $[\alpha]_D^{25}$ −27.0° (*c* 2.0, EtOAc).

Correlation of (+)-(3S)-4e

A solution of (+)-(3*S*)-3-cyclohexylvalerolactone (**4***e*, 1.45 g, 7.1 mmol, $[\alpha]_D^{25}$ +4.3°) in dry ethanol (15 mL) was saturated with dry hydrogen bromide at 0°C and then kept at 20°C overnight. Saturated brine (50 mL) was then added and the mixture extracted with ether (3 × 50 mL). Evaporation of the dried ($MgSO_4$) ether solution followed by molecular distillation yielded (−)-*ethyl* (3*S*)-*5-bromo-3-cyclohexylpentanoate* (1.48 g), $[\alpha]_D^{25}$ −1.8°. The bromo ester (1.0 g, 3.4 mmol) and tri-*n*-butyltin hydride (1.1 g, 3.8 mmol) in dry benzene (25 mL) was stirred under nitrogen at 20°C for 12 h and then refluxed for 4 h. The solvent was then evaporated and the oil obtained heated with 10% ethanolic potassium hydroxide (20 mL) at 100°C for 2 h. The mixture was cooled, diluted with water (50 mL), acidified with concentrated hydrochloric acid, and extracted with ether. Evaporation of the dried ($MgSO_4$) ether extract and then distillation afforded *3-cyclohexylvaleric acid* (500 mg), bp 172–174°C/20 Torr (lit. (15) bp 160–161°C/18 Torr). This acid was treated with ethereal diazomethane to give (+)-*methyl* (3S)-*3-cyclohexylvalerate* (410 mg), bp 120°C/20 Torr, $[\alpha]_D^{25}$ +1.2° (*c* 1, EtOH), (lit. (16) for 3*R*-enantiomer, $[\alpha]_D^{25}$ −7.2° (*c* 1, EtOH)).

Kinetic Studies

The rates of HLADH-catalyzed oxidations of (±)-**3***a–g* were determined as described previously (1*a*). The results are summarized in Table 3.

Acknowledgements

This work was supported by the National Research Council of Canada. We also thank Hoffmann La-Roche for financial aid and for a generous gift of HLADH. We are grateful to Dr. H. Bruce Goodbrand for helpful discussion and for his contributions in developing the **4***g* degradation sequence.

1. (*a*) A. J. Irwin, K. P. Lok, K. W-C. Huang, and J. B. Jones. J. Chem. Soc. Perkin I, 1636 (1978); (*b*) A. J. Irwin and J. B. Jones. J. Am. Chem. Soc. **99**, 556 (1977); (*c*) A. J. Irwin and J. B. Jones. J. Am. Chem. Soc. **99**, 1625 (1977); (*d*) J. B. Jones and K. E. Taylor. Can. J. Chem. **54**, 2969 (1976); (*e*) H. M. Schwartz, W-S. Wu, P. W. Marr, and J. B. Jones. J. Am. Chem. Soc. **100**, 5199 (1978).
2. J. B. Jones and J. F. Beck. Tech. Chem. (N.Y.), **10**, 107 (1976).
3. J. Schmidlin and A. Wettstein. Helv. Chim. Acta, **46**, 2799 (1963).
4. G. Saucy, R. Borer, D. P. Trullinger, J. B. Jones, and K. P. Lok. J. Org. Chem. **42**, 3206 (1977).
5. C. Tsai. Can. J. Biochem. **46**, 381 (1968).
6. (*a*) A. I. Meyers and C. E. Whitten. Tetrahedron Lett. 1947 (1976); (*b*) A. I. Meyers, R. K. Smith, and C. E. Whitten. J. Org. Chem. **44**. In press.
7. K. B. Sharpless, M. W. Young, and R. F. Lauer. Tetrahedron Lett. 1979 (1973).
8. (*a*) K. Dalziel. *In* The enzymes. Vol. 11. 3rd ed. *Edited by* P. D. Boyer. Academic, New York, NY. 1975. pp. 1–60; (*b*) K. Dalziel and F. M. Dickinson. Biochem. J. **100**, 491 (1966); (*c*) K. Dalziel. Acta Chem. Scand. **11**, 397 (1957).
9. E. Hope and W. H. Perkin. J. Chem. Soc. **95**, 1361 (1909).
10. R. Koppang, A. C. Ranade, and H. Gilman. J. Organometal. Chem. **22**, 1 (1970).
11. Y. R. Naves, P. Ochsner, A. F. Thomas, and D. Lamparsky. Bull. Soc. Chim. Fr. 1608 (1963); C. B. Anderson and D. T. Sepp. Tetrahedron, **24**, 1707 (1968).
12. A. Burger and A. Hofstetter. J. Org. Chem. **24**, 1290 (1959).
13. J. E. Baldwin, D. H. R. Barton, and J. K. Sutherland. J. Chem. Soc. 1787 (1965).
14. B. Sjöberg. Acta Chem. Scand. **14**, 273 (1960).
15. A. Fredga. Ark. Kemi Mineral. Geol. B, **26**, 11 (1948); Ark. Kemi, **6**, 277 (1953).
16. M. J. Briene, C. Ouannes, and J. Jacques. Bull. Soc. Chim. Fr. 613 (1967).

The reaction products of *N*-alkylquinoxalines with 7,7,8,8-tetracyanoquinodimethane

HEIMO JÜRGEN KELLER, DIETRICH NÖTHE, AND MANFRED WERNER

Anorganisch-Chemisches Institut der Universität Heidelberg, Im Neuenheimer Feld 270, 6900 Heidelberg 1, Federal Republic of Germany

Received October 27, 1978

HEIMO JÜRGEN KELLER, DIETRICH NÖTHE, and MANFRED WERNER. Can. J. Chem. **57**, 1033 (1979).

Simple (1:1) and complex (2:3) TCNQ salts of the *N*-ethylquinoxalinium (NEQ) and *N*-methylquinoxalinium (NMQ) cations were prepared and characterized. In contradiction to earlier claims it was found that the 1:1 NMQ–TCNQ compound is *not* highly conducting but is a semiconductor. The triclinic crystals with unit cell dimensions $a = 4.79$, $b = 10.46$, $c = 7.60$ Å, $\alpha = 93.49$, $\beta = 110.92$, $\gamma = 82.69°$ show triplet exciton lines in the epr spectra indicating the occurrence of dimerized radicals in this solid. The high dc conductivity of the *simple* salt as reported earlier can only be attributed to a complex salt.

HEIMO JÜRGEN KELLER, DIETRICH NÖTHE et MANFRED WERNER. Can. J. Chem. **57**, 1033 (1979).

On a préparé et caractérisé des sels TCNQ simples (1:1) et complexes (2:3) des cations *N*-éthylquinoxalinium (NEQ) et *N*-méthylquinoxalinium (NMQ). En opposition avec des prétentions antérieures, on a trouvé que le composé 1:1 NMQ–TCNQ *ne conduit pas bien* l'électricité mais est plutôt un semi-conducteur. Les dimensions de la maille des cristaux tricliniques sont $a = 4.79$, $b = 10.46$, $c = 7.60$ Å, $\alpha = 93.49$, $\beta = 110.92$, $\gamma = 82.69°$; ces cristaux présentent des raies d'exciton triplet dans leur spectre rpe ce qui indique la présence de radicaux dimères dans le solide. La conductivité cd élevée du sel *simple* rapportée plus tôt ne peut être attribuée qu'à un sel complexe.

[Traduit par le journal]

Introduction

Only a very few simple (1:1) TCNQ salts of *nitrogen-containing* donors (including organic amines and *N*-heterocyclic compounds) are reported to show high electrical conductivity (1, 2). One can therefore assume that these exceptional salts crystallize in regular segregated stacks. The most famous of these rare examples, the one-dimensional conductor NMP–TCNQ (3–6), seems to contain systematic crystal impurities (7, 8) which could favor this special arrangement of molecular radical ions in the solid. This supposition is supported by the fact that NMP–TCNQ shows increased dc conductivity after substitution of some part of NMP^+ by the neutral molecule phenazine (9).

It was our task to establish whether NMP–TCNQ and the three other 1:1 nitrogen donor compounds with comparatively high electrical conductivities (4-hydroxy-2,3,5,6-tetramethylanilinium–TCNQ (1), 5,8-dihydroxyquinolinium–TCNQ (1), and *N*-methylquinoxalinium–TCNQ (2)) are in fact outstanding exceptions to the general rule, i.e., that 1:1 salts of TCNQ with nitrogen donors normally do not crystallize in segregated uniform stacks, or whether there are any exceptions at all. Therefore, we reinvestigated one of the reported examples of 'highly conducting' 1:1 TCNQ–nitrogen-donor salts, *N*-methylquinoxalinium-7,7,8,8-tetracyanoquinodimethanide (NMQ–TCNQ) (2), its ethyl homologue and some other TCNQ derivatives. This paper summarizes some of the results concerning the chemistry and physics of these compounds.

Experimental

Preparation of Compounds

NMQ–TCNQ

This compound was prepared essentially as described by Melby (2). The procedure was altered because of the oxygen sensitivity of the solutions! To a boiling solution of 0.317 g (1.5 mmol) Li–TCNQ (which was prepared from LiI and TCNQ in CH_3CN) in 30 mL dry ethanol, was added *N*-methylquinoxaliniumiodide (NMQ–I) (0.408 g, 1.5 mmol) in 15 mL hot ethanol. The mixture was allowed to cool to room temperature. A microcrystalline *violet* product which was isolated after the filtration, was washed with a few millilitres of methanol and finally with ether. The yield was as described by Melby (2): 88%, mp 177°C (dec.). *Anal.* calcd. for NMQ–TCNQ, $C_{21}H_{13}N_6$: C 72.19, H 3.75, N 24.05; found: C 72.16, H 3.82, N 24.13.

For recrystallization (about 1 g in 100 mL acetonitrile) only absolutely oxygen- and moisture-free solvents could be used. All the procedures were carried out in a nitrogen atmosphere. After recrystallization and slow cooling in a Dewar flask, reddish-purple, shiny prisms up to an inch in size were obtained. All of them were *twinned* as shown by their X-ray and esr data.

$(NMQ)_2(TCNQ)_3$

TCNQ (0.204 g, 1 mmol) and NMQ–TCNQ (0.349 g, 1 mmol) were dissolved in 25 mL hot dry acetonitrile in a

0008-4042/79/091033-04$01.00/0

nitrogen atmosphere. The solution was filtered while hot and allowed to cool slowly to room temperature. Black needles with a metallic lustre separated and were filtered, washed with ether, and dried in a desiccator over $CaCl_2$. Recrystallization from acetonitrile and heatless drying in high vacuum did not change the properties of the isolated solid. The yield was 95%, mp 193°C (dec.). *Anal.* calcd. for NMQ(TCNQ)$_2$, $C_{33}H_{17}N_{10}$: C 71.60, H 3.10, N 25.30; calcd. for (NMQ)$_2$(TCNQ)$_3$·CH_3CN, $C_{56}H_{33}N_{17}$: C 71.25, H 3.52, N 25.22; calcd. for (NMQ)$_2$(TCNQ)$_3$, $C_{54}H_{30}N_{16}$: C 71.83, H 3.35, N 24.82; found: C 71.10, H 4.05, N 25.43; C 71.31, H 3.96, N 25.42;[1] C 72.09, H 3.54, N 24.61.[2]

N-*Ethylquinoxalinium–TCNQ (NEQ–TCNQ)*

A boiling solution of Li–TCNQ (0.317 g, 1.5 mmol) in 30 mL ethanol and a hot solution of NEQ iodide (0.429 g, 1.5 mmol, prepared as described previously (10)) in 15 mL ethanol were filtered under N_2 while hot, poured together, and *cooled rapidly*. The black lustrous, microcrystalline platelets which formed were filtered, washed with a few millilitres of methanol, and finally with ether, yield 63%, mp 139°C. *Anal.* calcd. for NEQ–TCNQ, $C_{22}H_{15}N_6$: C 72.71, H 4.16, N 23.13; found: C 72.52, H 4.40, N 23.03.

Slow cooling of the reaction mixture and recrystallization of the primary product yields only products containing appreciable amounts of the complex salt.

(NEQ)$_2$(TCNQ)$_3$

TCNQ (0.102 g, 0.5 mmol) and NEQ–TCNQ (0.182 g, 0.5 mmol) were dissolved together in 30 mL boiling acetonitrile (in an N_2 atmosphere!). The solution was filtered while hot and allowed to cool slowly to room temperature. The black crystals were washed with methanol and ether after filtration, yield 70%, mp 198–200°C. *Anal.* calcd. for: (NEQ)$_2$(TCNQ)$_3$·CH_3CN, $C_{58}H_{57}N_{17}$: C 71.67, H 3.84, N 24.50; (NEQ)(TCNQ)$_2$, $C_{34}H_{19}N_{10}$: C 71.97, H 3.35, N 24.68; (NEQ)$_2$(TCNQ)$_3$, $C_{56}H_{54}N_{16}$: C 72.24, H 3.68, N 24.07; found: C 71.72, H 3.48, N 24.52; C 71.78, H 3.47, N 24.45;[3] C 72.14, H 3.59, N 23.93.[4] These results show that on the basis of the analyses alone a clear decision cannot be made as to whether the composition of the complex salt is 1:2 or 2:3 (see Discussion).

Quinoxalinium–TCNQ (NHQ–TCNQ)

Attempts to synthesize a TCNQ salt of the protonated quinoxaline NHQ^+ were carried out on the basis of quinoxalinium iodide (NHQ–I) and perchlorate (NHQ–ClO_4) (obtained by direct reaction of quinoxaline dissolved in ethanol with an excess of the respective concentrated acid). Mixing the alcoholic solutions of these salts with alcoholic solutions of Li–TCNQ did not lead to the TCNQ salt. On the contrary, the deep green colour of the dissolved TCNQ anion disappeared immediately and, after a short period of time, greenish-yellow platelets precipitated. These platelets were identified as a mixture of TCNQ and H_2TCNQ. The experimental results suggest the following reaction

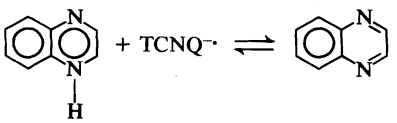

$$+ [HTCNQ^{\cdot}] \rightleftharpoons \tfrac{1}{2}H_2TCNQ + \tfrac{1}{2}TCNQ$$

which is similar to the reaction of $TCNQ^-$ with mineral acids (1). This result suggests that quinoxaline is too weak a base to form NHQ–TCNQ compounds in the usual way.

When the yellow solutions containing quinoxalinium salts and Li–TCNQ were cooled the color changed to green. This suggests that at lower temperatures the ionic forms are more stable. Accordingly, on quenching a solution of quinoxaline, TCNQ, and H_2TCNQ (2:1:1) in $CHCl_3$ in a liquid nitrogen bath a precipitate formed consisting of a mixture of greenish yellow crystals and a few violet crystals. The shiny violet platelets seem to be the 1:1 salt of NHQ–TCNQ.

Conductivity

The dc conductivity was measured on pressed pellets of about 0.3-mm thickness under a pressure of 1500 kPa. Resistivities of pressed powders frequently are about four orders of magnitude larger than values of single crystals measured along the radical chain direction.

Electron Paramagnetic Resonance Data

The epr spectra were taken on a Bruker B–ER 418 spectrometer with an nmr gaussmeter for field calibration and a DANA 320 D microwave frequency counter.

Discussion

The *N*-methyl- and *N*-ethylquinoxalinium ions form simple (1:1) and complex salts with TCNQ. Though the quinoxalinium salts are structurally similar to the *N*-alkylphenazinium ions, the chemistry is quite different predominantly owing to the reduced basicity of quinoxaline.

The experimental results clearly suggest that as already considered by Melby (2), a highly-conducting 1:1 NMQ–TCNQ adduct does not exist. The high conductivity reported for the 1:1 salts is possibly caused by an admixture of the complex salt in the 1:1 sample. The results prove that the 1:1 phase, which can be obtained in high purity by the usual (nevertheless more elaborate) methods, is a semiconductor (pressed pellet conductivity $4 \times 10^{-5}\ \Omega^{-1}\ cm^{-1}$) and has properties quite different from those reported by Melby (2). During the preparation of the 1:1 compound there was no evidence of another pure and conducting 1:1 phase. A *conducting* sample was then obtained by recrystallizing the pure NMQ–TCNQ in contact with the air. This sample had properties very similar to the ones mentioned by Melby (2). Whether this compound actually contains high amounts of the complex salt or only some neutral TCNQ 'impurities' in the stacks (which would give rise to partially charged TCNQ chains) was not investigated further. The formation of a sample contaminated with a complex salt can easily be explained in terms of the oxidation of $TCNQ^-$ anions to neutral TCNQ by air, which could result in the final precipitation of the complex salt. The latter compound is in fact a better conductor (pressed-pellet dc conductivity $4 \times 10^{-3}\ \Omega^{-1}\ cm^{-1}$ as compared to $4 \times 10^{-5}\ \Omega^{-1}\ cm^{-1}$ of the pure compound).

Typical epr spectra of NMQ–TCNQ at 230 K are

[1]Recrystallized from acetonitrile and dried in high vacuum.
[2]After heating the sample in high vacuum for 3 h to 120°C.
[3]Recrystallized from acetonitrile and dried under high vacuum.
[4]After heating the sample in high vacuum for 3 h to 120°C.

FIG. 1. Single crystal epr spectra of NMQ–TCNQ at 230 K. Spectra of three different crystal orientations (rotation of the crystal around an axis perpendicular to the field direction) which show the angular dependence of the triplet exciton splittings are drawn. The central peak corresponds to the 'impurity' peak.

shown in Fig. 1. Apart from the strong central line, sharp triplet exciton lines occur. The two different 'exciton' pairs are apparently due to the *twinning* of the crystal. The figure shows the spectra of three different crystal orientations, with the higher pair of peaks consecutively far apart from each other (*a*), closer together (*b*), and finally almost coinciding with the central $S = \frac{1}{2}$ peak (*c*).

This evidence of triplet excitons (which can be observed at room temperature too) proves that a kind of radical dimer exists in the lattice and can be thermally activated. Systems of this type cannot be expected to have high electrical conductivities.

As mentioned above, all the crystals obtained from NMQ–TCNQ were twinned. Therefore a full structure determination could not be carried out. Nevertheless we obtained the unit cell dimensions from single crystal X-ray data. The crystals are triclinic with $a = 4.79$, $b = 10.46$, $c = 7.60$ Å, $\alpha = 93.49$, $\beta = 110.92$, $\gamma = 82.69°$, and unit cell volume 352.7 Å.

The complex salt, which was obtained in very high yield by the usual methods, seems to be a 2:3 salt. The problems of varying stoichiometry and inclusion of solvent molecules for the complex TCNQ salts was recently discussed in connection with very similar donors (11, 12).

The pronounced differences in the behaviour of the semiconducting 1:1 and the highly conducting 2:3 compounds can easily be observed by comparing their ir spectra. The 1:1 compound shows highly resolved spectra with many typical and sharp peaks (most prominent the $\nu_{C\equiv N}$ at 2180 cm^{-1}) whereas the ir bands of the 2:3 compound are hidden under a broad and intense *electronic* absorption which is typical of all 'metallic' donor acceptor complexes (for a recent example see ref. 13; 16). The pressed pellet conductivity for this compound is 9×10^{-3} Ω^{-1} cm^{-1}, which fits well with previous reports on similar complexes (14).

The *N*-ethyl derivatives were investigated because of the special behaviour of *N*-ethylphenazinium–TCNQ (15). The chemical and physical behaviour of NEQ–TCNQ is very similar to that of NMQ–TCNQ.

The 1:1 adduct shows a pressed pellet conductivity of 4×10^{-5} Ω^{-1} cm^{-1}. The ir spectra with a $\nu_{C\equiv N}$ of 2180 cm^{-1} indicate, as seen above, no major electronic absorption in contrast to the 2:3 adduct which has a conductivity of 5×10^{-3} Ω^{-1} cm^{-1} and a very broad electronic absorption in the ir. The epr spectrum of the complex salt consists of a single line with a very anisotropic line width.

Acknowledgements

This work was supported by Deutsche Forschungsgemeinschaft (DFG) through grant No. Ke 135/18. We would like to thank Dr. H. Endres for the interpretation of the X-ray data.

1. L. R. MELBY, R. J. HARDER, W. R. HERTLER, W. MAHLER, R. E. BENSON, and W. E. MOCHEL. J. Am. Chem. Soc. **84**, 3374 (1962).
2. L. R. MELBY. Can. J. Chem. **43**, 1448 (1965).
3. F. FUJII, I. SHIROTANI, and H. NAGANO. Bull. Chem. Soc. Jpn. **50**, 1726 (1977).

4. M. A. BUTLER, F. WUDL, and Z. G. SOOS. Phys. Rev. B, **12**, 4708 (1975).
5. Z. G. SOOS and D. J. KLEIN. *In* Molecular association. Vol. 1. *Edited by* R. Foster. Academic Press, New York, NY. 1975.
6. J.-J. ANDRÉ, A. BIEVER, and F. GAUTIER. Ann. Phys. 145 (1976).
7. (*a*) H. J. KELLER, D. NÖTHE, W. MORONI, and Z. G. SOOS. J. Chem. Soc. Chem. Commun. 331 (1978); (*b*) H. J. KELLER, W. MORONI, D. NÖTHE, V. SEIFRIED, and M. WERNER. *In* Molecular metals. NATO-ARI-Series. *Edited by* W. E. Hatfield. Plenum Press, New York, NY. In print.
8. D. J. SANDMAN. J. Am. Chem. Soc. **100**, 5230 (1978).
9. J. S. MILLER and A. J. EPSTEIN. J. Am. Chem. Soc. **100**, 1639 (1978).
10. R. F. SMITH, W. J. REBEL, and T. N. BEACH. J. Org. Chem. **24**, 205 (1959).
11. M. MURAKAMI and S. YOSHIMURA. Bull. Chem. Soc. Jpn. **48**, 157 (1975).
12. S. FLANDROIS, P. LIBERT, and P. DUPIUS. Phys. Status Solidi, A, **28**, 411 (1975).
13. Z. G. SOOS, H. J. KELLER, W. MORONI, and D. NÖTHE. J. Am. Chem. Soc. **99**, 5040 (1977).
14. W. MORONI. Ph.D. Dissertation, University of Heidelberg, Heidelberg. 1977.
15. B. MOROSIN, H. J. PLASTAS, L. B. COLEMAN, and J. M. STEWART. Acta Crystallogr. B, **34**, 540 (1978).
16. R. C. WHELAND and J. L. GILLSON. J. Am. Chem. Soc. **98**, 3916 (1976).

Electronic excited states of small ring compounds. VII. Bicyclo[2.1.0]pentanes by the photocycloaddition of 1,2,3-triphenylcyclopropene to fumaro- and maleonitrile[1]

P. C. WONG AND D. R. ARNOLD[2]

Photochemistry Unit, Department of Chemistry, The University of Western Ontario, London, Ont., Canada N6A 5B7

Received September 11, 1978

P. C. WONG and D. R. ARNOLD. Can. J. Chem. **57**, 1037 (1979).

Irradiation of the charge-transfer complex between 1,2,3-triphenylcyclopropene (**1**) and fumaronitrile (**7**) and maleonitrile (**8**) leads to formation of bicyclo[2.1.0]pentane cycloaddition products (**9, 10, 11**) and the photoene product (**12**). These products were also formed when the reaction was photosensitized (triplet–triplet transfer). The structure of the adducts was established by analysis of ^{13}C and ^{1}Hmr spectra. Nuclear Overhauser effect studies were also useful. The triplet energies of **7** and **8** (E_T ca. 50 kcal mol^{-1}) were determined by studying the photosensitized isomerization as a function of sensitizer triplet energy. The thermal stability of the new bicyclo[2.1.0]pentanes has been studied, particularly with regard to the isomerization resulting from cleavage of the central [0] bond in these strained systems. The mechanism of the photocycloaddition reactions is discussed.

P. C. WONG et D. R. ARNOLD. Can. J. Chem. **57**, 1037 (1979).

L'irradiation du complexe de transfert de charge entre le triphényl-1,2,3 cyclopropène (**1**) et le fumaronitrile (**7**) et le maléonitrile (**8**) conduit à la formation de produits de cycloaddition bicyclo[2.1.0]pentane (**9, 10, 11**) et du produit (**12**) photoène. Ces produits se forment aussi lorsque la réaction est photosensibilisée (transfert triplet–triplet). On a déterminé la structure des adduits grâce à une analyse des spectres rmn ^{13}C et ^{1}H. Des études d'effet Overhauser nucléaire se sont aussi avérées utiles. On a déterminé les énergies triplet de **7** et de **8** (E_T ca. 50 kcal/mol) en étudiant l'isomérisation photosensibilisée en fonction de l'énergie du sensibilisateur triplet. On a étudié la stabilité thermique des nouveaux bicyclo[2.1.0]pentanes en particulier en ce qui a trait à l'isomérisation résultant du clivage de la liaison [0] centrale de ces systèmes tendus. On discute du mécanisme des réactions de photocycloaddition.

[Traduit par le journal]

Introduction

We have previously reported (1*b*,*c*) that the direct irradiation of the charge-transfer complex between 1,2,3-triphenylcyclopropene (**1**) and dimethyl fumarate (**2**) gives the bicyclo[2.1.0]pentane (**3**) (reaction [1]). Only one of the six possible stereoisomeric adducts was obtained as a primary product from this reaction, that having the ester groups *trans* and the phenyl at carbon-5 *exo*. This result could be taken as an indication that this type of cycloaddition reaction favours retention of the configuration of the olefin in the product. It was, however, impossible to test this hypothesis by using the isomeric olefin since no adduct was obtained when the weaker charge-transfer band of (**1**) and dimethyl maleate (**6**) was irradiated.[3] The possibility, therefore, remained that

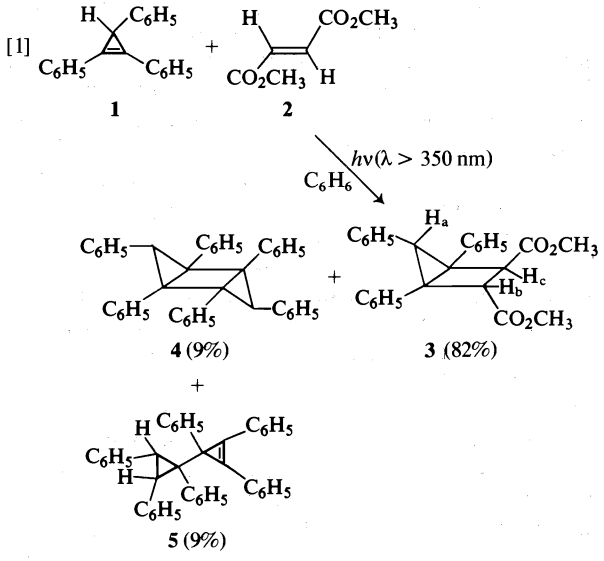

the observed product stereochemistry was controlled by thermodynamic rather than kinetic factors. The determination of the factors which control the product stereochemistry is important not only from the practical standpoint of defining the synthetic utility, but also for an understanding of the mech-

[1]Contribution No. 192 from the Photochemistry Unit. This article is dedicated to Professor E. Havinga, on the occasion of his 70th birthday (May 7th, 1979). Part 6 of this series is ref. 1*a*.

[2]To whom correspondence should be addressed. Department of Chemistry, Dalhousie University, Halifax, N.S. B3H 4J3.

[3]It is important to recall that the dimethyl maleate – dimethyl fumarate isomerization was not efficient under these conditions (1*c*).

0008-4042/79/091037-13$01.00/0

anism of this reaction. The proposed mechanism involved the cyclopropene triplet as the reactive species and thus a concerted cyclization would seem unlikely. Retention of stereochemistry could alternatively be explained as the result of rapid closure of a 1,4-diradical intermediate with a rate competitive with bond rotation.

Our search for a pair of isomeric olefins which would provide further examples of this type of reaction and allow a test of the stereospecificity led to fumaro- and maleonitrile (**7** and **8**). These dinitriles are more reactive dienophiles and 1,3-dipolarophiles than are the analogous diesters (2 and references cited therein). Furthermore, they have lower reduction potentials (3) so we expected they would form stronger charge-transfer complexes with **1**, complexes which would absorb at longer wavelengths and thus allow more efficient excitation.

In this paper, we report the results of a study of the photocycloaddition of **1** with the dinitriles **7** and **8**, brought about by irradiation of the charge-transfer band. We have characterized the bicyclo[2.1.0]pentane products and have also studied the thermal isomerization which results from cleavage of the [0] bond of these strained systems.

In contrast with the previous results with the isomeric diesters **2** and **6**, which were configurationally stable, the dinitriles **7** and **8** undergo comparatively rapid isomerization upon irradiation of the charge-transfer complex. In a search for an explanation for this difference in behaviour, we have studied the photosensitized (triplet–triplet transfer) isomerization of both the diesters and the dinitriles and conclude that the triplet energy of both of the dinitriles (E_T **7** and **8** ca. 50 kcal mol^{-1}) is considerably lower than that of the diesters (E_T **2** $\sim$ 61 kcal mol^{-1}, E_T **6** $>$ 72 kcal mol^{-1}) (4).

While this work was in progress, Farid and coworkers reported (5) a similar reaction involving the photocycloaddition of methyl 1,2-diphenylcyclopropene-3-carboxylate to dimethyl fumarate sensitized by triplet–triplet transfer. Their results and interpretation are in substantial agreement with ours. Furthermore, they were able to isolate and characterize the isomeric bicyclo[2.1.0]pentane, having the methyl ester groups *cis*, which gave an indication that reaction of the cyclopropene triplet did not occur with complete retention of the olefin configuration. Other pertinent results from their work will be mentioned in the Discussion.

Results

A benzene solution of **7** (0.3 *M*) and **1** (0.3 *M*) has long wavelength absorption not present in the spectrum of the individual components at the same concentration (Fig. 1). We assign this long wavelength absorption to the charge-transfer transition of the complex between **7** and **1**. Similar results were observed with **8** instead of **7**. The absorption spectra of both complexes tail about the same and extend to longer wavelength than do the complexes between either **2** or **6** and **1**.

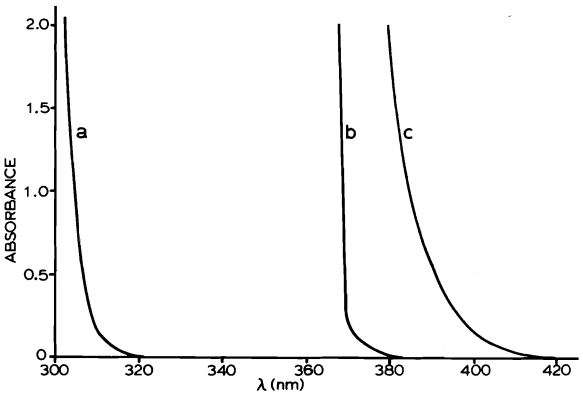

FIG. 1. Absorption curves for (*a*) **7** (0.3 *M*), (*b*) **1** (0.3 *M*), and (*c*) **7** and **1** (each 0.3 *M*) in benzene solution. Similar results were obtained using **8** instead of **7**.

Excitation of the charge-transfer band can be achieved by irradiation, with a medium pressure mercury vapour lamp, through a chemical solution filter (*A*) which absorbs light of wavelengths shorter than 350 nm.

A solution of **1** and **7** was irradiated through this filter solution and the progress of the reaction followed by proton nuclear magnetic resonance (^{1}Hmr) spectroscopy. After 24 h irradiation, all the cyclopropene had been consumed and the product mixture consisted of the tricyclohexane dimer of **1** (**4**), the bicyclo[2.1.0]pentane adducts **9**, **10**, and **11**, and the photoene product **12** (reaction [2]). Analysis of the ^{1}Hmr spectrum during the course of the reaction indicated that all of these products were primary products, although the ratio of products was not constant, and that the starting dinitrile **7** isomerized rather rapidly to a mixture of the isomers (**7**:**8**, 65:35).

When **1** and maleonitrile (**8**) were irradiated under these conditions, the same products resulted; however, the proportion of adducts **10** and **11**, having the cyano groups *cis*, was larger. Again, the starting dinitrile isomerized during the course of the irradiation until a photostationary state (**7**:**8**, 60:40) was obtained.

The cycloaddition reaction can be photosensitized (triplet–triplet transfer). For these experiments, a benzene solution of **1** (0.3 *M*), **7** (0.3 *M*), and thioxanthen-9-one (0.01 *M*, E_T = 65 kcal mol^{-1}) or fluoren-9-one (0.01 *M*, E_T = 53 kcal mol^{-1}) was

[2] 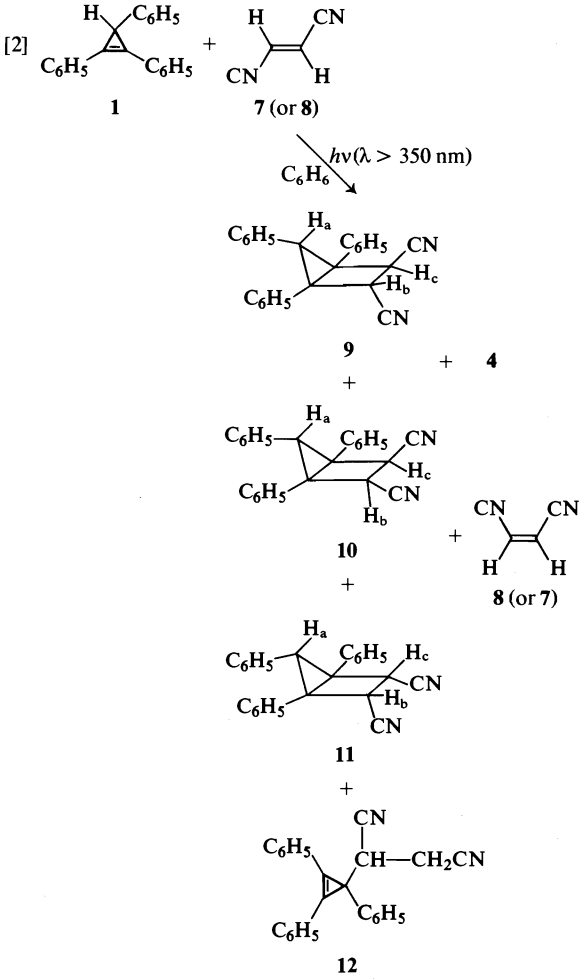

irradiated through a chemical solution filter (*B*) which absorbs all wavelengths shorter than 358 nm. Under these conditions, the sensitizer absorbs most of the light. Using thioxanthen-9-one as sensitizer, after only 2-h irradiation, 89% of **1** was consumed, the same products (**8–12**) were obtained, only in a different ratio, and the dimer **5** was also formed. The ratio of the unreacted **7** and **8** was again 60:40.

The reaction mixtures from each of the above irradiations were separated by column chromatography to provide products for structural analysis. The yields of products, obtained under these varying conditions were accurately determined by quantitative ^{1}Hmr of the crude reaction mixtures and are summarized in Table 1. The isolated yields and material balance were generally good and are reported in the Experimental.

Some control experiments were carried out to confirm that these reactions were reactions of the excited state. Heating a sealed tube of a toluene solution of **1** (0.075 *M*) and **7** (0.15 *M*) at 120°C for 2 weeks gave a good yield (95%) of the dimer **5** and none of the other products. A benzene solution of **1** and **7** was refluxed, under nitrogen, and small portions of a free-radical chain initiator (azobisisobutyronitrile) were added over a 2-day period. The starting materials were largely recovered; the only product identified was the dimer **5** (~2%) present in amounts expected from the thermal (nonchain) reaction.

All three bicyclo[2.1.0]pentane adducts (**9**, **10**, and **11**) were thermally unstable. Heating adduct **9** in benzene solution at 65°C gave complete rearrangement to the corresponding phenyl-in isomer **13** (reaction [3]). The progress of this reaction was

[3] 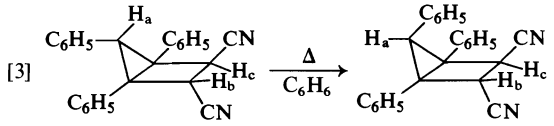

9 $t_{1/2}$ = 9.5 h at 65°C — **13**

followed by ^{1}Hmr and the half-life of **9** was 9.5 h under these conditions.

Adduct **10** is even more thermally labile. We were, in fact, unable to obtain **10** free from the corresponding phenyl-in isomer **14**. Heating a reaction mixture from the photosensitized (thioxanthen-9-one) irradiation of **1** and **7** for 1 h at 65°C gave rise to an equilibrium mixture of adducts **10** and **14** (ca. 1:3) among the other products. Adduct **14** is relatively stable in the crystalline form and since it is much less soluble than **10** in a mixture of chloroform–hexane, it can be obtained essentially pure upon crystallization from this solvent. Refluxing a benzene solution of **14** for 2 h gave an equilibrium mixture of **10** and **14** (23:77) (reaction [4]).

[4] 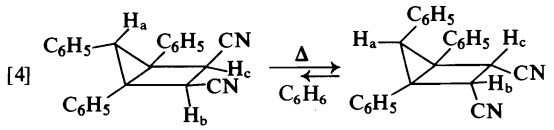

10 (23%) — **14** (77%)

Adduct **11** was stable by comparison with **9** and **10**. Prolonged heating (24 h at 75°C) in benzene-d_6 resulted in decomposition of **11** to products which, from an analysis of the ^{1}Hmr spectra, did not include the isomeric bicyclo[2.1.0]pentane and which were not further characterized.

Proof of Structure of the Adducts

The structural assignments for the bicyclo[2.1.0]-pentane adducts (**9–11**, **13**, and **14**) was based largely upon an analysis of their nuclear magnetic resonance spectra, both ^{13}C and ^{1}H. This series represents all but one of the six possible stereoisomers, the missing member is the isomer having the 5-phenyl and both

TABLE 1. Yields of products from reaction [1]

Reaction conditions	Product yields (%) (Unreacted) 1[a]	7[b]	8[b,c]	4[a,c]	5[a]	9[a]	10[a]	11[a]	12[a]
1 + 7	92.0	94.2	~0.4	~0.2	0	2.0	0.5	0.5	0.5
	74.0	78.1	~3.0	~1.4	0	8.0	1.3	1.0	2.0
	56.7	65.7	~9.0	~3.9	0	14.0	2.5	2.0	4.0
	29.5	40.6	~14.2	~8.0	0	28.0	6.2	3.0	8.0
	0.0	16.2	~9.4	~17.5	0	44.5	7.3	4.4	15.3
1 + 8[d]	6.6	24.4	~16.6	~18.2	0	23.7	11.8	6.7	17.0
1 + 7 + thioxanthen-9-one	43.4	43.6	~22.8	~13.2	8.4	10.0	7.7	1.9	8.8
	11.0	24.0	~16.0	~14.0	10.0	15.9	12.5	4.0	22.4
	0.0	21.3	~10.3	~16.0	10.0	17.3	12.6	4.0	22.8
1 + 7 + fluoren-9-one	76.0	84.6	~11.0	~4.2	2.3	7.0	3.0	0.8	4.5
	53.2	60.7	~14.8	~11.8	4.0	11.8	5.7	1.5	8.0
	33.0	53.6	~13.7	~13.8	4.5	13.8	5.9	2.1	8.9
	17.8[e]	42.6	~17.8	~19.2	8.2	17.8	8.3	2.8	15.1

[a]Calculated referring to the starting cyclopropene (**1**).
[b]Calculated referring to the starting olefins.
[c]Approximate values estimated from closely situated peaks in the ^{1}Hmr.
[d]Same kind of time-dependent product evolution observed as with **1** + **7**.
[e]Precipitate (mostly **12** and **4**) formed in reaction mixture.

cyano groups *endo*. Isomerization of **11** might have afforded this isomer; however, it was not detected and it seems reasonable that **11** is strongly favoured at equilibrium.

Details of the nmr spectra are reported in the Experimental. Only the salient features which distinguish each isomer will be discussed here. Consider first the isomeric pair **9** and **13**. The lack of symmetry in these isomers was obvious from both the ^{13}C and ^{1}Hmr spectra. Three features of the spectra allow the distinction between **9** and **13**. First, there is the long range 'w-coupling' observed between H_a and H_b for one of the isomers which is consistent with the geometry of **13**. Second, there is a 4% enhancement in the intensity of the signal assigned to H_a owing to the nuclear Overhauser effect (nOe) when H_b of the other isomer was double irradiated. This is an indication of the proximity of these nuclei and is consistent with **9**. The third observation is that the signals due to the protons in the aromatic region of the ^{1}Hmr spectrum of **9** appear as a series of multiplets over a broad region whereas the absorption in this region of **13** is a relatively narrow multiplet. This observation is reminiscent of the early report of the ^{1}Hmr of *cis*- and *trans*-1,2-diphenylcycloalkanes (6). The protons in the aromatic region of the *cis*-isomers appear as a multiplet whereas the *trans*-isomers have a relatively sharp singlet in this region. The multiplet was attributed to restricted rotation of the phenyl group in the more hindered (*cis*) isomers. This explanation is consistent with the relative stability of **9** and **13**; **9**, being the less stable isomer, has restricted rotation of the phenyl group and the multiplet absorption in the aromatic region. This correlation is also useful for assigning configurations of the other isomers, those having the phenyl on the apical carbon in the *exo* position (**10** and **11**) have a series of multiplets in the aromatic region while the corresponding (more stable) *endo*-phenyl isomer **14** has a relatively narrow multiplet.

The relatively simple ^{1}Hmr and ^{13}Cmr spectra of the other isomers are consistent with the more symmetric structures, **10**, **11**, and **14**. The assignment of structure **11**, that is, the isomer having both the phenyl in the 5-position and the cyano groups *exo* was made possible by the observation of a nuclear Overhauser effect. The intensity of the signal assigned to the proton on carbon-5 (H_a) increased (18%) when the protons on carbon 2 and 3 (H_b and H_c) were double irradiated.

The relationship between **10** and **14** was made apparent from the observation that they interconvert by inversion about the central [0] bond. In neither isomer is the proton on carbon-5 (H_a) significantly coupled to the protons H_b and H_c. The choice between them was made on the basis of the observed series of multiplets in the aromatic proton region of the ^{1}Hmr spectrum of **10**, while a relatively narrow multiplet is observed in this region of **14**. Furthermore, the relative stability of **10** and **14** is consistent with the assigned structures.

The structure of **12** was assigned on the basis of spectral (ir, mass, and ^{1}Hmr) characteristics. There is a close similarity of the ^{1}Hmr spectrum of **12** and that of phenylsuccinodinitrile (7). The structures of **4**

TABLE 2. Stationary states of the olefin pairs with various sensitizers

Sensitizer[a]	E_T (kcal mol^{-1})[b]	Maleonitrile (%)[c]	Dimethyl maleate (%)
Xanthen-9-one	74	39	67
1,3,5-Triacetylbenzene	74	41	—
Acetophenone	73.7	33	—
4,4′-Dimethoxybenzophenone	69.8[d]	34	91.6
Benzophenone	69.2[d]	44	96.0
4,4′-Dicyanobenzophenone	66.2[d]	39	97.9
Thioxanthen-9-one	65.5	38	—
2-Acetylfluorene	61	42	97
2-Acetonaphthone	59	38	55[f]
Benzil	53.4	40	—
Fluoren-9-one	53	36	—[g]
Phenanthrenequinone	49	45	—
Pyrene	48	52[f]	65[f]
1,2-Benzanthracene	47	36[f]	—
Acridine	45.3	40[f]	89[f]
Phenazine	43.8	[e]	—
9,10-Dibromoanthracene	40.2	33	0

[a]Sensitizer concentration was 0.01 *M* and olefin concentration was 0.05 *M*.
[b]Values taken from ref. 9 unless otherwise noted.
[c]Derivation for 2–4 runs were ± 2%.
[d]Values taken from O—O band of phosphorescence spectra in EPA at 77 K.
[e]Not isomerized on prolonged irradiation.
[f]Relatively slow compared to the high energy sensitizers.
[g]Too slow to give possible estimation.

and **5** were established by direct comparison (^{1}Hmr, ir) with authentic samples (8).

For reasons which will be made clear below, estimates of the triplet energies of **7** and **8** were required. An attempt was made to observe direct $S_0 \rightarrow T$ absorption by utilizing the external heavy atom effect. The absorption spectra of the dinitriles (**7** and **8**) (0.3 *M*) were measured in ethyl iodide solution. Both solutions were visibly yellow but the spectra showed only structureless absorption tailing out beyond 450 nm (<63.5 kcal mol^{-1}). Since it is impossible to determine the onset of such tailing, no definite conclusions can be drawn from these spectra.

The triplet state energy of an alkene can sometimes be determined by observing the variation of the stationary state in the photosensitized *cis–trans* isomerization as a function of sensitizer triplet energy. This approach has been successfully applied to the closely related diethyl maleate – diethyl fumarate esters by Hammond and his co-workers (4). The photostationary states established upon irradiation of benzene solutions containing the dinitriles **7** and **8** and various sensitizers were measured and are recorded in Table 2. In every case, the stationary state was approached from both directions. With some sensitizers complications arose as the result of instability of the sensitizer and/or the formation of a light absorbing residue on the surface of the irradiation vessel. For instance, phenanthrenequinone was particularly unstable as a sensitizer and the formation of a residue was a serious problem in the case of 1,2-benzanthracene and acridine. To minimize these complications, mixtures of the dinitriles close to the stationary state were used instead of the pure isomers so that shorter irradiation times were required to reach the stationary state.

The efficiency of the isomerizations were qualitatively similar, comparable irradiation times were required to reach the stationary state, with the higher energy sensitizers; that is, with sensitizers having a triplet energy of 49 kcal mol^{-1} or greater.

Since the reported work (4) on the diesters used the ethyl derivatives and our studies have involved the methyl esters, we determined the photostationary states of **2** and **6** with a few sensitizers. In this case, the approach to stationary states became appreciably slower using sensitizers having a triplet energy below 61 kcal mol^{-1}. These results are also reported in Table 2.

Discussion

In our previous report, we proposed a mechanism for reaction [1] which involved initial excitation of the charge-transfer complex followed by an intersystem-crossing process which led to formation of the cyclopropene triplet. Product formation was attributed to the reactivity of the cyclopropene triplet. This mechanism is also applicable to reaction [2]; however, there are significant differences between the behaviour of the diesters and that of the dinitriles. Scheme 1, for reaction [2] starting with **1** and **7**, is abbreviated to illustrate only those steps which lead to products. The differences in behaviour between the diesters and the dinitriles can be explained in the

TABLE 3. Half-wave oxidation and reduction potentials obtained by cyclic voltammetry[a]

Compound	$E_{1/2}^{red}$ (V)[b]	$E_{1/2}^{ox}$ (V)[b]
Fumaronitrile	−1.63	[c]
Maleonitrile	−1.63	[c]
Dimethyl fumarate	−1.79	[c]
Dimethyl maleate	−2.05	[c]
1,2,3-Triphenylcyclopropene	[d]	1.01

[a]Pt electrode, tetraethylammonium perchlorate (TEAP, 0.1 *M*) in acetonitrile solutions, vs. $Ag/AgNO_3$ (0.1 *M*) electrode.
[b]Taken as 0.03 V before the anodic peak potential and 0.03 V before the cathodic peak potential. All the oxidative and reductive processes observed above were irreversible, the half-wave potentials were estimated using the 100 mV/s sweep rate.
[c]No observed signal through scanning voltage from 0 to −2.2 V.
[d]No observed signal through scanning voltage from 0 to +2.2 V.

context of Scheme 1, as the result of the lower reduction potentials, the lower triplet energies, and the greater reactivity of the dinitriles in comparison to the diesters.

The reduction potentials of the diesters **2** and **6** and the dinitriles **7** and **8** are listed in Table 3. The dinitriles, since they have significantly lower reduction potentials than either of the diesters, should be better electron acceptors and the resulting charge-transfer complexes with **1** should absorb at longer wavelengths. The observations are consistent with these predictions. Charge-transfer complex formation between **6** and **1** is barely detectable in the long wavelength region of the absorption spectra of the mixture (1*b*). On the other hand, the charge-transfer complexes between both **7** and **8** and **1** are obvious from the extended absorption in this region (Fig. 1).

Step 1 $\quad \mathbf{1} + \mathbf{7} \rightleftharpoons [\mathbf{1}\text{–}\mathbf{7}]$

Charge-transfer complex formation

Step 2 $\quad [\mathbf{1}\text{–}\mathbf{7}] \xrightarrow{h\nu} [\mathbf{1}\text{–}\mathbf{7}]^*$

Excitation of the charge-transfer absorption band

Step 3*a* $\quad [\mathbf{1}\text{–}\mathbf{7}]^* \dashrightarrow \mathbf{1}^3 + \mathbf{7}$

Deactivation of the excited charge-transfer complex to give the cyclopropene triplet

Step 3*b* $\quad [\mathbf{1}\text{–}\mathbf{7}]^* \dashrightarrow \mathbf{1} + \mathbf{7}^3$

Deactivation of the excited charge-transfer complex to give the triplet of fumaronitrile

Step 4 $\quad \mathbf{1}^3 + \mathbf{7} \rightarrow [\dot{\mathbf{1}}\text{–}\dot{\mathbf{7}}]^3 \dashrightarrow \mathbf{9}\text{—}\mathbf{12}$

Reaction of the cyclopropene triplet, via 1,4-diradical intermediate(s) to yield adducts

Step 5 $\quad \mathbf{1}^3 + \mathbf{1} \rightarrow [\dot{\mathbf{1}}\text{–}\dot{\mathbf{1}}]^3 \dashrightarrow \mathbf{4} + \mathbf{5}$

Reaction of the cyclopropene triplet, via 1,4-diradical intermediate(s) to yield dimers

Step 6 $\quad \mathbf{7}^3 \rightarrow \alpha\mathbf{7} + (1 - \alpha)\mathbf{8}$

Isomerization of the fumaronitrile triplet

SCHEME 1

The use of filter solution *A*, which absorbs light of wavelength less than 350 nm, ensures that the excitation process involves predominantly, if not exclusively, the charge-transfer transition of the complex (step *2* in Scheme 1). The triphenylcyclopropene (**1**) does have absorption which tails out beyond 370 nm, so some direct excitation may occur; however, the cyclopropene alone is stable to direct irradiation (i.e., no dimers form) and the intersystem crossing process from the singlet of **1** has a quantum yield of less than 10^{-3} (8*a*). Furthermore, direct excitation of **1**, followed by complex formation between the singlet of **1** and **7** might give a species identical with that obtained by direct excitation of the charge-transfer complex (10).

Step *3* in Scheme 1 represents the deactivation pathway of the excited state of the charge-transfer complex which leads to formation of the triplet of one or both of the components of the complex. Most of the precedents for this process comes from photophysical studies where the triplet of one of the components of the charge-transfer complex or exciplex has been detected by flash spectroscopy or by phosphorescence (11). Surprisingly few examples of this potentially useful phenomena have been recognized in the area of preparative organic photochemistry (12).

In spite of the significant number of charge-transfer complexes studied by the photophysical techniques, it remains difficult to predict whether the triplet of a component of the complex will form upon irradiation. In the case of the complex between **1** and **2** it is clear that the irradiation gave only the triplet of **1**. This follows from the fact that the adduct **3** and the cyclopropene dimers **4** and **5** were obtained while isomerization of **2** was not observed. However, irradiation of the charge-transfer complex between **1** and **7** (or **8**) gives the triplet of both **1** (step 3*a*) and **7** (or **8**) (step 3*b*) since isomerization of the dinitrile was observed.

It seems likely that this difference can be attributed, at least in part, to the differences in triplet

TABLE 4. The application of the Weller equation to these systems

Reactants						
D	A	Solvent	$E_{1/2}^{ox}$ (D) (V)[a]	$E_{1/2}^{red}$ (A) (V)[a]	$\Delta^1E_{0,0}$ (D), (kcal mol^{-1})	ΔG (kcal mol^{-1})[e]
1	**2**	CH_3CN	1.01	−1.79	82.4[c]	−19.1
		C_6H_6	—	—	82.4	+5.5
1	**7** (or **8**)	CH_3CN	1.01	−1.63	82.4	−22.9
		C_6H_6	—	—	82.4	+0.2
Naphthalene	**7** (or **8**)	CH_3CN	1.19[b]	−1.63	92.0[d]	−27.4
		C_6H_6	—	—	92.0	−3.7

[a]Reference electrode $Ag/AgNO_3$ (0.1 *M*).
[b]See ref. 14. Value corrected to our system by subtracting 0.35 V.
[c]Value taken from overlapping of absorption and fluorescence spectra.
[d]See ref. 15.
[e]The Coulombic attraction terms are 0.056 and 0.90 eV for acetonitrile and benzene, respectively. The $\Delta\Delta F_{solv}$ is 1.91 eV from acetonitrile to benzene.

energy of **2** and **7** (and **8**). It may well be that while the excited state of the corresponding charge-transfer complexes can deactivate to give the triplet of **1** (E_T ca. 53 kcal mol^{-1}),[4] **7** (and **8**) (E_T ca. 50 kcal mol^{-1}), not enough energy is available to give the triplet of **2** (E_T = 61 kcal mol^{-1}). Since the large difference in triplet energy between the diesters and the dinitriles was unexpected, we will return to this point later.

There are several mechanisms which could apply to this intersystem crossing process; mixing of states which increase the probability of intersystem crossing, dipole–dipole or dispersion interactions, caged radical ion pair formation followed by back electron transfer, electron transfer between solvent-separated radical ions, etc. Although our results do not allow us to choose positively from among these possible explanations, we favour a mechanism involving the caged radical ion pair. It seems unlikely, in view of our use of nonpolar solvent, that solvent-separated radical ions are involved; yet, because of the large differences in oxidation and reduction potential of the components of the complex, it is reasonable to suggest considerable electron transfer in the complex and a radical–ion pair is not unlikely.

An estimate of the free-energy change associated with radical ion pair formation can be obtained by applying the concepts developed by Weller and his group (13). The Weller equation is shown in eq. [5].

$$[5]\quad \Delta G = ((E_{(D/D^+)} - E_{(A/A^-)} - (e_0^2/\varepsilon\alpha) + \Delta\Delta F_{solv})) - \Delta^1E_{0,0}$$

This empirical equation allows an estimate of the free-energy change (ΔG) for the electron transfer between a donor (D) and an acceptor (A) molecule within an encounter complex, based upon the oxidation potential of the donor and the reduction potential of the acceptor. The Coulombic attraction term takes into account the fact that the charges (e_0) remain within the encounter distance (α ca. 7 Å) in the solvent dielectric (ε). Since the oxidation and reduction potentials are measured in high dielectric solvents (e.g., acetonitrile, ε = 37) and the photochemical reaction is carried out in nonpolar solvents (benzene, ε = 2.28), a solvent correction term ($\Delta\Delta F_{solv}$) must be applied. The energy available ($\Delta^1E_{0,0}$) is the singlet energy.

The Weller equation is strictly applicable only to systems where no charge-transfer complex exists between the ground state molecules. Nevertheless, when the association constant for the charge-transfer complex is small (i.e., the binding energy between the components is weak), as it must be between **1** and **2**, **7** and **8**, the energy required for the electron transfer (the term in parentheses) is essentially the same and if the singlet energy of one of the components is used, the calculated free-energy change can be taken as a maximum (i.e., most favourable) value.

Table 4 lists the values which we have used in eq. [5] and the calculated ΔG values for the systems **1** and **2**, and **1** and **7** and **8**. Values have been calculated for both acetonitrile (where no solvent correction term is required) and benzene solution. The large negative values calculated when acetonitrile is the solvent leads to the prediction that radical–ion pair formation is favourable. Even for the benzene solutions, the calculated values are only slightly positive and we take this as an indication that radical–ion pair formation is possible in these systems as well.

There is a brief report in the literature which greatly influenced our thinking regarding the mechanism of step 3. Taylor[5] has studied the photo-

[4]Although **1** fluoresces strongly upon irradiation in rigid media at 77 K, we were unable to detect phosphorescence emission even when ethyl iodide was added to the solvent. This estimate was made by analogue with the reported triplet energy of methyl 1,2-diphenylcyclopropene-3-carboxylate which was determined by the Hammond–Herkstroeter method (5).

[5]G. N. Taylor. Private communication and unpublished results cited by Roth (16*a*).

chemically induced dynamic nuclear polarization (CIDNP) of the system naphthalene and **7** (16). Irradiation of a dilute solution of naphthalene and fumaronitrile (**7**) in acetonitrile-d_3 gave enhanced absorption of the protons on **7** and emission was observed for the protons of maleonitrile (**8**). This result was interpreted in terms of the radical–ion pair mechanism. The enhanced absorption of the protons on **7** results from back electron transfer within the singlet radical–ion pair, whereas the emission of the protons of **8** results from back electron transfer within the triplet radical–ion pair producing initially the triplet of **7** which can then isomerize to give **8**. Although it seems likely that a similar mechanism pertains during step 3, particularly in view of the similarities in the calculated free energy for the electron transfer processes (Table 4), we were unable to detect nuclear polarization upon irradiation of an acetonitrile-d_3 solution of **1** and **7**. Details of these attempts are given in the Experimental. It should also be mentioned that as a result of more recent advances in the theory of CIDNP, the mechanism originally proposed no longer uniquely explains the results.

Both of the isomeric dinitriles **7** and **8** react with the triplet of **1**. This is in contrast with the isomeric diesters **2** and **6** where the adduct is formed only with dimethyl fumarate (reaction [1]) (1*b*). The observed ratio of adducts to cyclopropene dimer (**4**) indicates that the reactivities of both **7** and **8** are comparable to that of **2**.

The ratio of one-to-one adducts (**9–12**) to cyclopropene dimers (**4** and **5**) was larger when the charge-transfer complex was irradiated than when the cyclopropene triplet was generated by photosensitization. This is consistent with previous results which were attributed to the cyclopropene triplet being formed next to the dinitrile upon irradiation of the charge-transfer complex and a rate of reaction of the cyclopropene triplet with the dinitrile which is competitive with diffusion (1*b*).

Although reaction [2] is not stereospecific with regard to the configuration of the vicinal cyano group, it is clear that there is some preference for retention of configuration (Table 1). These observations are in accord with the suggestion that the rate of ring closure of the intermediate 1,4-diradical which is formed initially in the triplet state (step 4 in Scheme 1), is competitive with the rate of bond rotation. There is adequate precedent for this behaviour (17).

The bicyclo[2.1.0]pentanes **9**, **10**, and **11** all have the phenyl on the apical carbon (carbon-5) in the *exo* position. This regiospecificity was also observed upon addition of **1** to **2** (reaction [1]) and to maleic anhydride (1*b*). Apparently, the phenyl on carbon-3 of the triplet of **1** hinders the formation of the initial bond on the same side even though the favoured configuration of the final product is the *endo*-phenyl isomer.

Reactions [3] and [4] provide additional examples of the isomerization of bicyclo[2.1.0]pentanes which illustrate the rate acceleration resulting from phenyl substitution at the bridge head. The half-life of **9**, 9.5 h at 65°C, is comparable to that of the analogous diester **3**, $t_{1/2} = 5$ h at 65°C (1*b*), which also rearranges to the phenyl-in isomer. The difference in thermodynamic stability between **9** and **13** favours **13** to such an extent that **9** was not detected at equilibrium. In contrast, the *cis*-dinitriles **10** and **14** are of similar stability with **14** only slightly favoured at equilibrium (reaction [4]). The isomer of **11** was not detected; this is perhaps not surprising since the apical phenyl and both nitriles would be forced *endo* in this isomer.

In addition to the bicyclo[2.1.0]pentane adduct, the adduct **12** was also obtained as a major product. A possible mechanism for formation of **12** involves hydrogen migration of the 1,4-diradical in competition with ring closure. The alternative concerted photoene process seems unlikely since this product was also obtained in the triplet sensitized reactions. Ring closure and hydrogen migration of 1,4-diradical intermediates has been proposed as the mechanism to account for the formation of the cyclopropene dimers **4** and **5** from the triplet of **1** (8). We have pointed out before that this explanation is not entirely satisfactory because the ratio of **4** to **5** is dependent upon the concentration of **1** (1*b*). Now, we find that **4**, but not **5**, is formed in reaction [2]. Clearly, different intermediates must be involved in the competitive formation of **4** and **5**. The reaction cannot simply be as shown in step 5 of Scheme 1.

It seemed possible that **5** and/or **12** could be products of a free-radical chain reaction; however, this was ruled out after control experiments indicated that neither **5** nor **12** was produced thermally in a chain initiated reaction. These control experiments also confirm that **5** does result from a thermal, non-chain, ene-reaction of **1** and that **7** does not compete with **1** via this mechanism. It should also be mentioned that the analogous ene-reaction product incorporating **2** was not observed from reaction [2]; however, Farid and co-workers (5), obtained this type of product from the triplet sensitized reaction of methyl 1,2-diphenylcyclopropene-3-carboxylate and **2**. Obviously, the factors which determine the ratio of these two types of products remains to be defined.

The Triplet Energy of Fumaro- and Maleonitrile

At the onset of this work, there was little indication in the literature as to what the triplet energy of fumaro- and maleonitrile might be. It was known that the triplets of butyrophenone (E_T = 72 kcal mol^{-1}), acetone (E_T = 78–80 kcal mol^{-1}), and benzophenone (E_T = 68 kcal mol^{-1}) were quenched at the diffusion controlled rate by fumaronitrile and so these results at least establish an upper limit for the triplet energy of this isomer (18, 19). It was also known that irradiation of ketones with a triplet energy that of biacetyl (E_T = 55 kcal mol^{-1}) and fluoren-9-one (E_T = 53 kcal mol^{-1}) could lead to some isomerization of fumaronitrile but the photostationary state was not reported and there was no mention of the efficiency of these isomerizations (18). The photo-CIDNP results mentioned earlier were the most informative in this regard, since they require that the triplet energy of both fumaro- and maleonitrile be less than that of naphthalene (E_T = 61 kcal mol^{-1}) (16).

In Table 2 are listed the photosensitized stationary state ratios of isomers **2**–**6** and **7**–**8** as a function of triplet energy of the sensitizer. The Saltiel plots of these data are shown in Fig. 2 (20).

Notice first that our results for the dimethyl esters are similar to those reported by Hammond and coworkers (4) for the diethyl esters. Energy transfer to dimethyl maleate (**6**) is apparently less than diffusion controlled when the triplet energy of the sensitizer is less than 70 kcal mol^{-1} and efficient energy transfer to dimethyl fumarate (**2**) requires a sensitizer having a triplet energy greater than 61 kcal mol^{-1}.

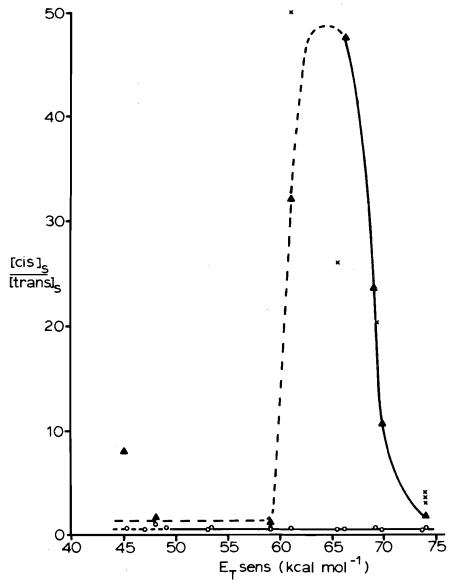

FIG. 2. Saltiel plots for ▲ dimethyl maleate and fumarate, × diethyl maleate and fumarate (4), and ⊙ maleonitrile and fumaronitrile.

No isomerization was induced when fluoren-9-one was the sensitizer and the isomerization observed when pyrene and acridine were used as sensitizers was relatively inefficient and of unknown mechanism. Rapid isomerization of **6** to **2** occurred when 9,10-dibromoanthracene was used as the sensitizer and the resulting mixture, i.e. >99% **2**, was identical to the thermodynamic equilibrium. Irradiation of this sensitizer is known to lead to carbon–bromine bond homolysis and the resulting bromine atoms could subsequently catalyze the thermal isomerization (21).

The behaviour of the isomeric dinitriles is obviously very different. The photosensitized stationary state is insensitive to variation in sensitizer triplet energy. Isomerization does, however, become relatively inefficient with sensitizers having a triplet energy less than 49 kcal mol^{-1} and no isomerization was observed with the sensitizer having triplet energy 44 kcal mol^{-1}. Our interpretation of these results is that the triplet energy of both **7** and **8** is approximately 50 kcal mol^{-1}.

Since it is known that sensitizers having a triplet energy between 68–78 kcal mol^{-1} are quenched at the diffusion-controlled rate by **7** and since the photostationary state is invariant over this range, it can be assumed that **8** also quenches these sensitizers at the diffusion limit. The fraction of triplets (**7**, **8**)[3] that decay to fumaronitrile (step 6 of Scheme 1) can be deduced from the photostationary state ratio established with these high energy triplet sensitizers: $\alpha = 0.61$.

Again in this case, isomerization was relatively rapid when 9,10-dibromoanthracene was the sensitizer. We believe the resulting mixture arises from a bromine atom catalyzed reaction and reflects the thermodynamic stability (33% **8** at 10°C; ΔG = 0.4 kcal mol^{-1}). The thermodynamic equilibrium has been established in a thermal reaction (180°C), catalyzed by iodine. The reported equilibrium value (33.8% **8**) (22) was based upon isolated yields and differs from the value we obtain (43.5% **8** at 180°C; ΔG = 0.2 kcal mol^{-1}) by vpc analysis of the crude reaction mixture. We believe it is fortuitous that the thermodynamic equilibrium is so similar to the photosensitized stationary state value.

No explanation was offered in the original work (4) for why diethyl maleate has such a high triplet energy relative to the fumarate. Since steric and electronic repulsions strongly (4.22 kcal mol^{-1}) (23) favour the *trans*-isomer in the ground state, the difference in the planar triplet state energies must be

proportionally larger; that is, the 'planar' triplet of diethyl maleate must be more than 16 kcal mol^{-1} above the 'planar' triplet of diethyl fumarate. To our knowledge the cause of this large difference has remained unexplained. Obviously, little or no difference exists between the triplet energy of **7** and **8**.

We were surprised that the triplet energies of the dinitriles were so much lower than that of the *trans*-diesters; we had assumed that **2**, **7**, and **8** would have similar triplet energies with the triplet of **6** being exceptionally high. This reasoning was based on the fact that both carbomethoxy and cyano substitution lowers the triplet energy of benzene by the same extent; methyl benzoate and cyanobenzene have essentially the same triplet energies (24). Baird (25) has proposed an empirical approach for estimating the energy of the 'twisted' π,π^* triplet of conjugated alkenes.[6] To use this approach to compare the relative triplet energies of two alkenes, one considers the relative stabilities of the pairs of radicals resulting from twisting each of the π bonds by 90°. From the reported heats of formation of the cyanomethyl radical (27) and fumaronitrile (28) the estimate of the 'twisted' triplet energy of fumaronitrile is 38.9 kcal mol^{-1}, similar to that of stilbene (37.8 kcal mol^{-1} (25)). The 'planar' triplet energy of *trans*-stilbene (49 kcal mol^{-1} (4)) is also close to that of the dinitriles. Unfortunately, the required thermodynamic data are not available for an estimate of 'twisted' triplet energy of the diesters.

An analysis based upon electron spin resonance hyperfine splitting, suggests that electron delocalization is much greater with the cyano than with the carbomethoxy substituted radicals (29).

It therefore seems likely that conjugation of the alkyl oxygen nonbonding pairs of electrons with the carboxyl carbonyl decreases the extent of conjugation of the carbonyl with the carbon–carbon double bond in the ground state and with the unpaired electrons in the triplet. This explanation gains some support from the relatively large reduction potential of the diesters (3), and the observation that rotation about the alkyl oxygen – carboxyl carbonyl carbon in the radical anion is relatively slow (30).

Experimental

General

Fumaronitrile (Aldrich Chemical Co.) was freshly sublimed under vacuum before use. Maleonitrile was prepared by thermal isomerization of fumaronitrile catalyzed with iodine (22), and was isolated by fractional distillation, column chromatography on neutral alumina (Woelm) eluting with a 1:1 mixture of benzene and hexane, followed by recrystallization from ether–pentane. 1,2,3-Triphenylcyclopropene was prepared using the method described by Breslow and Chang (31).

Dimethyl fumarate (Aldrich Chemical Co.) was recrystallized once from methanol.

Dimethyl maleate (Eastman Kodak Co.) was fractionally distilled twice before use.

The sensitizers thioxanten-9-one, 4,4′-dimethoxybenzophenone, 1,3,5-triacetylbenzene, 2-acetylfluorene, and phenazine (Aldrich Chemical Co.); benzophenone (Fisher Scientific Co.); benzil and 1,4-benzanthracene (BDH Chemical Co.); xanthen-9-one, 9,10-dibromoanthracene, fluoren-9-one 2-acetonaphthone, phenanthrene quinone, and pyrene (Eastman Kodak Co.); 4,4′-dicyanobenzophenone (32); were either repeatedly recrystallized or sublimed under vacuum until they gave a sharp melting point and showed a single spot on thin-layer chromatography using silica gel plates.

Thiophene-free benzene was obtained using the procedure employed by Wagner (19). The melting points were determined on a Thermolyne hot-stage microscope and were corrected. The combustion analyses were performed by Chemalytics Inc., Tempe, Arizona.

Mass spectra were obtained from a Varian Mat 311A mass spectrometer and are reported as *m/e* (relative intensity); only parent molecular-ion peak and the base peak are reported.

The infrared spectra were run in KBr disk on a PE-621 infrared spectrometer using the 1601 cm^{-1} absorption band of polystyrene for calibration. The ^{1}Hmr spectra were obtained either on a Varian T-60 or a Varian XL-100 spectrometer. The chemical shifts are taken as the centre of multiplets referring to tetramethylsilane and the coupling constants are the result of first-order analysis.

The ultraviolet absorption spectra were recorded on a Cary 118 spectrometer using 1.0-cm quartz cuvettes.

The ^{13}Cmr spectra were determined using a Varian XL-100-15 system operation at 25.2 MHz in the Fourier transform mode with 2000 Hz sweep widths, the peak positions were determined to ± 1 Hz reference to internal tetramethylsilane. Off-resonance decoupling was employed to confirm assignments for methylene, methine, and quarternary carbons.

All irradiations were performed using a General Electric Co. 1-kW medium pressure mercury vapour arc lamp with a quartz cooling jacket (Photochemical Research Associates). All solutions were placed in Pyrex irradiation vessels flushed with dry nitrogen and sealed with rubber septums. The irradiation vessels were immersed in a constant temperature bath maintained at 10°C.

Filter Solution A

$BiCl_3$ (200 mg) was dissolved in 10% HCl (150 mL) and this solution was placed in a container such that there was at least 1 cm of filter solution shielding the irradiation vessel. The long wavelength cut off is 350 nm. This filter solution was photolabile and was replaced after each 24-h irradiation.

Filter Solution B

Same as filter solution *A* except that a more concentrated solution of $BiCl_3$ was employed (1000 mg $BiCl_3$ in 150 mL 10% HCl). The long wavelength cut off is 358 nm.

Oxidation and Reduction Potential Measurements

Cyclic voltammetric data were obtained using a three-electrode cell with a Princeton Applied Research Electrochemistry System model 170. The working electrode was a platinum sphere sealed into glass and the counter electrode was a platinum wire. A $Ag/AgNO_3$ (0.1 *M*) electrode was used as a reference electrode and 0.1 *M* tetraethylammonium perchlorate as supporting electrolyte. The solvent was acetonitrile.

[6]Semiempirical molecular orbital calculations of the triplet energy ('planar') of both **7** and **8** range between 41.4 and 61.5 kcal mol^{-1} (26).

CIDNP Experiment

The light source was an Oriel Corporation 200-W HgXe lamp focused and passed down through a light pipe into the solution in a 5-mm nmr tube. The signals were detected by a Varian XL-100 ^{1}Hmr spectrometer. No CIDNP signal was found under the following conditions although we were able to reproduce Taylor's result (footnote 5 and ref. 16) under similar conditions: a CD_3CN (or C_6D_6) solution of **1** (18.6 m*M*) and **7** (13 m*M*) or a solution containing **1** (0.1 *M*) and **7** (0.1 *M*) in CD_3CN. Solutions were deaerated by purging thoroughly with dry nitrogen.

Irradiation of 1,2,3-Triphenylcyclopropene and Fumaronitrile

A solution containing 1,2,3-triphenylcyclopropene (3.0 g, 11.1 mmol) and fumaronitrile (0.9 g, 11.5 mmol) in 40 mL of benzene was irradiated through filter solution *A*. After 120-h irradiation, the ^{1}Hmr spectrum of the reaction mixture revealed that all the cyclopropene had been consumed. Remaining was a complex mixture of adducts, cyclopropene dimer, and the unreacted fumaronitrile together with maleonitrile.

Benzene was removed under vacuum and the residue was charged onto a column of silica gel (Woelm activity III) and eluted with hexane–benzene. The first component to be eluted was the hexaphenyltricyclohexane dimer **4** (546 mg, 18.2%), followed by the unreacted fumaronitrile, which sublimed readily as the solvent was being taken off. Adduct **9** (806 mg, 20.8%) was not stable under the column condition and had partially isomerized to the corresponding phenyl-in isomer **13**. Maleonitrile was next to be eluted and sublimed while the solvent was being evaporated. Adduct **10** isomerized to give an equilibrium mixture of **10** and **14** (202 mg, 5.2%). The photoene adduct **12** (431 mg, 13.9%) came next. The last component to be eluted was adduct **11** (100 mg, 2.6%). All of the above yields were isolated yields of pure compounds calculated on the bases of starting cyclopropene.

Since the adducts are labile to heat and/or silica gel, direct measurement of yields by ^{1}Hmr was conducted on the crude reaction mixture using cyclohexane as an internal standard. A benzene (0.5 mL) solution of 1,2,3-triphenylcyclopropene (0.3 *M*) and fumaronitrile (0.3 *M*) was irradiated for 24 h through filter solution *A*. The ^{1}Hmr spectra revealed that all the cyclopropene had been consumed. The calculated yields accounted for 89% of the cyclopropene consumed: dimer **4** (17.5%), adduct **9** (44.5%), adduct **10** (7.3%), adduct **11** (4.4%), the ene-product **12** (15.3%). The starting nitrile(s) was 75% consumed and the ratio of fumaronitrile to maleonitrile remaining was 65:35. Neither adduct **13** nor **14** was present in this reaction mixture.

Adduct **9** was purified by recrystallization from $CHCl_3$–hexane to give colourless rhombic crystals: mp 188–190°C; ir (KBr) ν: 3040, 2970, 2250 (m), 1600, 1495, 1442, 1160, 1080, 1030, 1000, 920, 850 cm^{-1}; ^{1}Hmr δ($CDCl_3$): 3.25 (H_a, s, 1H), 3.45 (H_b, d, 1H, J_{bc} = 4.5 Hz), 3.80 (H_c, d, 1H, J_{bc} = 4.5 Hz), 6.40–7.40 (m, 15H, the pattern of this multiplet was common to the phenyl-out adducts so far observed which divided into three groups of multiplets with the lowest field group being the largest); ^{1}Hmr δ(C_6D_6): 2.85 (H_a, s, 1H), 2.35 (H_b, d, 1H), 3.00 (H_c, d, 1H), 6.15–7.10 (m, 15H); no nOe effect was observed in $CDCl_3$ on H_a upon irradiating H_c, however, a 4% nOe enhancement of H_a was observed upon irradiating H_b in C_6H_6 while the intensity of H_c remained unchanged; ^{13}Cmr chemical shifts ($CDCl_3$): 43.6 (bridgehead carbons), 36.48 (methine carbons), 39.95 (apex carbon), 116.4 and 117.3 (cyanocarbons), 133.4 (one of the aryl carbons attached directly to the bicyclopentane nucleus), 126.6–132.0 (other aromatic carbons); ms (70 eV): 346 (95, M^+), 319 (100). *Anal.* calcd. for $C_{25}H_{18}N_2$: C 86.68, H 5.24; found: C 86.59, H 5.44. *Mol. Wt.* calcd. for $C_{25}H_{18}N_2$: 346.14699; found (mass spectroscopic): 346.14616.

Heating of adduct **9** in benzene at 65°C for 72 h gave complete rearrangement to the phenyl-in adduct **13** which, upon recrystallization from ether–hexane, gave colourless rhombic crystals: mp 141–143°C; ir (KBr) ν: 3030, 2965, 2255, 2245, 1600, 1500, 1445, 1320, 1190, 1125, 1075, 1030 cm^{-1}; ^{1}Hmr δ($CDCl_3$): 3.8 (H_b, d, 1H, J_{bc} = 5.35 Hz), 3.9 (H_a, broad s, 1H, J_{ac} = 1 Hz), 4.4 (H_c, q, J = 1 and 5.35 Hz), 7.4–7.9 (m, 15H). The same pattern was observed in C_6D_6 δ: 2.4 (d, 1H), 2.5 (broad s, 1H), 3.0 (q, 1H), 6.0–7.0 (m, 15H); since H_b and H_a overlapped, nOe was not attempted; ^{13}Cmr chemical shifts ($CDCl_3$): 40.3 and 42.2 (bridgehead carbons), 30.6 and 31.1 (methine carbons), 40.0 (apex carbon), 115.3 and 117.6 (cyanocarbons), 135.4 (one of the aryl carbons attached directly to bicyclopentane nucleus), 126.9–131.0 (other aromatic carbons); ms (70 eV): 346 (48, M^+), 319 (100). *Anal.* calcd. for $C_{25}H_{18}N_2$: C 86.68, H 5.24; found: C 86.41, H 5.49. *Mol. Wt.* calcd. for $C_{25}H_{18}N_2$: 346.14699; found (mass spectroscopy): 346.14633.

Adduct **10** was never isolated since isomerization occurred under mild conditions; on the other hand, the isomer, adduct **14**, readily crystallized from the mixture in $CHCl_3$–hexane: mp 215–217°C; ir (KBr) ν: 3065, 2248, 1600, 1500, 1450, 1280, 1085, 1032, 930, 830 cm^{-1}; ^{1}Hmr δ($CDCl_3$): 3.4 (s, 3H), 7.0–7.7 (m, 15H), the singlet at 3.4 was not split upon addition of a shift reagent Eu(fod)$_3$III; ^{1}Hmr δ(C_6D_6): 1.7 (s, 2H), 2.1 (s, 1H), 6.0–6.8 (m, 15H); ^{13}Cmr chemical shift ($CDCl_3$): 41.8 (bridgehead carbons), 31.8 (methine carbons), 40.2 (apex carbon), 116.3 (cyanocarbons), 133.5 and 131.0 (aryl carbons directly attached to bicyclopentane nucleus), 128.5–130.1 (other aromatic carbons); ms: 346 (81, M^+), 319 (100). *Anal.* calcd. for $C_{25}H_{18}N_2$: C 86.68, H 5.24; found: C 86.48, H 5.20.

Refluxing adduct **14** in benzene for 2 h gave an equilibrium mixture consisted of adduct **10** (23%) and adduct **14** (77%). The ir (KBr), ms, and tlc of this mixture was essentially the same as adduct **14** alone; however, ^{1}Hmr and ^{13}Cmr spectral assignments for adduct **10** can be obtained by subtracting the peaks due to adduct **14** from the spectra of the mixture: ^{1}Hmr δ($CDCl_3$): 3.55 (s, 1H), 3.8 (s, 2H), 6.4–7.8 (m, 15H, same pattern as adduct **3**); ^{1}Hmr δ(C_6D_6): 2.3 (s, 2H), 3.1 (s, 1H), 6.0–7.0 (m, 15H); ^{13}Cmr chemical shift ($CDCl_3$): 43.2 (bridgehead carbons), 35.0 (methine carbons), 38.4 (apex carbon), 115.0 (cyano carbons), 133.2 and 132.2 (aryl carbons attached directly to bicyclopentane nucleus), 126.0–130.3 (other aromatic carbons). Another piece of evidence supporting this thermodynamic equilibrium was the observation that, after crystals of **14** had been removed, the mother liquid which initially consisted of 72% of adduct **10** and 28% of adduct **14**, reverted to the equilibrium composition after 11 days at room temperature.

Adduct **11** was recrystallized from $CHCl_3$–EtOH to give shiny plates: mp 191–193°C (dec.); ir (KBr) ν: 3040, 2960, 2245, 1600, 1500, 1445, 1075, 1035, 925, 762, 700 cm^{-1}; ^{1}Hmr δ($CDCl_3$): 2.9 (H_a, s, 1H), 3.6 (H_b, s, 2H), 6.2–7.2 (m, 15H, same pattern as adduct **9**); ^{1}Hmr δ(C_6D_6): 1.6 (s, 1H), 2.0 (s, 2H), 5.6–6.8 (m, 15H); nOe ($CDCl_3$): irradiating H_a gave 7.3% enhancement of the methine protons and an 18% enhancement of H_a was observed when the methine protons were irradiated. ^{13}Cmr chemical shift ($CDCl_3$): 44.6 (bridgehead carbons), 36.8 (methine carbons), 41.8 (apex carbon), 115.9 (cyano carbons), 133.8 (one of the aryl carbons directly attached to bicyclopentane nucleus), 126.4–131.7 (other aromatic carbons); ms: 346 (75, M^+), 319 (100). *Anal.* calcd. for $C_{25}H_{18}N_2$: C 86.68, H 5.24; found: C 86.56, H 5.45. This adduct was also thermally unstable in solution. Upon heating

at 75°C in C_6D_6 for 24 h, the solution turned from colourless to red-brown, the ^{1}Hmr spectrum showed that **11** had been consumed, remaining was a singlet at $\delta(C_6D_6)$ 2.9 and a multiplet at 6.3–7.4 in the ratio ca. 1:10. No further attempt was made to characterize this product(s).

Compound **12** was colourless cubic crystals after recrystallization from $CHCl_3$–EtOH: mp 207–208°C; ir (KBr) ν: 3030, 2960, 2260, 2245, 1825, 1600, 1495, 1445, 1310, 1160, 1070, 1000, 960, 803 cm^{-1}; ^{1}Hmr $\delta(CDCl_3)$: 2.55 (d, 2H, J = 7 Hz), 4.3 (t, 1H, J = 7 Hz), 6.8–7.9 (m, 15H); ^{1}Hmr $\delta(C_6D_6)$: 1.2 (d, 2H), 2.9 (t, 1H), 6.2–7.4 (m, 15H); ms: 346 (9, M^+), 267 (100). *Anal.* calcd. for $C_{25}H_{18}N_2$: C 86.68, H 5.24; found: C 86.86, H 5.41. This compound was thermally stable and no change was observed upon heating at 75°C in C_6D_6 solution for 24 h.

Irradiation of 1,2,3-Triphenylcyclopropene and Maleonitrile

A solution containing 1,2,3-triphenylcyclopropene (80.4 mg, 0.3 mmol), maleonitrile (23.4 mg, 0.3 mmol) in benzene (1 mL) was irradiated through filter solution *A*. After irradiating for 47 h, analysis of the ^{1}Hmr spectrum revealed 94.4% of the cyclopropene had been consumed. The same products were found as in irradiation of the cyclopropene with fumaronitrile except the product ratios were different: adduct **9** (25.4%), adduct **10** (12.6%), adduct **11** (7.2%), compound **12** (18.2%), dimer **4** (19.5%). These yields are corrected for the unreacted cyclopropene and represent an 84% material balance. The ratio of the unreacted fumaronitrile and maleonitrile was 60:40.

Irradiation of 1,2,3-Triphenylcyclopropene and Fumaronitrile in the Presence of Thioxanthen-9-one

A solution of 1,2,3-triphenylcyclopropene (40.2 mg, 0.15 mmol), fumaronitrile (11.7 mg, 0.15 mmol), and thioxanthen-9-one (1 mg, 0.005 mmol) in benzene (0.5 mL) was irradiated through filter solution *B*. After 2 h, the ^{1}Hmr spectrum revealed that 89% of the cyclopropene had been consumed. The same products (and one additional) were obtained as upon direct irradiation: adduct **9** (17.9%), adduct **10** (14.0%), adduct **11** (4.7%), compound **12** (25.2%), dimer **4** (24.3%), and dimer **5** (11.8%). These yields were corrected for the cyclopropene unreacted and thus, 98% of the starting cyclopropene was accounted for. The ratio of the unreacted fumaronitrile and maleonitrile was 60:40. Essentially, the same results were obtained when fluoren-9-one was used as sensitizer.

Attempted Thermal Reactions of 1,2,3-Triphenylcyclopropene with Fumaronitrile

A solution of 1,2,3-triphenylcyclopropene (20 mg, 0.075 mmol), fumaronitrile (12 mg, 0.15 mmol) in toluene (1 mL) was sealed after three cycles of freeze–thaw and was then heated in an oil bath at 120°C. After heating for 450 h, most of the cyclopropene (>95%) was consumed while fumaronitrile remained unchanged. The sole product identified with ^{1}Hmr and tlc was dimer **5**.

A solution containing **1** (200 mg) and AIBN (10 mg) in benzene (5 mL) was refluxed under a nitrogen atmosphere. After 3 h, ^{1}Hmr and tlc showed small amount of **5** had been formed (half-life of AIBN at this temperature is ~1 h). Portions of AIBN (total 10 mg) were added after each 6 h. After 47 h of refluxing, ^{1}Hmr revealed ~2% of **5** as the sole product. A control experiment was performed in the absence of AIBN. After 48 h, approximately same amount of **5** was obtained.

Photostationary States of Photosensitized Isomerization of Fumaronitrile, Maleonitrile, Dimethyl Fumarate, and Dimethyl Maleate

Preliminary studies were conducted at higher concentration of fumaronitrile (0.3 *M*) and dimethyl fumarate (0.2 *M*) with the concentration of sensitizers being 0.05 *M* in benzene followed by ^{1}Hmr. Irradiations were done using a 0-51 Corning glass filter (cut off at 360 nm). The photostationary state was taken as the constant *cis–trans* ratio obtained upon prolonged irradiation.

To minimize possible complications, such as blocking of light due to polymer formation or sensitization other than triplet–triplet energy transfer from the lowest triplet excited state of the sensitizer, experiments were conducted at lower concentrations of quencher (0.05 *M*) and sensitizers (0.01 *M*). In these experiments, isomerization was followed by vapour phase chromatography (vpc) (PYE 140 vpc with a 5 ft 10% DEGS column at 175°C for the nitriles and 170°C for the esters). The response factors for the corresponding isomers were almost the same and the ratios were determined by weighing the peak areas. Also, 0.05 *M* of the synthetic mixtures close to the photostationary state were irradiated in the presence of 0.01 *M* sensitizer. In these experiments, no further change of the ratio of the *cis–trans* isomers occurred after a short period of irradiation. The results are listed in Table 2. In most of the cases, the two procedures gave the same (within experimental error) ratio of isomers.

Acknowledgements

We gratefully acknowledge the assistance of Dr. S. K. Wong in obtaining the photo CIDNP spectra. This work was supported by a grant from the National Research Council of Canada.

1. (*a*) R. M. MORCHAT and D. R. ARNOLD. J. Chem. Soc. Chem. Commun. 743 (1978); (*b*) D. R. ARNOLD and R. M. MORCHAT. Can. J. Chem. **55**, 393 (1977); (*c*) D. R. ARNOLD and R. M. MORCHAT. Afinidad, **34**, 276 (1977).
2. R. HUISGEN, R. GRASBEY, and J. SAVER. *In* The chemistry of alkenes. *Edited by* S. Patai. Interscience Inc., New York, NY. 1964. p. 919.
3. (*a*) P. J. ELVING and C. TEITELBAUM. J. Am. Chem. Soc. **71**, 3916 (1949); (*b*) S. K. SMIRNOV, I. G. SEVASTIJANOVA, A. P. TOMILOV, L. A. FEDOROVA, and O. G. STRUKOV. Zh. Org. Khim. **5**, 1392 (1969); (*c*) J. P. PETROVICH, H. M. BAIZER, and M. R. ORT. J. Electrochem. Soc. **116**, 743 (1969); (*d*) L.-S. R. YEH and A. J. BARD. J. Electrochem. Soc. **124**, 189 (1977); (*e*) V. J. PUGLISI and A. J. BARD. J. Electrochem. Soc. **119**, 829 (1972).
4. G. S. HAMMOND, J. SALTIEL, A. A. LAMOLA, N. J. TURRO, J. S. BRADSHAW, D. O. COWAN, R. C. COUNSELL, V. VOGT, and C. DALTON. J. Am. Chem. Soc. **86**, 3197 (1964).
5. K. A. BROWN-WENSLEY, S. L. MATTES, and S. FARID. J. Am. Chem. Soc. **100**, 4162 (1978).
6. D. Y. CURTIN, H. GRUEN, Y. G. HENDRICKSON, and H. E. KNIPMEYER. J. Am. Chem. Soc. **83**, 4838 (1961).
7. P. SCHULER and H. HENSINGER. Photochem. Photobiol. **24**, 307 (1976).
8. (*a*) C. D. DEBOER, D. H. WADSWORTH, and W. C. PERKINS. J. Am. Chem. Soc. **95**, 861 (1973); (*b*) H. DÜRR. Justus Liebigs Ann. Chem. **723**, 102 (1969).
9. P. S. ENGEL and B. M. MONROE. Adv. Photochem. **8**, 245 (1971).
10. M. ITOH, S. FURUYA, and T. OKAMOTO. Bull. Chem. Soc. Jpn. **50**, 2509 (1977).
11. (*a*) S. NAGAKURA. *In* Excited states. Vol. 2. *Edited by* E. C. Lim. Academic Press, New York, NY. 1975. pp. 322–383; (*b*) M. OTTOLENGHI. Acc. Chem. Res. **6**, 153 (1973); (*c*) N. ORBACH and M. OTTALENGHI. *In* The exciplex. *Edited by* M. Gordon and W. R. Ware. Academic Press Inc., New

York, NY. 1975. pp. 75–111; (*d*) K. B. EISENTHAL. J. Chem. Phys. **45**, 1850 (1966).
12. (*a*) R. FOSTER. Organic charge-transfer complexes. Academic Press, New York, NY. 1969. Chapt. 11; (*b*) A. GUPTA and G. S. HAMMOND. J. Am. Chem. Soc. **97**, 254 (1975).
13. (*a*) A. WELLER. *In* The exciplex. *Edited by* M. Gordon and W. R. Ware, Academic Press Inc., New York, NY. 1975. pp. 23–38; (*b*) D. REHM and A. WELLER. Isr. J. Chem. **8**, 259 (1970); (*c*) A. WELLER and K. ZACHARIASSE. Molecular luminescence. *Edited by* E. C. Lim. W. A. Benjamin Inc., New York, NY. 1969. p. 895 (part II).
14. E. S. PYSH and N. C. YANG. J. Am. Chem. Soc. **85**, 2124 (1963).
15. J. BIRKS. Photophysics of aromatic molecules. John Wiley and Sons, New York, NY. 1970. p. 70.
16. (*a*) H. D. ROTH. Mol. Photochem. **5**, 91 (1973); (*b*) G. L. CLOSS and M. S. CZEROPSKI. J. Am. Chem. Soc. **99**, 6127 (1977); (*c*) J. BARGON. J. Am. Chem. Soc. **99**, 8350 (1977).
17. (*a*) P. D. BARTLETT and N. A. PORTER. J. Am. Chem. Soc. **90**, 5317 (1968); (*b*) K. R. KOPECKY and S. EVANI. Can. J. Chem. **47**, 4041 (1969).
18. J. C. DALTON, P. A. WRIEDE, and N. J. TURRO. J. Am. Chem. Soc. **92**, 1318 (1970).
19. I. E. KOCHEVAR and P. J. WAGNER. J. Am. Chem. Soc. **94**, 3859 (1972).
20. J. SALTIEL, J. D'AGOSTINO, E. D. MEGARITY, L. METTS, K. R. NEUBERGER, M. WRIGHTON, and O. C. ZAFIRIOU. Organic photochemistry. Vol. 3. *Edited by* O. L. Chapman. Marcel Dekker, Inc., New York, NY. 1973. Chapt. 1.
21. P. S. ENGEL and B. M. MONROE. Adv. Photochem. **8**, 245 (1971).
22. G. E. FICKEN, R. P. LINSTEAD, E. STEPHEN, and M. WHALLEY. J. Chem. Soc. 3879 (1958).
23. R. B. WILLIAMS. J. Am. Chem. Soc. **64**, 1395 (1942).
24. D. R. ARNOLD, J. R. BOLTON, G. E. PALMER, and K. V. PRABHU. Can. J. Chem. **55**, 2728 (1977).
25. N. C. BAIRD. Mol. Photochem. **2**, 53 (1970).
26. C. LEIBOVICI and L. DE BROGLIE. C.R. Acad. Sci. Ser. C, **270**, 1507 (1970).
27. K. D. KING and R. D. GODDARD. Int. J. Chem. Kinet. **7**, 837 (1975).
28. R. H. BOYD, K. R. GUHA, and R. WUTHRICH. J. Phys. Chem. **71**, 2187 (1967).
29. (*a*) H. FISCHER. Z. Naturforsch. Teil A, **19**, 866 (1964); (*b*) H. FISCHER. Z. Naturforsch. Teil A, **202**, 428 (1965).
30. (*a*) S. F. NELSEN and J. P. GILLESPIE. J. Org. Chem. **40**, 2391 (1975); (*b*) A. J. BARD, V. J. PUGLISI, J. V. KENKEL, and A. LOMAX. Faraday Discuss. Chem. Soc. **56**, 353 (1973).
31. R. BRESLOW and H. W. CHANG. J. Am. Chem. Soc. **83**, 2367 (1961).
32. R. W. R. HUMPHREYS and D. R. ARNOLD. Can. J. Chem. **55**, 2286 (1977).

A nuclear magnetic resonance study of pyridoxal phosphate – metal ion interactions. II. Binding of manganese(II)[1]

TENKASI S. VISWANATHAN[2] AND TERRENCE J. SWIFT

Department of Chemistry, Case Western Reserve University, Cleveland, OH 44106, U.S.A.

Received August 8, 1978

TENKASI S. VISWANATHAN and TERRENCE J. SWIFT. Can. J. Chem. **57**, 1050 (1979).

The line width and spin–lattice relaxation rates of phosphorus and proton nuclei in PLP have been measured as a function of temperature in the presence of Mn(II) using pulsed nmr methods. The T_{1M} of ^{31}P in PLP–Mn(II) is very close to the T_{1M} values of β- and γ-phosphorus atoms in ATP–Mn(II) at ~40°C. The T_1 data of ^{31}P and ^1H have been interpreted in terms of the dipolar interaction between the electron and nuclear spins. With the assumption that the Mn(II) interacts directly with the phosphate of PLP the rotational correlation time τ_c at 38°C was calculated to be 7.6×10^{-10} s from phosphorus T_1 data. This τ_c value was subsequently used to calculate metal–proton distances from proton T_1 and T_2 data. The results lead to the conclusion that the phosphate-bound metal interacts directly with the aldehyde oxygen in a 1:1 PLP–Mn(II) complex. The linewidth of the ^{13}C resonances of PLP in the presence of Mn(II) supports this conclusion. The structure assigned for PLP–Mn(II) complex is in conformity with the structure for PLP–Co(II) complex.

TENKASI S. VISWANATHAN et TERRENCE J. SWIFT. Can. J. Chem. **57**, 1050 (1979).

On a mesuré les largeurs des raies et les taux de relaxation spin–réseau des noyaux de phosphore et du proton du PLP en fonction de la température en présence de Mn(II) en faisant appel à des méthodes de rmn pulsée. Les valeurs de T_{1M} du ^{31}P dans le PLP–Mn(II) sont très près des valeurs de T_{1M} des atomes de phosphore β et γ dans l'ATP–Mn(II) à ~40°C. On a interprété les données de T_1 pour le ^{31}P et le ^1H en termes d'interactions dipolaires entre les spins électronique et nucléaire. En faisant l'hypothèse que le Mn(II) interagit directement avec le phosphate du PLP, on a calculé que le temps de corrélation rotationnelle, τ_c, à 38°C est égal à 7.6×10^{-10} s à partir des données de T_1, pour le phosphore. On a ultérieurement utilisé cette valeur de τ_c pour calculer les distances métal–proton à partir des données de T_1 et T_2 pour le proton. Les résultats conduisent à la conclusion que le métal lié au phosphore interagit directement avec l'oxygène de l'aldéhyde dans un complexe 1:1 PLP–Mn(II). Les largeurs des raies des résonances ^{13}C du PLP en présence de Mn(II) sont en accord avec ces conclusions. La structure attribuée au complexe PLP–Mn(II) est conforme à la structure du complexe PLP–Co(II).

[Traduit par le journal]

Introduction

The metal complexes of Schiff bases derived from pyridoxal phosphate (PLP) (**1**) have been well studied because of their importance as model systems for PLP-catalyzed enzymatic reactions such as transamination and deamination (1). Pyridoxal phosphate itself has considerable affinity for divalent metal ions and only a limited number of studies (2, 3) have been reported on these complexes. The recent report by Farago *et al.* (3) describes these complexes as insoluble and probably polymeric solids.

Nuclear magnetic resonance is one of the powerful techniques used in the determination of binding sites, when the ligand in question possesses more than one binding site. Paramagnetic metal ions, in particular, cause large changes in the chemical shifts and relaxation rates of the neighbouring nuclei making the metal ion an exceptionally good probe of its environment. We have used a combination of ^{31}P, ^1H, and ^{13}C nmr studies to find the nature of the divalent metal ion complexes of PLP. The results presented in this report are useful in assigning an unambiguous structure for the PLP–Mn(II) complex.

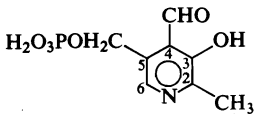

1 Pyridoxal phosphate

Experimental

Pyridoxal phosphate was purchased from Sigma Chemical Co. and it was found to be free of paramagnetic impurities. Measurements of proton line widths were done at 60 MHz at 37°C on a Varian A60A nmr spectrometer. Measurements of proton spin–lattice relaxation times and all the ^{13}C and ^{31}P nmr determinations were done on a Varian XL-100 in the

[1]Based on the Ph.D. Thesis of T.S.V., Case Western Reserve University, 1975.

[2]Address correspondence to this author at the Chemistry Department, Simon Fraser University, Burnaby, B.C., Canada V5A 1S6.

0008-4042/79/091050-06$01.00/0

pulsed FT mode. The temperature of the A60A and XL-100 probes were determined by inserting a calibrated thermometer inside the spectrometer cavity. The T_1 determinations were done by the inversion–recovery method. Usually 10 different τ values were taken with the largest τ value about three times the null point. The error in the T_1 values obtained in this study varied from 3 to 10%.

Internal tetramethylammonium (TMA) chloride was used as the reference for ^1H and ^{13}C nmr studies. The reference used for ^{31}P nmr was hexamethylphosphoramide (HMPA) contained in a coaxial tube. All nuclear resonances with frequency greater than the resonance frequency of the reference material were given positive sign for the chemical shift.

Theory

The effects on the nmr spectrum of a ligand molecule exchanging between the first coordination sphere of a paramagnetic metal ion and the free solution are described by the equations of Swift and Connick (4) and Luz and Meiboom (5). The contributions T_{1p}^{-1} and T_{2p}^{-1} by the metal ion to the observed relaxation rates are determined by the relaxation times of the resonances in the bound state, T_{1M} and T_{2M}, the fraction of the coordinated ligand, f, and the average residence time of the ligands in the bound form, τ_m:

$$[1] \qquad T_{1p}^{-1} = f/(T_{1M} + \tau_M)$$

$$[2] \qquad T_{2p}^{-1} = f/\tau_M\left[\frac{T_{2M}^{-1}(T_{2M}^{-1} + \tau_M^{-1}) + \Delta\omega_M^2}{(T_{2M}^{-1} + \tau_M^{-1})^2 + \Delta\omega_M^2}\right]$$

where $\Delta\omega_M$ is the shift between the resonances of free and bound ligand at the slow exchange limit (4).

Shulman *et al.* (6) modified the Solomon–Bloembergen equations (7, 8) to describe the relaxation of the ligand bound to the Mn(II) ion:

$$[3] \qquad T_{1M}^{-1} = \frac{2}{5}\left[\frac{S(S+1)g^2\beta^2\gamma_I^2}{r^6}\right]\tau_c$$

$$[4] \qquad T_{2M}^{-1} = \frac{7}{15}\left[\frac{S(S+1)g^2\beta^2\gamma_I^2}{r^6}\right]\tau_c + \frac{1}{3}\left[\frac{S(S+1)A^2}{\hbar^2}\right]\tau_e$$

where γ_I is the magnetogyric ratio, $A/\hbar$ is the scalar coupling constant between the nucleus and the electron, and r is the nuclear–electron distance. The dipolar correlation time τ_c and the scalar correlation time τ_e are given by:

$$[5] \qquad \tau_c^{-1} = \tau_s^{-1} + \tau_M^{-1} + \tau_r^{-1}$$

$$[6] \qquad \tau_e^{-1} = \tau_s^{-1} + \tau_M^{-1}$$

where τ_s is the electron spin relaxation time and τ_r is the rotational correlation time. In deriving [3] and [4] it has been assumed that $(\omega_s\tau_c)^2 \gg 1$ and $(\omega_s\tau_e)^2 \gg 1$, where ω_s is the resonance frequency of the electron.

Results and Discussion

Phosphorus Nuclear Magnetic Resonance Studies

The temperature dependence of the normalised paramagnetic contribution to the relaxation rates $(fT_{1p})^{-1}$ and $(fT_{2p})^{-1}$ of the phosphorus resonance of PLP–Mn(II) are shown in Fig. 1. The following features are noticeable in the curves. (*i*) As the temperature is raised $(fT_{2p})^{-1}$ passes through a maximum at 54°C and then decreases with further increase in temperature. (*ii*) The value of $(fT_{2p})^{-1}$ at its maximum is about 150 times larger than the value of $(fT_{1p})^{-1}$ at the same temperature. (*iii*) Increase in temperature causes decrease in the value of $(fT_{1p})^{-1}$ in the temperature range studied.

Since $T_{2p}^{-1} \gg T_{1p}^{-1}$ for the phosphorus resonance in PLP–Mn(II), it follows that $\tau_M^{-1} \gg T_{1M}^{-1}$ at the temperature of maximum $(fT_{2p})^{-1}$ or higher. At 54°C and above one would expect the value of T_{1p}^{-1} to reflect truly the weighted average longitudinal relaxation rate. Figure 2 shows the linear dependence of T_{1p}^{-1} and T_{2p}^{-1} of the phosphorus resonance of PLP on the concentration of added Mn(II) ion at 69°C. Little shifting of the phosphorus resonance was observed.

From the measured T_{1p}^{-1} values, it is possible to calculate the distance of the phosphorus atom from the Mn(II) ion using [3]. A knowledge of the magnitude of the dipolar correlation time τ_c is essential for the calculation of r. However, qualitative conclusions may be drawn by comparing the results for PLP–Mn(II) with results published for similar complexes

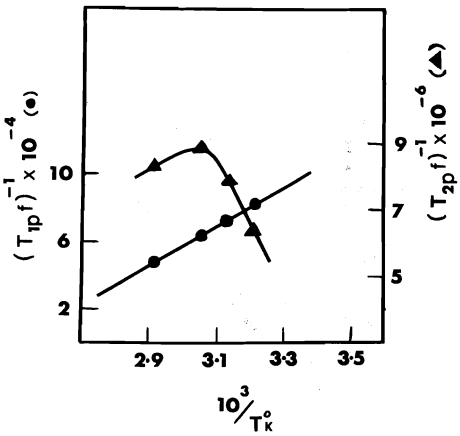

FIG. 1. The temperature dependence of $(fT_{2p})^{-1}$ and $(fT_{1p})^{-1}$ of the ^{31}P resonance of PLP–Mn(II) complex at 40.5 MHz. The pD of the solution was 7.0 and the concentration of PLP was 0.75 *M*. Mn(II) was added to yield a [Mn(II)] to [PLP] ratio of 1.33×10^{-5}.

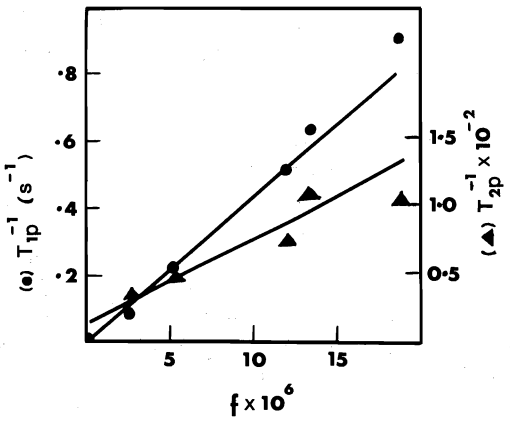

FIG. 2. The dependence of T_{1p}^{-1} and T_{2p}^{-1} of the ^{31}P resonance of PLP on the concentration of the added Mn(II) at 69°C.

such as ATP–Mn(II). The value of 0.8×10^5 s^{-1} for $(fT_{1p})^{-1}$ of phosphorus in PLP–Mn(II) is in excellent agreement with a value of 1×10^5 for the β- and γ-phosphorus resonances of ATP–Mn(II) at 40°C. Since ATP and PLP are similar in size, their rotational correlation times should have similar magnitude. With that assumption the conclusion is that the nature of the Mn–phosphate interaction is similar for Mn–ATP and Mn–PLP, namely, direct binding.

Since 'direct binding' of Mn(II) to the phosphate of PLP is a reasonable conclusion from our results, one can use the values of g, S (10, 11), and r (12) available in the literature for $LiMnPO_4$ to calculate the correlation time for PLP–Mn(II). For $g = 2.0$, $S = 5/2$, and $r = 3.3$ Å, the value of τ_c is 4.4×10^{-10} s at 69°C, 6×10^{-10} s at 54°C, and 7.6×10^{-10} s at 38°C.

Measurement of $(fT_{2p})^{-1}$ in the temperature range studied does not provide any binding structure information since $T_{2M}^{-1} \approx \tau_M^{-1}$ at temperatures as high as 69°C. Since in this slow exchange limit [2] reduces to $fT_{2p} = \tau_M$, the exchange rate may be calculated from the line width measurement. The average residence time of PLP molecules in the coordination sphere of Mn(II) at 38°C is 0.16 μs and τ_M has an activation energy of 5.6 kcal/mol.

Proton Nuclear Magnetic Resonance Studies

The addition of Mn(II) to a solution of PLP at pD 6.2 does not cause any significant shift of any of the proton resonances. However, selective broadening of the proton resonances does take place. The maximum broadening was observed for the formyl proton resonance. The line broadening of the 6-H proton was about half of that observed for the formyl proton whereas the 2-methyl proton broadening was only one-fifth of the broadening of the formyl proton. The dependence of the line width at half-height of these and the solvent (HDO) proton resonances on the concentration of the added Mn(II) at 37°C are shown in Fig. 3. The temperature dependences of the logarithm of the full line width at half-height of the 2-methyl, 6-H, and the solvent HDO resonances are shown in Fig. 4. This figure shows that at 37°C the observed line widths of all these protons are the weighted average values. The

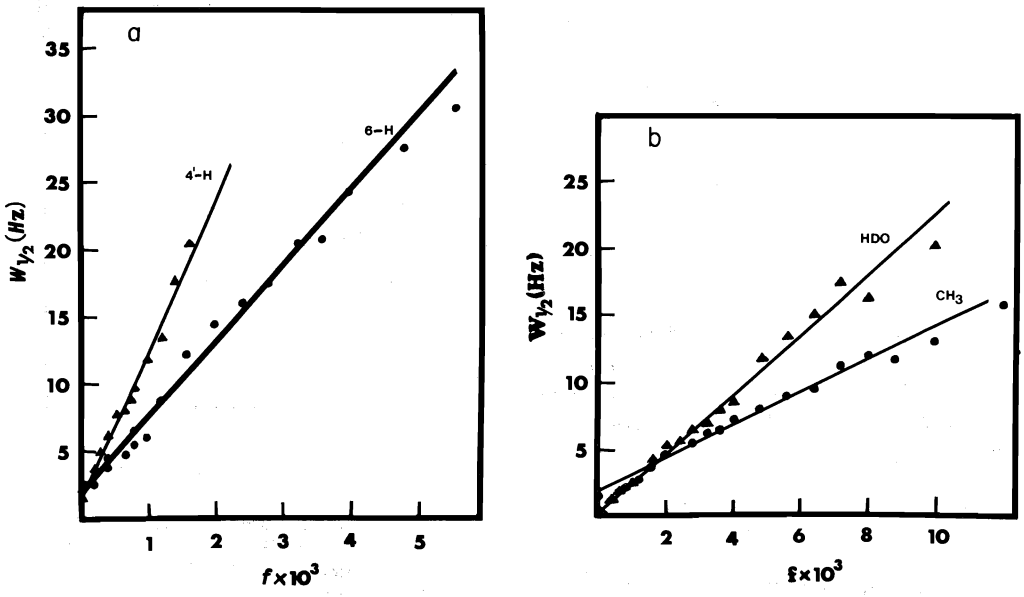

FIG. 3. The full line width at half-height of the proton resonances of PLP (0.25 M) at pD 6.2 and at 37°C as a function of the Mn(II) concentration: (*a*) 4-CHO and 6-H protons and (*b*) 2-methyl and solvent (HDO) protons.

TABLE 1. The transverse and longitudinal relaxation rates (s^{-1}) and metal–nuclei distances (Å) for the PLP–Mn(II) complex

Nuclei	$(fT_{2p})^{-1}$ at 60 MHz	r	$(fT_{1p})^{-1}$ at 100 MHz	r
4-CHO proton	1.7×10^4	6.0	9.6×10^3	6.4
5-CH_2 proton[a]	—	—	2.2×10^4	5.6
6-H proton	8.7×10^3	6.7	9.0×10^3	6.5
2-CH_3 proton[b]	1.9×10^3	8.6	—	—
Phosphorus	—	—	8×10^4	3.3[c]

[a]The measurement of line widths is complicated by the coupling of ^{31}P to the 5-CH_2 resonance.
[b]The T_1 value of the methyl resonance was not measured.
[c]Assumed for a direct binding of Mn(II) to phosphate.

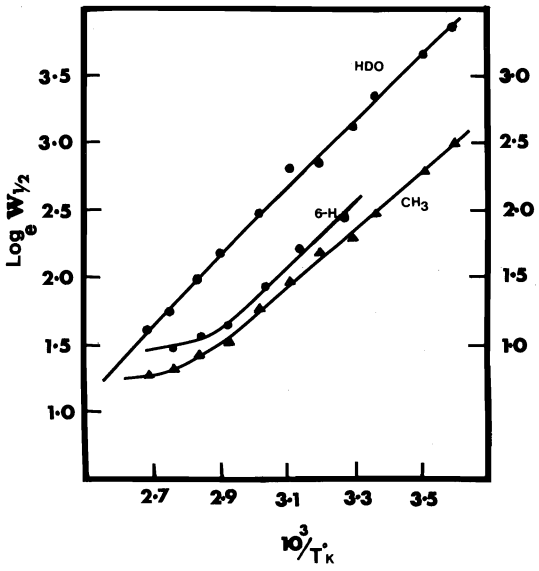

FIG. 4. The temperature dependence of the full line width at half-height of the solvent HDO (right scale) and the 6-H and 2-methyl (left scale) proton resonances of PLP–Mn(II) at pD 6.2. The [Mn(II)] to [PLP] ratio, f, was 1.4×10^{-3} for 6-H proton and 4×10^{-3} for 2-methyl and HDO protons. The concentration of PLP was 0.25 M.

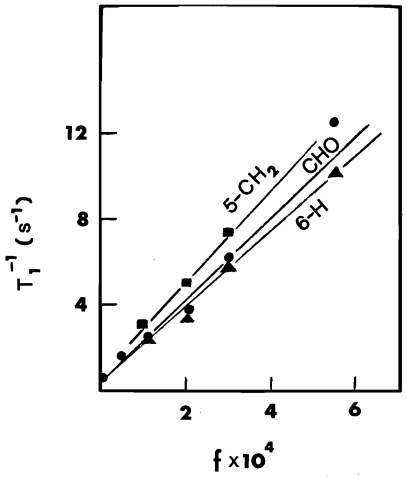

FIG. 5. The dependence of the observed T_1^{-1} of the 5-methylene, 4-CHO, and the 6-H proton resonances (100 MHz) of PLP (0.25 M) at 35°C on the ratio of [Mn(II)] to [PLP].

temperature dependence of $(fT_{2p})^{-1}$ of the formyl proton (not shown) exhibits a maximum at ~40°C. Consequently, the line width of the formyl proton may have some contributions from rate effects and it yields an upper limit for T_{2M}^{-1}.

The T_1 relaxation times of the 4-CHO, 6-H, and 5-CH_2 proton resonances were also measured at 37°C. However, these measurements were done at 100 MHz. The dependence of the observed T_1^{-1} for these protons on the concentration of the added Mn(II) is shown in Fig. 5. The large HDO peak at the center of the proton spectrum of PLP introduced some spectral phasing problems, especially when the T_1 run was in the complete control of the computer. Consequently, only peaks to the low field side of the HDO peak were plotted for T_1 determination. Thus, the T_1 values of the 2-methyl protons were not determined. The extrapolated T_2^{-1} and T_1^{-1} values at 60 and 100 MHz, respectively, of the proton resonances in the 1:1 PLP–Mn(II) complex are shown in Table 1. The $(fT_{2p})^{-1}$ for 6-H is slightly lower than the $(fT_{1p})^{-1}$ of this proton. This is spurious since $T_1^{-1} \leq T_2^{-1}$ for all systems without exception and may be the result of experimental uncertainties. However, the significant point is that the values of $(fT_{1p})^{-1}$ and $(fT_{2p})^{-1}$ are comparable indicating that the spin–lattice relaxation of the proton resonances in PLP–Mn(II) are controlled by the dipolar mechanism. Consequently, the expression for T_{2M}^{-1} of the protons in the PLP–Mn(II) complex is:

$$[7] \qquad T_{2M}^{-1} = 7/15[S(S+1)g^2\beta^2\gamma_I^2 r^{-6}\tau_c]$$

The expression for T_{1M}^{-1} is given by [3]. Thus, the ratio of T_{2M}^{-1} to T_{1M}^{-1} would be 7:6 or approximately unity.

The proton relaxation data could be used to calculate the metal–proton distances using [3] and [7] and from a knowledge of the rotational correlation time. It was shown by Sternlicht *et al.* (9) that the P—O—

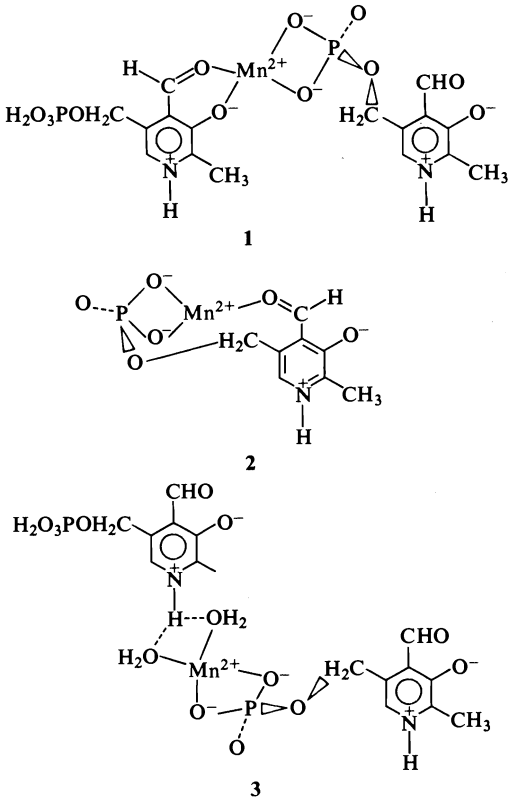

FIG. 6. Scheme of three possible PLP–Mn(II) complexes.

Mn—OH_2 chain is rigid relative to its axis and the fastest motion is a tumbling of that chain. The tumbling may be isotropic since the 1:1 PLP–Mn(II) complex lacks symmetry elements. Under these circumstances, the correlation time for all the PLP protons would be the same as the ^{31}P correlation time. The metal–proton distances calculated from [3] and [7] with a τ_c value of 7.6×10^{-10} s are tabulated in Table 1. Since the value of τ_c may be in error owing to certain assumptions made in its calculation, no significance could be given to the absolute magnitudes of these metal–proton distances.

The metal–proton distances tabulated in Table 1 are extremely valuable in arriving at a structure for the PLP–Mn(II) complex. The shortest distance from the metal is observed for 5-CH_2 protons, which strongly supports our conclusion that Mn(II) binds directly to the phosphate. There are three possibilities for the phosphate-bound metal to interact with the ring: (*i*) The metal may bind to both 4-CHO and 3-O^- functional groups of another PLP molecule in a 2:1 PLP–Mn(II) complex. (*ii*) The metal may interact only with the aldehyde oxygen in a 1:1 complex. (*iii*) The metal may interact with the heterocyclic nitrogen in a 2:1 or a 1:1 complex.

The third possibility is less likely since the nitrogen remains protonated at the pD employed (6.2) in our studies. Table 1 also reveals that the 2-methyl protons are more than 2 Å units farther away from the metal ion than the 4-CHO proton, which will be inconsistent with this model. The first possibility would place the methyl protons closer to the Mn(II) than the 6-H proton, which is inconsistent with the observed *r* values. The second model would place the metal closest to the methylene protons. The 6-H and 4-CHO protons would be nearly equidistant with the latter closer to the metal ion and the methyl protons would be quite far away from the metal ion. The average *r* values of 5.6, 6.4, 6.6, and 8.6 Å for 5-CH_2, 4-CHO, 6-H, and the 2-methyl protons observed in our results entirely supports this model. The next question would be whether complex **2** is a majority species? Potentiometric studies of Mn(II) and PLP at a total PLP concentration of 0.001 *M* indicate (14) that a 1:1 complex is formed and the stability constant of the complex indicates a definite interaction with the ring. However, it is possible that a sequential binding mechanism exists. The metal may be bound tightly to the phosphate all the time and this metal–phosphate complex exchange rapidly with complex **2**, which may account for less than 100% of Mn(II) in solution, a situation similar to the Mn–ATP complex in solution (13). Our evidence does not rule out this possibility.

Carbon Nuclear Magnetic Resonance Studies

The gradual addition of Mn(II) to a 0.75 *M* PLP solution at 35°C produces selective broadening of the carbon resonances of PLP. Figures 7*a* and 7*b* show the aromatic region of the ^{13}C nmr spectrum of PLP before and after Mn(II) was added to obtain a

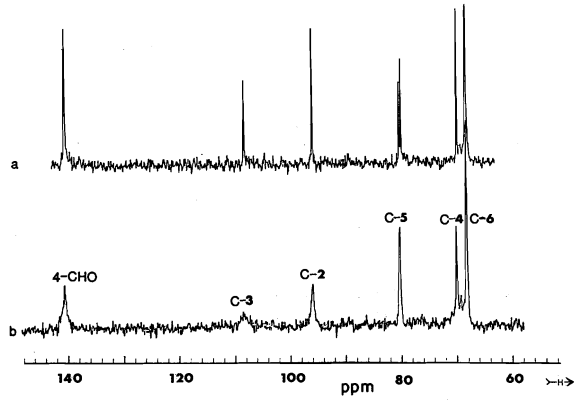

FIG. 7. The aromatic region of the ^{13}C nmr spectrum of 0.75 *M* PLP solution at pD 7.0: (*a*) metal-free solution and (*b*) after addition of Mn(II) to $f = 5.33 \times 10^{-4}$. The broadening of the side-chain carbon resonances, 5-methylene and 2-methyl, by Mn(II) present to this concentration was negligible.

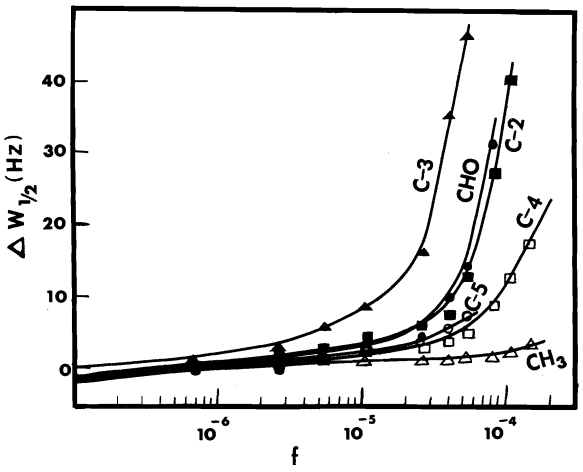

FIG. 8. The dependence of the full line width at half-height of the C-3, C-2, 4-CHO, C-4, C-5, and 2-methyl carbon resonances (25.16 MHz) of PLP (0.75 *M*) at pD 7.0 and at temperature 35°C on the logarithm of the [Mn(II)] to [PLP] ratio.

[Mn(II)] to [PLP] ratio of 5.33×10^{-4}. The C-3 carbon broadening is the largest, followed closely by the 4-CHO and C-2 broadenings. A plot of the full line width at half-height of the C-2, C-3, C-4, C-5, 2-CH_3, and 4-CHO resonances, caused by the addition of Mn(II) against log *f* is shown in Fig. 8. The C-5, C-6, and 5-CH_2 resonances have a small coupling to the ^{31}P making accurate measurement of their line widths difficult. However, rough measurements showed that the line broadening follows the order C-3 $\gg$ 4-CHO $\approx$ C-2 $\gg$ C-5 $\approx$ C-4 $\gg$ C-6 $\approx$ 5-CH_2 > 2-CH_3. Very little shifting was observed for any of the carbon resonances even for large amounts of added Mn(II). The temperature dependence of the ^{13}C line widths was not studied.

The ATP–Mn(II) complex was studied in detail with the use of ^{13}C nmr by Kuntz *et al.* (13). These authors showed that the transverse relaxation of the ^{13}C resonances of ATP–Mn(II) is dominated by the scalar mechanism. Hence, the Solomon–Bloembergen equation describing T_{2M}^{-1} for the carbon resonances reduces to:

$$[8] \qquad T_{2M}^{-1} = S(S+1)A^2\tau_e/3\hbar^2$$

Thus, relative values of T_{2M}^{-1} do not have any relationship to the metal–carbon distances. The T_{2M}^{-1} values rather indicate the extent of spin delocalisation to these carbon atoms. The large T_{2M}^{-1} observed for the C-3 may be the result of covalent binding of Mn(II) to the 4-CHO and subsequent spin transport by the resonance of the *o*-hydroxyaldehyde functional group. The value of $(fT_{2p})^{-1}$ for C-3 in PLP–Mn(II) is about 25 times larger than the $(fT_{2p})^{-1}$ for C-5 and C-8 resonances of ATP–Mn(II). In ATP the C-5 and C-8 carbons are α to the heterocyclic nitrogen to which Mn(II) was shown to form a covalent bond (13). Thus, the large values observed for T_{2p}^{-1} of the carbon resonances of PLP–Mn(II) probably indicate covalent binding of the metal ion to the ring.

In conclusion, the present ^{31}P, ^{1}H, and ^{13}C nmr study of the PLP–Mn(II) system indicates a structure for the metal–PLP complex in which the metal ion is simultaneously bound to the phosphate and the aldehyde oxygen. A similar structure has been proposed for the PLP–Co(II) complex (Swift and Viswanathan, to be published) and other divalent metal ion complexes of pyridoxal phosphate.

1. E. E. SNELL and D. E. METZLER. J. Am. Chem. Soc. **77**, 2431 (1955).
2. T. S. VISWANATHAN. Ph.D. Thesis, Case Western Reserve University, Cleveland, OH. 1975.
3. M. E. FARAGO, M. M. MCMILLAN, and S. S. SABIR. Inorg. Chim. Acta, **14**, 207 (1975).
4. T. J. SWIFT and R. E. CONNICK. J. Chem. Phys. **37**, 307 (1962).
5. Z. LUZ and S. MEIBOOM. J. Chem. Phys. **40**, 2686 (1964).
6. R. G. SHULMAN, H. STERNLICHT, and B. J. WYLUDA. J. Chem. Phys. **43**, 3116 (1965).
7. I. SOLOMON. Phys. Rev. **99**, 559 (1955).
8. N. BLOEMBERGEN. J. Chem. Phys. **27**, 572 (1957).
9. H. STERNLICHT, R. G. SHULMAN, and E. W. ANDERSON. J. Chem. Phys. **43**, 3123 (1965).
10. J. M. MAYS. Phys. Rev. **131**, 38 (1963).
11. J. M. MAYS. Phys. Rev. **108**, 1090 (1957).
12. S. GELLER and J. L. DURAND. Acta Crystallogr. **13**, 325 (1960).
13. G. P. P. KUNTZ, Y. LAM, and G. KOTOWYCZ. J. Am. Chem. Soc. **96**, 1834 (1974).
14. T. N. BRIGGS. Ph.D. Thesis, Case Western Reserve University, Cleveland, OH. 1976.

Synthesis of a thioanalogue of neamine. The reaction of nitrosochloroadducts of glycals with thiols

GERRY KAVADIAS,[1] ROBERT DROGHINI, YVON PÉPIN,[2] MARCEL MÉNARD, AND PHILIPPE LAPOINTE

Bristol Laboratories of Canada, 100 Industrial Boulevard, Candiac, P.Q., Canada J5R 1J1

Received October 20, 1978

GERRY KAVADIAS, ROBERT DROGHINI, YVON PÉPIN, MARCEL MÉNARD, and PHILIPPE LAPOINTE. Can. J. Chem. **57**, 1056 (1979).

The reaction of the dimeric 4-*O*-acetyl-6-azido-2,3,6-trideoxy-2-nitroso-α-D-*ribo*-hexopyranosyl chloride **2** with cyclohexanethiol and 2-propanethiol is stereospecific and produces the corresponding 2-hydroxyimino-1-thio-α-D-*erythro*-hexopyranosides **3***a* and **3***c* in high yields. Acetylation of the oxime **3***a* followed by reduction with borane, then by reduction with sodium borohydride and acetylation gave cyclohexyl 2,6-diacetamido-4-*O*-acetyl-2,3,6-trideoxy-1-thio-α-D-*ribo*-hexopyranoside (**4***b*). By a similar sequence of reactions, the oxime **3***c* was converted to isopropyl 2,6-dibenzamido-4-*O*-benzoyl-2,3,6-trideoxy-1-thio-α-D-*ribo*-hexopyranoside (**4***c*).

Condensation of the nitrosochloro adduct **2** with (1*S*,2*S*,4*R*,5*R*)-2,4-diethoxycarbonylamino-5-hydroxycyclohexanethiol (**5***c*) gave the α-D-thioglycoside **6***c* which, after acetylation followed by reduction and removal of the protective groups, yielded (1*S*,2*S*,4*R*,5*R*)-2,4-diamino-5-hydroxycyclohexyl 2,6-diamino-2,3,6-trideoxy-1-thio-α-D-*ribo*-hexopyranoside (**7***c*), a thioanalogue of neamine.

GERRY KAVADIAS, ROBERT DROGHINI, YVON PÉPIN, MARCEL MÉNARD et PHILIPPE LAPOINTE. Can. J. Chem. **57**, 1056 (1979).

La réaction du chlorure du *O*-acétyl-4 azido-6 tridéoxy-2,3,6 nitroso-2 α-D-*ribo*-hexopyrannosyle dimère **2** avec le cyclohexanethiol et le propanethiol-2 est stéréospécifique et conduit aux hydroxyimino-2 thio-1 α-D-*érythro*-hexopyrannosides **3***a* et **3***c* correspondants avec de bons rendements. L'acétylation de l'oxime **3***a*, suivie par une réduction avec le borane, puis par une réduction avec le borohydrure de sodium et une acétylation conduit au diacétamido-2,6 *O*-acétyl-4 tridéoxy-2,3,6 thio-1 α-D-*ribo*-hexopyrannoside de cyclohexyle (**4***b*). Utilisant les mêmes réactions, on peut transformer l'oxime **3***c* en dibenzamido-2,6 *O*-benzoyl-4 tridéoxy-2,3,6 thio-1 α-D-*ribo*-hexopyrannoside d'isopropyle (**4***c*).

La condensation de l'adduit chloro-nitroso **2** avec le (1*S*,2*S*,4*R*,5*R*) diéthoxycarbonylamino-2,4 hydroxy-5 cyclohexanethiol (**5***c*) conduit à l'α-D-thioglycoside **6***c* qui, après une acétylation suivie d'une réduction et de l'élimination des groupes protecteurs, fournit le diamino-2,6 tridéoxy-2,3,6 thio-1 α-D-*ribo*-hexopyrannoside de (1*S*,2*S*,4*R*,5*R*) diamino-2,4 hydroxy-5 cyclohexyle (**7***c*), un thioanalogue de la néamine.

[Traduit par le journal]

In continuation of our research program in the area of aminocyclitol antibiotics (1), we thought it desirable to explore the synthesis and biological properties of thio analogues of the clinically important antibiotics. The target structures were the kanamycins, gentamicins, tobramycin, etc., in which one or both of the glycosidic oxygens have been replaced by a sulfur atom(s). These novel structures have not been reported previously.

The present paper describes the synthesis of a thioanalogue of neamine, namely the (1*S*,2*S*,4*R*,5*R*)-2,4-diamino-5-hydroxycyclohexyl 2,6-diamino-2,3,6-trideoxy-1-thio-α-D-*ribo*-hexopyranoside (**7***c*).

Several problems are associated with the preparation of 1-thio-α-glycosides such as **7***c* and related compounds, the most important of which are: (*a*) a glycosidation process to yield selectively the α-glycosidic structure, (*b*) the availability of thio analogues of 2-deoxystreptamine as the aglycon components in the synthesis; and (*c*) the selection of protective groups which could easily be removed at the end of the synthesis in the presence of sulfur.

1-Thioglycosides (2) can be prepared by several methods, the most important of which are: (*i*) by reaction of an aldose with a thiol under strongly acidic conditions (3) yielding mixtures of 1,2-*cis*- and 1,2-*trans*-isomers; (*ii*) by the Helferich reaction (4) involving the reaction of a fully acetylated sugar with a thiol in the presence of a Lewis acid (5); (*iii*) from the reaction of *O*-acetylglycosyl halides with an alkali salt of a thiol (6); and (*iv*) by *S*-alkylation of 1-thio sugars with alkyl halides (7). None of the above procedures could be adopted for the synthesis of **7***c* for obvious reasons.

A promising potential route for the preparation of

[1]Author to whom correspondence may be addressed.

[2]On sabbatical leave; present address: Université du Québec à Montréal.

0008-4042/79/091056-08$01.00/0

7*c* appeared to be the reaction of the nitrosochloro adduct **2** with the aminothiol **5**. It is well known that the reaction of nitrosochloro adducts of glycals with alcohols, also known as the Lemieux–Nagabhushan reaction (8–19), produces selectively the α-glycosides in most cases and can be used to prepare 2-amino- and 2-hydroxyglycosides. A similar reaction, however, of nitrosochloro adducts of glycals with thiols has not been described previously and in order to determine its utility for the synthesis of the 1-thio-α-D-glycoside **7***c*, the reaction of the nitrosochloro adduct **2** with cyclohexanethiol and 2-propanethiol were examined first.

4-*O*-Acetyl-3-deoxy-6-*O*-tosyl-D-glucal (**1***a*) was prepared by a literature procedure (20); on treatment with sodium azide in dimethylformamide (DMF) a 50% yield of 4-*O*-acetyl-6-azido-3,6-dideoxy-D-glucal (20) (**1***b*) was obtained. Treatment of the glucal **1***b* with nitrosyl chloride in methylene chloride gave the dimeric 4-*O*-acetyl-6-azido-2,3,6-trideoxy-2-nitroso-α-D-*ribo*-hexopyranosyl chloride (20) (**2**) in high yield.

Condensation of the nitrosochloro adduct **2** with cyclohexanethiol in DMF at 23°C in the presence of 2,2,6,6-tetramethylpiperidine (TMP) afforded cyclohexyl 4-*O*-acetyl-6-azido-2,3,6-trideoxy-2-hydroxyimino-1-thio-α-D-*erythro*-hexopyranoside (**3***a*) in high yield. The ^{1}Hmr spectrum of **3***a* showed two anomeric proton singlets at δ 5.8 and 6.51, in a ratio of 10:1, presumably due to *E*- and *Z*-oxime isomers, respectively. This assumption was based on a previous report (14) that the anomeric proton of the *E*-isomer of 2-hydroxyimino-α-glucopyranosides resonates at higher field than that of the *Z*-isomer. Acetylation of the oxime **3***a* produced the acetate **3***b* which on reduction with borane (16) in tetrahydrofuran followed by acetylation gave a mixture of cyclohexyl 2-acetamido-4-*O*-acetyl-6-azido-2,3,6-trideoxy-1-thio-α-D-*ribo*-hexopyranoside (**4***a*) and cyclohexyl-2,6-diacetamido-4-*O*-acetyl-2,3,6-trideoxy-1-thio-α-D-*ribo*-hexopyranoside (**4***b*). The reduction of **3***b* with borane had caused partial reduction of its azide function. For identification purposes the two products were separated by chromatography on a silica gel column. Reduction of the azido group in **4***a* with sodium borohydride in isopropanol (21) followed by acetylation provided **4***b*. The yield of **4***b* based on the oxime acetate **3***b* was 50%. These reactions are summarized in Scheme 1. Structural assignment to **4***a* as the α-D-*ribo*-isomer was based on ^{1}Hmr spectroscopy. The ^{1}Hmr spectrum of **4***a* (Fig. 1) showed a doublet at δ 5.39 ($J_{1,2}$ = 5 Hz) due to the anomeric proton. It also showed a double triplet at δ 2.16 ($J_{2,3_e} = J_{3_e,4}$ = 5 Hz, J_{vic} = 12 Hz) due

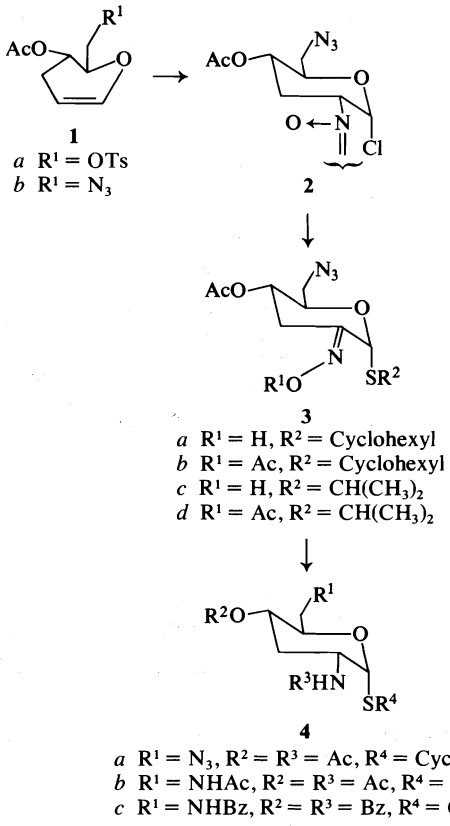

(Ac = $COCH_3$; Bz = COC_6H_5; Ts = $CH_3C_6H_4SO_2$)

SCHEME 1

to the equatorial H-3 indicating that this proton was coupled with two adjacent axial protons. It also exhibited an octet at δ 4.44 ($J_{1,2} = J_{2,3_e}$ = 5 Hz, $J_{2,3_a}$ = 13 Hz, $J_{2,NH}$ = 8 Hz) with band intensities ratio of 1:2:2:3:3:2:2:1, due to H-2, in good agreement with a theoretical first-order spectrum (Fig. 2) for this proton. These spectral data are in complete accord with the structure assigned to **4***a*. The ^{1}Hmr spectrum of **4***b* was also in agreement with that expected for the assigned structure.

Treatment of the nitrosochloro adduct **2** with 2-propanethiol in dimethylformamide in the presence of 2,2,6,6-tetramethylpiperidine produced isopropyl 4-*O*-acetyl-6-azido-2,3,6-trideoxy-2-hydroxyimino-1-thio-α-D-*erythro*-hexopyranoside (**3***c*). Acetylation of the oxime **3***c* gave the oxime acetate **3***d*. Reduction of **3***d* with borane in tetrahydrofuran (16) followed by reduction with sodium borohydride in isopropanol (21), to reduce the azide function, and benzoylation gave a 32% yield of isopropyl 2,6-dibenzamido-4-*O*-benzoyl-2,3,6-trideoxy-1-thio-α-D-*ribo*-hexopyranoside (**4***c*). The ^{1}Hmr spectrum of **4***c* was interpreted via extensive decoupling experiments (Fig. 3). It

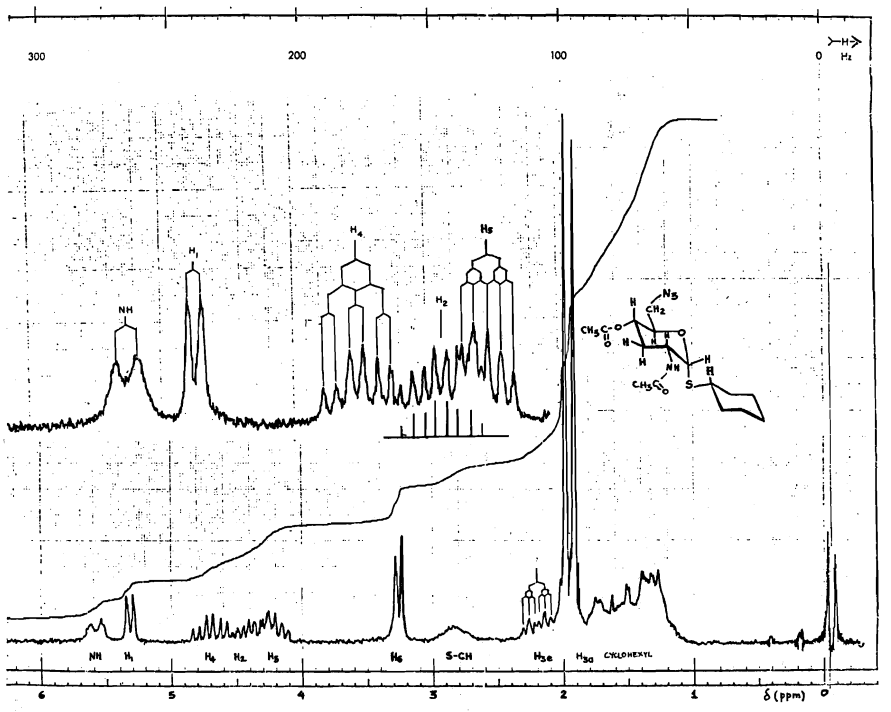

FIG. 1. The ^{1}Hmr spectrum at 100 MHz of cyclohexyl 2-acetamido-4-*O*-acetyl-6-azido-2,3,6-trideoxy-1-thio-α-D-*ribo*-hexopyranoside in deuteriochloroform.

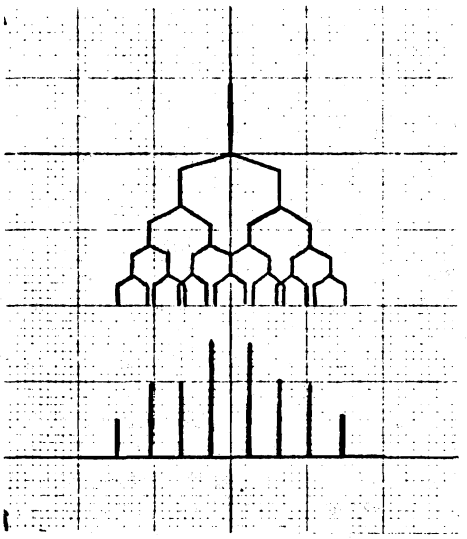

FIG. 2. Theoretical spectrum of H-2 in **4***a* calculated from the coupling constants $J_{2,3_a} = 13$, $J_{2,NH} = 8$, $J_{1,2} = 5$. $J_{2,3_e} = 5$ Hz.

exhibited a doublet at δ 5.51 ($J_{1,2}$ = 5 Hz) due to the anomeric proton, a double triplet at δ 1.81 (J_{vic} = 15 Hz, $J_{2,3_a} = J_{3_a,4}$ = 11 Hz) due to the axial H-3, and a double triplet at δ 2.52 (J_{vic} = 13 Hz, $J_{2,3_e} = J_{3_e,4}$ = 4.5 Hz) due to the equatorial H-3. The above data can only be consistent with the α-D-*ribo*-configuration for **4***c*. The preparation of the above model α-D-thioglycosides from the nitrosochloro adduct **2** demonstrated as anticipated that this process could successfully be applied to prepare thioanalogues of aminocyclitol antibiotics.

The preparation of **7***c* (Scheme 2) was then undertaken. The aminothiol **5***b* was prepared by our previously published method (22). Condensation of the nitrosochloro adduct **2** with the aminothiol **5***b* in dimethylformamide in the presence of 2,2,6,6-tetramethylpiperidine gave an 82% yield of the crystalline oxime **6***a*. The ^{1}Hmr spectrum of **6***a* showed a one-proton singlet at δ 5.85 due to the anomeric proton and, on the basis of precedents (14) discussed above, the *E*-configuration was assigned to this product. Acetylation of the oxime **6***a* afforded the acetate **6***b* which on reduction with borane in tetrahydrofuran gave a complex mixture of products due to the reduction of the oxime, of the azido and of the benzamido groups. The *N*-benzoyl protective group in **5***b* was then replaced with *N*-ethoxycarbonyl group.

Treatment of the nitrosochloro adduct **2** with **5***c* in dimethylformamide in the presence of 2,2,6,6-tetramethylpiperidine afforded an 80% yield of crystalline oxime **6***c*. Acetylation of **6***c* produced the acetate **6***d* which, on reduction with borane in tetrahydrofuran (16) followed by acetylation, gave a

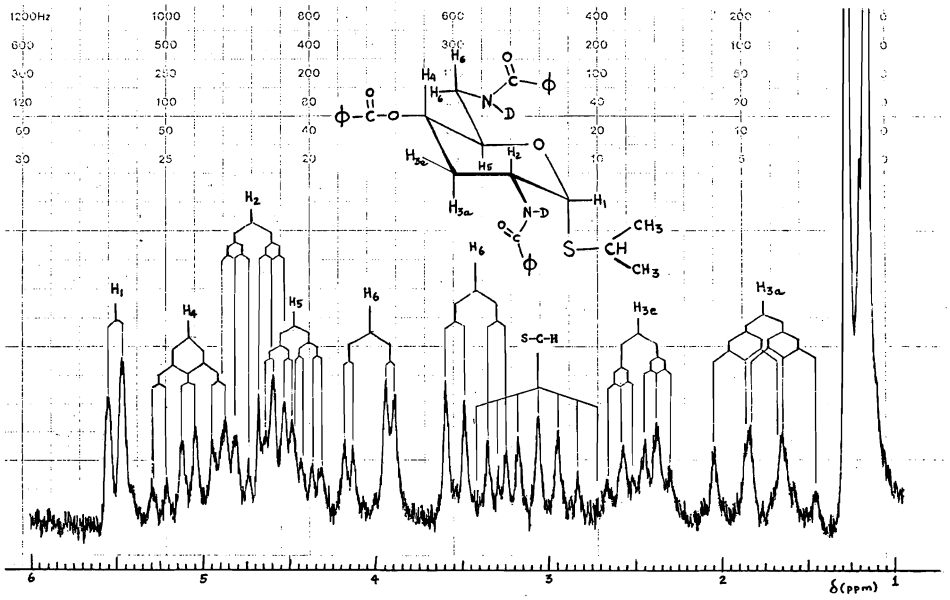

FIG. 3. The ^{1}Hmr spectrum at 60 MHz of isopropyl 2,6-dibenzamido-4-*O*-benzoyl-2,3,6-trideoxy-1-thio-α-D-*ribo*-hexopyranoside in deuteriochloroform. The amide protons have been exchanged with deuterium (D_2O, trifluoroacetic acid).

mixture of the 6-azido compound **7***a* and of the 6-acetamido product **7***b*. Hydrogenation of this mixture in methanol – acetic anhydride solvent mixture in the presence of platinum oxide catalyst afforded crystalline **7***b* in 30% yield based on the oxime **6***c*. The structure of **7***b* was established by chemical and spectroscopic means. Desulfurisation of **7***b* with Raney nickel in ethanol gave **8** thus establishing that **7***b* was a thioglycoside. The ^{1}Hmr spectrum of **7***b* contained a doublet at δ 5.43 due to

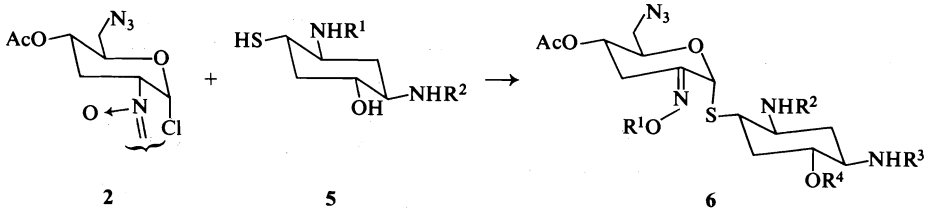

2 **5** **6**

a $R^1 = R^2 = H$
b R^1 = Bz, R^2 = Cbe
c $R^1 = R^2$ = Cbe

a $R^1 = R^4 = H$, R^2 = Bz, R^3 = Cbe
b $R^1 = R^4$ = Ac, R^2 = Bz, R^3 = Cbe
c $R^1 = R^4 = H$, $R^2 = R^3$ = Cbe
d $R^1 = R^4$ = Ac, $R^2 = R^3$ = Cbe

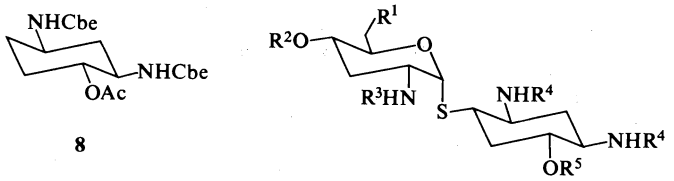

8 **7**

a $R^1 = N_3$, $R^2 = R^3 = R^5$ = Ac, R^4 = Cbe
b R^1 = NHAc, $R^2 = R^3 = R^5$ = Ac, R^4 = Cbe
c $R^1 = NH_2$, $R^2 = R^3 = R^4 = R^5 = H$

(Cbe = $CO_2C_2H_5$; Bz = COC_6H_5; Ac = $COCH_3$)

SCHEME 2

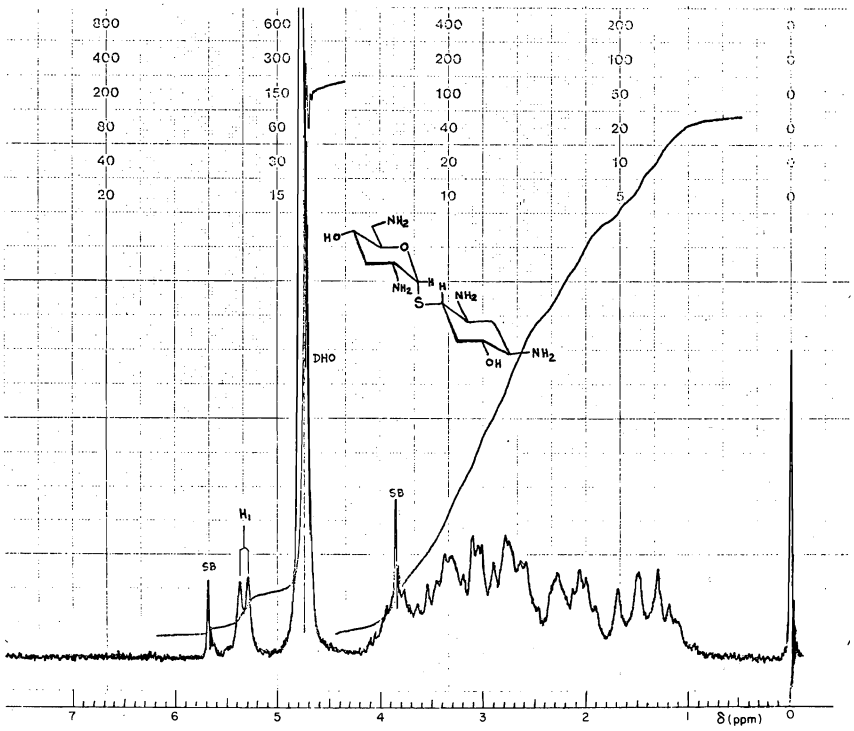

FIG. 4. The ^{1}Hmr spectrum of **7***c* at 60 MHz in D_2O.

the anomeric proton with a coupling constant of 5 Hz consistent with an α-D-*ribo*-configuration.

Removal of the protective groups in **7***b* by basic hydrolysis gave **7***c*. The ^{1}Hmr spectrum of **7***c* (Fig. 4) confirmed the assigned structure and exhibited a doublet at 5.35 (J = 5 Hz) due to the anomeric proton.

Compound **7***c* exhibited no significant antibiotic activity against 32 test organisms. At a concentration of 250 μg/mL compound **7***c* showed no inhibition in the growth of *Staphylococcus aureus*. The minimum inhibitory concentration (MIC) of neamine against this organism was 8 μg/mL.

Experimental

The melting points were determined on an Electrothermal melting point apparatus and are not corrected. The ir spectra were recorded on a Unicam SP-200G grating ir spectrometer. ^{1}Hmr spectra were obtained at 60 or 100 MHz with either a Varian EM-360A or an HA-100 spectrometer. Tetramethylsilane (for solutions other than deuterium oxide) and sodium 4,4-dimethyl-4-silapentane-1-sulfonate (for solution of deuterium oxide) were used as internal standards. Thin-layer chromatography (tlc) was carried out on microscope slides coated with silica gel and the spots were visualized with iodine or sulfuric acid. Optical rotations were measured with a Perkin-Elmer Model 141 polarimeter. The analyses were performed by Micro-Tech Laboratories, Skokie, IL.

*4-O-Acetyl-6-azido-3,6-dideoxy-D-glucal (**1**b)*

This product was prepared by a modified literature procedure (20) as follows. To a solution of 4-*O*-acetyl-3-deoxy-6-*O*-tosyl-D-glucal (**1***a*) (34.5 g, 0.11 mol) in dry dimethylformamide (400 mL) at 80°C, was added sodium azide (14 g, 0.22 mol) and the mixture stirred for 1 h maintaining the temperature between 75 and 80°C. The reaction mixture was poured into ice water (400 mL) and extracted with methylene chloride (3 × 150 mL). The combined extracts were washed successively with saturated sodium bicarbonate solution and water and dried (Na_2SO_4). Removal of the solvent by evaporation gave 19.7 g of a dark-colored syrup which on tlc (silica, 20% ethyl acetate in petroleum ether) showed three spots of R_f 0.48, 0.35 (major, **1***b*), and 0.25. The crude product was purified by column chromatography on silica gel (1 kg) using 20% ethyl acetate in petroleum ether as eluent to give 10.5 g (50%) of 4-*O*-acetyl-6-azido-3,6-dideoxy-D-glucal (**1***b*) as an oil; ir (neat): 2100, 1715, 1660 cm^{-1}; ^{1}Hmr ($CDCl_3$) δ: 2.06 (s, 3H, OAc), 2.0–2.7 (m, 2H, H-3), 3.45 (d, 2H, H-6, J = 4.5 Hz), 4.00 (d of t, 1H, H-5, $J_1 = J_2 = 4.5$, $J_3 = 8$ Hz), 4.71 (d of d of d, 1H, H-2, $J_1 = 6$, $J_2 = 4.5$, $J_3 = 3$ Hz), 4.98 (d of t, 1H, H-4, $J_1 = J_2 = 8$, $J_3 = 6$ Hz), 6.39 (d of t, 1H, H-1, $J_1 = J_2 = 2$, $J_3 = 6$ Hz).

*4-O-Acetyl-6-azido-2,3,6-trideoxy-2-nitroso-α-D-ribo-hexopyranosyl Chloride (**2**)*

This product was prepared by a modified literature procedure (20) as follows. The glucal **1***b* (3.0 g, 15.2 mmol) was dissolved in dry methylene chloride (60 mL) in a 250 mL three-neck flask equipped with a low temperature thermometer and gas inlet and outlet tubes. Nitrogen was passed through the magnetically stirred solution while it was cooled to −70°C in a Dry Ice – acetone mixture. To this solution was added a cold solution of nitrosyl chloride (3.2 g, 49 mmol) in methylene chloride (20 mL) and the mixture was stirred for 1 h under nitrogen while the temperature was slowly increased to −20°C.

The reaction mixture was filtered to remove some solid impurities and evaporated to give 3.6 g (90%) of **2** as a gum; ^{1}Hmr ($CDCl_3$) δ: 2.10 (s, 3H, OAc), 6.75 (m, 1H, H-1).

This material, soon after its preparation, was used without further purification in the glycosidation reaction.

*Cyclohexyl 4-O-Acetyl-6-azido-2,3,6-trideoxy-2-hydroxyimino-1-thio-α-*D*-erythro-hexopyranoside (3a)*

A solution of 1.52 g (5.8 mmol) of **2**, 1.5 mL of 2,2,6,6-tetramethylpiperidine and 1.3 mL of cyclohexanethiol in 5 mL of dry DMF was stirred at 23°C for 3 h. The reaction mixture was evaporated and the residue was dissolved in ether (100 mL). The ether solution was washed with 10% hydrochloric acid (100 mL) and water and, after drying, was evaporated to give 1.95 g (99%) of the oxime **3*a*** as a syrup. A sample (1.0 g) was chromatographed on a silica gel column using chloroform as eluent. The *E*-isomer was eluted first giving 630 mg as an oil; $[\alpha]_D^{23}$ +105° (*c* 1.0, EtOH); ir (neat): 3330, 2090, 1730 cm^{-1}; ^{1}Hmr ($CDCl_3$) δ: 2.09 (s, 3H, OAc), 5.80 (s, 1H, H-1).

The *Z*-isomer was eluted next, to give 70 mg of material as an oil; $[\alpha]_D^{23}$ +121° (*c* 0.5, EtOH); ir (neat): 3320, 2090, 1730 cm^{-1}; ^{1}Hmr ($CDCl_3$) δ: 2.10 (s, 3H, OAc), 6.51 (s, 1H, H-1).

*Cyclohexyl 2-Acetoxyimino-4-O-acetyl-6-azido-2,3,6-trideoxy-1-thio-α-*D*-erythro-hexopyranoside (3b)*

A solution of 0.63 g (1.84 mmol) of the oxime **3*a*** (*E*-isomer) and 1.6 mL of acetic anhydride in 4 mL of anhydrous pyridine was left at 23°C for 20 h. The reaction mixture was diluted with ether and washed first with 10% sodium bicarbonate solution and then with water and dried. Removal of the solvent by evaporation left a syrup (0.68 g) which was chromatographed on silica gel with chloroform to give 0.58 g (82%) of the acetate **3*b*** as a syrup $[\alpha]_D^{23}$ +151° (*c* 0.7, EtOH); ir (neat): 2100, 1770, 1740 cm^{-1}; ^{1}Hmr ($CDCl_3$) δ: 2.10 and 2.18 (2s, 6H, OAc), 5.94 (s, 1H, H-1).

*Cyclohexyl 2,6-Diacetamido-4-O-acetyl-2,3,6-trideoxy-1-thio-α-*D*-ribo-hexopyranoside (4b)*

To a solution of 0.26 g (0.68 mmol) of the oxime acetate **3*b*** in 5 mL of anhydrous THF at 0°C under nitrogen was added a 1 *M* solution of borane in THF (7 mL). After the addition of borane, the cooling bath was removed and the reaction mixture was stirred at room temperature for 3 h. The excess borane was decomposed by dropwise addition of methanol (10 mL) at 0°C, the reaction mixture was diluted with methylene chloride, and washed with water. After drying, the solvent was removed *in vacuo* to give 220 mg of a syrup. This product was dissolved in dry pyridine (4 mL), acetic anhydride (2 mL) was added and the solution let stand at 23°C for 3 h. The reaction mixture was diluted with methylene chloride and washed successively with 10% sodium bicarbonate solution and water. After drying, the solvent was removed *in vacuo* to give 280 mg of a syrup. Thin-layer chromatography (5% MeOH in $CHCl_3$) showed two spots of R_f 0.55 (**4*a***) and 0.4 (**4*b***). This material was chromatographed on silica gel using ether as eluent. The azido compound **4*a*** was eluted first; 80 mg, mp 148°C; $[\alpha]_D^{23}$ +151° (*c* 0.6, EtOH); ir (Nujol): 3320, 2090, 1730, 1650 cm^{-1}; ^{1}Hmr ($CDCl_3$) at 100 MHz δ: 1.2–1.8 (m, 11H, cyclohexyl and H-3$_a$), 1.90 (s, 3H, NHAc), 1.98 (s, 3H, OAc), 2.16 (d of t, 1H, H-3$_e$, J_{vic} = 12 Hz, $J_{2,3_e} = J_{3_e,4}$ = 5 Hz), 2.90 (m, 1H, S—C—H), 3.31 (d, 2H, H-6, *J* = 5 Hz), 4.26 (d of t, 1H, H-5, $J_1 = 10$, $J_2 = 5$, $J_3 = 5$ Hz), 4.44 (octet, 1H, H-2, $J_{1,2} = J_{2,3_e} = 5$, $J_{2,3_a} = 13$, $J_{2,NH} = 8$ Hz), 4.77 (d of t, 1H, H-4, $J_{3_a,4} = J_{4,5} = 10$, $J_{3_e,4} = 5$ Hz), 5.39 (d, 1H, H-1, $J_{1,2} = 5$ Hz), 5.64 (d, 1H, NH, *J* = 8 Hz).

The second product was the amide **4*b***, 60 mg, mp 229–230°C (MeOH); $[\alpha]_D^{23}$ +178° (*c* 0.5, EtOH); ir (Nujol) 3320, 3300, 1730, 1640 cm^{-1}; ^{1}Hmr ($CDCl_3$) at 100 MHz, δ: 1.0–2.0 (m, 11H, cyclohexyl and H-3$_a$), 2.0 (s, 6H, NAc), 2.05 (s, 3H, OAc), 2.29 (d of t, 1H, H-3$_e$, J_{vic} = 8, $J_{2,3_e} = J_{3_e,4}$ = 5 Hz), 2.82 (m, 1H, S—C—H), 3.43 (d, 2H, H-6, *J* = 4 Hz), 4.16 (d of t, 1H, H-5, $J_1 = J_2 = 10$, $J_3 = 4$ Hz), 4.35 (octet, 1H, H-2, $J_{1,2} = J_{2,3_e} = 5$, $J_{2,3_a} = 13$, $J_{2,NH} = 8$ Hz), 4.64 (d of t, 1–H, H-4, $J_{3_a,4} = J_{4,5} = 10$, $J_{3_e,4} = 5$ Hz), 5.30 (d, 1H, H-1, $J_{1,2} = 5$ Hz), 5.76 (m, 2H, NH). *Anal.* calcd. for $C_{18}H_{30}N_2O_5S$: C 55.62, H 7.71, N 7.40; found: C 56.00, H 7.83, N 7.25.

The azide **4*a*** (80 mg) and sodium borohydride (80 mg) were dissolved in dry isopropanol (4 mL) and the solution was heated under reflux for 18 h. The reaction mixture was diluted with water and extracted with methylene chloride. The organic extracts, after drying were evaporated to give a syrup (60 mg). This product was acetylated with acetic anhydride in pyridine to give 72 mg (86%) of **4*b***, mp 229–230°C, identical in all respects with the product described above. This material was combined with the one above to give a total of 132 mg of **4*b***, which corresponds to a 50% yield based on the oxime acetate **3*b***.

*Isopropyl 2,6-Dibenzamido-4-O-benzoyl-2,3,6-trideoxy-1-thio-α-*D*-ribo-hexopyranoside (4c)*

A solution of 2.6 g (10 mmol) of **2**, 2 mL (20 mmol) of 2-propanethiol and 3.3 mL of 2,2,6,6-tetramethylpiperidine in 40 mL of dry dimethylformamide was stirred at 23°C for 2 h. The reaction mixture was diluted with ether and washed successively with water, 1 *N* hydrochloric acid, and water and dried. Removal of the solvent by evaporation gave the oxime **3*c*** as a syrup. Thin-layer chromatography (ether) showed a major spot of R_f 0.73 and three minor ones with R_f 0.66, 0.51, and 0.42.

The above product and acetic anhydride (5 mL) were dissolved in pyridine (20 mL) and the solution let stand at 23°C for 16 h. The reaction mixture was diluted with methylene chloride and the solution washed with 10% sodium bicarbonate and water and dried. Removal of the solvent by evaporation gave 3.1 g (91% based on **2**) of the acetylated oxime **3*d***. Thin-layer chromatography (ether–hexane (4:1)) showed a major spot of R_f 0.48 (**3*d***) and a minor of R_f 0.34.

The above oxime acetate **3*d*** (3.1 g) was dissolved in dry THF (40 mL) and the solution, blanketed with nitrogen, was cooled to 0°C. A solution of 1 *M* borane in THF (60 mL) was added and the solution stirred at room temperature, under nitrogen, for 3 h. The excess borane reagent was decomposed with methanol and the reaction mixture was evaporated. The residue and sodium borohydride (1.5 g) were dissolved in dry isopropanol (40 mL) and the solution was heated under reflux for 18 h. After cooling to room temperature, Dowex 1-X8 resin (OH^- form) was added and the mixture stirred at 23°C for 2 h. The mixture was filtered and the filtrate evaporated to dryness. The residue was dissolved in pyridine (20 mL), benzoic anhydride was added, and the mixture stirred at 23°C for 18 h. The reaction mixture was poured into ice water and the solid precipitate collected. Recrystallization from methanol gave 1.7 g (32% based on **2**) of **4*c***, mp 212–217°C; ir (Nujol): 3320, 1730, 1720, 1640 cm^{-1}; ^{1}Hmr ($CDCl_3$) of the *N*-deuterated product, δ: 1.27 (d, 6H, CH_3, *J* = 7 Hz), 1.81 (d of t, 1H, H-3$_a$, J_{vic} = 13 Hz, $J_{2,3_a} = J_{3_a,4}$ = 11 Hz), 2.52 (d of t, 1H, H-3$_e$, J_{vic} = 13, $J_{2,3_e} = J_{3_e,4}$ = 4.5 Hz), 3.08 (m, 1H, S—C—H), 3.44 (d of d, 1H, H-6, J_1 = 14.5, J_2 = 6.5 Hz), 4.05 (d of d, 1H, H-6, J_1 = 14.5, J_2 = 3 Hz), 4.50 (octet, 1H, H-5, $J_1 = 10$, $J_2 = 6.5$, $J_3 = 3$ Hz), 5.09 (d of t, 1H, H-4, $J_{3_a,4} = J_{4,5} = 10.5$, $J_{3_e,4} = 4.5$ Hz), 5.51 (d, 1H, H-1, $J_{1,2} = 5$ Hz), 7.22–8.15 (m, 15H, ArH). *Anal.* calcd. for $C_{30}H_{32}N_2O_5S$: C 67.65, H 6.05, N 5.26; found: C 67.42, H 5.93, N 5.34.

(1S,2S,4R,5R)-2,4-Diethoxycarbonylamino-5-hydroxycyclohexanethiol (5c)

To a stirred solution of 3.05 g (13 mmol) of the hydrochloride salt of **5a** (22) in 30 mL water, under nitrogen atmosphere, was added 7.65 g (91 mmol) of sodium bicarbonate to liberate the free base. After gas evolution ceased, 10 mL methanol was added. To this mixture was added dropwise (10 min) a solution of 4.2 g (39 mmol) of ethyl chloroformate in 6.5 mL dry acetone and the reaction mixture was stirred at room temperature for 1.5 h. The solids which were formed were collected by filtration and dried to give 3.6 g of a mixture of **5c** and its *S*-carbethoxy derivative. This product was added to a 1 *N* solution of sodium hydroxide in 80% ethanol (25 mL) and the mixture stirred at room temperature for 30 min under nitrogen. The solution was diluted with ethanol (25 mL), neutralized with Dowex 50W-X8 cation exchange resin (12 g), and evaporated to give 2.3 g (58%) of **5c**, mp 200–202°C; $[\alpha]_D^{25}$ +16.5° (*c* 1.0, pyridine); ir (Nujol): 3300, 1700, 1550 cm^{-1}. *Anal.* calcd. for $C_{12}H_{22}N_2O_5S$: C 47.04, H 7.24, N 9.14, S 10.46; found: C 47.03, H 7.34, N 9.08, S 10.30.

(1S,2S,4R,5R)-2-Benzamido-4-ethoxycarbonylamino-5-hydroxycyclohexyl 4-O-Acetyl-6-azido-2,3,6-trideoxy-2-hydroxyimino-1-thio-α-D-erythro-hexopyranoside (6a)

A solution of 3.4 g (13 mmol) of freshly prepared **2**, 4.4 g (13 mmol) of **5b** (22) ($[\alpha]_D^{25}$ +33.4°) and 2.25 g (16 mmol) of 2,2,6,6-tetramethylpiperidine in 25 mL of dry dimethylformamide was stirred for 2 h at room temperature under a nitrogen atmosphere. Thin-layer chromatography on alumina plates with 10% ethanol in chloroform as eluent showed one spot of R_f 0.46 (**6a**). The reaction mixture was poured into ice water (200 mL) and the solids were collected by filtration, washed with water, and dried to give 6.0 g (82%) of **6a**. A sample (1.85 g) was recrystallized from ethanol to give 0.8 g of **6a**, mp 198–200°C (dec.); $[\alpha]_D^{25}$ +134° (*c* 0.7, DMF); ir (Nujol): 3450, 3300, 2100, 1750, 1680, 1640, 1540 cm^{-1}; ^{1}Hmr (DMSO-d_6) δ: 1.17 (t, 3H, CH_3, J = 7 Hz), 2.0 (s, 3H, OAc), 4.0 (q, 2H, CH_2 of CO_2Et, J = 7 Hz), 5.85 (s, 1H, H-1), 7.3–8.0 (m, 5H, ArH). *Anal.* calcd. for $C_{24}H_{32}N_6O_8S$: C 51.05, H 5.71, N 14.88, S 5.66; found: C 51.10, H 5.70, N 14.85, S 6.46.

Preparation of the Oxime Acetate (6b)

A solution of 4.36 g (7.7 mmol) of **6a** (mp 198–200°C) and 6.4 mL of acetic anhydride in 24 mL of dry pyridine was stirred at room temperature for 24 h. The mixture was poured into cold water (400 mL) and the solids collected by filtration, washed with water, and dried under vacuum (100°C, 2 h) to give 4.16 g (83%) of **6b**, mp 177–181°C; $[\alpha]_D^{25}$ +96.7° (*c* 1.0, $CHCl_3$); ir (Nujol): 3300, 2100, 1780, 1730, 1680, 1630, 1540 cm^{-1}; ^{1}Hmr ($CDCl_3$) δ: 1.20 and 4.07 (t and q for CO_2Et), 2.0, 2.08 and 2.13 (3s, 9H, Ac), 5.97 (s, 1H, H-1), 7.2–8.0 (m, 5H, ArH). *Anal.* calcd. for $C_{28}H_{36}N_6O_{10}S$: C 51.84, H 5.59, N 12.96, S 4.94; found: C 51.72, H 5.54, N 13.02, S 4.96.

(1S,2S,4R,5R)-2,4-Diethoxycarbonylamino-5-hydroxycyclohexyl 4-O-Acetyl-6-azido-2,3,6-trideoxy-2-hydroxyimino-1-thio-α-D-erythro-hexopyranoside (6c)

A solution of 2.9 g (11 mmol) of freshly prepared **2**, 3.36 g (11 mmol) of **5c**, and 1.55 g (11 mmol) of 2,2,6,6-tetramethylpiperidine in 22 mL dry dimethylformamide was stirred for 2 h at room temperature under nitrogen atmosphere. The solution was diluted with water (150 mL) and stirred for 15 min. The crystalline product which was formed was collected by filtration, washed with water (3 × 30 mL), and dried *in vacuo* at 100°C to give 3.82 g (65%) of **6c**, mp 167–171°C. The combined filtrate and washings were extracted with chloroform (3 × 80 mL). The chloroform extracts were combined, washed with water (5 × 100 mL), dried, and evaporated. The syrupy residue, on trituration with ether (30 mL), solidified. The crystalline product was collected by filtration, washed with ether, and dried to give 0.86 g of **6c**. Both crops showed on tlc (alumina, 10% EtOH–CH_2Cl_2) a single spot of R_f 0.44. The two crops were combined to yield 4.68 g (80%) of **6c**; $[\alpha]_D^{25}$ +132° (*c* 0.9, DMF); ir (Nujol); 3450, 3300, 3200, 2100, 1750, 1695, 1540 cm^{-1}; ^{1}Hmr ($CDCl_3$–DMSO-d_6) δ: 1.27 (t, 6H, CH_3, J = 7 Hz), 2.08 (s, 3H, OAc), 4.13 (q, 4H, CH_2 of CO_2Et), 5.75 (s, 1H, H-1). *Anal.* calcd. for $C_{20}H_{32}N_6O_9S$: C 45.10, H 6.06, N 15.78, S 6.02; found: C 45.05; H 5.81, N 15.95, S 6.37.

(1S,2S,4R,5R)-2,4-Diethoxycarbonylamino-5-acetoxycyclohexyl 2,6-Diacetamido-4-O-acetyl-2,3,6-trideoxy-1-thio-α-D-ribo-hexopyranoside (7b)

A solution of 5.7 g (10.7 mmol) of the oxime **6c** and 8 mL of acetic anhydride in 35 mL dry pyridine was left at room temperature for 24 h. Water (5 mL) was added to decompose the excess of acetic anhydride. The reaction mixture was diluted with chloroform (200 mL) and washed with water (5 × 200 mL). The chloroform solution, after drying, was evaporated to give 6.3 g (95%) of the oxime acetate **6d** as a foam. Examination by tlc (10% ethanol in chloroform) showed a single spot of R_f 0.61; $[\alpha]_D^{25}$ +65.7° (*c* 1.0, $CHCl_3$); ^{1}Hmr ($CDCl_3$) δ: 1.23 and 1.29 (2t, 6H, $CO_2CH_2CH_3$), 2.08, 2.12, and 2.22 (3s, 9H, CH_3CO), 4.13 and 4.20 (2q, 4H, CO_2CH_2-CH_3), 5.9 (s, 1H, H-1).

The oxime acetate **6d** (6.3 g, 10.2 mmol) was dissolved in dry tetrahydrofuran (25 mL) and the solution, blanketed with nitrogen, was cooled to 0°C with stirring. A 1 *M* solution of borane in tetrahydrofuran (100 mL) was added gradually and after the addition was completed, the cooling bath was removed, and the reaction mixture was stirred at room temperature for 3 h. The excess of borane reagent was destroyed by dropwise addition of methanol (80 mL) at 0°C and the solution evaporated *in vacuo*. The residue was dissolved in methanol (50 mL), the solution evaporated, and the process repeated once more. The resultant syrupy product was dissolved in a methanol–water mixture (5:1, 120 mL), 20 g of Rexyn 201 (anion exchange resin, OH^- form) was added and the mixture was stirred at room temperature for 1.5 h to decompose the borane–amine complex. The resin was filtered off and washed with a hot solution of concentrated ammonium hydroxide (2 mL) in ethanol (100 mL). The filtrate and washings were combined and evaporated *in vacuo* to give 3.9 g of product as a foam. Examination of this product by tlc using NH_4OH–EtOH–$CHCl_3$ (1:5:5) as eluent showed two major spots of R_f 0.23 and 0.32 and two minor ones of R_f 0.59 and 0.81. The ir spectrum showed only a comparatively small azide band.

The above product (3.9 g) and acetic anhydride (10 mL) were dissolved in dry pyridine (30 mL) and the solution was stirred at room temperature for 20 h. The reaction mixture was diluted with chloroform (200 mL) and washed with water (3 × 200 mL). The chloroform solution, after drying, was evaporated *in vacuo* to give 3.7 g of product as a foam. Inspection by tlc (silica, 10% EtOH–$CHCl_3$) showed the substance to contain two major components (R_f 0.19 and 0.41) and three other minor components.

The above product (3.70 g) and acetic anhydride (40 mL) were dissolved in methanol (150 mL). To this solution was added platinum oxide catalyst (0.8 g) and the mixture was hydrogenated in a Paar apparatus at room temperature and an

initial pressure of 50 psi for 2 h. The reaction mixture was filtered through a bed of activated charcoal (2.5 cm × 4.5 cm id) and the cake was washed with ethanol (4 × 25 mL). The combined filtrate and washings were evaporated *in vacuo* to give 3.2 g of solid material. This product was mixed with ethyl acetate (30 mL) and the mixture was refluxed with stirring for 20 min then cooled to room temperature and the crystalline precipitate collected to give 1.98 g (30% based on the oxime **6***c*) of **7***b*. Thin-layer chromatography (10% EtOH–$CHCl_3$) showed one major spot of R_f 0.20 (**7***b*) and traces of another component with R_f 0.40. The analytical sample was prepared by recrystallization from ethanol – ethyl acetate, mp 266–267°C; $[\alpha]_D^{25}$ +106° (*c* 1.0, DMF); ir (Nujol): 3310, 1740, 1690, 1650, 1550 cm^{-1}; ^{1}Hmr (DMSO-d_6) δ: 1.15 and 1.20 (2t, 6H, CH_3 of CO_2Et), 1.80, 1.83, 1.97, and 2.0 (4s, 12H, Ac), 3.93 and 4.03 (2q, 4H, CH_2 of CO_2Et), 5.43 (d, 1H, H-1, $J_{1,2}$ = 5 Hz). *Anal.* calcd. for $C_{26}H_{42}N_4O_{11}S$: C 50.47, H 6.84, N 9.06, S 5.18; found: C 50.26, H 6.77, N 9.13, S 5.32.

*(1S,2S,4R,5R)-2,4-Diamino-5-hydroxycyclohexyl 2,6-Diamino-2,3,6-trideoxy-1-thio-*α*-*D*-ribo-hexopyranoside (7c)*

To a 2.4 *N* solution of sodium hydroxide in ethanol (10 mL) was added 0.5 g (0.8 mmol) of **7***b* and the mixture was heated under reflux under nitrogen with stirring for 19 h. Examination by tlc (silica, MeOH – concentrated NH_4OH – $CHCl_3$, 4:2:1) showed several spots indicating incomplete hydrolysis. The solvent was removed by evaporation, replaced with water (10 mL), and the solution was heated under reflux under nitrogen for 25 h. The reaction mixture was neutralized with an equivalent amount of hydrochloric acid (1 *N*, 24 mL) and filtered to remove some insoluble matter. The filtrate was evaporated *in vacuo* and the solid residue extracted twice with boiling ethanol (25 and 10 mL). The combined ethanol extracts were evaporated to give 0.5 g of a solid product. Thin-layer chromatography showed two spots of R_f 0.39 (**7***c*) and 0.65. This material was chromatographed on Rexyn 102 (NH_4^+, 13 g) and resin eluted successively with water (100 mL), 0.1 *N* ammonium hydroxide (400 mL), and 1 *N* ammonium hydroxide (400 mL). Fractions of 15 mL were collected in tubes. The fractions containing **7***c* (tubes 19–48) were combined and evaporated to give 150 mg of **7***c*. This product was further purified by chromatography on silica gel plates using MeOH – concentrated NH_4OH – $CHCl_3$ (4:2:1) as eluent to give **7***c* as an amorphous solid; ^{1}Hmr (D_2O) δ: 5.35 (d, 1H, anomeric, *J* = 5 Hz). *Anal.* calcd. for $C_{12}H_{26}N_4O_3S \cdot \frac{1}{2}H_2O$: C 47.04, H 8.55, N 18.28, S 10.46; found: C 45.90, H 8.52, N 17.18, S 9.80.

Desulfurization of 7b

To a solution of 100 mg of **7***b* in 10 mL ethanol was added Raney nickel catalyst (~0.5 g) and the mixture heated under reflux with stirring for 1.5 h. The reaction mixture was filtered and the catalyst was washed with boiling ethanol. The combined filtrate and washings were evaporated to give 90 mg of a solid product. Thin-layer chromatography (10% ethanol in chloroform) showed two major spots of R_f 0.57 (**8**) and 0.21, and three minor of R_f 0.35, 0.32, and 0.28. The product was chromatographed on silica gel plates (10% ethanol–chloroform as eluent) to give 30 mg of **8**, mp 110–112°C, resolidified and melted at 150–151°C; ^{1}Hmr ($CDCl_3$) δ: 1.27 and 4.13 (t and q for CO_2Et), 2.08 (s, 3H, OAc). *Anal.* calcd. for $C_{14}H_{24}N_2O_6$: C 53.15, H 7.65, N 8.85; found: C 53.26, H 7.63, N 8.79.

Acknowledgment

One of us (Y.P.) is very grateful to the National Research Council of Canada for a Senior Industrial Fellowship.

1. G. KAVADIAS, P. DEXTRAZE, R. MASSÉ, and B. BELLEAU. Can. J. Chem. **56**, 2086 (1978).
2. (*a*) D. HORTON and D. H. HUTSON. Adv. Carbohydr. Chem. **18**, 123 (1963); (*b*) W. PIGMAN and D. HORTON. The carbohydrates chemistry and biochemistry. 2nd ed. Vol. 1A. Academic Press, New York, NY and London. 1972.
3. (*a*) L. HOUGH and M. I. TAHA. J. Chem. Soc. 2042 (1956); (*b*) J. FRIED and D. E. WALZ. J. Am. Chem. Soc. **71**, 140 (1949); (*c*) E. ZISSIS, A. L. GLINGMAN, and N. K. RICHTMYER. Carbohydr. Res. **2**, 461 (1966); (*d*) J. SCHNEIDER, H. H. LIU, and Y. C. LEA. Carbohydr. Res. **39**, 156 (1975).
4. B. HELFERICH and E. SCHMITZ-HILLEBRECHT. Ber. Dtsch. Chem. Ges. **66**, 378 (1933).
5. (*a*) C. D. HURD and W. A. BONNER. J. Org. Chem. **11**, 50 (1946); (*b*) M. L. CHAMLA and O. P. BAHL. Carbohydr. Res. **32**, 25 (1974); (*c*) J. SCHNEIDER and Y. C. LEE. Carbohydr. Res. **30**, 405 (1973).
6. (*a*) E. M. MONTGOMERY, N. K. RICHTMYER, and C. S. HUDSON. J. Org. Chem. **11**, 301 (1946); (*b*) B. HELFERICH, H. GRUNEWALD, and F. LANGENHOFF. Ber. **86**, 873 (1953); (*c*) M. BLANC-MUESSER, J. DEFAYE, and H. DRIGUEZ. Tetrahedron Lett. 4307 (1976).
7. (*a*) W. SNEIDER, R. GILLE, and K. EISFELD. Ber. **61**, 1244 (1928); (*b*) M. CERNY and J. PACAK. Chem. Listy, **52**, 2090 (1958); Collect. Czech. Chem. Commun. **24**, 2566 (1959).
8. R. U. LEMIEUX, T. L. NAGABHUSHAN, and I. K. O'NEILL. Tetrahedron Lett. 1909 (1964).
9. R. U. LEMIEUX and T. L. NAGABHUSHAN. Tetrahedron Lett. 2143 (1965).
10. R. U. LEMIEUX and S. W. GUNNER. Can. J. Chem. **46**, 397 (1968).
11. R. U. LEMIEUX, T. L. NAGABHUSHAN, and S. W. GUNNER. Can. J. Chem. **46**, 405 (1968); T. L. NAGABHUSHAN. Can. J. Chem. **48**, 257 (1970).
12. R. U. LEMIEUX, T. L. NAGABHUSHAN, and K. JAMES. Can. J. Chem. **51**, 1 (1973).
13. R. U. LEMIEUX, T. ITO, K. JAMES, and T. L. NAGABHUSHAN. Can. J. Chem. **51**, 7 (1973).
14. R. U. LEMIEUX, R. A. EARL, K. JAMES, and T. L. NAGABHUSHAN. Can. J. Chem. **51**, 19 (1973).
15. R. U. LEMIEUX, K. JAMES, and T. L. NAGABHUSHAN. Can. J. Chem. **51**, 27 (1973).
16. R. U. LEMIEUX, K. JAMES, T. L. NAGABHUSHAN, and Y. ITO. Can. J. Chem. **51**, 33 (1973).
17. R. U. LEMIEUX, K. JAMES, and T. L. NAGABHUSHAN. Can. J. Chem. **51**, 42 (1973).
18. R. U. LEMIEUX, K. JAMES, and T. L. NAGABHUSHAN. Can. J. Chem. **51**, 48 (1973).
19. R. U. LEMIEUX, T. L. NAGABHUSHAN, K. J. CLEMETSON, and L. C. N. TUCKER. Can. J. Chem. **51**, 53 (1973).
20. M. KUGELMAN, A. K. MALLAMS, and H. F. VERNAY. J. Chem. Soc. Perkin I, 1126 (1976).
21. L. F. FIESER and M. FIESER. Reagents for organic synthesis. Vol. I. John Wiley and Sons Inc., New York, NY. 1967. p. 1052.
22. G. KAVADIAS and R. DROGHINI. Can. J. Chem. **56**, 2743 (1978).

Intramolecular alkylation of α,β-unsaturated ketones: a study of the effect of substrate structure and experimental conditions on the site of alkylation

EDWARD PIERS[1] AND MICHAEL ZBOZNY

Department of Chemistry, University of British Columbia, 2075 Wesbrook Mall, Vancouver, B.C., Canada V6T 1W5

AND

DONALD C. WIGFIELD

Department of Chemistry, Carleton University, Ottawa, Ont., Canada K1S 5B6

Received November 30, 1979

EDWARD PIERS, MICHAEL ZBOZNY, and DONALD C. WIGFIELD. Can. J. Chem. **57**, 1064 (1979).

The syntheses of 4a-(3-chloropropyl)- (**22**), 4a-(3-iodopropyl)- (**23**), and 4a-mesyloxymethyl-4,4a,5,6,7,8-hexahydro-2(3*H*)-naphthalenone (**24**) are described. The results obtained from the intramolecular alkylation of each of these compounds under a variety of experimental conditions are summarized in Tables 1 and 2. It was found that alkylative cyclization of compounds **22** and **23** gave varying amounts of two products, one (**34**) resulting from α′ alkylation and the other (**35**) being derived from α alkylation. In contrast, intramolecular alkylation of the enone **24** produced only the γ alkylation product **11**, or afforded a mixture of **11** and the α alkylation product **41**. The intramolecular alkylation results are discussed in terms of Scheme 5.

EDWARD PIERS, MICHAEL ZBOZNY et DONALD C. WIGFIELD. Can. J. Chem. **57**, 1064 (1979).

On décrit les synthèses des (chloro-3 propyl)-4a (**22**), (iodo-3 propyl)-4a (**23**) et mésyloxyméthyl-4a hexahydro-4,4a,5,6,7,8 (3*H*)-naphtalénones-2 (**24**). Les résultats obtenus lors de l'alkylation intramoléculaire de chacun de ces composés dans diverses conditions expérimentales sont résumés dans les Tableaux 1 et 2. On a trouvé que la cyclisation alkylante des composés **22** et **23** conduit à des quantités variables de deux produits, l'un, **34**, provenant d'une alkylation en α′ et l'autre, **35**, dû à une alkylation en α. Par ailleurs, l'alkylation intramoléculaire de l'énone **24** ne fournit que le produit **11**, correspondant à une alkylation en γ, ou à un mélange de **11** et du produit d'alkylation α, **41**. On discute des résultats d'alkylations intramoléculaires en termes du Schéma 5.

[Traduit par le journal]

Introduction

The intermolecular alkylation of α,β-unsaturated ketones has been, and continues to be, a very important reaction in the area of synthetic organic chemistry. It appears to be quite well established that, in general, treatment of an enone (e.g., **1**, see Scheme 1) with a strong, nonnucleophilic base (e.g., lithium diisopropylamide) under aprotic conditions, results in the kinetically controlled formation of the α′ enolate anion **2**. If alkylation of the latter is fast compared with enolate anion equilibration, it is possible to obtain the α′ alkylation product **3** in good yield.[2] On the other hand, if a compound such as **1** is treated with a base under conditions (e.g., in the presence of a protic solvent) which promote enolate anion equilibration (thermodynamic control), the more stable (compared with **2**) dienolate anion **4** is obtained. Alkylation of **4** occurs preferentially at the α carbon, affording **5** as the primary alkylation product.[3]

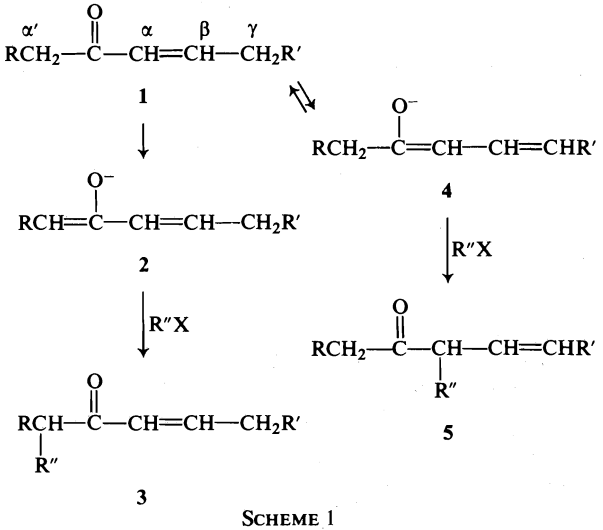

SCHEME 1

In contrast to the number of reported studies concerning the intermolecular alkylation of α,β-unsaturated ketones, the intramolecular variant of this type of reaction has received relatively little attention. Nevertheless, on the basis of the few examples which

[1]Author to whom correspondence should be addressed.

[2]For some examples, see ref. 1.

[3]For a general discussion regarding this type of reaction, see ref. 2.

0008-4042/79/091064-11$01.00/0

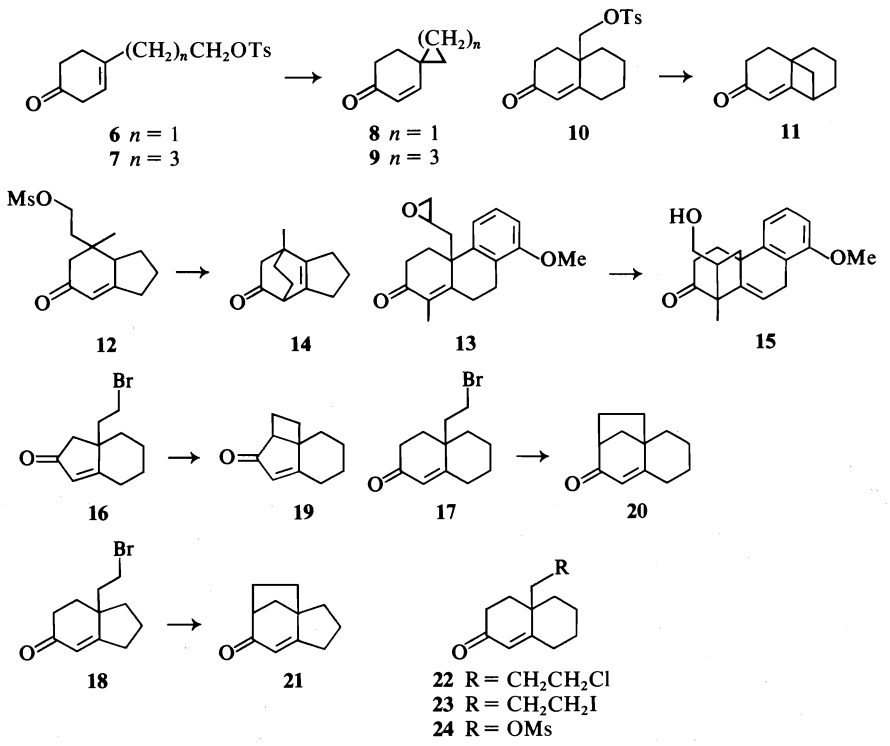

SCHEME 2

can be found scattered throughout the chemical literature, it is clear that every possible mode of cyclization has been observed. For example, treatment of the keto tosylates **6** and **7** (see Scheme 2) with sodium hydride in refluxing dioxan containing a small amount of *tert*-butyl alcohol gave, in fairly low yields, the γ alkylation products **8**[4] and **9**, respectively (3). In similar fashion, the substituted octalone **10**, upon treatment with potassium *tert*-butoxide in hot *tert*-butyl alcohol, gave the enone **11** as the only intramolecular alkylation product (5).[5] On the other hand, intramolecular alkylation of the substrates **12** (sodium hydride in hot dimethoxyethane containing a small amount of ethanol) (7) and **13** (potassium *tert*-butoxide in hot benzene) (8) afforded as the major products the α alkylated materials **14** and **15**, respectively. Finally, in what has been to date the most extensive single study of the intramolecular alkylation of enones, Cargill and Jackson (9) showed that treatment of the bromo ketones **16–18** with potassium *tert*-butoxide in *tert*-butyl alcohol resulted in the exclusive (or nearly exclusive) formation of the α′ alkylation products **19–21**, respectively.

[4]For other examples of γ alkylation involving the closure of three-membered rings, see ref. 4.

[5]For similar γ alkylations of 19-mesyloxy-(or tosyloxy-)-Δ[4]-3-keto steroids, see ref. 6.

The examples cited above indicate that substrate structure has a marked effect on the site of intramolecular alkylation of α,β-unsaturated ketones. However, we were intrigued by the following question: is it possible to control the site of alkylation within a given substrate by varying reaction conditions and/or by varying the nature of the leaving group? Clearly, an affirmative answer to this question would have potentially useful repercussions in synthesis (particularly in the area of natural product synthesis), since alkylation at different positions would give rise to products with distinctly different carbon skeletons. To our knowledge, no study aimed at obtaining an answer to the above question has as yet been reported. In this paper, we describe the preparation and intramolecular alkylation of the substituted octalones **22–24**. The results obtained clearly show that, with these substrates at least, it is indeed possible to (partially) control the site of intramolecular alkylation by varying experimental conditions.

Preparation of 4a-(3-Chloropropyl)- (22), 4a-(3-Iodopropyl)- (23), and 4a-Mesyloxymethyl-4,4a,5,6,7,8-hexahydro-2(3*H*)-naphthalenone (24)

The two substituted octalones **22** and **23** were prepared from 2-allylcyclohexanone (**25**) (10) via a

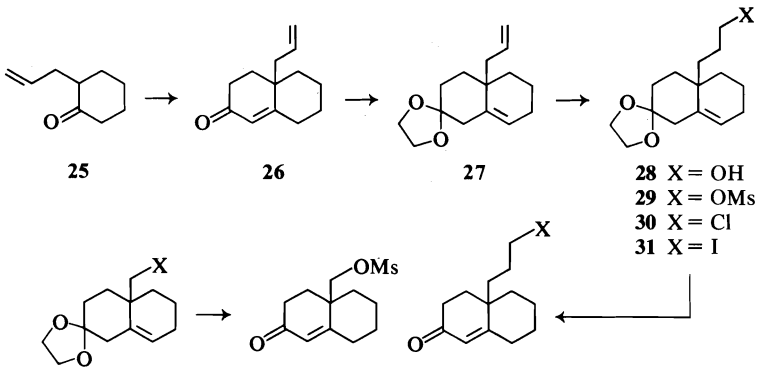

SCHEME 3

straightforward sequence of reactions as outlined in Scheme 3. Robinson annelation of **25** with methyl vinyl ketone by means of a procedure very similar to that reported by Marshall and Fanta (11) gave the octalone **26** which, upon subjection to standard ketalization conditions (ethylene glycol, *p*-toluenesulfonic acid, benzene), afforded the ketal diene **27**. Site-selective hydroboration of the latter with disiamylborane (12), followed by oxidation of the resultant trialkylborane intermediate with alkaline hydrogen peroxide, gave the olefinic alcohol **28**, which was converted (methanesulfonyl chloride, triethylamine, dichloromethane) into the corresponding mesylate **29**. Treatment of **29** with lithium chloride in refluxing acetone followed by hydrolysis (sulfuric acid in aqueous acetone) of the resultant ketal chloride **30** afforded the substituted octalone **22**. In similar fashion, the ketal mesylate **29** was also converted into the iodo compound **23**.

The known ketal alcohol **32** (13) served as a convenient starting material for the mesyloxymethyl octalone **24**. Thus, treatment of the former compound with methanesulfonyl chloride – triethylamine in dichloromethane gave the crystalline ketal mesylate **33** which, upon hydrolysis with sulfuric acid in aqueous acetone, afforded the desired octalone **24**.

Characterization of Intramolecular Alkylation Products

Before discussing the results obtained from the intramolecular alkylation of the octalones **22**–**24**, it is appropriate to make a few remarks regarding the characterization of the products of these reactions. Theoretically, three possible products could have been obtained from the alkylative cyclization of the octalones **22** and **23**: the enone **34** (derived from α′ alkylation), the β,γ-unsaturated ketone **35** (α alkylation), and the enone **36** (γ alkylation) (see Scheme 4). In fact, subjection of **22** and **23** to intramolecular alkylation under a variety of experimental conditions (*vide infra*) afforded only two different products. On the basis of spectral data obtained from pure samples of these products, it was clear that one of them was the β,γ-unsaturated ketone **35**, the product of α alkylation. However, although **35** could be distinguished readily from the other possible products **34** and **36**, a similar distinction between the latter two compounds (both α,β-unsaturated ketones) was not at all straightforward, since one would expect the spectral data obtained from these two substances to be very similar. This problem of determining the identity of the second alkylation product was solved by means of chemical transformations.

Subjection of the α alkylation product **35** to a modified Wolff–Kishner reduction procedure (14) gave the tricyclic olefin **37**. Allylic oxidation of the latter with chromium trioxide – dipyridine complex in dichloromethane (15) afforded the α,β-unsaturated ketone **36**, the compound which would have been derived from γ alkylation of the octalones **22** and **23**. Spectral data clearly showed that the oxidation product **36** was different from the α,β-unsatu-

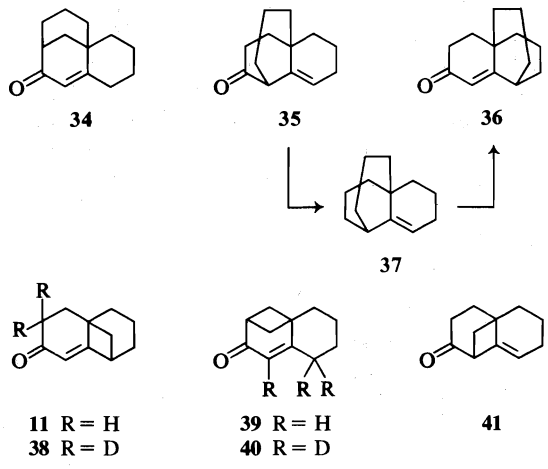

SCHEME 4

rated ketone **34** which was obtained from the alkylation reactions.

When the mesyloxymethyl octalone **24** was subjected to intramolecular alkylation under a variety of experimental conditions (*vide infra*), the sole product obtained in most cases was the α,β-unsaturated ketone **11** (γ alkylation). This compound had been obtained and characterized previously by Mukharji and Ganguly (5). To further confirm the structural assignment, compound **11** was subjected to base-catalyzed deuteration. Mass spectral analysis of the product **38** showed that two deuterium atoms had been incorporated into the molecule. It is clear that if the original alkylation product had been that derived from α′ alkylation (the α,β-unsaturated ketone **39**), the deuteration experiment would have produced the trideuterio derivative **40**.

Intramolecular alkylation of **24** with potassium *tert*-butoxide in hexamethylphosphoramide (*vide infra*) gave a major product different from **11**. Spectral analysis of this material showed clearly that it was the β,γ-unsaturated ketone **41**, the product of α alkylation.

Intramolecular Alkylation Studies. Results and Discussion

The two halo enones **22** and **23** were subjected to intramolecular alkylation under a variety of experimental conditions and the results are summarized in Table 1. In similar fashion, the results obtained from alkylative cyclization of the mesyloxy enone **24** are tabulated in Table 2.

From the data summarized in Tables 1 and 2, it is clear that there was considerable variation in the relative amounts of α′, α, and γ alkylation, this variation depending on the nature of the substrate and on the experimental conditions used. On the one hand, it is of interest to try to understand the product ratio variation for each individual substrate as a function of reaction conditions. Even more intriguing, however, is the extraordinary contrast between the internal alkylations of compounds **22** and **23** as compared with those of the enone **24**. The former substrates yielded varying amounts of α and α′ alkylation but no γ alkylation, whereas the latter substance gave only α and γ alkylation products (no α′ alkylation).

The framework in which one must endeavor to understand these intramolecular alkylations is given in Scheme 5. The main features of this scheme may be summarized as follows. Deprotonation of the ketone **42** can, in principle, give rise either to the α′ enolate anion **43** or to the resonance delocalized dienolate anion **44**. It has been well established that kinetically controlled deprotonation takes place on the α′ position to give an anion of the type **43** (1) but that the thermodynamically more stable anion is that

TABLE 1. Intramolecular alkylation of 4a-(3-chloropropyl)- (**22**) and 4a-(3-iodopropyl)-4,4a,5,6,7,8-hexahydro-2(3*H*)-naphthalenone (**23**)

Entry	Substrate	Base	Solvent	Added reagent	Reaction conditions	Product yield[a]		Product ratio[b]
						glc	Isolated	**34:35**
1	**22**	Me_3COK	Me_3COH	—	rt,[c] 4 h	80	78	12:88
2	**22**	Me_3COK	Me_3COH	18-Crown-6	rt, 15 min	72	71	5:95
3	**22**	Me_3COK	THF[d]	—	rt, 4 h	74	70	85:15
4	**22**	Me_3COK	THF	18-Crown-6	rt, 15 min	52	51	65:35
5	**22**	Me_3COK	HMPA[e]	—	rt, 15 min	65	64	19:81
6	**22**	Me_3COLi	Me_3COH	—	reflux, 6 h	81	77	39:57[f]
7	**22**	LDA–HMPA[g]	THF	—	rt, 3 h	56	55	>99:<1
8	**22**	Me_3COK	Me_3COH–THF (40:60)	18-Crown-6	−78°C, 30 min; rt, 15 min	62	61	<1:>95[h]
9	**23**	Me_3COK	Me_3COH	—	rt, 15 min	100	94	>99:<1
10	**23**	Me_3COK	Me_3COH	18-Crown-6	rt, 15 min	91.5	90	78:22
11	**23**	Me_3COK	Me_3COH–THF (40:60)	—	−78°C, 30 min; rt, 15 min	67	65	74:20[i]

[a]Gas–liquid chromatographic and isolated yields were determined as described in the Experimental. Appropriate, separate control experiments showed that the products **34** and **35** were stable under the various reaction conditions employed.
[b]Product ratios were determined by glc analysis. All experiments were done in duplicate and the numbers given are average values. The ratios obtained from individual experiments did not vary by more than ±2%.
[c]rt = room temperature.
[d]THF = tetrahydrofuran.
[e]HMPA = hexamethylphosphoramide.
[f]The product mixture contained 4% of a compound of unknown structure.
[g]LDA–HMPA = lithium diisopropylamide complexed with hexamethylphosphoramide.
[h]The product mixture contained ~5% of a compound of unknown structure.
[i]The product mixture contained ~6% of a compound of unknown structure.

TABLE 2. Intramolecular alkylation of 4a-mesyloxymethyl-4,4a,5,6,7,8-hexahydro-2(3*H*)-naphthalenone (**24**)

Entry	Base	Solvent	Added reagent	Reaction conditions	Product yield[a] glc	Product yield[a] Isolated	Product ratio[b] **11**:**41**
1	Me_3COK	Me_3COH	—	rt,[c] 20 h	77	74	>99:<1
2	Me_3COK	Me_3COH	18-Crown-6	rt, 45 min	73	71	>99:<1
3	Me_3COK	THF[d]	—	rt, 20 h	63	60.5	>99:<1
4	Me_3COLi	Me_3COH	—	reflux, 20 h	79	74	>99:<1
5	LDA–HMPA[e]	THF	—	reflux, 48 h	96	92	>99:<1
6	Me_3COK	HMPA[f]	—	rt, 1 h	74	73	20:80
7	Me_3COK	HMPA	18-Crown-6	rt, 30 min	78	75	8:92

[a]Gas–liquid chromatographic and isolated yields were determined as described in the Experimental. Appropriate, separate control experiments showed that the products **11** and **41** were stable under the various reaction conditions employed.
[b]Product ratios were determined by glc analysis. All experiments were done in duplicate and the numbers given are average values. The ratios obtained from individual experiments did not vary by more than ±2%.
[c]rt = room temperature.
[d]THF = tetrahydrofuran.
[e]LDA–HMPA = lithium diisopropylamide complexed with hexamethylphosphoramide.
[f]HMPA = hexamethylphosphoramide.

of the type **44**, reached by subsequent proton transfer equilibration. Anion **43** would subsequently alkylate to give the α′ products (**34** or **39**) and anion **44** would alkylate to afford either or both of the α (**35**, **41**) and γ (**36**, **11**) alkylation products. It is clear, then, that the competition between rates of anion equilibration and of alkylation may represent a key point in understanding these reactions. Consideration of the various individual results follow.

(a) Internal Alkylation of Compound 22

(i) Use of LDA–HMPA in THF (Table 1, Entry 7)

Under conditions where equilibration of the anion **43** does not occur, it is clear that the only possible internal alkylation product is the α′ product **34**. The title conditions are known to meet this criterion (1) and, indeed, the experimental results confirm exclusive formation of compound **34**.

(ii) Use of Me_3COK in Me_3COH (Table 1, Entry 1)

At the other end of the reaction condition spectrum, the conditions involving potassium *tert*-butoxide in the protic solvent *tert*-butyl alcohol are known to effect equilibration between ions of the type

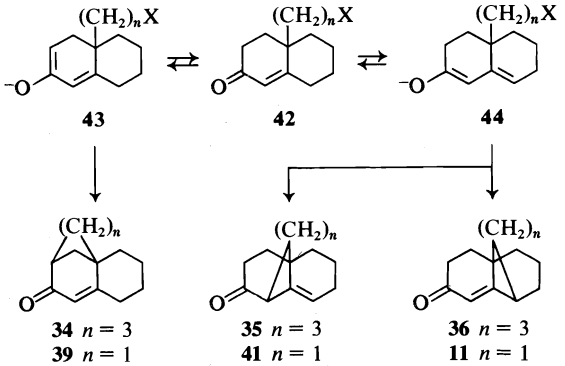

SCHEME 5

43 and **44** (2). Equilibration of this sort does not, however, necessarily allow for an *a priori* prediction of which product (α′ or α,γ) would predominate. Even though ion **44** predominates, it would still be possible for α′ alkylation to be significant, or even predominate, if α′ alkylation happened to be a substantially lower energy barrier process (Curtin–Hammett principle (16)). As it happens, the experimentally obtained result was an 88:12 ratio in favor of α alkylation; two explanations are possible for the significant amount of α′ alkylation. On the one hand, anion equilibration might be complete and this product ratio might simply represent the alkylation of the equilibrium mixture as indicated above (Curtin–Hammett). On the other hand, the significant amount of α′ alkylation product might be derived from significant remaining amounts of α′ anion **43**, owing to incomplete anion equilibration. Although this one result obviously does not allow distinction between these possibilities, consideration of subsequent results favours the second explanation and the following results will be discussed in terms of the rate competition between anion equilibration and anion alkylation.

(iii) Use of Me_3COK in THF (Table 1, Entry 3)

The use of tetrahydrofuran as solvent (entry 3) in place of *tert*-butyl alcohol (entry 1) essentially reversed the α to α′ product ratio, giving an 85:15 ratio in favor of α′ alkylation. This result is clearly consistent with slower anion equilibration in the aprotic solvent and thus an increased alkylation to equilibration rate ratio of the initially formed anion (**43**).

(iv) Effect of Cation and of Cation-complexing Solvents and Reagents (Table 1, Entries 2, 4, 5, 6, 8)

Use of these reagents had a substantial and expected effect on the rate of reaction, as represented crudely by the time required for completion of the

alkylation (Tables 1 and 2). Use of cation complexing reagents either as additive (18-crown-6) or solvent (hexamethylphosphoramide) increased the activity of the anion and decreased the required reaction time to 15 min or less. In contrast, decreasing the activity of the anion by the greater coordination of Li^+ led to the necessity of a 6-h reflux to complete the alkylation reaction. Inspection of the results shows that the α to α′ product ratio is correlated with this experimentally variable anion activity. Proceeding from entry 1 to entry 2, it is seen that the effect of 18-crown-6 was to increase the α to α′ product ratio from a value of 88:12 to 95:5. Similarly, in aprotic solvents the relative amount of α alkylation product **35** increased from 15% (tetrahydrofuran, entry 3) to 35% (addition of 18-crown-6, entry 4) and up to 81% when hexamethylphosphoramide was used as total solvent (entry 5). In contrast, proceeding from entry 1 to entry 6, it is seen that the retarding effect of the lithium cation reduced the α to α′ product ratio from 88:12 to 57:39.

These results are characterized by greater anion activity being associated with an increased α to α′ product ratio and diminished anion activity being associated with a decreased α to α′ product ratio. The simplest rationalization of these results appears to be in terms of competition between the rate of equilibration of the anion **43** to anion **44** with the rate of alkylation. This is a classic case of competition between the anion acting as a base or as a nucleophile, respectively, and the results are consistent with the idea that increased anion activity accelerated both equilibration and alkylation, but that the rate of equilibration was affected to a greater extent than that of alkylation. Thus, for example, in circumstances where the anion activity was increased, this caused increased equilibration relative to alkylation and resulted in an increased α to α′ product ratio.

It should be emphasized that the above generalizations, although they appear to be the most reasonable rationalization of the experimental results, are based only on product ratios and approximate times for completion of reaction and should not be confused with a proven explanation. They do, however, at least provide a useful framework within which product ratios may be predicted and experimentally manipulated. Consideration of these generalizations, for example, leads to the use of the combination of experimental conditions and low temperature for increased selectivity, in order to achieve an alkylation in which α′ alkylation is entirely suppressed (Table 1, entry 8).

(b) Internal Alkylation of Compound ***23****. Effect of Leaving Group*

Continuing the consideration of these internal alkylations in terms of the rate competition between anion equilibration and alkylation, it is clear that the nature of the leaving group would have a more clear-cut and predictable effect. Although the variation of conditions mentioned above affected the rates of both equilibration *and* alkylation, the nature of the leaving group would, to a first approximation, affect only the rate of alkylation. The prediction of the effect of increasing the leaving group ability of X (cf. **42**) by the use of iodine in the place of chlorine (17), is that the rate of alkylation would be increased relative to that of equilibration, thus giving rise to increased α′ alkylation. The experimental results indicate a dramatic shift in this direction. Comparison of entry 9 with entry 1 (Table 1) shows that under identical experimental conditions, compound **23** (chloride as leaving group) gave 88% α alkylation while enone **23** (iodide as leaving group) produced only the α′ alkylation product. To explore the degree to which the latter result could be manipulated, conditions which caused increased α alkylation in the case of compound **22** were applied to **23** (entries 10, 11). Some α alkylation product was indeed obtained under these conditions but a maximum of only 22%.

(c) The Absence of γ Alkylation

Although the dienolate anion **44** could, in principle, alkylate both at the α and at the γ position,[6] no detectable amounts of γ alkylation product were formed in the internal alkylation of compounds **22** and **23**. One of us has previously found it useful to consider the *C*- vs. *O*-alkylation of ambident anions in terms of the nature of the transition state (18) and the same type of consideration seems appropriate also in this regioselectivity question. If the transition state of the alkylation process were essentially reactantlike, a dominating factor in determining the α to γ product ratio would be the electron density at these positions in the anion **44** and thus one would expect predominant formation of the α alkylation product **35**. If, on the other hand, the transition state were productlike, factors affecting product stability would also be felt in the transition state, and thus, for purely kinetic reasons, one would obtain the more stable product, in this case the conjugated ketone arising from γ alkylation (compound **36**).

In this framework, the experimental observation of exclusive α alkylation is unremarkable. The product-determining reaction involves the conversion of a reactive intermediate **44** into a stable product (**35** and/or **36**). Application of Hammond-postulate (19) reasoning to this situation leads to the expectation

[6]It is also conceivable that both anions **43** and **44** could undergo *O*-alkylation. However, these processes would result in the formation of compounds having a double bond at a bridgehead.

of a reactantlike transition state and, therefore, α alkylation.

(d) Internal Alkylation of Compound **24**

(i) Use of Me_3COK in Me_3COH (Table 2, Entry 1)

Intramolecular alkylation of the mesyloxy enone **24** under these conditions gave exclusively the γ alkylation product **11**. This result is in sharp contrast to the alkylative cyclization of compounds **22** and **23** under the same conditions (Table 1, entries 1, 9). In the case of compound **24**, not only was α′ alkylation completely suppressed but the product derived from the dienolate anion **44** ($n = 1$) was exclusively the γ alkylation product **11**, whereas with **44** ($n = 3$, derived from **22**) only α alkylation occurred.

(ii) Other Conditions

Use of other reaction conditions (Table 2, entries 2, 3, 4, 5), which had caused variation of the alkylation product ratio in the case of compound **22** caused no variation when applied to compound **24**. In each case the only detectable alkylation product was that of γ alkylation, compound **11**. Most noteworthy is the reaction employing lithium diisopropylamide as base, conditions which gave 100% α′ alkylation of compound **22** (Table 1, entry 7). These conditions gave no reaction with compound **24** at room temperature, and when forced, using a 2-day reflux, again gave exclusively γ alkylation (Table 2, entry 5).

(iii) Absence of α′ Alkylation

The absence of α′ alkylation in the case of compound **24**, a striking difference in comparison with the behaviour of the enones **22** and **23**, requires comment. The fact that using lithium diisopropylamide as base, conditions which normally give rapid and exclusive α′ alkylation, gave no reaction except under forcing conditions, clearly indicates a substantial barrier to internal α′ alkylation in the case of compound **24**. Molecular models indicate the probable origin of this barrier to be steric interaction between the leaving mesylate group and the axial hydrogen at C-6. (cf. **45**). The recent formulation of the Baldwin

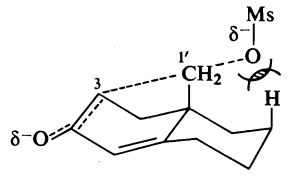

45

rules (20) have highlighted the critical importance of maintaining the appropriate geometry in displacement reactions. In the case of α′ alkylation of compound **24** this is the angle C-3—C-1′—OMs, which must be 180° (cf. **45**). Since both C-3 and C-1′ are more or less fixed in space, the direction of leaving of the mesylate group is rigidly controlled and heads directly to within the van der Waals radius of the axial hydrogen at C-6. Postulation of this steric repulsion to leaving is clearly a rationalization similar to the suggestion of Brown and co-workers to the leaving of 2-*endo* substituents from norbornyl derivatives (21). It is noteworthy that although the angles of departure of the mesylate group in α and γ alkylation of compound **24** are also fixed, the line of departure does not encounter such steric interference. In addition, the flexibility of the three-carbon side chain in compounds **22** and **23** renders the steric hindrance factor irrelevant for these substances. Thus, the resistance to α′ alkylation is peculiar to compound **24**.

(iv) Predominant γ Alkylation

In the alkylative cyclization of compounds **22** and **23**, the competition between α and γ alkylation was totally in favor of the α pathway. We rationalized this observation in terms of a reactantlike transition state, based on a Hammond postulate analysis (see (c), above). Clearly in order to account for the fact that internal alkylation of **24** under conditions summarized in Table 2, entries 1–5, gave only γ alkylation product, this rationalization must be modified. For a reactantlike transition state, the ideal conditions are the reaction of a reactive intermediate, via a small barrier, to a stable product. Although these conditions are met in the internal alkylation of compounds **22** and **23**, there are two modifying factors which must be considered in the alkylation of compound **24**. Firstly, because of the formation of the strained four-membered ring, the energy barrier to reaction is increased and, secondly, for the same reason, the stability of the product is reduced. Thus, the reaction has a higher activation energy and is less exothermic, and the Hammond postulate prediction is that of a transition state that is less reactantlike. Evidently the transition state shift in going from compounds **22** and **23** to compound **24** was sufficiently large so that the product stability factor in the transition state predominated over the electron density factor.

(v) Formation of the α Alkylation Product

If the above transition state argument has any validity, then the way in which it might be possible to induce α alkylation of the mesyloxy enone **24** would be to use conditions in which the transition state would be more reactantlike. Two factors are significant here: the energy barrier to reaction and the exothermicity of the process. The former can be reduced and the latter increased simultaneously by using conditions which would generate a more reactive anion. This approach proved to be successful. When **24** was treated with potassium *tert*-butoxide

in hexamethylphosphoramide (Table 2, entry 6), the predominant process became that of α alkylation (ratio of **41**:**11** = 80:20). Addition of 18-crown-6 to render the anion even more 'free' further increased this ratio to 92:8 (Table 2, entry 7).

Conclusions

It was found that internal alkylation of compounds **22** and **23** involved a competition between α and α′ alkylation. This competition is most easily rationalized in terms of competition between the relative rates of anion equilibration and irreversible alkylation. Exclusive formation of α′ product required either a good leaving group (compound **23**) or conditions in which anion equilibration was suppressed (lithium diisopropylamide in aprotic solvent). Predominant formation of the α product required a poorer leaving group (compound **22**), and the maximum reactivity of the anion, since fortunately, increased anion reactivity (hexamethylphosphoramide, 18-crown-6) apparently increased the rate of anion equilibration more than it did the rate of alkylation. No γ alkylation of compounds **22** and **23** was observed; this can be rationalized in terms of a reactantlike transition state.

Internal alkylation of compound **24** was apparently governed by entirely different considerations. Steric requirements of the leaving group are considered to be responsible for the total lack of α′ alkylation. Furthermore, the strain induced by the formation of the four-membered ring is considered to give rise to a less reactantlike transition state, leading to the exclusive formation of the γ alkylation product under most conditions. Raising the anion reactivity (hexamethylphosphoramide, 18-crown-6) can, apparently, restore some of the reactantlike nature of the transition state, leading to α alkylation predominating to the extent of 92%.

It is clear from the results described in this paper that it is indeed possible to control, at least to some extent, the site of intramolecular alkylation of a specific α,β-unsaturated ketone. Since each different mode of internal alkylation produces a product possessing a distinctive carbon skeleton, it is also clear that this control has obvious synthetic implications.

Experimental

General

Melting points were determined on a Fisher-Johns melting point apparatus and are uncorrected. Infrared spectra were recorded on a Perkin-Elmer model 710 spectrophotometer. Proton magnetic resonance spectra were measured using Varian Associates spectrometers, models T-60 and/or HA-100 or XL-100. Signal positions are given in δ units, with tetramethylsilane as the internal standard; the multiplicity, integrated peak areas and proton assignments are indicated in parentheses. High resolution mass spectrometric measurements were recorded on an A.E.I. model MS-50 mass spectrometer. Gas–liquid chromatographic analyses were carried out with a Hewlett-Packard model 5832A gas chromatograph containing a 6 ft × 0.125 in. column (5% OV-17 on 80–100 mesh HP Chromosorb W). Microanalyses were performed by Mr. P. Borda, Microanalytical Laboratory, University of British Columbia, Vancouver, B.C.

Preparation of Substrates for Intramolecular Alkylation Studies

*4a-Allyl-4,4a,5,6,7,8-hexahydro-2(3*H*)-naphthalenone (26)*

To a cold (−10°C), efficiently stirred mixture of 3 *N* methanolic sodium methoxide (3 mL) and 2-allylcyclohexanone (**25**) (10) (100 g, 0.72 mol) were added, over a period of 2 h, 54 g (0.77 mol) of methyl vinyl ketone. The reaction mixture was stirred at −10°C for 24 h. The thick, creamy mixture was diluted with water and the resultant mixture was extracted thoroughly with ether. The combined ether extract was washed with brine and dried over anhydrous magnesium sulfate. Removal of the ether gave ~180 g of crude oil. This material was dissolved in 5% methanolic sodium methoxide and the resulting solution was refluxed for 2 h and then cooled. The base was neutralized by addition of glacial acetic acid and the solvent was removed under reduced pressure. The residue was dissolved in ether and the resultant solution was washed with brine and dried over anhydrous magnesium sulfate. Removal of the solvent gave a yellow oil. Distillation of the latter gave 50 g of 2-allylcyclohexanone, bp 100–105°C/19 Torr, and 46 g (67%, based on unrecovered starting material) of the octalone **26**, bp 110–115°C/0.4 Torr; ir (film): 1675, 1620, 910 cm^{-1}; ^1H nmr ($CDCl_3$) δ: 0.95–2.88 (diffuse, 14H), 4.77–6.17 (diffuse, 4H). *Anal.* calcd. for $C_{13}H_{18}O$: C 82.06, H 9.53; found: C 81.90, H 9.77.

Preparation of the Ketal Diene 27

A solution of the octalone **26** (5 g, 26.3 mmol), ethylene glycol (4.6 ml, 75.0 mmol), and *p*-toluenesulfonic acid (100 mg) in 160 mL of benzene was refluxed under a Dean–Stark water separator for 18 h. The cooled solution was washed successively with aqueous sodium bicarbonate and brine, and dried over anhydrous magnesium sulfate. Removal of the solvent, followed by distillation (air bath temperature 135–145°C/0.5 Torr) of the residual oil, gave 5.5 g (92%) of the ketal diene **27**; ir (film): 1640, 1090, 905 cm^{-1}; ^1H nmr ($CDCl_3$) δ: 3.92 (s, 4H, ketal protons), 4.76–6.10 (diffuse, 4H, olefinic protons). *Exact mass* calcd. for $C_{15}H_{22}O_2$: 234.1618; found: 234.1620.

Preparation of the Ketal Alcohol 28

To a cold (0°C), stirred solution of 2-methyl-2-butene (14.3 mL, 0.131 mol) in 100 mL of tetrahydrofuran under an atmosphere of nitrogen was added 6.72 mL (0.065 mol) of borane – dimethyl sulfide complex. After the solution had been allowed to stir at 0°C for 1 h, a solution of the ketal diene **27** (5.0 g, 0.021 mol) in 40 mL of tetrahydrofuran was added. The resulting reaction mixture was allowed to stir at room temperature for 2 h and was then cooled again to 0°C. To this cold solution was added, successively and dropwise, 85 mL of 3 *N* aqueous sodium hydroxide and 85 mL of 30% aqueous hydrogen peroxide. The resulting mixture was allowed to warm to room temperature and was stirred for 3 h. Most of the solvent was removed under reduced pressure and the residual material was diluted with water and then thoroughly extracted with ether. The combined ether extract was washed with brine and dried over anhydrous magnesium sulfate. Removal of the solvent gave an oil which was subjected to column chromatography on silica gel. Elution with mixtures of petroleum ether and ether produced 4.6 g (70%) of the ketal alcohol **28** as a colorless oil. An analytical sample of this material, obtained by preparative glc, exhibited ir (film): 3450, 1090 cm^{-1}; ^1H nmr

($CDCl_3$) δ: 3.60 (poorly resolved t, 2H, —CH_2OH), 3.98 (s, 4H, ketal protons), 5.46 (broad m, 1H, olefinic proton). *Exact mass* calcd. for $C_{15}H_{24}O_3$: 252.1726; found: 252.1726.

*Preparation of 4a-(3-Chloropropyl)-4,4a,5,6,7,8-hexahydro-2(3H)-naphthalenone (**22**)*

To an ice cold solution of the ketal alcohol **28** (3 g, 11.9 mmol) and methanesulfonyl chloride (1.5 g, 13 mmol) in 80 mL of dry dichloromethane was added, dropwise, 1.8 g of triethylamine. The solution was allowed to stir under an atmosphere of nitrogen for 1 h and then poured into ice water. The resultant mixture was extracted with dichloromethane. The combined extract was washed with water and dried over anhydrous magnesium sulfate. Removal of the solvent gave 3.8 g (97%) of the crude ketal mesylate **29** which exhibited ir (film): 1450, 1350, 1170, 1090 cm^{-1}; ^1H nmr ($CDCl_3$) δ: 3.03 (s, 3H, —OSO_2CH_3), 3.98 (broad s, 4H, ketal protons), 4.28 (t, 2H, —CH_2—OMs, J = 7 Hz), 5.50 (broad m, 1H, olefinic proton). This material was not purified further.

A solution of the crude ketal mesylate **29** (3.8 g, 11.2 mmol) and anhydrous lithium chloride (2.5 g, 60 mmol) in dry acetone was refluxed for 18 h. Most of the solvent was removed under reduced pressure and the residual material was diluted with water and then thoroughly extracted with ether. The combined ether extract was washed with brine and dried over anhydrous magnesium sulfate. Removal of the solvent gave the crude ketal chloride **30** (2.8 g, 87% from the ketal alcohol **28**) as a slightly yellow oil. This material, which was not purified further, exhibited ir (film): 1450, 1090 cm^{-1}; ^1H nmr ($CDCl_3$) δ: 3.50 (m, 2H, —CH_2Cl), 3.97 (s, 4H, ketal protons), 5.47 (m, 1H, olefinic proton).

To a solution of the crude ketal chloride **30** (2.8 g, 10.4 mmol) in 20% aqueous acetone was added 0.3 mL of sulfuric acid and the resulting solution was refluxed for 14 h. After the solution had been cooled, solid sodium bicarbonate was added and most of the solvent was removed under reduced pressure. The residual mixture was diluted with water and then thoroughly extracted with ether. The combined ether extract was washed with water and dried over anhydrous magnesium sulfate. Removal of the solvent gave a crude oil which was subjected to column chromatography on silica gel. Elution of the column with mixtures of petroleum ether and ether afforded 2.1 g (78% from the ketal alcohol **28**) of the chloro octalone **22**, which was further purified by distillation (air bath temperature 125–130°C/0.03 Torr). This material exhibited ir (film): 1660, 1620, 1450 cm^{-1}; ^1H nmr ($CDCl_3$) δ: 1.07–2.60 (diffuse, 16 H), 3.57 (m, 2H, —CH_2Cl), 5.82 (broad s, 1H, olefinic proton). *Exact mass* calcd. for $C_{13}H_{19}{}^{35}ClO$: 226.1124; found: 226.1120.

*Preparation of 4a-(3-Iodopropyl)-4,4a,5,6,7,8-hexahydro-2(3H)-naphthalenone (**23**)*

A stirred solution of the crude ketal mesylate **29** (1.2 g, 3.6 mmol), sodium iodide (18 mmol), and sodium bicarbonate (4 mmol) in acetone was refluxed for 20 h. Most of the solvent was removed under reduced pressure. The residual material was diluted with water and then thoroughly extracted with ether. The combined ether extract was washed successively with water, brine, aqueous sodium thiosulfate, and water, and dried over anhydrous magnesium sulfate. Removal of the solvent afforded the crude ketal iodide **31**. This material was dissolved in 40 mL of 10% aqueous acetone and 0.15 mL of sulfuric acid was added to the resultant solution. The solution was refluxed for 18 h. After solid sodium bicarbonate had been added to the cooled solution, most of the solvent was removed under reduced pressure. The residual material was diluted with water and then extracted thoroughly with ether. The combined ether extract was washed with water and dried over anhydrous magnesium sulfate. Removal of the solvent afforded a white crystalline material which, upon recrystallization from a mixture of petroleum ether and ether, gave 350 mg (36%) of the iodo octalone **23** as white needles, mp 60–61°C; ir ($CHCl_3$): 1665, 1620 cm^{-1}; ^1H nmr ($CDCl_3$) δ: 1.03–2.57 (diffuse, 16 H), 3.17 (m, 2H, —CH_2I), 5.73 (broad s, 1H, olefinic proton). *Exact mass* calcd. for $C_{13}H_{19}IO$: 318.0484; found: 318.0482.

*Preparation of 4a-Mesyloxymethyl-4,4a,5,6,7,8-hexahydro-2(3H)-naphthalenone (**24**)*

To a cold (0°C), stirred solution of the ketal alcohol **32** (13) (2.24 g, 10 mmol) and methanesulfonyl chloride (12 mmol) in 70 mL of dichloromethane under an atmosphere of nitrogen was added, dropwise, 18 mmol of triethylamine. After the solution had been allowed to stir at 0°C for 45 min, it was poured into ice water and the resulting mixture was extracted thoroughly with dichloromethane. The combined extract was dried over anhydrous magnesium sulfate. Removal of the solvent afforded a quantitative yield of the crude ketal mesylate **33** as an oily solid. An analytical sample of **33**, obtained by recrystallization of a small amount of this material from ether – petroleum ether, exhibited mp 102–102.5°C; ir ($CHCl_3$): 1350. 1170, 1090, 940 cm^{-1}; ^1H nmr ($CDCl_3$) δ: 3.00 (s, 3H, —OSO_2CH_3), 3.84 (s, 4H, ketal protons), 4.20 (m, 2H, —CH_2OMs), 5.60 (m, 1H, olefinic proton). *Exact mass* calcd. for $C_{14}H_{22}O_5S$: 302.1188; found: 302.1173.

To a solution of the crude ketal mesylate **33** (obtained as described above) in 60 mL of 10% aqueous acetone was added, dropwise, 1 mL of sulfuric acid, and the resulting solution was refluxed for 24 h. Solid sodium bicarbonate was added to the cooled solution and most of the acetone was removed under reduced pressure. The residual material was diluted with water and extracted with ether. The combined extract was washed with brine and dried over anhydrous magnesium sulfate. Removal of the solvent, followed by recrystallization of the resulting crystalline material from carbon tetrachloride – hexane, gave 1.75 g (68% from the ketal alcohol **32**) of the mesyloxy octalone **24**, mp 98–99°C; ir ($CHCl_3$): 1670, 1620, 1350, 1170, 980, 940 cm^{-1}; ^1H nmr ($CDCl_3$) δ: 3.00 (s, 3H, —OSO_2CH_3), 4.33 (s, 2H, —CH_2OMs), 5.80 (s, 1H, olefinic proton). *Exact mass* calcd. for $C_{12}H_{18}O_4S$: 258.0926; found: 258.0918.

Intramolecular Alkylation Experiments

Base: Potassium tert-*Butoxide; Solvent:* tert-*Butyl Alcohol (Table 1, Entries 1,2,9,10; Table 2, Entries 1, 2)*

To a solution of potassium *tert*-butoxide (2.0 mmol) and, where appropriate, 18-crown-6 (2.0 mmol) in dry *tert*-butyl alcohol (20 mL) under an atmosphere of nitrogen was added a solution of the appropriate octalone (**22**, **23**, or **24**) (1.0 mmol) in 20 mL of dry *tert*-butyl alcohol and the resulting solution was stirred at the desired temperature for the designated length of time. The solution was poured into ice cold 0.1 *N* hydrochloric acid and the resultant mixture was extracted thoroughly with ether. The combined extract was washed successively with water and brine and dried over anhydrous magnesium sulfate. Removal of the solvent afforded a crude oil which was subjected to glc analysis in order to determine the ratio of products. At this point, 1.0 mmol of a standard compound (10-methyl-$\Delta^{1(9)}$-octal-2,5-dione, Wieland–Miescher ketone (22))[7] was added to the crude product and the resultant mixture was analyzed by glc to determine the (glc) yield of the products.

[7]This compound was chosen as a standard because it was found to possess a glc molar response factor (thermal conductivity detector) essentially identical with those of the various alkylation products. Also, its retention time was different from that of each of the alkylation products.

Finally, the entire mixture was subjected to bulb-to-bulb distillation under reduced pressure and the isolated yield of the products was determined by subtracting the weight of the standard compound which had been added from the total weight of distilled material.[8]

Base: Potassium tert-*Butoxide; Solvent: Tetrahydrofuran (Table 1, Entries 3, 4; Table 2, Entry 3)*

A solution of potassium *tert*-butoxide (2.0 mmol) in 20 mL of *tert*-butyl alcohol was distilled, under an atmosphere of nitrogen, until most of the alcohol had been removed. The remaining solvent was removed by warming the flask under reduced pressure (vacuum pump). To the residual potassium *tert*-butoxide was added successively 20 mL of dry tetrahydrofuran, 18-crown-6 (2.0 mmol, when desired) and a solution of 1.0 mmol of the appropriate octalone (**22** or **24**) in 20 mL of tetrahydrofuran. After the resultant solution had been stirred at the desired temperature for the appropriate length of time, it was subjected to work-up and analysis procedures identical with those described above.

Base: Potassium tert-*Butoxide; Solvent: Hexamethylphosphoramide (Table 1, Entry 5; Table 2, Entries 6, 7)*

To 2.0 mmol of dry potassium *tert*-butoxide (prepared as described above) under an atmosphere of nitrogen was added successively 20 mL of dry hexamethylphosphoramide, 2.0 mmol of 18-crown-6 (when desired), and a solution of 1.0 mmol of the appropriate octalone (**22** or **24**) in 20 mL of dry hexamethylphosphoramide. After the resultant solution had been stirred at the desired temperature for the designated length of time, it was subjected to work-up and analysis procedures identical with those described above, except that product extraction was done with petroleum ether instead of with ether.

Base: Potassium tert-*Butoxide; Solvent:* tert-*Butyl Alcohol – Tetrahydrofuran (40:60) (Table 1, Entries 8, 11)*

To a cold (−78°C), stirred solution of potassium *tert*-butoxide (2.0 mmol) and, where appropriate, 18-crown-6 (2.0 mmol) in 32 mL of a 1:1 mixture of dry *tert*-butyl alcohol and dry tetrahydrofuran, under an atmosphere of nitrogen, was added slowly a solution of 1.0 mmol of the appropriate octalone (**22** or **23**) in 8 mL of dry tetrahydrofuran. After the resultant solution had been stirred at −78°C for 30 min, it was allowed to warm to room temperature and then stirred for an additional 15 min. Work-up and analysis procedures were identical with those described above.

Base: Lithium tert-*Butoxide; Solvent:* tert-*Butyl Alcohol (Table 1, Entry 6; Table 2, Entry 4)*

To 20 mL of dry *tert*-butyl alcohol, under an atmosphere of nitrogen, was added successively 2.0 mmol of *n*-butyllithium (hexane solution) and a solution of 1.0 mmol of the appropriate octalone (**22** or **24**) in 20 mL of dry *tert*-butyl alcohol. After the resultant solution had been refluxed for the designated length of time, it was cooled and subjected to work-up and analysis procedures identical with those described above.

Base: Lithium Diisopropylamide; Solvent: Tetrahydrofuran (Table 1, Entry 7; Table 2, Entry 5)

To a stirred solution of diisopropylamine (2.2 mmol) and hexamethylphosphoramide (2.0 mmol) in 20 mL of dry tetrahydrofuran, under an atmosphere of nitrogen, was added 2.0 mmol of *n*-butyllithium (hexane solution). A solution of 1.0 mmol of the appropriate octalone (**22** or **24**) in 20 mL of dry tetrahydrofuran was added and the resultant reaction mixture was kept at the required temperature for the designated period of time. The solution was cooled to 0°C and subjected to work-up and analysis procedures identical with those described above.

Isolation and Characterization of Intramolecular Alkylation Products

The α,β-Unsaturated Ketone ***34***

Distillation (air bath temperature 115–125°C/0.2 Torr) of the crude product obtained from an experiment as summarized in Table 1, entry 9, afforded (94%) the tricyclic α,β-unsaturated ketone **34** as a clear colorless oil which exhibited one peak on glc; ir (film): 1670, 1618 cm^{-1}; ^1H nmr ($CDCl_3$) δ: 0.73–2.70 (diffuse, 17H), 6.02 (s, 1H, vinyl proton). *Exact mass* calcd. for $C_{13}H_{18}O$: 190.1357; found: 190.1363.

The β,γ-Unsaturated Ketone ***35***

The distilled product obtained from an experiment as summarized in Table 1, entry 2 (ratio of **34**:**35** ≈ 5:95) was subjected to column chromatography on silica gel. Elution of the column with ether – petroleum ether gave a pure sample of the tricyclic β,γ-unsaturated ketone **35**; ir (film): 1710 cm^{-1}; ^1H nmr ($CDCl_3$) δ: 0.90–2.63 (diffuse, 16H), 2.87 (broad s, 1H), 5.56 (t, 1H, olefinic proton, J = 4.0 Hz). *Exact mass* calcd. for $C_{13}H_{18}O$: 190.1357; found: 190.1352.

Wolff–Kishner Reduction of the β,γ-Unsaturated Ketone ***35***

To 25 mL of anhydrous diethylene glycol, under an atmosphere of nitrogen, was added 0.84 g (36.5 mmol) of sodium metal and the mixture was stirred until all of the sodium had reacted. Anhydrous hydrazine (prepared by refluxing hydrazine hydrate over sodium hydroxide) was distilled directly into the resulting solution until the latter refluxed freely at 165°C. The solution was cooled and 470 mg (2.47 mmol) of the tricyclic ketone **35** was added. The mixture was refluxed for 12 h and excess hydrazine was distilled (the distillate was saved) from the mixture until the internal temperature of the latter reached 210°C. Refluxing was then continued for an additional 8 h. The mixture was cooled, combined with the distillate (see above), and then poured into water. The resulting mixture was extracted with petroleum ether. The combined extract was washed with water and dried over anhydrous magnesium sulfate. Removal of the solvent gave a colorless oil which upon distillation (air bath temperature 135–140°C/7.0 Torr) afforded 0.35 g (90%) of the tricyclic olefin **37**; ir (film): 1665 cm^{-1}; ^1H nmr ($CDCl_3$) δ: 1.13–2.50 (diffuse, 19H), 5.30 (t, 1H, olefinic proton, J = 4.0 Hz). *Exact mass* calcd. for $C_{13}H_{20}$: 176.1565; found: 176.1572.

Preparation of the α,β-Unsaturated Ketone ***36***

To a solution of chromium trioxide – dipyridine complex (16.7 mmol) in 40 mL of dry dichloromethane, under an atmosphere of nitrogen, was added a solution of the tricyclic olefin **37** (0.195 g, 1.11 mmol) in 5 mL of dichloromethane. The resulting mixture was stirred at room temperature for 6 h, was filtered through Celite, and the filtrate was passed through a short column of activity III neutral alumina. The column was washed with additional volumes of dichloromethane. The combined eluant was washed successively with water, 3 *N* hydrochloric acid, and water and then dried over anhydrous magnesium sulfate. Removal of the solvent followed by distillation (air bath temperature 135°C/0.2 mm) of the residual oil gave 0.180 g (86%) of the tricyclic α,β-unsaturated ketone **36** as a colorless oil; ir (film): 1670, 1630 cm^{-1}; ^1H nmr ($CDCl_3$) δ: 1.13–2.83 (diffuse, 17H), 5.78 (s, 1H, olefinic proton). *Exact mass* calcd. for $C_{13}H_{18}O$: 190.1357; found: 190.1357.

[8]The boiling point of the Wieland–Miescher ketone was very near to, although somewhat lower than, those of the various alkylation products.

The α,β-Unsaturated Ketone ***11***

The crude product obtained from an experiment as summarized in Table 2, entry 1, was distilled (hot box) under reduced pressure, affording, in 74% yield, the pure tricyclic α,β-unsaturated ketone **11** (5); ir (film): 1660 cm^{-1}; ^1H nmr ($CDCl_3$) δ: 5.75 (s, 1H, olefinic proton). *Exact mass* calcd. for $C_{11}H_{14}O$: 162.1045; found: 162.1038.

The β,γ-Unsaturated Ketone ***41***

The crude product obtained from an experiment as summarized in Table 2, entry 7, was distilled (hot box) under reduced pressure, affording, in 75% yield, a clear oil which was shown (glc analysis) to consist of two components in a ratio of approximately 92:8. Subjection of this mixture to preparative glc gave a very small amount of the minor component (identical with the enone **11**) and a sample of the pure tricyclic β,γ-unsaturated ketone **41**; ir (film): 1720 cm^{-1}; ^1H nmr ($CDCl_3$) δ: ~2.5 (m, 2H, $-CH_2C(=O)-$), 3.55 (t, 1H, $-CH-C(=O)-$), 5.35 (t, 1H, olefinic proton). *Exact mass* calcd. for $C_{11}H_{14}O$: 162.1045; found: 162.1053.

Deuteration of the α,β-Unsaturated Ketone ***11***

To a solution of 40 mg of the α,β-unsaturated ketone **11** in 1.0 mL of 1,2-dimethoxyethane was added 0.5 mL of deuterium oxide and a catalytic amount of potassium hydroxide. The solution was stirred at room temperature for 3 days. A small amount of acetic acid was added and the resultant mixture was extracted with ether. The combined extract was washed successively with water, aqueous sodium bicarbonate and brine, and dried over anhydrous magnesium sulfate. Removal of the solvent, followed by distillation (hot box, reduced pressure) of the residual oil gave 32 mg of the dideutero derivative **38**. *Exact mass* calcd. for $C_{11}H_{12}D_2O$: 164.1170; found: 164.1164.

Acknowledgement

Financial assistance from the National Research Council of Canada is gratefully acknowledged.

1. R. A. Lee, C. McAndrews, K. M. Patel, and W. Reusch. Tetrahedron Lett. 965 (1973); K. M. Patel and W. Reusch. J. Org. Chem. **40**, 1504 (1975); G. Stork and R. L. Danheiser. J. Org. Chem. **38**, 1775 (1973); L. Nedelec, J. C. Gasc, and R. Bucourt. Tetrahedron, **30**, 3263 (1974); M. Tanabe and D. F. Crowe. J. Chem. Soc. Chem. Commun. 564 (1973); A. G. Schultz and D. S. Kashdan. J. Org. Chem. **38**, 3814 (1973); G. Stork, G. A. Kraus, and G. A. Garcia. J. Org. Chem. **39**, 3459 (1974); B. H. Toder, S. J. Branca, R. K. Dieter, and A. B. Smith III. Synth. Commun. **5**, 435 (1975).
2. H. O. House. Modern synthetic reactions. 2nd ed. W. A. Benjamin, Inc., Menlo Park, CA. 1972. pp. 555–558.
3. J. H. Fassnacht and N. A. Nelson. J. Org. Chem. **27**, 1885 (1962); M. T. Wuesthoff and B. Rickborn. J. Org. Chem. **33**, 1311 (1968).
4. R. B. Bates, G. Büchi, T. Matsuura, and R. R. Shaffer. J. Am. Chem. Soc. **82**, 2327 (1960); G. Büchi, J. M. Kauffman, and H. J. E. Loewenthal. J. Am. Chem. Soc. **88**, 3403 (1966); G. Büchi, W. Hofheinz, and J. V. Paukstelis. J. Am. Chem. Soc. **91**, 6473 (1969).
5. P. C. Mukharji and A. N. Ganguly. Tetrahedron, **25**, 5281 (1969).
6. J. J. Bonet, H. Wehrli, and K. Schaffner. Helv. Chim. Acta, **45**, 2615 (1962); O. Halpern, P. Crabbé, A. D. Cross, I. Delfin, L. Cervantes, and A. Bowers. Steroids, **4**, 1 (1964).
7. C. Mercier, A. R. Addas, and P. Deslongchamps. Can. J. Chem. **50**, 1882 (1972).
8. P. Grafen, H. J. Kabbe, O. Roos, G. D. Diana, T. Li, and R. B. Turner. J. Am. Chem. Soc. **90**, 6131 (1968).
9. R. L. Cargill and T. E. Jackson. J. Org. Chem. **38**, 2125 (1973).
10. G. Stork, A. Brizzolara, H. Landesman, J. Szmuszkovic, and R. Terrell. J. Am. Chem. Soc. **85**, 207 (1963).
11. J. A. Marshall and W. I. Fanta. J. Org. Chem. **29**, 2501 (1964).
12. H. C. Brown, A. K. Mandal, and S. U. Kulharni. J. Org. Chem. **42**, 1392 (1977).
13. W. G. Dauben and J. B. Rogan. J. Am. Chem. Soc. **79**, 5002 (1957).
14. D. H. R. Barton, D. A. J. Ives, and B. R. Thomas. J. Chem. Soc. 2056 (1955).
15. W. G. Dauben, M. Lorber, and D. S. Fullerton. J. Org. Chem. **34**, 3587 (1969).
16. L. P. Hammett. Physical organic chemistry. 2nd ed. McGraw-Hill Book Co., New York, NY. 1970. pp. 119, 120.
17. R. E. Davis. J. Am. Chem. Soc. **87**, 3010 (1965).
18. D. C. Wigfield. Can. J. Chem. **48**, 2120 (1970).
19. G. S. Hammond. J. Am. Chem. Soc. **77**, 334 (1955).
20. J. E. Baldwin, R. C. Thomas, L. I. Kruse, and L. Silberman. J. Org. Chem. **42**, 3846 (1977).
21. H. C. Brown. The nonclassical ion problem. Plenum Press, New York, NY. 1977. pp. 127ff.
22. P. Wieland and K. Miescher. Helv. Chim. Acta, **33**, 2215 (1950); S. Ramachandran and M. S. Newman. Org. Synth. **41**, 38 (1961).

A study of ^{14}N relaxation and nitrogen–proton spin coupling in Watson–Crick base pair models through Fourier transform measurements on NH proton spin–lattice relaxation in the rotating frame

MICHAEL E. MOSELEY AND PETER STILBS

Department of Physical Chemistry, Uppsala University, Box 532, S-751 21 Uppsala, Sweden

Received August 14, 1978

MICHAEL E. MOSELEY and PETER STILBS. Can. J. Chem. **57**, 1075 (1979).

Indirect measurements of nitrogen-14 nuclear spin–lattice relaxation times and direct proton coupling constants are presented together with carbon-13 T_1 data for a series of alkyl-substituted nucleic acid bases and mixtures thereof in DMSO-d_6. With the exception of the guanine NH nitrogen, which possibly experiences a decrease in the electric field gradient upon complexation with cytosine, no indications of significant changes in the electronic environment around the nitrogen nuclei were found for any combination of bases. Forsén–Hoffman spin saturation transfer experiments on the NH and NH_2 protons are also presented.

MICHAEL E. MOSELEY et PETER STILBS. Can. J. Chem. **57**, 1075 (1979).

On rapporte des mesures indirectes de temps de relaxation spin–nucléaire réseau de l'azote-14 et des mesures directes de constantes de couplage du proton ainsi que des données de T_1 pour le ^{13}C pour une série de bases d'acides nucléiques substitués par des groupes alkyles et de leurs mélanges dans le DMSO-d_6; aucune des combinaisons de bases ne semble conduire à des changements importants dans l'environnement électronique autour du noyau d'azote. On rapporte aussi des expériences de transferts de saturation de spin de Forsén–Hoffman sur des protons NH et NH_2.

[Traduit par le journal]

Introduction

Despite a great body of knowledge concerning the static structure of the inherent specific interaction between complementary nucleic acid bases, in which adenine specifically hydrogen bonds with thymine and cytosine with guanine, very little is known about the dynamic properties of the base pairs or of how the bonding influences the electronic character of the amino and imino moieties involved in the interaction. Although other factors than hydrogen bonding (stacking, hydrophobic forces, etc.) probably contribute to the specificity of interaction, it has been shown by Shoup *et al.* (1) and by Katz and Penman (2) that significant amino and imino ^1H downfield shifts occur in mixtures of complementary bases in solution but not for noncomplementary base pairs. Such downfield ^1H shifts are characteristic of hydrogen bonding and do reflect changes in the electronic environment of the NH groups involved. Since ^{14}N spin relaxation times and direct ^{14}N–^1H spin couplings also reflect such changes we have found it to be of interest also to investigate their behaviour under similar conditions.

The present paper therefore concerns measurements of ^{14}N relaxation times (T_{1N}) and direct proton–nitrogen spin coupling constants ($^1J_{^{14}N-H}$) made on the nucleic acid base derivatives 9-ethylguanine (henceforth denoted as G), 9-methyladenine (A), 1-methylcytosine (C), and 1-methylthymine (T) and mixtures thereof in water-free DMSO-d_6 solutions, employing the technique presented earlier (3) utilizing Fourier transform measurements of NH proton spin–lattice relaxation in the rotating frame (spin locking, $T_{1\rho}$).

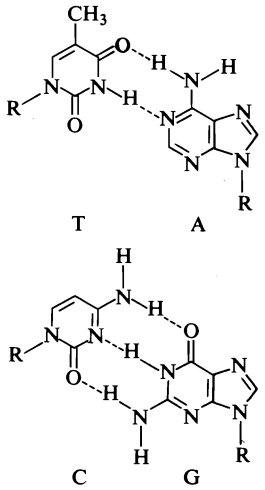

FIG. 1. The complementary base pairs G + C and A + T.

The $T_{1\rho}$ method for indirect determination of relaxation times and spin–spin couplings for quadrupolar nuclei embodies measurements of T_1 and $T_{1\rho}$ for (usually) directly bonded spin $\frac{1}{2}$ nuclei (see

0008-4042/79/091075-05$01.00/0

refs. 3–5). $T_{1\rho}$ is essentially T_1 measured at a very low field (B_1 instead of B_0), and thus becomes sensitive to the intensity of magnetic field fluctuations at an angular frequency of ω_1 ($=\gamma B_1$) instead of ω_0 ($=\gamma B_0$). Owing to common spectrometer design this will typically be in the kHz range. Sources of extraneous magnetic field fluctuations in this frequency range are, for example, (partially collapsed) spin couplings between the spin $\frac{1}{2}$ nuclei being studied and a rapidly relaxing (usually quadrupolar) nucleus. Assuming a spin coupling of J Hz, a quadrupolar relaxation time of T_{1q} s, and a spin of I makes $1/T_{1\rho}$ for the spin $\frac{1}{2}$ nucleus larger than its $1/T_1$ value by an amount shown in [1] (4, 5):

$$[1]\quad 1/T_{1\rho(sc)} = 1/T_{1\rho(obs)} - 1/T_1 = (\pi J)^2 \tfrac{4}{3}(I(I+1))\frac{T_{1q}}{1+(\omega_1 T_{1q})^2}$$

Here $1/T_{1\rho(sc)}$, the relaxation effect due to scalar coupling with the quadrupolar nucleus, is seen to depend on the strength of the B_1 field, provided that $\omega_1 T_{1q}$ is significant with regard to unity. Under these circumstances a study of the ω_1 dependence of $T_{1\rho}$ does give information about both T_{1q} and J. If $\omega_1 T_{1q}$ is close to zero, T_{1q} can still be evaluated, however, provided that J can be estimated independently.

Another possible source of magnetic field fluctuations in the kHz range is chemical exchange between nonequivalent sites and exchange rates and shift differences can be measured in a similar fashion (4–6). When both mechanisms are present simultaneously an analysis of the $T_{1\rho}$ data becomes uncertain and difficult, a factor which has been very troublesome in the present work (*vide infra*). Initial attempts to study the unsubstituted nucleosides were discontinued owing to disturbing proton exchange effects and it was also found necessary to prepare the samples under anhydrous conditions to eliminate possible proton exchange effects with water. Alternative approaches, which would eliminate this problem, are to study the $T_{1\rho}$ of ring carbon-13 nuclei or fluorine-19 in fluorinated analogues. However, in both cases more than one nitrogen will contribute to their $T_{1\rho}$ relaxation, making the analysis complicated and uncertain.

Experimental

The nucleoside base derivatives 1-methylcytosine (C) and 9-methyladenine (A) were obtained from Vega-Fox Biochemicals. 1-Methylthymine (T) was obtained from Pfaltz and Bauer Research Chemicals and 9-ethylguanine (G) was obtained from Sigma Chemical Co. Deuterated dimethyl sulphoxide (DMSO-d_6), purchased from Ciba-Geigy, was dried with 4 A molecular sieves and transferred to a vacuum line storage bulb through standard vacuum line techniques.

Samples were prepared by first degassing weighed amounts of the bases in 5-mm medium-wall tubes and then DMSO-d_6 was distilled over from the storage bulb to make the concentrations 0.1 M for each derivative. In addition, samples of T and G were prepared at 0.2 M as well (denoted 2T and 2G). 9-Ethyladenine (A) was only sparingly soluble in DMSO-d_6, to an estimated concentration of 0.07 M.

Chemical shifts were measured using the center of the DMSO-d_5 signal as an internal reference, and later adding the observed shift of DMSO-d_5 relative to TMS to these values.

Traces of water in the samples were found to be negligible and usually not observable in the proton spectra.

All measurements were made by Fourier transform methods on a JEOL FX-100 pulsed nmr spectrometer with double quadrature detection under control of the JEOL Autostacking program. The method of measurement, as well as the data analysis and error estimation were carried out as previously described (3, 6) noting that for each sample, $T_{1\rho}$ for each NH and NH_2 proton signal was measured from 15 spectra at each of six ω_1 values in the range 2600 to 18000 rad/s and that all quoted error limits correspond to a 90% confidence interval, encompassing only random error limits.

Forsén–Hoffman spin saturation transfer experiments (7) were carried out on all samples having two or more exchangeable proton types (NH, NH_2) and average proton lifetimes in each site were estimated.

Carbon-13 relaxation times for all ring methine carbons were measured for the same samples by the progressive saturation method. Each determination embodied the measurement of 11 spectra, each of 11 000 accumulations, at an observed temperature of 25°C.

Results and Discussion

Hydrogen-bond-induced Shifts and Proton Exchange Effects

The data in Table 1 present changes in amino and imino proton shifts for all combinations of bases, confirming earlier studies (1, 2). As previously pointed out (1, 2) the bases are already strongly hydrogen bonded in DMSO and the shift changes thus to reflect even more pronounced hydrogen bonding conditions. The pair interaction G + C is very significant whereas the A + T interaction is

TABLE 1. Interaction shifts upon base pairing

	δ				
Base	G-NH	G-NH_2	T-NH	A-NH_2	C-NH_2
G	(10.53)[a]	(6.43)[a]			
2G	0.02	0.01			
T			(11.17)[a]		
2T			0.02		
A				(7.16)[a]	
C					(6.93)[a]
G + C	0.98	0.46			0.34
G + A	0.00	0.00		0.01	
G + T	0.00	0.00	0.01		
A + T			0.00	0.01	
T + C			0.02		0.00
C + A				0.00	0.00

[a]The shift of this signal is taken as a reference and downfield shifts are denoted positive.

not. Although it may be possible to get more clear-cut results on solvents which do not form hydrogen bonds (2), this was not possible in the present study due to solubility reasons and to increased exchange rates for protons bonded to nitrogen.

Since the application of the present method relies on very slow exchange of the studied protons, an investigation of their lifetimes was carried out through Forsén–Hoffman spin saturation transfer experiments (7). Reliable data could be obtained for signals not too closely spaced and are summarized in Table 2. Proton exchange for G-NH protons is most severe with C-NH_2 protons and probably also with T-NH protons. Interestingly, exchange of G-NH_2 protons is invariably slow in all systems. Exchange between T-NH and G-NH_2 protons is very pronounced though considerably slower between T-NH protons and A-NH_2 protons.

A similar study on a few base combinations was recently presented by Iwahashi and Kyogoku (9) with much the same results. While information of this kind could have significant chemical implications, we must emphasize that it does not in any way prove that proton exchange occurs within a *base pair* as suggested in ref. 9. NH and NH_2 proton lifetimes at 25°C are of the order of a second although the lifetimes of the base pairs are probably less than a millisecond, since only averaged sets of ^1H nmr signals are observed.[1] Therefore, many other proton exchange pathways are possible, including exchange through trace impurities.

Nitrogen-14–Proton Spin Coupling Constants ($^1J_{^{14}N-H}$) and Nitrogen-14 Relaxation Times (T_{1N}) in Nucleic Acid Base Derivatives

In nucleic bases where the nitrogen-14 nucleus is directly linked to a proton the nuclei yield large direct spin couplings on the order of 65 Hz, characteristic of sp^2-type nitrogens (10, 11).[2] The measured coupling constants are given in Table 3 for each base or combination thereof. Nothing from the data seems to indicate any experimentally significant difference in the coupling constants between imino and amino groups in each base either alone in varying concentrations or upon admixture of bases, ruling out possible changes in nitrogen hybridization.

The data within parentheses in Tables 3 and 4 are *apparent* values, obtained from an analysis of proton T_1 and $T_{1\rho}$ data for signals shown (by the previously mentioned Forsén-Hoffman experiments) to be subject to significant proton exchange with no account for thereby induced effects on $T_{1\rho}$. The real significance of these data is unclear, since to our knowledge no theory presently exists for effects of slow exchange combined with averaging of N–H coupling on $T_{1\rho}$. All original T_1 and $T_{1\rho}$ data are given in the Appendix and can be used together with the data in Tables 1 and 2 to calculate more reliable data with the appearance of such a theory.[3]

TABLE 2. Estimated site lifetimes from Forsén-Hoffman measurements

	Lifetime (s)				
Base	G-NH	G-NH_2	T-NH	A-NH_2	C-NH_2
G	>7	>3[a]			
2G	>7	>3[a]			
G + C	≈0.02[b]	>3			0.13
G + A	>7	>3		>5	
G + T	[c]	>3	[c]		
A + T			1.1[d]	1.1[d]	
T + C			0.03		0.07
C + A				[e]	[e]

[a]This is the lower limit estimated from the observation of no significant saturation effect and a T_1 of 0.25 s. However, since the lifetime of a G-NH proton appears to be >7 s, the lower limit must be considerably higher, probably >15 s.
[b]Experimentally uncertain value. The G-NH_2 lifetime which can be more accurately determined, suggests a G-NH lifetime of the order of 0.06 s.
[c]Partial overlap prevented measurement. Signals were significantly broadened; significant proton exchange is suspected (<0.05 s).
[d]These apparently inconsistent values arise from the lower A concentration (cf. Experimental).
[e]Partial overlap. No significant signal broadening. Proton exchange is suspected to be slow (>5 s).

Changes in the electronic environment of the interacting nitrogen as well as changes in rotational behaviour affect nitrogen-14 relaxation times. The dominant relaxation mechanism is quadrupolar relaxation (8) and in the present mobility range relaxation rates are given by [2]:

$$[2]\quad \frac{1}{T_{1q}} = \frac{1}{T_1} = \frac{1}{T_2} = \frac{3}{8}\left(\frac{e^2qQ}{\hbar}\right)^2\left(1+\frac{\eta^2}{3}\right)\tau_c$$

Here eq is the electric field gradient at the nitrogen nucleus, η is the assymetry parameter of the field gradient, eQ is the electric quadrupole moment of ^{14}N, and τ_c is the rotational correlation time. Since changes in relaxation behaviour can be due to either changes in the electronic environment or changes in the rotational rate of the molecules, independent estimates of τ_c must be made in order to enable an interpretation of the data in Table 4. These estimates

[1]Compare with the results in Fig. 4 of ref. 2.

[2]The original relations given in refs. 10 and 11 concern ^{15}N nuclei for which the coupling constants are $(\gamma(^{15}N)/\gamma(^{14}N)) = 1.402$ times larger.

[3]The C-NH_2 data should also be corrected for $T_{1\rho}$ contributions from hindered internal rotation of the amino group (1, 12). However, since our DMSO solutions cannot be cooled much below 25°C and since a comparison between our spectra and those of Shoup *et al.* (1, 12) clearly indicates that $\delta\nu$ and (or) τ_c for this process are highly solvent dependent, this is not possible in the present study. It is clear, however, that this $T_{1\rho}$ contribution is much smaller in the present study than in the spectra at 25°C given in ref. 12.

TABLE 3. Nitrogen-14–proton spin–spin coupling constants in nucleic acid base derivatives[a]

	J^{14}_{N-H} (H_3)				
Bases	G-NH	G-NH_2	T-NH	A-NH_2	C-NH_2
G	63.0±0.6	67.5±0.3			
2G	63.2±0.4	68.1±0.7			
T			64.5±0.4		
2T			65.3±0.1		
A				64.6±0.6	
C					62.9±0.5
G + C	(58.9±1.2)	66.4±1.0			(68.4±1.0)
G + A	68.3±0.5	62.5±2.3		64.4±0.2	
G + T	(62.2±1.0)	69.1±2.5	(61.0±0.6)		
A + T			(75.7±1.2)	(64.6±1.0)	
T + C			(67.4±0.4)		(68.4±0.5)
C + A				63.1±1.2	63.1±0.4

[a]Values within parentheses are subject to systematic errors (see text).

TABLE 4. Nitrogen-14 relaxation times (T_{1N}) in nucleic acid base derivatives[a]

	T_{1N} (μs)				
Bases	G-NH	G-NH_2	T-NH	A-NH_2	C-NH_2
G	113.5±4.2	62.4±1.2			
2G	104.7±1.5	56.9±1.3			
T			303.9±8.6		
2T			229.9±1.0		
A				117.8±3.8	
C					171.7±5.0
G + C	(140.5±16.1)	45.1±2.0			(116.7±6.3)
G + A	127.0±4.1	76.0±12.7		117.0±1.0	
G + T	(161.9±6.1)	62.1±6.4	(178.2±4.2)		
A + T			(186.0±12.2)	(114.5±8.5)	
T + C			(263.7±6.3)		(191.0±5.0)
C + A				120.4±5.7	129.1±3.3

[a]Values within parentheses are subject to systematic errors (see text).

TABLE 5. Carbon-13 spin–lattice relaxation times (T_1) for ring methine carbons in nucleic acid base derivatives

	T_1					
Base	G	T	A_2	A_8	C_5	C_6
G	0.39±0.06					
T		0.60±0.05				
A			1.21±0.92	0.68±0.08		
C					0.88±0.15	0.71±0.09
G + C	0.27±0.02				0.39±0.03	0.40±0.03
G + A	0.39±0.04		0.48±0.34	0.57±0.20		
G + T	0.37±0.02	0.62±0.04				
A + T		0.67±0.08	0.42±0.08	0.60±0.27		
T + C		0.65±0.06			0.72±0.11	0.59±0.09

have been made through interpretation of the carbon-13 T_1 measurements of the ring methine carbons which are summarized in Table 5.

Combining data of Tables 4 and 5 makes possible for example, the deduction that the 30% T_{1N} decrease of the G-NH_2 nitrogen in the G + C mixture is due to decreased molecular mobility. Although somewhat speculative, some comment can be made about the corresponding G-NH and C-NH_2 data. The $T_{1\rho}$ data for the ^1H signals are affected by the same proton exchange effect but still the apparent (*vide supra*) T_{1N} values show opposite trends.

The C-NH_2 T_{1N} decrease can be explained by decreased mobility but the G-NH increase might

possibly be due to a decreased electric field gradient upon complexation. No major T_{1N} or carbon-13 T_1 changes were observed upon admixture of any non-complementary base pairs and unfortunately no reliable T_{1N} data could be obtained for the A + T pair due to the mentioned proton exchange effects.

The data can similarly be used to estimate relative electric field gradients at the nitrogens by inserting τ_c data deduced from carbon-13 T_1 measurements in [2].[4] Information of this kind is not readily obtained from direct nitrogen-14 nmr and nqr studies owing to the low concentrations and the large number of nitrogens contributing to the spectra. It is seen that the T-NH nitrogen experiences a lower field gradient than does the G-NH nitrogen. The field gradient is also higher at the G-NH_2 nitrogen than either the A- or C-NH_2 nitrogens.

Acknowledgements

We wish to thank Dr. G. Bergson for putting the spectrometer at our disposal and Dr. U. Obenius for technical assistance. Financial support provided by the Swedish Natural Science Research Council is also gratefully acknowledged.

1. R. R. SHOUP, H. T. MILES, and E. D. BECKER. Biochem. Biophys. Res. Commun. **23**, 194 (1966).
2. L. KATZ and S. PENMAN. J. Mol. Biol. **15**, 220 (1966).
3. M. E. MOSELEY and P. STILBS. Can. J. Chem. **56**, 1302 (1978).
4. N. BODEN. *In* Determination of organic structures by physical methods. Vol. 4. *Edited by* F. C. Nachod and J. J. Zuckerman. Academic Press, New York, NY. 1971.
5. T. C. FARRAR and E. D. BECKER. Pulse and Fourier transform nmr. Academic Press, New York and London. 1971.
6. P. STILBS and M. E. MOSELEY. J. Magn. Reson. **31**, 55 (1978).
7. J. W. FALLER. *In* Determination of organic structures by physical methods. Vol. 5. *Edited by* F. C. Nachod and J. J. Zuckerman. Academic Press, New York, NY. 1973.
8. J. M. LEHN and J. P. KINTZINGER. *In* Nitrogen nmr. *Edited by* M. Witanowski and G. A. Webb. Plenum Press, London and New York. 1971.
9. H. IWAHASHI and Y. KYOGOKU. Nature, **271**, 278 (1978).
10. G. BINSCH, J. B. LAMBERT, B. W. ROBERTS, and J. D. ROBERTS. J. Am. Chem. Soc. **86**, 5564 (1964).
11. A. J. R. BOURN and E. W. RANDALL. Mol. Phys. **8**, 567 (1964).
12. R. R. SHOUP, E. D. BECKER, and H. T. MILES. Biochem. Biophys. Res. Commun. **43**, 1350 (1971).

[4]The effects of the asymmetry parameter η are expected to be relatively minor and constant in the series. Typical η are ≈ 0.3 in similar compounds (6).

Appendix

Observed proton T_1 and $T_{1\rho}$ at 25°C

		$^1HT_{1\rho}$ (s)					
Base proton	$^1HT_1$ (s)	$\omega_1 = 17500^a$	$\omega_1 = 12800$	$\omega_1 = 9500$	$\omega_1 = 6600$	$\omega_1 = 4650$	$\omega_1 = 2600$
G-NH	0.77	0.27	0.19	0.15	0.11	0.093	0.083
G-NH_2	0.27	0.14	0.12	0.11	0.099	0.094	0.086
2G-NH	0.71	0.26	0.19	0.15	0.11	0.096	0.087
2G-NH_2	0.25	0.13	0.12	0.11	0.098	0.094	0.092
T-NH	1.69	0.61	0.37	0.24	0.13	0.075	0.043
2T-NH	2.08	0.51	0.32	0.20	0.12	0.080	0.051
A-NH_2	0.49	0.23	0.17	0.13	0.10	0.082	0.073
C-NH_2	0.54	0.27	0.19	0.14	0.10	0.081	0.059
G + C, G-NH	0.33	0.19	0.16	0.13	0.11	0.10	0.069
G-NH_2	0.19	0.12	0.11	0.10	0.10	0.097	0.097
C-NH_2	0.32	0.16	0.13	0.10	0.086	0.071	0.060
G + A, G-NH	0.71	0.23	0.17	0.13	0.097	0.079	0.064
G-NH_2	0.26	0.17	0.12	0.11	0.098	0.092	0.091
A-NH_2	0.49	0.22	0.17	0.13	0.10	0.084	0.076
G + T, G-NH	1.21	0.38	0.24	0.20	0.11	0.088	0.068
G-NH_2	0.27	0.13	0.12	—	0.099	0.093	0.091
T-NH	1.20	0.38	0.25	0.19	0.13	0.091	0.066
A + T, T-NH	1.17	0.27	0.17	0.12	0.083	0.059	0.041
A-NH_2	0.47	0.21	0.16	0.13	0.10	0.085	0.072
T + C, T-NH	0.75	0.35	0.23	0.17	0.11	0.072	0.043
C-NH_2	0.76	0.30	0.20	0.14	0.096	0.070	0.049
A + C, A-NH_2	0.48	0.23	0.17	0.13	0.10	0.090	0.073
C-NH_2	0.52	0.25	0.19	0.14	0.10	0.083	0.065

[a]ω_1 is the proton resonance frequency in the rotating frame and is expressed in radians per second.

Interaction entre les réactifs lanthanidiques et les bases de Lewis: Application à l'analyse conformationnelle d'alcools cyclohexaniques

JAMES BOUQUANT,[1] ALAIN MAUJEAN ET JOSSELIN CHUCHE

Laboratoire de Chimie Organique Physique, Centre de Spectroscopie moléculaire, E.R.A. 688 associée au C.N.R.S., B.P. 347, 51062 Reims, France

Reçu le 14 juillet 1978

JAMES BOUQUANT, ALAIN MAUJEAN et JOSSELIN CHUCHE. Can. J. Chem. **57**, 1080 (1979).

Une méthode de détermination des paramètres intrinsèques K et Δ de complexes réactif lanthanidique–substrat a été étendue aux molécules conformationnellement mobiles. Ces paramètres déterminés pour une série d'alcools cyclohexaniques secondaires (cyclohexanol et méthyl-2 cyclohexanol) et tertiaires (méthyl-1 cyclohexanol et éthyl-1 cyclohexanol) complexés par $Eu(DPM)_3$ et $Yb(DPM)_3$ ont permis de déterminer les constantes d'équilibre conformationnelles entre les espèces libres d'une part, et les espèces complexées d'autre part.

Les résultats obtenus pour les espèces libres sont en bon accord avec ceux obtenus par d'autres méthodes physico-chimiques. Pour les espèces complexées, un déplacement de l'équilibre conformationnel important est observé dans le cas des faibles valeurs des quotients d'association.

Pour la première fois, le groupement *tert*-butyle du réactif $Yb(DPM)_3$ a été utilisé comme sonde conformationnelle.

JAMES BOUQUANT, ALAIN MAUJEAN, and JOSSELIN CHUCHE. Can. J. Chem. **57**, 1080 (1979).

A method for the determination of the intrinsic parameters K and Δ for lanthanide–substrate complexes has been extended to conformationally mobile molecules. These parameters, determined for a series of secondary cyclohexane alcohols (cyclohexanol and 2-methylcyclohexanol) and for tertiary alcohols (1-methylcyclohexanol and 1-ethylcyclohexanol) complexed with $Eu(DPM)_3$ and $Yb(DPM)_3$ lead to the determination of the conformational equilibrium constants between the free species on one part and the complexed species on the other.

The results obtained for the free species are in good agreement with those obtained by other physicochemical methods. For the complexed species an appreciable shift of conformational equilibrium is noted for low values of the association constants.

For the first time, the *tert*-butyl group of $Yb(DPM)_3$ has been used as a conformational probe.

[Journal translation]

Introduction

Ces dernières années les réactifs de déplacement chimique ont été très utilisés pour déterminer la configuration de substrats conformationnellement homogènes (1, 2); par contre, les résultats relatifs à des systèmes conformationnellement mobiles sont beaucoup moins nombreux. Les études portent, en particulier, sur la rotation des amides (3–5) et des amino esters (6), systèmes pour lesquels la barrière énergétique entre les rotamères est assez élevée. Dans l'étude des équilibres conformationnels pour lesquels il existe un échange rapide, il est admis que les variations des déplacements chimiques avec la concentration du réactif paramagnétique sont à relier aux populations et aux déplacements chimiques intrinsèques des conformères; ces derniers sont ceux de composés modèles complexés (7–10) ou évalués (11–17) en utilisant l'équation de MacConnell–Robertson (18). Toutefois, on peut remarquer que ces méthodes supposent que l'aptitude à se complexer des différentes espèces en équilibre rapide est la même et que le chélate n'a pas d'effet sur cet équilibre. Cette hypothèse ne semble pas toujours vérifiée: en effet, un déplacement des équilibres rotationnels (3–6, 19) et conformationnels (7, 13 et références citées, 14, 20–23) a été mis en évidence en présence de réactif. En ce qui concerne les alcools cyclohexaniques, objets de ce travail, il a été montré (24, 25) que la valeur de la constante d'interaction dépend fortement de la position axiale ou équatoriale de l'hydroxyle. Dans une note précédente (26), nous avons décrit la première étude quantitative d'un équilibre conformationnel qui tient compte d'un éventuel déplacement de l'équilibre conformationnel par le réactif.

Nous nous proposons ici de compléter cette étude en montrant que la méthode de détermination des paramètres caractéristiques de l'interaction entre les réactifs lanthanidiques et les bases de Lewis, développée précédemment (27), peut s'appliquer aux molécules conformationnellement mobiles. Les paramètres apparents (K et Δ) ainsi obtenus, permet-

[1]Cette publication constitue une partie de la thèse de Doctorat ès-Sciences soutenue par J.B.

0008-4042/79/091080-09$01.00/0

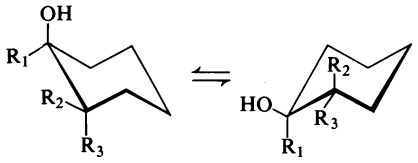

	R_1	R_2	R_3
1	H	H	H
2	H	CH_3	H
3	H	H	CH_3
4	CH_3	H	H
5	CH_2—CH_3	H	H

SCHÉMA 1

tent de calculer la constante d'équilibre conformationnel entre les espèces libres d'une part, et complexées d'autre part.

Le modèle proposé sera ensuite testé sur des alcools cyclohexaniques conformationnellement mobiles substitués ou non en positions 1 et 2 (Schéma 1).

Le choix de ces substrats se justifie dans la mesure où les constantes d'équilibre conformationnel sont connues ou peuvent être estimées. Leur connaissance nous permettra de dégager un certain nombre de critères pour apprécier la validité des valeurs obtenues. Nous montrerons, également, l'intérêt de changer de réactif ou de solvant dans une telle étude.

Modèle proposé

Le modèle proposé s'applique à un nombre quelconque de conformères, toutefois pour simplifier, nous considèrerons seulement le cas de deux conformères S_a et S_e pour le substrat S. Dans l'hypothèse de la formation de complexes de stoechiométrie 1:1 (25) en présence d'un réactif de déplacement chimique, on peut postuler l'existence des équilibres suivants:

$$\begin{array}{ccc} S_a + R & \overset{K_1}{\rightleftharpoons} & S_e + R \\ \Big\downarrow\uparrow K_a & & \Big\downarrow\uparrow K_e \\ S_aR & \overset{K_c}{\rightleftharpoons} & S_eR \end{array}$$

K_a, K_e d'une part, K_1 et K_c d'autre part, sont respectivement les constantes d'association de S_a et S_e avec R et d'équilibres conformationnels des formes libres et associées.

Désignons par C^0 et C les concentrations initiales et à l'équilibre, et par δ et δ_{RS} respectivement les déplacements chimiques mesurés en référence interne des conformères libres et complexes. Le déplacement chimique observé est alors donné par la relation [1]:

$$[1] \quad \delta_{obs} = \frac{C_{S_a}\delta_a + C_{S_e}\delta_e + C_{RS_a}\delta_{RS_a} + C_{RS_e}\delta_{RS_e}}{C_S^0}$$

Nous admettrons que δ_a et δ_e peuvent être assimilés au déplacement chimique du substrat libre ($\delta_a \simeq \delta_e \simeq \delta_0$) qui est la moyenne pondérée de ces deux valeurs.[2] Dans ces conditions, l'expression du déplacement chimique induit par le réactif s'écrit:

$$[2] \quad \delta_{ind} = \delta_{obs} - \delta_0 = \frac{C_{RS_a}\Delta_a + C_{RS_e}\Delta_e}{C_S^0}$$

Dans cette expression $\Delta_a = \delta_{RS_a} - \delta_0$ et $\Delta_e = \delta_{RS_e} - \delta_0$, sont les déplacements chimiques intrinsèques des noyaux engagés dans le complexe.

En outre, la loi d'action de masse permet de relier les concentrations entre elles:

$$[3] \quad K_a = \frac{C_{RS_a}}{C_{S_a}C_R}; \quad K_e = \frac{C_{RS_e}}{C_{S_e}C_R}$$
$$K_1 = \frac{C_{S_e}}{C_{S_a}}; \quad K_c = K_1\frac{K_e}{K_a}$$

Après combinaisons des éqs [2] et [3] nous obtenons:

$$[4] \quad \delta_{ind}(1 + K_1)(\Delta_a + K_c\Delta_e) = K_a(\Delta_a + K_c\Delta_e - \delta_{ind}(1 + K_c)) \times (C_R^0(\Delta_a + K_c\Delta_e) - \delta_{ind}C_S^0(1 + K_c))$$

Si les concentrations initiales en réactif et en substrat sont maintenues égales (27), l'éq. [4] s'écrit:

$$[5] \quad \delta_{ind} = -\left(\frac{(\Delta_a + K_c\Delta_e)(1 + K_1)}{K_a(1 + K_c)^2}\right)^{1/2}\left(\frac{\delta_{ind}}{C_S^0}\right)^{1/2} + \frac{\Delta_a + K_c\Delta_e}{1 + K_c}$$

Il apparaît que la courbe représentative de la fonction $\delta_{ind} = f(\delta_{ind}/C_S^0)^{1/2}$ est une droite de pente P_m et d'ordonnée à l'origine Δ_m

$$[6] \quad P_m = -\left(\frac{(\Delta_a + K_c\Delta_e)(1 + K_1)}{K_a(1 + K_c)^2}\right)^{1/2}$$

$$[7] \quad \Delta_m = \frac{\Delta_a + K_c\Delta_e}{1 + K_c}$$

Posons $K_m = \Delta_m/P_m{}^2$

$$[8] \quad K_m = \frac{K_a(1 + K_c)}{(1 + K_c)}$$

où K_m et Δ_m sont les paramètres intrinsèques apparents du complexe S–Eu(DPM)$_3$.

Après combinaisons des éqs [7] et [8], nous ob-

[2]La différence $\delta_a - \delta_e$ est de quelques hertz, alors que les déplacements chimiques induits sont comprise entre 10 et 20 ppm.

tenons les expressions suivantes:

$$[9] \qquad K_1 = \frac{K_a - K_m}{K_m - K_e}$$

$$[10] \qquad K_1 = \frac{K_a(\Delta_a - \Delta_m)}{K_e(\Delta_m - \Delta_e)}$$

$$[11] \qquad K_c = \frac{K_e}{K_a} K_1 = \frac{\Delta_a - \Delta_m}{\Delta_m - \Delta_e}$$

Ces équations sont formellement analogues à celles proposées par Stolow (28) et Eliel et Luckack (29) respectivement dans le cas de la protonation des amines et de mesures cinétiques de la solvolyse de tosylates de cyclohexyle.

Ces relations indiquent clairement que la connaissance des déplacements chimiques intrinsèques permet uniquement de calculer K_c. Les paramètres des conformères nécessaires à l'évaluation de K_1 peuvent être estimés à partir d'une étude de la complexation de composés modèles semblables.

Quelle que soit la méthode utilisée pour évaluer les paramètres intrinsèques, ceux-ci sont déterminés avec une incertitude fonction de la nature du substrat du réactif ou du solvant (25). Les constantes d'équilibre conformationnel K_1 ou K_c seront acceptables à la condition nécessaire que la variable X_a ou X_e (notée $X_{a/e}$) soit significativement différente de X_m (X désigne le quotient d'association ou le déplacement chimique intrinsèque). Les deux variables $X_{a/e}$ et X_m étant calculées dans deux échantillons indépendants, la condition précédente sera vérifiée (30) si la variable aléatoire:

$$X_d = \frac{X_{a/e} - X_m}{\sigma_{(X_{a/e} - X_m)}}$$

ne suit pas une loi de Student.

Dans l'expression ci-dessus, $\sigma_{X_{a/e} - X_m}$ représente l'écart type estimé de la différence $X_{a/e} - X_m$.

En d'autres termes, $X_{a/e} - X_m$ sera significativement différent de zéro si la condition $X_d > t_{\nu,\alpha}$ ou $z = X_d/t_{\nu,\alpha} > 1$ est vérifiée. La borne $t_{\nu,\alpha}$ donnée par la table de Student, est atteinte dans moins de $\alpha\%$ des cas pour ν degrés de liberté ($\nu = n_{a/e} + n_m - 4$: expression dans laquelle n représente le nombre de mesures de la variable $X_{a/e}$ ou X_m).

Determination des paramètres intrinsèques

Nous savons que la précision de mesure des paramètres intrinsèques est fonction de la grandeur des quotients d'association (27). Il était donc intéressant de comparer les complexations des cyclohexanols avec, d'une part $Eu(DPM)_3$[3] (association la plus forte), et d'autre part $Yb(DPM)_3$ (association la plus faible) (25).

[3](DPM)H = tétraméthyl-2,2,6,6 heptane dione-3,5.

Réactif de déplacement chimique Eu(DPM)$_3$

Les valeurs des quotients d'association et des déplacements chimiques intrinsèques des complexes $Eu(DPM)_3$–cyclohexanols conformationnellement mobiles (**1** à **5**) en solution dans le chloroforme deutérié sont reportées dans le tableau 1. Dans ce même tableau sont également rappelés les paramètres intrinsèques des *tert*-butyl-4 cyclohexanols homologues qui ont été étudiés (25) dans les mêmes conditions expérimentales. Ces alcools sont notés (tableau 1) avec un indice a ou e pour rappeler la position axiale ou équatoriale de la fonction alcool.

La comparaison des résultats fait apparaître que les valeurs des paramètres intrinsèques obtenues pour les alcools conformationnellement mobiles sont toujours comprises entre celles des dérivés tertiobutylés. En ce qui concerne l'alcool tertiobutylé $\mathbf{3}_a$, homologue de la conformation *trans* di-axiale de l'isomère **3**, il n'a pas pu être isolé; toutefois, pour l'alcool $\mathbf{3}_a$, le méthyle axial étant trans à l'hydroxyle, l'influence de ce méthyle sur la complexation doit être faible, voire nulle (25). De ce point de vue, il est à prévoir pour l'isomère $\mathbf{3}_a$ des valeurs des paramètres intrinsèques proches de celles du *tert*-butyl-4 cyclohexanol *cis* ($K = 323\ M^{-1}$ et $\Delta = 26.49$ ppm calculées (25) à partir de l'hydrogène en position 1). On peut d'ailleurs remarquer que les paramètres intrinsèques de **3** sont bien compris entre ceux de cet alcool et de l'alcool $\mathbf{3}_e$.

Réactif de déplacement chimique Yb(DPM)$_3$

Dans les conditions expérimentales utilisées ($C_R^0 = C_S^0$), ce réactif présente l'inconvénient de provoquer des élargissements de raies tels que nous perdons l'information relative à la multiplicité de ces raies. Cet élargissement explique pourquoi nous nous sommes limités à la détermination des déplacements chimiques des raies des radicaux méthyle et *tert*-butyle. En effet, seules ces raies peuvent être mesurées avec une précision acceptable.

En outre, les quotients d'association avec $Yb(DPM)_3$ étant plus faibles que ceux avec $Eu(DPM)_3$ (25), nous avons pu envisager l'étude d'une part des alcools **1**, **4** et **5** dans le tétrachlorure de carbone et d'autre part des alcools **1** et **5** dans le chloroforme deutérié.

La comparaison des valeurs des paramètres intrinsèques (K et Δ, tableau 2) à celles rapportées dans le tableau 1 fait apparaître clairement que les déplacements chimiques avec $Yb(DPM)_3$ sont environ 3.5 fois plus grands que ceux observés avec $Eu(DPM)_3$. Quant aux quotients d'association, ils restent inférieurs à ceux de $Eu(DPM)_3$ même lorsque le solvant est le tétrachlorure de carbone. Par contre, nous retrouvons des propriétés communes pour ces deux réactifs, à savoir: (*i*) le *tert*-butyl-4 cyclohexanol *cis*

TABLEAU 1. Paramètres intrinsèques des complexes Eu(DPM)$_3$–cyclohexanol (**1–5**) en solution dans le chloroforme deutérié*

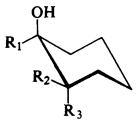

No†	N‡	R_1	R_2	R_3	K (M^{-1}) R_1	K (M^{-1}) R_2	K (M^{-1}) R_3	Δ (ppm) R_1	Δ (ppm) R_2	Δ (ppm) R_3
1$_a$	1				324 ± 16			26.47 ±0.11		
1	1	H	H	H	301 ±172	—	—	24.8 ±1.3	—	—
1$_e$	1				243 ± 18			24.34 ±0.20		
2$_a$	1				166.8± 7.5	164.8± 7.2		26.3 ±0.16	10.607±0.062	
2	1	H	CH_3	H	174.3± 9.5	172.6± 8.1	—	25.93 ±0.18	10.653±0.063	—
2$_e$	1				271 ± 75	260 ±16		25.4 ±3.2	10.82 ±0.18	
3	1	H	H	CH_3	177 ± 21	—	169.7±7.7	24.86 ±0.33	—	10.208±0.057
3$_e$	1				172 ± 17		165.2±7.1	24.31 ±0.30		10.318±0.061
4$_a$	1				70.4± 2.7			16.63 ±0.15		–
4	1	CH_3§	H	H	94.2± 3.7	—	—	16.32 ±0.13	—	—
4$_e$	1				124.1± 5.1			15.95 ±0.12		
5$_a$	2				49.6± 2.6			15.62 ±0.21		
5	3	CH_2§	H	H	72.2± 3.5	—	—	14.95 ±0.15	—	—
5$_e$	2				100.2± 2.5			14.483±0.058		
5$_a$	2				50.0± 2.6			8.14 ±0.11		
5	3	CH_3§	H	H	73.0± 3.8	—	—	8.814±0.098	—	—
5$_e$	2				99.6± 3.3			10.648±0.062		

*Les erreurs statistiques sont calculées pour des limites de confiance de 95%.
†Les alcools conformationnellement mobiles sont notés sans indice. Les *tert*-butyl-4 cyclohexanols homologues sont notés avec un souscrite a ou e pour rappeler la position axiale ou équatoriale de la fonction alcool.
‡N = nombre d'expériences independantes.
§Protons observés.

interagit plus fortement que le *trans*; (*ii*) les valeurs des paramètres intrinsèques des alcools mobiles sont situées entre celles des alcools homologues conformationnellement homogènes, excepté pour le déplacement chimique du méthyle de l'alcool **4**.

Dans le tableau 2 sont également consignés des résultats originaux relatifs aux paramètres intrinsèques des *tert*-butyles du ligand DPM. Il avait été observé (31), qualitativement, que l'addition de substrat à $Eu(FOD)_3$ entraînait un déplacement de la résonance des *tert*-butyles du réactif vers les champs forts. Nous avons envisagé une étude quantitative de ce déplacement dans le but de trouver éventuellement une voie d'accès aux quotients d'association. En particulier, avec $Yb(DPM)_3$, la variation du déplacement chimique des *tert*-butyles est suffisante pour déterminer les paramètres intrinsèques correspondant à ce groupement. En examinant les résultats, on constate un excellent accord entre les quotients d'association déterminés à partir du réactif ou du substrat (tableau 2). Remarquons dès maintenant que cette concordance peut être intéressante d'un point de vue pratique pour l'étude de la complexation de substrats pour lesquels les noyaux ont une raie de résonance très large (mesure imprécise du déplacement chimique) ou pas de raie de résonance.

Les valeurs des déplacements chimiques intrinsèques des *tert*-butyles du réactif sont indépendantes du solvant mais, par contre, sont influencées par une interaction stérique entre le substrat et le réactif. En effet, pour un alcool de configuration donnée, le déplacement chimique intrinsèque est d'autant plus grand que le substituant porté par le carbone 1 est plus volumineux (comparer entre eux $\mathbf{1}_a$, $\mathbf{4}_a$ et $\mathbf{5}_a$ ou $\mathbf{1}_e$, $\mathbf{4}_e$ et $\mathbf{5}_e$). En outre, pour deux alcools épimères en 1, on observe entre les déplacements un écart qui croît avec l'encombrement stérique du substituant (comparer $\mathbf{1}_a$ et $\mathbf{1}_e$, puis $\mathbf{4}_a$ et $\mathbf{4}_e$, et enfin $\mathbf{5}_a$ et $\mathbf{5}_e$). Ce résultat peut être interprété comme un changement de géométrie du réactif complexé (31, 32). En l'absence de substrat, il existe une interaction réactif–solvant puisque le déplacement chimique des groupements *tert*-butyles, mesurés par rapport à une référence interne de cyclohexane, sont respectivement de -91 ± 0.3 Hz dans le tétrachlorure de carbone et de -107.5 ± 0.3 Hz dans le chloroforme deutérié.

Dans le cas de $Eu(DPM)_3$, l'écart $\Delta_a - \Delta_e$ des valeurs extrêmes des déplacements chimiques intrinsèques ($\Delta(\mathbf{1}_a) = 26 \pm 3$ Hz; $\Delta(\mathbf{1}_e) = 26 \pm 5$ Hz; $\Delta(\mathbf{4}_a) = 39 \pm 3$ Hz et $\Delta(\mathbf{4}_e) = 33 \pm 3$ Hz à 60 MHz) des groupements *tert*-butyles du réactif sont plus faibles que ceux déterminés avec $Yb(DPM)_3$; ce qui semble confirmer l'origine stérique plutôt qu'électronique de ces effets (rayon ionique de Eu^{3+} superieur à celui de Yb^{3+}. Ce faible écart exclut l'utilisation des groupements *tert*-butyles de $Eu(DPM)_3$ pour des études quantitatives.

Analyse conformationnelle

L'évaluation des paramètres X_a ou X_e intervenant dans les éqs [9] à [11] ne peut pas se déduire de l'étude à basse température du complexe $Eu(DPM)_3$–substrat conformationnellement mobile. En effet, on n'observe jamais qu'un seul signal très large à -120°C pour le cyclohexanol **1** complexé, élargissement de la raie de résonance attribué à un ralentissement de la relaxation électronique (3). Les valeurs de ces paramètres peuvent être déduites des dérivés *cis* et *trans tert*-butylés en 4 conformationnellement homogènes. Cette approximation est justifiée dans la mesure où la présence d'un groupement *tert*-butyle en position équatoriale a une influence négligeable sur les valeurs de ces paramètres intrinsèques. Nous avons constaté, en effet, que deux alcools de même configuration mais appartenant respectivement à la série stéroïdique et cyclohexanique ont des valeurs de K et Δ très voisines (25). En remplaçant dans les éqs [9] à [11] les différents paramètres par leurs valeurs extraites des tableaux 1 et 2, nous pouvons calculer les constantes d'équilibre conformationnel des alcools **1** à **5**. Nous en déduisons alors directement la différence d'enthalpie libre calculée par la relation classique:

$$\Delta G^0 = -RT \log K$$

Les résultats obtenus avec les alcools cyclohexaniques secondaires et tertiaires sont rassemblés respectivement dans les tableaux 3 et 4. Dans ces tableaux, nous avons éliminé les valeurs de ΔG^0 calculées à partir des paramètres pour lesquels z est inférieur à l'unité au seuil 5% (*vide supra*). On constate en effet que ces valeurs comparées à celles de la littérature sont aberrantes.

D'une manière générale, nous remarquons que les valeurs de $\Delta G_1{}^0$ calculées à partir des valeurs des quotients d'association sont en bon accord, alcool **1** excepté, avec celles relevées dans la littérature et rappelées dans les tableaux. Dans le cas du cyclohexanol, le $z_{K_a - K_m}$ inférieur à 1 est dû à la faible différence entre les valeurs des quotients d'association (tableaux 1 et 2) et à une grande incertitude sur leurs déterminations. En effet, nous avons montré (27) que les erreurs sur la détermination des K sont d'autant plus grandes que les valeurs de ceux-ci sont plus élevées. La diminution de ces paramètres par utilisation de $Yb(DPM)_3$ et du chloroforme deutérié entraîne une meilleure détermination de ΔG^0.

En ce qui concerne les alcools tertiaires, nous ne connaissons pas de valeurs de $\Delta G_1{}^0$ déterminées par d'autres méthodes dans des solvants "inertes" à une température voisine de 40°C. Cependant, on peut

TABLEAU 2. Paramètres intrinsèques des complexes Yb(DPM)$_3$–cyclohexanol (**1**, **4** et **5**)*

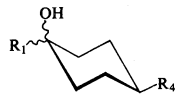

No	R_1	R_4	K (M^{-1}) R_1	K (M^{-1}) R_4	K (M^{-1}) DPM	Δ (ppm) R_1	Δ (ppm) R_4	Δ (ppm) DPM
			Solvant: tétrachlorure de carbone					
$\mathbf{1}_a$	H (équat.)	*t*Bu	‡	150 ±24	155 ±13	‡	10.60 ±0.34	−2.859±0.052
1	H	H	‡	—	152 ±14	‡	—	−2.948±0.045
$\mathbf{1}_e$	H (axial)	*t*Bu	‡	156 ±12	105.3 ± 8.7	‡	6.66 ±0.10	−2.994±0.058
$\mathbf{4}_a$	CH_3 (équat.)	*t*Bu	15.88†±0.62	16.12†± 0.76	15.89± 0.96	56.5† ±1.5	7.43†±0.24	−4.63 ±0.12
4	CH_3	H	23.2† ±2.0	—	27.0 ± 1.7	57.0† ±2.4	—	−4.040±0.086
$\mathbf{4}_e$	CH_3 (axial)	*t*Bu	38.9† ±1.7	39.4† ± 2.1	39.1 ± 4.6	54.13†±0.73	8.09†±0.14	−3.79 ±0.14
$\mathbf{5}_a$	CH_2‖ | CH_3 (équat.)	*t*Bu	8.88 ±0.67 8.73 ±0.67	8.8 ± 1.4	8.5 ± 1.3	55.9 ±2.1 27.8 ±1.1	5.98 ±0.48	−5.62 ±0.43
5	CH_2‖ | CH_3	H	16.52 ±0.73 16.17 ±0.73	—	15.5 ± 1.0	52.62 ±0.93 29.91 ±0.54	—	−4.76 ±0.14
$\mathbf{5}_e$	CH_2‖ | CH_3 (axial)	*t*Bu	27.2 ±2.3 25.6 ±3.3	26.1 ± 3.3	24.8 ± 2.2	52.4 ±1.4 36.6 ±1.7	7.94 ±0.35	−4.21 ±0.14
			Solvant: chloroforme deutérié					
$\mathbf{1}_a$	H (équat.)	*t*Bu	‡	31.6 ± 2.3	30.4 ±4.4	‡	10.30 ±0.28	−2.73 ±0.15
1	H	H	‡	—	24.1[(b)]±1.5	‡		−2.929†±0.065
$\mathbf{1}_e$	H (axial)	*t*Bu	‡	23.3† ± 1.1	21.3[(b)]±1.3	‡	6.89†±0.13	−2.972†±0.075
$\mathbf{5}_a$	CH_2 | CH_3‖ (équat.)	*t*Bu	§	2.24 ± 0.72	2.41 ±0.76	§	5.8 ±1.4	−5.4 ±1.2
5	CH_2 | CH_3‖	H	§ 2.9 ±1.7	—	3.44 ±0.44	§ 33 ±13	—	−4.89 ±0.40
$\mathbf{5}_e$	CH_2 | CH_3‖ (axial)	*t*Bu	4.5 ±2.8 4.7 ±2.9	4.59 ± 0.54	5.05 ±0.81	54 ±22 37 ±15	7.93 ±0.64	−4.13 ±0.43

*Les erreurs statistiques sont calculées au risque 5%.
†Valeur obtenue par moyenne pondérée des valeurs de deux expériences indépendantes.
‡Raie trop large pour être repérée avec précision.
§Recouvrement des raies.
‖Protons observés.

TABLEAU 3. Variation d'enthalpie libre de cyclohexanols secondaires libres et complexés par $Ln(DPM)_3$

Alcool	Ln	Solvant	Groupement	X	$z_{(x_a - x_m)}$	$z_{(x_m - x_e)}$	Enthalpie libre* ΔG_1^0	Enthalpie libre* ΔG_c^0
Cyclohexanol†	Eu	$CDCl_3$	H(1)	Δ	7.0	1.8	−0.99	−0.81
	Eu	$CDCl_3$	H(1)	*K*	0.7	1.7		
	Yb	CCl_4	*t*Bu(DPM)	Δ	2.1	1.0	−0.65	−0.41
	Yb	CCl_4	*t*Bu(DPM)	*K*	0.3	4.6		
	Yb	$CDCl_3$	*t*Bu(DPM)	Δ	2.4	0.6		
	Yb	$CDCl_3$	*t*Bu(DPM)	*K*	2.8	2.0	−0.49	−0.27
Methyl-2 cyclohexanol *cis*‡	Eu	$CDCl_3$	H(1)	Δ	2.6	<1§		
	Eu	$CDCl_3$	H(1)	*K*	1.0	≫1§	1.60	1.29
	Eu	$CDCl_3$	CH_3(2)	Δ	0.9	<1§		
	Eu	$CDCl_3$	CH_3(2)	*K*	1.2	≫1§	1.51	1.22

*Les valeurs de ΔG^0 sont exprimées en kcal/mol à 41°C.
†Les valeurs de ΔG^0 (T °C) de **1** relevées dans la littérature (réfs 33–35) sont comprises entre −0.6 (25°C) et −1.17 (−76°C) kcal/mol.
‡Sipos et coll. (36) proposent une valeur de ΔG^0 (25°C) = 1.5 kcal/mol.
§La valeur de z est estimée à partir des intervalles de confiance (tableau 1).

TABLEAU 4. Variation d'enthalpie libre de cyclohexanols tertiaires libres et complexés par $Ln(DPM)_3$

Alcool	Ln	Solvant	Groupement	X	$z_{(x_a - x_m)}$	$z_{(x_m - x_e)}$	Enthalpie libre* ΔG_1^0	Enthalpie libre* ΔG_c^0
Methyl-1 cyclohexanol†	Eu	$CDCl_3$	CH_3(1)	*K*	8.4	7.7	0.14	−0.21
	Eu	$CDCl_3$	CH_3(1)	Δ	2.5	3.4	0.47	
	Yb	$CDCl_3$	*t*Bu(DPM)	*K*	9.2	5.3	0.06	−0.50
	Yb	$CDCl_3$	*t*Bu(DPM)	Δ	6.4	3.1	0.04	−0.53
Ethyl-1 cyclohexanol‡	Eu	$CDCl_3$	CH_2—CH_3(1)	*K*	7.0	8.1	0.13	−0.31
	Eu	$CDCl_3$	CH_2—CH_3(1)	Δ	3.4	4.0	0.21	−0.23
	Eu	$CDCl_3$	CH_2—CH_3(1)	*K*	6.8	6.1	0.09	−0.34
	Eu	$CDCl_3$	CH_2—CH_3(1)	Δ	5.8	20	1.06	
	Yb	CCl_4	CH_2—CH_3(1)	*K*	14	9.9	0.21	−0.49
	Yb	CCl_4	CH_2—CH_3(1)	Δ	2.8	0.2		
	Yb	CCl_4	CH_2—CH_3(1)	*K*	13	5.2	0.15	−0.52
	Yb	CCl_4	CH_2—CH_3(1)	Δ	3.5	6.0	1.38	
	Yb	$CDCl_3$	*t*Bu(DPM)	*K*	2.3	2.9	0.28	−0.18
	Yb	$CDCl_3$	*t*Bu(DPM)	Δ	0.7	2.1		
	Yb	CCl_4	*t*Bu(DPM)	*K*	6.6	5.8	0.17	−0.50
	Yb	CCl_4	*t*Bu(DPM)	Δ	3.6	4.4	0.40	

*Les valeurs de ΔG^0 sont exprimées en kcal/mol à 41°C.
†Valeurs de ΔG^0 comprises entre +0.21 (25°C) et 0.41 (−80°C) kcal/mol (réfs 37 et 34).
‡ΔG^0 = +0.47 kcal/mol à −82°C dans le sulfure de carbone (34).

s'attendre à ce que les différences d'énergie libre pour les molécules **5** et **6** soient comparables, car il est généralement admis que les énergies libres des groupes méthyles et éthyles sont équivalentes (35 et références citées). Nous observons effectivement que nous pouvons attribuer aux alcools tertiaires **4** et **5** une valeur moyenne, calculée à partir des quotients d'association, de ΔG_1^0 = 0.16 kcal/mol. Cette valeur indépendante du réactif ou du solvant est comparable à celles de 0.21 et 0.24 kcal/mol déterminées par équilibration de **4** en présence respectivement d'acide acétique (37) et d'acide perchlorique (38) en solution aqueuse. Par contre, elle est très inférieure à la valeur de 0.41 kcal/mol obtenue par intégration des raies de résonance magnétique nucléaire des deux conformères (34 et références citées) à basse température.

Quant aux valeurs de ΔG_1^0 calculées à partir des déplacements chimiques, l'accord entre les valeurs observées et attendues est beaucoup moins satisfaisant. On constate en général pour une même expérience que la valeur de $z_{\Delta_a/_e - \Delta_m}$ est alors inférieure à $z_{K_a/_e - K_m}$ à l'exception du méthyle de **5** (tableau 4). Dans ce dernier exemple, il est vraisemblable que la conformation de la chaine éthyle dans les conformères axiaux et équatoriaux diffère de celle des composés modèles complexés par le réactif, l'effet étant moins sensible pour le groupement méthylène du radical éthyle.

Des valeurs de ΔG^0 plus précises pourraient être

déterminées en considérant des groupements éloignés du site fonctionnel tels que H(2)*trans* ou H(3)*cis*. Cependant, en présence de $Eu(DPM)_3$ et $Yb(DPM)_3$, nous observons, à 60 MHz, un recouvrement des raies de ces hydrogènes cyclohexaniques, en particulier dans les isomères conformationnellement mobiles.

Dans les tableaux 3 et 4, nous avons uniquement rapporté les valeurs de ΔG_c^0 calculées à partir des valeurs des paramètres qui donnaient les valeurs de ΔG_1^0 les plus proches des valeurs attendues. En présence de réactif paramagnétique, nous observons toujours un déplacement de l'équilibre conformationnel qui s'accompagne d'une diminution de la différence d'enthalpie libre à l'exception du cyclohexanol. Compte tenu de [11], l'importance du déplacement croît avec le rapport K_e/K_a et nous constatons que le réactif le moins complexant $Yb(DPM)_3$ déplace davantage l'équilibre que $Eu(DPM)_3$. L'équilibre ne sera pas déplacé lorsque $K_e = K_a$, condition souvent admise implicitement mais rarement vérifiée.

Conclusion

La méthode de détermination des paramètres intrinsèques K et Δ des complexes réactif–substrat, développée précédemment (27) a été étendue à celle des molécules conformationnellement mobiles. Les paramètres déterminés dans le cas des cyclohexanols ont permis de calculer des différences d'enthalpie libre ΔG_1^0 comparables à celles atteintes par d'autres techniques physico-chimiques. Ces résultats obtenus par utilisation de réactifs de pouvoir complexant très différent nous autorisent à accorder un seuil de confiance élevé à la grandeur des paramètres intrinsèques.

Les valeurs les plus satisfaisantes de ΔG_1^0 ont été déterminées à partir des quotients d'association. D'un point de vue pratique, s'il y a discordance, pour un complexe donné, entre les valeurs de ΔG_1^0 obtenues à partir de K et de Δ, le choix doit s'effectuer par référence au test statistique. La validité de ce test sera renforcée en augmentant le nombre d'expériences indépendantes (minimisation des erreurs systématiques).

Pour la première fois, à notre connaissance, nous avons utilisé le groupement *tert*-butyle du réactif comme "sonde conformationnelle."

Enfin, nous avons constaté, dans tous les cas étudiés, un déplacement de l'équilibre conformationnel des molécules complexées, d'autant plus grand que le quotient d'association est plus faible. Aussi, toute étude structurale par résonance magnétique nucléaire de molécules conformationnellement mobiles en présence de réactif devra être précédée d'une connaissance approfondie de l'aptitude à se complexer des différentes espèces en équilibre.

Partie expérimentale

Synthèse et purification des cyclohexanols

La préparation des alcools, à l'exception du cyclohexanol qui est d'origine commerciale (Merck), a été décrite précédemment (39). Avant utilisation, les cyclohexanols ont été purifiés par chromatographie en phase vapeur (cpv) puis sublimés.

En ce qui concerne la séparation des stéréoisomères du méthyl-2 cyclohexanol-1, leur séparation a dû être envisagée à partir des éthers silylés correspondants, obtenus avec un rendement quantitatif selon le protocole décrit par Corey et Venkateswarlu (40). Ces éthers silylés sont séparés par cpv sur colonne Carbowax 20 M (15%, $\frac{3}{8}$) à 70°C. Chaque stéréoisomère authentique est ensuite soumis à une hydrolyse acétique selon le protocole décrit par Corey et Venkateswarlu (40).

Préparation des échantillons

La préparation des solutions et les conditions d'enregistrement des spectres de rmn sur Varian A 60 A sont analogues à celles décrites précédemment (27).

1. A. F. Cockerill, G. L. O. Davies, R. C. Harden et D. M. Rackman. Chem. Rev. **73**, 553 (1973).
2. R. E. Sievers. Nuclear magnetic resonance, shift reagents. Academic Press, New York, NY. 1973.
3. H. N. Cheng et H. S. Gutowsky. J. Am. Chem. Soc. **94**, 5505 (1972).
4. R. A. Fletton, G. F. H. Green et J. E. Page. J. Chem. Soc. Chem. Commun. 1134 (1972).
5. H. Kessler et M. Molter. J. Am. Chem. Soc. **98**, 5969 (1976).
6. H. Kessler et M. Molter. Angew. Chem. Int. Ed. Engl. **12**, 1011 (1973).
7. T. P. Forrest, D. L. Hooper et S. Ray. J. Am. Chem. Soc. **96**, 4286 (1974).
8. K. L. Servis, D. J. Bowler et C. Ishiic. J. Am. Chem. Soc. **97**, 73 (1975).
9. K. L. Servis et D. J. Bowler. J. Am. Chem. Soc. **95**, 3392 (1973); **97**, 80 (1975).
10. J. T. Groves et M. Van der Puy. Tetrahedron Lett. 1949 (1975).
11. R. Perraud et J. L. Pierre. Bull. Soc. Chim. Fr. Pt. 2, **11**, 2615 (1974).
12. K. L. Servis et D. J. Patel. Tetrahedron, **31**, 1359 (1975).
13. P. Finocchiaro, A. Recca, W. G. Bentrude, H. W. Tan et K. C. Yee. J. Am. Chem. Soc. **98**, 3537 (1976).
14. A. J. Dale. Acta Chem. Scand. Ser. B, **30**, 255 (1976).
15. D. Doskocilova et B. Schneider. J. Mol. Struct. **31**, 337 (1976).
16. Y. Kodama, K. Nishihato et M. Nishio. J. Chem. Res. (S), **4**, 102 (1977).
17. D. J. Raber, M. D. Johnston, Jr. et M. A. Schwalke. J. Am. Chem. Soc. **99**, 7671 (1977).
18. H. M. MacConnell et R. E. Robertson. J. Chem. Phys. **29**, 1361 (1958).
19. K. L. Williamson, D. R. Clutter, R. Emch, M. Alexander, A. E. Burroughs, C. Chua et M. E. Bogel. J. Am. Chem. Soc. **96**, 1471 (1974).
20. W. G. Bentrude, H. W. Tan et K. C. Yee. J. Am. Chem. Soc. **94**, 3264 (1972).

21. A. J. DALE. Acta Chem. Scand. **26**, 2985 (1972).
22. N. PLATZER, J. J. BASSELIER et P. DEMERSEMAN. Bull. Soc. Chim. Fr. Pt. 2, **5**, 1717 (1973).
23. T. SATO et K. GOTO. J. Chem. Soc. Chem. Commun. 494 (1973).
24. M. D. JOHNSTON, JR., B. L. SHAPIRO, M. J. SHAPIRO, J. W. PROULX, A. D. GODWIN et H. L. PEARCE. J. Am. Chem. Soc. **97**, 542 (1975).
25. J. BOUQUANT. Thèse Doctorat ès Sciences, Reims. 1978.
26. J. BOUQUANT, M. WUILMET, A. MAUJEAN et J. CHUCHE. J. Chem. Soc. Chem. Commun. 778 (1974).
27. J. BOUQUANT et J. CHUCHE. Bull. Soc. Chim. Fr. Pt. 2, 959 (1977).
28. R. D. STOLOW. J. Am. Chem. Soc. **81**, 5806 (1959).
29. E. L. ELIEL et C. A. LUCKACK. J. Am. Chem. Soc. **79**, 5986 (1957).
30. A. ROSENGARD. Probabilités et statistiques en recherche scientifique, Dunod. 1972. p. 190.
31. J. REUBEN. J. Am. Chem. Soc. **95**, 3534 (1973).
32. D. SCHWENDIMEN et J. I. ZINK. Inorg. Chem. **11**, 3051 (1972).
33. E. L. ELIEL et E. C. GILBERT. J. Am. Chem. Soc. **91**, 5487 (1969).
34. J. MOULINES, J. P. BATS et M. PETRAUD. Tetrahedron Lett. 2971 (1972).
35. J. A. HIRSCH. *Dans* Topics in stereochemistry. Tome 1. *Edité par* N. L. Allinger et E. L. Eliel. Wiley Interscience, New York, NY. 1967. p. 204.
36. F. SIPOS, J. KRUPICKO, M. TICHY et J. SICHER. Coll. Czech. Chem. Commun. **27**, 2079 (1962).
37. J. J. UEBEL et H. W. GOODWIN. J. Org. Chem. **33**, 3317 (1968).
38. N. L. ALLINGER et C. D. LIANG. J. Org. Chem. **33**, 3319 (1968).
39. J. FICINI et A. MAUJEAN. Bull. Soc. Chim. Fr. 219 (1971).
40. E. J. COREY et A. VENKATESWARLU. J. Am. Chem. Soc. **94**, 6190 (1972).

Isotope effects in nucleophilic substitution reactions. II. Secondary α-deuterium kinetic isotope effects: a criterion of mechanism?

KENNETH CHARLES WESTAWAY[1] AND SYED FASAHAT ALI

Department of Chemistry, Laurentian University, Sudbury, Ont., Canada P3E 2C6

Received August 1, 1978

KENNETH CHARLES WESTAWAY and SYED FASAHAT ALI. Can. J. Chem. **57**, 1089 (1979).

A very large secondary α-deuterium kinetic isotope effect of 1.179 ± 0.007 (1.086 ± 0.003 per α-deuterium) has been observed for the S_N2 reaction of thiophenoxide ion with benzyldimethylphenylammonium ion in DMF at 0°C. This large isotope effect which is far outside the range reported for S_N2 reactions, is attributed to the fact that the extraordinarily large steric crowding around the Cα—H bonds in the substrate is reduced in the S_N2 transition state. The structure of the transition state is shown to be consistent with this hypothesis.

KENNETH CHARLES WESTAWAY et SYED FASAHAT ALI. Can. J. Chem. **57**, 1089 (1979).

Dans la réaction S_N2 de l'ion thiophénolate avec l'ion benzyldiméthylphénylammonium dans le DMF à 0°C, on a observé un effet isotopique cinétique secondaire du deutérium en alpha qui est très grand 1.179 ± 0.007 (1.086 ± 0.003 par deutérium α). Cet effet isotopique important, qui est à l'extérieur des valeurs rapportées pour des réactions S_N2, peut être attribué au fait que l'encombrement stérique qui est particulièrement important au niveau des liaisons Cα—H dans le substrat est réduit dans l'état de transition S_N2. On démontre que la structure de l'état de transition est en accord avec cette hypothèse.

[Traduit par le journal]

The magnitude of secondary α-deuterium kinetic isotope effects has been widely accepted as a criterion for distinguishing between nucleophilic substitution reactions at saturated carbon which react by way of a carbonium ion mechanism, eq. [1],

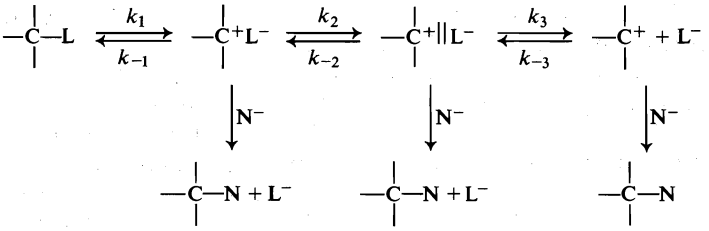

[1]

and those reacting by the one-step S_N2 mechanism (1 and ref. 2, pp. 104–137), eq. [2]

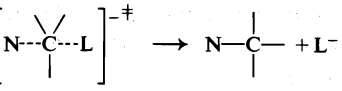

[2]

The criterion simply stated, is that large secondary α-deuterium kinetic isotope effects, i.e. $(k_H/k_D)_\alpha$ of ≥ 1.07 per α-deuterium for a primary alkyl iodide, Table 1, identifies a carbonium ion mechanism whereas isotope effects of less than 1.04 per α-deuterium for a primary substrate (3) (including inverse isotope effects) indicate that the reaction proceeds by the S_N2 mechanism.

Unfortunately, the magnitude of these isotope effects does not remain constant for a particular substrate. For example, the magnitude of the isotope effect changes significantly when (*i*) the leaving group is changed (3, 4) and also (*ii*) with a shift in the rate-determining step of a carbonium ion reaction (ref. 2, p. 137). In fact, maximum secondary α-deuterium kinetic isotope effects are observed when the formation of the solvent-separated ion pair or the free carbonium ion, i.e. when the k_2 or the k_3 step in [1], is rate determining. Smaller isotope effects of about 75% of the maximum values are observed when formation of the intimate ion pair (the k_1 step) is rate determining (ref. 2, p. 137), Table 1. Finally, the magnitude of these isotope effects can be changed to a smaller extent (1–2% per α-deuterium) by a change in solvent (5, 6).

Although the magnitude of the secondary α-deuterium kinetic isotope effects for S_N2 reactions also

[1]Author to whom all correspondence should be addressed.

0008-4042/79/091089-09$01.00/0

TABLE 1. Maximum secondary α-deuterium kinetic isotope effects for S_N reactions of primary substrates which react by way of a carbonium ion mechanism

Leaving group	Maximum $(k_H/k_D)_\alpha$ per α-deuterium (k_2 or k_3 rate determining)	$(k_H/k_D)_\alpha$ per α-deuterium if ionization (k_1) is rate determining
OTs, OBs	1.23	1.17
F	1.22	1.16
Cl	1.15	1.11
Br	1.125	1.09
I	1.09	1.07
NO_3	≥1.18	≥1.14

varies with the leaving group,[2] the variations are much smaller than those observed in carbonium ion reactions (ref. 2). This criterion of mechanism is successful in spite of these variations because the isotope effects for S_N2 reactions are significantly smaller (≤1.04 per α-deuterium) than those found for reactions involving carbonium ion intermediates.

Although many workers have measured secondary α-deuterium kinetic isotope effects for S_N reactions with the leaving groups shown in Table 1, only two isotope effects have been measured for S_N reactions of quaternary ammonium ions. Ko and Leffek (7) found very large secondary α-deuterium kinetic isotope effects (k_H/k_D) of 1.12 and 1.10 per α-deuterium at 30°C for the reaction between bromide ion and benzyldimethylphenylammonium ion in chloroform and acetone, respectively, eq. [3]. These isotope

$$3PhCH_2\overset{+}{N}(CH_3)_2PhBr^- \rightleftarrows \underset{\text{'A'}}{[(PhCH_2\overset{+}{N}(CH_3)_2Ph)_2Br^-]^+} + [PhCH_2\overset{+}{N}(CH_3)_2PhBr_2]^-$$

$$[3]\ \text{'A'} \xrightarrow{\text{slow}} \left[\begin{array}{c} PhCH_2 \quad (CH_3)_2NPh \\ Br^- \\ PhCH_2\overset{+}{N}(CH_3)_2Ph \end{array}\right]^+ \xrightarrow{\text{fast}} PhCH_2Br + (CH_3)_2NPh + PhCH_2\overset{+}{N}(CH_3)_2Ph$$

effects are considerably larger than those observed for S_N2 reactions and Leffek and Ko very reasonably concluded that these reactions must involve the formation of a carbonium ion intermediate in the slow step of the reaction. Based on this and other evidence (8, 9) these authors proposed that the reaction followed an 'ionic internal nucleophilic substitution' mechanism involving the triple ion 'A' shown in [3] (7, 10).

Although large secondary α-deuterium kinetic isotope effects should be observed for this mechanism, the formation of a benzyl carbonium ion seemed unlikely for several reasons. First, subsequent studies showed that quaternary ammonium salts could react in dipolar aprotic solvents by an S_N2 mechanism (11). Second, the reverse of these reactions, the Menshutkin reaction, occurs by an S_N2 process (12) and the principle of microscopic reversibility requires that the forward reaction also be an S_N2 process. Finally, all the experimental evidence except for the secondary α-deuterium kinetic isotope effects, is equally consistent with a mechanism where the substitution occurs in a one-step S_N2 reaction within the triple ion, 'A,' eq. [4].

$$[4]\ \text{'A'} \longrightarrow \left[\begin{array}{c} \quad Ph\ H \\ \delta^- \diagdown\ \diagup\ \delta^+ \\ Br\cdots C \cdots N(CH_3)_2Ph \\ \quad\ | \\ \quad H \\ PhCH_2\overset{+}{N}(CH_3)_2Ph \end{array}\right]^{\ddagger +} \downarrow \quad PhCH_2Br + (CH_3)_2NPh + PhCH_2\overset{+}{N}(CH_3)_2Ph$$

If the reaction occurs by the mechanism shown in [4], very large secondary α-deuterium kinetic isotope effects result when dimethylaniline is the leaving group and the criterion of mechanism based on the magnitude of these isotope effects fails.

It was important to measure a secondary α-deuterium kinetic isotope effect for an S_N2 reaction of a quaternary ammonium salt to learn if this criterion of mechanism applied to these reactions. Westaway and Poirier (11) have demonstrated that the reaction of benzyldimethylphenylammonium ion with thiophenoxide ion at 0°C in DMF is an S_N2 process, eq. [5].

$$[5]\ PhS^- + PhCH_2\overset{+}{N}(CH_3)_2Ph \longrightarrow \left[\begin{array}{c} \quad H\ Ph \\ \delta^- \diagdown\ \diagup\ \delta^+ \\ PhS\cdots C \cdots N(CH_3)_2Ph \\ \quad\ | \\ \quad H \end{array}\right]^{\ddagger} \downarrow \quad PhSCH_2Ph + (CH_3)_2NPh$$

The secondary α-deuterium kinetic isotope effect was determined for this reaction in order to test the hypothesis that an isotope effect of ≤1.04 per α-deuterium is observed for all S_N2 reactions.

[2]The magnitudes of secondary α-deuterium kinetic isotope effects for S_N2 reactions will also be affected by a change in the nucleophile.

Results and Discussion

The secondary α-deuterium kinetic isotope effect for the reaction shown in [5] was measured using the competitive technique (11, 13, 14). The isotope effect was calculated using [6].

$$[6] \qquad (k_H/k_D)_\alpha = \frac{\ln (1 - f)}{\ln \left(1 - \left(\frac{R_0}{R_f}\right) f\right)}$$

where f is the extent of reaction expressed as a fraction, R_0 is the ratio of the undeuterated to dideuterated quaternary ammonium salt in the reactant, and R_f is the ratio of the undeuterated to dideuterated benzyl phenyl sulfide in the product after small extents of reaction (15). The isotope effect per α-deuterium is the square root of the value obtained from [6]. The initial concentrations of the undeuterated and dideuterated quaternary ammonium salts in the reactant were determined from the weights of the undeuterated and deuterated quaternary salts and the deuterium content of the deuterated quaternary ammonium salt.[3] The ratio of undeuterated to dideuterated benzyl phenyl sulfide was determined in a mass spectrometric analysis of the product. The fraction of reaction was determined in a gas chromatographic analysis using the internal standard technique (11). The results are presented in Table 2.

The secondary α-deuterium kinetic isotope effect measured for small fractions of reaction for the S_N2 reaction of benzyldimethylphenylammonium ion with thiophenoxide ion at 0°C is 1.179 ± 0.007 or 1.086 per α-deuterium. The magnitude of this isotope effect is significantly larger than the maximum value of the isotope effect for S_N2 reactions, $k_H/k_D = 1.082$ or 1.04 per α-deuterium. The magnitude of this unexpectedly large isotope effect was confirmed by measuring the isotope effect at large fractions of reaction even though these isotope effects are less accurate. The isotope effects at high fractions of reaction are less accurate because (*i*) the differences between the isotopic ratios of the reactant and product are smaller (15) and thus the error in the R_0/R_f ratio, eq. [6], is larger and (*ii*) because the fraction of reaction cannot be determined as accurately at high extents of reaction. A Duncan's test (16) shows that the isotope effects measured at 36 and 63% of completion (Table 2) are not significantly different at the 96% confidence level from those measured for lower fractions of reaction. In addition, there is no trend in the isotope effects with fraction of reaction and this rules out a systematic error in the analyses. The constant value of this isotope effect over a wide range of fractions of reaction illustrates that the isotope effect for this reaction is $k_H/k_D = 1.179$ (1.086 per α-deuterium).

This secondary α-deuterium kinetic isotope effect is much larger than the upper limit of 1.04 per α-deuterium for S_N2 reactions and the criterion of mechanism based on the magnitude of this isotope effect fails, at least in the case where the leaving group is *N*,*N*-dimethylaniline. The very large isotope effect found in this study suggests that the maximum value of the isotope effect for S_N2 reactions will have to be carefully established when large, bulky leaving groups such as quaternary ammonium, sulfonium, or possibly even nitrate or arenesulfonate are involved in the reaction. Although the result of this study clearly illustrates that the magnitude of secondary α-deuterium isotope effects cannot be used as an absolute criterion of mechanism for S_N reactions, it does not totally destroy the usefulness of these isotope effects. The maximum value of 1.04 per α-deuterium is probably valid for most of the small or medium sized leaving groups in Table 1.

It is interesting to speculate on the reason for the very large isotope effect observed in the S_N2 reaction between benzyldimethylphenylammonium ion and thiophenoxide ion. The magnitude of secondary α-deuterium kinetic isotope effects is primarily determined by the changes that occur in the Cα—H out-of-plane bending vibration when the reactant is converted to the transition state (2, pp. 104–137, 17, 18). In an S_N reaction involving a carbonium ion intermediate, eq. [1], the Cα—H bonds are more sterically crowded in the tetrahedral substrate than in the transition state whether the formation of an ion pair or the free carbonium ion is rate determining. The Cα—H out-of-plane bending vibrations will be of lower frequency (energy) in the transition state of the rate-determining step and the zero point energy difference between the Cα—H and Cα—D out-of-plane bending vibrations will be smaller (19), Fig. 1*a*. A large normal isotope effect is observed for these reactions. For an S_N2 reaction, the opposite is true. Here the out-of-plane bending vibrations are usually of higher energy in the more sterically crowded trigonal bipyramidal transition state than in the tetrahedral reactant. The zero point energy difference is larger in the transition state and a small or inverse isotope effect is observed, Fig. 1*b*.

In the S_N2 reaction of the benzyldimethylphenylammonium ion the situation is again different. The bulky phenyl group and the extremely large leaving group (*N*,*N*-dimethylaniline, is even larger than a *tert*-butyl group) on the α-carbon place the Cα—H bonds in the reactant in an extremely crowded environment. Thus, the Cα—H out-of-plane bending vibrations in the substrate would be very high energy

[3]See Experimental for details.

TABLE 2. Secondary α-deuterium kinetic isotope effect for the S_N2 reaction of thiophenoxide ion with benzyldimethylphenylammonium ion in DMF at 0°C

Wt. ratio of undeuterated to deuterated substrate	$\frac{PhCH_2\overset{+}{N}(CH_3)_2Ph}{PhCD_2\overset{+}{N}(CH_3)_2Ph}$ (R_0)[a]	$\frac{PhCH_2SPh}{PhCD_2SPh}$ (R_f)	Fraction of reaction[b] (f)	k_H/k_D	k_H/k_D per α-D
$\frac{0.18630}{0.19272}$	0.99260	1.1468	0.187	1.172	1.083
$\frac{0.19455}{0.19489}$	1.0250	1.1858	0.171	1.173	1.083
$\frac{0.19380}{0.19250}$	1.0337	1.2035	0.218	1.186	1.089
$\frac{0.17017}{0.16544}$	1.0562	1.2267	0.220	$\frac{1.183}{1.179\pm0.007}$[c]	$\frac{1.088}{1.086\pm0.0032}$[c]
$\frac{0.16776}{0.16546}$	1.0411	1.1725	0.356	1.158	1.076
$\frac{0.16708}{0.16261}$	1.0550	1.1570	0.627	1.163	1.078

[a]This mole ratio was calculated on the basis that 98.1% of the deuterated quaternary salt was dideuterated at the α-carbon (see Experimental).
[b]These values were obtained by correcting the observed fraction of reaction for the error in the recovery of the product.
[c]The error limits are the standard deviation.

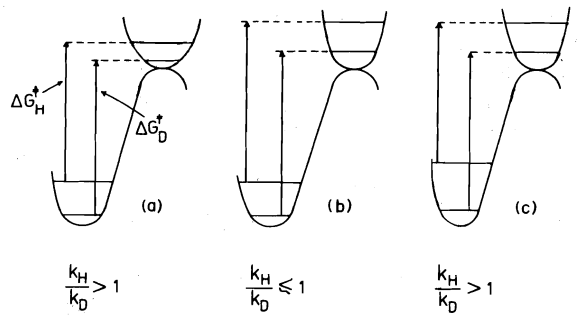

FIG. 1. The reaction coordinate diagram for (*a*) an S_N reaction with a carbonium ion intermediate, (*b*) an S_N2 reaction, and (*c*) an S_N2 reaction of a substrate that is very sterically crowded around the α-carbon.

and an unusually large zero point energy difference would be observed. In this circumstance, the zero point energy difference might be smaller in the transition state and a normal kinetic isotope effect would be found, Fig. 1*c*. This would be particularly likely if the $C\alpha\text{---}\overset{\delta-}{S}$ and the $C\alpha\text{---}\overset{\delta+}{N}$ bonds in the transition state were significantly longer than the normal $C\alpha\text{—}\overset{+}{N}$ and Cα—S bonds of the reactant and product respectively (20).[4]

Finally, it is worth noting that the steric explanation of the very large isotope effect in this S_N2 reaction is supported by the work of Kaplan and Thornton (21). These investigators concluded that the secondary α-deuterium kinetic isotope effects in the closely related S_N2 reaction between *N*,*N*-dimethyl-d_6-aniline and methyl *p*-toluenesulfonate was caused by steric crowding in the transition state.

Structure of the Transition State

Nitrogen (leaving group) kinetic isotope effects and Hammett ρ values have been used to determine the lengths of the Cα---N and Cα---S bonds in this S_N2 transition state. In a previous study the nitrogen (leaving group) kinetic isotope effect was found to be 1.0200 ± 0.0007 (11). This isotope effect which is approximately half of the theoretical maximum nitrogen isotope effect, shows that the Cα—N bond is significantly weaker in the S_N2 transition state. Thus, the Cα---N bond is reasonably long in the transition state. This conclusion was supported by the magnitude of the Hammett ρ value for reactions with different *para* substituents on the phenyl ring of the leaving group, i.e., where the rates of reaction for *para*-substituted phenylbenzyldimethylammonium ion were used to prepare a Hammett plot (11). In fact, the ρ value of +2.04 is approximately half of the value obtained for an equilibrium protonation of *para*-substituted dimethylanilines (11). This also suggests a substantial weakening of the Cα—N bond in the transition state and it can be concluded that the Cα—N bond is substantially longer in the transition state than in the reactant.

An estimate of the length of the Cα—S bond in the transition state was obtained in the following manner. Hudson and Klopman (22) reported the rate constants for the S_N2 reactions of several *para*-substituted thiophenoxide ions with several different *para*-substituted benzyl bromides eq. [7].

[7]

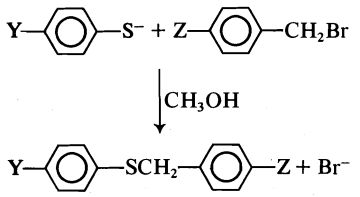

Y = OCH_3, CH_3, H, Cl, Br, and OAc
Z = OCH_3, CH_3, H, Br, and NO_2

When the log k/k_0 values calculated for the reactions of several *para*-substituted thiophenoxide ions with a particular *para*-substituted benzyl bromide were plotted against the sigma value of the *para* substituent on the thiophenoxide ion, good Hammett plots were obtained. The correlation coefficients for the Hammett plots for the five different benzyl bromides of [7] averaged 0.97 with extreme values of 0.95 and 0.99 (23). A consideration of the ρ values obtained in these Hammett plots led to the idea that the magnitude of the ρ value is inversely related to the length of the S---Cα bond in the transition state. If the S---Cα bond is almost fully formed in the transition state, the sulfur atom will be almost neutral. This means there will be a large change in the charge on the sulfur in going to the transition state and a large ρ value would be observed. Conversely, a long S---Cα bond would lead to a small ρ value.

The rate constants for the S_N2 reaction of *para*-substituted thiophenoxide ions with benzyldimethylphenylammonium ion are given in Table 3. The Hammett ρ value is −1.70 ± 0.047[5] with a correlation coefficient of 0.990. This ρ value is approximately half the magnitude of the Hammett ρ value of 3.30 (correlation coefficient = 0.997) calculated from the ionization constants of *para*-substituted thiophenols (24), eq. [8]. The relatively small ρ value of −1.70 for the S_N2 reaction indicates that there is a

[4]Although this large normal secondary α-deuterium kinetic isotope effect could also be a result of a transition state that is much looser (has longer S---Cα and Cα---N bonds) than other S_N2 transition states, the above explanation is preferred because (*i*) there is no evidence to suggest that this transition state is looser than normal (in fact other information from studies in our lab indicate that this is not the case) and (*ii*) because the study by Kaplan and Thornton (21) indicates that steric crowding is present in closely related S_N2 reactions.

[5]Standard deviation.

TABLE 3. Rate constants for the reaction of *para*-substituted thiophenoxide ions with benzyldimethylphenylammonium ion at 0°C in DMF

Para substituent on the thiophenoxide ion	$k \times 10^2$ (L mol^{-1} s^{-1})
—OCH_3	4.62
—CH_3	2.43
—H	1.28
—Cl	0.613

relatively small change in charge on the sulfur atom in going to the transition state. This in turn, means that the S—Cα bond formation is far from complete, i.e., that the S---Cα bond is fairly long in the transition state of this S_N2 reaction.

[8] 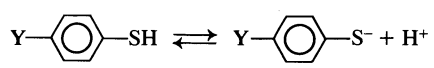

Combining the information about the S---Cα bond with that for the Cα---N bond leads to a complete (albeit qualitative) model of the transition state for the S_N2 reaction between benzyldimethylphenylammonium ion and thiophenoxide ion. In fact, both the S---Cα and Cα---N bonds are reasonably long in the transition state. Any increase in the length of the Cα—N bond moves the very bulky $(CH_3)_2NC_6H_5$ group away from the alpha carbon and reduces the steric crowding around the Cα—H bonds. The Cα---N bond is reasonably long in the transition state and thus the steric crowding around the Cα—H bonds will be markedly reduced from that in the substrate.[6,7] Normally, this reduction in steric crowding is balanced by an increase in steric crowding caused by the approach of a nucleophile. In this reaction, however, the S---Cα bond is also long in the transition state and the nucleophile will not increase the steric crowding around the Cα—H bonds significantly.[8] The net effect would be a much less crowded environment for the Cα—H bonds in the transition state. This means that the frequency of the Cα—H out-of-plane bending vibrations will be less in the transition state. The zero point energy difference for the Cα—H and Cα—D bonds will be lower than that in the reactant and a normal isotope effect should be observed. Thus, the hypothesis that this unusually large secondary α-deuterium kinetic isotope effect is caused by an inordinately large steric crowding around the α-carbon in the substrate which is relieved in going to the transition state, is supported by the structure of the transition state for this reaction.

Finally, it is worth noting that the secondary α-deuterium kinetic isotope effect of 1.179 measured in this study compares very well with the isotope effects of 1.20 in chloroform and 1.25 in acetone[9] measured by Leffek and Ko (7) for the reaction of the same substrate with bromide ion. The close agreement between the isotope effects for the bromide ion and the thiophenoxide ion reactions suggests that both of the reactions occur by the same mechanism, i.e., the one-step S_N2 mechanism. Thus, it is reasonable to conclude that the reaction with bromide ion in chloroform and acetone occurs by an internal S_N2 mechanism (an S_N2 reaction within the triple ion, eq. [4]) and not by the carbonium ion mechanism shown in [3].

The carbonium ion mechanism for the bromide ion reaction is unlikely for another reason. The smallest secondary α-deuterium kinetic isotope effect expected for a carbonium ion reaction is $k_H/k_D = 1.07$ per α-deuterium (Table 1). The isotope effects measured by Leffek and Ko for this reaction; $k_H/k_D =$ 1.10 and 1.12 per α-deuterium, are only slightly larger than the smallest possible value. In fact, a very large isotope effect (larger than most of the isotope effects in Table 1) would be expected if the benzyldimethylphenylammonium ion was converted into a benzyl carbonium ion during the reaction. This would occur for several reasons. First, calculations by Hartshorn and Shiner (26) have shown that the maximum secondary α-deuterium kinetic isotope effect for the reaction of a quaternary ammonium ion is large (approximately 1.19 per α-deuterium). Thus, an isotope effect of at least 1.14 per α-deuterium ($k_H/k_D = 1.30$) would be observed even if the ionization step were fully rate determining (2, p. 137). In fact, an even larger isotope effect than 1.14 per

[6]The Cα—H out-of-plane bending absorption occurs at 1487 cm^{-1} in the benzyldimethylphenylammonium ion. This is significantly higher energy than the corresponding absorptions in benzyl compounds with smaller leaving groups and hence less crowded environments at the α-carbon. For example, the Cα—H out-of-plane bending vibrations occur at 1440 cm^{-1} for benzyl chloride, 1448 cm^{-1} for benzyl bromide, 1460 cm^{-1} for benzyl formate, 1460–1490 cm^{-1} for benzyl-*tert*-butyl sulfone, 1485 cm^{-1} for benzyltrimethylammonium ion, and 1490 cm^{-1} for dibenzyldimethylammonium ion (25).

[7]For most S_N2 reactions the leaving group will be smaller than dimethylaniline and the reduction in the steric crowding around the Cα—H bonds will be smaller.

[8]This is the first transition state where the length of the nucleophile–α-carbon bond has been estimated. Comparisons with other systems are therefore impossible.

[9]The isotope effect for the reaction with thiophenoxide ion in DMF was measured at 0°C whereas the isotope effect for the reactions with bromide ion were measured at 30°C. The temperature effects on secondary alpha deuterium kinetic isotope effects are small (2, 7). The isotope effect for the reaction with thiophenoxide ion at 30°C would be approximately 1.17.

α-deuterium would be expected for a carbonium ion reaction because (*i*) the leaving group is extremely large and the initial state will be sterically crowded, (*ii*) the relief of steric crowding associated with the lengthening of the Cα—N bond of the very bulky leaving group is not replaced by an increased crowding from the approaching nucleophile (see Fig. 1), and (*iii*) because leaving group kinetic isotope effect studies have shown that the α-carbon leaving group bond is longer in the transition state of a carbonium ion reaction than in an S_N2 reaction (27, 28). Thus, the secondary α-deuterium kinetic isotope effects for the reaction are not large enough to be consistent with the formation of a benzyl carbonium ion intermediate.

In conclusion, this study has shown (*i*) that the magnitude of secondary α-deuterium kinetic isotope effects cannot be used as an absolute criterion of mechanism particularly for reactions of substrates with large, bulky leaving groups. (*ii*) The complete modelling of the S_N2 transition state for the reaction between benzyldimethylphenylammonium ion and thiophenoxide ion has shown that the structure of the transition state is consistent with the large normal isotope effect observed in this reaction. (*iii*) This study has also shown that the maximum value of secondary α-deuterium kinetic isotope effects for S_N2 reactions is more dependent on the leaving group than was previously suggested (2, pp. 104–137). This means that the maximum value of the isotope effect for S_N2 reactions will have to be established for each leaving group before the criterion of mechanism based on the magnitude of these isotope effects can be used with complete confidence. Finally, (*iv*) these results suggest that the reaction between benzyldimethylphenylammonium ion and bromide ion in chloroform and acetone also occurs by way of an S_N2 mechanism within the triple ion.

Experimental

Materials

The preparation of benzyldimethylphenylammonium nitrate, sodium thiophenoxide, and the solvent, *N*,*N*-dimethylformamide, are described elsewhere (11). The benzyl-1,1-d_2-dimethylphenylammonium nitrate was prepared from benzyl-1,1-d_2 bromide and *N*,*N*-dimethylaniline using the method described for the undeuterated compound (11). The benzyl-1,1-d_2 bromide was prepared in two steps. First, 25.5 g (0.177 mol) of ethyl benzoate was reduced with 4.0 g (0.095 mol) of lithium aluminum deuteride (Merck) in anhydrous ether to give 18.5 g (88%) of benzyl-1,1-d_2 alcohol (13). An nmr analysis indicated that the alcohol was 99% deuterated at the α-carbon. Next, anhydrous hydrogen bromide gas (Matheson) was bubbled through a solution containing 18.0 g (0.163 mol) of the alcohol in 50 mL of benzene for 3 h. The benzene layer was separated, washed with water and dried over anhydrous $CaCl_2$. The benzene was removed on the rotary evaporator and the product distilled to give 17.2 g (61%) of benzyl-1,1-d_2 bromide, bp 56°C (3 Torr), lit. (29) bp 56°C (3 Torr). An nmr analysis indicated the bromide was 99% deuterated. The 4.5 g (64% yield) of pure benzyl-1,1-d_2-dimethylphenylammonium nitrate, mp 157–157.5°C lit. (11) mp 157–158°C), produced from 4.0 g (0.023 mol) of benzyl-1,1-d_2 bromide and 3.1 g (0.026 mol) of *N*,*N*-dimethylaniline was also 99% deuterated. A mass spectrometric analysis showed that the quaternary ammonium salt was 98.1% dideuterated and 1.9% monodeuterated at the 1-position (*vide infra*).

The undeuterated benzyl phenyl sulfide standard required for the mass spectrographic analysis was prepared previously (11). The deuterated standard, benzyl-1,1-d_2 phenyl sulfide, was prepared by refluxing 2.3 g (0.013 mol) of the benzyl-1,1-d_2 bromide with sodium thiophenoxide in ethanol for 3 h. The sodium thiophenoxide was formed when 2.64 g (0.024 mol) of benzenethiol reacted with the sodium ethoxide produced from 0.58 g (0.025 mol) of sodium and 15 mL of degassed, anhydrous ethanol. Most of the ethanol was removed on the rotary evaporator and 100 mL of cold water was added. The solid that precipitated was filtered and recrystallized from ethanol. The purified yield was 1.10 g (41%), mp 42°C (lit. (30) mp 42°C). The amount of deuterium on the α-carbon was determined in a mass spectrometric analysis (*vide infra*).

The *para*-substituted sodium thiophenoxides used to determine the rate constants for the Hammett plot were prepared using the procedure described for sodium thiophenoxide (11). The yield of the sodium *p*-chlorothiophenoxide was significantly lower (60%) than that of the other salts.

Secondary α-Deuterium Kinetic Isotope Effect

This isotope effect was measured by the competitive technique (11, 13). The reactions were carried out using the procedure described in the section entitled 'Kinetic Measurements' in ref. 11 except that the reactant was a mixture of almost equal quantities of the deuterated and undeuterated benzyldimethylphenylammonium nitrate. The amounts of *dideuterated* and undeuterated quaternary ammonium salts in the starting material were calculated from the weights of the deuterated and undeuterated substrate and the percentage (98.1%) of the dideuterated compound in the deuterated benzyldimethylphenylammonium nitrate. The deuterium content of the deuterated quaternary ammonium salt was estimated by mass spectrometry (*vide infra*). The reactions were stopped after fractions of reaction ranging from 17 to 63% of completion by pouring the reaction mixture into 1400 mL of cold (0°C) pH 12 water. The product, a mixture of deuterated and undeuterated benzyl phenyl sulfide, was extracted from this mixture.[10] The fraction of reaction was estimated from the results of a gas chromatographic analysis of the sulfide (11). The volume of the ether solution used in the gas chromatographic analysis was reduced to approximately 0.25 mL by evaporating the ether in a stream of nitrogen and the ratio of the undeuterated to dideuterated benzyl phenyl sulfide determined by mass spectrometry (*vide infra*). The isotope effect was calculated using [6].

Mass Spectrometric Analyses

The amount of dideuterated quaternary ammonium salt in the deuterated substrate (required in the calculation of R_0 in [6]) was determined in a mass spectrometric analysis of the benzyl phenyl sulfide recovered (11) from reactions taken 100% to completion. The ratio of undeuterated to dideuterated

[10]Control experiments using synthetic mixtures showed that 93 ± 3% of the benzyl phenyl sulfide was recovered. This error in the recovery was taken into account in calculating the fraction of reaction.

benzyl phenyl sulfide in the product of reactions taken part way to completion (R_f in [6]) were also determined by a mass spectrometric analysis of benzyl phenyl sulfide. These analyses involved injecting 25 μL of the concentrated ether solutions containing the benzyl phenyl sulfide produced in the reaction (*vide supra*), into the liquid inlet system of a Dupont 21-491 double focussing mass spectrometer. The oven temperature was 140°C and the source temperature was 180°C. The ionizing voltage was 70 eV. The actual analyses were done by adjusting the sensitivity so that the largest of the *m/e* 200 and 202 peaks was expanded to nearly full scale on the galvanometric recorder (the concentration of benzyl phenyl sulfide was large enough so that a low sensitivity was used). The *m/e* 200–202 peaks were scanned 12 times using a scan speed of 200 s/decade and a chart speed of 0.5 in./s. The sample was pumped out and the background run at high sensitivity until there was no signal in the 200–202 mass range. The same sample was then reinjected and scanned 12 more times. The heights of the appropriate peaks were measured to the nearest hundredth of an inch and the ratio of the peaks calculated with the largest peak (either the *m/e* 200 or 202 peak) given a height of 100. The average ratio from all the scans for a particular sample was used in [9] and [10] to calculate the ratio of undeuterated to dideuterated benzyl phenyl sulfide in the sample.

$$[9] \qquad H_{200} = d_0 + \left(\frac{a}{100}\right)d_2$$

$$[10] \qquad H_{202} = \left(\frac{b}{100}\right)d_0 + d_2$$

H_{200} and H_{202} are the heights of the *m/e* 200 and 202 peaks, respectively, d_0 is the percentage of undeuterated sulfide, d_2 is the percentage of the dideuterated sulfide, a is the height of the *m/e* 200 peak from the deuterated benzyl phenyl sulfide, and b is the height of the *m/e* 202 peak for the undeuterated benzyl phenyl sulfide. The parameters a and b were determined by running samples of the deuterated and undeuterated benzyl phenyl sulfide at least twice during the analyses of the samples obtained from different experiments. It is worth noting that the monodeuterated substrate does not interfere in the analysis because it is converted to monodeuterated benzyl phenyl sulfide which gives a peak at *m/e* 201.

The amount of dideuterated substrate in the benzyl-1,1-d_2-dimethylphenylammonium nitrate was determined in two ways: (*i*) by determining the relative heights of the *m/e* 201 (monodeuterated) and 202 (dideuterated) peaks of the benzyl phenyl sulfide produced when a reaction of the deuterated quaternary ammonium salt was taken 100% to completion, and (*ii*) by determining the term c (eq. [11]) which makes the ratio of undeuterated to dideuterated benzyl phenyl sulfide obtained when a mixture of undeuterated and deuterated benzyldimethylphenylammonium nitrate was reacted 100% to completion, equal to the weight ratio of the undeuterated to deuterated substrate in the reactant.

$$[11] \qquad \frac{\text{wt. undeuterated reactant}}{\text{wt. deuterated reactant}} = c\left(\frac{\text{undeuterated product}}{\text{dideuterated product}}\right)$$

The term c is in fact, the fraction of dideuterated material in the deuterated quaternary ammonium salt. The results from five different reactions showed that the benzyl-1,1-$d_2$dimethylphenylammonium nitrate was 98.1 ± 0.7% dideuterated at the 1 position. This value was used to calculate the ratio of undeuterated to dideuterated quaternary ammonium salt (R_0) in the starting material of the isotope effect experiments. The percentage of the dideuterated benzyldimethylphenylammonium nitrate in the deuterated substrate was confirmed when it was found that the benzyl-1,1-d_2 phenyl sulfide produced from the benzyl-1,1-d_2 bromide used in the synthesis fo the deuterated quaternary ammonium salt, was also 98% dideuterated. In fact, the results from 11 different experiments using the two methods described above, indicated that the benzyl-1,1-d_2 phenyl sulfide was 97.7 ± 0.5% dideuterated.

The undeuterated to dideuterated ratio for the benzyl phenyl sulfide in the product from reactions taken part way to completion (R_f) was determined using the ether solution from the gas chromatographic analysis (*vide supra*).

Hammett ρ Value

The procedure used to measure the rate constants required for the Hammett plot has been described (11). The only difference was that the colour which developed at the end point in the titration of the substituted thiophenoxide ions varied from pink to blue. A purple colour is observed at the end point when sodium thiophenoxide is titrated.

Acknowledgements

The authors wish to thank Dr. E. J. Monahan, Past President of Laurentian University, and the National Research Council of Canada for the financial support required to complete this study. The authors also wish to thank Mr. M. Zavitz who synthesized the deuterated compounds.

1. V. F. Raaen, T. Juhlke, F. J. Brown, and C. J. Collins. J. Am. Chem. Soc. **96**, 5928 (1974).
2. V. J. Shiner, Jr. *In* Isotope effects in chemical reactions. Am. Chem. Soc. Monograph 166. *Edited by* C. J. Collins and N. S. Bowman. Van Nostrand-Reinhold, New York, NY. 1971.
3. K. Humski, V. Sendijarevic, and V. J. Shiner, Jr. J. Am. Chem. Soc. **96**, 6187 (1974).
4. K. M. Koshy. Ph.D. Dissertation, University of Alberta, Calgary, Alta. 1973. pp. 33 and 126.
5. H. Stecker and H. Elias. Chem. Ber. **102**, 1270 (1969).
6. V. J. Shiner, Jr., M. W. Rapp, and H. R. Pinnick, Jr. J. Am. Chem. Soc. **92**, 232 (1970).
7. E. C. F. Ko and K. T. Leffek. Can. J. Chem. **49**, 129 (1971).
8. K. T. Leffek and F. H. C. Tsao. Can. J. Chem. **46**, 1215 (1968).
9. J. T. Burns and K. T. Leffek. Can. J. Chem. **47**, 3725 (1969).
10. E. C. F. Ko and K. T. Leffek. Can. J. Chem. **50**, 1297 (1972).
11. K. C. Westaway and R. A. Poirier. Can. J. Chem. **53**, 3216 (1975).
12. K. T. Leffek and A. F. Matheson. Can. J. Chem. **50**, 986 (1972).
13. K. C. Westaway and A. N. Bourns. Can. J. Chem. **50**, 2332 (1972).
14. K. C. Westaway. Tetrahedron Lett. 4229 (1975).
15. J. Bigeleisen and M. Wolfsberg. Adv. Chem. Phys. **1**, 15 (1959).
16. R. G. D. Steel and J. H. Torrie. Principles and procedures of statistics. McGraw Hill Co., Toronto, Ont. 1960. pp. 101–115.
17. J. Bron. Can. J. Chem. **52**, 903 (1974).
18. V. J. Shiner, Jr., M. W. Rapp, E. A. Halevi, and M. Wolfsberg. J. Am. Chem. Soc. **90**, 7171 (1968).

19. K. B. WIBERG. Physical organic chemistry. J. Wiley and Sons, New York, NY. 1964. p. 351.
20. T. W. BENTLEY and P. VON R. SCHLEYER. Adv. Phys. Org. Chem. **14**, 1 (1977).
21. E. D. KAPLAN and E. R. THORNTON. J. Am. Chem. Soc. **89**, 6644 (1967).
22. R. F. HUDSON and G. KLOPMAN. J. Chem. Soc. 1062 (1962).
23. S. F. ALI. M.Sc. Dissertation, Laurentian University, Sudbury, Ont. 1976. pp. 106–109.
24. B. D. ENGLAND and D. H. MACLENNAN. J. Chem. Soc. B, 696 (1966).
25. C. J. PUCHERT. The Aldrich library of infrared spectra. Aldrich Chemical Co. Inc., Milwaukee, WI. 1970. Spectra 444-H, 445-A, 753-A, 840-A, 587-F, and 589-A.
26. S. R. HARTSHORN and V. J. SHINER, JR. J. Am. Chem. Soc. **94**, 9002 (1972).
27. D. G. GRACZYK and J. W. TAYLOR. J. Am. Chem. Soc. **96**, 3255 (1974).
28. J. BIGELEISEN and M. WOLFSBERG. J. Chem. Phys. **22**, 1264 (1954).
29. E. D. HUGHES and C. K. INGOLD. J. Chem. Soc. 57 (1933).
30. R. L. SHINER, H. C. STRUCT, and W. J. JORISON. J. Am. Chem. Soc. **52**, 2066 (1930).

Kinetics and mechanism of decarboxylation of some pyridinecarboxylic acids in aqueous solution. III. 3-Hydroxy- and 3-aminopyridine-2-carboxylic acids

GERALD E. DUNN, HARALD F. THIMM, AND RAJANI K. MOHANTY[1]

Department of Chemistry, University of Manitoba, Winnipeg, Man., Canada R3T 2N2

Received September 5, 1979

GERALD E. DUNN, HARALD F. THIMM, and RAJANI K. MOHANTY. Can. J. Chem. **57**, 1098 (1979).

Pseudo-first-order rate constants for the decarboxylation of 3-hydroxy- and 3-aminopicolinic acids in aqueous solution at 150°C were determined and plotted as a function of acidity. Each rate profile has a maximum at an acidity well above the isoelectric point and this is attributed to decarboxylation of an intermediate protonated at the 2-position, analogous to the intermediates involved in the decarboxylation of salicylic and anthranilic acids. There is also a shoulder on each rate profile at a lower acidity corresponding to the isoelectric point where the Hammick ylide mechanism has a rate maximum in most picolinic acid decarboxylations. It is concluded that 3-hydroxy- and 3-aminopicolinic acids decarboxylate by the ylide mechanism at low acidity and by the protonation mechanism at higher acidities. In agreement with this interpretation, the ^{13}C kinetic isotope effect in 3-hydroxypicolinic acid decarboxylation is 2.0% on the ylide part of the curve, 1.3% where decarboxylation of the protonated intermediate is rate determining, and drops to 0.4% in the intermediate region. Comparison of the rate constants for ylide decarboxylation with those for other 3-substituted picolinic acids shows that 3-hydroxy and 3-amino substituents facilitate decarboxylation, probably by their inductive and field effects on the developing negative charge at the 2-position of the transition state.

GERALD E. DUNN, HARALD F. THIMM et RAJANI K. MOHANTY. Can. J. Chem. **57**, 1098 (1979).

On a déterminé les constantes de vitesse de pseudo-premier ordre pour la décarboxylation des acides hydroxy-3 et amino-3 picoliniques en solution aqueuse à 150°C et on a tracé la courbe qui les relie à l'acidité. Pour chaque profil de vitesse, il existe un maximum à une acidité bien au dessus du point isoélectrique et on l'attribue à la décarboxylation d'un intermédiaire protoné en position 2, analogue aux intermédiaires impliqués dans la décarboxylation des acides salicyclique et anthranilique. On note aussi un épaulement sur chaque profil de vitesse, à une acidité plus basse que celle du point isoélectrique, où la vitesse pour le mécanisme ylide de Hammick est maximale pour les décarboxylations de la plupart des acides picoliniques. On en conclut que les acides hydroxy-3 et amino-3 picoliniques se décarboxylent par un mécanisme ylide à faible acidité et par un mécanisme de protonation à des acidités plus élevées. En accord avec cette interprétation, l'effet isotopique cinétique ^{13}C observé lors de la décarboxylation de l'acide hydroxy-3 picolinique est égal à 2% dans la portion ylide de la courbe, à 1.3% lorsque la décarboxylation implique un intermédiaire dans l'étape qui détermine la vitesse et tombe à 0.4% dans la région intermédiaire. Une comparaison des constantes de vitesse pour la décarboxylation par l'intermédiaire d'ylides avec celles d'autres acides picoliniques substitués en position 3 montre que les substituants hydroxy-3 et amino-3 facilitent la décarboxylation, probablement grâce à leurs effets inductifs et de champs sur la charge négative qui se développe en position 2 de l'état de transition.

[Traduit par le journal]

Introduction

The preceding papers in this series reported that the pH dependence of the first-order rate constants for decarboxylation of picolinic acid (1) and 3-benzoyl-, 3-carboxyl-, 3-bromo-, and 3-nitropicolinic acids (2) in aqueous solution fit the mechanism proposed by Dyson and Hammick (3) for decarboxylation of picolinic acid in nonaqueous solvents, as shown in reaction [1]. This mechanism requires that the first-order rate constant be a maximum at the isoelectric pH and that there be a ^{13}C kinetic

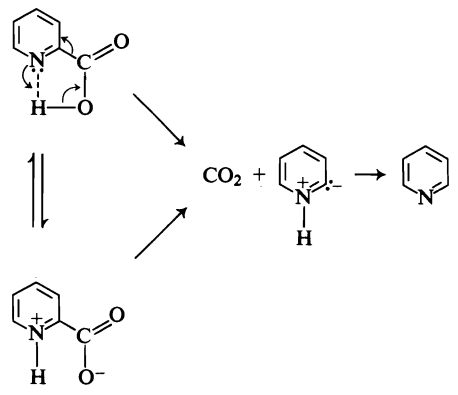

[1]

[1]On leave of absence from Ravenshaw College, Cuttack, Orissa, India.

0008-4042/79/091098-07$01.00/0

[2] 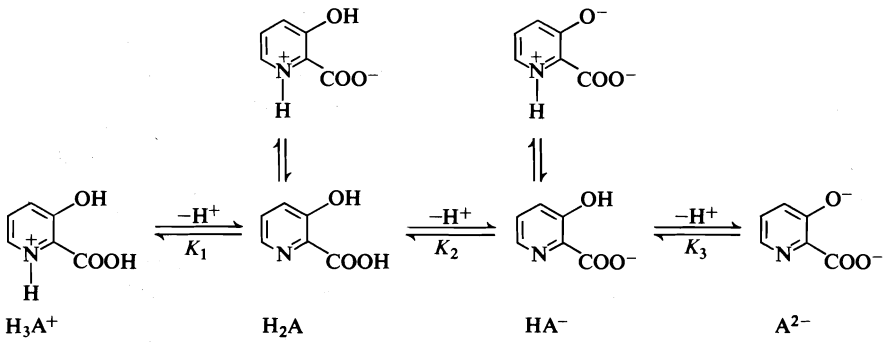

isotope effect at all pH's, both of which criteria were satisfied (1, 2). However, the pH–rate profiles for 3-hydroxy- and 3-aminopicolinic acids do not have maxima at their isoelectric pH's, so they were assumed to proceed by some mechanism other than [1]. The present paper reports an investigation of the mechanism of decarboxylation of these two acids.

Results and Discussion

3-Hydroxypicolinic Acid

The successive ionization constants of 3-hydroxypicolinic acid are defined in eq. [2]. Dutt *et al.* (4) report $pK_2 = 5.17$ and $pK_3 = 10.76$ at 25°C and ionic strength $\mu = 0.10$. Potentiometrically, we find $pK_2 = 5.21$ and $pK_3 = 10.74$ at 25°C and $\mu = 1.0$. The concentration maximum for HA^- under these conditions is therefore at pH 8.0. The value of K_1 is not known but, since pK_1 for picolinic acid is 1.08 (5) and an *ortho* hydroxy group increases the ionization constant of benzoic acid by 1.2 pK units, one may estimate pK_1 for 3-hydroxypicolinic acid as probably in the vicinity of zero. This puts the concentration maximum for H_2A in the vicinity of pH 2.6. Consequently, if 3-hydroxy, like other picolinic acids, decarboxylates in zwitterionic form by the Hammick mechanism (1, 2), there should be rate maxima at pH 2.6, or 8, or both.

The decarboxylation of 3-hydroxypicolinic acid in buffered aqueous solution is found to be first order with respect to substrate and the pseudo-first-order rate constants are recorded in Table 1. It is seen that the maximum rate constant occurs, not at either concentration maximum, but near pH 0. The rate constants are plotted against acidity in Fig. 1, which shows that the rate profile is not symmetrical, as would be the case if only one species were decarboxylating, but has a distinct shoulder at approximately pH 2.5. This suggests that H_2A may be decarboxylating by the Hammick mechanism at the concentration maximum as expected but there is evidently an additional mechanism for decarboxylation which has its rate maximum at a pH lower than either of the concentration maxima. The rate maximum at high acidity is reminiscent of the decarboxylation of aminobenzoic acids, where the rate maximum occurs a few pH units below the isoelectric pH (6, 7). In these cases decarboxylation takes place from intermediates in which the carbon α to the carboxyl group is protonated before decarboxylation. The pH–rate profile for 3-hydroxypicolinic acid may then be accounted for by a Hammick-type decarboxylation of H_2A in the pH range 2–5, which is overwhelmed by electrophilic substitution by proton at higher acidities.

TABLE 1. Pseudo-first-order rate constants for decarboxylation of 3-hydroxypicolinic acid in aqueous solution at 150°C

pH or H_A (25°C)	Buffer	$k \times 10^6$ (s^{-1})[a]
5.45	HCl, NaH_2PO_4, Na_2HPO_4	0.92±0.01
4.93	HCl, NaH_2PO_4, Na_2HPO_4	1.68±0.01
4.48	HCl, NaH_2PO_4, Na_2HPO_4	2.56
4.14	NaH_2PO_4	3.25±0.01
3.61	HCl, NaH_2PO_4	4.40±0.04
3.33	HCl, NaH_2PO_4	5.11
2.82	HCl, NaH_2PO_4	5.76±0.02
2.27	HCl, NaH_2PO_4	6.13±0.03
2.11	HCl, NaH_2PO_4	6.03±0.02
2.03	HCl, NaH_2PO_4	6.13±0.02
1.20	HCl, KCl	7.52
1.00	HCl, KCl	8.15±0.08
0.52	HCl, KCl	10.2
0.30	HCl, KCl	11.9
0	HCl	13.3
−1.05	H_2SO_4	8.08±0.04
−1.72	H_2SO_4	3.29±0.15
−2.19	H_2SO_4	1.49±0.07
−3.38	H_2SO_4	0.36±0.04

[a]Average of two runs ± maximum deviation. Constants with no deviation listed are from single runs.

The Hammick part of the decarboxylation may be represented by eq. [3].

[3] 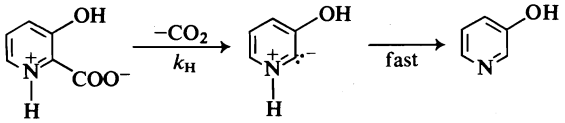

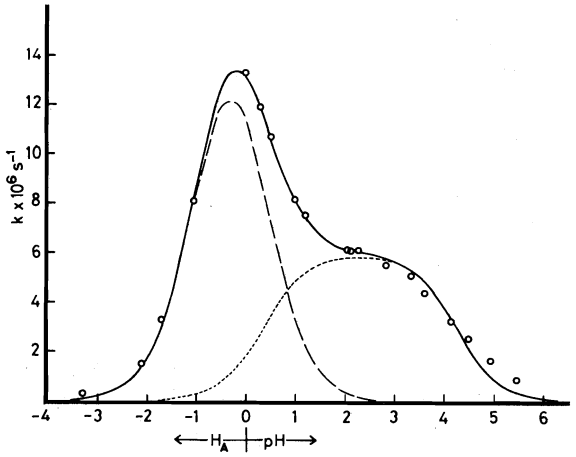

FIG. 1. Pseudo-first-order rate constants for the decarboxylation of 3-hydroxypicolinic acid in aqueous solution at 150°C. Circles represent experimental points. The solid line is generated by [12], the dashed line by [11], and the dotted line by [5].

The equilibrium concentration of H_2A is given by [4], in which [C] represents the total stoichiometric concentration of substrate.

$$[4] \qquad [H_2A] = \frac{[C]}{\frac{[H^+]}{K_1} + 1 + \frac{K_2}{[H^+]}}$$

The pseudo-first-order rate constant for this part of the decarboxylation is therefore given by [5].

$$[5] \qquad k_{ylide} = \frac{k_H}{\frac{[H^+]}{K_1} + 1 + \frac{K_2}{[H^+]}}$$

The protonation mechanism analogous to that found for the amino- and hydroxybenzoic acids is given by [6]. Applying the steady-state approximation to ($[H_3A^*] + [H_2A^*]$) and recognizing that K_3 is negligible at pH < 5, one obtains [7] as the expression for the dependence of the pseudo-first-order rate constant for this part of the decarboxylation upon acidity.

[6]

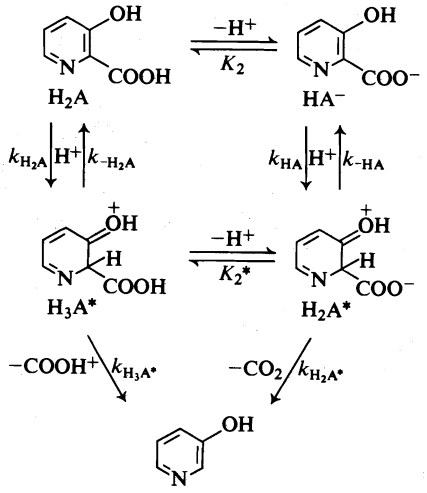

$$[7] \qquad k_{prot} = \frac{k_{H_2A}[H^+] + k_{HA}K_2}{\frac{[H^+]}{K_1} + 1 + \frac{K_2}{[H^+]}} \times \frac{k_{H_3A^*}[H^+] + k_{H_2A^*}K_2^*}{(k_{-H_2A} + k_{H_3A^*})[H^+] + (k_{-HA} + k_{H_2A^*})K_2^*}$$

As in the aminobenzoic acid case (6, 7), the mechanism can be simplified with the aid of ^{13}C kinetic isotope effects. Table 2 shows the ^{13}C kinetic isotope effects in the decarboxylation of 3-hydroxypicolinic acid at various pH's. There is a distinct isotope effect in the pH range 2–5. This is as expected, since we postulate the Hammick mechanism (eq. [5]) to predominate in this region and its rate-determining step is C—C bond breaking. In the acidity range 0 to −3 where the protonation mechanism (eq. [7]) should predominate, the isotope effect is small at low acidity, probably zero when the effect from the overlapping Hammick mechanism is subtracted, and increases at high acidities. This is the pattern shown by aminobenzoic acids decarboxylating by the protonation mechanism, and can be interpreted in the same way.

With the observation that in mechanism [6] the only C—C bond-breaking steps (and therefore the only ones which can produce ^{13}C kinetic isotope effects) are $k_{H_2A^*}$ and $k_{H_3A^*}$, the interpretation is as follows. At low acidity [7] reduces to [8]

$$[8] \qquad k = \frac{k_{HA}k_{H_2A^*}[H^+]}{k_{-HA} + k_{H_2A^*}}$$

so that the observed rate constant increases with acidity, as observed. However, since the isotope effect is small in this region, k_{-HA} must be small compared to $k_{H_2A^*}$, indicating that H_2A^* decarboxylates faster than it deprotonates.

At high acidity [7] reduces to [9]

TABLE 2. ^{13}C kinetic isotope effects in the decarboxylation of 3-hydroxypicolinic acid in aqueous solution at 150°C

	% isotope effect	
pH or H_A (25°C)	Observed[a]	Calculated from [12]
4.35	2.03±0.04	2.00
2.32	1.96	2.00
0.15	0.50±0.01	0.42
−0.92	0.38	0.48
−1.95	0.62	0.90
−2.18	1.26	1.00

[a]Percentage isotope effect = $(k_{12}/k_{13} - 1)100$ ± average deviation of three runs. Where no deviations are listed, results are from a single run.

[9] $$k = \frac{k_{H_2A}K_1k_{H_3A^*}}{k_{-H_2A} + k_{H_3A^*}}$$

so that the observed rate constant should level off at high acidity. In fact, however, the rate constant decreases at high acidity. To account for this we postulate that, as in the aminobenzoic acid case, $k_{H_3A^*}[H^+] < k_{H_2A^*}K_2^*$; i.e. that the COOH group in H_3A^* ionizes to COO^- in H_2A^* before decarboxylating. With this assumption, [7] at high acidity becomes [10].

[10] $$k = \frac{k_{H_2A}K_1k_{H_2A^*}K_2^*}{(k_{-H_2A} + k_{H_3A^*})[H^+]}$$

Then, in order to account for the large ^{13}C kinetic isotope effect at high acidity, we postulate that $k_{-H_2A} > k_{H_3A^*}$. Putting these three assumptions ($k_{-HA} > k_{H_2A^*}$, $k_{H_3A^*}[H^+] < k_{H_2A^*}K_2^*$, $k_{H_3A^*} < k_{-H_2A}$) into [7] produces [11].

[11] $$k_{prot} = \frac{k_{H_2A}[H^+] + k_{HA}K_2}{\frac{[H^+]}{K_1} + 1 + \frac{K_2}{[H^+]}} \times \frac{1}{\frac{k_{-H_2A}}{k_{H_2A^*}K_2^*}[H^+] + 1}$$

The overall expression for the dependence of rate constant upon pH is then obtained by combining [5] and [11] to give [12].

[12] $$k = k_{ylide} + k_{prot} = \frac{\left(k_{H_2A} + \frac{k_Hk_{-H_2A}}{k_{H_2A}K_2^*}\right)[H^+] + k_{HA}K_2 + k_H}{\left(\frac{k_{-H_2A}}{k_{H_2A^*}K_2^*}[H^+] + 1\right)\left(\frac{[H^+]}{K_1} + 1 + \frac{K_2}{[H^+]}\right)}$$

To fit the data of Table 1 to eq. [12] it is necessary to assume some acidity function for protonation at acidities above pH 0, where [12] reduces to [13].

[13] $$\log k = \log\left(\frac{k_{H_2A}k_{H_2A^*}K_2^*}{k_{-H_2A}} + k_H\right)K_1 + pH$$

In this range the pH term must be replaced by an acidity function, but the proper function is not known. However, since most acidity functions are proportional to H_0 (8), pH may be replaced by nH_0. A plot of log k vs. H_0 for the high acidity points gives a straight line with $n = 0.46$. This slope is similar to that obtained for the decarboxylation of pyrimidinecarboxylic acids (9) and corresponds roughly to that for the acidity function H_A. Therefore, in Fig. 1 rate constants at high acidities are plotted against H_A.

Also using H_A at high acidities, the data of Table 1 were fitted to [12] by an iterative least-squares computer program (10) with the results shown in Table 3. The curve generated by [12] with the data of Table 3 is shown as the solid line in Fig. 1. It can be seen that the fit of the experimental points to the curve is reasonably good and that the values of pK_1 and pK_2 at 150°C obtained from the kinetic data are in reasonable agreement with the values at 25°C. As is the case with other picolinic acids (1), pK_1 is not much affected by the rise in temperature but pK_2 is decreased by about 1 pK unit. The tailing of the points at pH's above 4 suggests that the monoanion, HA^-, may also be decarboxylating, as is the case with picolinic acid itself (1), but the number of experimental points in this region is not sufficient to justify the additional complexity that inclusion of this mode of decarboxylation would produce in [12].

TABLE 3. Rate and equilibrium constants at 150°C calculated from [12] and the data of Tables 1 and 4

Parameter	3-Hydroxypicolinic acid	3-Aminopicolinic acid
$k_{H_2A} + \frac{k_Hk_{-H_2A}}{k_{H_2A^*}K_2^*}$	4.04×10^{-5}	4.26×10^{-6}
$k_{HA}K_2 + k_H$	5.92×10^{-6}	3.27×10^{-5}
K_1 (pK_1)	0.441 (0.36)	2.12×10^{2} (−2.33)
K_2 (pK_2)	5.62×10^{-5} (4.25)	3.09×10^{-2} (1.51)
$\frac{k_{-H_2A}}{k_{H_2A^*}K_2^*}$	9.74×10^{-2}	4.49×10^{-3}

It is apparent from the shape of the curve in Fig. 1 that at pH > 3 the ylide mechanism predominates over the protonation mechanism, so that the rate profile should be represented in this region by [5]. In this same region [12] reduces to [14], which means

[14] $$k = \frac{k_{HA}K_2 + k_H}{\frac{[H^+]}{K_1} + 1 + \frac{K_2}{[H^+]}}$$

that $k_{HA}K_2$ must be negligible compared to k_H, or $k_H = 5.92 \times 10^{-6}\ s^{-1}$. This makes it possible to draw separate rate profiles of the ylide and protonation mechanisms, as shown by the dotted lines in Fig. 1.

Furthermore, multiplying the value of k_H by the value of the last parameter in Table 3 and comparing the result with the value of the first parameter in Table 3 shows that the second term in the first parameter is negligible. Equation [12] can therefore be reduced to [15]. The final mechanism, of which

[15] $$k = \frac{k_{H_2A}[H^+] + k_H}{\left(\frac{k_{-H_2A}}{k_{H_2A}K_2^*}[H^+] + 1\right)\left(\frac{[H^+]}{K_1} + 1 + \frac{K_2}{[H^+]}\right)}$$

[15] is the kinetic expression, is a combination and

[16]

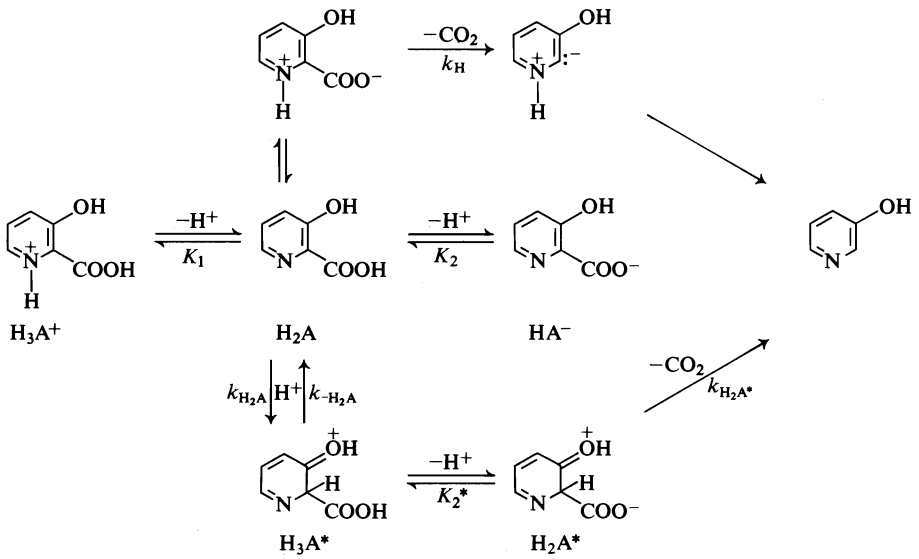

simplification of reactions [2], [3], and [6] which may be represented by [16].

In the pH region 6 to 2.5 H_2A is decomposing by the ylide mechanism, k_H represents the rate-determining step with a ^{13}C isotope effect and k increases as $[H_2A]$ increases. As pH decreases from 2.5 to 0.5, $[H_2A]$ remains relatively constant but k continues to increase because H_2A is being protonated to H_3A^* which decarboxylates rapidly via H_2A^*; k_{H_2A} is the rate-determining step, so there is no ^{13}C isotope effect. From pH 0.5 to $H_A = -3$ the rate of protonation of H_2A to H_3A^* exceeds the rate of decarboxylation of H_2A^* so that the rate-determining step is $k_{H_2A^*}$ which has a ^{13}C kinetic isotope effect; k decreases as H_2A^* (which is now in tautomeric equilibrium with H_2A) is increasingly converted to H_3A^+ which does not decarboxylate.[2]

This mechanism, as represented by [12], can be used to predict changes in the ^{13}C kinetic isotope effect with pH. Assuming isotope effects of 2% in k_H and 1% in $k_{H_2A^*}$, one calculates the isotope effects shown in Table 2. The agreement between calculated and observed isotope effects at a particular pH is only fair but the trend is correct and the difference between observed and calculated values is probably not much outside the experimental error, particularly when the naive treatment of acidity functions is considered.

In summary, then, the proposed mechanism agrees satisfactorily with the rate vs. pH profile, the expected ionization constants at 150°C, and the variation of ^{13}C kinetic isotope effect with pH. Obviously these observations can not prove the mechanism to be correct, but they do show that it is consistent with the data, and it is consistent also with what is known about the mechanisms of decarboxylation of hydroxybenzoic and picolinic acids.

3-Aminopicolinic Acid

The protonation equilibria for 3-aminopicolinic acid are shown in [17], omitting the zwitterionic forms. Literature values for pK_2 and pK_3 are 1.22 and 7.20, respectively, without reference to ionic strength (11). Potentiometrically, in 1 *M* KCl we found $pK_2 = 1.53$ and $pK_3 = 7.09$. No doubt pK_1 would be considerably negative.

The pseudo-first-order rate constants for 3-aminopicolinic acid are shown in Table 4 and plotted against pH in Fig. 2. It is seen that the pH vs. rate profile has a similar shape to that for 3-hydroxypicolinic acid, except that the ring-protonation mechanism contributes relatively more to the total rate in the amino acid case. The data were fitted to [12] by the same procedure used for the hydroxy acid, with the results shown in Table 3.

As in the hydroxypicolinic acid case, the shape of the rate profile suggests that $k_{HA}K_2$ is negligible compared to k_H, so that the overall rate constants can be separated into their ylide and protonation

[2]A referee suggests that H_3A^+ is at all times in tautomeric equilibrium with H_3A^*, which decarboxylates directly by loss of $COOH^+$ without the intermediacy of H_2A^*. To account for the decreasing rate at high acidity he postulates that the equilibrium constant for the tautomerism between H_3A^+ and H_3A^* changes with the medium so as to decrease $[H_3A^*]$ as acidity increases. This is, of course, a possible interpretation but we prefer the one in the text because the referee's mechanism requires an unpredictable change in the tautomeric equilibrium constant, because it requires that protonation at a carbon site be always rapid and because 3-hydroxypicolinic acid is following the same pattern as anthranilic acid (6), for which the rate decrease occurs at much lower acidity (pH 1.5 to 0) where no such dramatic medium effect is possible.

[17]

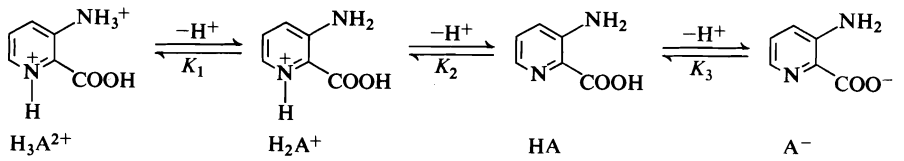

components by means of eqs. [5] and [11] as shown by the dotted lines in Fig. 2.

Finally, it should be noted that the decarboxylation study of 3-hydroxy- and 3-aminopicolinic acids was originally undertaken as part of a study of the effect of 3-substituents on the rates of decarboxylation by the ylide mechanism (2) but that the 3-hydroxy and 3-amino acids had to be eliminated from the study because of the intrusion of the protonation mechanism. Now that rate constants for the ylide component of the decarboxylation of these acids are available, they are compared with those from other 3-substituted picolinic acids (2) in Table 5.

TABLE 4. Pseudo-first-order rate constants for decarboxylation of 3-aminopicolinic acid in aqueous solution at 150°C

pH or H_A (25°C)	Buffer	$k \times 10^6$ (s^{-1})[a]
4.18	NaH_2PO_4	1.41
3.91	HCl, NaH_2PO_4	1.60
3.43	HCl, NaH_2PO_4	1.74±0.02
3.13	HCl, NaH_2PO_4	3.83±0.04
1.70	HCl, KCl	10.7
1.00	HCl, KCl	26.7±0.1
0.66	HCl, KCl	30.3±0.2
0.30	HCl, KCl	33.6
0	HCl	38.0±0.2
−0.45	H_2SO_4	41.9
−1.05	H_2SO_4	61.4
−1.71	H_2SO_4	150
−2.23	H_2SO_4	253
−3.38	H_2SO_4	52.6

[a]Average of two runs ± maximum deviation. Constants with no deviation listed are from single runs.

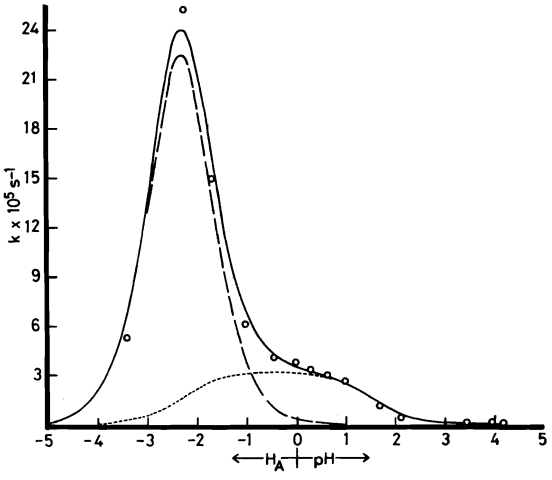

FIG. 2. Pseudo-first-order rate constants for the decarboxylation of 3-aminopicolinic acid in aqueous solution at 150°C. Circles represent experimental points. The solid line is generated by [12], the dashed line by [11], and the dotted line by [5].

TABLE 5. First-order rate constants for the decarboxylation of 3-substituted picolinic acids by the Hammick mechanism in aqueous solution at ionic strength 1.0

Substituent	Temperature (°C)	k_H (s^{-1})
Amino	150	3.2×10^{-5}
Hydroxy	150	5.9×10^{-6}
Methyl	150	4.0×10^{-6}
None	150	1.1×10^{-6}
Benzoyl	150	$\geq 4.5 \times 10^{-4}$
Carboxyl	150	$\geq 1.2 \times 10^{-3}$
	95	3.3×10^{-6}
Bromo	95	1.5×10^{-5}
Nitro	95	$\geq 1 \times 10^{-3}$

From the earlier set of rate constants (2) it was observed that all 3-substituents increase the rate of decarboxylation by the ylide mechanism and it was concluded that 3-substituents exert their influence largely by inductive or field effects tending to stabilize negative charge at the 2-position of the ylide. But, since 3-methyl also accelerates the decarboxylation, it was felt that steric interaction with the carboxyl group must favor decarboxylation. The new data for 3-hydroxy and 3-amino substituents confirm that the electronic component of the 3-substituent effect is largely inductive since they, like 3-carboxyl, 3-benzoyl, 3-bromo, and 3-nitro substituents accelerate decarboxylation. It is surprising that the 3-amino substituent should have a larger inductive effect than 3-hydroxy but it must be remembered that substituents also affect the zwitterionic distribution of protons within the various species and that it may well be the protonated amino group which has the large inductive effect.

Experimental

3-Hydroxypicolinic acid was a commercial product (Aldrich). The synthesis of 3-aminopicolinic acid has been described previously (2), as have the methods of measuring rates (2) and ^{13}C kinetic isotope effects (12). All pH's were measured with an Orion digital pH meter, Model 801. In the negative region H_A values (13) were calculated from density measurements of sulfuric acid solutions.

Acknowledgments

The authors are grateful to Dr. J. L. Charlton for help with the computer-assisted curve fitting, and to the National Research Council of Canada for financial support.

1. G. E. DUNN, G. K. J. LEE, and H. F. THIMM. Can. J. Chem. **50**, 3017 (1972).
2. G. E. DUNN and H. F. THIMM. Can. J. Chem. **55**, 1342 (1977).
3. P. DYSON and D. L. HAMMICK. J. Chem. Soc. 1724 (1937); M. F. R. ASHWORTH, R. P. DAFFERN, and D. L. HAMMICK. J. Chem. Soc. 809 (1939).
4. N. K. DUTT, G. S. SANYAL, and K. NAG. J. Indian Chem. Soc. **45**, 334 (1968).
5. R. F. EVANS, E. F. G. HERINGTON, and W. KYNASTON. Trans. Faraday Soc. **49**, 1284 (1953).
6. G. E. DUNN, P. LEGGATE, and I. E. SCHEFFLER. Can. J. Chem. **43**, 3080 (1965).
7. A. V. WILLI and P. VILK. Z. Phys. Chem. (Frankfurt am Main), **59**, 189 (1968).
8. K. YATES and R. A. MCCLELLAND. J. Am. Chem. Soc. **89**, 2686 (1967).
9. G. E. DUNN, E. A. LAWLER, and A. B. YAMASHITA. Can. J. Chem. **55**, 2478 (1977).
10. D. F. DETAR. Comput. Programs Chem. **4**, 71 (1972).
11. V. D. CANIC, M. B. ANCHELKOVIC, and V. B. GOLUBOVIC. Glas. Hem. Drus. Beograd, **21**, 65 (1956); Chem. Abstr. **54**, 8815 (1960).
12. G. E. DUNN and S. K. DAYAL. Can. J. Chem. **48**, 3349 (1970).
13. K. YATES, J. B. STEVENS, and A. R. KATRITZKY. Can. J. Chem. **42**, 1957 (1964).

COMMUNICATIONS

A new type of *Lycopodium* alkaloid. The $C_{30}N_3$ alkaloids from *Lycopodium lucidulum*

WILLIAM A. AYER, LOIS M. BROWNE, YUJI NAKAHARA, AND MOTOO TORI
Department of Chemistry, University of Alberta, Edmonton, Alta., Canada T6G 2G2
AND
LOUIS T. J. DELBAERE
Department of Biochemistry, University of Alberta, Edmonton, Alta., Canada T6G 2G2

Received December 14, 1978

WILLIAM A. AYER, LOIS M. BROWNE, YUJI NAKAHARA, MOTOO TORI, and LOUIS T. J. DELBAERE. Can. J. Chem. **57**, 1105 (1979).

The structures of lucidine B, dihydrolycolucine, and lycolucine, representatives of a new type of *Lycopodium* alkaloid, have been determined, mainly on the basis of an X-ray crystallographic study of a derivative (*N,O*-di-*p*-bromobenzoyltetrahydrodeoxyoxolucidine B) of lucidine B. Dehydrogenation of lucidine B gives dihydrolycolucine which in turn has been prepared from lycolucine.

WILLIAM A. AYER, LOIS M. BROWNE, YUJI NAKAHARA, MOTOO TORI et LOUIS T. J. DELBAERE. Can. J. Chem. **57**, 1105 (1979).

On a déterminé les structures de la lucidine B, de la dihydrolycolucine et de la lycolucine, représentatifs d'un nouveau type d'alcaloïde du *Lycopodium*, en se basant principalement sur une étude de diffraction de rayons-X effectuée sur un dérivé (la *N,O*-di-*p*-bromobenzoyltétrahydrodésoxyoxolucidine B) de la lucidine B. La déshydrogénation de la lucidine B conduit à la dihydrolycolucine qui a pu être préparée à son tour à partir de la lycolucine.
[Traduit par le journal]

In 1963 we described the separation of the alkaloids of *Lycopodium lucidulum* into strong and weak bases (1). The strong bases have been the subject of two further reports (2, 3). In 1968 the separation of the weak bases, which constitute about 80% of the total alkaloids, was described in more detail and the structure of one of these bases, luciduline (**1**), was reported (4). Luciduline, however, is one of the minor components of the weak base fraction and considerable work in these (5, 6) and other (7) laboratories has been devoted to the separation and identification of the remaining alkaloids. We have succeeded in characterizing several different $C_{30}N_3$ alkaloids from this source (5, 6) and now wish to report the structures of three of these alkaloids, representatives of a distinctively new type of *Lycopodium* alkaloid.

Separation of the weak bases of *L. lucidulum* was accomplished by countercurrent distribution between chloroform (moving phase) and saturated aqueous potassium hydrogen tartrate (stationary phase) followed by extensive column and thin layer chromatography over alumina.[1] Two isomeric alkaloids $C_{30}H_{49}N_3O$, named lucidine A and lucidine B, were isolated, along with a compound $C_{30}H_{43}N_3O$ (lycolucine) and a compound $C_{30}H_{45}N_3O$ (dihydrolycolucine).[2]

Structure **2** is proposed for lucidine B on the basis of an X-ray crystallographic study of the derivative **3** (*N,O*-di-*p*-bromobenzoyltetrahydrodeoxyoxolucidine B) prepared from lucidine B as described below. The presence of the tertiary $\rangle N—COCH_3$ and $\rangle N—CH_3$ groups in lucidine B are readily established by spectroscopic methods (ir, ^{1}Hmr). The presence of the fully substituted imino group is revealed by the ease of $NaBH_4$ reduction to dihydrolucidine B which, unlike lucidine B, shows NH absorption in the ir, and by the presence of a C=N absorption band (1643 cm^{-1}) in desacetyllucidine B (**4**), prepared by acid catalyzed hydrolysis of lucidine B. When a chloroform solution of lucidine B is stirred in the presence of air, a more polar com-

[1]Details of the separation procedure will be provided in the full paper. They may also be found in refs. 5 and 6.

[2]Several other $C_{30}N_3$ alkaloids, not yet fully characterized, are also present. Copies of the infrared spectra of the four alkaloids mentioned are available from the Depository of Unpublished Data. Photocopies may be obtained, at a nominal charge, from the Depository of Unpublished Data, CISTI, National Research Council of Canada, Ottawa, Ont., Canada K1A 0S2.

0008-4042/79/091105-03$01.00/0

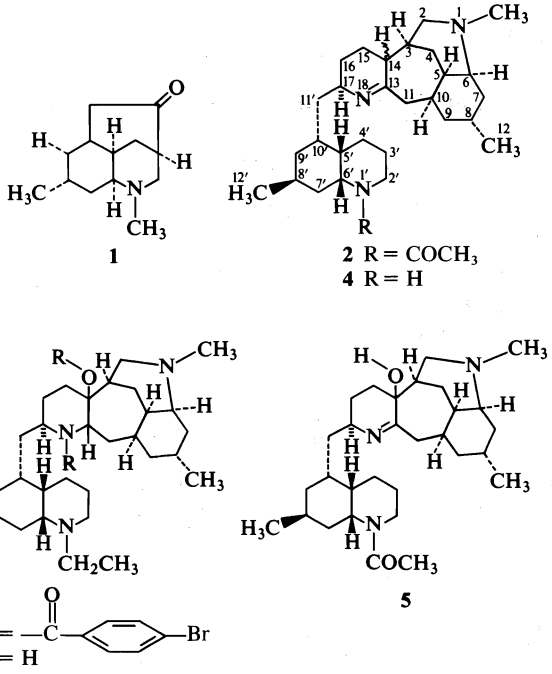

1

2 R = $COCH_3$
4 R = H

5

3 R = —C(=O)—C$_6$H$_4$—Br
6 R = H

pound $C_{30}H_{49}N_3O_2$ ('oxolucidine B'), **5**, is formed. Spectroscopic studies indicate the presence of a tertiary hydroxyl in oxolucidine B, and the X-ray structure reveals its position. Facile aerial oxidation of cyclic imines is well precedented (8). Treatment of **5** with lithium aluminum hydride in tetrahydrofuran brings about reduction of the imino group and the *N*-acetyl group and provides 'tetrahydrodeoxyoxolucidine B', **6**. Acylation of **6** with *p*-bromobenzoyl chloride in pyridine provided the first crystalline derivative in this series, *N*,*O*-di-*p*-bromobenzoyltetrahydrodeoxyoxolucidine B, **3**, mp 203–205°C (from ethyl acetate).[3] The complete structure of **3** was determined by an X-ray crystallographic study. Compound **3** crystallized in the monoclinic system with the following crystal data:

$C_{44}H_{59}N_3O_3Br_2$ fw = 837.8
$P2_1$, a = 11.340(1), b = 15.859(2), c = 12.922(3) Å, β = 115.5°, V = 2097.6 Å^3, Z = 2, ρ_o = 1.30 g/cm^3, ρ_c = 1.32 g/cm^3. Radiation Ni-filtered CuKα, λ = 1.5406 Å, temperature 22°C. Data collected: hkl, $\bar{h}kl$, $h\bar{k}l$, $\bar{h}\bar{k}l$ with $3° \leq 2\theta \leq 50°$ and hkl, $\bar{h}kl$ with $50° \leq 2\theta \leq 103°$. A total of 2435 reflections comprised the data set.

The solution of the structure involved examining the Patterson map to obtain the positions of the two bromine atoms of the molecule. Structure factors calculated for these bromine atoms produced an R index ($R = [\sum_{hkl}||F_o| - |F_c||]/[\sum_{hkl}|F_o|]$, where F_o and F_c are the observed and calculated structure factors, respectively) of 0.374. Twelve additional atoms, corresponding to two six-membered rings in chair conformations, were chosen from a subsequent difference Fourier map. The quantity minimized was $\sum_{hkl}\omega(|F_o| - k|F_c|)^2$, where ω is the weight and k is the scale factor relating to the observed and calculated structure amplitudes, in the CRYLSQ program of the X-RAY 70 system (9). The positions of the remaining nonhydrogen atoms were obtained by continually phasing on larger molecular fragments and calculating difference maps. After full matrix isotropic refinement of all of the 52 nonhydrogen atoms of the molecule, the R index was 0.186. Further blocked anisotropic refinement produced an R index of 0.097. Twelve hydrogen atoms were located on subsequent difference maps and were assigned isotropic temperature factors based on their peak heights. The hydrogen atom positional parameters (but not the temperature factors) were included in subsequent blocked refinement. Convergence was achieved at an R index of 0.087.

The choice of the enantiomorph was checked by converting the y/b values of these final atomic coordinates to $-y/b$ values; the corresponding structure factor calculation produced an R index of 0.131. Application of Hamilton's significance test

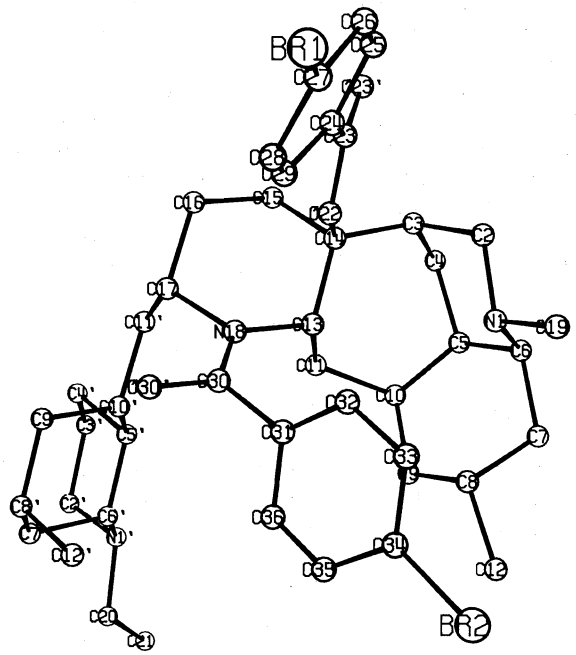

FIG. 1. Perspective view of *N*,*O*-di-*p*-bromobenzoyltetrahydrodeoxyoxolucidine B.

[3]Compound **3**, which does not show a molecular ion in the mass spectrum, gave a satisfactory C, H, N combustion analysis. Molecular formulas for the other compounds described herein were determined by high-resolution mass spectrometry.

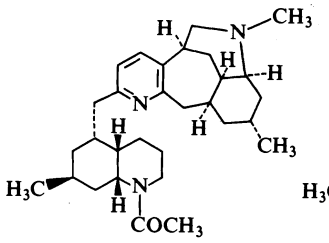

7

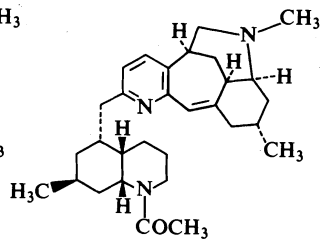

8

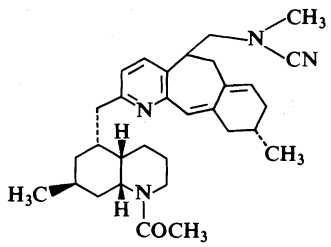

9

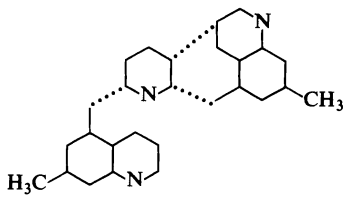

10

(10) shows that the original coordinates correspond to the correct enantiomorph of the molecule to a confidence level >99.5%.[4] A perspective drawing of **3** is shown in Fig. 1.

Dihydrolycolucine shows the properties of a 2,3,6-trisubstituted pyridine (λ_{max} 276 nm (ε 8500), $\lambda_{max}^{H^+}$ 279 nm (ε 13 400), AB quartet at δ 7.30 and δ 6.84 (J = 8 Hz)) and is assigned structure **7**. Dehydrogenation of lucidine B (**2**) with 5% Pd–C in refluxing isoquinoline gives, among other products, dihydrolycolucine (**7**), confirming the stereochemical features depicted for **7**.

Lycolucine, mp 198–200°C, on mild catalytic hydrogenation affords dihydrolycolucine (**7**). The uv spectrum (λ_{max} 261 nm (ε 8800), 272 nm (ε 7800), and 300 nm (ε 10 200)) indicates the extra unsaturation is conjugated to the pyridine ring and the ^{1}Hmr spectrum shows the presence of a single olefinic proton (δ 6.60, s). Treatment of lycolucine with cyanogen bromide in chloroform gives the *N*-cyanodiene **9** (λ_{max} 230, 282, 294, 309 nm), and establishes that the double bond in lycolucine (**8**) is located between C-10 and C-11, and not between C-10′ and C-11′.

It is interesting to note that the structures of these new alkaloids may be derived formally by attaching two (enantiomeric) $C_{11}N$ units (compare with **1**) to a piperidine ring as indicated by the broken lines in **10**. The fusion of a single $C_{11}N$ unit to a piperidine ring is found in the *Lycopodium* alkaloid phlegmarine (7).

Acknowledgements

We wish to thank Dr. Martin Cowie for his help in collecting the X-ray data, Prof. D. B. MacLean for a quantity of crude bases of *L. lucidulum*, and the National Research Council of Canada for financial support.

1. W. A. Ayer, J. A. Berezowsky, and D. A. Law. Can. J. Chem. **41**, 649 (1963).
2. W. A. Ayer, B. Altenkirk, R. H. Burnell, and M. Moinas. Can. J. Chem. **47**, 449 (1969).
3. W. A. Ayer and B. Altenkirk. Can. J. Chem. **47**, 499 (1969).
4. W. A. Ayer, N. Masaki, and D. S. Nkunika. Can. J. Chem. **46**, 3631 (1968).
5. D. S. Nkunika. Ph.D. Thesis, University of Alberta, Edmonton, Alta. 1967.
6. L. F. Ball. Ph.D. Thesis, University of Alberta, Edmonton, Alta. 1971.
7. L. Nyembo, A. Goffin, C. Hootelé, and J.-C. Braekman. Can. J. Chem. **56**, 851 (1978).
8. L. A. Cohen and B. Witkop. J. Am. Chem. Soc. **77**, 6595 (1955).
9. J. M. Stewart, F. A. Hundell, and J. C. Baldwin. The X-RAY 70 system. Computer Science Center, University of Maryland, College Park, MD. 1970.
10. W. C. Hamilton. Acta Crystallogr. **18**, 502 (1965).

[4]Tables of atomic parameters, bond lengths and angles, and structure factors are available, at a nominal charge, from the Depository of Unpublished Data, CISTI, National Research Council of Canada, Ottawa, Ont., Canada K1A 0S2.

Micellar super-structure in magnetically aligned lyotropic liquid crystals studied by light scattering[1]

PAULO C. ISOLANI, LEONARD W. REEVES,[2] AND J. ATILIO VANIN

Instituto de Química, Universidade de São Paulo, Caixa Postal 20780, São Paulo, Brasil and Department of Chemistry, University of Waterloo, Waterloo, Ont., Canada N2L 3G1

Received October 12, 1978

PAULO C. ISOLANI, LEONARD W. REEVES, and J. ATILIO VANIN. Can. J. Chem. **57**, 1108 (1979).

Depolarized components of laser light scattering patterns have been investigated for type II lyotropic liquid crystals. These patterns are characterized by intensity maxima and minima with constant angular separation. By using the Bragg equation, a set of distances typical for lamellar arrays can be derived. Two possible models are proposed to explain the results: the first is that the distances are related to the average diameter of lyomesomorphic micelles not accessible to low angle X-ray studies and the second model is a repeating hyperstructure of micellar microdomains.

PAULO C. ISOLANI, LEONARD W. REEVES et J. ATILIO VANIN. Can. J. Chem. **57**, 1108 (1979).

On a étudié les composantes dipolarisées des modèles de diffusion de la lumière laser pour des cristaux liquides lyotropes de types II. Ces modèles sont caractérisés par des maxima et minima d'intensité entre lesquels on observe des séparations angulaires constantes. Faisant appel à l'équation de Bragg, on a pu dériver un ensemble des distances typiques pour des arrangements lamellaires. On propose deux modèles pour expliquer les résultats: pour le premier, on fait l'hypothèse que les distances sont reliées au diamètre moyen des micelles lyomesomorphiques qui ne sont pas accessibles aux études par rayons-X aux petits angles alors que le second modèle est une hyperstructure de microdomaines micellaires qui se répètent.
[Traduit par le journal]

Introduction

In the last few years, Reeves and co-workers have been studying magnetically aligned lyotropic liquid crystals by means of nmr spectroscopy (1–11). The structure of most of these mesophases is not known and a tentative classification based on magnetic properties was proposed by Reeves *et al.* (6). This work reports a new contribution to the study of lyomesophases, in the sense that an attempt is made to clarify how the organized micellar arrays behave in magnetic fields by means of light scattering studies.

Light scattering phenomena, showing interference due to particle size in micellar or macromolecular solutions, were extensively studied during the 1940 decade by protein chemists (12). Friberg *et al.* used light scattering to distinguish between normal and inverted micelles in amphiphilic micellar solutions (13). Light scattering in thermotropic nematic and cholesteric liquid crystals have also been studied (14–18). Recently, Ribota reviewed the results in thermotropic smectic mesophases (19).

We have investigated intensity measurements of depolarized scattered light by lyotropic type II liquid crystals (6) and its dependence on the angle of scattering and sample orientation in magnetic fields.

Experimental

Scattering Studies

Light scattering experiments were carried out in a home-made apparatus. A Spectra-Physics model 155 helium-neon laser was used as a light source. The laser beam passed through a polarizer before incidence on the sample, which was kept in a 5 mm diameter high quality nmr tube. Scattered light passed through a narrow pass-band interference filter for 6328 Å wavelength (Oriel Optics, 90 Å FWHM), a second polarizer crossed with respect to the first, and was detected by a photo-multiplier (RCA No. 4832) placed immediately behind a 10 μm slit.

Sample, interference filter, second polarizer, slit, and photo-multiplier were placed in a closed box mounted on a goniometer which allowed angular readings. Sample position coincided with the center of the goniometer and it could be kept immobile with respect to the laser beam as well as rotating with the detector.

A HP model 6516a DC power supply was used for the photo-multiplier. Optimum signal-to-noise ratios were attained at 800 V. Current was measured by a Keithley model 616 digital electrometer. Typical currents were in the range of 10^{-7} A. Scattering patterns were obtained by plotting the photo-multiplier current as function of the scattering angle.

Optical birefringence was measured by a Zeiss universal polarizing microscope.

Sample Preparation

Typical percent weight compositions of samples are the following: Sample A: 36% sodium decanoate, 6% KCl,

[1]Work partially presented at the 29th Annual Meeting of the Brazilian Society for the Advancement of Science (SBPC), São Paulo, July 1977.

[2]Visiting Professor since 1967, Universidade de São Paulo.

0008-4042/79/091108-03$01.00/0

4% decanol, and 64% water. Sample B: 37% sodium decylsulfate, 6% Na_2SO_4, 6% *n*-decanol, and 51% water. Sample C: 36% sodium dodecanoate, 6% KCl, and 68% water.

Sample alignment was achieved in the 23.5 kG magnet of a Varian XL-100-12 NMR spectrometer, with or without sample spinning of a high precision 5 mm nmr tube. It was observed that liquid crystalline samples of this kind, once oriented in a magnetic field, keep their alignment at room temperature for several months. Samples were removed from the magnet without shaking and placed in the light scattering apparatus. All the experiments were performed in an air-conditioned room with temperature 23 ± 1°C.

Results

Figure 1 shows a typical pattern of depolarized scattered light. This specific lyomesophase was sample A, oriented in the 23.5 kG magnet overnight with sample spinning, as for a conventional nmr experiment. Angular measurements show maxima and minima in light intensity separated by well defined angles.

The angular separations between those maxima showed no modifications by varying slightly (about 2%) the relative concentrations of the sample constituents, as far as it still was a type II lyotropic liquid crystal. There was also no change with the direction of polarization of incident light. These separations were shown to vary only with the nature of the detergent headgroup in the mesophase. It is important to emphasize that the intensity of depolarized scattered light was observed to be much lower with respect to scattered polarized light; thus, only by using a crossed second polaroid was it possible to observe the diffractogram.

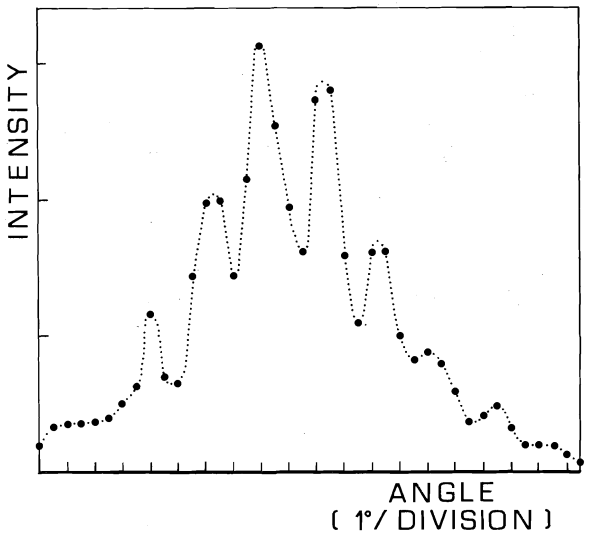

FIG. 1. Pattern of depolarized scattered light from sample A. Relative depolarized scattering intensity versus angle of diffracted laser light. Diffraction patterns have also been photographed in each case.

Measurements on sample A showed sharp maxima separated by 2° ± 15′ angle. By using the Bragg equation, $\lambda = 2d \sin \theta$, a set of *d* spacing values was obtained, with the relation 1:0.50:0.33:0.25:0.20, which are characteristic of lamellar arrays with 9.2 ± 1.2 μm periodicity. Sample C gave the same periodicity within experimental error. Lyomesophases of sodium decylsulfate (sample B) also gave sharp scattering maxima, but not as well defined as for sample A. For this mesophase, the scattering pattern shows an angular separation of 1° ± 15′. Using again the Bragg equation, these data can be fitted to a lamellar array of periodicity 19 ± 4 μm. The intensity of scattered light and the definition of intensity maxima were observed to be strongly dependent on the alignment of samples. Unoriented samples showed the same angular separation between maxima, though the observed pattern was very diffuse and sometimes not observable. All samples after stationary alignment in a magnetic field showed intense scattering and good maxima definition when the laser beam coincided with the direction of the steady magnetic field. Incidence in the perpendicular direction showed less sharp maxima and lower intensity of scattered light. Samples aligned by spinning in the magnetic field have shown the greatest light scattering intensity and the best maxima definition. All samples, when examined in a polarizing microscope, were characterized as optically monoaxial, showing negative birefringence.

Discussion

Extensive low-angle X-ray diffraction studies on samples of the same composition of sample B indicate that the structure of this kind of lyomesophase can be explained by a model consisting of arrays of disc-shaped lamellar micelles of about 38 Å thickness, corresponding to the length of two chains, with long range orientational but not positional order. The separation between micelles is in the range 54 to 92 Å and is filled with water. These distances are obtained directly from the low-angle X-ray diffractogram (20, 21).

The effect of the magnetic field is to align the normal to the disc surface (the so-called director) perpendicularly to the magnetic field force lines. Samples oriented in stationary magnetic fields have micellar directors in all directions perpendicular to the field. In the cylindrical tube of high quality, usually employed for nmr studies, the directions perpendicular to the liquid crystal/glass interface are favoured and therefore the distribution of the directors in the plane perpendicular to the magnetic field direction is not uniform. Samples which are aligned

by spinning the nmr tube perpendicular to the magnetic field have directors oriented perpendicularly to the force lines and parallel to the spinning axis. Obviously, unoriented samples have directors in all possible directions in space, but some cooperative effects between neighbour micelles or wall effects can induce local order over short ranges.

The pattern of scattered light can be explained by one of the following models: (*i*) The greatest dimension of the micelle or the average disc diameter, not accessible for investigation by low angle X-ray diffraction, might be responsible for the periodicity and give rise to the characteristic distance detected by visible light scattering. This hypothesis is supported by the fact that no X-ray scattering is observed in a direction perpendicular to the orienting magnetic field (20). In this respect also the analysis of the diffractogram widths in the low angle X-ray study (20, 21)[3] indicates a disc size greater than 1000 Å. (*ii*) The micelles may be packed in a super-superstructure, which could be called a hyperstructure or micellar microdomain. These hyperstructures could have a size corresponding to the distance obtained in this work and they might be disposed in a lamellar array.

Observations of samples in the polarizing microscope showed evidence of the micellar orientation between cover and slide. The observed optical monoaxial pattern suggested that in this thin layer of liquid crystal surface orientation makes the disc-shaped micelles stay in a position parallel (and, consequently, the directors perpendicular) to the glass surface. Further experiments in type I lyomesophases are in progress and the results will be reported briefly.

Acknowledgements

We wish to acknowledge gratefully Professor José M. Riveros for use of his laboratory and equipment. We also wish to thank Drs. Lia Queiroz do Amaral and Vera R. Paoli Monteiro for helpful discussions. This work was made possible by grants of the Conselho Nacional de Desenvolvimento Científico e Tecnológico of Brazil (CNPq) to the laboratory of Professor J. M. Riveros and from CNPq/National Research Council of Canada (NRCC) to L.W.R.

[3]Also M. R. Tavares, C. A. Pimental, and L. Q. do Amaral. Private communications.

1. L. W. Reeves, J. S. de Cara, M. Suzuki, and A. S. Tracey. Mol. Phys. **25**, 1481 (1973).
2. L. W. Reeves, A. S. Tracey, and M. M. Tracey. J. Am. Chem. Soc. **95**, 3799 (1973).
3. D. M. Chen, K. Radley, and L. W. Reeves. J. Am. Chem. Soc. **96**, 5251 (1974).
4. L. W. Reeves, M. Suzuki, and J. A. Vanin. Inorg. Chem. **15**, 1035 (1976).
5. Y. Lee and L. W. Reeves. Can. J. Chem. **53**, 161 (1975).
6. K. Radley, L. W. Reeves, and A. S. Tracey. J. Phys. Chem. **80**, 174 (1976).
7. F. Y. Fujiwara and L. W. Reeves. J. Am. Chem. Soc. **98**, 6790 (1976).
8. D. M. Chen, F. Y. Fujiwara, and L. W. Reeves. Can. J. Chem. **55**, 2396 (1977).
9. D. M. Chen, F. Y. Fujiwara, and L. W. Reeves. Can. J. Chem. **55**, 2404 (1977).
10. D. M. Chen and L. W. Reeves. J. Am. Chem. Soc. **94**, 4384 (1972).
11. L. W. Reeves, F. Y. Fujiwara, and M. Suzuki. Am. Soc. Symp. Ser. **34**, 55 (1976).
12. P. Doty and J. T. Edsall. Adv. Protein Chem. **6**, 37 (1951).
13. S. Friberg, L. Rydhag, and G. Lindblom. J. Phys. Chem. **77**, 1280 (1973).
14. D. Krishnamurti and H. S. Subramanya. Mol. Cryst. Liq. Cryst. **14**, 209 (1971).
15. T. Haller and J. D. Litster. Mol. Cryst. Liq. Cryst. **12**, 277 (1971).
16. J. Adams, W. E. Haas, and J. J. Wysocki. Mol. Cryst. Liq. Cryst. **8**, 9 (1969).
17. G. R. Alms, T. D. Gierke, and W. H. Flygare. J. Chem. Phys. **61**, 4083 (1974).
18. T. D. Gierke and W. H. Flygare. J. Chem. Phys. **61**, 2231 (1974).
19. R. Ribota. *In* Proceedings of the Third International Conference on Light Scattering in Solids. *Edited by* M. Balkanski, R. C. C. Leite, and S. P. S. Porto. Flammarion, Paris. 1976. p. 713.
20. Myriam R. Tavares. M.Sc. Dissertation, Instituto de Física, Universidade de São Paulo. 1978.
21. M. R. Tavares, C. A. Pimentel, and L. Q. do Amaral. Suppl. to Acta Crystallogr. A**34**, S188 (1978).

Absorption and magnetic circular dichroism spectra of metal-free phthalocyanine in ultraviolet-transparent solvents

KATHERINE A. MARTIN AND MARTIN J. STILLMAN[1]

Department of Chemistry, University of Western Ontario, London, Ont., Canada N6A 5B7

Received October 30, 1978

KATHERINE A. MARTIN and MARTIN J. STILLMAN. Can. J. Chem. **57**, 1111 (1979).

Absorption and magnetic circular dichroism spectra of metal-free phthalocyanine (H_2Pc) have been recorded over the range 270–800 nm. The use of solvents transparent in the 270–400 nm region allows the observation for the first time of the B band spectral envelope of H_2Pc in solution. The mcd spectrum clearly indicates that the complex $(NH_4)_2Pc$ is formed when ammonia is bubbled through a solution of H_2Pc in dimethyl sulphoxide. The multi-transition nature of the B band region is identified as a property of the phthalocyanine π electron system rather than arising from charge transfer between the ring and a central metal cation.

KATHERINE A. MARTIN et MARTIN J. STILLMAN. Can. J. Chem. **57**, 1111 (1979).

On a enregistré, entre 270 et 800 nm, les spectres d'absorption et de dichroïsme circulaire magnétique de la phtalocyanine (H_2Pc) ne contenant pas de métal. Utilisant des solvants qui n'absorbent pas entre 270 et 400 nm, on a pu observer pour la première fois la bande B, enveloppe spectrale de H_2Pc en solution. Le spectre de dcm indique clairement qu'il y a formation du complexe $(NH_4)_2Pc$ lorsqu'on fait barbotter de l'ammoniac dans une solution de H_2Pc dans le diméthylsulfoxyde. On a identifié que la nature multitransitionnelle de la bande dans la région B est une propriété du système d'électrons π de la phtalocyanine et qu'elle n'est pas due à un transfert de charge entre le cycle et un cation métallique central.
[Traduit par le journal]

The numerous calculations reported in the literature describing the electronic states in the phthalocyanine molecule (1–4) contrast with the paucity of data of a systematic nature that can be used to check the accuracy of these theoretical predictions. In particular, two problems are evident from a survey of both the calculations and the available spectra. (*i*) The perturbation of the central metal cations' orbitals on the ring π orbitals results in considerable variation in the observed MPc spectra (5–7); (*ii*) even with the same metal cation at the centre of the phthalocyanine ring, the effect of solvent and axially coordinating ligand can cause dramatic changes to the intensities and band energies of the major features of a "typical" phthalocyanine spectrum (5–8).

The key to this problem appeared to us to be the measurement of the spectra of a wide range of phthalocyanine complexes in a single solvent in which axial ligation effects on the π spectrum could be studied. It is clear from the calculations that we must attempt to include $\pi \rightarrow \pi^*$ transitions to 250 nm (3). For unlike the analogous porphyrin spectra the 250–380 nm region in the phthalocyanines is characterized by a series of broad, overlapping bands in both solution (6, 7) and solid state spectra (9, 10). In addition, magnetic circular dichroism spectra (mcd) should be included to provide polarization and angular momentum data to aid in the assignment (7, 10, 11).

Clearly an important spectrum in this survey is that of metal-free phthalocyanine as this will allow identification of both metal and ligand effects. Phthalocyanines are notoriously insoluble, in most spectroscopically-useful solvents. We have shown previously that it is possible to obtain the spectra of a large range of MPc complexes in dimethyl sulphoxide (DMSO) (7), and these experiments have been extended by us and others (12, 13) to include dimethyl acetamide (DMA), and dimethyl formamide (DMF). No spectra of H_2Pc in such solvents have been reported to our knowledge.

Solid state spectra, both from crystals in the β phase (14), and sublimed thin films in the α phase (9, 10), are available, but ligand effects cannot be studied readily due to extensive broadening and Davydov splitting (10). While vapour phase absorption experiments (15) have yielded spectra in the uv region (down to 200 nm), it is unlikely that ligand binding studies would be successful at these elevated temperatures. Solution spectra of H_2Pc have been reported in α-chloronaphthalene (5), where the two-banded Q band in the 670–690 nm region characterizes the D_{2h} symmetry resulting from the substitution of the metal, M^{2+}, by two protons, unfortunately the uv region is almost totally obscured

[1]To whom all correspondence should be addressed.

0008-4042/79/091111-03$01.00/0

in this solvent. Whalley (16) reported that H_2Pc exhibited a D_{4h} spectrum in pyridine, but, yet again, the solvent absorption in uv region restricted the analysis. Our data do confirm her characterization of the chromphoric species as the pyridinium salt.

Absorption and mcd spectra of H_2Pc between 270 nm and 720 nm in DMSO and DMA have been obtained by two methods. Figure 1 shows the spectra recorded after the addition of very dilute HCl to a solution of Li_2Pc in DMA at room temperature. A similar absorption spectrum is produced by dissolving multiply-sublimed H_2Pc in DMSO at 150°C, in this case there is a red-shift of 2 nm compared with the acid-produced spectrum. The band centres in the absorption are 693, 660, 638 (sh), 633 (sh), 600, 360 (sh), 333, 305, and 285 nm (sh) for H_2Pc in DMSO. When ammonia gas is bubbled vigorously through a solution of H_2Pc in DMSO the absorption and mcd spectra shown in Fig. 2 are obtained, with new band centres at 669, 638 (sh), 603, 380 (sh), and 367 nm. This species is stable at room temperature for several hours. Spectra with a similar visible region band envelope are obtained when other nitrogen donor ligands are added to H_2Pc in either DMA or DMSO (13).

We suggest that the chromophoric species in each of these complexes is the Pc^{2-} ion, thus with ammonia we have $(NH_4^+)_2Pc^{2-}$. Bubbling nitrogen gas through the ammonia saturated solution for 30 min displaces the bound ammonia. The absorption spectrum now reverts to its original form, which is characterized by two bands in the Q region at 693 and 660 nm.

The mcd spectra clearly indicate the difference in the symmetry between the two phthalocyanine complexes (H_2Pc in DMSO and H_2Pc + NH_3(g) in DMSO), supporting our assignment of H_2Pc as the molecular species in Fig. 1 and Pc^{2-} as the species in Fig. 2. It is perhaps reasonable to suggest that the $(NH_4)_2Pc$ spectrum, with its D_{4h}, 18π electron ring unperturbed by the asymmetric protons of the H_2Pc species, will most closely resemble a 'pure' phthalocyanine spectrum.

If this is the case, then we have, for the first time, a clear indication of the complex nature of the B region at 340 nm. The mcd spectra support the view that these absorption bands are all centred on the ring, which implies that there are at least three distinct states in this region arising from the π molecular orbitals. Until now it has been impossible to separate unambiguously the ring $\pi \rightarrow \pi^*$ transitions, from charge transfer transitions between the ring, the metal cation and/or the axial ligands.

The presence of a multi-transition envelope in the B region has not been generally discussed in the literature. With the advent of mcd spectroscopy the details of this region have become much clearer.

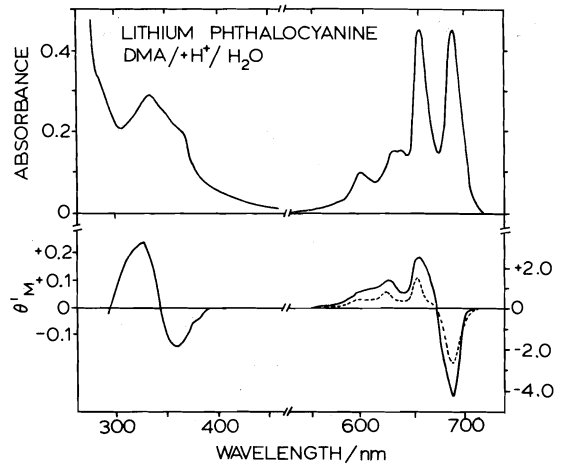

FIG. 1. Absorption and mcd of H_2Pc in DMA prepared by the addition of dilute acid to a solution of Li_2Pc. A magnetic field of 5.0 T was used for the mcd.

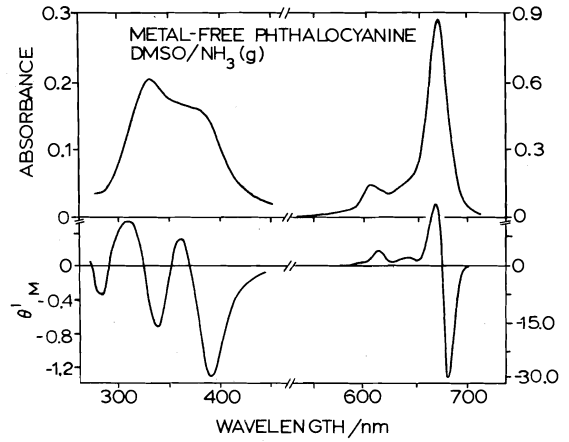

FIG. 2. Absorption and mcd of $(NH_4)_2Pc$ in DMSO prepared by bubbling NH_3(g) into a solution of H_2Pc. A magnetic field of 5.5 T was used for the mcd in the uv region and 1.4 T in the visible region.

Dale (6) used the ordering of states given by Weiss *et al.* (17) to assign the band envelope observed in this region in the spectrum of FePc complexes in DMSO. These data give a B band energy of between 25 000 cm^{-1} (400 nm) in $FePc(CN)_2$ and 29 000 cm^{-1} (345 nm) in FePc, and an N band energy close to 31 000 cm^{-1} (323 nm) for each species studied. These values are far from the energies observed in the vapour phase (15), however, the effect of the Fe^{2+} cation is still unknown. In our experiments we have extended the accessible wavelength range with DMSO to 260 nm, in doing so we have observed a band close to 270 nm for a wide range of complexes (7, 13). This transition, part of which is quite clear

in the mcd spectrum of $(NH_4)_2Pc$, Fig. 2, as a negative lobe at ca. 283 nm, lies close to the N band assigned by Edwards and Gouterman (15). We consider that the band envelope observed in the 330 nm region arises from at least two degenerate $\pi \rightarrow \pi^*$ transitions associated with the configurations that give rise to the B band.

Acknowledgements

The authors acknowledge the financial support of the National Research Council of Canada and a Province of Ontario Graduate Scholarship (to K.A.M.).

1. A. HENRIKSSON and M. SUNDBOM. Theor. Chim. Acta, **27**, 213 (1972).
2. A. M. SCHAFFER and M. GOUTERMAN. Theor. Chim. Acta, **25**, 62 (1972).
3. A. J. MCHUGH, M. GOUTERMAN, and C. WEISS, JR. Theor. Chim. Acta, **24**, 346 (1972).
4. M. GOUTERMAN. *In* The porphyrins. Vol. III. *Edited by* D. Dolphin. Academic Press. 1978.
5. A. B. P. LEVER. Adv. Inorg. Radiochem. **7**, 27 (1965).
6. B. W. DALE. Trans. Faraday Soc. **65**, 331 (1969).
7. M. J. STILLMAN and A. J. THOMSON. J. Chem. Soc. Faraday Trans. II, **70**, 790 (1974); **70**, 804 (1974).
8. W. CLACK and J. R. YANDLE. Inorg. Chem. **11**, 1738 (1972).
9. B. R. HOLLEBONE and M. J. STILLMAN. Chem. Phys. Lett. **29**, (2), 284 (1972).
10. B. R. HOLLEBONE and M. J. STILLMAN. J. Chem. Soc. Faraday Trans. II. In press.
11. A. J. MCCAFFERY and P. N. SCHATZ. J. Chem. Soc. Q. Rev. **23**, 552 (1969).
12. A. B. P. LEVER and J. P. WILSHIRE. Inorg. Chem. **17**, 1145 (1978).
13. K. A. MARTIN and M. J. STILLMAN. Unpublished work.
14. L. E. LYONS, J. R. WALSH, and J. W. WHITE. J. Chem. Soc. 167 (1960).
15. L. EDWARDS and M. GOUTERMAN. J. Mol. Spectrosc. **33**, 292 (1970).
16. M. WHALLEY. J. Chem. Soc. 866 (1961).
17. C. WEISS, H. KOBAYASHI, and M. GOUTERMAN. J. Mol. Spectrom. **11**, 108 (1965).

Canadian Journal of Chemistry
Published by
THE NATIONAL RESEARCH COUNCIL OF CANADA

Journal canadien de chimie
Publié par
LE CONSEIL NATIONAL DE RECHERCHES DU CANADA

Volume 57 Number 10 May 15, 1979 Volume 57 numéro 10 15 mai 1979

On the interpretation of measured rotational and vibrational relaxation times. III. Failure of the mixture rule for non-dilute gases

HUW O. PRITCHARD, NABIL I. LABIB, AND ARUNACHALAM LAKSHMI
Centre for Research in Experimental Space Science, York University, Downsview, Ont., Canada M3J 1P3

Received October 26, 1978

HUW O. PRITCHARD, NABIL I. LABIB, and ARUNACHALAM LAKSHMI. Can. J. Chem. **57**, 1115 (1979).

The rotation–vibration relaxation of a mixture of a diatomic gas (approximately simulating hydrogen) with an inert gas is studied both by direct integration, and by an approximate linearised normal-mode method. It is shown that although the linearised normal-mode approximation is a powerful aid to understanding these processes, its numerical accuracy is limited to high dilutions (e.g. 1% of X_2 in M) and to times shorter than the final relaxation time.

Direct numerical integration of the relaxation equations for various mixture ratios shows that the plot of vibrational relaxation rate constant vs. mole fraction x is non-linear, and that the slope of this plot near $x = 0$ can be correlated with the rates of the R–R processes, *not* the V–V processes as is normally assumed. A brief discussion is presented of the conditions under which the linear mixture rule for relaxation is rigorously obeyed: as is the case for chemical reaction, these conditions are impossibly stringent.

An appendix presents a comparison of the transition probabilities used in this series of papers with those recently obtained by Tarr and Rabitz for the relaxation of hydrogen in argon.

HUW O. PRITCHARD, NABIL I. LABIB et ARUNACHALAM LAKSHMI. Can. J. Chem. **57**, 1115 (1979).

On a étudié la relaxation rotation–vibration d'un mélange d'un gaz diatomique (simulant l'hydrogène) avec un gaz inerte par une intégration directe ainsi que par une méthode approximative du mode normal linéaire. On montre que même si l'approximation du mode normal linéaire est très utile pour comprendre ces processus, son exactitude numérique est limitée à hautes dilutions (environ 1% de X_2 dans M) et à des temps plus courts que le temps final de relaxation.

Une intégration numérique directe des équations de relaxation pour divers rapports de mélange montre que la courbe reliant la constante de vitesse de la vibration de relaxation et la fraction molaire (x) n'est pas linéaire et que la pente de cette courbe près de $x = 0$ peut être reliée aux taux des processus R–R et *non pas* aux processus V–V comme il est généralement supposé. On présente une brève discussion des conditions où la règle des mélanges linéaires pour la relaxation est suivie d'une façon rigoureuse: comme c'est le cas pour la réaction chimique, ces conditions sont très strictes.

Dans un appendice, on présente une comparaison des probabilités de transitions qui sont utilisés dans cette série de communications avec celles récemment obtenues par Tarr et Rabitz pour la relaxation de l'hydrogène dans l'argon.

[Traduit par le journal]

Introduction

The two preceding papers in this series (1, 2) have been devoted to the problem of understanding the nature of the rotation–vibration relaxation process for a system of diatomic molecules infinitely diluted in an inert-gas bath. In the absence of a detailed set of vibrational and rotational transition probabilities for any molecule, calculations were conducted using two hypothetical sets of transition probabilities, one termed the "standard" set which, it was hoped, would mimic the behaviour of H_2, and the other termed a "modified" set which was intended to

0008-4042/79/101115-07$01.00/0

mimic the behaviour of a typical diatomic molecule. As time passes, more information is becoming available concerning the required transition probabilities for H_2 itself and it would appear that, at 1500 K, our so-called "standard" set couples the rotational and vibrational relaxations a little too strongly: an analysis of this problem is presented in the Appendix.

However (anticipating the results presented below), because of the partial failure of the linearised normal-mode approach, most of the conclusions of this paper were derived from numerical integration of the relaxation equations; these equations are stiff and an increase in the separation of characteristic times for rotational and vibrational relaxation would automatically bring with it a corresponding increase in the computing time required to perform the necessary integrations. Consequently, this work continues to use the "standard" set of T–V, T–R, and T–VR transition probabilities used previously, essentially for three reasons: first to minimise computing costs, second to facilitate comparison with the earlier work, and third because at the low temperature of 500 K considered here, it does not obscure any of the essential features of the H_2/M relaxation process. The model used in this work, therefore, consists of this "standard" set of transition probabilities describing the relaxation of H_2 in M at infinite dilution, as summarized[1] in Table I(1), together with an additional non-linear term in each differential equation for the ith population n_i, viz.,

$$[1]\quad \frac{dn_i}{dt} = [M]Z\sum_k (P_{k\to i}n_k - P_{i\to k}n_i) + Z'\sum_{jkl}(P_{kl\to ij}n_k n_l - P_{ij\to kl}n_i n_j)$$

In eq. [1], [M] is the number density of the inert gas atoms, n_i is the number density of H_2 molecules in state i, Z and Z' are the collision numbers for M and H_2 and for H_2 and H_2 respectively, $P_{i\to k}$ is the transition probability per collision between M and H_2 of a transfer from state i to state k, and $P_{ij\to kl}$ is the probability of a simultaneous transfer in two colliding H_2 molecules from states i and j to states k and l.

The values chosen for the $P_{ij\to kl}$ transition probabilities at 500 K were taken from the calculations of Zarur and Rabitz (3), and, in order to generalise them to all required transitions in the system, were fitted to the empirical formula

$$[2]\quad P_{ij\to kl} = 0.006\exp[-(0.002|\Delta\varepsilon| + 2.5|\Delta J|)]$$

where $|\Delta\varepsilon|$ is the energy difference in cm^{-1} for any *exothermic* process and $|\Delta J|$ is the net change in J for the two partners; this parametrisation fits the results of Zarur and Rabitz reasonably closely. Endothermic and exothermic processes are of course related by the detailed balancing relationships

$$[3a]\quad \tilde{n}_i\tilde{n}_j P_{ij\to kl} = \tilde{n}_k\tilde{n}_l P_{kl\to ij}$$

$$[3b]\quad \tilde{n}_i P_{ij\to kj} = \tilde{n}_k P_{kj\to ij}$$

$$[3c]\quad \tilde{n}_i P_{i\to k} = \tilde{n}_k P_{k\to i}$$

where $\tilde{n}_i$ etc. represent the equilibrium number densities at the temperature of the heat bath.

In order to keep the size of the problem within reasonable bounds, the temperature for study was chosen to be 500 K so that truncation at 10 levels was permissible; also, because of the intrinsic interest of the $v = 1, J = 1$ level in laser-schlieren experiments, the calculations were again performed on the odd-J system, i.e. *ortho*-hydrogen. Likewise, because of the rapid decay of eq. [2] with $|\Delta\varepsilon|$, no values of $P_{ij\to kl}$ were calculated for $|\Delta\varepsilon| > 1000\ cm^{-1}$, which is acceptable at this temperature. Moreover, to facilitate some analysis of the results (since the linear mixture law does not necessarily hold for X_2 at infinite dilution in a mixture of two inert gases) it was assumed that as far as all T–V, T–R, and T–VR processes are concerned, H_2 and M have the same efficiencies, i.e.

$$[4]\quad ZP_{i\to k} = Z'P_{ij\to kj} \text{ for all } j$$

Linearised Normal Mode Results

Equation [1] can easily be put in normal-mode form by assuming that in the second term, n_j and n_l can be replaced by their equilibrium values $\tilde{n}_j$ and $\tilde{n}_l$, respectively, and by performing the appropriate summations: this transforms [1] into the form

$$[5]\quad \frac{dn_i}{dt} = (\mathbf{A} + x\bar{\mathbf{B}})n_i = \bar{\mathbf{C}}n_i$$

where x is the mole fraction of H_2 in the mixture. Note that in this representation, the matrix $\mathbf{A}$ contains all the T–VR processes for H_2–H_2 collisions: the matrix $\mathbf{A}$ really is

$$[6]\quad \mathbf{A} = (1 - x)\mathbf{A} + x\mathbf{A}'$$

since by eq. [4], $\mathbf{A} \equiv \mathbf{A}'$; thus the matrix $\bar{\mathbf{B}}$ contains only transition probabilities $P_{ij\to kl}$ for which k and l differ from i and j. One would expect this linearised form to be extremely accurate for small temperature changes, or for the final approach to equilibrium, especially so as $x \to 0$. Examination of the normal-mode diagrams generated from the solution of eq. [5] shows that, for $x = 0.01$ or 0.02, they are imperceptibly different (if the comparison is made

[1]Equations, figures, and tables located in Parts I and II (refs. 1 and 2) will henceforth be denoted by a Roman prefix indicating the Part number, followed by the number of the equation, etc., in parentheses.

visually) from each other, or from the normal-mode diagrams such as we have published previously (1, 2) for the infinitely dilute system; see, e.g., Fig. I(1). Moreover, in a given relaxation, e.g. a temperature step from 300 to 500 K, or from 499.5 to 500 K, the corresponding relaxation strengths ξ_i (as defined in eq. I(10)) are only slightly different for the three cases $x = 0$, 0.01, and 0.02. This is consistent with Shuler's observation almost 20 years ago (4) that the inclusion of these non-linearities does not alter the essential pattern of the relaxation.

Examination of the magnitudes of the eigenvalues themselves, however, yields an unexpected result which restricts the general usefulness of the linearised normal-mode technique. Apart from the zero eigenvalue, which is required by conservation, all the other eigenvalues move to a slightly more negative value, as required by the appropriate addition theorem. Most eigenvalues move by only a small amount, varying between 0.1 and 0.2%; however, the last eigenvalue (hereinafter designated simply as λ) representing the final vibrational part of the relaxation (see e.g. M_{14} of Fig. I(1)) is approximately doubled as x goes from 0 to 0.01, and is moved almost as much again when x goes from 0.01 to 0.02. This was not expected since the vibrational relaxation time of H_2 should not be grossly sensitive to the mole fraction x, and in fact it can easily be shown to be an artefact by direct numerical integration of eq. [1]. This integration gives the population evolution directly, and thus the evolution of the energy

$$[7] \qquad \Delta E(t) = E(t) - E_{\text{Boltzmann}}$$

of the system; the required relaxation time is then derived simply as the numerical derivative

$$[8] \qquad \tau_{\text{vib}}^{-1} \equiv -\lambda = \mathrm{d} \ln \Delta E(t)/\mathrm{d}t$$

For $x = 0.01$ and 0.02, the final relaxation times (τ_{vib}) are only very slightly different from the unperturbed value (i.e. for $x = 0$) as expected: the actual magnitudes of the differences will be discussed in detail later in this paper.

Comparison of the population and energy evolutions calculated from the linearised normal modes and by direct integration is quite interesting. Both calculations agree well (better than 1% in any particular value) right through almost to the end of the rotational part of the relaxation, but then they begin to differ because of the incorrect long-time behaviour of the linearised form, eq. [5]. If the temperature change is very small, e.g. 499.5 → 500 K, this deficiency can be patched up by artificially adjusting the last non-zero eigenvalue back to the proper value (given by eq. [8]) or else to the unperturbed value, since these two quantities differ by so little; however, for larger temperature jumps, this trick will not work since the eigenvectors and eigenvalues of $\bar{\mathbf{C}}$ are now no longer mutually consistent,[2] and some calculated populations go negative in the very early stages of the relaxation. In view of these limitations, we will not discuss this linearised form of the master equation any further in this paper, except in-so-far as it helps to throw light on the nature of the relaxation process; other than that, it would appear that its usefulness as a computational technique would be limited to exploring ultrasonic rotational relaxation measurements. The only discussions of which we are aware concerning the conditions for linearisation of vibrational relaxation equations are for the special case of mixtures of harmonic oscillators (4–6).

Some Simple Results Concerning Population Evolution at Early Times

There has been considerable interest over the years in the concept of canonical invariance in relaxation processes (5, 7, 8), but as more integration results become available, it becomes clear that canonical invariance is likely to be a rather unusual occurrence. It turns out to be a very common occurrence for some populations to set off in the wrong direction once the relaxation is allowed to commence, before turning around and approaching their final equilibrium values: alternatively, some populations overshoot and approach their final equilibrium values from the "wrong" direction; examples and explanations of these occurrences were given in Part II. In the non-dilute case, there are two additional sources for these "false starts" and overshoots, which can be understood relatively easily in algebraic terms. The dominant fluxes for X_2/X_2 collision processes are usually those of the kind

$$X_2(i) + X_2(i) \rightarrow X_2(i+1) + X_2(i-1)$$

where i denotes either a rotational or a vibrational quantum number. We can write the *initial* fluxes for these processes as

$$[9] \quad \delta_i \equiv F_{ii \rightarrow i+1,i-1} = P_{ii \rightarrow i+1,i-1} m_i^2 + P_{i+1,i-1 \rightarrow ii} m_{i+1} m_{i-1}$$

[2]It appears that this large shift of the vibrational relaxation eigenvalue is an interference effect. If we choose other non-physical sets of $P_{i \rightarrow k}$, e.g. the present ones truncated to tridiagonal form, the set corresponding to the tridiagonal sum rule (eq. [8] of ref. 19), or the full matrix of probabilities given by eq. [16*a*] of ref. 9 (cf. Fig. I(5)), the last non-zero eigenvalue is hardly changed on going from the matrix $\mathbf{A}$ to matrix $\bar{\mathbf{C}} = \mathbf{A} + 0.01\bar{\mathbf{B}}$ (cf. eq. [5]). None of these forms possesses a normal mode which is clearly recognisable as "vibrational", as is M_9 of Fig. I(1). However, when a more physically realistic set of transition probabilities is used, so that the slowest mode of relaxation is essentially vibrational, then there is interference between this and M_4' of $\bar{\mathbf{B}}$ in Fig. 2, resulting in a large shift in the combined eigenvalue.

where the m_i etc. represent the equilibrium number densities at the starting temperature; because of detailed balancing, eq. [3*a*], we then find that

$$[10]\quad \delta_i \equiv F_{ii\rightarrow i+1,i-1} = \text{constant } m_i^2\left(\frac{m_{i+1}m_{i-1}}{m_i^2}\frac{\tilde{n}_i^2}{\tilde{n}_{i+1}\tilde{n}_{i-1}} - 1\right)$$

We imagine a change to take place from T_i (with equilibrium populations m_{i-1}, m_i, and m_{i+1}) to T_f (with equilibrium populations $\tilde{n}_{i-1}$, $\tilde{n}_i$, $\tilde{n}_{i+1}$): then it is simple to show that for a harmonic oscillator, for all i (except the highest and the lowest in the system of levels) δ_i is zero, whereas for a Morse oscillator δ_i is always negative if $T_i > T_f$, and for a rigid rotor δ_i is always positive if $T_i > T_f$ (with the respective signs reversed if $T_i < T_f$).

Numerical Experiments for Non-dilute Relaxing Systems

Equation [1] was solved numerically for a series of hypothetical mixtures of M and X_2, X_2 being taken to have the same energy-level structure as *ortho*-H_2. In order to circumvent complications from the failure of the mixture rule for the relaxation of X_2 in a mixture of M and M′, M and X_2 (≡M′) were assumed to have identical T–VR transition rate constants for collisions with X_2, cf. eq. [4]; these were derived from eq. [16] of ref. 9, cf. Table I(1) for a selection of numerical values. For collisions between pairs of X_2 molecules, the transition probabilities were those appropriate to H_2/H_2 collisions, parametrised as eq. [2]. The initial distribution for each relaxation calculation, following our earlier work (2), was assumed to be one in which the population distribution was appropriate to the temperature of 500 K, except that the population of the $v = 1, J = 1$ state was increased by a factor of 100, to simulate a typical laser-schlieren relaxation experiment.

Figure 1 shows the results of these calculations, expressed as $-\lambda$, the rate constant for the final approach of the internal energy to the equilibrium value, found by using eq. [8]. It can be seen that the vibrational relaxation time, even for this idealised model, does not obey the mixture rule, and the plot is rather similar to those obtained by Glänzer (10) for nitric oxide – argon mixtures. In the special case of H_2 – inert-gas mixtures, there have been two sets of experiments: those of Dove and Teitelbaum (11) which show a linear relationship between $|\lambda|$ and x_{H_2} for $x_{H_2} > 0.35$ — very much as we find in Fig. 1; and those of Audibert, Joffrin, and Ducuing (12) which show a linear portion over most of the range of mole fraction, but a definite downward curvature as $x_{H_2} \rightarrow 0$. In the remainder of this section, we devote

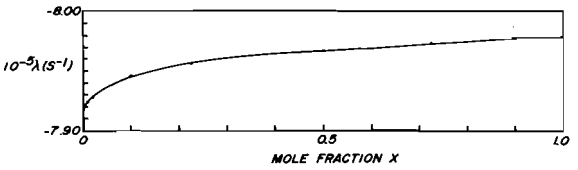

FIG. 1. Plot of $-\lambda = \tau_{vib}^{-1}$ for mixture of M and X_2, with a total number density of 3.5×10^{19} particles cm^{-3}. The T–VR transition rates are constrained to be identical for collisions of both M and X_2 with X_2, and are defined by the "standard" set of probabilities, eq. [16] of ref. 9. The TVR–TVR transition rates are defined by eq. [2].

our attention to the problem of deducing the physical meaning of the slope of this line, $d\lambda/dx$.

If the mixture rule is obeyed, then following the traditional arguments (13, 14) we would have

$$[11]\quad \lambda = (1-x)\lambda^{M/X_2(T-VR)} + x\lambda^{X_2/X_2(T-VR)} + x\lambda^{X_2/X_2(TVR-TVR)}$$

which, since we have taken identical transition rate matrices for the first two terms, reduces to

$$[12]\quad \lambda = \lambda^0 + x\lambda'$$

where λ^0 is the eigenvalue at infinite dilution and λ' is the $\lambda^{X_2/X_2(TVR-TVR)}$ of eq. [11]. Thus, the plot in Fig. 1 would be expected to be a straight line whose slope $d\lambda/dx$ would give the (so-called) V–V relaxation rate constant. Examination of the matrix of energy fluxes at a time $t = |\lambda^{-1}|$ reveals that by far the largest energy flux is due to the transitions $(v = 1, J = 1) \leftrightarrow (v = 0, J = 1)$ and $(v = 1, J = 3) \leftrightarrow (v = 0, J = 3)$ as expected; the energy fluxes for bimolecular collisions are dominated by two processes in the $v = 0$ manifold

$$[13]\quad J = 3 + J = 3 \leftrightarrow J = 1 + J = 5$$

$$[14]\quad J = 3 + J = 5 \leftrightarrow J = 1 + J = 7$$

The relative importance of these bimolecular processes varies with x (the ratio of [13]/[14] being about 1.15 at $x = 0.01$ and about 2.52 at $x = 1$), as also does their absolute importance, being about 0.2% of the total energy flux at $x = 0.01$ and 5% of it at $x = 1$.

Because of network-like effects, the final value of λ is very insensitive indeed to arbitrary variations in individual values of $P_{ij\rightarrow kl}$, and the only meaningful correlation we have been able to find is that if the values of $P_{ij\rightarrow kl}$ are doubled for *all* processes like [13] and [14] *having* a net $\Delta J = 0$, then the initial slope of the λ vs. x curve doubles from $-5.0_5 \times 10^4\ s^{-1}$ to $-1.0 \times 10^5\ s^{-1}$ at $x = 0$. Doubling of other subsets of the $P_{ij\rightarrow kl}$ has only insignificant effect on the initial slope of $d\lambda/dx$. This clearly identifies $|d\lambda/dx|_{x=0}$ as the mean rate constant for R–R processes of the

types [13], [14], etc. This identification is strongly confirmed by our normal-mode analysis. Figure 2 shows the form of the normal modes for the linearised perturbation matrix $\bar{\mathbf{B}}$ of eq. [5]. It can be seen that three of the "effective modes" are vibrational in character, i.e. M_2', M_3', and M_4', and that they are among the fastest modes; the remainder are all rotational in character, with the two slowest having time constants of -5.1×10^4 and $-3.6 \times 10^4\ s^{-1}$, respectively. If we now imagine a hypothetical relaxation in which only the matrix $\bar{\mathbf{B}}$ is operative (i.e. all the $P_{i\to k}$ and $P_{ij\to kj}$ are put equal to zero in eq. [1]) then 90% of the relaxation strength is carried by the mode M_8', and most of the rest by M_5' and M_6'. Since M_5' and M_6' both have time constants of the order of $-1 \times 10^6\ s^{-1}$, and since M_9' which involves $v = 0, J = 9$ is (therefore) not used, this hypothetical relaxation appears to have a time constant of $-5.1 \times 10^4\ s^{-1}$, virtually exactly the value derived from the initial slope of $d\lambda/dx$. This, in our view, conclusively identifies the quantity $|d\lambda/dx|_{x=0}$ as the rate constant for R–R relaxation,[3] and were it not for doubts about the validity of the mixture rule for two different monatomic gases, one might now be able to deduce an approximate R–R relaxation rate constant for H_2/H_2 collisions from the laser-schlieren data of Audibert *et al.* (12). For somewhat different reasons, that the rotational and vibrational relaxations are expected to be better separated, and that the temperature regime is very different from that considered here, we cannot identify at this stage the significance of the initial slope in Glänzer's nitric oxide – argon experiment (10) without undertaking further model calculations designed to reproduce the behaviour of such mixtures at 2500 K.

Having discerned the meaning of $|d\lambda/dx|_{x=0}$ in this model calculation, we have now to identify the meaning of the slope at other values of x. To this end, we examined the sensitivity of λ to variations in the $P_{ij\to kl}$ for $x = 0.75$ and $x = 1$. Doubling all of the probabilities of the J-conserving transitions (like [13] and [14]) raises the relaxation rate minutely, but has the same effect at both concentrations, so that $|d\lambda/dx|_{x\to 1}$ remains unchanged at $1.9 \times 10^3\ s^{-1}$. On the other hand, doubling all the transition probabilities for which $\Delta v = \pm 1$ does almost double the slope, to $3.2 \times 10^3\ s^{-1}$, suggesting that we are dealing here with an R–V property. However, there is no eigenvalue of the linearised relaxation matrix $\bar{\mathbf{B}}$ smaller than $-3 \times 10^4\ s^{-1}$ and, moreover, the vibrational components of this "effective" relaxation have time constants of the order of $-6 \times 10^5\ s^{-1}$ or faster: consequently, although $|d\lambda/dx|_{x\to 1}$ appears from our sensitivity tests to be the R–V relaxation rate constant, this conclusion is not corroborated by our (admittedly imperfect) normal-mode analysis.

The Linear Mixture Rule

The current state of theoretical knowledge concerning the linear mixture rule as it applies to chemical reaction was summarised recently by Boyd (15). He concluded that the conditions for rigid adherence to the mixture rule are impossibly stringent, and the problem remains as to how to predict the conditions under which experimentally observable deviations from the rule may be expected. As an eigenvalue problem, internal relaxation is really no different from chemical reaction, and so we may expect the same considerations to apply: perhaps a useful clue is that the linear mixture rule for reaction appears to hold to acceptable accuracy when the V–V transition rates are small compared with the T–V rates, but it fails badly when they are large (16). Experimental tests of the linear mixture rule in relaxation over large ranges of composition are few, and the results were summarised at the beginning of the preceding section.

Before we can take any particular experiment and try to interpret the meaning of $d\lambda/dx$, as we have been able to do for the limiting case $|d\lambda/dx|_{x=0}$ in this work, we have to know how much of the curvature in the λ vs. x plot is due to the simple failure of the linear mixture rule for the T–V or T–VR relaxations alone — in other words, if we exclude all non-linear terms, how curved will be the plot considering the relaxation as $[(1 - x)M + X_2] + [xM' + X_2]$? As Boyd showed for the reaction case, the conditions for zero curvature are impossibly stringent, and we have found only two.[4] The first is when *each* T–VR (or T–V) transition probability for X_2 in collision with M′ is the *same multiple* of the corresponding probability for X_2 with the other partner M; our simplifica-

[3]One might argue, on inspection of Fig. 2, that the truncation scheme has excluded some very important states, namely $v = 2, J = 1$ and 3, so that processes of the type $X_2(v = 0,J) + X_2(v = 2,J) \leftrightarrow 2X_2(v = 1,J)$ are missing. We have repeated a selection of these calculations with a different set of 10 levels, including these two but excluding $v = 0, J = 9$ and 11. The results are only insignificantly different from those already discussed, as would be expected since processes of this type are unimportant in H_2 at these temperatures. In our laser-schlieren simulation calculation, the energy flux for this reaction is about 10^{-7} of that for $M + X_2(v = 1,J) \leftrightarrow M + X_2(v = 0,J)$. This would not be the case for heavier molecules and/or higher temperatures.

[4]It is trivial to show that if the matrix A_M governing the relaxation of X_2 at infinite dilution in M *commutes* with the matrix $A_{M'}$ governing the relaxation of X_2 at infinite dilution in M′, then the mixture rule will hold for the relaxation of X_2 at infinite dilution in mixtures of M and M′ (the examples cited here both fall into this class); otherwise, the mixture rule cannot hold rigorously (15).

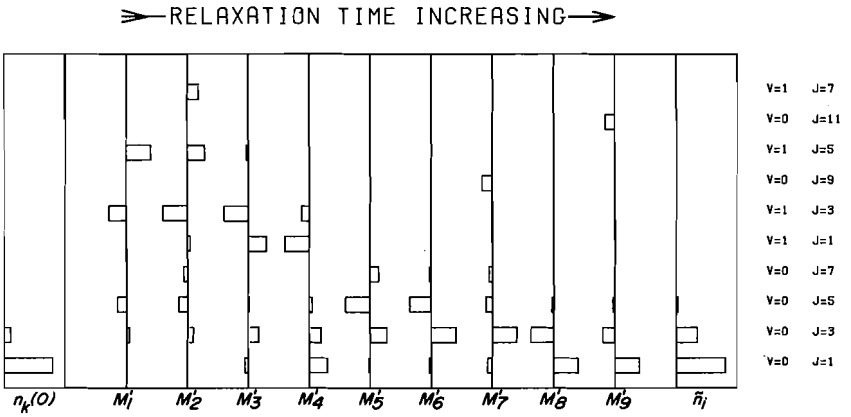

FIG. 2. Effective normal modes for the linearised TVR–TVR transition matrix $\bar{\mathbf{B}}$; for details of how to interpret these diagrams, see ref. 1.

tion, eq. [4], is a special case of this condition. The second occurs when *one set* of T–VR (or T–V) probabilities (say for M′) obeys the special form of the sum rule for which all the non-zero eigenvalues ($\lambda^{M'}$) are degenerate, i.e. eq. [42] of ref. 17. This happens because of a special feature, that no matter what the value of x is (provided that $x_{M'} \neq 1$), the eigenvectors of the combined relaxation matrix $\mathbf{A}$

$$[15] \qquad \mathbf{A} = (1 - x)\mathbf{A}_M + x\mathbf{A}_{M'}$$

are always the same as those of $\mathbf{A}_M$: this being the case, all the eigenvalues of $\mathbf{A}$ (except the one at zero) are shifted by the same amount, i.e.

$$[16] \quad \lambda_{n-1} = \lambda_{n-1}{}^{M} = \lambda_{n-1}{}^{M'} = 0,$$
$$\text{otherwise } \lambda_i = (1 - x)\lambda_i{}^{M} + x\lambda^{M'}$$

Clearly, a new program of calculations of a much more specific nature needs to be undertaken: in the first place, we must know under what conditions *observable* departures from the linear mixture rule *for* T–VR *relaxation only* will occur for systems of interest, specifically at the present time H_2 or NO admixed with inert gases. When this has been achieved, it will then be necessary to superimpose on these calculations the non-linear terms, and explore the relationships between the slope $d\lambda/dx$ and the R–R, V–V, or VR–VR relaxation rates, as may be appropriate, for the particular temperature and set of energy-level spacings in question.

Acknowledgements

This work was supported by the National Research Council of Canada; we also wish to thank Andrew Yau for continued assistance, and Herschel Rabitz for providing detailed sets of transition probabilities in machine-readable form.

1. H. O. PRITCHARD and N. I. LABIB. Can. J. Chem. **54**, 329 (1976).
2. H. O. PRITCHARD. Can. J. Chem. **54**, 2372 (1976).
3. G. ZARUR and H. RABITZ. J. Chem. Phys. **60**, 2057 (1974).
4. K. E. SHULER. J. Chem. Phys. **32**, 1692 (1960).
5. I. OPPENHEIM, K. E. SHULER, and G. H. WEISS. Adv. Mol. Relaxation Processes, **1**, 13 (1967).
6. S. TSUCHIYA and T. KOJIMA. Tenth Shock Tube Symposium, Kyoto, Japan. 1975. p. 587.
7. H. O. PRITCHARD. Specialist periodical reports, reaction kinetics. Vol. 1. The Chemical Society, London. 1975. p. 243.
8. A. W. YAU and H. O. PRITCHARD. Can. J. Chem. **55**, 1588 (1977), and references therein.
9. T. ASHTON, D. L. S. MCELWAIN, and H. O. PRITCHARD. Can. J. Chem. **51**, 237 (1973).
10. K. GLÄNZER. Chem. Phys. **22**, 367 (1977).
11. J. E. DOVE and H. TEITELBAUM. Chem. Phys. **6**, 431 (1974).
12. M. M. AUDIBERT, C. JOFFRIN, and J. DUCUING. Chem. Phys. Lett. **19**, 26 (1973).
13. K. F. HERZFELD and T. A. LITOVITZ. Absorption and dispersion of ultrasonic waves. Academic Press, New York. 1959.
14. T. L. COTTRELL and J. C. MCCOUBREY. Molecular energy transfer in gases. Butterworths, London. 1961.
15. R. K. BOYD. Can. J. Chem. **55**, 802 (1977).
16. D. L. S. MCELWAIN and H. O. PRITCHARD. J. Am. Chem. Soc. **92**, 5027 (1970).
17. A. W. YAU and H. O. PRITCHARD. Can. J. Chem. **56**, 1389 (1978).
18. S. M. TARR and H. RABITZ. J. Chem. Phys. **68**, 642 (1978); **68**, 647 (1978).
19. A. W. YAU and H. O. PRITCHARD. Can. J. Chem. **55**, 737 (1977).

Appendix

Recently, Tarr and Rabitz (18) have published details of calculations on T–V, T–R, and T–VR transitions amongst the first 27 states of *para*-H_2 for temperatures of 1000, 2000, and 2500 K. We have interpolated these probabilities to 1500 K in order to make a comparison of the best currently available

theoretical data with our assumed "standard" and "modified" sets of probabilities. The level structure for even J is somewhat different from that of odd J, with the first 20 levels ranging only up to ($v = 0, J = 14$), ($v = 1, J = 12$), and ($v = 2, J = 8$) instead of ($v = 0, J = 15$), ($v = 1, J = 11$), ($v = 2, J = 7$), and ($v = 3, J = 3$); however, with due allowance for the substitution of $v = 3$ levels for the topmost J-levels of $v = 1$ and $v = 2$, the normal-mode diagrams for our two sets of assumed probabilities with even J are exactly what one would expect by inspection of the already published odd-J diagrams, i.e. Figs. I(4) and II(3) respectively. The normal-mode diagram for the transition probabilities of Tarr and Rabitz is very similar indeed to that for our "modified" set: fifteen of the nineteen modes are clearly recognisable as being the same, and they come out in precisely the same order in both cases. The differences between the diagrams are two-fold. First, the modes for our "modified" set tend to couple non-adjacent J states a little too strongly — for example, referring to Fig. II(3), the $v = 2, J = 5$ component of M_1 would be at least a factor of two too large. Second, where the modes are not immediately recognisable as being the same, our "modified" set modes have a somewhat more complex structure: this is immaterial in practice since there is virtually no traffic carried by these modes (i.e. ξ_i is minute) in any practical relaxation; these very complex modes appear to be unphysical.

The net result is that the *qualitative* form of the normal modes used in the relaxation of H_2 at infinite dilution at 1500 K would be virtually indistinguishable whether our "modified" set of probabilities or those of Tarr and Rabitz were used. The relaxations would not be the same, however, since although the modes have the same ordering of time constants, the grouping of the time constants is rather different. The points of similarity and difference are best shown by comparing the contributions of the various modes to a practical relaxation, and this is done in Fig. 3 for all three sets of probabilities, for a sudden heating from 300–1500 K. It is clear that the probabilities of Tarr and Rabitz are intermediate between our "standard" set and our "modified" set[5] in respect of the uncoupling of the rotational and vibrational relaxations, and that in fact, to produce virtually indistinguishable relaxation behaviour at 1500 K, all

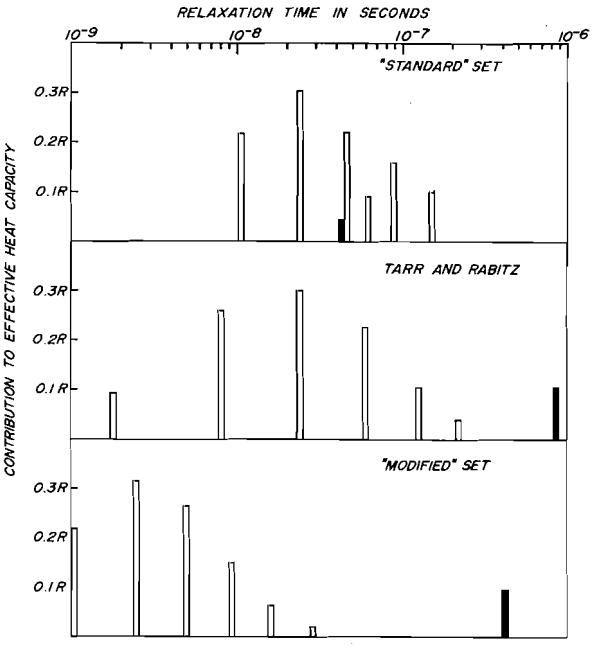

FIG. 3. Normal-mode analysis of a relaxation of *para*-H_2, at infinite dilution in M, from $T_i = 300$ K to $T_f = 1500$ K. From top to bottom, the transition probabilities are those of the "standard" set used throughout this series of papers (i.e. eq. [16] of ref. 9), those of Tarr and Rabitz (18) and those of our "modified" set (derived from the "standard" set by multiplying all T–R transition rates by 10 and dividing all other transition rates by 10). In all cases $\Sigma_i \eta_i = 1.136$ R, the mean heat capacity of *para*-H_2 between 300 and 1500 K; also, the component of the relaxation which is essentially vibrational in character is indicated by shading.

that would be necessary would be to take our "standard" set (i.e. eq. [16] of ref. 9), leave the rotational (i.e. T–R) probabilities unchanged, but multiply all probabilities for which v changes by a factor of about 0.05.

Returning to the problem of the present investigation where we have limited our calculations for the sake of feasibility to $T = 500$ K, we could simply take our "standard" set of transition probabilities and scale all the vibrational components by one-twentieth. However, because of step-length restrictions, this would make our integrations lengthier and costlier by a factor of at least 10. Moreover, it is unnecessary from the point of view of understanding the physics of the relaxation since at 500 K, even with our "standard" set of probabilities, the rotational and vibrational relaxations separate, and the final group of non-zero eigenvalues does correspond to the vibrational part of the relaxation, cf. Fig. I(1) and also the lengthy discussion of laser–schlieren experiments in Part II (2).

[5]In Fig. II(2), due to an accidental interchange of two cards in the computer program, the bottom two panels of the figure should be displaced to the left by a factor of 2.8 in t: this alters the details, although not the overall principle, of the discussion of this diagram in the first fifteen lines of p. 2377.

Etude chimique et spectroscopique du système $B(SCH_3)_3$–$B(NCS)_3$

HABIB-RAMAN ATCHEKZAI, HENRI MONGEOT ET JACQUES DAZORD

Université Claude Bernard, Lyon I, Laboratoire de Physico Chimie Minérale I associé au CNRS no 116, 43, Boulevard du 11 novembre 1918, 69621 Villeurbanne, France

ET

JEAN-PIERRE TUCHAGUES

Laboratoire de Chimie de Coordination, 205, Route de Narbonne, BP 4142, 31030 Toulouse, France

Reçu le 10 octobre 1978

HABIB-RAMAN ATCHEKZAI, HENRI MONGEOT, JACQUES DAZORD et JEAN-PIERRE TUCHAGUES. Can. J. Chem. **57**, 1122 (1979).

Le triméthylthioborate $B(SMe)_3$ réagit à la température ordinaire avec le triisothiocyanatoborane $B(NCS)_3$ pour donner des mélanges contenant $B(SMe)_3$, les dérivés mixtes $B(NCS)(SMe)_2$ et $B(NCS)_2(SMe)$ en faible concentration et des dérivés d'association. Les composés précédents ne sont pas isolables par suite de l'existence d'équilibres chimiques. Les données de rmn, de spectrométrie ir et de spectrométrie de masse sont reportées. Des structures faisant intervenir des liaisons donneur–accepteur S–B entre les monomères sont proposées pour les dérivés d'association $\{B(NCS)_2(SMe)\}_2$, $\{B(NCS)_2(SMe)\}_2\{B(NCS)_3\}$ et $\{B(NCS)_2(SMe)\}_2\{B(NCS)_3\}_2$. La réaction de ces composés avec la triméthylamine conduit à la formation de $Me_3NB(NCS)_3$ et $Me_3NB(NCS)_2(SMe)$. La même réaction avec le diméthyl-sulfure est incomplète et ne conduit qu'à la formation de $Me_2SB(NCS)_3$. Les acidités décroissent dans l'ordre $B(NCS)_3 > B(NCS)_2(SMe) > B(NCS)(SMe)_2 > B(SMe)_3$. Cette décroissance explique la dimérisation de $B(NCS)_2(SMe)$ a lieu, contrairement à celle de $B(NCS)(SMe)_2$.

HABIB-RAMAN ATCHEKZAI, HENRI MONGEOT, JACQUES DAZORD, and JEAN-PIERRE TUCHAGUES. Can. J. Chem. **57**, 1122 (1979).

Reaction of trimethylthioborate, $B(SMe)_3$, with triisothiocyanatoborane, $B(NCS)_3$, at room temperature gives mixtures containing $B(SMe)_3$, the mixed compounds $B(NCS)(SMe)_2$ and $B(NCS)_2(SMe)$ in low concentration, and association compounds. The previous compounds cannot be isolated due to equilibria being set up. Mass spectrometry, infrared and nmr data are reported. Structures involving S–B donor–acceptor bonds between the monomers are proposed for the association compounds $\{B(NCS)_2(SMe)\}_2$, $\{B(NCS)_2(SMe)\}_2\{B(NCS)_3\}$, and $\{B(NCS)_2(SMe)\}_2\{B(NCS)_3\}_2$. Reaction of these compounds with trimethylamine yields $Me_3NB(NCS)_3$ and $Me_3NB(NCS)_2(SMe)$. The same reaction with dimethylsulphide is incomplete and yields only $Me_2SB(NCS)_3$. Acidity strength decreases in the order $B(NCS)_3 > B(NCS)_2(SMe) > B(NCS)(SMe)_2 > B(SMe)_3$. This trend explains why dimerization of $B(NCS)_2(SMe)$ occurs whereas $B(NCS)(SMe)_2$ is unassociated.

Introduction

Le pseudo-halogène NCS est bien connu pour présenter de nombreuses analogies avec les halogènes. Ses propriétés chimiques sont considérées comme intermédiaires entre celles de l'iode et du brome (1). Le triisothiocyanate de bore $B(NCS)_3$ a généralement un comportement voisin de celui des halogénures de bore autres que BF_3 avec lesquels il donne d'ailleurs des réactions de redistribution (2, 3). Le triméthylthioborate $B(SMe)_3$ conduit facilement à des redistributions, en particulier avec les halogénures de bore BX_3 (4, 5); il y a alors formation de $BX(SMe)_2$ et $BX_2(SMe)$ ainsi que du dimère $\{BX_2(SMe)\}_2$. La tendance à la dimérisation augmente de l'iode au chlore. Nous avons entrepris l'étude du système $B(SMe)_3$–$B(NCS)_3$ en vue de le comparer aux systèmes $B(SMe)_3$–BX_3.

Résultats

Le mélange à la température ordinaire de $B(NCS)_3$ et $B(SMe)_3$ en solution dans des solvants inertes (CS_2, CCl_4, ...) conduit à des redistributions immédiates; les systèmes ainsi obtenus contiennent les deux dérivés libres $B(NCS)_2(SMe)$ et $B(NCS)(SMe)_2$ mais ceux-ci, et en particulier le premier, sont toujours en concentration très faible par suite de la formation de dérivés d'association. Ces dérivés d'association se forment en quantité d'autant plus importante que le mélange contient une forte proportion d'isothiocyanate. A titre d'exemple, le mélange de $B(NCS)_3$ avec une faible quantité de $B(SMe)_3$ ne conduit pratiquement qu'à la formation de produits d'association alors qu'à l'opposé, on obtient des solutions diluées qui ne laissent apparaître en rmn ^{11}B que les composés $B(NCS)(SMe)_2$ et

0008-4042/79/101122-05$01.00/0

$B(SMe)_3$, le rapport $B(NCS)(SMe)_2/B(SMe)_3$ pouvant dépasser 9%. Dans ce dernier cas, ces mélanges sont obtenus soit par mélange de $B(NCS)_3$ et $B(SMe)_3$, soit, beaucoup plus lentement, par la réaction:

$$B(SMe)_3 + AgNCS \rightarrow B(NCS)(SMe)_2 + AgSMe$$

Les deux dérivés $B(NCS)(SMe)_2$ et $B(NCS)_2(SMe)$ ont été caractérisés par spectrométrie de masse à partir de leurs pics moléculaires, par rmn ^{11}B et ^1H (voir tableau 1) et par spectrométrie infrarouge (voir tableau 2). Ces dérivés, comme tous ceux dans lesquels le bore est lié au groupe NCS possèdent une structure *iso*. Signalons comme preuve le fait que leur spectre infrarouge s'apparente respectivement à celui de $BX_2(NCS)$ et de $BX(NCS)_2$. C'est ainsi que pour ces derniers les vibrations de valence CN apparaissent respectivement vers 2045 et 2010 cm^{-1} (3) et qu'un effet isotopique $^{10}B^{11}B$ d'environ 10 cm^{-1} est observé vers 800 cm^{-1} sur νC═S, aussi bien pour BCl_2NCS et BBr_2NCS[1] que pour $B(SMe)_2(NCS)$. Les valeurs des déplacements chimiques observées en rmn ^{11}B sont également en bon accord avec une structure du même type que dans $B(NCS)_3$.

TABLEAU 1. Déplacements chimiques[a] observés sur les composés non associés et leurs complexes (en ppm)

Composé	rmn ^{11}B	rmn ^1H	rmn ^{13}C
$B(SCH_3)_3$	+42[b]	+2.25	+12.5
$B(NCS)(SCH_3)_2$	+27.3	+2.31	—
$B(NCS)_2(SCH_3)$	+8	+2.35	—
$B(NCS)_3$	−13.5[c]	—	+141.5
$Me_3NB(SCH_3)_3$	+21[d]	—	—
$Me_3NB(NCS)(SCH_3)_2$	+ 7	—	—
$Me_3NB(NCS)_2(SCH_3)$	−14	—	—
$Me_3NB(NCS)_3$	−28	—	—
$Me_2SB(NCS)_3$	−30.5		

[a]Les valeurs des déplacements chimiques sont comptées négativement quand les pics se situent vers les champs forts par rapport à l'étalon (rmn ^{11}B étalon externe $B(OMe)_3$, rmn ^1H et ^{13}C étalon interne $Si(CH_3)_4$).
[b]La valeur donnée dans la littérature est −43 ppm (9).
[c]Il s'agit de la valeur obtenue à partir de $B(NCS)_3$ pur en solution dans CS_2 (3).
[d]Valeur obtenue pour un mélange équimoléculaire de Me_3N et $B(SMe)_3$.

L'existence des produits d'association a été mise en évidence par rmn ^{11}B et ^1H et par des mesures de masse molaire au moyen de la tonométrie. Des tentatives de distillation n'ont pas permis d'isoler de produits purs. Toutes les réactions observées sont réversibles; nous avons pu rendre compte de la totalité des phénomènes observés à partir des équilibres suivants:

$$B(NCS)_3 + 2B(SMe)_3 \rightleftarrows 3B(NCS)(SMe)_2$$

$$2B(NCS)_3 + B(SMe)_3 \rightleftarrows 3B(NCS)_2(SMe)$$

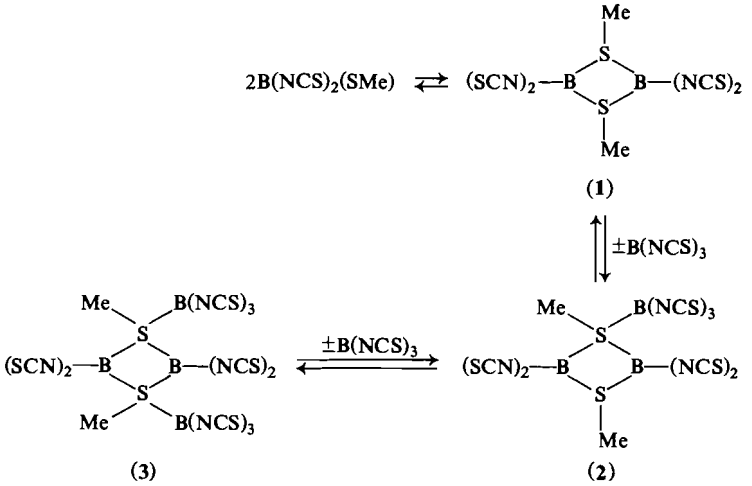

Etude des dérivés d'association

Le composé $B(NCS)_2(SMe)$ se dimérise de la même façon que ses homologues halogénés $BX_2(SMe)$ (4, 5). Cependant les phénomènes observés ne se limitent pas à une simple dimérisation. En effet, l'étude des mélanges $B(NCS)_3$–$B(SMe)_3$ dans un rapport molaire $B(NCS)_3/B(SMe)_3$ compris entre 0 et 4 montre que le degré d'association moyen dans les composés d'association est compris entre 2 et 3.2 environ. D'autre part, le rapport NCS/SMe dans ces composés est supérieur à 2 ce qui suggère la possibilité de fixation d'une ou deux molécules

[1]Etude du champ de force des molécules BX_2NCS à publier.

TABLEAU 2. Fréquence des principales bandes infrarouge observées[c]

$B(NCS)_2(SMe)$[a]	$B(NCS)(SMe)_2$[a]	Produit d'association[b]	Attribution
2025 TF	2070 TF	2020 à 2060 TF	νCN
1302 TF			$\nu_a{}^{10}BN_2$
1275 f			$\nu_a{}^{11}BN_2$
	1238 f		$\nu^{10}BN$
	1212 m		$\nu^{11}BN$
		1070 à 1165 F	$\nu_s BN_2$
	800 f		νC═S (^{10}B)
	790 m		νC═S (^{11}B)
		730 à 760 F	νC═S

[a]Le faible nombre de bandes répertoriées pour $B(NCS)_2(SMe)$ et $B(NCS)(SMe)_2$ est dû à la faible concentration de ces produits dans les mélanges.
[b]Le produit d'association 1 donne une bande à 2060 cm^{-1}.
[c]Le spectre de $B(SMe)_3$ étant connu (8), il n'a pas été reporté ici. TF = très forte, F = forte, m = moyenne, f = faible, tf = très faible.

$B(NCS)_3$ sur ce dimère. La formation de ces dérivés est réversible; c'est ainsi qu'ils se dégradent très rapidement lorsqu'on les met en solution dans $B(SMe)_3$ pour redonner $B(NCS)(SMe)_2$. Les déterminations de masses molaires ne sont plus possibles pour des solutions riches en $B(NCS)_3$ par suite de la formation connue (3, 6) du polymère insoluble $\{B(NCS)_3\}_n$.

L'étude des spectres d'absorption infrarouge de ces dérivés nous montre que les vibrations de valence νCN se trouvent dans la région 2020–2070 cm^{-1}. Leur fréquence n'a donc subi qu'une élévation très faible par suite de l'association ce qui indique que les groupes NCS ne sont pas modifiés. De plus la très légère augmentation de fréquence observée suggère que le bore est passé de l'état tricoordiné à l'état tétracoordiné; nous avons en effet noté un phénomène analogue (7) dans l'étude des complexes $R_3NBX_n(NCS)_{3-n}$ avec $n = 0, 1, 2$.

L'évolution des spectres de rmn ^{11}B du système $B(SMe)_3$–$B(NCS)_3$ est représentée sur la fig. 1. Quand on ajoute progressivement $B(NCS)_3$ à $B(SMe)_3$, il apparait successivement dans la partie du spectre située vers les champs forts par rapport à $B(OMe)_3$ des pics larges pour $\delta = -27$, -23.5, -19 et -14.6 ppm. Le premier pic est attribué au composé **1**, la dimérisation de $B(NCS)_2(SMe)$ se traduisant par un fort déplacement vers les champs forts. Le pic situé à -23.5 ppm est attribué aux deux atomes de bore appartenant au cycle du composé **2**. Le fait qu'un atome de soufre du cycle devienne tétravalent entrainant un léger déblindage du bore. Le pic observé à -19 ppm est attribué aux deux atomes cycliques du composé **3**, les deux atomes de soufre du cycle étant cette fois tétravalents. Enfin, le pic situé à -14.6 ppm appartient à $B(NCS)_3$ libre, le déplacement chimique observé est en effet très voisin de celui déterminé pour $B(NCS)_3$ seul; de plus,

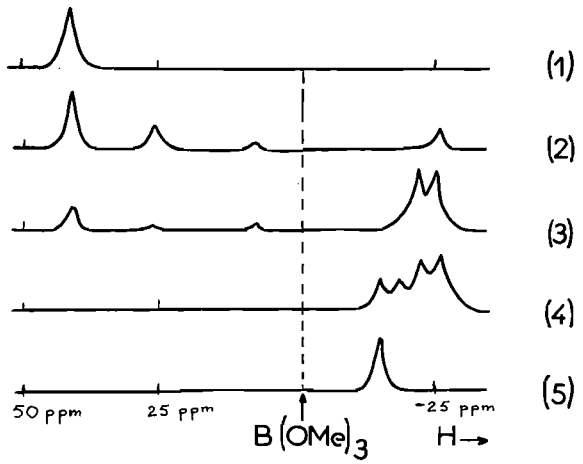

FIG. 1. Evolution des spectres de rmn ^{11}B du système $B(SMe)_3$–$B(NCS)_3$ en solution dans CS_2: (*1*) $B(SMe)_3$ pur, (*2*) $\{B(NCS)_3\}/\{B(SMe)_3\} = 0.28$, (*3*) $\{B(NCS)_3\}/\{B(SMe)_3\} = 2$, (*4*) $\{B(NCS)_3\}/\{B(SMe)_3\} = 5$, (*5*) $B(NCS)_3$ pur.

l'étude des spectres infrarouge a permis d'établir avec certitude que l'existence de ce composé dans les mélanges est liée à la présence du pic situé à -14.6 ppm. Nous pensons par ailleurs que les atomes de bore de $B(NCS)_3$ liés aux atomes de soufre cycliques dans les composés **1** et **2** sont peu différents les uns des autres, et donnent lieu à des déplacements chimiques voisins de -27 ppm. Cette valeur est en effet peu différente de celle obtenue avec les complexes $Me_3NB(NCS)_3$ et $Me_2SB(NCS)_3$ (voir tableau 1). De plus on observe un léger élargissement du pic situé à -27 ppm quand on ajoute des quantités croissantes de $B(NCS)_3$ à un mélange.

En rmn du proton, les spectres des produits d'association évoluent également en fonction de la composition du mélange. Quand on ajoute progressivement $B(NCS)_3$ à une solution de $B(SMe)_3$ il apparait d'abord un massif centré vers $+2.74$ ppm

puis progressivement un second massif vers +3 ppm alors que les pics du premier massif diminuent d'intensité pour devenir très faibles. Nous attribuons le premier massif aux groupes CH_3 liés à un soufre tricoordiné, et le second à ceux liés à un soufre tétracoordiné. La multiplicité des pics trouve sa justification dans le fait que chaque composé peut exister sous deux formes isomères. Il est à noter que Siebert et coll. (5) observent pour $BI_2(SMe)$ et son dimère des pics à +2.73 et +3.12 ppm. Nous obtenons un écart identique (0.39 ppm) entre la position du pic de $B(SMe)(NCS)_2$ (+2.25 ppm) et celle de son dimère (+2.74 ppm).

Réactions de complexation avec Me_3N et Me_2S

Dans le but d'avoir des indications complémentaires sur le système $B(SMe)_3$–$B(NCS)_3$, nous avons étudié les réactions de Me_3N et Me_2S avec $B(SMe)_3$, $B(NCS)_3$ ainsi que les produits formés en les mélangeant. $B(SMe)_3$ conduit avec Me_3N à un complexe instable, qui est facilement détruit par élimination de l'amine en portant simplement le produit sous vide à la température ordinaire. Par suite d'une réaction d'échange rapide, on n'observe qu'un seul pic en rmn ^{11}B quand on mélange Me_3N avec $B(SMe)_3$ en excès. La position de ce pic est intermédiaire entre celle de $B(SMe)_3$ libre et celle observée avec un mélange équimolaire de deux réactifs (voir tableau 1). Nous avons également observé un phénomène d'échange rapide en rmn du proton.

Dans les mêmes conditions $B(NCS)_3$ donne un complexe stable; celui-ci réagit d'ailleurs dans une faible proportion avec $B(SMe)_3$ suivant:

$$Me_3NB(NCS)_3 + B(SMe)_3 \rightarrow Me_3NB(NCS)_2(SMe) + B(NCS)(SMe)_2$$

ce qui montre que le complexe $Me_3NB(NCS)_2(SMe)$ est plus stable que $Me_3NB(NCS)(SMe)_2$. Il est à noter que la complexation d'un mélange s'accompagne d'une redistribution des groupes NCS et SMe. C'est ainsi que la complexation des produits résultant du mélange de $B(NCS)_3$ et $B(SMe)_3$ dans un rapport 2 (voir fig 1, spectre *3*) conduit presque exclusivement à $Me_3NB(NCS)(SMe)_2$.

Les mêmes réactions de complexation effectuées à partir de Me_2S n'ont permis de montrer que l'existence de $Me_2SB(NCS)_3$. Contrairement à Me_3N qui dissocie presque complètement les dérivés d'association, Me_2S qui est une base plus faible ne réagit que partiellement sur les produits d'association pour donner $Me_2SB(NCS)_3$. Le produit 1 subsiste dans ces conditions.

L'étude de ces réactions de complexation montre que le pouvoir accepteur du bore dans les composés $B(NCS)_n(SMe)_{3-n}$ augmente avec n. Ceci explique que seul $B(NCS)_2(SMe)$ se dimérise avec formation du cycle B_2S_2. Ce cycle renferme deux liaisons donneur–accepteur S–B que l'on rencontre également dans Me_2S–$B(NCS)_3$.

Discussion

D'après les structures que nous avons proposées pour les composés **1**, **2** et **3**, la formation des produits d'association résulte de liaisons donneur–accepteur. Le fait que leur formation soit concurrencée par des réactions de complexation avec une base de Lewis justifie bien l'existence de ce type de liaison. Les déplacements chimiques observés en rmn ^{11}B rendent également bien compte du fait que le bore joue un rôle d'accepteur. Par contre, il peut paraître surprenant que seul le soufre lié au groupe méthyl intervienne en tant que donneur, alors que, ni l'azote, ni le soufre des groupes NCS ne sont concernés. Cette hypothèse repose sur les considérations suivantes: en premier lieu l'étude des spectres infrarouge ne révèle aucune modification des groupes NCS. D'autre part, l'étude des spectres de rmn ^1H permet de classer les groupes CH_3 en deux types; il est logique de penser que c'est l'environnement du soufre auquel ils sont liés qui en est responsable plutôt que celui des groupes NCS beaucoup plus éloignés. Enfin, ceci est conforme au fait que $B(NCS)_3$ en solution est exclusivement sous forme de monomère.

Au sujet de $B(NCS)_3$, nous avons signalé qu'il avait tendance à former des polymères solides, mais il s'agit de composés très stables qu'il n'est plus possible de dissocier par l'action d'une amine. Il semble d'ailleurs que les molécules de $B(NCS)_3$ soient liées entre elles par des liaisons C—N, ce qui expliquerait la présence dans leur spectre infrarouge d'une bande forte et large entre 1550 et 1600 cm^{-1}. Or les spectres des produits d'association dont il est question ici ne renferment aucune bande de ce type.

Le système étudié diffère des systèmes BX_3–$B(SMe)_3$ par la formation des composés **2** et **3**. Si on fait abstraction de ce phénomène, il est assez voisin du système BBr_3–$B(SMe)_3$, en particulier en ce qui concerne les proportions relatives de produits libres et associés.

Partie expérimentale

$B(NCS)_3$ préparé par réaction de BBr_3 sur AgNCS (3) a été caractérisé à partir de ses spectres de rmn ^{11}B et infrarouge ainsi que par des mesures de masse molaire. $B(SMe)_3$ a été obtenu par action de MeSH sur BCl_3 en présence de Et_3N en solution dans l'éther (10). Il a été caractérisé à partir de son spectre de rmn ^{11}B (9), de son spectre infrarouge (8) et de mesures de masse molaire.

Les complexations par Me_3N ont été réalisées à basse température. L'amine (produit commercial contenu dans une bouteille métallique) est introduite par petites fractions à l'aide d'une rampe à vide dans une ampoule contenant les produits à complexer. Au cours de l'introduction, l'ampoule est à la température de l'air liquide, on la laisse ensuite revenir à la température ambiante tout en agitant le mélange. Cette opération est répétée jusqu'à ce qu'on se trouve en présence d'un excès d'amine. Les complexations, portant sur des quantités de produit allant de 1 g à 10 g, ont lieu indifféremment en présence ou non de solvant (CH_2Cl_2 ou CS_2). Dans le cas de la complexation par Me_2S, la réaction n'est pas violente et on ajoute lentement à la température ordinaire le sulfure liquide à une solution du produit à complexer maintenue sous agitation.

Les produits étudiés étant hydrolysables, toutes les manipulations sont été effectuées à l'abri de l'air.

Détermination des masses molaires

Le solvant utilisé a été dans tous les cas CS_2. Sa tension de vapeur a été déterminée à 0°C et 25°C par mesure directe à l'aide d'un manomètre à mercure. Aucune variation notable du degré d'association n'a été décelée entre ces deux températures.

Spectrométrie de masse

Les spectres ont été enregistrés à l'aide d'un appareil A.E.I. MS 902 à double focalisation avec une énergie d'ionisation de 70 eV. Nous avons introduit les produits par ballon chauffé tout en verre (all glass heated inlet system) à des températures allant de 25°C à 90°C. La température doit être d'autant plus élevée que le mélange est riche en $B(NCS)_3$. La source était dans tous les cas maintenue à 70°C. En plus des pics moléculaires de $B(SMe)_3$, $B(NCS)(SMe)_2$, $B(NCS)_2(SMe)$ et $B(NCS)_3$, des fragments dûs à $B(SMe)_3$ (11) on note la présence des ions $\{SB(NCS)(SCH)_3\}^+$, $\{NB(SCH_3)_2\}^+$ et $\{B(NCS)(SCH_3)\}^+$ qui proviennent de la fragmentation de $B(NCS)(SMe)_2$.

Spectrométrie infrarouge

Les spectres ont été enregistrés à l'aide d'un spectromètre Perkin-Elmer modèle 457, les cellules à liquide utilisées étaient munies de fenêtres en CsI.

Résonance magnétique nucléaire

Les spectres ont été enregistrés à l'aide d'un appareil Varian X.L.100 avec une fréquence de 32.1 MHz pour les noyaux ^{11}B et ^{13}C, et avec un appareil Varian A60A à la fréquence de 60 MHz pour les noyaux ^1H.

Détermination de la composition d'un mélange

Pour déterminer la composition d'un mélange à l'équilibre, nous avons tenu compte des quantités de $B(NCS)_3$ et $B(SMe)_3$ introduites au départ (celles-ci sont déterminées par pesée), des mesures de masse molaire, et des courbes intégrales en rmn ^{11}B. A titre d'exemple, nous reportons ci-dessous les résultats obtenus pour un mélange dont le spectre est représenté fig. 1, spectre *3*. Pour une composition de départ en millimoles de: $B(SMe)_3$: 10, $B(NCS)_3$: 20.49, CS_2: 844.54, les surfaces de pics de rmn ^{11}B sont à l'équilibre: $B(SMe)_3$: 6.29, $B(NCS)(SMe)_2$: 4.19, $B(NCS)_2(SMe)$: 5.59, produits d'association: 83.91. Compte-tenu de la présence de monomères, on obtient pour les produits d'association la formule empirique $B(NCS)_{2.22}(SMe)_{0.78}$. En admettant que ceux-ci sont constitués des composés **1**, **2** et **3**, le rapport NCS/SMe précédent correspond à un degré d'association de 2.6 ou encore à la formule empirique $\{B(NCS)_2(SMe)\}_2\{B(NCS)_3\}_{0.6}$. Les mesures de masse molaire effectuées sur la même solution ont permis de déterminer un degré d'association de 2.5, ce qui, comptetenu de la présence de 16% environ de molécules non associées conduit pour les produits d'association à un degré d'association de 2.8. Etant données l'instabilité des solutions de $B(NCS)_3$ et l'imprécision dans les dosages par rmn ^{11}B, ces résultats peuvent être considérés comme compatibles.

Remerciements

Nous remercions Monsieur Simeon, Service du Professeur Delmau, Université Lyon I, d'avoir enregistré la plupart de nos spectres de rmn.

Nous remercions également Monsieur Desruaz, Maître-Assistant du Laboratoire de Chimie Analytique de la Faculté de Pharmacie de Lyon, d'avoir enregistré nos spectres de masse.

1. A. A. NEWMAN. Chemistry and biochemistry of thiocyanic acid and its derivatives. Academic Press, London, New York, San Francisco. 1975. p. 19.
2. M. F. LAPPERT, H. PYSZORA et M. RIEBER. J. Chem. Soc. 4256 (1965).
3. J. DAZORD, H. MONGEOT, H. ATCHEKZAÏ et J. P. TUCHAGUES. Can. J. Chem. **54**, 2135 (1976).
4. J. GOUBEAU et H. W. WITTMEIER. Z. Anorg. Allg. Chem. **270**, 16 (1952).
5. W. SIEBERT, F. R. RITTIG et M. SCHMIDT. J. Organomet. Chem. **22**, 511 (1970).
6. D. B. SOWERBY. J. Am. Chem. Soc. **84**, 1831 (1962).
7. H. MONGEOT, J. DAZORD, H. ATCHEKZAÏ et J. P. TUCHAGUES. Synth. React. Inorg. Met.-Org. Chem. **6**, 191 (1976).
8. H. VAHRENKAMP. J. Organomet. Chem. **28**, 181 (1971).
9. R. H. CRAGG, J. P. N. HUSBAND et A. F. WESTON. J. Inorg. Nucl. Chem. **35**, 3685 (1973).
10. B. M. MIKHAILOV et YU. N. BUBNOV. Izv. Akad. Nauk SSSR, Otd. Khim. Nauk, 1378 (1962).
11. R. H. CRAGG, J. F. J. TODD et A. F. WESTON. J. Chem. Soc. Dalton Trans. **13**, 1373 (1972).

Etude des mobilités ioniques dans les mélanges eau–hexaméthylphosphotriamide (HMPT) à 25°C. II. Application de la théorie de Zwanzig au comportement des ions monovalents

JEAN-YVES GAL,[1] CHRISTINE LAVILLE, FRANÇOISE PERSIN ET MICHEL PERSIN

Laboratoire de Chimie Analytique, Université des Sciences et Techniques du Languedoc, Place E. Bataillon, 34060, Montpellier Cédex, France

ET

JEAN-CLAUDE BOLLINGER ET THÉOPHILE YVERNAULT

Laboratoire de Chimie Générale et Analytique, U.E.R. Sciences, Limoges, 123 Rue Albert Thomas, 87060, Limoges Cédex, France

Reçu le 16 août 1978

JEAN-YVES GAL, CHRISTINE LAVILLE, FRANÇOISE PERSIN, MICHEL PERSIN, JEAN-CLAUDE BOLLINGER et THÉOPHILE YVERNAULT. Can. J. Chem. **57**, 1127 (1979).

On a mesuré la conductibilité électrique de 19 électrolytes 1-1 MX (M = alcalin, ammonium quaternaire; X = halogénure perchlorate, nitrate) dans les mélanges eau–hexaméthylphosphotriamide à 25°C. A l'aide de l'hypothèse de l'équimobilité des ions dans Bu_4NBPh_4, on a déduit les conductibilités individuelles pour 17 ions monovalents dans ces mélanges. Après une critique des méthodes traditionnellement utilisées, nous montrons que seule la théorie de Zwanzig permet, à partir de ces résultats, d'aborder objectivement le problème des interactions ion–solvant. Cependant, cette théorie ne permet pas, dans l'état actuel de son développement, d'élucider la totalité des problèmes puisque Zwanzig considère le déplacement de l'ion nu mais elle permet de bien distinguer, selon la mobilité d'un ion, la nature des interactions entre celui-ci et le solvant.

JEAN-YVES GAL, CHRISTINE LAVILLE, FRANÇOISE PERSIN, MICHEL PERSIN, JEAN-CLAUDE BOLLINGER, and THÉOPHILE YVERNAULT. Can. J. Chem. **57**, 1127 (1979).

The electrical conductibilities of 19 1-1 MX electrolytes (M = alkaline, quaternary ammonium; X = perchlorate, halide, nitrate) in water–hexamethylphosphotriamide mixtures at 25°C has been measured. The individual conductibilities of 17 monovalent ions in these mixtures were calculated using the hypothesis of ion equimobility in Bu_4NBPh_4. Following a critical review of the traditionally used methods, it has been shown that, from these results, Zwanzig's theory alone allows the objective assessment of ion–solvent interactions. However, this theory at its present state of development cannot be used to elucidate all the problems (because Zwanzig considers the displacement of the free ion) but it does distinguish the nature of the interactions between an ion and the solvent, depending on the mobility of that ion.

Introduction

Les mélanges eau–hexaméthylphosphotriamide (HMPT) sont caractérisés par de fortes interactions entre les deux solvants. La variation importante de la viscosité en fonction de la composition du mélange nous a conduits à poursuivre dans ces milieux, l'étude des mobilités ioniques que nous avions entreprise dans le HMPT pur dans une étude précédente (1). Nous avons alors abordé le problème de la solvatation des ions dans les mélanges eau–HMPT en utilisant l'ensemble de nos résultats. En raison de l'incapacité des méthodes routinières à donner un ensemble cohérent de conclusions sur la sphère de solvatation des ions, nous nous sommes proposés d'appliquer la théorie de Zwanzig (2, 3) pour étudier le comportement des ions à partir de leur conductivité équivalente limite.

Partie expérimentale

L'origine et la purification des sels et du solvant ont été indiquées précédemment (1). Nous avons aussi indiqué notre façon d'opérer et les réserves en ce qui concerne la rusticité de notre appareillage.

Les mélanges eau–HMPT sont obtenus par pesée. Les solutions mères ont été contrôlées par dosage (méthodes électrochimiques variées ou spectrophotométrie de flamme selon les cas).

Les résultats publiés pour chaque mélange sont déduits, pour chaque sel, de 3 à 6 séries de 15 mesures sur des solutions de concentration $C = 4 \times 10^{-4}$ à 10^{-2} mol L^{-1}. Nous avons tracé pour chaque sel des graphes $\Lambda_0 = f(X_{HMPT})$ où Λ_0 est la conductibilité limite équivalente et X_{HMPT} la fraction molaire en HMPT. Les valeurs retenues sont issues du lissage de ces courbes, nous ne pouvons donc fournir les tableaux de mesures des conductivités en fonction des concentrations.

On estime pour les Λ_0 une incertitude de ± 0.05 Ω^{-1} cm^2 mol^{-1}.

Propriétés physiques des mélanges eau–HMPT

L'évolution des propriétés physiques des mélanges eau–HMPT avec leur composition a été récemment discutée (4–10). Il apparaît clairement que les deux solvants ont une grande affinité l'un pour l'autre, les variations d'enthalpie, d'enthalpie libre et d'entropie d'excès étant toujours négatives

[1]Auteur à qui toute correspondance doit être adressée.

0008-4042/79/101127-09$01.00/0

(4, 7), cette dernière permettant de supposer une organisation plus grande dans les mélanges que dans les solvants purs.

On peut calculer l'enthalpie de solvatation de l'eau dans le HMPT pur (8). La valeur trouvée ($\Delta H = -52.7$ kJ mol^{-1}) semble indiquer de la part du HMPT un pouvoir accepteur du proton encore supérieur à celui du DMSO (11). Par des mesures de temps de relaxation des protons Kessler et coll. (6, 10) confirment la stabilisation de la structure des mélanges eau–HMPT, essentiellement dans les milieux riches en eau, le maximum étant situé pour une fraction molaire en HMPT de l'ordre de 0.15. La variation de la viscosité (6–8) nous a semblé en tous points remarquable. Sur la fig. 1, on peut observer une très forte augmentation de la viscosité des mélanges par rapport aux solvants purs.

Ce phénomène est atténué lorsqu'on élève la température mais il reste néanmoins bien plus important que celui observé pour les mélanges d'eau et de solvants courants (fig. 1). La viscosité est maximale pour une fraction molaire en HMPT de l'ordre de 0.2, ce qui semble confirmer une stabilité maximum des mélanges dans ce domaine.

En fait, le comportement général des mélanges eau–HMPT est compatible avec le modèle proposé par Franks et Ives (14) pour les mélanges eau–éthanol et repris depuis par de nombreux auteurs pour d'autres mélanges eau–solvant (15–20). Aux fortes teneurs en eau, les interactions entre les molécules d'eau se trouveraient renforcées par la présence du HMPT, les structures tétraédriques seraient stabilisées. La faible variation du facteur de Kirkwood dans les milieux riches en eau (8) indique que la structure de l'eau n'est pas défaite par les premiers apports en HMPT, ce qui est confirmé par Saumagne et coll. (21) dans l'infrarouge. Dans le cas du HMPT, ce maximum de structuration de l'eau résulterait d'une part de l'influence hydrophobe des groupements méthyle et d'autre part de la forte polarité de cette molécule et de son encombrement stérique. Les molécules de HMPT seraient emprisonnées dans le réseau des molécules d'eau qu'elles auraient renforcé. Ce modèle explique bien l'augmentation constante du volume molaire partiel du HMPT (8) quand X_{HMPT} augmente (phénomène que l'on n'observe pas avec les solvants donnant eux-mêmes des liaisons hydrogènes (11, 22, 23)). Dans ce domaine, les propriétés solvatantes du HMPT devraient être faibles et l'on pourrait s'attendre à une solvatation préférentielle des ions par l'eau.

Lorsque X_{HMPT} augmente, les agrégats d'eau sont progressivement remplacés par des agrégats mixtes de composition dépendant de la teneur en HMPT.

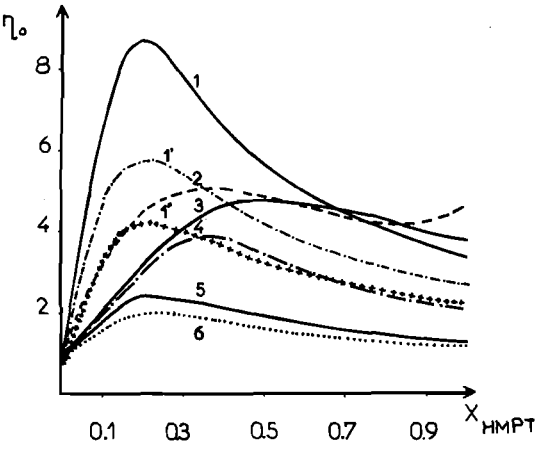

FIG. 1. Viscosité en centipoises de différents mélanges en fonction de X fraction molaire en composé organique. (*1*) Eau–HMPT à 25°C; (*1'*) eau–HMPT à 35°C; (*1''*) eau–HMPT à 45°C; (*2*) eau–terbutanol à 25°C (15); (*3*) eau–NMA à 30°C (12); (*4*) eau–DMSO à 25°C (13); (*5*) eau–éthanol à 25°C (16); (*6*) eau–dioxane à 25°C (15, 16).

Si on retient pour rayon de sphère rigide la molécule d'eau 1.37 Å (24) et 3.36 Å pour celui de la molécule de HMPT (25), il est clair que ϕ_{HMPT} la fraction volumique de HMPT augmente beaucoup pour de faibles augmentations de X_{HMPT} et le milieu doit rapidement se comporter peu différemment du HMPT lui-même. On peut mettre alors en évidence dans l'infrarouge des complexes $H_2O(HMPT)_2$ et $H_2O(HMPT)$ (21) et également $\{H^+(HMPT)_4\}OH^-$ qui a été confirmé par conductométrie et rmn de ^1H et ^{31}P (9). L'étude des variations de la constante diélectrique (4, 5, 10, 26) en fonction des X_{HMPT} n'a pas révélé une quelconque singularité des mélanges eau–HMPT. Par contre, le calcul à partir de ces résultats de la constante diélectrique d'excès (7, 8) met bien en évidence une augmentation de l'orientation des dipoles de l'eau dans le domaine riche en eau (fig. 2).

Il nous a semblé intéressant d'effectuer des mesures de mobilités ioniques dans les mélanges eau–HMPT essentiellement en raison des fortes variations de la viscosité en fonction de la teneur en HMPT. Nous verrons lors de l'interprétation de nos résultats selon la théorie de Zwanzig combien le comportement diélectrique d'un mélange de solvants est important et combien il est nécessaire d'en tenir compte lorsque l'on veut relier les valeurs des mobilités des ions à leur état de solvatation.

Etude des mobilités ioniques dans les mélanges eau–HMPT à 25°C

Nous avons indiqué dans notre précédent mémoire (1) comment nous déterminons la conductivité

TABLEAU 1. Valeurs des constantes physiques et des constantes α, β, E_1, E_2 (27) pour les différents mélanges étudiés à 25°C

	0.05	0.1	0.2	0.3	0.4	0.6	1
χ_0 (10^6 Ω^{-1} cm^{-1})	3.3	1.6	1.0	0.8	0.32	0.37	—
ρ^a (g cm^{-3})	1.0370	1.0430	1.0440	1.0410	1.0364	1.0292	1.0199
η^a (cP)	3.622	6.767	8.639	7.636	6.423	4.838	3.350
D^b	67	57.40	44.90	38.20	34.60	31.03	29.20
α	0.291	0.367	0.530	0.675	0.783	0.922	1.057
β	16.12	9.30	8.25	10.10	12.60	17.70	26.737
E_1	0.8498	1.351	2.824	4.585	6.17	8.555	11.266
E_2	6.9	5.00	6.40	10.10	14.60	24.10	41.74

[a]Nous-mêmes.
[b]D'après Clechet *et al.* (4).

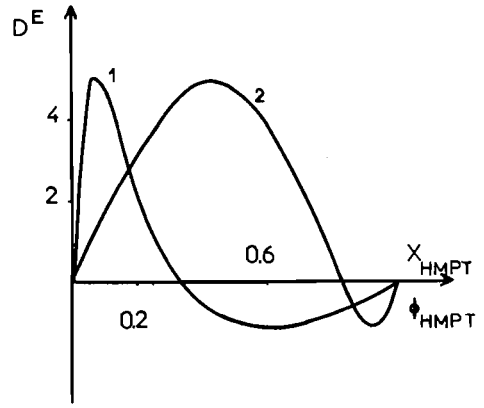

FIG. 2. Variation de la constante diélectrique d'excès D_E à 25°C: (*1*) en fonction de X_{HMPT}; (*2*) en fonction de ϕ_{HMPT}.

équivalente limite des sels en utilisant l'équation de Fuoss–Onsager (27). Nous résumons dans le tableau 1 les constantes correspondant aux mélanges étudiés et dans le tableau 2 les valeurs de conductivités équivalentes limites obtenues pour l'ensemble des sels étudiés.

La fig. 3 montre bien que l'addition de HMPT à l'eau diminue considérablement la conductivité des sels, ce qui est compatible avec la forte augmentation de la viscosité. Lorsque celle-ci diminue, la conductivité n'augmente pas dans les mêmes proportions, ce qui montre bien déjà que la viscosité n'est pas le seul facteur important.

Pour atteindre les valeurs des conductivités équivalentes limites ioniques, nous avions dans notre premier mémoire (1), considéré que dans le HMPT pur:

$$\tfrac{1}{2}\Lambda_0(Bu_4NBBu_4) = \lambda_0(Bu_4N^+) = \lambda_0(Bu_4B^-)$$

En fait, le tétrabutylborate de tétrabutylammonium est trop peu soluble dans les milieux riches en eau pour pouvoir servir de référence. Nous avons dû avoir recours à une autre hypothèse de travail en utilisant le tétraphénylborate de tétrabutylammonium, soit:

$$\Lambda_0(Bu_4NBPh_4) = \Lambda_0(Bu_4NX) + \Lambda_0(NaBPh_4) - \Lambda_0(NaX)$$

$$\tfrac{1}{2}\Lambda_0(Bu_4NBPh_4) = \lambda_0(Bu_4N^+) = \lambda_0(Ph_4B^-)$$

où X est I, Br et ClO_4.

Cette méthode conduit à augmenter encore l'incertitude absolue sur $\lambda_0(Bu_4N^+)$. Nous avons dans le tableau 3 comparé les résultats tirés de ces deux hypothèses de travail. Il apparaît dans les milieux riches en HMPT où la première méthode est applicable, que les résultats obtenus à l'aide de la seconde peuvent être considérés comme satisfaisants dans le cadre de notre étude. Nous rapportons dans le tableau 4, l'ensemble des valeurs de conductivités ioniques équivalentes limites trouvées pour les différents mélanges eau–HMPT étudiés. Il semblerait que la mobilité des anions dépende plus de la viscosité du milieu. Par ailleurs, pour l'ensemble des ions, au-delà d'une fraction molaire en HMPT de l'ordre de 0.3, on peut remarquer que la mobilité varie peu et qu'elle est très nettement inférieure aux valeurs correspondant à l'eau pure. Les mélanges eau–HMPT ne permettent donc pas d'obtenir des milieux très conducteurs du courant électrique.

Interprétation des résultats, étude de la solvatation des ions

L'utilisation de valeurs de mobilités ioniques pour aborder l'étude des interactions ion–solvant conduit à classer les méthodes de travail en deux catégories.

1. Méthodes conventionnelles

Elles reposent sur l'hypothèse que l'ion est sphérique et qu'il est entouré d'une sphère de solvatation qu'il entraîne dans son déplacement. La composition de la sphère de solvatation dépend de la nature de l'ion et des proportions des deux cosolvants. Dans une première étape, le mélange de solvant est assimilé à un milieu continu. Selon la composition de la sphère de solvatation les λ_0 seront différents et de ce fait les mesures de conductivités

TABLEAU 2. Conductivité équivalente limite des sels à 25°C (Λ_0 en Ω^{-1} cm^2 mol^{-1})

	X_{HMPT} =							
Sels	0	0.05	0.1	0.2	0.3	0.4	0.6	1
Me_4NClO_4	111.6	27.0	14.0	10.6	11.1	12.5	15.5	23.4
Et_4NClO_4	99.4	23.3	12.4	9.9	10.3	12.3	16.2	25.2
Pr_4NClO_4	90.4	21.2	10.6	8.8	9.5	11.1	15.0	22.5
Bu_4NClO_4	86.5	19.8	9.6	7.8	9.9	10.6	14.2	21.7
$LiClO_4$	105.2	25.3	11.4	8.5	9.1	10.1	13.0	21.0
$NaClO_4$	117.2	31.0	16.1	10.9	10.8	11.5	14.2	21.3
$KClO_4$	140.7	36.0	18.3	12.2	11.8	12.8	15.0	21.3
$RbClO_4$	145.0	37.9	18.8	12.6	11.9	12.8	15.1	21.9
$CsClO_4$	144.5	36.3	18.5	12.1	11.9	12.9	15.4	22.1
NaCl	126.3	42.0	22.9	13.6	12.0	12.7	16.0	
NaBr	128.0	42.0	22.4	13.4	12.4	13.1	15.7	23.8
NaI	126.8	36.3	19.6	11.9	12.0	12.6	15.0	22.2
$NaNO_3$	121.4	40.8	22.1	13.5	12.7	14.0	17.4	25.5
NaF	105.4	46.5	18.8	8.4		Trop peu soluble		
$NaBPh_4$		21.7	12.5	8.1	7.4	7.2	8.0	
Bu_4NBr	97.3	30.8	15.9	10.3	10.6	12.2	15.7	24.2
Bu_4NI	96.1	25.2	13.0	9.2	10.1	11.7	15.1	22.6
Bu_4NBBu_4			7.7	4.6	5.3	6.3	8.4	12.3
$AgNO_3$	133.3	42.9	22.0	13.1	12.2	14.2	17.8	25.1

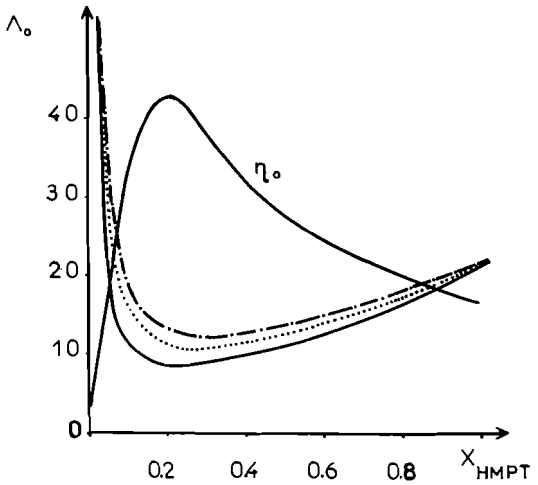

FIG. 3. Variation de Λ_0 (Ω^{-1} cm^2 mol^{-1}) de perchlorates en fonction de X_{HMPT}: — $LiClO_4$; ····· $KClO_4$, $RbClO_4$, $CsClO_4$; ··· $NaClO_4$.

ioniques constituent une approche de l'étude de la solvatation des ions par les mélanges de solvants.

Ces méthodes ont été largement utilisées et toutes conduisent à des contradictions que les auteurs ont levées en ajoutant des hypothèses supplémentaires. Le milieu ambiant ne serait plus un continuum, mais sa structure au voisinage d'un ion dépendrait de la nature de cet ion. En définitive, ces méthodes permettent bien de retrouver ce que l'on cherche à obtenir a priori: les cations sont plus solvatés par les solvants polaires, les anions sont plus solvatés par les solvants protiques, les gros anions polarisables peuvent être solvatés par les solvants polaires aprotiques.

On peut citer les études qui consistent: à tracer les variations de λ_0 en fonction de la viscosité, en négligeant les phénomènes diélectriques (12, 20, 34–36); à étudier les variations du produit de Walden $\lambda_0\eta_0$ en fonction de la fraction molaire (14, 15, 18, 37–39); à calculer le volume de solvatation des ions selon la méthode de Robinson et Stokes que nous avons exposée dans notre précédent mémoire (1, 14, 15, 18, 37–39).

Nous avons utilisé ces différentes méthodes dans les mélanges eau–HMPT (40). Nos résultats sont bien cohérents avec ce qui a été publié dans d'autres mélanges, mais nous ne pensons pas qu'ils permettent de faire avancer le problème, c'est pourquoi nous

TABLEAU 3. Comparaison des valeurs de $\lambda_0(Bu_4N^+)$ déduites de $\Lambda_0(Bu_4NBBu_4)$ (hypothèse I) et de $\Lambda_0(Bu_4NBPh_4)$ (hypothèse II) (Ω^{-1} cm^2 equiv.$^{-1}$)

	$\lambda_0(Bu_4N^+)$	
X_{HMPT}	Hypothèse I	Hypothèse II
0	—	19.3
0.05	—	5.3
0.1	3.85	3.0
0.2	2.35	2.5
0.3	2.65	2.78
0.4	3.15	3.2
0.6	4.20	4.0
1	6.15	6.15

TABLEAU 4. Conductivité équivalente limite des ions à 25°C (λ_0 en Ω^{-1} cm^2 equiv.$^{-1}$)

	X_{HMPT} =								
Ions	0	0.05	0.1	0.2	0.3	0.4	0.6	1	R_c (Å)
Li^+	38.7	10.8	5.2	3.2	3.0	2.7	3.0	5.3	0.74[b]
Na^+	50.0	16.5	9.5	5.6	4.6	4.1	4.0	5.7	1.01[b]
K^+	73.5	21.5	11.7	6.9	5.6	5.4	4.8	5.7	1.32[b]
Rb^+	77.8	23.4	13.1	7.3	5.7	5.2	4.9	6.3	1.48[c]
Cs^+	77.3	21.8	11.9	6.8	5.7	5.5	5.2	6.5	1.69[c]
Ag^+	61.9	18.6	9.3	5.1	4.4	4.2	4.4	5.3	1.13[d]
Me_4N^+	44.4	12.5	7.4	5.3	4.9	5.1	5.3	7.8	2.77[e]
Et_4N^+	32.2	8.8	5.8	4.6	4.1	4.6	6.0	9.5	3.42[e]
Pr_4N^+	23.2	6.7	4.0	4.5	3.3	3.7	4.8	6.9	3.97[e]
Bu_4N^+	19.3	5.3	3.0	2.5	2.8	3.2	4.0	6.1	4.37[c]
ClO_4^-	67.2	14.5	6.6	5.3	6.1	7.4	10.2	15.6	2.45[f]
NO_3^-	71.4	24.3	12.6	7.9	8.0	9.9	13.3	20.1	1.88[c]
Cl^-	76.3	25.5	13.4	8.0	7.4	8.6	12.0	19.7[a]	1.82[b]
Br^-	78.0	25.5	12.9	7.8	7.8	9.0	11.7	18.1	1.98[b]
I^-	76.8	19.8	10.0	6.7	7.3	8.5	11.0	16.8	2.24[b]
F^-	55.4	30.0	9.3	2.8		Trop peu soluble			1.36[c]

[a]Valeurs de Prue et coll. (28).
[b]Valeurs de Waddington (29).
[c]Valeurs de Nightingale (30).
[d]Valeurs de Goldschmidt (31).
[e]Valeurs de Desnoyers et coll. (32).
[f]Valeurs de Halliwell et Nyburg (33).

préférons exposer l'interprétation de nos mesures de mobilités ioniques en se référant à la théorie de Zwanzig (2, 3).

2. Méthode basée sur l'exploitation de la théorie de Zwanzig

Nous avons récemment rappelé cette théorie dans le cadre de son application dans le HMPT pur (25).

La loi de Stokes (41) ne traduisant pas parfaitement le comportement hydrodynamique des ions (36), une correction à cette loi a été proposée par Fuoss (42) et évaluée quantitativement par Boyd (43) et Zwanzig (2). Ils ont calculé une force diélectrique de friction en supposant que le déplacement relatif entre l'ion et un élément de volume de solvant était constant. Cette force de friction provient de l'énergie produite par l'ion orientant les dipoles de solvant qu'il rencontre lors de son déplacement. Ce calcul tient compte du retard dû à la relaxation des dipoles autour de l'ion en mouvement.

Quelques années plus tard, la vitesse relative d'un ion et d'un solvant dépendant de la distance entre l'ion et un élément de volume du solvant, Zwanzig (3) a revu sa théorie. Il vient à distinguer le cas où les molécules de solvant n'adhèrent pratiquement pas à la surface de l'ion (slipping = glissement parfait) et le cas où les dipoles de solvant proches de l'ion sont retenus plus ou moins longtemps près de l'ion (sticking = adhésion).

L'équation résultante du produit de Walden devient alors:

$$\lambda_0\eta_0 = \frac{ZeF}{AR_c + (B/R_c^3)}$$

où $A = A_v\pi$ représente les forces de freinage hydrodynamique dues au milieu. Et

$$B = A_D \frac{(Ze)^2(\varepsilon_0 - \varepsilon_\infty)\tau}{\varepsilon_0(2\varepsilon_0 + 1)\eta_0}$$

les forces de friction diélectrique. Z étant la charge de l'ion, F le Faraday, R_c le rayon cristallin de l'ion, ε_0 la constante diélectrique du solvant, ε_∞ la constante diélectrique à fréquence infinie, η_0 la viscosité du solvant, τ le temps de relaxation diélectrique, A_v et A_D des constantes respectivement égales à 6 et 3/8 dans le cas du "sticking" et 4 et 3/4 dans le cas du "slipping".

Il est important de bien remarquer qu'à ce jour la théorie de Zwanzig suppose que l'ion, positif ou négatif, se déplace dans un milieu continu et que le rayon pris en compte par Zwanzig est le rayon cristallin. Cela veut dire que, sans nier les phénomènes de solvatation, l'auteur suppose que les ions ne se déplacent pas en entraînant avec eux leur "sphère" de solvatation mais qu'ils la reconstituent de proche en proche.

Dans le cas du glissement parfait, l'échange ion–solvant est infiniment rapide, l'adhésion correspond au cas où la vitesse de déplacement de l'ion dépend de la cinétique de cet échange.

L'analyse sommaire de l'équation de Zwanzig

montre que pour les gros ions, le terme en R_c sera prépondérant et que ce sera le terme $1/R_c^3$ pour les petits ions. Cela conduit à prévoir un maximum pour les courbes $\lambda_0\eta_0 = f(1/R_c)$. Ce maximum a bien été observé sur les courbes expérimentales (44–47). Lorsque le terme en R_c est prépondérant on retrouve l'expression de la loi de Stokes. Le déplacement des ions est alors limité principalement par les forces de friction hydrodynamique.

Dans le cas des petits ions, ces dernières deviennent progressivement négligeables devant les forces dues aux interactions diélectriques.

L'application de la théorie de Zwanzig pour les cations a été effectuée dans l'eau, le méthanol, l'éthanol et l'acétonitrile par Kay et Evans (48) en 1966. Plus récemment Fernandez-Prini et Atkinson (47) en 1971 se sont intéressés à cette théorie dans l'eau et d'autres solvants polaires et dipolaires aprotiques.

Ces auteurs ont constaté que le maximum des mobilités calculé d'après la théorie correspondait au maximum expérimental pour les solvants dipolaires aprotiques à condition de considérer le cas du "glissement parfait". Pour les solvants polaires la théorie prévoit la position du maximum sauf dans le formamide.

Ils concluent également que dans les solvants aprotiques dipolaires, les mobilités des ions ammoniums quaternaires sont en accord avec la théorie de Zwanzig et celle de la loi de Stokes. Ils admettent donc que le déplacement de ces ions est essentiellement contrôlé par des forcés de friction hydrodynamique.

Pour les cations alcalins ces auteurs ont constaté que les courbes expérimentales se situaient toujours au-dessus des courbes théoriques quels que soient les solvants. La théorie prévoit donc un freinage plus important que les résultats expérimentaux ne le font apparaître. L'écart d'autre part est plus important pour les courbes obtenues dans les solvants protiques et particulièrement dans l'eau. Ces auteurs montrent également que l'excès de mobilité observé est d'autant plus grand que l'ion est plus petit, la théorie de Zwanzig donnerait alors trop d'importance au terme relatif à la force de friction diélectrique.

Nous avons représenté sur les figs 4 et 5 les courbes $\lambda_0\eta_0 = f(1/R_c)$ relatives aux différents cations et anions que nous avons étudiés dans les mélanges eau–HMPT. Nous constatons qu'elles présentent toutes un maximum comme le prévoit la théorie de Zwanzig, que les courbes obtenues pour les mélanges de fraction molaire $X_{HMPT} < 0.15$ sont situées au-dessus de celles de l'eau, que pour les mélanges de fraction molaire $X_{HMPT} > 0.15$ plus le mélange est

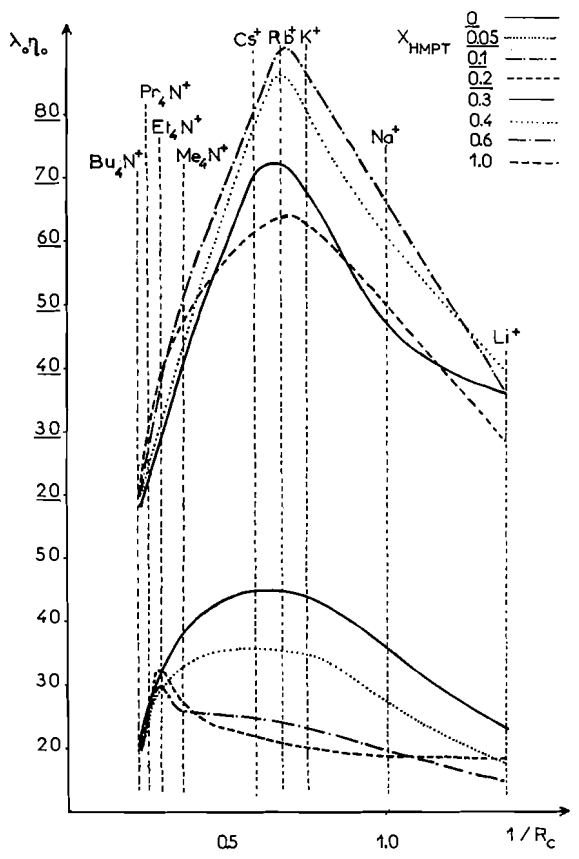

FIG. 4. Variation du produit $\lambda_0\eta_0$ (Ω^{-1} cm^2 equiv.$^{-1}$ cP) des cations en fonction de $1/R_c$.

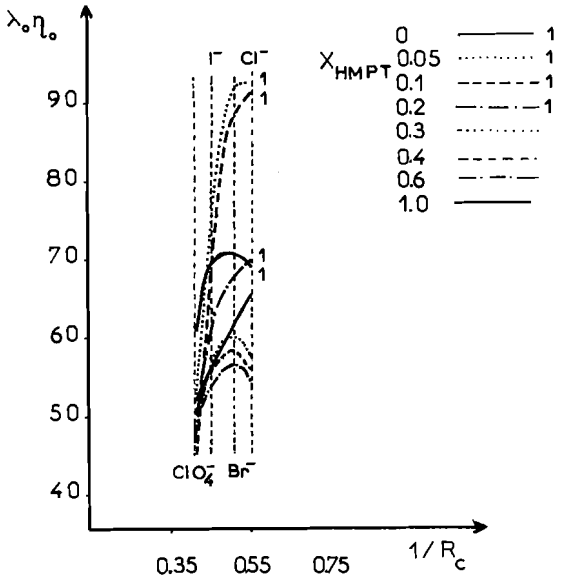

FIG. 5. Variation des produits $\lambda_0\eta_0$ (Ω^{-1} cm^2 equiv.$^{-1}$ cP) des anions en fonction de $1/R_c$.

riche en HMPT, plus la courbe $\lambda_0\eta_0 = f(1/R_c)$ s'aplatit.

On peut d'après ces constatations considérer que l'ion est moins freiné dans les mélanges riches en eau que dans l'eau ou les autres mélanges eau–HMPT. On peut concevoir que cet excès des mobilités des ions dans ces mélanges par rapport à l'eau serait dû à une diminution des interactions diélectriques ion–solvant par suite des propriétés physiques particulières des mélanges dans ce domaine. On a vu en effet que ces milieux étaient plus structurés que l'eau par suite d'interactions dipole–dipole importantes entre la molécule d'eau et la molécule de HMPT (8–10). L'on peut donc peut-être envisager que les forces de friction diélectrique qui s'exercent entre les molécules de solvant et l'ion seraient plus faibles que si les molécules de solvant n'interagissaient pas. Dans les milieux riches en HMPT, le ralentissement plus important des ions peut provenir d'une augmentation des forces de freinage aussi bien hydrodynamique que diélectrique étant donné la polarité du HMPT et l'encombrement stérique de sa molécule.

L'analyse des courbes $\lambda_0\eta_0 = f(1/R_c)$ montre que les ions Cs^+, Rb^+, K^+ situés aux environs du maximum, c'est-à-dire à la limite des zones de prédominance, subissent l'influence plus ou moins importante des forces de friction hydrodynamique ou diélectrique selon le mélange.

Dans les mélanges de fraction molaire $X_{HMPT} = 0.05$, 0.1 et 0.2, le plus gros cation alcalin Cs^+, de par sa position, semble obéir plutôt à la loi de Stokes. Il subirait davantage l'influence de la viscosité que dans les autres milieux. Dans les milieux riches en HMPT, les gros ions alcalins sont situés bien à droite du maximum. Si l'on considère que le HMPT est un composé très polaire, dans les milieux où il sera en excès par rapport à l'eau on peut envisager que les forces de friction diélectrique entre l'ion et le solvant deviennent de plus en plus importantes au fur et à mesure que la teneur en HMPT du milieu augmente. On constate que même l'ion Me_4N^+ dans ces milieux très riches en HMPT est à droite du maximum. Cet ion semble donc subir principalement des interactions diélectriques dans ces milieux.

Dans cette zone intermédiaire où la viscosité et la constante diélectrique influent plus ou moins selon la composition du solvant et selon l'ion se trouvent également situés les anions.

Il convient d'ajouter que les anions ne se placent pas sur la même courbe que les cations, ce qui est contraire à la théorie. Ce résultat n'est pas propre aux mélanges eau–HMPT, Kay et coll. rapportent que cela a été observé dans tous les solvants (44). Wolynes (49) a récemment noté que seule une théorie moléculaire pourrait tenir compte de l'influence de la charge de l'ion. Dans les mélanges eau–HMPT étant donnée l'allure des courbes, il semble que dans les mélanges riches en eau ($X_{HMPT} < 0.2$) la viscosité joue un rôle plus important que la constante diélectrique sur le déplacement des anions ClO_4^-, I^-, Br^-. Par contre, dans les mélanges à plus forte teneur en HMPT, les forces de friction diélectrique augmentant, les plus petits anions, Cl^- et Br^- subiraient plus leur influence.

En définitive, la théorie de Zwanzig ne peut donner dans son expression actuelle des informations sur la sphère de solvatation des ions.

Par contre, la distinction entre les forces de freinage hydrodynamique et les forces de freinage de nature diélectrique permet de bien mettre en évidence les différences d'interactions entre les ions et les mélanges selon la nature de ces ions et leur rayon cristallographique et selon les proportions relatives des deux cosolvants. Les contradictions apparentes relevées lors de l'exploitation conventionnelle des résultats peuvent être expliquées si l'on se réfère à la théorie de Zwanzig.

3. Retour sur les méthodes conventionnelles

Nous avons reporté sur la fig. 6 les courbes $\lambda_0 = f(\eta_0)$ des différents ions étudiés. Ces courbes présentent deux parties, la partie supérieure correspondant

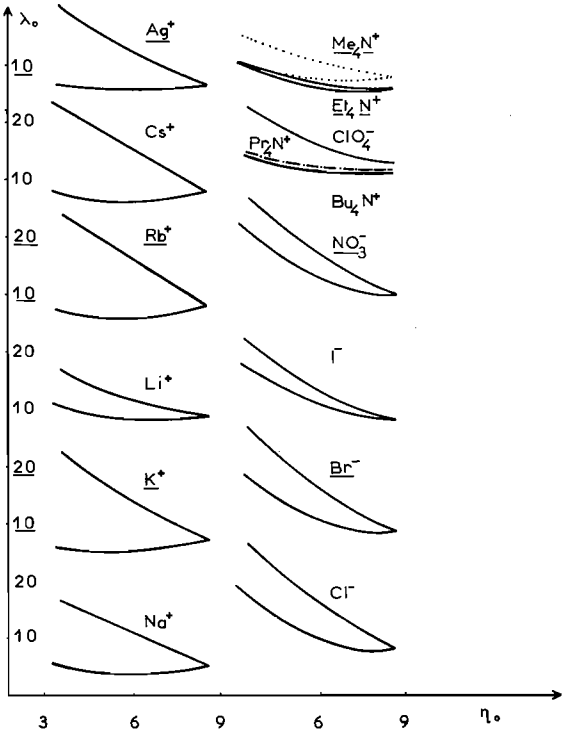

FIG. 6. Courbes $\lambda = f(\eta)$ de différents ions.

aux milieux riches en eau. Pour les gros cations ammoniums quaternaires, l'angle des deux parties des courbes est nul ce qui conduit à conclure que la viscosité est le facteur prédominant. C'est bien ce que l'on retrouve avec la théorie de Zwanzig, mais ici sans faire l'hypothèse que les ions ammoniums quaternaires ne sont pas solvatés. Cela est beaucoup plus conforme aux travaux récents où l'on envisage une solvatation de ces ions pour expliquer certaines de leurs propriétés aux interfaces (50, 51). Pour les cations alcalins on constate une croissance de l'angle avec la taille du cation que l'on ne saurait expliquer par une augmentation de la solvatation des gros ions par le HMPT.

En fait, cette croissance est due à une élévation de la branche de courbe relative aux milieux riches en eau. Il semblerait que si l'importance des forces diélectriques est sensiblement la même pour tous ces cations dans les milieux riches en HMPT, elle serait plus faible pour les plus gros cations dans les mélanges riches en eau, c'est bien ce que nous avons vu.

Pour les anions, plus l'anion est gros et plus l'angle est petit et c'est la courbe relative aux milieux riches en HMPT qui varie le plus.

Les gros anions ClO_4^- et I^-, plus proches de la zone où la viscosité a un effet prédominant sur le déplacement des ions, sembleraient influencés davantage par ce facteur que les petits anions Br^-, Cl^-. Par contre, ces derniers ions subiraient en plus un effet supplémentaire dû aux forces de friction diélectrique. Ces forces de freinage supplémentaires pourraient expliquer que la mobilité des plus petits anions dans les mélanges riches en HMPT soit inférieure à celle qu'ils possèdent dans les milieux plus riches en eau.

Ainsi la théorie de Zwanzig permet semble-t-il d'apporter une explication simple aux problèmes que nous posaient l'interprétation des courbes $\lambda_0 = f(\eta_0)$.

Il peut être également intéressant d'étudier l'évolution du produit de Walden en fonction de la fraction molaire en HMPT en tenant compte de l'analyse des résultats selon la théorie de Zwanzig.

Pour les cations alcalins et les petits anions au voisinage de $X_{HMPT} = 0.2$, les courbes $\lambda_0\eta_0 = f(X_{HMPT})$ présentent un maximum comme c'est le cas dans tous les autres mélanges eau–solvant (fig. 7).

Il semble qu'il ne soit pas indispensable d'invoquer une désolvatation spéciale des ions dans le domaine du voisinage du maximum du produit de Walden ni une destructuration du milieu. En effet, dans la zone riche en eau, nous avons envisagé une diminution des interactions diélectriques entre l'ion et le solvant. Cette baisse des forces de friction diélectrique vis-à-vis des petits ions pourrait par conséquence entraîner une croissance de leur mobilité, celle-ci dépendant en effet beaucoup de ces forces. Vers les milieux plus riches en HMPT, l'addition de ce composé induirait un effet inverse par suite de la polarité élevée du HMPT.

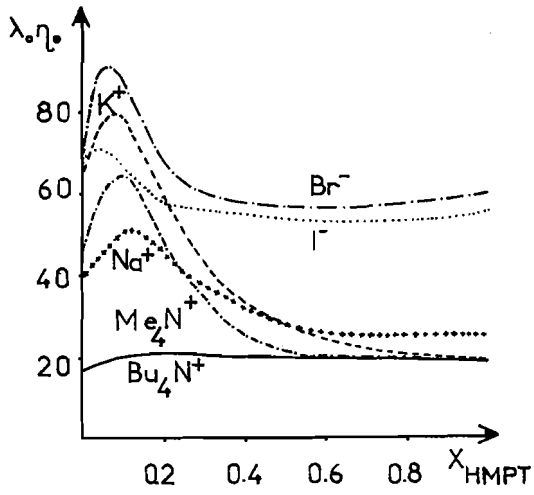

FIG. 7. Variation de $\lambda_0\eta_0$ (Ω^{-1} cm^2 equiv.$^{-1}$ cP) de quelques ions en fonction de X_{HMPT}.

Pour les anions ClO_4^-, I^- et le cation Bu_4N^+, l'absence de maximum marqué des courbes $\lambda_0\eta_0 = f(X_{HMPT})$ est en accord avec le fait que le déplacement de ces ions dépendrait davantage des forces hydrodynamiques et dans ce cas la théorie de Zwanzig prévoit aussi une invariance du produit de Walden.

Conclusion

Il ressort de notre travail que les mesures de mobilités ioniques effectuées dans les mélanges eau–HMPT ne permettent pas d'élucider les problèmes de la solvatation des ions mais que l'application de la théorie de Zwanzig permet de rendre compte de la répartition des influences de la viscosité et de la constante diélectrique d'un solvant sur ces mobilités.

De nombreux auteurs et récemment Kay et coll. (44) considèrent que les méthodes conductométriques ne peuvent apporter des informations sur la solvatation que par la détermination des constantes de dissociation des sels. Il n'est pas toujours possible d'atteindre ces constantes par des mesures de conductivité, d'autres méthodes électrochimiques peuvent être utilisées (40), nous en rendrons compte dans un prochain mémoire. Mais il convient bien de relever que les mesures de mobilités ioniques sont des données cinétiques alors que les constantes thermodynamiques sont déterminées à l'équilibre. Une corrélation des résultats ne peut être envisagée de façon systématique.

1. J. C. BOLLINGER, T. YVERNAULT, J. Y. GAL et F. PERSIN. Can. J. Chem. **54**, 3060 (1976).
2. R. ZWANZIG. J. Chem. Phys. **38**, 1603 (1963).
3. R. ZWANZIG. J. Chem. Phys. **52**, 3625 (1970).
4. J. JOSE, R. PHILIPPE et P. CLECHET. Can. J. Chem. Eng. **53**, 88 (1975).
5. YU. M. KESSLER. M. G. FORMICHEVA, N. M. ALPATOVA et V. P. EMELIN. Zh. Strukt. Khim. **13**, 517 (1972).
6. YU. M. KESSLER *et al.* Zh. Strukt. Khim. **16**, 797 (1975).
7. F. PERSIN. Thèse de Spécialité, Montpellier. 1975.
8. J. Y. GAL et F. PERSIN. C.R. Acad. Sci. **282**C, 1025 (1976).
9. M. ZIEGLER, H. ROSEMEYER, H. WINKLER et G. MODZEL. Talanta, **23**, 718 (1976).
10. V. S. GONCHAROV *et al.* Zh. Fiz. Khim. **51**, 789 (1977).
11. F. RALLO, F. RODANTE et P. SILVESTRONI. Thermochim. Acta, **1**, 311 (1970).
12. J. F. CASTEEL et E. S. AMIS. J. Chem. Eng. Data, **19**, 121 (1974).
13. J. P. MOREL. Bull. Soc. Chim. Fr. 1405 (1967).
14. F. FRANKS et D. J. G. IVES. Q. Rev. **20**, 1 (1966).
15. T. L. BROADWATER et R. L. KAY. J. Phys. Chem. **74**, 3802 (1970).
16. R. L. KAY et T. L. BROADWATER. Electrochim. Acta, **16**, 667 (1971).
17. F. ACCASCINA, R. DE LISI et M. GOFFREDI. Electrochim. Acta, **15**, 1209 (1970).
18. J. JUILLARD, J. P. MOREL et L. AVEDIKIAN. J. Chim. Phys. **5**, 787 (1972).
19. R. SMITS, P. VANDENWINKEL, D. L. JUILLARD et J. P. MOREL. Anal. Chem. **45**, 339 (1973).
20. E. S. AMIS et J. F. CASTEEL. J. Electrochem. Soc. **117**, 213 (1970).
21. A. LE NARVOR, E. GENTRIC et P. SAUMAGNE. Can. J. Chem. **49**, 1933 (1971).
22. R. A. HOVERMALE, P. G. SEARS et W. K. PLUKNETT. J. Chem. Eng. Data, **8**, 490 (1963).
23. R. REYNAUD. Bull. Soc. Chim. Fr. 532 (1972).
24. N. DESROSIERS et M. LUCAS. J. Phys. Chem. **78**, 2367 (1974).
25. J. C. BOLLINGER, T. YVERNAULT, J. Y. GAL et F. PERSIN. C.R. Acad. Sci. **287**C, 101 (1978).
26. J. Y. GAL. Travaux non publiés.
27. R. M. FUOSS et F. ACCASCINA. Electrolytic conductance. Interscience, New York, NY. 1959. pp. 191–205, 207–247.
28. E. M. HANNA, A. D. PETHYBRIDGE, J. E. PRUE et D. J. SPIERS. J. Solution Chem. **3**, 563 (1974).
29. T. C. WADDINGTON. Trans. Faraday Soc. **62**, 1482 (1966).
30. E. R. NIGHTINGALE, JR. J. Phys. Chem. **63**, 1381 (1959).
31. V. M. GOLDSCHMIDT. Chem. Ber. **60**, 1263 (1927).
32. N. DESROSIERS et J. E. DESNOYERS. Can. J. Chem. **54**, 3800 (1976).
33. N. F. HALLIWELL et S. C. NYBURG. J. Chem. Soc. 4603 (1960).
34. N. GOLDENBERG et E. S. AMIS. Z. Phys. Chem. Neue Folge, **31**, 3 (1962).
35. A. THAN et E. S. AMIS. Z. Phys. Chem. Neue Folge, **58**, 196 (1968).
36. N. G. FOSTER et E. S. AMIS. Z. Phys. Chem. Neue Folge, **7**, 360 (1956).
37. J. JUILLARD, J. P. MOREL, R. SMITH et D. L. MASSART. Bull. Soc. Chim. Belg. **82**, 7 (1973).
38. R. L. KAY et T. L. BROADWATER. J. Solution Chem. **5**, 57 (1976).
39. G. PETRELLA, A. SACCO, M. CASTAGNOLO, M. DELLA MONICA et A. DE GIGLIO. J. Solution Chem. **6**, 13 (1977).
40. C. LAVILLE. Thèse de Spécialité, Montpellier. 1978.
41. H. S. FRANK et W. Y. WEN. Discuss. Faraday Soc. **24**, 133 (1957).
42. R. M. FUOSS. Proc. Natl. Acad. Sci. U.S. **45**, 807 (1959).
43. R. H. BOYD. J. Chem. Phys. **35**, 1281 (1961).
44. R. L. KAY, D. F. EVANS et M. A. MATESICH. *In* Solute solvent interactions. Vol. 2. *Rédigé par* J. F. Coetzee et C. D. Ritchie. M. Dekker, New York, NY. 1976. p. 105.
45. P. BRUNO, M. DELLA MONICA et E. RIGHETTI. J. Phys. Chem. **77**, 1258 (1973).
46. R. L. KAY, G. P. CUNNINGHAM et D. F. EVANS. *In* Hydrogen bonded solvent systems. A. K. Covington, P. Jones Taylor et Francis Ltd., Londres. 1968. p. 249.
47. R. FERNANDEZ-PRINI et G. ATKINSON. J. Phys. Chem. **75**, 239 (1971).
48. R. L. KAY et D. F. EVANS. J. Phys. Chem. **70**, 2325 (1966).
49. P. G. WOLYNES. J. Chem. Phys. **68**, 473 (1978).
50. R. M. DIAMOND. J. Phys. Chem. **67**, 2513 (1963).
51. J. PIRO, R. BENNES et E. BOU KARAM. J. Electroanal. Chem. **57**, 399 (1974).

Studies on the adsorption and the association of cytidine sulphate at the dropping mercury electrode with phase-sensitive ac-polarography

YASSEIN M. TEMERK

Chemistry Department, Faculty of Science, Assiut University, Assiut, Egypt

Received June 5, 1978

YASSEIN M. TEMERK. Can. J. Chem. 57, 1136 (1979).

The adsorption and association of cytidine sulphate have been studied by using phase-sensitive ac-polarography in acidic buffer solution (pH 3.24) at the dropping mercury electrode. At low bulk concentrations, adsorbed molecules of cytidine sulphate at maximal adsorption potential (−0.7 V) are orientated in 'dilute' adsorption layer planar to the electrode surface where the interaction of π-electrons with interface favours adsorption. At bulk concentrations above a threshold value (6.6×10^{-3} *M*), the stacking interactions between vertically oriented molecules lead to association and formation of a compact layer; and a pit is observed. The concentration dependence of the ac-capacity current at a maximal adsorption potential (−0.7 V) shows a two-step Frumkin isotherm due to association of the adsorbed molecules. The adsorption parameters are computed and discussed.

YASSEIN M. TEMERK. Can. J. Chem. 57, 1136 (1979).

On a étudié l'adsorbtion et l'association du sulfate de cytidine en faisant appel à la polarographie-ca sensible aux phases, en solution acide tamponnée à un pH de 3.24 au niveau de l'électrode à goutte de mercure. A des concentrations globales faibles, les molécules de sulfate de cytidine adsorbées, au potentiel d'adsorbtion maximal (−0.7 V), sont orientées dans des couches d'adsorbtion "diluées" qui sont dans le plan de la surface de l'électrode où l'interaction des électrons π avec l'interface favorise l'adsorbtion. A des concentrations globales supérieures à une valeur de seuil (6.6×10^{-3} *M*), les interactions d'entassement entre les molécules orientées verticalement conduisent à une association et à la formation d'une couche compacte; on observe un creux. L'influence de la concentration sur le courant de capacité ca à un potentiel d'adsorbtion maximal (−0.7 V) suggère l'existence d'une isotherme de Frumkin en deux étapes qui est due aux molécules adsorbées. On a évalué les paramètres d'adsorbtion et on les discute.

[Traduit par le journal]

Introduction

The nucleic acids are substances of paramount biological and physiological significance. In the living cell, nucleic acids come into contact with various types of boundaries such as the surface of ribosomes and nuclear membranes. Interactions of nucleic acid with charge biological interfaces involve several specific processes with adsorption being the initial stage (1). Since both the charged interfaces found in biological systems, such as cell surfaces, and nucleic acid are very complex macromolecular assemblies (2, 3), it seems prudent to study the adsorption and interfacial orientations of the bases occurring in nucleic acids and derivatives of analogous structure. The surface of a cell has been compared to a liquid–solid interface like an electrode (4).

The adsorption properties of some bases, nucleosides and mononucleotides, present in the nucleic acid have been studied at the mercury electrode (5–17). Previous investigations have been made by Vetterl and co-workers (5–9) on pyrimidine and purine bases and nucleotides and by Elving and co-workers (10–13) on adenine and cytosine mono- and oligonucleotides using measurement of the changes of the double layer capacity with the impedance bridge or by means of total ac-polarography. Recently Nürnberg and co-workers (14–16) and Kinoshita *et al.* (17) have determined the adsorption parameters of cytosine, adenine, and deoxyadenine mononucleotides by out-of-phase ac-polarography and single sweep voltametry.

In the present paper the adsorption stages and the association of cytidine sulphate at charged interfaces have been investigated by using phase-sensitive ac-polarography. This investigation is focussed on the interfacial behaviour of adsorbed molecules of cytidine sulphate when the surface is covered by a rather 'dilute' coverage in contrast to the properties of the film stage resulting at higher bulk concentrations. No work on this salt of cytidine from the present standpoint has been published.

Experimental

(a) Chemicals and Solutions

Cytidine sulphate was a commercial sample from Serva, Heidelberg, FRG. A McIlvaine buffer brought to constant ionic strength of 0.5 *M* by addition of KCl was used as a sup-

0008-4042/79/101136-05$01.00/0

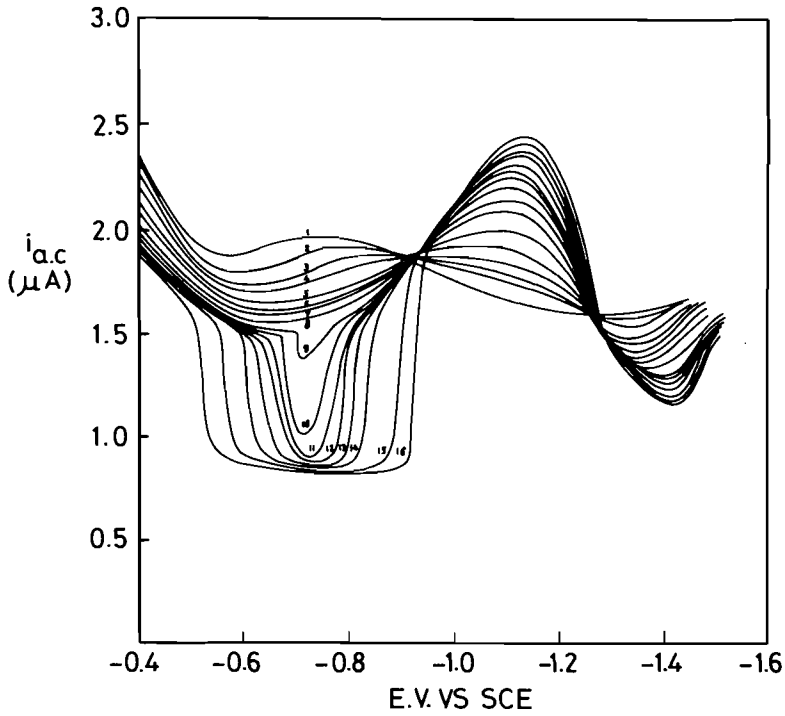

FIG. 1. AC-capacity current curves for cytidine sulphate at DME. 0.5 *M* McIlvaine buffer, pH 3.24, drop time 5 s, scan rate 2 m V s^{-1}, frequency 330 Hz, amplitude 5 m V_{pp} phase angle 90°, 5°C, curve (*1*), 0.0; (*2*), 4 × 10^{-5}; (*3*), 8 × 10^{-5}; (*4*), 1.7 × 10^{-4}; (*5*), 3.3 × 10^{-4}; (*6*), 8.1 × 10^{-4}; (*7*), 1.4 × 10^{-3}; (*8*), 3.2 × 10^{-3}; (*9*), 6.0 × 10^{-3}; (*10*), 6.6 × 10^{-3}; (*11*), 7.0 × 10^{-3}; (*12*), 7.7 × 10^{-3}; (*13*), 8.5 × 10^{-3}; (*14*), 9.0 × 10^{-3}; (*15*), 1.3 × 10^{-2}; (*16*), 2.2 × 10^{-2} *M* cytidine sulphate.

porting electrolyte. The pH was measured with an Orion digital pH meter, Model 701. All chemicals were reagent grade, KCl was Merck "Suprapur". Triply distilled water was used for preparing all solutions. The cytidine sulphate content of the polarographed sample was determined with a Unicam SP 800 Spectrophotometer at 279 nm.

(b) Apparatus and Method

The ac-polarographic measurements were carried out with a PAR Analyzer, Model 170, in a thermostated Metrohm cell with a three electrode system. Phase-sensitive ac-polarograms corresponding to the out-of-phase component of the total ac response were recorded at 90°, amplitude 5 mV (peak-to-peak), scan rate of dc ramp 2 mV s^{-1}, and a fixed medium frequency of 330 Hz.

The electrocapillary maximum potential was measured with a streaming type capillary electrometer similar to that used originally by Grahame (18).

The dropping mercury electrode used had the following characteristics: mercury flow rate $m = 0.229$ mg s^{-1}, natural drop time $t = 22.2$ s at open circuit in 1 *M* KCl and at a height of the mercury reservoir $h = 82.5$ cm. The drop time was controlled by mechanical detachment of the drop. The reference electrode was an Ingold saturated calomel electrode, and a platinum coil served as auxiliary electrode. All measurements were performed at 5°C.

Results and Discussion

Phase-sensitive ac-polarograms of cytidine sulphate in acidic buffer solution (pH 3.24) at the dropping mercury electrode are shown in Fig. 1. The recorded out-of-phase ac-component (90° phase angle) reflects, due to its strict proportionality to the differential double layer capacity (19), in potential ranges where no faradaic response occurs.

For relatively low bulk concentrations of cytidine sulphate (4 × 10^{-5} *M* – 4 × 10^{-3} *M*), the ac-polarograms indicate a progressive decrease of the capacitive ac signal around electrocapillary zero charge E_{ecm} (−0.54 V (sce) for the supporting electrolyte), corresponding to progressive coverage of the electrode surface by the 'dilute' adsorption layer. However, at cytidine sulphate concentrations at or above the threshold value (6.6 × 10^{-3} *M*), a sudden sharp decrease in an ac-capacity current is observed at a maximal adsorption potential .−0.7 V giving a very sharply defined pit. With increasing bulk concentration the pit grows in depth up to a saturation value and also in extension with respect to more positive and more negative potentials. The conclusions of Vetterl and co-workers (5–9) and Nürnberg and co-workers (14–16) suggest that the pit reflects the association of the oriented molecules on the electrode surface by intermolecular attraction forces and

formation of a compact layer. The broad peak following at more negative potentials (−1.1 V) is caused by a re-orientation of the adsorbed cytidine sulphate. This ac-peak which is also observed with cytidine (16), adenine mono-nucleotides (14, 15), denatured (20) and native DNA and related biosynthetic polynucleotides (21), is due to a structural rearrangement of the adsorbed species. It was established that in DNA this peak is specifically connected with a rearrangement of cytosine and adenine moieties of the adsorbed biopolymer. Closer inspection of this peak shows that the height of the peak measured (Δi_{ac}) varies linearly with frequency (up to 420 Hz) of the superimposed alternating voltage and presents a constant phase angle of 90°. These characteristics correspond to a peak of a nonfaradaic nature and the phenomenon is purely capacitive. After the re-orientation peak at more negative potential (around −1.35 V), an extended minimum capacitance is observed indicating a lateral adsorption of cytidine sulphate on the cathodic area. The rise of the response at more negative potentials (−1.4 V) is caused by a faradaic response due to cytidine sulphate reduction in an adsorbed state.

Further quantitative studies on the adsorption and the association of cytidine sulphate could be elucidated by plotting Δi_{ac}, the decrease of the capacitive ac-current with respect to the i_{ac} value of the blank supporting electrolyte for a given bulk concentration, as a function of bulk concentration of cytidine sulphate (C). The plot of Δi_{ac} vs. C at the maximal adsorption potential −0.7 V indicates a two-step isotherm (curve *a*, Fig. 2), corresponding to two adsorption stages of cytidine sulphate on the electrode surface. The first stage, which gives rise to the inflexion point at bulk concentration 2.0×10^{-4} M, reflects the 'dilute' adsorption layer for relative low bulk concentrations of cytidine sulphate. Above the threshold concentration value 6.6×10^{-3} M, one obtains the second stage, which is due to strong lateral interactions and high interaction coefficients between the adsorbed molecules giving rise to a compact layer of the adsorbed cytidine sulphate on the electrode surface. It is concluded that at maximal adsorption potential (−0.7 V) cytidine sulphate is oriented in a dilute adsorption layer planar to the electrode surface where the interaction of π-electron with the interface favours the adsorption. With the increase of the bulk concentration above the threshold value, the stacking interactions between vertically oriented molecules lead to association and formation of a compact layer in the pit region. The ratio at full coverage for the first and second step of isotherm indicates that the number of adsorbed molecules for the dilute layer is increased by a factor

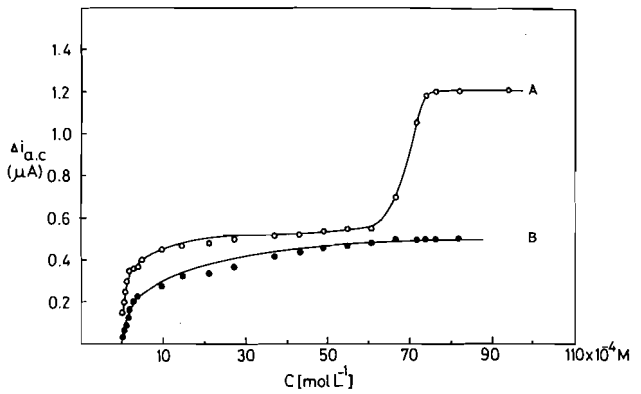

FIG. 2. Dependence of the capacity current decrease Δi_{ac} on the bulk concentration of cytidine sulphate, 0.5 McIlvaine buffer, pH 3.24, curve (*a*), adsorption potential −0.7 V; curve (*b*), adsorption potential −1.35 V, other conditions as in Fig. 1.

of 2.4 for the compact layer. This is in good agreement with the conclusions of Parsons (22) and Damaskin *et al.* (23) that the number of water molecules displaced from the surface by adsorption of a hydrophobic species is doubled for a change in adsorption orientation from the planar to the vertical position.

The concentration dependence of the ac-capacity current Δi_{ac} has the form of a one-step isotherm for the extended cathodic capacitance minimum at −1.35 V (curve *b*, Fig. 2). This indicates that the association of the adsorbed molecules of cytidine sulphate takes place only at potentials more positive than the re-orientation peak where the pit occurs. On the other hand, at potentials more negative than −1.2 V the adsorbed molecules of cytidine sulphate are more accessible to reduction via the cytosine moiety than to association on the electrode surface.

The dependence of the ac-capacity current per unit area of the dropping mercury electrode on the drop time (t) is of considerable interest. The curves are obtained at a maximal adsorption potential −0.7 V (Fig. 3). The horizontal curves *1* and *2* indicate the independence of ac-capacity current on the drop time for rather low bulk concentrations. This reflects the adsorption equilibrium of cytidine sulphate on the electrode surface for dilute adsorption layer. However, for concentrations larger than the threshold value where the pit occurs on ac-polarograms, a decrease of the ac-capacity current is observed (curve *3*, Fig. 3), indicating a slow adsorption process due to re-arrangement of the surface layer from a dilute state to a compact state. At very large bulk concentrations a compact layer is already formed and the adsorption equilibrium is attained more rapidly

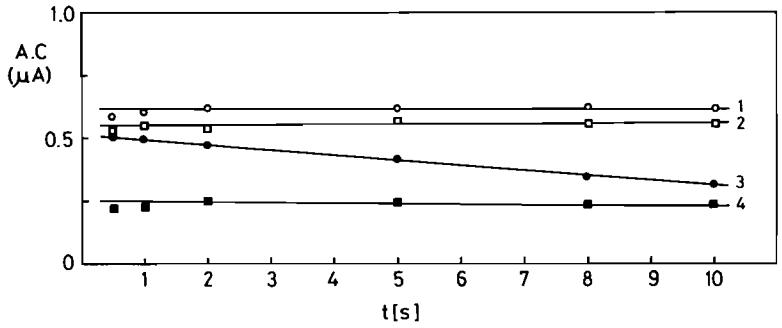

FIG. 3. Time dependence of the out-of-phase component of ac-current. pH 3.24, adsorption potential $E_s = -0.7$ V, concentration of cytidine sulphate: (*1*), 4.0×10^{-5} *M*; (*2*), 3.5×10^{-4} *M*; (*3*), 7.0×10^{-3} *M*; (*4*), 2.2×10^{-2} *M* cytidine sulphate, other conditions as in Fig. 1.

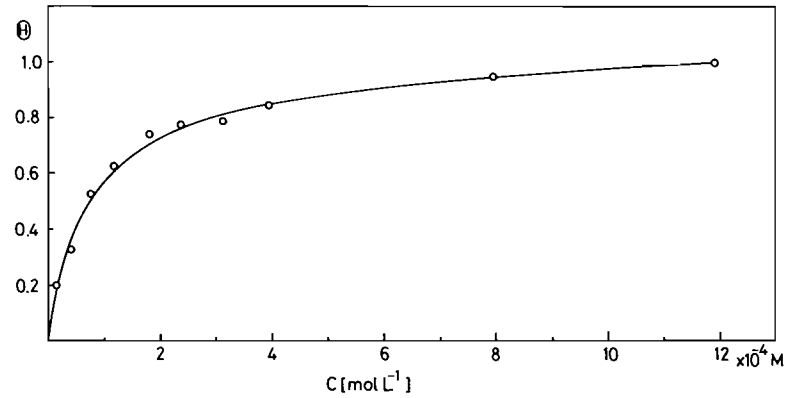

FIG. 4. Dependence of surface coverage Θ on the bulk concentration of cytidine sulphate for dilute layer, pH 3.24, adsorption potential $E_s = -0.7$ V, Θ is calculated from the results of out-of-phase ac-polarography. Other conditions as in Fig. 1.

(curve *4*, Fig. 3). A similar phenomenon has been observed previously for the formation of a compact layer of cytidine at the HDME (16). The result shown in Fig. 3 indicates that the ac-readings corresponding to 'dilute' adsorption layer are well equilibrium values. Accordingly, the following adsorption parameters are computed for the 'dilute' adsorption layer.

In order to calculate the adsorption parameters for the dilute adsorption layer at maximal adsorption −0.7 V, the equilibrium values of the ac-capacity current at a given bulk concentration were measured and the degree of coverage Θ was calculated using the relation

$$[1] \quad \Theta = (C_0 - C)/(C_0 - C_m) = \Delta i_{ac}/(\Delta i_{ac})_m$$

where *C*'s are the differential capacities in the supporting electrolyte (C_0), at a given bulk concentration of cytidine sulphate (C), and at bulk concentrations corresponding to full coverage (C_m), Δi_{ac} is the decrease of the capacitive ac-current (with respect to the i_{ac}-value of the blank supporting electrolyte) for a given bulk concentration and $(\Delta i_{ac})_m$ is the maximal decrease corresponding to full coverage. The concentration dependence of the surface coverage for the 'dilute' adsorption layer is shown in Fig. 4. It has been found that the experimental data fit well a Frumkin adsorption isotherm given by eq. [2].

$$[2] \quad BC = [\Theta/(1 - \Theta)] \exp(-2a\Theta)$$

where Θ is the degree of coverage, a the interaction coefficient, b the adsorption coefficient, and C the bulk concentration of cytidine sulphate.

The interaction coefficient a was determined from the slope of the logarithmic plot of the Frumkin isotherm and the adsorption coefficient B from the values at half coverage (Θ = 0.5). The free energy of adsorption ($-\Delta\bar{G}^0$) was then calculated from the adsorption coefficient B (Θ = 0.5) according to eq. [3].

$$[3] \quad B = \frac{1}{55.5} \exp\left(\frac{-\Delta\bar{G}^0}{RT}\right)$$

The calculated values of the adsorption parameters of cytidine sulphate for the 'dilute' adsorption layer at pH 3.24 are: adsorption coefficient, 8.7 ×

10^3 L/mol; interaction coefficient, 0.48; free energy of adsorption, 7.27 kcal/mol; bulk concentration at half coverage ($C_{\Theta=0.5}$), 7×10^{-5} M; pit potential, -0.70 V, orientation potential, -1.1 V. The moderately high positive interaction coefficient a for the 'dilute' layer indicates moderate lateral attractive interaction of adsorbed molecules. The rather large adsorption coefficient of cytidine sulphate is quite common behaviour for heterocyclic compounds as has been shown previously (24) for pyridine derivatives. The low value of adsorption energy $-\Delta\bar{G}^0$ indicates that the deviation from adsorption equilibrium is minimized and that equilibrium is established at relatively low bulk concentration of cytidine sulphate.

Acknowledgement

The author expresses his gratitude to the Alexander Von Humboldt Foundation for financial support to purchase the Polarographic Analyzer PAR equipment.

1. B. JANIK and R. G. SOMMER. Biopolymers, **12**, 2903 (1973).
2. D. E. COMINGS. Am. J. Hum. Genet. **20**, 440 (1968).
3. S. GILMOUR. New Sci. **65**, 390 (1975).
4. E. PALECEK. *In* Progress in nucleic acid research and molecular biology. Vol. 9. *Edited by* J. N. Davidson and W. E. Cohn. Academic Press, New York. 1969. p. 31.
5. V. VETTERL. Collect. Czech. Chem. Commun. **31**, 2105 (1966).
6. V. VETTERL. J. Electroanal. Chem. **19**, 169 (1968).
7. V. VETTERL. Biophysik, **5**, 255 (1968).
8. U. RETTER, H. JEHRING, and V. VETTERL. J. Electroanal. Chem. **57**, 391 (1974).
9. V. VETTERL and E. KOVARIKOVA. Chem. Nucleic Acid Components, **1**, 93 (1975).
10. B. JANIK and P. J. ELVING. Chem. Rev. **68**, 295 (1968).
11. B. JANIK and P. J. ELVING. J. Am. Chem. Soc. **92**, 235 (1970).
12. G. DRYHURST and P. J. ELVING. Talanta, **16**, 855 (1969).
13. J. WEBB, B. JANIK, and P. J. ELVING. J. Am. Chem. Soc. **95**, 991 (1973); **95**, 8495 (1973).
14. D. KRZNARIC, P. VALENTA, and H. W. NÜRNBERG. J. Electroanal. Chem. **65**, 863 (1975).
15. P. VALENTA, H. W. NÜRNBERG, and D. KRZNARIC. Bioelectrochem. Bioenerg. **3**, 418 (1976).
16. Y. M. TEMERK, P. VALENTA, and H. W. NÜRNBERG. J. Electroanal. Chem. In press.
17. H. KINOSHITA, S. D. CHRISTIAN, and G. DRYHURST. J. Electroanal. Chem. **83**, 151 (1977).
18. D. C. GRAHAME, E. M. COFFIN, and J. I. CUMMINGS. Office of Naval Research. Tech. Report No. 2. 1950.
19. H. JEHRING. Elekrosorptions analyse mit der Wechselstrampolarographie. Akademie Verlag, Berlin. 1974.
20. P. VALENTA and P. GRAHMANN. J. Electroanal. Chem. **49**, 41 (1974).
21. P. VALENTA, H. W. NÜRNBERG, and P. KLAHRE. Bioelectrochem. Bioenerg. **1**, 487 (1974); **2**, 204 (1975).
22. J. M. PARRY and R. PARSONS. J. Electrochem. Soc. **113**, 992 (1966).
23. B. B. DAMASKIN, S. L. DYATKINA, and S. L. PETROCHENKO. Elektrohimiya, **5**, 935 (1969).
24. R. G. BARRADAS and P. G. HAMILTON. Can. J. Chem. **43**, 2468 (1965).

Characterization of autohydrolysis aspen (*P. tremuloides*) lignins. Part 1. Composition and molecular weight distribution of extracted autohydrolysis lignin

MIRANDA G. S. CHUA AND MORRIS WAYMAN

Department of Chemical Engineering and Applied Chemistry, University of Toronto, Toronto, Ont., Canada M5S 1A4

Received November 2, 1978

MIRANDA G. S. CHUA and MORRIS WAYMAN. Can. J. Chem. 57, 1141 (1979).

Extractive-free aspen wood meal was subjected to autohydrolysis at 195°C for 5 min to 2 h, and the lignin extracted with 90% dioxane. Extracted autohydrolysis lignin was found to be higher in carbon but lower in hydrogen and oxygen content than aspen milled wood lignin. The methoxyl content was also lower than the reference lignin. These differences have been attributed to condensation and incorporation into the lignin of non-lignin components. A lignin extractability curve with a maximum delignification at autohydrolysis time of 30–40 min was found. From molecular weight distribution studies the ratio of high molecular weight to low molecular weight materials varied for the different extracted lignins and reached a maximum at autohydrolysis time of 40 min. A mechanism of depolymerization/repolymerization of the lignin via carbonium ions has been proposed. *p*-Hydroxybenzoic acid is postulated as contributing to the extractability of aspen lignin by acting as a blocking agent.

MIRANDA G. S. CHUA et MORRIS WAYMAN. Can. J. Chem. 57, 1141 (1979).

On a soumis de la sciure de bois de tremble (ne contenant plus de produits pouvant être extraits) à une autohydrolyse à 195°C pour des temps allant de 5 min à 2 h puis on en a extrait la lignine par du dioxanne à 90%. On a trouvé que la lignine extraite de l'autohydrolyse contient plus de carbone et moins d'hydrogène et d'oxygène que la lignine provenant de bois de tremble broyé. La quantité de méthoxyle qui y est contenue est aussi plus faible que celle contenue dans la lignine de référence. On a attribué ces différences à la condensation et à l'incorporation dans la lignine de composants qui ne sont pas des lignines. On a déterminé une courbe permettant d'évaluer la facilité d'extraction de la lignine; elle présente un maximum de délignification à des temps d'autohydrolyse de 30 à 40 min. En se basant sur des études de distribution de masses moléculaires, on a déterminé que le rapport des produits de masses moléculaires élevées/produits de masses moléculaires plus faibles varie suivant les différentes lignines extraites et qu'il atteint un maximum à un temps d'autohydrolyse de 40 min. On propose un mécanisme de dépolymérisation/repolymérisation de la lignine par l'intermédiaire de carbocations. On croit que l'acide *p*-hydroxybenzoïque facilite l'extraction de la lignine de tremble en agissant comme agent bloqueur.

[Traduit par le journal]

Introduction

Autohydrolysis (1, 2) of wood with water or steam at elevated temperature and pressure is catalysed by the organic acids formed from the wood components during the hydrolysis. The chemical changes which take place during autohydrolysis in the three main constituents of wood (hemicelluloses, cellulose, and lignin) are very much dependent on the temperature and the time at temperature. The hemicelluloses are hydrolysed to soluble sugars by the organic acids, mainly acetic acid derived from the acetylated polysaccharides present in wood. However, under more drastic conditions secondary reactions occur which result in the formation of furfural, hydroxymethyl furfural, and their precursors by the dehydration of pentoses and hexoses (3–5). The reactive precursor besides undergoing self-polymerization can participate in condensation reactions with lignin (refs. 5–10, ref. 11, pp. 287–295, 395–399).

Lignin degradation and modification during autohydrolysis has been reported by various investigators. In their studies of prehydrolysis kraft pulping, Traynard and Eymery (12) and Richter (13, 14) observed that the treatment of wood with water at high temperatures in prehydrolysis affected the lignin and its subsequent behaviour in kraft pulping. Work in this laboratory has shown that the solubility of lignin in 90% dioxane after autohydrolysis is a maximum over a narrow time range at each temperature between 165°C and 215°C. Goldschmid (15) and Stanek (16) found and identified monomeric lignin degradation products present in autohydrolysis liquor. Modification of the lignin remaining in the wood after autohydrolysis is indicated by its subsequent extractability by various organic solvents (12, 17) and dilute alkali as was found in this laboratory. It has also been observed that softwood lignins are much more affected by prehydrolysis treatment than hardwood lignins (14).

Studies on the steaming of wood have centred

0008-4042/79/101141-09$01.00/0

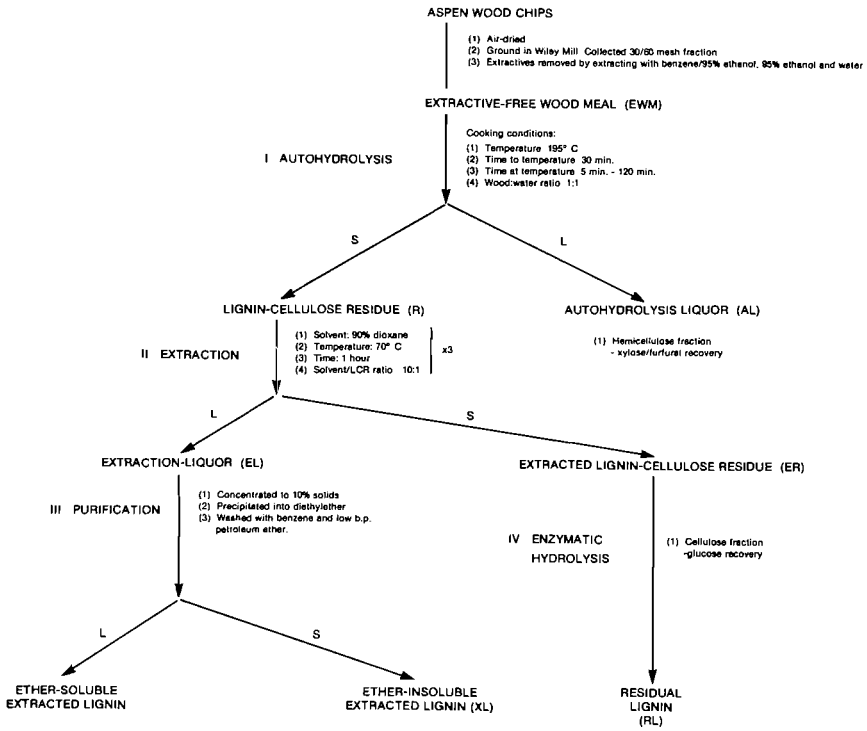

FIG. 1. Flow-chart of overall process involving the following four stages: I, autohydrolysis; II, extraction; III, purification; IV, enzymatic hydrolysis.

mainly on the hemicellulose fraction, for example, in the production of furfural (ref. 11, pp. 272–331) and on the cellulose fraction, as in the case of prehydrolysis pulping (14) and lately as a possible pretreatment before enzyme saccharification of the cellulose in wood (18). Thus far there has been very little comprehensive work with regard to the effect of steaming on the lignin component.

The purpose of this present work was to characterize the lignin obtained on autohydrolysis with a view to elucidating the mechanism involved in lignin depolymerization and repolymerization. In addition, it is hoped that such characterization would further the utilization of the autohydrolysis lignin which represents a potential source of renewable phenolic compounds, as well as medically interesting compounds (46).

The overall process used to obtain the extracted autohydrolysis lignin (XL) and the residual autohydrolysis lignin (RL) involved the four stages of autohydrolysis, extraction, purification, and enzyme hydrolysis as outlined in Fig. 1. The present paper deals with the chemical composition and the physical characterization of the extracted autohydrolysis lignin.

Results

Extractives

The percentage of extractives in aspen wood meal on extracting with benzene/95% ethanol (2:1), 95% ethanol, and water was 2.7% based on dry aspen wood meal. It was necessary to work with extractive-free wood meal (EWM) to avoid difficulties in interpreting results as lignans and polyphenolic extractives have similar chemical properties to lignin.

Autohydrolysis (Fig. 1)

The pH of the autohydrolysis liquors from the different cooking times at 195°C was between 3.2–3.4, and xylose contents ranged from 0.3–6.2% based on EWM for the longest to the shortest cook, representing less than 40% of the xylose potentially obtainable from aspen. This indicated that 195°C may not be the optimum temperature for hemicellulose recovery since the bulk of the hemicellulose is degraded. The lignocellulosic residue (R) yields were between 69 and 73%.

Extraction of R with 90% dioxane resulted in isolating the extractable lignin (XL) portion leaving behind the insoluble lignin fraction termed residual lignin (RL). Yields of extracted lignocellulosic resi-

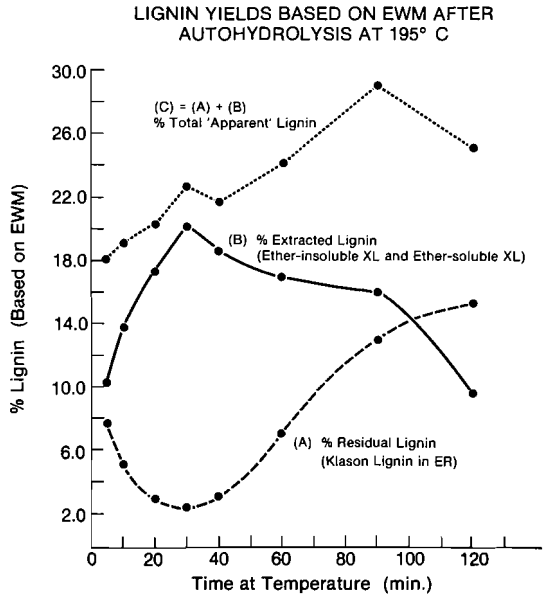

FIG. 2. Lignin yields based on EWM after autohydrolysis at 195°C.

due (ER) were between 50–61% based on EWM, and pH of the extraction liquor varied from 4.0–5.2.

A characteristic delignification trend as indicated by curve *A* in Fig. 2[1] was obtained, with maximum lignin extactability represented by minimum Klason lignin left in ER in the 30-min cook. Curve *A* suggests that during autohydrolysis two types of reactions are occurring. Initially the faster reaction, depolymerization of the native lignin by acidic hydrolysis, predominates, accounting for the solubility of the lignin in the solvent. However, as heating continues, condensation/repolymerization reactions take over, resulting in increasing amounts of insoluble residual lignin.

Curve *B* in Fig. 2 represents the total lignin recovered after extraction and purification by precipitation into ether. It represents both the ether-soluble and ether-insoluble (the bulk of the material) extracted lignin. Curve *C* is the sum of curves *A* and *B* and has been termed total 'apparent' lignin because it contains another component which is not lignin. This is substantiated by the fact that the Klason lignin content in the original aspen wood meal is 17.6%, but as shown in Fig. 2 the amount of 'apparent' lignin ranges from 18.1% upwards to 29.0%. The data support Klemola's (3) postulate that reactive hemicellulose degradation products, such as furfural and its precursors, can react with the lignin during autohydrolysis, thereby accounting for the apparent increase in lignin content. This also explains the low yield of xylose obtained in the autohydrolysis liquor mentioned earlier.

Elemental Analyses of Extracted Autohydrolysis Lignin (XL) (Table 1)

Using aspen milled wood lignin (MWL) purified according to the method of Lundquist *et al.* (19) as the reference lignin, two trends were observed. First the C-content of the extracted lignins is higher than the reference lignin whereas the H and O contents are consistently lower. These changes in C, H, and O can result from (*a*) condensation reactions which involve the elimination of water; and/or (*b*) they can also be associated with incorporation into the lignin of entities having higher C to H/O ratios during autohydrolysis; and/or (*c*) the initial preferential removal of syringyl to guaiacyl units at the shorter autohydrolysis times.

The second significant observation is that the methoxyl content per C_9 unit decreases gradually with increasing cooking time. This could be attributed to demethoxylation of the lignin during autohydrolysis, as is indicated by the presence of methanol (0.5–0.6% based on EWM or 2.5–3.0% based on lignin) found in the autohydrolysis liquor (20). Also, Klemola identified six catechol derivatives among the low-molecular degradation products, suggesting demethylation during the course of steam hydrolysis as catechols have not been identified in wood protolignins (21). Another explanation would point again to the inclusion of so-called non-lignin components, in all probability carbohydrate degradation products, which would also contribute to the decreasing percentage of methoxyl content observed. Pepper and Siddiqueullah (22) in their work with acidolysis lignins encountered similar C, H, O changes and lowering of methoxyl content with increasing acidolysis time. They attributed the differences to either non-homogeneity of protolignin or to inclusions of non-lignin (carbohydrate) residues. Finally, a variation of the proportion of syringyl to guaiacyl units in the extracted lignins would again account for the observed methoxyl content trend. All this implies that the extracted lignins are modified lignins, different from milled wood lignin, which has been widely accepted as representative of protolignin.

The rate of change in C% and OCH_3% in the first 30–40 min of autohydrolysis is 7–8 times greater than for the next 80 min. It is interesting to note that the transition point is the same as in delignification (Fig. 2) and molecular weight distribution (Fig. 4).

[1]Data in support of Fig. 2 are available, at a nominal charge, from the Depository of Unpublished Data, CISTI, National Research Council of Canada, Ottawa, Ont., Canada K1A 0S2.

TABLE 1. Elemental analysis of milled wood lignin (MWL)* and extracted lignin (XL) (carbohydrate-free basis)

Sample no.	C%	H%	O%	OCH_3%	C_9 formula	OCH_3/C_9 unit	Molecular weight of average lignin unit	% Carbohydrate in lignin
MWL	59.50	6.25	34.25	21.54	$C_9H_{8.70}O_{3.05}(OCH_3)_{1.47}$	1.47	211.2	2.5
XL-5	60.41	5.69	33.92	20.55	$C_9H_{7.54}O_{3.00}(OCH_3)_{1.37}$	1.37	206.1	3.9–4.8
XL-10	60.75	5.90	33.35	19.46	$C_9H_{8.06}O_{2.96}(OCH_3)_{1.27}$	1.27	203.2	1.2–1.8
XL-20	61.55	5.70	32.75	18.58	$C_9H_{7.67}O_{2.88}(OCH_3)_{1.19}$	1.19	198.8	0.5–0.6
XL-30	62.78	5.52	31.61	17.74	$C_9H_{7.27}O_{2.71}(OCH_3)_{1.11}$	1.11	193.3	0.5–0.8
XL-40	62.62	5.66	31.72	16.74	$C_9H_{7.69}O_{2.78}(OCH_3)_{1.04}$	1.04	192.4	0.5–0.5
XL-60	62.79	5.52	31.69	16.80	$C_9H_{7.40}O_{2.76}(OCH_3)_{1.04}$	1.04	192.1	0.4–0.9
XL-90	62.70	5.50	31.80	15.98	$C_9H_{7.49}O_{2.82}(OCH_3)_{0.99}$	0.99	191.6	0.4–0.9
XL-120	63.45	5.69	30.86	15.58	$C_9H_{7.79}O_{2.68}(OCH_3)_{0.95}$	0.95	188.2	0.5–0.9

*Aspen milled wood lignin purified according to the method by Lundquist (19) was prepared by Mr. J. H. Lora.

Molecular Weight Distribution (MD) of XL by Gel Permeation Chromatography (Fig. 3)

Gel permeation chromatography has proved to be a fast and effective method of fractionating polymers according to molecular size. In applying gel permeation chromatography to the study of MD of extracted lignins, the analytical system used by Obiaga and Wayman (23, 24) employing Sephadex G-100 (a dextran gel) swollen in dimethyl sulphoxide (DMSO) was again used. DMSO, a good lignin solvent, swells Sephadex G-100 to a greater extent than water (25), and adsorption effects of the lignin on the gel are absent. The hydrodynamic volume of lignin in DMSO is different from globular protein or dextran in aqueous buffer, and conventional calibration standards are of little use. To calibrate the column, lignin samples of known molecular weight have been used. However, in using one column of a single pore size for fractionating a polydisperse polymer like lignin, molecular weights and polydispersities obtained from the chromatograms are only approximate, because separation is incomplete. In spite of this inherent limitation, substantial information can be derived by comparing the XL chromatograms.

A prominent and common feature to all the XL chromatograms shown in Fig. 3 is the distinct dual-peaked character of the elution pattern, which clearly indicates that the XL are highly polydisperse. Broadly speaking the chromatograms can be divided into two fractions, namely, a high molecular weight at fraction number 20 and a low molecular weight portion at fraction number between 50–65, termed HML and LML respectively. The different XL have different amounts of HML and LML materials. Especially interesting is the observed increase in HML material from autohydrolysis time of 5 min to 40 min, with subsequent decrease of the peak thereafter.

It was found that although the quantity of XL injected was the same for all samples, the areas obtained for the chromatograms were slightly different. This can probably be attributed to different absorptivities for the different samples and for individual fractions. The absorptivities increased from 17.5 L g^{-1} cm^{-1} for XL-5 to 24.9 L g^{-1} cm^{-1} for XL-120, compared to 13.6 L g^{-1} cm^{-1} for MWL. The absorptivities for HML and LML were 16.9 and 23.8 L g^{-1} cm^{-1}, respectively. Due to this, analyses have been made based on the comparison of areas and on ratios of HML:LML which will enable one to follow the solubilization, degradation, and repolymerization processes taking place during autohydrolysis. Figure 4 illustrates the increase of the HML to LML materials in the extracted lignin with autohydrolysis time, reaching a maximum HML:LML ratio of 0.6 at 30–40 min, which is also the region of maximum lignin extractability. In order to compare the amounts of HML to LML generated based on original wood, the areas under the HML and LML peaks were multiplied by factors proportional to the yield of purified extracted lignin at each autohydrolysis time. The soluble HML material was found to increase, again reaching a maximum at the region of maximum delignification, followed by a decrease corresponding to an increase in the amount of insoluble residual lignin. This suggests that soluble HML is recondensing to form insoluble lignin. The LML fraction has two maxima, one at autohydrolysis time of 30 min and the other at 90 min. The first maximum is related to the initial extraction of low molecular weight material and the second, at longer autohydrolysis time, to degradation of HML under the more drastic conditions.

Acidolysis lignins of known molecular weights and polydispersities were used to calibrate the Sephadex G-100 column as is shown in Fig. 5. However, it was not possible to obtain a complete calibration curve of molecular weight vs. retention volume for the system, because the HML ($\overline{M}_w$ = 196 000) is above the exclusion limit of the gel used. In comparing the

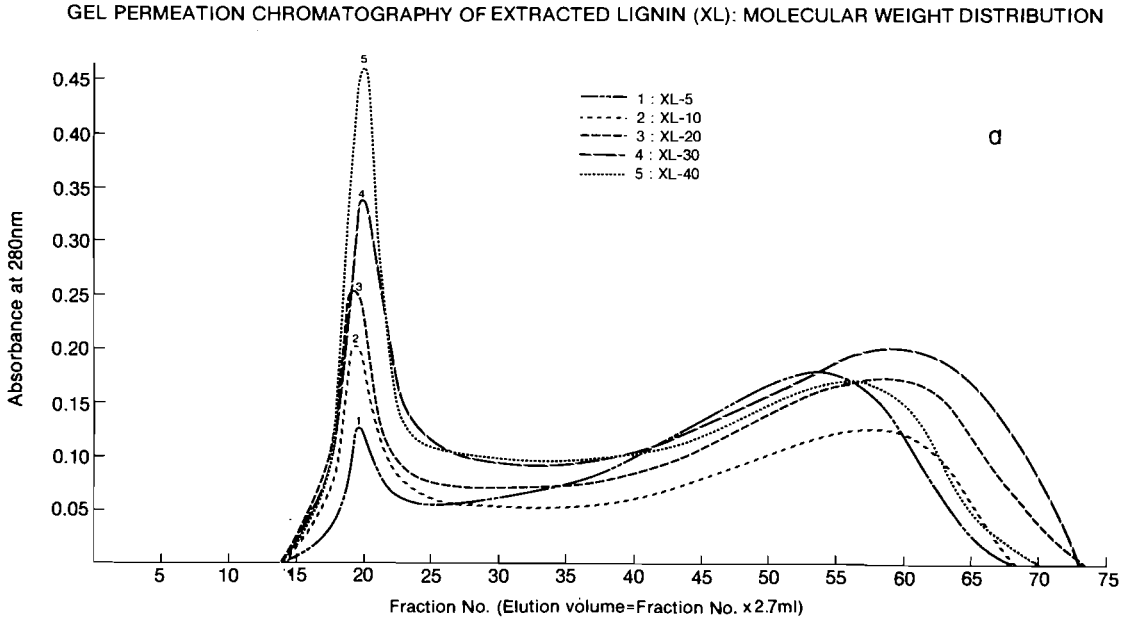

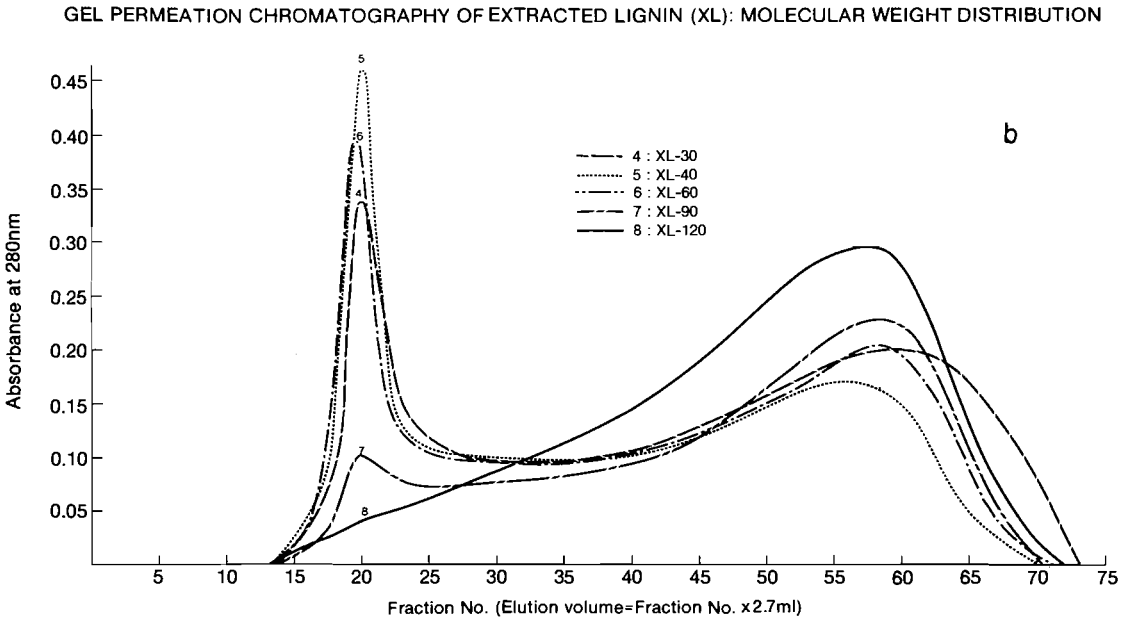

FIG. 3. Gel permeation chromatography of extracted lignin (XL): molecular weight distribution.

chromatograms of MWL and XL-40, it would appear that autohydrolysis resulted in the formation of more HML material. This has been substantiated by work in this laboratory with MWL under autohydrolysis conditions, which showed initial building-up of HML material followed by a decrease.

Table 2 contains the molecular weight determinations and polydispersities for XL's and MWL. The weight average molecular weight, $\overline{M}_w$, was determined for samples XL-40, XL-120, HML, and MWL. Using the $\overline{M}_w$ obtained for XL-40 and XL-120 together with the intrinsic viscosity measurements for all XL, and applying the Mark–Houwink equation, $\overline{M}_w$ was calculated for the other XL. Although reservations with regard to the absolute value of the numbers based on two measurements

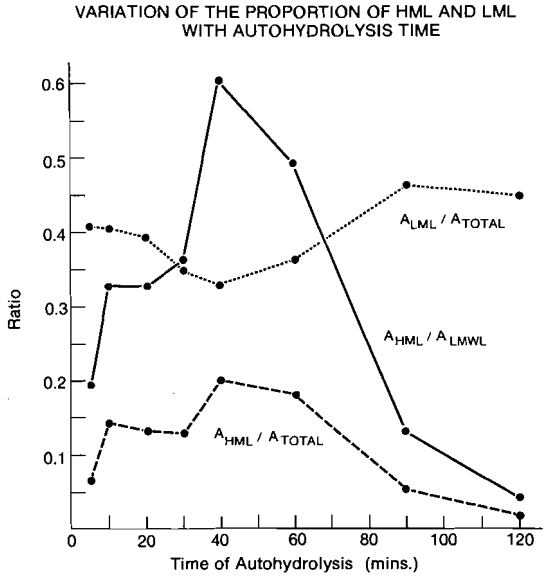

FIG. 4. Variation of the proportion of HML and LML with autohydrolysis time.

and the assumption that the Mark–Houwink relationship applies for XL, the values of $\bar{M}_w$ and the polydispersities so generated do not contradict, but supplement the trends observed for the MWD patterns obtained from gel permeation chromatography studies as shown in Figs. 3 and 5. The $\bar{M}_n$, $\bar{M}_w$ and the polydispersities increase for the first 30–40 min of autohydrolysis and decrease thereafter.

These molecular weight numbers and polydispersities are higher than observed for kraft lignins (24, 26) but more similar to the values obtained for lignosulphonates (27). This is indicative of the difference in mechanisms between alkaline pulping and acid pulping resulting in cleavage of different bonds in lignin and therefore varying molecular weight. Gierer (28) in his review of the reactions of lignin during pulping discussed in detail the mechanisms of alkaline and acid pulping.

It is interesting to note that the HML material has a $\bar{M}_w$ of 196 000. On the other hand, the XL-40 (which has the highest proportion of HML:LML material) has an average $\bar{M}_w$ of only 16 000. This means that the actual number of HML molecules in each of the XL is quite small.

In using the Mark–Houwink equation, $[\eta] = KM^a$, the value of a was found to be about 1.6, whereas alkali lignin and lignosulphonates believed to have spherical conformations had values of 0.1–0.5. In addition, linear and branched polymers like cellulose and xylan had a values of between 0.75 to 1.15 (29). The high value of a obtained suggests that the extracted lignin has a linear rather than a spherical conformation.

Discussion

From MD studies, it has been shown that increasing amounts of soluble HML material are being extracted with increasing autohydrolysis time up to the region of maximum lignin extractability. This phenomenon of successively extracting more higher molecular weight material as the cook proceeds is a common observation for both alkaline and acid delignification processes (30–32) and oxidized lignin (33). However, different interpretations have been placed on such MD patterns from chemically prepared lignin. The presence of a maximum over the time range considered suggests that the depolymerization/repolymerization reactions of lignin during autohydrolysis are taking place via a consecutive series of reactions, with the existence of an intermediate species which can be maximized. Alkaline nitrobenzene oxidation studies have also shown that XL increases in degree of condensation with autohydrolysis time. This implies that the soluble HML, although still extractable, is highly condensed, formed probably from the condensation of low molecular weight depolymerized lignin. This is related to the disappearance of the initial LML peak, which is associated with the appearance of the maximum of the HML peak. It is thus seen that repolymerization of lignin can be regarded as a succession of condensations leading eventually to the formation of insoluble residual lignin. Thus, soluble HML is postulated to be the intermediate species in the formation of insoluble residual lignin from depolymerized lignin. Scheme 1 illustrates the postulated pathway of depolymerization/repolymerization reactions of lignin during autohydrolysis.

As has been established by various authors (34–37), cleavage of lignin bonds under acidic conditions involves the formation of resonance-stabilised carbonium ions. In addition, carbonium ions are also strong electrophiles with the ability to participate in substitution forming carbon–carbon bonds with the aromatic C-1 or C-6 atom. Lignin depolymerization and condensation can be viewed as proceeding via a carbonium ion mechanism resulting in the observed extractability and repolymerization.

In autohydrolysis studies (1), aspen lignin has been found to be the most readily extractable compared with lignin of other hardwoods and softwoods studied. Aspen lignin is almost unique in that it contains large amounts of *p*-hydroxybenzoate groups, up to about 10% by weight (38–40). The ease of extractability of aspen lignin may thus be related to the presence of these *p*-hydroxybenzoate groups. *p*-Hydroxybenzoic acid, from hydrolysis of the *p*-hydroxybenzoate groups, can act as a blocking agent, preventing the self-condensation of lignin carbonium ions to-

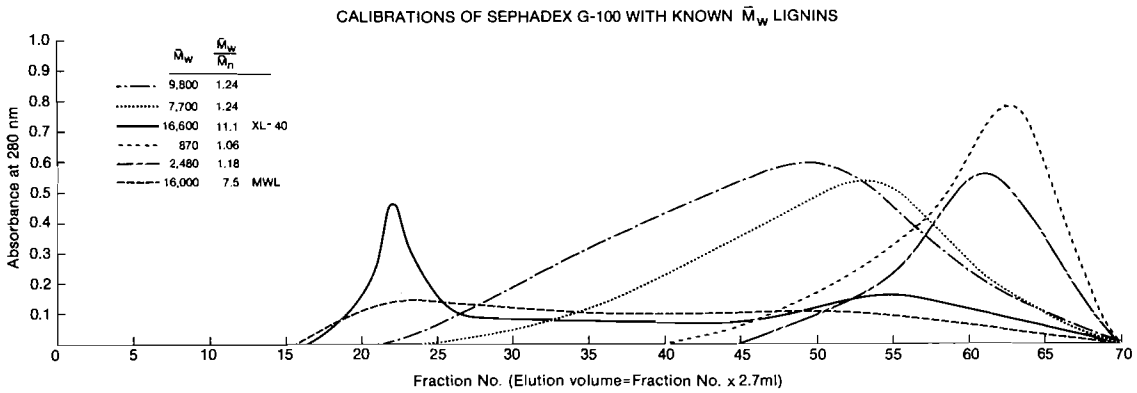

FIG. 5. Calibrations of Sephadex G-100 with known $\overline{M}_w$ lignins.

TABLE 2. Intrinsic viscosity η, $\overline{M}_n$, $\overline{M}_w$, and polydispersity of milled wood lignin (MWL) and extracted lignin (XL)

Sample no.	η dL/g (in DMF)	No. average molecular weight $\overline{M}_n$	Weight average molecular weight $\overline{M}_w$	Polydispersity $\overline{M}_w/\overline{M}_n$
MWL	—	2 120	16 000*	7.5
XL-5	0.082	1 320	10 900	8.3
XL-10	0.109	1 370	13 100	9.6
XL-20	0.133	1 480	14 800	10.0
XL-30	0.162	1 560	16 800	10.8
XL-40	0.159	1 490	16 600*	11.1
XL-60	0.124	1 390	14 200	10.2
XL-90	0.072	1 090	10 000	9.2
XL-120	0.050	970	8 000*	8.2

*$\overline{M}_w$ for MWL, HML, XL-40, and XL-120 were determined by Mr. W. Q. Yean on the Beckman Spinco Model E Ultracentrifuge. $\overline{M}_w$ for HML was 196 000. The other $\overline{M}_w$ were calculated from the Mark–Houwink equation $[\eta] = KM^a$, using K and a values derived by solving the simultaneous equations for samples XL-40 and XL-120.

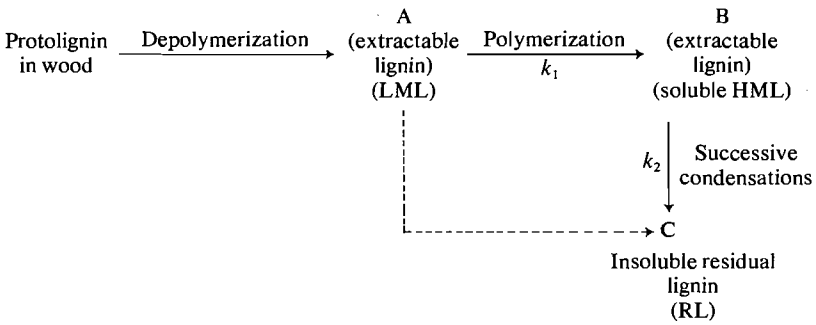

SCHEME 1. Representation of depolymerization/repolymerization reactions of lignin. The soluble HML passes through a maximum. LML = low molecular weight lignin, $\overline{M}_w < 8\,000$; soluble HML = soluble high molecular weight lignin, $\overline{M}_w \sim 196\,000$.

wards the formation of insoluble residual lignin, thereby allowing the lignin to be extractable. Wayman and Lora (2) have shown that during autohydrolysis, some aromatic additives acting as blocking agents are effective in preventing self-condensation to insoluble lignin and enhance the extractability of the lignin.

Experimental

(a) Preparation of Extracted Autohydrolysis Lignin

The wood used in these experiments was aspen. Extractive-free wood meal (EWM) was prepared according to TAPPI standard T12 m-59. Autohydrolysis of 30 g of EWM for each run (with a wood:water ratio 1:1) was carried out in 300 mL pressure vessels equipped with pressure gauge, thermocouple and safety valve. The pressure vessel was heated in a silicone

oil bath maintained at 195°C. Preheating time as indicated by the thermocouple and pressure gauge was 30 min. After heating for a further 5 min to 2 h, the pressure vessel was cooled by immersing in ice–water, the contents removed, washed with boiling water, and filtered. Washing was repeated 3 times to ensure complete removal of hemicellulose and its degradation products.

The lignocellulosic residue (R) was air-dried and batch extracted with 10 times its weight of 90% dioxane at 70°C for 1 h. After three extractions, the residue was thoroughly washed with boiling water, air-dried, and its Klason lignin content determined. This value represented the residual lignin left in the pulp after autohydrolysis. The three extracts, containing the extracted lignin, were combined and concentrated in a Buchi Rotovapor-R vacuum evaporator to approximately 1/10 its original volume. To displace the initial water present in the solvent system, pure dioxane was added and the solution concentrated further until a final solution of approximately 10% lignin in dioxane was obtained.

Purification was carried out by precipitating the above solution dropwise into anhydrous diethyl ether, stirring vigorously. The precipitation was done in stages. To 200 mL of ether 5–6 mL of solution was added, the solution centrifuged at 1500 rpm for 5 min, the supernatant decanted, 200 mL of fresh ether added, and a further 5–6 mL of solution added. The procedure was repeated until all the solution was precipitated. The precipitate was washed twice with fresh ether, twice with pure benzene, and twice with low-boiling petroleum ether. The lignin, in the form of a brown powdery material, was air-dried to remove traces of petroleum ether and stored in a vacuum desiccator. The supernatant ether was collected and vacuum evaporated to recover the low molecular weight lignin components. The yields of both products were determined.

(b) Elemental Analyses, Methoxyl Determination of Extracted Lignin, and % Carbohydrate in the Extracted Lignin

Lignin samples were analysed for C, H, and methoxyl content by Schwarzkopf Microanalytical Laboratory, Inc., New York.

The % carbohydrate in the extracted lignin was determined by measuring the amount of sugar present in the final hydrolysis liquor after Klason analysis. Two methods of sugar analysis were used: (*i*) dinitrosalicyclic acid (41) and (*ii*) phenol – sulphuric acid method (42).

(c) Analytical Gel Permeation Chromatography

The column used for molecular weight distribution (MD) analysis consisted of Sephadex G-100 swollen in dimethyl sulphoxide, packed in a Pharmacia solvent resistant glass column SR 25/45 with two polytetrafluoroethylene (PTFE) flow adaptors attached to the column ends. A Marriotte flask served as solvent reservoir as well as maintaining the elution rate through the column at 18 mL/h by adjusting its height. Sample injection was via a Sarle sample applicator valve assembly with a sample loop of 0.3 mL. The concentration of the sample injected was 3.5 mg/mL. The column was run on upward flow. The column effluent was continuously monitored at 280 nm with an ISCO UA-5 Absorbance Monitor (Instrumentation Specialties Co.) equipped with a micro-flowcell of capacity 10 μL and 5 mm light path length. The fractions were collected in a 2.7 mL siphon which had a manometer electrode assembly which triggered an event marker producing a spike of the chromatogram each time the siphon was filled and the contents dumped into a fraction collector. A complete chromatogram giving the MD pattern was obtained after 11 h.

(d) Preparative Gel Permeation Chromatography

For preparation of narrow molecular weight fractions a Pharmacia K50/100 column with two PTFE flow adaptors, packed with Bio-Gel A 0.5 m 50–100 mesh was used. The Bio-Gel A was obtained pre-swollen in 0.001 *M* Tris-EDTA buffer. The buffer was displaced in stages by 25%, 50%, and finally 75% dioxane. The preparative column was run with 75% dioxane as eluant for convenience of recovery of the lignin after fractionation. The flow and monitoring scheme was essentially the same as for the analytical column, except that the injection was via a Pharmacia SA-5 sample applicator and a 10 mL siphon was used.

Samples of approximately 100–120 mg of XL-40 in 1.5 mL of 75% dioxane were run through the column until sufficient material was collected for the high molecular weight peak (fractions 19–21). Flow rate was maintained at 58 mL/h and total elution time was 7 h. The collected fraction labelled high molecular weight lignin (HML) was concentrated in a vacuum evaporator and recovered as in (*a*) for lignin purification. The sample was used for weight average molecular weight determination.

(e) Beckman Spinco Model E Analytical Equilibrium Ultracentrifuge, $\overline{M}_w$

The weight average molecular weight of samples MWL, XL-40, XL-120, and HML were determined using the short-column sedimentation equilibrium technique on a Beckman Spinco Model E analytical ultracentrifuge. The determinations were carried out by Mr. W. Q. Yean at McGill University, using a reported procedure (43, 44).

(f) Ultraviolet Absorptivity at 280 nm

A Unicam SP 1700 spectrophotometer was used to determine the extinction coefficients of milled wood lignin (MWL) and XL at 280 nm. The samples were dissolved in DMSO and the spectra obtained relative to the solvent.

(g) Determination of Number Average Molecular Weight, M_n and Intrinsic Viscosity, η

The number average molecular weight of MWL and XL were determined using a Hewlett-Packard Model 302B vapor pressure osmometer. Samples in the concentration range 8–60 g/L in dimethyl formamide were run and the average of triplicate determinations at each concentration was taken. The dimethyl formamide was dried over anhydrous sodium sulphate and distilled before use. The instrument was calibrated using benzil (MW 210). An experimental value of 354 for curcumin was obtained giving a 4% error. The working temperature was 80°C and steady state was reached after 6 min. The molar concentration constant for the system was 12.35.

The intrinsic viscosities of the extracted lignin were determined using an automatic recording capillary viscometer (45). Measurements were made in dimethyl formamide at 25°C with solutions of about 0.1 g/dL concentration.

Acknowledgments

The authors wish to thank the National Research Council of Canada for both the award of an NRCC postgraduate scholarship to one of them (M.G.S.C.) and for a research grant which supported this investigation. The authors also wish to thank Mr. J. H. Lora for the sample of milled wood lignin used in this work, and for helpful discussion of the results.

1. J. H. LORA and M. WAYMAN. Tappi, **61** (6), 48 (1978).
2. M. WAYMAN and J. H. LORA. Tappi, **61** (6), 55 (1978).
3. A. KLEMOLA and G. A. NYMAN. Pap. och. Trä. **10**, 595 (1966).
4. B. W. WILSON. Aust. J. Council Sci. Ind. Res. **20**, 258 (1947).
5. H. HOSAKA, H. SUZUKI, A. NUNOMURA, T. UESUGI, H. TAKAHASHI, M. HONGO, and I. HASEGAWA. Report of the Hokkaido Forest Products Research Institute, No. 15, 32 (1959).
6. D. F. ROOT, J. F. SAEMAN, J. F. HARRIS, and W. K. NEILL. For. Products J. **9**, 158 (1959).
7. K. SCHONEMANN. *In* Chemical reaction engineering. Vol. 1. *Edited by* K. Rietema. *In* The international series of monographs on chemical engineering. Pergamon Press, London. 1957. pp. 171–175.
8. D. MENEGHINI and I. SORGATO. Ric. Sec. Progr. Teen. **13**, 756 (1943).
9. A. W. SOHN and P. O. LENEL. Das Pap. **3**, 109 (1949).
10. O. C. BOCKMAN. Nor. Skogind. **16**, 320 (1962).
11. A. P. DUNLOP and F. N. PETERS. The furans. Reinhold Publishing Corp., New York. 1953.
12. P. TRAYNARD and A. EYMERY. Holzforschung, **9** (6), 173 (1955).
13. G. RICHTER. Tappi, **38**, 129 (1955).
14. G. RICHTER. Tappi, **39**, 193 (1956).
15. O. GOLDSCHMID. Tappi, **38**, 728 (1955).
16. D. A. STANEK. Tappi, **41**, 601 (1958).
17. D. J. BRASCH and K. W. FREE. Tappi, **48**, 245 (1965).
18. M. A. MILLETT, A. J. BAKER, and L. D. SATTER. *In* Enzymatic Conversion of Cellulosic Materials: Technology and Applications, Biotechnology and Bioengineering Symposium No. 6. Interscience Publishers, New York. 1976. p. 125.
19. K. LUNDQUIST, B. OHLSSON, and R. SIMONS. Sven. Papperstidn. **80**(5), 143 (1977).
20. J. H. LORA. M.A.Sc. thesis, University of Toronto, Toronto, Ont. 1976.
21. A. KLEMOLA. Suom. Kemistil. B**41**, 83 (1968).
22. J. M. PEPPER and M. SIDDIQUEULLAH. Can. J. Chem. **39**, 1454 (1961).
23. T. I. OBIAGA and M. WAYMAN. J. Appl. Polym. Sci. **18**, 1943 (1974).
24. M. WAYMAN and T. I. OBIAGA. Can. J. Chem. **52**, 2102 (1974).
25. Pharmacia Fine Chemicals. Sephadex: Gel filtration in theory and practice.
26. J. MARTON and T. MARTON. Tappi, **47**, 471 (1964).
27. V. F. FELICETTA, A. AHOLA, and J. L. MCCARTHY. J. Am. Chem. Soc. **78**, 1899 (1956).
28. J. GIERER. Sven. Papperstidn. **73**(18), 571 (1970).
29. K. V. SARKANEN and C. H. LUDWIG. Lignins. Wiley Interscience, New York. 1971. pp. 702–705.
30. W. Q. YEAN and D. A. I. GORING. Sven. Papperstidn. **71**, 739 (1968).
31. E. NOKIHARA *et al.* J. Am. Chem. Soc. **79**, 4495 (1957).
32. B. LEOPOLD. Acta. Chem. Scand. **6**, 64 (1952).
33. H. I. BOLKER, H. E. W. RHODES, and K. S. LEE. J. Agric. Food Chem. **25**, 708 (1977).
34. E. ADLER, K. LUNDQUIST, and G. E. MIKSCHE. Adv. Chem. Ser. **59**, 22 (1966).
35. J. C. PEW. J. Am. Chem. Soc. **74** (11), 2850 (1952).
36. K. LUNDQUIST and R. LUNDGREN. Acta Chem. Scand. **26** (5), 2005 (1972).
37. G. GELLERSTEDT and J. GIERER. Acta Chem. Scand. B**29** (5), 561 (1975).
38. D. C. C. SMITH. J. Chem. Soc. 2347 (1955).
39. I. A. PEARL, D. L. BEYER, B. JOHNSON, and S. WILKINSON. Tappi, **40**, 374 (1957).
40. J. NAKANO, A. ISHIZU, and N. MIGITA. Tappi, **44**, 30 (1961).
41. G. L. MILLER. Anal. Chem. **3**, 426 (1959).
42. M. DUBOIS, K. GILLIS, J. K. HAMILTON, P. A. REBERS, and F. SMITH. Anal. Chem. **28**, 350 (1956).
43. W. Q. YEAN and D. A. I. GORING. J. Appl. Polym. Sci. **14**, 1115 (1970).
44. A. REZANOWICH, W. Q. YEAN, and D. A. I. GORING. Sven. Papperstidn. **66**, 141 (1963).
45. T. KILP, B. HOUVENAGEL-DEFOORT, W. PANNING, and J. E. GUILLET. Rev. Sci. Instrum. **47** (12), 1496 (1976).
46. R. M. KAY, S. M. STRASBERG, C. N. PETRUNKA, and M. WAYMAN. Abstracts, Annual Meeting American Chemical Society, Miami, 1978.

Spin trapping of the $\cdot CO_2^-$ radical in aqueous medium

JOHN R. HARBOUR AND MICHAEL L. HAIR

Xerox Research Centre of Canada Limited, 2480 Dunwin Drive, Mississauga, Ont., Canada L5L 1J9

Received November 6, 1978

JOHN R. HARBOUR and MICHAEL L. HAIR. Can. J. Chem. 57, 1150 (1979).

The $\cdot CO_2^-$ radical has been generated by photolysis of a solution of sodium peroxydisulfate containing sodium formate and by hydrogen abstraction using $TiCl_3$ and H_2O_2 in the presence of sodium formate. In both cases, the inclusion of DMPO resulted in the formation of a spin adduct with $a^N = 15.8$ G, $a_\beta^H = 19.1$ G, and $g = 2.0058$ which is assigned to the $\cdot CO_2^-$ adduct. In addition the DMPO adduct of $SO_4^{-\cdot}$ is presented. Finally, it is shown that DMPO can react with anionic radicals and that the resultant spin adducts are themselves highly dissociated.

JOHN R. HARBOUR et MICHAEL L. HAIR. Can. J. Chem. 57, 1150 (1979).

On a pu généré le radical $\cdot CO_2^-$ en photolysant une solution de peroxydisulfate de sodium contenant du formate de sodium et par enlèvement d'hydrogène faisant appel à du $TiCl_3$ et du H_2O_2 en présence de formate de sodium. Dans chacun des cas, l'inclusion de DMPO conduit à la formation d'un adduit de spin avec $a^N = 15.8$ G, $a_\beta^H = 19.1$ G et $g = 2.0058$ que l'on attribue à l'adduit du $\cdot CO_2^-$. De plus on présente l'adduit du $SO_4^{-\cdot}$ avec le DMPO. Finalement on montre que le DMPO peut réagir avec des radicaux anioniques et que les adduits de spin qui en résultent sont eux-mêmes très dissociés.

[Traduit par le journal]

Introduction

The use of spin trapping has been steadily increasing during the past few years. The technique has found application in biological systems (1–3), pigment dispersions (4, 5), polymer systems (6), and studies of chemical reaction mechanisms (7). One particular spin trap, 5,5′-dimethyl-1-pyrroline-1-oxide (DMPO) which was introduced by Janzen and Liu (8) in 1973, has been found to be particularly useful since the hyperfine splitting constants of the adducts depend strongly on the nature of the radical trapped and exhibit sufficient variation to make identification of different radicals relatively easy. In addition this trap is extensively soluble in water (as well as other solvents) and is uncharged.

The utility of the trapping technique depends to a large extent on the number of radical adducts which have been characterized in terms of the hyperfine splitting constants. Janzen and Liu (8) have compiled a list of various radical adducts of DMPO in benzene. However, in relation to the biological applications of spin trapping, it is important to consider the aqueous environment and the types of radicals which may exist in and derive from water. The initial effort in this area identified the formation of the hydroxyl ($\cdot OH$) and superoxide (O_2^-) radical adducts of DMPO (9). This was followed by the utilization of these results in a photochemical study of chlorophyll in micelles (2) and of both chloroplasts (1) and chromatophores (2). We have now extended this list to include the $\cdot CO_2^-$ radical which derives from the biologically important carbon dioxide (CO_2). This radical was generated by two independent means and trapped with DMPO in aqueous medium.

Experimental

The electron spin resonance (esr) and photochemical equipment have been previously described (9). DMPO was synthesized and purified prior to use by vacuum distillation. Sodium persulfate ($Na_2S_2O_8$), sodium formate, hydrogen peroxide, and titanium trichloride (15% w/v) were used as received from BDH Chemicals Ltd. The water was double distilled from an all glass apparatus.

Results and Discussion

Chawla and Fessenden (10) have shown that photolysis of an aqueous peroxydisulfate ($S_2O_8^{2-}$) solution in the presence of sodium formate results in the generation of the $\cdot CO_2^-$ radical. The $SO_4^{-\cdot}$ radical anion is initially formed according to reaction [1].

$$[1] \qquad S_2O_8^{2-} \xrightarrow{h\nu} 2SO_4^{-\cdot}$$

This radical is a good one-electron-transfer oxidizing agent. Hence it reacts with formate ion according to reaction [2].

$$[2] \qquad SO_4^{-\cdot} + HCO_2^- \rightarrow HSO_4^- + \cdot CO_2^-$$

This photochemical system can therefore serve as a generator of $\cdot CO_2^-$ radicals.

When DMPO was added to a solution of $S_2O_8^{2-}$ and the system photolyzed, an esr signal was observed which presumably results from the trapping of the $SO_4^{-\cdot}$ radical (see Fig. 1). Large signal intensities ($\sim 10^{-4}$ *M*) could be generated within several

0008-4042/79/101150-03$01.00/0

FIG. 1. The esr spectrum resulting from photolysis of an aqueous $Na_2S_2O_8$ (3×10^{-3} *M*) solution containing DMPO (~1 *M*). The $^{\bullet}OH$ adduct (1:2:2:1) is superimposed upon the $SO_4^{-\bullet}$ spectrum (see text).

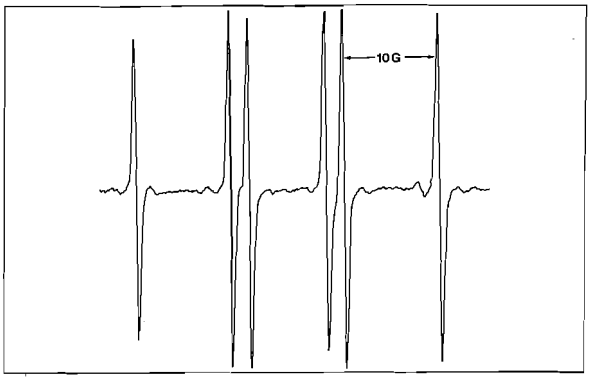

FIG. 2. The esr spectrum of the $^{\bullet}CO_2^-$ adduct of DMPO generated by $TiCl_3$ and H_2O_2.

seconds of photolysis and this observation can be contrasted to the absence of any signal under similar photolysis of a DMPO blank. This signal has $a^N = 13.9$ G, $a_\beta^H = 10.1$ G, $a_{\gamma_1}^H = 1.3$ G, $a_{\gamma_2}^H = 0.9$ G, and $g = 2.0062$. This radical is rather unstable decaying under these conditions with a decay time, τ, (time to 1/e of the initial value) of ~20 s.

As can be seen from Fig. 1, a small amount of $^{\bullet}OH$ radical adduct could also be detected. This radical has also been observed by Chawla and Fessenden (10) when $S_2O_8^{2-}$ was irradiated in the presence of the fumarate spin trap. They argued that $^{\bullet}OH$ results from the reaction

[3] $$SO_4^{-\bullet} + OH^- \rightarrow SO_4^{2-} + {}^{\bullet}OH$$

The hydroxyl radical adduct of DMPO is quite stable under these conditions as contrasted to the $SO_4^{-\bullet}$ adduct. Hence the apparent equal production of both adducts seen in Fig. 1 only reflects the fact that much of the $SO_4^{-\bullet}$ adduct has decayed away.

Addition of sodium formate to the solution yields a new esr signal upon irradiation (Fig. 2). This signal has $a^N = 15.8$ G, $a_\beta^H = 19.1$ G, and $g = 2.0058$ and is assigned to the $^{\bullet}CO_2^-$ adduct which is formed according to reaction [2]. The $SO_4^{-\bullet}$ adduct signal is much diminished under these conditions and can be reduced further by additional formate. This demonstrates that the $^{\bullet}CO_2^-$ results from a reaction with $SO_4^{-\bullet}$ and in fact competes with the DMPO for the available $SO_4^{-\bullet}$ radicals.

A second method for production of $^{\bullet}CO_2^-$ exists and has been used to confirm the assignment. The system Ti^{3+}–H_2O_2 is known (11) to oxidize formate in both acidic and basic media. The hydroxyl radical is first produced

[4] $$Ti^{3+} + H_2O_2 \rightarrow 2{}^{\bullet}OH$$

and this subsequently reacts with the formate

[5] $$^{\bullet}OH + HCO_2^- \rightarrow H_2O + {}^{\bullet}CO_2^-$$

In acidic solutions the $^{\bullet}CO_2H$ radical is formed whereas in neutral or basic solutions the $^{\bullet}CO_2^-$ radical is generated.

Addition of Ti^{3+} into a solution of H_2O_2 containing DMPO results in a strong $^{\bullet}OH$ radical adduct signal. However, when formate is initially present, an esr signal is generated which is identical to that shown in Fig. 2. Hence, as expected from reaction [4], this system produces the $^{\bullet}CO_2^-$ adduct.

Both of these independent methods of generation of the $^{\bullet}CO_2^-$ radical lead to the same signal in the presence of DMPO. This strongly suggests that the radical being observed is the adduct of the $^{\bullet}CO_2^-$ radical. Chawla and Fessenden (10) have demonstrated that the $^{\bullet}CO_2^-$ radical is a carbon-centered radical with $g = 2.00045$ and $\Delta H_{pp} \sim 2.3$ G. The signal we assign to the $^{\bullet}CO_2^-$ adduct reflects that the radical trapped was indeed a carbon-centered radical. This can be deduced from the facts that a_β^H is quite large, no a_γ^H is observed and $g = 2.0058$.

It is worth noting that the spin trap DMPO is reacting with ionic radicals in this work. The pK of $^{\bullet}CO_2H$ is less than 2 which implies that essentially all of the radical is present in the ionized form ($^{\bullet}CO_2^-$). Similarly the $SO_4^{-\bullet}$ radical is an anion. The present study therefore demonstrates that anionic radicals can be trapped with DMPO. This may also have been the case with O_2^- in water (4) but the fact that it has a pK of 4.6 leads to uncertainty as to which species was actually being trapped. Finally, once these adducts are formed, a new equilibrium is established. For example, the spin adduct of CO_2^- is a carboxylic acid. Since this acid derives from a salt, the spin adduct is present as the salt of a weak acid. Assuming a dissociation constant of $\sim 1 \times 10^{-5}$ and a concen-

tration of $\sim 1 \times 10^{-4}$ M, the spin adduct will be predominantly (>99%) in the ionized state.

Acknowledgements

We thank Professor James R. Bolton and the University of Western Ontario for the use of the esr facilities.

1. J. R. HARBOUR and J. R. BOLTON. Biochem. Biophys. Res. Commun. **52**, 803 (1975).
2. J. R. HARBOUR and J. R. BOLTON. Photochem. Photobiol. **38**, 231 (1978).
3. A. N. SAPRIN and L. H. PIETTE. Arch. Biochem. Biophys. **180**, 480 (1977).
4. J. R. HARBOUR and M. L. HAIR. J. Phys. Chem. **81**, 1791 (1977).
5. J. R. HARBOUR and M. L. HAIR. J. Phys. Chem. **82**, 1397 (1978).
6. T. SATO and T. OTSU. Makromol. Chem. **178**, 1941 (1977).
7. E. G. JANZEN. Acc. Chem. Res. **4**, 31 (1971).
8. E. G. JANZEN and J. I-P. LIU. J. Magn. Reson. **9**, 510 (1973).
9. J. R. HARBOUR, V. CHOW, and J. R. BOLTON. Can. J. Chem. **52**, 3549 (1974).
10. O. P. CHAWLA and R. W. FESSENDEN. J. Phys. Chem. **79**, 2693 (1975).
11. R. O. C. NORMAN and B. C. GILBERT. Adv. Phys. Org. Chem. **5**, 53 (1967).

Formation of aminals from amines via Pummerer rearrangement

SUMAN RAKHIT, MICHAEL GEORGES, AND JEHAN F. BAGLI
Chemistry Department, Ayerst Laboratories, Montreal, P.Q., Canada H3C 3J1

Received November 27, 1978

SUMAN RAKHIT, MICHAEL GEORGES, and JEHAN F. BAGLI. Can. J. Chem. **57**, 1153 (1979).

Reaction of 2-amino-3-nitropyridine with acid chlorides in the presence of dimethyl sulfoxide and a tertiary base, such as pyridine, unexpectedly yielded the aminal *N,N'*-bis(3-nitro-2-pyridinylimino)methylene **5**. A similar aminal **6** formed when 2-amino-5-nitropyridine was treated under the same conditions. However, simple aminopyridines such as 2-aminopyridine or 2-amino-6-methylpyridine gave only the 2-*N*-methylenethiomethyl derivatives. It was proved that the aminals are formed by the attack of a suitable base on the *N*-methylenethiomethyl intermediates with expulsion of methyl mercaptan. The formation of these unusual aminals may be explained to be taking place via a Pummerer type rearrangement.

SUMAN RAKHIT, MICHAEL GEORGES et JEHAN F. BAGLI. Can. J. Chem. **57**, 1153 (1979).

La réaction de l'amino-2 nitro-3 pyridine avec des chlorures d'acide en présence de DMSO et d'une base tertiaire comme la pyridine conduit d'une façon surprenante à l'aminal, *N,N'*-bis(nitro-3 pyridinyl-2 imino)méthylène (**5**). Il y a formation d'un aminal semblable (**6**) lorsqu'on fait réagir l'amino-2 nitro-5 pyridine dans les mêmes conditions. Toutefois des aminopyridines simples comme l'amino-2 pyridine ou l'amino-2 méthyl-6 pyridine ne conduisent qu'à des dérivés *N*-méthylènethiométhyles-2. On a prouvé que les aminals se forment par une attaque d'une base appropriée sur des intermédiaires *N*-méthylènethiométhyles avec l'expulsion de méthylmercaptan. La formation de ces aminals surprenants peut être expliquée par une transposition du type Pummerer.

[Traduit par le journal]

Activation of DMSO (dimethyl sulfoxide) by a variety of electrophiles such as acetic anhydride and related compounds is well documented (1). The intermediate complex **1** is known to decompose via a Pummerer rearrangement to yield an acyloxsulfonium salt of type **2**. These intermediates readily react with nucleophile generated from alcohols leading to thiomethyl ethers (2). Analogous reaction of the reactive intermediate **2** in the presence of an amine would be expected to yield hemithiomethyl aminals. However, such compounds have hitherto not been reported.

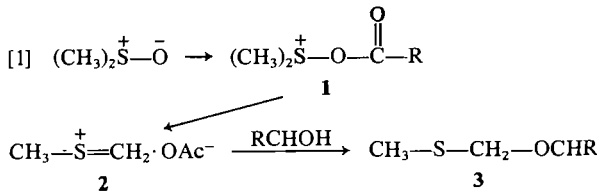

In a synthetic programme involving acylation of aminopyridines, 2-amino-3-nitropyridine was reacted with ethyl oxalyl chloride in pyridine at room temperature in the presence of DMSO as a cosolvent. Surprisingly, the desired oxamate represented only the minor component of the reaction mixture. The major product obtained from this reaction was crystallized from acetone (mp 198–200°C; $C_{11}H_{10}N_6O_4$, *m/e*: 290 (M^+)). The nmr spectrum in DMSO-d_6 showed six aromatic protons at δ 6.8–8.3 and two methylene protons of an aminal at δ 5.4 (t, J = 5.5 Hz) that collapsed to a singlet after D_2O exchange. The ir spectrum showed no carbonyl absorption. The above spectral data could be best accommodated by the structure **5**. This structure was further confirmed by X-ray crystallographic studies[1] and is represented as in Fig. 1*a*.

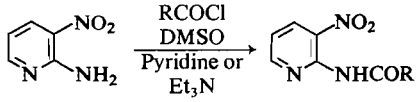

minor
4

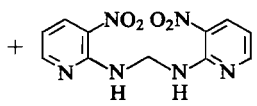

major
5

To test the scope of this unusual reaction, several 2-aminopyridines were allowed to react under the same conditions. 2-Amino-5-nitropyridine gave the aminal **6** (mp 267–268°C; $C_{11}H_{10}N_6O_4$, *m/e* 290 (M^+)). In contrast, 2-aminopyridine and 2-amino-6-methylpyridine yielded the hemithiomethyl aminal derivatives **7** (mp 61–63°C; $C_7H_{10}N_2S$, *m/e* 154 (M^+))

[1]The structure was determined by three dimensional X-ray crystallography by Drs. A. W. Hanson and C. Huber of the National Research Council of Canada, Ottawa. Details will be published elsewhere. Further information is obtainable from A. W. Hanson.

0008-4042/79/101153-04$01.00/0

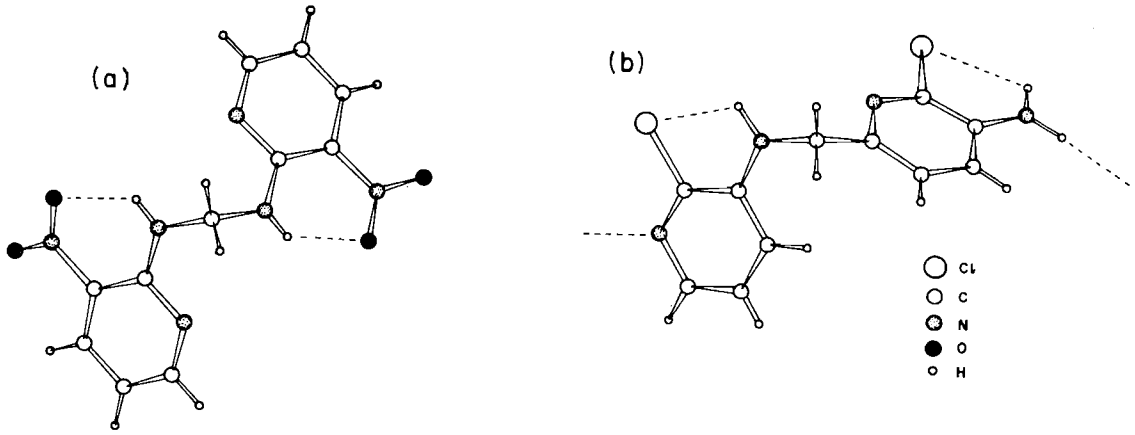

FIG. 1. Perspective view of (*a*) compound **5** and (*b*) compound **15**.

and **8** (oil; $C_8H_{12}N_2S$, *m/e* 168 (M^+)) respectively, along with some acylated products.

The absence of the aminal in the reaction of DMSO – acid chloride with 2-aminopyridine or 2-amino-6-methylpyridine suggested that the hemithiomethyl aminals were the progenitors in the formation of the aminal. When a time course study was performed of the reaction of 2-amino-3-nitropyridine and DMSO – ethoxalyl chloride in either DMSO or CH_2Cl_2 in the presence of Et_3N, and the reaction quenched at half-time, it was possible to isolate the corresponding hemithiomethyl aminal derivative **9** (mp 90–92°C; $C_7H_9N_3O_2S$, *m/e* 199 (M^+); nmr DMSO-d_6 δ: 2.15 (s, —SCH_3), 4.65 (d, N—CH_2—S, J = 7 Hz collapsing to a singlet after exchange with D_2O). This intermediate disappeared in time with the corresponding increase in the yield of the aminal at the end of the reaction. Also, when the isolated hemithiomethyl aminal **9** was heated at 80°C with 2-amino-3-nitropyridine in DMSO, the aminal **5** was obtained in quantitative yield.

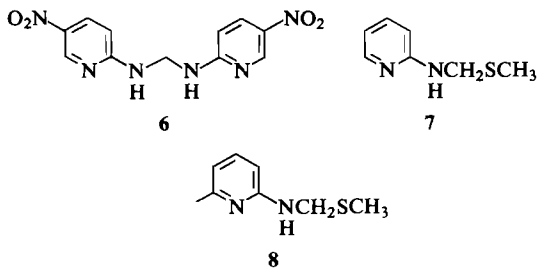

6 **7** **8**

The establishment of the precursor of aminal formation in this reaction suggested its potential utility for the synthesis of mixed aminals using various combinations of hemithiomethyl aminal derivatives and amines. When compounds **7** or **8** were treated with 2-amino-3-nitropyridine in DMSO or CH_2Cl_2 in the presence or absence of Et_3N at 80°C, no mixed aminal was formed. The products were identified as **9** and **5**. However, when the *N*-methylenethiomethyl derivative **10** was allowed to react with 2-amino-3-nitropyridine under the conditions described above, the corresponding mixed aminal **11** (mp 212–214°C; $C_{11}H_{10}N_6O_4$, *m/e* 290 (M^+)) was obtained in 30% yield.

Formation of the hemithiomethyl aminal **9** and

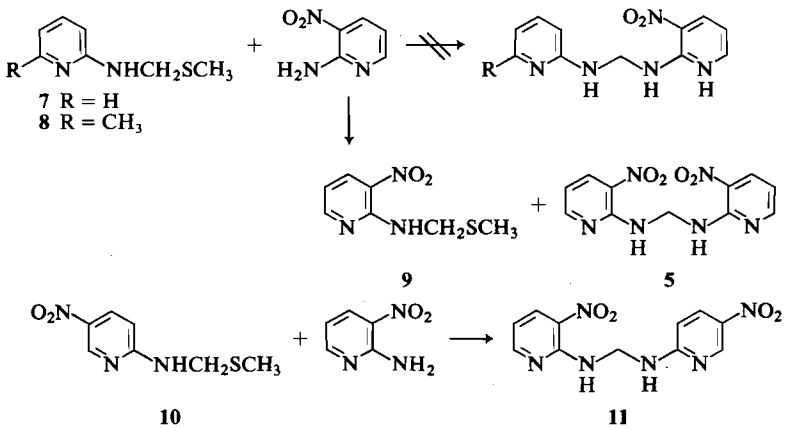

10 **11**

aminal **5** in the above reaction must follow a pathway similar to that reported for the formation of methylenethiomethyl ethers **3**. Thus the intermediate **2**, must be quenched by a molecule of amine to generate the hemithiomethyl aminal. The thiomethyl compound must then react with amine to lead to aminal and methyl mercaptan. The second step appears to be dependent on the base strength of the attacking and leaving nucleophile as demonstrated by the reaction of **7** to **9**.

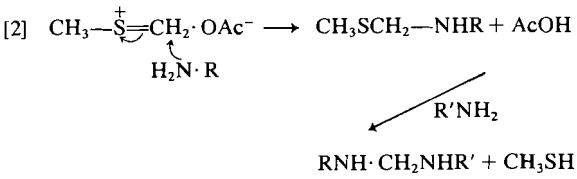

On the other hand, when 2-chloro-3-aminopyridine was treated with DMSO – ethoxalyl chloride in DMSO containing Et_3N, it produced the methylenethiomethyl derivative **12**, the acylated product **13**, and a small amount of a compound (mp 217–219°C; $C_{11}H_{10}N_4Cl_2$, *m/e*: 268, 270, 272 (M^+, $M^+ + 2$, $M^+ + 4$)). The nmr spectrum showed only five aromatic protons, one of them being a quartet at 7.56 ($J_1 = 4.5$ and $J_2 = 1.5$ Hz). This precludes the structure **14**, the expected product formed similar to **5**. It also showed three (2 + 1) exchangeable protons

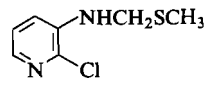

12

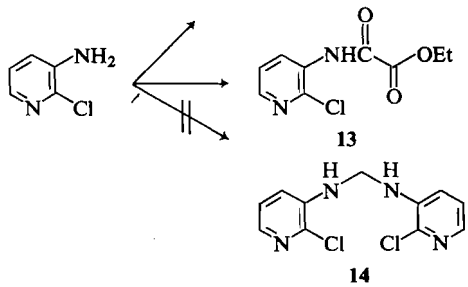

13

14

attributable to NH protons and a two proton doublets for CH_2NH (δ 4.41 (2H, d, $J = 6$ Hz)) collapsing to a singlet after D_2O exchange; ir ($CHCl_3$) ν: 3495, 3439, and 3400 cm^{-1}. These data strongly suggested structure **15** for the new compound. This product could be obtained in better yield (30%) by heating the methylenethiomethyl derivative **12** with the hydrochloride salt of the base in DMSO at 80°C for 10 min. The structure of **15** was finally established by X-ray crystallography[1] and is represented in Fig. 1*b*.

Acylation of **15** by acetic anhydride in methanol yielded the monoacetate **16** (mp 169–171°C; $C_{13}H_{12}N_4OCl_2$, *m/e*: 310, 312, 314 (M^+, $M^+ + 2$, $M^+ + 4$)).

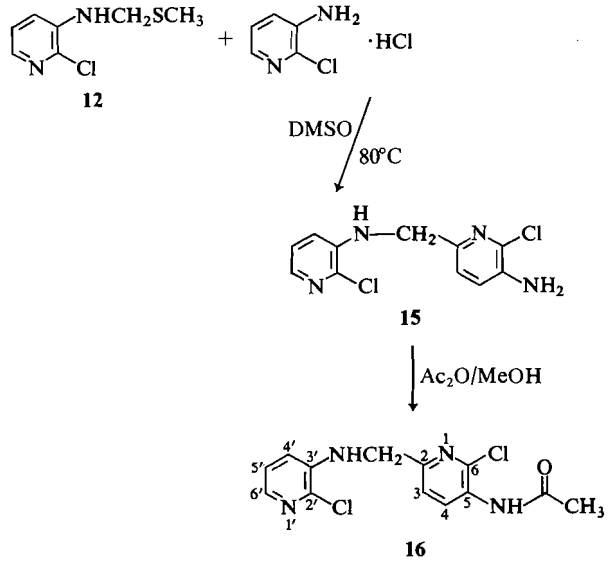

16

The nmr spectrum of **16** was very informative: it showed three proton singlets at δ 2.12 (—CH_3CO), a two-proton doublet at δ 4.41 for CH_2NH, collapsing to a singlet after D_2O exchange. The five aromatic protons could be assigned as follows according to their splitting patterns. Two *ortho*-coupled protons at δ 7.25 (H3) and 8.03 (H4) ($J = 8.5$ Hz), one proton (H5′) as doublet of a doublet at δ 7.10 ($J_{5'6'} = 4.5$, $J_{5'4'} = 8$ Hz) one proton (H6′) as two doublets (*ortho* and *meta* coupled) at 7.56 ($J_{5'6'} = 4.5$, $J_{4'6'} = 1.5$ Hz). These data are clearly indicative of structure **16**, and hence the structure of **15** follows from them.

Experimental

Melting points were determined in a Thomas Hoover-Unimelt apparatus and are uncorrected. Infrared (ir) spectra were recorded on a Perkin Elmer model 225 spectrophotometer in chloroform solution or as a mull. The proton magnetic spectra (^{1}Hmr) were measured on a Varian CFT-20 spectrometer using tetramethylsilane as internal standard. Mass spectra (ms) were determined on a LKB 9000-S spectrometer.

N,N′-Bis(3-nitro-2-pyridinyl)methanediamine (5)

Ethoxalyl chloride 1.37 g (0.01 mol) was added slowly to cold dimethyl sulfoxide (10 mL). This mixture was then added to a solution of 2-amino-3-nitropyridine 1.36 g (0.01 mol) in dimethyl sulfoxide (10 mL). The reaction mixture was allowed to stir at room temperature for a period of 18 h, when tlc showed disappearance of the starting material. The mixture was poured into ice water and the resulting precipitate was collected, washed with water and air dried to give 1.4 g of the desired product (98% yield). A portion was crystallized from acetone, mp 198–200°C; ^{1}Hmr (DMSO) δ: 5.4 (t, 2H, $J = 5.5$ Hz, $HNCH_2NH$, collapsing to singlet after exchange), 6.8–8.3 (m, 6H, aromatic); ir (mull) ν_{max}: 3420 (NH), 1505, and 1350 cm^{-1} (NO_2); ms (170°C) *m/e* 290 (M^+). *Anal.* calcd. for $C_{11}H_{10}N_6O_4$: C 45.52, H 3.45, N 28.97; found: C 45.49, H 3.37, N 29.25.

N-[(Methylthio)methyl]-2-pyridineamine (7)

Ethoxalyl chloride (6.8 g) was added to cold dimethyl

sulfoxide (4.0 g). The resulting mixture was then added to a solution of 2-aminopyridine (4.7 g) in 200 mL of benzene containing triethylamine (5 g). The mixture was heated under reflux for a period of 3 h. It was cooled and washed successively with cold 2 *N* HCl and water, dried over anhydrous sodium sulfate, and filtered. Removal of solvent *in vacuo* yielded an oil that was purified by chromatography over silica gel using 5% acetone, methylene chloride as eluant. The appropriate fractions were mixed to yield 2.5 g of desired product; mp 61–63°C; ^{1}Hmr ($CDCl_3$) δ: 2.05 (s, SCH_3), 4.4 (d, J = 6.5 Hz, $NHCH_2$ collapsing to singlet after D_2O exchange), 6.2–7.9 (m, 4H, aromatic); ms *m/e* 154 (M^+). *Anal.* calcd. for $C_7H_{10}N_2O_2S$: C 54.54, H 6.54, N 18.17; found: C 54.53, H 6.70, N 17.99.

*5-Nitro-*N*-[(methylthio)methyl]-2-pyridinamine (10)*

Ethoxalyl chloride (4.08 g) was added to cold dimethyl sulfoxide (2.5 mL). This mixture was added to a solution of 2-amino-5-nitropyridine (4.17 g) in benzene (50 mL) containing triethylamine (4 mL). The mixture was refluxed for a period of 6 h, after which it was washed with water and dried over anhydrous sodium sulfate and filtered. Removal of solvent yielded a mixture of solids that was chromatographed over silica gel using 3% ethyl acetate in methylene chloride as eluant. Appropriate fractions were collected to yield 1.8 g (30% yield) of the desired product; mp > 250°C; ^{1}Hmr (DMSO) δ: 2.15 (s, 3H, SCH_3), 4.45 (d, 2H, J = 7 Hz, NH—CH_2 collapsing to singlet after D_2O exchange), 6.5 (d, 1H, J = 8 Hz, aromatic), 7.9 (dd, 1H, J_1 = 2 Hz, J_2 = 8 Hz), 8.6 (d, 1H, J = 2 Hz, aromatic); ir (mull) ν_{max}: 3420 (NH), 1505, and 1350 cm^{-1} (NO_2); ms *m/e* 199 (M^+). *Anal.* calcd. for $C_7H_9N_3O_2S$: C 42.21, H 4.55, N 21.10; found: C 42.10, H 4.39, N 20.92.

N,N′-*Bis(5-nitro-2-pyridinyl)methane Diamine (6)*

This product was synthesized exactly in the same manner as described for **5** excepting that the reaction mixture was refluxed for 18 h. After the reaction was over, the solution was cooled and poured into ice. The resulting precipitate was collected, washed thoroughly with water and dried. It was further purified by chromatography over silica gel using 5% ethyl acetate – methylene chloride as eluant. The appropriate fractions were mixed to give the desired product in a yield of 70%. It was crystallized from methylene chloride – acetone; mp 267–268°C; ^{1}Hmr (DMSO) δ: 5.4 (t, 2H, J = 5.5 Hz, $NHCH_2NH$, collapsing to singlet after D_2O exchange); ir (mull) ν_{max}: 3420 (NH), 1505, and 1350 cm^{-1} (NO_2); ms *m/e* 290 (M^+). *Anal.* calcd. for $C_{11}H_{10}N_6O_4$: C 45.52, H 3.45, N 28.97; found: C 45.70, H 3.45, N 29.30.

N-*(3-Nitro-2-pyridinyl)*-N′-*(5-nitro-2-pyridinyl)methane Diamine (11)*

A mixture of 2-amino-3-nitropyridine (1.39 g) and 2-*N*-methylenethiomethyl-5-nitropyridine (2.0 g) in 10 mL dimethyl sulfoxide was refluxed for a period of 6 h. After this, the reaction mixture was cooled and poured into ice water. The resulting precipitate was collected, washed thoroughly with water, and air dried. The mixture was chromatographed over silica gel using methylene chloride as solvent. Identical fractions were mixed together to give three products. The first fraction (0.1 g) was identified as 2-*N*-methylenethiomethyl-3-nitropyridine **9**; mp 90–92°C; ^{1}Hmr ($CDCl_3$) δ: 2.1 (s, 3H, SCH_3), 4.3 (d, 2H, $NHCH_2$), 6.5–7.2 (m, 2H, aromatic), 7.9 (dd, 1H, J_1 = 2, J_2 = 8 Hz, aromatic); ms *m/e* 199 (M^+). *Anal.* calcd. for $C_7H_9N_3O_2S$: C 42.21, H 4.55, N 21.10; found: C 42.46, H 4.55, N 21.44.

The second fraction (0.2 g) was identified as the *N,N′*-bis(3-nitro-2-pyridinyl)methane diamine **5**; mp 198–200°C (identical nmr and ir spectra and no depression in melting point on admixture with the authentic sample).

The third fraction (1.1 g) was identified as the desired product; mp 212–214°C; ^{1}Hmr (DMSO) δ: 5.4 (t, 2H, J = 5.5 Hz, $NHCH_2NH$), 6.7–7 (m, 4H, aromatic), 8.2 (dd, 2H, J_1 = 2, J_2 = 9 Hz, aromatic); ms *m/e* 290 (M^+). *Anal.* calcd. for $C_{11}H_{10}N_6O_4$: C 45.52, H 3.45, N 28.97; found: C 45.27, H 3.42, N 28.87.

*2-Chloro-*N*-[(methylthio)methyl]-3-pyridinamine (12)*

To a cooled mixture of dimethyl sulfoxide (5.5 g) and dry tetrahydrofuran (75 mL), acetyl chloride (5.5 g) was added. To this solution triethylamine (14.1 g) and 3-amino-2-chloropyridine (6.4 g) were added successively. The reaction mixture was refluxed for 18 h, after which the solvent was removed under reduced pressure. The residual oil was purified by chromatography over silica gel using 20% ethyl acetate – methylene chloride as eluant, thus giving 8.8 g of the desired product as an oil (yield 93%); ^{1}Hmr ($CDCl_3$) δ: 2.12 (s, 3H, SCH_3), 4.36 (d, 2H, J = 6.6 Hz, $NHCH_2$), 7.06 (m, 2H, aromatic), 7.25 (dd, 1H, J_1 = 4, J_2 = 1.5 Hz, aromatic); ms *m/e* 188 (M^+). *Anal.* calcd. for $C_7H_9N_2SCl$: C 44.56, H 4.77, N 14.85; found: C 45.27, H 4.84, N 14.36.

*5-Amino-*N*-(2-chloro-3-pyridinyl)-6-chloropyridine-2-methanamine (15)*

A solution of 2-chloro-3-*N*-methylenethiomethylpyridine **12** (3.8 g) and 2-chloro-3-aminopyridine hydrochloride (3.3 g) in dimethyl sulfoxide (5 mL) was heated at 80°C for a period of 15 min. The cooled reaction mixture was poured into ether. The ether layer was decanted off and discarded. The resulting oil was washed several times with ether. The residue was chromatographed over silica gel using 20% ethyl acetate in methylene chloride as eluant. Appropriate fractions were mixed together to give 1.7 g of the desired product (30% yield); mp 127–129°C (methylene chloride – hexane); ^{1}Hmr ($CDCl_3$) δ: 4.45 (d, 2H, J = 6 Hz, NH—CH_2), 6.75–7.15 (m, 4H, aromatic), 7.7 (dd, 1H, J_1 = 4.5, J_2 = 1.5 Hz, aromatic); ms *m/e*: 268, 272, 274 (M^+, $M^+ + 2$, $M^+ + 4$). *Anal.* calcd. for $C_{11}H_{10}N_4Cl_2$: C 49.25, H 3.73, N 20.90; found: C 48.93, H 3.73, N 20.90.

*5-Acetamido-*N*-(2-chloro-3-pyridinyl)-6-chloropyridine-2-methanamine (16)*

A solution of **15** (200 mg) in pyridine (5 mL) and acetic anhydride (1.5 mL) was stored at room temperature for a period of 18 h. Excess of anhydride was decomposed by adding methanol under cooling and the mixture was poured into ice water. The resulting precipitate was collected, washed with water, and air dried to give a brown powder that was purified by chromatography over silica gel using 20% ethyl acetate – methylene chloride as eluant. Thus 150 mg of the desired product was obtained (65% yield); mp 169–171°C (methylene chloride – hexane); ^{1}Hmr (DMSO) δ: 2.12 (s, 3H, CH_3CO), 4.41 (d, 2H, J = 6 Hz, $NHCH_2$), 6.85 (dd, 1H, J_1 = 8, J_2 = 1.5 Hz), 7.10 (dd, 1H, J_1 = 8, J_2 = 4.5 Hz), 7.25 (d, 1H, J = 8.5 Hz), 7.56 (dd, 1H, J_1 = 4.5, J_2 = 1.5 Hz), 8.03 (d, 1H, J = 8.5 Hz); ms *m/e*: 310, 312, 314 (M^+, $M^+ + 2$, $M^+ + 4$). *Anal.* calcd. for $C_{13}H_{12}N_4OCl_2$: C 50.32, H 3.87, N 18.06; found: C 50.08, H 3.69, N 18.13.

Acknowledgments

The authors are grateful to Dr. G. Schilling and his associates for the analytical and spectral data.

1. (*a*) J. D. Albright and L. Goldman. J. Am. Chem. Soc. **89**, 2416 (1967); (*b*) J. D. Albright. J. Org. Chem. **39**, 1977 (1974).
2. K. Yamada, J. Kato, H. Nagase, and Y. Hirata. Tetrahedron Lett. 65 (1976).

Oxidation products of *N*-substituted imines and ketone hydrazones in the presence of sodium in ether: new and convenient syntheses of diimines and substituted aryl diazomethanes

B. P. GIRI, G. PRASAD, AND K. N. MEHROTRA

Department of Chemistry, Banaras Hindu University, Varanasi 221005, India

Received September 21, 1978

B. P. GIRI, G. PRASAD, and K. N. MEHROTRA. Can. J. Chem. **57**, 1157 (1979).

Several diimines have been synthesised from the reaction of substituted imines with sodium in dry ether followed by bubbling in oxygen and subsequent protonation. A probable mechanistic route for the formation of products through the dimerisation of initially formed anion radicals is presented and an alternative route, through the dimerisation of radicals formed by hydrogen abstraction from starting imine, has been excluded by substituent labelling experiments. Ketone hydrazones on treatment with sodium in ether and subsequent air oxidation gave substituted diazomethanes in excellent yields (88–95%).

B. P. GIRI, G. PRASAD et K. N. MEHROTRA. Can. J. Chem. **57**, 1157 (1979).

On a synthétisé plusieurs diimines en faisant d'abord réagir des imines substituées avec du sodium dans l'éther anhydre puis en y faisant barbotter de l'oxygène et finalement en protonant. On a présenté un mécanisme probable pour la formation de produits par l'intermédiaire de la dimérisation des radicaux anions qui se forment initialement; on a exclu un autre mécanisme possible impliquant une dimérisation des radicaux formés par l'enlèvement d'hydrogène de l'imine de départ en se basant sur des études impliquant le marquage des substituants. Si l'on traite des hydrazones de cétones par du sodium dans l'éther, puis qu'on oxyde le tout par de l'air, on obtient des diazométhanes substitués avec d'excellents rendements (88–95%).

[Traduit par le journal]

The reductive dimerisation of substituted anils either by the reaction of active metals (Li, Na, and K) in nonaqueous solvents (1) or of aluminium in moist ether (2) has been reported. This procedure has been extended to *N*-substituted imines (3). It was considered necessary to observe the effect of added oxygen before protonation of the sodium salt in the reaction of several substituted imines with sodium in dry ether. In the present paper we describe this modified procedure which leads to a new and more convenient synthetic route to substituted diimines. This one-step method has a distinct superiority over the conventional method, the condensation of 1,2-ethanediamines and carbonyl compounds, as the preparation of 1,2-ethanediamines alone would involve several steps. Similar treatment of ketone hydrazones leads to the formation of substituted diazomethanes in excellent yields.

Results and Discussion

The product mixture obtained with benzaldehyde *N*-benzylimine (**1***a*; Ar = Ar′ = C_6H_5, R = H) was separated by repeated (4–5) fractional crystallisation from ethanol; it consisted of *meso*- and *dl*-*N*,*N*′-dibenzylidene-1,2-diphenylethylenediamine (**2***a*; 17% each). Authentic samples of *meso*- and *dl*-**2***a* were prepared according to the method reported (4) and were identical to the products (ir, nmr, and mp). Catalytic hydrogenation of *meso*- and *dl*-**2***a* gave *meso*- and *dl*-*N*,*N*′-dibenzyl-1,2-diphenyl-1,2-diaminoethane (5), respectively (ir, nmr, and also mp in case of *meso* product, Table 1).

The probable reaction sequence for the formation of *meso*- and *dl*-diimines can be as shown in Scheme 1.

The radical anion formed by an electron transfer from sodium to imine **1***a* dimerises. The dianion may exist in equilibrium with the dicarbanion which may take up 2 molecules of oxygen; loss of hydroperoxide ions would lead to the diimines **2***a*. A similar equilibrium between the amide ion, obtained from aminoalkylsilanes in the presence of traces of *n*-butyllithium, and the isomeric carbanion has been proposed (6). The elimination of hydroperoxide ions has been suggested in the formation of diazomethanes from the reaction of ketone hydrazones with methyl lithium (7).

An alternative route for the formation of diimines (**2***a*) could be through the dimerisation of the intermediate radical formed by a possible hydrogen abstraction from the imine as shown in Scheme 2. This mechanistic route could be tested by labelling experiments.

Benzaldehyde *N*-(*p*)-methylbenzylimine (**1***b*; Ar = C_6H_5, Ar′ = $pCH_3C_6H_4$, and R = H) when simi-

0008-4042/79/101157-05$01.00/0

TABLE 1. Conversion of imines **1** to diimines **2**

Imine 1	Ar	Ar′	R	Product 2 Yield (%)	Melting point (°C)	Molecular formula	Elemental analysis (%) Found C	H	N	Calculated C	H	N
a	C_6H_5	C_6H_5	H	*meso* 17	164–165 (lit. (4) 164–165)	$C_{28}H_{24}N_2$	86.18	6.46	7.06	86.58	6.19	7.22
				dl 17	149–151 (lit. (4) 151–152)		86.24	6.50	6.90			
b	C_6H_5	$pCH_3C_6H_4$	H	*meso* 11	184–185	$C_{30}H_{28}N_2$	86.22	6.56	6.66	86.54	6.73	6.73
				dl 11	172–173		86.16	6.62	6.81			
c	C_6H_5	C_6H_5	C_6H_5	*dl* 45	228–229	$C_{40}H_{32}N_2$	88.63	6.11	5.08	88.89	5.92	5.20
d	$pCH_3C_6H_4$	C_6H_5	C_6H_5	*dl* 45	215–216	$C_{42}H_{36}N_2O_2$	84.00	6.00	4.67	84.12	6.16	4.47
e	$pClC_6H_4$	C_6H_5	C_6H_5	*meso* 10	Liquid	$C_{40}H_{30}N_2Cl_2$	78.83	5.12	4.73	78.95	4.93	4.60
				dl 8	223–224		78.63	4.89	4.73			

larly treated as **1***a* gave two products which were separated by repeated fractional crystallisation and characterised as *meso*- and *dl*-*N*,*N*′-di-*p*-methylbenzylidene-1,2-diphenylethylenediamine (**2***b*; 11% each) on the basis of analytical and spectral (uv, ir, and nmr) data. The structure of *meso*-**2***b* was confirmed by comparison (ir and undepressed mixture melting point) with an authentic sample obtained from the condensation of *meso*-1,2-diphenyl-1,2-diaminoethane (4) with *p*-methylbenzaldehyde. This excludes the mechanistic route for the formation of diimines given in Scheme 2.

Similar treatment of benzaldehyde and *p*-methoxybenzaldehyde *N*-benzhydrylimines (**1***c* and *d*) gave *dl*-*N*,*N*′-dibenzhydrylidene-1,2-diphenylethylenediamine (**2***c*) and *dl*-*N*,*N*′-dibenzhydrylidene-1,2-di-*p*-methoxyphenylethylenediamine (**2***d*), respectively, whereas the *p*-chlorobenzaldehyde *N*-benzhydrylimine (**1***e*) afforded both *meso*- and *dl*-*N*,*N*′-dibenzhydrylidene-1,2-di-*p*-chlorophenylethylenediamine (**2***e*) The *dl*-isomers of **2***c*, *d*, and *e* show a common feature in their nmr spectra (Table 2). Four aromatic protons in each appeared at higher field (between δ 6.47–6.62) as compared with the chemical shifts of

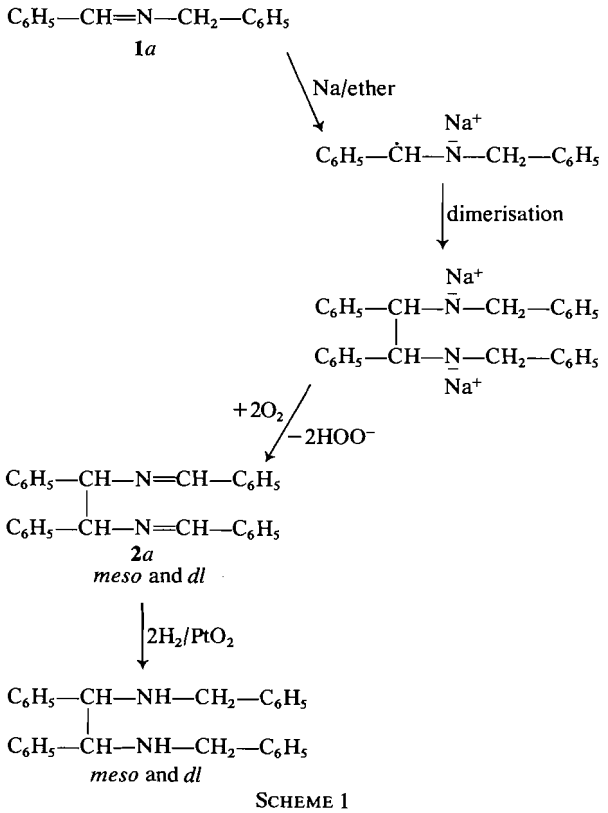

SCHEME 1

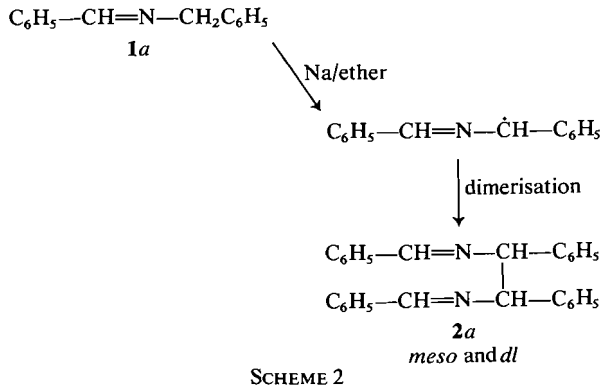

SCHEME 2

TABLE 2. Spectral data of diimines **2**

Compound	Ultraviolet λ_{max} (EtOH) (nm)	Infrared $\nu_{C=N}$ (cm^{-1})	Nuclear magnetic resonance δ (ppm)
meso-**2***a*	251	1640 (Nujol)	(CCl_4): 4.70 (s, 2H, CH), 7.30 and 7.65 (m, 20H, aromatic), 7.95 (s, 2H, —N=CH—)
dl-**2***a*	248	1640 (Nujol)	(CCl_4): 4.63 (s, 2H, CH), 7.30 and 7.70 (m, 20H, aromatic), 8.27 (s, 2H, —N=CH)
meso-**2***b*	260	1645 (Nujol)	($CDCl_3$): 2.32 (s, 6H, CH_3), 4.75 (s, 2H, CH), 7.30 (m, 18H, aromatic), 7.95 (s, 2H, —N=CH—)
dl-**2***b*	259	1645 (Nujol)	($CDCl_3$): 2.23 (s, 6H, CH_3), 4.75 (s, 2H, CH), 7.30 (m, 18H, aromatic), 7.92 (s, 2H, —N=CH—)
dl-**2***c*	253	1625 (KBr)	($CDCl_3$): 4.95 (s, 2H, CH), 6.50 (m, 4H, aromatic), 7.33 (m, 26H, aromatic)
dl-**2***d*	254	1630 (KBr)	($CDCl_3$): 3.72 (s, 6H, OCH_3), 4.80 (s, 2H, CH), 6.62 (m, 4H, aromatic), 7.25 (m, 24H, aromatic)
meso-**2***e*	254	1660 (neat)	($CDCl_3$): 5.57 (s, 2H, CH), 7.25 (m, 24H, aromatic), 7.75 (m, 4H, aromatic)
dl-**2***e*	255	1630 (KBr)	($CDCl_3$): 4.80 (s, 2H, CH), 6.47 (m, 4H, aromatic), 7.25 (m, 24H, aromatic)

remaining aromatic protons (δ 7.25–7.33). On catalytic hydrogenation the *dl*-diimines (**2***c* and *d*) in separate experiments gave *dl*-dihydrodimers of imines (ir and mmp) (5). The formation of diimines with benzaldehyde N-substituted imines can be as shown in Scheme 3.

Ketone hydrazones (**3***a–f*) on similar treatment, as described for imines, gave substituted diazomethanes (**4***a–f*) in 88–95% yield. The structural assignment of the products **4***a–f* was made on the basis of similarity of ir spectra (9, 10) and melting points (Table 3) and also by conversion to their respective azines **5***a–f*

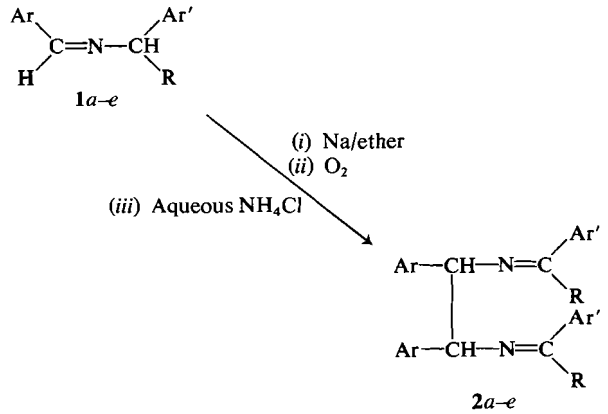

	Ar	Ar'	R
a	C_6H_5	C_6H_5	H
b	C_6H_5	$C_6H_4CH_3p$	H
c	C_6H_5	C_6H_5	C_6H_5
d	$C_6H_4OCH_3p$	C_6H_5	C_6H_5
e	C_6H_4Clp	C_6H_5	C_6H_5

SCHEME 3

which were characterised on the basis of spectral data (Table 4). The formation of diazomethanes can be as shown in Scheme 4.

Electron transfer from sodium to hydrazones **3***a–f* and loss of sodium hydride may lead to the anion *m*. When oxygen or air was not bubbled through the reaction mixture, protonolysis of *m* gave the starting ketone hydrazones (**3***a–f*). Addition of oxygen to *m* and loss of hydroperoxide ion would lead to the substituted diazomethanes (**4***a–f*). A similar mechanism has been proposed in the oxidation of benzophenone hydrazone anion formed by the reaction of methyl lithium in tetrahydrofuran (7). The above method provides a useful and convenient method for synthesising substituted diazomethanes in better yields in comparison with the earlier methods (7 and 8).

Experimental

Melting points were obtained on a Büchi apparatus (capillary method) and have been uncorrected. Infrared spectra were recorded on a Perkin-Elmer 720 spectrometer. Ultraviolet spectra were obtained in 95% ethanol on a Cary-14 spectrophotometer. Proton nuclear magnetic resonance data were obtained on a Varian A-60D spectrometer using TMS as internal standard.

Preparation of Imines

The starting imines were prepared by the condensation of an equimolar mixture of carbonyl compound and aliphatic amine as reported in the literature (11, 12) and characterised on the basis of ir, uv, and nmr data.

Preparation of Ketone Hydrazones

The ketone hydrazones were prepared by the condensation of ketone (2.0 g) with hydrazine hydrate (2.0 g) in 1 mL of *n*-butanol (13) and characterised by ir, uv, and nmr data.

TABLE 3. Conversion of ketone hydrazones **3** to diazomethanes **4**

Hydrazones 3	Ar	R	Product 4 Yield (%)	Melting point (°C)	Ultraviolet λ_{max} (EtOH) (nm)	Infrared $\nu_{C=N=N}$ (cm^{-1})	Nuclear magnetic resonance ($CDCl_3$) δ (ppm)
a	C_6H_5	C_6H_5	93	Liquid (lit. (10) 30)	526, 288	2030 (lit. (9))	6.90 (m, H, aromatic)
b	C_6H_5	$C_6H_4OCH_3p$	94	51–52	527, 317	2030	7.18 (m, 9H, aromatic), 3.70 (s, 3H, OCH_3)
c	$C_6H_4CH_3p$	$C_6H_4CH_3p$	93	106–107 (lit. (10) 107)	541, 284	2030	7.23 (m, 8H, aromatic), 2.35 (s, 6H, CH_3)
d	$C_6H_4OCH_3p$	$C_6H_4OCH_3p$	95	110–111 (lit. (10) 112)	556, 280	2030	6.91 (m, 8H, aromatic), 3.68 (s, 6H, OCH_3)
e	C_6H_5	CH_3	89	Liquid	521, 270	2104 (lit. (9))	7.29 (m, 5H, aromatic), 2.40 (s, 3H, CH_3)
f	C_6H_5	$C_6H_4NMe_2p$	88	80–82 (lit. (15) 82–84)	530, 285	2030	7.21 (m, 9H, aromatic), 2.97 (s, 6H, N—CH_3)

General Procedure for Preparation of Diimines 2

Pieces of sodium (1.0 g, 0.044 g at.) were slowly added to dry ether (40 mL) with stirring under a nitrogen atmosphere. Stirring was continued and the contents were heated under reflux for 2 h. A solution of the imine (1.0 g) in dry ether (40 mL) was added dropwise. The reaction mixture was stirred and heated under reflux for 3–12 h. Oxygen gas was passed through for 15 min and the mixture was allowed to cool. Unreacted pieces of sodium were removed by filtration. The ethereal suspension was treated with 10% aqueous ammonium chloride and the organic layer was washed twice with water and dried over sodium sulfate. The solvent was removed on a rotary evaporator and the residual material was crystallised from methanol. The products were separated by repeated

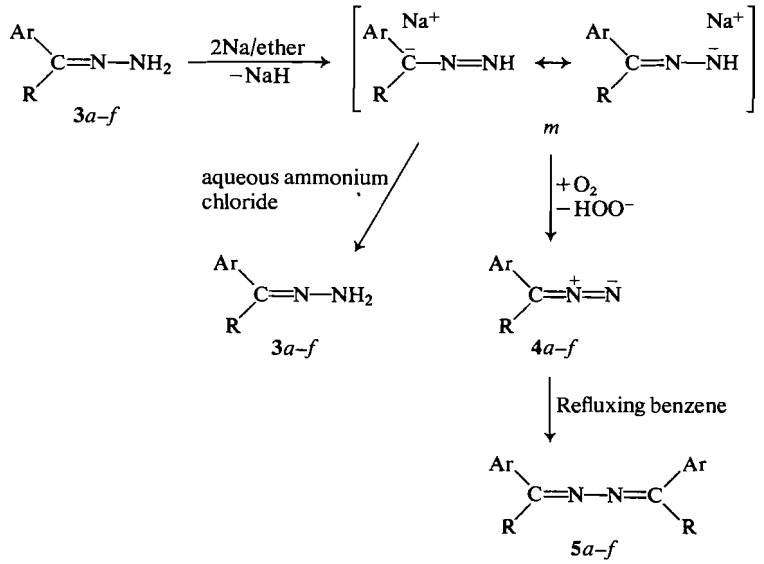

	Ar	R
a	C_6H_5	C_6H_5
b	C_6H_5	$C_6H_4OCH_3p$
c	$C_6H_4CH_3p$	$C_6H_4CH_3p$
d	$C_6H_4OCH_3p$	$C_6H_4OCH_3p$
e	C_6H_5	CH_3
f	C_6H_5	$C_6H_4NMe_2p$

SCHEME 4

TABLE 4. Spectral data of azines **5**

Compound **5**	Melting point (°C)	Infrared (Nujol) $\nu_{C=N}$ (cm^{-1})	Ultraviolet λ_{max} (EtOH) (nm)	Nuclear magnetic resonance ($CDCl_3$) δ (ppm)
a	162–163 (lit. (14) 163–164)	1605	310(sh), 278, 230	7.3 (m, H, aromatic)
b	130–131 (lit. (15) 131–132)	1605	326, 278, 252	3.74 (s, 6H, OCH_3), 7.24 (m, 18H, aromatic)
c	192–194 (lit. (16) 193–194)	1605	315, 250	2.35 (d, 12H, CH_3), 7.25 (m, 16H, aromatic)
d	179–180 (lit. (16) 181–182)	1603	335, 278, 224	3.82 (d, 12H, OCH_3), 7.15 (m, 16H, aromatic)
e	121–122 (lit. (14) 121–122)	1604	290 (sh), 256	2.30 (s, 6H, CH_3), 7.85 (m, 10H, aromatic)
f	194–195 (lit. (17) 194–195)	1605	366, 248	2.98 (s, 12H, N—CH_3), 7.00 (m, 18H, aromatic)

NOTE: These compounds gave satisfactory C, H, N analyses C ±0.34, H ±0.20, N ±0.15.

fractional crystallisation from ethanol. The analytical results are given in Table 1 and the spectral data of the products in Table 2.

*General Procedure for Preparation of Diazomethanes **4** and Azines **5***

In this procedure a solution of the hydrazone (2.0 g) in dry ether (75 mL) was used in place of imine. The red-violet product obtained was dissolved in *n*-hexane (25 mL) and filtered to remove any unreacted hydrazones. The solid products were crystallised from *n*-hexane. When air or oxygen was not bubbled into the reaction mixture and the sodium salt was washed with aqueous ammonium chloride, the starting hydrazones were recovered almost quantitatively.

The benzene solution of diaryldiazomethanes **4***a–f* was heated at reflux temperature till complete disappearance of red-violet coloration. The solvent was removed on a rotary evaporator and the residue was crystallised from ethanol to give the azines.

Acknowledgements

We thank Professor O. P. Malhotra for providing facilities and the Council of Scientific and Industrial Research, New Delhi for financial support to B.P.G.

1. J. J. EISCH, D. D. KASKA, and C. J. PETERSON. J. Org. Chem. **31**, 453 (1966); J. G. SMITH and I. Ho. J. Org. Chem. **37**, 653 (1972).
2. O. ANSELMINO. Chem. Ber. **11**, 623 (1908); W. STIIHMER and G. MESSWARB. Arch. Pharm. **286**, 211 (1953).
3. K. N. MEHROTRA and B. P. GIRI. Synthesis, 489 (1977).
4. G. GROSSMANN. Chem. Ber. **22**, 2298 (1889); F. FEIST. Chem. Ber. **27**, 213 (1894).
5. K. N. MEHROTRA and B. P. GIRI. Indian J. Chem. B, **15**, 1106 (1977).
6. J. M. DUFF and A. G. BROOK. Can. J. Chem. **55**, 2589 (1977).
7. W. FISCHER and J. P. ANSELME. J. Am. Chem. Soc. **89**, 5312 (1967).
8. J. B. MILLER. J. Org. Chem. **24**, 560 (1959).
9. C. PECILE, A. FOFFANI, and S. GHERSETTI. Tetrahedron, **20**, 823 (1964).
10. R. BALTZLY, N. B. MEHTA, P. B. RUSSELL, R. E. BROOKS, E. M. GRIVSKY, and A. M. STEINBERG. J. Org. Chem. **26**, 3672 (1961).
11. R. JUDAY and H. ADKINS. J. Am. Chem. Soc. **77**, 4559 (1955).
12. M. MICHAELIS. Chem. Ber. **26**, 2169 (1883).
13. A. SCHÖNBERG, A. E. KADER, and A. E. M. A. SAMMOUR. J. Am. Chem. Soc. **79**, 6020 (1957).
14. D. B. MOBBS and H. SUSCHITZKY. J. Chem. Soc. C, 175 (1971).
15. R. HÜTTEL, J. RIEDL, H. MARTIN, and K. FRANKE. Chem. Ber. **93**, 1425 (1960).
16. D. BETHELL, A. R. NEWALL, and D. WHITTAKER. J. Chem. Soc. B, 23 (1971).
17. H. H. SZMANT and C. MCGINNIS. J. Am. Chem. Soc. **74**, 240 (1952).

Mass spectra of bis(trimethylsilyl)- and bis(trimethylgermyl)carbodiimide

JOHN E. DRAKE, BORIS M. GLAVINČEVSKI, H. ERNEST HENDERSON, AND CLARA WONG

Department of Chemistry, University of Windsor, Windsor, Ont., Canada N9B 3P4

Received July 26, 1978

JOHN E. DRAKE, BORIS M. GLAVINČEVSKI, H. ERNEST HENDERSON, and CLARA WONG. Can. J. Chem. **57**, 1162 (1979).

The mass spectral fragmentation patterns of bis(trimethylsilyl)- and bis(trimethylgermyl)carbodiimides are compared. Metastable confirmed transitions involve elimination of neutral fragments apparently containing Si=N and/or Si=C bonds. The fragmentation pathways are similar for the germyl analogue but no proof of a fragment containing a Ge=C bond was observed.

JOHN E. DRAKE, BORIS M. GLAVINČEVSKI, H. ERNEST HENDERSON et CLARA WONG. Can. J. Chem. **57**, 1162 (1979).

On compare les types de fragmentation en spectrométrie de masse des bis(triméthylsilyl) et bis(triméthylgermyle) carbodiimides. Des transitions confirmées par des ions métastables impliquent l'élimination de fragments neutres contenant apparemment des liaisons Si=N et/ou Si=C. Les voies de fragmentation sont semblables dans le cas des analogues germylés; toutefois on n'a obtenu aucune preuve permettant de confirmer la présence d'un fragment contenant une liaison Ge=C.

[Traduit par le journal]

In a recent publication, we reported the synthesis, characterisation, and reactivity of various silyl- and germylcarbodiimides (1). Of these, only $(H_3GeN:)_2C$ has been analysed by mass spectrometry and from the observed ion fragments the existence of several rearrangement ions was deduced (2). The existence of both positively charged and neutral fragments containing an Si=C bond has been postulated in mass spectroscopic studies of organosilicon compounds (3, 4), as has the formation of species containing the Si=N bond in the spectra of silazanes (5). The two trimethyl derivatives $Me_3SiNCNSiMe_3$ and $Me_3GeNCNGeMe_3$ were selected for a comparative study of their fragmentation pathways to avoid problems of interpretation that might arise from 'hydrogen stripping' in the hydrido analogues. The carbodiimide skeleton could provide a basis for interesting rearrangements and also for the formation of intermediates involving double bonds to silicon or germanium.

Experimental

The mass spectra were obtained using a Varian MAT CH5 double focusing spectrometer, of reversed geometry, equipped with an INCOS 2000 computer system. The spectra were recorded at 70 eV. The metastable transitions were observed in the field free region by scanning the accelerating voltage (1–3 kV) at constant electric sector voltage (285 kV) and magnetic strength. The *m/e* value of the daughter ion is known to the nearest mass unit. It was possible, under special conditions, in the normal electron-impact spectrum, to record the silicon compound under high resolution to 0.001 eV. A linear least-squares iterative computer program (SMASABD)[1] was used to fit theoretical polyisotopic patterns of our compounds to the experimental data, and another program (MASPEC)[1] was used to calculate the theoretical polyisotopic clusters of each ion fragment. In 'clusters' involving silicon, the presence of M, M − 1, or M − 2 peaks could be readily discerned; typical average deviations obtained from the SMASABD program were ca. 1.0 for silicon species but closer to ca. 5.0 for germanium clusters.

$Me_3SiNCNSiMe_3$ and $Me_3GeNCNGeMe_3$ were prepared as described previously and their purity checked by their vibrational and ^1H nmr spectra (1). Carbodiimides are readily hydrolysed to the oxides, so great care must be taken to avoid any contact with moisture when the mass spectra are recorded.

Results and Discussion

The major features of the fragmentation patterns of $Me_3SiNCNSiMe_3$ and $Me_3GeNCNGeMe_3$ are very similar and surprisingly simple. If only those peaks with an ion count greater than 5% of the base peak are considered, then the main ions present are

$$Me_3SiNCNSiMe_3^+ \rightarrow Me_3SiNCNSiMe_2^+ \rightarrow Me_3Si^+$$

for the silane and

$$Me_3GeNCNGeMe_3^+ \rightarrow Me_3GeNCNGeMe_2^+ \rightarrow Me_3Ge^+ \rightarrow MeGe^+$$

for the germane. Table 1 includes all those peaks which have an ion count greater than 1% of the base peak and which are clearly part of a silicon- or germanium-containing ion.

In the course of investigating the metastable-supported fragmentation pathways for $Me_3SiNCNSiMe_3$ (Table 2) it becomes apparent that the loss of neutral species containing Si=C or Si=N bonds can readily account for the majority of features in Scheme 1. The

[1]SMASBD and MASPEC were obtained from J. Miller of Chemistry Department, Brock University.

0008-4042/79/101162-05$01.00/0

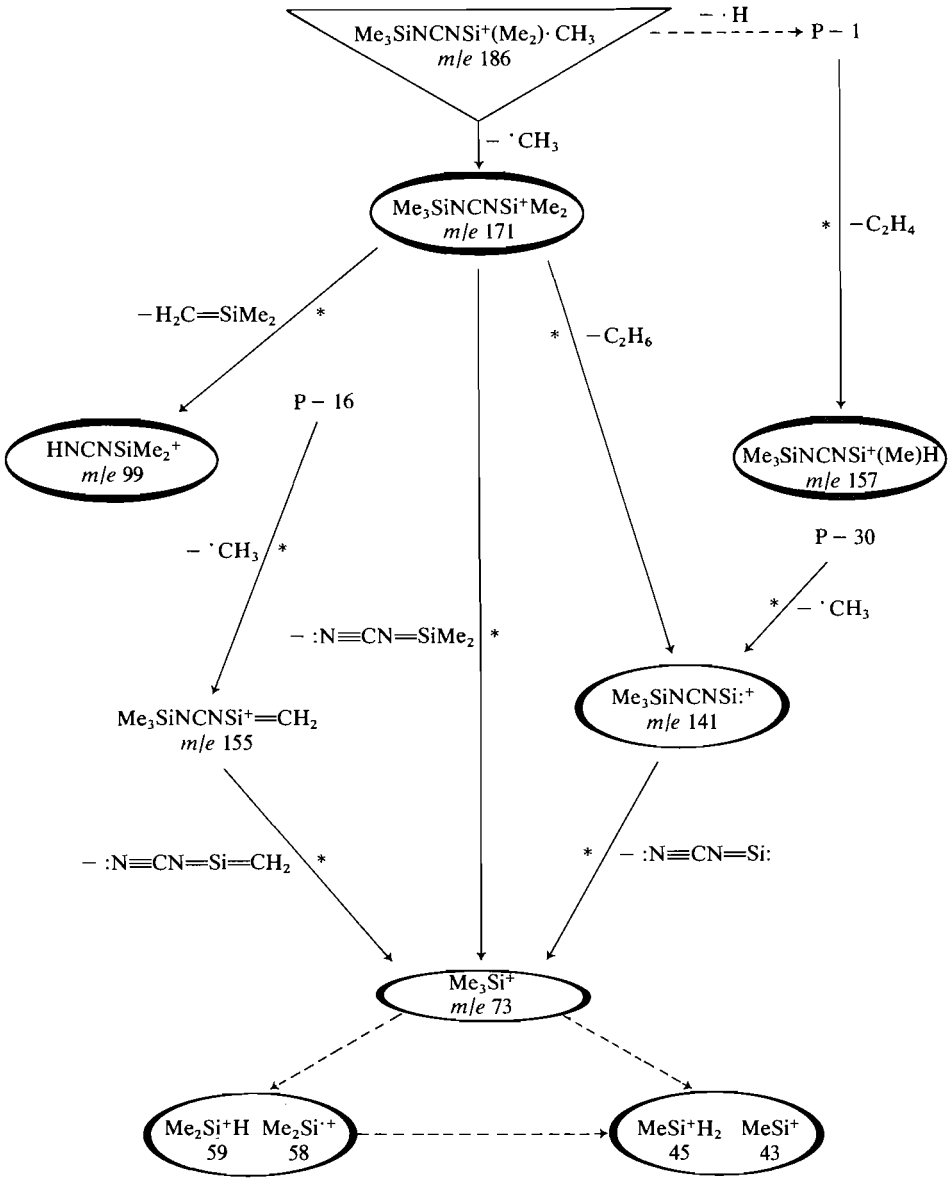

SCHEME 1. Fragmentation pattern for bis(trimethylsilyl)carbodiimide

formation of Me_3Si^+ arises from the loss of neutral fragments that apparently contain a Si=N bond and for which similar and reasonable electronic structures can be proposed. The transfer of charge to the 'other end' of the molecule should be a relatively simple mechanism given the delocalized nature of the π-bonding system in the SiNCNSi skeleton. Unfortunately, we were unable to get accurate determination of the parents of the ion below Me_3Si^+. Clusters containing one and two methyl groups attached to silicon are mixtures. The relative peak intensities suggest that the ions Me_2SiH^+ (*m/e* 59.024; calcd. 59.0317) and Me_2Si^+ can be detected in a ratio of ca. 3:1 as are the ions $MeSiH_2^+$ (*m/e* 44.98; calcd. 45.0161) and $MeSi^+$ (*m/e* 42.96; calcd. 43.0004). The genesis of the intermediates at *m/e* 157, 155, and 141 leads to metastable-confirmed transitions which apparently arise from 'parents' that have one hydrogen atom less than an ion that is seen in the main spectrum. These parents at *m/e* 185, 170, and 156 show insignificant abundances in the normal running mode and the origins of the latter two are unknown. The signal corresponding to *m/e* 99 is seen at 99.0219 under higher resolution which indicates

TABLE 1. The mass spectra of bis(trimethylgermyl)- and bis(trimethylsilyl)carbodiimide

	M = Ge			M = Si		
Ion family	*m/e*	Int	%RA	*m/e*	Int	%RA
	270	34				
	272	138				
	273	34				
	274	297				
	275	45				
$Me_3MNCNMMe_3^+$	276	289	9.58	186	1 430	7.66
	277	65		187	233	
	278	200		188	103	
	279	5		189	15	
	280	66				
	255	359				
	256	2				
	257	907				
	258	235				
	259	1 874				
	260	424				
$Me_3MNCNMMe_2^+$	261	1 922	68.43	171	13 631	73.15
	262	523		172	2 212	
	263	1 382		173	1 019	
	264	187		174	126	
	265	456		175	16	
	266	9				
	267	48				
$Me_3SiNCNSi^+{=}CH_2$				155	337	
				156	52	2.66
$Me_3SiNCNSi^+(CH_3)H$				157	198	
				158	24	
				159	8	
	227	29?				
	229	29				
	230	7				
$Me_3MNCNM{:}^+$	231	44	1.76	141	211	1.04
	232	4		142	17	
	233	43		143	13	
	234	6				
	235	33				
	236	3				
	237	17				
$Me_2SiNCNH^+$				99	221	2.43
$Me_2Si_2N^+$				100	292	
				101	37	
				102	14	
	115	354				
	116	10				
	117	542				
	118	117				
Me_3M^+	119	577	15.14	73	1 718	8.17
	120	22		74	136	
	121	173		75	43	
				76	3	
	100	37				
	101	19				
	102	51				
	103	57				
Me_2M^+	104	59	2.13	58	79	1.28
Me_2MH^+	105	23		59	217	
	106	16		60	11	
	85	53				
	86	2				
	87	99				
	88	40				

TABLE 1 (*Concluded*)

Ion family	M = Ge			M = Si		
	m/e	Int	%RA	*m/e*	Int	%RA
MeM^+	89	169	3.36	43	211	3.61
	90	8		44	93	
$MeMH_2^+$	91	41		45	501	
	92	2		46	12	
				47	20	
				48	3	

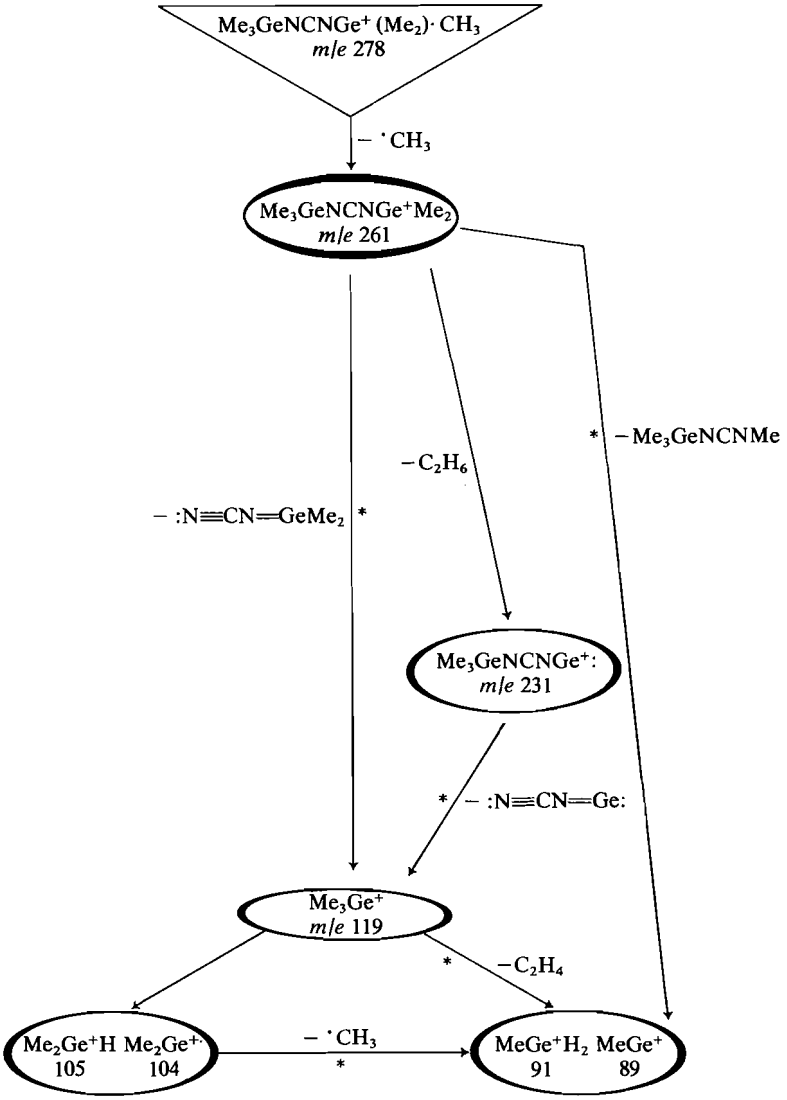

SCHEME 2. Fragmentation pattern for bis(trimethylgermyl)carbodiimide

the presence of $Me_2SiNCNH^+$ (*m/e* calcd. 99.0378) rather than Me_3SiNC^+ (*m/e* calcd. 99.0504). The former ion requires the loss of the neutral fragment $CH_2{=}SiMe_2$, whereas the latter requires the formation of two odd-electron scission products. It is difficult to assign unambiguously the species of *m/e* 100. The peak is of low intensity, making metastable and high resolution work less reliable. The metastable studies show an array of poorly characterised parent ions (Table 2) and in high resolution spectra there is

TABLE 2. Metastable transitions

Daughter *m/e*	Parent *m/e*
(a) $Me_3SiNCNSiMe_3$	
73	141, 155, 171*
99	171
100	115, 127, 141, 155, 172
141	156,* 171*
155	170*
157	185*
(b) $Me_3GeNCNGeMe_3$	
89	104, 117
119	233, 263*

*Peaks of good intensity are marked with an asterisk.

an indication of peaks of even lower intensity at *m/e* 100.03 and possibly at 99.96 in addition to the main one at 99.9954. Thus it seems clear that more than one species is present, one of which could be $Me_2Si_2N^+$ (*m/e* calcd. 100.0039) resulting from the loss of HCN (from *m/e* 127) and MeCN (from *m/e* 147). The formation of rearrangement ions of this type was suggested in the mass spectrum of $H_3GeNCNGeH_3$ (2) but there was no indication of the corresponding species, $Me_2Ge_2N^+$, in the spectrum of $Me_3GeNCNGeMe_3$.

The polyisotopic nature of germanium results in the mass spectrum of $Me_3GeNCNGeMe_3$ being potentially more complex than that of the silicon analogue. This not only leads to difficulty in assessing the degree of 'hydrogen-loss' in simple species such as Me_2Ge^+ compared with Me_2GeH^+, but also makes metastable work more difficult, because relatively few *m/e* values have significantly high intensities. Nevertheless, we can establish some metastable-confirmed transitions and suggest a probable pattern (Scheme 2) based on a comparison with the silicon analogue. The principal route is again the loss of methyl group to give the P − 15 ion followed by loss of a large neutral fragment to give Me_3Ge^+. This neutral fragment can be written as with the silicon analogue, as involving a double bond from the group IV element to nitrogen. Equally well, it may be written in a Zwitterion form which avoids the necessity of involving a π-bond to germanium, namely as $^-$:N=C=N—Ge^+Me_2 rather than as :N≡C—N=$GeMe_2$. This is also true of the fragment :N≡C—N=Ge: which can be written as :$^-$N=C=N—Ge^+:. It is interesting to note that there is no indication, either in the main spectrum or the metastable studies, of the intermediate $Me_3GeNCNGe{=}CH_2^+$ (*m/e* 245 for ^{74}Ge) which would contain a double bond between germanium and carbon, even though the corresponding pathway certainly exists in the silane. The presence of $HNCNGeMe_2^+$ and/or Me_3GeNC^+ (*m/e* 145 for ^{74}Ge) cannot be ruled out completely because very weak peaks were detected in the region of *m/e* 141 to 145 but they did not correspond to a typical germanium cluster. The elimination of C_2H_6 from $Me_3GeNCNGeMe_2^+$ is similar to that noted from Me_2GeCl^+ in the spectrum of Me_3GeCl (6) and the corresponding transition in the silicon analogue is metastable-confirmed. The elimination of C_2H_4 from Me_3Ge^+ is a well established pathway (6, 7).

Acknowledgements

We thank the Natural Sciences and Engineering Research Council of Canada for financial support and one of us (J.E.D.) thanks Professor N.B.H. Jonathan of the University of Southampton for providing facilities during a sabbatical leave.

1. J. E. DRAKE, R. T. HEMMINGS, and H. E. HENDERSON. J. Chem. Soc. Dalton, 336 (1976).
2. S. CRADOCK and E. A. V. EBSWORTH. J. Chem. Soc. A, 1423 (1968).
3. YU. A. USTYNUK, P. I. ZAKHAROV, and A. A. AZIZOV. Dokl. Akad. Nauk SSSR, **220**, 856 (1975).
4. Y. NAKACLAIRA, Y. KOBAYASHI, and H. SAKURAI. J. Organomet. Chem. **63**, 79 (1973).
5. J. SILBIGER, C. LIFSHITZ, J. FUCHS, and A. MANDELBAUM. J. Am. Chem. Soc. **89**, 4308 (1967).
6. F. GLOCKLING and J. R. C. LIGHT. J. Chem. Soc. A, 717 (1968).
7. D. B. CHAMBERS and F. GLOCKLING. J. Chem. Soc. A, 735 (1968).

Bound complex and triple collision mechanisms for diatom dissociation and recombination

NEIL SNIDER
Department of Chemistry, Queen's University, Kingston, Ont., Canada K7L 3N6
Received November 22, 1978

NEIL SNIDER. Can. J. Chem. **57**, 1167 (1979).

A method was devised for estimating relative contributions to atom recombination from the bound complex and triple collision mechanisms. The method is based on three assumptions: a collinear model is valid, recrossings of a suitably chosen transition state surface equally affect both contributions to the recombination rate, and the two contributions correspond to crossings of parts of the transition state surface which differ only in total energy. Ratios of the rate constants for recombination by the two mechanisms were calculated for a classical model of Br and I atom recombination in rare gases. The ratios had already been obtained for the model from three-dimensional trajectory calculations. The results disagreed by as much as a factor of ten for helium as the third body, but they were within 50% or better for xenon. It was argued that the discrepancies are largely due to a breakdown of the second of the foregoing assumptions. The formula for the rate constant for recombination by both mechanisms together was extended to three dimensions at the expense of introducing an adjustable parameter. The extended formula was found to give results in agreement with the trajectory calculation to within 30% or better.

NEIL SNIDER. Can. J. Chem. **57**, 1167 (1979).

On a developpé une méthode qui permet d'évaluer les contributions relatives à la recombinaison d'un atome par des mécanismes de liaison complexe et de collision triple. La méthode est basée sur trois hypothèses: un modèle colinéaire est valable, les recoupements d'une surface d'état de transition choisie judicieusement affecte d'une façon égale les deux contributions à la vitesse de recombinaison et les deux contributions correspondent à des recoupements de portions de la surface de l'état de transition qui ne diffèrent que dans leur énergie totale. On a calculé les rapports des constantes de vitesse pour la recombinaison par les deux mécanismes pour un modèle classique de recombinaison d'atomes de Br et de I dans des gaz rares. On a déjà obtenu les rapports pour le modèle à partir de calculs de trajectoires tridimensionnelles. Les résultats diffèrent par des facteurs pouvant atteindre 10 lorsque l'hélium est le troisième corps; dans le cas du xénon les résultats ne diffèrent que par 50% ou moins. Il est proposé que ces différences sont dues en grande partie à l'insuffisance de la deuxième hypothèse. On a étendu la formule de la constante de vitesse pour la recombinaison par les deux mécanismes aux trois dimensions en faisant intervenir un paramètre ajustable. On a trouvé que la formule étendue conduit à des résultats en accord à 30% ou mieux avec les calculs de trajectoire.

[Traduit par le journal]

Introduction

The simplest mechanism for gas phase recombination of two atoms A in the presence of an inert diluent M is a termolecular process

[1] $$2A + M \rightarrow A_2 + M$$

However, in practice, diluent gases are never completely inert, and the formation of bound species AM is always a possibility. Theories of the rate of recombination have been formulated (1, 2) wherein AM plays a central role,

[2] $$A + 2M \leftrightharpoons AM + M \quad \text{rapid equilibrium}$$
$$AM + A \rightarrow A_2 + M$$

Reaction [1] has come to be known as the "triple collision" mechanism for recombination, and reactions [2] as the "bound complex" mechanism (3).

In the reverse process, dissociation of A_2, the final step in the collisional excitation of A_2 to the dissociated state may be either the break-up of A_2,

[3] $$A_2 + M \rightarrow 2A + M$$

or exchange,

[4] $$A_2 + M \rightarrow AM + A$$

Reaction [3] is the reverse of [1], and [4] is the reverse of the second step of [2]. By detailed balancing the ratio of rates of [1] and [3] is equal to the ratio of rates of [2] and [4]. It follows that the recombination rate via the triple collision mechanism relative to the recombination rate via the bound complex mechanism is equal to the branching ratio for the possible reactions of M with A_2.

If M is one of the rare gases, the A—M bond is generally weak, and AM is not easy to detect experimentally. Thus, it is that there are no experimental data concerning the relative rates of [1] and [2] in this case. What are available are results of trajectory

0008-4042/79/101167-10$01.00/0

calculations for Br atoms and I atoms recombining in the presence of He, Ar, and Xe (3, 4). These studies indicate that for M = Ar, Xe the bound complex mechanism predominates at low temperatures, the triple collision mechanism at high temperatures whereas for M = He the triple collision mechanism predominates at all temperatures of interest.

The primary objective of the present work is to develop and test a method for estimating the relative rates of dissociation and recombination via the two aforementioned mechanisms. Three approximations are introduced over and above those of the trajectory studies. First, the problem is reduced to one dimension. Second, the dynamics are simplified as per transition state theory (5). Third, the contributions to the rate from the two mechanisms are identified with fluxes across parts of the transition state surface which differ only in total energy. The potential energy surfaces are assumed to be the same as those used in the above cited trajectory studies (6), and comparisons are made with the ratios of triple collision and bound complex contributions to the equilibrium rate of recombination k_r^{eq} from these studies. One thereby eliminates uncertainties due to lack of knowledge of the potential energy surfaces, to the need to correct for non-equilibrium effects, and to the need to correct for quantum effects. Discrepancies between the estimated values of the branching ratios and those calculated from trajectories can be due only to the three approximations mentioned previously.

A secondary objective of this work is to test a simple method for extending collinear results for k_r to three dimensions (7). The extended results can be compared directly to the values of k_r^{eq} obtained from trajectories. This comparison will provide some indication of the amount of inaccuracy which results from simplification of the dynamics.

Formulation of the Theory

Transition State Theory

The following derivation makes reference to reactions [3] and [4]. Extension to reactions [1] and [2] is effected by a straightforward application of the principle of detailed balancing. Semiclassical transition state theory has recently been formulated in one dimension (8) for the reaction scheme represented by [3] and [4]. The theory expresses the rate constant for the overall disappearance of A_2 by reactions [3] and [4] in terms of a phase space function $\mathcal{O}$. This function is a unit step function, and its discontinuity occurs at the surface in phase space which has been chosen to be the transition state.

In the just mentioned theory, the classical limiting expression for the sum of rate constants for reactions [3] and [4] is obtained by combining eqs. [13] and [15] of ref. 8,

$$[5]\quad k_3 + k_4 = \mathcal{I}_{Int}^{-1}(\beta/2\pi\mu)^{1/2} \times \int \{\mathcal{O}, H\}\theta(-\{\mathcal{O}, H\}) \exp(-\beta H)\, dpdq$$

where $\mathcal{I}_{Int}$ is the phase integral for the vibrational degree of freedom of A_2, β is the reciprocal of Boltzmann's constant times temperature, μ is the reduced mass of the A_2–M pair, H is the Hamiltonian for the system with the center of mass taken to be at rest, $\{\ \}$ denotes Poisson bracket, θ is the unit step function, and p and q are the momenta and coordinates for the two degrees of freedom of the collinear, three-atom system with fixed center of mass. It is to be noted that the integral on the right of [5] is essentially a surface integral since the Poisson bracket of $\mathcal{O}$ contains as a factor a Dirac delta function which is non-zero only at the transition state. Provided only that the transition state surface entirely separates the A_2 + M region from the rest of the phase space, eq. [5] gives an upper bound to the exact classical $k_3 + k_4$ for the same model (5).

The transition state surface to be assumed in the present work resembles the one employed in the original version of the variational theory of three-body recombination (9). This surface is defined differently in different regions of phase space. In the region for which a function $f(q)$ is negative, i.e. the region which by definition of f includes reactant-like configurations, it is the surface along which H_{Int}, the Hamiltonian for the vibrational degree of freedom of isolated A_2, is equal to D, the dissociation energy. In the region for which H_{Int} is less than D, it is the surface along which f is zero. The function $\mathcal{O}$ is then given by

$$[6]\qquad \mathcal{O} = \theta(D - H_{Int})\theta(-f)$$

In the present work the explicit form of f to be assumed differs from that of ref. 9 although, as in ref. 9, it is made to depend on a variational parameter. The explicit form of f used in the present work will be discussed later along with the rationale underlying its choice.

Partitioning of the Surface

The desired branching ratio Γ is given by

$$\Gamma = k_3/k_4$$

Equation [5] cannot provide this ratio. The transition state surface can be divided into a part through which pass trajectories which contribute to [3] and another part through which pass trajectories which contribute to [4]. However, one does not know how to effect this partitioning of the surface without actually computing the trajectories. Lacking trajectories, one must resort to a reasonable assumption.

Before discussing the partitioning which was here

assumed, it is to be noted that the law of conservation of energy imposes limits on that portion of the surface through which reactive trajectories may pass and also on the portion through which dissociative trajectories may pass. Let ε_∞ be the binding energy of isolated AM. Then for H less than $D - \varepsilon_\infty$ no reaction can take place, and for H between $D - \varepsilon_\infty$ and D only reaction [4] can occur. Thus the integration in [5] is restricted to that part of the surface for which H is greater than $D - \varepsilon_\infty$, and the integral over the part for which H lies between $D - \varepsilon_\infty$ and D may contribute only to k_4.

The simplest assumption one can make is that trajectories which pass through that part of the surface for which H is greater than D contribute *entirely* to [3]. This assumption is the one which was finally adopted in the present work. It leads to an upper bound to k_3 because all trajectories which contribute to [3] *must* pass through that part of the surface for which H is greater than D. The assumption seems physically reasonable in those cases for which A–M attractive forces are weak. In such a case it seems unlikely that many trajectories for which H is greater than D would contribute to reaction [4]. If the A–M attractive forces are strong, however, the assumption probably breaks down because many trajectories which cross the transition state surface are likely to be deflected into the AM + A region and to have their excess energy channeled into relative AM − A translation. Nevertheless, in those cases for which calculations are reported here, the A–M attractive forces are weak.

Formula for the Branching Ratio

The branching ratio is thus assumed to be a ratio of integrals over portions of the transition state surface which differ only in total energy. As the first step in the evaluation of these integrals, explicit coordinates are chosen. These are R, the distance from M to the center of mass of A_2 and r, the A–A distance, both conveniently mass weighted,

$$[7] \quad r = (2b)^{1/2} r_{AA} \qquad R = (2b)^{-1/2}(r_{AM} + \tfrac{1}{2} r_{AA})$$

In [7], r_{AA} is the A–A distance, r_{AM} is the distance between M and the nearest A, and b is given by

$$[8] \quad b = (1 + 2m_A/m_M)^{1/2}$$

where m_A and m_M are the masses of the designated atoms. In terms of these coordinates the Hamiltonian for the vibration of isolated A_2 is given by

$$[9] \quad H_{Int} = p_r^2/2\bar{\mu} + V_0(r)$$

and the total Hamiltonian is given by

$$[10] \quad H = (p_R^2 + p_r^2)/2\bar{\mu} + V_0(r) + V_1(R, r)$$

where $\bar{\mu}$ is given by

$$[11] \quad \bar{\mu} = \tfrac{1}{2} b\mu = m_A/b$$

and p_R, p_r are the momenta conjugate to the designated coordinates.

With $\mathcal{O}$ given by [6] and coordinates given by [7], the Poisson bracket in the integrand of [5] becomes

$$[12] \quad \{\mathcal{O},H\} = -\bar{\mu}^{-1}\left[p_r \frac{\partial V_1}{\partial r} \delta(D - H_{Int})\theta(-f) + \left(\frac{\partial f}{\partial r} p_r + \frac{\partial f}{\partial R} p_R\right)\delta(-f)\theta(D - H_{Int})\right]$$

where δ denotes the Dirac delta function. Substituting [12] into [5] and applying the assumption of the previous section concerning the parts of the integral which contribute to k_3 and k_4, one obtains

$$[13] \quad k_3 = (\beta\mathcal{I}_{Int})^{-1}(b/2)^{1/2} \int (F_3 + G_3)dR$$
$$k_4 = (\beta\mathcal{I}_{Int})^{-1}(b/2)^{1/2} \int (F_4 + G_4)dR$$

where F_3 and G_3 are given by

$$[14a] \quad F_3(R) = (2\pi)^{-1/2}(\beta/\bar{\mu})^{3/2} \int dr\, \delta(-f) \int dp_R dp_r \left(\frac{\partial f}{\partial r} p_r + \frac{\partial f}{\partial R} p_R\right)\theta\left(\frac{\partial f}{\partial r} p_r + \frac{\partial f}{\partial R} p_R\right) \times \theta(D - H_{Int})\theta(H - D)\exp(-\beta H)$$

$$[14b] \quad G_3(R) = (2\pi)^{-1/2}(\beta/\bar{\mu})^{3/2} \int dr\, \theta(-f) \int dp_R dp_r\, p_r \frac{\partial V_1}{\partial r}\theta\left(p_r \frac{\partial V_1}{\partial r}\right)\delta(D - H_{Int})\theta(H - D)\exp(-\beta H)$$

The functions F_4 and G_4 differ from F_3 and G_3 in that $\theta(H - D)$ in [14] is replaced by $\theta(H - D + \varepsilon_\infty)\theta \times (D - H)$. The branching ratio is given by

$$[15] \quad \Gamma = [\int (F_3 + G_3)dR]/[\int (F_4 + G_4)dR]$$

It is to be noted that the F's and G's are dimensionless. Since $\beta\mathcal{I}_{Int}$ has the units of time, it is clear from [13] that k_3 and k_4 have the units of velocity, as they should.

Integrations over r, p_R, and p_r in [14] require no special skill, only a certain amount of care. The mathematical manipulations involved are described in the Appendix. The zero of energy is taken to be the energy of the three atoms at infinite separation and at rest. Hence, D is set to zero. For F_3 and F_4 one obtains

$$[16a]\quad F_3(R) = (\{Z[\beta V_0(r_+)\csc^2\phi_+] - Z[\beta V(R,r_+)]\}\sec\phi_+ \exp[-\beta V_0(r_+)] - \{Z[\beta V_0(r_+)\operatorname{ctn}^2\phi_+] - Z[\beta V_1(R,r_+)]\} + 2(-\beta V_0(r_+)/\pi)^{1/2}\tan|\phi_+|\exp[\beta V_0(r_+) \times \operatorname{ctn}^2\phi_+])\exp[-\beta V_1(R,r_+)] \quad \text{for} \quad V_1(R,r_+) \geq V_0(r_+)\operatorname{ctn}^2\phi_+$$

$$= 2(-\beta V_0(r_+)/\pi)^{1/2}\tan|\phi_+| \quad \text{for} \quad V_1(R,r_+) < V_0(r_+)\operatorname{ctn}^2\phi_+$$

$$[16b]\quad F_4(R) = (\{Z[\beta V(R,r_+)] - Z[\beta V_c(R,r_+)]\}\sec\phi_+\exp[-\beta V_0(r_+)] - Z[\beta V_1(R,r_+)]) \times \exp[-\beta V_1(R,r_+)] \quad \text{for} \quad V_1(R,r_+) \geq V_0(r_+)\operatorname{ctn}^2\phi_+$$

$$= (\{Z[\beta V_0(r_+)\csc^2\phi_+] - Z[\beta V_c(R,r_+)]\}\sec\phi_+\exp[-\beta V_0(r_+)] - Z[\beta V_0(r_+)\operatorname{ctn}^2\phi_+] + 2(-\beta V_0(r_+)/\pi)^{1/2}\tan|\phi_+|\,\theta[-V_0(r_+)]\{\exp[\beta V_1(R,r_+)] - \exp[\beta V_0(r_+)\csc^2\phi_+]\})\exp[\beta V_1(R,r_+)] \quad \text{for} \quad V_1(R,r_+) < V_0(r_+)\operatorname{ctn}^2\phi_+$$

The function Z is defined by

$$[17]\qquad Z(\chi) = 2\pi^{-(1/2)}\,\theta(-\chi)\gamma(3/2, -\chi)$$

where γ denotes the incomplete gamma function. The function $r_+(R)$ is obtained by solving the equation

$$f(R,r) = 0$$

for r. The angle ϕ_+ is given by

$$[18]\qquad \tan\phi_+ = \mathrm{d}r_+/\mathrm{d}R$$

The potential functions V and V_c are given by

$$V = V_0 + V_1 \quad V_c = V + \varepsilon_\infty$$

For G_3 and G_4 one obtains

$$[19a]\quad G_3(R) = \pm\{1 - Z[\beta V_1(R,r_-)]\}\exp[-\beta V_1(R,r_-)] + 2\sum_m \pm\{1 - Z[\beta V_1(R,r_m)]\} \times \exp[-\beta V_1(R,r_m)] \pm \{1 - Z[\beta V_1(R,r_+)]\}\exp[-\beta V_1(R,r_+)]$$

$$[19b]\quad G_4(R) = \pm Z[\beta V_1(R,r_-)]\exp[-\beta V_1(R,r_-)] + 2\sum_m \pm Z[\beta V_1(R,r_m)]\exp[-\beta V_1(R,r_m)] \pm Z[\beta V_1(R,r_+)]\exp[-\beta V_1(R,r_+)]$$

where r_- is the value of r for which V_0 changes sign and is understood to be less than r_+. The r_m's are values of r between r_- and r_+ at which V_1 has maxima or minima. The plus signs in [19] apply at values of r for which V_1 is a minimum; the minus signs apply at maxima.

To proceed further, one needs explicit expressions for V_0, V_1, and f. In general these expressions will be such that the R-integration must be done numerically.

Extension to Three Dimensions

In the present work it is assumed that the one-dimensional k_3 and k_4 differ from their three-dimensional analogs by factors which are the same for both. It follows from this assumption that [15] may be used to estimate branching ratios for the corresponding three-dimensional system. Such is not the case for the rate constants themselves.

A fairly simple method for generalizing one-dimensional values of the recombination rate constant to three dimensions has been proposed (7). The result is given by eq. [14] of the just mentioned reference,

$$[20]\quad k_r = \frac{R_g\sigma h^3 X^*}{n\pi^2 m_A k\theta_r}\left(1 + \frac{2m_A}{m_M}\right)^{1/2}\tilde{T}^{1/n-1} \times \gamma(n^{-1}, \beta\varepsilon_c)r\sum_i P_{N+1,i}\exp(-\beta\varepsilon_i)$$

where R_g is the ratio of electronic degeneracies for the ground states of A_2 and 2A, σ is a hard sphere collision cross section, k is Boltzmann's constant, θ_r is the characteristic rotational temperature of A_2,

and $\tilde{T}$ is $(\beta D_e)^{-1}$. The parameters X^*, n, and ε_c characterize the angular momentum dependence of the height of the centrifugal barrier for a rotating Morse oscillator of well depth D_e. The way in which X^*, n, and ε_c are calculated is described in ref. 7. At low temperatures one can safely make the approximation

$$[21] \qquad n^{-1}\gamma(n^{-1},\beta\varepsilon_c) = \Gamma(1 + n^{-1})$$

where (in this section only) Γ denotes gamma function. The factor r is the non-equilibrium correction, which is set equal to one if k_r is assumed to be k_r^{eq}. The sum in [20] is related to the rate constant for the total disappearance of A_2,

$$[22] \quad \sum_i P_{N+1,i} \exp(-\beta\varepsilon_i) = \bar{u}^{-1} Q_{Int}(k_3 + k_4)$$

where Q_{Int} is the partition function for the vibrational degree of freedom of A_2, and $\bar{u}$ is the mean relative velocity of A_2–M pairs.

In the classical limit Q_{Int} is $h^{-1}\mathscr{I}_{Int}$. Hence, from [13] and [22] one obtains

$$[23] \quad \sum_i P_{N+1,i} \exp(-\beta\varepsilon_i) = (\pi b\mu/\beta)^{1/2}h^{-1} \times \int (F_3 + F_4 + G_3 + G_4)\,dR = (2\pi m_A \tilde{T} D_e/b)^{1/2}h^{-1}\mathscr{I}$$

In the second line of [23], [11] has been used, and $\mathscr{I}$ denotes the integral in the foregoing line. Combining [8], [20], [21], and [23] and using the standard formula (10) for θ_r of a diatomic molecule in terms of m_A and the internuclear distance r_e, one obtains

$$[24] \quad k_r^{eq} = 4\pi R_g X^* \Gamma(1 + n^{-1}) r_0^2 r_e^2 \times (2\pi D_e/m_A)^{1/2} \tilde{T}^{(1/n - 1/2)} b^{1/2} \mathscr{I}$$

where r_0 is the hard sphere collision diameter. The parameters n and X^* are fixed for given Morse parameters r_e and α. The only adjustable parameter in [24] is therefore r_0. Equation [24] gives the rate constant for recombination in three dimensions by reactions [1] and [2] together. In its derivation the tacit assumption has been made that k_3 and k_4 in three dimensions both differ from their one-dimensional analogs by the same factor. In this respect the derivation is consistent with the derivation of the branching ratio in the preceding section.

Explicit Formula for r_+

The function $r_+(R)$ is obtained by solving the equation

$$f(R,r) = 0$$

for r. Hence, the choice of a specific functional form for r_+ implies a choice of f. The graph of r_+ in the r–R plane represents that portion of the transition state surface which is most easily visualized.

The explicit form of r_+ to be used in the present study was motivated by several considerations. The first is that it must represent a curve which completely separates the A_2 + M region of configuration space from the AM + A region. Another is that it should be simple. A third is that it should depend on a parameter in order to allow some flexibility of choice. The potential energy surfaces assumed in the present work either have no saddle point or, at most, a saddle point of negligible height with respect to the AM + A valley. Hence, in the present study one cannot be guided in the standard way in one's choice of the transition state. The final, somewhat arbitrary condition on r_+ is that for some value of the parameter it should represent the transition state for a symmetric potential surface with a saddle point.

The above considerations led to the choice

$$r_+ = \tfrac{1}{3} bR + a\,\sigma_\infty/R$$

where a is the parameter, and σ_∞ is the equilibrium internuclear distance for isolated AM. In the present study a was chosen such as to minimize $k_3 + k_4$. Hence, it is not an adjustable parameter.

Numerical Results

Numerical evaluation of the integrals on the right of [13] was carried out using a subroutine based on Simpson's rule. All of the a-dependence of the rate constants is in these integrals. In a typical case, evaluation of $\mathscr{I}$ at five to ten values of a was sufficient to locate the minimum. As can be seen from eq. [19], the computation of G_3 and G_4 entails the location of relative maxima and minima in V_1. These extrema were found using a slightly modified version of Harwell Subroutine VD02A. The calculations reported here were done on a B6700, but it was found that calculations of this type can be performed satisfactorily on a PDP1103.

Thirty cases, six A_2–M combinations at each of five temperatures, were studied. They are the same as those reported in ref. 4. The potential function assumed is potential B of ref. 6. Morse functions with the standard Br_2 and I_2 parameters were used for V_0. For the sake of ready reference, these parameters are included in Table 1. Also for the sake of ready reference, the additional parameters which enter into V_1 are presented in Table 2. These parameters are the same as those used in ref. 4, thus making the results of this study and that one strictly comparable. The potential energy surface for Br_2 + Ar is depicted in Fig. 1. The potential surfaces for the other five A_2 + M combinations are qualitatively much the same.

TABLE 1. Electronic degeneracy factors, Morse potential parameters and parameters derived therefrom for the isolated molecules

A_2	R_g	α (nm^{-1})	r_e (nm)	D_e (kJ/mol)	n	X^*
Br_2	1/16	19.7	0.228	192	1.37	2.54
I_2	1/16	18.6	0.267	150	1.34	2.59

TABLE 2. Assumed potential parameters for A_2–M interactions

A_2	M	σ_0 (nm)	σ_∞ (nm)	ε_0 (kJ/mol)	ε_∞ (kJ/mol)
Br_2	He	0.3081	0.288	0.35	0.6
	Ar	0.3506	0.332	1.19	2.5
	Xe	0.3853	0.362	1.61	2.9
I_2	He	0.3328	0.308	0.39	0.8
	Ar	0.3752	0.355	1.35	2.5
	Xe	0.4100	0.390	1.84	2.9

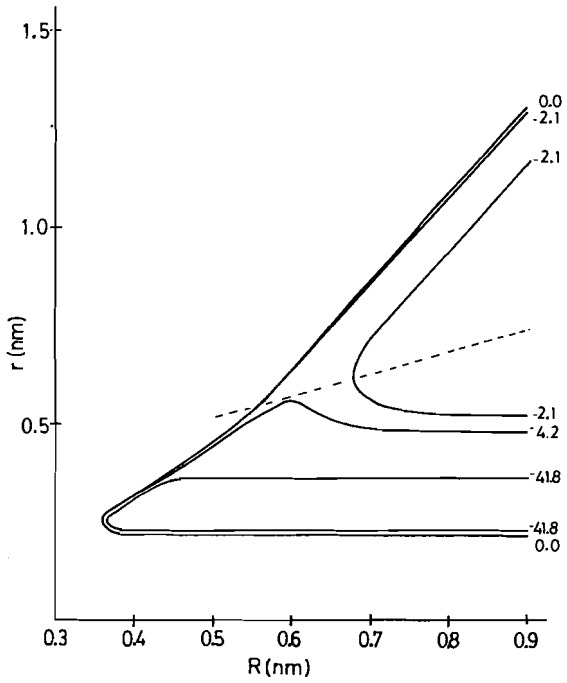

FIG. 1. Assumed potential energy surface for Br_2–Ar collisions. Note that the contours are not equally spaced in energy. The dashed line indicates the $r_+(R)$ curve for T = 1500 K.

In Table 3 the branching ratios calculated in the present study are presented along with those calculated in ref. 4. Agreement is seen to be fair for M = Xe and for M = Ar but poor for M = He. Also shown in Table 3 are the values of a, denoted a_m, for which the sum $k_3 + k_4$ is minimized. The resulting curve of $r_+(R)$ for Br_2 + Ar at 1500 K is shown in Fig. 1. In all cases a_m decreases somewhat with increasing temperature, but the resulting shift in $r_+(R)$ is never great.

The data of Table 3 are shown graphically in Fig. 2 as a plot of $\log_{10} \Gamma$ vs. $\log_{10} \beta\varepsilon_\infty$. The results of ref. 4 for M = Xe, Ar and the results of the present study all lie close to a straight line of slope $-3/2$. Interestingly, a $(\beta\varepsilon_\infty)^{-3/2}$ dependence of Γ was also found in three-dimensional trajectory studies of N_2 + Ar and Cl_2 + Ar (11). Finally, it can be seen from the scatter in the results from ref. 4 that some of the discrepancy between those results and the present ones is due to random numerical errors in the trajectory calculations.

Table 4 shows values of k_r^{eq} given by eq. [24] along with corresponding values from ref. 4. Also shown are the values of r_0, these having been obtained from a least-squares fit of the k_r^{eq}'s of ref. 4 to eq. [24]. Agreement of the k_r^{eq}'s is generally better than agreement of the Γ's, but it still must be regarded as only fair since an adjustable parameter has been used. Again, random errors in the trajectory calculations seem to be causing part of the disagreement. The best fit values of r_0 are smaller than the corresponding σ_0's of Table 2. This would be expected since transition state theory gives an upper bound. It is also to be noted that the r_0's do not increase in the same order as do the σ_0's, the values for M = He being most notably out of line.

Discussion

The results of the present study are in fair agreement with the results of a three-dimensional trajectory study of the same model (4) for the cases M = Xe, Ar. Agreement is poor for M = He. The discrepancies may be due to one or more of the three simplifying assumptions adopted in the present study. It will here be argued that the largest discrepancies between the results of this work and those of ref. 4, i.e. the discrepancies in the Γ's for M = He,

TABLE 3. Comparison of calculations of relative rates of reaction via triple collision and bound complex mechanisms for a model of halogen recombination in inert gases

				Γ	
A_2	M	T(K)	a_m (nm)	Eq. [13]	Ref. 4
Br_2	He	200	0.55	4.0	21
		300	0.54	7.0	31
		600	0.50	17	56
		1000	0.50	35	460
		1500	0.47	68	1520
Br_2	Ar	200	0.26	0.51	0.56
		300	0.25	0.97	1.28
		600	0.24	2.6	4.9
		1000	0.23	5.0	8.5
		1500	0.21	8.7	20
Br_2	Xe	200	0.20	0.36	0.22
		300	0.18	0.71	0.43
		600	0.16	1.85	1.06
		1000	0.15	3.7	2.8
		1500	0.14	5.9	4.8
I_2	He	200	0.65	2.8	18.9
		300	0.60	5.0	23
		600	0.57	13.3	141
		1000	0.54	24	220
		1500	0.52	41	360
I_2	Ar	200	0.30	0.51	0.36
		300	0.30	0.99	0.77
		600	0.30	2.6	3.9
		1000	0.25	4.9	7.6
		1500	0.25	8	18.0
I_2	Xe	200	0.25	0.36	0.22
		300	0.20	0.71	0.39
		600	0.20	1.92	1.04
		1000	0.18	3.7	3.4
		1500	0.17	6.1	5.3

are due to a breakdown of the fundamental assumption of classical transition state theory.

From Table 4 one sees that the k_r^{eq}'s calculated in the present study agree fairly well with those calculated in ref. 4. The method of calculation used in the present study is based on a simple extension of one-dimensional results to three dimensions. This extension changes both k_3 and k_4 by the same factor. The implication is that a one-dimensional calculation should suffice to determine Γ. One therefore has evidence (albeit inconclusive) for the validity of using the analogous collinear model in calculations of Γ. Another bit of evidence is the $\beta\varepsilon_\infty$-dependence of Γ as shown in Fig. 2. It seems reasonable to suppose that the displacement of the trajectory values for M = He from a straight line is due to dynamical effects. It is less likely that the phase integrals of three-dimensional transition state theory differ in such an essential way from those of the one-dimensional theory that the resulting values

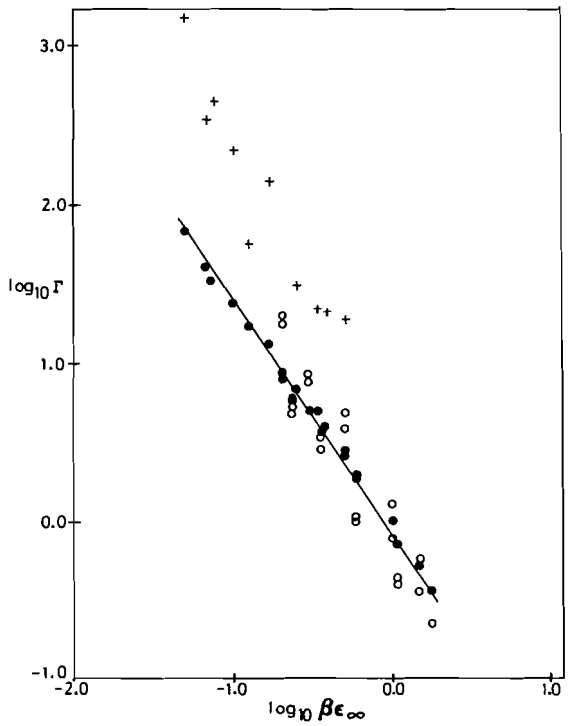

FIG. 2. log–log plot of the branching ratios from ref. 4 and from the present work. Filled circles represent results of the present work; open circles, results from ref. 4 for M = Xe, Ar; crosses, results from ref. 4 for M = He.

of log Γ as a function of log $\beta\varepsilon_\infty$ lie close to a straight line in the one case but not in the other. Thus the reduction to a collinear model does not appear to cause the large discrepancies between the Γ's calculated in the present work and those calculated in ref. 4.

As already mentioned, the assumed partitioning of the transition state surface is such as to give an upper bound to k_3 but not k_4. Since Γ is defined as k_3/k_4, it follows that this assumption as to the partitioning of the surface is more likely to overestimate Γ than to underestimate it. However, in the cases of worst disagreement the present calculations grossly underestimate Γ. One is therefore not inclined to ascribe these discrepancies to a breakdown of the assumption as to the partitioning of the surface.

One is left with the fundamental assumption of classical transition state theory, and at this point one should recall the physical significance of this assumption (5). The assumption is entirely valid provided that all trajectories which cross the transition state surface cross it only once. The more recrossings of the surface there are, the larger is the amount by which the transition state theory approximation overestimates the rate constant.

TABLE 4. Comparison of calculations of equilibrium rate constants for a model of halogen recombination in inert gases

				k_r^{eq} (10^9 L^2/mol^2 s)	
A_2	M	r_0 (nm)	T (K)	Eq. [22]	Ref. 4
Br_2	He	0.194	200	1.23	1.10
			300	1.09	1.00
			600	1.00	1.03
			1000	1.00	1.16
			1500	1.00	1.07
Br_2	Ar	0.145	200	2.3	2.2
			300	1.40	1.42
			600	0.85	0.84
			1000	0.68	0.81
			1500	0.60	0.78
Br_2	Xe	0.172	200	3.9	4.0
			300	2.2	2.3
			600	1.23	1.18
			1000	0.95	0.77
			1500	0.83	0.58
I_2	He	0.212	200	1.57	1.31
			300	1.32	1.26
			600	1.18	1.31
			1000	1.16	1.27
			1500	1.16	1.33
I_2	Ar	0.174	200	2.9	2.8
			300	1.79	1.74
			600	1.09	1.11
			1000	0.89	1.09
			1500	0.82	0.97
I_2	Xe	0.181	200	4.0	4.0
			300	2.3	2.5
			600	1.27	1.06
			1000	0.96	0.86
			1500	0.85	0.67

It is reasonable to suppose that multiple crossings are most likely through that portion of the transition state surface which has been associated with the bound complex mechanism (11). There the total energy is lower, and hence, the effect of the A–M attractive forces is larger. This effect very likely manifests itself in more complicated trajectories which make more crossings of the transition state surface.

It may be noted in passing that one can now advance a plausible explanation for the relatively large values of r_0 obtained for M = He. As mentioned in the previous section, the ratio of r_0 to σ_0 is a rough indication of the amount by which the trajectory value of k_r^{eq} is reduced relative to the transition state theory value, said reduction being due to recrossings. In the case of M = He the contribution to the overall rate from reaction [4] is relatively small. Since this is the contribution expected to be most reduced by recrossings, the overall reduction due to recrossings is expected to be smaller in this case.

The very large values of Γ for M = He are an indication that the relative contributions from reaction [4] which are already smallest at the level of transition state theory are also most greatly diminished due to recrossings. However, the cause is probably different in the two cases. At the level of transition state theory a small contribution from [4] is most likely due to a small value of ε_∞, as is indicated by Fig. 2. The further reduction due to recrossing is more likely due to the small mass of He. One may ascribe at least some of the complexity of the recrossing trajectories to incipient vibration of AM. The frequency of this vibration increases as the reduced mass of AM decreases. Hence, it seems reasonable that the smaller mass of He should cause more recrossing of that part of the transition state surface which has been associated with the bound complex mechanism.

It should be emphasized that the foregoing arguments are no more than plausible. Only a thoroughgoing analysis of the trajectories for the model would rigorously account for the discrepancies between the results of the present work and those of ref. 4.

The method described herein provides fairly reliable values of relative rates for recombination by reactions [1] and [2] in cases where AM is weakly bound and the masses of A and M are large. Although the method requires considerably less computation than do the trajectories, the amount of computation which it does entail still seems excessive in view of the simplicity of the final results, as indicated by Fig. 2. A search for further simplifications therefore seems in order, and the results reported here are mainly of interest in that they illustrate the discrepancies which arise as a consequence of more fundamental approximations.

Acknowledgments

This work was supported by a grant from the National Research Council of Canada. A discussion of the preliminary results with Professor George Burns was quite helpful. Assistance with the computations was provided by Mr. John Aitkens, Mr. Robert MacPherson, Mr. Derek Cheung, and Mr. Kevan Kristjanson.

1. D. L. BUNKER and N. DAVIDSON. J. Am. Chem. Soc. **80**, 5090 (1958).
2. G. PORTER and J. A. SMITH. Proc. R. Soc. London, **A261**, 28 (1961).
3. W. H. WONG and G. BURNS. J. Chem. Phys. **59**, 2974 (1973).

4. D. T. CHANG and G. BURNS. Can. J. Chem. **54**, 1535 (1976).
5. E. WIGNER. J. Chem. Phys. **5**, 720 (1937); Trans. Faraday Soc. **34**, 29 (1938); J. C. KECK. Adv. Chem. Phys. **13**, 85 (1967).
6. A. G. CLARKE and G. BURNS. J. Chem. Phys. **55**, 4717 (1971).
7. N. SNIDER. Can. J. Chem. **55**, 3464 (1977).
8. N. SNIDER. J. Chem. Phys. **69**, 3540 (1978).
9. J. C. KECK. J. Chem. Phys. **32**, 1035 (1960).
10. T. L. HILL. Introduction to statistical thermodynamics. Addison-Wesley Publishing Co., Reading, MA. 1960. p. 154.
11. V. H. SHUI. J. Chem. Phys. **57**, 1704 (1972).

Appendix

The object of this section is to show how eqs. [16] and [19] follow from [14]. Derivation of [19] is simpler and will be considered first. Substitution in [14*b*] of [10] for H, replacement of p_r by H_{Int} via [9], and integration over H_{Int} gives

$$G_3 = (\beta/2\pi\bar{\mu})^{1/2} \int dr\, \theta(-f)\theta(-V_0)|\partial\beta V_1/\partial r| \exp(-\beta V_1) \int dp_R\, \theta(p_R^2/2\bar{\mu} + V_1) \exp(-\beta p_R^2/2\bar{\mu})$$

The equation for G_4 is the same except in that $\theta(p_R^2/2\bar{\mu} + V_1)$ is replaced by $\theta(p_R^2/2\bar{\mu} + V_1 + \varepsilon_\infty) \times \theta(-p_R^2/2\bar{\mu} - V_1)$. The first of the foregoing factors is practically redundant since V_1 almost always exceeds $-\varepsilon_\infty$. Substitution of t^2 for $\beta p_R^2/2\bar{\mu}$ gives

$$G_3 = \pi^{-1/2} \int dr\, \theta(-f)\theta(-V_0)|\partial\beta V_1/\partial r| \exp(-\beta V_1) \int dt\, \theta(t^2 + \beta V_1) \exp(-t^2)$$

When V_1 is negative, the interval $-(-\beta V_1)^{1/2} \leq t \leq (-\beta V_1)^{1/2}$ is excluded from the range of t-integration by the unit step function. Hence, one obtains

[A1] $$G_3 = \int dr\, \theta(-f)\theta(-V_0)|\partial\beta V_1/\partial r| \exp(-\beta V_1)\,[1 - \operatorname{erf}(-\beta V_1)^{1/2}\,\theta(-\beta V_1)]$$

and similarly for G_4

[A2] $$G_4 = \int dr\, \theta(-f)\theta(-V_0)|\partial\beta V_1/\partial r| \exp(-\beta V_1) \operatorname{erf}(-\beta V_1)^{1/2}\,\theta(-\beta V_1)$$

where erf denotes error function.

Recalling the definitions of r_+ and r_-, one sees that the step function $\theta(-V_0)\theta(-f)$ implies limits of r_+ and r_- for the r-integration. Replacing r by βV_1 as the variable of integration, one obtains a sum of integrals each with a maximum in βV_1 as upper limit and an adjacent minimum in βV_1 as lower limit. Equation [17] and two integrations by parts give

[A3] $$\int_0^{-\chi\theta(-\chi)} \operatorname{erf}(-t)^{1/2}\, e^{-t}\, dt = 4\pi^{-1/2}\, e^{-\chi} \int^{(-\chi)^{1/2}\theta(-\chi)} \exp(-u^2)\, du = Z(\chi)\, e^{-\chi}$$

Thus eqs. [A1]–[A3] yield eq. [19].

Preparatory to evaluation of the integral in [14*b*], define ϕ by the relation

$$\tan\phi = (\partial r/\partial R)_f$$

from which follow

[A4] $$\frac{\partial f}{\partial R} = -\left[\left(\frac{\partial f}{\partial R}\right)^2 + \left(\frac{\partial f}{\partial r}\right)^2\right]^{1/2} \sin\phi$$

$$\frac{\partial f}{\partial r} = \left[\left(\frac{\partial f}{\partial R}\right)^2 + \left(\frac{\partial f}{\partial r}\right)^2\right]^{1/2} \cos\phi$$

Furthermore, from eq. [18] one obtains

[A5] $$\tan\phi_+ = \left(\frac{\partial r}{\partial R}\right)_{f=0}$$

From eqs. [A4] and the definition of r_+ follows the relation

[A6] $$\bar{\mu}^{-1}\left(\frac{\partial f}{\partial r}p_r + \frac{\partial f}{\partial R}p_R\right)\delta(-f) = \bar{\mu}^{-1}(p_r\cos\phi - p_R\sin\phi)\sec\phi\,\delta(r - r_+)$$

Next let s and α be given by

[A7]
$$s^2 = \bar{\mu}^{-2}(p_R^2 + p_r^2)$$
$$\cos\alpha = (\bar{\mu}s)^{-1}(p_r\cos\phi - p_R\sin\phi)$$

Insertion of [9], [10], [A6], and [A7] into [14*b*] gives

[A8]
$$F_3 = (\beta\bar{\mu})^{3/2}(2\pi)^{-1/2}\int dr\,\delta(r - r_+)\sec\phi\,\exp(-\beta V)\int ds\,s^2\theta(\tfrac{1}{2}\bar{\mu}s^2 + V)\exp(-\tfrac{1}{2}\beta\bar{\mu}s^2) \times \int_{-\pi/2}^{\pi/2} d\alpha\cos\alpha\,\theta[-\tfrac{1}{2}\bar{\mu}s^2\cos^2(\phi - \alpha) - V_0]$$

In the corresponding equation for F_4, $\theta(\frac{1}{2}\bar{\mu}s^2 + V)$ is replaced by $\theta(\frac{1}{2}\bar{\mu}s^2 + V_c)\theta(-\frac{1}{2}\bar{\mu}s^2 - V)$ where V and V_c are defined in the text.

The limits for the α-integration in [A8] are $-\pi/2$ and $\pi/2$ for V_0 less than $-\frac{1}{2}\bar{\mu}s^2$. For V_0 between $-\frac{1}{2}\bar{\mu}s^2$ and $-\frac{1}{2}\bar{\mu}s^2\sin^2\phi$ the limits become $\phi + \arccos z$, $\pi + \phi - \arccos z$ for ϕ less than zero and $\phi - \pi + \arccos z$, $\phi - \arccos z$ for ϕ greater than zero where z is given by

$$z = (-2V_0/\bar{\mu}s^2)^{1/2}$$

For V_0 between $-\frac{1}{2}\bar{\mu}s^2\sin^2\phi$ and zero the integral breaks into two parts, one with limits $-\pi/2$, $\phi - \arccos z$ and the other with limits $\phi + \arccos z$, $\pi/2$. For V_0 greater than zero the integral is zero. Hence, on integration over α and substitution of t^2 for $\frac{1}{2}\beta\bar{\mu}s^2$, eq. [A8] becomes

$$F_3 = 4\pi^{-1/2}\int dr\,\delta(r - r_+)\theta(-V_0)\sec\phi\,\exp(-\beta V)\Big[\int_0^{(-\beta V_0\csc^2\phi)^{1/2}} t^2\theta(t^2 + \beta V)\exp(-t^2)\,dt - \cos\phi\int_{(-\beta V_0)^{1/2}}^{(-\beta V_0\csc^2\phi)^{1/2}} t(t^2 + \beta V_0)^{1/2}\,\theta(t^2 + \beta V)\exp(-t^2)\,dt + (-\beta V_0)^{1/2}\sin|\phi| \times \int_{(-\beta V_0\csc^2\phi)^{1/2}}^{\infty} t\theta(t^2 + \beta V)\exp(-t^2)\,dt\Big]$$

The first integral in brackets can be evaluated using [A3] as can the second after substituting

$$u^2 = t^2 + \beta V_0$$

The last integral is trivial as is the integral over r. The final result is seen to be eq. [16*a*].

For F_4 one obtains after integration over α

[A9]
$$F_4 = 4\pi^{-1/2}\int dr\,\delta(r - r_+)\theta(-V_0)\sec\phi\,\exp(-\beta V)\Big[\int_0^{(-\beta V_0\csc^2\phi)^{1/2}} t^2\theta(t^2 + \beta V_c) \times \theta(-t^2 - \beta V)\exp(-t^2)\,dt - \cos\phi\exp(\beta V_0)\int_0^{(-\beta V_0\operatorname{ctn}^2\phi)^{1/2}} u^2\theta[u^2 + \beta(V_1 + \varepsilon_\infty)] \times \theta(-u^2 - \beta V_1)\exp(-u^2)\,du + \tfrac{1}{2}\sqrt{-\beta V_0}\sin|\phi|\int_{(-\beta V_0\csc^2\phi)^{1/2}}^{\infty}\theta(w + \beta V_c) \times \theta(-w - \beta V)\,e^{-w}\,dw\Big]$$

Recalling that V_1 can be assumed to be always greater than $-\varepsilon_\infty$ and using [A3] and [A5], one readily reduces [A9] to [16*b*].

The enol content of simple carbonyl compounds: an approach based upon pK_a estimation

J. PETER GUTHRIE[1]

Department of Chemistry, University of Western Ontario, London, Ont., Canada N6A 5B7

Received June 16, 1978

J. PETER GUTHRIE. Can. J. Chem. 57, 1177 (1979).

Rate constants for oxygen-base-catalyzed enolization of di- and tricarbonyl compounds can be correlated by a Marcus equation, with hydroxide requiring a slightly different curve from other oxyanions. Data for monocarbonyl compounds fall on a slightly different, but similar, set of curves. The equilibrium constants for enolization for a set of monocarbonyl compounds were derived from recent work in this laboratory. These correlations permit estimation of pK_a^{Keto} for a number of other monocarbonyl compounds from kinetics data in the literature. Elaboration of methods previously developed permits estimation of pK_a^{Enol}. From the values of pK_a^{Enol} and pK_a^{Keto}, pK_{Enol} can be derived. It is pointed out that pK_a^{Keto} for acetone and acetophenone can be determined from the kinetics of the reaction with hypochlorite in base; the values so derived are in good agreement with those used in this work. pK_{Enol} values are reported for: 1,3-dichloroacetone, 2.0; 1,1-dichloroacetone, 4.9; ethyl pyruvate, 4.2; bromoacetone, 3.5; chloroacetone, 3.7; 1-phenyl-2-propanone, 4.5 (CH_2); 7.2 (CH_3); *p*-nitroacetophenone, 7.1; ethyl levulinate, 5.6; methoxyacetone, 6.9 (CH_2); 7.6 (CH_3); benzalacetone, 7.6; *p*-methoxyacetophenone, 7.8; 3-methyl-2-butanone, 8.0 (CH); 2,4-dimethyl-3-pentanone, 9.4.

J. PETER GUTHRIE. Can. J. Chem. 57, 1177 (1979).

Les constantes de vitesse de l'énolisation catalysée par des bases oxygénées de composés di- et tricarbonylés peuvent être reliées par une équation de Marcus dans laquelle l'hydroxyde demande une courbe légèrement différente de celle des autres oxyanions. Les données pour les composés monocarbonylés tombent sur un ensemble de courbes légèrement différentes mais semblables. On a déduit les constantes d'équilibre pour l'énolisation d'un ensemble de composés monocarbonylés, à partir d'un travail récent de notre laboratoire. Ces corrélations permettent d'évaluer le $pK_a^{Céto}$ d'un certain nombre d'autres composés monocarbonylés à partir des données cinétiques que l'on peut trouver dans la littérature. Une élaboration des méthodes développées antérieurement permet d'évaluer le pK_a^{Enol}. A partir des valeurs de pK_a^{Enol} et $pK_a^{Céto}$, on peut obtenir le pK_{Enol}. On met en évidence que les $pK_a^{Céto}$ de l'acétone et de l'acétophénone peuvent être déterminés à partir de la cinétique de la réaction de l'hypochlorite en milieu basique; les valeurs ainsi obtenues sont en bon accord avec celles utilisées dans ce travail. On rapporte des valeurs de pK_{Enol} pour le: dichloro-1,3 acétone, 2.0; dichloro-1,1 acétone, 4.9; pyruvate d'éthyle, 4.2; bromoacétone, 3.5; chloroacétone, 3.7; phényl-1 propanone-2, 4.5 (CH_2); 7.2 (CH_3); *p*-nitroacétophénone, 7.1; lévulinate d'éthyle, 5.6; méthoxyacétone, 6.9 (CH_2); 7.6 (CH_3); benzalacétone, 7.6; *p*-méthoxyacétophénone, 7.8; méthyl-3 butanone-2, 8.0 (CH); diméthyl-2,4 pentanone-3, 9.4.

[Traduit par le journal]

Introduction

The problem of determining the enol content of simple carbonyl compounds has proven to be difficult and intractable. Early attempts to measure the enol content of such compounds as acetone (1, 2) have been shown to be subject to serious systematic errors (3, 4). Even the most modern variations on the halogen titration method (4) lead to results which are sometimes in conflict with the conclusions of other less direct measurements (5–7). Only very recently has it been possible to determine the enol content of some simple ketones by an indirect kinetic approach (8, 9) and this method requires specialized apparatus and considerable labor. We have presented in recent papers (7, 10) two general methods for evaluating the enol content of carbonyl compounds. This paper presents a third method which permits a great many further equilibrium constants to be evaluated from data in the literature.

It has been common practice for many years, following a suggestion of Bell (11), to estimate the pK_a for the keto form of carbonyl compounds from the rate of proton abstraction, using some form of rate equilibrium correlation. We have refined this procedure and have found that it is not permissible to use the correlation line for di- and tricarbonyl compounds for monocarbonyl compounds as has been done in the past (11, 12). By taking advantage of the work described in the earlier papers (7, 10), we can generate a correlation between rate and equilib-

[1]Alfred P. Sloan Fellow, 1975–1979.

0008-4042/79/101177-09$01.00/0

TABLE 1. Rate and equilibrium constants for reactions of oxygen bases with carbonyl compounds of known pK_a[a]

Carbonyl compounds	pK_a	Base[b]	pK_a[c]	log k_{corr}[d]	log K_{corr}[e]	b[f]
		(*a*) Oxyanion bases, other than hydroxide				
$CH_3COCH(Br)COCH_3$	7.0[g]	ClA	2.87	−0.22[h]	−4.13	8.02
		*m*NB	3.45	0.51[h]	−3.55	7.61
		Glyc	3.88	0.22[h]	−3.12	8.15
		βClP	4.10	0.57[h]	−2.90	7.91
		OBz	4.21	0.67[h]	−2.75	7.90
		PhA	4.31	0.82[h]	−2.69	7.78
		OAc	4.75	0.65[h]	−2.25	8.19
		OPiv	5.05	1.08[h]	−1.95	7.91
$(CH_3OOC)_3C—H$	7.8[i]	ClA	2.82	−0.34[i]	−5.2	7.52
		βClP	4.10	0.49[i]	−4.0	7.37
		OAc	4.75	0.81[i]	−3.3	7.45
		OPiv	5.05	0.79[i]	−3.1	7.58
$Ph—CO—CH_2—CO—CH_3$	8.52[g]	ClA	2.87	−0.74[h]	−6.82	6.91
		*m*NB	3.45	0.08[h]	−6.24	6.42
		Glyc	3.88	−0.80[h]	−5.81	7.62
		βClP	4.10	0.07[h]	−5.59	6.85
		OBz	4.21	0.09[h]	−5.48	6.90
		OAc	4.75	0.21[h]	−4.94	7.11
		OPiv	5.05	0.52[h]	−4.64	6.97
$CH_3—CO—CH_2—CO—CH_3$	8.87[i]	ClA	2.87	−0.78[h]	−6.30	7.29
		*m*NB	3.45	−0.42[h]	−5.85	7.20
		For	3.75	0.06[j]	−5.42	6.97
		Glyc	3.88	−0.33[h]	−5.42	7.37
		βClP	4.10	−0.19[h]	−5.07	7.44
		OBz	4.21	−0.10[h]	−4.96	7.41
		PhA	4.31	0.21[j]	−4.86	7.15
		OAc	4.75	0.26[j]	−4.42	7.36
		OPiv	5.05	0.26[h]	−4.12	7.54
		Cac	6.19	1.74[j]	−2.98	6.69
		*p*CNP	7.95	2.44[j]	−0.92	7.09
		*o*ClP	8.48	2.90[j]	−0.69	6.75
		*m*ClP	9.02	2.81[j]	−0.15	7.11
		PhO	10.00	3.48[j]	+0.83	6.93
		Gluc	12.3	4.00[j]	+3.13	7.48
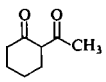	9.9[i]	OAc	4.75	−1.30[i]	−5.7	8.20
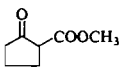	10.52[k]	Pi^-	2.12	−1.29[k]	−8.40	6.40
		ClA	2.87	−1.24[k]	−7.65	6.88
		Glyc	3.88	−0.71[k]	−6.64	7.00
		OAc	4.75	−0.15[k]	−5.77	6.97
		OPiv	5.05	0.01[k]	−5.47	6.99
$CH_3COCH_2COOCH_2CH_3$	10.68[g]	ClA	2.87	−1.72[h]	−8.11	7.08
		*m*NB	3.45	−1.26[h]	−7.43	7.00
		Glyc	3.88	−1.16[h]	−7.10	7.17
		OBz	4.21	−0.90[h]	−6.77	7.11
		PhA	4.31	−0.78[h]	−6.67	7.05
		OAc	4.75	−0.62[h]	−6.23	7.17
		OPiv	5.05	−0.44[h]	−5.93	7.17
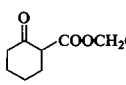	10.94[r]	ClA	2.87	−3.49[k]	−8.65	8.63
		Glyc	3.88	−2.89[k]	−7.64	8.65
		OAc	4.75	−2.27[k]	−6.77	8.55
		OPiv	5.05	−2.08[k]	−6.47	8.54
$CH_3—CO—CH(CH_3)—CO—OCH_2CH_3$	12.70[g,l]	Cl_2A	1.48	−4.47[m]	−11.22	7.86
		ClA	2.87	−3.52[m]	−9.83	7.84
		βClP	3.98	−2.75[m]	−8.72	7.78
		OAc	4.75	−2.49[m]	−9.95	6.57
		OPiv	5.05	−2.24[m]	−7.65	7.96
		$Pi^=$	7.21	−1.40[m]	−5.59	8.37
$(CH_3CH_2OOC)_2CH_3$	13.3[g]	Pi^-	2.12	−3.89[n]	−11.18	7.22
		ClA	2.87	−3.44[n]	−10.43	7.29
		Glyc	3.88	−2.75[n]	−9.42	7.28

TABLE 1 (*Concluded*)

Carbonyl compounds	pK_a	Base[b]	pK_a[c]	log k_{corr}[d]	log K_{corr}[e]	b[f]
		OAc	4.75	−1.95[n]	−8.55	7.02
		OPiv	5.05	−1.73[n]	−8.25	7.00
		Pi=	7.21	−0.83[n]	−6.09	7.47
$CH_3COCH_2SO_3^-$	13.6[i]	ClA	2.87	−5.16[i]	−11.4	8.50
		OAc	4.75	−3.65[i]	−9.6	8.14
		OPiv	5.05	−3.62[i]	−9.4	8.25
$(-O_3SCH_2)_2CO$	13.85[o]	ClA	2.87	−4.66[o]	−10.99	8.25
		Glyc	3.88	−3.96[o]	−9.97	8.22
		OAc	4.75	−3.40[o]	−9.10	8.22
					Average	7.50±0.56
	(*b*) Hydroxide ion as base					
$CH_3COCH_2COCH_3$	8.87[i]	OH^-	15.74	4.30[i]	6.57	8.67
$CH_3COCH_2COOCH_2CH_3$	10.68[g]	OH^-	15.74	3.53[p]	4.76	8.69
$CH_3COCHCOOCH_2CH_3$ (CH$_3$ on CH)	12.70[g,l]	OH^-	15.74	2.03[p]	3.04	9.43
$CH_3COCH_2SO_3^-$	13.6[i]	OH^-	15.74	2.11[i]	1.8	8.79
					Average	8.89±0.36
	(*c*) Water as catalyst					
$CH_3COCH(Br)COCH_3$	7.0[g]	H_2O	−1.74	−3.38[h]	−8.7	8.47
$(CH_3OOC)_3CH$	7.8[i]	H_2O	−1.74	−3.57[i]	−9.5	8.13
$CH_3COCH_2COCH_3$	8.87[j]	H_2O	−1.74	−3.52[j]	−10.91	7.00
$PhCOCH_2COCH_3$	9.39[g]	H_2O	−1.74	−4.00[h]	−11.43	7.14
	9.9[i]	H_2O	−1.74	−5.09[i]	−11.6	8.27
	10.52[k]	H_2O	−1.74	−4.38[h]	−12.26	6.88
$CH_3COCH_2COOCH_2CH_3$	10.68[g]	H_2O	−1.74	−4.96[h]	−12.72	7.19
$CH_3COCHCOCH_3$ (CH$_3$ on CH)	11.0[g]	H_2O	−1.74	−5.76[m]	−12.7	8.18
	10.94[r]	H_2O		−6.74[m]	−13.26	8.87
$CH_3COCH(COOCH_2CH_3)_2$	12.70[g,l]	H_2O		−6.70[m]	−14.44	7.81
$(CH_3CH_2OOC)_2CH_2$	13.30[g]	H_2O		6.68[n]	−15.34	6.87
$CH_3COCH_2SO_3^-$	13.6[i]	H_2O		−7.74[i]	−15.6	8.05
						7.74±0.69

[a] In water at 25°C.
[b] Abbreviations used are: Cl_2A, dichloroacetate; Pi$^-$, dihydrogenphosphate; ClA, monochloroacetate; *m*NB, *m*-nitrobenzoate; For, formate; Glyc, glycolate (2-hydroxyacetate); βClP, β-chloropropionate; OBz, benzoate; PhA, phenyl acetate; OAc, acetate; OPiv, pivalate (2,2-dimethylpropanoate); Cac, cacodylate (dimethylarsinate); Pi=, monohydrogenphosphate; *p*CNP, *p*-cyanophenoxide; *o*ClP, *o*-chlorophenoxide; *m*ClP, *m*-chlorophenoxide; PhO, phenoxide; Gluc, anion of glucose.
[c] pK_a for the conjugate acid of the base: values taken from the paper reporting the rate constants.
[d] Observed rate constant, corrected for the number of equivalent hydrogens, M^{-1} s^{-1}.
[e] Equilibrium constant for the reaction of the base with the carbonyl compound to give the enolate, corrected for the number of equivalent enolizable hydrogens.
[f] 'Intrinsic barrier' calculated from [1]; see text.
[g] Reference 20.
[h] Reference 21.
[i] Reference 22.
[j] Reference 23.
[k] Reference 24.
[l] Assumed to be the same as for $CH_3COCH(C_2H_5)COOC_2H_5$.
[m] Reference 25.
[n] Reference 26.
[o] Reference 27.
[p] Reference 28.
[q] Reference 29.
[r] Reference 30.

rium constants for monocarbonyl compounds, and use this to estimate pK_a values for the keto tautomers of numerous additional compounds.

Procedures for estimating the pK_a values of alcohols on the basis of substitutent effects have been developed and widely used (13). We have extended this approach to give estimates of the pK_a of enols. If the pK_a for both the keto and the enol tautomer are known, then the equilibrium constant for enolization, K_{Enol}, is also known, since by definition:

$$K_{Enol} = K_a^{Keto}/K_a^{Enol}$$

This procedure does not lead to precise estimates of the enol content but it does give answers of useful accuracy and has the advantage of being extremely simple.

Results and Discussion

In Table 1 are collected data for oxygen base catalyzed enolizations of carbonyl compounds for which the pK_a is measurable by titration. To apply rate equilibrium correlations, it is important to have sets of reactions with transition states identical as to atoms undergoing changes in bonding, and charge type of reactants and products; accordingly, the data are divided into reactions catalyzed by oxyanions other than hydroxide, reactions catalyzed by hydroxide, and uncatalyzed (or water-catalyzed) reactions. There are also some data for amine-catalyzed reactions but since these only refer to simple enolization for tertiary amines and the set of data for tertiary-amine-catalyzed reactions was comparatively small, these catalysts were not considered in this initial examination of the method.

All of the rate and equilibrium constants were corrected for the number of enolizable hydrogens. The data were fitted to the simplest of the equations derived by Cohen and Marcus (14) to correlate rate and equilibrium constants:

$$[1] \qquad \log k = 10 - b[1 - (\log K/4b)]^2$$

This equation assumes that reaction involves diffusion together of catalyst and substrate (with a rate constant of $10^{10}\ M^{-1}\ s^{-1}$ (15)) reaction within the encounter complex, and diffusion apart of the products. The parameter b, the 'intrinsic barrier,' is defined as the barrier to reaction when $\log K = 0$; in the treatment used here the intrinsic barrier includes both the free energy of activation required to achieve proton transfer and also the free energy cost of forming the, presumably very weak, hydrogen bond between catalyst and substrate. More elaborate equations derived by Marcus (14) include a 'work term' which allows for this latter contribution; however, inclusion of a work term necessarily increased the number of parameters. As will be seen below the available data are satisfactorily described by the simple equation used, and show no systematic deviations which would justify the inclusion of an additional parameter.

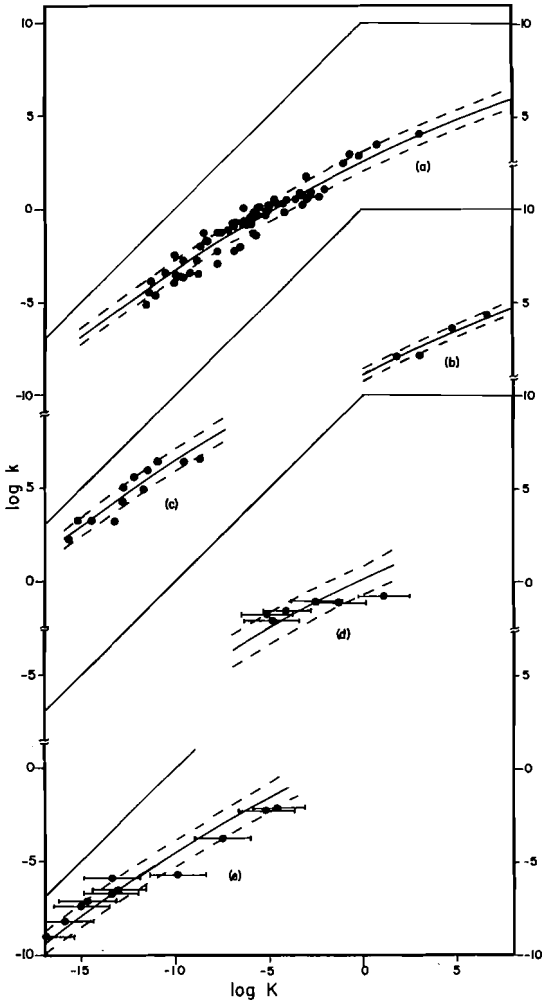

FIG. 1. Marcus plots for base-catalyzed enolization; for each curve the line corresponding to the best value of b (solid lines) and b plus or minus one standard deviation (dashed lines) are shown. Scales are offset by increments of 5–10 log units as indicated in order to avoid overlap. (*a*) Oxyanions other than hydroxide with di- or tricarbonyl compounds; (*b*) hydroxide with di- or tricarbonyl compounds; (*c*) water with di- or tricarbonyl compounds; (*d*) hydroxide with monocarbonyl compounds; (*e*) oxyanions other than hydroxide with monocarbonyl compounds.

The data for oxyanion bases other than hydroxide are found in Table 1*a*; Fig. 1 shows that these data are satisfactorily described by [1] with a b value of 7.50 ± 0.56. (A value of b was calculated for each point and all of the b values were averaged.) For any single substrate the scatter would be less.

In Table 1*b* are collected data for hydroxide-cata-

TABLE 2. Rate and equilibrium constants for the reaction of oxyanion bases with monocarbonyl compounds[a]

Compound	pK_a^{Enol} [b]	pK_{Enol} [b]	pK_a^{Keto} [b]	Base[c]	log K[d]	log k[e]	b[f]
			(*a*) Hydroxide ion as base				
CH_3CHO	11.2(1.0)	5.3(6)	16.5(1.2)	OH^-	−1.3	−1.11[g]	10.47
$(CH_3)_2CH—CHO$	11.8(1.0)	2.8(1.1)	14.6(1.5)	OH^-	+1.1	−0.76[h]	11.30
CH_3COCH_3	11.8(1.0)	7.2(0.9)[n]	19.0(1.3)	OH^-	−4.1	−1.54[i]	9.38
$CH_3—CH(H)—COCH_3$	12.1(1.0)	8.3(1.0)	20.5(1.4)	OH^-	−5.1	−1.72[j]	9.00
$CH_3—CH_2COCH_2CH_3$	12.1(1.0)	7.8(1.0)[o]	19.9(1.4)	OH^-	−4.8	−2.02[k]	9.47
$PhCOCH_3$	11.0(1.0)	6.7(1.0)	17.7(1.4)	OH^-	−2.5	−1.09[l]	9.80
						Average	9.90±0.85
			(*b*) Oxyanion bases other than hydroxide				
$(CH_3)_2CH—CHO$	11.8(1.0)	2.8(1.1)	14.6(1.5)	OAc	−9.9	−5.72[h]	10.17
				PhO	−4.6	−2.14[h]	9.70
				*p*ClP	−5.2	−2.26[h]	9.48
				*p*NP	−7.5	−3.78[h]	9.67
	12.1(1.0)	5.7(1.1)	17.8(1.5)	OAc	−13.4	−6.71[m]	8.72
				OPiv	−13.1	−6.51[m]	8.73
$(CH_2)_2CO$ (H)	11.8(1.0)	7.2(0.9)	19.0(1.3)	ClA	−16.9	−9.08[n]	8.54
				Glyc	−15.9	−8.20[n]	8.36
				OAc	−15.0	−7.39[n]	8.17
				OPiv	−14.7	−7.17[n]	8.17
				Cl_3P	−13.4	−5.90[n]	7.75
						Average	8.86±0.78

[a]In water, at 25°C; values in parentheses are estimated standard deviations.
[b]From reference 7.
[c]Abbreviations and pK_a values as in Table 1.
[d]Logarithm of the equilibrium constant for the reaction of hydroxide with the carbonyl compound to give the enolate, corrected for the number of equivalent hydrogens.
[e]Logarithm of the rate constant for hydroxide catalyzed enolization, corrected for the number of equivalent hydrogens.
[f]The 'intrinsic barrier' parameter from [1]; see text.
[g]Rate constants for enolization reactions: The rate constant for the reaction of hydroxide ion with acetaldehyde reported by Bell (31) was corrected for hydration (32).
[h]Rate constants for the reactions of various bases with 2-deuterioisobutyraldehyde at 35°C were reported by Hine *et al.* (33); these were corrected for hydration (33); corrected to 25°C assuming that the value of $\Delta S^{\ddagger}$ is independent of the base used and is the same as that for hydroxide catalyzed enolization of diisopropyl ketone, for which $\Delta S^{\ddagger}$ was calculated from the data in ref. 34; and corrected for the isotope effect by using a value estimated from the rate constant by means of the correlation reported by Kresge *et al.* (35).
[i]The rate constant for the reaction of hydroxide with butanone was calculated from that for detritiation reported in ref. 36, using an isotope effect assumed to be the same as for *p*-methyl acetophenone (37) which has a very similar k_T.
[j]Reference 38.
[k]Reference 39.
[l]Reference 37.
[m]Reference 40.
[n]A value of 8.84 (0.9) can be calculated from data in refs. 8 and 9.
[o]A value of 8.02 (0.9) can be calculated from data in refs. 8 and 9.

lyzed enolizations. Figure 1 shows that these data are satisfactorily described by a b value of 8.89 ± 0.38. Unfortunately there are relatively few data for this process; this is a consequence of the very rapid reactions involved, so that only the limited number of laboratories equipped for fast kinetics can measure the rate constants. It is common to find that hydroxide ion does not fit Brønsted plots for oxyanion catalysts and this is borne out by the distinctive b value observed. One is tempted to speculate that the larger b value for hydroxide may represent the greater cost in lost solvation energy on forming the very weak hydrogen bond between hydroxide and substrate relative to the other oxyanions.

In Table 1*c* are collected data for water catalyzed enolizations. These reactions were assumed to represent general base catalyzed reaction. Figure 1 shows that the data are satisfactorily described by a b value of 7.74 ± 0.69. Although this is in fact indistinguishable from the value observed for oxyanions, it seems unwise to average them or to assume that this identity of b values is a general phenomenon, since the charge types of the reactions are so different: neutral plus neutral to anion plus cation, as opposed to anion plus neutral to neutral plus anion.

Earlier papers in this series (7, 10) reported evaluation by two independent methods of equilibrium constants for enolization of a number of simple carbonyl compounds. For these compounds equilibrium constants can now be correlated. The data employed are found in Table 2. Table 2*a* reports the available data for hydroxide-catalyzed enolization; Fig. 1 shows that these data are described by a b value of 9.90 ± 0.85. It is apparent that these equilibrium constants are significantly less precise than the titrimetric values used for polycarbonyl compounds and that the fit is distinctly poorer. On

TABLE 4. pK enol values for simple carbonyl compounds, predicted by estimating pK_a^{Keto} and pK_a^{Enol}

Carbonyl compound[a]	Base[b]	Log k^{corr} [c]	pK_a^{Keto} [d]	Av pK_a^{Keto}	pK_a^{Enol} [e]	pK_{Enol} [f]
$(ClCH_2)_2CO$	ClA	−3.53[g]	11.22			
	Glyc	−2.90[g]	11.20	1.04	9.0	2.0
	OAc	−2.23[g]	10.95	±0.20		
	OPiv	−1.97[g]	10.80			
$CH_3—CO—CCl_2$ (H)	ClA	−4.09[h]	12.12			
	OAc	−2.66[h]	11.67	11.00	6.2	4.8
	OPiv	−2.28[h]	11.33	±1.46		
	OH^-	+3.24[h]	8.86			
$CH_3COCOOC_2H_5$	ClA	−4.84[i]	13.30			
	βClP	−4.08[i]	13.33	13.35	9.2	4.2
	OAc	−3.71[i]	13.34	±0.05		
	OPiv	−3.52[i]	13.39			
$CH_3CO—CHBr$ (H)	ClA	−5.43[h]	14.19			
	Glyc	−5.04[h]	14.61			
	OAc	−4.24[h]	14.24	13.72	10.3	3.4
	OPiv	−4.09[h]	14.30	±1.38		
	OH^-	+2.21[h]	11.27			
$CH_3COCH—Cl$ (H)	ClA	−5.62[h]	14.49			
	Glyc	−4.85[h]	14.32			
	OAc	−4.06[h]	13.95	14.05	10.4	3.6
	OPiv	−3.82[h]	13.87	±0.70		
	Cl_3Ph	−2.36[h]	12.82			
	HO^-	+0.55	14.83			
$Ph—CH(H)—CO—CH_3$	HO^-	+0.01[j]	15.91		11.8	4.1
O_2N-C$_6$H$_4$-$CO—CH_2$ (H)	HO^-	−0.37[k]	16.67		10.0	6.7
$CH_3—CO—CH(H)—CH_2—COOCH_2CH_3$	Man	−7.55[l]	17.84			
	βClP	−6.98[l]	17.72	17.74	12.1	5.6
	OAc	−6.49[l]	17.66	±0.09		
	OPiv	−6.22[l]	17.56			
$CH_3O—CH(H)—CO—CH_3$	*p*NP	−5.11[m]	17.98			
	PhO	−3.12[m]	17.69	18.49	11.8	6.7
	HO^-	−1.62[m]	19.04	±0.76		
		−1.72[n]	19.23			

the other hand the available data do appear to conform to [1].[2] The b values for mono- and for polycarbonyl compounds are not demonstrably different, although it appears likely that with more and better data they would be shown to differ; in particular the low values of b for the monocarbonyl compounds are found for the equilibrium constants which are least reliable, namely those for methyl ethyl ketone and diethyl ketone, where free energies of formation of the enol ethers were either estimated or derived by indirect means. Furthermore the set of data for polycarbonyl compounds is very small.

Table 2*b* reports the available data for oxyanion catalyzed enolization; Fig. 1 shows that these data are described by a b value of 8.86 ± 0.78. This value seems to be clearly different from that observed for the polycarbonyl compounds[3] and lends support to the belief that the b values for hydroxide-catalyzed reactions will also turn out to be different.

The advantage of having performed these correlations is that they can now be used to calculate unknown equilibrium constants for enolate formation from rate constants for enolization. This is not particularly useful for polycarbonyl compounds where direct measurement is normally possible but is of great potential value for simple monocarbonyl compounds where the enol content is not readily determined.

The procedure employed is to calculate equilibrium constants for all enolizations for which rate constants are available, using the b values for monocarbonyl

[2]A referee has pointed out that the trend of the data for monocarbonyl compounds is in the direction expected if the 'work term' in the Marcus equation is larger than for diffusion alone; although we agree, we feel that the data are too few and of too low precision to justify inclusion of an additional parameter; caution in the use of these correlations for extrapolation is indicated and it would clearly be very desirable to have more data for reactive monocarbonyl compounds.

[3]The mean values are different at the 99% confidence level by the t-test (51).

TABLE 4 (*Concluded*)

Carbonyl compound[a]	Base[b]	Log k^{corr} [c]	pK_a^{Keto} [d]	Av pK_a^{Keto}	pK_a^{Enol} [e]	pK_{Enol} [f]
Ph—CH_2—CO—CH_2 (H)	HO^-	−1.21[g]	18.27		11.5	6.7
Ph—CH=CH—CO—CH_2 (H)	HO^-	−1.28[g]	18.41		11.2	7.2
MeO—C$_6$H$_4$—CO—CH_2 (H)	HO^-	−1.35[h]	18.54		11.1	7.4
CH_3OCH_2CO—CH_2 (H)	*p*NP	−5.04[m]	17.87			
	PhO	−3.10[m]	17.65	18.29		
	HO^-	−1.92[m]	19.59	±0.88	10.9	7.4
		−1.08[q]	18.03			
$(CH_3)_2C$—$COCH_3$ (H)	OAc	−7.89[r]	19.17			
	HO^-	−2.71[s]	21.01	20.33	12.4	7.9
		−2.59[t]	20.80	+1.00		
$((CH_3)_2C)_2CO$ (H)	HO^-	−2.98[q]	21.48		12.4	9.1

[a]The hydrogen removed in enolate formation is indicated; compounds are listed in increasing order of pK_a^{Keto}.
[b]Abbreviations and pK_a values for the bases as in Table 1, with the following additions: *p*NP, *p*-nitrophenol, $pK_a = 7.14$ (ref. 50); Cl_3P, 2,4,6-trichlorophenol, $pK_a = 6.41$ (ref. 41); Man, mandelic acid, $pK_a = 3.40$ (ref. 45).
[c]Rate constants (corrected as necessary) are for reactions of the unhydrated carbonyl compound in water at 25°C and are calculated per hydrogen.
[d]Calculated from the curves in Fig. 1 and then corrected for number of equivalent hydrogens, so that apparent pK_a values are obtained. Average values are reported, with error limits reflecting both scatter in the data and the imprecision of the correlation in Fig. 1.
[e]Estimated as described in the text.
[f]$pK_{Enol} = pK_a^{Keto} - pK_a^{Enol}$ and is $-\log K_{Enol}$.
[g]Reference 42; corrected for hydration as described in ref. 42.
[h]Reference 41; corrected for hydration as described in ref. 42.
[i]Reference 43; corrected for hydration as described in ref. 44.
[j]Calculated from the rate constant for detritiation (ref. 36) assuming that k_H/k_T is the same as for pNO_2—C_6H_6—$COCH_3$, i.e. 18.2 (ref. 37).
[k]Reference 37.
[l]Reference 45.
[m]Reference 46; the rate constants were corrected for the temperature change from 35 to 25°C by assuming that the entropy of activation is the same as for the reactions of hydroxide with acetone (ref. 47) and for the primary deuterium isotope effect by using a value for this effect estimated from the rate constant using the correlation reported by Kresge *et al.* (35).
[n]Calculated from the rate constants for detritiation (ref. 36) assuming that k_H/k_T is the same as for *p*-chloroacetophenone, i.e. 14.8 (ref. 37).
[o]Calculated from the rate constant for detritiation (ref. 36) assuming that k_H/k_T is the same as for *m*-methylacetophenone, i.e. 15.8 (ref. 37).
[p]Calculated from the rate constant for detritiation (ref. 36) assuming that k_H/k_T is the same as for *p*-methylacetophenone, i.e. 14.8 (ref. 37).
[q]Calculated from the rate constant for detritiation (ref. 36) assuming that k_H/k_T is the same as for acetophenone, i.e. 15.1 (ref. 37).
[r]Reference 48; the data were corrected from 41.85 to 25°C, assuming that relative rates would be the same at both temperatures, using acetone as a standard; the rate constant for acetone was taken from ref. 38.
[s]Reference 49; the rate constants reported in this paper were measured in 2:1 dioxane–water at 32°C; it was assumed that relative rates would be the same in water at 25°C; acetone was used as a standard (ref. 38).
[t]Calculated from the rate constant for detritiation (ref. 36) assuming that k_H/k_T is the same as for acetone, i.e. 13.1. (Calculated using k_H from ref. 38 and k_T from ref. 47.)

compounds; then from the known pK_a values for the catalysts, the pK_a^{Keto} values can be calculated. These are averaged for each compound, using data for all bases which have been studied. There are in some cases serious discrepancies, amounting to 1 or 2 pK_a units; however, since error analysis suggests that the pK_a^{Keto} values cannot be better than ±2 pK_a units, given the nature of the correlations and the data, this is not a basis for rejecting the method but simply an illustration of its imperfections.

The scatter of the estimated pK_a^{Keto} values is indicated by the standard deviations calculated for the average pK_a^{Keto} values; in all cases this is less than the 2 pK unit uncertainty expected for each value. The final values of pK_{Enol} are assumed to be uncertain by about 2 pK units; this error arises mainly from the uncertainty in the enol content of the monocarbonyl compounds used to determine b and can only be reduced by more precise determination of these enol contents. Rate equilibrium correlations cannot be precise when the structural variation is close to the reaction site, as in the present case. On the other hand, such correlations are not of much utility unless they apply over a wide range of reactivity; there is thus a sort of uncertainty principle which dictates that one can have precise correlations over such a narrow range of structural types as to have little predictive utility, or one can have approximate correlations over wide ranges of structural types which are of considerable predictive utility. The present correlation falls in the latter category; by analogy with the behaviour shown by the polycarbonyl compounds, which obey [1] over a range of 15 powers of 10 in equilibrium constant, we expect that the correlation of monocarbonyl compounds, which is closely similar, will be of similar wide applicability, although the data presently available are over a narrower range of equilibrium constants than is desirable.

To calculate pK_{Enol} from pK_a^{Keto} it is necessary to estimate pK_a^{Enol}. In a recent paper (7) methods were developed to do this, making use of the analogies of

alcohol and phenol pK_a values for which well accepted linear free energy relations linking pK_a and σ^* or σ are available. For an enol **I**, the effects of

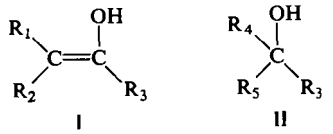

I II

substituents R_1 and R_2 upon the enol pK_a are assumed to be the same as the effects of the same substituents in the *ortho* position of a phenol upon the pK_a of the phenol. For R_1 the analogy is obviously very close; for R_2 it is less so and the assumption that the effects are the same must introduce an error. However, since the largest ΔpK_a for a substituent (chloro) is 1.4, and the difference in ΔpK_a between *cis*- and *trans*-chloro seems unlikely to be a large fraction of this, the error will not be prohibitively large. For R_3 the effect on the enol pK_a is assumed to be the same as for the effect upon the alcohol pK_a in **II**, which is estimated using the correlation with σ^* of Takahashi *et al.* (13). The ΔpK_a values and related data are contained in Table 3 which has been deposited within the Depository of Unpublished Data.[4] The starting point for the estimations is the pK_a of the enol of acetophenone, which have been recently evaluated by Novak and Loudon (16) as 11.0. Since the zero point for σ^* is methyl and not phenyl, a more convenient reference point for calculations is the enol of acetone, which can be estimated to have pK_a of 11.8 from the difference in σ^* for methyl and phenyl. The pK_a^{Enol} values so estimated are found in Table 4, as are the pK_{Enol} values we calculate.

In this connection it is of interest that there is a check upon the pK_a^{Keto} values deduced for acetone and acetophenone. Dubois and Toullec (8, 9) have demonstrated that the reaction of the enol of acetone with halogens is diffusion controlled, since the rate constants for the reaction of the enol with chlorine, bromine, or iodine are identical. It is reasonable to anticipate that the rate constant for the reaction of the enolate would be even faster and that even for a slightly less reactive halogenating agent such as hypochlorous acid the reaction of the enolate would be diffusion controlled. Many years ago, in a study which has not received the attention it deserves, Bartlett and co-worker (17, 18) investigated the base catalyzed chlorination of ketones and demonstrated a change in kinetic form from zero order in halogen to first order in halogen with increasing concentration of hydroxide ion. Furthermore the kinetics for the pseudo-second-order reaction of ketone and halogen required both a water catalyzed and a hydroxide catalyzed path; i.e.,

$$v = k_{obs}\,[\text{halogen}]\,[\text{ketone}] \qquad k_{obs} = a + b[OH^-]$$

In alkaline aqueous solutions of chlorine the major species is ClO^-. The kinetic term proportional to hydroxide concentration is clearly due to the reaction of enolate ion with hypochlorite; this reaction between two anions would be expected to be fast but not diffusion controlled. The hydroxide independent term is most reasonably ascribed to reaction of enolate with hypochlorous acid; the kinetically equivalent reaction of enol with hypochlorite should be much slower than the reaction of the enolate but the two terms in the rate law are of similar magnitude in 0.1 *N* NaOH.

If we assume the above interpretation of the rate law and that the reaction of enolate with hypochlorous acid is diffusion controlled, then the rate constant for this reaction is given by:

$$k_{obs} = k_{diff}K_a^{Keto}/K_a^{HOCl}$$

and

$$K_a^{Keto} = k_{obs}K_a^{HOCl}/k_{diff}$$

Bartlett's (17, 18) kinetics were performed at 35°C; K_a^{HOCl} at 35°C was calculated from the thermodynamic parameters tabulated by Larson and Hepler (19); k_{diff} was taken as $10^{10}\ M^{-1}\ s^{-1}$ (15). Then from the rate constants for the hydroxide independent contribution to the reaction rate the pK_a^{Keto} values for acetone and acetophenone can be calculated as 19.1 and 18.0 (at 35°C) in remarkably good agreement with the values deduced from the values for pK_a^{Enol} and pK_{Enol} given in a recent paper (7), namely 19.0 and 17.7, respectively (at 25°C). It appears that the hypochlorite method should be a very powerful tool for determining pK_a^{Keto} in aqueous solution.

The results in Table 2 for pK_a^{Keto} are relatively unsurprising and show the sorts of effects which one would have intuitively expected. The values predicted for pK_{Enol}, on the other hand are frequently quite surprising. It is to be hoped that independent means can be found to check some of these values to test the validity of our method. In particular, the contrast between 1,1- and 1,3-dichloroacetone is quite striking, since one would not have expected that having the second chlorine *not* attached to the enol double bond would favor enolization more than having it attached. This can be rationalized in terms of the beneficial effects of avoiding steric congestion which is imposed on the 1,1-isomer. Steric effects appear in both pK_a^{Enol} and pK_a^{Keto} but are automatically allowed for by our empirical method for

[4]Copies of material on deposit may be obtained, at a nominal charge, from the Depository of Unpublished Data, CISTI, National Research Council of Canada, Ottawa, Ont., Canada K1A 0S2.

evaluating pK_a^{Keto}; there should be little or no steric effect upon pK_a^{Enol}. Although the methods which we have used to estimate pK_a^{Enol} are admittedly crude, it seems highly unreasonable that they can be grievously in error.

The principal reason why an approach such as the present one has not been proposed before is probably that there has been, until very recently, no unambiguous independent value for the pK_a for any simple enol which could be used as a starting point for estimating pK_a values for other enols. Now that one such value has been reported by Novak and Loudon (16), it is possible to estimate such pK_a values with considerable confidence that they are at least approximately correct, because of the considerable body of knowledge concerning the effects of substituents on the pK_a values of various classes of compounds.

Conclusions

By the methods outlined in this paper, it is possible to estimate the pK_{Enol} for any carbonyl compound for which kinetic data for oxyanion catalyzed enolization are available at 25°C in water.

Acknowledgements

I wish to thank the National Research Council of Canada, the Alfred P. Sloan Foundation, and the Academic Development Fund of the University of Western Ontario for financial support of this research.

1. G. SCHWARTZENBACH and C. WITTWER. Helv. Chim. Acta, **30**, 669 (1947).
2. A. GERO. J. Org. Chem. **19**, 1760 (1954).
3. J. E. DUBOIS and G. BARBIER. Bull. Soc. Chim. Fr. 682 (1965).
4. R. P. BELL and P. W. SMITH. J. Chem. Soc. B, 241 (1966).
5. J. HINE and K. ARATA. Bull. Chem. Soc. Jpn. **49**, 3085 (1976).
6. J. HINE and K. ARATA. Bull. Chem. Soc. Jpn. **49**, 3089 (1976).
7. J. P. GUTHRIE and P. A. CULLIMORE. Can. J. Chem. **57**, 240 (1979).
8. J. TOULLEC and J. E. DUBOIS. Tetrahedron, **29**, 2851 (1973).
9. J. E. DUBOIS and J. TOULLEC. Tetrahedron, **29**, 2859 (1973).
10. J. P. GUTHRIE. Can. J. Chem. **57**, 797 (1979).
11. R. P. BELL. Trans. Faraday Soc. **39**, 253 (1943).
12. R. P. BELL. The proton in chemistry. 2nd ed. Cornell University Press, Ithaca, NY. 1973. p. 203.
13. S. TAKAHASHI, L. A. COHEN, H. K. MILLER, and E. G. PEAKE. J. Org. Chem. **36**, 1205 (1971).
14. (*a*) A. O. COHEN and R. A. MARCUS. J. Phys. Chem. **72**, 4249 (1968); (*b*) R. A. MARCUS. J. Am. Chem. Soc. **91**, 7224 (1969).
15. M. EIGEN. Angew. Chem. Int. Ed. Engl. **3**, 1 (1964).
16. M. NOVAK and G. M. LOUDON. J. Org. Chem. **42**, 2494 (1977).
17. P. D. BARTLETT. J. Am. Chem. Soc. **56**, 967 (1934).
18. P. D. BARTLETT and J. R. VINCENT. J. Am. Chem. Soc. **57**, 1596 (1935).
19. J. W. LARSON and L. G. HEPLER. *In* Solute–solvent interactions. *Edited by* J. F. Coetzee and C. D. Ritchie. Marcel Dekker, NY. 1969.
20. R. G. PEARSON and R. L. DILLON. J. Am. Chem. Soc. **75**, 2439 (1953).
21. R. P. BELL, E. GELLES, and E. MILLER. Proc. R. Soc. London Ser. A, **198**, 310 (1949).
22. R. P. BELL and D. J. BARNES. Proc. R. Soc. London Ser. A, **318**, 421 (1970).
23. M. L. AHRENS, M. EIGEN, W. KRUSE, and G. MAASS. Ber. Bunsenges. Phys. Chem. **74**, 380 (1970).
24. R. P. BELL and M. C. GOLDSMITH. Proc. R. Soc. London Ser. A, **216**, 322 (1952).
25. R. P. BELL and J. E. CROOKS. Proc. R. Soc. London Ser. A, **286**, 285 (1965).
26. R. P. BELL, D. H. EVERETT, and H. C. LONGUET-HIGGINS. Proc. R. Soc. London Ser. A, **186**, 433 (1946).
27. R. P. BELL, G. R. HILLIER, J. W. MANFIELD, and D. G. STREET. J. Chem. Soc. B, 827 (1967).
28. R. BROUILLARD and J. E. DUBOIS. J. Org. Chem. **39**, 1137 (1974).
29. M. L. EIDINOFF. J. Am. Chem. Soc. **67**, 2072 (1945); **67**, 2073 (1945).
30. R. P. BELL and D. C. VOGELSONG. J. Chem. Soc. 243 (1958).
31. R. P. BELL. J. Chem. Soc. 1637 (1937).
32. J. L. KING. J. Am. Chem. Soc. **89**, 3524 (1967).
33. J. HINE, J. G. HOUSTON, J. H. JENSEN, and J. MULDERS. J. Am. Chem. Soc. **87**, 5050 (1965).
34. R. A. LYNCH, S. P. VINCENTI, Y. T. LIN, L. D. SMUCHER, and S. C. SUBBA RAO. J. Am. Chem. Soc. **94**, 8351 (1972).
35. A. J. KRESGE, D. S. SAGATYS, and H. L. CHEN. J. Am. Chem. Soc. **99**, 7228 (1977).
36. A. KANKAANPERA, L. OINONEN, and P. SALOMAA. Acta Chem. Scand. A, **31**, 551 (1977).
37. J. R. JONES, R. E. MARKS, and S. C. SUBBA RAO. Trans. Faraday Soc. **63**, 111 (1967).
38. R. P. BELL and H. C. LONGUET-HIGGINS. J. Chem. Soc. 636 (1946).
39. R. P. BELL, G. R. HILLIER, J. W. MANSFIELD, and D. G. STREET. J. Chem. Soc. B, 827 (1967).
40. G. E. LIENHARD and T. C. WANG. J. Am. Chem. Soc. **91**, 1146 (1969).
41. R. P. BELL and O. M. LIDWELL. Proc. R. Soc. London Ser. A, **176**, 88 (1940).
42. R. P. BELL and J. HANSSON. Proc. R. Soc. London Ser. A, **255**, 214 (1960).
43. R. P. BELL and H. F. H. RIDGEWELL. Proc. R. Soc. London Ser. A, **298**, 178 (1967).
44. Y. POCKER, J. E. MEANY, and C. ZADOROJNY. J. Phys. Chem. **75**, 792 (1971).
45. R. P. BELL and P. DE MARIA. Trans. Faraday Soc. **66**, 930 (1970).
46. J. HINE, K. G. HAMPTON, and B. C. MENON. J. Am. Chem. Soc. **89**, 2664 (1967).
47. J. R. JONES. Trans. Faraday Soc. **61**, 95 (1965).
48. J. JULIEN and N. T. LAI. Bull. Soc. Chim. Fr. 3948 (1970).
49. J. WARKENTIN and C. BARNETT. J. Am. Chem. Soc. **90**, 4629 (1968).
50. W. P. JENCKS and J. REGENSTEIN. *In* Handbook of biochemistry. 1st ed. *Edited by* H. A. Sober. Chemical Rubber Co., Cleveland, OH. 1968.
51. R. M. BETHEA, B. S. DURAN, and T. L. BOULLION. Statistical methods for engineers and scientists. Marcel Dekker, New York, NY. 1975.

Photochemical and thermal rearrangements of some 3*H*-pyrazoles[1]

WILLIAM J. LEIGH AND DONALD R. ARNOLD[2]

Photochemistry Unit, Department of Chemistry, University of Western Ontario, London, Ont., Canada N6A 5B7

Received November 24, 1978

WILLIAM J. LEIGH and DONALD R. ARNOLD. Can. J. Chem. **57**, 1186 (1979).

Low temperature (−70°C) irradiation of 3,3,4,5-tetramethyl-3*H*-pyrazole (**2***a*) leads to the formation of the 1,2-diazabicyclo[2.1.0]pent-2-ene (**3***a*), as has been reported previously. Irradiation of 3,3-dimethyl-4,5-diphenyl-3*H*-pyrazole (**2***b*) under identical conditions did not result in formation of the analogous product but lead instead to formation of the cyclopropene via decomposition of the vinyl diazo compound. The thermal rearrangements of **2***a* and a series of 5-aryl-3,3-dimethyl-4-phenyl-3*H*-pyrazoles (**2***b–d*) lead to formation of the 4*H*-pyrazoles **6***a–d* and the *N*-methylpyrazoles **5***a–d*, resulting from competitive methyl migrations to carbon and nitrogen. The Arrhenius parameters for the rearrangement of **2***b* were determined. Decomposition of the methiodides derived from the 4*H*-pyrazoles **6***a–d* leads to formation of the *N*-methylpyrazoles **5***a–d*; the mechanism of this decomposition was examined by high temperature ^{1}Hmr spectroscopy. The *N*-methylpyrazoles were synthesized by independent routes and the structures were assigned with the aid of lanthanide shift reagents, ^{1}Hmr solvent shift studies, and ^{13}Cmr spectroscopy. The thermodynamic equilibria of the isomeric *N*-methylpyrazoles were determined and found to be influenced by a small substituent effect. The photochemical and thermal behaviour of 3*H*-pyrazoles is discussed and compared to that of 1-pyrazolines.

WILLIAM J. LEIGH et DONALD R. ARNOLD. Can. J. Chem. **57**, 1186 (1979).

L'irradiation à basse température (−70°C) du tétraméthyl-3,3,4,5 3*H*-pyrazole (**2***a*) conduit à la formation du diaza-1,2 bicyclo[2.1.0] pentène-2 (**3***a*) comme il a été rapporté antérieurement. L'irradiation du diméthyl-3,3 diphényl-4,5 3*H*-pyrazole (**2***b*) dans des conditions semblables ne conduit pas à la formation du produit analogue mais plutôt à la formation d'un cyclopropène par l'intermédiaire de la décomposition du composé vinyldiazo. Les transpositions thermiques de **2***a* et d'une série d'aryl-5 diméthyl-3,3 phényl-4 3*H*-pyrazoles (**2***b–d*) conduisent à la formation des 4*H*-pyrazoles (**6***a–d*) et des *N*-méthylpyrazoles (**5***a–d*) provenant de migrations compétitives de méthyles vers le carbone ou l'azote. On a déterminé les paramètres d'Arrhénius pour la transposition de **2***b*. La décomposition des méthiodures des 4*H*-pyrazoles **6***a–d* conduit à la formation des *N*-méthylpyrazoles **5***a–d*; on a étudié le mécanisme de cette décomposition par spectroscopie rmn ^{1}H à haute température. On a synthétisé les *N*-méthylpyrazoles par d'autres méthodes et on a attribué leurs structures grâce aux déplacements induits par les lanthanides, à des études de déplacements chimiques induits par les solvants et par spectroscopie rmn ^{13}C. On a déterminé les équilibres thermodynamiques des *N*-méthylpyrazoles isomères et on a trouvé qu'ils sont influencés par des petits effets de substituants. On discute des comportements photochimique et thermique des 3*H*-pyrazoles et on les compare à ceux des pyrazolines-1.

[Traduit par le journal]

Introduction

The photochemical and thermal reactions of 1-pyrazolines (**1**) have been extensively studied. Although some questions may still remain regarding the details of the mechanism(s), the overall course of the reaction is, predictably, extrusion of nitrogen followed by formation of the cyclopropane and/or propylene for both modes of activation (reaction [1]) (1). The photochemical and thermal behaviour of the analogous 3*H*-pyrazoles (**2**) is much less well understood and is clearly not yet fully predictable. Four types of reactions have been described for derivatives of this system. The two modes of activation invariably lead to different types of products in each case. Reactions [2] and [3] have been observed upon photochemical excitation and reactions [4] and [5] are typical thermal reactions.

Reaction [2], formally a photochemically allowed 4π*e* disrotatory electrocyclic ring closure (2), has been observed only upon irradiation at low temperature (< −40°C), presumably because the 1,2-diazabicyclo[2.1.0]pent-2-ene product (**3**) is thermally unstable and reverts to the starting material at higher temperatures. The only reported examples of this reaction involve fully alkylated 3*H*-pyrazoles (3). The more common photochemical reaction is formation of the vinyl diazo compound (reaction [3]) (4 and references cited therein). This reaction can be

[1]Contribution No. 210 from the Photochemistry Unit, University of Western Ontario.

[2]Address correspondence to this author, Department of Chemistry, Dalhousie University, Halifax, N.S. B3H 4J3.

0008-4042/79/101186-15$01.00/0

[1] 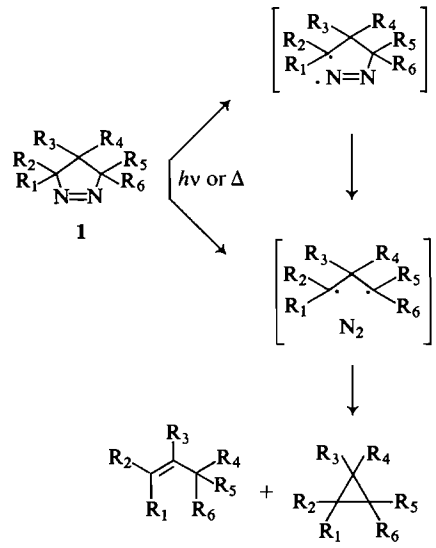

viewed as a 6e electrocyclic ring opening. Photochemical decomposition of the vinyl diazo compound (**4**) then leads to the cyclopropene, whereas thermal activation can lead to decomposition to give the cyclopropene (4) and/or to a concerted recyclization back to the 3*H*-pyrazole (5, 6). In those cases studied in detail, there was little or no direct loss of nitrogen from the 3*H*-pyrazole; that is, without the intermediacy of the vinyl diazo compound (4). Similarly, to our knowledge, there is no report of a photochemical sigmatropic rearrangement of a 3*H*-pyrazole.

Reactions [4] and [5] can be thermally allowed suprafacial [1,5]-sigmatropic rearrangements, although other mechanisms may be involved under some conditions (6). There are now numerous reports of these reactions in the literature (7–9). Usually, one of the possible products (**5** or **6**) predominates to the exclusion of the other, although

[2] 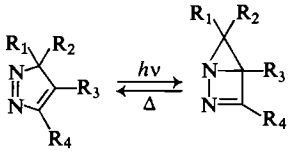

a R_1–R_4 = CH_3
b $R_1 = R_2 = CH_3$, $R_3 = R_4 = C_6H_5$
c $R_1 = R_2 = CH_3$, $R_3 = C_6H_5$, R_4 = 4-(NC)C_6H_4
d $R_1 = R_2 = CH_3$, $R_3 = C_6H_5$, R = 4-(CH_3O)C_6H_4

[3] 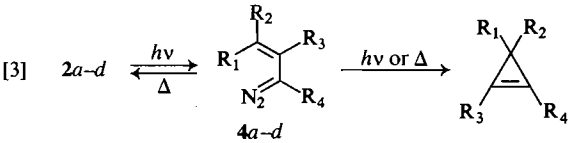

[4] 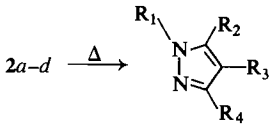

[5] 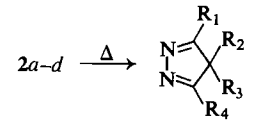

there have been two recent reports of competitive rearrangements (9, 10). In view of the facile thermal loss of nitrogen from the 1-pyrazolines, it is surprising that this reaction is not an important thermal reaction of 3*H*-pyrazoles. We know of only two, rather special, examples (5*b*, 9).

In this paper, we report the results of a study of the photochemical and thermal reactions of the 3*H*-pyrazoles, **2***a–d*. Results from the series **2***b–d* allow an assessment of the importance of electronic factors on reactions [4] and [5]. The kinetic parameters for the competitive [1,5]-sigmatropic rearrangements of **2***b* have been measured and the competition between these rearrangements and loss of nitrogen is discussed in light of these results.

Results

The 3*H*-pyrazoles **2***a–d* were known compounds, prepared as part of our earlier study, by the reaction of hydrazine and the corresponding α,β-unsaturated ketones followed by oxidation of the 2-pyrazolines (4).

The irradiation of **2***a*, at low temperature, has been studied previously (**3***a*, *b*) and our results agree with those reported. The proton magnetic resonance spectra (^{1}Hmr) of the irradiated solution, kept at low temperature, indicates the 1,2-diazabicyclo[2.1.0]pent-2-ene, **3***a* (R_1–R_4 = CH_3) was formed in high yield. When this solution was allowed to warm to room temperature, the ^{1}Hmr spectrum indicated almost quantitative reversion to starting material; there was a small amount (<5%) of tetramethylcyclopropene also detected. When **2***b* was irradiated under comparable low temperature conditions, no diazabicyclopentene was detected; 3,3-dimethyl-1,2-diphenylcyclopropene was observed (^{1}Hmr). When the irradiation of the 3*H*-pyrazoles **2***a–d* was carried out at 10°C, first the vinyl diazo compounds (**4***a–d*) and subsequently the cyclopropenes were produced in high yield (4). We found no evidence in any case for formation of a rearrangement product.

The thermal rearrangement studies were carried

TABLE 1. The rate of rearrangement of **2***a–d* in diphenyl ether solution

Compound	T (°C)	$10^5 \times k_{dec}$ (s^{-1})	$10^5 \times k_5$ (s^{-1})	**6**:**5**
2*a*	182.0	8.7±0.3	—	[a]
2*b*	173.1	3.1±0.2	2.6±0.3	9.9
	179.8	5.5±0.1	4.6±0.3	10.4
	182.6	6.6±0.2	5.3±0.5	10.4
	191.8	14.4±0.2	12.0±0.3	10.5
	192.2	14.1±0.4	11.6±0.4	9.8
	193.8	17.5±1.1	14.7±0.9	9.8
	195.0	18.3±0.3	15.4±0.7	9.8
	199.9	26.2±1.0	22.8±1.0	9.1
2*c*	*193.8*	30.3±0.8	—	9.8
2*d*	*193.8*	14.9±0.3	—	6.9

[a]An accurate value cannot be given because of the competitive isomerization of **6***a* to **5***a* at this temperature. A minimum ratio is **6***a*:**5***a* ≥ 35.

out in degassed, sealed tubes with diphenyl ether as solvent. Progress of the reaction was followed by ^{1}Hmr spectroscopy. When **2***a* was heated at 182°C, reaction was essentially complete after 11 h and *N*-methylpyrazole, **5***a* (R_1–R_4 = CH_3, 36%), and 4*H*-pyrazole, **6***a* (R_1–R_4 = CH_3, 64%), were produced. Continued heating (ca. 50 h) of this mixture resulted in complete conversion of **6***a* to **5***a*. The rate of disappearance of **2***a*, determined from the integrated ^{1}Hmr spectra, followed first-order kinetics (Table 1). The rate constant and product ratio were the same, within experimental error, when diphenyl ether – pyridine (10:1) was the solvent. The products (**6***a* and **5***a*) were identified by comparison of their spectra (ir, ^{1}Hmr) with those of authentic samples of the known compounds.

The thermal (194°C, 6 h) rearrangement of **2***b–d* also leads to the formation of two products, **5***b–d* and **6***b–d*. The other possible *N*-methylpyrazoles (**5***e–g*) were *not* detected in these reaction mixtures. In these cases, both of the products, **5***b–d* and **6***b–d*, were stable to further heating at this temperature so the product ratios reflect the relative rates of formation. The rate of disappearance of the 3*H*-pyrazoles and the product ratios were determined by integrating the ^{1}Hmr spectra. The rate of reaction of **2***b* was also studied as a function of temperature. These results are summarized in Table 1.

The products from these thermal rearrangements were isolated by column chromatography; they are all new compounds. The structure assigned to the 4*H*-pyrazoles **6***b–d* was first suggested by a comparison of their spectra (ir, ^{1}Hmr, and uv) with those of similar known compounds; these data are summarized in the Experimental. Treatment of **6***a–d* with methyl iodide leads to formation of the 4*H*-pyrazolium iodides **7***a–d*, which were also fully characterized. When compounds **7***b–d* were heated to their melting points under vacuum, methyl iodide was lost and the *N*-methylpyrazoles **5***b–d* were obtained in essentially quantitative yield. When **7***a* was subjected to the same conditions, **5***a* was obtained along with an appreciable quantity of its methiodide **9***a*. The position of the *N*-methyl substituent in compounds **7***b–d* was assigned partially from the fact that thermal decomposition gives only the analogous *N*-methylpyrazoles **5***b–d*. Furthermore, the ^{1}Hmr spectra of the series **7***a–d* show the expected small coupling of the *N*-methyl protons with the adjacent methyl group which is shifted significantly downfield.

We wondered if the *N*-methyl substituent in **7***a–d* could equilibrate between the nitrogens before the thermal decomposition, although the isomeric salts were never detected. This possibility was tested by studying the ^{1}Hmr spectrum of **7***a* at high temperature (80–150°C). The shape and position of the two singlets due to the methyls at carbons 3 and 5 remained unchanged even at 150°C. Furthermore, double irradiation of either the C-3 or C-5 methyl signals had no measurable effect on the integrated intensity of the other at this temperature. We conclude that any exchange of the methyl group between nitrogen-1 and -2 must be slow relative to the proton nuclear spin relaxation process. The formation of the *N*-methylpyrazole, methyl iodide, and 1,2,3,4,5-pentamethylpyrazolium iodide and the concomitant disappearance of **7***a* was clearly evident during the time required to carry out this ^{1}Hmr study at these temperatures.

The isolation of the *N*-methylpyrazoles **5***b–d* from reaction [7] effectively rules out the occurrence of any unsuspected rearrangement during the course of reactions [5], [6], or [7].

The gross structures of the *N*-methylpyrazoles **5***b–d* were established by comparison of their spectra (ir, ^{1}Hmr) with those of the products from an alternative synthesis. Condensation of methyl hydrazine with the 1,2-diaryl-1,3-butanediones (**8***b*, *d*, and *h*)

[6] 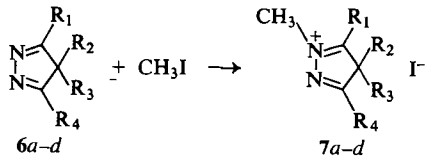

6*a–d* 7*a–d*

[7] 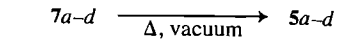

[8] 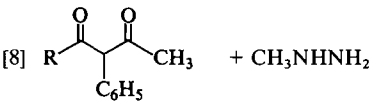

8

b R = C_6H_5
d R = 4-(CH_3O)C_6H_4
h R = 4-BrC_6H_4

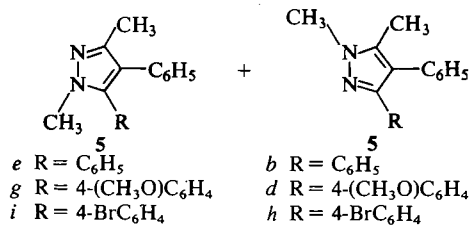

5

e R = C_6H_5
g R = 4-(CH_3O)C_6H_4
i R = 4-BrC_6H_4

5

b R = C_6H_5
d R = 4-(CH_3O)C_6H_4
h R = 4-BrC_6H_4

[9] 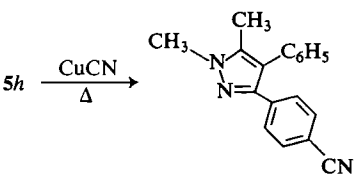

5c

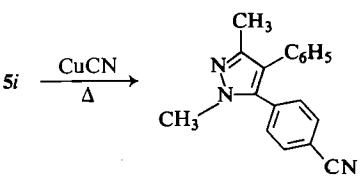

5f

gave the *N*-methylpyrazoles **5***b*, *d*, *e*, *g*, *h*, and *i* (reaction [8]). We were unable to synthesize the *para*-cyano diketone (see Experimental), so the *para*-cyano pyrazoles **5***c* and *f* were obtained by treatment of the *para*-bromo derivatives (**5***h* and *i*) with cuprous cyanide (reaction [9]). The isomeric pairs were separated by column chromatography.

The assignment of structure of the isomers was made largely on the basis of nuclear magnetic resonance studies; both ^{13}Cmr and ^{1}Hmr spectra were used. There are distinct differences in the spectra which allow the isomers to be divided into the two series **5***b–d* and **5***e–g*. Solvent and shift reagent studies on the ^{1}Hmr spectra of the isomeric pair **5***b* and **5***e* were then particularly useful for distinguishing the two series.

The spectra of **5***b* and **5***e* in the presence of varying amounts of the lanthanide shift reagents, Eu(fod)$_3$ and Pr(fod)$_3$, are summarized in Figs. 1 and 2. The *N*-methyl protons in **5***b* are shifted ca. 1.3 ppm by Eu(fod)$_3$ and 2.7 ppm by Pr(fod)$_3$,[3] while the *C*-methyl protons are shifted to a considerably lesser extent (0.6 and 0.7 ppm by Eu(fod)$_3$ and Pr(fod)$_3$, respectively). Two of the aromatic protons, presumably the *ortho*-protons of the 3-phenyl group, undergo shifts of ca. 1.0 ppm by Eu(fod)$_3$ and 4.6 ppm by Pr(fod)$_3$. On the other hand, the *N*-methyl and *C*-methyl protons in **5***e* are *both* shifted ca. 6.8 ppm by Eu(fod)$_3$ and 6.6 ppm by Pr(fod)$_3$, while the aromatic protons are relatively unaffected.

Elguero and co-workers obtained similar results in a study of the effect of the dipivalomethides of Co^{II}, Ni^{II}, Eu^{III}, and Pr^{III} on the ^{1}Hmr spectra of 1,3-dimethyl-, 1,5-dimethyl-, and 1,3,5-trimethylpyrazole, all of which have been well characterized (11*a*). Their results are consistent with complexation of the shift reagent at the unsubstituted nitrogen atom of the pyrazole ring; methyls in the 1- and 3-positions are shifted roughly equally and to a much greater extent than is a 5-methyl substituent. They also observed a shift in the position of the *ortho*-phenyl protons in 1-phenylpyrazole.

The magnitude of the pseudocontact shifts effected by the addition of a lanthanide shift reagent are due both to the relative distances between the substrate protons and the paramagnetic centre in the shift reagent – substrate complex and the degree of association of the substrate and shift reagent in solution (11*b*). Although the former is more important for our purposes, it can be seen from the data in Figs. 1 and 2 that the degree of association of **5***b* with both Eu(fod)$_3$ and Pr(fod)$_3$ is smaller than that of **5***e* with the two shift reagents. This may indicate that **5***e* exhibits a somewhat greater degree of Lewis basicity than does **5***b*, although we have no other evidence to support this conclusion. Further, it appears that Pr(fod)$_3$ is a somewhat better complexing agent with **5***b* than is Eu(fod)$_3$.

Further support for the identities of pyrazoles **5***b–i* comes from the solvent shift studies. Elguero and Jacquier observed remarkable consistencies in the ^{1}Hmr spectra of a number of 1,3- and 1,5-dimethylated pyrazole derivatives as a function of solvent (11*c*). In deuteriochloroform, they observed a small difference in chemical shift between 3-methyl

[3]Extrapolated to equimolar concentrations of pyrazole and shift reagent Pr(fod)$_3$, tris(6,6,7,7,8,8,8,-heptafluoro-2,2-dimethyl-3,5-octanedionato)praseodymium (see Figs. 1 and 2).

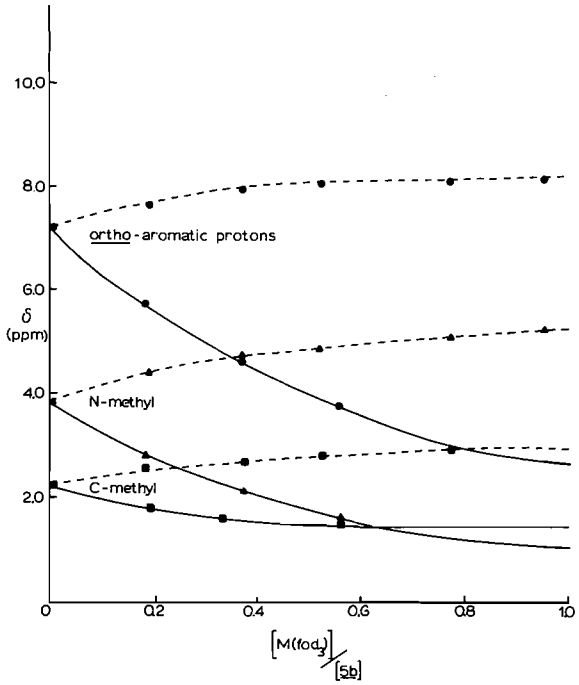

FIG. 1. ^{1}Hmr shift reagent study of **5***b* using Pr(fod)$_3$ (—) and Eu(fod)$_3$ (----).

and 5-methyl protons, with the 5-methyl protons occurring at higher field than 3-methyl protons. The differences in chemical shift in benzene solution are even more distinct; they found 3-methyl protons at 2.15–2.25 ppm and 5-methyl protons at 1.4–1.7 ppm. Although the methyl proton chemical shifts of **5***b–i* in deuteriochloroform are entirely consistent with their generalizations, the spectra in deuteriobenzene are far more illuminating owing to the greater differences observed. As can be seen in Table 2, the ^{1}Hmr spectra of **5***b*, *c*, *d*, and *h* all show methyl singlets in the range 1.62–1.71 ppm, while the corresponding signals in the spectra of **5***e*, *f*, *g*, and *i* occur in the range 2.35–2.46 ppm.

^{13}Cmr spectroscopy has also been shown to be useful for distinguishing isomeric pyrazoles of this type (11*d*). Table 2 lists the positions of the *C*- and *N*-methyl carbons in the 25.2 MHz ^{13}Cmr spectra of **5***b–i* in deuteriochloroform solution; certain generalizations are again apparent. It can be seen that 3-methyl carbons occur in the range 12.4–12.6 ppm, while 5-methyl carbons fall in the 9.7–10.0 ppm range. The *N*-methyl carbon shieldings cannot be placed in such characteristic frequency ranges, although it can be seen that within each isomer pair the *N*-methyl carbon in the 1,5-dimethyl isomer occurs at higher field than that of the 1,3-dimethyl isomer by 0.2–0.4 ppm.

The difference in thermodynamic stability between

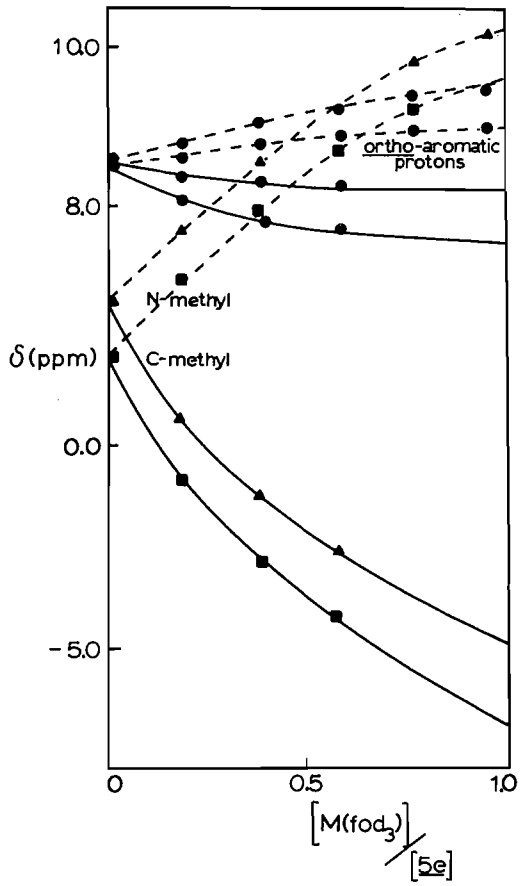

FIG. 2. ^{1}Hmr shift reagent study of **5***e* using Pr(fod)$_3$ (—) and Eu(fod)$_3$ (----).

the isomeric *N*-methylpyrazoles was determined. Equilibrium was established when the individual isomers were heated in diphenyl ether solution with methyl iodide added as a catalyst (reaction [10]). The consistency of the relative stability of the isomeric pairs, i.e., **5***b–d* more stable than **5***e–g*, constitutes additional evidence for the proposed structural assignments.

Discussion

The photochemical electrocyclic reactions of compounds having the 1,2-diaza-1,3-diene chromophore have not received much attention. There are, however, enough examples reported to indicate that this is an interesting and potentially fruitful research area; reactions [11] (3*a*, *b*), [12] (12), and [13] (13) illustrate this point. Reactions [2], [11], and [13] can be viewed as 4πe electrocyclic ring closures, while reaction [12] is a 6e electrocyclic process. Analogous reactions in the carbocyclic series are, of course, well known (14).

To our knowledge, there are no examples of direct

TABLE 2. ^1H and ^{13}C nuclear magnetic resonance data for pyrazoles **5***b–i*

Compound	100 MHz ^{1}Hmr		25.2 MHz ^{13}Cmr
	$CDCl_3$	C_6D_6	$CDCl_3$
5*b*	2.19(s, 3H)	1.67(s, 3H)	
	3.83(s, 3H)	3.25(s, 3H)	9.932
	7.20(m, 10H)	7.18(m, 8H), 7.89(m, 2H)	36.249
5*c*	2.24(s, 3H)	1.62(s, 3H)	
	3.92(s, 3H)	3.22(s, 3H)	9.996
	7.36(m, 9H)	6.97(d, 2H), 7.59(d, 2H)	36.662
		7.16(m, 5H)	
5*d*	2.21(s, 3H)	1.71(s, 3H)	
	3.75(s, 3H)	3.27(s, 3H)	9.776
	3.86(s, 3H)	3.30(s, 3H)	36.503
	6.79(d, 2H), 7.36(d, 2H)	6.73(d, 2H), 7.79(d, 2H)	
	7.32(m, 5H)	7.24(m, 5H)	
5*h*	2.22(s, 3H)	1.64(s, 3H)	
	3.87(s, 3H)	3.22(s, 3H)	10.016
	7.30(m, 9H)	7.17(m, 5H)	36.408
		7.20(d, 2H), 7.58(d, 2H)	
5*e*	2.30(s, 3H)	2.44(s, 3H)	
	3.72(s, 3H)	3.41(s, 3H)	12.659
	7.18(m, 10H)	7.03(s, 5H)	36.801
		7.12(m, 5H)	
5*f*	2.32(s, 3H)	2.35(s, 3H)	
	3.81(s, 3H)	3.27(s, 3H)	12.420
	7.13(m, 5H)	6.64(d, 2H), 6.87(d, 2H)	37.179
	7.31(d, 2H), 7.63(d, 2H)	7.12(m, 5H)	
5*g*	2.34(s, 3H)	2.46(s, 3H)	
	3.75(s, 3H)	3.22(s, 3H)	12.715
	3.80(s, 3H)	3.46(s, 3H)	36.722
	6.88(d, 2H), 7.20(d, 2H)	6.62(d, 2H), 6.96(d, 2H)	
	7.16(m, 5H)	7.17(m, 5H)	
5*i*	2.32(s, 3H)	2.41(s, 3H)	
	3.77(s, 3H)	3.31(s, 3H)	12.552
	7.18(m, 5H)	6.43(d, 2H)	36.897
	7.08(d, 2H), 7.50(d, 2H)	7.12(m, 7H)	

[10]

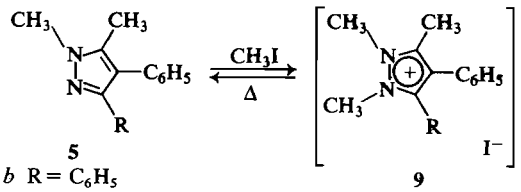

5

b R = C_6H_5
c R = 4-(NC)C_6H_4
d R = 4-(CH_3O)C_6H_4

9

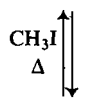

At equilibrium
5*b*/**5***e* = 4 (200°C)
5*c*/**5***f* = 3(210°C)
5*d*/**5***g* = 12.5(210°C)

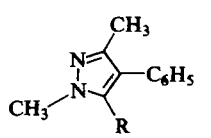

5

e R = C_6H_5
f R = 4-(NC)C_6H_4
g R = 4-(CH_3O)C_6H_4

loss of nitrogen upon irradiation of this chromophore. It is not suprising that neither concerted loss of nitrogen nor cleavage to give the vinyl and diazenyl radicals occurs; the central carbon–nitrogen bond must be rather strong in the ground state and even more bonding in the excited state. On the other hand, photochemically-induced homolytic cleavage to give the α,β-unsaturated diazenyl and alkyl radicals is not unlikely and may in fact account for the formation of **4** in reaction [3].

It seems likely that, in the case of **2***a*, reaction [2] is competing with reaction [3] and, at 10°C, the occurrence of the thermal reversion of **3***a* to **2***a* accounts for the ultimate high yield of cyclopropene upon irradiation at this temperature. We were unable to detect **3***b* from the irradiation of **2***b* at −77°C but cannot rule out the possibility that **3***b* would revert back to **2***b* at a rate fast enough to preclude its detection at this temperature. It is also pertinent to recall

[11] 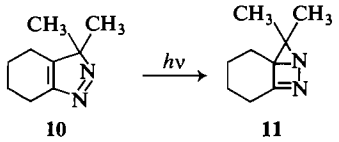

10 11

[12] 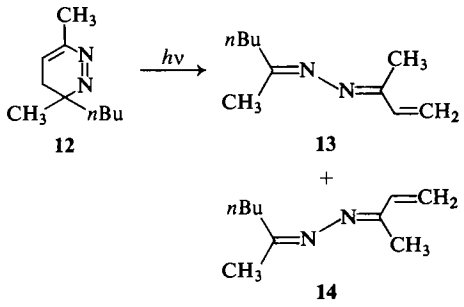

12 13 14

[13] 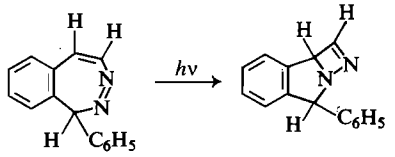

15 16

that reaction [3] occurs with **2***b–d* at ca. 10 K (4), although no attempt was made to detect **3***b–d* at this temperature. Clearly, the factors which influence the competition between reactions [2] and [3] have yet to be determined.

Reactions [4] and [5] are best described as thermally-allowed competitive suprafacial [1,5]-sigmatropic rearrangements. The evidence supporting this mechanism is, briefly: (*i*) the rate of rearrangement of **2***a,b* is not affected by the addition of base; (*ii*) the major products (**6***a–d*) are the result of kinetic, not thermodynamic, control; (*iii*) the rates of reactions [4] and [5] are relatively insensitive to substituent effects throughout the series **2***a–d*; (*iv*) the kinetic analysis of the rearrangement of **2***b* is consistent with a concerted reaction; and (*v*) these reactions are similar to those of the carbocyclic analog 5,5-dimethylcyclopenta-1,3-diene, whose rearrangement has been shown to occur by a concerted mechanism (reaction [14]) (15).

[14] 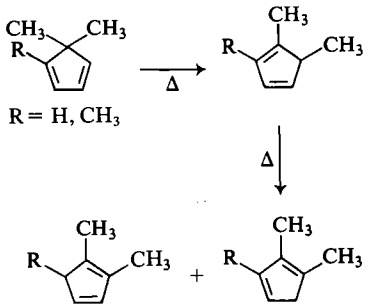

R = H, CH_3

The relative rates of reactions [4] and [5] of **2***a–d* favour reaction [5] in every case. The substituents on **2***b–d* have little influence on this ratio; however, the formation of the 4*H*-pyrazole is particularly favoured in the case of **2***a*. This is in spite of the fact that the *N*-methylpyrazoles are much more thermodynamically stable than the 4,4-disubstituted isomers. The resonance energy of pyrazole itself has been calculated to be ca. 10 kcal mol^{-1} (16). Obviously then, the transition state for reaction [4] must resemble the starting material and not the final product. There are several factors which may influence the relative rates of these two reactions. Perhaps the most important consideration is the fact that suprafacial migration from carbon-3 to nitrogen-2 renders the nitrogen tetrahedral; conformational and electronic reorganization must take place before the aromatic stabilization can develop. If this is so, it seems likely that, *in the absence of aromatic stabilization*, the bonding arrangement in **6**, with two relatively strong carbon–nitrogen double bonds, is more stable than that in **5**. Furthermore, the steric repulsion of the vicinal groups R_3 and R_4 in **2** is decreased when migration occurs toward carbon-4.

The observation that only one of the two isomeric *N*-methylpyrazoles **5***b–d* is formed during reaction [4] is consistent with a concerted [1,5]-sigmatropic rearrangement. This is particularly meaningful since the relative thermodynamic stability of the two isomers is only slightly in favour of **5***b–d*; product formation is therefore controlled by kinetic factors.

There is a consistent substituent effect on the absolute rate of reaction within the limited series **2***b–d*. Expressed in terms of the usual Hammett relationship, a plot of the rate of disappearance of **2***b–d* as a function of the substituent constant σ_p gives a straight line with slope $\rho = +0.33$ (correlation coefficient 0.998). This substituent effect is also reflected on the rate of appearance of the corresponding 4*H*-pyrazoles. The small magnitude of the effect and the accuracy of the experimental data do not allow an evaluation of the variation in rate of the minor reaction [4]. This small positive ρ is consistent with a concerted reaction.

Figure 3 is an Arrhenius plot of the rate of rearrangement of **2***b* to **5***b* and **6***b* as a function of temperature. The kinetic parameters from this data are summarized in Table 3. Included in the table are the Arrhenius parameters for the thermal rearrangement of the analogous carbocyclic systems, 5,5-dimethylcyclopentadiene (15) and 1,5,5-trimethylcyclopentadiene (reaction [14]) (17, 18).

We are now in a position to comment upon the competition between thermal loss of nitrogen and

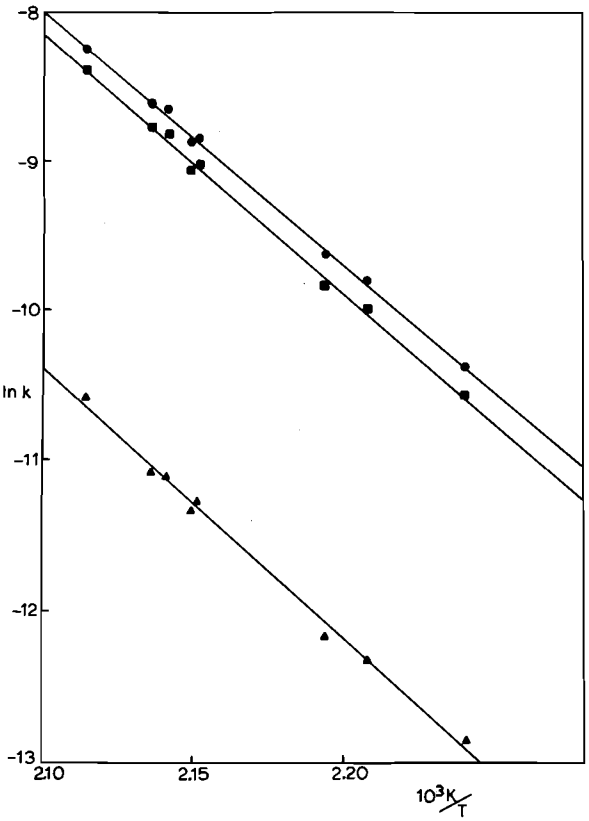

FIG. 3. Arrhenius plot for the thermal rearrangement of **2***b* in diphenyl ether: ●, disappearance of **2***b*; ■, appearance of **6***b*; ▲, appearance of **5***b*.

TABLE 3. Arrhenius parameters for the thermal rearrangement of **2***b*

Reaction	E_a(kcal mol^{-1})[a]	$\Delta S^{\ddagger}$ (eu)[a]	Correlation coefficient
[4][b]	35.6±1.1	−7.0±2.3	0.9973
[5]	34.2±0.7	−5.6±1.6	0.9987
[4] + [5]	33.4±0.5[c]	−6.7±1.0[c]	0.9993
	(34.3±1.0)[d]		
[14] R = H	43.3±2.4	3.0±3	—
[14] R = Me	40.3 (16)	−4 (16)	—
	(43.8) (17)	(0.7) (17)	

[a]It has been pointed out (20) that for the temperature range studied and the error inherent in nmr measurements (5%), the error in $\Delta S^{\ddagger}$ is ca. 3 eu and in E_a, ca. 1.2 kcal mol^{-1}. The errors listed are those estimated from least squares analysis of our data.

[b]The rate constants for reaction [4] were calculated from the measured rate constants for reaction [5] and the product ratios (6:5 = k_5/k_4).

[c]Determined from the rate constants for disappearance of **2***b* ($k_{dec} = k_4 + k_5$).

[d]Calculated from $E_{a,4+5} = (k_4E_{a,4} + k_5E_{a,5})/(k_4 + k_5)$; the value given is the mean of eight calculations.

[1,5]-sigmatropic rearrangement of 3*H*-pyrazoles. We know of only two reported examples of the thermal loss of nitrogen from a 3*H*-pyrazole (**5***b*, 9). Russian workers have reported (9) that the thermal decomposition of methyl and ethyl 3,3,5-triphenyl-3*H*-pyrazole-4-carboxylate (**2***j*) in *o*-xylene gave the products of [1,5]-sigmatropic rearrangement to both nitrogen (**5***j*) and carbon (**6***j*), as well as the cyclopropene **17**, (reaction [15]) (9). The closely related dimethyl 3,3-diphenyl-3*H*-pyrazole-4,5-dicarboxylate (**2***k*) has also been studied (7*b*); however, no mention was made of the cyclopropene in this case. This apparent dichotomy may simply be the result of differences in experimental conditions. The formation of the cyclopropene **17** from **2***j* was observed upon heating in *o*-xylene, reaction being complete after 40 min at 140°C. When this reaction was carried out using acetic acid as solvent (80–90°C, 3 h), **17** was

[15]

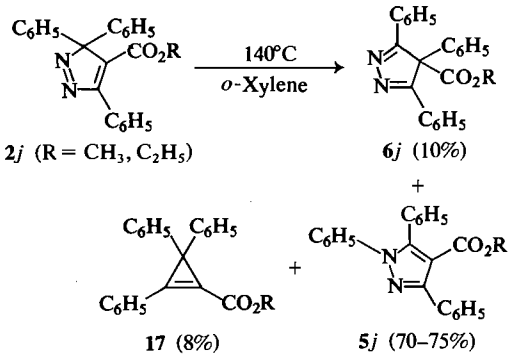

not reported among the products. Acetic acid (118°C) was also used in the study of the rearrangement of **2***k*. It seems likely that either in acetic acid the cyclopropene is formed but is unstable (the material balance was poor) or the rearrangement is catalyzed by acetic acid and at the lower temperatures used the loss of nitrogen simply does not compete. Both acid-catalyzed ring opening of cyclopropenes and acid-catalyzed rearrangement of 3*H*-pyrazoles are well documented (7, 19). In fact, the first reported example of the rearrangement of a 3*H*-pyrazole used acetic acid as solvent (7*a*); perhaps for this reason, acetic acid has usually been used. It may be that cyclopropenes would have been recognized as minor products had the rearrangements been examined in other solvents.

The other reported example of the loss of nitrogen

[16]

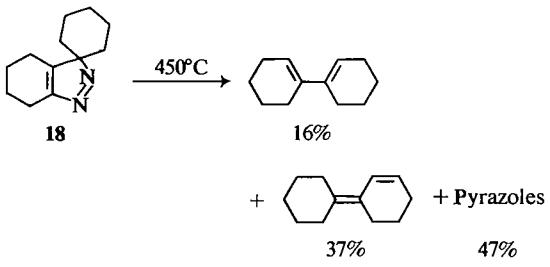

from a 3*H*-pyrazole is the flash vacuum pyrolysis (450°C) of **18**, reaction [16] (5*b*). These high temperature conditions may very well increase the relative importance of the higher activation energy process.

In the thermal decomposition of 1-pyrazolines (reaction [1]), the bulk of the evidence indicates that both carbon–nitrogen bonds are breaking at the transition state (21). This appears to be the case even when the two incipient radical sites differ considerably in stability. Simultaneous cleavage of both carbon–nitrogen bonds in 3*H*-pyrazoles seems highly unlikely. As mentioned previously, the difference between the two carbon–nitrogen bond dissociation energies must be very large in this case. In the analogous alkyl phenyl azo compounds, there is good evidence that only one carbon–nitrogen bond cleaves (reversibly) to give the alkyl and phenyl diazenyl radicals thermally (22). Therefore, it seems likely that the transition state for thermal ring opening in 3*H*-pyrazoles would involve predominantly the breaking of only the carbon-3–nitrogen-2 bond. Notice that the initially formed carbon-centred radical from **2***a–d* would be a tertiary alkyl radical, not allylic until bond rotation becomes possible. On the other hand, in the case of **2***j* where cyclopropene is a significant thermal decomposition product, the initially formed carbon-centred radical is 'bisbenzylic.' With these concepts in mind, we can now compare the reported kinetic parameters for the thermal decomposition of 3,3-dimethyl-1-pyrazoline (**1***a*; R_1–R_4 = H, R_5 = R_6 = CH_3) (1*a*) with those we have measured for **2***b*.

The activation energy for the decomposition of **1***a* (reaction [1]), E_a = 40 kcal mol^{-1}, and the entropy change, ΔS = 10.8 eu, are to be compared with E_a = 33.4 kcal mol^{-1} and ΔS = −6.7 eu for the rearrangement (reactions [4] and [5]) of **2***b*. Even though the activation energy for the decomposition of **1***a* via reaction [1] is considerably higher than that for rearrangement of **2***b*, the rate of decomposition is significantly faster; $k_{\text{dec } 1a}$ = 2.04 × 10^{-3} s^{-1} [4] vs. $k_{\text{dec } 2b}$ = 2.62 × 10^{-4} s^{-1} at 200°C. This is of course the result of the very much larger increase in entropy upon decomposition of **1***a*. The large positive value of ΔS for reaction [1] of **1***a* is consistent with simultaneous cleavage of both carbon–nitrogen bonds at the transition state. Since the transition state for the thermal loss of nitrogen from 3*H*-pyrazoles would involve cleavage of only the one carbon–nitrogen bond, a considerably smaller ΔS value would be involved. If we take 40 kcal mol^{-1} as a reasonable value of the activation energy for carbon–nitrogen bond cleavage in **2***b*,[5] we can calculate what the frequency factor would have to be for this reaction to occur at a rate approximately 3% (the limit of detection by ^{1}Hmr) of that of the rearrangement at the same temperature; log A is calculated to be 13.5. This corresponds to $\Delta S^{195°C} \sim 0.3$, which is again a reasonable value for a reaction of this type. At higher temperatures, the cleavage reaction would then increase in importance; in fact, at 450°C, the temperature at which the flash vacuum pyrolysis of **18** was carried out (reaction [16]), the ratio of the rate constants for rearrangement versus cleavage of **2***b* would be $k_{\text{rearr}}/k_{\text{cleav}} \sim 2.8$. The combination of a high activation energy and a small positive ΔS for the cleavage process allows the [1,5]-sigmatropic rearrangement(s) to compete with loss of nitrogen at lower temperatures.

Tautomeric equilibria in heterocycles has received a great deal of attention in the literature; a number of techniques have been applied to the determination of tautomeric composition in the N—H pyrazole series (23). Most of these methods involve comparison of physical and/or spectral properties of an N—H pyrazole with those of the 1- and 2-methylated derivatives, yet the isomeric equilibria in *N*-alkyl pyrazoles has received little attention.

In the course of our study of the thermal rearrangement of **2***b–d*, we found it necessary to determine the thermodynamic equilibrium constants; we found a small but significant substituent effect on the equilibrium constants for the 1,5- and 1,3-dimethylpyrazole pairs **5***b,c*; *c,f*; *d,g*. The usual Hammett plot of equilibrium constant (K = [1,5-isomer]/[1,3-isomer]) as a function of σ_p for the substituents (H, OMe, CN) on the 3(5)-aryl group reveals a linear relationship with slope ρ = +0.78 (correlation coefficient 0.996).

Elguero *et al.* (23) have pointed out the lack of any dependable criteria for the prediction of tautomeric composition in N—H pyrazoles. They were, however, able to make a qualitative correlation between the tendency of a substituent to occur in the 3- or 5-position and the sign of the Hammett σ_m for that substituent. Electron-donating groups appear to prefer the 5-position, whereas electron-withdrawing groups prefer the 3-position. The situation is complicated by the fact that hydrogen bonding (forming dimeric species) can contribute significantly to the relative tautomeric stability, particularly in nonpolar solvents. Our results with the *N*-methyl derivatives **5***b–g* agree with this qualitative correlation; the

[4]Calculated from reported Arrhenius parameters.

[5]Since the initially formed radical is *not* allylic, and inductive effects are known to have little effect on bond dissociation energies, the energetics of this process can be reasonably approximated by those found for the decomposition of **1***a*.

1,5-dimethyl isomers are favoured in all cases, presumably owing to the fact that all three aryl substituents are electron-withdrawing inductively. It is the *relative* position of the equilibria that is instructive in our case, and it can be seen that the presence of an electron-withdrawing aryl substituent favours the 1,5-dimethyl isomer more than does an electron-donating aryl substituent.

Conclusions

3*H*-Pyrazoles undergo two types of photochemical reaction, a 4πe electrocyclic ring closure and cleavage to give the vinyl diazo compounds. Since the former has been observed only with fully alkylated 3*H*-pyrazoles, the factors governing the relative importance of the two reactions are not well understood.

3*H*-Pyrazoles undergo three types of thermal reactions; two competitive [1,5]-sigmatropic rearrangements, and cleavage followed by loss of nitrogen. Cleavage of the N-1—C-5 bond becomes more important when radical stabilizing groups are present at C-5 or at high temperatures.

Isomeric (tautomeric) equilibria in *N*-methyl (N—H) pyrazoles are partially governed by the electronic characteristics of substituents in the 3- and 5-positions; electron-withdrawing substituents prefer the 3-position.

^{1}Hmr shift reagent studies, solvent shift studies, and ^{13}Cmr spectroscopy are all useful techniques for the differentiation of isomeric 1,3- and 1,5-dimethylpyrazoles.

Experimental

All melting points are corrected. ^{1}Hmr spectra were recorded on either a Varian HA-100 or Varian XL-100 spectrometer and are reported in parts per million downfield from TMS. ^{13}Cmr and ^{19}Fmr spectra were recorded on a Varian XL-100 nmr spectrometer and are reported in parts per million downfield from TMS and parts per million upfield from $CFCl_3$, respectively. Infrared spectra were recorded on a Perkin-Elmer 621 grating infrared spectrometer and are reported in wavenumbers, calibrated against the 1601.8 cm^{-1} polystyrene absorption. Ultraviolet–visible absorption spectra were recorded on a Cary 118 spectrometer and are reported in nanometers. A Fisher Proportional Temperature Control Unit with an insulated silicon oil (Dow Corning 210-H) bath was used in the kinetic studies. Temperatures were recorded using a copper–constantan thermocouple.

The 3*H*-pyrazoles **2***b–d* were prepared by an adaptation of the method of Williams and Dolbier (4, 24).

3,3,4,5-Tetramethyl-3*H*-pyrazole (**2***a*) was prepared by the method of Closs and Heyn (25). Yield from the pyrazoline was 52% (bp 40°C/2.6 Torr). The compound discolours when stored at −25°C and it was therefore redistilled before use.

Low Temperature Irradiation of 2a

A freshly distilled sample of **2***a* (0.05 g, 4.4×10^{-4} mol) was dissolved in methylene chloride (Fisher Spectrograde, 1.0 mL) in a Pyrex nmr tube and placed in a quartz Dewar containing Dry-Ice and acetone. The sample was irradiated with a 450-W medium pressure mercury vapour lamp (Hanovia) for 45 min. The ^{1}Hmr spectrum, taken at room temperature, indicated the formation of the 1,2-diazabicyclo-[2.1.0]pent-2-ene (> 60% yield) (**3***a, b*). The ir spectrum, also at room temperature, had the C=N stretching band at 1604 cm^{-1}. Allowing the solution to sit at room temperature regenerated the 3*H*-pyrazole (^{1}Hmr, ir).

Low Temperature Irradiation of 2b

3,3-Dimethyl-4,5-diphenyl-3*H*-pyrazole (**2***b*, 0.02 g, 9.7×10^{-5} mol) was dissolved in methylene chloride and irradiated as above for 1 h. The tube was transferred without warming to the precooled probe (−70°C) of the XL-100 nmr spectrometer. The ^{1}Hmr spectrum was that of 1,1-dimethyl-2,3-diphenylcyclopropene; no other products were detected.

Thermal Rearrangement of 2a

Freshly distilled **2***a* (0.03 g, 2.4×10^{-4} mol) was dissolved in diphenyl ether (distilled, 0.6 mL), degassed (four freeze–pump–thaw cycles), and sealed in an nmr tube. The tube was heated at 182°C for 11 h; progress of the reaction was monitored by ^{1}Hmr. Concentration vs. time data were obtained by normalizing the integrated intensity of the 3-methyl singlet of **2***a* against the total integrated intensity of the 1–4 ppm region. After 11 h, the reaction mixture consisted of **5***a* and **6***a* in the ratio 1:2, accounting for at least 75% of the material present; **2***a* had completely disappeared at this point. Continued heating for another 40 h resulted in the complete disappearance of **6***a*; the ^{1}Hmr spectrum showed the presence of **5***a*. Chromatography on a silica gel column yielded **5***a* as a colourless oil (0.02 g, 60%) which was identified by spectral comparisons with literature data (26). 4*H*-Pyrazole **6***a* was identified by heating a degassed, sealed tube of **2***a* (0.12 g) in benzene (0.3 mL) at 192°C for 4.5 h; the ^{1}Hmr spectrum at this point revealed the mixture consisted of 11% **2***a* and 85% **6***a* and **5***a* in the ratio 36:1. The tube was opened and the solvent evaporated to a brown oil (0.12 g); the major peaks in the ir spectrum matched the ir spectrum of an authentic sample of **6***a*.

A third sample of **2***a* (0.030 g) in diphenyl ether – pyridine (10:1, 0.6 mL) was degassed, sealed, and heated at 182°C as above. The rate of rearrangement of **2***a* in this case was the same as above (10.4×10^{-5} s^{-1}), within experimental error.

The 3*H*-pyrazoles **2***b–d* were purified by column chromatography (alumina) followed by three recrystallizations from hexane. Kinetic parameters were obtained by heating 0.5 mL portions of a solution of the 3*H*-pyrazole (3.8×10^{-3} mol) and mesitylene (0.13 g, 1.1×10^{-3} mol) in diphenyl ether (10 mL), which were degassed (four freeze–pump–thaw cycles) and sealed in nmr tubes. The mesitylene was used as an internal standard and was shown to be unreactive under these experimental conditions. Concentration vs. time data were obtained by recording the ^{1}Hmr spectra over at least 20 time intervals and measuring the intensity of the 3*H*-pyrazole methyl peak normalized against the mesitylene integral. The resultant plots of ln [I] vs. t in all cases yielded a straight line through at least four half-lives. The Arrhenius parameters for the rearrangement of **2***b* were obtained from a least-squares analysis of the first-order rate constants for disappearance of starting material as a function of temperature.

The possibility of an acid-catalyzed rearrangement was discounted by conducting the rearrangement in the presence of hexamethylenediamine at 192°C. Neither the rate of rearrangement nor the product distribution differed from the rearrangement in the absence of base at this temperature.

Preparative-scale Thermolyses: 2b–d

Thermal Rearrangement of 2b

A solution of **2***b* (0.10 g, 4.1×10^{-4} mol) in benzene (0.5 mL) was degassed and sealed in an nmr tube. The tube was

heated at 200°C for 16 h; progress of the reaction was followed by ^{1}Hmr and was essentially complete after 4 h. The crude reaction mixture was chromatographed on a silica gel (10 g) column with hexane–benzene and benzene–ether mixtures (starting with pure hexanes and increasing the proportion of benzene by 10% every 500 mL eluted). Pyrazole **5***b* (0.010 g, 10%) was eluted with pure benzene and identified by comparison with an authentic sample (*vide infra*). 4*H*-Pyrazole **6***b* (0.083 g, 81%) was eluted with ether (10%) – benzene and recrystallized twice from ether–hexane, mp 122–123.5°C; ir (KBr): 3070(m), 2985(m), 1579(m), 1520(s), 1498(m), 1446(m), 755(s), 763(s), 692(s, br); uv λ_{max} (ethanol): 277 (14 100); λ_{max} (hexane): 274 (12 000); ^{1}Hmr ($CDCl_3$) δ: 1.66 (s, 3H), 1.98 (s, 3H), 7.32 (m, 10H); *Anal.* calcd. for $C_{17}H_{16}N_2$: C 82.22, H 6.50, N 11.28; found: C 82.26, H 6.68, N 11.09.

Thermal Rearrangement of **2**c

A solution of **2***c* (0.048 g, 1.76×10^{-4} mol) in benzene (0.3 mL) was degassed and sealed in an nmr tube. The tube was heated at 200°C as above for 16 h. The crude reaction mixture was chromatographed on a silica gel (5 g) column with benzene–ether mixtures. Pyrazole **5***c* (0.005 g, 10%) was eluted with ether (2%) and **6***c* (0.036 g, 75%) with pure ether. Pyrazole **5***c* was identified by comparison with an authentic sample (*vide infra*). 4*H*-Pyrazole **6***c* was further purified by sublimation (120°C/0.1 Torr) and one recrystallization from absolute alcohol, mp 162–162.5°C; ir (KBr): 3070(w), 2230(s), 1568(m), 1496(m), 1380(w), 1270(w), 860(s), 848(s), 759(s), 700(s), 559(s); uv λ_{max} (ethanol): 284 (15 000); λ_{max} (hexane): 285 (16 500); ^{1}Hmr ($CDCl_3$) δ: 1.69 (s, 3H), 2.03 (s, 3H), 7.08 (m, 2H), 7.37 (m, 3H), 7.59 (d, 2H), 7.78 (d, 2H). *Anal.* calcd. for $C_{18}H_{15}N_3$: C 79.09, H 5.53; found: C 79.13, H 5.79.

Thermal Rearrangement of **2**d

A solution of **2***d* (0.050 g, 2.8×10^{-4} mol) in benzene (0.3 mL) was degassed, sealed, and heated as above for 16 h. Chromatography on silica gel (5 g) with hexane–benzene and benzene–ether mixtures afforded **5***d* (0.008 g, 16%), which was eluted with ether (2%) – benzene and identified by comparison with an authentic sample (*vide infra*). Pyrazole **6***d* (0.041 g, 82%) was eluted with ether (15%) – benzene and recrystallized three times from hexanes, mp 119–119.5°C; ir (KBr): 2840(w), 1604(s), 1578(m), 1503(s), 1418(s), 1309(s), 1248(s), 1172(s), 1033(s), 832(s), 763(m), 697(s); uv λ_{max} (ethanol): 307 (20 400); λ_{max} (hexane): 296 (19 100); ^{1}Hmr ($CDCl_3$) δ: 1.69 (s, 3H), 2.00 (s, 3H), 3.83 (s, 3H), 6.96 (d, 2H), 7.28 (m, 2H), 7.55 (m, 3H), 7.82 (d, 2H). *Anal.* calcd. for $C_{18}H_{18}N_2O$: C 77.67, H 6.52, N 10.07; found: C 77.78, H 6.46, N 9.79.

4*H*-Pyrazoles **6***b–d* were identified by comparison of their spectral properties with those of **6***a* and 3-phenyl-4,4,5-trimethyl-4*H*-pyrazole. Particularly diagnostic is the medium intensity C=N stretching band at 1570–1580 cm^{-1} in the ir spectra. The uv spectrum of **6***b* in hexane is almost identical to that of 3-phenyl-4,4,5-trimethyl-4*H*-pyrazole (λ_{max} (hexane): 271 (14 100)).

Preparation of 4H-*Pyrazolium Iodides (*7a–d*)*

*1,3,4,4,5-Pentamethyl-*4H*-pyrazolium Iodide (*7a*)*

A solution of **6***a* (0.18 g, 1.42×10^{-3} mol) in methyl iodide (4 mL) was refluxed on the steam bath for 15 min, resulting in the formation of a colourless precipitate. Anhydrous ether (3 mL) was added, and the mixture was filtered. The precipitate was washed with ether (2 × 0.5 mL) and dried, yielding the product as colourless crystals (0.36 g, 1.4×10^{-3} mol, 97%) which were recrystallized twice from absolute alcohol, mp 180–183°C (dec); ir (KBr): 2975(w), 1640(m), 1595(s), 1469(m), 1441(m), 1391(m), 1297(m), 790(m), 692(m); uv λ_{max} (ethanol): 222 nm (14 000); ^{1}Hmr ($CDCl_3$) δ: 1.63 (s, 6H), 2.32 (s, 3H), 2.99 (m, 3H), 4.16 (m, 3H).

Heating the salt (0.14 g, 5.4×10^{-4} mol) to its melting point under vacuum for 5 min resulted in the formation of an orange oil which bubbled vigorously, and a colourless oil which condensed on the walls of the flask. The orange oil crystallized on cooling. The ^{1}Hmr spectrum ($CDCl_3$) of this mixture showed it to contain 1,3,4,5-tetramethylpyrazole (δ: 1.85 (s, 3H), 2.10 (br s, 6H), 3.65 (s, 3H)) and 1,2,3,4,5-pentamethylpyrazolium iodide (δ: 4.10 (br s, 6H), 2.37 (br s, 6H), 1.98 (s, 3H)) (27) in the ratio 1:2. The material balance was poor (0.09 g), probably owing to loss of the 1,3,4,5-tetramethylpyrazole by vaporization.

*1,4,5-Trimethyl-3,4-diphenyl-*4H*-pyrazolium Iodide (*7b*)*

A solution of **6***b* (0.10 g, 4.0×10^{-4} mol) in methyl iodide (3 mL) was refluxed for 2 h, during which time a yellow precipitate formed. Anhydrous ether (3 mL) was added and the mixture was filtered. The yellow precipitate was washed with ether (2 × 0.5 mL) and dried (0.14 g, 3.5×10^{-4} mol, 87%). The material was further purified by three recrystallizations from chloroform–ether alternated with three recrystallizations from absolute alcohol to yield yellow crystals of **7***b*, mp 154.5–155°C (dec.); ir (KBr): 1637(m), 1547(s), 1495(m), 1444(s), 1157(w), 1076(w), 774(s), 698(s), 636(m); uv λ_{max} (ethanol): 219 (22 800), 299 (9700); ^{1}Hmr ($CDCl_3$) δ: 2.20 (s, 3H), 2.78 (br s, 3H), 4.42 (br s, 3H), 7.26 (m, 10H). *Anal.* calcd. for $C_{18}H_{19}N_2I$: C 55.40, H 4.91, N 7.18; found: C 54.77, H 5.01, N 7.35.

Heating the methiodide (0.05 g, 1.3×10^{-4} mol) to its melting point under vacuum resulted in the vigorous release of methyl iodide and formation of **5***b* (0.03 g, 1.2×10^{-4} mol, 91%).

*3-(4-Cyanophenyl)-4-phenyl-1,4,5-trimethyl-*4H*-Pyrazolium Iodide (*7c*)*

A solution of **6***c* (0.10 g, 3.7×10^{-4} mol) in methyl iodide (3 mL) was refluxed on the steam bath for 2 h, which resulted in the formation of a yellow precipitate. Work-up as above yielded the product as yellow crystals (0.11 g, 2.6×10^{-4} mol, 71%) which were further purified by five recrystallizations from absolute alcohol – anhydrous ether, mp 142.5–143°C (dec.); ir (KBr): 2229(s), 1626(s), 1575(m), 1535(s), 1498(m), 1442(m), 859(s), 702(s), 597(s); uv λ_{max} (ethanol): 217 (sh, 28 400), 250 (sh, 11 100), 355(sh, 11 000), 390 (12 600); ^{1}Hmr ($CDCl_3$) δ: 2.28 (s, 3H), 2.79 (br s, 3H), 4.42 (br s, 3H), 7.25 (m, 4H), 7.59 (s, 5H). *Anal.* calcd. for $C_{19}H_{18}N_3I$: C 54.95, H 4.37, N 10.12; found: C 54.84, H 4.50, N 10.31.

Heating the methiodide (0.06 g, 1.5×10^{-4} mol) to its melting point under vacuum resulted in vigorous release of methyl iodide and the formation of **5***c* (0.03 g, 1.1×10^{-4} mol, 75%).

*3-(4-Methoxyphenyl)-4-phenyl-1,4,5-Trimethyl-*4H*-pyrazolium Iodide (*7d*)*

A solution of **6***d* (0.09 g, 3.4×10^{-4} mol) in methyl iodide (2.5 mL) was refluxed for 1 h, during which time a bright yellow precipitate was formed. Addition of anhydrous ether, filtration, washing (anhydrous ether), and drying yielded the product as bright yellow crystals (0.11 g, 2.5×10^{-4} mol, 75%). The material was further purified by one recrystallization from absolute ethanol and three recrystallizations from chloroform–ether, mp 181.5–182°C (dec.); ir (KBr): 2930(w), 1608(s), 1529(s), 1510(s), 1427(m), 1263(s), 1176(s), 842(m), 790(m); uv λ_{max} (ethanol): 215 (sh, 24 300), 245 (sh, 6400), 340 (12 200). ^{1}Hmr ($CDCl_3$) δ: 2.20 (s, 3H), 2.77 (br s, 3H), 3.77 (s, 3H), 4.32 (br s, 3H), 6.73 (d, 2H), 7.21 (m, 5H), 7.45

(d, 2H). *Anal.* calcd. for $C_{19}H_{21}N_2OI$: C 54.30, H 5.04, N 6.67; found: C 53.86, H 5.07, N 6.96.

Heating the methiodide (0.02 g, 5.2×10^{-5} mol) to its melting point under vacuum resulted in vigorous release of methyl iodide and formation of **5***d* (0.01 g, 4.7×10^{-5} mol, 89%) which contained less than 8% of the other isomer.

*Preparation of 4,5-Diphenyl-1,2,3-trimethylpyrazolium Iodide (***9***b)*

Pyrazole **5***b* (0.05 g, 2.0×10^{-4} mol) was dissolved in methyl iodide (0.5 mL), placed in an nmr tube, degassed (four freeze–pump–thaw cycles) and the tube was sealed. The mixture was heated at 100°C for 4 h. Evaporation of the excess methyl iodide yielded the product as yellow crystals (0.07 g, 1.9×10^{-4} mol, 96%) which were recrystallized twice from chloroform–ether affording colourless plates of **9***b*, mp 224–225°C (dec.); ir (KBr): 1550(m), 1460(s), 1441(m), 1424(m), 1400(s), 1346(s), 791(s), 766(s), 708(s); uv λ_{max} (ethanol): 215 (15 000), 255 (sh, 4000); ^{1}Hmr ($CDCl_3$) δ: 2.49 (br s, 3H), 4.19 (br s, 3H), 4.39 (br s, 3H), 7.18 (m, 5H), 7.38 (s, 5H). *Anal.* calcd. for $C_{18}H_{19}N_2I$: C 55.40, H 4.91, N 7.18; found: C 55.57, H 4.83, N 6.83.

Compound **9***b* was also synthesized in 97% yield from **5***e* as above.

Thermolysis of **9***b* (0.05 g, 1.3×10^{-4} mol) at its melting point under vacuum resulted in vigorous bubbling and the formation of a colourless oil (0.03 g, 1.2×10^{-4} mol, 95%). The nmr spectrum showed the oil to be a 4:1 mixture of **5***b* and **5***e*.

High Temperature ^{1}H Nuclear Magnetic Resonance Spectrum of **7**a

The ^{1}Hmr spectrum of **7***a* in DMF-d_6 was examined at five temperatures between 80–150°C by heating a sealed tube in the probe of the XL-100 nmr spectrometer. No broadening or coalescence of any of the signals was observed at these temperatures. No decrease in intensity of the C-3 or C-5 methyl singlets was observed upon double irradiation of the C-5 or C-3 methyl singlets. The spectrum was complicated by the steady decomposition of **7***a* to give **5***a*, methyl iodide, and 1,2,3,4,5-pentamethylpyrazolium iodide.

Preparation of **5**b–i

Desoxybenzoin Enol Acetate

The procedure is that of Barnes *et al.* (28). A mixture of desoxybenzoin (15.0 g, 0.08 mol) and potassium acetate (30 g, 0.31 mol) in acetic anhydride (300 mL) was refluxed for 1 h in a 500-ml round-bottom flask equipped with magnetic stirrer, condenser, and drying tube. The resultant dark brown liquid was allowed to cool slightly, poured into water (1.4 L), and then stirred at room temperature for 0.5 h. The resulting brown crystalline suspension was extracted with ether (3 × 200 mL). The combined ether extracts were washed repeatedly with a saturated aqueous solution of sodium bicarbonate until CO_2 evolution had ceased, followed by one wash with water (100 mL). The dark brown solution was then dried over anhydrous magnesium sulphate and filtered. Evaporation of solvent afforded a dark brown oil (16.3 g) which crystallized upon addition of methanol. The crystals were filtered, washed with methanol, and dried. Reduction of the mother liquors afforded an additional quantity of product. A second recrystallization from methanol afforded the product as slightly brown crystals (12.4 g, 0.05 mol, 68%, mp 102–103°C (lit. (28) mp 101°C).

4-Methoxydesoxybenzoin Enol Acetate

This was prepared by refluxing 4-methoxydesoxybenzoin (10.1 g, 0.045 mol) and potassium acetate (20 g, 0.20 mol) in acetic anhydride (140 mL) for 18 h. Following work-up (as above), the product was recrystallized once from ethanol to afford brown crystals (5.89 g, 0.022 mol, 49%, mp 82–87°C, lit. (28) mp 88°C).

4-Bromodesoxybenzoin Enol Acetate

This was prepared by refluxing 4-bromodesoxybenzoin (10.1 g, 0.04 mol) and potassium acetate (20 g, 0.20 mol) in acetic anhydride (140 mL) for 20 h. Work-up and subsequent recrystallization from ethanol–water afforded the product as brown crystals (6.1 g, 0.02 mol, 61%, mp 104–106°C). Chromatography on a silica gel column with 1:1 benzene – petroleum ether followed by two recrystallizations from ethanol afforded the compound as colourless crystals (mp 107–108°C); ir (KBr): 1751(s), 1489(m), 1395(m), 1373(m), 1227(s), 1215(s), 1070(s), 1040(s), 1010(s), 939(m), 858(m), 851(m), 817(s), 754(s), 704(s), 573(m); uv λ_{max} (ethanol): 294 (25 000), 225 (10 100); λ_{max} (hexane): 292 (27 400), 223 (12 100); ^{1}Hmr ($CDCl_3$) δ: 2.28 (s, 3H), 6.67 (s, 1H), 7.42 (m, 9H). *Anal.* calcd. for $C_{16}H_{13}O_2Br$: C 60.59, H 4.13; found: C 60.87, H 4.20.

4-Cyanodesoxybenzoin Enol Acetate

This was prepared by refluxing 4-cyanodesoxybenzoin (8.14 g, 0.037 mol), and potassium acetate (10 g, 0.10 mol) in acetic anhydride (150 mL) for 1 h. Work-up and recrystallization from ethanol afforded the product as yellow crystals (6.94 g, 0.026 mol, 70%, mp 107–109°C). Column chromatography of a portion of the product on silica gel with benzene yielded the enol acetate as colourless crystals which were recrystallized twice from ethanol (mp 110–111°C); ir (KBr): 3028(w), 2223(s), 1752(s), 1601(s), 1371(s), 1211(s, br), 1178(s), 1040(s), 821(s), 745(m), 691(s); uv λ_{max} (ethanol): 230 (11 800), 308 (27 400); λ_{max} (hexane): 227 (11 100), 302 (25 000); ^{1}Hmr ($CDCl_3$) δ: 2.33 (s, 3H), 6.81 (s, 1H), 7.48 (m, 5H), 7.66 (s, 4H). *Anal.* calcd. for $C_{17}H_{13}NO_2$: C 77.55, H 4.98; found: C 77.67, H 4.97.

Synthesis of 1-Aryl-2-phenyl-1,3-butanediones (29)

1,2-Diphenyl-1,3-butanedione

Desoxybenzoin enol acetate (10.0 g, 0.04 mol) and acetyl chloride (1.5 mL, 0.02 mol) were dissolved in 1,2-dichloroethane (25 mL) in a 250 mL three-necked round-bottom flask fitted with overhead stirrer, gas inlet tube, and reflux condenser with drying tube ($CaCl_2$). The solution was cooled to 0°C in an ice bath and BF_3 (purified by bubbling through concentrated H_2SO_4) was let into the flask at such a rate so as to keep the mixture below the reflux temperature.

The BF_3 was absorbed rapidly for the first 15 min, at which time the brown mixture solidified; an additional quantity of dichloroethane (25 mL) was added. The reaction mixture was stirred at 0°C under a BF_3 atmosphere for 3 h.

A solution of sodium acetate (7.0 g, 0.09 mol) in water (25 mL) was added and the dichloroethane was distilled off on the steam bath. The aqueous mixture was refluxed for another 0.5 h, during which time a yellow oil formed. The mixture was cooled and extracted with ether (3 × 50 mL). The combined organic fractions were washed once with saturated aqueous bicarbonate (20 mL), once with water (20 mL), dried over anhydrous sodium sulphate, and filtered. Evaporation of solvent yielded a light yellow liquid (11.4 g); methanol (25 mL) was added and the subsequent solution was cooled. The product was isolated as slightly yellow crystals (enol form, 7.4 g, mp 86–89°C (lit. (30) mp 88–89°C)). Reduction of the mother liquors afforded slightly yellow plates (diketo form, 1.6 g, mp 76–80°C (lit. (29, 30) mp 76–77°C)). Total yield was 90%.

1-(4-Methoxyphenyl)-2-phenyl-1,3-butanedione

This was prepared as above from 4-methoxydesoxybenzoin enol acetate (0.39 g, 1.4×10^{-3} mol) and acetyl chloride (0.01 mL) in 1,2-dichloroethane (1 mL). Following sodium acetate hydrolysis, the product was extracted with benzene. Evaporation of solvent afforded brown crystals (0.39 g) which were shown by ^{1}Hmr to consist of the difluoroborate ether of the diketone (major), the diketone (two tautomeric forms), and 4-methoxydesoxybenzoin. The mixture was chromatographed on a silica gel (30 g) column with hexanes (10%) – benzene. First isolated from the column were yellow crystals of the difluoroborate ether (0.22 g, 6.8×10^{-4} mL, 47%), which were recrystallized once from ether–benzene and once from ethanol (mp 141–144°C); ir (KBr): 2848(w), 1600(s), 1580(s), 1550(s), 1463(br, s), 1439(m), 1342(s), 1265(s), 1179(s), 1059(br, s), 1022(s), 846(m), 775(m), 704(m), 558(m); uv λ_{max} (ethanol): 364 (16 000), 240 (5600); λ_{max} (hexane): 358 (26 400), 240 (7500); ^{1}Hmr ($CDCl_3$) δ: 2.17 (s, 3H), 3.80 (s, 3H), 6.71 (d, 2H), 7.33 (m, 7H); ^{19}Fmr ($CDCl_3$–$CFCl_3$): −140.1 ppm from $CFCl_3$. *Mass ion* calcd.: 316.1078; found: 316.1080. *Anal.* calcd. for $C_{17}H_{15}BF_2O_3$: C 64.59, H 4.78; found: C 64.72, H 4.61.

Next was isolated 4-methoxydesoxybenzoin (0.04 g) and finally a yellow oil (0.08 g); spectral data (^{1}Hmr, ir) identified it as a 1:2 mixture of the β-diketone and one of its enol forms; ir (KBr): 2920(w), 2840(w), 1720(m), 1670(m), 1602(s), 1510(m), 1422(w), 1264(s), 1173(s), 1030(m); uv λ_{max} (ethanol): 335 (sh, 1700), 286 (11 000), 235 (sh, 10 500); λ_{max} (hexane): 330 (sh, 1800), 277 (11 700), 220 (sh, 12 000); ^{1}Hmr ($CDCl_3$) β-diketone δ: 2.14 (s, 3H), 3.73 (s, 3H), 5.45 (s, 1H), 6.70 (d, 2H), 7.73 (d, 2H), 7.20 (m, 5H); enol δ: 1.94 (s, 3H), 3.65 (s, 3H), 6.45 (d, 2H), 7.18 (m, 7H), 18.9 (s, 1H).

Refluxing the difluoroborate ether (0.035 g, 1.1×10^{-4} mol) in methanol (4 mL) for 2.5 h, followed by evaporation of solvent, yielded a yellow oil (0.034 g). The ^{1}Hmr spectrum showed it to be a roughly equal mixture of the β-diketone and enol, plus a small amount of unreacted starting material. Chromatography on a silica gel column with benzene gave 0.010 g of the β-diketone–enol mixture as a yellow oil whose ir spectrum (KBr) matched that given above.

1-(4-Bromophenyl)-2-phenyl-1,3-butanedione

This was prepared as above from 4-bromodesoxybenzoin enol acetate (5.133 g, 0.016 mol) and 4 drops acetyl chloride in 1,2-dichloroethane (13 mL). A longer hydrolysis time was required in this case (1.5 h) since after 0.5 h a considerable amount of a black solid, insoluble in organic solvents, remained. Extraction with benzene–ether (1:1) and subsequent work-up yielded a brown-red solid (5.55 g); the ^{1}Hmr spectrum showed it to consist of the β-diketone and 4-bromodesoxybenzoin in the ratio 2:1. Repeated washings of the solid with anhydrous ether was effective in removing the desoxybenzoin, leaving impure crystals of 1-(4-bromophenyl)-2-phenyl-1,3-butanedione (2.76 g, 8.7×10^{-3} mol, 54%) which was used without further purification for the preparation of the pyrazoles.

The combined ether filtrates were evaporated and the residue was dissolved in hot ethanol and then cooled. The resulting crystals were filtered, washed, and dried, and identified as 4-bromodesoxybenzoin (1.52 g). The evaporated mother liquors were then chromatographed on a silica gel column, eluting with 10% hexanes in benzene. Initial fractions contained the desoxybenzoin; subsequent fractions containing the diketone were combined and recrystallized five times from 95% ethanol to yield light yellow needles of 1-(4-bromophenyl)-2-phenyl-1,3-butanedione (enol form), mp 83.5–84.5°C; ir (KBr): 3061(w), 3035(w), 1712(br, w), 1676(br, m), 1583(br, s), 1482(m), 1395(m), 1070(s), 1010(s), 834(m), 702(s); uv λ_{max} (ethanol) 316 (11 500), 258 (11 900); λ_{max} (hexane): 316 (12 700), 242 (8800); ^{1}Hmr ($CDCl_3$) δ: 2.05 (s, 3H), 7.21 (m, 9H), 17.31 (s, 1H). *Anal.* calcd. for $C_{16}H_{13}O_2Br$: C 60.59, H 4.13; found: C 60.37, H 4.20.

Several attempts to synthesize 1-(4-cyanophenyl)-2-phenyl-1,3-butanedione from 4-cyanodesoxybenzoin enol acetate by the above method and variations thereof were unsuccessful; the starting material and/or 4-cyanodesoxybenzoin were recovered in every case.

Preparation of **5**b, d, e, g, h, i

The pyrazoles were prepared by refluxing the β-diketone with a 4–5 molar excess of anhydrous methyl hydrazine in benzene for 8–12 h. The ^{1}Hmr and ^{13}Cmr spectra of these compounds are summarized in Table 2.

For example, 1,2-diphenyl-1,3-butanedione (2.00 g, 8.8×10^{-3} mol) and methyl hydrazine (1.93 g, 0.042 mol) were dissolved in benzene (40 mL) in a 100-mL round-bottom flask equipped with condenser and magnetic stirrer. Reflux for 8 h gave a light yellow solution which was removed from the heat, dried (magnesium sulphate), and filtered. The solvent and excess methylhydrazine were removed on the rotary evaporator to yield a yellow oil (2.02 g, 92%). The ^{1}Hmr spectrum showed the mixture consisted of **5***b* and **5***e* in the ratio 2:3. The isomers were separated by chromatography on an alumina (150 g) column with hexane–ether mixtures (ether concentration was increased by 3% for every 1000 mL of solvent eluted until a 12% ether solution was reached). The first compound to be eluted was **5***e*, which was recrystallized twice from ether and identified as 1,3-dimethyl-4,5-diphenylpyrazole (*vide infra*), mp 134–134.5°C; ir (KBr): 3061(w), 2929(w), 1603(s), 1513(s), 1488(m), 1439(m), 1363(m), 1019(s), 994(s), 769(s), 593(s); uv λ_{max} (ethanol): 233 (14 500); λ_{max} (hexane): 239 (16 000). *Anal.* calcd. for $C_{17}H_{16}N_2$: C 82.22, H 6.50, N 11.28; found: C 82.39, H 6.71, N 11.08.

Mixtures of **5***b*, *e* were eluted next and finally **5***b* was eluted. The mixtures were combined and rechromatographed; **5***b* was recrystallized twice from ether and identified as 1,5-dimethyl-3,4-diphenylpyrazole (*vide infra*), mp 121–122°C; ir (KBr): 3047(w), 2952(w), 1603(sh), 1547(m), 1495(m), 1436(m), 1367(m), 1076(s), 967(s), 768(s), 705(s); uv λ_{max} (ethanol): 231 (16 200); λ_{max} (hexane): 237 (17 100). *Anal.* calcd. for $C_{17}H_{16}N_2$: C 82.22, H 6.50, N 11.28; found: C 82.22, H 6.59, N 11.40.

Preparation of **5**d *and* g

The difluoroborate ether of 1-(4-methoxyphenyl)-2-phenyl-1,3-butanedione (1.381 g, 4.4×10^{-3} mol) and methyl hydrazine (1.93 g, 0.042 mol) were dissolved in benzene (50 mL) and refluxed as above for 16 h. Work-up yielded slightly yellow crystals (1.13 g, 4.05×10^{-3} mol, 93%). The ^{1}Hmr spectrum of the crude product showed it to consist of **5***d* and *g* in the ratio 1:12. This mixture was chromatographed on an alumina (65 g) column with an ether (1%) – benzene solution. The first fractions eluted contained **5***g* (0.77 g), which was recrystallized twice from hexane to give colourless crystals which were identified as 1,3-dimethyl-5-(4-methoxyphenyl)-4-phenylpyrazole, mp 122.5–123°C; ir (KBr): 3023(w), 2969(w), 2828(w), 1612(m), 1517(s), 1493(m), 1460(m), 1375(m), 1022(s), 850(m), 764(s), 593(m); uv λ_{max} (ethanol): 239 (21 500), 255 (sh, 11 500); λ_{max} (hexane): 243 (19 600), 260 (sh, 13 300). *Anal.* calcd. for $C_{18}H_{18}N_2O$: C 77.67, H 6.52, N 10.07; found: C 77.65, H 6.60, N 10.19.

The remaining fractions from the column consisted of mixtures of **5***d* and *g* (0.34 g). This mixture was dissolved in hot hexane and cooled; **5***g* crystallized (0.17 g).

Pure **5***d* was isolated by heating **5***g* (0.20 g, 7.0×10^{-4} mol) and methyl iodide (0.04 mL, 7.0×10^{-4} mol) in benzene (2 mL) in a Carius tube (which had been degassed and sealed) at 220°C

for 1 h. Evaporation of the benzene and excess methyl iodide yielded the equilibrium mixture of **5***d* and *g* (0.20 g, 100%). Fractional recrystallization from hexane–ether, followed by sublimation (105°C, 2 Torr) and three recrystallizations from hexane–ether afforded **5***d* as colourless crystals (mp 96.5–97°C) which were identified as 1,5-dimethyl-3-(4-methoxyphenyl)-4-phenylpyrazole; ir (KBr): 2994(w), 2839(w), 1608(m), 1527(s), 1434(s), 1386(m), 1036(s), 843(s), 761(s), 589(m); uv λ_{max} (ethanol): 242 (14 500), 255 (sh, 13 100); λ_{max} (hexane): 245 (19 400), 257 (sh, 17 800). *Anal.* calcd. for $C_{18}H_{18}N_2O$: C 77.67, H 6.52; found: C 77.69, H 6.64.

Preparation of **5**h, i

1-(4-Bromophenyl)-2-phenyl-1,3-butanedione (2.73 g, 8.52 $\times 10^{-3}$ mol) and methyl hydrazine (3.27 g, 0.071 mol) were dissolved in benzene (50 mL) and refluxed as above for 18 h. Work-up yielded a red oil (2.78 g) which consisted of **5***h* and *i* (approximate ratio 1:12) and 4-bromodesoxybenzoin. The mixture was chromatographed on a silica gel column with benzene–hexane mixtures, which resulted in the isolation of 4-bromodesoxybenzoin (0.34 g). Elution with ether (1%) – benzene gave pure **5***h* (0.16 g, 4.86×10^{-4} mol, 6%) which was recrystallized twice from hexanes, yielding colourless crystals of 3-(4-bromophenyl)-1,5-dimethyl-4-phenylpyrazole, mp 122–123°C; ir (KBr): 3073(w), 2934(w, br), 1603(w), 1491(m), 1434(s), 1066(s), 1013(s), 964(s), 838(s), 696(s); uv λ_{max} (ethanol): 240 (17 100), 261 (sh, 14 000); λ_{max} (hexane): 243 (18 900), 263 (sh, 17 300). *Anal.* calcd. for $C_{17}H_{15}N_2Br$: C 62.40, H 4.62, N 8.56; found: C 62.38, H 4.45, N 8.48.

Continued elution with ether (1%) – benzene gave **5***i* (1.85 g, 5.62×10^{-3} mol, 66%) which was recrystallized twice from hexanes, affording colourless crystals of 5-(4-bromophenyl)-1,3-dimethyl-4-phenylpyrazole, mp 105–106°C; ir (KBr): 3068(w), 2935(w), 1601(m), 1487(m), 1370(m), 1074(m), 1015(s), 855(s), 765(s), 699(s); uv λ_{max} (ethanol): 230 (sh, 18 100), 237 (17 800); λ_{max} (hexane) 228 (16 200), 244 (16 100). *Anal.* calcd. for $C_{17}H_{15}N_2Br$: C 62.40, H 4.62, N 8.56; found: C 62.46, H 4.89, N 8.74.

Preparation of **5**c *(31)*

A dry DMF (2 mL) solution of **5***b* (0.18 g, 5.5×10^{-4} mol; contained ~20% **5***i*) and cuprous cyanide (0.11 g, 1.2×10^{-3} mol) in a 10-ml round-bottom flask fitted with air condenser, magnetic stirrer, and drying tube was refluxed for 11 h.

The brown reaction mixture was poured into hot aqueous 10% sodium cyanide and heated on the steam bath for 1 h, during which time a yellow-brown oil formed. After cooling, the oil was extracted with benzene (3 × 15 mL). The combined benzene fractions were washed with water (3 × 10 mL), dried over magnesium sulphate, and filtered. Evaporation of the solvent yielded a yellow oil (0.13 g, 4.7×10^{-4} mol, 85%) which was then chromatographed on a silica gel column with benzene (70%) – hexane. First to be eluted was **5***c*, which was recrystallized once from hexanes, affording colourless crystals of 3-(4-cyanophenyl)-1,5-dimethyl-4-phenylpyrazole, mp 143–144°C; ir (KBr): 2224(s), 1606(s), 1492(m), 1379(m), 1282(m), 1119(m), 853(s), 692(s), 551(s); uv λ_{max} (ethanol): 232 (sh, 17 000), 285 (16 000); λ_{max} (hexane): 227 (sh, 12 400), 244 (sh, 11 500), 282 (15 000). *Anal.* calcd. for $C_{18}H_{15}N_3$: C 79.09, H 5.53; found: C 78.89, H 5.76.

Preparation of **5**f

A dry DMF (3 mL) solution of **5***i* (0.75 g, 2.0×10^{-3} mol) and cuprous cyanide (0.23 g, 2.6×10^{-3} mol) was refluxed (11 h) in a 10-mL round-bottom flask fitted with air condenser, drying tube, and magnetic stirrer.

The slightly brown mixture was then poured into hot aqueous 10% sodium cyanide (25 mL) and heated on the steam bath for 1 h, during which time a white precipitate appeared and gradually redissolved, followed by the appearance of a yellow oil. The mixture was cooled and the oil was extracted with benzene (3 × 15 mL). The combined organic fractions were washed with water (3 × 10 mL), dried over magnesium sulphate, and filtered. Evaporation of solvent yielded a yellow oil (0.69 g) which was chromatographed on an alumina column with hexane–benzene mixtures and finally ether (1%) – benzene. A total of 0.39 g of the pyrazole was collected (1.44×10^{-3} mol, 72%) and was recrystallized twice from ether–hexane to afford colourless needles of 5-(4-cyanophenyl)-1,3-dimethyl-4-phenylpyrazole, mp 128–128.5°C; ir (KBr): 2230(s), 1612(s), 1602(s), 1519(m), 1376(m), 1020(m), 966(m), 826(s), 699(s), 596(s); uv λ_{max} (ethanol): 231 (15 400), 285 (sh, 6800); λ_{max} (hexane): 229 (17 400), 280 (8200). *Anal.* calcd. for $C_{18}H_{15}N_3$: C 79.09, H 5.53; found: C 78.87, H 5.31.

Catalyzed Thermal Equilibration of Isomeric N*-Methylpyrazoles*

Equilibria were established by heating degassed solutions of the pyrazoles **5***b–g* with methyl iodide (equimolar) in phenyl ether in sealed tubes for 6 days at 210°C. In the case of **5***b* and *e*, a small amount of **9** was used as catalyst instead of methyl iodide. The tubes were checked daily (^{1}Hmr), and at no time could the methiodides **9** be detected. The equilibrium ratios were estimated by ^{1}Hmr and are summarized in [10].

Acknowledgements

This work was supported by a grant from the National Research Council of Canada. We gratefully acknowledge the assistance of Dr. J. B. Stothers and Ms. C. Ducharme in obtaining the ^{13}Cmr spectra and Ms. H. Schroeder in obtaining the 100 MHz ^{1}Hmr spectra.

1. (*a*) R. J. Crawford and A. Mishra. J. Am. Chem. Soc. **88**, 3963 (1966); (*b*) R. J. Crawford and D. M. Cameron. Can. J. Chem. **45**, 691 (1967); (*c*) D. E. McGreer and I. M. E. Masters. Can. J. Chem. **47**, 3975 (1969).
2. R. B. Woodward and R. Hoffmann. Angew. Chem. Int. Ed. Engl. **8**, 781 (1969).
3. (*a*) G. L. Closs and W. A. Böll. J. Am. Chem. Soc. **85**, 3904 (1963); (*b*) G. L. Closs, W. A. Böll, H. Heyn, and V. Dev. J. Am. Chem. Soc. **90**, 173 (1968).
4. D. R. Arnold, R. W. Humphreys, W. J. Leigh, and G. E. Palmer. J. Am. Chem. Soc. **98**, 6225 (1976).
5. (*a*) D. W. Adamson and J. Kenner. J. Chem. Soc. 286 (1935); (*b*) J. T. Sharp, R. H. Findlay, and P. B. Thorogood. J. Chem. Soc. Perkin Trans. I, 102 (1975); (*c*) J. L. Brewbaker and H. Hart. J. Am. Chem. Soc. **91**, 711 (1969).
6. J. A. Pincock and K. P. Murray. Can. J. Chem. In press.
7. (*a*) J. van Alphen. Recl. Trav. Chim. Pays-Bas, **62**, 485 (1943); (*b*) R. Baumes, J. Elguero, R. Jacquier, and G. Tarrago. Tetrahedron Lett. 3781 (1973); (*c*) H. Dürr and W. Schmidt. Justus Liebigs Ann. Chem. 1140 (1974); (*d*) R. Hüttel, K. Franke, H. Martin, and J. Riedl. Chem. Ber. **93**, 1433 (1960); (*e*) G. Wittig and J. J. Hutchison. Justus Liebigs Ann. Chem. **741**, 89 (1970).
8. (*a*) M. Franck-Neumann and C. Buchecker. Tetrahedron Lett. 937 (1972); (*b*) M. Franck-Neumann and C. Buchecker. Angew. Chem. Int. Ed. Engl. **12**, 240 (1973); (*c*) M. Martin and M. Regitz. Justus Liebigs Ann. Chem. 1702 (1974); (*d*) L. L. Rodina, V. V. Bulusheva, T. G. Ekimova, and I. K. Korobitsyna. J. Gen. Chem. USSR,

10, 53 (1974); (*e*) D. SEYFERTH and T. C. FLOOD. J. Organometal. Chem. **29**, C25 (1971).
9. M. I. KOMENDANTOV and R. R. BEKMUKHAMETOV. Chem. Heterocycl. Compd. 68 (1975).
10. M. FRANCK-NEUMANN and C. DIETRICH-BUCHECKER. Tetrahedron Lett. 2069 (1976).
11. (*a*) R. CLARAMUNT, J. ELGUERO, and R. JACQUIER. Org. Magn. Reson. **3**, 595 (1971); (*b*) A. F. COCKERILL, G. L. O. DAVIES, R. C. HARDEN, and D. M. RACKHAM. Chem. Rev. **73**, 553 (1973); (*c*) J. ELGUERO and R. JACQUIER. J. Chim. Phys. **63**, 1242 (1966); (*d*) J. ELGUERO, C. MARZIN, and J. D. ROBERTS. J. Org. Chem. **39**, 357 (1974).
12. P. DE MAYO and M. C. USSELMAN. Can. J. Chem. **51**, 1729 (1973).
13. A. A. REID, J. T. SHARP, and S. J. MURRAY. Chem. Commun. 827 (1972).
14. (*a*) J. I. BRAUMAN, L. E. ELLIS, and E. E. VAN TAMELEN. J. Am. Chem. Soc. **88**, 846 (1966); (*b*) E. HAVINGA and J. L. M. A. SCHLATMANN. Tetrahedron, **16**, 146 (1961); (*c*) A. R. BREMBER, A. A. GORMAN, R. L. LEYLAND, and J. B. SHERIDAN. Tetrahedron Lett. 2511 (1970).
15. S. MCLEAN and D. M. FINDLAY. Can. J. Chem. **48**, 3107 (1970).
16. B. A. HESS, L. J. SCHAAD, and C. W. HOLYOKE. Tetrahedron, **31**, 295 (1975).
17. J. W. DE HAAN and H. KLOOSTERZIEL. Recl. Trav. Chim. Pays-Bas, **84**, 1594 (1965).
18. W. C. HERNDON and J. M. MANION. J. Org. Chem. **33**, 4504 (1968).
19. D. R. ARNOLD and R. M. MORCHAT. Chem. Commun. 743 (1978).
20. L. L. SCHALAGER and F. A. LOND. Adv. Phys. Org. Chem. **1**, 8 (1963).
21. (*a*) D. E. MCGREER and J. W. MCKINLEY. Can. J. Chem. **49**, 105 (1971); (*b*) R. J. CRAWFORD and M. OHNO. Can. J. Chem. **52**, 3134 (1974); (*c*) R. J. CRAWFORD, D. M. CAMERON, and H. TOKUNAGA. Can. J. Chem. **52**, 4025 (1974); (*d*) R. J. CRAWFORD and H. TOKUNAGA. Can. J. Chem. **52**, 4033 (1974).
22. (*a*) N. A. PORTER, M. E. LANDIS, and L. J. MARNETT. J. Am. Chem. Soc. **93**, 795 (1971); (*b*) N. A. PORTER, L. J. MARNETT, C. H. LOCHMÜLLER, G. L. CLOSS, and M. SHOBATAKI. J. Am. Chem. Soc. **94**, 3664 (1972).
23. J. ELGUERO, C. MARZIN, A. R. KATRITZKY, and P. LINDA. Adv. Heterocycl. Chem. Suppl. 1, 269 (1971).
24. W. M. WILLIAMS and W. R. DOLBIER, JR. J. Am. Chem. Soc. **94**, 3955 (1972).
25. G. L. CLOSS and H. HEYN. Tetrahedron, **22**, 463 (1966).
26. I. I. GRANDBERG, A. P. KRASNOSHCHEK, A. N. KOST, and G. K. FAIZOVA. J. Gen. Chem. USSR, **33**, 2521 (1963).
27. R. K. BRAMLEY, R. GRIGG, G. GUILFORD, and P. MILNER. Tetrahedron, **29**, 4159 (1973).
28. R. P. BARNES, S. R. COOPER, V. J. TULANE, and H. DELANEY. J. Org. Chem. **8**, 153 (1943).
29. F. G. YOUNG, F. C. FROSTICK, JR., J. J. SANDERSON, and C. R. HAUSER. J. Am. Chem. Soc. **72**, 3635 (1950).
30. H. O. HOUSE and D. J. RIEF. J. Am. Chem. Soc. **77**, 6525 (1955).
31. L. FRIEDMAN and H. SHECHTER. J. Org Chem. **26**, 2522 (1961).

Milieux hyperbasiques: Recherches sur les amides et lactames ω-halogénés. Essais de cyclisation

THÉRÈSE CUVIGNY, PIERRE HULLOT, PATRICK MULOT, MARC LARCHEVEQUE ET HENRI NORMANT

Laboratoire de Synthèse Organique associé au C.N.R.S., Université Pierre et Marie Curie, tour 44–45, 4, place Jussieu 75230, Paris, France

Reçu 14 août 1978

THÉRÈSE CUVIGNY, PIERRE HULLOT, PATRICK MULOT, MARC LARCHEVEQUE et HENRI NORMANT. Can. J. Chem. **57**, 1201 (1979).

Les amides ω-halogénés *N,N*-disubstitués linéaires conduisent aux amides cycliques avec de bons rendements sous l'action des dialkylamidures de lithium "activés." Cependant, la même réaction avec les amides ramifiés donne principalement des amides ω-éthyléniques.

Les γ-et δ-lactames *N*-substitués, porteurs en α d'une chaîne ω-halogénée, fournissent dans les mêmes conditions des spirolactames tandis que les ε-lactames conduisent à un mélange de lactames spiraniques et éthyléniques.

THÉRÈSE CUVIGNY, PIERRE HULLOT, PATRICK MULOT, MARC LARCHEVEQUE, and HENRI NORMANT. Can. J. Chem. **57**, 1201 (1979).

Linear halogenated *N,N*-disubstituted amides afford cyclic amides in good yields by reaction with 'activated' lithium dialkylamides. However, the same reaction with substituted amides gives mainly ω-ethylenic amides.

In the same way, *N*-substituted γ- and δ-lactams with an ω-halogenated chain in the α position afford pure spirolactams whereas the reaction of ε-lactams furnishes a mixture of spiro and ethylenic compounds.

Les *N,N*-dialkyl cyclanecarboxamides (**II**) sont en général isolés à partir des acides cyclanecarboxyliques ou des nitriles correspondants qu'il faut d'abord synthétiser (1). Une autre méthode emploie les sels de cycloalkyl amidinium formés à l'aide d'ène-diamines et de dihalogénures d'alkyle (2). Cependant, les *N,N*-dialkyl cyclobutanecarboxamides ne peuvent être obtenus par ce procédé.

Nous avons récemment décrit une synthèse directe de *N,N*-dialkylamides ω-chlorés (**I**) à partir d'amides tertiaires commerciaux (3). Une cyclisation intramoléculaire de ces composés pouvait conduire directement aux cycloalcane amides tertiaires (**II**) produits intéressants par leurs propriétés pharmacologiques (4) (inhibiteurs des effets psychotomimétiques du LSD entre autres).

D'autre part, les lactames chlorés **III**, également accessibles par notre méthode à partir des lactames commerciaux, pouvaient mener aux spirolactames **IV**:

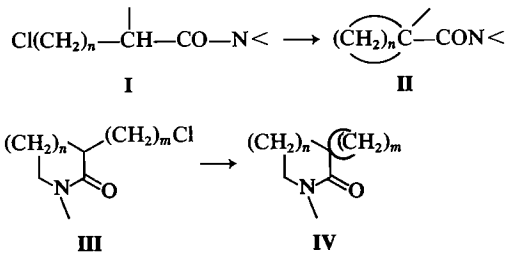

I **II**

III **IV**

Amides et lactames ω-halogénés

Ces amides et lactames ont été préparés selon la méthode que nous avons mise au point (3). La plupart sont décrits (3, 5), cependant nous avons été amenés à synthétiser quelques nouveaux amides et lactames ω-halogénés (tableau 1). Ils ont été obtenus par condensation des produits commerciaux avec des halogénures ω,ω′-chlorobromés. Quelques essais effectués avec le dichloro-1,4 butane ont fourni des rendements moyens (40–50%) en lactames chlorés. Le lactame *13* a été obtenu à l'aide du dibromo-1,4 butane, le lactame *14* à partir du lactame chloré correspondant par échange (iodure de sodium).

Essais de cyclisation des amides ω-chlorés

L'action d'une base forte, telle les dialkylamidures de lithium "activés" (3) préparés directement à partir du métal et de l'amine en milieu benzène–HMPT, sur les amides chlorés **A** pouvait conduire soit à un amide ω-éthylénique **B** par élimination d'une molécule d'hydracide, soit à l'amide cyclanique recherché **C** par cyclisation intramoléculaire, ces deux réactions étant compétitives. La présence du HMPT dans le milieu permettait d'envisager la cyclisation avec un halogénure aussi peu actif que le chloré.

Les essais ont été réalisés par action du diéthyl amidure de lithium "activé" sur l'amide ω-chloré maintenu aux températures indiquées dans le tableau II. A la fin de l'addition on laisse revenir le milieu à la température ambiante (essais *6*, *9*, *10* exceptés).

0008-4042/79/101201-05$01.00/0

TABLEAU 1. Amides $X(CH_2)_nCH(R)CON\langle R'R''$ à partir de $R{-}CH_2{-}CO{-}N\langle R'R''$

Essai	X	*n*	R	R′	R″	Rendement (%)
1	Cl	3	H	Me	Ph	55
2	Cl	4	H	Me	Me	60
3	Cl	3	C_3H_7	Me	Me	72
4	Cl	3	C_5H_{11}	Me	Me	60
5	Cl	3	C_5H_{11}	Me	Ph	47
6	Cl	4	iC_4H_9	Me	Me	68
7	Cl	3	$(CH_2)_2$		Me	68
8	Cl	3	$(CH_2)_3$		Me	84
9	Cl	4	$(CH_2)_3$		Me	81
10	Cl	4	$(CH_2)_4$		Me	80
11	Cl	*	$(CH_2)_2$		Me	50
12	Cl	*	$(CH_2)_3$		Me	84
13	Br	4	$(CH_2)_4$		Me	25†
14	I	4	$(CH_2)_4$		Me	80

*Les réactions sont effectuées avec $ClCH_2{-}CH(CH_3){-}CH_2Br$.
†Rendement faible dû à la formation de 65% de lactame éthylénique.

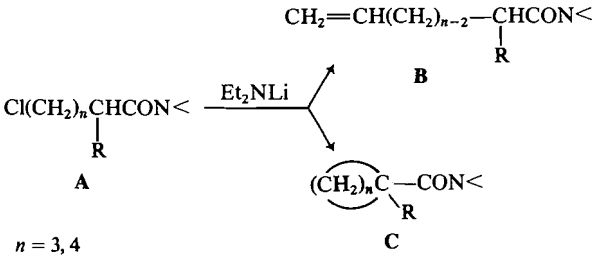

Amides linéaires ω-chlorés A (R = H)

Dans ce cas, la réaction majoritaire est la cyclisation et on atteint avec un rendement satisfaisant les amides cyclobutaniques et cyclopentaniques attendus (tableau 2, essais *1*, *2* et *3*). Les substituants portés par l'azote n'influent pas sur le cours de la réaction.

Amides ramifiés ω-chlorés A (R ≠ H)

Une ramification en α de la fonction amide modifie les résultats profondément. On isole dans la plupart des cas un mélange d'amide ω-éthylénique **B** et d'amide cyclanique **C** mais la réaction d'élimination l'emporte et nous n'avons pas réussi à augmenter la proportion d'amides cyclaniques quel que soit *n* (3 ou 4). On peut penser que l'empêchement stérique au niveau du carbone en α de la fonction est responsable de cette évolution différente de la réaction. Nous avons alors isolé des amides ω-éthyléniques purs (essais *4*, *7*, *10*, *11*). Là encore, les substituants portés par l'azote ne changent pas le cours de la réaction. Si la ramification se trouve en γ de la fonction amide et en β de l'halogène on obtient aussi un mélange d'amides éthylénique et cyclanique:

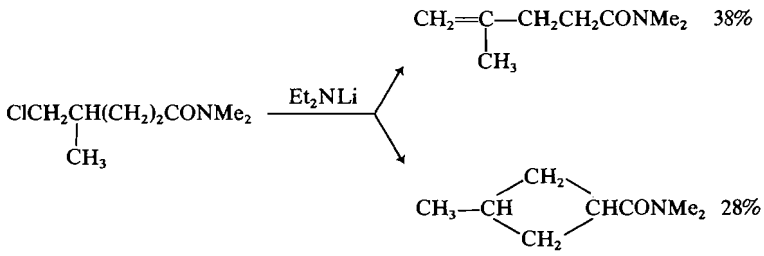

TABLEAU 2. Action du diéthyl amidure de lithium "activé" sur les amides ω-halogénés **A** → **B** + **C**

Essai	Amide initial	Température		Rendement (%)	
		Addition	Hydrolyse	**B**	**C**
1	$Cl(CH_2)_4CONMe_2$	−30°C	Ambiante	—	85
2	$Cl(CH_2)_4CON(Me)Ph$	−30°C	Ambiante	—	79
3	$Cl(CH_2)_5CONMe_2$	−30°C	Ambiante	—	60
4	$Cl(CH_2)_3CH(C_2H_5)CONMe_2$	−50°C	Ambiante	72	—
5	$Cl(CH_2)_3CH(iC_3H_7)CONMe_2$	−30°C	Ambiante	56	24
6	$Cl(CH_2)_3CH(iC_3H_7)CONMe_2$	−40°C	−40°C	64	20
7	$Cl(CH_2)_3CH(C_5H_{11})CONMe_2$	−30°C	Ambiante	56	—
8	$Cl(CH_2)_3CH(C_5H_{11})CON(Me)Ph$	−50°C	Ambiante	45	28
9	$ClCH_2CH(CH_3)(CH_2)_2CONMe_2$	−60°C	−50°C	38	28
10	$Cl(CH_2)_4CH(CH_3)CONMe_2$	−50°C	−50°C	76	—
11	$Cl(CH_2)_4CH(Et)CONMe_2$	−20°C	Ambiante	84	—

Essais de cyclisation des lactames halogénés en spirolactames

Nous avons étudié les γ, δ- et ε-lactames halogénés *N*-substitués:

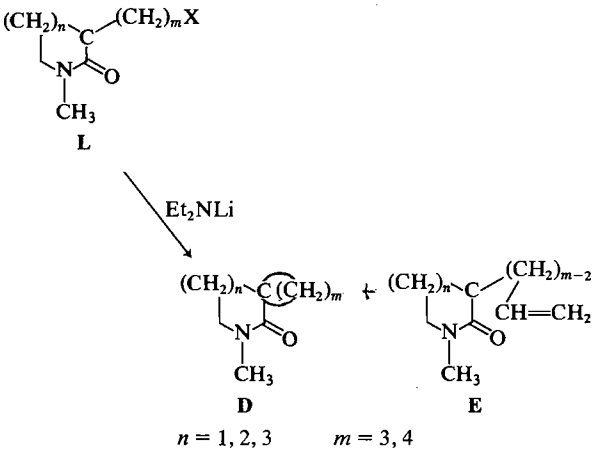

$n = 1, 2, 3$ $m = 3, 4$

Lors de tous les essais, nous avons additionné la base au lactame halogéné aux températures indiquées dans le tableau 3. La réaction de cyclisation intramoléculaire conduira à **D**, l'élimination d'une molécule d'hydracide à **E**. Les γ-lactames chlorés **L** ($n = 1$, $m = 3$ et 4) et les δ-lactames chlorés **L** ($n = 2$, $m = 3$ et 4) conduisent avec d'excellents rendements aux spirolactames **D**. Même le cycle cyclobutanique se forme aisément. Par contre, les ε-lactames **L** ($n = 3$, $m = 3$ et 4) ont fourni un mélange de **D** et de lactame éthylénique **E** si X = Cl, mais si X = Br ou I, la réaction d'élimination est totale.

Nous avons cependant constaté que, malgré une première substitution, la formation du carbanion en α du CO était aisée ainsi que l'alkylation ultérieure. Le lactame monosubstitué **G**, traité par un équivalent d'amidure activé, puis par l'iodure de méthyle a conduit au lactame dialkylé **H** avec un très bon rendement. Il est donc permis de penser que le demi échec rencontré lors de ces essais de cyclisation est dû, au moins en partie, à la conformation des ε-lactames.

TABLEAU 3. Action du diéthylamidure de lithium "activé" sur les lactames halogénés **L** → **D** + **E**

Essai	**L**			% **D**	% **E**
	n	*m*	X		
1	1	3	Cl	92	0
2	1	4	Cl	92	0
3	2	3	Cl	76	0
4	2	4	Cl	97	0
5	3	3	Cl	49	44
6	3	4	Cl	44	50
7	3	4	Br	0	85
8	3	4	I	0	83

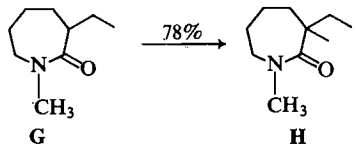

D'autre part, nous avons tenté la cyclisation des γ- et des δ-lactames chlorés **J** présentant une ramification en β du chlore, ce qui aurait permis d'atteindre les spirolactames substitués **K**. Seule la réaction d'élimination a lieu; on isole alors le composé vinylique **M** avec un rendement de 76%.

Conclusion

Ces essais de cyclisation des amides et lactames chlorés **I** et **III** ont permis la mise au point d'une synthèse directe d'amides tertiaires cyclobutaniques

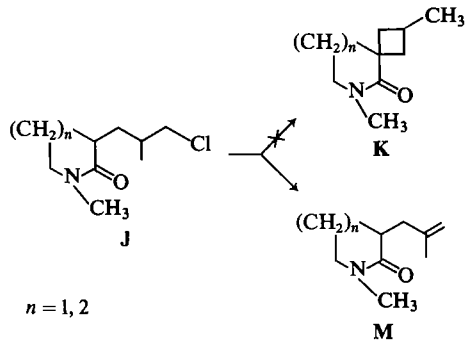

et cyclopentaniques et de γ- et δ-spirolactames dans d'excellentes conditions.

Partie expérimentale

La structure des différents produits a été confirmée par spectrographie infrarouge et rmn. Les spectres infrarouges ont été effectués avec un spectrophotomètre Perkin Elmer 457 sous forme de film. Les spectres rmn ont été enregistrés avec un appareil Perkin Elmer R 24 à 60 MHz sur des échantillons en solution dans le tétrachlorure de carbone et en utilisant le tétraméthyl silane comme référence interne. La pureté des produits a été contrôlée par cpv (colonne SE 30 de 2.5 m). Les analyses centésimales sont correctes à ±0.30% pour l'hydrogène et le carbone.

Amides ω-chlorés

Sauf indication contraire, suivre le mode opératoire décrit pour les amides linéaires, ramifiés ou cycliques (réf. 3).

Tableau 1

Essai 1

Métaller l'amide à −40°C, 15 min après la fin de l'addition couler le dérivé halogéné à −40°C et laisser revenir lentement à température ambiante; ir: 1640 cm^{-1} (C=O).

—pé 131°C/0.05 Torr; rmn δ: 2.05 (2H, t, CH_2CO), 3.20 (3H, s, NMe), 3.4 (2H, t, CH_2Cl), 7.3 (5H, m, C_6H_5).

Essai 2—pé 136°C/13 Torr; rmn δ: 2.21 (2H, t, CH_2CO), 2.98 (6H, d, NMe_2), 3.54 (2H, t, CH_2Cl).

Essai 3—pé 112°C/0.7 Torr; rmn δ: 2.97 (6H, d, NMe_2), 3.47 (2H, t, CH_2Cl).

Essai 4—pé 106°C/0.02 Torr; rmn δ: 3.00 (6H, d, NMe_2), 3.45 (2H, m, CH_2Cl).

Essai 5—pé 150°C/0.02 Torr; rmn δ: 3.15 (3H, s, NMe), 3.47 (2H, t, CH_2Cl), 7.35 (5H, m, C_6H_5).

Essai 6—pé 115°C/0.1 Torr; rmn δ: 0.89 (6H, d, Me_2CH), 3.00 (6H, d, NMe_2), 3.53 (2H, t, CH_2Cl).

Amides 1–6—ir: 1640 cm^{-1} (C=O).

Essai 7

Métaller le lactame à −20°C, revenir en 1½ h à +15°C, couler le carbanion ainsi formé sur le dérivé halogéné dilué de THF à −50°C, laisser à −50°C, 12 h; hydrolyser à −50°C; pé 97°C/0.05 Torr, ir: 1680 cm^{-1} (C=O); rmn δ: 2.78 (3H, s, NMe), 3.28 (2H, t, CH_2N), 3.58 (2H, t, CH_2Cl).

Essais 8, 9, 10 *et* 13

Métaller le lactame à −20°C, revenir en 1½ h à +15°C, couler le dérivé halogéné dilué de THF sur le carbanion maintenu à −50°C, laisser revenir à température ambiante.

Essai 8—pé 115°C/0.5 Torr; rmn δ: 2.85 (3H, s, NMe), 3.25 (2H, t, CH_2N), 3.50 (2H, t, CH_2Cl).

Essai 9—pé 121°C/0.5 Torr; rmn δ: 2.80 (3H, s, NMe), 3.25 (2H, t, CH_2N), 3.50 (2H, t, CH_2Cl).

Essai 10—pé 116°C/0.1 Torr; ir 1640 cm^{-1}; rmn δ: 2.85 (3H, s, NMe), 3.15 (2H, t, CH_2N), 3.45 (2H, t, CH_2Cl).

Essai 13—pé 136°C/0.5 Torr; ir 1640 cm^{-1}; rmn δ: 2.85 (3H, s, NMe), 3.25 (2H, t, CH_2N), 3.45 (3H, t, CH_2Br).

Essais 11 *et* 12

Métaller le lactame à +10°C, agiter 2 h à +15°C. Couler le carbanion sur le dérivé halogéné dilué de THF à −40°C, revenir en 12 h à température ambiante.

Essai 11—pé 108°C/0.1 Torr; ir 1680 cm^{-1}; rmn δ: 1.1 (3H, d, CH_3CH), 2.79 (3H, s, NMe), 3.25 (2H, t, CH_2N), 3.42 (3H, t, CH_2Cl).

Essai 12—pé 112°C/0.1 Torr; ir 1640 cm^{-1}; rmn δ: 1.05 (3H, d, CH_3CH), 2.78 (3H, s, NMe), 3.24 (2H, t, CH_2N), 3.42 (3H, t, CH_2Cl).

Essai 14

Traiter le dérivé chloré correspondant par INa dans le THF à reflux; on suit par chromatographie la disparition du produit initial; pé 145°C/0.5 Torr; ir 1640 cm^{-1}; rmn δ: 2.88 (3H, s, NMe), 3.15 (4H, m, CH_2N et CH_2I).

Tableau 2

Les températures d'addition et d'hydrolyse sont précisées dans le tableau 2. Les amides présentent une bande ir à 1640 cm^{-1} (C=O).

Essais 1, 2 *et* 3

Couler 0.04 mol de diéthyl amidure de lithium "activé" dilué de 40 mL de THF sur 0.027 mol d'amide chloré dilué de 10 mL de THF. Ramener à température ambiante, hydrolyser par l'eau glacée.

Essai 1—pé 107°C/13 Torr; rmn δ: 2.9 (6H, d, NMe_2).

Essai 2—pé 115°C/0.1 Torr; rmn δ: 3.2 (3H, s, NMe), 7.3 (5H, m, NPh).

Essai 3—pé 117°C/14 Torr; rmn δ: 2.95 (6H, d, NMe_2).

Essai 4

Couler 0.025 mol de diéthylamidure de lithium "activé" dilué de 30 mL de THF sur 0.025 mol d'amide chloré dilué de 10 mL de THF; ramener à température ambiante en 12 h; pé 110°C/13 Torr; rmn δ: 0.85 (3H, t, CH_3CH_2), 3.0 (6H, d, NMe_2), 5.05 (2H, m, $=CH_2$), 5.80 (H, m, =CH).

Essais 5, 6, 7 *et* 8

Addition de l'amide chloré sur 1 équiv. diéthylamidure de lithium "activé". Laisser revenir la nuit à température ambiante (essais *5* et *7*). Maintenir 24 h à −50°C (essais *6* et *8*).

Essais 5 *et* 6—Le mélange des amides cyclanique et éthylénique distille à 124°C/19 Torr. Le dosage rmn détermine le pourcentage de chacun.

Essai 7—pé 93°C/0.05 Torr; rmn δ: 0.90 (3H, t, CH_3CH_2), 2.95 (6H, d, NMe_2), 4.95 (2H, m, $=CH_2$), 5.65 (H, m, =CH).

Essai 8—pé 158°C/0.05 Torr; mélange d'amides dosé par rmn.

Essai 9

Addition de diéthylamidure de lithium "activé" sur 1 équiv. d'amide chloré; pé 117°C/15 Torr. Mélange d'amides dosé par rmn.

Essai 10

Addition du diéthylamidure de lithium "activé" sur 1 équiv. d'amide chloré. Maintenir la nuit à −50°C; pé 95°C/0.02 Torr; rmn δ: 0.85 (3H, t, CH_3CH_2), 3.25 (3H, s, NMe), 4.90 (2H, m, $=CH_2$), 5.55 (H, m, =CH), 7.40 (5H, m, NPh).

Essai 11

Addition de 0.025 mol d'amide chloré à 0.02 mol de diéthyl amidure de lithium activé. Ramener à température ambiante la nuit; pé 113°C/15 Torr; rmn δ: 1.05 (3H, d, CH_3CH), 2.95 (6H, d, NMe_2), 5.05 (2H, m, $=CH_2$), 5.65 (H, m, =CH).

Essais de cyclisation des lactames

Tableau 3

Additionner à −50°C 0.024 mol de diéthylamidure de lithium dilué de 30 mL de THF à 0.03 mol de lactame chloré

dilué de 80 mL de THF. Maintenir 12 h à −50°C et hydrolyser par l'eau glacée à la même température.

Essai 1—pé 68°C/0.02 Torr; rmn δ: 2.78 (3H, s, NMe), 3.25 (2H, t, CH_2N).

Essai 2—pé 72°C/0.01 Torr; rmn δ: 2.85 (3H, s, NMe), 3.30 (2H, t, CH_2N).

Essai 3—pé 128°C/13 Torr; rmn δ: 2.80 (3H, s, NMe), 3.25 (2H, t, CH_2N).

Essai 4—pé 140°C/13 Torr; rmn δ: 2.80 (3H, s, NMe), 3.25 (2H, t, CH_2N).

Essais 5 *et* 6—pé 97°C/0.1 Torr; mélange dosé par rmn.

Essais 7 *et* 8—pé 95°C/0.1 Torr; rmn δ: 2.9 (3H, s, NMe), 3.30 (2H, t, CH_2N), 4.90 (2H, m, $=CH_2$), 5.6 (H, m, =CH).

Synthèse de M—pé 78°C/0.01 Torr; rmn δ: 2.05 (3H, t, $CH_3—C=C$), 2.85 (3H, s, NMe), 3.30 (2H, t, $CH_2—N$), 4.80 (2H, s, $CH_2=C$).

1. J. M. Conia et J. Gore. C. R. Acad. Sci. **254**, 3708 (1962); M. Mousseron, J. Joullian et Y. Jolchine. Bull. Soc. Chim. Fr. 757 (1952).
2. C. F. Hobbs et H. Weingarten. J. Org. Chem. **39**, 918 (1974).
3. P. Hullot, Th. Cuvigny, M. Larcheveque et H. Normant. Can. J. Chem. **54**, 1098 (1976).
4. J. R. Smythies. Brevet Ger. no. 2,201,588 (Jul. 1972); *cited in* Chem. Abstr. **77**, 126125c (1972).
5. M. Larcheveque et P. Mulot. Can. J. Chem. **57**, 17 (1979).

The chlorosulfonyl moiety as a leaving group: hydride reduction of sulfonyl chlorides

HARVEY OWEN FONG, WILLIAM RAYNE HARDSTAFF, DENIS GEORGE KAY, RICHARD FRANCIS LANGLER,[1] RICHARD HERMAN MORSE, AND DEIG-NEVY SANDOVAL

Department of Chemistry, Dalhousie University, Halifax, N.S., Canada B3H 4J3

Received September 26, 1978

HARVEY OWEN FONG, WILLIAM RAYNE HARDSTAFF, DENIS GEORGE KAY, RICHARD FRANCIS LANGLER, RICHARD HERMAN MORSE, and DEIG-NEVY SANDOVAL. Can. J. Chem. **57**, 1206 (1979).

A series of γ-sulfone sulfonyl chlorides undergo a novel reduction upon reaction with lithium aluminum hydride to furnish the corresponding ethyl sulfones. The reactions appear to proceed in an S_N2 fashion with the chlorosulfonyl moiety functioning as the leaving group. In general sulfonyl chlorides furnish mercaptans as hydride reduction products.

A novel two-phase hydrolysis is shown to convert a thiol ester to a symmetric sulfide which involves hydrolysis and an S_N2 displacement in the aqueous phase.

HARVEY OWEN FONG, WILLIAM RAYNE HARDSTAFF, DENIS GEORGE KAY, RICHARD FRANCIS LANGLER, RICHARD HERMAN MORSE et DEIG-NEVY SANDOVAL. Can. J. Chem. **57**, 1206 (1979).

Une série de chlorures de γ-sulfone-sulfonyles subit une nouvelle réduction par réaction avec de l'hydrure de lithium et d'aluminium pour fournir les sulfones éthylées correspondantes. Les réactions semblent se produire par un mécanisme S_N2 dans lequel le groupe chlorosulfonyle agit comme nucléofuge. En général, les chlorures de sulfonyles conduisent aux mercaptans si on les soumets à une réduction par les hydrures.

On montre qu'une nouvelle hydrolyse en deux étapes permet de transformer un thioester en sulfure symétrique; la réaction implique une hydrolyse et une substitution S_N2 dans la phase aqueuse.

[Traduit par le journal]

Introduction

For some time, we have had an interest in the preparation and chemistry of sulfonyl chlorides (1–10). In principle, sulfonyl chlorides offer three potential sites for reactions with nucleophiles as shown below.

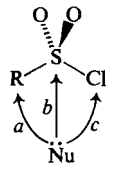

Pathway *c* involves sulfinate anion formation and has been suggested previously (5). Pathway *b* is an established pathway for the reaction of sulfonyl chlorides and represents the normal site of nucleophilic attack in sulfonate ester formation, when sulfenes do not intervene (11). To our knowledge, pathway *a* has not been observed or proposed previously.

Pathway *a* may be inferred as a possibility by analogy to other isomeric sulfur functional groups which can behave in the same way independently of the atoms by which the functional group is held in place. For example the following pair of cheletropic reactions are known (12, 13).

[1] 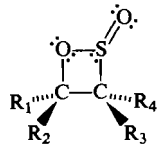 $\xrightarrow{\Delta}$ $R_1R_2C{=}CR_3R_4 + SO_2\uparrow$

[2] 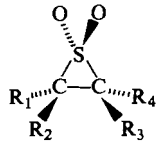 $\xrightarrow{\Delta}$ $R_1R_2C{=}CR_3R_4 + SO_2\uparrow$

Thus the extrusion of SO_2 proceeds in a facile way whether the second point of attachment is sulfur or oxygen. The chlorosulfonyl group is well known to be a good leaving group when attached by oxygen (14, 15) as shown below.

[3] 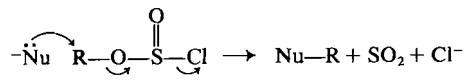

$\longrightarrow$ $Nu{-}R + SO_2 + Cl^-$

Hence, the possibility that the chlorosulfonyl moiety may function as a leaving group, whether it is attached by sulfur or oxygen, may be adduced. This possibility may have some immediate application in rationalizing the difficulties experienced in attempts to prepare sulfonyl chlorides, where the R group forms a particularly stable cation (16, 17). For

[1]To whom all correspondence should be addressed.

0008-4042/79/101206-08$01.00/0

example, we ourselves[2] have observed that 1-mercaptomethylnaphthalene forms 1-chloromethylnaphthalene upon chlorine–water oxidation under conditions which are known to furnish sulfonyl chlorides (6).

Results and Discussion

In connection with our ongoing studies of sulfide chlorinations (18), we wished to prepare some mercaptosulfones of the type: $RSO_2CH_2CH_2SH$. Our first attempt to prepare such a system utilized thiourea in standard fashion.

[4] $PhSO_2CH_2CH_2Cl \xrightarrow[(ii)\ ^-OH/H_2O]{(i)\ (NH_2)_2CS/EtOH} \times\!\!\rightarrow PhSO_2CH_2CH_2SH$

Since it is known that some sulfonyl chlorides can be converted into the corresponding mercaptans with lithium aluminum hydride (19, 20) we began the synthesis of the appropriate sulfone sulfonyl chlorides anticipating that they could be transformed into the desired mercaptosulfones with $LiAlH_4$. The general synthetic approach is outlined in Scheme 1.

Reaction of the sulfone sulfonyl chlorides **1***e*–**4***e* with lithium aluminum hydride furnished the corresponding ethyl sulfones as shown in [5].

[5] $RSO_2CH_2CH_2SO_2Cl \xrightarrow[THF]{LiAlH_4} RSO_2CH_2CH_3 + Li_2S$

1*e* R = Ph— **1***f*-**4***f*

2*e* R = CH_3CH_2—

3*e* R = CH_3—

4*e* R = $PhCH_2$—

Upon acidification of the reaction mixtures, H_2S was evolved.

The first problem raised by these results is that of the scope of the reaction. Mercaptans are the products observed upon reduction of aromatic sulfonyl chlorides (ref. 20, p. 124), which would be resistant to nucleophilic attack on the carbon to which the chlorosulfonyl group is attached. However, it seemed possible that chlorosulfonyl groups attached to sp^3 carbon might normally give complete reduction to the corresponding alkyl group upon treatment with lithium aluminum hydride. Such a possibility was readily discarded by the results from the reduction of 2,2-diphenylethanesulfonyl chloride, which furnished the mercaptan as the exclusive product.

[6] $Ph_2CHCH_2SO_2Cl \xrightarrow[THF]{LiAlH_4} Ph_2CHCH_2SH$

Consequently, the results observed for the hydride reductions of **1***e*–**4***e* are novel and not general whether or not the carbon bearing the chlorosulfonyl group is sp^3 hybridized.

We then began an examination of the mechanism of the reductions of **1***e*–**4***e*. Two reasonable possibilities were discernible, viz. (*i*) hydride induced elimination (E2 or $E1_{cb}$) followed by Michael-type addition of hydride to the intermediate vinyl sulfone or (*ii*) S_N2 displacement of the sulfur atom.

Our first attempt to distinguish between the two mechanistic schemes required the preparation of the dideuterated sulfone sulfonyl chloride **1***g* as shown in Scheme 2. Both mass spectrometry and nmr indicated that the sulfone sulfide **1***h* had incorporated ca. 94% deuterium at the carbon α to the sulfonyl group. Unfortunately, the mass spectrum of the sulfone sulfonyl chloride **1***g* did not show ions containing the methylene α to the sulfone sulfonyl group. However, the nmr of **1***g* indicated that no back-exchange had occurred during its preparation. Lithium aluminum hydride reduction of the dideuterated sulfone sulfonyl chloride **1***g* furnished phenyl ethyl sulfone which retained ca. 80% deuterium at the carbon α to the sulfonyl group. Work-up of this reaction involves the addition of water, so that there was a second opportunity for back-exchange before analysis of the product could be undertaken. In spite of these

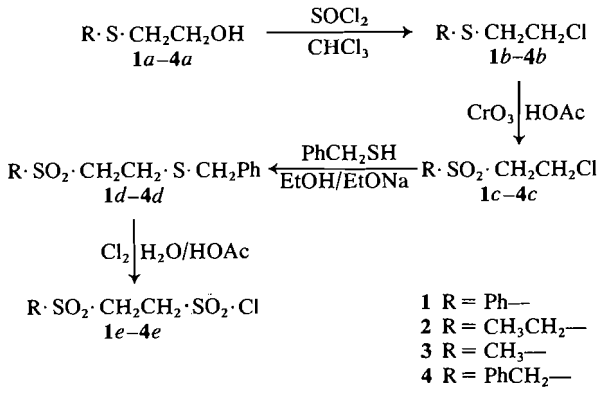

SCHEME 1

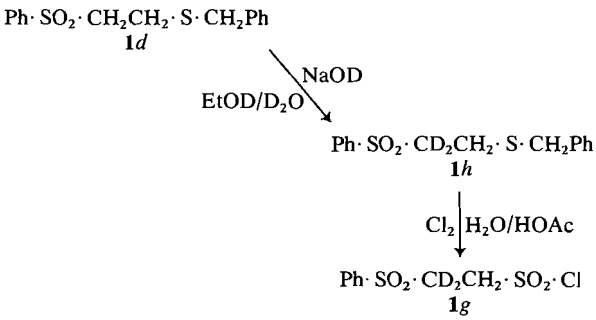

SCHEME 2

[2]H. O. Fong, R. F. Langler, and J. A. Pincock. Unpublished results.

difficulties, the labelling results indicate that somewhat more than half of the product formed without loss of label and that therefore the major pathway by which phenyl ethyl sulfone formed is an S_N2 displacement.

In our second approach, we have prepared phenyl vinyl sulfone and subjected it to standard hydride reduction conditions.[3] The product obtained was composed of oligomeric polysulfones which were separated on preparative tlc plates into three groups. The major band showed a very weak signal near δ 3.0 in its nmr, which could be attributed to a minor amount of phenyl ethyl sulfone (< 10% overall). The other bands showed no indication of phenyl ethyl sulfone by nmr or tlc. Consequently, it is now clear that an S_N2 displacement of sulfur is the near exclusive mode of formation of the ethyl sulfones.

The next point which we wished to clarify was the possible role of the sulfone sulfonyl groups in the reductions of **1***e*–**4***e*. To examine this question we have synthesized the sulfone sulfonyl chloride **9** which interposes another methylene between the sulfonyl groups. The complete synthesis of **9** is depicted in Scheme 3.

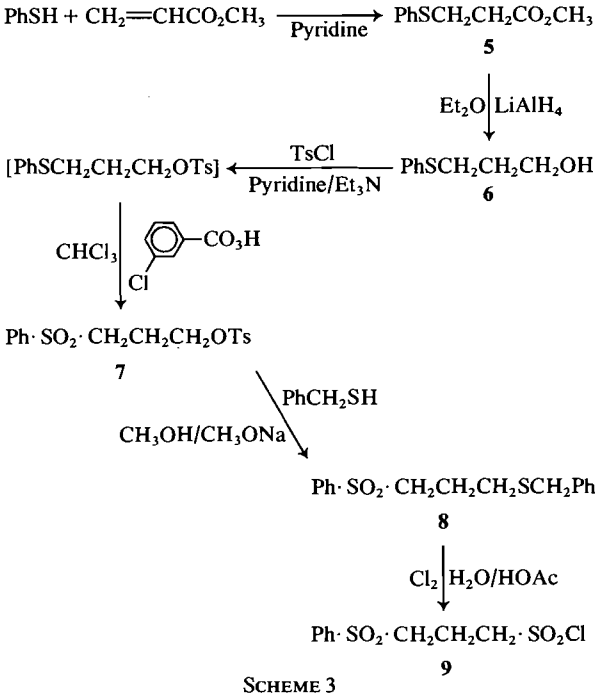

SCHEME 3

Treatment of the sulfone sulfonyl chloride **9** with lithium aluminum hydride furnished the mercaptosulfone **10**.

[3]Some vinyl sulfones may be satisfactorily reduced to the saturated sulfones with $LiAlH_4$ (21, 22).

[7] $PhSO_2CH_2CH_2CH_2SO_2Cl \xrightarrow[THF]{LiAlH_4}$ **9**

$PhSO_2CH_2CH_2CH_2SH \xrightarrow[MeOH/MeONa]{PhCH_2Cl}$ **8**

10

As expected **10** was readily converted into **8** under standard conditions.

The final problem remaining is that of the oxidation state of the sulfur atom when the carbon–sulfur bond is broken. By this time we had tentatively concluded that the chlorosulfonyl group was itself the leaving group displaced by hydride and that no preliminary reduction, for example to sulfinate anion, was necessary. Should this be the case, then another leaving group would be displaceable. Ideally a test case would involve a leaving group which was not capable of reduction before displacement, thereby removing the necessity of assuming that the chlorosulfonyl groups of **1***e*–**4***e* require conversion to another form before displacement can occur. We have chosen a chlorine atom as the leaving group.

[8] $PhSO_2CH_2CH_2Cl \xrightarrow[THF]{LiAlH_4} PhSO_2CH_2CH_3$

Consequently we have reached the view that these substitutions involve S_N2 displacements of the chlorosulfonyl group itself and that there must be some interaction between the reagent and the sulfone sulfonyl group. The most likely role for the sulfone sulfonyl group would be as an electron donor to the aluminum atom of the lithium aluminum hydride. This role would correspond to that of the carbonyl oxygen atom during a ketone reduction, viz. "$H:^-$ attacks carbon as the oxygen is complexing with released AlH_3" (23). Moreover aluminum hydrides generally form donor adducts with remarkable facility (24). The origin of the difference in behaviour of **1***e*–**4***e* and **9** would then lie with the fact that **1***e*–**4***e* would be able to form favorable six-membered transition states (as shown in Scheme 4) but **9** would

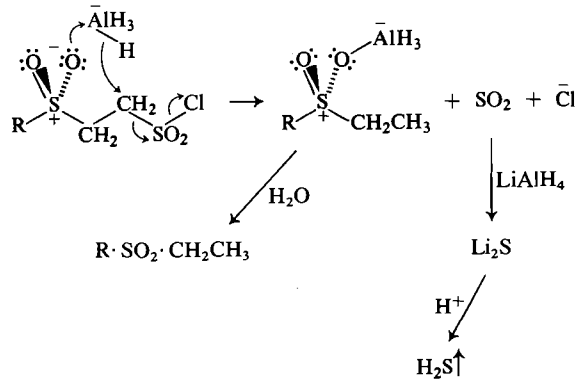

SCHEME 4

require an unfavourable seven-membered transition state and therefore reverts to typical behaviour, i.e., reduces to the mercaptan.

Scheme 5 depicts our final effort to establish a method for the preparation of the desired mercaptosulfones. We have prepared and hydrolyzed thiolacetate (**11**) in an attempt to obtain the mercaptosulfone corresponding to **1***e*.

Treatment of the hydrolysis product **12** with acetyl chloride failed to afford **11**, although the conditions employed are known to convert thiols to thiol acetates (25). A priori the isolation of a nonmercaptan from thiolacetate hydrolysis suggested that **12** was a disulfide since thiols are well known to be sensitive to air oxidation (26). However, (*i*) chlorine–water oxidation of the disulfide would have furnished 2 equiv. of the sulfone sulfonyl chloride **1***e*, whereas **12** actually furnished **1***e* in 60% yield on a 1:1 basis and (*ii*) peroxidation of **12** furnished the corresponding disulfone sulfoxide **13** and not the disulfone thiolsulfinate required if **12** were a disulfide.

Under the experimental conditions used for the hydrolysis of **11**, the organic phase (THF) was not miscible with the aqueous phase. When an hydrophobic thiol ester, benzyl thiol acetate, was subjected to the same reaction conditions, it was recovered unchanged. This result suggests that hydrolysis occurs in the aqueous phase and not in the 'wet' THF layer. Hydrolysis of **11** with an equivalent of benzyl chloride present in the THF layer furnished the disulfone sulfide **12** and unchanged benzyl chloride. Finally, as expected, substitution of methanol for THF, which provides an homogeneous reaction mixture, failed to divert the formation of **12** from **11**. These latter results indicate that the S_N2 displacement proceeds in the same phase as the hydrolysis step, and that the displacement proceeds faster than the hydrolysis.

Since thiol esters normally hydrolyze smoothly to furnish thiols and not sulfides, the relatively rapid

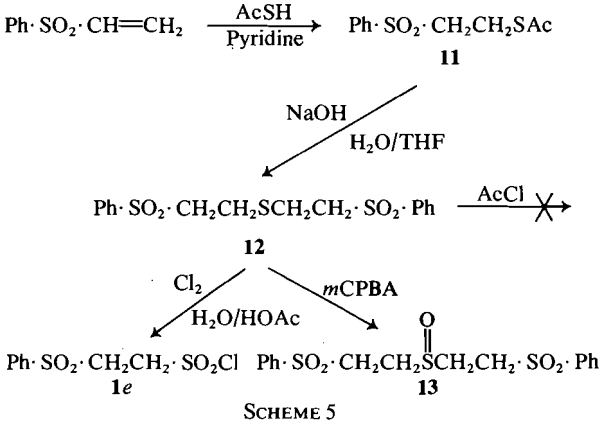

SCHEME 5

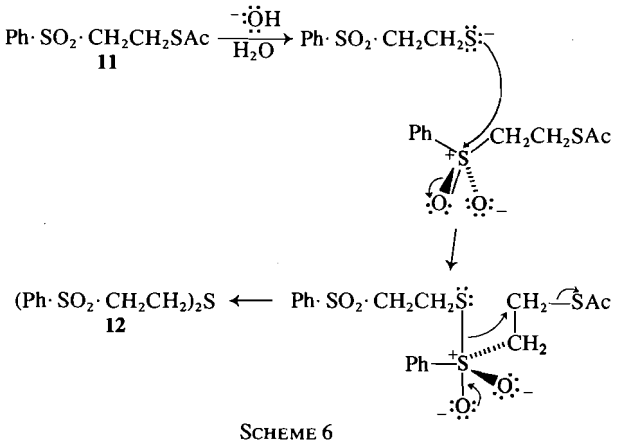

SCHEME 6

S_N2 displacement, in this case, must be subject to an unusual acceleration in rate. A role for the thiol ester sulfonyl group in accelerating the substitution reaction is shown in Scheme 6.

In conclusion, then, we have observed a novel sulfonyl chloride reduction reaction which appears to be the first reported case in which a chlorosulfonyl group, attached to carbon by sulfur, functions as a leaving group. We have also furnished details for the novel hydrolytic conversion of a thiol ester into a symmetric sulfide.

Experimental

General

The ir spectra were recorded on a Perkin-Elmer 237B grating spectrophotometer. The nmr spectra were obtained on a Varian T-60 instrument using TMS as the internal standard. The mass spectra were recorded on a Dupont-CEC model 21-104 mass spectrometer. The samples were directly introduced using an allglass probe and the spectra run at 30 eV with a source temperature of 150°C. Melting points were determined on a Fisher-Johns melting point apparatus and are uncorrected.

Chlorinations

The appropriate amount of sulfide was suspended in glacial acetic acid (25 mL) and water (3 mL) added. Cl_2 (ca. 200 mL/min) was bubbled into the reaction mixture for 0.5 h. Water (100 mL) was added and the resultant mixture washed with chloroform (five 100-mL aliquots). The combined organic layers were washed with 2.5% w/v NaOH (two 50-mL aliquots). After drying and concentration a crude residue was obtained.

Standard Work-up

A volume of water equal to the total volume of the reaction mixture was added to the reaction. Methylene chloride (three 100-mL portions) was used to extract the aqueous mixture. The combined organic layers were dried and concentrated affording crude product.

Preparation of Sulfide Alcohols ***1***a–***4***a

(i) ***1***a *and* ***2***a

Sodium metal (1 equiv.) was dissolved in absolute ethanol (150 mL) and the appropriate mercaptan (10 g) was added. The reaction mixture was cooled and 2-chloroethanol (1

equiv.) in absolute ethanol (50 mL) was added dropwise over 15 min. The reaction mixture was refluxed for 1 h and subjected to standard work-up.

$PhSCH_2CH_2OH$ (**1***a*) was rectified (10.48 g, bp 140°C/5 Torr); ir ($CHCl_3$): 3460 cm^{-1}; nmr ($CDCl_3$) δ: 7.40 (5H, s), 3.76 (2H, t), and 3.10 (3H, m); ms *m/e*: 154 (M^+, 100%), 123 (90%), 109 (36.5%) and 45 (85%).

$CH_3CH_2SCH_2CH_2OH$ (**2***a*) was rectified (13.06 g, bp 90°C/25 Torr); ir ($CHCl_3$): 3455 cm^{-1}; nmr ($CDCl_3$) δ: 3.60 (3H, m), 2.73 (2H, t), 2.40 (2H, q), and 1.16 (3H, t).

(ii) 3a and 4a

Sodium metal (1 equiv.) was dissolved in absolute ethanol (150 mL) and 2-mercaptoethanol (10 g) was added. The reaction mixture was cooled and methyl iodide or benzyl chloride (1 equiv.) in absolute ethanol (50 mL) was added dropwise over 15 min. The reaction mixture was stirred at ambient temperature overnight. Standard work-up afforded crude sulfide alcohol.

$CH_3SCH_2CH_2OH$ (**3***a*) was rectified (6.84 g, bp 81°C/37 Torr); ir ($CHCl_3$): 3460 cm^{-1}; nmr ($CDCl_3$) δ: 3.70 (3H,m), 2.66 (2H, m), and 2.03 (3H, s).

$PhCH_2SCH_2CH_2OH$ (**4***a*) was rectified (17.86 g, bp 161°C 4.2 Torr); ir ($CHCl_3$): 3465 cm^{-1}; nmr ($CDCl_3$) δ: 7.23 (5H, s), 3.70 (2H, s), 3.60 (2H, t), 2.96 (1H, s), and 2.56 (2H, t); ms *m/e*: 168 (M^+ 16.7%) and 91 (100%).

Preparation of Chlorosulfides **1**b–**4**b

The sulfide alcohol (15 g) was dissolved in chloroform (30 mL) and the solution brought to reflux. Thionyl chloride (1 equiv.) in chloroform (20 mL) was added dropwise over a period of 15 min. Upon completion of the addition the reaction mixture was refluxed for 3 h and the solvent evaporated.

$PhSCH_2CH_2Cl$ (**1***b*) was rectified (14.279 g, bp 111°C/5 Torr); nmr ($CDCl_3$) δ: 7.50 (5H, m), 3.75 (2H, m), and 3.30 (2H, m); ms *m/e*: 174 (18.6%) 172 (M^+, 56%) 123 (100%), and 109 (35%).

$CH_3CH_2SCH_2CH_2Cl$ (**2***b*) was rectified (14.95 g, bp 71°C/30 Torr); nmr ($CDCl_3$) δ: 3.63 (2H, t), 2.90 (2H, t), 2.63 (2H, q), and 1.30 (3H, t).

$CH_3SCH_2CH_2Cl$ (**3***b*) was rectified (14.340 g, bp 48°C/20 Torr); nmr ($CDCl_3$) δ: 3.63 (2H, t), 2.80 (2H, t), and 2.18 (3H, s).

$PhCH_2SCH_2CH_2Cl$ (**4***b*) was rectified (12.393 g, bp 138°C/220 Torr); nmr ($CDCl_3$) δ: 7.23 (5H, s), 3.70 (2H, s), 3.50 (2H, t), and 2.70 (2H, t); ms *m/e*: 188 (10%), 186 (M^+, 30%), and 91 (100%).

Preparation of Chlorosulfones **1**c–**4**c

A mixture of chromium trioxide (2.5 equiv.) and glacial acetic acid (100 mL) was vigorously stirred. A solution of the chlorosulfide (5 g) in glacial acetic acid (10 mL) was added over 5 min and the reaction maintained at 90–100°C for 0.5 h. Standard work-up afforded a mixture of crude chlorosulfone and acetic acid.

$PhSO_2CH_2CH_2Cl$ (**1***c*) was obtained by dissolving the crude concentrate in chloroform (200 mL) and washing the organic solution with 5% NaOH (100-mL aliquots) until the aqueous pH remained basic. The organic layer was dried ($MgSO_4$), filtered, and concentrated. The residue was recrystallized from 95% ethanol (4.930 g, mp 51–53°C); ir ($CHCl_3$): 1325 and 1150 cm^{-1}; nmr ($CDCl_3$) δ: 7.75 (5H, m) and 3.60 (4H, m); ms *m/e*: 206 (4.3%), 204 (M^+, 13.0%), 141 (50%), and 77 (100%).

$CH_3CH_2SO_2CH_2CH_2Cl$ (**2***c*) was rectified (5.018 g, bp 141°C/5 Torr); ir ($CHCl_3$): 1320 and 1125 cm^{-1}; nmr ($CDCl_3$) δ: 3.90 (2H, t), 3.40 (2H, t), 3.13 (2H, q), and 1.33 (3H, t); ms *m/e*: 130 (5.4%), 128 (16.8%), 65 (18.9%), 63 (52.6%), and 29 (100%).

$CH_3SO_2CH_2CH_2Cl$ (**3***c*) was rectified (2.763 g, bp 150°C/12 Torr); ir ($CHCl_3$): 1325 and 1150 cm^{-1}; nmr ($CDCl_3$) δ: 4.00 (2H, t), 3.50 (2H, t), and 3.18 (3H, s); ms *m/e*: 65 (33%) and 63 (100%).

$PhCH_2SO_2CH_2CH_2Cl$ (**4***c*) was obtained in the manner described above for **1***c*. The chlorosulfone was recrystallized from 95% ethanol (4.296 g, mp 90–91°C); ir ($CHCl_3$): 1320 and 1120 cm^{-1}; nmr ($CDCl_3$) δ: 7.46 (5H, s), 4.33 (2H, s), 3.83 (2H, t), and 3.30 (2H, t); ms *m/e*: 92 (8.8%) and 91 (100%).

Preparation of $PhSCH_2CH_2CO_2CH_3$ *(5)*

Benzenethiol (15.620 g) was dissolved in dry pyridine (100 mL) and methyl acrylate (19.8 g) added dropwise over 20 min. The reaction mixture was stirred at ambient temperature for 1.5 h. Chloroform (100 mL) was added and the resultant solution washed with 10% HCl (four 100-mL aliquots). The organic phase was dried ($MgSO_4$), filtered, and the solvent evaporated. The residue was distilled at reduced pressure (22.47 g, bp 113–115°C/2 Torr); ir ($CHCl_3$): 1740 cm^{-1}; nmr ($CDCl_3$) δ: 7.40 (5H, s), 3.70 (3H, s) 3.20 (2H, t), and 2.66 (2H, t); ms *m/e*: 196 (M^+, 100%), 136 (48.3%), 123 (86.5%), and 109 (52.8%).

Preparation of $PhSCH_2CH_2CH_2OH$ *(6)*

Lithium aluminum hydride (0.639 g) was covered with diethyl ether (20 mL) and the mixture refluxed for 0.5 h. The mixture was cooled to ambient temperature and a solution of the sulfide ester (**5**, 3.300 g) in diethyl ether (100 mL) added dropwise over 15 min. The reaction mixture was refluxed for 1 h and cooled to ambient temperature. Ethyl acetate (5 mL) was added dropwise, followed by 1% HCl (20 mL) added dropwise. Water (100 mL) was added and the layers separated. The aqueous layer was washed with methylene chloride (four 100-mL aliquots). The organic layers were dried and concentrated. The crude sulfide alcohol was rectified at reduced pressure, affording clean **6** (1.808 g, bp 130°C/2 Torr); ir ($CHCl_3$) 3650 and 3460 cm^{-1}; nmr ($CDCl_3$) δ: 7.40 (5H, s), 3.80 (2H, t), 3.06 (2H, t), and 1.90 (3H, m); ms *m/e*: 168 (M^+, 63%), 123 (22.2%), and 110 (100%).

Preparation of $PhSO_2CH_2CH_2CH_2OTs$ *(7)*

The sulfide alcohol (**6**) (11.054 g) was dissolved in a solution of dry pyridine (150 mL) and triethyl amine (6.645 g) and the reaction mixture cooled with an ice–water bath. *p*-Toluenesulfonyl chloride (12.544 g) was added in small portions over 5 min and the reaction mixture stirred at room temperature for 1 h. Methylene chloride (300 mL) was added and the solution washed with 10% HCl (100-mL aliquots) until the aqueous pH remained acidic. The organic layer was dried and concentrated affording crude sulfide tosylate as an oil.

The total crude sulfide tosylate was dissolved in chloroform (475 mL) and the solution cooled with an ice–salt–water bath. *m*-Chloroperbenzoic acid (85%, 26.580 g) was added in small portions over a 10-min period. The ice was allowed to melt and the reaction reached ambient temperature with overnight stirring. The reaction mixture was washed with 2.5% NaOH (100-mL aliquots) until the aqueous pH remained basic. The organic layer was dried and concentrated. Crude sulfone tosylate was recrystallized from 95% EtOH affording clean **7** (17.308 g, mp 82–84°C); ir ($CHCl_3$): 1370, 1320, 1175, and 1150 cm^{-1}; nmr ($CDCl_3$) δ: 7.76 (9H, m), 4.20 (2H, t), 3.26 (2H, t), 2.46 (3H, s), and 2.10 (2H, m); ms *m/e*: 354 (M^+, 14.2%), 183 (100%), 155 (53%), 143 (75%), and 91 (60%).

Preparation of the Sulfone Sulfides **1**d–**4**d

Sodium metal (2 equiv.) was dissolved in absolute ethanol (100 mL) and the appropriate chlorosulfone **1***c*–**4***c* (5 g) was added. The reaction mixture was stirred at room temperature

for 15 min and phenylmethanethiol (1 equiv.) was added. The reaction mixture was refluxed for 1 h, cooled, and subjected to standard work-up.

$PhSO_2CH_2CH_2SCH_2Ph$ (**1***d*) was recrystallized from 95% ethanol (5.849 g, mp 68–71°C); ir ($CHCl_3$): 1325 and 1150 cm^{-1}; nmr ($CDCl_3$) δ: 7.86 (5H, m), 7.33 (5H, s), 3.70 (2H, s), 3.26 (2H, m), and 2.73 (2H, m); ms *m/e*: 292 (M^+, 6.3), 150 (59%), 123 (34%), and 91 (100%). *Anal.* calcd. for $C_{15}H_{16}O_2S_2$: C 61.61, H 5.51; found: C 61.23, H 5.67.

$CH_3CH_2SO_2CH_2CH_2SCH_2Ph$ (**2***d*) was recrystallized from 95% ethanol (5.970 g, mp 42–45°C); ir ($CHCl_3$): 1320 and 1125 cm^{-1}; nmr ($CDCl_3$) δ; 7.33 (5H, s), 3.76 (2H, s), 2.96 (6H, m), and 1.33 (3H, t); ms *m/e*: 244 (M^+, 5%), 150 (21%), 123 (21%), and 91 (100%). *Anal.* calcd. for $C_{11}H_{16}O_2S_2$: C 54.06, H 6.59; found: C 54.21, H 6.65.

$CH_3SO_2CH_2CH_2SCH_2Ph$ (**3***d*) was recrystallized from 95% ethanol (5.636 g, mp 56–58°C); ir ($CHCl_3$): 1320 and 1140 cm^{-1}; nmr ($CDCl_3$) δ: 7.26 (5H, s), 3.70 (2H, s), and 3.00 (7H, m); ms *m/e*: 230 (M^+, 8.3%), 150 (26%), 123 (27%), and 91 (100%). *Anal.* calcd. for $C_{10}H_{14}O_2S_2$: C 52.14, H 6.12; found: C 51.94, H 5.87.

$PhCH_2SO_2CH_2CH_2SCH_2Ph$ (**4***d*) was recrystallized from 95% ethanol (4.325 g, mp 152–153°C); ir ($CHCl_3$): 1325 and 1120 cm^{-1}; nmr ($CDCl_3$) δ: 7.33 (5H, s), 7.20 (5H, s), 4.10 (2H, s), 3.63 (2H, s), and 2.80 (4H, m); ms *m/e* 306: (M^+, 2%), 150 (20%), 123 (11%), and 91 (100%). *Anal.* calcd. for $C_{16}H_{18}O_2S_2$: C 62.71, H 5.92; found: C 62.98, H 5.83.

*Preparation of $PhSO_2CH_2CH_2CH_2SCH_2Ph$ (**8**)*

Sodium metal (0.130 g) was dissolved in methanol (25 mL) and phenylmethanethiol (0.7 mL) added. The sulfone tosylate (**7**) (2.000 g) was added and the reaction mixture stirred at room temperature overnight. Standard work-up furnished crude **8** which was recrystallized from 95% ethanol (1.120 g, mp 53–55°C); ir ($CHCl_3$): 1320 and 1145 cm^{-1}; nmr ($CDCl_3$) δ: 7.86 (5H, m), 7.37 (5H, s), 3.70 (2H, s), 3.23 (2H, t), 2.53 (2H, t), and 2.03 (2H, m); ms *m/e*: 306 (M^+, 2.9%), 143 (16.7%), 123 (13.1%), and 91 (100%). *Anal.* calcd. for $C_{16}H_{18}O_2S_2$: C 62.71, H 5.92; found: C 62.90, H 5.87.

Preparation of $Ph_2CHCH_2SCH_2Ph$

Sodium metal (0.321 g) was dissolved in absolute ethanol (100 mL) and phenylmethanethiol (1.7 mL) added. The tosylate of 2,2-diphenylethanol (4.69 g) was added and the reaction mixture refluxed for 48 h. Standard work-up afforded crude sulfide. The crude material was chromatographed on silica gel (450 g) employing carbon tetrachloride elution (100-mL fractions). Fractions 34–63 were combined and concentrated affording clean sulfide (1.509 g) as an oil; nmr ($CDCl_3$) δ: 7.33 (15H, m), 4.13 (1H, t), 3.66 (2H, s), and 3.13 (2H, d); ms *m/e*: 304 (M^+, 48%), 167 (100%), and 91 (98%).

*Preparation of the Sulfonyl Chlorides **1**e → **4**e, **9**, and $Ph_2CHCH_2SO_2Cl$*

The following benzylic sulfides were chlorinated following the procedure outlined under Chlorinations.

The benzylic sulfide (**1***d*) (4.999 g) furnished $PhSO_2CH_2CH_2SO_2Cl$ (**1***e*) (3.285 g, mp 179–181°C) after recrystallization from chloroform; ir ($CHCl_3$): 1390, 1330, 1170, and 1150 cm^{-1}; nmr (CD_3COCD_3) δ: 7.90 (5H, m), 4.37 (2H, m), and 3.90 (2H, m); ms *m/e*: 141 (60.4%), 125 (18.6%), and 77 (100%). *Anal.* calcd. for $C_8H_9ClO_4S_2$: C 35.75, H 3.37; found: C 35.48, H 3.51.

The benzylic sulfide (**2***d*) (5.343 g) furnished $CH_3CH_2SO_2CH_2CH_2SO_2Cl$ (**2***e*) (1.612 g, mp 104–106°C) after recrystallization from carbon tetrachloride; ir ($CHCl_3$): 1390, 1330, 1170, and 1140 cm^{-1}; nmr ($CDCl_3$) δ: 4.20 (2H, m), 3.66 (2H, m), 3.16 (2H, q), and 1.43 (3H, t); ms *m/e*: 222 (20.3%), 220 (M^+, 61%), 185 (96.2%), and 156 (100%). *Anal.* calcd. for $C_4H_9ClO_4S_2$: C 21.77, H 4.11; found: C 21.86, H 4.04.

The benzylic sulfide (**3***d*) (5.006 g) furnished $CH_3SO_2CH_2CH_2SO_2Cl$ (**3***e*) (2.684 g, mp 126–127°C) after recrystallization from chloroform; ir (KBr): 1375, 1325, 1160, and 1145 cm^{-1}; nmr (CD_3COCD_3) δ: 4.63 (2H, m), 3.90 (2H, m) and 3.23 (3H, s); ms *m/e* 143 (15%), 107 (12%), and 79 (100%). *Anal.* calcd. for $C_3H_7ClO_4S_2$: C 17.43, H 3.41; found: C 17.52, H 3.35.

The benzylic sulfide (**4***d*) (4.980 g) furnished $PhCH_2SO_2CH_2CH_2SO_2Cl$ (**4***e*) (3.524 g, mp 191–192°C) after recrystallization from chloroform, ir (KBr): 1375, 1325, 1160, and 1145 cm^{-1}; nmr (CD_3CN) δ: 7.50 (5H, s), 4.50 (2H, s), 4.10 (2H, m), and 3.70 (2H, m); ms *m/e*: 91 (100%), 65 (12.2%) and 48 (4.5%). *Anal.* calcd. for $C_9H_{11}ClO_4S_2$: C 38.22, H 3.92; found: C 38.08, H 3.90.

The benzylic sulfide (**8**) (6.229 g) furnished $PhSO_2CH_2CH_2CH_2SO_2Cl$ (**9**) (3.951 g, mp 117–119°C) after recrystallization from chloroform; ir ($CHCl_3$): 1335, 1320, 1170, and 1155 cm^{-1}; nmr (CD_3COCD_3) δ: 7.86 (5H, m), 4.23 (2H, t), 3.57 (2H, t), and 2.43 (2H, m); ms *m/e*: 284 (2.3%), 282 (M^+, 7.1%), 141 (100%), and 77 (88%). *Anal.* calcd. for $C_9H_{11}ClO_4S_2$: C 38.22, H 3.92; found: C 38.41, H 3.81.

$Ph_2CHCH_2SCH_2Ph$ (1.504 g) furnished crude 2,2-diphenylethanesulfonyl chloride. The crude sulfonyl chloride was chromatographed on silica gel (150 g) employing carbon tetrachloride elution (100-mL fractions). Fractions 12–20 were concentrated and combined affording clean sulfonyl chloride (0.786 g); ir (CCl_4): 1340 and 1175 cm^{-1}; nmr ($CDCl_3$) δ: 7.40 (10H, s), 4.90 (1H, t), and 4.50 (2H, d); ms *m/e*: 282 (2.3%), 280 (M^+, 7.3%), 180 (94%), 139 (100%), and 77 (91%).

Lithium Aluminum Hydride Reductions

The reductions of **1***e*–**4***e*, phenyl ω-chloroethyl sulfone and 2,2-diphenylethanesulfonyl chloride were all carried out in the same manner as illustrated below by the procedure for the reduction of **2***e*.

Lithium aluminum hydride (0.576 g) was added to dry THF (10 mL) and the mixture refluxed for 0.5 h. The mixture was cooled to ambient temperature and a solution of $CH_3CH_2SO_2CH_2CH_2SO_2Cl$ (**2***e*) (1.031 g) in THF (40 mL) was added dropwise over 10 min. The resultant solution was refluxed for 1 h. Upon cooling to room temperature ethyl acetate (5 mL) was added dropwise, followed by 1% HCl (20 mL) added dropwise. Standard work-up afforded clean diethyl sulfone (0.550 g) which was identical to authentic material by nmr, ir, and ms.

Results for these experiments are shown in Table 1.

*Reduction of $PhSO_2CH_2CH_2CH_2SO_2Cl$ (**9**)*

The sulfone sulfonyl chloride (**9**) (0.9976 g) was reduced with lithium aluminum hydride (0.448 g) as described above. The product was the mercaptosulfone **10** (0.491 g) obtained as an oil; ir (CCl_4): 1325 and 1150 cm^{-1}; nmr ($CDCl_3$) δ: 7.86 (5H, m), 3.37 (2H, t), 2.63 (2H, m), 2.00 (2H, m), and 1.46 (1H, t); ms *m/e*: 216 (M^+, 2.5%), 152 (94.8%), 143 (100%), 77 (65.5%), and 74 (52.5%).

*Reaction of $PhSO_2CH_2CH_2CH_2SH$ (**10**) and Benzyl Chloride*

Sodium metal (0.043 g) was dissolved in methanol (25 mL) and $PhSO_2CH_2CH_2CH_2SH$ (0.400 g) added. Benzyl chloride (0.236 g) was added and the reaction mixture stirred at ambient temperature for 24 h. Standard work-up furnished crude sulfone sulfide which was chromatographed on silica gel (50 g) employing chloroform elution (50-mL fractions). Fractions 3–5 were concentrated and combined affording clean sulfone sulfide (**8**) (0.128 g) which was identical to authentic material by nmr, ir, and tlc.

TABLE 1. Yields for $LiAlH_4$ reductions of sulfonyl substrates

Substrate	Product	Yield (%)
$PhSO_2CH_2CH_2SO_2Cl$ (**1***e*)	$PhSO_2CH_2CH_3$	79.0
$CH_3CH_2SO_2CH_2CH_2SO_2Cl$ (**2***e*)	$(CH_3CH_2)_2SO_2$	96.1
$CH_3SO_2CH_2CH_2SO_2Cl$ (**3***e*)	$CH_3SO_2CH_2CH_3$	94.4
$PhCH_2SO_2CH_2CH_2SO_2Cl$ (**4***e*)	$PhCH_2SO_2CH_2CH_3$	71.7
$Ph_2CHCH_2SO_2Cl$	Ph_2CHCH_2SH	51.5
$PhSO_2CH_2CH_2Cl$	$PhSO_2CH_2CH_3$	79.5

Preparation of $PhSO_2CD_2CH_2SCH_2Ph$ (1h)

Sodium metal (0.037 g) was dissolved in 95% CH_3CH_2OD–D_2O (35 mL) and the sulfone sulfide (**1***d*) (3.557 g) added. The reaction mixture was refluxed for 24 h. The bulk of the solvent (30 mL) was distilled off and the residue cooled. The dideuterated sulfone sulfide (3.331 g) was filtered off and shown to be identical to undeuterated material by ir, mp, and mixture mp; nmr ($CDCl_3$) δ: 7.86 (5H, m), 7.33 (5H, s), 3.70 (2H, s), and 2.73 (2H, s). Deuterium incorporation was determined by mass spectrometry on the cluster of ions at *m/e* 150 → 155 which indicated $\%d_0 = 0, d_1 = 10.5, d_2 = 81.9, d_3 = 6.6$.

Preparation and Reduction of $PhSO_2CD_2CH_2SO_2Cl$ (1g)

$PhSO_2CD_2CH_2SCH_2Ph$ (3.006 g) was converted into $PhSO_2CD_2CH_2SO_2Cl$ (2.417 g) as described for the nondeuterated sulfide (**1***d*). The dideuterated sulfone sulfonyl chloride was shown to be identical with nondeuterated material by ir, mp, and mixture mp. The nmr showed the absence of the signal at δ 3.90 which is present in the nmr of **1***e*.

$PhSO_2CD_2CH_2SO_2Cl$ (1.001 g) was reduced with lithium aluminum hydride (0.472 g) as described previously for **1***e*. The dideuterated phenyl ethyl sulfone obtained showed a weak multiplet at ca. δ 3.0 for nondeuterated and monodeuterated phenyl ethyl sulfone. The mass spectrum indicated a deuterium incorporation of $\%d_0 = 7.9, d_1 = 39.0, d_2 = 52.0, d_3 = 0.9$.

Reaction of Phenyl Vinyl Sulfone with $LiAlH_4$

Phenyl vinyl sulfone (1.003 g) was treated with lithium aluminum hydride (0.741 g) as described above for the sulfonyl compounds of Table 1. The crude product (0.709 g) showed three spots R_f, 0.08, 0.22, and 0.52 when developed (2×) on silica gel tlc plates with chloroform. A portion of the crude product (0.600 g) was chromatographed on preparative tlc plates and the bands scraped. All three bands showed SO_2 stretching in the ir spectra indicating that the products were sulfones. Each band was homogeneous on tlc and showed abundant ions in the mass spectrum with *m/e* > 170. The nmr showed the absence of the methylene signal near δ 3.0 from phenyl ethyl sulfone for the bands at R_f 0.08 and 0.22. The material at R_f 0.52 (0.217 g) showed a weak signal near δ 3.0 which if attributed to phenyl ethyl sulfone would mean that less than 25% of the sample was phenyl ethyl sulfone and that therefore less than 10% of the starting phenyl vinyl sulfone had been converted into phenyl ethyl sulfone

Preparation of $PhSO_2CH_2CH_2SAc$ (11)

Phenyl vinyl sulfone (1.006 g) and thioacetic *S*-acid (0.502 g) were added to dry pyridine (25 mL) and the reaction mixture stirred at ambient temperature for 1 h. Chloroform (100 mL) was added and the resultant solution washed with 10% HCl (50-mL aliquots) until the aqueous pH remained acidic. The organic layer was dried and concentrated affording crude **11**. The crude thiol ester was chromatographed on silica gel (100 g) employing chloroform elution (100-mL fractions). Fractions 5–8 were combined and concentrated affording the thiol ester as an oil (1.435 g); ir ($CHCl_3$) 1695, 1320, and 1150 cm^{-1}; nmr ($CDCl_3$) δ: 7.93 (5H, m), 3.40 (4H, m), and 2.33 (3H, s); ms *m/e*: 125 (22.6%), 77 (27.1%) and 45 (100%).

Hydrolysis of Thiol Ester 11

The thiol ester **11** (0.999 g) was added to a mixture of THF (80 mL) and sodium hydroxide (0.259 g) in water (16 mL). The reaction mixture was stirred at ambient temperature and worked up as described above for the preparation of phenyl vinyl sulfone. The residue was recrystallized from 95% ethanol (40 mL) affording clean disulfone sulfide (**12**) (0.637 g, mp 116–118°C); ir ($CHCl_3$): 1325 and 1150 cm^{-1}; nmr ($CDCl_3$) δ: 7.90 (10H, m), 3.33 (4H, m), and 2.90 (4H, m); ms *m/e*: 230 (31%), 229 (30%), 201 (18.2%), 87 (57.3%), 86 (100%), and 77 (58.9%). *Anal.* calcd. for $C_{16}H_{18}O_4S_3$: C 51.86, H 4.89; found: C 51.89, H 4.71.

Chlorinolysis of 12

The disulfone sulfide **12** (1.004 g) was suspended in glacial acetic acid (25 mL) and water (3 mL). Cl_2 (ca. 200 mL/min) was bubbled into the solution for 0.5 h. The reaction mixture was worked-up as described for the preparation of sulfonyl chlorides **1***e*–**4***e*. The crude residue furnished two crops of crystalline sulfone sulfonyl chloride **1***e* (0.431 g) which was identical to previously obtained **1***e* by ir, nmr, mp, mixture mp, and tlc. The mother liquor contained only traces of **1***e* as indicated by tlc.

Preparation of Disulfone Sulfoxide 13

A solution of the disulfone sulfide **12** (0.506 g) in chloroform (25 mL) was cooled with an ice–water bath and *m*-chloroperbenzoic acid (85%, 0.272 g) was added in small portions over 5 min. The ice was allowed to melt and the reaction to reach room temperature while stirring overnight. Methylene chloride (200 mL) was added and the resultant solution washed with 1% NaOH (50 mL). The organic phase was dried and concentrated. The residue was recrystallized from 95% ethanol (100 mL) affording clean disulfone sulfoxide (0.469 g, mp 179–181°C; ir (KBr): 1320, 1150, and 1055 cm^{-1}; nmr (DMSO-d_6) δ: 7.57 (10H, m), 3.30 (4H, m), and 2.86 (4H, m); Cmr (DMSO-d_6) δ: 43.12 (t), 47.87 (t) 127.79 (d), 129.51 (d), 134.14 (d), 138.46 (s); ms *m/e*: 141 (42.5%), 125 (37%), 109 (13%), and 77 (100%). *Anal.* calcd. for $C_{16}H_{18}O_5S_3$: C 49.72, H 4.69; found: C 49.51, H 4.73.

Acknowledgements

The authors are indebted to Mr. W. S. Mantle for some technical assistance during the initial stages of this work. We thank Dr. J. H. Kim for running the mass spectra. We are grateful to Dalhousie University for financial support in the form of a grant from the Research Development Fund.

1. J. S. GROSSERT and R. F. LANGLER. Chem. Commun. 49 (1973).
2. J. S. GROSSERT, W. R. HARDSTAFF, and R. F. LANGLER. Chem. Commun. 50 (1973).
3. W. R. HARDSTAFF, R. F. LANGLER, and M. J. NEWMAN. Org. Mass Spectrom. **9**, 1156 (1974).
4. W. R. HARDSTAFF, R. F. LANGLER, J. LEAHY, and M. J. NEWMAN. Can. J. Chem. **53**, 2664 (1975).
5. J. R. JARDINE and R. F. LANGLER. J. Chromatog. **116**, 211 (1976).
6. R. F. LANGLER. Can. J. Chem. **54**, 498 (1976).
7. J. S. GROSSERT and R. F. LANGLER. Can. J. Chem. **55**, 407 (1977).
8. J. S. GROSSERT, W. R. HARDSTAFF, and R. F. LANGLER. Can. J. Chem. **55**, 421 (1977).
9. P. P. DAVIS, J. S. GROSSERT, R. F. LANGLER, and W. S. MANTLE. Org. Mass. Spectrom. **12**, 659 (1977).
10. R. F. LANGLER, Z. A. MARINI, and J. A. PINCOCK. Can. J. Chem. **56**, 903 (1978).
11. J. F. KING. Acc. Chem. Res. **8**, 10 (1975).
12. T. DURST and B. P. GIMBARZEVSKY. Chem. Commun. 724 (1975).
13. F. G. BORDWELL, J. M. WILLIAMS, E. B. HOYT, and B. B. JARVIS. J. Am. Chem. Soc. **90**, 429 (1968).
14. A. STREITWIESER and W. D. SCHAEFFER. J. Am. Chem. Soc. **79**, 379 (1957).
15. J. L. KICE. *In* The chemistry of organic sulfur compounds. *Edited by* N. Kharasch and C. Y. Meyers. Pergamon Press, London, Engl. 1966. p. 121.
16. M. S. KHARASCH, E. N. MAY, and F. R. MAYO. J. Org. Chem. **3**, 189 (1940).
17. R. H. ENGEBRECHT. Ph.D. Thesis, Oregon State University, Corvallis, OR. 1964.
18. T. P. AHERN, D. G. KAY, and R. F. LANGLER. Can. J. Chem. **56**, 2422 (1978).
19. F. G. BORDWELL and H. M. ANDERSEN. J. Am. Chem. Soc. **75**, 6019 (1953).
20. A. OHNO and S. OAE. *In* Organic chemistry of sulfur. *Edited by* S. Oae. Plenum Press, New York. 1977.
21. G. A. RUSSELL, H. D. BECKER, and J. SCHOEB. J. Org. Chem. **28**, 3584 (1963).
22. N. DUFORT and B. JODOIN. Can. J. Chem. **56**, 1779 (1978).
23. J. B. HENDRICKSON, D. J. CRAM, and G. S. HAMMOND. Organic chemistry. McGraw-Hill, New York, NY. 1970. p. 458.
24. F. A. COTTON and G. WILKINSON. Advanced inorganic chemistry. Interscience, New York, NY. 1966. p. 447.
25. R. F. LANGLER. Can. J. Chem. **49**, 481 (1971).

Kinetics of ion exchange of some complex cations on chromium ferrocyanide gel

ISHWARI P. SARASWAT,[1] SURESH K. SRIVASTAVA, AND ASHOK K. SHARMA

Department of Chemistry, University of Roorkee, Roorkee-247672, India

Received September 25, 1978

ISHWARI P. SARASWAT, SURESH K. SRIVASTAVA, and ASHOK K. SHARMA. Can. J. Chem. **57**, 1214 (1979).

The parameters effective diffusion coefficients, activation energies, and entropies of activation are reported for the exchange of the ammine-complex cations of cobalt, viz. $[Co(NH_3)_6]^{3+}$ and $[Co(en)_3]^{3+}$ (en = enthylenediamine) on chromium ferrocyanide gel in the H form. The values of these constants throw significant light on the possible structural changes in the exchanger framework caused by the introduction of these large size complex cations. Kinetic measurements have been made as the function of particle size of the exchanger, temperature, and solution concentration of the exchanging ions. The slow step governing the rate of exchange is diffusion of ions through the exchanger particles.

ISHWARI P. SARASWAT, SURESH K. SRIVASTAVA et ASHOK K. SHARMA. Can. J. Chem. **57**, 1214 (1979).

On rapporte les paramètres suivants: coefficients effectifs de diffusion, énergies d'activation et entropies d'activation pour l'échange des cobaltiamines du type $[Co(NH_3)_6]^{3+}$ et $[Co(en)_3]^{3+}$ (en = éthylènediamine) sur des gels de ferrocyanure de chrome sous forme H. Les valeurs de ces constantes jettent de la lumière sur les changements structuraux possibles dans le squelette de l'échangeur qui sont causés par l'introduction de ces cations complexes volumineux. On a effectué des mesures cinétiques en fonction de la grosseur des particules d'échangeur, de la température et de la concentration de la solution des ions qui s'échangent. L'étape lente déterminant la vitesse de l'échange est la diffusion des ions à travers les particules d'échangeurs.

[Traduit par le journal]

Introduction

The rate factor in ion-exchange adsorption is of recognized importance for the economic and industrial employment of ion-exchangers. The ion-exchange kinetics of simple metal cations, particularly of alkali and alkaline earth metal ions, on various minerals, inorganic exchangers, and organic resins have been studied by a number of workers (1–7). However, little attention seems to have been paid to the kinetics and mechanism of exchange of large cations or complex cations on inorganic exchangers. In continuation of our studies on the exchange behaviour of some simple cations with chromium ferrocyanide gel [CFC] reported earlier (8), the present article deals with the kinetic measurements for the exchange of some ammine complex cations of cobalt(III), viz., $[Co(NH_3)_6]^{3+}$ and $[Co(en)_3]^{3+}$ on the same substrate. To understand the mechanism and other theoretical aspects of the exchange process some kinetic and thermodynamic parameters like effective diffusion coefficients, activation energies, and entropies of activation are reported.

Experimental

All the chemicals used were of analytical grade and the solutions were prepared in double distilled water. Bausch and Lomb Spectronic-20 and Unicam-500 were used for spectrophotometric measurements.

Preparation and Analysis

Chromium ferrocyanide with exchange capacity 3.65 mequiv./g was prepared as reported earlier (9). The synthesized sample was subjected to chemical analysis, thermogravimetric analysis, ir, and X-ray measurements and the data agreed with the data reported for the compound (9) $K_6Cr_2[Fe(CN)_6]_3 \cdot 16H_2O$. The above exchanger of appropriate particle size was converted to H^+ form by the treatment with 1 *M* HCl solution for 48 h.

The hexammine cobalt(III) chloride and trisethylenediamine cobalt(III) chloride were prepared (10) by the standard methods. The purity of the samples was checked by ir spectra and by the gravimetric estimation of cobalt (11).

Particle Size

The exchanger was passed through different sieves and the fractions (100–170), (170–200), and (200–300) B.S.S. mesh sizes were collected. For each fraction, slides having about one hundred particles each were prepared and mounted on projector, Agfa Diamator m (Germany), to get fifty times magnification. The diameter of each magnified image was measured in two perpendicular directions and the mean particle radius was evaluated. No change in the radius of the particles was observed when kept in the water for 48 h.

Rate Measurements

The modified limited bath technique (5) was employed for kinetic measurements. A number of stoppered boiling test tubes each containing 20 mL of the solutions were thermostated at the desired temperatures. The weighed samples of exchanger (0.05 g and 0.10 g for $[Co(NH_3)_6]^{3+}$ and $[Co(en)_3]^{3+}$, respectively) were introduced into each tube. In all cases, the total amount of the exchanging ions in solution was more than

[1]Present address: Indian Co-operation Mission, Kathmandu, Nepal.

0008-4042/79/101214-04$01.00/0

the ion-exchange capacity of the exchanger sample. During the experiments the solutions were mechanically shaken. At predecided intervals of times, the tubes were taken out from the thermostat and exchange process was checked by immediate filtration. The experiments were carried out with three different particle sizes, at different solution concentrations, and at four or five different temperatures with the accuracy of ± 0.1°C.

Results and Discussion

The extent of exchange F, at time t, has been determined as:

$$[1] \qquad F = \frac{Q_t}{Q_\infty} = 1 - \frac{6}{\pi^2} \sum_{n=1}^{\infty} \frac{\exp -n^2 Bt}{n^2}$$

Here, Q_t and Q_∞ are the amounts exchanged at time t and ∞ or at equilibrium, respectively. B is the time co-ordinate of Boyd's equation (1) and is expressed in terms of the effective diffusion coefficient D_i and particle radius r as:

$$[2] \qquad B = \pi^2 D_i / r^2$$

For the observed values of F, corresponding Bt values as derived from eq. [1] are obtained from Reichenberg's table (2).

The plots of Bt vs. t (Figs. 1, 2, 3), above a definite solution concentration, are straight lines passing through the origin. In the present system of investigation, this shows the validity of Boyd's equation (1) and Reichenberg's test (2) developed for the particle diffusion-controlled kinetics. The increase in the slopes of the straight line plots, and hence in the rate of exchange, with the decrease in the particle radius (Fig. 2) and increase in the temperature (Fig. 3) further suggests that the rate of exchange is governed by the diffusion of exchanging ions within the exchanger particles.

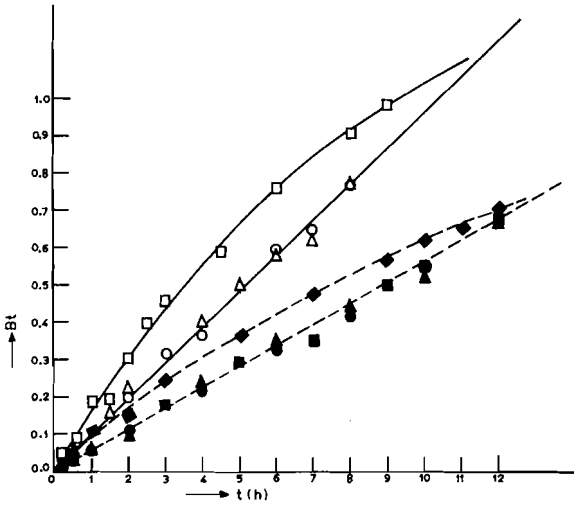

FIG. 1. Plots of Bt vs. t for $[Co(NH_3)_6]^{3+}$, solid lines, and $[Co(en)_3]^{3+}$, broken lines, using different solution concentration at 37.5°C on CFC ($r = 3.44 \times 10^{-3}$ cm): (△, ▲) 0.02 M; (○, ●) 0.01 M; (□, ■) 0.005 M; (◆) 0.0025 M.

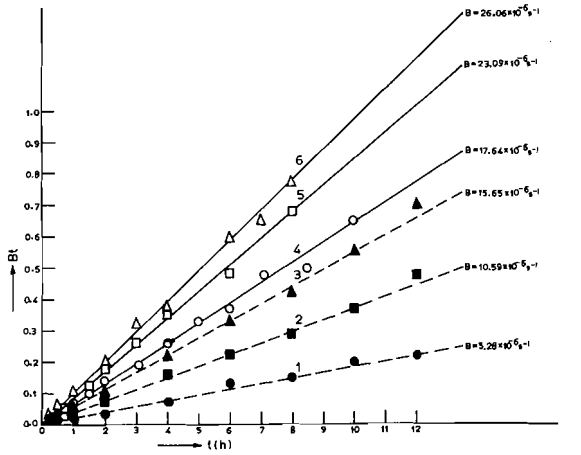

FIG. 2. Plots of Bt vs. t for $[Co(NH_3)_6]^{3+}$, solid lines, and $[Co(en)_3]^{3+}$, broken lines, using different particle sizes of CFC at 37.5°C: (1,4) $r = 6.79 \times 10^{-3}$ cm; (2,5) $r = 4.61 \times 10^{-3}$ cm; (3,6) $r = 3.44 \times 10^{-3}$ cm.

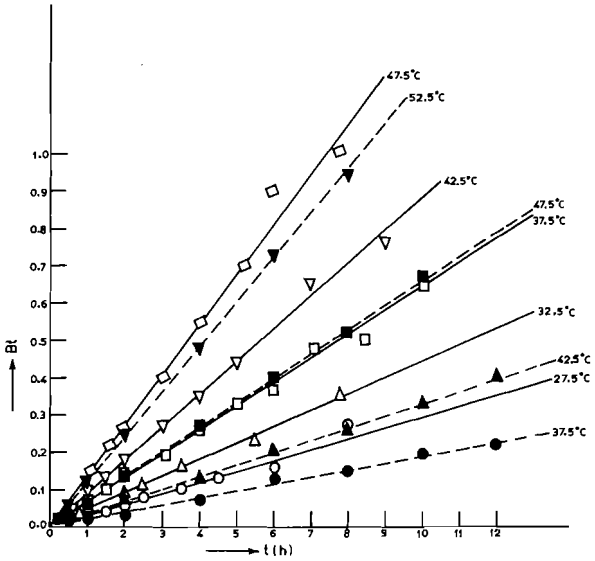

FIG. 3. Plots of Bt vs. t for $[Co(NH_3)_6]^{3+}$, solid lines, and $[Co(en)_3]^{3+}$, broken lines, at different temperatures using CFC ($r = 6.79 \times 10^{-3}$ cm).

It is clear from Fig. 1 that 0.01 M $[Co(NH_3)_6]^{3+}$ and 0.005 M $[Co(en)_3]^{3+}$ are the solution concentrations at and above which the Bt vs. t plots are straight lines and also the exchange rates are not concentration-dependent. This suggests that the particle-diffusion is the rate-controlling factor only at and above these concentrations. Although these concentrations are comparable with those required

for the particle-diffusion controlled kinetics of big ions on zirconium phosphate and oxide (12, 13) they are much lower than those observed for the simple cations on other exchangers (4, 7). In the present case, probably, the larger ionic sizes of complex cations and their slow rate of exchange decrease the possibility of the formation of a liquid film having significant concentration gradient around the exchanger-particles. Thus, even at lower solution concentrations, the prospects of film diffusion as the rate determining step are considerably minimized.

Figures 3 and 4 show an increase in the exchange rate with rise in temperature due to the increase in the mobility of the diffusing cations. The shape of the *F–t* curves (Fig. 4) indicates that the rate is initially rapid but slows down as the time passes. This behaviour is analogous to that observed by Heitner *et al.* (5) and Rawat *et al.* (7) for the exchange of simple cations on the H^+ form of chelating resin Bio-chelex-100 and Tantalum-arsenate respectively. However, the observations of Turse and Rieman (6) for the chemical-exchange of bivalent metal ions on Dowex A-1 are different.

The values of the time co-ordinate B are determined as the slopes of the straight line plots using the method of least-squares. The effective diffusion coefficient D_i at different temperatures calculated from B and exchanger radius (eq. [2]) are given in Table 1. Plots (Fig. 5) of the logarithm of D_i against $1/T(K^{-1})$ are straight lines indicating the validity of the Arrhenius equation:

$$[3] \qquad D_i = D_0 \exp(-E_a/RT)$$

From the slopes and intercepts, the energies of activation E_a and the D_0 respectively have been calculated using the method of least-squares.

The pre-exponential constant D_0 gives the entropy of activation $\Delta S^{\neq}$ (7, 14)

$$[4] \qquad D_0 = 2.72d^2 \frac{KT}{h} \exp\left(\frac{\Delta S^{\neq}}{R}\right)$$

where K and h are Boltzmann and Planck's constants, respectively, R (= 1.98 cal deg^{-1} mol^{-1}) is the gas constant, d (= 5 Å) is taken as the distance between the adjacent exchanging sites in the exchanger (7), and T is 273 K. The values of D_0, E_a, and $\Delta S^{\neq}$ are also recorded in Table 1.

The D_i values obtained for the exchange of $[Co(NH_3)_6]^{3+}$ are higher than that for the exchange of $[Co(en)_3]^{3+}$ (Table 1). It is because of the larger bulk of $[Co(en)_3]^{3+}$ ion that causes more hindrance to its entry into the solid phase and also retards its

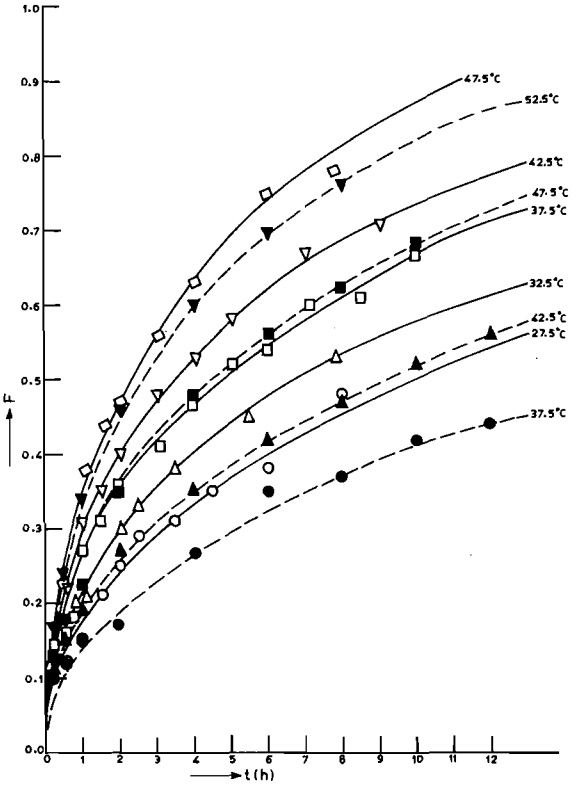

FIG. 4. Rate of exchange of $[Co(NH_3)_6]^{3+}$, solid curves, and $[Co(en)_3]^{3+}$, broken curves, at different temperatures using CFC ($r = 6.79 \times 10^{-3}$ cm).

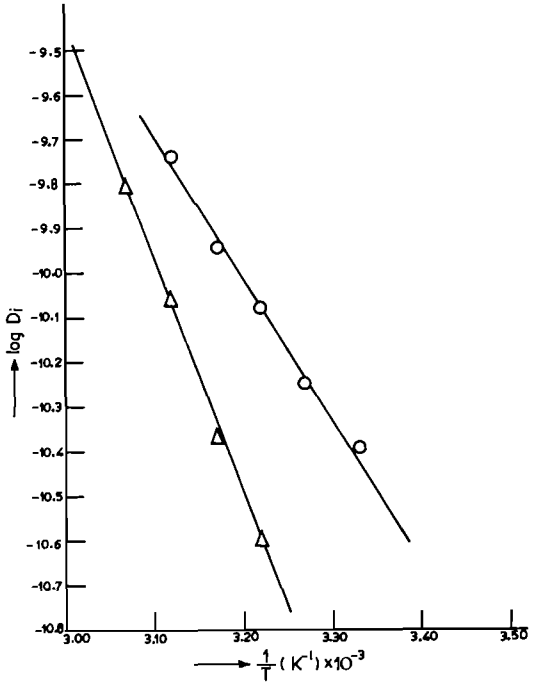

FIG. 5. Plots of log D_i vs. $1/T$; (○) for $[Co(NH_3)_6]^{3+}$ and (△) for $[Co(en)_3]^{3+}$.

TABLE 1. Parameters for the exchange on chromium ferrocyanide gel (radius of the exchanger particle $r = 6.79 \times 10^{-3}$ cm)

Exchanging system	Effective diffusion coefficient (D_i) $cm^2 s^{-1}$						D_0 ($cm^2 s^{-1}$)	Energy of activation (E_a) (kcal mol^{-1})	Entropy of activation ΔS^* (cal deg^{-1} mol^{-1})
	27.5 °C	32.5 °C	37.5 °C	42.5 °C	47.5 °C	52.5 °C			
$[Co(NH_3)_6]^{3+}/H^+$	41.06×10^{-12}	56.07×10^{-12}	82.48×10^{-12}	113.39×10^{-12}	181.20×10^{-12}	—	64.92×10^{-2}	14.05	+5.60
$[Co(en)_3]^{3+}/H^+$	—	—	24.69×10^{-12}	42.56×10^{-12}	87.07×10^{-12}	154.79×10^{-12}	$95.02 \times 10^{+5}$	25.00	+38.39

mobility within the pores of the exchanger particles. Here, it is to be noted that instead of 10^7 times higher value of D_0 for $[Co(en)_3]^{3+}$ as compared with D_0 value for $[Co(NH_3)_6]^{3+}$, the effective diffusion coefficient D_i is less for the former ion. It is due to the difference in the activation energy values of the two cations (Table 1).

In order to maintain the electroneutrality inside the exchanger, one complex cation must replace three mobile hydrogen ions from three exchanging sites. Thus, one complex cation inside the exchanger will reside between three neighbouring and relatively separated negative sites and will experience the coulombic force of attraction. This force of attraction will be greater for the more polarizable $[Co(en)_3]^{3+}$ ion than for the less polarizable $[Co(NH_3)_6]^{3+}$ ion (15). Thus the electrostatic contribution to the energy of activation will be higher in case of $[Co(en)_3]^{3+}$ ion. This explains higher value of activation energy for the $[Co(en)_3]^{3+}/H^+$ exchanging system. Moreover, these electrostatic forces may cause bending or coiling of the matrix that may be more in case of more polarizable cation $[Co(en)_3]^{3+}$. This deformation in the shape of the matrix will be associated with an increase in the total entropy of the system; and hence ΔS^* will be positive. This is what we observed.

Acknowledgements

We wish to thank Dr. Satish Kumar, Pool Officer, for helpful discussions. One of the authors (A.K.S.) is grateful to Council of Scientific and Industrial Research, New Delhi (India), for the award of Junior Research Fellowship.

1. G. E. BOYD, A. W. ADAMSON, and L. S. MYERS, JR. J. Am. Chem. Soc. **69**, 2836 (1947).
2. D. REICHENBERG. J. Am. Chem. Soc. **75**, 589 (1953).
3. D. E. CONWAY, J. H. S. GREEN, and D. REICHENBERG. Trans. Faraday Soc. **50**, 511 (1954).
4. G. H. NANCOLLAS and R. PATERSON. J. Inorg. Nucl. Chem. **22**, 259 (1961).
5. C. HEITNER-WIRGUIN and G. MARKOVITS. J. Phys. Chem. **67**, 2263 (1963).
6. R. TURSE and WM. RIEMAN. J. Phys. Chem. **65**, 1821 (1961).
7. J. P. RAWAT and P. S. THIND. J. Phys. Chem. **80**, 1384 (1976).
8. W. U. MALIK, S. K. SRIVASTAVA, R. P. SINGH, and S. KUMAR. J. Radioanal. Chem. **36**, 469 (1977).
9. W. U. MALIK, S. K. SRIVASTAVA, V. M. BHANDARI, and S. KUMAR. J. Inorg. Nucl. Chem. **38**, 342 (1976).
10. G. G. SCHLESSINGER. Inorganic laboratory preparations. Chemical Publishing Co., Inc., New York, NY. 1962. pp. 176–177 and 186–187.
11. A. I. VOGEL. A text book of quantitative inorganic analysis including elementary instrumental analysis. 3rd ed. Longmans. 1961. p. 530.
12. C. B. AMPHLETT, L. A. MCDONALD, and M. J. REDMAN. J. Inorg. Nucl. Chem. **6**, 236 (1958).
13. C. B. AMPHLETT, L. A. MCDONALD, and M. J. REDMAN. J. Inorg. Nucl. Chem. **6**, 220 (1958).
14. A. DYER and J. M. FAWCETT. J. Inorg. Nucl. Chem. **28**, 615 (1966).
15. F. HELFFERICH. Ion exchange. McGraw-Hill Book Company, Inc. 1962. pp. 162–163.

The adsorption of tri-*n*-butylphosphate at the *n*-dodecane–water interface[1,2]

NORMAN H. SAGERT, WOON LEE, AND MICHAEL J. QUINN

Research Chemistry Branch, Atomic Energy of Canada Limited, Whiteshell Nuclear Research Establishment, Pinawa, Man., Canada R0E 1L0

Received November 7, 1978

NORMAN H. SAGERT, WOON LEE, and MICHAEL J. QUINN. Can. J. Chem. **57**, 1218 (1979).

The adsorption of tri-*n*-butylphosphate (TBP) from *n*-dodecane to the *n*-dodecane–water interface has been studied as a function of TBP mole fraction up to 2.7×10^{-4} in the *n*-dodecane, and as a function of temperature from 293.15 K to 308.15 K. Free energies of adsorption were calculated from the results at low TBP mole fractions, where the surface pressures were linear with mole fraction. They were in the range −36.1 to −35.6 kJ/mol. The enthalpy of adsorption, determined from the variation of the free energies of adsorption with temperature, was −45.4 kJ/mol.

Several equations of state based on two-dimensional gas laws were applied to the results. The Schofield–Rideal equation described the results adequately but the simpler Volmer equation was inadequate especially at lower temperatures. Deviations from the Volmer equation were in the direction of higher surface pressure. A simple version of the two-dimensional solution model equation of state was not helpful.

NORMAN H. SAGERT, WOON LEE et MICHAEL J. QUINN. Can. J. Chem. **57**, 1218 (1979).

On a étudié l'adsorption du tri-*n*-butylphosphate (TBP) en solution dans le dodécane par des interfaces *n*-dodécane–eau; ces études ont été réalisées à des fractions molaires de TNP allant jusqu'à 2.7×10^{-4} dans le *n*-dodécane et à des températures allant de 293.15 à 308.15 K. On a calculé les énergies libres d'adsorption à partir des résultats obtenus aux faibles fractions molaires de TNP alors que les pressions superficielles sont linéaires avec la fraction molaire. Ces valeurs s'étalent de −36.1 à −35.6 kJ/mol. On a déterminé l'enthalpie d'adsorption, −45.4 kJ/mol, à partir de la variation des énergies libres d'adsorption en fonction de la température.

On a appliqué à nos résultats plusieurs équations d'état basées sur des lois des gaz bidimensionnelles. L'équation de Schofield–Rideal décrit les résultats d'une façon adéquate; toutefois l'équation plus simple de Volmer est inadéquate spécialement aux températures inférieures. Les déviations de l'équation de Volmer sont en direction d'une pression superficielle plus élevée. Une version plus simple d'une solution modèle bidimensionnelle de l'équation d'état ne s'est pas avérée utile.

[Traduit par le journal]

Introduction

This work on the adsorption of tri-*n*-butylphosphate (TBP) at the *n*-dodecane–water interface forms part of a program to study interfacial properties relevant to solvent extraction systems, especially those systems useful for separating the components of irradiated nuclear fuel. The interfacial properties have not been studied as intensively as the equilibrium distributions (1). TBP was selected as a solute since it is frequently used as an extractant and, since it is often used with a diluent such as kerosene, *n*-dodecane was chosen as the organic phase.

The adsorption of nonionic surfactants at hydrocarbon–water interfaces has received considerable attention in recent years (2). Most of the work has involved adsorption of *n*-alcohols at the *n*-alkane–water interface (3–5). Some adsorption studies using esters and diesters as solutes have also been reported (6). The adsorption of nonionic phosphates at hydrocarbon–water interfaces has received relatively little attention, although some studies of the adsorption of TBP at the benzene–water interface have been reported (7–9).

To calculate the thermodynamic properties of adsorption, we have investigated the adsorption of TBP at the *n*-dodecane–water interface at low TBP mole fractions and at a number of temperatures. These thermodynamic properties are essentially a measure of solute–subphase interactions (3). We have also investigated adsorption at higher TBP mole fractions to study the applicability of various equations of state to the adsorbed layer. These isotherms are useful in describing the nature of the interface itself. We examined equations of state, such as the Schofield–Rideal equation (10), which are derived by considering the adsorbed layer to have the properties of a two-dimensional gas, and examined a simple equa-

[1]AECL No. 6277.

[2]Presented in part at the 61st Chemical Conference of the Chemical Institute of Canada, Winnipeg, Man. June 1978.

0008-4042/79/101218-06$01.00/0

tion of state based on a two-dimensional solution model for the adsorbed layer (5, 11).

Experimental

Interfacial tensions were measured by the drop–volume method. Drops were formed on a stainless steel tip of 3.166 ± 0.001 mm radius and were aged at least 5 min. Volumes were measured with a 2500-mm³ Gilmont precision micrometer syringe fitted with a thermostatted barrel. The tip was located in a Ramé Hart closed thermostatted environmental chamber. Temperature control was to ±0.02 K and temperatures were known to ±0.05 K. This chamber was fitted with plane windows which allowed visual and photographic verification that the tip radius was the radius wetted by the liquid. Interfacial tensions were calculated using the Harkins and Brown correction curve (12). Interfacial tensions were reproducible to ±50 μN/m.

The *n*-dodecane was Phillips research grade. Before use it was passed through an alumina column. Its purity was better than 99.99 mol% as checked by gas chromatography. The water was triple distilled from Pyrex and had a final conductivity of 190 μS/m. No attempt was made to exclude CO_2. The TBP was Fisher purified grade, further purified by the method of Alcock *et al.* (13). This procedure involves shaking the TBP with dilute caustic solution and then distilling off some of the mixture to remove volatiles. Acidic impurities go into the aqueous phase. The TBP was then washed repeatedly with water, dried with a heat lamp, and stored over activated 12-mesh molecular sieve 4A.

A stock solution of TBP in *n*-dodecane was prepared. Appropriate amounts of stock solution were added to 5×10^{-5} m³ of *n*-dodecane plus 5×10^{-5} m³ of water in the environmental chamber to make up the required mole fraction in the *n*-dodecane. The system was then equilibrated by light shaking for 16 h. Since the distribution coefficient of TBP between *n*-dodecane and water is ~300 in favor of the *n*-dodecane (14), no correction was made for TBP dissolved in the water.

Densities were measured to within ±200 g/m³ using a 2.5×10^{-5} m³ pycnometer flask.

Results

n-*Dodecane–Water Interfacial Tensions*

Interfacial tensions of pure *n*-dodecane against water are shown in Fig. 1 as a function of temperature. Also shown are results of Aveyard and Haydon (15). Our results, while somewhat lower than those of Aveyard and Haydon, agree with theirs to within 150 μN/m. The temperature coefficient for our data is 85 ± 5 μN/(m K), based on a Students *t* distribution at the 95% confidence limit, compared with that of Aveyard and Haydon of 88 ± 9 μN/(m K) on the same basis. Thus our techniques gave results comparable with literature values.

Interfacial Adsorption of TBP

The adsorption of TBP at the *n*-dodecane–water interface was studied at 293.15, 298.15, 303.15, and 308.15 K for mole fractions of TBP in *n*-dodecane up to 2.74×10^{-4}, by measuring interfacial tensions. At these mole fractions, no significant changes in *n*-dodecane density were detected on adding TBP.

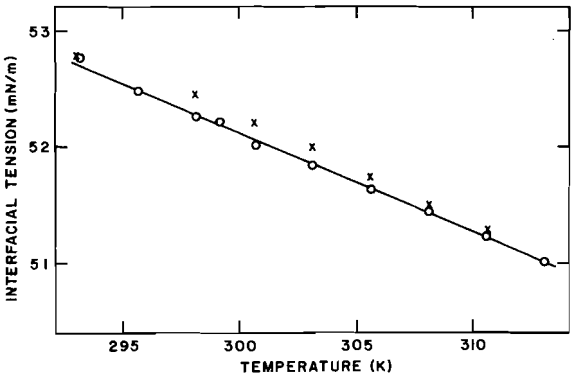

FIG. 1. Interfacial tensions at the *n*-dodecane–water interface as a function of temperature. The circles (○) represent our results and the crosses (×) represent those from ref. 15.

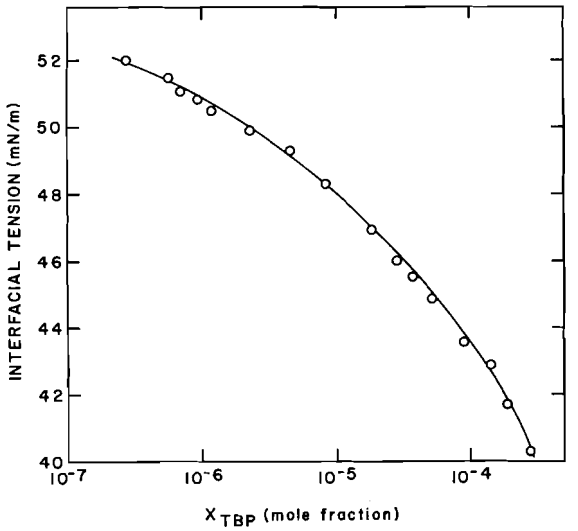

FIG. 2. Interfacial tensions at the *n*-dodecane–water interface on adding TBP to the *n*-dodecane. $T = 298.15$ K.

Results obtained at 298.15 K are shown in Fig. 2. The data at the four temperatures are expressed by eq. [1].

$$[1] \qquad \gamma = C_1 + C_2 \ln X + C_3 (\ln X)^2$$

where γ is the interfacial tension in mN/m and X is the mole fraction of TBP in the *n*-dodecane. The values of the constants, C_i, as determined by a second order least-squares fit are given in Table 1. These constants lead to fits of the data[3] which are within 0.2 mN/m. Additional measurements were made at 295.65, 300.65, and 305.65 K at TBP mole fractions up to 1.2×10^{-6}. The results in the region

[3]All the measured interfacial tensions are available, at a nominal charge, from the Depository of Unpublished Data, CISTI, National Research Council of Canada, Ottawa, Ont., Canada K1A 0S2.

TABLE 1. Coefficients in eq. [1] for adsorption of TBP at *n*-dodecane–water interface

T(K)	$10^3\ C_1$	$10^3\ C_2$	$10^4\ C_3$
293.15	6.681986	−5.422585	−2.771724
298.15	6.024138	−5.636496	−1.963373
303.15	5.623144	−5.812889	−1.597319
308.15	5.917435	−5.898650	−1.915968

of TBP mole fraction up to 1.2×10^{-6} are shown in Fig. 3, omitting the intermediate temperatures for clarity. Here, the interfacial pressure π, which is the interfacial tension in the absence of TBP less that in its presence, is plotted against the mole fraction of TBP.

Calculation of Molecular Areas

For moderately surface-active solutes adsorbed from dilute solutions, Aveyard and Briscoe (4) have shown that the simple form of the Gibbs adsorption equation (eq. [2]) may be used to calculate the area per molecule available at the interface.

$$[2] \qquad A = -kT(\partial\gamma/\partial \ln fX)^{-1}$$

In eq. [2] A is the area per molecule, k, the Boltzmann constant, and f, the activity coefficient for TBP in *n*-dodecane. This mole fraction activity coefficient approaches unity for dilute solutions.

Activity coefficients for dilute solutions of TBP in organic diluents have not been measured directly, to the best of our knowledge. However, activity coefficients measured from the distribution coefficients of TBP between water and kerosene (14, 16) indicate that the activity coefficients approach unity at the dilutions used here. Siekierski (17) has used an expression to correlate much TBP activity coefficient data which predicts an activity coefficient of 0.987 (present definition) at a mole fraction of 2.3×10^{-3} in *n*-dodecane. Although trialkylphosphates are known to associate through a system of dipole–dipole bonds, dimerization constants are small (2.9×10^{-3} m^3/mol for TBP in *n*-hexane (18)). Current knowledge on association in trialkylphosphate systems has been described recently by Kertes and Tsimering (19). In this work we will consider the activity coefficients as unity.

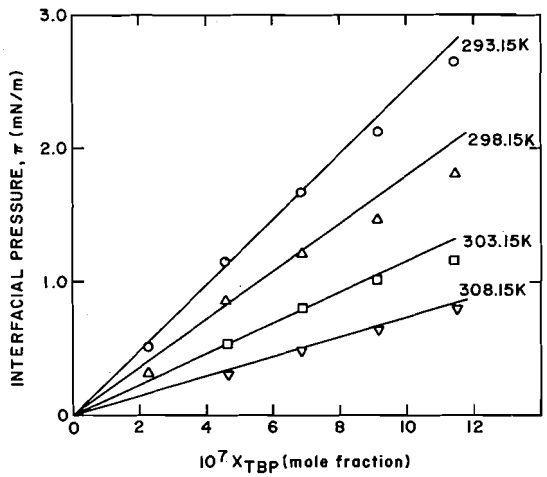

FIG. 3. Interfacial pressures as a function of mole fraction TBP in *n*-dodecane.

Using eqs. [1] and [2], the area per molecule may be calculated by eq. [3].

$$[3] \qquad A = -kT(C_2 + 2C_3 \ln X)^{-1}$$

Values of A were calculated at the experimentally used mole fractions, omitting the highest and lowest mole fraction of each set.

Discussion

Free Energies and Enthalpies of Adsorption

Standard free energies of adsorption, $\Delta_a\mu^\theta$ were calculated from eq. [4]

$$[4] \qquad \Delta_a\mu^\theta = -RT \ln (\pi/X)_0$$

where $(\pi/X)_0$ is the initial slope of the surface pressure curve when plotted against mole fraction of TBP in the *n*-dodecane (Fig. 3). The standard states were those of Aveyard and Briscoe (4). For the surface standard state they used a surface pressure of 1 mN/m. For the bulk standard state they used a hypothetical state, where the mole fraction of TBP was unity and the activity coefficient for TBP in *n*-dodecane was also unity. The free energies of adsorption, given in Table 2, range from −35.6 to −36.2 kJ/mol.

These free energies of adsorption are quite large and negative. For example, over the same temperature range, free energies of adsorption of octanol at the *n*-dodecane–water interface are in the range of −23.4 to −22.9 kJ/mol using the same standard states (4). It is thought (4, 5) that, at the oil–water interface, hydrocarbon chains are dissolved completely in the oil. The strong adsorption of *n*-alcohols has been attributed to polar group interactions as the

TABLE 2. Standard free energies of adsorption of TBP at the *n*-dodecane–water interface

T(K)	$-\Delta_a\mu^\theta$ (kJ/mol)
293.15	36.06
295.65	36.22
298.15	35.91
300.65	35.84
303.15	35.78
305.65	35.80
308.15	35.58

OH group is transferred from the oil to water. Our free energies for the adsorption of TBP from *n*-dodecane to the *n*-dodecane–water interface are about 12.7 kJ/mol more negative than those for adsorbing *n*-octanol from *n*-dodecane to the same interface. From this it might be inferred that the phosphate group of TBP has a greater tendency to interact with water than does the OH group of alcohols. Interactions between polar and self-associated liquids such as water and TBP are undoubtedly complex (19). Hydrogen bonding must be one of the major interactions between these species, especially in dilute solutions where a hydrogen-bonded equimolar hydrate is probably the major species (19–21). However, in dilute solution, hydrophobic stabilization of the water structure, the so-called "hydrophobic bonding" (22) has been shown to be very important in accounting for enthalpies of solution of trialkylphosphates in water (19). In more concentrated systems, which probably exist in the adsorbed phase, dipole–dipole interactions are likely important, because of the large dipole moment of TBP (23). Dimerization of TBP in more concentrated TBP–water systems is thought to occur through dipole–dipole interactions (18, 19, 21).

Although no exact tabular data are given, the work of Chifu, Andrei, and Tomoaia (7, 8) indicates that the free energy of adsorption of TBP from benzene to the benzene–water interface is much less negative than the values we have obtained for adsorption to the *n*-dodecane–water interface. This is in accord with evidence that there is some complexing between TBP and benzene (24). On the other hand, in their work, TBP mole fractions were high and activity coefficient corrections were not made.

Standard enthalpies of adsorption, $\Delta_a h^\theta$ were obtained from the temperature variation of the free energies (eq. [5]).

$$[5] \qquad \Delta_a h^\theta = \mathrm{d}(\Delta_a \mu^\theta/T)/\mathrm{d}(1/T)$$

The standard free energies of adsorption are shown in Fig. 4, plotted in the form suggested by eq. [5]. From Fig. 4, $\Delta_a h^\theta$ seems reasonably constant at -45.4 kJ/mol over this temperature interval.

It is interesting to compare this enthalpy for TBP adsorption from *n*-dodecane to the *n*-dodecane–water interface with the enthalpy of transfer of TBP from *n*-dodecane to water. The enthalpy of transfer of TBP from *n*-dodecane to water can only be estimated at the present time. By definition, this enthalpy is the enthalpy of solution of TBP in water minus the enthalpy of solution of TBP in *n*-dodecane. The latter enthalpy has been measured recently as $+7.4$ kJ/mol (25). However, the former enthalpy is not known. Recently, Kertes and Tsimering (19) measured the enthalpies of solution of trimethylphosphate (TMP)

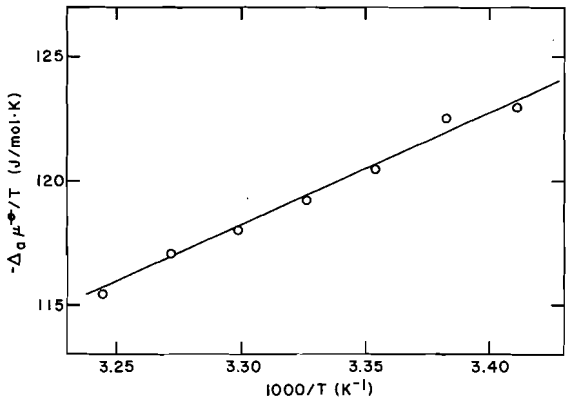

FIG. 4. Variation with temperature of the standard free energy of adsorption, $\Delta_a\mu^\theta$.

and triethylphosphate (TEP) in water and found large exothermic heats of solution with TEP giving the largest (most negative) enthalpy of solution. At infinite dilution, their values were -21.2 kJ/mol for TMP and -25.9 kJ/mol for TEP. Although they did not obtain an accurate value for the enthalpy of solution of tri-*n*-propylphosphate, they reported that it was larger (more negative) than that of TEP.

On the basis of a linear extrapolation of the TMP and TEP values, we estimated an enthalpy of solution for TBP of -35.5 kJ/mol. This is an absolute maximum (in the negative sense) since, as the hydrocarbon chains become very long, the enthalpy of solution will become less negative with increasing chain length (26). Therefore -42.9 kJ/mol may be taken as the absolute (negative) maximum for the enthalpy of transfer. Our observed enthalpy of adsorption of -45.4 kJ/mol for TBP with *n*-dodecane is of the order of, and somewhat larger than, this maximum enthalpy of transfer. Therefore the greater portion of the enthalpy of transfer seems accounted for when the TBP molecule reaches an equilibrium position in the interface, with, presumably, the phosphate group in the water. This situation is quite similar to that where *n*-octanol is the solute. In that case, the enthalpy of adsorption is -31.1 kJ/mol (4) and the enthalpy of transfer is about -26 kJ/mol, as determined from results of Aveyard and Mitchell (27) extrapolated to higher carbon chain lengths.

For the alcohols, the largest part of the enthalpy of transfer consists of an endothermic enthalpy of solution in *n*-dodecane with some contribution from a numerically smaller exothermic enthalpy of solution in water. Thus, it is relatively easy to rationalize the rough equivalence of the enthalpies of adsorption and transfer. However, with TBP, a large portion of the enthalpy of transfer comes from the exothermic enthalpy of solution in water, with a smaller contri-

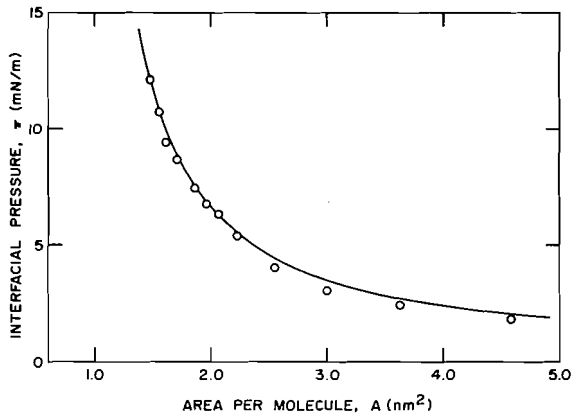

FIG. 5. Fit of surface pressure (π), area (A) data at 298.15 K to Schofield–Rideal equation using constants of Table 3.

bution from the endothermic enthalpy of solution in *n*-dodecane. This large enthalpy of solution in water has been ascribed (28) to "hydrophobic bonding" (22) where water structure is enhanced by the interaction of alkyl groups with the water. This hydration cage may involve about 30 water molecules (28). It would appear from this work that much of this structure is formed when the TBP molecule reaches its equilibrium position in the oil–water interface.

Surface Equations of State

The measured values of π and A can be fitted to two-dimensional equations of state which are analogous to the normal three-dimensional equations of state. The Schofield–Rideal equation (10) is frequently used.

$$[6] \qquad \pi(A - A_0) = ikT$$

Both A_0 and i are constants. The values obtained are given in Table 3 and a fit of the experimental data at 298.15 K is given in Fig. 5. The experimental data were not fitted by the usual $1/\pi$ vs. A plot, but rather, a non-linear, least-squares fitting routine (Chalk River Nuclear Laboratories CDC 6600 Fortran program LSQQ) based on Marquardt's method was used with eqs. [3] and [6] and the coefficients from Table 1 to reproduce the interfacial tension data. The errors given in Table 3 correspond to one standard deviation.

The values for A_0 of ≈ 0.9 nm^2 are similar to those at the benzene–water interface (0.97 and 1.14 nm^2) obtained by Tomoaia *et al.* (7) without and with added copper nitrate. Although A_0 is only a fitting constant, there is much evidence, for straight chain alcohols (5), at least, that it represents the static geometric area of the molecule at the interface. From molecular models, the area of the TBP molecule is ~ 1.0 nm^2, the exact area depending on the folding of the butyl groups.

TABLE 3. Constants of Schofield–Rideal equation

T (K)	A_0 (nm^2)	i
293.15	0.88±0.02	1.84±0.05
298.15	0.85±0.02	1.84±0.05
303.15	0.93±0.03	1.51±0.07
308.15	0.97±0.04	1.39±0.08

If the i in eq. [6] is 1.0 then the resulting equation is called the Volmer equation, and generally, our results do not fit the Volmer equation. The deviations observed (Table 3) may suggest extra repulsions in the monolayer rather than increased cohesion. Some of this repulsion could result from dipole–dipole interaction (29) if the adsorption forces are great enough to keep the dipoles aligned. Deviations from the Volmer equation could also arise from variation of A_0 with coverage, possibly due to changing orientation of TBP molecules in the interface. TBP molecules are more symmetric than the usual surfactant molecules making such changes possibly easier. On the other hand, the two-dimensional gas picture, which underlies the Volmer equation, may not be adequate for a solute such as TBP which is capable of restructuring the water phase (28).

Attempts were made to use a solution model for the surface (11). Generally, the simplifying assumption has to be made that the solute is located entirely in the *n*-dodecane. This assumption is clearly not a good one for TBP. If the *n*-dodecane – solute pair forms an ideal two-dimensional solution, then eq. [7] should hold (5). A similar equation has been used with some success by Fowkes (30).

$$[7] \qquad \pi = -\frac{kT}{\sigma_1} \ln\left(\frac{A - \sigma_2 + \sigma_1}{A - \sigma_2}\right)$$

In eq. [7] σ_1 and σ_2 are the surface areas of the solvent and solute, respectively. It would be expected that σ_1 and σ_2 would be quite different in this system. Unfortunately, it was not possible to fit our data using eq. [7]. When the data were plotted in the rearranged form suggested by Aveyard and Briscoe (5) and shown as eq. [8],

$$[8] \qquad [\exp(\pi\sigma_1/kT) - 1]^{-1} = A/\sigma_1 - \sigma_2/\sigma_1$$

all reasonable values of σ_1 gave ratios of σ_2/σ_1 between 2 and 3, but the slopes were always less than $1/\sigma_1$. The failure of the solution model may well result from the involvement of the water phase, if significant water restructuring takes place (28).

Acknowledgments

We thank D. G. Juhnke and R. J. Porth of the Chemical Technology Branch, WNRE for preparing

the purified TBP. We also thank our colleagues at WNRE for helpful advice.

1. Y. MARCUS and A. S. KERTES. Ion exchange and solvent extraction of metal complexes. John Wiley, New York. 1969.
2. R. AVEYARD and B. VINCENT. Prog. Surf. Sci. **8**, 59 (1977).
3. S. ROSS and E. S. CHEN. Ind. Eng. Chem. **57** (7), 40 (1965).
4. R. AVEYARD and B. J. BRISCOE. Trans. Faraday Soc. **66**, 2911 (1970).
5. R. AVEYARD and B. J. BRISCOE. J. Chem. Soc. Faraday I, **68**, 478 (1972).
6. R. AVEYARD and J. CHAPMAN. Can. J. Chem. **53**, 916 (1975).
7. M. TOMOAIA, Z. ANDREI, and E. CHIFU. Rev. Roum. Chim. **18**, 1547 (1973).
8. E. CHIFU, Z. ANDREI, and M. TOMOAIA. Ann. Chim. **64**, 869 (1974).
9. Z. ANDREI and E. CHIFU. Stud. Univ. Babes-Bolyai Chem. **21**, 10 (1976).
10. R. K. SCHOFIELD and E. K. RIDEAL. Proc. R. Soc. London, A**109**, 57 (1925).
11. E. H. LUCASSEN-REYNDERS. *In* Progress in surface and membrane science. Vol. 10. *Edited by* D. A. Cadenhead and J. F. Danielli. Academic Press, New York. 1976. pp. 253–360.
12. W. D. HARKINS and F. E. BROWN. J. Am. Chem. Soc. **41**, 499 (1919).
13. K. ALCOCK, S. S. GRIMLEY, T. V. HEALY, J. KENNEDY, and H. A. C. MCKAY. Trans. Faraday Soc. **52**, 39 (1956).
14. Y. MARCUS. Critical evaluation of some equilibrium constants involving organophosphorus extractants. Butterworths, London. 1974. p. 27.
15. R. AVEYARD and D. A. HAYDON. Trans. Faraday Soc. **61**, 2255 (1965).
16. Y. MARCUS. J. Phys. Chem. **65**, 1647 (1961).
17. S. SIEKIERSKI. J. Inorg. Nucl. Chem. **24**, 204 (1962).
18. D. M. PETKOVIĆ. J. Inorg. Nucl. Chem. **30**, 603 (1968).
19. A. S. KERTES and L. TSIMERING. J. Phys. Chem. **81**, 120 (1977).
20. C. J. HARDY, D. FAIRHURST, H. A. C. MCKAY, and A. M. WILLSON. Trans. Faraday Soc. **60**, 1626 (1964).
21. D. M. PETKOVIĆ and Z. B. MAKSIMOVIĆ. J. Inorg. Nucl. Chem. **39**, 2031 (1977).
22. F. FRANKS. *In* Water—a comprehensive treatise. Vol. 4. *Edited by* F. Franks. Plenum Press, New York. 1975. pp. 1–94.
23. D. M. PETKOVIĆ, B. A. KEZELE, and D. R. RAJIĆ. J. Phys. Chem. **77**, 922 (1973).
24. D. M. PETKOVIĆ and Z. B. MAKSIMOVIĆ. J. Inorg. Nucl. Chem. **38**, 297 (1976).
25. A. S. KERTES, L. TSIMERING, and F. GRAUER. J. Inorg. Nucl. Chem. **38**, 869 (1976).
26. R. AVEYARD and R. W. MITCHELL. Trans. Faraday Soc. **64**, 1757 (1968).
27. R. AVEYARD and R. W. MITCHELL. Trans. Faraday Soc. **65**, 2645 (1969).
28. S. LINDENBAUM, D. STEVENSON, and J. H. RYTTING. J. Solution Chem. **4**, 893 (1975).
29. C. J. F. BÖTTCHER. Theory of electric polarization. Vol. I. Dielectrics in static fields. Elsevier, Amsterdam. 1973. pp. 113–124.
30. F. M. FOWKES. J. Phys. Chem. **66**, 1863 (1962).

Anisotropic motion in 1-substituted adamantanes from ^{13}Cmr relaxation time data

HELMUT BEIERBECK, ROBERT MARTINO,[1] AND JOHN K. SAUNDERS
Département de Chimie, Université de Sherbrooke, Sherbrooke (Qué.), Canada J1K 2R1

Received August 31, 1978

HELMUT BEIERBECK, ROBERT MARTINO, and JOHN K. SAUNDERS. Can. J. Chem. **57**, 1224 (1979).

The carbon-13 relaxation time data and the calculated diffusion constants for several 1-substituted adamantane derivatives in various solvents are presented. The ratio of the diffusion constants for rotation about the principal axis relative to that about the two mutually perpendicular axes is found to vary significantly with substituent and to a lesser extent with solvent. The order for this ratio is $CO_2H > OH > NH_2 \approx Br$, which is interpreted in terms of the degree of association, either solute–solute or solute–solvent, and also the ease of rotation about the carbon–substituent bond.

HELMUT BEIERBECK, ROBERT MARTINO et JOHN K. SAUNDERS. Can. J. Chem. **57**, 1224 (1979).

Le temps de relaxation du carbone-13 de plusieurs dérivés d'adamantane substitués en position-1 a permis de calculer les constantes de diffusion pour la rotation autour de l'axe principal et autour des deux axes perpendiculaires à ce dernier. Le rapport de ces deux constantes de diffusion varie plus avec le substituent qu'avec le solvant. Ce rapport décroît dans l'ordre $CO_2H > OH > NH_2 \approx Br$, ce qui est interprété en termes d'association soit soluté–soluté soit soluté–solvant et aussi en termes de barrière de rotation autour de la liaison C—X.

^{13}C spin lattice relaxation times (T_1) have proven useful in the study of molecular dynamics of organic molecules in solution (1–4). The analysis of the T_1's for individual carbons leads to information on the overall molecular motion such as anisotropic behaviour (5–8) and thus on intermolecular interactions of the solute.

The dominant relaxation pathway for ^{13}C nuclei in the compounds studied is the dipole–dipole interaction between carbon and hydrogen. The relaxation rate thus depends principally on the number of attached hydrogens, and the modulation of the C—H bond vectors by molecular motion. If a C—H bond is situated parallel to a preferred axis of rotation, rotation about this axis does not modulate the C—H bond and the relaxation process for such a carbon is more efficient. This effect was observed in monosubstituted benzene derivatives (5). The T_1 value for the *para* carbon is shorter than for the *ortho* and *meta* since the *para* C—H bond is parallel to the C_2 axis. The 1-substituted adamantanes exhibit similar behaviour. The C—H *endo* bond of the δ carbons is parallel to the C_3 axis of rotation whereas the other C—H bonds are at angles of 60° or 90° to this axis. From the ^{13}C T_1 data, rotational diffusion constants may be derived by application of Woessner's equations (9) for axially symmetric ellipsoids.

We have determined relaxation times for a number of 1-substituted adamantanes in various solvents in order to study the effect of heterosubstituents on the anisotropy of the molecular motion and the interactions between solvents and heterosubstituents. The relaxation times are transformed into rotational diffusion constants which are compared with the macroscopic viscosity. For a molecule undergoing isotropic motion, the Stokes–Einstein expression (10) as modified by Gierer and Wirty (11) linking the diffusion constant with viscosity (η) is

$$\tau_c = (6R)^{-1} = 4\pi r^3 n f(r)/3kT$$

where τ_c is the effective rotational correlation time, R is the diffusion constant, r the molecular radius, and $f(r)$ is a correction factor, denoting the microviscosity factor which is defined (11) as

$$f(r) = [6(r_1/r) + (1 + r/r_1)^{-3}]^{-1}$$

where r_1 is the radius of solvent molecules. The correction factor was introduced to account for the observation that the Stokes–Einstein equation overestimates the magnitude of the rotational friction constant. In neat liquids, the above expression gives a value of approximately 1/6 for $f(r)$ whereas for a large number of associated and nonassociated liquids a value of 1/12 is found to be more compatible with experimental data (12). In solution, the situation is still more complex. In the ensuing discussion, we will compare the diffusion constant data, which gives insight into local fluid conditions, with the macroscopic viscosity which is averaged over the whole system and discuss qualitatively any marked discrepancies.

[1]Permanent address: U.E.R. de Chimie Organique, Université Paul Sabatier, 118 route de Narbonne, Toulouse, France.

0008-4042/79/101224-05$01.00/0

Results and Discussion

The T_1 data recorded as a function of solvent and viscosity are given in Table 1 as are the calculated rotational diffusion constants, R_1 and R_2. R_1 describes the rotation about the preferred axis, i.e. the C_3 axis. The T_1 values for the γ-carbons are always less than $2 \times T_1$ (β-carbons), due in part to the protons on the adjacent carbons contributing to the relaxation of the methine carbons to a greater extent than the β-carbons (13). This fact must be taken into account when calculating diffusion constants.

For the bromo derivative, the ratio of the diffusion constants, σ, varies between 1 and 2.95 whereas the ratio of the moments of inertia is 2.95. A plot of $(R_1)^{-1}$ versus viscosity is a straight line as illustrated in Fig. 1. Extrapolation to zero viscosity yields a value for R_1 of 1.2×10^{11} s^{-1} which differs significantly from the free rotation value of 1.7×10^{12} s^{-1} calculated using the moments of inertia and the equation derived by Bartoli and Litovitz (14), namely,

$$R_{free} = (9/2\pi)\,(kT/I)^{1/2}$$

This discrepancy, together with the σ values and the correlation of R_1 with viscosity, infer that molecular reorientation is diffusional in nature and that the inertial character is very small (15). The diffusion constant R_2, with one exception, decreases as the viscosity increases. The rate of rotation should be faster in $CDCl_3$ than in benzene according to viscosity whereas experimentally the reverse is observed. The value of R_2 will be dependent upon the solvation of the bromine relative to the hydrocarbon portion of the molecule as well as on viscosity. The small values of σ imply that there is no significant specific solvation of the bromine relative to the hydrocarbon moiety and that, with the exception of acetone, the principal reason for the anisotropic motion is a volume effect. In acetone the motion is essentially isotropic indicating that in this solvent, it is the hydrocarbon portion of the molecule which is the more strongly solvated.

For adamantan-1-ol, the molecular motion is quite anisotropic and σ varies from 3.3 in acetone to 9.5 in CD_3OD. There is no obvious correlation between viscosity and R_1 as can be seen in Fig. 1. The lack of correlation between R_2 and viscosity is to be expected since the OH group will be involved to a greater or lesser extent in hydrogen bonding either with other solute molecules or with the solvent. With the exception of acetone, the variation of σ as a function of solvent is reasonably small. In CCl_4, and to a lesser extent in $CDCl_3$, the molecule will exist in dimeric or polymeric forms due to intermolecular solute–solute hydrogen bonding, whereas in DMSO and CD_3OD the solute will exist essentially as solvated monomers. Due to the bulkiness of the adamantanyl moiety the associated species will most likely be the dimer with only limited access for the solvent to solvate the OH groups. The principal axis of rotation for the dimer will be almost parallel to the C_3 axis of rotation of the monomer with the center of gravity being between the two oxygens. The ratio of the volume[2] traced out by rotation about the major axis relative to the minor axis is approximately 1:2.5. Thus, based on volume considerations,[2] the value of σ should be about 2.5. However, rotation about the principal axis can occur via two mechanisms: rotation of the dimer as an entity or rotation about the C—O bond of the adamantanyl moiety. The experimental values of 6.5 and 7.2 infer that rotation about the C—O bond as well as the overall motion is important.

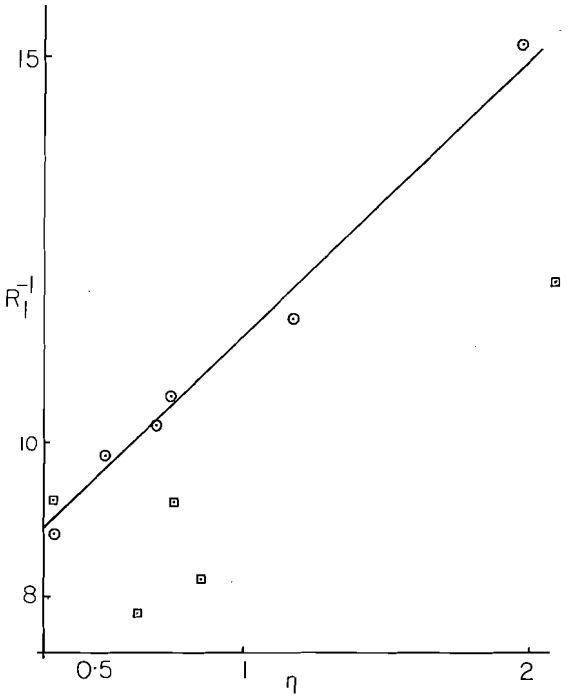

FIG. 1. Plot of $R_1^{-1} \times 10^{12}$ (s) versus viscosity, η (cP), for 1-bromoadamantane ○ and adamantan-1-ol □.

In order to have movement of the OH group in the more strongly solvating solvents, either the hydrogen bonds between the solvent and the OH group must be broken or the solvent molecules must rotate with the OH group. If the latter occurs, the

[2]Volumes were estimated from molecular models since the molecular volume so obtained correlated reasonably well with the experimental apparent molar volume.

centre of gravity of the molecular framework will approach the oxygen atom and the relative motion will be similar to that observed for solvents where the solute is involved in solute–solute interactions. Experimentally, the values of σ are 9.5 in CD_3OD and 6.7 in DMSO whereas in acetone it is only 3.3. This infers that the solute molecules are more strongly solvated in the former two solvents than in the latter. The value for acetone is an indication that the hydrogen bond formed between OH and the carbonyl group is significantly weaker than in either CD_3OD or DMSO, or that the solvent–solvent interactions are relatively weak. Similar results were obtained for phenol in acetone relative to other solvents (5).

The acid shows striking anisotropic behaviour with values of σ between 25 and 29. There is no correlation with viscosity, obviously due to extensive association in $CDCl_3$ and benzene. The amine exhibits quite different behaviour in that the motion is only slightly anisotropic. There is no correlation with viscosity since both R_1 and R_2 are largest in the most viscous solvent, CCl_4, and smallest in the least viscous solvent, CD_3OD.

In any discussion of the effect of association, whether by solvent or solute molecules, on the diffusion constants it is evident that R must be greater than k_{diss} (k_{diss} = rate constant for dissociation of the associated species) in order for evidence of association to be observed by T_1 measurements. As already mentioned, it appears that for the OH group, $R > k_{diss}$ for CD_3OD, DMSO, CCl_4, and $CDCl_3$ as solvents whereas in acetone the value of σ inferred that R and k_{diss} are of the same order of magnitude. For the amine in CCl_4, σ is very small and the rotation rates are faster than in the other solvents. This is a good indication that $k_{diss} > R$ for the dissociation of a solute–solute pair, that specific solvation of the NH_2 group by CCl_4 is minimal and that the T_1 values are essentially determined by the tumbling of a monomer. In other words, any solute–solute or solute–solvent pairs which are formed are too short-lived to be measured by this technique.

For 1-substituted adamantanes in which the substituents are engaged in strong intermolecular interactions, the value of σ will be large only if the barrier to rotation about the C—X bond is small. We have already discussed the case of X = OH where rapid rotation about the C—OH bond was suggested to explain the observed values. Although the barriers to rotation about the C—X bonds have not been determined for the compounds studied here, they are known in similar compounds (16). The barriers about C—CO_2H and C—OH are both relatively small, of the order of 2 and 4 kJ/mol, respectively (17, 18), whereas that for a C—NH_2 is significantly higher, namely 10 kJ/mol (18). Thus, for the acid, rotation about the C_3 axis of the molecule appears very rapid, due to the very low barrier to rotation about the C—CO_2H bond, even though the CO_2H group is 'fixed'. By contrast the amine exhibits smaller values of σ since the barrier is sufficiently high to restrict rotation about the C—NH_2 bond. Levy and Terpstra (19) studied benzoic acid as a 1 *M* solution in $C_2D_4Cl_2$ and found a tumbling ratio of 4.5, whereas in the adamantane derivative the value in $CDCl_3$ is 25.5. The R_2 values for the two compounds are within 20%. The tumbling ratios differ because the barrier to rotation in Ar—CO_2H is significantly higher than in the aliphatic compound due to overlap between the π electrons of the aromatic ring and the acid group. Comparison of each of the adamantane derivatives presented here with the corresponding aromatic compounds (5) shows that the degree of anisotropy is less in the latter since each of the heterosubstituents studied have either *p* or π electrons which overlap with the π electron system of the aromatic ring and increase the barrier.

For a spherical molecule, tumbling is characterized by the isotropic correlation time τ_c which represents the average of the overall molecular motion. For a nonspherical molecule undergoing anisotropic motion overall molecular motion is characterized by τ_{eff} (9), the trace of the tensor of the correlation times about the three mutually perpendicular axes. Values of τ_{eff} can be calculated using

$$1/\tau_{eff} = (1/3)(1/\tau_a + 1/\tau_b + 1/\tau_c)$$

where $\tau_a = (6R_2)^{-1}$, $\tau_b = (5R_2 + R_1)^{-1}$, and $\tau_c = (2R_2 + 4R_1)^{-1}$. The calculated τ_{eff} values for each molecule are also included in Table 1 with a plot of τ_{eff} versus viscosity being illustrated in Fig. 2 for the bromo and hydroxy derivatives. For the bromo compound, the points lead to a reasonably straight line with the exception of acetone. For the OH group, a straight line is also obtained, but in this case it is CD_3OD which appears to be the exception. The value in CD_3OD is just outside the limits of experimental error. In a study of the T_1 values of the CH_3 carbons of *tert*-butyl alcohol as function of solvent, it was found (20) that $1/T_1$ gave an excellent correlation with viscosity for nonhydroxylated solvents whereas the points for H_2O, D_2O, CD_3OD, and $(CH_3)_3C$—OH were above the line with the deviation being more pronounced for H_2O and D_2O. This deviation was interpreted in terms of changes in solvent structure upon introduction of the *tert*-butyl alcohol molecules.

It may have been expected that R_1 would be

TABLE 1. T_1 and diffusion constant data for 1-substituted adamantanes

X	Solvent	Viscosity η (cP)	Volume[a]	T_1[b] β	γ	δ	Moment of inertia $I_{\|}$	$I_{\perp}$	ρ[c]	Diffusion constants[d] R_1	R_2	σ[e]	τ_{eff}[f]	τ_{eff}[g]/η
Br	CD_3OD	0.51	185	8.9	16.0	7.2	300	884	2.95	10.2	4.6	2.2	2.7	5.3
	C_6D_6	0.74	162	7.0	12.4	5.8				9.5	3.6	2.6	3.2	4.3
	$CDCl_3$	0.68	160	7.4	12.6	5.4				9.8	3.3	3.0	3.3	4.9
	CCl_4	1.16	189	6.8	11.6	5.1				8.6	3.1	2.8	3.6	3.1
	DMSO	1.95	163	5.4	9.4	4.2				6.6	2.7	2.5	4.4	2.2
	C_3D_6O	0.35	175	9.7	17.2	9.4				11.4	11.0	1.0	1.5	4.3
OH	CD_3OD	0.74	160	4.5	7.7	2.2	300	423	1.41	10.9	1.2	9.1	4.2	5.7
	$CDCl_3$	0.61	160	6.6	11.6	3.7				12.9	2.0	6.5	3.4	5.1
	CCl_4	0.83	176	5.6	10.2	3.3				12.2	1.7	7.2	3.6	4.3
	DMSO	2.05	168	4.4	7.2	2.4				8.5	1.3	6.7	5.1	2.5
	C_3D_6O	0.34	175	8.0	14.4	5.4				10.8	3.2	3.3	3.1	9.0
NH_2	CD_3OD	0.76	186	3.9	6.5	2.9	300	419	1.36	5.1	1.7	3.0	6.2	8.2
	$CDCl_3$	0.67	158	5.1	9.4	3.7				7.2	2.2	3.2	4.6	6.9
	CCl_4	0.89	172	9.1	16.4	8.2				8.4	5.7	1.5	2.6	2.9
CO_2H	CD_3OD	0.63	173	4.0	6.6	1.4	300	612	2.04	17.3	0.6	28	3.2	5.1
	$CDCl_3$	0.66	168	2.0	2.9	0.7				7.7	0.3	26	7.0	10.6
	C_6D_6	0.68	170	2.0	3.2	0.7				8.4	0.3	28	6.4	9.4
CH_2OH	$CDCl_3$	0.76	175	2.7	5.1	2.0	300	530	1.8	3.5	1.3	2.7	8.7	11.4

[a]Calculated apparent molar volume × 10^{-24} cm^3.
[b]In s ± 10% at 33 ± 1°C.
[c]$\rho = I_{\perp}/I_{\|}$.
[d]× 10^{10} s^{-1}.
[e]$\sigma = R_1/R_2$.
[f]× 10^{-11} s.
[g]× 10^{-9} cm^3 erg^{-1}.

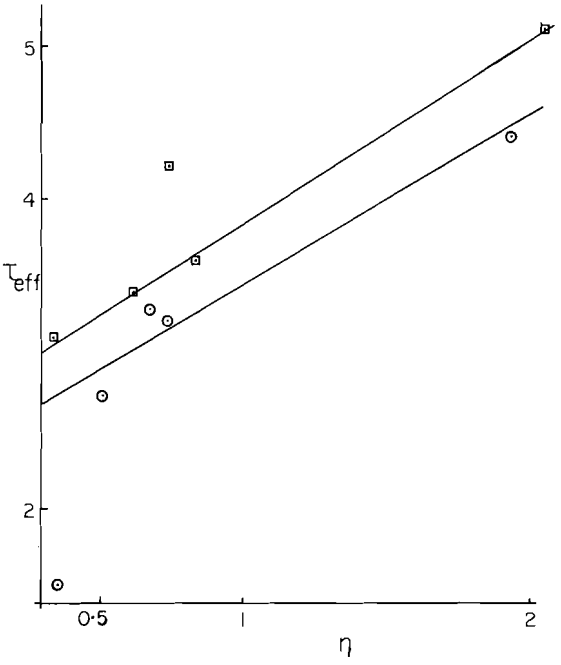

FIG. 2. Plot of $\tau_{eff} \times 10^{11}$ (s) versus viscosity, η (cP), for 1-bromoadamantane ○ and adamantan-1-ol □.

independent of the attached group, provided the barrier to rotation about the C—X bond is small, since the rotation being measured is that of the adamantanyl moiety. Inspection of the data shows that neither the value of R_1 nor R_2 is independent of X. If we examine CD_3OD as example, the values of R_2 (at the same viscosity) are 3.2, 1.2, and 0.6 × 10^{10} s^{-1} for Br, OH, and CO_2H, respectively, whereas the corresponding values for R_1 are 7.0, 11.4, and 17.3 × 10^{10} s^{-1}, i.e. when the diffusion constant about the non-principal axis is decreased there is a concomitant increase about the principal axis. The values of τ_{eff}/η are also given in Table 1. Inspection of these data with respect to solvent shows that (*a*) in CD_3OD, the values for Br, OH, and CO_2H have the same value within experimental error whereas that for NH_2 is significantly different; (*b*) in $CDCl_3$ the values for OH and Br are similar whereas those for NH_2 and CO_2H vary significantly; (*c*) in CCl_4 the values do not differ significantly; (*d*) in DMSO the values are within experimental error of one another whereas for benzene and acetone large deviations are observed. The difference in CD_3OD and $CDCl_3$ of the amine is due to the restriction of rotation about the C—NH_2 bond. The acid even in CD_3OD exists almost exclusively as the dimer (19). In $CDCl_3$ and benzene, the value of σ is the same as that obtained in CD_3OD whereas both R_1 and R_2 are smaller. These results suggest that the degree of association for the acid is significantly greater in the relatively non-polar solvents than in CD_3OD, i.e., the acid forms aggregates in non-polar solvents whose overall motion is less than the dimer.

The last entry in Table 1 differs from those described previously in that the C—X bond is no longer coincident with the principal axis of the molecule. The value of σ is 2.7 (cf. 6.5 for the 1-OH) and both R_1 and R_2 have decreased with the most dramatic decrease being that for R_1. The decrease in σ does not indicate that solvation or dimerization of the CH_2OH group relative to the OH group is less but rather that in the associated form, rotation about the C—O bond is significantly restricted. The molecules probably exist as dimers and if we consider the dimer as an ellipse then the relative rates based on volume would be predicted to be about 3:1 which is similar to the observed σ value of 2.7.

Experimental

All compounds used were obtained commercially and were studied without further purification. The T_1 data were obtained using a Bruker HX-90 spectrometer equipped with a Nicolet 1083 computer using the inversion recovery method as described previously (21). At least 15 t values were obtained for each carbon as well as a minimum of 4 S_∞ values. The T_1 values were then obtained using the standard least-squares plot of ln $(S(\infty) - S(t))$ versus time. The error limits are estimated at $\pm 10\%$, although the values were found to be reproducible to $\pm 5\%$. Recently Grant and co-workers (22) have shown that cross correlation terms can be important in the relaxation processes for CH_2 and CH_3 carbons and thus, treatment of the relaxation time data as a monoexponential can lead to errors in the calculated T_1 values. The consequences of this effect in the presented data should be a minimum in that our main interest is in the comparison of values and that all T_1 values were obtained from the same range of t values ($0.2T_1$ to $1.4T_1$). The T_1 data were then analysed by use of a computer program based on the equations of Woessner (9) for an axially symmetric ellipse. The program takes into account the relaxation contributions of all protons. Viscosities were measured using a Ubbelohde viscosimeter as described by Tuan and Fuoss (23).

Acknowledgments

The authors wish to express their appreciation to CNRC for generous financial support and to the "Cooperation Franco-Québécoise" for a "bourse post-doctorale" to one of us (R.M.).

1. R. A. Komoroski and G. C. Levy. J. Phys. Chem. **80**, 2410 (1976).
2. U. Edlund, C. Holloway, and G. C. Levy. J. Am. Chem. Soc. **98**, 5069 (1976).
3. A. Allerhand, D. Doddrell, and R. Komoroski. J. Chem. Phys. **55**, 189 (1971).
4. J. R. Lyerla and G. C. Levy. Top. Carbon-13 NMR Spectrosc. **1**, 79 (1974) and references cited therein.
5. G. C. Levy, J. D. Cargioli, and F. A. L. Anet. J. Am. Chem. Soc. **95**, 1528 (1973).
6. S. Berger, F. R. Kneissl, D. M. Grant, and J. D. Roberts. J. Am. Chem. Soc. **97**, 1805 (1975).
7. R. Somorjai and R. Deslauriers. J. Am. Chem. Soc. **98**, 6460 (1976).
8. T. D. Alger, D. M. Grant, and J. R. Lyerla. J. Phys. Chem. **75**, 2539 (1971).
9. D. E. Woessner. J. Chem. Phys. **37**, 647 (1962).
10. A. Einstein. Investigation on the theory of the Brownian motion. Dover, New York, NY. 1956. pp. 19–34.
11. A. Gierer and K. Wirtz. Naturforsch. A, **8**, 532 (1953).
12. J. A. Classel. J. Am. Chem. Soc. **91**, 4569 (1969).
13. K. F. Kuhlmann, D. M. Grant, and R. K. Harris. J. Chem. Phys. **52**, 3439 (1970).
14. F. J. Bartoli and T. A. Litovitz. J. Chem. Phys. **56**, 404 (1972); **56**, 413 (1972).
15. S. Grandjean and P. Laszlo. Mol. Phys. **30**, 413 (1975).
16. E. V. Ivash and D. M. Dennison. J. Chem. Phys. **21**, 1804 (1953).
17. W. Tabor. J. Chem. Phys. **27**, 974 (1957).
18. T. Nishikawa, T. Itoh, and K. Shimoda. J. Chem. Phys. **23**, 1735 (1955).
19. G. C. Levy and D. Terpstra. Org. Magn. Reson. **8**, 658 (1976).
20. O. W. Howarth. J. Chem. Soc. Faraday Trans. 2303 (1975).
21. J. W. ApSimon, H. Beierbeck, and J. K. Saunders. Can. J. Chem. **53**, 338 (1975).
22. L. C. Werbelow and D. M. Grant. Can. J. Chem. **55**, 1558 (1977).
23. D. F. T. Tuan and R. M. Fuoss. J. Phys. Chem. **67**, 1343 (1963).

The reaction of methylene radicals with methyl isocyanide

MARSHA T. J. GLIONNA AND HUW O. PRITCHARD
Chemistry Department, York University, Downsview, Ont., Canada M3J 1P3

Received October 10, 1978

MARSHA T. J. GLIONNA and HUW O. PRITCHARD. Can. J. Chem. **57**, 1229 (1979).

An exploratory study has been made of the gas-phase reactions of methylene radicals, generated by the photolysis of ketene near 3000 Å, with methyl, ethyl, and allyl isocyanides at room temperature.

With methyl isocyanide, the principal product at low pressure is ethyl cyanide, together with a few percent of methyl cyanide; ethyl isocyanide is also formed, increasingly so as the total pressure is increased. Reaction appears to take place through a vibrationally excited ethyl isocyanide intermediate, and approximate rate constants for each reaction pathway are derived. Isotopic studies suggest that the methylene radicals insert in the H_3C—NC bond of the methyl isocyanide.

MARSHA T. J. GLIONNA et HUW O. PRITCHARD. Can. J. Chem. **57**, 1229 (1979).

On a effectué une étude préliminaire des réactions en phase gazeuse des radicaux méthylènes, produits par photolyse d'un cétène près de 3000 Å, avec des isocyanures de méthyle, d'éthyle ou d'allyle à température ambiante.

Avec l'isocyanure de méthyle, à basse pression, le produit principal est le cyanure d'éthyle avec un faible pourcentage de cyanure de méthyle; il se forme aussi de l'isocyanure d'éthyle dont la quantité augmente avec l'augmentation de la pression. Il semble que la réaction se produise grâce à un intermédiaire vibrationnellement excité de l'isocyanure d'éthyle; on a évalué les constantes de vitesse approximatives de chacune des voies de réaction. Des études isotopiques suggèrent que les radicaux méthylènes s'insèrent dans la liaison H_3C—NC de l'isocyanure de méthyle.

[Traduit par le journal]

Introduction

In a recent series of chemical activation studies, Rabinovitch and co-workers (1–3) have generated vibrationally excited molecules in which there are two (almost isoenergetic) pathways for decomposition, in competition with collisional stabilisation. It would be interesting to extend this kind of approach to the study of a vibrationally excited molecule which could decompose by two reaction paths having *very* different critical energies. For example, vibrationally excited cyclopropyl isocyanide could isomerise to allyl isocyanide at excitation energies greater than about 60 kcal mol^{-1} and to cyclopropyl cyanide at excitation energies greater than about 40 kcal mol^{-1}; isomerisation of both functional groups is also possible. Unfortunately, the production of vibrationally excited cyclopropyl isocyanide molecules by addition of methylene radicals to vinyl isocyanide is not feasible because vinyl isocyanide is rather unstable, both to visible light and with respect to spontaneous polymerisation (4). Consequently, despite the fact that more isomerisation pathways exist, we undertook to explore the homologous reaction, methylene radicals plus allyl isocyanide, in search of the same kind of information. However, although the expected range of mass 81 cyanides and isocyanides was observed, and their relative proportions varied with the total pressure, detailed identification of each product was not pursued because, unexpectedly, the major product of the reaction was allyl cyanide. Since allyl cyanide was not formed photochemically from allyl isocyanide under our conditions, we undertook the study reported below to try to elucidate the nature of this catalysed isomerisation. In view of the tentative conclusion reached, that the principal reaction of methylene radicals with saturated isocyanide molecules is to insert in the R—NC bond, the proposed study of methylene radicals with allyl isocyanide appears to be rather intractable because some of the same reaction products may arise both from the addition to the double bond and from the insertion into the allyl—NC bond. We now proceed to present evidence for this insertion of methylene radicals into the R—NC bond, where R is methyl, and also some circumstantial evidence for the same process when R is ethyl.

Experimental

Methyl, ethyl, *n*-propyl, *s*-propyl, and allyl isocyanides were prepared from the appropriate *N*-alkyl formamide by the method of Casanova, Schuster, and Werner (5); except in the case of *N*-methyl formamide which was obtained commercially, the other *N*-alkyl formamides were prepared from ethyl formate and the corresponding amine by standard methods

0008-4042/79/101229-04$01.00/0

(6). Each isocyanide was purified by vapour-phase chromatography.

Methyl, ethyl, *n*-propyl, *s*-propyl, and allyl cyanides, used for identification and calibration purposes, were obtained commercially.

Ketene was prepared by the pyrolysis of acetic anhydride vapour at 400°C (7), and after separation by trap-to-trap distillation, was stored at liquid nitrogen temperature; the liquid was degassed each time before use. Dideuterioketene (CD_2CO) was prepared in an analogous manner from 99% acetic anhydride-d_6, obtained from Merck, Sharp and Dohme.

Photolysis experiments were conducted at room temperature in a 500 mL Pyrex glass vessel, using the unfiltered light from a 100 W high-pressure mercury lamp; during the filling of the reaction vessel and the analysis of the products, it was necessary to avoid condensing isocyanide and ketene together in liquid nitrogen, as they react immediately under these conditions. Products were identified by gas chromatography (using a Pennwalt 223 column at 70°C) coupled with mass spectrometry.

Results and Discussion

Our initial supposition was that methylene radicals, which commonly insert into C—H bonds in organic molecules (8), would react with methyl isocyanide to form a vibrationally hot ethyl isocyanide molecule.

[1] $$CH_2 + CH_3NC \rightarrow [C_2H_5NC]^*$$

This excited molecule would then isomerise to ethyl cyanide

[2] $$[C_2H_5NC]^* \xrightarrow{k_1} C_2H_5CN$$

at a rate which can be estimated according to unimolecular reaction theory (9), or be stabilised collisionally

[3] $$[C_2H_5NC]^* + M \xrightarrow{k_2} C_2H_5NC + M$$

Thus, the relative rates of formation of cyanide and isocyanide should obey the simple form

[4] $$R_{EtCN}\,[M]/R_{EtNC} = k_1/k_2 = \text{constant}.$$

At low pressures (5–10 Torr of methyl isocyanide, 1–5 Torr of ketene), the reaction product was almost exclusively ethyl cyanide, with small amounts of methyl cyanide and hydrogen cyanide amounting, respectively, to about 10% and 1% of the total product. Increasing the total pressure of the system by addition of up to 600 Torr of argon or nitrogen led to small but increasing yields of ethyl isocyanide; qualitatively, at least, this is consistent with the reaction scheme proposed above.

Likewise, the reaction of methylene radicals with ethyl isocyanide gives significant quantities of *n*-propyl cyanide and *n*-propyl isocyanide, but only minute traces of *s*-propyl cyanide and *s*-propyl isocyanide. Neither methyl cyanide nor ethyl cyanide reacts with methylene radicals, nor are any of the cyanides or isocyanides affected by the photolysis lamp in the absence of ketene (cf. also refs. 10 and 11 for more extensive information on the photochemical reactions of methyl isocyanide).

Returning to the reaction of methylene radicals with methyl isocyanide, the relative variations of the yields of ethyl cyanide and ethyl isocyanide can be shown to be consistent with the reaction scheme [1]–[3], at least semiquantitatively. Because of the need to avoid condensing reactant or product mixtures in liquid nitrogen, and because of the relatively high pressures of argon required to produce significant quantities of ethyl isocyanide, we chose simply to study the variation of product yields with varying ketene pressure at fixed isocyanide pressure, realising that this procedure is somewhat unconventional and very inefficient in the use of methylene radicals. Table 1 gives a summary of the results of four experiments carried out at different ketene pressures, but otherwise performed under the same conditions. It is clear that, in the penultimate column of this table, the relationship [4] holds quite well. If we assume collision diameters of 4.5 and 5.5 Å respectively for CH_2CO and $[C_2H_5NC]^*$, the appropriate collision number $Z = 4 \times 10^{-10}$ cm^3 molecule^{-1} s^{-1} at room temperature. We may also assume (9) that the rate constant for deactivation of vibrationally excited ethyl isocyanide, i.e. k_2, is 0.1 times the collision rate constant Z, whence the data in Table 1 give k_1 as approximately $2.2_5 \times 10^{10}$ s^{-1}.

By using the following thermochemical data (all relating to the gas phase at room temperature)

$$\Delta H_f(CH_3NC) \simeq 41 \text{ kcal mol}^{-1} \quad (12)$$

$$\Delta H_f(CH_2) \simeq 92 \text{ kcal mol}^{-1} \quad (13)$$

$$\Delta H_f(C_2H_5CN) \simeq 12 \text{ kcal mol}^{-1} \quad (14)$$

the overall reaction

[5] $$CH_3NC + CH_2 \rightarrow C_2H_5CN$$

is approximately 121 kcal mol^{-1} exothermic, and since the ΔH for isomerisation of ethyl isocyanide is about -22 kcal mol^{-1} (12, 15), this indicates that the newly formed ethyl isocyanide molecule in reaction [1] contains about 99 kcal mol^{-1} of internal energy. We may then estimate the rate constant k_1 for the isomerisation of such an excited molecule (16), treated as a collection of Morse oscillators[1] and rigid rotors with kinetic and spectroscopic properties as tabulated in ref. 9, to be approximately 4.1×10^{10} s^{-1}. We conclude that in view of both the uncertainties in the theoretical model and in the experimental method, the proximity of this figure to

[1]Alternatively, in the harmonic-oscillator rigid-rotor approximation, the estimated value would be about 6×10^{10} s^{-1} (16).

TABLE 1. Relative rates of formation of products in the reaction of methylene radicals with methyl isocyanide at room temperature

P_{CH_2CO} (Torr)	P_{total} (Torr)	R_{EtCN}/R_{EtNC} ($\equiv R$)	R_{MeCN}/R_{EtNC} ($\equiv R'$)	$P_{total} \times R$ ($\times 10^{-3}$)	$P_{total} \times R'$ ($\times 10^{-3}$)
590	595	28.8	(0.5)	17.2	—
305	310	54.9	(1.7)	17.1	—
152	157	124	7.9	19.5	1.2
80	85	192	16.0	16.3	1.4

our experimentally derived value of about 2×10^{10} s^{-1} lends support to our interpretation of the experimental process.

The last column in Table 1 may suggest that the ratio $R_{MeCN}[M]/R_{EtNC}$ is also constant, if one acknowledges the fact that at high pressures, the yield of methyl cyanide is too small to be measured accurately on the tail of the methyl isocyanide peak: thus, it appears that at these energies, there could be another reaction channel available

$$[6] \qquad [C_2H_5NC]^* \xrightarrow{k_3} CH_3CN + CH_2$$

with $k_3 \sim 1.7 \times 10^9$ s^{-1}. This would imply that at very high temperatures, the thermal decomposition of ethyl isocyanide should yield small amounts of methyl cyanide, as well as the normal product ethyl cyanide; methyl isocyanide would also be formed by the reverse of reaction [1], but would not live long enough to be detected by conventional kinetic techniques.[2] At the same time, at these high temperatures, one would expect the formation of large quantities of hydrogen cyanide, since this is a major product in the conventional pyrolysis of ethyl cyanide (17, 18); however, in our reaction, the yield of hydrogen cyanide was only of the order of 10–20% of that of the methyl cyanide, and we were unable to estimate a rate constant for the postulated third channel

$$[7] \qquad [C_2H_5NC]^* \rightarrow HCN + C_2H_4$$

The observations described so far are not inconsistent with the proposed reaction scheme [1]–[3], but they do not shed any light on the nature of the addition process [1], neither in respect of the site of attack nor in respect of the degree of excitation of the methylene radical involved. The addition of small quantities of air or oxygen to our reaction mixtures, commonly used (1, 2) to ensure that only singlet methylene radicals undergo reaction, suppressed the formation of all the products noted above. However, in view of the high reactivity of isocyanides in general (19) and the incipient free-radical nature of the proposed adduct $[C_2H_5NC]^*$, we do not feel that this observation is decisive, one way or the other. Thus, although we have been unable to demonstrate conclusively that we observed the reactions of *singlet* methylene radicals, the high pressures used in Table 1 would tend to support that assumption. However, from the mass-spectroscopic evidence we now describe, it appears to be reasonably certain that the overall addition process [1] may be regarded as an insertion into the R—NC bond rather than an insertion into a C—H bond, as is usually observed (8).

Using dideuterioketene as the source of radicals, samples of ethyl cyanide and methyl cyanide taken from low-pressure runs, and a sample of ethyl isocyanide taken from a high-pressure run, were subjected to mass-spectroscopic examination. These experiments show that (*i*) the ethyl cyanide and ethyl isocyanide formed both contain two D atoms as expected; (*ii*) the cracking patterns of these molecules show fairly unambiguously that the CD_2 radical inserts into the H_3C—NC bond: in the first place, mass peaks are present at $m/e = 42$ (CD_2CN^+) and 40 ($CDCN^+$ or CH_2CN^+), but there is no peak at $m/e = 41$ ($CHDCN^+$); moreover, there is a strong peak at $m/e = 15$ (CH_3^+), but nothing above background at mass values of 16 (CH_2D^+) or 17 (CD_2H^+). This conclusion is also supported by the absence of *s*-propyl products in the reaction of methylene radicals with ethyl isocyanide, as noted above; (*iii*) the methyl cyanide formed in the CD_2-labelled reaction [6] contains no deuterium atoms.

Acknowledgements

This work was supported by the National Research Council of Canada, and we would also like to acknowledge the benefit of considerable assistance from Drs. J. L. Collister, B. H. Khouw, and M. H. B. Vayjooee.

1. J. D. RYNBRANDT and B. S. RABINOVITCH. J. Phys. Chem. **75**, 2164 (1971).
2. J. F. MEAGHER, K. J. CHAO, J. R. BARKER, and B. S. RABINOVITCH. J. Phys. Chem. **78**, 2535 (1974).

[2]In this respect, it is interesting to note that the simple photolysis, under our conditions, of an unpurified commercial sample of ethyl cyanide gave small amounts of methyl cyanide, methyl isocyanide, and ethyl isocyanide, presumably through photosensitisation by an unknown impurity to form a hot ethyl cyanide molecule.

3. A. N. Ko, B. S. Rabinovitch, and K. J. Chao. J. Chem. Phys. **66**, 1374 (1977).
4. D. S. Matteson and R. A. Bailey. J. Am. Chem. Soc. **90**, 3761 (1968).
5. J. Casanova, R. E. Schuster, and N. D. Werner. J. Chem. Soc. 4280 (1963).
6. H. E. Baumgarten (*Editor*). Organic syntheses, collected volume 5. John Wiley, New York. 1973. p. 301.
7. P. G. Blake and A. Speis. J. Chem. Soc. Perkin II, 1879 (1974).
8. H. M. Frey. Prog. Reaction Kinet. **2**, 131 (1964).
9. A. W. Yau and H. O. Pritchard. Can. J. Chem. **56**, 1389 (1978).
10. D. H. Shaw and H. O. Pritchard. J. Phys. Chem. **70**, 1230 (1966).
11. J. T. Knudston and M. J. Berry. J. Chem. Phys. **68**, 4419 (1978).
12. M. H. B. Vayjooee, J. L. Collister, and H. O. Pritchard. Can. J. Chem. **55**, 2634 (1977).
13. JANAF Thermochemical Tables, Second Edition, National Bureau of Standards, Washington, DC. 1971.
14. D. R. Stull, E. F. Westrum, and G. C. Sinke. The chemical thermodynamics of organic compounds. John Wiley, New York. 1969.
15. P. Lemoult. C. R. Acad. Sci. Paris, **149**, 1602 (1909).
16. A. W. Yau. Unpublished results.
17. M. Hunt, J. A. Kerr, and A. F. Trotman-Dickenson. J. Chem. Soc. 5074 (1965).
18. P. N. Dastoor and E. U. Emovon. Can. J. Chem. **51**, 366 (1973).
19. D. H. Shaw and H. O. Pritchard. Can. J. Chem. **45**, 2749 (1967).

Chromium exchange between chromium(II) and benzylchromium(III) ions

M. PARRIS

Chemistry Department, Carleton University, Ottawa, Ont., Canada K1S 5B6

AND

A. W. ASHBROOK

Eldorado Nuclear Ltd., 400-255 Albert St., Ottawa, Ont., Canada K1P 5G8

Received August 8, 1978

M. PARRIS and A. W. ASHBROOK. Can. J. Chem. **57**, 1233 (1979).

The rate of first-order hydrogen-ion independent chromium isotope exchange between benzylchromium(III) and chromium(II) ions is $1.2 \times 10^{-2}\ M^{-1}\ s^{-1}$ at 0°C in a 70% methanol–water solvent, $\Delta S^{\ddagger} = -28.5$ eu, $\Delta H^{\ddagger} = 10.3$ kcal M^{-1}. For the corresponding exchange between benzylchromium(III) and *p*-chlorobenzylchromium(III) ions, these figures are $1.2 \times 10^{-3}\ M^{-1}\ s^{-1}$, −32.2 eu, and 10.9 kcal M^{-1}.

M. PARRIS et A. W. ASHBROOK. Can. J. Chem. **57**, 1233 (1979).

La vitesse du premier ordre de l'échange isotopique du chrome, indépendante des ions hydrogène, du benzylchrome(III) et du chrome(II) est égale à $1.2 \times 10^{-2}\ M^{-1}\ s^{-1}$ à 0°C dans un solvant à 70% méthanol/eau; le $\Delta S^{\ddagger} = 28.5$ ue et le $\Delta H^{\ddagger} = 10.3$ kcal M^{-1}. Pour l'échange correspondant entre les ions benzylchrome(III) et *p*-chlorobenzylchrome(III), ces valeurs sont respectivement $1.2 \times 10^{-3}\ M^{-1}\ s^{-1}$, −32.2 ue et 10.9 kcal M^{-1}.

[Traduit par le journal]

It has been suggested (1) that the mixed coupling upon reduction of mixed organic halides by chromous ion results from an inner sphere exchange,

[1] Benzyl Cr^{2+} + *benzyl halide

$$\rightleftharpoons \text{Benzyl halide} + \text{*benzyl } Cr^{2+}$$

occurring simultaneously with a coupling sequence,

[2] Benzyl Cr^{2+} + *benzyl halide

$$\rightleftharpoons \text{Benzyl *benzyl} + \text{halo } Cr^{2+}$$

The extent to which these two reactions occur together leads to the postulate that similar intermediates are involved in both reactions (2), in particular a four-centred transition state for the coupling reaction,

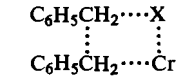

kinetically indistinguishable from that for the exchange,

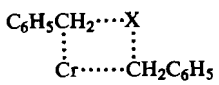

Evidence for the former transition state was apparently obtained when an optically-active *threo*-2,3-diphenylbutane resulted from the reduction of the α-phenethylchloride (2). It was of interest to determine the extent of exchange between two different benzylchromium(III) species: the more symmetric analogue of reactions [1] and [2],

[3] *Benzyl Cr^{2+} + benzyl *Cr^{2+} ⇌

$$\text{*Benzyl *}Cr^{2+} + \text{benzyl } Cr^{2+}$$

in order to assess the more symmetric four-centred transition state,

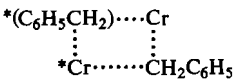

Experimental Section

Materials

Chromium(III) perchlorate stock solution was prepared from potassium dichromate, perchloric acid solutions by reduction with either ethanol or formic acid, and used to prepare chromium(II) solutions by reduction with zinc amalgam. The chromous solutions were always prepared immediately prior to their use, and always contained at least half as many gram-ions of Zn(II) as Cr(II).

^{51}Cr tracer was obtained from Atomic Energy of Canada Ltd. as a solution of sodium chromate. The tracer was added to an aliquot of the potassium dichromate and fumed with perchloric acid to remove any chloride.

1,1-Dimethyl-2-phenethylethanol (Eastman) was distilled, bp 62–64°C (1.5 mm), benzyl bromide (Eastman), 1,1-dimethyl-2-(*p*-chlorophenyl)ethanol, *p*-bromobenzyl bromide, *p*-methylbenzyl bromide, and *p*-methoxybenzyl bromide (Aldrich) were used without further purification.

Ion-exchange resin, Dowex 50-X2 and 50-X8, 100–200 mesh (Baker) was pretreated as follows: after removal of the fine material the remaining resin was warmed with a dilute alkaline solution of hydrogen peroxide, washed with dilute hydrochloric acid and then with water, and stored under 1 *m* perchloric acid.

*1,1-Dimethyl-2-(*p*-chlorophenyl)ethyl Hydroperoxide*

This was prepared by an adaptation of the method for 1,1-dimethyl-2-phenylethyl hydroperoxide (1). ***The preparation is***

0008-4042/79/101233-05$01.00/0

hazardous. Recrystallization from petroleum ether gave white needles, mp 51–52°C, yield 28%. Analysis by ceric titration showed greater than 99.5% hydroperoxide.

Apparatus

Ion-exchange columns were jacketted at 0°C. A well-type NaI crystal (1 × 1.5 in.) was used as a scintillation detector. Provision was made for continuous monitoring of the column eluate, fraction collection, and counting of individual samples. A Beckman model B spectrophotometer was used for chromium analyses on the column eluate.

Analysis

Chromium(II) concentrations were determined by ferric oxidation and ceric back-titration. Free acid was determined, after oxidation of any chromium(II) present, by passing an aliquot through an ion exchange column in the hydrogen ion form. Total chromium was determined spectrophotometrically at 372 nm, as chromate (3) after alkaline oxidation with hydrogen peroxide (4). The main chromium species (see Fig. 1*A*) separated from an exchange between benzylchromium(III) and chromium(II) ions, quenched by ferric ammonium sulphate, was found to be a sulphatochromium(III) ion plus a small (< 5%) amount of a disulphatochromium(III) ion, in addition to the hexaaquochromium(III) ion initially present. The sulphato complexes were identified by spectra (6) and by $CrSO_4$ analyses on the separated fractions. No ligated ethanol was found even when the benzylchromium(III) ion had been prepared originally in 90 vol.% ethanol–water at 0°C. Visually, oxidation of chromium(II) ion by ferric ammonium sulphate did not appear to be slower than by ferric perchlorate for which $k = 2 \times 10^3\ M^{-1}\ s^{-1}$ at 25°C, and the lack of ligated ethanol must reflect discrimination by chromium(II) ion against ethanol. Ethanol, bound and unbound, associated with chromic species was determined by the method of Kemp and King (5).

Determination of Rate Constants

1. Oxidation of Cr(II), Spectrophotometric Method

Solvent was measured into the capped, thermostatted cell and the appropriate reagent introduced by means of a hypodermic syringe.

2. Isotope Exchange Reactions

The general procedure used was as follows.

Exchange between Benzylchromium(III) Ion and Chromium(II) Ion

1,1-Dimethyl-2-phenethyl hydroperoxide or benzyl halide and solvent were nitrogen-flushed in a capped vessel. A stoichiometric quantity of chromium(II) perchlorate solution was added to produce the benzylchromium(III) ion. A known amount of labelled chromium(II) perchlorate solution was added and after a time the exchange was quenched by addition of a slight excess (2%) of oxygen-free ferric solution before injection of an aliquot into the ion-exchange column. The eluate activity was continuously monitored and Fig. 1 shows typical records obtained. In experiments in which ferric ammonium sulphate was used as the quenching reagent, the column was eluted initially with 1 *m* perchloric acid for the chromic sulphate species and then with 2 *m* perchloric acid for, first, the hexaquochromium(III) and, later, the benzylchromium(III) ion. In the case of ferric perchlorate quenching, 2 *m* perchloric acid was used throughout.

Exchange between Benzylchromium(III) Ion and p-Chlorobenzylchromium(III) Ion

Unsubstituted benzylchromium(III) ion was prepared from labelled chromium(II) ion and an aliquot of the unlabelled species injected into the labelled solution. After the required exchange time, an aliquot of the mixture was treated as before.

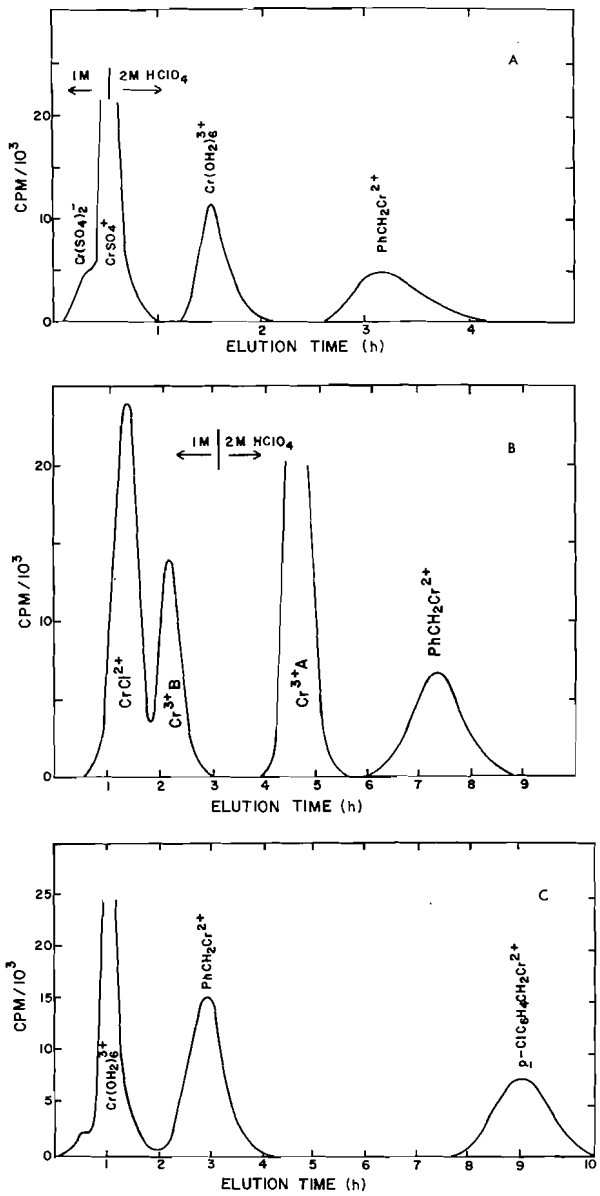

FIG. 1. (*A*) Elution of ^{51}Cr-containing species in the exchange between benzylchromium(III) and chromium(II) ions. (*B*) Elution of ^{51}Cr-containing species in the reaction between benzylchromium(III) ion and benzylchloride. (*C*) Elution of ^{51}Cr-containing species in the exchange between benzylchromium(III) and *p*-chlorobenzylchromium(III) ions.

Exchange between Benzylchromium(III) Ion and Hexaquochromium(III) Ion

The same general procedure was used, the labelled species being hexaaquochromium(III) ion.

3. Oxidation of Cr(II), Ion-exchange Method

In many cases it proved convenient to use an adaptation of the isotope exchange method in order to study the reaction

TABLE 1. Cr exchange between benzylchromium(III) and chromium(II) in 70 vol.% methanol – water

Exchange time (min)	Temperature (°C)	[Cr(II)] × 10^2	[$B_zCr(III)$]^a × 10^2	[$LiClO_4$]	[$HClO_4$]	k (M^{-1} s^{-1} × 10^2)
1	0	1.30	5.00	0.4	0.3	1.0_5
2	0	1.30	5.00	0.4	0.3	1.1_3
5	0	1.30	5.00	0.4	0.3	1.1_7
10	0	1.30	5.00	0.4	0.3	1.2_5
20	0	1.30	5.00	0.4	0.3	1.1_9
30	0	1.30	5.00	0.4	0.3	1.1_8
45	0	1.30	5.00	0.4	0.3	1.1_9
60	0	1.30	5.00	0.4	0.3	1.1_8
120	0	1.30	5.00	0.4	0.3	—
15	0	2.72	3.84	0.4	0.3	1.1_9
30	0	4.40	3.87	0.4	0.3	1.2_5
60	0	1.10	1.22	0.4	0.3	1.0_8
10	0	1.10	1.22	0.4	0.3	1.0_9
15	0	1.10	1.22	0.4	0.3	1.0_8
15	0	6.48	2.52	0.4	0.3	1.1_9
15	0	6.48	2.52	0.4	0.3	1.2_2
30	−10	6.35	2.52	0.4	0.3	0.51
30	−10	6.35	2.52	0.4	0.3	0.49
15	5	6.48	2.52	0.4	0.3	1.6_3
15	5	6.48	2.52	0.4	0.3	1.6_1
15	10	6.50	2.52	0.4	0.3	2.2_1
20	10	6.50	2.52	0.4	0.3	2.3_2
20	10	1.33	5.00	0.4	0.2	1.9_5
15	0	2.52	6.48	0.2	0.9	1.3_8
15	0	2.52	6.48	0.4	0.3	1.1_9
15	0	2.52	6.48	0.4	0.8	1.4_3
15	0	2.52	6.48	0.7	0.4	1.4_4
15	0	2.52	6.48	0.8	0.3	1.4_1
15	0	2.52	6.48	0.4^b	0.3	0.77

^{a}The benzylchromium(III) was prepared from $C_6H_5CH_2C(CH_3)_2OOH$ and thus there was present also an equivalent amount of $Cr(III)(H_2O)_6$.
^{b}Contains additionally 0.1 M LiCl.

between benzylchromium(III) ion and the benzyl halides. Labelled benzylchromium(III) ion was prepared from 1,1-dimethyl-2-phenylethyl hydroperoxide and labelled Cr(II), mixed with the benzyl halide, and used in ion-exchange chromatography as before.

Results and Discussion

Exchange Reactions

The rate R at which a chromium(III) species exchanges with chromium(II) follows the McKay exponential function

$$R = -\frac{[Cr(III)][Cr(II)]}{[Cr(III)] + [Cr(II)]} \frac{\ln(1 - F)}{t}$$

F is the extent to which distribution of the label between chromium species approaches the equilibrium value of 1 and, where the Cr(III) is originally inactive, is given by

$$F = \frac{S_{Cr(III)}{}^t}{S_{Cr(III)}{}^\infty} = \frac{S_{Cr(II)}{}^0 - S_{Cr(II)}{}^t}{S_{Cr(II)}{}^0 - S_{Cr(II)}{}^\infty}$$

$S_x{}^t$ being the specific activity of species x at time t.

For a second-order exchange rate

$$R = k\,[Cr(III)][Cr(II)]$$

Table 1 contains data for the exchange between benzylchromium(III), $B_zCr(III)_{aq}{}^{2+}$, and chromium(II), $Cr_{aq}{}^{2+}$, ions at various temperatures, acid and salt concentrations.

The exchange

[4] $B_zCr(III)_{aq}{}^{2+} + {}^*Cr(II)_{aq}{}^{2+} \rightleftharpoons B_z{}^*Cr(III)_{aq}{}^{2+} + Cr(II)_{aq}{}^{2+}$

could perhaps result from the successive reactions

[5] $Cr(III)_{aq}{}^{3+} + {}^*Cr(II)_{aq}{}^{2+} \rightleftharpoons {}^*Cr(III)_{aq}{}^{3+} + Cr(II)_{aq}{}^{2+}$

[6] $B_zCr(III)_{aq}{}^{2+} + {}^*Cr(III)_{aq}{}^{3+} \rightleftharpoons B_z{}^*Cr(III)_{aq}{}^{2+} + Cr(III)_{aq}{}^{3+}$

since hexaaquochromium(III) ion, $Cr(III)_{aq}{}^{3+}$, is present, formed coincidentally with the benzylchromium(III) species. However, the rate constant for reaction [5] is $\leq 2 \times 10^{-5}\ M^{-1}\ s^{-1}$. For reaction [6] the exchange rate in 70 vol.% methanol – water at 0°C, $[B_zCr(III)^{2+}] = 2.0 \times 10^{-2}\ m$, $[Cr(III)_{aq}{}^{3+}] = 5.0 \times 10^{-2}\ m$ was found to be very slow; after 1.5 h practically no exchange had occurred and an upper limit for the rate constant is calculable,

$\leq 3 \times 10^{-5}\ M^{-1}\ s^{-1}$. The average rate constant for reaction [4] at 0°C is $1.2_2 \times 10^{-2}\ M^{-1}\ s^{-1}$, $\Delta S^{\ddagger} = -28.5 \pm 1.1$ eu, and $\Delta H^{\ddagger} = 10.3 \pm 0.3$ kcal mol^{-1}.

Figure 1*B* illustrates how two apparently distinct chromium(III) species (Cr_A^{3+} and Cr_B^{3+}) are produced in the reaction between benzylchromium(III) ion and various benzyl halides. The rate of increase of $[Cr_B^{3+}]$ followed the rate of increase of $[CrX^{2+}]$, the initial product of reduction of the benzyl halide, $C_6H_5CH_2X$, by the chromous ion. When the reaction was allowed to proceed after complete decomposition of the benzylchromium(III) ion, $[Cr_B^{3+}]$ increased, $[CrX^{2+}]$ decreased, and $[Cr_A^{3+}]$ remained virtually unchanged. It is concluded that Cr_B^{3+} results from aquation of CrX^{2+} and Cr_A^{3+} from the original oxidation of chromium(II) ion by 1,1-dimethyl-2-phenylethyl hydroperoxide. The Cr_A^{3+} was identified as $Cr(III)(H_2O)_6^{3+}$ by its absorption spectrum, λ_{max} 407 and 573 nm (5). Determination of bound ethanol in the Cr_B^{3+} species on the other hand showed 0.5 to 0.8 mol ethanol per atom Cr.

Rate constants for exchange between two different benzylchromium species (see Fig. 1*C* and eq. [3], *benzyl = *p*-chlorobenzyl)

[7] $(B_z)Cr(III)_{aq}^{2+} + (p\text{-}ClB_z)^*Cr(III)_{aq}^{2+} \rightleftharpoons (B_z)^*Cr(III)_{aq}^{2+} + (p\text{-}ClB_z)Cr(III)_{aq}^{2+}$

were found to vary significantly with the ion elution-rate owing to that reaction which had occurred after injection into the ion-exchange column yet prior to separation thereon. There is no obvious way to arrest this exchange; however, at constant elution-rate the log $(1 - F)$ plots are linear with a $t = 0$ intercept less than 1. The unit intercept is restored by shifting the plot ca. 1/2 h, indicative of a reasonably constant separation time. At 0°C the half-time for exchange was typically ca. 4 h and the rate constant for reaction [7] was found to be $1.2 \times 10^{-3}\ M^{-1}\ s^{-1}$, $\Delta S^{\ddagger} = -32.2 \pm 1.6$ eu and $\Delta H^{\ddagger} = 10.9 \pm 0.3$ kcal mol^{-1}.

The reactions between benzylchromium and benzyl halides were studied at temperatures between 0 and 25°C, Table 2, and the rate of disappearance of benzylchromium monitored spectrophotometrically at 360 nm. For example

[8] $PhCH_2Cr_{aq}^{2+} + PhCH_2Br \rightarrow$ Products

[8*A*] $PhCH_2Cr_{aq}^{2+} + PhCH_2Cl \rightarrow$ Products

[9] $PhCH_2Cr_{aq}^{2+} + p\text{-}BrC_6H_4CH_2Br \rightarrow$ Products

Reaction [8] implies and includes the sequence:

[10] $PhCH_2C(CH_3)_2OOH + 2Cr_{aq}^{2+} \xrightarrow{k_1} PhCH_2Cr_{aq}^{2+} + (CH_3)_2CO + Cr_A^{3+}$

TABLE 2. Exchange rates between some substituted benzylchromium(III) and chromium(II) ions at 0°C[a]

[Species] × 10²		[Cr²⁺] × 10²	$k(M^{-1}s^{-1}) \times 10^2$
$C_6H_5CH_2Cr^{2+}$	2.52	6.48	1.20[e]
$p\text{-}BrC_6H_4CH_2Cr^{2+}$[b]	2.50	6.52	1.06
$p\text{-}MeC_6H_4CH_2Cr^{2+}$[c]	2.88	6.95	1.05
$p\text{-}MeOC_6H_4CH_2Cr^{2+}$[d]	2.28	6.85	1.11

[a] $[LiClO_4] = 0.4$, $[H^+] = 0.3$, 70 vol.% methanol – water.
[b] From *p*-Brbenzylbromide.
[c] From *p*-Mebenzylbromide.
[d] From *p*-MeObenzylbromide.
[e] Data from Table 1.

[11] $PhCH_2Cr_{aq}^{2+} + H_3O^+ \xrightarrow{k_2} PhCH_3 + Cr_A^{3+}$

[12] $PhCH_2Cr_{aq}^{2+} + PhCH_2Br \xrightarrow{k_3} PhCH_2CH_2Ph + CrBr_{aq}^{2+}$

[13] $CrBr_{aq}^{2+} \xrightarrow{k_4} Cr_B^{3+} + Br^-$

Reaction [9] implies and includes in addition the sequence:

[14] $PhCH_2Cr_{aq}^{2+} + p\text{-}BrC_6H_4CH_2Br \xrightarrow{k_5} p\text{-}BrC_6H_4CH_2CH_2Ph + CrBr_{aq}^{2+}$

[15] $PhCH_2Cr_{aq}^{2+} + p\text{-}BrC_6H_4CH_2Br \xrightarrow{k_6} PhCH_2Br + p\text{-}BrC_6H_4CH_2Cr_{aq}^{2+}$

[16] $p\text{-}BrC_6H_4CH_2Cr_{aq}^{2+} + PhCH_2Br \xrightarrow{k_7} p\text{-}BrC_6H_4CH_2CH_2Ph + CrBr_{aq}^{2+}$

[17] $p\text{-}BrC_6H_4CH_2Cr_{aq}^{2+} + p\text{-}BrC_6H_4CH_2Br \xrightarrow{k_8} p,p'\text{-}(BrC_6H_4CH_2)_2 + CrBr_{aq}^{2+}$

[18] $p\text{-}BrC_6H_4CH_2Cr_{aq}^{2+} + H_3O^+ \xrightarrow{k_9} p\text{-}BrC_6H_4CH_3 + Cr_A^{3+}$

The differential equations associated with these reaction schemes cannot be solved in closed form. Using known or estimated values for the rate constants k_1–k_9, a numerical integration by the Runge–Kutta method (8) confirmed that the observed spectrophotometric and concentration data are in agreement. The rate constants used were obtained as follows:

k_1: $10^3\ M^{-1}\ s^{-1}$ (1, 9);

k_2: calculated from experimental data for both the decrease in benzylchromium and the increase in Cr_A^{3+}, $2.3 \times 10^{-6}\ s^{-1}$ (2);

k_3, k_5, k_6, k_7, k_8: calculated from the initial rate of disappearance of the appropriate benzylchromium. These initial rates were practically the same for reactions [8] and [9]. Furthermore, organic product

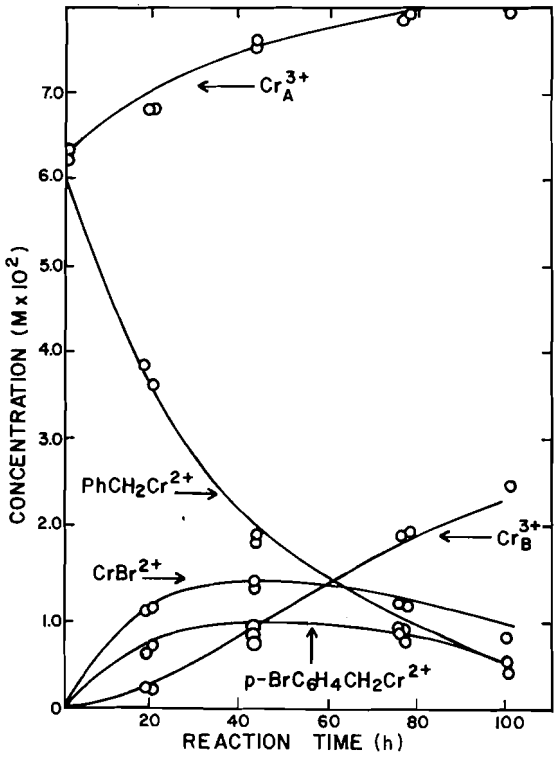

FIG. 2. Experimental (○) and calculated (—) concentrations for the reaction between benzylchromium(III) and *p*-bromobenzyl bromide at 0°C in 70 vol% methanol/water, $\mu = 0.5$, $[H^+] = 0.05$.

proportions from reactions between benzylchromium and several substituted benzyl halides were similar, indicating that reaction proportions, and so rates, are essentially the same. For the benzyl bromides, the rate constants used (at 0°C) were all $5.0 \times 10^{-5}\ M^{-1}\ s^{-1}$. For the chlorides the value of 1.0×10^{-7} was used.

k_4: aquation rate constants were calculated from available data. For chloropentaaquochromium(III) at 0°C, $[H^+] = 0.5$, a value $1.0 \times 10^{-8}\ s^{-1}$ was used (7) and for the bromo species, $2.0 \times 10^{-6}\ s^{-1}$ (10);

k_9: this was determined in the same way as k_2, $1.0 \times 10^{-6}\ s^{-1}$. The values for k_2 and k_9 used here, 2.3×10^{-6} and $1 \times 10^{-6}\ s^{-1}$, are comparable in ratio to the values at 28°C, 1.0×10^{-2} and $4.6 \times 10^{-3}\ s^{-1}$ from ref. 2. Figure 2 shows the experimental concentrations of reactants, intermediates and products for the reaction between benzylchromium(III) ion and *p*-bromobenzylbromide at 0°C, together with values calculated using these rate constants.

1. J. K. KOCHI and D. DAVIS. J. Am. Chem. Soc. **86**, 5264 (1964).
2. J. K. KOCHI and D. BUCHANAN. J. Am. Chem. Soc. **87**, 853 (1965).
3. E. DEUTSCH and H. TAUBE. Inorg. Chem. **8**, 1532 (1968).
4. G. W. HAUPT. J. Res. Natl. Bur. Stand. **48**, 414 (1952).
5. D. W. KEMP and E. L. KING. J. Am. Chem. Soc. **89**, 3433 (1967).
6. N. FOGEL, J. M. J. TAI, and Y. YARBOROUGH. J. Am. Chem. Soc. **84**, 1145 (1962).
7. T. W. SWADDLE and E. L. KING. Inorg. Chem. **4**, 532 (1965).
8. T. H. ESPENSON and O. J. PARKER. J. Am. Chem. Soc. **90**, 3689 (1968).
9. F. A. L. ANET and E. LEBLANC. J. Am. Chem. Soc. **79**, 2649 (1957).
10. F. A. GUTHRIE and E. L. KING. Inorg. Chem. **3**, 916 (1964).

A gas chromatographic detector based on the quenching of luminescence from a P_4/O_2 cold flame

WALTER A. AUE AND ZBIGNIEW M. MIELNICZUK[1]

5637 Life Sciences Centre, Dalhousie University, Halifax, N.S., Canada B3H 4J1

Received October 3, 1978

WALTER A. AUE and ZBIGNIEW M. MIELNICZUK. Can. J. Chem. **57**, 1238 (1979).

Gas chromatographic effluents were detected by their quenching effect on the luminescence of a steady 'cold flame', as provided by the gas-phase reaction of phosphorus vapor and oxygen. The response of organic compounds correlated with their 'ease of oxidation' in accordance with the literature, suggesting that such compounds act as oxygen atom scavengers in the branched-chain P_4/O_2 reaction.

Most substances showed linear response over one to two orders of magnitude, and minimum detectable amounts ranged from 2×10^{-9}g (benzaldehyde) to 2×10^{-4}g (dichloromethane). The detector temperature could be varied to (*a*) alter response ratios, i.e. selectivity, among some types of compounds; and (*b*) produce easily-obtained Arrhenius plots. However, the response (luminescence quenching) of most compounds was independent of temperature over a considerable range.

WALTER A. AUE et ZBIGNIEW M. MIELNICZUK. Can. J. Chem. **57**, 1238 (1979).

On a détecté des gaz qui s'écoulent d'un chromatographe grâce à leur effet d'amortissement sur la luminescence d'une "flamme froide" stationnaire fournie par une réaction en phase gazeuse de vapeurs de phosphore et d'oxygène. Le taux de composés organiques peut être relié à leur facilité d'oxydation; cette observation est en accord avec les suggestions faites dans la littérature à l'effet que de tels composés peuvent agir comme pièges pour des atomes d'oxygène dans la réaction de P_4 chaîne ramifiée/O_2.

La plupart des substances répondent d'une façon linéaire selon un ou deux ordres de grandeur; les quantités minimales que l'on peut détecter vont de 2×10^{-9}g (benzaldéhyde) jusqu'à 2×10^{-4}g (dichlorométhane). On peut faire varier la température du détecteur afin de (*a*) faire varier les rapports de réponse, soit la sélectivité entre quelques types de composés; et (*b*) produire des courbes d'Arrhénius qui peuvent être obtenues facilement. Toutefois, la réponse (l'amortissement de luminescence) de la plupart des composés est indépendante de la température sur une grande étendue.

[Traduit par le journal]

Introduction

The chemiluminescent oxidation of white phosphorus has been known for a few centuries. The origin of its glow or 'cold flame' has intrigued and challenged many a scientist, and the literature on the subject has become voluminous (1). Yet, this complex phenomenon is still not understood in all of its aspects.

Semenoff characterized the luminescent oxidation of phosphorus as an isothermal, branched-chain radical reaction (2). This interpretation fitted well the easily-observed, sharp upper and lower limiting pressures of oxygen, outside of which there occurs little if any luminescence. The light-emitting species is unknown (3), but kinetic investigations have established reasonable models based on the correlation of these limits to various experimental parameters.

The gas-phase oxidation of white phosphorus, according to Dainton and Kimberley (4), proceeds as follows:

[1] $P_4 + O_2 \rightarrow P_4O + O$ initiation

[2] $P_4 + O + M \rightarrow P_4O + M$ propagation

[3] $P_4O_n + O_2 \rightarrow P_4O_{n+1} + O$ branching, where $n = 1$–9

[4] $O + O_2 + M \rightarrow O_3 + M$ termination

[5] $O +$ inhibitor $\rightarrow$ termination

[6] $O +$ wall $\rightarrow$ termination

Reaction [2] is strongly exothermic and has no energy of activation; but $E_{(4)} = 4.3$ kcal (4).

The reaction of primary interest in the context of this paper is the gas-phase termination step [5]. It competes with the chain propagating reaction [2] for oxygen atoms, thereby lowering, in the experiments by Dainton and Kimberley, the upper limit of oxygen pressure.

The reasonable use of reaction [5] in a gas chromatographic detector cannot rely on the measurement of a limit, i.e. a glow/no glow criterion. Rather, the reactions have to proceed well within limits to obtain

[1]Present address: Institute of Food and Nutrition, Warsaw, Poland.

0008-4042/79/101238-06$01.00/0

linear response to the inhibitor (the gas chromatographic effluent). Since reactions [2] and [5] compete for oxygen atoms, the inhibitor should decrease the (intrinsic) luminescence of a steady P_4/O_2 cold flame.

Under reasonable gc detector conditions, a cold flame is best produced from an excess of P_4 vapor and extremely small (sub-ppm) levels of O_2. Thus reaction [4] is of minor importance. Furthermore, the cold flame is small and sharply defined under these circumstances much like the flame of an FID. Thus, reaction [6] does not occur.

Since P_4/O_2 chemiluminescence consists mainly of a continuum (3), spectral discrimination cannot be usefully employed. But without spectral discrimination, any luminescence arising from the reaction of gc effluents with O or O_3, will in effect oppose the quenching effect on P_4/O_2 chemiluminescence. It could, indeed, lead to a net increase in light emitted. Thus 'positive' gc peaks could be observed under these circumstances in contrast to the usual 'negative' ones.

Many luminescent reactions involving O and O_3 are known (5), and have given rise to various air pollution monitors and even a gc detector (6). Judging from these data, as well as from two of our own studies (7, 8), there should exist particular cases where the magnitude of such responses becomes large enough to be noticed. These should not, however, seriously impair the over-all performance of the proposed detector.

It is understood that the effect of inhibitors on the P_4/O_2 reaction, and the reaction rates of such substances with oxygen atoms produced by other means (9), correlate to what one may vaguely describe as their 'ease of oxidation'. This term should be understood in the traditional context of organic synthesis; indicating, for instance, that benzaldehyde is much easier oxidized than toluene. Translated to detector response, then, the former should yield a much larger signal than the latter. On this basis, an approximate prediction of response can be had for many compounds. Conversely, the detector could serve to compare and quantify, in an easy manner, the oxidation behavior of many organic structures.

This reciprocity, in our view, is important. It helps to justify further investigation of the effects of gas chromatographic effluents on the luminescence yield of the P_4/O_2 reaction. Thus we would expect this study to be of interest in the following three contexts.

First, the context of oxygen atom chemistry. Many studies have been concerned with this topic (9) but, mostly owing to technical difficulties, much remains to be learned. The P_4/O_2 system, in the clean, flow-through configuration of a gc detector, appears to offer a cheap and convenient source of oxygen atoms with luminescence as built-in indicator. Gas chromatographic measurements are rapid and easily performed over a wide temperature range, besides contributing the inherent advantage of a highly purified test compound.

Second, the context of biochemical oxidation. It seems reasonable to speculate that a detector based on the reaction of oxygen atoms with analyte molecules, could parallel in some of its responses biochemical reactivity.

Many anthropogenic substances depend on microsomal oxidation for activation, detoxification, etc. Their chemical 'ease of oxidation' has been more than once correlated with biological activity; especially for anticholinesterases and carcinogens (10).

To invoke such speculations may seem far-fetched. However, their realization would not lack precedent. Most of the substances that respond well in the electron capture detector (ECD) are of considerable biological activity (pesticides, steroids, etc.), and a causal relationship has been suggested (11).

If so, then a strong response from the ECD can pin-point an 'important' substance in screening experiments. It may lead, as it has done on several occasions in the past, to the discovery of potentially harmful trace components in complex environmental or biological extracts. Possibly the P_4/O_2 detector can play a similar role.

Third, and of primary importance for this paper, is the analytical context. It concerns the prospect of developing a gas chromatographic detector for some analytically difficult types of compounds; compounds for which a truly selective gc detector does not now exist. In technical terms, this task appeared but a logical extension of our recent experience with phosphorus vapor for the determination of molecular oxygen in gas streams (7).

Experimental

Three photometric detector prototypes, designated OD1, 2 and 3, were used in this study. The first, OD1, served initially in the detection of oxygen (hence the abbreviation OD) down to the 20 pg level (7). The P_4/O_2 chemiluminescence was monitored by a low-noise PM tube through a light guide in non-dispersive mode. The construction of the technically improved models OD2 and 3, which are better suited to the monitoring of organic analytes via quenching of the P_4/O_2 chemiluminescence, has been described in detail (8). The three detectors differ in mechanical and operational detail (ease of cleaning, temperature control, etc.) but not in basic design or function. This paper, in contrast to refs. 7 and 8, deals not with detector construction but with the characterization and possible interpretation of its responses.

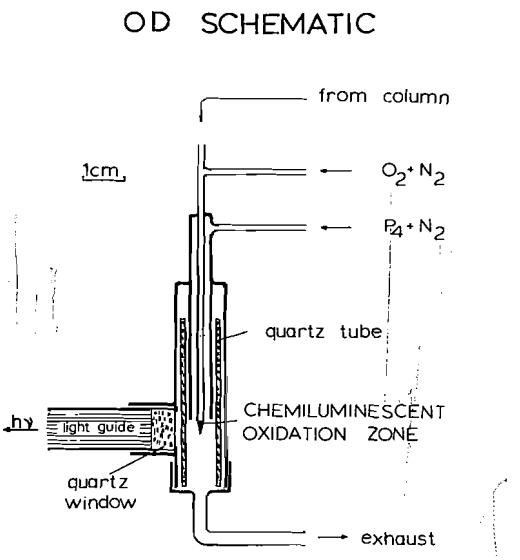

FIG. 1. Schematic detector cross section.

However, to allow facile orientation, the mostly used OD3 is shown in schematic representation in Fig. 1. P_4 vapor was supplied in a 20 mL/min stream of nitrogen, which had passed over liquid white phosphorus at 50°C. Oxygen was supplied by a minute stream of 'high purity' grade nitrogen (~14 ppm O_2), adjusted to produce a constant light level throughout the experiments. This level was established by prior signal/noise maximization.

Gas chromatographic conditions were essentially routine. A 150 × 0.2 cm id glass column packed with 3% OV-101 on Carbowax 20M-deactivated Chromosorb W, 100/120 mesh, was used with a 25 mL/min nitrogen flow. Test compounds were taken mostly from Chemical Standard Kits (Polyscience Corp. and Chem. Service) and used without further purification, provided not too many impurity peaks were noticed.

For calibration graphs, single compounds were injected at isothermal conditions. The temperature was chosen to produce approximately the same retention time for all compounds. For temperature dependence curves, typical solutes selected from preliminary runs were combined in one mixture, and chromatographed at four different dilutions with a standard temperature program. This was done to ensure that the values for the Arrhenius plot would be taken from within linear range.

On occasion, the column effluent was split to supply OD3 and a conventional FID simultaneously, or the FID exclusively. For comparison, OD3 was also operated with ozone as a reagent gas, or with a steady SiH_4/O_2 cold flame. The former served as tie-in to the work of Bruening and Concha (6), the latter provided a chemically different light source that was also quenched by column effluents (8). All other conditions were as indicated in the legends.

Results and Discussion

Most tested compounds produced response as expected, i.e. a decrease in the level of light reaching the photomultiplier tube (negative peaks). Positive peaks were observed occasionally, depending on the nature and concentration of the solute, and on detector conditions. Oxygen had to be present in the system for positive peaks to occur. Although interesting in their own right, these were not further evaluated in the context of this study. Also, no efforts were made to define any spectral features associated with the passage of peaks.

Table 1 lists most of the compounds that were used to test detector reponse. Values for molar response and linear range are deliberately given in one-digit

TABLE 1. Response and linear range

Compound	Response in mm peak height per mol injected (noise = 1 mm)	Linear range (g measured)
Benzaldehyde	2×10^{11}	$2\times10^{-9}-5\times10^{-8}$
Tetraethyllead	1×10^{11}	$5\times10^{-9}-4\times10^{-8}$
Piazselenole	1×10^{11}	$4\times10^{-9}-6\times10^{-8}$
p-Benzoquinone	1×10^{11}	$3\times10^{-9}-1\times10^{-7}$
Tetravinyltin	6×10^{10}	$1\times10^{-8}-1\times10^{-7}$
t-Butyldisulfide	5×10^{10}	$1\times10^{-8}-2\times10^{-7}$
Crotonaldehyde	4×10^{10}*	$1\times10^{-8}-5\times10^{-8}$
i-Butanol	4×10^{10}	$8\times10^{-9}-1\times10^{-7}$
l-Butanol	3×10^{10}	$1\times10^{-8}-1\times10^{-7}$
Dimethylsulfoxide	2×10^{10}	$1\times10^{-8}-2\times10^{-7}$
l-Pentanol	2×10^{10}	$1\times10^{-8}-1\times10^{-7}$
l-Hexanol	2×10^{10}	$1\times10^{-8}-2\times10^{-7}$
sec-Butanol	1×10^{10}	$3\times10^{-8}-2\times10^{-7}$
Mercaptoethanol	1×10^{10}	$3\times10^{-8}-9\times10^{-7}$
l-Octanethiol	7×10^{9}	$7\times10^{-8}-6\times10^{-7}$
Butyraldehyde	6×10^{9}	$9\times10^{-8}-3\times10^{-7}$
Valeraldehyde	6×10^{9}	$1\times10^{-7}-6\times10^{-7}$
Benzenethiol	5×10^{9}	$5\times10^{-8}-5\times10^{-7}$
t-Butanol	4×10^{9}	$4\times10^{-7}-6\times10^{-7}$
α-Pinene	4×10^{9}	$6\times10^{-8}-4\times10^{-6}$
t-Amyl alcohol	2×10^{9}	$1\times10^{-7}-8\times10^{-7}$
l-Octene	2×10^{9}	$1\times10^{-7}-1\times10^{-6}$
Phenol	1×10^{9}	$4\times10^{-7}-3\times10^{-6}$
2-Octanone	1×10^{9}	$2\times10^{-7}-9\times10^{-7}$
Fluorobenzene	6×10^{8}	$3\times10^{-7}-2\times10^{-6}$
Thiophene	3×10^{8}	$6\times10^{-7}-4\times10^{-5}$
n-Octane	2×10^{8}	$1\times10^{-6}-1\times10^{-5}$
Toluene	1×10^{8}	$3\times10^{-6}-9\times10^{-6}$
Benzene	3×10^{7}	$9\times10^{-6}-3\times10^{-4}$
Chlorobenzene	2×10^{7}	$2\times10^{-5}-2\times10^{-4}$
Bromobenzene	2×10^{7}	$2\times10^{-5}-8\times10^{-5}$
Dichloromethane	4×10^{6}	$3\times10^{-4}-8\times10^{-4}$

Compound	Response in mm peak height per mol injected	Comment
Diethylmercury	2×10^{10}	One point
Tetrahydrothiophene	1×10^{10}	Non-linear
Hexamethylditin	8×10^{9}	One point
Tetraethyltin	4×10^{9}	One point
Aniline	2×10^{9}	Non-linear
Anthracene	2×10^{9}	One point
Ferrocene	2×10^{9}	One point
Tetrabutylgermane	1×10^{9}	One point
α-Camphene	1×10^{9}	Non-linear
Phenanthrene	4×10^{8}	One point
Naphthalene	2×10^{8}	One point

*From linear range. Upper part of calibration curve non-linear, maximum response 7×10^{10}.

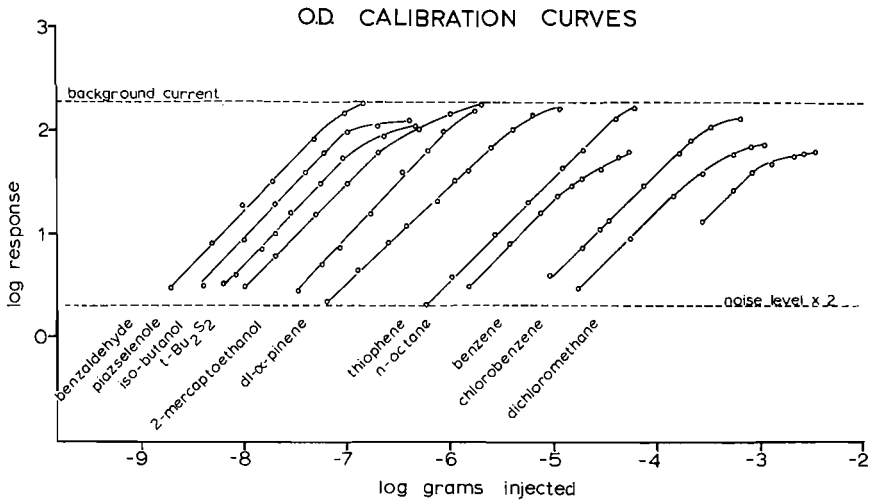

FIG. 2. Calibration curves for selected organic solutes quenching P_4/O_2 luminescence.

numbers, even though the short term reproducibility of peak heights was comparable to that obtained from other gc detectors. The sole purpose of Table 1 is to provide an approximate, general survey of the response obtained from various organic structures. While some approximate comparisons are thus reasonable to make, these data should not be used in a strictly quantitative context. It is easy enough to procure accurate comparisons with this detector on a peak area basis, (and it may, in fact, be very desirable to do so for studies of organic reactivity) but the necessary general precautions to ensure sample purity, guard against premature solute decomposition, etc. become extremely time-consuming when a large number of compounds is involved.

Hence, it has become common practice to forego such precautions in gc studies. While its limitations are obvious, that approach was clearly called for for an exploratory study such as this one.

Even with these limitations in mind, however, it is obvious from Table 1 that OD response relates to chemical structure, and that the 'ease of oxidation' criterion mentioned earlier plays a dominant role. Aldehydes and alcohols are among the best responding compounds; halogenated materials among the worst.

The first part of Table 1 lists a greater number of compounds for which full calibration curves have been established. The second part contains some more compounds that (*a*) did not show linear response or (*b*) were measured only at one concentration. In the former case, the numbers given for peak height per mole injected refer to the highest one measured. The three clearly non-linearly responding compounds, aniline, tetrahydrothiophene, and α-camphene showed slopes (in a log/log plot where slope 1 = linear) of 0.63, 0.84, and 2.0, respectively.

The linear range is given only as far as actually measured; extrapolation to $S/N = 2$ would have given slightly larger values in most cases. (This was done because a few compounds, notably dichloromethane, failed to show up at lower concentrations even though extrapolation of their calibration curves would have suggested otherwise). As can be seen from the few, typical examples shown in Fig. 2 and the numbers quoted in Table 1, compounds do differ in linear range. Furthermore, since the level of available light and the noise level are only two orders of magnitude apart, the linear ranges are of necessity very short.

It is interesting to compare, however approximate, the molar responses obtained for various types of compounds. For instance the series primary:secondary:tertiary butyl alcohols, with relative molar responses of 1:0.3:0.1 or anthracene:phenanthrene:naphthalene:toluene:benzene with relative responses of 1:0.2:0.1:0.05:0.02. These orders follow the general 'ease of oxidation', and various other examples can be found. Not surprisingly, results did deviate in a few cases from those expected. Little is known about the mechanism(s) involved, and there is always the possibility that oxidation of the analyte produces enough luminescence to reduce the observed P_4/O_2 flame quenching.

In general, the selectivity displayed towards alcohols, aldehydes, etc. should be helpful to the analyses of certain natural products, biofluids, and environmental samples. Most calibration curves, as judged by a few typical ones shown in Fig. 2, follow similar patterns.

There are exceptions, though-non-linear ones and those that flatten out relatively early. It ought to come as little surprise, however, that among the many compounds tested, some variation in mechanism should occur.

A similar statement can be made about the temperature dependence of response, shown in Fig. 3 as an Arrhenius plot for a few selected compounds. More than those shown were run and, as expected, similar structures did exhibit similar behavior.

From an analytical viewpoint, the relative response of a few compounds, say 2,4,4-trimethylpentene-2 and 1-hexanol, can be influenced by a judicious choice of detector temperature. Other compounds show little difference. Above a temperature around 140°C, response generally increases.

From a kinetic viewpoint, a different reaction mechanism would appear to take over above these temperatures. If we assume that the crucial step in quenching luminescence is the competition for oxygen atoms between reactions [5] and [2], then the slope of the lines in Fig. 3 should equal $-(E_A[5] - E_A[2])/2.3R$; provided the baseline current stays the same. If $E_A[2] = 0(4)$ and no other reaction interferes, the slope should be characteristic of the analyte reaction with oxygen atoms. Obviously this could not be applicable to the olefin, and would mean zero activation energy for (among other compounds not shown) benzaldehyde, and for octane and benzene in the lower temperature range. Thus, a difference in rates of some four orders of magnitude would have to be accounted for by the pre-exponential factor.

This seems quite unlikely. Maybe the simple, initial assumptions are incorrect; or perhaps the oxygen atoms are epithermal. Even though it is the quenching of the luminescence, and not the luminescence itself, that is being recorded, it follows the same trend as many chemiluminescent reactions, i.e. to exhibit little if any temperature dependence (12). The question of mechanism(s) remains unresolved.

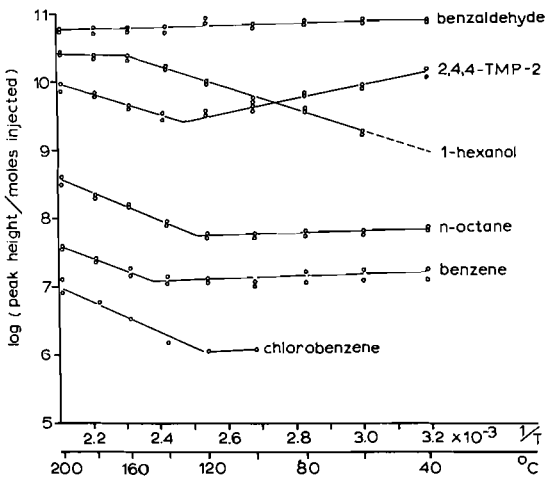

FIG. 3. Arrhenius plot for selected compounds.

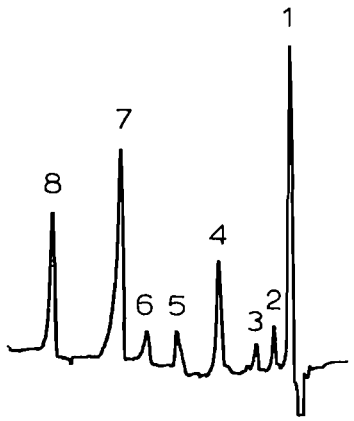

FIG. 4. Temperature programmed gc of selected analytes near their minimum detectable amounts. *1*: ~3 mg dichloromethane (solvent); *2*: 26 μg benzene; *3*: 150 ng 2,4,4-trimethylpentene (2); *4*: 13 μg *n*-octane; *5*: 50 μg chlorobenzene; *6*: unknown; *7*: 140 ng 1-hexanol; *8*: 26 ng benzaldehyde.

It may be added, however, that this exploratory study could not reasonably attempt, nor was it designed to provide, a definite answer to this question. Rather, the question was brought up to draw attention to an interesting problem, and to the relative ease with which a gc detector can provide relevant data.

Figure 4 shows a temperature programmed chromatogram of the six compounds used in the Arrhenius plot, at concentration levels not too far from minimum detectable limits. The figure demonstrates well the sensitivities and selectivities characteristic of the method.

A further demonstration of selectivity is provided in Fig. 5. The same mixture of compounds was detected by the OD operating in three different modes: the P_4/O_2 quenching mode discussed in this paper, an SiH_4/O_2 quenching mode (8), and an O_3-induced chemiluminescence mode (6, 8). Conventional FID detection was also included. In order to use the same mixture in all four cases and still detect all peaks in the FID, some compounds (e.g. *p*-quinone, piazselenole) had to exceed linear range in the OD, as may be noticed by the distorted peak shapes. The large differences among the four detection modes are readily apparent.

At present, the sensitivity of the OD for the best-responding analytes is close to that of the FID. More important, however, its selectivity favors easily oxidized compounds.

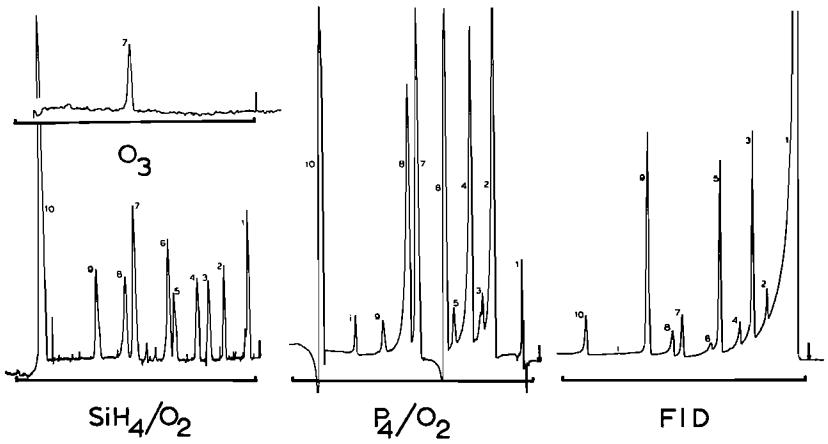

FIG. 5. Temperature programmed gas chromatography of selected compounds in the microgram range with four different detection modes. Injected for FID, P_4/O_2 quenching and SiH_4/O_2 quenching modes: *1*: 1 μL dichloromethane (solvent); *2*: 1.8 μg 1-pentanol; *3*: 4.3 μg *n*-nonane; *4*: 1.9 μg 1-hexanol; *5*: 3.8 μg *n*-decane; *6*: 3.5 μg *p*-quinone; *7*: 2.1 μg *tert*-butyldisulfide; *8*: 1.8 μg 1-octanol; *9*: 4.2 μg *n*-dodecane; *10*: 3.6 μg piazselenole; *i*: impurity. Fourfold amounts injected for O_3 luminescence mode. Recorder traces for the two quenching modes are inverted.

This property suggests its use on samples where the presence of such compounds is important, but is often obscured in the chromatogram by larger amounts of uninteresting co-eluates. One can speculate that aldehydes in air pollution samples, or in headspace from a variety of foods and beverages, may provide a case-in-point. It should also be interesting to examine volatiles in physiological fluids or breath in this manner.

Another possible use of the OD is operation in parallel with an FID. The OD/FID peak height ratio for a particular compound (normalized by means of an appropriate standard to account for day-to-day variation in the two detectors) should provide a very selective test of peak identity. To wit, this ratio should be fairly characteristic of a compound's nature, since such ratios can vary by more than four orders of magnitude (cf. Table 1), but could likely be determined with only a few percent relative standard deviation. The coincidence, within error limits, of the OD/FID ratios for an authentic standard and an analyte peak of the same retention, would greatly strengthen the assumption that the two compounds are indeed identical.

Acknowledgements

This research was supported by NRCC grant A9604 and a Dalhousie RDF grant for one of us (Z.M.M.). We appreciate the discussions with R. Stephens, and the skillful contributions of R. Myatt in steel and J. Mueller in quartz.

1. Gmelin's Handbook #16. Phosphorus. Part B. 1964. pp. 263–273.
2. N. SEMENOFF. Chemical kinetics and chain reactions. Clarendon Press, Oxford. 1935. pp. 163–199.
3. P. T. GILBERT. *In* Analytical flame spectroscopy. *Edited by* R. Mavrodineanu. Macmillan, Toronto. 1970. p. 253.
4. F. S. DAINTON and H. M. KIMBERLEY. Trans. Faraday Soc. **46**, 629 (1950).
5. A. FONTIJN, D. GOLOMB, and J. A. HODGESON. *In* Chemiluminescence and bioluminescence. *Edited by* M. J. Cormier, D. M. Hercules, and J. Lee. Plenum, New York. 1973. p. 393.
6. W. BRUENING and F. J. M. CONCHA. J. Chromatogr. **112**, 253 (1975).
7. Z. M. MIELNICZUK, C. G. FLINN, and W. A. AUE. Anal. Chem. **50**, 684 (1978).
8. Z. M. MIELNICZUK and W. A. AUE. J. Chromatogr. **166**, 1 (1978).
9. E. W. R. STEACIE. Atomic and free radical reactions. Vol. 2. 2nd ed. Reinhold Publ. Corp., New York. 1954.
10. S. K. HALL. Chemical structure and carcinogenicity. Chem. Can. 1977.
11. J. E. LOVELOCK. *In* Physical processes in radiation biology. Academic Press, New York. 1964. p. 183.
12. V. YA. SHLYAPINTOKH. Chemiluminescence techniques in chemical reactions. Consultants Bureau, New York. 1968. p. 8.

The azidonitration of tri-*O*-acetyl-D-galactal[1]

R. U. LEMIEUX AND R. M. RATCLIFFE[2]

Department of Chemistry, University of Alberta, Edmonton, Alta., Canada T6G 2G2

Received December 22, 1978

R. U. LEMIEUX and R. M. RATCLIFFE. Can. J. Chem. **57**, 1244 (1979).

Reaction of 3,4,6-tri-*O*-acetyl-D-galactal with excess ceric ammonium nitrate and sodium azide in acetonitrile produced 2-azido-1-nitrate addition products (53% β-*galacto*, 22% α-*galacto*, and 8% α-*talo*) and *N*-acetyl-3,4,6-tri-*O*-acetyl-2-azido-2-deoxy-α-D-galactopyranosylamine was formed, on hydrolysis, in 10% yield. The reaction product provides a convenient source of D-galactosamine and 3,4,6-tri-*O*-acetyl-2-azido-2-deoxy-α-D-galactopyranosyl halides. The crystalline β-chloride is also reported. The use of these glycosyl halides as reactants for the preparation of 2-azido-2-deoxy-α- and -β-D-galactopyranosides under conditions promoted by both mercuric cyanide and silver salts are reported.

R. U. LEMIEUX et R. M. RATCLIFFE. Can. J. Chem. **57**, 1244 (1979).

La réaction du tri-*O*-acétyl-3,4,6 D-galactal avec du nitrate d'ammonium cérique en excès et de l'azoture de sodium dans l'acétonitrile conduit aux produits d'addition azido-2 nitrate-1 (53% β-*galacto*, 22% α-*galacto* et 8% α-*talo*); par hydrolyse, il y a formation de la *N*-acétyltri-*O*-acétyl-3,4,6 azido-2 désoxy-2 α-D galactopyrannosylamine avec un rendement de 10%. Le produit de la réaction s'avère une source convenable de la D-galactosamine et des halogénures du tri-*O*-acétyl-3,4,6 azido-2 désoxy-2 α-D-galactopyrannosyle. On rapporte aussi la formation du chlorure β cristallin. On rapporte l'utilisation de ces halogénures de glycosyle comme réactifs dans la préparation des azido-2 désoxy-2 α- et β-D-galactopyrannosides dans des conditions favorisées par des sels de cyanure mercurique et d'argent.

[Traduit par le journal]

Introduction

The occurrence of building units derived from 2-acetamido-2-deoxy-α-D-galactopyranose, which are *O*-linked to either serine or threonine, in a wide variety of glycoproteins (1, 2) including glycophorin A (3), epiglycanin (4), antifreeze glycoproteins (5), and the human blood specific glycoproteins (6) is well documented. Both α- and β-glycosidic units derived from *N*-acetyl-D-galactosamine occur in the oligosaccharidic antigenic determinants of a number of glycosphingolipids (7). Thus, there has developed widespread interest in achieving chemical syntheses of oligosaccharides containing these groupings both for immunochemical and enzymological studies (8). However, the lack of a readily accessible supply of either D-galactosamine or of suitable progenitors has curtailed research in this biologically important area. This work was initiated primarily to achieve the syntheses of oligosaccharides related to the A blood determinants (9) but has been extended to the synthesis of the T, T_N (10), and other important human cell-surface antigenic determinants.

The major source of D-galactosamine is by way of the acid hydrolysis of chondroitin sulfate (11). Numerous synthetic methods have been described including the chain extension of D-lyxose (12, 13), inversion of C-4 of D-glucosamine (14), the addition of ammonia to 1,6;2,3-dianhydro-β-D-talopyranose (15) and by reduction of oximes obtained by way of the addition of nitrosyl chloride to tri-*O*-acetyl-D-galactal (16).

The preparation of α-D-galactosaminides by way of 2-oximo-α-D-*lyxo*-hexopyranosides (17) provided the first synthesis of an *N*-acetyl-α-D-galactosaminidic disaccharide (18). However, to date, this method is handicapped by the fact that reduction of the intermediate oxime to the *galacto* configuration cannot be achieved with a high degree of stereoselectivity. More recently, Paulsen and co-workers (19–22), utilized 6-*O*-acetyl-2-azido-3,4-di-*O*-benzyl-2-deoxy-β-D-galactopyranosyl chloride to synthesize the terminal trisaccharide of the Forssman antigenic determinant and a partial structure of the A human blood group determinant. Thus, the utility of the azide group as a nonparticipating 2-substituent in glycosyl halides to be engaged in Koenigs–Knorr type glycosidation reactions was established but, to become attractive, a more ready access to 2-azido-2-deoxyglycosyl halides was needed than is provided by the 10-stage process used by Paulsen and co-workers. The main purpose of this communication is to report a relatively simple five-stage process from D-galactose to obtain 3,4,6-tri-*O*-acetyl-2-azido-2-deoxy-D-galacto-

[1]Presented, in part, at the Carbohydrate Discussion Group of The Chemical Society, University of East Anglia, Norwich, England, April 18–20, 1977.

[2]University of Alberta Postdoctorate Fellow, 1975–1977, Research Associate, 1977–present.

0008-4042/79/101244-08$01.00/0

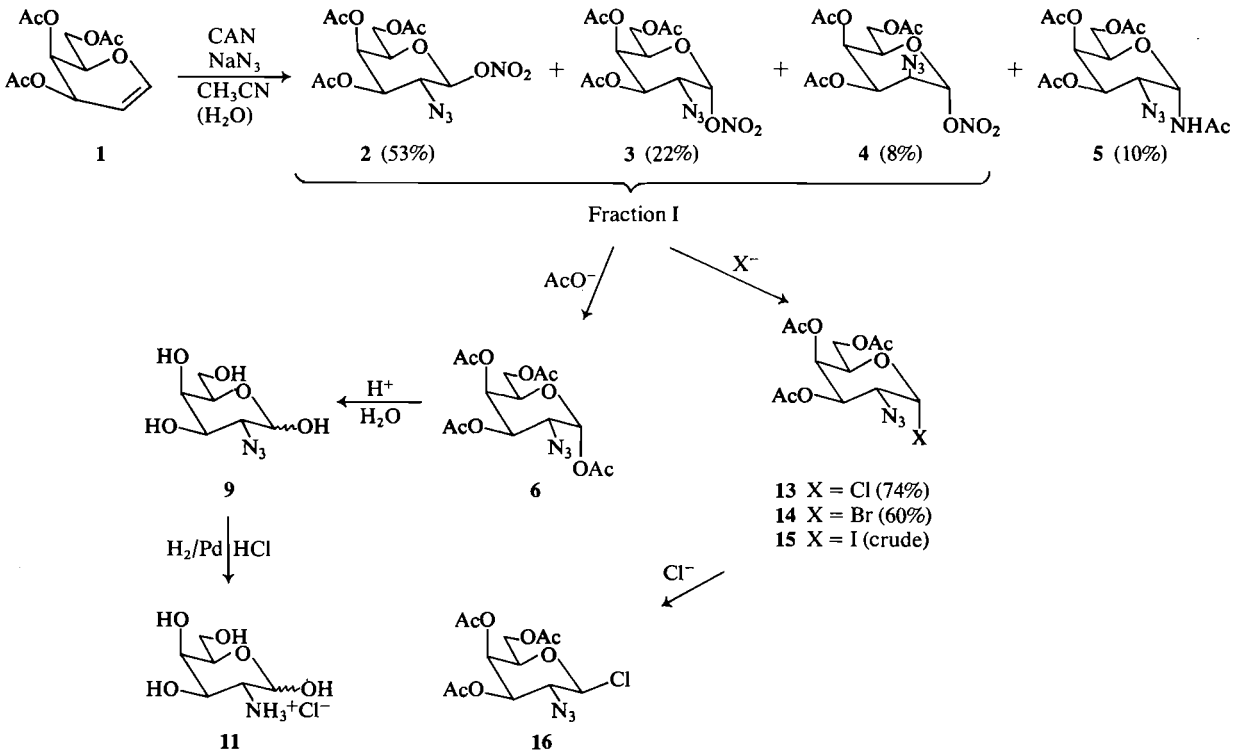

SCHEME 1. Azidonitration of D-galactal triacetate and some of the products derived therefrom.

pyranosyl halides. However, the method also provides ready access to D-galactosamine. The method appears generally applicable to *O*-protected glycals and is expected to find widespread application for the preparation of 2-azido-2-deoxyaldoses and their glycosides.

In 1971, Trahanovsky and co-workers (23, 24) reported the formation of α-azido-β-nitratoalkanes on treating alkenes with sodium azide and ceric ammonium nitrate in moist acetonitrile. The matter of central importance to the present application of this reaction was that the products obtained were consistent with the reaction being initiated by addition of an azide radical (23). Several mechanisms have been proposed (25) to rationalize the fate of the proposed azidoalkane radical intermediate. Although no reference could be found to the application of this 'azidonitration' reaction to vinyl ethers, it could be anticipated that a radical induced addition would follow the anti-Markovnikov route and, therefore, when applied to *O*-protected glycals would provide 2-azido-2-deoxyglycosyl nitrates. It may be mentioned that our attempts to induce free-radical addition of either ClN_3 or BrN_3 to *O*-acetylated glycals failed and only 1-azido-1-deoxy-2-halogeno-2-deoxy sugars were obtained. Further work in this regard was abandoned when a reaction involving chloroazide and with sulfuryl chloride as the radical initiator detonated with violence.

The more important aspects of this paper are outlined in Scheme 1. It is seen that, in the azidonitration of 3,4,6-tri-*O*-acetyl-D-galactal (**1**), 93% of the reaction products were identified and all of these products, as expected, contain the azide group at the 2-position with 85% of these products containing this group in the equatorial orientation (the *galacto* configuration). The similar azidonitration of other glycals will be reported separately (26). However, it is noteworthy at this point that the above-mentioned stereoselectivity appears related to the quasiaxial orientation of the 4-acetoxy group of **1** since the azidonitration of the acetates of D-xylal, D-glucal, and lactal all provided substantially lower yields of C-2 equatorial azide; namely, ratios of equatorial to axial isomer of 2, 1, and 3, respectively. This is in contrast to the ratio of 11 in the case of D-galactal triacetate. Thus, the development of a *syn*-diaxial interaction with an acetoxy group during the establishment of the azido group is more prohibitive than is the development of a *syn*-clinal interaction with a neighboring acetoxy group. It is not considered definite that the reaction is initiated by the attack of

the double bond by an azide radical rather than by a ceric–azide complex (23). The steric bulk of the latter could help to explain the stereochemical route of reaction. It is to be noted that it was necessary to use an excess of both CAN and sodium azide since some of these reagents are lost in the ceric oxidation of azide to nitrogen gas. The rate of this competing reaction appeared dependent on the concentration of the azide in solution. When *N*,*N*-dimethylacetamide was used as solvent, a solvent which rapidly provided a homogeneous reaction mixture, this competing reaction consumed all of the oxidant. It is possible that the reaction of CAN with azide ion to a ceric–azide species is rapid and that the azidonitration reaction is promoted relative to oxidation of the azide to nitrogen by a low concentration of azide ion.

Since the formation of the 1-acetamido product **5** requires water and the azidonitration was performed under strictly anhydrous conditions, this product must form during the isolation. Indeed, rapid tlc examination of the supernatant liquid of the reaction mixture provided no evidence of **5** in the reaction mixture. However, if this solution was worked up, **5** appeared in the product but the amount appeared less than that present when the solids were worked up separately. It is apparent, therefore, that the precursor of **5** is a relatively insoluble product. Azidonitration reactions in 10% aqueous acetonitrile (23) provided relatively poor yields of the azidonitrates in more complex reaction product mixtures. The 1-acetamido product **5** was readily separated from the azidonitrates **2**, **3**, and **4** by column chromatography using silica gel. The mixture of azidonitrates obtained in this way proved useful for the preparation of the 3,4,6-tri-*O*-acetyl-2-azido-2-deoxy-α-D-galactosyl halides (**13**, **14**, **15**). This mixture is referred to as the azidonitration reaction product fraction I.

One of the mechanisms suggested by Trahanovsky and Robbins (23) is that the initially formed azidoalkyl radical is oxidized to a carbonium ion which, in turn, accepts nitrate to form the azidonitrate. The formation of **5** would appear to be in line with this mechanistic pathway since the attack of the α-side of a carbonium ion (A) by nucleophilic acetonitrile to form a nitrilium ion (B) which in turn provides the precursor to **5** could be accounted for in this way. It seems evident, however, that any consideration of the mechanism for the azidonitration will need to take into account the tendency for the overall addition to provide *trans*-products of addition. Thus, the 1,2-*trans*-β-azidonitrate to 1,2-*cis*-α-azidonitrate ratios were 1.5, 2, 2, and 10 on azidonitration of the acetates of D-galactal, D-glucal, D-lactal, and D-xylal, respectively (26). These results do not appear likely to arise from attack by nitrate ion on intermediate

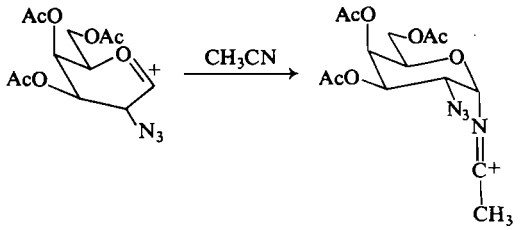

A B

glycosyl carbonium ions of type A (27). Furthermore, a reaction pathway involving a carbonium ion intermediate might be expected to give rise to appreciable yields of 2-azido-2-deoxyglycosyl azides but these were not detected in our reaction products.

Acetolysis of the crude β-azidonitrate **2**, obtained by removal of the α-nitrates **3** and **4** from fraction I by crystallization from ether, provided crystalline 1,3,4,6-tetra-*O*-acetyl-2-azido-2-deoxy-α-D-galactopyranose (**6**) which was readily recrystallized to high purity. As expected, hydrogenation of this compound led to migration of the 1-*O*-acetyl group to the developed amino group to form 2-acetamido-3,4,6-tri-*O*-acetyl-α-D-galactopyranose. It is considered interesting to note that an attempt to avoid this migration by performing the hydrogenation in the presence of acetic anhydride led to the formation of 2-(*N*-acetylacetamido-1,3,4,6-tetra-*O*-acetyl-2-deoxy-α-D-galactopyranose (**8**) in 30% yield. Di-*N*-acetylation of an amine is not expected to arise when using acetic anhydride in ethanol and therefore the formation of **8** must involve some intermediate which formed in the course of the hydrogenation. Deacetylation of **6** provided 2-azido-2-deoxy-D-galactose from which pure D-galactosamine hydrochloride was readily prepared. A process aimed at preparing this latter compound would appear to best proceed by way of anomerization of the crude reaction product using lithium nitrate in acetonitrile followed by crystallization of the α-azidonitrate **3**. However, since the product of the acetolysis of **3** (the β-anomer of **6**) resisted crystallization, this route was not explored in detail.

The main purpose of this investigation was to achieve syntheses of 3,4,6-tri-*O*-acetyl-2-azido-2-deoxy-D-galactopyranosyl halides (**13**, **14**, and **16**) to be used as reagents in the preparation of 2-azido- and 2-amino-2-deoxy-α- and -β-D-galactopyranosides. The α-chloride **13** and the α-bromide **14** were readily prepared in crystalline condition by replacement of the nitrate group of compounds **2** and **3** using an appropriate soluble halide salt and starting with fraction I. Lemieux and Hayami (28) reported the preparation of 2,3,4,6-tetra-*O*-acetyl-β-D-glucopyranosyl chloride in good yield by kinetic control of the reaction of 2,3,4,6-tetra-*O*-acetyl-α-D-gluco-

pyranosyl bromide with tetraethylammonium chloride. Paulsen *et al.* (22) used this method to prepare protected 2-azido-2-deoxy-β-D-galacto- and -glucopyranosyl chlorides. Reaction of the 2-azido-2-deoxy-α-bromide **14** with tetraethylammonium chloride provided the β-chloride **16** but observation of the progress of the reaction by ^{1}Hmr showed that the α-chloride **13** was forming to an appreciable extent prior to the disappearance of **14**. It was therefore decided to investigate the use of the more reactive 2-azido-2-deoxy-α-iodide **15** as starting material. This compound was most conveniently prepared as a crude syrup starting from fraction I and used directly in a very brief (2.5 min) reaction to form the β-chloride **16** which proved readily isolable by crystallization. The yield from 3,4,6-tri-*O*-acetyl-D-galactal (**1**) was 31%.

To assess the behavior of the glycosyl halides **13**, **14**, and **16** in glycosidation reactions, reactions were conducted under two set conditions using *tert*-butyl alcohol as a representative of a hindered alcohol and benzyl alcohol as a representative of a more reactive alcohol. The alcohols were also chosen, in part, to facilitate a study of the reaction products by ^{1}Hmr. Two of the most widely used conditions for glycosidation were examined; namely, reactions promoted by mercuric cyanide and using benzene–nitromethane as solvent (29) and by silver carbonate in conjunction with a soluble silver salt (30) which provides a labile glycosyl intermediate and using methylene chloride as solvent. Although silver perchlorate is often used, silver trifluoromethanesulfonate (31) was used in the present experiments. Although the α-bromide **14** provided a Koenigs–Knorr condensation in the presence of silver carbonate alone, the α- and β-chlorides **13** and **16** were too unreactive.

Under the Helferich conditions, the α-chloride **13** underwent extremely slow reaction with both alcohols since less than 10% glycoside formation was observed in the reaction time allowed (48 h at 50°C). However, reaction was complete in the case of the α-bromide but the stereoselectivity was poor with a ratio of near 1 for the α- and β-glycosides formed. The yield of both the α- and β-glycosides was excellent (92%) in the case of the reaction with benzyl alcohol but only 51% in the case of the more hindered *tert*-butyl alcohol. The lack of stereoselectivity very likely arose from anomerization of the α-bromide to the β-anomer which would be expected to provide α-glycoside (27). Certainly, the β-chloride **16** was anomerized to the α-chloride **13** when the β-chloride was used as starting material. In this case, reaction effectively ceased with the disappearance of the β-chloride. The reaction with benzyl alcohol provided a 70% yield of glycoside with an α/β ratio of 5, with 30% of the starting material being converted to the α-chloride. In the case of the reaction using *tert*-butyl alcohol, the product contained the α-chloride in 50% yield. The yield of glycoside was only 21% but the α/β ratio was greater than 10. It is thus evident that under the Helferich conditions, reactions of the β-chloride proceed with a high degree of inversion of the anomeric center but that anomerization catalyzed by liberated chloride ion can very adversely affect the yield, especially with hindered alcohols.

The glycosidation reactions promoted by silver salts proceeded to complete reaction of the glycosyl halide. The reactions of the α-halides provided poor stereoselectivity. The yields of β-glycoside were higher starting with the α-chloride (α/β ratio = 0.6) than with the α-bromide (α/β ratio = 1.1). Also, the yields of glycosides were higher starting with the α-chloride (97% and 80% with the benzyl and *tert*-butyl alcohols, respectively) than with the α-bromide (72% and 58% with the benzyl and *tert*-butyl alcohols, respectively). The total yields of glycoside were virtually the same starting with the β-chloride as those obtained starting with the α-chloride. However, the α/β ratios (near 1.7 in each case) were, as expected, more in favor of α-glycoside formation. It is expected that the rather low degree of stereoselectivity exhibited in all of these silver salt promoted glycosidation reactions is related to an important pathway of the reaction occurring by way of a dissociation of the glycosyl halide with silver ion assistance to an oxocarbonium ion which is not coordinated to alcohol.

Experimental

The general procedures and analytical methods used were the same as previously described (27).

Azidonitrations

Although the azidonitrations were examined under a wide variety of conditions, all those reported herein were performed at −15°C and in a dry nitrogen atmosphere by adding a 0.2 *M* solution of the *O*-acylated glycal in dry acetonitrile to a dry mixture of sodium azide and ceric ammonium nitrate (CAN) with relative molar amounts of these reagents at 1:1.5:3, respectively. As soon as the addition was completed, strong stirring was begun and continued until the presence of the glycal could no longer be detected by the examination of the supernatant. The reaction was performed behind a barrier under a wide range of conditions including changes in temperature, solvent and relative amounts of reactants. Although such changes caused appreciable changes in yield and the coloration of the product, no lack of control was experienced. Nevertheless, it must be realized that hazardous conditions may be encountered and all azidonitrations should be conducted with due caution. Furthermore, the use and disposal of sodium azide must be carefully controlled.

*Azidonitration of 3,4,6-Tri-*O*-acetyl-D-galactal (1)*

Compound **1** (21.1 g, 0.077 mol) in acetonitrile (420 mL)

was added to a mixture of sodium azide (7.50 g, 0.115 mol) and CAN (126.5 g, 0.281 mol). The resulting suspension was vigorously stirred with cooling until analysis by tlc (Skellysolve B – ethyl acetate (6:4), silica gel) of the supernatant liquid phase no longer showed the presence of compound **1**. At this time, normally after an 8- to 10-h reaction period, cold diethyl ether (500 mL) and water (500 mL) were added. The organic layer was separated and washed with ice-cold water (3 × 500 mL) prior to drying over anhydrous sodium sulfate. Evaporation of the solvent left a yellow syrup (21.0 g).

The ^{1}Hmr spectrum of this product showed doublet signals at 5.68, 6.35, and 6.21 ppm which were assigned to the anomeric protons of the following reaction products; 3,4,6-tri-*O*-acetyl-2-azido-2-deoxy-β-D-galactopyranosyl nitrate (**2**), 3,4,6-tri-*O*-acetyl-2-azido-2-deoxy-α-D-galactopyranosyl nitrate (**3**), and 3,4,6-tri-*O*-acetyl-2-azido-2-deoxy-α-D-talopyranosyl nitrate (**4**). This latter compound was not isolated and the assignment of the α-configuration is made on the basis that a solution of the reaction product in acetonitrile-*N,N*-dimethylformamide (4:1) which contained lithium nitrate (as described in detail below for the anomerization of **2** to **3**) caused no detectable change in the amount of the component responsible for the signal at 6.21 ppm which is assigned to **4**. The total intensity for the above-mentioned signals for anomeric hydrogens relative to the total signals attributable to *O*-acetyl groups required compounds **2**, **3**, and **4** to comprise near 75% of the reaction product and to be present in the ratios near 1:0.67:0.15, respectively. It will be seen below that *N*-acetyl-3,4,6-tri-*O*-acetyl-2-azido-2-deoxy-α-D-galactopyranosylamine (**5**) was also a major reaction product (10% yield) but its presence in the crude reaction product could not be detected by ^{1}Hmr.

To remove the acetamido compound **5** from the reaction product, the syrup (117 g) was dissolved in Skellysolve B – ethyl acetate (6:4) (300 mL) and immediately applied to a column (20 × 10 cm diameter) packed with solvent-wetted silica gel (400 g) and the chromatogram was developed with this same solvent system. The initial fractions (15 mL each) of the eluate which contained reaction products consisted of mixtures of the nitrates **2**, **3**, and **4**. The acetamido compound **5** was detected (tlc) after 30 such fractions had been collected and these initial fractions when combined and evaporated provided a mixture (68 g) of the nitrates **2**, **3**, and **4** which will be referred to hereafter as reaction product fraction I. The ratio of α-nitrate **3** to β-nitrate **2** in this product was normally close to 0.8, suggesting that some anomerization had occurred during the chromatographic separation. However, it is possible that the more reactive β-nitrate **2** underwent hydrolysis to a greater extent than did its α-anomer.

*3,4,6-Tri-*O*-acetyl-2-azido-2-deoxy-*β*-D-galactopyranosyl Nitrate (2)*

Trituration either of the above-described product from the azidonitration of tri-*O*-acetyl-D-galactal or of fraction I with diethyl ether caused a copious precipitation of a crystalline product which was removed by filtration. Evaporation of the ether left a syrup (12.6 g, 44% yield in the case of the crude product) which resisted crystallization although examination by tlc and ^{1}Hmr required this product to be about 80% pure title compound with the α-anomer (**3**) being the main contaminant; ir (film) ν_{max}: 2120 (N_3), 1650 (ONO_2) cm^{-1}; ^{1}Hmr ($CDCl_3$) δ: 5.60 (d, 1H, $J_{1,2}$ = 9.0 Hz, H-1), 5.42 (q, 1H, H-4), 5.08 (q, 1H, $J_{3,4}$ = 3.2 Hz, H-3), 3.82 (q, 1H, $J_{2,3}$ = 10.8 Hz, H-2), 2.18, 2.10, 2.03 (3s, 9H, $3CH_3$).

*3,4,6-Tri-*O*-acetyl-2-azido-2-deoxy-*α*-D-galactopyranosyl Nitrate (3)*

The crystalline product (8.3 g, 29% yield) which formed in the above-described treatment of the product from the azidonitration with ether was found to be the title compound mixed with the *talo*-isomer (**4**). This latter product proved difficult to remove by recrystallization. The pure title compound was best obtained by anomerization of **2**. The syrupy β-D-nitrate **2** (9.50 g, 25.5 mmol) was dissolved in a 4:1 (v/v) mixture (35 mL) of acetonitrile and *N,N*-dimethylformamide which contained anhydrous lithium nitrate (3.50 g, 50.1 mmol). After standing at room temperature for 41 h, the solution was diluted with dichloromethane (250 mL) before treatment with ice-cold water (3 × 125 mL). The organic layer was dried over sodium sulfate prior to evaporation to a syrup (9.0 g). This product crystallized from diethyl ether and was recrystallized to afford pure title compound **3**; mp 103–104°C, $[\alpha]_D^{25}$ +125° (*c* 1.0, $CHCl_3$); ir (film) ν_{max}: 2120 (N_3), 1650 (ONO_2) cm^{-1}; ^{1}Hmr ($CDCl_3$) δ: 6.35 (d, 1H, $J_{1,2}$ = 4.0 Hz, H-1), 5.49 (q, 1H, $J_{4,5}$ = 1.8 Hz, H-4), 5.24 (q, 1H, $J_{3,4}$ = 3.25 Hz, H-3), 4.12 (q, 1H, $J_{2,3}$ = 11.5 Hz, H-2), 2.18, 2.07, 2.02 (3s, 9H, $3CH_3$). *Anal.* calcd. for $C_{12}H_{16}N_4O_{10}$: C 38.30, H 4.29, N 14.89; found: C 38.52, H 4.32, N 14.69.

*N-Acetyl-3,4,6-tri-*O*-acetyl-2-azido-2-deoxy-*α*-D-galactopyranosylamine (5)*

The reaction product from the azidonitration was chromatographed on a silica gel column using Skellysolve B – ethyl acetate (6:4 v/v) as solvent. The nitrates **2**, **3**, and **4** appeared first in the eluate but were not separated. Further development of the column provided a fraction in 10% overall yield which crystallized readily from diethyl ether. Recrystallization provided pure title compound (**5**); mp 142–143.5°C, $[\alpha]_D^{25}$ +68.0° (*c* 1, $CHCl_3$); ir (Nujol) ν_{max}: 3380 (NH), 2120 (N_3) cm^{-1}; ^{1}Hmr (DMSO-d_6) δ: 8.84 (d, 1H, $J_{NH,1}$ = 10.0 Hz, NH), 5.78 (q, 1H, $J_{1,2}$ = 5.5 Hz, H-1), 5.47 (q, 1H, $J_{3,4}$ = 3.5 Hz, H-3), 5.24 (d, 1H, H-4), 4.21 (q, 1H, $J_{2,3}$ = 11.5 Hz, H-2), 2.11, 1.98, 1.96, 1.91 (4s, 12H, $4CH_3$). *Anal.* calcd. for $C_{14}H_{20}N_4O_8$: C 45.16, H 5.41, N 15.05; found: C 44.92, H 5.50, N 14.93.

As described below, acid hydrolysis provided 2-azido-2-deoxy-D-galactose. The α-configuration was assigned on the basis of the optical rotation relative to that for the 1-acetoxy analog (**6**) and the strong deshielding observed for H-3 (assigned by spin-decoupling experiments).

*1,3,4,6-Tetra-*O*-acetyl-2-azido-2-deoxy-*α*-D-galactopyranose (6)*

A suspension of the crude syrupy β-D-nitrate **2** (8.0 g, 0.021 mol) and anhydrous sodium acetate (3.44 g) in glacial acetic acid (50 mL) was heated to 100°C for 1 h (tlc showed no remaining starting material). The reaction mixture was diluted with dichloromethane (250 mL) and this mixture was successively treated with ice-cold water (200 mL), saturated aqueous sodium bicarbonate (2 × 100 mL), and water (125 mL). Drying and evaporation of the organic layer left a yellow solid (7.5 g, 94%). Recrystallization from diethyl ether provided pure title compound (**6**) (6.9 g, 85%); mp 114–115°C, $[\alpha]_D^{25}$ +91.7° (*c* 1.05, $CHCl_3$) (lit. (22) mp 117°C, $[\alpha]_D^{20}$ +109° ($CHCl_3$)); ir (film) ν_{max}: 2120 (N_3) cm^{-1}; ^{1}Hmr ($CDCl_3$) δ: 6.39 (d, 1H, $J_{1,2}$ = 3.6 Hz, H-1), 4.04 (q, 1, $J_{2,3}$ = 10.0 Hz H-2), 2.19, 2.09, 2.06 (3s, 12, $4CH_3$). *Anal.* calcd. for $C_{14}H_{19}N_3O_9$: C 45.04, H 5.13, N 11.26; found: C 44.88, H 5.11, N 11.15.

*2-Acetamido-1,3,4,6-tetra-*O*-acetyl-2-deoxy-*α*-D-galactopyranose (7) and its N-Acetyl Derivative (8)*

A solution of compound **6** (200 mg) in ethyl acetate (1 mL) was added to a suspension of 5% palladium-on-charcoal (80 mg) in ethanol containing acetic anhydride (0.25 mL). This mixture was hydrogenated at 1 atm and room tempera-

ture for 1 h. Examination by tlc using benzene – ethyl acetate – ethanol (5:5:1) showed the presence of two products. Removal of the catalyst and dilution with dichloromethane (5 mL) provided a solution which was washed with water (5 mL) before evaporation to a white solid (206 mg). The two components were separated by chromatography on a silica gel (20 g) column (20 × 2 cm) eluted with the above solvent system.

The first product to appear in the eluate was 2-*N*-acetylacetamido-1,3,4,6-tetra-*O*-acetyl-2-deoxy-α-D-galactopyranose (**8**) (68 mg, 30%); ^{1}Hmr ($CDCl_3$) δ: 6.32 (d, 1H, $J_{1,2}$ = 3.8 Hz, H-1), 5.72 (q, 1H, $J_{2,3}$ = 11.0 Hz, H-3), 5.53 (q, 1, $J_{3,4}$ = 3.5 Hz, H-4), 4.27 (q, 1, H-2), 2.36 (1s, 6, 2NAc), 2.16, 2.14, 2.04, 1.95 (4s, 12, $4CH_3$). These parameters are in good agreement with those reported for this compound by Pravdic and Fletcher (32).

The second fraction (100 mg, 43% yield) crystallized from ether; mp 177–178°C, $[\alpha]_D^{25}$ +99° (*c* 1, $CHCl_3$) (lit. (33) mp 178°C, $[\alpha]_D^{20}$ +102°). The ^{1}Hmr was in agreement with that reported by Tarasiejska and Jeanloz (34) for 2-acetamido-1,3,4,6-tetra-*O*-acetyl-2-deoxy-α-D-galactopyranose (**7**).

When the hydrogenation was performed under the same conditions except that the acetic anhydride was added after the reduction of the azide was complete, the product did not contain the *N*,*N*-diacetylamino compound (**8**) but was mainly 2-acetamido-3,4,6-tri-*O*-acetyl-2-deoxy-D-galactose.

*2-Azido-2-deoxy-*β-D-*galactose (**9**)*

A mixture of 1,3,4,6-tetra-*O*-acetyl-2-azido-2-deoxy-α-D-galactopyranose (**6**) (4.59 g) with 4 *N* aqueous hydrochloric acid (50 mL) was warmed until solution was complete and then left at room temperature for 15 h. After decolorization with charcoal, an equal volume of *n*-butanol was added and the solution was evaporated at 40°C to a yellow solid. Recrystallization from ethanol provided 2-azido-2-deoxy-β-D-galactose (**9**) (1.40 g, 56%): mp 161.5–163°C (dec.), $[\alpha]_D^{25}$ +76.9° (final) (*c* 0.98, H_2O); ir (Nujol) ν_{max}: 2130 (N_3) cm^{-1}; ^{1}Hmr (DMSO-d_6) δ: 4.30 (d, 1H, $J_{1,2}$ = 7.75 Hz, H-1); ^{13}Cmr (DMSO-d_6) δ: 95.5 (C-1). *Anal.* calcd. for $C_6H_{11}O_5N_3$: C 35.12, H 5.41, N 20.48; found: C 35.08, H 5.40, N 20.50.

Treatment of *N*-acetyl-3,4,6-tri-*O*-acetyl-2-azido-2-deoxy-α-D-galactopyranosylamine (**5**) (1.0 g) in the same manner also provided recrystallized title compound (**9**) (0.324 g, 58%).

*2-Acetamido-2-deoxy-*D-*galactose (**10**)*

2-Azido-2-deoxy-D-galactopyranose (**9**) (1.0 g) was dissolved in methanol (20 mL) containing acetic anhydride (1.5 mL) and hydrogenated at room temperature and 1 atm in the presence of 5% palladium-on-charcoal (0.25 g). After 8 h, examination by tlc indicated the formation of only one product which was isolated in the usual manner and crystallized from ethanol to provide the title compound (**10**) as an anomeric mixture, mp 108–110°C, $[\alpha]_D^{25}$ +79° (final), (*c* 1, H_2O) (lit. (33) for the α-anomer mp 120–122°C, $[\alpha]_D$ +115 → 80° (water)); ^{1}Hmr (D_2O) δ: 5.44 (d, $J_{1,2}$ = 3.50 Hz, H-1α), 4.86 (d, $J_{1,2}$ = 7.25 Hz, H-1β), 2.24 (s, $COCH_3$).

D-*Galactosamine Hydrochloride (**11**)*

2-Azido-2-deoxy-D-galactopyranose (**9**) (100 mg) was dissolved in aqueous 90% methanol (5 mL) which contained 1.5 equiv. of hydrochloric acid. Low pressure hydrogenation in the presence of 5% palladium-on-charcoal (25 mg) followed by the usual work-up provided a residue (100 mg) which examination by tlc developed with isopropanol – ammonium hydroxide – water (7:1:2) gave evidence for only one substance with the same mobility as that of an authentic sample of the title compound (**11**). Crystallization from ethanol–methanol gave pure D-galactosamine hydrochloride (**11**) (50 mg, 48%): mp 182–200°C (dec.), $[\alpha]_D^{25}$ +89.5° (*c* 1, water) (lit. (12) mp 178–190°C, $[\alpha]_D^{25}$ +91.5° (final)); ^{1}Hmr (D_2O) δ: 5.66 (d, $J_{1,2}$ = 3.50 Hz, H-1α), 5.07 (d, $J_{1,2}$ = 8.50 Hz, H-1β).

*2-Acetamido-*N*-acetyl-3,4,6-tri-*O*-acetyl-2-deoxy-α-D-galactosamine (**12**)*

N-Acetyl-3,4,6-tri-*O*-acetyl-2-azido-2-deoxy-α-D-galactopyranosylamine (**5**) (1.135 g) was dissolved in acetic acid (10 mL) for low pressure hydrogenation in the presence of 5% palladium-on-charcoal (0.30 g). After 12 h, acetic anhydride (1 mL) was added. Catalyst removal and evaporation provided a solid (1.05 g) which crystallized on trituration with diethyl ether. Recrystallization from ethyl acetate – diethyl ether provided the title compound (**12**) (0.990 g, 85%); mp 192–193°C, $[\alpha]_D^{25}$ +104.4° (*c* 1, $CHCl_3$); ^{1}Hmr (DMSO-d_6) δ: 8.44 (d, 1H, $J_{NH,1}$ = 10.0 Hz, NH), 7.80 (d, 1H, $J_{NH,2}$ = 8.4 Hz, NH), 5.60 (q, 1H, $J_{1,2}$ = 5.0 Hz, H-1), 2.12, 2.01, 1.94, 1.80 (4s, 15H, $5CH_3$); ^{13}Cmr ($CDCl_3$–DMSO-d_6 (7:3) v/v)) δ: 75.5 (C-1); *Anal.* calcd. for $C_{16}H_{24}O_9N_2$: C 49.48, H 6.22, N 7.21; found: C 49.67, H 6.12, N 6.94.

*2-Azido-3,4,6-tri-*O*-acetyl-2-deoxy-α-D-galactopyranosyl Chloride (**13**)*

The syrupy azidonitration product (fraction I) (0.377 g) was dissolved in acetonitrile (12 mL) which contained tetraethylammonium chloride (0.754 g). After 5 h, the ^{1}Hmr was constant and the solution was diluted with dichloromethane (25 mL) before treatment with water (2 × 10 mL). Solvent removal left a syrup (0.325 g), which was applied to a column (1 × 10 cm) of silica gel (3.5 g) for chromatographic separation using Skellysolve B – ethyl acetate (6:4). The α-D-chloride (**13**) (0.260 g, 74%) crystallized from diethyl ether – pentane; mp 86–88°C, $[\alpha]_D^{25}$ +145° (*c* 1, $CHCl_3$); ^{1}Hmr ($CDCl_3$) δ: 6.20 (d, 1H, $J_{1,2}$ = 3.9 Hz, H-1), 5.52 (q, 1H, $J_{4,5}$ = 1.4 Hz, H-4), 5.38 (q, 1H, $J_{3,4}$ = 3.2 Hz, H-3). *Anal.* calcd. for $C_{12}H_{16}N_3O_7Cl$: C 41.21, H 4.61, N 12.01, Cl 10.14; found: C 40.91, H 4.52, N 12.60, Cl 10.34.

The title compound **13** (3.0 g, 75%) was readily obtained by anomerization of 3,4,6-tri-*O*-acetyl-2-azido-2-deoxy-β-D-galactopyranosyl chloride (**16**) (4.0 g) in acetonitrile (80 mL) with tetraethylammonium chloride (13.2 g) at room temperature for 16 h. Passage through a short column of silica gel was again used to obtain the crystalline product.

The difference between the optical rotation for **13** reported above and that, $[\alpha]_D^{20}$ +39.1° (CH_3CN), recorded by Paulsen *et al.* (22) should be noted.

*3,4,6-Tri-*O*-acetyl-2-azido-2-deoxy-α-D-galactopyranosyl Bromide (**14**)*

Treatment of the product of the azidonitration (14.24 g) with a suspension of lithium bromide (16.53 g) in acetonitrile (140 mL) at room temperature for 3 h followed by product isolation as described for the preparation of **13**, provided a syrup (13.0 g). Chromatography on a column (4 × 48 cm) of silica gel which was developed with benzene (100 mL) and finally benzene – diethyl ether (1:1) gave 3,4,6-tri-*O*-acetyl-2-azido-2-deoxy-α-D-galactopyranosyl bromide (**14**) (8.98 g, 60% yield) which was recrystallized from diethyl ether – pentane; mp 97–98°C, $[\alpha]_D^{25}$ +188.6° (*c* 1.95, $CHCl_3$), $[\alpha]_D^{25}$ +172.6° (*c* 1, CH_3CN) (lit. (22) mp 90°C, $[\alpha]_D^{20}$ +104° (*c* 1.2, CH_3CN)); ^{1}Hmr ($CDCl_3$) δ: 6.47 (d, 1H, $J_{1,2}$ = 4.0 Hz, H-1), 5.49 (q, 1H, $J_{4,5}$ = 2.7 Hz, H-4), 5.33 (q, 1H, $J_{3,4}$ = 3.25 Hz, H-3), 4.48 (m, 1H, H-5), 3.96 (q, 1H, $J_{2,3}$ = 10.5 Hz, H-2), 2.14, 2.04, 2.02 (3s, 9H, $3CH_3$). *Anal.* calcd. for $C_{12}H_{16}N_3O_7Br$: C 36.56, H 4.09, N 10.66, Br 20.27; found: C 36.73, H 4.39, N 10.57, Br 20.27.

3,4,6-Tri-O-acetyl-2-azido-2-deoxy-β-D-galactopyranosyl Chloride (16)

A solution of lithium iodide (62.5 g) in acetonitrile (250 mL) was added in the dark to the product of the azidonitration (25.0 g). After 20 min at room temperature, dichloromethane (500 mL) and cold saturated aqueous sodium thiosulfate (500 mL) were added. The organic phase was separated and washed with ice-cold water (2 × 500 mL), dried over sodium sulfate, and evaporated *in vacuo* to a yellow foam. The ^{1}Hmr spectrum of a sample of this product indicated that it consisted of about 75% of 3,4,6-tri-*O*-acetyl-2-azido-2-deoxy-α-D-galactopyranosyl iodide (**15**); ^{1}Hmr ($CDCl_3$) δ: 6.87 (d, 1H, $J_{1,2}$ = 4.0 Hz, H-1), 5.18 (q, 1H, $J_{3,4}$ = 3.7 Hz, H-3), 3.34 (q, 1H, $J_{2,3}$ = 10.5 Hz, H-2). No attempt was made to purify this product.

Instead, it was treated immediately with a solution of tetraethylammonium chloride (11.0 g) in acetonitrile (57 mL). After vigorous shaking for 2.5 min at room temperature, the turbid mixture was diluted first with dichloromethane (150 mL) and then with 10% aqueous sodium thiosulfate (100 mL). The organic phase was then washed with water (100 mL), dried, and rapidly evaporated *in vacuo* to a syrup which was promptly triturated with diethyl ether. Crystalline 3,4,6-tri-*O*-acetyl-2-azido-2-deoxy-β-D-galactopyranosyl chloride (**16**) (11.3 g, mp 102–104°C) was deposited. The overall yield from the tri-*O*-acetyl-D-galactal used in the azidonitration was 31%; $[\alpha]_D^{25}$ −16.5° (*c* 1, $CHCl_3$): ir (Nujol) ν_{max}: 2120 (N_3) cm^{-1}; ^{1}Hmr ($CDCl_3$) δ: 5.37 (d, 1H, $J_{3,4}$ = 3.25 Hz, H-4), 5.13 (d, 1H, $J_{1,2}$ = 9.0 Hz, H-1), 4.84 (q, 1H, $J_{2,3}$ = 10.5 Hz, H-3), 3.82 (q, 1H, H-2), 2.15, 2.05, 2.03 (3s, 9H, $3CH_3$). *Anal.* calcd. for $C_{12}H_{16}N_3O_7Cl$: C 41.21, H 4.61, N 12.01, Cl 10.14; found: C 41.04, H 4.60, N 12.10, Cl 9.89.

The ^{1}Hmr data are in good accord with those reported by Paulsen *et al.* (22) for a syrupy product which was not further analyzed.

Glycosidation Reactions

In every case, a 10% molar excess of the alcohol (either benzyl alcohol or *tert*-butyl alcohol) over the glycosyl halide (1 mmol) was used and the reactions were conducted in the presence of Drierite (0.50 g). The reactions promoted by silver carbonate (3 mmol) and silver trifluoromethanesulfonate (0.05 mmol) employed dichloromethane (8 mL) as solvent and were conducted for 24 h at 5°C. The reactions promoted by mercuric cyanide (1.1 mmol) employed a 1:1 mixture of benzene and nitromethane (9 mL) as solvent and were conducted for 48 h at 50°C. The analyses of the reaction mixtures were made by isolation of the products in the usual manner using dichloromethane as the extracting solvent and then subjecting these syrupy products to examination by both ^{1}Hmr and ^{13}Cmr. The following signals were assigned: for the benzyl 3,4,6-tri-*O*-acetyl-2-azido-2-deoxy-D-galactopyranosides: ^{1}Hmr δ: 4.48 (d, $J_{1,2}$ = 8.2 Hz, H-1β), 5.20 (d, $J_{1,2}$ = 3.5 Hz, H-1α); ^{13}Cmr δ: 100.6 (C-1β), 97.1 (C-1α); and for the *tert*-butyl 3,4,6-tri-*O*-acetyl-2-azido-2-deoxy-D-galactopyranosides: ^{1}Hmr δ: 4.57 (d, $J_{1,2}$ = 8.0 Hz, H-1β) (H-1α signal was obscured); ^{13}Cmr δ: 97.3 (C-1β), 93.1 (C-1α). In the reactions involving the α-chloride **13** and promoted by mercuric cyanide, unreacted **13** remained and the amount of this material was estimated from the intensities of ^{1}Hmr doublet for H-1 ($J_{1,2}$ = 3.9 Hz) at 6.20 ppm and the ^{13}Cmr signal for C-1 at 92.8 ppm. This compound **13** also occurred in the reaction products from the mercuric cyanide promoted reactions of the β-chloride **16** (undoubtedly a product of anomerization of **16** by released chloride ion) and its formation effectively quenched the reaction. It was found that the relative intensities of the H-1 signals provided a ratio for the amounts of the α- and β-glycosides in good agreement with the ratio obtained by comparing the intensities of the signals for C-1. In the case of the *tert*-butyl glycosides the α/β ratio could also be estimated by comparison of the intensities for the signals of the *tert*-butyl groups at δ 1.30 (α-anomer) and 1.32 (β-anomer) ppm. The total yield of glycoside was estimated by comparison of the intensities of the signals present for the acetyl groups with those for the phenyl groups in the case of the benzyl glycosides and with those for the *tert*-butyl groups in the case of the *tert*-butyl glycosides.

Acknowledgements

The authors wish to acknowledge the financial support of the University of Alberta and the National Research Council of Canada (Grant A-172 to R. U. Lemieux), helpful discussions with Mr. Ole Hindsgaul, and the assistance of Mr. William Pettit in conducting the glycosidation reactions.

1. W. M. WATKINS. *In* Glycoproteins. *Edited by* A. Gottschalk. Elsevier, Amsterdam. 1972. p. 830.
2. P. VAITH and G. UHLENBRUCK. Z. Immun. Forsch. **154**, 1 (1978).
3. R. J. WINZLER. *In* Red cell membrane. *Edited by* G. A. Jamieson and T. J. Greenwalt. Lippincott, Philadelphia. 1969. p. 157.
4. J. F. CODINGTON, K. B. LINSLEY, and R. W. JEANLOZ. Carbohydr. Res. **40**, 171 (1975).
5. W. T. SHIER, Y. LIN, and A. L. DEVRIES. FEBS Lett. **54**, 135 (1975).
6. E. A. KABAT. *In* Blood and tissue antigens. *Edited by* D. Aminoff. Academic Press, New York. 1970. p. 187.
7. S.-I. HAKOMORI. Prog. Biochem. Pharmacol. **10**, 167 (1975).
8. R. U. LEMIEUX. Q. Rev. Chem. Soc. In press.
9. R. U. LEMIEUX and R. M. RATCLIFFE. Can. J. Chem. In preparation.
10. D. A. BAKER, R. M. RATCLIFFE, and R. U. LEMIEUX. Can. J. Chem. In preparation.
11. P. KARRER and J. MAYER. Helv. Chim. Acta, **20**, 407 (1937); M. L. WOLFROM and K. ONODERA. J. Am. Chem. Soc. **79**, 4737 (1957) and references therein.
12. R. KUHN and W. KIRSCHENLOHR. Justus Liebigs Ann. Chem. **600**, 126 (1956).
13. M. B. PERRY and A. C. WEBB. Can. J. Chem. **46**, 2481 (1968).
14. M. W. HORNER, L. HOUGH, and A. C. RICHARDSON. J. Chem. Soc. 1336 (1970).
15. S. P. JAMES, F. SMITH, M. STACEY, and L. F. WIGGINS. J. Chem. Soc. 625 (1946).
16. R. U. LEMIEUX and T. L. NAGABHUSHAN. Can. J. Chem. **46**, 401 (1968).
17. R. U. LEMIEUX, K. JAMES, T. L. NAGABHUSHAN, and Y. ITO. Can. J. Chem. **51**, 33 (1973).
18. R. U. LEMIEUX and R. V. STICK. Aust. J. Chem. **31**, 901 (1978).
19. H. PAULSEN, C. KÓLAŘ, and W. STENZEL. Angew. Chem. Int. Ed. Engl. **15**, 440 (1976).
20. H. PAULSEN. Pure Appl. Chem. **49**, 1169 (1977).
21. H. PAULSEN, W. STENZEL, and C. KÓLAŘ. Tetrahedron Lett. 2785 (1977).
22. H. PAULSEN, A. RICHTER, V. SINNWELL, and W. STENZEL. Carbohydr. Res. **64**, 339 (1978).

23. W. S. TRAHANOVSKY and M. D. ROBBINS. J. Am. Chem. Soc. **93**, 5256 (1971).
24. R. S. HANSEN and W. S. TRAHANOVSKY. J. Org. Chem. **39**, 570 (1974).
25. W. S. TRAHANOVSKY and J. CRAMER. J. Org. Chem. **36**, 1890 (1971).
26. R. U. LEMIEUX and R. M. RATCLIFFE. Can. J. Chem. In preparation.
27. R. U. LEMIEUX, K. B. HENDRIKS, R. V. STICK, and K. JAMES. J. Am. Chem. Soc. **97**, 4056 (1975).
28. R. U. LEMIEUX and J. HAYAMI. Can. J. Chem. **43**, 2162 (1965).
29. R. W. JEANLOZ and H. M. FLOWERS. J. Am. Chem. Soc. **84**, 3030 (1962).
30. M. L. WOLFROM, A. O. PITTET, and I. C. GILLAM. Proc. Natl. Acad. Sci. U.S.A. **47**, 700 (1961).
31. S. HANESSIAN and J. BANOUB. Carbohydr. Res. **53**, C13 (1977).
32. N. PRAVDIC and H. G. FLETCHER, JR. Croat. Chem. Acta, **39**, 71 (1967).
33. M. STACEY. J. Chem. Soc. 272 (1944).
34. Z. TARASIEJSKA and R. W. JEANLOZ. J. Am. Chem. Soc. **80**, 6325 (1958).

Studies of β-diketone complexes of rhenium. IX. The preparation and characterization of salts of the *trans*-dihalobis(pentane-2,4-dionato)rhenate(III) anion and an improved preparation of tris(pentane-2,4-dionato)rhenium(III)

C. J. L. Lock,[1] C. N. Murphy, and M. L. Turner

Institute for Materials Research, McMaster University, Hamilton, Ont., Canada L8S 4M1

Received September 12, 1978

C. J. L. Lock, C. N. Murphy, and M. L. Turner. Can. J. Chem. 57, 1252 (1979).

Salts of the anion $Re(C_5H_7O_2)Cl_2^-$ have been made by the reduction of both *cis*- and *trans*-$Re(C_5H_7O_2)Cl_2$ with a number of different reducing agents. The salts have been examined and characterized by physical methods. An improved preparation for $Re(C_5H_7O_2)_3$ is reported.

C. J. L. Lock, C. N. Murphy et M. L. Turner. Can. J. Chem. 57, 1252 (1979).

On a préparé des sels de l'anion $Re(C_5H_7O_2)Cl_2^-$ par réduction des $Re(C_5H_7O_2)Cl_2$ *cis* ainsi que *trans* par un certain nombre d'agents réducteurs. On a étudié les sels et on les a caractérisés par des méthodes physiques. On rapporte une méthode améliorée de préparation du $Re(C_5H_7O_2)_3$.

[Traduit par le journal]

Introduction

When attempting to reduce *trans*-$Re(C_5H_7O_2)_2Cl_2$, **A**, with either halide abstracting agents such as a zinc–methanol mixture or thallium acetylacetonate, Courrier (1) obtained blue-green solutions, which were air-unstable and from which no solid products were isolated. Subsequent work by us showed that the same colour could be produced in organic solvents by the action of a variety of reducing agents on **A** but again no solid products were isolated. The identity of the blue-green material was first indicated when a green solid was isolated by the reduction of **A** in benzene with sodium borohydride. The material dissolved in water giving a green solution which rapidly decolorized, with the precipitation of an orange solid, later shown to be **A**. It appeared as if the blue-green colour was a simple one-electron reduction product of **A**. This suggested alternate and more efficient methods of preparing salts of the $[Re(C_5H_7O_2)_2Cl_2]^-$ anion. We describe this work here.

Experimental

Analyses were performed by A. B. Gygli, Toronto, Ont. The infrared spectra in the region 4000–250 cm^{-1} were recorded on a Perkin Elmer #283 grating spectrophotometer. The samples were mixed with KBr and pressed into thin discs. In the region 250–100 cm^{-1}, the spectra were obtained using a Nicolet Model 7199 Fourier transform infrared spectrophotometer. A Mylar beam splitter was used. The optical path was flushed with dry N_2 and 100 interferrograms were recorded for each sample. The samples were ground into a mull with Nujol and sealed in a polyethylene bag under N_2. A Cary 14 spectrophotometer was used to record the electronic spectra of aqueous or CH_3CN solutions in the region 50 000–6000 cm^{-1}. Diffuse reflectance spectra in the region 36 000–4000 cm^{-1} were recorded on a Beckman DK2A recording spectrophotometer. Magnesium oxide was used as a reference. Measurements of the magnetic susceptibilities of powdered, solid samples were made by the Faraday method at three different field strengths. Calibration of the magnetic apparatus was accomplished using mercury tetrathiocyanatocobaltate(II) obtained from Eastman Organic Chemicals, Rochester, New York, and cupric sulfate pentahydrate (Baker Analyzed Reagent). Diamagnetic corrections were taken from Earnshaw (2). Mass spectra[2] were recorded on a Consolidated Electrodynamic Corporation mass spectrometer Model 21-110B. The samples were injected at 200°C. The electrical resistances of aqueous solutions of $K[Re(C_5H_7O_2)_2Cl_2]$ were measured in a N_2 atmosphere. This resistance was measured between two platinum electrodes about 1 cm apart. Reduction potentials were measured on a Princeton Applied Research Polarographic Analyzer, Model 174 operating in a DC mode. The potential was scanned from +0.5 to −1.0 V with respect to a saturated calomel electrode using two techniques (cathodic stripping voltammetry and single sweep voltammetry). The accuracy was checked by measuring the reduction potential for the reaction

$$Hg_2X_2 + 2e \rightarrow 2Hg + 2X^-$$

These were found to be 0.28 V (X = Cl) and 0.19 V (X = Br) compared with literature values (3) of +0.27 and 0.14 V, respectively.

The complexes $Re(C_5H_7O_2)_2X_2$ (X = Cl, Br) were prepared as described previously (4). Subsequent reactions were executed in a glove box under a nitrogen atmosphere. All solvents and reagents used were reagent grade. The solvents were deoxygenated by bubbling dry N_2 through them.

Thallium trans-*Dichlorobis(pentane-2-4-dionato)rhenate(III), Tl[Re(C₅H₇O₂)₂Cl₂]*

This complex was prepared by refluxing 1 mmol (0.45 g) of $Re(C_5H_7O_2)_2Cl_2$ with an equimolar amount of $Tl(C_5H_7O_2)$ (0.30 g) in ether for several hours. The resulting green solid was collected by filtration and dried *in vacuo*, yield 30%. *Anal.*

[1]Author to whom correspondence should be addressed.

[2]Mass spectra were recorded through the courtesy of Professor D. B. MacLean.

0008-4042/79/101252-05$01.00/0

calcd. (by hydrolysis and gravimetric determination as thallous chromate (5) and as $Re(C_5H_7O_2)_2Cl_2$, **A**): Tl 31.0, $Re(C_5H_7O_2)_2Cl_2$ 69.0; found: Tl 31 ± 1, $Re(C_5H_7O_2)_2Cl_2$ 69 ± 1. *Anal.* calcd. for precipitated A (M 455): C 26.4, H 3.1, Cl 15.6; found (M 420): C 26.2, H 3.6, Cl 17.5.

Sodium trans-*Dichlorobis(pentane-2,4-dionato)rhenate(III)*, *Na[Re(C₅H₇O₂)₂Cl₂]*

Several small shavings of sodium were added to a suspension of $Re(C_5H_7O_2)_2Cl_2$ (ca. 1 mmol) in acetonitrile (ca. 8 mL). The resulting deep green solution was separated from the unreacted rhenium(IV) complex by centrifuging and decanting. More solvent and sodium shavings were added to the unreacted complex and the process was repeated until additional shavings no longer resulted in the characteristic green color of the product. The product was then precipitated from solution by addition of ether and recrystallized from CH_3CN with ether, yield ~35%. *Anal.* calcd. for $C_{10}H_{14}Cl_2NaO_4Re$: C 25.1, H 3.0, Cl 14.8; found: C 24.9, H 3.1, Cl 14.7.

Potassium trans-*Dihalobis(pentane-2,4-dionato)rhenium(III)*, *K[Re(C₅H₇O₂)₂X₂] (X = Cl, Br)*

These green complexes were prepared in a manner identical to the preparation of $Na(Re(C_5H_7O_2)_2Cl_2]$ by using potassium shavings, yield ~30%. *Anal.* calcd. for $C_{10}H_{14}Cl_2KO_4Re$: C 24.3, H 2.9, Cl 14.3; found: C 24.3, H 3.0, Cl 14.2. *Anal.* calcd. for $C_{10}H_{14}Br_2KO_4Re$: C 20.6, H 2.4; found: C 20.9, H 2.7.

Tetraphenylarsonium trans-*Dichlorobis(pentane-2,4-dionato)-rhenate(III)*, *[(C₆H₅)₄As][Re(C₅H₇O₂)₂Cl₂]*

An aqueous solution of $K[Re(C_5H_7O_2)_2Cl_2]$ (ca. 1 mmol in 10 mL) was reacted with an aqueous solution of $[(C_6H_5)_4As]Cl$ (ca. 1 mmol in 10 mL). The product precipitated immediately. The product was purified by dissolving in dichloromethane followed by precipitation with diethylether. The product was analyzed by single crystal X-ray diffraction (6).

Preparation of Trispentane-2,4-dionatorhenium(III), *Re(C₅H₇O₂)₃*

(*a*) Dichlorobispentane-2,4-dionatorhenium(IV) (1 mmol, 0.45 g) and powdered zinc (1 mmol, 0.07 g) were stored in acetylacetone (~10 mL) under constant nitrogen flow. The solution rapidly turned bright green, then brown, and finally, after several minutes, to the deep maroon colour of $Re(C_5H_7O_2)_3$.

Ether (~20 mL) was added to the solution, which was then filtered through a fine sintered glass funnel on the vacuum line. The filtrate contained $Re(C_5H_7O_2)_3$ while unreacted $Re(C_5H_7O_2)_2Cl_2$, zinc, and zinc by-products were removed on the filter. $Re(C_5H_7O_2)_3$ was recovered from the solution by evaporation of the solvents under vacuum (yield ~50%).

(*b*) Dichlorobispentane-2,4-dionatorhenium(IV), (1 mmol, 0.45 g) in benzene solution was refluxed under nitrogen with zinc amalgam (~5 mL). In a few minutes a green solid was formed. After refluxing for several hours, the green solid redissolved giving a maroon solution of $Re(C_5H_7O_2)_3$. The purple solution was decanted from the amalgam and filtered to remove unreacted $Re(C_5H_2O_2)_2Cl_2$, zinc by-products, and rhenium metal. $Re(C_5H_7O_2)_3$ was recovered from solution by evaporation of benzene under vacuum (yield ~25%). *Anal.* calcd. for $C_{15}H_{21}O_6Re$: C 37.4, H 4.4; found (*a*): C 37.1, H 4.5; (*b*): C 37.0, H 4.4.

Results and Discussion

Addition of an alkali metal to *trans*-$Re(C_5H_7O_2)_2X_2$ (X = Cl, Br) in acetonitrile results in a one-electron reduction of the rhenium complex to give $M[Re(C_5H_7O_2)_2X_2]$ (M = Na or K). The reaction of $Tl(C_5H_7O_2)$ with $Re(C_5H_7O_2)_2Cl_2$ gives $Tl[Re(C_5H_7O_2)_2Cl_2]$. The reaction of $Re(C_5H_7O_2)_2X_2$ (X = Cl, Br, or I) with reducing agents to give similar salts appears to be more general than this, however. Although it was not possible to characterize the materials adequately, similar green products were obtained when using Zn, Zn amalgam, alkali metals, $NaBH_4$, or $LiAlH_4$ reacting with solutions of the Re(IV) complex in benzene or an ether. These complexes were all soluble in polar solvents such as acetonitrile, water, alcohol, or dimethyl sulphoxide and the aqueous solutions in air rapidly gave back $Re(C_5H_2O_2)_2X_2$. Where metals are the reductant the reduction involves a simple electron transfer but the reduction with the thallous salt must involve the concommitant formation of Tl(III). The reduction with the hydrides was more complex but likely involved hydrogen production.

Interestingly, the infrared spectra and X-ray diffraction patterns indicate that both *cis* and *trans* isomers of the Re(IV) complex give the same isomer of the Re(III) product. The thallium salt oxidized in the presence of air to give *trans*-$Re(C_5H_7O_2)_2Cl_2$ after several days. It is most likely, then, that the thallium salt is also the *trans* isomer and indeed the tetraphenylarsonium analogue has been shown to have this structure (6). The solid alkali metal salts of the chloro and bromo complexes also oxidize in the atmosphere to give $Re(C_5H_7O_2)_2X_2$ after several days. The solid Re(III) complexes are all stable indefinitely in the absence of oxygen. In aqueous medium, the reduction

$$Re(C_5H_7O_2)_2X_2 + e^- \rightarrow [Re(C_5H_7O_2)_2X_2]^-$$

occurs at virtually the same potential for both the chloro and bromo species (−0.28 and −0.29 V, respectively).

The alkali metal salts are soluble in water with $K[Re(C_5H_7O_2)_2Cl_2]$ behaving as a strong 1:1 electrolyte (Λ_0 = 106 cm² equiv^{-1} Ω^{-1}, infinite dilution; cf. NaCl Λ_0 126.5 cm² equiv^{-1} Ω^{-1}) (Fig. 1). This is consistent with a potassium cation and a $[Re(C_5H_7O_2)_2Cl_2]^-$ anion. The mass spectrum of $Tl[Re(C_5H_7O_2)_2Cl_2]$ (Table 1) does not show a parent ion peak; the highest peak occurs at *m/e* 455. This indicates a two-electron oxidation of the anion to give $[Re(C_5H_7O_2)_2Cl_2]^+$. The subsequent fragmentation of this ion is independent of its origin so that the mass spectrum of the thallium salt is very similar to that of the rhenium(IV) complex. The thallium salt has two additional peaks at *m/e* 205 and 203. The relative

TABLE 1. Mass spectral data for *cis*- and *trans*-$Re(C_5H_7O_2)_2Cl_2$ and for $Tl[Re(C_5H_7O_2)_2Cl_2]$

Fragment	*m/e*	Intensity		
		trans-$Re(C_5H_7O_2)_2Cl_2$	*cis*-$Re(C_5H_7O_2)_2Cl_2$	$Tl[Re(C_5H_7O_2)_2Cl_2]$
$Re(acac)_2Cl_2^+$	453, 455, 457*, 459	100	100	75
$Re(acac)_2Cl^+$	418, 420*, 422	6	5	8
$Re(acac)_2^+$	383, 385*	3	5	4
$ReCl(acac)(C_3H_4O)^+$	375, 377*, 379	—	5	<2
$ReO(acac)Cl_2^+$	370, 372, 374*, 376	<2	2	2
$Re(acac)Cl_2^+$	354, 356, 358*, 360	<2	2	<2
$ReO(acac)Cl^+$	335, 337*, 339	63	75	70
$Re(acac)Cl^+$	319, 321*, 323	<2	5	8
ReO(acac)	300, 302*	2	<2	4
$ReOCl_2^+$	271, 273, 275*, 277	5	7	4
$TlOH^+$	220, 222*	—	—	2
Tl^+	203, 205*	—	—	100

NOTE: Intensities given in terms of the strongest peak marked by an asterisk. In all cases, the isotope intensity ratios were as expected. acac is $C_5H_7O_2^-$.

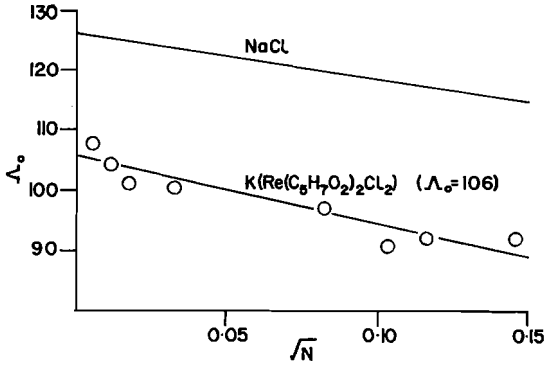

FIG. 1. Equivalent conductivity vs. $\sqrt{N}$ for NaCl and $K[Re(C_5H_7O_2)_2Cl_2]$.

intensities of these peaks are the same as the abundance of the two stable isotopes of thallium.

The infrared spectra of $M[Re(C_5H_7O_2)_2X_2]$ are listed in Table 2 for M = Na, X = Cl and M = K, X = Cl, Br. Also, some of the bands have been assigned empirically (see ref. 4). Assuming local C_{2h} symmetry, of the four Re—O stretching vibrations (A_g, B_{1g}, B_{2u}, and B_{3u}), only the vibrations of B_{2u} and B_{3u} symmetry will be ir active. It has previously been suggested (4) that bands observed around 463 and 250 cm^{-1} in $Re(C_5H_7O_2)_2X_2$ (X = Cl, Br) contain a large contribution from these modes. Similar bands observed around 450 and 250 cm^{-1} in each of the reduced species no doubt also contain a large contribution from these modes. It is noteworthy that the energies of these bands are similar for both the Re(IV) and the Re(III) complexes. It is likely then that the extra electron density in the reduced species is not associated with the ReO_4 moiety.

The Re—X stretching mode of B_{1u} symmetry is ir active and can be assigned to bands observed at 309 and 208 cm^{-1} in $Re(C_5H_7O_2)_2X_2$ (X = Cl and Br, respectively). In the reduced species these bands are found at 300 and 200 cm^{-1}, respectively. It is noted that for both the Re(IV) and the Re(III) complexes $\nu_{Cl}/\nu_{Br} \sim 1.5:1$. For a simple harmonic oscillator of a diatomic with the assumption that the force constant is the same for both Re—Cl and Re—Br the ratio of the frequencies is estimated (7) to be $\nu_{Cl}/\nu_{Br} \simeq 1.4$. The fairly close agreement between the observed and calculated ratios indicates that the Re—X stretching vibrations are fairly pure in both the Re(III) and Re(IV) complexes. If these Re—X vibrations are pure then their relative energies in the Re(IV) and Re(III) complexes should be indicative of the relative strengths of the Re—X bonds. Since the Re—X vibrations occur at slightly lower energy in the reduced species than in the Re(IV) complexes one would predict that the Re—X bond would be weaker and longer in the anions, as is observed (6).

The electronic spectra of the reduced species are summarized in Table 3. The numerous bands observed can be grouped into three regions. Region I contains bands of very high energy (greater than 35 000 cm^{-1}) and high extinction coefficients ($\sim$10 000 L mol^{-1} cm^{-1}). Region II contains bands of moderate energy (15 000–30 000 cm^{-1}) and moderately high extinction coefficients (2000–9000 L mol^{-1} cm^{-1}). Region III contains bands of relatively low energy (less than 15 000 cm^{-1}) and low extinction coefficients (100–400 L mol^{-1} cm^{-1}). A band observed around 30 000–36 000 cm^{-1} ($\varepsilon \sim$ 30 000 L mol^{-1} cm^{-1}) in many β-diketone complexes has been assigned (8) to transitions between π molecular orbitals of the β-diketone ligand. The complicated set of bands in region I is probably caused, at least in part, by this kind of ligand transition. The bands in

TABLE 2. Infrared spectra of $Na[Re(C_5H_7O_2)_2Cl_2]$, $K[Re(C_5H_7O_2)_2Cl_2]$, and $K[Re(C_5H_7O_2)_2Br_2]$*

$Na[Re(C_5H_7O_2)_2Cl_2]$	$K[Re(C_5H_7O_2)_2Cl_2]$	$K[Re(C_5H_7O_2)_2Br_2]$	Assignment
3085 w*	3085 w	3080 w	
	3000 w	3000 w	
2970 w	2950 sh	2950 sh	
2920 w	2920 w	2915 w	
		~1600 sh	
1520 s	1520 s	1515 s	ν_s(C—O)
	1490 sh		
1420 m	1420 m	1415 m	ν_{as}(C—C)
1355 s,bd	1360 s	1360 s	$\delta_s(CH_3)$
1330 sh	1330 sh		ν_{as}(C—O)
1280 m,sp	1280 m,sp	1280 s,sp	ν_s(C—C)
1190 w	1195 w	1190 w	δ(C—H)
1100 w,bd		1110 w,bd	
1025 sh			
1015 m	1020 m	1015 m	$\rho(CH_3)$
935 s	935 s	935 s	$\nu(C—CH_3)$
		920 s	
910 s	910 s	910 s	
		810 s	
802 s,sp	802 s,sp	800 s,sp	
765 w			
685 w	685 w	685 w	ν(M—O) + $\delta(C—CH_3)$ *or* δ(ring)
650 w	650 w	650 w	
625 s,sp	620 s,sp	620 s,sp	ν(M—O) + $\delta(C—CH_3)$ *or* δ(ring)
465 w	465 w		
450 m	450 m	450 m	ν(Re—O)
430 m	430 m	430 m	
300 s	300 s		ν(Re—Cl)
	268 s	285 m	
	258 s		
		205 sh	
		200 s	ν(Re—Br)
	159 m		
	154 m		
	133 s		
	129 s		

*Abbreviations: sh, shoulder; s, strong; m, medium; w, weak; bd, broad; sp, sharp.

TABLE 3. Electronic spectral data for $Na[Re(C_5H_7O_2)_2Cl_2]$, $K[Re(C_5H_7O_2)_2Cl_2]$, and $K[Re(C_5H_7O_2)_2Br_2]$

$Na[Re(C_5H_7O_2)_2Cl_2]$ reflectance (cm^{-1})	$K[Re(C_5H_7O_2)_2Cl_2]$					$K[Re(C_5H_7O_2)_2Br_2]$		
	Reflectance (cm^{-1})	CH_3CN		H_2O		Reflectance (cm^{-1})	CH_3CN	
		cm^{-1}	ε*	cm^{-1}	ε		cm^{-1}	ε
4 200	4 430					4 350		
7 410	7 410	7 550	170			7 335	7 670	95
10 990	11 430	10 500	325	11 500	365			
							15 385	9 090
15 870	16 670	14 900	7420	16 100	6 200	16 670	16 670	5 230
22 220	22 730	21 050	3150	22 700	2 570	22 220	21 740	3 295
30 300		30 300	4570	28 600	4 990	28 600	28 600	5 455
		36 400	9200	36 400	11 400	35 710	37 040	11 360
				37 700	10 300			
				40 800	9 800			
				44 400	9 600			

*ε is in L mol^{-1} cm^{-1}.

region II have extinction coefficients which are typical of metal → ligand or ligand → metal[3] charge transfer transitions (9). The strong band around 15 000 cm^{-1} results in the characteristic blue-green colour of the reduced species. The bands in region III are probably *d–d* transitions. The very low energy band ($\sim$4000 cm^{-1}) was too weak to be observed in solutions and its origin is unclear.

The reduced dichlorocomplexes exhibit room temperature magnetic susceptibilities which are typical of Re(III) in an octahedral environment (10) (1950×10^{-6} cgsu for M = Na and 2020 cgsu for M = K). Similarly, $K[Re(C_5H_7O_2)_2Br_2]$ has a room temperature magnetic susceptibility of 1370×10^{-6} cgsu.

The reduction of *trans*-$Re(C_5H_7O_2)_2Cl_2$ with zinc amalgam in aqueous medium results in a blue solution whose electronic spectrum is identical with that of an aqueous solution of $M[Re(C_5H_7O_2)_2Cl_2]$ (M = Na, K). This blue solution no doubt contains the $[Re(C_5H_6O_2)_2Cl_2]^-$ anion. In CH_3CN, however, this anion is formed only as an intermediate, the final product being $Re(C_5H_7O_2)_3$. The Zn(II) ions appear, then, to be catalyzing the formation of this latter complex. In aqueous solutions, the Zn(II) ion would be hydrated, thus poisoning the catalytic activity.

[3]The bands are probably ligand → metal charge transfer bands as they increase in energy as the formal oxidation state of the metal decreases.

Acknowledgement

We thank the National Research Council of Canada for financial support of this work.

1. W. D. Courrier. Ph.D Thesis, McMaster University, Hamilton, Ont. 1971.
2. A. Earnshaw. Introduction to magnetochemistry. Academic Press, New York, NY. 1968. pp. 5 and 6.
3. R. C. Weast (*Editor*). Handbook of chemistry and physics. 48th ed. The Chemical Rubber Co., Cleveland, OH. 1967–1968. p. D86.
4. W. D. Courrier, C. J. L. Lock, and G. Turner. Can. J. Chem. **50**, 1797 (1972).
5. A. I. Vogel. A textbook of quantitative inorganic analysis. Longmans, Green and Co. Ltd., London. 1961. p. 477.
6. C. J. L. Lock and C. N. Murphy. Acta Crystallogr. In press.
7. G. Herzberg. Spectra of diatomic molecules. 2nd ed. Van Nostrand, New York, NY. 1950. p. 75.
8. J. P. Fackler and F. A. Cotton. Inorg. Chem. **2**, 102 (1963).
9. A. B. P. Lever. Inorganic electronic spectroscopy. Elsevier Publishing Company, New York, NY. 1968. pp. 131, 224.
10. A. Earnshaw, B. N. Figgis, J. Lewis, and R. D. Peacock. J. Chem. Soc. 3132 (1961).

Structure et réactivité. III.[1] Evolutions stéréochimiques et chemins réactionnels des radicaux cyclohexyles substitués en 2 et cyclohexényles substitués en 3 (réaction de Kochi)

MAURICE MONNIER ET JEAN-PIERRE AYCARD[2]

Laboratoire de Chimie Organique Structurale, Université de Provence de Saint-Jérôme, 13397 Marseille Cedex 4, France

Reçu le 31 juillet 1978

MAURICE MONNIER et JEAN-PIERRE AYCARD. Can. J. Chem. 57, 1257 (1979).

L'étude de la réaction de chlorodécarboxylation par le tetracetate de plomb en présence de LiCl (réaction de Kochi) d'une série d'acides cyclohexaniques et cyclohexéniques montre que celle-ci s'accompagne d'une acétoxydécarboxylation. La proportion d'acétate formé augmente avec l'encombrement stérique du groupement R vicinal du centre radicalaire. La différence de stéréosélectivité de la formation des acétates et des chlorures est expliquée en considérant une évolution partielle à partir des conformères les moins stables.

MAURICE MONNIER and JEAN-PIERRE AYCARD. Can. J. Chem. 57, 1257 (1979).

The chlorodecarboxylation reaction (Kochi reaction) of a series of cyclohexane and cyclohexene carboxylic acids was investigated. Competitive acetoxy decarboxylation occurs, and the proportion of acetates is shown to increase with steric hindrance due to the R-substituent relative to the radical center. A partial evolution involving high energy conformers is suggested to explain the difference of stereoselectivities in the formation of acetates and chlorides.

Introduction

Sous l'action du tétracétate de plomb et d'un chlorure alcalin, un acide carboxylique est facilement décarboxylé et le radical ainsi formé évolue vers le chlorure d'alkyle ou vers l'acétate correspondant. Mise au point par Kochi (2), cette réaction a été particulièrement bien étudiée tant au point de vue de la synthèse que du mécanisme, mais seuls des travaux limités ont abordé l'aspect stéréochimique de cette réaction (3–5). Ce mémoire est une contribution à cet aspect de la réaction de Kochi.

Pour approfondir ces problèmes, il est indispensable d'utiliser des substrats cyclohexaniques étant donné les possibilités de comparaison avec d'autres réactions radicalaires induisant des faces diastéréotopiques (6–8) et en particulier l'excellente analyse de Gruselle et Lefort (9).

Avec ces substrats, il est également possible d'étudier l'influence des effets stériques sur la stéréosélectivité et en passant aux homologues cyclohexéniques nous sommes en mesure de faire varier ces effets stériques.

Résultats

Ils sont rapportés dans le Tableau 1. La première observation est l'identité de stéréosélectivité quelle que soit la stéréochimie des acides de départ. Ceci est tout à fait conforme avec l'hypothèse du passage par un même radical intermédiaire. La seconde constatation est celle de l'importance de l'évolution vers les acétates lorsque l'encombrement stérique augmente à proximité du site radicalaire; cette caractéristique de la réaction de Kochi n'avait pas encore été mise en évidence.

En série cyclohexanique, pour la réaction normale de formation des chlorures, les stéréosélectivités observées sont en faveur de l'isomère thermodynamiquement le moins stable, même pour le radical *tert*-butyl-2 cyclohexyle pour lequel le pourcentage de chlorure *trans* obtenu est très légèrement supérieur au pourcentage de chlorure *cis*. En effet, il a été montré que pour ces structures l'existence d'une interaction gauche *tert*-butyle-X déstabilise fortement l'isomère *trans* (0.3 kcal pour X = OH (10), 1.5 kcal pour X = CN (11)) par rapport à l'isomère *cis*.

En série cyclohexénique, pour le radical méthyl-3 cyclohexényle, le chlorure *trans*, vraisemblablement le plus stable (11), est formé préférentiellement; par contre, pour le radical *tert*-butyl-3 cyclohexényle nous obtenons le résultat inverse.

Pour la réaction "anormale" de formation des acétates, les stéréosélectivités sont en faveur de l'isomère thermodynamiquement le plus stable dans trois cas sur quatre; l'exception étant celle de la structure *tert*-butyl-2 cyclohexyle.

Enfin, avec la réaction de chlorodécarboxylation de l'acide cyclohexène-3 carboxylique optiquement actif (12), nous avons confirmé que le chlorure et les deux acétates formés ont perdu toute activité optique, ce qui est en accord avec le passage par un radical en interconversion rapide.

[1]Pour la partie II, voir réf. 1.

[2]Auteur à qui la correspondance doit être adressée.

0008-4042/79/101257-05$01.00/0

TABLEAU 1. Pourcentages des produits formés lors de la réaction de Kochi*

[11] RCOOH *cis* ou *trans* →		RCl *cis* (%)	RCl *trans* (%)	+ ROAc *cis* (%)	ROAc *trans* (%)
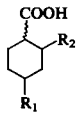	$R_1 = C(CH_3)_3$				
	$R_2 = H$	63	36	1	
	$R_2 = CH_3$	67	33	—	
	$R_1 = H$				
	$R_2 = CH_3$	50	33.7	4.7	11.6
	$R_2 = C(CH_3)_3$	32.7	33.5	5.6	28.2
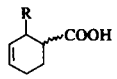	R = CH_3	36	54	2	8
	R = $C(CH_3)_3$	60	10	3	27
	R = H	83.8		16.2	14a / 2.2b

*a = acétoxy-4 cyclohexène; b = acétoxy-3 cyclohexène.

Discussion

La structure *tert*-butyl-4 cyclohexyle constitue une référence pour comparer les diverses réactions; la stéréosélectivité obtenue (27%) résulte d'une attaque axiale préférentielle et est tout à fait analogue à celles (30 à 40%) de la majorité des réactions qui conduisent au chlorure d'alkyle en passant par le radical *tert*-butyl-4 cyclohexyle (4, 9, 13); une stéréosélectivité plus marquée (60%) a toutefois été observée par Gruselle et coll. (9) lors de la décomposition thermique de peracides qui conduit aux alcools correspondants. Il est évident qu'au delà de ces petites différences qui résultent des comportements spécifiques des espèces chimiques opposées au radical, dans l'étape qui détermine les proportions des produits, la stéréosélectivité est essentiellement déterminée par la structure du radical. L'interprétation est fondée sur les hypothèses d'états de transition précoces et d'une prédominance des interactions d'éclipsage (attaque équatoriale) sur les interactions stériques (attaque axiale) c'est-à-dire, d'un modèle tout à fait similaire à celui de Cherest et Felkin (14). La première hypothèse est tout à fait satisfaisante compte tenu de la forte exothermicité de l'étape qui conduit du radical au chlorure d'alkyle. Dans cette série cyclohexanique la présence d'un groupement méthyle équatorial vicinal du centre radicalaire ne modifie que légèrement la stéréosélectivité; ce groupement méthyle équatorial a donc des contingences stériques pratiquement identiques vis-à-vis des deux types d'attaques (axiale et équatoriale).

La chlorodécarboxylation de l'acide méthyl-2 cyclohexane carboxylique présente une stéréosélectivité plus faible (20%), la diminution correspondante pouvant être attribuée à une évolution partielle à partir du conformère à méthyl axial du radical. A partir de cette hypothèse, et en considérant l'enthalpie libre conformationnelle du groupement méthyle égale à 1.6 kcal mol^{-1} dans le radical méthyl-2 cyclohexyle (par analogie avec l'équilibre conformationnel de la méthyl-2 cyclohexanone (15)); nous pouvons calculer (cf. partie expérimentale) les différences d'enthalpie libre entre les différents états de transition soit (en kcal mol^{-1}):

$$[1] \quad \begin{aligned} (G^{\ddagger})_E{}^e - (G^{\ddagger})_E{}^a &\simeq +0.5 \\ (G^{\ddagger})_A{}^e - (G^{\ddagger})_E{}^a &\simeq +1.5 \\ (G^{\ddagger})_A{}^a - (G^{\ddagger})_E{}^a &\simeq -0.5 \end{aligned}$$

Compte tenu des approximations, les valeurs obtenues ne constituent que des ordres de grandeurs. L'inégalité $\Delta G^{\ddagger}{}_A{}^a < \Delta G^{\ddagger}{}_A{}^e$ montre une réactivité importante du conformère à méthyl axial. Dans ces conditions, la formation du chlorure *trans* s'effectue essentiellement à partir du conformère thermodynamiquement le moins stable, alors que du fait de la relation $\Delta G^{\ddagger}{}_E{}^a \simeq \Delta G^{\ddagger}{}_A{}^e$ le chlorure *cis* peut être obtenu à partir des deux conformations (16).

Ces résultats peuvent être expliqués de la façon suivante. Un groupement méthyle équatorial vicinal du centre radicalaire désactive au même degré et l'attaque axiale et l'attaque équatoriale de sorte qu'il ne modifie pratiquement pas la stéréosélectivité, alors qu'un méthyl axial désactive l'attaque équatoriale.

Avec le radical *tert*-butyl-2 cyclohexyle, la réaction de formation des chlorures d'alkyle s'effectue avec une stéréosélectivité quasi nulle (1%); d'autre part, la proportion d'acétates concurrents est nettement augmentée, ce qui suggère une diminution des vitesses de la réaction de formation des chlorures.

$$[2] \quad R^{\cdot} \rightarrow RCl$$

Le premier de ces faits expérimentaux résulte soit d'une influence spécifique du groupement *tert*-butyle sur la vitesse d'attaque axiale sur le conformère équatorial, dont la diminution serait due à un encombrement stérique plus marqué, soit à une contribution d'un autre conformère. N'ayant aucun moyen de contrôler la validité de la première hypothèse, nous pouvons au moins montrer que la seconde est raisonnable. En effet, par analogie avec les données relatives à la *tert*-butyl-2 cyclohexanone, nous pouvons considérer que le radical *tert*-butyl-2 cyclohexyle présente un équilibre entre un conformère à groupement *tert*-butyle équatorial et un conformère twist 1–4 (cf. Fig. 1).

La structure du deuxième conformère n'a pas été prouvée mais elle est très raisonnable compte tenu des données récentes (17). Un calcul analogue au précédent permet d'accéder aux différences d'enthalpie libre entre états de transition.

$$[3] \qquad (G^{\neq})_E{}^e - (G^{\neq})_E{}^a \simeq +0.4$$
$$(G^{\neq})_T{}^e - (G^{\neq})_E{}^a \simeq -1.2 \text{ kcal mol}^{-1}$$

La stéréosélectivité du conformère twist (T) est considérée comme totale car l'évolution vers le chlorure *trans* n'implique pas d'interaction *syn*-1,3 avec l'un des méthyl du *tert*-butyle (cf. Fig. 1); il est alors logique que l'énergie d'activation correspondante soit très nettement inférieure à celle de la réaction du conformère équatorial.

La formation des acétates pourrait être due à une réaction de type S_N2, catalysée par le tetracétate de plomb, sur les chlorures formés. Différents essais de substitution dans les conditions de la réaction de Kochi nous ont permis d'écarter cette éventualité.

Ce problème pouvait aussi être abordé dans le cadre de l'hypothèse d'une évolution du radical vers le carbocation correspondant (2, 5). Des essais d'acétoxydécarboxylation en milieu ionique (18) ne nous ayant pas conduit à des résultats analogues à ceux de la réaction de Kochi, nous resterons dans le cadre d'une évolution directe à partir des radicaux pour tenter de dégager une interprétation cohérente des résultats.

La première remarque concerne une différence de comportements de radicaux *cis*-méthyl-2 *tert*-butyl-4 cyclohexyle et méthyl-2 cyclohexyle, le premier conduisant exclusivement aux chlorures, alors que le second conduit à 16.3% d'acétates. L'explication la plus simple est que ces acétates résultent essentiellement de l'évolution à partir du conformère à méthyl axial; cela expliquerait également la stéréosélectivité (42%) en faveur de l'acétate *trans* (attaque axiale sur le conformère à méthyl axial). Cette interprétation implique que la réaction de formation des acétates est plus sensible aux effets stériques que celle qui conduit aux chlorures, ce qui est en accord avec le renforcement de la stéréosélectivité (67%) quand c'est le radical *tert*-butyl-2 cyclohexyle qui évolue vers les acétates correspondants. Ce renforcement de stéréosélectivité nous permet également d'éliminer l'hypothèse d'un état de transition plus tardif pour la réaction conduisant aux acétates; en effet, pour les *tert*-butyl-2 acétoxycyclohexane c'est l'isomère *cis* qui est thermodynamiquement le plus stable (10).

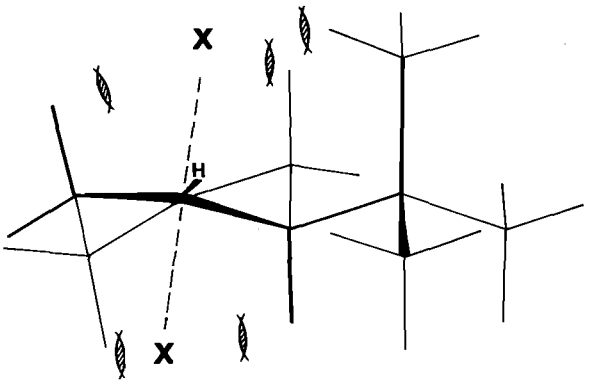

FIG. 1. Conformère twist du radical *tert*-butyl-2 cyclohexyle.

Enfin, pour l'évolution des radicaux cyclohexényles vers les chlorures les résultats sont a priori contradictoires; pour l'homologue *tert*-butylé, la stéréosélectivité (72%) est fortement en faveur du chlorure *cis* thermodynamiquement le moins stable (11), c'est-à-dire un comportement analogue à celui observé dans la série cyclohexanique. Au contraire le radical méthyl-3 cyclohexényle évolue vers le chlorure *trans* thermodynamiquement le plus stable; ce dernier résultat s'explique si l'on admet que l'équilibre conformationnel de ce radical est en faveur du conformère à méthyl pseudo-axial. Cette hypothèse ne semble pas déraisonnable; elle nous conduira à développer une analyse conformationnelle de ce type de structure.

Conclusion

La chlorodécarboxylation de Kochi est donc accompagnée d'une réaction parasite qui est une acétoxydécarboxylation et qui devient relativement importante lorsque les radicaux intermédiaires disposent d'un groupement encombrant au voisinage du site radicalaire. Les deux réactions sont examinées du point de vue de leur stéréosélectivité; elles sont généralement opposées mais peuvent être interprétées simplement en considérant une évolution partielle à partir des conformères les moins stables.

Partie expérimentale

Les spectres ir et rmn ont été enregistrés sur des appareils Perkin-Elmer modèle 377 et Varian EM 360 respectivement. Les analyses chromatographiques ont été effectuées sur des appareils Girdel 3000 ou Aérograph 90P.

Identification des composés

Les différents produits de réaction sont séparés par cppv et identifiés par spectroscopie infrarouge et par rmn (largeur de bande du proton *gem* du groupement fonctionnel). Le chloro-4 cyclohexène a été identifié à l'aide des spectres ir (19) et rmn déjà décrits. L'identification des acétoxy-3 et -4 cyclohexènes a été effectuée par comparaison avec des échantillons authentiques obtenus par estérification des cyclohexène-2,ol et cyclohexène-3,ol.

Les *tert*-butyl-3 X-4 cyclohexènes ont été identifiés par analyse des spectres rmn des composés trideutériés en position 3,6,6.

L'examen des constantes de couplage montre que les dérivés *cis* sont conformationnellement homogènes alors que les dérivés *trans* présentent un équilibre conformationnel.

L'identification des dérivés cyclohexéniques a d'autre part été confirmée par la comparaison de leurs produits d'hydrogénation avec les dérivés cyclohexaniques précédemment obtenus.

Paramètres des composés synthétisés

tert-*Butyl-2 chlorocyclohexanes*

Cis: ^{1}Hmr ($CDCl_3$) δ: 1 (s, 9H, C-2—t*Bu*), 1.0–2.2 (m, 9H, ring), 4.7–4.5 (m, 1H, *H*—C-1—Cl).

Trans: ^{1}Hmr ($CDCl_3$) δ: 1.05 (s, 9H, C-2—t*Bu*), 1.05–2.6 (m, 9H, ring), 4.2–3.6 (m, 1H, *H*—C-1—Cl).

tert-*Butyl-2 acétoxy cyclohexanes*

Cis: ^{1}Hmr ($CDCl_3$) δ: 0.9 (s, 9H, C-2—t*Bu*), 0.9–2.2 (m, 9H, ring), 2.07 (s, 3H, O—CO—*CH*$_3$), 5.03–5.23 (m, 1H, *H*—C-1—O—CO—CH_3).

Trans: ^{1}Hmr ($CDCl_3$) δ: 0.9 (s, 9H, C-2—t*Bu*), 0.9–2.2 (m, 9H, ring), 2.07 (s, 3H, O—CO—*CH*$_3$), 4.5–5 (m, 1H, *H*—C-1—O—CO—CH_3).

Méthyl-2 chlorocyclohexanes

Cis: ir (20); ^{1}Hmr ($CDCl_3$) δ: 1.1 (d, 3H, C-2—*CH*$_3$), 1.2–2.13 (m, 9H, ring), 4.23–4.43 (m, 1H, *H*—C-1—Cl).

Trans: ir (20); ^{1}Hmr ($CDCl_3$) δ: 1.1 (d, 3H, C-2—*CH*$_3$), 0.9–2.43 (m, 9H, ring), 3.31–3.83 (m, 1H, *H*—C-1—Cl).

Méthyl-2 acétoxycyclohexanes

Cis: ^{1}Hmr ($CDCl_3$) δ: 1 (d, 3H, C-2—*CH*$_3$), 1–2 (m, 9H, ring), 2.1 (s, 3H, O—CO—*CH*$_3$), 4.9–5.1 (m, 1H, *H*—C-1—O—CO—CH_3).

Trans: ^{1}Hmr ($CDCl_3$) δ: 1 (d, 3H, C-1—*CH*$_3$), 1–2 (m, 9H, ring), 2.1 (s, 3H, O—CO—*CH*$_3$), 4.1–4.6 (m, 1H, *H*—C-1—O—CO—CH_3).

Méthyl-3 chloro-4 cyclohexènes

Cis: ir ν_{max}: 1653 (m, C=C), 680–646 (S, C—Cl); ^{1}Hmr ($CDCl_3$) δ: 1.3 (d, 3H, C-3—*CH*$_3$), 1.7–2.75 (m, 7H, ring), 4–4.3 (m, 1H, *H*—C-4—Cl), 5.03–5.7 (m, 2H, *H*—C=C—*H*).

Trans: ir ν_{max}: 1653 (m, C=C), 680 (w, C—Cl); ^{1}Hmr ($CDCl_3$) δ: 1.16 (d, 3H, C-3—*CH*$_3$), 1.76–1.28 (m, 7H, ring), 3.63–4.1 (m, 1H, *H*—C-4—Cl), 5.4–6 (m, *H*—C=C—*H*).

Méthyl-3 acétoxy-4 cyclohexènes

Cis: ^{1}Hmr ($CDCl_3$) δ: 0.8–1.4 (m, 3H, C-3—*CH*$_3$), 0.8–2.6 (m, 7H, ring), 1.93 (s, 3H, O—CO—*CH*$_3$), 4.17–4.3 (m, 1H, *H*—C-4—O—CO—CH_3), 5.3–5.6 (m, 2H, *H*—C=C—*H*).

Trans: ^{1}Hmr ($CDCl_3$) δ: 0.95 (d, 3H, C-3—*CH*$_3$), 0.8–2.6 (m, 7H, ring), 1.95 (s, 3H, O—CO—*CH*$_3$), 4.23–4.4 (m, 1H, *H*—C-4—O—CO—CH_3), 5.3–5.6 (m, 2H, *H*—C=C—*H*).

tert-*Butyl-3 X-4 cyclohexènes*-d_3 *3,6,6* (cf. Schéma 1) (*X* = *Cl*)

Cis: ir ν_{max}: 1652 (m, C=C), 659 (S, C—Cl); ^{1}Hmr ($CDCl_3$) δ: 1 (s, 9H, C-3—t*Bu*), 1.84 (d, 2H, C-5—*H*-4—*H*-5), 4.31 (m, 1H, $^3J_{34} = {}^3J_{35}$ = 4.2 Hz, C-4—*H*-3), 5.61 (m, 1H, $^3J_{ij}$ = 10.5 Hz, $^4J_{3i}$ = 1.2 Hz, C-2—*H*-*i*), 5.78 (d, 1H, $^3J_{ij}$ = 10.5 Hz, C-1—*H*-*j*).

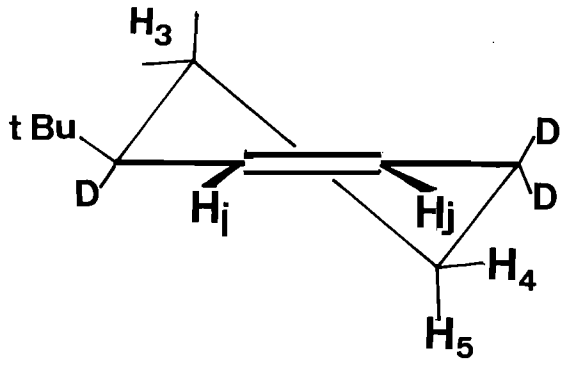

SCHÉMA 1

Trans: ir ν_{max}: 1654 (m, C=C), 630–668 (S, C—Cl).

tert-*Butyl-3 X-4 cyclohèxenes*-d_3 (cf. Schéma 1) (*X* = *OAc*)

Trans: ^{1}Hmr ($CDCl_3$) δ: 1 (s, 9H, C-3—t*Bu*), 1.58 (m, 1H, J_{34} = 8.3 Hz, C-5—*H*-4), 1.78 (m, 1H, $^3J_{35}$ = 3.6 Hz, J_{45} = −12.8 Hz, C-5—*H*-5), 4.90 (m, 1H, C-4—*H*-3), 5.58 (d, 1H, $^3J_{ij}$ = 10.4 Hz, C-2—*H*-*i*), 5.68 (d, 1H, $^3J_{ij}$ = 10.4 Hz, C-1—*H*-*j*).

Obtention des composés

Les acides de départ ont été obtenus par saponification des esters correspondants (11).

L'hydrogénation catalytique a été effectuée sur Pd/C 5% Fluka dans l'éthanol sous 1 atm.

La réaction de chlorodécarboxylation a été effectuée suivant le mode opératoire décrit par Kochi (2). Les rendements (acétates + chlorures) après séparation par cppv sont de 50% pour les dérivés méthylés et de 70% pour les dérivés *tert*-butylés.

Le tétracétate de plomb a été obtenu suivant la méthode de Vogel (21).

Séparation des composés

Les R-3 X-4 cyclohexènes (R = CH_3, $C(CH_3)_3$; X = Cl, OAc) ont été séparés sur une colonne de Carbowax 6000 de 2.5 m, diamètre 9.6 mm/colonne 115°C/débit 150 mL/min.

Les R-2 X-1 cyclohexanes (X = Cl, OAc; R = CH_3, $C(CH_3)_3$) ont été séparés sur une colonne de Réoplex 400 de 2.5 m, diamètre 9.6 mm/colonne 120°C/débit 120 mL/min.

Les acétoxy-1 *tert*-butyl-4 cyclohexane et chloro-1 *tert*-butyl-4 cyclohexane ont été séparés sur une colonne de tricresyl phosphate de 2.5 m, diamètre 9.6 mm/colonne 90°C/débit 120 mL/min.

Les chromatographies analytiques ont été effectuées sur des colonnes analogues.

Calcul des énergies libres des états de transition

Soient k_E^e et k_E^a les constantes de vitesse pour l'attaque sur le radical à groupement R équatorial et k_A^e et k_A^a celles pour l'attaque sur le radical à groupement R axial (cf. Schéma 2). La lettre minuscule désigne la face d'entrée, la majuscule la position du groupement.

La différence des différences d'énergie libre de l'état de transition suivant les attaques est pour chaque conformère

$$[4] \qquad \Delta\Delta G^{\ddagger}_E = \Delta G^{\ddagger}{}_E{}^e - \Delta G^{\ddagger}{}_E{}^a$$

$$[5] \qquad = -RT \ln (k_E{}^e/k_E{}^a)$$

$$[6] \qquad \Delta\Delta G^{\ddagger}_A = \Delta G^{\ddagger}{}_A{}^a - \Delta G^{\ddagger}{}_A{}^e$$

$$[7] \qquad = -RT \ln (k_A{}^a/k_A{}^e)$$

La réaction ayant un contrôle cinétique, le rapport des

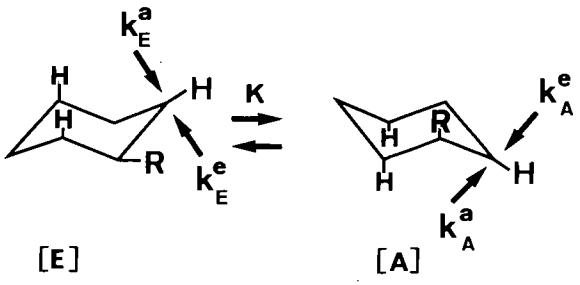

SCHÉMA 2

produits formés est égal au rapport de leurs vitesses de formation:

$$[8]\qquad \frac{[cis]}{[trans]}=\frac{\mathrm{d}[cis]/\mathrm{d}t}{\mathrm{d}[trans]/\mathrm{d}t}=\frac{k_E^a[E]+k_A^e[A]}{k_E^e[E]+k_A^a[A]}$$

$$=\frac{k_E^a+k_A^eK}{k_E^e+k_A^aK}\quad\text{avec}\quad K=[A]/[E]$$

La détermination de K à partir de la différence d'enthalpie libre ΔG^0 du radical permet de déterminer les différences d'énergie libre dans les états de transitions des différents conformères.

$$[9]\qquad \Delta\Delta G^{\ddagger}_{cis}=\Delta G^{\ddagger}_{E^a}-\Delta G^{\ddagger}_{A^e}=-RT\ln a\quad a=k_E^a/k_A^e$$

$$[10]\qquad \Delta\Delta G^{\ddagger}_{trans}=\Delta G^{\ddagger}_{E^e}-\Delta G^{\ddagger}_{A^a}=-RT\ln b$$

$$b=k_E^e/k_A^a$$

Pour le calcul des différences d'énergie libre: pour R = CH_3 le rapport k_E^e/k_E^a est tiré de nos résultats alors que le rapport k_A^a/k_A^e a été tiré des travaux de Cruselle et Lefort (8) sur la décomposition thermique de peracides cyclohexaniques. Pour R = $(CH_3)_3$—C nous avons considéré $k_A^e = 0$.

Remerciements

Les auteurs remercient les rapporteurs pour leurs suggestions et leurs remarques constructives.

1. L. PIZZALA, J. P. AYCARD et H. BODOT. J. Org. Chem. **43**, 1013 (1978).
2. J. K. KOCHI. J. Org. Chem. **30**, 3265 (1965).
3. J. K. KOCHI. Free radicals. Vol. 1. *Editeur*: J. K. Kochi. Wiley Interscience, New York, NY. 1973. p. 591.
4. R. D. STOLOW et T. W. GIANTS. Tetrahedron Lett. 695 (1971); R. D. STOLOW et T. W. GIANTS. J. Am. Chem. Soc. **93**, 3536 (1971).
5. M. L. MIHAILOVIC, J. BOSNJAK et Z. CEKOVIC. Bull. Acad. Serbe Arts, **14**, 91 (1976).
6. F. R. JENSEN, L. H. GALE et J. E. RODGERS. J. Am. Chem. Soc. **90**, 5793 (1968).
7. P. BOLDT, L. SCHULZ, U. KLINSMANN, H. KOSTER et W. THIELECKE. Tetrahedron, **26**, 3591 (1970).
8. M. GRUSELLE, J. FOSSEY, D. LEFORT, C. LAMARRE et J. C. RICHER. Can. J. Chem. **54**, 905 (1976); M. GRUSELLE. Thèse d'état, Université de Paris, France. 1975.
9. M. GRUSELLE, M. TICHY et D. LEFORT. Tetrahedron, **28**, 3885 (1972).
10. D. J. PASTO et R. D. RAO. J. Am. Chem. Soc. **92**, 5151 (1970).
11. J. P. AYCARD et H. BODOT. Can. J. Chem. **51**, 741 (1973).
12. O. CEDER et B. HANSON. Acta Chem. Scand. **24**, 2693 (1970).
13. F. D. GREENE, C. CHU et J. WALIA. J. Am. Chem. Soc. **84**, 2463 (1962).
14. M. CHEREST et H. FELKIN. Tetrahedron Lett. 2205 (1968).
15. N. L. ALLINGER et H. M. BLATTER. J. Am. Chem. Soc. **83**, 994 (1961).
16. D. C. WIGFIELD et D. J. PHELPS. J. Am. Chem. Soc. **96**, 543 (1974).
17. R. VIANI, J. LAPASSET, J. P. AYCARD, R. LAFRANCE et H. BODOT. Acta Crystallogr. **34**, 1190 (1978).
18. B. C. C. CANTELLO, J. M. MELLOR et G. SCHOLES. J. Chem. Soc. Perkin Trans. II, 1589 (1973).
19. F. FERNANDES-GOMES, O. D. UL'YANOVA et YU. PENTIN. Russ. J. Phys. Chem. **47**, 252 (1973).
20. U. KH. AGAEV, A. T. ALYEV, S. Z. RIZAEVA et YU. A. PENTIN. Zh. Prikl. Spectrosk. **19**, 739 (1973).
21. A. I. VOGEL. Practical organic chemistry. Longmans, London, England. 1962.

Canadian Journal of Chemistry
Published by
THE NATIONAL RESEARCH COUNCIL OF CANADA

Journal canadien de chimie
Publié par
LE CONSEIL NATIONAL DE RECHERCHES DU CANADA

Volume 57 Number 11 June 1, 1979

Volume 57 numéro 11 1 juin 1979

Complexation of cadmium(II) with water- and soil-derived fulvic acids: effect of pH and fulvic acid concentration

ROBERT A. SAAR AND JAMES H. WEBER[1]

Department of Chemistry, Parsons Hall, University of New Hampshire, Durham, NH 03824, U.S.A.

Received November 21, 1978

ROBERT A. SAAR and JAMES H. WEBER. Can. J. Chem. **57**, 1263 (1979).

We studied the conditional stability constants of cadmium(II) bound to fulvic acid derived from water and soil, and found that (1) stability constants increased with increasing pH, and (2) stability constants decreased as we increased the fulvic acid concentration toward 70 mg/L. The second effect does not occur for the copper(II)–fulvate system. Conformational changes that occur when a fulvic acid solution becomes more concentrated apparently weaken sites that are otherwise more accessible to weak-binding cadmium. From pH 4 to 8, the overall conditional stability constant increases from 1.4 to 12 × 10^3 for water-derived fulvic acid and from 1.7 to 43 × 10^3 for soil-derived fulvic acid. Increases in fulvic acid concentration from 20 mg/L to 70 mg/L halve the conditional stability constant at a given pH.

ROBERT A. SAAR et JAMES H. WEBER. Can. J. Chem. **57**, 1263 (1979).

Nous avons étudié les constantes de stabilité conditionnelles du cadmium(II) lié à de l'acide fulvique provenant d'eau et de sel et nous avons trouvé que (1) les constantes de stabilité augmentent avec le pH et (2) les constantes de stabilité diminuent lorsque nous augmentons la concentration de l'acide fulvique vers 70 mg/L. On ne note pas le second effet avec le système cuivre(II)/fulvate. Les changements conformationnels qui se produisent lorsqu'une solution d'acide fulvique devient plus concentrée semblent affaiblir les sites qui sont autrement plus accessibles au cadmium qui se lie faiblement. Du pH = 4 à 8, la constante de stabilité conditionnelle globale augmente de 1.4 à 12 × 10^3 pour l'acide fulvique provenant d'eau et de 1.7 à 43 × 10^3 pour l'acide fulvique provenant du sol. Lorsqu'on porte la concentration de l'acide fulvique de 20 mg/L à 70 mg/L à un pH donné, on réduit la constante de stabilité conditionnelle de moitié.

[Traduit par le journal]

Introduction

Fulvic acid (FA) is the fraction of naturally occurring humic matter that remains in solution at low pH. Its properties, particularly its ability to bind heavy metals, have been studied, but most fulvic acid for these studies has been extracted from soils (1–7). Work on humic materials extracted from natural waters is usually done on the total dissolved humic matter (fulvic and humic acids), not just on aquatic fulvic acid (6, 8–11).

Our group has isolated fulvic acids from river water (WFA) and from a podzol soil (SFA), and has carefully characterized them chemically and spectroscopically (12–14). This study describes the complexation of Cd^{2+} to these well-characterized samples. Many workers have noted that complexation of heavy metals to fulvic acid increases as the pH of the solution rises (3, 5, 6). The literature also shows decreased heavy-metal binding by fulvic acid as the ionic strength of the solution increases (10).

A third variable, largely overlooked, is the fulvic acid concentration itself. Fulvic acid is characterized as a polyelectrolyte (7), a class of molecules that changes conformation at different concentrations (15). Measurements by Reuter (16) on aquatic humic substances show a rapid increase in reduced viscosity (specific viscosity per unit concentration) as the humic material was diluted below about 100 mg/L

[1]To whom all correspondence should be addressed.

0008-4042/79/111263-06$01.00/0

at pH 7. He attributes the reduced-viscosity increase at low concentration to uncoiling of the humic structure. This uncoiling, or increase in apparent size of an average humic or fulvic acid molecule, may make sites more available for heavy-metal binding. As shown in gel permeation chromatographic studies (17), raising the pH or lowering the ionic strength also increases the apparent molecular size.

We designed our study to measure the effect of pH and fulvic acid concentration on the binding of Cd^{2+} (a highly toxic metal ion) to our WFA and SFA. Previous work in our group shows that copper(II) – fulvic acid binding is pH dependent (18). However, we had not observed that fulvic acid concentration affected the binding of Cu^{2+}. We employed Cd^{2+}, hoping it would be more sensitive than Cu^{2+} to conformational changes made by varying the polyelectrolyte (fulvic acid) concentration.

We analyzed free-metal concentration with ion-selective electrodes (ISE), an *in situ* method, because of difficulties with other techniques. Since our FA samples have average molecular weights below 700 amu (13), dialysis tubing we tried could not fully separate free and bound metal for analysis by atomic absorption spectrophotometry. Ultrafiltration with an Amicon UM05 membrane separates well enough, but requires too much time and fulvic acid.

Gel filtration chromatography is used for binding studies (19), but the aromaticity of our fulvic acids may interact non-ideally with the chromatographic resins (20). The surface activity of fulvic acid makes many voltammetric techniques difficult (21, 22), although aqueous humic matter apparently does not adsorb on the membranes of ion-selective electrodes (9).

Experimental

Materials

Fulvic acid. An earlier paper (12) describes the isolation and characterization of our soil- and water-derived fulvic acids.

Cadmium(II) solutions. Fisher SO-C-118 certified atomic absorption standard (1000 ppm) diluted with potassium nitrate electrolyte.

Copper(II) solutions. Orion copper(II) nitrate (0.1000 ± 0.005 *M*) standard, diluted with electrolyte.

Electrolyte. Mallinckrodt purified granular potassium nitrate crystals, dissolved in double deionized water.

KOH. Baker reagent grade 45% KOH, diluted with double deionized water or electrolyte, whichever gave the ionic strength closest to the experiment.

Apparatus

We measured the Cd^{2+} and Cu^{2+} concentrations with Orion model 94-48 and 94-29 solid-state ion-selective electrodes. The reference portion of a Corning model 476050 combination electrode was the reference for the ion-selective electrodes; a second Corning combination electrode monitored pH. Two Orion model 701A pH/mV meters recorded simultaneously free-metal concentration and pH.

We titrated into a Princeton Applied Research (Princeton, NJ, U.S.A.) model 9301 water jacketed cell. A P.M. Tamson circulating water bath maintained the temperature for all experiments at 25.0 ± 0.2°C. A magnetic stirring bar and stirrer maintained solution homogeneity.

Procedures

We titrated with either a cadmium-ion solution or a fulvic acid solution. For those experiments where metal-ion solution was the titrant, we placed 25.0 mL of the pH-adjusted fulvic acid solution, prepared daily in 0.1 *M* KNO_3, in the jacketed cell. We then added aliquots of the Cd^{2+} solution, also prepared that day from the concentrated metal-ion standards, with Gilson Pipetman variable pipets. To maintain pH within ± 0.03 pH units, we added small volumes of KOH solutions. We calibrated the ion-selective electrodes by adding standard metal-ion solutions to the electrolyte before and after each titration. Because the cadmium ion ISE has a small pH dependence, we calibrated that electrode at the pH of the day's work by adding KOH as needed.

For experiments where fulvic acid was titrant, we placed 25.0 mL of 0.1 *M* KNO_3 in the jacketed cell and added several aliquots of standard metal-ion solution to form a calibration curve. After adding the last metal aliquot, we began the titration with fulvic acid without changing the solution in the cell. Again, we adjusted the pH as necessary. We list the conditions for both types of experiment in Table 1.

ISE response flattens below about 10^{-6} *M* free metal so we computer fitted a polynomial of the form

$$\log [M^{2+}] = \sum_{i=0}^{n} a_i(mv)^i$$

to the calibration curves. $[M^{2+}]$ is the free metal ion concentration, *mv* is the millivolt reading from the ISE, a_i are the polynomial regression coefficients, and *n* is the order of the polynomial.

Calculations

We first tried to divide the binding sites on the fulvic acid into classes (such as strong, weak, and very weak) by the Scatchard method of analysis (23). Although we found 1.0 ± 0.3 sites per average fulvic acid molecule, the sites did not fall into well-defined classes with a given equilibrium constant for each. We observed a continuous variation in site strengths with respect to Cd^{2+}, which would explain the lack of clear breaks in our Scatchard plots.

Gamble and co-workers have demonstrated that fulvic acids contain acid functional groups with similar, but not identical pK_a values (7). The acid strength of these groups decreases as the degree of ionization increases. Work by several groups has shown that salicylic acid-type structures are the sites of copper chelation (24–26). We assume that such sites are available for cadmium(II) binding as well.

We expect that the extent of binding, and hence the stability constant for the cadmium–fulvate system will depend on pH and degree of association of metal and fulvic acid. The salicylic-type sites are similar but not identical, so the overall stability constant is a weighted average of the stability constants for each increment of chelating sites. The reaction at the *i*th

TABLE 1. Experimental conditions for cadmium – fulvic acid titrations

Water-derived fulvic acid (WFA)			Soil-derived fulvic acid (SFA)		
pH	Titrant	Solution in cell	pH	Titrant	Solution in cell
6.0	5.27×10^{-3} *M* WFA	$1.6–1.9\times10^{-5}$ *M* Cd^{2+}	6.0	5.20×10^{-3} *M* SFA	1.9×10^{-5} *M* Cd^{2+}
8.0	5.91	4.9	8.0	5.04	4.9
4.0[a]	1.03×10^{-3} *M* Cd^{2+}	5.5×10^{-4} *M* WFA	4.0[a]	1.67×10^{-3} *M* Cd^{2+}	5.4×10^{-4} *M* SFA
5.0[a]	1.53	5.5	5.0[a]	1.67	5.4
6.0[a]	1.99	5.9	6.0[a]	2.67	5.6
7.0[a]	2.69	5.7	7.0[a]	2.67	5.9
8.0[a]	3.30	5.8	8.0[a]	4.15	5.4
7.0[b]	0.215	0.279	6.0[b]	0.108	0.30
7.0[b]	0.357	0.559	6.0[b]	0.209	0.61
7.0[b]	0.756	1.06	6.0[b]	0.395	1.3
7.0[b]	2.14	3.18	6.0[b]	1.07	2.4
			6.0[b]	1.68	4.1

[a]Series of experiments where pH was the variable.
[b]Series of experiments where fulvic acid concentration was the variable.

type of chelating site is

$$[1] \qquad HFA_i^- + Cd^{2+} \rightarrow Cd\text{–}FA_i + H^+$$

Here, HFA_i^- is the *i*th type of fulvic acid binding site without metal, Cd^{2+} represents the free cadmium ion and Cd–FA_i is the *i*th type of cadmium–fulvate 1:1 complex. We define the incremental conditional stability constant K_i:

$$[2] \qquad K_i = [Cd\text{–}FA_i]/[HFA_i^-][Cd^{2+}]$$

The overall conditional stability constant K is

$$[3] \qquad K = \sum_{i=1}^{k} [HFA_i^-]K_i \Big/ \sum_{i=1}^{k} [HFA_i^-]$$

The weighting factors $[HFA_i^-]$ will change with pH and possibly with concentration of fulvic acid. Further, the overall conditional stability constant K will vary depending on the proportion of sites occupied by metal. With cadmium ions occupying the strongest sites at low metal-to-fulvic-acid ratios, each added increment of Cd^{2+} will go to successively weaker chelation sites so that K will drop. We calculated the overall stability constant K for various levels of cadmium loading, that is, for various values of $[Cd\text{–}FA]/C_{FA}$, where C_{FA}, the total fulvic acid concentration, equals $[HFA^-] + [Cd\text{–}FA]$. Our Scratchard analysis showed approximately one site per fulvic acid molecule, so we assumed that 1:1 complexes predominate. We used the expression

$$[4] \qquad K = [Cd\text{–}FA]/[HFA^-][Cd^{2+}]$$

for the conditional stability constant. Since total cadmium concentration, C_{Cd}, is

$$[5] \qquad C_{Cd} = [Cd\text{–}FA] + [Cd^{2+}]$$

$$[6] \qquad K = [Cd\text{–}FA]/(C_{FA} - [Cd\text{–}FA])[Cd^{2+}]$$

Results and Discussion

Tables 2 and 3 show the effect of pH and fulvic acid concentration on K for our water- and soil-derived fulvic acids. These K values are taken from the high $[Cd\text{–}FA]/C_{FA}$ part of those titrations where cadmium-ion solution is the titrant. $[Cd\text{–}FA]/C_{FA}$ represents the average number of cadmium ions bound per fulvic acid molecule. Figures 1–4 show that much higher stability constants exist early in the titration (at low $[Cd\text{–}FA]/C_{FA}$), due to the few strongest fulvic acid sites to which the cadmium ions from the first few titration aliquots bind.

TABLE 2. Effect of pH on cadmium – fulvic acid conditional stability constants*

	$K\times10^{-3}$	
pH	WFA	SFA
4.0	1.4	1.7
5.0	3.0	6.3
6.0	4.8	12
7.0	8.1	21
8.0	12	43

*All titrations have fulvic acid concentrations of 5 to 6×10^{-4} *M* and 0.1 *M* KNO_3 supporting electrolyte at 25°C.

TABLE 3. Effect of fulvic acid concentration on cadmium – fulvic acid conditional stability constants

[WFA] $\times 10^4$ *M*[a]	$K\times10^{-3}$	[SFA] $\times 10^4$ *M*[b]	$K\times10^{-3}$
0.28	8.8	0.30	29
0.56	6.5	0.61	24
1.06	2.5	1.3	18
3.18	4.4	2.4	13
		4.1	14
		5.6	12

[a]Titrations done at pH 7.0 in 0.1 *M* KNO_3.
[b]Titrations done at pH 6.0 in 0.1 *M* KNO_3.

Much useful information appears in our log K vs. [Cd–FA]/C_{FA} graphs. The high [Cd–FA]/C_{FA} values represent an average of all the sites involved during titration and indicate the type of fulvic acid sample and experimental conditions. The somewhat lower log K values for WFA compared to SFA may be explained by its lower phenol OH content: 5.2 meq/g for SFA and 4.3 meq/g for WFA (12). This confirms the assumption that salicylic acid functional groups are the sites of binding (24–26).

It is clear from Figs. 1 and 2 that fulvic acid isolated from either water or soil binds Cd^{2+} more strongly as the pH is raised. There is a roughly two-fold increase in the binding constant, K, for each pH unit increase. These two figures also show that for lower pH values, the stability constant K becomes constant at lower levels of metal loading, that is, at lower [Cd–FA]/C_{FA}.

Figures 3 and 4 show the effect of fulvic acid concentration on its ability to complex metal ions. For both types of fulvic acids, we see higher conditional stability constants in the more dilute solutions. The dependence of stability constant on concentration occurs for solutions below about 1×10^{-4} M (about

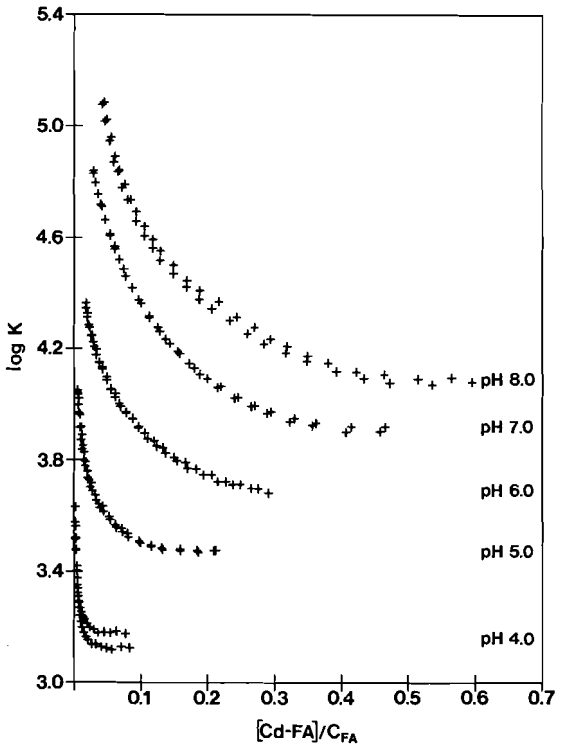

FIG. 1. Conditional stability constants for water-derived fulvic acid as a function of pH. Data represent replicate titrations at each pH.

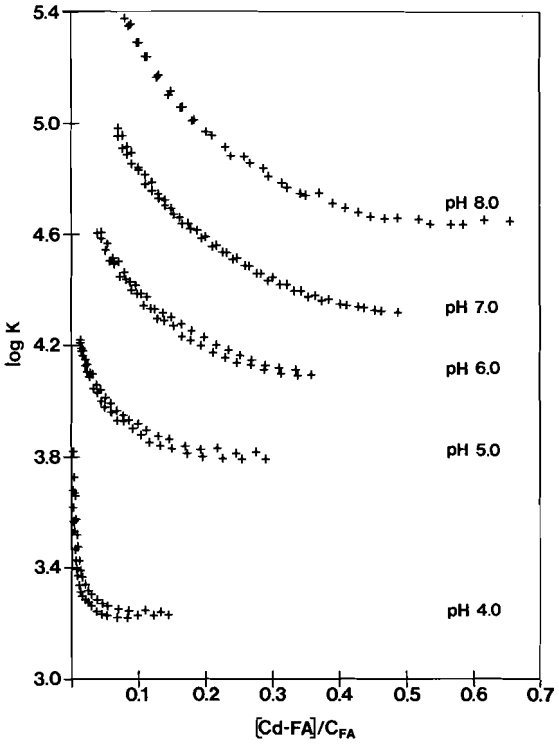

FIG. 2. Conditional stability constants for soil-derived fulvic acid as a function of pH. Data represent replicate titrations at each pH.

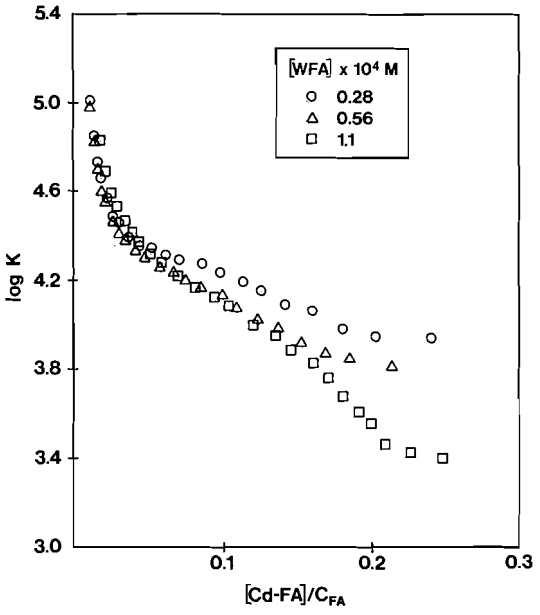

FIG. 3: Conditional stability constants at pH 7.0 for water-derived fulvic acid (WFA) at three different WFA concentrations.

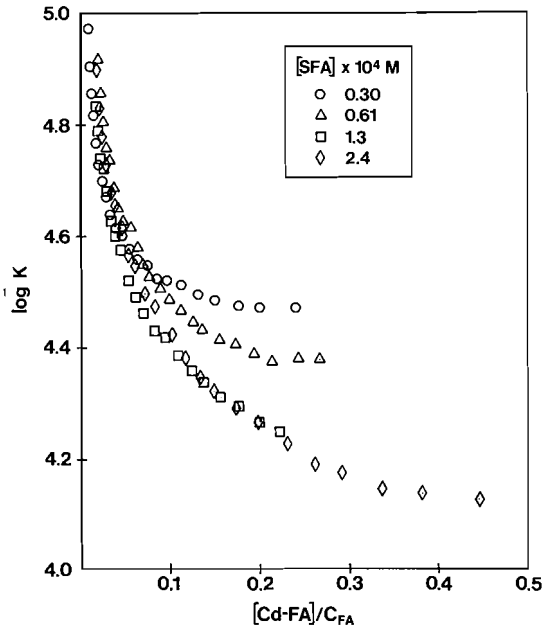

FIG. 4. Conditional stability constants at pH 6.0 for soil-derived fulvic acid (SFA) at four different SFA concentrations.

60–70 mg/L) using the molecular weights of 644 amu for SFA and 626 amu for WFA (13). This concentration corresponds well to the concentration range where Reuter found that reduced viscosities of aquatic humus change with concentration (16), that is, below about 100 mg/L. The higher reduced viscosity of dilute solutions may imply that the humus molecules are uncoiled or in an 'open' conformation.

Studies in our group (18) and the work of others (1–3, 5, 10, 27, 28) show that Cu^{2+} binds more strongly to fulvic and humic acids than Cd^{2+} does. We surmise that the conformational changes (decrease in apparent molecular size) that result from increasing the concentration of fulvic acids are forceful enough to block some potential Cd^{2+} binding sites. However, the stability of Cu^{2+} with the fulvate binding sites is great enough to overcome this relatively weak conformational blocking. We conclude that the intramolecular attractions (forces) involved here are stronger than those in Cd–FA complexation, but weaker than those in Cu–FA complexation. We expect that metal ions like Pb^{2+} that bind to simple organic ligands much as Cu^{2+} does (29) would not have stability constants that depend on fulvic acid concentration. Similarly, we anticipate that weak binding metals like Zn^{2+} would have concentration-dependent K values.

The data from reverse titrations (those where a fulvic acid solution is the titrant) confirm the concentration effect for cadmium. Early in such a titration, the stability constant drops after each addition of FA, but then levels off and begins to increase again toward the end of the titration (data represented by triangles in Fig. 5). This confirms that fulvic acid binding to cadmium is strongest when FA is most dilute (early in this type of titration). As we add more aliquots of FA titrant, its concentration in the cell increases and the K value drops. However, as we add more FA, the ratio of FA to Cd^{2+} increases, so that Cd^{2+} ions have an ever widening choice of sites on the fulvic acid for binding. The metal ions will bind preferentially to the strongest sites, so as we add more fulvic acid, the average K value increases.

The result is that the selection of titrant (FA or Cd^{2+}) makes a significant difference in the shape of the binding curve for cadmium due to the fulvic acid concentration effect. Figure 5 shows the two curve shapes for WFA at pH 6.0. Curve shapes for the SFA–cadmium system also depend on the titrant chosen and are very similar to those for WFA shown in Fig. 5. In contrast, we observed no FA concentration effect for the copper–fulvate system and our curves for both types of titration have the same shape, that is, K always increases when adding FA or K always decreases when titrating with Cu^{2+}.

We believe that fulvic acid concentration should be considered as an important variable when investi-

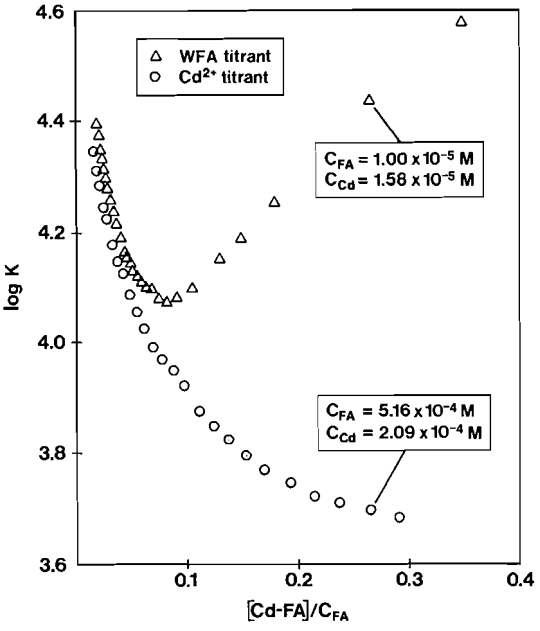

FIG. 5. Two pH 6.0 titrations, one each with WFA and Cd^{2+} as titrant. Reagent concentrations are shown for an experimental point in each titration with approximately equal $[Cd\text{–}FA]/C_{FA}$.

gating the transport of weakly bound metals like cadmium in natural systems. We have demonstrated that on a per-mole basis, fulvic acid binds cadmium most strongly when FA is in low concentration. Graphs such as those in Figs. 1–4 help to calculate the proportion of free and bound metal ion (cadmium ion in this case) for a given pH, for a range of fulvic acid concentrations and at different [Cd–FA]/C_{FA} values. If we assume that U.S. average river water has 10–13 mg/L of dissolved humic substances (30) and about 1 μg/L of Cd^{2+} (31), the low [Cd–FA]/C_{FA} parts of our figures would be most suitable. However, areas with much heavy-metal pollution might be best represented by the high [Cd–FA]/C_{FA} portions of these graphs. We observe finally that fulvic acids extracted from water and soils behave very similarly with respect to Cd^{2+} complexation.

Acknowledgements

This work was partly supported by National Science Foundation grant OCE 77-08390. We thank Rob O'Neil for experimental assistance.

1. F. J. Stevenson. Soil Sci. **123**, 10 (1977).
2. F. J. Stevenson. Soil Sci. Soc. Am. J. **40**, 665 (1976).
3. T. Takamatsu and T. Yoshida. Soil Sci. **125**, 377 (1978).
4. V. Cheam. Can. J. Soil Sci. **53**, 377 (1973).
5. V. Cheam and D. S. Gamble. Can. J. Soil Sci. **54**, 413 (1974).
6. B. Brady and G. K. Pagenkopf. Can. J. Chem. **56**, 2331 (1978).
7. D. S. Gamble. Can. J. Chem. **48**, 2662 (1970).
8. J. Gardiner. Water Res. **8**, 23 (1974).
9. J. Buffle, F.-L. Greter, and W. Haerdi. Anal. Chem. **49**, 216 (1977).
10. R. F. C. Mantoura, A. Dickson, and J. P. Riley. Estuarine Coastal Mar. Sci. **6**, 387 (1978).
11. P. Beneš, E. T. Gjessing, and E. Steinnes. Water Res. **10**, 711 (1976).
12. J. H. Weber and S. A. Wilson. Water Res. **9**, 1079 (1975).
13. S. A. Wilson and J. H. Weber. Chem. Geol. **19**, 285 (1977).
14. S. A. Wilson and J. H. Weber. Anal. Lett. **10**(1), 75 (1977).
15. H.-G. Elias. Macromolecules **1**. Structure and properties. Plenum, New York, NY. 1977. p. 352*ff*.
16. J. H. Reuter. Geol. Soc. Am. Abstr. **9**(7), 1140 (1977).
17. E. T. Gjessing. Schweiz. Z. Hydrol. **33**, 592 (1971).
18. W. T. Bresnahan, C. L. Grant, and J. H. Weber. Anal. Chem. **50**, 1675 (1978).
19. R. F. C. Mantoura and J. P. Riley. Anal. Chim. Acta, **78**, 193 (1975).
20. B. Gelotte. J. Chromatogr. **3**, 330 (1960).
21. A. M. Bond and G. Hefter. J. Electroanal. Chem. **31**, 477 (1971).
22. P. L. Brezonik, P. A. Brauner, and W. Stumm. Water Res. **10**, 605 (1976).
23. G. Scatchard. Ann. N.Y. Acad. Sci. **51**, 660 (1949).
24. R. S. Beckwith. Nature, **184**, 745 (1959).
25. S. S. Khanna and F. J. Stevenson. Soil Sci. **93**, 298 (1962).
26. M. Schnitzer and S. I. M. Skinner. Soil Sci. **96**, 86 (1963).
27. R. D. Guy and C. L. Chakrabarti. Can. J. Chem. **54**, 2600 (1976).
28. S. Ramamoorthy and D. J. Kushner. Nature, **256**, 399 (1975).
29. A. E. Martell and R. M. Smith. Critical stability constants. Vol. 3. Other organic ligands. Plenum, New York, NY. 1977.
30. J. H. Reuter and E. M. Perdue. Geochim. Cosmochim. Acta, **41**, 325 (1977).
31. W. H. Durum, J. D. Hem, and S. G. Heidel. U.S. Geol. Surv. Circ. 643 (1971).

The reactions of atomic oxygen with 1-propanol and 2-propanol

A. L. AYUB AND JOHN M. ROSCOE[1]

Department of Chemistry, Acadia University, Wolfville, N.S., Canada B0P 1X0

Received August 16, 1978

A. L. AYUB and JOHN M. ROSCOE. Can. J. Chem. 57, 1269 (1979).

The reactions of $O(^3P)$ with *n*-propanol and isopropanol were studied as a function of temperature. The absolute rate constants for these reactions, in the units M^{-1} s^{-1}, obey the following relations.

$$O + n\text{-propanol: } \ln k = 20.49 \pm 0.09 - (1.5 \pm 11\%) \times 10^3/T$$

$$O + \text{isopropanol: } \ln k = 19.58 \pm 0.07 - (1.1 \pm 13\%) \times 10^3/T$$

The activation energies of these reactions are similar to those of the corresponding reactions of methanol and ethanol, although some dependence on the strength of the α-C—H bond is discernible. The nearly constant pre-exponential factors for the reactions of methanol, ethanol, *n*-propanol, and isopropanol suggest that no special steric effects are present in the reactions of these compounds with $O(^3P)$. Mechanisms are discussed for the reactions of *n*-propanol and isopropanol with $O(^3P)$.

A. L. AYUB et JOHN M. ROSCOE. Can. J. Chem. 57, 1269 (1979).

On a étudié les réactions de $O(^3P)$ avec les *n*- et isopropanols en fonction de la température. Les constantes absolues de vitesse de ces réactions, en M^{-1} s^{-1}, obéissent aux relations suivantes:

$$O + n\text{-propanol: } \ln k = 20.49 \pm 0.09 - (1.5 \pm 11\%) \times 10^3/T$$

$$O + \text{isopropanol: } \ln k = 19.58 \pm 0.07 - (1.1 \pm 13\%) \times 10^3/T$$

Les énergies d'activation de ces réactions sont semblables à celles des réactions correspondantes du méthanol et de l'éthanol même si l'on peut discerner une relation avec la force de la liaison α-C—H. Le fait que les facteurs pré-exponentiels sont presque constants pour les réactions du méthanol, éthanol, *n*-propanol et isopropanol suggère qu'il n'existe pas d'effets stériques spéciaux lors de la réaction de ces composés avec $O(^3P)$. On discute des mécanismes de réaction des *n*- et isopropanols avec $O(^3P)$.

[Traduit par le journal]

Earlier work on the reactions of $O(^3P)$ with alcohols has established the importance of attack by the O atom on the hydrogens at the α-carbon atom of the alcohol (1–5). However, absolute rate constants over a range of temperatures are available only for the reactions of $O(^3P)$ with methanol and ethanol (4, 5). Kinetic data are also available for the reaction of 2-propanol with $O(^3P)$ at 298 K (3). The work presented here was undertaken to compare the Arrhenius parameters for abstraction of a hydrogen atom from the α-carbon atom of a primary and a secondary alcohol, and to investigate the possibility of steric effects in the reactions of $O(^3P)$ with alcohols.

Experimental

The experimental methods used in this work have been described in detail elsewhere (5). Briefly, the reactions were studied in a conventional fast flow system. The $O(^3P)$ was produced by adding NO to $N(^4S)$ atoms formed in a microwave discharge through N_2. The $O(^3P)$ concentrations were measured by determining the intensity of emission from excited NO_2 produced by a small amount of NO in excess of that required to completely consume the $N(^4S)$. The purification procedures for the NO and N_2 are described in detail elsewhere (5). The rate constants and product analyses were independent of the amount of excess NO.

Both *n*-propanol and isopropanol were refluxed with magnesium turnings in the presence of a small amount of I_2 to remove water. The alcohols were then purified further by fractional distillation until no impurities could be detected by gas chromatography. Their purity was estimated to be better than 99.999%.

Reaction products were analysed both by gas chromatography and by mass spectrometry. In the gas chromatographic analyses, the condensable products were collected in traps cooled in liquid nitrogen. They were then analysed on an 8-foot column of 10% Carbowax on Chromosorb W and on an 8-foot column packed with Porapak Q, using an F and M model 700 gas chromatograph with a flame ionization detector.

The mass spectrometric analyses were made by sampling through a molecular leak located in the reaction vessel. The mass spectra were obtained with a CEC model 21-104 single focussing mass spectrometer which was operated at sufficiently low ionizing voltages that interference due to fragmentation was minimal. Corrections for the small amount of residual fragmentation could easily be made.

Computer simulation of the reactions was done on a DEC-10 computer using a Fortran program described by Stabler and Chesick (6). This program was found to give

[1]To whom all correspondence should be addressed.

0008-4042/79/111269-05$01.00/0

reliable results when tested on several mechanisms which are generally regarded as being accurate and for which extensive experimental data are available.

Results and Discussion

Kinetics

The absolute rate constants[2] for the reactions of $O(^3P)$ with *n*-propanol and isopropanol are given in Table 1 and the temperature dependence of these rate constants is shown in Fig. 1. The stoichiometric coefficients in Table 2 were not used in calculating the absolute rate constants. Since $\Delta[O]/\Delta[ROH]$ is much less than unity, and in view of the calculated effects of possible secondary reactions which are discussed later, it may be concluded that secondary reactions do not result in significant loss of $O(^3P)$. Thus, the measured rate constants are, in fact, the absolute rate constants.

The activation energy for the reaction of $O(^3P)$ with isopropanol is slightly less than that for the corresponding reaction of *n*-propanol. This might be expected since the α-C—H bond energy in isopropanol should be less than the α-C—H bond energy in *n*-propanol.

The Arrhenius preexponential factors for the reactions of $O(^3P)$ with *n*-propanol and isopropanol are similar. They are also similar to those reported earlier for the reactions of $O(^3P)$ with methanol (4, 5) and ethanol (5). This suggests that there is no significant 'steric effect' on the rate constant for the reactions of $O(^3P)$ with alcohols having up to three carbon atoms. This insensitivity to structure has been reported for reactions of $O(^3P)$ with other organic compounds containing oxygen (7). The relatively small preexponential factors for these reactions have been interpreted as indicating that $O(^3P)$ preferentially attacks the O-atom in the molecule. This electrophilic attack would result in relatively few collisions having the correct geometry for abstraction of the α-H atom from the alcohols studied here. There is considerable evidence that such abstraction is the initial step in the reactions of $O(^3P)$ with alcohols (2–5) and the electrophilic nature of $O(^3P)$ has been discussed elsewhere (7, 8).

Reaction Mechanism

The analytical data for the reactions of $O(^3P)$ with *n*-propanol and isopropanol are given in Table 2. Water and pinacol were also found in the products of the reaction of isopropanol with $O(^3P)$, but their yields were not measured. Based on these data and earlier work (2–5), the following reactions serve as the nucleus for describing the reactions of $O(^3P)$ with these alcohols.

[1] $O + C_3H_7OH \rightarrow C_3H_6OH + OH$

[2] $OH + C_3H_7OH \rightarrow C_3H_6OH + H_2O$

[3] $2C_3H_6OH \rightarrow C_3H_7OH + C_3H_6O$

[4] $2C_3H_6OH \rightarrow$ glycol

[2]Tables of the kinetic data from which these rate constants were calculated are available, at a nominal charge, from the Depository of Unpublished Data, CISTI, The National Research Council of Canada, Ottawa, Ont., Canada K1A 0S2.

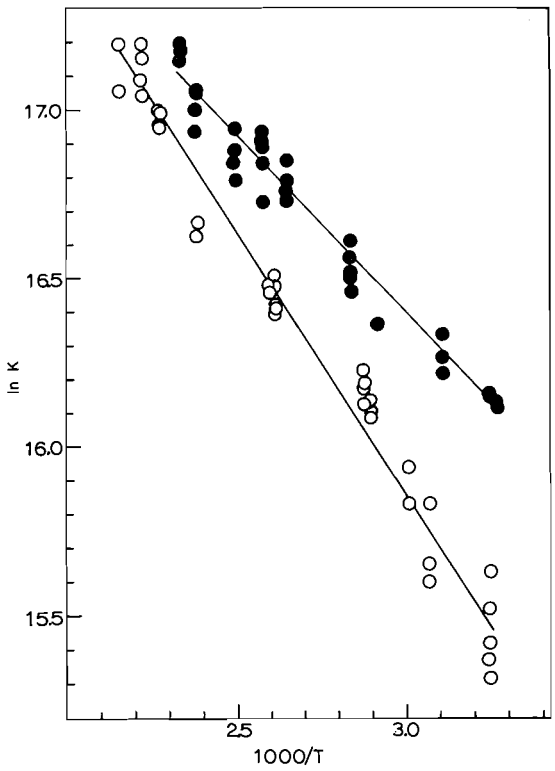

FIG. 1. Arrhenius plots for the reactions of $O(^3P)$ with *n*-propanol (○) and isopropanol (●).

TABLE 1. Absolute rate constants for O + ROH*

O + n-C_3H_7OH		O + iso-C_3H_7OH	
T (K)	$k \times 10^{-7}$ (L mol^{-1} s^{-1})	T (K)	$k \times 10^{-7}$ (L mol^{-1} s^{-1})
463	2.8±0.2	428	2.9±0.1
449	2.7±0.2	419	2.4±0.1
439	2.3±0.1	400	2.1±0.1
419	1.7±0.1	388	2.1±0.1
385	1.4±0.1	378	2.0±0.1
381	1.4±0.1	352	1.5±0.1
347	1.06±0.05	343	1.3±0.1
345	1.00±0.03	322	1.17±0.05
332	0.79±0.04	308	1.02±0.02
326	0.66±0.06	306	1.02±0.02
308	0 52+0 06		

*ln $k(n\text{-}C_3H_7OH) = 20.49 \pm 0.09 - (1.5 \pm 0.2) \times 10^3/T$; correlation coefficient = 0.98; ln k(iso-C_3H_7OH) = $19.58 \pm 0.07 - (1.1 \pm 0.1) \times 10^3/T$; correlation coefficient = 0.98. All rate constants are within two standard deviations of the regression line. The uncertainties represent one standard deviation. Pressures in these experiments ranged from 1.0 to 1.5 Torr. $[ROH]_0/[O]_0$ ranged from about 10 to 100.

TABLE 2. Analytical data*

Reaction	[ROH]/[O]	Δ[O]/Δ[ROH]	[ROH]/[O]	[RCH:O]/Δ[O]	[$(CH_3)_2C$:O]/Δ[O]
O + *n*-C_3H_7OH	41.7	0.55	29.4	0.107	—
	41.5	0.48	25.5	0.161	—
	41.3	0.53	25.3	0.163	—
	39.5	0.41	21.8	0.121	—
	39.2	0.45	18.2	0.175	—
	32.8	0.59	17.2	0.195	—
	32.8	0.58	17.2	0.168	—
	20.5	0.42	14.8	0.123	
		0.50±0.07		*0.15±0.03*	
O + iso-C_3H_7OH	54.4	0.61	30.8	0.07	0.49
	42.9	0.57	28.0	0.08	0.46
	38.0	0.50	27.2	0.07	0.35
	31.5	0.49	23.3	0.08	0.38
	29.8	0.60	22.0	—	0.51
	25.6	0.50	18.9	—	0.38
	25.5	0.64	5.73	—	0.43
	22.0	0.46	—	—	—
	21.5	0.61	—	—	—
	18.0	0.74	—	—	—
	15.4	0.51	—	—	—
		0.57±0.06		*0.075±0.006*	*0.43±0.05*

*Average values in italics.

While no glycol could be detected in the products of the reaction of $O(^3P)$ with *n*-propanol, and only a small amount of pinacol was recovered in the corresponding reaction of isopropanol, these products could easily have been lost on the walls of the apparatus.

The possibility of $O(^3P)$ consumption by the carbonyl product, C_3H_6O, and by OH was examined for each reaction by numerical integration of the appropriate rate equations. The additional reactions required for this analysis are

[5] $$O + C_3H_6O \rightarrow C_3H_5O + OH$$

[6] $$C_3H_5O + C_3H_7OH \rightarrow C_3H_6OH + C_3H_6O$$

[7] $$O + OH \rightarrow O_2 + H$$

Rate constants for reactions [2], [5], and [7] were taken from the literature (7, 9–11). Our value of k_1 was used and all other rate constants were made at least ten times as large as k_2. The ratio k_3/k_4 was adjusted to give the observed yield of the carbonyl compound. The calculations were then repeated with k_5 and k_6 set to zero, and then with k_7 set to zero as well. In the reaction of $O(^3P)$ with *n*-propanol, the inclusion of reaction [7] increased the overall rate constant by 5% and inclusion of reactions [5] and [6] altered the overall rate constant by 10%. In the reaction of $O(^3P)$ with isopropanol, the corresponding values were 0.3% and 1%. These calculations were made with a 50-fold excess of alcohol over $O(^3P)$, which is typical of our experimental conditions. Such estimates are likely to represent an upper limit on the effects of secondary reactions since the reactions of OH with the carbonyl compounds are also likely to be fast but were neglected for lack of kinetic data. It should therefore be safe to assume that reactions [5] to [7] played a negligible role in our experiments, within the uncertainties evident in Table 1. At least partial confirmation of this was found in a few experiments in which the ratio of $O(^3P)$ to alcohol was varied from 5 to 100. The calculated rate constant at 298 K was dependent on alcohol concentration until about a 15-fold excess of alcohol was used. Beyond this point, the rate constant was independent of alcohol concentration within experimental error. As expected, the smaller alcohol concentrations gave a substantially larger rate constant than was obtained with 20- to 100-fold excess of alcohol. Consumption of $O(^3P)$ by the α-alkanol radicals could not be estimated by the above method because of the lack of kinetic data. However, such reactions are unlikely to have been important since they would have made the yield of the carbonyl compound and relative consumption of $O(^3P)$ greater than the observed values. Participation by such reactions would have made the measured rate constants too large, and may have been responsible for the downward curvature of some of the pseudo first order plots which extended to relatively long reaction times.

Comparison of the Reactions of $O(^3P)$ with Alcohols

The reactions of $O(^3P)$ with C_1 to C_3 alcohols seem to follow the same general mechanism, although under the conditions in which we studied the reaction of $O(^3P)$ with methanol the reaction of $O(^3P)$ with OH seemed to be important (5). This is presumably

TABLE 3. Comparison of available kinetic data for reactions of $O(^3P)$ with alcohols*

Alcohol	$k_{298} \times 10^{-7}$ (M^{-1} s^{-1})	$A \times 10^{-9}$ (M^{-1} s^{-1})	ΔE_a (kJ mol^{-1})	Method	Reference
CH_3OH	0.825	1.45±0.10	12.8±1.2	Discharge flow, chemiluminescence	5
CH_3OH	1.71	1.70±0.66	11.4±2.3	Discharge flow, esr	4
C_2H_5OH	5.27	0.670±0.078	6.3±1.7	Discharge flow, chemiluminescence	5†
C_2H_5OH	7.48			Hg sensitization, product analysis	2
n-C_3H_7OH	0.510	0.792±0.075	12.5±1.4	Discharge flow, chemiluminescence	This work
iso-C_3H_7OH	0.796	0.319±0.023	9.1±1.2	Discharge flow, chemiluminescence	This work
iso-C_3H_7OH	11.2			Hg sensitization, product analysis	3

*The uncertainties indicated represent one standard deviation.
†The results have been corrected as explained in the text.

due to the relatively small rate constant for the competing reaction of OH with methanol (9) and to the experimental limitations on the concentration of methanol relative to $O(^3P)$.

If the general mechanism proposed by Kato and Cvetanović (2, 3) and outlined here applies to the reaction of $O(^3P)$ with ethanol, the stoichiometric coefficient used to convert the measured rate constants for that reaction to absolute values (5) must be corrected for regeneration of ethanol by the disproportionation of the α-alkanol radical. When this is done, all the absolute rate constants reported in our earlier work on this reaction (5) must be multiplied by a factor of 1.6. This makes our absolute rate constant at 298 K in better agreement with that reported by Kato and Cvetanović (2) (Table 3). The revised temperature dependence of this rate constant is then given by $\ln k = 20.3 \pm 0.2 - (760 \pm 27\%)/T$.

The discrepancy between our results for the reaction of isopropanol with $O(^3P)$ and those of Kato and Cvetanović (3) is more serious and more difficult to understand. Although their experiments were made with a much larger excess of alcohol than was possible in our work, the effects of secondary reactions under our conditions were estimated to be negligible. Moreover, any such secondary reactions would have made our rate constants too large, while they are actually about an order of magnitude smaller than the value reported by Kato and Cvetanović based on competitive measurements using 1-butene. We are unable to detect any systematic errors in either our experiments or our calculations which could have caused this discrepancy. The kinetic measurements were made on two different flow systems by two persons working independently. The results obtained were in good agreement. The stoichiometry measurements were also made by two persons on two different flow systems, one equipped with a gas chromatograph and the other with a mass spectrometer. Again, the results obtained on the two systems were in good agreement. Clearly, further independent work is needed to resolve this question.

While the preexponential factors for the reactions of the alcohols are similar, a small but systematic dependence on the number of α-C—H bonds is discernible. When the preexponential factors are divided by the number of α-C—H bonds, the variation among the resulting values is random and is within experimental error. From this, it appears that apart from a statistical effect, there are no special steric influences in the reactions of $O(^3P)$ with the alcohols. No conclusions can be drawn from the activation energies for these reactions because their combined uncertainties are greater than the small differences among them. It seems, however, that the reported activation energy for the reaction of $O(^3P)$ with ethanol (5) may be somewhat too small since one would expect a value comparable to that for the corresponding reaction with n-propanol and larger than that for the reaction of $O(^3P)$ with isopropanol.

Acknowledgment

Financial support for this work was provided by the National Research Council of Canada.

1. L. I. AVRAMENKO, R. V. KOLESNIKOVA, and N. L. KUZNETSOVA. Izv. Akad. Nauk SSR Otd. Khim. Nauk, 599 (1961).
2. A. KATO and R. J. CVETANOVIĆ. Can. J. Chem. **45**, 1845 (1967).
3. A. KATO and R. J. CVETANOVIĆ. Can. J. Chem. **46**, 235 (1968).
4. H. F. LEFEVRE, J. F. MEAGHER, and R. B. TIMMONS. Int. J. Chem. Kinet. **4**, 103 (1972).

5. C. M. OWENS and J. M. ROSCOE. Can. J. Chem. **54**, 984 (1976).
6. R. N. STABLER and J. P. CHESICK. Int. J. Chem. Kinet. **10**, 461 (1978).
7. J. H. LEE and R. B. TIMMONS. Int. J. Chem. Kinet. **9**, 133 (1977).
8. R. J. CVETANOVIĆ. Can. J. Chem. **38**, 1678 (1960).
9. R. OVEREND and G. PARASKEVOPOULOS. J. Phys. Chem. **82**, 1329 (1978).
10. D. L. SINGLETON, R. S. IRWIN, and R. J. CVETANOVIĆ. Can. J. Chem. **55**, 3321 (1977).
11. A. A. WESTENBERG, N. DE HAAS, and J. M. ROSCOE. J. Phys. Chem. **74**, 3431 (1970).

Erratum: Crystal and molecular structures of 2,2,4,4,6,8,8-heptamethyl-6-methylamino-1,3,5-triaza-2,4,6,8(P^V)-tetraphosphorin and 2,2,4,4,6,8,8-heptamethyl-6-methylamino-7-benzoyl-1,3,5-triaza-2,4,6,8(P^V)-tetraphosphorin

HARRY P. CALHOUN, RICHARD T. OAKLEY, NORMAN L. PADDOCK, STEVEN J. RETTIG, AND JAMES TROTTER
Department of Chemistry, University of British Columbia, 2075 Wesbrook Mall, Vancouver, B.C., Canada V6T 1W5

Received February 27, 1979
(Ref.: Can. J. Chem. **56**, 2833 (1978))

The caption to Fig. 1 should read: "Molecular structures of (*a*), **2***a* (occupancy factor 0.3); (*b*), **2***b* (occupancy factor 0.7); and (*c*), **4**."

A carbon-13 nuclear magnetic resonance study of benzyl cyanide

RODERICK E. WASYLISHEN AND BRIAN A. PETTITT
University of Winnipeg, Winnipeg, Man., Canada R3B 2E9

Received October 20, 1978

RODERICK E. WASYLISHEN and BRIAN A. PETTITT. Can. J. Chem. **57**, 1274 (1979).

Spin–lattice relaxation times are reported for the cyano, methylene, and ring carbons in liquid benzyl cyanide at selected temperatures between 215 and 406 K. The rotation of the molecule is modelled on the diffusion of a prolate spheroid and the following features are deduced: (*1*) rotation of the aromatic ring about the long axis of the molecule is about 3 times faster than rotation of this axis, (*2*) rotation of the —CH_2CN group about the long axis is about 1.5 times faster than the aromatic ring, and (*3*) activation energies associated with the temperature dependence of the $^{13}C—^1H$ dipolar relaxation rates agree with the hydrodynamical prediction of 3.6 kcal/mol associated with the temperature dependence of the ratio shear viscosity – temperature.

Linewidths of the cyano carbon resonance are shown to result from scalar coupling with ^{14}N.

Spin–spin coupling constants involving the cyano and methylene carbons are reported and compared with those calculated at the INDO level of molecular orbital theory.

RODERICK E. WASYLISHEN et BRIAN A. PETTITT. Can. J. Chem. **57**, 1274 (1979).

On rapporte les temps de relaxation spin–réseau des carbones du cyano, du méthylène et du cycle du cyanure de benzyle liquide à des températures déterminées entre 215 et 406 K. On peut imaginer le modèle pour la rotation de la molécule sur la base d'une diffusion d'une sphéroïde allongée et l'on a pu déduire les caractéristiques suivantes: (*1*) la rotation du cycle aromatique autour de son axe le plus long est environ 3 fois plus rapide que la rotation de cet axe, (*2*) la rotation du groupe —CH_2CN autour de son axe le plus long est environ 1.5 fois plus rapide que celle du noyau aromatique et (*3*) les énergies d'activation associées avec le fait que les taux de relaxation dipolaire $^{13}C—^1H$ dépendent de la température sont en bon accord avec la prédiction hydrodynamique de 3.6 kcal/mol qui est associée avec la relation entre la température et le rapport viscosité de cisaillement – température.

L'élargissement des raies de résonance du carbone du cyano provient d'un couplage scalaire avec le ^{14}N.

On rapporte les constantes de couplage spin–spin impliquant les carbones cyano et méthylène et on les compare avec celles calculées au niveau INDO de la théorie des orbitales moléculaires.

[Traduit par le journal]

Introduction

The rotational modes of a molecule usually constitute the 'lattice' that gives rise to the time dependence of the relaxation terms in the nuclear spin Hamiltonian; hence the widespread use of T_1 experiments in the study of liquid state rotational dynamics. The complexities of the liquid state rarely permit the interpretation of such experiments in any other than the crude terms of the rotational diffusion model, in which molecular rotations are regarded as the result of unspecified intermolecular torques fluctuating on a very short timescale. The model is generally accepted as a satisfactory framework within which the rates of rotation in the various modes of 'large' molecules can be compared. For example, the ^{14}N, ^{13}C, and ^2H resonances of acetonitrile, CH_3CN, have been thoroughly studied (1–7). At room temperature, CD_3CN rotates approximately 9 times faster about its C_3 axis than about axes perpendicular to this symmetry axis; and the two types of motion are characterized by activation energies (E_a's) of 0.8 kcal/mol and 1.7 kcal/mol, respectively (2). The present paper is concerned with the ^{13}C spin–lattice relaxation times of benzyl cyanide (C_6H_5—CH_2CN, Fig. 1), a derivative of acetonitrile, which exists as a liquid over a broad temperature range (249 to 507 K at atmospheric pressure). In addition $^{13}C,^{13}C$ coupling constants involving the methylene and cyano carbons are reported and compared with those calculated using the INDO semiempirical molecular orbital theory.

Previous nmr work on benzyl cyanide includes a variable temperature study of the ^{14}N linewidths by Wallach (8), and measurements of the temperature and pressure dependences of ^2H relaxation times of benzyl-4-d_1 cyanide and α,α-dideuterobenzyl cyanide by Jonas and co-workers (9–11). In their analyses, they emphasized the internal rotation of the —CH_2CN group (E_a = 2.9 kcal/mol), assuming this to be superimposed on isotropic overall rotation

0008-4042/79/111274-05$01.00/0

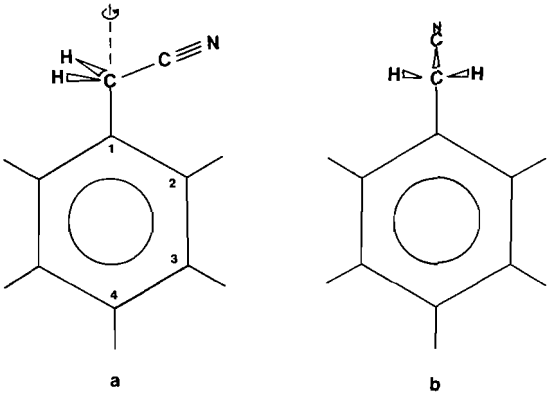

FIG. 1. Benzyl cyanide conformations.

(E_a = 3.3 kcal/mol). In a recent study, Schaefer *et al.* (12) measured the six-bond coupling constant between the methylene and *para* protons of 3,5-dichlorobenzyl cyanide and the analogous $^1H,^{19}F$ coupling constant in *p*-fluorobenzyl cyanide, from which they inferred a barrier height of approximately 0.35 kcal/mol for the twofold intramolecular potential of the $—CH_2CN$ group, the more stable conformation having the cyano group out of the aromatic plane (Fig. 1*b*). They also used the *ab initio* (STO-3G) molecular orbital scheme with partial geometry optimization to show that this quantity is less than 1 kcal/mol.

In the present paper, recognition of the grossly stochastic nature of the rotational diffusion model and the relatively weak interaction between the $C_6H_5—$ and $—CH_2CN$ fragments leads us to emphasize the anisotropy of the rotation and to regard any systematic effects that may result from the intramolecular potential as outside the scope of this picture, lost in the fluctuations of the number, momentum, and energy densities of the fluid.

Experimental

Benzyl cyanide (>98% purity) was obtained from the Aldrich Chemical Company and benzyl cyanide-*8*-^{13}C (i.e. ^{13}CN) and benzyl cyanide-*7*-^{13}C (i.e. $^{13}CH_2$) were obtained from Petrochem. The ^{13}C enriched samples were diluted with ordinary benzyl cyanide, 5% by volume cyclohexane-d_{12} was added to provide an internal lock, and the samples were degassed by the freeze–pump–thaw technique under vacuum and sealed.

Proton-decoupled ^{13}C spectra were obtained on a Varian CFT-20 spectrometer equipped with an 8 mm variable temperature probe. The spin–lattice relaxation times were measured using the inversion–recovery pulse sequence (d – 180° – t – 90°), where d is a delay time ($d > 5T_1$) and t is a variable time. T_1's of the methylene and aromatic carbons were measured independently using a sweep width of 125 Hz. Typically, 50 transients were accumulated for the methylene carbon (unenriched) and 16 to 25 transients for the ring carbons. Free induction signals were weighted slightly by an exponential weighting factor before being Fourier transformed. The 90° pulse width was 17 μs.

Nuclear Overhauser enhancement factors (nOe's) were measured using the gated proton decoupler with $d > 10T_1$ (^{13}C).

$^{13}C,^{13}C$ spin–spin coupling constants were measured using acquisition times > 10 s and are accurate to ±0.1 Hz.

Results and Discussion

^{13}C Spin–Lattice Relaxation Times and Rotational Diffusion Coefficients

Aromatic and Methylene Carbons

The dipolar part of the ^{13}C spin–lattice relaxation rate due to N identical, directly bonded protons is related to a reorientational correlation time, τ_2, in the extreme narrowing approximation by (13*a*)

$$[1] \qquad \frac{1}{T_1} = N\left(\frac{\gamma_C\gamma_H\hbar}{r^3}\right)^2 \tau_2$$

where γ_C and γ_H are the gyromagnetic ratios of ^{13}C and the proton, $2\pi\hbar$ is Planck's constant, and r is the C—H bond length. The rotational dynamics of the molecule are assumed to be adequately represented by the diffusion of a prolate spheroid with major axis passing through the $C_6H_5—CH_2CN$ bond. The rotation of this axis is characterized by a rotational diffusion coefficient, $D_\perp$, and the $C_6H_5—$ and $—CH_2CN$ groups are treated as rigid fragments in relative rotation about this axis, characterized by diffusion coefficients $D_\parallel$ and $D_\parallel'$, respectively. Woessner (14) has shown that the two coefficients are related to the correlation time by

$$[2] \quad \tau_2 = \frac{A}{6D_\perp} + \frac{B}{D_\parallel + 5D_\perp} + \frac{C}{4D_\parallel + 2D_\perp}$$

where $A = \frac{1}{4}(3\cos^2\theta - 1)^2$, $B = 3\sin^2\theta\cos^2\theta$, and $C = 3/4\sin^4\theta$, θ being the angle between the C—H vector and the major axis of the spheroid. Equation [2] explicitly refers to the $C_6H_5—$ group, and replacement of $D_\parallel$ by $D_\parallel'$ makes it applicable to the $—CH_2CN$ group. Because $\theta = 0$ for the *para* carbon (C_4), $\tau_2(C_4) = 1/6D_\perp$, such that the T_1 of this carbon is sufficient to determine $D_\perp$. The *ortho* (C_2) and *meta* (C_3) carbons both have $\theta = 60°$, so this model requires that their T_1's be equal. Standard geometries are assumed: the methylene carbon (C_m) is assigned the tetrahedral angle and r = 1.09 Å, and the aromatic r = 1.08 Å.

Table 1 displays the measured T_1's and the diffusion coefficients derived from them. The important features of this table can be summarized as follows: (*a*) $T_1(C_2) = T_1(C_3)$ within experimental error, (*b*) over 125 *K* temperature range, the T_1's and diffusion

TABLE 1. ^{13}C spin–lattice relaxation times and rotational diffusion coefficients[a]

T (K)	$T_1(C_2)$ (s)	$T_1(C_3)$ (s)	$T_1(C_4)$ (s)	$T_1(C_m)$ (s)	$D_\perp$ (rad^2 ps^{-1})	$D_\parallel$ (rad^2 ps^{-1})	$D_\parallel'$ (rad^2 ps^{-1})	$D_\parallel/D_\perp$	$D_\parallel'/D_\parallel$
251	1.85	1.85	1.10	1.14	0.0042	0.013	0.016	3.1	1.2
265	2.55	2.68	1.62	2.02	0.0061	0.018	0.034	3.0	1.9
277	4.02	4.05	2.40	2.67	0.0091	0.029	0.041	3.2	1.4
292	5.90	5.84	3.75	3.85	0.014	0.040	0.055	2.9	1.4
307	8.00	8.00	4.67	5.05	0.018	0.059	0.076	3.3	1.3
327	11.1	11.3	6.97	7.11	0.026	0.078	0.10	3.0	1.3
338	12.0	12.5	7.59	9.10	0.029	0.086	0.15	3.0	1.7
353	14.4	14.3	8.93	10.0	0.034	0.10	0.16	2.9	1.6
377	16.7	16.7	11.4	12.1	0.043	0.14	0.18	3.2	1.3

[a]All nOe factors are 2.0 within experimental error. Estimated error ±10% in the T_1's.

coefficients change by an order of magnitude, (*c*) the aromatic ring rotates about the major axis of the molecule approximately 3 times faster than the axis itself, and (*d*) the —CH_2CN group rotates about the major axis approximately 1.5 times faster than the aromatic ring. The constancy of $D_\parallel/D_\perp$ is in accordance with simple hydrodynamical theory (15), which predicts that this ratio is determined by the molecular geometry. The value for benzyl cyanide is similar to those of *tert*-butylbenzene, phenylacetylene, and biphenyl (13*b*).

Plots of $1/T_1$ on a logarithmic scale versus reciprocal temperature for the aromatic and methylene carbons all give activation energies of 3.5 ± 0.3 kcal/mol. Simple hydrodynamical theory predicts that this quantity can be equated to the activation energy associated with the ratio η/T, where η is the shear viscosity (15). This prediction is upheld by published viscosity data for benzyl cyanide (16), which, when plotted as $\ln(\eta/T)$ versus $1/T$, gives a good straight line with a slope corresponding to an E_a = 3.6 kcal/mol.

The quantity $D_\parallel' - D_\parallel$ ($\simeq \frac{1}{2}D_\parallel$ in this case) is the rate of diffusive rotation of the —CH_2CN group with respect to the aromatic ring (17). In general, this quantity is probably determined by a complicated interplay of inter- and intramolecular effects; but some investigators have attempted to equate the activation energy associated with its temperature dependence to the barrier to internal rotation (18). The data in Table 1 is not accurate enough for such treatment, but in any case we regard the procedure as inadequate. The relationships between transport coefficients and more fundamental molecular properties are very elaborate (19), and features as complicated as the geometric variation of the total energy of a polyatomic molecule require techniques of a precision as yet unattempted by the most ambitious kinetic theorists.

Cyano Carbon

Spin–lattice relaxation times were measured for the cyano carbon, and the components due to dipolar coupling with protons, T_1^d, were extracted with the corresponding nOe factors (13*a*), giving the results in Table 2. T_1' is a relaxation time associated with the total rate of relaxation due to mechanisms other than ^{13}C—^1H dipolar coupling. Ln $(1/T_1^d)$ and ln $(1/T_1')$ are plotted versus reciprocal temperature in Fig. 2, from which it was determined that the former has E_a = 3.6 kcal/mol. T_1^d has contributions from the *ortho* and methylene protons, and studies of acetonitrile (5) and cyanoacetylene (20) suggest that protons on adjacent molecules may also contribute.

T_1' represents the combined effects of spin–rotation coupling, ^{13}C—^{14}N dipolar coupling, scalar coupling (of the second kind), chemical shift anisotropy, and possibly traces of paramagnetic species such as O_2 (13). Rough calculations show that ^{13}C—^{14}N dipolar coupling and chemical shift anisotropy, which have the same temperature dependence as the ^{13}C—^1H dipolar coupling, are expected to contribute, whereas the scalar mechanism can be discounted. The high temperature behaviour of T_1' is consistent with the spin–rotation mechanism, but this effect is difficult to quantify for a nucleus in an unsymmetrical environment.

Although it makes no contribution to T_1, the

TABLE 2. Spin–lattice relaxation times and nOe factors for the cyano ^{13}C

T (K)	T_1[a] (s)	η[b]	T_1^d (s)	T_1' (s)
251	17.9	1.34	26.6	55.1
265	31.6	1.32	47.5	94.0
277	38.0	1.28	59.0	107
291	61.5	1.17	105	148
304	65.6	1.17	112	158
320	81.8	1.13	144	189
334	97.3	0.98	198	191
340	90.6	1.08	167	198
353	109	0.81	267	183
368	109	0.68	319	165
386	112	0.60	371	160
406	105	0.41	511	133

[a]Estimated error ±10% in the T_1's.
[b]Estimated error ±0.05 in the nOe factors.

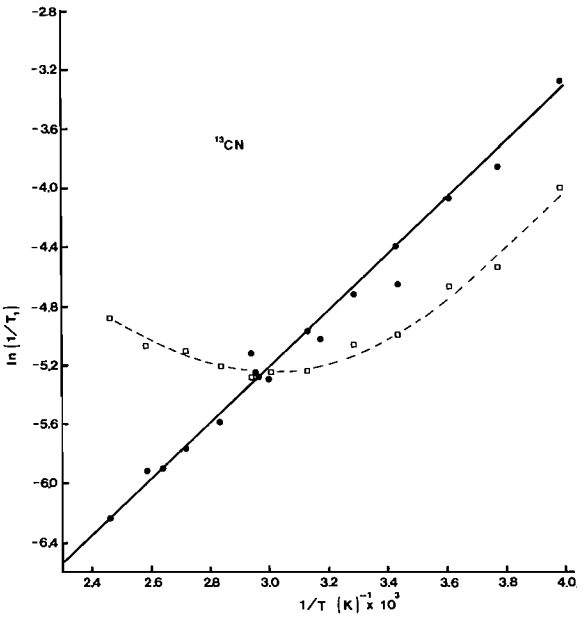

FIG. 2. The temperature dependence of the observed relaxation rates for the cyano ^{13}C in benzyl cyanide: the circles and solid line represent the ^{13}C—^{1}H dipolar component, and the squares and broken line represent the component due to other mechanisms.

scalar mechanism is very effective in the relaxation of the transverse component of the cyano ^{13}C magnetization. In this case, the spin–spin relaxation time, T_2^{sc}, is related to the ^{14}N spin–lattice relaxation time, $T_1(^{14}N)$, by (13*a*)

$$[3] \qquad \frac{1}{T_2^{sc}} = \frac{1}{T_1^{sc}} + \frac{8}{3}\pi^2 J^2 T_1(^{14}N)$$

where T_1^{sc} is very large and J is the ^{13}C—^{14}N spin–spin coupling constant. Since $\nu_{1/2} = (\pi T_2)^{-1}$ and it can be assumed that $T_1(^{14}N) = T_2(^{14}N)$ for rapid relaxation of the nitrogen, [3] can be approximated as

$$[4] \qquad \nu_{1/2}(^{13}C) \simeq \frac{8}{3}\frac{J^2(^{13}C—^{14}N)}{\nu_{1/2}(^{14}N)}$$

in terms of half-height linewidths. $J(^{13}$C—^{15}N) is -17.5 Hz in acetonitrile and -16.4 Hz in propionitrile (21), so we have estimated $J(^{13}$C—^{14}N) in benzyl cyanide as $\simeq -16\gamma(^{14}N)/\gamma(^{15}N) = 11.4$ Hz. Estimating ^{14}N linewidths from a graph in ref. 8 and using [4] we have calculated cyano ^{13}C linewidths which are in good agreement with experiment. For example, at 303, 378, 423, and 443 K the calculated (observed) values in Hz are 0.9 (1.2), 1.7 (1.7), 2.6 (2.3), and 3.0 (2.9), respectively.[1]

A few reservations about the analysis presented here should be stated. It is not completely certain that multispin effects (22) are absent in decoupled ^{13}C spectra, but we have made the usual assumption that single exponential recovery of the magnetization (as observed) is due to the mechanisms discussed above. More importantly, the choice of axes for the diagonalized rotational diffusion tensor was made heuristically, and the inertial and dipolar properties of the molecule due to the —CN group are thereby oversimplified. Also, it has been shown (23) that $D_{\parallel,\perp}$ is quite sensitive to small changes in molecular geometry. With these limitations in mind, we believe that the observed anisotropy, relative motion of the C_6H_5— and —CH_2CN groups, and hydrodynamically determined temperature dependence are significant features of the rotational dynamics.

$^{13}C,^{13}C$ Spin–Spin Coupling Constants

Cyano Carbon

Observed and calculated ^{13}C,^{13}C coupling constants involving the cyano carbon are listed in Table 3. The calculated values are Fermi contact contributions at the INDO–MO–FPT level of approximation (24–26) for the conformation in which the C≡N bond is in the plane of the benzene ring (Fig. 1*a*) and the conformation derived from this by rotation through 90° about the C_6H_5—CH_2CN bond (Fig. 1*b*). Standard geometries were used in all calculations (26).

The value 57.2 Hz observed for $^1J(CH_2,CN)$ in benzyl cyanide is similar to the value 56.6 Hz observed in acetonitrile (7), and the calculated values are substantially larger than those observed for both molecules (27, 28). Agreement might be improved if the orbital-dipolar (OD) and spin-dipolar (SD) contributions were included, but Blizzard and Santry (28) have estimated these terms to be only -2.56 and 0.57 Hz respectively in acetonitrile.

The value of $^2J(CN,C)$ in benzyl cyanide is only 3.53 Hz, in contrast to a value of 33.0 Hz reported for propionitrile (7). The INDO–MO–FPT procedure

TABLE 3. Observed and INDO–FPT calculated values of $^nJ(^{13}CN,^{13}C)$ in benzyl cyanide

Coupling constant	Observed values[a] (Hz)	Calculated values (Hz)	
		a	*b*
$^1J(CN,CH_2)$	57.2	76.30	74.96
$^2J(CN,C_1)$	3.53	−8.34	−9.39
$^3J(CN,C_2)$	3.37	3.35	3.60
$^3J(CN,C_6)$	3.37	5.65	3.60
$^4J(CN,C_3)$	≤0.3	−0.32	−2.51
$^4J(CN,C_5)$	≤0.3	0.00	−2.51
$^5J(CN,C_4)$	≃0.3	0.23	2.73

[a]Estimated error is ±0.1 Hz.

[1]Observed linewidths have been corrected for magnetic field inhomogeneity, estimated error ±0.3 Hz.

TABLE 4. Observed and INDO–FPT calculated values of $^nJ(^{13}CH_2,^{13}C)$ in benzyl cyanide

Coupling constant	Observed values[a] (Hz)	Calculated values (Hz)	
		a	*b*
$^1J(CH_2,C_1)$	44.25	48.29	48.09
$^2J(CH_2,C_2)$	4.05	−4.72	−4.89
$^2J(CH_2,C_6)$	4.05	−4.82	−4.89
$^3J(CH_2,C_3)$	3.61	5.15	4.80
$^3J(CH_2,C_5)$	3.61	5.10	4.80
$^4J(CH_2,C_4)$	≤0.6	−2.10	−1.78

[a]Estimated error ±0.1 Hz.

predicts −8.9 Hz in propionitrile, similar to the value for benzyl cyanide. If this large difference between the two molecules is real, then it appears that the combined OD and SD contributions to ^2J(C,C) are very different.

The general behaviour of ^3J(C,C) as a function of dihedral angle has been investigated (29–33) and shown to be quite different for saturated systems than for systems with π character in the coupling path. That this quantity is not very useful in conformational analysis (30) is reflected in the similarity of its values for *a* and *b* (Fig. 1).

The values of ^4J(C,C) and ^5J(C,C) suggest that *a* contributes more than *b* to the averages, but the more accurate STO-3G calculations (12) of the energy of the free molecule do not support this. Long range H,H couplings are reasonably well reproduced by INDO–MO–FPT calculations (34), but the absence of good model compounds make such an assessment for C,C difficult.

Methylene Carbon

Values of $^nJ(CH_2,C)$ observed for benzyl cyanide are given in Table 4 along with those calculated by the INDO–MO–FPT method. The observed values are similar to those of toluene, benzyl alcohol, and benzyl chloride (35). The calculated values are not very sensitive to the orientation of the methylene group. The large values calculated for $^4J(CH_2,C)$ may indicate the importance of the OD and SD terms, but are more likely to result from limitations in the INDO approximation.

Acknowledgements

Ted Schaefer's encouragement and Werner Danchura's patience are gratefully acknowledged, as is the financial support of the National Research Council of Canada.

1. T. T. BOPP. J. Chem. Phys. **47**, 3621 (1967).
2. W. T. HUNTRESS. Adv. Magn. Reson. **4**, 27 (1970).
3. A. OLIVSON, E. LIPPMAA, and J. PAST. Eesti NSV Tead. Akad. Toim. Fuus. Mat. **16**, 390 (1967).
4. A. P. ZENS and P. D. ELLIS. J. Am. Chem. Soc. **97**, 5685 (1975).
5. T. K. LEIPERT, J. H. NOGGLE, and K. T. GILLEN. J. Magn. Reson. **13**, 158 (1974).
6. E. VON GOLDHAMMER, H.-D. LIIDEMANN, and A. MIILLER. J. Chem. Phys. **60**, 4590 (1974); **61**, 3493 (1974).
7. G. A. GRAY, G. E. MACIEL, and P. D. ELLIS. J. Magn. Reson. **1**, 407 (1969).
8. D. WALLACH. J. Phys. Chem. **73**, 307 (1969).
9. R. A. ASSINK, J. DE ZWAAN, and J. JONAS. J. Chem. Phys. **56**, 4975 (1972).
10. M. FURY and J. JONAS. J. Chem. Phys. **65**, 2206 (1976).
11. J. DE ZWAAN and J. JONAS. J. Chem. Phys. **77**, 1768 (1973).
12. T. SCHAEFER, W. DANCHURA, W. NIEMCZURA, and J. PEELING. Can. J. Chem. **56**, 2442 (1978).
13. (*a*) J. R. LYERLA and G. C. LEVY. Topics in ^{13}C NMR. Vol. 1. Wiley-Interscience, New York, NY. 1974. (*b*) G. C. LEVY, J. D. CARGIOLI, and F. A. L. ANET. J. Am. Chem. Soc. **95**, 1527 (1973).
14. D. E. WOESSNER. J. Chem. Phys. **37**, 647 (1962).
15. R. E. WASYLISHEN, B. A. PETTITT, and W. DANCHURA. Can. J. Chem. **55**, 3602 (1977) and references therein.
16. F. J. WRIGHT. J. Chem. Eng. Data, **6**, 454 (1961).
17. D. E. WOESSNER and B. S. SNOWDEN. Adv. Mol. Relaxation Processes, **3**, 181 (1972).
18. D. E. AXELSON and C. E. HOLLOWAY. Can. J. Chem. **54**, 2820 (1976); H. NAKANISHI and O. YAMAMOTO. Chem. Phys. Letts. **35**, 407 (1975); J. R. LYERLA and G. C. LEVY. Topics in ^{13}C NMR. Vol. 1. Wiley-Interscience, New York, NY. 1974. p. 131.
19. D. A. MCQUARRIE. Statistical Mechanics. Harper and Row, New York, NY. 1973.
20. N. M. SZEVERENYI, R. R. VOLD, and R. L. VOLD. Chem. Phys. **18**, 28 (1976).
21. G. A. GRAY. Ph.D. Dissertation. University of California, Davis, CA. 1967.
22. L. G. WERBELOW and D. M. GRANT. Adv. Magn. Reson. **9**, 189 (1977).
23. J. W. BLUNT and J. B. STOTHERS. J. Magn. Reson. **27**, 515 (1977).
24. J. A. POPLE, J. W. MCIVER, JR., and N. S. OSTLUND. Chem. Phys. Lett. **1**, 465 (1967).
25. J. A. POPLE, J. W. MCIVER, JR., and N. S. OSTLUND. J. Chem. Phys. **49**, 2960 (1968); **49**, 2965 (1968).
26. J. A. POPLE and D. L. BEVERIDE. Approximate molecular orbital theory. McGraw-Hill Book Co., New York, NY. 1970.
27. G. E. MACIEL, J. W. MCIVER, JR., N. S. OSTLUND, and J. A. POPLE. J. Am. Chem. Soc. **92**, 11 (1970).
28. (*a*) A. C. BLIZZARD and D. P. SANTRY. J. Chem. Phys. **55**, 950 (1971). (*b*) A. C. BLIZZARD and D. P. SANTRY. J. Chem. Phys. **58**, 4714 (1973).
29. J. L. MARSHALL and D. E. MILLER. J. Am. Chem. Soc. **95**, 8305 (1973).
30. J. L. MARSHALL, L. G. FAEHL, A. M. IHRIG, and M. BARFIELD. J. Am. Chem. Soc. **98**, 3406 (1976).
31. M. BARFIELD, I. BURFITT, and D. DODDRELL. J. Am. Chem. Soc. **97**, 2631 (1975).
32. D. DODDRELL, I. BURFITT, J. B. GRUTZNER, and M. BARFIELD. J. Am. Chem. Soc. **96**, 1241 (1974).
33. R. E. WASYLISHEN. *In* Annual reports on NMR spectroscopy. Vol. 7. *Edited by* G. A. Webb. Academic Press, New York, NY. 1977. p. 245.
34. J. KOWALEWSKI. *In* Progress in NMR spectroscopy. Vol. 11. *Edited by* J. W. Emsley, J. Feeney, and L. H. Sutcliffe. Pergamon Press, Oxford. 1977. p. 1.
35. A. M. IHRIG and J. L. MARSHALL. J. Am. Chem. Soc. **94**, 1756 (1972).

The photoelectron spectra of the methylbromamines and unsubstituted bromamines[1]

D. COLBOURNE, D. C. FROST, C. A. MCDOWELL, AND N. P. C. WESTWOOD

Department of Chemistry, University of British Columbia, 2075 Wesbrook Mall, Vancouver, B.C., Canada V6T 1W5

Received January 3, 1979

D. COLBOURNE, D. C. FROST, C. A. MCDOWELL, and N. P. C. WESTWOOD. Can. J. Chem. 57, 1279 (1979).

HeI photoelectron spectra are reported for pure gas-phase samples of the unstable methylbromamines, CH_3NHBr, CH_3NBr_2, and $(CH_3)_2NBr$. Results are also presented for the unsubstituted bromamines NH_2Br and $NHBr_2$ obtained as products from a gas-phase mixing of NH_3 and Br_2. The spectra are compared with those of the corresponding chloramines.

D. COLBOURNE, D. C. FROST, C. A. MCDOWELL et N. P. C. WESTWOOD. Can. J. Chem. 57, 1279 (1979).

On rapporte les spectres photoélectroniques, HeI, d'échantillons gazeux purs des méthylbromamines instables, CH_3NHBr, CH_3NBr_2 et $(CH_3)_2NBr$. On présente aussi des résultats pour les bromamines non-substituées NH_2Br et $NHBr_2$ que l'on a obtenues comme produits par mélange en phase gazeuse de NH_3 et Br_2. On compare les spectres avec ceux des chloramines correspondantes.

[Traduit par le journal]

Introduction

The simple unsubstituted bromamines, $NH_{3-n}Br_n$, are known to be rather unstable molecules (4–6), and for this reason have not been as extensively studied as the analogous chloramines (5, 6). Monobromamine (NH_2Br) has been prepared in ether solution by reaction of ammonia and bromine at 0°C (7) or −60°C (8), and dibromamine ($NHBr_2$) results from a modification of the same procedure (9, 10). The absorption spectra of ether solutions of these compounds indicates that there exists an equilibrium between bromamine, ammonia, and dibromamine (11). The preparation of both species in aqueous solution has been claimed (12, 13), identification being based on ultraviolet absorption spectrometry. These claims were later substantiated (14), and the presence of nitrogen tribromide (NBr_3) was also postulated. Only monobromamine has been prepared in the gas phase (15), following reaction of a large excess of ammonia with bromine diluted with nitrogen.

N-Bromoalkylamines are considerably more stable (16); the methylbromamines, although not isolated, have previously been prepared in aqueous solution (17), and as such have been studied by infrared (17) and ultraviolet (11, 17) absorption spectrometry. Similar studies, conducted in ether solution (11) indicate that an equilibrium between CH_3NHBr, CH_3NBr_2, and free amine occurs. Dimethylbromamine, $(CH_3)_2NBr$, is the only methylbromamine that has previously been prepared in the gas phase (15), albeit from a mixture of gaseous dimethylamine and bromine, where one of the components is always in excess. In summary, therefore, all of the unsubstituted and methylated bromamines are unstable, and have never been characterized in the gas phase. Methylation increases the stability.

We previously studied the HeI and NeI photoelectron (PE) spectra of the unsubstituted chloramines (NH_2Cl, $NHCl_2$, and NCl_3) and the methyl substituted chloramines (CH_3NHCl, CH_3NCl_2, and $(CH_3)_2NCl$) (2, 3), and now wish to extend this to the PE spectra of the bromo analogues. Our purpose is twofold: first, to obtain information on the electronic structures of these bromamines and relate them to those of the chloramines, and secondly, to illustrate how relatively pure samples of these molecules may be produced for gas-phase investigation. Thus following our earlier work on the chloramines (2, 3), the methylbromamines are prepared as volatile components of a solution reaction, and the unsubstituted monobromamine is prepared via a gas phase mixing reaction. Evidence for the formation and detection of dibromamine is presented. During the course of this work a paper was published on the PE spectrum of NH_2Br (18*a*) and subsequent to the completion of this manuscript, a paper on CH_3NHBr and CH_3NBr_2 also appeared in the literature (18*b*). All three species were obtained as constituents of Br_2/NH_3 (or CH_3NH_2) mixtures in the gas-phase, and the resultant "clean" spectra were obtained by spectrum stripping procedures. Here we present the PE spectra of *pure* gas-phase samples.

[1]Part III of a series. For parts I and II, see refs. 2 and 3. Part IV is ref. 1.

0008-4042/79/111279-07$01.00/0

Experimental

(a) Methylbromamines

These were prepared in aqueous solution by mixing a solution of sodium hypobromite, NaOBr, with the appropriate amine solution. The temperature was maintained at 0°C. The methylbromamine thus formed was sufficiently volatile *in vacuo* to be led directly into the ionization chamber of the PE spectrometer (19) via a $CaCl_2$ trap to remove excess water.

(*i*) Preparation of the NaOBr solution: Br_2 was added slowly to a 20% NaOH solution at room temperature until there was an excess of halogen. This solution was kept in the dark at −10°C until required.

(*ii*) CH_3NHBr: an excess of 40% methylamine solution was added quickly to the hypobromite solution. As we have previously observed for CH_3NHCl (3), the ratio of amine:hypohalite for optimum yields was found to be critical, since insufficient amine results in the formation of CH_3NBr_2. Best yields were obtained at a pH of about 9.

(*iii*) CH_3NBr_2: 40% methylamine solution was added dropwise with stirring to the hypobromite solution. The dibromo-substituted species was formed under these conditions when the amine was not in excess (pH ~ 7).

(*iv*) $(CH_3)_2NBr$: 40% dimethylamine solution was added to the hypobromite solution until alkaline (pH ~ 10).

(*v*) Sampling: a similar technique to that used for the chloramines (2, 3) was found to be appropriate here; the volatile component from the solution was led directly into the PE spectrometer (19) via a $CaCl_2$ U-trap maintained at −37°C. Spectra were calibrated using the known ionization potentials (IP's) of CH_3I, H_2O, N_2, and Ar.

(b) Monobromamine (and Dibromamine)

Extensive experiments to prepare and sample the unsubstituted bromamines from aqueous solution were unsuccessful. Rapid decomposition in solution prevented the observation of any gas-phase bromamine. Nitrogen was observed in abundance. Similar results were obtained using a variety of solvents. Thus a direct gas-phase synthesis was devised, based on the generator used previously for the monochloramine synthesis (2, 20) which involved mixing of Br_2 and NH_3. NH_2Br is easily produced by this method (see later, and refs. 15 and 18*a*). The NH_3:Br_2 ratio, the flow rate, and temperature were all extensively varied in an attempt to improve the yield of gas-phase dibromamine, since the previous work (2, 3) indicated that substantial amounts of di- and even tri-chloramine are produced by this method.

Results

The HeI PE spectra of CH_3NHBr, CH_3NBr_2, and $(CH_3)_2NBr$ are shown in Fig. 1 *a*, *b*, and *c*, respectively. The spectra are relatively clean, the only contaminant being a trace of water evidenced by the sharp peak at 12.62 eV. Certain bands in each of the spectra show resolvable vibrational structure (listed in Table 1).

Spectra of NH_2Br in the presence of excess Br_2 (21) and excess NH_3 (22) are shown in Fig. 2 *a* and *b*, respectively, with expansions of the first region under the same conditions shown in Fig. 3 *a* and *b*. The first band of NH_2Br shows resolvable fine structure (Fig. 4).

All IP's and associated vibrational structure are given in Table 1 for the methylbromamines and Table 2 for the unsubstituted bromamines. The weak

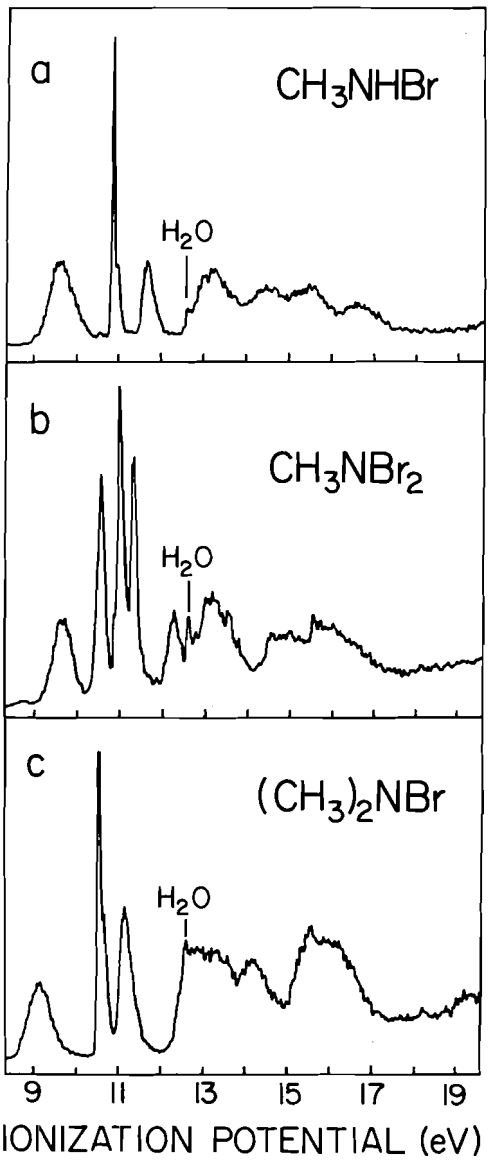

FIG. 1. The HeI photoelectron spectra of (*a*) CH_3NHBr, (*b*) CH_3NBr_2, and (*c*) $(CH_3)_2NBr$.

Franck–Condon factors for the adiabatic transition of the first band may mean that the quoted adiabatic IP's are in error by one vibrational quantum. Error limits are given in Tables 1 and 2 together with the proposed assignments.

Assignments

(a) Methylbromamines

The assignments for the methylbromamines are based partly on the expected shifts for bromination of an amine, and partly on the previous results for the analogous methylchloramines (3). Since there appear to be no changes in the sequence of orbital energies (assuming Koopmans' theorem (23)) for

TABLE 1. Experimental vertical IP's and assignments[a] for CH_3NHBr, $(CH_3)_2NBr$, and CH_3NBr_2

CH_3NHBr[b]			$(CH_3)_2NBr$[b]			CH_3NBr_2[c]		
IP (eV)	v′ (cm^{-1})	Assignment	IP (eV)	v′ (cm^{-1})	Assignment	IP (eV)	v′ (cm^{-1})	Assignment
(9.12)			(8.61)			(9.15)		
9.60		10*a*	9.14		8*a*′	9.62		8*a*′
10.86	830	9*a*	10.55	320 1040	5*a*″	10.56		5*a*″
11.68		8*a*	11.18		7*a*′	11.02	300	7*a*′
13.22		7*a*	12.84		4*a*″	11.33		4*a*″
14.64		6*a*	13.33		6*a*′	12.28		6*a*′
15.63		5*a*	14.20		3*a*″	13.19		3*a*″
16.66		4*a*	15.55		5*a*′	14.88		5*a*′
			16.08		2*a*″	15.78		2*a*″
			16.36		4*a*′	16.30		4*a*′

[a]Adiabatic IP's in parentheses. Valence level numbering. Vibrational structure ±50 cm^{-1}.
[b]First three IP's, ±0.02 eV, the rest ±0.05 eV.
[c]First five IP's, ±0.02 eV, the rest ±0.05 eV.

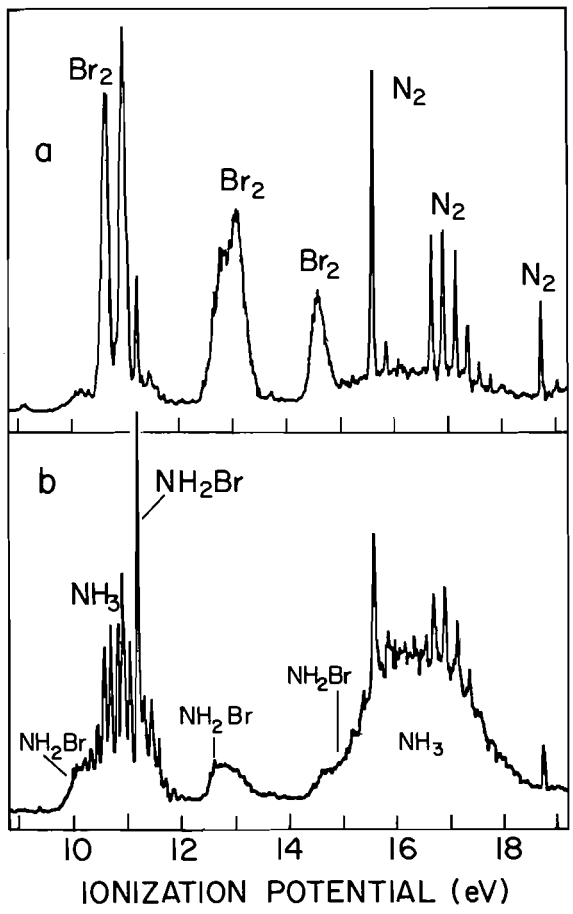

FIG. 2. HeI photoelectron spectra of the $NH_3 + Br_2$ gas-phase reaction. (*a*) Excess Br_2 and (*b*) excess NH_3.

these methylbromamines, we prefer not to discuss them in detail, except to point out any unusual features. A comparison of Fig. 1 with Fig. 3 of ref. 3 will illustrate the direct correspondence of the IP's. The numerical values are summarized in the correlation diagram, Fig. 5. The results are in good agreement with the recent spectra obtained by spectrum stripping from mixtures (18*b*) (apart from an interchange of the closely spaced 7*a*′ and 4*a*″ orbitals).

Certain features of the spectra and the numerical values are worth considering. First, as expected, all IP's of the methylbromamines are lower than those of the corresponding methylchloramines. The effect is more pronounced for those bands involving considerable Br 4*p* character, i.e. the halogen lone pairs, and the *n*N + *n*X combinations. Secondly, all bands in the methylbromamines are more spread out than the corresponding bands in the methylchloramines. The individual IP's become more apparent, especially in the CH_3 region (>12.5 eV), where the location and assignment of individual IP's were more difficult in the case of the methylchloramines. We also note that the third and fourth bands of CH_3NBr_2 are now completely separated, whereas in $NHCl_2$ they are essentially degenerate, and only slighly separated in CH_3NCl_2. Thirdly, there are some slight variations in the vibrational fine structure observed on the sharp second bands of CH_3NHBr and $(CH_3)_2NBr$ compared to the corresponding structure on the methylchloramines. This structure was not observed in the recently published work (18*b*). Specifically, the observed structure on the second band of CH_3NHBr is 830 ± 50 cm^{-1}, and cannot therefore correspond to an N—Br stretching frequency, since the value for CH_3NHCl^+ is 750 ± 50 cm^{-1} (3). We prefer to assign this mode in both cases to an N—C stretching frequency (895, 875 cm^{-1} in the molecular ground state of CH_3NHCl (24)). On the second band of $(CH_3)_2NBr$, two progressions are resolvable, one of 320 ± 50 cm^{-1} not previously seen on the corresponding band of $(CH_3)_2NCl$, and the other of 1040 ± 50 cm^{-1}, corresponding to the excitation of

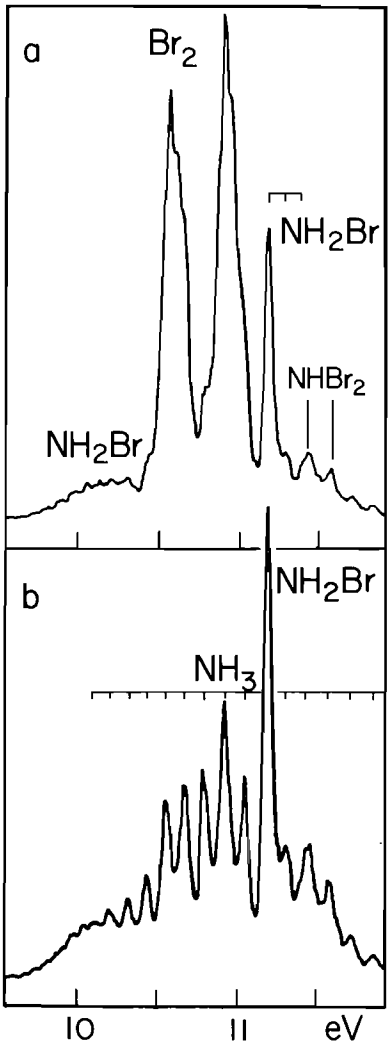

FIG. 3. Expansion of the 10–12 eV region in the gas-phase reaction of NH_3 and Br_2. (*a*) Excess Br_2 and (*b*) excess NH_3.

960 ± 50 cm^{-1} in $(CH_3)_2NCl^+$. The latter is either a reduced CH_3 deformation (1200–1150 cm^{-1} in molecular $(CH_3)_2NBr$ (25)) or an NC_2 stretching frequency (900 cm^{-1} in molecular $(CH_3)_2NBr$). The value of 320 cm^{-1} could be a reduced N—Br stretching frequency (525 cm^{-1} in $(CH_3)_2NBr$), although this seems unlikely in view of the non-bonding nature of this transition. The more plausible alternative is an NC_2 deformation (390 cm^{-1} for molecular $(CH_3)_2NCl$ (25)).

As mentioned above, the third and fourth bands of CH_3NBr_2 are now well separated, and the third band now shows some vibrational structure, 300 ± 50 cm^{-1}, the assignment of which is probably similar to that of $(CH_3)_2NBr$. Such structure was not observed on the corresponding bands of $NHCl_2$ or CH_3NCl_2 due to the overlapping of the peaks.

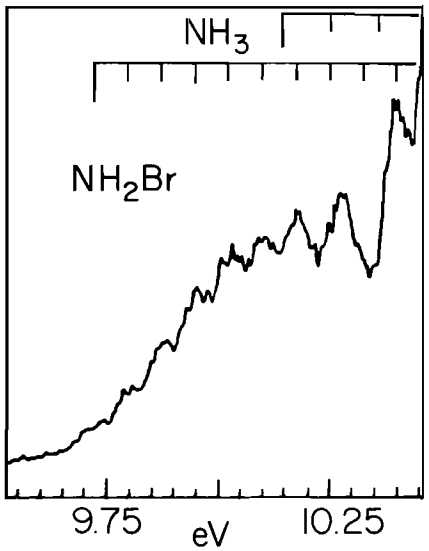

FIG. 4. Detail of the first band in the PE spectrum of NH_2Br.

(b) Monobromamine and Dibromamine

The PE spectrum of monobromamine should show five bands, directly analogous to those of monochloramine (2, 3). The spectra which are obtained from a gas-phase reaction of Br_2 and NH_3 always involve the presence of one of these components (e.g. Fig. 2*a*, excess Br_2, Fig. 2*b*, excess NH_3), and so values for only the first four IP's can be given with any certainty since the remaining band is of low intensity (see NH_2Cl (2)) and obscured by the broad ^2E state of NH_3^+ (15–18 eV) (22).

The first band (Fig. 4) with adiabatic and vertical IP's of 9.74 and 10.18 eV corresponds to an N—Br antibonding combination decreased by 0.34 eV from the corresponding band of NH_2Cl, and ~0.70 eV from the corresponding band of NH_3. It retains the broad envelope of a nitrogen lone pair, but the downward shift implies considerable Br 4*p* involvement. As with the first band of NH_2Cl there is a distinct vibrational progression, a mean value of 650 ± 50 cm^{-1} being observed (compare NH_2Cl, 760 ± 40 cm^{-1}) (2). The only vibrational data available for NH_2Br are those involving νN—Br (540 cm^{-1}) (6) and this is certainly a possible excitation since the orbital is N—Br antibonding. The other alternative which we considered for NH_2Cl (2) is a reduced value of the H_2N—Br bending frequency (estimated to be ~800 cm^{-1} in the molecular ground state).

The second band (Fig. 3) with coincident adiabatic and vertical IP's (11.19 eV) is sharp and intense, analogous to the corresponding bands in NH_2Cl (2) and the methylbromamines, CH_3NHBr and $(CH_3)_2NBr$ (Fig. 1). It retains the non-bonding character and is shifted from the corresponding band in NH_2Cl by −0.73 eV. From a careful study of

TABLE 2. Experimental vertical IP's and assignments[a] for NH_2Br together with predicted vertical IP's for $NHBr_2$

NH_2Br			$NHBr_2$		
IP (eV)	ν' (cm^{-1})	Assignment	Predicted IP[b]	Observed IP	Assignment
(9.72)					
10.18	650	$5a'$	10.15		$6a'$
11.19	840	$2a''$	10.96		$4a''$
12.69		$4a'$	11.42	11.43	$5a'$
15.0		$3a'$	11.67	11.57	$3a''$
			13.35		$4a'$

[a]Adiabatic IP in parentheses. Valence level numbering. Vibrational structure ± 50 cm^{-1}.
[b]Obtained by IP ($NHCl_2$) × IP(CH_3NBr_2)/IP(CH_3NCl_2).

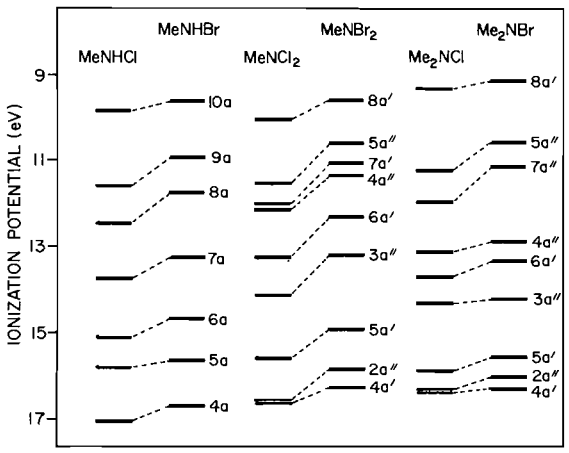

FIG. 5. Correlation diagram for the complete series of methylchloramines and methylbromamines. Valence level numbering.

many spectra under varying Br_2:NH_3 ratios, it is apparent that there are three other much weaker peaks in this region which are not associated with either Br_2 or NH_3. One (at 11.29 eV) is definitely associated with this intense second band and is assigned to a vibrational component at 840 ± 50 cm^{-1}, probably corresponding to the H_2N—Br bending frequency. From intensity changes, the other two peaks at 11.43 and 11.57 eV are not associated with this ionization event, and are therefore tentatively assigned to bands belonging to the third and fourth IP's of dibromamine, $NHBr_2$. Our rationale for this is twofold: these two bands increase in intensity with excess Br_2, and as we have previously observed (2), the reaction of excess gaseous Cl_2 with NH_3 leads to the formation of the dichloro- species. Finally, the observed values of 11.43 and 11.57 eV are very close to the predicted values for the third and fourth bands of $NHBr_2$ (see below). NBr_3 can be excluded on these grounds.

The third band of NH_2Br, the N—Br bonding combination, retains the same band envelope as the corresponding band of NH_2Cl, and is shifted by -0.81 eV to give a vertical IP of 12.69 eV. The spectrum shown in Fig. 2 shows a slight trace of residual Br_2 ($^2\Pi_{1/2\,u}$) (21) on the high energy side of this band.

The fourth IP is located at the onset of the band due to the ^2E state of NH_3^+ (22) and partially overlaps the $^2\Sigma_g^+$ state of Br_2^+ (21). We can, however, estimate a vertical IP of 15.0 ± 0.1 eV, the corresponding band of NH_2Cl occurring at 15.72 eV with a similar weak, broad Franck–Condon profile. The weaker fifth band, which occurs in NH_2Cl at 17.50 eV, is not observed here, since it occurs directly under the broad second band of NH_3. Previous work (18), also involving a gas-phase reaction of NH_3 and Br_2, gives a spectrum very similar to that reported here. The IP's are in relatively good agreement, a spectrum stripping procedure also locating the fifth IP at 16.93 eV. There is a slight discrepancy in the absolute position of the sharp second band, and the magnitude of the associated vibrational frequency. The latter is particularly confused by the presence of the bands due to $NHBr_2$.

Discussion

As mentioned above, and as illustrated in Fig. 5, the PE spectra of all the methylbromamines follow directly from those of the corresponding methylchloramines after incurring the usual shift due to replacement of Cl by Br. The mixing between orbitals is considerable for these low symmetry molecules, and thus all IP's show appropriate shifts dependent upon the extent of Br $4p$ involvement. The increased separation of most of the bands allows individual IP's beyond 12.5 eV to be assigned with more certainty although the deepest lying levels in CH_3NBr_2 and $(CH_3)_2NBr$ are still not completely separated. The proposed assignments are given in Table 1.

The unsubstituted bromamines are considerably more unstable than the methylated derivatives, and so PE spectra could not be obtained completely free of precursors. All attempts to prepare NH_2Br from solution resulted in spontaneous formation of solid

NH_4Br and the evolution of nitrogen. Even in the gas-phase reaction of NH_3 and Br_2 it was noted that high yields of NH_2Br resulted in increased formation of nitrogen. However, NH_2Br shows four IP's in the PE spectrum, similar in appearance and expected position to those of NH_2Cl (2). In addition, under certain conditions with excess Br_2 we were able to produce small amounts (estimated to be $<5\%$) of a new species (peaks at 11.43 and 11.57 eV) which we believe to be $NHBr_2$. By scaling the IP values for $NHCl_2$ by the ratio of the shifts for CH_3NCl_2 and CH_3NBr_2 we can predict a PE spectrum for $NHBr_2$, which should be close to the experimental spectrum. The numerical values are given in Table 2, together with the observed values; the agreement is remarkably good, and the correlation diagram (Fig. 6) shows the anticipated spacings between the first five bands. Also included in this correlation diagram, to complete the series of *N*-dihalamines, is difluoramine, NHF_2, the PE spectrum of which we have recently obtained (1).

The effect of Br and CH_3 substitution upon the absolute position (vertical IP) of the first band of NH_3 is summarized in Fig. 7. Here horizontal and vertical arrows refer to replacement of H by CH_3 or Br respectively. The diagonal arrows correspond to replacement of Br by CH_3. As we have previously noted for the chloramines (3), the first IP of NH_3 is substantially destabilized by the antibonding halogen interaction. However, from the observed shifts of Fig. 7, we may estimate vertical IP's for $NHBr_2$ and NBr_3, the former result being in good agreement with that estimate by the scaling method (Fig. 6 and Table 2). Again, the diagonal relationships are the most consistent, the replacement of any Br atom by a

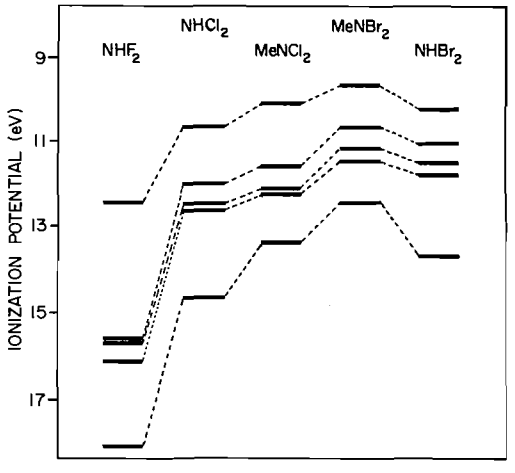

FIG. 6. Correlation diagram for the dihalamines, NHX_2 (X = F, Cl, and Br), and the methyldihalamines, CH_3NX_2 (X = Cl and Br).

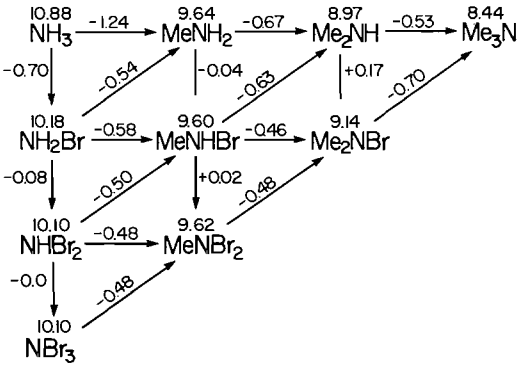

FIG. 7. Effect of Me and Br substitution upon the first IP's of substituted ammonias. Horizontal arrows, replacement of H by Me; vertical arrows, replacement of H by Br; diagonal arrows, replacement of Br by Me. Estimated values for $NHBr_2$ and NBr_3.

CH_3 group decreasing the first IP by a factor of 0.56 ± 0.14 eV (compare 0.78 ± 0.1 eV for the chloramines (3)).

From this work it seems unlikely that a pure sample of $NHBr_2$ for gas-phase investigation may ever be prepared, although it is possible that a spectrum stripping procedure similar to that used for NH_2Br (18) may be feasible in order to obtain a "clean" PE spectrum. $NHCl_2$ itself is prone to decompose when pure, although we have succeeded in obtaining impurity free spectra of this species (3). Addition of methyl groups does however confer substantial stability as we have seen for the methylbromamines. In the light of our recent work on the PE spectra of several halo and methyl substituted ammonias, we offer here an estimate of the gas-phase stability of these molecules based on their rates of decomposition, viz., $(CH_3)_2NCl > CH_3NCl_2 \sim (CH_3)_2NBr > CH_3NHCl > CH_3NBr_2 > CH_3NHBr > NH_2Cl > NCl_3 > NHCl_2 \gg NH_2Br > NHBr_2$. This is somewhat subjective, but hopefully useful to those wishing to investigate further these interesting compounds.

Acknowledgement

The financial support of the National Research Council of Canada is gratefully acknowledged.

1. D. COLBOURNE, D. C. FROST, C. A. MCDOWELL, and N. P. C. WESTWOOD. To be published.
2. D. COLBOURNE, D. C. FROST, C. A. MCDOWELL, and N. P. C. WESTWOOD. J. Chem. Phys. **68**, 3574 (1978).
3. D. COLBOURNE, D. C. FROST, C. A. MCDOWELL, and N. P. C. WESTWOOD. J. Chem. Phys. **69**, 1078 (1978).
4. J. JANDER, E. KURZBACH, and E. SCHMID. Chem. Soc. Special Publications, **10**, 65 (1957).
5. P. KOVACIC, M. K. LOWERY, and K. W. FIELD. Chem. Rev. **70**, 639 (1970).
6. J. JANDER and U. ENGELHARDT. *In* Developments in inorganic nitrogen chemistry. Vol. 2. *Edited by* C. B. Colburn. Elsevier, Amsterdam. 1973.

7. W. MOLDENHAUER and M. BURGER. Ber. Dtsch. Chem. Ges. **62**, 1615 (1929).
8. G. H. COLEMAN, H. SOROOS, and C. B. YAGER. J. Am. Chem. Soc. **55**, 2075 (1933).
9. G. H. COLEMAN, C. B. YAGER, and H. SOROOS. J. Am. Chem. Soc. **56**, 965 (1934).
10. G. H. COLEMAN and G. E. GOHEEN. Inorg. Synth. **1**, 62 (1939).
11. J. JANDER and C. LAFRENZ. Z. Anorg. Allg. Chem. **349**, 57 (1967).
12. J. K. JOHANNESSON. Chem. Ind. London, 97 (1958).
13. J. K. JOHANNESSON. J. Chem. Soc. 2998 (1959).
14. H. GALAL-GORCHEV and J. C. MORRIS. Inorg. Chem. **4**, 899 (1965).
15. D. F. CLEMENS, W. WOODFORD, E. DELLINGER, and Z. TYNDALL. Inorg. Chem. **8**, 998 (1969).
16. A. W. HOFMANN. Ber. Dtsch. Chem. Ges. **16**, 558 (1883).
17. V. L. HEASLEY, P. KOVACIC, and R. M. LANGE. J. Org. Chem. **31**, 3050 (1966).
18. (*a*) E. NAGY-FELSOBUKI, J. B. PEEL, and G. D. WILLETT. J. Electron Spectrosc. Relat. Phenom. **13**, 17 (1978); (*b*) F. CARNOVALE, E. NAGY-FELSOBUKI, J. B. PEEL, and G. D. WILLETT. J. Electron Spectrosc. Relat. Phenom. **14**, 163 (1978).
19. D. C. FROST, S. T. LEE, C. A. MCDOWELL, and N. P. C. WESTWOOD. J. Electron Spectrosc. Relat. Phenom. **12**, 95 (1977).
20. H. H. SISLER, F. T. NETH, R. S. DRAGO, and D. YANEY. J. Am. Chem. Soc. **76**, 3906 (1954).
21. A. B. CORNFORD, D. C. FROST, C. A. MCDOWELL, J. L. RAGLE, and I. A. STENHOUSE. J. Chem. Phys. **54**, 2651 (1971).
22. J. W. RABALAIS, L. KARLSSON, L. O. WERME, T. BERGMARK, and K. SIEGBAHN. J. Chem. Phys. **58**, 3370 (1973).
23. T. KOOPMANS. Physica, **1**, 104 (1934).
24. R. G. LAUGHLIN. Chemiker-Zeitung/Chem. App. **11**. 383 (1968).
25. W. WEISS and A. SCHMIDT. Z. Anorg. Allg. Chem. **433**, 207 (1977).

Reactions of the tetrasulfur pentanitride(-1) ion with halogens: synthesis, spectroscopic characterization, and crystal structure of pentasulfur hexanitride

T. CHIVERS AND J. PROCTOR

Department of Chemistry, The University of Calgary, Calgary, Alta., Canada T2N 1N4

Received January 9, 1979

T. CHIVERS and J. PROCTOR. Can. J. Chem. **57**, 1286 (1979).

Pentasulfur hexanitride, S_5N_6, has been prepared in good yield by the reaction of $[n\text{-}Bu_4N^+][S_4N_5^-]$ with bromine (or iodine) in methylene chloride at 0°C. In contrast, the tetrasulfur pentanitride(−1) ion reacts smoothly with chlorine to give S_4N_5Cl, while the reaction with sulfuryl chloride produces S_4N_5Cl *and* S_5N_6 and the reaction with thionyl chloride produces a mixture of S_3N_2O, $S_3N_2O_2$, S_4N_4, and S_5N_6. Pentasulfur hexanitride is an air-sensitive, explosive, yellow-orange solid which sublimes at ca. 45°C/10^{-2} Torr without significant decomposition. It has been characterised by infrared, Raman, uv–visible, and mass spectra and by a single crystal X-ray structure determination. The crystals are monoclinic and belong to the space group $C2/c$, $a = 8.787(2)$, $b = 11.190(2)$, $c = 7.427(2)$ Å, $\beta = 106.46(2)°$, $V = 700.3(5)$ Å^3, $Z = 4$, $D_c = 2.317$ g cm^{-3}. The refined structure ($R_w = 0.040$) has twofold symmetry and resembles a basket in which an —N=S=N— unit (d(S—N) = 1.54 Å) is the handle which bridges an S_4N_4 cradle via S—N single bonds (d(S—N) = 1.70 Å). The introduction of this bridge widens one of the S---S transannular separations in S_4N_4 to 3.94 Å while the other is shortened to 2.43 Å. Thus, the S_4N_4 cradle can be viewed as two five-membered rings fused at the S—S bond.

T. CHIVERS et J. PROCTOR. Can. J. Chem. **57**, 1286 (1979).

On a préparé l'hexanitrure de pentasoufre, S_5N_6, avec de bons rendements par réaction du $[n\text{-}Bu_4N]^+[S_4N_5^-]$ avec du brome (ou de l'iode) dans le chlorure de méthylène à 0°C. Par ailleurs, l'ion pentanitrure de tétrasoufre (−1) réagit facilement avec le chlore pour donner le S_4N_5Cl alors que la réaction du chlorure de sulfuryle fournit du S_4N_5Cl *et* du S_5N_6 et que la réaction du chlorure de thionyle conduit à un mélange de S_3N_2O, $S_3N_2O_2$, S_4N_4 et S_5N_6. L'hexanitrure de pentasoufre est un solide jaune orange, sensible à l'air et explosif qui se sublime à environ 45°C/10^{-2} Torr sans se décomposer d'une façon importante. On l'a caractérisé grâce à ses spectres infrarouge, Raman, uv–visible et de masse et par une détermination de structure sur un cristal unique. Les cristaux sont monocliniques, groupe d'espace $C2/c$, $a = 8.787(2)$, $b = 11.190(2)$, $c = 7.427(2)$ Å, $\beta = 106.46(2)°$, $V = 700.3(5)$ Å^3, $Z = 4$, $D_c = 2.317$ g cm^{-3}. La structure affinée ($R_w = 0.040$) présente un axe de symétrie binaire et ressemble à un panier dans lequel une unité —N=S=N— (d(S—N) = 1.54 Å) est l'anse qui relie un S_4N_4 en cale par l'intermédiaire de liaisons simples S—N (d(S—N) = 1.70 Å). L'introduction de ce pont élargit une des séparations transannulaires S---S dans le S_4N_4 jusqu'à une valeur de 3.94 Å alors que l'autre est raccourci à 2.43 Å. On peut donc visualiser le S_4N_4 en cale sous la forme de deux cycles à cinq chainons reliés par une liaison S—S.

[Traduit par le journal]

Introduction

Although a number of sulfur nitrides have been known for many years (1), the development of their chemistry has, until recently, been slow and unsystematic. The central molecule of this chemistry is the tetramer, S_4N_4, which was first discovered in 1835 (2) but was not structurally characterised until 1963 (3). Thiazyl monomer, SN, is a radical with only a transient existence in the gaseous phase (1). The reactive, square planar dimer, S_2N_2, can be obtained by passing S_4N_4 vapor over silver wool and is an important precursor for the synthesis of polythiazyl, $(SN)_x$ (4, 5). This fascinating polymer and its halogenated derivatives have been the focus of attention of many of the recent studies of S—N compounds due to their metallic properties and superconducting behaviour (6, 7). The only other *unsaturated*[1] sulfur nitride known is S_4N_2, for which a structure with nitrogen atoms in the 1,3 positions of a six-membered ring has been established by a variety of physical techniques (8). However, the suggestion that the ring has a planar conformation awaits confirmation by X-ray crystallography (9).

In addition to these neutral molecules a rapidly growing number of binary S—N ions have been structurally characterised. The cations $S_3N_2^+$ (10), $S_4N_3^+$ (11), $S_4N_4^{2+}$ (12), $S_4N_5^+$ (13), and $S_5N_5^+$ (14) and the anions $S_3N_3^-$ (15) and $S_4N_5^-$ (16) belong to this group. As part of a study of the redox chemistry

[1]"Unsaturated" refers to sulfur nitrides in which the nitrogen atoms are two coordinate.

0008-4042/79/111286-08$01.00/0

of S_4N_5 cage species, we have investigated the oxidation of the $S_4N_5^-$ ion by halogens and certain halogen-containing reagents. We expected the formation of some novel halogenated sulfur nitrides. Instead, we found that pentasulfur hexanitride, S_5N_6, is a frequent product of these reactions. In this paper we describe the full details of various syntheses, the spectroscopic characterization and X-ray crystal structure determination of this new sulfur nitride (for a preliminary communication, see ref. 17).

Experimental

General Procedures

Acetonitrile, carbon tetrachloride, and methylene chloride were dried over phosphorus pentoxide and freshly distilled before use. All distillations of solvents and reagents and all reactions were carried out under nitrogen (99.99%; passed through Ridox and phosphorus pentoxide) or under vacuum. All glassware was flame-dried before use.

Chlorine (Matheson, 99.5%) and iodine (Fisher, resublimed grade) were used as received. Bromine (Baker) was stored over phosphorus pentoxide and potassium bromide before use. Thionyl chloride (Baker, bp 75–77°C) was purified by refluxing with linseed oil (10% by volume) for 2 h and was distilled prior to use. Sulfuryl chloride (Alfa, 99%) was distilled (large forerun discarded) and pumped under vacuum at room temperature until colorless before use. Sulfur dichloride (Matheson, Coleman and Bell, Technical) was doubly distilled under a static vacuum in a glass vacuum line from a vessel at 20°C to a receiver at −78°C. Sulfur monochloride (Alfa) was purified by distillation (large forerun discarded).

$Na^+S_4N_5^-$ was prepared from S_4N_4 and sodium azide in ethanol, and converted to n-$Bu_4N^+S_4N_5^-$ by treatment with tetra-*n*-butylammonium hydroxide (Eastman, 1 *M* in methanol) (18).

Instrumentation

Infrared spectra were recorded as Nujol mulls, using CsI windows (4000–250 cm^{-1}) or polythene discs (650–40 cm^{-1}),on a Perkin Elmer 467 spectrophotometer or a Digilab FTS 16 instrument, respectively. Raman spectra were obtained on samples sealed in glass capillaries under nitrogen using Argon (514.5 nm) and He/Ne (632.8 nm) lasers with a Jarrell-Ash spectrophotometer. Mass spectra were recorded on a Varian CH5 instrument operating at 70 eV. Ultraviolet–visible spectra were recorded for solutions made up in a Vacuum Atmospheres dry-box on a Cary 15 spectrophotometer. Elemental analyses were performed by Analytische Laboratorium, Engelskirchen, W. Germany. The X-ray crystal structure determination of S_5N_6 was carried out by Dr. Jan Troup of the Molecular Structure Corporation, TX.

The Synthesis of Pentasulfur Hexanitride, S_5N_6

(a) From the reaction of n-$Bu_4N^+S_4N_5^-$ *with Bromine*

Bromine (0.065 g, 0.404 mmol) in methylene chloride (30 mL) was added dropwise (20 min) with rapid stirring to a solution of n-$Bu_4N^+S_4N_5^-$ (0.284 g, 0.645 mmol) in methylene chloride (20 mL) at 0°C. After 5.5 h a *trace* of white precipitate was filtered off and shown to be an ammonium salt by its infrared spectrum. Partial removal of the solvent from the filtrate under vacuum produced an orange-yellow precipitate. The orange supernatant solution was decanted by pipette and the product was washed with cold (−20°C) methylene chloride. The product was recrystallised from methylene chloride at −78°C to give pentasulfur hexanitride (0.092 g, 0.376 mmol, 73% based on S). *Anal.* calcd. for N_6S_5: N 34.39, S 65.61; found: N 34.65, S 65.29.

CAUTION: It is strongly recommended that samples of S_5N_6 be handled in small quantities and with great care since the material will explode if subjected to friction, e.g., in the preparation of infrared mulls.

The infrared spectrum of S_5N_6 (Nujol) showed bands at 1306vw, 1193vw, 1088sh, 1066s, 1030s, 968w, 938s, 852s, 835w, 807vw, 694m, 648s, 621w, 573s, 554m, 500s, 463w, 433m, 418w, 388s, 327vw cm^{-1}. The Raman spectrum, obtained with either 514.5 or 632.8 nm excitation, showed bands at 1028s, 927w, 770w, 675s, 535m, 494w, 423s, 388w, 354w, 312w, 269vs, 225s, 160vs, and 130m cm^{-1}. Removal of solvent from the decanted orange solution yielded a red oil which became a dry yellow-orange powder after pumping in vacuo for 48 h at 23°C. This powder was identified as n-$Bu_4N^+Br_3^-$ by mp 69–70°C (lit: 72.5–74°C) and comparison of the infrared and Raman spectra with those of an authentic sample prepared by the literature method (19). The Raman spectra of both the product and the authentic sample of n-$Bu_4N^+Br_3^-$ in acetonitrile showed a strong band at 160 cm^{-1} corresponding to the ν_1 vibration of Br_3^- (cf. 162 cm^{-1} in $C_6H_5NO_2$ and 163 cm^{-1} in $CHCl_3$) (20). The far infrared spectrum showed a strong band at 194 cm^{-1} ($\nu_3(Br_3^-)$) cf. lit.: 193 cm^{-1} (20).

(b) From the Reaction of n-$Bu_4N^+S_4N_5^-$ *with Iodine*

Excess solid iodine (0.219 g, 0.842 mmol) was added to a stirred solution of n-$Bu_4N^+S_4N_5^-$ (0.098 g, 0.223 mmol) in methylene chloride (50 mL) at 23°C. After 4 h the solution was still dark purple. Slow removal of solvent *in vacuo* caused the precipitation of an orange solid as the solution cooled down. The supernatant solution was decanted by pipette and the product was washed with cold methylene chloride (3 mL), dried *in vacuo* for several hours and identified as pure S_5N_6 by comparison of its infrared and Raman spectra with those of an authentic sample. Removal of solvent and excess iodine *in vacuo* from the decanted solution yielded blue-black crystals identified as $Bu_4N^+I_3^-$ by mp 67.5–68°C (lit: 70–70.5°C) (21) and by comparison of its infrared and Raman spectra with those of an authentic sample prepared according to the literature (21). The Raman spectra of solutions in acetonitrile showed a strong band at 110 cm^{-1}, corresponding to the ν_1 vibration of I_3^- (cf. 104–108 cm^{-1} for other $R_4N^+I_3^-$ salts (R = Me, Et, *n*-Pr)) (22). The far infrared spectrum showed a strong band at 135 cm^{-1} ($\nu_3(I_3^-)$) cf. 132–138 cm^{-1} for other $R_4N^+I_3^-$ salts (22).

Reaction of $Na^+S_4N_5^-$ with Chlorine

Chlorine gas (0.041 g, 1.16 mmol) was condensed into a glass vessel containing $Na^+S_4N_5^-$ (0.125 g, 0.566 mmol) as a slurry in methylene chloride (25 mL). The reaction mixture was stirred at −78°C for 20 min. The white precipitate was filtered off and identified as sodium chloride containing a trace of unreacted $Na^+S_4N_5^-$. Solvent was removed from the filtrate and the greenish-yellow solid residue was pumped *in vacuo* for 10 h and then identified as pure S_4N_5Cl (0.060 g, 0.257 mmol) by comparison of its infrared spectrum with that of an authentic sample (13).

Reaction of $Na^+S_4N_5^-$ with Thionyl Chloride

Thionyl chloride (0.313 g, 2.64 mmol) in methylene chloride (25 mL) was added dropwise over 20 min to a slurry of $Na^+S_4N_5^-$ (0.569 g, 2.52 mmol) in methylene chloride (25 mL). The color of the solution became blood red im-

mediately. After completion of the addition, the solution was stirred for 30 min and the insoluble white solid, presumably sodium chloride, was filtered off. The volume of the filtrate was reduced to 5 mL *in vacuo*, and then the supernatant solution was decanted from the orange solid which precipitated as the solution cooled down. This product was washed with cold methylene chloride (3 × 2 mL) and, after drying at 35°C/10^{-2} Torr for 12 h, it was identified as pure S_5N_6 by its infrared spectrum.

Complete removal of solvent from the decanted filtrate produced a black residue containing yellow crystals. Sublimation of this residue at 25–30°C/10^{-2} Torr *for 1 h* gave bright yellow crystals of $S_3N_2O_2$ which had mp 95–96°C (lit: 100–101°C) (23) and an infrared spectrum, which showed bands at 1184vs, 1040s, 1017w, 998m, 685s, 658m, 507m, and 363s cm^{-1}, identical to that of a sample prepared by the method described by Brauer (24). Further sublimation at 30–40°C/10^{-2} Torr for several hours yielded S_4N_4, identified by its characteristic infrared spectrum.

After removal of S_5N_6 by crystallisation, the two products, $S_3N_2O_2$ and S_4N_4, are readily separated by the sublimation procedure described above if the $SOCl_2/Na^+S_4N_5^-$ molar ratio is slightly greater than one. However, when this ratio falls below one a fourth product, a red oil, is also formed. This oil sublimes readily at 20°C/10^{-2} Torr and was identified as S_3N_2O by comparison of its infrared spectrum with that of an authentic sample prepared by the method of Roesky and coworkers (25). The spectrum showed bands at 1180m, 1123m, 1107s, 1040sh, 972s, 749sh, 719s, 700sh, 660s, 580m, 557m, 495s, 387s, 377s, 321m cm^{-1}.

The *trace* of black residue which remains after removal of the other products by sublimation could not be identified. It consistently decomposed to S_4N_4 within 1–2 days on storage in a nitrogen atmosphere at room temperature.

Reaction of $Na^+S_4N_5^-$ with Sulfuryl Chloride

Sulfuryl chloride (0.092 g, 0.680 mmol) in methylene chloride (30 mL) was added dropwise over 15 min to a stirred slurry of $Na^+S_4N_5^-$ (0.151 g, 0.681 mmol) at 0°C. The colour of the solution became orange during the addition. After 2.5 h of stirring, the solution was filtered and solvent was removed from the filtrate to give a bright yellow powder shown by its infrared spectrum to be a mixture of S_5N_6 and S_4N_5Cl. Slow sublimation at 45–50°C/10^{-2} Torr gave S_5N_6, contaminated with a trace of black material, as the sublimate. The residue was S_4N_5Cl (infrared spectrum) (13).

X-ray Crystal Structure Determination

Crystal Preparation

A sample of S_5N_6, recrystallised from methylene chloride, was dissolved in carbon disulfide. Slow removal of solvent from this solution *in vacuo* yielded yellow prisms as the solution cooled down. The dimensions of the crystal used in this study were 0.15 × 0.15 × 0.20 mm. All manipulations were carried out under an atmosphere of dry nitrogen due to the sensitivity of S_5N_6 to oxidation by air.

Crystal Data

S_5N_6, $M = 244.36$, monoclinic. For calculation of cell constants, 25 reflections were computer-centered and the setting angles were refined by least-squares. The following systematic absences were observed: $h0l$, $l \neq 2n$. The cell constants are $a = 8.787(2)$, $b = 11.190(2)$, $c = 7.427(2)$ Å, $\beta = 106.46(2)°$, $V = 700.3(5)$ Å^3, $Z = 4$, $D_c = 2.317$ g cm^{-3}. The space group was $C2/c$, confirmed by refinement.

X-ray Measurements

The goniometer was mounted on an Enraf-Nonius CAD4 automated diffractometer under the control of a PDP 11/45 computer. Intensity data were collected at 23 ± 1°C using graphite monochromated MoK_α radiation ($\lambda = 0.71073$ Å) and a θ–2θ scan rate varying from 3 to 20°/min, depending on the intensity of the reflection. The scan range was from 2θ ($MoK_{\alpha 1}$) − 0.6° to 2θ ($MoK_{\alpha 2}$) + 0.6°. A counter aperture width of 2.0 mm, a crystal-to-detector distance of 21 cm, and an incident-beam collimator diameter of 2.0 mm were used in this study. Stationary-crystal stationary-counter background counts were taken at each end of the scan range. The ratio R of scan time to background counting time was 2.0. Of the 800 reflections collected in the range $0° < 2\theta(MoK_\alpha) < 60°$, 781 unique reflections with $I > 3\sigma(I)$ were retained as observed and corrected for Lorentz and polarization effects. Three representative reflections were measured periodically to check crystal and electronic stability, but no significant change in intensity was observed. The linear absorption coefficient of this compound is 15.24 cm^{-1} for MoK_α radiation and corrections for absorption, extinction, or changes in the intensity of the standard reflections were unnecessary.

Solution and Refinement of the Structure

The structure was solved by direct methods. Using 110 reflections ($E_{min} = 1.40$) and 1927 phase relationships, a total of 8 phase sets were produced. From an E-map prepared from the phase set showing the best probability statistics a total of 5 atoms were located. These atoms were included in least-squares refinement, resulting in agreement factors (defined below) of $R_1 = 0.26$ and $R_2 = 0.33$. The remaining atoms were located in succeeding difference Fourier syntheses. The structure was solved in space group Cc and later was determined to have two-fold symmetry so that it could be refined in the centrosymmetric space group $C2/c$.

In full-matrix least-squares refinement the function minimized was $\Sigma w(|F_o| - |F_c|)^2$ where the weight w is defined as $4F_o^2/\sigma^2(F_o^2)$. Scattering factors were taken from Cromer and Waber (26). Anomalous dispersion effects were included in F_c; the values of $\Delta f'$ and $\Delta f''$ were those of Cromer and Lieberman (27). Only the 630 reflections having $F_o^2 > 3\sigma(F_o^2)$ were used in the refinement. The following values pertain to the final cycle of least-squares refinement:

$$R_1 = \Sigma ||F_o| - |F_c|| / \Sigma F_o = 0.033$$

$$R_2 = [\Sigma w(|F_o| - |F_c|)^2 / \Sigma w F_o^2]^{1/2} = 0.040$$

For the six atoms studied, the number of variable parameters considered was 51. The esd of an observation of unit weight was then 1.102, while the maximum parameter shift was 0.03 times its esd.

The final difference Fourier map showed no significant residual electron density. Plots of $\Sigma w(|F_o| - |F_c|)^2$ versus F_o and $\lambda^{-1} \sin\theta$ showed no unusual trends. The final positional parameters and anisotropic thermal parameters are shown in Table 1. A list of observed and calculated structure factor amplitudes and a complete list of bond angles are available in the supplementary material.[2]

Results and Discussion

Preparation of Pentasulfur Hexanitride

The reaction of an excess of iodine with *n*-$Bu_4N^+S_4N_5^-$ in methylene chloride proceeds slowly at 23°C to give S_5N_6 and *n*-$Bu_4N^+I_3^-$. When bromine is used as the oxidizing agent, however, the

[2]Complete set of data is available, at a nominal charge, from the Depository of Unpublished Data, CISTI, National Research Council of Canada, Ottawa, Ont., Canada K1A 0S2.

TABLE 1

(*a*) Final positional parameters, with esd's, for S_5N_6

Atom	*x*	*y*	*z*
S(1)	0.00000(0)	0.08128(10)	0.2500(0)
S(2)	−0.04516(10)	0.28541(8)	0.4947(1)
S(3)	−0.14092(9)	0.42844(7)	0.1696(1)
N(1)	−0.0218(4)	0.1432(3)	0.4256(4)
N(2)	−0.1823(3)	0.3515(3)	0.3321(4)
N(3)	0.1166(3)	0.3593(3)	0.5097(4)

(*b*) Anisotropic thermal parameters (in Å²) for S_5N_6[a]

Atom	B_{11}	B_{22}	B_{33}	B_{12}	B_{13}	B_{23}
S(1)	0.01089(14)	0.00335(8)	0.0137(2)	0.0000(0)	0.0057(3)	0.0000(0)
S(2)	0.01271(10)	0.00492(6)	0.0101(1)	−0.0030(1)	0.0114(2)	−0.0014(2)
S(3)	0.00839(8)	0.00425(5)	0.0126(1)	0.0027(1)	0.0038(2)	−0.0009(2)
N(1)	0.0147(4)	0.0041(2)	0.0130(5)	−0.0018(5)	0.0096(7)	0.0010(6)
N(2)	0.0085(3)	0.0056(2)	0.0174(5)	0.0001(5)	0.0115(6)	−0.0010(6)
N(3)	0.0109(4)	0.0051(2)	0.0100(4)	−0.0039(5)	0.0003(7)	0.0007(6)

[a]The form of the anisotropic thermal parameter is exp $(-B_{11}h^*h^* + B_{22}k^*k^* + B_{33}l^*l^* + B_{12}h^*k^* + B_{13}h^*l^* + B_{23}k^*l^*)$.

reaction takes place even at 0°C to yield S_5N_6 and n-$Bu_4N^+Br_3^-$. Both these synthetic routes produce pure S_5N_6 in good yield, but the reaction with bromine is preferred since it proceeds more quickly and the course of the reaction can be followed by observing the change in color of the solution from dark red to pale orange. It should be noted that small amounts of ammonium salts, identified by their infrared spectra, are also formed if the solvents are not scrupulously dry (cf. ref. 28).

In contrast, the reaction of a slurry of $Na^+S_4N_5^-$ in methylene chloride with chlorine at −78°C occurs rapidly to give S_4N_5Cl, which contains the cation $S_4N_5^+$ (13), and sodium chloride. Wolmershäuser and Street have recently pointed out (28) that bromination of S_4N_4 occurs in a different, and more complicated, manner from chlorination. The products depend markedly on the reaction conditions and either linear polymers of the type $(SNBr_y)_x$ (7, 29) or the cyclic compound $S_4N_3Br_3$ can be obtained (28). Both the linear and cyclic products contain the Br_3^- ion (28). It is apparent that the formation of the linear polymer involves an irreversible ring-opening of S_4N_4 (29), and in the reaction of S_4N_4 with *excess* bromine some evidence for the formation of the volatile monomer NSBr has been presented (28). In the present work, the conversion of $S_4N_5^-$ to $S_4N_5^+$ by chlorine can be viewed as a two electron oxidation which is manifested in the opening up of the unbridged S---S bond (2.71 Å) in the anion (16) to a non-bonding distance (ca. 4 Å) in the cation (13). It is possible that the reactions of $S_4N_5^-$ with the milder oxidizing agents, Br_2 and I_2, occur via a one electron oxidation to give the radical, $S_4N_5^{\bullet}$, but we have no evidence for this intermediate. Since a substantial rearrangement of the skeletal atoms occurs in the conversion of $S_4N_5^-$ to S_5N_6 further speculation on the reaction mechanism will be deferred until information of the dynamic behaviour of S—N cages in solutions is available from ^{15}N nmr studies.

The reaction of $Na^+S_4N_5^-$ with thionyl chloride at 0°C in methylene chloride was complex. In addition to sodium chloride, four products S_4N_4, S_5N_6, $S_3N_2O_2$, and S_3N_2O were separated and identified when the molar ratio $SOCl_2/Na^+S_4N_5^-$ was less than one. When this ratio exceeded one, S_3N_2O was not detected among the products possibly due to its conversion to $S_3N_2O_2$ by thionyl chloride, a reaction which was shown to occur in a separate experiment. Banister and Padley have reported that S_4N_4 reacts with thionyl chloride to give $S_3N_2O_2$ and S_4N_3Cl (30), but this cannot be the source of $S_3N_2O_2$ in the $S_4N_5^-/SOCl_2$ reaction since S_4N_3Cl was not identified among the products.

The reaction of sulfuryl chloride with $Na^+S_4N_5^-$ proceeded slowly to give a mixture of S_5N_6 and S_4N_5Cl, separable by sublimation. Presumably SO_2 was evolved during the reaction, since no sulfur–nitrogen oxides were obtained.

Physical Properties and Crystal Structure of Pentasulfur Hexanitride

Pure S_5N_6 ranges in color from yellow for powdered samples to orange for crystals. *The solid is explosive and great care should be taken to avoid friction or sudden heating when handling samples.* S_5N_6 can be sublimed without significant decomposition at 45–50°C/10^{-2} Torr, but the sublimate

TABLE 2. Interatomic distances and esd's for S_5N_6

Atoms	Distance (Å)	Atoms	Distance (Å)
S(1)—S(2)	3.014(1)	S(3)—N(2)	1.606(3)
S(1)—S(2)′	3.014(1)	S(3)—N(2)′	2.971(3)
S(2)—S(3)	2.819(1)	S(3)—N(3)	2.976(3)
S(2)—S(3)′	2.802(1)	S(3)—N(3)′	1.606(3)
S(3)—S(3)′	2.425(2)	N(1)—N(1)′	2.741(5)
S(1)—N(1)	1.536(3)	N(1)—N(2)	2.711(4)
S(1)—N(1)′	1.536(3)	N(1)—N(3)	2.699(4)
S(2)—N(1)	1.702(3)	N(2)—N(3)	2.585(4)
S(2)—N(2)	1.623(3)	N(2)—N(3)′	2.760(4)
S(2)—N(3)	1.621(3)		

TABLE 3. Selected bond angles with esd's in S_5N_6[a]

Bonds	Angle (deg)	Bonds	Angle (deg)
N(1)—S(1)—N(1)′	126.3(2)	S(3)—S(3)′—N(3)	92.9(1)
N(1)—S(2)—N(2)	109.2(2)	N(2)—S(3)—N(3)′	118.5(2)
N(1)—S(2)—N(3)	108.6(2)	S(1)—N(1)—S(2)	137.1(2)
N(2)—S(2)—N(3)	105.7(2)	S(2)—N(2)—S(3)	121.7(2)
S(3)′—S(3)—N(2)	92.7(1)	S(2)—N(3)—S(3)′	120.6(2)

[a]A complete list of bond angles is available as supplementary material (see footnote 2).

is accompanied by a trace of unidentified black material. A sample heated in a sealed capillary tube under nitrogen decomposed over the range 130–165°C. Analytically pure samples of S_5N_6 can be obtained by recrystallization from methylene chloride or carbon disulfide below 0°C, but decomposition of such solutions at 23°C is indicated by noticeable darkening during 12 h and exposure to air results in the immediate precipitation of a white ammonium salt (infrared spectrum). Solid samples of S_5N_6 can be stored for months in an inert atmosphere without significant decomposition but turn black within 2–3 min in air.

The structure of S_5N_6, determined by X-ray crystallography, is shown in Fig. 1. The important interatomic distances are shown in Table 2 and some selected bond angles have been included in Table 3. The structure resembles a basket in which an —N=S=N— unit (S(1)—N(1) = 1.54 Å) bridges two sulfur atoms of an S_4N_4 cradle via S—N single bonds (S(2)—N(1) = 1.70 Å). Within the cradle neither the variation of S—N distances (1.606–1.623 Å) nor the average S—N distance are significantly different from those found for S_4N_4 (1.619–1.633 Å) (31). The introduction of the bridge does, however, have a marked influence on the transannular S---S interactions of S_4N_4. One of the S—S distances (S(2)—S(2)′) is forced to open out to 3.93 Å while the other one becomes significantly shorter (S(3)—S(3)′ = 2.43 Å) than it is in S_4N_4 (2.58 Å (3), 2.59 Å (31)). As a result, the S_4N_4 cradle can be viewed as two fused five-membered rings, a structure

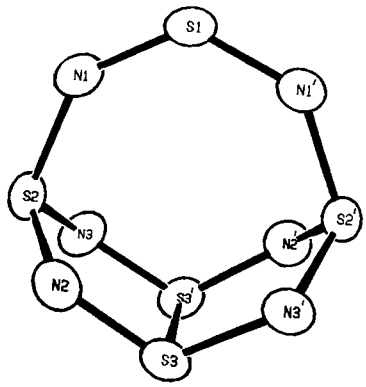

FIG. 1. X-ray structure of S_5N_6 showing symmetry related atoms labeled with primes.

which has been considered for $S_4N_4^{2+}$ (32) but has not been found in practice. It is now well established that a variety of derivatives of the five-membered S_3N_2 ring (33, 34), are obtained from the reactions of S_4N_4 with various oxidizing agents. Moreover, the mechanism proposed for the formation of $S_3N_2^+$ by the oxidation of S_4N_4 with arsenic pentafluoride invokes the formation of S_3N_2 rings after the loss of one electron by S_4N_4 (10). Thus, the incipient formation of five-membered rings in S_5N_6 is particularly significant.

Table 4 summarizes the least-squares planes and the dihedral angles between various planes in S_5N_6. From this data it can be seen that the almost planar group of atoms S(2)N(1)S(1)N(1)′S(2)′ is at 87–88° to the planes containing N(2)S(3)S(3)′N(3) and

TABLE 4

(*a*) Least-squares planes

Atom in plane	Distance from plane (Å)	Other atoms	Distance from plane (Å)
Plane *1*: $-0.8979X + 0.0063Y - 0.4401Z = -0.2974$			
S(1)	−0.008	N(2)	1.347
N(1)	−0.050	N(2)′	−1.326
N(1)′	0.042	S(3)	1.228
S(2)	0.058	S(3)′	−1.196
S(2)′	−0.046	N(3)	−1.232
		N(3)′	1.254
Plane *2*: $0.2630X - 0.8556Y - 0.4458Z = -5.0412$			
S(3)	−0.019	S(2)	0.360
S(3)′	0.033		
N(2)	0.016		
N(3)	−0.030		
Plane *3*: $0.2574X + 0.8649Y - 0.4309Z = 3.2363$			
S(3)	−0.021	S(2)′	−0.391
S(3)′	0.036		
N(3)′	0.013		
N(2)′	−0.028		
Plane *4*: $0.2920X - 0.7992Y - 0.5254Z = -4.9694$			
S(3)	0.038		
S(3)′	0.060		
N(2)	−0.089		
N(3)	−0.166		
S(2)	0.146		
Plane *5*: $0.3214X + 0.7969Y - 0.5115Z = 2.7925$			
S(3)	−0.102		
S(3)′	−0.001		
N(2)′	0.132		
N(3)′	0.125		
S(2)′	−0.143		

(*b*) Dihedral angles between planes

Plane No.	Plane No.	Angle (deg)
1	*2*	−87.4
1	*3*	−87.9
1	*4*	−87.9
1	*5*	−86.6
2	*3*	−61.3
2	*4*	5.8
2	*5*	−68.3
3	*4*	−67.1
3	*5*	7.1
4	*5*	−74.1

N(2)′S(3)′S(3)N(3)′. The sulfur atoms S(2) and S(2)′ are a significant distance (0.36 and 0.39 Å, respectively) out of the latter two planes.

It is obvious from Fig. 1 that certain atoms in S_5N_6 are related by a C_2 symmetry axis which passes through S(1) and bisects S(3)—S(3)′. An alternative view of S_5N_6 is to consider S(2) and S(2)′ as the apical atoms of a distorted trigonal bipyramid (tbp) of sulfur atoms. Thus, the equatorial atoms would be S(1), S(3), and S(3)′. The six edges of the tbp joining axial and equatorial sulfur atoms are bridged by nitrogen atoms, while the three edges connecting equatorial sulfur atoms are unbridged. It is clear from inspection of a model that three equivalent configurations of S_5N_6, in which the atomic groups N(1)S(1)N(1)′ or N(2)S(3)N(3)′ or N(3)S(3)′N(2)′ alternately occupy the bridge position, could exist. Thus, *in solution* this S—N cage could exhibit fluxional behaviour with these three configurations as the interconverting forms. ^{15}N nmr studies would be

extremely useful in providing information on this point.

Bonding in Pentasulfur Hexanitride

Different approaches to a description of the bonding in electron-rich S—N cages have been reported in the literature. Banister has suggested that the bonding in S_4N_4 can be satisfactorily rationalized in terms of localized two centre bonds (35). Thus, the 44 valence electrons of S_4N_4 are allocated to lone pairs on each of the sulfur and nitrogen atoms, a bond pair to each S—N linkage and the remaining six electron pairs to the six S—S bonds of the S_4 tetrahedron. In preliminary communications (13, 17) we have adopted this approach to rationalize the structures of $S_4N_5^-$, $S_4N_5^+$, and S_5N_6. In contrast, molecular orbital calculations (36) allow only two transannular S—S bonds in S_4N_4 and assign the additional four electron pairs to non-bonding electron pairs on the nitrogen atoms (36*b*). Very recent *ab initio* Hartree Fock Slater SCF calculations on S_4N_4 support the view of only two S—S bonds in S_4N_4, the presence of only one S—S bond in $S_4N_5^-$, and no S—S bonds in $S_4N_5^+$ (37). A full account of these calculations is in preparation.

Spectroscopic Characterization of Pentasulfur Hexanitride

The uv–visible spectrum of S_5N_6 (in CH_2Cl_2) shows two smooth absorption bands at λ_{max} 375 (ε ca. 5×10^3 L mol^{-1} cm^{-1}) and 250 nm (ε ca. 6×10^4 L mol^{-1} cm^{-1}). The mass spectrum obtained at an ionizing voltage of 70 eV and probe temperature of 70°C showed no parent ion peak. Strong peaks at *m/e* 92 ($S_2N_2^+$), 78 (S_2N^+), 64 (S_2^+), and 46 (SN^+), in addition to a medium intensity peak at 138 ($S_3N_3^+$; cf. S_4N_4 (38)) and very weak peaks at 184 ($S_4N_4^+$) and 198 ($S_4N_5^+$) were observed. The infrared and Raman spectra of S_5N_6 are summarized in the Experimental section. Certain structural features of S_5N_6 should give rise to characteristic bands in the vibrational spectra. For example, the short bonds of the —N=S=N— bridge should give rise to infrared bands at relatively high frequencies. Thus, the strong bands at 1066 and 1030 cm^{-1} can probably be assigned to the asymmetric and symmetric stretching vibrations, respectively, of the —N=S=N— unit. The latter band shows a coincidence in the Raman spectrum (1028s cm^{-1}) as expected for a symmetric vibration. The S—S bond, S(3)—S(3)′, should exhibit a very strong band in the Raman spectrum and a frequency of <300 cm^{-1} can be predicted from the bond length of 2.43 Å (39). Thus, the band at 269 cm^{-1} is tentatively assigned to ν(S—S) (cf. 213 cm^{-1} for ν(S—S) in S_4N_4) (40).

Conclusions

Pentasulfur nitride is readily obtained in good yield by the oxidation of the $S_4N_5^-$ ion with Br_2 or I_2. This novel sulfur nitride has a structure in which an —N=S=N— unit bridges two sulfur atoms of an S_4N_4 cradle. The unexpected discovery of S_5N_6 provides an alternative starting point for the attempted synthesis of hitherto unsuspected sulfur–nitrogen cage species or linear polymers.

Acknowledgements

We are grateful to the National Research Council of Canada for financial support and, in particular, to Dr. Jan Troup of the Molecular Structure Corp., who carried out the X-ray crystal structure determination of S_5N_6. We also wish to thank Drs. R. Kydd and C. Lau for assistance in obtaining the Raman spectra and Mr. T. Smithson for recording the far infrared spectra.

1. H. G. Heal. Adv. Inorg. Radiochem. **15**, 375 (1972).
2. W. Gregory. J. Pharm. **21**, 315 (1835).
3. B. D. Sharma and J. Donohue. Acta Crystallogr. **16**, 891 (1963).
4. C. M. Mikulski, P. J. Russo, M. S. Saran, A. G. MacDiarmid, A. F. Garito, and A. J. Heeger. J. Am. Chem. Soc. **97**, 6358 (1975).
5. M. J. Cohen, A. F. Garito, A. J. Heeger, A. G. MacDiarmid, C. M. Mikulski, M. S. Saran, and J. Kleppinger. J. Am. Chem. Soc. **98**, 3844 (1976).
6. M. Akhtar, C. K. Chiang, A. J. Heeger, J. Milliken, and A. G. MacDiarmid. Inorg. Chem. **17**, 1539 (1978), and references therein.
7. G. B. Street, R. L. Bingham, J. I. Crowley, and J. Kuyper. J. Chem. Soc. Chem. Commun. 464 (1977) and references therein.
8. J. Nelson and H. G. Heal. J. Chem. Soc. A, 136 (1971).
9. R. R. Adkins and A. G. Turner. J. Am. Chem. Soc. **100**, 1383 (1978).
10. (*a*) R. J. Gillespie, P. R. Ireland, and J. Vekris. Can. J. Chem. **53**, 3147 (1975); (*b*) H. W. Roesky and A. Hamza. Angew. Chem. Int. Ed. Engl. **15**, 226 (1976).
11. T. N. Guru Row and P. Coppens. Inorg. Chem. **17**, 1670 (1978).
12. R. J. Gillespie, D. R. Slim, and J. D. Tyrer. J. Chem. Soc. Chem. Commun. 253 (1977).
13. T. Chivers and L. Fielding. J. Chem. Soc. Chem. Commun. 212 (1978).
14. (*a*) H. W. Roesky, W. Grosse-Bowing, I. Rayment, and H. M. M. Shearer. J. Chem. Soc. Chem. Commun. 735 (1975); (*b*) A. J. Banister, J. A. Durant, I. Rayment, and H. M. M. Shearer. J. Chem. Soc. Dalton, 928 (1976).
15. (*a*) J. Bojes and T. Chivers. J. Chem. Soc. Chem. Commun. 391 (1978); (*b*) J. Bojes, T. Chivers, W. G. Laidlaw, and M. Trsic. J. Am. Chem. Soc. To be published.
16. W. Flues, O. J. Scherer, J. Weiss, and G. Wolmershäuser. Angew. Chem. Int. Ed. Engl. **15**, 379 (1976).
17. T. Chivers and J. Proctor. J. Chem. Soc. Chem. Commun. 642 (1978).
18. J. Bojes and T. Chivers. Inorg. Chem. **17**, 318 (1978).
19. A. I. Popov and R. E. Buckles. Inorg. Synth. **5**, 176 (1957).

20. W. G. PERSON, G. R. ANDERSON, J. H. FORDEMWALT, H. STAMMERECH, and R. FORNERIS. J. Chem. Phys. **35**, 908 (1961).
21. M. KAHN, A. J. FREEDMAN, and C. G. SCHULZ. Inorg. Synth. **5**, 167 (1957).
22. F. W. PARRETT and N. J. TAYLOR. J. Inorg. Nucl. Chem. **32**, 2458 (1970).
23. D. A. ARMITAGE and A. W. SINDEN. Inorg. Chem. **11**, 1151 (1972).
24. G. BRAUER. Handbook of preparative inorganic chemistry. Vol. 1. Academic Press, NY. 1963. p. 370.
25. H. W. ROESKY, W. SCHAPER, O. PETERSEN, and T. MULLER. Chem. Ber. **110**, 2695 (1977).
26. D. T. CROMER and J. T. WABER. International tables for X-ray crystallography. Vol. IV. Kynoch Press, Birmingham, England. In preparation.
27. D. T. CROMER and D. LIEBERMAN. J. Chem. Phys. **53**, 1891 (1970).
28. G. WOLMERSHÄUSER and G. B. STREET. Inorg. Chem. **17**, 2685 (1978).
29. M. AKHTAR, C. K. CHIANG, A. J. HEEGER, J. MILLIKEN, and A. G. MACDIARMID. Inorg. Chem. **17**, 1539 (1978).
30. A. J. BANISTER and J. S. PADLEY. J. Chem. Soc. A, 1437 (1967).
31. M. L. DELUCIA and P. COPPENS. Inorg. Chem. **17**, 2336 (1978).
32. A. J. BANISTER and J. A. DURRANT. J. Chem. Res. M, 1928 (1978).
33. R. STEUDEL, F. ROSE, R. REINHARDT, and H. BRADACZEK. Z. Naturforsch. **32B**, 488 (1977).
34. H. W. ROESKY, W. SCHAPER, O. PETERSEN, and T. MULLER. Chem. Ber. **110**, 2695 (1977).
35. A. J. BANISTER. Nature Phys. Sci. **239**, 69 (1972).
36. (*a*) R. GLEITER. J. Chem. Soc. A, 3174 (1970); (*b*) M. S. GOPINATHAN and M. A. WHITEHEAD. Can. J. Chem. **53**, 1343 (1975); (*c*) D. R. SALAHUB and R. P. MESSMER. J. Chem. Phys. **64**, 2039 (1976); (*d*) W. R. SALANECK, J. W-P LIN, A. PATON, C. B. DUKE, and G. P. CEASAR. Phys. Rev. B, **13**, 4517 (1976); (*e*) K. TANAKA, T. YAMABE, A. NODA, K. FUKUI, and H. KATO. J. Phys. Chem. **82**, 1453 (1978).
37. W. G. LAIDLAW and M. TRSIC. Private communication.
38. I. S. BUTLER and T. SAWAI. Can. J. Chem. **55**, 3838 (1977).
39. R. STEUDEL. Z. Naturforsch. **30B**, 281 (1975).
40. J. BRAGIN and M. V. EVANS. J. Chem. Phys. **51**, 268 (1969).

Polarographic reduction of phenolphthalein, cresolphthalein, thymolphthalein, and α-naphtholphthalein in aqueous and nonaqueous ethanolic solutions

MOHAMED M. GHONEIM[1] AND MOHAMED A. A. ASHY[2]

Chemistry Department, Faculty of Science, Tanta University, Tanta, A.R. Egypt

Received June 26, 1978

MOHAMED M. GHONEIM and MOHAMED A. A. ASHY. Can. J. Chem. **57**, 1294 (1979).

The polarographic reduction of phenolphthalein, cresolphthalein, thymolphthalein, and α-naphtholphthalein has been studied in ethanolic Britton–Robinson buffer series (pH 2–12), non-aqueous ethanolic medium, and water–ethanol mixtures. The compounds are reduced through a single $2e^-$ wave in non-aqueous medium and aqueous buffered solutions of pH < 9 or $1e^-$ steps for pH > 9. The nature of the waves, mechanism of the electrode reaction, and kinetic parameters has been considered.

MOHAMED M. GHONEIM et MOHAMED A. A. ASHY. Can. J. Chem. **57**, 1294 (1979).

On a étudié la réduction polarographique de la phénolphtaléine, de la crésolphtaléine de la thymolphtaléine et de l'α-naphtolphtaléine dans une série de tampons éthanoliques de Britton–Robinson (pH 2 à 12), dans un milieu éthanolique non-aqueux et dans des mélanges eau–éthanol. La réduction des composés, dans les milieux non-aqueux et dans des solutions aqueuses tamponnées à des pH < 9, se produit au cours d'une vague unique impliquant $2e^-$ ou par des étapes de $1e^-$ pour des pH > 9. On a considéré la nature des vagues, le mécanisme de la réaction à l'électrode et les paramètres cinétiques.

[Traduit par le journal]

Introduction

Phenolphthalein and related compounds in solution were considered by Kolthoff (1) to exist in different hydration and ionic forms in equilibrium. It was concluded that the lactone form of phenolphthalein (2) is not reducible at the dropping mercury electrode, at least not at potentials less negative than that at which the wave of the supporting electrolyte appeared. The hydrated forms are reduced along a single two-electron reduction wave. The reduction of the red form, however, occurred in two one-electron steps. No thorough investigation of polarographic work on the phenolphthalein derivatives is available, also the exact mechanism of the polarographic reduction of phenolphthalein is not completely understood. The main reason is that the nature of the species present in aqueous solutions of different pH values is not known, and that there is no hard evidence for the existence of the forms participating in its colour change. A comprehensive study on the kinetics and mechanism of electroreduction of phenolphthalein or its derivatives is lacking in literature.

In the present study, we report the current–voltage curves of four phenolphthaleins in aqueous and nonaqueous ethanolic solutions as well as an attempt made to clarify the nature of the waves and to evaluate the kinetics of the electrode process.

[1]To whom all correspondence should be addressed.

[2]Permanent address: Chemistry Department, Faculty of Science, King Abdulaziz University, Jeddah, Saudi Arabia.

Experimental

Stock solutions (10^{-2} mol L^{-1}) of phenolphthalein, cresolphthalein, thymolphthalein, or α-naphtholphthalein were prepared by dissolving the compounds (AR grade) in purified ethanol. The polarographic behaviour of these compounds was studied (*a*) in Britton–Robinson (3) buffer series of pH 2–12 containing different percentages of ethanol (25–35 vol%); (*b*) in non-aqueous ethanolic solution, and (*c*) in water–ethanol mixtures. In the media (*b*) and (*c*), 0.1 *M* LiCl was used as a supporting electrolyte. Ethanolic solutions of benzoic acid and sodium hydroxide, respectively, were used as proton-donor and as a base in the case of non-aqueous medium (*b*).

The prepared depolarizer solution (1.25 mL) was placed in a 25 mL calibrated flask and brought to the mark by adding solutions (*a*), (*b*), or (*c*) so that the final solution had 5×10^{-4} *M* of the depolarizer. The test solution was then transferred to the polarographic cell then deaerated with pure argon. An inert atmosphere was maintained over the solution during the reduction.

The polarograms were recorded with a pen recording Radiometer Polarograph (Polariter PO4 g). The electrode assembly E64 with a SCE (K 505) as anode and the dropping mercury electrode as cathode was used. The capillary characteristic in 0.1 *M* KCl (open circuit) were: $t = 3.54$ s drop^{-1} and $m = 2.575$ mg s^{-1} at a mercury height of 50 cm. A Corning research pH-meter, Model 12 accurate to ±0.01 pH unit, was used. All the potentials are referred to SCE at 25°C.

Owing to the limiting solubility of these compounds in aqueous buffered solutions, the measurements were carried out in solutions containing at least 25 vol% of ethanol to keep the compounds in solutions.

Results and Discussion

(*A*) *Behaviour in Aqueous Buffered Solutions*

Considering the number of waves observed at various pH values (2–12) and the variation of the

0008-4042/79/111294-05$01.00/0

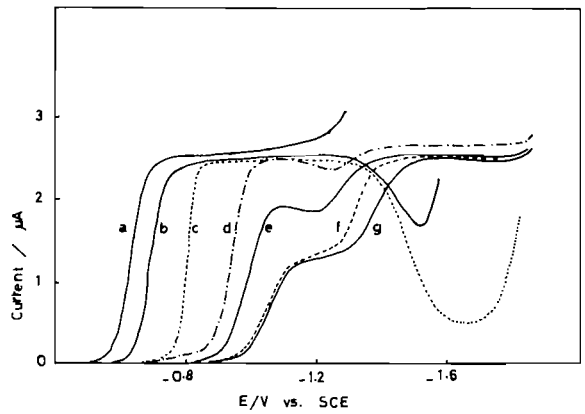

FIG. 1. Polarograms of 5×10^{-4} *M* cresolphthalein in 25 vol% ethanolic aqueous buffered solutions of pH: (*a*) 2.89; (*b*) 4.5; (*c*) 7.02; (*d*) 9.79; (*e*) 10.3; (*f*) 11.0; and (*g*) 11.51.

limiting current with pH, three polarographic trends are observed (cf. Fig. 1).

(*a*) In solutions of pH values < 8.5, a single $2e^-$ wave is observed, its height being pH-independent (e.g. Fig. 1, curves *a–c*). At pH values 3.5 to 8.5, the limiting current decreased to a minimum value in the potential range of about -1.6 to -1.7 V. However, before the flat minimum is attained, the wave of the supporting electrolyte appeared (2). The $E_{1/2}$–pH dependence of the single wave denotes that the H^+ ions are involved in the electrode reaction.

(*b*) In solutions of pH 8.5 to 10.5, two reduction waves of unequal heights are observed (e.g. Fig. 1, curves *d* and *e*). The height of the second wave gradually increases at the expense of the first one with increasing pH until both attain equal heights at pH values $\geq$ 10.5. The plots of i_1 as a function of pH for both waves yield typical dissociation and association curves. This behaviour indicates that the electrode reaction is governed by the rate of proton transfer which becomes slower at higher pH values. The descending or ascending parts of the i_1–pH curves shift to lower pH values in the presence of an increasing amount of ethanol (25–35%). This means that the rate of proton transfer becomes slower as the polarity of the medium is lowered.

(*c*) In media of pH values above 10.5, two $1e^-$ waves of equal height are obtained. The $E_{1/2}$ of the second wave is pH-dependent whereas that of the first wave is not (Fig. 1, curves *f* and *g*).

(*B*) *Behaviour in Non-aqueous Ethanolic Medium or Water–Ethanol Mixtures*

In 99.7% ethanolic solutions, phenolphthalein and its derivatives are reduced through a single two-electron wave (Fig. 2*A*, curve *a*); its height equalling that of the wave obtained in aqueous buffered

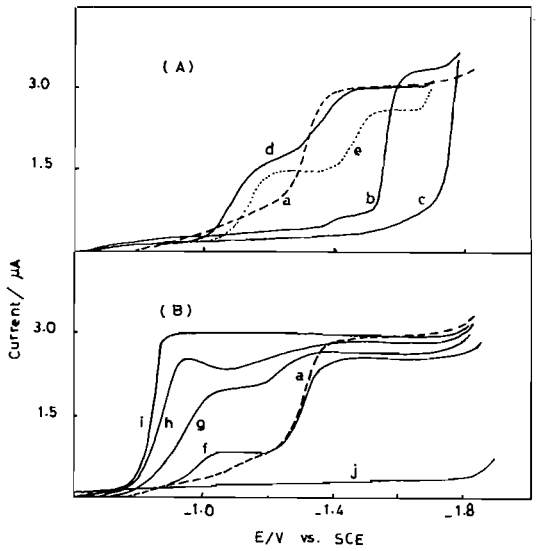

FIG. 2. Polarographic wave of 5×10^{-4} *M* phenolphthalein in non-aqueous ethanolic solution (curve *a*). (*A*) Effect of benzoic acid and sodium hydroxide on wave (*a*): (*b*) 10^{-4}, (*c*) 4×10^{-4} *M* benzoic acid; and (*d*) 10^{-3}, (*e*) 1.1×10^{-2} *M* NaOH. (*B*) Effect of increasing proportion of water in the ethanolic medium on wave (*a*): (*f*) 48; (*g*) 68; (*h*) 75; (*i*) 87 vol% water, and (*j*) residual current (non-aqueous).

solutions of pH < 8.5. The $E_{1/2}$ of this wave lies at more negative potential (-1.31 V) due to decreased availability of protons in non-aqueous ethanolic medium. The height of the wave is also proportional to the concentration of the depolarizer in solution.

The addition of benzoic acid, as a proton-donor, to ethanolic solution of phenolphthalein or its derivatives causes retardation, then complete elimination of the reduction wave (Fig. 2*A*, curves *b* and *c*). On the other hand, addition of sodium hydroxide turned the solution red and gave rise to polarograms of two one-electron waves similar to those obtained in aqueous buffered media of pH > 9 (Fig. 2*A*, curves *d* and *e*). This behaviour indicates that the presence of acid or base, respectively, leads to the formation of the non-reducible lactone form (I) or the electroactive red forms (V and VIII) through an acid–base equilibrium.

In water–ethanol mixtures, the polarograms (Fig. 2*B*) show the development of a prewave, at more positive potentials, on increasing the water percentage (Fig. 2*B*, curves *f–i*). This prewave attains the full height of the original polarogram when the media contain at least 80 vol% of water. This wave is preceded by a maximum, but this is easily eliminated when the solution is made 10^{-4}% with respect to Triton X-100. Enhancement of the reduction on increasing the water content in the medium is due to

TABLE 1. Data obtained for the depolarizers in aqueous buffered media containing 25 vol% ethanol

pH	Slope[a] S_1 (mV)	Slope[a] S_2 (mV)	Z_{H^+}	α $n_a = 1$	α $n_a = 2$	$k_{f,h}^0$ (cm/s)	ΔG^* (kcal/mol)	Notes
				(a) Phenolphthalein				
2.82	55	45	0.8	1.07	0.49	4.1×10^{-10}	83.7	1st wave
5.15	45	45	1	1.31	0.66	3.3×10^{-13}	101.6	1st wave
7.13	45	45	1	1.31	0.66	4.2×10^{-16}	118.3	1st wave
10.40	70	71	1	0.84	0.42	5.3×10^{-14}	106.1	1st wave
	80	91	1.1	0.74	0.37	2.1×10^{-16}	120.1	2nd wave
11.48	87	—	—	0.68	0.34	2.0×10^{-13}	102.8	1st wave
	78	91	1.2	0.76	0.38	9.9×10^{-15}	110.4	2nd wave
				(b) α-Naphtholphthalein				
4.61	40	45	1.1	1.48	0.74	1.4×10^{-12}	98.0	1st wave
7.13	40	45	1.1	1.48	0.74	1.2×10^{-15}	115.6	1st wave
9.46	70	90	1.3	0.84	0.42	6.38×10^{-13}	99.9	1st wave
11.85	85	—	—	0.69	0.35	1.4×10^{-12}	97.9	1st wave
	75	67	0.9	0.79	0.39	7.5×10^{-19}	134.0	2nd wave
				(c) Cresolphthalein				
4.50	45	45	1	1.31	0.66	1.6×10^{-11}	91.8	1st wave
7.02	37	45	1.2	1.60	0.80	4.9×10^{-18}	129.5	1st wave
9.79	50	45	0.9	1.18	0.59	1.4×10^{-17}	126.8	1st wave
11.50	65	—	—	0.91	0.45	1.16×10^{-15}	115.8	1st wave
	80	83	1	0.74	0.37	1.2×10^{-17}	127.1	2nd wave
				(d) Thymolphthalein				
5.25	45	45	1	1.31	0.66	7.1×10^{-13}	99.5	1st wave
10.50	65	63	1	0.91	0.45	3.2×10^{-13}	101.7	1st wave
11.74	80	—	—	0.74	0.37	1.7×10^{-13}	103.1	1st wave
	80	78	1	0.74	0.37	6.7×10^{-18}	128.7	2nd wave

[a] $S_1 = \Delta E_{d,e}/\Delta \log i/(i_d - i)$; $S_2 = \Delta E_{1/2}/\Delta pH$.

the increased availability of protons (from water) in a medium which is still more or less neutral. Also the addition of water facilitates the transformation of depolarizer molecules from the non-reducible lactone form (I) to the reducible hydrated form (II*a*).

These results support the idea (2) that the lactone form (I) is not reducible at the dropping mercury electrode at least at potentials more positive than that at which the wave of the supporting electrolyte appears.

Nature of the Waves

The effect of pressure at mercury head on the limiting current showed that the reduction process of the four depolarizers is mainly diffusion-controlled with a small kinetic contribution. The value of the exponent x in the relation i_l = constant $\times$ h^x amounts to 0.45–0.5.

Analysis of the waves applying the fundamental equation for polarographic waves (4) indicated that the reduction process proceeds in an irreversible manner. The values of transfer coefficient (α) and αn_a are determined from the slopes (S_1) of E_{de} vs. log $i/(i_d - i)$ plots at different pH values (Table 1). The most probable α-values are obtained for $n_a = 2$ at pH < 8.5 and $n_a = 1$ for the pH range above 10.5.

The $E_{1/2}$–pH plots of the first and second waves for the different depolarizers consist of three or two segments, respectively (Fig. 3). The breaks in these plots lie at pH values of ~8.5 and ~10.5 which correspond to those at which the reduction behaviour is changed. The number of protons (Z_{H^+}) participating in the rate-determining step is determined by using the relation:

$$Z_{H^+} = (\Delta E_{1/2}/\Delta pH)\,(\alpha n_a/0.059) = S_2/S_1$$

and is found to be, approximately, one (Table 1). Accordingly, the rate-determining step of the electrode process would involve one proton and two electrons (pH < 8.5) or one proton and one electron (pH ≥ 10.5). For intermediate pH values (8.5–10.5) both sequences are contributing in varying proportions.

According to the foregoing results, the reduction of any of the depolarizers under study at the electrode surface can be explained by the following schemes:

(*a*) In aqueous solutions of pH < 8.5 and non-aqueous media (Scheme 1)

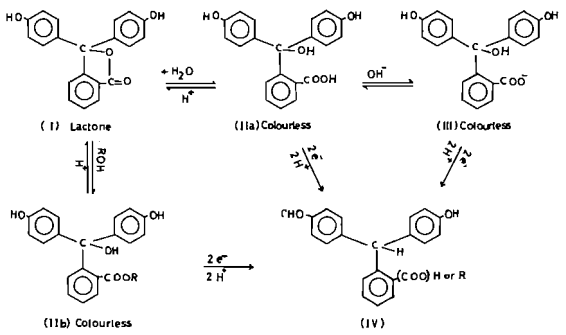

SCHEME 1

The dominant species within these media is II*a* and III (aqueous) or II*b* (non-aqueous) forms (5); each one can be reduced through a two-electron step.

(*b*) In solutions of pH values 8.5–10.5 (Scheme 2)

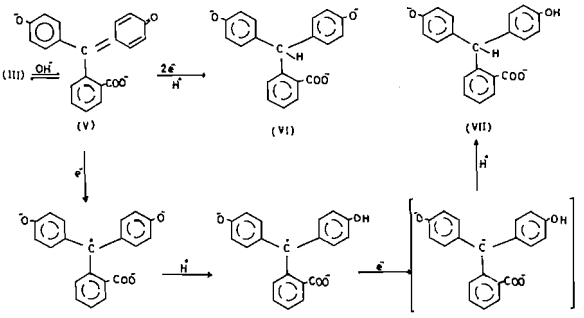

SCHEME 2

The number of protons participating in the electrode process is, approximately, one (first wave); the second small wave is slightly pH-dependent. The processes according to Scheme 2 are considered to compete within this pH range.

(*c*) In solutions of pH values > 10.5 (Scheme 3)

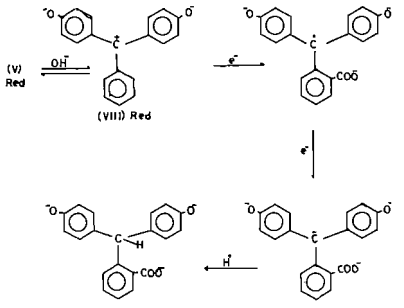

SCHEME 3

The $E_{1/2}$ of the first step is independent of pH while that of the second step is pH-dependent. The mechanism is shown in Scheme 3.

The Electrode Reaction

The polarographic behaviour of the depolarizers in buffer solutions indicates that they belong to the category of organic compounds where $E_{1/2}$ and i_l are pH-dependent. The change of the reduction current with the pH of the medium leading to the splitting of the reduction wave was explained by Zuman (6). The main factors considered to govern the current changes are:

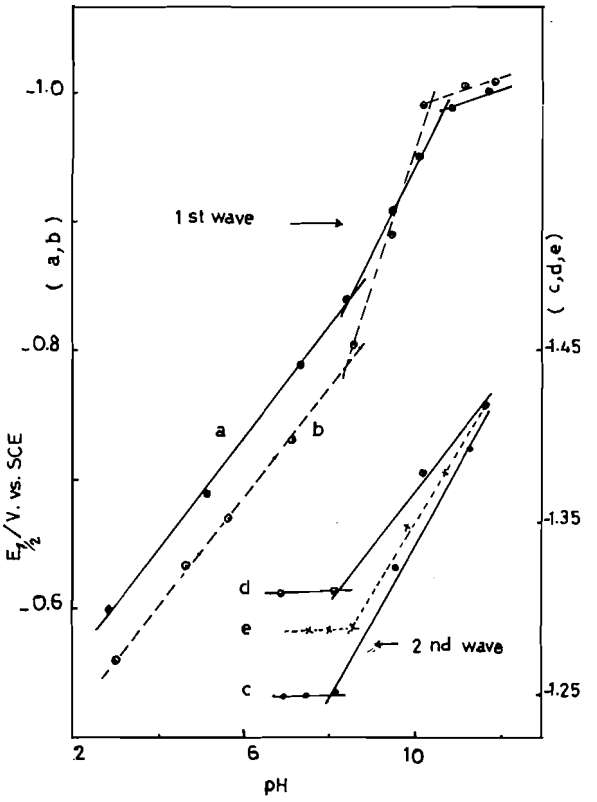

FIG. 3. $E_{1/2}$–pH curves of phenolphthalein (*a* and *c*); α-naphthalphthalein (*b* and *d*) and cresolphthalein (*e*). Curves *c*, *d*, and *e* are shifted three pH units to the right side of the scale.

(*i*) The existence of an acid–base equilibrium:

$$BH^- \underset{k_r}{\overset{k_d}{\rightleftharpoons}} B^{2-} + H^+$$

for which the variation of the current with pH is governed by the relation (7):

$$[1] \quad pH = \log 0.886\left(\frac{k_r t_1}{K}\right)^{1/2} + \log\left(\frac{i_l - i_{HB^-}}{i_{HB^-}}\right)$$

which is a modified form of the Koutecky equation (8).

(*ii*) Change of current due to chemical transformation. The probable chemical transformation with increasing pH in analogy to the case of fluorescein (9) is the formation of triphenyl carbonium ion

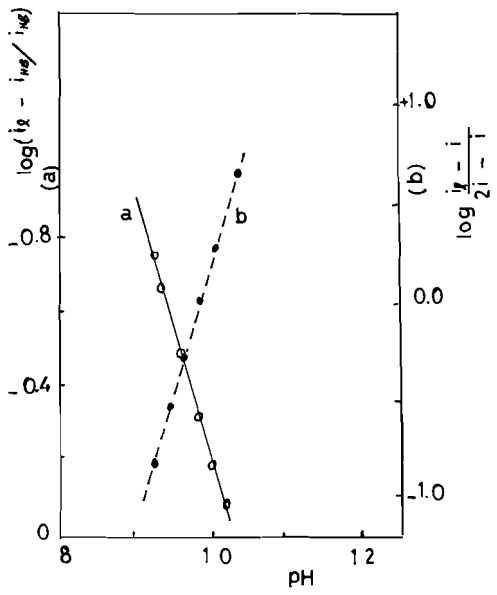

FIG. 4. Application of eqs. [1] and [2] for phenolphthalein.

(V $\rightleftharpoons$ VIII), the reduction of which proceeds to a free radical through one electron, whereas the overall reduction process corresponds to two electrons.

(*iii*) The existence of two electroactive forms which differ in the number of electrons consumed in the electrode reaction. In this case, the change of current with pH should follow the relation (6, 7):

$$[2] \quad \mathrm{pH} = \log 0.886\left(\frac{k_r t_1}{K}\right)^{1/2} - \log\left(\frac{i_1 - i}{2i - i_1}\right)$$

The plots of log $[(i_1 - i_{HB^-})/i_{HB^-}]$ or log $[(i_1 - i)/(2i - i_1)]$ vs. pH yield straight lines (e.g. Fig. 4), indicating the validity of eqs. [1] and [2].

Accordingly it may be concluded that the change in the reduction current of the depolarizers under investigation would depend on the three mentioned factors, which recalls the case of fluorescein (7).

According to the above findings, the electrode sequence for the reduction of the compounds under investigation in buffered solutions can be given as follows:

$$[3a] \quad (\mathrm{P})_{ox}^{-} + e^{-} \xrightarrow{E_1} P_1^{-2}$$

$$[3b] \quad P_1^{-2} + H^{+} \overset{K_1}{\rightleftharpoons} P_1H^{-} \text{ (pH-dependent)}$$

$$[4a] \quad P_1H^{-} + e^{-} \xrightarrow{E_2} P_2^{-2}$$

$$[4b] \quad P_2^{-2} + H^{+} \overset{K_2}{\rightleftharpoons} \text{Reduction product (pH-dependent)}$$

Processes [3*a*]–[4*b*] occur at lower pH values (<8.5) through one two-electron step. As the pH increases the protonation step [3*b*] slows down and the second reduction step [4*a*] is attained at higher potential, leading to separation of the two steps ($E_1 \neq E_2$). The lowering of i_1 at the first wave is due to slowed rate of protonation of the intermediate radical anion (P_1^{2-}).

Values of kinetic parameters ($k_{f,h}^0$, ΔG^*, αn_a, and α) of the electrode reaction were calculated as explained previously (10–12). The values of rate constant ($k_{f,h}^0$) are smaller than 3×10^{-5} cm/s denoting an irreversible process. On increasing pH of the medium $k_{f,h}^0$ decreases and energy of activation (ΔG^*) increases (Table 1), denoting a more difficult electron transfer and consequently a more difficult reduction process.

1. I. M. KOLTHOFF. J. Phys. Chem. **35**, 1433 (1931).
2. I. M. KOLTHOFF and D. J. LEHMICKE. J. Am. Chem. Soc. **70**, 1879 (1948).
3. H. T. S. BRITTON. Hydrogen ions. 4th ed. Chapman and Hall, London. 1952. p. 338.
4. L. MEITES. Polarographic techniques. Interscience publishers, New York. 1965. p. 240.
5. A. M. HASSANEIN. M.Sc. Thesis, Al-Azhar University, A.R. Egypt. 1979.
6. P. ZUMAN. The elucidation of organic electrode processes. Academic Press, New York. 1969. pp. 28–39.
7. F. M. SALEM, R. M. ISSA, and A. M. HINDAWEY. Anal. Chim. Rome, **64**, 735 (1974).
8. J. KOUTECKY. Collect. Czech. Chem. Commun. **28**, 829 (1963).
9. R. M. ISSA, F. M. ABDEL-HALIM, and A. A. HASSANEIN. Electrochim. Acta, **14**, 561 (1969).
10. J. KOUTECKY. Chem. Listy, **47**, 323 (1953); Collect. Czech. Chem. Commun. **18**, 597 (1953).
11. I. M. ISSA, A. A. EL-SAMAHY, and M. M. GHONEIM. Electrochim. Acta, **16**, 1655 (1971).
12. M. M. GHONEIM. Monats. Chem. **109**, 661 (1978).

Thermal decomposition of diazirines in the presence of *m*-chloroperoxybenzoic acid. A method to determine the partitioning of reaction pathways

MICHAEL T. H. LIU AND IWAO YAMAMOTO[1]

Department of Chemistry, University of Prince Edward Island, Charlottetown, P.E.I., Canada C1A 4P3

Received April 25, 1978

MICHAEL T. H. LIU and IWAO YAMAMOTO. Can. J. Chem. 57, 1299 (1979).

The oxidation of various diazirines by *m*-chloroperoxybenzoic acid as well as the activation parameters for these reactions have been investigated. The oxidation products and the information derived from kinetic studies indicate that the oxidation does not take place on the diazirine ring as expected but rather on the decomposition products of the diazirines. The oxidation products obtained are shown to be characteristic of the diazirine decomposition by carbenic and diazo pathways and thus the measurement of the oxidation products provides a measure of the partitioning of the two reaction pathways for diazirine decomposition.

MICHAEL T. H. LIU et IWAO YAMAMOTO. Can. J. Chem. 57, 1299 (1979).

On a étudié l'oxydation de diverses diazirines par l'acide *m*-chloroperbenzoïque de même que les paramètres d'activation de ces réactions. Les produits d'oxydation et l'information que l'on tire des études cinétiques indiquent que l'oxydation ne se produit pas sur le cycle diazirine tel qu'attendu mais plutôt sur les produits de décomposition des diazirines. On montre que les produits d'oxydation obtenus sont caractéristiques de la décomposition de la diazirine par des voies carbéniques et diazo et la mesure des produits d'oxydation fournit donc une mesure de la repartition entre les deux voies réactionnelles pour la décomposition de la diazirine.

[Traduit par le journal]

Introduction

The chemistry of diazirines has been characterized by the facile thermal decomposition which generates carbenes (1–4), and generally low reactivity when compared with the linear isomers (5). Schmitz (4, 5), Lau (6), and more recently Bradley, Evans, and Stevens (7) have shown diazirines to be insensitive towards a wide range of compounds. The direct oxidation of the nitrogen–nitrogen double bond of the diazirine system is not known but the ozonisation of methyl-vinyldiazirine has been reported (8). The product of this oxidation process was an etherhydroperoxide which contained the original three member ring. It was hoped that in the present experiments the unknown azoxy analog could be made so that a new class of compounds would be available; the kinetic and mechanistic implications would be obvious. As well, extensive *ab initio* SCF-MO calculations with a double-zeta basis set of Gaussian type orbitals have been carried out for diazirine and diazirine *N*-oxide (9).

The present paper is an extension of previously reported work (10) in which the oxidation of chlorophenyldiazirine by *m*-chloroperoxybenzoic acid (MCPBA) gave benzoyl chloride. The results suggested that the *N*-oxide of the diazirine may be generated but that it decomposes under the conditions of the reaction. The formation of benzoyl chloride in the chlorophenyldiazirine oxidation was rationalized by the following mechanism:

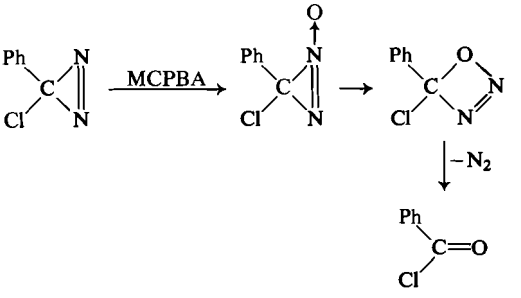

It is to be noted that an intermediate, 1,2,3-oxadiazete, is formed prior to the formation of benzoyl chloride. This mechanism receives some support from the work of Snyder *et al.* (11) on the oxidation of diazobasketene with MCPBA to give the *N*-oxide which rearranged readily in boron trifluoride etherate. In view of the considerable interest in this area of chemistry, we decided to investigate the oxidation of several diazirines by various oxidants and in particular by MCPBA. Kinetic studies on the oxidation of phenyl-*n*-butyldiazirine and chlorophenyldiazirine by MCPBA in various solvents were also conducted.

Results and Discussion

The reactivity of diazirine towards a range of

[1]On sabbatical leave (1977–1978) from Department of Chemistry, Shinshu University at Ueda, Nagano 386, Japan.

0008-4042/79/111299-05$01.00/0

oxidants has been examined. Chlorophenyldiazirine is recovered almost unchanged after treatment with basic hydrogen peroxide and peracetic acid. The negative results with the above oxidants may at first appear to result from the milder reaction temperature as compared with the positive results with MCPBA. It will be shown later in this discussion that the negative results are really due to the inertness of the diazirine ring and not at all due to the effect of temperature. As well the relative degree of the oxidizing powers of the reagents used has no effect. The thermal decomposition of phenyl-*n*-butyldiazirine (**1**) in DMSO solvent has been investigated in detail by us and the intermediate formation of the diazo compound, 1-phenyl-1-diazopentane has been detected and the intermediate has been isolated. The decomposition of **1** and the subsequent decomposition of its product, 1-phenyl-1-diazopentane to give *cis* and *trans* 1-phenyl-1-pentenes (ratio *cis*:*trans* = 1:5) provide an interesting illustration of consecutive reactions (12).

In the oxidation of **1** by MCPBA in chlorobenzene and in 1,2-dichloroethane solvents, the products were *cis* and *trans* 1-phenyl-1-pentene oxides and valerophenone. In the oxidation reaction it was noted that the color of the solution was yellowish throughout the experiment and the characteristic red-color due to the formation of the diazo intermediate was not observed. As we could see no red color, we were led to believe that the oxidation was indeed taking place on the diazirine ring. If this were the case, the formation of the four-atom ring, 1,2,3-oxadiazete would be inevitable. This particular four-atom ring has been postulated in the decomposition of nitrosoimines (13) but has not been isolated. In view of its similarity to the 1,2-dioxetane system (14, 15), we were hoping that the 1,2,3-oxadiazete ring would produce excited carbonyl molecules (excited valerophenone in this case) which would luminesce. However, since the photo product acetophenone from valerophenone (resulting from a Norrish type II reaction) was not found in the above oxidation experiment, it was decided that the proposed mechanism would have to be examined more carefully.

Up to this point, we could not provide sufficient evidence to propose an unequivocal mechanism for the oxidation of diazirines. We have extended our investigation to determine the activation parameters for the oxidation of **1** by MCPBA in chlorobenzene and in 1,2-dichloroethane. In all kinetic experiments the concentrations of diazirine and MCPBA were both 0.05 *M* in chlorobenzene and in 1,2-dichloroethane, respectively. The results for the oxidation of **1** in chlorobenzene by MCPBA show that the reaction is not second-order as expected but rather the reaction is first-order. In fact, the first-order plot gave an excellent straight line even up to 80% reaction. Similar results were obtained for the reaction of **1** and MCPBA in 1,2-dichloroethane. Also, the first-order rate constants determined by N_2 evolution and separately by a uv spectrophotometric method agreed within 4%. The first-order rate constants for these reactions are tabulated in Table 1 and the oxidation products in various solvents are given in Table 2. The first-order rate constant at 99.8°C for the reaction of equimolar concentration of **1** and MCPBA in chlorobenzene was 6.31×10^{-4} s^{-1}. Additional experiments at the same temperature with a four-fold increase in MCPBA gave 6.50×10^{-4} s^{-1}. It is evident that the rate of reaction is not a function of MCPBA concentration. From the least-squares analysis of the rate constants in Table 1, the following activation parameters for **1** were obtained: in chlorobenzene, $\Delta H^{\ddagger} = 27.0$ kcal mol^{-1}, $\Delta S^{\ddagger} = -1.2$ cal deg^{-1} mol^{-1} and in 1,2-dichloroethane, $\Delta H^{\ddagger} = 27.6$ kcal mol^{-1}, $\Delta S^{\ddagger} = 0.74$ cal deg^{-1} mol^{-1}. Examination of these parameters reveals that they are merely the parameters for the decomposition of phenyl-*n*-butyldiazirine, the values of which have been reported already (12). When further kinetic studies were carried out using chlorophenyldiazirine and MCPBA in 1,2-dichloroethane, good first-order plots were obtained over the temperature range of 50–70°C. The following activation parameters for chlorophenyldiazirine were derived: $\Delta H^{\ddagger} = 25.8$ kcal mol^{-1} and $\Delta S^{\ddagger} = 1.7$ cal deg^{-1}

TABLE 1. Rate constants for the oxidation of phenyl-*n*-butyl diazirine by MCPBA in chlorobenzene and in 1,2-dichloroethane

(*a*) Chlorobenzene

T (°C)	$k \times 10^4$ (s^{-1})	Method
105.0	10.5	N_2
102.4	8.51	N_2
99.8	6.31	N_2
94.0	3.40	N_2
88.0	1.68	N_2
81.6	0.996	N_2

(*b*) 1,2-Dichloroethane

T (°C)	$k \times 10^5$ (s^{-1})	Method
79.5	8.71	N_2
76.5	6.76	N_2
72.9	3.85	N_2
66.8	1.86*	N_2, uv
63.5	1.24	N_2
61.3	0.95*	N_2, uv

*Average value of k measured by N_2 evolution and by uv.

TABLE 2. % Distribution of products for the decomposition of phenyl-*n*-butyldiazirine in various solvents

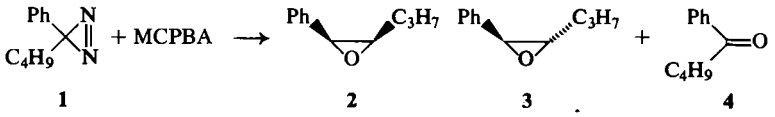

1 2 3 4

T (°C)	Solvent	2	3	4
105	PhCl	6	37	57
102.4	PhCl	9	31	59
100	PhCl	7	39	54
99.8	PhCl	9	40	51
99.8	PhCl*	6	44	50
94	PhCl	7	37	56
88	PhCl	5	30	65
81.6	PhCl	5	32	63
78	1,2-Dichloroethane	7	43	50
78	$PhNO_2$	2	23	75

*Diazirine/MCPBA = 1/4.

mol^{-1}, in agreement with our earlier finding (16). These various kinetic results suggest that the oxidation by MCPBA does not take place on the ring but rather on the products of the decomposition. If the diazirine *N*-oxide were to be made, it would probably require a new synthetic route.

In order to account for the products of the reaction the following mechanism is postulated:

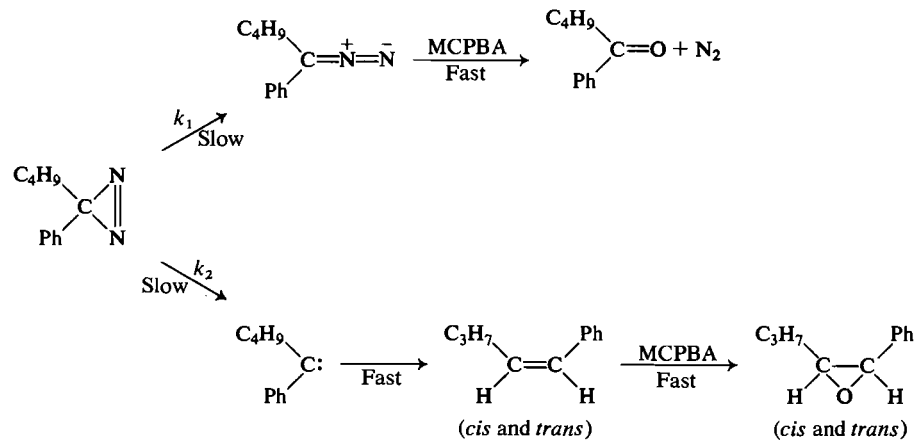

In pathway [1], the diazirine is isomerized to diazomethane which is rapidly consumed by MCPBA to give the corresponding ketone. In a control experiment, we have synthesized 1-phenyl-1-diazopentane independently and reacted it with MCPBA in chlorobenzene at room temperature, the distinct red-color of the diazo compound was completely removed in a few seconds with vigorous evolution of nitrogen. This result shows that the reaction requires little or no activation energy.[2] Analysis showed that valerophenone was the only product and therefore, 1-phenyl-1-diazopentane does not react with MCPBA to yield 1-phenyl-1-pentene or 1-phenyl-1-pentene oxide.

In pathway [2], the diazirine decomposes directly to give a carbene intermediate which rearranges to *cis* and *trans* 1-phenyl-1-pentenes which in turn are further oxidized to *cis* and *trans* 1-phenyl-1-pentene oxides by MCPBA. In a separate experiment conducted by heating a mixture of *cis* and *trans* 1-phenyl-1-pentenes (*cis*:*trans* = 1:10.8) and MCPBA in chlorobenzene at 100°C for 40 min, the products were *cis* and *trans* 1-phenyl-1-pentene oxides (*cis*:*trans* = 1:11.3). This indicates that all the *cis*-olefin is converted to the *cis*-epoxide and *trans*-olefin

[2]This conclusion is substantiated by the reaction of peroxybenzoic acid (in 1,2-dichloroethane) with diazodiphenylmethanes (ref. 17) for which the activation parameters were found to be $\Delta H^{\ddagger} = 5.8$ kcal mol^{-1}, $\Delta S^{\ddagger} = -40.0$ cal deg^{-1} mol^{-1}.

to *trans*-epoxide. This conclusion was again supported by the epoxidation of *trans*-stilbene with MCPBA which was shown to be a fast reaction even at room temperature (18). Thus the yields of the epoxides and of the ketones provide a measure of the partitioning of the two reaction paths. Our experiments show that in the decomposition of phenyl-*n*-butyldiazirine in chlorobenzene, MCPBA can be used as a trapping agent for the intermediate formation of olefin and for the diazo compound. The yields of the epoxides and of the valerophenone are approximately 50% each. This is to say that the decomposition of **1** in chlorobenzene is 50% carbenic and 50% via the diazo process. The percentage by each pathway does not appear to be very sensitive to temperature since the product ratio of ketone to epoxides is approximately the same at all temperatures (somewhat large values occur at the lowest temperatures). It was found that the ketone to epoxides ratio did not vary, even for a 4-fold increase in MCPBA concentration. In another non-polar solvent such as 1,2-dichloroethane, the ratio of ketone to epoxides is found to be very similar to the ratio when chlorobenzene was the solvent. However, in a more polar solvent, such as nitrobenzene, the decomposition of **1** occurs 75% by the diazo pathway and 25% by the carbenic pathway. In an even more polar solvent, DMSO, the pathway leading to 1-phenyl-1-diazopentane accounts for as much as 90% of the products (12). The concerted decomposition of **1** to give phenyl-*n*-butylcarbene is only of minor importance in this case (12). It is likely that the 1-phenyl-1-diazopentane is stabilized in the presence of polar solvent molecules. The solvent dependence of the decomposition pathways in the diazirine system is not well understood because there has been no method which could provide a good measure for the partitioning of the two reaction pathways. If the decomposition pathways in diazirine are indeed solvent dependent as it would appear to be in the present case, then a comparison of the decomposition pathways in diazo compound would be very interesting. In the decomposition of diethyl diazosuccinate (19), it was found that the diazo compound decomposes via a carbenic pathway in non-polar solvent, a diazonium pathway in protic solvent and a carbenoid pathway in acetic acid solvent. However, the participation of dual pathways in a given solvent is also possible in the thermal decomposition of a diethyl diazosuccinate (19).

If one examines the activation parameters for the decomposition of **1** in chlorobenzene ($\Delta H^{\ddagger} = 27.0$ kcal mol^{-1} and $\Delta S^{\ddagger} = -1.2$ cal deg^{-1} mol^{-1} where the decomposition of **1** is 50% diazo – 50% carbenic) and in DMSO ($\Delta H^{\ddagger} = 27.3$ kcal mol^{-1} and $\Delta S^{\ddagger} = -0.32$ cal deg^{-1} mol^{-1} where the decomposition of **1** is 90% diazo – 10% carbenic (12)), one observes that the enthalpies of activation in both solvents are very similar. This would imply that the $\Delta H^{\ddagger}$ values for

[*a*] 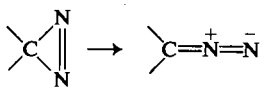

and for

[*b*] 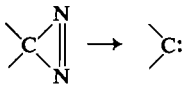

are very similar in these two competitive processes. The results could also be interpreted to suggest that the $\Delta H^{\ddagger}$ value for process [*b*] is very large in DMSO solvent. However, in view of the solvent studies carried out in the thermal decomposition of chloroethyldiazirine (20), where the activation energies were found to be similar in a variety of solvents, this latter hypothesis does not seem to hold. Despite the fact that process [*a*] involves the breaking of one C—N bond and process [*b*] involves the breaking of two C—N bonds, the entropy of activation is nearly identical for the two elementary processes. This implies that the activated complex must be very much alike for both pathways. The element of single vs. double bond breaking must occur after the transition state and the transition state must resemble the diazirine in structure. This is substantiated by the fact that the $\Delta S^{\ddagger}$ values are very small; this indicates that no additional free rotations are developed in the transition state.

In conclusion, the pathway for the thermal decomposition of diazirine appears to be dependent on (*1*) the nature of the substituents on the diazirine ring, (*2*) the stability of the intermediate diazo compound, and (*3*) the ability of the solvent molecules to stabilize the intermediate (carbene or diazo compound) formed in the decomposition.

Experimental

The ir, nmr, and uv spectra were obtained with Perkin-Elmer Model 137, Varian T-60, and Unicam SP800 respectively. The vpc analyses were carried out using a Perkin-Elmer model F-11 equipped with a hydrogen flame detector.

Since the oxidation products for all the diazirines were common compounds, they were identified by comparing their ir and nmr spectra with authentic samples.

The chlorophenyldiazirine and phenyl-*n*-butyldiazirine were prepared according to methods described previously (12, 21).

The rates of reaction of various diazirines (0.05 *M*) with *m*-chloroperoxybenzoic acid (0.05 *M*) in 1,2-dichloroethane were determined by measuring the disappearance of diazirine according to standard spectrophotometric techniques (16) and by measuring the nitrogen evolution as a function of time. For the spectrophotometric experiments, the first-order rate constants were determined graphically from the plot of log $(D_t - D_\infty)$ vs. time, where D_t is the optical density at the

wavelength of observation (369 nm for phenyl-*n*-butyldiazirine and 390 nm for chlorophenyldiazirine) and D_∞ corresponds to that of complete reaction. For the nitrogen evolution experiments the first-order rate constants were determined graphically from the plot of log $(V_\infty - V_t)$ vs. time, where V_∞ is the volume of nitrogen measured at infinite time and V_t is that at time t. The first-order plots obtained in both methods were linear to at least 80% reaction.

Purification of m-*Chloroperoxybenzoic Acid (18)*

Peracid (3.5 g) (Aldrich 85%) was suspended in 91.1 mL of phosphate buffer solution (pH 7.5) and stirred for 2 h. The product, a white powder, was filtered, washed with distilled water (3 × 100 mL), and the powder was dried under reduced pressure for 2 days. The purity of MCPBA was determined by iodometric titration, which showed 99 ± 1% assay.

Preparation of 1-Diazo-1-phenyl-pentane

Valerophenone-*p*-toluene sulfonylhydrazone (6.6 g, 0.02 mol) was dissolved in 20 mL of distilled pyridine in a 100 mL round bottom flask equipped with a condenser and NaOH drying tube. Sodium methoxide (1.08 g, 0.02 mol) was added to this solution and the mixture was stirred at 75–80°C for 20 min. The contents were poured into 200 mL of ice–water and extracted with pentane (2 × 100 mL). The combined organic fractions were washed with water, dried, and concentrated *in vacuo* to give 2.15 g of dark red oil. The ir of this material showed an intense band at 2040 cm^{-1} (diazo $>C=N_2$).

Several diazirine oxidation experiments were carried out but only the oxidation with *m*-chloroperoxybenzoic acid gave positive results.

1. Basic Hydrogen Peroxide

Chlorophenyldiazirine (1.0 g), 30 mL of 50% hydrogen peroxide, and 4.0 g KOH were stirred at 40°C for 10 h. The resulting mixture was extracted with ether and almost all of the diazirine was recovered. A small amount of diazirine will decompose under these experimental conditions.

2. Peracetic Acid

A solution of 1.0 g chlorophenyldiazirine in 15 mL glacial acetic acid and 5 mL of 30% H_2O_2 was stirred at 40°C for 5 h. The solution was cooled, neutralized with NaOH, and extracted with CH_2Cl_2. Most of the diazirine was recovered.

3. m-*Chloroperoxybenzoic Acid*

(*a*) The reaction was carried out by refluxing 1.55 g of chlorophenyldiazirine and 2.06 g *m*-chloroperoxybenzoic acid in $CHCl_3$ for 5 h. The resulting solution was worked up quickly under basic conditions. Chromatographic analysis of the products indicated the presence of benzoyl chloride (45–50%), benzaldehyde (40%) and a trace amount of benzoic acid. The components were identified by comparing their ir and tlc with those of authentic samples. Benzoyl chloride was converted to benzamide, mp 130°C and benzaldehyde to its 2,4-dinitrophenylhydrazone, mp 237°C. The formation of benzaldehyde was attributed to the decomposition of unreacted starting material during aqueous work-up.

(*b*) Phenyl-*n*-butyldiazirine (200 mg) and 200 mg of *m*-chloroperoxybenzoic acid in 20 mL chlorobenzene were mixed and heated to reflux for 20 h. The color of the solution was yellowish throughout the experiment. The solution was washed with 2 × 20 mL saturated $NaHCO_3$, followed by 2 × 50 mL H_2O. After drying and evaporation in vacuo, 200 mg of yellow oil remained. Vapour phase chromatographic analysis on a 12 ft, 20% Carbowax column at 150°C showed that the products were valerophenone and *cis* and *trans* 1-phenyl-1-pentene oxides. ^1H nmr ($CDCl_3$) δ: 1.00 (t, 3, J = 6 Hz, CH_3), 1.20–1.80 (m, 4, methylenes), 6.92 (bm, 1, H—C—C_3H_7), 3.60 (d, 1, J = 2 Hz, H—C—C_6H_5), 7.35 (s, 5, aromatics). ms (70 eV) *m/e* (relative intensity): 162.122 (70, M^+, $C_{11}H_{14}O$), 133 (90, M—CHO), 119 (38, M—C_3H_7), 105 (85), 91 (100, M—C_4H_7O).

Acknowledgements

Financial support from the National Research Council of Canada and the Senate Research Committee is gratefully acknowledged. We wish to thank W. Y. Kwan for technical assistance.

1. S. Braslavsky and J. Heicklen. Chem. Rev. **77**, 473 (1977).
2. H. Meier and K.-P. Zeller. Angew. Chem. Int. Ed. **16**, 835 (1977).
3. W. Kirmse. Carbene chemistry. Academic Press, New York, NY. 1971.
4. E. Schmitz. Angew. Chem. Int. Ed. **3**, 333 (1964).
5. E. Schmitz. Advances in heterocyclic chemistry. Vol. 2. Academic Press, New York. 1963. pp. 126–130.
6. A. Lau. Spectrochim. Acta, **20**, 97 (1964).
7. G. F. Bradley, W. B. L. Evans, and I. D. R. Stevens. J. Chem. Soc. Perkins II, 1214 (1977).
8. E. Schmitz and C. Hörig. Chem. Ber. **100**, 2101 (1967).
9. R. J. Boyd and A. Gupta. Abstracts, 61st Canadian Chemical Conference, Winnipeg, Manitoba, June 1978.
10. M. T. H. Liu and J. C. W. Li. Tetrahedron Lett. 1329 (1974).
11. J. P. Synder, L. Lee, and D. G. Farnum. J. Am. Chem. Soc. **93**, 3816 (1971).
12. M. T. H. Liu and B. M. Jennings. Can. J. Chem. **55**, 3596 (1977); B. M. Jennings and M. T. H. Liu. J. Am. Chem. Soc. **98**, 6416 (1976).
13. K. Akiba and N. Inamoto. Heterocycles, 7, 1131 (1977).
14. K. R. Kopecky and C. Mumford. Can. J. Chem. **47**, 709 (1969).
15. N. J. Turro, P. Lecktken, N. W. Schore, G. Schuster, H. C. Steinmetzer, and A. Yekta. Acc. Chem. Res. 7, 97 (1974).
16. M. T. H. Liu and K. Toriyama. J. Phys. Chem. **76**, 797 (1972).
17. R. Curci, F. Di Furia, and F. Marcuzzi. J. Org. Chem. **36**, 3774 (1971).
18. N. N. Schwartz and J. H. Blumbergs. J. Org. Chem. **29**, 1976 (1964).
19. M. T. H. Liu, O. Banjoko, Y. Yamamoto, and I. Moritani. Tetrahedron, **31**, 1645 (1975).
20. M. T. H. Liu and D. H. T. Chien. Can. J. Chem. **52**, 246 (1974).
21. W. H. Graham. J. Am. Chem. Soc. **87**, 4396 (1965).

The fine structure of the Kolmogoroff–Avrami theorem

ARTHUR SMITH
Department of Mathematics, Carleton University, Ottawa, Ont., Canada K1S 5B6
AND
STEPHEN FLETCHER
Department of Chemistry, Carleton University, Ottawa, Ont., Canada K1S 5B6

Received September 13, 1978

ARTHUR SMITH and STEPHEN FLETCHER. Can. J. Chem. **57**, 1304 (1979).

The fundamental processes underlying phase changes at electrode surfaces are often described in terms of the Kolmogoroff–Avrami theorem.

Some aspects of the 'fine structure' of this theorem are considered. Particular attention is paid to the case of two-dimensional nucleation and growth under the influence of an applied electrode potential (equivalent to supersaturation). A probabilistic analysis is presented for circularly-symmetric nuclei which obviates the need for concepts such as 'overlap' between emergent nuclei. The concept of a 'collision front' is introduced which is defined as the line of contact along which neighbouring nuclei collide. It is shown that for instantaneous nucleation (potentiostatic double step method) the extended set of collision fronts constitutes a net composed of irregular convex polygons. The properties of this net are investigated in some detail. In particular, the extent of applicability of the Kolmogoroff–Avrami equation is delineated, the distribution of collisional polygons is calculated, and an approximate treatment for the variance of the surface coverage function is presented. The general approach exposes clearly the relationship between the single nucleus and the multinuclear situations.

ARTHUR SMITH et STEPHEN FLETCHER. Can. J. Chem. **57**, 1304 (1979).

On considère quelques aspects de la structure fine de ce théorème. On attache une attention particulière au cas de la nucléation bi-dimensionnelle et à la croissance sous l'influence d'un potentiel d'électrode appliqué (équivalent à la sursaturation). On présente une analyse, basée sur le calcul des probabilités, pour des noyaux circulairement symétriques; ceci permet d'obvier à la nécessité de concepts comme celui du recouvrement entre des noyaux qui émergent. On introduit le concept d'un "front de collision" qui est défini comme la ligne de contact le long de laquelle des noyaux voisins entrent en collision. On montre que, dans le cas de la nucléation instantanée (méthode du double saut potentiostatique), l'ensemble étendu des ponts de collision constitue un filet composé de polygones convexes irréguliers. On a étudié, en détail, les propriétés de ce filet. En particulier, on a délimité la portée d'application de l'équation Kolmogoroff–Avrami, on a calculé la distribution des polygones collisionnels et on présente un traitement approximatif de la variation de la fonction exprimant la surface couverte. L'approche générale expose clairement la relation entre le noyau unique et les situations multinoyaux.

[Traduit par le journal]

General Introduction

Although a great deal of experimental data relating to electrolytic crystal growth has been accumulated over the years, the fundamental processes underlying phase changes at electrode surfaces are not completely understood in detail. However, the general picture is clear and involves a number of well-established concepts. In particular, when an overpotential ($\eta = E - E_0$) is applied to a given electrode surface then the adunit concentration at that surface rapidly increases. These adunits arise following an electron-transfer process between the electrode surface and a suitably labile species; this will usually be a metal ion in the case of metal deposition and will be surface atoms themselves in the case of anodic film formations. The result of such an increase in the adunit concentration is that the adunits begin to form clusters with a distribution of sizes and stabilities (1). The larger clusters (nuclei) tend to grow while the smaller clusters (embryos) tend to diminish in size. The clusters with an equal probability of both growing and diminishing are of particular interest and are called critical nuclei. The steady-state properties of critical nuclei are usually derived from thermodynamic (2) or atomistic (3) considerations. On the other hand, nuclei larger than the critical size are the subject of kinetic investigations.

The emergence and subsequent growth of nuclei is a complex problem, for which two rather different lines of approach may be discerned in the literature. One of these approaches is the macroscopic mod-

0008-4042/79/111304-15$01.00/0

elling of polynuclear nucleation, which has proved useful in the interpretation of electrochemical experiments (4). The other theoretical approach has been to conduct (microscopic) Monte-Carlo simulations of events occurring at the atomic level (5), and these may be compared with crystal growth from the gas phase. Both approaches have met with success in their particular areas of applicability, but nevertheless a number of theoretical disparities exists between them. These disparities arise because of the different assumptions inherent in the two models. These assumptions, in turn, are necessary because of considerations of mathematical tractability in the macroscopic case, and because of limited computer resources in the Monte-Carlo case. Because of the assumptions made, discrepancies also exist between the individual models and actual experimental data.

In the case of Monte-Carlo simulations only small elements of surface may be considered in a given computer experiment, so that it is necessary to employ cyclical boundary conditions (5). The use of such boundary conditions necessarily precludes the observation of the simultaneous collision of large numbers of nuclei. However, this is the very state of affairs with which the macroscopic models concern themselves. Their strategy for dealing with such multi-centre collisions is to invoke the Avrami theorem (6), with the result that the 'fine structure' of events on the electrode surface is lost and even the probabilistic aspect of nucleation (so evident in Monte-Carlo simulations) is to some extent obscured.

The purpose of the present work is to investigate some microscopic consequences of the assumption of a macroscopic model of polynuclear nucleation. We do this for the case of two-dimensional nucleation, in which N_0 nuclei are effectively nucleated at $t = 0$ and thereafter grow uniformly across the electrode surface (4). Both exact solutions and computer-simulated data are calculated and compared. In particular, the 'fine structure' of the two-dimensional nucleation and growth model is investigated in detail to see how far geometrical properties of individual nuclei may be recovered. It is hoped that the results obtained will lead to more complete modelling of real situations, for example, the extension of present theory to polycrystalline substrates. Also a clearer comparison of macroscopic (geometric) and microscopic (Monte-Carlo) models may ultimately evolve via considerations of this sort. Because of the probabilistic nature of the present work, some of the results presented will also be relevant to such varied problems as the effect of electrode boundaries on nucleation and growth phenomena, the measurement of noise on microelectrodes, and the elucidation of the exact extent of applicability of the Avrami theorem to crystal growth kinetics.

Before considering the problem in detail, some fundamental aspects of two-dimensional nucleation are briefly considered which are pertinent to both microscopic and macroscopic models. The geometrical 'fine structure' of the macroscopic model is then calculated from first principles.

The Nucleation Rate

Nucleation consists in the formation of nuclei of critical size from a distribution of sub-critical clusters. As clusters larger than the critical size grow out, so the distribution re-adjusts towards its original condition, thus perpetuating the nucleation process. Clusters can grow via two possible processes. The first is the addition of individual adunits (atoms, ions) at the periphery of clusters. The second process is the addition of smaller clusters to larger clusters. Because the critical nucleus size is usually small, however, this latter route is statistically improbable, because the distances between subcritical nuclei are usually large compared to their diameters. Therefore it is considered that growth occurs only via the addition of individual growth units (7). Now, suppose an overpotential is applied to an electrode surface. The adunit concentration increases rapidly to a new value characteristic of that overpotential, and if the overpotential is large enough then critical nuclei emerge which become experimentally observable as a finite rate of nucleation. Thus, provided the nucleation process occurs isothermally, we may write for the steady-state of nucleation (7)

$$[1] \quad \langle A \rangle = \langle A_n \rangle = \langle A_{n+1} \rangle = \ldots \qquad n = 1, 2, 3, \ldots$$

$$[2] \quad \langle A \rangle = \omega_n{}^{+}\langle C_n \rangle - \omega_{n+1}{}^{-}\langle C_{n+1} \rangle$$

where A is the steady-state rate of nucleation, n is the number of adunits per cluster, C_n are the concentrations of clusters containing n adunits, and $\omega_n{}^{+}$ and $\omega_n{}^{-}$ are the (suitably averaged) probabilities that single adunits are added or subtracted from a cluster containing n adunits. Equation [2] may be solved for $\langle A \rangle$ provided the probabilities $\omega_n{}^{+}$ and $\omega_{n+1}{}^{-}$ are specified. In the most general case, on a thermodynamic view (2)

$$[3] \quad \frac{\omega_n{}^{+}}{\omega_{n+1}{}^{-}} = \exp\left[\frac{\Delta G_n}{kT} - \frac{\Delta G_{n+1}}{kT}\right]$$

in which ΔG_n is the increase in Gibbs free energy of the system when n adunits from the bulk phase form a cluster of n adunits on the electrode surface. By substituting [3] in [2] and using the boundary con-

dition $\langle C_\infty \rangle = 0$ one obtains

$$[4] \quad \frac{\langle C_1 \rangle}{\langle A \rangle} = \sum_{n=1}^{\infty} \left[\omega_n^+ \exp\left(\frac{-\Delta G_n}{kT}\right) \right]^{-1}$$

ΔG_n is a maximum for the cluster of critical size, and it is usually assumed that this maximum is sharp as a function of n. In this case, calling the number of adunits in the critical nucleus $\bar{n}$, the $\bar{n}$th term provides the major contribution to the sum of eq. [4]. Combining all other contributions in a single term Z, the Zeldovich factor (2), simple rearrangement gives

$$[5] \quad \langle A \rangle = Z\omega_{\bar{n}}^+ \langle C_1 \rangle \exp\left(\frac{-\Delta G_{\bar{n}}}{kT}\right)$$

This equation therefore relates the expectation value of the steady-state nucleation rate to three potential-dependent parameters; Z, $\omega_{\bar{n}}^+$ and $\Delta G_{\bar{n}}$. To evaluate the exact potential-dependence of $\langle A \rangle$, however, is not simple because Z and $\Delta G_{\bar{n}}$ are strongly dependent on the model chosen for the clusters. Also $\omega_{\bar{n}}^+$ is only an average quantity, in reality depending on the configuration and types of sites available at the peripheries of the critical nuclei. Monte-Carlo simulations aside, one method for circumventing these difficulties is to suppose that $\bar{n}$ is large (>50 adunits, say) so that $\Delta G_{\bar{n}}$ has a simple, macroscopic, thermodynamic significance. Upon further assuming a circular, two dimensional nucleus (2) then

$$[6] \quad Z^2 = \frac{\Delta G_{\bar{n}}}{4\pi(\bar{n})^2 kT}$$

so that [5] becomes

$$[7] \quad \langle A \rangle = \left(\frac{\Delta G_{\bar{n}}}{4\pi(\bar{n})^2 kT}\right)^{1/2} \omega_{\bar{n}}^+ \langle C_1 \rangle \exp\left(\frac{-\Delta G_{\bar{n}}}{kT}\right)$$

For the case of the deposition of a metal ion onto a substrate of the same metal, Budevski (8) has estimated $\langle A \rangle$ from eq. [7] with the result that

$$[8] \quad \langle A \rangle = K' \exp\left[\frac{(1-\alpha)zF\eta}{RT}\right]\sqrt{\eta} \times \exp\left[\frac{-b\Omega\bar{\varepsilon}^2}{zekT} \cdot \frac{1}{\eta}\right]$$

where K' is a constant, e is the electronic charge, α is the transfer co-efficient, z is the number of electrons transferred, R is the gas constant, T is the absolute temperature, k is the Boltzmann constant, ε is the mean value of the specific periphery energy of the edge of a cluster, Ω is the area occupied by an adunit on the surface of the cluster, b is a geometrical constant, and η is the overpotential. This equation is expected to hold at low overpotentials in the absence of surface diffusion. An alternative expression, valid at high overpotentials, has been calculated by Milchev *et al.* (9) using atomistic, rather than thermodynamic, arguments. This approach yields

$$[9] \quad \langle A \rangle = K'' \exp\left\{\frac{(\bar{n}+1-\alpha)ze}{kT}\eta\right\}$$

where K'' is approximately constant. Comparable expressions may also be obtained for the formation of anodic films by taking the surface free energy terms of the emergent crystalline phase into account in the evaluation of $\Delta G_{\bar{n}}$.

The essential features of eqs. [8] and [9] are that a given expectation value of the steady-state rate of nucleation is associated with a given overpotential, and that the dependence of $\langle A \rangle$ on η is likely to be very strong. These facts mean that experimental and theoretical analyses of electrochemical nucleation will necessarily be complex unless performed at constant overpotential. Also the number of nuclei will, in general, vary as a function of time.

If the nuclei arise independently of each other, then we may assume the nucleation process to be Poissonian, so that the probability of forming one nucleus in time dt is

$$[10] \quad P = \lambda \exp(-\lambda t)\, dt$$

where λ is a constant equal to $\langle A \rangle S'$, S' being the area of the electrode surface. If the number density of nuclei is sufficiently large, then stochastic variations will be unimportant and the overall process may be regarded as deterministic. That is, $A = \langle A \rangle$.

The Growth of Two-dimensional Nuclei

Following Fleischmann and Thirsk (4), we shall assume that any given nucleus has circular symmetry and is of fixed height h. Also, it is supposed that the critical nucleus size is small so that radial growth begins at $r = 0$ when $t = 0$, where r is the radius of the growing nucleus. When the slow step in the overall growth process is at the edge of the nucleus, the observed current density, following a potential step from a potential of no-growth to one of growth, may be expressed as (4)

$$[11] \quad i = nFh\left(\frac{\rho}{M}\right)\frac{ds}{dt} = \pi nFh\left(\frac{M}{\rho}\right)Ak^2t^2$$

Here s is the fractional surface coverage of the electrode, M is the gram-formula weight of the species composing the nuclei, ρ is the density of the nuclei, and k is a suitably averaged rate describing the radial growth. Experimental observation of growth of this type may be simplified in practice by the use of the double potential step method (10). In this case a large overpotential step is applied to the electrode for a short period of time, followed by a

second step to a lower overpotential. The first step serves to nucleate and grow a large number of supercritical nuclei which continue to grow at the lower overpotential (provided the first step was of sufficient duration for the nuclei to achieve a size which is stable at the lower overpotential). The advantage of this technique is that so many nuclei are nucleated at the first overpotential that their number is effectively constant at the second overpotential. In this case, eq. [11] becomes

$$[12] \quad i = nFh\left(\frac{\rho}{M}\right)\frac{ds}{dt} = 2\pi nFh\left(\frac{M}{\rho}\right)Nk^2t$$

where N is the number of nuclei nucleated at the higher overpotential. N obviously depends in this case on the overpotential of the first step, and on the time spent at that overpotential. Equation [12] is usually referred to as describing 'instantaneous' nucleation because the nucleation takes place effectively at $t = 0$. Also, it should be noted that eq. [11] is derived on the basis that nuclei do not mutually interfere as they grow, i.e., the boundaries of adjacent nuclei are far apart. However, as the nuclei become large the probability of collisions increases drastically, so that some sort of interference becomes inevitable. Usually, it is assumed that at points at which the periphery of one nucleus impinges on another, then growth ceases.[1] The particular advantage of this 'impinge-and-stop' hypothesis is that it allows the calculation of the $i(t)$ response to a potential step even when nuclei collide, provided the remaining periphery of a collided nucleus continues to grow in the same way after the collision as before it. This assumption allows the application of a geometrical, probabilistic, theorem to the electrode surface in order to modify eq. [12]. This theorem is due to Kolmogoroff (11) and Avrami (6). It states that for a locally random distribution of nuclei,

$$[13] \quad \langle S\rangle = 1 - \exp(-S_{ex})$$

Here S is the (fractional) surface coverage of the plane by the collided nuclei, and S_{ex} is the (fractional) surface coverage that would have been observed had the nuclei not collided. Note that as $S_{ex} \to 0$, $\langle S\rangle/S_{ex} \to 1$ and that as $S_{ex} \to \infty$, $\langle S\rangle \to 1$. Now, from [12] and [13] we see

$$[14] \quad i = nFh\left(\frac{\rho}{M}\right)\frac{dS}{dt} = nFh\left(\frac{\rho}{M}\right)\frac{dS_{ex}}{dt}\exp(-S_{ex})$$

which shows

$$[15] \quad i = 2\pi nFhN\left(\frac{M}{\rho}\right)k^2t\exp\left[-\pi\left(\frac{M}{\rho}\right)^2Nk^2t^2\right]$$

This useful solution, first obtained by Fleischmann and Thirsk (4), is therefore the amended version of eq. [12] so that the collision of nuclei has been taken into account. Naturally, eq. [15] has limitations, particularly those introduced via the Kolmogoroff–Avrami theorem, and it is of interest to determine precisely what these are. Therefore, we shall now consider the effect of both a finite number of nuclei and the effect of a finite growth region on the validity of eqs. [13] and [15].

The Kolmogoroff–Avrami Theorem

Equation [13] is central to the macroscopic (geometrical) treatment of nucleation and subsequent growth of 2-D phases, and therefore its range of validity should be examined. (In fact, eq. [13] may be generalized in n-dimensional space (6), but for convenience we shall restrict ourselves to the two-dimensional problem.) In a forthcoming paper (12), we shall prove that the Kolmogoroff–Avrami theorem may, under rather specific circumstances, overestimate $\langle S\rangle$ for certain growth rates and geometries of nuclei. However, suffice it to say for the present that for the instantaneous (and progressive) nucleation and growth of geometrically regular nuclei (circles, squares, etc.), which have identical spatial orientations and conserve their geometry as they grow, then the Avrami theorem applies within the mathematical limitations of eq. [13].

In the present work, we are concerned with the mathematical limitations of eq. [13] for two-dimensional instantaneous nucleation, in a situation where the number of nuclei (N) is finite and these nuclei are confined to a finite region A' of an area A in the two-dimensional plane. We shall regard N and A as 'large' in order to perform statistical operations, but not so large that the probability that S differs from its mean $\langle S\rangle$ by any appreciable amount is almost zero. In particular, we suppose that N centres are deposited in a convex region A' at time $t = 0$, each centre having a uniform probability $d\sigma/A$ of being in an element $d\sigma$ of area within A'.

Suppose now that each centre grows as a circular nucleus of radius r at time t, and that all the nuclei grow until they meet an edge of A' or another nucleus, at which stage growth in that direction stops, but growth in other directions is unaffected. Then S is a random variable and in theory, given the distribution of the centres, the probability distribu-

[1]Although this is probably reasonable for many cases of electrochemical crystal growth, it should be pointed out that other situations are, in fact, possible. For instance, coalescence may occur in the deposition of liquids such as mercury. Also, nuclei may 'bounce off' each other when they are deposited on liquid substrates (such as amalgams), or local competition for adatoms might slow growth in regions where centres interact.

tion function of S at time t could be calculated. This task is daunting to say the least, so we shall be content to check how valid [13] is as a measure of $\langle S \rangle$ and work towards the calculation of the variance of S.

In the outlined model there is the odd fact that S is totally deterministic for both small and large t, since $S = N\pi r^2/A$ for r small enough, since there is no overlap, and $S = 1$ for r large enough, since even a single nucleus would eventually cover A'.

Now, eq. [13] applies strictly to the limiting case $N \to \infty$, $A \to \infty$, $N/A = \rho$ where ρ is the uniform density of centres, so that in fact

$$S_{ex} = \lim \sum_{i=1}^{N} S_i/A$$

the limit being in the above sense, and where S_i is the area of the ith nucleus. For the geometry of nuclei described above, we may assign the probability that a point P in A' chosen at random will be in S_i'. This probability is clearly $\hat{S}_i/A$ where $\hat{S}_i$ is the area of $S_i' \cap A'$. Thus the probability that P belongs to at least one of the S_i' is

$$[16] \qquad q = 1 - \prod_{i=1}^{N} (1 - \hat{S}_i/A)$$

Evidently $q = \langle S \rangle$, so we now examine to what extent eq. [13] is a reasonable approximation to eq. [16].

Suppose that $\sum_{i=1}^{N} \hat{S}_i^2/A^2$ is small, so that the approximation $1 - \hat{S}_i/A = \exp(-\hat{S}_i/A)$ is valid, and that $\sum_{i=1}^{N} (S_i - \hat{S}_i)/A$ is also small so that overlap of the S_i' with A' is negligible. Then from [16]

$$\langle S \rangle = 1 - \prod_{i=1}^{N} (1 - \hat{S}_i/A) \simeq 1 - \exp\left(\sum_{i=1}^{N} -\hat{S}_i/A\right)$$

$$\simeq 1 - \exp\left(\sum_{i=1}^{N} -S_i/A\right) = 1 - \exp(-S_{ex})$$

Now if $\sum_{i=1}^{N} \hat{S}_i/A$ is as large as 3, although the relative error in approximating [16] by [13] is large, this is unimportant since both formulae predict a surface coverage of more than 95%. Hence we may assume $\sum_{i=1}^{N} \hat{S}_i/A \simeq 1$. In this general scheme there exists the possibility that some $\hat{S}_i$ are of the order of A_i which would make [16] deviate strongly from [13]. We therefore further assume that the $\hat{S}_i$ are of comparable magnitude (as in the case of circular nuclei each of radius r) and hence that $\hat{S}_i = O(A/N)$. Then

$$\sum_{i=1}^{N} \hat{S}_i^2/A^2 = O\left(\frac{1}{N}\right)$$

which is small for large N. For $\sum(S_i - \hat{S}_i)/A$ to be small it is necessary that $S_i = \hat{S}_i$ for a sufficiently large number of i. *Thus if the centres are uniformly distributed we expect only* $O(\sqrt{N})$ *of the* S_i' *to have parts outside* A'. This conjecture is dealt with in more detail later. Given the conjecture it follows that the error due to edge effects is $O(1/\sqrt{N})$ and so is generally bigger than the effect due the finiteness of N. Note that these two effects *tend to mask each other* in the sense that

$$1 - \exp\left(\sum_{i=1}^{N} -\hat{S}_i/A\right) < 1 - \exp\left(\sum_{i=1}^{N} -S_i/A\right)$$

while

$$1 - \prod_{i=1}^{N} (1 - \hat{S}_i/A) > 1 - \exp\left(\sum_{i=1}^{N} -\hat{S}_i/A\right)$$

It is important to know just how small N can be and still apply the simpler equation [13] instead of [16]. As an example suppose $S_i = A/N$ and $\hat{S}_i = A/2N$. Equation [13] gives $\langle S \rangle = 1 - e^{-1} = 0.63$ while [16] gives

$$\langle S \rangle = 1 - \left(1 - \frac{1}{N}\right)^{N - \sqrt{N}} \left(1 - \frac{1}{2N}\right)^{\sqrt{N}}$$

which has the values 0.57, 0.58, 0.59, 0.60, 0.61, for $N = 4, 9, 16, 25, 36, 49$, respectively.

In this section we note finally the case of N and A infinite, but ρ finite. This can be dealt with directly in terms of "nearest neighbour" theory (13), at least when the S_i' are circular and of the same radius r. Thus the probability that a point P is covered is simply the probability that at least one centre is within r of P, and this is $1 - \exp(-\pi\rho r^2)$. Since $\pi\rho r^2 = S_{ex}$, we recover [13].

Collision Fronts

Let us further consider the case when each S_i' is a circle of radius r. The radius is a function of time t, and is zero at $t = 0$. Suppose there is a set T of N centres. Each centre P becomes a circular nucleus which grows into a definite region R_p', determined uniquely by A' and the set T, until the region R_p' is completely filled. Thus A' is divided into precisely N regions (see Fig. 1).

Evidently a knowledge of the region R_p' will help towards the ultimate goal of describing the probability distribution function of the fractional surface coverage.

Firstly note R_p' may be described mathematically as

$$[17] \qquad R_p' = S_p' \cap A'$$

where

$$[18] \qquad S_p' = \bigcap_{\substack{Q \in T \\ Q \neq P}} H_{pq}$$

and where H_{pq} is the half plane containing the point

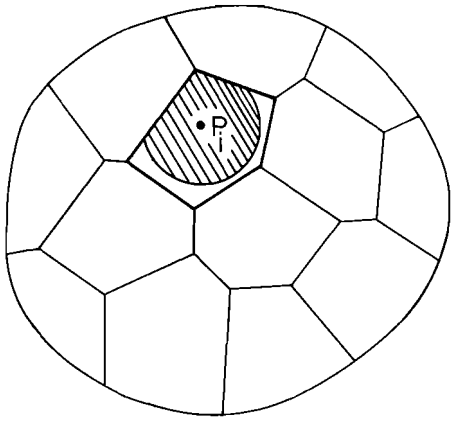

FIG. 1. Typical collision-front geometry illustrating the net of irregular convex m-gons. The nucleus centre P_i expands until the polygon surrounding P_i is filled.

P of T and whose edge is the perpendicular bisector of the line joining P to another point Q of T. *From* [17] *we see* R_p' *is a convex region (being the intersection of convex regions) and further* S_p' *is bounded by a polygon so that* R_p' *is also bounded by a polygon if* $S_p' \subset A'$.

The above regions are bounded by *collision fronts*, i.e. lines of contact of nuclei growing into each other. Even in the limiting case $N \to \infty, A' \to \infty, A/N = \rho$, any particular region R_p' remains finite in size, since with a uniform distribution of centres in the plane, the probability that a finite region of area B is devoid of points of T is $e^{-\rho B}$. Hence the probability of an infinite area devoid of points of T is zero, though arbitrarily large areas can occur.

Although the region R_p' is described in terms of all the members of T it is clear that only a finite subset T_p of T contributes to R_p', in the sense that some points of T could be removed without altering R_p'.

The characterization of T_p will be discussed in the next section, but first we turn to the problem of finding the distribution of the number of sides of a typical R_p'. This in itself is difficult, but to obtain the mean number of sides is not so difficult and oddly enough depends rather weakly on the actual distribution of T and is essentially a topological property of dividing the region A' in a certain way.

Consider again Fig. 1. It represents N regions, a number E of edges, and a number V of vertices where edges meet. It is easy to prove by an inductive argument that $(N + V - E)$ is topologically invariant and has value 1. (In Fig. 1, $N = 13$, $V = 24$, $E = 36$.) *The region* A′ *is divided in a special way since exactly three edges emanate from each vertex.* This statement holds with probability 1 since if four or more edges emerged from a vertex then at least four of the randomly distributed set of points T would lie on a circle. Therefore, since any edge connects two vertices, it follows directly that $V = 2E/3$ and so

$$E = 3(N - 1) \qquad [19]$$

Thus the total number of edges of all the regions R_p' is $2E - A(N)$, where $A(N)$ is the number of edges on the boundary of A'. Hence the mean number of sides M of a region R_p' is

$$M = 6(1 - 1/N) - A(N)/N \qquad [20]$$

This shows that $M < 6$ and

$$\lim_{N \to \infty} M = 6 \qquad [21]$$

provided only that $A(N) = o(N)$ as $N \to \infty$; so the dependence of this result on the distribution of T is indeed weak.

We now prove $A(N) = O(\sqrt{N})$ which yields [21] and completes the discussion of the effect of boundaries on the validity of the Kolmogoroff–Avrami theorem. The general approach is to imagine travelling out from a point P of T, and then deciding whether we first hit a collision front l_Q (associated with another point Q of T) or the boundary of A'.

Let P be a point of T, and let $l(\theta)$ be a straight line emanating from P in the direction θ relative to some fixed direction. *There will be no edge of* R_p' *encountered between* P *and* X (*where* X *is a point of* $1(\theta)$ *a distance* x *from* P) *provided the circle centre* X *radius* x *contains no point of* T *in its interior.* This is proved in the next section on the characterization of T_p. The probability that such a circle exists is $\exp(-\pi\rho x^2)$. Thus if $f(\theta)$ is the distance of P to the boundary of A', then the probability that l meets the boundary before meeting l_Q for some Q is $\exp(-\pi\rho f^2(\theta))$. Hence the probability of at least one of the lines $l(\theta)$ meeting the boundary of A' first is

$$\frac{1}{2\pi}\int_0^{2\pi} \exp[-\pi\rho f^2(\theta)]\,d\theta \leq \exp(-\pi\rho r_p^2)$$

where r_p is the closest distance of P to the boundary.

Let O be any fixed point of A' and R its closest distance to the boundary of A'. Assume that $R \to \infty$ as $A \to \infty$. Then $A \geq \pi R^2$. The proportion of points of T a distance s to $s + ds$ from O is $2\pi\rho s ds$. Hence the proportion of points which 'see' the boundary of A' along some line is $\leq 2\pi\rho s ds \times \exp[-\pi\rho(R - s)^2]$. Thus the expected number of points of T which see a boundary is

$$\leq \int_0^R 2\pi\rho s \exp[-\pi\rho(R - S)^2]\,dS$$

$$\leq 2\pi\rho R\int_0^\infty \exp(-\pi\rho s^2)\,dS = \pi R\sqrt{\rho}$$

$$\leq (A\pi\rho)^{1/2} = (\pi N)^{1/2}$$

As $A \rightarrow \infty$ the probability that a point of R_p' sees more than one boundary edge $\rightarrow 0$. Thus we have proved that $A(N) = O(\sqrt{N})$ as $N \rightarrow \infty$. Hence as $N \rightarrow \infty$ [20] becomes.

$$M = 6 + O(1/\sqrt{N}) \quad [22]$$

where the error is always negative. In a necessarily finite computer simulation, the difference between M and 6 would be an indicator of the magnitude of the boundary effect. However, the limiting version of [22] may be arrived at in an entirely different way, as we shall show after a discussion of the set T_p.

The Set T_p

Consider the case when A is large so that edge effects may be neglected. Under these circumstances, the set T_p of contributors to R_p' is determined uniquely by the following theorem: *The point* W *of* T *is a member of* T_p *if and only if there is a circle* C *with no points of* T *in its interior but with* P *and* W *on its circumference.*

First suppose such a circle C exists (see Fig. 2). Its centre X is on the perpendicular bisector L of PW. We need to show some part of L is a side of R_p', and to do this it is sufficient to show the point X must be on the boundary. Recalling the definition of R_p' in terms of intersections of half planes (eq. [18]), and noting that C is the locus of all possible contributors Y to R_p' such that X is on an edge of H_{py}, it follows that X is a point of the half plane M_{pu} of any contributor U which lies outside C. Thus X is contained in the intersection of all such half planes H_{pu}. Hence X is a point of R_p' and lies necessarily on the boundary.

Given that W is a contributor, the circle C may be constructed as follows. Some part of L is on the boundary of R_p' and in particular contributes a vertex Z of R_p'. Now define C as the circle centre Z radius ZP (which passes through W). Then C contains no contributors in its interior, since if it did, Z would cease to be a vertex.

An immediate corollary of the above theorem, illustrated in Fig. 3, is that the nearest neighbour A to P belongs to T_p. For we may take C as the circle with AP as diameter, which is contained in the circle centre P radius AP, which by definition does not contain points of T in its interior. Figure 4 illustrates the fact that even the second nearest neighbour to P may not be a member of T_p.

Knowing one member of T_p allows us to construct the whole set T_p by the following algorithm. Consider A to be vertically above P and draw the perpendicular bisector of AP. Starting at the point of intersection of AP with this bisector and proceeding to the right draw the largest circle with centre

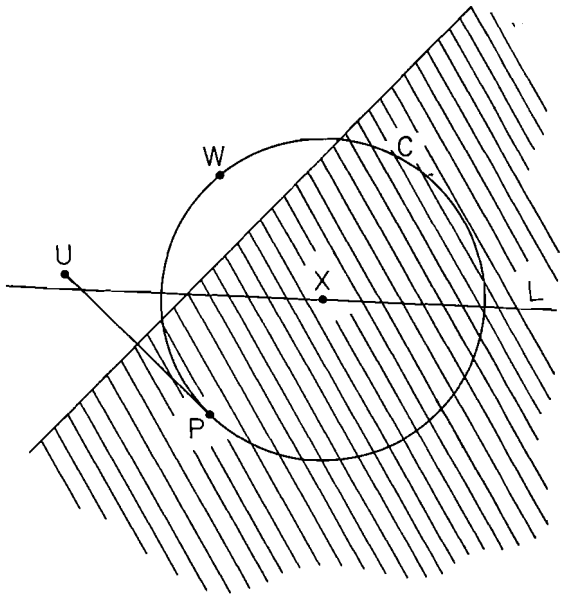

FIG. 2. Illustrating the fact that point W of T is a member of T_p if and only if there is a circle C with no points of T in its interior but with P and W on its circumference.

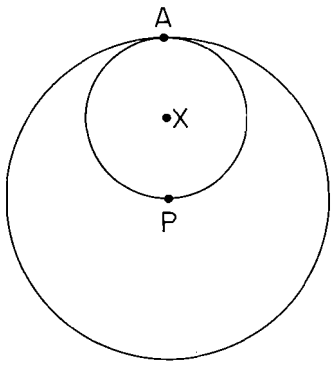

FIG. 3. Illustrating the fact that the nearest neighbour A to P belongs to T_p.

on the bisector which contains no point of T in its interior but does contain A, P, and a different point B of T on its circumference. Then B is a member of T_p (Fig. 5).

Replacing A by B, B by C in the above statement we obtain a third member C of T_p. Proceeding in a clockwise fashion the process ends when an apparently new point of T_p turns out to be A. The above construction is unique with probability 1.

The union of all construction circles above defines a unique region Q_p' whose boundary contains all the members of T_p and whose interior contains no member of T except P.

It is easy to see that $Q_p > 4R_p$ where Q_p is the area of Q_p'. However, the ratio Q_p/R_p can be

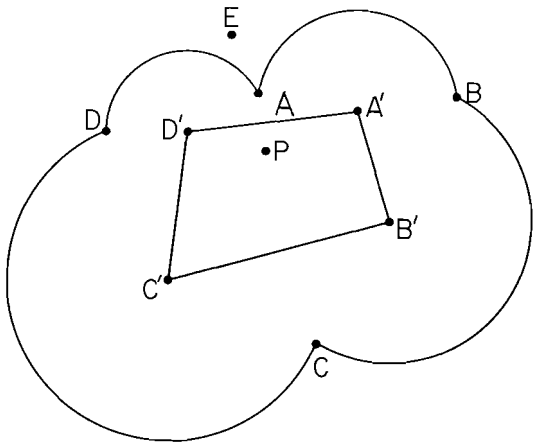

FIG. 4. The nearest neighbour A to P necessarily belongs to T_p and hence is always a contributor to the polygon. But the second nearest neighbour (in this case E) is not necessarily a contributor.

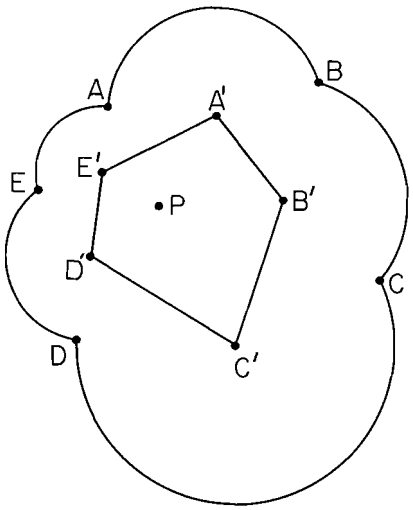

FIG. 5. Given P, the set $T_p\{A,B,C,D,E\}$ determines both R' (i.e. the polygon $A'B'C'D'E'$) and the region Q' (i.e. the union of circles, centres the vertices of R', passing through P).

arbitrarily large when R_p' is highly asymmetric (see Fig. 6). The quantity Q_p must figure in any exact calculation of the probability P_n that R_p' has precisely n sides.

The Distribution of Contributors

Suppose we are given P and another point W of T a distance $2d$ from P, we now seek the probability that W is a member of T_p. This information is useful for two reasons. Firstly, since we expect the probability to decay with d, a knowledge of the actual law of decay would allow the partition of the plane into essentially independent parts (in the sense that within some specified distance of P the probability is

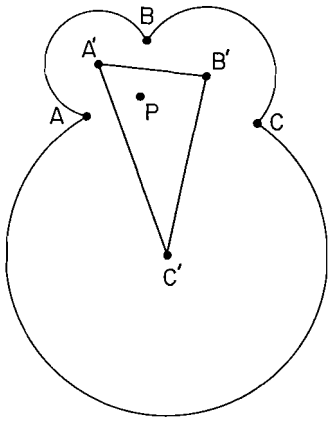

FIG. 6. The ratio Q/R is always >4. But if R' has an elongated shape then this ratio can be much larger, thus rendering the shape less likely to occur than a centrally symmetric shape.

very small of a member of T_p being further from P than that specified distance). Secondly, knowledge of the probability would yield the density of contributors at any point.

To find the probability it is necessary to use the criterion for W to be a member of T_p. Now W will not be a member of T_p if every circle with P, W on its circumference contains a point of T. Let $Q(x,y)$ be the probability that all circles passing through P and W with centres a distance $\leq y$ to the right of PW and all circles passing through P and W with centres a distance $\leq x$ to the left of PW contain a point of T.

Referring to Fig. 7 consider the two circles $PAWB$ (centre X) and $PCWD$ (centre Y), the distance of whose centres from PW are y and $y + dy$ respectively.

Let $E(x,y)$ be the event of which $Q(x,y)$ is the probability. *Then* E(x,y) *occurs if and only if either* E(x,y+dy) *occurs or if circle* PCWD *is devoid of points of* T *while the area* PAWC *contains a point of* T.

To prove this observe that if $E(x,y+dy)$ occurs then $E(x,y)$ occurs by definition. If, however, $PCWD$ contains no point of T (so $E(x,y+dy)$ fails to occur) and $PAWC$ contains a point of T, then this point is

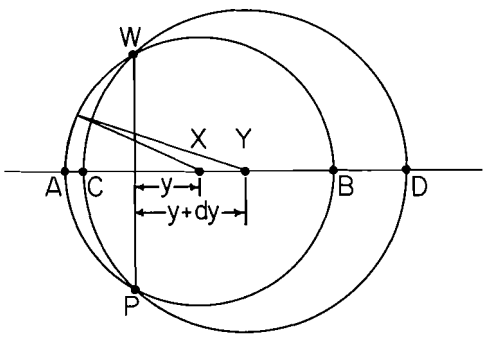

FIG. 7. Construction used in determining the probability that, given P, another point W is a member of T_p.

common to all circles passing through P and W with centres $\leq y$ from PW, to the right of PW. This point is also common to all circles passing through P and W with centres to the left of PW. Thus the event $E(x,y)$ occurs.

Further, if $E(x,y)$ occurs then either $E(x,y+\mathrm{d}y)$ occurs or if it does not there must be a point of T in area $PAWC$.

We have thus proved that

$$Q(x,y) = Q(x,y+\mathrm{d}y) + (\text{probability no point of } T \text{ is in } PCWD) \times (\text{probability a point of } T \text{ is in } PAWC)$$

Let the area of $PAWC$ be $f(y)\mathrm{d}y$. The radius of the circle $PCWD$ is $\{(y+\mathrm{d}y)^2 + d^2\}^{1/2}$. Hence the probability there is no point of T in $PCWD$ is $\exp\{-\rho\pi[(y+\mathrm{d}y)^2 + d^2]\}$ and so

$$Q(x,y) = Q(x,y+\mathrm{d}y) + \rho \exp\{-\rho\pi[(y+\mathrm{d}y)^2 + d^2]\} f(y)\mathrm{d}y$$

Dividing by $\mathrm{d}y$ and letting $\mathrm{d}y \to 0$ we obtain the differential equation

$$[23] \quad \partial Q/\partial y = -\rho f(y) \exp[-\pi\rho(y^2 + d^2)]$$

Solving [23] gives

$$[24] \quad Q(x,y) = Q(x,0) - \rho \exp(-\pi\rho d^2) \times \int_0^y \exp(-\pi\rho v^2) f(v)\,\mathrm{d}v$$

By symmetry we also have

$$[25] \quad Q(x,y) = Q(0,y) - \rho \exp(-\pi\rho d^2) \times \int_0^x \exp(-\pi\rho v^2) f(v)\,\mathrm{d}v$$

Putting $y = 0$ in [25] and substituting for $Q(x,0)$ in [24] gives

$$[26] \quad Q(x,y) = Q(0,0) - \rho \exp(-\pi\rho d^2) \times \left\{ \int_0^x \exp(-\pi\rho v^2) f(v)\,\mathrm{d}v + \int_0^y \exp(-\pi\rho v^2) f(v)\,\mathrm{d}v \right\}$$

Now $Q(0,0)$ is the probability that the circle diameter PW contains a point of T and thus

$$[27] \quad Q(0,0) = 1 - \exp(-\pi\rho d^2)$$

Hence from eqs. [26], [27]

$$[28] \quad Q(\infty,\infty) = 1 - \exp(-\pi\rho d^2) - 2\rho \exp(-\pi\rho d^2) \int_0^\infty \exp(-\pi\rho v^2) f(v)\,\mathrm{d}v$$

It is straightforward to calculate $f(y)$ and we obtain

$$[29] \quad f(y) = 2(d - y \tan^{-1} d/y)$$

Hence if $g(d)$ is the probability that a member of T a distance $2d$ from P is a member of T_p then $g(d) = 1 - Q(\infty,\infty)$, so from eqs. [28], [29]

$$[30] \quad g(d) = \exp(-\pi\rho d^2) + 4\rho \exp(-\pi\rho d^2) \times \int_0^\infty (d - x \tan^{-1} d/x) \exp(-\pi\rho x^2)\,\mathrm{d}x$$

Equation [30] may be expressed in either of the two forms

$$[31] \quad g(d) = 2d\sqrt{\rho} \exp(-\pi\rho d^2) + \operatorname{erfc}(d\sqrt{\pi\rho})$$

$$[32] \quad g(d) = 1 - 4\pi\rho^{3/2} \int_0^d t^2 \exp(-\pi\rho t^2)\,\mathrm{d}t$$

The form [31] shows $g(d)$ decreases steadily from 1 to 0 as d increases from 0 to ∞.

From [30] we may calculate the density of contributors a distance r to $r + \mathrm{d}r$ from P as $2\pi\rho r g \times (r/2)\mathrm{d}r$. Then the expected number of contributors to R_p' is

$$[33] \quad M = 2\pi\rho \int_0^\infty r \exp(-\pi\rho r^2/4)\,\mathrm{d}r + 8\pi\rho^2 \times \int_0^\infty \int_0^\infty r\left(\frac{r}{2} - x \tan^{-1}\frac{r}{2x}\right) \times \exp\left[-\pi\rho\left(x^2 + \frac{r^2}{4}\right)\right] \mathrm{d}x\mathrm{d}r$$

The transformation $x = R\cos\theta$, $r = 2R\sin\theta$ allows the evaluation of the second integral to be made while the first integral has value 4. Hence

$$[34] \quad M = 4 + 32\pi\rho^2 \int_0^\infty R^3 \exp(-\pi\rho R^2)\,\mathrm{d}r \times \int_0^{\pi/2} \sin\theta(\sin\theta - \theta\cos\theta)\,\mathrm{d}\theta$$

The expected result $M = 6$ follows using integration by parts. This result was obtained before by topological arguments (eq. [21]).

We can then regard $f(r) = (\pi\rho/3)rg(r/2)$ as the probability density of contributors at a distance r from P. The mean distance of a contributor to R_p' from P is

$$\int_0^\infty r f(r)\,\mathrm{d}r = \rho^{-1/2}\left(\frac{1}{2} + \frac{8}{9\pi}\right)$$

as is easily verified. This compares with the mean distance of the nearest neighbour to P, viz.

$$\int_0^\infty r[2\pi\rho r \exp(-\pi\rho r^2)]\,dr = \tfrac{1}{2}\rho^{-1/2}$$

(ref. 13). Thus the mean distance of a contributor is only about one and a half times that of the nearest neighbour, showing that although the shape of a region R_p' depends on the whole distribution of centres, the influence of centres outside a few units of $\rho^{-1/2}$ from P on R_p' is weak in the probabilistic sense.

The Distribution of Polygons

It would also be of interest to obtain both the probability P_m that a given region R_p' is a polygon with m sides (an m-gon) and the distribution of the sizes of m-gons for a given m, since these quantities are required for any detailed study of the distribution function for the surface coverage.

So far we have the result

$$[35] \qquad \sum_{m=3}^{\infty} mP_m = 6$$

Consider now a vertex of any polygon. By symmetry it can be seen that the mean value of an external angle of a polygon is $\pi/3$, which indicates that hexagons will predominate. Although this turns out to be true, the computer simulation described later indicates that approximately 25% m-gons are pentagons as compared to only 29% hexagons, so the predominance is not striking. (Geometrically, hexagons, pentagons, and heptagons will tend to have m-gons of a similar type as neighbours, simply because the sum of the interior angles of an m-gon depends on m.)

Suppose a polygon is chosen at random. One way to determine the number of sides is to proceed round the polygon counting the sum of the external angles. If after m such steps the sum is less than 2π, it is certain the polygon has at least $m + 1$ sides. If this experiment is repeated a large number of times, the probability Q_m that a polygon chosen at random has at least m sides is determined. Then $P_m = Q_{m-1} - Q_m$, $m = 3, 4, \ldots$.

Because the external angles of a polygon are not independent, P_m cannot be determined from the knowledge of the distribution of a single external angle taken at random.

However, suppose we let $\tau(\varphi)d\varphi$ be the probability that an external angle of a polygon taken at random has a value in the range $\varphi \to \varphi + d\varphi$. Let $P_n(\theta)d\theta$ be the probability that the sum of n such angles, regarded as independent, is in the range θ to $\theta + d\theta$. Then put

$$[36] \qquad Q_n = \int_0^{2\pi} P_n(\theta)\,d\theta$$

Thus Q_n is actually the probability that the sum of n random variables with given distribution $\tau(\theta)$ has a value $<2\pi$. This will be different from the probability actually required, namely the probability (Q_n') that a polygon has at least n sides. But a knowledge of Q_n gives us a measure of the interdependence of polygons and, as it turns out, the asymptotic behaviour of P_n for large n.

Now $P_n(\theta)$ is obtained by a convolution; which, using Fourier transforms, yields

$$[37] \quad P_n(\theta) = \frac{1}{2\pi}\int_{-\infty}^{\infty} e^{ik\theta}\left(\int_0^{\pi} \tau(\varphi)\, e^{-ik\varphi}\,d\varphi\right)^n dk$$

where it is noted that $\tau(\varphi) = 0$ for $\varphi < 0$ and $\varphi > \pi$. To obtain $\tau(\varphi)$ consider how a vertex O of a polygon is constructed. Let P_1, P_2, P_3 be three points of the set T, each of which contributes to the polygons belonging to the other two. Also, the vertex (O) is common to the three polygons. Referring to Fig. 8, the external angle φ of the polygon belonging to P_1 is the angle between OQ_2 and Q_3O. Since $OQ_2P_1Q_3$ is a cyclic quadrilateral $\varphi = \angle Q_2P_1Q_3 = \angle P_3P_1P_2 = \frac{1}{2}\angle P_2OP_3$. Thus if $\varphi_1 = \angle P_1OP_2$ and $\varphi_2 = \angle P_1OP_3$, then $\varphi = \frac{1}{2}|\varphi_1 - \varphi_2|$. Let us make the reasonable assumption that φ_1 and φ_2 are uniformly distributed in $[0,2\pi]$. Then

$$\tau(\varphi) = \left(\frac{1}{2\pi}\right)^2 \frac{d}{d\varphi}R(\varphi)$$

where $R(\varphi)$ is the region in the $\varphi_1\varphi_2$ plane determined by $0 \le \varphi_1 \le 2\pi$, $0 \le \varphi_2 \le 2\pi$, $|\varphi_2 - \varphi_1| \le 2\varphi$. This gives

$$R(\varphi) = 0,\ \varphi \le 0$$

$$R(\varphi) = 4\pi^2 - (2\pi - 2\varphi)^2,\ 0 \le \varphi \le \pi$$

$$R(\varphi) = 4\pi^2,\ \varphi \ge \pi$$

and hence

$$[38] \qquad \tau(\varphi) = (2/\pi^2)(\pi - \varphi),\ 0 \le \varphi \le \pi$$

Substituting [38] into [37] gives

$$[39] \quad P_n(\theta) = \left(\frac{2}{\pi^2}\right)^n \frac{1}{2\pi}\int_{-\infty}^{+\infty} \frac{e^{ik\theta}}{k^{2n}} \times (1 - ik\pi - e^{-ik\pi})^n\,dk$$

Let $f(k) = e^{ik\theta}(1 - ik\pi - e^{-ik\pi})^n$. Note $f(k)/k^{2n}$ has a removable singularity at $k = 0$, as does

$$f(-k)/k^{2n} \equiv f^*(k)/k^{2n}$$

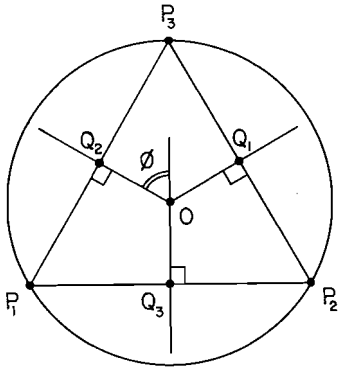

FIG. 8. Geometry of the vertex (O) of a polygon. The points P_1,P_2,P_3 are the centres of nuclei belonging to a set T, each of which contributes to the polygons belonging to the other two.

Also, expanding $\{(1 - ik\pi) - e^{-ik\pi}\}^n$ by the binomial theorem shows that

$$f(k) = e^{ik\theta}(1 - ik\pi)^n + g_1(k,\theta)$$

where for $\theta < \pi$, $g_1^*(k,\theta)$ decays exponentially as $k \to \infty$ in the upper half of the complex plane. Then

$$[40] \qquad P_n(\theta) = \left(\frac{2}{\pi^2}\right)^n \frac{1}{2\pi} \int_{-\infty}^{+\infty} \frac{h(k)}{k^{2n}} dk$$

where $h(k) = e^{ik\theta}(1 - ik\pi)^n + g_1^*(k,\theta)$ and the expression [40] is a Cauchy principal value integral. For $0 < \theta < \pi$, [40] may be evaluated by contour integration giving

$$[41] \quad P_n(\theta) = \left(\frac{2}{\pi^2}\right)^n \frac{1}{2\pi} \pi i \operatorname{res} \left\{\frac{h(k)}{k^{2n}}\right\}_{k=0}$$

$$= \left(\frac{2}{\pi^2}\right)^n \frac{i}{2} \operatorname{res} \left\{\frac{h(k) - f^*(k)}{k^{2n}}\right\}$$

$$= \left(\frac{2}{\pi^2}\right)^n \frac{i}{2} \times \operatorname{res} \left\{\frac{(1 - ik\pi)^n e^{ik\theta} - (1 + ik\pi)^n e^{-ik\theta}}{k^{2n}}\right\}_{k=0}$$

$$= -\left(\frac{2}{\pi^2}\right)^n \frac{1}{(2n-1)!} \times \mathcal{I}\{(D + i\theta)^{2n-1}(1 - ik\pi)^n\}|_{k=0}$$

where $\mathcal{I}$ denotes 'imaginary part of' and $D = d/dk$.

Equation [41] may be written in the real form

$$[42] \quad P_n(\theta) = \left(\frac{2}{\pi^2}\right)^n \frac{1}{(2n-1)!} \times (D + \theta)^{2n-1}(k\pi - 1)^n|_{k=0}$$

For $\pi < \theta < 2\pi$ the above procedure is modified slightly and we write

$$f(k) = e^{ik\theta}(1 - ik\pi)^n - n(1 - ik\pi)^{n-1} e^{ik(\theta-\pi)} + g_2(k,\theta)$$

where $g_2^*(k,\theta)$ decays exponentially in the upper half plane.

Corresponding to [42], the formula

$$[43] \quad P_n(\theta) = \left(\frac{2}{\pi^2}\right)^n \frac{1}{(2n-1)!} \times \{(D + \theta)^{2n-1}(k\pi - 1)^n + n(D + \theta - \pi)^{2n-1}(k\pi - 1)^{n-1}\}_{k=0}$$

is obtained. Thus

$$[44] \quad Q_n = \left(\frac{2}{\pi^2}\right)^n \frac{1}{(2n-1)!} \left\{\int_0^{2\pi} (D + \theta)^{2n-1} \times (k\pi - 1)^n|_{k=0} d\theta + n \int_\pi^{2\pi} (D + \theta - \pi)^{2n-1} \times (k\pi - 1)^{n-1}\right\}_{k=0} d\theta = \frac{2^n}{(2n)!} \times \{(D + 2)^{2n} z^n + n(D + 1)^{2n} z^{n-1}\}_{z=-1}$$

where now $D = d/dz$.

Finally, [44] gives

$$[45] \qquad Q_n = 2^n n! \sum_{r=0}^{n} \frac{(2^{n+r} - r)(-1)^r}{r!(n-r)!(n+r)!}$$

The first few values of Q_n are easy to obtain; $Q_2 = 1$, $Q_3 = 89/90$, $Q_4 = 115/126$, $Q_5 = 9329/12600$, etc. This then gives $P_3 = 1/90$, $P_4 = 8/105$, etc.

The graph of P_n versus n is illustrated in Fig. 9, where it is compared with a similar graph obtained by simulation. It is evident that the calculated values of P_n differ from the simulation values on two main counts. Firstly no account is taken in the above calculation of the fact that m-gons with $m = 5, 6, 7$ tend to occur in clusters, which makes these polygons occur more frequently than is calculated on the basis of independent polygons. Secondly no account is taken of the fact, discovered by the simulation experiment, that the mean size of an m-gon ($\bar{A}_m$) tends to increase linearly with m, an approximation being $(m-2)/4\rho$. This effect reduces the frequency of occurrence of polygons with m large as compared with the above calculations, because large deviations from the local density ρ are required as well as large deviations from the mean ($\pi/3$) of the external angle for such m-gons.

This latter observation gives us an upper bound on the decay with m of the actual probability of the occurrence of an m-gon.

We need only calculate the asymptotic form of

$Q_n - Q_{n+1}$. To do this we return to the integral form of Q_n rather than [45]. Now from [36] and [39] we have

$$[46] \quad Q_n = \left(\frac{2}{\pi^2}\right)^n \frac{1}{2\pi} \int_{-\infty}^{+\infty} \left(\frac{e^{2\pi ik} - 1}{ik}\right) \times \left(\frac{1 - ik\pi - e^{-ik\pi}}{k^2}\right)^n dk$$

For n large, only contributions to the integral near $k = 0$ are significant. We may therefore expand the second factor about $k = 0$, and re-express it in exponential form giving

$$[47] \quad Q_n - Q_{n+1} \sim \frac{1}{2\pi} \int_{-\infty}^{+\infty} \left(\frac{e^{2\pi ik} - 1}{ik}\right) \times \left[1 - \frac{2}{\pi^2 k^2}(1 - ik\pi - e^{-ik\pi})\right] \times (e^{-nik\pi/3 - nk^2\pi^2/12})\, dk$$

$$\sim \frac{1}{2\pi} \int_{-\infty}^{+\infty} (2\pi)\left(\frac{ik\pi}{3}\right) \times \exp(-nik\pi/3 - nk^2\pi^2/12)\, dk$$

$$= \frac{i\pi}{3} e^{-n/3} \int_{-\infty}^{+\infty} k \exp\left[\frac{-n\pi^2}{12}\left(k + \frac{2i}{\pi}\right)^2\right] dk$$

$$= \frac{2}{3} e^{-n/3} \int_{-\infty}^{+\infty} \exp\left[\frac{-n\pi^2}{12}\left(k + \frac{2i}{\pi}\right)^2\right] dk$$

$$= \frac{4}{(3\pi n)^{1/2}} e^{-n/3}$$

Thus P_n decays at least exponentially with n.

The Variance of S

It is evident from the preceding considerations that an analytical solution to the problem of finding the probability distribution function for nuclei growing at random in a large but finite region is well nigh impossible. Approximations can however be made.

In Fig. 10 a typical region R_i' is depicted in the case when all nuclei would be circles of radius r at time t if allowed to grow unimpeded. Let G_i' with area G_i be the area of the intersection of R_p' with the circle centre P_i radius r.

Now

$$[48] \quad S = \frac{1}{A} \sum_{i=1}^{N} G_i$$

which is exact. From [48] and the discussion of the Kolmogoroff–Avrami theorem

$$[49] \quad \langle S \rangle = \frac{N}{A} \langle G_i \rangle + O(1/\sqrt{N})$$

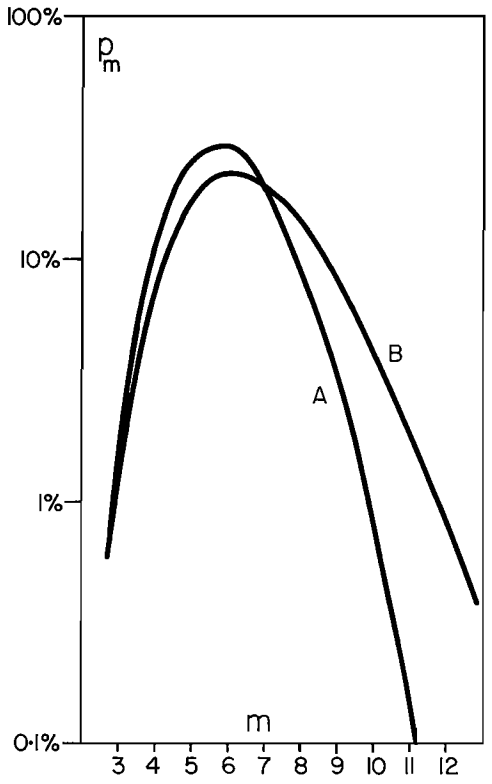

FIG. 9. The distribution of the number of sides of random m-gons (logarithmic scale). (A) Computer-simulated net, (B) according to eq. [45].

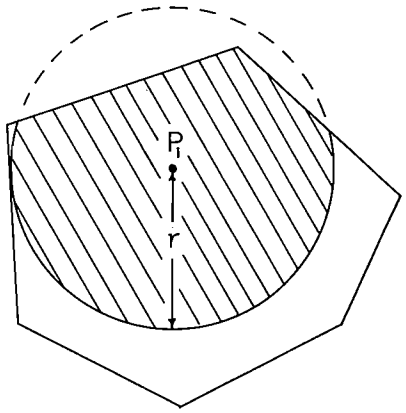

FIG. 10. The shape of a typical nucleus and its collision fronts.

Thus for N large enough, from [49] and [13] specialised to the case of circular nuclei

$$[50] \quad \langle G_i \rangle = \frac{1}{\rho}[1 - \exp(-\pi\rho r^2)]$$

Now

$$A = \sum_{i=1}^{N} R_i$$

so to order $1/\sqrt{N}$

$$[51] \qquad \langle R_i \rangle = 1/\rho$$

Thus $\langle G_i \rangle$ behaves as expected. For r small enough $G_i = \pi r^2$ and for r large enough $G_i = R_{p_i}$. For intermediate values of r all the geometric details of R_{p_i}' need to be considered.

Obviously the mean shape of R_{p_i}' is a circle. If it were a circle of radius x, and P_i were in the centre of this circle, then G_i would be πr^2 for $r \leq x$ and πx^2 for $r \geq x$. Thus a good model of the growth of a circular nucleus into a typical region R_i' would be one where x was a random variable such that $\langle G_i \rangle$ is given by [50] and $\langle R_i \rangle$ by [51]. For the moment let x be the distance between a centre P and a point Q on a collision front in an arbitrary direction. The circle centre Q radius QP necessarily has no point of T in its interior. Hence the probability that $x \leq y$ is $1 - \exp(-\pi\rho y^2)$. This suggests that we replace R_i' by a circle of radius x and probability distribution function $F_x(y) = 1 - \exp(-\pi\rho y^2)$, $y \geq 0$. Then

$$[52] \quad \langle R_i \rangle = \langle \pi x^2 \rangle = \int_0^\infty (2\pi\rho x)\pi x^2 \exp(-\pi\rho x^2)\, dx = 1/\rho$$

and

$$\langle G_i \rangle = \int_0^r (2\pi\rho x)(\pi x^2) \exp(-\pi\rho x^2)\, dx + \int_r^\infty (2\pi\rho x)(\pi x^2) \exp(-\pi\rho x^2)\, dx = \frac{1}{\rho}[1 - \exp(-\pi\rho r^2)]$$

Thus the replacement of R_i' by a circle with a radius with the above probability distribution does not alter $\langle G_i \rangle$ nor $\langle R_i \rangle$.

If we were to regard the circles R_i' as independent we get immediately that

$$\langle S \rangle = \rho\langle G_i \rangle = 1 - \exp(-\pi\rho r^2)$$

and

$$[53] \quad \langle (S - \langle S \rangle)^2 \rangle = (\rho^2/N)\langle (G_i - \langle G_i \rangle)^2 \rangle = (1/N)[1 - 2\pi\rho r^2 \exp(-\pi\rho r^2) - \exp(-2\pi\rho r^2)]$$

It is easy to see that the right hand side of [53] increases with r to value $1/N$. In the truly finite case, of course, the limiting value of the variance σ^2 is zero. The difference is accounted for when we realise that

$$A = \sum_{i=1}^{N} R_i$$

is a fixed quantity, and if we regard the R_i as random variables, A becomes a random variable. In spite of this difference, the way in which σ^2 varies with r at least for $\pi r^2 \ll A$ should follow the law [53]. A direct computer simulation of the distribution of the random variable S seems required to clear up to what extent [53] is valid.

Computer Simulation

For a random distribution of instantaneously-nucleated circular nuclei in a plane, the complete set of extended collision fronts constitutes a 'net' composed of irregular convex m-gons. Each m-gon represents the complete collision-front encountered by a single nucleus. The properties of the set of m-gons will obviously determine the shape of the i–t transient observed experimentally, and consequently is of fundamental importance. Also, investigation of the properties of such m-gons will provide insight into the limitations of the Avrami theorem as encountered, say, in measurement of electrochemical noise.

The simulation was built as follows. On the interval $[-1,+1]$ in both the x and y directions in the plane, 10^3 nuclei were distributed at co-ordinates determined by a random number generator. The area of the plane was thus 4 square units. The density of nuclei in any random element of the plane was such that it approached the expectation density of the complete plane. That is, the distribution was uniform.

Next, a second interval was defined $[-0.7,+0.7]$ in both the x and y directions in the plane which bounded a square box of 2 square units. Only nuclei inside this inner box were used as centres for calculations, but nuclei outside the box could be used for the calculation of collision fronts. This precaution was teleologically necessary to prevent m-gons 'spilling' outside $[-1,+1]$. On the rare occasions that a given nucleus spilled over anyway, the program recognised the m-gon and rejected it.

Since the area considered was half the total area, then approximately 500 nuclei could be examined per run. For each nucleus it was necessary to order its nearest neighbours in terms of their distances in polar co-ordinates, and then compute collision fronts individually until the complete m-gon had been calculated. Various properties of the resultant m-gons could then be established as desired. Note that the resultant density was $>2/500$ because some m-gons necessarily spilled over the inner box. The overall weighted average density, ρ, was 4.2×10^{-3}.

The first property of the m-gons investigated was the distribution of the number of sides. This is expressed as a percentage of all m-gons (P_m) in Fig. 9. The m-gons with more than a 5% probability of occurrence are those having 4, 5, 6, 7, and 8 sides. The expected number of sides, calculated earlier (eqs. [21] and [33]) was found to be 6. The overall weighted average number of sides, calculated for 24 000 nuclei, was found to be 5.999.

The average area of individual m-gons was also calculated. The result is shown in Fig. 11 which plots the average area as a function of m. An approximately linear relationship is found in accordance with

$$[54] \qquad \bar{A}_m \simeq (m - 2)/4\rho, \; m \geq 3$$

where ρ is the average density and $\bar{A}_m$ is the average area of an m-gon. This result explains, at least partially, the rapid diminution of P_m in Fig. 10 for $m > 8$. Obviously the probability of a single nucleus existing in a large 'open space' (i.e. $\bar{A}_m$ large) diminishes rapidly as m increases, because the overall distribution of other nuclei is uniform. Not a single 15-gon was recorded in 24 000 nuclei.

The area distribution of all nuclei was also calculated. In this case, 6000 nuclei were considered. The number of nuclei having areas between intervals of 4×10^{-4} area units were counted, and the results plotted versus the interval number (Fig. 12). A smooth distribution is found which rises rapidly to a maximum (at $A \simeq 4 \times 10^{-3}$ area units) and then exhibits a tailing region. The tailing region becomes statistically insignificant for the chosen number of nuclei (6000) above $A \simeq 1.2 \times 10^{-2}$ area units.

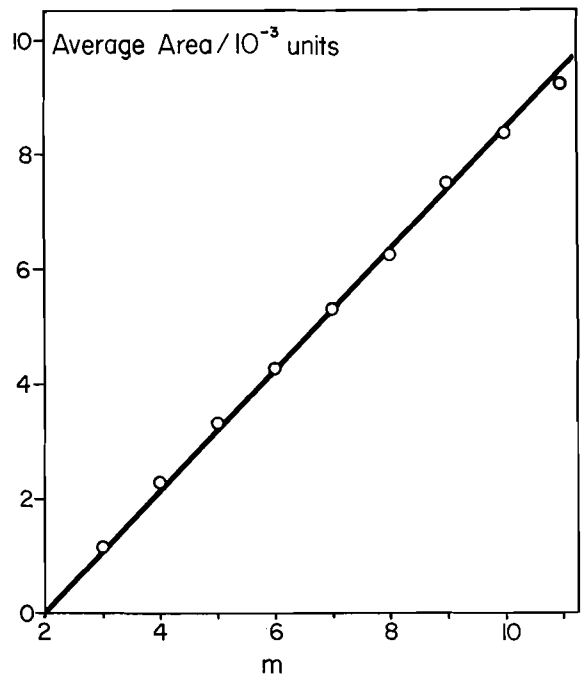

FIG. 11. The average area of individual m-gons. Points are computer simulated data. The solid line is from eq. [54].

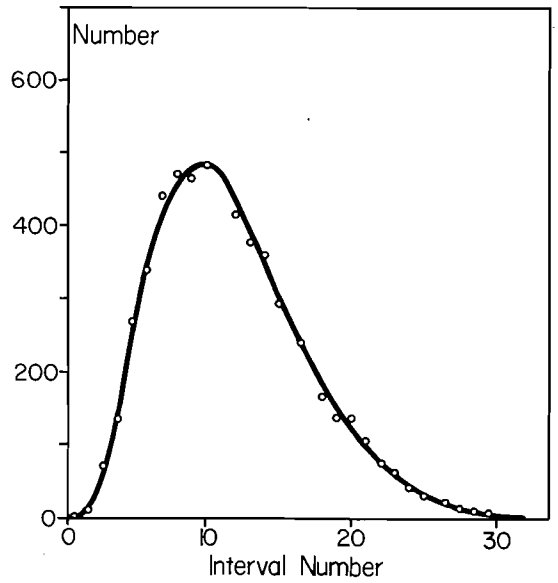

FIG. 12. The area distribution of m-gons (from computer simulation).

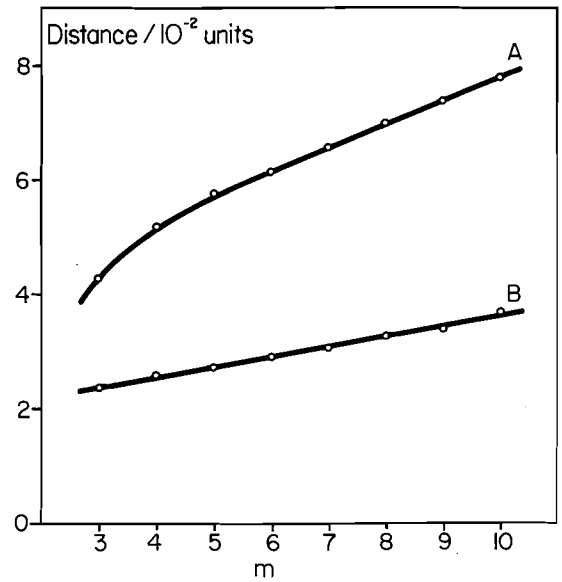

FIG. 13. The average distance from the centre P of a nucleus to (A) furthest vertex of a polygon and (B) nearest vertex of a polygon.

The properties of vertices of the m-gons were also examined. In particular, the average distances of nearest and furthest vertices from centre P were calculated for $n < 10$ from a sample of 6000 n-gons. The result is shown in Fig. 13. The average distance

of the nearest vertex of an m-gon varies linearly with m, while the average distance of the furthest vertex shows a more complex dependence. This dependence is probably $O(m^{1/2})$, meaning that m-gons containing a large number of sides would tend towards the circular.

Conclusions

A particularly useful area in which theories of two-dimensional nucleation and growth may be confronted with experimental data is in the study of electrocrystallization phenomena. However, a complication lies in elucidating the effects of electrode potential on the various nucleation parameters (the nucleation rate, the probability of addition or subtraction of adunits to a nucleus, etc.). It is well-known that these difficulties can be circumvented to some extent by the judicious application of the (potentiostatic) double potential step method. The theory of this method was briefly reviewed. It was then shown that for circularly symmetric nuclei the fine structure of events at the electrode surface could be quantified in some detail. In particular both stochastic and geometric properties of nuclei were calculated. These properties were then compared to the predictions of the Kolmogoroff–Avrami theorem, which is widely used in macroscopic theories of 2-D nucleation and growth to describe the mutual collision of randomly-distributed nuclei.

It was found that the Kolmogoroff–Avrami theorem broke down when either the number of nuclei was finite, or nuclei were confined within a finite area with fixed boundaries. The magnitude of the errors arising from the use of the Kolmogoroff–Avrami theorem in these circumstances was calculated. (Another possibility, namely that the Kolmogoroff–Avrami theorem may break down for certain geometries and growth rates of nuclei, other than circular, will be considered in a future publication.)

In the present work the concept of a *collision front* was also introduced, this being defined as the line of contact along which nuclei collide. This concept was used throughout to replace the older idea of 'overlap' between growing nuclei (6). It was shown that for a random distribution of instantaneously nucleated circular nuclei in a plane, the complete set of extended collision fronts constituted a 'net' composed of irregular convex m-gons. Each m-gon then represented the complete collision-front encountered by a single nucleus.

The properties of a set of m-gons in a given plane were then described, and it was shown that the average number of sides approached 6 as the number of nuclei approached infinity. The magnitude of the 'edge effect', due to boundaries of the plane, was shown to be $O(\sqrt{N})$.

A set T_p was then defined, which was composed of those nuclei which impinged on a given nucleus in such a way that the collision fronts constituted the unique m-gon into which the given neuclus grew. Some properties of this set were described, and in particular the distribution of contributors to T_p was calculated. The mean distance of contributors to the m-gon of a given nucleus was also calculated, and was compared with the mean distance of the nearest neighbour.

The distribution of m-gons was then investigated, with some interesting results. First of all, the distribution of 'random' m-gons was calculated and an explicit formula given. Comparison of this result with a computer-simulated 'net' of m-gons then showed that a clustering phenomenon occurred in the real situation, such that 5, 6, and 7-gons tended to be surrounded by other 5, 6, and 7-gons. Nevertheless the departure from 'ideal randomness' was not too great (Fig. 9). At large values of n (>13, say), the probability of observing a given m-gon was shown to decay at least exponentially with m.

An approximate treatment was then given for the variance of S, i.e. the surface coverage of the plane at some time t for a given growth law. The general approach here was to replace the real situation of circular nuclei growing into a set of m-gons with a hypothetical situation of circular nuclei growing into circular regions having a certain probability distribution function. The probability distribution function used was a natural choice and preserved the mean value properties of the real situation.

Finally, some computer-simulated data were reported which verified the concepts used in the body of the text. An additional fact which emerged from the computed data was that the average size of m-gons varied approximately linearly with m.

1. T. Erdey-Gruz and M. Volmer. Z. Phys. Chem. **157**, 165 (1931).
2. J. B. Zeldovich. Acta Physicochim. URSS, **18**, 1 (1943).
3. D. Walton. J. Chem. Phys. **37**, 2182 (1962).
4. M. Fleischmann and H. R. Thirsk. Advances in electrochemistry and electrochemical engineering. Vol. 3. *Edited by* P. Delahay. Wiley, Interscience. 1963.
5. G. H. Gilmer. Faraday Symposium No. 12, Dec. 1977. In press.
6. M. Avrami. J. Chem. Phys. **7**, 1103 (1939); **8**, 212 (1940); **9**, 177 (1941).
7. F. C. Frank. J. Cryst. Growth, **13/14**, 154 (1972).
8. E. B. Budevski. *In* Progress in surface and membrane science. Vol. II. *Edited by* D. A. Cadenhead and J. F. Danielli. Academic Press, NY. 1976. p. 71.
9. A. Milchev, S. Stoyanov, and R. Kaischev. Thin Solid Films, **22**, 255 (1974); **22**, 267 (1974).
10. R. Kaischev, A. Scheludko, and G. Bliznakov. Bull. Acad. Bulgare Sci. Phys. **1**, 137 (1950).
11. A. N. Kolmogoroff. Bull. Acad. Sci. URSS/Sci. Math. Nat. **3**, 355 (1937).
12. S. Fletcher and A. Smith. To be published.
13. P. Hertz. Math. Ann. **67**, 387 (1909).

Vapour pressure and calorimetric data for the solution of sulfur dioxide in aprotic solvents

ROBERT L. BENOIT AND ETELA MILANOVA

Département de Chimie, Université de Montréal, C.P. 6210, Succ. A, Montréal (Qué.), Canada H3C 3V1

Received December 15, 1978

ROBERT L. BENOIT and ETELA MILANOVA. Can. J. Chem. 57, 1319 (1979).

Vapour–liquid equilibrium data for dilute sulfur dioxide solutions in sixteen solvents were derived from total vapour pressure measurements at 25°C. The SO_2 enthalpies of solution at infinite dilution ΔH^0 were determined at 25°C by direct calorimetry. The solvents used belong to the aprotic class. The ΔH^0 values (kcal mol^{-1}) are for the non-polar solvents, isooctane (−3.5), cyclohexane (−3.5), *n*-heptane (−3.8), benzene (−5.8), and for the polar solvents, 1,2-dichloroethane (−5.5), nitromethane (−6.2), nitrobenzene (−6.3), acetonitrile (−6.7), ethyl acetate (−7.1), sulfolane (−7.3), propylene carbonate (−7.5), trimethyl phosphate (−8.9), tetrahydrofuran (−9.4), dimethylformamide (−10.9), pyridine (−11.6), dimethylsulfoxide (−13.0). Out of three correlation methods which we tested to account for our data in non-polar solvents, the Hildebrand solubility parameter treatment gives the best results. The SO_2 enthalpies of solution, ΔH^0, in the polar solvents are discussed in terms of solvent basicity. There is a good correlation between the ΔH^0 values, which relate to the basicity of the bulk solvent, and the solvent 'donor number' which is a molecular basicity parameter.

ROBERT L. BENOIT et ETELA MILANOVA. Can. J. Chem. 57, 1319 (1979).

On a déduit de mesures de pression de vapeur totale à 25°C des données sur l'équilibre vapeur–liquide de solutions diluées d'anhydride sulfureux dans seize solvants. Les enthalpies de solution de SO_2 à dilution infinie ΔH^0 ont été déterminées à 25°C par calorimétrie directe. Les solvants étudiés font partie de la classe aprotonique. Les valeurs de ΔH^0 (kcal mol^{-1}) sont pour les solvants non-polaires, isooctane (−3.5), cyclohexane (−3.5), *n*-heptane (−3.8), benzene (−5.8) et pour les solvants polaires, 1,2-dichloroéthane (−5.5), nitrométhane (−6.2), nitrobenzène (−6.3), acétonitrile (−6.7), acétate d'éthyle (−7.1), sulfolane (−7.3), carbonate de propylène (−7.5), phosphate de triméthyle (−8.9), tétrahydrofuranne (−9.4), diméthylformamide (−10.9), pyridine (−11.6), diméthylsulfoxyde (−13.0). Des trois méthodes de corrélation que nous avons considérées pour rendre compte de nos données avec les solvants non-polaires, celle utilisant les paramètres de solubilité d'Hildebrand donne le meilleur résultat. Les enthalpies de solution de SO_2, ΔH^0, dans les solvants polaires sont reliées à la basicité des solvants. On observe une bonne corrélation entre les valeurs de ΔH^0 qui sont reliées à la basicité du liquide, et le "nombre donneur" des solvants qui caractérise la basicité moléculaire.

The recovery and concentration of dilute sulfur dioxide from gaseous effluents produced by stationary sources are an environmental and industrial problem of increasing importance (1). Some of the wet chemical processes being developed to remove SO_2 use non-aqueous absorbents (2). This lends interest to the establishment of data on the free energy and enthalpy changes for the absorption of gaseous SO_2 in solvents. Such thermodynamic data for the solvents which belong to the aprotic class have further value, because in these media SO_2 is cleanly and easily reduced, chemically or electrochemically, to the radical ion $SO_2^{-\cdot}$ and its dimer the dithionite ion. This reduction reaction is used to advantage in the preparation of industrially important alkali dithionites (3) and in the operation of the Li–SO_2 high density energy battery (4). Finally, additional data on the solution of SO_2, a polar gas, should be valuable to test the applicability of various theories and correlations which are being developed to account for the properties of solutions of gases in liquids (ref. 5 and references cited therein).

Available literature data on vapour–liquid equilibria of SO_2–solvent systems are fairly extensive but scattered (6). Results are often reported for SO_2 in the form of Henry's constants or infinite dilution activity coefficients as determined by gas–liquid chromatography (7, 8). SO_2 solubilities are also given (9, 10). Extensive total vapour pressure measurements have been used to calculate the excess Gibbs function G^E (11) for some solvents. Less recent data are found in Frank's review (12). The enthalpies of solution of SO_2 have been determined for only a few solvents and, except for dimethylaniline (13), from the temperature dependence, often within a limited range, of vapour pressure or solubility.

This paper reports vapour–liquid equilibrium data derived from total vapour pressure measurements at 25°C on sixteen SO_2–solvent systems at low SO_2 concentrations. The SO_2 enthalpies of solution at

0008-4042/79/111319-05$01.00/0

infinite dilution were also determined at 25°C by direct calorimetry. The solvents used for this study belong to the aprotic class and were selected to cover a wide range of basicity (14) so that the effect of this solvent property could be assessed.

Experimental

Apparatus and Procedure

Solution vapour pressures at 25°C were measured with a precision quartz spiral gauge (Texas Instruments). The experimental set-up has been described before (15). The SO_2 partial pressures were obtained from the total equilibrium vapour pressures by subtracting the solvent vapour pressure calculated according to Raoult's law. The SO_2 mole fractions of the solutions were below 0.1 and the SO_2 partial pressures below 150 mm Hg.

The gas calorimeter and procedure used have been given previously (15). The calculated enthalpies of solution per mole of SO_2 at 25°C were within experimental errors independent of the SO_2 concentration (0.03–0.18 M). The enthalpies of solution reported, which are averages of usually 3–4 determinations, are assumed to be equivalent to the SO_2 enthalpies of solution at infinite dilution ΔH^0. Reproducibility was 0.1–0.2 kcal mol^{-1}; however, with dimethylsulfoxide the standard deviation was unexplicably high: 0.91 kcal mol^{-1} for seven determinations.

For both types of measurements the SO_2 concentrations in the solvents were determined iodometrically after flooding with water immediately after each experiment. Methanol was used when required to insure miscibility. In the case of pyridine, an addition of acid preceded that of iodine.

Materials

The solvents were reagent grade, or distilled before use, and dried over 4A activated molecular sieves. Anhydrous sulfur dioxide from Canadian Liquid Air was 99.98% pure.

Results and Discussion

The partial pressures P_{SO_2} (mm Hg) at 25°C are plotted in Fig. 1 as a function of the SO_2 molar concentration C_{SO_2} for 13 solvents. The curves are linear at low C_{SO_2}, usually below 0.5 M, and the corresponding proportionality constants are expressed as $H = P_{SO_2}/X_{SO_2}$, where P_{SO_2} is in atm and X_{SO_2} is the SO_2 mole fraction calculated from C_{SO_2} and the density of the solvent. Since the fugacity corrections are less than 0.3%, in view of the low pressures used for extrapolation, H is simply Henry's law constant. Our average deviations in H vary according to the volatility and basicity of the solvents. For basic pyridine where the solvent vapour pressure P_S is near 20 mm Hg and P_{SO_2} varies up to 7 mm Hg, the average deviation is 11%, but for basic dimethylsulfoxide with $P_S \sim 0.60$ mm Hg and $P_{SO_2} \leq 8$ mm Hg the deviation is lower, 6.4%. For weakly basic nitrobenzene, $P_S \sim 0.3$ mm Hg and $P_{SO_2} \leq 110$ mm Hg, the deviation is 0.7% but for acetonitrile, $P_S \sim 85$ mm Hg and $P_{SO_2} \leq 100$ mm Hg, the deviation is higher, 1.8%. Values of H are reported in Table 1 together with literature data for

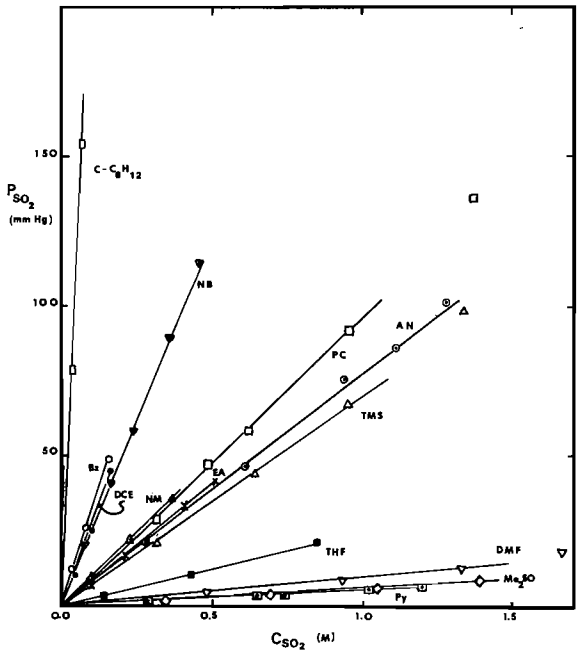

FIG. 1. SO_2 partial pressure for SO_2 solutions in aprotic solvents as a function of SO_2 molar concentration at 25°C. Pyridine (⊡, Py), dimethylsulfoxide (◇, Me_2SO), dimethylformamide (▽, DMF), tetrahydrofuran (■, THF), sulfolane at 30°C (△, TMS), acetonitrile (⊙, AN), ethyl acetate (×, EA), propylene carbonate (□, PC), nitromethane (◬, NM), nitrobenzene (▽, NB), 1,2-dichloroethane (●, DCE), benzene (○, Bz), cyclohexane (□, *c*-C_6H_{12}).

the solvents studied here and other solvents of interest. Our value for Me_2SO compares well with a previous value (7). Our value for nitrobenzene compares well with one out of three previous values (7, 8, 17). We believe that our static vapour pressure method leads to more reliable values of H; at any rate the chromatographic method appears to give widely different results where a comparison is possible such as for $C_6H_5NO_2$ (7, 8, 17).

In order to calculate the thermodynamic functions for the solution of SO_2, we take as standard states, for gaseous SO_2 that state in which SO_2 has unit atmosphere pressure, and for SO_2 as solute, that hypothetical state in which SO_2 has unit mole fraction. Then assuming ideal behaviour of the gas, the free energy of solution of SO_2 is given by:

$$\Delta G^0 = RT \ln H$$

Table 2 contains the values of ΔG^0 thus obtained, as well as ΔG^0 values calculated from reported SO_2 solubility data (10). These latter values are more positive than ours when the solubility of SO_2 is large, as is apparent when we compare data for nitromethane and acetonitrile. These differences arise because the SO_2–solvent systems studied

TABLE 1. Henry's law constants for SO_2 in polar and non-polar aprotic solvents at 25°C

Solvent	H (atm)
Dimethylsulfoxide	0.109 (0.117)†
Pyridine	0.088
Dimethylformamide	0.172
Tetrahydrofuran	0.392
Propylene carbonate	1.51 (1.20)†
Sulfolane*	1.01
Ethyl acetate	1.09
Acetonitrile	1.91
Nitrobenzene	3.18 (1.64)†, (3.43)‡, (2.96)§
Nitromethane	2.33
1,2-Dichloroethane	4.23
Isooctane	20.3
Cyclohexane	28.3
n-Heptane	16.5‖
Benzene	4.51
n-Hexadecane	12.9†
Decahydronaphthalene	18.8†

*At 30°C.
†Reference 7.
‡Reference 8.
§Reference 17.
‖Reference 18.

exhibit a positive deviation from Henry's law for increasing values of X_{SO_2}.

Our values for ΔH^0, the SO_2 enthalpy of solution, are listed in Table 2. In order to ascertain the validity of our direct calorimetric measurements, we also determined ΔH^0, for the solvent acetonitrile, from the dependence of Henry's law constant, H, on temperature. The values of H (atm) for 4–6 SO_2 concentrations ($0.2 < C_{SO_2} < 1.3\ M$) and three temperatures were as follows: 15.00°C, $H = 1.31$; 25.00°C, $H = 1.94$; 35.00°C, $H = 2.83$. ΔH^0 thus calculated, -6.8 kcal mol^{-1}, compares satisfactorily with the calorimetric values -7.1 ± 0.2 kcal mol^{-1} (five determinations). Furthermore, our calorimetric value -3.8 kcal mol^{-1} for the solvent *n*-heptane is identical with that calculated by Christian *et al.* (18) from their vapour pressure measurements at 10, 20, and 30°C. As expected, the ΔH^0 values deduced from the temperature coefficient of the SO_2 solubility are in rather poor agreement with our calorimetric ΔH^0 values. For example, we obtained for MeCN and benzene as solvents -7.1 and -5.8 kcal mol^{-1}, respectively, to be contrasted with -9.9 (10) and -6.7 kcal mol^{-1} (12) calculated from solubility. Our -7.1 kcal mol^{-1} value for ethyl acetate also suggests that $\Delta H^0 = -4.1$ kcal mol^{-1} for methyl acetate (12) is probably in error. Plotting our values of ΔH^0 against ΔG^0 both of which were independently determined, rather than plotting ΔS^0 vs. ΔG^0 or ΔH^0 vs. ΔS^0, in order to test for a simple "enthalpy–entropy relationship" (19), the slope of the correlation line is 2.91 and the correlation coefficient is only 0.973. However, the points do appear to follow a smooth (although non-linear) curve which could be used to estimate one thermodynamic parameter if the other one were known.

TABLE 2. Enthalpy and free energy of solution of SO_2 in aprotic solvents and water at 25°C

Polar solvents	ΔH^0 (kcal mol^{-1})	ΔG^0 (kcal mol^{-1})	ΔS^0 (eu)
Dimethylaniline (DMAn)*	−15.0	−1.74	−44.5
Dimethylsulfoxide (Me_2SO)	−13.0	−1.30	−39.2
Pyridine (Py)	−11.6	−1.43	−34.1
Dimethylformamide (DMF)	−10.9	−1.03	−33.1
Tetrahydrofuran (THF)	−9.4	−0.55	−29.7
Trimethylphosphate (TMP)	−8.9		
Propylene carbonate (PC)	−7.5	+0.24	−26.0
Acetone†		+0.25	
Sulfolane (TMS)‡	−7.3	+0.01	−24.5
Ethyl acetate (EA)	−7.1	−0.05	−23.7
Methyl acetate†		+0.30	
Acetonitrile (AN)	−7.1	+0.38	−25.1
		+0.74‖	
Nitrobenzene (NB)	−6.3	+0.68	−23.4
		+0.89‖	
Nitromethane (NM)	−6.2	+0.50	−22.5
		+0.82‖	
1,2-Dichloroethane (DCE)	−5.5	+0.85	−21.3
		+0.89‖	
Chlorobenzene†		+0.92	
Water¶	−6.26	+2.26	−28.6

Non-polar solvents	ΔH^0 (kcal mol^{-1})	ΔG^0 (kcal mol^{-1})	ΔS^0 (eu)
n-Hexadecane§	−3.0	+1.60	−15.3
Isooctane	−3.5	+1.77	−17.6
Cyclohexane	−3.5	+1.98	−18.3
		+1.95‖	
n-Heptane	−3.8	+1.66	−18.3
Carbon tetrachloride†		+1.54	
Benzene (Bz)†	−5.8	+0.88	−22.4
	~−6.7	+0.82	−25.2
		+1.05‖	

*Reference 13. Obtained from solubility and calorimetric data.
†Reference 12. Calculated from previous workers' solubility data.
‡At 30°C.
§Calculated from solubility data in ref. 9.
‖Calculated from solubility data in ref. 10.
¶Calculated from solubility data and previous workers' conductivity data in ref. 25.

Turning to the results in Table 2, for the free energy of solution of SO_2 in the aprotic solvents, it is of interest to compare these ΔG^0 values in terms of deviations from Raoult's law. Taking $P^0 = 3.77$ atm for the vapour pressure of pure SO_2 at 25°C (8) and correcting for the non-ideality of the gas, the free energy of solution of SO_2 is calculated as $+0.79$ kcal mol^{-1} for an ideal system. Then, the systems involving the non-polar solvents, cyclohexane, *n*-heptane, isooctane, *n*-hexadecane, decahydronaphthalene, carbon tetrachloride, exhibit positive deviations

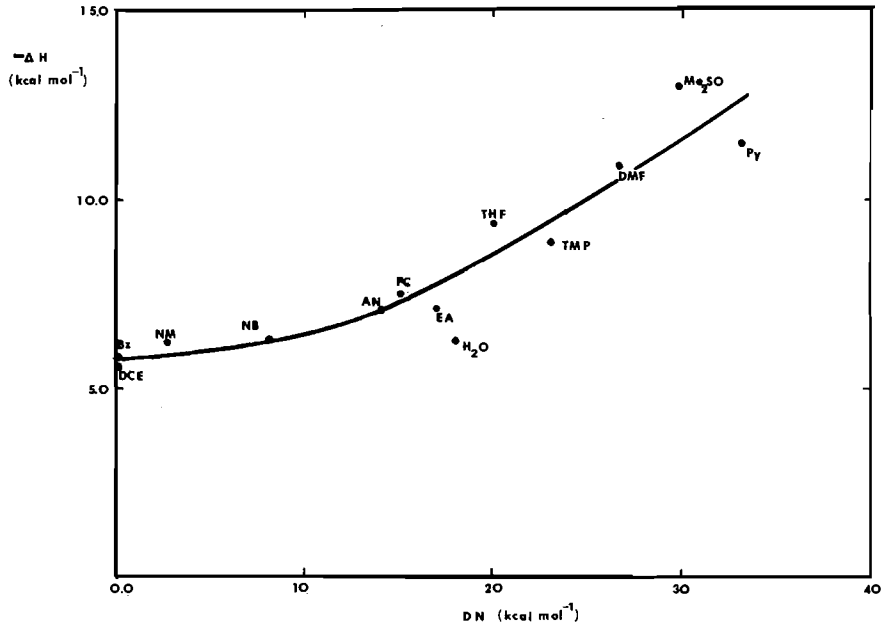

FIG. 2. Correlation between the enthalpy of solution of SO_2 in aprotic solvents and the donor number of the solvents.

from Raoult's law. Benzene, chlorobenzene, 1,2-dichloroethane, and nitrobenzene show only small deviations while all other polar aprotic solvents exhibit negative deviations from Raoult's law. These latter deviations can be attributed in the main to strong chemical interactions[1] between solute SO_2 and the basic solvent molecules.

Attempts were made to determine to what extent three correlation methods relating the solubility behaviour of gases in liquids (ref. 20 and references cited therein) to molecular parameters could account for our results with at least the three simpler non-polar solvents cyclohexane, *n*-heptane, and benzene. In both the free volume theory (20) and Pierotti's scaled particle theory, the calculated ΔG^0 and ΔH^0 values were found to be very sensitive to the solute and solvent molecular parameters whose values appear to differ widely according to the method used for their determination. Furthermore, both theories could not account for the observed higher SO_2 solubility in benzene. Hildebrand's solubility parameter method (ref. 21 and references cited therein) leads to better agreement between calculated and experimental values though the corresponding H values still differ by an average factor of 2. There again, uncertain values of molecular parameters, V_2^L, the partial molar volume of solute SO_2, as well as δ_2, the SO_2 solubility parameter, introduce a large uncertainty on calculated values of H.

Turning now to interactions of a chemical nature between solute SO_2 and solvent, it is of interest to try to account for such interactions in terms of acid–base reactions between SO_2, a Lewis acid, and basic solvent molecules. With this purpose in mind, we have plotted in Fig. 2 our values of ΔH^0, the SO_2 enthalpy of solution against an enthalpy parameter characterizing the basicity of the solvent molecules (14). We have taken as basicity parameter the widely used Gutman's donor number (DN) (22) which is minus the enthalpy of adduct formation between $SbCl_5$, a Lewis acid, and basic molecules as determined in dilute solution in 1,2-dichloroethane. The correlation between ΔH^0 and DN is good considering first that ΔH^0 relates to the basicity of the bulk solvent while DN relates to the basicity of isolated solvent molecules (14) and second that SO_2 is a "borderline" acid while $SbCl_5$ is a hard acid in Pearson's classification. The value $\Delta H^0 = -5.5$ kcal mol^{-1} for DN = 0 (1,2-dichloroethane) is remarkably close to the heat of condensation of SO_2 at 25°C, -5.4 kcal mol^{-1}. Then, if the enthalpy change for the solution of gaseous SO_2 in a solvent at 25°C is viewed as a two-step process, first condensation of SO_2 then followed by mixing of liquid SO_2 with the solvent, the previous observation indicates a very small heat of mixing of liquid SO_2 with 1,2-dichloroethane. This is somewhat unexpected considering the polar nature of both solute and solvent molecules. On the other hand, the ΔH^0 values (Table 2) for the non-polar solvents *n*-hexadecane, isooctane, cyclohexane, and *n*-heptane, all presumably with DN = 0, are all near -3.5 kcal mol^{-1}, so that this time the contribution of the heat of mixing is large and near

[1]No correlation was found between the ΔH^0 values and the dipole moment of the solvent molecules.

+2 kcal mol^{-1}. However, the calculation of this heat of mixing from the solubility parameters δ_1, δ_2, and V_2^L gives values which, although depending on the values selected for the parameters δ_2 and V_2^L, are respectively lower than +1.0 kcal mol^{-1} for isooctane, +0.7 for *n*-heptane, and +0.5 for cyclohexane. It thus appears that we cannot account simply for the heat of solution of SO_2 in these inert non-polar solvents.

In view of the preceding it is perhaps not surprising that in the correlation between ΔH^0 and DN some representative points are off the line by as much as 1.0 kcal mol^{-1} because of the effect of non-chemical interactions between SO_2 and solvent molecules. The position of the correlation line for DN $\geq$ 30 is in doubt because of the opposing values of ΔH^0 and DN for Me_2SO and pyridine, the solution enthalpy of SO_2 being more negative (although the margin of error is uncomfortably high) in Me_2SO than in pyridine, while the opposite is true for the enthalpy of reaction with $SbCl_5$. Reasons for this reversal may be that SO_2 and $SbCl_5$ do not interact with the same basic site in either the Me_2SO or pyridine molecules. DN (pyridine) could also be too large if the reaction between $SbCl_5$ and pyridine involved additional complex ionization of $SbCl_5$ or of the adduct. Among the solvents listed in Table 2, it is dimethylaniline which has the highest $-\Delta H^0$ value, 15.0 kcal mol^{-1}, as well as the lowest Henry constant. It is noteworthy that dimethylaniline is the non-aqueous absorbant used industrially to recover SO_2 from waste smelter gases (ref. 2 and references cited therein). It is apparent from Fig. 2 that the spread in the $-\Delta H^0$ values for the different solvents is some five times smaller than for the DN values. This is largely due to the fact that SO_2 is a much weaker Lewis acid than $SbCl_5$, in this respect SO_2 ranks even slightly weaker than I_2 (23). $SbCl_5$ is thus a better discriminating Lewis acid to differentiate bases in inert media such as 1,2-dichloroethane, but SO_2 has the advantage that it can be used to assess the basicity of bulk solvents because it does not give any complex ionization reaction with the more basic solvents as $SbCl_5$ does (14). That the representative point for the protic solvent H_2O (DN = 16.4 (24)) falls off the line in Fig. 2 is not unexpected and using for H_2O the value DN = 33, which is supposed to characterize the basicity of bulk water (22), makes matters even worse. This emphasizes the difficulty in relating bulk basicity to molecular basicity for protic solvents (14). However, assuming that water basicity plays a major part in determining the heat of solution of SO_2 in water,[2] our ΔH^0 data suggest that the basicity of bulk water is low and near that of nitrobenzene; interestingly, the same result holds for I_2, another non H-bonding molecular acid, since the heats of solution of solid I_2 are, respectively, +5.2 kcal mol^{-1} (H_2O) and +4.7 kcal mol^{-1} ($C_6H_5NO_2$).

[2]The major species in aqueous solution is SO_2 (ref. 26 and references therein).

Acknowledgements

The financial assistance of the National Research Council of Canada is gratefully acknowledged. We thank Professor F. Kimmerle for bringing ref. 10 to our attention, and S. Y. Lam and D. Dubois for carrying out parts of the experimental work.

1. H. M. Malin, Jr. Environ. Sci. Technol. **6**, 688 (1972).
2. K. Semrau. *In* Sulfur removal and recovery from industrial processes. *Edited by* J. B. Pfeiffer. Adv. Chem. Ser. 139 (1975).
3. R. G. Rinker and S. Lynn. Ind. Eng. Chem. Prod. Res. Dev. **8**, 338 (1969).
4. J. O. Besenhard and G. Eichinger. J. Electroanal. Chem. **68**, 1 (1976).
5. E. Wilhelm and R. Battino. Chem. Rev. **73**, 1 (1973).
6. D. F. Cooper and J. W. Smith. J. Chem. Eng. Data, **19**, 133 (1974).
7. J. Y. Lenoir, P. Renault, and H. Renon. J. Chem. Eng. Data, **16**, 340 (1971).
8. A. S. Bogeatzes and D. P. Tassios. Ind. Eng. Chem. Process Des. Dev. **12**, 274 (1973).
9. K. K. Tremper and J. M. Prausnitz. J. Chem. Eng. Data, **21**, 295 (1976).
10. H. Sano. Nippon Kagaku Zasshi, **89**, 362 (1968).
11. J. W. Lorimer, B. C. Smith, and G. H. Smith. J. Chem. Soc. Faraday Trans. I, 2232 (1975).
12. H. S. Frank and M. W. Evans. J. Chem. Phys. **13**, 507 (1945).
13. J. Balej and A. Regner. Collect. Czech. Chem. Commun. **21**, 1545 (1956); **21**, 1553 (1956).
14. R. L. Benoit and C. Louis. *In* The chemistry of non-aqueous solvents. Vol. VA. *Edited by* J. J. Lagowski. Academic Press, New York, NY. 1978.
15. S. Y. Lam, C. Louis, and R. L. Benoit. J. Am. Chem. Soc. **98**, 1156 (1976).
16. R. Domain, M. Rinfret, and R. L. Benoit. Can. J. Chem. **54**, 2101 (1976).
17. Battelle Memorial Institute. Applicability of organic liquids to gases. Report No. PB-183513 (1969), quoted in ref. 8.
18. J. Grundnes and S. D. Christian. J. Am. Chem. Soc. **90**, 2239 (1968).
19. O. Exner. (*a*) Collect. Czech. Chem. Commun. **38**, 799 (1973); (*b*) Prog. Phys. Org. Chem. **10**, 411 (1973).
20. K. Gotoh. Ind. Eng. Chem. Fundam. **15**, 269 (1976).
21. A. F. M. Barton. Chem. Rev. **75**, 731 (1975).
22. V. Gutmann and R. Schmid. Coord. Chem. Rev. **12**, 263 (1974).
23. E. Milanova and R. L. Benoit. Can. J. Chem. **55**, 2807 (1977).
24. G. Olofsson and I. Olofsson. Tetrahedron, **29**, 1711 (1973).
25. H. F. Johnstone and P. W. Leppla. J. Am. Chem. Soc. **56**, 2233 (1934).
26. J. P. Guthrie. Can. J. Chem. **57**, 454 (1979).

Pyrolysis of cyclopentane behind reflected shock waves

BANSI L. KALRA,[1] STUART A. FEINSTEIN,[2] AND DAVID K. LEWIS[3]

Department of Chemistry, Colgate University, Hamilton, NY 13346, U.S.A.

Received May 23, 1978

BANSI L. KALRA, STUART A. FEINSTEIN, and DAVID K. LEWIS. Can. J. Chem. 57, 1324 (1979).

Gas samples containing either 0.20% or 1.0% cyclopentane plus 0.25% *tert*-butyl alcohol in argon have been heated to 1185–1257 K in a single pulse shock tube. The previously studied dehydration of the alcohol was used as an internal standard reaction for temperature measurement. Pyrolysis of the cyclopentane yielded a broad spectrum of C_1–C_5 hydrocarbon products; however, the products and their concentration ratios were in good agreement with those recently reported by Tsang, in a comparative rate study of cyclopentane pyrolysis vs. cyclohexene decyclization. Thus strong support is offered for Tsang's proposed complex mechanism involving (*a*) molecular isomerization to 1-pentene and subsequent degradation of that product, (*b*) molecular decomposition to cyclopropane and ethene, followed by isomerization of cyclopropane to propene, and (*c*) induced decomposition to a variety of C_1–C_5 hydrocarbons plus H_2 via hydrogen atom abstraction from cyclopentane by various radicals generated from 1-pentene. The only significant disagreement with Tsang's study is a ~40° temperature discrepancy; possible sources of this are discussed.

BANSI L. KALRA, STUART A. FEINSTEIN et DAVID K. LEWIS. Can. J. Chem. 57, 1324 (1979).

On a chauffé des échantillons gazeux contenant soit 0.20% ou 1.0% de cyclopentane plus 0.25% d'alcool *tert*-butylique dans l'argon à des températures allant de 1185 à 1257 K dans un tube de chocs à pulsation unique. On a utilisé la déshydratation étudiée antérieurement comme réaction de référence interne pour la mesure de la température. La pyrolyse du cyclopentane fournit une grand nombre d'hydrocarbures de C_1 à C_5; toutefois la nature des produits et les rapports de leurs concentrations sont en bon accord avec ceux rapportés par Tsang dans une étude comparée des vitesses de pyrolyse du cyclopentane vs la décyclisation du cyclohexène. Nos résultats militent donc fortement en faveur du mécanisme complexe proposé par Tsang qui implique (*a*) une isomérisation moléculaire fournissant du pentène-1 et une dégradation subséquente de ce produit, (*b*) une décomposition moléculaire en cyclopropane et en éthène et (*c*) une décomposition induite en une variété d'hydrocarbures de C_1 à C_5 plus du H_2 par l'intermédiaire d'enlèvements d'atomes d'hydrogène du cyclopentane par divers radicaux formés à partir du pentène-1. La seule différence importante avec l'étude de Tsang a trait à une différence d'environ ~40°; on discute des sources possibles de cette différence.

[Traduit par le journal]

Introduction

Kinetic and thermodynamic parameters for thermal decompositions of hydrocarbon molecules are of interest on theoretical grounds (1), and because of the eventual usefulness of such information for numerical modeling of cracking and combustion reactions. We have been studying a number of small cyclic alkanes and alkenes at high temperatures in chemical shock tubes (2–4). This series included a brief unpublished study of cyclopentane at ~1200–1250 K via the comparative rate single-pulse technique, using *tert*-butyl alcohol as the internal standard.

Recently, Tsang (5) reported the results of an extensive and careful comparative single-pulse shock tube study of cyclopentane pyrolysis at 1050–1250 K, in which he used the decomposition of cyclohexene to ethene and 1,3-butadiene as the internal standard. He proposed a complex radical mechanism which provided a very satisfactory fit to his data. Arrhenius parameters determined for various steps in the overall process are in reasonable agreement with earlier studies of those specific reactions and/or with thermochemical predictions.

Tsang chose his experimental conditions so as to minimize the effects of interaction between the cyclopentane pyrolysis and the reference or possible impurity reactions; and there is nothing in his data or results to suggest that his efforts were unsuccessful. Nevertheless, our existing data, we feel, provide a further opportunity to confirm the probable reliability of Tsang's results, since they are derived from a different apparatus and standard reaction. The

[1]Alfred P. Sloan Teaching-Research Postdoctoral Fellow, 1974–1975.

[2]Petroleum Research Fund Undergraduate Research Assistant, 1975.

[3]To whom all correspondence should be addressed.

0008-4042/79/111324-05$01.00/0

purpose of this report is to compare our measured product yields with those reported by Tsang, and to draw attention to areas of agreement or disagreement and comment on their significance.

Experimental Section

The 2.54 cm id Pyrex single-pulse shock tube used for our comparative rate experiments has been previously described (6). Reaction products were analyzed on Varian Aerograph Model 1440-20 and Model 90-P gas chromatographs. The previously characterized reaction *tert*-butyl alcohol → isobutene + water (7) was used as the reference reaction. Both the cyclopentane (K and K Laboratories) and the *tert*-butyl alcohol (Brothers Chemical Co.) were subjected to an extensive pre-purification process consisting of a series of degassings at 77 K and distillations from slush baths. Gas chromatographic analysis for hydrocarbon impurities indicated probable final purity of > 99.99% for each reactant. Reaction mixtures were prepared in stainless steel tanks at $p > 1$ atm, with Ultra-High Purity grade argon (Matheson) diluent, at least three days before use.

Reactant sample compositions and experimental conditions are summarized in Table 1.

TABLE 1. Summary of experimental conditions

Set	%⬠	%*t*-BuOH	P_1(Torr)*	T_5 (K)†	τ(μs)
A	0.201	0.250	65–83	1186–1255	~800
B	1.00	0.25	57.5–77	1217–1256	~800

*Pressures in shock tube sample section before heating.
†Temperatures behind reflected shocks, deduced from isobutene yields, measured reaction times τ, and the previously measured rate constants for *tert*-butyl alcohol → isobutene + H_2O: $\log (k, s^{-1}) = 14.6 - 66\,200/4.576T$ (ref. 7).

Results

The following gases were found in product samples: hydrogen, methane, ethane, ethene, propene, allene, isobutene, *tert*-butyl alcohol, 1,3-butadiene, 1-pentene, cyclopentane, cyclopentene, and cyclopentadiene. Earlier studies of *tert*-butyl alcohol pyrolysis (7, 8) and a few runs on cyclopentane plus argon mixtures in the present study indicated that the isobutene was produced solely from the alcohol and that the 1,3-butadiene and C_5 products came only from the cyclopentane. The C_1, C_2, and C_3 products were produced primarily from cyclopentane, but with minor contributions from *tert*-butyl alcohol and its primary decomposition product, isobutene.

Graphs have been drawn of $\log_{10}$ $\{([\text{product}]_t/[⬠]_0) \times 100\}$ vs. $1/T$ (K) for each cyclopentane product. Examples for ethene, propene, allene, and butadiene appear in Fig. 1. Here, $[\text{product}]_t$ represents concentration of the product in the post-shock sample, and $[⬠]_0$ represents initial cyclopentane concentration for that run. The quantity within the { } is the percent product relative to initial reactant. This presentation is similar to a first-order rate plot; coincidence of the data representing different percentage mixtures would indicate first-order dependence on cyclopentane for production of a particular product. The lines through the groups of data in Fig. 1 were determined by linear least-squares analysis, with all variance assigned to the *y*-axis variable.

Also shown in Fig. 1 are least-squares lines through the product yields reported by Tsang (5) for comparable reaction times. The symbol on each line represents the upper limit of the temperature range covered by Tsang with the respective sample mixture. Extension of the line to the left of the symbol assumes that Tsang's results can be reliably extrapolated upward by 50–100 K as required. Since Tsang used cyclohexene decyclization as his comparative rate standard and deduced reaction temperatures from 1,3-butadiene yields, he was not able to determine production rates for that product from cyclopentane. And since Tsang's cyclopentane/cyclohexene reactant ratio was 100/1, we were concerned that the contribution of 1,3-butadiene from the subject molecule might be comparable to that from the standard, resulting in calculated temperatures higher than actual reaction temperatures. To assess this possibility, we have shown in Fig. 1*d* the expected percentage of 1,3-butadiene from cyclohexene, relative to initial cyclopentane concentration, as a function of temperature under the conditions of Tsang's experiments. The calculated values were based on the Arrhenius parameters for cyclohexene decyclization previously reported by Tsang (9). As can be seen, cyclohexene was probably the only significant source of butadiene at $T < 1200$ K.

Discussion

A comparison of the results of the two independent studies indicates good agreement in terms of products produced and their concentration ratios. Tsang did report small amounts of cyclopropane, which we did not observe; however, it is probable that this material was produced in our study but not recognized since its retention time and that of allene on our column were identical. Overall, it appears that the cyclopentane pyrolysis was proceeding via essentially the same mechanism in both studies, with no overwhelming effect from the comparative rate standard, from impurities, or from other experimental artifacts.

Considering both sets of data, there appears to be a trend toward decreasing reaction order at lower reactant percentages. Tsang's data from mixtures containing 0.4 to 5% cyclopentane show apparent

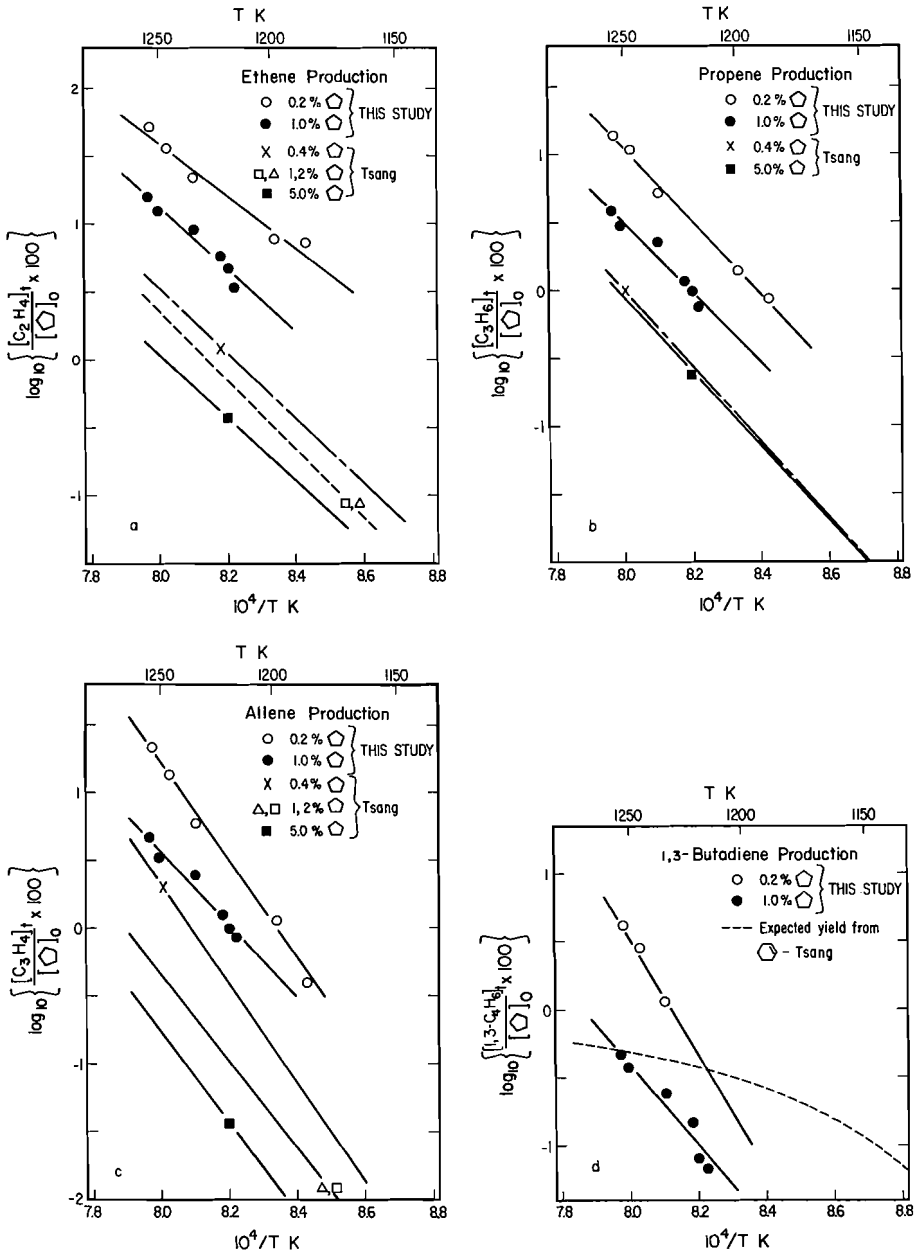

FIG. 1. (*a*) log (% C_2H_4) produced relative to initial concentration of cyclopentane as a function of $1/T$; (*b*) log (% C_3H_6) produced relative to initial concentration of cyclopentane as a function of $1/T$; (*c*) log (% C_3H_4) produced relative to initial concentration of cyclopentane as a function of $1/T$; (*d*) log (% 1,3-C_4H_6) produced relative to initial concentration of cyclopentane as a function of $1/T$.

reaction orders for production of most products between 0 and 1. Our data, from 0.2 to 1% mixtures give approximately zero order dependence on reactant for all C_1–C_4 products. This overall behavior is consistent with the speculation that the bulk of C_1–C_4 products are the result of induced decomposition of cyclopentane and subsequent reactions caused by relatively invariant quantities of impurities present in the comparative rate standard or diluent gas, or introduced into sample mixtures during the gas handling process.

A third area for comparison is the apparent extent of reaction in comparable percentage (1%) mixtures, at comparable reaction times and temperatures. Product % vs. inverse temperature plots (Fig. 1) for ethene, propene, and allene show a

40 ± 10 K discrepancy between the two studies. The larger than average difference (50° vs. 40°) for allene is consistent with our expectation that there was a small cyclopropane contribution to the allene analysis in our work, and the smaller than average (30° vs. 40°) difference for propene suggests that Tsang's propene production data from 1% mixtures may be slightly high. Lowering that line slightly would give about the same reaction order for propene production that we observed.

The ~40° difference may be attributed to (*a*) differences in impurity levels or other unknown factors, which differently affect the rates of cyclopentane pyrolysis in the two shock tubes, or (*b*) errors in temperature calculations on one or both shock tubes resulting from the choice of different comparative rate standard reactions or from non-ideal shock tube behavior. As described above, it seems unlikely that (*a*) is the dominant cause for the observed difference in rates. Possibility (*b*) will now be considered.

Tsang has previously studied the cyclohexene decyclization in comparative rate shock tube experiments against three other unimolecular reactions (9–11). The cleanliness of the reaction up to 1200 K and the close agreement among the three studies suggests that there can be very little error in Tsang's cyclopentane study temperature calculations attributable to incorrect Arrhenius parameters. However, a possible source of error in Tsang's study is induced decomposition of the standard molecule by radicals that must have been present. Tsang has measured rates of fragmentation of cyclohexyl radical generated from *tert*-butyl cyclohexane (12) and from induced decomposition of cyclohexane (13), but there is inadequate information available to estimate the extent of induced decomposition of cyclohexene relative to that of cyclopentane, in a mixture of the two. If the same relative percentages of each reactant suffered induced decomposition, which seems a reasonable assumption, then a small but not negligible fraction of the cyclohexene loss could be attributed to the induced channel.

Since the Arrhenius parameters for *tert*-butyl alcohol pyrolysis used for temperature calculations in the present work were determined from a study of *tert*-butyl alcohol vs. cyclohexene (7), less than 5° of the apparent difference between Tsang's and our cyclopentane data can be attributed to errors in these parameters. A possible source of error in the present work is further reaction of the isobutene product or direct bond breaking, rather than molecular elimination, of the alcohol. In our earlier study of *tert*-butyl alcohol (7), we found allene and propene formed as side products above 1150 K. The allene/isobutene ratio was 0.1 at 1200 K, at which temperature about 30% of the alcohol was reacted; and the ratio increased with temperature. Tsang (8) has suggested that these two side products arise from decomposition of isobutene. If so, our calculated temperatures from apparent isobutene yields may be up to 10 degrees too low at ~1200 K. Mintz and Cvetanović (14) have proposed that the C_3 side products result from a C—C bond breakage of the alcohol:

$$t\text{-}C_4H_9OH \rightarrow \dot{C}H_3 + (CH_3)_2\dot{C}OH$$

Either of the above processes, if important, would produce an error that rapidly increases with temperature. However, the divergence between Tsang's extrapolated and our actual C_2–C_4 product percentages appears essentially constant over the 1200–1250 K range. Breakage of the C—O bond also appears likely, considering the similarity between C—C and C—O single-bond strengths:

$$t\text{-}C_4H_9OH \rightarrow t\text{-}\dot{C}_4H_9 + \dot{O}H$$
$$\hookrightarrow i\text{-}C_4H_8 + \dot{H}$$

This parallel channel for isobutene formation would result in a positive rather than negative temperature error. Overall, the most probable significant effect of either C—C or C—O bond breaking processes is not a large change in isobutene yield, but rather an increase in the induced decomposition of cyclopentane due to the production of radicals. The ~0 order rates of C_1–C_4 hydrocarbon production in our experiments supports this interpretation.

A potential source of significant error in shock tube experiments is the cold boundary layer that grows in thickness from the walls into the reacting gas. In comparative rate experiments, the inclusion of improperly heated gas in the product samples affects the calculated rate constants of both reference and subject reactions. The more nearly identical the Arrhenius parameters of the two reactions, the more nearly exact is the cancellation of the error. Although both Tsang's shock tube and our own are of small diameter (1 in. id), we have both avoided use of the reaction time extending tailored interface technique, and used similar short dwell times in the interest of minimizing boundary layer influence. A further argument against extreme influence of boundary layer growth is the fact that we are routinely able to achieve conversion rates $\gtrsim$95% for unimolecular reactions of organic species within the ~800 μs dwell time with sufficiently hot shocks.

Considering the above factors and the quite linear offset of our rate data from that reported by Tsang, we feel the most probable source of the offset is induced decomposition of cyclopentane caused by

tert-butyl alcohol-generated radicals in our study. However, from the ~40° magnitude of the offset, it seems possible that Tsang's reported temperatures might be 0–15° higher than actual values, the error being caused by induced decomposition of his internal standard. If so, correction of his comparative rate data would result in a small upward adjustment of all pre-exponential factors deduced from his analysis. The correction would not appreciably change apparent activation energies, his enthalpy analysis of reactants, intermediates and products, or the mechanistic interpretations he has presented.

Acknowledgements

We would like to acknowledge support of this research by the Alfred P. Sloan Foundation and by the Donors of the Petroleum Research Fund, administered by the American Chemical Society. We also thank Dr. Tsang for providing a pre-print of his cyclopentane study.

1. S. W. BENSON. Thermochemical kinetics. 2nd ed. John Wiley, New York. 1976.
2. P. JEFFERS, D. LEWIS, and M. SARR. J. Phys. Chem. **77**, 3037 (1973).
3. D. LEWIS, S. FEINSTEIN, and P. JEFFERS. J. Phys. Chem. **81**, 1887 (1977).
4. D. LEWIS, M. SARR, and M. KEIL. J. Phys. Chem. **78**, 436 (1974).
5. W. TSANG. Int. J. Chem. Kinet. **X**, 599 (1978).
6. D. K. LEWIS, S. E. GEISLER, and M. S. BROWN. Int. J. Chem. Kinet. **X**, 277 (1978).
7. D. K. LEWIS, M. KEIL, and M. SARR. J. Am. Chem. Soc. **96**, 4398 (1974).
8. W. TSANG. J. Chem. Phys. **40**, 1498 (1964).
9. W. TSANG. Int. J. Chem. Kinet. **VIII**, 173 (1976).
10. W. TSANG. J. Chem. Phys. **42**, 1805 (1965).
11. W. TSANG. Int. J. Chem. Kinet. **II**, 311 (1970).
12. W. TSANG. J. Phys. Chem. **76**, 143 (1972).
13. W. TSANG. Int. J. Chem. Kinet. **X**, 1119 (1978).
14. K. J. MINTZ and R. T. CVETANOVIĆ. Can. J. Chem. **51**, 3386 (1973).

Differential equation for transport along parallel linear successions of identical symmetrical potential barriers

M. J. DIGNAM

Department of Chemistry, University of Toronto, Toronto, Ont., Canada M5S 1A1

Received September 26, 1978

M. J. DIGNAM. Can. J. Chem. **57**, 1329 (1979).

The differential equation for transport of non-interacting species along parallel paths, each consisting of a linear succession of identical symmetrical potential barriers, is expanded as an infinite series in the derivatives of the electrostatic potential and concentration. The first order expression is shown to represent the model adequately for all but extremely high space charge concentrations and/or extreme departures from steady-state conditions. Under the appropriate limiting conditions it reduces to the well-known linear transport equation, and to the Mott–Cabrera equation, but extends these to higher concentrations since the formulation forbids hops into occupied sites. The treatment leads to a concentration independent diffusion coefficient, but to a concentration dependent mobility.

M. J. DIGNAM. Can. J. Chem. **57**, 1329 (1979).

On a étendu l'équation différentielle décrivant le transport d'espèces qui n'interagissent pas et qui suivent des chemins parallèles, chacun correspondant à une série linéaire de barrières de potentiel symétriques et identiques, sous forme d'une série infinie de dérivés du potentiel électrostatique et de la concentration. On montre que l'expression du premier ordre représente adéquatement le modèle pour tous les cas exceptés ceux relatifs aux concentrations extrêmement élevées de charges spatiales et ceux où les conditions s'écartent d'une façon extrême d'un état stationnaire. Sous des conditions limites appropriées, elle est réduite à l'équation bien connue des transports linéaires et à l'équation de Mott–Cabrera; elle étend toutefois ces équations à des concentrations plus élevées puisque la formulation empêche des sauts vers des sites occupés. Ce traitement conduit à un coefficient de diffusion qui est indépendant de la concentration mais une mobilité qui dépend de la concentration.

[Traduit par le journal]

Introduction

The purpose of this paper is to derive the differential equation for transport of non-interacting species, in general carrying a charge, along parallel paths each consisting of a linear succession of identical symmetrical potential barriers. Although the transport model itself is well-known (1–3), the development of the differential equation of transport for the model, in a general way, was first published by Dignam, Young, and Goad in 1973 (4). This paper extends the earlier treatment both by including the effect of site depletion and by deriving the full second order correction to the first order approximation. The latter allows the range of applicability of the first order equation to be defined for all values of the field strength. The general transport equation has found its main application in the areas of metal oxidation, including anodic oxidation (2–8). Recently, Fromhold has been particularly active in this field, mainly in determining the accumulative effects of space charge on transport processes, through a step-by-step integration of a difference equation for the transport process. (For a review of this work see ref. 8.) In this paper, a differential equation of transport is derived from a difference equation, and its range of validity assessed. For many problems, it is easier and/or more informative to work from the differential equation of transport.

Derivation of Transport Equation

The model is one in which the mobile ionic species must surmount a succession of identical, symmetrical, potential barriers, of height U, and distance from minimum to maximum a. We suppose that:

(*1*) The problem can be treated as a one-dimensional one.

(*2*) Discreteness of charge effects can be neglected in relation to space charge effects which are treated in a continuum fashion.

(*3*) All interaction forces between the mobile species may be neglected except for coulomb forces, which are handled through space charge, as above, and a hard sphere type of force which prevents two species from occupying the same potential well.

(*4*) The height of a potential barrier situated at position x in the presence of an electric field resulting from a combination of space charge and an external

0008-4042/79/111329-06$01.00/0

potential difference is

$$U + qV_x - qV_{x\pm a}$$

where q is the charge on the ion, V the local electrostatic potential at the position indicated by the subscript, the $-$ and $+$ signs being chosen for barrier crossing in the $+x$ and $-x$ directions respectively.

On the basis of elementary rate theory, the net particle flux in the $+x$ direction, J, is thus given by the following:

$$[1]\quad J = m_{x-a}(1 - m_{x+a}/M)\nu \times \exp[-(U + qV_x - qV_{x-a})/kT] - m_{x+a}(1 - m_{x-a}/M)\nu \times \exp[-(U + qV_x - qV_{x+a})/kT]$$

where ν is the particles attempt frequency, $m_{x\pm a}$ the concentration per unit area of mobile species situated near the potential minimum at $x \pm a$, and M the number of sites per unit area for such species at the potential minima. The factors $(1 - m_{x\pm a}/M)$ are included to exclude hops into occupied sites.

The concentrations per unit area may be replaced by concentrations per unit volume through the substitutions

$$[2]\quad m_{x\pm a} = 2an_{x\pm a}$$
$$M = 2aN$$

We define the following dimensionless parameters

$$c = n/N = m/M$$
$$p = qV/kT$$
$$[3]\quad s = x/a$$
$$j = J/[2a\nu N \exp(-U/kT)]$$
$$\varepsilon = qaE/kT = -\mathrm{d}p/\mathrm{d}s$$

where $E = -\partial V/\partial x$ and is the electric field strength.

Equation [1] can now be written

$$[4]\quad j = -\exp(-p_s)[c_{s+1}(1 - c_{s-1})\exp(p_{s+1}) - c_{s-1}(1 - c_{s+1})\exp(p_{s-1})]$$

Setting

$$[5]\quad \alpha = c/(1 - c) = n/(N - n)$$

eq. [4] reduces to

$$[6]\quad j = -\exp(-p_s)[(\alpha\exp(p))_{s+1} - (\alpha\exp(p))_{s-1}]/(1 + \alpha)_{s+1}(1 + \alpha)_{s-1}$$

Taylor series expansions of the functions $(\alpha\exp(p))_{s\pm1}$ and $(1 + \alpha)_{s\pm1}$ about s convert eq. [6] to

$$[7]\quad j = -\frac{2\exp(-p)\{\sinh\partial/\partial s\}(\alpha\exp(p))}{[\{\exp\partial/\partial s\}(1 + \alpha)][\{\exp(-\partial/\partial s)\}(1 + \alpha]}$$

where the terms in braces are operators.

Using the identity

$$\{[\exp(-p)](\partial/\partial s)[\exp(p)]\} \equiv -\{\varepsilon - \partial/\partial s\}$$

it follows that

$$\{[\exp(-p)](\partial/\partial s)^n[\exp(p)]\} \equiv \{[\exp(-p)](\partial/\partial s)[\exp(p)]\}^n \equiv (-1)^n\{\varepsilon - \partial/\partial s\}^n$$

so that eq. [7] may be written

$$[8]\quad j = 2[\{\sinh(\varepsilon - \partial/\partial s)\}\alpha]/[(1 + \alpha)^2 + (1 + \alpha)\alpha'' - \alpha'^2 + \cdots]$$

where the prime denotes differentiation by s.

Factoring $(\varepsilon - \partial/\partial s)$ from the operator, eq. [8] reduces to

$$[9]\quad j = 2[\hat{O}(\varepsilon\alpha - \alpha')]/[(1 + \alpha)^2 + (1 + \alpha)\alpha'' - \alpha'^2 + \cdots]$$

where

$$[10]\quad \hat{O} \equiv \sum_{l=1,3,5,\ldots} (\varepsilon - \partial/\partial s)^{l-1}/l!$$

In order to expand j in terms of increasing order in the derivatives of p and α, $\hat{O}$ must be expanded in terms of increasing order in $\partial/\partial s$. To this end we define $\hat{T}_i^{l-1}$ to be all terms in the expansion of $(-1)^i\{\varepsilon - \partial/\partial s\}^{l-1}$ of order i in $\partial/\partial s$ so that

$$[11]\quad \{\varepsilon - \partial/\partial s\}^{l-1} \equiv \sum_{i=0}^{l-1} (-1)^i\hat{T}_i^{l-1}$$

Since ε and $\partial/\partial s$ do not commute, $(\varepsilon - \partial/\partial s)^n$ cannot be expanded using the binomial theorem. The following procedure is used to obtain $\hat{T}_0{}^n$, $\hat{T}_1{}^n$, $\hat{T}_2{}^n$, ..., $\hat{T}_i{}^n$.

$\hat{T}_0{}^n$ represents the term zero order in $\partial/\partial s$ in the expansion of $(\varepsilon - \partial/\partial s)^n$ and is clearly given by ε^n.

$\hat{T}_1{}^n$ is the term first order in $\partial/\partial s$ in the expansion of $-(\varepsilon - \partial/\partial s)^n$. It is made up of n terms, corresponding to the n factors from which $\partial/\partial s$ may be selected. A typical term is given by $\varepsilon^{n-1-K}(\partial/\partial s)\varepsilon^K$. That is, there is a total of n factors in each term, $n-1$ consisting of ε, the remaining one being $-\partial/\partial s$. Thus $\hat{T}_1{}^n$ is given by

$$\hat{T}_1{}^n = \sum_{K=0}^{n-1} \varepsilon^{n-1-K}(\partial/\partial s)\varepsilon^K = \sum_{K=0}^{n-1} T_0{}^{n-1-K}(\partial/\partial s)\varepsilon^K$$

$\hat{T}_2{}^n$ represents the sum of all terms arising from the different ways of selection $-\partial/\partial s$ from two of the n factors in $(\varepsilon - \partial/\partial s)^n$. If one of the derivatives is selected from the $(K+1)$th factor from the right hand side, and the other from one of the factors to the left of it, then a typical term belonging to this subset has the form

$$[\varepsilon^{n-K-2-j}(\partial/\partial s)\varepsilon^j](\partial/\partial s)\varepsilon^K$$

The sum of all such terms having the right hand derivative selected from the $(K+1)$th term from the right is obtained by summing over j from 0 to $n-K-2$. But

$$\sum_{j=0}^{n-K-2} \varepsilon^{n-K-2-j}(\partial/\partial s)\varepsilon^j = \hat{T}_1{}^{n-K-1}$$

Finally, summing over K we have

$$\hat{T}_2{}^n = \sum_{K=0}^{n-2} T_1{}^{n-K-1}(\partial/\partial s)\varepsilon^K$$

If a third differential operator is selected from the $(K+1)$th position from the right, the other two on the left of it, then by the same process of reasoning it follows that all terms belonging to $T_3{}^n$ having this form, sum to $\hat{T}_2{}^{n-K-1}(\partial/\partial s)\varepsilon^K$ so that $\hat{T}_3{}^n$ is given by

$$\hat{T}_3{}^n = \sum_{K=0}^{n-3} T_2{}^{n-K-1}(\partial/\partial s)\varepsilon^K$$

Repeated application of this process leads to the following general recursive relationship.

$$[12] \quad \hat{T}_i{}^n = \sum_{K=0}^{n-i} \{T_{i-1}{}^{n-1-K}(\partial/\partial s)\varepsilon^K\} \quad i \geq 1$$

If we had begun by selecting the terminal differential operator from the left rather than from the right hand side, an equivalent expression would have been obtained in which the factors $\hat{T}_{i-1}{}^{n-1-K}$ and ε^K are interchanged in eq. [12]. This is the form of the equivalent relationship derived in ref. 4. (A typographical error appears in eq. [2.18], ref. 4: $T_{i-1}{}^k$ should read $T_{i-1}{}^{k+i-2}$.)

We can now write

$$[13] \quad \hat{T}_0{}^n = \varepsilon^n$$

while $\hat{T}_1{}^n$ is given by

$$\hat{T}_1{}^n = \sum_{K=0}^{n-1} \varepsilon^{n-1-K}(\partial/\partial s)\varepsilon^K$$

$$= \sum_{K=0}^{n-1} \varepsilon^{n-1-K}\varepsilon^K(\partial/\partial s) + \varepsilon' \sum_{K=0}^{n-1} \varepsilon^{n-1-K}K\varepsilon^{K-1}$$

On carrying out the summation

$$[14] \quad \hat{T}_1{}^n = \binom{n}{1}\varepsilon^{n-1}(\partial/\partial s) + \binom{n}{2}\varepsilon'\varepsilon^{n-2}$$

where

$$\binom{n}{K} = n!/K!(n-K)!$$

In principal all higher order terms can be evaluated in the same way.

Expanding $\hat{O}$ now in terms of increasing order in $\partial/\partial s$, i.e.

$$[15] \quad \hat{O} = \sum_{i=0}^{\infty} (-1)^i \hat{O}_i$$

we have from eqs. [10] and [11]

$$[16] \quad \hat{O}_i = \sum_{l \geq i}^{\infty} T_i{}^{l-1}/l!$$

where l is restricted to odd integer values. Thus

$$[17] \quad \hat{O}_0 = \sum_{l=1,3,5,\ldots} \frac{1}{l!}\binom{l-1}{0}\varepsilon^{l-1}$$

$$[18] \quad \hat{O}_1 = \left(\sum_{l=3,5,\ldots} \frac{1}{l!}\binom{l-1}{1}\varepsilon^{l-2}\right)\frac{\partial}{\partial s} + \left(\sum_{l=3,5,\ldots} \frac{1}{l!}\binom{l-1}{2}\varepsilon^{l-3}\right)\varepsilon'$$

However,

$$[19] \quad \sum_{l \geq K+1} \frac{1}{l!}\binom{l-1}{K}\varepsilon^{l-1-K} = \frac{1}{K!}\sum_{l=1,3,5,\ldots} \frac{(l-1)(l-2)\ldots(l-K)}{l!}\varepsilon^{l-K-1} = \frac{1}{K!}\sum_{l=1,3,5} \frac{1}{l!}\frac{d^K}{d\varepsilon^K}(\varepsilon^{l-1})$$

$$= \frac{1}{K!}\frac{d^K}{d\varepsilon^K}\left[\varepsilon^{-1}\sum_{l=1,3,5} \frac{\varepsilon^l}{l!}\right] = \frac{1}{K!}\left[\frac{d^K}{d\varepsilon^K}\left(\frac{\sinh\varepsilon}{\varepsilon}\right)\right]$$

Thus

[20] $$\hat{O}_0 = (\sinh \varepsilon)/\varepsilon$$

and

[21] $$\hat{O}_1 = \left[\frac{d}{d\varepsilon}\left(\frac{\sinh \varepsilon}{\varepsilon}\right)\right]\frac{\partial}{\partial s} + \frac{1}{2!}\left[\frac{d^2}{d\varepsilon^2}\left(\frac{\sinh \varepsilon}{\varepsilon}\right)\right]\varepsilon'$$

Upon retaining only up to first order derivatives, the first order expansion of j is obtained from eqs. [9] and [20] and is given by

[22] $$j_1 = \frac{2(\varepsilon\alpha - \alpha')}{(1+\alpha)^2}\left(\frac{\sinh \varepsilon}{\varepsilon}\right)$$

For the model chosen, elementary statistical mechanics gives for the electrochemical potential of the mobile defects, $\bar{\mu}$, the result (see Appendix)

[23] $$\bar{\mu} = \mu^0 + kT \ln \alpha + qV$$

where μ^0 is the standard chemical potential. Thus from eqs. [23] and [3]

[24] $$(\varepsilon\alpha - \alpha') = -\frac{\alpha}{kT}\left(\frac{\partial \bar{\mu}}{\partial s}\right)$$

so that upon conversion to conventional variables eq. [22] can be written

[25] $$J_1 = -\frac{DN\alpha}{kT(1+\alpha)^2}\left(\frac{\partial \bar{\mu}}{\partial x}\right)\frac{\sinh (qaE/kT)}{(qaE/kT)}$$

where

[26] $$D = 4a^2\nu \exp(-U/kT)$$

For $qaE/kT \ll 1$, eq. [25] reduces to the familiar linear transport equation,

[27] $$J_1 = -\frac{DN\alpha}{kT(1+\alpha)^2}\left(\frac{\partial \bar{\mu}}{\partial x}\right) = -\frac{D\partial n}{\partial x} + nvE$$

where $v = qD(1 - n/N)/kT$. Thus D and v are the diffusion coefficient and mobility, respectively, for this model. Note that although D is independent of concentration for this model, v is independent of concentration only if $n/N \ll 1$.

In the absence of an activity gradient, on the other hand, eq. [25] reduces to

[28] $$J_1 = [4a\nu n(1 - n/N)][\exp(-U/kT)] \times \sinh qaE/kT$$

which for $n \ll N$ is identically the Mott–Cabrera conduction equation (5).

Realm of Validity of First Order Equation

We next examine under what conditions the second order terms and presumably higher order terms can be neglected. We do so first for the case $\alpha \ll 1$ so that j_1 may be written as

[29] $$j_1 = 2(\alpha\varepsilon - \alpha')(\sinh \varepsilon)/\varepsilon$$

It is easily shown (4) that eq. [29] is exact for this model for $\alpha \ll 1$, and for $\varepsilon' = 0 = j'$, i.e. for steady-state transport in the absence of space charge. We now consider the contribution of the term $\hat{O}_1(\alpha\varepsilon - \alpha')$ to steady-state transport in the presence of space charge, so the $\varepsilon' \neq 0$ but $j' = 0$. Setting

[30] $$(\alpha\varepsilon - \alpha') = \beta \text{ and } (\sinh \varepsilon)/\varepsilon = Y$$

[31] $$\hat{O}_1\beta = \frac{dY}{d\varepsilon}\beta' + \frac{1}{2}\frac{d^2Y}{d\varepsilon^2}\beta\varepsilon'$$

or alternatively

[32] $$(\hat{O}_1\beta)/(\hat{O}_0\beta) = \frac{d \ln Y}{d\varepsilon}(\ln \beta)' + \frac{1}{2}\frac{1}{Y}\frac{d^2Y}{d\varepsilon^2}\varepsilon'$$

We now eliminate $(\ln \beta)'$ from the second order correction, using the first order approximation. Thus from eq. [29]

[33] $$\ln(j_1/2) = \ln Y + \ln \beta$$

so that upon differentiating by s and setting $j_1' \simeq 0$ we get

[34] $$0 \simeq \frac{d \ln Y}{d\varepsilon}\varepsilon' + (\ln \beta)'$$

Equation [32] can now be written as

[35] $$\hat{O}_1\beta/\hat{O}_0\beta = [\tfrac{1}{2} + (\coth \varepsilon)(1/\varepsilon - \coth \varepsilon)]\varepsilon'$$

The expression for j for steady-state conduction, correct to second order terms, thus becomes

[36] $$j_2 = 2(\varepsilon\alpha - \alpha')[(\sinh \varepsilon)/\varepsilon][1 - (\hat{O}_1\beta)/(\hat{O}_0\beta)]$$

For ε in $(-\infty, +\infty)$, $(\hat{O}_1\beta)/(\hat{O}_0\beta)$ lies in $[-\frac{1}{2}\varepsilon', \frac{1}{6}\varepsilon']$ so that the condition that this second order correction term may be neglected is that $|\varepsilon'/2|$ be small compared to unity. This will be met typically for space charge concentrations up to about 10^{20} electron charges per cm^3.

To avoid any possible confusion on the implications of this statement, we point out that it does not mean that in dealing with ion transport processes space charge need not be considered unless it exceeds 10^{20} electron charges cm^3. This would of course be a totally erroneous interpretation of the

above result. In any given physical problem, eq. [22] must be combined with Poisson's equation, and integrated, to give the net flux as a function of the boundary conditions. This has been done for certain cases to obtain analytical solutions (see, for example, ref. 4).

Another approach to treating physical problems exists, and has been extensively exploited by Fromhold (8). Fromhold's procedure is to use the difference equation, eq. [1] (less the factors $1 - m_{x\pm a}$) along with Gauss' theorem, in a step-by-step numerical calculation to obtain numerical solutions for particular boundary conditions. While such a procedure certainly has merit, where it is possible to obtain them, analytical solutions are usually more informative. Of course, not all situations can be handled analytically, but even when analytical solutions cannot be obtained, it is often easier to carry out numerical calculations using a differential equation for transport rather than a difference equation. This is generally the case for thick films. The point made above is that the differential equation of transport, eq. [22], is a satisfactory approximation to the difference equation (which itself is approximate) provided that the space charge concentration does not exceed about 10^{20} e/cm^2.

In order to evaluate the conditions under which the second order term in the denominator of eq. [9] may be neglected, we proceed as before by evaluating it from the first order approximation. Upon rearranging eq. [22] one obtains:

$$[37] \qquad -\alpha' = \alpha^2 + (2A - \varepsilon)\alpha + A$$

where

$$A = \tfrac{1}{2} j_1 \varepsilon / \sinh \varepsilon$$

Equation [37] may be solved readily if A and ε are treated as constants. For $|\tfrac{1}{2}\varepsilon'| \ll 1$, a condition already shown to be necessary for the validity of the first order expression, A and ε will in fact be nearly constant over short distances (i.e. for $\Delta S \gtrsim 10$ say). As the procedure is tedious, and the result not unexpected, we give only the result. For low field strengths, $\alpha''/(1 + \alpha)$ and $[\alpha'/(1 + \alpha)]^2$ are much smaller than unity everywhere except perhaps very close (relative to total thickness) to one or both of the boundaries. For high field strengths again they are much smaller than unity everywhere except perhaps very close (much less than one jump distance) to the boundary away from which the defects move. It has been shown previously (9) that for high field strengths, c varies only slowly with position except perhaps near the entrance boundary, so the present result is not surprising.

In summary, it appears that for all practical purposes the first order equation, eq. [22], represents the model satisfactorily provided that transport conditions do not depart radically from steady-state conditions and that space charge is not too high, i.e. $\varepsilon' \gtrsim 0.2$. An interesting consequence of forbidding hops into occupied sites is that while the form of the diffusion coefficient is unaltered, the mobility becomes a function of concentration.

1. N. F. Mott and R. W. Gurney. Electronic processes in ionic crystals. 2nd ed. Oxford University Press. 1957. pp. 40–43.
2. L. Young. Anodic oxide films. Academic Press, London. 1961. pp. 13–17.
3. A. T. Fromhold, Jr. and E. L. Cook. J. Appl. Phys. **38**, 1546 (1967).
4. M. J. Dignam, D. J. Young, and D. G. W. Goad. J. Phys. Chem. Solids, **34**, 1227 (1973).
5. N. F. Mott and N. Cabrera. Rep. Prog. Phys. **12**, 163 (1948).
6. D. J. Young and M. J. Dignam. J. Phys. Chem. Solids, **34**, 1235 (1973).
7. M. J. Dignam. *In* Oxides and oxide films. Vol. 1. *Edited by* J. W. Diggle. Marcel Dekker, Inc., New York. 1972. Chapt. 2.
8. A. T. Fromhold, Jr. *In* Oxides and oxide films. Vol. 3. *Edited by* J. W. Diggle and A. K. Vijh. Marcel Dekker, Inc., New York. 1976. Chapt. 1.
9. M. J. Dignam. J. Phys. Chem. Solids, **29**, 249 (1968).
10. R. A. Swalin. Thermodynamics of solids. Wiley, New York. 1962.

Appendix

The Form of the Electrochemical Potential for the Mobile Species

The following derivation of the electrochemical potential for the mobile species follows very closely textbook treatments of Schotky defects in monatomic crystals (see e.g. ref. 1, pp. 28–31 or ref. 10).

For consistency with the transport model treated in the main body of the paper, we assign the following properties to the system: (*1*) There are N sites per unit volume for the mobile defects. A given site may only be empty or singly occupied. (*2*) There is no direct interaction energy between pairs of defects, so that the chemical part of the enthalpy per defect is independent of n. The electrostatic part of the enthalpy is treated in a continuum model, which takes care of the electrostatic part of the interaction energy of the defects. (This is the assumption on which the transport equation was developed.) (*3*) The addition of a defect to the transport medium may alter the existing vibrational frequencies of the medium and introduce new ones. That is to say, there will be in general a thermal entropy change associated with the process. Since there is by postulate no direct interaction between defects, this thermal entropy change per defect will be independent of the number of defects. (*4*) In addition to the thermal

entropy terms, there will be a configurational entropy arising from the number of ways n identical defects can be arranged on N distinguishable sites. We derive first the chemical potential for uncharged defects, and deal with the electrostatic part of the electrochemical potential at the end.

From (*1*) to (*4*) above, the Gibbs free energy for unit volume of the transport medium containing n defects is given by:

$$[A1] \qquad G = G^0 + n\Delta\bar{H} - nT\Delta\bar{S}_v - kT \ln P$$

where G^0 is the free energy prior to introducing the defect, $\Delta\bar{H}$ the enthalpy increase, and $\Delta\bar{S}_v$ the thermal entropy increase per defect added at constant temperature and pressure, and $k \ln P$ the configurational entropy, with P being the statistical weight.

P is the number of microscopically distinguishable ways in which the n identical defects can be arranged in the N available positions, and is given by

$$[A2] \qquad P = N!/[(N - n)!n!]$$

The use of Stirling's formula then gives

$$[A3] \qquad \ln P = N \ln N - (N - n) \ln (N - n) - n \ln n$$

Substituting [A3] into [A1], and evaluating $\mu = (\partial G/\partial n)_{T,\text{pressure}}$, one obtains

$$[A4] \qquad \mu = \Delta\bar{H} - T\Delta\bar{S}_v + kT \ln \left(\frac{n}{N - n}\right)$$

$$[A5] \qquad = \mu^0 + kT \ln \alpha$$

where $\alpha = n/(N - n)$ and is the thermodynamic activity of the mobile defects, as noted in the body of the paper.

If the defects carry a charge q, and reside in a region of electrostatic potential V, then the electrochemical potential is obtained from the chemical potential in the usual way by simply adding the electrostatic potential energy per defect, i.e.

$$[A6] \qquad \bar{\mu} = \mu_0 + kT \ln \alpha + qV$$

If the mobile defects are assigned a polarizability $\bar{\alpha}$, there is then an additional energy term, $-\frac{1}{2}\bar{\alpha}E^2$, to be added to the expression for $\bar{\mu}$, but this term is small for all but extremely large values of E (7). The inclusion of this polarization energy term is not warranted in the present context.

Crystal and molecular structure of (η^3-2-methylallyl)[dimethyl(ethanolamino)-(3,5-dimethyl-1-pyrazolyl)gallato(*N*(2),*N*(3),*O*)]dicarbonylmolybdenum, $[Me_2Ga(N_2C_5H_7)(OCH_2CH_2NH_2)]Mo(CO)_2(\eta^3\text{-}C_4H_7)$

KENNETH S. CHONG, STEVEN J. RETTIG, ALAN STORR, AND JAMES TROTTER

Department of Chemistry, University of British Columbia, 2075 Wesbrook Mall, Vancouver, B.C., Canada V6T 1W5

Received November 7, 1978

KENNETH S. CHONG, STEVEN J. RETTIG, ALAN STORR, and JAMES TROTTER. Can. J. Chem. **57**, 1335 (1979).

Crystals of (η^3-2-methylallyl)[dimethyl(ethanolamino)(3,5-dimethyl-1-pyrazolyl)gallato-(*N*(2),*N*(3),*O*)]dicarbonylmolybdenum are triclinic, $a = 7.6047(5)$, $b = 10.882(1)$, $c = 12.633(1)$ Å, $\alpha = 77.07(1)$, $\beta = 89.19(1)$, $\gamma = 71.91(1)°$, $Z = 2$, space group $P\bar{1}$. The structure was solved by Patterson and Fourier syntheses and was refined by full-matrix least-squares procedures to $R = 0.024$ and $R_w = 0.030$ for 3835 reflections with $I \geq 3\sigma(I)$. The crystal structure consists of discrete molecular units, each linked to four others by weak N—H···O hydrogen bonds (N···O = 3.129(3) and 3.137(4) Å). The Mo atom is in a distorted octahedral environment with the η^3-C_4H_7 ligand occupying one of the six coordination sites as a π-donating ligand. Important bond distances (corrected for libration) are: Mo—C(allyl), 2.335(3), 2.372(3), 2.324(3); Mo—C(O), 1.902(3) and 1.961(2); Mo—O, 2.269(2); Mo—N(pz), 2.222(2); Mo—N(amino), 2.285(2); Ga—O, 1.924(2); Ga—N, 2.006(2); and Ga—C, 1.968(4) and 1.981(4) Å.

KENNETH S. CHONG, STEVEN J. RETTIG, ALAN STORR et JAMES TROTTER. Can. J. Chem. **57**, 1335 (1979).

Les cristaux du (η^3 méthyl-2 allyl)[diméthyl(éthanolamino)(diméthyl-3,5 pyrazolyl-1) gallato (*N*(2),*N*(3),*O*)] dicarbonyl de molybdène sont tricliniques $a = 7.6047(5)$, $b = 10.882(1)$, $c = 12.633(1)$ Å, $\alpha = 77.07(1)$, $\beta = 89.19(1)$, $\gamma = 71.91(1)°$, $Z = 2$, groupe d'espace $P\bar{1}$. On a résolu la structure par des synthèses de Patterson et de Fourier et on l'a affinée par la méthode des moindres carrés (matrice complète) jusqu'à des valeurs de $R = 0.024$ et $R_w = 0.030$ pour 3835 réflexions avec $I \geq 3\sigma(I)$. La structure cristalline comporte des unités moléculaires définies reliées à quatre autres par des liaisons hydrogènes N—H···O faibles (N···O = 3.129(3) et 3.137(4) Å). L'environnement de l'atome de Mo est un octaèdre déformé dans lequel le ligand η^3-C_4H_7 occupe un des six sites de coordination sous forme de ligand donnant des électrons π. Les distances de liaisons importantes (corrigées pour la libration) sont: Mo—C(allyl), 2.335(3), 2.372(3), 2.324(3), Mo—C(O), 1.902(3) et 1.961(2), Mo—O, 2.269(2), Mo—N(pz), 2.222(2), Mo—N(amino), 2.285(2), Ga—O, 1.924(2), Ga—N, 2.006(2) et Ga—C, 1.968(4) et 1.981(3) Å.

[Traduit par le journal]

Introduction

The synthesis and coordinating properties of the anionic ligands **1** have been discussed in previous publications (1–3). The ligands represent part of an ongoing program investigating a range of anionic gallate ligands and their coordinating abilities towards transition metal species. The present paper describes the crystal structure analysis of the complex $[Me_2Ga(N_2C_5H_7)(OCH_2CH_2NH_2)]Mo(CO)_2(\eta^3\text{-}C_4H_7)$. The structure confirms our earlier predictions (3) regarding the *fac* nature of the tridentate gallate ligand in this type of octahedral complex and also establishes the position of substitution of the η^3-C_4H_7 moiety. Bond length data and ν_{CO} stretching frequencies are discussed in conjunction with similar data for the related complexes described earlier, $[MeGa(N_2C_3H_3)_3]Mo(CO)_2(\eta^3\text{-}C_3H_5)$, **2** (4), and $[MeGa(N_2C_5H_7)_2(OH)]Mo(CO)_2(\eta^3\text{-}C_4H_7)$, **3** (5).

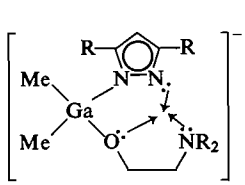

1 (R = H, Me)

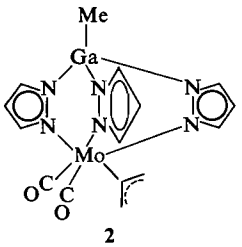

2

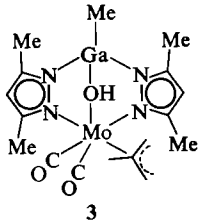

3

0008-4042/79/111335-06$01.00/0

Experimental

The title compound was prepared and characterized as described previously (3). Crystals suitable for X-ray study were obtained by recrystallization from benzene. The crystal chosen was mounted in a general orientation and had dimensions of ca. 0.35 × 0.44 × 0.48 mm. Unit-cell parameters were refined by least-squares on 2 sin θ/λ values for 25 reflections measured on a diffractometer with MoK_α radiation (λ = 0.71073 Å). Crystal data (at 22°C) are:

$C_{15}H_{26}GaMoN_3O_3$ fw = 462.05
Triclinic, a = 7.6047(5), b = 10.882(1), c = 12.633(1) Å, α = 77.07(1), β = 89.19(1), γ = 71.91(1)°, V = 966.9(2) Å^3, Z = 2, ρ_c = 1.587 g cm^{-3}, $F(000)$ = 468, $\mu(MoK_\alpha)$ = 21.2 cm^{-1}. Absent reflections: none. Space group $P\bar{1}$ (C_i^1, No. 2) from structure analysis. Cell reduction failed to locate a cell of higher symmetry, reduced cell is given above.

Intensities were measured with graphite monochromatized MoK_α radiation on an Enraf-Nonius CAD4-F diffractometer. An ω scan at 0.91–6.71° min^{-1} over a range of (0.85 + 0.35 tan θ) degrees in ω (extended by 25% on both sides for background measurement) was employed. Data were measured to 2θ = 55°. The intensities of 3 check reflections, measured every 3600 s throughout the data collection, did not vary by more than 1%. After data reduction, an absorption correction was applied using the Gaussian integration method (6, 7). Transmission factors ranged from 0.455 to 0.524. Of the 4413 independent reflections measured, 3835 (87%) had intensities greater than 3σ(I) above background where $\sigma^2(I) = S + 2B + (0.04(S - B))^2$ with S = scan count and B = background count.

Analysis was initiated in the centrosymmetric space group $P\bar{1}$ on the basis of the E-statistics. The positions of the molybdenum and gallium atoms were determined from the Patterson function and those of the remaining non-hydrogen atoms from a subsequent difference map. After full-matrix least-squares refinement of all non-hydrogen atoms with anisotropic thermal parameters to R = 0.034, a difference map gave positions for all 26 hydrogen atoms which were included in all subsequent cycles of refinement with isotropic thermal parameters. The scattering factors of ref. 8 were used for non-hydrogen atoms and those of ref. 9 for hydrogen atoms. Anomalous scattering factors from ref. 10 were used for the Mo and Ga atoms. The weighting scheme, $w = 1/\sigma^2(F)$ where $\sigma^2(F)$ is derived from the previously defined, $\sigma^2(I)$ gave uniform average values of $w(|F_o| - |F_c|)^2$ over ranges of $|F_o|$ and was employed in the final stages of refinement. An isotropic Type I extinction correction (Thornley–Nelmes definition of mosaic anisotropy with a Lorentzian distribution) was applied (11–13). The final value of g was 0.61(7) × 10^4. Convergence was reached at R = 0.024 and R_w = 0.030 for 3835 reflections with $I \geq 3\sigma(I)$. For all 4418 reflections R = 0.030 and R_w = 0.031.

On the final cycle of refinement the mean and maximum parameter shifts corresponded to 0.14 and 1.1σ respectively. The mean error in an observation of unit weight was 0.9875. A final difference map showed maximum fluctuations of ±0.95 e Å^{-3} near the heavy atoms and ±0.25 e Å^{-3} elsewhere (carbon peak heights on earlier maps had heights of 5–9 e Å^{-3}). The final positional and thermal parameters appear in Tables 1 and 2[1] respectively. Measured and calculated structure factors have been placed in the Depository of Unpublished Data.[1]

[1]The structure factor table and Table 2 (thermal parameters) are available, at a nominal charge, from the Depository of Unpublished Data, CISTI, National Research Council of Canada, Ottawa, Ont., Canada K1A 0S2.

TABLE 1. Final positional parameters (fractional × 10^4, Mo and Ga × 10^5, H × 10^3) with estimated standard deviations in parentheses

Atom	x	y	z
Mo	37659(2)	45588(2)	26260(1)
Ga	43367(4)	16566(3)	17611(2)
O(1)	2351(3)	6612(2)	4014(2)
O(2)	−483(3)	5062(3)	2522(2)
O(3)	5446(2)	3021(2)	1750(1)
N(1)	3468(3)	2739(2)	3714(2)
N(2)	3478(3)	1690(2)	3262(2)
N(3)	6607(3)	3697(3)	3532(2)
C(1)	2880(3)	5813(3)	3495(2)
C(2)	1094(3)	4869(3)	2505(2)
C(3)	2170(5)	2372(5)	722(3)
C(4)	6229(7)	−67(4)	1767(4)
C(5)	5171(4)	6027(3)	1614(2)
C(6)	3333(4)	6494(3)	1218(2)
C(7)	2664(4)	5594(3)	842(2)
C(8)	2813(3)	2503(2)	4713(2)
C(9)	2418(4)	1310(3)	4904(2)
C(10)	2835(4)	842(3)	3973(2)
C(11)	7379(4)	2612(3)	2030(3)
C(12)	7700(4)	2447(3)	3238(3)
C(13)	2020(7)	7834(4)	1290(4)
C(14)	2605(5)	3411(4)	5464(3)
C(15)	2645(7)	−383(4)	3713(4)
H(Na)	719(5)	430(4)	340(3)
H(Nb)	653(4)	362(3)	420(3)
H(3a)	257(8)	243(6)	−1(6)
H(3b)	124(8)	315(6)	76(5)
H(3c)	152(7)	181(5)	81(4)
H(4a)	702(7)	−46(5)	245(4)
H(4b)	697(8)	13(6)	128(5)
H(4c)	554(6)	−68(5)	175(4)
H(5a)	606(4)	538(3)	129(2)
H(5b)	565(5)	658(4)	199(3)
H(7a)	349(4)	496(3)	57(3)
H(7b)	148(5)	584(3)	59(3)
H(9)	197(5)	89(3)	555(3)
H(11a)	789(4)	328(3)	163(2)
H(11b)	806(4)	178(3)	179(2)
H(12a)	726(4)	175(3)	359(2)
H(12b)	904(5)	223(3)	346(3)
H(13a)	72(6)	781(4)	143(3)
H(13b)	220(6)	845(5)	69(4)
H(13c)	243(5)	806(4)	186(3)
H(14a)	170(5)	419(4)	523(3)
H(14b)	355(6)	368(4)	557(3)
H(14c)	222(6)	310(5)	614(4)
H(15a)	382(7)	−97(5)	346(4)
H(15b)	194(8)	−70(6)	417(5)
H(15c)	211(6)	−14(5)	302(4)

The ellipsoids of thermal motion for the non-hydrogen atoms are shown in Fig. 1. The thermal motion has been analysed in terms of the rigid-body modes of translation, libration, and screw motion (14) using the computer program MGTLS. The rms standard error in the temperature factors σU_{ij} (derived from the least-squares analysis) is 0.0014 Å^2. Analysis of all non-hydrogen atoms except the carbonyl oxygen atoms O(1) and O(2) gave physically reasonable rigid-body parameters (rms ΔU_{ij} = 0.0040 Å^2). The appropriate bond distances have been corrected for libration (15), using

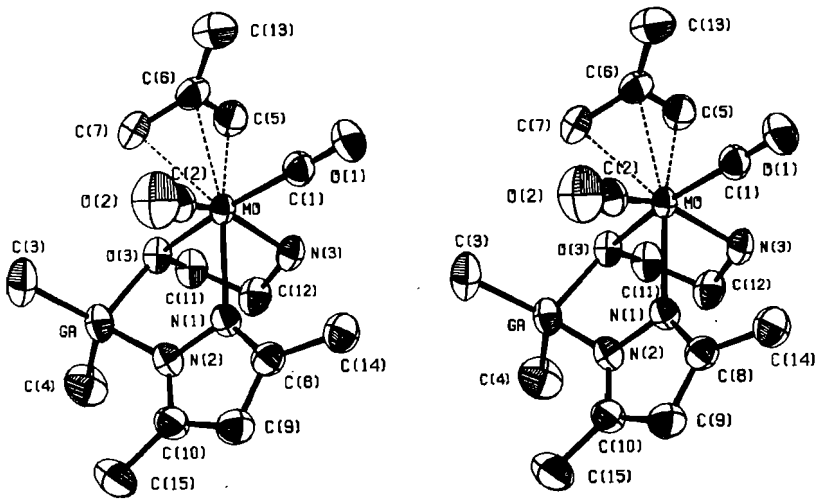

FIG. 1. Stereo view of the (η^3-2-methylallyl)[dimethyl(ethanolamino)(3,5-dimethyl-1-pyrazolyl)gallato(*N(2),N(3),O*)]dicarbonylmolybdenum molecule, 50% ellipsoids are shown for the non-hydrogen atoms. Hydrogen atoms have been omitted for the sake of clarity.

TABLE 3. Bond lengths (Å) with estimated standard deviations in parentheses

(*a*) Non-hydrogen atoms

	Length			Length	
Bond	Uncorr.	Corr.	Bond	Uncorr.	Corr.
Mo —O(3)	2.263(2)	2.269	O(3) —C(11)	1.422(3)	1.424
Mo —N(1)	2.217(2)	2.222	N(1) —N(2)	1.384(3)	1.387
Mo —N(3)	2.278(2)	2.285	N(1) —C(8)	1.351(3)	1.352
Mo —C(1)	1.898(3)	1.902	N(2) —C(10)	1.339(3)	1.339
Mo —C(2)	1.956(2)	1.961	N(3) —C(12)	1.482(4)	1.484
Mo —C(5)	2.331(3)	2.335	C(5) —C(6)	1.388(4)	1.391
Mo —C(6)	2.370(3)	2.372	C(6) —C(7)	1.402(4)	1.405
Mo —C(7)	2.320(3)	2.324	C(6) —C(13)	1.511(5)	1.512
Ga —O(3)	1.919(2)	1.924	C(8) —C(9)	1.390(4)	1.391
Ga —N(2)	2.002(2)	2.006	C(8) —C(14)	1.490(4)	1.492
Ga —C(3)	1.963(4)	1.968	C(9) —C(10)	1.379(4)	1.382
Ga —C(4)	1.977(4)	1.981	C(10)—C(15)	1.491(4)	1.492
O(1)—C(1)	1.174(3)	1.174	C(11)—C(12)	1.511(4)	1.514
O(2)—C(2)	1.152(3)	1.152			

(*b*) Bonds involving hydrogen atoms

Bond	Length
N—H	0.83(3) and 0.88(4)
C(pz)—H	0.96(3)
C(allyl)—H	0.89–1.00(3) (Mean 0.94(5))
C(sp^3)—H	0.87–1.02(3–7) (Mean 0.94(5))

shape parameters q^2 of 0.08 for all atoms involved. Corrected bond lengths are given in Table 3 along with the uncorrected values. Corrected bond angles differ by less than 0.1° from the uncorrected values listed in Table 4. Intra-annular torsion angles in the five-membered chelate rings are given in Table 5 and details of the hydrogen bonding are given in Table 6.

Results and Discussion

The crystal structure of $[Me_2Ga(N_2C_5H_7)(OCH_2CH_2NH_2)]Mo(CO)_2(\eta^3\text{-}C_4H_7)$ consists of discrete molecules, each linked to four others by an extensive network of weak N—H···O hydrogen bonds involv-

TABLE 4. Bond angles (deg) with estimated standard deviations in parentheses

(*a*) Non-hydrogen atoms

Bonds	Angle (deg)	Bonds	Angle (deg)
O(3)—Mo—N(1)	80.4(1)	N(2)—Ga —C(4)	110.0(2)
O(3)—Mo—N(3)	74.7(1)	C(3)—Ga —C(4)	121.2(2)
O(3)—Mo—C(1)	167.2(1)	Mo —O(3) —Ga	111.9(1)
O(3)—Mo—C(2)	114.0(1)	Mo —O(3) —C(11)	112.9(2)
O(3)—Mo—C(5)	87.5(1)	Ga —O(3) —C(11)	117.4(2)
O(3)—Mo—C(6)	99.2(1)	Mo —N(1) —N(2)	118.3(1)
O(3)—Mo—C(7)	79.5(1)	Mo —N(1) —C(8)	132.7(2)
N(1)—Mo—N(3)	79.5(1)	N(2)—N(1) —C(8)	106.8(2)
N(1)—Mo—C(1)	101.1(1)	Ga —N(2) —N(1)	119.9(2)
N(1)—Mo—C(2)	77.5(1)	Ga —N(2) —C(10)	131.2(2)
N(1)—Mo—C(5)	159.8(1)	N(1)—N(2) —C(10)	108.9(2)
N(1)—Mo—C(6)	164.0(1)	Mo —N(3) —C(12)	111.3(2)
N(1)—Mo—C(7)	130.9(1)	Mo —C(1) —O(1)	178.2(2)
N(3)—Mo—C(1)	93.0(1)	Mo —C(2) —O(2)	174.3(2)
N(3)—Mo—C(2)	153.4(1)	Mo —C(6) —C(5)	71.3(2)
N(3)—Mo—C(5)	81.7(1)	Mo —C(6) —C(7)	70.6(2)
N(3)—Mo—C(6)	115.9(1)	Mo —C(6) —C(13)	122.5(2)
N(3)—Mo—C(7)	135.5(1)	C(5)—C(6) —C(7)	116.3(3)
C(1)—Mo—C(2)	78.6(1)	C(5)—C(6) —C(13)	123.4(3)
C(1)—Mo—C(5)	87.3(1)	C(7)—C(6) —C(13)	119.9(3)
C(1)—Mo—C(6)	83.0(1)	N(1)—C(8) —C(9)	109.4(2)
C(1)—Mo—C(7)	108.0(1)	N(1)—C(8) —C(14)	123.0(2)
C(2)—Mo—C(5)	122.5(1)	C(9)—C(8) —C(14)	127.5(2)
C(2)—Mo—C(6)	88.3(1)	C(8)—C(9) —C(10)	105.8(2)
C(2)—Mo—C(7)	70.9(1)	N(2)—C(10)—C(9)	109.0(2)
O(3)—Ga —N(2)	92.4(1)	N(2)—C(10)—C(15)	121.8(3)
O(3)—Ga —C(3)	109.0(1)	C(9)—C(10)—C(15)	129.2(3)
O(3)—Ga —C(4)	111.5(2)	O(3)—C(11)—C(12)	109.9(2)
N(2)—Ga —C(3)	108.9(1)	N(3)—C(12)—C(11)	108.2(2)

(*b*) Angles involving hydrogen atoms

Bonds	Angle (deg)
R—N—H	109–113(2–3)
R—C(pz)—H	127(2) and 127(2)
C—C(allyl)—H	117–120(2)
R—C(sp^3)—H	104–121(2–4)
H—N—H	99(3)
H—C(allyl)—H	117(3) and 118(3)
H—C(sp^3)—H	90–125(2–5)

ing the carbonyl oxygen atoms (N···O = 3.129(3) and 3.137(4) Å are in the range of 2.55–3.25 Å normally observed for N—H···O hydrogen bonds, see Table 6). All other intermolecular distances correspond to normal van der Waals contacts.

The X-ray crystallographic analysis confirms unequivocally the tridentate chelating character of the gallate ligand and also the *fac* nature of its coordination in this type of complex, an arrangement predicted earlier from ir studies (3). The Mo atom is in a distorted octahedral environment with the η^3-C_4H_7 ligand occupying one of the six coordination sites as a π-donating ligand. As predicted on the basis of molecular model studies (3), the η^3-C_4H_7 is situated *trans* to the pyrazolyl nitrogen atom (see Fig. 1). The steric requirements of the gallate ligand in the present structure force the η^3-C_4H_7 ligand to have an orientation 'opposite' to

TABLE 5. Intra-annular torsion angles (deg)

Bond	Angle obs.	Bond	Angle obs.
	Five-membered chelate rings		
Mo —O(3)	38.9(1)	Mo —O(3)	−14.6(2)
O(3)—Ga	−36.3(1)	O(3) —C(11)	41.1(2)
Ga —N(2)	14.7(1)	C(11)—C(12)	−53.8(3)
N(2)—N(1)	14.3(2)	C(12)—N(3)	40.2(2)
N(1)—Mo	−30.9(1)	N(3) —Mo	−14.8(2)

TABLE 6. Hydrogen-bond data* (distances in Å and angles in deg)

D—H···A	H···A	D···A	∠DHA	∠XAH†
N(3)—H(Na)···O(2)[1]	2.35(4)	3.137(4)	149(3)	144(1)
N(3)—H(Nb)···O(1)[2]	2.36(3)	3.129(3)	155(3)	124.8(8)

*Superscripts refer to atoms at positions: [1] $1 + x, y, z$; [2] $1 - x, 1 - y, 1 - z$.
†Atom X is bonded to atom A.

TABLE 7. Carbonyl group geometry (distances in Å and angles in deg) and ν_{co} (cm^{-1}) for $LMo(CO)_2X$ complexes*

L	X	ν_{CO}	M—C	C—O	M—C—O	Ref.
$HB(N_2C_3H_3)_3$	η^3-C_4H_7	1958	1.959	1.150	177.3	16
		1874	1.958	1.151	177.8	
$MeGa(N_2C_3H_3)_3$	η^3-C_3H_5	1948	1.948	1.162	177.2	4
		1860	1.936	1.166	176.5	
$MeGa(N_2C_5H_7)_2OH$	η^3-C_4H_7	1940	1.931	1.177	173.5	5
		1850	1.917	1.174	173.7	
$Me_2Ga(N_2C_5H_7)(OCH_2CH_2NH_2)$	η^3-C_4H_7	1933	1.961	1.152	174.3	This
		1840	1.902	1.174	178.2	work

*ν_{CO} for cyclohexane solutions.

that observed in **2** (4), **3** (5), and the related boron complex $[HB(N_2C_3H_3)_3]Mo(CO)_2(\eta^3\text{-}C_4H_7)$ (16); i.e. the substituent on the central carbon of the allyl group is directed toward, rather than away from, the two carbonyl groups. As a result of methyl–carbonyl repulsions the central Mo—C(allyl) distance is significantly longer than the two other Mo—C(allyl) distances. This is in contrast to the structures of **2**, **3**, and most other η^3-allyl structures (17, 18, and references therein) where the central M—C bond is the shortest of the three. Tilt angles and other parameters describing the mode of allyl coordination to the metal atom have been calculated; δ^1, δ^2, and *h* (defined in ref. 17 and calculated assuming the 'coordination plane' to be normal to the Mo—C(1) vector) are 118.6°, 111.3°, and 0.30 Å respectively and the parameters τ and β (defined in ref. 18) are 117.6° and 90.4°. All of these parameters are intermediate with respect to the observed ranges (17, 18) although the tilt angles δ^1 and τ are both higher than the mean values for these parameters (115° for both δ^1 and τ). All of the other allyl complexes listed (17, 18) in which the central M—C(allyl) bond is longer than the others have higher than average tilt angles. The distance from the Mo atom to the centre of mass of the three coordinated allyl carbon atoms, *D'*, is 2.103 Å which is at the long end of the 2.02–2.10 Å range observed for d^4-M(allyl)L_5 complexes (18).

The Mo—N(pz) bond *trans* to the allyl ligand is shortened to 2.222(2) Å relative to corresponding distances of 2.242(4) Å in **3** and 2.232(3) Å in **2**. The Mo—O distance of 2.269(2) Å agrees well with the value of 2.272(4) Å in **3**. The Mo—N(amino) distance is 2.285(2) Å.

It is noteworthy that the carbonyl C—O bond lengths are significantly different in the present structure with the C—O bond *trans* to the oxygen atom of the gallate ligand being 0.022(4) Å longer than the C—O bond *trans* to the amino nitrogen donor atom. The Mo—C(O) distances also reflect this effect with the Mo—C(O) bond *trans* to oxygen being much shorter than that *trans* to the amino nitrogen (1.902(3) vs. 1.961(2) Å). The differences between the Mo—C(O) and C—O distances probably arise from a combination of structural *trans* effects and steric effects, the latter being most important in this case as C(2) is forced well away from an 'ideal' coordination site. There are two significant intramolecular non-bonded contacts, both of which involve the ethanolamine moiety (H(5a)···H(11a) = 2.23(4), and H(4b)···H(11b) = 2.41(6) Å). As in the structures of **2** and **3** (4, 5) the M—C—O bond angles are significantly non-linear (178.2(2) and 174.3(2)°), an effect almost certainly arising from packing forces and intramolecular steric effects. Deviations of this magnitude are quite common in this type of carbonyl complex (16, 19, 20).

The ν_{CO} frequencies for the title complex listed in Table 7, along with those for related compounds, are the lowest in the series and based on previous arguments (4, 5), might be expected to result in longer C—O bond distances. The data, however, do not reveal the expected values of ~1.18 Å for these distances but rather two very different C—O bond lengths, the shorter of the two being almost the same as the C—O distance in the boron complex $[HB(N_2C_3H_3)_3]Mo(CO)_2(\eta^3\text{-}C_4H_7)$ (16) which displays much higher ν_{CO} frequencies.

The gallium atom is tetrahedrally coordinated to two methyl groups (Ga—C = 1.968(4) and 1.981(4) Å), the oxygen atom of the ethanolamine moiety (Ga—O = 1.924(2) Å), and to a pyrazolyl nitrogen atom (Ga—N = 2.006(2) Å). Bond angles at gallium range from 92.4° in the chelate ring to 121.2(2)° between the methyl groups. The bond lengths involving gallium are as expected (ref. 1 and references therein). The difference between the two Ga—C bond lengths, although not statistically significant, may be caused by the steric interaction between the C(4) methyl group and the ethanolamine moiety mentioned above.

Steric factors are responsible for a slight but significant non-planarity of the pyrazolyl ring (χ^2 = 9.2 for the five ring atoms) and as in related structures (4, 5) the metal atoms are considerably displaced from the mean plane of the pyrazolyl ring (Mo by 0.4985(2) and Ga by 0.0116(3) Å). The trivalent oxygen atom has distinctly pyramidal coordination geometry (mean bond angle at O is 114.1°). The allyl group is significantly non-planar, the central carbon atom being displaced 0.04 Å from the C(5)C(7)C(13) plane. Other bond lengths and angles in the molecule assume normal values.

Acknowledgments

We thank the National Research Council of Canada for financial support and the University of British Columbia Computing Centre for assistance.

1. K. S. Chong, S. J. Rettig, A. Storr, and J. Trotter. Can. J. Chem. **56**, 1212 (1978).
2. K. S. Chong, S. J. Rettig, A. Storr, and J. Trotter. Can. J. Chem. **55**, 4166 (1977).
3. K. S. Chong and A. Storr. Can. J. Chem. **57**, 167 (1979).
4. K. R. Breakell, S. J. Rettig, D. L. Singbeil, A. Storr, and J. Trotter. Can. J. Chem. **56**, 2099 (1978).
5. K. R. Breakell, S. J. Rettig, A. Storr, and J. Trotter. Can. J. Chem. **57**, 139 (1979).
6. P. Coppens, L. Leiserowitz, and D. Rabinovich. Acta Crystallogr. **18**, 1035 (1965).
7. W. R. Busing and H. A. Levy. Acta Crystallogr. **22**, 457 (1967).
8. D. T. Cromer and J. B. Mann. Acta Crystallogr. Sect. A, **24**, 321 (1968).
9. R. F. Stewart, E. R. Davidson, and W. T. Simpson. J. Chem. Phys. **42**, 3175 (1965).
10. D. T. Cromer and D. Liberman. J. Chem. Phys. **53**, 1891 (1970).
11. P. J. Becker and P. Coppens. Acta Crystallogr. Sect. A, **30**, 129 (1974); **30**, 148 (1974); **31**, 417 (1975).
12. P. Coppens and W. C. Hamilton. Acta Crystallogr. Sect. A, **26**, 71 (1970).
13. F. R. Thornley and R. J. Nelmes. Acta Crystallogr. Sect. A, **30**, 748 (1974).
14. V. Schomaker and K. N. Trueblood. Acta Crystallogr. Sect. B, **24**, 63 (1969).
15. D. W. J. Cruickshank. Acta Crystallogr. **9**, 747 (1956); **9**, 754 (1956); **14**, 896 (1961).
16. E. M. Holt, S. L. Holt, and K. J. Watson. J. Chem. Soc. Dalton Trans. 2444 (1973).
17. C. F. Putnik, J. J. Welter, G. D. Stucky, M. J. D'Aniello, Jr., B. A. Sosinsky, J. F. Kirner, and E. L. Muetterties. J. Am. Chem. Soc. **100**, 4107 (1978).
18. J. A. Kaduk, A. T. Poulos, and J. A. Ibers. J. Organomet. Chem. **127**, 245 (1977).
19. G. H. Barnett, M. K. Cooper, M. McPartlin, and G. B. Robertson. J. Chem. Soc. Dalton Trans. 587 (1978).
20. S. F. A. Kettle. Inorg. Chem. **4**, 1661 (1965).

Gas phase observation of the first overtone of the H—F stretching fundamental in hydrogen bonded complexes

J. W. BEVAN,[1] B. MARTINEAU, AND C. SANDORFY

Département de Chimie, Université de Montréal, Montréal (Qué.), Canada H3C 3V1

Received December 8, 1978

J. W. BEVAN, B. MARTINEAU, and C. SANDORFY. Can. J. Chem. 57, 1341 (1979).

First overtones of H—F and D—F stretching vibrations in hydrogen bonded complexes with dimethylether, diethylether, and acetone have been measured in the gas phase. The assignment of the observed bands is discussed together with previously made observations on the fundamentals. Anharmonicity constants of the order of -200 and -100 cm^{-1} are determined for the most probable assignments from the available data for the H—F and D—F stretching vibrations (ν_1) while their values in the "free" H—F and D—F molecules are -90 and -46 cm^{-1} respectively. The spectra are compatible with a coupling constant between the ν_1 and the bridge stretching vibration (ν_3) of the order of $+70$ cm^{-1}.

J. W. BEVAN, B. MARTINEAU et C. SANDORFY. Can. J. Chem. 57, 1341 (1979).

Les premières harmoniques des vibrations de valence H—F et D—F dans les complexes formés avec le diméthyléther, le diéthyléther et l'acétone ont été mesurées dans l'état gazeux. L'attribution des bandes observées est discutée conjointement avec celle des fondamentales. La constante d'anharmonicité de la vibration de valence H—F et D—F (ν_1) augmente considérablement en conséquence de la formation de liaisons hydrogène. La constante de couplage entre ν_1 et la vibration de valence du pont (ν_3) semble être environ 70 cm^{-1}.

Introduction

Anharmonicity is a fundamental quantity for the understanding of the nature of H-bonding. This was recognized twenty years ago by Bratos and Hadži (1) and by Sheppard (2). All existing theories of H-bonding imply anharmonicity directly or indirectly. It is not intended here to review these theories; we only mention the most recent treatments of the problem that are known to us: those by Robertson (3), by Sokolov and Savelev (4), and by Bouteiller and Maréchal (5).

Let us consider the simple triatomic model X—H---Y and let ν_1, ν_2, and ν_3 be the frequencies of the X—H stretching, X—H bending, and XH---Y stretching vibrations respectively. In the linear model ν_2 is degenerate. However, in most actual systems it will give rise to an out-of-plane and an in-plane bending vibration. Disregarding the out-of-plane bending mode the mechanical anharmonicity can be characterized, to the second order, by the anharmonicity constants X_{11}, X_{22}, and X_{33} for the three normal vibrations and the coupling constants X_{12}, X_{13}, and X_{23}.

In this approximation a vibrational term is:

$$[1]\quad G(v_1, v_2, v_3) = \omega_1(v_1 + \tfrac{1}{2}) + \omega_2(v_2 + \tfrac{1}{2}) + \omega_3(v_3 + \tfrac{1}{2}) + X_{11}(v_1 + \tfrac{1}{2})^2 + X_{22}(v_2 + \tfrac{1}{2})^2 + X_{33}(v_3 + \tfrac{1}{2})^2 + X_{12}(v_1 + \tfrac{1}{2})(v_2 + \tfrac{1}{2}) + X_{13}(v_1 + \tfrac{1}{2}) \times (v_3 + \tfrac{1}{2}) + X_{23}(v_2 + \tfrac{1}{2})(v_3 + \tfrac{1}{2})$$

and the frequencies of given bands are obtained from:

$$[2]\quad \nu = G(v_1',v_2',v_3') - G(v_1'',v_2'',v_3'')$$

(see Herzberg (6)).

By far the most important constant is X_{13}; its value is a measure of the coupling between the X—H and XH---Y stretching motions on which most hydrogen bond theories are based. The other constants are also important, however; they contribute in determining the frequencies and intensities of the vibrations and the changes that are produced in these quantities by environmental effects; they are needed for a more complete knowledge of the potential surface. This work reports new information on two of these constants: X_{11} and X_{13}.

The experimental determination of anharmonicity constants entails the measurement of overtones and combination tones. A number of such investigations have been carried out in solution (7–11) (for a review see ref. 12). Solvent effects, however, might affect the frequencies of fundamentals, overtones, and combination tones to different degrees. Thus results obtained in solution apply only approximately to isolated hydrogen bonds.

Gas phase studies of hydrogen bonded complexes

[1]Present address: Department of Chemistry, Texas A and M University, College Station, TX 77843, U.S.A.

0008-4042/79/111341-09$01.00/0

enable these systems to be investigated free from solvent perturbations. The initial gas phase infrared studies of H—F and H—Cl hydrogen bonded stretching fundamentals by Arnold and Millen (13) and by Bertie and Millen (14) have been extended and numerous other systems have been examined (15–19). However, to our knowledge no gas phase data exist for the first or higher overtones of these vibrations, presumably due to their apparent weakness.

The present investigation represents an attempt to observe the first overtone (v_1^{02}) of the high frequency H-bonded stretching fundamental in the gas phase so that an estimate of the anharmonicity constant X_{11} can be made. At the same time an attempt is made to identify ($2v_1 + v_3$) type combination bands. The ir spectra of dimethylether, diethylether, and acetone with hydrogen fluoride were chosen for study because they form relatively strong volatile complexes whose fundamentals had been the subject of previous investigation (13–19). Several deuterated analogues were also studied to provide additional information.

Experimental

All near-infrared spectra of the hydrogen bonded overtones were recorded with a Cary-17 spectrometer and a corrosion resistent Wilks multireflection cell. Gold surfaced mirrors and calcium fluoride windows were employed with a variable cell pathlength of 0.75 to 20 m. Certain of the corresponding fundamentals were recorded in a 10 cm cell using a Perkin-Elmer 621 spectrometer.

Hydrogen fluoride was purchased from Matheson while deuterium fluoride and d_{10} diethyl ether were obtained from Merck, Sharpe and Dohme of Canada. They were used without further purification.

There is always a danger in these experiments of having >O:---H—F---H—F type complexes present in addition to >O:---H—F. However, we varied the relative pressures of the proton donor and acceptor between wide limits without observing significant changes in the spectra.

Results

When hydrogen fluoride and ethers or acetone are mixed together an intense new feature, not present in the spectra of the components, appears in the spectrum of the mixture. Subtraction spectra of the regions of interest are recorded in Figs. 1–7. These bands show considerable similarity to those of the fundamental H—F stretching vibration previously recorded by Millen *et al.* (13, 14). The main bands observed could be attributed to overtone or combination bands of the hydrogen bonded complexes. The absence of other new bands at lower frequencies in all mixtures effectively rules out overtones and combination tones involving vibrations with frequencies less than 2000 cm^{-1}. Mixtures of the perdeuterated electron donors with hydrogen fluoride show practically no change in the position of overtone and combination bands involving H—F vibrations while, naturally, they displace those involving C—H motions. Additional support to the assignment of the strongest bands in these spectra to the first overtone of the H-bonded H—F stretching vibration is provided by the similarity of their profile to the corresponding fundamental. The v_H/v_D ratio can be used to confirm individual assignments.

Similar spectra have been obtained for common species of the donors with deuterium fluoride. The positions of the band maxima are recorded in Table 1, while the data calculated from these using eq. [2] are given in Table 2. Several other weak features

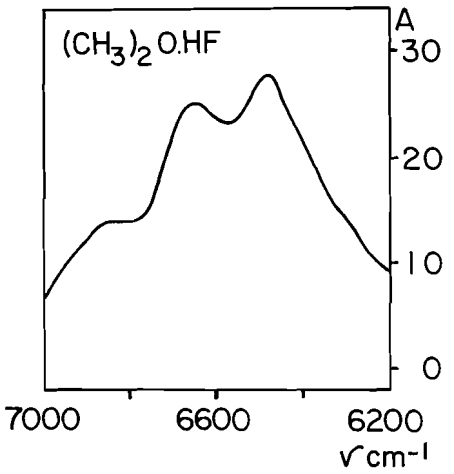

FIG. 1. A part of the gas phase near-infrared spectrum of the $(CH_3)_2O{\cdot}HF$ complex. Pressure: dimethylether 55 Torr, hydrogen fluoride 30 Torr. Optical path: 14.25 m. Absorbance in arbitrary units against frequency in cm^{-1}.

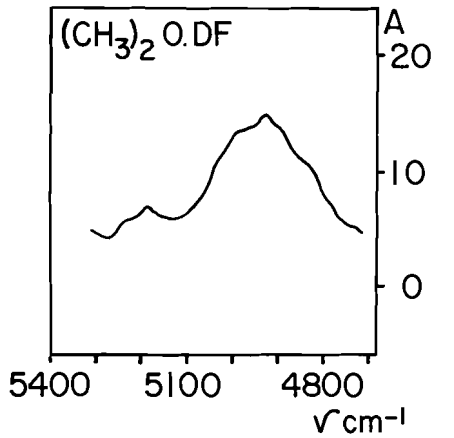

FIG. 2. A part of the gas phase near-infrared spectrum of the $(CH_3)_2O{\cdot}DF$ complex. Pressure: dimethylether 55 Torr, deuterium fluoride 30 Torr. Optical path: 18.75 m. Absorbance in arbitrary units against frequency in cm^{-1}.

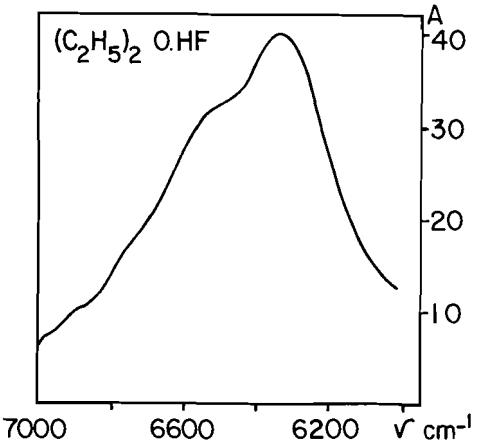

FIG. 3. A part of the gas phase near-infrared spectrum of the $(C_2H_5)_2O{\cdot}HF$ complex. Pressure: diethylether 55 Torr, hydrogen fluoride 30 Torr. Optical path: 17.25 m. Absorbance in arbitrary units against frequency in cm^{-1}.

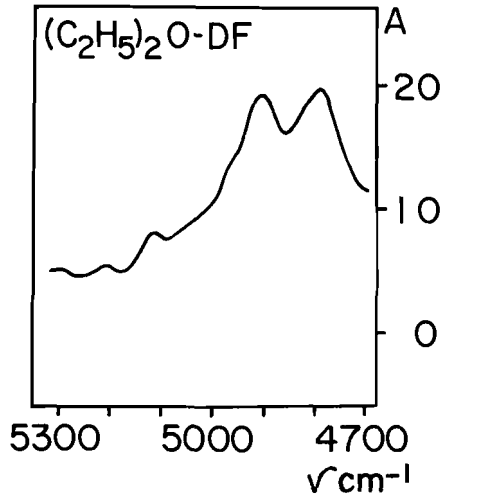

FIG. 4. A part of the gas phase near-infrared spectrum of the $(C_2H_5)_2O{\cdot}DF$ complex. Pressure: diethylether 55 Torr, deuterium fluoride 30 Torr. Optical path: 12.75 m. Absorbance in arbitrary units against frequency in cm^{-1}.

associated with the H-bonded species have been observed but their low intensity and diffuseness precluded further study.

The observed bands would exhibit an extensive and complicated structure under high resolution. Relatively low resolution studies like those presented here must necessarily restrict the extent and quality of the information obtained. Notwithstanding this limitation it is possible to utilize these data to estimate hydrogen bonded vibrational frequencies and anharmonicity constants.

Discussion

The interpretation of our results depends on the

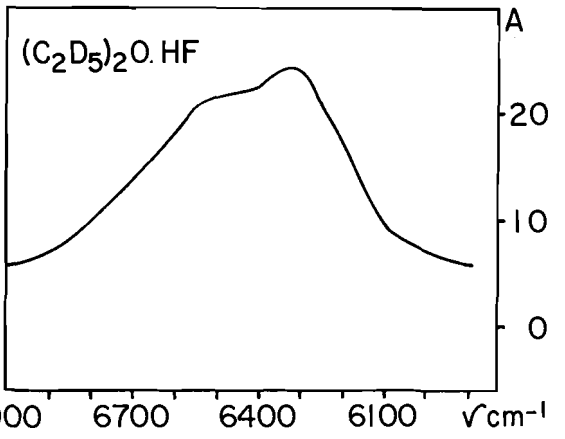

FIG. 5. A part of the gas phase near-infrared spectrum of the $(C_2D_5)_2O{\cdot}HF$ complex. Pressure diethylether-d_{10} 55 Torr, hydrogen fluoride 30 Torr. Optical path: 11.25 m. Absorbance in arbitrary units against frequency in cm^{-1}.

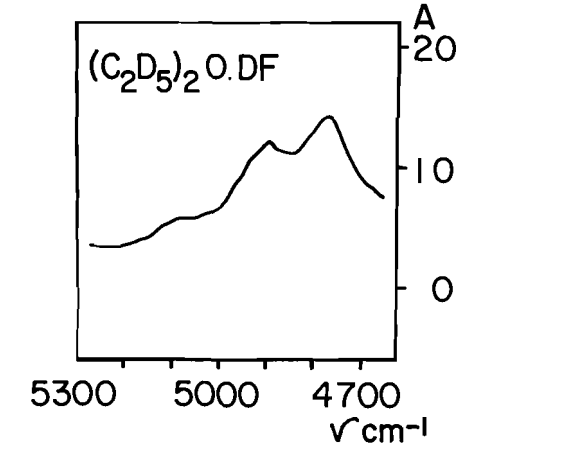

FIG. 6. A part of the gas phase near-infrared spectrum of the $(C_2D_5)_2O{\cdot}DF$ complex. Pressure: diethylether-d_{10} 55 Torr, deuterium fluoride 30 Torr. Optical path: 12.75 m. Absorbance in arbitrary units against frequency in cm^{-1}.

assignments of the observed peaks to the various possible combination bands. The combinations between ν_1 and ν_3 are often represented by Stepanov's (20, 21) Franck–Condon-like diagram. In this respect, Sheppard pointed out many years ago (2) that "because of the anharmonicity of the νXH vibration, the H atom will move on average nearer to Y in the ($v_1 = 1$) excited state, and consequently the hydrogen bond will become stronger". Thus the upper potential energy curve has a deeper minimum than the lower one, and its minimum occurs at a lower value of ν_{XY}. (See also Gallagher (22).) While there is little doubt about the validity of his suggestion, we have to examine its consequences for the relative intensities of the combination bands (subbands).

Initial considerations according to usual Franck–

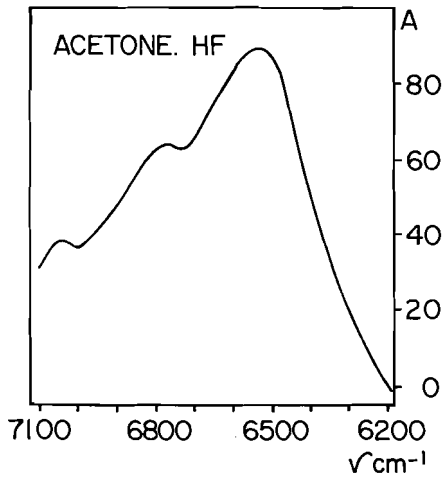

FIG. 7. A part of the gas phase near-infrared spectrum of the $(CH_3)_2CO{\cdot}HF$ complex. Pressure: acetone 55 Torr, hydrogen fluoride 30 Torr. Optical path: 6.75 m. Absorbance in arbitrary units against frequency in cm^{-1}.

Condon reasoning should make a transition other than (1,0) ← (0,0) vertical, and therefore the most intense one. (In each bracket the first number indicates the vibrational quantum number v_1 of ν_1 and the second number the vibrational quantum number v_3 of ν_3.) It is pertinent to note, however, that the Franck–Condon principle is less valid in this case than for electronic transitions. While an electronic transition might be a thousand times faster than a vibrational one, a much smaller factor should exist between ν_1 and ν_3. Under the circumstances non-vertical transitions could have quite appreciable

TABLE 1. Apparent band maxima (in italics) and pronounced shoulders in the near-infrared spectra of H-bonded complexes of ethers or acetone with HF or DF

Complex	Wavenumbers in cm^{-1}					
$(CH_3)_2O$–HF	6290	6400	*6485*†	*6650*†	6850‡	6950‡
$(CH_3)_2O$–DF	4840	4890†	*4930**†	4980	5045	5190
$(C_2H_5)_2O$–HF		6150	*6335*†	6525	6725	6900
$(C_2H_5)_2O$–DF			*4780*†	*4900*†	4970	5120
$(C_2D_5)_2O$–HF	6025	6200	*6325*‡	6450	*6525*‡	6725
$(C_2D_5)_2O$–DF		4700	*4770*†	*4900*‡	4970	5090
$(CH_3)_2CO$–HF		6330	*6530*†	*6765*†	6900	*7045*†

*See text.
†Estimated error of frequency maximum ±25 cm^{-1}.
‡Estimated error of frequency maximum ±50 cm^{-1}.

probabilities. In addition, the Franck–Condon diagram should not make us forget that we are dealing with combination tones. For example, (1,1) ← (0,0) is a binary combination, $(\nu_1 + \nu_3)$. Thus when we say that the (1,1) ← (0,0) band is more intense than the (1,0) ← (0,0) band this implies that the combination is more intense than the fundamental. While this might be the case, it requires a large value for X_{13} (and/or considerable electrical anharmonicity). At the $v_1 = 2$ level the (2,1) ← (0,0) band is a ternary combination. While the intensity of $\nu_1{}^{02}$ depends on X_{11} that of $(2\nu_1 + \nu_3)$ depends on both X_{11} and X_{13}. Also, the non-linearity of the rate of change in the dipole moment, electrical anharmonicity, is likely to contribute significantly to the intensity of combination bands. If M is the variable dipole moment, Q_1 and Q_3 the normal coordinates for vibration of frequencies ν_1 and ν_3, and the subscript e refers to the equilibrium geometry,

$$[3] \qquad M = M_e + \left(\frac{\partial M}{\partial Q_1}\right)_e Q_1 + \left(\frac{\partial M}{\partial Q_3}\right)_e Q_3 + \frac{1}{2}\left(\frac{\partial^2 M}{\partial Q_1{}^2}\right)_e Q_1{}^2 + \frac{1}{2}\left(\frac{\partial^2 M}{\partial Q_3{}^2}\right)_e Q_3{}^2 + \left(\frac{\partial^2 M}{\partial Q_1 \partial Q_3}\right)_e Q_1 Q_3 + \ldots$$

While the intensity of the fundamentals depends relatively little on electrical anharmonicity that of combination tones can receive a large contribution from it if the mixed derivative in eq. [3] is large and it can be either positive or negative (see ref. 23). Unfortunately, there does not seem to be any information available on the latter for hydrogen bonded systems. Then all we can say is that the validity of the Sheppard shift of the potential minimum for $v_1 = 1$ does not necessarily imply that the (1,0) ← (0,0) band is weak. It may or may not be the strongest of the subbands in given cases.

A further comment we have to make concerns the difficulty of using the temperature effect for identifying (1,0) ← (0,1), (1,0) ← (0,0), (1,1) ← (0,0), etc., bands (18, 19). Thomas (16, 17) has shown that all these bands receive a large part of their intensity from hot bands of the $(\nu + v\nu_i - v\nu_i)$ type. The recent calculations of Robertson (3) which take account of Franck–Condon factors and the Boltzmann distribution but not electrical anharmonicity substantiate this strikingly (Tables 1 and 4 in ref. 3). For the $(CH_3)_2O{\cdot}HCl$ system at 300 K, the intensity of the (1,0) ← (0,1) difference band, 0.39 on a relative scale, receives 0.16 from hotter bands; the (1,0) ← (0,0) overtone band with an intensity of 0.80 receives

TABLE 2. The frequencies of the HF or DF stretching fundamental (ν_1^{01}) and its first overtone (ν_1^{02}), the anharmonicity constant X_{11} (also in cm^{-1}), and the respective isotopic ratios. Based on assignments given in section *a*

Complex	ν_1^{01}*	ν_H/ν_D	ν_1^{02}	ν_H/ν_D	X_{11}
$(CH_3)_2O$–HF	3470†	1.366 (±0.014)	6485	1.334 (±0.012)	−228 (±28)
$(CH_3)_2O$–DF	2540		4860‡		−110 (±28)
$(C_2H_5)_2O$–HF	3405†	1.362 (±0.014)	6335	1.325 (±0.012)	−237 (±28)
$(C_2H_5)_2O$–DF	2500		4780		−110 (±28)
$(C_2D_5)_2O$–HF	3400	1.360 (±0.014)	6325	1.326 (±0.017)	−237 (±40)
$(C_2D_5)_2O$–DF	2500		4770		−115 (±28)
$(CH_3)_2CO$–HF	3470†		6530		−205 (±28)

*Estimated errors of band maxima ±15 cm^{-1}.
†From Arnold and Millen (13).
‡See text.

TABLE 3. The frequencies of the HF or DF stretching fundamental (ν_1^{01}) and its first overtone (ν_1^{02}), the anharmonicity constant X_{11} (also in cm^{-1}), and the respective isotopic ratios. Based on assignments given in section *d*

Complex	ν_1^{01}	ν_H/ν_D	ν_1^{02}	ν_H/ν_D	X_{11}
$(CH_3)_2O$–HF	3470†	1.366 (±0.014)	6650‡	1.349 (±0.012)	−145 (±28)
$(CH_3)_2O$–DF	2540		4930‡		−75 (±28)
$(C_2H_5)_2O$–HF	3405†	1.362 (±0.014)	6525‡	1.347 (±0.012)	−142 (±28)
$(C_2H_5)_2O$–DF	2500		4845*‡		−77 (±28)
$(C_2D_5)_2O$–HF	3400	1.360 (±0.014)	6525§	1.347 (±0.012)	−137 (±40)
$(C_2D_5)_2O$–DF	2500		4845*‡		−77 (±28)
$(CH_3)_2CO$–HF	3470†		6660‡		−140 (±28)

*See text.
†From Arnold and Millen (13).
‡Estimated errors ±25 cm^{-1}.
§Estimated errors ±50 cm^{-1}.

0.135 from hot bands and the (1,1) ← (0,0) summation band, with an intensity of 1.00 receives 0.54 from hot bands. This means that the subband at the high frequency side of the 'pure overtone' should be as or more sensitive to temperature change than the one at its low frequency side.

However, as Robertson has pointed out, conditions are significantly different for X—D systems. Because of lesser amplitude and mechanic anharmonicity the Sheppard shift is expected to be much less. This would tend to make the (1,0) ← (0,0) band the most intense one. Robertson's calculations on $(CH_3)_2O{\cdot}DCl$ at 300 K illustrate this: the (1,0) ← (0,1) difference, the (1,0) ← (0,0) and (1,1) ← (0,0) summation bands have relative intensities 0.39, 1.10, and 1.00 respectively. (With the corresponding hot bands contributing 0.24, 0.30, and 0.72.)

The frequencies of the bands in wavenumbers and the more pronounced shoulders which appear in the overtone spectra are listed in Table 1. The numbers in italics relate to the observed band maxima, all other numbers represent shoulders. These values together with fundamentals determined by Arnold and Millen (13) and by Thomas (16) were used to construct Tables 2 and 3.

(*a*) Table 2 is based on the assumption that the well defined band of lowest wavenumber belongs to the pure fundamental, ν_1^{01}, and pure overtone, ν_1^{02},

at the fundamental and overtone levels respectively. (The values marked by † are taken from Arnold and Millen (13).)

The first observation from the data of Table 2 is that by using the frequencies of the respective HF and DF fundamentals we obtain isotopic ratios very close to 1.36. Since the harmonic ratio is 1.380 this is quite satisfactory and lends support to Arnold and Millen's original assignments for the fundamentals. This implies that despite the Sheppard shift, the (1,0) ← (0,0) band is still the most intense.

The overtones yield the isotopic ratios shown in the fourth column of Table 2. They are close to 1.33. This is also quite satisfactory from the point of view of the assignments made in constructing Table 2. (To the second order the ratio of the harmonic frequencies (ω) is, for a purely diatomic oscillator equal to the square root of the inverse ratio of the reduced masses whereas the ratio of the anharmonicity constants like X_{11} is equal to the ratio of the reduced masses themselves.) Therefore, since the overtones depend more strongly on the X_{11} and since the latter are larger for HF than for DF, the overtones are expected to yield lower isotopic ratios.

$$[4] \qquad \nu_1^{01} = \omega_1 + 2X_{11}$$

$$[5] \qquad \nu_1^{02} = 2\omega_1 + 6X_{11}$$

We can compute the X_{11} from [6]:

$$[6] \qquad X_{11} = \nu_1^{02}/2 - \nu_1^{01}$$

They are somewhat above $-200\ cm^{-1}$ for the HF complexes. Since the free HF vibrator has an X_{11} value equal to $-90\ cm^{-1}$ (5, 24), this corresponds to a greater than twofold increase. The ethylether–DF complexes give about $-110\ cm^{-1}$. This then leads to an isotopic ratio of about two (or slightly higher) for the X_{11}, close to the ratio of the reduced masses despite the large experimental error. However, with dimethylether–DF we encounter a difficulty. With the apparent maximum of the overtone $X_{11} = -75\ cm^{-1}$ is obtained. This would lead to an unreasonably high isotopic ratio for the X_{11}, about 3.0. It is significant that there is a conspicuous difference between the overtone spectra of the diethylether–DF and dimethylether–DF complexes. The former contains two well defined bands with nearly equal intensities (Figs. 4 and 6) at about 4770 (or 4780) and 4900 cm^{-1} while the latter has a single maximum at 4930 cm^{-1} (Fig. 2). It is possible that the 4930 band is actually double and that the single apparent peak is created by mutual overlap between two bands located near 4860 and 4980 cm^{-1}. The one of lower frequency (4860 cm^{-1}) would give a value of X_{11} similar to that of the diethylether–DF complexes. Since the X_{11} of free DF is $-46\ cm^{-1}$ (5, 23) the increases upon H-bond formation would be again somewhat larger than twofold. Thus a coherent picture is obtained.

However, we still have to make an estimate for the coupling constant X_{13}. This requires assignments for the other bands found in the overtone spectrum. In Arnold and Millen's spectrum of $(C_2H_5)_2O{\cdot}HF$ (13) there are, in addition to the strong band at 3405 cm^{-1}, two weaker bands at 3655 and 3225 cm^{-1} respectively. Following Arnold and Millen's initial assignment, we can assign 3655 to the summation tone $(\nu_1 + \nu_3)$ and 3225 to the $(\nu_1 - \nu_3)$ difference tone. It is important to remember in this respect that while the frequency of a difference tone is the simple difference of the frequency of the two fundamentals:

$$[7] \qquad (\nu_1 - \nu_3) = \nu_1^{01} - \nu_3^{03}$$

the summation tone involves the coupling constant:

$$[8] \qquad (\nu_1 + \nu_3) = \nu_1^{01} + \nu_3^{01} + X_{13}$$

In this case the frequency difference $3405 - 3225 = 180\ cm^{-1}$ is practically the same as the $\nu_3 = 175\ cm^{-1}$ measured by Thomas (16). On the other hand we obtain:

$$X_{13} = 3655 - (3405 + 180) = +70\ cm^{-1}$$

where the positive sign reflects the Sheppard shift. The band at 3655 is also present in our $(C_2D_5)_2O{\cdot}HF$ spectrum but the shoulder near 3220 cm^{-1} is ill-resolved.

The same result is obtained from Millen's $(CH_3)_2O{\cdot}HF$ spectrum with his original assignments. In addition to the strong 3470 cm^{-1} band there are weaker bands at 3300 and 3710 cm^{-1}. The difference $3470 - 3300 = 170\ cm^{-1}$ still compares well with Thomas' 185 cm^{-1}. The coupling constant turns out to be again:

$$X_{13} = 3710 - (3470 + 170) = +70\ cm^{-1}$$

For acetone–HF, Arnold and Millen (13) found the strongest peak at 3470 with weaker subbands at 3580, 3700, and 3280 and 3380 cm^{-1}. However, 3580 cannot be $(\nu_1 + \nu_3)$ and 3380 cannot be $(\nu_1 - \nu_3)$ (being too close to 3470 cm^{-1}). The remaining bands give $3470 - 3280 = 190\ cm^{-1}$ for the difference tone and

$$X_{13} = 3700 - (3470 + 190) = +40\ cm^{-1}$$

It is believed that in reality it must be somewhat higher. The X_{13} value of about $+70\ cm^{-1}$ for the ether–HF complexes is believed to be about correct.

If so, the same constant should be obtainable from the overtone spectra. Taking $\nu_3 = 180\ cm^{-1}$ and $X_{13} = 70\ cm^{-1}$, $(2\nu_1 + \nu_3)$ should be about 320

cm^{-1} higher than ν_1^{02} since

[9] $$(2\nu_1 + \nu_3) = \nu_1^{02} + \nu_3^{01} + 2X_{13}$$

Now, if we have a look at the overtone spectra (Figs. 1, 3, 5, 7) we see immediately that we find the band of second highest frequency much closer to the first one. For the diethylether–HF complexes the 6335 (or 6325) cm^{-1} band is followed by a very broad shoulder at the high frequency side. By prospection the second band can be located at about 6525 cm^{-1}. The band is well resolved for dimethylether–HF with a peak at 6650 cm^{-1}. Thus for the latter the interval between the first and second peaks is only $6650 - 6485 = 165\ cm^{-1}$. With the above location of the bands it is less than 200 cm^{-1} for the diethylethers. The somewhat surprising conclusion is that if the first band is ν_1^{02}, the second band cannot be $(2\nu_1 + \nu_3)$. In consequence we have to think about combinations involving the bridge deformation (wagging) vibration (let us call it ν_4). In the case of acetone–HF, Arnold and Millen (13) estimated the frequency of this band to about 100 cm^{-1}. With a frequency of this order and a positive X_{14} coupling constant of about 30 or 40 cm^{-1} the observed intervals could be explained. (See, for the similar case of alcohols, Asselin and Sandorfy, ref. 25.) The $(2\nu_1 + \nu_3)$ combination then should be looked for at higher frequencies, about 6650 for the diethylether–HF and 6800–6850 cm^{-1} for dimethylether–HF and acetone–HF. Actually, there are weaker bands or shoulders at the right places but there are other shoulders as well and we cannot make firm assignments. It is relevant in the respect that for $(C_2H_5)_2O$–HCl Bertie and Falk (18) estimated the frequency of the wagging band as 50 cm^{-1} and found combinations between ν_1 and ν_4. They have shown that for $(CH_3)_2O$–HCl the main features in the fundamental region are due to $\nu_1 \pm n\nu_3$ whereas for $(CH_3)_2O$–DCl they appear to be due to $\nu_1 \pm n\nu_4$. This is a situation similar to the one we find. Arnold and Millen (13) also invoked ν_4 to explain the 3580 and 3380 cm^{-1} bands of acetone–HF. (Thomas (16), however, does not mention these in connection with the ether–HF complexes.)

Now we turn to the ether–DF complexes. At the fundamental level, the high frequency sides of the bands at 2500 or 2540 cm^{-1} always have a broad shoulder extending to about 50–100 cm^{-1} which might again be due to $(\nu_1 + \nu_4)$ type combinations. Unfortunately, the weakness of these spectra and the closeness of the CH bands did not enable us to locate $(\nu_1 + \nu_3)$ type combination bands.

Arnold and Millen (13) found for $(CD_3)_2O$–DF (which was not available to us) the fundamental at about 2550 and a weaker band at 2770 cm^{-1}. While these values could only be estimated they yield a plausible value for the X_{13} of the DF complex:

$$X_{13} = 2770 - (2550 + 185) = +35\ cm^{-1}$$

(The value of ν_3 is from Thomas (16).)

As mentioned above at the overtone level $(C_2H_5)_2O$–DF and $(C_2D_5)_2O$–DF have two well defined bands separated by $4900 - 4780 = 120\ cm^{-1}$ and $4900 - 4770 = 130\ cm^{-1}$ respectively. Now, this interval is much too small: the two bands cannot be ν_1^{02} and $(2\nu_1 + \nu_3)$. According to [9] the wavenumber of the summation tone should be $4780 + 185 + (2 \times 35) = 5035\ cm^{-1}$ instead of 4900 cm^{-1}. The interval of 120 or 130 cm^{-1} could be explained again by $(2\nu_1 + \nu_4)$ combinations involving the bridge wagging vibration.

There is an interesting possibility which is compatible with the assignments made in this section. If we take the best resolved bands (6485 and 6650 for dimethylether–HF and 4770 (4780) and 4900 for diethylether–DF) we can still assign 6485 and 4770 (or 4780) to the pure overtone ν_1^{02} and 6650 and 4900 to (2,1) ← (0,1). Indeed, the frequency of the latter is $\nu_1^{02} + 2X_{13}$ and the observed intervals 165 cm^{-1} and 120 cm^{-1} are just slightly larger than twice the X_{13} values inferred from the fundamentals. Like this combinations with ν_4 would not be involved.

Three alternative interpretations of the spectra are possible.

(*b*) We can take the second bands in the overtone spectra (6525 for diethylether–HF and 6650 for dimethylether–HF) with 4780, 4770, and (the inferred) 4860 for dimethylether–DF. This would, however, yield isotopic ratios around 1.365 for the *overtones* and this is certainly too high.

(*c*) We can take the second bands in the overtone spectra as ν_1^{02} for both the HF and DF complexes. (4900 cm^{-1} for diethylether–DF.) This would give isotopic ratios for the X_{11} close to 3.0 which is much too high.

(*d*) There seems to exist another consistent way of assigning the subbands in the overtone spectra. One could suppose that in the HF complexes the first band is 'hot': (2,0) ← (0,1) and that the second band is the pure ν_1^{02}. (6650 cm^{-1} for dimethylether–HF, 6525 cm^{-1} for the two diethylether–HF complexes, and 6765 cm^{-1} in acetone–HF (Table 3).) This appears to be plausible for two reasons. First, as said above the Sheppard shift would favor this assignment. Second, the shift from the (2,0) ← (0,0) to the (2,0) ← (0,1) bands is $6650 - 6485 = 165$, $6525 - 6335 = 190$, $6525 - 6325 = 200\ cm^{-1}$, $6765 - 6530 = 235\ cm^{-1}$, in the above order. Except for acetone they are close to the wavenumbers of ν_3^{01} determined by Thomas. With these assignments, since

[10] $[(2,0) \leftarrow (0,1)] = \nu_1^{02} - \nu_3^{01}$

one obtains that X_{11} is about $-140\ cm^{-1}$ (Table 3).

The ether–DF complexes do not fit into this scheme, however. As mentioned above the two bands are separated by only 120 or 130 cm^{-1}. This is significantly less than ν_3^{01}. Thus while the two bands cannot be interpreted as the pure overtone and the summation tone they cannot be interpreted as the difference tone and the pure overtone either.

In other words, it is readily seen that, for example, $4770 + 165 = 4935\ cm^{-1}$, so that negative X_{13} would be required according to [9] to bring this back to 4900 cm^{-1}, about $X_{13} = -35\ cm^{-1}$. This would contradict Sheppard's principle. The same can be applied to the complexes with HF. For example, if for $(C_2H_5)_2O{\cdot}HF$ the bands at 6335 and 6525 cm^{-1} were ν_1^{02} and $(\nu_1 + \nu_3)$ respectively since the interval between them is just about equal to ν_3^{01}, the coupling constant would be practically zero. With no anharmonic coupling most known theories on hydrogen bonding would also come to zero.

One could, however, suppose that the 4900 and 4770 (or 80) bands are the sum and difference tones of ν_1^{02} and the bridge wagging vibration ν_4 with a wavenumber of about 50 or 60 cm^{-1} so that ν_1^{02} would be located near their midpoint but closer to the band of lower wavenumber. This assumption would give X_{11} values of the order of $-75\ cm^{-1}$ for the diethylether–DF as well as for dimethylether–DF taking this time the apparent maximum for the latter (4930 cm^{-1}). This would amount to a coherent picture as can be seen from the data of Table 3. It is strange, however, that for obtaining it we have to take the midpoint of the two bands for the DF complexes but the bands of higher wavenumber for the HF complexes. This is not impossible. That the pure overtone is the second band for the HF complexes but the first one for the DF complexes would be in line with the larger amplitude (and anharmonicity) of the HF vibration and the larger Sheppard-shift it causes. If the scheme of Table 3 did apply the increase in X_{11} would still be sizeable, about -140 cm^{-1} for HF instead of $-90\ cm^{-1}$ for the free vibrator and $-75\ cm^{-1}$ for DF instead of $-46\ cm^{-1}$. This latter scheme is of a rather artificial character, however. In view of all the different considerations we regard the initial assignment of the spectra (*a*, Table 2) as the most probable which we can propose from the available data.

Conclusions

Despite the difficulties encountered in the interpretation of our results some noteworthy points emerge.

(*1*) The observed isotopic ratios confirm Arnold and Millen's original assignments for the fundamentals.

(*2*) The existence of the Sheppard shift does not make it impossible for the 0–0 band to be the most intense one.

(*3*) The $\nu_1 + \nu_3$ type combinations are not necessarily the strongest bands in the spectrum. In particular stretching and bridge-bending or $(1,1) \leftarrow (0,1)$ type combinations seem to be prominent in overtone spectra. These conditions can vary from case to case.

(*4*) The values of the anharmonicity constants depend, of course, on the assignments we make but in every case a sizeable increase for X_{11} is obtained upon H-bonding. While the overtone spectra did not make it possible to obtain new values for the coupling constant X_{13}, Millen's values (about $+70\ cm^{-1}$ for HF complexes) seem to be of the right order of magnitude.

(*5*) The sizeable (although not dramatic) increase in X_{11} upon H-bond formation supports, in a general way, the order of magnitude of the values obtained for associated alcohols and some other systems *in solution* (7–12). Their X_{11} also underwent a significant increase upon H-bond formation although to a lesser extent than the HF complexes treated in this paper.

Acknowledgements

The acquisition of a Wilks 20 m variable long path gas cell was made possible for us by a grant from the "Fonds annuel de soutien de l'Université de Montréal" for which we express our sincere thanks. Financial assistance from the National Research Council of Canada and the Ministère de l'Education du Québec is also acknowledged.

1. S. Bratos and D. Hadži. J. Chem. Phys. **27**, 991 (1957).
2. N. Sheppard. *In* Hydrogen bonding. *Edited by* D. Hadži. Pergamon Press, London. 1959. p. 85.
3. G. N. Robertson. Philos. Trans. R. Soc. London, **286**, 25 (1977).
4. N. D. Sokolov and V. A. Savelev. Chem. Phys. **22**, 383 (1977).
5. Y. Bouteiller and E. Marechal. In press.
6. G. Herzberg. Molecular spectra and molecular structure. Vol. I. Spectra of diatomic molecules. Van Nostrand, New York. 1950. Chapt. 3; Vol. II. Infrared and Raman spectra of polyatomic molecules. Van Nostrand, New York. 1945. Chapt. 3.
7. M. Asselin and C. Sandorfy. J. Mol. Struct. **8**, 145 (1971).
8. C. Bourdéron and C. Sandorfy. J. Chem. Phys. **59**, 2527 (1973).
9. J. J. Péron and C. Sandorfy. J. Chem. Phys. **65**, 3153 (1976).
10. M. C. Bernard-Houplain and C. Sandorfy. J. Chem. Phys. **56**, 3412 (1972).

11. R. BICCA DE ALENCASTRO. Can. J. Chem. **50**, 3594 (1972).
12. C. SANDORFY. *In* The hydrogen bond. Vol. 2. *Edited by* P. Schuster, G. Zundel, and C. Sandorfy. North-Holland, Amsterdam. 1976. Chapt. 13.
13. J. ARNOLD and D. J. MILLEN. J. Chem. Soc. 503 (1965); 510 (1965).
14. J. E. BERTIE and D. J. MILLEN. J. Chem. Soc. 497 (1965); 514 (1965).
15. R. K. THOMAS and SIR H. THOMPSON. Proc. R. Soc. London, A**316**, 303 (1970).
16. R. K. THOMAS. Proc. R. Soc. London, A**322**, 137 (1971).
17. R. K. THOMAS. Proc. R. Soc. London, A**325**, 133 (1971).
18. J. E. BERTIE and M. V. FALK. Can. J. Chem. **51**, 1713 (1973).
19. J. C. LASSÈGUES and P. V. HUONG. Chem. Phys. Lett. **17**, 444 (1972).
20. B. I. STEPANOV. Zh. Fiz. Khim. **19**, 507 (1945).
21. B. I. STEPANOV. Zh. Fiz. Khim. **20**, 408 (1946).
22. K. J. GALLAGHER. *In* Hydrogen bonding. *Edited by* D. Hadži. Pergamon Press, London. 1959. p. 45.
23. T. DI PAOLO, C. BOURDÉRON, and C. SANDORFY. Can. J. Chem. **50**, 3161 (1972).
24. R. M. TALLEY, H. M. TAYLOR, and A. H. NIELSEN. Phys. Rev. **77**, 529 (1950).
25. M. ASSELIN and C. SANDORFY. Can. J. Chem. **49**, 1539 (1971).

Hydrogen bonding and vapor pressure isotope effect of ethanethiol

JERZY SZYDLOWSKI[1] AND HANS WOLFF

Physikalisch-chemisches Institut, Universität Heidelberg, 6900 Heidelberg, Federal Republic of Germany

Received September 15, 1978

JERZY SZYDLOWSKI and HANS WOLFF. Can. J. Chem. **57**, 1350 (1979).

The vapor pressure ratios of ethanethiol and ethanethiol-d_1 between 223 and 323 K can be represented by the relation

$$\ln P_D/P_H = -5116.67\ K^2/T^2 + 34.032\ K/T - 0.04804$$

The P_D/P_H vs. T curve increases initially and reaches a flat maximum at 293 K; at higher temperatures there is an apparent decrease. This behavior can be explained by the superposition of predominantly the normal effect of the intermolecular vibrations and the SH and SD torsion vibrations, and the inverse effect of the SH and SD stretching vibrations. Contrary to the value of 0.91 reported previously, P_D/P_H values of 1.002 to 1.008 confirm that for weakly hydrogen-bonded substances and their deuterium-bonded analogues a negligibly normal or a slightly inverse vapor pressure isotope effect should be observed.

JERZY SZYDLOWSKI et HANS WOLFF. Can. J. Chem. **57**, 1350 (1979).

On peut représenter les rapports des tensions de vapeur de l'éthanethiol et de l'éthanethiol-d_1 entre 223 et 323 K par la relation

$$\ln P_D/P_H = -5116.67\ K^2/T^2 + 34.032\ K/T - 0.04804$$

La courbe du rapport P_D/P_H vs T augmente au début et atteint un maximum à 293 K; à des températures plus élevées, il semble se produire une diminution. On peut expliquer ce comportement par la superposition d'un effet normal prédominant des vibrations intermoléculaires et des vibrations de torsion SH et SD et l'effet inverse des vibrations de valence SH et SD. Contrairement à la valeur de 0.91 rapportée antérieurement, les valeurs de P_D/P_H de 1.002 à 1.008 confirment que dans le cas de substances faiblement liées par des liaisons hydrogène et celui de leurs analogues liés par des deutérium, on devrait observer un effet isotopique de la tension de vapeur qui est légèrement inverse ou faiblement normal.

[Traduit par le journal]

While valuable results have been obtained from investigations of the vapor pressure isotope effect on hydrogen bonding of water, alcohols, amines, carboxylic acids, etc. (1–3), such information is lacking in the case of thiols. Hobden *et al.* (4) have reported the P_D/P_H ratio of 0.91 at 298 K from the vapor pressures of C_2H_5SH and C_2H_5SD. According to the relationship developed between hydrogen bonding and vapor pressure isotope effect (1–3) this value appears too low for a substance with weak hydrogen bonding, such as ethanethiol (5, 6). Reliable and more complete data over a wide temperature range are required in order to obtain further insight into the vapor pressure behavior of thiols. Therefore, the vapor pressures of C_2H_5SH and C_2H_5SD and their ratios were determined between 223 and 323 K.

Ethanethiol (purchased in pure form from Fluka) was dried over molecular sieve, previously heated under vacuum at 300°C, and then purified by low temperature distillation in a spinning band column. Ethanethiol-d_1 was prepared by the exchange reaction of pure C_2H_5SH with D_2O using a specially designed column; a four stage exchange, prior to the further purification as for C_2H_5SH, yielded a purity of C_2H_5SD better than 99%.

The pressures of C_2H_5SH and C_2H_5SD between 293 and 323 K were measured with a quartz manometer. In the range 223–293 K the pressures of C_2H_5SH were determined with a mercury manometer, and the pressure differences $\Delta P = P(C_2H_5SD) - P(C_2H_5SH)$ with a differential mercury manometer; the pressures of C_2H_5SD resulted from $P(C_2H_5SH)$ and ΔP. The sample cell (two sample cells in difference measurements) and the quartz manometer with its connections to the sample cell in measurements above room temperature were thermostated by the method described in previous vapor pressure investigations of binary mixtures (7, 8). The drift of the sample temperature during a measurement was less than 0.02 K, and a cathetometer was used to determine the pressure differences. This led to an accuracy of 0.2 Torr in the pressure determinations with the quartz manometer and of 0.02 Torr with the differential mercury manometer.

The results of the determinations are listed in

[1]Permanent address: Department of Chemistry, University of Warsaw, Zwirki i Wigury 101, 02-069 Warsaw, Poland.

0008-4042/79/111350-04$01.00/0

Table 1. The pressures of C_2H_5SH are in agreement with those of McCullough *et al.* (9) between 273 and 323 K and can be represented over the entire experimental temperature range of 223–323 K by the equation

$$[1] \quad \log P/\text{Torr} = -64261.1\ \text{K}^2/T^2 - 1039.10\ \text{K}/T + 6.92908$$

The pressures of C_2H_5SD, which are reported for the first time (Table 1), can be represented over the same temperature range by the equation[2]

$$[2] \quad \log P/\text{Torr} = -66468.8\ \text{K}^2/T^2 - 1024.43\ \text{K}/T + 6.90840$$

The P_D/P_H ratios were found to be 1.002 to 1.008 between 223 and 323 K and can be represented by the relation

$$[5] \quad \ln P_D/P_H = -(5116.67 \pm 295.21)\ \text{K}^2/T^2 + (34.032 \pm 2.165)\ \text{K}/T - (0.04804 \pm 0.00394)$$

A two parameter equation of the $A/T^2 + B/T$ type fits badly the experimental results at high and low temperatures.

The P_D/P_H vs. T curve (Fig. 1) initially increases and reaches a flat maximum at 293 K; at higher temperatures there is an apparent decrease. This significant behavior can be explained by the superposition of a weak normal vapor pressure isotope effect which rapidly converges to unity, and of a somewhat greater inverse effect which slowly converges to unity. In eq. [5] the weak normal effect can be associated with the $1/T^2$ term which in light of the theory of the vapor pressure isotope effect (10–13) is related to the low-lying vibrations, in particular the intermolecular vibrations. The somewhat greater inverse effect can be associated with the $1/T$ term which is related to the high-lying intramolecular vibrations. However, the situation is more complicated because the constant term, being due to temperature dependence and anharmonicity of the vibrations as well as to other complications, is comparable in the order of its magnitude to the $1/T$ and the $1/T^2$ terms.

According to infrared and Raman measurements of the internal frequencies (14–16) only stretching and torsion vibrations of the sulfhydryl group show changes on condensation which noticeably differ for the normal and the deuterated compound. Therefore, the use of these vibrations for the internal frequencies should be sufficient to approximately evaluate the equation for the vapor pressure ratio (10–13). In its simplified form based on the cell model for the liquid and neglecting anharmonicities etc., this equation gives P_D/P_H as function of 6 external frequencies of the condensed phase and of $3N - 6$ internal frequencies of the gaseous as well as of the condensed phase (eq. [13] of ref. 12).

The values of 2599/2590 and 2558 cm^{-1} of the stretching vibrations and of 191 and 215 cm^{-1} of the torsion vibrations may be applied for the two phases of C_2H_5SH. The corresponding frequencies of C_2H_5SD are 1888/1883 and 1860 cm^{-1} and 150 and 169 cm^{-1} (14–16) (169 cm^{-1} from the relation $(\nu_{gas}^{H} - \nu_{liq}^{H})/\nu_{gas}^{H} = (\nu_{gas}^{D} - \nu_{liq}^{D})/\nu_{gas}^{D}$). Assuming no large error occurs due to differences in the equilibrium of *trans* and *gauche* conformers, the factor with which the internal frequencies enter the P_D/P_H ratio is found to be 1.025–1.021 between 270 and 320 K. From these values and the measured P_D/P_H values (Table 1) the factor with which the external frequencies enter the ratio is determined to be 0.983–0.987.

The contribution of the three translations computed from

$$[6] \quad \alpha_{tr} = \exp\left\{\frac{1}{24}\left(\frac{hc}{kT}\right)^2 \sum_{i=1}^{3} \left(\nu_i'^2\left[1 - \frac{M'}{M}\right]\right)\right\}$$

(M′ and M are the molecular weights of C_2H_5SH and C_2H_5SD) for the Debye temperature of 129.4 K (9) is negligible; therefore, the values of 0.983–0.987 are due to the contribution of the three librations. Defining the cube root of the product of the three different librations as mean libration, $\bar{\nu}_i$, and the cube root of the product of the three different moments of inertia as mean moment of inertia, $\bar{I}$, the relation

$$[7] \quad \bar{\nu}_i/\bar{\nu}_i' = (\bar{I}'/\bar{I})^{1/2} = 0.979$$

can be assumed, where the moments of inertia for the calculation of $(\bar{I}'/\bar{I})^{1/2}$ have been taken from literature (17, 18) (the value of 0.979 is the average of $(\bar{I}'/\bar{I})^{1/2}$ of the *trans* and *gauche* conformers). From

[2]The Antoine equations, mostly used in the representation of vapor pressure data but physically less significant, are for C_2H_5SH for the temperature range of 223–293 K

[3*a*] $\log P/\text{Torr} = 7.10235 - 1156.08/(T/\text{K} - 34.237)$

and for the temperature range of 293–323 K

[3*b*] $\log P/\text{Torr} = 6.93273 - 1074.83/(T/\text{K} - 42.912)$

The corresponding equations of C_2H_5SD for the range of 223–293 K are

[4*a*] $\log P/\text{Torr} = 7.09984 - 1151.74/(T/\text{K} - 34.849)$

and for the range of 293–323 K

[4*b*] $\log P/\text{Torr} = 6.91033 - 1051.47/(T/\text{K} - 44.508)$

TABLE 1. Results of vapor pressure measurements of the pair C_2H_5SH/C_2H_5SD*

T/K	P_H/Torr†	ΔP/Torr	P_D/P_H	T/K	P_H/Torr	ΔP/Torr	P_D/P_H
224.86	10.6_2	0.02	1.0019	276.18	210.7_3	1.67	1.0079
230.46	16.4_0	0.04	1.0024	278.24	231.3_5	1.85	1.0080
232.81	19.2_2	0.06	1.0031	278.32	232.1_9	1.86	1.0080
233.06	19.5_4	0.07	1.0036	278.80	237.2_4	1.97	1.0083
235.46	22.8_8	0.08	1.0035	280.26	253.1_6	2.01	1.0079
236.02	23.7_3	0.10	1.0042	280.36	254.2_9	2.07	1.0081
237.92	26.8_0	0.13	1.0049	282.16	275.2_0	2.18	1.0079
239.22	29.1_0	0.15	1.0052	282.50	279.3_0	2.25	1.0081
240.64	31.7_9	0.14	1.0044	283.30	289.1_6	2.35	1.0081
242.32	35.2_5	0.19	1.0054	283.80	295.4_6	2.47	1.0084
242.68	36.0_4	0.20	1.0055	285.26	314.5_1	2.55	1.0081
242.88	36.4_8	0.22	1.0060	286.28	328.4_1	2.74	1.0083
244.98	41.3_9	0.24	1.0058	287.36	343.6_7	2.71	1.0079
245.42	42.4_8	0.25	1.0059	288.56	360.7_1	2.94	1.0082
248.16	49.8_8	0.30	1.0060	289.00	367.2_6	3.06	1.0083
248.56	51.0_5	0.32	1.0063	290.92	396.9_9	3.24	1.0082
251.68	60.9_6	0.40	1.0066	291.02	398.5_9	3.33	1.0084
252.74	64.6_8	0.44	1.0068	291.76	410.5_9	3.47	1.0085
253.12	66.0_5	0.43	1.0065	292.91	429.8_0	3.47	1.0081
254.96	73.0_8	0.50	1.0068	293.80	445.1_6	(3.6_5)	1.0082
255.68	76.0_0	0.57	1.0075	294.44	456.4_7	(3.8_9)	1.0085
257.26	82.7_4	0.62	1.0075	297.15	507.1_3	(4.5_5)	1.0090
257.84	85.3_4	0.67	1.0079	299.15	547.1_6	(4.8_7)	1.0089
259.68	94.0_4	0.73	1.0078	301.15	589.6_5	(5.2_1)	1.0088
262.96	111.3_8	0.84	1.0075	303.15	634.7_1	(5.5_6)	1.0088
263.02	111.7_3	0.87	1.0078	305.15	682.4_4	(5.9_4)	1.0087
265.80	128.4_9	1.02	1.0079	307.15	732.9_7	(6.3_4)	1.0086
265.82	128.6_2	0.98	1.0076	309.15	786.3_9	(6.7_6)	1.0086
268.62	147.5_9	1.14	1.0077	311.15	842.3_2	(7.2_1)	1.0086
268.88	149.4_6	1.18	1.0079	313.15	902.3_8	(7.6_9)	1.0085
272.00	173.5_3	1.41	1.0081	315.15	965.1_8	(8.1_9)	1.0085
272.70	179.3_5	1.41	1.0079	317.15	1031.3_4	(8.7_2)	1.0085
274.34	193.6_2	1.55	1.0080	319.15	1100.9_8	(9.2_9)	1.0084
274.54	195.4_2	1.55	1.0079	321.15	1174.2_1	(9.8_9)	1.0084
275.28	202.2_1	1.65	1.0082	323.15	1251.1_7	(10.5_2)	1.0084

*P_H = pressure of C_2H_5SH; ΔP = difference of the pressures P_D of C_2H_5SD and P_H of C_2H_5SH; measured pressure differences are without parentheses; pressure differences calculated from $P(C_2H_5SD)$ and $P(C_2H_5SH)$ are within parentheses; P_D/P_H = measured vapor pressure ratio.
†1 Torr = 0.13332 kPa.

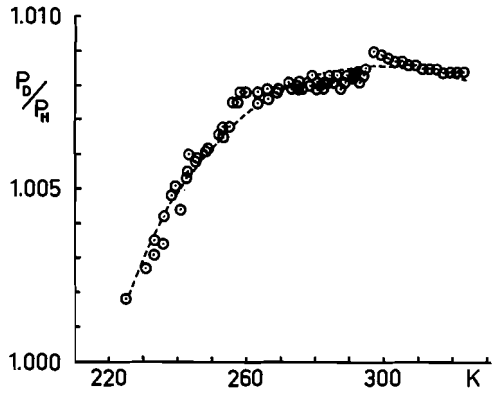

FIG. 1. Vapor pressure ratio P_D/P_H of ethanethiol and ethanethiol-d_1 as function of the temperature; ○ measured points; --- ratios calculated according to eq. [5].

[7] and the contribution of the three librations (eq. [13] of ref. 12) with the values of 0.983–0.987, $\overline{\nu_i'}$ is calculated as 350–360 cm^{-1}, and $\overline{\nu_i}$ as 340–350 cm^{-1}.

There is no doubt that the high values obtained can be considered only as rough approximations of the actual values due to their sensitivity to small frequency errors and the considerable simplifications involved in these calculations. Nevertheless, the results permit the interpretation that the superposition predominantly of the normal effect of the intermolecular vibrations and the SH and SD torsion vibrations and of the inverse effect of the SH and SD stretching vibrations leads to the measured vapor pressure ratio curve.

It may be added that the P_D/P_H ratio at 293 K has been determined to be 1.010 for CH_3SH and CH_3SD (19) and 1.014 for H_2S and D_2S (20); the 293 K

value of C_2H_5SH and C_2H_5SD is 1.008. The result for ethanethiol, therefore, is in reasonable agreement with the data for other sulfhydrides, while there exists a considerable difference in relation to the oxygenic analogue of ethanethiol; the P_D/P_H ratio of ethanol is lowered to about 0.94 (21) as a consequence of its strong hydrogen bonding. Contrary to the large normal vapor pressure isotope effect reported previously, the high accuracy of the present measurements on ethanethiol confirms that for weakly hydrogen-bonded substances and their deuterium-bonded analogues only a negligibly normal or a slightly inverse effect should be observed.

Acknowledgements

We gratefully acknowledge support of this work by Deutsche Forschungsgemeinschaft, Bad Godesberg, by Fonds der Chemie, Frankfurt, and by BASF, Ludwigshafen. J.S. would like to express his gratitude to Deutscher Akademischer Austauschdienst for a fellowship.

1. G. JANCSO and W. A. VAN HOOK. Chem. Rev. **74**, 689 (1974).
2. I. B. RABINOVICH. Influence of isotopy on the physicochemical properties of liquids. Consultants Bureau, New York. 1970.
3. H. WOLFF. Vapor pressure studies on hydrogen and deuterium bonding. *In* The hydrogen bond. *Edited by* P. Schuster, G. Zundel, and C. Sandorfy. North-Holland Publishing Co., Amsterdam. 1976. p. 1227.
4. F. W. HOBDEN, E. P. JOHNSTON, L. R. P. WELDON, and G. L. WILSON. J. Chem. Soc. 61 (1939).
5. S. M. MARCUS and S. J. MILLER. J. Am. Chem. Soc. **88**, 3719 (1966).
6. A. J. BARNES, H. E. HALLAM, and J. D. R. HOWELLS. Trans. Faraday Soc. **68**, 737 (1972).
7. H. WOLFF and H.-E. HÖPPEL. Ber. Bunsenges. Phys. Chem. **72**, 1173 (1968).
8. H. WOLFF and O. SCHILLER. To be published.
9. J. P. MCCULLOUGH, D. W. SCOTT, H. L. FINKE, M. E. GROSS, K. D. WILLIAMSON, R. E. PENNINGTON, G. WADDINGTON, and H. M. HUFFMAN. J. Am. Chem. Soc. **74**, 2801 (1952).
10. J. BIGELEISEN. J. Chem. Phys. **34**, 1485 (1961).
11. J. BIGELEISEN. J. Chim. Phys. **60**, 35 (1963).
12. M. J. STERN, W. A. VAN HOOK, and M. WOLFSBERG. J. Chem. Phys. **39**, 3179 (1963).
13. W. A. VAN HOOK. J. Chem. Phys. **44**, 234 (1966).
14. D. M. SMITH, J. P. DEVLIN, and D. W. SCOTT. J. Mol. Spectrosc. **25**, 174 (1968).
15. J. R. DURIG, W. H. BUCY, C. J. WURREY, and L. CARREIRA. J. Phys. Chem. **79**, 988 (1975).
16. J. SZYDLOWSKI and H. WOLFF. To be published.
17. M. HAYASHI, H. IMASHI, and K. KUWADA. Bull. Chem. Soc. Jpn. **47**, 2382 (1974).
18. J. NAKAGAWA, K. KUWADA, and M. HAYASHI. Bull. Chem. Soc. Jpn. **49**, 3420 (1976).
19. J. SZYDLOWSKI and H. WOLFF. Unpublished results.
20. E. C. W. CLARKE and D. N. GLEW. Can. J. Chem. **48**, 764 (1970).
21. I. KISS, G. JÁKLY, G. JANCSÓ, and H. ILLY. Acta Chim. Acad. Hung. **51**, 65 (1967).

Isotope effects in nucleophilic substitution reactions. III. The effect of changing the leaving group on transition state structure in S_N2 reactions

KENNETH CHARLES WESTAWAY[1] AND SYED FASAHAT ALI

Department of Chemistry, Laurentian University, Sudbury, Ont. Canada P3E 2C6

Received August 21, 1978

KENNETH CHARLES WESTAWAY and SYED FASAHAT ALI. Can. J. Chem. **57**, 1354 (1979).

The nucleophilic substitution reactions of a series of 4-substituted phenylbenzyldimethylammonium ions with thiophenoxide ions at 0°C in *N,N*-dimethylformamide have been used to demonstrate how a change in the leaving group alters the structure of the S_N2 transition state. Heavy atom (nitrogen) kinetic isotope effects, secondary α-deuterium kinetic isotope effects and Hammett ρ values provide qualitative descriptions of both the nucleophile–α-carbon and α-carbon – leaving group bonds in the transition states of these reactions. The results indicate that changing to a better leaving group causes the bond between the α-carbon and the nucleophile to be much more fully formed while the bond to the leaving group is essentially unchanged. The results are discussed in the light of current theories of substituent effects on S_N2 reactions and a possible explanation for the surprising results (*i*) that the greatest effect is in the bond more remote from the point of structural change and (*ii*) that more nucleophilic assistance is required to displace a better leaving group is given.

KENNETH CHARLES WESTAWAY et SYED FASAHAT ALI. Can. J. Chem. **57**, 1354 (1979).

On a utilisé les réactions de substitutions nucléophiles d'une série d'ions X-4 phénylbenzyldiméthylammonium avec les ions thiophénolates à 0°C dans le *N,N*-diméthylformamide pour démontrer l'influence d'un changement dans le nucléofuge sur la structure de l'état de transition S_N2. Les effets isotopiques cinétiques des atomes lourds (azote), les effets isotopiques cinétiques secondaires des deutérium en α et les valeurs ρ de Hammett fournissent des descriptions qualitatives des liaisons nucléophile – carbone en alpha et carbone en alpha groupe nucléofuge dans les états de transition de ces réactions. Les résultats indiquent que si l'on utilise un meilleur nucléofuge la liaison entre le carbone alpha et le nucléophile devient plus développée alors que la liaison vers le groupe nucléofuge est pratiquement inchangée. On discute des résultats à la lumière des théoriques actuelles des effets de substituants sur les réactions S_N2 et l'on propose une explication plausible pour les résultats surprenants: (*i*) que l'effet est le plus grand dans la liaison la plus éloignée du point de changement structural et (*ii*) qu'il faut plus d'aide de la part du nucléophile pour déplacer un meilleur nucléofuge.

[Traduit par le journal]

Introduction

Although the mechanisms of the simple one-step (S_N2) nucleophilic substitution reaction at saturated carbon, eq. [1], have been investigated for over half

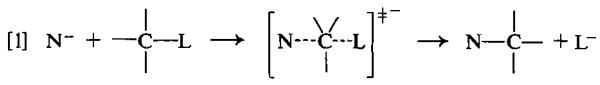

[1]

a century, there are still some questions that remain unanswered. One of these questions is: How does a change in the nucleophile, N^-, the substrate, or the leaving group, L^-, affect the structure of the transition state of an S_N2 reaction? In fact, rate studies (1, 2), secondary α-deuterium kinetic isotope effects (3–5), thermodynamic properties (6, 7), heavy atom (carbon (5, 8), nitrogen (9, 10), sulfur (11–13), chlorine (14–15), and bromine[2]) kinetic isotope effects, and linear free energy relationships (2, 9, 10) have been used in studies on a wide range of reactions in an effort to determine how the structure of the reactants affects the structure of the S_N2 transition states. In addition, several theoretical studies (18–23) have predicted the answer to this question. In spite of these studies, the question has not been resolved completely. This has happened for two reasons. First, changes in the structure of either the nucleophile or the leaving group cause large changes in several properties of the reacting molecule. For example, even changing the leaving group from chloride ion to bromide ion causes large changes in (*i*) the force constant of the Cα—L bond, (*ii*) the polarizability of the leaving group, (*iii*) the dipole moment of the Cα—L bond, (*iv*) the Cα—L bond length, (*v*) the size of the leaving group changing the steric crowding at the reaction center, and (*vi*) the solvation of both the substrate and the transition state. These changes make comparisons between different reactions difficult to interpret and it is impossible to indicate why the observed changes

[1]Author to whom all correspondence should be addressed.

[2]J. W. Taylor. Private communication.

0008-4042/79/111354-14$01.00/0

occur. The second difficulty is that these studies have not provided enough information so that detailed models of the transition states could be constructed. For example, almost all of these studies have only provided information about the Cα--L transition state bond length and the lengths of the other bond(s) in the transition state have either been ignored or inferred from the predictions of theoretical models (18–22) which have not been tested experimentally.

In this study, eq. [2], the structure of the nucleophile, the substrate, or the leaving group can be altered without changing the properties of the reactants significantly. For example, changing the substituent Z in the leaving group will not change the Cα—N bond length, the size of the leaving group at the reaction center, or the polarizability of the leaving atom. In addition, the changes in the Cα—N bond strength, the dipole moment of the Cα—N bond, and the solvation of the substrate and the transition state would be small or zero. Thus, the effect of a change resulting from a change in the structure of the leaving group can be determined and related to one property: the electron donating or withdrawing ability of the substituent. The second advantage of this system is that the combination of leaving group (nitrogen) kinetic isotope effects, secondary α-deuterium kinetic isotope effects, and Hammett ρ values has led to complete (albeit qualitative) structures for the S_N2 transition states for three different leaving groups. This removes the uncertainty associated with the other studies and provides the answer to the question of how the structure of the transition state varies with a change in the leaving group of an S_N2 reaction.

Results and Discussion

The reactions used in this study were followed by titrating the unreacted thiophenoxide ion with Hg(II) ion (24). The data was consistent with a second order reaction that was first order in each reactant. The kinetics and a Hammett ρ value of −1.70 associated with a change of the X group (eq. [2]) in the reaction with phenylbenzyldimethylammonium ion indicated that the Cα—S bond was formed in the transition state of the slow step of the reaction (9, 10). A Hammett ρ value of +2.04 when the Z substituent in the leaving group was varied and a nitrogen kinetic isotope effect of 1.0200 showed that the Cα—N bond was breaking in the transition state of the rate-determining step (9). These results were only consistent with the one-step S_N2 mechanism (9, 10, 25).

The products of the reaction, benzylphenyl sulfide and *N*,*N*-dimethylaniline, were recovered from reactions taken to completion and analyzed by gas chromatography using the internal standard technique (benzylphenyl sulfide) (26) and the micro-Kjeldahl technique (*N*,*N*-dimethylaniline) (9). These analyses showed that the products were formed quantitatively. This demonstrates that the kinetic isotope effects and rate constants measured in this study are those of the S_N2 reaction shown in [2].

Kinetic Studies

The second order rate constants for four different *para*-substituted thiophenoxide ions with each of the *p*-methoxyphenyl-, the phenyl-, and the *p*-chlorophenylbenzyldimethylammonium ions are given in Table 1. Each rate constant is the average of the value obtained from at least four separate kinetic runs. The rate constant for the reaction between *p*-methoxythiophenoxide ion and *p*-chlorophenylbenzyldimethylammonium ion was too fast to be measured by the titrimetric method used to follow these reactions.

The rate constant is altered significantly by a change in leaving group. Changing the substituent Z

TABLE 1. Second order rate constants for the S_N2 substitution reactions of *para*-substituted phenylbenzyldimethylammonium ions with *para*-substituted thiophenoxide ions at 0°C in DMF

Substituent (Z) on the *N*-phenyl group	*k* (L/mol min) for substituent (X) on the thiophenoxide ion			
	—OCH_3	—CH_3	—H	Cl
—OCH_3	0.835	0.465	0.256	0.135
—H	2.77	1.46	0.770	0.368
—Cl	—	5.33	2.26	0.971

from methoxy to hydrogen causes a threefold increase in rate while a tenfold increase in rate is observed for the more electron withdrawing chlorine substituent. Thus, the best leaving group from a kinetic point of view is the weakest base, *p*-chloro-*N*,*N*-dimethylaniline. This is, in fact, what is expected (27, 28).

The best nucleophile for each substrate is the *p*-methoxythiophenoxide ion. The reactivity decreases regularly as the substituent X becomes more electron withdrawing. This occurs because more electron withdrawing substituents lower the electron density on the sulfur atom of the nucleophile (29).

Nitrogen Kinetic Isotope Effect

The nitrogen kinetic isotope effects for the reactions of the *p*-methoxyphenyl-, the phenyl-, and the *p*-chlorophenylbenzyldimethylammonium nitrates with sodium thiophenoxide at 0°C were calculated using [3] (9).

$$[3] \qquad \frac{k^{14}}{k^{15}} = \frac{\ln (1 - f)}{\ln (1 - (R_0/R_f)f)}$$

where f is the fraction of quaternary ammonium salt that has reacted, R_0 is the $^{14}N/^{15}N$ ratio of the ammonium nitrogen in the starting material and R_f is the corresponding ratio in the product (the *para*-substituted *N*,*N*-dimethylaniline) recovered after fractions of reaction ranging from 16–38% completion. The fraction of reaction, f, was the average of the percent reaction found in the gas chromatographic analysis of the benzylphenyl sulfide and the micro-Kjeldahl analysis of the *para*-substituted *N*,*N*-dimethylaniline recovered from a reaction mixture (9). The R_0 value was obtained by measuring the $^{14}N/^{15}N$ ratio in the product recovered from reactions taken 100% to completion. The $^{14}N/^{15}N$ ratios for [3] were obtained in a mass spectrometric analysis of the nitrogen gas that was produced when the ammonium sulfate from the micro-Kjeldahl analysis was oxidized with sodium hypobromite (9). The results of these experiments are given in Table 2.

The isotope effects are all large. In fact, they are approximately half of the theoretical maximum nitrogen kinetic isotope effect at 0°C[3] and indicate that there is substantial Cα—N bond rupture in the transition states of these reactions.

The relative lengths of the Cα--N bonds in the three transition states can be estimated from the magnitudes of these isotope effects (12–14). Theoretical calculations (31, 32) indicate that the magnitude of heavy atom (leaving group) kinetic isotope effects

[3]The maximum nitrogen kinetic isotope effect of 1.04 at 0°C was calculated using a Cα—N^+ absorption frequency of 1003 cm^{-1} (30).

TABLE 2. Nitrogen kinetic isotope effects for the S_N2 substitution reactions of *para*-substituted phenylbenzyldimethylammonium nitrate with sodium thiophenoxide at 0°C in DMF

Para-substituent (Z) on the leaving group	Experiment No.	Fraction of reaction (%)[a]	k^{14}/k^{15}
—OCH_3	1	21.5	1.0193
	2	25.8	1.0201
	3	17.6	1.0198
	4	19.1	1.0195
	5	22.5	1.0200
			1.01974 ± 0.00034[b]
—H	1	16.6	1.0200
	2	16.6	1.0197
	3	21.3	1.0191
	4	21.7	1.0203
	5	22.0	1.0200
	6	37.8	1.0212
			1.0200 ± 0.0007[b]
—Cl	1	18.2	1.0197
	2	18.5	1.0204
	3	18.4	1.0197
	4	17.0	1.0190
	5	23.8	1.0216
	6	31.1	1.0207
			1.0202 ± 0.0009[b]

[a]Based on the average of the yields of benzylphenylsulfide and *N*,*N*-dimethylaniline.
[b]Standard deviation.

increases as the amount of the Cα—L bond rupture in the transition state increases.[4] This relationship is predicted because the last term in the square brackets of Bigeleisen's equation (34) is smaller for a longer Cα--L transition state bond, eq. [4]. The terms μ_{14}^*

$$[4] \qquad \frac{k^{14}}{k^{15}} = \frac{\mu_{14}^*}{\mu_{15}^*}\left[1 + \sum_i^{3n-6} G(\mu_i)\Delta u_i - \sum_i^{3n-7} G(\mu_i^*)\Delta\mu_i^*\right]$$

and μ_{15}^* are the reaction coordinate frequencies of the transition state containing the C—^{14}N and C—^{15}N bonds respectively. The $\sum_i^{3n-6} G(\mu_i)\Delta\mu_i$ term gives the difference in the vibrational energies of the nitrogen-14 and nitrogen-15 quaternary ammonium salts. $\sum_i^{3n-7} G(\mu_i^*)\Delta\mu_i^*$ is the corresponding term for the transition states.

An initial consideration of the results in Table 2 shows that the three isotope effects are not statistic-

[4]Theoretical calculations by Sims and co-workers (33) show that hydrogen bonding between a protic solvent and a negatively charged leaving group, e.g., Cl^-, can reduce the magnitude of a leaving group kinetic isotope effect (with respect to that expected for a particular α-carbon – leaving group transition state bond length) significantly. This reduction in the magnitude of the isotope effect should be very small in the reactions reported in this paper because a nonhydrogen bonding solvent (DMF) is used and because the leaving group has a slight positive charge in the transition state.

ally different. In spite of this, the isotope effects do increase slightly as the substituent Z on the leaving group is changed from methoxy to the more electron withdrawing chlorine. This suggests that the Cα—N bond length is the same in all three transition states or increases very slightly as the substituent changes from methoxy to chlorine.

Unfortunately, the interpretation of these isotope effects is not simple. The difficulty arises because the N—C(phenyl) bond becomes stronger as the Cα—N bond breaks.[5] Thus, some of the Cα—N vibrational energy that has been lost in going to the transition state is partially replaced by the increased vibrational energy associated with the strengthening of the N—C(phenyl) bond. The last term in [4] will not be reduced as much as expected for a particular Cα--N bond length and the slope of the 'magnitude of the kinetic isotope effect versus extent of Cα—N bond rupture in the transition state' curve will be lower (Fig. 1).[6] This suggests that the small, regular increases observed in the nitrogen kinetic isotope effects are indicative of slightly longer Cα--N transition state bonds in the reactions with more electron withdrawing substituents. This interpretation of the results is strengthened because the N—C(phenyl) bond strengthening effect should be most important, i.e., the observed nitrogen kinetic isotope effect will be smaller, when the substituent on the leaving group is chlorine, the most electron withdrawing substituent used in this study (Fig. 1*c*). Thus, the best interpretation of these results is that the Cα--N transition state bond becomes slightly longer as the substituent Z changes from methoxy to hydrogen to chlorine.

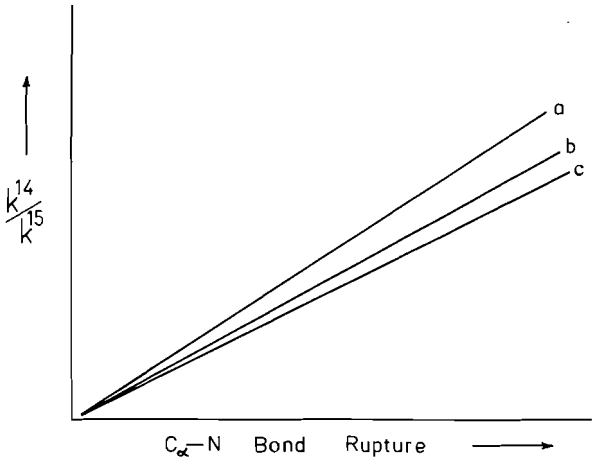

FIG. 1. Nitrogen kinetic isotope effect versus extent of Cα—N bond rupture in the transition state (*a*) for a system where there is no interaction between the developing lone pair of electrons on the dimethylamino group and the benzene ring of the leaving group, (*b*) for a system where there is conjugation between the dimethylamino group and the benzene ring of the leaving group, and (*c*) for a system where the conjugation between the dimethylamino group and the benzene ring is increased by an electron withdrawing substituent Z in the leaving group.

Secondary α-Deuterium Kinetic Isotope Effects

The secondary α-deuterium kinetic isotope effects were also determined by the competitive technique (9,10), i.e., by reacting approximately equal amounts of the *para*-substituted phenylbenzyl-1,1-d_2-dimethylammonium nitrate and the corresponding undeuterated quaternary ammonium salt to extents of reaction varying from 17–27% completion. The isotope effect was calculated using [3]. The fraction of reaction *f* was calculated from the results of a gas chromatographic analysis of the product (benzyl-1,1-d_2-phenyl sulfide and benzylphenyl sulfide) using the internal standard technique (9, 26). The ratio of the undeuterated/dideuterated benzylphenyl sulfide in the product of reactions taken part way to completion, R_f, was determined in a mass spectrometric analysis of the benzylphenyl sulfide. The ratio of undeuterated/dideuterated *para*-substituted phenylbenzyldimethylammonium ion, R_0, was obtained from the weights of the undeuterated and deuterated quaternary ammonium salts and the percentage of dideuterated material (98.1%) in the

[5]The conjugation between the dimethylamino group and the benzene ring in the product (a *para*-substituted *N,N*-dimethylaniline) makes the N—C(phenyl) bond in the product (and to a lesser degree in the transition state) stronger than that in the substrate where the lone pair of electrons are not available. The absorption frequencies of the Cα—N bond of the substrate and the N—C(phenyl) bond of the product are 1000 and ~1330 cm^{-1} respectively.

[6]This phenomenon has been reported for carbon-13 kinetic isotope effects in the S_N1 reactions of 1-phenylethylbromides (35, 36) and for a carbon-13 equilibrium isotope effect for the dissociation of triphenylmethylchloride into triphenylmethyl carbonium ion (37). In these cases, the vibrational energies from the increased bonding in the CH_3—Cα and the Cα—C(phenyl) bonds in the carbonium ions (the increase in frequency was ~200–300 cm^{-1} per bond or a bond order of ~1.2 (CH_3—$C\alpha^+$) and 1.5 ($C\alpha^+$—C(phenyl) (L. B. Sims, private communication)) was sufficient to balance or even overcome the loss of vibrational energy resulting from the rupture of the C–halogen bond (vibrational frequency ~500–600 cm^{-1}) and small (35, 36) and inverse (36, 37) isotope effects were observed. The increased bonding in the N—C(phenyl) bond should have a much smaller effect on the nitrogen kinetic isotope effects measured in this study because (*a*) only one bond increases its vibrational energy in the transition state, (*b*) the Cα—N bond is much stronger than a C–halogen bond so the loss of vibrational energy will be greater, (*c*) the amount of Cα—N bond rupture and thus N—C(phenyl) bond strengthening (this uses the same pair of electrons) are smaller in an S_N2 transition state than in an S_N1 transition state (39, 40), and (*d*) the amount of N—C(phenyl) bond strengthening should be smaller than that observed for the $C\alpha^+$—C(phenyl) bond where the demand for electrons by the positively charged carbon is greater.

TABLE 3. Secondary α-deuterium kinetic isotope effects for the reactions between *para*-methoxyphenyl-, phenyl-, and *para*-chlorophenylbenzyl-1,1-d_2-dimethylammonium nitrates and thiophenoxide ion at 0°C in DMF

Substituent (Z) in the leaving group	Weight of undeuterated / deuterated substrate	$\frac{PhCH_2N^+(CH_3)_2C_6H_4Z^a}{PhCD_2N^+(CH_3)_2C_6H_4Z}$ (R_0)	$\frac{PhCH_2SPh}{PhCD_2SPh}$ (R_f)	Fraction[b] of reaction (f)	k_H/k_D	k_H/k_D per α-D
—OCH_3	0.13873/0.14596	0.9759	1.1422	0.274	1.201	1.096
	0.18265/0.18408	1.0188	1.2306	0.204	1.233	1.111
	0.18337/0.18417	1.0223	1.1935	0.184	1.186	1.089
	0.18328/0.18626	1.0104	1.1988	0.204	1.209	1.100
					1.207±0.020	1.099±0.009
—H	0.18630/0.19272	0.9926	1.1468	0.187	1.172	1.083
	0.19455/0.19489	1.0250	1.1858	0.171	1.173	1.083
	0.19380/0.19250	1.0337	1.2035	0.218	1.186	1.089
	0.17017/0.16544	1.0562	1.2267	0.220	1.183	1.088
					1.179±0.007	1.086±0.003
—Cl	0.19173/0.19440	1.0127	1.1455	0.215	1.148	1.072
	0.19642/0.19781	1.0196	1.1608	0.214	1.156	1.075
	0.18007/0.17977	1.0285	1.1772	0.225	1.165	1.079
	0.19394/0.18884	1.0545	1.1796	0.204	1.133	1.065
					1.151±0.014	1.073±0.0056

[a]The deuterated substrate was 98.1% dideuterated at the α-carbon.
[b]The fraction of reaction was corrected for the error in the recovery of the product.

deuterated substrate. The secondary α-deuterium kinetic isotope effects for the reaction of the *p*-methoxyphenyl-, the phenyl-, and the *p*-chlorophenylbenzyldimethylammonium ion with thiophenoxide ion at 0°C in DMF are given in Table 3.

An examination of the isotope effects in Table 3 shows that (*i*) all three isotope effects are significantly larger than the maximum secondary α-deuterium kinetic isotope effect (k_H/k_D = 1.08 or 1.04 per α-deuterium) expected for an S_N2 reaction (41) and (*ii*) that the magnitude of these isotope effects decreases as a more electron withdrawing substituent Z is added to the leaving group.

Unusually large secondary α-deuterium kinetic isotope effects are observed in these S_N2 reactions because the exceptionally large steric crowding around the Cα—H bonds in the substrates is reduced substantially in going to transition states with fairly long Cα--N and S--Cα bonds.[7] Thus, the zero point energy difference for the Cα—H and Cα—D out-of-plane bending vibrations will be much smaller in the transition state than in the reactant and large normal deuterium kinetic isotope effects would be expected for these reactions (10, 25).

More important, however, is the regular[8] decrease that is observed in the isotope effects as the substituent Z in the leaving group is changed from methoxy to chlorine. Unfortunately, no one has been able to suggest how the magnitudes of secondary α-deuterium kinetic isotope effects are related to the structure of S_N2 transition states (16). Thus the meaning of the trend in these isotope effects cannot be interpreted with certainty.

A consideration of the trend in the isotope effects in Table 3 has led the authors to propose that the magnitude of secondary α-deuterium kinetic isotope effects from closely related S_N2 reactions can be used to determine the structure of the transition state. Several workers have shown that the magnitude of secondary α-deuterium kinetic isotope effects is primarily determined by the changes that occur in the Cα—H out-of-plane bending vibrations when the substrate is converted into the transition state (42–44). In fact, the energy of these bending vibrations is directly related to the amount of steric crowding around the Cα—H bonds. A change of the substituent Z in the leaving group occurs several bonds away from the reaction center and obviously will not affect the steric crowding around the Cα—H bonds in the substrate. Thus the energy (frequency) of these vibrations and the zero point energy dif-

[7]The steric crowding around the reacting atoms in the initial states of the *p*-methoxyphenyl-, the phenyl, and the *p*-chlorophenylbenzyldimethylammonium ions will be identical. Moreover, the very similar nitrogen kinetic isotope effects and Hammett ρ values for substitution in the nucleophile (*vide infra*) observed for these reactions indicate that the transition states are similar.

[8]The magnitude of the isotope effect decreases by 3% when the change in the Hammett σ values of the substituent Z is $0.27 = |\sigma_{OCH_3} - \sigma_H|$ and $0.23 = |\sigma_H - \sigma_{Cl}|$.

ference ($\frac{1}{2}h\nu$) for the Cα—H and Cα—D out-of-plane bending vibrations will be the same for all three substrates. This means the trend observed in these isotope effects is caused by differences in the steric crowding around the Cα—H bonds in the transition states with Z equal to methoxy, hydrogen, and chlorine. The energy of the transition state Cα—H out-of-plane bending vibrations will be directly related to the amount of steric crowding around the Cα—H bonds. The amount of steric crowding around the Cα—H bonds in the trigonal bipyramidal transition state can only be altered significantly by changing the length of one or both of the nucleophile–α-carbon or α-carbon – leaving group bonds. Thus if either or both of the nucleophile–α-carbon and α-carbon – leaving group bonds were shorter in the transition state, the steric crowding around the Cα—H bonds would be larger and the energy of the out-of-plane bending vibrations would be increased (Fig. 2). This means the zero point energy difference between the Cα—H and Cα—D bonds will also be larger and a smaller kinetic isotope effect would be observed (Fig. 2*c*). These bond changes which decrease the nucleophile – leaving group distance in the transition state lead to a decrease in the magnitude of the secondary α-deuterium kinetic isotope effect. It follows that a larger nucleophile – leaving group distance in the transition state produces lower energy Cα—H bending vibrations and a larger isotope effect (Fig. 2*a*). Thus, the magnitude of the secondary α-deuterium kinetic isotope effect should be a measure of the nucleophile – leaving group distance in an S_N2 transition state.[9]

The data obtained in theoretical calculations of S_N2 transition states (23, 44) provides evidence to support this use of secondary α-deuterium kinetic isotope effects. Bron (44) has calculated secondary α-deuterium kinetic isotope effects for the S_N2 hydrolysis of benzyl bromide. Isotope effects were calculated for a wide range of transition state structures, i.e., many O—Cα bond order/Cα—Br bond order = n_1/n_2 ratios representing reactant-like, intermediate, and product-like transition states were used in the calculations. For all n_1/n_2 ratios, the magnitude of the isotope effect decreased linearly as the total bond order $n_t = n_1 + n_2$ increased from zero to 1.5. Since an increase in n_t means that both

[9]This method of estimating transition state structure may not be useful in every case. It would be difficult, if not impossible, to relate the magnitude of the isotope effect to transition state structure if a substituent change causes one bond to become longer and the second bond to shorten. It would also fail in cases where the change in substituent altered the steric crowding at the α-carbon of the substrate.

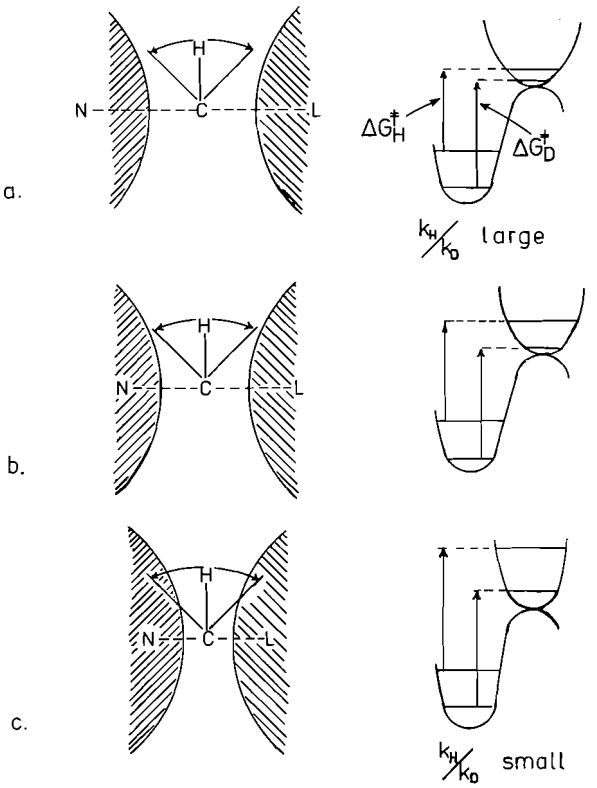

FIG. 2. The effect of a change in the nucleophile – leaving group (N—L) distance on the zero point energy difference between the Cα—H and Cα—D out-of-plane bending vibrations in an S_N2 transition state and hence on the magnitude of the secondary α-deuterium kinetic isotope effect.

O—Cα and Cα—Br bond orders are increased (the O—Cα and Cα—Br bonds become shorter), the isotope effect decreases as the O—Br distance is decreased. This is precisely the relationship proposed above. Similar calculations by Sims and coworkers (23) predict that the same relationship between the magnitude of the isotope effect and the nucleophile – leaving group distance in the transition state, exists. Thus it would appear that the magnitude of the secondary α-deuterium kinetic isotope effects measured in this study can be used to obtain the sulfur–nitrogen distance in the transition states with the substituent Z in the leaving group equal to methoxy, hydrogen, and chlorine.

The magnitude of the secondary α-deuterium kinetic isotope effects in Table 3 decreases when a more electron withdrawing substituent is in the leaving group. The relationship proposed above suggests that the largest S—N distance exists in the transition state with Z equal to methoxy. The smallest S—N distance is found in the transition state with Z equal to chlorine.

TABLE 4. The influence of a change of substituent, Z, in the leaving group on the transition state structure of an S_N2 reaction

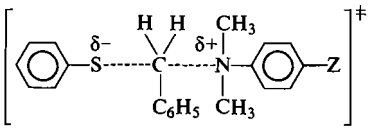

Para-substituent (Z) on the leaving group	k^{14}/k^{15}	Relative Cα—N bond length in transition state	$(k_H/k_D)_\alpha$	Relative S—N distance in transition state	Relative transition state structure
—OCH_3	1.0197	C-----N	1.207	S----------N	S--------C-----N
—H	1.0200	C------N	1.179	S--------N	S-----C------N
—Cl	1.0202	C-------N	1.151	S----N	S--C-------N

Combining these results with those from the nitrogen kinetic isotope effect study provides a qualitative estimate of both the nucleophile–α-carbon and the α-carbon – leaving group bonds in the transition states for the reactions with the different leaving groups. The nitrogen isotope effects indicated that the Cα—N bonds were the same length or showed a very slight, but regular, increase as the substituent Z was changed from methoxy to hydrogen to chlorine. The secondary α-deuterium kinetic isotope effects on the other hand showed that the sulfur–nitrogen distance decreased as more electron withdrawing substituents were placed in the leaving group (Table 4). Since the Cα—N bond in the transition state stays the same or becomes slightly longer as the S—N distance is decreasing, it must be concluded that the S—Cα bond length decreases as the substituent Z is changed from methoxy to chlorine. A second requirement is that the decrease in the S—Cα transition state bond length caused by a change to a more electron withdrawing substituent Z, must be greater than the increase in the Cα—N transition state bond. The relative structures of the three S_N2 transition states are shown in Table 4.

These changes in the structure of the transition states were surprising for two reasons: (*i*) the greatest change in the length of a transition state bond occurs in the bond more remote from the point of structural change and (*ii*) the best leaving group kinetically the *p*-chloro-*N*,*N*-dimethylaniline, requires the strongest push from the nucleophile, i.e., has the shortest S—Cα bond in the transition state. This result is surprising because it was expected that a better leaving group would require much less assistance from the nucleophile, i.e., less nucleophile–α-carbon bond formation. This would require an earlier transition state with a longer S—Cα bond and a shorter Cα—N bond. In fact, the opposite has been found.

Hammett ρ *Values*

It seemed necessary to confirm the above results for two reasons. Firstly, the structures of the transition states were completely unexpected and secondly because the conclusions were based on a new use of secondary α-deuterium kinetic isotope effects. In particular, it was important to confirm the lengths of the S—Cα bonds in the transition states of these reactions. In a recent publication Westaway and Ali (10) have shown that the Hammett ρ value obtained by changing the *para*-substituent in the nucleophile, i.e., in the thiophenoxide ion, can be used to estimate the length of the nucleophile–α-carbon bond in the transition state of an S_N2 reaction. Briefly, a large Hammett ρ value indicates that the charge on the nucleophile has changed markedly in going to the transition state. This means that a large portion of the electron density on the nucleophile has been used to form the nucleophile–α-carbon bond, i.e., the nucleophile–α-carbon bond must be short in the transition state. Conversely, a small Hammett ρ value would indicate a long weak nucleophile–α-carbon bond in the transition state.

The Hammett ρ values associated with changing the *para*-substituent in the thiophenoxide ion (changing X (eq. [2]) from methoxy to methyl, hydrogen, and chlorine) were determined for each substrate (the *p*-methoxyphenyl-, the phenyl-, and the *p*-chlorophenylbenzyldimethylammonium ion) at 0°C in DMF. The rate constants in Table 1 were used to determine these ρ values. The three ρ values, their standard deviation, and correlation coefficients are given in Table 5.

Two points are worth noting. First, all the Hammett ρ values are negative. This is expected because the sulfur atom of the nucleophile is more positively charged in the transition state of all three reactions. The second, and more important observation, is that the magnitude of the ρ values increases

TABLE 5. Hammett ρ values for the reactions of *para*-substituted thiophenoxide ions with *para*-methoxy-, *para*-hydrogen-, and *para*-chlorophenylbenzyldimethylammonium nitrates at 0°C in DMF

Substituent (Z) on the leaving group	ρ[a]	Correlation coefficient
$-OCH_3$	-1.536 ± 0.045	0.988
—H	-1.702 ± 0.047	0.990
—Cl	-1.834 ± 0.016	0.996

[a]The error limits are the standard deviation.

as the substituent in the leaving group is changed from methoxy to chlorine. This indicates that the largest change in the charge on the sulfur atom has occurred in the reaction where Z is chlorine. The smallest change of charge on the sulfur is found in the reaction where Z is methoxy. Since the change in charge varies inversely with the length of the S—Cα transition state bond, it can be concluded that the longest S—Cα bond is in the transition state with Z equal to methoxy. The shortest S—Cα bond is observed when Z is chlorine.

These results are in complete agreement with those based on the magnitude of the secondary α-deuterium kinetic isotope effect. The two methods used to estimate the relative lengths of the S—Cα transition state bonds are based on two completely different types of experimental data. Thus, the agreement provides very strong support for the results, i.e., that changing to a better leaving group, from a kinetic point of view (a more electron withdrawing substituent Z), causes a slight increase in the length of the Cα—N bond and a large decrease in the S—Cα bond in the transition state. The agreement also substantiates the new use of the secondary α-deuterium kinetic isotope effects to determine the nucleophile – leaving group distance in an S_N2 transition state.

Comparison of Experimental Results and Theoretical Predictions

Several workers have published theories which predict how changes in substituents will affect the structure of S_N2 transition states. The results of this investigation provide, for the first time, a good test of these theories.

The first method for predicting transition state structure was Hammond's 'thermal postulate'[10] (the Bell–Evans–Polanyi principle (45)). Hammond's postulate predicts that changing to a better leaving group from a kinetic point of view,[11] should lead to a more reactant-like transition state, i.e., with a longer S—Cα and a shorter Cα—N bond in the transition state. This is not observed. The experimental results indicate that changing to a better leaving group (Z equal to chlorine) leads to a tighter or more product-like transition state with a much shorter S—Cα bond and slightly longer Cα—N bond.

The second attempt to explain substituent effects in S_N2 transition states by Swain and Thornton (19) has been replaced by Thornton's reacting bond rule' (20). In this theory the substituent effects are determined by considering the effect of the change in substituent on the transition state stretching vibrations perpendicular (A) and parallel (B) to the reaction coordinate. Application of the 'reacting bond rule' to a transition state with a more electron withdrawing substituent in the leaving group (20) indicates that both the S—Cα and Cα—N bonds will be longer for the perpendicular vibration. A longer S—Cα bond and a shorter Cα—N bond are predicted for the parallel vibration. Since the S—Cα bond is longer for both vibrations, a longer S—Cα bond would be expected in the transition state with the better leaving group. The effect on the Cα—N bond is different for the two vibrations, however, and it is difficult to predict the change that will occur in the Cα—N transition state bond when the leaving group is altered. Recent studies by Winey and Thornton (47) on the structure of the transition states of concerted E2 elimination reactions have indicated that the relative perpendicular and parallel contributions are of comparable magnitude. If the parallel and perpendicular contributions are also equal for S_N2 reactions, changing to a better leaving group would still lead to a transition state with a longer S—Cα bond. The Cα—N bond on the other hand would not be changed significantly. The experimental results indicate (*i*) that the S—Cα bond is more sensitive to a change in the leaving group than the Cα—N bond and (*ii*) that the Cα—N bond becomes slightly longer and the S—Cα bond significantly shorter when a better leaving group is present. The reacting bond rule predicts correctly that the S—Cα bond will change more than the Cα—N bond.

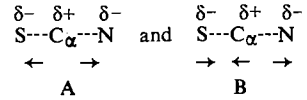

[10]Although Hammond's postulate has been used to predict changes in the structure of S_N2 transition states, this use has been criticized (46).

[11]A more stable *para*-substituted *N,N*-dimethylaniline is produced when a more electron withdrawing substituent Z is present in the leaving group. The energy of the reactants would not be changed significantly by a change in Z (45).

Moreover, if the perpendicular effect is slightly more important than the parallel effect, a slightly longer Cα—N bond would be observed when a better leaving group is present. Unfortunately, the reacting bond rule predicts a longer S—Cα bond and a shorter S—Cα bond is found. In fact, the experimental results are not predicted by any combination of the parallel and perpendicular effects.

Harris and Kurz (21) have modified Thornton's reacting bond rule in an effort to improve the results predicted for a change of substituent in the substrate. In spite of these modifications, the Harris–Kurz theory predicts the same changes in transition state structure for a change in the leaving group as Thornton's rule. Thus, the Harris-Kurz theory also fails in the same way to predict the experimental results.

Critchlow (22) devised a method to determine the energy and structure of S_N2 transition states from estimates of the energies of the carbonium ion and pentavalent (N—C—L) intermediates of the hypothetical stepwise reactions. Critchlow's theory predicts that the major change will occur in the bond more remote from the point of structural change, i.e., in the S—Cα bond. In particular, changing to a better leaving group is expected to give a transition state with a longer S—Cα bond. The Cα—N bond on the other hand should not change significantly. While the S—Cα bond does change more than the Cα—N bond when the leaving group is changed, the change in the S—Cα bond is opposite to that predicted. The experimental results indicate that a better leaving group leads to a transition state with a shorter S—Cα bond.

The most recent method of predicting substituent effects was suggested by Sims *et al.* (23). They proposed the use of a More O'Ferrall type of energy surface (48) (Fig. 3) to predict the changes that occur in the structure of the transition state when a substituent in the substrate, the nucleophile, or the leaving group is changed. The energy of the reactants, products, and the two possible intermediates, the carbonium ion and the pentavalent N—C—L complex, are represented at the corners of the energy surface. The X and Y axes represent changes in the α-carbon – leaving group (Cα—N) bond and the nucleophile–α-carbon (S—Cα) bond, respectively. The contours show the lowest energy pathway, i.e., the reaction coordinate, through the energy surface. The transition state is designated by a star.

The effect of changing a substituent in one of the reactants is determined by considering how this change would affect the energies of the reactants, the products, and the two possible intermediates. The benzyl carbonium ion intermediate and substitution product (benzylphenyl sulfide) are identical for all three leaving groups. Thus, the change in the energy of the carbonium ion (lower right corner) and the products (top right corner) resulting from a change in the leaving group is caused by the different energies of the leaving groups, i.e., the *para*-substituted *N*,*N*-dimethylanilines. Changing to a better leaving group (an *N*,*N*-dimethylaniline with a more electron withdrawing substituent) will lower the energy of the bottom right and top right corners of the energy surface by the same amount. Lowering the top right corner will cause the transition state to move back towards the reactant along the diagonal between reactants and products, a parallel effect. Lowering the bottom right corner of the energy surface would cause the transition state to move to the right, a perpendicular effect. The parallel effect will lead to a longer S—Cα bond and a shorter Cα—N bond in the transition state. The perpendic-

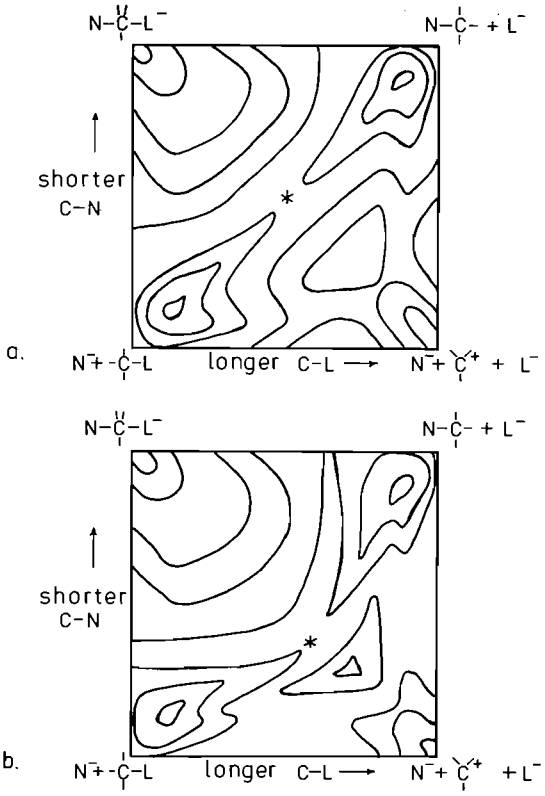

FIG. 3. Potential energy surface for a concerted (S_N2) nucleophilic substitution reaction with a symmetrical transition state (*a*) and showing the effect of changing to a better leaving group (*b*).

ular effect would lead to a longer S—Cα bond and a longer Cα—N bond. If the perpendicular effect were slightly larger than the parallel effect,[12] the transition state should have a longer S—Cα bond and a slightly longer Cα—N bond when a better leaving group is present.[13] This, like Thornton's, Kurz's, and Critchlow's theories, suggests that the more remote S—Cα transition state bond length will change more with a change to a better leaving group than the closer Cα—N bond. It also suggests correctly that the Cα—N bond should be slightly longer in the transition state. Unfortunately, it also predicts that the S—Cα bond should be longer in the transition state and a shorter bond is observed.

Thus, none of the theories predict the changes in transition state structure that are observed experimentally. Thornton's reacting bond rule (provided that the perpendicular and parallel effects are of comparable magnitudes), Kurz's theory, Critchlow's theory, and Sim's More O'Ferrall type of energy surface all predict that the largest change in transition state structure will occur in the more remote S—Cα bond rather than in the closer Cα—N bond. Only Sim's More O'Ferrall type of energy surface and Thornton's reacting bond rule can predict the small increase that is observed in the length of the Cα—N transition state bond. Finally, none of the theories predicts the direction of the change in the S—Cα bond.

The discrepancy between the theoretical predictions and the experimental results is disturbing. This discrepancy may occur for several reasons. (*1*) The theories are based on the enthalpy changes associated with the change of substituent and completely ignore entropy effects. (*2*) The theories only allow shifts of the electron density within a bond when a substituent is changed. In fact, a substituent change may cause the electron density in one bond to be transferred into an adjacent bond. This would be most likely to occur with the weak bonds in the transition state. (*3*) The theories predicting substituent effects do not consider any change in bonding with substituents on the α-carbon. If the bonding between the benzene ring and the α-carbon changed as the substituent Z in the leaving group were changed, the theories would be expected to fail. (*4*) The theories do not consider the effect of changing the relative energies of the nucleophile–α-carbon and α-carbon – leaving group bonds. Unfortunately, it is impossible to suggest which, if any, of these suggestions causes the failure to predict the experimental results.

Although the experimental results are not those suggested by the theories for predicting how changes in substituents affect the structures of S_N2 transition states, the authors believe that it would be premature to conclude that the theories are wrong. In fact, there may be some special, unsuspected properties which cause the reactions used in this study to respond to a substituent change in an unusual or unexpected way. It is also possible that the interpretation of the experimental results is not correct.[14] These results do,

[12]The perpendicular effect should be larger because lowering the energy of the right corner will distort the energy surface more than lowering the energy of the upper right corner. This occurs because the diagonal of the diagram is longer than the *x*-axis of the diagram.

[13]Substitution in the substrate that stabilizes the carbonium ion will lead to similar changes in the Cα—L and N—Cα transition state bonds, i.e., a perpendicular effect towards the lower right corner. Changing to a better nucleophile would lower the energy of the pentavalent intermediate and the product and shorten the α-carbon – leaving group bond and cause little or no change in the nucleophile–α-carbon bond.

[14]One of the referees has suggested a different but possible explanation of the experimental results. The referee suggests that the Cα—N transition state bond is not affected by a change in substituent Z. The smaller secondary α-deuterium kinetic isotope effect obtained when a more electron withdrawing substituent Z is present is observed because of an increase in the conjugation of the electrons of the partly broken Cα—N bond (the developing lone pair of electrons) with the N-phenyl ring. This would flatten the $(CH_3)_2NPh$ leaving group in a plane perpendicular to the S--Cα--N axis and move the two *N*-methyl and the *N*-phenyl groups closer to the Cα—H bonds. The area available for the Cα—H out-of-plane bending vibrations would be reduced in the same way as reducing the S—N distance in the transition state and a smaller α-deuterium kinetic isotope effect would be observed. The larger ρ values observed when a more electron withdrawing substituent is present in the leaving group is attributed to the greater electrostatic interaction between the more positive nitrogen (the nitrogen will be more electron deficient when Z is more strongly electron withdrawing) and the negatively charged sulfur atom in the transition state. This assumes that the increased electrostatic interaction has little or no effect on transition state structure. Finally, the faster rate of reaction observed when a more electron withdrawing substituent Z is present in the leaving group is a result of the extra stability arising from the increased conjugation between nitrogen and the *N*-phenyl group. Thus, all of the experimental results obtained when the leaving group is altered are attributed to a change in the conjugation between the nitrogen and the *N*-phenyl group rather than to a change in transition state structure. This means there is no significant change in either the Cα—N or S—Cα transition state bond lengths when the leaving group is altered and this system is not capable of testing Thornton's reacting bond rule or the other theories which predict how changes in substituents affect the structure of S_N2 transition states.

Although this alternate explanation is possible, the authors believe it is less likely than the interpretation presented above. This is for several reasons. (*1*) It seems more reasonable to conclude that the Cα—N bond is slightly longer in the transition state with a more electron withdrawing substituent Z. This is particularly true if the conjugation between the nitrogen and the *N*-phenyl group changes significantly when the substituent is altered. Moreover, a significant change in conjuga-

however, illustrate the need for more experimental results that can test these theories. We are currently examining other systems in order to learn whether the theories are correct or whether they need to be modified. In any case, the usefulness of these theories for other types of reactions is not compromised by the results of this study.

Supporting Evidence from Other Reactions

The results obtained in this study, i.e., that changing to a better leaving group leads to a transition state with a much shorter nucleophile–α-carbon bond and a slightly longer Cα—N bond, are believed to be general and not specific to this system. Although complete evidence to support this conclusion is not available, several published reports do concur with the results obtained in this study.

Ballistreri *et al.* (2) have measured the Hammett ρ values for the Menshutkin reactions between *para*-substituted anilines and benzyl halides. They found that the magnitude of the Hammett ρ values decreased as poorer leaving groups were placed in the molecule; the ρ value decreased from −1.46 when iodide ion was in the leaving group, to −1.40 when the leaving group was bromide ion, and to −0.87 for the poorest leaving group, chloride ion. Thus the largest change in the charge on the nitrogen of the nucleophile occurs with the best leaving group. This means the shortest N—Cα transition state bond occurs with the best leaving group and the longest N—Cα bond is found with the poorest leaving group. These results are in perfect agreement with those from the Hammett ρ study of the reactions between thiophenoxide ion and the *para*-substituted phenylbenzyldimethylammonium ions. Unfortunately, the lengths of the Cα–halogen bond are not known and a complete comparison of the transition states in these two studies is impossible.

Weaker evidence of a similar type is available from the Menshutkin reaction of *para*-substituted *N,N*-dimethylanilines and methyl iodide. A very large Hammett ρ value of −3.30 is observed for this S_N2 reaction (9). This ρ value is almost as large as that reported for an equilibrium protonation of *N,N*-dimethylaniline (9) and indicates that the N—Cα bond formation is almost complete in the transition state. In fact, a very short N—Cα bond would be expected in this reaction because iodide ion is a good leaving group.

Cromartie and Swain (50) measured the entering group chlorine isotope effects for the reaction of chloride ion with ethylene oxide under neutral (eq. [5]) and acidic conditions (eq. [6]). The chlorine

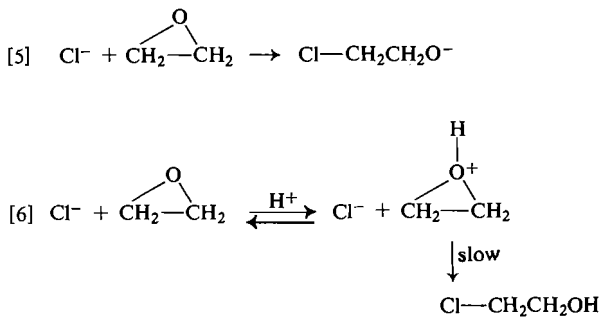

isotope effect was 1.00245 when the reaction was carried out under acidic conditions and 1.00280 in neutral medium. A smaller entering group chlorine kinetic isotope effect is expected for the transition state with the greatest amount of Cl—Cα bond formation because the second term in the square brackets of Bigeleisen's isotope effect equation (eq. [4]) is almost zero[15] and the third term is larger when the carbon–chlorine bond formation is more complete in the transition state. Cromartie and Swain expected a longer Cl—Cα bond in the transition state for the reaction with a better leaving group, i.e., the reaction in acidic medium. The isotope effects which were not consistent with their expectations were rationalized in the following manner. The loss in hydrogen bonding between the chloride ion and the solvent would obviously be

tion between the nitrogen and the *N*-phenyl group would be expected to cause some change in the Cα—N transition state bond length. This is not predicted by the referee's interpretation of the results. (*2*) It is difficult to believe that a change in substituent Z that changes the electrostatic interaction between the nitrogen and the sulfur enough to increase the ρ value would not lead to a change in transition state structure (particularly of the weaker S—Cα transition state bond). (*3*) It is not clear whether the tetrahedral character of the nitrogen in anilines would be altered by the change in *para*-substituents used in this study. Different studies have shown (*1*) that the amino group in 4-fluoroaniline is slightly more tetrahedral than it is in analine (49); (*2*) that the electron density on the amino nitrogen of 4-chloroaniline and aniline is almost the same (53); this suggests the structures of the amino groups are almost identical in these two compounds; (*3*) that the infrared N—C(phenyl) stretching absorption is the same for 4-methoxy- and 4-chloroaniline. These results suggest that the structure of the amino group in anilines is not altered significantly when the *para*-substituent is changed from methoxy to hydrogen or chlorine even though a full lone pair of electrons is available for delocalization into the phenyl group. The observation that the amino group in crystalline 4-chloroaniline is almost coplanar with the benzene ring (54) supports the referee's argument. In any case, any changes in the structure of the amino nitrogen in the transition states will be much smaller than those in the anilines because the developing lone pair of electrons on the nitrogen are not completely free to delocalize into the N-phenyl group. (*4*) Finally, other results obtained in our laboratory are more consistent with the interpretation presented in the main body of the paper.

[15]This term will have a small value because the chloride ion forms weak hydrogen bonds with water (33, 51).

greater in the transition state with a shorter Cl—Cα bond and Cromartie and Swain proposed that the loss in vibrational energy caused by the loss of hydrogen bonding would be greater than the increase in vibrational energy from the formation of the Cl—Cα bond. This would mean that the term in the square brackets of [4] would be smaller when the C—Cl bond formation was more complete in the transition state. While the loss in hydrogen bonding between the chloride ion and the solvent will undoubtedly lower the magnitude of the entering group chlorine kinetic isotope effects (33, 51), this effect should be almost identical for these two reactions which have very similar (long) Cl—Cα bonds in the transition state (52). In fact, a more likely explanation of these entering group chlorine kinetic isotope effects is that there is a shorter Cl—Cα bond length (more complete Cl—Cα bond formation) in the transition state of the reaction with the better leaving group.

The data in the above examples and the results of this study indicate that the nucleophile–α-carbon bond will be shorter in the transition state of the reaction with a better leaving group. It is worth noting that these results were obtained from three completely unrelated methods: secondary α-deuterium kinetic isotope effects, Hammett ρ values determined from reactions in which the *para*-substituent of the nucleophile was changed, and entering group chlorine kinetic isotope effects. Unfortunately, these results do not give any information to indicate whether the α-carbon – leaving group bond is slightly longer in the transition state of a reaction with a better leaving group or whether the more remote nucleophile–α-carbon bond responds more to a change in the leaving group than the nearer α-carbon – leaving group bond.

This study has shown that changing to a better leaving group will (*i*) change the nucleophile–α-carbon bond to a greater extent than the α-carbon – leaving group bond and (*ii*) that the nucleophile must be closer to the α-carbon to displace a better leaving group, i.e., that the transition state will be more product-like. Although the reasons for these two observations are not apparent, tentative suggestions which qualitatively explain the observed results can be given. The greater change in the S—Cα bond in the reactions between the thiophenoxide ion and the *para*-substituted phenylbenzyldimethylammonium ion may occur because a large increase in the amount of bond formation of the weaker[16] S—Cα bond would be required to provide the energy to increase the length of the stronger Cα—N bond slightly.[17] Experiments to determine if this is the case or whether the greater sensitivity in the more remote bond is a general property of S_N2 transition states as Critchlow's theory and the energy surface approach of Sims *et al.* suggest have been started in this laboratory.

The second problem is explaining why a shorter S—Cα transition state bond is observed when a better leaving group is present in the molecule. A possible explanation for this observation is that although the nucleophile must be present to help displace the leaving group, the position of the nucleophile in the transition state (the S—Cα bond length) is determined by the need to reduce or eliminate any positive charge on the α-carbon. Introducing a more electron withdrawing substituent into the leaving group (making a better leaving group) will lower the electron density in the weak transition state bonds and increase the positive charge on the ammonium nitrogen and to a lesser extent, the α-carbon. Since any increase in the positive charge on the α-carbon would be expected to increase the energy of the transition state and reduce the rate of reaction, a better leaving group must not increase the charge on the α-carbon significantly. In fact, other workers have suggested that the positive charge on the α-carbon is small in S_N2 transition states (16, 38). The increased need for electron density at the α-carbon resulting from the introduction of the electron withdrawing substituent is most readily obtained by bringing the nucleophile closer to the α-carbon, i.e., a shorter S—Cα bond will increase the electron density at the α-carbon more than a long S—Cα bond. Substituting a more electron donating group in the leaving group would have the opposite effect. The electron density on the α-carbon would be increased, the need for electrons from the nucleophile would be decreased, and a longer S—Cα transition state bond would be observed. While this suggestion is consistent with the experimental results, it cannot be supported with any solid evidence and is purely speculative.

Conclusions

(*1*) This study has shown that the magnitude of secondary α-deuterium kinetic isotope effects can be used to determine the structure of S_N2 transition states. In particular, the nucleophile – leaving group distance has been found to be inversely related to the magnitude of these isotope effects. (*2*) This study has

[16]The S—C bond in sulfides has a stretching frequency between 600 and 700 cm^{-1} (17), whereas the C—N stretching frequency is approximately 1000 cm^{-1} (*vide supra*).

[17]Theoretical calculations by Sims *et al.* (31) suggest that a more product-like transition state will be observed when the α-carbon–nucleophile bond becomes weaker than the α-carbon – leaving group bond.

also shown that S_N2 transition states of carefully designed systems can be modelled qualitatively in sufficient detail to allow the substituent effects on both the nucleophile–α-carbon and α-carbon – leaving group bonds to be determined. (*3*) Finally, this investigation has shown that changing to a better leaving group changes the length of the nucleophile–α-carbon bond more than the α-carbon – leaving group bond and leads to a more product-like transition state where nucleophile–α-carbon bond formation is much more complete and α-carbon – leaving group bond rupture is slightly more advanced.

Experimental

Materials

The *p*-methoxyphenyl-, *p*-chlorophenyl-, and phenylbenzyldimethylammonium nitrates were prepared for an earlier study (9). The *p*-methoxyphenyl-, *p*-chlorophenyl-, and phenylbenzyl-1,1-d_2-dimethylammonium nitrates were synthesized from the same sample of benzyl bromide-1,1-d_2 (10) using the methods described for the undeuterated compounds. The deuterated substrates were purified as described in ref. 9. The melting points were within 1°C of the values reported for the undeuterated compounds. A deuterium analysis (10) indicated that these deuterated quaternary ammonium salts were 98.1% dideuterated and 1.9% monodeuterated at the 1-position. The purification of the solvent, *N*,*N*-dimethylformamide (9), and the preparation of the *para*-substituted sodium thiophenoxides have been described (10).

Kinetic Measurements and Isotope Effects

The procedures used in measuring the rate constants and the nitrogen kinetic isotope effects were identical to those described in ref. 9. The secondary α-deuterium kinetic isotope effects were measured using the procedure in ref. 10.

Acknowledgements

The authors wish to thank Dr. E. J. Monahan, past President of Laurentian University, and the National Research Council of Canada for the financial support required to complete this study. The authors also wish to thank Mr. M. Zavits and Mr. E. Moro who helped in the synthesis of the deuterated and undeuterated *para*-substituted phenylbenzyldimethylammonium nitrates and Mr. M. Gravelle who helped develop many of the experimental techniques used in this study. The authors also wish to thank Professor E. R. Thornton for his very helpful suggestions.

1. R. F. Hudson and G. Klopman. J. Chem. Soc. 1062 (1962).
2. F. P. Ballistreri, E. Maccarone, and A. Mamo. J. Org. Chem. **41**, 3364 (1976).
3. V. J. Shiner, Jr., M. W. Rapp, and H. R. Pinnick, Jr. J. Am. Chem. Soc. **92**, 232 (1970).
4. K. M. Koshy and R. E. Robertson. J. Am. Chem. Soc. **96**, 914 (1974).
5. V. F. Raaen, T. Juhlke, F. J. Brown, and C. J. Collins. J. Am. Chem. Soc. **96**, 5928 (1974).
6. E. C. F. Ko and A. J. Parker. J. Am. Chem. Soc. **90**, 6447 (1968).
7. K. M. Koshy, R. E. Robertson, G. S. Dyson, and S. Singh. Can. J. Chem. **54**, 3614 (1976).
8. H. Yamataka and T. Ando. Tetrahedron Lett. 1059 (1975).
9. K. C. Westaway and R. A. Poirier. Can. J. Chem. **53**, 3216 (1975).
10. (*a*) K. C. Westaway and S. F. Ali. Can. J. Chem. **57**, 1089 (1979). (*b*) S. F. Ali. M.Sc. Thesis, Laurentian University, Sudbury, Ont. 1976.
11. C. G. Swain and E. R. Thornton. J. Org. Chem. **26**, 4808 (1961).
12. M. P. Friedberger and E. R. Thornton. J. Am. Chem. Soc. **98**, 2861 (1976).
13. R. T. Hargreaves, A. M. Katz, and W. H. Saunders, Jr. J. Am. Chem. Soc. **98**, 2614 (1976).
14. E. P. Grimsrud and J. W. Taylor. J. Am. Chem. Soc. **92**, 739 (1970).
15. R. C. Williams and J. W. Taylor. J. Am. Chem. Soc. **95**, 1710 (1973).
16. K. C. Westaway. Can. J. Chem. **56**, 2691 (1978).
17. L. J. Bellamy. The infra-red spectra of complex molecules. J. Wiley and Sons Inc., New York, NY. 1960. p. 353.
18. G. S. Hammond. J. Am. Chem. Soc. **77**, 334 (1955).
19. C. G. Swain and E. R. Thornton. J. Am. Chem. Soc. **84**, 817 (1962).
20. E. R. Thornton. J. Am. Chem. Soc. **89**, 2915 (1969).
21. J. C. Harris and J. L. Kurz. J. Am. Chem. Soc. **92**, 349 (1970).
22. J. E. Critchlow. J. Chem. Soc. Faraday Trans. 1, **68**, 1774 (1972).
23. L. B. Sims, G. W. Burton, and D. M. Brubaker. 173rd American Chemical Society, National Meeting, New Orleans, LA, March, 1977; D. M. Brubaker, Ph.D. Thesis, University of Arkansas, Fayetteville, Arkansas, AR. 1978.
24. D. C. Gregg, P. E. Bouffard, and R. Barton. Anal. Chem. **33**, 269 (1961).
25. K. C. Westaway. Tetrahedron Lett. 4229 (1975).
26. S. Dal Nogare and R. S. Juvet, Jr. Gas–liquid chromatography. Interscience, New York, NY. 1962. p. 256.
27. J. March. Advanced organic chemistry: Reactions, mechanisms, and structure. 2nd ed. McGraw-Hill Book Co., Toronto, Ont. 1977. p. 325.
28. W. H. Saunders, Jr. Ionic aliphatic reactions. Prentice-Hall Inc., Englewood Cliffs, NJ. 1965. p. 41.
29. J. March. Advanced organic chemistry: Reactions mechanisms, and structure. 2nd ed. McGraw-Hill Book Co., Toronto, Ont. 1977. p. 322.
30. L. Melander. Isotope effects on reaction rates. Ronald Press, New York, NY. 1960. p. 20.
31. L. B. Sims, A. Fry, L. T. Netherton, J. C. Wilson, K. D. Reppond, and S. W. Crooke. J. Am. Chem. Soc. **94**, 1364 (1972).
32. W. H. Saunders, Jr. Chim. Scr. **8**, 27 (1975).
33. G. W. Burton, L. B. Sims, J. C. Wilson, and A. Fry. J. Am. Chem. Soc. **99**, 3371 (1977).
34. J. Bigeleisen. J. Chem. Phys. **17**, 675 (1949).
35. J. Bron and J. B. Stothers. Can. J. Chem. **47**, 2506 (1969).
36. J. Bron and J. B. Stothers. Can. J. Chem. **46**, 1435 (1968).
37. A. J. Kresge, N. N. Lichtin, K. N. Rao, and R. E. Weston, Jr. J. Am. Chem. Soc. **87**, 437 (1965).
38. A. Streitweiser, Jr. Solvolytic displacement reactions. McGraw-Hill, New York, NY. 1962. p. 15.
39. D. G. Graczyk and J. W. Taylor. J. Am. Chem. Soc. **96**, 3255 (1974).

40. J. BIGELEISEN and M. WOLFSBERG. J. Chem. Phys. **22**, 1264 (1954).
41. H. HUMSKI, V. SENDIJAREVIC, and V. J. SHINER, JR. J. Am. Chem. Soc. **96**, 6187 (1974).
42. V. J. SHINER, JR. *In* Isotope effects in chemical reactions. A.C.S. Monograph 166. *Edited by* C. J. Collins and N. S. Bowman. Van Nostrand-Reinhold, New York, NY. 1971. Chapt. 2, pp. 104–137.
43. V. J. SHINER, JR., M. W. RAPP, E. A. HALEVI, and M. WOLFSBERG. J. Am. Chem. Soc. **90**, 7171 (1968).
44. J. BRON. Can. J. Chem. **52**, 903 (1974).
45. M. J. DEWAR. The molecular orbital theory of organic chemistry. McGraw Hill, New York, NY. 1969. pp. 284–288.
46. D. FARCASIU. J. Chem. Educ. **52**, 76 (1975).
47. D. A. WINEY and E. R. THORNTON. J. Am. Chem. Soc. **97**, 3102 (1975).
48. R. A. MORE O'FERRALL. J. Chem. Soc. B, 274 (1970).
49. A. HASTIE, D. G. LISTER, R. L. MCNEIL, and J. K. TYLER. Chem. Commun. 108 (1970).
50. T. H. CROMARTIE and C. G. SWAIN. J. Am. Chem. Soc. **98**, 2962 (1976).
51. K. REPPOND. Ph.D. Thesis, University of Arkansas, Fayetteville, AR. 1974.
52. T. H. CROMARTIE and C. G. SWAIN. J. Am. Chem. Soc. **98**, 545 (1976).
53. P. HAMPSON, A. MATHIAS, and R. WESTHEAD. J. Chem. Soc. B, 397 (1971).
54. C. T. YIM, M. A. WHITEHEAD, and D. H. LO. Can. J. Chem. **46**, 3595 (1968).

The crystal and molecular structure of *cis*-dichloro(2,2′-*o*-phenylenebisbenzothiazole)copper(II)

RICHARD G. BALL AND JAMES TROTTER

Department of Chemistry, University of British Columbia, 2075 Wesbrook Mall, Vancouver, B.C., Canada V6T 1W5

Received November 14, 1978

RICHARD G. BALL and JAMES TROTTER. Can. J. Chem. **57**, 1368 (1979).

The molecular structure of *cis*-dichloro(2,2′-*o*-phenylenebisbenzothiazole)copper(II) has been determined by single crystal X-ray diffractometry. The crystal is monoclinic, $P2_1/n$, $a = 8.408(1)$, $b = 15.819(1)$, $c = 14.229(2)$ Å, $\beta = 93.19(1)°$, and $Z = 4$. The structure has been refined by full-matrix least-squares techniques on F, using 3316 unique reflections for which $F^2 > 3\sigma(F^2)$, to a final agreement factor of 0.028. The complex adopts an approximately square planar coordination geometry with the Cu bound to two *cis* Cl atoms and the N atoms of the chelating benzothiazole ligand. The mean Cu—N and Cu—Cl distances are 2.016(6) and 2.217(6) Å, respectively.

RICHARD G. BALL et JAMES TROTTER. Can. J. Chem. **57**, 1368 (1979).

On a déterminé la structure moléculaire du *cis*-dichloro(2,2′-*o*-phénylènebisbenzothiazole)-cuivre(II) par diffraction de rayons-X d'un cristal unique. Les cristaux sont monocliniques, $P2_1/n$, $a = 8.408(1)$, $b = 15.819(1)$, $c = 14.229(2)$ Å, $\beta = 93.19(1)°$ et $Z = 4$. On a affiné la structure sur F par la méthode des moindres carrés (matrice complète) en faisant appel à 3316 réflexions indépendantes pour lesquelles $F^2 > 3\sigma(F^2)$ jusqu'à un facteur d'accord final de 0.028. Le complexe adopte une géométrie de coordination qui est approximativement plan carré; le cuivre est lié à deux atomes de Cl *cis* et aux atomes de N du ligand chélatant benzothiazole. Les distances moyennes Cu—N et Cu—Cl sont respectivement 2.016(6) et 2.217(6) Å.

[Traduit par le journal]

Introduction

It has been postulated that ligands which have imidazole or thioether functionality are important in modelling type I and type III copper metalloproteins (1). The bifunctional benzothiazole ligand, 2,2′-*o*-phenylenebisbenzothiazole (OBT), has both pseudo-imidazole and thioether groups and is potentially capable of binding to a metal by either the N or S atoms. Benzothiazole itself also has this capability but investigations of its complexes with first row transition metals show it to be N bonded if it does not act as a bridging bidentate ligand (2).

A spectroscopic investigation of the Co(II), Cu(II), and Zn(II) complexes of 2,2′-*o*-phenylenebisbenzothiazole was initiated to discover the bonding mode and the stereochemistry of the complexes containing this ligand (3). However, it proved impossible to determine unambiguously whether the $Cu(OBT)Cl_2$ complex was N or S bonded, and we undertook the X-ray crystallographic examination of the complex to resolve this ambiguity and to determine the precise stereochemistry about the Cu atom.

Experimental

Dark green crystals of *cis*-dichloro(2,2′-*o*-phenylenebisbenzothiazole)copper(II) were kindly supplied by L. K. Thompson. Preliminary Weissenberg and precession photography indicated the crystal possessed monoclinic symmetry. The crystal data, as determined by film and diffractometer methods, are:

$C_{20}H_{12}Cl_2CuN_2S_2$ fw = 478.91

Monoclinic, $a = 8.408(1)$, $b = 15.819(1)$, $c = 14.229(2)$ Å, $\beta = 93.19(1)°$, $V = 1889.42$ Å^3, $Z = 4$ (22°C, MoK_α, $\lambda = 0.71073$ Å), $\mu = 15.83$ cm^{-1}, $\rho_o = 1.699(2)$ g cm^{-3} (by flotation in CCl_4 and $CHBr_3$), $\rho_c = 1.683$ g cm^{-3}. Systematic absences; $h0l$, $h + l \neq 2n$; $0k0$, $k \neq 2n$. Space group $P2_1/n$, an alternative setting of $P2_1/c$ (C_{2h}^5, No. 14).

The crystal chosen for data collection had dimensions of ca. 0.15 × 0.19 × 0.44 mm and was bounded by 12 faces of the forms {121}, {12$\bar{2}$}, {010}, and {001}. It was mounted on an Enraf-Nonius CAD-4 computer controlled diffractometer in a non-specific orientation with the long dimension of the crystal, the normal to (12$\bar{2}$), approximately along the spindle axis. Cell constants and an orientation matrix were obtained from a least-squares refinement of the setting angles of 16 reflections in the range $38 < 2\theta < 48°$. Crystal mosaicity was checked by the ω scan technique, and the average width at half-weight for the 3 reflections examined was 0.12°.

The intensity data were collected using the ω–2θ scan technique in which both the scan range and aperture width were functions of tan θ. Three reference reflections were used as a check on machine and crystal stability. Crystal orientation was checked every 100 reflections by recentering 3 reflections which were well separated in reciprocal space. If the deviation of the scattering vectors exceeded 0.05° automatic recentering and least-squares refinement of the orientation matrix and cell dimensions were carried out. Data collection parameters are given in Table 1. Over the course of data collection the reference reflections showed only random fluctuations and the unit cell parameters did not change significantly.

Corrections for Lorentz and polarization effects were applied

0008-4042/79/111368-04$01.00/0

TABLE 1. Experimental conditions

Radiation: MoK$_\alpha$, graphite monochromator
Scan range: (0.60 + 0.347 tan θ)°, extended 25% on either side for backgrounds
Scan speed: variable between 0.7 and 10.1 deg min^{-1} to give $I/\sigma(I) \geq 20$
Aperture: (2.0 + 0.50 tan θ) × 4 mm, 173 mm from crystal
Data collected: $\pm h, k, l$ to $2\theta = 60°$
Standards: 1 9 11, $\bar{7}$ 0 9, $\bar{1}$ 4 13; measured every hour of exposure time

during data reduction.[1] The standard deviation, $\sigma(I)$, is calculated from

$$\sigma(I) = [\text{Int} + 4(\text{BL} + \text{BH}) + (pI)^2]^{1/2}$$

where Int is the total integrated intensity, BL and BH are the low and high angle background counts, and the value for p was 0.03. Of the 5681 intensities measured, there were 3316 independent reflections which had $I > 3\sigma(I)$ and these were used in the structure solution and refinement.

Structure Solution and Refinement

The positional parameters for the Cu atom were derived from a three dimensional Patterson synthesis. Two cycles of full-matrix least-squares refinement of the positional parameters and scale factor followed by calculation of a difference Fourier synthesis revealed the positions of the two Cl atoms and one of the S atoms. A least-squares refinement of the atomic parameters and calculation of a difference Fourier synthesis resulted in location of the remaining non-hydrogen atoms.

Refinement of atomic parameters was carried out by full-matrix least-squares techniques on F minimizing the function $\Sigma w(|F_o| - |F_c|)^2$ where $|F_o|$ and $|F_c|$ are the observed and calculated structure factor amplitudes, respectively. The weighting factor w is given by $w = 4F_o^2/\sigma^2(F_o^2)$. The scattering factors for Cu^{2+}, Cl^-, S, N, and C were calculated from the coefficients for the scattering curve (4), while those for H were from Stewart *et al.* (5). The f' and f'' corrections for anomalous dispersion were those of Cromer and Liberman (6) and were included for the Cu, Cl, and S atoms. After two cycles of refinement, in which all the atoms were assigned anisotropic thermal parameters, the agreement factors were $R_1 = \Sigma(||F_o| - |F_c||)/\Sigma|F_o| = 0.045$ and $R_2 = (\Sigma w(|F_o| - |F_c|)^2/\Sigma w(F_o)^2)^{1/2} = 0.070$. At this time a difference Fourier showed peaks of positive electron density for all twelve H atoms present in the molecule. These were included in subsequent cycles and their positional and isotropic thermal parameters refined. Prior to the final cycles of refinement an absorption correction, using the Gaussian integration method, was applied to all 4881 data with $F^2 > 0$ and, in addition, as it appeared that some of the data suffered from extinction effects an isotropic extinction parameter (7) was refined during the final cycles.

The model was refined to convergence and in the final cycle no parameter shift exceeded 0.6 times its estimated standard deviation. The final agreement factors, for 293 variables and 3316 data with $F^2 > 3\sigma(F^2)$, were $R_1 = 0.028$ and $R_2 = 0.037$ (including the data with $0 < F^2 < 3\sigma$ in the refinement produced no significant improvement in either the atomic parameters or their esd's while the agreement factors increased to $R_1 = 0.059$ and $R_2 = 0.041$). The error in an observation of unit weight is 1.3 electrons. An analysis of R_2 in terms of $|F_o|$, $\lambda^{-1}\sin\theta$, and combinations of Miller indices showed no significant trends. A difference Fourier synthesis calculated from the final structure factors contained no features of chemical significance. The highest peak, with fractional coordinates (0.250 −0.077, −0.234), is located 0.73 Å from the Cu atom and has an electron density of 0.35 e Å^{-3}. The final atomic positional parameters are presented in Table 2, while the thermal parameters are listed in Table 3.[2] A listing of F_o and F_c is given in Table 4.[2]

TABLE 2. Final positional parameters (fractional × 10^4) with estimated standard deviations in parentheses

Atom	x	y	z
Cu	1718.8(4)	−865.7(2)	−2584.8(2)
Cl(1)	1636(1)	−1727(1)	−3817(1)
Cl(2)	−157(1)	−1551(1)	−1858(1)
S(1)	1650(1)	1089.6(5)	−285(1)
S(2)	4309(1)	1324.0(5)	−3854(1)
N(1)	2073(3)	−128(1)	−1442(2)
N(2)	3230(3)	−59(1)	−3185(2)
C(1)	2873(4)	742(2)	−3331(2)
C(2)	1378(4)	1155(2)	−3091(2)
C(3)	757(3)	1119(2)	−2190(2)
C(4)	1522(3)	645(2)	−1398(2)
C(5)	606(4)	1654(2)	−3784(2)
C(6)	−769(4)	2090(2)	−3610(3)
C(7)	−1376(4)	2049(2)	−2738(3)
C(8)	−606(4)	1580(2)	−2027(3)
C(9)	4744(3)	−251(2)	−3493(2)
C(10)	5510(4)	−1032(2)	−3420(2)
C(11)	7036(4)	−1096(3)	−3734(3)
C(12)	7769(4)	−407(3)	−4141(3)
C(13)	7020(4)	358(3)	−4243(2)
C(14)	5494(4)	437(2)	−3897(2)
C(15)	2696(3)	−407(2)	−567(2)
C(16)	3413(4)	−1190(2)	−387(2)
C(17)	4024(4)	−1352(2)	516(3)
C(18)	3907(4)	−756(2)	1227(3)
C(19)	3177(4)	6(2)	1068(2)
C(20)	2563(4)	184(2)	156(2)
HC(5)	1009(40)	1673(21)	−4373(24)
HC(6)	−1335(45)	2438(24)	−4073(27)
HC(7)	−2309(42)	2335(22)	−2610(24)
HC(8)	−1046(39)	1530(20)	−1430(24)
HC(10)	4996(40)	−1503(22)	−3199(24)
HC(11)	7576(50)	−1616(27)	−3687(30)
HC(12)	8899(49)	−498(25)	−4298(28)
HC(13)	7377(50)	833(25)	−4530(31)
HC(16)	3433(42)	−1577(22)	−878(25)
HC(17)	4515(42)	−1826(23)	654(25)
HC(18)	4428(46)	−892(22)	1802(28)
HC(19)	3088(46)	384(24)	1495(28)

[1]The computer programs used include local modifications of the following: full-matrix least-squares, ORFLS by W. R. Busing, K. O. Martin, and H. A. Levy; Patterson and Fourier synthesis, FORDAP by A. Zalkin; function and errors, ORFFE by W. R. Busing, K. O. Martin, and H. A. Levy; crystal structure illustrations, ORTEP by C. K. Johnson; absorption correction, BICABS by F. H. Allen and S. J. Rettig.

[2]Table 3 (thermal parameters) and the structure factor table are available, at a nominal charge, from the Depository of Unpublished Data, CISTI, National Research Council of Canada, Ottawa, Ont., Canada K1A 0S2.

TABLE 5. Selected bond distances and angles

Bond	Distance (Å)	Bond	Distance (Å)
Cu—Cl(1)	2.218(1)	S(2)—C(14)	1.724(3)
Cu—Cl(2)	2.216(1)	N(1)—C(4)	1.310(3)
Cu—N(1)	2.010(2)	N(1)—C(15)	1.395(3)
Cu—N(2)	2.023(2)	N(2)—C(1)	1.316(3)
S(1)—C(4)	1.730(3)	N(2)—C(9)	1.402(4)
S(1)—C(20)	1.727(3)	C(1)—C(2)	1.474(4)
S(2)—C(1)	1.721(3)	C(3)—C(4)	1.471(4)

Bonds	Angle (deg)	Bonds	Angle (deg)
Cl(1)—Cu—Cl(2)	94.40(3)	N(1)—Cu—N(2)	84.66(9)
Cl(1)—Cu—N(1)	173.01(7)	Cl(2)—Cu—N(2)	170.16(7)
C(4)—S(1)—C(20)	90.0(1)	C(1)—S(2)—C(14)	90.0(1)
S(1)—C(4)—N(1)	114.8(2)	S(2)—C(1)—N(2)	115.1(2)
C(4)—N(1)—C(15)	111.6(2)	C(1)—N(2)—C(9)	111.2(2)
N(1)—C(15)—C(20)	113.7(2)	N(2)—C(9)—C(14)	113.5(2)
C(15)—C(20)—S(1)	109.8(2)	C(9)—C(14)—S(2)	110.1(2)
N(2)—C(1)—C(2)	125.5(3)	N(1)—C(4)—C(3)	125.4(2)
C(1)—C(2)—C(3)	123.8(2)	C(2)—C(3)—C(4)	123.2(2)
Cu—N(1)—C(4)	123.0(2)	Cu—N(2)—C(1)	122.0(2)
Cu—N(1)—C(15)	124.7(2)	Cu—N(2)—C(9)	126.7(2)

Structure Description

A perspective view of the molecule including the atom numbering scheme is presented in Fig. 1. Selected bond distances and angles are listed in Table 5 and some weighted least-squares planes are given in Table 6.

The Cu atom is coordinated to two *cis* Cl atoms and is N bonded to the two benzothiazole groups of the OBT ligand. The coordination geometry of the Cu atom is slightly tetrahedrally distorted from square planar. This distortion is indicated by a dihedral angle of 9.63° between the Cu—Cl(1)—Cl(2) and Cu—N(1)—N(2) planes and the relative displacements of the N atoms from the Cu—Cl(1)—Cl(2) plane (Table 6). The mean Cu—Cl distance of 2.217(1) Å is at the short end of the range of distances, 2.20–2.27 Å, commonly observed for ter-

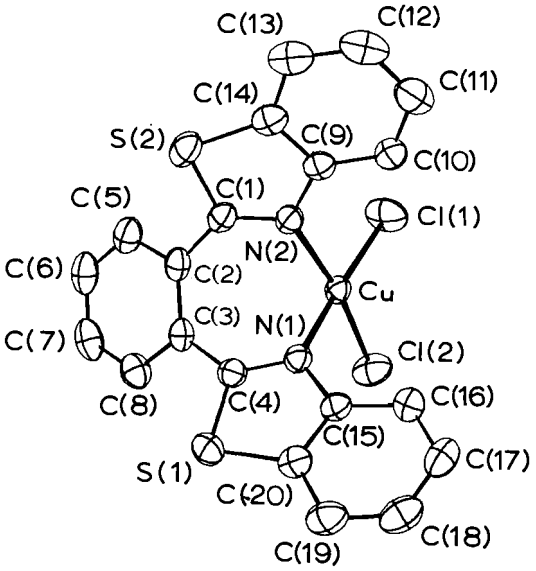

FIG. 1. Perspective view of the dichloro(2,2′-*o*-phenylenebisbenzothiazole)copper(II) molecule. Atoms are represented by 50% probability thermal ellipsoids and the hydrogens have been omitted.

TABLE 6

(*a*) Selected weighted least-squares planes

Plane *1*. $-0.674x + 0.578y - 0.460z + 0.212 = 0$
Atoms in plane: Cu, Cl(1), Cl(2)
Atoms not in plane: N(1) −0.213(2),[a] N(2) 0.241(2)

Plane *2*. $-0.757x + 0.572y - 0.315z + 0.877 = 0$
Atoms in plane: Cu, N(1), N(2)
Atoms not in plane: Cl(1) −0.250(1), Cl(2) 0.292(1)

Plane *3*. $-0.541x - 0.790y - 0.288z + 0.943 = 0$
Atoms in plane: C(2) 0.006(3), C(3) 0.003(3), C(5) −0.013(3), C(6) 0.004(3), C(7) 0.011(3), C(8) −0.013(3)

Plane *4*. $0.900x + 0.385y - 0.206z - 2.017 = 0$
Atoms in plane: S(1) −0.001(1), N(1) −0.002(2), C(4) 0.036(3), C(15) −0.019(3), C(16) −0.018(3), C(17) 0.017(3), C(18) 0.034(4), C(19) 0.002(4), C(20) −0.022(3).

Plane *5*. $-0.356x - 0.241y - 0.903z - 3.041 = 0$
Atoms in plane: S(2) −0.003(1), N(2), 0.009(2), C(1) −0.007(3), C(9) 0.015(3), C(10) −0.008(3), C(11) −0.047(4), C(12) −0.019(4), C(13) 0.042(3), C(14) 0.035(3)

[a]Perpendicular distance above (+) or below (−) the plane in Å.

(*b*) Interplanar angles (deg)

Planes	Angle	Planes	Angle	Planes	Angle
1–2	9.63	3–4	137.01	3–5	49.95

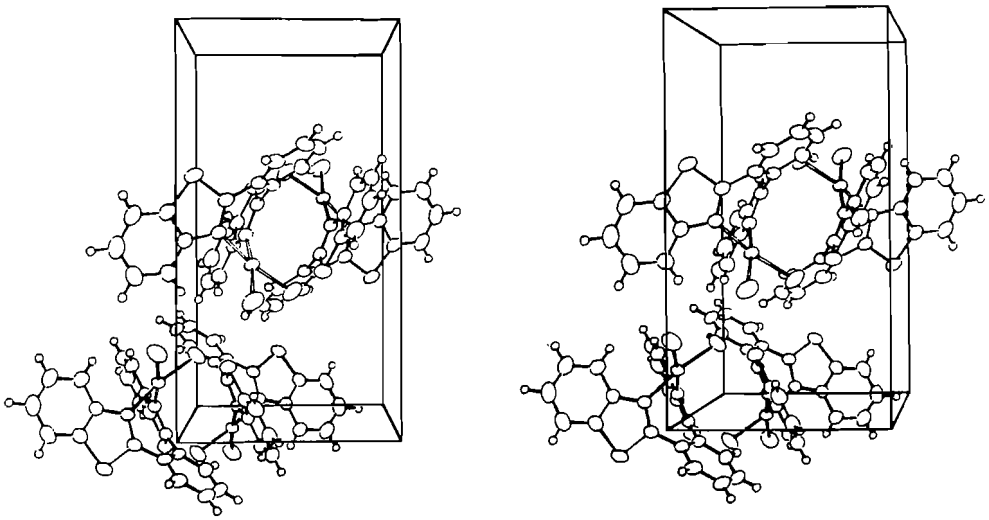

FIG. 2. Stereoview of a unit cell content. The view is along *c*, with *a* running horizontally to the right and *b* vertical.

minal Cu—Cl bonds (8–13). The mean Cu—N distance of 2.016(3) Å is normal in comparison with other structures (8–10, 14, 15).

The internal geometries of the two benzothiazole moieties do not show any significant differences and are comparable to structures observed for uncoordinated benzothiazole molecules (16, 17). The benzothiazole groups are close to being planar (Table 6) and are inclined by approximately 45°, with respect to the mean plane of the phenylene ring linking them.

The three phenylene rings in the molecule do not display any significant distortions from an ideal geometry; the mean bond distance and angle in each ring are 1.39(1) Å and 120(2)°, respectively. The mean C—H bond length of 0.93(4) Å is normal for sp^2 type carbon atoms.

A stereoview of a unit cell showing the packing of the molecules is presented in Fig. 2. An analysis of the intermolecular distances indicates there are no unusual intermolecular contacts, with the closest distance of approach being 2.83(4) Å between Cl(2) and HC(7) at $(-0.5 - x, -0.5 + y, -0.5 - z)$. There does not appear to be any interaction with the Cu atom along directions axial to the square plane which would imply pseudo-octahedral coordination to the Cu atom. This is presumably a result of the steric bulk of the OBT ligand above and below the coordination plane of the metal atom.

Acknowledgments

We thank the National Research Council of Canada for financial support of this work and the University of British Columbia Computing Centre for assistance.

1. A. R. AMUNDSEN, J. WHELAN, and B. BOSNICH. J. Am. Chem. Soc. **99**, 6730 (1977), and references therein.
2. E. J. DUFF, M. N. HUGHES, and K. J. RUTT. J. Chem. Soc. A, 2354 (1968); N. N. Y. CHAN, M. GOODGAME, and M. J. WEEKS. J. Chem. Soc. A, 2499 (1968).
3. J. C. T. RENDELL and L. K. THOMPSON. Can. J. Chem. In press.
4. International Tables for X-Ray Crystallography. Vol. IV. Kynoch Press, Birmingham, England. 1972. p. 99.
5. R. F. STEWART, E. R. DAVIDSON, and W. T. SIMPSON. J. Chem. Phys. **42**, 3175 (1965).
6. D. T. CROMER and D. LIBERMAN. J. Chem. Phys. **53**, 1891 (1970).
7. F. R. THORNLEY and R. J. NELMES. Acta Crystallogr. Sect. A, **30**, 748 (1974).
8. E. D. ESTES and D. J. HODGSON. J. Chem. Soc. Dalton Trans. 1168 (1975).
9. R. A. BREAM, E. D. ESTES, and D. J. HODGSON. Inorg. Chem. **14**, 1672 (1975).
10. E. D. ESTES, W. E. ESTES, W. E. HATFIELD, and D. J. HODGSON. Inorg. Chem. **14**, 106 (1975).
11. V. F. DUCKWORTH and N. C. STEPHENSON. Acta Crystallogr. Sect. B, **25**, 1795 (1969).
12. R. D. WILLETT and C. CHOW. Acta Crystallogr. Sect. B, **30**, 207 (1974).
13. W. STAHLIN and H. R. OSWALD. Acta Crystallogr. Sect. B, **27**, 1368 (1971).
14. E. SLETTEN and A. APELAND. Acta Crystallogr. Sect. B, **31**, 2019 (1975).
15. P. DE MEESTER and A. C. SKAPSKI. J. Chem. Soc. Dalton Trans. 424 (1973).
16. M. FEHLMANN. Acta Crystallogr. Sect. B, **26**, 1736 (1970).
17. J. P. CHESICK and J. DONOHUE. Acta Crystallogr. Sect. B, **27**, 1441 (1971).

Crystal structure of dichlorobis(1-methylcytosine)cadmium(II)

CAROLE GAGNON AND ANDRÉ L. BEAUCHAMP
Département de Chimie, Université de Montréal, Montréal (Qué.), Canada H3C 3V1
AND
DUC TRANQUI
Laboratoire de Cristallographie, CNRS, 166 X, 38042 Grenoble Cedex, France

Received December 18, 1978

CAROLE GAGNON, ANDRÉ L. BEAUCHAMP, and DUC TRANQUI. Can. J. Chem. **57**, 1372 (1979).

Crystals of $CdCl_2$(1-methylcytosine)$_2$ belong to space group *Cc*, with $a = 10.571(7)$, $b = 24.35(2)$, $c = 7.097(3)$ Å, $\beta = 57.33(4)°$, and $Z = 4$. The structure was refined over 1988 independent reflections to an *R* factor of 0.026. The structure consists of monomeric molecules in which cadmium has a (4 + 2)-coordination. Four strong bonds, two Cd—Cl (2.497, 2.485 Å) and two Cd—N(3) (2.281, 2.296 Å), define an approximate tetrahedron around the metal. Two carbonyl oxygens take part in weak Cd—O bonding interactions (2.677, 2.780 Å). The amino groups form only very weak intramolecular hydrogen bonds with chlorine and the difference $> 30°$ between angles Cd—N(3)—C(4) and Cd—N(3)—C(2) is ascribed to Cd—O bonding. Similar effects for other metal complexes are discussed in terms of steric hindrance of the amino group and bonding of the carbonyl group.

CAROLE GAGNON, ANDRÉ L. BEAUCHAMP et DUC TRANQUI. Can. J. Chem. **57**, 1372 (1979).

Les cristaux de $CdCl_2$(méthyl-1 cytosine)$_2$ appartiennent au groupe d'espace *Cc* et les paramètres de maille sont $a = 10.571(7)$, $b = 24.35(2)$, $c = 7.097(3)$ Å, $\beta = 57.33(4)°$ et $Z = 4$. Les paramètres structuraux ont été affinés au moyen de 1988 réflexions indépendantes jusqu'à un facteur *R* de 0.026. La structure est constituée de molécules monomères dans lesquelles le cadmium possède une coordination (4 + 2). Quatre liaisons fortes, soit deux Cd—Cl (2.497, 2.485 Å) et deux Cd—N(3) (2.281, 2.296 Å) définissent un tétraèdre déformé autour du métal. Deux atomes d'oxygène de groupes carbonyles participent à une faible interaction liante Cd—O (2.677, 2.780 Å). Les liaisons hydrogènes formées par les groupements amino sont très faibles et la différence $> 30°$ qu'on observe entre les angles Cd—N(3)—C(4) et Cd—N(3)—C(2) est attribuée à la présence d'une liaison Cd—O. On discute d'effets analogues rapportés pour d'autres complexes métalliques en rapport avec l'effet stérique du groupe amino et la formation de liaisons avec le groupe carbonyle.

Introduction

The crystal structure of a $HgCl_2$ addition compound with 1-methylcytosine (MC) was reported in an earlier paper (1). Mercury was found to bind to N(3) as expected and some bonding with the adjacent carbonyl oxygen was inferred from the Hg—O distance. In order to assess the influence of the carbonyl group, complexes with cadmium and zinc were synthesized. The present paper describes the structure of a 2:1 addition compound between MC and $CdCl_2$.

When this work was undertaken, crystal structures had been published for two Cd(II) complexes with cytidine 5′-monophosphate (CMP) (2, 3). Recently, we became aware of X-ray work on a third compound (4) in which metal–base interactions are quite similar to ours.

Experimental

Crystal Data

$C_{10}H_{14}CdCl_2N_6O_2$ fw = 433.7

Monoclinic, space group *Cc*, $a = 10.571(7)$, $b = 24.35(2)$, $c = 7.097(3)$ Å, $\beta = 57.33(4)°$, $V = 1537.8$ Å^3, $Z = 4$ formula units per cell, $D_c = 1.873$ g cm^{-3}, $D_o = 1.90$ cm^{-3} (flotation in ethylene bromide – chlorobenzene) $\lambda(MoK\bar{\alpha}) = 0.71068$ Å, $\mu(MoK\alpha) = 18.0$ cm^{-1}, $t = 23°C$.

Preparation

$CdCl_2 \cdot 2\frac{1}{2}H_2O$ and 1-methylcytosine (Het-Chem. Co.) were dissolved (1:2 molar ratio) in the minimum of hot water and the mixture was slowly cooled to room temperature. The colorless crystals so obtained were suitable for X-ray work. The specimen selected for data collection had many faces and its shape was nearly spherical with a 'diameter' of 0.15–0.18 mm.

Crystallographic Measurements

A set of precession photographs showed the monoclinic Laue symmetry and the systematic absences (*hkl*, $h + k \neq 2n$; *h0l*, $l \neq 2n$) were consistent with space groups *Cc* and *C*2/*c*. Final cell parameters were obtained by least-squares refinement of the setting angles for 15 reflections centered in the counter aperture of a Syntex $P\bar{1}$ automatic diffractometer. As a check, oscillation photographs taken on the diffractometer along each axis showed the expected symmetry and spacing. The unit cell used to solve the structure has an acute angle, but a more conventional cell with $\beta = 123.67°$ can be defined by reversing *b* and either *a* or *c*.

All *hkl* and *hkl̄* reflections within a sphere $2\theta \leq 60°$ were measured with the $\theta/2\theta$ scan technique. The scan speed (from

0008-4042/79/111372-05$01.00/0

1° to 24° (2θ)/min) was selected according to peak height by the autocollection program. The 2θ scans were from [2θ($K\alpha_1$) − 1.2]° to [2θ($K\alpha_2$) + 1.2]°. Background counts were taken at each limit of the scan and the background time-to-scan time ratio was 0.4. Three standard reflections measured every 45 reflections showed fluctuations within ±3% from their respective means. The reduced set of data consisted of 2227 unique reflections. A total of 1988 reflections with net intensities $I \geq 3\sigma(I)$, where I and $\sigma(I)$ are defined as previously (5), were used to solve the structure. They were corrected for Lorentz and polarization effects. No absorption correction was applied because of the low absorption coefficient and the nearly spherical shape of the crystal. A transmission range 0.72–0.76 was expected from preliminary calculations on sample points in the reflection sphere.

Resolution of the Structure

The centrosymmetric space group was first assumed. In group $C2/c$, cadmium should occupy a special position of symmetry 2 or $\bar{1}$. The inversion centers were ruled out from a Patterson synthesis and Cd was positioned on equipoint *4e* with $y = 0.38$ ($x = 1/2$ and $z = 1/4$ by symmetry). At this point, a Fourier map phased on Cd should have unambiguously revealed at least some of the remaining atoms. Instead, overlapping images were obtained, indicating that the space group was Cc. Cadmium was left at the above coordinates and one cytosine ring could be sorted out from overlapping images. The rest of the structure was progressively constructed from structure factor calculations and Fourier maps. When all nonhydrogen atoms were located, the structure was isotropically refined using full-matrix least-squares. The R factor $\Sigma\,||F_o| - |F_c||/\Sigma\,|F_o|$ was 0.084 (unit weights).

Anisotropic refinement was carried out by block-diagonal least-squares. All hydrogen atoms in the plane of the ring were visible on the Fourier map and they were isotropically refined. Those of the methyl groups were not found. An isotropic secondary extinction coefficient (6) was also refined. Individual weights w based on counting statistics (7) were used at the latest stage of the refinement. Convergence was attained with $R = 0.026$ and $R_w = \{\Sigma\, w(|F_o| - |F_c|)^2/\Sigma\, w|F_o|^2\}^{1/2} = 0.033$. A final difference Fourier map showed no peaks higher than 0.6 e Å^{-3}.

In order to establish the absolute structure, all coordinates were changed into $\bar{x}$, $\bar{y}$, $\bar{z}$ and refinement was continued. Under the same conditions as above, the structure refined to $R = 0.028$ and $R_w = 0.036$. Those higher values indicate that the original model is to be preferred.

The refined coordinates are given in Table 1. Lists of structure factors and temperature factors are available upon request.[1] The scattering curves used were those of Cromer and Waber (8) for nonhydrogen atoms and of Stewart *et al.* (9) for hydrogen. Anomalous scattering coefficients $\Delta f'$ and $\Delta f''$ for Cd and Cl were taken from Cromer (10). The computer programs are listed elsewhere (1).

Description of the Structure and Discussion

The crystal contains individual $CdCl_2(MC)_2$ neutral molecules in which cadmium is (4 + 2)-coordinated (Fig. 1). Four strong bonds (2Cd—Cl and 2Cd—N) define a distorted tetrahedron (Table 2). The coordination sphere also includes two loosely bound oxygen atoms of carbonyl groups.

TABLE 1. Refined fractional coordinates (× 10^4, Cd × 10^5, H × 10^3) of $CdCl_2(MC)_2$

Atom	*x*	*y*	*z*
Cd	50000	37982(1)	25000
Cl(1)	6025(2)	3496(1)	−1430(2)
Cl(2)	7120(2)	4297(1)	2302(3)
N(11)	668(4)	4520(2)	4938(7)
C(11)	−750(7)	4231(3)	5647(13)
C(12)	1966(5)	4217(2)	4163(8)
O(12)	1964(5)	3706(1)	4074(8)
N(13)	3284(4)	4485(2)	3487(7)
C(14)	3343(5)	5040(2)	3510(7)
N(14)	4645(5)	5283(2)	2811(9)
C(15)	2007(7)	5359(2)	4259(9)
C(16)	721(6)	5087(2)	4954(9)
N(21)	3238(5)	2648(2)	7868(7)
C(21)	2473(7)	2792(3)	10274(9)
C(22)	3774(5)	3074(2)	6309(8)
O(22)	3533(5)	3561(2)	6869(6)
N(23)	4577(5)	2941(2)	4081(7)
C(24)	4824(5)	2418(2)	3380(9)
N(24)	5611(6)	2319(2)	1201(8)
C(25)	4166(7)	1978(2)	5044(11)
C(26)	3410(7)	2115(2)	7195(10)
H(141)	542(10)	507(4)	186(14)
H(142)	473(7)	556(2)	279(10)
H(15)	210(7)	570(2)	423(10)
H(16)	−17(11)	536(4)	497(15)
H(241)	597(11)	263(5)	18(15)
H(242)	578(6)	195(2)	66(9)
H(25)	401(9)	156(3)	501(13)
H(26)	291(7)	181(2)	841(10)

Coordination of Cadmium

Crystal structures are known for a number of chloro complexes (11), but only a few of them contain non-bridging chlorine as observed here. For four-coordinated tetrahedral compounds, the typical Cd—Cl distance is 2.46 Å (e.g. $CdCl_4^{2-}$, 2.432–2.465 Å (12); $CdCl_2(\phi_3P)_2$, 2.440 and 2.504 Å (13)). Significantly longer distances are found in six-coordinated species (e.g. $CdCl_6^{4-}$, 2.588, 2.617, 2.765 Å (14)). The intermediate Cd—Cl bond lengths observed in this compound (2.497(1) and 2.485(2) Å) are consistent with (4 + 2)-coordinated cadmium.

The Cd—N bond lengths (2.281(4) and 2.296(4) Å) are in the normal range observed with a variety of ligands (11). It is noteworthy that complexes with similar ligands show greater Cd—N distances when five or six donor atoms are strongly bonded: 2.327 Å, CMP (2); 2.36 Å, CMP (3); 2.37 Å, guanosine 5′-monophosphate (15); 2.33 Å, CMP (4).

[1]The supplementary material includes a list of temperature factors, a table of structure factors, and a list of interatomic distances and bond angles in the individual ligands. It is available, at a nominal charge, from the Depository of Unpublished Data, CISTI, National Research Council of Canada, Ottawa, Ont., Canada K1A 0S2.

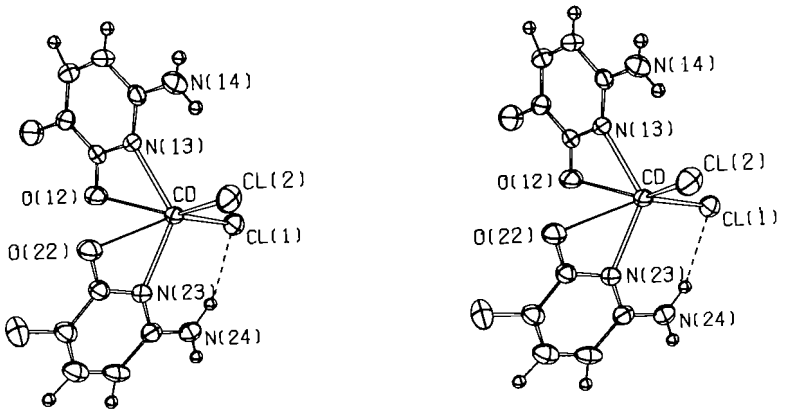

FIG. 1. Molecular structure of $CdCl_2(MC)_2$. The ellipsoids correspond to 50% probability. Hydrogen atoms are represented by spheres of arbitrary size.

TABLE 2. Distances and angles around cadmium

Atoms	Distances (Å)	Bonds	Angle (deg)
Cd—Cl(1)	2.497(1)	Cl(1)—Cd—Cl(2)	104.28(5)
Cd—Cl(2)	2.485(2)	Cl(1)—Cd—N(13)	110.7(1)
Cd—N(13)	2.281(4)	Cl(1)—Cd—N(23)	97.5(1)
Cd—N(23)	2.296(4)	Cl(2)—Cd—N(13)	101.7(1)
Cd—O(12)	2.780(6)	Cl(2)—Cd—N(23)	113.8(1)
Cd—O(22)	2.677(4)	N(13)—Cd—N(23)	127.1(2)
		Cl(1)—Cd—O(12)	97.8(1)
		Cl(1)—Cd—O(22)	149.5(1)
		Cl(2)—Cd—O(12)	150.7(1)
		Cl(2)—Cd—O(22)	96.4(1)
		N(13)—Cd—O(12)	51.8(1)
		N(13)—Cd—O(22)	86.3(1)
		N(23)—Cd—O(12)	81.5(1)
		N(23)—Cd—O(22)	53.1(1)
		O(12)—Cd—O(22)	72.3(1)

The upper limit for a Cd—O bond length appears to be ~2.40 Å (11). Much greater distances (2.780(6) and 2.677(4) Å) are observed here. The carbonyl oxygens cannot be considered as fully bonded to cadmium, but it is difficult to assess the degree of bonding interaction involved. The role of exocyclic groups will be further discussed hereafter.

The Ligand

Bond lengths and angles do not differ significantly between the two independent ligands and average values are shown in Fig. 2. At the present level of accuracy (0.007 Å and 0.4°), the bond lengths are similar to those of the uncoordinated ligand (16). Two angles near N(3) seem to be somewhat affected in the same way as in $Hg_2Cl_4(MC)_2$ (5): N(3)—C(4)—C(5) (119.9°) and C(2)—N(3)—C(4) (121.5°) have changed by −1.6 and +1.0° with respect to the corresponding values in free MC.

The six-membered ring of ligand **1** is planar within 3σ. Two of its substituents are significantly

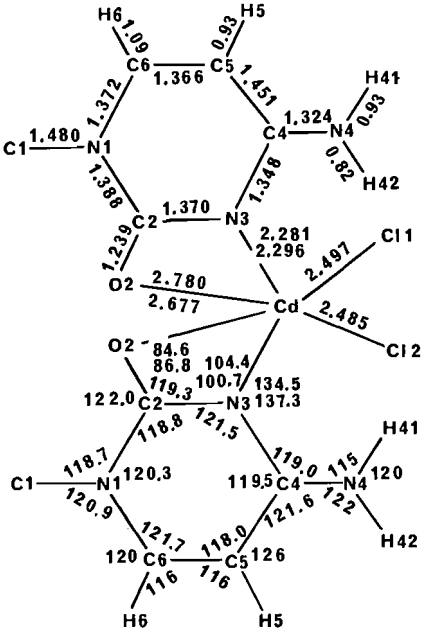

FIG. 2. Interatomic distances and bond angles in $CdCl_2(MC)_2$. Average values over the two independent ligands are shown. Individual values are part of the supplementary material. The standard deviations are: 0.005–0.010 Å and 0.4–0.6°, except where hydrogen is involved, 0.1 Å and 5°.

out of the plane: O(2), 0.039(5) Å and Cd, −0.023(2) Å. Ligand **2** is more distorted. All exocyclic groups are considerably distant from the best plane through the ring: C(1), 0.111(8); O(2), −0.092(6); N(4), 0.041(7); and Cd, −0.200(2) Å. The corresponding ring atoms show maximum departures of 4σ on the same side of the plane as their exocyclic atom.

Hydrogen Bonding and Packing

The only intramolecular H-bond (N(24)—H(242)···Cl(1)) is much weaker than in $Hg_2Cl_4(MC)_2$:

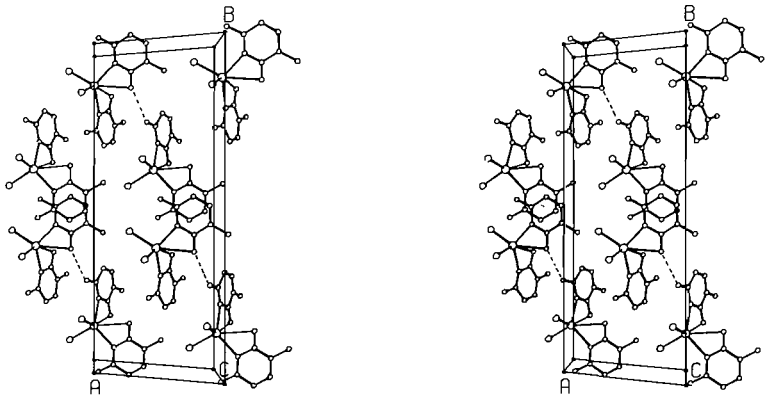

FIG. 3. Stereo view of the molecular packing in $CdCl_2(MC)_2$. The dotted lines represent intermolecular H-bonds.

N(24)—Cl(1) = 3.318(5) Å, C(24)—N(24)—Cl(1) = 108.0(4)°, Cd—Cl(1)—N(24) = 77.3(1)°. Amino group N(14) is not involved in H-bonding, the nearest potential acceptor, Cl(2), is found at 3.423(6) Å. Inspection of Fig. 1 reveals that much stronger N—H···Cl interactions could be achieved if the ligands were rotated in their own planes about N(13) and N(23) respectively. Of course, this would move the carbonyl groups away from cadmium and disrupt any oxygen–metal bond. The weakness or absence of H-bonds is considered as evidence for a greater stabilisation by Cd—O interaction than by amino–Cl H-bonding.

Figure 3 shows a projection of the unit cell. Base stacking, a common feature with this type of ligand, is observed for both independent MC ligands with an interplanar distance of ~3.55 Å. On the other hand, intermolecular H-bonding occurs only to a limited extent. The only strong H-bond involves N(24)—H(241) and O(12) $(1/2 + x, 1/2 - y, -1/2 + z)$: N(24)—O(12) = 2.867(6) Å, C(24)—N(24)—O(12) = 126.4(4)°, C(12)—O(12)—N(24) = 148.9(4)°. Both chlorine atoms form normal van der Waals contacts with methyl groups and hydrogens of the cytosine ring.

Role of Exocyclic Groups

As shown in Fig. 4, exocyclic groups on both adjacent ring positions interfere with a metal atom approaching N(3). Some repulsion is expected with an amino hydrogen when the metal moves along the bisector of the external C(2)—N(3)—C(4) angle. This situation, which is assumed to achieve maximum overlap with the lone pair of N(3), is referred to hereafter as $\Delta = 0$ (where Δ is the difference between angles M—N(3)—C(2) and M—N(3)—C(4)). If Δ becomes 7.5°, M and H will just touch. Such considerations hold only if no other ligands on the metal create steric hindrance *in the cytosine plane*. The

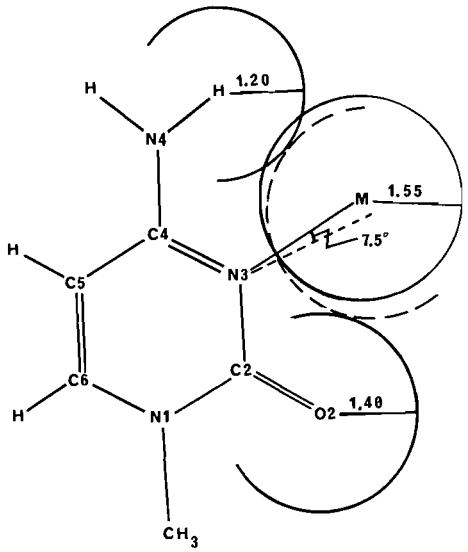

FIG. 4. Steric effect of exocyclic groups on metal coordination to N(3). Ligand geometry was taken from ref. 16 and an M—N(3) distance of 2.10 Å was used. The van der Waals radius of M (1.55 Å) is similar to the value proposed by Grdenic for mercury (17).

square planar Pt(II) complexes with methylcytosine (18) and cytidine (19), where $\Delta = 9.8$ and 7.6° respectively, fulfill those conditions. In both cases, the coordination plane is approximately perpendicular to the ligand, suppressing any steric effects of other ligands.

Copper resembles platinum to a certain extent in forming four strong bonds in a plane roughly perpendicular to the cytosine moiety. However, whereas Pt(II) has no appreciable affinity for a fifth ligand, Cu(II) is well known to assume (4 + 1)- and (4 + 2)-coordination by forming weaker bonds above and below the plane of the four strong ones. From the consistency of this pattern in Cu com-

plexes, Marzilli and Kistenmacher (21) have concluded that such interactions are important in copper–cytosine complexes. Recently, evidence for coordination at O(2) has been obtained from Raman and ^{13}C nmr spectra (22). Cu—O(2) bonding increases Δ to values much greater than with Pt(II): 14.7, 21.4 (23), 17.5 (24), 22.2 (25), 18.8, 12.9° (26).

In the present Cd complex, Δ values of 30.1 and 36.5° are observed. It is unlikely that they result from packing forces producing similar large effects on both independent ligands. As pointed out earlier, intramolecular H-bonding involving amino groups is very weak, although it would have been sterically feasible to promote H-bonding at the expense of Cd—O interactions. We believe that the high Δ values in this structure and in $Hg_2Cl_4(MC)_2$ ($\Delta = 24°$) (5) are due to metal–O(2) bonding interactions.

Nevertheless, they are only weak bonds. Strong metal–O(2) bonds have been reported for two compounds. In a Mn(II)–CMP complex (27), the cytosine moiety is bonded via O(2) only with an Mn—O distance of 2.08 Å. In $AgNO_3 \cdot MC$, silver is bonded to N(3) of one ligand and O(2) of another, with distances Ag—N = 2.225 and Ag—O = 2.367 (28). A feature common to both structures is the metal—O(2)—C(2) angle of ~150°. That value is estimated from the figures in preliminary communications, atomic coordinates not being available yet. In contrast, that angle is restricted to ~85° in chelates. Pullman and co-workers (29) have calculated an electrostatic molecular potential-energy map for cytosine. They have predicted maximum basicity at 55° from the C=O bond. According to their Fig. 2, this statement has to be interpreted as meaning that the optimum M—O(2)—C(2) angle is 125°. In addition, potential energy seems to change only slowly in the range 110–180°. This can explain that stronger bonds are formed in the Mn(II) and Ag(I) complex compared with other compounds where four-membered chelate formation requires angles well outside of that range. It is noteworthy that in two methylthyminato (MT) complexes showing strong metal–oxygen bonds, the M—C—O angles are in the above range: $[(NH_3)_4Pt_2(MT)_2]^{2+}$ (30), Pt—O = 2.012, 2.037 Å, angle = 129.5, 130.6°; Ag(MT) (31), Ag—O 2.333, 2.512 Å, angles 127.6, 121.9°.

Acknowledgments

We are very grateful to Dr. F. D. Rochon for permission to use the Syntex diffractometer and valuable assistance during data collection. We wish to thank Dr. R. Bau who kindly made his results on the Cd–CMP structure available to us prior to publication.

1. M. Authier-Martin and A. L. Beauchamp. Can. J. Chem. **55**, 1213 (1977).
2. D. M. L. Goodgame, I. Jeeves, C. D. Reynolds, and A. C. Skapski. Biochem. J. **151**, 467 (1975).
3. G. R. Clark and J. D. Orbell. J. Chem. Soc. Chem. Commun. 697 (1975).
4. J. K. Shiba and R. Bau. Inorg. Chem. **17**, 3484 (1978).
5. M. Authier-Martin, J. Hubert, R. Rivest, and A. L. Beauchamp. Acta Crystallogr. B**34**, 273 (1978).
6. W. H. Zachariasen. Acta Crystallogr. **16**, 1139 (1963).
7. G. H. Stout and L. H. Jensen. X-ray structure determination. MacMillan Co., New York. 1968. p. 457.
8. D. T. Cromer and J. T. Waber. Acta Crystallogr. **18**, 104 (1965).
9. R. F. Stewart, E. R. Davidson, and W. T. Simpson. J. Chem. Phys. **42**, 3175 (1965).
10. D. T. Cromer. Acta Crystallogr. **18**, 17 (1965).
11. I. D. Brown (*Editor*). Bond index to the determinations of inorganic crystal structure (BIDICS). 1970–1977.
12. M. F. Richarson, K. Franklin, and D. M. Thompson. J. Am. Chem. Soc. **97**, 3204 (1975).
13. A. F. Cameron, K. P. Forrest, and G. Ferguson. J. Chem. Soc. A, 1286 (1971).
14. J. T. Veal and D. J. Hodgson. Inorg. Chem. **11**, 597 (1972).
15. K. Aoki. Acta Crystallogr. B**32**, 1454 (1976).
16. D. Voet and A. Rich. Prog. Nucleic Acid Res. Mol. Biol. **10**, 183 (1970).
17. D. Grdenic. Q. Rev. **19**, 303 (1965).
18. C. J. L. Lock, R. A. Speranzini, and J. Powell. Can. J. Chem. **54**, 53 (1976).
19. R. Melanson and F. D. Rochon. Inorg. Chem. **17**, 679 (1978).
20. S. Louie and R. Bau. J. Am. Chem. Soc. **99**, 3874 (1977).
21. L. G. Marzilli and T. J. Kistenmacher. Acc. Chem. Res. **10**, 146 (1977).
22. L. G. Marzilli, R. C. Stewart, C. P. Van Vuuren, B. de Castro, and J. P. Caradonna. J. Am. Chem. Soc. **100**, 3967 (1978).
23. T. J. Kistenmacher, D. J. Szalda, and L. G. Marzilli. Acta Crystallogr. B**31**, 2416 (1975).
24. D. J. Szalda, L. G. Marzilli, and T. J. Kistenmacher. Inorg. Chem. **14**, 2076 (1975).
25. D. J. Szalda and T. J. Kistenmacher. Acta Crystallogr. B**33**, 865 (1977).
26. M. Sundaralingam and J. A. Carrabine. J. Mol. Biol. **61**, 287 (1971).
27. M. A. Aoki. Chem. Commun. 748 (1976).
28. L. G. Marzilli, T. J. Kistenmacher, and M. Rossi. J. Am. Chem. Soc. **99**, 2797 (1977).
29. R. Bonaccorsi, A. Pullman, E. Scrocco, and J. Tomasi. Theor. Chim. Acta, **24**, 51 (1972).
30. C. J. L. Lock, H. J. Peresie, B. Rosenberg, and G. Turner. J. Am. Chem. Soc. **100**, 3371 (1978).
31. F. Guay and A. L. Beauchamp. To be published.

Synthesis of long-chain coumarines and 2*H*-chromenes. Spectral and monolayer properties[1]

H. P. POMMIER, J. BARIL, I. GRUDA, AND R. M. LEBLANC

Groupe de Recherche en Biophysique, Département de Chimie-Biologie, Université du Québec à Trois-Rivières, Trois-Rivières, P.Q., Canada G9A 5H7

Received October 16, 1978

H. P. POMMIER, J. BARIL, I. GRUDA, and R. M. LEBLANC. Can. J. Chem. **57**, 1377 (1979).

Several coumarines and 2*H*-chromenes containing one or two long-chain substituents were synthesized and their spectroscopic properties (uv, nmr) were investigated. All compounds were studied at the air–water interface. Five of them give a monolayer which is characterized by the pressure–area isotherm. An interpretation of the isotherms is discussed in relation to the molecular structure.

H. P. POMMIER, J. BARIL, I. GRUDA et R. M. LEBLANC. Can. J. Chem. **57**, 1377 (1979).

La synthèse d'une série de coumarines et de 2*H*-chromènes substitués par une ou deux chaînes grasses est décrite. Les composés sont caractérisés par leurs propriétés physiques et spectroscopiques. Toutes les substances ont été étudiées à l'interface air–eau. Cinq d'entre elles présentent les caractéristiques d'une monocouche suite à l'examen de leur isotherme de pression de surface. Une interprétation des isothermes est donnée en fonction de la structure moléculaire.

Introduction

The monolayer organization of natural photosensitive pigments seems to favour the energetic transformations occurring during irradiation. Also for some synthetic compounds it has been found that their reactivity in monolayer assemblies is quite different from their behaviour in solution (1).

In order to study the specificity of photochemical or photophysical reactions in monolayers in comparison with the same reactions in solutions and (or) in solid films, we needed some model compounds. These compounds have to be photosensitive, for example, photochromic and (or) to possess some luminescence characteristics. They also have to contain a polar head and one or more nonpolar hydrophobic substituents, i.e., they must be amphipatic which is the essential structural requirement for the formation of a monolayer at the air–water interface.

We have recently synthesized some photochromic long-chain spiroindolinopyrans (2), and the monolayer properties of these compounds have been investigated in this laboratory (to be published). The surface pressure – area isotherms for most compounds in this series exhibited inflections due probably to some conformational changes during compression.

To avoid the possibility of conformational changes we looked for other model compounds with a more rigid, one-plane, polar head. Photochromic 2*H*-benzopyrans (chromenes) (3, 4) as well as coumarines which are fluorescent seemed to have all the necessary features. An additional interesting feature of these compounds is their presence in many natural plant products (5).

Since the known chromenes and coumarines are not amphipatic, we had to modify their structure by introducing long aliphatic chains. In this paper, we report the synthesis of a number of long-chain coumarines and chromenes with their spectral and monolayer properties. In the case of spectral properties, the λ_{max} and the extinction coefficients in various solvents were determined. The monolayer properties of the synthesized compounds are discussed on the basis of the experimentally determined pressure–area isotherms. An interpretation of the isotherms is proposed in relation to the molecular structure.

Results and Discussion

Synthesis

The relative position of the polar head and the non-polar tail in a molecule is a very important factor for the formation of a monolayer. Another essential factor is the hydrophile–lipophile balance of a molecule. It was, therefore, interesting to synthesize several coumarines and chromenes containing one or more long chains in different positions in the ring.

Long-chain Coumarines

Scheme 1 shows the method which has been used in order to introduce a long-chain aliphatic substituent into the coumarine.

Starting materials are the easily available hydroxycoumarines. Long chains are introduced by the *n*-hexadecyl *p*-toluenesulfonate according to a general method used for alkylation of different phenols and

[1]Part II of photochromic studies in monolayers.

0008-4042/79/111377-07$01.00/0

TABLE 1. Yields and physical properties of long-chain coumarines

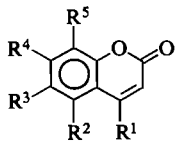

2

Compound	R^1	R^2	R^3	R^4	R^5	Yield (%)	Melting point (°C)	Thin layer chromatography R_f (solvent)
2*a*	$OC_{16}H_{33}$	H	H	H	H	52	83.2	0.5 ($CHCl_3$)
2*b*	CH_3	H	H	$OC_{16}H_{33}$	H	69	68	0.6 (CCl_4 + $CHCl_3$, 1:1)
2*c*	CH_3	H	H	$OC_{16}H_{33}$	$OC_{16}H_{33}$	80	85.4	0.7 (CCl_4 + $CHCl_3$, 1:1)
2*d*	CH_3	$OC_{16}H_{33}$	H	$OC_{16}H_{33}$	H	50	73	0.5 (C_6H_6)
2*e*	CH_3	H	NO_2	$OC_{16}H_{33}$	H	33	145	0.3 (C_6H_6)

other compounds containing an active hydrogen (6). We significantly improved the yield of the reaction with some modifications of the original method (see Experimental).

Table 1 shows yields and physical properties of the synthesized long-chain coumarines. Compound **2***e* was prepared by nitration of **2***b*.

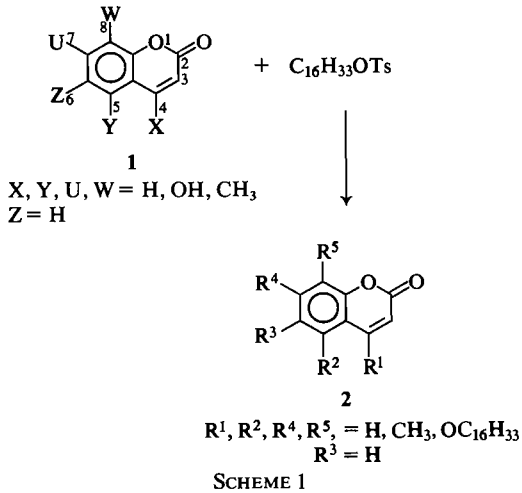

SCHEME 1

Long-chain Chromenes

Many papers describing the synthesis of 2*H*-chromenes have been published (5, 7–12). However, most of the methods give poor yields and necessitate long procedures or difficult work-up. Many side products are present in the reaction mixtures which make the isolation and purification of the chromenes very difficult. We adapted three of the known methods for the synthesis of long-chain chromenes.

Method A

2,2-Dialkyl 2*H*-chromenes may be obtained in the reaction between a coumarine and 2 mol of a Grignard reagent, as shown in Scheme 2.

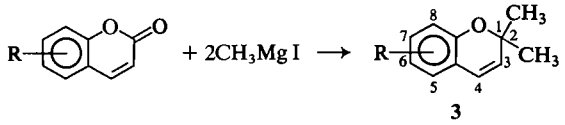

SCHEME 2

According to the literature (5, 7), the nature of the products depends upon the reaction conditions and varies with the character of substituents present in the molecule of the starting coumarine. Long-chain coumarines **2** add 2 mol of methylmagnesium iodide in anhydrous ether at 0°C. Nevertheless, some side products are also formed and the chromenes have to be purified by chromatography on silica gel columns followed by crystallization. Chromenes which have been synthesized by method *A* have one or two long chains attached by an ether linkage at carbons -5, -7, or -8.

Method B

In order to prepare chromenes with a long-chain substituent attached by a C—C link at carbon-3, we followed the method given by Arrigo (12) who has described the preparation of 3-substituted chromenes in a Lewis acid catalyzed reaction between tertiary alkyl chlorides and *o*-hydroxybenzaldehydes. The alkyl chloride used in our case was the 2-chloro-2-methylnonadecane prepared from the corresponding tertiary alcohol. The reaction was carried out with

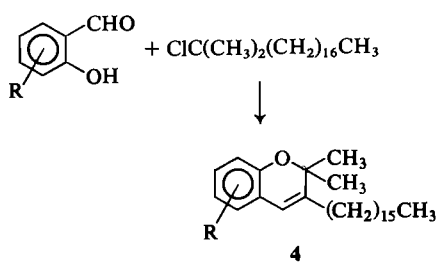

SCHEME 3

salicylaldehyde, 3-methoxysalicylaldehyde, and 5-nitrosalicylaldehyde.

Products have been purified by chromatography on silica gel columns followed by crystallization, except for **7***c* for which only crystallization was done. The yields were poor, which is not uncommon when a long aliphatic chain is present in the starting compound.

Method C

o-Hydroxybenzaldehydes may be converted into benzopyrylium salts as shown in Scheme 4 by an acid catalyzed condensation with ketones (7). Some benzopyrilium salts are reported to react with Grignard reagents to give chromenes (7).

Also in this reaction the formation of several side products is reported and the choice of the reaction conditions is very important. In ethereal solution at low temperature, which is the condition reported for the synthesis of several benzopyrylium salts, we found that the nonadecanone does not react with *o*-hydroxybenzaldehydes. When the reaction was carried out with 3-methoxysalicylaldehyde in ethanol at room temperature, 3-hexadecyl-2-methyl-5-methoxybenzopyryliumperchlorate was obtained. This salt reacts with methylmagnesium iodide to give the 2,2-dimethyl-3-hexadecyl-5-methoxy-2*H*-chromene which is identical with the product obtained by method *B*. Table 2 gives yields and physical properties of the long-chain chromenes synthesized by the three methods. Spectral characteristics of synthesized compounds are given in Table 3.

Monolayer

The results are presented as diagrams of the surface pressure – area isotherms (π–*A* isotherm). Figure 1 illustrates the π–*A* isotherms for compounds **2***b* and **2***c*. Figure 2 gives the isotherms for compounds **7***b*,

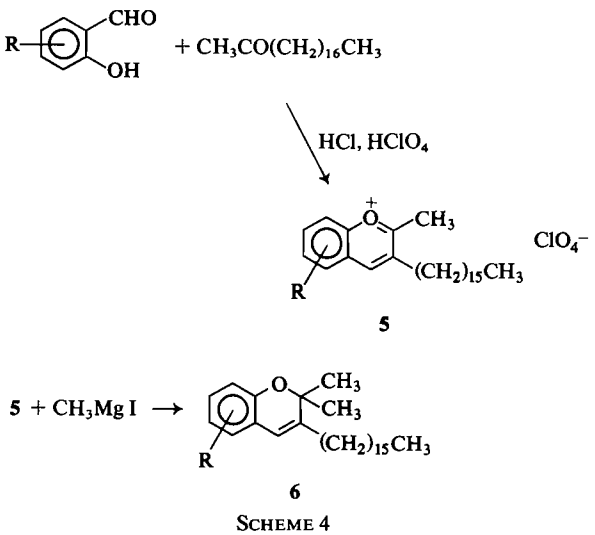

SCHEME 4

TABLE 2. Yields and physical properties of long-chain 2*H*-chromenes

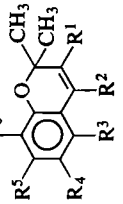

Compound	R^1	R^2	R^3	R^4	R^5	R^6	Yield (%) (method)	Melting point (°C)	Thin layer chromatography R_f (solvent)
7a	$C_{16}H_{33}$	H	H	H	H	H	5 (*B*)	61	0.83 (CCl_4)
7b	$C_{16}H_{33}$	H	H	H	H	OCH_3	14 (*B*); 48*(*C*)	69	0.77 (CCl_4 + $CHCl_3$, 1:1)
7c	$C_{16}H_{33}$	H	H	NO_2	H	H	20 (*B*)	85	0.38 (CCl_4)
7d	H	CH_3	H	H	$OC_{16}H_{33}$	H	72 (*A*)	47	0.70 ($CHCl_3$ + CCl_4, 1:1)
7e	H	CH_3	H	H	$OC_{16}H_{33}$	$OC_{16}H_{33}$	61 (*A*)	48	0.62 (CCl_4)
7f	H	CH_3	$OC_{16}H_{33}$	H	$OC_{16}H_{33}$	H	47 (*A*)	45	0.60 (isooctane + CCl_4, 1:1)

*Yield of the Grignard reaction.

TABLE 3. Spectral characteristics of long-chain coumarines and 2*H*-chromenes

Compound	Solvent	λ_{max}, nm (log ε)*
2*a*	Isooctane	213 (4.59); 254 sh; 263 (4.09); 274 (4.04); 294 sh; 303 (3.84); 316 sh
	Ethanol	213 (4.54); 257 sh; 264 (4.06); 276 (4.04); 303 (3.83); 312 sh
2*b*	Cyclohexane	216 (4.65); 240 (3.91); 250 (3.79); 278 (3.92); 288 (3.98); 310 (4.12); 318 (4.14); 337 sh
2*c*	Cyclohexane	220 sh; 247 (3.95); 257 (3.94); 303 (4.16); 314 sh
2*d*	Cyclohexane	212 (4.45); 242 (3.89); 252 (3.83); 307 (4.16); 313 (4.15); 328 sh
	Ethanol	212 (4.47); 245 (3.85); 254 (3.82); 321 (4.22)
2*e*	Cyclohexane†	260; 294; 307; 321; 328 sh
7*a*	Cyclohexane	219 (4.40); 258 sh; 266 (3.80); 275 (3.74); 306 (3.65); 315 sh
	Ethanol†	218; 256 sh; 265; 275; 304; 315 sh
7*b*	Cyclohexane	228 (4.20); 233 sh; 263 sh; 270 (3.77); 281 (3.64); 310 (3.08)
	Ethanol	226 (4.18); 269 (3.66); 280 (3.61); 306 (3.04)
7*c*	Cyclohexane	226 (4.16); 264 (4.35); 272 sh; 303 (3.77); 341 (3.72)
	Ethanol	227 (4.17); 233 sh; 270 (4.30); 278 sh; 305 (3.79); 347 (3.75)
7*d*	Isooctane	220 (4.43); 271 (3.89); 277 sh; 304 (3.88); 313 sh
	Ethanol	218 (4.34); 271 (3.88); 277 sh; 304 (3.85); 313 sh
7*e*	Cyclohexane	223 (4.47); 272 (4.04); 282 sh; 300 (3.59); 316 sh
	Ethanol	223 (4.49); 272 (4.03); 280 sh; 300 (3.60); 312 sh
7*f*	Isooctane	233 (4.65); 240 sh; 278 (4.41)

*In the calculation of log ε, the concentrations are in the range 10^{-4}–10^{-5}.
†For compounds having very low solubility, only λ_{max} is given.

7*d*, and **7***e*. When the maximum surface pressure was kept below the collapse region, all the isotherms studied were reversible within experimental error. These results favour the suggestion that only a monolayer is present at the air–water interface. For compound **7***c*, we found no reversibility in the π–*A* isotherms as shown in Fig. 3. The low values of the area per molecule for this compound suggest either the formation of a film or the result of film loss due to the penetration of the hydrocarbon chain in the subphase.

The limiting area per molecule for the coumarines **2***b* and **2***c* are, respectively, 24.3 and 44.5 Å^2/molecule. For the 2*H*-chromenes **7***b*, **7***d*, and **7***e*, the limiting areas are, respectively, 53.7, 25.3, and 26.5 Å^2/molecule.

For some coumarines, we observed an instability of the film. No isotherm was obtained for coumarines **2***a*, **2***d*, and **2***e*. Comparing the structure of compound **2***a* with compound **2***b*, we have for compound **2***a* the position of the long-chain alkoxy group in the same ring as the two other oxygens, whereas the long-chain alkoxy group in compound **2***b* is situated on the same side as the two oxygens in the coumarine structure. As we found a solid-type isotherm for compound **2***b* with a limiting area of 24.3 Å^2 molecule^{-1} (see Fig. 1), we may suggest that the presence of a long chain at C-7 is important to stabilize the film. The introduction of OR at C-4 may solubilize the film due to the presence of hydrophilic groups in the same ring causing instability in the surface pressure measurements as we noted for compound **2***a*. Addition of nitro group at C-6 (compound **2***e*) to the structure of compound **2***b* also imparts an instability to the isotherm. We were not able to compress the film from **2***e* to obtain the characteristic π–*A* curve. For compounds **2***c* and **2***d*, two long-chain alkoxy groups were fixed in the benzene ring. The compound **2***c*, with the alkoxy groups in the *ortho* position, gives an isotherm with a limiting area of 44.5 Å^2 molecule^{-1} which is approximately twice the value obtained for compound **2***b*. The behaviour of the isotherm presents a liquid-type monolayer for surface pressure below $\sim$15 mN m^{-1} and a solid type at a higher surface pressure. The hydrophobic interaction between the fatty alkoxy groups may explain the surface pressure characteristics of the monolayer.

In the case of compound **2***d*, the long-chain alkoxy groups are in the *meta* position; an instability in the film was observed during compression. To explain this result, we suggest the possibility that the two-long chain alkoxy groups are essentially uncorrelated in regard to direction in space. The molecule is then coiled; hence, in this structure there is no possibility for forming a stable monolayer.

Similar behaviour is observed for the 2*H*-chromenes. For example, the introduction of a nitro group causes instability of the film (compound **7***c*) (Fig. 3), as well as for compound **7***f*, in which two long chains are present in the *meta* position. A solid

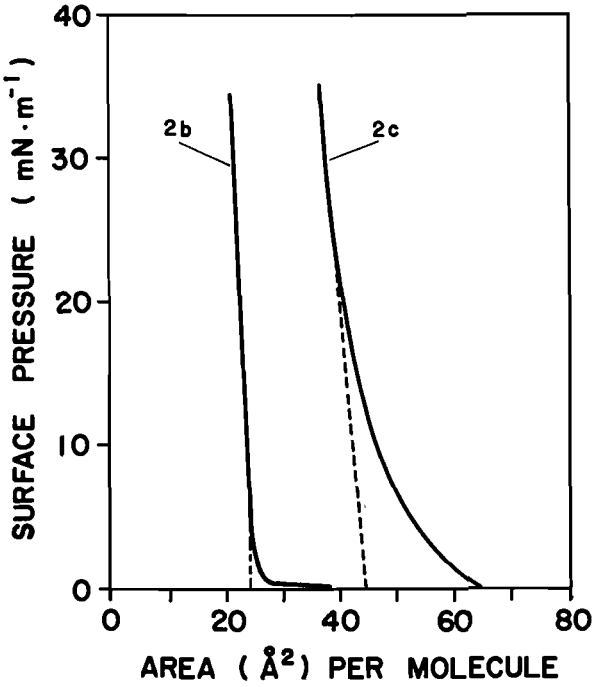

FIG. 1. Pressure–area isotherms of compounds 2*b* and 2*c*.

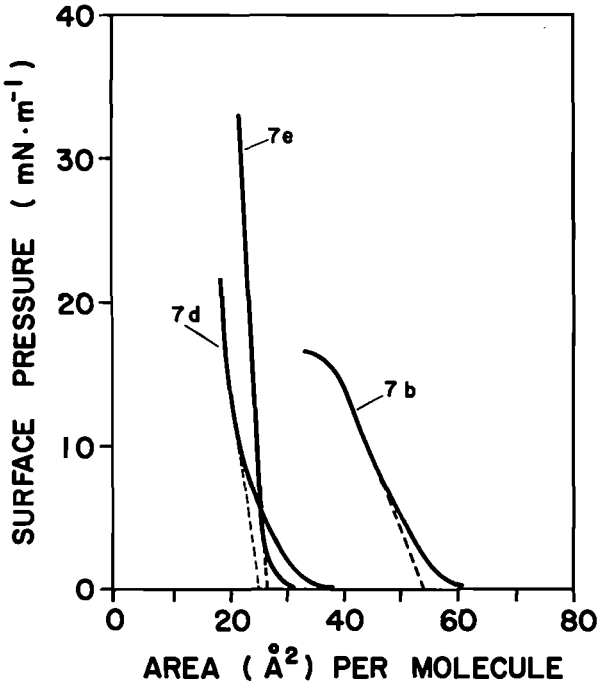

FIG. 2. Pressure–area isotherms of compounds 7*b*, 7*d*, and 7*e*.

film is obtained for compound 7*d* with an $A_{\pi=0}$ = 25.3 Å^2 molecule^{-1} as for the corresponding coumarine (compound 2*b*). In this case, one can see that the carbonyl group is not essential in the formation of a solid monolayer. For compounds 2*c* and 7*e*, the structures are identical, except for the carbonyl group in compound 2*c*. The π–*A* isotherms show differences in the limiting area per molecule and in the state of the monolayer. The absence of a carbonyl group facilitates the formation of a solid monolayer as we see in Fig. 2 (compound 7*e*).

When the molecule had only one oxygen as in the case of compound 7*a*, we were not able to get a stable monolayer. To increase the polarity of the molecule, we introduced the methoxy group at C-8 (compound 7*b*). A stable monolayer is formed which presents the characteristic of a liquid-state film as shown in Fig. 2.

In view of these observations, some structural characteristics in the benzopyran series may be pointed out for the formation of a stable monolayer at the air–water interface: (*i*) one or two aliphatic chains (C_{16}) is necessary for the formation of a monolayer; in the case of two chains, they must be in the *ortho* position to have a stable film; (*ii*) the alkoxy group, a weak hydrophilic group, favours the stability of the monolayer, which is not the case for a strong hydrophilic group such as —NO_2; (*iii*) the position of the polar atoms has some effect on the stability of the film, polar atoms on the same side of the molecule giving a stable monolayer.

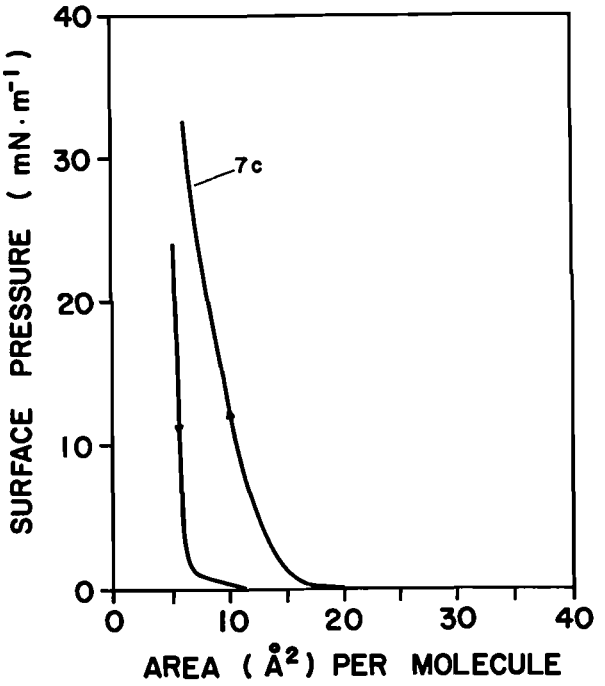

FIG. 3. Hysteresis curves for compound 7*c*.

From our monolayer work, the coumarines 2*b*, 2*c* and the corresponding 2*H*-chromenes 7*d*, 7*e* are good

TABLE 4. Analytical data of coumarines and chromenes

Compound	Analyses: Calculated C	Calculated H	Calculated N	Found C	Found H	Found N	Nuclear magnetic resonance (solvent, δ)
2a	77.72	9.84	—	77.88	10.02	—	$CDCl_3$, 0.80 (t, 3H, CH_3), 1.20 (m, 28H, CH_2), 4.00 (t, 2H, OCH_2), 5.68 (s, 1H, olefinic), 7.05–7.85 (m, 4H, aromatic)
2b	78.00	10.00	—	78.14	10.24	—	CCl_4, 0.80 (t, 3H, CH_3), 1 20 (m, 28H, CH_2), 2.25 (app.s, 3H, CH_3), 3.88 (t, 2H, OCH_2), 5.90 (app. s, 1H, olefinic), 6.55–7.40 (m, 3H, aromatic)
2c	78.75	11.25	—	78.30	11.28	—	CCl_4, 0.80 (t, 6H, CH_3), 1.20 (m, 56H, CH_2), 2.20 (app.s, 3H, CH_3), 3.90 (t, 4H, OCH_2), 5.82 (app.s, 1H, olefinic), 6.60 (d, 1H, aromatic), 7.00 (d, 1H, aromatic)
2d	78.75	11.25	—	78.87	11.42	—	$CDCl_3$, 0.80 (t, 6H, CH_3), 1.20 (m, 56H, CH_2), 2.45 (app.s, 3H, CH_3), 3.85 (t, 4H, OCH_2), 5.82 (app.s, 1H, olefinic), 6.28 (d, 2H, aromatic)
2e	70.11	8.76	3.15	70.39	8.95	2.88	$CDCl_3$, 0.80 (t, 3H, CH_3), 1.25 (m, 28H, CH_2), 2.40 (app.s, 3H, CH_3), 4.13 (t, 2H, OCH_2), 6.25 (app.s, 1H, olefinic), 6.98 (s, 1H, aromatic), 8.20 (s, 1H, aromatic)
7a	84.38	11.46	—	84.23	11.60	—	CCl_4, 0.80 (t, 3H, CH_3), 1.18 (m, 28H, CH_2), 1.28 (s, 6H, $2CH_3$), 2.00 (m, 2H, CH_2), 5.90 (app.s, 1H, olefinic), 6.40–6.90 (m, 4H, aromatic)
7b	81.16	11.11	—	81.26	11.45	—	CCl_4, 0.80 (t, 3H, CH_3), 1.20 (m, 28H, CH_2), 1.32 (s, 6H, $2CH_3$), 1.95 (m, 2H, CH_2), 3.65 (s, 3H, OCH_3), 5.85 (app.s, 1H, olefinic), 6.35–6.55 (m, 3H, aromatic)
7c	75.52	10.02	3.26	75.18	10.35	—	CCl_4, 0.85 (t, 3H, CH_3), 1.28 (m, 28H, CH_2), 1.45 (s, 6H, $2CH_3$), 2.18 (m, 2H, CH_2), 6.08 (app.s, 1H, olefinic), 6.75 (d, 1H, aromatic), 7.70–7.80 (m, 2H, aromatic)
7d	81.16	11.11	—	80.34	11.02	—	CCl_4, 0.80 (t, 3H, CH_3), 1.20 (m, 34H, CH_2 and $2CH_3$), 1.83 (app.s, 3H, CH_3), 3.73 (t, 2H, OCH_2), 5.05 (app.s, 1H, olefinic), 6.10–6.88 (m, 3H, aromatic)
7e	80.73	11.93	—	80.32	12.00	—	CCl_4, 0.80 (t, 6H, CH_3), 1.20 (m, 62H, CH_2 and $2CH_3$), 1.82 (app.s, 3H, CH_3), 3.80 (m, 4H, OCH_2), 5.12 (app.s, 1H, olefinic), 6.18 (d, 1H, aromatic), 6.58 (d, 1H, aromatic)
7f	80.73	11.93	—	80.63	11.84	—	CCl_4, 0.80 (t, 6H, CH_3), 1.20 (m, 62H, CH_2 and $2CH_3$), 1.95 (app.s, 3H, CH_3), 3.70 (m, 4H, OCH_2), 4.92 (app.s, 1H, olefinic), 5.80 (app.s, 2H, aromatic)

model compounds to compare photophysical and photochemical properties in monolayer, film, and solution.

Experimental

Melting points are uncorrected. Microanalyses were performed by Schwarzkopf Microanalytical Lab., New York, NY. The nmr spectra were recorded at 60 MHz using a Perkin Elmer R-12 spectrometer with TMS as standard. The absorption spectra were measured with a Colman 124 spectrometer. The extinction coefficients were calculated in the range of 10^{-4}–10^{-5} *M*; Spectrograde solvents were used. The purity of synthesized compounds was checked by tlc; all coumarines and chromenes presented one spot in two or three solvents.

In the monolayer experiments, a surface balance based on the technique of Langmuir–Adam for detection of the change in surface pressure was used. The trough and the pressure sensing unit (0.200 mN m^{-1} deg^{-1}) has been described elsewhere (13). The float was attached to the edges of the trough by flexible gold foil strips. The sensitivity of the unit was better than 0.1 mN m^{-1}.

The spreading solvent was certified grade *n*-hexane and the sub-phase water was adjusted to pH 5.3 with potassium phosphate, 10^{-3} *M*. The water used for experiments was obtained from a quartz distillation apparatus. The water temperature was maintained at 24.0 ± 0.5°C.

Prior to compression, the surface was cleaned carefully on both sides of the float to eliminate film-forming impurities. The investigated solutions were deposited on the surface (approximately 100 μL depending on the compounds studied) with a Hamilton microsyringe and equilibrated for 20 min before compression. The rate of compression was kept low, i.e., 3.0 $Å^2$ $molecule^{-1}$ min^{-1}.

The pressure–area isotherms were duplicated more than three times. Reproducibility of the results was within 1–2 $Å^2$ $molecule^{-1}$ and ±0.2 mN m^{-1}.

Hexadecyloxycoumarines

A mixture of 0.025 mol of a mono(di)-hydroxycoumarine

with 0.025 (0.050) mol of sodium hydroxide in 20 mL of water was added to a warm solution of 0.025 (0.050) mol of *n*-hexadecyl tosylate in 80 mL of ethanol. The resulting mixture was refluxed for 8 h. Cold water (100 mL) was added and ethanol evaporated. After cooling, the mixture was filtered and the solid was washed several times with water and recrystallized in acetone.

7-Hexadecyloxy-4-methyl-6-nitrocoumarine

To a cold solution of 4 g (0.01 mol) of 7-hexadecyloxy-4-methylcoumarine in concentrated sulfuric acid (100 mL) was added slowly 1.2 g of 70% nitric acid. The mixture was stirred at 0°C for 3 h, poured on ice, and filtered. The solid was washed with water and purified by recrystallization in acetone followed by chromatography on a silica gel column with benzene as eluent.

2H-Chromenes

Method A

A suspension of 0.01 mol of the appropriate hexadecyloxycoumarine in anhydrous ether was added slowly at 0°C to 0.02 mol of methylmagnesium iodide in anhydrous ether. The reaction mixture was stirred at 0°C for 5 h and hydrolyzed with a NH_4Cl–HCl solution. The ethereal layer was washed with water, dried, and the solvent evaporated. The residue was recrystallized in ethanol and further purified by chromatography on a silica gel column. The elution was performed with solvents used for tlc (Table 2).

Method B

To 1.05 g of melted $ZnCl_2$, a solution of 0.025 mol of the appropriate salicylaldehyde and 0.025 mol of 2-chloro-2-methylnonadecane in chloroform (15 mL) was added. The mixture was refluxed for 20 h, cooled, washed several times with water, dried ($CaCl_2$), and the solvent evaporated. The residue was purified on a silica gel column with petroleum ether as eluent and recrystallized in ethanol. In the case of **7***c*, no chromatography was done; the product was recrystallized in hexane and in ethanol.

Method C

3-Hexadecyl-2-methyl-8-methoxypyrylium perchlorate—A solution of 10 g (0.066 mol) of 3-methoxysalicylaldehyde, 18.5 g (0.066 mol) of 2-nonadecanone, and 22 g (0.131 mol) of 70% perchloric acid in ethanol (200 mL) was treated with hydrogen chloride gas during 20 h. The mixture was filtered and the solid washed successively with ether, hexane, and chloroform, and finally recrystallized in chloroform; 10 g (30.4%) of yellow solid, mp 185–186°C, of the pyrylium perchlorate was obtained; nmr ($CDCl_3$) δ: 0.88 (t, J = 4.5 Hz, 3H, CH_3), 1.26 (m, 28H, CH_2), 2.96 (t, J = 7.5 Hz, 2H, CH_2), 3.20 (s, 3H, 2-CH_3), 4.08 (s, 3H, OCH_3), 7.51–7.98 (m, 3H, aromatic), 9.32 (s, 1H, aromatic).

2,2-Dimethyl-3-hexadecyl-8-methoxy-2H-chromene—A suspension of 1.4 g (0.0028 mol) of 3-hexadecyl-2-methyl-8-methoxypyrylium perchlorate in anhydrous ether was added to a cooled solution of Grignard reagent prepared from 0.07 g of Mg (0.0029 mol) and 0.9 g (0.0028 mol) of methyl iodide in anhydrous ether. The reaction mixture was stirred at room temperature for 1 h and hydrolysed with a NH_4Cl–HCl solution. The ethereal layer was separated, dried, and the solvent evaporated; 0.7 g (48%) of 2,2-dimethyl-3-hexadecyl-8-methoxy-2*H*-chromene, mp 49–62°C, was obtained. The crude product was purified by chromatography on a silica gel column with a mixture of CCl_4 and $CHCl_3$ (1:1) as eluent.

After recrystallization in ethanol, pure 2,2-dimethyl-3-hexadecyl-8-methoxy-2*H*-chromene, mp 69°C, was obtained. The compound was identical with the appropriate chromene obtained by method *B*.

The analytical data of all synthesized compounds are given in Table 4.

Acknowledgements

We thank Mr. G. Munger, Mr M. Granger, and Miss I. Dupont for the help given in the present work. Financial assistance from the Ministère de l'Education du Québec (FCAC) and the National Research Council of Canada is gratefully acknowledged.

1. I. Gruda and R. M. Leblanc. Can. J. Chem. **54**, 576 (1976).
2. H. Kuhn, D. Möbius, and H. Bücher. *In* Physical methods of chemistry. Vol. 1. *Edited by* A. Weissberger and B. W. Rossiter. Wiley Interscience, New York, NY. 1972. Part IIIB.
3. R. S. Becker and J. Michl. J. Am. Chem. Soc. **88**, 5931 (1966).
4. J. Kolc and R. S. Becker. J. Phys. Chem. **71**, 4045 (1967); Photochem. Photobiol. **12**, 383 (1970).
5. F. M. Dean. Naturally occurring oxygen ring compounds. Butterworths, London. 1963.
6. D. A. Shirley and W. H. Reedy. J. Am. Chem. Soc. **73**, 458 (1951).
7. S. Wawzonek. *In* Heterocyclic compounds. Vol. 2. *Edited by* R. C. Elderfield. John Wiley and Sons, Inc., New York, NY. 1951. pp. 277–342.
8. E. E. Schweizer, A. T. Wehman, and D. M. Nyez. J. Org. Chem. **38**, 1583 (1973).
9. G. Cardillo, R. Cricchio, and L. Merlini. Tetrahedron, **27**, 1875 (1971).
10. C. E. Cook and C. E. Twine. J. Chem. Soc. Chem. Commun. 791 (1968).
11. W. K. Anderson and E. J. LaVoie. J. Org. Chem. **38**, 3832 (1973).
12. J. T. Arrigo. U.S. Patent No. 2,984,525 (1961); Chem. Abstr. **56**, 3460 (1962).
13. R. M. Leblanc, G. Galinier, A. Tessier, and L. Lemieux. Can. J. Chem. **52**, 3723 (1974).

Rearrangement studies with ^{14}C. XLIII. The acetolysis of trianisyl[2-^{14}C]vinyl bromide

CHOI CHUCK LEE, URSULA WEBER, AND CRAIG A. OBAFEMI

Department of Chemistry and Chemical Engineering, University of Saskatchewan, Saskatoon, Sask., Canada S7N 0W0

Received December 7, 1978

CHOI CHUCK LEE, URSULA WEBER, and CRAIG A. OBAFEMI. Can. J. Chem. **57**, 1384 (1979).

Acetolyses of trianisyl[2-^{14}C]vinyl bromide (**1**-Br-*2*-^{14}C) were carried out in the presence of various amounts of added NaOAc or NaOAc and LiBr. Scramblings of the isotopic label from C-2 to C-1 arising from 1,2-anisyl shifts in the trianisylvinyl cation were observed in both the reaction product and the recovered, unconsumed reactant. The results indicate that the relative contribution of the 1,2-shift process is decreased with an increase in the amount of NaOAc or LiBr, in support of a mechanism involving formation of the dissociated trianisylvinyl cation which will competitively undergo 1,2-anisyl shift to give scrambling, be captured by Br^- ion and return to scrambled starting material, and be captured by OAc^- ion to give scrambled product. The results are also compared with previous data from solvolyses of triphenyl[2-^{14}C]vinyl bromide and the differences are discussed.

CHOI CHUCK LEE, URSULA WEBER et CRAIG A. OBAFEMI. Can. J. Chem. **57**, 1384 (1979).

On a effectué l'acétolyse du bromure de trianisyl[2-^{14}C]vinyle (**1**-Br-*2*-^{14}C) en présence de quantités diverses de NaOAc ou de NaOAc et de LiBr. On a observé des échanges des isotopes marqueurs du C-2 vers C-1 provenant de transpositions-1,2 des anisyles dans le cation trianisylvinyle tant dans le produit de la réaction que dans le réactif récupéré qui n'avait pas réagit. Les résultats indiquent que la contribution relative aux transpositions-1,2 diminue avec une augmentation de la quantité de NaOAc ou de LiBr; ceci est en accord avec un mécanisme impliquant la formation du cation trianisylvinyle dissocié qui subira des réactions compétitives soit de transpositions-1,2 donnant lieu à des échanges des isotopes soit des réactions où l'ion est piégé par du Br^- et donne lieu à une réaction de retour redonnant le produit de départ où il s'est produit des échanges ou des réactions où l'ion est piégé par des ions OAc^- qui fournissent des produits où il s'est effectué un échange. On compare aussi ces résultats à ceux obtenus antérieurement lors de la solvolyse du bromure de triphényl[2-^{14}C]vinyle et on discute des différences.

[Traduit par le journal]

The degenerate rearrangement arising from a 1,2-anisyl shift across the double bond in the trianisylvinyl (tris(*p*-methoxyphenyl)vinyl)) cation was first reported from this laboratory in 1975 (1). For example, in the reaction of trianisyl[2-^{13}C]vinyl bromide (**1**-Br-*2*-^{13}C) with HOAc–AgOAc, ^{13}C nmr analysis of the product showed about 20% scrambling of the label from C-2 to C-1 (1). Similarly, using D-labeling and ^{1}H nmr analysis, Rappoport and co-workers (2) found that the NaOAc buffered acetolysis of 1,2-dianisyl-2-*p*-($^2H_3$)methoxyphenylvinyl bromide (**1**-Br-methoxy-d_3) gave $35 \pm 2\%$ rearrangement[1] arising from 1,2-anisyl shifts. It was also noted that when the NaOAc buffered acetolysis was carried out in the presence of an excess of Bu_4NBr, $4 \pm 1.5\%$ rearrangement was observed in the recovered reactant (2). Earlier, Rappoport and Gal (3) had reported that the unbuffered acetolysis of **1**-Br gave irregular kinetics and extensive blackening, while in the NaOAc buffered acetolysis, the first order rate constant decreased markedly as the reaction proceeded during a given run. In the presence of added Bu_4NBr, a large common ion rate depression was observed and it was concluded that the acetolysis of **1**-Br took place via the dissociated trianisylvinyl cation, which could be captured competitively by the leaving group and by the lyate ion (3).[2] In the present work, further studies were undertaken on the acetolysis using trianisyl[2-^{14}C]vinyl bromide (**1**-Br-*2*-^{14}C). The extents of scrambling were determined in both the reaction product and unconsumed reactant at different stages of the reaction, carried out with added NaOAc or NaOAc and LiBr, in order to provide more scrambling data on the role of the trianisylvinyl cation in relation to its rearrangement and return processes.

1-Br-*2*-^{14}C was synthesized in the same way as in the preparation of **1**-Br-*2*-^{13}C (1), except that ^{14}C instead of ^{13}C was used as the label. The acetolyses of **1**-Br-*2*-^{14}C were carried out in 9:1 HOAc–Ac_2O in the presence of 2 or 20 equiv. of NaOAc, or in the

[1]With **1**-Br-methoxy-d_3, 100% rearrangement corresponds to the formation of 33.3% of the rearranged product. On this basis, the 20% scrambling observed in the work with **1**-Br-*2*-^{13}C corresponds to 40% rearrangement.

[2]A book providing a general review on vinyl cations is now in preparation (9).

0008-4042/79/111384-04$01.00/0

presence of 2 equiv. of NaOAc and various amounts of LiBr as recorded in Table 1. Since the reaction rate would decrease markedly at the later stages of the reaction because of returns and since added Br^- ions would further slow down the rate (3), for each set of experiments with a given amount of NaOAc or NaOAc and LiBr, preliminary studies were made with inactive materials to determine the time required to give about 25, 50, or 75% reaction as measured by titration of the liberated Br^- ions. In the active runs, these reaction times were utilized together with an experiment using a prolonged reaction time. Because of 1,2-anisyl shifts in the trianisylvinyl cation and returns from the ion to covalent starting material, the ^{14}C-label would be scrambled over the C-1 and C-2 positions in both the reaction product, trianisyl[1,2-^{14}C]vinyl acetate (**1**-OAc-*1,2*-^{14}C), and the unconsumed reactant, trianisyl[1,2-^{14}C]vinyl bromide (**1**-Br-*1,2*-^{14}C). Upon two successive treatments of the product and unconsumed reactant with $LiAlH_4$ as described previously (1), the **1**-OAc-*1,2*-^{14}C was converted to 1,2,2-trianisyl[1,2-^{14}C]ethanol (**2**-*1,2*-^{14}C) (1) and, at the same time, the unconsumed **1**-Br-*1,2*-^{14}C was transformed to trianisyl[1,2-^{14}C]ethene (**3**-*1,2*-^{14}C) (4). After separation through an alumina column, the **2**-*1,2*-^{14}C was oxidized (5) to give dianisyl[^{14}C]ketone (**4**-^{14}C), and the difference in activity between **4**-^{14}C and **3**-*1,2*-^{14}C gave the extent of scrambling from C-2 to C-1 in the reaction product. Degradation of the **3**-*1,2*-^{14}C was effected by ozonolysis, again giving rise to **4**-^{14}C and hence the extent of scrambling in the recovered unconsumed reactant. The results are summarized in Table 1.

The results in Table 1 can be interpreted by the mechanism shown in Scheme 1, in which RX and R′X designate, respectively, the original substrate, **1**-Br-*2*-^{14}C, and the isotopically rearranged **1**-Br-*1*-^{14}C, RY and R′Y designate the isotopically unrearranged and rearranged **1**-OAc-*2*-^{14}C and **1**-OAc-*1*-^{14}C, derived from the unrearranged and rearranged trianisyl[2-^{14}C]vinyl and trianisyl[1-^{14}C]vinyl cations, and k_r, k_{-1} and k_p, respectively, are the rate constants for the 1,2-anisyl shift, the return process, and the product formation. The rates for the return process and production formation would also be dependent on $[Br^-]$ and $[OAc^-]$, respectively. As stated in paper XLII of this series (6), a steady state treatment for the processes in Scheme 1 will give the relationship depicted in [1].

$$[1]\quad \frac{d[R'Y]/dt}{d[RY]/dt} = \frac{(k_{-1} + k_p)[R'X] + k_r([RX] + [R'X])}{(k_{-1} + k_p)[RX] + k_r([RX] + [R'X])}$$

TABLE 1. Acetolyses of 15 m*M* trianisyl[2-^{14}C]vinyl bromide in the presence of added NaOAc or NaOAc and LiBr at 120 ± 2°C

Expt.	[NaOAc] (m*M*)	[LiBr] (m*M*)	Reaction time (h)	Approx. % reaction	Specific activity[a] (dpm/mmol)								Scrambling from C-2 to C-1 (%)			
					Reaction product				Recovered reactant				Reaction product		Recovered reactant	
					$An_2CHCHOHAn$		An_2CO[b]		$An_2C{=}CHAn$		An_2CO[b]					
					Run 1	Run 2	Run 1	Run 2	Run 1	Run 2	Run 1	Run 2	Run 1	Run 2	Run 1	Run 2
1	30		5	25	177 000		160 000		149 000		148 000		9.6		0.7	
2	30		10	50	89 000	609 000	80 000	546 000	206 000	472 000	196 000	454 000	10.1	10.3	4.9	3.8
3	30		70	75	236 000	136 000	195 000	112 000	207 000	108 000	165 000	86 300	17.4	17.6	20.3	20.1
4	30		100	90	112 000	294 000	85 500	223 000	704 000	144 000	501 000	101 000	23.7	24.1	28.8	29.9
5	300		3	50	470 000	298 000	434 000	275 000	291 000	204 000	290 000	203 000	7.7	7.7	0.3	0.5
6	300		30	95	178 000	90 000	159 000	81 000	85 000	78 000	80 000	73 000	10.7	10.0	5.9	6.4
7	30	30	21	25	87 800		81 900		41 900		41 700		6.7		0.5	
8	30	30	64	50	231 000	286 000	210 000	262 000	362 000	322 000	348 000	309 000	9.1	8.4	3.9	4.0
9	30	30	135	75	142 000	439 000	120 000	373 000	276 000	176 000	225 000	145 000	15.5	15.0	18.5	17.6
10	30	30	384	85	741 000	182 000	458 000	113 000	161 000	182 000	81 200	89 400	38.2	37.9	49.6	50.9
11	30	60	77	50	797 000	177 000	735 000	163 000	267 000	261 000	257 000	252 000	7.8	7.9	3.7	3.4
12	30	60	384	80	272 000	242 000	185 000	168 000	302 000	226 000	166 000	121 000	32.0	30.6	45.0	46.5
13	30	100	135	50	175 000	325 000	163 000	303 000	218 000	236 000	212 000	229 000	6.9	6.8	2.8	3.0
14	30	100	432	70	182 000	153 000	146 000	118 000	333 000	312 000	199 000	192 000	19.8	22.9	40.2	38.5
15	30	300	96[c]	20	250 000		239 000		46 600		46 100		4.4		1.1	

[a]Measured by a liquid scintillation counter.
[b]Assayed as the oxime.
[c]The reaction mixture blackens on further heating.

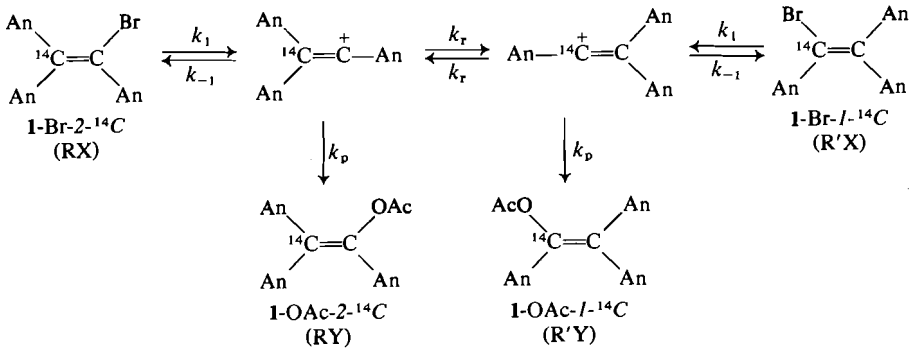

SCHEME 1

Since the ratio of the rates of formation of the rearranged and unrearranged products is dependent on [RX] and [R'X] as shown in [1], the amount of scrambling in the product is expected to increase with increasing extents of reaction. This expectation is in agreement with the observed results (Table 1) which show that for a given set of experimental conditions, the scrambling in the product does increase with an increase in reaction time. For example, when the acetolysis was carried out in the presence of 2 equiv. of NaOAc with no added LiBr (experiments 1–4), for reactions ranging from about 25 to 90%, the increasing amounts of scrambling in the product ranged from 9.6 to 24.1% (19.2 to 48.2% rearrangement). In the experiment on the NaOAc buffered acetolysis of **1**-Br-methoxy-d_3 (2), the observed 35 ± 2% rearrangement is also within this range.

The observation of scrambling in the recovered reactant indicates definitely the occurrence of returns from both the isotopically unrearranged and rearranged ions to covalent starting material. Again using experiments 1–4 as an illustration, in the earlier stages of the reaction (experiments 1 and 2), the scrambling in the recovered reactant is less than that found in the corresponding product and this is to be expected since there would be a relatively large amount of unchanged reactant remaining in the reaction mixture. In the later stages of the reaction (experiments 3 and 4), the scrambling in the recovered reactant is higher than that in the corresponding product. Most probably, the occurrence of many cycles of ionization, 1,2-shift, and return will lead to the accumulation of a greater amount of the rearranged reactant in the recovered, unconsumed substrate.

In experiments 5 and 6, an increase in the amount of NaOAc from 2 to 20 equiv. resulted in a decrease in the extent of scrambling for both the product and recovered reactant (compare experiments 5 and 6 with experiments 2 and 4). Similar effects of added OAc^- in decreasing the extent of rearrangement have been previously reported. For example, the 20% rearrangement of the 1-phenyl-2,2-di-*p*-tolylvinyl cation to the more stable 2-phenyl-1,2-di-*p*-tolylvinyl cation, observed in the decomposition in HOAc of 1-phenyl-2,2-di-*p*-tolylvinylphenyltriazene, was found to be completely suppressed by the presence of a 10 molar equiv. of KOAc (7). Similarly, in the decomposition in HOAc of trianisyl[2-^{14}C]vinylphenyltriazene, the isotopic scrambling arising from 1,2-anisyl shifts in the trianisylvinyl cation was decreased from about 38 to 17% by the presence of 1.7 equiv. of NaOAc (8). Such results from the decomposition of triazenes, which presumably took place via the diazonium ions, were interpreted as indicating that the 1,2-aryl shift occurred in the dissociated triarylvinyl cation. The presently observed decrease in rearrangement arising from an increased acetate concentration may, therefore, be regarded as a further confirmation that the acetolysis of **1**-Br proceeds via the dissociated trianisylvinyl cation which undergoes 1,2-shifts competitively with captures by nucleophiles. An increased OAc^- concentration will, therefore, enhance the rate of capture of the trianisylvinyl cation, thereby decreasing the relative amount of 1,2-anisyl shifts.

When the acetolysis was carried out in the presence of 2 equiv. of NaOAc and various amounts of LiBr (experiments 7–15), except in the cases involving prolonged reaction times, there was generally a further reduction in the extent of scrambling when compared with analogous experiments without the presence of added LiBr. This again fits the mechanism given in Scheme 1 since there would be further competition between the 1,2-shift in the dissociated trianisylvinyl cation and its capture by the additional Br^- ions. In the experiments with prolonged reaction times (experiments 10, 12, and 14), the recovered reactant showed extensive scramblings, indicative of a high rate for the return process and the repeated cycles of ionization, 1,2-shift, and return gave rise to the accumulation of a completely or nearly completely scrambled residual unconsumed reactant. In experiments 10 and 12, these cycles of ionization, 1,2-shift, and return even resulted in a higher extent of scrambling in the product than the scrambling in the

product from experiment 4, which involved the use of 2 equiv. of NaOAc and a long reaction time but without the added LiBr.

It is of interest to compare the present results with those observed from our recent study with triphenyl[2-^{14}C]vinyl bromide (**5**-Br-*2*-^{14}*C*) (6). The solvolysis of **5**-Br-*2*-^{14}*C* in HOAc–NaOAc was too slow and experiments were carried out with various combinations of HOAc and H_2O. In HOAc–H_2O, no scrambling was found in the recovered reactant. In the reaction product, the extent of scrambling remained the same regardless of the extent of reaction and was unaffected by the presence of added NaOAc or NaBr. A mechanism simpler than Scheme 1 and without involving the return process was sufficient to account for those results (6). It was also suggested that the 1,2-phenyl shift in the triphenylvinyl cation may have occurred in the ion-pair stage rather than in the dissociated ion since added OAc^- or Br^- did not affect the extent of scrambling. In the solvolysis of **5**-Br-*2*-^{14}*C* in 2,2,2-trifluoroethanol (TFE) buffered with lutidine (6), scrambling was found in both the product and recovered reactant. An interesting difference between the present results and those obtained from the trifluoroethanolysis of **5**-Br-*2*-^{14}*C* is that after about 30 or 60% reaction with **5**-Br-*2*-^{14}*C*, the scrambling in the product and in the recovered reactant was found to be the same (6). This finding suggests that in the triphenylvinyl system, k_r for the 1,2-phenyl shift is relatively unimportant when compared with k_{-1} and k_p for the return and product forming processes. Once the rearranged triphenyl[1-^{14}C]vinyl cation or ion pair is formed, the ratio of the rearranged to unrearranged ions or ion pairs will determine the ratio of their products, [R′Y]/[RY], as well as the recovered reactants, [R′X]/[RX], because interconversion between the rearranged and unrearranged ions or ion pairs, the k_r process, is relatively small. However, for the trianisylvinyl system, k_r is not unimportant when compared with k_{-1} or k_p, and from [1] the scramblings in the product and in the recovered reactant are not the same (Table 1). This interpretation of the difference between the triphenylvinyl and trianisylvinyl systems appears to be quite reasonable since the migratory aptitudes for the 1,2-shifts would be much larger for the anisyl than the phenyl group.

Experimental

*Acetolysis of Trianisyl[2-^{14}C]vinyl Bromide (***1***-Br-2-^{14}C)*

The acetolysis of **1**-Br-*2*-^{14}*C* was carried out in the presence of various amounts of NaOAc or NaOAc and LiBr as indicated in Table 1. A typical experiment is described below.

A solution of 64 mg (0.15 mmol) of **1**-Br-*2*-^{14}*C*, 26 mg (0.30 mmol) of NaOAc, and 25 mg (0.30 mmol) of LiBr in 10 mL of glacial acetic acid containing 10% acetic anhydride in a sealed tube was heated at 120 ± 2°C for the desired length of time. The tube was then cooled in ice, opened, and the contents poured into 200 mL of ether containing ordinary **1**-Br and **1**-OAc (about 100 mg each) as carriers. The ether solution was washed three times with 50 mL portions of water and then with a saturated $NaHCO_3$ solution. After drying over $MgSO_4$, the ether was removed by distillation, leaving a residue containing the reaction product, trianisyl[1,2-^{14}C]vinyl acetate (**1**-OAc-*1,2*-^{14}*C*), and any unconsumed reactant, trianisyl[1,2-^{14}C]vinyl bromide (**1**-Br-*1,2*-^{14}*C*).

Work-up Procedure

The residual mixture of **1**-OAc-*1,2*-^{14}*C* and **1**-Br-*1,2*-^{14}*C* was treated twice successively with $LiAlH_4$ as previously described (1). After one $LiAlH_4$ reduction, **1**-OAc-*1,2*-^{14}*C* gave a mixture of 1,2,2-trianisyl[1,2-^{14}C]ethanone and 1,2,2-trianisyl[1,2-^{14}C]ethanol (**2**-*1,2*-^{14}*C*) (1), while **1**-Br-*1,2*-^{14}*C* was converted to 1,2,2-trianisyl[1,2-^{14}C]ethene (**3**-*1,2*-^{14}*C*) (4). After the second reduction, a mixture of **2**-*1,2*-^{14}*C* and **3**-*1,2*-^{14}*C* was obtained. This mixture was passed through a 30 cm × 2 cm diameter column packed with adsorption alumina (Fisher Scientific Co.). The **3**-*1,2*-^{14}*C* was first eluted with 90% petroleum ether (bp 40–60°C) and 10% ether, and the **2**-*1,2*-^{14}*C* was then recovered after a change to $CHCl_3$ as eluant.

Degradation of **2**-1,2-^{14}C *and* **3**-1,2-^{14}C

After the addition of appropriate amounts of inactive carrier if needed, **2**-*1,2*-^{14}*C* was oxidized with $KMnO_4$ to give dianisyl[^{14}C]ketone (**4**-^{14}*C*) in the same way as described in earlier work (5, 8).

The **3**-*1,2*-^{14}*C*, again with added carrier if needed, was degraded by ozonolysis to give **4**-^{14}*C*. Typically, a stream of oxygen–ozone mixture, containing about 8% O_3, from an ozone generator was passed through a stirred and cooled solution of 500 mg (1.5 mmol) of **3**-*1,2*-^{14}*C* in 100 mL of ethyl acetate for 1 h. The solvent was removed in a rotary evaporator and the residual crude ozonide was heated under reflux for 2 h with a mixture of 48 mL of H_2O, 2 mL of HOAc, and 10 mg of Zn dust. After cooling, the mixture was extracted three times with ether, and the combined extract was dried over $MgSO_4$ before the ether was removed by distillation. The residue was then passed through the 15 cm × 2 cm diameter alumina column, with 90% petroleum ether(bp 40–60°C) – 10% ether as eluant. Unreacted **3**-*1,2*-^{14}*C* was eluted first, followed by a small amount of *p*-methoxybenzaldehyde. The desired ketone, **4**-^{14}*C*, was eluted last, the recovery being 200 mg (55%).

Acknowledgements

The financial support given by the National Research Council of Canada and valuable comments from Professor Z. Rappoport are gratefully acknowledged.

1. M. Oka and C. C. Lee. Can. J. Chem. **53**, 320 (1975).
2. Y. Houminer, E. Noy, and Z. Rappoport. J. Am. Chem. Soc. **98**, 5632 (1976).
3. Z. Rappoport and A. Gal. Tetrahedron Lett. 3233 (1970).
4. C. C. Lee and U. Weber. J. Org. Chem. **43**, 2721 (1978).
5. C. C. Lee, A. J. Cessna, B. A. Davis, and M. Oka. Can. J. Chem. **52**, 2679 (1974).
6. C. C. Lee and E. C. F. Ko. Can. J. Chem. **56**, 2459 (1978).
7. W. M. Jones and F. W. Miller. J. Am. Chem. Soc. **89**, 1960 (1967).
8. C. C. Lee and E. C. F. Ko. Can. J. Chem. **54**, 3041 (1976).
9. P. J. Stang, Z. Rappoport, M. Hanack, and L. R. Subramanian. Vinyl cations. Academic Press, New York, NY. In press.

Total synthesis of δ-(L-α-aminoadipyl)-L-cysteinyl-D-valine (ACV), a biosynthetic precursor of penicillins and cephalosporins

SAUL WOLFE AND MARK GORDON JOKINEN

Department of Chemistry, Queen's University, Kingston, Ont., Canada K7L 3N6

Received December 11, 1978

SAUL WOLFE and MARK GORDON JOKINEN. Can. J. Chem. 57, 1388 (1979).

The title compound has been synthesized as its disulfide by a classical route from the fully protected precursor *N*-BOC-*S*-trityl-δ-(L-α-aminoadipyl)-L-cysteinyl-D-valine bisbenzhydryl ester. Deprotection has been achieved by oxidative removal of the trityl group with iodine, followed by removal of BOC and benzhydryl using trifluoroacetic acid. The final product is obtained in 23% overall yield from D-valine.

SAUL WOLFE et MARK GORDON JOKINEN. Can. J. Chem. 57, 1388 (1979).

On a synthétisé le composé mentionné dans le titre sous forme de disulfure par une voie classique à partir du précurseur complètement protégé qui est l'ester bisbenzhydrylique de la *N*-BOC *S*-trityl δ-(L-α-aminoadipyl) L-cystéinyl D-valine. On a effectué la déprotection en faisant suivre l'élimination du groupe tritylе grâce à une oxydation avec de l'iode suivi par l'enlèvement des groupes BOC et benzhydryles à l'aide d'acide trifluoroacétique. On a obtenu le produit final avec un rendement global de 23% à partir de la D-valine.

[Traduit par le journal]

The biosyntheses of Penicillin N (**1***a*) by *Cephalosporium acremonium*, and of Isopenicillin N (**1***b*) by *Penicillium chrysogenum*, proceed via the common tripeptide precursor δ-(L-α-aminoadipyl)-L-cysteinyl-D-valine (**2**) (ACV) (1). Although many of the details of the biosynthesis of ACV from the amino acid precursors L-α-aminoadipic acid, L-cysteine, and L-valine have been established (1), the specific processes by which the tripeptide is transformed to the oxidation level of penicillin remain unknown. Thus it has not yet been possible to relate the stereochemical observations, that the pro-S hydrogen of cysteine is removed (2), and that the C5—N (2) and C2—S bonds (3) of penicillin are formed with retention of configuration, to proven chemical mechanisms. The principal reason for the lack of progress on this aspect of the problem is that studies of the fate of ACV and (or) the role of post-ACV intermediates require that protoplasts or protoplast lysates (4) derived from *P. chrysogenum* or *C. acremonium* be employed in the biosynthetic experiments. The required techniques have only become available in recent years, as a result of the important work of Abraham and his co-workers (5).

There are, therefore, two prerequisites for any planned investigation of the oxidative stages of penicillin biosynthesis. The first is a protoplast or protoplast lysate system that will convert ACV efficiently into penicillin; the second is a supply of labelled ACV. We wish to disclose a new total synthesis of ACV (as its disulfide), which makes this compound readily available for biosynthetic studies.

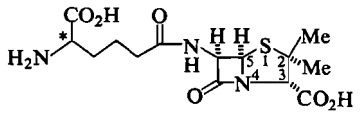

1

a (D-configuration at *C)
b (L-configuration at *C)

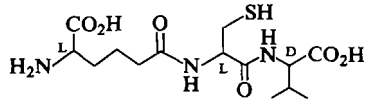

2

In this synthesis, the final product and most of the intermediates have been obtained in crystalline form and have been characterized fully.

Four syntheses of ACV and (or) its stereoisomers have been reported previously in the literature (6–9). Two of these (6, 7) were directed specifically towards the LLL isomer; however, the experimental details of Rudinger's synthesis (6) have not yet been presented, and spectroscopic and analytical data were not given for the peptide intermediates and the final product of Bauer's synthesis (7). Only the synthesis of Fawcett *et al.* (9) has been accompanied by full experimental details and microanalytical data for the various intermediates. In this latter work, three separate deprotecting steps were needed, and the final product was obtained in 8.5% yield from the fully protected tripeptide.

The syntheses of Adriaens *et al.* (8) and Fawcett *et al.* (9) include an alkaline hydrolysis of a protected

0008-4042/79/111388-09$01.00/0

tripeptide. In the work of Adriaens, this removes the benzyl ester of the intermediate **3**; in the work of Fawcett, the alkaline hydrolysis removes the ethyl and 4-methoxybenzyl esters from the intermediate **4**. In our hands, the removal of esters by alkaline hydrolysis led to problems.[1] Thus, exposure of **5** to ethanolic sodium hydroxide led to loss of the α-aminoadipyl residue; application of the same conditions to **6**, followed by removal of the *tert*-butoxycarbonyl (BOC) protecting groups with trifluoroacetic acid, led to a mixture of products. As a result of these failures, a successful synthesis was designed in which all carboxyl and amino protecting groups were removed in a single, acidic step. This synthesis is summarized in Scheme 1.

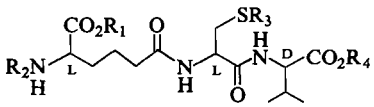

3 $R_1 = PhCH_2, R_2 = PhCH_2OCO, R_3 =$ disulfide, $R_4 = H$

4 $R_1 = p\text{-}CH_3OC_6H_4CH_2, R_2 = p\text{-}CH_3OC_6H_4CH_2OCO, R_3 = AcNHCH_2, R_4 = Et$

5 $R_1 = PhCH_2, R_2 = H, R_3 = PhCH_2, R_4 = H$

6 $R_1 = PhCH_2, R_2 = t\text{-BOC}, R_3 =$ disulfide, $R_4 = PhCH_2$

Benzhydryl and BOC protection were employed for the carboxyl and amino groups, respectively, and the trityl group for the protection of sulfur. As a test of the various procedures, D-valine was first protected and deprotected, as shown in Scheme 2, and L-cystinyl-bis-D-valine was synthesized, as shown in Scheme 3. In this latter synthesis, oxidative cleavage of the trityl group from benzhydryl-*N*-BOC-*S*-trityl-L-cysteinyl-D-valinate was accomplished in over 75% yield, using iodine in methanol containing pyridine (10).

As shown in Scheme 4, DL-α-aminoadipic acid was prepared by the amidomalonic ester procedure described by Abraham and his co-workers (11), and resolved enzymatically as the *N*-chloroacetyl derivative (12). The α-benzhydryl ester was then synthesized by treatment of the *p*-toluenesulfonic acid salt with 1 equiv. of diphenyldiazomethane (13). This reaction, based upon a literature precedent with the β-naphthalenesulfonic acid salt of glutamic acid (14), afforded a mixture of unreacted diacid and the α-benzhydryl ester, from which the ester could be isolated without difficulty. The introduction of the BOC protecting group was performed using 2-*tert*-butoxycarbonyloximino-2-phenylacetonitrile (BOC-ON) (15) in the presence of dicyclohexylamine. This minor modification of the recommended procedure (15) has been found to be generally applicable to the synthesis of BOC-amino acids.[2]

The BOC-protected cysteinylvaline peptide shown in Scheme 3 was unsuitable for an ACV synthesis because of the difficulties (16) associated with the selective removal of the BOC group from **7** (see Scheme 3) prior to coupling with the aminoadipic acid moiety. Therefore, in the ACV synthesis, the *N*,*S*-dityrityl derivative of L-cysteine (17) was coupled to the benzhydryl ester of D-valine. The *N*-trityl group of the resulting material (**8**; see Scheme 1) could be removed selectively with aqueous acetic acid, and the product isolated as the hydrochloride salt. Conversion to fully protected ACV (**9**; see Scheme 1) was achieved using EEDQ (18) as the coupling agent.

A problem with the use of the *N*-trityl group in peptide synthesis is the steric crowding which is introduced at the adjacent carboxyl group. This causes a reduction in the rate of the peptide coupling reaction (19). Nevertheless, *N*,*S*-ditritylcysteine has been coupled successfully with many amino acid esters, via the active *N*-hydroxysuccinimide ester **10** (17, 20). However, despite these literature precedents, initial experiments suggested that the direct coupling of **10** with the benzhydryl ester of D-valine was extremely slow, and did not proceed to completion.[3] The problem was overcome by addition of the active ester aminolysis catalyst 1,2,4-triazole to the reaction mixture (21), which allowed the synthesis of **8** under mild conditions.

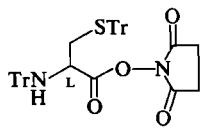

10

Certain N,S-diprotected cysteine esters have been found to undergo racemization under the conditions required for peptide coupling (22). It was, therefore, necessary to check the stability of **10** under the conditions of its coupling to the valine moiety. No racemization was observed.

Oxidative removal of the *S*-trityl group from **9** proceeded in 64% yield, and treatment of the resulting bis-δ-(*N*-BOC-L-α-aminoadipyl)-L-cystinyl-bis-D-valine tetrabenzhydryl ester (**11**; see Scheme 1)

[1]M. G. Jokinen, P. Mathiaparanam, and S. Wolfe. Unpublished results.

[2]J. D. Greenhorn, M. G. Jokinen, and S. Wolfe. Unpublished results.

[3]M. G. Jokinen and S. Wolfe. Unpublished results. See also ref. 19, p. 138.

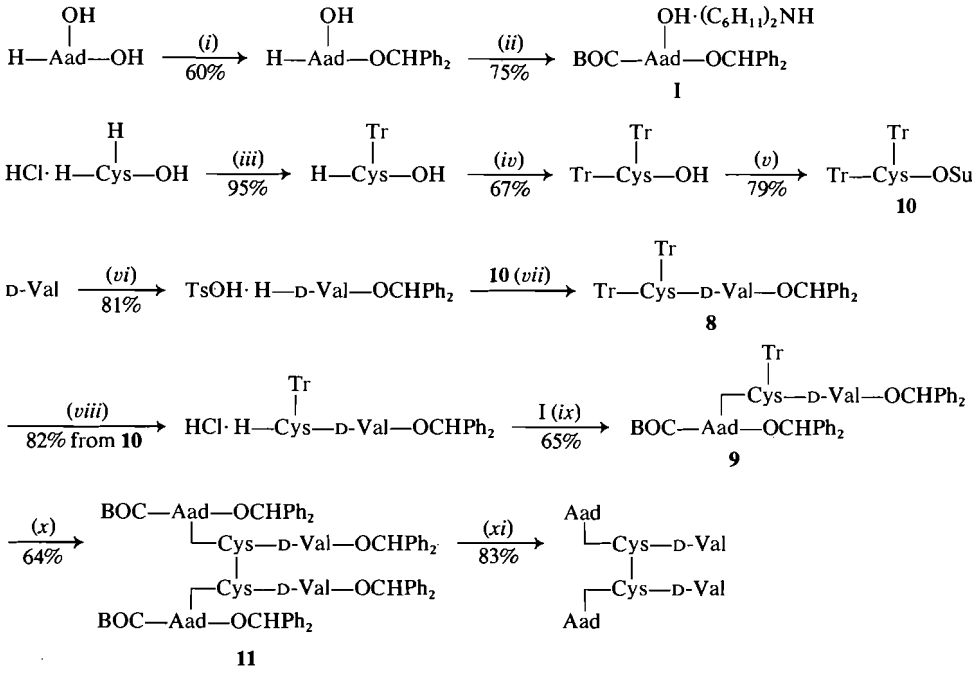

SCHEME 1. Reagents: (*i*) TsOH; Ph_2CN_2–DMF; (*ii*) BOC-ON, EtOH, dicyclohexylamine; (*iii*) TrOH, TFA; (*iv*) TrCl, Et_2NH; (*v*) *N*-hydroxysuccinimide, DCC; (*vi*) TsOH; Ph_2CN_2–DMF; (*vii*) 1,2,4-triazole, Et_3N; (*viii*) HOAc–H_2O; then HCl–EtOH; (*ix*) EEDQ; (*x*) I_2–MeOH–pyridine; (*xi*) TFA, anisole.

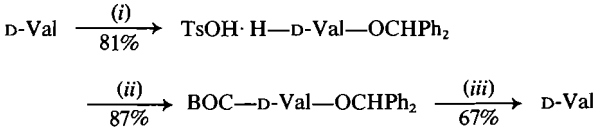

SCHEME 2. Reagents: (*i*) TsOH; Ph_2CN_2–DMF; (*ii*) BOC-ON–Et_3N; (*iii*) TFA.

with trifluoroacetic acid and anisole led to crystalline ACV-disulfide in 83% yield. The overall yield of this compound from D-valine is ca. 23%. As reported by Adriaens *et al.* (8), the disulfide is converted to ACV itself upon reduction with dithiothreitol (23).

Experimental

General

The ir spectra were taken on a Perkin-Elmer 180 spectrometer. Proton nmr spectra were recorded on a Varian Anaspect EM360, or a Varian T-60. Chemical shifts are reported in δ values relative to tetramethylsilane or 2,2-dimethyl-2-sila-pentane-5-sulfonate as internal standards, and in deuteriochloroform unless otherwise noted. Microanalyses were carried out by Galbraith Laboratories, Knoxville, Tennessee. Melting points were determined on a Meltemp apparatus. Optical rotations were obtained on a Perkin-Elmer 141 polarimeter. Thin layer chromatography was performed on pre-coated Brinkmann silica gel 60 F-254 plates with aluminum or glass backing. Spots were observed under short wave ultraviolet light, or were visualized with ninhydrin or iodine vapour. Magnesium sulfate and sodium sulfate were used as drying agents. Solvents were distilled before use, and were dried, as required, by literature procedures.

DL-α-*Aminoadipic Acid (11, 25)*

γ-Chlorobutyronitrile (Aldrich, purity 95%, 51.7 g, 0.50 mol) was added at room temperature to a solution of sodium iodide (90 g, 0.60 mol) in distilled acetone (200 mL) containing some glass boiling granules (24). A precipitate began to form within minutes. The mixture was refluxed for 24 h, cooled to room temperature, and the precipitated salt was removed by suction filtration and dried (28.4 g, 97% of theory). The filtrate was concentrated below 30°C under reduced pressure, and the residual slurry was dissolved in commercial anhydrous ether. After filtration, the ether was removed to yield crude γ-iodobutyronitrile as a clear yellow oil. This was purified by fractional distillation, bp 83–86°C/1–2 Torr, to give 83.7 g (86%) as a clear, colourless liquid; ir: 2240 cm^{-1} (—C≡N stretch); ^{1}Hmr (CCl_4): $Cl(CH_2)_3CN$: 3.64 (2H, t, 6), 1.90–2.80 (4H, m); $I(CH_2)_3CN$: 3.28 (2H, t, 6), 1.90–2.80 (4H, m).

A solution of sodium methoxide (Aldrich, 18.0 g, 0.33 mol, 1.1 equiv.) in 75 mL absolute ethanol was added dropwise and with mechanical stirring to a solution of diethylacetamidomalonate (DAM) (65.1 g, 0.30 mol) in 240 mL ethanol. The resulting mixture was extremely viscous. γ-Iodobutyronitrile (78.0 g, 0.40 mol, 1.33 equiv.), in ethanol (50 mL), was then added dropwise and with vigorous stirring. After the addition was complete, the mixture was refluxed for 6 h. The solvent was removed and the residual slurry was taken up in 100 mL of ethyl acetate, followed by water and sufficient 10% citric acid to adjust the aqueous phase to about pH 4. The aqueous phase was removed, and the organic phase was washed with water (3 × 100 mL). After drying over anhydrous magnesium sulfate, and removal of the ethyl acetate, 11.66 g of iodobutyronitrile was recovered from the residual oil by fractional distillation. The yield of crude alkylated product was 79.33 g, and its ^{1}Hmr spectrum indicated some contamination with $I(CH_2)_3CN$ and DAM.

The crude product (44.5 g) was dissolved in 480 mL of

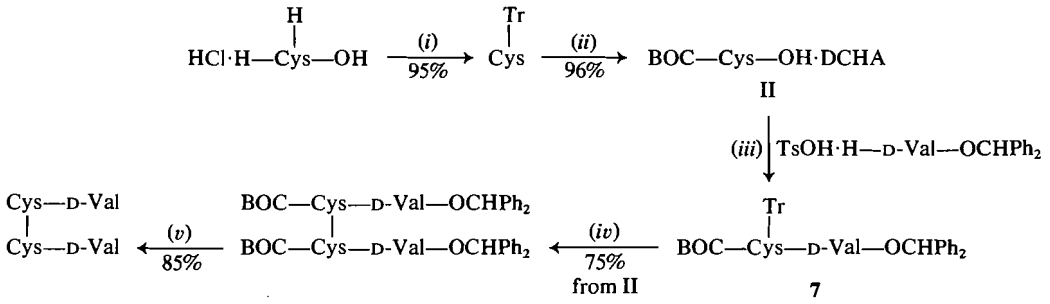

SCHEME 3. Reagents: (*i*) TrOH, TFA; (*ii*) BOC-ON–Et_3N; (*iii*) *N*-methylmorpholine, EEDQ; (*iv*) I_2, MeOH, pyridine; (*v*) TFA.

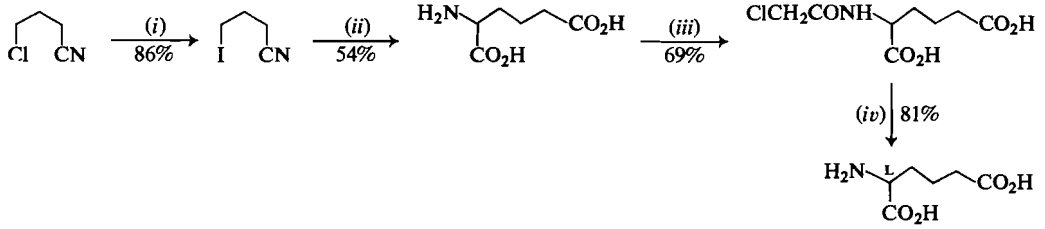

SCHEME 4. Reagents: (*i*) NaI–Me_2CO; (*ii*) diethylacetamidomalonate–NaOEt; then 8 *N* HCl; (*iii*) *p*-nitrophenylchloroacetate; (*iv*) hog kidney acylase I.

8 *N* hydrochloric acid, and the solution was refluxed for 10 h. Removal of the solvent yielded a crystalline slurry which was dissolved in 50 mL of water. The pH was adjusted to 2.9 with aqueous sodium hydroxide and the resulting precipitate was collected, dried, and dissolved in 100 mL of water with the aid of aqueous sodium hydroxide. The clear solution (pH 6) was then acidified to pH 2.9 with concentrated hydrochloric acid, and an equal volume of ethanol was added. The DL-α-aminoadipic acid was collected after refrigeration, and dried, 14.8 g (54% from diethylacetamidomalonate). The material was positive to ninhydrin; ir (KBr): 1640, 1665 cm^{-1}; ^{1}Hmr (D_2O + Na_2CO_3 + DSS): 3.25–3.6 (1H, m), 2.4–2.1 (2H, m), 1.9–1.4 (4H, m).

p-*Nitrophenyl Chloroacetate (26)*

Monochloroacetic acid (18.8 g, 0.20 mol) and *p*-nitrophenol (27.8 g, 0.20 mol) were dissolved in 400 mL of ethyl acetate, and the solution was cooled to 0°C. Dicyclohexylcarbodiimide (43.8 g, 0.21 mol), in ethyl acetate (100 mL), was added in one portion, with stirring. Dicyclohexylurea precipitation began within a minute. After 20 min, the ice bath was removed, and the solution was stirred for another 2 h. Oxalic acid (0.5 g) was added, and the solution was stirred a further 15 min. The urea and oxalic acid were then removed by filtration and the ethyl acetate filtrate was evaporated to dryness to yield the crude product. This was recrystallized twice from absolute ethanol to yield pale brown *p*-nitrophenyl chloroacetate (36.12 g, 84%), mp 95–98°C (Meltemp); ^{1}Hmr: 8.25 (2H, d, 9), 7.31 (2H, d, 9), 4.37 (2H, s); ir: 1780–1760, 1515, 1335 cm^{-1}.

DL-α-*Chloroacetylaminoadipic Acid (26, 27)*

DL-α-Aminoadipic acid (8.06 g, 50 mmol) and sodium hydroxide (3.0 g, 75 mmol) were dissolved in 50 mL of distilled water, and the solution was cooled to room temperature (pH 9.9). Acetone (25 mL) was then added, with stirring. A solution of *p*-nitrophenyl chloroacetate (12.52 g, 61 mmol) in 25 mL of dry acetone was added dropwise with vigorous stirring during a 2 h period, with concurrent addition of 3 *N* NaOH to maintain the pH at 9.5. After the addition was complete, and the pH had ceased to fall, concentrated hydrochloric acid was added carefully to lower the pH to 7.0. The solution was concentrated to half its original volume and an orange precipitate was removed. The pH was then lowered to 5.5, and the solution was extracted with ethyl acetate (4 × 100 mL), and the organic phase was discarded. The aqueous phase was concentrated to about 50 mL, acidified to pH 1–1.5, and extracted again with ethyl acetate (2 × 50 mL, 2 × 20 mL). The combined extracts were then dried over anhydrous magnesium sulfate and evaporated. The residual yellow oil was triturated with hexane to give a pale brown solid (9.95 g). Recrystallization from ethyl acetate – hexane afforded 8.11 g (69%), mp 129–131.5°C (Meltemp) (lit. (11) mp 129–130°C); ir (KBr): 3370 (s), 1690–1750 (b), 1600–1640 cm^{-1}; ^{1}Hmr ($CDCl_3$ + 3 drops DMSO-d_6): 11.56 (2H, s), 7.53 (1H, d, 8), 4.7–4.3 (1H, m), 4.07 (2H, s), 2.30 (2H, t, 6), 2.1–1.4 (4H, m).

L-α-*Aminoadipic Acid (28)*

Racemic *N*-chloroacetylaminoadipic acid (6.02 g, 25 mmol) and potassium dihydrogen phosphate (0.68 g, 5 mmol) were suspended in 100 mL of water, and brought into solution by the addition of 3 *N* sodium hydroxide. The pH was adjusted to 7.0, 250 mg of hog kidney acylase I was added, and the solution was stirred for 22 h. The enzyme was removed by careful heating of the solution to boiling for 5 min, followed by filtration. The solution was concentrated to 50 mL, the pH adjusted to 2.9 with hydrochloric acid, and 150 mL of ethanol was then added. After refrigeration for 24 h, the crude L-α-aminoadipic acid was collected, dried, and recrystallized from water–ethanol: 1.65 g (81%); $[\alpha]_D$ + 23.5° (*c* 2, 5 *N* HCl) (lit. (28) +25°). The material was positive to ninhydrin.

The D-α-chloroacetylaminoadipic acid was recovered by removal of ethanol from the original filtrate, acidification to pH 1, and extraction with ethyl acetate. Workup in the usual manner and recrystallization from ethyl acetate – hexane gave 2.33 g (77%), mp 99–100°C.

L-α-*Aminoadipic Acid* α-*Benzhydryl Ester (14)*

L-α-Aminoadipic acid (2.65 g, 16.5 mmol) and *p*-toluene-

sulfonic acid monohydrate (3.29 g, 17.3 mmol) were dissolved in water (20 mL), with warming. The solvent was removed under reduced pressure, and the residue was recrystallized from acetone–methanol(1:1)–ether: 5.40 g (98%). The L-α-aminoadipic acid *p*-toluenesulfonate (5.32 g, 16.0 mmol) was dissolved in reagent grade dimethylformamide (8 mL) at 40°C, and diphenyldiazomethane (3.10 g, 16.0 mmol), in dimethylformamide (4 mL), was added in several portions over 5 min, with vigorous stirring. Evolution of gas occurred, and the red colour faded rapidly to a faint yellow (29). After a further 5 min of stirring, sodium acetate (4 g) in water (20 mL) was added, and the product crystallized out. After standing overnight at 4°C, the product was collected, washed thoroughly with water and ether, and dried: 2.49 g. The aqueous phase of the washings was evaporated to dryness *in vacuo*, and the residue was redissolved in water (50 mL). A second crop of product was collected and washed with aqueous potassium phosphate (pH 7) to remove traces of aminoadipic acid. The combined yield was 3.24 g (60%), mp 124–128°C. This was raised to 133–134.5°C after brief boiling in absolute ethanol. The aqueous washings of the reaction were combined, concentrated, the pH adjusted to 3, and three volumes of methanol were added to give 0.29 g (11%) of L-α-aminoadipic acid.

Analytical tlc of the aminoadipic acid benzhydryl ester (silica gel 60, ninhydrin) showed single spots in (*a*) water–methanol–pyridine (1:2:1), $R_f = 0.61$ (yellow spot); (*b*) 95% ethanol – concentrated aqueous ammonia (10:1), $R_f = 0.13$ (violet spot); (*c*) 95% ethanol – glacial acetic acid (20:1), $R_f = 0.61$ (yellow spot). Under the same conditions, α-aminoadipic acid showed R_f values of 0.52, 0.71, 0.14, respectively. $[\alpha]_D = -11°$ (*c* 2, CH_3OH, 0.1 dm cell, with 1 equiv. of *p*-toluenesulfonic acid monohydrate added); ir (KBr): 1747 cm^{-1} (ester); ^{1}Hmr (DMSO-d_6 + TMS, Fourier transform)[4]: 7.36 (10H, m), 6.79 (1H, s), 3.60–3.33 (1H, m), 2.38–2.03 (2H, m), 1.75–1.33 (4H, m). *Anal.* calcd. for $C_{19}H_{21}NO_4$: C 69.70, H 6.47; found: C 68.95, H 6.46.

N-BOC-L-α-aminoadipic acid α-Benzhydryl Ester δ-Dicyclohexylammonium Salt

L-α-Aminoadipic acid α-benzhydryl ester (1.635 g, 5.00 mmol) was suspended in methanol (10 mL). A clear solution resulted when dicyclohexylamine (1.04 mL, 5.25 mmol) was added. Then BOC-ON (1.30 g, 5.25 mmol, 1.05 equiv.) was added, and the pale yellow solution was stirred at room temperature for 24 h. The methanol was then removed *in vacuo*, diethyl ether (50 mL) was added, and, after chilling at −20°C, the precipitated product was collected, washed with ether, and dried: 2.26 g (75%), mp 153.0–155.5°C, raised to 156.5–157.5°C after one recrystallization from ethanol–ether. $[\alpha]_D = -20.5°$ (*c* 2, methanol, 0.1 dm cell); ir (KBr): 1740 (ester), 1700 cm^{-1} (urethane); ^{1}Hmr (free acid[5]): 11.3–10.9 (1H, br s, exchanges with D_2O), 7.33 (10H, s), 6.95 (1H, s), 5.20 (1H, d, 7.8, exchanges with D_2O), 4.70–4.13 (1H, m, unaltered with D_2O), 2.57-2.13 (2H, m), 1.97–1.57 (4H, m), 1.42 (9H, s).

Analytical tlc (silica gel): the free acid showed a single spot (R_f 0.74) in 95% ethanol – glacial acetic acid (20:1), visible with short wave uv, and positive to ninhydrin after treatment with one drop of concentrated hydrochloric acid. *Anal.* calcd. for $C_{36}H_{52}N_2O_6$: C 71.02, H 8.61; found: C 70.67, H 8.74.

D-*Valine Benzhydryl Ester* p-*Toluenesulfonic Acid Salt (29)*

D-Valine (1.0 equiv.) and *p*-toluenesulfonic acid monohydrate (1.05 equiv.) were dissolved in water. The solution was evaporated to dryness under reduced pressure, and the residue recrystallized from warm acetone–ether. The salt (5.83 g, 20 mmol) was dissolved in reagent grade dimethylformamide (5 mL), and the solution was warmed to approximately 50°C. Crude diphenyldiazomethane (DDM) (5.82 g, 30 mmol) was mixed with sufficient dimethylformamide to make 7.5 mL of solution and this solution was then added slowly (one drop every 4–5 s) to the vigorously stirred solution of the amino acid salt. Evolution of gas occurred, with the red colour fading immediately to faint yellow. The red colour began to persist as 1 equiv. of DDM was approached, and persisted for some minutes at slightly more than 1 equiv. The solution was then transferred to a 250 mL flask, and 150 mL of diethyl ether were added. A white solid precipitated immediately from the faintly pink solution. After chilling overnight at −20°C, the product was collected by filtration, washed with ether, and dried *in vacuo*. It was then recrystallized from absolute methanol – anhydrous diethyl ether, giving 7.43 g (81%, lit. (29) 77% with a different work-up), mp 175.5–177.0°C (lit. (26) 170–171°C, from acetonitrile); ir (KBr): 1743 cm^{-1}; ^{1}Hmr ($CDCl_3$): 7.68 (2H, d, 8.2), 7.1–7.5 (10H, m), 6.8–7.1 (3H, m), 4.0 (1H, d, 3.6), 2.05–2.50 (4H, m), 0.82 (3H, d, 6.8), 0.80 (3H, d, 7.0); $[\alpha]_D = +20.2°$ (*c* 2, CH_3OH, 0.1 dm cell).

N-*BOC-D-valine Benzhydryl Ester*

D-Valine benzhydryl ester *p*-toluenesulfonic acid salt (2.28 g, 5.0 mmol) was suspended in ethyl acetate (15 mL), and triethylamine (0.73 mL, 5.25 mmol), followed by BOC-ON (1.35 g, 5.50 mmol), were added. The mixture was stirred for 23 h at room temperature, and then extracted successively with 10% potassium hydrogen sulfate (2 × 20 mL), saturated sodium chloride (1 × 20 mL), 5% sodium carbonate (2 × 20 mL), and saturated sodium chloride (1 × 20 mL). The organic phase was dried over anhydrous magnesium sulfate and evaporated to give an oil which crystallized upon seeding and scratching. The crude product was recrystallized from methanol to give 1.39 g (72%) of white needles, mp 110–111°C. A further 0.28 g was obtained by addition of water to the methanol mother liquor, mp 109–110.5°C (total yield 87%); $[\alpha]_D = +19.5°$ (*c* 2, $CHCl_3$); ir (KBr): 3370(s), 1727(s), 1697(s); ^{1}Hmr: 7.28 (10H, s), 6.90 (1H, s), 5.03 (1H, d, J = 9 Hz, exchanges with D_2O), 4.33 (1H, q, 9,4; D_2O: d, J = 4 Hz), 2.5–1.8 (1H, m), 3.08 (9H, s), 0.92 (3H, d, 8), 0.80 (3H, d, 8). *Anal.* calcd. for $C_{23}H_{29}NO_4$: C 72.03, H 7.62; found: C 71.90, H 7.62.

Deprotection of N-*BOC-D-valine Benzhydryl Ester*

To a mixture of trifluoroacetic acid (10.5 mL, distilled from phosphorous pentoxide) and anisole (1.1 mL, distilled *in vacuo* from anhydrous calcium chloride) was added *N*-BOC-D-valine benzhydryl ester (1.34 g, 3.5 mmol). The material dissolved immediately, with evolution of gas, to give a clear yellow solution. This was stirred for 1 h at room temperature, during which time a yellow precipitate formed. The trifluoroacetic acid was removed *in vacuo*, and the residue was dissolved

[4]The compound was insufficiently stable under acidic ($CDCl_3$ + 1 drop CF_3COOH) or basic (D_2O + Na_2CO_3 + DSS) conditions for a successful nmr, and was poorly soluble under neutral conditions.

[5]The free acid was generated by partition of the salt (0.61 g, 1 mmole) between ethyl acetate (5 mL) and 10% aqueous potassium hydrogen sulfate (5 mL). The aqueous phase was removed, and the organic phase was washed a second time with aqueous acid (5 mL), once with saturated sodium chloride solution (5 mL), and dried over sodium sulfate. After removal of the solvent *in vacuo* and trituration of the residual oil with petroleum ether, the free acid solidified and was collected: 0.42 g (98%). Treatment of an ether solution of the acid with dicyclohexylamine regenerated the original salt, indicating that no ester isomerization had occurred.

in ether (75 mL). The trifluoroacetic acid salt of D-valine did not precipitate, and the ether solution was, therefore, concentrated to 20 mL and extracted with water (2 × 50 mL). The combined aqueous extracts were back-extracted once with ether (20 mL), and evaporated *in vacuo* to give about 1 mL of clear, colourless oil. This was diluted to about 5 mL with water, and pyridine was added dropwise until the pH (initially about 0) was raised to 5–6. Absolute ethanol (10 mL) was added, and the precipitated D-valine was collected after chilling at 5°C for several hours: 0.27 g (67%). The material was identical to authentic valine on thin layer chromatography (R_f 0.61 on silica gel in 2:1 isopropanol–water, ninhydrin, with the sample applied in aqueous TFA), and by ^{1}Hmr; $[\alpha]_D = -46°$ (*c* 1, glacial acetic acid, 0.1 dm cell) (lit. (30) $[\alpha]_D = +47.2°$ for the L-isomer).

N-*BOC*-S-*trityl*-L-*cysteine Dicyclohexylammonium Salt*

L-Cysteine hydrochloride hydrate (2.64 g, 15 mmol) was converted to the anhydrous form by dissolution in 15 mL of absolute methanol followed by evaporation to dryness *in vacuo*. The procedure was repeated twice with chloroform to yield cysteine hydrochloride. Trityl alcohol (3.90 g, 15 mmol) and anhydrous trifluoroacetic acid (27 mL) were added and the mixture, which had immediately turned dark red, was stirred at room temperature for 15 min. Some insoluble material was still present, and the trifluoroacetic acid was, therefore, removed under reduced pressure and the procedure repeated with a further 10 mL. After an additional 15 min, no insoluble material remained. The solvent was removed *in vacuo* at room temperature to yield a yellow foam. Anhydrous diethyl ether (25 mL) was added and the solution was evaporated. This ether addition–evaporation was repeated, and saturated aqueous sodium bicarbonate (50 mL) was then added to the foam, which was transformed into a flocculent white precipitate. After refrigeration overnight, this was collected and dried to yield crude *S*-trityl-L-cysteine, which was used without purification in the next step.

The *S*-trityl-L-cysteine was dissolved in a mixture of dioxane (10 mL) and water (5 mL) with the aid of 10 *N* sodium hydroxide. The final pH was 10.2. BOC-ON (Aldrich, 4.06 g, 16.5 mmol) in dioxane (5 mL) was added in one portion, and the pH was returned to 10.2 with sodium hydroxide. The solution was then stirred for 6 h at room temperature. The pH fell only very slowly during this period (10.2 to 9.9). No further base was added. The dioxane was then removed *in vacuo* to yield a viscous yellow solution. Water (30 mL) was added, and the mixture was extracted with diethyl ether (2 × 30 mL) and acidified to pH 3 by addition of solid citric acid. The acidified solution was extracted with ether (3 × 30 mL), and these latter extracts were combined, dried over magnesium sulfate, and dicyclohexylamine (15 mmol, 2.98 mL) in ether (5 mL) was added. A white precipitate formed immediately. After refrigeration at −20°C for 1 day, the product was collected and dried *in vacuo*: 7.83 g (84%), mp 211–212°C (dec.) (lit. (31) mp 210–211°C); $[\alpha]_D$ +23° (0.1 dm cell, *c* 1, methanol) (lit. (31) $[\alpha]_D$ +23.8°); ir (KBr): 3238, 1698, 1624 cm^{-1} (salt); ^{1}Hmr (free acid): 9.5 (1H, m), 7.5–6.9 (15H, m), 4.8 (1H, m), 4.1 (1H, m), 2.60 (2H, d, 5.5), 1.40 (9H, s).

Alternatively, *S*-tritylcysteine (1.093 g, 3 mmol) was suspended in chloroform (6 mL), and dicyclohexylamine (0.66 mL, 3.3 mmol, 99% pure) was added to yield a clear solution. BOC-ON (Aldrich, 0.81 g, 3.3 mmol) was added in one portion, and the solution was stirred at room temperature for 18 h. The chloroform was then removed under reduced pressure to yield a viscous yellow oil, to which was added diethyl ether (50 mL). After chilling at −20°C, the white precipitate was collected, washed with ether, and dried to give 1.782 g (96%) of product, mp 207–211°C; $[\alpha]_D = +23.8°$ (*c* 1, CH_3OH, 1.0 dm cell).

Bis-N-*BOC*-L-*cystinyl-bis*-D-*valine Bisbenzhydryl Ester (7)*

N-BOC-*S*-trityl-L-cysteine dicyclohexylammonium salt (3.04 g, 4.9 mmol) was converted to the free acid by partition between ethyl acetate (25 mL) and 10% aqueous potassium hydrogen sulfate (25 mL), followed by a second washing of the organic phase with aqueous potassium hydrogen sulfate, and then brine (25 mL). The organic layer was dried over anhydrous sodium sulfate, and to the solution was added D-valine benzhydryl ester *p*-toluenesulfonic acid salt (2.46 g, 5.39 mmol, 1.1 equiv.), *N*-methylmorpholine (0.55 g, 5.39 mmol), EEDQ (1.27 g, 5.15 mmol, 1.05 equiv.), and ethyl acetate (25 mL). After 2 days at room temperature, the solution was washed successively with 10% aqueous potassium bisulfate (3 × 40 mL), saturated sodium chloride (1 × 40 mL), saturated sodium bicarbonate (2 × 40 mL), and saturated sodium chloride (1 × 40 mL). It was then dried over anhydrous sodium sulfate and evaporated to yield a foam: 3.51 g (98% crude yield).

To a solution of the foam (3.29 g, 4.52 mmol) in methanol (20 mL) and pyridine (1 mL, 12 mmol) was added a solution of iodine (1.20 g, 4.73 mmol, 1.05 equiv.) in methanol (10 mL). A precipitate began to form within 2 min, and additional methanol (20 mL) was added to facilitate stirring. After 1 h of stirring at room temperature, the precipitate was collected and washed with methanol. To the filtrate was added 10% aqueous sodium bisulfite to destroy residual iodine. The filtrate was concentrated *in vacuo*, and additional sodium bisulfite was added to yield a precipitate, which was collected and combined with the first precipitate. The crude product (the dipeptide disulfide and trityl methyl ether) was dissolved in chloroform (60 mL), washed once with water (20 mL), dried over anhydrous sodium sulfate, and evaporated. Petroleum ether (30 mL) was added to the residual white solid, and the dipeptide was recovered by filtration, after grinding of the powder with the solvent: 1.90 g. Recrystallization from chloroform–methanol gave 1.66 g (75% from *N*-BOC-*S*-trityl-L-cysteine), mp 167–169°C, $[\alpha]_D = +30°$ (*c* 2, $CHCl_3$, 0.1 dm cell). The material travelled as a single spot, R_f 0.80, on aluminum-backed silica gel G plates in 1:1 ethyl acetate – petroleum ether, visible with short wave ultraviolet; not positive to ninhydrin, but became positive after heating with a drop of trifluoroacetic acid (yellow spot); ir (KBr): 3330, 3310, 1734 (ester), 1677 (urethane), 1646 cm^{-1} (amide); ^{1}Hmr: 7.44 (1H, d, J = 10 Hz, exchanges with D_2O), 7.26 (10H, s), 6.88 (1H, s), 5.54 (1H, d, J = 9 Hz, exchanges with D_2O), 4.88–4.52 (2H, m), 3.02–2.92 (2H, m), 2.45–2.00 (1H, m), 1.42 (9H, s), 0.90 (3H, d, J = 7 Hz), 0.84 (3H, d, J = 7 Hz). *Anal.* calcd. for $C_{52}H_{66}N_4S_2O_{10}$: C 64.30, H 6.85; found: C 64.25, H 7.08.

L-*Cystinyl-bis*-D-*valine*

To a mixture of trifluoroacetic acid (10 mL, distilled from phosphorus pentoxide) and anisole (1.0 mL, distilled *in vacuo* from anhydrous calcium chloride) was added 7 (1.65 g, 1.70 mmol). The material dissolved immediately, with evolution of gas, to give a clear, yellow solution. This was stirred for 1 h at room temperature, during which time a yellow precipitate formed. The trifluoroacetic acid was removed *in vacuo*, and ether (60 mL) was added to the residue. A precipitate formed, but it dissolved immediately upon the addition of water (40 mL). After agitation of the mixture, the aqueous phase was removed, and the ether phase was extracted a second time with water (40 mL). The combined aqueous extracts were evaporated *in vacuo* to yield a glassy foam. This was dissolved in water (4 mL), and pyridine was added dropwise until the pH

(initially about 0) was raised to 5–6. A white precipitate formed almost immediately. Absolute ethanol (8 mL) was added, and the precipitated L-cystinyl-bis-D-valine was collected after chilling at 5°C for several hours: 0.63 g (85%); $[\alpha]_D = +88°$ (*c* 2, 2 *N* HCl, 0.1 dm cell); ir (KBr): 1687, 1630, 1570–1510 cm^{-1}; ^{1}Hmr (trifluoroacetic acid + TMS): 8.3–7.3 (4H, m, contains d, $J = 8$ Hz; all exchange with TFA-*d*), 5.2–4.6 (2H, m, contains q, $J = 4.5$ Hz, 8 Hz: with TFA-*d*, 2H, m, contains d, $J = 4.5$ Hz), 3.50 (2H, d, 6), 2.8–2.0 (1H, m), 1.13 (6H, d, 6). Analytical tlc (silica gel): R_f 0.58 (applied as the trifluoroacetate salt; 2:1 isopropanol–water), 0.17 (applied as the free dipeptide in water; *n*-butanol – acetic acid – water, 4:1:4). The compound was visible with short wave uv, and gave a yellow spot with ninhydrin. *Anal.* calcd. for $C_{16}H_{30}N_4O_6S_2 \cdot 2H_2O$: C 40.49, H 7.22, N 11.81; found: C 40.42, H 6.96, N 11.57.

N,S-*Dityrityl*-L-*cysteine*

S-Tritylcysteine (3.63 g, 10 mmol) was suspended in methylene chloride (30 mL), and the mixture was cooled in ice. A homogeneous solution resulted when diisopropylamine (3.0 mL, 21 mmol, distilled from potassium hydroxide) was added. Solid triphenylmethyl chloride (2.93 g, 10.5 mmol, recrystallized from benzene plus acetyl chloride) was then added in five portions over 10 min, with continued cooling, and the solution was stirred for 2.5 h at room temperature. Additional methylene chloride (10 mL) was added at 90 min to facilitate the stirring. The solvent was removed under reduced pressure and the residue was triturated with water (100 mL) for 1 h. Then additional water (50 mL) and diethyl ether (50 mL) were added, whereupon the insoluble material solidified, 5.92 g. Recrystallization from hot chloroform – diethyl ether yielded 5.07 g (72%) of off-white solid, mp 169–175°C (dec.).

For conversion to the free acid, the salt (2.00 g, 2.83 mmol) was partitioned between ethyl acetate (30 mL) and 5% aqueous potassium hydrogen sulfate (20 mL). The organic phase was washed again with potassium bisulfate (20 mL), water (20 mL), and then dried over anhydrous sodium sulfate and evaporated. The residual oil was triturated with petroleum ether, to yield 1.68 g (98%) of the free acid as an amorphous solid, mp 111–119°C (dec.). This was crystallized from benzene – petroleum ether: 1.59 g (93%), mp 116–118°C (dec.) (lit. (17) mp 125–128°C); $[\alpha]_D = +71°$ (*c* 1, CH_3OH) (lit. (17) $[\alpha]_D = +70°$); ir (KBr): 1703 cm^{-1}; ^{1}Hmr (CCl_4 + TMS): 7.9–6.5 (30H, m), 3.47–3.03 (1H, m), 2.60–2.23 (2H, m).

N,S-*Dityrityl*-L-*cysteine* N-*Hydroxysuccinimide Ester (**10**)*

N,S-Dityrityl-L-cysteine (2.88 g, 4.75 mmol) and *N*-hydroxysuccinimide (0.60 g, 5.23 mmol, 1.1 equiv.) were dissolved in dimethoxyethane (4 mL). The solution was cooled in ice, and dicyclohexylcarbodiimide (1.08 g, 5.23 mmol, 1.1 equiv.) in dimethoxyethane (2 mL) was added, followed by more dimethoxyethane (2 mL). Dicyclohexylurea began to precipitate almost immediately. The solution was warmed to room temperature by allowing the ice to melt, and was stirred for a total of 19 h. The urea was then collected, washed with dimethoxyethane and dried (1.12 g, 96% of theory). Evaporation of the mother liquors afforded a golden oil which solidified, upon scratching and chilling with isopropanol (20 mL), to give, after drying *in vacuo*, 3.73 g of a pale yellow solid (20). The ^{1}Hmr spectrum of this material indicated the presence of between one and two solvated molecules of isopropanol. The crude product was recrystallized from benzene – petroleum ether (17) to give 2.94 g of white crystals (79%, lit. (17) 89%, one benzene molecule solvate), mp 119–125°C (dec.) (lit. (17) mp 130°C), $[\alpha]_D = +62°$ (*c* 2, $CHCl_3$) lit. (17) $[\alpha]_D = +64°$); ir (KBr): 1796(w), 1763(m), 1730(s); ^{1}Hmr: 7.7–6.9 (36H, m, approximately 6H removable by evaporation of the nmr sample), 4.0–3.5 (1H, m), 2.8–2.3 (7H, m, 1H exchanges with D_2O).

Rotation of N,S-*Dityrityl*-L-*cysteine* N-*Hydroxysuccinimide Ester in Ethyl Acetate Containing Triethylamine*

Two solutions of *N,S*-dityrityl-L-cysteine *N*-hydroxysuccinimide ester (50 mg/mL) in 9:1 (v:v) ethyl acetate – triethylamine were prepared. To one of these was added 1 equiv. (5 mg/mL) of 1,2,4-triazole. Each solution was kept at room temperature, and its optical rotation was measured periodically. The results are shown in Table 1.

In tetrahydrofuran in the presence of triethylamine, *N*-carbobenzoxy-*S*-benzyl-L-cysteine *N*-hydroxysuccinimide ester is reported (22) to have a second order racemization rate constant, $K_{rac} = 4.88 \times 10^{-3} M^{-1}$ s^{-1}. This would result in almost total racemization within 20 min.

S-*Trityl*-L-*cysteinyl*-D-*valine Benzhydryl Ester Hydrochloride*

D-Valine benzhydryl ester *p*-toluenesulfonic acid salt (1.51 g, 3.3 mmol, 1.2 equiv.) was partitioned between ethyl acetate (6 mL) and 5% sodium carbonate (6 mL). The aqueous phase was separated, and the organic phase was washed once with saturated sodium chloride (6 mL) and dried over anhydrous sodium sulfate. The solution was then mixed with *N,S*-dityrityl-L-cysteine *N*-hydroxysuccinimide ester (2.15 g, 2.75 mmol), and ethyl acetate (4 mL), triethylamine (0.38 mL, 2.75 mmol), and 1,2,4-triazole (0.19 g, 2.75 mmol) were added. The solution was stirred at room temperature for 36 h and then, after dilution with ethyl acetate (10 mL), was washed successively with 10% potassium hydrogen sulfate (3 × 20 mL) saturated sodium chloride (1 × 20 mL), saturated sodium bicarbonate (3 × 20 mL), and saturated sodium chloride (1 × 20 mL). It was then dried over anhydrous sodium sulfate and evaporated to give 2.50 g of a foam. Analytical chromatography on silica gel (ethyl acetate – petroleum ether – pyridine 50:40:10) showed a major uv positive spot at R_f 0.88, and minor spots at R_f 0.70, 0.15. The crude product (**8**) was detritylated without purification.

The crude dipeptide (2.50 g) was dissolved in reagent grade glacial acetic acid (16 mL), and water (4 mL) was added dropwise with stirring (32). A white gum precipitated during the course of the addition. After the addition of the water, the mixture was agitated for 1 h, and by this time the gum had partially dissolved. The clear supernatant was decanted and retained. The gum was redissolved in acetic acid (16 mL), and a clear homogeneous solution resulted when this was added dropwise to the supernatant. Water (4 mL) was added dropwise to the mixture and the resulting clear solution was stirred for an additional 30 min at room temperature. More water (28 mL) was then added slowly, and the precipitated triphenylmethanol was removed by filtration and dried (0.71 g, 99% of theory). The cloudy filtrate was evaporated *in vacuo* below 35°C to give a clear oil which was dissolved in ethyl acetate (100 mL). This solution was washed with saturated sodium bicarbonate (2 × 100 mL), saturated sodium chloride (1 × 50 mL), dried over anhydrous sodium sulfate, and concentra-

TABLE 1. Optical rotation measurements

Time (h)	$[\alpha]_D$ (no triazole) (°)	Time (h)	$[\alpha]_D$ (triazole added) (°)
0	+36.4	0	+40.6
1	+36.2	0.75	+41.8
2	+37.0	4.5	+42.0
11	+37.6	24	+41.4
35	+39.2	52	+41.2

ted *in vacuo* to about 20 mL. A solution of hydrogen chloride in absolute ethanol (2.38 *M*, 1.20 mL, 1.05 equiv.) was added dropwise with shaking, and the solvent was removed *in vacuo* to give a foam which solidified upon trituration with petroleum ether (20 mL): 1.50 g (82%) of the dipeptide ester hydrochloride, mp 80–98°C (dec.); $[\alpha]_D = +26°$ (*c* 2, $CHCl_3$); ir (KBr): 1728 (ester), 1680 cm^{-1} (amide); ^{1}Hmr: 8.8–7.6 (4H, m, exchanges with D_2O), 7.6–6.9 (25H, m), 6.82 (1H, s), 4.8–4.4 (1H, m; D_2O d, $J = 4.5$ Hz), 4.3–3.7 (1H, m; D_2O shifted to 4.0–3.6δ), 3.0–2.6 (2H, m), 2.5–1.9 (1H, m), 0.9–0.6 (6H, m).

*Fully Protected ACV (**9**)*

N-BOC-α-benzhydryl-L-α-aminoadipic acid, freed from the dicyclohexylamine salt (853 mg, 1.4 mmol) in the usual manner, was mixed with *S*-trityl-L-cysteinyl-D-valine benzhydryl ester hydrochloride (928 mg, 1.4 mmol) in ethyl acetate (5 mL). Triethylamine (0.195 mL, 1.4 mmol), and EEDQ (371 mg, 1.5 mmol) were added, and the mixture was stirred at room temperature for 30 h. It was then diluted with ethyl acetate (5 mL), and extracted successively with 10% potassium hydrogen sulfate (2 × 5 mL), saturated sodium chloride (1 × 5 mL), saturated sodium bicarbonate (2 × 5 mL), and saturated sodium chloride (1 × 5 mL). After drying of the organic phase over anhydrous sodium sulfate, evaporation yielded a foam, which solidified upon trituration with petroleum ether: 1.24 g. The crude product was recrystallized from ethyl acetate – petroleum ether to give 0.95 g (65%) of fully protected ACV, mp 97.5–101°C; $[\alpha]_D = -8°$ (*c* 2, $CHCl_3$); ir (KBr): 1736(s), 1704(w), 1680(m), 1647(s) cm^{-1}; ^{1}Hmr: 7.6–7.1 (35H, m), 6.89 (2H, s), 6.63 (1H, d, $J = 9$ Hz, exchanges with D_2O), 4.55 (1H, q, 9,4; D_2O d, $J = 4$ Hz), 4.4–3.9 (2H, m), 2.8–2.5 (2H, m), 2.2–1.1 (16H, m), 0.85 (3H, d, 7.5), 0.73 (3H, d, 7.5). Analytical tlc (silica gel): R_f 0.78 (50:50 petroleum ether – ethyl acetate), 0.63 (60:35:5 petroleum ether – ethyl acetate – diethylamine). The compound was visible with short wave uv, was negative to ninhydrin, and became positive to ninhydrin after heating with a drop of trifluoroacetic acid. *Anal.* calcd. for $C_{64}H_{67}N_3O_8S$: C 74.03, H 6.51, N 4.05, S 3.09; found: C 74.13, H 6.76, N 3.89, S 3.27.

*Detritylation of **9***

Fully protected ACV (2.08 g, 2.00 mmol) was dissolved in ethyl acetate (20 mL), and methanol (40 mL) was added with stirring. Pyridine (0.65 mL, 8 mmol), followed by iodine (0.517 g, 2.04 mmol), in methanol (5 mL), were added, and the mixture was allowed to stand for 1 h at room temperature. No precipitate had formed by this time, and analytical tlc indicated that the reaction was proceeding more slowly than expected. The solution was therefore concentrated to a volume of 10 mL, and methanol (30 mL) was added. A precipitate began to form within 2 h, and it was collected after additional stirring for 23 h. The solid was washed with methanol and then dissolved in chloroform (20 mL), and decolourized by shaking with 10% aqueous sodium bisulfite (20 mL). Evaporation of the methanol washings yielded 102 mg (5%) of unreacted **9**, mp 98–105°C. The chloroform layer was separated, and the aqueous phase was extracted with additional chloroform (10 mL). The combined chloroform extracts were dried over anhydrous sodium sulfate, filtered, and evaporated to yield a foam: 1.37 g. Trituration of the foam with petroleum ether removed trityl methyl ether and gave 1.13 g of solid, which was recrystallized from methanol to yield the product: 1.02 g (64%), mp 139–140.5°C; $[\alpha]_D = +7°$ (*c* 2, $CHCl_3$, 0.1 dm cell); ir (KBr): 1736(s), 1710(m), 1680(m), 1638(s) cm^{-1}; ^{1}Hmr: 8.46 (1H, d, $J = 9$ Hz), 7.5–7.1 (20H, m), 6.87 (2H, s), 6.53 (1H, d, 8), 5.6–5.4 (1H, br s), 5.15 (1H, d, 8, exchanges with D_2O), 4.7–4.5 (1H, m), 4.5–4.25 (1H, br s), 3.1–2.8 (2H, m), 2.4–1.3 (16H, m), 1.10–0.80 (6H, m). Analytical tlc (silica gel): R_f 0.71 (50:50 petroleum ether – ethyl acetate), 0.79 (19:1 methanol–diethylamine). The compound was revealed with short wave uv, and became ninhydrin-positive after treatment with trifluoroacetic acid. No other spots were revealed with either treatment. *Anal.* calcd. for $C_{90}H_{104}N_6O_{16}S_2$: C 68.00, H 6.59, N 5.29, S 4.03; found: C 67.46, H 6.66, N 5.19, S 4.17.

ACV Disulfide

To a mixture of trifluoroacetic acid (3.6 mL, distilled from phosphorous pentoxide) and anisole (0.36 mL, distilled *in vacuo* from anhydrous calcium chloride) was added bis-δ-(*N*-BOC-L-α-aminoadipyl)-L-cystinyl-bis-D-valine tetrabenzhydryl ester (639 mg, 0.4 mmol). The material dissolved immediately, with evolution of gas, to give a clear, yellow solution. A yellow precipitate formed within a few minutes. The mixture was stirred for 1 h at room temperature. The trifluoroacetic acid was then removed *in vacuo* below 30°C, and the residual yellow slurry was dissolved in water (10 mL) and diethyl ether (20 mL). The aqueous phase was removed, filtered to remove a small amount of solid, and the ether phase was washed again with water (5 mL). The combined aqueous fraction was concentrated *in vacuo* below 30°C to about 1 mL, and then further under high vacuum overnight to 0.5 g of a glassy foam. This was dissolved in water to give about 2 mL of solution, and the pH was adjusted to 2.9 with 10% aqueous pyridine. A precipitate formed quickly, and the mixture was diluted to 10 mL with absolute ethanol. After 6 h at 4°C, the precipitate was collected and dried *in vacuo*: 240 mg (83%) of white crystalline solid, mp 236–237°C (dec.); $[\alpha]_D = -11°$ (*c* 2, 2 *N* HCl) (lit. (8) $[\alpha]_D = -9.5°$ (*c* 2, 2 *N* HCl)); ir (KBr): 1700(m), 1630(s), 1520(s) cm^{-1}; ^{1}Hmr (TFA + TMS): 8.1–7.2 (5H, m; exchanges with TFA-*d*), 5.4–4.9 (1H, m; with TFA-*d*, vague triplet, $J = 6$ Hz), 4.9–4.2 (2H, m; with TFA-*d*: 1H, d, $J = 4$ Hz at 4.72δ, and 1H, m at 4.6–4.3δ), 3.5–3.0 (2H, d, $J = 6$ Hz), 2.9–1.75 (7H, m), 1.13 (6H, d, 7). Analytical tlc (silica gel): R_f 0.20 (applied as the trifluoroacetate salt; *n*-butanol – acetic acid – water 4:1:4). The compound was visible with short wave uv, and gave a red spot with ninhydrin. *Anal.* calcd. for $C_{28}H_{48}N_6O_{12}S_2 \cdot 1.5H_2O$: C 44.73, H 6.84, N 11.18, S 8.53; found: C 44.66, H 7.03, N 10.91, S 8.47.

Acknowledgements

We thank the National Research Council of Canada for financial support of this research, and the Province of Ontario and Queen's University for the award of scholarships.

1. D. J. ABERHART. Tetrahedron, **33**, 1545 (1977); E. P. ABRAHAM. *In* Recent advances in the chemistry of β-lactam antibiotics. Chemical Society Special Publication No. 28. The Chemical Society, London, Engl. 1977. p. 1.
2. D. J. MORECOMBE and D. W. YOUNG. J. Chem. Soc. Chem. Commun. 198 (1975); D. J. ABERHART, J. Y. R. CHU, and L. J. LIN. J. Chem. Soc. Perkin Trans. I, 2517 (1975).
3. N. NEUSS, C. H. NASH, J. E. BALDWIN, P. A. LEMKE, and J. B. GRUTZNER. J. Am. Chem. Soc. **95**, 3797 (1973); H. KLUENDER, C. H. BRADLEY, C. J. SIH, P. FAWCETT, and E. P. ABRAHAM. J. Am. Chem. Soc. **95**, 6149 (1973); D. J. ABERHART and L. J. LIN. J. Chem. Soc. Perkin Trans. I, 2320 (1974).
4. J. ANNÉ, H. EYSSEN, and P. DE SOMER. Arch. Microbiol. **98**, 159 (1974).
5. P. A. FAWCETT, P. B. LODER, M. J. DUNCAN. T. J. BEESLEY, and E. P. ABRAHAM. J. Gen. Microbiol. **79**, 293 (1973).

6. J. RUDINGER. Coll. Czech. Chem. Commun. **27**, 2246 (1962).
7. K. BAUER. Z. Naturforsch. **25B**, 1125 (1970).
8. P. ADRIAENS, B. MEESSCHAERT, W. WUYTS, H. VANDERHAEGHE, and H. EYSSEN. Antimicrob. Agents Chemotherapy, **8**, 638 (1975).
9. P. A. FAWCETT, J. J. USHER, J. A. HUDDLESTON, R. C. BLEANEY, J. J. NISBET, and E. P. ABRAHAM. Biochem. J. **157**, 651 (1976).
10. B. KAMBER and W. RITTEL. Helv. Chim. Acta, **51**, 2065 (1968).
11. P. W. TROWN, B. SMITH, and E. P. ABRAHAM. Biochem. J. **86**, 284 (1963).
12. J. P. GREENSTEIN. *In* Advances in protein chemistry. Vol. 9. *Edited by* M. L. Anson, K. Bailey, and J. T. Edsall. Academic Press, New York, NY. 1954. p. 122.
13. L. I. SMITH and K. L. HOWARD. Org. Synth. Coll. Vol. **III**, 351 (1955).
14. J. TAYLOR-PAPADIMITRIOU, C. YOVANIDIS, A. PAGANOU, and L. ZERVAS. J. Chem. Soc. C, 1830 (1967).
15. M. ITOH, D. HAGIWARA, and T. KAMIYA. Tetrahedron Lett. 4393 (1975).
16. R. G. HISKEY and J. B. ADAMS, JR. J. Am. Chem. Soc. **87**, 3969 (1965).
17. B. KAMBER, H. BRÜCKNER, B. RINIKER, P. SIEBER, and W. RITTEL. Helv. Chim. Acta, **53**, 556 (1970).
18. B. BELLEAU and G. MALEK. J. Am. Chem. Soc. **90**, 1651 (1968).
19. E. SCHRÖDER and K. LÜBKE. *In* The peptides. Vol. I. Academic Press, New York, NY. 1965. pp. 45–47.
20. R. G. HISKEY, L. M. BEACHAM, and V. G. MATL. J. Org. Chem. **32**, 2472 (1972).
21. H. C. BEYERMAN, W. MAASSEN VAN DEN BRINK, F. WEYGAND, A. PROX, W. KÖNIG, L. SCHMIDHAMMER, and E. NINTZ. Recl. Trav. Chim. **84**, 213 (1965).
22. J. KOVACS, G. L. MAYERS, R. H. JOHNSON, R. E. COVER, and U. R. GHATAK. J. Chem. Soc. Chem. Commun. 53 (1970).
23. W. W. CLELAND. Biochemistry, **3**, 480 (1964).
24. N. J. LEONARD and W. E. GOODE. J. Am. Chem. Soc. **72**, 5404 (1950).
25. J. W. THANASSI. J. Org. Chem. **36**, 3019 (1971).
26. S. C. WARREN, G. G. F. NEWTON, and E. P. ABRAHAM. Biochem. J. **103**, 891 (1967).
27. M. CLAESEN, A. VLIETINCK, and H. VANDERHAEGHE. Bull. Soc. Chim. Belg. **77**, 587 (1968).
28. J. P. GREENSTEIN, S. M. BIRNBAUM, and M. C. OTEY. J. Am. Chem. Soc. **75**, 1994 (1953).
29. A. A. ABODERIN, G. R. DELPIERRE, and J. S. FRUTON. J. Am. Chem. Soc. **87**, 5469 (1965).
30. J. C. SHEEHAN and V. J. GRENDA. J. Am. Chem. Soc. **84**, 2417 (1962).
31. L. ZERVAS and I. PHOTAKI. J. Chem. Soc. C, 2683 (1970).
32. B. KAMBER. Helv. Chim. Acta, **56**, 1370 (1973).

Total synthesis of 14β-hydroxy-4,9(11)-androstadiene-3,17-dione

ANDRZEJ ROBERT DANIEWSKI,[1] PETER S. WHITE, AND ZDENEK VALENTA
Department of Chemistry, University of New Brunswick, Fredericton, N.B., Canada E3B 5A3

Received February 16, 1979

ANDRZEJ ROBERT DANIEWSKI, PETER S. WHITE, AND ZDENEK VALENTA. Can. J. Chem. **57**, 1397 (1979).

The title compound **8**, a potential intermediate in the total synthesis of cardiac-active principles and other polyfunctional steroids, is prepared in nine steps using methyl vinyl ketone and 2-methylcyclohexane-1,3-dione as starting materials and acetylene and 2-methylcyclopentane-1,3-dione as additional sources of carbon atoms. In a crucial aldol condensation leading to the closure of steroid ring *C*, an efficient asymmetric induction by one chiral center leads to the establishment of three new chiral centers.

Since the total synthesis of equilenin by Bachman, Cole, and Wilds in 1939 (1), the challenge presented by the preparation of more complex steroids has led during the past forty years to spectacular advances in synthetic methodology and in synthetic regio- and stereocontrol.[2] Interest in steroid total synthesis continues unabated because of the possibility of the discovery of new compounds with important biological activity and because of the continuing challenge in finding the simplest possible synthetic pathways.

We wish to report a synthesis of dione **8** in which known (3) intermediate **5** containing one chiral center is, after the introduction of a C(6)—C(7) double bond,[3] converted by an aldol condensation into the 14β-hydroxyandrostane derivative **7** containing four chiral centers. The chiral starting material, dione **1**, is accessible in two steps from methyl vinyl ketone and 2-methylcyclohexane-1,3-dione in an asymmetric synthesis using (*S*)-proline (6, 7). Racemic **1** was used for the synthesis reported in this communication. The previously reported (8) treatment of **1** with lithium acetylide followed by hydrogenation in pyridine solution (9) gives allyl alcohol **3**.

Treatment of **3** with thionyl chloride in methylene chloride and dimethyl formamide at −60°C to −40°C gave crude chlorocompound **4** which was not purified because of its instability. Compound **4** in dimethyl formamide was treated sequentially with sodium iodide and with the sodium salt of 2-methylcyclopentane-1,3-dione in methanol. The resulting racemic trione **5**, mp 79–81°C, was obtained in 69% yield based on **3**.[4] Dehydrogenation of **5** with DDQ in dioxane containing HCl (10) gave crude triene **6** which on treatment with sodium methoxide in anhydrous methanol for 2 h at room temperature gave tetracyclic triene **7**, mp 219–225°C (dec.), in a 30% yield based on **5**.[5] No isomeric tetracyclic compound could be isolated.[5] Finally, hydrogenation of **7** with 2% Pd on $SrCO_3$ in benzene and ethanol gave (*d,l*)-**8**, mp 170–172°C, in 85% yield.

The structure of compound **8** was established by X-ray diffraction.

A four-step sequence performed on **8** and involving Li–NH_3 reduction, reoxidation of secondary alcohols,

[1]On leave of absence from the Institute of Organic Chemistry of the Polish Academy of Sciences, Warsaw, Poland.

[2]For comprehensive reviews, see ref. 2.

[3]The ring *A* aromatic analogue of **5** was, following the key discovery by Ananchenko and Torgov in 1959 (4), converted in several laboratories (5) into estrone and its derivatives in a sequence so remarkably simple that we are presently able to use an adapted estrone synthesis as a one-term preparation in an introductory undergraduate laboratory (Ž. Stojanac and G. Reid, unpublished). Unfortunately, the crucial cyclization of steroid ring *C* of this sequence does not work without the activation by the aromatic ring or an equivalent (e.g. enol ether) and the method can thus not be used as such for the synthesis of C(10)-methylated steroids.

[4]Optically active **5** is known (3). Our procedure using chloride **4**, iodide exchange, and methanol improves the yield significantly.

[5]Crude **6** contains ~20% of **5** from which it cannot conveniently be separated by chromatography. A maximum yield of 40% for the conversion **5** → **7** was realized in a longer sequence involving bromination and dehydrobromination of the enol-acetate of **5**. **6** was also prepared by an alternative sequence in which **3** was first converted by DDQ in 72% yield to 6,7-dehydro-**3**, mp 101–102°C.

0008-4042/79/111397-02$01.00/0

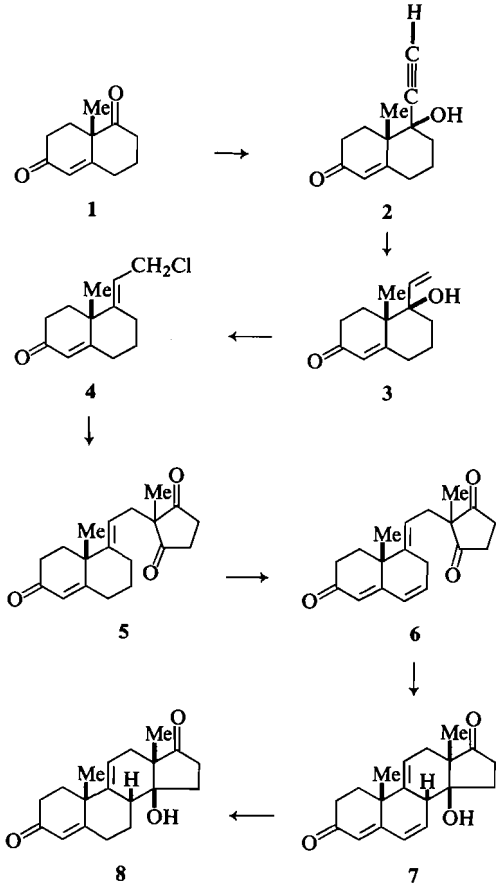

catalytic hydrogenation (Pt/HOAc), and acetylation gave racemic 3β-acetoxy-14β-hydroxyandrostan-17-one, mp 182–184°C, nmr values of which agree with those reported for the optically active compound (11).

The specificity of cyclization **6** → **7**, involving only one out of eight theoretically possible transition states, probably arises from a particularly favourable angle of attack (12) indicated in formula **9**.[6]

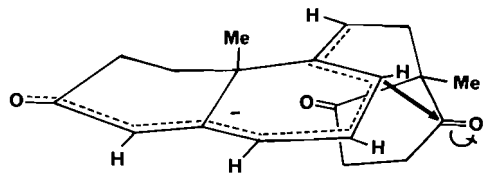

The presence of the 14β-hydroxyl group and additional functionality in compounds **7** and **8**, the relative efficiency and brevity of the synthetic sequence, and the ready availability of starting material **1** in chiral form (6, 7) should make the reported androstane derivatives suitable as intermediates in total syntheses of cardiac-active principles (13) and other polyfunctional steroids.

[6]Kinetic control of the reaction is probable, but not rigorously proven.

Acknowledgements

The authors thank the National Research Council of Canada for financial support. Useful discussions concerning many aspects of steroid chemistry with Drs. G. Saucy and N. Cohen and their colleagues in Hoffmann-La Roche Co., Nutley, New Jersey, are gratefully acknowledged.

1. W. E. Bachmann, W. Cole, and A. L. Wilds. J. Am. Chem. Soc. **61**, 974 (1939).
2. A. A. Akhrem and Yu. A. Titov. Total steroid synthesis. Am. ed. Plenum Press, New York, NY. 1970; R. T. Blickenstaff, A. C. Ghosh, and G. C. Wolf. Total synthesis of steroids. Academic Press, New York, NY. 1974; R. Pappo. *In* The chemistry and biochemistry of steroids. Intra-Science Research Foundation, Santa Monica, CA, Research Reports Vol. 3, Nos. 1 and 2, 1969. p. 123; G. Saucy and N. Cohen. MTP Int. Rev. Sci., Ser. One, **8**, 1 (1973); N. Cohen. Acc. Chem. Res. **9**, 412 (1976).
3. J. Ruppert, U. Eder, and R. Wiechert. Chem. Ber. **106**, 3636 (1973).
4. S. N. Ananchenko and I. V. Torgov. Dokl. Akad. Nauk SSSR, **127**, 553 (1959).
5. S. N. Ananchenko and I. V. Torgov. Tetrahedron Lett. 1553 (1963); D. J. Crispin and J. S. Whitehurst. Proc. Chem. Soc. London, 22 (1963); T. Miki, K. Hiraga, and T. Asako. Proc. Chem. Soc. London, 139 (1963); H. Smith, G. A. Hughes, and G. H. Douglas. Experientia, **19**, 394 (1963); T. B. Windholz, J. H. Fried, and A. A. Patchett. J. Org. Chem. **28**, 1092 (1963).
6. W. Ger. Patent 2102623. Priority date Jan. 21, 1970; Z. G. Hajos and D. R. Parrish. J. Org. Chem. **39**, 1615 (1974); J. Gutzwiller, P. Buchschacher, and A. Fürst. Synthesis, 167 (1977).
7. W. Ger. Patent 2014757. Priority date March 20, 1970; U. Eder, G. Sauer, and R. Wiechert. Angew. Chem. Int. Ed. Engl. **10**, 496 (1971).
8. I. N. Nazarov and I. A. Gurvich. Zh. Obshch. Khim. **25**, 956 (1955); M. S. Newman, S. Ramachandran, S. K. Sankarappa, and S. Swaminathan. J. Org. Chem. **26**, 727 (1961).
9. S. Swaninathan, J. P. John, and S. Ramachandran. Tetrahedron Lett. 729 (1962).
10. A. B. Turner and H. J. Ringold. J. Chem. Soc. C, 1720 (1967); C. C. Beard. *In* Organic reactions in steroid chemistry. Vol. 1. *Edited by* J. Fried and J. A. Edwards. van Nostrand Reinhold Co., New York. 1972, p. 308.
11. R. Kasai, S. Sakuma, S. Kawanishi, and J. Shoji. Chem. Pharm. Bull. Jpn. **20**, 1869 (1972); F. Sondheimer, S. Burnstein, and R. Mechoulam. J. Am. Chem. Soc. **82**, 3209 (1960).
12. H. B. Bürgi, J. D. Dunitz, J. M. Lehn, and G. Wipff. Tetrahedron, **30**, 1563 (1974); J. E. Baldwin. Chem. Commun. 734 (1976).
13. L. F. Fieser and M. Fieser. Steroids. Reinhold Publishing Corp., New York. 1959. p. 727.

Stereocontrolled Diels–Alder reactions with a bifunctional dienophile

MASATOSHI KAKUSHIMA AND DANIEL G. SCOTT

Department of Chemistry, University of New Brunswick, Fredericton, N.B., Canada E3B 5A3

Received February 5, 1979

MASATOSHI KAKUSHIMA and DANIEL G. SCOTT. Can. J. Chem. **57**, 1399 (1979).

In the Diels–Alder cycloaddition of electron-rich dienes to methyl *E*-4-oxobutenoate, the formyl group controls both regio- and stereoselectivity. Secondary overlap considerations are used to explain these results.

MASATOSHI KAKUSHIMA et DANIEL G. SCOTT. Can. J. Chem. **57**, 1399 (1979).

Lors de la cycloaddition selon Diels–Alder de dièmes riches en électrons sur l'oxo-4 buténoate de méthyle (*E*), le groupe formyle contrôle la régio- ainsi que la stéréo-sélectivité. On fait appel à des considérations de recouvrements secondaires pour expliquer ces résultats.

[Traduit par le journal]

Regioselectivity of Diels–Alder reactions has been successfully predicted by frontier molecular orbital theory in the case of relatively simple systems (1). However, controversy has arisen on the subject of the importance of secondary overlap on the stereochemical outcome of the reaction (2–4). In this communication, we hope to demonstrate how secondary overlap considerations may enhance the synthetic utility of Diels–Alder reactions.

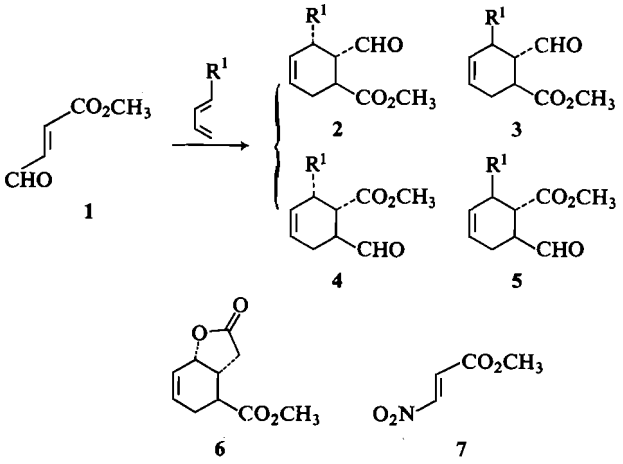

As summarized in Table 1, the addition of electron-rich dienes to methyl *E*-4-oxobutenoate (**1**) produces the isomer **2** as the major adduct.[1] It is evident that the formyl group of **1** controls regioselectivity better than the methoxycarbonyl group. Interestingly, Danishefsky *et al.* (6) have reported that the nitro group of **7** completely controls regioselectivity in such additions. The magnitudes of the LUMO coefficients at C-2 and C-3 of both **1** and **7** as listed in Table 2 agree with the observed regioselectivity. There is, however, a large difference in character between a formyl group and a nitro group: the nitro group of **7** fails to control *endo* stereoselectivity (6), while the formyl group of **1** does control it. This difference can be rationalized as follows. As shown in Table 2, the difference in the magnitudes of the LUMO coefficients at C-1 and *N* of **7** is larger than that in the magnitudes of the LUMO coefficients at C-1 and C-4 of **1**, which would normally lead to the nitro group being *endo* due to a secondary attractive

[1]The structure of **2***c* ($R^1 = OSi(CH_3)_3$) was established as follows. Hydrolysis followed by treatment with pyrrolidine gave a conjugated aldehyde: ir ($CHCl_3$) 1672, 1720, and 2720 cm^{-1}; λ_{max} (EtOH) 300 nm (log ε 4.2). Homologation of **2***c* with $(C_6H_5)_3P{=}CHOCH_3$ followed by hydrolysis gave an epimeric mixture of hemiacetals, which was then oxidized to the γ-lactone **6**: ir (CCl_4) 1730 and 1785 cm^{-1}. The overall yield of the conversion **1** → **6** is 58%. The stereochemistry of **2***b* ($R^1 = OCH_3$) and **2***c* was determined by comparison of the 220 MHz nmr spectra with the spectrum of **2***a* ($R^1 = CH_3$) (5) and both product ratios were based on the integration of the aldehydic protons. Oxidation of **2***b* with Jones' reagent followed by treatment with CH_2N_2 gave a mixture of the corresponding dimethyl esters in a ratio of 5:1.

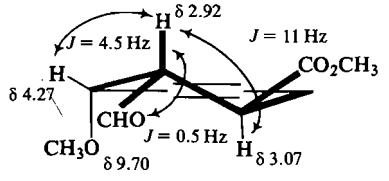

2*b*

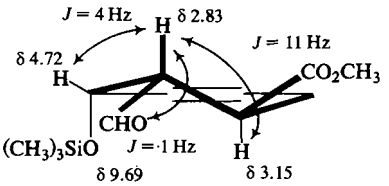

2*c*

0008-4042/79/111399-03$01.00/0

TABLE 1. The addition of 1-substituted dienes to **1**

R^1	Conditions	Total yield (%)	Product ratio (%)			
			2	**4**	**3**	**5**
CH_3	CH_2Cl_2, 40°C, 35 h	>90	54	15	9	22
OCH_3	CH_2Cl_2, 25°C, 48 h	>90	80	3	17(**3** + **5**)	
$OSi(CH_3)_3$	CH_2Cl_2, 40°C, 48 h	>90	83	17(**3** + **4** + **5**)		

TABLE 2. The computational data[a] for **1** and **7**

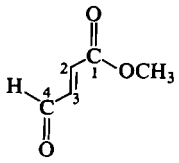

1

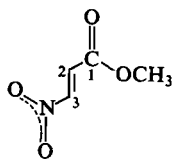

7

	LUMO					Exclusion shells			
	Eigenvalues	Eigenvectors ($2P_z$)				Gross orbital charges ($2P_z$)[b]			
Compound	(au)	C-1	C-2	C-3	C-4(*N*)	C-1	C-2	C-3	C-4(*N*)
1	0.169	0.300	0.519	−0.508	−0.343	0.927	0.996	0.951	0.937
7	0.139	0.261	0.517	−0.480	−0.360	0.939	0.942	1.024	1.228

[a]MO method: *ab initio* STO-3G (14); standardized geometrical parameters were employed (15).
[b]In units of electrons.

interaction (2), but closed-shell repulsion[2] due to the large exclusion shell[3] at *N* of **7** must counteract this attraction. The experimental results (*endo*:*exo* ≃ 1:1) (6) indicate that the closed-shell repulsion should be of the same order of magnitude as the secondary attractive interaction.[4] Since the exclusion shell at C-4 of **1** is much smaller than that at *N* of **7**, the secondary attractive interaction overcomes closed-shell repulsion and the isomer **2** is therefore preferred.

As demonstrated by the formyl group of **1**, a substituent with a large LUMO coefficient and a small exclusion shell is most likely to assume *endo* geometry. A quantitative assessment of several effects (terminal (1, 3) and secondary (2) attractive interactions and closed-shell repulsion (7)) on the stereochemical outcome of Diels–Alder reactions is clearly difficult.[5] However, careful model studies with MO calculations will make it possible to advance our understanding of cycloadditions.[7]

The combination of different electron-attracting groups on the dienophile (*E* or *Z*), as indicated above, opens a way to the stereo-specific construction of synthetically useful cyclohexenes. The preparation of several types of dienes has been reported (13).

Acknowledgments

We would like to express our sincere appreciation to Professor Z. Valenta for his encouragement, suggestions, and ample financial support. Also we thank Professor F. Grein for helping us with the computations and Mr. D. J. Burnell for enlightening discussions.

1. K. N. HOUK. J. Am. Chem. Soc. **95**, 4092 (1973); K. N. HOUK and R. W. STROZIER. J. Am. Chem. Soc. **95**, 4094 (1973); K. N. HOUK. Acc. Chem. Res. **8**, 361 (1975).
2. P. V. ALSTON, R. M. OTTENBRITE, and D. D. SHILLADY. J.

[2]Salem (7) derived an expression for the total energy of interaction as a function of the total repulsive energy due to the "exclusion shell" around each atom, and the total attractive energy, due to the mixing of occupied orbitals on one molecule with unoccupied orbitals on the other. Closed-shell repulsion has also been discussed in detail by other groups (8).

[3]Since the coefficients of $2P_z$ orbitals are discussed for attractive interactions by FMO theory (1–4), the gross orbital charges of $2P_z$ orbitals should be considered for repulsive interactions.

[4]Alston (2) has also reported that the reactions with β-nitrostyrene produce almost 1:1 mixtures of the *endo* and *exo* isomers.

[5]Other effects, such as steric attraction (9), schizophrenic tendency (10), steric (11) and attractive effects on primary bond-forming termini (12), nuclear-nuclear repulsion[6] and solvent effect, may have to be considered.

[6]A point from a referee.

[7]Details on the two opposing effects in a model system will be reported shortly.

Org. Chem. **38**, 4075 (1973); P. V. ALSTON and R. M. OTTENBRITE. J. Org. Chem. **40**, 1111 (1975); P. V. ALSTON, R. M. OTTENBRITE, and T. COHEN. J. Org. Chem. **43**, 1864 (1978); T. COHEN, R. J. RUFFNER, D. W. SHULL, W. M. DANIEWSKI, R. M. OTTENBRITE, and P. V. ALSTON. J. Org. Chem. **43**, 4052 (1978).
3. O. EISENSTEIN, J. M. LEFOUR, N. T. ANH, and R. F. HUDSON. Tetrahedron, **33**, 523 (1977).
4. I. FLEMING, J. P. MICHAEL, L. E. OVERMAN, and G. F. TAYLOR. Tetrahedron Lett. 1313 (1978).
5. M. KAKUSHIMA, J. ESPINOSA, and Z. VALENTA. Can. J. Chem. **54**, 3304 (1976).
6. S. DANISHEFSKY, M. P. PRISBYLLA, and S. HINER. J. Am. Chem. Soc. **100**, 2918 (1978).
7. L. SALEM. J. Am. Chem. Soc. **90**, 543 (1968); **90**, 553 (1968).
8. P. CARAMELLA, K. N. HOUK, and L. N. DOMELSMITH. J. Am. Chem. Soc. **99**, 4511 (1977) and references therein.
9. R. HOFFMANN, C. C. LEVIN, and R. A. MOSS. J. Am. Chem. Soc. **95**, 629 (1973).
10. K. N. HOUK, L. N. DOMELSMITH, R. W. STROZIER, and R. T. PATTERSON. J. Am. Chem. Soc. **100**, 6531 (1978).
11. F. BOHLMANN, W. MATHAR, and H. SCHWARZ. Chem. Ber. **110**, 2028 (1977).
12. R. B. WOODWARD and T. J. KATZ. Tetrahedron, **5**, 70 (1959).
13. B. M. TROST, S. A. GODLESKI, and J. IPPEN. J. Org. Chem. **43**, 4559 (1978) and references therein.
14. W. J. HEHRE, W. A. LATHAN, R. DITCHFIELD, M. D. NEWTON, and J. A. POPLE. Program No. 236, QCPE **10**, 236 (1973).
15. J. A. POPLE and M. GORDON. J. Am. Chem. Soc. **89**, 4253 (1967).

Canadian Journal of Chemistry
Published by
THE NATIONAL RESEARCH COUNCIL OF CANADA

Journal canadien de chimie
Publié par
LE CONSEIL NATIONAL DE RECHERCHES DU CANADA

Volume 57 Number 12 June 15, 1979 Volume 57 numéro 12 15 juin 1979

The thermal chemistry of vinyldiazo compounds as a method for the generation of vinylmethylenes

JAMES A. PINCOCK and KIM P. MURRAY
Department of Chemistry, Dalhousie University, Halifax, N.S., Canada B3H 4J3

Received October 30, 1978

JAMES A. PINCOCK and KIM P. MURRAY. Can. J. Chem. **57**, 1403 (1979).

The thermal chemistry of a series of substituted 1-aryl-3-methyl-2-phenyl-1-diazobut-2-enes has been examined. These vinyldiazo compounds react in two parallel pathways: cyclization to a 3-aryl-5,5-dimethyl-4-phenyl-5*H*-pyrazole or loss of nitrogen and cyclization to a 1-aryl-2-phenyl-3,3-dimethylcyclopropene presumably by a vinylmethylene intermediate. The kinetics of these processes reveal quite different substituent effects. The relation of these results to the stability of the vinylmethylene produced and to the singlet photochemistry of cyclopropene derivatives is discussed.

JAMES A. PINCOCK et KIM P. MURRAY. Can. J. Chem. **57**, 1403 (1979).

On a étudié la thermochimie d'une série d'aryl-1 méthyl-3 phényl-2 diazo-1 butènes-2 substitués. Ces composés vinyldiazo réagissent par deux voies parallèles: une cyclisation conduisant à l'aryl-3 diméthyl-5,5 phényl-4 5*H*-pyrazole ou une perte d'azote et une cyclisation en aryl-1 phényl-2 diméthyl-3,3 cyclopropène probablement par un intermédiaire vinylméthylène. Des études cinétiques de ces processus révèlent des effets de substituants importants. On discute de la relation qui existe entre ces résultats et la stabilité du vinylméthylène qui est produit ainsi que la photochimie singulet des dérivés du cyclopropène.

[Traduit par le journal]

Introduction

The photochemical reactivity of the singlet excited state of cyclopropene derivatives has generally been explained in terms of σ bond cleavage and the chemistry of the vinyl methylenes formed (1–3). However, recent results for cases with unsymmetrical substitution on the double bond (1, 2, 4, 5) have led to considerable speculation as to the effect of these substituents on ring cleavage. Some examples are summarized in reactions [1] to [4].

[1][1]

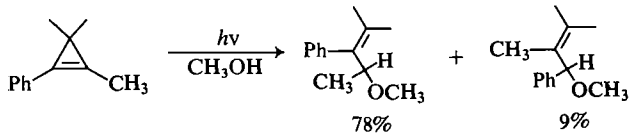

[2][2]

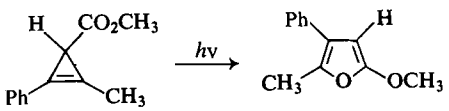

[1]Reference 1.
[2]Reference 2.

0008-4042/79/121403-08$01.00/0

[3][3]

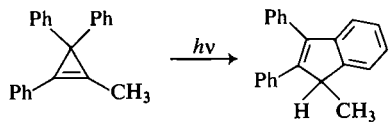

[4][4]

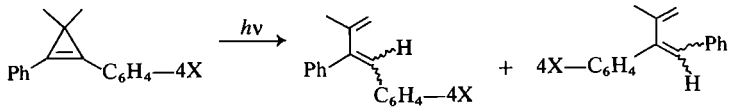

X = OCH_3	74%	26%
X = CN	<2%	98%

The first three cases indicate that σ bond cleavage is occurring on the methyl rather than the phenyl substituted side; the last example gives cleavage on the side that is substituted by the better electron donating aromatic ring. Zimmerman has suggested (4) that the reactions do not involve vinylmethylenes but rather housane biradicals.

[5]

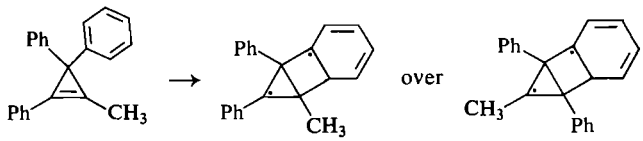

Ring cleavage is then controlled by the better delocalization of odd electron density by phenyl over methyl (note reaction [5]). This mechanism cannot apply to the cases (reactions [1] and [4]) that do not have π-systems at carbon 3. Moreover, optically active cyclopropenes (reaction [2]) have been shown to racemize photochemically (2) and this is more compatible with a planar vinylmethylene intermediate than the non-planar biradical. Padwa *et al.* (1) have invoked, among several explanations, inductive destabilization by phenyl substitution at the developing biradical formed by σ bond cleavage as the controlling factor. This explanation does not hold for Arnold's results (reaction [4]) since both methoxy and cyano should be inductively electron-withdrawing and therefore cleavage at the unsubstituted phenyl side should be preferred for both substrates. Clearly a better understanding of substituent effects on vinylmethylene stability is required before these results can be interpreted.

Besides the evidence for singlet photochemistry, vinylmethylenes have attracted considerable recent interest both on theoretical grounds (6–9) and as intermediates in the thermal (10) chemistry of cyclopropenes. As has been discussed several times their properties are expected to be complicated because there should be several low-lying states of similar energy as a result of the two free valences at the methylene carbon. These are summarized in Fig. 1.

The non-planar **1***a*, a singlet biradical, is the suggested transition state for thermal σ bond cleavage of cyclopropenes (6, 10). Although a triplet **1***a* is possible, excited triplet cyclopropenes do not in general (for some exceptions, note ref. 4) react by bond cleavage but instead dimerize (12). As well, for suitably substituted cyclopropenes, polar cleavage to zwitterion **1***b*:**1***c* might be preferred. For the planar vinylmethylene, **2**, four states are again possible: a singlet and triplet corresponding to **2***a* and two singlets **2***b* (designated 2π (6) or σ^2 (9)) and **2***c* (4π or p^2). Both calculations and esr results (13, 14) give triplet **2***a* as the most stable state. Singlet **2***a* correlates with **1***a* and is the likely first-formed intermediate in the thermal reactions of cyclopropenes (10). Padwa *et al.* have observed that a 1-methyl-2-phenylcyclopropene cleaves thermally at the phenyl substituted σ bond (1) as expected based on arguments of delocalization. The most stable singlet by calculations (6) is **2***b*. The correlation between singlet excited cyclopropenes and the possible vinylmethylenes is not as yet clear.

Vinylmethylenes can also be generated by the

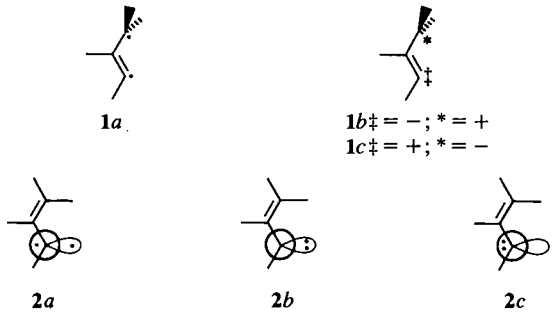

FIG. 1. Geometries and electronic configurations of vinylmethylene.

[3]Reference 4.
[4]Reference 5.

thermal decomposition of vinyldiazo compounds (3). Rate constants for this process should be directly related to vinylmethylene stabilities. This is not necessarily true for the photochemical and thermal results for cyclopropenes where the process leading to vinylmethylenes may be complicated by reversibility (2, 10). In view of this, we have examined the thermal chemistry of the vinyldiazo compounds **3***a*–**3***e* as a method of assessing substituent effects on vinylmethylene stabilities.

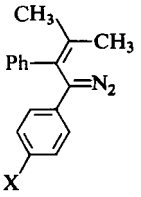

3*a* X = OCH_3
3*b* X = CH_3
3*c* X = H
3*d* X = Br
3*e* X = CN

Results and Discussion

Preparation of 1-Aryl-3-methyl-2-phenyl-1-diazobut-2-enes

As has been reported previously, vinyldiazo compounds **3** can be generated by photolysis of the corresponding 5*H*-pyrazoles **4** (3, 13). This must be done with filtered light in order to avoid photochemical decomposition of the diazo compound to 1-aryl-2-phenyl-3,3-dimethylcyclopropenes, **5**. The conversion is easily monitored by ^{1}H nmr spectroscopy and the photolysis terminated when the relative amount of **3** is at a maximum (see Experimental). The 5*H*-pyrazoles were prepared by the sequence shown in Scheme 1: **4***a*, **4***c*, and **4***e* are known (3, 13); **4***b* and **4***d* are new compounds.

[6]

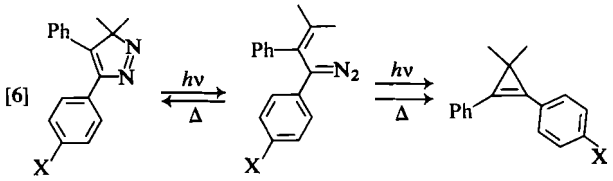

4*a*–*e* **3***a*–*e* **5***a*–*e*

Thermal Decomposition of 1-Aryl-3-methyl-2-phenyl-1-diazobut-2-enes

Initial attempts at obtaining rate constants for the thermal decomposition of **3***c* were by ^{1}H nmr spectroscopy. The sealed tube from the photolysis (see Experimental) was placed in a constant temperature bath, removed at suitable times and quenched in an ice bath. Integration then gave the ratio of **3***c*:**4***c*:**5***c*. However, the error of the integrations lead to considerable scatter in the rate plots. As well this method required ~10 mg per run and was somewhat wasteful of the pyrazole. We therefore switched to a spectrophotometric method which relied on the strong absorption bond of diarylcyclopropenes at ~330 nm ($\varepsilon > 10^4$). Since the rates were followed at temperatures (65–98°C) where solvent volatility would be a problem, sealed ampoules were used.

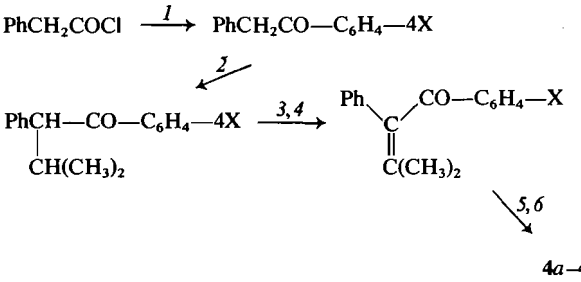

SCHEME 1. Synthesis of 1-aryl-3-methyl-2-phenyl-1-diazobut-2-enes. *1*, $AlCl_3$, C_6H_5—X; *2*, *t*-BuO^-K^+, $(CH_3)_2CHBr$; *3*, Br_2/CCl_4; *4*, LiCl/DMF; *5*, NH_2NH_2; *6*, Br_2/KOH.

The preliminary ^{1}Hmr kinetic runs indicated two facts. First from the ratio of **3***c*:**4***c*:**5***c* as a function of time, it was obvious that both **4***c* and **5***c* were products from the thermal chemistry of **3***c*. As shown in reaction [7], this is an example of the well known

[7]

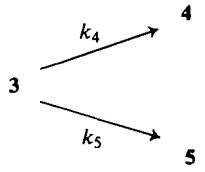

(15) first-order parallel reaction where the observed rate constant is obtained from $d[5]/dt = k_{obs}[5]$ and $k_{obs} = k_4 + k_5$. At 330 nm all these species are absorbing but, since both processes are first-order, the $A - A_\infty$ method will give values proportional to the concentration of **5**. To obtain the individual rate constants, k_4 and k_5, the product ratio must be determined separately (see Experimental).

The second feature of the preliminary runs was the obvious variation in the rate constants in benzene as solvent. However, as has been reported earlier, thermal decompositions of diazo compounds are often variable because of spurious catalysis (16). In fact, from qualitative observations, **3***c* was known to be more stable in benzene if pyridine was added (3), suggesting that trace acid is the problem. The rate of decomposition of **3***c* was therefore measured spectrophotometrically at 88.9°C in benzene with 1%, 3%, and 5% pyridine. At a given concentration of pyridine the runs were quite reproducible. The rate constants were very similar for 3 and 5% pyridine but

TABLE 1. Rate constants (k_{obs}) for the thermal decomposition of 1-aryl-3-methyl-2-phenyl-1-diazobut-2-ene (**3***a*–**3***e*) in 5% pyridine/benzene

Substrate		$k_{obs} \times 10^4$ (s^{-1})[a]			
No.	X	67.1°C	78.6°C	88.9°C	97.0°C
3*a*	4-OMe	0.96±0.06	4.3±0.2	10.7±0.4	22.8±0.8
3*b*	4-Me	0.65±0.04	2.5±0.1	7.8±0.1	13.8±0.5
3*c*	H	0.55±0.02	2.4±0.1	7.4±0.1	16.6±0.2
3*d*	4-Br	0.90±0.06	3.0±0.1	9.3±0.2	19.0±0.6
3*e*	4-CN	—	7.3±0.6	—	—

[a]Errors quoted are the mean deviation of from two to four runs.

TABLE 2. Product ratios, rate constants $k_4 \times 10^4$ (s^{-1}) and $k_5 \times 10^4$ (s^{-1}) for the thermal decomposition of **3***a*–**3***e*

	67.1°C			78.6°C			88.9°C			97.0°C		
X	%**4**	k_4	k_5	%**4**	k_4	k_5	%**4**	k_4	k_5	%**4**	k_4	k_5
4-OMe	40	0.58	0.38	47	2.3	2.0	54	5.0	5.7	49	11.7	11.1
4-Me	49	0.34	0.31	50	1.3	1.3	55	3.5	4.3	52	6.6	7.2
4-H	70	0.16	0.39	66	0.82	1.6	65	2.6	4.8	70	5.0	11.6
4-Br	70	0.27	0.63	72	0.84	2.2	68	3.0	6.3	70	5.7	13.3
4-CN	—	—	—	>95	<0.4	>6.9	—	—	—	—	—	—

about 30% greater with 1% pyridine. Therefore all other runs reported are in 5% pyridine/benzene.

Rate constants (k_{obs}) (at four different temperatures) for four of the five diazo compounds (**3***a*–**3***d*) are reported in Table 1. Photolysis of the *p*-cyano pyrazole **4***e* gives only very low concentrations of the corresponding diazo compound (13). Therefore the change in cyclopropene concentration during pyrolysis is quite small and the total absorbance change was only about 0.1. The deviation in the rate constants was obviously greater than that for all other substrates. Since this makes it difficult to obtain reliable activation parameters, this substrate was only studied at one temperature.

The ratio of the two products from the pyrolysis of **3** was obtained by careful ^{1}H nmr integration (see Experimental) and is reported as % cyclopropene (**4**) in Table 2. This allows k_{obs} to be separated into k_4 and k_5; these values are also in Table 2. Since the error in the product ratios is estimated at 5% (see Experimental) and the error in k_{obs} approximately 5%, the error in the individual rate constants is estimated at 10%. For **3***e* (4-cyano) no pyrazole product could be detected, so only an upper and lower limit for k_4 and k_5 respectively is available.

From the rate/temperature data activation parameters for both k_4 and k_5 can be calculated for **3***a*–**3***d* by the usual ln k/T vs. $1/T$ plot (Table 3). As has been discussed (ref. 17, p. 8), for a 30° temperature range and 10% error in rate constants, the error in $\Delta H^{\neq}$ is approximately 1.2 kcal M^{-1} and in $\Delta S^{\neq}$ 3 eu.

The most obvious feature of the rate constants reported in Table 2 is that the substituent effects are quite small for both k_4 and k_5. Since the errors in these values are about 10%, reliable quantitative interpretation of these effects may be difficult. However qualitatively, the trends in k_4 and k_5 are quite different. Thus as the substituents change from electron-donating to electron-withdrawing k_4 tends to decrease whereas the k_5 values go through a minimum for **3***b* (X = CH_3). The k_4 values will be discussed first.

As shown in reaction [6], k_4 represents the rate of thermal return of the diazo compound **3** to the 5*H*-pyrazole, **4**. Since this is a unimolecular ring closure, the transition state should have fewer degrees of freedom than the starting material leading to a negative $\Delta S_4^{\neq}$. As shown in Table 3, this is in general true except for the small positive value for **3***d* (X = Br). From an orbital viewpoint the closure of **3** to **4** might be regarded as a 6 electron 1,5-cycloaddition (ref. 18, p. 38). However, as shown in Fig. 2, this process is not the same as normal cycloadditions where out-of-plane π bonds are converted to in-plane σ bonds by rotation of the termini. In fact only a rotation at C_1 is required to give overlap with an in-plane π bond at N_5.[5] The other lobe of the N_4—N_5 π bond becomes a lone pair at N_4.

A very similar process, the conversion of vinylazide to triazole (reaction [8]), has been examined by *ab initio* MO calculations (19). The least energy path involves initial bending of the N_3—N_4—N_5 bond,

[5]These numbers refer to the Figure and are not the same as those used for nomenclature.

TABLE 3. Activation values $\Delta H^{\ddagger}$ and $\Delta S^{\ddagger}$ for the thermal decomposition of **3***a*–**3***e*[a]

X	$\Delta H_4^{\ddagger}$ (kcal M^{-1})	$\Delta S_4^{\ddagger}$ (eu)	$\Delta H_5^{\ddagger}$ (kcal M^{-1})	$\Delta S_5^{\ddagger}$ (eu)
4-OMe	24	−8	27	+2
4-Me	24	−8	29	+5
H	25	−7	27	+2
4-Br	26	+2	27	+2

[a]Estimated errors are 1.2 kcal M^{-1} in $\Delta H^{\ddagger}$ and 3 eu in $\Delta S^{\ddagger}$ (ref. 17, p. 8).

development of the long pair on N_4 and positive charge on N_5. Very little change in the charge distribution of the out-of-plane π systems occurs during this stage. The transition state is passed as C_1 rotates and electron density is transferred from the π system to the σ bond forming.

Assuming that this reaction (reaction [8]) is a

[8] 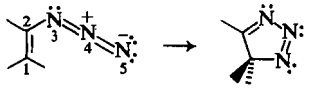

reasonable model for the conversion of **3** to **4**, the substituent effects can be explained. Thus, electron-withdrawing substituents on a phenyl group at C_3 (Fig. 2) stabilize negative charge and make the conversion of out-of-plane π electron density into the in-plane σ bond more difficult. Thus, k_4 decreases from **3***a* to **3***e*. According to these arguments substitution at C_1 should have the same effect. This is confirmed by the results of Brewbaker and Hart (20) on the rates for the conversion of a series of 1-aryl-3-diazopropenes, **6**, to the corresponding pyrazoles, **8** (presumably via 5*H*-pyrazoles, **7** (reaction [9])).

[9] 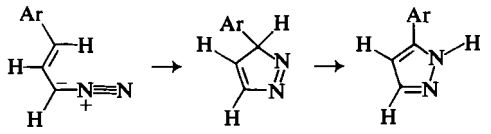

6 **7** **8**

In fact Hammett plots using σ^- give $\rho^- = -0.4$ ($r = 0.998$) for cyclization of **6** and $\rho^- = -0.5$ ($r = 0.93$) for **3***a*–**3***e*. (The very poor correlation for our results is partially accounted for because only an upper limit for k_4 for 4-CN could be obtained.) The comparison between the results of Brewbaker and Hart (20) and those reported here can be extended. Thus only pyrazoles are formed from **6** whereas there is competition between pyrazole formation, **4**, and loss of nitrogen to give cyclopropene, **5**, for the case of **3**. Moreover the cyclizations of **3** occur about 10^3 times as slow. This decrease in rate probably results from steric inhibition to ring closure by dimethyl substitution at C_1 particularly if the ring closure is

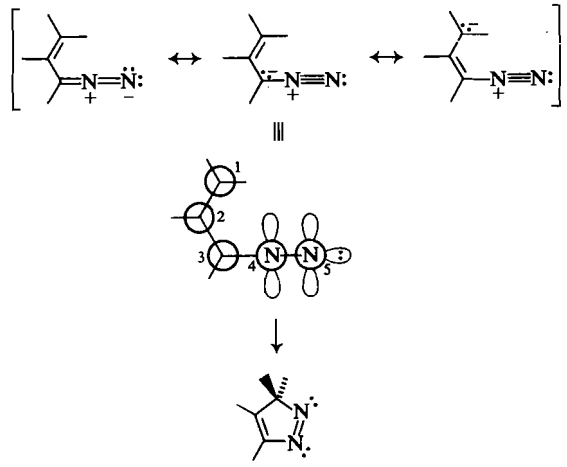

FIG. 2. Conversion of vinyldiazomethane to 5*H*-pyrazole.

initiated by bending of the C_3—N_4—N_5 bond. Since the competition between pyrazole and cyclopropene formation is quite close for **3**, not surprisingly when the pyrazole rates increase as in **6** no cyclopropene is formed.

The kinetics of the second process for **3**, loss of nitrogen to form cyclopropene **5**, presumably via a vinylmethylene intermediate will now be discussed. As shown in Table 3 this process is characterized by small positive $\Delta S^{\ddagger}$ values. Since this is a unimolecular dissociation, the entropy should be positive but a higher value might be expected (21). However, the thermal decomposition of diphenyldiazomethane has been clearly shown to be a simple unimolecular dissociation to nitrogen and diphenylmethylene and also has $\Delta S^{\ddagger}$ values close to zero (16, 22). That the reaction does not involve large charge separation for **3***c* is indicated by the observation that the rate is only 25% greater in acetonitrile:5% pyridine than in benzene:5% pyridine.

As shown in Table 2, the k_5 rate constant is a minimum for **3***b* (X = CH_3) and is faster for both electron-withdrawing and the better electron-donating substituent, OCH_3. An explanation for this order requires a more careful examination of the electronic details of the loss of nitrogen from **3**.

As discussed by Woodward and Hoffmann loss of nitrogen from a diazo compound is a cheleotropic reaction that is forbidden if it occurs in the linear mode (ref. 18, p. 152). As shown in Fig. 3*a*, this results because the electrons in the σ bond breaking correlate with the new lone pair at nitrogen and a "doubly excited" p^2 state (9) of methylene is formed. The same analysis is true for vinyldiazo compounds (Fig. 3*b*) where the vinylmethylene formed will be **2***c*.

In their recent paper on vinylmethylene, Davis, Goddard, and Bergman have stated that "extrusion

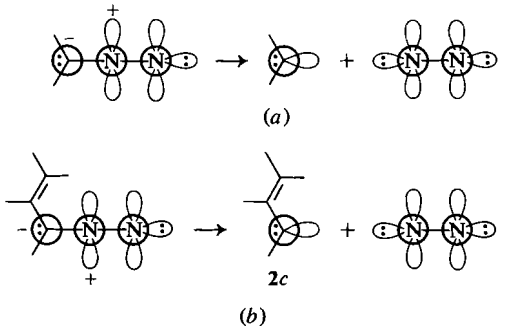

FIG. 3. (*a*) Loss of nitrogen from diazomethane, (*b*) loss of nitrogen from vinyldiazomethane.

of nitrogen from a vinyl diazo compound should lead directly to" **2***b* (6). This seems an oversimplification of the process but can be rationalized in two ways. First, the conversion of **2***c* to **2***b* will be exothermic and should have little or no activation barrier. As shown in reaction [10], this is true because

[10] 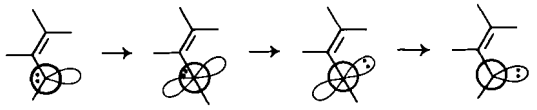

conversion of **2***c* to **2***c* (linear) only results in decrease in *s* character for an empty orbital. The occupied *p* orbital is still of the allyl type. The rotation converting **2***c* (linear) to **2***b* (linear) should also be isothermal since the orbital system is now allyl plus non-bonded *p* and the occupancy simply changes from non-bonded allyl to non-bonded *p*. Bending **2***b* has been shown by calculation to be exothermic, as expected, by 18.1 kcal/*M* (6). Therefore, although the linear loss of nitrogen gives **2***c*, the first-formed species should be converted rapidly to **2***b*. The second possibility is that loss of nitrogen occurs in a non-linear fashion (ref. 18, p. 152) and is thus symmetry allowed. In fact, recent calculations for diazomethane (24) have shown that the barrier to loss of nitrogen disappears completely if the restriction of C_{2v} symmetry is removed. The singlet ground state of methylene is then formed directly. Regardless of whether the decomposition of **3** occurs by formation of **2***c* and then **2***b* or directly to **2***b*, the electronic distribution is such that the π-system is electron-rich and the σ-system electron-deficient (**2***c*) or *vice versa* (**2***b*).[6] It is interesting that the final product of these thermal reactions is cyclopropene **5** although **2***c* does not correlate with **5** (6). The vinylmethylene **2***b* does correlate with **5** and yet the ratio of formation of cyclopropene relative to H migration products is about 10:1 (10). For **2***b* this ratio must be at least 20:1 since no other products are observed.

The discussion above provides an explanation for the substituent effect for the thermal loss of nitrogen from **3**. The substituted phenyl group can conjugate with either an electron-deficient or an electron-rich orbital on the methylene carbon. The substituent therefore can stabilize the transition state for reaction for both electron-donating and electron-withdrawing cases.

A very similar order has been observed for the thermal decomposition of diphenyldiazomethanes where for monophenyl substitution all groups accelerate the reactions over H (23). A similar explanation was used in this case. In fact a plot of log *k* versus σ^+ for resonance electron-donating substituents and σ^- for electron-withdrawing gives very similar curves for both substrates (Fig. 4). The observation that **3** looses nitrogen about fifteen times as fast as diphenyldiazomethane means that the vinyl group is better at stabilizing the carbene center than phenyl although this may be very dependent on the conformation of the groups at the carbene carbon.

Finally, a comparison between these results for the generation of vinylmethylenes by thermolysis of **3** and those from the photochemical cleavage of cyclopropenes should be made. The closest comparison is

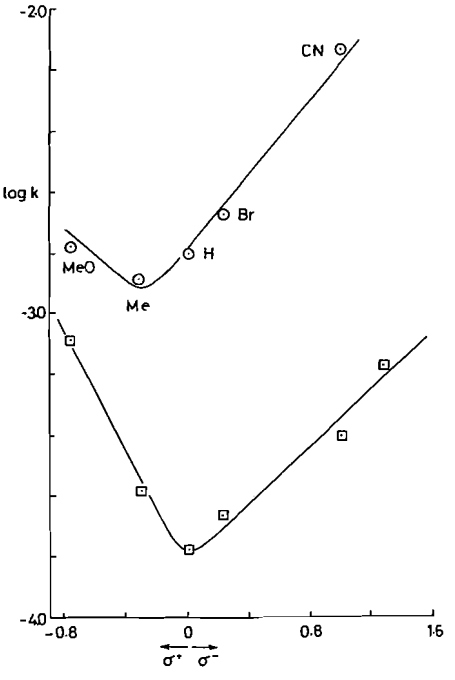

FIG. 4. Hammett plots for the conversion of **3***a*–**3***e* to **5***a*–**5***e* (○) and for the loss of nitrogen from diphenyldiazomethane (□) (25).

[6]Note that photochemical decomposition of **3** gives triplet **2** (13) but the multiplicity of the excited state involved is unknown and the intermediacy of singlet **2** is not ruled out.

with the results of Arnold (5) (reaction [4]). Obviously, the substituent effects are not the same since the photochemical results suggest that the vinylmethylene formed is more stable the better the electron-donating ability of the substituent. Perhaps the photochemical selectivity is being controlled by reversibility of vinylmethylene formation (2) in competition with the rates of hydrogen migration. A second possibility is that the substituent effects on the bond order in the excited singlet of the cyclopropene (11) are different from those on the vinylmethylene intermediate; that is, that the potential energy surfaces cross. The suggestion of Padwa *et al.* (1) that inductive destabilization by an electron-withdrawing phenyl group conjugated to the double bond of the cyclopropene and not to the developing radical center as σ bond cleavage occurs makes use of this possibility. Note that for the rate of decomposition of **3** inductively electron-withdrawing substituents (—Br, —OCH_3, —CN) are faster than H and the electron-donating CH_3 is slower.

Clearly, there is no simple explanation for all the results for both cyclopropene reactivity and vinylmethylene generation from vinyldiazo compounds. Only more extensive studies on these systems will indicate whether a single explanation exists or whether different substituent patterns and conditions lead to different mechanisms.

Experimental

Preparation of Substituted Pyrazoles

3-(4-Cyanophenyl)-5,5-dimethyl-4-phenyl-5*H*-pyrazole and 3-(4-methoxyphenyl)-5,5-dimethyl-4-phenyl-5*H*-pyrazole were prepared according to the published procedure (13). The new pyrazoles, 3-(4-bromophenyl) and 3-(4-methylphenyl), were prepared by the same six-step sequence. The physical properties for them and the precursor α,β-unsaturated ketones are given below.

1-(4-Bromophenyl)-3-methyl-2-phenyl-2-buten-1-one: bp (bulb-to-bulb distillation) 110°C/2 Torr; nmr δ1.83 (3H,s), 1.92 (3H,s), 7.37 (5H,bs), 7.77 (4H,dd). *Anal.* calcd. for $C_{17}H_{15}OBr$: C 64.77, H 4.81, Br 25.35; found: C 64.65, H 5.04, Br 25.24.

1-(4-Methylphenyl)-3-methyl-2-phenyl-2-buten-1-one: purified by sublimation: mp 106–107°C; nmr δ1.77 (3H,s), 1.86 (3H,s), 2.35 (3H,s), 7.31 (5H,bs), 7.38 (dd). *Anal.* calcd. for $C_{18}H_{18}O$: C 86.35, H 7.26; found: C 86.31, H 7.21.

3-(4-Bromophenyl)-5,5-dimethyl-4-phenyl-5*H*-pyrazole; purified by sublimation: mp 128–130°C; nmr δ1.55 (6H,s), 7.2–7.8 (9H,m); ir (CCl_4) 2970, 2930, 1460, 1330 cm^{-1}; uv (MeOH) 305 (ε, 5 700), 245 (ε, 17 700); mass spectrum (parent ion plus intensities greater than 20% of base peak), 328 (12), 326 (12), 300 (57), 298 (57), 285 (92), 283 (92), 220 (46), 204 (100), 203 (61), 202 (50), 101 (26), 100 (39). *Anal.* calcd. for $C_{17}H_{15}BrN_2$: C 62.39, H 4.63, Br 24.42, N 8.56; found: C 62.27, H 4.81, Br 24.20, N 8.39.

3-(4-Methylphenyl)-5,5-dimethyl-4-phenyl-5*H*-pyrazole; purified by sublimation: mp 106–107°C; nmr δ1.50 (6H,s), 2.35 (3H,s), 7.1–7.9 (9H,m); ir (CCl_4) 2970, 2920, 1450, 1330, 1170 cm^{-1}, uv (MeOH) 305 (ε, 4 900), 240 mm (ε, 16 900); mass spectrum 262 (4), 234 (40), 220 (20), 219 (100), 204 (21). *Anal.* calcd. for $C_{18}H_{18}N_2$: C 82.39, H 6.93, N 10.68; found: C 82.38, H 6.98, N 10.61.

Preparation of 1-Aryl-3-methyl-2-phenyl-1-diazobut-2-enes

The pyrazole (~10 mg) was dissolved in 0.4 mL of 5% pyridine in benzene-d_6 and sealed in a Pyrex nmr tube after three freeze–pump–thaw cycles. The sample was then irradiated using Filter System A (13) and a 200 W Hanovia medium-pressure mercury-arc lamp. The appearance of the diazo compound was apparent from the red colour of the sample and could be monitored quantitatively by nmr spectroscopy. As reported previously (13) the diazo compound could not be generated without some conversion to the corresponding cyclopropene. Typical compositions at the termination of irradiation were: substrate, % pyrazole, % diazo, % cyclopropene: 4-CH_3O, 10, 69, 21; 4OCH_3, 8, 78, 14; H, 20, 50, 30; 4-Br, 36, 45, 19; 4-CN, 39, 19, 42. These compositions were determined by averaging multiple integrations (five forward and five reverse) using a Varian T-60 spectrometer. The average deviation is approximately 1–2%.

Product Composition for the Thermal Decomposition of 1-Aryl-3-methyl-2-phenyl-1-diazobut-2-enes

The sealed nmr tubes containing the diazo compound solutions were placed in a constant temperature bath until the red colour of the diazo compound had disappeared. The yields of cyclopropene and pyrazole were then determined by multiple nmr integrations. The % yields as reported in Table 2 were then calculated from the difference before and after thermolysis. Since they are obtained from the difference in two nmr integrations the error is approximately 5%.

Kinetics of the Thermal Decomposition of 1-Aryl-3-methyl-2-phenyl-1-diazobut-2-enes

Solutions of $\sim 10^{-4}$ *M* in the diazo compound were prepared by diluting the nmr samples to 400 mL with 5% pyridine in benzene. Samples were then sealed in 5 mL ampoules (10 per kinetic run). (Since diazo compounds decompose in visible light, these dilute solutions could only be used reliably if the ampoules were wrapped in aluminum foil.) The ampoules were placed in a constant temperature bath for the kinetic run and quenched in ice water at appropriate times.

The absorbance of the solutions was then measured at 335 mm (355 mm for the 4-cyano compound) to monitor the appearance of the 1-aryl-2-phenyl-3,3-dimethylcyclopropene. For the 4-cyano compound the total absorbance change was only ~0.1 absorbance units and measurements were taken using a Unicam SP-800 Spectrophotometer with a scale expander. All others were taken with a Hitachi Coleman 124 Spectrophotometer. First-order rate constants were then obtained by the usual ln $(A - A_\infty)$ method with points taken for two half-lives; correlation coefficients were always greater than 0.99. A typical run for aryl = phenyl (t = 97.0°C) gave: time (abs); 0 (0.638), 120 s (0.708), 240 (0.770), 360 (0.820), 480 (0.871), 600 (0.897), 720 (0.925), 960 (0.960), ∞ (1.050): $k = 1.63 \times 10^{-3}$ s^{-1} (r = 0.999). The average values of at least two runs for each substrate at each temperature are listed in Table 1.

Acknowledgements

We would like to thank Professor D. R. Arnold for a generous gift of 4-cyano pyrazole as well as helpful discussions, and Brent Amero, Jim Hancock, and Fred Northrup for the initial ^1H nmr kinetic work. The financial support of the National Research Council of Canada is gratefully acknowledged.

1. A. PADWA, T. J. BLACKLOCK, D. GETMAN, N. HATANAKA, and R. LOZA. J. Org. Chem. **43**, 1481 (1978).
2. J. A. PINCOCK and A. MOUTSOKAPAS. Can. J. Chem. **55**, 979 (1977).
3. J. A. PINCOCK, R. MORCHAT, and D. R. ARNOLD. J. Am. Chem. Soc. **95**, 7536 (1973).
4. H. E. ZIMMERMAN and J. M. AASEN. J. Org. Chem. **43**, 1493 (1978).
5. R. M. MORCHAT and D. R. ARNOLD. Chem. Commun. 743 (1978).
6. J. H. DAVIS, W. A. GODDARD, and R. G. BERGMAN. J. Am. Chem. Soc. **99**, 2427 (1977).
7. J. A. PINCOCK and R. J. BOYD. Can. J. Chem. **55**, 2482 (1977).
8. L. SALEM and W. D. STOHRER. Personal communication.
9. R. HOFFMANN, G. D. ZEISS, and G. W. VAN DINE. J. Am. Chem. Soc. **90**, 1485 (1968).
10. E. J. YORK, W. DITTMAR, J. R. STEVENSON, and R. G. BERGMAN. J. Am. Chem. Soc. **95**, 5680 (1973).
11. H. E. ZIMMMERMAN and T. R. WELTER. J. Am. Chem. Soc. **100**, 4131 (1978).
12. C. D. DEBOER, D. H. WADSWORTH, and W. C. PERKINS. J. Am. Chem. Soc. **95**, 861 (1973).
13. D. R. ARNOLD, R. W. HUMPHREYS, W. LEIGH, and G. E. PALMER. J. Am. Chem. Soc. **98**, 6225 (1976).
14. R. S. HUTTON, M. L. MANION, H. D. ROTH, and E. WASSERMAN. J. Am. Chem. Soc. **96**, 4680 (1974).
15. A. A. FROST and R. G. PEARSON. Kinetics and mechanisms. J. Wiley and Sons, New York. 1961. p. 160.
16. D. BETHELL, D. WHITTAKER, and J. D. CALLISTER. J. Chem. Soc. 2466 (1965).
17. L. L. SCHALEGER and F. A. LONG. *In* Advances in physical organic chemistry. Vol. 1. *Edited by* V. Gold. Academic Press, New York. 1963.
18. R. B. WOODWARD and R. HOFFMANN. The conservation of orbital symmetry. Verlag Chimie, GmbH, Weinheim, Germany. 1970.
19. L. A. BURKE, G. LEROY, M. T. NGUYEN, and M. SANA. J. Am. Chem. Soc. **100**, 3668 (1978).
20. J. L. BREWBAKER and H. HART. J. Am. Chem. Soc. **91**, 711 (1969).
21. K. B. WIBERG. Physical organic chemistry. J. Wiley and Sons, Inc., New York. 1964. p. 387.
22. G. MURGULESCU and T. ONCESCU. J. Chim. Phys. **58**, 508 (1961).
23. (*a*) R. J. MILLER, L. S. YANG, and H. SHECHTER. J. Am. Chem. Soc. **99**, 938 (1977); (*b*) R. J. MILLER and H. SHECHTER. J. Am. Chem. Soc. **100**, 7920 (1978).
24. J. LIEVIN and G. VERHAEGEN. Theor. Chim. Acta Berlin, **45**, 269 (1977).

Analytical potentiometric and spectroscopic study of the equilibria in the aqueous nickel(II)–triethylenetetramine and nickel(II)–D-penicillamine systems

STUART H. LAURIE AND DIANA H. PRIME
The School of Chemistry, Leicester Polytechnic, P.O. Box 143, Leicester, England
AND
BIBUDHENDRA SARKAR[1]
The Research Institute, The Hospital for Sick Children, Toronto, Ont., Canada M5G 1X8 and the Department of Biochemistry, University of Toronto, Ont., Canada M5S 1A8

Received January 3, 1979

STUART H. LAURIE, DIANA H. PRIME, and BIBUDHENDRA SARKAR. Can. J. Chem. **57**, 1411 (1979).

The complexation of nickel(II) with triethylenetetramine and D-penicillamine has been examined in 0.15 *M* NaCl solution at 25°C by a combined potentiometric–spectroscopic approach. Trien (A) forms the following complexes with Ni(II): MA, MA_2, MH_2A_2, M_2A_3, M_2HA_3, and $M_2H_2A_3$ with overall log stability constants: 14.34, 20.64, 37.28, 40.05, 49.20, and 55.02, respectively. Their concentrations as a function of pH are presented and their likely structures discussed. In contrast, D-penicillamine forms the species MA and MA_2 only. The latter species, which is the only species from pH 5.8 to 10.0, is shown to be square-planar via coordination of the N, S atoms of the ligand molecules. The overall log stability constants of MA and MA_2 are 11.22 and 22.71, respectively. The significance of these results in relation to the effectiveness of these ligands in preventing nickel toxicity in rats is discussed.

STUART H. LAURIE, DIANA H. PRIME et BIBUDHENDRA SARKAR. Can. J. Chem. **57**, 1411 (1979).

On a étudié la complexation du nickel(II) par la triéthylènetétramine et la D-pénicillamine dans des solutions 0.15 *M* en NaCl à 25°C en faisant appel à des méthodes potentiométrique et spectroscopique. Le trien (A) forme les complexes suivants avec le Ni(II): MA, MA_2, MH_2A_2, M_2A_3, M_2HA_3 et $M_2H_2A_3$ avec des constantes de stabilité logarithmiques globales respectives de 14.34, 20.64, 37.28, 40.05, 49.20 et 55.02. On présente leurs concentrations en fonction du pH et on discute de leurs structures les plus probables. Par ailleurs la D-pénicillamine ne forme que les espèces MA et MA_2. Cette dernière espèce, qui est la seule à se former à des pH de 5.8 à 10.0, est plan-carré par coordination des atomes N et S des molécules de ligand. Les constantes de stabilité logarithmiques de MA et MA_2 sont respectivement 11.22 et 22.71. On discute de la signification de ces résultats en relation avec l'efficacité de ces ligands à prévenir la toxicité du nickel dans les rats.

[Traduit par le journal]

Introduction

There is a great deal of concern regarding the health hazards caused by excessive intake of metals due to occupational exposure or environmental pollution. A study has shown that the serum nickel in the healthy inhabitants of Sudbury, Ontario, the site of the largest open-pit nickel mines in North America, was double that of healthy inhabitants of Hartford, Connecticut, a city with a relatively low environmental concentration of nickel (1). Industrial hazards of nickel workers are greatly eliminated by making better working conditions (2). However, a recent investigation of workers at a nickel refinery in Norway found that the degree of epithelial keratinization was more pronounced in the nickel exposed group than in the controls (3).

In our program of studying the biological transport of metals and its removal we have undertaken a detailed investigation with nickel(II). Recent studies have revealed that the organic ligands triethylenetetramine (trien) and D-penicillamine (Pen) were the most effective in prevention of death after a single parenteral injection of $NiCl_2$ in rats (4). Interestingly, the same two ligands have been found to be the most effective, among the many examined, for the removal of accumulated copper from patients of Wilson's disease (5). The complex equilibria of these ligands with copper(II) ions have recently been examined by us (6).

There is a general agreement on the formation of a 1:1 complex between Ni(II) and trien, but there exists some confusion over other species present, particularly above pH 7. This can be attributed partly to the use of impure trien in some instances and also to the lack of the necessary mathematical

[1]To whom correspondence should be addressed at the Hospital for Sick Children, Toronto, Ont., Canada M5G 1X8.

0008-4042/79/121411-07$01.00/0

or computing facilities necessary to solve the species present, especially in the earlier work. The Ni(II)–Pen system, with no inherent redox reactions, is considerably simpler than the Cu(II)–Pen system (6), and has been studied by a number of earlier workers, some using the racemic form of the ligand, while with others the optical form used was not mentioned. The particular isomer used is important since only the D optical isomer is used medically (the L form is toxic) and the differences in the species formed in metal complexation can arise from stereoselectivity effects.

We have now re-examined the aqueous Ni(II)–trien and Ni(II)–D-Pen systems, because of their importance, by the combined analytical potentiometric–spectroscopic method (7, 8) which has been so successfully applied to other systems (9–12). In this paper we present the results of this study.

Experimental Section

Materials

AnalaR $NiCl_2 \cdot 6H_2O$ was used to prepare stock Ni(II) solutions. They were analyzed for Ni(II) content by the EDTA back-titration method employing standard $ZnSO_4 \cdot 7H_2O$ solutions. Trien–4HCl was purified as previously described (11). D-Penicillamine (Koch-Light 'Puriss' grade) was kept under vacuum at 0°C and used without further purification, tlc (*n*-butanol:acetone:water:acetic acid, 4:3:2:1) gave only a single spot. All other reagents were of 'AnalaR' or equivalent grade. All solutions were prepared from doubly-deionized CO_2-free water and kept under an oxygen-free atmosphere.

Analytical Potentiometry

Potentiometric titrations were carried out as described earlier (11) at 25 ± 0.05°C in 1.5 *M* NaCl solutions containing sufficient HCl so that the starting pH was below that of either the first deprotonation or the beginning of complexation.[2] A notable feature of the Ni(II)–trien system was the slow equilibration in the pH region 4.4–6.2.

Spectroscopic Measurements

Spectra were recorded using solutions containing 0.15 *M* NaCl thermostatted at 25 ± 0.1°C. A Cary 15 recording spectrophotometer and 5 cm cells were used to obtain the spectra of the Ni(II)–trien solutions. For the Ni(II)–Pen solutions a Unicam SP800 spectrophotometer was used with 1 cm and 3 cm cells.

Computational Procedures

The previously described programs PLOT-2, GUESS-2, and LEASK-2 (7) were substantially modified to facilitate data handling and reduce costly computer time.

PLOT-2: The polynomial fitting to obtain the $\delta H^+/\delta C_X$ curves was replaced with a numerical fitting method. This change eliminates problems found with polynomial 'over-fitting' and means the titration data can now be treated in a single computer run, considerably reducing computational time.

GUESS-2: Calculation of the species concentration factor ($p.m^p h^q a^r$) was carried out in log mode so as to avoid elimination of viable species by the computer due to the concentration factors being outside the computer's precision limits. This problem was particularly acute with the highly protonated dinuclear Ni(II)–trien species.

LEASK-2 was replaced with two programs using different minimization procedures. The first uses the Gauss–Newton minimization procedure which has the advantage of rapid convergence even with initial 'wild' guesses of the stability constants. Use of matrices in the convergence routine required this program to be written in a double-precision mode. The second program uses the Newton–Raphson minimization procedure which is more accurate than the Gauss–Newton procedure but will only converge if the initial guesses are close to the true values. These procedures have previously been used in this area and their advantages outlined (13). The advantages of using more than one minimization routine is that the chances of reading false minima (e.g. saddle points) are greatly reduced. Both programs are considerably faster to run than the earlier LEASK versions which employed a polynomial fitting procedure. The computations were carried out using a series GE400 computer (Toronto) and a Burroughs B6700 computer (Leicester).[3]

Results

Stability Constants and Species Distribution

The general equilibrium involving a metal ion M, a proton H, and a ligand A can be written in the form of reaction [1].

$$[1] \qquad pM + qH + rA \rightleftarrows M_pH_qA_r$$

The stabilities of the species formed may be expressed as their stoichiometric equilibrium constants β_{pqr} in terms of concentrations at constant ionic strength, temperature, and pressure as in eq. [2]

$$[2] \qquad \beta_{pqr} = [M_pH_qA_r]/m^p h^q a^r$$

where m, h, and a are the concentrations of free metal ion, hydrogen ion, and completely deprotonated ligand, respectively. The proton-liberation data and the amounts of unchanged reagents were determined by processing the original titration data with the computer program PLOT-2. The data so obtained were then processed by programs GUESS-2 and LEASK-2 to obtain the distribution of the species and their stability constants. A detailed account of the data processing has been previously reported (9–11).

Proton–Triethylenetetramine System

The pK values of the ligand at 25°C and in 0.15 *M* NaCl solution were obtained in an earlier study (11). The values obtained were 3.59, 6.77, 9.22, and 9.81, and these were used in this study.

[2]The concentrations used, pH titration curves, and proton displacement of pH curves can be obtained as supplementary material from Dr. B. Sarkar.

[3]The original programs and their derivations have been the subject of two recent communications (ref. 30, *a* and *b*). The former report confirms, with a few caveats, the general applicability of the analytical potentiometric method, the latter report is critical, but relates to modified versions of the computer programs. Some of the problems highlighted in these papers have been solved by the replacement of the polynomial procedures in the programs used here. These are to be published in the near future.

Proton–Triethylenetetramine–Nickel(II) System

From the metal and ligand variation titrations, using PLOT-2, pM and pA values were obtained for the concentrations Ni(II) = 2.00×10^{-4} M and trien = 8.022×10^{-4} M over the pH range 3.40–10.00 (in 0.20 steps). The input for the GUESS-2 program was $p = 1, 2; q = -2, -1, 0, +1, +2, +3$; $r = 1, 2, 3$. Of the 19 species processed, only 6 were found to give a good fit to the titration data: MA, MA_2, M_2A_3, MHA_2, M_2HA_3, and $M_2H_2A_3$. In the region pH 3.40–4.80, other protonated species (MHA, MH_2A, and MH_2A_2) were evident, but only at insignificant concentrations.

The β values obtained and the species distributions are given in Table 1 and Fig. 1 respectively.

The formation of the MA species in the pH range 4.4–6.2 corresponds to the observed slow equilibration region of the titration curves. The formation of this species is known to be relatively slow and has been studied kinetically in the pH 5.0–7.0 range (15, 16). The slow rate of formation is attributed to the rate of ring closure around the Ni(II) ion. There was no evidence for the formation of hydroxy species below pH 10.

Visible Absorption Spectroscopy of the Proton–Triethylenetetramine–Nickel(II) Systems

Solutions with Ni(II):trien = 1:4 were used to obtain the spectra as a function of pH. The measurements were made using Ni(II) concentrations of $1.2–25 \times 10^{-3}$ M. Representative spectra showing the strong pH dependence are given in Fig. 2. Resolution of these spectra into contributions from different species was achieved using the Beer–Lambert law, eq. [3], as previously described (11):

$$[3] \qquad A_l^{\lambda} = \sum^{i} \varepsilon_{\lambda,i} l [M_p H_q A_r]_i$$

The ε value was determined for each species at 20 nm intervals. Spectra were resolved at pH 5.07, 7.55, and 9.52 for all species except $M_2H_2A_3$. At pH 5.07 account was taken of the substantial amount of free Ni_{aq}^{2+}. After obtaining ε values for all species, except those for the species $M_2H_2A_3$, over the

TABLE 1. log stability constant (β_{pqr}) of complex species $M_pH_qA_r$ (M = Ni(II), A = triethylenetetramine) in 0.15 M NaCl at 25°C

Species			log β_{pqr}	
p	q	r	This work[a]	Literature values
1	0	1	14.34 (0.02)	14.35,[f] 13.92,[g] 14.1,[h] 14.0,[i] 13.82[j]
1	1	1	[b]	19.03,[f] 18.64,[g] 18.5[j]
1	2	1	[b]	[c,k]
1	−1	1	[d]	[c,l]
1	−2	1	[d]	[c,l]
1	0	2	20.64 (0.02)	19.97[m]
1	1	2	[b]	[d]
1	2	2	37.28 (0.06)	[d]
2	0	1	[d]	15.98[f]
2	0	3	40.05 (0.06)	35.45[f]
2	1	3	49.20 (0.10)	43.99[f]
2	2	3	55.02 (0.10)	[d]
3	0	2	[d]	5.63[e,m]

[a]Figures in parentheses are 'estimated' errors, standard deviations only ±5%.
[b]Observed as an insignificant species (see text).
[c]Observed but no β value measured.
[d]Not observed.
[e]Only at Ni(II):trien ratios > 1.
[f]25°C, 1.0 M KNO_3 (18).
[g]Extrapolated from spectroscopic measurements at 25°C from ref. 26.
[h]25°C, 0.1 M NaCl (27).
[i]20°C, 0.1 M KCl (28).
[j]25°C, 0.1 M $NaClO_4$ (14).
[k]Reference 15.
[l]Reference 29.
[m]30°C and 0.1 M KCl + KNO_3 (19).

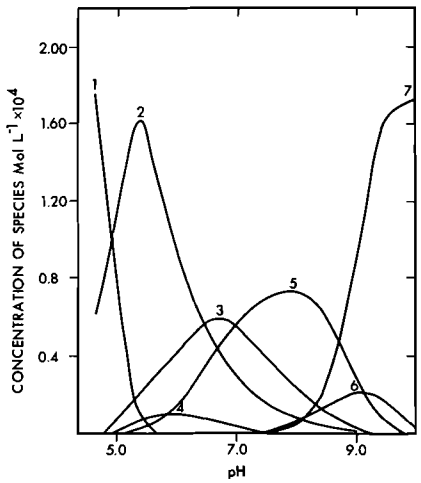

FIG. 1. Species distribution as a function of pH for nickel(II)–triethylenetetramine solution of Ni, 2.00×10^{-4} M; trien, 8.022×10^{-4} M; NaCl, 0.15 M; T = 25°C; *1*, M^{2+}; *2*, MA; *3*, MH_2A_2; *4*, $M_2H_2A_3$; *5*, M_2HA_3; *6*, M_2A_3; *7*, MA_2.

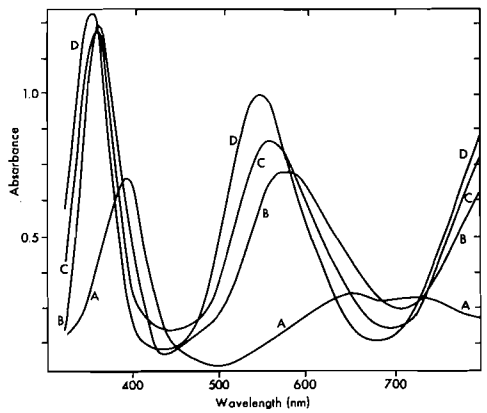

FIG. 2. Visible absorption spectra of nickel(II)–triethylenetetramine solutions as a function of pH. Ni(II), 0.025 M; trien, 0.101 M; NaCl, 0.15 M; T = 25°C, 5 cm pathlength. *A*, pH 3.98_6; *B*, pH 5.07_1; *C*, pH 7.55_3; *D*, pH 9.52_3.

300–800 nm range, the resolved spectrum of $M_2H_2A_3$ was then obtained from the observed spectrum at pH 6.70 using the ε values obtained for the other species. All six species gave an excellent fit to the observed spectra. The individual spectra are shown in Figs. 3 and 4.

For all species two peaks were evident. These are as expected for octahedrally coordinated Ni(II) ion. There is no evidence of any square-planar Ni(II) ion. The peaks in the 500–600 nm and the 340–360 nm regions can be assigned to $^3A_{2g} \rightarrow {}^3T_{1g}$ (F) and $^3A_{2g} \rightarrow {}^3T_{1g}$ (P) electronic transitions of octahedral symmetry. The corresponding transition for $Ni(H_2O)_6^{2+}$ are at 650–720 nm (doublet) and 395 nm, respectively. The occurrence of this doublet for the aquo ion and its disappearance upon replacement of H_2O with a nitrogen-donor ligand has been well documented (16), as also has the shift of λ_{max} to shorter wavelengths with increases in ε values as H_2O ligands are replaced by nitrogen-donor ligands. The resolved spectra show these expected features. A

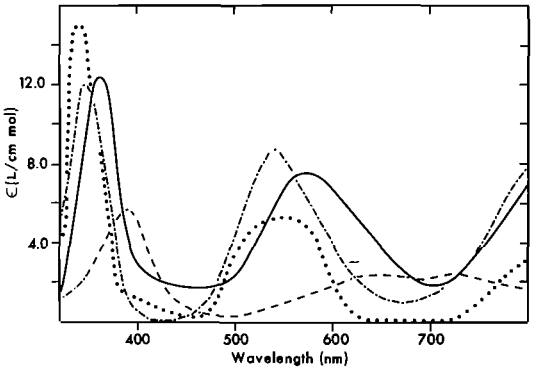

FIG. 3. Visible absorption spectra of $Ni^{2+}{}_{(aq)}$(observed), ---; and those of the species MA, —; MA_2, ·····; and MH_2A_2, ··· (computed from the spectra given in Fig. 2); NaCl, 0.15 *M*; $T = 25°C$.

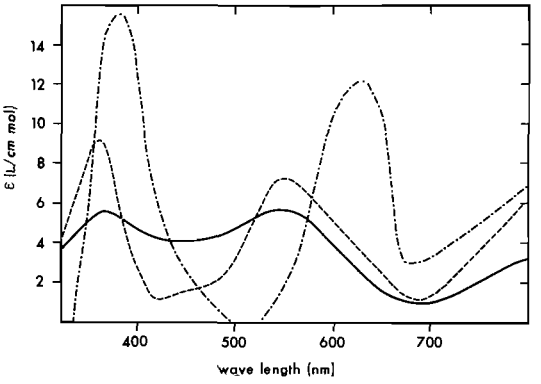

FIG. 4. Computed visible absorption spectra of the dinuclear species M_2A_3, —; M_2HA_3, ---; $M_2H_2A_3$, ·····; NaCl, 0.15 *M*; $T = 25°C$ (molar extinction coefficients based on per *M* Ni(II)).

third *d–d* transition ($^3A_{2g} \rightarrow {}^3T_{2g}$) is expected above 800 nm (~900 nm for the trien complexes). The beginning of this peak can be seen above 700 nm (the third peak for $Ni(H_2O)_6^{2+}$ is at 1100 nm).

Proton–D-Penicillamine System

Titrations were carried out over the range pH 1–12. The proton equilibrium (β_{031}) at the lower pH region was treated by the Henderson–Hasselbach equation. The two equilibria over the range pH 8–11 were solved by treating the titration data with PLOT-2 to obtain $\delta H^+/\delta C_A$, from which the average number of bound protons, $\bar{n}_H$, at each pH value was calculated, since:

$$[4] \qquad \bar{n}_H = 2 - (\delta H^+/\delta C_A)$$

The total number of bound protons in this region being two. The two equilibrium constants were then obtained via expression [5]

$$[5] \quad \bar{n}_H = \beta_{011}(1 - \bar{n}_H)[H^+] + \beta_{021}(2 - \bar{n}_H)[H^+]^2$$

Using increments of 0.20 pH units, simultaneous sets of eq. [5] were solved by program LEASK-2 to obtain the constants β_{011} and β_{021} of the species HA and H_2A respectively. The values obtained, given as pK_a values for ease of comparison with literature values, are presented in Table 2.

Proton–D-Penicillamine–Nickel(II) System

Data processing was as for trien system, using Ni(II) = 1.00×10^{-3} *M* and Pen = 4.00×10^{-3} *M* over the pH range 3.00–10.00 (in 0.20 steps), although significant metal binding only occurred above pH 4.4. The input range for GUESS-2 was $p = 1, 2$; $q = -2, -1, 0, +1, +2, +3$; $r = 1, 2, 3$. LEASK-2 reduced the number of species over the pH range 4.4–10.0 to just two, MA and MA_2. The stability constants obtained are shown in Table 2 and the species distribution in Fig. 5.

Visible Absorption Spectroscopy of the Proton–D-Penicillamine–Nickel(II) System

Consistent with the potentiometric results of a single species above pH 5.8, the visible absorption spectrum (300–800 nm) was found to be invariant over the range pH 5.8–10.0 (Fig. 6). The spectra were recorded with solutions containing a Ni:Pen ratio of 1:4, using Ni(II) concentrations over the range $1.0 \times 10^{-3} - 5.0 \times 10^{-2}$ *M*. Resolution of spectra at lower pH, in order to obtain the spectrum of the 1:1 species, was not attempted because this species is only formed to a minor extent (see Fig. 5). The red color of the Ni–Pen solutions and their spectra are in marked contrast to those of the blue Ni–trien system, and suggest a square-planar configuration for $Ni(Pen)_2$. Two electronic transitions are expected

TABLE 2. pK_a and log stability constants (β_{pqr}) of complex species $M_pH_qA_r$ (M = Ni(II), A = D-penicillamine) in 0.15 *M* NaCl at 25°C

Species			This work		
p	*q*	*r*	pK_a	log β_{pqr}	Literature values
0	1	1	10.60 (0.02)[a]		10.46,[b] 10.43,[c] 10.68,[d] 10.66[e]
0	2	1	8.08 (0.02)		7.79,[b] 7.88,[c] 8.13,[d] 7.93[e]
0	3	1	1.99 (0.03)		2.44,[b] 1.90[e]
1	0	1		11.22 (0.02)	11.40,[b] 11.11,[c] 10.75,[d] 10.63[e]
1	0	2		22.71 (0.01)	22.30,[b] 21.79,[c] 22.89,[d] 23.02[e]

[a]'Estimated' error, standard deviation ± 1%.
[b]0.15 *M* KNO_3, 25°C (20).
[c]0.10 *M* KNO_3, 25°C (21).
[d]0.10 *M* $NaClO_4$, 20°C (22).
[e]0.10 *M* KCl, 25°C (23).

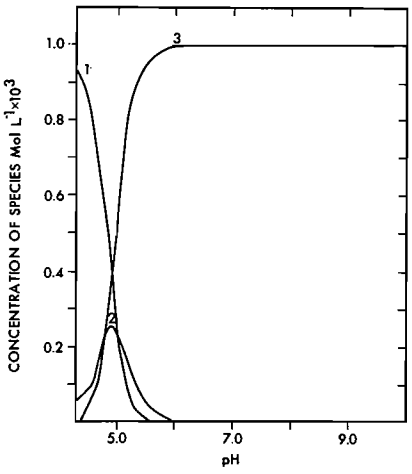

FIG. 5. Species distribution as a function of pH for nickel(II)–D-penicillamine solution of Ni(II), 1.00 × 10^{-3} *M*; Pen, 4.00 × 10^{-3} *M*; NaCl, 0.15 *M*; *T* = 25°C. *1*, M^{2+}; *2*, MA; *3*, MA_2.

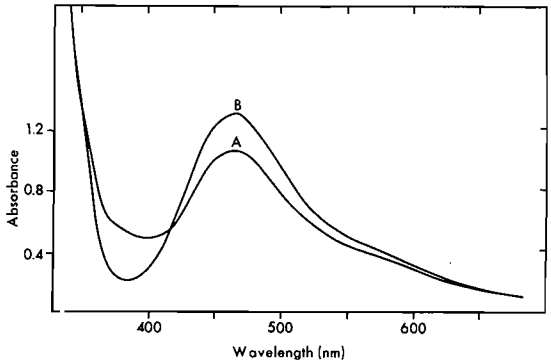

FIG. 6. Visible absorption spectra of nickel(II)–D-penicillamine solutions as a function of pH. Ni(II), 0.010 *M*; D-Pen, 0.040 *M*; NaCl, 0.15 *M*; *T* = 25°C, 1 cm pathlength. *A*, pH 5.40; *B*, pH 5.8–10.0.

(17) for a square planar Ni(II) system: $^1A_{1g} \rightarrow {}^1A_{2g}$ in the region 660–430 nm ($\varepsilon \sim$ 50–500 L cm^{-1} mol^{-1}), and $^1A_{1g} \rightarrow {}^1B_{1g}$ in the region of 430–370 nm (ε variable). For $Ni(Pen)_2$ three transitions are evident, a very intense band below 300 nm (presumably a ligand → metal charge transfer transition), a band with a maximum absorbance at 463 ± 2 nm (ε = 127), and from the asymmetry of the band at 463 nm a further, weaker, band is evident at approximately 560 nm. The latter band is tentatively assigned to the $^1A_{1g} \rightarrow {}^1A_{2g}$ transition and the band at 463 nm to the $^1A_{1g} \rightarrow {}^1B_{1g}$ transition.

Discussion

The results presented here show the aqueous Ni(II)–trien system to be complex. Only one other report (18) has indicated the complexity of this system. Most of the earlier work has listed the species MA and MHA as being the major species. However, our species distribution (Fig. 1) shows that MA is only a major species in the pH 5.0–6.5 region. The species MHA is only evident in our studies as a possible species below pH 5, but must be insignificant since most of the Ni(II) is in the form of the aquo complex below pH 5. In support of this, Margerum and co-workers (14), from kinetic measurements, also found only 50% of the Ni(II) to be complexed at pH 5.0. The stability constant of the MA species is in good agreement with earlier determinations (see Table 1). Reports of this species being the major one above pH 7 can be attributed to lack of consideration of species other than mononuclear ones. A survey of the literature in fact shows inconsistencies in interpretation at large trien:Ni(II) ratios (18).

Intuitively, with Ni(II) having six coordination sites and trien having only four donor atoms, one would expect bis-chelated or bridged systems to form above pH 7 in the presence of excess trien. Indeed,

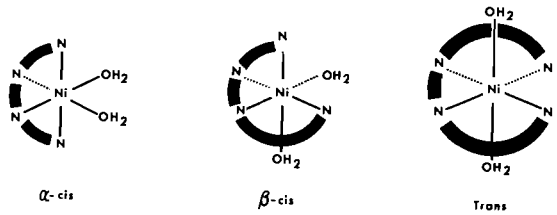

FIG. 7. Possible structures of $[Ni(trien)(H_2O)_2]^{2+}$.

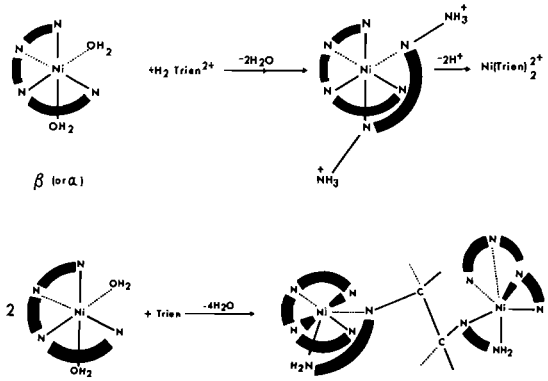

FIG. 8. Formation of MH_2A_2, MA_2, M_2A_3.

the formation of polymeric Ni(II) species in which an octahedral environment is maintained is well known and is often referred to as one of the 'anomalies' of Ni(II) chemistry (16). Earlier workers (18, 19) have reported some of these species, their stability constants given in Table 1, are in fair agreement with ours.

The resolved visible absorption spectra indicate all the species to be octahedral. The species MA must therefore have the stoichiometry $[Ni(trien)(H_2O)_2]^{2+}$, with the possible structures shown in Fig. 7.

The *cis* isomers (α and β) are likely to be the more important structures: firstly, the trien is less strained than in the planar configuration required for the *trans* isomer; secondly, two available *cis* coordination sites are necessary for the formation of the species MH_2A_2, MA_2, and M_2A_3 as depicted in Fig. 8. The species M_2A_3 makes maximum use of the available metal coordination sites and the available ligands donor atoms. Molecular models show that a trien molecule can bridge the two pairs of *cis* sites on adjacent $[Ni(trien)(H_2O)_2]^{2+}$ ions, resulting in the central

$$\diagdown N—CH_2—CH_2—N \diagup$$

moiety being elongated and the two methylene groups having a staggered conformation with respect to each other. Formation of the species M_2HA_3 from M_2A_3 must involve protonation at a coordination site with consequent breaking of the Ni—$\overset{+}{N}$ bond. This is consistent with the observed spectral differences between these species.

In contrast with the Ni(II)–trien system the Ni(II)–Pen system is exceedingly simple, only two species being formed over the pH range 4–10. The first species MA is only a minor one at lower pH (Fig. 5), while above pH 5.8 all the Ni(II) is in the form of the species MA_2. The finding of just two species is consistent with earlier reports (20–23); the stability constants are in excellent agreement (Table 2) considering the different conditions and the use of racemic penicillamine by others (22). In fact, Ritsma and Jellinek (23) have observed a small stereoselectivity effect which enhances the stability of the racemic complex, [Ni(D-Pen)(L-Pen)] over that of the optically active forms. An interesting feature of this system is the finding of $K_2 > K_1$, a reverse of the usual order.[4] The spectroscopic measurements show that this can be attributed to the enhancement of stability gained by the formation of a square-planar MA_2 species, in which the Pen ligands act as bidentate *S,N*-donor ligands rather than in the expected tridentate fashion. A similar conclusion regarding the square-planar configuration of MA_2 for both D-Pen and the much studied, L-cysteine, has been reached by others (24, 25).

L-Cysteine, which is closely related to penicillamine (penicillamine = β,β-dimethylcysteine), is a naturally occurring amino acid and an important metal-binding agent in blood serum. A comparison of the binding properties of D-penicillamine and L-cysteine with Ni(II) is therefore important. Both form MA and MA_2 species in aqueous solution, the latter in both cases being a red, square-planar complex.

The stability constants for the MA and MA_2 species are greater, by a factor of approximately 10 in each case for the D-Pen system, presumably reflecting the influence of the two methyl substituents adjacent to the thiol group in Pen. The methyl groups also exert a steric influence in that no polynuclear species are observed with D-Pen, in contrast to the finding of polynuclear species with L-cysteine, by Perrin and Sayce (22), of the type M_2A_3 and M_3A_4.

As previously indicated, both D-Pen and trien have been found to be the most effective of a number of chelating agents in preventing nickel toxicity in rats. The results presented here show that these ligands are, as was well known, very effective chelating agents of Ni(II), but a number of additional features are also shown to be of importance. Thus, at ratios

[4]The enhancement of the stability of MA_2 over MA is also evident from the species distribution curves (Fig. 5) where it is evident that the MA species exists only in a narrow band of the pH region. We are grateful to a referee for pointing this out.

of trien/Ni(II) > 1 and at the physiological pH of 7.4, trien chelates Ni(II) in a number of ways, i.e. as the species M_2HA_3, MH_2A_2, MA, plus the minor species M_2A_3, MA_2, and $M_2H_2A_3$. The efficiency of trien as a therapeutic agent therefore lies in its flexibility in being able to adopt a number of configurations. In contrast, D-penicillamine, at high Pen/Ni(II) exclusively forms $Ni(Pen)_2^{2-}$, this complex gains additional stability by adopting a square-planar configuration. Complexes of Ni(II) involving D-penicillamine are also more stable than those formed with the related, naturally occurring amino acid, L-cysteine.

Acknowledgements

Part of the research was supported by a grant from the Medical Research Council of Canada and was carried out by S. H. Laurie as a Visiting Scientist Awardee of the Hospital for Sick Children. The authors thank particularly Drs. D. A. Armitage and R. G. Linford, School of Chemistry, Leicester Polytechnic, for the conversions and rewriting of the computer programs.

1. M. D. McNeely, M. W. Neckay, and F. W. Sunderman, Jr. Clin. Chem. **18**, 992 (1972).
2. E. J. Mastromatteo. Occup. Med. **9**, 127 (1967).
3. W. Torjussen and L. A. Solberg. Acta Otolaryngol. **82**, 266 (1976).
4. E. Horak, F. W. Sunderman, Jr., and B. Sarkar. Res. Commun. Chem. Pathol. Pharmacol. **14**, 153 (1976).
5. J. M. Walshe. Lancet, **II**, 1401 (1969).
6. B. Sarkar, A. Sass-Kortsak, R. Clarke, S. H. Laurie, and P. Wei. Proc. R. Soc. Med. **70**, Suppl. 3, 13 (1977).
7. B. Sarkar and T. P. A. Kruck. Can. J. Chem. **51**, 3541 (1973).
8. B. Sarkar. J. Ind. Chem. Soc. **54**, 117 (1977).
9. T. P. A. Kruck and B. Sarkar. Can. J. Chem. **51**, 3563 (1973).
10. T. P. A. Kruck, S. Lau, and B. Sarkar. Can. J. Chem. **54**, 1300 (1976).
11. S. H. Laurie and B. Sarkar. J. Chem. Soc. Dalton, 1822 (1977).
12. D. A. Brown, M. V. Chidambaram, J. J. Clarke, and D. M. McAleese. Bioinorg. Chem. **9**, 255 (1978).
13. P. Gans and A. Vacca. Talanta, **21**, 45 (1974).
14. D. W. Margerum, D. B. Rorabacher, and J. F. G. Clarke. Inorg. Chem. **2**, 667 (1963).
15. G. A. Melson and R. G. Wilkins. J. Chem. Soc. 2663 (1963).
16. F. A. Cotton and R. G. Wilkinson. *In* Advanced inorganic chemistry. 3rd ed. J. Wiley and Sons. 1972. p. 894.
17. A. B. P. Lever. *In* Inorganic spectroscopy. Elsevier. 1968.
18. P. C. Dunningan. Ph.D. Thesis, Ohio University. 1975; Chem. Abstr. **83**, 169 (1975).
19. H. B. Jonassen, G. G. Hurst, R. B. LeBlanc, and A. W. Meinbohm. J. Phys. Chem. **56**, 16 (1952).
20. E. J. Kuchinkas and Y. Rosen. Arch. Biochem. Biophys. **97**, 370 (1962).
21. G. R. Lenz and A. E. Martell. Biochem. **3**, 745 (1964).
22. D. D. Perrin and I. G. Sayce. J. Chem. Soc. A, 53 (1968).
23. J. H. Ritsma and F. Jellinek. Recl. Trav. Chim. **91**, 923 (1972).
24. J. E. Letter and R. B. Jordan. J. Am. Chem. Soc. **97**, 2381 (1975).
25. D. F. S. Natusch and L. J. Porter. J. Chem. Soc. A, 2527 (1971), and references therein.
26. V. M. Myl'mikova and K. V. Astaklov. Russian J. Phys. Chem. **45**, 186 (1977).
27. C. N. Reilly and R. W. Schmid. *In* 'Stability constants' special publication No. 17, The Chemical Society, London. *Edited by* L. G. Sillen and A. E. Martell. 1964.
28. G. Schwarzenbach. Helv. Chim. Acta, **33**, 974 (1950).
29. H. B. Jonassen and H. Thielemann. Z. Anorg. Allg. Chem. **320**, 274 (1963).
30. (*a*) R. Guevremont and D. L. Rabenstein. Can. J. Chem. **55**, 4211 (1977); (*b*) T. B. Field and W. A. E. McBryde. **56**, 1202 (1978).

Estimation of the fraction of dative structure in molecular complexes using Hammett ρ values

BO-LONG POH

School of Chemical Sciences, Universiti Sains Malaysia, Penang, Malaysia

Received August 8, 1978

BO-LONG POH. Can. J. Chem. **57**, 1418 (1979).

A simple method of estimating the fraction of dative structure in molecular complexes using Hammett ρ values is given. A physical interpretation of the parameter m in the equation, $h\nu = mI_D + n$, relating the charge-transfer energy, $h\nu$, of a molecular complex and the ionization potential, I_D, of the donor is given.

BO-LONG POH. Can. J. Chem. **57**, 1418 (1979).

On rapporte une méthode simple, basée sur des valeurs de ρ de Hammett, permettant d'évaluer la fraction de la structure dative de complexes moléculaires. On fournit une interprétation physique du paramètre m de l'équation $h\nu = mI_D + n$ permettant de relier l'énergie de transfert de charge, $h\nu$, d'un complexe moléculaire et le potentiel d'ionisation, I_D, du donneur.

[Traduit par le journal]

Introduction

A considerable amount of work has been done on molecular complexes. Several books (1–4) on this subject have been published. According to Mulliken's theory (5) a molecular complex is formed between an electron donor and an electron acceptor. In the ground state the wave function Ψ_N of a 1:1 donor–acceptor organic complex formed from neutral molecules has the form of eq. [1]. The symbols D and A denote donor and acceptor respectively, Ψ_0 is the wave function of the no-bond structure, Ψ_1 is the wave function of the dative structure in which there is a transfer of an electron from the donor to the acceptor, a and b are coefficients. The excited state wave function Ψ_V is given by eq. [2] where a^* and b^* are coefficients.

$$[1] \quad \Psi_N = a\Psi_0(D, A) + b\Psi_1(D^+—A^-)$$

$$[2] \quad \Psi_V = -b^*\Psi_0(D, A) + a^*\Psi_1(D^+—A^-)$$

Currently, there are two common methods (ref. 3, chapt. 6) of estimating the fraction of dative structure in the ground state of molecular complexes. One method is based upon infrared frequency shifts and the other method is based on dipole moment data. Both methods are quite complicated to use and they also involve some major assumptions (ref. 3, chapt. 6).

The relationship between the energy, $h\nu$, of a charge-transfer transition from the ground state, Ψ_N, to the excited state, Ψ_V, and the ionization potential, I_D, of the donor was given by Briegleb and Czekalla (7) in the form of eq. [3] where h is Planck's constant and C_1 and C_2 are constants for a given acceptor. Later, it was found that eq. [4] which expresses a

$$[3] \quad h\nu = I_D - C_1 + C_2/(I_D - C_1)$$

$$[4] \quad h\nu = mI_D + n$$

linear relationship between $h\nu$ and I_D is valid for many complexes (8, 9). There are two problems (2, 3, 7, 8) associated with the use of eq. [4]. The first one is the deviation of the slope m from unity. The deviation increases as the complex becomes stronger. In the case of amine–iodine complexes the deviation is large and various reasons have been given to account for it (10–12). The second problem is the choice of the correct set of m and n values for often more than one value each for m and n could fit the observed values of $h\nu$.

This paper is presented with two aims. The first aim is to give a simple method of estimating the fraction, F_1, of dative structure in molecular complexes using [5] where ρ_{CT} is the Hammett (13) ρ value relating the equilibrium constants of a series of molecular complexes formed from a closely related series of donors with a common acceptor and ρ_{Ref} is the Hammett ρ value of a model system which has a full positive charge developed on the donors.

$$[5] \quad F_1 = \rho_{CT}/\rho_{Ref}$$

The second aim is to give a physical interpretation to the slope m of eq. [4] to account for its deviation from unity.

Results and Discussion

Equation [5] is applied to molecular complexes formed from a series of methyl-substituted benzenes as donors with a variety of acceptors. The ρ value for the ionization potentials of benzenes is taken to be ρ_{Ref} since the cation of the substituted benzene (**1**) is a good model for the corresponding donor in the dative structure (**2**) of the molecular complex. This

0008-4042/79/121418-03$01.00/0

TABLE 1. Fraction of dative structure in benzene complexes

No.	Acceptor	Solvent	ρ Value	ρ Source of data	n^a	r^b	F_1 This work[k]	F_1 Literature value
1.	Bromine	CCl_4	−0.48	Ref. 19	3	0.999	0.033	0.04[c,h]
2.	Iodine monochloride	CCl_4	−1.55	Ref. 20	3	0.866	0.105	0.11,[c,h] 0.10,[d,h] 0.11,[e,h]
3.	Iodine	CCl_4	−0.54	Ref. 20	7	0.978	0.036	0.075[c,h]
4.	Iodine monobromide	CCl_4	−0.58	Ref. 21	6	0.956	0.039	—
5.	*s*-Trinitrobenzene	$CHCl_3$	−0.52	Ref. 22	4	0.931	0.036	0.021,[f,i] 0.038[g,i]
6.	Tetracyanoethylene	CH_2Cl_2	−0.98	Ref. 23	6	0.986	0.067	0.062,[f,j] 0.067[g,j]
7.	Chloranil	CCl_4	−0.59	Ref. 24	3	0.999	0.040	0.041[f,j]
8.	Carbon tetrachloride	CCl_4	−0.62	Ref. 25	4	0.986	0.042	—
9.	Dinitrobenzene	CCl_4	−0.41	Ref. 26	4	0.972	0.028	—
10.	Fluoranil	CCl_4	−0.76	Ref. 27	7	0.994	0.052	—
11.	Nitroform	Cyclohexane	−0.87	Ref. 28	9	0.992	0.059	—
12.	Trinitrotoluene	CCl_4	−0.48	Ref. 26	5	0.977	0.033	—

[a]Number of points used in correlations.
[b]Correlation coefficient.
[c]For benzene.
[d]For toluene.
[e]For *p*-xylene.
[f]For durene.
[g]For hexamethylbenzene.
[h]Reference 3, pp. 67–68.
[i]Reference 29.
[j]Reference 30.
[k]Calculated from eq. [5] with $\rho_{Ref} = -14.7$.

value of ρ_{Ref} is −14.7 (14). The values of ρ_{CT} for the equilibrium constants for molecular complexes formation were calculated from the usual Hammett plots using σ_p^+ values taken from Okamoto and

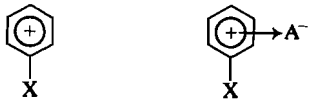

1 2

Brown (15) and assuming additive substituent effects of the methyl group. On the whole the plots are good (Table 1) and the F_1 values compare well with literature values obtained from infrared frequency shifts and dipole moments. The inherent assumption in eq. [5], that molecular complexes formed from a closely related series of donors with a common acceptor have the same amount of dative structure, is supported by the few available literature results. For examples, the complexes of iodine monochloride with benzene, toluene, and *p*-xylene all have 11% dative structure (Table 1), and complexes of iodine monochloride with pyridine and 3,5-dibromopyridine have 30% dative structure (16).

Actually the ρ_{Ref} value used must be from the same solvent in which the equilibrium constants of molecular complexes were measured. However, such data are not available. The fact that the gas phase value of −14.7 works well in our method probably indicates that the ρ values in chlorinated methanes (the solvents used in molecular complex studies) are close to −14.7 (17).

The underlying principle of eq. [5] is that ρ_{CT} is essentially determined by the dative structure because the donor in the dative structure has a positive charge on it whereas the no-bond structure is expected to have a negligible effect on the magnitude of ρ_{CT} because the donor in the no-bond structure is an uncharged species. We can see an analogous situation in the large ρ values for ion producing reactions and small ρ values for free radical reactions in which no charge is developed.

We shall now derive eq. [4] from a combination of two Hammett equations. The Hammett equation correlating the charge-transfer energies of a series of molecular complexes (2) is given by eq. [6]

$$[6] \qquad (h\nu_x - h\nu_0)/(2.3RT) = \rho_{h\nu}\sigma$$

where the subscripts x and 0 denote the substituted and unsubstituted donors respectively, R is the gas constant, and T is the absolute temperature. The Hammett equation correlating the ionization potentials of the same series of donors is given by eq. [7] (I and $h\nu$ are expressed in the same unit).

$$[7] \qquad (I_x - I_0)/(2.3RT) = \rho_{IP}\sigma$$

A combination of eqs. [6] and [7] yields

$$[8] \qquad h\nu_x = (\rho_{h\nu}/\rho_{IP})I_x + h\nu_0 - (\rho_{h\nu}/\rho_{IP})I_0$$

which is analogous to eq. [4] with

$$[9] \qquad m = \rho_{h\nu}/\rho_{IP}$$

$$[10] \qquad n = h\nu_0 - (\rho_{h\nu}/\rho_{IP})I_0$$

TABLE 2. A comparison of calculated and observed values of m and n

No.	Complex[a]	m		n	
		Calculated[h]	Observed	Calculated[i]	Observed
1.	Benzenes–TNB	0.93	0.89[b]	−4.2	−4.3[b]
2.	Benzenes–IBr	0.92	0.84[c]	−4.2	−3.3[c]
3.	Benzenes–Chloranil	0.92	0.89[d]	−4.8	−4.3[d]
4.	Benzenes–I_2	0.86	0.87[b]	− 3.7	−3.6[e]
5.	Benzenes–TCNE	0.87	0.83[e]	−4.8	−4.4[f]
6.	Benzenes–ICl	0.78	0.68[f]	−2.8	−1.8[g]
7.	Amines–I_2	0.30	0.35[g]	2.4	1.9[g]

[a]TNB = trinitrobenzene; TCNE = tetracyanoethylene; Nos. 1, 2, 3, 4, and 6 in CCl_4, No. 5 in CH_2Cl_2, and No. 7 in heptane.
[b]Reference 31.
[c]Calculated from data of ref. 21.
[d]Reference 18.
[e]Reference 6.
[f]Calculated from data of ref. 20.
[g]Calculated from data of ref. 12.
[h]Calculated using eq. [11]; F_1 values taken from Table 1 except No. 7 with $F_1 = 0.35$ (ref. 3, p. 68).
[i]Calculated using eq. [12] with ν_0 and I_0 values taken from the references listed under the column for n.

In eq. [5] only the ground state of the molecular complex is involved and ρ_{CT} is determined by the dative structure. In eq. [8] both the ground and excited states of the molecular complex are involved. Therefore, $\rho_{h\nu}$ is determined by the difference in the fraction of dative structures in these two states, that is, $F_1^* - F_1$ where the superscript * indicates the excited state. The factor $F_1^* - F_1$ is equivalent to $1 - 2F_1$ (ref. 3, chapt. 1). Therefore, we obtain

$$[11] \qquad m = 1 - 2F_1$$

$$[12] \qquad n = h\nu_0 - (1 - 2F_1)I_0$$

Table 2 gives the m and n values calculated from eqs. [11] and [12], respectively, for several molecular complexes. They are in good agreement with the observed values reported in the literature. Therefore, eqs. [11] and [12] provide a method of predicting the slope m and the intercept n of the commonly used eq. [4], and thereby overcome the problem of choosing the correct set of m and n values. Equation [11] further gives a physical meaning to m, in contrast to the earlier suggestion that it has no theoretical significance (2, 3). We also can see that unit m is a special case — when F_1 is zero.

Acknowledgement

The author thanks Universiti Sains Malaysia for financial support in this work.

1. L. J. ANDREWS and R. M. KEEFER. Molecular complexes in organic chemistry. Holden-Day, San Francisco. 1964.
2. R. FOSTER. Organic charge-transfer complexes. Academic Press, London. 1969.
3. R. S. MULLIKEN and W. B. PERSON. Molecular complexes: a lecture and reprint volume. Wiley-Interscience, New York. 1969.
4. C. N. R. RAO, S. N. BHAT, and P. C. DWIVEDI. *In* Applied spectroscopy review. Vol. 5. Marcel Dekker, New York. 1972.
5. R. S. MULLIKEN. J. Am. Chem. Soc. **74**, 811 (1952).
6. E. M. VOIGT and C. REID. J. Am. Chem. Soc. **86**, 3930 (1964).
7. G. BRIEGLEB and J. CZEKALLA. Z. Elektrochem. **63**, 6 (1959).
8. H. M. MCCONNELL, J. S. HAM, and J. R. PLATT. J. Chem. Phys. **21**, 66 (1959).
9. R. FOSTER. Tetrahedron, **10**, 96 (1960).
10. J. COLLIN. Z. Elektrochem. **64**, 936 (1960).
11. K. TOYODA and W. B. PERSON. J. Am. Chem. Soc. **88**, 1629 (1966).
12. H. YADA, J. TANAKA, and S. NAGAKURA. Bull. Chem. Soc. Jpn. **33**, 1660 (1960).
13. L. P. HAMMETT. Physical organic chemistry. McGraw-Hill, New York. 1940.
14. P. LINDA, G. MARINO, and S. PIGNATARO. J. Chem. Soc. B, 1585 (1971); G. F. KRABLE and G. L. KEARNS. J. Phys. Chem. **66**, 436 (1962).
15. Y. OKAMOTO and H. C. BROWN. J. Org. Chem. **22**, 485 (1953).
16. W. B. PERSON. *In* Spectroscopy and structure of molecular complexes. Plenum Press, London. 1973. p. 28.
17. B.-L. POH. Can. J. Chem. **57**, 255 (1979).
18. R. FOSTER. Nature, London, **183**, 1253 (1959).
19. R. M. KEEFER and L. J. ANDREWS. J. Am. Chem. Soc. **72**, 4677 (1950).
20. L. J. ANDREWS and R. M. KEEFER. J. Am. Chem. Soc. **74**, 4500 (1950).
21. R. D. WHITAKER and H. H. SISLER. J. Phys. Chem. **67**, 523 (1963).
22. A. BIER. Recl. Trav. Chim. **75**, 866 (1956).
23. R. E. MERRIFIELD and W. D. PHILLIPS. J. Am. Chem. Soc. **80**, 2778 (1958).
24. T. E. HUNTER and D. H. NORFOLK. Spectrochim. Acta, A**25**, 193 (1969).
25. M. L. MCGLASHAN, D. STUBLEY, and H. WATTS. J. Chem. Soc. A, 673 (1969).
26. N. B. JURINSKI and P. A. D. DE MAINE. J. Am. Chem. Soc. **86**, 3217 (1964).
27. N. M. D. BROWN, R. FOSTER, and C. A. FYFE. J. Chem. Soc. B, 406 (1967).
28. J. HOMER and P. J. HUCK. J. Chem. Soc. A, 277 (1968).
29. G. BRIEGLEB and J. CZEKALLA. Z. Elektrochem. **59**, 184 (1955).
30. G. BRIEGLEB, J. CZEKALLA, and G. RENAS. Z. Phys. Chem. Frankfurt am Main, **30**, 333 (1961).
31. R. S. MULLIKEN and W. B. PERSON. Ann. Rev. Phys. Chem. **13**, 107 (1962).

In-plane and out-of-plane conformational preferences of the sulfhydryl group in some halothiophenol derivatives

TED SCHAEFER AND WILLIAM J. E. PARR
Department of Chemistry, University of Manitoba, Winnipeg, Man., Canada R3T 2N2
Received November 10, 1978

TED SCHAEFER and WILLIAM J. E. PARR. Can. J. Chem. **57**, 1421 (1979).

Long-range spin–spin coupling constants between sulfhydryl protons and ring protons in some halothiophenol derivatives in CCl_4 solutions are reported. In contrast to the corresponding phenol derivatives, substantial amounts of out-of-plane conformers are present at 305 K for all but 2,6-dichlorothiophenol. The *cis* and *trans* conformers differ by only about 0.2 kcal/mol in free energy for 2,4-dibromothiophenol and 2,4-dichlorothiophenol, in good agreement with a recent analysis of the dipole moment observed for the latter compound. The barrier to internal rotation of the sulfhydryl group is considerably smaller than for a hydroxyl group and rough estimates are given for the barrier in a few compounds. For example, the barrier in 2,3,5,6-tetrafluorothiophenol is lower than in 2,6-dichlorothiophenol. STO-3G MO calculations overestimate the internal barrier to rotation of the sulfhydryl group, but yield charge densities for this group which indicate that a major cause of the relative weakness of its intramolecular hydrogen bonds resides in its lack of polarity.

TED SCHAEFER et WILLIAM J. E. PARR. Can. J. Chem. **57**, 1421 (1979).

On rapporte les constantes de couplage à longue distance entre les protons sulfhydryles et ceux du cycle de quelques dérivés halothiophénols en solution dans le CCl_4. Par opposition aux résultats obtenus avec les dérivés phénoliques correspondants, il en résulte que, dans tous les cas, excepté le dichloro-2,6 thiophénol, des quantités importantes de conformères qui ne sont pas dans le plan à 305 K. L'énergie libre des conformères *cis* et *trans* ne diffère que par 0.2 kcal/mol dans le cas des dibromo-2,4 et dichloro-2,4 thiophénols; ce résultat est en bon accord avec une analyse récente du moment dipolaire observé pour ce dernier composé. La barrière à la rotation interne du groupe sulfhydryle est beaucoup plus faible que dans le cas du groupe hydroxyle et l'on donne des évaluations grossières pour cette rotation dans quelques composés. Par exemple, la barrière dans le tétrafluoro-2,3,5,6 thiophénol est plus basse que dans le dichloro-2,6 thiophénol. Des calculs de OM STO-3G donnent une évaluation trop élevée pour la barrière interne à la rotation du groupe sulfhydryle; toutefois les densités de charge qu'ils fournissent indiquent que la cause principale de la faiblesse relative de ses liaisons hydrogène intramoléculaires provient de son manque de polarité.

[Traduit par le journal]

Introduction

It has been shown (1–4) that the use of stereospecific long-range spin–spin coupling constants between hydroxyl and ring protons or ^{19}F nuclei in halophenol derivatives is perhaps one of the best ways to determine the conformational preferences of the hydroxyl group. For example, for 2,4-dihalophenols there exists little doubt that in CCl_4 or C_6H_{12} solution greater than 90% of **1** exists in the form **1***a* (*cis*) near room temperature.

For the corresponding halothiophenol derivatives,

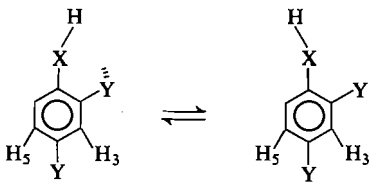

cis **1***a* X = O, S *trans* **1***b* X = O, S

their remains some ambiguity about the conformational populations so that the existence of so-called intramolecular hydrogen bonding of the S—H group to an *ortho* halogen substituent remains in doubt.

For example, an infrared study of 2,4-dichlorothiophenol in CCl_4 solution (5) gave no evidence for an intramolecular hydrogen bond, whereas another such study (6) indicated intramolecular hydrogen bonding in *o*-chlorothiophenol. Dipole moments in benzene solution of *o*-chlorothiophenol (7) and of 2,4-dichlorothiophenol (8), respectively, indicate about 70 and 50% abundance of the *cis* form (8). Other workers (6) suggest 95 ± 5% of the intramolecularly bonded forms for *o*-chlorothiophenol in CCl_4 at 298 K. In the latter study (6) the infrared and proton chemical shift data did not prove the existence of *cis* forms for the *o*-halothiophenols (in our opinion).

CNDO/2 MO calculations predict stronger intramolecular hydrogen bonds in *o*-chloro- and *o*-bromo-

0008-4042/79/121421-05$01.00/0

thiophenol than in the corresponding phenols, whereas an STO-3G MO calculation favours the *trans* conformer of *o*-chlorothiophenol by 2.8 kcal/mol (9).

In this paper we examine the proton magnetic resonance spectra in the absence of intermolecular proton exchange of some polyhalothiophenol derivatives dissolved in CCl_4. The long-range coupling constants involving the sulfhydryl proton demonstrate that intramolecular hydrogen bonding is considerably weaker than in the corresponding phenol derivatives. *Ab initio* MO calculations on some dichlorothiophenols and on 2,4-dichlorophenol are somewhat helpful in rationalizing the differences in conformational preferences.

Experimental

The compounds came from Aldrich Chemical Co.; 5 mol% solutions in CCl_4, containing some tetramethylsilane, were degassed by the freeze–pump–thaw method. Pellets of molecular sieve were sealed into the sample tube and prevented intermolecular sulfhydryl proton exchange, although some samples were kept for several weeks before the sulfhydryl proton resonances became sharp multiplets.

Weak irradiation experiments (10) gave the relative signs of coupling constants, determining spectra which were repeatedly calibrated at sweep rates of 0.02 Hz/s and a dispersion of 1 Hz/cm on HA100 and DA60I spectrometers operating in the frequency sweep mode. Frequency markers were placed at intervals of 5 Hz or less. The proton spectra were recorded at 305 K and the ^{19}F spectra at 301 K.

The proton resonance spectra of 2,5-dichloro- and of 2,4-dichlorothiophenol were also recorded for 1 mol% solutions in CCl_4.

Molecular orbital calculations at the *ab initio* STO-3G level (11) were performed on an IBM 370/158 system.

Results and Discussion

Spectral Analysis

The calibrated ^1H and ^{19}F magnetic resonance spectra were analyzed with the computer program LAME (12, 13). The error in the spectral parameters is thought to be 0.02 Hz or less, the numerical data for a typical analysis being given in Table 1. The signs of the coupling constants are given on the basis of $^3J_o^{H,H} > 0$, $^3J_o^{HF} > 0$, and $^3J_o^{F,F} < 0$ (14). The other spectral parameters of interest in this study are presented in Table 2.

The analysis of the proton spectrum of 3,5-dichlorothiophenol was impossible because of chemical shift equivalence. A similar occurrence is known for *p*-chlorothiophenol (15). The long-range couplings to the sulfhydryl proton in 2,5-dichloro- and in 3,4-dichlorothiophenol were the same in 1 and 5 mol% solutions. The sulfhydryl proton chemical shifts were not significantly different at the two concentrations, indicating negligible self-association. The chemical shifts of the S—H proton of thiophenol at 5 mol% (16) and at infinite dilution in CCl_4 (17) differ by only 0.03 ppm.

Extent of Intramolecular Hydrogen Bonding

In 2,4-dichlorophenol, $^5J_m^{H_3,OH} = J_3$ is not observable, whereas $^5J_m^{H_5,OH} = J_5$ is 0.46 Hz (1), suggesting that the compound exists almost solely in form **1***a* as a 4.9 mol% solution in CCl_4. Now, in 2,4-dichlorothiophenol (Table 2) J_3 is 0.30 ± 0.02 Hz and J_5 is 0.24 ± 0.02 Hz. On the assumption that J_3 vanishes for **1***a*, that J_5 vanishes for **1***b*, and that $J_3 = J_5$ in **1***b* and **1***a*, respectively,[1] one has $\Delta G^0 = G^0_{1b} - G^0_{1a} = -RT \ln J_5/J_3 = -0.14 \pm 0.12$ kcal/mol. In other words, the *trans* form is slightly more stable than the *cis* form. A similar calculation for 2,4-dibromothiophenol yields $\Delta G^0 = G^0_{1b} - G^0_{1a} = -0.17 \pm 0.12$ kcal/mol.

Apparently, the *cis* conformer of 2,4-dichlorothiophenol is $45 \pm 5\%$ abundant at 305 K, in close agreement with the 50% abundance deduced from the most recent dipole moment study (8). It is also of interest that a similar abundance of the *cis* conformer occurs in 2-methoxythiophenol (18).

No comparison between J_3 and J_5 can be made for the 2,5-disubstituted derivatives in Table 2. However, it is clear that substantial amounts of the *trans* conformers of 2,5-dichloro- and 2,5-dibromothiophenol exist under the experimental conditions.

The Population of Conformers with an Out-of-plane Sulfhydryl Bond

The twofold barrier to internal rotation in phenol is 3.5 kcal/mol (19, 20). In consequence, $^6J_p^{H,OH}$ is very small at 305 K (21) because this coupling very likely displays a $\sin^2\theta$ dependence, θ being the angle by which the O—H bond twists out of the plane of the phenyl group.[2] In thiophenol, however, ^6J is -0.33 Hz (16) in CCl_4 solution. It has been used to derive a twofold barrier to rotation about the C—S bond, amounting to 1.1 ± 0.3 kcal/mol (16) and in reasonable agreement with a barrier of 0.8 kcal/mol deduced from torsional data in the gas phase (22).

[1]This assumption for $^5J_m^{H,OH}$ has led to self-consistent intramolecular equilibrium constants for a variety of phenol derivatives and to agreement with conformational preferences deduced by other methods (1–4).

[2]It could have been argued that a decrease in θ implies an increase in the conjugation of the oxygen atom with the π-electron system of the ring. A π-electron coupling mechanism operating via the partially double C···O bond would then enhance the magnitude of $^6J_p^{H,OH}$ at $\theta = 0$. However, a $\sin^2\theta$ dependence of $^6J_p^{H,OH}$ is compatible with a σ–π electron coupling mechanism in which the spin polarization of the σ electrons in the O—H bond is transferred to the π system by a 'hyperconjugative' interaction. The latter is most effective where the O—H bond occupies a plane perpendicular to the benzene plane, i.e., when $\theta = 90°$.

TABLE 1. Proton* and fluorine† chemical shift and coupling‡ parameters for 2,3,5,6-tetrafluorothiophenol in CCl_4

Parameter	Value	Parameter	Value
ν_{SH}	369.50	$^4J_m^{F_3,F_5}$	−0.427(8)
$\nu_{2,6}$	3161.331(4)	$^4J_m^{H,F}$	7.326(8)
$\nu_{3,5}$	3209.240(4)	$^5J_p^{F,F}$	11.915(6)
ν_4	684.084(6)	$^4J_o^{F,SH}$	0.367(8)
$^3J_o^{F,F}$	−21.586(5)	$^5J_m^{F,SH}$	0.451(8)
$^3J_o^{H,F}$	9.604(8)	$^6J_p^{H,SH}$	−0.108(12)
$^4J_m^{F_2,F_6}$	−1.424(8)	rms deviation	0.023§

*In Hz at 100 MHz to low field of internal tetramethylsilane at 305 K.
†In Hz to high field of internal CF_3CCl_3 at 56.4 MHz at 301 K (20 mol% in CCl_4).
‡In Hz; numbers in parentheses indicate the standard deviation in the last figure.
§For the fluorine iteration.

The value of 1.1 kcal/mol depends on the assumption that ^6J varies as $\sin^2\theta$. It was estimated that ^6J ($\theta = 90°$) is −1.05 Hz. A value of ^6J ($\theta = 90°$) of −0.97 Hz would reproduce the gas phase barrier.

The observed ^6J of −0.17 Hz in 2,5-dichlorothiophenol means that out-of-plane conformations are appreciably populated. The potential function for internal rotation of the S—H bond in this molecule must contain at least onefold and twofold terms, V_1 and V_2 (23). The former measures the energy difference between the *cis* and *trans* planar conformers and, by analogy to the 2,4-dichloroisomer, is probably less than 0.2 kcal/mol (see ^5J values in Table 2). One may write (23)

$$[1]\quad V(\theta) = V_1(1 - \cos\theta)/2 + V_2(1 - \cos 2\theta)/2$$

Here, $\theta = 0°$ for the *cis* conformer, **1***a*.

If $V_2 \gg V_1$, a treatment in terms of a twofold barrier (16) has some meaning. Writing $\langle\sin^2\theta\rangle$ as 0.17/0.97 for 2,5-dichlorothiophenol (see Table 2) yields V_2 as 2.4 ± 0.8 kcal/mol; the quoted error recognizes the approximate nature of this model.

The value of −0.12 Hz for ^6J in the corresponding bromine derivative then indicates a V_2 of 3.0 ± 1.0 kcal/mol.

Of course, it is conceivable that in the *cis* conformer the S—H bond is held mainly in-plane by electrostatic interaction with the *ortho* C–halogen bond and that the ^6J arises mainly from out-of-plane conformations in the *trans* conformer. It would then be expected, however, that V_1 be considerably larger than the value indicated by the equilibrium populations found above and by the most recent dipole moment studies (8), which surmised the existence of out-of-plane conformations of the S—H group in 2,4-dichlorothiophenol.

2,6-Dichlorothiophenol

$^6J_p^{SH,H}$ is less than 0.05 Hz in this compound, implying that the twofold barrier to internal rotation is appreciably larger than 3 kcal/mol (16), and that out-of-plane conformations are inappreciably populated at 305 K in CCl_4 solution. It is assumed, of course, that the substituents do not alter the $\sin^2\theta$ dependence of ^6J_p, a very good assumption in the corresponding toluene derivatives (24) and, apparently, in a variety of phenol derivatives (1–4).

In CCl_4 solution, the chemical shift of the S—H proton in benzenethiol is 3.23 ppm (16). In 2,6-dichlorothiophenol the S—H resonance shifts to low field by 1.28 ppm (Table 2) and such shifts have been taken as an indicator[3] of intramolecular hydrogen bonding (6, 25). On the other hand, the O—H resonance at infinite dilution of phenol in CCl_4 is 4.25 ppm at 305 K (26, 27). In 2,6-dichlorophenol (5 mol% in CCl_4 at 305 K) the O—H peak occurs at 5.66 ppm; the low-field shift is 1.41 ppm. It is accepted that a relatively strong intramolecular hydrogen bond exists in the phenol derivative (20) although no V_2 has been derived. For pentachlorophenol in solution, torsion data yield a V_2 of 6.3 kcal/mol (28), almost 3 kcal/mol higher than in phenol.

The present nmr data on 2,6-dichlorothiophenol are consistent with a V_2 of greater than 3 kcal/mol, an increase of greater than 2 kcal/mol relative to thiophenol. It is improbable that V_2 is as large as in the phenol derivative, however. Thus, our STO-3G calculations (see below) find a charge density of 0.996 electron on the S—H hydrogen atom, compared to only 0.762 electron on the O—H hydrogen atom in the *cis* conformation of 2,4-dichlorophenol. If the hydrogen bond is mainly electrostatic in nature (29, 30), these calculations suggest a weak hydrogen bond in the thiophenol derivative. The comparable magnitudes of the low-field shifts of the O—H and S—H proton resonances do not necessarily indicate similar strengths of intramolecular hydrogen bonds (31, 32).

2,3,5,6-Tetrafluorothiophenol

CNDO/2 and STO-3G calculations (9) agree that the intramolecular hydrogen bond in *o*-fluorothiophenol is about half the strength of that in *o*-fluorophenol. The CNDO/2 calculations (9) also yield a much weaker bond in *o*-fluorothiophenol than in *o*-chlorophenol. Similarly, V_2 in pentafluorophenol is 3.5 kcal/mol (33), compared to 6.3 kcal/mol in pentachlorophenol (although it should be remembered that a *para* fluoro substituent decreases the barrier in phenol by 0.3 to 0.4 kcal relative to a para *chloro* substituent (34)).

[3]The insignificant changes in the chemical shifts of the S—H protons in 2,4- and 3,4-dichlorothiophenol on dilution from 5 to 1 mol% in CCl_4 suggest negligible intermolecular association between solute molecules at these concentrations, in agreement with infrared studies of thiophenol derivatives (5).

TABLE 2. Sulfhydryl proton chemical shifts* and long-range spin–spin coupling constants† in some halothiophenol derivatives

Compound	ν_{SH}	$^4J_o^{SH,H}$	$^5J_m^{SH,H_3}$	$^5J_m^{SH,H_5}$	$^6J_p^{SH,H_4}$
2,4-DiCl	379.10	<0.05	0.30	0.24	—
2,5-DiCl	385.18	<0.07	0.26	—	−0.17
2,6-DiCl	450.67	—	0.36	0.36	<0.05
3,4-DiCl	335.19	−0.37‡	—	0.24	—
2,4-DiBr	388.07	<0.05	0.24	0.18	—
2,5-DiBr	392.51	−0.07	0.29	—	−0.12

*In Hz at 100 MHz and 305 K for 5 mol% solutions in CCl_4; to low field of internal tetramethylsilane.
†In Hz, with an accuracy of 0.02 Hz.
‡$^4J_o^{SH,H_2}$ is −0.38 Hz and $^4J_o^{SH,H_6}$ is −0.37 Hz, i.e., the couplings are equal to within experimental error.

All these data are consistent with the ^6J_p of −0.11 Hz in the tetrafluoro derivative (Table 1). V_2 is therefore smaller than in 2,6-dichlorothiophenol, in which a ^6J_p could not be observed. An estimate of V_2 is 3.0 ± 1.0 kcal/mol in the thiophenol derivative. Note that the chemical shift of the S—H proton resonance is 3.70 ppm, considerably upfield of the 4.51 ppm in 2,6-dichlorothiophenol.

That the S—H proton approaches the *ortho* fluorine atom less closely on average in the tetrafluorothiophenol than in the analogous phenol derivative is suggested by the positive value of $^4J_o^{F,SH}$. Its magnitude is only 0.37 Hz. An approach of the S—H proton and the ^{19}F nucleus to well within a distance corresponding to the sum of the van der Waals radii of the corresponding atoms, would undoubtedly lead to a large, negative, coupling constant (2, 35). This would be a result of the so-called through-space coupling mechanism, arising from direct interaction between the orbitals in the atoms containing the ^1H and ^{19}F nuclei (35–38). Thus, $^4J_o^{F,OH}$ in *o*-fluorophenol is calculated by INDO MO FPT as −4.5 Hz when the H,F distance is in the vicinity of 2.2 Å in the *cis* conformation (35), in very good agreement with a measured $^4J_{cis}^{F,OH}$ of −4.4 Hz in an *o*-fluorophenol derivative (2) and with an average $^4J^{F,OH}$ (*cis* and *trans*) of −2.5 Hz in 2,3,5,6-tetrafluorophenol (2). An increase in the H,F distance to 2.5 Å yields a positive calculated $^4J^{F,OH}$. Furthermore, as the O—H bond twists out-of-plane the calculated $^4J^{F,OH}$ rapidly increases, not only because of the decreased H,F distance but also because the σ–π mechanism ($\sin^2\theta$ dependence) makes a positive contribution to $^4J^{F,OH}$ (the hyperfine interaction constant, Q_{CF}, is positive in contrast to Q_{CH}).

That $^4J^{F,SH}$ is +0.37 Hz in 2,3,5,6-tetrafluorothiophenol is therefore consistent with the observed, finite $^6J_p^{SH,H}$ and with the observation of a relatively small low-field shift of the S—H proton in this compound.

3,4-Dichlorothiophenol

As the barrier to internal rotation in *para*-substituted thiophenols decreases, the magnitude of $^4J_o^{SH,H}$ increases, ranging from −0.70 Hz in 4-aminothiophenol to −0.20 Hz in 4-nitrothiophenol (16). ^4J_o is −0.37 Hz in 3,4-dichlorothiophenol (Table 2), within experimental error of its values in thiophenol and 4-bromothiophenol (16), suggesting an internal barrier of 1.0 ± 0.3 kcal/mol (note that the couplings to the two *ortho* protons are equal).

The very small magnitudes of ^4J_o in the other compounds in Table 2 are consistent with appreciably larger internal barriers as suggested in previous sections. However, distortions of the S—H group and and intrinsic substituent effect on ^4J_o from an electronegative or bulky *ortho* substituent may well be present, which may alter the magnitudes of ^4J_o in an unknown way.

Molecular Orbital Calculations

The STO-3G MO calculations with a standard geometry (39) yielded an internal barrier of 2.8 kcal/mol, clearly much too high and comparable to the overestimate of 1.7 kcal/mol for phenol (34). Optimization of the geometry of the S—H bond gave a CSH bond angle of 95.8° (CNDO/2 yields 98° (9)) and a C—S bond length of 1.762 Å. The predicted barrier increased to 3.5 kcal/mol, however.

The geometry optimization consumed 1.5 h of cpu time, so that a limited number of other calculations were performed.[4] In 2,6-dichlorothiophenol, the planar conformation had an optimized CSH angle of 94.5°, indicating, by comparison with thiophenol, that intramolecular attraction (hydrogen bonding to the C—Cl dipole) decreases the CSH angle. This indication is supported by the calculated hydrogen atom charges, which are 1.029 electrons in thiophenol (optimized geometry) and 0.996 electrons in the 2,6-dichloro derivative. In other words, one has a S^+—H^- dipole in thiophenol itself.

In 2,4-dichlorothiophenol, the STO-3G calculations found the *trans* form as more stable than the *cis* form for both standard and optimized geometries, in contradiction to experiment, and reminiscent of

[4]Kollmann and co-workers (9) have compiled an extensive set of CNDO/2 and STO-3G calculations on *ortho*-substituted phenols and thiophenols.

recent calculations on *o*-chlorothiophenol (9). Further calculations were contraindicated. The calculation on the 2,4-dichlorophenol, mentioned above, assumed a standard geometry.

A CSH bond angle of 96°, C—S, S—H, and C—F bond lengths of 1.80, 1.34, and 1.35 Å, respectively, together with an otherwise standard geometry, implies a H,F distance of 2.22 Å for a planar conformation of 2,3,5,6-tetrafluorothiophenol. Therefore a large, negative $^4J^{F,SH}$ might be expected. However, a MINDO/3 optimization on thiophenol (40) gave a CSH angle of 102.3°. Such a bond angle, together with some out-of-plane motion of the S—H bond and perhaps a small increase of the CCF bond angle, might very well increase the average H,F distance to such an extent that the highly distance-sensitive through-space coupling becomes small in magnitude.

It does appear that the primary reason for the relatively weak intramolecular hydrogen bonds in thiophenol derivatives is the small polarity of the S—H bond (41). Intermolecular hydrogen bonding would therefore also be weak relative to phenol, as observed (42).

Acknowledgment

We are grateful to the National Research Council of Canada for financial assistance.

1. J. B. Rowbotham and T. Schaefer. Can. J. Chem. **52**, 3037 (1974).
2. J. B. Rowbotham, M. Smith, and T. Schaefer. Can. J. Chem. **53**, 986 (1975).
3. T. Schaefer and J. B. Rowbotham. Can. J. Chem. **54**, 2243 (1976).
4. T. Schaefer and K. Chum. Can. J. Chem. **56**, 1788 (1978).
5. J. G. David and H. E. Hallam. Spectrochim. Acta, **21**, 841 (1965).
6. T. Kobayashi, A. Yamashita, Y. Furuya, R. Horie, and M. Hirota. Bull. Chem. Soc. Jpn. **45**, 1494 (1972).
7. H. Lumbroso, D. M. Bertin, and N. Marziano. Bull. Soc. Chim. Fr. 540 (1966).
8. H. Lumbroso, J. Curé, and C. G. Andrieu. J. Mol. Struct. **43**, 87 (1978).
9. S. W. Dietrich, E. C. Jorgensen, P. A. Kollman, and S. Rothenberg. J. Am. Chem. Soc. **98**, 8310 (1976).
10. R. Freeman and W. A. Anderson. J. Chem. Phys. **37**, 2053 (1962).
11. W. J. Hehre, W. A. Lathan, R. Ditchfield, M. D. Newton, and J. A. Pople. Quantum Chemistry Program Exchange, **10**, 236 (1974).
12. S. M. Castellano and A. A. Bothner-By. J. Chem. Phys. **41**, 3863 (1974).
13. C. W. Haigh and J. M. Williams. J. Mol. Spectrosc. **32**, 398 (1969).
14. W. B. Moniz and E. Lustig. J. Chem. Phys. **50**, 1905 (1969).
15. S. H. Marcus and S. I. Miller. J. Phys. Chem. **68**, 331 (1964).
16. W. J. E. Parr and T. Schaefer. J. Magn. Reson. **25**, 171 (1977).
17. S. H. Marcus and S. I. Miller. J. Phys. Chem. **73**, 453 (1969).
18. T. Schaefer and T. A. Wildman. Can. J. Chem. **57**, 450 (1979).
19. (*a*) E. Mathier, D. Welti, A. Bauder, and H. H. Gunthard. J. Mol. Spectrosc. **37**, 63 (1971). (*b*) J. C. Evans. Spectrochim. Acta, **16**, 1382 (1960).
20. W. G. Fateley and G. L. Carlson. Pure Appl. Chem. **36**, 109 (1973).
21. T. Schaefer, J. B. Rowbotham, and K. Chum. Can. J. Chem. **54**, 3666 (1976).
22. N. W. Larsen and F. M. Nicolaisen. J. Mol. Struct. **22**, 29 (1974).
23. G. L. Carlson and W. G. Fateley. J. Phys. Chem. 77, 1157 (1973).
24. T. Schaefer, L. J. Kruczynski, and W. J. E. Parr. Can. J. Chem. **54**, 3210 (1976).
25. M. Hiroto and R. Hoshi. Tetrahedron, **25**, 5953 (1969).
26. T. Gramstad and E. D. Becker. J. Mol. Struct. **5**, 253 (1970).
27. A. J. Dale and T. Gramstad. Spectrochim. Acta, Part A, **28**, 639 (1972).
28. J. H. S. Green, D. J. Harrison, and C. P. Stockley. J. Mol. Struct. **33**, 307 (1976).
29. A. Igawa and H. Fukutome. Bull. Chem. Soc. Jpn. **47**, 34 (1974).
30. H. Umeyama and K. Morokuma. J. Am. Chem. Soc. **99**, 1316 (1977).
31. P. A. Kollman and L. C. Allen. Chem. Rev. **72**, 283 (1972).
32. L. C. Allen. J. Am. Chem. Soc. **97**, 6921 (1975).
33. J. H. S. Green and D. J. Harrison. J. Chem. Thermodyn. **8**, 529 (1976).
34. L. Radom, W. J. Hehre, J. A. Pople, G. L. Carlson, and W. G. Fateley. J. Chem. Soc. Chem. Commun. 308 (1972).
35. T. Schaefer and J. B. Rowbotham. Chem. Phys. Lett. **29**, 633 (1974).
36. T. Schaefer, K. Chum, K. Marat, and R. E. Wasylishen. Can. J. Chem. **54**, 800 (1976).
37. J. Hilton and L. H. Sutcliffe. Prog. Nucl. Magn. Reson. Spectrosc. **10**, 27 (1975).
38. R. E. Wasylishen and M. Barfield. J. Am. Chem. Soc. **97**, 4545 (1975).
39. J. A. Pople and M. Gordon. J. Am. Chem. Soc. **89**, 4254 (1967).
40. M. J. S. Dewar, D. H. Lo, and C. A. Ramsden. J. Am. Chem. Soc. **97**, 1311 (1975).
41. H. Lumbroso and D. M. Bertin. Bull. Soc. Chim. Fr. 532 (1966).
42. S. H. Marcus and S. I. Miller. J. Am. Chem. Soc. **88**, 3719 (1966).

The ^{13}C chemical shifts of various methylgermanium derivatives

JOHN E. DRAKE, BORIS M. GLAVINČEVSKI, ROBYN E. HUMPHRIES, AND ABDUL MAJID
Department of Chemistry, University of Windsor, Windsor, Ont., Canada N9B 3P4

Received November 9, 1978

JOHN E. DRAKE, BORIS M. GLAVINČEVSKI, ROBYN E. HUMPHRIES, and ABDUL MAJID. Can. J. Chem. **57**, 1426 (1979).

This paper reports ^{13}C chemical shifts for 20 methylgermanium compounds. These shifts are correlated against (*i*) the electronegativity of halogen in the Me_3GeX compounds, (*ii*) the calculated charge on the carbon atom, (*iii*) the ^1H shifts of the methyl protons, and (*iv*) the ^{13}C shifts for the analogous carbon, silicon, and tin compounds.

JOHN E. DRAKE, BORIS M. GLAVINČEVSKI, ROBYN E. HUMPHRIES et ABDUL MAJID. Can. J. Chem. **57**, 1426 (1979).

Dans ce travail, on rapporte les déplacements chimiques du ^{13}C de 20 composés méthylgermanium. On a établi une corrélation entre ces déplacements chimiques et (*i*) l'électronégativité de l'halogène présent dans les composés Me_3GeX, (*ii*) la charge calculée sur l'atome de carbone, (*iii*) les déplacements chimiques ^1H des protons des groupes méthyles et (*iv*) les déplacements chimiques du ^{13}C des composés analogues du carbone, du silicium et de l'étain.
[Traduit par le journal]

Introduction

Although numerous methylgermane derivatives have been described in the literature and their ^1H nmr spectra have been reported, no systematic study of their ^{13}C nmr spectra has appeared. By contrast, there have been recent ^{13}C nmr studies of organosilicon compounds (1–3) and, of course, ^{13}C nmr spectroscopy is a widely used structural tool for which many empirical correlations between ^{13}C chemical shifts and structural features have been developed (4, 5).

As an aid to understanding the chemistry of germanium compounds, we provide herein a tabulation of ^{13}C nmr chemical shifts for a variety of methylgermanium derivatives. We also include ^1H chemical shifts of the germanium compounds and the ^{13}C chemical shifts of the corresponding carbon, silicon, and tin compounds (1, 2, 4, 6–17) where available. For carbon compounds, the ^{13}C chemical shifts of the central carbon are not included in the data. These would have appropriately been correlated with ^{73}Ge chemical shifts which are not yet available.

Results and Discussion

From an inspection of the data on the halide derivatives (Table 1), it is immediately apparent that within any series of methylgermanium halides, the degree of deshielding, as represented by the value of the ^{13}C chemical shift, exhibits an inverse dependency on the electronegativity of the halogen substituent. For the series Me_3GeX (X = F, Cl, Br, I) this inverse dependency is remarkably, and probably fortuitously, linear as is shown by the insert in Fig. 1. The linearity is maintained when the plot is made using the calculated charge on the carbon atom rather than electronegativity (Fig. 1). The latter plot also serves to illustrate that, by contrast, an increase in the number of halogen, electronegative substituents does cause an increased deshielding of the remaining methyl carbon atoms. The figure also emphasizes that differences resulting from a change in the number of like substituents on germanium are much larger than differences resulting from a change in the nature of a substituent. The comparative data show that these general features are also observed for the corresponding halides in the Me_3MX, Me_2MX_2, and $MeMX_3$ species, when M = Si (1, 2) or C (4). Moreover, in the corresponding lead compounds this trend is reversed (29). but no explanation for this difference in behaviour has been presented. The ^1H chemical shifts of the methyl groups in silicon, germanium, and tin methyl halides also exhibit an inverse dependency on the electronegativity of the halogen (4, 8, 18). The trends in silicon analogues have been attributed to halogen → silicon (*p–d*) π-bonding (19). However, the same trends can be noted in germanium and tin compounds where (*p–d*) π-bonding is said to be less important (8), as well as in the carbon analogues where it must be nonexistent. It has been suggested that the trends in the ^1H chemical shifts are explainable in terms of a major contribution from diamagnetic anisotropy and (or) dispersion effects on the ligands (8, 18). It is perhaps glib to suggest that the ^{13}C chemical shifts observed herein result from the same factors because it is apparent, to quote from work on the silicon

0008-4042/79/121426-05$01.00/0

TABLE 1. Nuclear magnetic resonance spectral data for Me_3MX, Me_2MX_2, and $MeMX_3$ species

No.‡	X	δ_C (methyl)* M = C	M = Si	M = Ge	M = Sn	δ_H*, M = Ge
1	CH_3	31.5[a]	0	−0.65	−9.3[b]	0.13
2	H	24.3[a]	−2.65[c]	−4.38	−11.8[d]	0.21
3	F	—	0.18[f]	1.34	—	0.51[e]
4	Cl	33.6[a]	3.25[f]	4.78	0.0[d]	0.78[e]
5	Br	36.5[a]	4.16[f]	5.65	−0.1[d]	0.88[e]
6	I	40.6[a]	4.84[f]	7.9	—	0.98[e]
7	OMe†	—	−1.35[f]	−1.52	−5.7[g]	0.33[h]
8	SEt†	—	—	1.6	−4.3[g]	0.46[i]
9	CN†	36.5[a]	−2.53[p]	−1.23	—	0.56[j]
10	SBu^t†	—	—	3.51	—	0.50[k]
11	SPh†	32.0[a]	2.0[l]	1.95	−3.6[g]	0.40[k]
12	SeEt†	—	—	2.01	—	0.55[m]
4	Cl_2	39.6[a]	6.6[f]	10.72	—	1.14[j]
5	Br_2	44.2[a]	—	15.05	8.6[d]	1.44[j]
6	I_2	—	12.97[f]	16.57	—	1.91[j]
7	$(OMe)_2$†	—	−4.7[f]	−3.14	—	0.36[n]
4	Cl_3	46.3[a]	9.82[f]	15.92	—	1.58[o]
5	Br_3	—	—	20.37	—	1.98[o]
6	I_3	—	21.1[f]	26.37	—	2.61[o]
7	$(OMe)_3$†	—	−9.36	−7.43	—	0.51

NOTES: [a]ref. 4, [b]ref. 6, [c]ref. 2, [d]ref. 7, [e]ref. 8, [f]ref. 1, [g]ref. 9, [h]ref. 10, [i]ref. 11, [j]ref. 12, [k]ref. 13, [l]ref. 14, [m]ref. 15, [n]ref. 16, [o]ref. 17, [p]supplied by one of the referees.

*All ^{13}C and ^1H chemical shifts are in ppm with reference to TMS; positive values denote downfield shifts.

†The following additional ^{13}C shifts are reported: Me_3GeOCH_3 50.78; $Me_3GeSCH_2CH_3$ 19.07; $Me_3GeSCH_2CH_3$ 20.89; Me_3GeCN 125.96; $Me_3GeSC(CH_3)_3$ 43.65; $Me_3GeSC(CH_3)_3$ 35.47; Me_3GeSPh, C_m 128.95, C_p 127.05, C_o 136.22 C—S 129.9; $Me_3GeSeCH_2CH_3$ 18.77; $Me_3GeSeCH_2CH_3$ 11.43; $Me_2Ge(OCH_3)_2$ 50.95; $MeGe(OCH_3)_3$ 51.1; Me_3SiCN 126.14.

‡The numbering system is used as a key to Figs. 2–4.

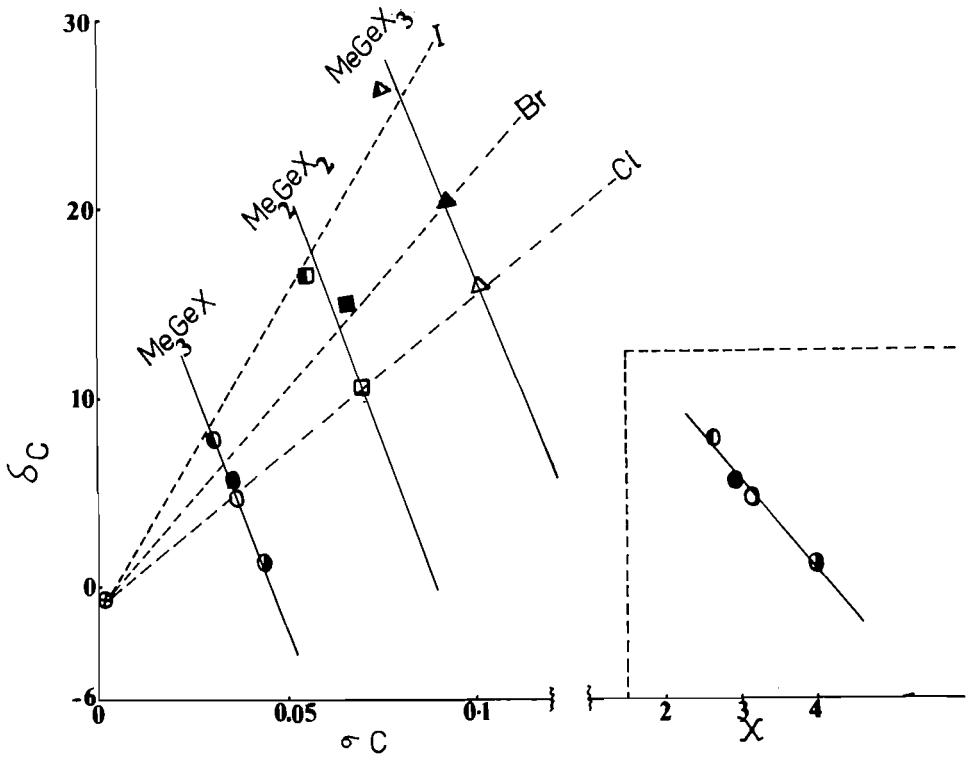

FIG. 1. ^{13}C chemical shifts, δ_C (ppm) as a function of the calculated charge on carbon, σC (and in parenthesis as a function of Pauling electronegativity, *X*) for the compounds Me_4Ge ⊗, Me_3GeF ◑, Me_3GeCl ○, Me_3GeBr ●, Me_3GeI ◐, Me_2GeCl_2 □, Me_2GeBr_2 ■, Me_2GeI_2 ◧, $MeGeCl_3$ △, $MeGeBr_3$ ▲, $MeGeI_3$ ◭.

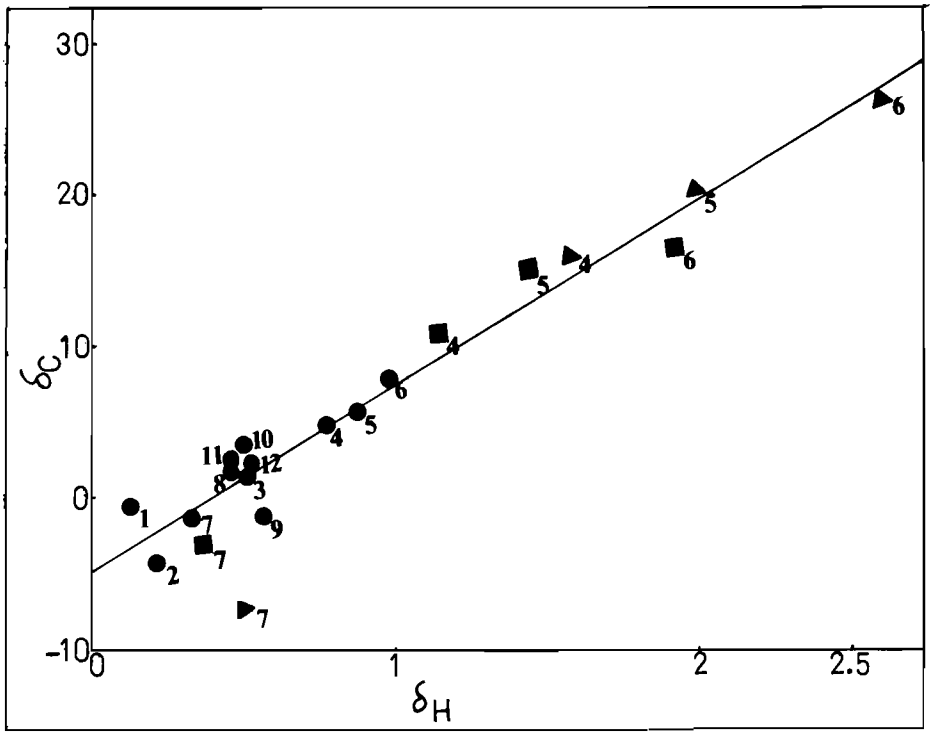

FIG. 2. ^{13}C chemical shifts (ppm) as a function of the ^{1}H chemical shifts (ppm) for various methylgermanes. The key to the numbering is in Table 1 with Me_3GeX ●, Me_2GeX_2 ■, and $MeGeX_3$ ▲. The correlation is $\delta_C = 12.7\delta_H - 5.55$.

compounds, that the reason for this β-effect is not clear (2).

However, as can be seen from Fig. 2, there is, in general, a linear relationship between the ^{13}C and ^{1}H chemical shifts within these germanium compounds which can be stated as fitting the equation $\delta_C = 12.7\delta_H - 5.55$. The linear correlation again suggests that similar factors are responsible for the observed trends in the ^{13}C and ^{1}H chemical shifts.

A correlation is presented in Fig. 3 of the ^{13}C chemical shifts of the methyl groups in germanium compounds, plotted against the corresponding shifts in similar carbon, silicon, and tin analogues. The data in two cases give slopes close to unity and may be correlated by the following linear relationships:

$$\delta_C(Ge) = 0.97\delta_C(C) - 29.68 = 0.92\delta_C(Sn) + 5.80$$

This suggests that the ^{13}C β-shifts for most of these compounds of carbon, germanium, and tin are controlled mainly by similar effects such as magnetic anisotropy or dispersion effects of ligands and hyperconjunction rather than effects such as (*p–d*) π-bonding, which if present, might be expected to differ for each group IV element. However, the silicon system, for which the latter effect is invoked most frequently, shows a significant deviation from a slope of unity, with $\delta_C(Ge) = 1.20\delta_C(Si) + 1.30$. Thus, we have yet another example of the behaviour of germanium being more like carbon than silicon.

The anomalous behaviour of successive methoxy group substitution compared with halide substitution, which was noted in discussing Fig. 2, is further illustrated by Fig. 4. The general features of this figure are remarkably similar to that recently reported for a variety of methylsilicon derivatives (1).

Experimental

Chloro- and bromomethylgermanes were obtained commercially (Alfa Inorganics) as was tetramethylgermane. The preparations of the other germanium compounds have been described in the literature (12, 13, 20–27). The purity was checked from their ir, Raman, and ^{1}H nmr spectra. Where there was sufficient quantity of material, the compounds were recorded as neat liquids (Me_3GeX and Me_2GeX_2; X = Cl, Br, I) or in deuteriochloroform (Me_3GeF) in 5 mm tubes. However, all of the other samples were sealed in capillaries which were then placed in the 5 mm nmr tubes containing deuteriochloroform (as lock) and TMS (as internal standard).

The spectra were all obtained using the Bruker CPX100 multinuclear pulsed Fourier transform NMR spectrometer operating at 22.64 MHz at a probe temperature of 35°C. All spectra were recorded under ^{1}H noise-decoupling conditions.

The charges on carbon in Fig. 1 were calculated by the EESOP method assuming varying degrees of *s*-character on fluorine (0%), chlorine (11%), bromine (16%), and iodine (19%) (28).

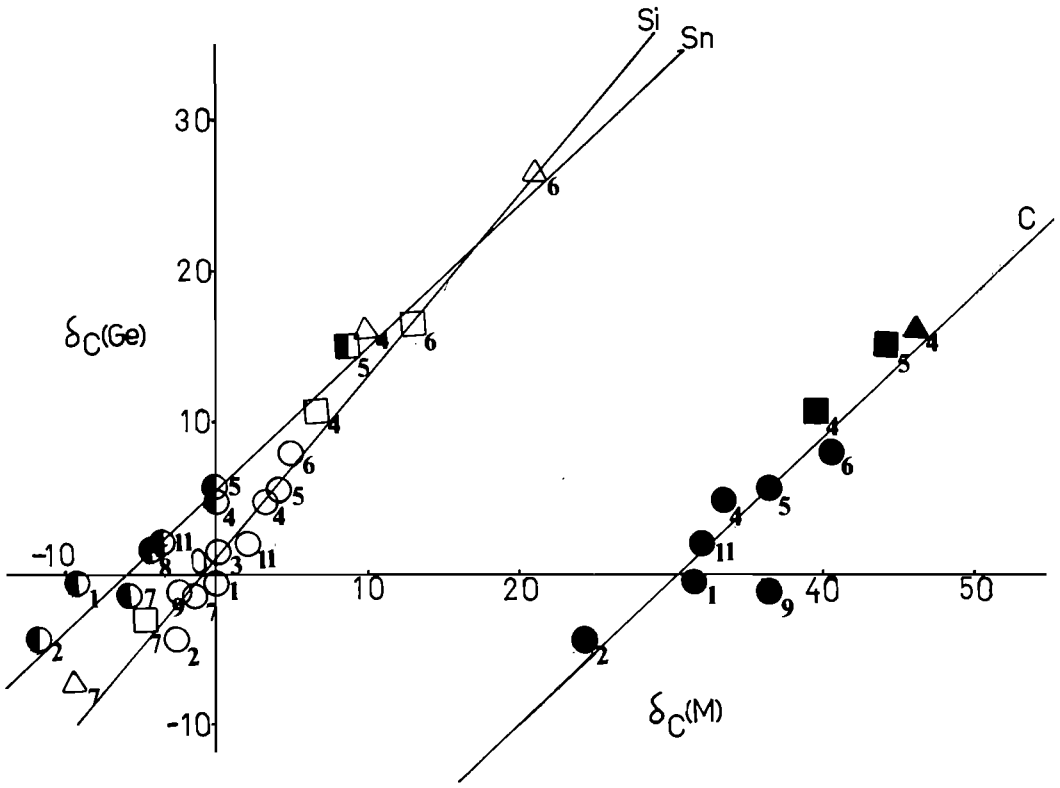

FIG. 3. The ^{13}C chemical shifts (ppm) of methylgermanium derivatives as a function of the ^{13}C chemical shifts (ppm) of the corresponding carbon, silicon, and tin analogues. The key to the numbering is shown in Table 1, with Me_3MX (M = C ●, Si ○, Sn ◐); Me_2MX_2 (M = C ■, Si □, Sn ◧); and $MeMX_3$ (M = C ▲, Si △). Correlations are given by $\delta_C(Ge) = 0.97\delta_C(C) - 29.68 = 1.20\delta_C(Si) + 1.30 = 0.92\delta_C(Sn) + 5.80$.

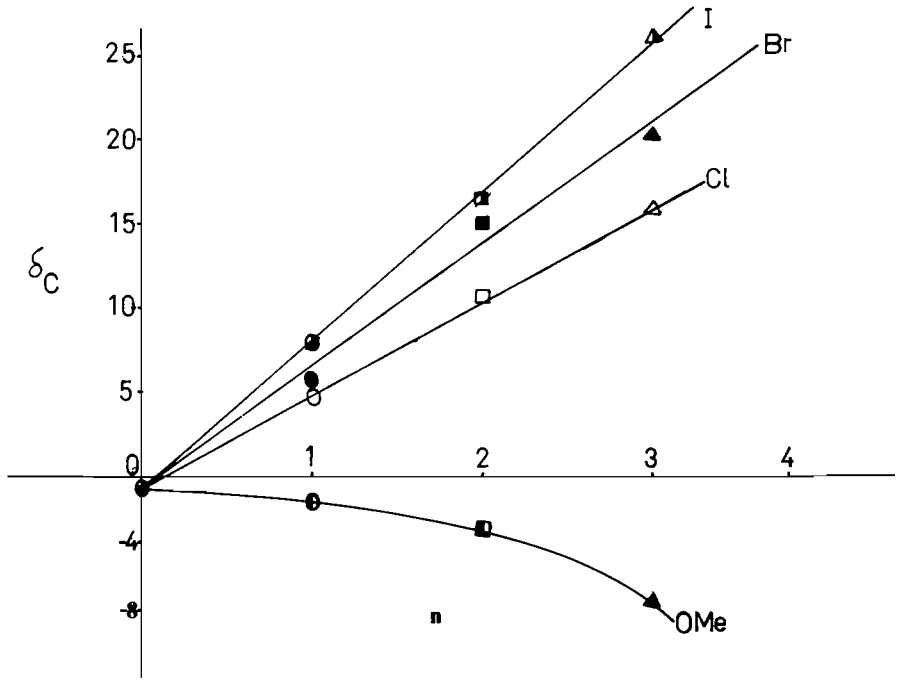

FIG. 4. Variation in ^{13}C chemical shifts of the methylgermanium resonance of $Me_{4-n}GeX_n$ as a function of the successive replacement of methyl by X = Cl ○□△, Br ●■▲, I ◑◨◭, and OMe ◐◧◮, with Me_4Ge ⊗.

Acknowledgement

We thank the Natural Sciences and Engineering Research Council of Canada for financial support.

1. P. E. RAKITA and L. S. WORSHAM. Inorg. Nucl. Chem. Lett. **13**, 547 (1977).
2. R. K. HARRIS and B. J. KIMBER. J. Magn. Reson. **17**, 174 (1975).
3. R. K. HARRIS and B. J. KIMBER. Org. Magn. Reson. **7**, 460 (1975).
4. J. B. STOTHERS. Carbon-13 NMR spectroscopy. Academic Press, New York, NY. 1972.
5. P. S. PREGOSIN and E. W. RANDALL. Determination of organic structures by physical methods. Vol. 4. Academic Press, New York, NY. 1971. p. 263.
6. M. H. CHISHOLM and S. GODELSKI. Progr. Inorg. Chem. **20**, 299 (1976).
7. T. N. MITCHELL. J. Organomet. Chem. **59**, 189 (1973).
8. H. SCHMIDBAUR and I. RUIDISCH. Inorg. Chem. **3**, 559 (1964).
9. V. S. PETROSYAN. Progr. Nucl. Magn. Reson. Spectrosc. **11**, 115 (1977).
10. C. YODER and R. SCHENCK. J. Inorg. Nucl. Chem. **33**, 2697 (1971).
11. J. E. DRAKE, B. M. GLAVINČEVSKI, and H. E. HENDERSON. Inorg. Nucl. Chem. Lett. **13**, 565 (1977).
12. G. K. BARKER, J. E. DRAKE, and R. T. HEMMINGS. Can. J. Chem. **52**, 2622 (1974).
13. J. E. DRAKE, R. T. HEMMINGS, and H. E. HENDERSON. J. Chem. Soc. Dalton Trans. 366 (1976).
14. S. PIGNATARO, L. LUNAZZI, C. A. BOICELLI, R. DIMARINO, A. RICCI, A. MANZINI, and R. DANIELE. Tetrahedron Lett. No. 52, 5341 (1972).
15. J. W. ANDERSON, G. K. BARKER, J. E. DRAKE, and M. RODGER. J. Chem. Soc. Dalton Trans. 1716 (1973).
16. K. M. ABRAHAM and J. R. VAN WAZER. J. Inorg. Nucl. Chem. **37**, 541 (1975).
17. J. E. DRAKE, R. T. HEMMINGS, and C. RIDDLE. J. Chem. Soc. A, 3359 (1970).
18. E. V. VAN DEN BERGHE and G. P. VAN DER KELEN. J. Organometal. Chem. **6**, 515 (1966); **26**, 207 (1971); **59**, 175 (1973).
19. H. SCHMIDBAUR. J. Am. Chem. Soc. **85**, 2336 (1963).
20. D. F. VAN DE VONDEL. J. Organometal. Chem. **3**, 400 (1975).
21. J. E. DRAKE, B. M. GLAVINČEVSKI, R. T. HEMMINGS, and H. E. HENDERSON. Inorg. Synth. **18**, 154 (1978).
22. J. W. ANDERSON, G. K. BARKER, A. J. F. CLARK, J. E. DRAKE, and R. T. HEMMINGS. Spectrochim. Acta, Part A, **30**, 1081 (1974).
23. J. W. ANDERSON, G. K. BARKER, J. E. DRAKE, and R. T. HEMMINGS. Can. J. Chem. **49**, 2931 (1971).
24. J. E. DRAKE, B. M. GLAVINČEVSKI, and H. E. HENDERSON. Synth. React. Inorg. Met. Org. Chem. **8**, 7 (1978).
25. F. WATARI. J. Mol. Struct. **32**, 285 (1976).
26. D. A. ARMITAGE and A. TARASSOLI. Inorg. Nucl. Chem. Lett. **9**, 1225 (1973).
27. A. MARCHAND, M.-T. FOREL, M. LEBEDEFF, and J. VALADE. J. Organometal. Chem. **26**, 69 (1971).
28. J. E. DRAKE, C. RIDDLE, H. E. HENDERSON, and B. M. GLAVINČEVSKI. Can. J. Chem. **54**, 3876 (1976).
29. T. N. MITCHELL, J. GMEHLING, and F. HUBER. J. Chem. Soc. Dalton Trans. 960 (1978).

Stereoselective synthesis of β-substituted α,β-unsaturated esters by dialkylcuprate coupling to the enol phosphate of β-keto esters

FUK-WAH SUM AND LARRY WEILER[1]

Department of Chemistry, University of British Columbia, Vancouver, B.C., Canada V6T 1W5

Received November 2, 1978

FUK-WAH SUM and LARRY WEILER. Can. J. Chem. 57, 1431 (1979).

The anions from β-keto esters or β-diketones were reacted with diethyl phosphorochloridate to yield the corresponding enol phosphates. These enol phosphates were coupled with dialkylcuprates to produce the β-substituted α,β-unsaturated esters or ketones in good yield. Starting from acyclic β-keto esters this sequence was used to stereoselectively generate tri- and tetrasubstituted olefins.

FUK-WAH SUM et LARRY WEILER. Can. J. Chem. 57, 1431 (1979).

On a fait réagir les anions de β-cétoesters ou de β-dicétones avec le phosphorochloridate de diéthyle et l'on a obtenu les phosphates énoliques correspondants. On a effectué une réaction de copulation de ces phosphates énoliques avec des cuprates de dialkyles pour conduire, avec de bons rendements, aux cétones ou aux esters α,β-non saturés substitués en β. En appliquant cette série de réactions à des esters β-cétoniques acycliques, on a obtenu stéréosélectivement des oléfines tri- et tétrasubstituées.

[Traduit par le journal]

In the past decade there has been wide interest in developing new methods to synthesize tri- and tetrasubstituted alkenes in a stereoselective fashion (1). These alkenes have been very useful in the synthesis of a range of natural products, including insect pheromones and terpenes. Recently, we have been investigating methods to utilize β-keto esters in the synthesis of these types of natural products. Dianions of β-keto esters can be trapped by a variety of electrophiles at the γ-carbon (2). These methods have been useful in the synthesis of acetogenins in which the β-keto ester moiety is directly incorporated into the final product (for some examples see ref. 3). On the other hand, conversion of the ketone of a β-keto ester into a methylated olefin as shown in [1] would then constitute a method to incorporate an isoprene unit in a synthetic scheme. The utility of this transformation would be further enhanced if any alkyl group could be used in place of the methyl group in [1].

[1] 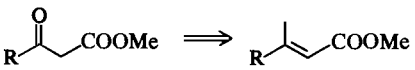

Casey and co-workers (4) have reported that acyclic β-keto esters can be stereoselectively converted into either the (*E*) or (*Z*) enol acetates which then undergo a stereospecific reaction with lithium dimethylcuprate. These reactions were applied in a synthesis of geraniol (4*a*) and (*Z*,*Z*)-7-methyl-3-propyl-2,6-decadien-1-ol (5). This sequence involves treating acyclic β-keto esters with isopropenyl acetate and *p*-toluenesulfonic acid at high temperature to obtain the (*Z*) enol acetates (4, 5). Unfortunately these strong acid conditions severely limit the functionality which may be incorporated in R of [1]; indeed this sequence has only been successful when R is a hydrocarbon. Recently, we have prepared the enol acetates of several cyclic β-keto esters and we find that they do not couple with dialkylcuprates. At low temperatures enol acetate is recovered, and at higher temperature or after prolonged reaction times the acetate is cleaved to yield a mixture of cyclic β-keto ester and enol acetate. House and co-workers (6) have shown that cuprate additions to α,β-unsaturated systems are governed by the ease of electron transfer to the conjugated system. This can be estimated from the reduction potential of the substrate. The reduction potential of the ester (**1**) is −2.50 V (6*a*) and House suggests that

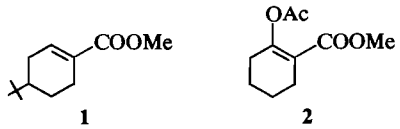

1 **2**

a β-acetoxy substituent has about the same effect on the reduction potential as a β-hydrogen substituent (6*b*). Thus we would estimate the reduction potential of the enol acetate **2** to be −2.5 V. Since it has been found that the α,β-unsaturated carbonyl compounds will react with lithium dimethylcuprate if the reduction potential of the unsaturated carbonyl compound is in the range −1.3 to −2.3 V (6*c*), it is not totally unexpected that **2** and related enol acetates do not react with lithium dimethylcuprate.

[1]Author to whom correspondence should be addressed.

0008-4042/79/121431-11$01.00/0

Two groups (7, 8) have reported that β-thiol α,β-unsaturated esters undergo a stereospecific coupling with dialkylcuprates. Unfortunately the β-thiol α,β-unsaturated esters are not readily available from β-keto esters as shown in [2]. In the case of methyl

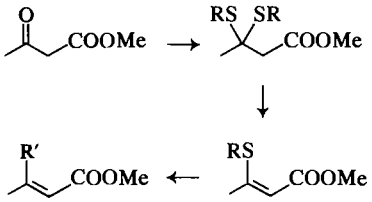

[2]

acetoacetate the desired vinyl sulfide can be prepared by a base catalyzed or thermal elimination from the thioketal (see [2]). However, in the case of more complex β-keto esters, particularly cyclic β-keto esters, the β,γ-unsaturated ester was often the major product from this reaction (9). Kobayashi and Mukaiyama (8*b*) overcame this difficulty by preparing acyclic vinyl sulfides from acetylenic esters as in [3]. It is clear that this route could not be used for α-substituted or cyclic systems.

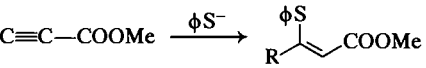

[3]

We also considered the use of β-halo α,β-unsaturated esters in a coupling reaction with dialkylcuprates. The very considerable success in the preparation of β-halo enones from β-diketones (10) and the coupling of dialkylcuprates with these systems (10*a*, 11) augured well for the β-halo α,β-unsaturated esters. However, we have been unable to efficiently convert β-keto esters into the corresponding β-halo α,β-unsaturated ester under a variety of conditions (also see ref. 10*a*). In cases where reaction did occur the product was often a mixture of *gem*-dihalo ester, desired β-halo ester, and γ-halo compound. Bryson (12) has prepared a β-iodo α,β-unsaturated ester by an internal solvolytic addition of the halide to an α,β-acetylenic ester. Again this method is not generally applicable.

Clearly there is a need for a simple, efficient, and general method to convert β-keto esters into β-substituted α,β-unsaturated esters. It is known that the enol phosphate of a ketone reacts with a dialkylcuprate to give the corresponding alkene (13). Thus we considered the synthesis and coupling of the enol phosphates of β-keto esters.

Treatment of methyl acetoacetate with sodium hydride and diethyl phosphorochloridate in ether (14) gave the enol phosphate **3** in 97% isolated yield. The vpc analysis of this material shows only one isomer and this was assigned the (*Z*) stereochemistry by comparing the proton nmr spectrum of enol phosphate **3** with that reported for the (*E*) and (*Z*) isomers of the enol dimethylphosphate of methyl acetoacetate (15). Coupling of the enol phosphate **3** with lithium dimethylcuprate gave the ester **4** in over 80% isolated yield.

This sequence was extended to include the β-keto esters in Table 1. Every β-keto ester we have investigated gave the corresponding enol phosphate in essentially quantitative yield. In the case of acyclic compounds the product was a single isomer by vpc and spectroscopic analysis, and this isomer was invariably the (*Z*) isomer using the above conditions. These enol phosphates can then be coupled with 1.5 to 3 equiv. of lithium dialkylcuprates at low temperature to produce the corresponding alkenes in good yield (Table 1).

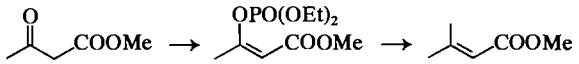

3 **4**

Several interesting points can be seen from this data. First, the coupling of primary dialkylcuprates has been successful with *every* combination of cuprate and enol phosphate we have tried. Note, for example, that the methyl 2-cyclohexanonecarboxylate (**10**) was converted into the alkene **22** in 94% yield (Table 1, entry 12) which can be compared to the complete failure of the enol acetate route (*vide supra*) with keto ester **10**. In the coupling with lithium di-*n*-butylcuprate often it was advantageous to use 1-bromobutane to quench the reaction (Table 1, entries 11 and 15). Secondary alkylcuprates proceed in poor yield (Table 1, entry 16) and tertiary alkylcuprates do not add to these enol phosphates under the above conditions. However, with excess di-*tert*-butylcuprate and at higher temperatures the enol phosphate from **10** can be converted into the ketone **26** in 80% yield (Table 1, entry 17). There is some evidence that the ester is attacked first to give the ketone **31**,

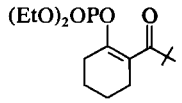

31

which then undergoes a coupling reaction with excess dialkylcuprate to give **26**.

Second, note that the coupling proceeds in the case of highly substituted systems (Table 1, entry 18). The keto ester **11** is readily prepared according to [4]. The dianion of methyl acetoacetate (2*a*) was alkylated with 1-bromo-3-methyl-2-butene to give **32** in 85% yield and **32** was then cyclized in almost quantitative yield with stannic chloride to give the keto ester **11**. The ester **27** is an obvious terminal unit for the syn-

TABLE 1. Preparation of β-substituted α,β-unsaturated esters from β-keto esters

No.	β-Keto ester	Cuprate	Product (yield)[a]	
1	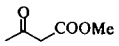	2 equiv. $LiMe_2Cu$	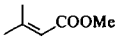 **4**	(83%)
2	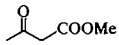	2 equiv. $LiEt_2Cu$	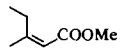 **13**	(90%)[b] ($Z:E$ = 5:1)[b]
3	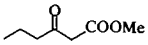 **5**	2 equiv. $LiMe_2Cu$	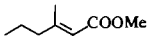 **14**	(83%) (>94%E)[b]
4	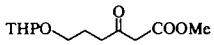 **6**	2 equiv. $LiMe_2Cu$	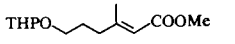 **15**	(94%) (>90%E)
5	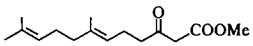 **7**	2 equiv. $LiMe_2Cu$	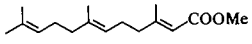 **16**	(91%) (>89%E)
6	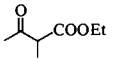 **8**	1.5 equiv. $LiMe_2Cu$	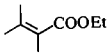 **17**	(85%)
7	**8**	2 equiv. $Li(nBu)_2Cu$ + nBuBr	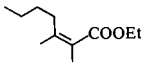 **18**	(72%) (>86%Z)
8	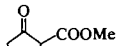 **9**	3 equiv. $LiMe_2Cu$	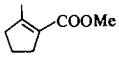 **19**	(85%)
9	**9**	2 equiv. $LiEt_2Cu$	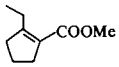 **20**	(52%)
10	**9**	2 equiv. $Li(nBu)_2Cu$	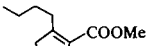 **21**	(67%)
11	**9**	2 equiv. $Li(nBu)_2Cu$ + nBuBr	**21**	(80%)
12	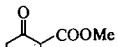 **10**	1.5 equiv. $LiMe_2Cu$	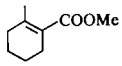 **22**	(94%)
13	**10**	2 equiv. $LiEt_2Cu$	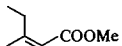 **23**	(79%)
14	**10**	2 equiv. $Li(nBu)_2Cu$	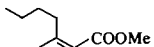 **24**	(54%)
15	**10**	2 equiv. $Li(nBu)_2Cu$ + nBuBr	**24**	(73%)
16	**10**	2 equiv. $Li(sBu)_2Cu$	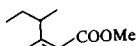 **25**	(20%)

TABLE 1 (*Concluded*)

No.	β-Keto ester	Cuprate	Product (yield)[a]	
17	**10**	4 equiv. $Li(tBu)_2Cu$	 **26**	(80%)
18	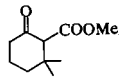 **11**	2 equiv. $LiMe_2Cu$	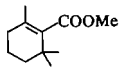 **27**	(92%)
19	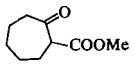 **12**	2 equiv. $LiMe_2Cu$	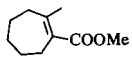 **28**	(98%)
20	**12**	2 equiv. $LiEt_2Cu$	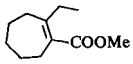 **29**	(79%)
21	**12**	2 equiv. $Li(nBu)_2Cu$ + $nBuBr$	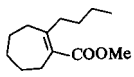 **30**	(81%)

[a]All yields are for isolated product and represent the overall yield for the two-step sequence.
[b]Determined by vpc. Because we were not always able to unambiguously identify the isomeric alkene in these vpc analyses, the percentage of the major isomer represents a lower limit in the stereoselectivity.

TABLE 2. Preparation of β-substituted α,β-unsaturated ketones from β-diketones

No.	β-Diketone	Cuprate	Product (yield)[a]	
1		2 equiv. $LiMe_2Cu$		(83%)
2		1.1 equiv. $LiMe_2Cu$		(92%)
3		2 equiv. $Li(tBu)_2Cu$		(83%)
4		1.1 equiv. $LiMe_2Cu$		(84%)
5		2 equiv. $LiMe_2Cu$		(74%)

[a]All yields are for isolated product and represent the overall yield for the two-step sequence.

thesis of carotenoids and retinals. Entries 6 and 7 of Table 1 also show that the reaction can be used to synthesize acyclic tetrasubstituted alkenes.

[4] 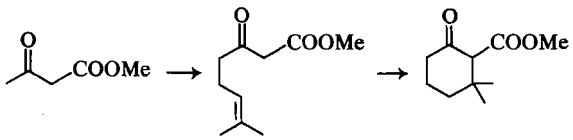

32 **11**

The third point to note is that the enol phosphate is prepared by a base catalyzed method and hence can be used with acid sensitive groups, for example Table 1, entry 4. In fact the dianion reactions (2) can be quenched directly with diethyl phosphorochloridate as shown in [5]. We have extended this to the multistep sequence shown in [6] in which the alkene **33** was obtained in 68% overall *without* isolation of any intermediates in a one-pot sequence in-

TABLE 3. Spectral data for enol phosphates of β-keto esters in Table 1

Enol phosphate	Infrared (cm^{-1})	Nuclear magnetic resonance (δ)	Mass spectra *m/e* (relative intensity)
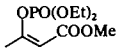	1725 1675 1030	1.38(d of t, J = 7 and 1.5 Hz, 6H), 2.17(m, 3H), 3.67(s, 3H), 4.23(qn, J = 7 Hz, 4H), and 5.27(m, 1H)	43(36), 67(30), 99(100), 109(26), 113(26), 127(64), 155(67), 164(70), 179(25), 192(53), 207(21), 220(70), and 252(34). *Anal.* calcd. for $C_9H_{17}PO_6$: 252.0763; found: 252.0739
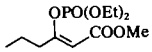	1725 1660 1035	0.95(t, J = 7 Hz, 3H), 1.35(bt, J = 7 Hz, 6H), 1.8(m, 2H), 2.2(m, 2H), 3.65(s, 3H), 4.21(qn, J = 7 Hz, 4H), and 5.28(s, 1H)	99(51), 101(38), 113(24), 127(5), 155(100), 220(23), 248(23), and 280(20). *Anal.* calcd. for $C_{11}H_{21}PO_6$: 280.1075; found: 280.1075
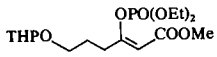	1730 1670 1030	1.36(t, J=7 Hz, 6H), 1.2–2 (m, 8H), 2.53(b t, J=7 Hz, 2H), 3.2–4(m, 2H), 3.65 (s, 3H), 4.22(qn, J=7 Hz, 4H), 4.50(b s, 1H), and 5.33(s, 1H)	85(17), 99(20), 111(25), 127(18), 142(42), 155(100), 219(10), 251(8), 279(6), 296(5), 349(2), and 380(·1). *Anal.* calcd. for $C_{15}H_{26}PO_7$(P−OMe): 349.1416; found: 349.1443
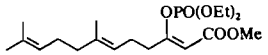	1730 1670 1030	1.35(t, J=7 Hz, 6H), 1.60(s, 6H), 1.67(s, 3H), 1.6–2.6(m, 8H), 3.65(s, 3H), 4.23(qn, J=7 Hz, 4H), 5(m, 2H), and 5.30(s, 1H)	99(63), 127(50), 155(100), 192(14), 202(13), 220(28), 234(20), 252(25), 287(18), 319(4), 343(3), 357(5), and 388(12). *Anal.* calcd. for $C_{19}H_{33}PO_6$: 388.2015; found: 388.2024
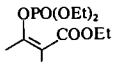	1720 1030	1.1–1.5(m, 9H), 1.83(m, 3H), 2.10(m, 3H), and 3.8–4.4(m, 6H)	43(45), 53(25), 70(20), 81(35), 99(100), 109(15), 127(70), 150(25), 155(75), 178(50), 206(40), 234(75), and 280(30). *Anal.* calcd. for $C_{11}H_{21}PO_6$: 280.1076; found: 280.1076
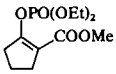	1710 1660 1035	1.38(t, J=7 Hz, 6H), 1.88(b qn, J=7 Hz, 2H), 2.4–3(m, 4H), 3.67(s, 3H), and 4.20(qn, J=7 Hz, 4H)	55(15), 81(8), 99(11), 101(17), 109(11), 113(14), 129(10), 141(7), 162(7), 190(100), 218(38), 246(60), and 278(12). *Anal.* calcd. for $C_{11}H_{19}PO_6$: 278.0919; found: 278.0918
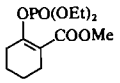	1715 1660 1030	1.35(t, J=7 Hz, 6H), 1.6(m, 4H), 2.3(m, 4H), 3.68(s, 3H), and 4.15(qn, J=7 Hz, 4H)	41(11), 55(14), 176(13), 204(100), 232(35), 260(67), and 292(10). *Anal.* calcd. for $C_{12}H_{21}PO_6$: 292.1076; found: 292.1087
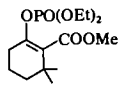	1725 1625 1030	1.15(s, 6H), 1–1.7(m, 4H), 1.31(t, J=7 Hz, 6H), 2.4 (m, 2H), 3.70(s, 3H), and 4.10(qn, J=7 Hz, 4H)	99(10), 127(8), 137(10), 217(28), 232(24), 245(17), 260(25), 273(28), 288(100), and 320(7). *Anal.* calcd. for $C_{14}H_{25}PO_6$: 320.1389; found: 320.1403
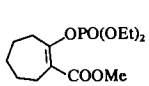	1720 1660(sh) 1030	1.34(t, J=7 Hz, 6H), 1.7(m, 6H), 2.2–2.8(m, 4H), 3.71(s, 3H), and 4.13(qn, J=7 Hz, 4H)	41(13), 55(15), 99(33), 113(9), 127(22), 155(21), 190(20), 218(50), 245(42), 274(100), and 306(9). *Anal.* calcd. for $C_{13}H_{23}PO_6$: 306.1232; found: 306.1242

volving dianion generation and alkylation, followed by phosphorochloridate quench and addition to the dialkylcuprate.

Finally, we note the very high stereoselectivity in the case of acyclic enol phosphates. In no case is the stereoselectivity less than 80% and it is usually considerably higher (Table 1, entries 2–5 and 7). In all cases investigated the alkyl group of the dialkylcuprate replaces the phosphate with retention of geometry. It is not clear what the origin of the stereoselectivity is in this reaction. However, dialkylcuprates react with vinyl halides via a substitution

TABLE 4. Spectral data for enol phosphates of β-diketones in Table 2

Enol phosphate	Infrared (cm^{-1})	Nuclear magnetic resonance (δ)	Mass spectra *m/e* (relative intensity)
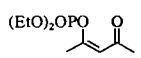	1695 1615 1025	1.36(t, J=7 Hz, 6H), 2.18(s, 3H) 2.33(s, 3H), 3.9–4.4(m, 4H), and 6.18(b s, 1H)	43(83), 67(28), 85(23), 99(58), 100(28), 127(58), 155(100), 165(21), 193(9), 221(6), and 236(27). *Anal.* calcd. for $C_9H_{17}PO_5$: 236.0814; found: 236.0834
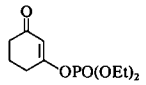	1675 1630 1030	1.37(t, J=7 Hz, 6H), 1.7–2.7(m, 6H), 4.17(q, J=7 Hz, 4H), and 5.86(b s, 1H)	67(45), 99(49), 102(100), 104(34), 127(45), 130(50), 145(17), 155(73), 161(20), 164(17), 179(12), 192(22), 220(22), 235(14), and 248(49). *Anal.* calcd. for $C_{10}H_{17}PO_5$: 248.0814; found: 248.0790
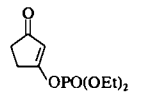	1710 1610 1030	1.38(t, J=7 Hz, 6H), 2.3–2.9 (m, 4H), 4.2(m, 4H), and 5.78(b s, 1H)	45(22), 53(85), 81(66), 99(19), 116(100), 117(78), 129(22), 145(60), 161(22), 179(19), and 234(19). *Anal.* calcd. for $C_9H_{15}PO_5$: 234.0657; found: 234.0649
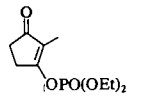	1710 1660 1030	1.38(t, J=7 Hz, 6H), 1.67(m, 3H), 2.3–2.6(m, 2H), 2.6–3(m, 2H), and 4.22(qn, J=7 Hz, 4H)	45(28), 67(55), 81(19), 117(100), 119(45), 130(70), 145(85), 161(13), 179(8), 235(9), and 248(5). *Anal.* calcd. for $C_{10}H_{17}PO_5$: 248.0814; found: 248.0817

reaction in which the alkyl group replaces the halides with retention of geometry about the double bond (16). Although simple enol phosphates couple with dialkylcuprates (13), there is no report of any stereoselectivity in the examples cited in this work.

The stereochemistry of the alkenes **13–18** was determined from their nmr spectra. In particular, the chemical shift of β-methyl groups in α,β-unsaturated esters is δ 2.1–2.2 for a β-methyl group *cis* to a carboxymethyl group and δ 1.8–1.9 for a *trans* β-methyl group (8*a*, 12, 17, 18). The ^1H nmr spectra for the alkenes **13–18** are given in Table 5 and all of the stereochemical assignments are consistent with the above observations. In addition, the ^{13}C nmr spectrum of the tetrahydropyranyl ether **15** had a signal at δ 16.2 due to the β-methyl carbon. In the corresponding *E* alcohol the ^{13}C-resonance of the β-methyl carbon is at 19.2 whereas the isomeric *Z* alcohol from **15** has a signal at δ 25.5 due to the β-methyl group (12).

[5] 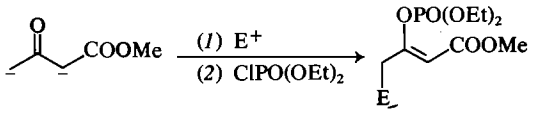

[6] 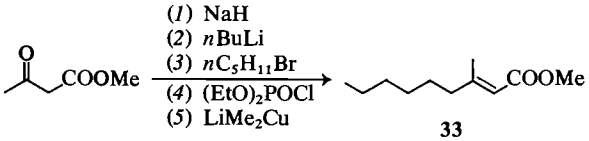

33

The benefits enumerated above should make this new route to α,β-unsaturated esters a very useful tool in the stereoselective synthesis of more complex compounds. Using this methodology, methyl farnesoate was prepared in over 86% yield from geranyl bromide which compares with a 38% overall yield of methyl farnesoate using the thioether sequence (8*b*). Also, compound **15** (Table 1, entry 4) has been used in a synthesis (18) of the butterfly compound **34** (19).

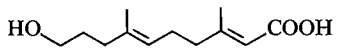

34

In each of these syntheses the isoprene unit **35** is stereoselectively added to a chain in an overall sense as shown in [7].

In addition we have extended this method to the β-diketones shown in Table 2. The enol phosphates of these β-diketones were formed in almost quantitative yield using the above procedure for β-keto esters. Occasionally it was advantageous to use triethylamine as base in place of sodium hydride because of

[7] 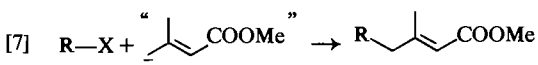

35

insolubility of the sodium enolates in the reaction medium (Table 2, entries 4 and 5). These enol phosphates also reacted with dialkylcuprates to give the corresponding β-substituted α,β-unsaturated ketones.

TABLE 5. Spectral data for β-substituted α,β-unsaturated esters from Table 1

Ester	Infrared (cm^{-1})	Nuclear magnetic resonance (δ)	Mass spectra *m/e* (relative intensity)	Analysis or reference
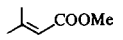	1715 1655 1150	1.88(s, 3H), 2.15(s, 3H), 3.65(s, 3H), and 5.63(b s, 1H)	55(45), 83(100), and 114(47)	[a]
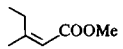	1715 1650 1155	1.06(t, J=7 Hz, 3H, $E+Z$), 1.83(d, J=2 Hz, Z), 2.13(m, E), 2.61(q, J=7 Hz, E), 3.63(s, 3H, $E+Z$), and 5.58(m, 1H, $E+Z$)	41(55), 43(32), 74(35), 97(100), and 128(80)	[b]
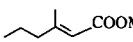	1715 1650 1155	0.88(t, J=7 Hz, 3H), 1.2–1.7(m, 2H), 2(m, 2H), 2.13(d, J=2 Hz, 3H), 3.63(s, 3H), and 5.60(b s, 1H)	41(55), 43(45), 55(55), 57(48), 69(35), 83(100), 111(100), 125(40), 121(40), 122(45), and 142(45)	*Anal.* calcd. for $C_8H_{14}O_2$: C 67.57, H 9.92; found: C 67.28, H 10.12[c]
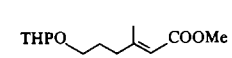	1715 1650 1155 1030	1.2–2.4(m, 10H), 2.13(b s, 3H), 3–4(m, 4H), 3.63(s, 3H), 4.50(m, 1H), and 5.63(m, 1H)	41(10), 81(10), 85(100), 109(8), 112(6), 127(9), 141(8), 158(20), and 242(0·1)	*Anal.* calcd. for $C_{13}H_{22}O_4$: C 64.44, H 9.12; found: C 64.23, H 9.24
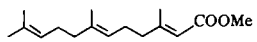	1715 1650 1155	1.60(s, 6H), 1.67(s, 3H), 1.8–2.3(m, 8H), 2.15(d, J=1.5 Hz, 3H), 3.65(s, 3H), 5.0(m, 2H), and 5.62(b s, 1H)	41(53), 69(100), 81(43), 114(54), 136(32), 137(30), 207(20), 219(17), and 250(35)	[d]
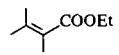	1705 1105	1.27(t, J=7 Hz, 3H), 1.8(b s, 6H), 1.97(s, 3H), and 4.14(q, J=7 Hz, 2H)	41(65), 69(57), 96(69), 97(88), 99(46), 114(20), 127(10), and 142(100)	*Anal.* calcd. for $C_8H_{14}O_2$: C 67.57, H 9.92; found: C 67.46, H 9.85[e]
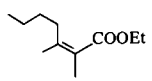	1700 1640 1105	0.90(t, 3H), 1.28(t, J=7 Hz, 3H), 1–1.6(m, 4H), 1.77(s, 3H), 1.83(s, 3H), 2.3(b t, J=6 Hz, 2H), and 4.13(q, J=7 Hz, 2H)	41(48), 43(30), 69(48), 102(30), 109(80), 127(47), 139(100), 155(18), 169(17), and 184(63)	*Anal.* calcd. for $C_{11}H_{20}O_2$: C 71.70, H 10.94; found: C 71.42, H 10.98
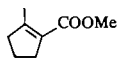	1700 1645 1120	1.5–2.2(m, 2H), 2.10(b s, 3H), 2.2–2.8(m, 4H), and 3.70(s, 3H)	81(95), 109(100), 125(30), and 140(95)	*Anal.* calcd. for $C_8H_{12}O_2$: C 68.55, H 8.63; found: C 68.32, H 8.90[f]
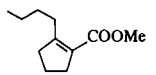	1700 1640 1120	0.9(m, 3H), 1–2(m, 6H), 2.2–2.7(m, 6H), and 3.67(s, 3H)	41(25), 67(25), 79(30), 81(42), 93(40), 121(55), 140(50), 151(58), 153(100), and 182(86)	*Anal.* calcd. for $C_{11}H_{18}O_2$: 182.1307; found: 182.1278

TABLE 5 (*Continued*)

Ester	Infrared (cm^{-1})	Nuclear magnetic resonance (δ)	Mass spectra *m/e* (relative intensity)	Analysis or reference
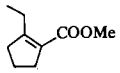	1705 1640 1120	1.01(t, J=7 Hz, 3H), 1.5–2.1 (m, 2H), 2.2–2.8(m, 6H), and 3.68(s, 3H)	41(33), 43(21), 55(25), 67(38), 79(33), 91(33), 95(88), 122(74), 123(92), 139(18), and 154(100)	*Anal.* calcd. for $C_9H_{14}O_2$: 154.0994; found: 154.1000
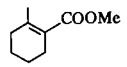	1700 1640	1.3–1.7(m, 4H), 1.97(b s, 3H), 1.8–2.4(m, 4H), and 3.69(s, 3H)	67(16), 79(22), 89(33), 90(100), 122(32), 123(34), 139(10), and 154(75)	*Anal.* calcd. for $C_9H_{14}O_2$: C 70.10, H 9.15; found: C 69.96, H 9.31
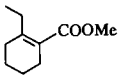	1705 1640 1085	1.03(t, J=7 Hz, 3H), 1.4–1.7(m, 4H), 1.9–2.5(m, 6H), and 3.68(s, 3H)	41(30), 55(22), 67(50), 79(46), 109(75), 136(84), 137(58), and 168(100)	*Anal.* calcd. for $C_{10}H_{16}O_2$: C 71.39, H 9.59; found: C 71.20, H 9.80
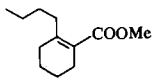	1705 1630 1085	0.9(m, 3H), 1.1–1.9(m, 8H), 2–2.6 (m, 6H), and 3.67(s, 3H)	79(66), 94(65), 95(75), 107(50), 122(38), 135(85), 154(41), 165(100), and 196(100)	*Anal.* calcd. for $C_{12}H_{20}O_2$: C 73.43, H 10.27; found: C 73.20, H 10.20
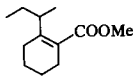	1710 1630	0.90(t, J=7 Hz, 3H), 0.97(d, J=7 Hz, 3H), 1–2.4(m, 10H), 2.5–3.2(sextet, J=7 Hz, 1H), and 3.66(s, 3H)	41(30), 79(36), 81(32), 107(50), 128(34), 137(85), 149(60), 165(85), 167(55), and 196(100)	*Anal.* calcd. for $C_{12}H_{20}O_2$: 196.1463; found: 196.1474
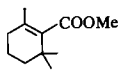	1710 1070	1.08(s, 6H), 1.2–2(m, 6H), 1.64(s, 3H), and 3.69(s, 3H)	77(8), 79(10), 81(9), 107(48), 123(67), 135(100), 151(25), 167(80), and 182(36)	*Anal.* calcd. for $C_{11}H_{18}O_2$: C 72.49, H 9.95; found: C 72.20, H 9.87
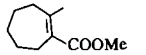	1705 1635 1110	1.2–1.9(m, 6H), 1.99(s, 3H), 2–2.6(m, 4H), and 3.67(s, 3H)	41(25), 55(18), 67(38), 79(22), 81(25), 93(41), 108(47), 109(72), 125(18), 136(36), 137(39), 153(15), and 168(100)	*Anal.* calcd. for $C_{10}H_{16}O_2$: C 71.39, H 9.59; found: C 71.14, H 9.55
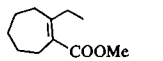	1700 1635 1115	1.04(t, J=7 Hz, 3H), 1.2–1.9 (m, 6H), 2–2.6(m, 6H), and 3.69(s, 3H)	41(46), 55(38), 67(40), 79(41), 81(85), 93(80), 107(34), 108(27), 121(27), 122(43), 123(55), 150(88), 151(52), and 182(100)	*Anal.* calcd. for $C_{11}H_{18}O_2$: C 72.49, H 9.95; found: C 72.70, H 10.14

TABLE 5 (*Concluded*)

Ester	Infrared (cm^{-1})	Nuclear magnetic resonance (δ)	Mass spectra *m/e* (relative intensity)	Analysis or reference
	1710 1640 1115	0.93(m, 3H), 1–1.9(m, 10H), 2–2.6(m, 6H), and 3.69(s, 3H)	41(40), 55(28), 67(30), 79(33), 81(25), 93(38), 95(56), 107(32), 108(42), 109(38), 121(38), 125(20), 136(30), 149(90), 168(31), 179(66), and 210(100)	*Anal.* calcd. for $C_{13}H_{22}O_2$: C 74.24, H 10.54; found: C 74.14, H 10.44

[a] I. Heilbron (*Editor*). Dictionary of organic compounds. Vol. 2. Eyre and Spottiswood Ltd., London, Engl. 1965. p. 1136.
[b] Reference 18*a*.
[c] Reference 18*b*.
[d] Reference 8*b*.
[e] J. C. Sheehan and J. H. Beeson. J. Am. Chem. Soc. **89**, 362 (1967).
[f] S. J. Rhoads, J. K. Chattopadhyay, and E. E. Waali. J. Org. Chem. **35**, 3352 (1970).

This reaction appears to go with equal facility using primary and tertiary dialkylcuprates (Table 2, entry 3) unlike the above case where the tertiary dialkylcuprate could not be coupled with the enol phosphate of β-keto esters. These results (Table 2) would indicate that the enol phosphate – dialkylcuprate coupling sequence would complement the excellent methods available (10) to prepare β-halo enones and couple these compounds with dialkylcuprates (11).

Experimental

All ir spectra were recorded in $CHCl_3$ solution using a Perkin Elmer Model 700 spectrophotometer, and were calibrated with the 1601 cm^{-1} band of polystyrene. The ^1H nmr spectra were recorded in $CDCl_3$ solution on either a Varian model T-60 or HA-100 spectrometer. The signal positions are reported using the δ scale with tetramethylsilane as internal standard. The multiplicity, coupling constants, and integrated peak areas are indicated in parentheses after each signal. The mass spectra were obtained using an Atlas CH-4B mass spectrometer, and high resolution determinations were obtained using an AEI MS-9 or MS-50 mass spectrometer. Both instruments were operated at an ionizing potential of 70 eV. Elemental microanalyses were performed by Mr. Peter Borda, University of British Columbia. The silica gel used was obtained from E. Merck and that used for thin layer chromatography (tlc) was the grade PF_{254}, whilst that used for column chromatography was the 100–200 mesh ASTM (Fisher). Vapor phase chromatographic analyses were performed on a Hewlett-Packard Model 5830-A using 6 ft × $\frac{1}{8}$ in. columns of 3% OV-17 and 3% OV-101. Ether and tetrahydrofuran (THF) were freshly distilled from lithium aluminum hydride before use.

Preparation of Enol Phosphates of β-*Keto Esters*

A solution of 1.0 equiv. of the β-keto ester in dry ether was added to a suspension of 1.1 equiv. of sodium hydride in ether, all under nitrogen and at 0°C. After stirring for 15–20 min at 0°C (or 10 min at room temperature), 1.1 equiv. of diethyl phosphorochloridate (Aldrich) was introduced and stirring was continued for 1–2 h at room temperature. For reactions of less than 5 mmol scale, the reaction mixture was stirred with excess solid ammonium chloride for 20 min, filtered through Celite, and the solvent evaporated under reduced pressure. For reactions of larger than 5 mmol scale, the reaction mixture was quenched with aqueous ammonium chloride. The ether solution was then washed with saturated sodium bicarbonate solution, dried over magnesium sulfate, filtered, and the solvents removed under reduced pressure. The enol phosphate was pure by spectroscopic and chromatographic analysis, and it was used directly in the dialkylcuprate coupling reaction. The spectral data for these enol phosphates are given in Table 3.

Preparation of Enol Phosphates of β-*Diketones*

Method *A* was identical to the above procedure for β-keto esters.

Method *B* for those β-diketones which had an insoluble monosodium salt involved treating a suspension of 1.0 equiv. of the β-diketone in ether with 1.1 equiv. of triethylamine and 1.1 equiv. of diethyl phosphorochloridate for 20 h at room temperature. The reaction mixture was filtered, washed with 10% sodium bicarbonate and brine, dried over magnesium sulfate, filtered, and the solvents removed under reduced pressure. The enol phosphate was pure by spectroscopic and chromato-

TABLE 6. Spectral data for β-substituted enones from Table 2

Enone	Infrared (cm^{-1})	Nuclear magnetic resonance (δ)	Mass spectra *m/e* (relative intensity)	Analysis or reference
	1690 1615	1.85(d, J=1 Hz, 3H), 2.16(s, 6H), and 6.03(m, 1H)		[a]
	1660	1.95(b s, 3H), 1.5–2.5(m, 6H), and 5.80(b s, 1H)	54(38), 82(93), and 110(100)	[b]
	1655 1610	1.12(s, 9H), 1.7–2.5(m, 6H), and 5.88(s, 1H)	41(22), 67(20), 81(24), 96(90), 109(100), 124(60), 137(20), and 152(78)	[b]
	1700 1670 1620	2.13(b s, 3H), 2.2–2.7(m, 4H), and 5.88(q, J=1 Hz, 1H)	40(38), 41(28), 53(60), 67(66), 81(64), 95(48), and 96(100)	[c]
	1735 1695 1650	1.68(s, 3H), 2.03(b s, 4H), and 2.38(s, 3H)	41(16), 67(71), 95(38), and 110(100)	[d]

[a] J. B. Conant and N. Tuttle. Org. Syn. Coll. Vol. I, 345 (1932).
[b] Reference 11*b*.
[c] I. Heilbron (*Editor*). Dictionary of organic compounds. Vol. 4. Eyre and Spottiswood Ltd., London, Engl. 1965. p. 2177.
[d] S. Dev and C. Rai. J. Indian Chem. Soc. 34, 270 (1957).

graphic analysis and it was used directly in the dialkylcuprate coupling reaction. The spectral data for these enol phosphates are given in Table 4.

Coupling of Enol Phosphates with Dialkylcuprates

Preparation of Dialkylcuprates

(*i*) $LiMe_2Cu$: 2.0 equiv. of methyllithium in ether was added to a suspension of 1.0 equiv. of cuprous iodide (CuI) in ether under nitrogen and at 0°C. This solution was used directly.

(*ii*) $LiEt_2Cu$: 2.0 equiv. of ethyllithium in benzene was added to a suspension of 1.0 equiv. of CuI in ether under nitrogen and at −78°C. The resulting black mixture was stirred at −78°C for 30 min and used.

(*iii*) $Li(nBu)_2Cu$: 2.0 equiv. of *n*-butyllithium in hexane was added to a suspension of 1.0 equiv. of CuI in ether under nitrogen and at −47°C. The resulting dark brown solution was stirred at −47°C for 15 min before use.

(*iv*) $Li(sBu)_2Cu$: 2.0 equiv. of *sec*-butyllithium in cyclohexane was added to a suspension of 1.0 equiv. of CuI in ether under nitrogen and at −23°C. The dark black mixture was stirred at −23°C for 15 min before use.

(*v*) $Li(tBu)_2Cu$: 2.0 equiv. of *tert*-butyllithium in pentane was added to a suspension of 1.0 equiv. of CuI in ether under nitrogen and at −47°C. The dark black mixture was stirred at −47°C for 30 min before use.

Dialkylcuprate Coupling

One equivalent of the enol phosphate in ether was added to a cooled, −47°C to −98°C, solution of the dialkylcuprate (1.5–4 equiv.) prepared as above. The resulting mixture was stirred at low temperature for 1–4 h and worked up by pouring it into saturated ammonium chloride solution. The aqueous layer was extracted with ether. The extracts were combined, washed with dilute ammonia in brine and then brine, dried over magnesium sulfate, filtered, and the solvent removed under reduced pressure. The product was purified by chromatography or Kugelrohr distillation. The spectral data for the product esters are given in Table 5, and those for the α,β-unsaturated ketones are given in Table 6.

*Preparation of Methyl Farnesoate (**16**)*

The dianion of methyl acetoacetate (60 mmol) was generated with sodium hydride (66 mmol) and *n*-butyllithium (60 mmol) in the usual manner (2*a*). Then 50 mmol of geranyl bromide was added to the dianion solution at 0°C. After 1 h at 0°C the reaction was worked up (2*a*) to yield 12.6 g of alkylation product which was distilled at 90–92°C/0.02 Torr to give 12.0 g (95%) of **7**.

The keto ester **7** (30 mmol) was converted into 11.45 g of enol phosphate by the general procedure above. A solution of 60 mmol of lithium dimethylcuprate was prepared as above, cooled to −78°C, and treated with a solution of enol phosphate (11.45 g) in 10 mL of ether. This mixture was stirred at −78°C for 2 h and at −47°C for 1 h. The reaction mixture was worked up as described above to yield 7.4 g of crude product which was Kugelrohr distilled at 96–98°C/0.2 Torr to yield 6.83 g (91%) of methyl farnesoate (**16**).

*One-pot Preparation of Methyl (Z)-3-Methyl-2-nonenoate (**33**)*

The dianion of methyl acetoacetate (1.0 mmol) was generated (2*a*) in 3 mL of THF and treated with 1.1 mmol of 1-bromopentane at 0°C. The reaction mixture was stirred at 0°C for 10 min, warmed to room temperature for 25 min, and finally cooled to 0°C again. Diethyl phosphorochloridate (1.1 mmol) was added, and the resulting mixture was stirred at room temperature for 2 h. The enol phosphate solution was cooled to −78°C and added to 2.0 mmol of lithium dimethylcuprate in ether at −78°C. This reaction mixture was held at −78°C for 1¼ h, then at −47°C for 40 min and worked up as above. The crude product (177 mg) was purified by tlc to yield 125 mg (68%) of the unsaturated ester **33** which was characterized by ir: 1710 and 1650 cm^{-1}; nmr δ: 0.87 (b t, J = 6 Hz, 3H), 1.1–1.8 (m, 8H), 2.13 (d, J = 1.8 Hz, 3H), 1.8–2.4 (m, 2H), 3.64 (s, 3H), and 5.6 ppm (m, 1H); ms *m/e* (relative intensity): 41 (17), 55 (18), 82 (20), 83 (20), 110 (30), 114 (100), 127 (40), 153 (25), and 184 (16). *Anal.* calcd. for $C_{11}H_{20}O_2$: C 71.70, H 10.94; found: C 71.59, H 10.75.

*Methyl 6,6-Dimethyl-2-cyclohexanone Carboxylate (**11**)*

The dianion of methyl acetoacetate (2*a*) was alkylated with

3,3-dimethylallyl bromide on a 0.1 mmol scale to yield 15.7 g (85%) of alkylated β-keto ester **32**, bp 67–68°C/0.1 Torr. A solution of 9.2 g (50 mmol) of ester **32** in 10 mL of methylene chloride was added to a solution of 6.4 mL (55 mmol) of stannic chloride in about 150 mL of methylene chloride cooled in ice. The resulting solution was stirred at room temperature for 18½ h. Finally the solution was poured into ice-cold water. The aqueous phase was extracted with ether and the extracts were combined, washed with water and brine, dried over magnesium sulfate, filtered, and the solvents removed under reduced pressure. The crude product was distilled at 64–66°C/0.1 Torr to yield 8.46 g (92%) of cyclized ester **11** which was characterized by ir: 1750 (sh), 1730, and 1710 cm^{-1}; nmr δ: 1.02 (s, 3H), 1.08 (s, 3H), 1.2–2.1 (m, 4H), 2.1–2.7 (m, 2H), 3.13 (s, 1H), and 3.65 ppm (s, 3H); ms *m/e* (relative intensity): 41 (87), 43 (96), 55 (100), 69 (79), 74 (74), 83 (85), 100 (68), 111 (58), 137 (53), 141 (19), 153 (38), 169 (20), and 184 (26). *Anal.* calcd. for $C_{10}H_{16}O_3$: C 65.19, H 8.75; found: C 65.0, H 8.55.

Acknowledgements

We are grateful to the National Research Council of Canada and the University of British Columbia for financial support of this work.

1. (*a*) D. J. Faulkner. Synthesis, 175 (1971); (*b*) J. Reucroft and P. G. Sammes. Q. Rev. **25**, 135 (1971).
2. (*a*) S. N. Huckin and L. Weiler. J. Am. Chem. Soc. **96**, 1082 (1974); (*b*) S. N. Huckin and L. Weiler. Can. J. Chem. **52**, 1343 (1974); (*c*) S. N. Huckin and L. Weiler. Can. J. Chem. **52**, 2157 (1974); (*d*) P. E. Sum and L. Weiler. Chem. Commun. **91**, (1977); (*e*) P. E. Sum and L. Weiler. Can. J. Chem. **55**, 996 (1977).
3. (*a*) D. Seebach and H. Meyer. Angew. Chem. Int. Ed. Engl. **13**, 77 (1974); (*b*) T. M. Harris, T. P. Murray, C. M. Harris, and M. Gumulka. Chem. Commun. 362 (1974); (*c*) J. F. Kingston and L. Weiler. Can. J. Chem. **55**, 785 (1977).
4. (*a*) C. P. Casey and D. F. Marten. Synth. Commun. **3**, 321 (1973); (*b*) C. P. Casey, D. F. Marten, and R. A. Boggs. Tetrahedron Lett. 2071 (1973); (*c*) C. P. Casey and D. F. Marten. Tetrahedron Lett. 925 (1974).
5. C. Ouannès and Y. Langlois. Tetrahedron Lett. 3461 (1975).
6. (*a*) H. O. House, L. E. Huber, and M. J. Umen. J. Am. Chem. Soc. **94**, 8471 (1972); (*b*) H. O. House and J. M. Wilkins. J. Org. Chem. **43**, 2443 (1978); (*c*) H. O. House. Acc. Chem. Res. **9**, 59 (1976) and references therein.
7. G. H. Posner and D. J. Brunelle. Chem. Commun. 907 (1973).
8. (*a*) S. Kobayashi, H. Takei, and T. Mukaiyama. Chem. Lett. 1097 (1973); (*b*) S. Kobayashi and T. Mukaiyama. Chem. Lett. 1425 (1974).
9. (*a*) D. Paquer and S. Smadja. Recl. Trav. Chim. Pays-Bas, **95**, 172 (1976); (*b*) L. Morin, D. Paquer, and S. Smadja. Recl. Trav. Chim. Pays-Bas, **95**, 179 (1976) and references therein.
10. (*a*) R. D. Clark and C. H. Heathcock. J. Org. Chem. **41**, 636 (1976); (*b*) E. Piers and I. Nagakura. Synth. Commun. **5**, 193 (1975).
11. (*a*) E. Piers, C. K. Lau, and I. Nagakura. Tetrahedron Lett. 3233 (1976); (*b*) E. Piers and I. Nagakura. J. Org. Chem. **40**, 2694 (1975).
12. T. A. Bryson. Tetrahedron Lett. 4923 (1973).
13. L. Blaszczak, J. Winkler, and S. O'Kuhn. Tetrahedron Lett. 4405 (1976).
14. R. E. Ireland and G. Pfister. Tetrahedron Lett. 2145 (1969).
15. (*a*) T. R. Fukoto, E. O. Hornig, R. L. Metcalf, and M. Y. Winton. J. Org. Chem. **26**, 4620 (1961); (*b*) J. E. Thompson. J. Org. Chem. **30**, 4276 (1965).
16. G. H. Posner. Org. React. **22**, 253 (1975).
17. L. M. Jackson and S. Sternhell. *In* Applications of nuclear magnetic resonance spectroscopy in organic chemistry. 2nd ed. Pergamon Press, Headington Hill Hall, Oxford, Engl. 1969. Chapt. 3.
18. (*a*) K. H. Dahm, B. M. Trost, and H. Röller. J. Am. Chem. Soc. **89**, 5292 (1967); (*b*) N. Khan, D. E. Loeber, T. P. Toube, and B. C. L. Weedon. J. Chem. Soc. Perkin Trans. I, 1457 (1975).
19. F. W. Sum and L. Weiler. Chem. Commun. 985 (1978).
20. J. Meinwald, A. M. Chalmers, T. E. Pliske, and T. Eisner. Tetrahedron Lett. 4893 (1968).

Photoisomerization of protonated cyclohex-2-enones

RONALD F. CHILDS,[1] KENNETH E. HINE, AND FREDERICK A. HUNG
Department of Chemistry, McMaster University, Hamilton, Ont., Canada L8S 4M1

Received October 5, 1978

RONALD F. CHILDS, KENNETH E. HINE, and FREDERICK A. HUNG. Can. J. Chem. 57, 1442 (1979).

Protonated 4,4-dimethylcyclohex-2-enone, **1***H*, has been shown to isomerize on irradiation in FSO_3H at −85°C to give protonated 6,6-dimethylbicyclo[3.1.0]hexan-2-one, **5***H*, and protonated 3-isopropylcyclopent-2-enone, **4***H*. The protonated bicyclic ketone **5***H* was found to be both thermally and photochemically labile, in both instances rearranging to **4***H*. The first order rate constant for the thermal isomerization of **5***H* to **4***H* at −60°C was 1.73×10^{-4} s^{-1}. As **5***H* was shown to be photolabile in the presence of **1***H*, it was not possible to establish whether **4***H* was a primary photoproduct of **1***H*. No photoisomerizations of protonated cyclohex-2-enone and protonated 4-methylcyclohex-2-enone could be detected. The photoisomerization of protonated $\Delta^{1,9}$-10-methyl-2-octalone has been re-examined at low temperature in an attempt to detect tricyclic products.

RONALD F. CHILDS, KENNETH E. HINE et FREDERICK A. HUNG. Can. J. Chem. 57, 1442 (1979).

On a trouvé que la diméthyl-4,4 cyclohexène-2 one (**1***H*) protonée s'isomérise par irradiation dans le FSO_3H à −85°C pour fournir la diméthyl-6,6 bicyclo[3.1.0]hexanone-2 protonée (**5***H*) et de l'isopropyl-3 cyclopentène-2 one protonée (**4***H*). On a trouvé que la cétone bicyclique protonée **5***H* est labile thermiquement ainsi que photochimiquement et que chaque fois elle se transpose en **4***H*. La constante de vitesse du premier ordre de l'isomérisation thermique de **5***H* en **4***H* à −60°C est égale à 1.73×10^{-4} s^{-1}. Comme on a montré que **5***H* est photolabile en présence de **1***H*, on n'a pas pu déterminer si **4***H* est un photoproduit primaire de **1***H*. On n'a pas pu détecter de photoisomérisations de la cyclohexène-2 one protonée ou de la méthyl-4 cyclohexène-2 one. On a réétudié la photoisomérisation de la $\Delta^{1,9}$-méthyl-10 octalone-2 protonée à basse température afin d'essayer de détecter des produits tricycliques.

[Traduit par le journal]

We have recently reported that protonated acyclic α,β-unsaturated carbonyl compounds undergo photoinduced stereomutation about the carbon–carbon double bond on irradiation in super-acid media, eq. [1] (1). This photoisomerization, which takes place with protonated aldehydes, ketones, acids, and esters, eventually leads to the establishment of a photostationary state between the two stereoisomers. No other products were detected under the reaction conditions used although more recent work in our laboratories suggests that a photoinduced isomerization may also be occurring about the carbon–oxygen bond in these systems (2).

[1] 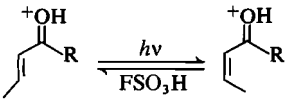

R = H, Me, OH, OMe

With the incorporation of the chromophore of these unsaturated carbonyl compounds into a ring system, isomerism about the double bond will become more difficult to achieve and other photoreactions could become more important. For this reason we have examined and report here the photoisomerization of some protonated cyclohexenones. Cornell and Filipescu (3) have recently described the photorearrangement of protonated 10-methyloctalone, a system which incorporates a protonated cyclohexenone. However, the results reported here differ from their observations in that, working at low temperatures, a bicyclic product has been detected.

Results and Discussion

Ketones **1**, **2**, and **3** were dissolved in FSO_3H to give solutions of the corresponding hydroxy cations **1***H*, **2***H*, and **3***H* respectively. The ^1H nmr spectrum of **3***H* was very similar to that described previously (4) while those of **1***H* and **2***H* were entirely consistent with the assigned structures (Table 1). FSO_3H solutions of these cations were stable at room temperature and could be quenched with methanol–bicarbonate slurry to regenerate the original ketones. The ultraviolet spectrum of **3***H* has been reported by Zalewski and Dunn (5) and those of **1***H* and **2***H* were recorded in 96% H_2SO_4.

Samples of **1***H* in FSO_3H were irradiated at −60°C in thin walled nmr tubes with light from an unfiltered medium pressure mercury lamp. The

[1]Author to whom all correspondence should be addressed.

0008-4042/79/121442-04$01.00/0

TABLE 1. ^{1}H nmr spectra of protonated ketones[a]

Compound	Chemical shift (ppm)						
	C_1H	C_2H	C_3H	C_4H	C_5H	C_6H	CH_3
1*H*	—	6.74d	8.28d	—	2.09	3.29	1.32
2*H*	—	6.84d	8.42d	—	1.7–3.3	—	1.36d
3*H*	—	6.88d	9.27	2.87	2.25	8.15t	—
4*H*	—	6.85	—	3.29	3.29	3.20h[c]	1.35d
5*H*[b]	2.0–3.5	—	2.0–3.5	2.0–3.5	2.0–3.5	—	1.52

[a]All spectra obtained in FSO_3H at −60°C unless otherwise noted. $(CH_3)_4N^+$ as an internal standard taken as 3.1δ; d, doublet, t, triplet, h, heptet.
[b]FSO_3H–SO_2ClF solvent at −85°C.
[c]Isopropyl proton.

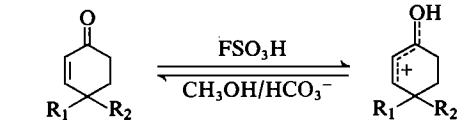

1 $R_1 = R_2 = CH_3$ — **1***H* λ_{max} 275 nm, log ε 3.96
2 $R_1 = H$; $R_2 = CH_3$ — **2***H* λ_{max} 274 nm, log ε 3.96
3 $R_1 = R_2 = H$ — **3***H* λ_{max} 271 nm, log ε 3.97

formation of a new cation was detected by ^{1}H nmr and this was identified as **4***H* (Table 1). Quenching the acid solution after irradiation gave ketone **4** with properties identical with those of an authentic sample (6). Reprotonation of **4** in FSO_3H gave **4***H*.

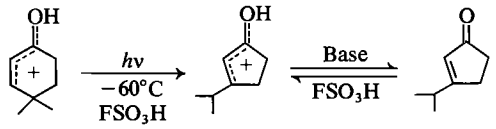

The photoisomerization of **1** in *tert*-butanol gives **4** together with bicyclic ketone **5** (6). To check whether **5***H* was also being formed on irradiation of **1***H*, it was necessary to establish that **5***H* would have been stable under the reaction conditions.

Protonation of **5** using a FSO_3H–SO_2ClF mixture (1:3) at −100°C gave a cation whose ^{1}H nmr spectrum was entirely consistent with the formation of **5***H* (Table 1). This acid solution could be quenched with a methanol–bicarbonate mixture at −78°C to give back **5** together with some **4**. Cation **5***H* was found to be thermally unstable and to isomerize quantitatively to give **4***H*. At −60°C, the first order rate constant for this process was found to be 1.73×10^{-4} s^{-1} ($\Delta G^{\ddagger}$ = 15.9 kcal/mol).

As a typical photoisomerization of **1***H* took several hours, it would not have been possible to detect **5***H* under the reaction conditions used. Accordingly, the photoisomerization of **1***H* was repeated taking care that the temperature of the sample did not rise above −85°C at any time during the irradiation or subsequent monitoring by ^{1}H nmr. After 3 h irradiation both **4***H* (25%) and **5***H* (10%) were detected in the reaction mixture. Quenching this acid solution at low temperature yielded both **4** and **5**.

Under the conditions employed in the above experiment, it would seem very unlikely that **4***H*

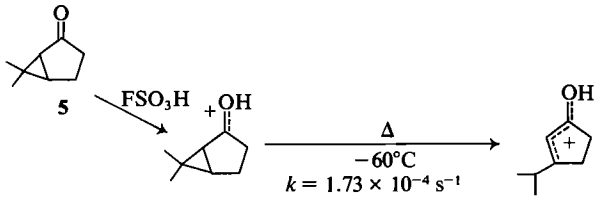

arises from a thermal isomerization of **5***H*. At −85°C, the half life for rearrangement of **5***H* would be of the order of 200 h, which is much longer than the 3 h used in the irradiation.

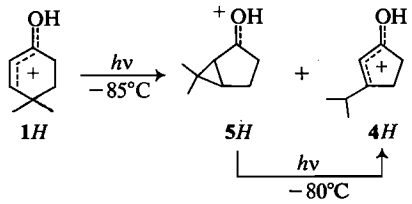

To test whether **4***H* arises by a secondary photoisomerization of **5***H*, the photochemistry of the latter cation was examined. Irradiation of a FSO_3H solution of **5***H* at −80°C caused it to isomerize to **4***H*. This photoisomerization of **5***H* to **4***H* proceeded with an efficiency comparable to that of **1***H* to **4***H* and **5***H*. Irradiation of a mixture of **1***H* and **5***H* indicated that **5***H* was photolabile *even in the presence* of **1***H*. It is not clear at this stage whether or not **4***H* is indeed a primary photoproduct of **1***H*.

In the contrast to the reactivity of **1***H* on irradiation, both **2***H* and **3***H* were remarkably unreactive. Photolysis of solutions of these cations under conditions comparable to those used for **1***H* did not induce any detectable isomerization.

The photoisomerization of **1***H* described above closely parallels the rearrangements reported for the neutral ketone (6, for recent reviews see ref. 7). This type of photoisomerization of cyclohexenones is thought to proceed via a triplet state of π,π^* character (8). The basicities of cyclohexenones are such that they are essentially completely protonated in FSO_3H (5). Consequently, with the n-electron pair being bound to a proton, the lowest excited states of the protonated enones will also most likely be of π,π^* character (10). The multiplicity of the excited state involved in the photoisomerization of **1***H* is not known.

One possible route for the photoisomerization of **1***H* to **4***H* and **5***H* involves the initial formation of **6** as an intermediate. In the ground state the orbital overlap between the p-lobe on C_3 of **1***H* and the electron in the C_4C_5 bond is poor (11). Photoexcitation of **1***H* would likely lead to a twisting about the C_2C_3 bond (1, 12) and so facilitate the 1,2-alkyl shift to give **6**. The difference in behaviour of **1***H*, **2***H*, and **3***H* could possibly be attributed to the thermodynamic differences in energy between a cation such as **6** and its twisted allyl precursor.

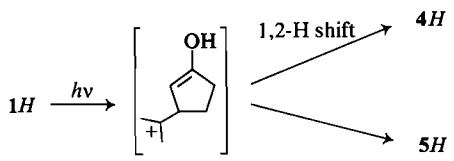

6

The extreme thermal lability of **5***H* raises some interesting questions regarding the photoisomerization of protonated 10-methyloctalone, **7***H*, recently reported by Cornell and Filipescu (3). The only product detected on irradiation of **6***H* at ambient temperature was **8***H* and no cyclopropyl containing products were observed, eq. [2].

[2] 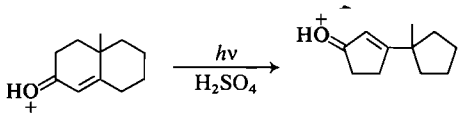

7*H* **8***H*

The photochemistry of **7** has been extensively studied. In *tert*-butanol, the principal product is the tricyclic ketone **9**, eq. [3] (13). Again, a triplet state of π,π^* character has been implicated in this isomerization.

[3] 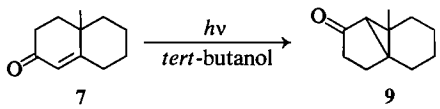

7 **9**

In view of the results obtained here, it would seem possible that **9***H* is also a photoproduct of **7***H* and the previous failure to detect it would stem from its thermal instability. To check this we have examined the protonation of **9** at low temperatures.

Dissolution of **9** in FSO_3H was carried out at $-78°C$ and an ^1H nmr spectrum of the solution obtained at $-80°C$. The spectrum so obtained showed no evidence for the presence of **9***H* but rather three rearrangement products were observed. These isomeric cations were **7***H* (25%), **8***H* (35%), and an unidentified cation, **10***H* (40%). This latter cation exhibited amongst other resonances signals attributable to a single vinyl proton at 6.47 δ and methyl group at 2.33 δ. All attempts to recover a pure sample of the ketone corresponding to this cation were unsuccessful.

The thermal instability of **9***H* is such that it clearly could not have been detected as a photoproduct in reactions carried out at room temperature nor indeed using our low temperature equipment (low temperature limit $-85°C$). Evidence against the intervention of **9***H* in the photoisomerization of **7***H* is suggested in that no products corresponding to **10***H* were reported. However, irradiation of the FSO_3H solution of **7***H*, **8***H*, and **10***H*, obtained by rearrangement of **9***H*, under similar conditions to those previously described (3), caused **10***H* to be converted to **8***H*. As a consequence, only a relatively low concentration of **10***H* might be expected during the photoisomerization of **7***H*. Careful examination of the ^1H nmr spectra of the partially photorearranged solution of **7***H* in fact showed reproducible but low concentrations of **10***H* ($<5\%$) to be present.

Overall, the question as to whether or not **9***H* is a photoproduct of **7***H* remains open. However, it is apparent that a close parallel exists between the photoreactions of cyclohexenones and their protonated derivatives.

Experimental

General

^1H nmr spectra were recorded on Varian HA100 or T60 spectrometers. Probe temperatures were measured using a non-spinning thermocouple inserted in a sample taken at the appropriate depth in the probe. Ultraviolet spectra were obtained on a Cary 14 instrument. Gas chromatography was carried out on a Varian A90-P3 preparative instrument using a 15% Carbowax 20 M column, and a Varian 3700 analytical instrument.

Protonations were carried out directly in nmr tubes, extracting the appropriate ketone from CH_2Cl_2 into the acid medium at low temperature ($-78°C$ with FSO_3H, $-100°C$ with FSO_3H–SO_2ClF). Tetramethyl ammonium chloride was added to the cation solutions as an internal standard.

Most irradiations were carried out using the low temperature equipment previously described (14) and a Toshiba 125 W medium pressure mercury lamp. Clear, thin wall nmr tubes were used and these transmitted light down to ca. 260 nm. Temperatures were monitored during the photoreactions with a glass encased thermocouple junction inserted into the acid

medium. The photoisomerization of **7***H* was carried out using a circular arrangement of 1.3-W, RPR 3000 A lamps (Southern New England Ultraviolet Co., Middletown, CT), surrounding a sample held at low temperature in an unsilvered Dewar.

Quenches of the acid solutions were carried out by adding the acid to a rapidly stirred slurry of methanol and sodium bicarbonate at −78°C. The resulting mixture was allowed to warm to ca. −20°C when water was added and the organic products extracted into ether. The products were identified by their ^{1}H nmr spectra and glpc retention times.

Materials

Fluorosulfuric acid (Allied Chemicals) was treated as previously described (15). The ketones **1** (9, 16), **2** (9), **4**, **5** (6), **7** (3), and **9** (13) were prepared by standard procedures.

Photoisomerization of **1**H

1 (5 mg) was dissolved in FSO_3H (0.5 mL) in an nmr tube and irradiated for 3 h using the equipment described above. The ^{1}H nmr spectrum (recorded at −85°C) of the resulting mixture indicated that **1***H* (65%), **4***H* (25%), and **5***H* (10%) were present. The reaction mixture was quenched and the organic extract analyzed by glpc. Both **4** and **5** were shown to be present in a 3:1 ratio.

Photoisomerization of **5**H

5 (5 mg) in FSO_3H (0.5 mL) was irradiated at −85°C for 2 h. The ^{1}H nmr spectrum of the resulting solution showed a mixture of **5***H* (35%) and **4***H* (65%) to be present.

Photoisomerization of **5**H *and* **1**H

A mixture of **1***H* (70%) and **5***H* (30%) was prepared in FSO_3H and assayed by ^{1}H nmr at −85°C. The solution was irradiated for 3.5 h and again subjected to ^{1}H nmr analysis. The composition found was **1***H* (12%), **5***H* (14%), and **4***H* (74%).

Photoisomerization of **7**H

A sample of **7** (5 mg) in FSO_3H was irradiated for 5 h at −65°C using the apparatus described above. The ^{1}H nmr spectrum of the resulting solution showed signals at δ 6.44 (vinyl H) and 1.22 (CH_3) attributable to **7***H*; at δ 6.67 (vinyl H) and 1.19 (CH_3) attributable to **8***H*; and δ 6.48 (shoulder, vinyl H) and 2.33 (CH_3) attributable to **10***H*. The ratio of **7***H* to **8***H* to **10***H* by integration was 55:40:5.

Protonation of **9**H

9 (5 mg) was dissolved in FSO_3H at −78°C and the ^{1}H nmr spectrum recorded at −80°C within 10 min. Only **7***H* (25%), **8***H* (35%), and **10***H* (40%) (chemical shifts given above) were detected. The reaction mixture was quenched and the products examined by analytical glpc using both Carbowax 20 M and silicone oil, SE 30, columns. Using a variety of conditions, it was not possible to separate **7** and **10** from each other.

Irradiation of a mixture of **7**H, **8**H, *and* **10**H

A solution of the above cations, prepared by protonation of **9** (5 mg) in FSO_3H, was irradiated under identical conditions to those used above for the isomerization of **7***H*. After 3 h irradiation the ratio of **7***H* to **8***H* to **10***H* had changed from 25:35:40 to 26:48:26.

Acknowledgement

We are grateful to the National Research Council of Canada for financial support.

1. R. F. Childs, E. F. Lund, A. G. Marshall, W. J. Morrisey, and C. V. Rogerson. J. Am. Chem. Soc. **98**, 5924 (1976).
2. R. F. Childs and M. E. Hagar. J. Am. Chem. Soc. **101**, 1052 (1979).
3. D. G. Cornell and N. Filipescu. J. Org. Chem. **42**, 3331 (1977).
4. H. Hogeveen. Recl. Trav. Chim. Pays-Bas, **87**, 1295 (1968); G. A. Olah, Y. Halpern, Y. K. Mo, and G. Liang. J. Am. Chem. Soc. **94**, 3554 (1972).
5. R. I. Zalewski and G. E. Dunn. Can. J. Chem. **46**, 2469 (1968).
6. O. L. Chapman, T. A. Rettig, A. A. Griswold, A. I. Dutton, and P. Fitton. Tetrahedron Lett. 2049 (1963).
7. K. Schaffner. Tetrahedron, **30**, 1891 (1974); O. L. Chapman and D. S. Weiss. *In* Organic photochemistry. Vol. 3. *Edited by* O. L. Chapman. Marcel Dekker, New York, NY. 1973. p. 197.
8. W. G. Dauben, W. A. Spitzer, and M. S. Kellog. J. Am. Chem. Soc. **93**, 3674 (1971).
9. W. G. Dauben, G. W. Schaffner, and N. D. Vietmeyer. J. Org. Chem. **33**, 4060 (1968).
10. R. Rusakowicz, G. W. Byers, and P. A. Leermakers. J. Am. Chem. Soc. **93**, 3263 (1971).
11. D. M. Brouwer and H. Hogeveen. Recl. Trav. Chim. Pays-Bas, **89**, 211 (1970); P. Vogel, M. Saunders, W. Thielecke, and P. v. R. Schleyer. Tetrahedron Lett. 1429 (1971).
12. J. J. McCullough, H. Ohorodnyk, and D. P. Santry. J. Chem. Soc. Chem. Commun. 570 (1970); A. Devaquet. J. Am. Chem. Soc. **94**, 5160 (1972); W. C. Herndon. Mol. Photochem. **5**, 253 (1973); N. C. Baird and R. M. West. Mol. Photochem. **5**, 209 (1973).
13. H. E. Zimmerman, R. G. Lewis, J. J. McCullough, A. Padwa, S. W. Staley, and M. Semmelhack. J. Am. Chem. Soc. **88**, 1965 (1966); D. Bellus, D. R. Kearns, and K. Schaffner. Helv. Chim. Acta, **52**, 971 (1969); P. Margaretha and K. Schaffner. Helv. Chim. Acta, **56**, 2884 (1973).
14. R. F. Childs, M. Sakai, B. D. Parrington, and S. Winstein. J. Am. Chem. Soc. **96**, 6403 (1974).
15. K. E. Hine and R. F. Childs. J. Am. Chem. Soc. **99**, 3289 (1973).
16. K. L. Cook and A. J. Waring. J. Chem. Soc. Perkin Trans. **1**, 529 (1973).

Effets des substituants dans les spectres de rmn de benzhydrols substitués en présence de Eu $(dcm)_3$

JOËL CAPILLON ET LILIANE LACOMBE

Laboratoire de Chimie Organique des Hormones, G.R. n° 20 du CNRS, Collège de France, 11 Place Marcelin Berthelot, 75231 Paris Cedex 05, France

Reçu le 16 novembre 1978

JOËL CAPILLON et LILIANE LACOMBE. Can. J. Chem. **57**, 1446 (1979).

Des benzhydrols chiraux, mono ou disubstitués en *para*, ont été étudiés par rmn en présence du réactif de déplacement chiral Eu$(dcm)_3$. L'influence des constantes d'association lanthanide–substrat et des facteurs géométriques a été déterminée séparément. La non-équivalence observée ne peut être reliée à une différence des constantes d'association mais est dûe à une différence de structure des complexes lanthanide–substrat qui varie avec la nature électronique des substituants. De plus on établit une règle de détermination de configuration absolue pour ce type de composé.

JOËL CAPILLON and LILIANE LACOMBE. Can. J. Chem. **57**, 1446 (1979).

Para mono- or disubstituted chiral benzhydrols have been studied by nmr in the presence of Eu$(dcm)_3$. The influence of association constants and structural parameters has been assessed separately. The observed nonequivalence cannot be related to a difference between the association constants but is primarily due to a difference between the geometries of the lanthanide–substrate complexes, correlated with the electronic nature of the substituents. A rule for the determination of the absolute configuration of such compounds has been established.

Au cours de travaux précédents (1), nous avons été amenés à effectuer des déterminations de pureté optique d'alcools aromatiques chiraux substitués en *para*, par rmn en présence d'un réactif de déplacement chiral. Pour une série de composés voisins, nous avions envisagé de relier les sens de non-équivalence observés aux configurations absolues et nous avions remarqué que le sens de la non-équivalence dépendait du caractère électrodonneur ou électroattracteur du substituant. C'est ainsi que dans la série des benzhydrols monosubstitués en *para*, en présence[1] de Eu$(dcm)_3$ le signal du proton benzylique de l'énantiomère *R* se déplace plus rapidement que celui de l'énantiomère *S* lorsque le substituant est électrodonneur alors que l'on observe le phénomène inverse lorsque le substituant est électroattracteur. De même en présence[2] de Eu$(tfc)_3$ on observe un changement du sens de la non-équivalence opposé à celui observé avec Eu$(dcm)_3$. En ce qui concerne les signaux des protons aromatiques on ne retrouve pas le phénomène observé par Mosher *et al.* (4) dans son étude de l'action[3] de Eu$(hfbc)_3$ sur des alcools chiraux L_1CHOHL_2: lorsque le complexe chiral produit une non-équivalence sur les signaux des protons de L_1 et L_2 Mosher avait noté que le sens de la non-équivalence restait le même quels que soient L_1 et L_2 ($\Delta\delta_R - \Delta\delta_S < 0$). Cette constatation lui a permis de suggérer une règle de détermination de la configuration absolue des alcools secondaires chiraux. Dans notre cas, en présence de Eu$(dcm)_3$, $\Delta\delta_R - \Delta\delta_S > 0$ pour les signaux du noyau substitué tandis que $\Delta\delta_R - \Delta\delta_S < 0$ pour les signaux du noyau non substitué. De plus, dans la série des phényléthylcarbinols $ArCHOHCH_2CH_3$, en présence de Eu$(dcm)_3$, le sens de la non-équivalence des signaux du groupe méthyle varie selon le caractère électrodonneur ou électroattracteur du substituant porté en *para* par le noyau aromatique. Ces quelques remarques nous ont incités à étudier plus en détail ces effets de substituants.

La non-équivalence observée dépend à la fois de la différence de stabilité entre les complexes diastéréoisomères formés et de la différence de structure entre ces complexes. Il est possible d'évaluer séparément les contributions de ces deux facteurs en analysant de deux manières distinctes les déplacements induits: d'une part la méthode de Williams (6) qui permet d'apprécier les différences de constantes d'association; d'autre part la méthode de Kelsey (7) et ApSimon *et al.* (8) qui fournit des informations sur la structure des complexes lanthanide–substrat. On peut noter que ces méthodes d'analyse sont possibles quelle que soit la quantité de compétiteur qui se trouve en solution (y compris l'eau) et dans notre cas quelle que soit la pureté optique du substrat.

Cette double analyse n'est valable que si les déplacements induits sont dûs à des complexes

[1] Eu$(dcm)_3$ = tris(d,d-dicamphoylmethanato)europium III (2).

[2] Eu$(tfc)_3$ = tris(d-trifluoroacetyl-3 camphorato)europium III (3).

[3] Eu$(hfbc)_3$ = tris(d-heptafluorobutanoyl-3 camphorato)-europium III (5).

0008-4042/79/121446-05$01.00/0

TABLEAU 1. Déplacements chimiques des benzhydrols étudiés et sens des non-équivalences $\Delta\delta_R - \Delta\delta_S$ en présence de $Eu(dcm)_3$

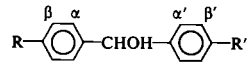

			H benz.		Hα		Hα′		Hβ		Hβ′	
			δ_0	$\Delta\delta_R - \Delta\delta_S$	δ_0	$\Delta\delta_R - \Delta\delta_S$	δ_0	$\Delta\delta_R - \Delta\delta_S$	δ_0	$\Delta\delta_R - \Delta\delta_S$	δ_0	$\Delta\delta_R - \Delta\delta_S$
1	$R = OCH_3$	$R' = H$	5.593	+	7.117	+	7.202	−	6.173	+	7.202	−
2	$R = CH_3$	$R' = H$	5.602	+	7.107	+	7.198	−	7.011	+	7.198	[a]
3	$R = Br$	$R' = H$	5.562	−	7.108	+	7.198	−	7.346	+	7.198	[a]
4	$R = CF_3$	$R' = H$	5.685	−	7.398	+	7.228	−	7.510	+	7.228	[a]
5	$R = CF_3$	$R' = CH_3$	5.641	−	7.373	+	7.062	−	7.497	+	7.062	+
6	$R = Br$	$R' = CF_3$	5.657	+	7.130	+	7.383	−	7.390	+	7.529	−

[a]Non observé.

lanthanide–substrat de stoechiométrie 1:1. Goering *et al.* (3) ont établi que le réactif chiral $Eu(tfc)_3$, donnait aussi un complexe de stoechiométrie 1:2. Une étude analogue n'a pas été effectuée au sujet du réactif $Eu(dcm)_3$. Cependant des observations qualitatives montrent que les complexes 1:2 éventuels interviennent peu dans les déplacements induits, surtout s'il y a en même temps une grande dilution du substrat et une grande concentration du lanthanide (9, 10). Ces considérations nous ont amenés à utiliser pour notre étude le réactif $Eu(dcm)_3$.

Méthode

On prépare dans CCl_4, avec le TMS comme référence interne, une solution 0.2 *M* de benzhydrol partiellement dédoublé et de configuration absolue connue (1). A cette solution on ajoute des petites quantités successives non pesées de $Eu(dcm)_3$.[4] L'enregistrement du spectre est effectué à 30°C sur un spectrographe Varian HA 100, 30 min après chaque addition de $Eu(dcm)_3$ de façon à ce que les équilibres soient atteints. On mesure au fréquencemètre les déplacements chimiques. Les déplacements initiaux et les sens de non-équivalence $\Delta\delta_R - \Delta\delta_S$ sont regroupés dans le Tableau 1.

Etude des constantes d'association

D'après les travaux de Williams (6) et Roth (12), le rapport des déplacements induits entre le signal d'un proton *i* d'un substrat A ($\Delta\delta_A{}^i$) et celui d'un proton *j* de B est

$$[1] \qquad \frac{\Delta\delta_A{}^i}{\Delta\delta_B{}^j} = \frac{K_B - K_A}{K_B \Delta_B{}^j}\Delta\delta_A{}^i + \frac{K_A \Delta_A{}^i}{K_B \Delta_B{}^j}$$

où K_A et K_B représentent les constantes d'association des complexes lanthanide–substrat et Δ_A et Δ_B les déplacements induits limites c'est-à-dire la différence entre le déplacement chimique de l'espèce totalement associé et celui de l'espèce libre.

Pour un couple d'énantiomères *R* et *S*, si on compare deux protons structuralement identiques ($i = j$), [1] peut être transformé pour faire apparaître la non-équivalence $\Delta\delta_R{}^i - \Delta\delta_S{}^i$:

$$[2] \qquad \frac{\Delta\delta_R{}^i - \Delta\delta_S{}^i}{\Delta\delta_R{}^i} = \frac{K_R - K_S}{K_R}\frac{\Delta_S{}^i - \Delta\delta_S{}^i}{\Delta_R{}^i} + \frac{\Delta_R{}^i - \Delta_S{}^i}{\Delta_R{}^i}$$

Cette équation montre que la contribution des constantes d'association au phénomène de non-équivalence diminue lorsque le degré de complexation augmente ($\Delta\delta_S{}^i \to \Delta_S{}^i$). Ce type de facteur pourrait donc être négligé si l'on pouvait atteindre un très grand degré d'association. Dans notre cas cela n'est pas possible, certainement parce que l'association benzhydrol–$Eu(dcm)_3$ est faible, et nous avons dû évaluer la différence des constantes d'association.

En appliquant [2], on obtient des droites de pente $-(K_R - K_S)/K_R\Delta_R{}^i$. Cette étude a été effectuée sur les signaux des protons benzylique, α et α′, les déplacements induits des signaux des protons β et β′ étant trop faibles pour être analysés valablement (Tableau 2).

Les valeurs obtenues sont très faibles et montrent que les différences des constantes d'association ont, dans le cas des benzhydrols, une influence mineure sur le sens de la non-équivalence. Ce résultat est confirmé par la comparaison des signes des Tableaux 1 et 2. Pour les protons benzyliques et pour la moitié des protons aromatiques, les signes sont opposés ce qui démontre que, pour ces protons, les effets structuraux imposent le sens de la non-équivalence malgré l'effet contraire des effets d'association.

TABLEAU 2. Etude des constantes d'association: $(K_R - K_S)/K_R\Delta_R{}^i$ tiré des pentes[a] des droites de [2]

	H benz.	Hα	Hα′
1	−0.0006	−0.0024	−0.0005
2	−0.0003	−0.0017	+0.0008[b]
3	+0.0009	+0.0014	+0.0037
4	+0.0024	+0.0036	+0.0054
5	+0.0028	+0.0047	+0.0070
6	−0.0014	−0.0027	−0.0023

[a]Valeurs obtenues par la méthode des moindres carrés.
[b]Valeur aberrante.

[4]Nous remercions le Dr A. Schoofs et le Dr Huynh pour leur préparation du complexe $Eu(dcm)_3$.

Facteurs structuraux

Relations intermoléculaires

Puisque les effets d'association sont peu importants, [1] peut être simplifiée:

$$[3] \qquad \Delta\delta_R{}^i/\Delta\delta_S{}^j \simeq \Delta_R{}^i/\Delta_S{}^j$$

Cette nouvelle relation montre que le rapport des déplacements induits de deux signaux quelconques d'énantiomères différents est proportionnel au rapport des déplacements limites, lequel traduit les effets structuraux.

L'inversion du sens de la non-équivalence du proton benzylique quand on remplace un substituant électrodonneur par un substituant électroattracteur, nous a suggéré l'idée que les facteurs structuraux peuvent être reliés aux σ_p de Hammett des substituants. Nous avons donc porté les rapports $\Delta\delta_R/\Delta\delta_S$ pour le proton benzylique en fonction des σ_p. Pour les benzhydrols monosubstitués, nous trouvons une droite (Fig. 1). On retrouve bien que $\Delta\delta_R/\Delta\delta_S = 1$ pour $\sigma_p = 0$ c'est-à-dire pour le benzhydrol nonsubstitué. A l'aide de cette droite, on peut prédire la configuration absolue de benzhydrols monosubstitués connaissant le σ_p du substituant.

Relations intramoléculaires

La relation [3] n'est valable qu'en première approximation. L'étude de la non-équivalence nous a montré qu'il y avait des différences de structure entre les complexes L*S* et L*R*. Pour comprendre ces phénomènes, il est intéressant d'étudier les facteurs structuraux propres à chaque complexe.

Kelsey (7) et ApSimon *et al.* (8) ont montré que le déplacement observé d'un proton *i* pouvait être relié au déplacement induit d'un proton *j* de la même molécule par la relation:

$$[4] \qquad \delta_A{}^i = (\Delta_A{}^i/\Delta_A{}^j)\,\Delta\delta_A{}^j + \delta_{A_0}{}^i$$

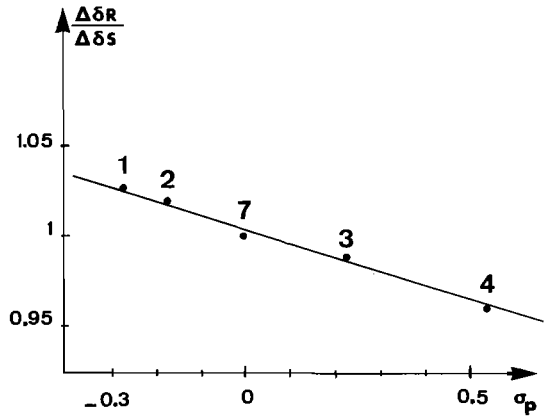

FIG. 1. Variation du rapport des déplacements induits des protons benzyliques de chaque couple d'énantiomère en fonction des σ_p.

D'après McConnell et Robertson (13) et en faisant l'hypothèse généralement admise que les facteurs angulaires sont négligeables (14), la pente de [4] est proportionnelle au rapport du cube des distances r_j^3/r_i^3. Cette simplification est particulièrement justifiée si on compare les déplacements des protons α et α′ de chaque énantiomère (Tableau 3).

Les rapports des déplacements limites sont différents de 1. Ceci indique que l'europium n'est pas à la même distance des protons α et des protons α′. D'autre part, la valeur de ces rapports varie avec la nature des substituants. Comme précédemment, on peut relier les rapports des déplacements limites aux σ_p de Hammett. Dans le cas des composés monosubstitués, on obtient une droite pour les énantiomères *S* et une autre pour les énantiomères *R* (Fig. 2). Ces droites sont à peu près parallèles et les valeurs à l'origine sont 1.142 et 0.868. Ces dernières valeurs sont inverses l'une de l'autre. Or dans le benzhydrol non substitué **7** ($\sigma_p = 0$) les protons α énantiotopes deviennent diastéréotopes (15) en présence du réactif chiral $Eu(dcm)_3$, et ils présentent une forte anisochronie. Le rapport des déplacements limites mesurés par la même méthode est 1.152 ou son inverse 0.868 selon le sens dans lequel ce rapport est calculé. On retrouve la valeur calculée à partir de la Fig. 2. Ce résultat nous a amenés à considérer que la substitution du benzhydrol **7** perturbe l'anisochronie observée en présence de $Eu(dcm)_3$ entre les protons des noyaux aromatiques Pro *R* et Pro *S* (16).

Cette perturbation peut s'exprimer uniquement en fonction de la différence d'électronégativité des substituants des noyaux. Pour cela nous avons utilisé une représentation spatiale unique de tous les composés étudiés même les composés disubstitués. Si on appelle X le substituant porté par le noyau Pro *R* et Y le substituant porté par le noyau Pro *S* (Fig. 3), on peut décrire tous les énantiomères de tous les benzhydrols étudiés à partir d'une seule repré-

TABLEAU 3. Rapport des déplacements induits,[a] pente des droites $\delta^{\alpha}_{obs} = f(\Delta\delta^{\alpha'})$

	$\Delta^{\alpha}/\Delta^{\alpha'}$	
	R	*S*
1	1.040	0.785
2	1.101	0.825
3	1.221	0.933
4	1.317	1.022
5	1.366	1.064
6	1.040	0.807

[a]Ces valeurs sont obtenues par la méthode des moindres carrés $\rho^2 > 0.999$.

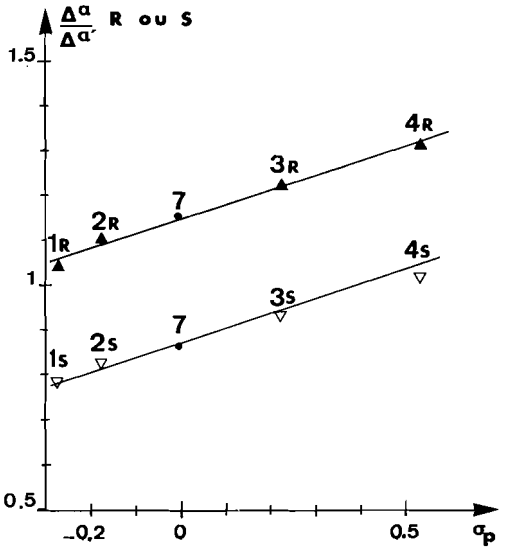

FIG. 2. Variation du rapport des déplacements induits des protons aromatiques de chaque énantiomère en fonction des σ_p.

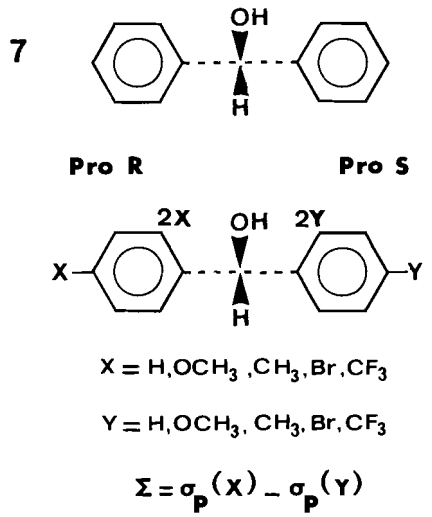

FIG. 3. Représentation spatiale des benzhydrols étudiés utilisée pour la définition de Σ.

sentation spatiale du carbone asymétrique. Par exemple, l'énantiomère *R* du composé **1** sera dans notre nouvelle représentation celui où X = OCH_3 et Y = H. Il n'est plus possible d'utiliser la nomenclature α et α′ que nous avons employé jusqu'ici. Maintenant, pour les énantiomères *R*, les protons α s'appelleront 2X et α′, 2Y et pour les énantiomères *S*, les protons α s'appelleront 2Y et α′, 2X.

On peut alors attribuer à chaque composé un paramètre Σ qui rend compte de la différence d'électronégativité entre le noyau dérivant du noyau Pro *R* et celui dérivant du noyau Pro *S*. Ce paramètre Σ peut être obtenu aisément à partir des σ_p de Hammett des substituants en faisant la différence $\Sigma = \sigma_p(X) - \sigma_p(Y)$. Cette définition entraîne que deux énantiomères ont des Σ de même grandeur mais de signes opposés.

La perturbation de l'anisochronie dûe aux substituants peut être exprimée en reliant Δ^{2X}/Δ^{2Y} au paramètre Σ. En effet $\Delta^{2X}/\Delta^{2Y} = \Delta^{\alpha}/\Delta^{\alpha'}$, pour les énantiomères *R* et $\Delta^{2X}/\Delta^{2Y} = \Delta^{\alpha'}/\Delta^{\alpha}$ pour les énantiomères *S*. On obtient à partir des données relatives aux benzhydrols **1** à **7** une droite (Fig. 4) d'origine 1.15 correspondant à X = Y, valeur proche de celle déterminée expérimentalement pour **7**. Nous avons vérifié que l'on obtenait la même valeur de ce rapport pour deux autres benzhydrols disubstitués symétriques (Σ = 0); pour X = Y = OCH_3, $\Delta^{2X}/\Delta^{2Y} = 1.145$ et pour X = Y = Cl, $\Delta^{2X}/\Delta^{2Y} = 1.148$.

Cette représentation permet aussi de déterminer la configuration absolue de benzhydrols mono- ou disubstitués en *para*: soit un énantiomère d'un benzhydrol portant deux substituants A et B: ou bien A est sur le noyau Pro *R* défini précédemment et alors Δ^{2A}/Δ^{2B} doit se placer sur la droite de la Fig. 4 à la valeur correspondant à $\Sigma = \sigma_p(A) - \sigma_p(B)$; ou bien B est sur le noyau Pro *R* et alors Δ^{2B}/Δ^{2A} doit correspondre à la valeur $\sigma_p(B) - \sigma_p(A)$. Cette méthode est applicable même si l'on ne dispose que d'un seul des énantiomères.

Puisque le rapport des déplacements induits, c'est-à-dire le rapport des distances, est supérieur à 1 lorsque X = Y, cela signifie que pour les benzhydrols symétriques, le noyau Pro *R* paraît plus proche de l'europium que le noyau Pro *S*. La distance de l'europium aux noyaux aromatiques varie selon l'électronégativité des substituants: le noyau Pro *R* devenu porteur du substituant X paraît d'autant plus proche de l'europium que ce substituant est électronégatif ou bien le noyau porteur du groupe Y paraît d'autant plus éloigné de l'europium que le substituant est électrodonneur. Tout se

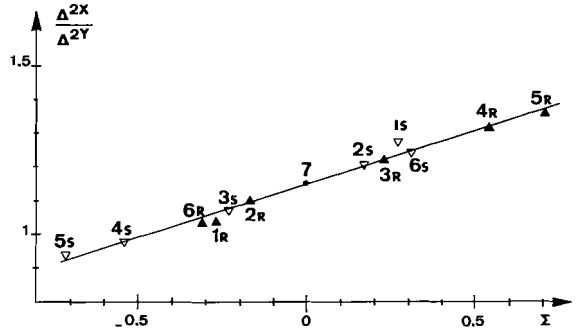

FIG. 4. Variation du rapport des déplacements induits des protons aromatiques de chaque énantiomère en fonction du paramètre Σ (voir texte).

passe comme si un substituant donneur augmentait "l'encombrement" d'un noyau aromatique tandis qu'un substituant attracteur le diminuait. Un substituant d'un noyau aromatique, du seul fait de son électronégativité peut produire des modifications notables de la structure du complexe; lorsque le substrat et le réactif sont chiraux, il en résulte que le phénomène de non-équivalence observé peut se représenter différemment selon la nature du substituant. Il devient évident que la prudence est désormais nécessaire lorsqu'on veut assimiler un composé substitué à un composé non substitué. Comme c'est déjà le cas en synthèse asymétrique (1, 11), les effets électroniques des substituants sur les manifestations de la chiralité ne peuvent plus être négligés.

1. J. CAPILLON et J. P. GUETTE. Tetrahedron. Sous presse.
2. M. D. MCCREARY, D. W. LEWIS, D. L. WERNICK et G. M. WHITESIDES. J. Am. Chem. Soc. **96**, 1038 (1974).
3. H. L. GOERING, J. N. EIKENBERRY et G. S. KOERMER. J. Am. Chem. Soc. **92**, 6979 (1970).
4. G. R. SULLIVAN, D. CIAVARELLA et H. S. MOSHER. J. Org. Chem. **39**, 2411 (1974).
5. R. R. FRASER, M. A. PETIT et J. K. SAUNDERS. Chem. Commun. 1450 (1971).
6. D. E. WILLIAMS. Tetrahedron Lett. 1345 (1972).
7. D. K. KELSEY. J. Am. Chem. Soc. **94**, 1766 (1972).
8. J. W. APSIMON, H. BEIERBECK et A. FRUCHIER. Org. Magn. Reson. **8**, 483 (1976) et références citées.
9. J. REUBEN. J. Am. Chem. Soc. **95**, 3534 (1973).
10. M. D. JOHNSTON, B. L. SHAPIRO, M. J. SHAPIRO, T. W. PROULX, A. D. GODWIN et H. L. PEARCE. J. Am. Chem. Soc. **97**, 542 (1975).
11. W. H. PIRKLE, M. S. HOEKSTRA et W. H. MILLER. Tetrahedron Lett. 2109 (1976).
12. K. ROTH. Anal. Chem. **48**, 2277 (1976).
13. H. M. MCCONNELL et R. E. ROBERTSON. J. Chem. Phys. **29**, 1361 (1958).
14. A. F. COCKERILL, G. O. DAVIES, R. C. HARDEN et D. M. RACKHAM. Chem. Rev. **73**, 553 (1973).
15. M. RABAN et K. MISLOW. Topics in stereochemistry. Vol. 1. Interscience Publishers, New York, NY. 1966. p. 1.
16. K. R. HANSON. J. Am. Chem. Soc. **88**, 2731 (1966).

Pyrones. IV.[1] Phacidin, a fungal growth inhibitor from *Potebniamyces balsamicola* Smerlis var. *boycei* Funk

GERALD ARTHUR POULTON[2] AND TERRY DONALD CYR

Department of Chemistry, University of Victoria, Victoria, B.C., Canada V8W 2Y2

AND

ELEANOR E. MCMULLAN

Department of the Environment, Canadian Forestry Service, Pacific Forest Research Centre, Victoria, B.C., Canada V8Z 1M5

Received December 22, 1978

GERALD ARTHUR POULTON, TERRY DONALD CYR, and ELEANOR E. MCMULLAN. Can. J. Chem. 57, 1451 (1979).

Phacidin, an antifungal antibiotic, isolated from the canker fungus *Potebniamyces balsamicola* Smerlis var. *boycei* Funk is shown to be 2-methoxy-6-nonanoyl-4*H*-pyran-4-one-3-carboxaldehyde. Carbon-13 nmr spectra of phacidin and several related γ-pyrones are discussed.

GERALD ARTHUR POULTON, TERRY DONALD CYR et ELEANOR E. MCMULLAN. Can. J. Chem. 57, 1451 (1979).

On a démontré que la structure de la phacidine, un antibiotique fongicide isolé du champignon chancre *Potébniamyces balsamicola* Smerlis var. *boycei* Funk, est le méthoxy-2 nonanoyl-6 4*H* pyrannone-4 carboxaldéhyde-3. On discute des spectres RMN du ^{13}C de la phacidine et de plusieurs γ-pyrones qui lui sont liées.

[Traduit par le journal]

Introduction

The fungus *Potebniamyces balsamicola* Smerlis var. *boycei* Funk, responsible for a bark disease in *Abies grandis* (Dougl.) Lindl. (1), produces in culture (2) a pale yellow crystalline substance, phacidin. Subsequent testing of this substance revealed (3) promising in vitro activity against a variety of dermatophytes, systemic dimorphic and opportunistic fungi, and yeasts of medical importance. The choice of 6-methoxy-5-nonanoyl-4*H*-pyran-4-one-2-carboxaldehyde (**2**) as the structure best representing phacidin was made (4) on the basis of an examination of the spectra and on the basis of reactivity analogous to that observed in the literature. The structural assignment must now be revised on the basis of more recent chemical and spectroscopic evidence.

Experimental

Nuclear magnetic resonance data were obtained on a Perkin Elmer R12A (60 MHz) or R32 (90 MHz) instrument (proton) or Nicolet TT-14 (15.1 MHz) instrument (carbon) in $CDCl_3$ solution and are referenced to TMS. Mass spectra were obtained using the Hitachi – Perkin Elmer RMU-7E, ultraviolet spectra on the Beckman SP800, and infrared spectra on Beckman IR20 and Unicam SP1000 instruments.

2-Ethoxy-, 2-methoxy-, and 3-bromo-2-ethoxy-6-methyl-4*H*-pyran-4-one (compounds **5**, **6**, **7** respectively) were prepared as described previously (5).

Phacidin (1)

Pure phacidin was isolated from cultures of *P. balsamicola* as described previously (2), as yellow needles, mp 112–113°C; ν_{max} (KBr): 3110 (w), 2975 (sh), 2040 (s), 2870 (s), 1730 (m), 1700 (s), 1690 (m), 1620 (m), 1530 (m), 1520 (s), 1480 (m), 1387 (m), 1340 (m), 1239 (m), and 1041 cm^{-1} (w); λ_{max} (EtOH) (log ε): 224 (4.20), 274 (3.43), and 342 nm (3.90); nmr δ_H: 10.17 (1H, s), 7.11 (1H, s), 4.11 (3H, s), 2.96 (2H, t, J = 6.7 Hz), 2.0–1.1 (12H, m), and 0.88 ppm (3H, t, J = 6.1 Hz); δ_C: see Table 1; ms *m/e* (relative intensity): 294.151 (3%; M^+, $^{12}C_{16}{}^1H_{22}{}^{16}O_5$ requires 294.147), 266 (3.5), 154 (9), 153.020 (100; $^{12}C_7{}^1H_5{}^{16}O_4$ requires 153.019), 141 (4), 126 (2), 125 (9), 121 (4), 93 (4), 85 (2), 71 (3), 69 (5), 59 (4), 57 (5), 55 (3), 53 (3), 43 (5), 41 (5), 39 (2), and 29 (3). *Anal.* calcd. for $C_{16}H_{22}O_5$: C 65.29, H 7.53; found: C 65.10, H 7.62.

Oxidation of Phacidin

To ruthenium tetroxide solution (from ruthenium trichloride trihydrate (3.6 mL of a 2% solution, 2.8×10^{-4} mol) and sodium hypochlorite (29 mL of a 0.5% solution) (6*a*)) were added dropwise phacidin (0.075 g, 2.55×10^{-4} mol) in dichloromethane (20 mL) and sodium hypochlorite (6%, added in quantity sufficient to maintain a yellow reaction mixture). When addition was finished, the mixture was acidified with dilute HCl, extracted with dichloromethane, the extracts dried ($MgSO_4$), filtered, and evaporated to give, after purification, *n*-nonanoic acid[3] (0.013 g, 33%), δ_H 2.33 (2H, t), 1.8–2.1 (12H, m), and 0.88 ppm (3H, t); ν_{max} 3400–2400 (br), 2950 (sh), 2920 (s), 2850 (m), 1712 (s), 1448 (m), 1410 (m), 1280 (m), 1108 (w), and 925 cm^{-1} (m); *m/e* 158.125, $^{12}C_9{}^1H_{18}{}^{16}O_2$ requires 158.131.

2-Methoxy-6-nonanoyl-4H-pyran-4-one (3)

Phacidin (75 mg, 0.26 mmol) and tris(triphenylphosphine)-

[1]For Part III in this series, see ref. 5.

[2]Author to whom all correspondence should be addressed.

[3]Identified by spectral comparison with an authentic sample prepared from 1-bromooctane by a Grignard reaction.

0008-4042/79/121451-05$01.00/0

TABLE 1. ^{13}C nmr chemical shifts (ppm) and coupling constants (Hz) of phacidin and related compounds

Compound	Values	Data for carbon: 2	3	4	5	6	7	8	9	10	11	12	13	14	15	16	OCH_3
1, R = CHO	δ_C	160.2	105.9	172.9	97.0	158.5	193.5	38.3	23.1	29.2	29.3	29.1	31.8	22.7	14.1	186.3	58.4
	$^1J_{CH}$				*175.3*			*123.6*	*127.5*	*125.1*	*125.1*	*125.1*	*125.5*	*127.5*	*124.6*	*186.2*	*148.4*
	$^2J_{CH}$		*24.5*	*m*			*m*										
	$^3J_{CH}$	*2.5*	*4.2*			*1.4*											
3, R = H	δ_C	162.4	103.7	169.9	93.6	154.8	193.9	38.2	23.1	29.1	29.1	29.1	31.8	22.7	14.1		56.5
	$^1J_{CH}$		*176.0*		*169.4*												
	$^3J_{CH}$		*5.35*		*4.0*												
4, R = Br	δ_C	158.5	96.6	165.6	97.5	154.0	193.4	38.2	23.2	29.1	29.1	29.1	31.8	22.7	14.1		57.9
	$^1J_{CH}$				*174.2*												
	$^3J_{CH}$		*6.6*														

1

2

3

4

5

6

7

chlororhodium (6*b*) (235 mg, 0.27 mmol) were dissolved in benzene (10 mL) and refluxed with stirring until no starting material remained. The precipitated rhodium carbonyl was removed by filtration, the benzene evaporated, and the crude product thus obtained purified by chromatography. 2-Methoxy-6-nonanoyl-4*H*-pyran-4-one was colourless needles, mp 120–121°C (95% EtOH); ν_{max} (KBr): 3080 (w), 2950 (sh), 2920 (5), 2850 (m), 1730 (s), 1710 (s), 1630 (m), 1520 (m), 1465 (m), 1390 (s), 1310 (m), 1235 (m), 1080 (m), 985 (m) and 940 cm^{-1} (m); λ_{max} (EtOH) (log ε): 220 (4.07), 255 (3.12), and 307 nm (3.50); nmr δ_H: 6.72 (1H, d, J = 2.4 Hz), 5.69 (1H, d, J = 2.4 Hz), 3.84 (3H, s), 2.87 (2H, t, J = 7.4 Hz), 1.85–1.0 (12H, m), and 0.88 ppm (3H, t, J = 6.0 Hz); δ_C: see Table 1; ms *m/e* (relative intensity): 266.156 (3; $M^{\ddagger}$; $^{12}C_{15}{}^{1}H_{22}{}^{16}O_4$ requires 266.152), 238 (5), 169 (4), 168 (6), 140 (2), 127 (3), 126 (21), 125 (100), 101 (1), 99 (1), 97 (3), 95 (2), 83 (2), 81 (1), 71 (3), 69 (31), 67 (2), 57 (5), 55 (7), 53 (6), 43 (11), 41 (15), 39 (7), and 29 (12).

*3-Bromo-2-methoxy-6-nonanoyl-4*H*-pyran-4-one (4)*

Phacidin (25.0 mg, 0.085 mmol) was dissolved in methanol (2.5 mL) and treated with an excess of a solution of bromine water (saturated, 1 mL). The crude product was separated by dichloromethane extraction and recrystallized: 3-bromo-2-

TABLE 2. ^{13}C nmr chemical shifts of ring carbons of some γ-pyrones

Compound	Values for carbon: 2	3	4	5	6	Ref.
5	168.1	89.3	181.5	112.6	161.4	This work
6	167.4	89.9	181.7	112.7	161.5	This work
7	162.5	90.4	175.4	111.8	159.8	This work
Colletotrichitin	163.5	106.0	177.1	120.2	160.8	13
Spectinabilin	162.1	99.1	180.6	119.9	155.2	10
Aureothin	163.8	99.9	183.6	120.6	156.2	14
Tridachione	160.1*	97.8	181.1	118.4	161.1*	15

*Assignments may be reversed.

methoxy-6-nonanoyl-4*H*-pyran-4-one, mp 79–80°C (aqueous EtOH); 24.2 mg (82%); ν_{max} (KBr): 3085 (w), 2920 (s), 2860 (m), 1730 (s), 1710 (s), 1643 (s), 1570 (m), 1470 (m), 1420 (s), 1350 (w), 1270 (s), 1180 (w), 1005 (s), and 990 cm^{-1} (s); λ_{max} (EtOH) (log ε): 226 (4.21) and 337.5 nm (3.99); nmr δ_H: 7.02 (1H, s), 4.06 (3H, s), 2.91 (2H, t, J = 6.7 Hz), 1.9–1.1 (12H, m), and 0.90 ppm (3H, br t); δ_C: see Table 1; ms *m/e* (relative intensity): 345 (7, M^+), 343 (7, M^+), 264 (3), 247 (11), 245 (10), 236 (5), 206 (8.5), 205 (100), 204 (8.5), 203 (100), 177 (7), 175 (8), 149 (31), 147 (34), 141 (6), 125 (11), 124 (25), 95 (3), 94 (5), 93 (4), 71 (13), 69 (12), 66 (24), 59 (8), 57 (25), 55 (30), 53 (22), 43 (48), 41 (43), 39 (15), and 29 (29).

Discussion

The presence of a γ-pyrone (4*H*-pyran-4-one) nucleus in phacidin was inferred (4) from the observed infrared absorptions at 1690 (C=O), 1620, 1530, 1520 (C=C), and 1235 cm^{-1} (C—O—C) and from the ultraviolet maxima at 224 (log ε 4.20), 274 (3.43), and 342 nm (3.90). In general, γ-pyrones are found to exhibit their first carbonyl band in the 1675–1650 cm^{-1} region, the position being somewhat variable, depending upon substituent nature and solvent (7), while α-pyrones absorb in the 1740–1720 cm^{-1} range (7, 8). We felt that our data were best rationalized by a γ-pyrone structure, and this was supported by the fact that γ-pyrone ultraviolet spectra generally reveal intense absorption maxima in the 245–275 nm region (9), although differentiation between α- and γ-pyrone isomers becomes difficult unless both isomers are available. The mass spectrum of phacidin is also in agreement with that expected for γ-pyrones (10, 11), showing two successive losses of carbon monoxide:

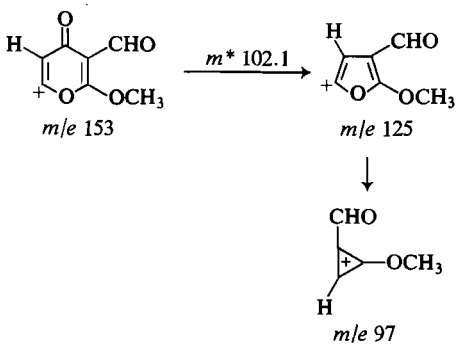

Confirmatory evidence for the existence of the γ-pyrone nucleus in phacidin has been obtained from the carbon magnetic resonance spectra:[4] the C4 carbon resonates at 172.9 ppm (see Table 1), well within the normal range of 171–184 ppm observed for γ-pyrone carbonyl carbons (ref. 12 and references in Table 2). Similarly, the α-carbon resonances (158.5 and 160.2 ppm) and the β-carbon resonances (97.0 and 105.9 ppm) are typical of γ-pyrones (β-range normally 88–120 ppm; α-range normally 139–167 ppm (ref. 12 and Table 2)).[5]

The substitution pattern of the γ-pyrone ring may be readily identified from spectral and chemical evidence. The substituents are: (*i*) a hydrogen (one-proton singlet, δ_H 7.11 ppm), (*ii*) a methoxyl group (δ_H 4.11 ppm (3H, s); δ_C 58.4 ppm ($^1J_{C-H}$ = 148.4 Hz)), (*iii*) an aldehyde, and (*iv*) a *n*-nonanoyl moiety. The aldehyde group is inferred from the infrared (2870, 1730 cm^{-1}), proton nmr (10.17 ppm, 1H, s), and carbon nmr spectra (186.3 ppm, $^1J_{C-H}$ = 186.2 Hz), and confirmed by the formation of a phenylhydrazone (4) and by ready decarbonylation with tris(triphenylphosphine)chlororhodium (6*b*) (discussed below). The nonanoyl group may be inferred from the spectra (ν_{max} 1700 cm^{-1}; δ_H 0.88 (3H, t), 1.1–2.0 (12H, m), and 2.96 ppm (2H, t); δ_C 193.5 (—CO—), plus 7 triplet resonances between 22.7 and 38.3 ppm (see Table 1 for assignments) and 14.1 ppm (q, —CH_3)), and from the isolation and identification of nonanoic acid as the sole isolable product from the oxidation of phacidin (4). The location of the unsubstituted γ-pyrone carbon can be readily made from the observed carbon–proton coupling in the gated spectrum: the resonance at 97.0 ppm exhibits a coupling constant ($^1J_{C-H}$ = 175.3 Hz), similar to those observed[6] for β-protons. This agrees with the argument which was previously advanced

[4]Obtained through the kind cooperation of Dr. John Walter, Atlantic Regional Laboratory, National Research Council of Canada, Halifax.

[5]Normal chemical shift values for α-pyrones are: α 137–165 ppm, β 87–116 ppm, and C=O 157–162 ppm (16).

[6]$^1J_{C-H}$ (β) typically 166–169 Hz, $^1J_{C-H}$ (α) 197–202 Hz (12).

(4), which identified the 7.11 ppm proton magnetic resonance absorption as being due to a β-proton deshielded by an adjacent carbonyl substituent.[7] Thus, the partial structure **8** may be assigned.

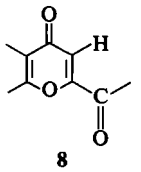

8

The nature of this carbonyl substituent may be deduced from the results of some chemical investigations with phacidin. Treatment of phacidin with tris-(triphenylphosphine)chlororhodium effects smooth decarbonylation (*6b*), producing 2-methoxy-6-nonanoyl-4*H*-pyran-4-one (**3**). Interpretation of the carbon magnetic resonance spectra of phacidin and its decarbonylated analogue can only adequately be made using the structure **1**. In phacidin, the β-carbon signal seen at 105.9 ppm appears in the gated spectrum as a double doublet, with coupling constants of 24.5 and 4.2 Hz. The latter is similar to the typical values (5.1–6.0 Hz) observed (12) for three-bond coupling between C3 and H5 in a series of simple pyrones; the former, larger coupling can then only be reasonably explained if it represents a two-bond coupling between C3 and the proton on the attached aldehyde group. This placement of the aldehyde at position 3 is confirmed by the cmr spectra of the decarbonylated compound, which show δ_C 103.7 ($^1J_{C-H}$ = 176.0 Hz, $^3J_{C-H}$ = 5.35 Hz) and 93.6 ppm ($^1J_{C-H}$ = 169.4 Hz, $^3J_{C-H}$ = 4.0 Hz) and δ_H 6.72 and 5.69 ppm (both 1H, d, J = 2.4 Hz[8]), signals characteristic of a 2,6-disubstituted γ-pyrone. This result unequivocally rules out the structure **2**, in which the deformylated compound would now have one α- and one β-proton, whose chemical shifts would be considerably different and where the coupling constant would be larger.[8] The methoxyl group must then be at position 2 and phacidin is thus 2-methoxy-6-nonanoyl-4*H*-pyran-4-one-3-carboxaldehyde (**1**).

On the basis of this structure for phacidin, the remaining spectra and chemical transformations may be rationalized. Explanation of the mass spectral behaviour is straightforward: the molecular ion undergoes predominant cleavage with loss of the side chain to yield the base peak at *m/e* 153; subsequent fragmentations of this ion have been discussed. Minor fragmentation pathways from the molecular ion involve two sequential CO losses (metastable ion peaks observed at 240.7 and 212.9). The nonanoyl side chain ion (*m/e* 141) and the ions derived from its decomposition ($C_nH_{2n+1}CO$ and $C_nH_{2n-1}CO$ series) are prevalent in the low molecular weight region of phacidin and its derivatives.

Treatment of phacidin with bromine in aqueous methanol results in the replacement of the aldehyde group by a bromine atom. This can be seen by the change in the mass spectrum (molecular weight and fragmentation pattern) and from the carbon magnetic resonance: the aldehyde signal disappears, and that due to C3 shifts upfield to 96.6 ppm (appearing now as a doublet, $^3J_{C-H}$ = 6.6 Hz). This reaction is not without precedent, as Nohara *et al.* (18) have reported the room temperature conversions of chromone-3-carboxaldehyde (**9**) to the corresponding 3-chloro- and 3-bromo-compounds (**10**).

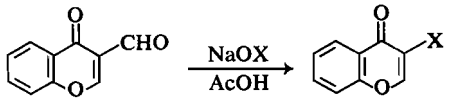

(ref. 18)

9 **10**

The biogenesis of phacidin may also be easily rationalized, since some naturally occurring α-methoxy-γ-pyrones have been shown (see, for example, refs. 13, 14) to be produced from polyketide routes.

It is therefore likely that phacidin is produced from a heptaacetate precursor which undergoes the appropriate cyclizations, alkylations, and modifications:

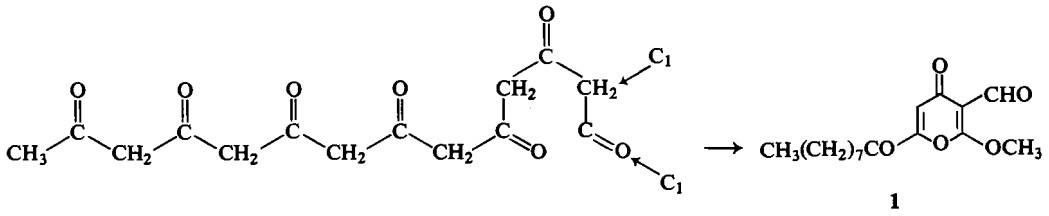

1

[7]The 'normal' position of a β-hydrogen (4) is in the 5.9–6.5 ppm range; a carbonyl substituent at the adjacent α-position, for example in comenaldehyde methyl ether, results in a deshielding of the proton and a shift of the resonance to 6.97 ppm.

[8]J_{H3-H5} = 2.68 Hz, J_{H2-H3} = 6.3 Hz in γ-pyrone (17).

Methylation at oxygen and ring alkylation by intermediates from the 'one-carbon' pool have been shown (13) to occur in pyrones, and a parallel biogenetic route may be assumed here.

NOTE ADDED IN PROOF: Recent synthetic evidence has shown that the decarbonylated product **3** is 6-nonanoyl-4-methoxy-2*H*-pyran-2-one. Although a rearrangement occurred (previously observed with 2-methoxy-4*H*-pyran-4-ones) and the assignment of chemical shifts (see Table 1) must necessarily be altered, this reassignment does not invalidate the arguments relating to disposition of substituents in phacidin.

Acknowledgements

Financial support from the Natural Sciences and Engineering Research Council and the University of Victoria is gratefully acknowledged. We are also very grateful to the National Research Council of Canada, Atlantic Regional Laboratory, and to Dr. John Walter, for providing the 25.2 MHz carbon magnetic resonance spectra of phacidin.

1. A. FUNK. Can. J. Bot. **47**, 751 (1969); **48**, 1023 (1970).
2. A. FUNK and E. E. MCMULLAN. Can. J. Microbiol. **20**, 422 (1974).
3. A. S. SEKHON and A. FUNK. J. Antimicrobiol Chemother. **3**, 95 (1977).
4. G. A. POULTON, M. E. WILLIAMS, and E. E. MCMULLAN. Tetrahedron Lett. 2611 (1974).
5. T. D. CYR and G. A. POULTON. Can. J. Chem. **56**, 1796 (1978).
6. L. F. FIESER and M. FIESER. Reagents for organic synthesis. (*a*) Vol. 3. John Wiley and Sons Ltd., New York, NY. 1972. p. 243, (*b*) Vol. 1. John Wiley and Sons Ltd., New York, NY. 1967. p. 1252.
7. D. HERBST, W. B. MORS, O. R. GOTTLIEB, and C. DJERASSI. J. Am. Chem. Soc. **81**, 2427 (1959).
8. K. NAKANISHI. Infrared absorption spectroscopy — practical. Holden-Day Inc., San Francisco, CA. 1962. p. 204.
9. A. I. SCOTT. Interpretation of the ultraviolet spectra of natural products. Pergamon Press, Oxford, Engl. 1964. pp. 140–147.
10. K. KAKINUMA, C. A. HANSON, and K. L. RINEHART, JR. Tetrahedron, **32**, 217 (1976).
11. Q. N. PORTER and J. BALDAS. Mass spectrometry of heterocyclic compounds. Wiley-Interscience, New York, NY. 1971. pp. 139–147.
12. C. A. KINGSBURY, M. CLIFFTON, and J. H. LOOKER. J. Org. Chem. **41**, 2777 (1976).
13. Y. KIMURA, M. GOHBARA, and A. SUZUKI. Tetrahedron Lett. 4615 (1977).
14. M. YAMAZAKI, Y. MAEBAYASHI, H. KATOH, J. OHISHI, and Y. KOYAMA. Chem. Pharm. Bull. **23**, 569 (1975).
15. C. IRELAND, D. J. FAULKNER, B. A. SOLHEIM, and J. CLARDY. J. Am. Chem. Soc. **100**, 1002 (1978).
16. W. V. TURNER and W. H. PIRKLE. J. Org. Chem. **39**, 1935 (1974).
17. C. T. MATHIS and J. H. GOLDSTEIN. Spectrochim. Acta, **20**, 871 (1964).
18. A. NOHARA, K. UKAWA, and Y. SANNO. Tetrahedron Lett. 1999 (1973).

Stereochemistry of the Bucherer–Bergs and Strecker reactions of tropinone, *cis*-bicyclo[3.3.0]octan-3-one and *cis*-3,4-dimethylcyclopentanone

GREGORIO G. TRIGO, CARMEN AVENDAÑO, AND EMILIA SANTOS

Department of Organic and Pharmaceutical Chemistry, School of Pharmacy, Universidad Complutense, Madrid-3, Spain

AND

JOHN T. EDWARD AND SIN CHEONG WONG

Department of Chemistry, McGill University, Montreal, P.Q., Canada H3A 2K6

Received June 19, 1978[1]

GREGORIO G. TRIGO, CARMEN AVENDAÑO, EMILIA SANTOS, JOHN T. EDWARD, and SIN CHEONG WONG. Can. J. Chem. 57, 1456 (1979).

The tropane-3-spiro-5′-hydantoin (α isomer) obtained from tropinone by the Bucherer–Bergs reaction has been shown by ^{13}C nmr and X-ray diffraction studies to have the 4′-carbonyl group in the equatorial position; the β isomer, obtained via the Strecker reaction, has this group axial. The results of these two reactions on *cis*-bicyclo[3.3.0]octan-3-one and on *cis*-3,4-dimethylcyclopentanone show, on the basis of the ^1H nmr, ^{13}C nmr, and X-ray diffraction studies of the products, a stereochemical course related to the preferred conformation of the cyclopentane rings.

GREGORIO G. TRIGO, CARMEN AVENDAÑO, EMILIA SANTOS, JOHN T. EDWARD et SIN CHEONG WONG. Can. J. Chem. 57, 1456 (1979).

On a démontré, au moyen d'études de rmn ^{13}C et de diffraction de rayons-x, que la tropane-3-spiro-5′-hydantoïne (isomère α), obtenue de la tropinone au cours de la réaction Bucherer–Bergs, possède le groupe carbonyle-4′ dans la position équatoriale; l'isomère β, obtenu par la réaction Strecker, possède ce groupement en position axiale. Les structures des produits isomères fournis par le *cis*-bicyclo[3.3.0]octan-3-one et par le cyclopentanone-*cis*-3,4-diméthyle ont été établies par des études semblables. Le chemin stéréochimique des deux réactions est conditionné par la conformation préférée des anneaux cyclopentaniques.

Introduction

The Bucherer–Bergs reaction of aldehydes or ketones with ammonium carbonate and sodium cyanide to form hydantoins (1) and the alternative Strecker reaction via amino nitriles (2) can lead, with some ketones, to different (α and β) products. The stereochemistry of the α and β isomers has been studied by several workers, with conflicting conclusions (3–11). However, this conflict was resolved by the work of Edward and Jitrangsri (11) who explained, by a detailed consideration of reaction mechanisms, how the same amino nitrile could yield either the α- or the β-hydantoin, according to reaction conditions. They concluded that the Bucherer–Bergs reaction of substituted cyclohexanones yields as the major product the isomer (α) with the 4′-carbonyl group of the spiro-hydantoin ring in the less sterically hindered position, while the Strecker reaction yields as the major product the isomer (β) with this carbonyl group in the more sterically hindered position (the EJ rule).

The present work was undertaken to test this rule by establishing the configurations of the isomeric spiro-hydantoins obtained from tropinone (**1**), *cis*-bicyclo[3.3.0]octan-3-one (**4**), and *cis*-3,4-dimethylcyclopentanone (**9**). The preparation of some of these spiro-hydantoins has already been reported (12, 13).

Experimental

All melting points were taken in open capillary tubes and are uncorrected. The ^1H nmr spectra have been recorded on a Perkin Elmer R-24A (60 MHz) spectrometer. The ^{13}C nmr spectra were determined on a Bruker 22.63 MHz spectrometer. Infrared spectra were determined using a Perkin Elmer 577 spectrophotometer.

Materials

Tropinone (**1**) was synthesized by the Robinson–Schöpf method, previously modified by Findlay (14). *cis*-Bicyclo[3.3.0]octan-3-one (**4**) was obtained following the Linstead and Meade scheme (15) as modified by us (13). *cis*-3,4-Dimethylcyclopentanone (**9**) was obtained, with the *trans*-isomer, by catalyzed hydrogenation of 3,4-dimethyl-2-cyclopentenone following the Conia and Leriverend scheme (16). The *cis*- and *trans*-3,4-dimethylcyclopentanones were first separated by analytical gas chromatography on a Perkin Elmer F-20 chromatograph, using a Carbowax 1500 column (4 m length and $\frac{1}{8}$ in. diameter), Chromosorb W-80-100 as support, 130°C of column temperature, nitrogen as carrier gas and 20 mL/min flowing. Retention times (uncorrected): *trans*-isomer 8.35 min; *cis*-isomer 10.4 min. Preparative gas chromatography, using a Perkin Elmer F-21, with a Carbowax 1500 column of 5 m length, nitrogen as carrier gas, 9 s of injection time, and isothermic conditions at 145°C, yielded the two separated isomers.

[1]Revision received January 26, 1979.

0008-4042/79/121456-06$01.00/0

Tropane-3-spiro-5′-hydantoins (2 and 3)

Bucherer and Strecker products were prepared by the methods previously described (12).

cis-*Bicyclo[3.3.0]octane-3-spiro-5′-hydantoins (5 and 6)*

Bucherer and Strecker products were prepared by the methods previously described (13).

cis-*Bicyclo[3.3.0]octane-3-spiro-5′-(1′,3′-diacetylhydantoin) (β Isomer)*

A solution of *cis*-bicyclo[3.3.0]octane-3-spiro-5′-hydantoin (β isomer; **5**) (0.7 g) in acetic anhydride (73.6 mL) was heated under reflux for 12 h. After the solvent was removed by evaporation under reduced pressure, the residue was crystallized from absolute ethanol; mp 105–110°C (50%); ν_{max} (KBr): 1815, 1785, 1760, and 1700 ($\nu_{C=O}$) cm^{-1}; $\delta(CDCl_3)$: 2.6 (s, 6H, two acetyls). *Anal.* calcd. for $C_{14}H_{18}N_2O_4$: C 60.43, H 6.47, N 10.07; found: C 60.17, H 6.55, N 9.81.

cis-*Bicyclo[3.3.0]octane-3-spiro-5′-(3′-acetylhydantoin) (α Isomer)*

A mixture (50 mg) of **5** (60%) and **6** (40%) (from the Bucherer reaction) was heated as above in acetic anhydride. The residue, recovered in poor yield after recrystallization from water, melted at 138–140°C; ν_{max} (KBr): 3220, 3110 (ν_{N-H}), 1795, 1760, 1690 ($\nu_{C=O}$) cm^{-1}. *Anal.* calcd. for $C_{12}H_{16}N_2O_3$: C 61.00, H 6.83, N 11.86; found: C 61.32, 61.53, H 7.22, 7.15, N 11.92, 11.87.

cis-*3,4-Dimethylcyclopentane-3-spiro-5′-hydantoins (10 and 11)*

(a) Bucherer Product

A solution of *cis*-3,4-dimethylcyclopentanone (0.6 g), potassium cyanide (0.6 g), and ammonium carbonate (7.5 g) in ethanol (20 mL) and water (20 mL) was heated under reflux at 50–55°C for 5 h. After cooling, the precipitated solid was filtered off, washed with water, and recrystallized from methanol; mp 298–299°C (31%); ν_{max} (KBr) 3200 ($\nu_{N1'-H}$), 3070 and 3120 ($\nu_{N3'-H}$), and 1745 and 1780 ($\nu_{C=O}$) cm^{-1}. *Anal.* calcd. for $C_9H_{14}N_2O_2$: C 59.34, H 7.74, N 15.37; found: C 59.50, H 7.78, N 15.09.

(b) Strecker Product

cis-3,4-Dimethylcyclopentanone (4.5 g) was stirred with potassium cyanide (3 g) and ammonium chloride (2.2 g) in water (33 mL) and ethanol (25 mL), at room temperature for 7 days. The solvents were removed under reduced pressure, the residue was extracted with ether, and the extract was dried ($MgSO_4$). Passage of dry hydrogen chloride gave 1-amino-*cis*-3,4-dimethylcyclopentanecarboxynitrile hydrochloride; mp 157–158°C (27%). A solution of this crude aminonitrile hydrochloride (1 g) and potassium cyanate (2.1 g) in acetic acid (18 mL) and water (9 mL) was heated at 100°C under reflux for 1 h. The reaction mixture was heated with concentrated hydrochloric acid (9 mL) for 30 min. The mixture was diluted with water, cooled, and the crude product was filtered off and recrystallized from methanol; mp 291–292°C (77%); ν_{max} (KBr): 3200 ($\nu_{N1'-H}$), 3080 and 3100 ($\nu_{N3'-H}$), and 1745 and 1775 ($\nu_{C=O}$) cm^{-1}. *Anal.* calcd. for $C_9H_{14}N_2O_2$: C 59.34, H 7.74, N 15.37; found: C 59.60, H 7.64, N 15.43.

Results and Discussion

We have found that the Strecker reaction with tropinone (**1**) furnished exclusively one isomer (β) and the Bucherer–Bergs reaction exclusively another isomer (α). The structures of the two isomers were established from the ^{13}C nmr data.

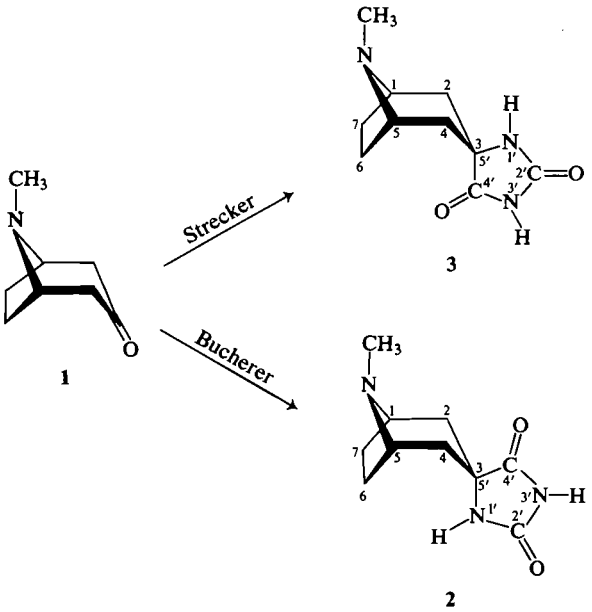

The isomers must differ in having the 4′-carbon atom equatorial in one (**2**) and axial in the other (**3**) isomer. In **2** the 4′-carbon will be *gauche* with respect to all four hydrogen atoms at C2 and C4, but in **3** it will be *anti* with respect to two of them. We must expect then that the vicinal coupling constant, $^3J_{^{13}C-^1H}$, should be greater, and hence the ^{13}C peak broader, in **3** than in **2**.

The ^{13}C nmr spectra of α and β isomers (Table 1) were obtained in 85% D_2SO_4 solution since solubilities in the usual solvents were too small. In this solvent the hydantoins will exist as the monoprotonated or diprotonated cations (17), so that the peaks for 2′- and 4′-carbon atoms will be at very low field. The distinction between these positions is possible from the fact that the 4′-, but not the 2′-carbon, spin couples with hydrogen atoms at positions 2 and 4 of the cycloheptane ring.

The 4′-carbon peak of the β isomer had a half-width of 17 Hz, as compared with a half-width of 10 Hz for the 4′-carbon peak of the α isomer. This indicates that the β isomer has the structure **3** and the α isomer the structure **2**.

Since these structural assignments have now been confirmed by X-ray diffraction (18), this work can be considered a confirmation both of the use of ^{13}C nmr for structural diagnosis, and of the EJ rule quoted above.

To utilize this rule to predict the stereochemistry of the Bucherer–Bergs and Strecker reactions with cyclopentanones is more difficult than with anchored cyclohexanones, since the question of which face of

TABLE 1. ^{13}C chemical shifts (ppm, downfield from TMS) and coupling constants (Hz) of tropane-3-spiro-5′-hydantoins **2** and **3**

	2 (Bucherer product)		**3** (Strecker product)	
	δ	$^1J_{(^{13}C-^1H)}$	δ	$^1J_{(^{13}C-^1H)}$
C3(C5′)	57.0 (s)	—	55.4 (s)	—
C2=C4	36.3 (t)	130	34.2 (t)	133
C1=C5	60.2 (d)	150	60.8 (d)	153
C6=C7	20.3 (t)	137	20.4 (t)	137
CH_3	37.1 (q)	143	36.4 (q)	143
C2′	156.7 (s)	—	155.8 (s)[a]	—
C4′	175.5 (s)[b]	—	174.8 (s)[c]	—

[a]Half-width of peak with or without spin-decoupling 12 Hz.
[b]Half-width of peak with spin-decoupling 4 Hz; without spin-decoupling 10 Hz.
[c]Half-width of peak with spin-decoupling 5 Hz; without spin-decoupling 17 Hz.

the molecule is more sterically hindered depends on the preferred conformation of the cyclopentane ring.

The only cyclopentane ketones thus far studied have been (±)-camphor and (±)-norcamphor (3, 19). Tager and Christensen (20) showed by X-ray diffraction that the amino acid formed on hydrolysis of the Bucherer hydantoin from (±)-norcamphor had the carboxyl group *exo*, sterically more accessible (21), while the amino acid formed on hydrolysis of the Strecker amino nitrile had the carboxyl *endo*, sterically less accessible, in conformity with the EJ rule.

The steric characteristics of (±)-norcamphor are unambiguous because of its rigid structure. However, *cis*-bicyclo[3.3.0]octan-3-one (**4**) is conformationally mobile, so that application of the EJ rule is difficult. If the ketone has the envelope–envelope conformation shown in **4**, then the rule would indicate the structures **5** for the Strecker product and **6** for the Bucherer product.

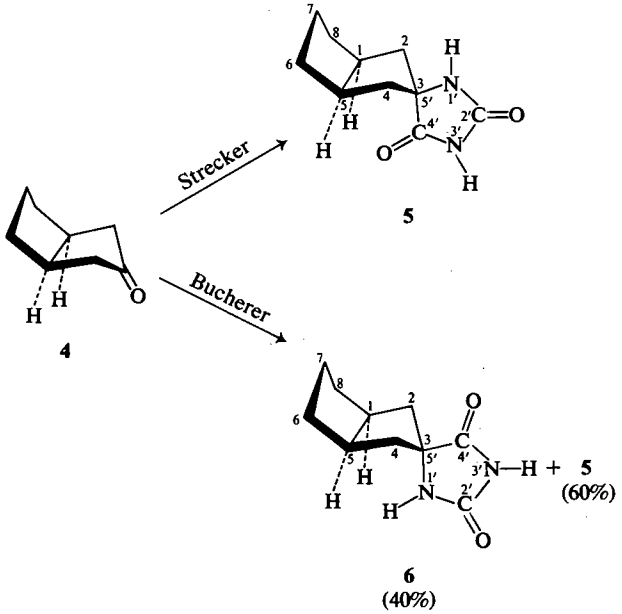

The ^{13}C nmr spectra (Table 2) indicate the Strecker product to be a pure compound B, but the Bucherer product, in spite of a sharp melting point, to be a mixture of 60% B + 40% of an isomeric compound A.[2] It was not necessary to separate this mixture in order to establish the structure of A, since its nmr spectrum could be obtained by comparison of the spectrum of the mixture with that of pure B. The chemical shifts and *J* values of A and B are listed in Table 2. The isomers differ in the extent to which the 4′-carbon is coupled with protons on vicinal carbon atoms, as shown by the varying half-widths of the spin-coupled systems (18 Hz for B as opposed to 6 Hz for A). This indicates the structure **5** for B and **6** for A if, indeed, *cis*-bicyclo[3.3.0]octane ring has the conformation shown in **4**–**6**. While it would be difficult to deduce this conformation a priori, it has been established by X-ray crystallography (22) for the Strecker product B. This study confirms the structure **5** for B, with the angles indicated. The plane of the hydantoin ring bisects the angle formed by the C2, C3, and C4 carbon atoms.

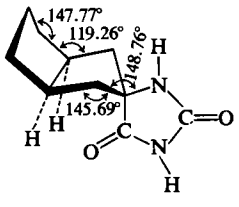

5

These structures accord with the results of acetylation experiments (cf. ref. 11). B reacted with acetic anhydride to give a diacetyl derivative, as would be expected of **5** (11). Under the same conditions, the 40:60 mixture of A and B from the Bucherer reaction

[2]The same composition of the Bucherer–Bergs product is indicated in its ^1H nmr spectrum, which shows two peaks for the 1′-hydrogen atom with relative intensities 6:4 (see Table 3); the spectrum of the Strecker product shows only one 1′-hydrogen peak having the same chemical shift as the peak of the major isomer from the Bucherer–Bergs reaction.

TABLE 2. ^{13}C chemical shifts (ppm, downfield from TMS) and coupling constants (Hz) of *cis*-bicyclo[3.3.0]octane-3-spiro-5′-hydantoins

	Bucherer products					
	5		**6**		Strecker product (**5**)	
	δ	$^1J_{(^{13}C-^1H)}$	δ	$^1J_{(^{13}C-^1H)}$	δ	$^1J_{(^{13}C-^1H)}$
C3(C5′)	88.4 (s)	—	90.4 (s)	—	88.4 (s)	—
C2=C4	55.2 (t)	133	57.3 (t)	133	55.2 (t)	133
C1=C5	55.7 (d)	137	56.6 (d)	133	55.6 (d)	133
C6=C8	46.7 (t)	129	46.2 (t)	—	46.6 (t)	129
C7	38.8 (t)	129	38.4 (t)	—	38.7 (t)	129
C2′	174.4 (s)[a]	—	174.6 (s)[a]	—	174.4 (s)[a]	—
C4′	193.4 (s)[b,c]	—	192.2 (s)[b,d]	—	193.4 (s)[b,e]	—

[a]Half-width of peak with and without spin-decoupling 3 Hz.
[b]Half-width of peak with spin-decoupling 3 Hz.
[c]Half-width of peak without spin-decoupling 18 Hz.
[d]Half-width of peak without spin-decoupling 6 Hz.
[e]Half-width of peak without spin-decoupling 14.5 Hz.

TABLE 3. ^1H chemical shifts of *cis*-bicyclo[3.3.0]octane-3-spiro-5′-hydantoins

		δ	
Products	Solvent	N3′—H	N1′—H
Bucherer	F_3C–COOH	9.45	7.75, 7.40
Bucherer	D_3C–SO–CD_3	10.54	8.32, 7.86
Strecker	F_3C–COOH	9.42	7.40
Strecker	D_3C–SO–CD_3	10.35	7.86

gave in low yield a monoacetyl derivative, evidently derived from **6** in which the axial N(1)—H is hindered.[3]

The results above show the limitations of the EJ rule when applied to conformationally mobile systems. Assuming for simplicity only envelope–envelope conformations for bicyclo[3.3.0]octanes, the aminonitrile progenitors of the Strecker and Bucherer products have the structures **7** or **8**; the different conformations of these isomers are shown in Scheme 1. Because of the small steric requirements of the nitrile as compared with the amino group (23), the conformation *7a* should be considerably more stable than *7b*; furthermore, the aminonitrile **7** should be considerably more stable than its isomer **8**, which in its more stable conformation (*8b*) has the nitrile group opposed by two quasi-axial methylene groups, while in *7a* it is opposed by two quasi-axial hydrogen atoms. These considerations accord with the fact that the Strecker product is derived wholly, as expected, from **7**. However, 60% of the Bucherer product is also derived from **7**, probably reacting via the conformation *7b*, and only 40% from **8**, probably reacting via the conformation *8a*, for reasons discussed earlier (11). It would be expected that the product ratio would be a complicated function of the relative proportions of *7a*, *7b*, *8a*, *8b*, and of their relative rates of reaction and of interconversion (the major product probably being formed by the route *7a* → *7b* → hydantoin).

It seems likely that the mutual repulsion of the two methyl groups in *cis*-3,4-dimethylcyclopentanone (**9**) will disfavour the envelope and favour a half-chair conformation in which the upper face will be the more sterically hindered. Consequently, the EJ rule predicts **10** as the major product of the Bucherer–Bergs reaction and **11** as that of the Strecker reaction (with the proviso that for this conformationally

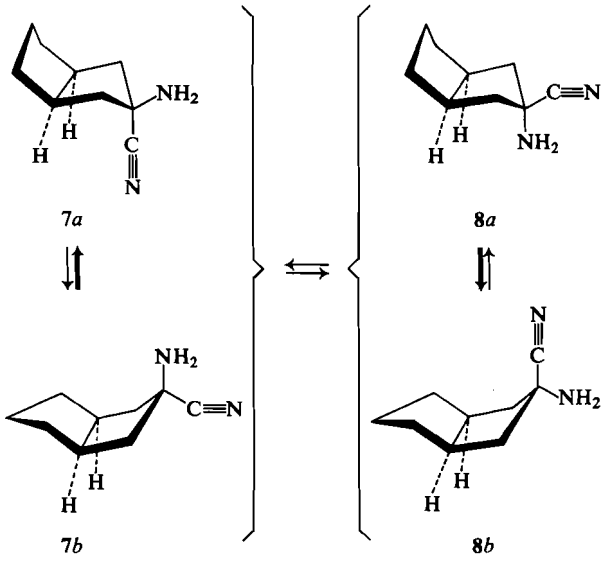

SCHEME 1

[3]The hydantoins have high melting points and low solubilities because of strong hydrogen bonding (N—H···O=C) in the crystal. Melting points fall and solubilities increase dramatically with acetylation of the N—H groups. In the present instance the monoacetyl **6** (which retains one N—H group) is evidently considerably less soluble than the more abundant diacetyl **5**. Since hydantoins are readily recovered from their acetyl derivatives by hydrolysis, acetylation may prove a useful technique in separating α and β isomers.

TABLE 4. ^{13}C chemical shifts (ppm, downfield from TMS) and coupling constants (Hz) of *cis*-3,4-dimethylcyclopentane-1-spiro-5′-hydantoins **10** and **11**

	Bucherer product				Strecker product			
	C[a] (**10**)		D (**11**)		D[a] (**11**)		C (**10**)	
	δ	$^1J_{(^{13}C-^1H)}$	δ	$^1J_{(^{13}C-^1H)}$	δ	$^1J_{(^{13}C-^1H)}$	δ	$^1J_{(^{13}C-^1H)}$
C1(C5′)	85.8 (s)	—	86.9 (s)	—	87.1 (s)	—	85.9 (s)	—
C2=C5	58.1 (t)	133	59.0 (t)	—	58.3 (t)	133	57.4 (t)	133
C3=C4	51.7 (d)	133	51.2 (d)	—	50.7 (d)	133	51.1 (d)	133
CH_3	28.8 (q)	125	28.8 (q)	—	28.2 (q)	125	28.2 (q)	125
C2′	174.7 (s)[b]	—	[h]	—	174.6 (s)[c]	—	174.6 (s)[c]	—
C4′	196.4 (s)[d,e]	—	[h]	—	194.0 (s)[d,f]	—	195.1 (s)[d,g]	—

[a]Major product of reaction.
[b]Half-width of peak with and without spin-decoupling 3 Hz.
[c]Half-width of peak with and without spin-decoupling 4 Hz.
[d]Half-width of peak with spin-decoupling 4 Hz.
[e]Half-width of peak without spin-decoupling 12.5 Hz.
[f]Half-width of peak without spin-decoupling 9 Hz.
[g]Poor resolution in spin-coupled spectrum.
[h]Peaks too small for accurate measurement.

mobile system the results will not be clear-cut). In fact, the ^1H nmr spectra of both Bucherer–Bergs and Strecker products show them to be mixtures of two isomers (C and D) having chemical shift values for the 1′-hydrogen atom at 8.0 and 8.2 δ respectively. The Bucherer product was about 90%, and the Strecker product about 40% C. The ^1H chemical shifts for the other protons (N3′—H, 11 (s); CH_3, 0.9 (d); remaining protons, 1.4–2.4 δ) were identical in C and D.

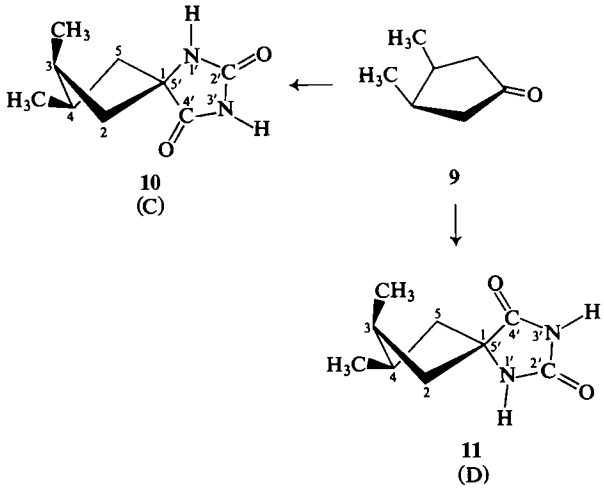

10 (C) ← **9** → **11** (D)

The ^{13}C nmr spectra also indicate 90% C in the Bucherer and 64% D in the Strecker product. The Bucherer product is slightly less soluble in 85% D_2SO_4 than the Strecker product, and so was dissolved in 90% D_2SO_4. This difference in acid concentration accounts for the slight differences in chemical shift values of C and D in the two products shown in Table 4. The isomers differ in the extent of coupling of the 4′-carbon atom with protons on vicinal carbon atoms, so that the half-widths of the spin-coupled systems are 9 Hz for D as opposed to 12.5 Hz for C.

We now consider arguments for identifying C with **10** and D with **11**.

Examination of Dreiding or Fieser models of **10** and **11** shows that these compounds probably exist as the conformers **10***a*/**10***b* and **11***a*/**11***b* in mobile equilibrium (Scheme 2): this would explain why only one nmr peak is observed for the two methyl groups of **10** and **11**. The models of **10***a* and **10***b* indicate the dihedral angles reported in Table 5 for the C4′C5′ bond with the C—H bonds on C2 and C5. The models (which are sensitive to Baeyer strain but not to torsional strain or nonbonded interactions) indicate the same dihedral angles for **11***a*/**11***b*; however, these structures ignore the nonbonded interaction between the 4′-carbonyl oxygen and the *quasi*-axial methyl at C3 or C4. This interaction must be very considerable (11). If one bends the oxygen away from the methyl group, the dihedral angles recorded in Table 5 for **11***a*/**11***b* can be measured on the models.[4] The curve relating the $^3J_{^{13}C-H}$ coupling constant to dihedral angle (24) is qualitatively similar to the familiar curve for $^3J_{H-H}$ (25). Using such a curve, it can be readily established that the angles reported in Table 5 require the C4′ peak of **10** to be broader than that of **11**, thus identifying C as **10** and D as **11**.

These results are in agreement with the EJ rule if one takes account of the weaker stereochemical preferences found in reactions of cyclopentanones as compared with cyclohexanones. The hydantoins **11** and **10** will be formed from the aminonitriles **12** and **13** as shown in Scheme 3. Because the amino and

[4]The angles recorded in Table 5 can be only very approximate, but almost certainly give the correct trends. The result of the argument which follows, is not affected by small variations in the dihedral angles from those reported in Table 5.

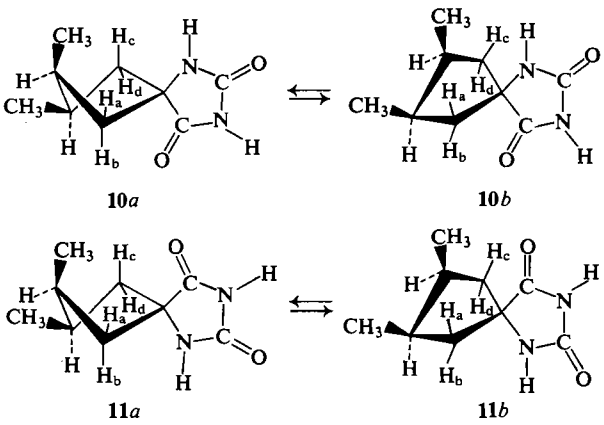

10*a* 10*b*

11*a* 11*b*

SCHEME 2

TABLE 5. Approximate values of dihedral angles (deg) made by the C5′—C4′ bond with vicinal C—H bonds of **10***a*/**10***b* and **11***a*/**11***b*

C—H	**10***a*	**10***b*	**11***a*	**11***b*
C2—H_a	15	15	20	45
C2—H_b	135	105	100	75
C5—H_c	15	15	45	20
C5—H_d	105	135	75	100

nitrile groups at the 1-position are not axial or equatorial, the preference for **12** over **13** is slight, and hence the preponderance of **11** over **10** in the Strecker product (which reflects the proportions of **12** and **13** (11)) is also slight. On the other hand, interference between the C=NH group with one axial methyl group in **14** will be much more serious than interference between this group and an axial hydrogen atom in **15**, and so the stereoselectivity of the Bucherer reaction in favour of **10** over **11** is higher.

It is evident that the stereochemical preferences of biased cyclopentanones are much less pronounced than those of biased cyclohexanones, but that the EJ rule is effective in indicating trends. Further studies of substituted cyclopentanones are needed to confirm the highly tentative conclusions reached above.

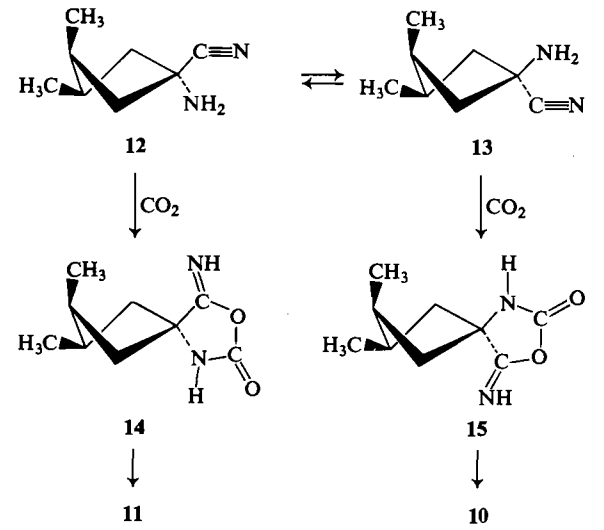

12 **13**

14 **15**

11 **10**

SCHEME 3

Acknowledgments

We remain most grateful to Professor A. S. Perlin, who initially suggested ^{13}C nmr studies as a means of establishing configurations, and to Dr. N. Cyr, who made the spectral measurements. We thank the National Research Council of Canada for financial support of part of the work described and the Spanish government for a F.P.I. Scholarship (to E. Santos).

1. H. T. BUCHERER and W. STEINER. J. Prakt. Chem. **140**, 291 (1934); H. T. BUCHERER and V. A. LIEB. J. Prakt. Chem. **141**, 5 (1934).
2. W. T. READ. J. Am. Chem. Soc. **44**, 1746 (1922).
3. H. L. HOYER. Chem. Ber. **83**, 491 (1950).
4. H. C. BRIMELOW and C. H. VASEY. Chemical Industries Ltd., Brit. Patent No. 807,678 (21 January 1959); Chem. Abstr. **53**, 12303 (1959).
5. L. MUNDAY. J. Chem. Soc. 4372 (1961).
6. H. C. BRIMELOW, H. C. CARRINGTON, C. H. VASEY, and W. S. WARING. J. Chem. Soc. 2789 (1962).
7. R. J. CREMLYN and M. CHISHOLM. J. Chem. Soc. C, 2269 (1967).
8. Y. MAKI and T. MASUGI. Chem. Pharm. Bull. Tokyo, **21**, 685 (1973).
9. H. C. CARRINGTON. J. Chem. Soc. 681 (1947).
10. H. C. CARRINGTON, C. H. VASEY, and W. S. WARING. J. Chem. Soc. 396 (1959).
11. J. T. EDWARD and C. JITRANGSRI. Can. J. Chem. **53**, 3339 (1975).
12. G. G. TRIGO and M. MARTINEZ. Pharm. Mediterranea, **10**, 643 (1974).
13. G. G. TRIGO and C. AVENDAÑO. Pharm. Mediterranea, **10**, 627 (1974).
14. S. P. FINDLAY. J. Org. Chem. **22**, 1385 (1957).
15. R. P. LINSTEAD and E. M. MEADE. J. Chem. Soc. 935 (1934).
16. J. M. CONIA and M. L. LERIVEREND. Bull. Soc. Chim. Fr. 2981 (1970).
17. W. I. CONGDON and J. T. EDWARD. Can. J. Chem. **50**, 3767 (1972).
18. P. SMITH-VERDIER, F. FLORENCIO, and S. GARCIA-BLANCO. Acta Crystallogr. Sect. B, **33**, 3381 (1977).
19. R. J. CREMLYN and M. CHISHOLM. J. Chem. Soc. C, 1762 (1967).
20. H. S. TAGER and H. N. CHRISTENSEN. J. Am. Chem. Soc. **94**, 968 (1972).
21. H. C. BROWN. Chem. Br. 199 (1966).
22. P. SMITH-VERDIER, F. FLORENCIO, and S. GARCIA-BLANCO. Rocasolano Institute, Consejo Superior de Investigaciones Cientificas Madrid. In press.
23. E. L. ELIEL, N. L. ALLINGER, S. J. ANGYAL, and G. A. MORRISON. Conformational analysis. John Wiley, New York, NY. 1967. p. 44.
24. A. S. PERLIN. *In* Isotopes in organic chemistry. Vol. 3. *Edited by* E. Buncel and C. C. Lee. Elsevier, New York, NY. 1977. p. 171.
25. J. R. DYER. Applications of absorption spectroscopy of organic compounds. Prentice-Hall, Englewood Cliffs, NJ. 1965. p. 117.

Benzocyclobutyl phenyl sulfone. An evaluation of its potential as a precursor to substituted benzocyclobutenes and *ortho*-quinodimethanes

BARBARA D. GOWLAND AND TONY DURST

Department of Chemistry, University of Ottawa, Ottawa, Ont., Canada K1N 9B4

Received December 15, 1978

BARBARA D. GOWLAND and TONY DURST. Can. J. Chem. **57**, 1462 (1979).

Benzocyclobutyl phenyl sulfone has been converted to several 7-substituted benzocyclobutenes via reaction of its α-sulfonyl carbanion with typical electrophiles followed by desulfonylation with Na/Hg in methanol. Two benzocyclobutenes carrying remote terminal vinyl groups have been isomerized to tricyclic ring systems upon heating at 250°C. The *o*-quinodimethane obtained from thermolysis of benzocyclobutyl phenyl sulfone in toluene at 250°C is not trapped by maleic anhydride but by the solvent toluene in a Friedel–Crafts type alkylation.

BARBARA D. GOWLAND et TONY DURST. Can. J. Chem. **57**, 1462 (1979).

On a transformé la benzocyclobutyl phénylsulfone en plusieurs benzocyclobutènes substitués en position 7 par l'intermédiaire de la réaction de son carbanion α-sulfonyle avec des électrophiles appropriés suivie d'une désulfonylation avec Na/Hg dans le méthanol. On a isomérisé deux benzocyclobutènes, portant des groupes vinyles terminaux éloignés, en systèmes tricycliques par chauffage à 250°C. Le *o*-quinodiméthane que l'on obtient par thermolyse de la benzocyclobutyl phénylsulfone dans le toluène à 250°C ne peut pas être piégée par l'anhydride maléique; le toluène agissant comme solvant le piège toutefois par une alkylation de type Friedel–Crafts.

[Traduit par le journal]

Introduction

o-Quinodimethanes, generated thermally from benzocyclobutenes, have been used effectively, especially by groups led by Oppolzer (1) and Kametani (2) for the rapid and highly stereoselective assembly of certain steroid and alkaloid ring systems.

A key intermediate in these approaches is the benzocyclobutyl nitrile **1** and aryl substituted derivatives thereof. These nitriles are generally converted into the amide **2** or iodide **3** for use in the alkaloid (1) and steroid (1*b*, 2) syntheses respectively.

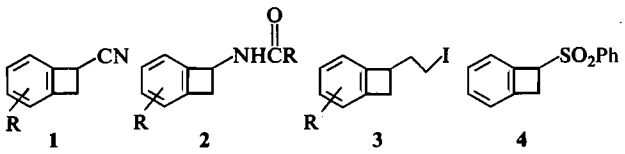

1 **2** **3** **4**

As part of our work on the use of sulfones in organic synthesis (3) we decided to investigate the potential of benzocyclobutyl phenyl sulfone, **4**, as a reagent in this area.

We had felt that the sulfone **4** might provide a number of key advantages over the nitrile **1** in the preparation of substituted benzocyclobutenes which could be thermolyzed to polycyclic ring systems. For example, alkylation of **4** via its anion followed by desulfonylation should yield the substituted benzocyclobutenes **5**. Similar reactions have been reported for **1** (4), but the reductive removal of the CN group requires more stringent conditions (Li or Na in amines) than that of the $PhSO_2$ group (Na/Hg in buffered methanol) (5).

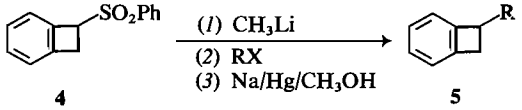

4 **5**

Synthesis of Benzocyclobutyl Phenyl Sulfone (4)

Benzocyclobutyl phenyl sulfone had previously been prepared by Bunnett and Skorcz (6) from *o*-chlorophenylacetic acid following Scheme 1. This synthesis featured an intramolecular benzyne cyclization and is thus difficult to carry out on a large scale. It was therefore decided to first investigate other potential routes to **4** which might be more suitable for a large scale synthesis. These attempts are briefly described below. Unfortunately none were successful and we had to revert, with some modifications, to the Bunnett and Skorcz synthesis.

One of our approaches to **4** involved the base-catalyzed elimination of HCl from the chloro sulfone **8**. It was hoped that the intermediate **9** from such an elimination might cyclize to **4** in the same way that the debromination of α,α,α′,α′-tetrabromo-*o*-xylene with NaI afforded, via an *o*-quinodimethane intermediate, a dibromobenzocyclobutene (7). The chloro sulfone **8**, mp 75–77°C, was prepared in 42% yield by refluxing sodium benzenesulfinate with bis-1,2-

0008-4042/79/121462-06$01.00/0

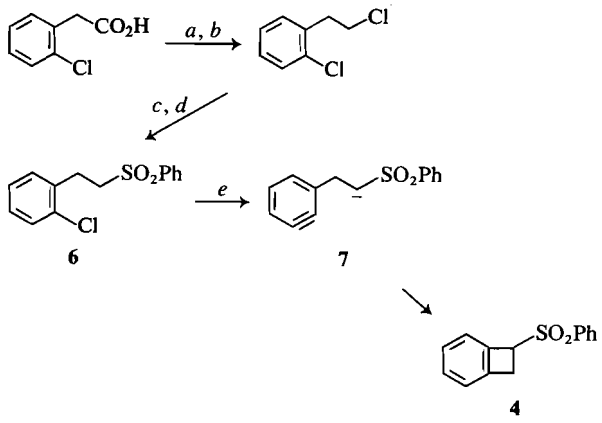

SCHEME 1. Reagents: (*a*) $LiAlH_4$, (*b*) $SOCl_2$–pyridine, (*c*) PhS^-Na^+, (*d*) H_2O_2, (*e*) $NaNH_2/NH_3$.

(chloromethyl)benzene in methanol for 1 day. The elimination of HCl from **8** was attempted with lithium diisopropylamide at −78°C, CH_3Li at 0°C or 25°C, and NaOH under phase-transfer conditions. In each case a yellow-coloured solution was generated but only a polymeric product was isolated. Possibly the presumed intermediate **8***a* is trapped by the α-sulfonyl carbanion of the starting material in an oligomerization reaction. Attempts to trap **8***a* with Δ-1-cyclohexenylpyrrolidine were unsuccessful.

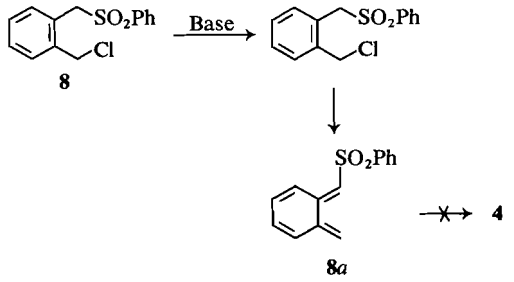

Loudon *et al.* (8) have reported that the flash vacuum thermolysis of α-chloro-*o*-xylene at 630°C afforded 68% of benzocyclobutene. Similar treatment of **8** at 500°C/0.06 Torr gave an inseparable mixture of products containing no **4** while thermolysis at lower temperatures (400°C) yielded mixtures including some recovered starting material.

In a reinvestigation of the Bunnett and Skorcz route we attempted to prepare the benzyne precursor **6** by alkylation of α-lithiomethyl phenyl sulfone with *o*-bromobenzyl bromide. Many experimental variations of this reaction were attempted (see Experimental section); however, in all cases mixtures of mono- and dialkylation products, together with the starting materials, were recovered. In contrast, the alkylation of $PhS(O)CH_2Li$ with *o*-chlorobenzyl bromide afforded the expected sulfoxide in 82% isolated yield, oxidation of which gave 91% of **6**. The 75% overall yield of **6** in this two-step procedure can be compared with the 60% overall yield of **6** achieved in 4 steps by Bunnett and Skorcz.

The cyclization of **6** to **4** requires careful control of the stoichiometry of base to substrate. When the KNH_2/**6** ratio was 2:1 no benzocyclobutyl phenyl sulfone was obtained. Instead, the major reaction products were *o*-chlorostyrene **9** and a crystalline material, $C_6H_{14}Cl_2$, mp 51–53°C, to which we assigned the structure **10** mainly on the basis of the proton nmr spectrum (see Experimental section). A

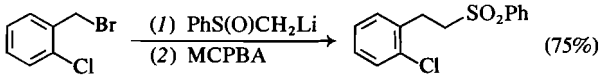

proposal accounting for both **9** and **10** is given in Scheme 2.

The use of 4 equiv. of KNH_2 per equivalent of **6** did give **4** in an average yield of about 35% (8 runs), together with 15% of isomeric amino sulfones due to the trapping of the benzyne intermediate **7**, or its protonated equivalent with $^-NH_2$.

The different behavior of the sulfone **6** in the presence of either 2 or 4 equiv. of KNH_2 can be explained in the following manner. In the presence of one or somewhat more than 1 equiv. of KNH_2 the α-sulfonyl anion **6***a* would be expected to be formed preferentially. This anion should be stable under the reaction conditions and in equilibrium with the starting material. A slow competitive β-elimination of $PhSO_2^-$ from **6** by the action of

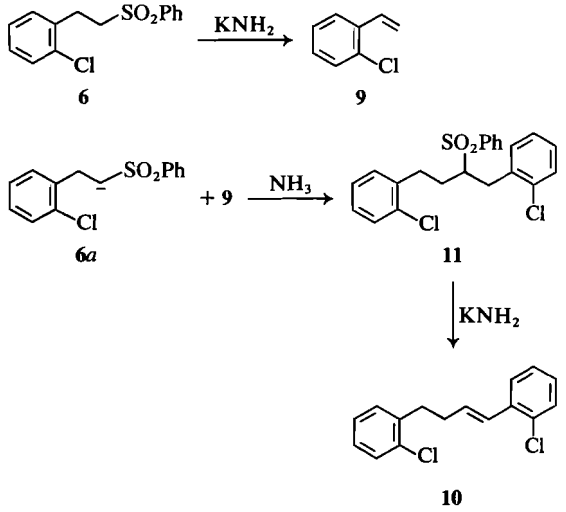

SCHEME 2

TABLE 1. Preparation of 7-substituted benzocyclobutenes (4 → 12 → 5)

Series	Electrophile	Yield (%) 12	5
a	D_2O	98	96*
b	CH_3I	82	—
c	$BrCH_2CH{=}CH_2$	81	95
d	$Br(CH_2)_2CH{=}CH_2$	67	—
e	$I(CH_2)_3CH{=}CH_2$	79	93
f	$Br(CH_2)_4CH{=}CH_2$	62	96
g	Acetone	58†	—
h	Styrene oxide	30†	—

*Desulfonylation was carried out on nondeuterated material.
†Nuclear magnetic resonance yield. The product could not be separated from 4.

$^-NH_2$ (9) would yield *o*-chlorostyrene. Addition of the anion **6***a* to *o*-chlorostyrene should give the sulfone **11** from which **10** can be obtained via a β-elimination. Under these conditions benzyne formation would be expected to be slow.

As the amount of base is increased most of **6** would be converted to the monoanion **6***a*. Sufficient $^-NH_2$ would still be present to produce the benzyne intermediate **7** at a reasonable rate, intramolecular trapping of which yields **4**. The use of an $NaNH_2$/**4** ratio of greater than 4 was not investigated since it was felt that this would produce mainly the amination products. Reaction of **4** with either 2 or 4 equiv. of lithium 2,2,6,6-tetramethylpiperidide (11) did not generate any of the benzocyclobutene **4**.

Preparation of 7-Substituted Benzocyclobutenes

Reaction of **4** with CH_3Li at −78°C in dry tetrahydrofuran (THF) under N_2 rapidly generated a yellow-coloured solution containing the α-sulfonyl anion of **4** as evidenced by reaction with D_2O, CH_3I, and several alkyl bromides (Table 1). Typical aliphatic chlorides or epoxides did not react efficiently with this anion.[1] Each of the alkylated products was characterized by elemental analysis and infrared and ^1H nmr spectra, the latter showing a characteristic isolated AB quartet in the 3.2–3.8 ppm region. The reductive removal of the $PhSO_2$ group from the alkylated derivatives **12** was carried out using a slightly modified version of the Trost procedure (5).

[1]The anion of **4** decomposed overnight and yielded a mixture of nonpolar crystalline substances, mp 103–112°C. The nmr spectrum of this mixture showed two singlets at δ = 3.52 and 3.80 as well as aromatic protons from 7.0–7.4 ppm. The infrared indicated the absence of any sulfonyl moiety. The highest *m/e* peak in the ms of the mixture occurred at *m/e* = 204 suggestive of a possible 'dimer' of benzocyclobutadiene resulting from a β-elimination of $PhSO_2^-$ from some unionized **4**. The structure of the compounds in this mixture remain to be determined.

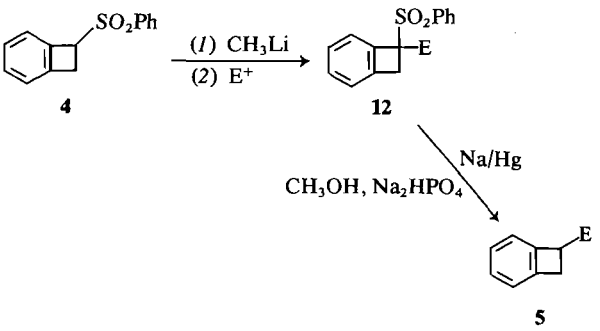

The yields of the desulfonylated products **5** were greater than 90% (Table 1).

Thermolysis of Benzocyclobutyl Phenyl Sulfones

Benzocyclobutyl phenyl sulfone **4** was thermolyzed at 250°C in a sealed tube as a toluene solution containing excess maleic anhydride. The reaction conditions chosen were similar to those used by Kametani *et al.* (13) who reported the trapping of the *o*-quinodimethane intermediate **13** from 7-cyano-7-methylbenzocyclobutene with maleic anhydride in 65% yield. In contrast to the Kametani results the only isolable product from the thermolysis of **4** had not incorporated maleic anhydride, but rather toluene. The product, obtained in 25% yield after preparative thin layer chromatography, was shown to be an isomer mixture, **14**. The nmr spectrum of **14** showed peaks at 2.18 and 2.28 (2 singlets, total 3H), 3.80 (s, 2H), 4.29 (s, 2H), and 7.0–7.8 (m, 13H), while the infrared indicated sulfone bands at 1125 and 1300 cm^{-1}. A plausible route for the formation of **14** involves a rather novel Friedel–Crafts alkylation of toluene by the *o*-quinodimethane intermediate **15**. As expected, **14** was best obtained if **4** was thermolyzed in toluene at 250°C in the absence of maleic anhydride. Prolonged heating of **4** in cyclohexane at 250°C with maleic anhydride gave decomposition but none of the desired Diels–Alder product. The reason for the difference in the behavior of the intermediates **13** and **15** toward maleic anhydride is not obvious since cyano and sulfonyl groups have similar electron withdrawing character.

Thermolysis of the substituted benzocyclobutyl phenyl sulfone **12***f* gave only the styrene derivative **16** resulting from a 1,5-sigmatropic shift of a hydrogen in the *o*-quinodimethane intermediate **17**. No evidence of any trapping by the remote olefinic group was observed. 1,5-Hydrogen shifts in *o*-quinodimethanes are known to be facile (13).

Thermolysis of the 7-Substituted Benzocyclobutenes

The two benzocyclobutenes (**5***e*, *f*), carrying remote vinyl groups isomerized cleanly to the tricyclic products **18** and **19** when thermolyzed in

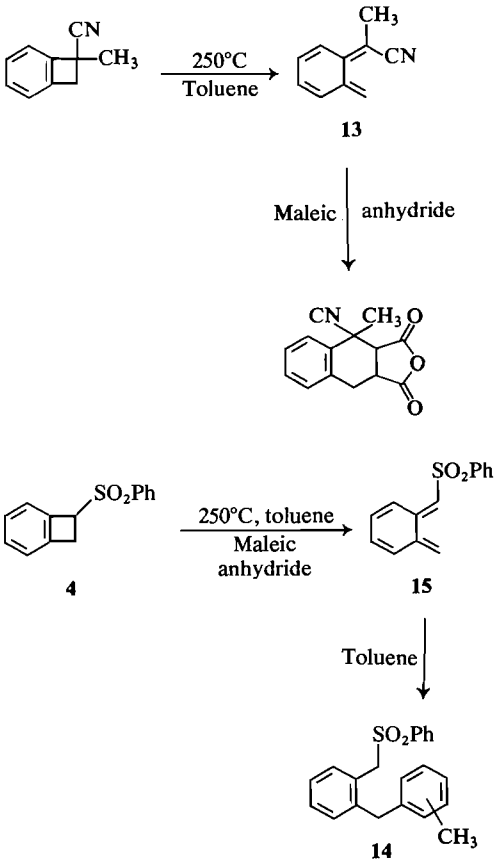

cyclohexane. Vapor phase chromatographic analysis of the isomerized product indicated that **19** was probably formed as a single stereoisomer while **18**

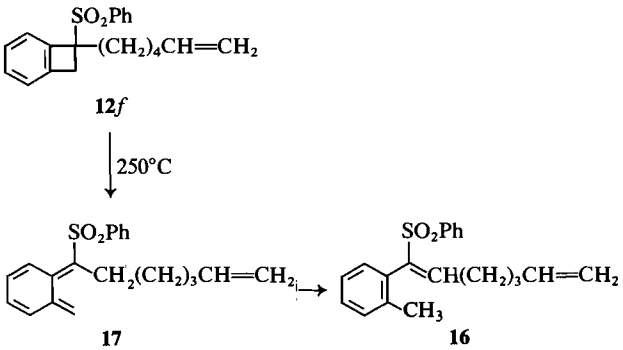

was obtained as an isomeric mixture. No detailed stereochemical assignments were attempted with these products.

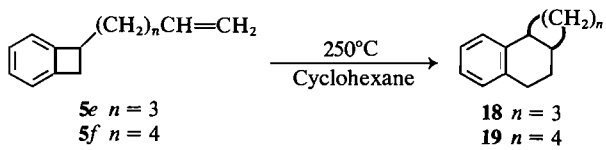

Conclusions

Benzocyclobutyl phenyl sulfone **4** can easily be converted into a number of substituted benzocyclobutenes via reaction of its α-sulfonyl carbanion with electrophiles followed by desulfonylation. Some of the benzocyclobutenes thus obtained are suitable for conversion into polycyclic ring systems. The method is of somewhat limited value since the present synthesis of **4** is not suitable for large scale work. The *o*-quinodimethane derived from the thermolysis of **4** does not react with a typical dienophile such as maleic anhydride; it appears to behave like a highly electron deficient diene.

Experimental

Melting points were taken on a Thomas Hoover melting point apparatus and are uncorrected. Infrared spectra were obtained on Beckman IR-20 or Unicam SP 1100 spectrophotometers. Nuclear magnetic resonance spectra were taken on Varian Associates HA-100 and T-60A spectrometers. Chemical shifts are reported in ppm downfield from internal TMS. The term 'work-up' refers to quenching a reaction mixture with excess H_2O, extraction with CH_2Cl_2, drying of the organic extracts over anhydrous $MgSO_4$, and evaporation of the solvent under reduced pressure. The silica gel used for column chromatography was 60–200 mesh Baker silica gel.

1-(Chloromethyl)-2-(phenylsulfonylmethyl)benzene (8)

Sodium benzenesulfinate (2.8 g, 17 mmol) and 1,2-bis-(chloromethyl)benzene (3.0 g 17 mmol) were refluxed in 100 mL of methanol for 1 day. The cooled reaction mixture was diluted with 100 mL of H_2O and extracted with 4 × 20 mL of CH_2Cl_2. Chromatography of the crude product on silica gel using 1:3 ethyl acetate – hexane gave 2.02 g (42%) of **8** as colourless crystals, (CH_2Cl_2–hexane), mp 75–77°C; nmr δ: 4.57 (s, 2H), 4.70 (s, 2H), 6.9–8.0 (m, 9H); ir: 1305 and 1120 cm^{-1}; ms *m/e*: M^+ 282, 280. *Anal.* calcd. for $C_{14}H_{13}ClO_2S$: C 60.00, H 4.64; found: C 59.94, H 4.70.

Reaction of 8 with Bases

The chloro sulfone **8** (0.5 g) was reacted with 1:1 equivalents of LDA in THF at −78°C. The reaction mixture turned yellow and then orange-red. After 30 min of reaction at −78°C work-up gave a product whose nmr showed very broad absorption indicative of a polymeric product.

Essentially the same results were obtained when **8** was reacted under phase-transfer conditions, or with CH_3Li either at −78°C or at +25°C.

Attempted Trapping of the Intermediate 9 with N-1-Cyclohexenylpyrrolidine

Chloro sulfone **8** (0.20 g) and the above enamine (0.12 g) were dissolved in 15 mL CH_2Cl_2 and stirred with 15 mL 50% NaOH containing benzyltriethylammonium chloride. After 24 h the reaction mixture had turned yellow and **8** was absent as shown by analytical tlc. Attempts to purify the 0.3 g of crude product were not successful.

Reaction of PhS(O)CH_2Li with o-Chlorobenzyl Chloride

To a solution of LDA (38 mmol) in THF at 0°C was added 4.74 g (34 mmol) of $PhS(O)CH_3$. The bright yellow solution was stirred for 5 min and then treated with 6.93 g (34 mmol) of *o*-chlorobenzyl chloride for 25 min. The bright purple solution was worked up in the usual manner and produced, after column chromatography, 7.3 g (82%) of chloro sulfoxide.

This chloro sulfoxide was oxidized with *meta*-chloroperbenzoic acid in refluxing CH_2Cl_2. Work-up, after the more polar sulfoxide was absent by tlc, gave 91% of the chloro sulfone **6**, mp 44–46°C (lit. (6) mp 45–47°C).

Reaction of $PhSO_2CH_2Li$ with o-Bromobenzyl Bromide

To 4.0 g (25 mmol) phenyl methyl sulfone in 80 mL of THF and 0°C was added 28 mmol of CH_3Li giving a bright yellow solution. Following 5 min of reaction time, 6.4 g (25 mmol) of *o*-bromobenzyl bromide was added which resulted in a dark brown solution. Usual work-up following 24 h of reaction time gave 8.45 g of crude product which was chromatographed on 130 g of silica with increasing proportions of ethyl acetate in hexanes. In order of elution there was obtained 0.68 g of 1,3-di(*o*-bromophenyl)-2-(phenylsulfonyl)propane (nmr δ: 2.8–3.5 (m, 4H), 4.1–4.3 (m, 1H), 6.1–8.1 (m, H)); 1.3 g (16%) of 2-(*o*-bromophenyl)ethyl phenyl sulfone (nmr δ: 2.6–3.7 (m, 4H), 6.7–8.1 (m, 9H)); and considerable amounts of recovered $PhSO_2CH_3$.

The above reaction was repeated in the presence of hexamethylphosphoramide or by adding $PhSO_2CH_2Li$ to *o*-bromobenzyl bromide in THF at −78°C. The yield of the desired monoalkylation product could not be significantly increased.

*Reaction of the Chloro Sulfone **6** with $4KNH_2$; Preparation of **4***

A solution of KNH_2 was prepared by dissolving K metal in liquid ammonia. A trace of powdered ferric nitrate was used as a catalyst. To this solution was added all at once 0.25 equiv. of the sulfone **6** giving an orange-brown solution. The reaction mixture was stirred for 10 min and then quenched with ammonium nitrate. The ammonia was allowed to evaporate and the reaction mixture was worked up. The crude reaction product was purified by silica gel column chromatography. Elution with a 1:4 ethyl acetate – hexane gave **4**, mp 102–103°C, from benzene-hexane (lit. (5) mp 103.5–104.5°C). The yields in **8** different reactions carried out on a 20 mmol scale varied from 30–40%; nmr δ: 3.52 (d, J = 4 Hz, 2H), 4.92 (t, J = 4 Hz, 1H), 6.9–8.0 (m, 9H); ir: 1120, 1290 cm^{-1}; ms *m/e*: M⁺ = 244. *Anal.* calcd. for $C_{14}H_{12}O_2S$: C 68.85, H 4.86; found: C 68.94, H 4.92.

When the above reaction was carried out using only $2KNH_2$ per mole of **6**, the nmr spectrum of the crude product showed the presence of *o*-chlorostyrene and the product **12**. Chromatography on silica gel resulted in loss of the styrene and isolation of **12**, mp 51–53°C; nmr δ: 2.4–3.0 (m, 4H), 6.0–6.4 (doublet of triplets, J = 16 and 7 Hz, 1H), 6.8 (d, J = 16 Hz, 1H), 7.0–7.6 (m, 8H); ir: 960 cm^{-1}. *Anal.* calcd. for $C_{16}H_{14}Cl_2$: C 69.32, H 5.09; found: C 69.25, H 5.04.

*Generation of the α-Lithio Derivative of **4** and Reactions with Electrophiles*

Compound **4** was dissolved in THF at −78°C and reacted with 1.1 equiv. of CH_3Li. A bright yellow solution formed immediately. This solution was treated with electrophiles at −78°C and then allowed to warm to room temperature. The products were isolated by the usual work-up and purified by chromatography on silica gel.

(*a*) D_2O. 98%; nmr δ: 3.51 (s, 2H), 6.9–8.0 (m, 9H).

(*b*) CH_3I. Reaction time 15 min (82% isolated yield); mp 61–63°C, off-white solid; nmr δ: 1.84 (s, 3H), 3.12 (d, J = 14 Hz, 1H), 3.74 (d, J = 14 Hz, 1H), 6.9–7.0 (m, 9H); ir: 1290 (s) 1120 (s) cm^{-1}; ms *m/e*: M⁺ 258. *Anal.* calcd. for $C_{15}H_{14}O_2S$: C 69.74, H 5.46; found: C 69.53, H 5.53.

(*c*) $BrCH_2CH{=}CH_2$. Reaction time 15 min, oil, 81%; nmr δ: 2.6–3.1 (m, 2H), 3.23 (d, J = 14 Hz, 1H), 3.54 (d, J = 14 Hz, 1H), 4.85–5.25 (m, 2H), 5.35–5.83 (m, 1H), 6.8–7.9 (m, 9H); ir: 1295 (s), 1130 (s), 975 (m), 905 (m); ms *m/e*: M⁺ = 284. *Anal.* calcd. for $C_{17}H_{16}O_2S$: C 71.80, H 5.67; found: C 71.82, H 5.57.

(*d*) $Br(CH_2)_2CH{=}CH_2$. Reaction time, 16 h, oil, 67%; nmr δ: 1.9–2.7 (m, 4H), 3.25 (d, J = 14 Hz, 1H), 3.58 (d, J = 14 Hz, 1H), 4.8–5.1 (m, 2H), 5.5–6.0 (m, 1H), 6.8–7.9 (m, 9H); ir: 1295 (s), 1135 (s), 985 (m), 900 (m) cm^{-1}. *Anal.* calcd. for $C_{18}H_{18}O_2S$: C 72.45, H 6.08; found: C 72.38, H 6.05.

(*e*) $I(CH_2)_3CH{=}CH_2$. Reaction time 0.5 h, oil, 79%; nmr δ: 1.1–1.6 (m, 2H), 1.9–2.5 (m, 4H), 3.22 (d, J = 15 Hz, 1H), 3.54 (d, J = 15 Hz, 1H), 4.8–5.15 (m, 2H), 5.5–6.0 (m, 1H), 6.8–7.8 (m, 9H); ir: 1290 (s), 1130 (s), 980 (m), 905 (m) cm^{-1}. *Anal.* calcd. for $C_{19}H_{20}O_2S$: C 73.04, H 6.45; found: C 73.06, H 6.50.

(*f*) $Br(CH_2)_4CH{=}CH_2$. Reaction time 0.5 h, colourless solid, mp 57–58°C, 62%; nmr δ: 1.1–1.8 (m, 4H), 1.8–2.6 (m, 4H), 3.22 (d, J = 14 Hz, 1H), 3.52 (d, J = 14 Hz, 1H), 4.80–5.1 (m, 2H), 5.5–6.0 (m, 1H), 6.8–7.9 (m, 9H); ir: 1295 (s), 1130 (s), 980 (m), 900 (m); ms *m/e*: M⁺ 326. *Anal.* calcd. for $C_{20}H_{22}O_2S$: C 73.58, H 6.79; found: C 73.13, H 6.69.

(*g*) Styrene oxide. Reaction time 24 h; the product was a mixture of the unknown nonpolar benzocyclobutene dimer (see footnote 1), unreacted **4**, and presumed product (nmr). The desired product and unreacted **4** could not be separated by chromatography.

(*h*) Acetone. Reaction time 15 min at −78°C; the remaining starting material and product (4:6 ratio) by nmr could not be separated; nmr of the product by difference: 1.37 (s, 3H), 1.67 (s, 3H), 3.55 (d, J = 14 Hz, 1H), 3.67 (d, J = 14 Hz, 1H) 6.8–7.8 (m, 9H). When the reaction was allowed to warm to room temperature prior to quenching with H_2O only unreacted **4** was obtained, presumably due to reversal of the condensation reaction.

*Reaction of **4** with CH_3Li*

To 0.2 g (0.82 mmol) of **4** at −78°C in 15 mL of THF was added 0.90 mmol of CH_3Li. The reaction mixture was allowed to stir at room temperature for 24 h. Work-up gave 0.06 g of a nonpolar product, mp 103–112°C. Vapor phase chromatographic analysis indicated the presence of two components of similar retention time; nmr (of the mixture) δ: 3.52 (s), 3.80 (s), 7.06–7.40 (m); ms *m/e*: M⁺ 204.

When **4** was reacted with about 2 equiv. of CH_3Li, starting material was recovered after a 24 h reaction period.

Desulfonylation of the α-Alkylated Benzocyclobutyl Phenyl Sulfones

All desulfonylations were carried out by treating 1 equiv. of sulfone dissolved in 10 mL of dry methanol containing Na_2HPO_4 with excess 6% Na/Hg amalgam at room temperature. Amalgam was added until tlc confirmed the absence of starting material. The reaction times were about 0.5 h. The reaction mixture was diluted with 10 mL of saturated NaCl solution and worked up in the usual manner. The products obtained are described below. All products were obtained as colorless oils.

(*a*) Benzocyclobutene, 96%; nmr δ: 2.97 (s, 4H), 6.6–7.5 (m, 4H) (14).

(*b*) 7-(2′-*n*-Propenyl)benzocyclobutene, **5***c* 95%; nmr δ: 2.45 (m, 2H) 2.80 (dd, J = 14 and 2 Hz, 1H), 3.35 (dd, J = 14 and 2 Hz, 1H), 3.35–3.8 (m, 1H), 4.95–5.25 (m, 2H), 5.7–6.2 (m, 1H) 7.0–7.3 (m, 4H); ms *m/e*: M⁺ 144.

(*c*) 7-(4′-*n*-Pentenyl)benzocyclobutene, **5***e* 93%; nmr δ: 1.4–1.9 (m, 4H), 2.0–2.30 (m, 2H), 2.74 (dd, J = 14 and 2 Hz, 1H), 3.35 (dd, J = 14 and 2 Hz, 1H) 3.3–3.6 (m, 1H), 4.8–5.2 (m, 2H), 5.5–6.1 (m, 1H), 7.0–7.3 (m, 4H). *Anal.* calcd. for $C_{13}H_{16}$: C 90.64, H 9.36; found: C 90.84, H 9.41.

(*d*) 7-(5′-*n*-Hexenyl)benzocyclobutene, **5***f* 96%; nmr δ: 1.2–1.9 (m, 6H), 1.9–2.3 (m, 2H), 2.75 (dd, J = 14 and 2 Hz, 1H), 3.25 (dd, J = 14 and 2 Hz, 1H), 3.25–3.6 (m, 1H), 4.8–5.2 (m, 2H), 5.6–6.1 (m, 1H), 7.0–7.3 (m, 4H). *Anal.* calcd. for $C_{14}H_{18}$: C 90.26, H 9.74; found: C 89.95, H 9.69.

Thermolysis of Benzocyclobutyl Phenyl Sulfone (4)

Compound **4** (0.13 g, 0.51 mmol) and maleic anhydride (0.087 g, 0.9 mmol) were heated in 3 mL of toluene in a sealed tube at 250°C for 15 h. Upon cooling 0.078 g of maleic anhydride was recovered by filtration. The remaining material was chromatographed on silica gel plates using 3:1 hexane – ethyl acetate as eluent. A major fraction was recovered which on recrystallization from CH_2Cl_2–hexane gave 0.043 g (25%) of **14**, mp 116–118°C; nmr δ: 2.18, 2.28 (2s, 3H), 3.80 (s, 2H), 4.29 (s, 2H), 6.6–7.8 (m, 13H); ir: 1300 (s), 1125 (s) cm^{-1}; ms *m/e*: M^+ 336. *Anal.* calcd. for $C_{21}H_{20}O_2S$: C 74.97, H 5.99; found: C 74.78, H 6.11.

Thermolysis of **4** in toluene in the absence of maleic anhydride gave a similar result.

Thermolysis of 0.15 g of **4** and 0.87 g of maleic anhydride in 2 mL of cyclohexane for 10 h at 250°C gave a crude product from which diphenyl disulfide was obtained as the only identifiable product.

Thermolysis of 12f

Compound **12*f*** (0.07 g) was heated in 3 mL of cyclohexane in an evacuated sealed tube at 250°C for 20 h. Purification of the crude product on silica gel plates (3:1 hexane – ethyl acetate) gave **16** in 59% yield; nmr δ: 1.5–2.1 (m, 9H), 4.8–5.0 (m, 2H), 5.2–5.9 (m, 1H), 6.7–6.9 (m, 1H), 6.9–7.7 (m, 9H). *Anal.* calcd. for $C_{20}H_{22}O_2S$: C 73.58, H 6.79; found: C 73.12, H 6.62.

Thermolysis of 7-(4′-n-Pentenyl)benzocyclobutene

This compound (0.031 g) was thermolyzed in cyclohexane at 250°C for 24 h. Purification on silica gel plates using hexane as eluent gave 74% of tricyclic material (**18**); nmr δ: 1.2–3.2 (m, 12H), 7.0–7.22 (m, 4H). *Anal.* calcd. for $C_{13}H_{16}$: C 90.64, H 9.36; found: C 91.10, H 8.96. Vapor phase chromatographic analysis on a 2.0 m SE-30 column gave a nonsymmetrical peak suggestive of two isomers.

Thermolysis of 7-(5′-n-Hexenyl)benzocyclobutene

Heating of 0.082 g of the above compound in 3 mL of cyclohexane as above resulted in the isolation of 0.063 g of tricyclic compound **19** after preparative tlc separation; nmr δ: 0.9–3.0 (m, 14H), 7.0–7.4 (m, 4H). *Anal.* calcd. for $C_{14}H_{18}$: C 90.26, H 9.74; found: C 89.96, H 9.61. Vapor phase chromatographic analysis, as for **18**, gave a single symmetrical peak suggestive of one isomer.

Acknowledgement

Continued financial support by the National Research Council of Canada is gratefully acknowledged.

1. (*a*) W. Oppolzer. J. Am. Chem. Soc. **93**, 3833 (1971); 3834 (1971); (*b*) W. Oppolzer, K. Battig, and M. Petrizilka. Helv. Chim. Acta, **61**, 1945 (1978); (*c*) W. Oppolzer. Synthesis, 793 (1968).
2. T. Kametani, H. Nemoto, H. Ishidawa, K. Shiroyama, H. Matsumoto, and K. Fukumoto. J. Am. Chem. Soc. **99**, 3461 (1977).
3. B. Corbel, J. M. Decesare, and T. Durst. Can. J. Chem. **56**, 505 (1978).
4. J. A. Skorcz and F. E. Kaminski. J. Med. Chem. **8**, 732 (1965).
5. B. M. Trost, H. C. Arndt, P. E. Strege, and T. R. Verhoeven. Tetrahedron Lett. 3477 (1976).
6. J. F. Bunnett and J. A. Skorcz. J. Org. Chem. **27**, 3836 (1962).
7. M. P. Cava and D. R. Napier. J. Am. Chem. Soc. **79**, 1701 (1957).
8. A. G. Loudon, A. Maccoll, and S. K. Wong. J. Am. Chem. Soc. **91**, 7577 (1969).
9. P. C. Conrad and P. L. Fuchs. J. Am. Chem. Soc. **100**, 347 (1978).
10. P. A. Argabright, J. E. Hofman, and A. Schriesheim. J. Org. Chem. **30**, 3233 (1965).
11. R. A. Olofson and C. M. Dougherty. J. Am. Chem. Soc. **95**, 581 (1973).
12. (*a*) M. P. Cava and M. M. Mitchell. Cyclobutadiene and related compounds. Academic Press, New York, NY. 1967. p. 209; (*b*) G. F. Emerson, L. Watts, and R. Petit. J. Am. Chem. Soc. **87**, 131 (1965).
13. T. Kametani, M. Tsubuki, Y. Shiratori, Y. Katò, H. Nemoto, M. Ihara, and K. Fukomoto. J. Org. Chem. **42**, 2672 (1977).
14. R. J. Spangler, B. G. Berkmann, and J. H. Kim. J. Org. Chem. **42**, 2989 (1977).

Determination of $\Delta H_{f298}^0(C_{12}F_{10},g)$ from studies of the combustion of decafluorobiphenyl in oxygen and calculation of $D(C_6F_5—C_6F_5)$

STANLEY JAMES W. PRICE[1] AND HENRY J. SAPIANO

Department of Chemistry, University of Windsor, Windsor, Ont., Canada N9B 3P4

Received December 22, 1978

STANLEY JAMES W. PRICE and HENRY J. SAPIANO. Can. J. Chem. 57, 1468 (1979).

The heat of formation of decafluorobiphenyl has been determined by the direct combustion method previously developed and used for hexafluorobenzene and related compounds. As in the hexafluorobenzene case the combustion of decafluorobiphenyl in oxygen yields CO_2, CF_4, and F_2. With a ten-fold excess of oxygen the CO_2 to CF_4 ratio is 5.85 ± 0.08. A full material balance was obtained. The value of $\Delta H_{f298}^0(C_{12}F_{10},g) = -1263.2 \pm 5.1$ kJ mol^{-1} may be combined with $\Delta H_{f298}^0(C_6F_5,g) = -387.4 \pm 12.0$ kJ mol^{-1} to give $D(C_6F_5—C_6F_5) = 488.4 \pm 24.5$ kJ mol^{-1}. Also with $\Delta H_{f298}^0(C_6F_6,g) = -945.6 \pm 8.0$ kJ mol^{-1} ΔH_{298}^0 for reaction [3]

[3] $$C_6F_5—C_6F_5(g) + F_2(g) \rightarrow 2C_6F_6(g)$$

is calculated to be -628.0 ± 16.8 kJ mol^{-1}.

STANLEY JAMES W. PRICE et HENRY J. SAPIANO. Can. J. Chem. 57, 1468 (1979).

On a déterminé la chaleur de formation du décafluorobiphényle par la méthode de combustion directe développée antérieurement et appliquée à l'hexafluorobenzène et à des composés apparentés. Comme dans le cas de l'hexafluorobenzène, la combustion du décafluorobiphényle dans l'oxygène fournit du CO_2, du CF_4 et du F_2. Lorsqu'on utilise un excès d'oxygène égal à dix fois les quantités requises, le rapport CO_2 à CF_4 est égal à 5.85 ± 0.08. On a établi un bilan complet des réactifs. La valeur de $\Delta H_{f298}^0(C_{12}H_{10},g) = -1263.2 \pm 5.1$ kJ mol^{-1} peut être combinée avec $\Delta H_{f298}^0(C_6H_5,g) = -387.4 \pm 12.0$ kJ mol^{-1} pour conduire à $D(C_6F_5—C_6F_5) = 488.4 \pm 24.5$ kJ mol^{-1}. Utilisant aussi la valeur de $\Delta H_{f298}^0(C_6F_6,g) = -945.6 \pm 8$ kJ mol^{-1}, on peut calculer que le ΔH_{298}^0 pour la réaction [3]

[3] $$C_6F_5—C_6F_5(g) + F_2(g) \rightarrow 2C_6F_6(g)$$

est égal à -628.0 ± 16.8 kJ mol^{-1}.

[Traduit par le journal]

Introduction

To date no thermodynamic study for the heat of formation of decafluorobiphenyl has been reported. The heat of formation of a variety of compounds containing the pentafluorophenyl group has been reported by Cox *et al.* (1, 2). To ensure complete combustion and minimize the formation of tetrafluoromethane as a product, hydrogen containing organic materials were added to the crucible.

The present paper describes the measurement of the heat of combustion of decafluorobiphenyl in a steel bomb with the compound contained in a steel crucible. The combustion was done under anhydrous conditions and without the use of any auxiliary materials. With approximately a ten-fold excess of oxygen, complete combustion is easily obtained and the only products are CO_2, CF_4, and F_2.

Experimental

Materials

(*i*) Decafluorobiphenyl was supplied by the Imperial Smelting Corporation Limited and was used without further purification. The melting point was found to be 68°C in agreement with the reported value of 68°C (3). The mass spectrum of decafluorobiphenyl was taken and found to be similar to that reported by Cotter (4). The $^{12}C^{13}C$ peak ratios at *m/e* values of 167, 167.5, 334, and 335 tend to confirm Cotter's observation that the 167 peak is due virtually exclusively to $C_{12}F_{10}^{2+}$. Cotter found no formation of the $C_6F_5^+$ ion. No mass fragments heavier than those corresponding to the molecular ion were found in the mass spectrum of the sample.

Sublimation pressure measurements (5) over the range of 24 to 49°C are adequately represented by

[1] $$\log_{10} P(\text{cm}) = 4.0777 - 4056.0/T + 2.927 \log_{10} T$$

The resulting heat of sublimation and average heat capacity differences (vapour − solid) are $\Delta H_{298}^0 = 84.9$ kJ mol^{-1} and $\langle \Delta C_p$, 25 to 49°C$\rangle = 24.33$ J deg^{-1} mol^{-1}.

(*ii*) CO_2, CF_4, and F_2 were obtained from the Matheson Chemical Company and were used without further purification.

Apparatus and Calorimetric Procedure

The apparatus and procedure used for the main combustion process were identical to those previously used for C_6F_5Br (6), C_6F_{10}, and C_6F_{12} (7). A Parr model 1004C steel bomb and steel crucible were again used for the combustion process.

Over the time interval required to place the weighed sample into the bomb no measureable loss of decafluorobiphenyl sample from the crucible in which it was weighed was observed.

[1]To whom all correspondence should be addressed.

0008-4042/79/121468-03$01.00/0

TABLE 1. Combustion data and calculated enthalpy of formation for decafluorobiphenyl[a]

Mass $C_{12}F_{10}$ (g)	ΔT_{cor} (°C)	CO_2/CF_4[b] (by gc)	CO_2 collected (g)	F_2 collected (g)	% Theoretical yields C	% Theoretical yields F	$\Delta H_{f298}^0(C_{12}F_{10},g)$ (kJ mol^{-1})
1.245	0.9073	5.82	1.677	0.222	99.9	101.6	−1266.7
1.054	0.7669	5.88	1.421	0.184	99.8	100.3	−1266.9
1.338	0.9777	5.78	1.830	0.226	101.5	101.5	−1262.3
1.176	0.8578	5.84	1.582	0.203	99.6	100.3	−1261.0
1.327	0.9664	5.88	1.803	0.225	100.6	98.7	−1263.1
1.410	1.0288	5.86	1.922	0.242	100.9	100.4	−1260.6
1.088	0.7940	5.84	1.504	0.189	102.4	102.4	−1260.6
1.212	0.8824	5.88					−1264.0
							Mean −1263.2±5.1[c]

[a]Additional typical data (see ref. 14 for notation); E, ign/J = 13.3, $E(J)(-t_c)$/J = −15977.8, E_c^0/M(compound)/J g^{-1} = −12979.5.
[b]Molar ratio.
[c]Error limits are twice the standard deviation of the mean.

Analysis of Reaction Products

The analytical procedures for CO_2, CF_4, and F_2 have been described elsewhere (8–10). Mass spectra were obtained using a Varian MAT CH5-DF Spectrometer controlled by an INCOS computer system. A Bausch and Lomb Spectronic 100 was used to determine iron with 1,10-phenanthroline (11).

Results and Discussion

The experimental results for decafluorobiphenyl are shown in Table 1. In the combustion of $C_{12}F_{10}$ in the steel bomb the formation of a green coloration was observed as in the case of C_6F_5Br (6). The amount of Fe(II) and Fe(III) fluoride after combustion was determined using a colorimetric procedure (11). Approximately 1.30 mg of iron fluorides were formed, of which roughly 80% was FeF_2. The correction to the heat of formation of $C_{12}F_{10}$ caused by the formation of FeF_2 and FeF_3 was less than 2.5 kJ mol^{-1}.

The only detectable products of combustion are CO_2, CF_4, and F_2, with the exception of the small quantities of iron fluorides. These products were identified and quantitatively determined in the same manner reported for the products of combustion of C_6F_{10} and C_6F_{12} (7).

The column used was a 6 ft × 1/4 in. od Porapak Q column (25°C, He carrier, 48 cm^3/min). Calibrations were carried out using O_2–CF_4 and O_2–CO_2 mixtures. If pure CO_2 is used the CO_2 calibration is unaffected. If pure CF_4 is used the net result is that the relative response factor for CF_4 is increased by 3.5% resulting in a value for $\Delta H_{f298}^0(C_{12}F_{10},g)$ which is about 32.6 kJ mol^{-1} too high.

Based on the observed products and the average CO_2/CF_4 molar ratio of 5.85 the combustion reaction of decafluorobiphenyl may be written

[2] $C_{12}F_{10} + 10.248O_2 \rightarrow 10.248CO_2 + 1.752CF_4 + 1.496F_2$

With the exception of $C_{12}F_{10}$ all reactants and products are in the gaseous state. The decafluorobiphenyl is present in the bomb as a solid at the time of combustion.

No detectable heat of mixing was observed when F_2, O_2, CF_4, and CO_2 were mixed under anhydrous conditions (10).

For calculation of $\Delta H_{f298}^0(C_{12}F_{10},g)$, the standard heats of formation of the combustion products were taken as $\Delta H_{f298}^0(CO_2,g) = -393.512$ kJ mol^{-1} (12) and $\Delta H_{f298}^0(CF_4,g) = -933.0$ kJ mol^{-1} (13). The heat of sublimation of $C_{12}F_{10}$ was taken as $\Delta H_{298}^0 = 84.9$ kJ mol^{-1} (5).

Based on the preceding data and an estimated correction to standard state of 5.0 kJ mol^{-1}, $\Delta H_{f298}^0(C_{12}F_{10},g) = -1263.2 \pm 5.1$ kJ mol^{-1}. Using this value and $\Delta H_{f298}^0(C_6F_5,g) = -387.4$ kJ mol^{-1} (4) the value for $D(C_6F_5—C_6F_5) = 488.4$ kJ mol^{-1}.

It is also possible to calculate the enthalpy change for reaction [3].

[3] $C_6F_5—C_6F_5(g) + F_2(g) \rightarrow 2C_6F_6(g)$

With $\Delta H_{f298}^0(C_6F_6,g) = -945.6$ kJ mol^{-1}, ΔH_{298}^0 for this reaction is −628.0 kJ. This high negative value reflects both the weakness of the F—F bond in F_2 and the high C—F bond dissociation energy in hexafluorobenzene.

For reaction [4], based on $\Delta H_{f298}^0(C_6H_5F,g) = -116.0$ kJ mol^{-1} (15)

[4] $C_6H_5—C_6H_5(g) + F_2(g) \rightarrow 2C_6H_5F(g)$

and $\Delta H_{f298}^0(C_{12}H_{10},g) = 182.3$ kJ mol^{-1} (15), $\Delta H_{rx} = -414.3$ kJ. The difference between this result and that for reaction [3], 214 kJ, is within 6 kJ of that estimated from $D(C_6F_5—F) = 637.2$ kJ mol^{-1} (8) and $D(C_6F_5—C_6F_5)$ and from $D(C_6H_5—F) =$

514.6 kJ mol^{-1} (16) and $D(C_6H_5—C_6H_5)$ = 463.7 kJ mol^{-1} (15, 16).

Acknowledgements

The authors wish to thank Mr. Ahti Koski for his help in this work. This work has been supported by an operating grant from the Natural Sciences and Engineering Research Council of Canada.

1. J. D. Cox, H. A. Gundry, and A. J. Head. Trans. Faraday Soc. **60**, 653 (1964).
2. J. D. Cox, H. A. Gundry, D. Harrop, and A. J. Head. J. Chem. Thermodyn. **1**, 77 (1969).
3. Highly fluorinated aromatic and alicyclic compounds. Imperial Smelting Company, St. Andrews Road, Avonmouth, Bristol BS119HP, England.
4. J. L. Cotter. J. Chem. Soc. 1520 (1965).
5. L. G. Radchenko and A. I. Kitaigorodskii. Zh. Fiz. Khim. **48**(11), 2702 (1974).
6. M. J. Krech, S. J. W. Price, and H. J. Sapiano. Can. J. Chem. **55**, 4222 (1977).
7. S. J. W. Price and H. J. Sapiano. Can. J. Chem. In press.
8. M. J. Krech, S. J. W. Price, and W. F. Yared. Can. J. Chem. **50**, 2935 (1972).
9. M. J. Krech, S. J. W. Price, and W. F. Yared. Can. J. Chem. **51**, 2673 (1973).
10. M. J. Krech, S. J. W. Price, and W. F. Yared. Can. J. Chem. **52**, 2673 (1974).
11. H. H. William, L. L. Merrit, and J. A. Dean. Instrumental methods of analysis. 4th ed. D. Van Nostrand Company Inc., New York, NY. 1969. p. 104.
12. F. D. Rossini *et al.* Selected values of chemical thermodynamic properties. Natl. Bur. Stand. (U.S.), Tech. Note No. 270-3. 1968.
13. E. Greenberg and W. H. Hubbard. J. Phys. Chem. **72**, 222 (1968).
14. J. Coops, R. S. Jessup, and K. Vannes. *In* Experimental thermochemistry. Vol. 1. *Edited by* F. D. Rossini. Interscience, New York. 1956.
15. J. B. Pedley and J. Rylance (*Editors*). Sussex – N.P.L. computer analysed thermochemical data: organic and organometallic compounds. University of Sussex. 1977.
16. G. A. Chamberlain and E. Whittle. Trans. Faraday Soc. **67**, 2077 (1971).

Effect of temperature on the fluorescence quenching by *N*-bromosuccinamide of tryptophan residues in proteins

BRANKO F. PETERMAN AND KEITH J. LAIDLER

Department of Chemistry, University of Ottawa, Ottawa, Ont., Canada K1N 9B4

Received January 2, 1979

BRANKO F. PETERMAN and KEITH J. LAIDLER. Can. J. Chem. 57, 1471 (1979).

The quenching of tryptophan fluorescence by *N*-bromosuccinamide was studied by the fluorescence stopped-flow technique over a temperature range of 5 to 35°C in order to compare the reactivities of tryptophan residues in various molecules. The highest rates and lowest activation energies were found with the simple molecule *N*-acetyltryptophanamide. The hormone glucagon, which contains a single tryptophan residue, showed a somewhat lower rate and higher activation energy. α-Chymotrypsin, which has three groups of tryptophan residues in different environments, gave three rate constants which were lower than those with the other compounds, and the activation energies were correspondingly higher. There was a linear relationship between enthalpy of activation and the Gibbs energy of activation, the proportionality factor being 6.7. This indicates a $\Delta H^* - \Delta S^*$ compensation, with an isokinetic temperature of 350 K. The compensation is discussed in the light of the steric effects.

BRANKO F. PETERMAN et KEITH J. LAIDLER. Can. J. Chem. 57, 1471 (1979).

On a étudié le piégeage de la fluorescence du tryptophane par la *N*-bromosuccinamide par la technique de fluorescence à flux stoppé à des températures allant de 5 à 35°C afin de comparer la réactivité de résidus de tryptophane dans diverses molécules. On a trouvé que les vitesses les plus rapides et les énergies d'activation les plus basses sont associées à la molécule simple, *N*-acétyltryptophanamide. L'hormone glucagone, qui contient un seul résidu tryptophane simple, présente une vitesse un peu plus basse et une énergie d'activation un peu plus élevée. L'α-chymotrypsine qui contient trois tryptophanes dans des environnements différents, présente trois constantes de vitesse qui sont plus faibles que celles des autres composés et les énergies d'activation sont proportionnellement plus élevées. Il existe une relation linéaire entre l'enthalpie d'activation et l'énergie libre d'activation de Gibbs; le facteur de proportionalité est de 6.7. Ceci indique que le ΔH^+ et le ΔS^+ se compensent; la température isocinétique est de 350 K. On discute de la compensation à la lumière des effets stériques.

[Traduit par le journal]

Introduction

In a previous paper (1) we have shown that kinetic studies of the quenching by *N*-bromosuccinamide (NBS) of the fluorescence of tryptophan provide valuable information about the environments of tryptophan residues in proteins. The quenching of the fluorescence of *N*-acetyl-L-tryptophanamide (*N*-AcTrpNH$_2$), the tripeptide Gly-Trp-Gly, and apocytochrome *c*, all of which contain a single tryptophan residue, was found to follow simple second-order kinetics (first-order in NBS and first-order in the tryptophan-containing compound). The enzyme α-chymotrypsin contains eight tryptophan residues per molecule, and the X-ray study (2) shows that six are at the surface and two buried in the interior of the molecule. Three of the six surface residues have the indole rings protruding out of the molecule, and the remaining three are pointing inwards. The tryptophan residues thus fall into three groups, and our quenching kinetics studies showed that there are three relaxation times which can be identified as corresponding to the three groups.

Since quenching by NBS occurs with half-lives of less than 100 ms, significant conformational changes in the protein molecules are unlikely, and the technique therefore appears to provide a valuable tool for obtaining supporting conformational evidence. Because of enthalpy–entropy compensation effects, Gibbs energies of activation, and therefore rate constants, are frequently less sensitive to structural factors than are enthalpies or energies of activation. We have therefore made a study of the temperature dependence of the rate constants for the quenching reactions, and the results are described and discussed in the present paper. The work has been done with *N*-AcTrpNH$_2$ and α-chymotrypsin, and also with the hormone glucagon. This polypeptide, which plays an important physiological role in stimulating the action of adenylate cyclase, contains a single tryptophan residue which previous fluorescence studies (3, 4) have shown to be largely exposed to the solvent. In the crystalline state glucagon has an α-helical arrangement (5) but in aqueous solution it appears to exist as a flexible chain (3, 6).

0008-4042/79/121471-04$01.00/0

Experimental

Materials

N-Bromosuccinamide was purchased from Fisher Chemical Co., *N*-acetyl-L-tryptophanamide from Sigma Chemical Co., α-chymotrypsin (3 × crystallized) from Worthington Biochemical Co., and glucagon from Research Plus Laboratories. Since glucagon suspended in HCl solution at pH ~ 2.5 did not dissolve completely, it was filtered on a Sephadex G-25 column equilibrated with sodium phosphate buffer at pH 7.0 and an ionic strength of 0.05 *M*. Undissolved material, which eluted first from the column, was followed by dissolved glucagon, as judged from the absorption spectrum. The fractions with a high A_{280}/A_{240} ratio (~1.6) were pooled and used for subsequent experiments.

Spectroscopic Measurements

Absorption measurements were carried out with a Pye-Unicam model SP 1800 spectrophotometer. The concentrations of proteins were determined spectrophotometrically using the following absorption coefficients: α-chymotrypsin, ε (282) = $5.15 \times 10^4\ M^{-1}\ cm^{-1}$ (7) and glucagon, ε (280) = $8.05 \times 10^3\ M^{-1}\ cm^{-1}$ (8).

Kinetic Measurements

Kinetic measurements were made with a Durrum stopped-flow instrument as previously described (1). All samples were excited at 296 nm and the emitted light was selected by a Corning 0-54 filter. The temperature was controlled to ±0.2°C by a Haake model KT 33 constant temperature circulator, and was measured at various positions by a Yellow Springs Instrument Co. telethermometer. Rate measurements were made at temperatures from 5 to 35°C. The records of fluorescence vs. time were captured by a Biomation recorder, displayed on an oscilloscope screen, and photographed, the records then being transferred to semilogarithmic graph paper. Analysis of the results was as explained in ref. 1. Maximum errors were estimated from a number of results obtained under identical conditions; the first-order rate coefficients were always within ±10% of the average value, and this maximum deviation is about twice the standard deviation.

Results

As in the previous studies (1) the fluorescence quenching of *N*-AcTrpNH$_2$ by NBS followed simple second-order kinetics. The Arrhenius plot for the quenching of the fluorescence of *N*-AcTrpNH$_2$ is shown in Fig. 1. The activation energy E_a is 7.3 ± 0.8 kcal mol^{-1}, and Table 1 lists other kinetic parameters at 25.0°C, calculated using the equations (9)

$$[1] \qquad \Delta H^{\ddagger} = E_a + RT$$

$$[2] \qquad \Delta G^{\ddagger} = -RT \ln [k(T)h/kT]$$

$$[3] \qquad \Delta S^{\ddagger} = (\Delta H^{\ddagger} - \Delta G^{\ddagger})/T$$

where R is the gas constant, h Planck's constant, k the Boltzmann constant, and $k(T)$ the rate constant at 25.0°C.

The fluorescence quenching of glucagon also followed simple second-order kinetics, and the Arrhenius plot is included in Fig. 1. The kinetic parameters are listed in Table 1.

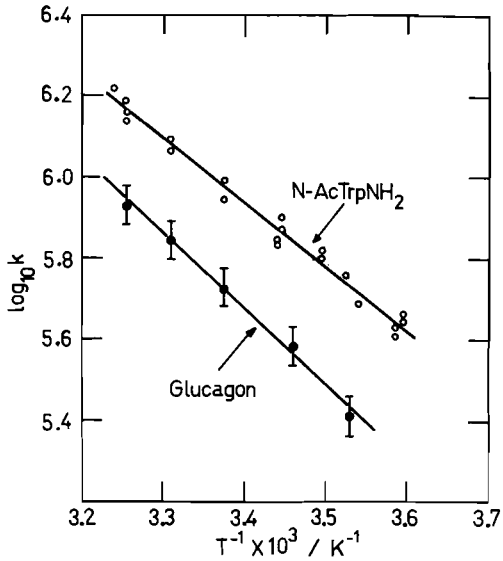

FIG. 1. Arrhenius plots for the reaction between *N*-bromosuccinamide and *N*-acetyltryptophanamide, and between *N*-bromosuccinamide and glucagon. The concentration of NBS was $5 \times 10^{-5}\ M$ for the *N*-AcTrpNH$_2$ experiments and $10 \times 10^{-5}\ M$ for the glucagon experiments. The concentrations of *N*-AcTrpNH$_2$ and glucagon were $5 \times 10^{-6}\ M$. The reactions took place in a sodium phosphate buffer, pH 7.0, at an ionic strength of 0.05 *M*.

The quenching of the fluorescence of α-chymotrypsin shows three second-order relaxations (1), and the corresponding Arrhenius plots are displayed in Fig. 2. The rate constants and other kinetic parameters are shown in Table 1.

Discussion

The order of the rate constants and the Gibbs energies of activation, $\Delta G^{\ddagger}$, can be related to the structures involved. The highest rate constant is found with *N*-AcTrpNH$_2$, where there is little steric shielding of the tryptophan residue. In glucagon there is somewhat more shielding by the rest of the protein molecule which probably forms a flexible chain (3, 6), and the rate constant is ~0.67 of the value with *N*-AcTrpNH$_2$. This ratio is consistent with the ratio of ~0.59 found with quenching by acrylamide (4).

The amplitudes for the three second-order components found in the α-chymotrypsin quenching are in the approximate ratio of 3:3:2 and, as discussed in our previous paper (1), are attributed to the three types of tryptophans in α-chymotrypsin. The fastest component presumably corresponds to reaction between NBS and the surface residues having exterior indole rings. The fact that the rate constant ($2.3 \times 10^5\ dm^3\ mol^{-1}\ s^{-1}$) is significantly less than that with glucagon suggests that even these exterior indole rings are more shielded by the protein matrix. The

TABLE 1. Kinetic parameters for the quenching of the fluorescence of tryptophan-containing compounds by NBS at 25°C*

Compound	k (25°C) ($dm^3\ mol^{-1}\ s^{-1}$)	E_a (kcal mol^{-1})	$\Delta H^{\ddagger}$ (kcal mol^{-1})	$\Delta G^{\ddagger}$ (kcal mol^{-1})	$\Delta S^{\ddagger}$ (cal $K^{-1}\ mol^{-1}$)
N-AcTrypNH$_2$	$(1.0\pm0.1)\times10^6$	7.3±0.8	7.9±0.8	9.2±0.05	−4.4±0.5
Glucagon	$(5.8\pm0.5)\times10^5$	8.4±1.2	9.0±1.3	9.5±0.1	−1.7±0.5
α-Chymotrypsin					
Fast relaxation	$(2.3\pm0.2)\times10^5$	16.7±1.4	17.3±1.5	10.1±0.1	24±3
Intermediate relaxation	$(7.6\pm0.7)\times10^4$	18.7±1.6	19.3±1.6	10.8±0.1	28±3
Slow relaxation	$(1.6\pm0.2)\times10^4$	21.0±1.8	21.6±1.8	11.7±0.1	33±3

*The errors indicated are maximum deviations, obtained from a number of duplicate experiments. The standard deviations, calculated using the method of least squares, are about one half of the maximum deviations.

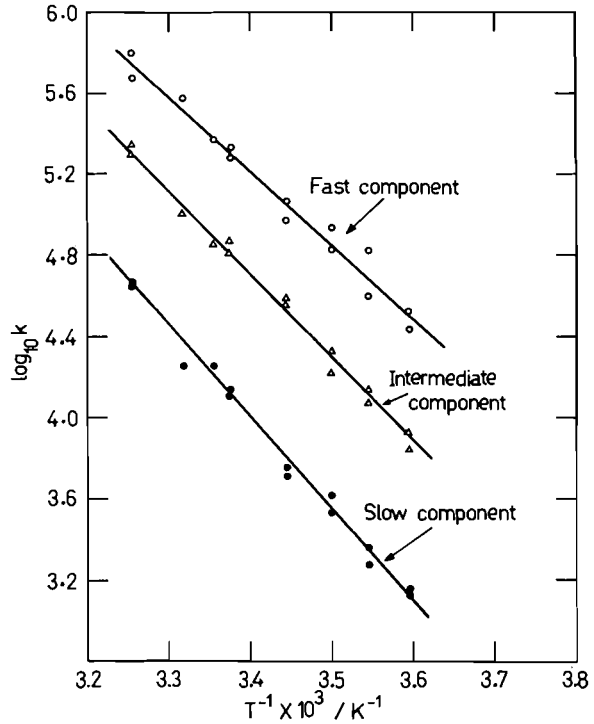

FIG. 2. Arrhenius plots for the reaction between *N*-bromosuccinamide and the tryptophan residues in α-chymotrypsin. The three plots are for the three kinetic components, as indicated. Concentrations of reactants: α-chymotrypsin, $6.2\times10^{-7}\ M$; NBS, $10\times10^{-5}\ M$. Buffer as indicated in Fig. 1.

intermediate relaxation is attributed to the three surface tryptophans whose indole rings are pointing inwards, and the slow relaxation to the two tryptophan residues which are buried inside the protein molecule.

The differences between the five reactions are greatly magnified if we consider the variations in E_a (or $\Delta H^{\ddagger}$) instead of the variations in k (or $\Delta G^{\ddagger}$). This is shown by the plot in Fig. 3*a* of $\Delta H^{\ddagger}$ against $\Delta G^{\ddagger}$. The points lie satisfactorily on a straight line, the equation for which is

[4] $$\Delta H^{\ddagger} = 6.7\Delta G^{\ddagger} + \text{constant}$$

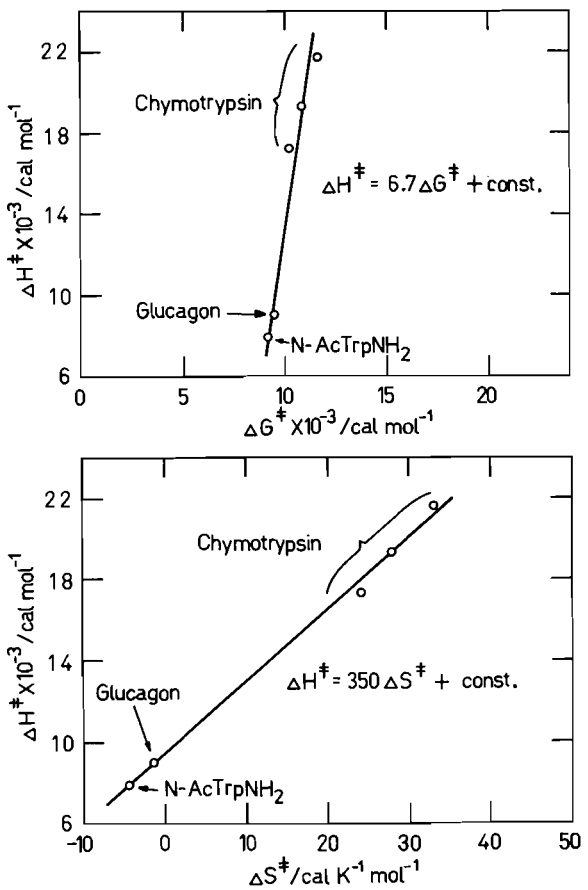

FIG. 3. (*a*), A plot of the enthalpy of activation against the Gibbs energy of activation at 25°C, for the five reactions. (*b*), A plot of the enthalpy of activation against the entropy of activation.

There is thus a magnification by 6.7 when the enthalpies (or energies) of activation are used, and the latter thus provide a much more sensitive measure of the behaviour of tryptophan groups in proteins.

Since $\Delta G^{\ddagger} = \Delta H^{\ddagger} - T\Delta S^{\ddagger} = \Delta H^{\ddagger} - 298\Delta S^{\ddagger}$ (at 25°C) it follows from eq. [4] that

[5] $$\Delta H^{\ddagger} = 350\Delta S^{\ddagger} + \text{constant}$$

if $\Delta H^{\ddagger}$ is in the units cal mol^{-1} and $\Delta S^{\ddagger}$ in the units cal K^{-1} mol^{-1}. This relationship is shown in Fig. 3*b*. If the experiments were (hypothetically) carried out at 350 K, the compensation or isokinetic temperature, the rates would all be approximately the same, since there would then be complete compensation between $\Delta H^{\ddagger}$ and $T\Delta S^{\ddagger}$. However, the compensation temperature is of no simple significance.

Compensation effects are frequently observed (10–12), and have been interpreted (13) as due to solvent and steric effects. A change in vibrational frequency brings about parallel changes in H/T and in S, and the compensation is greater for the higher frequency. In the reactions studied in this investigation, a tryptophan residue which is sterically protected from the NBS will react with a higher activation energy. At the same time there will be a loosening of the vibrations in the activated complex, and a corresponding increase in entropy which will partly compensate for the increase in activation energy.

The present results thus provide an additional example in which measurements of activation energies provide more sensitive information than rate measurements at a single temperature.

1. B. F. PETERMAN and K. J. LAIDLER. Biochim. Biophys. Acta. In press.
2. J. J. BIRKTOFT and D. M. BLOW. J. Mol. Biol. **68**, 187 (1972).
3. M. EDELHOCH and R. E. LIPPOLDT. J. Biol. Chem. **244**, 3876 (1969).
4. M. R. EFTINK and C. A. GHIRON. Biochemistry, **15**, 672 (1976).
5. K. SASAKI, S. DOCKERILL, D. A. ADAMIAK, I. J. TICKLE, and T. BLUNDELL. Nature, **257**, 751 (1975).
6. B. PANIJPAN and W. B. GRATZER. Eur. J. Biochem. **45**, 547 (1974).
7. W. J. DREYER, R. D. WADE, and H. NEURATH. Arch. Biochem. Biophys. **59**, 145 (1955).
8. M. C. LIN, D. E. WRIGHT, V. J. HRUBY, and M. RODBELL. Biochemistry, **14**, 1554 (1975).
9. K. J. LAIDLER. Theories of chemical reaction rates. McGraw-Hill, New York. 1969. pp. 76–79.
10. K. J. LAIDLER and H. EYRING. Ann. N.Y. Acad. Sci. **39**, 303 (1940).
11. R. LUMRY and S. RAJENDER. Biopolymers, **9**, 1125 (1970).
12. U. BORGMAN, K. J. LAIDLER, and T. W. MOON. Can. J. Biochem. **53**, 1196 (1975).
13. K. J. LAIDLER. Trans. Faraday Soc. **55**, 1725 (1959).

Synthesis of *exo*- and *endo*-brevicomin and frontalin

PHAIK-ENG SUM AND LARRY WEILER[1]

Department of Chemistry, University of British Columbia, Vancouver, B.C., Canada V6T 1W5

Received January 9, 1979

PHAIK-ENG SUM and LARRY WEILER. Can. J. Chem. **57**, 1475 (1979).

The dianion of methyl acetoacetate is alkylated at the γ-carbon with homoallylic bromides. The resulting alkenes are epoxidized and then cyclized with a Lewis acid to produce esters of 6,8-dioxabicyclo[3.2.1]octane. These esters can be hydrolyzed and decarboxylated in a novel reaction. This methodology has been applied to a stereospecific synthesis of the title compounds. In addition, one of the intermediates in the *exo*-brevicomin synthesis can be resolved to provide the natural (+)-pheromone.

PHAIK-ENG SUM et LARRY WEILER. Can. J. Chem. **57**, 1475 (1979).

Le dianion de l'acétoacétate de méthyle peut être alkylé au niveau du carbone γ par des bromures homoallyliques. Les alcènes qui en résultent peuvent être époxydés et ensuite cyclisés à l'aide d'un acide de Lewis pour fournir des esters du dioxa-6,8 bicyclo[3.2.1] octane. On peut hydrolyser ces esters et les décarboxyler dans une réaction nouvelle. On a appliqué cette méthodologie à une synthèse stéréospécifique des composés sus-mentionnés. De plus, un des intermédiaires de la synthèse de l'*exo*-brévicomine peut être résolu pour fournir la (+)-phéromone naturelle.

[Traduit par le journal]

Recently we have been interested in using acyclic β-keto esters to form cyclic compounds. Five-membered carbocyclic compounds were prepared in our synthesis of jasmone (1) and a prostaglandin intermediate (2). In addition other groups have reported the cyclization of β-keto esters in prostaglandin syntheses (3). In these reactions the cyclization occurs at a sp^2 carbon as shown in [1]. We have

[1] 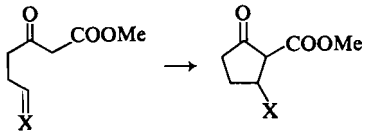

also been able to generate six-membered carbocyclic rings by cyclization of an appropriately substituted β-keto ester in an approach to the synthesis of resistomycin (4). White and co-workers have found that the olefinic β-keto ester **1** undergoes the Lewis acid catalyzed cyclization shown in [2] (5). These

[2] 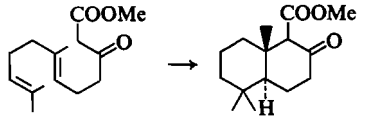

1

results illustrate the utility of acyclic β-keto esters to form five- and six-membered rings.

We were also interested in investigating the cyclization of epoxy β-keto esters. In the case of the epoxide **2** we found that acid or Lewis acid catalyzed reactions gave only the O-cyclized product **3**.[2] Here

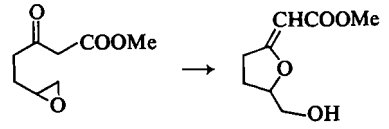

2 **3**

we would like to report our results on the homologous epoxide **4** and some substituted derivatives of **4**. The epoxide **4** was readily prepared by alkylating the dianion of methyl acetoacetate (6) with 4-bromo-1-butene and epoxidizing the resulting alkene to give **4** in 60% overall yield. This same epoxide could be

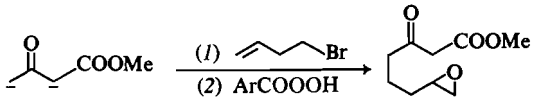

4

synthesized by alkylating the dianion of methyl acetoacetate with 4-bromo-1,2-epoxybutane. However, the yields in this one-step sequence were usually lower than the above two-step sequence. The epoxide **4** underwent an isomerization on heating. Subsequently we found that this isomerization could be effected in 85% yield by treating **4** with boron trifluoride etherate. The structure of the isomerization product was readily identified from the spectral data. The salient points were the observation of a single carbonyl band in the infrared at 1740 cm^{-1}, which we assigned to an ester. The nmr spectrum of the isomerization product had a three-proton singlet at δ 3.68 due to the methyl group of an ester. The meythlene of the β-keto ester **4** was replaced by an

[1]To whom all correspondence should be addressed.

[2]J. Liu, F. W. Sum, and L. Weiler. Unpublished results. 1975.

0008-4042/79/121475-06$01.00/0

apparent singlet at δ 2.73. In addition there were two low-field signals at δ 3.8 and δ 4.5 attributed to three protons on carbon atoms attached to an oxygen atom. These structural features were combined to lead to **5** as the product of this isomerization.

Compound **5** contains the 6,8-dioxabicyclo[3.2.1]-octane skeleton (7) which is the basic framework of

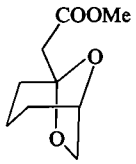

5

several bark beetle sex pheromones. *exo*-Brevicomin was isolated and found to have structure **6** by Silverstein and co-workers (8). This material is the aggregating pheromone of the bark beetle, *Dendroctonus brevicomis*, which attacks western pine trees. Subsequently, the *endo* isomer **7** was found to be a minor component in the natural pheromone mixture produced by *D. brevicomis*. Shortly after these reports on the brevicomin isomers frontalin, which is the sex pheromone of the bark beetle, *Dendroctonus frontalis*, that attacks southern pine trees, was found to have structure **8** (9). These three pheromones all

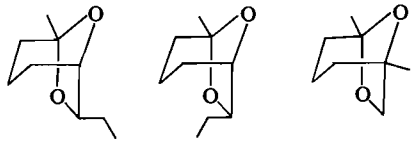

6 **7** **8**

have the 6,8-dioxabicyclo[3.2.1]octane skeleton and all three have been the object of several synthetic (for brevicomin, see ref. 10; for frontalin, see ref. 11) and entomological studies (12) because of their unusual structures and interesting biological properties. Hence we turned our attention to the preparation of pheromones **6**–**8** using the above β-keto ester cyclization.

The synthesis of these pheromones is outlined in Scheme 1. In the synthesis of frontalin (**8** = **13***C*), the dianion of methyl acetoacetate was alkylated with 4-bromo-2-methyl-1-butene (**9***C*), prepared from the commercially available 2-methyl-1-buten-4-ol and phosphorus tribromide, to give an 83% yield of the γ-alkylated product which was epoxidized with *m*-chloroperbenzoic acid to produce **10***C* in 71% yield from methyl acetoacetate. The $BF_3 \cdot Et_2O$ catalyzed cyclization of **10***C* produced **11***C* in 95% yield. To convert **11***C* into frontalin we must remove the carbomethoxy group on the side chain. This was accomplished as follows. The ester **11***C* was hydro-

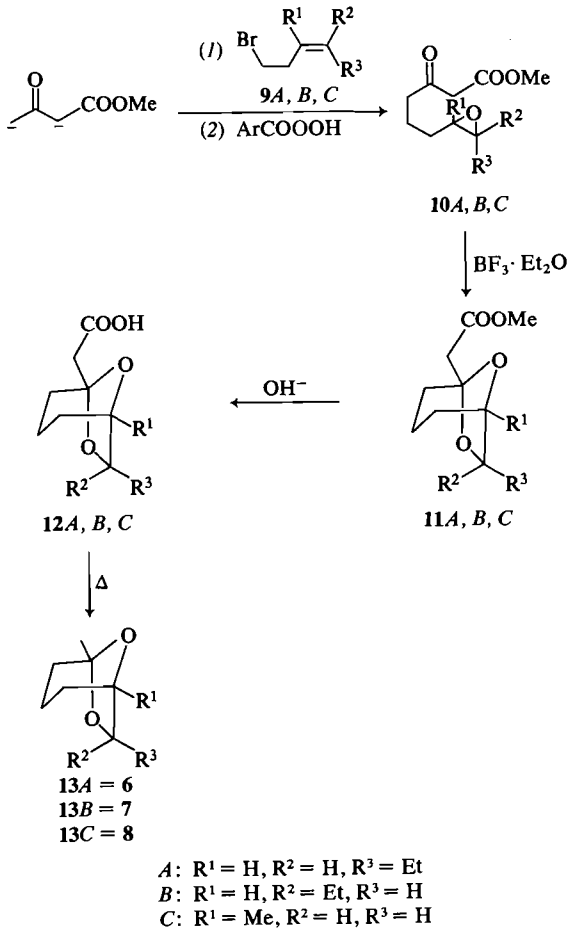

SCHEME 1. Syntheses of *exo*- and *endo*-brevicomin and frontalin.

lyzed in 88% yield by aqueous alkaline and the resulting carboxylic acid **12***C* underwent a smooth thermal decarboxylation (Kugelrohr oven at 220°C, 5 min) to give an 85% yield of frontalin (**13***C*). The rather facile decarboxylation of acid **12***C* may be due to participation of one of the ketal oxygens as shown below (reaction [3]). A similar mechanism was pro-

[3]

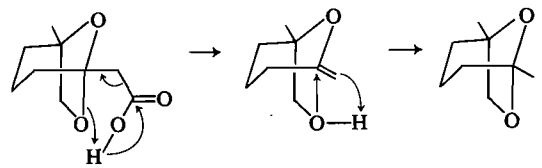

posed by Atkinson and Miller (13) for the decarboxylation of acid **14** in [4]. Hydrolysis and decarboxylation of ester **5** produced 5-methyl-6,8-dioxabicyclo[3.2.1]octane in 73% yield for the two steps.

The synthesis of *endo*-brevicomin (**13***B*) was accomplished along similar lines as that of frontalin

[4] 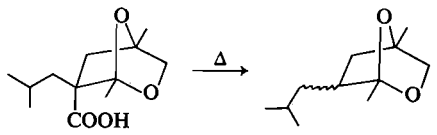

14

(Scheme 1). Specifically, the dianion of methyl acetoacetate was alkylated (83% yield) with *E*-1-bromo-3-hexene (**9***B*) and the resulting alkene was epoxidized (87% yield) to give **10***B* which was cyclized to **11***B* in 91% yield. We could not detect any of the isomeric *exo*-isomer **12***A* in this cyclization. A number of earlier syntheses of *endo*- or *exo*-brevicomin have involved a thermal or acid catalyzed cyclization of a keto epoxide to generate the 6,8-dioxabicyclo[3.2.1]octane skeleton (8, 10). However, these conditions usually produced a mixture of *endo*- and *exo*-brevicomin. This Lewis acid catalyzed cyclization of the β-keto esters **10***A* (*vide infra*) and **10***B* can be effected in high yield and high stereospecificity. We suggest that the high stereospecificity in the cyclizations of **10***A* and **10***B* may be related to the significantly higher enol content of a β-keto ester relative to a simple ketone. The ketal ester **11***B* was converted into *endo*-brevicomin by hydrolysis (95%) and thermal decarboxylation (85%) as above. There was no detectable epimerization during the thermal decarboxylation which is consistent with the mechanism proposed in [3].

Finally the synthesis of *exo*-brevicomin (**13***A*) was also carried out as shown in Scheme 1. The overall yield of *exo*-brevicomin (**13***A*) from methyl acetoacetate and *Z*-1-bromo-3-hexene (**9***A*) was ca. 58%. In addition to the overall efficiency and high stereospecificity in this route we have found an added bonus. Namely, the carboxylic acid function in **12** provides a useful handle to achieve the resolution of this intermediate and hence achieve a synthesis of *both* enantiomers of **13** from a single intermediate. Often a comparison of the biological activity of the racemic attractant relative to each enantiomer can provide fascinating insight into the insect receptor sites (14). To date the lack of a useful handle has prevented the resolution of an intermediate late in the synthesis of frontalin or brevicomin. Efficiency requires that the resolution be applied as late as possible in the synthesis since we desire *both* enantiomers. Syntheses of optically active frontalin (11*c*, *e*) and brevicomin (10*d*, *i*) from a chiral precursor have been reported and the synthesis of the two enantiomers of frontalin via resolution of an intermediate has been reported (11*b*). However, we are not aware of any synthesis of (+) and (−)-*exo*-brevicomin by resolution of a synthetic intermediate; thus we investigated the possibility of resolving the carboxylic acid **12***A*. Although there are a variety of methods to resolve carboxylic acids, many of which could be applied here, we only investigated a single method to demonstrate the feasibility of this approach. We chose to resolve **12***A* via formation of the α-methylbenzylammonium salts since both enantiomers of the resolving agent are readily available (15, 16). Two recrystallizations of the (+)-α-methylbenzylammonium salt of **12***A* gave a 40% yield of a salt mp 110–115°C. This salt was hydrolyzed in aqueous acid to liberate the free acid **12***A* which was thermally decarboxylated as above to yield (+)-*exo*-brevicomin, $[\alpha]_D^{25} = +52°$ (c = 0.12 g/mL, Et_2O) which compares with the reported rotation of $[\alpha]_D^{26} = +84.1°$ (c = 2.2, Et_2O) for natural (+)-*exo*-brevicomin (10*d*). This would indicate that we have achieved a 62% resolution of **12***A*.

Experimental

All ir spectra were recorded in $CHCl_3$ solution using a Perkin Elmer model 700 spectrophotometer and were calibrated with the 1601 cm^{-1} band of polystyrene. The ^1H nmr spectra were recorded in $CDCl_3$ solution on either a Varian model T-60 or HA-100 spectrometer. The signal positions are reported using the δ scale with tetramethylsilane as internal standard. The multiplicity, coupling constants, and integrated peak areas are indicated in parentheses after each signal. The mass spectra were obtained using an Atlas CH-4B mass spectrometer and high resolution determinations were obtained using an AEI MS-9 or MS-50 mass spectrometer. Both instruments were operated at an ionizing potential of 70 eV. The silica gel used was obtained from E. Merck and that used for thin-layer chromatography (tlc) was the grade PF_{254}, whilst that used for column chromatography was the grade finer than 200 mesh ASTM. Elemental microanalyses were performed by Mr. Peter Borda, University of British Columbia.

Epoxide 4

The dianion of methyl acetoacetate (6) was alkylated with 4-bromo-1-butene to give in 79% yield methyl 3-oxo-7-octenoate, bp 60°C/0.1 Torr; ir: 1745, 1720, 1650, and 920 cm^{-1}; nmr δ: 1.5–2.3 (m, 4H), 2.51 (t, J = 7 Hz, 2H), 3.38 (s, 2H), 3.68 (s, 3H), 4.7–5.2 (m, 2H), and 5.3–6.1 (m, 1H); ms *m/e* (relative intensity): 170(29), 138(16), 129(13), 116(100), 101(54), 97(53), 84(32), 74(60), 69(43), 59(37), 55(32), 43(45), and 41(57). *Anal.* calcd. for $C_9H_{14}O_3$: C 63.51, H 8.29; found: C 63.51, H 8.37.

A sample of 1.01 g of 85% *m*-chloroperbenzoic acid (5.5 mmol) was added to a solution of 0.850 g (5.0 mmol) of the above olefinic ester in ca. 20 mL dry CH_2Cl_2 at 0°C. The reaction mixture was stirred at 0°C for ½ h and then at room temperature for an additional 20 h. The reaction was quenched with saturated aqueous $NaHSO_3$ and the aqueous layer was extracted with 2 × 50 mL Et_2O. The extracts were combined, washed with aqueous $NaHCO_3$ and brine, dried over $MgSO_4$, and the solvents removed under reduced pressure. The resulting oil was distilled (Kugelrohr) at 90°C/0.7 Torr to yield 0.696 g (75%) of epoxide **4**; ir: 1745 and 1720 cm^{-1}; nmr δ: 1.1–2.0 (m, 4H), 2.3–3 (m, 5H), 3.40 (s, 2H), and 3.68 (s, 3H); ms (*a*): high resolution calcd. for $C_9H_{14}O_4$: 186.0892

amu; found: 186.0912; (*b*) *m/e* (relative intensity): 186(15), 155(21), 124(15), 117(15), 116(21), 113(25), 101(100), 74(28), 69(50), 59(57), 55(61), 43(57), and 41(71).

*Cyclization of Epoxide **4** to Ketal **5***

A solution of 0.093 g (0.50 mmol) of ester **4** in 12 mL dry CH_2Cl_2 under N_2 was treated with 0.1 mL distilled $BF_3{\cdot}Et_2O$ and the resulting solution was stirred at room temperature for 2 h. The reaction was quenched with water and the aqueous layer was extracted several times with Et_2O. The extracts were combined, dried ($MgSO_4$), and the solvents removed under reduced pressure to yield an oil which was distilled (Kugelrohr) at 93°C/0.5 Torr to yield 0.079 g (85%) of cyclic ketal **5**; ir: 1740 cm^{-1}; nmr δ: 1.1–2.1 (m, 6H), 2.73 (s, 2H), 3.68 (s, 3H), 3.8 (m, 2H), and 4.5 (m, 1H); ms (*a*): high resolution calcd. for $C_9H_{14}O_4$: 186.0908 amu; found: 186.0889; (*b*) *m/e* (relative intensity): 186(32), 155(23), 113(13), 101(100), 87(23), 74(15), 59(16), 57(13), and 41(11).

5-Methyl-6,8-dioxabicyclo[3.2.1]octane

A solution of 0.093 g (0.50 mmol) ester **5** in 5 mL MeOH and 3 mL of 50% KOH was refluxed for 3 h. This solution was acidified with dilute HCl and extracted several times with ether. The extracts were combined and worked up as above to give 0.075 g (87%) of the acid, mp 77–79°C. The crude acid (0.026 g, 0.15 mmol) was placed in a small Kugelrohr tube which was then inserted into a preheated (220°C) Kugelrohr oven. The chromatographically pure 5-methyl-6,8-dioxabicyclo[3.2.1]octane, distilled within 8 min at that temperature and 1 atm. A total of 0.0192 g (84%) of product was obtained; ir: 2990, 1390, 1015, and 840 cm^{-1}; nmr δ: 1.41 (s, 3H), 1.3–2 (m, 6H), 3.8 (m, 2H), and 4.5 (m, 1H); ms (*a*): high resolution calcd. for $C_7H_{12}O_2$: 128.0837 amu; found: 128.0837; (*b*) *m/e* (relative intensity): 128(30), 100(15), 86(24), 68(12), 58(18), 47(14), 43(100), and 41(16).

*Z-1-Bromo-3-hexene (**9**A)*

The dianion of 3-butyn-1-ol, prepared using $LiNH_2$ in liquid NH_3, was alkylated with ethyl bromide to give 3-hexyn-1-ol in ca. 75% yield. A mixture of 4.16 g (41 mmol) of 3-hexyn-1-ol, 0.2 g of 5% Pd-on-$BaSO_4$, and 3 drops of freshly distilled quinoline in 50 mL MeOH was hydrogenated at atmospheric pressure. After 2 h the hydrogenation was stopped and the MeOH was removed under reduced pressure. The crude product was dissolved in Et_2O, washed with dilute HCl, and distilled to yield 3.4 g (82%) of *Z*-3-hexen-1-ol, bp 74°C/15 Torr.

A solution of 8.5 g of *Z*-3-hexen-1-ol in 10 mL anhydrous Et_2O was added dropwise to a cooled (−30°C) mixture of 7.6 g of PBr_3 and 0.43 g of pyridine in 40 mL of Et_2O. The reaction mixture was stirred at −30°C for 1 h, and then at room temperature for 5 h. The reaction was quenched with ice and water, and the aqueous layer was extracted several times with Et_2O. The extracts were combined, washed with 5% $NaHCO_3$, then brine, dried ($MgSO_4$), filtered, and the solvent removed under reduced pressure. This product was distilled at 65°C/15 Torr to yield 6.3 g (46%) of *Z*-1-bromo-3-hexene (**9***A*) (17); ir: 3000, 2910, and 1265 cm^{-1}; nmr δ: 0.98 (t, J = 7 Hz, 3H), 2.03 (qn, J = 7 Hz, 2H), 2.63 (q, J = 7 Hz, 2H), 3.32 (t, J = 7 Hz, 2H), and 5–5.75 (sym. m, 2H); ms *m/e* (relative intensity): 164(25), 162(25), 83(88), 82(31), 68(25), 67(33), 55(100), and 41(89).

E-*1-Bromo-3-hexene (**9**B)*

A solution of 9.8 g (0.10 mol) of 3-hexyn-1-ol, prepared as above, in 50 mL anhydrous Et_2O was added dropwise to a solution of 8.81 g of sodium in 500 mL ammonia. The reaction was stirred at −35°C for 4 h, quenched with 12 g of NH_4Cl, and the ammonia was allowed to evaporate. The residue was treated with 250 mL of ice cold water and the aqueous layer was extracted with 4 × 300 mL Et_2O. The extracts were combined and worked up to yield 8.7 g (87%) of *E*-3-hexen-1-ol which distilled at 72–74°C/15 Torr. This alcohol (6.0 g, 0.060 mol) was converted into 5.4 g (56%) of *E*-1-bromo-3-hexene (**9***B*) (18) as above; bp 78–80°C/15 Torr; ir: 3000, 2925, and 970 cm^{-1}; nmr δ: 0.98 (t, J = 7 Hz, 3H), 1.7–2.7 (m, 4H), 3.2–3.7 (m, 2H), and 5–5.8 (m, 2H); ms *m/e* (relative intensity): 164(21), 162(22), 83(77), 82(38), 69(28), 67(38), 55(81), and 41(100).

*4-Bromo-2-methyl-1-butene (**9**C)*

2-Methyl-1-buten-4-ol (1.4 g, 16 mmol) was converted into 1.0 g (42%) of bromide **9***C* (19) as above and Kugelrohr distilled at 105°C/760 Torr.

*Alkylation of the Dianion of Methyl Acetoacetate with Bromide **9***

A solution of the dianion from 0.35 g (3.0 mmol) of methyl acetoacetate was generated (6) in THF and alkylated with a solution of 0.52 g (3.2 mmol) of *Z*-1-bromo-3-hexene (**9***A*) in ½ mL THF at 0°C. The reaction mixture was stirred at 0°C for 2 h and at room temperature for an additional 3 h. It was then quenched with dilute HCl, and extracted several times with ether. The extracts were combined and worked up to yield 0.52 g (88%) of methyl *Z*-3-oxo-7-decenoate which distilled (Kugelrohr) at 70°C/0.8 Torr; ir: 1745, 1715, 1650, and 1630 cm^{-1}; nmr δ: 0.96 (t, J = 7 Hz, 3H), 1.4–2.2 (m, 6H), 2.53 (t, J = 7 Hz, 2H), 3.41 (s, 2H), 3.72 (s, 3H), and 4.9–5.5 (m, 2H); ms *m/e* (relative intensity): 198(10), 180(25), 129(22), 117(22), 116(100), 101(22), 82(84), 67(68), 55(41), and 41(46). *Anal.* calcd. for $C_{11}H_{18}O_3$: C 66.64, H 9.15; found: C 66.56, H 9.24.

In a similar manner 2.32 g (0.020 mol) of methyl acetoacetate was converted into 3.27 g (83%) of methyl *E*-3-oxo-7-decenoate which distilled (Kugelrohr) at 81°C/0.1 Torr; ir: 1745, 1720, 1660, 1630, and 970 cm^{-1}; nmr δ: 0.94 (t, J = 7 Hz, 3H), 1.2–2.1 (m, 6H), 2.48 (t, J = 7 Hz, 2H), 3.39 (s, 2H), 3.70 (s, 3H), and 5.2–5.4 (m, 2H); ms *m/e* (relative intensity): 198(32), 180(32), 125(21), 117(21), 116(100), 101(30), 82(83), 67(65), and 55(21). *Anal.* calcd. for $C_{11}H_{18}O_3$: C 66.64, H 9.15; found: C 66.65, H 9.05.

Methyl 7-methyl-3-oxo-7-octenoate was prepared as above in 83% yield. The product, bp 75°C/0.3 Torr, was characterized by ir: 1745, 1715, 1650, 1635, and 890 cm^{-1}; nmr δ: 1.69 (s, 3H), 1.6–2.1 (m, 4H), 2.49 (t, J = 7 Hz, 2H), 3.40 (s, 2H), 3.70 (s, 3H), and 4.65 (m, 2H); ms *m/e* (relative intensity): 184(24), 166(18), 129(37), 117(34), 116(75), 111(35), 101(37), 74(100), 69(58), 68(56), 59(42), 55(77), 43(87), and 41(57). *Anal.* calcd. for $C_{10}H_{16}O_3$: C 65.19, H 8.75; found: C 65.20, H 8.75.

*Epoxidation of Alkenes to Produce **10***

A solution of 0.198 g (1.0 mmol) of methyl *Z*-3-oxo-7-decenoate, from above, in 6 mL dry CH_2Cl_2 was cooled to ca. 14°C and treated with 0.236 g (1.3 mmol) of *m*-chloroperbenzoic acid and 0.213 g (1.5 mmol) of anhydrous NaH_2PO_4. The reaction mixture was stirred at room temperature for 9 h and then quenched with saturated $NaHSO_3$. The aqueous layer was extracted with 2 × 25 mL Et_2O; the extracts were combined, washed with $NaHCO_3$, and worked up to yield 0.185 g (87%) of epoxide **10***A* which was homogeneous by tlc. The epoxide **10***A* distilled (Kugelrohr) at 93°C/0.15 Torr and was characterized by the following spectral data: ir: 1745 and 1715 cm^{-1}; nmr δ: 1.02 (t, J = 7 Hz, 3H), 1.3–2 (m, 6H), 2.5–3.1 (m, 4H), 3.42 (s, 2H), and 3.70 (s, 3H); ms *m/e* (relative intensity): 214(15), 159(21), 156(57), 141(25), 139(41), 124(100),

116(37), 101(55), 97(71), 96(69), 83(55), 69(52), 59(52), 57(60), 55(72), 43(78), and 41(77). *Anal.* calcd. for $C_{11}H_{18}O_4$: C 61.66, H 8.47; found: C 61.38, H 8.25.

In a similar fashion 1.78 g (9.0 mmol) of methyl *E*-3-oxo-7-decenoate was epoxidized in 87% yield to give **10***B* which was distilled (Kugelrohr) at 96°C/0.1 Torr; ir: 1745 and 1720 cm^{-1}; nmr δ: 0.98 (t, J = 7 Hz, 3H), 1.2–2 (m, 6H), 2.35–2.7 (m, 4H), 3.43 (s, 2H), and 3.72 (s, 3H); ms *m/e* (relative intensity): 214(16), 184(20), 156(56), 141(22), 124(100), 116(59), 114(45), 113(44), 101(91), 97(68), 96(76), 59(51), 57(51), 55(67), 43(66), and 41(66). *Anal.* calcd. for $C_{11}H_{18}O_4$: C 61.66, H 8.47; found: C 61.38, H 8.57.

Epoxide **10***C* was also prepared as above in 86% yield and it was found to distill (Kugelrohr) at 95°C/0.7 Torr; ir: 1745 and 1720 cm^{-1}; nmr δ: 1.30 (s, 3H), 1.5–1.8 (m, 4H), 2.53 (s, 2H), 2.55 (t, J = 7 Hz, 2H), 3.39 (s, 2H), and 3.68 (s, 3H); ms (*a*): high resolution calcd. for $C_{10}H_{16}O_4$: 200.1042 amu; found: 200.1035; (*b*) low resolution *m/e* (relative intensity): 200(13), 170(17), 169(25), 164(20), 129(28), 127(30), 111(54), 101(65), 85(49), 81(42), 72(47), 69(40), 59(44), 55(68), 43(100), and 41(50).

*Cyclization of Epoxides **10** to Bicyclic Ketals **11***

Four drops of distilled $BF_3{\cdot}Et_2O$ were added to a solution of 0.072 g (0.33 mmol) of epoxide **10***A* in 2 mL dry CH_2Cl_2. This reaction mixture was stirred under N_2 at room temperature for 2 h, then quenched with water, and the aqueous phase was extracted with 3 × 15 mL Et_2O. The extracts were combined and worked up to yield 0.066 g (92%) of **11***A* which distilled (Kugelrohr) at 90°C/0.15 Torr for analysis. The crude material was homogeneous by tlc and had the following spectral data: ir: 1740 cm^{-1}; nmr δ: 0.89 (t, J = 7 Hz, 3H), 1.3–2.0 (m, 8H), 2.71 (s, 2H), 3.67 (s, 3H), 3.91 (t, J = 6 Hz, 1H), and 4.15 (bs, 1H); ms *m/e* (relative intensity): 214(10), 183(15), 141(9), 124(10), 115(10), 114(100), 101(31), 85(50), 68(19), 59(17), 57(15), and 41(18). *Anal.* calcd. for $C_{11}H_{18}O_4$: C 61.66, H 8.47; found: C 61.54, H 8.35.

In a similar fashion 1.28 g (6.0 mmol) of epoxide **10***B* was cyclized to 1.17 g (91%) of bicyclic ketal **11***B* which was distilled (Kugelrohr) at 96°C/0.1 Torr; ir: 1740 cm^{-1}; nmr δ: 0.97 (t, J = 7 Hz, 3H), 1.2–2 (m, 8H), 2.73 (s, 2H), 3.68 (s, 3H), 3.7–4.1 (m, 1H), and 4.1–4.3 (m, 1H); ms *m/e* (relative intensity): 214(26), 196(31), 184(47), 156(75), 141(33), 124(66), 114(61), 113(53), 101(100), 96(61), 85(55), 68(59), 59(54), and 41(51). *Anal.* calcd. for $C_{11}H_{18}O_4$: C 61.66, H 8.47; found: C 61.36, H 8.29.

Finally, 0.080 g (0.40 mmol) of epoxide **10***C* was cyclized under the above conditions to yield 0.076 g (95%) of ketal **11***C* which was Kugelrohr distilled at 90°C/0.1 Torr; ir: 1740 cm^{-1}; nmr δ: 1.32 (s, 3H), 1.5–1.9 (m, 6H), 2.72 (s, 2H), 3.40 (d, J = 7 Hz, 1H), 3.66 (s, 3H), and 3.88 (d, J = 7 Hz, 1H); ms *m/e* (relative intensity): 200(32), 169(29), 111(15), 101(59), 100(100), 72(70), and 43(59). *Anal.* calcd. for $C_{10}H_{16}O_4$: C 59.98, H 8.05; found: C 59.86, H 7.96.

*Hydrolysis of Esters **11** to Acids **12***

A solution of 0.214 g (1.0 mmol) of ester **11***A* in 5 mL MeOH and 6 mL 50% aqueous KOH was refluxed for 3 h, then cooled, acidified with aqueous HCl, and extracted several times with Et_2O. The extracts were combined and worked up to yield 0.189 g (95%) of acid **12***A*. The crude material was used directly in the decarboxylation and this acid was characterized by the following data: ir: 2400–3400, 1750, 1715 cm^{-1}; nmr δ: 0.90 (t, J = 7 Hz, 3H), 1.3–2.2 (m, 8H), 2.77 (s, 2H), 3.97 (t, J = 6 Hz, 1H), 4.18 (bs, 1H), and 9.72 (bs, 1H); ms (*a*): high resolution calcd. for $C_{10}H_{16}O_4$: 200.1049 amu; found: 200.1049; (*b*) low resolution *m/e* (relative intensity): 200(3), 124(11), 114(100), 87(26), 85(82), 68(28), 57(25), and 43(25).

The ester **11***B* (0.107 g, 0.50 mmol) was hydrolyzed in a similar fashion to yield 0.095 g (95%) of acid **12***B*; ir: 2400–3500, 1765, 1715 cm^{-1}; nmr δ: 0.98 (t, J = 7 Hz, 3H), 1.2–2.1 (m, 8H), 2.77 (s, 2H), 3.8–4.15 (m, 1H), 4.26 (bs, 1H), and 8.6 (bs, 1H); ms (*a*): high resolution calcd. for $C_{10}H_{16}O_4$: 200.1049 amu; found: 200.1045; (*b*) low resolution *m/e* (relative intensity): 200(3), 192(14), 156(21), 149(14), 142(14), 124(12), 114(36), 98(45), 71(26), 57(25), 44(47), 43(100), and 41(29).

The ester **11***C* (0.030 g, 0.15 mmol) was hydrolyzed as above to yield 0.025 g (88%) of acid **12***C*; ir: 2400–3600, 1755, 1715 cm^{-1}; nmr δ: 1.34 (s, 3H), 1.5–1.9 (m, 6H), 2.78 (s, 2H), 3.48 (d, J = 7 Hz, 1H), 3.95 (d, J = 7 Hz, 1H), and 9.52 (bs, 1H); ms (*a*): high resolution calcd. for $C_9H_{14}O_4$: 186.0892 amu; found: 186.0895; (*b*) low resolution *m/e* (relative intensity): 186(10), 156(13), 111(24), 100(100), 87(23), 72(79), and 43(42).

*Decarboxylation of Acids **12***

exo-*Brevicomin (**13**A)*

The crude acid **12***A* (0.100 g, 0.50 mmol) was placed in a Kugelrohr tube and inserted into a preheated (220°C) Kugelrohr oven. A colourless oil distilled within 8 min at atmospheric pressure to yield 0.068 g (87%) of *exo*-brevicomin (**13***A*) which had spectral data identical to that reported for **13***A* (8, 10).

endo-*Brevicomin (**13**B)*

In a similar fashion 0.060 g (0.30 mmol) of carboxylic acid **12***B* was decarboxylated to yield 0.040 g (85%) of *endo*-brevicomin (**13***B*) which had spectral data identical to that reported for **13***B* (10).

*Frontalin (**13**C)*

Finally 0.019 g (0.10 mmol) of crude acid **12***C* was decarboxylated to yield 0.012 g (85%) of frontalin (**13***C*) which had spectral data identical to that reported for **13***C* (11).

*Resolution of Carboxylic Acid **12**A*

A solution of 0.400 g (2.0 mmol) of carboxylic acid **12***A* in 10 mL dry CH_2Cl_2 was treated with 0.242 g (2.0 mmol) of (+)-α-methylbenzylamine. The mixture was stirred at room temperature and the solvent removed. The resulting solid was recrystallized from ether–hexane. After two such recrystallizations 0.180 g of salt, mp 110–115°C, was obtained. This salt was dissolved in 10% aqueous HCl and extracted several times with ether. The extracts were combined and worked up to yield 0.100 g of partially resolved **12***A*, $[\alpha]_D^{25}$ + 39.8° (0.20 g/mL, Et_2O). This acid (0.100 g) was decarboxylated as above to yield 0.060 g of (+)-*exo*-brevicomin, $[\alpha]_D^{26}$ +52° (0.12 g/mL, Et_2O).

Acknowledgements

We are grateful to the National Research Council of Canada and the University of British Columbia for financial support of this work.

1. P. E. Sum and L. Weiler. Can. J. Chem. **56**, 2301 (1978).
2. G. R. Rickards. M.Sc. Thesis, University of British Columbia, Vancouver, B.C. 1977.
3. (*a*) J. Martel, E. Toromanoff, J. Mathieu, and G. Nomine. Tetrahedron Lett. 1491 (1972); (*b*) K. Kondo, T. Umemoto, Y. Takahataka, and D. Tunemoto. Tetrahedron Lett. 113 (1977); (*c*) D. F. Taber. J. Am. Chem. Soc. **99**, 3513 (1977); (*d*) J. Buendia and M. Vivat. Ger. Patent No. 2,657,347; Chem. Abstr. **87**, 117633 (1977); (*e*) J.

BUENDIA and J. SCHALBAR. Ger. Patent No. 2,653,604; Chem. Abstr. **87**, 151759 (1977).
4. (*a*) J. F. KINGSTON and L. WEILER. Can. J. Chem. **55**, 785 (1977); (*b*) J. F. KINGSTON. Ph.D. Thesis, University of British Columbia, Vancouver, B.C. 1974.
5. R. W. SKEEAN, G. L. TRAMMELL, and J. D. WHITE. Tetrahedron Lett. 525 (1976).
6. (*a*) S. N. HUCKIN and L. WEILER. J. Am. Chem. Soc. **96**, 1082 (1974); (*b*) L. WEILER. J. Am. Chem. Soc. **92**, 6702 (1970).
7. B. P. MUNDY, K. B. LIPKOWITZ, and G. W. DIRKS. Heterocycles, **6**, 51 (1977).
8. R. M. SILVERSTEIN, R. G. BROWNLEE, T. E. BELLAS, D. L. WOOD, and L. E. BROWNE. Science, **159**, 889 (1968).
9. G. W. KINZER, A. F. FENTIMAN, JR., T. F. PAGE, JR., R. L. FOLTZ, J. P. VITÉ, and G. B. PITMAN. Nature, **221**, 477 (1969).
10. (*a*) H. H. WASSERMAN and E. H. BARBER. J. Am. Chem. Soc. **91**, 3674 (1969); (*b*) T. E. BELLAS, R. G. BROWNLEE, and R. M. SILVERSTEIN. Tetrahedron, **25**, 5149 (1969); (*c*) J. KNOLLE and H. J. SCHAFER. Angew. Chem. Int. Ed. Engl. **14**, 758 (1975); (*d*) K. MORI. Tetrahedron, **30**, 4223 (1974); (*e*) P. J. KOCIENSKI and R. W. OSTROW. J. Org. Chem. **41**, 398 (1976); (*f*) K. B. LIPKOWITZ and B. P. MUNDY. J. Org. Chem. **41**, 373 (1976); (*g*) N. T. BYROM, R. GRIGG, and B. KONGKATHIP. J. Chem. Soc. Chem. Commun. 216 (1976); (*h*) J. L. COKE, H. J. WILLIAMS, and S. NATARAJAN. J. Org. Chem. **42**, 2380 (1977); (*i*) H. H. MEYER. Justus Liebigs Ann. Chem. 732 (1977).
11. (*a*) B. P. MUNDY, R. P. OTZENBERGER, and A. R. DEBERNARDIS. J. Org. Chem. **36**, 2390 (1971); (*b*) K. MORI. Tetrahedron, **31**, 1381 (1975); (*c*) D. R. HICKS and B. FRASER-REID. J. Chem. Soc. Chem. Commun. 869 (1976); (*d*) H. OHRUI and S. EMOTO. Agric. Biol. Chem. **40**, 2267 (1976); (*e*) P. D. MAGNUS and G. ROY. J. Chem. Soc. Chem. Commun. 297 (1978).
12. (*a*) J. P. VITÉ. Naturwissenschaften, **63**, 550 (1976); (*b*) D. L. WOOD and W. D. BEDARD. Proceedings of XVth International Congress of Entomologists, Washington, DC. 1976. pp. 643–652.
13. R. S. ATKINSON and J. E. MILLER. J. Chem. Soc. Chem. Commun. 35 (1977).
14. O. L. CHAPMAN, K. C. MATTES, R. S. SHERIDAN, and J. A. KLUN. J. Am. Chem. Soc. **100**, 4878 (1978).
15. A. W. INGERSOLL. Organic Syntheses. Coll. Vol. II. John Wiley and Sons, New York, NY. 1943. p. 506.
16. A. AULT. Organic Syntheses. Coll. Vol. V. John Wiley and Sons, New York, NY. 1973. p. 932.
17. H. STETTER and H. KUHLMANN. Synthesis, 379 (1975).
18. M. JULIA, S. JULIA, and T. S. YU. Bull. Soc. Chim. Fr. 1849 (1961).
19. A. MAERCKER and K. WEBER. Justus Liebigs Ann. Chem. **756**, 43 (1972).

Strong hydrogen bonding in oxime solvates of tetra-*n*-butylammonium fluoride

JAMES H. CLARK[1]

Department of Chemistry, University of Exeter, Exeter EX4 4QD, England

Received November 1, 1978

JAMES H. CLARK. Can. J. Chem. 57, 1481 (1979).

Four stable, crystalline oxime solvates of tetra-*n*-butylammonium fluoride have been prepared, characterised, and studied by ^1H, ^{13}C, and ^{19}F nmr, infrared, and ultraviolet spectroscopy. All of the complexes crystallise from solution as the disolvates, $Bu_4NF(oxime)_2$. The spectroscopic changes accompanying solvate formation are interpreted on the basis of strong hydrogen bonding between the fluoride anion and the oxime hydroxyl.

JAMES H. CLARK. Can. J. Chem. 57, 1481 (1979).

Quatre produits de solvatation stables et cristallins d'oxime par le fluorure de tétra *n*-butylammonium ont pu être préparés, caractérisés et étudiés par rmn. ^1H, ^{13}C et ^{19}F et par spectroscopies infrarouge et ultraviolette. Tous les complexes cristallisent de la solution sous forme de produits de double solvatation $Bu_4NF(oxime)_2$. On a interprété les changements spectroscopiques qui accompagnent la formation des produits de solvatation sur la base d'une liaison hydrogène importante entre l'anion fluorure et l'hydroxyle de l'oxime.

[Traduit par le journal]

In recent years, a number of complexes of the type $AH\cdots B^-$ where AH is an electron acceptor hydrogen bonded to an electron donor anion B^-, have been studied by a wide variety of spectroscopic and nonspectroscopic techniques (1–6). When AH is a strong H-bond electron acceptor such as a carboxylic acid or phenol and B a strong H-bond electron donor such as a small halide or carboxylate anion, the resulting complex is unusually stable and the spectroscopic and nonspectroscopic manifestations of H-bonding are exaggerated providing the opportunity for more detailed and more informative investigations of the H-bonding phenomenon.

This article describes the preparation and study of four novel AHB^- H-bonded complexes of the type $Bu_4N^+F^-\cdots(HON{:}CR^1R^2)_2$ (**1** to **4**). The four oximes selected represent examples of (*a*) a saturated oxime (**4**); (*b*) an aromatic oxime (**3**); (*c*) an aromatic oxime containing an additional H-bond electron acceptor site (**2**); and (*d*) a nonaromatic oxime containing a conjugated double bond system and an H-bond electron donor site (**1**). The solvates are good candidates for H-bonding investigations in that they are reasonably air-stable and may be recrystallised unchanged from aprotic solvents.

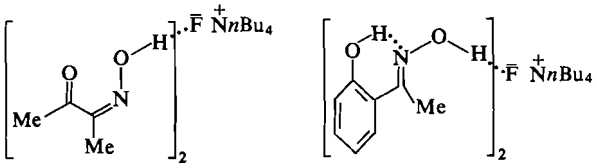

1

2

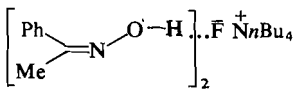

3

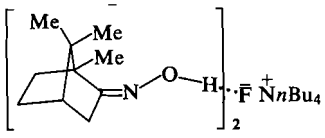

4

Experimental

^1H nmr spectra were recorded on JEOL MH-100 (100 MHz) and Perkin Elmer R10 (60 MHz) spectrometers. Variable temperature ^1H nmr spectra were recorded on the JEOL MH-100. ^{13}C nmr spectra were recorded on a JEOL JNM PS-100 spectrometer operating at 25.15 MHz using ca. 0.5 *m* solutions and Me_4Si as internal standard. ^{19}F nmr spectra were recorded on a JEOL JNM PS-100 spectrometer operating at 94.1 MHz using ca. 0.5 *m* solutions (MeCN). The ^{19}F nmr spectra were referenced to a separate sample of C_6F_6 and the chemical shifts quoted here are therefore, approximate. Addition of C_6F_6 to the sample solutions resulted in changes in sample colour and in the sample spectra (see later). Infrared spectra were recorded on a Perkin Elmer 357 spectrometer. Solid samples were run as Nujol and hexachlorobutadiene mulls and as evaporated thin films on NaCl discs. Ultraviolet spectra were run on Unicam SP1800 and Perkin Elmer 402 spectrophotometers; all samples were run in acetonitrile solution and those containing fluoride were prepared by vigorously shaking the oxime–MeCN solution with a labile Drifluor reagent (see later) followed by filtration. Melting points were recorded on a Mettler FP5 digital temperature read-out using a Mettler FP52 hot stage and are uncorrected.

Tetra-*n*-butylammonium fluoride was prepared by neutralisation of the commercial hydroxide (40% aqueous) with 40% hydrofluoric acid. Acetophenoxime (mp 58°C) and 2-hydroxyacetophenoxime (mp 116.5°C) were prepared from the

[1]Present address: Department of Chemistry, University of York, Heslington, York YO1 5DD, England.

0008-4042/79/121481-07$01.00/0

respective ketones by reaction with hydroxylamine (from the hydrochloride + NaOH) in aqueous ethanol; the reaction mixtures were poured into cold dilute hydrochloric acid, filtered, and the solids recrystallised from benzene – petroleum ether. *dl*-Camphoroxime and 2,3-butanedionemonoxime were commercial samples recrystallised from benzene – petroleum ether before use. The purified oximes gave the following nmr characteristics. 2,3-Butanedionemonoxime: δ_H 10.20 (1H, s, OH), 2.49 (3H, s, MeCO) and 2.07 ppm (3H, s, MeCN—); δ_C 198.0 (C=O), 157.1 (C=N), 25.1 (*Me*CO), and 8.1 ppm (*Me*CN—). 2-Hydroxyacetophenoxime: δ_H 11.98 (1H, s, OH), 8.74 (1H, s, br, OH), ca. 7.1 (2H, m, ring CH), ca. 6.9 (2H, m, ring CH), and 2.29 ppm (3H, s, Me); δ_C 159.3 (C—OH), 157.1 (C=N), 130.7, 127.6, 119.4, 118.7, 117.1 (ring carbons), and 10.7 ppm (Me). Acetophenoxime: δ_H 10.04 (1H, s, OH), ca. 7.6 (2H, m, ring CH), 7.36 (3H, m, ring CH), and 2.33 ppm (3H, s, Me); δ_C 155.9 (C=N), 136.4, 129.2, 128.4, 126.0 (ring carbons), and 12.4 ppm (Me). *dl*-Camphoroxime: δ_H 9.47 (1H, s, OH), 2.55 (1H, 2 × tr, CH), ca. 1.9–1.1 (6H, m, $3CH_2$), 1.04 (3H, s, Me), 0.95 (3H, s, Me), and 0.83 ppm (3H, s, Me); δ_C 169.6 (C=N), 51.8, 48.3, 43.7, 33.1, 32.7, 27.3, 19.5, 18.6, and 11.1 ppm.

Labile Difluor reagents were prepared by treating chromatographic grade acidic alumina or commercial porous glass beads (10 g) with 20% aqueous tetra-*n*-butylammonium fluoride (20 g) followed by evaporation under reduced pressure to constant weight (14 g; 1 g ≡ 1 mmol $\overline{F}$).

All other materials were commercial products and were purified, where necessary, by normal methods.

*Preparation of Tetra-*n*-butylammonium Fluoride – 2,3-Butanedionemonoxime Disolvate (1)*

2,3-Butanedionemonoxime (0.011 mol in 20 g tetrahydrofuran) was added to a concentrated aqueous solution of tetra-*n*-butylammonium fluoride (0.01 mol) and the mixture was slowly evaporated with stirring, at ca. 50°C under reduced pressure until no further ebullition occurred. The mixture was then cooled in ice to provide a solid which was washed with cold ether and recrystallised from a little *N,N*-dimethylformamide, washed with ether, and dried at 0.1 Torr (30°C) to give fine colourless crystals of the disolvate **1** (1.95 g, 0.0042 mol, 76%), mp 80.0–80.6°C; δ_H 14.06 (2H, s, OH, concentration dependent), ca. 3.3 (8H, m, CH_2N), 2.34 (6H, s, MeCO) 1.88 (6H, s, MeCN—), ca. 1.5 (16H, m, $—(CH_2)_2—$) and 0.99 ppm (12H, tr, Me). On standing for ca. 1 week, the $CDCl_3$ solution showed the OH peak reduced to $<\frac{1}{2}$ of its original intensity and broadened; a strong peak at δ 7.3 ppm (> 2H, s, $CHCl_3$) and the peak at 2.34 weakened and overlapping with a new peak at δ 2.32 (tr, J = 2.4 Hz, CH_2D—); δ_C 198.5 (C=O), 154.5 (C=N), 58.6 (CH_2N), 24.8 (*Me*CO), 23.9 ($—CH_2—$), 19.7 (CH_2Me), 13.6 ($MeCH_2$), and 7.8 (*Me*CN—); δ_F (C_6F_6) 26.9 ppm (s, br). *Anal.* calcd. for $C_{24}H_{50}N_3O_4F$: C 62.2, H 10.8, N 9.1; found: C 61.7, H 9.9, N 9.0.

*Preparation of Tetra-*n*-butylammonium Fluoride – 2-Hydroxyacetophenoxime Disolvate (2)*

2-Hydroxyacetophenoxime (0.02 mol in 20 g tetrahydrofuran) was added to a concentrated aqueous solution of tetra-*n*-butylammonium fluoride (0.012 mol) and the mixture evaporated at ca. 70°C under reduced pressure (rotary evaporator) until no further ebullition occurred. The mixture was then cooled in an ice bath and washed with cold ether (2 × 100 cm^3) to give a white solid which was recrystallised from dimethylformamide (Et_2O), washed with ether, and dried at 0.1 Torr (30°C) to give the disolvate **2** (3.4 g, 0.006 mol, 60%); mp 92.3°C; δ_H 13.22 (4H, s, br, OH, concentration dependent), ca. 7.2 (4H, m, ring CH), ca. 6.8 (4H, m, ring CH), ca. 3.1 (8H, m, CH_2N), 2.24 (6H, s, MeCN—), 1.40 (16H, m, $—(CH_2)_2—$), and 0.86 ppm (12H, tr, Me). On standing for ca. 1 week, the $CDCl_3$ solution showed the OH peak reduced to $<\frac{1}{2}$ of its original intensity and broadened and a strong, new peak at δ 7.3 ppm (> 2H, s, $CHCl_3$). δ_C: 158.2 (C—OH), 155.3 (C=N), 129.0, 126.7, 119.9, 118.1, 116.7 (ring carbons), 58.1 (CH_2N), 23.7 (CH_2), 19.5 ($MeCH_2$), 13.5 ($MeCH_2$), and 10.4 ppm (*Me*CN—); δ_F (C_6F_6): 26.7 ppm (s, br). *Anal.* calcd. for $C_{32}H_{54}N_3O_4F$: C 68.2, H 9.6, N 7.4; found: C 66.0, H 9.2, N 7.1.

*Preparation of Tetra-*n*-butylammonium Fluoride – Acetophenoxime Disolvate (3)*

Acetophenoxime (0.01 mol in 20 g tetrahydrofuran) was added to a concentrated aqueous solution of tetra-*n*-butylammonium fluoride (0.01 mol) and the mixture evaporated with stirring, at 50–60°C under reduced pressure until no further ebullition occurred. Dimethylformamide (10 cm^3) was added and the solution evaporated at 60°C under reduced pressure for a further 15 min. The residue was washed with cold ether (2 × 50 cm^3) and the resulting solid recrystallised from dimethylformamide, washed with ether and dried at 0.1 Torr (30°C) to give crystals of the disolvate **3** (2.0 g, 0.0038 mol, 76%), mp 88.2°C (sample freezes on standing at this temperature and melts at 103.2–104°C; cooling and reheating the sample gives a mp of 103–104°C); δ_H (MeCN solvent): 11.1 (2H, s, br, OH, concentration dependent), 7.48 (4H, m, ring CH), 7.12 (6H, m, ring CH), 3.16 (8H, m, CH_2N), 2.12 (6H, s, Me), 1.32 (16H, m, $—(CH_2)_2—$), and 0.82 ppm (12H, tr, $MeCH_2$). The ^1H nmr spectrum in $CDCl_3$ shows no OH signal and a peak at δ 7.18 ppm (ca. 2H, s, $CHCl_3$); δ_C: 151.3 (C=N), 138.3, 128.0, 127.8, 125.5 (ring carbons), 58.1 (CH_2N), 23.8 (CH_2), 19.5 ($MeCH_2$), 13.6 ($MeCH_2$), and 11.6 ppm (*Me*CN—); δ_F (C_6F_6): 36.3 ppm (s). *Anal.* calcd. for $C_{32}H_{54}N_3O_2F$: C 72.3, H 10.1, N 7.9; found: C 72.0, H 9.9, N 7.9.

*Preparation of Tetra-*n*-butylammonium Fluoride –* dl*-Camphoroxime Disolvate (4)*

dl-Camphoroxime (0.01 mol in 20 g tetrahydrofuran) was added to concentrated aqueous tetra-*n*-butylammonium fluoride (0.01 mol) and the mixture evaporated with stirring, at 50–60°C, under reduced pressure until no further ebullition occurred. The resulting solid was recrystallised from dimethylformamide and then twice from dry diethyl ether followed by drying at 0.1 Torr (30°C) to give white needles of the disolvate **4** (1.8 g, 0.003 mol, 60%); mp 179–181°C; δ_H (MeCN solvent): ca. 11 (2H, s, br, OH, concentration dependent), 3.34 (8H, m, CH_2N), 2.48 (2H, 2 × tr, CH), ca. 1.8–1.1 (28H, m, CH_2), 1.01 (6H, s, Me), ca. 1.0 (12H, tr, $MeCH_2$), 0.93 (6H, s, Me), and 0.80 ppm (6H, s, Me). The ^1H nmr spectrum in $CDCl_3$ shows no OH peak and a new peak at δ 7.34 ppm (ca. 2H, s, $CHCl_3$); δ_C: 167.2 (C=N), 58.4 (CH_2N), 51.3, 48.1, 43.8, 33.2, 33.0, 27.4, 24.0 (CH_2CH_2N), 19.7 (Me?), 19.5 ($MeCH_2$), 18.6 (Me?), 13.8 ($MeCH_2$), and 11.4 ppm (Me?); δ_F (C_6F_6): 37.1 ppm (s). *Anal.* calcd. for $C_{36}H_{70}N_3O_2F$: C 72.6, H 11.7, N 7.1; found: C 71.7, H 11.4, N 7.1.

Results and Discussion

All of the solvates prepared crystallise from solution as the disolvates irrespective of the initial concentrations of fluoride and oxime. Attempts to synthesize crystalline monosolvates by using deliberate excesses of the fluoride were unsuccessful. This is not without precedent for fluorides since it has been reported that crystals of $KF(CH_3CO_2H)_2$ grow from $KF–CH_3CO_2H$ solutions (1). All of the disolvates are soluble in common polar aprotic

TABLE 1. Hydroxyl proton nmr chemical shifts (ppm)

1		2		3		4	
Complex[a]	Parent oxime[a]	Complex[a]	Parent oxime[a]	Complex[b]	Parent oxime[a]	Complex[b]	Parent oxime[a]
12.0[c,d]	10.20	11.1[c,d]	12.00, 8.94	11.1[c,f]	10.04	ca. 11[c,f]	9.47
13.32[e]		12.15[e]					
13.47[f]		12.36[f]					
14.06[g]		12.60[g]					

[a]$CDCl_3$ solvent.
[b]MeCN solvent.
[c]Very broad.
[d]Concentration 0.1 *m*.
[e]Concentration 0.3 *m*.
[f]Concentration 0.5 *m*.
[g]Concentration 1.0 *m*.

solvents such as dimethylformamide and acetonitrile but only **4** is soluble in diethyl ether.

Proton Magnetic Resonance Spectra

The ^1H nmr chemical shifts of the H-bonding protons of several strongly H-bonded anionic complexes have been reported (2, 4, 7). The commonly observed effect on the H-bonding proton resonance on going from the self-associated electron acceptor to the anionic complex is a deshielding (downfield shift) one which is usually assumed to reflect an increase in strength of the H-bond. The chemical shifts of the H-bonding protons of **1**–**4** along with the corresponding values for the parent oximes are summarised in Table 1. All of the hydroxyl proton signals observed (with the possible exception of the intramolecularly H-bonded phenolic proton in the parent oxime of **2**) are concentration (and temperature) dependent and although some care was taken to ensure that each pair of spectra (complex and oxime) were run at approximately the same concentration (and temperature), the results are only meant to illustrate trends and should not be considered on a strict quantitative basis.

In all cases, the H-bonding proton experiences a net deshielding effect on going to the anionic complex which presumably reflects a strengthening in the H-bond to the oxime hydroxyl. It is interesting to note that **2** shows only one hydroxyl proton signal whereas its parent oxime shows two distinct signals under the same conditions.

The most striking observation made with these spectra is that **3** and **4** do not show a hydroxyl proton signal in $CDCl_3$ but instead show a strong chloroform signal at ca. 7.2–7.3 ppm. No other changes were apparent in the spectra on going from MeCN to $CDCl_3$. This suggests that these complexes undergo rapid H–D exchange with $CDCl_3$ (eq. [1]).

[1] $$—OH\cdots\bar{F} + CDCl_3 \rightleftharpoons —OD\cdots\bar{F} + CHCl_3$$

The hydroxyl proton chemical shifts for **3** and **4** were recorded in MeCN and addition of $CDCl_3$ to these solutions was found to result in immediate loss of the OH signal and its replacement by a strong, sharp singlet at 7.2–7.3 ppm. It was also discovered that allowing **1** and **2** to stand in $CDCl_3$ over a period of several days resulted in a marked increase in intensity of the $CHCl_3$ signal while the OH signals became very weak.

Furthermore, the spectrum of **1** in $CDCl_3$, after a long period, showed a marked reduction in intensity of the *Me*CO signal and the appearance of a new triplet ($J \sim 2.4$ Hz) the central band of which is ca. 0.02 ppm upfield from the original *Me*CO signal. This is in excellent agreement with Tiers reported ^1H nmr on α-toluene-d_1 which showed a triplet ($J = 2.38$ Hz) due to $—CH_2D$ slightly upfield from that of the methyl in toluene-h_8 (8). The behaviour of **1** in $CDCl_3$ may be explained by a fluoride induced enolisation (9) of the MeCO group allowing incorporation of deuterium into the methyl group via H–D exchange at the hydroxyl group (eq. [2]).

[2] 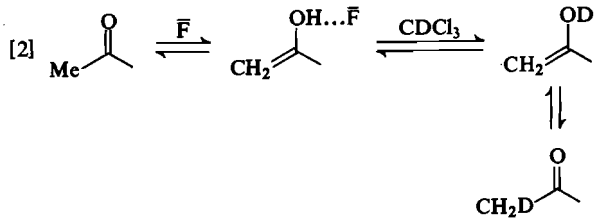

Variable temperature ^1H nmr studies on **1** and **2** in $CDCl_3$ showed little change[2] in δ(OH) whereas variable concentration studies showed an appreciable fall in δ(OH) with decreasing concentration of **1** and **2**. These changes may be readily interpreted in terms of dissociation of the complexes to free oxime and fluoride (eq. [3]).

[3] $$\bar{F}(oxime)_2 \rightleftharpoons \bar{F}(oxime) + oxime \rightleftharpoons \bar{F} + 2oxime$$

Fluorine-19 Magnetic Resonance Spectra

The ^{19}F nmr chemical shifts of **1**–**4** in MeCN solution are reported in Table 2. The values represent a large downfield shift (ca. 140–150 ppm) relative to

[2]δ(OH) remains constant to ±0.2 ppm for both complexes over the temperature range −24 to +28°C (0.1, 0.3, and 0.5 *m*).

TABLE 2. Fluorine-19 nmr chemical shifts (ppm)[a]

1	2	3	4
26.9(s,br)[b]	26.7(s,br)[b]	36.3(s)[b]	37.1(s)[b]
31.7(s)[c]	32.0(s)[c]	38.0(s)[c]	37.9(s)[c]

[a]δ (C_6F_6) = 0 ppm (external reference); MeCN solvent.
[b]Ambient temperature.
[c]−25°C.

the free fluoride ion (10, 11). An appreciable deshielding of the electron donor on formation of a strong H-bond is to be expected.

It is interesting to note that on addition of C_6F_6 to the sample solutions, the fluoride peak broadens and shifts to higher magnetic fields ($\Delta\delta$ = 1–5 ppm). In addition to this, several new peaks appear near the C_6F_6 signal. The position and complexity of the new peaks suggest that we may be observing nucleophilic attack by the oxime, the nucleophilicity of which will be enhanced by H-bonding to fluoride (6, 12, 13), on the C_6F_6. The results of a more detailed investigation on these and related systems will be reported elsewhere.

Carbon-13 Magnetic Resonance Spectra

Carbon-13 nmr offers the opportunity to observe long range effects of H-bonding in the solvates **1–4**. Among the relatively few reported spectroscopic investigations of long range effects of H-bonding, carbon-13 spin–lattice relaxation studies on H-bonded long chain alcohols (14) and chlorine-35 nuclear quadrupole resonance studies on H-bonded chlorocarboxylic acids (15) are outstanding, demonstrating the value of investigating electron structure modifications of nucleii that are not in the immediate vicinity of the H-bond.

The chemical shifts of the carbons closest to the H-bonds ($\rangle C{=}N{-}$) are given in Table 3 along with the differences in chemical shifts with respect to those of the corresponding parent oximes ($\delta(C{=}N)_{complex} - \delta(C{=}N)_{oxime}$). The observed shielding effect experienced on going from the oxime to its fluoride complex is relatively small but significant and is to be expected for a nucleus close to the H-bonding site of an associated electron acceptor. The methyl carbons α to the C=N group in **1–3** also experience a small shielding effect on fluoride solvation. Full details of the ^{13}C nmr spectra of **1–4** and of their parent oximes are given in the Experimental.

Infrared Spectra

The positions of the most important bands in the ir spectra of **1–4** and of the parent oximes are given in Table 4.

The most pronounced changes in the spectra on going from the oxime to the fluoride solvate occur in the 4000–1800 cm^{-1} region, that is, in the position of the ν_s(OH) bands. In all four cases, the broad bands centred at 3350–3200 cm^{-1} and due to the stretching vibrations of the self-associated oximes, disappear or are considerably reduced in intensity. The spectrum of **4** shows a new, very broad band at ca. 2700 cm^{-1} which represents a shift of some 900 cm^{-1} relative to the free oxime[3] (a $\Delta\nu_s$ consistent with strong anionic H-bonding (6)). In the spectra of **1–3** there are several new bands in the 2700–1800 cm^{-1} region as compared to the spectra of the parent oximes, although of these only **3** showed a pronounced new band at above 2300 cm^{-1}. These features are in line with type 1 H-bonds using Joesten and Schaads classification (16) having overlapping ν_s bands above 1800 cm^{-1} and being typical of the asymmetric double-minimum-potential function kind of H-bond. Thus, these H-bonds are apparently weaker than some other $\bar{F}\cdots H{-}O{-}$ H-bonds such as those in fluoride – carboxylic acid systems (1) and than the $\bar{O}\cdots H{-}O{-}$ H-bonds in some acid salts of very acidic oximes (17) which show broad bands below 1800 cm^{-1} and represent a vibration of a very strong H-bond characterised by a single potential function. It should also be emphasised that some of the bands above 1800 cm^{-1} may be due to overtones, combinations, or to proton transfer. The ir picture shows all possible H-bonds and contributions from $F{-}H\cdots\bar{O}$ cannot be ruled out although it does seem that significant contributions from $(F\cdots H\cdots F)^-$ can be discounted since some of its characteristic vibrations appear to be absent in all of the spectra recorded (18).

The relative intensities and positions of the two broad hydroxyl stretching bands in the spectrum of 2-hydroxyacetophenoxime suggest that the band at ca. 3340 cm^{-1} is due to intermolecular association (probably $\nu_s(OH\cdots O)$) while that under the strong ν_s(CH) band is due to intramolecular association ($\nu_s(OH\cdots N)$) (19). It is interesting to note that on going to **2**, the former band is absent while the latter band appears to be only slightly displaced. It would seem, therefore, that while the intermolecular association of this oxime is disrupted by the highly localised electron density of the fluoride anion, the intramolecular association remains intact (eq. [4]).

The absence of bands in the 2600–1700 cm^{-1} region of the spectrum of **4** is outstanding and suggests that this complex contains an H-bond of a quite different type from those in **1–3**. This may be due to the ability of **1–3** to delocalise their negative charges by way of their conjugated double bond systems, e.g., [5].

[3]A weak, sharp band at ca. 3600 cm^{-1} is visible in spectra of *dl*-camphoroxime dissolved in an inert (in an H-bonding sense) solvent and may be assigned to the hydroxyl stretching vibration of the monomeric oxime.

TABLE 3. Carbon-13 nmr chemical shifts of $\geq C{=}N-$ in **1–4** (δ_C) and changes in shifts relative to parent oximes (Δ_C)[a] (ppm)

1		**2**		**3**		**4**	
δ_C	Δ_C	δ_C	Δ_C	δ_C	Δ_C	δ_C	Δ_C
154.5	−2.5	155.3	−1.9	151.3	−4.7	167.2	−2.4

[a] $\Delta_C = (\delta(C{=}N)_{complex} - \delta(C{=}N)_{oxime})$.

TABLE 4. Characteristic ir absorption frequencies

	ν_s(OH)	ν_s(C=O)	ν_s(C=N)	ν_b(OH)[a]	ν_t(OH)	ν_s(NO)
MeCOC(:NOH)Me	3200(vs,br)	1668(vs,br)		1370(sh)	800(m)	1015(vs)
1 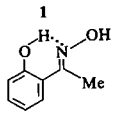	2210(s,br) 1875(vs,br)	1676(vs,br)		1378(sh)	890(m)	1040(vs)
	3340(s,br) 3100–2800[b]		1633(m)	1375(sh)	783(m)	1018(vs)
2	3050–2700[b] 2170(s,br) 1850(vs,br)		1620(sh)	1375(sh)	880(m)	1020(vs)
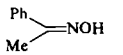	3220(s,br)			1368(sh)		927(ms) 917(ms)
3	2670(s,br) 2200(s,br) 1900(s,br)		1620(m)	1370(sh)	885(m)	938(ms)
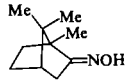	3290(vs,br)		1685(m)	1370(sh)	722(s,br)	925(s)
4	2700(vs,br)		1675(m)	1370(sh)	895(sh)	953(s) 932(s)

[a] Located by observing effect of deuteration.
[b] Under ν_s(CH); sh, shoulder.

[4] 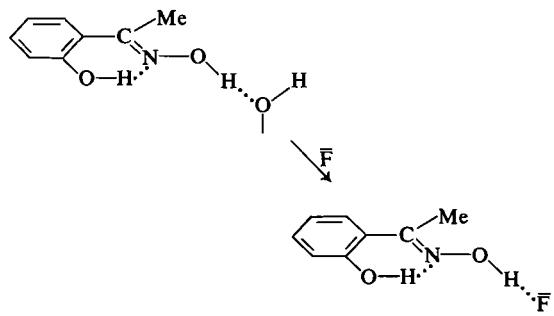

The spectral changes in the out-of-plane torsional mode ν_t, of the H-bond electron acceptor caused by H-bond formation are often quite spectacular, though rarely as pronounced as those seen with ν_s. For each of the complexes studied, one medium-strong band below 1000 cm^{-1} is at a significantly higher frequency than in the spectra of the corresponding parent oxime ($\Delta\nu_t > 90\ cm^{-1}$) and these bands are assigned to the ν_t vibrations. The positions of these bands and their movement on increasing H-bond strength are in line with previous studies on the strongly H-bonded *N*-methylpyridinium-2-aldoxime salts (20), as are the positions and small movements of the in-plane bending modes, ν_b.

[5] 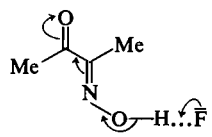

The small but significant positive frequency shifts in the ν_s(NO) bands on going from oxime to fluoride solvate are also consistent with previous studies on oximes (20) and are consistent with increased electron density on the oxygen atom due to stronger H-bonding.

It was noted earlier that solution of **3** or **4** in $CDCl_3$ appeared, by ^1H nmr, to result in deuteration of the oxime. Infrared studies on these systems confirm this observation and suggest that in dilute solution ($CDCl_3$), the complexes are largely dissociated since the position of the most intense bands (2400 cm^{-1} for **4** and 2350 cm^{-1} for **2**) are consistent with the self-associated forms ($\nu_s(OH)_{oxime}/\nu_s(OD)_{obs}$ = 1.37 for **4** and **3**). Evaporation of these solutions restores the original spectra with only weak bands due to the deuterated forms remaining. Results of a more detailed investigation of dilution effects on the ir spectra of the solvates will be reported in a later article.

Ultraviolet Spectra

Since the very low concentrations normally re-

quired for recording electronic spectra would almost certainly result in significant dissociation of the complexes, it was necessary to consider an alternative approach to obtaining information on the effect of strong anionic H-bonding on the electronic spectra of oximes. In a recent communication, a novel source of anhydrous quaternary ammonium fluoride was described where the fluoride was supported on a porous, surface hydroxylated, polymeric support such as silica gel (21). For our purposes, we required a source of anhydrous tetra-*n*-butylammonium fluoride which would be effective in an aprotic medium such as acetonitrile. We have found that while silica supported Bu_4NF loses little, if any, of its fluoride in such media, analogous reagents involving acidic alumina and finely ground porous glass beads behave as an excellent source of fluoride in acetonitrile. We have termed these reagents 'labile drifluors' in keeping with the previous nomenclature (21).

There is a paucity of reliable electronic spectroscopic data on oximes. Orenski studied a number of saturated and unsaturated oximes and concluded that while the former usually shows a strong π–π^* band near 200 mμ, the latter show their strong π–π^* band near 240 mμ (22). The one saturated oxime we have studied here, *dl*-camphoroxime, appears to show only a weak ($\varepsilon = 1.1 \times 10^2$) band at 228 mμ which undergoes considerable enhancement in intensity but only slight change in position on addition of a large excess of available fluoride ($\varepsilon \sim 10^4$, $\lambda = 231$ mμ).

Spectacular changes occur in the ultraviolet spectra of 2,3-butanedionemonoxime and 2-hydroxyacetophenoxime on addition of fluoride. The former oxime shows a strong ($\varepsilon \sim 7 \times 10^3$) π–π^* band at 225 mμ which steadily increases in intensity and in wavelength ($\lambda_{max} = 231$ mμ) on increasing the amount of available fluoride. As the fluoride concentration increases, a new band appears at 302 mμ ($\varepsilon \sim 3 \times 10^3$).

There have been numerous reports of small changes in the wavelengths of the π–π^* bands of protic species on varying the H-bond electron donor ability of the medium (23) but dramatic changes such as that observed here are less well known. The growth of the new high wavelength band presumably reflects the formation of the anionic complex. More precisely, it may well be that the new band is due to a significant contribution from the proton transfer species [6] to the H-bonded complex since it has been reported that 2-nitrosophenol shows a strong π–π^* band at ca. 300 mμ (23).

The ultraviolet absorption spectrum of 2-hydroxyacetophenoxime shows bands at 228 mμ ($\varepsilon \sim 6 \times 10^3$) and at 305 mμ ($\varepsilon \sim 3 \times 10^3$) in addition to the

[6] 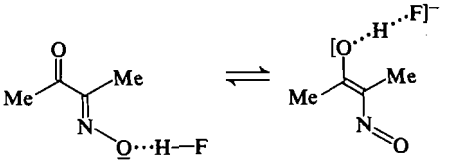

complex pattern of bands between 240 and 260 mμ characteristic of an aromatic molecule. The low wavelength band is enhanced in intensity and shifts to higher wavelength ($\lambda_{max} \sim 231$ mμ) on addition of fluoride while the band at 305 mμ does not change significantly in position or intensity and a new, broad band appears at ca. 357 mμ. In the presence of a large excess of available fluoride, the band at 357 mμ is pronounced ($\varepsilon \sim 4 \times 10^3$) and accompanied by a very broad, complex band at 245–270 mμ with a shoulder at ca. 300 mμ. The growth of the new band at 357 mμ presumably reflects the formation of the anionic complex.

Summary

The crystalline fluoride solvates **1**–**4** show spectroscopic features characteristic of strong H-bonding. The H-bonding is between the hydroxyl group of the oxime and the fluoride anion and is probably of the asymmetric double-minimum-potential function kind although complex **4** shows somewhat different infrared and solvent-stability characteristics which may be due to an absence of conjugation in this particular species. All of the complexes will exchange with $CDCl_3$ although only very slowly in the cases of **1** and **2**. Complex **1** appears to be capable of incorporating deuterium into its MeCO group via MeCO enolisation and there is further spectroscopic evidence for this complex to support the existence of contributing structures containing a C-hydroxyl group.

Acknowledgements

The author is indebted to Mr. V. Sik and Mr. E. Underwood for running many of the nmr spectra and to Professor Jack Miller for his valuable advice and encouragement which was aided by a NATO collaborative research grant (to JHC, JM, and Dr. J. Emsley).

1. J. Emsley. J. Chem. Soc. A, 2511 (1971); 2702 (1971).
2. J. H. Clark and J. Emsley. J. Chem. Soc. Dalton Trans. 2154 (1973); 1125 (1974).
3. R. P. Taylor and I. D. Kuntz. J. Phys. Chem. **74**, 4573 (1970).
4. F. Y. Fujiwara and J. S. Martin. J. Am. Chem. Soc. **96**, 7625 (1974).
5. W. Kolodziejski and Z. Kecki. J. Mol. Struct. **29**, 27 (1975).
6. J. H. Clark and J. M. Miller. J. Am. Chem. Soc. **99**, 498 (1977).

7. R. G. JONES and J. R. DYER. J. Am. Chem. Soc. **95**, 2465 (1973).
8. G. V. D. TIERS. J. Chem. Phys. **29**, 963 (1958).
9. J. H. CLARK. J. Chem. Soc. Perkin Trans. II, 1326 (1978).
10. C. DEVERELL, K. SCHAUMBURG, and H. BERNSTEIN. J. Chem. Phys. **49**, 1276 (1968).
11. G. SVENTICKIJ and G. SAVOSKINA. Jad. Magnifnyj Rezon. **3**, 85 (1969).
12. R. E. BANKS, D. R. CHOUDHURY, R. N. HASZELDINE, and C. OPPENHEIM. J. Organomet. Chem. C20 (1972).
13. J. H. CLARK and J. M. MILLER. Can. J. Chem. **56**, 141 (1978).
14. J. R. LYERIA and G. C. LEVY. *In* Topics in ^{13}C N.M.R. spectroscopy. Vol. 1. *Edited by* G. C. Levy. Wiley-Interscience, New York, NY. 1974. Chapt. 3; E. BREITMAIER, K.-H. SPOHN, and S. BERGER. Angew. Chem. Int. Ed. Engl. **14**, 144 (1975); U. EDLUND, C. HOLLOWAY, and G. C. LEVY. J. Am. Chem. Soc. **98**, 5069 (1976) and references therein.
15. J. PIETRZAK and B. NOGAJ. Acta Phys. Polon. **A52**, 77 (1977); R. J. LYNCH, T. C. WADDINGTON, T. A. O'SHEA, and J. A. S. SMITH. J. Chem. Soc. Faraday Trans. II, 1980 (1976); H. CHIHARA, A. INABA, N. NAKAMURA, and T. YAMAMOTO. J. Phys. Soc. Jpn. **35**, 1480 (1973).
16. M. D. JOESTEN and L. J. SCHAAD. Hydrogen bonding. Marcel Dekker, New York, NY. 1974.
17. D. S. JACKSON. J. Chem. Soc. B, 785 (1969).
18. R. NEWMAN and R. M. BADGER. J. Chem. Phys. **19**, 1207 (1951).
19. B. N. LASKONIN, V. V. YAKSHIN, and A. M. MIROKHIN. Dokl. Akad. Nauk SSSR, **210**, 353 (1973); Chem. Abstr. **79**, 65325k (1973).
20. R. J. MESLEY and D. F. WARDLEWORTH. Spectrochim. Acta, Part A, **26**, 1753 (1970).
21. J. H. CLARK. J. Chem. Soc. Chem. Commun. 789 (1978).
22. P. J. ORENSKI and W. D. CLOSSON. Tetrahedron Lett. 3629 (1967).
23. A. BURAWOY, M. CAIS, J. T. CHAMBERLAIN, F. LIVERSEDGE, and A. R. THOMPSON. J. Chem. Soc. 3727 (1955).

A study of trapped electrons in $LiCl/D_2O$ and other aqueous glasses at temperatures down to 2 K by radiolysis, pulse radiolysis, photolysis, and stimulated luminescence

NORMAN V. KLASSEN AND GEORGE G. TEATHER

Division of Physics, National Research Council of Canada, Ottawa, Ont., Canada K1A 0R6

AND

FERNAND KIEFFER

Laboratoire de Physico-Chimie des Rayonnements de l'Université de Paris – Sud, associé au C.N.R.S., 91405 Orsay, France

Received December 14, 1978

NORMAN V. KLASSEN, GEORGE G. TEATHER, and FERNAND KIEFFER. Can. J. Chem. **57**, 1488 (1979).

Pulse radiolysis of 9.5 *M* $LiCl/D_2O$ glass at 6 K produces both types of trapped electrons, e_{vis}^- and e_{ir}^-, just as it does at 75 K. However, going from 75 K to 6 K increases the initial yield of e_{ir}^- and decreases its decay rate, while the yield of e_{vis}^- decreases and its decay rate increases. These results are attributed to fast trap-to-trap tunnelling of e_{vis}^- from unrelaxed traps at 6 K and slower tunnelling from deeper traps at 75 K while the e_{ir}^- traps seem to relax within 100 ns even at 6 K. In 12 *M* $LiCl/D_2O$ at 4–10 K the initial e_{vis}^- band with $\lambda_{max} = 625$ nm decays considerably over minutes revealing a stable band with $\lambda_{max} = 695$ nm. The stimulation spectrum and absorption spectrum of this stable band indicate a bound–free transition of 2.0 eV and a bound–bound transition of 1.8 eV. Similar measurements of e_{vis}^- at 77 K indicate a bound–free transition of 2.6 eV and a bound–bound transition of 2.1 eV. Tryptophan was photolyzed in 9.5 *M* $LiCl/D_2O$ at 2 K to produce e_{ir}^-.

NORMAN V. KLASSEN, GEORGE G. TEATHER et FERNAND KIEFFER. Can. J. Chem. **57**, 1488 (1979).

La radiolyse pulsée de verres de $LiCl/D_2O$ 9.5 *M* à 6 K produit, comme à 75 K, les deux types d'électrons piégés, e_{vis}^- et e_{ir}^-. Cependant en passant de 75 à 6 K, on voit augmenter le rendement initial de e_{ir}^- et diminuer sa vitesse de déclin, tandis que le rendement de e_{vis}^- diminue et que sa vitesse de déclin augmente. Ces résultats sont attribués à un transfert rapide de e_{vis}^- par effet tunnel de piège à piège à partir de pièges non relaxés à 6 K et à un transfer plus lent à partir de pièges plus profonds à 75 K, tandis que les pièges de e_{ir}^- semblent être déjà relaxés avant 100 ns même à 6 K. Dans $LiCl/D_2O$ 12 *M* à 4–10 K la bande initiale de e_{vis}^-, de $\lambda_{max} = 625$ nm, décroît pendant plusieurs minutes pour laisser subsister une bande stable de $\lambda_{max} = 695$ nm. Le spectre de stimulation et le spectra d'absorption correspondant à cette bande stable indiquent une transition état lié – état non lié de 2.0 eV et une transition état lié – état lié de 1.8 eV. Des mesures semblables concernant e_{vis}^- à 77 K indiquent une transition état lié – état non lié de 2.6 eV et une transition état lié – état lié de 2.1 eV. La photolyse du tryptophan dans $LiCl/D_2O$ 9.5 *M* à 2 K conduit à la formation de e_{ir}^-.

Introduction

Recently it was found by pulse radiolysis that substantial yields of two distinct types of trapped electrons, e_{vis}^- and e_{ir}^-, are formed at low temperatures in some aqueous glasses and in both pure and doped ice crystals (1–3). The species e_{vis}^- is the oft-studied species with an optical absorption band centered around 600 nm. The species e_{ir}^- has an absorption band whose maximum has not yet been measured but has been estimated to be ~ 3600 nm in aqueous glasses and ~ 2950 nm in ice. In some aqueous glasses e_{ir}^- was not found but the formation of both e_{vis}^- and e_{ir}^- in pure ice indicates that neither species requires the presence of solutes. Two very recent studies show that in $LiCl/D_2O$ (4) and in BeF_2/D_2O (5) glasses e_{vis}^- is associated with water molecules involved in the solvation shell of the Li^+ and the Be^{2+} ions whereas e_{ir}^- is associated with free water. The production of e_{ir}^-, as well as e_{vis}^-, in aqueous glasses and ice made with H_2O (6) shows that e_{ir}^- is not restricted to D_2O matrices.

The evidence for the assignment of the infrared band to a trapped electron, e_{ir}^-, is of three types: (*a*) it was found (1, 2, 4) that the electron scavengers SeO_4^{2-}, Cu^{2+}, CrO_4^{2-}, and $(CH_3)_2CO$ both reduced the initial yield and increased the decay rate of e_{ir}^-; (*b*) in ethylene glycol/D_2O (2) and BeF_2/D_2O (5) glasses at 76 K and in D_2O ice at 4 K (7) a portion of the e_{ir}^- decays to become e_{vis}^-; (*c*) in several aqueous glasses at 77 K a luminescence is found to accompany the decay of e_{ir}^- and this luminescence has also been produced by laser photolysis of e_{vis}^- at 77 K. Presumably e_{vis}^- was photoionized by laser photolysis and, in part, retrapped as e_{ir}^- which then decayed to produce the luminescence (8, 9).

In this study we have investigated e_{vis}^- and e_{ir}^-

0008-4042/79/121488-12$01.00/0

further, primarily in $LiCl/D_2O$ glasses in which both species are produced in good yield and appear to decay independently of one another. Both radiolysis of aqueous glasses and photolysis of glasses containing tryptophan were used to produce trapped electrons. Optical absorption measurements, coupled with decay kinetics, were carried out between 2 K and 90 K on both the nanoseconds to milliseconds time scale and the minutes time scale. Spectral stimulation measurements of e_{vis}^- and e_{ir}^- were carried out between 4 K and 77 K.

Experimental

All solutions were prepared with D_2O (99.7% isotopic purity) obtained from Merck, Sharp and Dohme. Solutes were reagent grade, used without purification. Samples were deaerated with argon for the absorption measurements and by the freeze–pump–thaw method for the stimulation spectra measurements. Samples were sealed off and plunged into liquid nitrogen, or otherwise rapidly cooled, to produce a glass. Radiolysis experiments were carried out with windowless samples or with 5 mm Suprasil cells, while 1 mm Suprasil cells were used for the absorption measurements following photoionization. Stimulation spectra were measured either in 3 mm id quartz tubes or in a 0.24 mm Suprasil cell. The latter was made by inserting a 0.76 mm spacer into a 1 mm cell. The $LiCl/D_2O$ and $NaOD/D_2O$ glasses were free or almost free of cracks. The ethylene glycol/D_2O (EG/D_2O) glasses were badly cracked.

Pulse radiolysis experiments were carried out as described earlier (2, 3) with the exception that the samples were irradiated in a Janis model 8DT Super Varitemp cryostat in which the samples were cooled with a flow of cold helium gas (10). The temperature was maintained within ± 0.5 K of the desired value by a Lake Shore Cryotronics model DRC-70C temperature controller and the temperature of the sample was measured with a silicon diode sensor situated very close to the sample. Pulses, 40 ns in duration, of 35 MeV electrons were used, each pulse delivering about 12 krad. Dosimetry was done by comparing each sample to 9.5 *M* $LiCl/D_2O$ irradiated at 72–73 K for which $G\varepsilon_{650} = 1.96 \times 10^4\ M^{-1}\ cm^{-1}$ at 100 ns (4).[1] It was assumed that the electron density of 9.5 *M* $LiCl/D_2O$ glass is constant from 6 K to 90 K. Variations of dose from pulse to pulse were measured with a secondary emission monitor. Absorption measurements at 450 nm $\leq \lambda \leq$ 1000 nm were made with an EG&G SHS-100 Si photodiode, at $\lambda \leq 450$ nm with a Philips XP-1003 photomultiplier and at $\lambda \geq 1000$ nm with a Barnes A-100 room temperature InAs detector. Spectra were measured by the split light beam technique. When measuring decay kinetics over more than 1 μs an interference filter restricted the analyzing light entering the sample to the wavelength being examined. It was determined that this procedure reduced photobleaching of trapped electrons by the analyzing light to negligible proportions.

The absorption measurements made on the minutes time scale were carried out with a Cary 17 spectrophotometer. In a Cary 17 the analyzing wavelength is selected before the light passes through the sample, thus avoiding the bleaching of trapped electrons by the analyzing light. Once in the spectrophotometer, the sample was not moved during the experiment. Absorption measurements were made before and after photolysis to determine the absorption spectrum produced by photolysis. Photolysis of tryptophan was carried out with an 8 W low pressure Hg lamp and bleaching was done with a tungsten halogen lamp both of which could be inserted into the sample compartment. At all other times the sample compartment was sealed from room light. The background absorbance of the matrix for radiolyzed samples at wavelengths >800 nm was measured after complete optical bleaching of the trapped electrons. At wavelengths <800 nm a residual absorbance, probably due to Cl_2^-, defied bleaching. Therefore the background below 800 nm was assumed to be that of an unirradiated solution of 12 *M* LiCl at room temperature which has a practically flat absorption spectrum between 300 nm and 800 nm. For experiments at 2 K the sample was immersed in liquid helium cooled by pumping. Experiments at 4–10 K employed the method of cooling by helium gas.

The method of measuring stimulation spectra has already been described (11, 12). The sample was held in an Oxford Instruments optical cryostat and immersed in liquid helium for studies at 4 K and immersed in liquid nitrogen for 77 K. Intermediate temperatures were obtained by cooling with cold helium gas. The phosphorescence intensity was measured with a photomultiplier using the full phosphorescence emission without any wavelength filtering.

Results and Discussion

Production of e_{vis}^- and e_{ir}^- by Tryptophan Photolysis at 2 K

We wished to find a system in which e_{ir}^- could be easily produced by methods other than radiolysis and in which e_{ir}^- could be studied on the minutes time scale. The system chosen was 9.5 *M* $LiCl/D_2O/5 \times 10^{-4}$ *M* L-tryptophan at 2 K. A 5 min uv photolysis of this glass produced spectrum *A* of Fig. 1, with an absorbance at 2500 nm typically in the range 0.1 to 0.2. Several minutes were needed to measure a complete spectrum during which time a small amount of isothermal decay occurred. Corrections were made for this decay on the basis of several consecutive spectral determinations. Spectra *A*, *B*, *C*, and *D* of Fig. 1 all represent spectra corrected to 1 min after the end of photolysis.

The uv photolysis of L-tryptophan (tryp) has been studied in several aqueous glasses at 77 K (13). When tryp was photoionized at 77 K in 9 *M* $LiCl/H_2O$ glass, both the tryptophan cation ($tryp^+$) with absorption maxima at 615, 560, and 340 nm (13) and e_{vis}^-, whose absorption maximum is known to be 590 nm (14), were produced. Our pulse radiolysis experiments with 9.5 *M* LiCl at 6 K indicate the likelihood of a very small yield of e_{vis}^- relative to that of e_{ir}^- when measured on the minutes time scale at 2 K. Thus spectrum *A* with λ_{max} at 330, 564, and 620 nm seems to be satisfactorily accounted for by $tryp^+$ and e_{vis}^-. There is no sign of the tryptophan

[1]Measurements made with a more precise instrument now lead us to believe that the temperature stated to be 76 K in refs. 1–4 was actually 72–73 K.

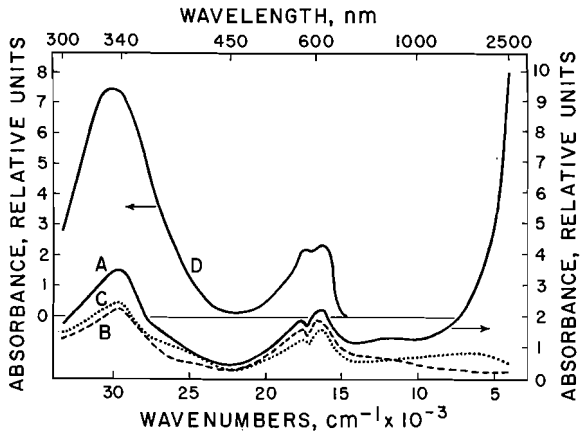

FIG. 1. Spectra *A*, *B*, and *C* were obtained at 2 K from a single sample prepared from an argon bubbled solution of 9.5 *M* LiCl/D_2O containing 5×10^{-4} *M* L-tryptophan. Spectrum *A* represents the absorption spectrum following a 5 min uv photolysis. Spectrum *B* shows the effect on *A* of partial bleaching with infrared light. Spectrum *C* shows the effect on *B* of partial bleaching with the full light of a projector lamp. Spectra *A*, *B*, and *C* are all plotted on the same relative absorbance scale and are corrected to correspond to 1 min after the end of photolysis, using kinetic data such as shown in Fig. 2. Spectrum *D*, on a different relative absorbance scale, represents the spectrum a few minutes after a 5 min photolysis of a glass prepared from a similar solution saturated with N_2O.

radical ($\lambda_{max} = 320$ and 500 nm) (15) nor the triplet state of tryptophan ($\lambda_{max} \sim 460$ nm) (16). We cannot discount the possibility of a small contribution of the tryptophan anion ($tryp^-$) ($\lambda_{max} \sim 350$ nm) (16). In addition, there is an intense infrared absorption. Above 1300 nm this absorption has a shape identical to that of e_{ir}^- as presented in ref. 2. This is further, strong evidence that the ir band is due to a trapped electron since no other species seems to be common to the uv photolysis of 9.5 *M* LiCl/D_2O/5×10^{-4} *M* tryp glass and the radiolysis of the LiCl/D_2O, $MgCl_2/D_2O$, and ethylene glycol/D_2O glasses. Ultraviolet photolysis is not expected to lead to the trapped exciton pair, $D_2O^+ \ldots e^-$.

After measuring spectrum *A*, the sample was bleached for 1 min with a 500 W projector lamp run at a dull glow and shielded from the sample with a 2 mm Chance-Pilkington filter type OX-5 which transmits mainly the infrared. The result was spectrum *B*. Thus, e_{ir}^- was completely bleached with great ease. The concomitant small decrease in the visible bands and larger decrease in the uv band are interpreted as a loss of $tryp^+$ due to reaction with bleached e_{ir}^- and some retrapping of bleached e_{ir}^- as e_{vis}^-. Finally, the sample was bleached for 1 min with the lamp at a dull glow but no OX-5 filter. The result was spectrum *C*. The result of this partial bleaching with the full light is not completely clear. The decrease in the visible band presumably represents a loss of e_{vis}^- and of $tryp^+$ with which it reacted. The small growth in the uv may be due to the production of $tryp^-$ by the reaction of bleached e_{vis}^- with tryp. The small band produced in the infrared is of unknown origin.

In another experiment, a glass made from 9.5 *M* LiCl/5×10^{-4} *M* tryp which had been saturated with N_2O at 2 atm was photolyzed for 5 min at 2 K. The result was spectrum *D* which shows that, in the presence of this electron scavenger, e_{ir}^- is not found. Neither do we believe that e_{vis}^- is present in spectrum *D*. This assumption is justified by the fact that the ratio of the visible absorbance maxima to the uv absorbance maximum is identical to that reported for the uv photolysis of tryp in 9 *M* HCl glass at 77 K (13) where e_{vis}^- would not be expected due to rapid reaction with H_3O^+.

We are now in a position to test the validity of the extinction coefficient, ε, measured previously for e_{ir}^- in ethylene glycol/D_2O glass at 1400 nm as $\varepsilon_{1400} = 5.7(\pm 0.8) \times 10^3\ M^{-1}\ cm^{-1}$ (2) which can be converted into $\varepsilon_{2500} = 3.1\ (\pm 0.5) \times 10^4$. For ε_{564}-($tryp^+$) we use $2700\ M^{-1}\ cm^{-1}$ (15). For $\varepsilon_{564}(e_{vis}^-)$ we use $1.6 \times 10^4\ M^{-1}\ cm^{-1}$ based on $\varepsilon_{max}(e_{vis}^-) = 2 \times 10^4\ M^{-1}\ cm^{-1}$ (2) and the long term spectrum of e_{vis}^- in 12 *M* LiCl at 4–10 K (see below). We assume that spectrum *D* represents $tryp^+$. We further assume that in spectrum *A* the uv band is due solely to $tryp^+$ but that the visible bands are comprised of $tryp^+$ plus e_{vis}^-. We then calculate that $\varepsilon_{2500}(e_{ir}^-) = 3.5 \times 10^4\ M^{-1}\ cm^{-1}$ if the yield of $tryp^+$ equals the sum of e_{vis}^- plus e_{ir}^- in spectrum *A*. Hence, we have determined $\varepsilon(e_{ir}^-)$ by a different method in a LiCl glass and find a value consistent with the previous determination in an ethylene glycol glass. This is further evidence that e_{ir}^- is the same species in the various glasses in which it has been produced. Several measures might be taken to make the method described here more reliable if they do not result in a significant reduction of the absorptions to be measured. The possible formation of $tryp^-$ might be countered by using a lower concentration of tryp and filtering the photolyzing light to reduce bleaching of e_{vis}^- and e_{ir}^-. The yield of e_{ir}^- relative to that of e_{vis}^- might be increased by using 6 *M* LiCl.

The isothermal changes in absorbance were measured following a 5 min photolysis of 9.5 *M* LiCl/5×10^{-4} *M* tryp at 2 K. These results are shown in Fig. 2. Photobleaching was avoided by passing the analyzing light through the sample for only a few seconds to measure each of the data points shown. A slow decay of $tryp^+$, as represented by the absorbance at 330 nm, was observed and a somewhat faster decay of e_{ir}^- was measured at 2300 nm. The growth at 580 nm and 620 nm could be due

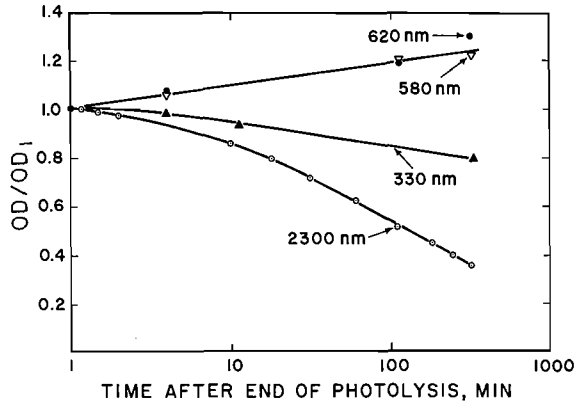

FIG. 2. The isothermal changes in absorbance with time at several wavelengths after a 5 min uv photolysis at 2 K of a glass prepared from an argon bubbled solution of 9.5 *M* $LiCl/D_2O$ containing 5×10^{-4} *M* tryptophan. OD_1 is the absorbance 1 min after photolysis.

to the reaction $e_{ir}^- \rightarrow e_{vis}^-$ and/or a spectral shift in the e_{vis}^- band. The actual growth of e_{vis}^- would be greater than the apparent growth measured at 580 and 620 nm because the absorbance changes contain both the growth of e_{vis}^- and the decay of $tryp^+$. A balance between loss of trapped electrons and $tryp^+$ cannot be made without postulating some production of $tryp^-$.

Pulse Radiolysis of 9.5 M *LiCl at 6–90 K*

The optical absorption spectra in 9.5 *M* LiCl measured at 100 ns at 6 K and 73 K are shown in Fig. 3. The ir band with $\lambda_{max} > 2400$ nm is due to e_{ir}^-, the band with $\lambda_{max} = 625$ nm to e_{vis}^-, and the band with $\lambda_{max} = 340$ nm is probably due mostly to Cl_2^-. Assuming no changes in extinction coefficients with change in temperature, the result of lowering the temperature from 73 K to 6 K is, roughly speaking, to double $G(e_{ir}^-)$ and to halve $G(e_{vis}^-)$ and $G(Cl_2^-)$. The ir band and the 625 nm band were analytically separated from one another as described in ref. 2 into a Lorentzian form for the ir band and a Gaussian form for the 625 nm band at $\lambda > 625$ nm.

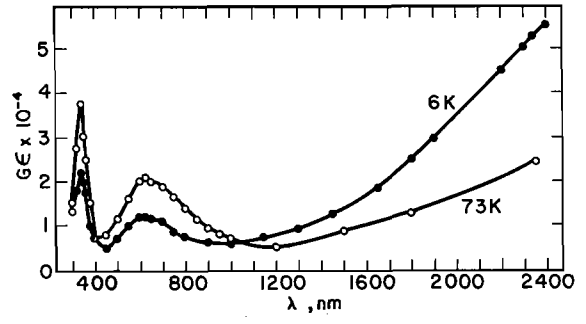

FIG. 3. Optical absorption spectra in 9.5 *M* $LiCl/D_2O$ at 6 K and 73 K measured 100 ns after the start of a 40 ns pulse.

When separated in this fashion both the e_{vis}^- and e_{ir}^- bands at 100 ns were found to have about the same shape at 6 K as at 73 K. Despite this similarity we shall show later that the visible band is probably composed of two bands (at least) which have different temperature dependent characteristics. One of the bands appears to be a relatively minor component in 9.5 *M* LiCl so we shall first discuss the results in terms of a unique visible band.

Although the absorption bands of e_{ir}^- and e_{vis}^- at 100 ns have similar shapes at 73 K and 6 K, the temporal stabilities of these two species are reversed. The decay of e_{vis}^-, represented by its absorbance at 650 nm, and of e_{ir}^-, represented by its absorbance at 2300 nm, are plotted in Fig. 4 for temperatures between 6 K and 90 K. Interference filters prevented bleaching of the trapped electrons by the analyzing light. As the temperature is lowered e_{ir}^- decays more slowly and its yield is greater. The reverse holds true for e_{vis}^- except that it decays faster at 90 K than at 75 K. In one experiment at 6 K we observed a small initial increase of 8% in the absorbance at 2300 nm. We were never able to reproduce this growth.

A detailed study of the decay of the e_{vis}^- band at 6 K and 73 K is shown in Fig. 5. The time intervals for the two temperatures are quite different, being 100 ns to 1 μs at 6 K, and 100 ns to 500 μs at 73 K. The ordinate represents the percentage of the absorbance lost over the appropriate time interval after corrections for the blank and e_{ir}^-. The decay at 73 K takes place mostly at $\lambda > \lambda_{max}$ whereas the

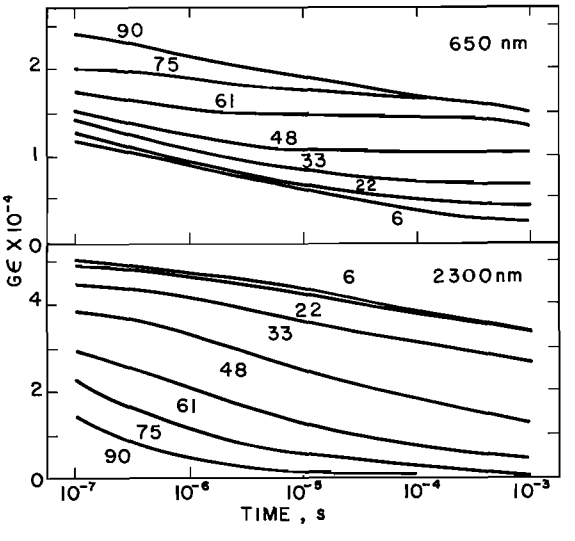

FIG. 4. Decay of e_{vis}^- (measured at 650 nm) and decay of e_{ir}^- (measured at 2300 nm) in the temperature range 6 K to 90 K. Temperatures are indicated beside each curve. No correction has been made for absorbance due to e_{ir}^- at 650 nm.

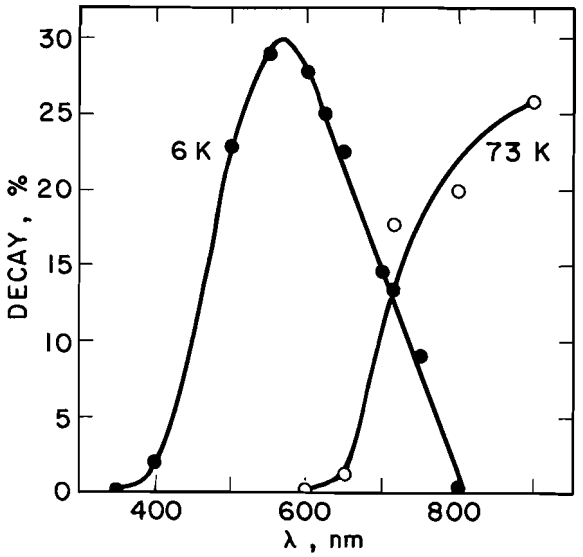

FIG. 5. Decay of the absorption band of e_{vis}^- as a function of wavelength. At 6 K the decay plotted occurred between 100 ns and 1 μs after the start of a 40 ns pulse. At 73 K the decay plotted occurred between 100 ns and 500 μs. A correction has been applied at each wavelength for the contribution of e_{ir}^-.

fractional decay at 6 K is peaked near λ_{max}. These fractional decay patterns mean that at 73 K the first spectral change in the e_{vis}^- band is a loss of intensity at $\lambda > \lambda_{max}$, perhaps due to the decay of a separate absorption band on the red side of the spectrum as suggested for BeF_2/D_2O glasses (5). At 6 K the decay observed causes the absorption band to become broader with little change in λ_{max}.

We shall consider several possible explanations for the increase in the decay rate of e_{vis}^- with decrease in temperature. One possibility is that e_{vis}^- is, on average, trapped closer to reactive species at 6 K than at 73 K. However, there is evidence in hydrocarbon glasses that the initial distributions of e_t^- are similar at 6 K and 77 K (10). Moreover, this possibility seems inconsistent with the slower decay of e_{ir}^- with decrease in temperature. Another possibility is that a reactive species such as D_3O^+, which seems to react more rapidly with e_{vis}^- than with e_{ir}^- (2), is more mobile at 6 K than at 73 K. This possibility does not explain why the absorption band decays preferentially in the vicinity of λ_{max}. Nor is it explained by the hypothesis that direct tunnelling of e_{vis}^- to reactant is faster at 6 K than at 73 K because of shallower, less relaxed, traps at 6 K. The explanation which we prefer is that e_{vis}^- at 6 K, 100 ns, exists in unrelaxed traps and that the visible absorption band is the composite of many bands representing the depth distribution of the naturally occurring traps. Apparently e_{vis}^- in the most abundant traps has λ_{max} = 625 nm (Fig. 3) and it is in the same wavelength region that decay occurs most rapidly (Fig. 5). Being in unrelaxed traps, e_{vis}^- is able to tunnel relatively freely from an occupied trap to an unoccupied trap of the same depth. The frequency of tunnelling will be greater for those e_{vis}^- absorbing near λ_{max} because they represent the most abundant traps. Increasing the movement of e_{vis}^- increases the rate at which it will disappear by reaction with a reactive species. Direct tunnelling of trapped electrons in glasses has been discussed by Miller (17). Buxton and Kemsley (14) have suggested that trap-to-trap tunnelling occurs in $LiCl/H_2O$ at low temperatures. Rice and Pilling (18) have discussed the effect of trap relaxation on trap-to-trap tunnelling. We suggest that trap relaxation for at least the first millisecond at 6 K is small enough to permit e_{vis}^- to tunnel from trap-to-trap.

Looking at Fig. 4 we can see a decrease in the 650 nm decay rate, the timing of which depends on the temperature. At 6 K we do not see any flattening of the curve, at 22 K it occurs at ~200 μs, at 33 K at ~100 μs, at 48 K at ~10 μs, at 61 K at ~2 μs, and at 75 K it presumably occurs before 100 ns. In fact, at 73 K a small sharp decay of ~3% is observed at $\lambda < \lambda_{max}$ over the period 100–200 ns. This may represent partly a flattening of the decay curve of e_{vis}^- and partly the decay of e_{ir}^- which probably makes a small contribution to the absorbance at 650 nm. We suggest that the time at which the decay curves flatten is approximately the time required for trap relaxation to substantially reduce the rate of trap-to-trap tunnelling. According to this model the 100 ns value of $G(e_{vis}^-)$ increases with increasing temperature due to the increasing rate of trap relaxation. For the same reason $G(e_{vis}^-)$ is higher at 90 K than at 75 K. At the higher temperatures we propose that thermally activated decay of e_{vis}^- also occurs as evidenced by a sudden steepening of the decay curves in Fig. 4. This sets in at ~100 μs at 61 K, ~300 ns at 75 K, and before 100 ns at 90 K. At 90 K the glass is still well below the glass transition temperature of 145 K measured for 9.5 *M* $LiCl/H_2O$ (19).

The trends of decay rates and yields of e_{ir}^- are opposite to those for e_{vis}^-. We speculate that e_{ir}^- is in relaxed traps by 100 ns at 6 K. Increased decay before 100 ns would account for the smaller values of $G(e_{ir}^-)$ at higher temperatures. We propose that the increased decay rate at higher temperatures is due to thermally assisted tunnelling. Rice and Pilling (18) have stated that phonon-assisted trap-to-trap tunnelling might be a significant factor by 10^{-2} s at 150 K for a trap relaxation energy of less than 0.2 eV. A trap relaxation energy of less than 0.2 eV for e_{ir}^-

does not seem unreasonable based on a trap depth ≤ 0.5 eV as estimated from its stimulation spectrum (below). The reason why the e_{ir}^- trap relaxes so much faster than the e_{vis}^- trap may reflect the much different environments of the two traps. It is believed that e_{ir}^- is associated with amorphous water in the glass whereas e_{vis}^- is associated with D_2O bound to Li^+ (4). It is expected that molecular motion of the water molecules in the potential field of the Li^+ ion will require more energy than will motion of the water molecules making up the e_{ir}^- traps. This effect will be particularly noticeable at low temperatures.

If e_{ir}^- was in a relaxed state during all the observations carried out it is possible to estimate very roughly an activation energy for the thermally assisted decay. Bearing in mind that tunnelling is a likely transport mechanism and that tunnelling is strongly distance dependent and removes first the e_{ir}^- trapped closest to a reactant, any meaningful calculation of activation energies must apply to the same distance distribution at all temperatures. We assume, for purposes of calculation, that the initial yield of e_{ir}^- and the initial distance distribution of e_{ir}^- with respect to species with which it may react are independent of temperature. We further assume that the distance distribution will be the same for the same value of $G\varepsilon$ regardless of temperature. We have compared the decay rates measured at $G\varepsilon = 2.2 \times 10^4$ over a range of temperatures. This value of $G\varepsilon$ is reached at 100 ns at 75 K, at 600 ns at 61 K, at 20 μs at 48 K and, by extrapolation, at ~20 ms at 33 K. Between 22 K and 6 K there seems to be an activation energy of zero indicating that simple, temperature-independent, tunnelling may predominate at these temperatures. An Arhennius plot of the decay rates above 22 K measured at $G\varepsilon = 2.2 \times 10^4$ yields an activation energy of 0.3 kcal/mol (0.01 eV). An activation energy of ~0.04 eV was estimated for the temperature dependent decay rate of e_t^- between 60 K and 77 K in methylcyclohexane glass (20), another system in which infrared absorbing trapped electrons probably decay by tunnelling.

It is not known which species react with e_{vis}^- and e_{ir}^-. Likely candidates are D_2O^+, D_3O^+, OD, and Cl_2^-. These are produced in the following reactions:

$$D_2O \rightsquigarrow D_2O^+ + e^-$$
$$D_2O^+ + D_2O \rightarrow D_3O^+ + OD$$
$$D_2O^+ + Cl^- \rightarrow D_2O + Cl$$
$$OD + Cl^- \rightarrow OD^- + Cl$$
$$Cl + Cl^- \rightarrow Cl_2^-$$

$G(Cl_2^-)$ was calculated from the absorbance at 340 nm assuming that $\varepsilon_{max} = 8.8 \times 10^3\ M^{-1}\ cm^{-1}$ (21). Corrections were made for the contribution of e_{vis}^- at 340 nm assuming that its absorption band resembles that of e_{vis}^- in an ethylene glycol/D_2O glass (2). Values calculated for $G(Cl_2^-)$ at 100 ns are 3.4 at 73 K and 2.2 at 6 K. The value of 3.4 at 73 K is in disagreement with the value of 2.57 reported previously (4).[1] The reason for this discrepancy is not known and has not yet been examined in more detail. Cl_2^- does not seem to be an important reactant in the decay of trapped electrons. For example, the absorbance at 350 nm decayed by 4% from 100 ns to 1 ms at 73 K and remained constant from 100 ns to 1 μs at 6 K. Over the same time intervals considerable decay of trapped electrons occurred (Fig. 4). It is possible that the uv band is partly due to $ClOH^-$ which has $\varepsilon_{max} = 3.7 \times 10^3\ M^{-1}\ cm^{-1}$ at 350 nm in aqueous solution (21).

Values of $G(e_{vis}^-)$, $G(e_{ir}^-)$, and $G(Cl_2^-)$ at 100 ns are tabulated in Table 1.

Radiolysis of 12 M LiCl/D_2O

Pulse radiolysis measurements on 12 *M* LiCl at 6 K led to the 100 ns spectrum shown in Fig. 6. Values of $G(e_{vis}^-)$ and $G(e_{ir}^-)$ are given in Table 1. Below the 100 ns spectrum in Fig. 6, and on the same scale of $G\varepsilon$, is shown the amount by which $G\varepsilon$ decreased between 100 ns and 1 μs. For example, a decrease in $G\varepsilon$ of 21% was measured at 600 nm. At 600 nm and 715 nm filters were used to check that bleaching by the analyzing light did not contribute to the measured decay.

The pulse radiolysis results for 12 *M* LiCl and for 9.5 *M* LiCl are similar. In both glasses the 100 ns yield of e_{vis}^- is lower at 6 K than at 73 K while the

TABLE 1. Values of $G(e_{vis}^-)$, $G(e_{ir}^-)$, and $G(Cl_2^-)$ in LiCl/D_2O at 100 ns

Temperature (K)	G		
	e_{vis}^-[a]	e_{ir}^-[b]	Cl_2^-[c]
	9.5 *M* LiCl/D_2O		
90	1.20	0.56	
75	0.98	0.90	3.40
61	0.84	1.13	
48	0.71	1.47	
33	0.65	1.71	
22	0.56	1.89	
6	0.53	1.94	2.23
	12 *M* LiCl/D_2O		
73	1.46[d]	0.36[d]	
6	0.76	1.29	

[a]Assuming $\varepsilon_{max} = 2 \times 10^4\ M^{-1}\ cm^{-1}$ and corrected for e_{ir}^- by using the spectra of e_{vis}^- and e_{ir}^- in ref. 2.
[b]Using $\varepsilon_{1400} = 5.7 \times 10^3\ M^{-1}\ cm^{-1}$ to calculate $\varepsilon_{2300} = 2.6 \times 10^4\ M^{-1}\ cm^{-1}$ from band analysis of e_{ir}^- in $MgCl_2$ glass (2).
[c]Using $\varepsilon_{340} = 8.8 \times 10^3\ M^{-1}\ cm^{-1}$ (21) and corrected for e_{vis}^- using spectrum in ref. 2.
[d]Taken from Gillis, Teather, and Buxton (4).[1]

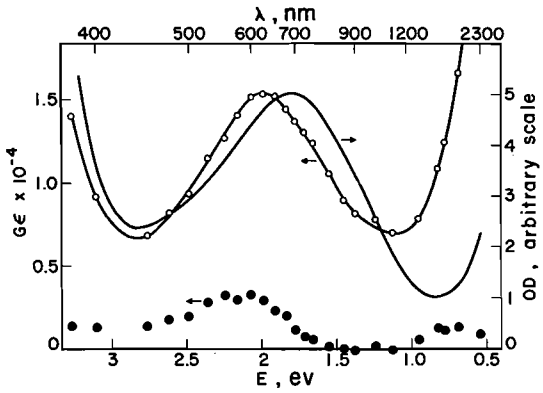

FIG. 6. Optical spectra and spectral changes in irradiated 12 *M* $LiCl/D_2O$ glass. ○ represents the absorption spectrum at 6 K measured 100 ns after the start of a 40 ns pulse. The loss (not the resultant absorption) observed to occur in this spectrum between 100 ns and 1 μs is shown by ●. The — line represents the absorption spectrum measured 50 min after irradiating a sample with 25 pulses, the sample being maintained constantly at 4–10 K.

yield of e_{ir}^- is larger. The spectral shapes of e_{vis} and e_{ir}^- are similar in both glasses. The initial decay at 6 K is faster in the visible than in the infrared. The decay was 16% at 650 nm between 100 ns and 1 μs in 12 *M* LiCl at 6 K compared to 23% in 9.5 *M* LiCl. This greater stability in 12 *M* LiCl, also evidenced by measurements to 1 ms, seems to be related to a stable underlying band in the visible at 6 K.

An experiment was carried out in which a 12 *M* LiCl sample was given 25 pulses in quick succession and kept in the dark during transfer to the Cary 17 spectrophotometer. The temperature was kept between 4–10 K at all times. The absorption spectrum was measured 50 min after irradiation and is shown in Fig. 6. A rough calculation was possible which indicated that the loss of absorbance between 100 ns and 50 min was nil in the uv, ~55% at 600 nm, ~35% at 715 nm, and ~90% at 2300 nm. At 600 nm and 715 nm these decays correspond roughly to that actually measured between 100 ns and 1 ms which leads us to believe that the decay in the visible band is largely complete by 1 ms. The stable band is similar to the 100 ns spectrum but is red shifted with $\lambda_{max} = 695$ nm. We have insufficient data to make more than a rough estimate but it seems that the stable band may represent ~40% of the visible band at 6 K, 100 ns. In 9.5 *M* LiCl this is reduced to perhaps 20% based on the decay at 650 nm over the first millisecond. After measuring the absorption spectrum for 12 *M* LiCl the sample was bleached by several exposures to 633 nm light from a 5 W He–Ne laser. The visible band appeared to bleach homogeneously. At the same time the infrared band increased presumably due to retrapping of photoionized e_{vis}^- as e_{ir}^-.

Information on the two bands making up e_{vis}^- is still very limited. Their broadness is consistent with their being trapped electrons. It is possible that the 695 nm band at 6 K may be related to the more rapid decay observed in 9.5 *M* LiCl at $\lambda > \lambda_{max}$ at 76 K, i.e., the 695 nm band may be less stable at 76 K than at 6 K in the same way that e_{ir}^- is. The 695 nm band may be similar to the "red wing" and/or "red band" in BeF_2/D_2O glasses (5). The "red wing" and "red band" have values of λ_{max} which seem to depend on the concentration of BeF_2 but which lie in the region 600 nm to 900 nm. They are believed to represent e_t^- and they form part of the larger "visible" band. The spectrum of e_{vis}^- in ethylene glycol/H_2O may also be composed of two bands. Higashimura *et al.* (22) have reported that λ_{max} for e_t^- at 77 K was 585 nm if the radiolysis was carried out at 77 K and 660 nm if carried out at 4 K.

Thus, it appears that e_{vis}^- in 12 *M* LiCl is composed mostly of the species which is predominant in 9.5 *M* LiCl but, in addition, there exists a significant fraction of another type of trapped electron. The relationship between these two components, if any exists, is not yet clear.

Stimulation Spectra of e_{vis}^- and e_{ir}^-

Stimulation spectra of e_{vis}^- and e_{ir}^- were measured in several aqueous glasses at 4 K and 77 K. The procedure followed was to photolyze a glassy sample containing 5×10^{-4} *M* tryp for 1 min with uv light from a low pressure Hg lamp. The light was first passed through a Corning 7-54 filter and a water filter to reduce bleaching of e_{ir}^- by infrared light. Photolysis ionized tryp producing $tryp^+$, e_{vis}^-, and e_{ir}^-. Beginning several minutes later, when isothermal luminescence from the sample had decreased sufficiently, the stimulation spectrum was determined by illuminating the sample with 0.3 s light pulses at wavelengths selected by a monochromator and measuring the intensity of the stimulated luminescence 0.2 s later with a photomultiplier and recording the oscilloscope trace photographically. The stimulating light came from a xenon arc, the pulse was produced with a mechanical shutter system and the timing of the sequence was exactly reproduced for each light pulse. At each wavelength the monochromator slits were set so that the same number of photons reached the sample. The correct slit widths were determined in a separate experiment with a radiation flux meter in the sample position. Each light pulse photoionized some of the trapped electrons absorbing at the wavelength used causing a very small fraction of the trapped electrons to decay by reaction with $tryp^+$. This reaction produced triplet tryptophan which phosphoresces largely in the visible (23). We measured a phosphorescence

lifetime of 6.5 ± 0.1 s in 9.5 *M* LiCl/5 × 10^{-4} *M* tryp at both 4 K and 77 K, in agreement with the reported lifetime of 6.6 s (23). This confirmed that we were measuring only the phosphorescence of triplet tryptophan when exciting at $\lambda > 500$ nm. For $\lambda < 500$ nm a small amount of more rapid decay was observed and corrections were made for this. A plot versus wavelength of the maximum phosphorescence intensity measured at each wavelength constitutes the stimulation spectrum. Barring significant changes in transmission of the stimulating light through the sample caused by absorption by the cell, the glassy matrix and the trapped species, the number of photons absorbed by trapped electrons was proportional to their absorbance at each wavelength. It was found that e_{ir}^- decayed noticeably during the measurement of a complete spectrum. A lesser decay occurred for e_{vis}^-. These decays were corrected for by measuring the spectrum several times and interpolating the results at each wavelength to construct a stimulation spectrum representing a single instant of time. This also avoids the possible problem of a change in the quantum yield of phosphorescence with change in the concentration of trapped electrons.

Stimulation spectra are akin to photobleaching spectra but instead of measuring the decrease in trapped electrons caused by photolysis one measures only the emission caused by those electrons which are photoreleased and react with $tryp^+$ to produce triplet tryptophan which phosphoresces. Absorption of light by $tryp^+$ does not result in phosphorescence. In this way we were able to study e_{vis}^- without interference from $tryp^+$ which absorbs in the same wavelength region.

For each sample a stimulation spectrum was measured on the unphotolyzed sample in order to correct for direct excitation of tryp molecules. This correction was only significant below 500 nm. The stimulation spectra and their decay characteristics were reproducible from experiment to experiment when using tubular cells but the absolute intensities were irreproducible, presumably due to variations in the output of the photolysis lamp. As usual, D_2O glasses were used to avoid the stronger near-ir absorption of light found in H_2O matrices.

(a) e_{ir}^- in LiCl Glasses

The open circles in Fig. 7 constitute the stimulation spectrum measured at 4 K for 9.5 *M* LiCl/5 × 10^{-4} *M* tryp contained in a 3 mm id tube. Beyond 1300 nm dips appear in the spectrum due to absorption of the stimulating light by the matrix. The decay of the stimulation spectrum was uniform between 1000 nm and 2300 nm indicating that, over this range at least, the decay of a single species, e_{ir}^-, was being observed. The decay rate was close to that measured by

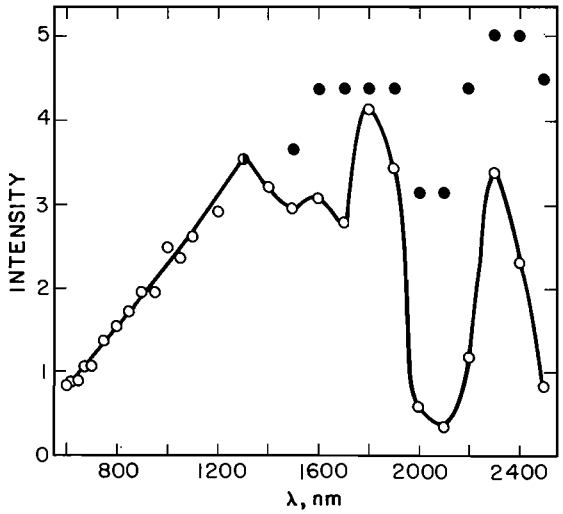

FIG. 7. Stimulation spectrum of e_{ir}^- at 4 K. ○ refers to the intensity (arbitrary units) measured in 9.5 *M* LiCl/D_2O/5 × 10^{-4} *M* tryp corrected to 30 min after the start of a 1 min photolysis. ● refers to 6 *M* LiCl/D_2O/5 × 10^{-4} *M* tryp in a 0.24 mm cell corrected to 10 min and normalized to agree with the open circles at 1300 nm.

absorption at 2300 nm at 2 K as shown in Fig. 2. Thus, those e_{ir}^- stimulated to react with $tryp^+$ and produce phosphorescence seem to represent the bulk of e_{ir}^- as measured by absorption. In other words, the stimulation method seems to sample adequately the total population of e_{ir}^-. The shape of the stimulation spectrum from 600 nm to 1300 nm, if corrected for the presence of e_{vis}^-, is very similar to the absorption spectrum of e_{ir}^-. The correction for e_{vis}^- could be made from kinetic measurements because e_{vis}^- was found to decay more slowly than e_{ir}^-. The relatively small yield of e_{vis}^- and its slower decay is consistent with the absorption measurements described above.

In order to reduce absorption of the stimulating light by the matrix we used a 0.24 mm sample of 9.5 *M* LiCl in a flat cell. The result was a stimulation spectrum with less pronounced dips but it did not prove to be an ideal sample because it always cracked badly and e_{ir}^- decayed much faster than in the cylindrical sample. The result was a spectrum dominated by e_{vis}^-. We obtained similar, but more reliable, results in the infrared with a 0.24 mm sample of 6 *M* LiCl. Gillis, Teather, and Buxton (4) have shown that the yield and stability of e_{ir}^- is increased on going from 9.5 *M* LiCl to 6 *M* LiCl at 76 K while the yield of e_{vis}^- is decreased. The stimulation spectrum in 6 *M* LiCl is shown in Fig. 7 as the closed circles which are normalized to the open circles at 1300 nm. Calculations indicate that, even in the thin sample, appreciable light absorption by the matrix took place at 2300 nm so we were still

unable to determine the true shape of the stimulation spectrum of e_{ir}^- at $\lambda > 1300$ nm. Thinner samples were not practical due to the smallness of the signal.

(b) e_{vis}^- in LiCl Glasses

The stimulation spectrum of e_{vis}^- at 4 K in 9.5 *M* LiCl, even when measured after many minutes in the 0.24 mm cell, was still difficult to disentangle from that of e_{ir}^-. However, similar and more reliable results which were obtained with a cylindrical sample of 12 *M* LiCl at 4 K are shown in Fig. 8. Gillis, Teather, and Buxton (4) have shown that, at 76 K, the yield of e_{vis}^- is increased and that of e_{ir}^- is decreased on going from 9.5 *M* LiCl to 12 *M* LiCl. Indeed, the 4 K stimulation spectrum in Fig. 8 does show a much smaller contribution of e_{ir}^- than the spectrum in Fig. 7. The λ_{max} of the stimulation spectrum at 4 K is 625 nm as compared to the absorption maximum of 695 nm at 4–10 K in Fig. 6.

The stimulation spectrum of e_{vis}^- in 9.5 *M* LiCl was also measured at 77 K. Once again, a similar but more reliable spectrum was measured in 12 *M* LiCl. This spectrum is shown, as corrected to 20 min, in Fig. 8 as open circles. This spectrum is very similar to the photoconductivity spectrum reported by Rice and Kevan (24) for 10 *M* $LiCl/H_2O$ glass at 85 K. The long term absorption spectrum at 77 K in 12 *M* $LiCl/D_2O$ has not been measured so we must compare the stimulation spectrum in Fig. 8 with its $\lambda_{max} \sim 475$ nm to the absorption spectrum in 9.5 *M* $LiCl/H_2O$ which has $\lambda_{max} = 590$ nm (14).

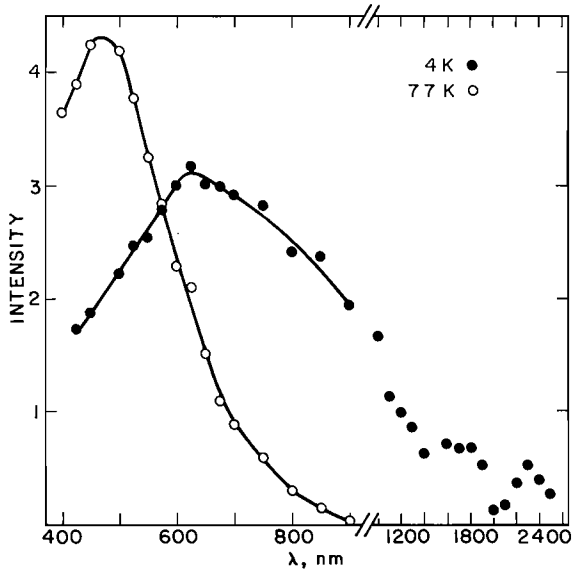

FIG. 8. Stimulation spectra in 12 *M* $LiCl/D_2O/5 \times 10^{-4}$ *M* tryp corrected to 20 min after the start of a 1 min photolysis. ● were measured at 4 K and ○ were measured at 77 K. The intensity units for each curve are arbitrary and independent of one another.

The intensity units in Fig. 8 are arbitrary and independent for each curve. The decrease in intensity on going from 450 nm to 400 nm at 77 K is believed to be real but this region of the spectrum is complicated since at $\lambda \leq 600$ nm the measured stimulation intensity grew slightly for the first 20 min and then decayed. At $\lambda > 600$ nm only decay was observed. The reason for this behaviour is not known but it might be associated with the shift in the absorption spectrum which sees λ_{max} change from a value of 625 nm at 100 ns to a long term value of 590 nm (14). A growth in the visible region, measured by absorption, has already been noted (see Fig. 2). Since e_{ir}^- decays rapidly at 77 K it is not surprising that the stimulation spectrum was zero above 1000 nm.

(c) Trap Depths and Relaxation Energies

The spectrum of the quantum yield for photoionization of e_{vis}^- in 12 *M* LiCl at 77 K can be obtained by dividing the stimulation intensity by the optical absorption. Assuming an absorption spectrum similar to that of 9.5 *M* LiCl (14), the result is a low quantum efficiency for photoionization at $\lambda > \lambda_{max}$ followed by a sharp rise from ~ 600 nm to ~ 500 nm and a broad maximum at ~ 450 nm. A similar sharp rise, setting in at λ_{max}, in the quantum efficiency of photoconductivity in 10 *M* $LiCl/H_2O$ at 85 K (24) was interpreted to mean that the optical absorption is due to bound–bound transitions above λ_{max} and to bound–free (continuum) transitions below λ_{max}.

Thus, the long term absorption band of e_{vis}^- at 77 K seems to be made up of a bound–bound transition from which photoionization is inefficient and a bound–free transition represented by the stimulation band, similar to an analysis of the e_{vis}^- band in EG/D_2O shown in ref. 2. We shall assume that these two transitions belong to the same trapped electrons. Thus, the maximum of the absorption band of e_{vis}^- at 77 K (590 nm, 2.1 eV) (14) represents the energy of the transition from the ground state to the first excited state for the most abundant trap depth. The energy of the transition from the ground state to the continuum for the most abundant trap depth is the maximum of the stimulation spectrum (475 nm, 2.6 eV). This places the first excited state 0.5 eV below the continuum. We are neglecting more refined details such as autoionization, tunnelling from a bound excited state to the continuum, and changes in λ_{max} due solely to temperature changes. Similarly, we can separate the absorption spectrum measured at 50 min, 4–10 K (Fig. 6) into a bound–bound transition with $\lambda_{max} = 695$ nm (1.8 eV) and, from its stimulation spectrum, a bound–free transition with $\lambda_{max} = 625$ nm (2.0 eV).

If we knew the energy of the bound–free transition of the unrelaxed e_{vis}^- precursor to the 77 K relaxed state we could calculate the relaxation energy. We are inclined to believe that the unrelaxed state in question is represented by the rapidly decaying component at 6 K in Fig. 5 for which the rapid decay prevents a determination of the stimulation spectrum. However, it is unlikely that the bound–free transition would correspond to an energy less than the λ_{max} of the absorption spectrum at 100 ns which is 625 nm (2.0 eV) at both 73 and 6 K. Hence we estimate that the relaxation energy of the major component of the e_{vis}^- band is ≤ 0.6 eV.

The composite picture of e_{vis}^- in $LiCl/D_2O$ glasses presented by the various techniques employed here is that the predominant species is in an unrelaxed trap at 6 K, 100 ns but in a partially relaxed trap at 77 K, 100 ns. Another band is present, at least in 12 *M* LiCl. The characteristics of this second band are ill-defined at present. We do not know whether decay of the second band at 77 K contributes to the shift of λ_{max} from 625 nm to 590 nm at long times. Both bands, under the conditions in which their stimulation spectra can be measured, show both bound–bound and bound–free transitions. The relaxation energy of the predominant species at 77 K is ≤ 0.6 eV. We recognize that we have postulated $\lambda_{max} = 625$ nm for both non-relaxed e_{vis}^- at 6 K, 100 ns and for partially relaxed e_{vis}^- at 73 K, 100 ns. Since it is not known whether the transitions at 100 ns are bound–bound or bound–free and since the maximum spectral shift on complete relaxation at 77 K is only from 625 nm to 590 nm we do not feel that any conclusions can be drawn from the similarity of λ_{max} at 6 K and 77 K at 100 ns.

We believe that the present evidence, while not conclusive, is incompatible with the idea that the energies of the ground state levels of e_{vis}^- and e_{ir}^- could be very similar. This idea was recently commented on with regard to possible tunnelling from e_{vis}^- to e_{ir}^- (4). Briefly stated, we conclude that the ground state for e_{vis}^- in relaxed traps at 77 K is 2.6 eV below the continuum. The maximum of the stimulation spectrum of e_{ir}^- could not be reliably determined because of matrix absorption but an upper energy limit is 0.5 eV (2400 nm) based on Fig. 7. The higher energy portion of the stimulation band is presumably due to transitions from the ground state to higher levels in the continuum and/or a range of trap depths. If we neglect changes in energy levels due solely to temperature changes we place the ground state of e_{ir}^- at 77 K at ~ 0.5 eV, far from the 2.6 eV level of the ground state in e_{vis}^- but, interestingly, close to the level of the first bound excited state in e_{vis}^-. A much deeper trap depth for e_{vis}^- than for e_{ir}^- has also been deduced by Rice, Dolivo, and Kevan (25).

(d) Temperature Dependent Tunnelling of e_{ir}^-

The decrease in the stimulation spectrum between 10 min and 50 min after the start of a 1 min photolysis was measured at 1800 nm at several temperatures. The percent decay was found to be relatively independent of temperature but the intensity at 10 min was clearly smaller the higher the temperature. The decay was 30% at 4 K, 28% at 20 K, 35% at 32 K, and $35(\pm 5)\%$ at 46 K. It must not be construed from this temperature independent decay that the tunnelling rate constant is temperature independent. To be valid, a comparison of tunnelling rate constants at different temperatures is best made for identical e_t^--reactant distance distributions and identical e_t^- trap depth distributions. If we assume that the initial yield and distance distribution of e_{ir}^- is independent of temperature between 4 K and 77 K, as seems to be the case for glassy hydrocarbons (10), we conclude that the higher the temperature the smaller the fraction of the original e_{ir}^- left at 10 min. Given the strong distance dependence of tunnelling, this implies that the higher the temperature, the greater is the average e_{ir}^--reactant distance at 10 min. We conclude, once again, that the tunnelling rate constant between 4 K and 46 K is temperature dependent. Phonon-assisted tunnelling of e_{ir}^- has already been mentioned.

(e) Ethylene Glycol Glass

We measured the stimulation spectra in EG/D_2O (50/50 by volume) glasses containing 5×10^{-4} *M* tryp. The EG was protiated, not deuterated. The spectra at 4 K and 77 K are shown in Fig. 9. They provide little information about e_{ir}^-. The low intensity above 1800 nm is due to a low concentration of e_{ir}^- and/or matrix absorption of the stimulating light. The stimulation spectrum of e_{vis}^- at 4 K seems to be shifted to slightly shorter wavelengths as compared to the absorption spectrum of e_{vis}^- at 4 K (26) bearing in mind the difficulty in separating the e_{vis}^- and e_{ir}^- contributions in both cases. This suggests that a considerable fraction of the absorption band is due to a bound–free transition. The stimulation spectrum of e_{vis}^- at 77 K is also shown in Fig. 9 and is consistent with the reported photoconductivity spectrum (24). From it and the absorption spectrum at 77 K (27) we calculate a relative quantum efficiency curve the same as that reported by Moan (28) for photobleaching of e_{vis}^- in EG/H_2O/tryp glass at 77 K.

(f) NaOD Glass

A cursory examination was made of the stimulation spectrum of 10 *M* $NaOD/D_2O/5 \times 10^{-4}$ *M*

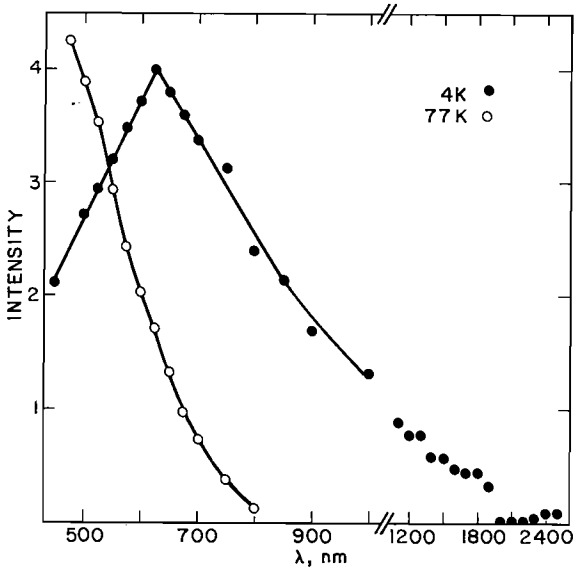

FIG. 9. Stimulation spectra measured in EG/D_2O glasses (50/50 by volume) containing 5×10^{-4} *M* tryp. ● were measured at 4 K, 25 min after the start of a 1 min photolysis. ○ were measured at 77 K, 30 min after the start of a 1 min photolysis. The intensity units for each curve are arbitrary and independent of each other.

tryp. The results at 4 K and 77 K are shown in Fig. 10. The luminescence decay in this glass was not the simple phosphorescence of triplet tryptophan. Two decays, one with lifetime ~1.4 s and another with lifetime ~4.8 s seemed to be present. In Fig. 10 we have plotted the maximum value of the total measured stimulated emission. The intensities measured in 10 *M* NaOD were weak and the measurements less reliable than in the EG and LiCl glasses but they are sufficiently interesting to warrant inclusion in this report because they demonstrate a case in which the stimulation spectrum and the absorption spectrum at 77 K (26) are very similar, indicating a bound–free transition. This conclusion has already been drawn from the similarity of the wavelength dependence of photo-current in irradiated 10 *M* NaOH to the absorption spectrum (24). The apparent differences between the stimulation spectra at 4 K and 77 K are not considered to be outside experimental error.

An indication that the absorption spectrum in 10 *M* NaOD is not due solely to one transition comes from preliminary results at both 4 K and 77 K which indicate that photobleaching with light at $\lambda > \lambda_{max}$ caused more bleaching at λ than at wavelengths $< \lambda_{max}$. This suggests that the absorption spectrum is due to at least two trap depths, one of which is more easily bleached than the other as reported for BeF_2/D_2O glasses at 76 K (5).

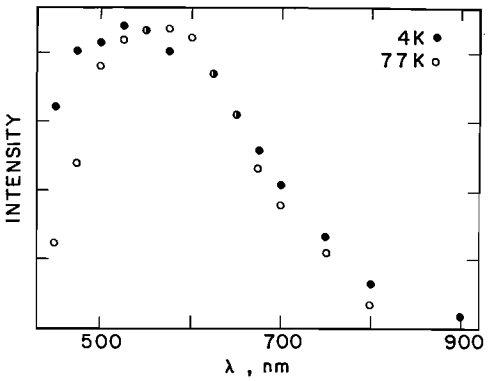

FIG. 10. Stimulation spectra measured in 10 *M* NaOD/D_2O/5×10^{-4} *M* tryp. ● were measured at 4 K between 10 and 20 min after the start of a 1 min photolysis. ○ were measured at 77 K between 20 and 30 min after the start of a 1 min photolysis. The intensity units for each curve are arbitrary and are independent of each other.

Summary of e_{ir}^- and e_{vis}^- in LiCl Glass

(a) e_{ir}^-

1. The production of the infrared band by photoionization of tryptophan further substantiates its assignment to a trapped electron, e_{ir}^-.

2. The spectrum of e_{ir}^- in LiCl/D_2O seems to be essentially the same as in EG/D_2O even to the value of its extinction coefficient ($\varepsilon_{2500} = 3.1\ (\pm 0.5) \times 10^4\ M^{-1}\ cm^{-1}$).

3. The ground state of e_{ir}^- is ≤ 0.5 eV below the continuum while the calculated value of λ_{max} is 3600 nm (0.34 eV).

4. The e_{ir}^- trap seems to be substantially relaxed by 100 ns even at 6 K.

5. The decay of e_{ir}^- is temperature independent between 6 K and 22 K and presumably occurs by tunnelling. Above 22 K the decay is temperature dependent, possibly involving phonon-assisted trap-to-trap tunnelling given the strong possibility that the relaxation energy of e_{ir}^- is small.

(b) e_{vis}^-

1. The spectrum of e_{vis}^- is probably composed of at least two distinct bands.

2. The predominant band in 9.5 *M* LiCl and 12 *M* LiCl decays faster at 6 K than at 75 K probably because it relaxes more slowly at 6 K, allowing trap-to-trap tunnelling to occur.

3. The predominant band at long times at 77 K has a bound–bound transition with maximum intensity at 2.1 eV and a bound–free transition with maximum at 2.6 eV. The relaxation energy is believed to be ≤ 0.6 eV.

4. The second band of e_{vis}^- is more prominent in 12 *M* than in 9.5 *M* LiCl. It has been isolated at 6 K where it is much more stable than the predominant

band, probably due to faster relaxation. It has a bound–bound transition maximum at 1.8 eV and a bound–free maximum at 2.0 eV.

Acknowledgements

We wish to thank J. Rolfe for the generous loan of the Cary 17 spectrophotometer and the cryostat used with it and to thank M. Buchanan for her invaluable assistance with this apparatus. We wish also to gratefully acknowledge many interesting discussions with J. Menigaux and C. Lapersonne-Meyer. The extent of the pulse radiolysis data was only made possible by the very generous assistance of C. Ross with the computer-related data collection and processing.

1. G. V. Buxton, H. A. Gillis, and N. V. Klassen. Chem. Phys. Lett. **32**, 533 (1975).
2. G. V. Buxton, H. A. Gillis, and N. V. Klassen. Can. J. Chem. **54**, 367 (1976).
3. G. V. Buxton, H. A. Gillis, and N. V. Klassen. Can. J. Chem. **55**, 2385 (1977).
4. H. A. Gillis, G. G. Teather, and G. V. Buxton. Can. J. Chem. **56**, 1889 (1978).
5. T. Q. Nguyen, D. C. Walker, and H. A. Gillis. J. Chem. Phys. **69**, 1038 (1978).
6. H. A. Gillis, N. V. Klassen, and G. Trudel. To be published.
7. H. Hase and K. Kawabata. J. Chem. Phys. **65**, 64 (1976).
8. H. A. Gillis and D. C. Walker. J. Chem. Phys. **65**, 4590 (1976).
9. T. Q. Nguyen and D. C. Walker. J. Chem. Soc. Faraday Trans. I, **73**, 1958 (1977).
10. N. V. Klassen and G. G. Teather. J. Phys. Chem. **83**, 326 (1979).
11. A. Déroulède. J. Lumin. **3**, 302 (1971).
12. F. Kieffer, C. Meyer, and J. Rigaut. J. Chim. Phys. **68**, 1741 (1971).
13. J. Moan and O. Kaalhus. J. Chem. Phys. **61**, 3556 (1974).
14. G. V. Buxton and K. G. Kemsley. J. Chem. Soc. Faraday Trans. I, **71**, 568 (1975).
15. J. F. Baugher and L. I. Grossweiner. J. Phys. Chem. **81**, 1349 (1977).
16. W. A. Volkert, R. R. Kuntz, C. A. Ghiron, R. F. Evans, R. Santus, and M. Bazin. Photochem. Photobiol. **26**, 3 (1977).
17. J. R. Miller. J. Chem. Phys. **56**, 5173 (1972).
18. S. A. Rice and M. J. Pilling. Prog. React. Kinet. **9**, 93 (1978).
19. C. A. Angell and E. J. Sare. J. Chem. Phys. **52**, 1058 (1970).
20. P. Cordier, F. Kieffer, C. Lapersonne-Meyer, and J. Rigaut. Proceedings of the Fifth International Congress of Radiation Research, July 1974. p. 426.
21. G. G. Jayson, B. J. Parsons, and A. J. Swallow. J. Chem. Soc. Faraday Trans. I, **69**, 1597 (1973).
22. T. Higashimura, M. Noda, T. Warashina, and H. Yoshida. J. Chem. Phys. **53**, 1152 (1970).
23. H. B. Steen. Photochem. Photobiol. **6**, 805 (1967).
24. S. A. Rice and L. Kevan. J. Phys. Chem. **81**, 847 (1977).
25. S. A. Rice, G. Dolivo, and L. Kevan. J. Chem. Phys. **68**, 4864 (1978).
26. H. Hase, M. Noda, and T. Higashimura. J. Chem. Phys. **54**, 2975 (1971).
27. H. B. Steen. *In* Electron–solvent and anion–solvent interactions. *Edited by* L. Kevan and B. Webster. Elsevier Scientific Publishing Co., New York, NY. 1976. p. 175.
28. J. Moan. Int. J. Radiat. Phys. Chem. **5**, 293 (1973).

Electron spin resonance study of radical adducts of unsaturated dicarboxylic and tricarboxylic acids

BABATUNDE B. ADELEKE[1] AND JOSHUA A. FANIRAN
Department of Chemistry, University of Ibadan, Ibadan, Nigeria

Received October 16, 1978

BABATUNDE B. ADELEKE and JOSHUA A. FANIRAN. Can. J. Chem. 57, 1500 (1979).

An esr study of the addition reactions of $^{\bullet}OH$, $CO_2^{-\bullet}$, $SO_3^{-\bullet}$, and $^{\bullet}PO_3^{2-}$ radicals to the anions of aconitic, itaconic, and chelidonic acids is reported. There was an electron transfer reaction between $CO_2^{-\bullet}$ and chelidonic acid anion. The phosphite radical reacted with chelidonic acid to produce two types of radicals resulting from addition to C=C and the oxygen of the carbonyl group in the acid. The radical adducts of the anions of aconitic and itaconic acids exhibited extensive linebroadenings due to hindered internal rotations. The barrier to internal rotations is shown to be the repulsive forces between the negative charges on the various substituents.

BABATUNDE B. ADELEKE et JOSHUA A. FANIRAN. Can. J. Chem. 57, 1500 (1979).

On rapporte une étude rpe des réactions d'addition des radicaux $^{\bullet}OH$, $CO_2^{-\bullet}$, $SO_3^{-\bullet}$, et $^{\bullet}PO_3^{2-}$ aux anions des acides aconitique, itaconique et chélidonique. Il se produit une réaction de transfert d'électron entre le $CO_2^{-\bullet}$ et l'anion de l'acide chélidonique. Le radical phosphite réagit avec l'acide chélidonique pour conduire à deux types de radicaux provenant d'additions au niveau du C=C et de l'oxygène du groupe carbonyle de l'acide. Les adduits radicalaires des anions des acides aconitique et itaconique présentent des élargissements de raie qui sont importants et qui proviennent d'empêchement aux rotations internes. On a montré que la barrière aux rotations internes est due aux forces répulsives entre les charges négatives sur les divers substituants.

[Traduit par le journal]

Introduction

Many transient organic free radicals have been generated in aqueous flow medium for esr study by the reactions of $^{\bullet}OH$ with reactive organic substances (1–4). The hydroxyl radical is usually produced in a flow system by the reaction of Ti(III) with hydrogen peroxide. Norman *et al.* and others have extensively used this method to generate various types of radicals for esr studies (2, 5–7). Among the many systems studied by Norman and co-workers is radical addition to maleic acid (6, 7).

Chawla and Fessenden used the fumarate ion as a spin trap for a number of radicals including $SO_4^{\bullet-}$, $^{\bullet}NH_2$, and $^{\bullet}PO_4^{2-}$ radicals (8), while Neta produced radicals for esr studies by the reaction of fumarate ions with e_{aq}, $H^{\bullet}$, $^{\bullet}OH$, carboxyl radicals, and a series of alkyl radicals (8). More recently Steeken and Lyda have used fumarate and maleate ions as spin traps for acyl radicals (8). Fessenden and Neta studied the reactions of hydrated electrons with some unsaturated dicarboxylic acids including chelidonic acid (10) while Kirino and Fessenden have studied the addition of $^{\bullet}S^-$ and $^{\bullet}OH^-$ radicals to the anion of itaconic acid (10). Apart from maleic (4, 6–9) and fumaric (8) acids, few esr studies of radical addition to other unsaturated dicarboxylic and tricarboxylic acids have been reported.

In this article we report an esr study of addition reactions of $^{\bullet}OH$, $SO_3^{-\bullet}$, $CO_2^{-\bullet}$ and $^{\bullet}PO_3^{2-}$ radicals to the anions of aconitic, itaconic, and chelidonic acids. The radicals generated in alkaline medium were very persistent. This is presumably because of the high negative charges on the radicals. As a result of this high persistency, enough concentration of some radicals was obtained to observe, at natural abundance ratio, ^{13}C splittings.

Results and Discussion

Itaconic Acid

When $^{\bullet}OH$ radical was generated in the presence of itaconic acid, the observed esr spectrum depended on both the concentration of the acid and the pH of the medium. It was obvious that more than one radical type was present. A similar observation was made by Fischer *et al.* (1) in their esr study of hydrogen abstraction from succinic acid. They showed that rapid and reversible proton transfer reactions between the radicals and the acid molecules was responsible for the observation.

At a pH of 9.5 and itaconic acid concentration of 0.5 g/L, a spectrum attributable to radical **I** was observed. The *g*-value and splitting constants

[1]To whom all correspondence should be addressed.

0008-4042/79/121500-06$01.00/0

TABLE 1. Radical structures and their esr parameters

Number	Radical structure	a_α^H (G)	a_β^H (G)	a^{others}	g
I	$CH_2(CO_2^-)\dot{C}(CO_2^-)CH_2OH$		21.45 (2H) 14.21 (2H)	$a_{OH}^H = 0.40$	2.0032
II	$(^-O_2CCH_2)_2\dot{C}CO_2^-$		14.02 (4H)	$a_\gamma^{13}C(2) = 17.94$ $a_\beta^{13}C(2) = 10.81$ $a_\beta^{13}C(1) = 12.42$	2.0032
III	$(HO_2CCH_2)_2\dot{C}CO_2H$		14.71 (4H)		2.0032
IV	$^-O_2CCH_2\dot{C}(CO_2^-)CH_2SO_3^-$		12.01*(2H) 13.92*(2H)	$a_\beta^{13}C(1) = 12.46$ $a_\beta^{13}C(1) = 11.66$ $a_\beta^{13}C(1) = 10.75$ $a_\gamma^{13}C(1) = 18.41$	2.0030
V	$^-O_2CCH_2\dot{C}(CO_2^-)CH_2PO_3^{2-}$		14.8*(2H) 12.1 (2H)	$a^P = 71.6$	2.0032
VI	$^-O_2CCH_2COH(CO_2^-)\dot{C}HCO_2^-$	20.06 (1H)		$a_\gamma^H = 0.54$ (1H) $a_{OH}^H = 0.22$	2.0032
VII	$^-O_2CCH_2\dot{C}(CO_2^-)CHOH(CO_2^-)$		12.31 (1H) 5.35 (1H) 0.84 (1H)		2.0032
VIII	$HO_2CCH_2\dot{C}(CO_2H)CHOH(CO_2H)$		14.77 (1H) 4.69 (1H) 1.39 (1H)		2.0032
IX	$^-O_2CCH_2\dot{C}(CO_2^-)CH(CO_2^-)_2$		13.80*(2H) 9.57 (1H)		2.0033
X	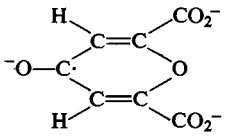		1.26 (2H)		2.0038
XI	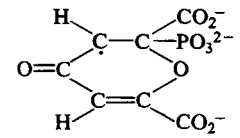	9.6 (1H)		$a_\gamma^H = 1.8$ (1H) $a^P = 81.6$	2.0035
XII	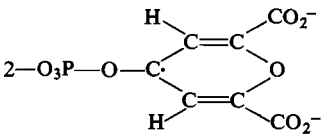		5.8 (2H)	$a^P = 62.4$	2.0031

*The value given is one-half the observed line separation.

(Table 1) are in good agreement with the values reported by Kirino and Fessenden (10), however, they did not observe the —OH proton splitting constant. The lines corresponding to $M_I = 0$ of both triplets were broadened with respect to the other lines.

The inclusion of sodium formate in the system resulted in the observation of the spectrum shown in Fig. 1*a*. The spectrum conforms to that of four equivalent protons in which the lines corresponding to $M_I = \pm 1$ are broadened. The spectrum is assigned to radical **II**, Table 1. Laroff and Fessenden (11) obtained a spectrum similar to that of Fig. 1*a*, except that the $M_I = \pm 1$ lines were broadened beyond detection. They assigned the spectrum to radical **II**, which they obtained during the continuous in situ radiolysis of the anion of 1,2,3-propane tricarboxylic acid. Our values of both the proton and ^{13}C splitting constants are in good agreement with theirs. The broadened lines became sharper with increasing temperature, but at 50°C the expected 1:4:6:4:1 ratio was not attained. However, at pH of 3, the spectrum in Fig. 1*b* was obtained. The intensity ratio approximates closely to that expected from four equivalent protons. The spectrum is that of radical **III** in Table 1.

The spectrum recorded when the sulphite anion radical was generated in the presence of itaconate anion consisted of four lines of equal intensity and one broader and less intense line at $g = 2.0030$. This

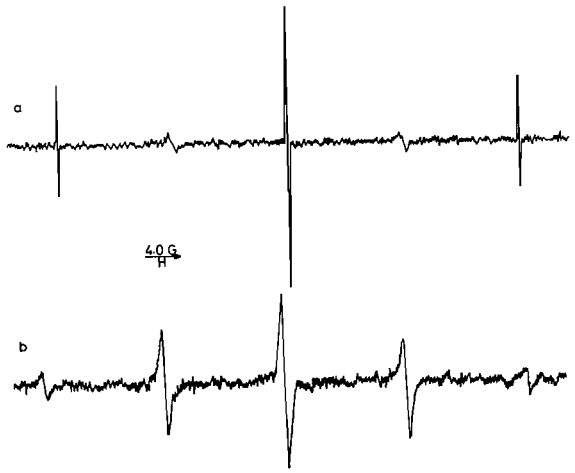

FIG. 1. Electron spin resonance spectrum of (*a*) $(^{-}O_2C\text{-}CH_2)_2\dot{C}CO_2^{-}$; (*b*) $(HO_2CCH_2)_2\dot{C}CO_2H$.

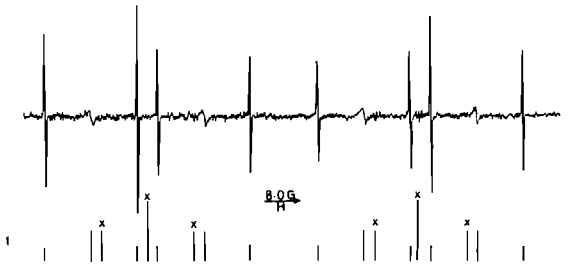

FIG. 2. Electron spin resonance spectrum and stick plot of $^{-}O_2CCH_2\dot{C}(CO_2^{-})CH_2PO_3^{2-}$. The asterisked lines are broadened beyond detection.

one line is due to the sulphite anion radical (6). The four lines spectrum is analysed in terms of a pair of two equivalent protons, in which the centre line of each triplet was broadened beyond detection. The parameters and the suggested structure of radical **IV** are shown in Table 1.

Figure 2 is the spectrum recorded for the adduct of $^{\bullet}PO_3^{2-}$ with itaconic acid at pH of 9.5. The large doublet is associated with phosphorus. Here again, the centre line of each triplet is broadened but the centre line of the triplet with larger splitting constant is broadened beyond detection. The spectrum is assigned to radical **V**.

From the values of a_β^H in $(^{-}O_2CCH_2)_2\dot{C}CO_2^{-}$, the hyperfine splitting constants which are much different from 14 G are assigned to the methylene protons of $—CH_2X$ in $^{-}O_2\dot{C}CH_2\dot{C}(CO_2^{-})CH_2X$ where X is OH, SO_3^{-}, or PO_3^{2-}. We note that the values of a_β^H in all the radicals reported above are less than the value expected for a freely rotating β methyl group (12).

Aconitic Acid

Three radicals **VI, VII,** and **VII**(*b*) can be identified from the reaction of $^{\bullet}OH$ with aconitic acid at pH of 9.8 (Fig. 3). The determined parameters and the structures of radicals **VI** and **VII** are recorded in Table 1.

Radical **VI** was generated previously during the photolysis of sodium citrate (13) and in situ radiolysis of the anion of 1,2,3-propane tricarboxylic acid (11). It is interesting to note that the two γ methylene protons of radical **VI** are non-equivalent. This agrees with the observation of Norman *et al.* that methylene protons which are adjacent to a chiral centre are magnetically non-equivalent (14).

Radical **VII** is the major $^{\bullet}OH$ adduct of the anion of aconitic acid (Fig. 3*a*). The smallest splitting did not decrease either in deuterium oxide or in the presence of a mineral acid. This suggests that all the splitting constants in this radical can be assigned to the three β-protons of the radical. It is not clear why the methylene protons of the $—CH_2CO_2^{-}$ group in this radical unlike in the OH adduct of itaconate are not equivalent. It is observed that the two outermost lines are broadened compared to the inner lines.

We are unable to suggest a structure for radical **VII**(*b*) which has a large doublet of 34.74 G and a smaller doublet of 1.01 G.

At pH of 2, radical **VIII** and the unknown radical with $a^H = 38.35$ G were observed (Fig. 3*b*).

The spectrum observed when carbon dioxide

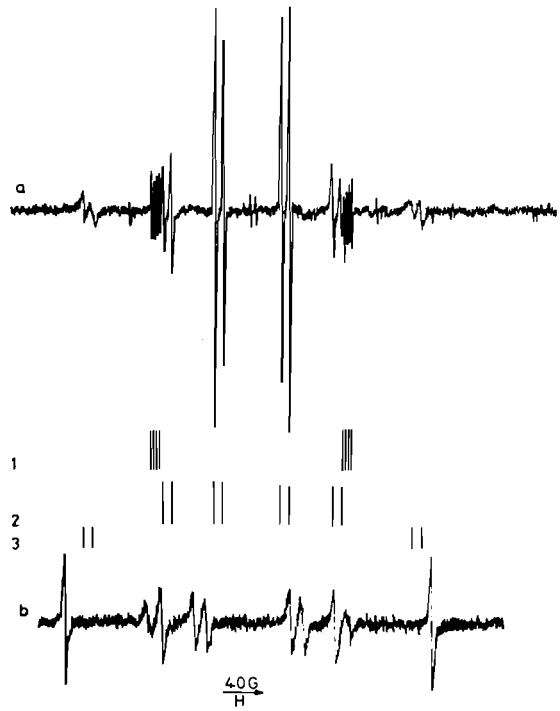

FIG. 3. Electron spin resonance spectrum of $^{\bullet}OH$ adduct of aconitic acid at (*a*) pH of 9.8; (*b*) pH of 2.0. (*1*) Stick plot for $^{-}O_2CCH_2COH(CO_2^{-})\dot{C}HCO_2^{-}$; (*2*) stick plot for $^{-}O_2CCH_2\text{-}\dot{C}(CO_2^{-})CHOH(CO_2^{-})$; (*3*) stick plot for radical **VII**(*b*).

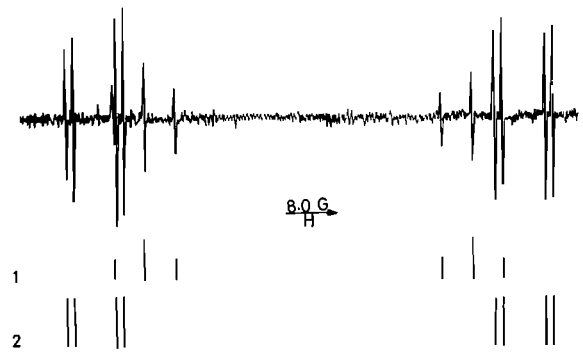

FIG. 4. Electron spin resonance spectrum of $\cdot PO_3^{2-}$ adducts of chelidonic acid in alkaline medium; (*1*) stick plot for radical **XII**; (*2*) stick plot for radical **XI**.

radical anion reacted with the anion of aconitic acid consisted of four lines. The parameters and the suggested structure for radical **IX** are given in Table 1.

The sulphite radical anion was generated in the presence of aconitic acid anion. No other esr spectrum was observed besides those of the sulphite radical anion and radical **VII**. Apparently $SO_3^{\cdot -}$ did not add to aconitic acid. A similar observation was made by Norman and Storey (6).

The spectrum obtained when $\cdot PO_3^{2-}$ reacted with aconitic acid could not be unambiguously analysed, though the large doublet characteristic of phosphorus was obvious.

Chelidonic Acid

No esr spectrum was observed when either ·OH or $SO_3^{-\cdot}$ was generated in the presence of the anion of chelidonic acid.

A three line spectrum with intensity ratio of 1:2:1 was obtained by the reaction of $CO_2^{-\cdot}$ with chelidonic acid. The radical is identified as **X** in Table 1.

Neta and Fessenden (10) produced radical **X** by the addition of hydrated electrons to the anion of chelidonic acid. Our values of a_β^H and g are in good agreement with theirs. In the present study radical **X** must have been produced by an electron transfer from $CO_2^{-\cdot}$ to the acid. The carbon dioxide radical anion has been shown to be an effective one-electron reducing agent for carbonyl-containing compounds (18).

Two radicals (Fig. 4) identified as **XI** and **XII** were produced by the addition of $\cdot PO_3^{2-}$ to chelidonic acid at pH of 9.5.

Structure **XI** is suggested by the observation of the hyperfine constant of the γ-proton. The appearance of a 1:2:1 triplet in the spectrum of radical **XII** suggests that the radical possesses a C_2 axis and the structure of the radical must be similar to that of radical **X**. The value of ^{31}P splitting constant in radical **XII** appears to be large compared with a^P of straight chain aliphatic radicals (15), which possess similar $\cdot COPO_3^{2-}$ structure. The relatively large value of a^P in radical **XII** indicates the existence of hyperconjugation interaction between the unpaired electron and the phosphorus atom. Such hyperconjugation interaction has been used to explain the increase in the splitting due to the ^{31}P nucleus from 1.3 G in the *p*-benzosemiquinone-1-phosphate radical to 20 G in 2,3,5,6-tetrachloro-1,4-benzosemiquinone-1-phosphate radical (16). Phosphorus splitting constants of 57.79 G, 56.58 G, and 46.6 G have been observed by Ingold *et al.* in radicals possessing the $\cdot CN[(EtO)_2PO]$ structure (17). In the two instances cited above steric hindrance forces the P—O and P—N bonds into a plane in which the phosphorus atom is optimally positioned for hyperconjugation interaction with the unpaired electron. In the present study the repulsive forces between PO_3^{2-} and the two CO_3^{2-} groups in radical **XII** might serve the same purpose as the steric hindrance in the substituted benzosemiquinone 1-phosphate (16) and the substituted α-aminoalkyl radicals (17). Previously we have observed the addition of diphenyl phosphino radical to the carbonyl oxygen of 2,6-di-*tert*-butyl-*p*-benzoquinone (18).

Generally the dependence of a_β^H upon the dihedral angle θ, between the β-C—H bond and the *p*-orbital containing the unpaired electron is given by

$$a_\beta^H = A + B\cos^2\theta$$

where A and B are constants. The minimum value (13–15 G) of a_β^H occurs when the radical is fixed in a conformation with $\theta = 60°$ (12, 19). Thus the values of a_β^H for the $SO_3^{-\cdot}$, $CO_2^{-\cdot}$, and $\cdot PO_3^{2-}$ radical adducts of itaconate and $CO_2^{-\cdot}$ radical adduct of aconitic acid suggest that the radicals exist in the preferred conformation **1** or **2**.

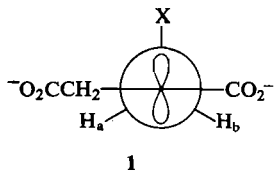

1

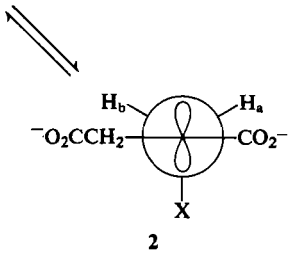

2

This is supported by the increase of a_β^H with increasing temperature (Table 2).

It is noteworthy to observe that the values of 12 G for a_β^H when X is SO_3^- or PO_3^{2-} are less than the

TABLE 2. Variation of a_β^H with temperature

(*a*) $^-O_2CCH_2\dot{C}(CO_2^-)CH(CO_2^-)_2$

Temperature (°C)	a_β^H $CH_2CO_2^-$	a_β^H $CH(CO_2^-)_2$
24	13.90	9.58
43	14.04	9.77

(*b*) $^-O_2CCH_2\dot{C}(CO_2^-)CH_2SO_3^-$

Temperature (°C)	a_β^H $CH_2CO_2^-$	a_β^H $CH_2SO_3^-$
13	13.88	11.96
36	13.97	12.04
44	14.02	12.06

predicted minimum. Similar observation was made in the study of β-mercapto alkyl radicals (12). The unusually low values of a_β^H were explained by a model in which the β-sulfur atom is displaced from its tetrahedral position toward the *p*-orbital. Possibly the same type of distortion might be responsible for the very low values of a_β^H of $-CH_2PO_3^{2-}$ and $-CH_2SO_3^-$ methylene protons.

The value (21.45 G) of a_β^H of the $-CH_2OH$ methylene protons in radical **I** and its decrease with increasing temperature suggest that the $-CH_2OH$ group assumes conformation **3** or **4** in the radical.

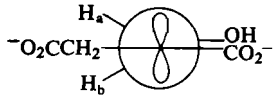

3

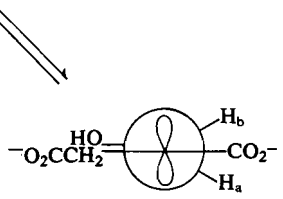

4

The line broadenings observed in the radicals reported here are not unique. Kochi and Krusic (12) and Norman *et al.* (7) have observed similar effects. Such line broadenings result from hindered internal rotation. Exchanges between conformations **1** and **2** or **3** and **4** as shown above at a rate comparable to the difference in the a_β^H splitting constants in the two corresponding conformations would lead to the broadening of the lines associated with $M_I = 0$ of the triplets. These line broadenings are virtually absent in the protonated radicals (Figs. 1*b*, 3*b*). This shows that the barrier to internal rotation in these radicals is mainly the repulsive forces between the negatively charged substituents.

Experimental

Electron spin resonance spectra were recorded on Varian E-4 spectrometer with 100 kHz modulation. The mixing chamber was the Varian E-249 liquid flow mixing chamber which allows the mixing of two reactants. The instrument was calibrated using the $^\cdot PO_3^{2-}$ radical adduct of maleate ion (7). The *g*-values were measured by comparison with DPPH (20) and are corrected for second order effect (21). The temperature of the solutions was varied by the appropriate use of ice or heater. The temperature of the solution as it left the mixing chamber was recorded. The pH of the effluent solution is reported.

For the generation of the $^\cdot OH$ adduct in alkaline medium, the two solutions which were mixed contained (*a*) 12.5 mL/L of 12.5% (w/v) titanium trichloride solution, 9 g/L of disodium ethylenediamine tetraacetate, EDTA, and the pH of solution adjusted to 8.5 with concentrated ammonia solution. (*b*) 0.5–3 g/L of an unsaturated acid, 2 mL/L of 30% hydrogen peroxide, and pH of solution adjusted to 9–11 with ammonia.

In the study of $SO_3^{-\cdot}$ or $CO_2^{-\cdot}$ reactions 30 g/L of sodium sulphite or sodium formate respectively was included in solution (*a*). For $^\cdot PO_3^{2-}$ radical, 10 g/L of phosphorus acid was included in solution (*b*).

The reactions in acid medium were carried out without EDTA in solution (*a*) and the pH of both solutions were adjusted to values of 2–3 with sulphuric acid.

Itaconic acid (L. Light and Co.) and chelidonic acid (L. Light and Co.) were used as supplied. Aconitic acid was prepared from citric acid using the literature method (22). All other chemicals were from BDH company.

Acknowledgment

The authors are grateful to the referees for their helpful comments.

1. H. FISCHER, H. K. HELLWEGE, and M. LEHNIG. Ber. Bunsenges. Phys. Chem. **72**, 1166 (1968).
2. A. J. DOBBS, B. C. GILBERT, and R. O. C. NORMAN. J. Chem. Soc. Perkin II, 786 (1972).
3. P. SMITH, R. A. KABA, and P. B. WOOD. J. Phys. Chem. **78**, 117 (1974).
4. A. L. J. BECKWITH. Aust. J. Chem. **25**, 1887 (1972).
5. A. L. J. BECKWITH and R. O. C. NORMAN. J. Chem. Soc. B, 400 (1969).
6. R. O. C. NORMAN and P. M. STOREY. J. Chem. Soc. B, 1009 (1971).
7. B. C. GILBERT, J. P. LARKIN, R. O. C. NORMAN, and P. M. STOREY. J. Chem. Soc. Perkin II, 1508 (1972).
8. OM P. CHAWLA and R. W. FESSENDEN. J. Phys. Chem. **79**, 2693 (1975); P. NETA. J. Phys. Chem. **75**, 2570 (1971); S. STEEKEN and M. LYDA. J. Phys. Chem. **81**, 2201 (1977); N. H. ANDERSON, A. J. DOBBS, D. J. EDGE, R. O. C. NORMAN, and P. R. WEST. J. Chem. Soc. B, 1004 (1971).
9. W. I. DIXON, J. FOXALL, and G. H. WILLIAMS. J. Chem. Soc. Faraday II, 1614 (1974).
10. P. NETA and R. W. FESSENDEN. J. Phys. Chem. **76**, 1957 (1972); Y. KIRINO and R. W. FESSENDEN. J. Phys. Chem. **79**, 837 (1975).

11. G. P. LAROFF and R. W. FESSENDEN. J. Chem. Phys. **55**, 5000 (1971).
12. P. J. KRUSIC and J. K. KOCHI. J. Am. Chem. Soc. **93**, 846 (1971); P. J. KRUSIC, P. MEAKIN, and J. P. JESSON. J. Phys. Chem. **75**, 3438 (1971).
13. H. ZELDES and R. LIVINGSTON. J. Am. Chem. Soc. **93**, 1082 (1971).
14. B. C. GILBERT, J. P. LARKIN, and R. O. C. NORMAN. J. Chem. Soc. Perkin II, 1272 (1972).
15. A. SAMUNI and P. NETA. J. Phys. Chem. **77**, 2425 (1973); E. A. C. LUCKEN. J. Chem. Soc. A, 1354 (1966).
16. B. T. ALLEN and A. BOND. J. Phys. Chem. **68**, 2439 (1964).
17. R. A. KABA, D. GRILLER, and K. U. INGOLD. J. Am. Chem. Soc. **96**, 6202 (1974).
18. B. B. ADELEKE and J. K. S. WAN. Unpublished results.
19. D. GRILLER and K. U. INGOLD. J. Am. Chem. Soc. **96**, 6715 (1974).
20. P. B. AYSCONGH. Electron spin resonance in chemistry. Methuen and Co. Ltd. 1967. p. 156.
21. R. W. FESSENDEN. J. Chem. Phys. **37**, 747 (1962).
22. A. H. BLATT. Organic syntheses, collective volume 2. John Wiley and Sons, Inc. 1969. p. 12.

Reactions at the nitrogen atoms in azafluorene systems

KRYSTIAN KLOC, JACEK MŁOCHOWSKI, AND ZDZISŁAW SZULC

Institute of Organic and Physical Chemistry, Technical University, 50-370 Wrocław, Poland

Received August 30, 1978

KRYSTIAN KLOC, JACEK MŁOCHOWSKI, and ZDZISŁAW SZULC. Can. J. Chem. **57**, 1506 (1979).

Isomeric azafluorenones have been oxidized to *N*-oxides with H_2O_2 in acetic acid or in the presence of Na_2WO_4.

In the same manner monoazafluorenes have been converted into azafluorene *N*-oxides, but oxidation of diazafluorenes led first to diazafluorenones which then formed diazafluorenone *N*-oxides. Azafluorenones and azafluorenes are readily *N*-methylated with CH_3I to give methiodides. The relations between the rate constants of *N*-methylation and structural factors have been discussed.

KRYSTIAN KLOC, JACEK MŁOCHOWSKI et ZDZISŁAW SZULC. Can. J. Chem. **57**, 1506 (1979).

Les azafluorénones isomères sont oxydées en *N*-oxydes par H_2O_2 en présence d'acide acétique ou en présence de Na_2WO_4. De la même façon on a converti les monoazafluorènes en azafluorène *N*-oxydes, alors que l'oxydation de diazafluorènes conduit à la formation de diazafluorènones qui fournissent ensuite les diazafluorénones *N*-oxydes. Les azafluorénones et azafluorènes sont aisément méthylés avec CH_3I. On discute des vitesses de la *N*-méthylation en fonction de la structure.

Introduction

The chemistry of nitrogen analogues of fluorene and fluorenone is of interest because of the high biological activity and the possibility of pharmaceutical application, as well as the synthetic significance of this little known class of compounds (1, 2). In connection with a general study of the chemistry of polycyclic azines we have previously reported a convenient synthesis of unsubstituted azafluorenones starting from mono- and diazaphenanthrenes (3). Azafluorenones were simply converted into azafluorenes by adopting the Wolff–Kishner reduction procedure (4).

The aim of the present work has been to investigate oxidation and alkylation at nitrogen azafluorenes and azafluorenones, and to obtain hitherto unknown *N*-oxides as well as *N*-methiodides.

There are only a few reported examples of *N*-alkylation of azafluorenes and azafluorenones (5–8). The *N*-oxidation of this class of compounds has been reported only for the cases of 4-azafluorene to 4-azafluorene *N*-oxide (9) and of 3-methyl-2-azafluorene to 3-methyl-2-azafluorene *N*-oxide (10). Analogously, 11*H*-indene[1,2-b]quinoline **1** gives 85% of the corresponding *N*-oxide **2**, but its isomer, 11*H*-indene[2,1-b]quinoline **3**, is oxidized to the corresponding oxo-compound **4** (11).

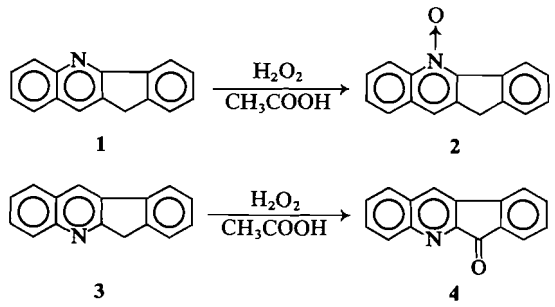

1 **2** **3** **4**

Results and Discussion

We have examined the reactions of 1- and 4-monoazafluorenones **5** and **6** with hydrogen peroxide in benzene – acetic acid medium and found that they gave corresponding *N*-oxides **7** and **8**.

Under similar conditions, after 18 h, 1,8-diazafluorenone **9** gave 1,8-diazafluorenone 1,8-dioxide **10** in 47% yield, and 2,5-diazafluorenone **11** gave 2,5-diazafluorenone 2,5-dioxide **12** in 9% yield only. Oxidation of 1,5- and 4,5-diazafluorenones **13** and **14** led to tarry unidentified products in which no *N*-oxides were detected.

Adopting the procedure reported by Hamada and Takeuchi (12) and oxidizing the studied compounds with H_2O_2 in the presence of Na_2WO_4 we obtained 2,5-diazafluorenone 2,5-dioxide **12** (30%), 4,5-diazafluorenone 4-oxide **15** (22%), as well as 1,5-diazafluorenone 5-oxide **16** (37%).

The structure of **16** was confirmed by its ^1H nmr spectrum and comparison with the starting base **13**. The H-4 proton is deshielded by the *N*-oxide group and its signal is shifted to lower field by about

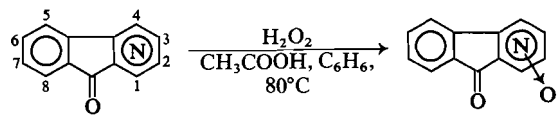

5 1-*N*
6 4-*N*

7 1-*N*
8 4-*N*

0008-4042/79/121506-05$01.00/0

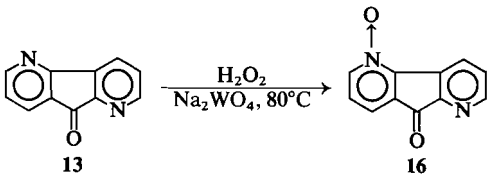

13 16

0.55 ppm. Similar effects were observed in other *N*-oxides (13).

The presence of N→O groups was confirmed by the ir spectra in which the position of stretching bands occurring at 1200–1300 cm^{-1} in accord with the data obtained for other *N*-oxides (14).

By oxidizing 4-azafluorene **18** with hydrogen peroxide in acetic acid – benzene mixture, we obtained 4-oxide **20** as reported in the literature (9). 1-Azafluorene **17** was oxidized to 1-oxide **19** and neither azafluorenone nor its *N*-oxide was detected, although in the case of the similar compound **3** the active methylene group was oxidized to give **4** (11).

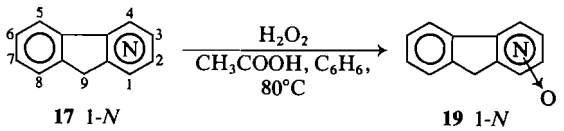

17 1-*N* **19** 1-*N*
18 4-*N* **20** 4-*N*

Nevertheless, 1,8-diazafluorene **21** was oxidized in the first step to 1,8-diazafluorenone **9** which was simultaneously converted to 1,8-diazafluorenone 1,8-dioxide **10**.

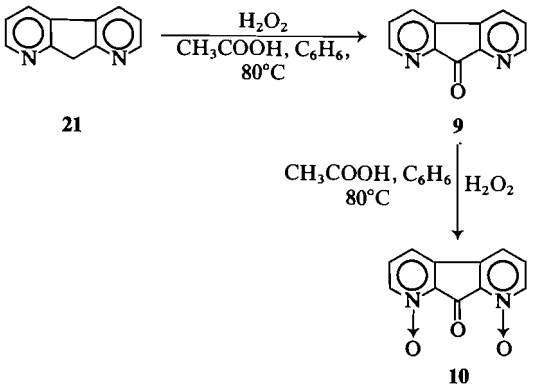

21 **9** **10**

Analogously, 1,5-, 2,5-, and 4,5-diazafluorenes **22**, **23**, and **24** were oxidized to the corresponding azafluorenones and then to their *N*-oxides which immediately underwent decomposition in acetic acid medium.

When reaction was carried out with H_2O_2 in the presence of Na_2WO_4, the diazafluorenone *N*-oxides **12** (9%), **15** (7%), and **16** (16%) were isolated. The above experiments are evidence that in diazafluorenes, where two pyridine rings exert a strong electron withdrawing effect on the methylene group; this group is more active than are nitrogen atoms. No significant steric effects were observed in contrast to nitrogen analogues of phenanthrene (14). We carried out the *N*-methylation of azafluorenes **17**, **18**, **21**, **22**, **23**, and **24** as well as azafluorenones **5**, **6**, **9**, **11**, **13**, and **14**. The reaction was performed with methyl iodide in benzene solution under reflux. The results of *N*-methylation and the properties of the products are listed in Table 1.

The structure of the synthesized products was confirmed by ^1H nmr spectroscopy and comparison of the spectra with those of starting bases (3, 4), although the structure of *N*-methyl derivatives of monoazafluorenes, monoazafluorenones, and symmetrical diazacompounds are unequivocal.

In the case of 1,5-diazafluorene **22** only 1-methiodide **30** was formed and in the ^1H nmr spectrum the downfield signals were similar to **26**, and not to **28**. The product could not be a mixture of two monomethiodides because the $-CH_3$ protons would not be equivalent, and two singlets would be seen in the spectrum. On the other hand, 1,5-diazafluorenone formed mainly 1-methiodide **29**, admixture with about 20% of the 5-isomer. In the ^1H nmr spectrum two upfield singlets of $-CH_3$ groups (δ = 4.86 and 4.72 ppm, 1:4) occurred. The 4.86 ppm signal was similar to **27** and the 4.72 ppm to **25**. The downfield signals were more similar to **25** than to **27**.

In the same manner we found that 2,5-diazafluorene **23** and 2,5-diazafluorenone **11** were methylated at the 2-position to give **33** and **34**.

The rate constants were also established for the *N*-methylation of monoaza- and symmetric diazafluorenones and azafluorenes, and are listed in Table 2.

The data obtained show that the azafluorenes are more reactive as compared to azafluorenones, this fact being probably due to the electron withdrawing effect of the carbonyl group decreasing nucleophilicity of the nitrogen atoms. The second nitrogen atom in diazacompounds **9**, **14**, **21**, and **24** also decreases the electron density on the other one and reactivities of **9** or **21** are similar to that of **5** or **17**. Otherwise one would have expected that double the number of nitrogen atoms in the molecule would have doubled the rate constants.

4-Azacompounds **6** and **18** are less reactive than 1-isomers **5** and **17** because the H-5 atom could cause steric hindrance. When the ≡C—H group in the 5-position is replaced by a nitrogen atom (compounds **14** and **24**) reactivity increases, and this fact can probably be assigned to the high electron density at the reaction center, which is due to the proximity of the nonbonding orbitals of both N atoms and to

TABLE 1. Results of the syntheses of azafluorene and azafluorenone *N*-methiodides

Compound	Yield (%)	mp (°C)	^{1}H nmr†	Elemental analysis (% I) Calcd.	Found
1-Methyl-1-azafluorenone iodide **25**	71	200–201 (dec.)	9.25 (dd, J = 5 Hz and 1.5 Hz, 1H, H-2), 9.15 (dd, J = 8 Hz and 1.5 Hz, 1H, H-4), 8.23–8.62 (m, 2H, H-5 and H-8), 8.22–8.76 (m, 3H, H-3, H-6, H-7), 4.78 (s, 3H, —CH_3)	39.30	39.00
1-Methyl-1-azafluorene iodide **26**	93	205–207 (dec.)	8.89 (dd, J = 5 Hz and 2 Hz, 1H, H-2), 8.78 (dd, J = 8 Hz and 2 Hz, 1H, H-4), 8.10–8.50 (m, 1H, H-5), 7.55–7.95 (m, 4H, H-3, H-6—H-8), 4.62 (s, 3H, —CH_3), 3.72 (s, 2H, =CH_2)	41.05	40.09
4-Methyl-4-azafluorenone iodide **27**	11 (55*)	Dec. above 255	9.26 (dd, J = 5 Hz and 1.5 Hz, 1H, H-3), 8.97 (dd, J = 8 Hz and 1.5 Hz, 1H, H-1), 8.52–8.70 (m, 1H, H-5), 8.15–8.42 (m, 4H, H-2, H-6—H-8), 4.95 (s, 3H, —CH_3)	39.30	39.20
4-Methyl-4-azafluorene iodide **28**	87	Dec. above 278	8.50 (dd, J = 5 Hz and 2 Hz, 1H, H-3), 8.42 (dd, J = 7 Hz and 2 Hz, 1H, H-1), 8.15–8.27 (m, 1H, H-5), 7.65–7.87 (m, 4H, H-2, H-6—H-8), 4.75 (s, 3H, —CH_3), 4.30 (s, 2H, =CH_2)	41.05	40.96
1-Methyl-1,5-diazafluorenone iodide **29**	27 (51*)	Dec. above 233	9.20 (dd, J = 5 Hz and 1.5 Hz, 1H, H-2), 9.10 (dd, J = 8 Hz and 1.5 Hz, 1H, H-4), 9.05 (dd, J = 5 Hz and 2 Hz, 1H, H-6), 8.40–8.60 (m, 2H, H-3, H-8), 7.84 (dd, J = 8 Hz and 5 Hz, 1H, H-7), 4.72 (s, 3H, —CH_3)	39.20	38.98
1-Methyl-1,5-diazafluorene iodide **30**	98	222–224 (dec.)	9.12–9.35 (m, 2H, H-2, H-4), 8.87 (dd, J = 5 Hz and 1.5 Hz, 1H, H-6), 8.50–8.67 (m, 2H, H-3, H-8), 7.95 (dd, J = 8 Hz and 5 Hz, 1H, H-7), 4.98 (s, 3H, —CH_3), 4.72 (s, 2H, =CH_2)	40.91	40.72
1-Methyl-1,8-diazafluorenone iodide **31**	39	Dec. above 260	9.05–9.40 (m, 3H, H-2, H-4, H-7), 8.87 (dd, J = 8 Hz and 2 Hz, 1H, H-5), 8.50–8.75 (m, 1H, H-3), 8.10 (dd, J = 8 Hz and 5 Hz, 1H, H-6), 4.90 (s, 3H, —CH_3)	39.20	38.88
1-Methyl-1,8-diazafluorene iodide **32**	97	Dec. above 233	9.16 (dd, J = 5 Hz and 1.5 Hz, 1H, H-2), 9.05 (dd, J = 8 Hz and 1.5 Hz, 1H, H-4), 8.65–8.75 (m, 2H, H-5, H-7), 7.35–7.57 (m, 2H, H-3, H-6), 4.50 (s, 3H, —CH_3), 3.84 (s, 2H, =CH_2)	40.91	40.61
2-Methyl-2,5-diazafluorenone iodide **33**	98	Dec. above 260	9.68 (s, 1H, H-1), 9.51 (d, J = 6 Hz, 1H, H-3), 9.23 (dd, J = 5 Hz and 2 Hz, 1H, H-6), 8.76 (d, J = 6 Hz, 1H, H-4), 8.56 (dd, J = 8 Hz and 2 Hz, 1H, H-8), 8.03 (dd, J = 8 Hz and 5 Hz, 1H, H-7), 4.76 (s, 3H, —CH_3)	39.20	38.92
2-Methyl-2,5-diazafluorene iodide **34**	100	238–240 (dec.)	9.25 (s, 1H, H-1) 9.02 (d, J = 6 Hz, 1H, H-3), 8.70 (dd, J = 5 Hz and 1.5 Hz, 1H, H-6) 8.45 (d, J = 6 Hz, 1H, H-4), 8.35 (dd, J = 8 Hz and 1.5 Hz, 1H, H-8), 7.73 (dd, J = 8 Hz, and 5 Hz, 1H, H-7), 4.81 (s, 3H, —CH_3), 4.41 (s, 2H, =CH_2)	40.91	40.63
4-Methyl-4,5-diazafluorenone iodide **35**	93	248	9.42 (dd, J = 5 Hz and 1.5 Hz, 1H, H-3), 9.30 (dd, J = 5 Hz and 1.5 Hz, 1H, H-6), 9.07 (dd, J = 8 Hz and 1.5 Hz, 1H, H-1), 8.67 (dd, J = 8 Hz and 1.5 Hz, 1H, H-8), 8.47 (dd, J = 8 Hz and 5 Hz, 1H, H-2), 8.08 (dd, J = 8 Hz and 5 Hz, 1H, H-7), 5.12 (s, 3H, —CH_3)	39.20	39.03
4-Methyl-4,5-diazafluorene iodide **36**	99	227–229 (dec.)	9.00–9.20 (m, 3H, H-1, H-3, H-6), 8.60 (dd, J = 8 Hz and 2 Hz, 1H, H-8), 8.37 (dd, J = 8 Hz and 5 Hz, 1H, H-2), 7.97 (dd, J = 8 Hz and 5 Hz, 1H, H-7), 5.33 (s, 3H, —CH_3), 4.72 (s, 2H, =CH_2)	40.91	40.45

*After 60 h.

†The spectra of azafluorenone *N*-methiodides were measured in DMSO. The spectra of azafluorene *N*-methiodides except compound **28** were measured in D_2O and the spectrum of **28** in CF_3COOD–$CDCl_3$ (1:1).

the absence of the H-5 atom. Nevertheless, the influence of these factors is smaller than in the analogous azaphenanthrenes (15) because azafluorene molecules are more linear.

The synthesized *N*-oxides and *N*-methiodides of the azafluorenones were subjected to preliminary screening against bacteria and fungi in the same manner as was described for phenanthrolines (16). We have found that in all cases the *N*-derivatives exhibited higher activity than the free bases. Activity most similar to that of 1,10-phenanthroline and the widest antibacterial spectra were shown by 2,5-diazafluorenone 2,5-dioxide **12**, and *N*-methiodides of 1-azafluorenone **25**, 1-azafluorene **26**, and 1,8-diazafluorene **32** *N*-methiodides. Further investigations of the activity of azafluorenones, azafluorenes, and their derivatives are in progress.

Experimental

All melting points were taken with a Kofler apparatus and are uncorrected. The ir spectra (in KBr) were recorded with a Perkin Elmer 621 spectrophotometer, and nmr spectra with a Tesla BS-478/80 MHz spectrometer in D_2O, DMSO, $(CF_3)_2CO$, or $CDCl_3$–CF_3COOD solution, using HMDS as an external standard.

The reaction course, and their products were checked by tlc on silica gel using chloroform or ethyl acetate as eluents. The spots were visualized with Dragendorff reagent.

The starting azafluorenones and azafluorenes were synthesized from the appropriate azaphenanthrenes as described earlier (3, 4). The biological tests were performed in the Microbiology Department of the Medicinal Academy in Lublin. The screening method involved testing synthetic compounds against bacteria and fungi; the results are available from the Depository of Unpublished Data.[1]

1-Azafluorenone 1-Oxide (7)

To a solution of **5** (1.81 g, 10 mmol) in glacial acetic acid (10 mL) and benzene (10 mL), 30% hydrogen peroxide (3 mL) was added and the mixture was heated to gentle boiling. After 8 h, the second portion of 30% hydrogen peroxide (3 mL) was added and the reaction mixture was heated for an additional 6 h. After oxidation the reaction mixture was concentrated under reduced pressure to about 5 mL, water (20 mL) added, and the resulting mixture concentrated again. This procedure was repeated, and then the residue was evaporated to dryness. The crude product was recrystallized from ethanol–water yellow needles 69% yield, mp 221–223°C (dec.); ir (KBr) ν_{max}: 1720 (s, CO), 1285 cm^{-1} (s, NO). *Anal.* calcd. for $C_{12}H_7O_2N$: C 73.10, H 3.55, N 7.10; found: C 73.45, H 3.50, N 7.11.

4-Azafluorenone 4-Oxide (8)

This compound was obtained from **6** in the same manner as **7**, oxidation time being 8 h; orange needles, 68% yield, mp 257–259°C; ir (KBr) ν_{max}: 1720 (s, CO), 1285, and 1275 cm^{-1} (s, NO). *Anal.* calcd. for $C_{12}H_7O_2N$: C 73.10, H 3.55, N 7.10; found: C 73.40, H 3.45, N 6.79.

1,8-Diazafluorenone 1,8-Dioxide (10)

10 was obtained from **9** in the same manner as for **7**. After 10 h, the second portion of 30% hydrogen peroxide (3 mL) was added and reaction mixture was heated for an additional 6 h. The insoluble product was filtered and washed with hot ethanol; orange needles, 47% yield, mp 274–276°C (dec.); ir (KBr) ν_{max}: 1712 (s, CO), 1290, and 1270 cm^{-1} (s, NO). *Anal.* calcd. for $C_{11}H_6N_2O_3$: C 61.69, H 2.82, N 13.08; found: C 61.76, H 3.02, N 12.78.

2,5-Diazafluorenone-2,5-dioxide (12)

12 was obtained from **11** in the same manner as for **7**. The reaction was complete after 30 min and the product was isolated in 9% yield only. The following modification was also used. **11** (1.82 g, 10 mmol) was stirred at 50°C with the solution of $Na_2WO_4 \cdot 2H_2O$ (0.2 g) in 5% hydrogen peroxide (40 mL) until the starting material was dissolved completely. The reaction mixture was then allowed to stand for 12 h at room temperature and the insoluble product filtered off and recrystallized from water. Small red prisms decomposed in a range of 220–240°C; 30% yield; ir (KBr) ν_{max}: 1728 (s, CO), 1272, and 1245 cm^{-1} (s, NO). *Anal.* calcd. for $C_{11}H_6N_2O_3$: C 61.69, H 2.82, N 13.08; found: C 61.99, H 2.93, N 13.13.

4,5-Diazafluorenone 4-Oxide (15)

A suspension of **14** (1.82 g, 10 mmol) in 30% hydrogen peroxide (40 mL) with $Na_2WO_4 \cdot 2H_2O$ (0.1 g) was heated at 80°C with vigorous stirring for 1 h. The insoluble excess of the starting material was removed by filtration and the filtrate was extracted several times with chloroform and the extracts were checked chromatographically. The previous extracts containing a mixture of substrate and **15** were evaporated, the residue collected and added to unreacted substrate, and the oxidation repeated. The latter extracts containing solely *N*-oxide were collected and dried ($MgSO_4$). This compound **15** underwent decomposition on a column filled with silica gel or alumina and could be purified or separated chromatographically. Purification was effected by recrystallization from water; yellow needles decomposed above 230°C, 22% yield; ir (KBr) ν_{max}: 1725 (s, CO), 1294, and 1262 cm^{-1} (s, NO). *Anal.* calcd. for $C_{11}H_6N_2O_2$: C 66.66, H 3.05, N 14.14; found: C 66.40, H 2.91, N 13.76.

1,5-Diazafluorenone 5-Oxide (16)

16 was obtained from **13** similarly to **15**. The reaction was complete after 3 h, and the reaction mixture was extracted with chloroform. The extracts were dried ($MgSO_4$) and evaporated, and the residue separated chromatographically on a column filled with silica gel, using the mixture: ethyl acetate – methanol – chloroform (5:3:1) as eluent. The crude **16** was obtained from the former fractions and recrystallized from water; yellow needles, 37% yield, mp 240–242°C (dec.); ir (KBr) ν_{max}: 1732 (s, CO), 1270, and 1251 cm^{-1} (s, NO). *Anal.* calcd. for $C_{11}H_6N_2O_2$: C 66.66, H 3.05, N 14.14; found: C 66.36, H 3.06, N 14.17; ^1H nmr ($(CF_3)_2CO$) δ: 9.08 (dd, J = 8 Hz and 1.5 Hz, 1H, H-4), 8.94 (dd, J = 5 Hz and 1.5 Hz, 1H, H-2), 8.62 (dd, J = 5 and 1.5 Hz, 1H, H-6), 8.17 (dd, J = 8 Hz and 1.5 Hz, 1H, H-8), and 7.65–7.97 (m, 2H, H-3 and H-7).

1-Azafluorene 1-Oxide (19)

To a solution of **17** (1.0 g, 6 mmol) in glacial acetic acid (12 mL) and benzene (12 mL), 30% hydrogen peroxide (3 mL) was added and the mixture was refluxed for 2 h. Then the second portion of 30% hydrogen peroxide (1 mL) was added and the reaction mixture was heated for an additional 6 h, concentrated under reduced pressure to about 3 mL, water (15 mL) added, and the solution concentrated again. This procedure was repeated for the complete removal of acetic acid. The residue was evaporated to dryness and extracted with chloroform. The extracts were dried ($MgSO_4$) and evap-

[1]Photocopies may be obtained, at a nominal charge, upon request from the Depository of Unpublished Data, CISTI, National Research Council of Canada, Ottawa, Ont., Canada K1A 0S2.

orated. The crude product was recrystallized from methanol–water (5:1); yellow prisms, 54% yield, mp 142–143°C (dec.); ir (KBr) ν_{max}: 1255 and 1240 cm^{-1} (s, NO). *Anal.* calcd. for $C_{12}H_9NO$: C 78.66, H 4.95, N 7.64; found: C 78.31, H 4.80, N 7.52.

4-Azafluorene 4-Oxide (20)

20 was obtained from **18** in a similar manner as for **19** by oxidation for 10 h. The crude product was recrystallized twice from ethyl acetate; yellow needles, 45% yield, mp 164–165°C (lit. (9) mp 163–164°C); ir (KBr) ν_{max}: 1291 (s, NO), 1270 cm^{-1} (s, NO). *Anal.* calcd. for $C_{12}H_9NO$: C 78.66, H 4.95, N 7.64; found: C 78.51, H 5.08, N 7.54.

Oxidation of Diazafluorenones

Oxidation of 1,8-diazafluorenone **21** was carried out in a similar manner as for **9**, with 30% H_2O_2 in acetic acid – benzene solution. The product (19% yield) was identical with **10**.

Oxidation of 1,5-, 2,5-, and 4,5-diazafluorenes **22**, **23**, and **24** was performed in a similar manner as for the oxidation of diazafluorenones, with H_2O_2 in the presence of Na_2WO_4, and the corresponding *N*-oxides **12** (9% yield), **15** (7% yield), and **16** (16% yield) isolated.

General Procedure of N-*Methylation*

Azafluorene or azafluorenone (5 mmol) and methyl iodide (22.7 g, 160 mmol) were dissolved in 50 mL of benzene, refluxed for 6 h, and allowed to stand for an additional 12 h at room temperature. The precipitated *N*-methiodide was isolated by filtration and washed three times with small amounts of benzene. The crude **29** was recrystallized from water. Reaction yields and the characteristics of the products are given in Table 1.

In order to determine the rate constants, two series of measurements were run for each experiment, reacting the solution of 2.5 mmol of the starting base in benzene (25 mL) with 80 mmol of CH_3I for four short reaction times at the boiling point of the mixture. Amounts of the methiodides formed were established gravimetrically. The particular rate constants k were calculated using the formula for a second order reaction

$$kb(t_1 - t_2) = \ln [(a - x_1)/(a - x_2)] \qquad \text{when } b \gg a$$

where b = the methyl iodide concentration, a = the initial concentration of the substrate, x_1 = the loss of the substrate in time t_1, and x_2 = the loss of the substrate in time t_2. The average k values obtained with the accuracy ±2% are listed in Table 2.

TABLE 2. Rate constants of *N*-methylation of azafluorenones and azafluorenes

Azafluorenones	$k \times 10^5$ ($L \cdot mol^{-1} \cdot s^{-1}$)	Azafluorenes	$k \times 10^5$ ($L \cdot mol^{-1} \cdot s^{-1}$)
5	1.85	**17**	30.9
6	0.18	**18**	3.42
9	2.12	**21**	23.4
14	5.10	**24**	160

1. N. S. PROSTAKOV. Usp. Khim. **38**, 1710 (1969).
2. J. MŁOCHOWSKI and Z. SZULC. Wiad. Chem. **31**, 665 (1977).
3. K. KLOC, J. MŁOCHOWSKI, and Z. SZULC. Z. Prakt. Chem. **319**, 959 (1977).
4. K. KLOC, J. MŁOCHOWSKI, and Z. SZULC. Heterocycles, **9**, 849 (1978).
5. W. TRIEBS and J. BEGER. Ann. Chem. **652**, 212 (1962).
6. C. JUTZ, R. M. WAGNER, A. KRAATZ, and H.-G. LÖBERING. Ann. Chem. **5**, 874 (1975).
7. J. CROSSLAND and O. T. DYRNUM. Acta Chem. Scand. Ser. B, **30**, 358 (1976).
8. L. A. SUMMERS, J. F. ECKHARD, and N. G. KEATS. Z. Naturforsch. Teil B, **33**, 80 (1978).
9. R. F. PARCELL and F. P. HAUCK, JR. J. Org. Chem. **28**, 3468 (1963).
10. N. S. PROSTAKOV, A. W. WARLAMOV, G. A. WASILIEV, O. G. KESAREV, and G. A. URBINA. Khim. Geterotsikl. Soedin. 124 (1977).
11. N. H. CROMWELL and R. A. MITSCH. J. Org. Chem. **26**, 3812 (1961); **26**, 3817 (1961).
12. Y. HAMADA and J. TAKEUCHI. Chem. Pharm. Bull. **24**, 2769 (1976).
13. P. HAMM and W. v. PHILIPSBORN. Helv. Chim. Acta, **54**, 2363 (1971).
14. J. MŁOCHOWSKI and K. KLOC. Roczn. Chem. **47**, 727 (1973).
15. M. JASTRZĘBSKA-GLAPA, J. MŁOCHOWSKI, and W. SLIWA. Pol. J. Chem. In press.
16. M. TUSZKIEWICZ, E. PLESZCZYŃSKA, J. MŁOCHOWSKI, and Z. SKROWACZEWSKA. Med. Dosw. Mikrobiol. **27**, 11 (1975).

The decomposition of cyclobutanone vapor induced by infrared radiation from a pulsed CO_2 TEA laser[1]

M. H. BACK
Department of Chemistry, University of Ottawa, Ottawa, Ont., Canada K1N 9B4
AND
R. A. BACK
Division of Chemistry, National Research Council of Canada, Ottawa, Ont., Canada K1A 0R6

Received December 20, 1978

M. H. BACK and R. A. BACK. Can. J. Chem. **57**, 1511 (1979).

The decomposition of cyclobutanone vapor by infrared radiation from a pulsed CO_2 TEA laser at 9.552 μm has been studied at pressures from about 0.1 to 10 Torr. The main decomposition path was

[1] 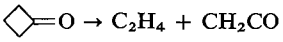

while the reaction

[2] 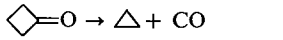

was much less important. Very minor amounts of propylene and acetylene were also observed. From the ratio of reaction [2] to reaction [1], information was obtained about the effective temperature of the decomposition and the energy of the decomposing molecules. With the laser beam unfocussed, the decomposition at pressures above about 3 Torr is adequately described as a thermal decomposition, controlled by the initial temperature attained and the rate of cooling of the irradiated gas. At lower pressures, and when the laser beam was focussed, direct excitation and decomposition of individual molecules by multiphoton absorption appears to be involved.

M. H. BACK et R. A. BACK. Can. J. Chem. **57**, 1511 (1979).

Opérant à des pressions de 0.1 à 10 Torr, on a étudié la décomposition de la vapeur de cyclobutanone par une radiation infrarouge émise par un laser TEA à CO_2 déclenché à 9.552 μm. La voie principale de décomposition est

[1] 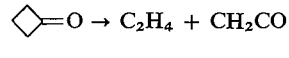

alors que la réaction

[2] 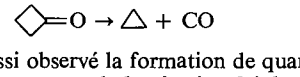

est moins importante. On a aussi observé la formation de quantités mineures de propylène et d'acétylène. En se basant sur le rapport de la réaction 2 à la réaction 1, on a obtenu des informations concernant la température effective de la décomposition et l'énergie des molécules qui se décomposent. Lorsque le rayon laser n'est pas bien focalisé, on peut décrire adéquatement la décomposition à des pressions supérieures à 3 Torr par une décomposition thermique qui est contrôlée par la température initiale obtenue et le taux de refroidissement des gaz irradiés. A des pressions inférieures et lorsque le rayon laser est bien focalisé, il semble que l'excitation et la décomposition directe de molécules individuelles par une absorbtion multiphoton soient impliquées.

[Traduit par le journal]

Introduction

The decomposition of gases by intense infrared radiation from pulsed lasers is the subject of widespread interest and investigation (1, 2). It is clear that many molecules can be excited beyond their dissociation limits, both at high pressures where collisional energy transfer dominates, and at low pressures where excitation of isolated molecules occurs essentially free of collisions. One of the more interesting questions in these systems is the energy distribution of the molecules that have been excited, particularly those that have been excited beyond their dissociation limits and decompose (1–6). Such energy distributions are obviously complex functions of radiation intensity, absorption coefficients, energy transfer (both inter- and intramolecular), and the rate of decomposition of molecules from various states of excitation above the dissociation energy.

One experimental approach to an estimate of energy distributions in such systems is the study of a

[1]NRCC No. 17348.

0008-4042/79/121511-07$01.00/0

molecule with two well-defined modes of decomposition with different threshold energies. A molecule that appears well suited to such a study is cyclobutanone. It is well established (7–10) from conventional thermal decomposition studies that there are two clean, nonradical unimolecular modes of decomposition:

[1] 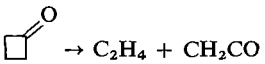 $\rightarrow C_2H_4 + CH_2CO$

[2] 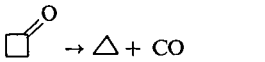 $\rightarrow \triangle + CO$

with rates given by the Arrhenius expressions[2]

$$k_1 = 3.60 \times 10^{14} \exp(-52\,000/RT)\ s^{-1}$$

and

$$k_2 = 2.34 \times 10^{14} \exp(-58\,000/RT)\ s^{-1}$$

The present paper describes a study of the decomposition of cyclobutanone vapor over a range of pressures and in both the focussed and unfocussed beams of a pulsed CO_2 TEA laser.

Experimental

Experiments were done in a cylindrical Pyrex reaction vessel, 10 cm long and 5 cm in diameter, fitted with plane salt windows attached with black wax. Infrared radiation was obtained from a Lumonics Model 203 pulsed CO_2 TEA laser, operating at about 0.5 Hz, with a $He/CO_2/N_2$ mix of 10/3/1.1, with the beam stopped down to a diameter of 1.3 cm. Incident and transmitted fluence were monitored with calibrated pyroelectric detectors and suitable beam splitters. Incident fluence was varied by inserting germanium flats in the laser beam. For experiments with a focussed beam, a NaCl lens with 5 cm focal length was placed immediately before the front window of the cell. All irradiations were done using the P(20) line at 9.552 μm, selected by an intracavity grating, which represented an optimum combination of laser intensity and absorption coefficient to give a maximum energy deposition in the cyclobutanone vapor. Maximum pulse energy was about 2 J.

Cyclobutanone was purchased from Aldrich Chemical Co. and used after simple degassing at −78°C on a conventional vacuum line. Blank experiments showed residual traces of ethylene and cyclopropane for which small corrections were made. The reaction vessel was attached to the vacuum line by a standard-taper joint, filled to the desired pressure, and removed for irradiation. After irradiation it was attached again to the vacuum line for analysis. Gases noncondensable at −210°C were removed through a solid-nitrogen trap, after which products volatile at −78°C were condensed and sealed into glass ampoules for gc analysis. The products ethylene, cyclopropane, propylene, and acetylene were analysed on a 6 m column of phenylisocyanate on Porasil at 40°C. Ketene, which is a probable product, was not detected by this analysis.

[2]These expressions are based on the measurements of k_1 by Das *et al.* (7) and on values of k_1/k_2 obtained by Blades (8). The later study by McGee and Schleifer (9) gave almost identical values of k_1, while their relative rate data when replotted with those of Blades show no significant differences and cover a much narrower range of temperature.

Results

Infrared Absorption Spectrum

The absorption spectrum of cyclobutanone vapor in the 10-μm region is shown in Fig. 1. The band at 1070 cm^{-1} has been assigned to ν_{24}, a B_2 rocking mode of the αCH_2 groups (11). All experiments were done using the P_{20} line of the CO_2 laser at 1059 cm^{-1} which lies on the low frequency shoulder of the absorption band (Fig. 1). The absorption at this frequency, based on measurements of incident and transmitted fluence of the unfocussed beam, showed a Beer's Law behaviour, i.e., log (incident fluence/transmitted fluence) varied linearly with cyclobutanone pressure corresponding to an effective decadic molar extinction coefficient of 23 $M^{-1}\ cm^{-1}$. Addition of inert gas (air or xenon) had no effect on the absorption.

Decomposition in the Unfocussed Beam

Products observed and measured were ethylene, cyclopropane, propylene, and acetylene, the latter two of very minor importance. Yields per pulse were independent of the number of pulses, showing that all products were of primary origin and that their secondary decomposition was not important. The fraction of the cyclobutanone decomposed was never more than 5% and usually much less.

Figure 2 shows a log–log plot of the dependence of the yield of ethylene on pressure of cyclobutanone,

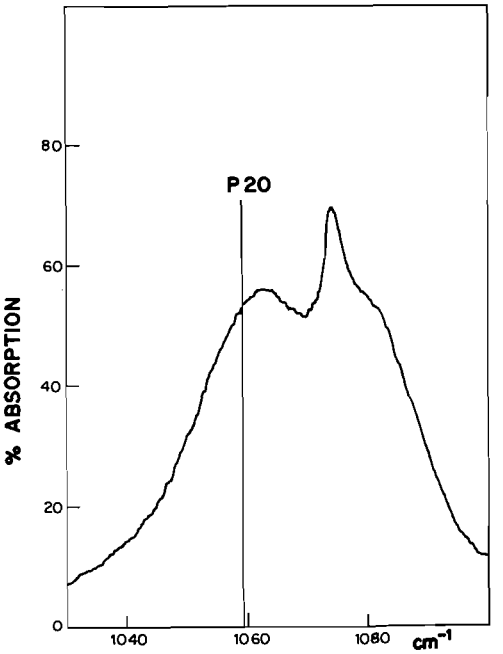

FIG. 1. Absorption spectrum of cyclobutanone vapor at 10 Torr pressure, in the 9–10 μm region.

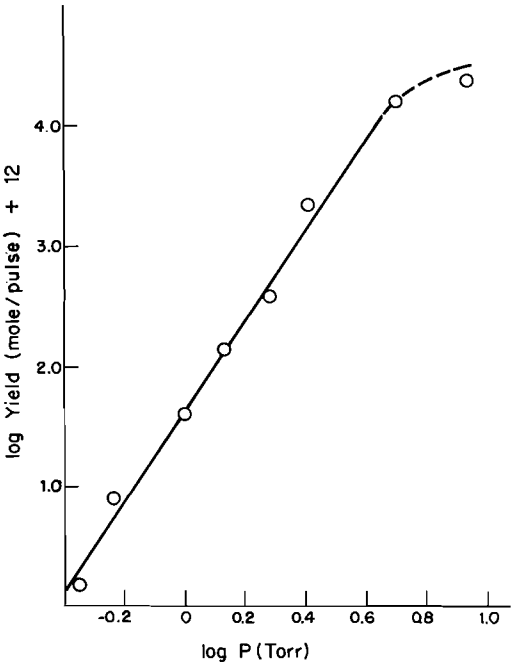

FIG. 2. Yield of ethylene per pulse vs. pressure of cyclobutanone from the unfocussed beam.

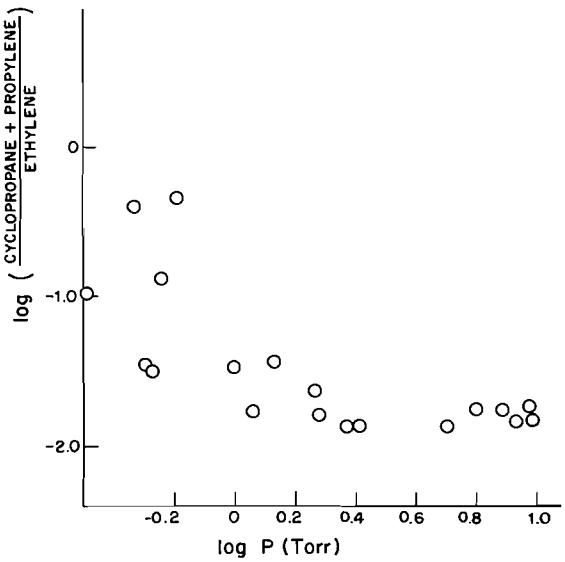

FIG. 3. Product ratio (cyclopropane + propylene)/ethylene vs. pressure of cyclobutanone from the unfocussed beam.

while Fig. 3 shows the variation of the (cyclopropane + propylene)/ethylene ratio. Yields of propylene varied from about 1% of the cyclopropane at pressures above 5 Torr to as high as 20% at the lowest pressures, with considerable scatter in the data. Acetylene formation was somewhat irregular, but usually less than 0.5% of the ethylene.

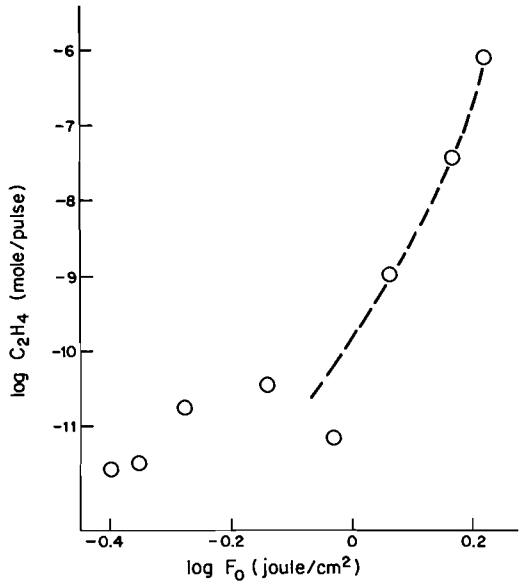

FIG. 4. Yield of ethylene per pulse vs. incident fluence; unfocussed beam, 9.5 Torr cyclobutanone.

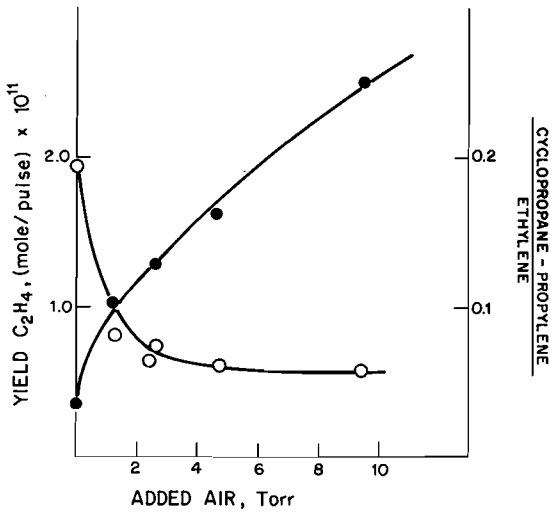

FIG. 5. Effect of added air on the product yields; unfocussed beam, 0.5 Torr cyclobutanone. ○ = ethylene; ● = (cyclopropane + propylene)/ethylene.

Figure 4 shows the dependence of the yield of ethylene on fluence at a constant pressure (9.5 Torr) of cyclobutanone. Figure 5 shows the effect of the addition of a nonabsorbing gas (air) on the yield of ethylene from 0.5 Torr of cyclobutanone, and the effect on the ratio (cyclopropane + propylene)/ethylene.

Decomposition in the Focussed Beam

Ethylene was again the major product of the decomposition detected and measured. The minor

products increased in importance in the focussed beam. The sum of cyclopropane + propylene increased to about 3.5% of the ethylene, while the propylene rose sharply to about 40% of the cyclopropane, with both these product ratios approximately independent of cyclobutanone pressure and incident fluence. The yield of acetylene increased markedly to about 4% of the ethylene at the maximum fluence employed. The ratio acetylene/ethylene was approximately independent of pressure, but varied almost linearly with incident fluence. Figure 6 shows the dependence of the ethylene yield on cyclobutanone pressure, while Fig. 7 shows its variation with fluence incident on the lens at a pressure of 0.14 Torr.

Discussion

It is useful to discuss the present results in terms of two limiting mechanisms. The first, which will predominate at high pressure and low fluence, can be described as a thermal decomposition of a hot gas approaching thermal equilibrium through collisional redistribution of energy. The second mechanism involves multiphoton absorption and dissociation of individual molecules essentially free of collisions, which can be expected to operate at low pressures and high fluence. Under conditions between these two extreme limits, some mixture of the two mechanisms will occur.

The results with the unfocussed laser at pressures above about 3 Torr of cyclobutanone point clearly to a system tending towards the first mechanism, a thermal decomposition, rather than a multiphoton dissociation. At the highest fluence employed, an average of about 4 photons per molecule were absorbed during the ~250 ns pulse, while at 3 Torr pressure each molecule would suffer on the average about 25 collisions during the same period. Collisional energy transfer would obviously compete effectively with excitation, and the direct accumulation in a single molecule of the 17 quanta necessary for dissociation would become very improbable. At lower fluence and higher pressure collisional processes would become even more dominant. To test the plausibility of a thermal decomposition model under such conditions, a simple calculation can be made of the maximum temperature to be expected in the irradiated gas. At a pressure of 9.5 Torr the average total energy absorbed in a single pulse at the highest fluence was 17.9 kcal/mol. The heat capacity of cyclobutanone was calculated by the group additivity method outlined by Benson and O'Neal (10) at intervals of 100°, and a graphical integration performed to estimate a temperature of 880 K at the end of the pulse, assuming thermal equilibration in the irradiated zone and negligible cooling. Temperatures estimated in this way are shown in Table 1 for all the experiments plotted in Fig. 4, and yields of ethylene are then plotted in Arrhenius form in Fig. 8, in which the linear portion corresponds to an activation energy of about 50 kcal/mol. The deviation from linearity at the lowest fluences may be genuine or may simply reflect the uncertainty in measurement

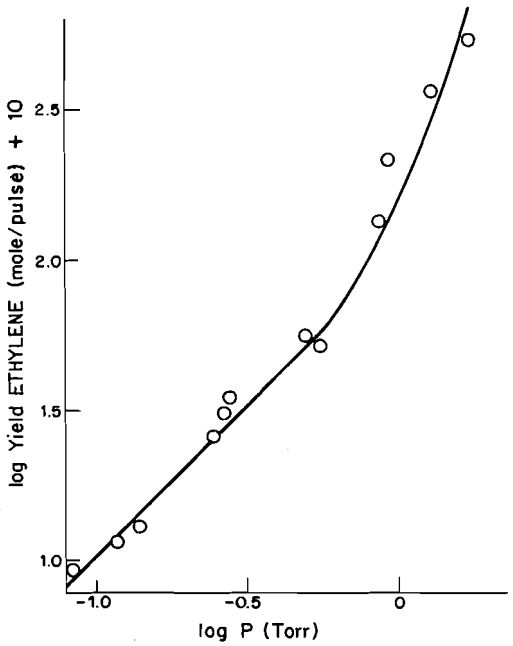

FIG. 6. Yield of ethylene per pulse vs. pressure of cyclobutanone in the focussed beam.

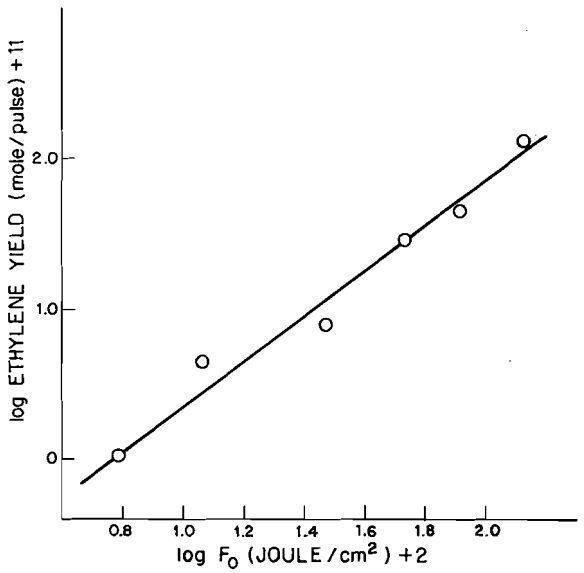

FIG. 7. Yield of ethylene per pulse vs. fluence incident on the lens; focussed beam, 0.13 Torr cyclobutanone.

TABLE 1. Thermal decomposition model for unfocussed beam

Expt. No.	F_0 (J/cm²)	C_2H_4 (mol/pulse)	T (K)	Reaction time (ms)
52	1.47	3.89×10^{-8}	816	1
53	1.65	1.30×10^{-7}	880	0.5
54	0.53	1.77×10^{-11}	486	
55	0.733	3.48×10^{-11}	558	
56	0.932	6.78×10^{-12}	628	3
57	0.444	3.14×10^{-12}	456	
58	0.40	2.84×10^{-12}	440	
59	1.16	1.12×10^{-9}	708	5

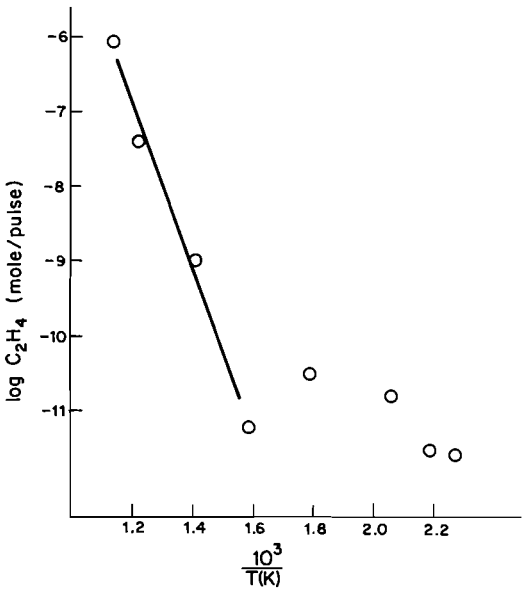

FIG. 8. Yield of ethylene per pulse as a function of estimated temperature in irradiated zone. The straight line corresponds to an activation energy of about 50 kcal/mol. Unfocussed beam, 9.5 Torr cyclobutanone.

of the very small yields. In the thermal decomposition model, the reaction time will be determined by the rate of cooling of the hot gas after the pulse. Effective reaction times required to account for the extent of decomposition observed can be estimated from the known Arrhenius parameters for k_1 and are shown in Table 1. A precise treatment of the system would require a complex integration of k_1 over time, temperature, and space. The magnitude of the activation energy, however, will dictate that most of the decomposition will occur within a few degrees of the maximum temperature achieved, so that the estimates of the latter in Table 1 may be a fair approximation to the temperature of the decomposition. The activation energy obtained from Fig. 8 is close to that established for reaction [1], and the effective times estimated are in reasonable accord with rough approximations of the rate of cooling by conduction of the hot gas. Thus the decomposition of cyclobutanone observed in the unfocussed beam at 9.5 Torr can be reasonably accounted for by a thermal decomposition model, although the limitations of such a simple treatment are obvious (3–6) and should be stressed.

The ratio of cyclopropane to ethylene can also be used to estimate the effective temperature of the decomposition. This ratio was approximately constant above 3 Torr (Fig. 3) with a value of 0.017 ± 0.002. From the Arrhenius relation reported by Blades (8) that $k_2/k_1 = 0.65 \exp(-6000/RT)$, this corresponds to a temperature of 830 ± 30 K. Uncertainty in the measurement of the rather small yields of cyclopropane make this an inaccurate estimate of temperature, but within these limitations the agreement with the data in Table 1 is reasonable. The same uncertainty in the measurement of cyclopropane obscured any systematic variation in the cyclopropane/ethylene ratio with fluence.

The strong pressure dependence of the reaction (Fig. 2) is also explicable by the thermal decomposition model. For the present weakly absorbing system, the energy absorbed per molecule and hence the temperature achieved at the end of the pulse should be roughly independent of pressure. The rate of cooling then becomes an important parameter and in cylindrical geometry with cooling by conduction, the integrated decomposition of the hot gas during the cooling period should be very roughly proportional to p^2. Blades observed that the decomposition of cyclobutanone was pressure dependent below 10 Torr at about 630 K (8), and at the higher temperatures achieved in the present study this effect would be enhanced and the decomposition would approach second order. A total pressure dependence of about p^3 or p^4 might therefore be expected, as was observed.

The effect of adding a nonabsorbing gas (air or xenon) to the system is also compatible with the thermal decomposition model. Interpretation of these experiments is not simple, as three different effects will be superimposed; (*i*), reduction in temperature through increased heat capacity of the system; (*ii*), slower cooling by conduction, just as in cyclobutanone itself; and (*iii*), enhancement of rates of reactions [1] and [2] if they are pressure dependent as suggested. The first effect should predominate, and indeed the rate of decomposition decreased as expected (Fig. 5), although the decrease was probably reduced by the latter two effects which act in the opposite direction. Surprisingly, formation of cyclopropane was reduced less than that of ethylene, so that the ratio cyclopropane/ethylene increased with

added gas (Fig. 5), the reverse of the effect expected from a reduction in temperature. The same effect was observed on the addition of xenon. A possible explanation lies in the greater pressure dependence of reaction [2] reported by Blades (8), which might outweigh the effect of reduced temperature.

At pressures below 3 Torr of cyclobutane in the unfocussed beam, the ratio (cyclopropane + propylene)/ethylene increased notably (Fig. 3), and a similar increase in the propylene/cyclopropane ratio was also observed. The thermal decomposition model does not predict a rise in temperature at low pressure, and it seems probable that these changes in the product ratios arise from the onset of some multiphoton dissociation as the pressure was reduced. If the decomposition of a cyclobutanone molecule energized by multiphoton absorption is a statistical process dependent only on the total energy content, as seems probable for a polyatomic molecule of this complexity (1–6), the change in product ratios at low pressure implies that the dissociating molecules have a much higher average energy content than those decomposing in the thermally equilibrated system at the same fluence. This could come about through a more efficient absorption of radiation, either an overall higher average absorption coefficient, or perhaps a stronger absorption at the higher energy levels which could lead to relatively higher populations at energies above the dissociation energy than found in a Boltzmann distribution. An alternative explanation is that only a fraction of the molecules (those in appropriate rotational levels) absorb radiation, and the absorbed energy remains more or less in this selected assembly of molecules which is thereby raised to a higher average energy content or 'temperature'. From an average value of cyclopropane/ethylene of about 0.1 at 0.5 Torr, an effective temperature of the dissociating molecules of about 1600 K can be estimated, which would require that the absorbed energy was effectively restricted to about half the molecules in the irradiated zone. The present level of understanding of multiphoton absorption does not permit a clear decision between the two suggested explanations.

The decomposition of cyclobutanone in the focussed beam showed a behaviour quite different from that found with unfocussed radiation. The dependence on pressure and fluence was much less sharp (Figs. 6 and 7), and the minor products, propylene, and acetylene, became much more important. All these features point to a decomposition occurring largely through multiphoton absorption by individual molecules, as might be expected at the high fluence and relatively low pressures in these experiments (pressure was limited by electrical breakdown at the focus). The 3/2 dependence on fluence (Fig. 7) has been attributed in other systems to a simple geometric effect arising when complete decomposition occurs within a reaction zone around the focus which is sharply defined by a threshold fluence (1, 2, 12). The very high dependence on fluence observed in the unfocussed beam (Fig. 4) will give rise to such a threshold behaviour, and there is no reason to doubt that this model applies to the present system. From the absolute yield of decomposition per pulse, a reaction zone of 0.09 cm^3 volume can be estimated at the maximum fluence employed, which corresponds to a double cone 3.4 cm long and 0.44 cm end diameter, and a threshold fluence of ~ 11 J/cm^2.

The first-order pressure dependence of the decomposition at low pressures is also indicative of a multiphoton dissociation, simply reflecting the number of molecules present in the reaction zone. The increasing pressure dependence above about 0.5 Torr suggests that a thermal decomposition mechanism is beginning to contribute to the reaction.

The source of the increased yields of the minor products in the focussed beam is not entirely clear. It was concluded that in the unfocussed beam, cyclopropane and propylene were primary in origin, arising from excitation of cyclobutanone to levels capable of yielding these products. For cyclopropane, Blades found an activation energy 6 kcal/mol higher than that for ethylene formation (8), and suggested that from theoretical estimates of its heat of formation (9), the C_3H_6 biradical (which could give rise to propylene) would require an additional 5 to 10 kcal/mol. The relative yields of ethylene, cyclopropane, and propylene in the unfocussed system are compatible with these activation energy differences operating in a thermal decomposition, with some contribution from direct multiphoton excitation at low pressure. The marked increase in yields of cyclopropane and propylene in the focussed beam could be explained by primary excitation of cyclobutanone to higher energy levels in the multiphoton process, operating at the much higher fluences of the focussed beam. However, secondary decomposition of cyclopropane or ethylene cannot be ruled out as sources of propylene and acetylene in the focussed beam, since cyclobutanone was almost completely decomposed in the reaction zone so that product concentrations became comparable to that of starting material. Both ethylene and cyclopropane absorb the 9.552 μm laser radiation, the former weakly, the latter strongly, and their decomposition by multiphoton absorption (13, 14) or perhaps by thermal processes following the pulse might be possible. In particular, formation of acetylene, which

was barely detectable in the unfocussed beam, and which would probably require a large additional excitation of cyclobutanone above the threshold for ethylene formation, is best explained in the focussed beam by a secondary decomposition of ethylene. The relatively small enhancement of the sum of the yields of cyclopropane + propylene on focussing the beam suggests that the energy content of the decomposing cyclobutanone molecules was not enormously higher than in the unfocussed beam, perhaps implying an energy distribution limited by rapid decomposition via reactions [1] and [2]. It is not clear whether propylene is primary or secondary in origin in the focussed beam.

1. R. V. AMBARTZUMIAN and V. S. LETOKHOV. Chemical and biochemical application of lasers. Vol. III. Academic Press, New York. 1977. p. 167.
2. N. BLOEMBERGEN and E. YABLONOVITCH. Phys. Today, **31**, 23 (1978); M. J. SCHULTZ and E. YABLONOVITCH. J. Chem. Phys. **68**, 3007 (1978).
3. I. OREF and B. S. RABINOVITCH. J. Phys. Chem. **26**, 2587 (1977).
4. S. H. BAUER. Chem. Rev. **78**, 147 (1978).
5. W. C. DANEN, W. D. MUNSLOW, and D. W. SETSER. J. Am. Chem. Soc. **99**, 6961 (1977).
6. W. TSANG, J. A. WALKER, W. BRAUN, and J. T. HERRON. Chem. Phys. Lett. **59**, 487 (1978).
7. M. N. DAS, F. KERN, T. D. COYLE, and W. D. WALTERS. J. Am. Chem. Soc. **76**, 6271 (1954).
8. A. T. BLADES. Can. J. Chem. **47**, 615 (1969).
9. T. H. MCGEE and A. SCHLEIFER. J. Phys. Chem. **76**, 963 (1972); **77**, 1317 (1973); A. T. BLADES and S. SANDHU. J. Phys. Chem. **77**, 1316 (1973).
10. S. W. BENSON and H. E. O'NEAL. Kinetic data on gas phase unimolecular reactions. NSRDS-NBS 21, Washington. 1970.
11. K. FREI and Hs. H. GUNTHARD. J. Mol. Spectrosc. **5**, 218 (1960); R. CATALIOTTI, M. G. GIORGINI, G. PALIANI, and A. POLETTI. Spectrosc. Lett. **7**, 563 (1974).
12. P. FETTWEIS and M. NEVE DE MEVERGNIES. Appl. Phys. **12**, 219 (1977); S. SPEISER and J. JORTNER. Chem. Phys. Lett. **44**, 399 (1976).
13. M. L. LESIECKI and W. A. GUILLORY. J. Chem. Phys. **66**, 4317 (1977).
14. N. C. PETERSON, R. G. MANNING, and W. BRAUN. J. Res. Natl. Bur. Stand. A, **83**, 117 (1978).

Gas-phase proton-transfer reactions of the hydronium ion at 298 K

GERVASE I. MACKAY, SCOTT D. TANNER, ALAN C. HOPKINSON, AND DIETHARD K. BOHME[1]

Department of Chemistry, York University, Downsview, Ont., Canada M3J 1P3

Received November 29, 1978

GERVASE I. MACKAY, SCOTT D. TANNER, ALAN C. HOPKINSON, and DIETHARD K. BOHME. Can. J. Chem. 57, 1518 (1979).

Rate constants measured with the flowing afterglow technique at 298 ± 2 K are reported for the proton-transfer reactions of H_3O^+ with CH_2O, CH_3CHO, $(CH_3)_2CO$, HCOOH, CH_3COOH, $HCOOCH_3$, CH_3OH, C_2H_5OH, $(CH_3)_2O$, and CH_2CO. Dissociative proton-transfer was observed only with CH_3COOH. The rate constants are compared with the predictions of various theories for ion–molecule collisions. The protonation is discussed in terms of the energetics and mechanisms of various modes of dissociation.

GERVASE I. MACKAY, SCOTT D. TANNER, ALAN C. HOPKINSON et DIETHARD K. BOHME. Can. J. Chem. 57, 1518 (1979).

On rapporte les constantes de vitesse à 298 ± 2 K, mesurées grâce à la technique de lueur d'écoulement, pour les réactions de transfert de proton de H_3O^+ avec CH_2O, CH_3CHO, $(CH_3)_2CO$, HCOOH, CH_3COOH, $HCOOCH_3$, CH_3OH, C_2H_5OH, $(CH_3)_2O$ et CH_2CO. On a observé la réaction de transfert dissociatif de proton que dans le cas du CH_3COOH. On compare les constantes de vitesse avec les valeurs prédites par diverses théories pour les collisions ion–molécule. On discute de la protonation en termes des énergies et des mécanismes de divers modes de dissociation.

[Traduit par le journal]

Introduction

Experimental studies of the gas-phase chemistry of the hydronium ion have not been extensive since its first observation in 1940 (1). This is somewhat surprising, particularly in view of the history of this ubiquitous ion in solution chemistry. The gas-phase measurements have generally been restricted to the kinetics and equilibria of three-body association reactions of the hydronium ion with H_2O molecules (2, 3). They were undertaken primarily to provide insight into fundamental aspects of the step-wise hydration of this ion, particularly as it is believed to proceed in and below the D-region of the earth's ionosphere (4, 5). The few measurements concerned with two-body reactions of H_3O^+ which have been reported were largely incidental to investigations directed towards the determination of the gas-phase proton affinity of H_2O (6), the systematic assessment of classical theories of ion–molecule collisions (7–9), and the identification of ion–molecule reactions which represent a sink for chlorofluoromethanes in the troposphere and stratosphere (10). We report here an extensive flowing afterglow study of the room-temperature kinetics and energetics of proton-transfer reactions of H_3O^+ which was undertaken primarily to provide a 'benchmark' for the solution chemistry of the hydronium ion and to set the stage for further gas-phase measurements designed to elucidate the influence of step-wise hydration on the chemical behaviour of H_3O^+ (11). Proton-transfer reactions of H_3O^+ are also of interest in several other diverse areas of chemistry including chemical ionization mass spectrometry (12), flame ion chemistry (13), and the ion chemistry of moist atmospheres (5).

Experimental

The majority of the measurements was carried out in a conventional flowing plasma mass-spectrometer (flowing afterglow) system which has been described previously (14). The reactant H_3O^+ ions were established in either a flowing helium or a flowing hydrogen plasma. Distilled water vapor was added to the helium upstream of the ion production region. In this mode the H_2O^+, OH^+, and H^+ ions produced, either directly by electron impact, or indirectly by reactions of helium ions and excited neutral atoms, undergo further reactions with H_2O to eventually produce H_3O^+. In a flowing hydrogen plasma H_3O^+ is established primarily by the fast proton-transfer reaction

$$[1] \qquad H_3^+ + H_2O \rightarrow H_3O^+ + H_2$$

with $k = (4.3 \pm 1) \times 10^{-9}$ cm^3 molecule^{-1} s^{-1} (15). In this case the distilled water vapor was added downstream of the ionizer in amounts sufficient to ensure the completion of reaction [1] prior to the reaction region further downstream.

A few of the measurements were carried out with the apparatus in the Selected Ion Flow Tube (SIFT) configuration modelled after the original design reported by Adams and Smith (16). In this configuration a differentially pumped quadrupole mass filter was interposed between the ion production and ion reaction regions. The H_3O^+ ions, after being produced in the conventional manner described above, were extracted from the ion production region through a 1 mm diameter orifice into the quadrupole mass filter which communicated

[1]To whom all correspondence should be addressed.

0008-4042/79/121518-06$01.00/0

TABLE 1. Energetics and measured rate constants (in units of 10^{-9} cm^3 molecule^{-1} s^{-1}) at 298 ± 2 K for proton-transfer reactions of H_3O^+ with molecules, M

M	$PA_{298}(M)^a$	Ref.	$-\Delta H_{298}{}^{0\,b}$	k^c	Ref.
H_2S	170.2±1.8	6	3.8±0.6	1.9±0.4	6
CH_2O	170.9±1.2	6	4.5±1.1	3.4±0.9(14)	
HCN	171.0±1.7	6	4.7±0.5	3.5±0.7	6
HCOOH	178.1±2	24	12±5	2.7±0.8(12)	
CH_3CHCH_2	180±2	9	14±5	1.5±0.3	25
CH_3NO_2	181±3	9	15±6	4.1±1.0	9
CH_3OH	181±3	9	15±6	2.8±0.7(7)	
CH_3CHO	185.4±2	24	19±5	3.6±0.9(12)	
C_2H_5OH	186.8±2	24	20±5	2.8±0.7(4)	
CH_3COOH	187.4±2	24	21±5	3.0±0.9(7)	
CH_3CN	187.4±2	24	21±5	4.7±0.7	8
$HCOOCH_3$	187.8±2	24	21±5	3.3±0.8(3)	
$(CH_3)_2O$	190.1±2	24	24±5	2.7±0.7(5)	
$(CH_3)_2CO$	193.6±1	26	27±4	3.9±1.0(7)	
CH_2CO	194.1±1	26	28±4	2.0±0.5(3)	
NH_3	200.4±2	24	34±5	2.4±0.5	7

[a]Proton affinity (in kcal mol^{-1}) corresponding to the formation of the lowest energy tautomer.
[b]Standard enthalpy change for proton transfer based on $PA_{298}(H_2O) = 166.4 \pm 2.4$ kcal mol^{-1} or direct equilibrium constant measurement (6).
[c]The mean value together with the estimated accuracy of the measurement. The number of measurements is given in parentheses. The precision of the measurements was observed to be better than ±15%.

with the flow tube through a 5 mm diameter gas entrainment orifice. After injection into the flow tube at ca. 40 eV, the H_3O^+ ions were allowed to thermalize by collision before they entered the reaction region 106 cm further downstream. In this way we could avoid the introduction of ion types other than H_3O^+ into the reaction region. This procedure also eliminated H_2O, the parent gas of H_3O^+, from the reaction region.

The reactant neutrals were added into the reaction region as vapors either in their pure form or diluted with helium. The determination of their flows required separate viscosity measurements as has been described (17). Rate constants were determined in the usual manner from measurements of the $m/e = 19$ signal as a function of addition of vapor into the reaction region (14). Product ion signals were measured concomitantly. The operating conditions in these experiments encompassed total gas pressures, P, in the range 0.258 to 0.509 Torr, average gas velocities, $\bar{v}$, in the range 6.7 to 8.2 × 10^3 cm s^{-1}, effective reaction lengths, L, of the order of 60 and 85 cm and a gas temperature, $T = 298 \pm 2$ K.

The vapors were derived from the following liquids: CH_3OH, HCOOH, and $(CH_3)_2CO$ (BDH chemicals, Analytical Reagent Grade), C_2H_5OH (Consolidated Alcohols, Absolute), CH_3CHO (BDH chemicals, Laboratory Reagent Grade, 99.0% min.), $HCOOCH_3$ (BDH chemicals, 98%), CH_3COOH (Anachemia Chemicals, Glacial, 99.7%), and $(CH_3)_2O$ (Matheson, 99.8% (typical)). CH_2O was prepared by the low pressure distillation of paraformaldehyde (Fisher Scientific, Purified Grade) by an adaptation of the method of Spence and Wild (18). Ketene was prepared by the pyrolysis of acetone at ca. 800 K. The monomeric gas was purified by passing it through a cold trap at 250 K (CCl_4 slush) and collecting it as a liquid at 144 K (pentane slush).

The flows of formic acid and acetic acid were corrected for dimerization using the dissociation equilibrium constants K_p (Torr) = 2.704 and 0.5458 respectively, at 299 K (19, 20). This correction was based on the reasonable assumption that the dimers were present in their equilibrium amounts both in the storage bulbs and prior to their entry into the reaction region. A separate experiment was performed to determine the extent of dimerization in ketene vapor. The infrared spectrum of a sample of ketene vapor was recorded over a period of several days and was compared to those of the ketene monomer (21, 22) and dimer (23). Over the range of pressure and storage time of our experimental gas samples, the mole fraction of dimer in the vapor phase appeared to be negligible.

Results and Discussion

Kinetics of Proton Transfer

The rate constants measured in this study for the reactions of H_3O^+ with oxygen bases are given in Table 1 along with several others which have been determined previously in this laboratory. The majority of these reactions appeared to proceed simply by the transfer of a proton without concomitant decomposition of the protonated product but followed by its solvation, primarily with the parent base. For example, as is evident from Fig. 1, the reaction of H_3O^+ with HCOOH produced $HCOOH_2^+$ as the only primary product ion which then reacted further by solvation to form the proton-bound formic acid dimer, $HCOOH_2^+ \cdot HCOOH$, presumably via three-body association according to the reaction

$$[2]\quad HCOOH_2^+ + HCOOH + M \rightarrow HCOOH_2^+ \cdot HCOOH + M$$

where M is a stabilizing third body which is primarily H_2 in these experiments. The rise in the hydrated ion $HCOOH_2^+ \cdot H_2O$ may be attributed primarily to the reaction of the hydrated H_3O^+ with HCOOH (11).

Proton transfer was observed to proceed in all cases with the rate constants spanning a range in

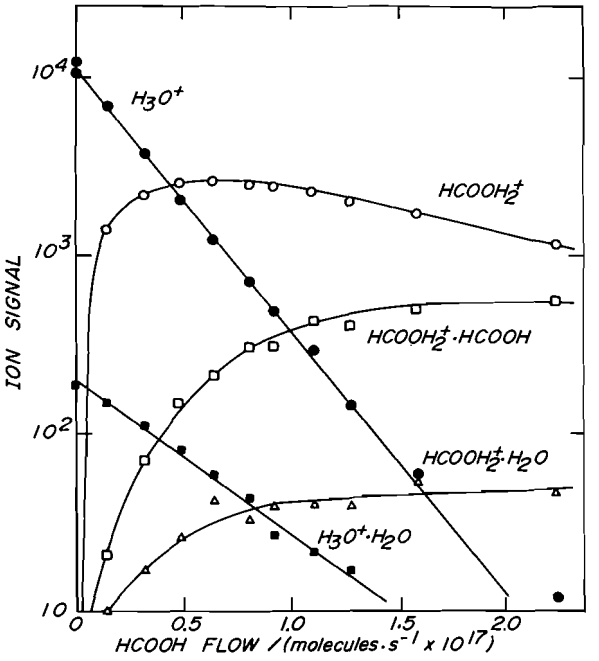

FIG. 1. The variation of the major positive ions observed upon the addition of formic acid vapor into a flowing H_2O–H_2 plasma in which H_3O^+ is initially a dominant ion. This decay of the H_3O^+ signal provides a rate constant of 2.4×10^{-9} cm^3 molecule^{-1} s^{-1}. $T = 298$ K, $P = 0.414$ Torr, $\bar{v} = 8.0 \times 10^3$ cm s^{-1}, and $L = 85$ cm.

values from 1.5 to 4.1×10^{-9} cm^3 molecule^{-1} s^{-1}. Surprisingly few other measurements are available for comparison. Interest in tropospheric and stratospheric ion chemistry prompted Fehsenfeld and co-workers to determine and report rate constants for the reaction of H_3O^+ with NH_3 for which (27) $k = (2.1 \pm 0.6) \times 10^{-9}$ cm^3 molecule^{-1} s^{-1} at 296 K, and with CH_2O and CH_3OH for both of which (28) $k = (2.2 \pm 0.9) \times 10^{-9}$ cm^3 molecule^{-1} s^{-1} at room temperature. These values are systematically lower than the corresponding values in Table 1, albeit there is agreement within the overall uncertainties reported for the two sets of measurements. The larger uncertainties associated with the reactions involving CH_2O and CH_3OH are attributed by these authors to the uncertainties associated with the measurement of the flow of these substances as vapors when derived from the liquid phase. The reaction of H_3O^+ with NH_3 has also been investigated with the ion cyclotron resonance technique by Huntress who reported (29) a value of $(2.20 \pm 0.12) \times 10^{-9}$ cm^3 molecule^{-1} s^{-1}. The remaining rate constants in Table 1 appear not to have been determined previously by other workers.

Figure 2 compares the proton-transfer rate constants listed in Table 1 with the capture rate constants predicted by various ion–molecule collision theories: the Langevin theory which ignores the influence of the permanent dipole moment of the molecule (30), the average-dipole-orientation (ADO) theory (the $\overline{\cos\theta}$ model) (31), the theory of Barker and Ridge (32), and the locked-dipole limit (33). The permanent dipole moments, μ_D, were all taken from the compilation of Nelson *et al.* (34). The polarizabilities, α, for H_2S, CH_2O, HCN, CH_3CHCH_2, CH_3OH, $(CH_3)_2CO$, and NH_3 were taken from existing compilations (35–37). The mean polarizabilities of the remaining molecules were calculated from bond and group polarizabilities (36) to be 3.09, 5.2, 4.40, 5.17, 5.03, 4.56, 5.90, 6.04, and 4.12 Å^3 for HCOOH, CH_3NO_2, CH_3CHO, C_2H_5OH, CH_3COOH, CH_3CN, $HCOOCH_3$, $(CH_3)_2O$, and CH_2CO, respectively. It is apparent from Fig. 2 that proton transfer to these molecules from H_3O^+ proceeds with essentially unit probability, in concert with the behaviour reported previously for other analogous systems (38). The small deviation of the measured proton-transfer rate constants from the calculated capture rate constants which is evident from Fig. 2 is reminiscent of similar deviations observed previously in our laboratory for other proton-transfer reactions. Barker and Ridge (32) have also discussed the implications of these deviations. No new substantial insight is evident from the comparison reported here, but the results do provide an additional useful data base for the assessment of any future developments in theories of ion–molecule collision and reaction.

Dissociative Proton Transfer

Most of the reactions of H_3O^+ listed in Table 1 appeared to proceed simply by proton transfer to form predominantly (>99%) MH^+. Only with CH_3COOH did the primary product spectrum include substantial amounts of ions other than MH^+ with lower values of *m/e*, evidently because of the dissociation of MH^+ according to

$$[3] \qquad H_3O^+ + M \rightarrow [MH^+]^* + H_2O$$

$$[3a] \qquad [MH^+]^* \rightarrow \text{products}$$

where the internal energy required for the unimolecular decomposition of $[MH^+]^*$ is provided by the deposition of a substantial fraction of the excess energy which is in the form of reaction exothermicity. The extent to which this decomposition may be moderated under our experimental conditions by collisional stabilization of $[MH^+]^*$ is uncertain; the influence of the H_2 bath pressure on the primary product spectrum was not investigated systematically. The excess energy available in the form of reaction exothermicity is given by the difference in the proton affinity of H_2O and M which is included in Table 1. It is possible, therefore, using thermo-

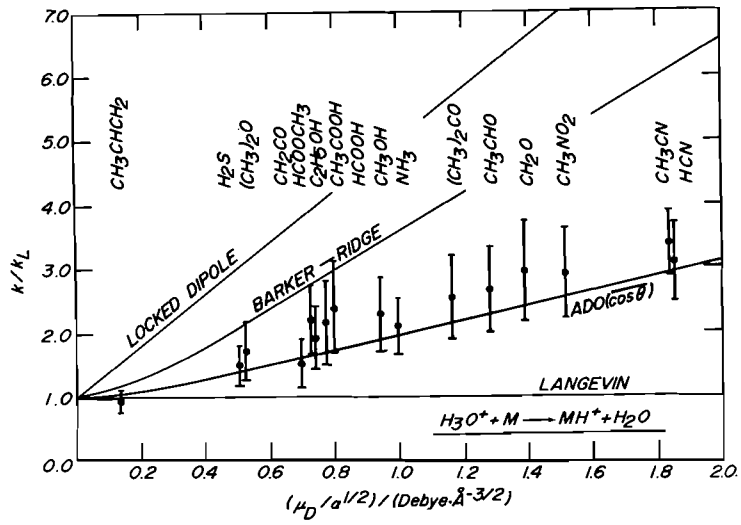

FIG. 2. A comparison of measured rate constants with capture rate constants predicted by various theories of collision for proton transfer reactions of H_3O^+ with polar molecules. The solid bars represent the estimated accuracy of the measurements. k_L is the collision rate constant determined from the Langevin expression.

TABLE 2. Energies (in kcal/mol) and energetically possible dissociative pathways

Molecule	Maximum excess energy available on protonation by H_3O^+	Possible dissociation reaction		
C_2H_5OH	20±4	$C_2H_5OH_2^+$	$\rightarrow C_2H_4OH^+ + H_2$	−18
$(CH_3)_2O$	24±5	$(CH_3)_2O^+H$	$\rightarrow CH_3CHOH^+ + H_2$	−9
			$\rightarrow CH_2OH^+ + CH_4$	−19
			$\rightarrow H_3O^+ + C_2H_4$	−23
$(CH_3)_2CO$	27±4	$(CH_3)_2C^+OH$	$\rightarrow CH_3CO^+ + CH_4$	−22
CH_3COOH	21±5	$CH_3COOH_2^+$	$\rightarrow CH_3CO^+ + H_2O$	0
HCOOH	12±5	$HCOOH_2^+$	$\rightarrow HCO^+ + H_2O$	−41
			$\rightarrow CO + H_3O^+$	−18
$HCOOCH_3$	22±5	$HCOO(CH_3)H^+$	$\rightarrow HCO^+ + CH_3OH$	−54
			$\rightarrow CH_3OH_2^+ + CO$	−16
			$\rightarrow CH_3CO^+ + H_2O$	−8

chemical data from the recent compilation of Rosenstock *et al.* (39), to calculate what dissociation reactions are feasible for each protonated base. The energetically possible dissociation pathways are listed in Table 2.

H_2 elimination from $C_2H_5OH_2^+$ to yield $C_2H_4OH^+$ (assumed to be protonated acetaldehyde) is, by analogy with vicinal elimination of H_2 from $CH_3OH_2^+$ (40), likely to have a kinetic barrier of approximately 20 kcal/mol and would therefore not be expected to occur. Furthermore, this mode of decomposition is not observed with the stronger acid HCO^+ (41).

The only thermodynamically possible dissociation products of $(CH_3)_2OH^+$ require generation of carbon bonds. These can only be achieved by large skeletal rearrangements and the large barriers normally accompanying such rearrangements would not be expected to be overcome by the relatively low exothermicity of the initial proton transfer reaction.

Dissociation of protonated acetone to form methane and the acetyl ion is possible thermodynamically but is mechanistically unlikely as it requires protonation at the methyl carbon (calculation of the exothermicity of the proton-transfer reaction is for protonation at the most basic site, in this case the oxygen atom). Protonation at a saturated carbon is a high energy process, while the alternative process, a 1,3-shift of the proton from the oxygen to the carbon accompanied by synchronous fission of the carbon–carbon bond will also have a high barrier.

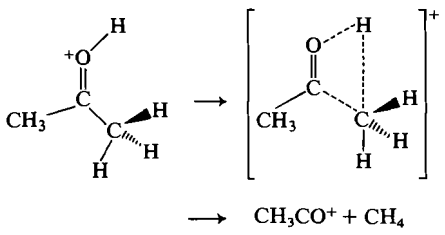

$\longrightarrow$ $CH_3CO^+ + CH_4$

Dissociative proton transfer to formic acid, acetic acid, and methyl formate should result in acylium ions and water or methanol via the $A_{Ac}1$ mechanism.

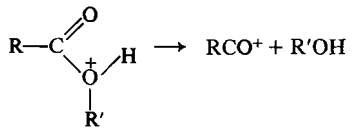

In the case of formyl derivatives subsequent proton transfer between HCO^+ and R'OH (R' = CH_3 or H) produces $R'OH_2^+$ and CO. However, this mechanism requires protonation at the energetically less accessible ether or hydroxy-oxygen. In solution two

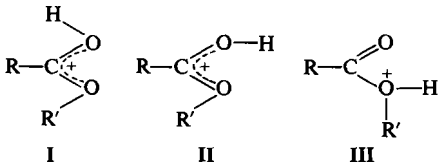

I II III

tautomers of $HCOOH_2^+$ (42) have been detected by proton nmr but these have been assigned structures **I** and **II**, both rotamers of carbonyl protonated formic acid. Benoit and Harrison (43), using ionization energy correlations, predict that the proton affinities of the hydroxy-oxygens of formic acid and acetic acid will be 26 ± 3 and 27 ± 3 kcal/mol respectively lower than those of the corresponding carbonyl oxygens. *Ab initio* molecular orbital calculations (44) similarly predict hydroxy-protonation of formic acid (**III**, R = R' = H) to be 25 kcal/mol less stable than the carbonyl-protonated tautomer (structure **I**). The exothermicities listed in Table 2 are for formation of the most stable carbonyl-protonated rotamer and the hydroxy-protonated tautomers, required as intermediates in the $A_{Ac}1$ fission mechanism, can only be attained if the exothermicities of the initial proton transfer are at least 25 kcal/mol. Clearly, then, when the protonating acid is H_3O^+ the $A_{Ac}1$ mechanism is not accessible to formic acid and is barely possible, within the error limits, for acetic acid. The observed 5% dissociation of acetic acid and the total lack of dissociation for formic acid are then entirely consistent with this mechanism. Protonation by the stronger acid HCO^+ is sufficient to increase the dissociation of acetic acid to 20% but does not cause formic acid dissociation (45). The even stronger acid, H_3^+, results in complete dissociation of both acetic and formic acids.

Protonation of the methoxy-oxygen of methyl formate, using the ionization energy correlation method (43), only requires ca. 22 kcal/mol more energy than that of the carbonyl group. Hence, in the unlikely event of all the exothermicity appearing as internal energy in the protonated ester, gas-phase protonation by H_3O^+ may occur at either oxygen. However, dissociation by the $A_{Ac}1$ mechanism would formally produce HCO^+ and CH_3OH, a process requiring 54 kcal/mol, and is therefore not possible. The final products from this mode of fission, CO and $CH_3OH_2^+$, are within the exothermicity of the initial proton transfer and it is possible to envisage a second proton transfer reaction occurring synchronously with the cleavage of the C—O bond, thereby lowering the overall barrier to the reaction. There is little evidence (46) of such a lowering as the stronger acids HCO^+ and CH_5^+ (reaction exothermicities 45 and 57 kcal/mol, respectively) also do not produce dissociation.

Acknowledgement

The authors wish to acknowledge the support of the National Research Council of Canada.

1. M. M. Mann, A. Hustrulid, and J. T. Tate. Phys. Rev. **58**, 340 (1940).
2. A. J. Cunningham, J. D. Payzant, and P. Kebarle. J. Am. Chem. Soc. **94**, 7627 (1972).
3. M. Meot-Ner and F. H. Field. J. Am. Chem. Soc. **99**, 998 (1977).
4. F. C. Fehsenfeld and E. E. Ferguson. J. Geophys. Res. **74**, 2217 (1969).
5. A. Good, D. A. Durden, and P. Kebarle. J. Chem. Phys. **52**, 222 (1970).
6. K. Tanaka, G. I. Mackay, and D. K. Bohme. Can. J. Chem. **56**, 193 (1978).
7. R. S. Hemsworth, J. D. Payzant, H. I. Schiff, and D. K. Bohme. Chem. Phys. Lett. **26**, 417 (1974).
8. G. I. Mackay, L. D. Betowski, J. D. Payzant, H. I. Schiff, and D. K. Bohme. J. Phys. Chem. **80**, 2919 (1976).
9. G. I. Mackay and D. K. Bohme. Int. J. Mass Spectrom. Ion Phys. **26**, 327 (1978).
10. F. C. Fehsenfeld, P. J. Crutzen, A. L. Schmeltekopf, C. J. Howard, D. L. Albritton, E. E. Ferguson, J. A. Davidson, and H. I. Schiff. J. Geophys. Res. **81**, 4454 (1976).
11. D. K. Bohme, G. I. Mackay, and S. D. Tanner. J. Am. Chem. Soc. To be published.
12. G. P. Arsenault. J. Am. Chem. Soc. **94**, 8241 (1972).
13. D. K. Bohme. *In* Kinetics of ion–molecule reactions. *Edited by* P. Ausloos. Plenum Press, New York, NY. 1979.
14. D. K. Bohme, R. S. Hemsworth, H. W. Rundle, and H. I. Schiff. J. Chem. Phys. **58**, 3504 (1973).
15. D. Betowski, J. D. Payzant, G. I. Mackay, and D. K. Bohme. Chem. Phys. Lett. **31**, 321 (1975).
16. N. G. Adams and D. Smith. Int. J. Mass Spectrom. Ion Phys. **21**, 349 (1976).

17. G. I. MACKAY, R. S. HEMSWORTH, and D. K. BOHME. Can. J. Chem. **54**, 1624 (1976).
18. R. SPENCE and W. WILD. J. Chem. Soc. 338 (1935).
19. M. D. TAYLOR and J. BURTON. J. Am. Chem. Soc. **74**, 4151 (1952).
20. M. D. TAYLOR. J. Am. Chem. Soc. 73, 315 (1951).
21. F. HALVERSON and V. Z. WILLIAMS. J. Chem. Phys. **15**, 552 (1947).
22. L. G. DRAYTON and H. W. THOMPSON. J. Chem. Soc. 1416 (1948).
23. J. R. DURIG and J. N. WILLIS. Spectrochim. Acta, **22**, 1299 (1966).
24. R. YAMDAGNI and P. KEBARLE. J. Am. Chem. Soc. **98**, 1320 (1976).
25. G. I. MACKAY, M. H. LIEN, A. C. HOPKINSON, and D. K. BOHME. Can. J. Chem. **56**, 131 (1978).
26. P. AUSLOOS and S. G. LIAS. Chem. Phys. Lett. **51**, 53 (1977).
27. F. C. FEHSENFELD and E. E. FERGUSON. J. Chem. Phys. **59**, 6272 (1973).
28. F. C. FEHSENFELD, I. DOTAN, D. L. ALBRITTON, C. J. HOWARD, and E. E. FERGUSON. J. Geophys. Res. **83**, 1333 (1978).
29. W. T. HUNTRESS. Ap. J. Supp. **33**, 495 (1977).
30. P. GIOUMOUSIS and D. P. STEVENSON. J. Chem. Phys. **29**, 294 (1958).
31. L. BASS, T. SU, W. J. CHESNAVICH, and M. T. BOWERS. Chem. Phys. Lett. **34**, 119 (1975); T. SU, E. C. F. SU, and M. T. BOWERS. J. Chem. Phys. **69**, 2243 (1978).
32. R. A. BARKER and D. P. RIDGE. J. Chem. Phys. **64**, 4411 (1976).
33. S. K. GUPTA, E. G. JONES, A. G. HARRISON, and J. J. MYHER. Can. J. Chem. **45**, 3107 (1967).
34. R. D. NELSON, D. R. LIDE, and A. A. MARYOTT. Natl. Stand. Ref. Data Ser. Natl. Bur. Stand. No. 10 (1967).
35. E. W. ROTHE and R. B. BERNSTEIN. J. Chem. Phys. **31**, 1619 (1959).
36. E. R. LIPPINCOTT and J. M. STUTMAN. J. Phys. Chem. **68**, 2926 (1964).
37. J. O. HIRSCHFELDER, C. F. CURTISS, and R. B. BIRD. Molecular theory of gases and liquids. Wiley, New York, NY. 1967.
38. D. K. BOHME. *In* Interactions between ions and molecules. *Edited by* P. Ausloos. Plenum Press, New York, NY. 1975.
39. H. M. ROSENSTOCK, K. DRAXL, B. W. STEINER, and J. T. HERRON. J. Phys. Chem. Ref. Data, **6** (1977).
40. W. T. HUNTRESS, D. K. SEN SHARMA, K. R. JENNINGS, and M. T. BOWERS. Int. J. Mass Spectrom. Ion Phys. **24**, 25 (1977).
41. S. D. TANNER, G. I. MACKAY, A. C. HOPKINSON, and D. K. BOHME. Int. J. Mass Spectrom. Ion Phys. **29**, 57 (1979).
42. G. A. OLAH, A. M. WHITE, and D. H. O'BRIEN. *In* Carbonium ions. Vol. IV. *Edited by* G. A. Olah and P. von R. Schleyer. Wiley-Interscience, New York, NY. 1973.
43. F. M. BENOIT and A. G. HARRISON. J. Am. Chem. Soc. **99**, 3980 (1977).
44. A. C. HOPKINSON, K. YATES, and I. G. CSIZMADIA. J. Chem. Phys. **52**, 1784 (1970).
45. G. I. MACKAY, A. C. HOPKINSON, and D. K. BOHME. J. Am. Chem. Soc. **100**, 7460 (1978).
46. A. C. HOPKINSON, G. I. MACKAY, and D. K. BOHME. Unpublished results.

Kinetics and mechanisms of some reactions of aqueous sodium bromite

C. L. LEE AND M. W. LISTER

Department of Chemistry, University of Toronto, Toronto, Ont., Canada M5S 1A7

Received September 7, 1978

C. L. LEE and M. W. LISTER. Can. J. Chem. **57**, 1524 (1979).

The kinetics of the reactions of aqueous bromite ions with basic aqueous solutions of iodide, sulphite, formate, and thiosulphate ions have been investigated. The products are, respectively, iodate, sulphate, and carbonate ions, and with thiosulphate either tetrathionate or sulphate depending on the conditions. The reaction with formate is autocatalytic, being catalysed by carbonate ions. All the reactions show some dependence on hydroxide concentration, and in general k(apparent) $= k_1 + k_2[OH^-]^{-1}$. The various rate constants have been obtained, as have the associated kinetic parameters. The relative rates of the reactions of bromite ions parallel those of the corresponding reactions of hypochlorite ions, but at 25°C K is smaller by a factor of roughtly 10^5.

C. L. LEE et M. W. LISTER. Can. J. Chem. **57**, 1524 (1979).

On a étudié la cinétique des réactions des ions bromites avec des solutions aqueuses basiques d'ions iodure, sulfite, formate et thiosulfate. Les produits sont respectivement les ions iodate, sulfate et carbonate; dans le cas du thiosulfate, on obtient soit du tétrathionate ou du sulfate suivant les conditions. La réaction avec le formate est autocatalytique puisqu'elle est catalysée par les ions carbonates. Toutes les réactions dépendent un peu de la concentration en ions hydroxyde et, d'une façon générale, k(apparent) $= k_1 + k_2[OH^-]^{-1}$. On a obtenu les diverses constantes de vitesse de même que les paramètres cinétiques qui leur sont associés. Les vitesses relatives des réactions des ions bromites sont parallèles à celles des réactions correspondantes des ions hypochlorites; toutefois, à 25°C, les vitesses sont plus faibles par un facteur de 10^5.

[Traduit par le journal]

Many investigations of the kinetics of groups of similar reactions have been made with the intention of relating the rate constants to other properties of the reagents, and thereby throwing some light on the details of the mechanisms of the reactions. Edwards (1, 2) applied this technique some time ago to the reactions of peroxides and it has, of course, been applied to many other reactions, both inorganic and organic. In particular, investigations of oxyhalogen ions have been made, in an attempt to discover whether the regularity of behaviour found for peroxides, and summarised in ref. 3, was duplicated elsewhere. Reactions of hypochlorous acid and hypochlorite ions (4, 5) with a series of reducing agents, and of hypobromous acid or hypobromite ions (6), have been investigated. There is evidently some similarity between the reactions of peroxides and of hypochlorites, and the same holds to a smaller degree with hypobromites.

The behaviour of the bromite ion is evidently of interest, both as a continuation of the above series, and also in itself, since it is an ion of which the chemistry has been studied relatively little. Its decomposition has been examined (7), and goes in several steps to bromate and bromide ions. The present paper deals with its reaction with various reducing ions, and as might be expected these reactions were all found to require at least two stages for completion. Comparisons with the reactions of other oxyhalogen ions will be made.

Experimental

Chemicals

Sodium Bromite

This was prepared as described in the earlier paper (7).

The following were all Fisher Scientific Co. certified reagent grade, with further treatment as noted.

Sodium Iodide

This was recrystallized once, and stock solutions were standardised by titration with silver nitrate.

Sodium Formate

This was recrystallized once, and stock solutions were standardised by titration with potassium permanganate.

Sodium Sulphite

To avoid the effect of any air oxidation, stock solutions were standardised just before use by adding excess iodine to an aliquot and titrating the excess with As_2O_3.

Sodium Thiosulphate

This was standardised by titration with iodine.

Sodium Hydroxide

The 50% solution was diluted as required.

Sodium Perchlorate

The Anachemia Chemical Company product was recrystallized, and dried to constant weight. Weighed amounts were added as required to control the ionic strength.

0008-4042/79/121524-07$01.00/0

Apparatus

In the experiments with iodide or formate ions, the appropriate solutions were mixed, and sealed in Pyrex glass ampoules. These were immersed in a silicone oil bath with the temperature controlled to ±0.02°C. At known times the ampoules were removed, rapidly cooled, and analysed as outlined below.

In experiments with sulphite or thiosulphate ions, a Durrum Stopped-Flow Spectrophotometer Model D110 was used. The wavelength drum was usually set to 296 nm, which is the absorption peak for bromite ions. The decay of the absorbance was followed on the oscilloscope. The final absorbance was also recorded by reactivating the oscilloscope after a sufficient interval of time. The time base was calibrated at intervals by pulses generated by a Tektronix, Type 184, Mark Time Generator. The temperature was controlled to ±0.05°C by a water bath surrounding the drive syringes.

Results

1. Reaction of Bromite and Iodide Ions

Preliminary experiments showed that the overall reaction in alkaline solution is

$$3BrO_2^- + 2I^- \rightarrow 3Br^- + 2IO_3^-$$

In the kinetic runs, solutions containing sodium bromite, iodide, hydroxide, and perchlorate were made up, kept at constant temperature, and at intervals the absorbances of the solutions were measured at wavelengths from 296 to 380 nm. The resulting spectra could not be explained on the assumption that only bromite and iodate ions were present as light absorbing species (the contribution of IO_3^- ions is very small). Various possible combinations of other absorbing species were examined, and it was found that good agreement with the observed spectra could be obtained, if it was assumed that absorbing species were bromite, hypoiodite, and triiodide ions. Previously published (8, 9) extinction coefficients were used. The concentration of hypobromite ions seemed to be negligibly small, presumably because, as was already known, they react rapidly with iodide ions.

During a typical run at 25°C with initial concentrations approximately: bromite 6.5×10^{-3} *M*, iodide 1.0×10^{-1} *M*, and hydroxide ions 5.0×10^{-2} *M*, the concentration of hypoiodite ions built up slowly to about 10^{-3} *M*, and triiodide ions (with a large extinction coefficient) to about 10^{-5} *M*. Triiodide ions are presumably formed by

$$IO^- + 2I^- + H_2O \rightleftharpoons I_3^- + 2OH^-$$

and the observed concentrations in the later stages of a run at 25°C, ionic strength 0.25 *M*, gave a roughly constant value for $[I_3^-][OH^-]^2/[IO^-][I^-]^2$ of 1.5×10^{-3}. It cannot be claimed that this is the equilibrium constant, since the concentrations are altering; however, it may be noted that Chia (ref. 10, see also ref. 14, p. 348) gave a value of 5×10^{-3} for this equilibrium constant at 25°C and zero ionic strength.

The concentrations of bromite ions were calculated from the absorbances on the assumption that hypoiodite and triiodide ions were the only other species contributing appreciably to the absorption. It was found that the concentrations fitted a rate law which was first order in both reagents, and if k is defined by

$$-\tfrac{1}{3}\frac{d[BrO_2^-]}{dt} = k[BrO_2^-][I^-]$$

this leads to

$$kt = \frac{1}{A}\ln\left(\frac{2x}{2x - A}\right) - \frac{1}{A}\ln\left(\frac{2x_0}{2x_0 - A}\right)$$

where $x = [BrO_2^-]$, initially x_0,

$$A = 2x_0 - 3[I^-]_0$$

k was obtained as the slope of the least mean squares line through the points in a plot of $(1/A)\ln(2x/(2x - A))$ against t.

The results are given in Table 1. The initial bromite concentrations ranged from 5 to 8×10^{-3}, in different runs, and runs were continued until about 50% of the original bromite remained. The initial iodide concentration varied from 8 to 12×10^{-2} *M*. In every case the ionic strength was 0.50 within 0.02. Values of k are given in Table 1, together with the standard deviation, σ_k, calculated in the usual way (11). These deviations are almost all in the range of 1 to 3%.

The value of k varies with hydroxide concentration, and a plot of k against $[OH^-]^{-1}$ was linear. If

TABLE 1. Apparent rate constants for the reaction of bromite and iodide ions

Run	T (°C)	[NaOH] (*M*)	k (M^{-1} s^{-1}) ($\times 10^{-5}$)	σ_k ($\times 10^{-5}$)
1	25.1	0.0506	14.15	0.32
2	25.1	0.0608	12.69	0.20
3	25.1	0.0760	11.01	0.09
4	25.1	0.1090	8.00	0.07
5	25.1	0.1100	8.22	0.08
6	25.1	0.1107	8.20	0.18
7	25.1	0.1125	7.60	0.15
8	25.1	0.1482	6.80	0.15
9	35.1	0.0506	32.01	1.56
10	35.1	0.0608	26.34	0.87
11	35.1	0.0800	20.33	1.04
12	35.1	0.1877	13.07	0.25
13	44.4	0.0506	66.54	1.51
14	44.4	0.0608	56.95	1.89
15	44.4	0.1106	35.08	1.19
16	44.4	0.1694	26.98	0.64

we write

$$k = k_1 + k_2[OH^-]^{-1}$$

the derived values of k_1, k_2 are given in Table 2. These lead to the following activation parameters, calculated for 35°C. k_1, $\Delta H_1^{\ddagger} = 48.5$ kJ mol^{-1}, $\Delta S_1^{\ddagger} = -169$ J K^{-1} mol^{-1}. The part of the reaction that depends on $[OH^-]^{-1}$ is probably a reaction of bromous acid. However, as thermodynamic data on the ionisation of bromous acid are not available, only an apparent $\Delta H^{\ddagger}$ can be calculated. Since the first reaction (k_1) is between two similarly charged ions, a negative $\Delta S_1^{\ddagger}$ might be expected, but the value found is surprisingly large, and suggests that other factors, such as orientation, must contribute to it.

The first step in the reaction is probably

$$BrO_2^- + I^- \rightarrow BrO^- + IO^-$$

for which ΔG^0 can be calculated from earlier data (7, 12) to be -44.6 kJ mol^{-1}; followed by the known reaction

$$BrO^- + I^- \rightarrow Br^- + IO^- \qquad \Delta G^0 = -53.3 \text{ kJ mol}^{-1}$$

Hypoiodite ions are known to decompose readily to iodate and iodide; although the direct reaction

$$BrO_2^- + IO^- \rightarrow Br^- + IO_3^-$$

is possible so far as ΔG^0 (-230 kJ mol^{-1}) is concerned.

2. Reaction of Bromite and Sulphite Ions

The overall reaction was (as might be expected):

$$BrO_2^- + 2SO_3^{2-} \rightarrow Br^- + 2SO_4^{2-}$$

The reaction was found to be first order in both reagents, which leads to the equation

$$kt = \frac{1}{B}\ln\left(\frac{2x}{2x - B}\right) - \frac{1}{B}\ln\left(\frac{2x_0}{2x_0 - B}\right)$$

where $x = [BrO_2^-]$, initially x_0

$$B = [2x_0] - [SO_3^{2-}]_0$$

k was obtained as the slope of the least mean squares line through the points on a plot of $(1/B)\ln(2x/(2x - B))$ against t.

The results are given in Table 3. The plots from which k was obtained were always good straight lines, as shown by the fairly small values of σ_k. It can be seen that k varies with $[OH^-]$, and it was found that k plotted against $[OH^-]^{-1}$ also gives a straight line. If we write $k = k_1 + k_2[OH^-]$, and take the slope and intercept to get k_2 and k_1, we obtain the results in Table 4. This table also gives the standard deviations of these constants.

These values make the activation parameters for k_1, $\Delta H_1^{\ddagger} = 44.3$ kJ mol^{-1}, $\Delta S_1^{\ddagger} = -85$ J K^{-1} mol^{-1}. As before, the part in k_2 is probably a reaction of bromous acid, and hence only an apparent rate constant and activation enthalpy can be calculated. The part in k_1 has a negative $\Delta S^{\ddagger}$ of a size that is reasonable for a reaction of ions of charge -1 and -2. The fairly small $\Delta H^{\ddagger}$ is also not sur-

TABLE 3. Apparent rate constants for the reaction of bromite and sulphite ions

Run	T (°C)	[NaOH] (M)	k (M^{-1} s^{-1})	σ_k
1	25.1	0.0162	10.95	0.03
2	25.1	0.0269	8.11	0.08
3	25.1	0.0473	6.24	0.03
4	25.1	0.0187	9.99	0.09
5	25.1	0.0166	11.31	0.07
6	25.1	0.0439	6.18	0.04
7	25.1	0.0439	6.69	0.04
8	25.1	0.0250	8.52	0.09
9	25.1	0.0250	8.55	0.04
10	25.1	0.0459	6.69	0.06
11	25.1	0.0145	12.21	0.11
12	39.1	0.0459	15.99	0.05
13	39.1	0.0459	15.53	0.09
14	39.1	0.0250	21.87	0.08
15	39.1	0.0250	21.97	0.11
16	39.1	0.0145	29.77	0.21
17	39.1	0.0145	29.72	0.11
18	39.1	0.0354	18.56	0.07
19	39.1	0.0354	17.89	0.10
20	13.0	0.0145	4.77	0.014
21	13.0	0.0166	4.33	0.019
22	13.0	0.0208	3.84	0.019
23	13.0	0.0250	3.53	0.016
24	13.0	0.0354	2.97	0.011
25	13.0	0.0459	3.78	0.018
26	1.7	0.0354	1.38	0.006
27	1.7	0.0459	1.23	0.002
28	1.7	0.0145	2.13	0.013
29	1.7	0.0166	2.04	0.009

TABLE 2. Values of k_1 and k_2 for the reaction of bromite and iodide ions

T (°C)	k_1 (M^{-1} s^{-1}) (× 10^{-5})	σ_{k_1} (× 10^{-5})	k_2 (s^{-1}) (× 10^{-6})	σ_{k_2} (× 10^{-6})
25.1	2.75	0.3	5.9	0.25
35.1	5.4	1.7	13.0	1.2
44.4	9.6	0.6	28.8	0.4

TABLE 4. Values of k_1 and k_2 for the reaction of bromite and sulphite ions

T (°C)	k_1 (M^{-1} s^{-1})	σ_{k_1}	k_2 (s^{-1})	σ_{k_2}
1.7	0.82	0.05	0.0195	0.0010
13.0	1.82	0.05	0.042	0.001
25.1	3.73	0.20	0.121	0.004
39.1	9.71	0.37	0.295	0.008

prising, since the reaction

$$BrO_2^- + SO_3^{2-} \rightarrow BrO^- + SO_4^{2-}$$

which is presumably the first stage, has ΔH^0 equal to -326 kJ mol^{-1}, and $\Delta G^0 = -317$ kJ mol^{-1}, so it is a very exothermic reaction. It was already known (6) that the proposed second stage:

$$BrO^- + SO_3^{2-} \rightarrow Br^- + SO_4^{2-}$$

is rapid.

3. Reaction of Bromite and Formate Ions

Preliminary experiments showed that formate was oxidized to carbonate by the overall reaction:

$$BrO_2^- + 2HCO_2^- + 2OH^- \rightarrow Br^- + 2CO_3^{2-} + 2H_2O$$

It was also found that the rate of reaction accelerated at first before slowing down; see Fig. 1. This behaviour presumably arose from catalysis by the products, and experiment showed that carbonate, but not bromide, ions caused this acceleration. As will be seen later, the reduction in $[OH^-]$ would also speed up the reaction, but this would be a small effect. Accordingly a series of experiments was made in the virtual absence of carbonate, by adding barium nitrate which precipitated $BaCO_3$. The remaining solution was analysed for bromite.

The following mechanism is proposed for the reaction:

[*i*] $$2BrO_2^- \xrightarrow{k_1} BrO^- + BrO_3^-$$

[*ii*] $$BrO^- + BrO_2^- \xrightarrow{k_2} BrO_3^- + Br^-$$

[*iii*] $$BrO_2^- + HCO_2^- \xrightarrow{k_3} BrO^- + HCO_3^-$$

[*iv*] $$BrO^- + HCO_2^- \xrightarrow{k_4} Br_2^- + HCO_3^-$$

[*v*] $$HCO_3^- + OH^- \xrightarrow{k_5} CO_3^{2-} + H_2O$$

Reactions [*i*] and [*ii*] allow for the spontaneous decomposition of bromite ions, and the corresponding rate constants, k_1 and k_2 above, were already known (7). The rate constant for reaction [*iv*], k_4, was also known (6), and reaction [*v*], of course, is rapid. To apply this mechanism, if

$$x = [BrO_2^-] \quad y = [HCO_2^-] \quad z = [BrO^-]$$

then

$$-dx/dt = 2k_1x^2 + k_2xz + k_3xy$$

$$-dy/dt = k_3xy + k_4yz$$

$$-dz/dt = -k_1x^2 + k_2xz - k_3xy + k_4yz$$

Since our experiments indicated that hypobromite ions reacted considerably faster than bromite ions,

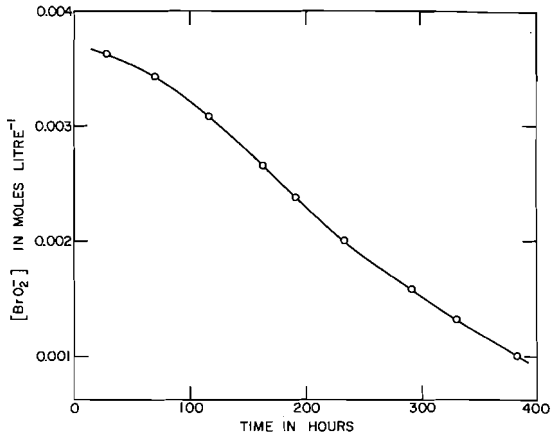

FIG. 1. $[BrO_2^-]$ plotted against time in a reaction of bromite and formate ions, without added carbonate or barium ions.

it was assumed that a steady state treatment could be applied to them; that is, $dz/dt = 0$. With this assumption these equations can be solved to give

$$q \ln \frac{x}{x_0} = -3\alpha\beta \ln \frac{\mu}{\mu_0} + \frac{n}{2\sqrt{m}} \times \ln \left\{ \frac{\mu\mu_0 + (\alpha+\beta-1)(\mu+\mu_0) + \sqrt{m}(\mu-\mu_0) + q}{\mu_0 + (\alpha+\beta-1)(\mu+\mu_0) - \sqrt{m}(\mu-\mu_0) + q} \right\} + \frac{\alpha+\beta}{2} \ln \left\{ \frac{\mu^2 + 2(\alpha+\beta-1)\mu + q}{\mu_0^2 + 2(\alpha+\beta-1)\mu_0 + q} \right\}$$

where $\mu = y/x$, initially μ_0; $\alpha = k_1/k_3$; $\beta = k_2/k_4$; $q = 3\alpha\beta - \alpha - \beta$; $n = \alpha^2 + \beta^2 - 4\alpha\beta + \alpha + \beta$; $m = \alpha^2 + \beta^2 - \alpha\beta - \alpha - \beta + 1$. In effect an iterative method was used in applying this equation, as follows. Since k_1, k_2, and k_4 were known from earlier work, only k_3 remained to be found. A value of k_3 was guessed, and hence x/x_0 could be calculated for any value of μ. The ratio of the changes in formate and bromite concentrations:

$$\frac{\Delta y}{\Delta x} = \frac{y_0 - y}{x_0 - x} = a$$

could thus be calculated. This quantity, the effective stoichiometry arising from all reactions, was found to be nearly constant in any one run; details are given in Table 5. If this quantity is constant, the differential equations can be solved to give

$$k_3t = \frac{1}{2ps} \left[(s+\alpha) \ln \left\{ \frac{r+s+p/x}{r+s+p/x_0} \right\} + (s-\alpha) \ln \left\{ \frac{r-s+p/x}{r-s+p/x_0} \right\} \right]$$

TABLE 5. Data for the reaction of sodium bromite and sodium formate in the presence of barium ions

Run	T(°C)	$[NaBrO_2]_0$	$[NaHCO_2]_0$	$[NaOH]_0$	a	10^6k_3	$10^6\sigma$
1	85.7	0.00410	0.0724	0.0138	1.395–1.44	1.95	0.06
2	85.7	0.00410	0.0724	0.0184	1.53 –1.56	2.00	0.04
3	85.7	0.00789	0.0714	0.0256	1.225–1.26	1.97	0.11
4	85.7	0.00632	0.0700	0.0212	1.26 –1.31	1.89	0.07
5	85.7	0.00722	0.0700	0.0212	1.33 –1.38	2.00	0.13
6	85.7	0.00789	0.1006	0.0234	1.42 –1.46	1.99	0.08
7	96.7	0.00670	0.0592	0.0422	1.14 –1.195	4.09	0.09
8	96.7	0.00412	0.0592	0.0407	1.08 –1.12	4.17	0.12
9	96.7	0.00412	0.0296	0.0407	1.05 –1.10	3.73	0.10
10	96.7	0.00658	0.0551	0.0296	1.085–1.13	3.99	0.11

where

$$p = y_0 - ax_0$$
$$r = \alpha + \beta + a$$
$$s^2 = \alpha^2 + \beta^2 - \alpha\beta$$

If we define

$$g(x) = (1/2ps)[(s + \alpha)\ln(r + s + p/x) + (s - \alpha)\ln(r - s + p/x)]$$

the equation above is: $k_3t = g(x) - g(x_0)$. Consequently $g(x)$ was plotted against t. These plots were found to be linear, and the slope of the best line through the points, which equals k_3, was found by the usual method of least squares. The k_3 so obtained was in general somewhat different from the originally assumed k_3. The calculations were therefore repeated until k_3 did not change appreciably on further repetition. It was checked that the change in the effective stoichiometry, a, during a run did not appreciably alter k_3; in fact, use of the initial or final values of a during any one run was found to give values of k_3 differing by 0.1% or less. Hence a value of a corresponding to the middle of each run was used.

Table 5 gives details of the initial conditions of each run, and the calculated values of a and k_3. The ionic strength throughout was close to 0.26 ($\pm$0.02). The other rate constants used in the calculations were: for 85.7°C, $k_1 = 7.81 \times 10^{-6}$, $k_2 = 2.30 \times 10^{-3}$, $k_4 = 9.09 \times 10^{-4}/[OH^-]$; for 96.7°C, $k_1 = 2.53 \times 10^{-5}$, $k_2 = 5.34 \times 10^{-3}$, $k_4 = 1.74 \times 10^{-3}/[OH^-]$. Average values of k_3 are $(1.97 \pm 0.04) \times 10^{-6}$ at 85.7°C and $(4.00 \pm 0.17) \times 10^{-6}\ M^{-1}\ s^{-1}$ at 96.7°C. The precision is only moderate, in part because of the considerable spontaneous decomposition of sodium bromite. These constants, though only for two temperatures, make $\Delta H^{\ddagger} = 68 \pm 9$ kJ mol^{-1}, $\Delta S^{\ddagger} = -166 \pm 20$ J K^{-1} mol^{-1}.

A similar series of runs was carried out with a fairly high concentration (0.05 M) of sodium carbonate present. This did not increase much during a run, since the initial bromite concentrations were about ten times smaller. The same method was applied in analysing the results, and the initial concentrations, and calculated values of a and k_3 are given in Table 6. The ionic strength was the same as before. It is evident that these values of k_3 depend on $[OH^-]$. A plot of k_3 against $[OH^-]^{-1}$ was approximately linear. If we write

$$k_3 = k_5 + k_6[OH^-]^{-1}$$

and use the average $[OH^-]$ during the period of measurement then the usual least-squares method gives values of k_5 and k_6 as in Table 7.

The part of the reaction contributed by k_6 presumably arises from the reaction of $HBrO_2 + HCO_2^-$, or $BrO_2^- + HCO_2H$. As before, it is impossible to go further in terms of bromous acid, but data are available on formic acid (13) for its ionisation over the temperature range 0 to 60°C at 5°C intervals. From these ΔG^0 of ionisation can be calculated, and ΔS^0 from $-\partial\Delta G^0/\partial T$. ΔS^0 varies quite considerably, and approximately linearly, with temperature; the same is true of ΔH^0. The values of ΔS^0 and ΔH^0 were extrapolated to the temperatures of the kinetic measurements. Similar data on the ionisation of water (ref. 14, p. 39) are available for a wide range of temperature, and hence the equilibrium constant, K_{eq}, for

$$HCO_2^- + H_2O \rightleftharpoons HCO_2H + OH^-$$

was calculated at each of the temperatures used in the kinetic measurements with the results: T = 85.7°C, $K_{eq} = 3.70 \times 10^{-9}$; 91.0°C, 5.20×10^{-9}; 96.7°C, 7.46×10^{-9}. If we write this part of the overall rate as $k_7[BrO_2^-][HCO_2H]$, then $k_7 = k_6/K_{eq}$, and resulting values of k_7 are given in the last column of Table 7. The activation parameters obtained are: k_5: $\Delta H^{\ddagger} = 167(\pm 4)$ kJ mol^{-1}; $\Delta S^{\ddagger} = 120(\pm 12)$ J K^{-1} mol^{-1}; k_7: $\Delta H^{\ddagger} = 63(\pm 11)$ kJ mol^{-1}; $\Delta S^{\ddagger} = 36(\pm 30)$ J K^{-1} mol^{-1}. The relative large positive values of $\Delta S^{\ddagger}$ are perhaps unexpected, but the mechanism of the catalysis by carbonate is unknown. In deducing k_7 above it was assumed that

TABLE 6. Data for the reaction of sodium bromite and sodium formate in the presence of 0.050 *M* sodium carbonate

Run	T (°C)	$[NaBrO_2]_0$	$[NaHCO_2]_0$	$[NaOH]_0$	a	10^5k_3	$10^5\sigma$
11	85.7	0.00595	0.0785	0.0218	1.90–1.92	1.88	0.04
12	85.7	0.00839	0.0785	0.0234	1.87–1.90	1.67	0.04
13	85.7	0.00575	0.0785	0.0308	1.87–1.90	1.41	0.05
14	85.7	0.00420	0.0785	0.0171	1.93–1.95	2.15	0.06
15	85.7	0.00575	0.1177	0.0399	1.90–1.92	1.22	0.13
16	85.7	0.00575	0.1308	0.0399	1.91–1.93	1.29	0.08
17	85.7	0.00420	0.1872	0.0153	1.94–1.96	2.17	0.19
18	85.7	0.00574	0.0654	0.0198	1.88–1.90	1.88	0.10
19	91.0	0.00720	0.0110	0.0380	1.89–1.92	2.88	0.03
20	91.0	0.00720	0.110	0.0234	1.92–1.94	3.80	0.19
21	91.0	0.00720	0.0544	0.0173	1.87–1.90	4.63	0.15
22	91.0	0.00720	0.0544	0.0379	1.80–1.83	2.84	0.06
23	91.0	0.00720	0.0652	0.0276	1.85–1.88	3.36	0.08
24	91.0	0.00720	0.0652	0.0276	1.87–1.89	3.76	0.06
25	96.7	0.00660	0.115	0.0464	1.77–1.79	5.86	0.17
26	96.7	0.00660	0.115	0.0285	1.93–1.95	6.80	0.57
27	96.7	0.00660	0.115	0.0173	1.72–1.73	9.31	0.78
28	96.7	0.00660	0.0557	0.0240	1.87–1.90	7.19	0.24
29	96.7	0.00660	0.0557	0.0195	1.89–1.92	9.08	0.53
30	96.7	0.00660	0.0557	0.0151	1.91–1.93	10.99	0.93
31	96.7	0.00503	0.0444	0.0400	1.84–1.88	6.27	0.62

all this part of reaction came from formic acid; apart from the possibility of a reaction of bromous acid, it should be mentioned that catalysis by bicarbonate, as well as carbonate ions, might be considered.

4. Reaction of Bromite and Thiosulphate Ions

Preliminary experiments showed that at least two overall reactions were possible between bromite and thiosulphate ions. If the initial concentration of thiosulphate ions was about ten times that of bromite ions, the ratio of thiosulphate to bromite ions consumed was close to, though always a little less than, four. This corresponds to the reaction

[1] $BrO_2^- + 4S_2O_3^{2-} + 2H_2O \rightarrow Br^- + 2S_4O_6^{2-} + 4OH^-$

Moreover this value of the ratio was only approached at low hydroxide concentration (0.05 *M* or less). The hydroxide produced in the reaction was an amount corresponding to reaction [1] only if it was rapidly titrated with acid; on standing less hydroxide was found, and after roughly an hour or more, the ratio of hydroxide produced to bromite consumed was close to 1.0. Probably the cause of these effects was the alkaline hydrolysis of tetrathionate ions, reported (15) to occur by

$$4S_4O_6^{2-} + 6OH^- \rightarrow 5S_2O_3^{2-} + 2S_3O_6^{3-} + 3H_2O$$

At lower ratios (2.5 or less) of thiosulphate to bromite ions, and roughly 0.1 *M* sodium hydroxide, the ratio of thiosulphate to bromite consumed was 0.5. Tests showed that sulphate had been produced, and one OH^- had reacted for each BrO_2^- reacting. This agrees with the reaction:

[2] $2BrO_2^- + S_2O_3^{2-} + 2OH^- \rightarrow Br^- + 2SO_4^{2-} + H_2O$

Preliminary kinetic experiments were made on the stopped flow spectrophotometer, with concentrations such that reaction [1] would greatly preponderate. With initial concentrations approximately: $[BrO_2^-] = 0.007\ M$, $[S_2O_3^{2-}] = 0.09\ M$, and $[OH^-] = 0.05\ M$, and 25°C, the bromite concentration had fallen virtually to zero in 10 s. At this instant the spectrum of the remaining solution agreed with that of sodium tetrathionate; sodium thiosulphate has extinction coefficients about 100 times smaller at the wavelengths used, which ranged from 296 to 380 nm, and so it contributes very little to the total absorbance. The absorbance was followed at intervals for about 3 min after mixing, and over the period from 20 to 180 s, the tetrathionate concentration decreased by an apparently first order reaction with a rate constant of 0.0082 s^{-1}. Thus, over the period of measurement in the kinetic runs (10 s or less), only a very small amount of thiosulphate could have been regenerated by hydrolysis of tetrathionate, and this was therefore ignored.

In the main series of runs, the absorbance at 350

TABLE 7. Values of rate constants in carbonate catalyzed reactions of bromite and formate ions

T (°C)	k_5 (M^{-1} s^{-1})	k_6 (s^{-1})	k_7 (M^{-1} s^{-1})
85.7	0.71×10^{-5}	2.05×10^{-7}	55.4
91.0	1.57×10^{-5}	4.39×10^{-7}	84.4
96.7	3.87×10^{-5}	8.02×10^{-7}	107.5

TABLE 8. Slope of plots of $-\mathrm{d} \ln [BrO_2^-]/dt$ against mean $[S_2O_3^{2-}]$

Temp.	Slope (s^{-1})	Mean $[OH^-]$ (M)	k_1	k_2
25.1	3.03	0.0182	2.39	0.013
25.1	2.94	0.0249		
25.1	2.67	0.0385		
25.1	2.75	0.0439		
25.1	2.58	0.0596		
25.1	2.29	0.1003		
35.9	6.34	0.0175	3.96	0.030
35.9	5.15	0.0228		
35.9	4.52	0.0367		
35.9	4.62	0.0774		
1.5	0.83	0.0208	0.71	0.0025
1.5	0.74	0.0798		

nm was followed. It was assumed that BrO_2^-, $S_2O_3^{2-}$, and $S_4O_6^{2-}$ contributed to the absorbance, and that the overall reaction was [1] above. Hence $[BrO_2^-]$ could be calculated for various time intervals. With thiosulphate in considerable excess, a plot of ln $[BrO_2^-]$ against t was found to be linear. The slopes of such plots were found by the usual method of least squares; the standard deviations in these slopes were always about 1%. By plotting these slopes against thiosulphate concentration (the concentration at the midpoint of the run was used), the rate was found to depend on the first power of the thiosulphate concentration. There was also a small spontaneous decomposition of bromite ions. The slope of the plots of $-\mathrm{d} \ln [BrO_2^-]/dt$ against mean $[S_2O_3^{2-}]$ are given in Table 8, as are also the mean $[OH^-]$ during each series of runs. These mean $[OH^-]$ values are averages of $[OH^-]$ at the midpoint of a series of runs with closely similar hydroxide concentration (the initial $[OH^-]$ were the same). There seems to be some dependence of rate on $[OH^-]$, but the differences are sufficiently small that, after allowing for the scatter in the points, the exact form of the dependence of rate on $[OH^-]$ cannot be deduced. If it is assumed that, as in other reactions, k(apparent) $= k_1 + k_2[OH^-]^{-1}$, then the values of k_1 and k_2 so obtained are also shown in Table 8. In obtaining k_1 and k_2 in Table 8, the points are weighted in proportion to the number of runs contributing to each point. The activation parameters are (for 25°C) k_1, $\Delta H_1^{\ddagger} = 33$ kJ mol^{-1}; $\Delta S_1^{\ddagger} = -120$ J K^{-1} mol^{-1}. The accuracy of these is not very high; perhaps for k_1, $\Delta H_1^{\ddagger} \pm 5$ kJ, $\Delta S_1^{\ddagger} \pm 20$ J K^{-1} mol^{-1}. However the general pattern of the reaction seems to be similar to other reactions of bromite ions.

Discussion

It is evident that bromite ions behave somewhat like the hypohalite ions as an oxidising agent, though they have the peculiarity that the reaction independent of $[OH^-]$ and that proportional to $[OH^-]^{-1}$ both contribute appreciably to the rate at ordinary hydroxide concentrations. This makes a detailed comparison difficult, but the following are all apparent rate k, for the rate proportional to $[OH^-]^{-1}$, for reactions at 25°C (extrapolated where necessary). Values of log k are given:

Oxidiser/reducer	SO_3^{2-}	I^-	HCO_2^-
ClO^-	3.93	1.96	−6.12
BrO_2^-	−0.92	−5.23	−10.73

The rates fall in the same order, with the bromite reactions about 10^5 slower. $\Delta H^{\ddagger}$ are also roughly parallel.

The reactions of bromite ions so far investigated were all first order in both reagents, and in the cases above are probably simple oxygen transfer reactions, followed by a similar reaction with hypobromite ions (or hypobromous acid). The reaction with thiosulphate is evidently complicated, and though it may also be an oxygen transfer reaction, at present this would simply be speculation.

1. J. O. EDWARDS. J. Am. Chem. Soc. **76**, 1540 (1954).
2. J. O. EDWARDS. J. Am. Chem. Soc. **78**, 1819 (1956).
3. J. O. EDWARDS. Peroxide reaction mechanisms. Interscience Publishers, New York, NY. 1962.
4. M. W. LISTER and P. ROSENBLUM. Can. J. Chem. **39**, 1645 (1961).
5. M. W. LISTER and P. ROSENBLUM. Can. J. Chem. **41**, 2727 (1963); **41**, 3013 (1963).
6. M. W. LISTER and P. E. MCLEOD. Can. J. Chem. **49**, 1987 (1971).
7. C. L. LEE and M. W. LISTER. Can. J. Chem. **49**, 1987 (1971).
8. O. HAIMOVICH and A. TREININ. Nature, **207**, 185 (1965).
9. A. D. AWTREY and R. E. CONNICK. J. Am. Chem. Soc. **73**, 1842 (1951).
10. Y. T. CHIA. UCRL 8311 (1958).
11. P. R. BEVINGTON. Data reduction and error analysis for the physical sciences. McGraw-Hill Book Co. 1969. p. 114.
12. W. M. LATIMER. The oxidation states of the elements and their potentials in aqueous solutions. 2nd ed. Prentice-Hall Inc. 1952.
13. M. LLOYD, V. WYCHERLEY, and C. B. MONK. J. Chem. Soc. 1786 (1951).
14. Stability Constants, Special Publication No 17. The Chemical Society, London. 1964.
15. V. M. GOEHRING, W. HELBING, and I. APPEL. Z. Anorg. Chem. **254**, 185 (1947).

Carbonyl oxygen exchange of glycol monoesters. Rate and equilibrium constants for the formation of a tetrahedral intermediate

R. A. McClelland, M. Ahmad, J. Bohonek, and S. Gedge

Department of Chemistry, University of Toronto, Scarborough College, West Hill, Ont., Canada M1C 1A4

Received December 1, 1978

R. A. McClelland, M. Ahmad, J. Bohonek, and S. Gedge. Can. J. Chem. **57**, 1531 (1979).

Kinetic investigations of the hydrolysis of the 2-phenyl-4,4,5,5-tetramethyl-1,3-dioxolenium ion and 2-phenyl-2-methoxy-4,4,5,5-tetramethyl-1,3-dioxolane furnish rate constants for all three reaction stages of the ortho ester hydrolysis: (*1*) generation of the dioxolenium ion, (*2*) hydration of this ion to form hydrogen ortho ester, and (*3*) breakdown of this species to pinacol monobenzoate. The equilibrium constant for stage (*2*) can also be obtained. This study complements a previous investigation of 2-phenyl-2-alkoxy-1,3-dioxolanes where similar information was obtained.

The rate constants for carbonyl oxygen exchange of the ester products of these reactions, pinacol monobenzoate and ethylene glycol monobenzoate, have been measured. This reaction is shown to proceed by a different mechanism to that normally associated with exchange of carboxylic acid derivatives: cyclization of the glycol monoester to form hydrogen ortho ester, followed by loss of the labelled exocyclic OH group to give 1,3-dioxolenium ion. Reversal of these steps, initiated by an unlabelled water molecule, results in exchange. The relationship of this mechanism with that of the ortho ester hydrolysis is obvious; it is shown that the exchange provides rate constants for the reverse of stage (*3*). This means that both the forward and reverse rates of this process have been obtained, and this provides the equilibrium constant.

R. A. McClelland, M. Ahmad, J. Bohonek et S. Gedge. Can. J. Chem. **57**, 1531 (1979).

Des études cinétiques de l'hydrolyse de l'ion phényl-2 tétraméthyl-4,4,5,5 dioxolénium-1,3 et du phényl-2 méthoxy-2 tétraméthyl-4,4,5,5 dioxolanne-1,3 ont permis d'établir les constantes de vitesse pour chacune des trois étapes de l'hydrolyse des ortho esters: (*1*) formation de l'ion dioxolénium, (*2*) hydratation de cet ion conduisant à l'ortho ester acide et (*3*) décomposition de cette espèce en monobenzoate de pinacol. On a pu aussi obtenir la constante d'équilibre pour l'étape (*2*). Cette étude complète un travail antérieur sur les phényl-2 alkoxy-2 dioxolannes-1,3 qui a fourni des informations semblables.

On a mesuré les constantes de vitesse d'échange d'oxygène du carbonyle des esters produits au cours de ces réactions, soit le monobenzoate de pinacol et le monobenzoate de l'éthylène glycol. On montre que cette réaction se produit par un mécanisme différent de celui qui est normalement associé avec l'échange de dérivés d'acides carboxyliques: cyclisation du monoester du glycol avec formation d'une ortho ester acide, suivie par la perte du groupe OH exocyclique marqué conduisant à un ion dioxolénium-1,3. Les étapes inverses, provoquées par l'addition d'eau ne contenant pas de marqueur, conduisent à l'échange. La relation entre ce mécanisme et celui de l'hydrolyse des ortho esters est évidente; on montre que l'échange fournit les constantes de vitesse pour l'inverse de l'étape (*3*). Ceci signifie que l'on a déterminé les vitesses dans les deux sens de la réaction et que l'on peut évaluer la constante d'équilibre.

[Traduit par le journal]

It has been established for some time now that the hydrolysis of carboxylic acid esters is accompanied by exchange of the carbonyl oxygen atom with solvent (1). This exchange occurs when the tetrahedral intermediate of this reaction returns to starting ester, rather than proceeds to product. The demonstration that hydrolysis is accompanied by such exchange is one of the principal pieces of evidence that there is a discrete tetrahedral addition intermediate in acyl transfer reactions (2).

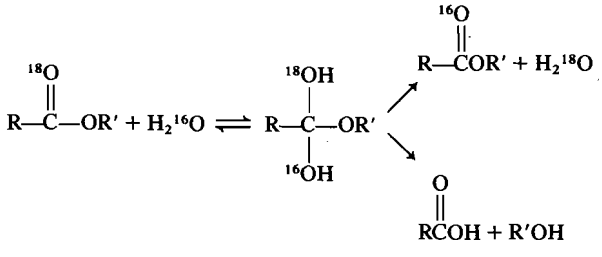

In experiments involving the hydrolysis of 2-aryl-2-alkoxy-1,3-dioxolane ortho esters we have found that it is possible to observe all three reaction stages (3, 4), thus verifying the general mechanism commonly proposed for such reactions.

The ultimate product of this reaction, an ethylene glycol monobenzoate ester, has in principle an additional route available for carbonyl oxygen exchange, namely **4** → **3** → **2** → **3** → **4**, where a solvent water molecule comes in at the **2** → **3** reaction stage. This sequence is of course intimately related to

0008-4042/79/121531-10$01.00/0

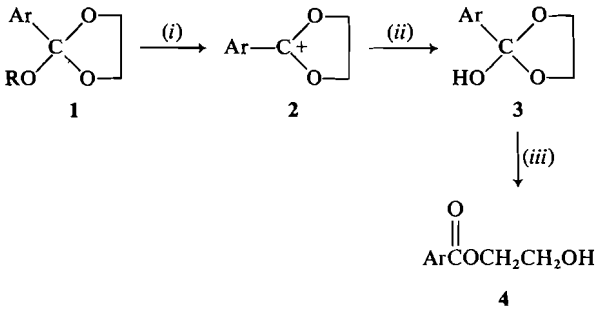

1 2 3 4

the last two reaction stages of the ortho ester hydrolysis. Our results on this latter system lead to the prediction that this exchange reaction is a reasonable one. This paper presents that argument and experimental results obtained with ethylene glycol monobenzoate and pinacol monobenzoate.

Experimental

Materials

Oxygen-18 water (83.1% ^{18}O or 92.2% ^{18}O) was obtained from Miles Research. Sulfuric acid solutions were prepared as previously described (5). 2-Phenyl-2-methoxy-1,3-dioxolane (**1***a*) (6), 2-phenyl-1,3-dioxolenium borofluorate (**2***a*) (7), and 2-phenyl-4,4,5,5-tetramethyl-1,3-dioxolenium borofluorate (**2***b*) (8) have been described.

2-Phenyl-2-methoxy-4,4,5,5-tetramethyl-1,3-dioxolane (**1***b*) was obtained by addition of the dioxolenium salt **2***b* to a sodium methoxide solution in methanol, as described for other ortho esters (7). Compound **1***b* had bp 75°C (0.2 Torr); nmr($CDCl_3$, TMS) δ: 7.2–7.7 (m, 5H), 3.03 (s, 3H), 1.38 (s, 6H), 1.13 (s, 6H). *Anal.* calcd. for $C_{14}H_{20}O_3$: C 71.16, H 8.53; found: C 71.17, H 8.59.

Ethylene glycol monobenzoate, **4***a*, and pinacol monobenzoate **4***b*, were prepared by stirring the ortho esters **1***a* and **1***b* in 0.1 *M* HCl for 30 min. The acid was neutralized with $NaHCO_3$, and the resultant suspension was extracted with ether. This was dried ($MgSO_4$), filtered, and the ester obtained by distillation. Ethylene glycol monobenzoate had bp 100°C (0.2 Torr). Pinacol monobenzoate had bp 85°C (0.1 Torr); nmr ($CDCl_3$, TMS) δ: 8–8.2 (m, 2H), 7.5–7.6 (m, 3H), 3.7 (s, 1H), 1.70 (s, 6H), 1.35 (s, 6H). *Anal.* calcd. for $C_{13}H_{18}O_3$: C 70.25, H 8.16; found: C 70.13, H, 8.37.

Ethylene glycol monobenzoate-carbonyl-^{18}O (92.2%) and pinacol monobenzoate-carbonyl-^{18}O (83.1%) were prepared by mixing ortho ester **1***a* or **1***b* (0.01 mol) with ^{18}O-water (0.011 mol), and adding *p*-toluene sulfonic acid (10 mg). The two phase system was stirred until it became homogeneous. Work-up followed the procedure outlined above for the unlabelled glycol monoester.

Kinetics of Exchange

Labelled glycol monoester (0.2 g) was dissolved in unlabelled aqueous solution (100 mL for **4***a*, 500 mL for **4***b*), and the solution placed in a thermostatted water bath (25°C). After an appropriate time this solution was extracted with ether, the ether extract washed with aqueous $NaHCO_3$, dried ($MgSO_4$), filtered, and the ether removed.

This sample was analyzed directly on an AEI model MS 902 mass spectrometer, equipped with a Vacuumetrics ratiometer. The relative intensity of two peaks in the mass spectrum of the glycol monoester was determined as the average of 40–50 measurements. For ethylene glycol monobenzoate the ratio of the peaks at *m/e* 125/123 was taken; for pinacol monobenzoate, 166/164. Neither ester shows a molecular ion in its mass spectrum; both exhibited strong signals at 107/105, but the ratio of these was found to vary with time. This was not the case with the peaks chosen for analysis.

The excess ^{18}O in a given sample was calculated using the formula (9)

$$\text{Excess } ^{18}O = 99.8\left(\frac{R - R_0}{1.002 + R - R_0}\right)$$

where R is the ratio of the two peaks of the sample in question, and R_0 is the ratio of the same two peaks in unlabelled material. This equation corrects relative peak intensities for natural isotopic variation, but it applies to a sample where one atom only is enriched, a point which will be addressed later. Rate constants for oxygen exchange were evaluated as slopes of plots of ln (excess ^{18}O) versus time. Table 1 shows the results of a representative run.

Hydrolysis of Ethylene Glycol Monobenzoate

The ester was dissolved in aqueous sulfuric acid, and the solution placed in a thermostatted water bath (25°C). At appropriate times a sample was withdrawn and its nmr spectrum immediately recorded on a Varian T60 nmr spectrophotometer. The quantities measured were the (integrated) area of the set of signals of the methylene protons of the ester (A_E) relative to the area of the sharp singlet of the ethylene glycol product (A_p). Rate constants were calculated as the slopes of plots of ln ($A_E/(A_p + A_E)$) versus time.

Hydroxy Ester – Dioxolenium Ion Equilibrium

Ultraviolet Method

A stock solution containing 2-phenyl-1,3-dioxolenium borofluorate (4×10^{-5} mol L^{-1}) in rigorously dry acetonitrile was prepared. This solution (3.0 μL) was added directly to a thermostatted uv cell containing exactly 3 mL of various sulfuric acid solutions, and the spectral change recorded at 265 nm, the wavelength corresponding to λ_{max} for the ion. A first-order decrease in absorbance is observed (below 80% H_2SO_4); first-order rate constants were evaluated as the slopes of plots of ln ($A - A_\infty$) vs. time. A plot of the A_∞ values vs. % H_2SO_4 was found to take the form of a titration curve. Above 80% H_2SO_4 the 2-phenyl-1,3-dioxolenium ion is in fact stable, and undergoes no hydrolysis. This is caused by the fact that the dioxolenium ion (**2***a*) and glycol monoester (**4***a*) equilibrate. Their ratio at equilibrium [**2**]/[**4**] was determined as $(A_\infty - A^4)/(A^2 - A_\infty)$, where A^4 is the absorbance of ester at 265 nm as determined from the A_∞ value in dilute acid (below 50% H_2SO_4) and A^2 is the absorbance of ion at 265 nm as determined in concentrated acid (above 85% H_2SO_4).

The approach to equilibrium was also followed starting with ester, for which an increase in absorbance is observed at 265 nm in solutions more concentrated than 67% H_2SO_4. Rate constants for this process, obtained as the slopes of plots of ln ($A_\infty - A$) versus time were found to be identical to rate

TABLE 1. Oxygen exchange of pinacol monobenzoate-^{18}O in 0.100 *M* HCl (25°C)

Time (h)	166/164	Excess ^{18}O (%)
0[a]	4.91 ±0.02	82.8
1.93	1.50 ±0.01	59.6
4.00	0.757±0.005	42.4
6.27	0.425±0.005	28.9
175.00	0.016±0.002	
Unlabelled	0.016±0.002	

[a]Labelled ester, before solution.

constants in the same acids obtained starting with dioxolenium ion.

Nuclear Magnetic Resonance Method

Ethylene glycol monobenzoate was dissolved in acids where the uv spectra suggest an appreciable concentration of ion at equilibrium. The formation of this ion could be easily seen from the appearance of a downfield singlet corresponding to the methylene protons of the ion. (This signal is not due to ethylene glycol, whose C—H protons are upfield from the methylene protons of the ester.) The ratio of ion to ester after attainment of equilibrium was calculated from the relative areas of the signals of the methylene protons in the two species. This ratio was within experimental error identical to the ratio obtained using uv spectroscopy.

Hydrolysis of Ortho Ester **1**b *and Ion* **2**b

In the pH region these species hydrolyze to pinacol monobenzoate. The kinetics for this hydrolysis were followed spectroscopically, using either a Unicam Sp 1800 spectrophotometer or a Durrum-Gibson stopped-flow apparatus. Studies involving the former were carried out by adding 3 μL of an acetonitrile solution of the substrate directly to a pre-equilibrated uv cell containing the aqueous solution. Studies with the latter were carried out by dissolving the substrate (ortho ester only in this case) in 0.002 *M* NaOH, and mixing this with an equal volume of the appropriate aqueous acid. In both cases changes in optical density as a function of time were monitored; wavelengths of 265 nm, λ_{max} for the dioxolenium ion, or 232 nm, λ_{max} for the ester product, were employed. First-order rate constants were evaluated as the slopes of plots of ln $(A - A_\infty)$ ($\lambda = 265$) or ln $(A_\infty - A)$ ($\lambda = 232$) versus time. All studies were carried out at 25°C, and ionic strength 0.1.

Results

2-Phenyl-4,4,5,5-tetramethyl-1,3-dioxolenium Ion

The above ion, as its borofluorate salt, was added in a very small amount of acetonitrile to aqueous solutions with pH 1.0–5.5, and the conversion to pinacol monobenzoate monitored by conventional uv spectroscopy. First-order rate constants for this process were obtained throughout this pH region following the absorbance increase due to the product ester at $\lambda = 232$ nm. In the more acidic solutions a signal due to the ion could also be seen at $\lambda = 265$ nm. First-order rate constants for the disappearance of this signal were also determined; these were found to be identical to the rate constants obtained following product appearance. The variation with pH of the observed rate constants will be described later. Buffer catalysis is also found; standard analysis reveals that both the acid and base component are catalytically active.

2-Phenyl-2-methoxy-4,4,5,5-tetramethyl-1,3-dioxolane

First-order rate constants for the hydrolysis of the above ortho ester were obtained following product appearance in solutions with pH > 6, and follow the rate law

$$k_{obs} = k_{H^+}{}^1[H^+] + k_0{}^1 + k_{HA}{}^1[HA]$$

with $k_{H^+}{}^1 = 3.1 \times 10^4\ M^{-1}\ s^{-1}$ and $k_0{}^1 \approx 1 \times 10^{-6}\ s^{-1}$. At pH 5–6, the first-order rate plots based on product appearance show marked deviations from linearity. At pH 1–5 the rate behaviour becomes identical in every respect to that observed with the 1,3-dioxolenium ion. This includes the fact that the ion itself can be detected in the more acidic solutions. Stopped-flow experiments, starting with the ortho ester in very dilute base and mixing with excess acid, show that this ion disappears in two phases (Fig. 1). The absorbance decrease which is observed in the experiments using conventional uv spectroscopy is preceded by a much faster decrease. This initial phase is also first order; rate constants follow the empirical equation $k_{obs} = a + b[H^+]$, with $a = 6 \times 10^2\ s^{-1}$ and $b = 2 \times 10^4\ M^{-1}\ s^{-1}$. The stopped-flow experiments also permit accurate measurement of the amount of dioxolenium ion which disappears in the two kinetic phases. A plot versus acidity of the absorbance change of the slow second phase divided by the total absorbance change takes the form of a titration curve for an acid with a pK value of 1.4, with the slow phase accounting for a greater proportion at high acid concentrations.

Hydroxy Ester – Dioxolenium Ion Equilibrium

The equilibrium between the 2-phenyl-1,3-dioxo-

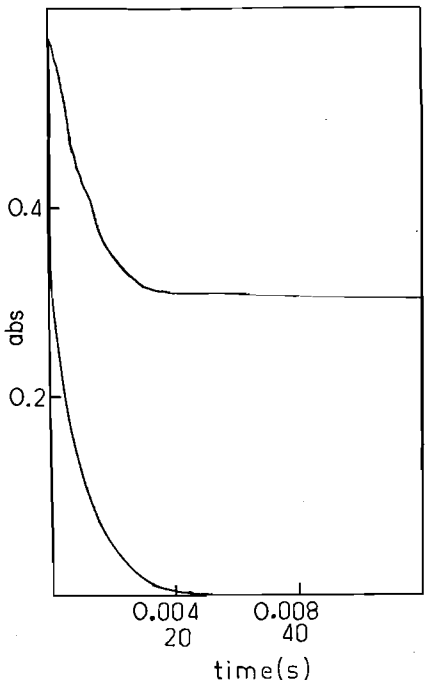

FIG. 1. Biphasic nature of the disappearance of dioxolenium ion ($\lambda = 265$) in the hydrolysis of 2-phenyl-2-methoxy-4,4,5,5-tetramethyl-1,3-dioxolane in 0.02 *M* HCl. The two traces were obtained in consecutive runs on the stopped-flow apparatus. The top and bottom timescales refer to the top and bottom traces respectively.

lenium ion and ethylene glycol monobenzoate was studied in 67–77% H_2SO_4 by determining

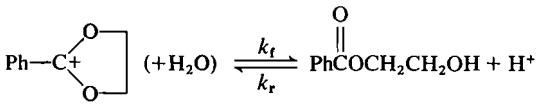

2 4

using uv and nmr spectroscopy, the ratio [**2**]/[**4**] as a function of acidity. A plot of the logarithm of this ratio versus the H_R acidity function was linear (correlation coefficient = 0.998), with a slope = −0.71 and an intercept of −8.68.

First-order rate constants could also be obtained for the approach to equilibrium, and are the same regardless of the direction of approach. These rate constants are given by $k_{obs} = k_f + k_r$; the ratio [**2**]/[**4**] = k_f/k_r, so that the individual rate constants k_f and k_r can be obtained. These are depicted in Fig. 5 (see Discussion).

Oxygen Exchange

Samples of the two glycol monoesters enriched with ^{18}O were prepared by hydrolyzing the corresponding ortho ester with ^{18}O enriched water, in the presence of a small amount of acid. It is important to establish that this reaction has produced only carbonyl labelled ester. This is obviously required if we are going to follow carbonyl exchange, and not some other process. We also require in the equation used to calculate ^{18}O content that any excess ^{18}O be present in only one oxygen. Finally and perhaps most importantly, our mechanistic interpretation of these ortho ester hydrolyses demands this result.

In principle the label could end up in two different oxygens.

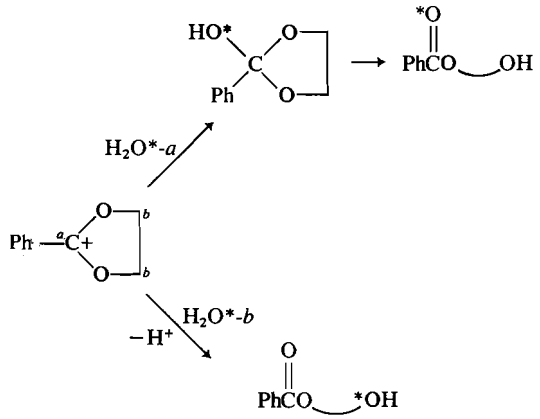

The peaks analyzed in the mass spectrum of each ester were fragments arising from loss of a group containing the hydroxyl oxygen. The analysis shows that all of the label of the reagent ^{18}O water is still present in these peaks, and therefore could not have gone into the β-hydroxy oxygen. For example 83.1% ^{18}O-water was used to prepare the labelled pinacol monobenzoate; the 166/164 fragment peaks analyzed show 83.0% label (see Table 1).

A second piece of evidence, perhaps less rigorous, is the observation that the label can be completely exchanged out with a large excess of unlabelled solvent (see, for example, Table 1). As we will show, there is a mechanism by which this can occur if the label is in the carbonyl oxygen. It is more difficult to account for this exchange if the label is in the hydroxy oxygen, since alcohol exchange is far too slow (10).

The labelled esters do exchange this oxygen when treated with unlabelled aqueous acid. Unlike ordinary esters, this exchange process occurs more rapidly than the ester undergoes hydrolysis and it is in fact possible to observe essentially complete exchange before the ester is completely destroyed. A typical exchange run is presented in Table 1. Excellent first-order plots for the exchange were obtained in all cases. The acid dependency of these rate constants is described in the Discussion.

Discussion

Ortho Ester Hydrolysis

We will discuss initially how it is possible to obtain kinetic information for the three reaction stages for the hydrolysis of the tetramethyl substituted ortho ester. Our results, and analysis, for the unsubstituted system are presented elsewhere (3, 4). Although the same kinetic information is eventually obtained in each case, experimentally slightly different approaches are used. This happens simply because in the tetramethyl system the rate of the last reaction stage is in the range of conventional uv spectroscopy. This means that it is possible to add the 1,3-dioxolenium ion directly to a uv cell, and observe the kinetics associated with the last reaction stage, in essentially a pure aqueous medium. With the unsubstituted ortho esters the later reaction stages are too fast for conventional uv spectroscopy, although they are in the range of stopped-flow instruments. However, because of the nature of our apparatus which mixes only in a 50:50 proportion, experiments starting directly with dioxolenium ion result in rate constants in a solvent which is 50% organic. To obtain rate data in water alone we were forced to rely on the fact that appropriate precursors which are stable in aqueous base hydrolyze at some acidity with rate-determining decomposition of the hydrogen ortho ester (3, 4).

First-order rate constants obtained in the hydrolysis of the 2-phenyl-4,4,5,5-tetramethyl-1,3-dioxolenium ion are depicted in Fig. 2. These, along with

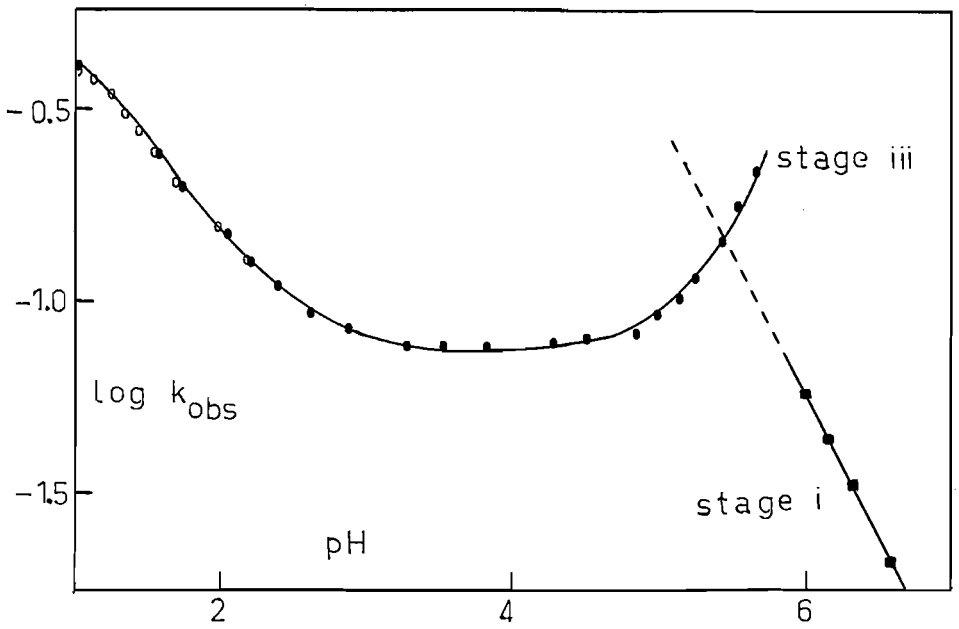

FIG. 2. First-order rate constants (μ = 0.1, 25°C) in the hydrolysis of 2-phenyl-4,4,5,5-tetramethyl-1,3-dioxolenium borofluorate ((●) λ = 232 nm; (○) λ = 265 nm, slow phase) and 2-phenyl-2-methoxy-4,4,5,5-tetramethyl-1,3-dioxolane ((■) λ = 232 nm). Rate constants for experiments starting with the ortho ester in solutions with pH < 5 are not shown but are identical, within experimental error, to those of the dioxolenium ion. All rate constants for solutions with pH > 3 are based on extrapolation to zero buffer concentration.

other observations, can be explained by postulating a rapid and reversible hydration of the ion followed by a slower decomposition of the hydrogen ortho ester to pinacol monobenzoate. This latter process is catalyzed by hydronium ion, water (no catalysis), and hydroxide ion, as well as general acids and general bases. We will define the rate constants for the three stages of a dioxolane ortho ester hydrolysis as indicated below.

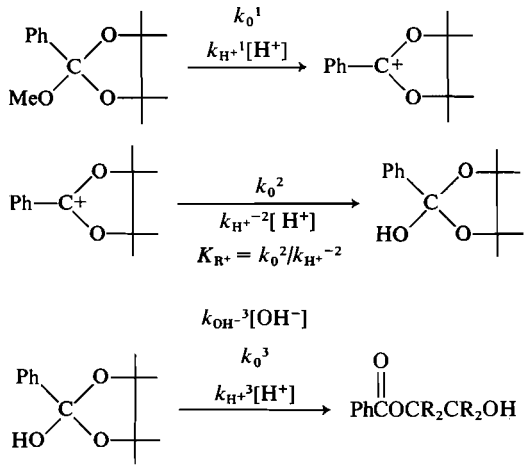

For the last two stages, the following rate law can be derived, assuming a rapid equilibrium between dioxolenium ion and hydrogen ortho ester. The

$$k_{obs} = \frac{k_{H^+}{}^3[H^+] + k_0{}^3 + k_{OH^-}{}^3[OH^-]}{1 + [H^+]/K_{R+}}$$

observed first-order rate constant k_{obs} refers to formation of pinacol monobenzoate, and the disappearance of the ion present after the equilibrium between ion and hydrogen ortho ester is established. Values of the four constants of this equation which best fit the experimental data of Fig. 2 are given in Table 2. The agreement of our kinetic analysis with

TABLE 2. Rate and equilibrium constants (25°C, μ = 0.1)

Constant	Tetramethyl	Unsubstituted
$k_{H^+}{}^1(M^{-1}\,s^{-1})$	3.1×10^4	5.4×10^{3d}
$k_0{}^2(s^{-1})$	6×10^2	1.7×10^{4d}
$k_{H^+}{}^{-2}(M^{-1}\,s^{-1})$	2×10^4	4.3×10^{3d}
pK_R	1.4[a]	−0.6[d]
	1.5[b]	
	1.4[c]	
$k_{H^+}{}^3(M^{-1}\,s^{-1})$	13	3×10^{2d}
$k_0{}^3(s^{-1})$	0.074	1.5[d]
$k_{OH^-}{}^3(M^{-1}\,s^{-1})$	2.0×10^7	6.0×10^{10d}
K^{-3}	3.7×10^{-5}	2.7×10^{-9}
$k_{H^+}{}^{-3}(M^{-1}\,s^{-1})$	4.8×10^{-4}	8.1×10^{-7}
$k_0{}^{-3}(s^{-1})$	2.7×10^{-6}	4.1×10^{-9}
$k_{OH^-}{}^{-3}(M^{-1}\,s^{-1})$	7.4×10^2	1.6×10^2

[a]Kinetic analysis.
[b]From $k_0{}^2/k_{H^+}{}^{-2}$.
[c]Spectroscopic.
[d]Reference 4.

the experimental observations can be seen by comparing in Fig. 2 the curve, which is calculated, with the experimental points. In simple terms the rate–pH profile exhibits regions corresponding to the hydronium ion catalysis, water catalysis, and hydroxide ion catalysis of the hydrogen ortho ester decomposition. Also a levelling off in rate at high acid concentration is apparent. This occurs because of a shift in the position of the equilibrium between the hydrogen ortho ester and dioxolenium ion, the latter species becoming favored in this equilibrium as the acidity is increased. In the solutions where significant amounts of dioxolenium ion and hydrogen ortho ester are present at equilibrium, the ion disappearance is biphasic. The initial kinetic phase corresponds to the rapid equilibration of the two species. This is followed by a considerably slower second phase as the ion in equilibrium with hydrogen ortho ester is siphoned off as the latter is converted to pinacol monobenzoate. In the experiments starting with the borofluorate salt of the ion, only the second phase is seen. These experiments are necessarily carried out on a conventional uv spectrophotometer, and are incapable of showing the much more rapid initial phase. In less acidic solutions, no uv signal due to the ion can be observed in these conventional uv experiments. Now the equilibrium favors hydrogen ortho ester, and the ion completely disappears in the rapid phase. However, although the ion does disappear rapidly, the appearance of product is much slower. This can only mean that there is some intermediate being formed and this must be the hydrogen ortho ester.

Considering now the situation starting one stage further back at the ortho ester, it can be concluded that only in solutions with pH > 6 is the first reaction stage the slow step in the overall hydrolysis. In more acidic solutions this stage becomes faster than the third stage, and what is observed (following product appearance) are the kinetics associated with this later stage. In other words, there is a change in the rate-limiting step in the overall hydrolysis, just as there is in the unsubstituted case (3, 4). Here, however, the evidence is very simple. In the more acidic solutions the kinetic behavior observed starting with ortho ester is identical to that observed starting with dioxolenium ion, one of the intermediates in its hydrolysis. Above pH 6 this is no longer the case, and the dioxolenium ion decomposes more rapidly than the ortho ester hydrolyses. The crossover in behavior is seen very clearly in Fig. 2, in the intersection of the two curves, the curve obtained at high pH representing the first stage, and the curve obtained at low pH representing the third stage. The reason for the changeover is also apparent; the first stage remains hydronium ion catalyzed throughout this pH region, whereas the third stage is catalyzed by water and hydroxide ion as well. It can also be noted that in the vicinity of the crossover point, first-order kinetics in product appearance are not obtained. The system is properly described here by the equations for two consecutive first-order reactions (see ref. 4 for a more detailed discussion of this point).

Stopped-flow experiments starting with ortho ester (Fig. 1) reveal the two step nature associated with the disappearance of the dioxolenium ion in the more acidic solutions. First-order rate constants for the initial phase must follow the rate law

$$k_{obs} = k_0^2 + k_{H^+}{}^{-2}[H^+]$$

so that the empirically determined constants $a = k_0^2$ and $b = k_{H^+}{}^{-2}$. The ratio $k_0^2/k_{H^+}{}^{-2}$ should also give pK_R and, in fact, the value so determined agrees well with that obtained in the kinetic analysis (Table 2).

A third measure of the value of pK_R, also in agreement, is produced by the titration curve representing the variation in the absorbance in the two kinetic phases. This is essentially a standard

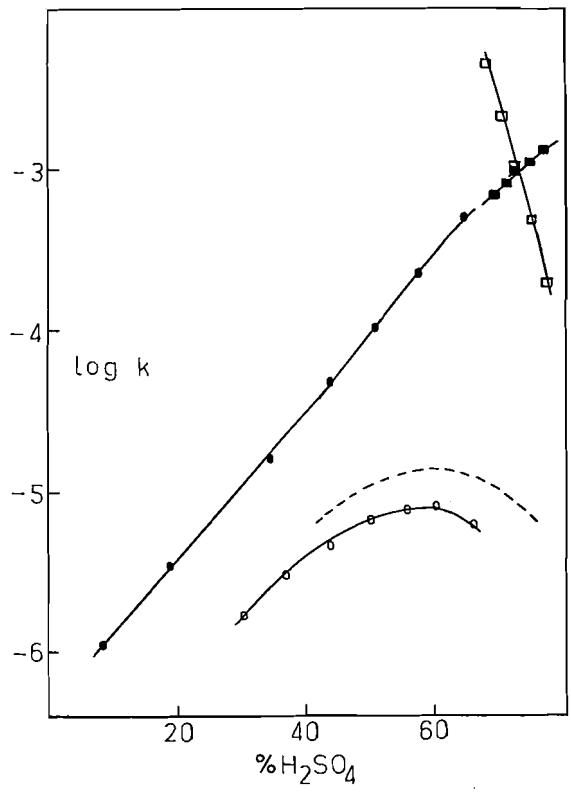

FIG 3. Rate constants for ethylene glycol monobenzoate. (●) Carbonyl oxygen exchange, (○) hydrolysis, (■) and (□) forward and reverse rate constants for the reversible cyclization to the 2-phenyl-1,3-dioxolenium ion, (--) rate constants for methyl benzoate hydrolysis (13).

spectroscopic approach, and is described in detail elsewhere (4).

Table 2 also contains values of the rate and equilibrium constants obtained for the unsubstituted system. The introduction of the four methyl substituents results in a 5–6-fold increase in the rate of the first reaction stage, as well as the reverse of stage 2. This is probably due to increased steric strain in the ortho ester (or hydrogen ortho ester), relative to the dioxolenium ion, brought about by the presence of the four methyl groups. This substitution also results, undoubtedly for the same reason, in a decrease by a factor of 28 in the rate constant for hydration of the ion. The combined effects result in a change in pK_R by 1.9 log units. That the steric effect is manifested more in the hydration direction (k_0^{-2}) than the dehydration direction ($k_{H^+}^{-2}$) implies that the transition state lies closer to the hydrogen ortho ester. This suggestion is consistent with previous observations of ortho ester hydrolysis, which imply an 'early' transition state in the reaction proceeding to the oxocarbonium ion (11, 12).

Carbonyl Oxygen Exchange

The cyclization mechanism for carbonyl oxygen exchange of a labelled glycol monoester is shown below, where for consistency we have maintained the same formulism for the rate constants.

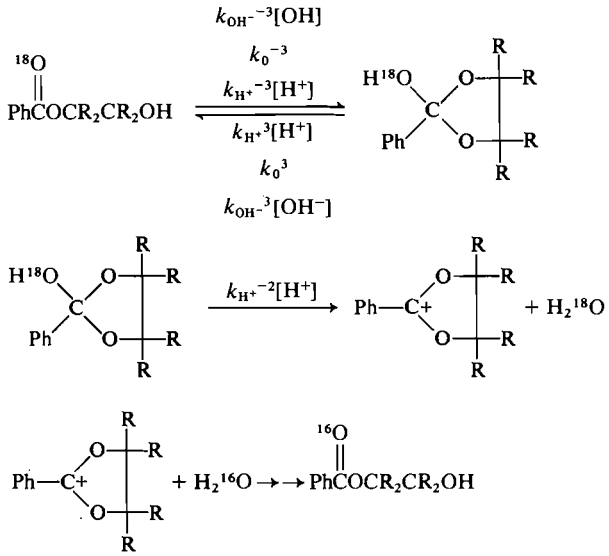

Under our experimental conditions, which involve the use of a large excess of unlabelled solvent, any dioxolenium ion that forms is trapped by unlabelled water. Thus we can assume that exchange occurs via the above mechanism whenever β-hydroxy ester is converted to dioxolenium ion. To observe this exchange there are two requirements: (*a*) hydrogen ortho ester formed on cyclization of the β-hydroxy ester must have some tendency to proceed on to dioxolenium ion, rather than revert immediately back, and (*b*) the cyclization reaction, which involves intramolecular addition of an OH group, must be able to compete with normal hydrolysis, i.e., the intermolecular addition of an OH group. It can immediately be predicted that in acid solutions, where the reversion of the hydrogen ortho ester to hydroxy ester occurs with acid catalysis, requirement (*a*) is met. As seen in our results on the ortho ester hydrolysis, acid-catalyzed ring opening of the hydrogen ortho ester is considerably slower than the acid-catalyzed cleavage of the exocyclic OH group ($k_{H^+}^{-2} > k_{H^+}^{3}$, Table 2).

Ethylene Glycol Monobenzoate

Figure 3 plots first-order rate constants for the carbonyl oxygen exchange of ethylene glycol monobenzoate as a function of sulfuric acid concentration. We suggest that these rate constants do represent the cyclization mechanism for exchange. The most convincing argument for this proposal comes from our observation that in acids more concentrated than 67% H_2SO_4 there is a detectable amount of the 2-phenyl-1,3-dioxolenium ion present in equilibrium with the hydroxy ester, and we have been able to measure the forward and reverse first-order rate constants associated with this equilibration. One of these rate constants refers specifically to the rate of formation of the 1,3-dioxolenium ion from the ester. We have pointed out that the cyclization exchange involves this very reaction. As can be seen in Fig. 3 there are two curves, one obtained in dilute acids for carbonyl oxygen exchange, and the other obtained in more concentrated acids where the cyclization is actually observed. Within experimental error these two curves are continuous functions of one another.

Another observation of significance is that the rate constants for exchange are greater than the rate constants for the hydrolysis. In all other examples of acid-catalyzed ester hydrolysis thus far investigated the reverse has been true (1, 2, 10, 13–17). Ethyl benzoate, for example, in 0.1 *M* HCl (33% dioxane:H_2O) exchanges its carbonyl oxygen one-fifth as fast as it hydrolyzes (1, 14). As can be seen in Fig. 3 the hydrolysis of ethylene glycol monobenzoate is in fact normal; its kinetic behavior is very similar to that shown in the hydrolysis of methyl benzoate (13). It is the exchange reaction of ethylene glycol monobenzoate which is abnormally rapid, and this occurs because of the different mechanism.

Also significant is a comparison of the rate profiles for hydrolysis and exchange. For the simple esters investigated in detail thus far (ethyl acetate (13) and isopropyl acetate (16)), the ratio of the rates of

hydrolysis and exchange has been found to be essentially constant as the sulfuric acid concentration is changed. For ethylene glycol monobenzoate, however, this is not the case, the ratio of exchange to hydrolysis increasing by a factor of about 10 over the range of acidities for which both processes were investigated. This can be accounted for in terms of two different mechanisms for the two processes.

The comparison can in fact be put on quantitative terms based on the following expressions for the first-order rate constants.

$$k_{ex} = \frac{k_{ex}^{0}}{K_{SH^+}} \frac{f_s a_{H^+}}{f_{s^*}^{ex}}$$

$$k_{hyd} = \frac{k_{hyd}^{0}}{K_{SH^+}} \frac{f_s a_{H_2O} a_{H^+}}{f_{s^*}^{hyd}}$$

These equations are obtained by assuming that the reactions occur by way of the protonated ester; all of the terms are defined in the normal way (17, 18). We have explicitly included in the expression for the hydrolysis rate constant the activity of water, this term representing the external water molecule which must be involved in this reaction. Dividing these equations, and taking logarithms, there is obtained the equation

$$\log k_{ex} - \log k_{hyd} = \log k_{ex}^{0} - \log k_{hyd}^{0} - \log a_{H_2O} + \log (f_{s^*}^{ex}/f_{s^*}^{hyd})$$

In fact, a plot of $\log k_{ex} - \log k_{hyd}$ versus $-\log a_{H_2O}$ is linear, with a slope of 1.05 (Fig. 4). This implies that $\log (f_{s^*}^{ex}/f_{s^*}^{hyd}) \approx 0$, or, in other words, that the activity coefficients for the two transition states vary with acidity in the same way. As will be shown in a later section, the rate of exchange in acid solutions is essentially equal to the rate of cyclization, so that $f_{s^*}^{ex}$ refers to the reaction of protonated carbonyl with the β-hydroxy group. Since in normal esters hydrolysis occurs more rapidly than exchange, the rate of formation of the hydrolysis tetrahedral intermediate is rate determining in that reaction, so that $f_{s^*}^{hyd}$ can be taken to refer to the reaction of the protonated carbonyl with a water molecule. Therefore, the two transition states are in fact very similar, the only difference being that one involves reaction with an internal nucleophile, while the other involves reaction with an external nucleophile. It is only necessary in considering the latter case to account explicitly for the activity of this nucleophile.

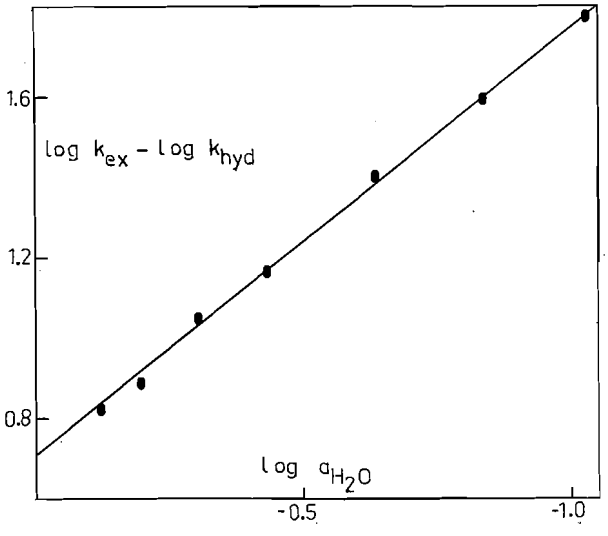

FIG. 4. Log k_{ex} − log k_{hyd} for ethylene glycol monobenzoate plotted as a function of log a_{H_2O}.

The intercept of Fig. 4 provides the relative rates in water of the intramolecular and intermolecular reactions. This is compared below with the same ratio for two related systems recently studied in our laboratories.

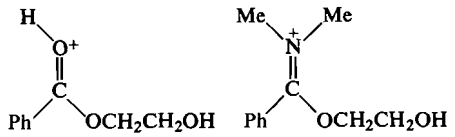

$\frac{k_{intra}}{k_{inter}}$ 5 ≈40 (ref. 19)

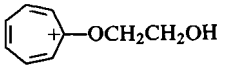

4.5 (ref. 20)

In all three cases the intramolecular reaction is favored, but the preference for it is not that great.

Pinacol Monobenzoate

With this ester, the exchange reaction is sufficiently rapid in the pH region that an extensive rate–pH profile could be obtained (see Fig. 5). Rates of hydrolysis were not determined; using data for *tert*-butyl benzoate (21), we estimate that in 0.1 *M* HCl the exchange of pinacol monobenzoate occurs 10 times more rapidly than its hydrolysis. Moreover, even if hydrolysis did occur, the normal carbonyl oxygen mechanism would still not be in operation, since this ester, being a tertiary ester, would probably hydrolyze by an $A_{A1}1$ mechanism (21). There can be little doubt then that the exchange observed arises via cyclization.

To account for the rate–pH profile we note that the rate of exchange can be set equal to the rate of formation of dioxolenium ion, and calculate this rate making a steady-state assumption in hydrogen ortho ester.

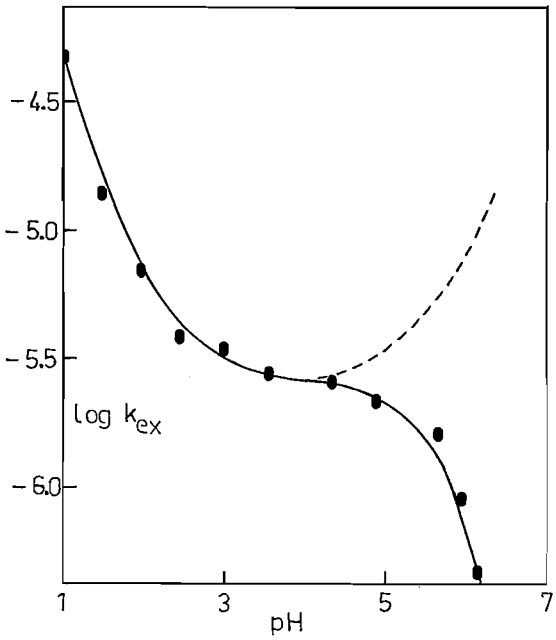

FIG. 5. Rate constants for the carbonyl oxygen exchange of pinacol monobenzoate (25°C, $\mu = 0.1$). The points are experimental, while the solid curve is calculated (see text). The dashed curve, which merges with the solid curve below pH 3.5, represents the variation in the rate constant for the cyclization step as a function of pH.

[1] $$k_{ex} = \frac{k_{H^+}{}^{-2}[H^+](k_{OH^-}{}^{-3}[OH^-] + k_0{}^{-3} + k_{H^+}{}^{-3}[H^+])}{k_{OH^-}{}^{3}[OH^-] + k_0{}^{3} + (k_{H^+}{}^{3} + k_{H^+}{}^{-2})[H^+]}$$

Although several rate constants not already obtained appear in this expression, there is in fact only one new unknown, since

$$k_{OH^-}{}^{-3}/k_{OH^-}{}^{3} = k_0{}^{-3}/k_0{}^{3} = k_{H^+}{}^{-3}/k_{H^+}{}^{3} = K^{-3}$$

Taking this into account, and rearranging

[2] $$K^{-3} = \frac{k_{ex}((k_{OH^-}{}^{3}[OH^-] + k_0{}^{3} + (k_{H^+}{}^{3} + k_{H^+}{}^{-2})[H^+])}{k_{H^+}{}^{-2}[H^+](k_{OH^-}{}^{3}[OH^-] + k_0{}^{3} + k_{H^+}{}^{3}[H^+])}$$

Values of K^{-3} obtained from this equation, using the rate constants of Table 2 are indeed constant, with a value of $K^{-3} = 3.7 \pm 0.5 \times 10^{-5}$. This can be used to calculate values for the three constants of the form k^{-3} (Table 2). The consistency of our analysis is seen in Fig. 5 from the agreement of the experimental data with the solid curve which has been calculated using [1].

In simple terms, this kinetic analysis can be broken down, showing that at pH 1–3.5 the carbonyl exchange is occurring with rate-determining cyclization, and $k_{ex} \approx k_{H^+}{}^{-3}[H^+] + k_0{}^{-3}$. The rate–pH profile contains an acid-catalyzed region giving way to a pH independent region. In these acidic solutions the hydrogen ortho ester has a large preference for cleavage of the exocyclic hydroxyl group over ring-opening to return to glycol monoester. Exchange therefore results on virtually every act of cyclization. In the pH region 3.5–4.5 there is, however, a change in rate-determining step. This occurs because the conversion of hydrogen ortho ester to glycol monoester becomes water catalyzed, and then hydroxide ion catalyzed, while its conversion to dioxolenium ion remains hydronium ion catalyzed. By about pH 5.0 the hydrogen ortho ester reverts to ester more readily, and the rate-limiting step in the exchange is the conversion to the dioxolenium ion. The rate constant for exchange is now given by $k_{ex} = K^{-3}k_{H^+}{}^{-2}[H^+]$ and the reaction now becomes acid-catalyzed again. It is interesting to note that the cyclization stage has, in fact, become hydroxide ion catalyzed by this point. This is seen by the dashed line in Fig. 5 which represents $k_{OH^-}{}^{-3}[OH^-] + k_0{}^{-3} + k_{H^+}{}^{-3}[H^+]$, and gives therefore the rate constant for cyclization. We can also point out that the exchange reaction should become pH independent at high pH, where the loss of the exocyclic OH group becomes non-catalyzed ($k_{ex} = K^{-3}k_0{}^{-2}$, where $k_0{}^{-2}$ = pH independent rate constant). That this process should occur can be predicted on the basis that a very similar reaction, the loss of the exocyclic OMe group from the ortho ester, becomes pH independent at high pH.

Glycol Monoester–Hydrogen Ortho Ester Equilibrium

For ethylene glycol monobenzoate, carbonyl oxygen exchange in dilute acids is very slow. We did obtain one rate constant in 0.1 *M* HCl (8.0×10^{-8} s^{-1}); using [2] this provides a value of $K^{-3} = 2.7 \times 10^{-9}$. This then allows the determination of the values for the constants k^{-3} (Table 2).

For both monobenzoates, the calculation of K^{-3} in acids as concentrated as 0.1 *M* HCl is, in fact, simpler than it seems on the basis of [2], since the terms in hydronium ion dominate, and $k_{H^+}{}^{3} < k_{H^+}{}^{-2}$. This means that essentially we are obtaining K^{-3} in this solution as the ratio of forward and reverse rate constants. This is possible despite the instability of the hydrogen ortho ester, since this species can be observed, starting with an appropriate precursor, and its rate of decomposition measured (the reverse rate). The forward process cannot be observed; we can, however, measure its rate using ^{18}O exchange.

The hydrogen ortho ester can be regarded as a tetrahedral intermediate, being the intermediate of a

TABLE 3. Free energies for cyclization of glycol monoesters

Reaction	ΔG^0 (kcal/mol) R = H[a]	R = Ph[b]
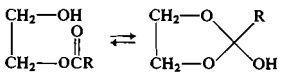	7.5	11.8
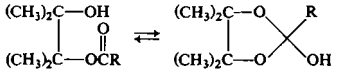	3.2	6.1

[a]Reference 23.
[b]This work.

degenerate intramolecular acyl transfer reaction. Although the equilibrium between the hydrogen ortho ester and the glycol monoester considerably favors the latter, our values of the equilibrium constant for their interconversion are actually measured quantities, with no assumptions or approximations. This represents the first direct measurement for such equilibrium constants. The numbers obtained, particularly that for the unsubstituted compound, reflect the expected instability of the tetrahedral intermediate relative to the carbonyl compound.

Recently, Guthrie has used a thermochemical method for calculating equilibrium constants for the formation of several types of tetrahedral intermediates (22, 23). The basic premise of his method involves the evaluation of the free energy change for the replacement of the OR group of a stable ortho acid derivative by an OH group, using a correlation based on cases where both species are stable. Although the actual compounds of our study have not been considered, the cyclization of several glycol monoesters was investigated. In Table 3 we compare Guthrie's results for formate derivatives with our numbers. Considering that the effect of replacing hydrogen by phenyl will disfavor the hydrogen ortho ester relative to the carbonyl, there is excellent consistency between the two sets of methods, since the formate esters are indeed predicted to cyclize considerably more readily. Both sets of data also show the much greater tendency for the pinacol monoester to cyclize. This has been attributed by Guthrie (23) to relief of steric compression on cyclization.

Acknowledgment

Financial support of the National Research Council of Canada is gratefully acknowledged.

1. M. L. BENDER. J. Am. Chem. Soc. **73**, 1626 (1951).
2. S. L. JOHNSON. Adv. Phys. Org. Chem. **5**, 237 (1967); W. P. JENCKS. Catalysis in chemistry and enzymology. McGraw-Hill, New York, NY. 1968. pp. 463–554; A. J. KIRBY. Comprehensive chemical kinetics. Vol. 10. *Edited by* C. H. Bamford and C. F. H. Tipper. Elsevier, New York, NY. 1972. p. 165.
3. M. AHMAD, R. G. BERGSTROM, M. J. CASHEN, A. J. KRESGE, R. A. MCCLELLAND, and M. F. POWELL. J. Am. Chem. Soc. **99**, 4827 (1977).
4. M. AHMAD, R. G. BERGSTROM, M. J. CASHEN, Y. CHIANG, A. J. KRESGE, R. A. MCCLELLAND, and M. F. POWELL. J. Am. Chem. Soc. In press.
5. K. YATES and R. A. MCCLELLAND. Can. J. Chem. **52**, 1098 (1974).
6. Y. CHIANG, A. J. KRESGE, P. SALOMAA, and C. I. YOUNG. J. Am. Chem. Soc. **96**, 4494 (1974).
7. Y. CHIANG, A. J. KRESGE, and C. I. YOUNG. Finn. Chem. Lett. 13 (1978).
8. H. MEERWEIN, V. HEDERICH, H. MORSCHEL, and K. WUNDERLICH. Justus Liebigs Ann. Chem. **635**, 1 (1960).
9. R. A. MCCLELLAND and M. AHMAD. J. Am. Chem. Soc. **99**, 5356 (1977).
10. D. SAMUEL and B. L. SILVER. Adv. Phys. Org. Chem. **3**, 123 (1965).
11. H. G. BULL, K. KOEHLER, T. C. PLETCHER, J. J. ORTIZ, and E. H. CORDES. J. Am. Chem. Soc. **93**, 3002 (1971).
12. R. A. MCCLELLAND and M. AHMAD. J. Am. Chem. Soc. **100**, 7031 (1978).
13. C. A. LANE, M. F. CHEUNG, and G. F. DORSEY. J. Am. Chem. Soc. **90**, 6492 (1968).
14. M. L. BENDER, R. D. GINGER, and J. P. UNIK. J. Am. Chem. Soc. **80**, 1044 (1958).
15. S. A. SHAIN and J. F. KIRSCH. J. Am. Chem. Soc. **90**, 5848 (1968).
16. R. A. MCCLELLAND. Ph.D. thesis, University of Toronto, Toronto, Ont. 1969.
17. K. YATES. Acc. Chem. Res. **4**, 136 (1971).
18. R. A. MCCLELLAND, T. A. MODRO, M. F. GOLDMAN, and K. YATES. J. Am. Chem. Soc. **97**, 5223 (1975).
19. R. A. MCCLELLAND and M. AHMAD. J. Org. Chem. In press.
20. R. A. MCCLELLAND, M. AHMAD, and G. MANDRAPILIAS. J. Am. Chem. Soc. **101**, 970 (1979).
21. C. A. BUNTON, J. H. CRABTREE, and L. ROBINSON. J. Am. Chem. Soc. **90**, 1258 (1968).
22. J. P. GUTHRIE. J. Am. Chem. Soc. **95**, 6999 (1973); **96**, 3608 (1974); Can. J. Chem. **53**, 898 (1975); **54**, 202 (1976).
23. J. P. GUTHRIE. Can. J. Chem. **55**, 3562 (1977).

COMMUNICATION

An interesting azirine induced reaction of the cyclopentadienyliron dicarbonyl dimer

HOWARD ALPER[1] AND TSUTOMU SAKAKIBARA

Department of Chemistry, University of Ottawa, Ottawa, Ont., Canada K1N 9B4

Received March 22, 1979

HOWARD ALPER and TSUTOMU SAKAKIBARA. Can. J. Chem. **57**, 1541 (1979).

Reaction of cyclopentadienyliron dicarbonyl dimer with a series of 2-arylazirines in anhydrous benzene (room temperature or 40°C, 41–96 h) affords cycloaddition products (pyrazines, isoxazoles) and the dimer of cyclopentadienone (1,8-diketo-4,7-methano-3a,4,7,7a-tetrahydroindene). The formation of the latter product is proposed to occur via a complex in which each cyclopentadienyl ring is π-complexed to one iron atom and σ-bound to another.

HOWARD ALPER et TSUTOMU SAKAKIBARA. Can. J. Chem. **57**, 1541 (1979).

La réaction du dimère du cyclopentadiénylferdicarbonyle avec une série d'aryl-2 azirines dans le benzène anhydre (t.a. ou 40°C, 41–96 h) conduit aux produits de cycloaddition (pyrazines, isoxazoles) et au dimère de la cyclopentadiènone (dicéto-1,8 méthano-4,7 tétrahydro-3a,4,7,7a indène). On croit que ce dernier produit se forme par l'intermédiaire d'un complexe dans lequel chaque cycle cyclopentadiènyle forme un complexe π avec un atome de fer et un complexe σ avec l'autre.

[Traduit par le journal]

Recent investigations have shown cobalt (eq. [1]) and Group VI (eq. [2]) metal carbonyls to be effective reagents for converting azirines to useful heterocycles via cycloaddition processes (1, 2). Several interesting complexes were obtained by the use of diiron enneacarbonyl as the reagent (3). In continuation of our exploration of azirine – metal carbonyl chemistry, we studied the reaction of the three-membered ring heterocycles with the cyclopentadienyliron dicarbonyl dimer (**1**). We now wish to report that the latter reaction results not only in cycloaddition of the azirine, but in an unusual reaction of the iron dimer.

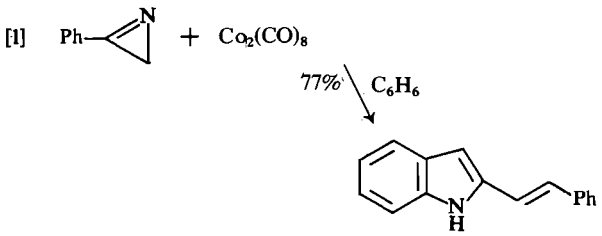

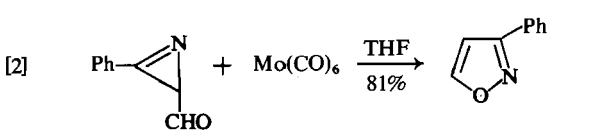

Treatment of 2-arylazirines (**2***a–c*) with half the molar amount of **1** in *dry* benzene (N_2 or Ar atmosphere) for 41–96 h at room temperature, or higher, followed by work-up in air, gave pyrazines (**3***a–c*) in modest yields (Table 1). A similar reaction, using **2***d* as the substrate, afforded 3-phenylisoxazole (see [2]) in 84% yield. These results indicate that the iron dimer is behaving in an analogous manner towards azirines as Group VI metal carbonyls (2).

A surprising product of most of these reactions, formed in as high as 38% yield, was the cyclopentadienone dimer **4**[2], identified on the basis of melting

TABLE 1. Products obtained from reaction of azirines with **1**[a]

Azirine	Reaction temperature (°C)	Reaction time (h)	Product yields[f] (%)		
			3[b]	**4**[c]	Other
2*a*	r.t.[g]	41	39	tr[g]	17[d]
	40	41	6	28	
2*b*	r.t.	72	16	8	
	40	72	15	5	
2*c*	r.t.	96	17	26	
2*d*	r.t.	41		38	84[e]

[a]The ratio of **2**:**1** used was 10:5 or 5:2.5 mmol.
[b]Yield is based on azirine reacted. Products were identified by comparison of melting points and spectral properties with those for authentic materials (2).
[c]Yield is based on $(C_5H_5Fe(CO)_2)_2$ reacted.
[d]A tetramer of the azirine. Its structure is not known, and it is not formed from reaction of **3** with **1**.
[e]3-Phenylisoxazole.
[f]Polymeric materials were also formed.
[g]Abbreviations: r.t. = room temperature; tr = trace.

[1]To whom all correspondence should be addressed.

[2]Product **4** is 1,8-diketo-4,7-methano-3a,4,7,7a-tetrahydroindene.

0008-4042/79/121541-03$01.00/0

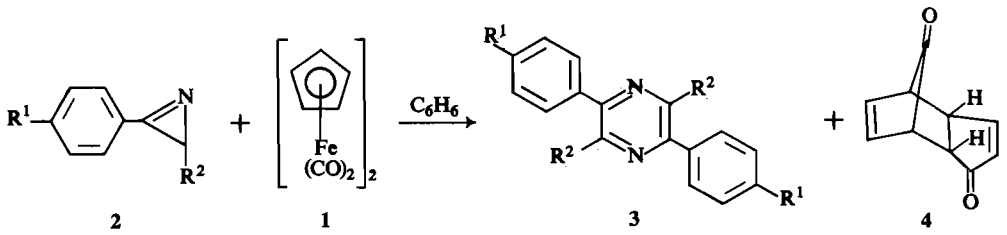

a $R^1 = R^2 = H$
b $R^1 = CH_3, R^2 = H$
c $R^1 = Br, R^2 = H$
d $R^1 = H, R^2 = CHO$

point (101–102°C, lit. (5) mp 102.0–102.5°C), elemental analysis (*anal.* calcd. for $C_{10}H_8O_2$: C 74.99, H 5.03; found: C 75.50, H 5.04), and spectral data ir γ_{CO} (KBr): 1788, 1720 cm^{-1} (5); ^{1}Hmr ($CDCl_3$) δ: 2.88t, 3.16m, 3.41m, 6.25m, 7.30m (5); uv λ_{max} (CH_3OH): 228, 328 nm (6); ms *m/e*: 160 $(M)^+$, 132 $(M - CO)^+$, 104 $(M - 2CO)^+$, 78 $(M - 2CO - C_2H_2)^+$ (7). The cyclopentadienone dimer was not formed in the absence of azirine, and use of a 10:1 ratio of **1**:**2***d* gave **4** in less than 2% yield.

The formation of the cyclopentadienone dimer may occur via initial azirine displacement of carbon monoxide from **1** to give **5** (Scheme 1, illustrated for **2***a*). Metalation with hydrogen transfer to the azirine (possibly by an iron hydride intermediate) would afford **6**, in which each iron atom is π-complexed to one cyclopentadienyl ring and σ-bonded to another. Oxidative cleavage of **6** (work-up) would give cyclopentadienone (7), which readily dimerizes (path *a*). It is also conceivable that loss of azirine would accompany metalation of **5** to give **8**, which could then collapse to **7** (path *b*).

Precedence exists for intermediates of type **6** and **8**, from the work by Tebbe and Parshall (8) on niobium and tantalum complexes and by Baker *et al.* (9) on a thorium(IV) complex. Cyclopentadienone is not formed prior to work-up of the above reactions since (*i*) no organometallic complexes of the dienone ligand were detected (10, 11) and (*ii*) cycloaddition

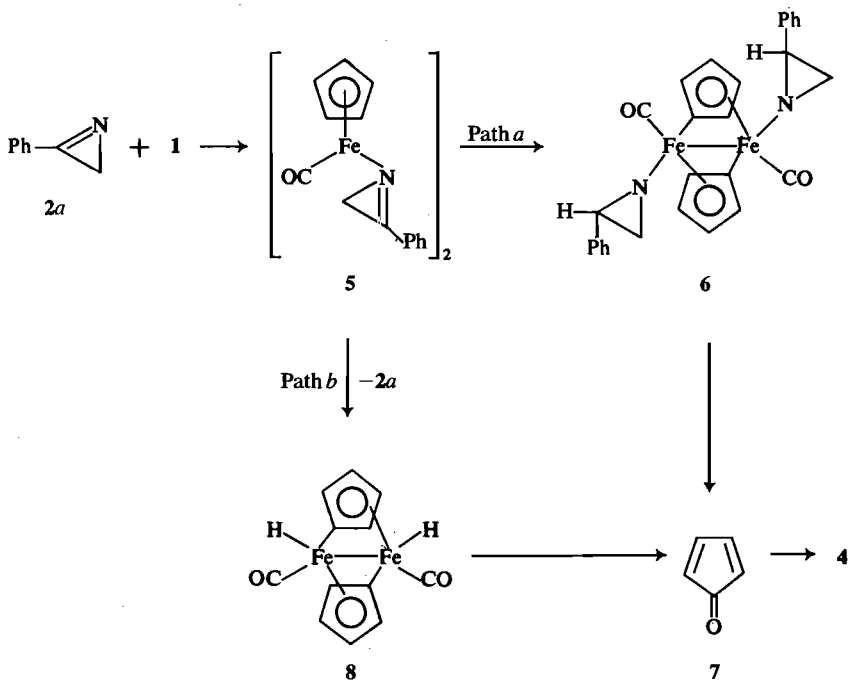

SCHEME 1

of any azirine with **7** would produce azepines, which were not isolated either (4).

The following general procedure was used. A mixture of the azirine (**2**) and cyclopentadienyliron dicarbonyl dimer (**1**) in *dry* benzene was stirred at room temperature until none of the azirine remained (by thin-layer chromatography, see Table 1 for reaction times). The solvent was then rotary evaporated to remove benzene. The residue was chromatographed on silica gel or Florisil. The pyrazine (**3***a*) or 3-phenylisoxazole was eluted with benzene–hexane, and the dimer of cyclopentadienone (**4**) was eluted with chloroform–ether.

Acknowledgements

We are grateful to the Natural Sciences and Engineering Research Council for support of this work. Dr. T. Sakakibara is a participant in the Japan–Canada Scientific Exchange Program.

1. H. ALPER and J. E. PRICKETT. Tetrahedron Lett. 2589 (1976).
2. H. ALPER, J. E. PRICKETT, and (in part) S. WOLLOWITZ. J. Am. Chem. Soc. **99**, 4330 (1977).
3. H. ALPER and J. E. PRICKETT. Inorg. Chem. **16**, 67 (1977).
4. V. NAIR and K. H. KIM. Heterocycles, **7**, 353 (1977) and references cited therein.
5. D. C. DE JONGH and R. Y. VAN FOSSEN. J. Org Chem. **37**, 1129 (1972).
6. E. BAGGIOLINI, E. G. HERZOG, S. IWASAKI, R. SCHORTA, and K. SCHAFFNER. Helv. Chim. Acta, **50**, 297 (1967).
7. D. C. DE JONGH, R. Y. VAN FOSSEN, and C. F. BOURGEOIS. Tetrahedron Lett. 271 (1967).
8. F. N. TEBBE and G. W. PARSHALL. J. Am. Chem. Soc. **93**, 3793 (1971).
9. E. C. BAKER, K. N. RAYMOND, T. J. MARKS, and W. A. WACHTER. J. Am. Chem. Soc. **96**, 7586 (1974).
10. W. HUBEL. *In* Organic syntheses via metal carbonyls. Vol. 1. *Edited by* I. Wender and P. Pino. Wiley-Interscience, New York, NY. 1968. p. 273.
11. H. ALPER and E. C. H. KEUNG. J. Am. Chem. Soc. **94**, 2144 (1972).

Canadian Journal of Chemistry

Published by
THE NATIONAL RESEARCH COUNCIL OF CANADA

Journal canadien de chimie

Publié par
LE CONSEIL NATIONAL DE RECHERCHES DU CANADA

Volume 57 Number 13 July 1, 1979 Volume 57 numéro 13 1 juillet 1979

A versatile synthesis of spirobenzylisoquinoline and phthalideisoquinoline alkaloids. Conversion of a phthalideisoquinoline to spirobenzylisoquinolines[1]

B. C. NALLIAH AND D. B. MACLEAN
Department of Chemistry, McMaster University, Hamilton, Ont., Canada L8S 4M1
H. L. HOLLAND
Department of Chemistry, Brock University, St. Catharines, Ont., Canada L2S 3A1
AND
R. RODRIGO
Department of Chemistry, Wilfrid Laurier University, Waterloo, Ont., Canada N2L 3C5

Received December 8, 1978

B. C. NALLIAH, D. B. MACLEAN, H. L. HOLLAND, and R. RODRIGO. Can. J. Chem. **57**, 1545 (1979).

Eight spirobenzylisoquinolines and four phthalideisoquinolines have been synthesized through 1,9-dehydrophthalideisoquinoline intermediates. The latter are reduced and rearranged in one step to spirobenzylisoquinolines of the corydaine–sibiricine type. The phthalideisoquinoline alkaloid hydrastine has been converted by *in vitro* methods to a spirobenzylisoquinoline in two steps.

B. C. NALLIAH, D. B. MACLEAN, H. L. HOLLAND et R. RODRIGO. Can. J. Chem. **57**, 1545 (1979).

On a synthétisé huit spirobenzylisoquinoléines et quatre phtalideisoquinoléines par l'intermédiaire de déhydro-1,9 phtalideisoquinoléines. Ces dernières se réduisent et se transposent en spirobenzylisoquinoléines du type corydaine–sibiricine en une étape. On a transformé l'alcaloïde phtalidéisoquinoléine, hydrastine, en une spirobenzylquinoléine par des méthodes *in vitro* impliquant deux étapes.

[Traduit par le journal]

The last decade has seen the isolation of a new group of benzylisoquinoline alkaloids whose structures are characterised by the presence of an indane moiety spiro fused at C1 of the isoquinoline system. Approximately 20 such spirobenzylisoquinoline alkaloids have been isolated and characterised (1) and all of them possess 'unsymmetrical' methylenedioxy substitution in the indane benzene ring (ring D). The five-membered ring of the indane moiety is often oxygenated at the benzylic positions with one or two substituents. In the latter case they may be identical hydroxyl groups in a *trans* disposition as in ochrobirine (**1**) and yenhusomine (**2**) (or *cis* as in raddeamine (**3**)) or nonidentical substituents as in corydaine (**4**), sibiricine (**5**), yenhusomidine (**6**), and raddeanone (**7**).

Many syntheses of these alkaloids have been developed (2) but variations of the indanedione and indanetrione approaches have hitherto been the most popular. Such methods, however, are in the main long and tedious, often beset with poor yields and are not especially suited to the preparation of alkaloids of the corydaine–sibiricine type because some differentiation of the two oxygenated positions of the five-membered ring C would have to be tailored into the C/D synthon. Recently these difficulties have in fact been overcome in a synthesis of corydaine (13).

Nevertheless, it still seemed desirable to develop a route to alkaloids such as **4**–**7** by devising a strategy

[1]Dedicated to the late Professor R. H. F. Manske.

0008-4042/79/131545-05$01.00/0

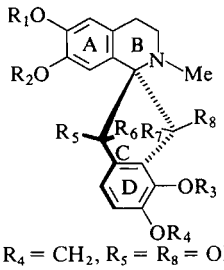

1 $R_1 + R_2 = R_3 + R_4 = CH_2$, $R_5 = R_8 = OH$, $R_6 = R_7 = H$
2 $R_1 = R_2 = Me$, $R_3 + R_4 = CH_2$, $R_5 = R_8 = OH$, $R_8 = R_7 = H$
3 $R_1 = R_2 = Me$, $R_3 + R_4 = CH_2$, $R_5 = R_7 = OH$, $R_6 = R_8 = H$
4 $R_1 + R_2 = R_3 + R_4 = CH_2$, $R_5 + R_6 = O$, $R_7 = H$, $R_8 = OH$
5 $R_1 + R_2 = R_3 + R_4 = CH_2$, $R_5 + R_6 = O$, $R_7 = OH$, $R_8 = H$
6 $R_1 = R_2 = Me$, $R_3 + R_4 = CH_2$, $R_5 + R_6 = O$, $R_7 = H$, $R_8 = OH$
7 $R_1 = R_2 = Me$, $R_3 + R_4 = CH_2$, $R_5 + R_6 = O$, $R_7 = OH$, $R_8 = H$
8 $R_1 = R_2 = R_3 = R_4 = Me$, $R_5 + R_6 = O$, $R_7 = H$, $R_8 = OH$
9 $R_1 = R_2 = R_3 = R_4 = Me$, $R_5 + R_6 = O$, $R_7 = OH$, $R_8 = H$
26 $R_1 + R_2 = CH_2$, $R_3 = R_4 = Me$, $R_5 + R_6 = O$, $R_7 = H$, $R_8 = OH$
27 $R_1 + R_2 = CH_2$, $R_3 = R_4 = Me$, $R_5 + R_6 = O$, $R_7 = OH$, $R_8 = H$

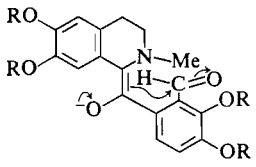

10

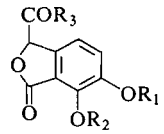

11 $R_1 = R_2 = Me$, $R_3 = OH$
14 $R_1 + R_2 = CH_2$, $R_3 = OH$
15 $R_1 + R_2 = CH_2$, $R_3 = NH_2$

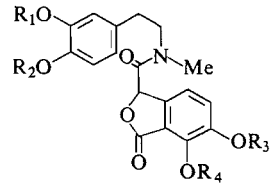

12 $R_1 = R_2 = R_3 = R_4 = Me$
18 $R_1 + R_2 = R_3 + R_4 = CH_2$
19 $R_1 = R_2 = Me$, $R_3 + R_4 = CH_2$

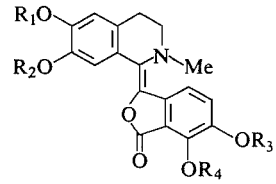

13 $R_1 = R_2 = R_3 = R_4 = Me$
16 $R_1 + R_2 = R_3 + R_4 = CH_2$
17 $R_1 = R_2 = Me$, $R_3 + R_4 = CH_2$
25 $R_1 + R_2 = CH_2$, $R_3 = R_4 = Me$

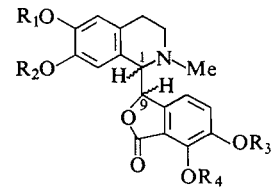

20 $R_1 + R_2 = R_3 + R_4 = CH_2$(1*S*, 9*S* and 1*R*,9*R*)
21 $R_1 + R_2 = R_3 + R_4 = CH_2$(1*S*,9*R* and 1*R*,9*S*)
22 $R_1 = R_2 = Me$, $R_3 + R_4 = CH_2$(1*S*,9*S* and 1*R*,9*R*)
23 $R_1 = R_2 = Me$, $R_3 + R_4 = CH_2$(1*S*,9*R* and 1*R*,9*S*)
24 $R_1 + R_2 = CH_2$, $R_3 = R_4 = Me$

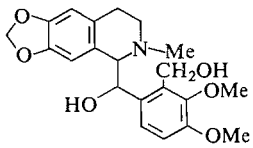

28

that would avoid this problem. The intramolecular aldol condensation of an intermediate such as **10** appeared to be an attractive solution to the problem. The epimeric mixture (e.g., **4** and **5** or **6** and **7**) that would result from such a process might be expected to be richer in **4** or **6**, thermodynamically more stable in view of their capacity (3, 4) for intramolecular hydrogen bonding.

This scheme was first investigated (5) with easily available model compounds. Meconin-α-carboxylic acid **11** (6) was converted to the amide **12** and cyclised to yield dehydrocordrastine **13** (7). Reduction of the latter with diisobutylaluminum hydride resulted in the production of an epimeric mixture of **8** and **9** in the ratio 6:7 presumably through an enolate such as **10**. This result confirmed the viability of the route but surprisingly provided the nonhydrogen bonded **9** in slightly larger quantities than the more stable epimer **8**.

Application (8) of this procedure to the synthesis of alkaloids **4**–**7** required the preparation of the phthalide-α-carboxylic acid **14**. Piperonal was carboxylated (9) and the resulting 2-carboxylic acid converted through the amide **15** to the required phthalide-α-carboxylic acid **14** in 31% overall yield. This acid was used as before to obtain the dehydrophthalideisoquinolines **16** and **17** through the amides **18** and **19**, respectively. The detection of a substantial nuclear Overhauser effect between the *N*-methyl group and the C6′ aromatic proton in **16** and **17** established the *E*-configuration of the double bond as shown. Catalytic hydrogenation of **16** and **17** provided the phthalideisoquinolines (±)-adlumidine (**20**), (±)-bicuculline (**21**) and (±)-adlumine (**22**),

(±)-corlumine (**23**), respectively. The individual components of each mixture were separated by chromatography and characterised by comparison with authentic samples.

The dehydrophthalides **16** and **17** upon treatment with diisobutylaluminum hydride in tetrahydrofuran at −10°C for 1 h underwent reduction and rearrangement as expected to yield mixtures of corydaine (**4**) – sibiricine (**5**) and yenhusomidine (**6**) – raddeanone (**7**), respectively, in total yields of approximately 65% in each case. The individual components of each pair were again separated by chromatography.

We have observed that the proportions of the individual diastereomers produced in each mixture varies with the time spent in the work-up procedure upon completion of the reaction. Thus the proportion of corydaine–yenhusomidine is increased if the treatment of the reaction mixture with methanol and saturated aqueous sodium sulfate, routinely done at completion of the reaction, is extended. Indeed it has been possible to equilibrate pure samples of sibiricine and raddeanone with corydaine and yenhusomidine, respectively, by exposure to methanolic potassium hydroxide. These mixtures were analysed by ^{1}Hmr spectroscopy; furthermore, the process is not a clean and entirely reproducible one, since other reactions presumably supervene. These results however, clearly point to the existence of a retro-aldol realdolisation sequence which is responsible for the generation of at least a part of the corydaine–yenhusomidine components of the mixtures.

The formation of the sibiricine–raddeanone components may result from the transition states in these instances possessing oxygen and nitrogen atoms *anti* to each other (they will have to be *syn* for the formation of corydaine–yenhusomidine) or from aluminum coordination to both negative oxygen atoms in the transition states or from both of these considerations. Such an aluminum coordinate complex, if it arises from the *E*-enolate could be a seven-membered cyclic species which must lead to the *anti* arrangement of the nitrogen and hydroxyl groups in the product. Indeed precedents do exist for such aluminum coordination in the aldol condensation (10).

Reduction of corydaine and yenhusomidine with sodium borohydride provided the *trans*-diols ochrobirine **1** and yenhusomine **2** in satisfactory yield.

The successful completion of this synthesis prompted us to investigate the possibility of applying the strategy for the conversion of a natural phthalide-isoquinoline to a spirobenzylisoquinoline. Thus hydrastine **24** was converted to its *N*-oxide with *m*-chloroperbenzoic acid and then treated with trifluoroacetic anhydride to provide dehydrohydrastine **25** which was similarly reduced and rearranged with diisobutylaluminum hydride to yield the spirobenzylisoquinolines **26** and **27**.

Alternatively, hydrastine diol **28** was oxidised with dimethyl sulfoxide – trifluoroacetic acid (12) and the product rearranged without isolation into the same epimeric mixture of **26** and **27** though now in different proportions. In the latter instance the more stable (H-bonded) isomer **26** predominated 5:4 whereas in the previous case **26** and **27** were isolated in 2:3 proportions. Such a result although not absolutely unambiguous, lends some credibility to the idea of aluminum coordination expressed above.

Experimental

Melting points were determined on a Fischer Mel-Temp apparatus and are uncorrected. The ^{1}Hmr spectra were recorded on a Varian HA-100 spectrometer in $CDCl_3$ with added TMS as the internal lock. Chemical shifts are reported in ppm (δ) from TMS. A Beckmann IR10 spectrometer was used to record the ir spectra.

*Dehydrocordrastine (**13**)*

The amide **12** (7) (4 g) was dissolved in a mixture of phosphorus oxychloride (24 mL) and acetonitrile (8 mL) and the resulting solution refluxed for 3 h. The red solution was cooled and evaporated to dryness. The residue was dissolved in methanol (10 mL), basified with 10% aqueous ammonia, and extracted with chloroform. The extract was washed, dried, and evaporated to dryness and the residue crystallised twice from methanol to afford pale yellow crystals (2.8 g), mp 140–142°C (lit. (7) mp 136–136.5°C); ir ν_{max} ($CHCl_3$): 1760 cm^{-1}; ^{1}Hmr: 8.02 (s, 1H), 7.86 and 7.22 (q, 2H, J_{AB} = 8.0 Hz), 6.56 (s, 1H), 4.08 (s, 3H), 3.92 (s, 3H), 3.88 (s, 3H), 3.84 (s, 3H), 3.20 (t, 2H), 2.80 (t, 2H), and 2.68 (s, 3H). *Anal.* calcd. for $C_{22}H_{23}NO_6$: C 66.49, H 5.83, N 3.52; found: C 66.65, H 5.72, N 3.61.

*Spirobenzylisoquinolines **8** and **9***

A solution of diisobutylaluminum hydride in hexane (1.5 mL, 15%) was added to a stirred solution of dehydrocordrastine (0.15 g) in dry toluene (30 mL) under an atmosphere of argon at −78°C. The resulting red solution was stirred at this temperature for 10 min. Acetone (0.5 mL) was then added and the solution allowed to come to room temperature. The reaction mixture was diluted with ether, water added, and the ether phase washed with water, dried and evaporated. Chromatography of the residue on silica gel in chloroform gave the two compounds which were crystallised from ether: **8**, mp 118–120°C (47 mg); **9**, mp 149–151°C (54 mg). Spectral data have been previously reported (5). *Anal.* calcd. for $C_{22}H_{25}NO_6$: C 66.15, H 6.31, N 3.50; found for **8**: C 66.08, H 6.49, N 3.48; found for **9**: C 65.93, H 6.30, N 3.38.

*3,4-Methylenedioxyphthalide-α-carboxamide (**15**)*

An aqueous solution (20 mL) of potassium cyanide (1.6 g) was added dropwise to a stirred suspension of 2-formyl-5,6-methylenedioxybenzoic acid (4 g) in water (20 mL) and a clear solution was obtained. On continued stirring (1 h) a white precipitate separated. The mixture on acidification (15% HCl, 10 mL) yielded a clear solution and on continued stirring another white precipitate separated. The mixture was heated to obtain a clear solution and the solution maintained at this

temperature for ten minutes until another precipitate begins to separate. The mixture was cooled, the solid separated by filtration and crystallized from aqueous methanol as white needles (3.84 g), mp 239–240°C; ir ν_{max} (Nujol): 3460, 3220, 1770, and 1650 cm^{-1}; ^{1}Hmr (DMSO-d_6): 7.89 (s, 1H), 7.60 (s, 1H), 7.32 and 7.12 (AB_q, 2H, J_{AB} = 8.0 Hz), 6.27 (s, 2H), 5.83 (s, 1H). *Anal.* calcd. for $C_{10}H_7O_5N$: C 54.28, H 3.19, N 6.36; found: C 54.26, H 3.24, N 6.31.

*3,4-Methylenedioxyphthalide-α-carboxylic Acid (**14**)*

A stirred suspension of the amide **15** (2 g) in concentrated hydrochloric acid (20 mL) was heated until a clear solution was obtained (ca. 75°C) and the solution maintained at this temperature for 5 min. The pale yellow crystals which separated on cooling were filtered and crystallized from aqueous acetone yielding white needles (1.35 g), mp 210°C; ir ν_{max} (Nujol): 1733 and 1790 cm^{-1}; ^{1}Hmr (DMSO-d_6): 7.31 and 7.11 (AB_q, 2H, J_{AB} = 8.0 Hz), 6.27 (s, 2H), 6.04 (s, 1H). *Anal.* calcd. for $C_{10}H_6O_6$: C 53.80, H 2.71; found: C 53.64, H 2.91.

N-*Methyl*-N-*[2′-(3″,4″-methylenedioxyphenyl)ethyl]-3,4-methylenedioxyphthalide-α-carboxamide (**18**)*

Oxalyl chloride (3 mL) was added to a solution of the acid **14** (2 g) in dry tetrahydrofuran (50 mL) and refluxed for 0.5 h. The solution was cooled, the solvent removed under reduced pressure, and the residue dried under vacuum for 1 h. The dried residue was dissolved in methylene chloride (30 mL) and added dropwise to a stirred solution of *N*-methylhomopiperonylamine (2 g) in methylene chloride (20 mL) and 10% sodium hydroxide (5 mL). Stirring was continued for 2 h, the mixture was acidified (10% hydrochloric acid), and the organic layer separated. The organic phase was successively washed with aqueous potassium carbonate, water, and dried (Na_2SO_4). The solvent was removed and the residue crystallized from methanol as colorless prisms (2.5 g), mp 155°C; ir ν_{max} ($CHCl_3$): 1665 and 1780 cm^{-1}; ^{1}Hmr: 7.10 and 6.90 (q, 2H, J_{AB} = 8.0 Hz), 6.67 (br s, 2H), 6.17 (s, 2H), 5.91 (s, 2H), 6.03 and 5.67 (s, 1H), 3.4–3.8 (m, 2H), 3.0 and 3.1 (s, 3H), 2.67–3.0 (m, 2H). *Anal.* calcd. for $C_{20}H_{17}O_7N$: C 62.66, H 4.44, N 3.66; found: C 62.45, H 4.25, N 3.58.

N-*Methyl*-N-*[2′-(3″,4″-dimethoxyphenyl)ethyl]-3,4-methylenedioxyphthalide-α-carboxamide (**19**)*

The experiment was carried out using the same reaction conditions and quantities as above with *N*-methyl-3,4-dimethoxyphenethylamine and the amide **19** was obtained as colorless prisms (2.3 g), mp 145–146°C; ir ν_{max} ($CHCl_3$): 1668 and 1780 cm^{-1}; ^{1}Hmr: 7.07 and 6.83 (q, 2H, J_{AB} = 8.0 Hz), 6.77 (br s, 2H), 6.13 (s, 2H), 6.03 and 5.57 (s, 1H), 3.83 (s, 6H), 3.5–3.8 (m, 2H), 3.10 and 3.0 (s, 3H), 3.10–2.7 (m, 2H); *Anal.* calcd. for $C_{21}H_{21}O_7N$: C 63.16, H 5.26, N 3.51; found: C 63.01, H 5.08, N 3.36.

*Dehydrobicuculline (**16**)*

Phosphorus oxychloride (10 mL) was added dropwise to a stirred refluxing solution of the amide **18** (1 g) in acetonitrile (30 mL) over a period of 30 min and the mixture was refluxed for 4 h. The solvent was removed under reduced pressure, the residue washed with petroleum ether and dissolved in the minimum quantity of cold methanol. The solution was basified (NH_4OH) and extracted with methylene chloride. The organic phase was washed with water and dried (Na_2SO_4). Upon removal of the solvent under reduced pressure a yellow residue remained which was crystallized from benzene–methanol as yellow needles (710 mg), mp 259°C; ir ν_{max} ($CHCl_3$): 1760 cm^{-1}; ^{1}Hmr: 7.90 (s, 1H), 7.71 and 7.24 (q, 2H, J_{AB} = 8.0 Hz), 6.62 (s, 1H), 6.18 (s, 2H), 5.96 (s, 2H), 3.18 (t, 2H), 2.83 (t, 2H), 2.72 (s, 3H). A 25% nOe was observed for the resonance at 7.71 ppm upon irradiation of the *N*-methyl signal at 2.72 ppm. *Anal.* calcd. for $C_{20}H_{15}O_6N$: C 65.75, H 4.11, N 3.84; found: C 65.93, H 4.29, N 3.68.

*Dehydrocorlumine (**17**)*

The experiment was carried out using the same conditions and quantities as above with the amide **19**. The residue crystallized from methanol – methylene chloride as golden flakes (750 mg), mp 218–219°C; ir ν_{max} ($CHCl_3$): 1765 cm^{-1}; ^{1}Hmr: 8.02 (s, 1H), 7.77 and 7.13 (q, 2H, J_{AB} = 8 Hz), 6.63 (s, 1H), 6.17 (s, 2H), 3.98 (s, 3H), 3.90 (s, 3H), 3.23 (t, 2H), 2.83 (t, 2H), 2.75 (s, 3H). *Anal.* calcd. for $C_{21}H_{19}O_6N$: C 66.14, H 4.99, N 3.67; found: C 66.36, H 5.02, N 3.58.

*(±)-Adlumidine (**20**) and (±)-Bicuculline (**21**)*

Platinum oxide (15 mg) was added to a solution of dehydrobicuculline **16** (100 mg) in acetic acid (30 mL) and shaken in a Parr apparatus under hydrogen at 30 psi. After hydrogen uptake had ceased the catalyst was removed by filtration and the filtrate evaporated to dryness. The residue was basified (NH_4OH), extracted with ether and the organic phase dried (Na_2SO_4). The ether was removed under reduced pressure and the residue chromatographed (silica gel, benzene–acetone (70:30)) yielding (±)-adlumidine (31 mg), mp 198–199°C, and (±)-bicuculline (32 mg), mp 215–216°C, identical with authentic samples.

*(±)-Adlumine (**22**) and (±)-Corlumine (**23**)*

The experiment was carried out using the same conditions and quantities as described previously and (±)-corlumine (28 mg), mp 175–176°C, (±)-adlumine (38 mg), mp 189–190°C, were isolated. They were identical with authentic samples.

*(±)-Sibiricine (**5**) and (±)-Corydaine (**4**)*

A solution of diisobutylaluminum hydride in hexane (1.5 mL, 20%) was added to a stirred solution of dehydrobicuculline **16** (0.15 g) in dry tetrahydrofuran (70 mL) under an atmosphere of nitrogen at −10°C and the stirring continued at this temperature for 1 h. Methanol (3 mL) was added and the solution was allowed to come to room temperature. A saturated solution of sodium sulfate (1 mL) was added to the solution and the stirring continued for 10 min. The precipitated salts were removed by filtration and the filtrate evaporated to dryness under reduced pressure. The residue was chromatographed (silica gel, benzene–acetone (7:3)) and the two components isolated and crystallized from methanol were corydaine (39 mg), mp 127–129°C, and sibiricine (62 mg), mp 223–225°C, whose ir and ^{1}Hmr spectra were identical with those of authentic samples.

*(±)-Raddeanone (**7**) and (±)-Yenhusomidine (**6**)*

The experiment was repeated using similar conditions as above and (±)-raddeanone (15 mg), mp 181–182°C, and (±)-yenhusomidine (83 mg), mp 239–240°C, were separated by chromatography. It was found that (±)-raddeanone was very unstable and rearranged to the more stable yenhusomidine making its isolation difficult. The ir and ^{1}Hmr spectra of the two compounds were identical with the spectra of the authentic materials (4).

*(±)-Ochrobirine (**1**)*

Sodium borohydride (150 mg) was added to a solution of corydaine **4** (60 mg) in methanol (20 mL) and the stirring continued for 24 h. The solution was acidified with acetic acid and the solvent removed under reduced pressure. The residue was basified (ammonia) and extracted with ether. The ether extract was dried ($MgSO_4$), evaporated to dryness, and the residue crystallized from methanol (24 mg), mp 235°C. The ir and

^{1}Hmr spectra were identical with the spectra of the authentic material.

(±)-Yenhusomine (2)

Sodium borohydride (150 mg) was added to a solution of yenhusomidine **6** (60 mg) in tetrahydrofuran (15 mL) and methanol (5 mL) and stirred for 24 h. The solution was acidified and the solvent removed under reduced pressure. The residue was basified (NH_4OH) and extracted with ether. The ether extract was dried ($MgSO_4$), evaporated to dryness, and the residue crystallized from methanol (28 mg), mp 223–225°C. The ir and ^{1}Hmr properties were identical with published (4) data.

Preparation of Dehydrohydrastine (25)

m-Chloroperbenzoic acid was added to a solution of hydrastine (800 mg) in dry tetrahydrofuran (50 mL) and stirred at ambient temperature for 24 h. The solution was cooled in ice, trifluoroacetic anhydride (2 mL) was added, and the mixture was stirred at this temperature for 0.5 h. Ammonium hydroxide (5 mL) was added and stirring was continued for another 15 min whereupon the solution turned deep orange. Water (50 mL) was added and the solution was extracted twice with methylene chloride (100 mL). The extract was dried (Na_2SO_4), evaporated under reduced pressure, and the residue crystallised from methanol as yellow needles (325 mg), mp 203°C (dec.); ir ν_{max} ($CHCl_3$): 1755 cm^{-1}; ^{1}Hmr: 7.98 (s, 1H), 7.93 and 7.33 (q, 2H, J_{AB} = 8 Hz), 6.64 (s, 1H), 5.96 (s, 2H), 4.13 (s, 3H), 3.94 (s, 3H), 3.21 (t, 2H), 2.82 (t, 2H), 2.71 (s, 3H). *Anal.* calcd. for $C_{21}H_{21}O_6N$: C 66.14, H 4.99, N 3.67; found: C 66.23, H 4.97, N 3.58.

Reduction of Dehydrohydrastine with Dibal-H

Dibal-H (1.5 mL, 20% in hexane) was added to a solution of dehydrohydrastine (150 mg) in dry tetrahydrofuran under a nitrogen atmosphere at −30°C and the mixture stirred for 1 h. Methanol (3 mL) was added to decompose the excess reducing agent and the mixture allowed to warm up to room temperature. A saturated solution of sodium sulfate (2 mL) was added and the mixture stirred for 0.5 h and filtered. The filtrate was evaporated to dryness under reduced pressure and the residue chromatographed (silica gel, benzene–acetone (7:3)). Two compounds were isolated and crystallised from methanol: **26** (42 mg), mp 164–165°C, and **27** (60 mg), mp 191–192°C; ^{1}Hmr compound **26**: 7.67 and 7.17 (q, 2H, J_{AB} = 8.0 Hz), 6.61 (s, 1H), 6.07 (s, 1H), 5.87 (br s, 2H), 5.07 (s, 1H), 4.07 (s, 3H), 4.00 (s, 3H), 3.5–2.5 (m, 4H), 2.33 (s, 3H); ^{1}Hmr compound **27**: 7.67 and 7.17 (q, 2H, J_{AB} = 8.0 Hz), 6.63 (s, 1H), 6.07 (s, 1H), 5.87 (s, 2H), 5.63 (br s, 1H), 4.08 (s, 6H), 3.5–2.7 (m, 4H), 2.40 (s, 3H). *Anal.* calcd. for $C_{21}H_{21}O_6N$: C 65.79, H 5.48, N 3.66; found for **26**: C 65.57, H 5.71, N 3.48; found for **27**: C 65.57, H 5.36, N 3.41.

Oxidation of Hydrastine Diol with Dimethyl Sulfoxide and Trifluoroacetic Anhydride

A solution of trifluoroacetic anhydride (630 mg, 30 mmol) in dry methylene chloride (5 mL) was added dropwise to a solution of dry dimethyl sulfoxide (312 mg, 4 mmol) in methylene chloride (5 mL) at −60°C (Dry Ice – acetone) and the mixture stirred at this temperature for 10 min. A solution of the diol **28** (387 mg, 1 mmol) in methylene chloride (10 mL) was added dropwise to the cold mixture and the stirring was continued for another 30 min. Triethylamine (4 mL) was added dropwise over a period of 10 min to the cold solution, then the cooling bath was removed and the reaction was allowed to warm up to room temperature (ca. 1 h). The solution was poured into water and extracted with methylene chloride (50 mL). The extract was dried (Na_2SO_4) was evaporated and the residue was chromatographed on silica gel (benzene–acetone–methanol, (7:2:1)) and the two epimeric spirobenzylisoquinolines were isolated and crystallised from methanol. The faster moving component (52 mg) and the slower moving component (41 mg) were identical with the two compounds **26** and **27**, respectively, obtained from the reduction of dehydrohydrastine with Dibal-H (*vide supra*).

Acknowledgments

We thank the National Research Council of Canada for support of this work. We are grateful to Professor Stewart McLean for informing us of his synthetic route to these alkaloids before publication (13).

1. F. SANTAVY. The Papaveraceae alkaloids. *In* The alkaloids. Vol. 17. *Edited by* R. H. F. Manske. Academic Press, New York. 1979. p. 385.
2. D. B. MACLEAN. Isr. J. Chem. **16**, 68 (1977).
3. KL. SL. BAISHEVA, D. A. FESENKO, B. K. ROSTOTSKII, and M. E. PEREL'SON. Khim. Prir. Soedin. **6**, 456 (1970); Chem. Abstr. **74**, 10343j (1971); D. A. FESENKO and M. E. PEREL'SON. Khim. Prir. Soedin. 7, 166 (1971); Chem. Abstr. **75**, 49381n (1971).
4. S.-T. LU, T-L SU, T. KAMETANI, and M. IHARA. Heterocycles, **3**, 301 (1975).
5. H. L. HOLLAND, D. B. MACLEAN, R. G. A. RODRIGO, and R. H. F. MANSKE. Tetrahedron Lett. 4323 (1975).
6. P. FRITSCH. Justus Liebigs Ann. Chem. **301**, 352 (1898).
7. R. D. HAWORTH and A. R. PINDER. J. Chem. Soc. 1776 (1950).
8. B. C. NALLIAH, D. B. MACLEAN, R. G. A. RODRIGO, and R. H. F. MANSKE. Can. J. Chem. **55**, 922 (1977).
9. F. E. ZIEGLER and K. W. FOWLER. J. Org. Chem. **41**, 1564 (1976).
10. E. A. JEFFREY, A. MEISTERS, and T. MOLE. J. Organomet. Chem. **74**, 373 (1974).
11. K. W. BENTLEY and A. W. MURRAY. J. Chem. Soc. 2491 (1963).
12. W. W. EPSTEIN and F. W. SWEAT. Chem. Rev. **67**, 247 (1967).
13. S. MCLEAN and D. DIME. Can. J. Chem. **55**, 924 (1977).

^{13}C nuclear magnetic resonance studies. 85. ^{13}C spectra of several ring-contracted and -expanded steroids[1,2]

VINOD DAVE AND J. B. STOTHERS

Department of Chemistry, University of Western Ontario, London, Ont., Canada N6A 5B7

Received November 27, 1978

VINOD DAVE and J. B. STOTHERS. Can. J. Chem. 57, 1550 (1979).

The ^{13}Cmr spectra of several cholestanes including 13 *A*-homo-*B*-nor derivatives, 11 *A*-homo derivatives, and 8 *B*-nor examples have been examined. In addition the ^{13}C data for a few of the corresponding androstanes and 16 precursors in the cholestane series are reported. Examples in both the 5α- and 5β-cholestane families were included. These results represent the first systematic examination of the ^{13}C spectra of *A*-homo-*B*-nor steroids and should be useful for the characterization of other members in each series. These data also permit some tentative conclusions regarding the favored conformation for the seven-membered ring in the *A*-homo derivatives.

VINOD DAVE et J. B. STOTHERS. Can. J. Chem. 57, 1550 (1979).

On a étudié les spectres rmn du ^{13}C de plusieurs cholestanes dont 13 dérivés *A*-homo *B*-nor, 11 dérivés *A*-homo et 8 dérivés *B*-nor. On rapporte de plus des données rmn du ^{13}C de quelques androstanes correspondants et de 16 précurseurs de la série cholestane. On a inclu des exemples des familles 5α- aussi bien que 5β-cholestanes. Ces résultats représentent le premier examen systématique de spectres rmn du ^{13}C de stéroïdes *A*-homo *B*-nor et ils devraient s'avérer utiles pour caractériser d'autres composés de chacune de ces séries. Ces données permettent aussi de tirer des conclusions provisoires concernant la conformation favorisée des cycles à sept chaînons des dérivés *A*-homo.

[Traduit par le journal]

Since the appearance of the original report describing the ^{13}C spectra of several steroids by Roberts' group in 1969 (1), literally dozens of papers have been published extending the examination to a wide variety of compounds within the family. For example, two recent reviews (2) include the complete shielding data for nearly 500 steroids. Within this body of data, however, there is a dearth of examples having the *A*-homo-*B*-nor, *A*-homo, or *B*-nor steroid skeleton. The ^{13}C spectra of a few members of the first of these three series were recorded as an aid to their characterization in connection with another study (3) and these results established that the ^{13}C spectra of *A*-homo-*B*-norcholestanes could be readily utilized to identify these derivatives in the presence of cholestanes. This finding led to a reexamination of several ring expansion processes to exploit the use of ^{13}C spectra for the determination of the true product compositions. Previously, the analyses of these products by other physical methods had led to conflicting results and, in some cases, rather startling conclusions. The reexamination with ^{13}Cmr analysis, however, gave a consistent, readily interpretable set of results (4). In the course of this project several additional compounds were required as synthetic intermediates and, thus, derivatives in each of the three series noted above became available. The ^{13}C spectrum of each sample was recorded and these results are presented in this paper. These data form the basis for the specific assignments noted in the accompanying paper for the signals which were employed for the product analyses. The results for the carbons in the A and B rings of the *A*-homo derivatives allow one to consider probable favored conformations for the seven-membered ring.

Experimental

Materials

With two exceptions, the compounds examined in this study have been described in the literature and the specific method of preparation employed for each compound is cited in the tables of shielding data. In a few cases, hydrogen–deuterium exchange at positions α to carbonyl groups was carried out to aid the spectral analysis (3). A sample of 6β-acetyloxy-5α-cholestan-3-one (**39**) was prepared from 3β-benzoyloxy-5α-cholestan-6-one by interchange of the carbonyl and ester functions using standard methods.[3]

A-*Homo-5β-cholestane (**15**)*

A mixture of *A*-homo-5β-cholestan-3-one and -4-one (**16** and **19**) was treated under Wolff–Kishner conditions. The crude product was chromatographed on a 10-g plate (SiO_2, hexanes) and the band at the solvent front gave **15** as a colorless oil (13 mg) whose ir spectrum exhibited no carbonyl absorption. ^{1}Hmr ($CDCl_3$) δ: 0.65, 0.81, 0.90 (3 methyl signals). *Exact mass* calcd. for $C_{28}H_{50}$: 386.3912; found (high resolution ms): 386.3908.

[1]This paper is dedicated to the memory of R. H. F. Manske.

[2]For Part 84 see ref. 28; Part 83, ref. 29; Part 82, ref. 30.

[3]E. W. Warnhoff. Unpublished work.

0008-4042/79/131550-07$01.00/0

Spectra

All ^{13}C spectra were obtained at 25.2 MHz with a Varian XL-100-15 system operating in the Fourier transform mode with square wave modulated proton decoupling at 100 MHz. Completely decoupled and off-resonance decoupled spectra were recorded for each compound in $CDCl_3$ solutions (10–20 mg in 0.2–0.3 mL of solution). In several cases, the shift dispersions produced by the sequential addition of 0.1–0.5 equiv. of $Eu(fod)_3$ were determined to aid the asssignment of specific signals. In most cases the operating conditions gave digital resolution of 0.02 ppm and the precision of the tabulated data is judged to be ± 0.05 ppm.

Results and Discussion

Most of the compounds included in this study are cholestane derivatives with substitution restricted to the A and B rings; consequently, the shieldings of the side chain carbons are the same in each case, while the shieldings of C-15, -16, and -17 fall into two groups depending on the size of the B ring. Thus the signals for C-15–C-27, with the exception of C-18 and -19, were readily identified for each of these compounds, and the assignments confirmed by the fact that these signals were least sensitive to the addition of $Eu(fod)_3$. These results are summarized in Table 1. For the four androstan-17β-ol derivatives, C-15, -16, and -17 were similarly easily identified with these signals appearing at 23.4, 30.6, and 81.9 ppm, respectively. Significant variations were observed for each of the remaining shieldings and these data are tabulated in the following groups: *A*-homo-*B*-norcholestanes **1–14**, Table 2; *A*-homo derivatives **15–27**, Table 3; *B*-norcholestanes **28–35**, Table 4; the cholestanes **36–51** and androstanes **52** and **53** which were encountered in the preparations and for which ^{13}C data have not been published are collected in Table 5. The numbering scheme for the *A*-homo and *B*-nor derivatives are given for the parent hydrocarbons **1**, **15**, and **28** below. The assignments listed

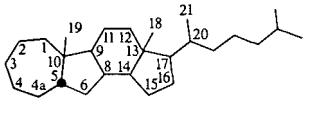

1

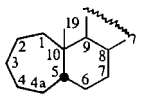

15

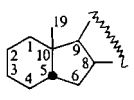

28

in these tables were based on the following considerations.

For C-11, -12, -13, and -14, the variations throughout the series could be expected to be small (2) and the line positions should be less affected by the addition of $Eu(fod)_3$ than those for the A- and B-ring carbons. The latter feature rendered the distinction between C-10 and C-13 straightforward. Of the methine carbons, C-5, -8, and -9, the shift reagent experiments permitted a ready distinction in addition to the expected pronounced shielding difference between C-8 and -9. In the *B*-nor derivatives the C-6 methylene signal was identified by its lesser sensitivity to added $Eu(fod)_3$ relative to the shifts exhibited by the A-ring methylene carbons. In most cases the C-18 and -19 methyl carbons were readily distinguished both by comparisons within each series and with the data for other related compounds; in many instances, this was confirmed by the difference in shift reagent effects. Thus the major assignment problem concerned the methylene signals arising from the A ring carbons.

TABLE 1. ^{13}C shieldings[a] in cholestane derivatives **1–51**

Compounds	C-15	C-16	C-17
1–14, 28–35	24.5	28.5	55.8
15–25, 36–51	24.2	28.3	56.3

[a]In ppm from internal TMS for $CDCl_3$ solutions; in all cases C-20 to C-27 absorb at 35.7, 18.7, 36.2, 23.9, 39.5, 28.0, 22.6, and 22.8 ppm, respectively.

The ^{13}C spectra of several methyl-substituted cycloheptanes, cycloheptanols, and cycloheptanones were examined by Christl and Roberts (21) who found that the results are in good agreement with predictions based on the twist-chair (TC) conformation for the ring. Since the conformational features revealed by earlier molecular mechanics calculations were presented by these authors, there seems no need to review the details here. Their shielding results led to a set of shielding effects for the various substituents on the ring carbons and these data provide a starting point for the present analysis. Although the TC form of cycloheptane is flexible and undergoes rapid pseudorotation between equivalent forms, the A ring in these *A*-homo steroids may be expected to favor a particular conformation. Having an angular C-19 methyl and ring fusion to the B ring, hydrocarbon **1**, the parent of the *A*-homo-*B*-nor-5β series, can be viewed as a '1,1,2-trialkylcycloheptane' and on the basis of the earlier work (21) probably adopts TC **54** preferentially with C-9 and -19 in isoclinal positions and C-6 in a pseudoequatorial orientation. In which case the shieldings of C-2, -3, and -4 would be expected to approximate those for C-6, -5, and -4, respectively, in 1,1,2-trimethylcycloheptane (**55**). The latter values are 22.8, 30.7, and 29.7 ppm, in reasonable agreement with the data for **1** as the two sets were obtained in different media.

TABLE 2. ^{13}C shieldings[a] of some *A*-homo-*B*-norcholestanes[b]

Compound	Series	Substrate	C-1	C-2	C-3	C-4	C-4a	C-5	C-6	C-8	C-9	C-10	C-11	C-12	C-13	C-14	C-18	C-19
1	5β	Nil	40.3	24.6	32.1	29.6	35.0	52.0	38.4	39.1	58.4	44.1	21.5	40.1	43.8	56.8	12.3	25.6
2[c]		3α-OH	35.7	30.5	69.9	31.8	26.5	51.1	38.4	40.2	57.4	43.5	21.4	40.0	43.7	56.6	12.3	25.5
3[c]		3-Oxo	32.0	40.5	215.3	44.2	28.2	50.0	38.7	39.2	57.8	43.0	21.5	39.8	43.9	56.5	12.3	24.3
4[c]		4-Oxo	35.2	20.0	44.4	213.7	47.8	45.3	38.4	40.0	57.6	43.6	21.4	39.8	43.8	56.5	12.3	23.8
5		Δ^{4a}	(38.5)	(26.7)	29.0	(27.8)	121.1	153.7	(38.9)	38.9	60.0	46.6	21.0	39.9	43.9	56.5	12.4	17.6
6[c]		3α-OH-Δ^{4a}	34.2	30.8	66.9	32.4	113.7	156.9	38.5	38.9	59.8	46.4	20.9	39.7	43.9	56.4	12.4	16.2
7[d]		3-Oxo-Δ^{4a}	35.5	41.5	209.7	43.4	111.8	153.6	37.6	38.3	58.7	45.7	21.0	39.6	44.0	56.2	12.4	17.7
8[c]		3α-OH-Δ^{5}	32.4	33.2	75.9	40.6	23.5	153.9	127.0	45.0	56.5	48.9	20.8	40.2	44.7	54.5	12.4	18.7
9[c]		3α-OH-5β-Me-$\Delta^{9(10)}$	19.6	39.8	75.9	33.5	35.3	49.2	43.8	43.0	136.7	140.0	22.1	39.6	43.2	58.6	11.0	26.7
10[c]		3-Oxo-5β-Me-$\Delta^{9(10)}$	19.8	43.1	214.1	39.4	35.9	49.3	44.5	43.4	137.1	138.6	22.3	39.5	43.2	58.5	11.1	24.7
11	5α	3-Oxo	32.5	41.4	215.1	43.9	24.2	51.7	34.9	38.5	59.7	44.6	21.6	39.9	43.8	56.7	12.5	12.5
12		3α,5α-Oxido	29.1	26.8	73.3	(28.6)	(28.3)	91.9	36.9	38.3	51.5	44.7	21.7	40.1	44.0	56.3	12.5	20.3
13[d]		3α,5α-Oxido-4a-oxo	30.9	26.0	70.6	44.2	216.3	90.2	36.1	38.5	56.6	45.9	21.2	39.5	44.2	56.4	12.3	16.8
14		*A*-Bishomo-4-oxo-Δ^{4b}	35.7	22.0	39.7	214.6	44.7[e]	151.2	37.6	39.0	58.1	45.9	21.0	40.0	43.8	56.2	12.3	20.3

[a]In ppm from internal TMS for $CDCl_3$ solutions; similar values in parentheses may be interchanged. For remaining shieldings see Table 1.
[b]For procedures employed for synthesis see ref. 3.
[c]Shifts caused by the addition of $Eu(fod)_3$ examined.
[d]Products from $^1H/^2H$ exchange at the α-positions (3) also examined.
[e]C-4b at 120.1 ppm.

TABLE 3. ^{13}C shieldings[a] of some *A*-homocholestanes and -androstanes

Compound	Series	Substrate	C-1	C-2	C-3	C-4	C-4a	C-5	C-6	C-7	C-8	C-9	C-10	C-11	C-12	C-13	C-14	C-18	C-19	Ref.[b]
15	5β	Nil	42.5	21.8	(30.8)	(30.9)	31.5	45.4	29.7	27.1	36.5	49.3	37.1	21.4	40.5	42.5	56.4	12.1	21.8	
16[c]		3-Oxo	35.0	37.5	214.9	42.8	26.6	46.6	30.2	26.0	36.0	43.5	37.8	21.2	40.1	42.7	56.4	12.1	23.6	4
17		3-Oxo-4-Br-Δ^{4}	35.1	37.3	197.4	125.0	150.7	44.0	25.8	26.6	35.3	50.8	37.8	21.3	39.9	42.5	55.9	12.0	18.7	4
18[c]		3-Oxo-Δ^{4a}	32.0	37.9	209.9	41.6	110.3	149.9	35.4	33.7	35.8	50.1	42.6	21.5	39.9	42.5	56.2	12.0	20.8	5
19		4-Oxo	39.3	16.3	41.4	214.6	44.5	45.9	29.9	26.5	35.9	43.4	37.4	21.2	40.2	42.7	56.4	12.1	22.7	4
20	5α	Nil	40.7	22.0	(27.0)	(28.0)	31.6	48.4	31.4	32.6	35.4	53.4	38.7	21.9	40.5	42.5	57.0	12.1	14.0	6
21[c]		3-Oxo	35.3	39.1	215.5	43.2	27.9	50.6	31.1	32.1	35.4	53.3	38.9	21.8	40.2	42.3	56.8	12.1	11.9	4
22		3-Oxo-4Br-Δ^{4}	31.0	38.0	197.2	124.5	151.5	47.1	27.3	31.4	35.6	49.5	38.6	22.6	40.1	42.6	56.5	12.2	18.5	6
23		3-Oxo-4-Cl-Δ^{4},Δ^{5}	30.2	38.0	194.5	128.9	(144.1)	143.4	(139.4)	32.5	31.2	47.5	38.2	21.7	39.7	42.4	56.8	12.0	19.4	7
24[c]		4-Oxo	42.5	19.0	43.2	214.6	47.9	43.7	31.5	32.2	35.0	54.1	39.1	21.7	40.2	42.3	56.6	12.0	12.3	4
25		3-Br-4-oxo-Δ^{2}	39.9	142.2	125.3	197.8	45.8	42.7	29.2	31.9	35.6	51.9	38.6	22.1	39.9	42.5	56.5	12.1	14.9	6
26[c]		3-Oxo[d]	35.4	39.0	215.6	43.1	27.8	50.5	30.9	31.6	35.3	53.4	39.0	21.3	36.9	42.8	51.2	11.2	11.9	4
27[c]		4-Oxo[d]	42.5	18.9	43.1	214.7	47.8	43.8	31.7	31.3	35.1	54.2	39.2	21.3	36.9	42.7	51.1	11.1	12.3	4

[a]See footnote *a*, Table 2.
[b]Procedure employed for synthesis.
[c]Shifts produced by addition of $Eu(fod)_3$ examined.
[d]Androstanes.

TABLE 4. ^{13}C shieldings[a] of some *B*-nor-5β-cholestanes

Compound	Substrate	C-1	C-2	C-3	C-4	C-5	C-6	C-8	C-9	C-10	C-11	C-12	C-13	C-14	C-18	C-19	Ref.[b]
28	Nil	33.2	19.0	21.9	29.9	45.3	36.0	39.6	54.0	40.3	21.6	40.1	44.2	57.1	12.4	24.8	8
29[c]	3-Oxo	32.4	35.3	214.7	44.4	44.3	38.4	40.1	55.2	39.8	21.6	39.8	43.8	56.2	12.3	24.9	3
30[c,d]	3-Oxo-4β,5β-methano	32.5	39.7	211.4	34.3	42.7	41.8	40.3	60.4	39.3	21.8	39.6	43.5	56.3	12.2	19.3	9
31[c]	3-Oxo-Δ^4	35.3	33.6	199.3	122.5	179.0	34.6	38.3	58.1	44.0	20.9	39.5	44.2	55.9	12.4	17.4	10
32[c]	3β-OH-Δ^5	37.3	32.0	71.6	36.6	149.0	125.4	46.2	62.5	44.8	21.2	40.1	44.5	54.5	12.3	15.0	10
33	3β-OAc-Δ^5	37.0	28.0	73.8	32.8	147.6	126.4	46.2	62.3	44.8	21.1	40.1	44.5	54.3	12.3	14.9	10
34[e]	3β-OAc-5β-OH-6β-CHO	28.1	24.5	70.3	42.2	83.6	51.5	39.3	64.5	45.6	21.6	39.6	44.6	56.0	12.5	18.2	10
35[f]	3β-OAc-5β-OH-6β-COOH	30.4	24.1	70.0	41.1	81.9	52.7	41.6	59.5	45.4	21.5	39.5	44.3	56.2	12.4	17.2	11

[a]See footnote *a*, Table 2.
[b]Procedure employed for synthesis.
[c]Shifts caused by addition of $Eu(fod)_3$ examined.
[d]Methano carbon at 23.6 ppm.
[e]Acetoxyl carbons at 21.4 and 169.7 ppm; formyl carbon at 203.8 ppm.
[f]Acetoxyl carbons at 21.4 and 170.6 ppm; carboxyl carbon at 178.1 ppm.

TABLE 5. ^{13}C shieldings[a,b] of some cholestanes and androstanes

Cpd	Series	Substrate	C-1	C-2	C-3	C-4	C-5	C-6	C-7	C-8	C-9	C-10	C-11	C-12	C-13	C-14	C-19	Other	Ref.[c]
36	5α	2α-Br-3-oxo	51.7	54.6	201.1	44.0	47.5	28.2	31.5	34.9	53.6	39.0	21.5	39.7	42.6	56.1	12.1		12
37		4α-Br-3-oxo	37.4	38.3	201.9	62.7	55.2	28.1	31.5	35.0	54.0	39.0	21.5	39.8	42.6	56.1	12.5		13
38		2α,4α-Br_2-3-oxo	51.2	51.8	186.2	60.0	55.4	28.0	31.3	34.8	53.9	41.0	21.6	39.6	42.5	56.0	13.2		14
39		3-Oxo-6β-OAc	38.0	36.2	211.2	41.4	47.5	72.7	39.4	30.8	53.5	35.7	21.3	39.8	42.7	55.9	14.4	21.2, 170.3	*f*
40		3,3-$(OMe)_2$	(35.5)	(28.4)	100.5	(35.1)	42.4	(28.5)	32.0	35.5	54.1	35.7	21.2	40.1	42.6	56.5	11.6	47.5	4
41[d]		(3*R*)-3-Spiro-2′-oxiran	35.9	29.3	58.6	36.0	43.7	28.7	31.9	35.5	54.1	35.5	21.1	40.1	42.6	56.5	11.3	53.5	15
42[d]		(3*S*)-3-Spiro-2′-oxiran	37.8	29.7	59.7	36.4	46.1	28.8	32.0	35.5	54.3	35.6	21.3	40.1	42.6	56.5	11.8	55.8	15
43		3-OMe-Δ^2	38.2	91.7	153.9	32.3	41.8	28.6	31.8	35.6	53.9	34.8	21.2	40.1	42.5	56.5	11.6	53.8	4
44		3-OAc-Δ^3	34.3	27.4	147.1	118.0	44.9	24.6	32.0	35.5	52.9	35.2	21.5	40.0	42.7	56.4	12.0	21.0, 169.5	16
45		3β-OH-Δ^4	35.3	29.5	67.9	123.4	147.5	33.1	32.2	36.0	54.5	37.3	21.0	39.9	42.5	56.2	18.9		17
46		3α-OH-Δ^4	31.7	27.9	64.2	120.7	150.2	32.8	32.4	35.8	54.1	37.5	21.5	39.9	42.5	56.2	18.1		17
47		3-Methylene-Δ^4	37.3	27.2	149.1	122.6	143.9	32.8	32.5	35.9	54.2	37.4	21.5	40.0	42.5	56.2	18.4	107.8	18
48	5β	2β-Br-3-oxo	49.4	53.2	202.4	41.9	45.2	25.7	26.3	35.6	41.3	38.8	21.5	40.0	42.7	56.4	22.4		19
49[d]		4β-Br-3-oxo	(36.8)	(36.6)	202.5	60.1	54.3	(25.1)	(25.6)	35.7	42.0	38.3	21.3	40.0	42.8	56.4	23.2		20*a*
49*a*		2β,4β-Br_2-3-oxo	48.9	50.4	193.8	57.5	54.2	24.9	25.6	35.7	42.7	40.7	21.5	39.9	42.7	56.2	22.9		20*b*
50		3,3-$(OMe)_2$	(33.0)	27.4	101.0	(33.5)	39.9	26.3	26.9	35.7	39.8	34.8	21.1	40.2	42.7	56.5	23.3	47.4	4
51		3-Oxo-4β,5β-methano	27.6	32.3	210.0	35.1	36.8	32.5	30.1	35.5	45.9	34.3	21.7	39.8	42.4	56.2	20.7	17.9	17
52[e]	5α	(3*R*)-3-Spiro-2′-oxiran-17β-OH	35.9	29.2	58.7	36.0	43.8	28.5	31.5	35.6	54.2	36.0	20.6	36.8	43.0	51.0	11.3	53.6	4
53[e]		3-OH-3-$MeOCH_2$-17β-OH	(30.2)	(28.4)	71.1	37.2	40.3	33.4	31.6	35.6	54.3	36.1	20.6	36.8	43.0	51.1	11.3	59.4, 82.0	4

[a]See footnote *a*, Table 2.
[b]For the cholestanes C-18 absorbs at 12.1 ppm; for the androstanes C-18 is at 11.2 ppm.
[c]Procedure employed for synthesis.
[d]Shifts produced by addition of $Eu(fod)_3$ examined.
[e]Androstanes.
[f]E. W. Warnhoff. Unpublished work.

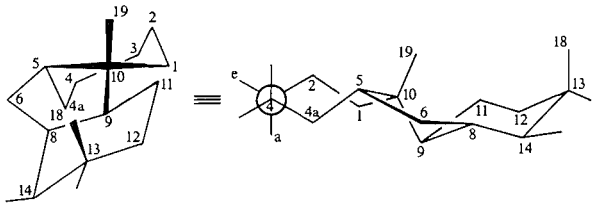

54

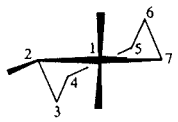

55

In addition C-1 in **1** which is *gauche* with respect to C-11 should be shielded relative to C-7 in **55** and an upfield shift of -3.6 ppm is indeed found. On the other hand, C-4a is deshielded by 2.6 ppm relative to C-3 in **55** but there is no obvious prediction for the change at C-4a, whereas the downfield shifts for C-5 and -10 in **1** vs. the C-2 and -1 shieldings (43.2 and 35.6) in **55** are as expected because of the β-effects of C-8 and -11. Even better correspondence is found between the A-ring methylene shieldings of **15** and those of **55** indicating that **15** probably adopts a TC form analogous to **54** with a six-membered ring.

Introduction of the 3α-hydroxyl as in **2** appears to require a conformational change for the A ring since in **54** the 3α-OH is axial and the observed shielding differences from those of **1** do not fit well for such substitution. For example, C-4 shifts downfield by only 2.2 ppm, and C-1 and -4a exhibit distinctly different upfield shifts. Inspection of molecular models indicates that the latter carbons should be shielded to comparable extents with 3α-OH substitution in **54**. On the other hand, TC **56** may be a major contributing form. Three methylene signals at 26.5, 30.5, and 31.8 ppm are much more strongly affected by $Eu(fod)_3$ than the others which is consistent with **56**

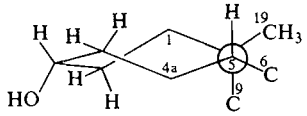

56

whereas the symmetry of **54** suggests that four signals should shift appreciably.

A recent analysis of the cycloheptanone system by St-Jacques *et al.* (22) led to the conclusion that these ketones favor twist-chair forms with the carbonyl group at position TC-2. Thus, **57** should be the favored arrangement for 4,4-dimethylcycloheptanone, the methylene shielding results (21) for which are indicated. A comparison of the results for **3** with the latter suggests that **58** is a major conformer for **3** as is 5β-**59** for **4**. The same comparison of **16** and **19** with **57** shows even better agreement indicating that the differences of 1–2 ppm between model **57** and the *B*-nor derivatives may arise, in part, from constraint owing to the presence of the five-membered ring. It may be noted that C-9 is shielded by -5.8 ppm in **16** relative to **15** but is little changed from **1** to **3**. From molecular models this difference in the two hydrocarbon–ketone pairs can be attributed to the change in B-ring size. With a six-membered B ring, the TC analogous to **58** places C-9 *gauche* with respect to C-2 and C-4a, whereas the TC form analogous to **54** has only one such interaction, C-9 with C-4a. This accounts nicely for the observed shift for C-9 between **16** and **15**. With five-membered B rings, however, C-9 is not *gauche* to any A-ring carbon in either **54** or **58** and its shielding would be expected to be similar in **1** and **3**, as observed. In any event, the methylene shieldings in **3**, **4**, **16**, and **19** seem consistent with forms **58** and 5β-**59**. The analogous comparison for the 5α-*A*-homoketones **11**, **21**, and **26** suggests **60** as a major contributing form with 5α-**59** important for **24** and **27**.

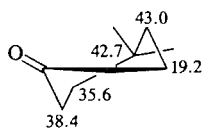

57

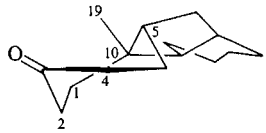

58

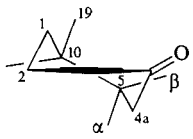

59

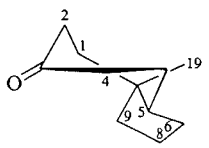

60

Apart from **12** and **13** which lack flexibility,[4] the remaining *A*-homo derivatives contain olefinic bonds. Compounds **5**, **6**, and **7** could exist preferentially in chair **61** or a more flexible twist-boat arrangement such as **62**. Although a clear distinction between these two possibilities cannot be made on the basis of the present results, it may be noted that a comparison of **6** with **5**, to assess the differences produced upon introduction of the 3α-OH group, indicates a significant upfield shift for both γ-carbons (C-1 and -4a) suggesting an axial disposition of the hydroxyl group in **6**. Furthermore, the carbinyl proton absorption in **6** exhibited a half width of

[4]A referee suggests that C-1 in these oxides has sufficient freedom of movement to alter the conformation of the A ring and produce the shielding differences found for C-9 and -19.

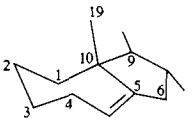

61

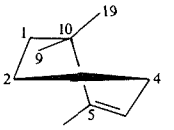

62

~9 Hz (3) which seems more compatible with **61** than **62**. A comparison of the carbonyl shieldings for **7** vs. **3** and **18** vs. **16** reveals upfield shifts of −5 ppm ascribable to homoconjugation in the unsaturated systems (23) and is consistent with **61** as the favored conformer.

Compounds **8–10** contain double bonds exocyclic to the *A*-homo ring and can be considered in the light of the results for substituted cycloheptanones cited above (22). On this basis **8** should favor TC **63**

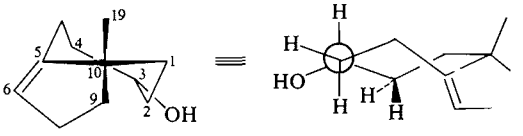

63

having C-9 and -19 at the isoclinal positions and the olefinic bond at the TC-2 position. In contrast to **54** this form places the hydroxyl group in an equatorial orientation with the carbinyl proton antiperiplanar with respect to a proton on each of C-2 and -4. However, this proton absorption has a half-width of ~11 Hz (3) which suggests that other conformations make significant contributions to the actual equilibrium mixture of conformers.

In the earlier study (3) concerning the chemistry of the *A*-homo-*B*-nor derivatives included in Table 2 it had been found that cleavage of **12** with $BF_3 \cdot Et_2O$–Ac_2O at room temperature afforded a single acetate which contained a fully substituted double bond rather than the desired acetate of **6**. Clearly a backbone rearrangement had occurred. Hydrolysis of the product to the alcohol whose ^{13}C spectrum was recorded established that the rearrangement was relatively simple. The ^{13}C signals included a series corresponding to those for C-13 to C-27 in many cholestanes (2) with one methyl (C-18) at 11.0 ppm. Furthermore, in the presence of $Eu(fod)_3$, the olefinic signals were more strongly affected than any of the methine signals apart from that for the carbinyl carbon. These findings show the alcohol to have structure **9** arising from a Westphalen-type of rearrangement as indicated in **64** (24). Alcohol **9**

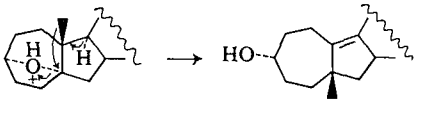

64 9

would be expected to exist preferentially in the conformation corresponding to the mirror image of **63** and it may be noted that the half width of the carbinyl proton absorption of ~20 Hz (3) fits nicely with this prediction. The ^{13}C shieldings for **10**, obtained by oxidation of **9**, indicate that the ketone favors a similar conformation.

The remaining *A*-homo derivatives lack suitable models for consideration of favored conformations but the signal assignments as listed seem the most probable. The results for the single bis-*A*-homo ketone **14** may be viewed similarly.

The *B*-nor compounds listed in Table 4 include the precursors, or derivatives, employed for the preparation of the several *A*-homo steroids discussed above. It is interesting to compare the shieldings for A- and B-ring carbons with those for the normal analogs. For example, a comparison of the data for *B*-nor-5β-cholestan-3-one (**29**) with those for 5β-cholestan-3-one (2) reveals that, in **29**, C-1 and -2 are more shielded whereas C-3 and -4 are deshielded. Presumably this reflects an enhancement of the *gauche* interaction between C-1 and -11 (and, perhaps, C-2 and -9) and the absence of a *gauche* interaction corresponding to that between C-4 and -7 in 5β-cholestan-3-one (see projections **65** and **66**). The

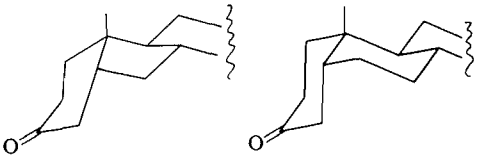

65 66

carbons of the *B*-nor ring appear at significantly lower fields than the corresponding centres in the normal B ring which is consistent with the somewhat enhanced deshielding effects found for some simple methyl substituted cyclopentanes (25) relative to results for the corresponding cyclohexanes (26). The assignments listed for the parent hydrocarbon **28** were obtained using the data for 5β-cholestane (2) and the differences observed between 5β-cholestan-3-one and **29**; thus, these assignments are tentative. The analogous comparison of **31–33** with the cholest-4-en-3-one, cholesterol and its acetate indicates that the shieldings of C-1, -2, and -3 are comparable in both systems while C-4 is somewhat shielded in the *B*-nor derivatives; each of the carbons in the B ring are significantly deshielded in the *B*-nor derivatives relative to the cholestane analogs which is the usual trend for cyclopentenes versus cyclohexenes. Finally, the data for aldol **34** and acid **35**, the parent derivatives for each of the *B*-nor compounds, are included in Table 4.

The stereochemistry of the A/B ring junction in each of these modified steroid skeletons is clearly revealed by the C-19 shieldings, as had been expected by analogy with the results for the natural steroids (2). A comparison of the data for 5α and 5β isomers such as **3** and **11**, **16** and **21**, **19** and **24** (**27**) shows that C-19 is deshielded by 10–12 ppm in the 5β structures, which is comparable to the findings for cholestane, coprostane and several of their derivatives (27).

The ^{13}C shieldings for 16 cholestanes and 2 androstanes are collected in Table 5 since these results provide information on the shielding effects of some substituents and substitution patterns which had not been reported previously.[5] These data should be helpful for the examination of related systems.

From the body of data for the *A*-homo derivatives included in this study, it is apparent that tentative conclusions can be drawn regarding the favored conformations of the seven-membered ring which are consistent with expectations based on the results for simpler systems for which definitive data are available. It may be noted that in each case there are characteristic signals which can be utilized to identify these derivatives in mixtures with other steroids. This can be helpful, both qualitatively and quantitatively, in monitoring the course of reactions involving these species as illustrated in the accompanying paper (4).

Acknowledgements

We are grateful for the financial support of the National Research Council of Canada and we thank Cheryl DuCharme for technical assistance.

1. H. J. Reich, M. Jautelat, M. T. Messe, F. J. Weigert, and J. D. Roberts. J. Am. Chem. Soc. **91**, 7445 (1969).
2. (*a*) J. W. Blunt and J. B. Stothers. Org. Magn. Reson. **9**, 439 (1977); (*b*) W. B. Smith. Annual reports on nmr spectroscopy. Vol. 8. *Edited by* G. A. Webb. Academic Press, New York. 1978.
3. V. Dave and E. W. Warnhoff. J. Org. Chem. **43**, 4622 (1978).
4. V. Dave, J. B. Stothers and E. W. Warnhoff. Can. J. Chem. This issue.
5. W. S. Johnson, M. Neeman, S. P. Birkeland, and N. A. Fedoruk. J. Am. Chem. Soc. **84**, 989 (1962).
6. J. Levisalles, G. Teutsch, and I. Tkatchenko. Bull. Soc. Chim. Fr. 3194 (1969).
7. S. A. G. de Graaf and U. K. Pandit. Tetrahedron, **30**, 1115 (1974).
8. G. H. R. Summers. J. Chem. Soc. 2908 (1959).
9. J. Joska, J. Fajkoš, and M. Budesinsky. Collect. Czech. Chem. Commun. **39**, 1914 (1974).
10. K. Tanabe, R. Hoyashi, and R. Takasaki. Chem. Pharm. Bull. **9**, 12 (1961).
11. K. Tanabe and Y. Morisawa. Chem. Pharm. Bull. **11**, 536 (1963).
12. L. F. Feiser and X. A. Dominguez. J. Am. Chem. Soc. **75**, 1704 (1953).
13. I. Malynowicz, J. Farkus, and F. Sorm. Collect. Czech. Chem. Commun. **25**, 1359 (1960).
14. R. M. Evans, J. C. Hamlet, J. S. Hunt, P. G. Jones, A. G. Long, J. F. Oughton, L. Stephenson, T. Walker, and B. M. Wilson. J. Chem. Soc. 4356 (1956).
15. J. D. Ballantine and P. J. Sykes. J. Chem. Soc. C, 731 (1970).
16. G. Stork, M. Nussim, and B. August. Tetrahedron Suppl. No. 8, Pt. 1, 105 (1966).
17. W. G. Dauben, P. Lang, and G. H. Berezin. J. Org. Chem. **31**, 3869 (1966).
18. F. Sondheimer and R. Mechoulam. J. Am. Chem. Soc. **79**, 5029 (1957).
19. J. Y. Satoh, K. Misawa, T. T. Takehashi, M. Hiruse, C. A. Huriuchi, S. Tsuji, and A. Hagitam. Bull. Chem. Soc. Jpn. **46**, 3155 (1973).
20. (*a*) A. Butenandt and A. Wolfe. Chem. Ber. **68**, 2091 (1935); (*b*) H. H. Inhoffen, G. Kolling, G. Koch, and I. Nebel. Chem. Ber. **84**, 361 (1951).
21. M. Christl and J. D. Roberts. J. Org. Chem. **37**, 3443 (1972).
22. M. St-Jacques, C. Vaziri, D. A. Frenette, A. Goursot, and S. Fliszar. J. Am. Chem. Soc. **98**, 5759 (1976).
23. J. B. Stothers, J. R. Swenson, and C. T. Tan. Can. J. Chem. **53**, 581 (1975).
24. J. M. Coxon, P. R. Hoskins, and T. K. Ridley. Aust. J. Chem. **30**, 1735 (1977).
25. M. Christl, H. J. Reich, and J. D. Roberts. J. Am. Chem. Soc. **93**, 3463 (1971).
26. D. K. Dalling and D. M. Grant. J. Am. Chem. Soc. **89**, 6612 (1967).
27. J. L. Gough, J. P. Guthrie, and J. B. Stothers. J. Chem. Soc. Chem. Commun. 979 (1972).
28. A. Stoessl and J. B. Stothers. Z. Naturforsch. **34c**, 87 (1979).
29. R. A. Dyllick-Brenzinger and J. B. Stothers. J. Chem. Soc. Chem. Commun. 108 (1979).
30. L. M. Browne, R. E. Klinck, and J. B. Stothers. Org. Magn. Reson. In press. 1979.

[5]Strictly speaking the results for **36** and **38** have been reported previously but apparently were inadvertently attributed to the corresponding β-bromo isomers (*2b*).

Ring expansion of cyclic ketones: The reliable determination of migration ratios for 3-keto steroids by ^{13}C nuclear magnetic resonance and the general implications thereof[1,2]

VINOD DAVE, J. B. STOTHERS, AND E. W. WARNHOFF

Department of Chemistry, University of Western Ontario, London, Ont., Canada N6A 5B7

Received November 27, 1978

VINOD DAVE, J. B. STOTHERS, and E. W. WARNHOFF. Can. J. Chem. 57, 1557 (1979).

Several ring-expansion reactions (diazomethane, diazoacetic ester, Tiffeneau–Demjanov, Baeyer–Villiger, and Schmidt) of 3-keto steroids have been reexamined to determine the true migration ratios for C-2 and C-4 in these unsymmetrical cyclohexanones. Migration ratios were measured to $\pm 3\%$ accuracy by integration of baseline-separated signals in the proton-decoupled ^{13}Cmr spectra of total reaction products. This underexploited method provides for the first time a way to get accurate migration ratios without loss of components during separation and without interference from excess starting material under conditions minimizing side reactions. In contrast to numerous literature reports, all but one of the 16 reactions studied were found to give nearly the same amount of both possible *A*-homo products. (The single exception was the only reaction in which the *A*-homo product reacts markedly faster than the starting material.) This simple, consistent $\sim 1:1$ pattern is that expected if migration is governed mainly by the electronic effect of the α- and α′-carbon atoms and not by any conformational or near-by-to-remote substituent effect.

VINOD DAVE, J. B. STOTHERS et E. W. WARNHOFF. Can. J. Chem. 57, 1557 (1979).

On a réétudié plusieurs réactions d'extension de cycles (diazométhane, esterdiazoacétique, Tiffeneau–Demjanov, Baeyer–Villiger et Schmidt) de céto-3 stéroïdes afin de déterminer les rapports réels de migration de C-2 et de C-4 dans ces cyclohexanones qui ne sont pas symétriques. On a mesuré ces rapports d'aptitudes à la migration avec une exactitude de $\pm 3\%$ en intégrant les signaux séparés à la base, des spectres rmn du ^{13}C découplés pour le proton, des produits totaux de réaction. Cette méthode sous-exploitée fournit pour la première fois une façon d'obtenir des rapports précis d'aptitudes à la migration sans perte de composants au cours de la séparation et sans interférence de la part du produit qui n'a pas réagi dans des conditions minimisant les réactions secondaires. Par opposition à de nombreux rapports publiés dans la littérature, on a trouvé, dans tous les 16 cas étudiés, à l'exception d'un, qu'il se forme des quantités égales des deux produits *A*-homo possibles. (La seule exception est notée dans la seule réaction dans laquelle le produit *A*-homo réagit beaucoup plus rapidement que le produit de départ). Ce résultat, $\sim 1:1$, obtenu d'une façon systématique est celui que l'on peut prévoir si la migration n'est gouvernée que par l'effet électronique des atomes de carbone α et α′ et non pas par un effet conformationnel ou d'un substituant proche ou éloigné.

[Traduit par le journal]

The ring expansion of cyclic ketones is a useful synthetic reaction, but it is frequently complicated by the problem of similar α- and α′-migratory aptitudes leading to two isomeric ring-expanded products which can be difficult to separate or analyze. This problem has been of most concern with unsymmetrical cyclohexanones, and a conspicuous example is the ring homologation of 3-keto steroids **1**. The conflicting reports (2–15) of varying product composition from this series of compounds has led to the postulation of remarkable differential migratory aptitudes and their equally remarkable rationalizations (4, 7, 13, 16). It has now become apparent, through the work of Jones and Price (15) and Levisalles *et al.* (10) on the homologation reactions, that most of the complexities are the result of analytical techniques inadequate for the task.

For example, initial reports of the formation of a majority (≥ 50–60%) of *A*-homo-4-ketone **4***a* (Scheme 1) from ring expansion of 5α-cholestan-3-one (**2***a*) by either diazomethane (CH_2N_2) (3) or by the Tif-

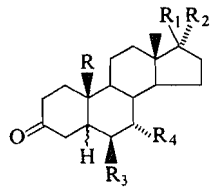

1

R = CH_3 or H
R_1 = OH, OAc, H, or 2-isooctyl
R_2 = OH, CH_3, or H
R_3 = OAc, H, or *p*-π
R_4 = OBz, H, or *p*-π

[1]This paper is dedicated to the memory of R. H. F. Manske.
[2]Part 86 of ^{13}C nuclear magnetic resonance studies of one of us (J.B.S.). For Part 85, see ref. 1.

0008-4042/79/131557-12$01.00/0

feneau–Demjanov method (amino alcohol diazotization) (2, 3) were based on analysis by alumina chromatography and infrared spectroscopy. Later, the additional use of ord was introduced by Jones and co-workers (4, 7) to determine the ratio of *A*-homo ketones in product mixtures from 3-keto steroids by comparison with the ord curves for the pure products. With the nearly inseparable products from 5α-cholestan-3-one, the ratio of 3-ketone **3***a* to 4-ketone **4***a* determined by this method was 21:79 ±3% (7). However, further investigation revealed that one or both of the reference samples **3***a* or **4***a* was apparently contaminated. Thus, Levisalles *et al.* (10) prepared these two ketones by methods leading unambiguously to pure specimens, and both they and Jones and Price (15) used these samples to recheck the ring-expansion ratio for **2***a* + CH_2N_2. Both groups found a new **3***a*:**4***a* ratio of 57:43 ±5% (10) ≈ 58.5:41.5 ±3% (15) in good agreement with ratios for other 3-keto steroids whose homologation products were more readily separated (see entries from ref. 7 in Table 1). The Tiffeneau–Demjanov expansion of 5α-cholestan-3-one was also checked by Levisalles *et al.* (10) who found the **3***a*:**4***a* product ratio to be 50:50 (Table 1, entry 7) comparable to the value found for CH_2N_2. In complete disagreement, Sykes and co-workers (13) reported concurrently that the 4-ketone **4***a* was the only *A*-homo ketone formed from either epimer of the amino alcohol **9**; the absence of *A*-homo-3-ketone **3***a* was judged by glpc comparison with authentic specimens of **3***a* and **4***a*. In a more recent repetition of the reaction, Jones and Price (15) have reaffirmed that both *A*-homo ketones are formed in slightly different proportions from each epimer of the amino alcohol **9** (Table 1, entries 8 and 9). It was desirable to have an independent check both on these conflicting accounts of the Tiffeneau–Demjanov reaction and on the CH_2N_2 reaction.

As can be appreciated from the foregoing, the analytical methods employed had inherent shortcomings. The use of ord requires both optical activity and the availability of both ring-expansion products in pure form; it also requires that *only* the two compounds of interest be present in the mixture to be analyzed. However, CH_2N_2 ring expansion usually produces small amounts of epoxides and polyhomologation products difficult to separate from the homo ketones. With CH_2N_2 another drawback of the chromatography–ord method of analysis is that the 3-keto starting material should be completely used up to simplify the product separation. In this way is introduced the additional complication of possible differential ring expansion of the initial *A*-homo ketones. Should the 3- and 4-ketones react

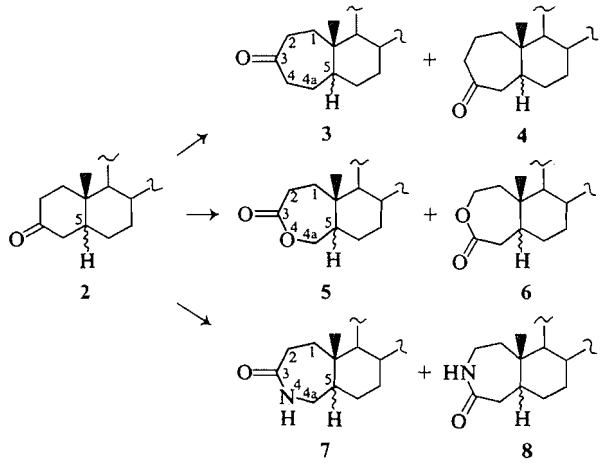

a 5α-Cholestane skeleton
b 5β-Cholestane skeleton
c 17β-Hydroxy-5α-androstane skeleton
d 6β-Acetoxy-5α-cholestane skeleton

SCHEME 1

at different rates, the final **3**:**4** ratio would not reflect the true migration ratio for the reaction of **2**. On the other hand, the use of glpc requires sufficiently different retention times for the two expansion products, a requirement not easily met for such closely similar high molecular weight compounds (15). Although the application of ^{1}Hmr spectra to the analysis of these product mixtures should be more successful, it depends on there being well-separated signals for the two isomers, and for 3-keto steroids very high magnetic fields may be needed to achieve separation (17).

A convenient, more recently available analytical method which does overcome all of the aforementioned difficulties is integration of appropriate peaks in the proton-decoupled ^{13}Cmr spectra of product mixtures. Although for smaller molecules peak areas are not necessarily proportional to numbers of nuclei, Wehrli (18, 19) has shown that for molecules as large and rigid as **2***a*, under non-saturating conditions the nuclear Overhauser effect in proton-decoupled spectra is complete and equal for all skeletal carbon atoms (including quaternary), and therefore signal integration can be used for quantitative analysis. Moreover, unlike the ord or glpc methods, the nature of ^{13}Cmr spectra reflects the structural identity of a mixture's components. We have found, in the course of examining the ^{13}Cmr spectra of some *A*-homo steroids (1, 20), that several of the lower-field signals in the 40–60 ppm region were well separated in isomeric *A*-homo compounds and their precursor. Fortunately, integration of these separated peaks in mixtures was not only reproducible in duplicate reactions, but with test mixtures

it was found to give reliable isomer ratios accurate to ±3%.[3] Hence, there were no complications from potentially unequal Overhauser effects (21). The absence of interfering absorptions from starting material meant that it was now possible to perform the CH_2N_2 ring expansions with a large excess of starting material remaining in order to minimize the likelihood of further reaction of initially formed *A*-homo ketones, a bothersome problem in some instances. Furthermore, if any side products such as epoxides and bishomo ketones should be formed to any significant (≥5%) extent, they would be readily detected by extra peaks in the low-field end (40–70 ppm) of the ^{13}Cmr spectrum, but they would not cause any difficulties with integration of carefully selected signals. The extent of mono- and polyhomologation could be estimated from the mass spectrum of the reaction product.[4] The advantages of the method were well demonstrated in examining the reactions of 3-keto steroids.

The first compound studied was 5α-cholestan-3-one (**2***a*) whose ^{13}Cmr spectrum has a region devoid of signals between 46 and 54 ppm (22). Authentic samples of **4***a* and **3***a* prepared by known methods (10, 23) (see Experimental) were used for ^{13}C peak assignments (1). Each of the *A*-homo ketones absorbed in the region free of **2***a* absorption, **3***a* at 50.6 (C-5) and 53.3 ppm (C-9), and **4***a* at 47.9 (C-4a) and 54.1 ppm (C-9). The accuracy of integration of these peaks was verified with three known mixtures of **3***a* and **4***a* (see Experimental). Limited ring expansion of the 3-ketone **2***a* with CH_2N_2 by both the *in situ* and *ex situ* procedures (see Experimental) gave a product containing 20–28% of *A*-homo ketones. Integration of the ^{13}C signal at 53.3 ppm relative to that at 54.1 ppm and of the peak at 47.9 ppm relative to that at 50.6 ppm gave the same **3***a*:**4***a* ratio of 58:42 ±3% (Table 1, entries 1, 2, and 5) in excellent agreement with the ord derived value of Levisalles *et al.* (10) and Jones and Price (15) (Table 1, entries 3 and 4), which therefore did represent the true kinetic migration ratio in spite of consumption of most of the starting ketone **2***a* in their reactions.

To test whether the initial *A*-homo ketones would show selectivity in the event of their reaction, a synthetic 50:50 mixture of **3***a* + **4***a* was treated to the extent of 15% reaction with CH_2N_2 generated *in situ*. ^{13}Cmr examination of the remaining *A*-homo ketones gave an altered **3***a*:**4***a* ratio of 57:43 ±3%, and consequently the 4-ketone is more reactive. The probable reason that this selectivity was not reflected in Levisalles's and Jones's ratios is that the reaction of CH_2N_2 with both **3***a* and **4***a* is slower than with **2***a*, and any excess CH_2N_2 may have been used up in polymerization.[5]

As independent confirmation that the Tiffeneau–Demjanov expansion of 5α-cholestan-3-one does indeed give both *A*-homo ketones, this reaction too was reexamined. Diazotization of a 30% α – 70% β mixture of hydroxyl epimers of amino alcohol **9** gave a product whose ^{13}Cmr spectrum revealed the presence of both **3***a* and **4***a* in the ratio of 43:57 (Table 1, entry 6) in reasonable agreement with the ord-derived values of Levisalles *et al.* (10) and Jones and Price (15) (Table 1, entries 7, 8, and 9). Apparently, as pointed out by Jones and Price (15), the very close glpc retention times for **3***a* and **4***a* used by Sykes and co-workers (13) did not permit resolution of mixtures of the two isomers.

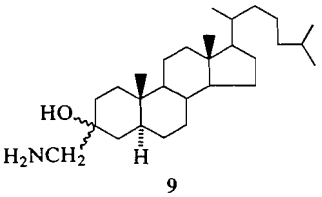

9

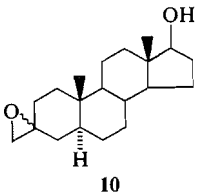

10

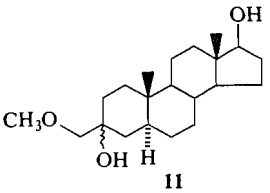

11

The next migration ratio determined was for a reported (7, 9, 15) ring expansion giving products more easily separated by chromatography, and for which the migration ratio determined by a combination of separation and ord should therefore be accurate provided that no by-products contaminated the ord samples. Ring expansion of an excess of 17β-hydroxy-5α-androstan-3-one (**2***c*) afforded a product containing 35–43% of *A*-homo ketones. The ^{13}C peaks were assigned (1) with the aid of authentic specimens of both products (7) separated by chromatography from a reaction in which all starting material had been consumed. In the spectrum of the mixture, the best separated peaks for integration were the signals at δ 27.8 in homo ketone **3***c* and at δ 18.9 in **4***c*. Values of the **3***c*:**4***c* ratio of 56:44 and

[3]The accuracy is probably better than that (±3–5%) estimated for the ord method (7, 10). Note also that integration of two or more peaks for each component provides an internal check.

[4]The extra CH_2 group or two would have a negligible effect on the vapour pressure of these large molecules.

[5]Note that the selectivity found (**4***a* reacts faster than **3***a*) is in the wrong sense to account for the originally reported **3***a*:**4***a* ratio of 21:79 (7) by further preferential reaction of initial *A*-homo products.

TABLE 1. Migration ratios for ring expansions of 3-keto steroids

Entry	Starting material	Reaction	3 C=O : 4 C=O ratio[a]	Analytical method	Ref.
1	5α-Cholestan-3-one (*2a*)	CH_2N_2 NMU[b] *in situ*	**58:42**	^{13}Cmr	[a]
2	5α-Cholestan-3-one (*2a*)	CH_2N_2 NMU[b] *ex situ*	**59:41**	^{13}Cmr	[a]
3	5α-Cholestan-3-one (*2a*)	CH_2N_2 NMU[b] *in situ*	57:43	ord	10
4	5α-Cholestan-3-one (*2a*)	CH_2N_2 NMU[b] *in situ*	58.5:41.5	ord	15
5	5α-Cholestan-3-one (*2a*)	CH_2N_2 Diazald[c] *in situ*	**58:42**	^{13}Cmr	[a]
6	5α-Cholestan-3-one (*2a*)	Tiffeneau–Demjanov 30%α-OH, 70%β-OH	**43:57**	^{13}Cmr	[a]
7	5α-Cholestan-3-one (*2a*)	Tiffeneau–Demjanov	50:50	ord	10
8	5α-Cholestan-3-one (*2a*)	Tiffeneau–Demjanov β-OH, α-CH_2NH_2	48:52	ord	15
9	5α-Cholestan-3-one (*2a*)	Tiffeneau–Demjanov α-OH, β-CH_2NH_2	63:37	ord	15
10	5α-Cholestan-3-one (*2a*)	DAE[f] and —COOEt	**46:54**	^{13}Cmr	[a]
11	5α-Cholestan-3-one (*2a*)	*m*-CPBA[d] Baeyer–Villiger	**55:45**	^{13}Cmr	[a]
12	5α-Cholestan-3-one (*2a*)	CF_3CO_3H Baeyer–Villiger	**58:42**	^{13}Cmr	[a]
13	5α-Cholestan-3-one (*2a*)	PPA[e] Schmidt	**50:50**	^{13}Cmr	[a]
14	17β-Hydroxy-5α-androstan-3-one (*2c*)	CH_2N_2 NMU[b] *in situ*	**56:44**	^{13}Cmr	[a]
15	17β-Hydroxy-5α-androstan-3-one (*2c*)	CH_2N_2 NMU[b] *in situ*	59:41	ord	7, 15
16	17β-Hydroxy-5α-androstan-3-one (*2c*)	Tiffeneau–Demjanov 3β-OH, 3α-CH_2NH_2	49.5:50.5	ord	15
17	17β-Hydroxy-5α-androstan-3-one (*2c*)	Tiffeneau–Demjanov 3α-OH, 3β-CH_2NH_2	61.5:38.5	ord	15
18	17β-Hydroxy-5α-androstan-3-one (*2c*)	*m*-CPBA[d] Baeyer–Villiger	**58:42**	^{13}Cmr	[a]
19	5β-Cholestan-3-one (*2b*)	CH_2N_2 NMU[b] *in situ*	**52:48**	^{13}Cmr	[a]
20	5β-Cholestan-3-one (*2b*)	DAE[f] and —COOEt	**47:53**	^{13}Cmr	[a]
21	5β-Cholestan-3-one (*2b*)	*m*-CPBA[d] Baeyer–Villiger	**58:42**	^{13}Cmr	[a]
22	5β-Cholestan-3-one (*2b*)	PPA[e] Schmidt	**51:49**	^{13}Cmr	[a]
23	17α-Hydroxy-5α-androstan-3-one	CH_2N_2 NMU[b] *in situ*	55:45	ord	7
24	5α-Androstan-3-one	CH_2N_2 NMU[b] *in situ*	58:42	ord	7
25	17β-Acetoxy-5α-androstan-3-one	CH_2N_2 NMU[b] *in situ*	55:45	ord	7
26	17β-Hydroxy-17α-methyl-5α-androstan-3-one	CH_2N_2 NMU[b] *in situ*	62:38	ord	7
27	17β-Hydroxy-5α-estran-3-one	CH_2N_2 NMU[b] *in situ*	60:40	ord	7
28	17β-Acetoxy-5α-estran-3-one	CH_2N_2 NMU[b] *in situ*	55:45	ord	7
29	17β-Hydroxy-5β-androstan-3-one	CH_2N_2 NMU[b] *in situ*	50:50	ord	7
30	17β-Hydroxy-5β-estran-3-one	CH_2N_2 NMU[b] *in situ*	61:39	ord	7
31	7α-Benzoyloxy-5α-cholestan-3-one	CH_2N_2 Diazald[c] *in situ*	60:40	ord	14
32	5α-Cholest-6-en-3-one	CH_2N_2 NMT[i] *ex situ*	60:40	^{1}Hmr	17
33	6β-Acetoxy-5α-cholestan-3-one	CH_2N_2 NMU[b] *ex situ*	**50:50**	^{13}Cmr	[a]
34	*B*-Nor-5β-cholestan-3-one	CH_2N_2 NMU[b] *in situ*	(*70:30*)[h]	^{13}Cmr	[a]
35	*B*-Nor-5β-cholestan-3-one	DAE[f] and —COOEt	**42:58**	^{13}Cmr	20
36	*trans*-2-Decalone	CH_2N_2 NMU[b] *in situ*	56:44	glpc	24
37	*trans*-2-Decalone	Tiffeneau–Demjanov 3β-OH, 3α-CH_2NH_2	50:50	glpc	24
38	*trans*-2-Decalone	Tiffeneau–Demjanov 3α-OH, 3β-CH_2NH_2	61:39	glpc	24

[a]Present work.
[b]*N*-Nitroso-*N*-methylurea.
[c]*N*-Nitroso-*N*-methyl-*p*-toluenesulfonamide.
[d]*m*-Chloroperbenzoic acid.
[e]Polyphosphoric acid.
[f]Ethyl diazoacetate.
[g]Numbers in boldface are from present work. For the ratios determined by ^{13}Cmr and ord the error limits are ±3%. See also footnote 3 and the ^{13}Cmr part of the Experimental.
[h]Not reliable because one or both products reacts faster than starting material.
[i]*N*-Nitroso-*N*-methylterephthalamide.

57:43 were obtained in this way from two reactions. Four lower-field signals at δ 47.8, 50.5, 53.4, and 54.2 were not sufficiently separated from starting material peaks for confident integration unless most of the **2***c* had been consumed. Therefore, a homologation carried to >90% consumption of **2***c* was chromatographed to separate the *A*-homo ketone mixture which was integrated over all six peaks to give a **3***c*:**4***c* ratio of 55:45, identical with the two-peak integration ratio within experimental error. The validity of the integrations was also checked with a known mixture. The **3***c*:**4***c* migration ratio of 56:44 (Table 1, entry 14) obtained by averaging the above results agrees within experimental error with the earlier reported value of 59:41 (7, 15).

For 5β-cholestan-3-one, the only reported (7) value of 78:22 (ord derived) for the **3***b*:**4***b* ring-expansion ratio was suspect because the almost 4:1 preference for C-4 migration deviated from the negligible preference now established for other 3-keto steroids. Accordingly, the reaction was re-examined. The ^{13}C absorption-free region was slightly shifted to 44–56 ppm for **2***b* (22). Limited ring expansion by the *in situ* method gave a product with 39–53% of starting material remaining.[6] Its ^{13}C signals were assigned by comparison with those of starting ketone **2***b* and of an authentic specimen of *A*-homo-5β-cholestan-3-one (**3***b*) prepared as shown in Scheme 2 (also see Experimental). The true **3***b*:**4***b* product ratio found by integration of baseline separated peaks at 46.6 ppm (C-5 of **3***b*) and 45.9 ppm (C-5 of **4***b*) was 52:48 in good agreement with the values of other 3-ketones.

There are two other reports in the literature which are at variance with the present findings. In ref. 6, only the *A*-homo 4-ketone[7] was isolated from the reaction of *B*-nor-5β-cholestan-3-one with CH_2N_2. Actually, both *A*-homo ketones were undoubtedly formed since the Tiffeneau–Demjanov expansion of the same *B*-nor ketone gave both *A*-homo-3- and -4-ketones (14), and since diazoacetic ester expansion gave a 42:58 ratio of *A*-homo-3- to -4-ketone after decarbethoxylation (20). Repetition of the reaction with CH_2N_2 to a limited extent gave a product containing 83.4% of unreacted *B*-nor ketone, 11.2% of *A*-homo ketone mixture, and surprisingly 5.3% of

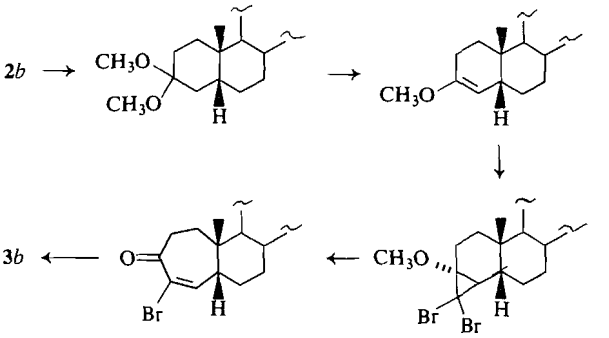

SCHEME 2

bis-*A*-homo ketones. Therefore, one or both of the *A*-homo ketones reacts considerably faster with CH_2N_2 than does the starting material. Consequently, the *A*-homo-3- to -4-ketone ratio found of ~70:30[7] probably does not represent the true migration ratio which should be closer to the 42:58 figure from the diazoacetic ester reaction (Table 1, entry 35).

The second anomalous case is that of 6β-acetoxy-5α-cholestan-3-one (**2***d*) from whose reaction with a large excess of CH_2N_2 + $AlCl_3$ only bis- and tris-homo products were isolated (12). However, from reaction with a limited amount of CH_2N_2 such that 69% of starting material remained, we find that both *A*-homo ketones are formed in a ratio not experimentally different from 50:50 by comparison of the integral of the ^{13}C signal at δ 75.3, which contains the absorption from C-6 of both *A*-homo ketones, with peaks at δ 30.0, 30.5, 51.9, and 53.0, each of which arises from only one of the *A*-homo ketones.

Therefore, for all of the 15 steroids whose ring homologation has been studied with care (see Table 1) there is either no preference or else a negligible preference for migration of C-4 over C-2, and the **3**:**4** ratio does not exceed 6:4 (or *vice versa*) in any case.[8] This is as would be expected in consideration of both C-2 and C-4 being secondary and there being no conformational migratory preference discernible from Dreiding models. It should also be noted that the C-19 methyl group and the steroid C- and substituted D-ring do not play a detectable role in determining the migration ratio since CH_2N_2 ring expansion of *trans*-2-decalone (**12**), a bicyclic model for 5α-3-keto steroids, also gave the same value of 56:44 for the **13**:**14** ratio (24). Likewise, the Tiffeneau–Demjanov rearrangement of each of the

[6]If ring expansion of the 5β-ketone **2***b* is carried to near completion, a much more complex mixture of products is apparent from the ^{13}Cmr spectrum than is the case with the 5α-ketone **2***a* under similar conditions.

[7]It is not clear which ketone isomer is meant in ref. 6; the structural formula is that of the *A*-homo-3-ketone but the name given in the Experimental is for the *A*-homo-4-ketone. Since excess CH_2N_2 was used and since the $[\alpha]_D$ was +21°, the product was probably the *A*-homo-3-ketone (20) in view of the present findings, even though its melting point was low.

[8]Strictly speaking, the homologations of the compounds listed in entries 23–31 of Table 1 should also be reexamined by the ^{13}Cmr method but the 1:1 pattern from all five different reactions examined by this technique in the present work now leaves no real doubt that the earlier ord results for these compounds (7) are substantially correct.

epimeric bicyclic amino alcohols **15** gave the same ratios as did the Tiffeneau-Demjanov rearrangement of the corresponding amino alcohols from 5α-cholestan-3-one and 17β-hydroxy-5α-androstan-3-one (compare entries 8, 9, 16, and 17 with 37 and 38 in Table 1).

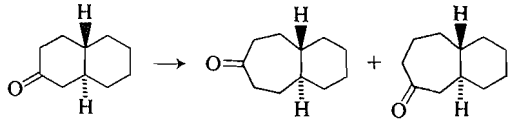

12 **13** **14**

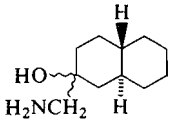

15

The consistency of the results emerging from these experiments prompted the scrutiny of related ring expansion reactions to see how widely the generalization held.

Homologation of ketones with diazoacetic ester (DAE) has become a useful alternative to the use of CH_2N_2 (25, 26). When both 5α- and 5β-cholestan-3-one were partially homologated with DAE–$Et_3O^+BF_4^-$ and decarbethoxylated,[9] the ratios of *A*-homo products were the same for both (Table 1, entries 10 and 20) and were changed slightly in favor of more 4-ketone relative to the CH_2N_2 reactions, but for all practical purposes the change is negligible.

The ring expansion of ketones to lactones by migration to oxygen in the Baeyer–Villiger reaction involves an intermediate **16** that is of the same type as in the diazoalkane reaction, and the simplest view would lead one to expect the same migration ratio for both reactions. Unfortunately, the Baeyer–Villiger cleavage of 3-keto steroids has been beset by the same difficulties found with the CH_2N_2 reactions. Most investigators report only the isolation of the 3-oxolactone **5** in yields as high as 76% (27–35) from peracid oxidation, but on reinvestigation some of these reactions have been shown to produce both lactones **5** and **6** (36). In other cases both lactones were found initially (37, 38). However, no accurate values for product ratios have been reported. Therefore, we have carried out the cleavage by *m*-chloroperbenzoic acid – $CHCl_3$ of 5α- and 5β-cholestan-3-one as well as 17β-hydroxy-5α-androstan-3-one. In each case both lactones were formed in a nearly 1:1 ratio. The different location of the introduced oxygen atom in the two lactones made unambiguous the assignment by chemical shift of the lowest-field sp^3-^{13}C signals in the ^{13}Cmr spectrum without the necessity of authentic samples of the lactones. For example, the lowest field sp^3-^{13}C peak in the spectrum of the 5α-cholestan-3-one product at 70.0 ppm can only be C-4a (O—CH_2—CH) of lactone **5***a*, while the next lowest sp^3-^{13}C peak at 64.7 ppm must be C-2 (O—CH_2—CH_2) of lactone **6***a* (39). These assignments were confirmed for the **2***a* reaction by preparation of pure lactone **5***a* (40) as described in the Experimental. Integration of the spectrum of the lactone mixture gave a **5***a*:**6***a* migration ratio of 55:45 (Table 1, entry 11), very nearly the same as the CH_2N_2 migration ratio with this ketone (Table 1, entries 1–5). The product ratios for the lactones from **2***b* and **2***c* (Table 1, entries 18 and 21) were likewise as easily determined[10] and were close to those for the corresponding CH_2N_2 reactions.

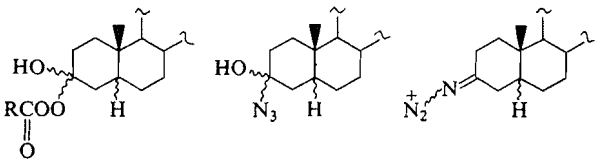

16 **17** **18**

Because different peracid oxidation conditions have been known to influence the proportion of cleavage products from some ketones, the oxidation of **2***a* was also done with CF_3CO_3H–$CHCl_3$, a much stronger peracid. Contrary to a previous report for this reagent (34), the migration ratio (Table 1, entry 12) was found to be essentially the same as for the *m*-chloroperbenzoic acid – $CHCl_3$ cleavage.

Finally, ring expansion to nitrogen was examined by means of the Schmidt reaction. The mechanistic evidence (41, 42) allows for the reaction to proceed to amide through either the tetrahedral intermediate **17**, analogous to those of the already mentioned ring expansion reactions, or else through *anti* rearrangement of the geometrical isomers of the diazoimonium ion **18**. Since the proportion of *syn* and *anti* isomers is determined by steric factors, and since the steric situation is the same for both isomers with these 3-keto steroids, either mechanism would be expected to lead to an approximately 1:1 ratio of products **7** and **8**. However, the Schmidt reaction with both 5α- and 5β-cholestan-3-one has been

[9]The crude β-keto esters were decarbethoxylated with water in sealed tubes at 150°C (26). Under these conditions the ketonic components underwent condensation reactions to some extent. Possibly these side reactions were acid catalyzed (by traces of boron compounds remaining?) because they were minimized by the addition of a small amount of $NaHCO_3$ to the water (see Experimental).

[10]With the 17β-hydroxy compound **2***c* care had to be taken to avoid an excess of peracid which oxidized the 17β-OH to a carbonyl group.

reported by Doorenbos and Wu (43) to yield only isomer **8**. Repetition of the reaction of the 5α- and 5β-ketones **2***a* and **2***b* according to their procedure gave products each of whose ^{13}Cmr spectra clearly showed the presence of both lactams **7** and **8** in similar amount. The assignment of ^{13}C peaks in each lactam mixture was made with the aid of spectra of pure **8***a* and **8***b* prepared as described below.

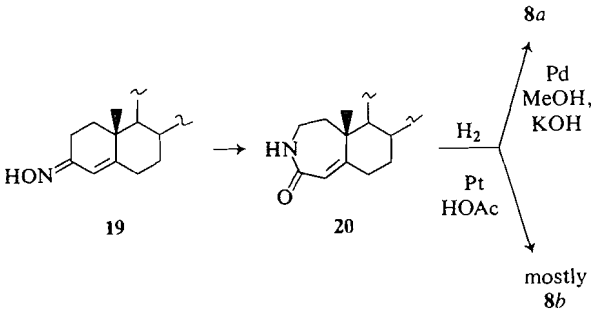

Beckmann rearrangement of the mixture of cholest-4-en-3-one oximes **19** at room temperature with $SOCl_2$ in dioxane results only in migration of the sp^3 C-2 to produce the unsaturated lactam **20** (44, 45). Hydrogenation over Pd/C in methanol–KOH gave the 5α-lactam **8***a* (44) whose *trans* A/B fusion was verified by its ^{13}C-19 methyl signal at 12.0 ppm (46). Hydrogenation of **20** over Pt in HOAc gave mostly the 5β-lactam **8***b* which was purified by thick-layer chromatography; the *cis* A/B fusion was confirmed by its ^{13}C-19 methyl peak at 23.3 ppm (46). With the ^{13}C signals identified in the Schmidt reaction mixtures, the 1:1 ratios given in entries 13 and 22 of Table 1 were calculated.[11]

In conclusion, we see that the supposedly widely differing results of various 3-keto steroid ring-expansion reactions actually fit a consistent pattern. Thus, for 16 of these similar unsymmetrical cyclohexanones (including 2-decalone) and five different reactions, ring expansion to C, N, and O gives a migration ratio of ~1:1. This simple outcome is to be expected if migration in all of these reactions is governed *mainly* by the electronic effect of the α- and α′-methylene groups and not by any conformational or long range effects. As a corollary, in each of the many cases in which the lactones and lactams from Baeyer–Villiger or Schmidt or even Beckmann reactions on 3-keto steroids have been prepared or used (on the assumption that pure compounds were involved) in structure assignments to other compounds or as starting materials for synthesis (*inter alia* 32, 34, 40, 47, 48), the conclusion or purity of product is dubious, and this implication of the present work will be considered in a subsequent paper.

[11]Although the ratios turned out to be exactly 50:50, assignment of signals to individual lactams gave assurance that the integrated peaks were not all from a single lactam.

Experimental

General

Reagents, instruments, and procedures are the same as in ref. 20 except for the following. Camag DSF-O silica gel was used for some tlc plates. Some ir spectra were recorded on a Perkin Elmer model 621 instrument. The samples of **2***a*, **2***b*, **2***c*, and **2***d* used were shown to be pure by ^{13}Cmr spectroscopy. Complete ^{13}Cmr assignments for the steroids in this work are given in ref. 1. The mass spectra for quantitative analysis of product mixtures were run at 25 eV to minimize fragmentation and maximize molecular ions. The figures in parentheses after the ion masses are the percentages of starting material and homo and bishomo products calculated from the ion intensities and estimated to be accurate to ±3%.

^{13}C Nuclear Magnetic Resonance Spectra

Spectra were obtained at 25.2 MHz with a Varian XL-100-15 system operating in the Fourier transform mode with square-wave modulated proton decoupling. Solutions were usually ~0.25 *M* in $CDCl_3$ and in no case exceeded 1.25 *M*; TMS was used as an internal reference. Wehrli has shown (18) that all carbons of the steroid ring system exhibit maximum and equal nOe's under appropriate operating conditions. With 2 or 2.5 kHz sweep widths, flip angles ≤45°, and pulse acquisition times of 0.8–1.0 s, our conditions insured that the protonated skeletal carbons gave full nOe's although the quaternary carbons were probably partially saturated. To achieve suitable signal-to-noise levels the number of scans varied from 10–50 K and 8 K transforms were used. Integrations were done both by the usual electronic means and by comparing the products of peak height × peak width at half-height for the best-separated signals in expanded traces of the region of interest. If peak separation permitted, two or more signals per component were integrated, and the results were averaged to obtain the reported composition data. Integrals were found to be reproducible to ±2% and, from control experiments, the composition of known mixtures of **3***a* and **4***a* was found to a precision of ±2%; in these controls the following signal areas were measured: **3***a*, 50.6 (C-5) and 53.3 ppm (C-9); **4***a*, 47.9 (C-4a) and 54.1 ppm (C-9). This led to the following results.

Mixture (mg)		3a		
3a	4a	By weight %	By integration	Average
12.0	36.0	25	26, 25, 27, 26	26
24.0	24.0	50	49, 49, 50, 49	49
36.0	12.0	75	76, 74, 76, 75, 74	75

On this basis, the compositions of the product mixtures are judged by the 4d rule to have precisions of 3%. Whenever possible, the crude mixtures of ring expansion products were not chromatographed before ^{13}Cmr spectroscopy to avoid any possibly unequal irreversible adsorption. Each CH_2N_2 and DAE ring expansion was done at least in duplicate, but only one experiment per ring expansion is described in the sequel.

General Procedure for In Situ *CH_2N_2 Reactions*

To a stirred (magnetic bar) solution of 100 mg of steroid, 30 mg of powdered KOH, 1 mL of MeOH, and 2 mL of ether at 0–5°C was added a known amount of CH_2N_2 precursor. When less than 100 mg was used, the amounts of MeOH and ether were reduced proportionately. Throughout the reaction

solid was present, initially the partially soluble CH_2N_2 precursor and later presumably potassium salts. After the two-phase mixture had been stirred at 5–8°C for 6 h, the solvents were evaporated in a stream of N_2. Water and 10% aqueous HCl were added, and the product was extracted with ether. The organic layer was washed with water, dried, and evaporated to leave the crude product which was examined by ^{13}Cmr and mass spectroscopy. The amount of CH_2N_2 precursor required to achieve partial homologation varied because of the limited solubility of the CH_2N_2 precursor and the competing polymerization side reaction of CH_2N_2. For the same reasons, a given level of homologation was difficult to reproduce in duplicate reactions.

(a) 5α-Cholestan-3-one + N-Methyl-N-nitrosourea (NMU)

From 100 mg (0.26 mmol) of **2***a* and 15 mg (0.15 mmol) of NMU was obtained 92 mg of colorless solid product, *m/e* 386 (72% of **2***a*) and 400 (28% of **2***a* + CH_2) with no detectable bis homologation at 414. ^{13}C peaks integrated: δ 47.9 (C-4a of **4***a*), 50.6 (C-5 of **3***a*), 53.3 (C-9 of **3***a*), and 54.1 ppm (C-9 of **4***a*) (Table 1, entry 1).

(b) 5α-Cholestan-3-one + Diazald

From 100 mg (0.26 mmol) of **2***a* and 94 mg (0.44 mmol) of Diazald was obtained 88 mg of colorless solid, *m/e* 386 (20.5% of **2***a*), 400 (78.7% of **2***a* + CH_2), and 414 (0.7% of **2***a* + 2 CH_2). ^{13}C peaks integrated: same as in (*a*) (Table 1, entry 5).

(c) A-Homo-5α-cholestan-3- and -4-ones (1:1) + NMU

From 20 mg (0.05 mmol) of **3***a* plus 20 mg (0.05 mmol) of **4***a* and 21 mg (0.20 mmol) of NMU was obtained 40 mg of colorless solid, *m/e* 400 (84% of **3***a* + **4***a*) and 414 (16% of **3***a* and **4***a* + CH_2) with no detectable amount of bis homologation product. ^{13}C peaks integrated: same as in (*a*); **3***a*:**4***a* ratio, 57:43 ± 3%.

(d) 5β-Cholestan-3-one + NMU

From 50 mg (0.13 mmol) of **2***b* and 15 mg (0.15 mmol) of NMU was obtained 47 mg of colorless solid, *m/e* 386 (53% of **2***b*), 382 and 400 (47% of **2***b* + CH_2 and its $M^+ - 18$ ion) with less than 0.5% of bis homologation. ^{13}C peaks integrated: δ 45.9 (C-5 of **4***b*) and 46.6 ppm (C-5 of **3***b*) (Table 1, entry 19).

(e) 17β-Hydroxy-5α-androstan-3-one + NMU

From 50 mg (0.17 mmol) of **2***c* and 12 mg (0.12 mmol) of NMU was obtained 44 mg of colorless solid, *m/e* 290 (65% of **2***c*) and 304 (35% of **2***c* + CH_2) with no more than 0.2% of bis homologation. ^{13}C peaks integrated (see Discussion): δ 18.9 (C-2 of **4***c*), 27.8 (C-4a of **3***c*), 47.8 (C-4a of **4***c*), 50.5 (C-5 of **3***c*), 53.4 (C-9 of **3***c*), and 54.2 ppm (C-9 of **4***c*). Duplicate reactions gave **3***c*:**4***c* ratios of 56:44 and 55:45 (Table 1, entry 14).

A synthetic mixture of 17.0 mg of **3***c* and 13.0 mg of **4***c* (ratio 56.6:43.4) was analyzed by integration of the same set of signals, and it gave a **3***c*:**4***c* ratio of 56:44.

(f) B-Nor-5β-cholestan-3-one + NMU

From 48 mg (0.13 mmol) of *B*-nor-5β-cholestan-3-one and 13 mg (0.13 mmol) of NMU was obtained 48 mg of colorless noncrystalline product, *m/e* 372 (83.4% starting material), 386 (11.2% of monohomo product), and 400 (5.3% of bishomo product). ^{13}C peaksi ntegrated: δ 47.8 (C-4a of the *A*-homo-4-ketone) and 50.0 ppm (C-5 of the *A*-homo-3-ketone) (Table 1, entry 34).

Ex Situ *Diazomethane Reactions*

(a) 5α-Cholestan-3-one

A solution of 100 mg of **2***a* in 1.5 mL of ether, 1.5 mL of MeOH, and 0.1 mL of water was treated with excess distilled ethereal CH_2N_2 at 5–8°C for 2 days. After evaporation of solvent, the residue was dissolved in ether, washed with water, dried, and concentrated to give 90 mg of colorless solid, *m/e* 400 (93% of **2***a* + CH_2) and 414 (7% of **2***a* + 2 CH_2) with no **2***a* remaining. ^{13}C peaks integrated: same as in (*a*) of the *in situ* reactions (Table 1, entry 2).

(b) 6β-Acetoxy-5α-cholestan-3-one

To a solution of 44 mg (0.10 mmol) of 6β-acetoxy-5α-cholestan-3-one in 0.75 mL of ether plus 0.75 mL of MeOH was added 0.3 mL of 0.33 *N* CH_2N_2 in ether and 1 drop of water. After 2 days at 5–8°C, solvent was evaporated to leave 44 mg of solid which gave two tlc spots. Since the ^{13}Cmr spectrum of the crude product was not suitable for integration, it was chromatographed on a 10-g preparative plate developed (2×) in benzene–ether (90:10). Extraction of the band at R_f 0.54 gave 32 mg of the major, more polar material, *m/e* 444 (79% of starting material) and 458 (21% of starting material + CH_2) with no detectable amount of bis homologation product. ^{13}C peaks integrated [relative peak area] δ: 30.0[177], 30.5[177], 51.9[163], 53.0[165], and 75.3 ppm [350] (Table 1, entry 33).

Preparative Reaction with 17β-Hydroxy-5α-androstan-3-one (2c)

To a stirred (magnetic bar) solution of 200 mg of **2***c* (Sigma Chemical Co.), 980 mg of powdered KOH, 3 mL of ether, and 3 mL of MeOH at 0–5°C was added 750 mg of *N*-methyl-*N*-nitroso-*p*-toluenesulfonamide during 10 min; the two-phase mixture was then stirred at 5°C for 6 h. After evaporation of most of the solvent in a stream of nitrogen, the residue was dissolved in ether, washed with water, dried, and concentrated to leave 186 mg of oily solid which was chromatographed on four preparative plates developed (3×) with benzene–ether (50:50).

Extraction of the band at R_f 0.76 gave 12 mg of a colorless oily mixture of oxides, probably **10**, ir: no C=O absorption. M^+ calcd. for $C_{20}H_{32}O_2$: 304.2402; found: 304.2405.

Extraction of the band at R_f 0.73 gave 25 mg of colorless solid. Recrystallization (2×) from EtOAc gave 8 mg of 17β-hydroxy-*A*-homo-5α-androstan-4-one (**4***c*), mp 196–199°C (lit. (7) mp 193.5–194.5°C); ^{1}Hmr ($CDCl_3$) δ: 0.74 (3H, s, CH_3), 0.88 (3H, s, CH_3), 2.41 (2H, m, band w = 16 Hz, ketone α-CH_2), 2.82 (1H, dd, J_{AX+BX} = 25 Hz, ketone α-H), and 3.64 ppm (1H, bt, J_{AX+BX} = 18 Hz, C*H*OH).

Extraction of the band at R_f 0.67 gave 44 mg of colorless solid. Recrystallization from MeOH (1×) and from EtOAc (1×) gave 13 mg of colorless plates of 17β-hydroxy-*A*-homo-5α-androstan-3-one (**3***c*), mp 207–210°C (lit. (4) mp 212–213°C). M^+ calcd. for $C_{20}H_{32}O_2$: 304.2402; found: 304.2404.

Extraction of the most polar band at R_f 0.52 gave 17 mg of colorless solid, *m/e* 336 (M^+) and 291 ($M - CH_3OCH_2$); ir ($CHCl_3$): 3700–3300 cm^{-1} (broad OH) and no C=O absorption; ^{1}Hmr ($CDCl_3$) δ: 0.73 (3H, s, CH_3), 0.76 (3H, s, CH_3), 3.18 (2H, s, —OCH_2—), 3.39 (3H, s, OCH_3), and 3.64 ppm (1H, bt, J_{AX+BX} = 18 Hz, C*H*OH). M^+ calcd. for $C_{21}H_{36}O_3$: 336.2664; found: 336.2665. The ^{13}Cmr spectrum was in agreement with structure **11**. The compound did not react with $NaIO_4$ or $Pb(OAc)_4$.

Tiffeneau–Demjanov Expansion of 5α-Cholestan-3-one

A mixture of epimeric amino alcohols **9** was made from **2***a* by the method of ref. 13 without purification of intermediates. Integration of the —CH_2N protons at δ 2.75 for the 3β-OH epimer and δ 2.55 for the 3α-OH epimer gave 70% β-OH and 30% α-OH. To a stirred (magnetic bar) solution of 110 mg (0.26 mmol) of the amino alcohol mixture in 2 mL of HOAc and 2 mL of ether at 0–5°C was added a solution of 400 mg (5.8 mmol) of $NaNO_2$ in 1 mL of water during 10 min. The reaction mixture was stirred at ~8°C for 1 h and at room temperature for 17 h. After dilution with water and extraction with ether, the organic layer was washed with water and 5%

aqueous $NaHCO_3$. Evaporation of the dried organic solution left 90 mg (86%) of oily solid, ir ($CHCl_3$): 1695 cm^{-1} (C=O); *m/e* 400 (M^+). ^{13}C peaks integrated: same as in (*a*) of the *in situ* CH_2N_2 reactions (Table 1, entry 6).

Diazoacetic Ester Reactions

*(a) 5α-Cholestan-3-one (***2a***)*

To a stirred (magnetic bar) solution of 100 mg (0.26 mmol) of **2***a* and 99 mg (0.52 mmol) of $Et_3O^+BF_4^-$ in 1 mL of CH_2Cl_2 at 0–5°C was added a solution of 59 mg (0.52 mmol) of DAE in 0.5 mL of CH_2Cl_2. The cooling bath was allowed to warm to room temperature, and the reaction mixture which slowly darkened was stirred for 7 h. After addition of 5% aqueous $NaHCO_3$, stirring was continued for 15 min. Evaporation of CH_2Cl_2 and partition of the residue between ether and water yielded a dark brown oil which was heated in a sealed glass tube at 150°C with 1 mL of water and 5 mg of $NaHCO_3$ for 1 h.[9] There was obtained 83 mg (83%) of amber oily ketone mixture, ir ($CHCl_3$): 1695 and 1705 cm^{-1} (C=O); *m/e* 386 (46% of **2***a*), 400 (51% of **2***a* + CH_2), 414 (1% of **2***a* + 2 CH_2), and 416 (2% of **2***a* + ?) (Table 1, entry 10).

*(b) 5β-Cholestan-3-one (***2b***)*

A reaction was carried out as in (a) on 50 mg of **2***b* and half quantities of the other reagents. There was obtained 46 mg (92%) of amber oily ketone mixture after decarbethoxylation, *m/e* 386 (31% of **2***b*), 382 and 400 (69% of **2***b* + CH_2 and its $M^+ - 18$ fragmentation ion). ^{13}C peaks integrated: same as (*d*) of the *in situ* reaction (Table 1, entry 20).

Synthesis of Authentic A-*Homo-5α-cholestan-4-one (***4a***)*

(a) 3,3-Dimethoxy-5α-cholestane

This dimethyl ketal was prepared by the method of Levisalles *et al.* (10). From 500 mg of **2***a* was obtained after recrystallization (4×) from ether–MeOH 228 mg (40%) of colorless granules, mp 77–79°C, $[\alpha]_D^{19}$ +35° (*c* 1.06, $CHCl_3$) (lit. (10) mp 78–80°C, $[\alpha]_D$ +24°); ir, no C=O absorption; ^{1}Hmr ($CDCl_3$) δ: 3.15 (3H, s, OCH_3) and 3.20 ppm (3H, s, OCH_3); *m/e* 432.4 (M^+).

(b) 3-Methoxy-5α-cholest-2-ene

The procedure of Levisalles *et al.* (10) was modified. The dimethyl ketal (125 mg) from (*a*) was evaporatively distilled in a tube at 200°C/1 Torr over a period of ~7 h. The solidified distillate was recrystallized (4×) from ether–methanol to give 35 mg (30%) of colorless plates of the enol ether, mp 98–100°C, $[\alpha]_D^{19}$ +69° (*c* 1.04, $CHCl_3$) (lit. (10) mp 100–101°C, $[\alpha]_D$ +61°); ir ($CHCl_3$): 1680 cm^{-1} (C=C of enol ether); ^{1}Hmr ($CDCl_3$) δ: 3.50 (3H, s, OCH_3) and 4.50 ppm (1H, bd, C=CH) M^+ calcd. for $C_{28}H_{48}O$: 400.3705; found: 400.3708.

On a larger scale (500 mg) the reaction was conducted by heating the ketal in a sealed tube at 200°C for 10–20 h.

(c) 2α,3α-Dibromomethylene-3β-methoxy-5α-cholestane

The procedure of Levisalles *et al.* (10) was used. The reaction of 92 mg of enol ether from (*b*) with dibromocarbene gave 50 mg (38%) of adduct, mp 128–130°C, $[\alpha]_D^{19}$ +51.5° (*c* 1.10, $CHCl_3$) (lit. (10) mp 137–138°C, $[\alpha]_D$ +44°); ir, no C=C absorption; ^{1}Hmr ($CDCl_3$) δ: 3.51 ppm (3H, s, OCH_3). M^+ calcd. for $C_{29}H_{48}Br_2O$: 572.2051; found: 572.2037.

*(d) 3-Bromo-*A*-homo-5α-cholest-2-en-4-one*

The AgOAc-catalyzed solvolysis of the dibromocarbene adduct (50 mg) from (*c*) was carried out according to the published procedure (10) to yield 20 mg (47%) of bromo enone, mp 108–110°C (lit. (10) mp 112–112.5°C); ir ($CHCl_3$): 1680 cm^{-1} (conjugated C=O); ^{1}Hmr ($CDCl_3$) δ: 4.79 ppm (1H, t, $|J_{AX} + J_{BX}| = 15$ Hz, C=CH). M^+ calcd. for $C_{28}H_{45}BrO$: 478.2633; found: 478.2639.

(e) A-*Homo-5α-cholestan-4-one (***4a***)*

The bromo enone (200 mg) from (*d*) and a larger scale run was hydrogenated in benzene over 10% Pd/C and Na_2CO_3 according to ref. 10 to yield 166 mg (99%) of colorless plates of **4***a* after recrystallization from MeOH, mp 96–99°C, $[\alpha]_D^{20}$ +107° (*c* 1.02, $CHCl_3$) (lit. (10) mp 96–97.5°C, $[\alpha]_D$ +103°); ir ($CHCl_3$): 1695 cm^{-1} (7-ring C=O). M^+ calcd. for $C_{28}H_{48}O$: 400.3705; found: 400.3701.

Synthesis of Authentic A-*Homo-5α-cholestan-3-one (***3a***)*

*(a) 4-Chloro-*A*-homocholesta-4,5-dien-3-one*

This compound was prepared in 13% yield from 1.0 g of cholest-4-en-3-one without purification of the pyrrolidine dienamine or dichlorocarbene adduct according to the procedure of ref. 23. The 148 mg of colorless plates had mp 138–140°C, $[\alpha]_D^{19.5}$ −147°C (*c* 1.04, $CHCl_3$) (lit. (23) mp 137.5–140°C); ir ($CHCl_3$): 1660 (conjugated C=O) and 1610 cm^{-1} (conjugated C=C); ^{1}Hmr ($CDCl_3$) δ: 6.04 (1H, bs, C=CH) and 7.10 ppm (1H, s, C=CH—C=C). M^+ calcd. for $C_{28}H_{43}ClO$: 430.3002; found: 430.3005.

(b) A-*Homo-5α-cholestan-3-one (***3a***)*

The chlorodienone (148 mg) from (*a*) was hydrogenated by the procedure of ref. 23 to give, after thick-layer chromatography and recrystallization from ether–MeOH, 72 mg of colorless needles of **3***a*, mp 83–84°C, $[\alpha]_D^{19}$ −21.6° (*c* 1.00, $CHCl_3$) (lit. (23) mp 81–82.5°C, lit. (14) $[\alpha]_D$ −21°); ir ($CHCl_3$): 1698 cm^{-1} (7-ring C=O). M^+ calcd. for $C_{28}H_{48}O$: 400.3705; found: 400.3708.

Synthesis of Authentic A-*Homo-5β-cholestan-3-one (***3b***)*

(a) 3,3-Dimethoxy-5β-cholestane

A solution of 50 mg of **2***b* and 2 mg of *p*-TsOH in 2.5 mL of MeOH was refluxed for 5 h. After basification with NaOMe–MeOH the reaction mixture was diluted with ether, washed with water, dried, and concentrated to leave 50 mg of a colorless oil (49); ir ($CHCl_3$): faint C=O at 1710 cm^{-1}; ^{1}Hmr ($CDCl_3$) δ: 3.14 (3H, s, OCH_3) and 3.21 ppm (3H, s, OCH_3). M^+ calcd. for $C_{29}H_{52}O_2$: 432.3967; found: 432.3957.

Analysis by tlc showed ~5% of **2***b* remaining; the ketal was used without further purification.

(b) 3-Methoxy-5β-cholest-3-ene

The dimethyl ketal (50 mg) from (*a*) was evaporatively distilled in a tube at 200°C/1 Torr over a period of 3 h to give 35 mg of viscous oily enol ether containing ~5% of **2***b* (49); ir ($CHCl_3$): 1667 (C=C of enol ether) and faint C=O at 1710 cm^{-1}; ^{1}Hmr ($CDCl_3$) δ: 3.53 (3H, s, OCH_3) and 4.24 ppm (1H, bs, C=CH). M^+ calcd. for $C_{28}H_{48}O$: 400.3705; found: 400.3697.

(c) 3β,4β-Dibromomethylene-3α-methoxy-5β-cholestane

To a stirred (magnetic bar) solution of 92 mg of enol ether from (*b*) in 2.5 mL of cyclohexane at 0–5°C was added 272 mg of KO *t*Bu followed by addition of a solution of 540 mg of $CHBr_3$ in 1.5 mL of cyclohexane during 3 min. The reaction mixture was allowed to warm to room temperature and was stirred for 1 h. Dilution with ether, washing with water, drying, and concentration left a viscous oil which was chromatographed on a preparative plate developed twice with hexanes. Extraction of the band at R_f 0.38 gave 82 mg (62%) of colorless solid. Recrystallization from ether–MeOH (1×) and from $CHCl_3$–MeOH (2×) gave glistening colorless plates of the dibromocyclopropyl steroid, mp 140–143°C (dec.), $[\alpha]_D^{20}$ +66° (*c* 0.90, $CHCl_3$); ir, no C=C absorption; ^{1}Hmr ($CDCl_3$) δ: 3.51 ppm (3H, s, OCH_3). M^+ calcd. for $C_{29}H_{48}Br_2O$: 572.2051; found: 572.2026. *Anal.* calcd. for $C_{29}H_{48}Br_2O$: C 60.83, H 8.45; found: C 60.98, H 8.46.

*(d) 4-Bromo-*A*-homo-5β-cholest-4-en-3-one*

A mixture of 59 mg of dibromocyclopropyl compound from (*c*), 30 mg of AgOAc, 2 mL of HOAc, and 2 drops of water was stirred (magnetic bar) and refluxed for 2 h. After evaporation

of HOAc and water, the $CHCl_3$-soluble material was chromatographed on a preparative plate developed in benzene–hexanes (75:25). Extraction of the band at R_f 0.40 gave 33 mg (67%) of colorless solid. Recrystallization from ether–MeOH (3×) afforded 23 mg of colorless needles of the bromo enone, mp 108–110°C, $[\alpha]_D^{19.5}$ −124° (*c* 0.80, $CHCl_3$); ir ($CHCl_3$): 1680 cm^{-1} (conjugated C=O); ^{1}Hmr ($CDCl_3$) δ: 7.07 (1H, d, J = 6.5 Hz, C=CH) ppm. M^+ calcd. for $C_{28}H_{45}BrO$: 476.2654; found: 476.2663. *Anal.* calcd. for $C_{28}H_{45}BrO$: C 70.41, H 9.50; found: C 70.58, H 9.45.

(e) A-Homo-5β-cholestan-3-one (3b)

A mixture of 98 mg of bromo enone from (*d*), 50 mg of 10% Pd/C, 50 mg of K_2CO_3, and 6 mL of benzene was hydrogenated with stirring (magnetic bar) at room temperature and atmospheric pressure for 17 h. The filtered solution was concentrated and chromatographed on a preparative plate developed with benzene–ether (95:5). Extraction of the band at R_f 0.44 gave 80 mg of colorless viscous oil which crystallized on standing. Recrystallization (2×) of a 68-mg portion from ether–MeOH gave 26 mg of colorless needles of pure **3***b*, mp 55.5–56°C, $[\alpha]_D^{19}$ +89° (*c* 0.88, $CHCl_3$); ir ($CHCl_3$): 1695 cm^{-1} (7-ring C=O). M^+ calcd. for $C_{28}H_{48}O$: 400.3705; found: 400.3697. *Anal.* calcd. for $C_{28}H_{48}O$: C 83.93, H 12.07; found: C 84.15, H 11.87.

Baeyer–Villiger Reactions

(a) 5α-Cholestan-3-one

A solution of 100 mg (0.26 mmol) of **2***a*, 100 mg (75%, 0.43 mmol) of *m*-chloroperbenzoic acid, and 3 mL of $CHCl_3$ was allowed to stand at room temperature for 36 h. The solution was washed with 10% aqueous Na_2SO_3, 5% aqueous $NaHCO_3$, water, and dried. Concentration left 94 mg (90%) of colorless solid lactone mixture **5***a* + **6***a* which gave a single tlc spot more polar than **2***a*, ir ($CHCl_3$): 1725 cm^{-1} (lactone C=O), *m/e* 402 (M^+). ^{13}C peaks integrated: δ 64.7 (C-2 of **6***a*) and 70.0 ppm (C-4a of **5***a*).

(b) 5β-Cholestan-3-one

A 100-mg sample of **2***b* oxidized as in (*a*) yielded 92 mg (88%) of colorless solid lactone mixture **5***b* + **6***b*; ir ($CHCl_3$): 1720 cm^{-1} (lactone C=O); *m/e* 402 (M^+). ^{13}C peaks integrated: δ 63.3 (C-2 of **6***b*) and 70.5 ppm (C-4a of **5***b*).

(c) 17β-Hydroxy-5α-androstan-3-one

A 50-mg sample (0.19 mmol) of **2***c* was oxidized with 48 mg (0.21 mmol) of *m*-chloroperbenzoic acid in 3 mL of $CHCl_3$ for 24 h to yield 48 mg (92%) of colorless solid lactone mixture **5***c* + **6***c* which contained ~20% of **2***c*; ir ($CHCl_3$) 1730 cm^{-1} (lactone C=O); *m/e* 306 (M^+). ^{13}C peaks integrated: δ 64.7 (C-2 of **6***c*) and 70.0 ppm (C-4a of **5***c*).

When 50 mg (0.19 mmol) of **2***c* was oxidized with 100 mg (0.43 mmol) of *m*-chloroperbenzoic acid for 2.5 days, the product was ~85% 17-oxo-A-ring lactones; *m/e* 304 (85%) and 306 (15%) (M^+).

(d) 5α-Cholestan-3-one + CF_3CO_3H

A solution of CF_3CO_3H made by stirring 0.1 mL of 63% H_2O_2 and 0.4 mL of $(CF_3C{=}O)_2O$ in 1 mL of CH_2Cl_2 at 5°C for 10 min was added to a solution of 125 mg of **2***a* in 2 mL of CH_2Cl_2 containing 250 mg of suspended Na_2HPO_4. The reaction was stirred (magnetic bar) at room temperature for 2 h. The organic solution was washed with 10% aqueous Na_2CO_3 and water, dried, and concentrated to leave 123 mg (95%) of oily solid lactone mixture **5***a* + **6***a* which was used for ^{13}C integration of the isolated peaks at δ 64.7 (C-2 of **6***a*) and 70.0 ppm (C-4a of **5***a*).

Authentic 4-Oxa-A-homo-5α-cholestan-3-one (5a)

(a) 2α-Bromo-A-homo-4-oxa-5α-cholestan-3-one

A solution of 200 mg (0.43 mmol) of 2α-bromo-5α-cholestan-3-one and 500 mg (~2 mmol) of *m*-chloroperbenzoic acid (Aldrich, 75%) in 5 mL of $CHCl_3$ was allowed to stand at room temperature. At the end of 4 h, tlc showed considerable starting material remaining, and two more 500-mg portions of the peracid were added during the next 4 h to increase the reaction rate. The $CHCl_3$ solution was washed thoroughly with 10% aqueous Na_2SO_3, saturated aqueous $NaHCO_3$ and water. Evaporation of the dried solution left 207 mg (100%) of colorless solid which gave a single tlc spot more polar than starting material. A 125-mg portion dissolved in 1 mL of CCl_4 was chromatographed on a column of 3 g of silica gel. Elution with hexanes–benzene (45:55) gave 79 mg of colorless solid. Recrystallization from acetone–hexanes (1×) and from ether – petroleum ether (1×) gave 34 mg of colorless needles of *bromo lactone*, mp 186–189°C, $[\alpha]_D^{20}$ −5.4° (*c* 1.60, $CHCl_3$) (lit. (40), mp 192–193°C, $[\alpha]_D$ −4.5°); ir ($CHCl_3$): 1750 cm^{-1} (lactone C=O); ^{1}Hmr ($CDCl_3$) δ: 3.82 (1H, d, 4a-H), 4.34 (1H, dd, 4a-H), and 4.96 ppm (1H, dd, 2β-H). The bromo lactone was a single pure isomer according to its ^{13}Cmr spectrum.

(b) Reductive Debromination

The method of Bolliger *et al.* (40) was used. A solution of $CrCl_2$ was made from 1.0 g of $CrCl_3{\cdot}6H_2O$, 2.0 g of Zn, and 1.6 g of $HgCl_2$ (50). To this stirred solution under N_2 was added a solution of 100 mg of the bromo lactone from (*a*) in 4 mL of HOAc, and the reaction mixture was stirred for 12 h. The product was isolated by ether extraction, and the ether solution was washed with aqueous $NaHCO_3$ and water. Evaporation of the dried solution left 64 mg (77%) of colorless solid. Recrystallization (3×) from $CHCl_3$–CH_3OH gave 23 mg of colorless needles of lactone **5***a*, mp 192–195°C (lit. (40), mp 199–200°C); ir ($CHCl_3$): 1725 cm^{-1} (lactone C=O); ^{1}Hmr ($CDCl_3$) δ: 3.68 (1H, d, 4a-H) and 4.29 ppm (1H, dd, 4a-H). M^+ calcd. for $C_{27}H_{46}O_2$: 402.3498; found: 402.3501. The ^{13}Cmr spectrum was that of a single lactone.

Schmidt Reactions

(a) 5α-Cholestan-3-one

The procedure of Doorenbos and Wu (43) was used. To a mixture of 1.25 g of polyphosphoric acid and 50 mg (0.13 mmol) of **2***a* at 65°C was added 10 mg (0.15 mmol) of NaN_3; the 65°C temperature was maintained for 12 h. After addition of ice, the mixture was basified with 50% aqueous NaOH and extracted with $CHCl_3$. The organic layer was washed with water, dried and concentrated. Since tlc examination of the product revealed some unreacted **2***a*, it was recycled through a second treatment with HN_3 as above to give 35 mg (67%) of colorless solid lactam mixture **7***a* + **8***a* (free of **2***a*), mp 262–264°C with a phase change ~230°C; ir ($CHCl_3$): 3430 (NH) and 1660 cm^{-1} (amide C=O); *m/e* 401 (M^+). ^{13}C peaks for integration: δ 21.0, 35.3, 44.4, 49.6, and 53.8 ppm from **7***a*; δ 21.3, 34.7, 42.0, 43.3, and 54.1 ppm from **8***a* (Table 1, entry 13).

(b) 5β-Cholestan-3-one

A 50-mg sample of **2***b* under the reaction conditions in (*a*) gave complete reaction after one treatment and yielded 45 mg (86%) of colorless solid lactam mixture **7***b* + **8***b* (free of **2***b*); ir ($CHCl_3$): 3430 (NH) and 1660 cm^{-1} (amide C=O); *m/e* 401 (M^+). ^{13}C peaks for integration: δ 27.0, 38.8, 42.2, 44.1, and 45.5 ppm from **7***b*; δ 26.0, 36.8, and 43.0 ppm from **8***b* (Table 1, entry 22).

Authentic Lactams 8a and 8b

(a) 3-Aza-A-homo-4a-cholesten-4-one (Part Structure 20)

The Beckmann rearrangement procedure of Mazur (51) was adapted. To a stirred (magnetic bar) solution of 300 mg of the oxime of 4-cholesten-3-one (~30% *syn*, ~70% *anti* OH:C=C)

in 4.5 mL of dry dioxane at 10°C was added 0.9 mL of freshly distilled $SOCl_2$. The cooling bath was allowed to warm to room temperature, and the dark yellow solution was stirred for 2 h. After addition of excess 5% aqueous $NaHCO_3$, the product was extracted with ether. Evaporation of the washed and dried organic solution left 285 mg of tan oily solid which was chromatographed on two preparative plates developed in EtOAc. Extraction of the band visible under uv on the lower half of the plate gave 160 mg of off-white solid. Recrystallization (2×) from benzene–acetone gave colorless granules of the *lactam* **20**, mp 245–247°C with a phase change ~220°C, $[\alpha]_D^{20}$ +24° (*c* 1.40, $CHCl_3$) (lit. (44, 52), mp 252–256°C, 255–260°C, $[\alpha]_D$ +20°); uv (MeOH): 222 (22 000) and 247 nm (20 000); ir ($CHCl_3$): 3440 (NH), 1660 (C=O), and 1625 cm^{-1} (conjugated C=C); ^{1}Hmr ($CDCl_3$) δ: 3.18 (2H, bm, O=$CNCH_2$), 5.75 (1H, bs, C=CH), and 6.55 ppm (1H, bs, NH). M^+ calcd. for $C_{27}H_{45}NO$: 399.3501; found: 399.3498.

*(b) 3-Aza-*A*-homo-5α-cholestan-4-one (**8**a)*

To a mixture of 100 mg of 10% Pd/C catalyst and 100 mg of powdered KOH in 5 mL of MeOH stirred (magnetic bar) under H_2 was added a solution of 100 mg of unsaturated lactam **20** in 25 mL of MeOH. After 12 h the catalyst was removed by filtration and the solvent evaporated. The residual solid was dissolved in $CHCl_3$, and the solution was washed with water, dried, and concentrated. Recrystallization (2×) from MeOH–$CHCl_3$ gave 42 mg of colorless granules of pure *lactam* **8***a*, mp 260–280°C (dec. and subl.) with a phase change to needles at ~210°C; when the melting point was taken in a sealed capillary, a narrower range, mp 280–282°C (dec.), was observed; $[\alpha]_D^{20}$ +35° (*c* 1.60, $CHCl_3$) (lit. (44) mp 294–296°C, $[\alpha]_D$ +41°); uv (MeOH) rising end absorption only; ir ($CHCl_3$): 3420 (NH) and 1660 cm^{-1} (amide C=O); ^{1}Hmr ($CDCl_3$) δ: 2.6–3.5 (2H, bm, O=$CNCH_2$) and 6.47 ppm (1H, bs, NH). M^+ calcd. for $C_{27}H_{47}NO$: 401.3658; found: 401.3655.

*(c) 3-Aza-*A*-homo-5β-cholestan-4-one (**8**b)*

To a mixture of 50 mg of PtO_2 in 1.5 mL of HOAc stirred (magnetic bar) under H_2 was added a solution of 140 mg of unsaturated lactam **20** in 4 mL of HOAc. After 18 h the catalyst was removed by filtration, and the product was isolated by partition between ether and water. The semi solid product was chromatographed on two preparative plates developed (3×) in EtOAc–MeOH (97:3). Extraction of the band at R_f 0.82 produced 78 mg of colorless solid which was recrystallized (2×) from MeOH to give 49 mg of colorless plates of pure *lactam* **8***b*, mp 230–232°C, $[\alpha]_D^{20}$ + 56.4° (*c* 1.00, $CHCl_3$); uv (MeOH) rising end absorption only; ir ($CHCl_3$): 3420 (NH) and 1655 cm^{-1} (amide C=O); ^{1}Hmr ($CDCl_3$) δ: 3.08 (2H, m, O=$CNCH_2$) and 6.18 ppm (1H, bs, NH). M^+ calcd. for $C_{27}H_{47}NO$: 401.3658; found: 401.3663.

Both **8***a* and **8***b* gave only 27 signals each in their ^{13}Cmr spectra.

Acknowledgements

We would like to thank the National Research Council of Canada for financial support, Cheryl DuCharme for the ^{13}Cmr spectra, Heather Schroeder for the 100 MHz ^{1}Hmr spectra, and Doug Hairsine for the mass spectra.

1. V. Dave and J. B. Stothers. Can. J. Chem. This issue.
2. M. W. Goldberg and H. Kirchensteiner. Helv. Chim. Acta, **26**, 288 (1943).
3. N. A. Nelson and R. N. Schut. J. Am. Chem. Soc. **81**, 6486 (1959).
4. J. B. Jones and P. Price. Can. J. Chem. **44**, 999 (1966).
5. G. D. Meakins and D. J. Morris. J. Chem. Soc. C, 394 (1967).
6. M. Nussim and Y. Mazur. Tetrahedron, **24**, 5337 (1968).
7. J. B. Jones and J. M. Zander. Can. J. Chem. **46**, 1913 (1968).
8. J. B. Jones and J. M. Zander. Can. J. Chem. **47**, 3501 (1969).
9. J. B. Jones and P. Price. Chem. Commun. 1478 (1969).
10. J. Levisalles, G. Teutsch, and I. Tkatchenko. Bull. Soc. Chim. Fr. 3194 (1969).
11. P. A. Hart and R. A. Sandmann. Tetrahedron Lett. 305 (1969).
12. H. Velgová and V. Černý. Coll. Czech. Chem. Commun. **35**, 2408 (1970).
13. J. D. Ballantine, J. P. Ritchie, and P. J. Sykes. J. Chem. Soc. C, 736 (1970).
14. M. Ephritikhine and J. Levisalles. Bull. Soc. Chim. Fr. 4331 (1971).
15. J. B. Jones and P. Price. Tetrahedron, **29**, 1941 (1973).
16. C. D. Gutsche and D. Redmore. Carbocyclic ring expansion reactions. Academic Press, New York. 1968. p. 76, *footnote* 232, and p. 87.
17. S. M. Sine, T. E. Conklin, and W. H. Okamura. J. Org. Chem. **39**, 3797 (1974).
18. F. W. Wehrli. Adv. Mol. Relaxation Processes, **6**, 149 (1974).
19. F. W. Wehrli and T. Wirthlin. Interpretation of carbon-13 nmr spectra. Heyden, London. 1976. p. 264.
20. V. Dave and E. W. Warnhoff. J. Org. Chem. **43**, 4622 (1978).
21. G. N. La Mar. J. Am. Chem. Soc. **93**, 1040 (1971).
22. J. W. Blunt and J. B. Stothers. Org. Magn. Reson. **9**, 439 (1977).
23. S. A. G. de Graaf and U. K. Pandit. Tetrahedron, **30**, 1115 (1974).
24. R. G. Carlson and N. S. Behn. J. Org. Chem. **33**, 2069 (1968).
25. W. T. Tai and E. W. Warnhoff. Can. J. Chem. **42**, 1333 (1964).
26. W. L. Mock and M. E. Hartman. J. Org. Chem. **42**, 459 (1977).
27. V. Burckhardt and T. Reichstein. Helv. Chim. Acta, **25**, 821, 1434 (1942).
28. V. Prelog, L. Ruzicka, P. Meister, and P. Wieland. Helv. Chim. Acta, **28**, 618 (1945).
29. L. Ruzicka, V. Prelog, and P. Meister. Helv. Chim. Acta, **28**, 1651 (1945).
30. E. Lederer, F. Marx, D. Mercier, and G. Perot. Helv. Chim. Acta, **29**, 1354 (1946).
31. S. Mori and F. Mukawa. Proc. Jpn. Acad. **31**, 532 (1955).
32. C. W. Shoppee and J. C. P. Sly. J. Chem. Soc. 3458 (1958).
33. N. L. Allinger and S. Greenberg. J. Org. Chem. **25**, 1399 (1960).
34. G. R. Pettit, B. Green, T. R. Kasturi, and U. R. Ghatak. Tetrahedron, **18**, 953 (1962).
35. S. Hara and N. Matsumoto. Yakugaku Zasshi, **85**, 48 (1965).
36. S. Hara, N. Matsumoto, and M. Takeuchi. Chem. Ind. (London), 2086 (1962).
37. H. Heymann and L. F. Fieser. Helv. Chim. Acta, **35**, 631 (1952).
38. T. Rull and G. Ourisson. Bull. Soc. Chim. Fr. 1579 (1958).
39. J. B. Stothers. Carbon-13 nmr spectroscopy. Academic Press, New York, NY. 1972. pp. 139–142.
40. J. E. Bolliger and J. L. Courtney. Aust. J. Chem. **17**, 440 (1964).

41. G. I. KOLDOBSKII, G. F. TERESHCHENKO, E. S. GERASIMOVA, and L. I. BAGAL. Russ. Chem. Rev. **40**, 835 (1971).
42. P. A. S. SMITH. *In* Molecular rearrangements. *Edited by* P. de Mayo. Interscience Publishers, New York, NY. 1963. pp. 507–527.
43. N. J. DOORENBOS and M. T. WU. J. Org. Chem. **26**, 2548 (1961).
44. C. W. SHOPPEE, G. KRÜGER, and R. N. MIRRINGTON. J. Chem. Soc. 1050 (1962).
45. I. FLEMING and R. B. WOODWARD. J. Chem. Soc. Perkin I, 1653 (1973).
46. J. L. GOUGH, J. P. GUTHRIE, and J. B. STOTHERS. J. Chem. Soc. Chem. Commun. 979 (1972).
47. A. M. MAIONE and M. G. QUAGLIA. Chem. Ind. (London), 230 (1977).
48. J. C. CRAIG and A. R. NAIK. J. Am. Chem. Soc. **84**, 3410 (1962).
49. D. N. KIRK and D. R. A. LEONARD. J. Chem. Soc. Perkin I, 1836 (1973).
50. G. ROSENKRANZ, O. MANCERA, J. GATICA, and C. DJERASSI. J. Am. Chem. Soc. **72**, 4077 (1950).
51. R. H. MAZUR. J. Org. Chem. **28**, 248 (1963).
52. N. J. DOORENBOS and H. SINGH. J. Pharm. Sci. **51**, 418 (1962).

Total synthesis of spirobenzylisoquinoline alkaloids. Part V. Generalized approach to the complete set of alkaloids[1,2]

DAVID DIME AND STEWART MCLEAN

Department of Chemistry, University of Toronto, 80 St. George Street, Toronto, Ont., Canada M5S 1A1

Received August 23, 1978

DAVID DIME and STEWART MCLEAN. Can. J. Chem. 57, 1569 (1979).

The strategy outlined previously has been developed to provide, in principle, routes to any known spirobenzylisoquinoline alkaloid. The generality has been demonstrated by the synthesis of the racemic forms of corydaine, yenhusomidine, corpaine, sibiricine, and raddeanone.

DAVID DIME et STEWART MCLEAN. Can. J. Chem. 57, 1569 (1979).

On a développé la stratégie décrite antérieurement afin de proposer en principe des voies permettant d'atteindre tous les alcaloïdes connus derivés de la spirobenzylisoquinoléine. On a démontré la généralité de la méthode par la synthèse des formes racémiques de la corydaïne de la yenhusomidine, de la corpaïne, de la sibiricine et de la raddéanone.

[Traduit par le journal]

It has been our goal to develop a synthetic strategy which could, with appropriate tactical modifications, provide a totally synthetic route to any possible spirobenzylisoquinoline alkaloid. We have previously outlined the strategy and described its application to the successful syntheses of (±)-ochotensimine (**1**) (1) and (±)-ochrobirine (**2**) (2). Alkaloids such as corydaine (**3**), yenhusomidine (**4**), sibiricine (**5**), and raddeanone (**6**) present a more challenging target since control of both functionality and stereochemistry at C-9 and C-14 is required in the synthesis. We have recently made a preliminary report (3) of our partial success in reaching this target with the syntheses of (±)-corydaine and (±)-yenhusomidine. We report now a more detailed account of these syntheses and an account of further developments that have allowed us to complete the generalization of the synthetic approach.

The synthetic strategy was based on the formation of the spirobenzylisoquinoline skeleton (**7**) by a Pictet–Spengler reaction of a suitably substituted indanedione (**8**) with an appropriate phenylethylamine derivative (**9**). This, in principle, maintains the functional differentiation between C-9 and C-14 and allows the development of the required functional groups with control of stereochemistry. For the synthesis of the alkaloids with two oxygen functions on the five-membered ring we chose to use the bromoindanedione **8** (X = Br), and 3,4-dihydroxyphenylethylamine **9** (R′ = R″ = H); the latter was used since our earlier work with this series of compounds indicated that, without the hydroxyl group *para* to the site of ring closure, yields in the Pictet–Spengler reaction were unsatisfactory. The bromoindanedione was unstable and was used as soon as it had been prepared. The product of the Pictet–Spengler reaction was amorphous and could not be characterized completely but on the basis of the eventual successful outcome of the synthetic sequence, it was assumed to be **7** (R = R′ = R″ = H; X = Br). Various spectroscopic data were in accord with this proposal and, furthermore, the nmr evidence indicated that the product was a single epimer but no conclusion could be reached from this evidence about its configuration. Displacement of the halogen by an external nucleophile was unsuccessful under a wide variety of conditions and a plan was then devised in which the nitrogen atom was acylated, with the intention that this would provide a nucleophile capable of partaking in an intramolecular displacement. It was recognized that this should be successful only if the intermediate were the correct epimer with the halogen *trans* to the nitrogen. The *N*-formyl derivative was treated with silver acetate in aqueous acetic acid and the desired transformation to an alcohol with the hydroxyl group *cis* to the nitrogen did indeed take place. This successful outcome led us to propose that the reaction had followed the anticipated path (Scheme 1).

Our present study was concerned first with probing further the apparent high degree of stereoselectivity in the Pictet–Spengler reaction that seemed to lead to a single epimer. Unfortunately, we have not made significant progress regarding this question but we have made a number of surprising discoveries that force us to revise our account (2) of the course of the

[1]Dedicated to the memory of Dr. R. H. F. Manske who isolated the first spirobenzylisoquinoline alkaloids.

[2]Taken from the Ph.D. Thesis of David Dime, University of Toronto, Toronto, Ont. 1978.

0008-4042/79/131569-10$01.00/0

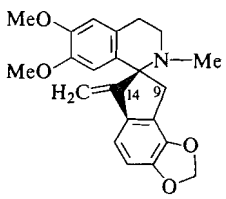

1[3]

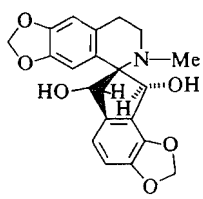

2

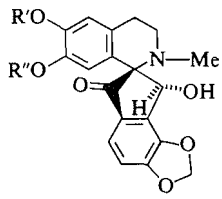

3 R′ + R″ = CH_2
4 R′ = R″ = Me
17 R′ = Me; R″ = H

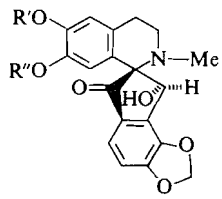

5 R′ + R″ = CH_2
6 R′ = R″ = Me

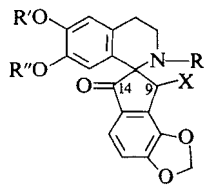

7

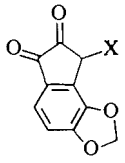

8

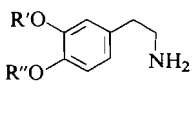

9

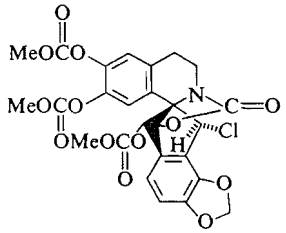

10

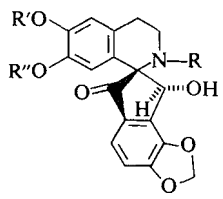

11 R = CHO; R′ = R″ = MeOCO
12 R = CHO; R′ + R″ = CH_2
13 R = CHO; R′ = R″ = Me
14 R = H; R′ + R″ = CH_2
16 R = R″ = H; R′ = Me

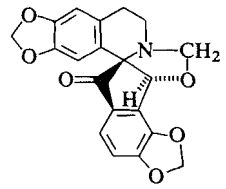

15

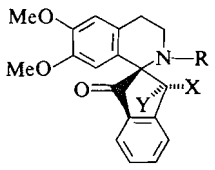

18 R = CHO; X = OH; Y = H
19 R = CHO; X = H; Y = OH
20 R = Me; X = OH; Y = H
21 R = Me; X = H; Y = OH

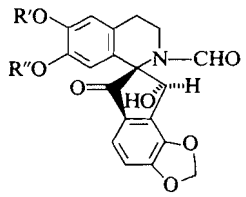

22 R′ = R″ = Me
23 R′ = R″ = CH_2

reactions we have described. Most of the compounds at this stage of the synthesis have been amorphous, and often unstable and difficult to characterize adequately. In a modification of the procedure we used to protect the phenolic hydroxyl groups, the Pictet–Spengler product was treated with methyl chloroformate under conditions that also carbomethoxylated the nitrogen. For the first time a beautifully crystalline product was obtained and presumed to be **7** (R = R′ = R″ = COOMe; X = Br). This was considered to be ideal for an investigation of its stereochemistry by X-ray crystal analysis. During this analysis (4) several disturbing features unfolded, not the least of which was the discovery that the molecule contained chlorine, not bromine. The final structure determination by the X-ray method showed further that the compound was not a ketone and not a simple urethane but had the more complex bridged structure **10**. This compound and its mode of formation are interesting in their own right, but the most significant feature for our present concern is that the configuration at C-9 (with a Cl substituent) is opposite to that we had assigned to related compounds in the original *N*-formyl series where we believed that C-9 carried a Br substituent. Furthermore, the chlorine was displaced by the treatment of **10** with silver fluoroborate in aqueous acetone. The product could not be properly characterized but it appears to be a mixture, possibly of epimers; the nmr spectrum, for example, shows signals appropriate for two kinds of C-9 protons (τ 4.47, 4.76) with a combined area of one proton. Nevertheless, when this intermediate was subjected to the sequence of reactions used in the *N*-formyl series (described below), the alkaloids corydaine (**3**) and yenhusomidine (**4**) were isolated. The most important observation for the present is that the displacement reaction took place on a molecule with the C-9 configuration of **10** and at

[3]The absolute configurations of natural (+)-ochotensimine (**1**) and (+)-ochrobirine (**2**) have been determined (12). Other configurations depicted in this paper are arbitrarily chosen for convenience and uniformity of presentation. All synthetic compounds are racemic.

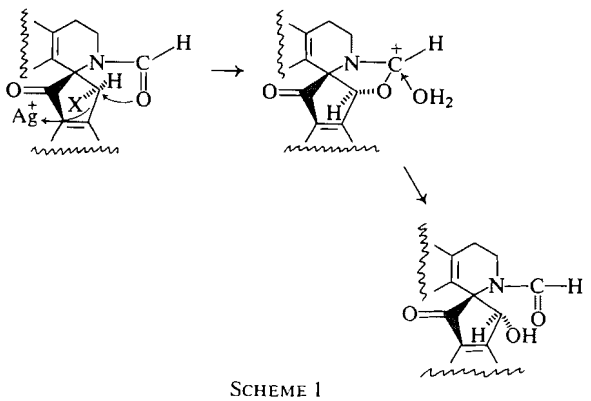

SCHEME 1

least a substantial part of the product was formed with retention of configuration.

These disconcerting results led us to examine more closely our intermediates in the original sequence (including a series of model compounds (2)), particularly with respect to the question of how and when chlorine had replaced bromine in the molecule. It became apparent that our original observation that compounds of form **7** are not susceptible to simple S_N2 displacement of the halogen was indeed correct and that replacement of bromine by chlorine had not taken place at this stage. The precursor **8** (X = Br) is, however, extremely susceptible to displacement of bromine by chlorine when treated with hydrochloric acid; the extreme ease of this reaction leads us to assume that it takes place by addition of HCl to the enol form of **8** followed by elimination of HBr from the adduct. It follows that the replacement of bromine by chlorine in the synthetic sequence took place through the action of the HCl used in the Pictet–Spengler reaction. As we have already pointed out, the products could not be adequately purified and were deemed unsuitable for microanalysis; no molecular ions were observed in the high resolution mass spectra and the ions of highest mass appeared to correspond to M − Br. Subsequently, differential Br/Cl analyses were carried out by standard procedures and it became clear that all of the Pictet–Spengler products were mixtures of bromo and chloro compounds, usually containing a substantial excess of the chloro compound; since replacement took place before the spiro product had formed and not after, the Br/Cl ratio in a given run depended on how long **8** had been in contact with HCl during the Pictet–Spengler reaction.

It follows that where we have previously described intermediates of form **7** (X = Br) we should replace this description by **7** (X = Cl/Br). It also follows that we can not come to a firm conclusion about the configuration of these compounds. It is still true that the nmr spectra suggest that only one epimer is present but the previous argument that led to the conclusion that this was the epimer sterically suitable for internal displacement is no longer valid. The X-ray crystal structure analysis of **10** provides the only firm evidence for the stereochemistry of any halo compound in this series, and this compound has the configuration opposite to that proposed previously (2), yet it still undergoes replacement of Cl by OH under the conditions described previously. A more satisfactory explanation for the success of this reaction must therefore be found.

The key reagent in the displacement reaction is the silver salt, which undoubtedly serves to 'pull off' the halogen from C-9. However, the 'push' from the *N*-formyl group shown in Scheme 1 is not obligatory. Compound **10** at least has the wrong configuration for this and still undergoes the reaction. Nevertheless, the presence of the *N*-acyl group is necessary for a successful completion of the desired reaction but we believe now that it serves rather a different function: the amide resonance makes the lone pair of electrons on nitrogen unavailable for direct attack at the carbonium centre (incipient or otherwise); when the amine is not acylated, this attack does take place and the aziridinium ion formed can subsequently reopen in a direction that leads to rearranged products. We also believe that the stereospecific formation of the hydroxyl group *cis* to the nitrogen shows that, once the halogen has been removed far enough, the ionic intermediate in Scheme 1 is indeed formed by internal attack of the electrons on the *N*-acyl oxygen atom, and that the remainder of the sequence proceeds as originally proposed. (It is possible that the bridged intermediate derived from 10 is not susceptible to this internal attack and a mixture of epimers results.) Our original synthetic sequence thus remains an experimentally viable route to intermediates with the stereochemistry of **11**, albeit for reasons different in detail from those originally postulated.

The continuation of the synthetic sequence required at this stage the deprotection of the catechol system and its conversion to the derivative present in the target alkaloid; the example of the formation of the methylenedioxybenzene **12** required for ochrobirine (**2**) has already been described (2). The dimethoxy analog **13** is available by methylation of the catechol with diazomethane. It is worth noting here that it is desirable to protect the sensitive β-hydroxy ketone during hydrolysis of the protecting groups under basic conditions, and that it is undesirable to hydrolyze the *N*-formyl group before methylation of the phenolic hydroxyl groups since the free amine in these compounds is especially susceptible to *N*-methylation by diazomethane.

In our earlier work (2), a difficulty arose at this stage and severely limited the generality of the synthesis: the Eschweiler–Clarke reaction, which had worked well in the ochotensimine synthesis (1), failed to convert **14**, the hydrolysis product of **12**, to corydaine (**3**). Direct reduction of the *N*-formyl group of **12** to *N*-methyl was accomplished with lithium aluminium hydride but inevitably the ketone was reduced at the same time. This provided a successful synthesis of ochrobirine (**2**) but unhappily removed the functional differentiation at C-9 and C-14 that we had carefully preserved through the synthesis, and syntheses by this route of alkaloids having one ketone and one alcohol function at these sites became impossible. It was presumed that the failure of the Eschweiler–Clarke reaction could be attributed to the interaction of the C-14 hydroxyl group with the moiety formed by reaction of formaldehyde with the adjacent amine centre. Confirmation of this proposal was forthcoming when a crystalline oxazolidine (**15**) was isolated when the amine **14** was treated with formaldehyde in the absence of formic acid. A variant of the Eschweiler–Clarke reductive methylation could now be designed: sodium cyanoborohydride reduced the oxazolidine in an acidic solution, where it presumably exists in equilibrium with the open hydroxy imminium intermediate, and the desired *N*-methylated product was obtained, with regeneration of the C-9 alcohol *cis* to the nitrogen and without reduction of the C-14 ketone. A general route to alkaloids of this substitution pattern was thus available and it was applied successfully to the synthesis of (±)-corydaine (**3**) and (±)-yenhusomidine (**4**).

One step in the route to yenhusomidine was the hydrolysis of the *N*-formyl intermediate **13** under acidic conditions. This normally proceeded without difficulty and in high yield, but on one occasion about half of the product had suffered hydrolysis of a methoxyl group as well as hydrolysis of the amide. The nmr spectrum showed that it was the higher field methoxyl group that had disappeared and that it was probably the phenol **16** that had been produced. This was the only occasion when the mild hydrolysis conditions normally used gave significant amounts of phenol but careful examination of the spectra of other batches of hydrolyzed material showed that small amounts had been produced in other runs. However, the production of a significant amount of this phenol on one occasion led us to seek and find more vigorous hydrolysis conditions under which significant amounts of the phenol could be obtained reproducibly. We are unable to advance a convincing argument based on either electronic or steric features to account for the observed selective hydrolysis of one methoxyl group; we would certainly not have been able to predict it. Compounds of form **7** (R′ = H; R″ = Me) are available from the Pictet–Spengler reaction (see above) whereas those of form **7** (R′ = Me; R″ = H) are not. The result we have observed serendipitously opens a route to the alkaloids with the latter substitution pattern. Thus when the phenol **16** was carried through the modified reductive methylation sequence described above, the alkaloid (±)-corpaine (**17**) was obtained.

Once we had shown that our synthetic strategy could provide routes to the alkaloids corydaine, yenhusomidine, and corpaine, we had to face an important stereochemical question, one which had been apparent to us from the start. These alkaloids are β-hydroxy ketones and epimers are possibly susceptible to equilibration by a sequence of retro-aldol and aldol condensations. If equilibration did take place, our earlier efforts to maintain steric control of reactions would have been wasted and the stereospecificity of our synthesis would be an illusion since the stereochemistry of the final products would simply be under the control of thermodynamics. A report from the laboratories of MacLean and Manske (5) indicated that our worst fears were justified: in the course of an imaginative and elegant synthesis of the spirobenzylisoquinoline alkaloids, they showed that the aldol–retro-aldol equilibration does take place under basic conditions and, even worse from our point of view, the more stable epimers are those such as **3** which we had synthesized. At this point we were pleased to receive a sample of natural corydaine (**3**) from the laboratory of M. E. Perel'son and to find that this material was optically active; this allowed us to dispose of the suggestion that all alkaloids of this group would probably be found to have racemized by equilibration during the isolation process. We were also able to follow semiquantitatively the rate of racemization of the alkaloid under a number of conditions. Racemization took place rapidly, as expected, in alkaline methanol, but in neutral or acidic solution the rate was very much lower. We were also pleased to find that racemized alkaloid showed mp 126–130°C, thus removing the apparent discrepancy between natural and synthetic material in this physical constant. The main value of this study was, however, the demonstration that the alkaloid could survive the conditions of the final steps of our synthetic sequence without equilibrating.

A way of testing more searchingly the stereospecificity of the final steps of our synthesis now presented itself and, at the same time, pointed to a procedure that could complete the generalization of

our synthesis and make available the epimers, such as **5** and **6**, that had initially appeared unavailable by our route. The model compound **18** was prepared from precursors described previously (2) in order to investigate the proposed procedure.

The ir spectrum of **18** in chloroform shows a broad peak at 2.84 μ, indicating that the hydroxyl group is hydrogen bonded. However, as the solution is progressively diluted, this band is replaced by a sharp peak at 2.76 μ and at high dilution the replacement is complete; as this change occurs, an amide peak at 6.07 μ grows at the expense of a peak at 6.24 μ and at high dilution the 6.24 μ peak is absent. It follows that the hydrogen bonding is not intramolecular and the factor that is believed to stabilize the *cis*-hydroxy amines such as **3** (5) is absent. When **18** was heated with anhydrous potassium carbonate in dry dimethylformamide, a mixture of the epimers **18** and **19** (the ratio varied with reaction conditions and was not optimized; a typical value is 40:60) was obtained. Partial separation of the mixture was possible by fractional crystallization; a crystalline sample of **18** was recovered but even the best sample of **19** was not completely pure and failed to crystallize, and in accord with previous observations (5), **19** readily underwent epimerization during crystallization attempts. The original mixture was, therefore, subjected to the sequence of reactions described for converting the *N*-formyl group to *N*-methyl. Hydrolysis of the amides in acidic methanol solution required a longer reflux time than in previous cases, probably because the *trans* isomer was not so readily hydrolyzed. The epimeric ratio remained constant, as judged by nmr spectroscopy, during this process. The mixture of amines was treated with formaldehyde in methanol, the pH was brought to 3, and reduction with sodium cyanoborohydride was carried out. A mixture of the required *N*-methyl compounds was obtained and no appreciable change in the epimeric ratio was observed.

Epimerization of the intermediates **12** and **13**, required for the synthesis of the actual alkaloids, proved to be more difficult than in the model series and it was necessary to modify the conditions used. The *N*-formyl compound was treated with lithium diisopropylamide and hexamethylphosphoramide in tetrahydrofuran at −78°C; the reaction mixture was then allowed to warm to room temperature and was stirred overnight. The mixture of epimers produced was then converted to the *N*-methyl analogs by the same reaction sequence as that used in the model series. The dimethoxy compound **13**, under the epimerizing conditions described, was converted to a mixture of epimers which contained 30% of the *trans* isomer **22**. This mixture afforded, after hydrolysis and methylation, the alkaloids (±)-yenhusomidine (**4**) and (±)-raddeanone (**6**), still in the ratio 70:30. Separation was again difficult because of the ease with which epimerization took place; a pure sample of the more stable epimer, yenhusomidine, could be obtained by fractional crystallization but only spectroscopic evidence could be obtained that the mother liquors were enriched in raddeanone and separation was effected only at an analytical level by hplc. In the same way **12** was converted through a mixture (70:30) of the starting compound and its epimer **23** to a mixture of (±)-corydaine (**3**) and (±)-sibiricine (**5**) in the same ratio. Pure corydaine could be isolated by fractional crystallization but, once again, sibiricine could be separated only at an analytical level by hplc of the mother liquors.

The success of the strategy has thus been established. It is capable, in principle, of providing rational synthetic routes to spirobenzylisoquinoline alkaloids of any substitution pattern or stereochemistry and it has been reduced to practice with the syntheses of the racemic modifications of ochotensimine (1), ochrobirine (2), corydaine, yenhusomidine, sibiricine, raddeanone, and corpaine by us and of ochotensine (6, 7), fumaricine, fumaritine, and fumariline (8) by others using the same approach.

Experimental

Melting points were determined on a Thomas-Kofler micro hot stage. Spectrometers used were a Perkin-Elmer 137 for ir spectra, a Unicam SP800A for uv spectra, a Varian T-60, Bruker WP-80, or Varian HA-100 for proton nmr spectra, a CEC 21-490 for mass spectra, an AEI MS-902 for accurate mass measurements, and a Roussel-Jouan Dichrographe II for cd spectra. Unless otherwise indicated, chloroform solutions were used to obtain ir spectra and the wavelengths (μ) of selected absorptions are reported, methanol solutions were used to obtain uv spectra and the wavelengths (λ_{max}, nm) of significant peaks are reported followed in parentheses by the extinction coefficient (ε), and chloroform-*d* solutions (with tetramethylsilane as internal standard) were used to obtain proton nmr spectra and chemical shifts are reported on the τ scale (60 MHz spectra are routinely reported) followed in parentheses by an indication of the multiplicity (initial letter) and the number of protons associated with it. The ms data reported are the *m/e* values of significant ions followed in parentheses by an indication of their abundance relative to the base peak (100%).[4]

The Model Series

3-Bromo-1,2-indanedione; Reaction with Hydrochloric Acid

When the bromoindanedione (209 mg), prepared as described previously (1, 2), was dissolved in 50 mL of ethanol containing 0.25 mL of concentrated hydrochloric acid and heated at 65°C under nitrogen for 13 h, and the reaction mixture was then diluted with 200 mL of water and extracted with

[4]Carbon-13 nmr spectra of pure compounds were recorded. Copies of these data may be obtained, at a nominal charge, from the Depository of Unpublished Data, CISTI, The National Research Council of Canada, Ottawa, Ont., K1A 0S2.

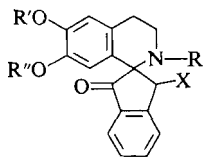

24

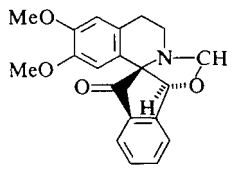

25

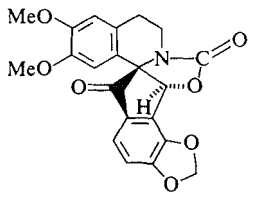

26

methylene chloride, an oil (122 mg) was obtained from the extract. No starting material remained and the product appeared to be 3-chloro-1,2-indanedione; ms: 182 (15), 180 (45).

Compound ***18***

The preparation of the unstable intermediate **24** (R = R′ = R″ = H; X = Cl/Br) from 3-bromo-1,2-indanedione and **9** (R′ = R″ = H) has been described previously (2). A solution of this compound in methanol was treated at 0°C with an excess of diazomethane dissolved in ether. The solution was allowed to come to room temperature and was stirred overnight in the absence of light. Excess diazomethane was destroyed with acetic acid and the solvent was removed under reduced pressure. (This method sometimes produced a considerable amount of *N*-methylated product.) The crude product was treated with acetic anhydride – formic anhydride in the manner described previously (2). A brown foam was isolated; recrystallization from methanol afforded white crystals, mp 181–182°C. This was a mixture of the halo compounds **24** (R = CHO; R′ = R″ = Me; X = Cl/Br); ir: 5.79, 5.99. *Anal.* calcd. for $C_{20}H_{18}NBrO_4$: C 57.70, H 4.36, N 3.36, Br 19.20; calcd. for $C_{20}H_{18}NClO_4$: C 64.60, H 4.88, N 3.77, Cl 9.54; found: C 64.06, H 4.63, N 3.77, Br 2.84, Cl 8.06.

This formamide (357 mg) was dissolved in 20 mL of nitromethane and stirred overnight with silver fluoroborate (700 mg) under a nitrogen atmosphere and with the exclusion of light. The reaction mixture was stirred for 10 min with aqueous sodium chloride and then filtered through Celite. The organic layer afforded **18** as a crystalline solid (311 mg) which, on recrystallization from methanol, formed white crystals, mp 202–206°C; ir: 2.76 (sharp), 2.84 (broad, absent at high dilution), 5.81, 6.07 (increases on dilution), 6.24 (absent at high dilution); uv; 212 (17 300), 238 (13 400), 288 (3300); nmr: 1.73 (s, 1), 2.0–2.7 (complex, 4), 3.33 (s, 1), 4.08 (s, 1), 4.78 (d, J = 12 Hz, D_2O addition produces s, 1), 5.8–7.5 (complex, 4), 6.13 (s, 3), 6.55 (s, 3), 6.87 (d, J = 12 Hz, 1, removed by D_2O addition); ms 354 (22), 353 (95), 335 (27), 325 (19), 324 (60), 308 (56), 307 (30), 280 (60), 279 (20), 248 (20), 221 (18), 220 (100). *Anal.* calcd. for $C_{20}H_{19}NO_5$: C 67.98, H 5.42, N 3.96; found: C 67.83, H 5.45, N 3.89.

The Oxazolidine ***25***

A solution of the formamide **18** (443 mg, 1.25 mmol) in 50 mL of 9:1 methanol – concentrated hydrochloric acid was refluxed under nitrogen for 5 h. The amine (420 mg, 1.25 mmol) was isolated from the reaction mixture after it had been cooled, diluted with 200 mL of water, made basic with solid sodium bicarbonate, and extracted with methylene chloride. Recrystallization from methanol of the product obtained from the extract gave white crystals, mp 182–183°C; ir: 3.10 (broad), 5.80; uv: 214 (15 200), 239 (16 800), 285 (5650), 343 (450); nmr: 2.0–2.6 (complex, 4), 3.67 (s, 1), 4.05 (s, 1), 5.00 (s, 1), 6.0–7.5 (complex, 4), 6.17 (s, 3), 6.40 (broad signal, removed by D_2O addition, 2), 6.57 (s, 3); ms: 326 (12), 325 (63), 324 (10), 323 (44), 322 (41), 321 (33), 320 (100), 308 (34), 307 (83), 306 (23), 305 (31), 292 (63), 276 (29), 266 (24), 264 (16), 262 (20), 248 (27), 220 (20), 192 (15), 190 (15), 105 (17), 89 (16), 79 (29), 77 (23), 76 (26), 52 (22), 51 (23), 44 (62). *Anal.* calcd. for $C_{19}H_{19}NO_4 \cdot \frac{1}{2}H_2O$: C 68.25, H 6.03, N 4.19; found: C 68.18, H 6.03, N 4.14.

A solution of this amine (321 mg, 0.96 mmol) in 200 mL of acetonitrile containing 2 mL of 37% aqueous formaldehyde was stirred at room temperature under nitrogen for 2 h. The solution was evaporated under reduced pressure, and the residue was dissolved in methylene chloride and washed with water. The organic layer yielded the oxazolidine **25** (306 mg, 91 mmol), which was recrystallized from methanol and obtained as white crystals, mp 160–163°C; ir: 5.82; uv: 214 (18 000), 242 (18 000), 286 (5500); nmr: 2.0–2.6 (complex, 4), 3.30 (s, 1), 4.00 (s, 1), 4.63 (s, 1), 5.59 (ABq; J = 7 Hz, internal (int.) chemical shift 21 Hz, 2), 6.5–7.5 (complex, 4), 6.12 (s, 3), 6.45 (s, 3); ms: 338 (22), 337 (100), 309 (24), 308 (84), 307 (45), 294 (45), 280 (90), 278 (37). *Anal.* calcd. for $C_{20}H_{19}NO_4$: C 71.20, H 5.68, N 4.15; found: C 71.15, H 5.77, N 4.08.

Compound ***20***

A solution of the oxazolidine **25** (208 mg, 0.62 mmol) and sodium cyanoborohydride (60 mg, 0.95 mmol) in 30 mL of methanol containing enough concentrated hydrochloric acid to bring it to pH 3 was stirred at room temperature under nitrogen for 1 h. The solution was diluted with 200 mL of water, made basic with solid sodium bicarbonate, and then thoroughly extracted with methylene chloride. The organic extract was washed with dilute sodium hydroxide and then with water, dried, and evaporated to dryness under reduced pressure. The product, **20** (209 mg, 0.62 mmol), was obtained as a crystalline solid which, after recrystallization from hexane–acetone, had mp 199–200°C; ir: 3.08 (broad), 5.82; uv: 213 (13 400), 243 (12 800), 286 (4750); nmr: 2.0–2.9 (complex, 4), 3.37 (s, 1), 3.92 (s, 1), 4.92 (s, 1), 5.62 (broad, 1), 6.4–7.5 (complex, 4), 6.13 (s, 3), 6.37 (s, 3), 7.81 (s, 3); ms: 340 (24), 339 (100), 324 (31), 296 (25), 294 (39), 280 (30). *Exact mass* calcd. for $C_{20}H_{21}NO_4$: 339.1462; found: 339.1470. *Anal.* calcd. for $C_{20}H_{21}NO_4$: C 70.77, H 6.24, N 4.13; found: C 70.53, H 6.16, N 4.22.

Epimerization Experiments

A mixture of compound **18** (118 mg) and anhydrous potassium carbonate (200 mg) in 15 mL of dry dimethylformamide was heated to 120–125°C with vigorous stirring under nitrogen for 1.3 h. The reaction mixture was poured into 200 mL of ice water and extracted with methylene chloride. The extract was washed with water, dried, and evaporated under reduced pressure. A yellow solid was obtained which was judged to consist of 40% of **18** and 60% of **19** on the basis of its nmr spectrum.

The mixture was hydrolyzed by refluxing in methanol – hydrochloric acid in the manner described above for pure **18** (see oxazolidine **25**), except that reflux was continued for 18 h. The product, a pale foam (78 mg) was judged, from its nmr spectrum, to contain the amine derived from **18** (described above) and its epimer in the ratio 40:60. Fractional crystallization of this material afforded a crystalline sample of the former amine, but the epimer was recovered from the mother liquor

as a noncrystalline residue; ir: 2.86 (sharp), 2.97 (sharp), 3.03 (broad), 5.83; nmr: 2.0–2.7 (complex, 4), 3.35 (s, 1), 4.42 (s, 1), 4.75 (s, 1), 6.3–7.5 (complex, 4), 6.33 (s, 3), 6.58 (s, 3), 7.62 (broad signal, removed by D_2O addition, 2). *Exact mass* calcd. for $C_{19}H_{19}NO_4$: 325.1317; found: 325.1320.

The 40:60 mixture of epimeric amines (27 mg) was dissolved in 6 mL of methanol, 0.2 mL of 37% aqueous formaldehyde was added, and the solution was stirred for 1 h at room temperature under nitrogen. The solution was brought to pH 3.5 by the addition of concentrated hydrochloric acid, sodium cyanoborohydride (6 mg) was added, and the stirring under nitrogen was continued for 1 h further. During this period the pH was maintained by the addition of hydrochloric acid as required. The reaction mixture was worked up in the manner previously described and the product was obtained as an oil (23 mg) which was judged on the basis of its nmr spectrum to contain compounds **20** and **21** in the ratio 40:60.

The 10,11-Methylenedioxyspirobenzylisoquinolines

*3-Bromo-4,5-methylenedioxy-1,2-indanedione (**8**; X = Br)*

This was prepared from *o*-vanillin by the method described previously (1, 2) with the following improvements. The 2,3-methylenedioxycinnamic acid intermediate was dissolved in aqueous sodium hydroxide and reduced quantitatively to the dihydro compound with hydrogen (40 psi) in the presence of 10% palladium–charcoal catalyst; the method of Kelly and Beckett (7) was used to convert the indanone to the indanedione.

Pictet–Spengler Reaction

The bromoindanedione **8** (X = Br) (1.847 g, 6.87 mmol) and β-(3,4-dihydroxyphenyl)ethylamine hydrochloride (2.38 g, 13.6 mmol) in 150 mL of dry ethanol were heated to 70°C under nitrogen for 24 h. The reaction mixture was cooled, poured into 150 mL of 3% hydrochloric acid, and extracted with methylene chloride. (The organic extract provided 650 mg of uncharacterizable material.) The aqueous solution was freeze-dried, the solid (3.52 g) obtained was dissolved in the minimum volume of boiling methanol, and the solution was then diluted with twice that volume of benzene. The excess starting amine hydrochloride precipitated as white crystals (1.074 g, 6.14 mmol). The spirobenzylisoquinoline hydrochloride product was obtained from the mother liquor as a brown oil (2.45 g) after evaporation of the solvent. A solution of this material in 40 mL of dry pyridine under nitrogen was cooled to −78°C and methyl chloroformate (1.50 mL, 19.3 mmol) was added dropwise to the solution. The reaction mixture was allowed to warm to room temperature and was stirred vigorously under nitrogen for 22 h. The solvent was removed under high vacuum and the residue was dissolved in 200 mL of methylene chloride, washed with brine, dried, and evaporated to dryness. The residue (2.46 g) was dissolved in 50 mL of dry methylene chloride and stirred under nitrogen with 10 mL of acetic-formic anhydride for 26 h. The solvent was removed under reduced pressure and the residue was dissolved in 200 mL of methylene chloride and washed with brine. The organic layer afforded, as a brown foam (2.52 g), **7** (R = CHO, R′ = R″ = COOMe, X = Cl/Br) which had the same spectroscopic characteristics as those reported previously (2).

*Displacement of Halogen: Compound **11***

Undried silver fluoroborate (5 g) was added to a solution of the above halo product (2.52 g) in 50 mL of nitromethane and the mixture was stirred under nitrogen with exclusion of light for 18 h. An excess of aqueous sodium chloride solution was added, stirring was continued for 5 min, and the mixture was filtered through Celite. The filter pad was washed with methylene chloride and water, and the combined organic layers were washed with water, dried, and evaporated to dryness under reduced pressure. The product (**11**) was obtained as a brown solid (2.29 g, 4.73 mmol) which, after recrystallization from acetone–ether, formed white crystals, mp 205–210°C; ir: 2.80 (sharp), 3.05 (shoulder), 5.62, 5.77, 6.00, 6.05, (shoulder); uv: 214 (21 200), 238 (22 400), 295 (8150), 313 (9400); nmr: 1.70 (s, 1), 2.77 (ABq, J = 8 Hz, int. chemical shift 27 Hz, 2), 2.80 (s, 1), 3.50 (s, 1), 3.78(s, 2), 4.72 (broadened d, J = 5 Hz, s after D_2O addition, 1), 5.8–7.5 (complex, 5, 4 after D_2O addition), 6.08 (s, 3), 6.14 (s, 3); ms: 467 (3), 453 (28), 377 (25), 350 (41), 349 (24), 334 (18), 323 (20), 322 (100), 59 (66). *Anal.* calcd. for $C_{23}H_{19}NO_{11}$: C 56.91, H 3.95, N 2.89; found: C 56.65, H 4.28, N 3.14.

*Compound **12***

The procedure used has been described previously (2). Compound **11** (1.000 g, 2.06 mmol) was converted to its tetrahydropyranyl ether (epimeric mixture) by treatment with 0.32 mL of dihydropyran in 60 mL of dry methylene chloride containing a trace of *p*-toluenesulfonic acid and the ester protecting groups were removed by hydrolysis with sodium bicarbonate in aqueous methanol, with care being taken to deoxygenate all solutions by continuous flushing with nitrogen. The catechol produced was dried in a 500-mL flask under high vacuum, anhydrous potassium carbonate (3.6 g), cupric oxide (1.8 g), and a stirring bar were added to the flask and the contents were dried under vacuum for a further 30 mins. Deoxygenated dimethylformamide (200 mL) and dry methylene iodide (2.0 mL) were then added and the mixture was heated at 120–125°C for 1.5 h. After it had cooled, the reaction mixture was filtered through Celite, the filter cake was washed with 200 mL of water and 200 mL of methylene chloride, and 500 mL of brine was added to the filtrate. The organic layer was separated, the aqueous layer was extracted with additional methylene chloride, and the combined organic extracts were worked up in the usual manner. The tetrahydropyranyl derivative of **12** was obtained as a light brown foam, which was dissolved in 100 mL of methanol containing 80 mL of 0.5 *N* hydrochloric acid and hydrolyzed in the manner described before (2). Compound **12** was obtained as white crystals (775 mg, 2.03 mmol) which, after recrystallization from acetone–methanol, had mp 190–193°C; ir: 2.86 (sharp), 5.78, 6.01; uv: 212 (13 000), 236 (14 900), 293 (7500), 308 (inflection 5350); nmr: 1.72 (s, 1), 2.76 (ABq, J = 8 Hz, int. chemical shift 27 Hz, 2), 3.37 (s, 1), 3.82 (s, 2), 3.98 (s, 1), 4.16 (ABq, J = 1.5 Hz, int. chemical shift 3 Hz, 2), 4.78 (d, J = 12 Hz, s after D_2O addition, 1), 5.6–7.5 (complex, 5, 4 after D_2O addition); ms: 381 (23), 364 (23), 363 (100), 352 (15), 336 (35), 335 (42), 334 (23), 320 (29), 308 (27), 307 (44), 278 (21), 277 (57), 249 (22), 163 (19). *Exact mass* calcd. for $C_{20}H_{15}NO_7$: 381.0847; found: 381.0846; calcd. for $C_{20}H_{13}NO_6$: 363.0757; found: 363.0771; calcd. for: $C_{19}H_{14}NO_6$: 352.0846); found: 352.0871; calcd. for $C_{19}H_{13}NO_5$: 335.0744; found: 335.0724; calcd. for $C_{19}H_{12}NO_5$: 334.0707; found: 334.0699; calcd. for $C_{18}H_{10}NO_5$: 320.0572; found: 320.0585; calcd. for $C_{11}H_{10}NO_3$: 204.0671; found: 204.0682. *Anal.* calcd. for $C_{20}H_{15}NO_7$: C 62.99, H 3.97, N 3.67; found: C 62.79, H 4.38, N 3.96.

*Compound **14***

A solution of the formamide **12** (120 mg, 0.315 mmol) in 20 mL of a 9:1 mixture of methanol and concentrated hydrochloric acid was refluxed for 5 h. The reaction mixture was poured into 100 mL of water, the solution was made basic with solid sodium bicarbonate, extracted with methylene chloride, and the extract was worked up in the usual manner. The amine

14 was obtained as crystals (112 mg, 0.314 mmol) which, after recrystallization from methanol, had mp 191–193°C; ir: 3.16 (broad), 5.85; uv: 212 (18 400), 237 (23 800), 294 (10 700), 308 (inflection 8400); nmr: 2.82 (ABq, J = 8 Hz, int. chemical shift 28 Hz, 2), 3.44 (s, 1), 3.83 (s, 2), 3.99 (s, 1), 4.20 (s, 2), 5.04 (s, 1), 5.9–7.7 (complex, 6, 4 after D_2O addition); ms: 353 (50), 336 (34), 335 (100), 334 (30), 320 (22), 306 (20). *Exact Mass* calcd. for $C_{19}H_{15}NO_6$: 353.0901; found: 353.0903. *Anal.* calcd. for $C_{19}H_{15}NO_6$: C 64.58, H 4.28, N 3.96; found: C 64.19, H 4.23, N 3.87.

The Oxazolidine 15

A solution of compound **14** (103 mg, 0.292 mmol) and 1.0 mL of 37% aqueous formaldehyde in 10 mL of methanol was stirred at room temperature under nitrogen for 1 h. The solvent was removed under reduced pressure and the residue was dissolved in 100 mL of methylene chloride, washed with water, and worked up in the usual way. Oxazolidine **15** was obtained as crystals (104 mg, 0.285 mmol) which, after recrystallization from acetone–ether had mp 240–247°C; ir: 5.80; uv: 212 (23 200), 237 (31 400), 295 (14 300), 314 (11 800); nmr: 2.74 (ABq, J = 8 Hz, int. chemical shift 27 Hz, 2), 3.35 (s, 1), 3.78 (narrow m, 2), 3.95 (s, 1), 4.72 (narrow m, 2), 4.66 (s, 1), 5.56 (ABq, J = 7 Hz, int. chemical shift 21 Hz, 2), 6.5–7.8 (complex, 4); ms: 365 (59), 337 (24,) 336 (100), 335 (79), 320 (27), 308 (66), 307 (19), 306 (31), 279 (20), 278 (40). *Exact Mass* calcd. for $C_{20}H_{15}NO_6$: 365.0897; found: 365.0895. *Anal.* calcd. for $C_{20}H_{15}NO_6$: C 65.75, H 4.14, N 3.83; found: C 65.48, H 4.34, N 3.57.

(±)-Corydaine 3

A solution of the oxazolidine **15** (16 mg; 0.044 mmol) and sodium cyanoborohydride (4 mg, 0.063 mmol) in 3 mL of methanol containing sufficient concentrated hydrochloric acid to bring it to pH 3 was stirred at room temperature under nitrogen for 1 h. The reaction mixture was diluted with 100 mL of water, made basic with solid sodium bicarbonate, and thoroughly extracted with methylene chloride. The extract afforded (±)-corydaine (**3**) as a solid (11 mg, 0.030 mmol) which, on recrystallization from ethanol, had mp 127–128°C. The spectroscopic (nmr, ir, ms) and tlc (four systems) characteristics of the synthetic material and of natural (+)-corydaine were identical. A sample of racemized natural corydaine (see below) was identical in every respect and the melting point was not depressed on admixture. A sample of (±)-corydaine synthesized by a different route (5) was also identical.

Compound 13

Compound **11** (500 mg, 1.03 mmol) was converted to its tetrahydropyranyl derivative and the ester groups were hydrolyzed as before (see under Compound **12**) but the catechol was not isolated; instead the methylene chloride extract was concentrated and then added to a solution of diazomethane (prepared from 7.5 g of *N,N'*-dimethyl-*N,N'*-dinitrosoterephthalamide (70% in mineral oil)) in ether at 0°C. The solution was allowed to warm to room temperature and was stirred overnight with exclusion of light. Sufficient glacial acetic acid was added to destroy the excess diazomethane, and the solution was evaporated to dryness under reduced pressure. The oil obtained was stirred under nitrogen with 50 mL of methanol and 40 mL of 0.5 *N* hydrochloric acid for 2.5 h; 200 mL of water was added and the mixture was extracted with methylene chloride. The extract afforded **13** as a solid product (390 mg, 0.982 mmol), which had mp 166–176°C after recrystallization from acetone–ether. The microanalyses of this material were unsatisfactory, the erratic values suggesting that samples were hydrated to varying degrees. Spectroscopic characteristics: ir: 2.87 (sharp), 5.80, 6.04, 6.20; uv: 212 (23 200), 235 (23 200), 290 (9850), 310 (7400); nmr: 1.77 (s, 1), 2.81 (ABq, J = 8 Hz, int. chemical shift 28 Hz, 2), 3.40 (s, 1), 3.87 (s, 2), 4.04 (s, 1), 4.79 (broad, 1), 5.6–7.5 (complex, 4), 6.17 (s, 3), 6.50 (s, 3); ms: 397 (25), 383 (30), 381 (20), 379 (75), 366 (25), 365 (100), 354 (10), 352 (27), 351 (76), 338 (47), 337 (70), 336 (55), 335 (30), 324 (26), 323 (46), 322 (40), 310 (33), 309 (32), 308 (20), 307 (25), 294 (30), 293 (20), 292 (30), 278 (21), 277 (55), 220 (25), 206 (27), 106 (34). *Exact Mass* calcd. for $C_{21}H_{19}NO_7$: 397.1155; found: 397.1149; calcd. for $C_{20}H_{17}NO_7$: 383.1007; found: 383.1009; calcd. for $C_{21}H_{17}NO_6$: 379.1010; found: 379.0965; calcd. for $C_{19}H_{16}NO_6$: 354.0932; found: 354.0887; calcd. for $C_{20}H_{17}NO_5$: 351.1132; found: 351.1158; calcd. for $C_{19}H_{15}NO_5$: 337.0943; found: 337.0935; calcd. for $C_{19}H_{14}NO_5$: 336.0868; found: 336.0864.

Yenhusomidine 4

The formamide **13** (200 mg, 0.504 mmol) was hydrolyzed in the manner described above in the preparation of **14**. The amine (186 mg, 0.504 mmol) isolated, after recrystallization from methanol–ether, had mp 183–184°C; ir: 3.18 (broad), 5.85; uv: 212 (20 300), 236 (28 800), 289 (10 800), 310 (8450); nmr: 2.78 (ABq, J = 8 Hz, int. chemical shift 28 Hz, 2), 3.39 (s, 1), 3.81 (s, 2), 3.97 (s, 1), 4.98 (s, 1), 5.9–7.7 (complex, 4), 6.18 (s, 3), 6.49 (s, 3); ms: 370 (23), 369 (100), 352 (33), 351 (85), 340 (20), 336 (40), 310 (28), 292 (23). *Exact Mass* calcd. for $C_{20}H_{19}NO_6$: 369.1208; found: 369.1204. *Anal.* calcd. for $C_{20}H_{19}NO_6$: C 65.03, H 5.19, N 3.79; found: C 64.73, H 5.35, N 3.69.

(On one occasion (see below) the hydrolysis gave a 50:50 mixture of the normal amine and the phenolic amine **16**.)

The amine (87 mg, 0.235 mmol) was stirred with 1 mL of 37% aqueous formaldehyde in 5 mL of acetonitrile at room temperature under nitrogen for 50 min. The oxazolidine (90 mg, 0.235 mmol), isolated in the manner described for **15**, was recrystallized from methanol and obtained as white crystals, mp 262–267°C; ir: 5.80; uv: 211 (15 800), 236 (22 200), 290 (8100), 314 (7350); nmr: 2.73 (ABq, J = 8 Hz, int. chemical shift 28 Hz, 2), 3.32 (s, 1), 3.77 (s, 2), 3.95 (s, 1), 4.63 (s, 1), 5.57 (ABq, J = 7 Hz, int. chemical shift 20 Hz, 2), 6.5–7.6 (complex, 4), 6.14 (s, 3), 6.40 (s, 3); ms: 381 (20), 352 (19), 351 (15), 324 (17), 86 (27), 85 (67), 84 (41), 83 (100). *Exact Mass* calcd. for $C_{21}H_{19}NO_6$: 381.1207; found: 381.1202. *Anal.* calcd. for $C_{21}H_{19}NO_6$: C 66.13, H 5.02, N 3.67; found: C 66.38, H 5.27, N 3.52.

The oxazolidine (100 mg, 0.262 mmol) was reduced with sodium cyanoborohydride (20 mg, 0.313 mmol) in 10 mL of methanol in the manner described above for the preparation of **3**. (±)-Yenhusomidine (**4**) was obtained as a solid (95 mg, 0.248 mmol) which, after recrystallization from methanol, had mp 239–241°C. Its spectroscopic characteristics (ir, uv, nmr, ms) were identical with those of natural yenhusomidine (9). The material was identical in all respects with (±)-yenhusomidine synthesized by a different route (5), and the melting point of a mixture of the two was not depressed.

Compound 16

In one run, the hydrolysis of formamide **13** (198 mg) in methanolic hydrochloric acid (see Yenhusomidine **4**, above) led to the isolation of a mixture of products (163 mg) which was separated by tlc on alumina with chloroform that had been treated with ammonia. This provided the previous dimethoxy amine (66 mg) and the phenolic amine **16** (51 mg) as a foam with the following characteristics: ir: 2.88 (sharp), 3.03 (sharp), 3.15 (broad), 5.83; nmr: 2.79 (ABq, J = 8 Hz, int. chemical shift 28 Hz, 2), 3.39 (s, 1), 3.80 (s, 2), 3.87 (s, 1), 5.01 (s, 1), 5.80 (broad signal, removed by D_2O addition, 3), 6.2–7.8 (complex, 4), 6.17 (s, 1); ms: 355 (45), 338 (35), 337 (100), 336 (42), 294 (28), 107 (25), 106 (40), 105 (27). *Exact Mass* calcd. for $C_{19}H_{17}NO_6$: 355.1062; found: 355.1056.

The formation of **16** in significant amounts under these conditions occurred only once. Reproducible results were obtained with the following hydrolysis conditions: a solution of the formamide **13** (25 mg) in 2 mL of acetic acid saturated with hydrogen bromide was refluxed under nitrogen for 1.5 h. The reaction mixture was cooled, diluted with 25 mL of water, made basic with solid sodium bicarbonate, and extracted thoroughly with methylene chloride. The extract afforded a 50:50 mixture of the two amines (13 mg).

Corpaine ***17***

A solution of the amine **16** (23 mg, 0.065 mmol) in 5 mL of acetonitrile containing 0.2 mL of acetonitrile was stirred at room temperature under nitrogen for 1.25 h. The oxazolidine (21 mg, 0.059 mmol) was isolated in the manner described for **15** and obtained as a white solid; ir: 2.86 (sharp), 5.79; nmr: 2.25 (ABq, J = 8 Hz, int. chemical shift 28 Hz, 2), 3.35 (s, 1), 3.77 (narrow m, 2), 3.83 (s, 1), 4.43 (broad, 1, removed by D_2O addition), 4.68 (s, 1), 5.58 (ABq, J = 7 Hz, int. chemical shift 20 Hz, 2), 6.2–7.6 (complex, 4), 6.12 (s, 3); ms: 368 (23), 367 (82), 339 (27), 338 (100), 337 (84), 324 (30), 323 (21), 322 (48), 310 (74), 308 (27), 294 (27), 292 (26), 281 (21), 280 (42). *Exact Mass* calcd. for $C_{20}H_{17}NO_6$: 367.1062; found: 367.1056.

The oxazolidine (20 mg, 0.054 mmol) was reduced with sodium cyanoborohydride (10 mg) in 10 mL of methanol in the manner described for the preparation of **3**. (±)-Corpaine (**17**) was obtained as a solid (20 mg, 0.053 mmol) which, after recrystallization from methanol, had mp 252–255°C. Its spectroscopic characteristics (ir, nmr, ms) were identical with those of natural corpaine (10). *Exact Mass* calcd. for $C_{20}H_{19}NO_6$: 369.1227; found: 369.1241; calcd. for $C_{20}H_{17}NO_5$: 351.1116; found: 351.1125; calcd. for $C_{19}H_{18}NO_5$: 340.1181; found: 340.1177; calcd. for $C_{19}H_{15}NO_5$: 337.0939; found: 337.0928; calcd. for $C_{19}H_{18}NO_4$: 324.1235; found: 324.1235; calcd. for $C_{11}H_{12}NO_3$: 206.0849; found: 206.0881.

Compound ***10***

The bromoindanedione **8** (X = Br) (1.134 g) and β-(3,4-dihydroxyphenyl)ethylamine hydrochloride (1.00 g) in 90 mL of dry ethanol were heated to 70°C under nitrogen for 24 h. The unstable product was isolated in the manner described above (see Pictet–Spengler Reaction), dissolved in 25 mL of dry pyridine, and treated as before with methyl chloroformate, except that excess methyl chloroformate (5.0 g) was employed and the treatment with methyl chloroformate was repeated twice (or until no free amine remained). The product (1.025 g) was a foam which formed crystals after it had been dissolved in methanol and treated with activated charcoal. Recrystallization from methanol afforded **10** as white crystals, mp 215–216°C; ir: 5.78; uv: 216 (28 600), 252 (3900), 297 (2800); nmr: 2.82 (s, 1), 2.91 (ABq, J = 8.5 Hz; int. chemical shift 8.5 Hz, 2), 3.33 (s, 1), 3.85 (s, 2), 4.43 (s, 1), 5.3–7.6 (complex, 4), 6.08 (s, 3), 6.15 (s, 3), 6.54 (s, 3); ms: 579 (5), 577 (15), 395 (23), 96 (99), 94 (100), 93 (20), 59 (29). *Anal.* calcd. for $C_{25}H_{20}NClO_{13}$: C 51.96, H 3.49, N 2.42, Cl 6.14; found: C 51.87, H 3.30, N 2.42, Cl 6.24.

Conversion of ***10*** *to Corydaine and Yenhusomidine*

A solution of **10** (527 mg) and silver fluoroborate (1.2 g) in 30 mL of acetone containing 2 mL of water was stirred at room temperature under nitrogen with the exclusion of light for 40 h. The solvent was removed under reduced pressure and the product was isolated in the standard way. This solid (467 mg), mp 199–201°C, appeared to be a mixture but it could not be characterized satisfactorily.

This material (175 mg) was converted to its tetrahydropyranyl derivative in the manner described above. The product (210 mg) was hydrolyzed to the catechol and this was converted to the methylenedioxybenzene in the manner described above (see Compound **12**). Hydrolysis of both the tetrahydropyranyl group and the amide were carried out at the same time under the conditions described above for the conversion of **12** to **14**. The product (166 mg) obtained was impure **14** and could be converted to (±)-corydaine by the sequence described above.

The above dehalogenated intermediate, mp 199–201°C, (188 mg) was converted to the catechol just described. This was treated with diazomethane as described previously (see Compound **13**) and the product was hydrolyzed under the conditions described for the conversion of **12** to **14** except that reflux was carried out for 10 h. The product (149 mg) was subjected to tlc on silica gel (with 96:4 methylene chloride – methanol) and separated into two components: the amine (67 mg) derived from **13**, which was converted to (±)-yenhusomidine, and a compound (67 mg) tentatively identified as the urethane **26** from its spectroscopic characteristics; ir: 5.77, 5.87; nmr: 2.72 (ABq, J = 8 Hz, int. chemical shift 25 Hz, 2), 3.35 (s, 1), 3.81 (s, 2), 3.91 (s, 1), 4.23 (s, 1), 5.6–7.4 (complex, 4), 6.15 (s, 3), 6.33 (s, 3); ms: 395 (24), 352 (25), 351 (100), 350 (15), 336 (50), 308 (15), 293 (19), 292 (50).

Sibiricine ***5***

A solution of the amide **12** (65 mg) in 20 mL of dry tetrahydrofuran was added dropwise to a solution of lithium diisopropylamide (prepared from 0.10 mL of dry diisopropylamine and 0.18 mL of 1.6 M n-butyllithium in hexane) in 10 mL of dry tetrahydrofuran at −78°C under nitrogen and 0.2 mL of hexamethylphosphoramide (freshly distilled from calcium hydride) was then added. The solution was stirred and allowed to warm to room temperature. After 20 h, the solution was poured into 100 mL of ice water, salt was added, and the mixture was thoroughly extracted with methylene chloride. The extract afforded a solid (65 mg) which was judged, from its nmr spectrum, to be a 70:30 mixture of **12** and **23**. This mixture was hydrolyzed under the conditions used to convert **12** to **14** (except that reflux was carried out for 17 h) and the solid product (53 mg) obtained was judged, from its nmr spectrum, to be a 70:30 mixture of **14** and its epimer. A solution of this material and 0.4 mL of 37% aqueous formaldehyde in 10 mL of acetonitrile was stirred at room temperature under nitrogen for 15 min. Sodium cyanoborohydride (20 mg) and 10 drops of glacial acetic acid were added, and stirring was continued for a further 1 h; 100 mL of water was added, the solution was made basic with solid sodium bicarbonate, and thoroughly extracted with methylene chloride. The product contained some unchanged amine, so it was subjected to another cycle of the methylation sequence. After this, the product was a solid (46 mg) which, from its nmr spectrum, was judged to be a 70:30 mixture of **3** and **5** (11). Recrystallization from methanol afforded crystalline **3** and the mother liquors were evaporated to provide a 55:45 mixture of **3** and **5**. This mixture was separated into its components by reversed phase hplc (Corasil C-18 in 90:10 water–methanol) at an analytical level.

Raddeanone ***6***

A solution of the amide **13** (40 mg) in 20 mL of dry tetrahydrofuran was treated with lithium diisopropylamide in the manner described above (see Sibiricine). The product was a mixture of **13** and **22** in the ratio 70:30, as judged from the nmr spectrum. The mixture was hydrolyzed as described above and the hydroxy amines were obtained as a 70:30 mixture. A solution of the mixture in 20 mL of methanol was treated with 0.2 mL of aqueous formaldehyde and reduced with sodium cyanoborohydride (10 mg) in the manner described for the model series (see Epimerization Experiments). The methylated

product (35 mg) consisted of a 70:30 mixture of (±)-yenhusomidine (**4**) and (±)-raddeanone (**6**), as judged from the nmr spectrum. Trituration of the mixture with acetone left a sample of yenhusomidine undissolved, and the solution contained raddeanone and yenhusomidine in the ratio 70:30. This mixture could be separated under the hplc conditions described above (see Sibiricine).

Racemization of Natural Corydaine

Corydaine, isolated by Perel'son *et al.* (ref. 10 and personal communication) by a procedure that avoided prolonged contact of the extract with a base, formed crystals, mp 189–189.5°C, $[\alpha]_D^{32}$ +145° (*c* 1.3, chloroform). We were provided with a sample of this material; as received, it had mp 175–186°C. A sample (1.3 mg) was dissolved in pure methanol at room temperature and its optical activity, measured by its circular dichroism between 360 and 450 nm, was plotted as a function of time. The decay in optical activity followed first-order kinetics and showed a half-life of about 500 h. A similar sample showed no measurable loss of optical activity when refluxed with 9:1 methanol – concentrated hydrochloric acid under nitrogen for 5 h.

A solution of natural corydaine (8 mg) in 10 mL of methanol containing a little potassium hydroxide was refluxed under nitrogen for 20 h. The recovered alkaloid (7.3 mg) was optically inactive and had mp 126–130°C.

Acknowledgements

Reference samples and spectra were received from the following: Drs. M. E. Perel'son and N. Margvelashvily (natural corydaine and corpaine), Professor T. Kametani (natural yenhusomidine and raddeanone), and Professor D. B. MacLean (synthetic corydaine and yenhusomidine). We are grateful to them for their generous cooperation. We thank the National Research Council of Canada for financial support of this work and for a scholarship (to D.D.), and the University of Toronto for an Open Fellowship (to D.D.).

1. S. McLean, M.-S. Lin, and J. Whelan. Tetrahedron Lett. 2425 (1968); Can. J. Chem. **48**, 948 (1970).
2. S. McLean and J. Whelan. Can. J. Chem. **51**, 2457 (1973).
3. S. McLean and D. Dime. Can. J. Chem. **55**, 924 (1977).
4. W. Wong-Ng and S. C. Nyburg. Can. J. Chem. **57**, 157 (1979).
5. B. C. Nalliah, D. B. MacLean, R. G. A. Rodrigo, and R. H. F. Manske. Can. J. Chem. **55**, 922 (1977).
6. H. Irie, T. Kishimoto, and S. Uyeo. J. Chem. Soc. C, 3501 (1968).
7. R. B. Kelly and B. A. Beckett. Can. J. Chem. **47**, 2501 (1969).
8. T. Kishimoto and S. Uyeo. J. Chem. Soc. C, 2600 (1969); 1644 (1971).
9. S.-T. Lu, T.-L. Su, T. Kametani, and M. Ihara. Heterocycles, **3**, 301 (1975).
10. D. A. Fesenko and M. E. Perel'son. Khim. Prir. Soedin, 7, 166; K. S. Baisheva, D. A. Fesenko, M. E. Perel'son, and B. K. Rostotskii. Khim. Prir. Soedin, **6**, 574 (1970).
11. R. H. F. Manske, R. Rodrigo, D. B. MacLean, D. E. F. Gracey, and J. K. Saunders. Can. J. Chem. **47**, 3585 (1969).
12. M. Shamma, J. L. Moniot, R. H. F. Manske, W. K. Chan, and K. Nakanishi. J. Chem. Soc. Chem. Commun. 310 (1972).

A new synthesis of spirovetivanes via the spiro acyloin intermediate[1]

TOSHIRO IBUKA, KENJI HAYASHI, HIROYUKI MINAKATA,
YOSHIKUNI ITO, AND YASUO INUBUSHI

Faculty of Pharmaceutical Sciences, Kyoto University, Sakyo-ku, Kyoto 606, Japan

Received November 28, 1978

TOSHIRO IBUKA, KENJI HAYASHI, HIROYUKI MINAKATA, YOSHIKUNI ITO, and YASUO INUBUSHI. Can. J. Chem. 57, 1579 (1979).

Ethyl-3-(1-ethoxycarbonyl-2,6-dimethylcyclohex-2-enyl)propionate **5** was stereoselectively synthesized. The diester **5** was spiroannulated by the acyloin condensation to give the bis(trimethylsiloxy) ether **11**. The ether **11** was hydrolyzed to provide the acyloins **6** and **12**. The acyloins **6** and **12** were elaborated into (±)-hinesol **1**, (±)-agarospirol **2**, (±)-β-vetivone **3**, and (±)-α-vetispirene **4**.

TOSHIRO IBUKA, KENJI HAYASHI, HIROYUKI MINAKATA, YOSHIKUNI ITO et YASUO INUBUSHI. Can. J. Chem. 57, 1579 (1979).

On a synthétisé le (éthoxycarbonyl-1 diméthyl-2,6 cyclohexène-2 yl)-3 propionate d'éthyle (**5**) d'une façon stéréosélective. On a provoqué une spirocyclosation de **5** par une condensation aux acyloïnes qui a conduit au bis(triméthylsiloxy) éther (**11**). L'hydrolyse de l'éther **11** fournit les acyloïnes **6** et **12**. On a pu transformer les acyloïnes **6** et **12** en (+)-hinésol (**1**), en (+)-agarospirol (**2**), en (+)-β-vétivone (**3**) et en (+)-α-vétispirène (**4**).

[Traduit par le journal]

The spirovetivanes possessing a spiro[4.5]decane framework (1) have been isolated from a variety of sources such as vetiver oil (2), the stress metabolites from infected potato tubers (3), the flue-cured Virginia tobacco (4), and the stress metabolites of *Datura stramonium* (5). Since Marshall and coworkers (6) reported that β-vetivone was a member of spirovetivanes rather than a hydroazulenone derivative, much attention, by many groups (1, 7–10), has been directed towards the efficient syntheses of these types of sesquiterpenes, owing to their unique structures and the increasing occurrence of spirovetivanes with interesting biological activity (3).

We have been interested in constructing stereoselectively the properly functionalized spiro[4.5]decane system which is generally suited for synthesis of spirovetivanes. The efficient synthesis of such sesquiterpenes as (±)-hinesol **1**, (±)-agarospirol **2**, (±)-β-vetivone **3**, and (±)-α-vetispirene **4** depends upon the stereoselective construction of the spirocycle and the regioselective introduction of the unsaturated bond into the spirocyclic compound (Scheme 1). The diester **5** is suitably substituted for the annulation to a functionalized spiro[4.5]decane key intermediate **6**, which may subsequently be elaborated to the natural spirovetivanes. We now detail the synthesis of racemic hinesol **1**, agarospirol **2**, β-vetivone **3**, and α-vetispirene **4**.

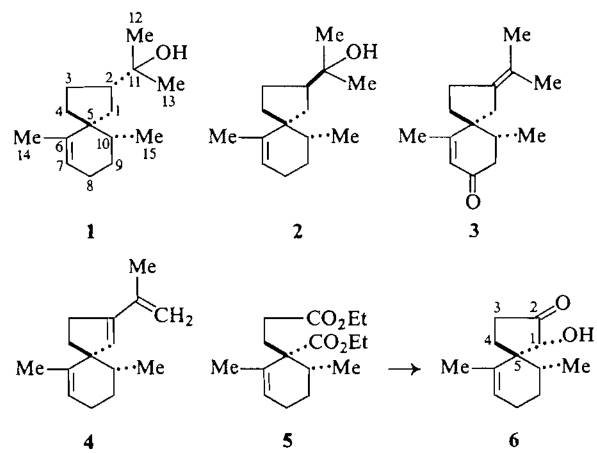

SCHEME 1

The keto ester **8**, prepared by the Diels–Alder reaction of 2,4-bis(trimethylsiloxy)-1,3-pentadiene (**7**) with ethyl crotonate followed by hydrolysis (11), was treated with ethanedithiol to afford the dithioacetal **9** which was subsequently reduced with Raney nickel to give the β,γ-unsaturated ester **10** (Scheme 2). Treatment of **10** with lithium diisopropylamide, and subsequent alkylation of the lithium enolate with ethyl β-bromopropionate provided the diester **5**. The high stereoselectivity of the alkylation reaction is probably a result of axial alkylation in which the bromide approaches the face of the molecule opposite to the pseudo axial C-10 methyl group. This high stereoselectivity was ascertained finally by the conversion of diester **5** to racemic hinesol **1**, which was identified by comparison with an authentic sample.[2]

[1]Dedicated to the memory of Professor R. H. F. Manske.

[2]We are grateful to Prof. I. Kitagawa, Osaka University, for his gift of an authentic natural hinesol.

0008-4042/79/131579-06$01.00/0

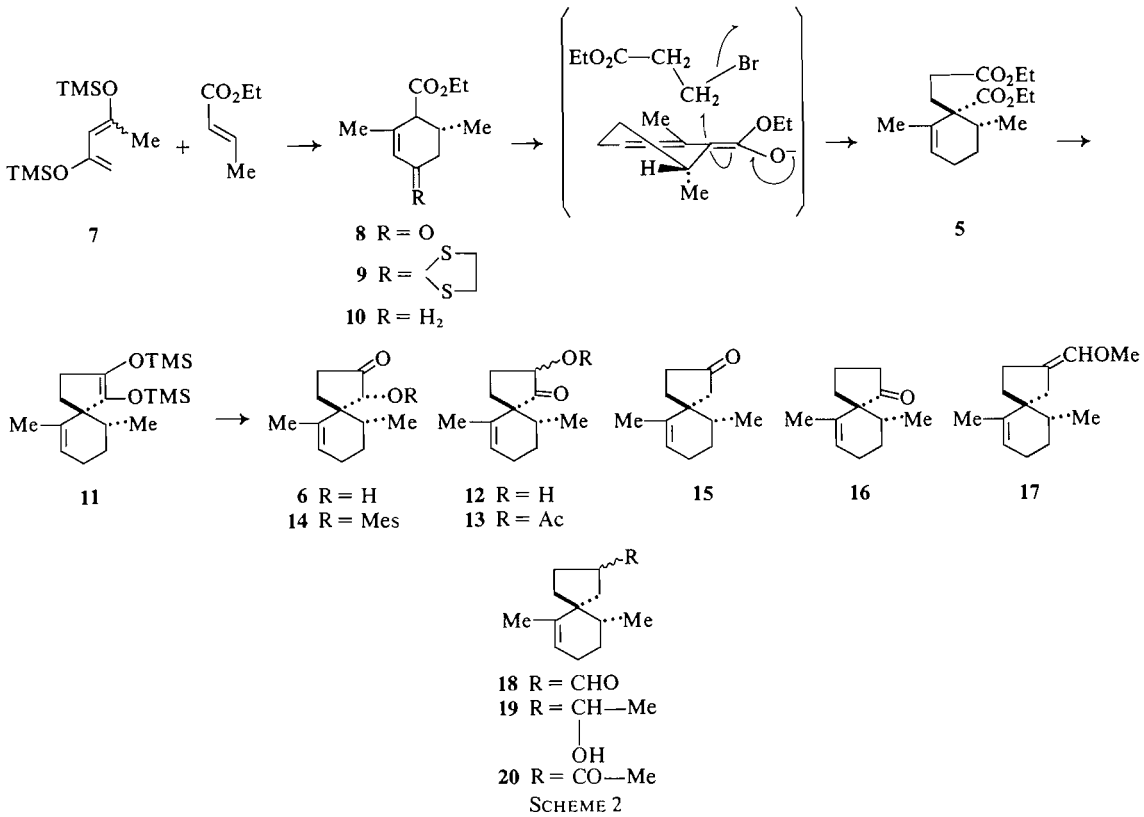

7

8 R = O
9 R = S, S
10 R = H_2

5

11

6 R = H
14 R = Mes

12 R = H
13 R = Ac

15

16

17

18 R = CHO
19 R = CH(OH)—Me
20 R = CO—Me

SCHEME 2

Acyloin condensation of the diester **5** was carried out at reflux in toluene employing sodium and trimethylchlorosilane to afford the bis(trimethylsiloxy) ether **11** in a 79% yield. The condition for hydrolysis of the bis(trimethylsiloxy) ether **11** was critical. Thus, hydrolysis of **11** in dry methanol under the conditions recommended (12) led to a mixture consisting of many inseparable products, but in tetrahydrofuran containing 10% hydrochloric acid at 0°C, a mixture of the crystalline spiro acyloin **6** and the unisolable isomeric acyloin **12** was obtained in ca. 100% yield. Although the isomeric acyloin **12** itself could not be isolated by chromatographic procedure on silica gel owing to its instability, the presence of **12** was easily detected by ^{1}H nmr analysis of the hydrolyzed product of **11**. The mother liquor removed from the crystalline **6** by filtration was concentrated and acetylated to give the stable acetyl derivative **13** of the acyloin **12**. The β-configuration of the C-1 hydrogen of **6** was confirmed by the observation of a nuclear Overhauser effect: irradiation at the frequency of the C-10 methyl group (δ 1.12) resulted in ca. 20% enhancement of the C-1 hydrogen signal at δ 4.05.

With the key spiro acyloin intermediate **6** in hand, we focused our efforts on the synthesis of the spirovetivane sesquiterpenes. Mesylation of **6**, followed by zinc – ammonium chloride reduction of the mesylate **14** in tetrahydrofuran afforded the spiro ketone **15** in a 99% yield. Spiro ketone **15** is a constituent of vetiver oil (13) and was recently synthesized in racemic form by Büchi *et al.* (8), Caine *et al.* (9), and Piers and Lau (10). The structure of **15** was confirmed by comparison of its ir and ^{1}H nmr spectra with those of an authentic sample (9).[3] The ketone **15** (19% yield), accompanied with the isomeric ketone **16** (38% yield), was also prepared from the keto acetate **13** by a known three-step sequence (14) involving reduction with sodium borohydride, mesylation, and elimination with potassium hydroxide.

To prepare (±)-hinesol (**1**) and (±)-agarospirol (**2**) from ketone **15**, it was necessary to introduce a three-carbon unit at the C-2 position. A Wittig reaction of **15** with methoxymethylenetriphenylphosphorane (59% yield) followed by hydrolysis of the enol methyl ether **17** with 10% hydrochloric acid gave the aldehyde **18** as an epimeric mixture. Without separation at this stage, **18** was converted into a 3:2 mixture of (±)-hinesol (**1**) and (±)-agarospirol (**2**)

[3]The authors express their thanks to Prof. D. Caine, Georgia Institute of Technology, U.S.A., for authentic ir and nmr spectra.

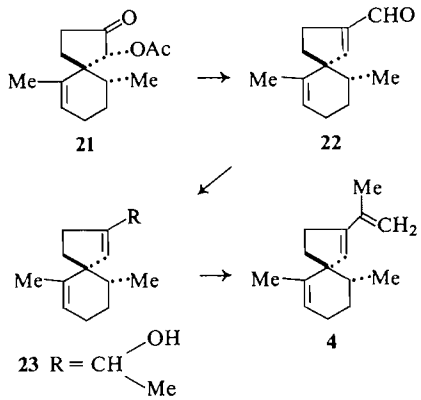

SCHEME 3

by the conventional method via the alcohol **19** and the methyl ketone **20**. Separation of the mixture of **1** and **2** is known to be troublesome and was achieved by repeated preparative thin-layer chromatography on silica gel. Synthetic (±)-hinesol (**1**) was identical with an authentic sample of natural hinesol (15)[2] by ir and ^{1}H nmr spectral comparison and by gas chromatographic analysis. The epimeric mixture of **1** and **2** was readily converted to (±)-β-vetivone (**3**), mp 44–46°C, according to the method of Marshall and Johnson (6). The spectral properties of synthesized (±)-β-vetivone (**3**) were completely in accord with the assigned structure.

To prepare (±)-α-vetispirene (**4**) from the key intermediate **6** (Scheme 3), it was necessary to introduce an isopropenyl group at C-2 and a double bond between C-1 and C-2. The acetate **21** derived from the spiro acyloin **6** was treated with methoxymethylenetriphenylphosphorane and then hydrolyzed with 10% hydrochloric acid in tetrahydrofuran to provide the α,β-unsaturated aldehyde **22**. (±)-α-Vetispirene **4** was prepared from **22** by a conventional four-step sequence (**22** → **23** → **24** → **25** → **4**) involving reaction with methyllithium, oxidation with Jones' reagent, treatment with methyllithium, and finally dehydration with 10-camphorsulfonic acid. The identity of the synthesized (±)-α-vetispirene **4** with an authentic sample was shown by comparison of their ir and ^{1}H nmr spectra.[3]

Experimental

All melting points were determined on a Yanagimoto micro-melting point apparatus and were uncorrected. The nmr spectra were obtained, unless otherwise specified, in deuteriochloroform containing tetramethylsilane as an internal standard with either a Varian A-60 or a JOEL JNM-FX-100 spectrometer, and chemical shifts were reported in δ values relative to tetramethylsilane. The abbreviations, s, d, t, q, and m in the nmr spectra signify singlet, doublet, triplet, quartet, and multiplet and the coupling constant (J) was measured in Hz. The nominal and the high resolution mass spectra were taken on a JOEL JMS-01SG-2 spectrometer equipped with a computer; M^+ signifies the molecular ion. Unless otherwise specified, the ir spectra were taken on a Shimadzu IR-400 spectrometer in chloroform. Gas chromatography was carried out on a 1.5% SE-30 or 10% FFAP on Chromosorb W (glass column, 1 or 3 m × 3 mm) with a Hitachi gas chromatograph model 063 and nitrogen as carrier gas (30 mL/min). Column chromatography was performed on silica gel (Mallinckrodt silicic acid, 100 mesh). Bulb-to-bulb distillation was carried out using a Büchi Kugelrohr distillation apparatus (type KR) and the temperatures recorded were oven temperatures. Unless otherwise stated, all the extracts were dried over anhydrous magnesium sulfate.

2,4-Bis(trimethylsiloxy)-1,3-pentadiene (7)

To a stirred mixture of triethylamine (61 g, 0.6 mol) and zinc chloride (2 g) was added a solution of acetylacetone (20 g, 0.2 mol) in a mixture of ether (100 mL) and benzene (100 mL) at 0°C. To the above mixture was added trimethylchlorosilane (64 g, 0.6 mol) under stirring and the mixture was stirred at room temperature for 48 h. Ether (500 mL) was added to the mixture and the filtrate of the mixture was concentrated under reduced pressure below 40°C. The resultant residue was distilled to give **7** (42 g, 86%) as a 1:1 mixture of 4*E* and 4*Z*; bp 73°C/3 Torr; nmr δ: 0.20 (36H, s, $Si(CH_3)_3$), 1.84 (3H, s, vinylic CH_3), 2.00 (3H, s, vinylic CH_3), 4.11 (2H, d, J = 3 Hz, olefinic protons), 4.31 (1H, m, olefinic proton), 4.71 (1H, s, olefinic proton), 4.76 (1H, m, olefinic proton), and 5.20 (1H, s, olefinic proton); ms *m/e*: 244 (M^+). *Anal.* calcd. for $C_{11}H_{24}O_2Si_2$: C 54.04, H 9.90; found: C 53.78, H 9.85.

The Keto Ester 8

A mixture of the diene **7** (4.9 g, 20 mmol), ethyl crotonate (3.42 g, 30 mmol), and xylene (6 mL) was heated at 180°C in a sealed glass tube for 5 days. After cooling, the mixture was mixed with 5% hydrochloric acid (3 mL) and tetrahydrofuran (10 mL) at 5°C for 1 h, and then extracted with ether. The extract was washed, dried, and evaporated *in vacuo* to leave a yellowish residue. Distillation of the residue gave the keto ester **8** (2.45 g); bp 133–135°C/3 Torr; nmr δ: 1.07 (3H, d, J = 6 Hz, secondary CH_3), 1.28 (3H, t, J = 7 Hz, $CO_2CH_2CH_3$), 1.95 (3H, m, vinylic CH_3), 4.23 (2H, q, J = 7 Hz, $CO_2CH_2CH_3$), and 5.93 (1H, m, olefinic proton); ir ν_{max}: 1729 and 1666 cm^{-1}; ms *m/e*: 196 (M^+). *Anal.* calcd. for $C_{11}H_{16}O_3$: C 67.32, H 8.22; found: C 67.18, H 8.38.

The Ethylene Dithioacetal 9

To the keto ester **8** (10 g) in methylene chloride (40 mL) were added ethanedithiol (5.76 g), boron trifluoride etherate (2 mL), and molecular sieves (3 g). The mixture was allowed to stand at room temperature for 5 days and then filtered. The filtrate was made alkaline with 3% ammonia and the methylene chloride layer was separated. The organic layer was washed, dried, and evaporated to leave the dithioacetal **9** (13 g, 94%). This product was used for the next step without purification. An analytical sample of **9** was obtained by silica gel column chromatography with chloroform; Kugelrohr distillation at 160–161°C/3 Torr; nmr δ: 1.02 (3H, d, J = 6 Hz, secondary CH_3), 1.27 (3H, t, J = 7 Hz, $CO_2CH_2CH_3$), 1.67 (3H, m, vinylic CH_3), 3.34 (4H, m, $S(CH_2)_2S$), 4.20 (2H, q, J = 7 Hz, $CO_2CH_2CH_3$), and 5.75 (1H, m, olefinic proton); ir ν_{max}: 1728 cm^{-1}. *Anal.* calcd. for $C_{13}H_{20}O_2S_2$: C 57.32, H 7.40; found: C 57.06, H 7.54.

The β,γ-Unsaturated Ester 10

To a solution of **9** (23 g) in dry tetrahydrofuran (200 mL) was added Raney W2 nickel (115 g) and the mixture was stirred at room temperature for 7 days. The mixture was

filtered and the solvent of the filtrate was evaporated *in vacuo* to leave an oily residue. The residue was extracted with ether, and the extract was washed, dried, and evaporated to leave an oil, which was distilled to give the β,γ-unsaturated ester **10** (9.44 g, 61%); bp 98–101°C/28 Torr; ir ν_{max}: 1720 cm^{-1}; nmr δ: 0.97 (3H, d, J = 6 Hz, secondary CH_3), 1.27 (3H, t, J = 7 Hz, $CO_2CH_2CH_3$), 1.64 (3H, m, vinylic CH_3), 4.18 (2H, q, J = 7 Hz, $CO_2CH_2CH_3$), and 5.59 (1H, m, olefinic H). *Anal.* calcd. for $C_{11}H_{18}O_2$: C 72.49, H 9.96; found: C 72.72, H 10.11.

The Diester **5**

To a solution of lithium diisopropylamide prepared from diisopropylamine (2.4 mL) and *n*-butyllithium (11 mL of 1.6 *M* *n*-hexane solution) in tetrahydrofuran (3 mL) was added a solution of **10** (1.82 g, 0.01 mol) in tetrahydrofuran (3 mL) at −70°C and the mixture was stirred at −70°C for 2 h. To the mixture were added hexamethylphosphoric triamide (1 mL) and ethyl β-bromopropionate (2.72 g, 0.015 mol), and the mixture was stirred at −30°C for 1 h and then at 0°C for 11 h. The mixture was acidified with 6% hydrochloric acid, concentrated *in vacuo* at room temperature and extracted with ether. The extract was successively washed with 2% sodium bicarbonate, 5% hydrochloric acid, and water. The solution was dried and concentrated to leave a yellow oil (1.5 g). Chromatography over silica gel with chloroform gave the starting material **10** (900 mg) and the diester **5** (570 mg, 40% based on the starting material consumed); Kugelrohr distillation at 128°C/5 Torr; ir ν_{max}: 1721 and 1715 cm^{-1}; nmr δ: 0.92 (3H, m, secondary CH_3), 1.25 (6H, t, J = 7 Hz, $CO_2CH_2CH_3$), 1.55 (3H, m, vinylic CH_3), 4.14 (2H, q, J = 7 Hz, $CO_2CH_2CH_3$), 4.16 (2H, q, J = 7 Hz, $CO_2CH_2CH_3$), and 5.73 (1H, m, olefinic H). *Anal.* calcd. for $C_{16}H_{26}O_4$: C 68.05, H 9.28; found: C 67.82, H 9.02.

The Bis(trimethylsiloxy) Ether **11**

To a refluxing mixture of dry toluene (200 mL) and sodium (11.3 g, 0.5 mol) was added a mixture of **5** (28.2 g, 0.1 mol) and trimethylchlorosilane (70 mL, 0.5 mol) with vigorous stirring under argon and the mixture was continuously stirred under reflux for 2 h. After cooling, the mixture was filtered and the residue was washed with dry ether. The filtrate and the washing were combined and concentrated *in vacuo*. Distillation of the residue under reduced pressure gave **11** (26.6 g, 79%) as a colorless oil; bp 123°C/5 Torr; ir ν_{max}: 1694, 869, and 850 cm^{-1}; nmr δ: 0.17 (9H, s, $Si(CH_3)_3$), 0.22 (9H, s, $Si(CH_3)_3$), 0.98 (3H, d, J = 6 Hz, CH_3 at C-10), 1.67 (3H, m, CH_3 at C-6), and 5.52 (1H, m, H at C-7); ms *m/e* (M^+), calcd. for $C_{18}H_{34}O_2Si_2$: 338.2096; found: 338.2084.

The Spiro Acyloin **6** *and the Keto Acetates* **13** *and* **21**

A mixture of **11** (26.6 g, 79 mmol), 10% hydrochloric acid (10 mL), and tetrahydrofuran (80 mL) was stirred at 0°C for 1 h and then concentrated at room temperature *in vacuo*. The residual oil was extracted with chloroform and the extract was washed, dried, and concentrated *in vacuo* to provide a semisolid (15.6 g). Recrystallization of the solid from chloroform gave the acyloin **6** as colorless needles (5.6 g, 34%); mp 115–118°C; ir ν_{max}: 3500 and 1742 cm^{-1}; nmr δ: 1.12 (3H, d, J = 6 Hz, CH_3 at C-10), 1.52 (3H, m, CH_3 at C-6), 2.75 (1H, d, J = 3.5 Hz, OH at C-1, disappeared by addition of deuterium oxide), 4.05 (1H, d, J = 3.5 Hz, H at C-1, this signal was changed to a singlet by addition of deuterium oxide), 5.53 (1H, m, H at C-7). *Anal.* calcd. for $C_{12}H_{18}O_2$: C 74.19, H 9.34; found: C 73.89, H 9.46.

The solvent of the mother liquor removed from the crystalline acyloin **6** by filtration was evaporated *in vacuo* to leave an oil (10 g) which was treated with pyridine (10 mL) and acetic anhydride (10 mL) in chloroform (30 mL) at 0°C for 48 h. The mixture was concentrated *in vacuo* and the residue was made alkaline with 3% ammonia, and then extracted with ether. The extract was washed, dried, and concentrated to leave an oil (11.7 g) which was chromatographed over silica gel (column 6 × 22 cm) with a 3:7 mixture of *n*-pentane and chloroform to yield the colorless oily keto acetate **13** in the first eluate (5.3 g, 43.6% based on the oil obtained from the mother liquor) and the colorless oily keto acetate **21** in the later eluate (1.9 g, 15.6% based on the oil obtained from the mother liquor).

The acetate **13**: Kugelrohr distillation at 110°C/5 Torr; ir ν_{max}: 1754 and 1737 cm^{-1}; nmr δ: 0.93 (3H, d, J = 6 Hz, CH_3 at C-10), 1.58 (3H, m, CH_3 at C-6), 2.12 (3H, s, $OCOCH_3$), 5.28 (1H, t, J = 10 Hz, H at C-1), and 5.63 (1H, m, H at C-7); M^+ calcd. for $C_{14}H_{20}O_3$: 236.1411; found (ms): 236.1364.

The acetate **21**: mp 64–68°C (**21** forms colorless prisms on standing in a refrigerator after Kugelrohr distillation): ir ν_{max}: 1757 and 1742 cm^{-1}; nmr δ: 1.00 (3H, d, J = 6 Hz, CH_3 at C-10), 1.59 (3H, m, CH_3 at C-7), 2.13 (3H, s, $OCOCH_3$), 5.38 (1H, s, H at C-1), and 5.48 (1H, m, H at C-7). *Anal.* calcd. for $C_{14}H_{20}O_3$: C 71.16, H 8.53; found: C 70.96, H 8.56.

The Keto Mesylate **14**

To the acyloin **6** (300 mg, 1.55 mmol) in chloroform (5 mL) were added pyridine (3 mL) and methanesulfonyl chloride (1.4 mL) at 0°C and the mixture was allowed to stand at 0°C for 48 h. The mixture was made alkaline with 3% ammonia and extracted with ether. The extract was washed with 5% hydrochloric acid, dried, and evaporated to leave a crystalline mass. Recrystallization of the mass from a 4:1 mixture of ether and chloroform gave **14** (405 mg, 96%) as colorless needles; mp 126–127°C; ir ν_{max}: 1759 cm^{-1}; nmr δ: 1.15 (3H, d, J = 6 Hz, CH_3 at C-10), 1.57 (3H, m, CH_3 at C-6), 3.27 (3H, s, SO_2CH_3), 5.09 (1H, s, H at C-1), and 5.48 (1H, m, H at C-6). *Anal.* calcd. for $C_{13}H_{20}O_4$: C 57.33, H 7.40; found: C 57.56, H 7.58.

The Spiro Ketone **15**

To a mixture of **14** (230 mg, 0.85 mmol) in methanol (9 mL) and tetrahydrofuran (1 mL) were added ammonium chloride (1 g) and zinc powder (3 g) with stirring. The mixture was stirred at room temperature for 2 h and then at 60°C for 6 h. The mixture was added to tetrahydrofuran (20 mL) and filtered and the residue was washed with ether. The filtrate and the washing were combined and concentrated *in vacuo* to leave an oil. The oil was extracted with ether and the extract was washed, dried, and evaporated to leave an oil. Chromatography of the oil on silica gel (column 2.5 × 17 cm) with methylene chloride gave **15** (150 mg, 99%). The spiro ketone **15**: Kugelrohr distillation at 128°C/15 Torr; ir ν_{max} (film): 1740 cm^{-1}; nmr δ (CCl_4): 0.90 (3H, d, J = 6 Hz, CH_3 at C-10), 1.64 (3H, m, CH_3 at C-6), and 5.37 (1H, m, H at C-7). *Anal.* calcd. for $C_{12}H_{18}O$: C 80.85, H 10.18; found: C 81.14, H 10.48.

The Spiro Ketones **15** *and* **16**

To the keto acetate **13** (700 mg) in a 9:1 mixture of methanol and water was added sodium borohydride (150 mg) with stirring at −10°C and the mixture was stirred for 30 min. After evaporation of the solvent *in vacuo*, the residue was made acidic with 5% hydrochloric acid and extracted with chloroform. The extract was washed, dried, and evaporated to leave a colorless oil (710 mg). To the above oil (710 mg) in chloroform (4 mL) were added pyridine (2 mL) and methanesulfonyl chloride (2 mL) at 0°C with stirring, and the mixture was kept

at 0°C for 24 h. The mixture was made alkaline with 3% ammonia and extracted with ether. The extract was successively washed with 5% hydrochloric acid and water, dried, and evaporated to leave a colorless oil (800 mg). The above oil (800 mg) in ethanol (10 mL) was added to 25% potassium hydroxide (2 mL), and the mixture was heated under reflux for 3 h under an atmosphere of argon. After evaporation of the solvent *in vacuo*, the residue was extracted with ether and the extract was washed, dried, and concentrated *in vacuo* to leave an oil. The oil was chromatographed on silica gel (column 10 × 30 cm) with methylene chloride to afford the spiro ketone **15** (100 mg, 19% based on the keto acetate **13**) and the isomeric spiro ketone **16** (200 mg, 38% based on **13**). The spiro ketone **15** was identified by ir, nmr, and gas chromatographic comparisons with those of an authentic sample prepared from **14**. The spiro ketone **16**: ir ν_{max}: 1719 cm^{-1}; nmr δ: 0.89 (3H, d, J = 6 Hz, CH_3 at C-10), 1.57 (3H, m, CH_3 at C-6), and 5.62 (1H, m, H at C-7). *Anal.* calcd. for $C_{12}H_{18}O$: C 80.85, H 10.18; found: C 80.92, H 10.42.

The Enol Methyl Ether ***17***

To a solution of the Wittig reagent prepared from methoxymethylenetriphenylphosphonium chloride (1.7 g, 5 mmol) and sodium hydride (120 mg, 5 mmol) in dimethyl sulfoxide (12 mL) was added **15** (176 mg, 1 mmol) in tetrahydrofuran (2 mL) at 0°C with stirring under an atmosphere of argon, and the mixture was stirred at 0°C for 17 h. The mixture was added to water (10 mL) and extracted with ether. The extract was successively washed with 2% hydrochloric acid, 3% ammonia, and water, dried and evaporated to leave an oily residue, which was purified by preparative thin-layer chromatography on silica gel developed with a 3:7 mixture of *n*-hexane and chloroform to yield **17** (120 mg, 59%) as a colorless oil; ir ν_{max}: 1690 cm^{-1}. M^+ calcd. for $C_{14}H_{22}O$: 206.1670; found (ms): 206.1660.

The Aldehyde ***18***

To a solution of **17** (140 mg, 0.68 mmol) in tetrahydrofuran (2 mL) was added 10% hydrochloric acid (2 mL) and the mixture was heated under reflux for 2 h. After evaporation of the solvent, the residue was extracted with ether. The extract was washed, dried, and evaporated to leave a yellow oily residue which was purified by preparative thin-layer chromatography on silica gel developed with a 4:1 mixture of chloroform and *n*-hexane to provide **18** (110 mg, 84%) as an epimeric mixture; Kugelrohr distillation at 95°C/5 Torr; ir ν_{max}: 2680 and 1718 cm^{-1}; nmr δ: 0.90 and 0.93 (3H, d, J= 6 Hz, CH_3 at C-10), 1.67 (3H, m, CH_3 at C-6), 2.75 (1H, m, H at C-1), 5.37 (1H, m, H at C-7), and 9.63 (1H, d, J = 3 Hz, CHO). M^+ calcd. for $C_{13}H_{20}O$: 192.1512; found (ms): 192.1495.

The Methyl Ketone ***20***

To an ethereal solution (3 mL) of 1.25 mol methyllithium in ether was added a solution of **18** (100 mg, 0.52 mol) in dry ether (2 mL) and the mixture was stirred at room temperature for 30 min. To the mixture was added water and then the solution was extracted with a 4:1 mixture of ether and chloroform. The extract was successively washed with 2% sodium bisulfite and water, dried, and evaporated to leave a yellow oil (100 mg). The above oil (100 mg) in acetone (5 mL) was oxidized with the Jones' reagent (0.3 mL) under stirring at room temperature. After evaporation of the solvent *in vacuo*, the residual oil was extracted with ether. The extract was washed, dried, and evaporated to provide a yellow oil which was purified by preparative thin-layer chromatography on silica gel developed with a 10:1 mixture of chloroform and *n*-hexane to provide **20** (33 mg, 31% based on **18**) as an epimeric mixture due to the C-2 chiral center. The methyl ketone **20**: Kugelrohr distillation at 145°C/8 Torr; ir ν_{max}: 1703 cm^{-1}; nmr δ: 0.89 and 0.93 (3H, d, J = 6 Hz, CH_3 at C-10), 1.68 (3H, m, CH_3 at C-6), 2.15 (3H, s, $COCH_3$), 2.92 (1H, m, H at C-2), and 5.33 (1H, m, H at C-7). M^+ calcd. for $C_{14}H_{22}O$: 206.1669; found (ms): 206.1669.

*(±)-Hinesol (**1**) and (±)-Agarospirol (**2**)*

To an ethereal solution (3 mL) of 1.25 mol methyllithium in ether was added a solution of **20** (370 mg, 1.8 mmol) in dry ether (3 mL) with stirring at −30°C. The solution was allowed to stand at room temperature for 5 min. To the mixture was added water, and the solution was extracted with a 4:1 mixture of ether and chloroform. The extract was washed with 2% sodium bisulfite and water, dried, and evaporated to leave an oily residue (330 mg, 83%) which was a 3:2 mixture of (±)-hinesol **1** and (±)-agarospirol **2** judging from gas chromatography on 10% FFAP on chromosorb W (3 mm × 3 m, column temperature 190°C, (±)-hinesol 12.4 min, (±)-agarospirol 12.0 min). The mixture was separated by repeated preparative thin-layer chromatography on silica gel (silica gel 60 F_{254}, Merck) developed with a 3:1 mixture of chloroform and *n*-hexane to give (±)-hinesol (**1**) and (±)-agarospirol (**2**).

(±)-Hinesol (**1**): Kugelrohr distillation at 99°C/5 Torr; ir ν_{max} (CCl_4): 3620, 3025, 2965, 2920, 2870, 2830, 1660, 1468, 1455, 1380, 1367, 947, and 915 cm^{-1}; nmr δ: 0.93 (3H, d, J = 6 Hz, CH_3 at C-10), 1.21 (6H, s, CH_3 at C-12 and C-13), 1.69 (3H, m, CH_3 at C-6), and 5.28 (1H, m, H at C-7). M^+ calcd. for $C_{15}H_{26}O$: 222.1983; found (ms): 222.2058. The ir and nmr spectra of (±)-hinesol **1** were indistinguishable from those of natural hinesol.

(±)-Agarospirol (**2**): Kugelrohr distillation at 99°C/5 Torr; ir ν_{max} (CCl_4): 3620, 3025, 2960, 2930, 2875, 2845, 1460, 1437, 1379, 1368, 931, and 910 cm^{-1}; nmr δ: 0.90 (3H, d, J = 6 Hz, CH_3 at C-10), 1.20 (6H, s, CH_3 at C-12 and C-13), 1.68 (3H, m, CH_3 at C-6), and 5.22 (1H, m, H at C-7). M^+ calcd. for $C_{15}H_{26}O$: 222.1982; found: 222.1979.

The Keto Acetates ***13*** *and* ***21***

To a stirred solution of **6** (500 mg, 2.6 mmol) in chloroform (2 mL) pyridine (2 mL) and acetic anhydride (2 mL) were added and the mixture was allowed to stand at room temperature for 18 h. The solvent and the excess reagents were evaporated *in vacuo*, and the residual oil was, after made alkaline with 3% ammonia, extracted with ether. The extract was successively washed with 5% hydrochloric acid, 3% ammonia, and water. The solution was dried and evaporated *in vacuo* to leave an oily residue (600 mg, 99%) which was a 10:24 mixture of **13** and **21**. The mixture was chromatographed on silica gel (column 3.8 × 21 cm) with chloroform to provide **13** in the first eluate and **21** in a later eluate. The keto acetates **13** and **21** were identified by ir and nmr spectral comparisons with those of authentic samples (*vide supra*).

The α,β-Unsaturated Aldehyde ***22***

To a solution of sodium methylsulfinylmethide prepared from sodium hydride (120 mg, 5 mmol) and dimethyl sulfoxide (4 mL) were added tetrahydrofuran (5 mL) and methoxymethylenetriphenylphosphonium chloride (1.7 g, 5 mmol) in dimethyl sulfoxide (6 mL). To the above reagent was added **21** (236 mg, 1 mmol) in tetrahydrofuran (3 mL) with stirring at 0°C and stirring was continued for 15 h. To the mixture was added ice water and the solution was extracted with ether. The extract was washed, dried, and evaporated *in vacuo* to provide an oily residue which was heated under reflux in a mixture of tetrahydrofuran (20 mL) and 10% hydrochloric acid (5 mL) for 1 h. After evaporating the solvent *in vacuo*, the residual oil was extracted with ether and

the extract was washed, dried, and evaporated to give an oily residue. Purification by preparative thin-layer chromatography over silica gel developed with a 1:1 mixture of *n*-hexane and chloroform gave **22** (13 mg, 7%); ir ν_{max}: 1678 and 1620 cm^{-1}; nmr δ: 0.90 (3H, d, J = 6 Hz, CH_3 at C-10), 1.57 (3H, m, CH_3 at C-6), 5.50 (1H, m, H at C-7), 6.62 (1H, t, J = 1.5 Hz, H at C-1), and 9.82 (1H, s, CHO). M^+ calcd. for $C_{13}H_{18}O$: 190.1356; found (ms): 190.1348.

The Methyl Ketone ***24***

Following the experimental procedure of the synthesis of the ketone **20**, the aldehyde **22** (55 mg, 0.29 mmol) was converted into the methyl ketone **24** (25 mg, 42%) by the conventional two-step sequence involving reaction with methyllithium and subsequent treatment with Jones' reagent. The methyl ketone **24**: ir ν_{max}: 1657 and 1610 cm^{-1}; nmr δ: 0.88 (3H, d, J = 6 Hz, CH_3 at C-10), 1.58 (3H, m, CH_3 at C-6), 2.31 (3H, s, $COCH_3$), 5.48 (1H, m, H at C-7), and 6.47 (1H, t, J = 1.5 Hz, H at C-1). M^+ calcd. for $C_{14}H_{20}O$: 204.1512; found (ms): 204.1497.

*(±)-α-Vetispirene (****4****)*

To a stirred ethereal solution of methyllithium (4 mL, 5 mmol) was added a solution of **24** (25 mg, 0.12 mmol) in dry ether (2 mL) at −30°C and the solution was stirred for 30 min. Water was added to the mixture and the solution was extracted with ether. The extract was washed with 5% sodium bisulfite and then with water, dried, and evaporated to leave **25** (27 mg, 95%) as a rather labile oil which was warmed at 50°C with 10-camphorsulfonic acid (5 mg) in dry benzene (1 mL) for 1 h. The mixture was extracted with ether and the extract was washed, dried, and evaporated to leave an oil which was purified by preparative thin layer chromatography on silica gel developed with *n*-hexane to provide (±)-α-vetispirene **4** (11 mg, 44%). The ir and nmr spectra of synthesized product were identical with those of an authentic sample.[3] (±)-α-Vetispirene **4**: ir ν_{max} (CCl_4): 3085, 3045, 3018, 1774, 1673, 1630, 1596, 1374, 1199, 1073, 1056, 880, and 840 cm^{-1}; nmr δ (CCl_4): 0.86 (3H, d, J = 6 Hz, CH_3 at C-10), 1.53 (3H, m, CH_3 at C-6), 1.90 (3H, d, J = 1.0 Hz, CH_3 at C-12) 4.83 (2H, d, J = 1.0 Hz, CH_2 at C-13), 5.30 (1H, m, H at C-7), and 5.44 (1H, m, H at C-1). M^+ calcd. for $C_{15}H_{22}$: 202.1719; found (ms): 202.1651.

Acknowledgement

This work was supported, in part, by a grant (No. 357604) from the Ministry of Education of Japan.

1. (*a*) J. A. MARSHALL, ST. F. BRADY, and N. H. ANDERSEN. *In* Progress in the chemistry of organic natural products. Vol. 31. Springer-Verlag, Wien and New York. 1974. pp. 283–371 and references cited therein; (*b*) C. H. HEATHCOCK. *In* The total synthesis of natural products. Vol. 2. *Edited by* J. ApSimon. John Wiley & Sons. 1973. pp. 466–474 and references cited therein.
2. (*a*) A. ST. PFAU and PL. A. PLATTNER. Helv. Chim. Acta, **23**, 768 (1940); (*b*) J. A. MARSHALL and P. C. JOHNSON. J. Am. Chem. Soc. **89**, 2750 (1967); (*c*) N. H. ANDERSEN and M. S. FALCONE. Chem. Ind. (London), 62 (1972).
3. (*a*) K. YAMADA, S. GOTO, H. NAGASE, and A. T. CHRISTENSEN. J. Chem. Soc. Chem. Commun. 554 (1977); (*b*) A. STOESSL, J. B. STOTHERS, and E. W. B. WARD. J. Chem. Soc. Chem. Commun. 431 (1975); (*c*) A. STOESSL, J. B. STOTHERS, and E. W. B. WARD. Can. J. Chem. **53**, 3351 (1975) and references cited therein; (*d*) D. T. COXON, K. R. PRICE, B. HOWARD, S. F. OSMAN, E. B. KALAN, and R. M. ZACHARIUS. Tetrahedron Lett. 2921 (1974).
4. R. C. ANDERSON, D. M. GUNN, J. M.-RUST, P. M.-RUST, and J. S. ROBERTS. J. Chem. Soc. Chem. Commun. 27 (1977).
5. G. I. BIRNBAUM, C. P. HUBER, M. L. POST, and J. B. STOTHERS. J. Chem. Soc. Chem. Commun. 330 (1976).
6. J. A. MARSHALL and P. C. JOHNSON. J. Org. Chem. **35**, 192 (1970).
7. (*a*) W. G. DAUBEN and D. J. HART. J. Am. Chem. Soc. **99**, 7307 (1977); (*b*) G. STORK, R. L. DANHEISER, and B. GANEM. J. Am. Chem. Soc. **95**, 3414 (1973); (*c*) E. WENKERT, B. L. BUCKWALTER, A. A. CRAVEIRO, L. SANCHEZ, and S. S. SATHE. J. Am. Chem. Soc. **100**, 1267 (1978); (*d*) M. MONGRAIN, J. LAFONTAINE, A. BÉLANGER, and P. DESLONGCHAMPS. Can. J. Chem. **48**, 3273 (1970); (*e*) K. YAMADA, K. AOKI, H. NAGASE, Y. HAYAKAWA, and Y. HIRATA. Tetrahedron Lett. 4967 (1973) and references cited therein.
8. G. BÜCHI, D. BERTHET, R. DECORZANT, A. GRIEDER, and H. HAUSER. J. Org. Chem. **41**, 3208 (1976).
9. (*a*) D. CAINE, A. A. BOUCUGNANI, S. T. CHAO, J. B. DAWSON, and P. E. INGWALSON. J. Org. Chem. **41**, 1539 (1976); (*b*) D. CAINE, A. A. BOUCUGNANI, and W. R. PENNINGTON. J. Org. Chem. **41**, 3632 (1976); (*c*) D. CAINE, A. A. BOUCUGNANI, C.-Y. CHU, S. L. GRAHAM, and T. L. SMITH, JR. Tetrahedron Lett. 2667 (1978).
10. E. PIERS and C. K. LAU. Synth. Commun. 495 (1977).
11. T. IBUKA, Y. ITO, Y. MORI, T. AOYAMA, and Y. INUBUSHI. Synth. Commun. 131 (1977).
12. J. J. BLOOMFIELD, D. C. OWSLEY, and J. M. NELKE. Org. Reactions, **23**, 305 (1976).
13. G. BÜCHI. Koryo, 99 (1978).
14. K. OKA and S. HARA. J. Am. Chem. Soc. **99**, 3857 (1977).
15. I. YOSHIOKA and T. KIMURA. Chem. Pharm. Bull. **13**, 1430 (1965).

Microbial hydroxylation of steroids. 6. Hydroxylation of C-6-substituted androst-4-ene-3,17-diones by *Rhizopus arrhizus* ATCC 11145[1]

HERBERT L. HOLLAND AND PETER R. P. DIAKOW

Department of Chemistry, Brock University, St. Catharines, Ont., Canada L2S 3A1

Received November 1, 1978

HERBERT L. HOLLAND and PETER R. P. DIAKOW. Can. J. Chem. **57**, 1585 (1979).

The products arising from the incubations of C-6α and C-6β chloro-, fluoro-, and methyl-substituted Δ^4-3-keto steroids with the C-6β hydroxylating fungus *Rhizopus arrhizus* ATCC 11145 have been identified, and their formation rationalised in terms of $\Delta^{3,5}$ enolic intermediates. The incubations of C-6 chloro and methyl $\Delta^{3,5}$ enol acetates with *R. arrhizus*, and the oxidations by *m*-chloroperoxybenzoic acid of the corresponding enol ethyl ethers have also been described. The relevance of the results so obtained to the mechanism of C-6β hydroxylation of Δ^4-3-keto steroids by *R. arrhizus* is discussed.

HERBERT L. HOLLAND et PETER R. P. DIAKOW. Can. J. Chem. **57**, 1585 (1979).

On a identifié les produits qui se forment par incubation de Δ^4 céto-3 stéroïdes (substitués en C-6α et C-6β par des chlore, fluor ou méthyle) avec les champignons hydroxylant en C-6β, *Rhizopus arrhizus* ATCC 11145 et l'on a rationalisé leur formation en termes d'intermédiaires énoliques $\Delta^{3,5}$. On décrit aussi les incubations des acétates énoliques $\Delta^{3,5}$ substitués en C-6 par un chlore ou un méthyle ainsi que les oxydations par l'acide *m*-chloroperbenzoïque des éthers énoliques éthyliques correspondants. On discute de la relation entre ces résultats et le mécanisme de l'hydroxylation en C-6β des Δ^4 céto-3 stéroïdes par le *R arrhizus*.

[Traduit par le journal]

Introduction

The microbial hydroxylation of the medicinally important 9-halo steroids at positions remote from the site of halogen substitution has been investigated (1, 2) and the C-11α hydroxylation of 6-halo steroids documented (1, 2) but there have been no reports concerning the incubation of *n*-halo steroids with fungi known to hydroxylate C-*n* of the corresponding unsubstituted steroid.

As part of our investigation into the mechanism of the C-6β hydroxylation of androst-4-ene-3,17-dione (**1***a*) (3, 4) by *Rhizopus arrhizus* ATCC 11145, we have incubated C-6-chloro- (**1***b*, **2***a*), C-6-fluoro- (**1***d*, **2***b*), and C-6-methyl- (**1***e*, **2***c*) substituted androst-4-ene-3,17-diones with this fungus. We have also studied the metabolism of the $\Delta^{3,5}$ enol acetates **4***a* and **4***b*, and the oxidation of the corresponding enol ethers **4***c* and **4***d* by *m*-chloroperoxybenzoic acid.

Results and Discussion

The results of the incubations with *R. arrhizus* are summarised in Table 1 (see also Experimental). The identification of known steroids was confirmed by a comparison of physical and spectral data with those of authentic samples. New steroids arising from C-11α hydroxylation (**1***c*, **1***f*, **1***g*, and **2***d*) were identified by spectral analysis (see Experimental), ^{1}Hmr data being typically diagnostic (5).

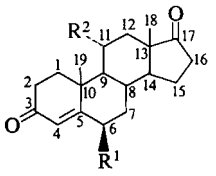

1

a $R^1 = R^2 = H$
b $R^1 = Cl, R^2 = H$
c $R^1 = Cl, R^2 = OH$
d $R^1 = F, R^2 = H$
e $R^1 = CH_3, R^2 = H$
f $R^1 = CH_3, R^2 = OH$
g $R^1 = F, R^2 = OH$

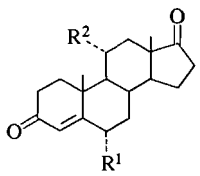

2

a $R^1 = Cl, R^2 = H$
b $R^1 = F, R^2 = H$
c $R^1 = CH_3, R^2 = OH$

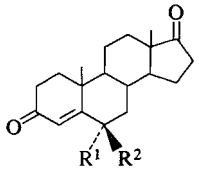

3

a $R^1 + R^2 = O$
b $R^1 = CH_3, R^2 = OH$

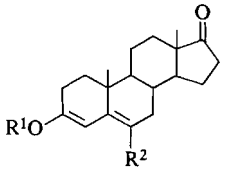

4

a $R^1 = Ac, R^2 = Cl$
b $R^1 = Ac, R^2 = CH_3$
c $R^1 = Et, R^2 = Cl$
d $R^1 = Et, R^2 = CH_3$

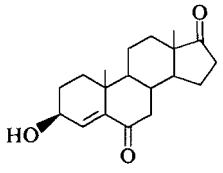

5

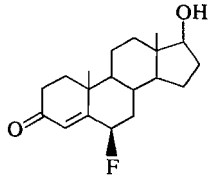

6

[1]Dedicated to the memory of R. H. F. Manske.

0008-4042/79/131585-03$01.00/0

TABLE 1. Results of incubations with *Rhizopus arrhizus*

Substrate	Amount incubated (mg)	Amount recovered (mg)	Products (% isolated)
1*b****	1500	650	**1***b* (2), **2***a* (2), **1***c* (3)
1*d**	1600	1200	**1***d* (17), **1***g* (2), **3***a* (1), **5** (1), **6** (2)
1*e*	500	419	**1***e* (40), **1***f* (17)
2*a*	2000	1100	**2***a* (32), **3***a* (1), **5** (0.5)
2*b*	1000	630	**2***b* (14), **3***a* (2)
2*c*	500	300	**2***c* (5), **2***d* (19)
4*a*	1500	560	**4***a* (4), **2***a* (1), **3***a* (3), **5** (2)
4*b*	150	104	**1***e* (40), **2***d* (16), **3***b* (14)

*Control incubations in the absence of fungus resulted in the recovery of starting material only.

The C-6β chloride **1***b* gave, along with some recovered starting material, small amounts of the corresponding C-6α chloride **2***a* and the product of C-11α hydroxylation, **1***c*, only. In contrast, the C-6β fluoride **1***d* gave, in addition to the C-11α-hydroxy steroid **1***g*, the Δ^4-3,6-dione **3***a*, the 3β-hydroxy-Δ^4-6-ketone **5**, and the product of reduction of the C-17 carbonyl, **6**; the reduction at C-17 of androst-4-ene-3,17-dione (**1***a*) by *R. arrhizus* has been reported (3). The corresponding C-6α-halo steroids **2***a* and **2***b* were recovered largely unchanged from incubation with *R. arrhizus*, although small amounts of **3***a* were formed in each case and the chloride **2***a* also gave the 3β-hydroxy Δ^4-6-ketone **5**.

The hydroxylation at C-6β of androst-4-ene-3,17-dione (**1***a*) by *R. arrhizus* is thought to proceed via the $\Delta^{3,5}$ enol intermediate (**7***a*) (3, 4, 6) and the results presented above may also be interpreted as involving the corresponding chloro and fluoro enols, **7***b* and **7***c*, respectively (Scheme 1). Protonation of an intermediate such as **7** would be expected to give the thermodynamically stable C-6α derivative; electrophilic oxidation will lead, via the halo hydrin **8** to **3***a*; and hydration, via **9**, will lead to **5**. The extent of protonation versus oxidation and/or hydration is presumably controlled by enzymic factors, which are unknown at the present time.

Support for the existence of the intermediate **7** is provided by the results of the incubation of the 6-chloro enol acetate **4***a*; the products of protonation (**2***a*), oxidation (**3***a*), and hydration (**5**) were isolated. Chemical analogy for the protonation and oxidation processes are provided by the *m*-chloroperoxybenzoic acid oxidation of the 6-chloro enol ether **4***c* (see refs. 3 and 6 for discussion of this reaction as a model for the C-6β hydroxylation process), where both **2***a* and **3***a* were formed.

The C-6-methyl substituted steroids **1***e* and **2***c* gave only the products of the C-11α hydroxylation (**1***f* and **2***d*, respectively), on incubation with *R. arrhizus*,

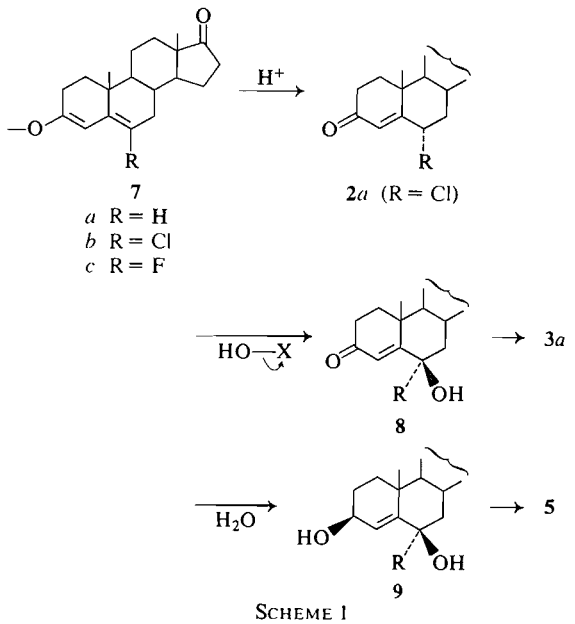

7
a R = H
b R = Cl
c R = F

2*a* (R = Cl)

8

9

SCHEME 1

although incubation of the corresponding enol acetate **4***b* did lead to the formation of a C-6β-hydroxylated steroid (**3***b*), in addition to C-11α hydroxylation. This observation has been interpreted as follows (7): C-6β hydroxylation occurs via the $\Delta^{3,5}$ enol and the fungus is able to hydrolyse and oxidise **4***b* to **3***b* but it lacks the ability to enolise either **1***e* or **2***c*. Chemical analogy for the enzymic oxidation of **4***b* is again provided by peracid oxidation of the corresponding enol ether (**4***d*), leading to **3***b* in moderate yield.

The results presented and discussed herein therefore support our earlier conclusion (3, 4) that the C-6β hydroxylation of androst-4-ene-3,17-dione by the fungus *R. arrhizus* involves an enolic intermediate. Studies with more sophisticated chemical model systems for this reaction are currently in progress.

Experimental

Apparatus, Materials, and Methods

The apparatus and techniques used were as previously described (3). Analytical samples were purified and final separation of **1***g*, **5**, and **6** performed by chromatography on a column of Whatman Partisil 20 silica gel (800 × 7.8 mm, eluent 0.5% methanolic chloroform) using a Perkin-Elmer series 3 high pressure liquid chromatograph. Incubations with *R. arrhizus* were performed as described (6).

Preparation of Substrates

The following were prepared by published procedures and gave satisfactory spectral and analytical data. 6β-Chloroandrost-4-ene-3,17-dione (**1***b*) (8), 6α-chloroandrost-4-ene-3,17-dione (**2***a*) (8), 6β-fluoroandrost-4-ene-3,17-dione (**1***d*) (9), 6α-fluoroandrost-4-ene-3,17-dione (**2***b*) (9), 6β-methylandrost-4-ene-3,17-dione (**1***e*) (10), 6α-methylandrost-4-ene-3,17-dione (**2***c*) (10), 3-acetoxy-6-methylandrosta-3,5-diene-17-

one (**4***b*) (11), 6-chloro-3-ethoxyandrosta-3,5-diene-17-one (**4***c*) (12), and 3-ethoxy-6-methylandrosta-3,5-diene-17-one (**4***d*) (13).

*3-Acetoxy-6-chloroandrosta-3,5-diene-17-one (**4**a)*

6α-Chloroandrost-4-ene-3,17-dione (5 g) was dissolved in a mixture of absolute ethyl acetate (800 mL), chloroform (100 mL), and acetic anhydride (100 mL), and then 70% aqueous perchloric acid (0.4 mL) added to the solution. The resulting dark green mixture was stirred at room temperature for 2 h and then washed (sodium bicarbonate, followed by water) and dried (sodium sulphate). After treatment of the solution with decolourising carbon and filtration, it was concentrated on a rotary evaporator at 40°C and then diluted with hexane (500 mL). The crystals which deposited after the resulting solution was cooled overnight at −20°C were collected by filtration and recrystallized from ethyl acetate – hexane to give 2.5 g of the title compound, mp 170–172°C; ir (KBr) ν_{max}: 1735, 1760 cm^{-1}; ^{1}Hmr (δ): 0.92 (3H, s, C-18H), 1.08 (3H, s, C-19H), 2.17 (3H, s, CH_3CO—), 6.33 (1H, s, C-4H); ms *m/e* (%): 322 (32), 320 (100), 307 (1.5), 305 (3.5), 285 (9). *Anal.* calcd. for $C_{21}H_{27}ClO_3$: C 69.51, H 7.50, Cl 9.77; found: C 69.31, H 7.47, Cl 9.63.

Incubations with R. arrhizus

Results of the incubations of **1**, **2**, and **4** are presented in Table 1. In all cases, products were isolated by chromatography as previously described (4). Physical and spectral data for hitherto unreported compounds are listed (*vide infra*); all other products were identified by comparison of physical and spectral data with those of authentic samples.

*6β-Chloro-11α-hydroxyandrost-4-ene-3,17-dione (**1**c)*—mp 189–192°C (dec.); ^{1}Hmr (δ): 1.01 (3H, s, C-18H), 1.62 (3H, s, C-19H), 4.20 (1H, sex., J = 10 and 5 Hz, C-11βH), 4.82 (1H, t, J = 3 Hz, C-6αH), 5.90 (1H, s, C-4H); ms *m/e* (%): 338 (6), 336 (15), 302 (100), 300 (39), 287 (36), 282 (50). *Anal.* calcd. for $C_{19}H_{25}ClO_3$ (M^+ 336.149 (^{35}Cl)): C 67.75, H 7.48, Cl 10.52; found (M^+ 336.155): C 67.72, H 7.37, Cl 10.39.

*11α-Hydroxy-6β-methylandrost-4-ene-3,17-dione (**1**f)*—mp 212–214°C; ^{1}Hmr (δ): 0.97 (3H, s, C-18H), 1.30 (3H, d, J = 8 Hz, C-6βCH_3), 1.44 (3H, s, C-19H), 3.9–4.3 (1H, m, C-11βH), 5.80 (1H, s, C-4H); ms *m/e* (%): 316 (90), 298 (100), 283 (32). *Anal.* calcd. for $C_{20}H_{28}O_3$: C 75.91, H 8.92; found: C 75.81, H 9.14.

*11α-Hydroxy-6α-methylandrost-4-ene-3,17-dione (**2**d)*—mp 225–227°C; ^{1}Hmr (δ): 0.96 (3H, s, C-18H), 1.13 (3H, d, J = 6.5 Hz, C-6αCH_3) 1.36 (3H, s, C-19H), 3.9–4.3 (1H, m, C-11βH), 5.87 (1H, d, J = 2 Hz, C-4H); ms *m/e* (%): 316 (83), 298 (100), 283 (25). *Anal.* calcd. for $C_{20}H_{28}O_3$ (M^+ 316.204): C 75.91, H 8.92; found (M^+ 316.205): C 75.67, H 9.0.

*6β-Fluoro-11α-hydroxyandrost-4-ene-3,17-dione (**1**g)*—R_f 0.20 (4% methanol–chloroform), 0.33 (2% methanol – ether), 0.15 (ether); mp 206–209°C (acetone–hexane); ^{1}Hmr δ: 1.00 (3H, s, C-19H), 1.47 (3H, d, J = 2 Hz, C-19H), 3.9–4.3 (1H, m, C-11βH), 5.06 (1H, d, J = 50 Hz, C-6αH), 5.93 (1H, d, J = 5.5 Hz, C-4H); ms *m/e* (%): 320 (100), 302 (77), 300 (50), 287 (37), 282 (55), 267 (73). M^+ calcd. for $C_{19}H_{25}FO_3$: 320.179; found: 320.181.

Oxidations with m-*Chloroperoxybenzoic Acid*

The following were oxidised using the procedure described previously (6) and gave the products indicated.

*6-Chloro-3-ethoxyandrosta-3,5-diene-17-one (**4**c)*

Oxidation of 0.696 g of **4***c* gave 6α-chloroandrost-4-ene-3,17-dione (**2***a*) (0.31 g, 50%), mp 215–217°C (lit. (8) mp 216–218°C); ^{1}Hmr (δ): 0.93 (3H, s, C-18H), 1.27 (3H, s, C-19H), 4.6–5.0 (1H, m, C-6βH), 6.43 (1H, d, J = 2 Hz, C-4H); ms M^+ 320/322; and androst-4-ene-3,6-17, trione (**3***a*) (0.107 g, 19%), mp 222–224°C (lit. (14) mp 217–219°C); ^{1}Hmr (δ): 0.94 (3H, s, C-18H), 1.21 (3H, s, C-19H), 6.21 (1H, s, C-4H); ms M^+ 320.

*3-Ethoxy-6-methylandrosta-3,5-diene-17-one (**4**d)*

Oxidation of 0.9 g of **4***d* gave 6α-methylandrost-4-ene-3,17-dione (**2***c*) (0.1 g, 12%), mp 165–166°C (lit. (10) mp 164–167°C); ^{1}Hmr (δ): 0.93 (3H, s, C-18H), 1.12 (3H, d, J = 6.5 Hz, C-6αCH_3), 1.23 (3H, s, C-19H), 5.86 (1H, d, J = 2 Hz, C-4H); ms M^+ 300; and 6β-hydroxy-6α-methylandrost-4-ene-3,17-dione (**3***b*) (0.48 g, 42%), mp 235–238°C (lit. (11) mp 237–239°C); ^{1}Hmr (δ): 0.95 (3H, s, C-18H), 1.42, 1.45 (each 3H, s, C-19 and C-6CH_3 H's), 6.06 (1H, s, C-4H); ms M^+ 316.

Acknowledgement

We thank the National Research Council of Canada for financial support.

1. W. Charney and H. L. Herzog. Microbial transformations of steroids. A handbook. Academic Press, New York. 1967.
2. L. L. Smith. Terpenes and steroids. Vol. 4. The Chemical Society, London. 1974. p. 394.
3. H. L. Holland and P. R. P. Diakow. Can. J. Chem. **56**, 694 (1978).
4. H. L. Holland and P. R. P. Diakow. Can. J. Chem. **57**, 436 (1979).
5. J. E. Bridgeman, P. C. Cherry, A. S. Clegg, J. M. Evans, Sir Ewart R. H. Jones, A. Kasal, V. Kumar, G. D. Meakins, Y. Morisawa, E. E. Richards, and P. D. Woodgate. J. Chem. Soc. C, 250 (1970).
6. H. L. Holland and B. J. Auret. Can. J. Chem. **53**, 2041 (1975).
7. H. L. Holland and B. J. Auret. Tetrahedron Lett. 3787 (1975).
8. H. Mori and J. Yamada. Chem. Pharm. Bull. **11**, 1418 (1961).
9. A. Bowers and H. J. Ringold. Tetrahedron, **3**, 14 (1958).
10. J. A. Campbell, J. C. Babcock, and J. A. Hogg. J. Am. Chem. Soc. **80**, 4717 (1958).
11. B. Ellis, S. P. Hall, V. Petrow, and D. M. Williamson. J. Chem. Soc. 22 (1962).
12. A. Ercoli. Br. Patent No. 911,740 (November 28, 1962); Chem. Abstr. **58**, 9180c (1963).
13. C. Burgess, D. Burn, J. W. Ducker, B. Ellis, P. Feather, A. K. Hiscock, A. P. Leftwick, J. S. Mills, and V. Petrow. J. Chem. Soc. 4995 (1962).
14. T. Rull and G. Ourisson. Bull. Soc. Chim. Fr. 1581 (1958).

The biosynthesis of protoberberine and related isoquinoline alkaloids[1]

HERBERT L. HOLLAND
Department of Chemistry, Brock University, St. Catharines, Ont., Canada L2S 3A1

PETER W. JEFFS AND THOMAS M. CAPPS
Paul M. Gross Chemical Laboratory, Department of Chemistry, Duke University, Durham, NC 27706, U.S.A.

AND

DAVID B. MACLEAN
Department of Chemistry, McMaster University, Hamilton, Ont., Canada L8S 4M1

Received December 15, 1978

HERBERT L. HOLLAND, PETER W. JEFFS, THOMAS M. CAPPS, and DAVID B. MACLEAN. Can. J. Chem. 57, 1588 (1979).

The biosynthesis of berberine and hydrastine (in *Hydrastis canadensis*), corydaline and protopine (in *Corydalis solida*), and ochotensimine and protopine (in *C. ochotensis*), has been investigated by the administration of [3-^{14}C]-3′,4′-dihydroxyphenylalanine ([3-^{14}C]DOPA). In all cases, incorporation of label was predominantly into the isoquinoline portion of the alkaloid. The role of DOPA in the early stages of isoquinoline alkaloid biosynthesis in these plants is discussed in the light of this and other relevant data. In addition, the later stages of corydaline biosynthesis have been studied by the administration of [9-*methoxy*-^{14}C]palmatine and -tetrahydropalmatine to *C. solida*, and the origin of the exocyclic carbons of ochotensimine further verified by feeding [*methyl*-^{14}C,^{3}H]methionine to *C. ochotensis*.

HERBERT L. HOLLAND, PETER W. JEFFS, THOMAS M. CAPPS et DAVID B. MACLEAN. Can. J. Chem. 57, 1588 (1979).

On a étudié la biosynthèse de la berbérine et de l'hydrastine (dans *Hydrastis canadensis*), de la corydaline et de la protopine (dans *Corydalis solida*) et de l'ochotensimine et de la protopine (dans *C. ochotensis*) en administrant de la [3-^{14}C]dihydroxy-3′,4′ phénylalanine ([3-^{14}C]DOPA). Dans tous les cas, l'incorporation du marqueur se fait principalement dans la portion isoquinoléine de l'alcaloïde. On discute du rôle de la DOPA dans les stades préliminaires de la biosynthèse des alcaloïdes de l'isoquinoléine dans ces plantes à la lumière de ces données et d'autres qui leur sont reliées. De plus, on a étudié les derniers stades de la biosynthèse de la corydaline en administrant des [*méthoxy*-9 ^{14}C]palmatine et -tétrahydropalmatine dans du *C. solida* et on a de plus vérifié l'origine des carbones exocycliques de l'ochotensimine en administrant de la [*méthyl*-^{14}C,^{3}H]méthionine au *C. ochotensis*.

[Traduit par le journal]

The biosynthesis of alkaloids of the benzylisoquinoline group (**1**) and of related alkaloids such as the protoberberines (**2**) has been extensively investigated (1). As shown in Scheme 1 two molecules of tyrosine (**3**) form the isoquinoline 'upper' and benzyl 'lower' portions of **1** whereas the protoberberines are derived from **1** and methionine. In the many isoquinoline systems that have been studied tyrosine has been shown to be incorporated almost equally into both the 'upper' and 'lower' portions of the molecule (1, 2).

The nature of the intermediates resulting from tyrosine during the biosynthesis of the benzylisoquinoline system has not, however, been fully established. It has been proposed that norlaudanosoline (**8***a*) may be derived from two molecules of tyrosine by either of the routes shown in Scheme 2 (1, 3) and that norlaudanosoline in turn serves as a precursor of other classes of isoquinoline alkaloids. It is well known that dopamine (**5**) is incorporated only into the upper portion of the alkaloids (1). Tyramine (**4**) can also serve as a precursor but it has been less extensively examined (4). DOPA (3,4-dihydroxyphenylalanine) **6** is a key intermediate in this scheme since it may lead both to dopamine, by decarboxylation, and to 3,4-dihydroxyphenylpyruvic acid (**7**) by transamination. The combination of **5** and **7** followed by decarboxylation provides the benzylisoquinoline **8***a* (3, 5, 6).

Although the incorporation of DOPA into isoquinoline alkaloids has been known for some time (7), its role in their formation is only now being clarified. Battersby *et al.* (8) reported that 96% of

[1]This paper is dedicated to the memory of our former coworker, R. H. F. Manske, who contributed so much to the chemistry of the isoquinoline alkaloids.

0008-4042/79/131588-10$01.00/0

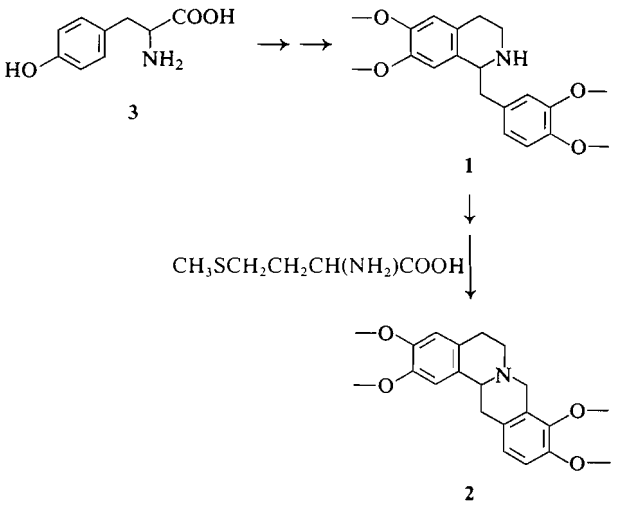

SCHEME 1. Biogenesis of the protoberberine skeleton

the radioactive label from [2-^{14}C]DOPA was located in the 'upper' portion of the aporphine alkaloid glaucine (**9**) and that similar incorporation into the alkaloids hasubanonine (**10**), protostephanine (**11**) (98 and 92%, respectively) (4), and into morphine (5) was observed. Similarly, Bhakuni and co-workers (3, 9) observed that 97% of the radioactivity of intact reticuline (**8***b*) isolated from *Litsea glutinosa* fed with [2-^{14}C]DOPA was located in the 'upper' half of the molecule. These results are consistent with a mechanism of benzylisoquinoline biosynthesis in which the predominant route of DOPA metabolism is via decarboxylation to dopamine. Wilson and Coscia (6) have recently reported that DOPA is incorporated into the 'lower' portion of norlaudanosoline carboxylic acid (**12**) and propose that the latter is an intermediate in the pathway for norlaudanosoline. This would indicate that although DOPA may be predominantly incorporated into benzylisoquinoline and derived alkaloids via dopamine, this mode of incorporation is not the unique pathway of DOPA metabolism and that, in all the cases quoted above, a small but significant proportion of DOPA may be incorporated into the 'lower' portion of the intact alkaloid.

In the present study, [3-^{14}C]DOPA was administered to plants which elaborate protoberberine, protoberberine-derived bases, and spirobenzylisoquinolines as major alkaloid components. The alkaloids examined were berberine (**13**) (10, 11) and hydrastine (**16**) (10, 11) in *Hydrastis canadensis*, corydaline (**19**) (2) and protopine (**21**) (7) in *Corydalis solida*, and ochotensimine (**24**) (2) and protopine in *Corydalis ochotensis*. The feeding experiments are summarized in Table 1. The intact alkaloids were degraded by established procedures (see refs. 2, 10, 11 and Experimental). These degradations are outlined in Schemes 3–7, and the results summarized in Tables 2–6.

In all cases examined, incorporation of DOPA was predominantly into the upper portion of the molecule. Since all the alkaloids examined have been shown to be derived from tyrosine, which is incorporated with approximately equal efficiency into both portions of the molecule, tyrosine cannot be metabolised *solely* via DOPA in its incorporation into the benzylisoquinoline system (see Scheme 2). The distribution of DOPA-derived label in the alkaloids is consistent with a pathway in which DOPA is metabolised predominantly by decarboxylation to **5** (9). The observation of Wilson and Coscia (6) that DOPA contributes to the lower portion of norlaudanosoline carboxylic acid (**12**) in *P. orientale* may mean that oxidation of DOPA to a keto acid such as **7** occurs to an appreciable extent in that plant. However, the specific function of the intermediate **7** in the formation of a benzyl isoquinoline or benzyl isoquinoline-derived alkaloid remains to be demonstrated: Bhakuni *et al.* (3) report the

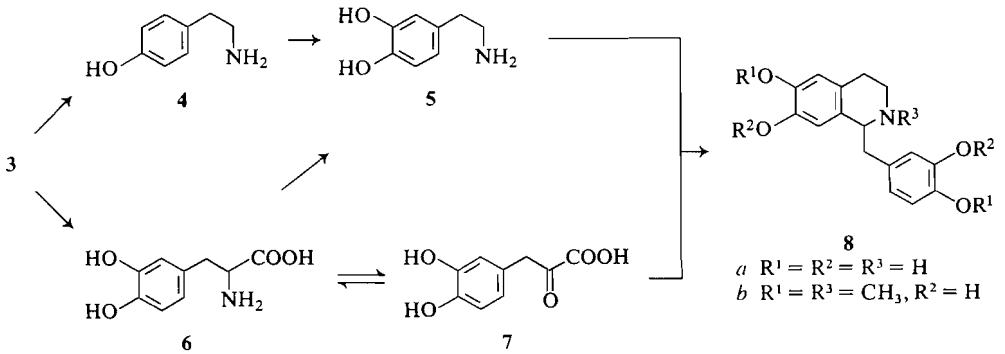

SCHEME 2. Biogenesis of the benzylisoquinoline skeleton

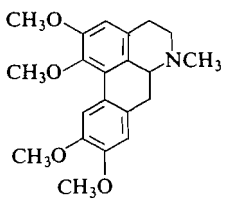

9

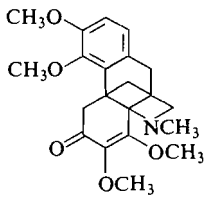

10

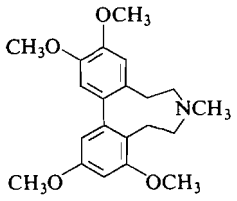

11

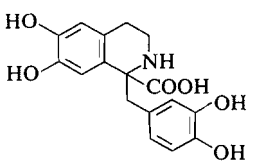

12

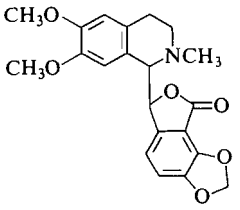

33

incorporation of [^{3}H]-**7** into reticuline but note that significant label (32%), presumably via transamination, appears in the upper portion. The interpretation of the results of experiments with DOPA must therefore necessarily be regarded as tentative until the roles of **7** and *p*-hydroxyphenylpyruvic acid in the production of benzyl isoquinolines are clarified.

We have also investigated the later stages of the biosynthesis of corydaline (**19**) in *C. solida* by the administration of (*RS*)-[9-*methoxy*-^{14}C]tetrahydropalmatine ([9-OCH_3-^{14}C]-**26**) and [9-*methoxy*-^{14}C]-palmatine ([9-OCH_3-^{14}C]-**27**). The synthesis of these alkaloids via palmatrubine (**28**) is outlined in Scheme 8. The corydaline fraction isolated from three separate feedings of [9-OCH_3-^{14}C]-**26** showed only slight activity, and radiochromatoscan analysis failed to detect significant activity associated with corydaline. Feeding of [9-OCH_3-^{14}C]-**27** as the hydroxide, however, yielded corydaline (**19**) which was labelled at the C-9 methoxyl carbon. Specific incorporation was demonstrated by degradation (Scheme 9, Table 7) of the resulting corydaline, via the tetradehydro salt (**29**), to corydalubine (**30**) and methyl iodide (isolated as methyl triethyl ammonium chloride), the latter accounting for 94% of the activity of the corydaline from which it was derived.

The incorporation of labelled **27**, but not **26**, into corydaline is explained in Scheme 10 on the basis of our earlier assumption (2) that the one carbon unit comprising C-13′ (derived from the *S*-methyl group of methionine (2)) is added to a didehydro protoberberine precursor such as **31**. The inability of *C. solida* to convert **26** into **31** is in accord with our demonstration (2) that extensive reversible oxidation and reduction of corydaline in *C. solida* does not occur (viz. retention of tritium from [*methyl*-^{3}H]-methionine at C-8 of corydaline); presumably the same is true of tetrahydropalmatine. We therefore regard **27** as functioning to provide **31** following reduction but not necessarily as an obligatory intermediate in the corydaline pathway. The stage in the pathway from **8***a* to **19** (see Schemes 2 and 10) at which the enamine functionality of **31** is introduced is unknown, and experiments to clarify this are currently under way.

As an extension of our earlier work on the biosynthesis of ochotensimine (**24**) in *C. ochotensis* (2),

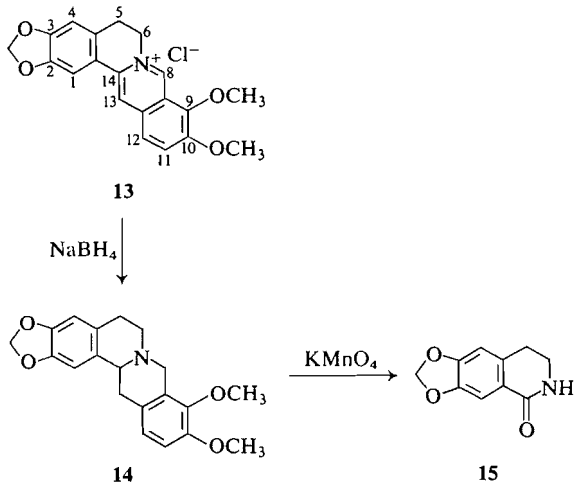

13 14 15

SCHEME 3. The degradation of berberine (**13**)

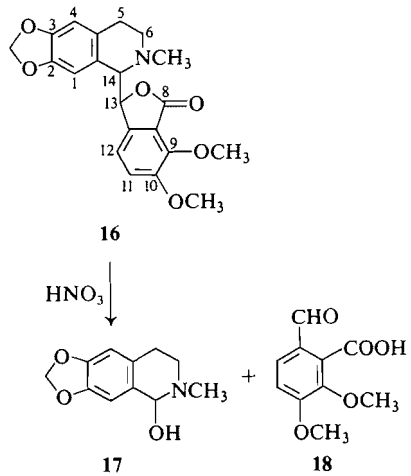

16 17 18

SCHEME 4. The degradation of hydrastine (**16**)

TABLE 1. Feeding of DL-[3-^{14}C]DOPA[a] to *C. solida*, *C. ochotensis*, and *H. canadensis*

Plant	Substrate activity			Product specific activity[b] (^{14}C) × 10^{-4} (dpm/mmol)				
	Specific (mCi/mmol)	Total (mCi)	Date	Corydaline	Protopine	Ochotensimine	Berberine	Hydrastine
Corydalis solida	61	0.05	May 1975	17.7	5.7	—	—	—
Corydalis ochotensis	52	0.05	July 1975	—	24.6	3.6	—	—
Hydrastis canadensis		0.05	June 1975	—	—	—	32.3	7.0

[a]Amersham/Searle.
[b]After appropriate dilution, detailed in the Experimental.

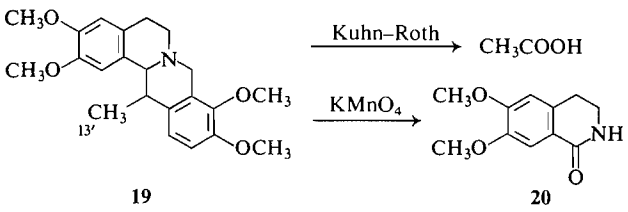

SCHEME 5. The degradation of corydaline (**19**) derived from DL-[3-^{14}C]DOPA

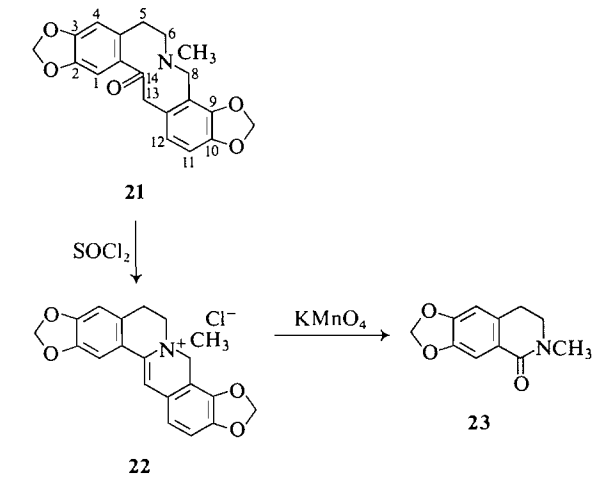

SCHEME 6. The degradation of protopine (**21**)

we have administered L-[*methyl*-^{3}H,^{14}C]methionine to this plant (Table 8): degradation of the resulting ochotensimine (Scheme 11, Table 9) followed established procedures (2, 12), and confirmed the intact derivation of the *O*-methyls, *N*-methyl, and C-13′-methylene from the *S*-methyl of methionine. The results also suggest, although do not confirm, the intact derivation of the C-8 methylene group from the same source. The ^{3}H/^{14}C ratio of **25**, which contains all the carbon and hydrogen atoms of ochotensimine, is identical with that of the precursor amino acid (cf. Table 8), whereas the ratio observed for the Hoffmann product **32** (6.5) is only 83% of that of **25**. Since the ^{3}H/^{14}C ratio of the *N*-methyl lost in this transformation is close to that of the precursor (7.4 ± 0.2 vs. 7.8 ± 0.1), this reduction in ^{3}H/^{14}C ratio can only be explained by an additional loss of ^{3}H relative to ^{14}C. The observed loss of 17% ^{3}H relative to ^{14}C is close to that which would result from the loss of two labelled hydrogen atoms in the conversion of **25** to **32** (10:12 = 83.3%). The reaction of the C-3 benzylic hydrogens of 1-indenes with base (the conditions for this transformation) is well known (e.g. ref. 13) so that loss of tritium from C-8 by base catalysed exchange during the production of **32** from **25** methiodide may well account for the observed ratios. The retention of tritium from L-[*methyl*-^{3}H]methionine at C-8 of ochotensimine would preclude a pathway of ochotensimine biosynthesis which involves a ring C oxygenated intermediate such as adlumine (**33**) but is consistent with other proposals for the derivation of ochotensimine (and related alkaloids) from the protoberberine system (2, and references therein).

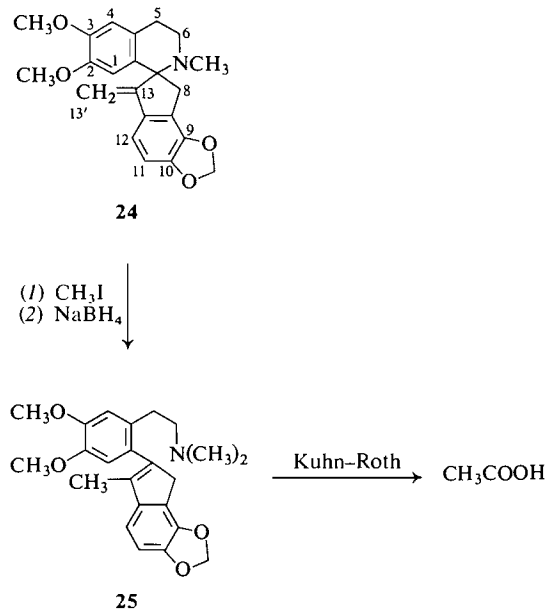

SCHEME 7. The degradation of ochotensimine derived from DL-[3-^{14}C]DOPA

TABLE 2. Distribution of label within berberine chloride derived from DL-[3-^{14}C]DOPA

Products	Carbon atoms of berberine chloride	Specific activity (dpm/mmol)	Relative specific activity (%)
Berberine chloride	All	$3.23 \pm 0.02 \times 10^5$	100 ± 1
(±)-Canadine	All	$3.39 \pm 0.03 \times 10^5$	104 ± 1
Lactam **15**	C-1–C-6, C-14	$3.20 \pm 0.02 \times 10^5$	99 ± 1

TABLE 3. Distribution of label within hydrastine derived from DL-[3-^{14}C]DOPA

Products	Carbon atoms of hydrastine	Specific activity (dpm/mmol)	Relative specific activity (%)
Hydrastine	All	$7.0 \pm 0.2 \times 10^4$	100 ± 3
Hydrastinine	C-1–C-6, C-14	$6.7 \pm 0.3 \times 10^4$	96 ± 4
Opianic acid	C-8–C-13	$0.08 \pm 0.12 \times 10^4$	1 ± 1

TABLE 4. Distribution of label within corydaline derived from DL-[3-^{14}C]DOPA

Products	Carbon atoms of corydaline	Specific activity (dpm/mmol)	Relative specific activity (%)
Corydaline	All	$1.77 \pm 0.08 \times 10^5$	100 ± 4
Corydaldine	C-1–C-6, C-14	$1.65 \pm 0.02 \times 10^5$	93 ± 1
Acetic acid (as α-naphthyl-amide)	C-13, C-13′	$0.19 \pm 0.3 \times 10^3$	0.1 ± 0.1

TABLE 5. Distribution of label within protopine derived from DL-[3-^{14}C]DOPA

Products	Carbon atoms of protopine	Specific activity (dpm/mmol)		Relative specific activity (%)	
		From *C. solida*	From *C. ochotensis*	From *C. solida*	From *C. ochotensis*
Protopine	All	$5.72 \pm 0.07 \times 10^4$	$2.46 \pm 0.02 \times 10^5$	100 ± 1	100 ± 1
N-Methyldihydro-coptisinium chloride	All	$5.52 \pm 0.1 \times 10^4$	$2.51 \pm 0.04 \times 10^5$	96 ± 2	102 ± 2
Oxyhydrastinine	C-1–C-6, C-14	$5.45 \pm 0.08 \times 10^4$	$2.55 \pm 0.04 \times 10^5$	95 ± 2	103 ± 2

TABLE 6. Distribution of label within ochotensimine derived from DL-[3-^{14}C]DOPA

Products	Carbon atoms of ochotensimine	Specific activity (dpm/mmol)	Relative specific activity (%)
Ochotensimine methiodide	All	$3.61 \pm 0.3 \times 10^4$	100 ± 4
Indene derivative **25**	All	$3.51 \pm 0.3 \times 10^4$	97 ± 4
Acetic acid (as α-naphthyl-amide)	C-13, C-13′	$1.2 \pm 0.8 \times 10^3$	4 ± 3

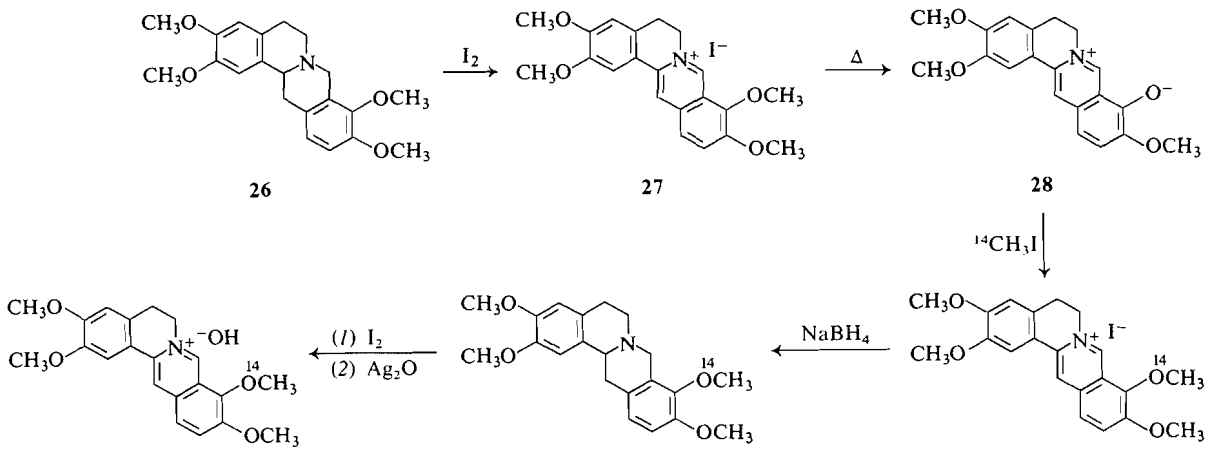

SCHEME 8. Synthesis of [9-OCH_3-^{14}C]-**26** and [9-OCH_3-^{14}C]-**27** hydroxide from (±)-tetrahydropalmatine (**26**)

TABLE 7. Feeding of (*RS*)-[9-*methoxy*-^{14}C]tetrahydropalmatine (**26**) and [9-*methoxy*-^{14}C]palmatine (**27**) to *Corydalis solida*

Substrate	Substrate activity		Date	Specific activities × 10^{-4} (dpm/mmol) (% total)		
	Specific (mCi/mmol)	Total (mCi)		Corydaline	Corydalubine	Methyltriethyl ammonium chloride
26	7.54	0.05	May 1977	3.6±0.2[a,b]	—	—
27	7.54	0.1	May 1978	6.1±0.1[c] (100±1)	0.33±0.2 (5±3)	5.75±0.1 (94±2)

[a]Typical value from three separate feeding experiments.
[b]Radiochromatoscan analysis failed to reveal significant activity associated with corydaline.
[c]After 40-fold dilution for degradation (see Experimental).

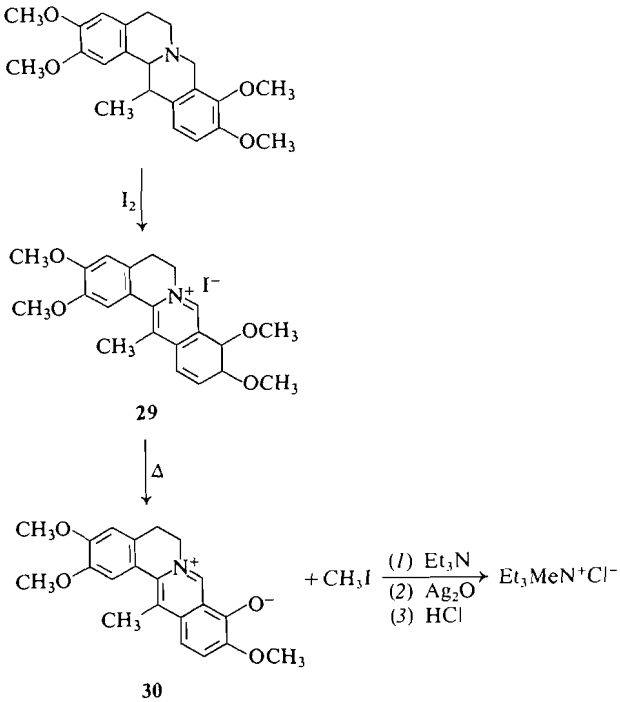

SCHEME 9. Degradation of corydaline derived from [9-OCH_3-^{14}C]palmatine

Experimental

Plants

Corydalis solida (2), *Corydalis ochotensis* (2), and *Hydrastis canadensis* (10) plants were propagated as described.

Synthesis of Labelled Alkaloids

(RS)-[9-methoxy-^{14}*C*]*Tetrahydropalmatine from* (±)-*Tetrahydropalmatine* (**26**)

Palmatine iodide (**27**)—(±)-Tetrahydropalmatine (3.55 g, 10 mmol) was dissolved in 95% ethanol (250 mL) containing iodine (3.81 g, 30 mmol) and refluxed for 3 h. The dark brown mixture was then treated with 5% sodium bisulphite (ca. 2 mL) and the mixture turned bright yellow within 30 s. The mixture was cooled in an ice bath to induce crystallization and the palmatine iodide removed by filtration. Recrystallization from MeOH–EtOAc yielded 4.60 g (96%) of the palmatine iodide as yellow needles; mp 240–242°C (lit. (14) 241°C).

Palmatrubine (**28**)—Palmatine iodide (1.0 g, 2.1 mmol) was mixed with urea (2 g) and ground into a fine powder. This powdered mixture was heated at 200°C in an oil bath for 30 min. Upon heating the mixture turned from bright yellow to a brilliant red colour. The resulting dark red solid was then poured into water (100 mL) and extracted into chloroform (4 × 50 mL). The combined organic extracts were washed with water (1 × 100 mL), dried over magnesium sulphate, and the solvent removed *in vacuo* to give a dark reddish solid. Recrystallization from absolute ethanol gave 650 mg (92%) of the palmatrubine (**28**) as red flakes; mp 288–292°C (lit. (15) 290–295°C).

(RS)-[9-methoxy-^{14}*C*]*Tetrahydropalmatine* (**26**)

The phenol betaine, palmatrubine (**28**) (35 mg, 0.1 mmol),

TABLE 8. Feeding of L-[*methyl*-^{3}H,^{14}C]methionine to *C. ochotensis*

Substrate	Nominal activity: Specific (mCi/mmol)	Nominal activity: Total (mCi)	Date	Ochotensimine: Weight (mg)	Ochotensimine: Specific activity (^{14}C) dpm/mmol × 10^{-6}	^{3}H/^{14}C ratio (measured)
L-[*methyl*-^{14}C]-methionine	56	0.1	July 1973	88	1.4±0.01[a]	7.8±0.1
L-[*methyl*-^{3}H]-methionine	5000	1.0				

[a]Determined after conversion to ochotensimine methiodide.

TABLE 9. Distribution of label within ochotensimine derived from methyl-[^{3}H,^{14}C]-methionine

Products	Carbon atoms of ochotensimine	Specific activity (^{14}C) dpm/mmol	Relative specific activity % (^{14}C)	^{3}H/^{14}C
Ochotensimine methiodide[a]	All	$1.4\pm0.1\times10^6$	—	—
Indene derivative **25**[b]	All	$2.8\pm0.2\times10^5$	100±1	7.8±0.1
Acetic acid (as α-naphthylamide)	C-13, C-13′	$5.1\pm0.2\times10^4$	18±1	7.6±0.1
Methylamine (as *N*-methyl-β-naphthoamide)	C-13′	$4.8\pm0.2\times10^4$	17±1	7.1±0.1
N-Methyl (as tetramethyl-ammonium chloride)	*N*-Methyl	$4.9\pm0.2\times10^4$	17±1	7.4±0.2
O-Methyls (as tetramethyl-ammonium chloride)	*O*-Methyls	$4.2\pm0.2\times10^4$	15±1	7.7±0.1
Styrene derivative **32**	All except *N*-methyl	$2.3\pm0.2\times10^5$	82±1	6.5±0.2

[a]From ochotensimine isolated without dilution with unlabelled alkaloid.
[b]Obtained from ochotensimine methiodide after dilution with unlabelled material.

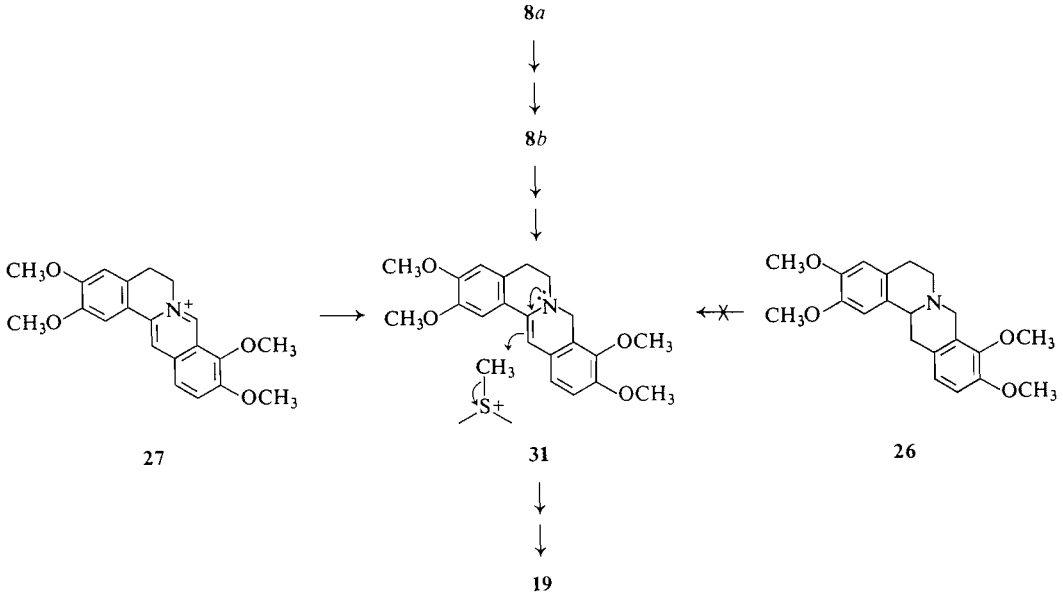

SCHEME 10. Introduction of the C-13 methyl of corydaline

was dissolved in dry DMF (3 mL) and placed on a high vacuum manifold. A break-seal ampule containing ^{14}C-labelled methyl iodide (1 mCi, 20 mCi/mmol) was also placed on the vacuum manifold. The reaction vessel containing the DMF solution was thoroughly cooled in Dry Ice – acetone and the system was evacuated to a pressure of 0.03 Torr with a rough pump. At this time liquid nitrogen was substituted for the Dry Ice – acetone bath and the break-seal container of methyl iodide was also cooled in liquid nitrogen. With the aid of an oil diffusion pump the system was further evacuated to a

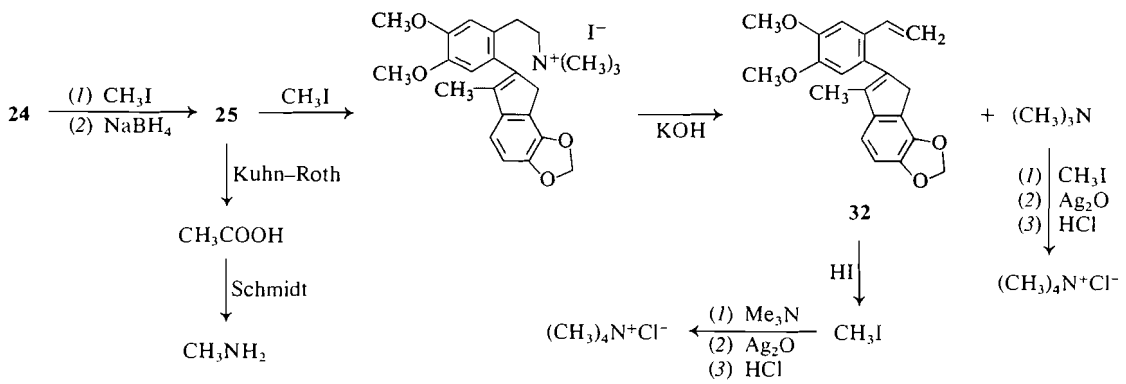

SCHEME 11. Degradation of ochotensimine derived from L-[*methyl*-^{3}H,^{14}C]methionine (Table 9).

pressure of ca. 10^{-5} Torr. At this time the break-seal was cracked, the liquid nitrogen removed from the break-seal ampule, and the radio-labelled methyl iodide was allowed to distill into the reaction mixture which was kept at liquid nitrogen temperature. The reaction flask was then sealed under vacuum and kept at room temperature for 6 days. At the end of this period the mixture was cooled in Dry Ice – acetone and an additional aliquot (2 mL) of inactive methyl iodide was added. The mixture was again sealed and kept at room temperature for 2 days during which time a yellow solid had precipitated. The DMF was removed *in vacuo* and this residue taken up in methanol–water (3:1, v/v 30 mL). The mixture was treated with excess sodium borohydride and stirred at room temperature overnight. The excess borohydride was quenched by slow addition of 10% hydrochloric acid and the mixture was concentrated *in vacuo* to remove the methanol. The resultant solution was diluted with water (75 mL), basified with solid potassium carbonate and extracted with chloroform (3 × 60 mL). The combined extracts were washed with water (50 mL) and dried over sodium sulphate. The solvent was removed *in vacuo* to yield a white powder which was radiochemically pure by tlc and radioscan. Recrystallization from methanol yielded 25 mg (70%) of 9-[OCH_3-^{14}C]-(±)-tetrahydropalmatine as white needles; specific activity 21.26 μCi/mg, 7.54 mCi/mmol.

[*9*-methoxy-^{14}*C*]*Palmatine (27) from* (RS)-[*9*-methoxy-^{14}*C*]-*Tetrahydropalmatine (26)*

(RS)-[*9-methoxy*-^{14}C]Tetrahydropalmatine (4.8 mg, 102 μC) was converted into [*9-methoxy*-^{14}C]palmatine iodide by the method described above. The salt so obtained was dissolved in distilled water (5 mL) and stirred with an excess of freshly prepared silver oxide with exclusion of light for a period of 1 h. The resulting yellow solution was decanted, combined with aqueous washings of the insoluble material, and used directly.

Administration of DL-[*3*-^{14}*C*]*DOPA (Table 1)*

The labelled material was administered by infusion into the stem as described (2, 10). Ascorbic acid (1 mg/mL) was added to the feeding solutions to prevent aerial oxidation.

Extraction of the Alkaloids

Corydalis solida

Six plants were exposed to the radioactive amino acid for 3 days. The total plant material was then harvested (fresh weight 130 g) and dried at 40°C for 72 h, yielding 34 g of dry plant material. The extraction then followed the procedure of Manske (16). Corydaline (300 mg) was added to fractions BC + EC of the extract and crystallization of the extract from methanol gave 270 mg of radioactive corydaline, which was purified by recrystallization from methanol followed by sublimation (140°C, 1 × 10^{-2} Torr). Protopine (150 mg) was added to fractions BS + ES and the resulting extract crystallized from methanol to give 94 mg of radioactive protopine. A further 200 mg of protopine was added to 50 mg of the radioactive sample, and this mixture was recrystallized from chloroform–methanol to give material for degradation.

Corydalis ochotensis

Five plants (fresh weight 203 g) were exposed to the labelled amino acid for 4 days, and harvested and dried as described above to give 46 g of dry plant material. This was extracted by the procedure of Manske (17) and ochotensimine isolated from fractions BC + EC and converted to the methiodide (124 mg) as described previously (2). The radioactive methiodide (50 mg) was diluted with carrier methiodide (200 mg) prior to degradation. Protopine (24 mg) was crystallized directly from fractions BS + ES. A further 230 mg of protopine was added to 20 mg of the labelled sample and the whole crystallized from chloroform–methanol to give material for degradation purposes.

Hydrastis canadensis

Three plants were exposed to radioactive tracer for 3 days and harvested to give a total of 626 g of fresh material. The dried roots (205 g) and aerial portion (32 g) were extracted as described (10) to give berberine chloride (3.76 g) and hydrastine (1.8 g).

Administration of (RS)-[*9*-methoxy-^{14}*C*]*Tetrahydropalmatine (26) and* [*9*-methoxy-^{14}*C*]*Palmatine (27) to* C. solida *(Table 7)*

In separate feeding experiments [9-OCH_3-^{14}C]-(**26**) and -(**27**) were each administered to three plants for a period of 4 days by the cotton wick method. Corydaline was extracted and purified by the procedure described above with the modification that only 30 mg of carrier corydaline was added to the extract. It was then further purified by preparative layer chromatography (silica gel, 2% methanolic chloroform).

Administration of [methyl-^{14}*C*,^{3}*H*]-*Methionine to* C. ochotensis *(Table 8)*

Following administration by the method used previously (2), *C. ochotensis* (fresh weight 230 g, dry weight 45 g) was extracted as described (2) to give ochotensimine (**24**) (88 mg).

Degradation of the Alkaloids

Degradation of Berberine Chloride Derived from DL-[*3*-^{14}*C*]*DOPA (Table 2)*

Conversion to (±)-*canadine*—Reduction of berberine chloride (1 g) with sodium borohydride in ethanol gave (±)-canadine (746 mg), mp 170–172°C from ethanol (lit. (18) mp 171°C).

Carbons 1–6, nitrogen, and carbon-14; oxidation of canadine to **15**—Oxidation of (±)-canadine (0.5 g) with potassium permanganate, by the method described below for the oxidation of corydaline to corydaldine, gave 6,7-methylenedioxy-1,2,3,4-tetrahydro-1-isoquinolinone. Sublimation at 70–80°C, 1.1×10^{-3} Torr, and crystallization from ether gave 32 mg, mp 180–182°C (lit. (19) mp 181–182°C).

Degradation of Hydrastine Derived from DL-[*3*-^{14}*C*]*DOPA (Scheme 4, Table 3)*

Hydrastine (400 mg) was converted to hydrastinine, 162 mg, mp 116–117°C (lit. (7) mp 116–117°C) and opianic acid, 23 mg, mp 143–145°C (lit. (10) mp 146°C) by the described procedure (10).

Degradation of Corydaline Derived from DL-[*3*-^{14}*C*]*DOPA (Scheme 5, Table 4)*

Carbon-13 and the C-methyl by oxidation—The Kuhn–Roth oxidation of corydaline and the conversion of the resulting acetic acid to *N*-acetyl-α-naphthylamide were performed as described (2).

Carbon 1–6, nitrogen, and carbon-14; oxidation of corydaline to corydaldine—Sodium hydroxide solution (15%) was added dropwise to a stirred solution of corydaline (100 mg) in 50 mL of aqueous sulfuric acid at 0°C until the mixture reached pH 5. A solution of potassium permanganate (180 mg) in water (10 mL) was then added and the resulting solution stirred at 0°C. After 2 h had elapsed the solution was heated to 50°C, adjusted to pH 10 (15% NaOH) and then filtered. The filtrate was extracted with chloroform and the extract washed with 5% HCl, dried and evaporated. The residue was purified first by preparative layer chromatography (Merck silica 60 F-254, 10% methanolic chloroform, R_f 0.5) and then by sublimation at 100°C, 2×10^{-2} Torr. Crystallization from ether gave 8.4 mg of corydaldine, mp 173–175°C (lit. (20) mp 175°C).

Degradation of Corydaline Derived from [*9*-methoxy-^{14}*C*]-*Palmatine (Table 7)*

9-O-Methyl by conversion to methyltriethylammonium chloride and corydalubine—Corydaline isolated from *C. solida* after administration of [*9-methoxy*-^{14}C]palmatine (10 mg) was diluted with unlabelled corydaline (400 mg) and the mixture so obtained treated as described for the preparation of palmatrubine (above), with the addition of nitrogen inlet and outlet tubes to the reaction flask. During the reaction a slow stream of nitrogen was passed through the flask and then through three traps each containing a solution of 0.5 mL triethylamine in 5 mL methanol at −78°C. When the reaction was complete, the material from the traps was combined, allowed to stand overnight at room temperature, and then evaporated in a stream of dry nitrogen. The residue was then converted to methyltriethylammonium chloride by reaction with silver oxide and HCl as described (2). The residue in the reaction flask was treated as described above and afforded corydalubine (230 mg).

Degradation of Protopine Derived from DL-[*3*-^{14}*C*]*DOPA (Scheme 6, Table 5)*

Conversion of protopine to N-methyldihydrocoptisinium chloride—This was performed by the method described (21). In a typical transformation 200 mg of protopine gave 136 mg of the desired salt, mp 210–213°C (dec.) (lit. (21) mp 215°C (dec.)).

Carbons 1–6, nitrogen, and carbon-14; oxidation of **22** *to oxyhydrastinine*—Potassium permanganate (100 mg) was added to a stirred suspension of **22** (100 mg) in water (50 mL) at 0°C. The solution was stirred for 2 h at 0°C and then heated to 50°C, basified to pH 10 (15% NaOH), and extracted with chloroform. The extract was washed with 5% HCl, dried and evaporated to give a residue which was purified first by preparative layer chromatography (Merck silica 60 F-254, 5% methanolic chloroform, R_f 0.6) and then by sublimation at 120°C, 5×10^{-2} Torr. Crystallization from ether gave oxyhydrastinine (11.2 mg), mp 96–98°C (lit. (22) mp 97–98°C).

Degradation of Ochotensimine (Schemes 7 and 11, Tables 6 and 9)

Carbon-13 and the exocyclic methylene—The degradation of ochotensimine methiodide to isolate C-13 and C-13′ as acetic acid and transformation of the latter into *N*-acetyl-α-naphthylamide was performed as described (2).

N-Methyl as tetramethylammonium chloride—The indene derivative **25** (150 mg), obtained from ochotensimine as described (2), was dissolved in a solution of ether (1 mL) and methanol (0.2 mL) containing methyl iodide (0.5 mL). The resulting solution was allowed to remain at room temperature for 24 h, and then at −20°C for a further 24 h. The crystals which deposited (220 mg) were then removed by filtration. A solution of **25** methiodide so obtained (200 mg) in 50% aqueous ethanol (30 mL) containing potassium hydroxide (1 g) was heated at 80°C for 4 h. A slow stream of nitrogen passed through the reaction flask into a series of three traps each containing 1 mL of 10% methyl iodide – ether (v/v). The material from the traps was combined and allowed to stand at room temperature for 24 h. The precipitate of tetramethylammonium iodide so obtained was converted to tetramethylammonium chloride (2) for counting.

1-Methyl-2(2′-vinyl-4′,5′-dimethoxyphenyl)-4,5-methylene dioxy-1-indene (32)—The aqueous ethanol solution from the Hoffmann degradation described above was poured onto water (20 mL) and extracted with chloroform. The extract was washed with 5% HCl, dried, and then evaporated. The residue was dissolved in chloroform and filtered through a column of silica gel to remove polar impurities. It was then evaporated and recrystallized from acetone–hexane to give **32** (120 mg), mp 140–142°C (lit. (12) mp 142–144°C). The sample was further purified for counting by sublimation at 100°C and 0.05 Torr.

Methoxyl methyls as tetramethylammonium chloride—Treatment of **32** (100 mg) with HI by the procedure described previously (2) gave tetramethylammonium iodide (18 mg) which was converted to tetramethylammonium chloride (2) for counting.

Determination of Radioactivity

Radioactivity was assayed by liquid scintillation counting (Mark 1 liquid scintillation computer, Model 6860, Nuclear Chicago). Samples were dissolved in methanol or water and the solution dispersed in a solution of Aquasol (New England Nuclear). Triplicate samples of each compound were counted under comparable conditions of quenching. For highly quenched samples the confidence limits of the quench correction curves were ±5%. Confidence limits shown in the tables are standard deviations of the mean.

Acknowledgements

We are greatly indebted to the late Dr. R. H. F. Manske of the University of Waterloo for providing generous samples of alkaloids and plant material, and for the provision of live plants of *Corydalis solida* and *Corydalis ochotensis* from his private garden in Guelph, Ontario. We are also grateful to the Royal Botanical Gardens, Hamilton, Ont., for the propagation of *Hydrastis canadensis*. This work was supported by the National Research Council of Canada.

1. I. D. SPENSER. *In* Comprehensive biochemistry. Vol. 20. *Edited by* M. Florkin and E. H. Stotz. Elsevier, Amsterdam. 1968. p. 231.
2. H. L. HOLLAND, M. CASTILLO, D. B. MACLEAN, and I. D. SPENSER. Can. J. Chem. **52**, 2818 (1974).
3. D. S. BHAKUNI, A. N. SINGH, S. TEWARI, and R. S. KAPIL. J. Chem. Soc. Perkin Trans. 1, 1662 (1977).
4. A. R. BATTERSBY, R. C. F. JONES, R. KAZLAUSKAS, C. POUPAT, C. W. THORNBER, S. RUCHIRAWAT, and J. STAUNTON. Chem. Commun. 773 (1974).
5. A. R. BATTERSBY, R. C. F. JONES, and R. KAZLAUSKAS. Tetrahedron Lett. 1873 (1975).
6. M. L. WILSON and C. J. COSCIA. J. Am. Chem. Soc. **97**, 431 (1975).
7. D. H. R. BARTON, R. H. HESSE, and G. W. KIRBY. J. Chem. Soc. 6379 (1965).
8. A. R. BATTERSBY, J. L. MCHUGH, J. STAUNTON, and M. TODD. Chem. Commun. 985 (1971).
9. S. TEWARI, D. S. BHAKUNI, and R. S. KAPIL. Chem. Commun. 554 (1975).
10. J. R. GEAR and I. D. SPENSER. Can. J. Chem. **41**, 783 (1963).
11. R. N. GUPTA and I. D. SPENSER. Can. J. Chem. **43**, 133 (1965).
12. S. MCLEAN, M.-S. LIN, and R. H. F. MANSKE. Can. J. Chem. **44**, 2449 (1966).
13. B. WEINSTEIN. J. Org. Chem. **26**, 4161 (1961).
14. K. FEIST and G. SANDSTEDE. Arch. Pharm. **256**, 1 (1918).
15. K. FEIST and G. L. DSCHU. Arch. Pharm. **263**, 294 (1925).
16. R. H. F. MANSKE. Can. J. Chem. **34**, 1 (1956).
17. R. H. F. MANSKE. Can. J. Res. B, **18**, 75 (1940).
18. R. H. F. MANSKE. *In* The alkaloids. Vol. 4. *Edited by* R. H. F. Manske. Academic Press, New York. 1954. p. 91.
19. W. H. PERKIN. J. Chem. Soc. **57**, 992 (1890).
20. J. J. DOBBIE and A. LAUDER. J. Chem. Soc. **75**, 670 (1899).
21. W. H. PERKIN. J. Chem. Soc. **109**, 815 (1916).
22. M. FREUND and W. WILL. Chem. Ber. **20**, 2400 (1887).

A convergent route to phthalideisoquinoline alkaloids via directed metalation of tertiary benzamides[1,2]

S. O. DE SILVA, I. AHMAD,[3] AND V. SNIECKUS

Guelph–Waterloo Center for Graduate Work in Chemistry, University of Waterloo, Waterloo, Ont., Canada N2L 3G1

Received January 2, 1979

S. O. DE SILVA, I. AHMAD, and V. SNIECKUS. Can. J. Chem. **57**, 1598 (1979).

Diastereomeric phthalideisoquinolines **8** and **9** have been synthesized by a route involving an amine-induced bromohomophthalic anhydride – phthalide-α-carboxamide rearrangement, **3** + **4** → **6**, as the key step. This rearrangement has been applied to the synthesis of the methoxylated phthalide-α-carboxamide **18** which has been converted into the dehydrophthalide **19** thereby achieving a formal synthesis of the phthalideisoquinoline alkaloids cordrastine I (**1***a*) and cordrastine II (**1***b*). The key intermediate in this sequence, 3,4-dimethoxyhomophthalic acid (**15**), has been efficiently prepared in two steps via directed lithiation of 2,3-dimethoxy-*N*,*N*-diethylbenzamide (**13**).

S. O. DE SILVA, I. AHMAD et V. SNIECKUS. Can. J. Chem. **57**, 1598 (1979).

On a synthétisé les phtalideisoquinoléines diastéréoisomères **8** et **9** en faisant appel, comme étape-clé, à une transposition induite par une amine d'un anhydride bromohomophtalique en phtalide α-carboxamide **3** + **4** → **6**. On a utilisé cette transposition pour la synthèse du phtalide α-carboxamide méthoxylé (**18**) qui peut être transformé en déhydrophtalide **19**; ces réactions complètent la synthèse formelle des alcaloïdes de la phtalideisoquinoléine, cordrastine I (**1***a*) et cordrastine II (**1***b*). On a préparé l'intermédiaire de cette série de réactions, l'acide diméthoxy-3,4 homophtalique (**15**), d'une manière efficace en deux étapes par une lithiation directe du diméthoxy-2,3 *N*,*N*-diéthylbenzamide (**13**).

[Traduit par le journal]

Cordrastine I (**1***a*) and cordrastine II (**1***b*) constitute early discoveries of the phthalideisoquinoline class of alkaloids which currently number about 15 bases elaborated by Berberidaceae, Fumariaceae, Papaveraceae, and Ranunculaceae plant families (2–5). Recent interest in this group derives from the discovery of biogenetically related B/C ring-opened alkaloids (4) the interconversion of representative members into other classes of alkaloids (3, 4), elucidation of biosynthetic pathways (6), and the finding that several alkaloids act as effective γ-aminobutyric acid (GABA) antagonists (4).

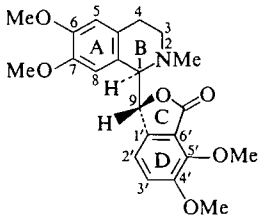

1*a*
Cordrastine I

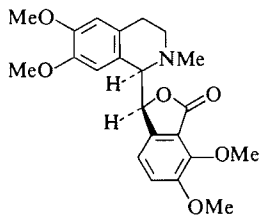

1*b*
Cordrastine II

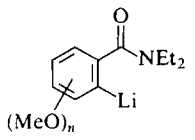

2

The isolation and structural elucidation of the cordrastines (**1**) was carried out by Manske (7) in a historical period when "new alkaloids were discovered at a rate that would make the discoverer of islands in the St. Lawrence envious" (8). Forty years later, Manske and co-workers also contributed to the development of a total synthesis of phthalideisoquinoline alkaloids (9), based on the classical Haworth–Pinder route (10), which constitutes one of the most efficient of the available routes reported to date (3, 4). Herein we describe a new synthesis[2,3] of phthalideisoquinolines which also proceeds via Haworth–Pinder intermediates but which involves the principle of directed metalation of substituted benzamides (**2**) (11) for the construction of the C/D ring fragment. An additional feature of our synthesis is a bromohomophthalic anhydride – phthalide-α-carboxamide rearrangement for the convergent assemblage of a skeleton embodying all the requisite atoms of cordrastine I (**1***a*) and cordrastine II (**1***b*) (Scheme 2).

Model Study (Scheme 1)

In connection with synthetic efforts towards the

[1]Dedicated to R. H. F. Manske, an early force and a continuing influence in Canadian Chemistry.

[2]Part of this work has been published in preliminary form; see ref. 1.

[3]Taken, in part, from the Ph.D. Thesis of I.A., University of Waterloo, Waterloo, Ont. 1975.

0008-4042/79/131598-08$01.00/0

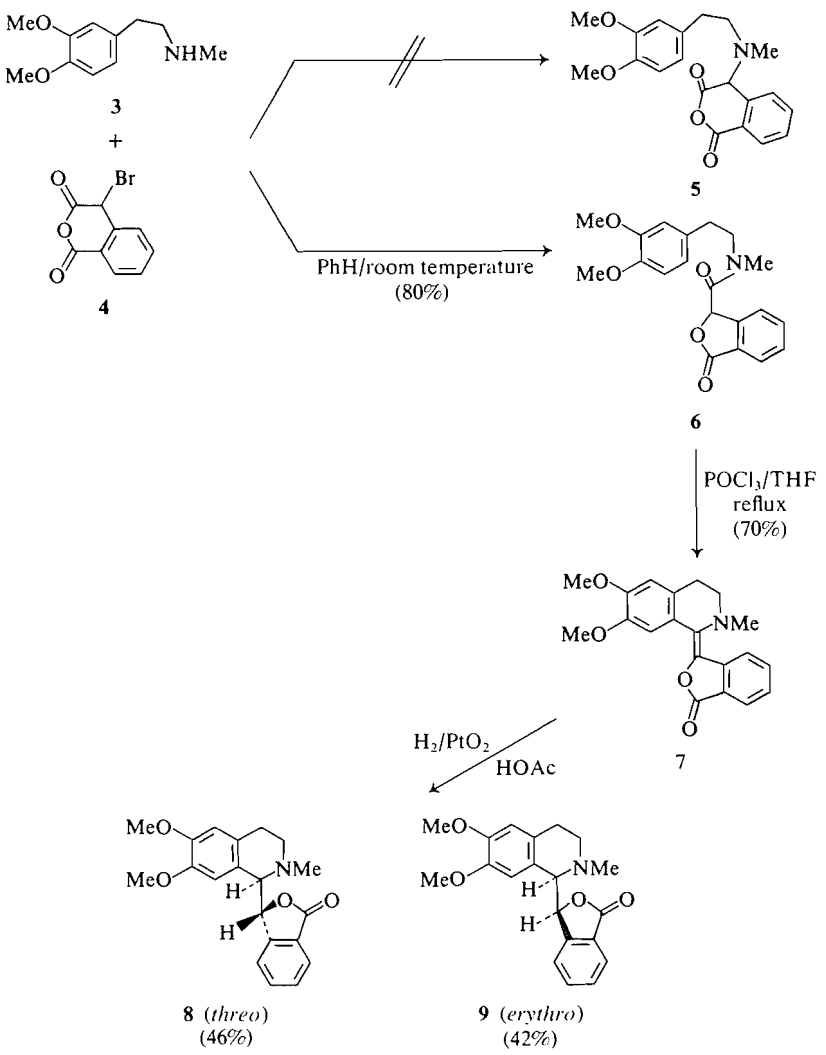

SCHEME I

rhoeadine alkaloids,[3] we observed that condensation of the phenethylamine **3** with bromohomophthalic anhydride (**4**), both readily available compounds (see Experimental), did not yield the required anhydride **5** but provided the rearranged phthalide-α-carboxamide **6** in good yield.[4] The structure of **6** was assigned by comparison of its spectral data[5] with those of the ring D dimethoxylated analogue **18**. Modified Bischler–Napieralski cyclization afforded the yellow dehydrophthalide **7** which upon catalytic hydrogenation gave a mixture of the phthalideisoquinolines **8** and **9**. These were easily separated by preparative tlc into the pure *threo* (**8**) (46%) and *erythro* (**9**) (42%) diastereomers. Stereochemical assignments were made by comparison of tlc behavior and ^{1}Hmr spectra of **8** and **9** with those of

[4]This rearrangement was foreshadowed by the observations that bromination of homophthalic anhydride in acetic acid gave **i**[3] and distillation of dimethyl α-bromohomophthalate produced the corresponding methyl ester **ii** (28).

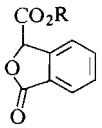

i R = H
ii R = Me

[5]An interesting feature of the ^{1}Hmr spectrum of **6** is the presence of two sets of doublets at δ 3.02, 3.13 and δ 5.64, 6.12 assigned to the NCH_3 and C-3 protons respectively of the two conformational isomers arising from restricted rotation about the amide bond. These signals were shown to collapse at + 69°C (sharp singlet) and + 74°C (broad peak, incomplete averaging).

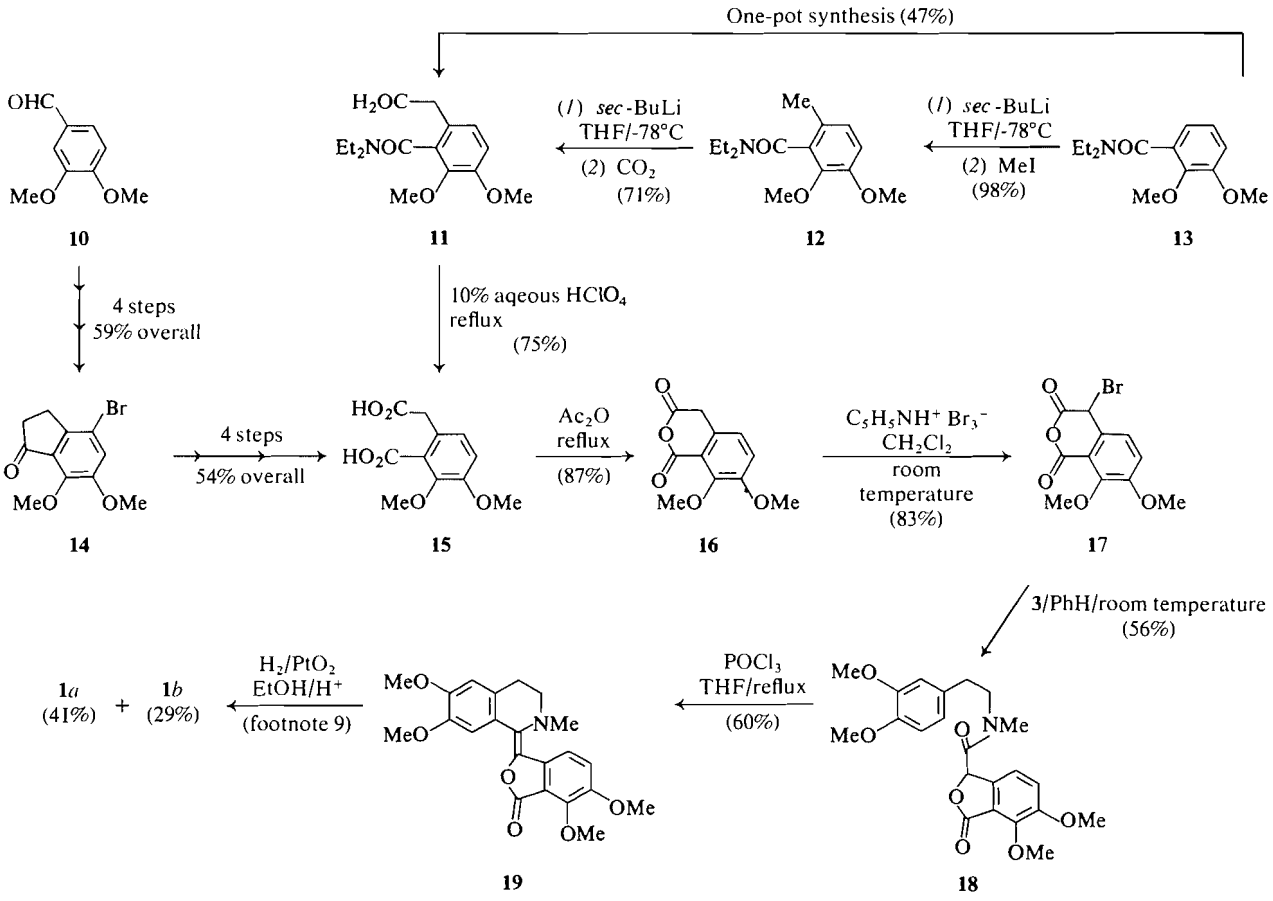

SCHEME 2

the corresponding diastereomeric cordrastines **1***a* and **1***b* (12). The faster moving diastereomer **8**, R_f = 0.7 (silica gel, $CHCl_3$–MeOH, 97:3), showed absorptions at δ 4.15 (d, J = 4 Hz), 5.76 (d, J = 4 Hz), and 6.38 (s) assigned to the C-1, C-9, and C-8 protons, respectively, whereas the other diastereomer **9**, R_f = 0.35, displayed corresponding signals at δ 4.08 (d, J = 4 Hz), 5.7 (d, J = 4 Hz), and 6.3 (s). The differences in R_f values and chemical shifts of **8** and **9** are mirrored in the corresponding tlc and ^{1}Hmr data of the diastereomeric cordrastine I (**1***a*) (R_f = 0.6) and cordrastine II (**1***b*) (R_f = 0.3) whose stereochemistry has been established (12). In particular, the highly characteristic C-8 proton which reflects the favored conformations of phthalideisoquinoline diastereoisomeric pairs (4) appears at lower field in the ^{1}Hmr spectrum of the *threo* isomer **8** (δ 6.38) compared to the *erythro* isomer **9** (δ 6.3) thus paralleling the values recorded for the cordrastine isomers **1***a* (δ 6.62) and **1***b* (δ 6.19) (12). The correspondence of the R_f values and ^{1}Hmr data for the pairs **8**,**1***a* and **9**,**1***b* supports the *threo* and *erythro* stereochemical assignments to **8** and **9**, respectively.

Cordrastines I and II (Scheme 2)

The applicability of the model bromohomophthalic anhydride – phthalide-α-carboxamide rearrangement, **3** + **4** → **6**, to the synthesis of the cordrastines I (**1***a*) and II (**1***b*) critically depended on the availability of 3,4-dimethoxyhomophthalic acid (**15**). This compound could be prepared by a tedious, multistep route from 3,4-dimethoxybenzaldehyde (**10**) via the bromoindanone intermediate **14** (Scheme 3).[6] Simplification and abbreviation of this classical route was achieved as a consequence of our work with *ortho*-lithiated *N*,*N*-diethylbenzamides (**2**) as useful intermediates for the synthesis of contiguously tri- and tetrasubstituted aromatic systems (11).

Directed lithiation of 2,3-dimethoxy-*N*,*N*-diethylbenzamide (**13**) with *sec*-butyllithium in THF provided a yellow homogeneous solution which upon treatment with methyl iodide afforded a quantitative

[6]This route consists of reactions from unrelated literature sources some of which have been improved to provide a higher overall yield of **15**. *Only* the significantly improved procedures are given in the Experimental (Scheme 3). For similar results, see ref. 13.

yield of the toluamide **12**. The ^{1}Hmr spectrum of compound **12** showed, *inter alia*, a collapsed AB pattern centered at δ 6.93 (2H) due to the aromatic protons and broad absorption at δ 0.87–1.42 (2 × t, 6H) and δ 2.87–3.83 (2 × q, 4H) due to the CH_2 and CH_3 protons, respectively, of the diethylamide function. The nonequivalency of the two sets of CH_2 and CH_3 protons is due to the amide restricted rotation phenomenon and strongly suggests that methylation has occurred *ortho* to the diethylamide function. Lithiation of **12** under similar conditions resulted in the formation of a deep purple solution of the *o*-toluoyl anion[7] which upon quenching with dry carbon dioxide gave the homophthalic acid amide **11**. The conversion of **13** into **11** was also achieved in a one-pot operation with attendant gain in convenience but some loss in overall efficacy. In this sequence, the second lithiation was carried out with *sec*-BuLi (1 equiv.) in the presence of $(i\text{Pr})_2\text{NH}$ (0.1 equiv.) as it was found that the use of *sec*-BuLi alone resulted in partial lithiation of the aromatic ring (presumably *ortho* to the 3-OMe group). The abbreviated synthesis of the homophthalic acid **15** was completed by perchloric acid hydrolysis of **11**.

Conversion of **15** into the C/D ring precursor (**17**) of the target alkaloids was readily effected by treatment with acetic anhydride to give the homophthalic anhydride **16** followed by bromination of the latter with pyridinium bromide perbromide. The unstable bromoanhydride **17** (ir ν_{max}: 1810, 1755 cm^{-1}; nmr δ: 6.10 (s, 1H, C-4 H))[8] was not purified but immediately treated with the phenethylamine **3** to give the phthalide-α-carboxamide **18**. Compound **18** was shown to be identical (mp, mixture mp, tlc, ir, and ^{1}Hmr) with an authentic sample[9] prepared by the Haworth–Pinder synthesis (10). The phenomenon of restricted rotation about the amide bond, already encountered in the model compound **6**, was again evident from the examination of the ^{1}Hmr spectrum of **18** (see Experimental). Bischler–Napieralski cyclization of **18** furnished the orange-yellow dehydrocordrastine (**19**) whose identity was established by comparison (mp, mixture mp, tlc, and ir) with an authentic sample.[9] Since **19** has been previously converted[9] (10) into cordrastine I (**1***a*) and cordrastine II (**1***b*), our work formally represents a new synthesis of these phthalideisoquinoline alkaloids.

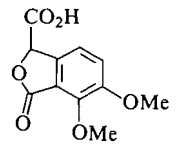

20

As demonstrated here and elsewhere (9, 11), oxygenated homophthalic anhydrides, e.g., **16**, and phthalide-α-carboxylic acids (**20**) are now readily available by directed metalation reactions. These developments elevate the original Haworth–Pinder route (10) to the stature of a general method for phthalideisoquinoline alkaloid synthesis.

Experimental

General Methods

Microanalyses were performed by A. G. Gygli, Toronto, Ont., and Baron Consulting Co., Orange, CT. Melting points were measured on Fisher-Johns and Büchi SMP-20 apparatus and are uncorrected. Infrared spectra were determined on a Beckmann IR-10 spectrometer. Ultraviolet spectra were recorded on an SP-800E ultraviolet spectrophotometer in methanol solution. Nuclear magnetic resonance spectra were obtained with a Varian T-60 spectrometer using tetramethylsilane as internal standard in deuteriochloroform unless otherwise indicated. Mass spectra were determined on an A.E.I. MS-30 double beam, double focussing mass spectrometer. For column chromatography, silica gel 60 (70-230 mesh) and aluminum oxide (neutral, activity 1) obtained from Brinkmann (Canada), and Florisil (60–100 mesh) purchased from Fisher Scientific Co. (Canada) were used. Silica gel GF-254 and aluminum oxide G (type E) adsorbents were used for thick-layer chromatography. *sec*-Butyllithium, as a solution in hexane, and tetramethylethylenediamine (TMEDA) were purchased from Aldrich Chemical Co. When used below, the phrase 'standard work-up' signifies that a given organic solution was dried (Na_2SO_4) and evaporated to dryness *in vacuo*.

4-Bromoisochroman-1,3-dione (4)

To a stirred solution of isochroman-1,3-dione (15) (0.8 g, 5 mmol) in anhydrous methylene chloride (7 mL) was added pyridinium bromide perbromide (1.6 g, 5 mmol) in one portion. The mixture which became homogeneous in a few minutes was further stirred for 1 h. The solvent was removed under reduced pressure at room temperature and the residue was stirred with anhydrous benzene (25 mL) for 0.5 h after which time the benzene solution was decanted. This process was repeated. The combined benzene solution was subjected to filtration to remove the suspension of pyridinium hydrobromide. The filtrate was concentrated *in vacuo* at room temperature to give 0.8 g (67%) of compound **4** as a pale yellow oil; ir (C_6D_6) ν_{max}: 1800 and 1765 cm^{-1} (anhydride); nmr (C_6D_6) δ: 6.20 (s, 1H, C-4 H), 7.7–8.13 (m, 4H, aromatic H). This compound was found to be unstable and rearranged to phthalide-α-carboxylic acid, mp 154–156°C (lit. (16) mp 151°C) when water was used in the work-up or when it was stored for 1 week. Owing to its instability, compound **4** was used in the next reaction on the same day.

N-Methyl-N-(β-3,4-dimethoxyphenylethyl)phthalide-α-carboxamide (6)

A solution of freshly prepared 4-bromoisochroman-1,3-

[7]Related, synthetically useful species may be derived from secondary *o*-toluamides (14*a* and references therein) and *o*-toluic acids (14*b*).

[8]The possibility that these data correspond to the rearranged 6,7-dimethoxyphthalide-α-carboxylic acid bromide (see footnote 4) was eliminated by synthesis of this compound and comparison of its spectral data with those of the isomeric **17** (see Experimental).

[9]H. L. Holland and D. B. MacLean. Unpublished results, McMaster University, Hamilton, Ont.

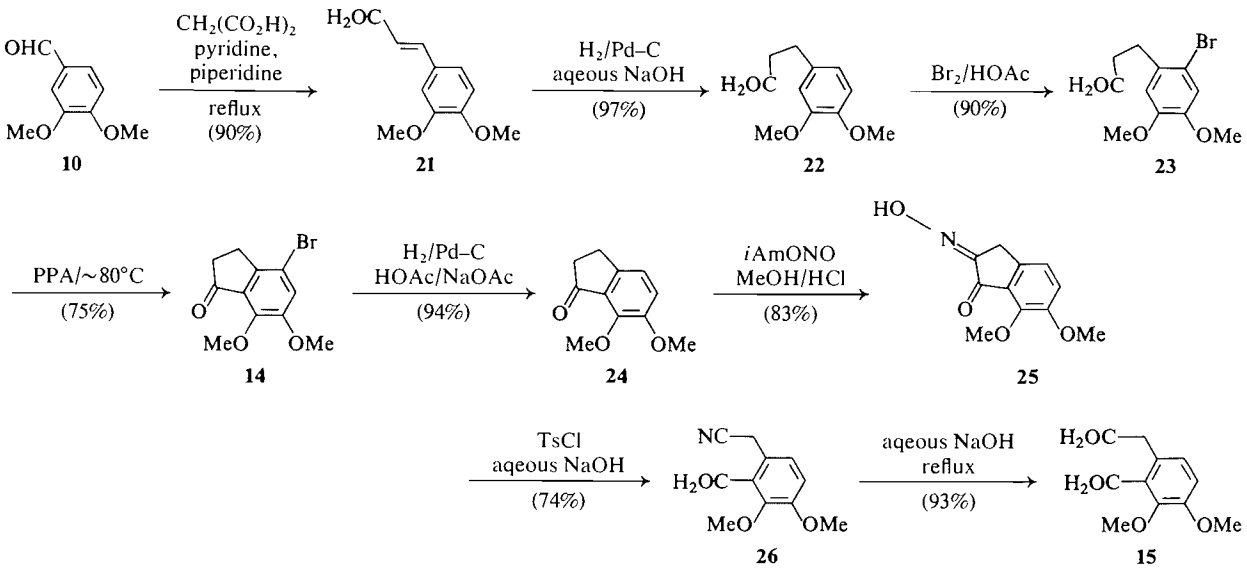

SCHEME 3

dione (**4**) (0.72 g, 3 mmol) in anhydrous benzene (10 mL) was added dropwise under nitrogen to a stirred solution of *N*-methyl-β-3,4-dimethoxyphenylethylamine (**3**) (17) (1.17 g, 6 mmol) in anhydrous benzene (18 mL). The mixture was stirred at room temperature for 1 h and the precipitated hydrobromide of **3** was removed by filtration. The filtrate was concentrated under reduced pressure to give a thick pale yellow oil which was purified by column chromatography (silica gel, $CHCl_3$–MeOH, 100:0.7). Initial fractions were combined and evaporated to dryness to give 0.85 g (80%) of compound **6** as a colourless syrup; ir ($CHCl_3$) ν_{max}: 1775 (γ-lactone), 1660 cm^{-1} (amide); nmr δ: 2.60–2.95 (m, 2H, —CH_2), 3.02, 3.13 (2 × s, 3H, NCH_3), 3.4–3.75 (m, 2H, —CH_2N), 3.8, 3.83, 3.88 (3 × s, 6H, 2 × OCH_3), 5.64 and 6.12 (2 × s, 1H, C-9 H), 6.8 (s, 3H, A ring aromatic H), 7.4–8.0 (m, 4H, D ring aromatic H); ms *m/e* (% relative intensity): 355 (41, M^+), 222 (26), 165 (78), 164 (100), 151 (100), 134 (24), 133 (100), 104 (28), 79 (41), 78 (41). *Anal.* calcd. for $C_{20}H_{21}NO_5$: C 67.60, H 5.90, N 3.94; found: C 67.38, H 6.16, N 3.80.

3-(3,4-Dihydro-6,7-dimethoxy-2-methyl-1(2H)isoquinolylidene)phthalide (7)

To a solution of *N*-methyl-*N*-(β-3,4-dimethoxyphenylethyl)phthalide-α-carboxamide (**6**) (0.5 g, 1.41 mmol) in dry THF (1 mL) was added freshly distilled phosphorous oxychloride (2.5 mL) and the mixture was refluxed on a steam bath for 3.5 h. The resulting dark red solution was cooled in an ice bath and treated by dropwise addition of a mixture of ammonium hydroxide and methanol (1:1) (2 mL). Water (4 mL) was added and the mixture was extracted with chloroform (3 × 25 mL). The organic extract was washed with water and treated by standard work up to give a dark red gum which when dissolved in methanol and allowed to stand overnight deposited 0.33 g (70%) of yellow crystals of compound **7**, mp 167–168.5°C; ir (KBr) ν_{max}: 1758 (lactone), 1594 cm^{-1} (C=C); uv λ_{max}: 219 (23 300), 307 (9600), 342 (11 600), 400 nm (16 000); nmr δ: 2.9 (s, 3H, NCH_3), 3.0–3.85 (m, 4H, —CH_2CH_2—), 4.05 (s, 3H, OCH_3), 4.15 (s, 3H, OCH_3), 6.9 (s) and 7.58–8.58 (m, 6H, aromatic H); ms *m/e* (% relative intensity): 338 (23), 337 (100, M^+), 280 (42), 278 (65). *Anal.* calcd. for $C_{20}H_{19}NO_4 \cdot \frac{1}{2}CH_3OH$: C 69.67, H 5.99, N 3.96; found: C 69.82, H 5.70, N 3.70.

(±)-threo- and -erythro-2-Methyl-6,7-dimethoxy-1-(phthalidyl)-1,2,3,4-tetrahydroisoquinolines (8 and 9)

To a suspension of powdered dehydrophthalide **7** (0.25 g, 0.74 mmol) in glacial acetic acid (25 mL) was added platinum oxide (10 mg) and the mixture was hydrogenated at room temperature and atmospheric pressure until hydrogen uptake ceased. The catalyst was removed by filtration and the colourless filtrate was evaporated to dryness under reduced pressure. The residual gum was neutralized with aqueous ammonium hydroxide and the resulting mixture was extracted with chloroform (3 × 25 mL). Standard work-up gave 0.25 g (96%) of a colourless syrup which was subjected to preparative tlc (silica gel, $CHCl_3$–MeOH, 97:3) to give the following two components.

Band 1

(±)-*threo*-2-Methyl-6,7-dimethoxy-1-(phthalidyl)-1,2,3,4-tetrahydroisoquinoline (**8**), 0.12 g (46%); R_f 0.7 (silica gel, $CHCl_3$–MeOH, 97:3); mp 168–170°C; ir (KBr) ν_{max}: 1760 cm^{-1} (γ-lactone); nmr δ: 2.66 (s, 3H, NCH_3), 2.2–3.4 (m, 4H, —CH_2CH_2—), 3.71 (s, 3H, OCH_3), 3.79 (s, 3H, OCH_3), 4.15 (d, J = 4 Hz, 1H, C-1 H), 5.76 (d, J = 4 Hz, 1H, C-9 H), 6.38 (s, 1H, C-8 H), 6.7 (s, 1H, C-5 H), 7.3–7.9 (m, 4H, D aromatic ring H); ms *m/e* (% relative intensity): 206 (100), 58 (67).

Picrate—Compound **8** (67.8 mg, 0.2 mmol) was dissolved in methanol (0.5 mL) and treated with a solution of picric acid (45.8 mg, 0.2 mmol) in methanol (0.5 mL). The mixture was refluxed on a steam bath for 15 min and cooled to give 105 mg (92%) of the picrate of **8** as yellow prisms, mp 198–200°C. *Anal.* calcd. for $C_{26}H_{24}N_4O_{11}$: C 54.93, H 4.26, N 9.86; found: C 54.87, H 4.41, N 9.77.

Band 2

(±)-*erythro*-2-Methyl-6,7-dimethoxy-1-(phthalidyl)-1,2,3,4-tetrahydroisoquinoline (**9**), 0.11 g (42%); R_f 0.35 (silica gel, $CHCl_3$–MeOH, 97:3); amorphous solid; ir ($CHCl_3$) ν_{max}: 1765 cm^{-1} (γ-lactone); nmr δ: 2.57 (s, 3H, NCH_3), 2.35–3.2 (m, 4H, —CH_2CH_2—), 3.63 (s, 3H, OCH_3), 3.85 (s, 3H, OCH_3), 4.08 (d, J = 4 Hz, 1H, C-1 H), 5.7 (d, J = 4 Hz, 1H, C-9 H), 6.3 (s, 1H, C-8 H), 6.6 (s, 1H, C-5 H), 6.8–7.05, 7.4–8.0 (m, 4H, D aromatic ring H); ms *m/e* (% relative intensity): 206 (100), 58 (67).

Picrate—Using the procedure described above, the picrate of **9** was prepared in 92% yield: yellow prisms, mp 208–210°C. *Anal.* calcd. for $C_{26}H_{24}N_4O_{11}$: C 54.93, H 4.26, N 9.86; found: C 55.10, H 4.26, N 9.78.

The mixture melting point of the two picrates was depressed (mp 176–188°C).

*Synthesis of 3,4-Dimethoxyhomophthalic Acid (**15**)*

(a) By a Classical Route (Scheme 3)

*3,4-Dimethoxycinnamic acid (**21**)*—A high yield (92%) procedure has been claimed (18) which apparently could not be reproduced (60%) (19). Following the Doebner reaction between 3,4-dimethoxybenzaldehyde and malonic acid as described by Koo *et al.* (20) furnished a 90% yield of compound **21**. A sample recrystallized from aqueous ethanol gave colourless needles, mp 180–181.5°C (lit. (19) mp 181–181.5°C); ir (KBr) ν_{max}: 3440 (br, OH) and 1682 cm^{-1} (C=O); nmr δ: 3.95 (s, 6H, 2× OCH_3), 6.3 (d, J = 16 Hz, 1H, —CH=C*H*CO_2H), 6.75–7.15 (m, 3H, aromatic H), 7.78 (d, J = 16 Hz, 1H, —C*H*=$CHCO_2H$).

*3,4-Dimethoxyphenylpropionic acid (**22**)*—Compound **22** has been previously obtained in 85% yield by reduction of **21** using sodium amalgam (21, 22). The hydrogenation procedure of McCorkindale *et al.* (23) was followed. From 5 g (24 mmol) of **21** there was obtained 4.9 g (97%) of compound **22**. A sample recrystallized from aqueous ethanol showed mp 95–96°C (lit. (21) mp 97°C); ir (KBr) ν_{max}: 2900 (br, OH), 1700 cm^{-1} (C=O); nmr δ: 2.40–3.20 (m, 4H, —CH_2CH_2—), 3.88 (s, 6H, 2× OCH_3), 6.80 (s, 3H, aromatic H), 8.90 (br s, 1H, OH).

*3-(2-Bromo-4,5-dimethoxyphenyl)propionic acid (**23**)*—Compound **23** was obtained in 90% yield by bromination of **22** according to a literature procedure (24). A sample recrystallized from aqueous ethanol showed mp 118–119°C (lit. (24) mp 118–119°C); ir (KBr) ν_{max}: 2930–2832 (br, OH), 1710 cm^{-1} (C=O); nmr δ: 2.45–3.15 (m, 4H, —CH_2CH_2—), 3.83 (s, 6H, 2× OCH_3), 6.78 (s, 1H, C-6 H), 7.0 (s, 1H, C-3 H), OH absorption was not detected.

*4-Bromo-6,7-dimethoxyindan-1-one (**14**)*—Friedel–Crafts cyclization of **23** using concentrated sulfuric acid (24) gave **14** in only 25% yield. We obtained **14** in 75% yield by using polyphosphoric acid under conditions which are essentially those recently described by Cushman and Dekow (13). A sample recrystallized from methanol showed mp 120–121°C (lit. (13) 118–120°C; lit. (24) mp 120–121°C); ir and nmr spectra identical with those reported (13).

*6,7-Dimethoxyindan-1-one (**24**)*—Compound **24** has been previously obtained from 2-carboxy-3,4-dimethoxybenzaldehyde (opianic acid) in four steps and unknown overall yield (25). A mixture of compound **14** (2 g, 7.4 mmol) and anhydrous sodium acetate (1 g) in glacial acetic acid (100 mL) was hydrogenated in the presence of 10% palladium-on-carbon (0.2 g) at room temperature and 50 psi until hydrogen uptake ceased. The catalyst was removed by filtration and the filtrate was evaporated to dryness under reduced pressure. The resulting residue was dissolved in water (25 mL) and extracted with ethyl acetate (2 × 50 mL). Standard work up gave an oil. Vacuum distillation afforded 1.33 g (94%) of compound **24** as a colourless oil, bp 188–190°C/20 Torr which crystallized, mp 40–42°C (lit. (25) mp 40–43°C); ir ($CHCl_3$) ν_{max}: 1703 cm^{-1} (C=O); nmr δ: 2.48–2.78 (m, 2H, —CH_2—), 2.86–3.2 (m, 2H, CH_2CO), 3.9 (s, 3H, OCH_3), 4.0 (s, 3H, OCH_3), 7.04 (d, J = 8 Hz, C-5 H), 7.24 (d, J = 8 Hz, C-4 H).

*2-Hydroxyimino-6,7-dimethoxyindan-1-one (**25**)*—The method of Schöpf *et al.* (25), also recently adopted by Cushman and Dekow (13), was employed using *iso*-amylnitrite as the nitrosating reagent. In this manner, compound **24** gave **25** in 83% yield, mp 208–209.5°C. (lit. (25) mp 208–210°C); ir (KBr): 1722 (C=O), 1650 cm^{-1} (C=N). This material was used in the next step without purification.

*2-Carboxy-3,4-dimethoxyphenylacetonitrile (**26**)*—The second-order Beckmann rearrangement of **25** was carried out according to the method of Gensler *et al.* (26) (see also ref. 13) to give compound **26** in 74% yield, mp 116–118°C (lit. (25) mp 97–99°C; lit. (26) mp 104–108°C); ir ($CHCl_3$) ν_{max}: 2320 (CN), 1745 cm^{-1} (C=O); nmr δ: 3.93 (s, 2H, —CH_2—), 4.0 (s, 6H, 2 × OCH_3), 7.0 (d, J = 8.5 Hz, C-5 H), 7.25 (d, J = 8.5 Hz, C-6 H).

*3,4-Dimethoxyhomophthalic acid (**15**)*—Base-catalyzed hydrolysis of **26** was carried out according to a literature method (25) (see also ref. 13) to give **15** in 93% yield, mp 117–118°C (lit. (25) mp 115–117°C); ir and nmr spectra in agreement with those reported (13).

*(b) By Directed Metalation of **13** (Scheme 2)*

*2,3-Dimethoxy-6-methyl-*N,N*-diethylbenzamide (**12**)*—A stirred solution of 2,3-dimethoxy-*N,N*-diethylbenzamide (bp 140°C/0.2 Torr) (27) (2.37 g, 10 mmol) and TMEDA (1.5 mL, 10 mmol) in dry tetrahydrofuran (200 mL) contained in a two-necked flask equipped with a gas inlet tube and a septum inlet and maintained under an atmosphere of dry nitrogen, was cooled to −78°C (Dry Ice – acetone bath). A solution (0.9 *M*) of *sec*-butyllithium in hexane (11.1 mL, 10 mmol) was slowly introduced through the septum inlet using a hypodermic syringe. The light yellow solution was stirred for 1 h at −78°C and dry methyl iodide (1.24 mL, 20 mmol) was injected into the flask. Stirring was continued for 6 h during which time the cooling bath warmed to room temperature. Evaporation of the reaction mixture under reduced pressure gave a gummy product which was suspended in water (200 mL) and extracted with methylene chloride (2 × 100 mL). Standard work up yielded an oil which upon vacuum distillation gave 2.4 g (98%) of compound **12**, bp 130°C/0.4 Torr; ir ($CHCl_3$) ν_{max}: 1625 cm^{-1} (amide); nmr δ: 0.87–1.42 (2 × overlapping t, 6H, $N(CH_2CH_3)_2$), 2.23 (s, 3H, $ArCH_3$), 2.87–3.83 (2 × overlapping q, 4H, $N(CH_2CH_3)_2$), 3.87 (s, 6H, 2× OCH_3), 6.93 (s, 2H, collapsed AB pattern, aromatic H). *Anal.* calcd. for $C_{14}H_{21}NO_3$: C 66.91, H 8.42, N 5.57; found: C 66.61, H 8.39, N 5.23.

*2-(*N,N*-Diethylcarboxamido)-3,4-dimethoxyphenylacetic acid (**11**)*—A solution of **12** (0.5 g, 2 mmol) in dry THF (200 mL) at −78°C prepared as for the synthesis of **11**, was treated with a solution (0.9 *M*) of *sec*-butyllithium in hexane (2.22 mL, 2 mmol) by slow injection through a septum cap using a hypodermic syringe. The resulting purple solution was stirred at −78°C for 0.5 h and allowed to warm to −60°C. The solution was blanketed with a stream of dry carbon dioxide passed through a syringe needle inserted into the septum cap. The purple color was discharged (3 min) to give a yellow solution but the carbon dioxide supply was maintained for 15 min. The solution was allowed to warm to room temperature and evaporated to yield a gum which was suspended in water (200 mL). The resulting mixture was extracted with methylene chloride (100 mL) and the aqueous layer was acidified (6 *N* HCl, 50 mL) and continuously extracted (24 h) with diethyl ether. Standard work up yielded 0.498 g of a semisolid which was recrystallized from benzene – petroleum ether (60–80°C) (1:1) to afford 0.42 g (71% of compound **11**), mp 107°C; ir ($CHCl_3$) ν_{max}: 1740 (CO_2H), 1580 cm^{-1} (amide); nmr δ: 0.87–1.42 (2 × overlapping t, 6H, $N(CH_2CH_3)_2$), 3.02–3.75 (m, 6H, CH_2CO_2H, $N(CH_2CH_3)_2$), 3.75 (s, 3H, OCH_3), 3.91 (s, 3H, OCH_3), 6.98 (d, 1H, J = 8 Hz, C-6 H), 7.2 (d, 1H, J = 8 Hz, C-5 H). *Anal.* calcd. for $C_{15}H_{21}NO_5$: C 61.00, H 7.17, N 4.74; found: C 60.91, H 7.02, N 4.42.

*One-pot synthesis of compound **11***—The procedure described for the preparation of **12** was followed up to and including the

methyl iodide addition step using the following quantities of reagents: compound **13** (237 mg, 1 mmol), dry THF (100 mL), *sec*-butyllithium (0.9 *M* solution in hexane, 1.12 mL, 1 mmol), methyl iodide (0.09 mL, 1.5 mmol). The mixture was allowed to warm to room temperature over 1 h and then heated at 60°C for 0.5 h in the presence of a continuous stream of dry nitrogen. The mixture was cooled to −60°C (gradual addition of Dry Ice to an acetone bath) and sequentially injected with freshly distilled diisopropyl amine (0.14 mL, 0.1 mmol) and a solution of *sec*-butyllithium in hexane (1.12 mL, 1 mmol). The resulting deep purple solution was stirred for 0.5 h and subjected to treatment with carbon dioxide and standard work up according to the description above for the conversion **12** → **11**. The crude product was chromatographed (silica gel, benzene–methanol–acetone, 9:1:1) to give 0.140 g (47%) of compound **11** which was shown to be identical (mp, tlc, nmr) with a sample prepared above by the two-step procedure.

*Hydrolysis of Compound **12**: 3,4-Dimethoxyhomophthalic acid (**15**)*—A suspension of the homophthalic acid amide **11** (120 mg) in 10% aqueous perchloric acid (40 mL) was refluxed for 40 h, cooled, and continuously extracted with diethyl ether. The ether layer was dried by azeotropic removal of water using benzene and evaporated to dryness yielding a gum which was recrystallized from benzene to give 74 mg (75%) of compound **15**, mp 117°C which was shown to be identical (mixture mp, ir, nmr) with a sample prepared by the classical method. decribed above.

*7,8-Dimethoxyisochroman-1,3-dione (**16**)*

A mixture of dry 3,4-dimethoxyhomophthalic acid (**15**) (0.5 g, 2.1 mmol) and acetic anhydride (4.5 mL) was refluxed for 3 h and evaporated to dryness under reduced pressure to give a pale yellow solid. Recrystallization from anhydrous benzene afforded 0.4 g (87%) of 7,8-dimethoxyisochroman-1,4-dione (**16**) as colourless plates, mp 103–105°C (lit. (24) mp 104–105°C); ir (KBr) ν_{max}: 1790, 1750 cm^{-1} (anhydride); nmr (acetone-d_6) δ: 3.87 (s, 3H, OCH_3), 3.9 (s, 3H, OCH_3), 4.14 (s, 2H, —CH_2—), 7.17, 7.47 (2 × d, J = 8.5 Hz, 2H, aromatic H).

*4-Bromo-7,8-dimethoxyisochroman-1,3-dione (**17**)*

To a solution of 7,8-dimethoxyisochroman-1,3-dione (**16**) (0.44 g, 2 mmol) in anhydrous methylene chloride (4 mL) was added pyridinium bromide perbromide (0.638 g, 2 mmol). Dissolution occurred in a few minutes. The mixture was stirred at room temperature for 1.5 h and then evaporated to dryness at reduced pressure and room temperature. The residue was stirred with anhydrous benzene (10 mL) for 15 min and the benzene solution was decanted. This process was repeated. The combined benzene extracts were subjected to filtration in order to remove remaining pyridinium hydrobromide. The filtrate was concentrated *in vacuo* at room temperature to give 0.58 g (83%) of compound **17** as an unstable oil (ir ($CHCl_3$) ν_{max}: 1810, 1755 cm^{-1} (anhydride); nmr (acetone-d_6) δ: 3.93 (s, 3H, OCH_3), 3.99 (s, 3H, OCH_3), 6.10 (s, 1H, C-4 H), 7.55 (s, 2H, aromatic H)) which was used without further purification in the next reaction.

That the above data correspond to structure **17** and are not due to the acid bromide of 6,7-dimethoxyphthalide-α-carboxylic acid (**20**) was shown by an unambiguous synthesis of the latter as follows.

Thionyl bromide (1 mL) was added to 6,7-dimethoxyphthalide-α-carboxylic acid (**20**) (20 mg) (11) placed in a flask equipped with a magnetic stirring bar and a drying tube, and the flask immersed in an ice bath. The mixture was stirred and allowed to warm to room temperature over 3 h. The excess thionyl bromide was removed under high vacuum to give the acid bromide of compound **20** as a gummy, highly moisture-sensitive material (22 mg, 87%); ir ($CHCl_3$) ν_{max}: 1780, 1770 cm^{-1} (γ-lactone); nmr (acetone-d_6) δ: 3.96 (s, 3H, OCH_3), 4.05 (s, 3H, OCH_3), 6.0 (s, 1H, C-3 H), 7.5 (collapsed AB pattern, 2H, aromatic H); mass spectrum *m/e* (% relative intensity) 301 (M^+, 3), 193 (—COBr, 72), 85 (97), 83 (97).

N-*Methyl*-N-*(β-3,4,-dimethoxyphenylethyl)meconine-α-carboxamide (**18**)*

A solution of freshly prepared **17** (0.58 g, 1.92 mmol) in anhydrous benzene (5 mL) was added dropwise under dry nitrogen to a stirred solution of *N*-methyl-β-3,4-dimethoxyphenylethylamine (**3**) (0.749 g, 3.84 mmol) in anhydrous benzene (8 mL). The mixture was stirred at room temperature for 1.5 h. The resulting precipitate of the hydrobromide of **3** was removed by filtration and the filtrate was diluted with benzene (25 mL) and washed with successive portions of dilute hydrochloric acid and water. The organic layer was dried (Na_2SO_4) and concentrated under reduced pressure to give a pale yellow syrup. Purification by preparative tlc (silica gel, $CHCl_3$–MeOH, 100:3) gave 0.45 g (56%) of compound **18** as an oil which crystallized from methyl alcohol in glistening white prisms, mp 123–125°C (lit. (10) mp 123–124°C); ir ($CHCl_3$) ν_{max}: 1780 (lactone), 1650 cm^{-1} (amide); nmr δ: 2.65–2.98 (m, 2H, —CH_2—), 3.07, 3.15 (2 × s, ~2:1, 3H, NCH_3), 3.51–4.2 (m, 14H, —CH_2N, 4 × OCH_3), 5.58, 6.03 (2 × s, ~2:1, 1H, phthalide-α-H), 6.67–7.25 (m, 5H, aromatic H). This compound was shown to be identical (mixture mp, tlc (silica gel, $CHCl_3$–MeOH, 100:3), and nmr) with an authentic sample provided by Professors D. B. MacLean and H. L. Holland.

*3-(3,4-Dihydro-6,7-dimethoxy-2-methyl-1(2H)-isoquinolylidene)-6,7-dimethoxyphthalide (Dehydrocordrastine) (**19**)*

To a solution of compound **18** (200 mg, 0.48 mmol) in anhydrous THF (0.5 mL) was added freshly distilled phosphorous oxychloride (1.2 mL) and the mixture was refluxed on a steam bath for 3.5 h. The resulting deep red solution was evaporated to dryness *in vacuo* to give a dark red syrup which was cooled in an ice bath and treated dropwise with a mixture of ammonium hydroxide and methanol (1:1) (1.2 mL). Water (2 mL) was added and the mixture was extracted with chloroform (3 × 30 mL). Standard work up gave a dark red gum which was crystallized from methanol to afford 120 mg (60%) of compound **19** as orange-yellow prisms, mp 139–141°C (lit. (10) mp 136–136.5°C); ir (KBr) ν_{max}: 1764 (lactone), 1600 cm^{-1} (C=C); uv λ_{max}: 225 (24 800), 307 (14 950), 330 (14 400), 404 nm (18 900); nmr δ: 2.65 (s, 3H, NCH_3), 2.76 (t, 2H, —CH_2—), 3.17 (t, 2H, —CH_2N), 3.8, 3.85, 3.89, 4.04 (4 × s, 12H, 4 × OCH_3), 6.54 (s, 1H, C-8 H), 7.18, 7.84 (2 × s, 2H, C-2′, C-3′ H), 7.97 (s, 1H, C-5 H); ms *m/e* (% relative intensity): 398 (28), 397 (M^+, 100), 382 (32), 364 (32), 341 (32), 339 (50), 309 (25), 199 (67). This compound was shown to be identical (mixture mp, ir, tlc (silica gel, $CHCl_3$–MeOH, 100:3), nmr) with an authentic sample provided by Professors D. B. MacLean and H. L. Holland.

Acknowledgements

We are grateful to Professor D. B. MacLean, McMaster University, and Professor H. L. Holland, Brock University, for authentic samples and several helpful exchanges of information. This work was supported by the National Research Council of Canada and by Bristol Laboratories.

1. S. O. DE SILVA, I. AHMAD, and V. SNIECKUS. Tetrahedron Lett. 5107 (1978).
2. F. SANTAVY. *In* The alkaloids. Vol. 12. *Edited by* R. H. F. Manske. Academic Press, New York, NY. 1970. p. 397.
3. M. SHAMMA. The isoquinoline alkaloids. Chemistry and pharmacology. Academic Press, New York, NY. 1972. p. 359.
4. M. SHAMMA and J. L. MONIOT. Isoquinoline alkaloid research 1972–1977. Plenum Press, New York, NY. 1978. p. 307.
5. T. KAMETANI. The isoquinoline alkaloids. Elsevier Publishing Co. Amsterdam. 1969. p. 136; T. KAMETANI. The isoquinoline alkaloids. Vol. 2. Elsevier Publishing Co., Amsterdam. 1972. p. 221.
6. A. R. BATTERSBY, J. STAUNTON, H. R. WILTSHIRE, B. J. BIRCHER, and C. FUGANTI. J. Chem. Soc. Perkin Trans. I, 1162 (1975).
7. R. H. F. MANSKE. Can. J. Res. **14** B, 325 (1936); R. H. F. MANSKE. Can. J. Res. **16** B, 81 (1938).
8. R. H. F. MANSKE. Chem. Can. **11**, 74 (1959).
9. B. C. NALLIAH, D. B. MACLEAN, R. G. A. RODRIGO, and R. H. F. MANSKE. Can. J. Chem. **55**, 922 (1977).
10. R. D. HAWORTH and A. R. PINDER. J. Chem. Soc. 1776 (1950).
11. S. O. DE SILVA, J. N. REED, and V. SNIECKUS. Tetrahedron Lett. 5099 (1978).
12. V. SMULA, N. E. CUNDASAWMY, H. L. HOLLAND, and D. B. MACLEAN. Can. J. Chem. **51**, 3287 (1973).
13. M. CUSHMAN and F. W. DEKOW. Tetrahedron, **34**, 1435 (1978).
14. (*a*) R. E. LUDT, J. S. GRIFFITHS, K. N. MCGRATH, and C. R. HAUSER. J. Org. Chem. **38**, 1668 (1973); (*b*) P. L. CREGER. J. Am. Chem. Soc. **92**, 1396 (1970); F. M. HAUSER and R. P. RHEE. J. Org. Chem. **42**, 4155 (1977).
15. O. GRUMMITT, R. EGAN, and A. BUCK. Org. Synth. Coll. Vol. III, 449 (1955).
16. T. S. STEVENS and J. L. WILSON. J. Chem. Soc. 2827 (1928).
17. W. W. SPEIR, V. MIHRANIAN, and J. L. MCLAUGHLIN. Lloydia, **33**, 15 (1970).
18. A. OLIVERIO. Rend. Semin. Fac. Sci. Univ. Cagliari, **1**, 117 (1931); Chem. Abstr. **27**, 4531 (1933).
19. F. B. WITTMER and L. C. RAIFORD. J. Org. Chem. **10**, 527 (1945).
20. J. KOO, M. S. FISH, G. N. WALKER, and J. BLAKE. Org. Synth. Coll. Vol. IV, 327 (1963).
21. W. H. PERKIN, JR. and R. ROBINSON. J. Chem. Soc. **91**, 1073 (1907).
22. R. D. HAWORTH, W. H. PERKIN, JR., and H. S. PINK. J. Chem. Soc. **127**, 1709 (1925).
23. N. J. MCCORKINDALE, A. W. MCCULLOCH, D. S. MAGRILL, B. CADDY, M. MARTIN-SMITH, S. J. SMITH, and J. B. STENLAKE. Tetrahedron, **25**, 5475 (1969).
24. R. D. HAWORTH, J. B. KOEPFLI, and W. H. PERKIN, JR. J. Chem. Soc. 548 (1927).
25. C. SCHÖPF, I. JACKH-TETTWEILER, G. MAYER, H. PERREY-FEHRENBACH, and L. WINTERHALDER. Justus Liebigs Ann. Chem. **544**, 77 (1940).
26. W. J. GENSLER, S. F. LAWLESS, A. L. BLUHM, and D. DERTOUZOS. J. Org. Chem. **40**, 733 (1975).
27. A. BARUFFINI, G. PAGANI, and G. CACCIALANZA. Farmaco, Ed. Sci. **29**, 317 (1974); Chem. Abstr. **81**, 73303h (1974).
28. H. O. BERNHARD. Ph.D. Thesis, University of Waterloo, Waterloo, Ont. 1971.

The biosynthesis of the Lythraceae alkaloids.[1,2] I. The lysine-derived fragment

RAM NATH GUPTA, PETER HORSEWOOD, SWE HOO KOO, and IAN D. SPENSER

Department of Chemistry, McMaster University, Hamilton, Ont., Canada L8S 4M1

Received August 30, 1978

RAM NATH GUPTA, PETER HORSEWOOD, SWE HOO KOO, and IAN D. SPENSER. Can. J. Chem. **57**, 1606 (1979).

The biosynthesis of decodine (**7**) and decinine (**9**), Lythraceae alkaloids containing a *trans*-fused quinolizidine nucleus, was studied in intact plants of *Decodon verticillatus* (L.) Ell. Nonrandom incorporation of radioactivity from ^{14}C-labelled samples of lysine, cadaverine, and Δ^1-piperideine was demonstrated by partial degradation. Pelletierine did not serve as a precursor of the alkaloids. It was also shown, by means of ^{3}H,^{14}C-labelled tracers, that the alkaloids are derived from L-lysine whereas pipecolic acid, which is present in the plant, is derived from D-lysine.

RAM NATH GUPTA, PETER HORSEWOOD, SWE HOO KOO et IAN D. SPENSER. Can. J. Chem. **57**, 1606 (1979).

On a étudié la biosynthèse, dans des plantes complètes de *Decodon verticillatus* (L.) Ell, de la décodine (**7**) et de la décinine (**9**), des alcaloïdes lythraceae contenant un noyau quinolizidine avec fusion *trans*. Faisant appel à une dégradation partielle, on a démontré que l'incorporation de la radioactivité provenant d'échantillons de lysine, de cadavérine et de Δ^1-pipéridéine se fait d'une façon qui ne relève pas du hasard. On n'a pas observé que la pelletierine puisse servir de précurseur pour ces alcaloïdes. On a aussi montré, en faisant appel à des marqueurs ^{3}H et ^{14}C que les alcaloïdes dérivent de la L-lysine alors que l'acide pipécolique qui est présent dans la plante provient de la D-lysine.

[Traduit par le journal]

Introduction

Several structural variants are known among the alkaloids of the family Lythraceae (Scheme 1) (for a review, see ref. 2). One major group comprises *cis*- and *trans*-fused phenylquinolizidinols, derivatized by esterification and phenol coupling (either C—C or O—C) with a C_6–C_3 phenylpropanoid acid. A second group are *cis*-fused phenylquinolizidinols which are further substituted by a C_6–C_4 unit. Thirdly, there are piperidine derivatives, disubstituted, at the two α-carbons, by C_6–C_4 units. The different groups are further characterized by stereochemical distinctions.

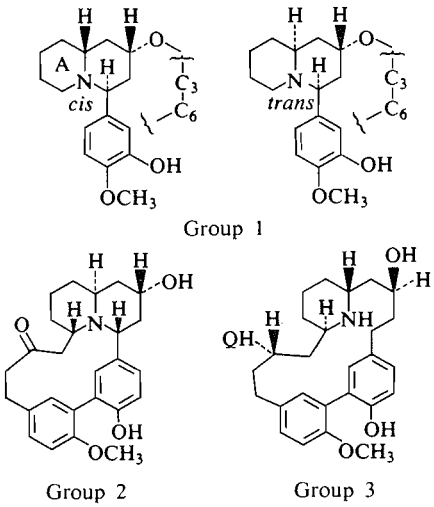

SCHEME 1. Alkaloids of the Family Lythraceae: group 1: *Decodon*-type alkaloids; group 2: *Lythrum*-type alkaloids; group 3: piperidine-type alkaloids.

The ring systems of the three structural types are biogenetically derivable (3, 4) (Scheme 2) from pelletierine (**4**) whose nucleus, in turn, has been shown to be generated from L-lysine (5), via cadaverine (6) and, presumably, Δ^1-piperideine (cf. refs. 7–10), and whose side chain originates from acetate (11–13). Biogenetically modelled syntheses of pelletierine have been reported (14). Mannich condensation of pelletierine with a C_6–C_1 unit, isovanillin, a reaction which has been employed in biomimetic synthesis (15–17), yields the phenylquinolizidinone (**6**). This compound, together with the corresponding alcohol, has been detected in *Heimia salicifolia* (16, 17). It represents the structural core of the first group of Lythraceae alkaloids. Introduction of a second α-side chain into pelletierine (cf. ref. 18), followed by condensation with two C_6–C_1 units, yields an intermediate from which alkaloids of the second and third groups may plausibly be derived.

We have tested the validity of the pelletierine hypothesis of the origin of the Lythraceae alkaloids of *Decodon verticillatus* by tracer experiments. Radioactivity from ^{14}C-labelled samples of lysine, cadaverine, and Δ^1-piperideine is indeed incorporated

[1]This paper is dedicated to the memory of R. H. F. Manske.

[2]A preliminary report of part of this work has been published (1).

0008-4042/79/131606-09$01.00/0

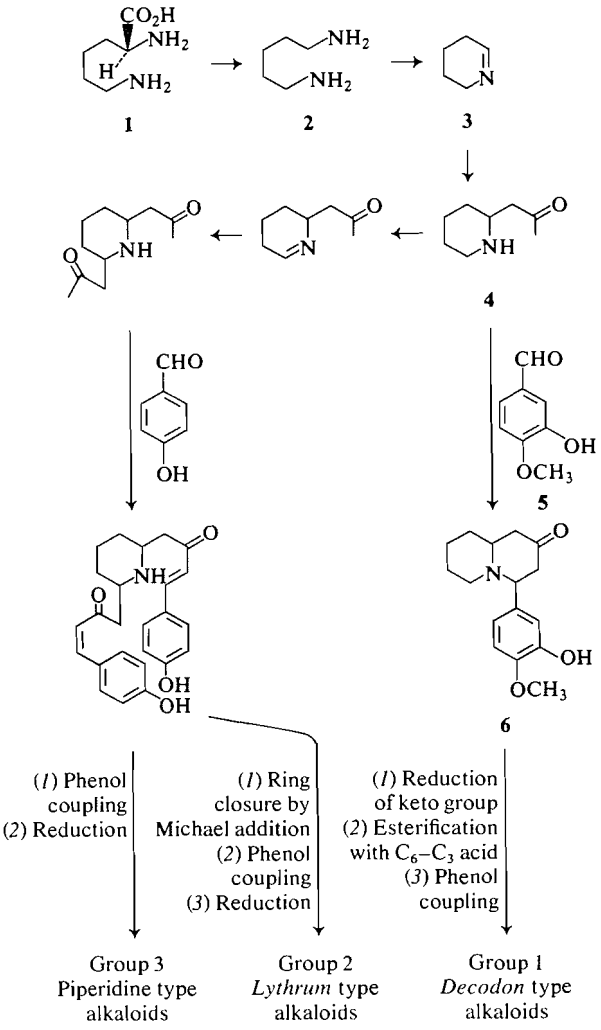

SCHEME 2. Biogenesis from pelletierine of the skeletons of the Lythraceae alkaloids (ignoring stereochemistry).

in predicted fashion into decodine and decinine. Contrary to prediction, however, pelletierine does not serve as a precursor.

Methods and Results

The plant species used in this investigation was *Decodon verticillatus* (L.) Ell. (water oleander). This is the species of the family Lythraceae from which alkaloids were first isolated by J. P. Ferris (19, 20). A voucher specimen is deposited in the herbarium of the Royal Botanical Gardens, Hamilton. For feeding experiments, stocks of the plant were transferred to the greenhouse from their native habitat in swampy areas of the botanical gardens. Tracers were administered to intact plants through wicks inserted into the stems of the plants. Two, three, or four stocks were used in each experiment. All feeding experiments were carried out in late June or early July, 3 or 4 weeks after fresh growth appeared. Biosynthesis of the major alkaloids does not appear to take place later in the season.

Specifically labelled samples of lysine (experiments 1–4), cadaverine (experiment 5), Δ^1-piperideine (experiment 6), and pelletierine (experiments 7 and 8) were administered, the plants were kept in contact with tracer for 3 days, and the aerial parts of the plants were harvested, dried, and ground. The underwater parts of the plant, which do not appear to contain alkaloids, were discarded. Alkaloids were extracted from the powdered leaves and stems. Decodine, and in most cases also decinine, was isolated by dilution with inactive carrier and purified to constant radioactivity. A summary of these experiments is presented in Table 1.

Decodine obtained from the experiments with labelled lysine, cadaverine, and Δ^1-piperideine was radioactive, as was the decinine which was also isolated from the experiments with lysine. To determine the distribution of ^{14}C, the labelled samples were degraded by chromic acid oxidation into the partial degradation products, β-alanine, γ-aminobutyric acid, and 2-piperidylacetic acid (Scheme 3).

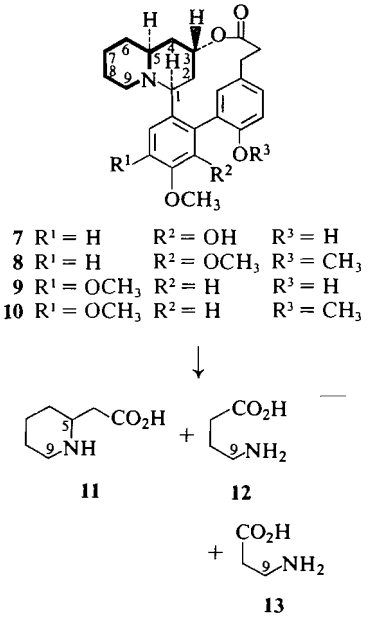

SCHEME 3. Degradation of decodine (**7**) and decinine (**9**). (For reasons which will be discussed in the second paper of this series, the numbering of the quinolizidine carbon atoms employed here is that used by Schöpf *et al.* (21) rather than that recommended by the Ring Index (22, RR1 1687) and used previously for the *Decodon* alkaloids.)

TABLE 1. Tracer experiments with *Decodon verticillatus*

Experiment No. (date)	Precursors	Nominal total activity, mCi	Nominal specific activity, mCi/mmol	Measured $^3H/^{14}C$ ratio	Weight of dry plant material (g)	^{14}C specific activity (dpm/mmol) $\times 10^{-4}$ of products after dilution with inactive material (mg)	
						Decodine	Decinine
1 (1969)	DL-[6-^{14}C]Lysine[a]	0.1	48	—	22	7.53±0.12 (600)[c]	7.53±0.12 (600)
2 (1969)	DL-[2-^{14}C]Lysine[b]	0.1	1.6	—	32	16.95±0.12 (650)[c]	28.80±0.42 (400)
3 (1973)	DL-[6-^{14}C]Lysine[a] DL-[4,5-$^3H_2$]Lysine[b]	0.1 1.0	48 3.3×10^4	5.17±0.07	14	166.4 ±1.1 (20)	115.0 ±1.0 (20)
4 (1972)	DL-[6-^{14}C]Lysine[a] L-[4-^{3}H]Lysine[b]	0.1 1.0	48 3.9×10^4	5.69±0.08	37	93.8 ±0.7 (10)	93.6±0.4 (10)
5 (1970)	[1,5-^{14}C]Cadaverine dihydrochloride[b]	0.05	13	—	17	11.19±0.18 (350)[c]	Not isolated
6 (1972)	[6-^{14}C]-Δ^1-Piperideine (from DL-[6-^{14}C]lysine)[a]	0.08 0.1	0.4 48	—	14	3.90±0.03 (300)	Not isolated
7 (1970)	*RS*-[6-^{14}C]Pelletierine (from DL-[6-^{14}C]lysine)[a] *RS*-[2′-^{14}C]Pelletierine (from ethyl [3-^{14}C]acetoacetate)[d]	0.03 0.2 0.05 0.13	0.4 48 0.5 4.7	—	45	Inactive (350)	Inactive (350)
8 (1973)	*RS*-[6-^{3}H]Pelletierine (from DL-[6-^{3}H]lysine)[b] *RS*-[2′-^{14}C]Pelletierine (from ethyl [3-^{14}C]acetoacetate)[d]	0.6 1.2 0.06 0.13	2.4 7.9×10^3 0.5 4.7	10.4±0.1	15	Inactive	Inactive (no carrier added)

[a]Commissariat à l'Energie Atomique, France.
[b]New England Nuclear.
[c]Assayed as dimethyldecodine.
[d]Amersham/Searle.

The specific activities of these degradation products, obtained from the samples of decodine and decinine from individual feeding experiments, are listed in Tables 2 and 3.

The samples of β-alanine and of γ-aminobutyric acid (isolated as their *N*-dinitrophenyl derivatives) obtained by oxidation of decodine and decinine, derived from [2-^{14}C]lysine (experiment 1) and [6-^{14}C]lysine (experiment 2), and of decodine from [1,5-^{14}C]cadaverine (experiment 5) in each case accounted for approximately one-half of the activity of the intact alkaloid from which they were derived. The sample of 2-piperidylacetic acid from the same experiments contained the entire activity of the intact alkaloid. Decodine, derived from [6-^{14}C]-Δ^1-piperideine (experiment 6), on the other hand, yielded γ-aminobutyric acid which, like the 2-piperidylacetic acid, maintained the total activity of the intact alkaloid.

The alkaloids, obtained from plants which had been kept in contact with labelled pelletierine (experiments 7 and 8), were not radioactive.

The ^{3}H/^{14}C ratio of the lysine administered in experiments 3 and 4 is compared with that of the samples of decodine and decinine as well as that of the pipecolic acid isolated from the plants (Table 4). The alkaloids and pipecolic acid maintained the ^{3}H/^{14}C ratio of the tracer in the experiment with DL-[^{3}H]lysine/DL-[^{14}C]lysine. In the experiment with L-[^{3}H]lysine/DL-[^{14}C]lysine, the pipecolic acid was rich in ^{14}C but had lost 97% of the ^{3}H relative to ^{14}C. The alkaloids, on the other hand, were found to have a ^{3}H/^{14}C ratio which was double that of the precursor.

Discussion

Biosynthesis of decodine and decinine from pelletierine and pelletierine precursors demands a predictable pattern of radioactivity from ^{14}C-labelled samples of lysine, cadaverine, Δ^1-piperideine and ring-labelled pelletierine, in ring A (i.e., C-5 to C-9,*N*) of the alkaloids. A degradation of the alkaloids was therefore required which generates fragments recognizably derived from that portion of the molecules. Chromic acid oxidation of the alkaloids yields such fragments (Scheme 3). They are 2-piperidylacetic acid (**11**) (C-3 to -9), γ-aminobutyric acid (**12**) (C-6 to -9), and β-alanine (**13**) (C-7 to -9). Pipecolic acid or δ-aminovaleric acid were not detected among the degradation products. The yield of the oxidation products was too low (1–2%) to permit the further chemical manipulation which is required to separate individual carbon atoms. It was not possible, therefore, to isolate C-5 and C-9, the

TABLE 2. Incorporation of precursors into decodine

Product	Experiment 1 DL-[6-^{14}C]lysine		Experiment 2 DL-[2-^{14}C]lysine		Experiment 5 [1-^{14}C]cadaverine		Experiment 6 [6-^{14}C]-Δ^1-piperideine	
	SA[a]	RSA[b]	SA[a]	RSA[b]	SA[a]	RSA[b]	SA[a]	RSA[b]
Dimethyldecodine (8)	7.53±0.12	100±1	16.95±0.12	100±1	11.19±0.18	100±2	3.90±0.03	100±1
DNP-β-alanine (13)	3.84±0.06	51±1	[c]	49±1	5.64±0.09	50±1	—	—
DNP-γ-aminobutyric acid (12)	3.84±0.06	51±1	8.40±0.18	50±1	—	—	4.02±0.06	103±2
DNP-2-piperidyl-acetic acid (11)	7.44±0.15	99±3	17.04±0.18	100±1	11.28±0.21	101±2	3.21±0.09	83±2

[a]Specific activity (dpm mmol^{-1}) × 10^{-4}.
[b]Relative specific activity (%) (dimethyldecodine = 100).
[c]The DNP-β-alanine (specific activity 4.38 (±0.06) × 10^4 dpm mmol^{-1}) was obtained by oxidation of a sample of dimethyldecodine (specific activity 8.94 (±0.15) × 10^4 dpm mmol^{-1}) which was prepared by carrier dilution of the sample, specific activity 16.95 (±0.12) × 10^4 dpm mmol^{-1}.

TABLE 3. Incorporation of lysine into decinine

Product	Experiment 1 DL-[6-^{14}C]lysine SA[a]	Experiment 1 DL-[6-^{14}C]lysine RSA[b]	Experiment 2 DL-[2-^{14}]lysine SA[a]	Experiment 2 DL-[2-^{14}]lysine RSA[b]
Decinine (9)	7.53±0.09	100±1	28.80±0.42	100±2
DNP-β-alanine (13)	4.14±0.09	55±1	15.39±0.33	53±1
DNP-γ-aminobutyric acid (12)	3.93±0.06	52±1	16.53±0.18	57±1
DNP-2-piperidyl-acetic acid (11)	7.98±0.12	106±2	29.10±0.39	101±2

[a]Specific activity (dpm mmol^{-1}) × 10^{-4}.
[b]Relative specific activity (%) (decinine = 100).

TABLE 4. Experiments with doubly ^{3}H/^{14}C labelled lysines

	Experiment 3 DL-[4,5-$^3H_2$]lysine/DL-[6-^{14}C]lysine		Experiment 4 L-[4-^{3}H]lysine/DL-[6-^{14}C]lysine	
	^{3}H/^{14}C ratio	% retention of ^{3}H relative to ^{14}C	^{3}H/^{14}C ratio	% of product derived from L-lysine[a]
Lysine	5.17±0.07		5.69±0.08	
Pipecolic acid	5.55±0.02	107±2	0.32±0.004	2.8±0.1
Decodine	5.40±0.04	104±2	11.36±0.07	100 ±2
Decinine	5.43±0.05	105±2	11.32±0.06	100 ±2

[a]See ref. 5. In an experiment with L-[^{3}H]substrate/DL-[^{14}C]substrate, % product derived from L-substrate = 50 (^{3}H/^{14}C in product)/(^{3}H/^{14}C in substrate).

sites within the alkaloids predicted to carry label derived from the chosen precursors, for individual radioactive assay. However, since β-alanine and γ-aminobutyric acid contain only one of these two carbon atoms (C-9), whereas 2-piperidylacetic acid contains both (C-5 and C-9), and since it can be assumed (cf. ref. 10) that none of the other carbon atoms of the isolated degradation products are likely to be sites of activity from the radiomers of lysine, cadaverine and Δ^1-piperideine which were tested as precursors, definite conclusions can nevertheless be drawn on the basis of this degradation, incomplete though it is.

The results of experiments 1 and 2 show that lysine is incorporated into decodine (Table 2) and decinine (Table 3) in a specific manner. When either [2-^{14}C]-lysine or [6-^{14}C]lysine served as the precursor, the entire radioactivity of the alkaloids was recovered in 2-piperidylacetic acid and was, therefore, located at C-5 or at C-9, or at both sites. One-half of the label was found in β-alanine and in γ-aminobutyric acid, and was therefore located at C-9. The other half must then be present at C-5. It can thus be inferred that a C_5 fragment comprising C-2 to C-6 of lysine is incorporated into ring A. Since distribution of activity within the alkaloids was the same when either [2-^{14}C]- or [6-^{14}C]lysine serves as substrate, the C_5 fragment must originate from lysine by way of a symmetrical intermediate.

The symmetrical mode of entry into the alkaloids of label from lysine (Scheme 4) is similar to that observed in the case of the lycopodium (9, 23) and lupine (24, 25) alkaloids.

It is known that the lysine-derived units of lycopodine (26), lupanine (27), and several piperidine alkaloids (5) originate from L-lysine, whereas pipecolic acid, isolated from the same sources, is derived from D-lysine (5, 26, 27). This is demonstrated by a tracer technique whereby the chirality of a precursor–product relationship is determined by the use of doubly labelled substrate. Provided intact incorporation of ^{3}H,^{14}C-labelled racemate of a substrate into a product has been shown to take place with maintenance of the ^{3}H/^{14}C ratio, it is possible to determine, by use of a multiply-labelled substrate in which one enantiomer is labelled with tritium, while the other is labelled not only with tritium but also with ^{14}C, which one of the enantiomers of the substrate is incorporated into the product (5).

The incorporation into decodine and decinine of an intact C_5 fragment (C-2 to C-6 of lysine) derived from lysine by decarboxylation, may be inferred from the results of the experiments with [2-^{14}C]- and [6-^{14}C]lysine (experiments 1 and 2). Experiment 3 (Table 4) shows that when DL-[4,5-$^3H_2$]lysine/DL-[6-^{14}C]lysine serves as the substrate, the ^{3}H/^{14}C ratio of the precursor is maintained in the alkaloids, as well as in the pipecolic acid which is isolated. The

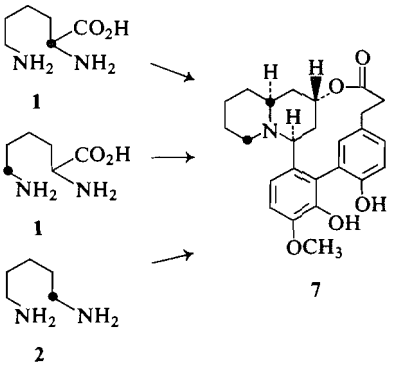

SCHEME 4. Incorporation of lysine (**1**) (experiments 1 and 2) and cadaverine (**2**) (experiment 5) into decodine (**7**).

necessary conditions for the determination of the chirality of the precursor-product relationship are thus met. The experiment with L-[4-^{3}H]lysine/DL-[6-^{14}C]lysine (experiment 4) then gives the required information.

Comparison of the $^3H/^{14}C$ ratios of substrate and products (experiment 4, Table 4) clearly indicates that decodine and decinine are derived from L-lysine, since their $^3H/^{14}C$ ratio was twice that of the administered lysine. Pipecolic acid, on the other hand, is derived largely, if not exclusively, from D-lysine, since it was rich in ^{14}C but contained little ^3H. These results are entirely analogous to those obtained with other plant species in which alkaloids are derived from L-lysine whereas L-pipecolic acid is generated from D-lysine (5, 26, 27).

Two other substrates whose incorporation into decodine was tested were [1,5-^{14}C]cadaverine (experiment 5) and [6-^{14}C]-Δ^1-piperideine (experiment 6). These compounds are regarded as intermediates on the route from lysine into pelletierine (6, 8, 9, 23), anabasine (6, 7), and other piperidine alkaloids. Both served as specific precursors of decodine.

Decodine derived from [1,5-^{14}C]cadaverine showed a distribution of label identical with that of the lysine-derived samples. Activity was equally divided among C-9 (β-alanine) and C-5 (2-piperidylacetic acid minus β-alanine) (experiment 5, Table 2). Since cadaverine is a symmetrical molecule, no other incorporation pattern is possible.

The distribution of activity in decodine derived from [6-^{14}C]-Δ^1-piperideine was entirely different. Label was confined to C-9 (γ-aminobutyric acid) (experiment 6, Table 2) (Scheme 5). This is consistent with the established evidence (7, 14) that the double bond in Δ^1-piperideine does not migrate from one side of the nitrogen to the other.

The fact that the individuality of C-6 of labelled Δ^1-piperideine is maintained within the product, whereas that of the corresponding carbon atom of lysine (C-6) and of cadaverine (C-1) are not, is not inconsistent with a route into the alkaloids from lysine via cadaverine and Δ^1-piperideine. It simply indicates that randomization of C-6 and C-2 of lysine takes place before the formation of Δ^1-piperideine, since, once the latter is formed, equilibration of the corresponding centres does not occur. The Δ^1-piperideine which is formed *in situ* from [2-^{14}C]- or [6-^{14}C]lysine and from [1,5-^{14}C]cadaverine is an equimolar mixture of [2-^{14}C]- and [6-^{14}C]-Δ^1-piperideine, incorporation of which into the alkaloids yields a different labelling pattern from that obtained when either [2-^{14}C]-Δ^1-piperideine or [6-^{14}C]-Δ^1-piperideine is supplied exogenously.

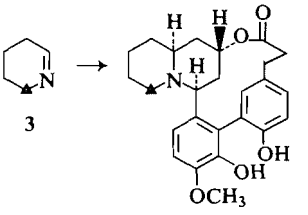

SCHEME 5. Incorporation of Δ^1-piperideine (**3**) into decodine (**7**) (experiment 6).

The specific incorporation, into predicted sites of ring A of the alkaloids, of radioactivity from labelled samples of L-lysine, cadaverine, and Δ^1-piperideine, compounds known or inferred to be precursors of pelletierine, is consistent with the pelletierine hypothesis of their origin (3). The ultimate test of the hypothesis is the specific incorporation into the alkaloids of labelled samples of pelletierine. Decodine and decinine, isolated from plants which had been treated with *RS*-[6,2′-$^{14}C_2$]pelletierine and *RS*-[6-^{3}H,2′-^{14}C]pelletierine (experiments 7 and 8, Table 1) were not radioactive, however.

The two negative experiments with pelletierine were carried out concurrently with experiments in which labelled alkaloids were obtained from other substrates (cadaverine (experiment 5) and lysine (experiment 3), respectively).[3] The conclusion was, therefore, unavoidable that the pelletierine hypothesis of the biosynthesis of decodine and decinine might have to be abandoned. Conclusive evidence against the pelletierine hypothesis, and in support of an alternative biogenetic hypothesis, will be presented in the second paper of this series.

[3]It can, of course, be argued that the alkaloids are formed from pelletierine which is synthesized endogenously from the substrates whose incorporation has been demonstrated, but that exogenously administered pelletierine does not reach the site of alkaloid biosynthesis in *Decodon verticillatus*. Such a contention can be neither proved nor disproved on the basis of tracer experiments with intact plants.

Experimental

Labelled Compounds

The samples of DL-[2-^{14}C]-, [6-^{14}C]-, [4,5-$^{3}H_2$]-, and [6-^{3}H]lysine, L-[4-^{3}H]lysine, [1,5-^{14}C]cadaverine, and ethyl [3-^{14}C]acetoacetate were obtained from commercial suppliers (see Table 1).

[6-^{14}C]-Δ^1-Piperideine (experiment 6) was prepared from DL-[6-^{14}C]lysine (8). *RS*-[6-^{14}C]- and [6-^{3}H]Pelletierine were synthesised by condensation of labelled Δ^1-piperideine, prepared, respectively, from DL-[6-^{14}C]- and [6-^{3}H]lysine, with inactive acetoacetic acid (14). *RS*-[2′-^{14}C]Pelletierine was obtained by condensation of [3-^{14}C]acetoacetic acid (prepared by hydrolysis of ethyl [3-^{14}C]acetoacetate) with Δ^1-piperideine, obtained from inactive DL-lysine (cf. ref. 8). The location of the label in the latter sample of pelletierine was confirmed by subjecting a small amount of the product ($\sim$0.5 μCi) to Kuhn–Roth oxidation, followed by Schmidt reaction of the resulting acetate.

Administration of Labelled Compounds to Decodon verticillatus *(Water Oleander)*

Decodon verticillatus plants were found in two colonies in swampy areas of Hendrie Valley and of Coote's Paradise, Royal Botanical Gardens, Hamilton. Plants from the colony in Hendrie Valley were used in the experiments from 1968–1972. The plants in this location were rooted in the muddy bottom of the swamp, generally in 3–4 ft of water. In the spring of 1973, the water level in this location was above 6 ft and the colony was wiped out. In later experiments, plants from Coote's Paradise were used. This colony is growing on a floating mat of roots and survived the high water. Plants used in feeding experiments were transported intact to the greenhouse where they were acclimatized for 1–2 weeks before administration of tracers.

All feeding experiments were performed in late June or early July, about 3 or 4 weeks after appearance of foliage, when shoots were approximately 1–1½ ft tall. Experiments later in the season yielded inactive decinine and decodine.

Preliminary experiments showed that administration of tracer solution to intact stocks by the wick method led to incorporation of label into decodine and decinine, whereas no incorporation was observed when cuttings from the same stocks were immersed in tracer solution, even though the tracer was readily absorbed by the cuttings.

In each tracer experiment, threads were inserted into 20 stems on 2–4 stocks. The ends of each thread were placed into a specimen tube attached to the stem by Scotch tape. A solution (10 mL) of the labelled compound was distributed among the specimen tubes, and was absorbed by the plants within 24 h. The plants were kept in contact with tracer for 3–5 days and were then harvested. The green stems and leaves were cut, dried for 2 days, and extracted as described below, to yield radioactive alkaloids. The roots were discarded since it was found in preliminary work that they contained little, if any, alkaloidal material.

The details of the feeding experiments are summarized in Table 1.

Radioactivity Measurements

In early experiments (before 1971, experiments 1, 2, 5) radioactivity was determined on samples of finite thickness on aluminum planchettes with a gas-flow system (model 4342, Nuclear Chicago). For plating, a 1% solution of collodion in dimethylformamide was used as a solvent. The usual corrections for background and selfabsorption were applied. The efficiency of the system for ^{14}C ($\sim$30%) was determined using sodium benzoate of known activity as a standard. Since 1971, radioactivity was assayed by liquid scintillation counting (Mark I liquid scintillation computer, model 6860, Nuclear Chicago Corporation). The efficiency of counting for ^{14}C and ^{3}H was determined by external standardization counting with ^{133}Ba. Samples for counting were dissolved in dioxane or methanol and dispersed in Aquasol (New England Nuclear) (10 mL). To determine the activity of the yellow DNP derivatives of the degradation products of the alkaloids (*vide infra*), the samples were decolorized before counting. Weighed samples (ca. 1 mg) of the DNP derivatives were dissolved in methanol (2 drops) in the liquid scintillation vial and aqueous sodium borohydride (1 *M*, 2 drops) was added. The solution decolorized within 5 min. Aquasol (10 mL) was then added. The confidence limits shown in the results (Tables 1–4) are standard deviation of the mean.

Isolation of Decodine (7), Decinine (9), and Pipecolic Acid

For large-scale isolation of inactive alkaloids, the procedure of Ferris *et al.* (20) was employed. In small-scale work with radioactive plants, several modified procedures were used.

In a typical experiment, the dried aerial parts (14 g) of the plants which had been kept in contact with tracer solution were ground to a fine powder in a blender (Osterizer Galaxie 10). The powder was moistened with aqueous ammonia (3% w/v, 10 mL) and was continuously extracted with chloroform for two days in a Soxhlet extractor. In the experiments in which pipecolic acid was to be isolated, the chloroform extract was washed once with dilute ammonia solution and this was used in the isolation of the amino acid (*vide infra*). The chloroform solution was evaporated *in vacuo* to a small volume (20 mL) and 2 *M* hydrochloric acid (20 mL) was added. The mixture was heated on a steam bath 15 min to boil off residual chloroform and the aqueous solution was decanted from the coagulated solids. Chloroform (10 mL) and 2 *M* hydrochloric acid was again added and the procedure repeated. After yet another extraction with 2 *M* hydrochloric acid, the combined acid extract (ca. 60 mL) was washed with ether (2 × 25 mL) and the ether layer was discarded. The aqueous layer was carefully basified with solid sodium bicarbonate (foaming) and extracted with chloroform (3 × 20 mL). The chloroform extract was dried (anhydrous Na_2SO_4) and evaporated *in vacuo*, leaving the crude alkaloids as a foam (155 mg).

The crude alkaloid extract (155 mg) was fractionated on a column (10-mm diameter) of neutral alumina (activity IV, 10 g). The following solvent sequence was used for elution of the alkaloids: petroleum ether (30–60°C); petroleum ether – benzene (1:4); benzene; benzene–chloroform (1:4); chloroform; 5% methanol in chloroform; and methanol. Twenty-five fractions, each containing 25 mL solvent, were collected. A small sample (ca. 5 μL) of each fraction was checked for radioactivity by liquid scintillation counting. The fractions were concentrated and chromatographed (silica gel GF 254 containing 4% KOH, developed with chloroform–methanol–diethylamine (10:1:1)). The fractions containing the same compounds were combined. In general, decinine was eluted from the column by petroleum ether – bezene (1:4) whereas decodine was found mostly in the benzene–chloroform (1:4) fractions. However, the elution sequence of these alkaloids from the column varied somewhat from experiment to experiment and depended on the activity and amount of alumina used and the size of the column. To conserve radioactive materials, inactive decodine, mp 195–197°C, and decinine, mp 223–225°C, obtained by extraction of *D. verticillatus* plants, was added to their respective fractions and the diluted product crystallized from methanol to constant radioactivity.

In further simplification of the separation method, the

crude alkaloid mixture was applied to several alumina plates (20 cm × 20 cm × 1.5 mm thickness, Merck F_{254} type T) using chloroform – 2% methanol as developing solvent. Four well-defined bands were observed under uv light. The corresponding bands from the several plates were combined and stirred overnight with chloroform–methanol (4:1) solution. Filtration and evaporation gave the alkaloids. The least polar band (R_f 0.65) gave crude decinine which crystallized as colourless needles from methanol. This was diluted with inactive decinine and crystallized to constant activity. Repeated chromatography was, in some cases, necessary to remove contaminating decamine from the decinine fraction.

The third least polar band (R_f 0.4) gave decodine as a nearly colourless residue. This crystallized from methanol and after dilution with inactive material, was crystallized to constant activity.

The specific activity of the samples of decodine and decinine so obtained in each experiment is shown in Table 1.

Isolation of Pipecolic Acid

The chloroform extracted plant material from experiments 3 and 4 was mixed with inactive dried ground plant material (8 g). Inactive DL-pipecolic acid (100 mg) was added as carrier and the mixture was placed in a large column. Hot water (400 mL) was percolated through the column and to this was added the ammonia solution obtained by washing the chloroform alkaloid extract (*vide supra*). The combined aqueous solution was evaporated to small volume and then taken to dryness under reduced pressure. Methanol (30 mL) was added to the dark residue and the solution left for 20 h with occasional shaking. Charcoal was added and the mixture was then filtered. The solution was evaporated, the residue dissolved in a little water (1 mL), and the solution applied to a column of Dowex 50W × 4 (H^+ form) (12 cm × 2.5 cm). The column was washed with water (120 mL). Amino acids were then eluted with 1 *M* ammonia until no further activity emerged (ca. 200 mL). The eluate was evaporated to dryness under reduced pressure and the residue dissolved in 6 *M* hydrochloric acid (4 mL). Sodium nitrite (0.5 g) was added in small portions and the solution left for 25 min when a further batch (0.3 g) of sodium nitrite was added in small portions. The solution was left at room temperature for 40 min and was then extracted with ether (3 × 10 mL). The ether extracts were evaporated and the yellow, oily residue dissolved in concentrated hydrochloric acid. The acid solution was heated on a steam bath for 15 min and finally taken to dryness under reduced pressure and the residue crystallized from methanol–ether. A solution of the purified pipecolic acid was applied to a column of Dowex 50W × 4 (H^+ form) (10 cm × 1.5 cm). The column was washed with water–methanol (9:1) and the column was then eluted with *M* ammonia until all activity had emerged. Evaporation of the solvent gave pipecolic acid which sublimed at 190°C and 10^{-1} Torr and was crystallized from methanol–ether, mp 266–268°C (lit. (28) mp 264°C (DL-pipecolic acid); lit. (29) mp 270°C (L-pipecolic acid)).

Degradation of Decodine (7) and Decinine (9)

Conversion of Decodine (7) to Dimethyldecodine (8)

Decodine (**7**) (300 mg) was dissolved in methanol (15 mL) and excess ethereal diazomethane (75 mL) was added. The mixture was kept in a cold room (0–4°C) for 2 days. The solvent was then removed. Methanol (10 mL) was added to the residue and the mixture was warmed on a steam bath and filtered. The methanolic filtrate was concentrated and dimethyldecodine (**8**) (308 mg) crystallized out. Repeated recrystallization from methanol yielded dimethyldecodine, mp 207–208°C (lit. (30) mp 206–207°C).

Chromic Acid Oxidation of Dimethyldecodine (8) and Decinine (9)

Dimethyldecodine (300 mg) was dissolved in hot sulfuric acid (30% v/v, 3 mL) and chromium trioxide (1.5 g) in water (3 mL) was added in several portions. The resulting mixture was heated under reflux with stirring for 48 h. The mixture was cooled and extracted with ether (3 × 10 mL). The ether layer was rejected. The aqueous layer was diluted with water (10 mL) and heated on the steam bath. Hot aqueous barium hydroxide solution was then added until the solution was neutral (pH 7). After 1 h, the mixture was filtered, the precipitate was washed with hot water (3 × 10 mL) and the combined filtrate and washings were concentrated *in vacuo*. Sodium carbonate (35 mg) and methanolic 2,4-dinitrofluorobenzene (10%, 1.5 mL) was added and the resultant mixture was allowed to stand for 2 h at room temperature with occasional stirring. The pH of the solution was maintained at 8–9 with additional sodium carbonate. At the end of 2 h, the solution was extracted with ether (3 × 8 mL) and the ether extract was discarded. The solution was then acidified by addition of 6 *M* hydrochloric acid and extracted with ether (3 × 10 mL). The dried (anhydrous Na_2SO_4) ether extract was evaporated to dryness. The deep yellow residue, containing the 2,4-dinitrophenyl (DNP) amino acids, was dissolved in methanol (0.5 mL) and applied to a silica gel plate (GF_{254}, 20 cm × 20 cm × 0.5 mm). Development with benzene – pyridine – acetic acid (40:10:1) led to the appearance of four well-separated bands. The major band (R_f 0.50) was identical with that of an authentic sample of *N*-2,4-dinitrophenyl-β-alanine. The band with an R_f value of 0.65 was identical with that of an authentic sample of *N*-2,4-dinitrophenyl-γ-aminobutyric acid while the top band (R_f 0.76) corresponded to *N*-2,4-dinitrophenyl-2-piperidylacetic acid. The minor band (R_f 0.22) was 2,4-dinitrophenol. The amino acid DNP derivatives were scraped off the plates separately and eluted from the absorbant with methanol. The methanolic extract (60 mL) of the DNP-β-alanine band (R_f 0.50) which was the most abundant, was evaporated to dryness. The residue was dissolved in dilute hydrochloric acid (6 *M*, 5 mL) and water (2 mL) was then added. The mixture was extracted with ether (3 × 10 mL). The ether layer was washed with water (8 mL), dried (anhydrous Na_2SO_4), and evaporated. The yellow residue was distilled at 160–170°C and 1×10^{-3} Torr when the DNP-β-alanine was obtained as a yellow crystalline solid, mp 140–142°C (lit. (31) mp 145–146°C), yield, 6 mg. The bands corresponding to DNP derivatives of γ-aminobutyric acid and 2-piperidylacetic acid were worked up separately in the same way to give pure DNP-γ-aminobutyric acid, mp 144–145°C (lit. (31) mp 145–146°C), yield, 3.5 mg; and DNP-2-piperidylacetic acid (presumably *S*), mp 139–143°C, rising to 148–151°C after repeated recrystallization from benzene, yield, 3.5 mg. *Anal.* calcd. for $C_{13}H_{15}N_3O_6$: C 50.48, H 4.89, N 13.59; found: C 50.70, H 4.96, N 13.56.

Direct oxidation of decodine by the same method yielded the same products, except that β-alanine was a minor and 2-piperidylacetic acid the major oxidation product.

Decinine was oxidized similarly to give the same amino acid derivatives.

Acknowledgements

We are indebted to Dr. J. P. Ferris, Department of Chemistry, Rensselaer Polytechnic Institute, Troy, New York, for authentic specimens from his collection of *D. verticillatus* alkaloids and for informing us of an improved isolation procedure (20), before publication. We are grateful to Mr. L. Laking,

Director, Royal Botanical Gardens, Hamilton, for permission to use plants from the colonies of *Decodon verticillatus* growing in his gardens, and to Dr. J. S. Pringle, taxonomist of the Royal Botanical Gardens, Hamilton, for authenticating the plant species. We thank Dr. A. I. Meyers, Department of Chemistry, Colorado State University, Fort Collins, Colorado, for a generous sample of 2-piperidylacetic acid. This work was supported by a grant from the National Research Council of Canada.

1. S. H. Koo, R. N. Gupta, I. D. Spenser, and J. T. Wróbel. Chem. Commun. 396 (1970).
2. J. T. Wróbel and W. M. Golebiewski. The alkaloids. Vol. 18. In press.
3. J. P. Ferris, C. B. Boyce, and R. C. Briner. Tetrahedron Lett. 5129 (1966).
4. H. Wright, J. Clardy, and J. P. Ferris. J. Am. Chem. Soc. **95**, 6467 (1973).
5. E. Leistner, R. N. Gupta, and I. D. Spenser. J. Am. Chem. Soc. **95**, 4040 (1973).
6. E. Leistner and I. D. Spenser. J. Am. Chem. Soc. **95**, 4715 (1973).
7. E. Leete. J. Am. Chem. Soc. **91**, 1697 (1969).
8. M. Castillo, R. N. Gupta, Y. K. Ho, D. B. MacLean, and I. D. Spenser. Can. J. Chem. **48**, 2911 (1970).
9. Y. K. Ho, R. N. Gupta, D. B. MacLean, and I. D. Spenser. Can. J. Chem. **49**, 3352 (1971).
10. W. M. Golebiewski and I. D. Spenser. J. Am. Chem. Soc. **98**, 6726 (1976).
11. H. W. Liebisch, N. Marekov, and H. R. Schütte. Z. Naturforsch. B, **23**, 1116 (1968).
12. R. N. Gupta and I. D. Spenser. Phytochemistry, **8**, 1937 (1969).
13. M. F. Keogh and D. G. O'Donovan. J. Chem. Soc. C, 1792 (1970).
14. R. N. Gupta and I. D. Spenser. Can. J. Chem. **47**, 445 (1969).
15. J. T. Wróbel and M. W. Golebiewski. Rocz. Chem. **45**, 705 (1971).
16. A. Rother and A. E. Schwarting. Experientia, **30**, 222 (1974).
17. A. Rother and A. E. Schwarting. Lloydia, **38**, 477 (1975).
18. M. F. Keogh and D. G. O'Donovan. J. Chem. Soc. C, 2470 (1970).
19. J. P. Ferris. J. Org. Chem. **27**, 2985 (1962).
20. J. P. Ferris, R. C. Briner, and C. B. Boyce. J. Am. Chem. Soc. **93**, 2953 (1971).
21. C. Schöpf, E. Schmidt, and W. Braun. Chem. Ber. B, **64**, 683 (1931).
22. A. M. Patterson, L. T. Capell, and D. F. Walker (*Editors*). The ring index. 2nd ed. American Chemical Society. Washington, DC. 1960.
23. M. Castillo, R. N. Gupta, D. B. MacLean, and I. D. Spenser. Can. J. Chem. **48**, 1893 (1970).
24. H. R. Schütte. *In* Biosynthese der Alkaloide. *Edited by* K. Mothes and H. R. Schütte. VEB Deutscher Verlag der Wissenschaften, Berlin. 1969. p. 324.
25. I. D. Spenser. *In* Comprehensive biochemistry. Vol. 20. *Edited by* M. Florkin and E. H. Stotz. Elsevier Publishing Co., Amsterdam. 1968. p. 231.
26. W. D. Marshall, T. T. Nguyen, D. B. MacLean, and I. D. Spenser. Can. J. Chem. **53**, 41 (1975).
27. E. Leistner and I. D. Spenser. Pol. J. Chem. **53** (1979). In press.
28. R. Willstätter. Chem. Ber. **29**, 389 (1896).
29. F. Mende. Chem. Ber. **29**, 2887 (1896).
30. J. P. Ferris. J. Org. Chem. **28**, 817 (1963).
31. K. R. Rao and H. A. Sober. J. Am. Chem. Soc. **76**, 1328 (1954).

The biosynthesis of the Lythraceae alkaloids.[1] II. The phenylalanine-derived fragments

PETER HORSEWOOD, W. MAREK GOLEBIEWSKI,[2] JERZY T. WROBEL,[2] IAN D. SPENSER, AND (IN PART) JONATHAN F. COHEN AND FRED COMER

Department of Chemistry, McMaster University, Hamilton, Ont., Canada L8S 4M1

Received December 14, 1978

PETER HORSEWOOD, W. MAREK GOLEBIEWSKI, JERZY T. WROBEL, IAN D. SPENSER, JONATHAN F. COHEN, and FRED COMER. Can. J. Chem. **57**, 1615 (1979).

Label from [1-^{14}C]-, [2-^{14}C]-, [3-^{14}C]-, and [1,3-^{14}C$_2$]phenylalanine is incorporated non-randomly into the Lythraceae alkaloids, decodine and decinine, in *Decodon verticillatus*. The incorporation pattern, determined by chemical degradation of the alkaloids, demonstrates incorporation of two intact C_6—C_3 units.

PETER HORSEWOOD, W. MAREK GOLEBIEWSKI, JERZY T. WROBEL, IAN D. SPENSER, JONATHAN F. COHEN et FRED COMER. Can. J. Chem. **57**, 1615 (1979).

Des marqueurs provenant de phénylalanines [1-^{14}C], [2-^{14}C], [3-^{14}C] et [1,3-^{14}C$_2$] s'incorporent d'un façon qui n'est pas au hasard dans les alcaloïdes lythracée, décodine et décinine, dans le *Decodon verticillatus*. Le schéma général de l'incorporation, tel que déterminé par la dégradation chimique des alcaloides, démontre qu'il y a incorporation de deux unités C_6—C_3 intactes.

[Traduit par le journal]

Introduction

Several biogenetic proposals (1–4) have been advanced to account for the origin of the phenylquinolizidine lactone alkaloids (e.g., decodine (**5**) and decinine (**6**)) found in several genera of the family Lythraceae (e.g., *Decodon verticillatus* (5, 6), *Heimia salicifolia* and *H. myrtifolia* (7–11), *Lagerstroemia indica* (12), and *Lythrum lanceolatum* (13)) (Scheme 1). Steps common to all the proposals are the reduction of a phenylquinolizidinone (**1**, or the corresponding *cis*-ring-fused isomer) to the corresponding phenylquinolizidinol (**2**), followed by insertion into the latter, by ester formation and phenol coupling, of a phenylpropanoid (C_6–C_3) unit (e.g., *p*-coumaric acid (**3**)) derived from phenylalanine via cinnamic acid.

Indeed, compounds corresponding in structure to the phenylquinolizidinone (**1**) (14), the phenylquinolizidinols (**2**, and its *cis*-fused isomer) (14, 15) and to phenylpropanoid esters of the latter (e.g. **4**) (16, 17) have been found in *H. salicifolia*.

The proposals differ in the suggested mode of biogenesis of the skeleton of the phenylquinolizidinone (**1**).

The skeleton is derivable, *inter alia*, from a polyketide chain (4 × C_2) and a C_6–C_1 unit (route A); or from a polyketide chain (3 × C_2) and a phenylpropanoid C_6–C_3 unit (route B). It is also derivable from pelletierine (itself generated from lysine and acetate (18, 19)) and a C_6—C_1 unit (route C); from pipecolic acid (derived from lysine (19, 20)) and a phenylpropanoid C_6—C_3 unit (route D); or from Δ^1-piperideine (derived from lysine (cf. refs. 21–24)) and a C_6—C_5 unit which is generated from a phenylpropanoid C_6—C_3 unit by chain extension with acetyl or malonyl CoA (route E) (Scheme 1).

The first paper of this series (25) dealt with the status of lysine and its metabolites in the biosynthesis of decodine (**5**) and decinine (**6**), phenylquinolizidine lactone alkaloids from *Decodon verticillatus*. In the present investigation, the question is examined whether it is a C_6—C_1 unit, or a C_6—C_3 unit, derived from phenylalanine, which is implicated in the biosynthesis of the phenylquinolizidinol system of the *Decodon* alkaloids.

It is shown that two intact C_6—C_3 units are incorporated into decodine and into decinine. One of these units supplies the phenylpropanoid C_6—C_3 unit of the lactone ring. The other supplies the phenyl ring and C-1, C-2, and C-3 of the phenylquinolizidinol system.

Methods and Results

Administration of tracers to plants of *Decodon verticillatus* (water oleander) and isolation of decodine (**5**) and decinine (**6**) was carried out by the methods described in the preceding paper (25).

Radioactive samples of the alkaloids were obtained from plants which had been kept in contact with [^{14}C]-labelled phenylalanine (experiments 9–12) and

[1]This paper is dedicated to the memory of R. H. F. Manske, on the first anniversary of his untimely death, September 1977.

[2]Present address: Department of Chemistry, University of Warsaw, Ul. Pasteura 1, 02-093 Warszawa, Poland.

0008-4042/79/131615-16$01.00/0

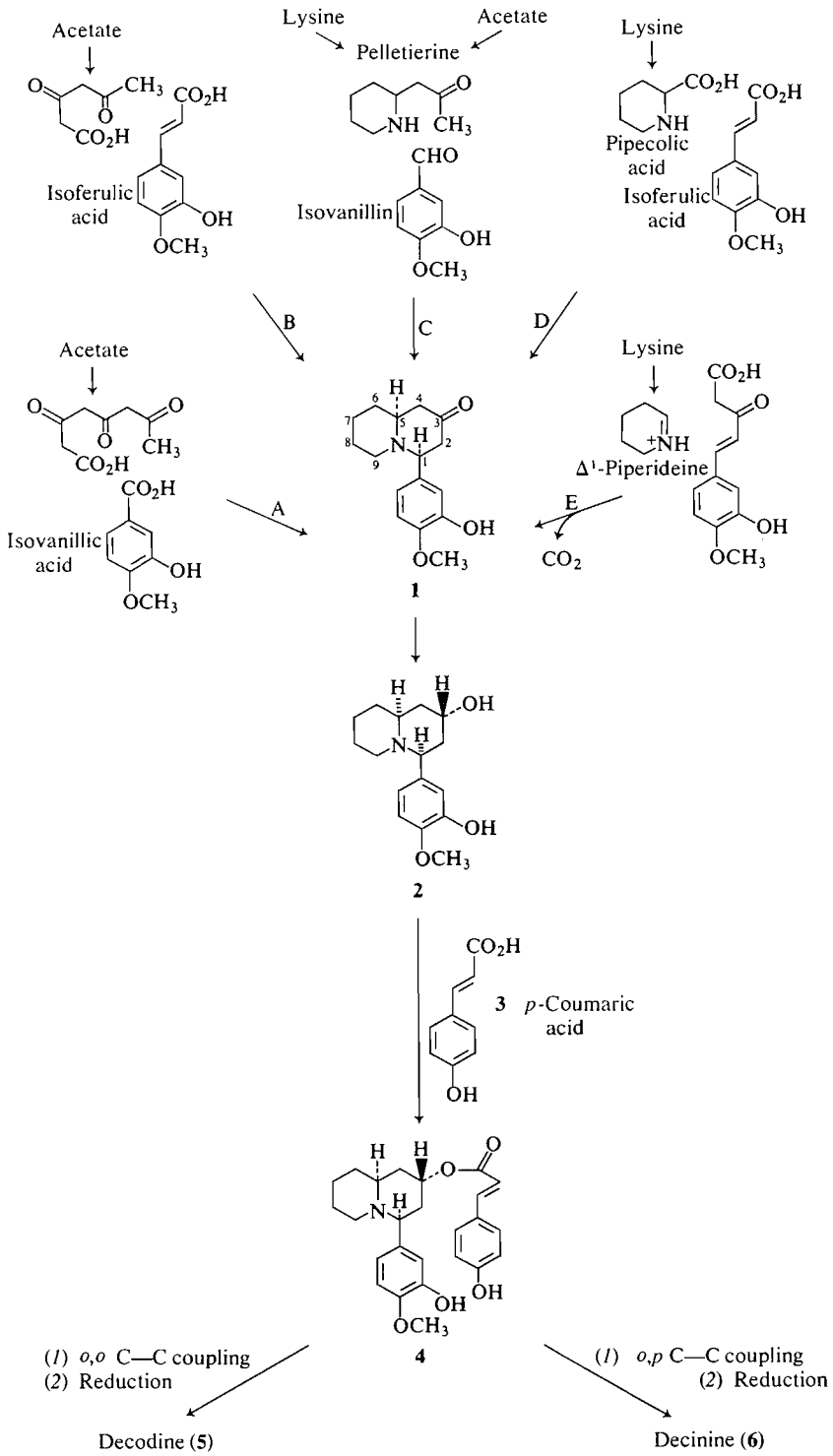

SCHEME 1. Five biogenetic routes (A–E) to decodine and decinine.

TABLE 1. Incorporation of precursors

Experiment No. (date)	Precursors	Nominal total activity (mCi)	Nominal specific activity (mCi/mmol)	Weight of dry plant material (g)	Specific activity (dpm per mmol) × 10^{-4} after dilution with inactive carrier (mg)	
					Decodine	Decinine
9 (1974)	DL-[1-^{14}C]Phenylalanine[a]	0.1	59	38	1.92±0.03 (600)	1.66±0.02 (180)
10 (1974)	DL-[2-^{14}C]Phenylalanine[a]	0.1	32	40	3.12±0.06 (400)	2.49±0.05 (300)
11 (1971)	DL-[3-^{14}C]Phenylalanine[b]	0.1	50	40	4.04±0.03 (400)	3.04±0.02 (400)
12 (1969)	DL-[1,3-$^{14}C_2$]Phenylalanine[d] from	0.2	4.0	22	8.07±0.09 (600)[e]	9.78±0.14 (400)
	DL-[1-^{14}C]phenylalanine[c] plus	0.1	2.1			
	DL-[3-^{14}C]phenylalanine[b]	0.1	48			
13 (1976)	[2-^{14}C]Malonic acid[c]	0.1	11.5	18	2.89±0.05 (600)	

[a]Amersham/Searle.
[b]Commissariat à l'Energie Atomique, France.
[c]New England Nuclear.
[d]The total activity due to each component of the intermolecularly doubly labelled material was determined prior to mixing. The activity due to [1-^{14}C]-phenylalanine accounted for 45.4(± 1.4)%, and due to [3-^{14}C]phenylalanine for 54.6(± 1.3%) of the total activity of the doubly labelled sample.
[e]Assayed as dimethyldecodine.

malonic acid (experiment 13). The details of the tracer experiments are presented in Table 1.

The distribution of radioactivity within the labelled alkaloids was determined by a series of partial degradation sequences designed to separate predicted sites of labelling. The reactions employed in the degradation of the labelled samples of decodine (Scheme 2) and decinine (Scheme 3) are fully described in the Experimental. The segments of the alkaloids demanding attention in tracer experiments with labelled phenylalanine are the two C_6—C_3 moieties, C-14 to C-19, C-13 to C-11 and C-20 to C-25, C-1 to C-3.[3]

The carbon atoms predicted as the sites of label when [3-^{14}C]phenylalanine served as the substrate (C-1, C-13) were secured by oxidative cleavage (3, 26). Permanganate oxidation of dimethyldecodine (**7**), obtained by methylation of decodine (**5**) (27), gave 4-methoxyisophthalic acid (**10**) (C-13 to C-20) (containing C-13 as the only carbon atom not originating from an aromatic nucleus) and hemipinic anhydride (**9**) (C-1, C-18, C-20 to C-25, OCH_3) (containing C-1 as the only 'nonaromatic' or nonmethoxy carbon) (27). Similarly, methyldecinine (**17**), obtained from decinine (**6**) (cf. ref. 7), gave 4-methoxyisophthalic acid (**10**) (C-13) (cf. ref. 26). The yield of the other desired oxidation product, 4,5-dimethoxyphthalic acid (**18**) (C-1) was too low to permit assay of radioactivity. In the course of the oxidative degradation of one sample of labelled decodine (experiment 11), a new dicarboxylic acid was isolated. The accurate mass of its dimethyl ester was found by high resolution mass spectrometry to be 360.119. This corresponds to that of the dimethyl ester of the expected biphenyldicarboxylic acid (**8**) (mass calcd. for $C_{19}H_{20}O_7$: 360.121) (cf. refs. 26, 28, 29).

The carbonyl carbon atom of the lactone ring (C-11) of each of the two alkaloids was obtained by phenylation of dimethyldecodine (**7**) and methyldecinine (**17**), respectively, with phenyl Grignard reagent (29). The diphenylcarbinols so obtained were dehydrated to the diphenylolefins (**11**) and (**19**), respectively, and these were subjected to chromic acid oxidation, yielding C-11 as benzophenone, which was isolated as the oxime.

Several steps were required to gain access to the carbinol carbon of the quinolizidine system (C-3) and the carbon (C-12) adjacent to the lactone carbonyl group. Lithium aluminium hydride reduction of dimethyldecodine (**7**) (27) and of methyldecinine (**17**) gave the corresponding diols **12** and **20**, respectively. Tosylation of the primary alcohol group, followed by lithium aluminium hydride reduction of the resulting tosylates **13** and **21**, respectively, yielded the corresponding desoxy derivatives, **14** and **22**. These were the key intermediates of the degradation sequences. Kuhn–Roth oxidation gave acetic acid isolated as the α-naphthylamide, derived from the ethyl group, C-11, C-12. Since C-11 is obtainable

[3]For a justification of the new numbering system for the phenylquinolizidine lactone alkaloids, employed here, see the Appendix.

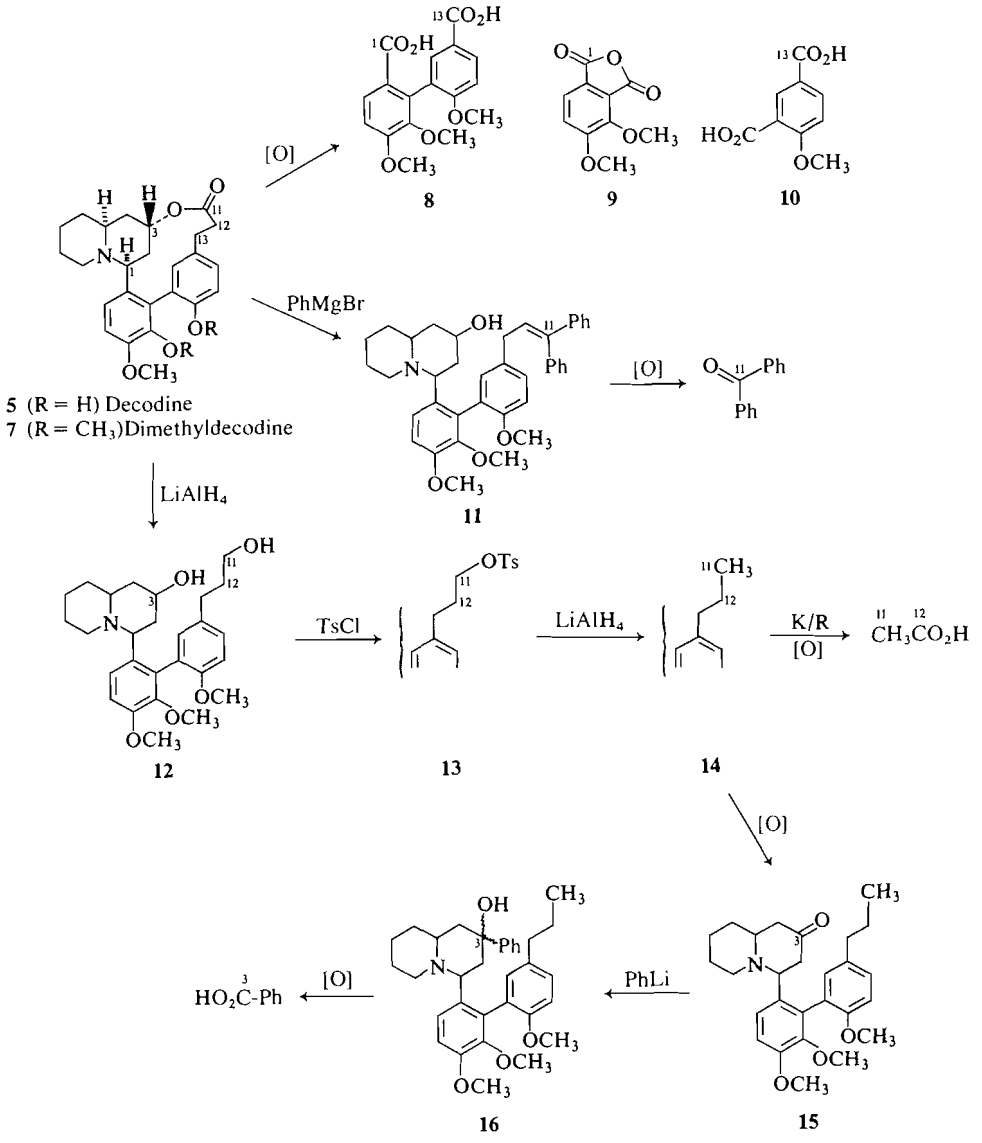

SCHEME 2. Degradation of decodine.

separately as benzophenone (see above), C-12 is thus accessible.

Mild oxidation of the desoxy derivatives **14** and **22**. yielded the corresponding ketones, **15** and **23**, respectively. Phenylation with phenyl lithium gave, in each case, a mixture of epimeric phenyl carbinols, **16** and **24**, respectively. Permanganate oxidation then yielded benzoic acid, i.e. C-3 of the alkaloids.

The results of the degradation of the labelled samples of decodine and of decinine derived from the experiments with radiomers of [^{14}C]phenylalanine are presented in Tables 2 and 3.

Decodine and decinine, isolated from plants kept in contact with DL-[1-^{14}C]phenylalanine (experiment 9) yielded benzophenone oxime (C-11) which contained approximately three-quarters and benzoic acid (C-3) which contained approximately one-quarter of the activity of the intact alkaloid from which they were derived. These two degradation products accounted for 99 ± 2 and $96\pm2\%$, respectively, of the total activity of the original alkaloids.

Decodine and decinine, isolated from plants to which DL-[2-^{14}C]phenylalanine (experiment 10) had been administered, yielded *N*-acetyl-α-naphthylamine (C-11, C-12) containing ca. two-thirds of the activity of the intact alkaloids. Since C-11 was shown, above, to be derived from the carboxyl carbon of phenylalanine, the activity derived from [2-^{14}C]phenyl-

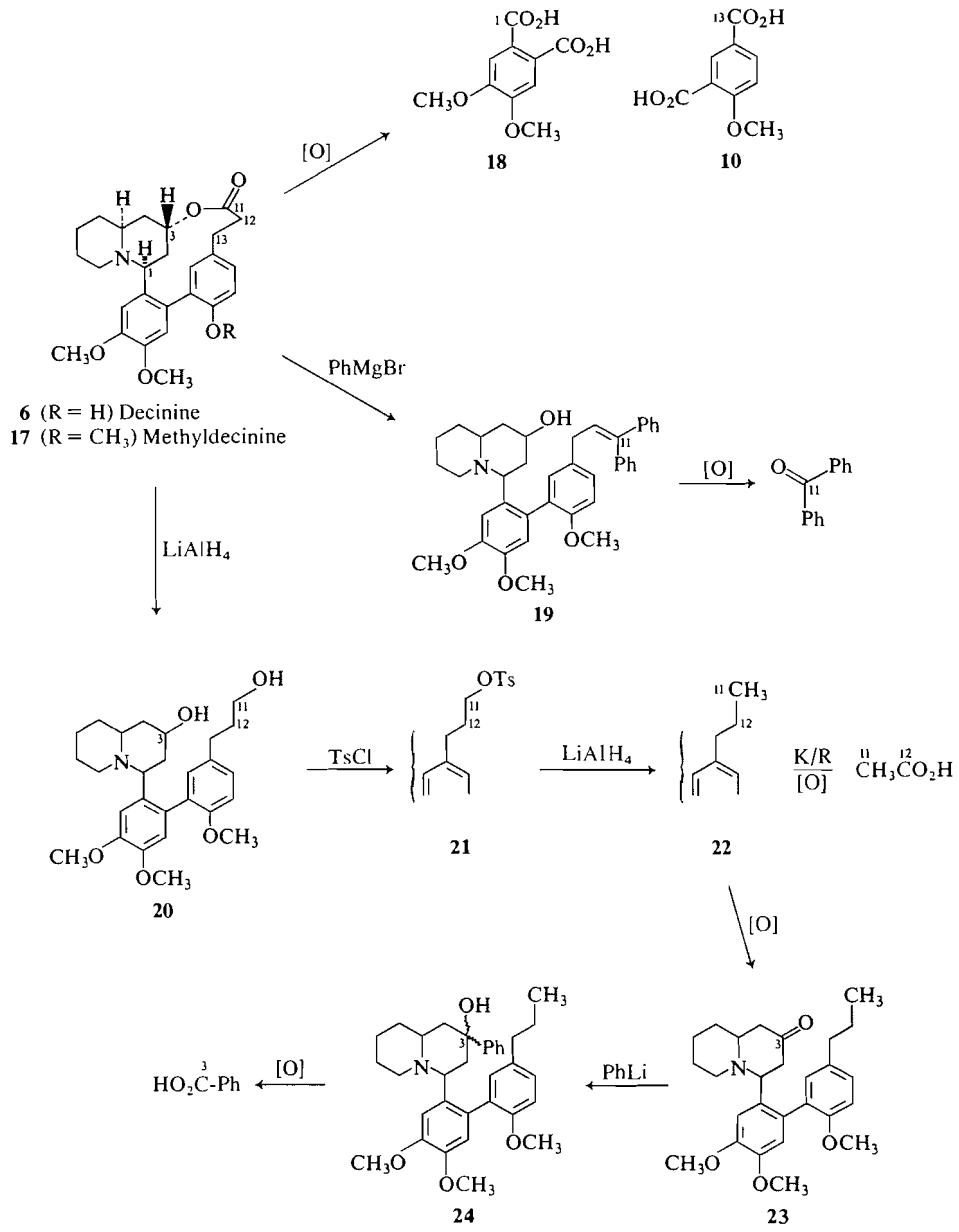

SCHEME 3. Degradation of decinine.

alanine must be present at C-12. The remaining one-third of the activity of the alkaloids was not accounted for, as attempts to develop a practicable degradation sequence yielding C-2 of the quinolizidine system were unsuccessful.

Decodine, from the experiment with DL-[3-^{14}C]-phenylalanine (experiment 11) gave the biphenyl derivative (**8**) (C-1 plus C-13, together with C-14 to C-25 and *O*-methyl) containing all the activity of the alkaloid (98±7%). Of this activity, approximately one-third was recovered in hemipinic anhydride (**9**), representing C-1, and the rest in 4-methoxyisophthalic acid (**10**), representing C-13.

Decodine from a doubly labelled sample of phenylalanine, DL-[1,3-$^{14}C_2$]phenylalanine (experiment 12), gave labelled benzophenone oxime (C-11) (25(±1)% of the activity of the original decodine), benzoic acid (C-3) (19(±2)%), 4-methoxyisophthalic acid (C-13) (30(±1)%), and hemipinic anhydride (C-1) (23(±2)%). The four degradation products account for the total activity of the intact decodine. Decinine, from the same feeding experiment, gave benzophenone oxime

TABLE 2. Incorporation of phenylalanine into decodine

		Precursor											
		Experiment 9 DL-[1-^{14}C]phenylalanine		Experiment 10 DL-[2-^{14}C]phenylalanine		Experiment 11 DL-[3-^{14}C]phenylalanine		Experiment 12 DL-[1,3-$^{14}C_2$]phenylalanine					
Product	C-atoms of decodine	SA[a]	RSA[b]	SA[a]	RSA[b]	SA[a]	RSA[b]	SA[a]	RSA[b]	SA[a]	RSA[b]	SA[a]	RSA[b]
Decodine (5)	All	1.92±0.03	100±2	1.51±0.03[c]	100±2	1.15±0.03[d]	100±3	—	—	—	—	—	—
Dimethyldecodine (7)	All	1.92±0.03	100±2	1.51±0.02	100±2	1.18±0.05	103±5	2.83±0.04[e]	100±1	4.23±0.08[e]	100±2	1.08±0.05[e]	100±5
Dimethyldecodine HCl salt	All	—	—	—	—	—	—	2.83±0.04	100±2	4.32±0.07	102±3	1.05±0.08	97±9
Benzophenone oxime	C-11	1.36±0.02	71±1	—	—	—	—	0.71±0.01	25±1[f]	—	—	—	—
Benzoic acid	C-3	0.54±0.01	28±1	—	—	—	—	—	—	—	—	0.20±0.02	19±2
Acetyl-α-naphthylamine	C-11, C-12	—	—	0.93±0.01	62±1	—	—	—	—	—	—	—	—
4-Methoxyisophthalic acid (10)	C-13 (also C-14 to C-20)	—	—	—	—	0.66±0.05	58±5	—	—	1.25±0.05	30±1[f]	—	—
Hemipinic anhydride (9)	C-1 (also C-18, C-20 to C-25, OCH_3)	—	—	—	—	0.38±0.03	33±3	—	—	0.99±0.08	23±2[f]	—	—
Biphenyl derivative (8)	C-1 plus C-13 (also C-14 to C-25, OCH_3)	—	—	—	—	1.13±0.08	98±7	—	—	—	—	—	—

[a]Specific activity (dpm mmol^{-1}) × 10^{-4}
[b]Relative specific activity (%) (decodine = 100)
[c]Derived from the sample of decodine, specific activity 3.12 (±0.06) × 10^4 dpm per mmol, by further dilution with inactive decodine.
[d]Derived from the sample of decodine, specific activity 4.04 (±0.03) × 10^4 dpm per mmol, by further dilution with inactive decodine.
[e]Derived from the sample of dimethyldecodine, specific activity 8.07 (±0.09) × 10^4 dpm per mmol, by further dilution with inactive dimethyldecodine.
[f]See footnote 4.

TABLE 3. Incorporation of phenylalanine into decinine

		Precursor											
		Experiment 9 DL-[1-^{14}C]phenylalanine				Experiment 10 DL-[2-^{14}C]phenylalanine		Experiment 12 DL-[1,3-$^{14}C_2$]phenylalanine					
Product	C-atoms of decinine	SA[a]	RSA[b]	SA[a]	RSA[b]	SA[a]	RSA[b]	SA[a]	RSA[b]	SA[a]	RSA[b]	SA[a]	RSA[b]
Decinine (6)	All	1.66±0.02	100±1	0.66±0.03[c]	100±5	2.49±0.05	100±2	8.13±0.09[d]	100±1	1.70±0.06[d]	100±4	9.78±0.14	100±1
Methyldecinine (17)	All	1.67±0.02	101±2	0.65±0.03	98±7	2.48±0.05	100±3	—	—	1.71±0.11	101±8	—	—
Benzophenone oxime	C-11	1.26±0.01	76±1	—	—	—	—	1.38±0.02	17±1	—	—	—	—
Acetyl-α-naphthylamine	C-11, C-12	—	—	—	—	1.63±0.04	66±2	—	—	—	—	—	—
Benzoic acid	C-3	—	—	0.13±0.01	20±1	—	—	—	—	0.48±0.07	28±4	—	—
4-Methoxyisophthalic acid (10)	C-13 (also C-14 to C-20)	—	—	—	—	—	—	—	—	—	—	2.10±0.05	21±1

[a]Specific activity (dpm mmol^{-1}) × 10^{-4}.
[b]Relative specific activity (%) (decinine = 100)
[c]Derived from the sample of decinine, specific activity 1.66 (±0.02) × 10^4 dpm per mmol, by further dilution with inactive decinine.
[d]Derived from the sample of decinine, specific activity 9.78 (±0.14) × 10^4 dpm per mmol, by further dilution with inactive decinine.

TABLE 4. Incorporation of 2-^{14}C-malonic acid into decodine

	C-atoms of decodine	SA[a]	RSA[b]
Decodine	All	2.89±0.05	100±2
2-Piperidylacetic acid	C-3 to C-9	2.84±0.05	98±2
β-Alanine	C-7 to C-9	1.13±0.05	39±2
γ-Aminobutyric acid	C-6 to C-9	1.28±0.03	44±1

[a]Specific activity (dpm mmol^{-1}) × 10^{-4}.
[b]Relative specific activity (%) (decodine = 100).

(C-11) (17(±1)%), benzoic acid (C-3) (28(±4)%), and 4-methoxyisophthalic acid (C-13) (21(±1)%).

A further experiment was performed with [2-^{14}C]-malonic acid as the tracer (experiment 13). Decodine which was isolated, was radioactive and was degraded by chromic acid oxidation and the partial degradation products, β-alanine (C-7 to C-9), γ-aminobutyric acid (C-6 to C-9) and 2-piperidylacetic acid (C-3 to C-9), were isolated as described in the preceding paper (25). The 2-piperidylacetic acid accounted for the entire activity of the intact alkaloid. The β-alanine and the γ-aminobutyric acid each contained approximately 40% of the total activity (Table 4).

Discussion

It has been known for almost 10 years that radioactivity from [3-^{14}C]phenylalanine is incorporated into cryogenine (**25**), a *Decodon*-type alkaloid, in *Heimia salicifolia* (3, 26). Partial degradation placed most of this activity into one or more of the carbon atoms of the two C_6—C_1 units, C-13 to C-19 and C-1, C-20 to C-25. In particular, it was shown that label was localized at C-13 (ca. 50%) and very probably at C-1 (ca. 33%). From these results it is reasonable to infer that phenylalanine supplies the two aromatic nuclei of cryogenine (**25**) together with one carbon atom adjacent to each, a conclusion which is consistent with any one of the five biogenetic schemes outlined in Scheme 1. To distinguish among the schemes the question must be answered whether the phenylalanine derived fragment which enters the quinolizidine nucleus is indeed a C_6—C_1 unit (routes A, C) or whether it is an intact C_6—C_3 unit (routes B, D, E).

The key to the solution of this problem is a controlled degradation of the carbon skeleton, capable of yielding products recognizably derived from C-2, C-3, C-11, and C-12 of the skeleton of the *Decodon* alkaloids. The reaction sequences discussed in the preceding section, which were devised for the degradation of decodine (**5**) (Scheme 2) and decinine (**6**) (Scheme 3), account for three of these four carbon atoms. Application of these reaction sequences to labelled samples of decodine and decinine, derived from feeding experiments with [1-^{14}C]- , [2-^{14}C]- , [3-^{14}C]- , and [1,3-$^{14}C_2$]phenylalanine yielded data (Tables 2 and 3 and preceding section) from which the desired information was deduced (Scheme 4).

The experiment with [3-^{14}C]phenylalanine (experiment 11) showed that the distribution of label within decodine (**5**) in *D. verticillatus* (C-13 58%, C-1 33%) was very similar to that found earlier in cryogenine (**25**) derived from the same precursor in *H. salicifolia* (C-13 61%, C-1 31%(3), C-13 46%, C-1 33% (26)), indicating a close correspondence in the origin of two alkaloids of different ring stereochemistry in two different plant species.

The experiment with [1-^{14}C]phenylalanine as the substrate (experiment 9) showed that even though the major fraction of activity within decodine (**5**) (71%) and within decinine (**6**) (76%) was located at C-11, i.e., at the carbonyl carbon of the lactone ring, label was not confined to this position. The remaining activity (28 and 20%, respectively) was present at C-3, i.e., at the carbinol carbon of the quinolizidine ring. In each case, these two carbon atoms, C-11 and C-3, accounted for the entire activity of the intact alkaloid. It can be inferred from this result that, in all probability, phenylalanine supplies two C_6—C_3 units to the skeleton of the *Decodon* alkaloids.

The result of the experiment with [2-^{14}C]phenylalanine (experiment 10) was consistent with this inference. Label was not confined to C-12 of the phenylpropanoid unit of decodine and of decinine. Only 62 and 66% of the total activity, respectively, was recovered from this site. The rest of the activity is presumably located at C-2 of the quinolizidine nucleus. It is a plausible supposition that this site is derived from the α-carbon of phenylalanine, since the adjacent carbon atoms, C-3 and C-1, have been shown (experiments 9 and 11) to be derived from the carboxyl carbon and from the β-carbon of phenylalanine, respectively. However, a degradation sequence capable of extracting C-2 of the quinolizidine system has not yet been realized and this assumption remains to be confirmed.

The fourth experiment with labelled phenylalanine (experiment 12) was intended to strengthen the evidence that 2 three-carbon chains, each representing an entire phenylalanine side-chain, enter the *Decodon* skeleton as intact units. The substrate was a sample of phenylalanine, intermolecularly doubly labelled at the carboxyl carbon and at the β-carbon of the side chain, with 45.4% activity at the carboxyl and 54.6% at the β-carbon (radioactivity ratio —CO_2H-β-CH_2 = (45.4±1.4)/(54.6±1.3) = 0.83±0.03) (see Table 1). Incorporation into decodine and decinine of the intact side chain from this doubly labelled phenylalanine would be demonstrated by the isolation of labelled alkaloids containing radioactivity at each of the four carbon atoms C-3, C-1, C-11, and

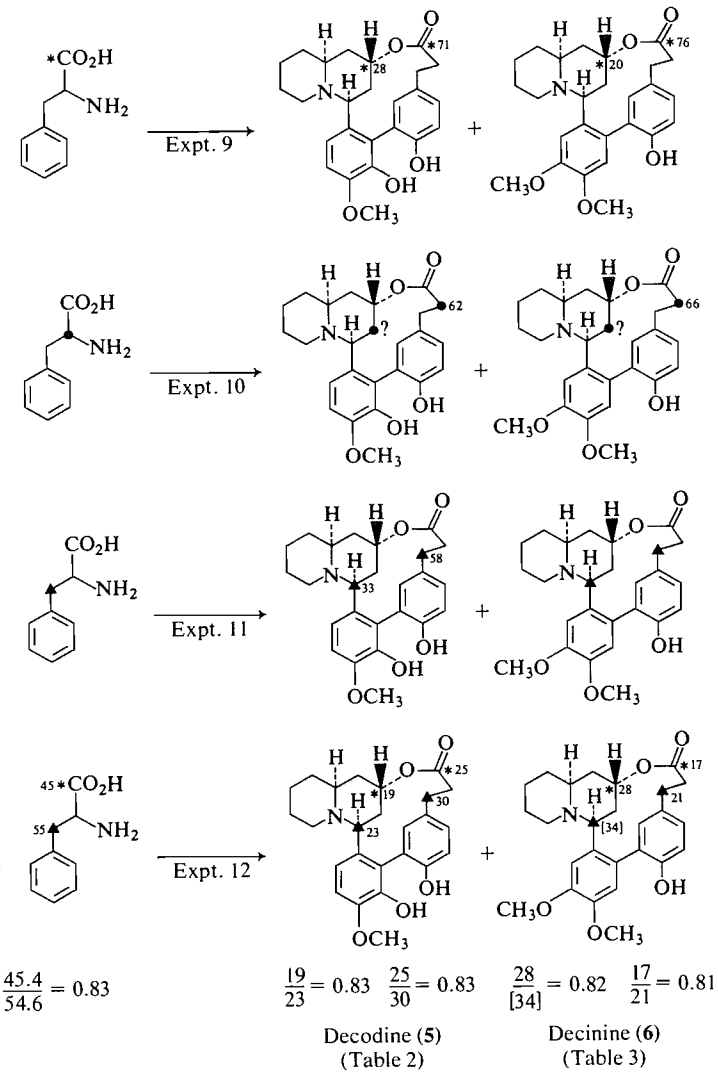

SCHEME 4. Incorporation pattern within decodine and decinine of radioactivity derived from [1-^{14}C]-, [2-^{14}C]-, [3-^{14}C]-, and [1,3-$^{14}C_2$]phenylalanine.

C-13 and at no other site, with a distribution such that the ratios of activities, C-3/C-1, and C-11/C-13, each equalled the ratio of activities —CO_2H/β-CH_2 within the doubly labelled phenylalanine serving as their precursor.

This was indeed observed:[4] each of the four predicted sites of labelling within the decodine obtained from this experiment (experiment 12) were isolated, and assayed for radioactivity (Table 2). The ratios of relative specific activities, calculated from these data (C-11/C-13 = $(25\pm1)/(30\pm1) = 0.83\pm0.04$; C-3/C-1 = $(19\pm2)/(23\pm2) = 0.83\pm0.11$), are in good agreement with the activity ratio of the substrate (0.83 ± 0.03, see above). As predicted, the activities

[4]A different result of this experiment was recorded in a preliminary communication (30). It was reported that the hemipinic anhydride obtained by degradation of decodine derived from the experiment with [1,3-$^{14}C_2$]phenylalanine (now referred to as experiment 12) accounted for 46% of the activity of the alkaloid. When, at a later date, degradation sequences were devised which made C-3 of decodine and decinine accessible, and it was found that radioactivity from [1-^{14}C]phenylalanine entered C-3 (experiment 9), the earlier result became suspect. Further doubt was cast on its validity when it was shown that the sample of decinine derived from [1,3-$^{14}C_2$]-phenylalanine also contained activity at C-3. It was fortunate that a sample, large enough to permit a complete reinvestigation, of the original decodine from the experiment with [1,3-$^{14}C_2$]phenylalanine remained in our possession. The data reported in the present paper (experiment 12, Table 2) are based on an entirely new set of degradation experiments. Since it is now evident that the earlier result was in error, the inference drawn from it (30) is untenable. Careful reexamination of the relevant laboratory records failed to disclose the origin of the erroneous result.

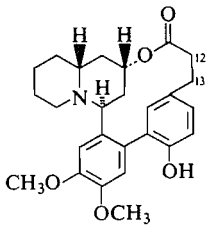

25 Cryogenine = Vertine
26 Decamine = 12,13-Dihydrovertine

at these four carbon atoms of decodine account for the total activity of the alkaloid (C-3 + C-1 + C-11 + C-13 = $(19\pm2) + (23\pm2) + (25\pm1) + (30\pm1) = 97\pm3\%$).[3]

In the case of decinine, only three of the four crucial carbon atoms were assayed directly (Table 3). Activity at the fourth site, C-1, could not be determined because of the low yield of the degradation product representing this carbon atom (4,5-dimethoxyphthalic acid (**18**)) (see Experimental) (cf. ref. 26). For the present calculation, activity at C-1 must be obtained by difference. Even so, the calculated ratios (C-11/C-13 = $(17\pm1)/(21\pm1) = 0.81\pm0.06$; C-3/C-1 = $(28\pm4)/\{100 - [(28\pm4) + (17\pm1) + (21\pm1)]\} = 0.82\pm0.16$), are in reasonable agreement with the $-CO_2H/\beta\text{-}CH_2$ ratio of the substrate (0.83 ± 0.03).

The results of the experiments with [1-^{14}C]-, [2-^{14}C]-, and [1,3-$^{14}C_2$]phenylalanine (experiments 9, 10, and 12) lead to the inference that two intact C_6—C_3 units are implicated in the biosynthesis of decodine and decinine. One of these gives rise to the phenylpropanoid moiety of the lactone ring, C-11 to C-19, the other to the segment C-3 to C-1, C-20 to C-25, of the phenylquinolizidine system of the alkaloids.

Since it thus appears that an intact C_6—C_3 unit is implicated in the biosynthesis of the phenylquinolizidine ring system (**1**), those biogenetic hypotheses which demand participation of a C_6—C_1 unit in its construction (routes A and C, Scheme 1) must be rejected. One of the hypotheses which is thus eliminated is the hitherto favoured route based on pelletierine (route C). Each of the remaining routes, B, D, and E, involves an intact phenylpropanoid moiety. They differ from each other in the postulated origin of the rest of the quinolizidine system.

In the preceding paper of this series (25), we showed that the C_5N unit, C-5 to C-9, N, of the quinolizidine system is derived from L-lysine, which is incorporated after loss of its carboxyl group, via cadaverine and Δ^1-piperideine. This earlier evidence eliminates route B, which invokes a polyketide precursor. It also disposes of route D which demands participation of pipecolic acid or of some other lysine metabolite containing the intact C_6 chain of lysine, since pipecolic acid in *D. verticillatus* was shown to be derived from D-lysine whereas the alkaloids incorporate a C_5N unit derived from L-lysine.

The remaining hypothesis, route E (Scheme 1) (2, 4) is the only one that is consistent with all the evidence now available on the mode of incorporation of phenylalanine, and of L-lysine and its metabolites. A more detailed outline of this route is shown in Scheme 5.

The scheme demands an extension of the side chain of the phenylpropanoid precursor by a two-carbon unit, supplied by a donor such as acetyl or malonyl CoA. A final experiment (experiment 13) with [2-^{14}C]malonic acid was performed in an attempt to test this prediction. Label from this substrate should enter C-4 of the quinolizidine system. The results of this experiment (Table 4), even though consistent with route E (Scheme 5), were inconclusive. As predicted, all activity of the decodine which was isolated was located within the fragment, C-3 to C-9, recovered as 2-piperidylacetic acid. Since C-3 has been shown to be derived from the carboxyl group of phenylalanine (experiment 9) and C-5 to C-9 from lysine (25), it might have been anticipated that all activity derived from [2-^{14}C]malonate might be confined to C-4, the predicted site. This was not so, however. Two other degradation products, β-alanine (C-7 to C-9) and γ-aminobutyric acid (C-6 to C-9), representing fragments of the lysine derived portion of the ring system, contained a significant fraction of the total activity (~40%). As lysine in plants originates by the diaminopimelic pathway (31) which delivers label from the methyl group of acetate into every carbon atom of its C_6 chain, but not with equal efficiency, and as malonate serves as an acetate donor, incorporation of label into the lysine-derived fragment of the molecule was not unexpected. What was unexpected was the high level of labelling within this moiety. As a consequence and since C-4, the carbon atom at issue, was not directly accessible, the results of this experiment are indicative rather than conclusive, and the origin of C-4 remains to be confirmed by direct experiment.

Several other aspects of the biosynthesis of the Lythraceae alkaloids which remain to be clarified deserve mention.

The first of these emerges from the present results. It concerns the variation in the distribution of label among the two phenylpropanoid units of each of the alkaloid samples obtained from experiments 9–12. In three of the four experiments (experiments 9–11), the lactone C_6—C_3 unit (C-11 to C-19) of each alkaloid sample contains approximately twice as much label as the phenylquinolizidine C_6—C_3 unit (C-1 to C-3, C-20 to C-25). A similar distribution was

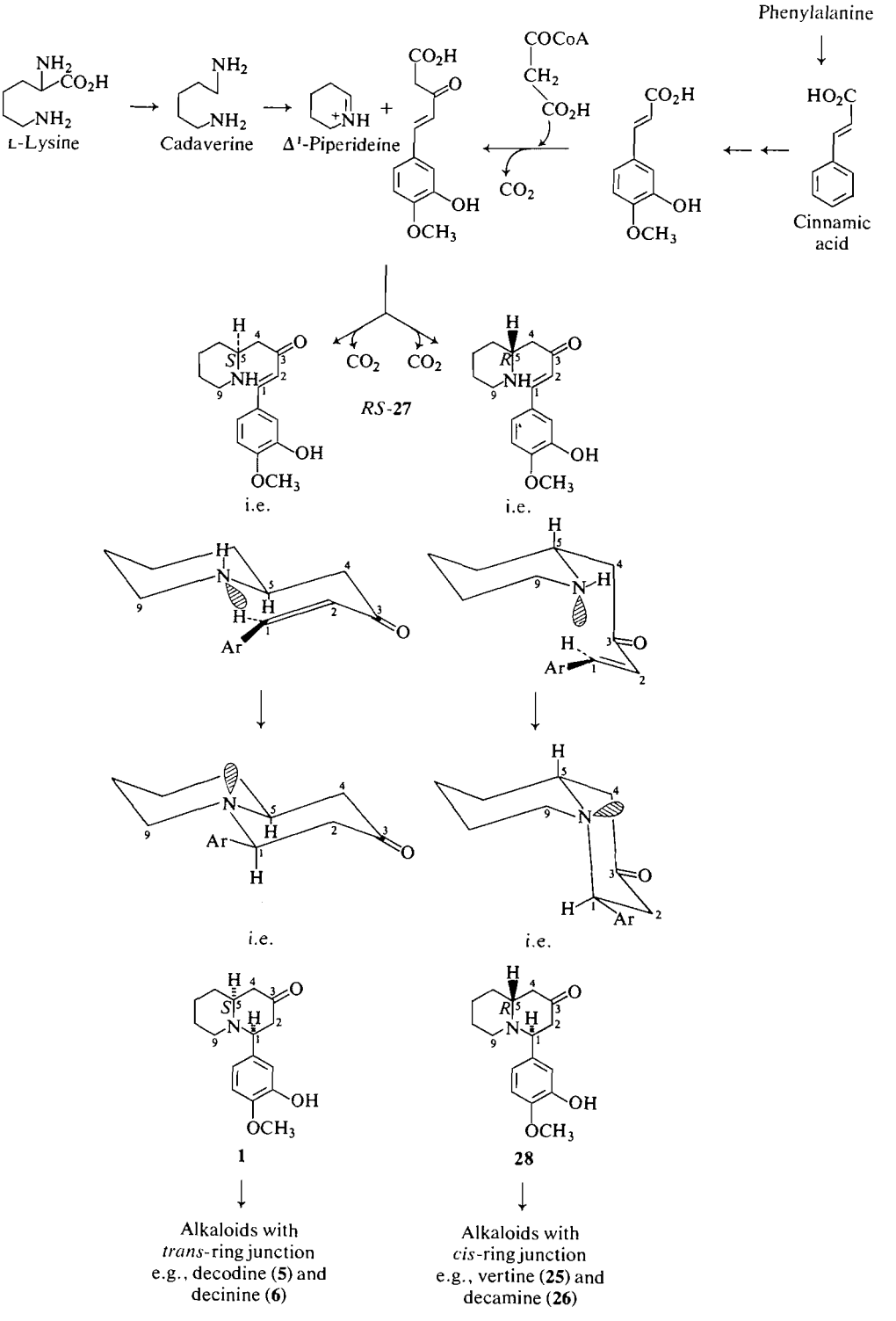

SCHEME 5. Biosynthesis of the phenylquinolizidine system.

found in cryogenine (**25**) in *H. salicifolia* (3, 26). The distribution of label in the alkaloids obtained in experiment 12 is entirely different. In the decodine from this experiment, activity is almost equally divided between the two C_6—C_3 units, the lactone phenylpropanoid unit being favoured to a slight extent. In the decinine, on the other hand, the distribution of activity is reversed, with the phenylquinolizidine unit containing almost twice as much label as the lactone C_6—C_3 unit.

Since the two C_6—C_3 units in each of the samples contain a different fraction of the total activity, the units, even though derived from the same substrate, must have entered the product by different routes (cf. ref. 32). Since the two alkaloids, isolated from the same experiment, show different distributions of label, a systematic study of the variation of this distribution with time over the seasonal growth period of the plant may throw light on the timing of the competing biosynthetic events which lead from the phenylquinolizidine intermediate (**1**) to the two alkaloids with common ring stereochemistry, decodine and decinine.

A second problem concerns the competing routes which lead, in the same plant, from the same substrate, to alkaloids with isomeric ring stereochemistry (e.g., decinine (**6**) and decamine (**26**) in *D. verticillatus* (5)). A possible derivation of diastereomeric phenylquinolizidines from common precursors is illustrated in Scheme 5. It is suggested that the stereochemistry at the ring junction (5-*S*-*trans*, e.g., decodine (**5**) or 5-*R*-*cis*, e.g., decamine (**26**)) is determined by the conformation of the lone pair (axial or equatorial) within the requisite enantiomer of the key intermediate, **27**. Intramolecular Michael addition yields the *S*-*trans*-phenylquinolizidinone (**1**) and the *R*-*cis*-phenylquinolizidinone (**28**), respectively. This model cannot explain the stereospecific utilization of the two conformers, i.e., conversion into alkaloids of the conformer with equatorial lone pair in the *S*-series but not in the *R*-series, and of the conformer with axial lone pair in the *R*-series but not in the *S*-series.

Finally, the origin of the Lythraceae alkaloids of the *Lythrum* and piperidine groups requires consideration. The only published proposal (13) concerning their biogenesis is based on pelletierine. In the light of the present evidence which eliminates pelletierine as a precursor of the *Decodon* group of Lythraceae alkaloids, it is tempting to seek a new model for the biogenesis of the other alkaloid groups, from precursors analogous to those now shown to yield the *Decodon* group. Such a model is shown in Scheme 6. It invokes intermediacy of a 2-substituted piperidine (**29**), analogous in structure to the *Decodon* intermediate **27**, and of a 2,6-disubstituted piperidine (**30**). The latter is analogous in structure (33) and, pre-

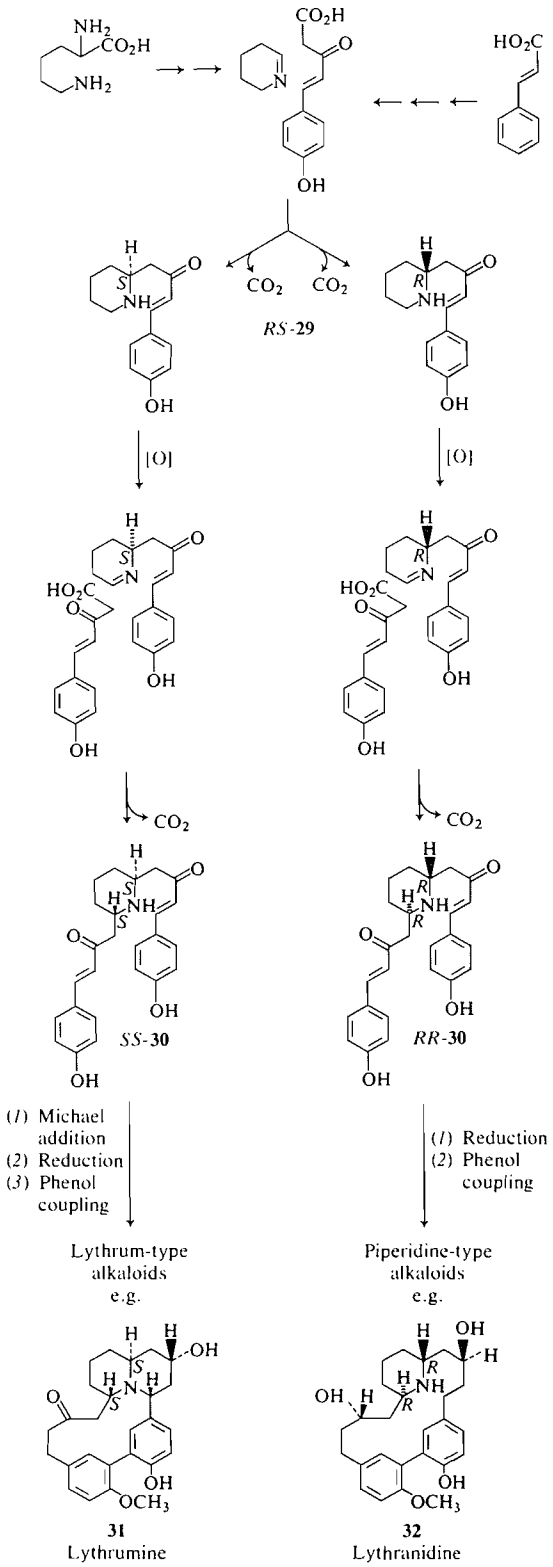

SCHEME 6. Biogenesis of the Lythrum and piperidine-type Lythraceae alkaloids.

sumably, in origin (34) to the lobelia alkaloids (e.g., lobeline (**33**)) and bears the same relationship to the intermediate **29** that lobeline (**33**) bears to sedamine (**34**) (35).

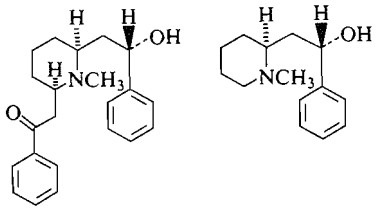

33 (−)-Lobeline

34 (−)-Sedamine

Experimental

Administration of Labelled Compounds to Decodon verticillatus *and Isolation of Decodine and Decinine*

These experiments were performed as described in the preceding paper (25). The details of the feeding experiments and the specific activities of the samples of decodine and decinine isolated from individual experiments are summarized in Table 1.

Determination of Radioactivity

Before 1971 (experiment 12) radioactivity was measured on samples of finite thickness on aluminum planchettes with a gas-flow Geiger system (Model 4342, Nuclear Chicago). For plating, a 1% solution of collodion in dimethylformamide was used as a solvent. The usual corrections for background and self-absorption were applied. The efficiency of the system for ^{14}C (~30%) was determined using sodium benzoate of known activity as a standard. Since 1971, radioactivity has been assayed by liquid scintillation counting (Mark 1 liquid scintillation computer, model 6860, Nuclear Chicago Corporation). The efficiency of counting was determined using ^{133}Ba as the external standard. Samples were dissolved in methanol and dispersed in Aquasol (New England Nuclear) (10 mL). The confidence limits shown in the results (Tables 1–4) are standard deviation of the mean.

Degradation of Labelled Samples

Degradation of Decodine Derived from [1-^{14}C]Phenylalanine

The Lactone Carbonyl Carbon (C-11) as Benzophenone Oxime

*Dimethyldecodine (**7**) (27)*—Decodine (300 mg) was methylated with diazomethane or with dimethyl sulfate. Dimethyldecodine was recrystallized from methanol; mp 206–207°C (lit. (27) mp 206–207°C); ^1H nmr ($CDCl_3$) δ: 3.70 (s, 3H, OCH_3), 3.72 (s, 3H, OCH_3), 3.88 ppm (s, 3H, OCH_3). To prepare dimethyldecodine hydrochloride the base was dissolved in ether, ethereal hydrogen chloride was added until precipitation was complete. The product was recrystallized from methanol, mp 256–262°C (dec.)

*Diphenylolefin (**11**) from dimethyldecodine (**7**)* (cf. ref. 29)—To a solution of phenylmagnesium bromide prepared from magnesium turnings (200 mg) and bromobenzene (0.85 mL, 1.27 g) in dry tetrahydrofuran, was added a solution of dimethyldecodine (180 mg) in dry tetrahydrofuran (8 mL). The mixture was heated 6 h under reflux. Water was added to destroy excess Grignard reagent, the magnesium salts were dissolved by adding ammonium sulfate and enough 1 *M* sulfuric acid to give pH 8. The mixture was extracted with ether (3 × 10 mL). Formic acid (5 mL, 90%) was added to the ether extract and the solution was heated 1 h on a steam bath. The cooled solution was washed with carbon tetrachloride (15 mL) and the organic layer discarded. The aqueous phase was concentrated to a small volume (ca. 2 mL) and basified with dilute sodium hydroxide solution. Extraction with ether (4 × 20 mL) followed by drying (anhydrous Na_2SO_4) and evaporation gave a foam (200 mg) whose tlc showed two spots. The two components were separated by chromatography on silica plates (20 × 20 cm × 2 mm thickness) using ether as developing solvent. The less polar product was recovered from the plates as a white foam (95 mg) which could not be obtained crystalline; ^1H nmr ($CDCl_3$) δ: 6.28 (t, J = 7 Hz, 1H, olefin), 7.25 ppm (m, 10H, 2 × phenyl).

*Oxidation of the diphenylolefin (**11**)*—Glacial acetic acid (4.5 mL) was added to a solution of the diphenylolefin (90 mg) in chloroform (0.8 mL). A solution of chromium trioxide (75 mg) in 85% aqueous acetic acid (4 mL) was added dropwise over 10 min to the stirred solution and stirring was continued for a further 1 h at room temperature. Methanol (1 mL) and, after a further 15 min, water (40 mL) was added and the solution extracted with ether (3 × 15 mL). The combined extracts were washed with water, dried (anhydrous Na_2SO_4) and evaporated, the remaining trace of acetic acid being removed by azeotropic distillation with benzene. The crystalline yellow residue (29 mg) showed a single spot on tlc which had the same R_f value as benzophenone. The residue was dissolved in ethanol (5 mL), pyridine (0.5 mL) and hydroxylamine hydrochloride (30 mg) were added, and this solution was heated under reflux for 2 h. The solvent was removed and the residue dissolved in a little methanol and filtered. Removal of the methanol gave benzophenone oxime as pale yellow needles (21 mg), mp 135–137°C (from methanol–water). The solid was dissolved in ether, the solution filtered, the ether removed, and the residue sublimed at 90°C and 10^{-1} Torr giving benzophenone oxime as colourless prisms, mp 142–143°C, (lit. (36) mp 144°C).

The Lactone Carbinol Carbon (C-3) as Benzoic Acid

*Tetrahydrodimethyldecodine (**12**) (27)*—Dimethyldecodine (260 mg) obtained by methylation of decodine (250 mg) was dissolved in dry ether (25 mL) and lithium aluminium hydride (200 mg) added in small portions over 15 min. The mixture was stirred at room temperature overnight, a little Celite was then added and excess lithium aluminium hydride destroyed by addition of water. The mixture was filtered, washed with ether and the residue heated with tetrahydrofuran and again filtered and washed. The combined filtrates were evaporated leaving a white foam (210 mg) which showed one spot on tlc. *Anal.* calcd. for $C_{27}H_{37}NO_5$: C 71.18, H 8.19, N 3.07; found: C 71.05, H 8.13, N 2.99; ms *m/e*: 455 (molecular ion), 454, 425.

O-*Tosyltetrahydrodimethyldecodine (**13**)*[5]—*p*-Toluenesulfonyl chloride (200 mg) was added to an ice cold solution of tetrahydrodimethyldecodine (210 mg) in freshly distilled dry pyridine (5 mL). The yellow solution was kept 16 h at 4°C when tlc showed one major product. The pyridine solution was poured into a cold, stirred saturated solution of sodium bicarbonate (40 mL) and stirred for 15 min. This solution was extracted with chloroform (3 × 20 mL) and the dried (anhydrous Na_2SO_4) extracts evaporated at room temperature under reduced pressure. The residual pyridine was removed at room temperature *in vacuo* to leave a pale yellow foam (280 mg); ^1H nmr ($CDCl_3$) δ: 2.43 ppm (s, 3H, aromatic methyl).

[5]The conditions employed here for the selective tosylation of a primary in the presence of a secondary alcohol are similar to those described by Johnson *et al.* (37).

Reduction of O-*tosyltetrahydrodimethyldecodine (**13**) to desoxytetrahydrodimethyldecodine (**14**)*—The above tosylate (275 mg) was dissolved in dry distilled tetrahydrofuran (20 mL) and lithium aluminium hydride (100 mg) was added in four portions over a 10 min period. The mixture was heated under reflux for 1 h when tlc showed three spots (one major) none of which corresponded to starting material. A little Celite was added to the cold mixture and the excess lithium aluminium hydride destroyed by the careful addition of water. The mixture was filtered and the solids stirred with hot tetrahydrofuran and again filtered. The combined filtrates were evaporated leaving a pale yellow oil (210 mg) which was dissolved in a little chloroform and applied to a neutral alumina column (12 × 1.5 cm, Activity 1). Fractions (20 mL) were eluted with ether. After elution of a small amount of a minor component, the major product emerged. Combination and evaporation of the fractions gave a colourless gum (154 mg) which was pure by ^{1}H nmr and on three tlc systems but could not be obtained crystalline; ^{1}H nmr ($CDCl_3$) δ: 0.93 (t, J = 7 Hz, 3H, CH_2CH_3) 2.58 (broad t, J = 7 Hz, 2H, Ar—CH_2), 3.57 (s, 3H, OCH_3), 3.71 (s, 3H, OCH_3), 3.89 ppm (s, 3H, OCH_3). *Anal.* calcd. for $C_{27}H_{37}NO_4$: C 73.77, H 8.49, N 3.19; found: C 73.82, H 8.20, N 3.30.

*Oxidation of desoxytetrahydrodimethyldecodine (**14**) to the corresponding ketone, dehydrodesoxytetrahydrodimethyldecodine (**15**)*—Standard Jones' reagent (0.9 mL) was added dropwise to an ice cold solution of the alcohol (**14**) (150 mg) in acetone. The cooled mixture was stirred 10 min, excess reagent was destroyed by addition of 2-propanol (1 mL), and the solution poured into 0.01 *M* hydrochloric acid (30 mL). The acid solution was washed with ether, basified with solid sodium bicarbonate, and extracted with ether (4 × 40 mL). The ether solution was dried ($MgSO_4$) and evaporated to yield a light yellow oil (83 mg). The residue which on tlc showed a trace of starting material and one major product, was purified by preparative thick layer chromatography on alumina with ether as the solvent. The major band (R_f 0.8) was eluted from the absorbant with ether, and the product (80 mg) was obtained as an almost colourless oil; ir 1730 cm^{-1}; ^{1}H nmr ($CDCl_3$) δ: 0.92 (t, J = 7 Hz, 3H, CH_2CH_3), 3.56, 3.68, 3.90 ppm (3 × s, 3H, 3 × OCH_3). *Anal.* calcd. for $C_{27}H_{35}NO_4$: mol. wt. 437.257; C 74.11, H 8.06, N 3.20; found: *m/e* 437.256; C 74.02, H 8.28, N 2.93.

If the reaction time is increased, a by-product showing a second carbonyl band at 1680 cm^{-1}, in addition to the band at 1730 cm^{-1} is obtained.

*Phenylation of the ketone, dehydrodesoxytetrahydrodimethyldecodine (**15**)*—The above ketone (77 mg) was carefully dried and dissolved in anhydrous ether in a 5 mL flask under nitrogen. Phenyllithium (1.9 *M*, 1 mL) was added to the stirred solution. After 1 h stirring at room temperature no starting material was detectable by tlc. The reaction was quenched with ice and the product extracted into chloroform. The chloroform solution was evaporated to yield a pale yellow oily residue (80 mg) which did not crystallize. *Anal.* calcd. for $C_{33}H_{41}NO_4$: C 76.86, H 8.01, N 2.72; found: C 76.65, H 8.20, N 2.59. Mass spectrum *m/e*: 515 (M^+), 499, 485, 454, 347. Thin-layer chromatography of the product on alumina revealed two bands, presumably due to the epimeric, equatorial and axial, phenylcarbinols (**16**).

*Oxidation of the phenylcarbinol (**16**)*—The phenylation product (75 mg) was dissolved in acetone and dispersed in water (15 mL). Acetone was removed at 80°C and potassium carbonate (1 g) was added to the stirred solution. Finely powdered potassium permanganate (2.5 g) was added in small portions over 6 h and the mixture refluxed 8 h with vigorous stirring and then kept overnight. Manganese dioxide was filtered off, washed with water (3 × 2 mL), the filtrate extracted with ether (3 × 10 mL), and the extracts discarded. The aqueous solution was acidified with 1 *M* sulfuric acid and decolourized with sodium bisulfite. Ether extraction and evaporation of solvent gave benzoic acid which was purified by sublimation at 40°C and 10^{-2} Torr. The yield of benzoic acid (10 mg) was 14% overall from decodine.

Degradation of Decodine Derived from [2-^{14}C]Phenylalanine

The α-Methylene Carbon (C-12) (Together with the Carbonyl Carbon (C-11)) of the Lactone Ring

*Kuhn–Roth oxidation of desoxytetrahydrodimethyldecodine (**14**)*—This derivative was prepared from dimethyldecodine via tetrahydrodimethyldecodine and *O*-tosyltetrahydrodimethyldecodine as described above in the sequence to separate the lactone carbinol carbon.

Desoxytetrahydrodimethyldecodine (142 mg) was dissolved in dilute sulfuric acid (4 *M*, 8 mL), in a small flask fitted with a condenser. A solution of chromium trioxide (2.5 g) in water (2 mL) was added by pipette down the condenser into the magnetically stirred mixture, which was then slowly heated to boiling under reflux for 2 h. The flask was cooled in ice and water washed down the condenser. The flask was fitted with a steam distillation head such that nitrogen could be bubbled through the solution and water added at the same rate as it distilled off. A total of 60 mL distillate was collected in 3 h and this was titrated with 0.1 *N* sodium hydroxide to pH 8 (2.0 mL). The titrated solution was then evaporated at 60°C overnight and the residue dissolved in water (1.5 mL). To this solution was added a solution of α-naphthylamine hydrochloride (25 mg) in water (1.5 mL) and 1-ethyl-3-(3-dimethylaminopropyl)carbodiimide (50 mg). The mixture was kept for 2 h and the resulting pink precipitate was extracted with chloroform (3 × 5 mL) and the concentrated extracts applied to a silica plate (20 × 5 cm, 2 mm thickness). The plate was developed with ether and showed three bands under uv. The band corresponding to *N*-acetyl-α-naphthylamine was removed and extracted with chloroform–methanol. The product (8 mg) was obtained as a white crystalline solid, which was further purified by sublimation at 130°C and 10^{-2} Torr. Yield 7 mg, mp 159–160°C (lit. (36) mp 160°C; (38) mp 159–160°C).

Degradation of Decodine Derived from [3-^{14}C]Phenylalanine

*4-Methoxyisophthalic Acid (**10**) and Hemipinic Anhydride (**9**) by Permanganate Oxidation of Dimethyldecodine (**7**) (26–28)*

Dimethyldecodine (200 mg) was dissolved in dilute sulfuric acid (1 *M*, 8 mL) and dilute sodium carbonate (1 *M*, 10 mL) was added (final pH 8.5) yielding a fine white precipitate of dimethyldecodine. Potassium permanganate (1.1 g) was added to the stirred suspension in small portions over a 4-h period and stirring was continued for a further 18 h. The solution was carefully (frothing!!) acidified with 2 *M* sulfuric acid and the excess potassium permanganate and precipitated manganese dioxide destroyed by the addition of sodium bisulfite. The resulting solution was extracted with ethyl acetate (4 × 20 mL). The dried extracts (anhydrous Na_2SO_4) were evaporated leaving a pale yellow residue (160 mg).

The above oxidation was repeated on a second sample of dimethyldecodine (200 mg) and a similar residue (170 mg) was obtained.

Thin-layer chromatography (silica, ethanol–water–ammonia (100:12:10)) showed each of the two oxidation residues to be a complex mixture of at least nine components. Preparative chromatography (silica, 20 × 20 cm × 2 mm plates) using the

above solvent system resolved the components into nine bands. Numbering from the solvent front, the sixth and seventh bands, containing the major components which in a preliminary run had been shown to correspond to 4-methoxyisophthalic acid and hemipinic acid, respectively, by comparison with authentic specimens, were eluted separately from the inert support with water. The extract was acidified and the product extracted into ethyl acetate (5 × 25 mL). Corresponding eluates from the two oxidations were combined.

The crude product from band six (41 mg) was sublimed at 155°C and 10^{-1} Torr to give 4-methoxyisophthalic acid (**10**) as a pale yellow solid which was crystallized from aqueous methanol and sublimed. Yield 3.5 mg, mp 260–265°C, undepressed by admixture with an authentic sample; (lit. (27) mp 258–263°C).

The crude hemipinic acid from band seven (21 mg) was sublimed at 130°C and 10^{-1} Torr to give hemipinic anhydride (9) as a white crystalline sublimate. This was crystallized from a very small amount of acetone to give colourless crystals (3 mg) mp 159–161°C, undepressed on admixture with authentic hemipinic anhydride; (lit. (27) mp 158–160°C; (36) 166–167°C).

During one of the radioactive runs (experiment 11) a third component of the mixture was obtained in larger quantity. This was presumably 2′,2,3-trimethoxybiphenyl-5′,6-dicarboxylic acid (**8**), mp 236–239°C after sublimation at 195°C and 5 × 10^{-2} Torr. Accurate mass measurement (CEC 21-110B) of the molecular ion of the corresponding dimethyl ester; *m/e* calcd. for $C_{19}H_{20}O_7$: 360.121; found: 360.119.

Degradation of Decodine from [1,3-$^{14}C_2$]Phenylalanine

Decodine (**5**) was converted into dimethyldecodine (**7**) which was degraded to benzophenone oxime (C-11) and to benzoic acid (C-3) as described for the degradation of the sample from [1-^{14}C]phenylalanine, and to 4-methoxyisophthalic acid (**10**) and hemipinic anhydride (**9**), as described for the degradation of the sample from [3-^{14}C]phenylalanine.

Degradation of Decinine Derived from [1-^{14}C]Phenylalanine

The Lactone Carbonyl Carbon (C-11) as Benzophenone Oxime

Methyldecinine (17) (cf. ref. 7)—Decinine (300 mg) was dissolved in methanol (15 mL) and excess diazomethane in ether (75 mL) was added. The mixture was kept in a cold room (4°C) for 2 days. Solvent was removed, methanol (10 mL) was added to the residue, and the mixture was warmed on a steam bath and filtered. The filtrate was concentrated and the product crystallized. Repeated recrystallization from methanol yielded methyldecinine (305 mg), mp 169–170°C (lit. (7) mp for methylated reduced lythrine, i.e., methyldihydrolythrine, i.e. methyldecinine (**17**) 173–175°C); ^{1}H nmr ($CDCl_3$) δ: 3.72, 3.83, 3.92 ppm (3 × s, 3H, 3 × OCH_3).

Benzophenone oxime from methyldecinine—Methyldecinine was converted to the diphenylcarbinol by treatment with phenylmagnesium bromide, and the diphenylcarbinol dehydrated to the corresponding diphenylolefin (**19**) (29) as described for decodine. The product was obtained as a frothy solid which was directly oxidized to benzophenone. The latter was converted into the oxime. The procedure and yields were similar to those reported in the corresponding decodine degradation.

The Lactone Carbinol Carbon (C-3) as Benzoic Acid

Tetrahydromethyldecinine (20) (cf. ref. 29)—Methyldecinine (140 mg) obtained by methylation of decinine (140 mg) was dissolved in dry ether (18 mL), and lithium aluminium hydride (130 mg) was added in small portions and the mixture stirred at room temperature overnight. Subsequent work-up followed that for the corresponding decodine derivative (*vide supra*). The product (135 mg) was obtained as a white foam; ^{1}H nmr ($CDCl_3$) δ: 2.68 (broad, t, J = 7 Hz, 2H, Ar—CH_2), 3.55 (t, J = 6 Hz, —CH_2OH), 3.70, 3.80, 3.92 ppm (3 × s, 3H, 3 × OCH_3).

O-*Tosyltetrahydromethyldecinine (21)*[5]—The above tetrahydromethyldecinine (135 mg) was tosylated with *p*-toluenesulfonylchloride (125 mg) in anhydrous pyridine (4 mL) in the manner described for the corresponding reaction in the decodine series. The product (167 mg) was a brown foam, which showed a single spot on tlc (alumina, chloroform).

Reduction of O-*tosyltetrahydromethyldecinine (21) to desoxytetrahydromethyldecinine (22)*—The above tosylate (165 mg) in anhydrous tetrahydrofuran (12 mL) was reduced with lithium aluminium hydride (70 mg) in the manner described for the corresponding reaction in the decodine series. The product was obtained as a yellow oil (133 mg) which was purified by chromatography on neutral alumina to yield a colourless foam (94 mg) which did not crystallize; ^{1}H nmr ($CDCl_3$) δ: 0.95 (t, J = 7 Hz, 3H, —CH_2CH_3), 2.60 (broad t, $J \sim$ 7 Hz, 2H, Ar—CH_2), 3.72, 3.83, 3.92 ppm (3 × s, 3H, 3 × OCH_3).

Oxidation of desoxytetrahydromethyldecinine (22) to the corresponding ketone, dehydrodesoxytetrahydromethyldecinine (23)—Standard Jones' reagent (0.55 mL) was added dropwise to a stirred, cooled solution of the above derivative (94 mg) in acetone (30 mL). Stirring was continued 10 min, excess Jones' reagent was destroyed with 2-propanol (1 mL), and hydrochloric acid (0.025 *M*, 90 mL) was added. Subsequent work-up was similar to that for the corresponding experiment in the decodine series, yield 49 mg; ir 1730 cm^{-1}; ms *m/e*: 437 (molecular ion) 422, 406; ^{1}H nmr ($CDCl_3$) δ: 0.92 (t, J = 7 Hz, 3H, —CH_2CH_3), 3.75, 3.84, 3.94 ppm (3 × s, 3H, 3 × OCH_3).

Phenylation of dehydrodesoxytetrahydromethyldecinine (23)—The ketone (49 mg) was phenylated with phenyllithium following the procedure described for the corresponding reaction in the decodine series. The product (45 mg), a mixture of epimeric phenylcarbinols (**24**), was not separated into components. Mass spectrum *m/e*: 515 (molecular ion), 485, 454.

Oxidation of the phenylcarbinol (24)—The phenylation product (43 mg) was oxidized with permanganate (1.5 g) in the presence of potassium carbonate in the manner described for the corresponding reaction in the decodine series. On work-up, benzoic acid was obtained and purified by sublimation, yield 5 mg.

Degradation of Decinine Derived from [2-^{14}C]Phenylalanine

The α-Methylene Carbon (C-12) (Together with the Carbonyl Carbon (C-11)) of the Lactone Ring

Kuhn–Roth oxidation of desoxytetrahydromethyldecinine (22)—Desoxytetrahydromethyldecinine was prepared from methyldecinine (**17**) via tetrahydromethyldecinine (**20**) and *O*-tosyltetrahydromethyldecinine (**21**), as described above. The Kuhn-Roth oxidation was carried out by the same procedure that was used in the corresponding degradation of desoxytetrahydrodimethyldecodine; yield of *N*-acetyl-α-naphthylamine 8 mg (from 300 mg decinine); mp 157–158°C.

Degradation of Decinine Derived from [1,3-$^{14}C_2$]Phenylalanine

4,5-Dimethoxyphthalic acid (18) and 4-Methoxyisophthalic Acid (10) from Methyldecinine (17) (26–28)

A suspension of methyldecinine (*17*) (200 mg) in dilute sulfuric acid (1 *M*, 8 mL) was made alkaline by adding 1 *M* sodium carbonate solution (10 mL) so that the pH of the solution was 8–8.5. Potassium permanganate (1.1 g) was added with stirring over a period of 4 h and stirring was continued for 20 h at room temperature. The solution was then acidified with 2 *M* sulfuric acid and the excess potassium permanganate and the precipitated manganese dioxide were decomposed

with sodium bisulfite. The resulting colourless solution was extracted with ethyl acetate (4 × 40 mL) and the organic layer washed, dried (anhydrous Na_2SO_4), and evaporated.

The residue (70 mg) was separated by preparative thin layer chromatography (silica, benzene–methanol–acetic acid 45:8:4). The major product, R_f 0.43, was eluted with water, the solution acidified with sulfuric acid (1 *M*) and extracted with ethyl acetate (3 × 25 mL). The organic layer was washed with water, dried (anhydrous Na_2SO_4) and evaporated and the crude product sublimed (160°C, 1 × 10^{-3} Torr) to yield 4-methoxyisophthalic acid (**10**); yield 6 mg; mp 260–265°C.

The other product which was detected on the tlc plate (R_f 0.25) was eluted similarly. This product had chromatographic properties corresponding to those of authentic 4,5-dimethoxyphthalic acid (**18**). The low yield (< 1 mg) precluded the use of this compound in radioactive determinations.

Degradation of Decodine Derived from [2-^{14}C]Malonic Acid

Chromic acid oxidation of decodine, and isolation of the resulting degradation products, 2-piperidylacetic acid, γ-aminobutyric acid and β-alanine, was carried out as described in the preceding paper (25).

Acknowledgements

We thank Mr. L. Laking, Director, and Dr. J. S. Pringle, Taxonomist, Royal Botanical Gardens, Hamilton, for their unfailing help and cooperation, without which this investigation could not have been undertaken. Financial support by the National Research Council of Canada is gratefully acknowledged.

1. J. P. Ferris, C. B. Boyce, and R. C. Briner. Tetrahedron Lett. 5129 (1966).
2. J. P. Rosazza, J. M. Bobbitt, and A. E. Schwarting. 5th International Symposium on the Chemistry of Natural Products, I.U.P.A.C., London 1968. Abstr. C8.
3. A. Rother and A. E. Schwarting. Chem. Commun. 1411 (1969).
4. J. P. Rosazza, J. M. Bobbitt, and A. E. Schwarting. J. Org. Chem. **35**, 2564 (1970).
5. J. P. Ferris. J. Org. Chem. **27**, 2985 (1962).
6. J. P. Ferris, R. C. Briner, and C. B. Boyce. J. Am. Chem. Soc. **93**, 2953 (1971).
7. R. N. Blomster, A. E. Schwarting, and J. M. Bobbitt. Lloydia, **27**, 15 (1964).
8. B. Douglas, J. L. Kirkpatrick, R. F. Raffauf, O. Ribeiro, and J. A. Weisbach. Lloydia, **27**, 25 (1964).
9. H.-G. Appel, A. Rother, and A. E. Schwarting. Lloydia, **28**, 84 (1965).
10. R. B. Hörhammer, A. E. Schwarting, and J. M. Edwards. Z. Naturforsch. B, **26**, 970 (1971).
11. R. H. Dobberstein, J. M. Edwards, and A. E. Schwarting. Phytochemistry, **14**, 1769 (1975).
12. J. P. Ferris, R. C. Briner, and C. B. Boyce. J. Am. Chem. Soc. **93**, 2958 (1971).
13. H. Wright, J. Clardy, and J. P. Ferris. J. Am. Chem. Soc. **95**, 6467 (1973).
14. A. Rother and A. E. Schwarting. Lloydia, **38**, 477 (1975).
15. A. Rother and A. E. Schwarting. Experientia, **30**, 222 (1974).
16. R. B. Hörhammer, A. E. Schwarting, and J. M. Edwards. J. Org. Chem. **40**, 656 (1975).
17. A. Rother and A. E. Schwarting. Phytochemistry, **17**, 305 (1978).
18. R. N. Gupta and I. D. Spenser. Phytochemistry, **8**, 1937 (1969).
19. E. Leistner, R. N. Gupta, and I. D. Spenser. J. Am. Chem. Soc. **95**, 4040 (1973).
20. R. N. Gupta and I. D. Spenser. J. Biol. Chem. **244**, 88 (1969).
21. E. Leete. J. Am. Chem. Soc. **91**, 1697 (1969).
22. M. Castillo, R. N. Gupta, Y. K. Ho, D. B. MacLean, and I. D. Spenser. Can. J. Chem. **48**, 2911 (1970).
23. Y. K. Ho, R. N. Gupta, D. B. MacLean, and I. D. Spenser. Can. J. Chem. **49**, 3352 (1971).
24. W. M. Golebiewski and I. D. Spenser. J. Am. Chem. Soc. **98**, 6726 (1976).
25. R. N. Gupta, P. Horsewood, S. H. Koo, and I. D. Spenser. Can. J. Chem. This issue.
26. A. Rother and A. E. Schwarting. Phytochemistry, **11**, 2475 (1972).
27. J. P. Ferris. J. Org. Chem. **28**, 817 (1963).
28. A. Rother, H.-G. Appel, J. M. Kiely, A. E. Schwarting, and J. M. Bobbitt. Lloydia, **28**, 90 (1965).
29. J. P. Ferris, C. B. Boyce, and R. C. Briner. J. Am. Chem. Soc. **93**, 2942 (1971).
30. S. H. Koo, F. Comer, and I. D. Spenser. Chem. Commun. 897 (1970).
31. B. L. Møller. Plant Physiol. **54**, 638 (1974).
32. J. R. Gear and I. D. Spenser. Nature, London, **191**, 1393 (1961).
33. H. Wieland and O. Dragendorff. Justus Liebigs Ann. Chem. **473**, 83 (1929).
34. M. F. Keogh and D. G. O'Donovan. J. Chem. Soc. C, 2470 (1970); D. G. O'Donovan, D. J. Long, E. Forde, and P. Geary. J. Chem. Soc. Perkin Trans. I, 415 (1975).
35. R. N. Gupta and I. D. Spenser. Can. J. Chem. **45**, 1275 (1967).
36. J. R. A. Pollock and R. Stevens (*Editors*). Dictionary of organic compounds. 4th ed. Eyre and Spottiswoode, London. 1965.
37. W. S. Johnson, J. C. Collins, Jr., R. Pappo, M. B. Rubin, P. J. Kropp, W. F. Johns, J. E. Pike, and W. Bartmann. J. Am. Chem. Soc. **85**, 1409 (1963); L. F. Fieser and M. Fieser. Reagents for organic synthesis. Vol. 1. John Wiley & Sons, New York. 1967. p. 1181.
38. E. Leete, H. Gregory, and E. G. Gros. J. Am. Chem. Soc. **87**, 3475 (1965).
39. J. P. Ferris, C. B. Boyce, R. C. Briner, B. Douglas, J. L. Kirkpatrick, and J. A. Weisbach. Tetrahedron Lett. 3641 (1966).
40. J. P. Ferris, R. C. Briner, C. B. Boyce, and M. J. Wolf. Tetrahedron Lett. 5125 (1966).
41. A. M. Patterson, L. T. Capell, and D. F. Walker. The ring index. 2nd ed. American Chemical Society. 1960.
42. E. Fujita, K. Fuji, K. Bessho, and S. Nakamura. Chem. Pharm. Bull. **18**, 2393 (1970).
43. E. Fujita and Y. Saeki. Chem. Commun. 368 (1971).
44. C. Schöpf, E. Schmidt, and W. Braun. Chem. Ber. **64B**, 683 (1931).

Appendix

Numbering of the Lythraceae Alkaloids

In view of the probable common biogenetic origin of the three structural groups of the Lythraceae alkaloids, a numbering system is desirable which is applicable to the *Decodon*-type alkaloids (group 1) (e.g., decodine (**5**) and vertaline (**35**)), as well as the *Lythrum*-type (group 2) (e.g., lythrumine (**31**)), and

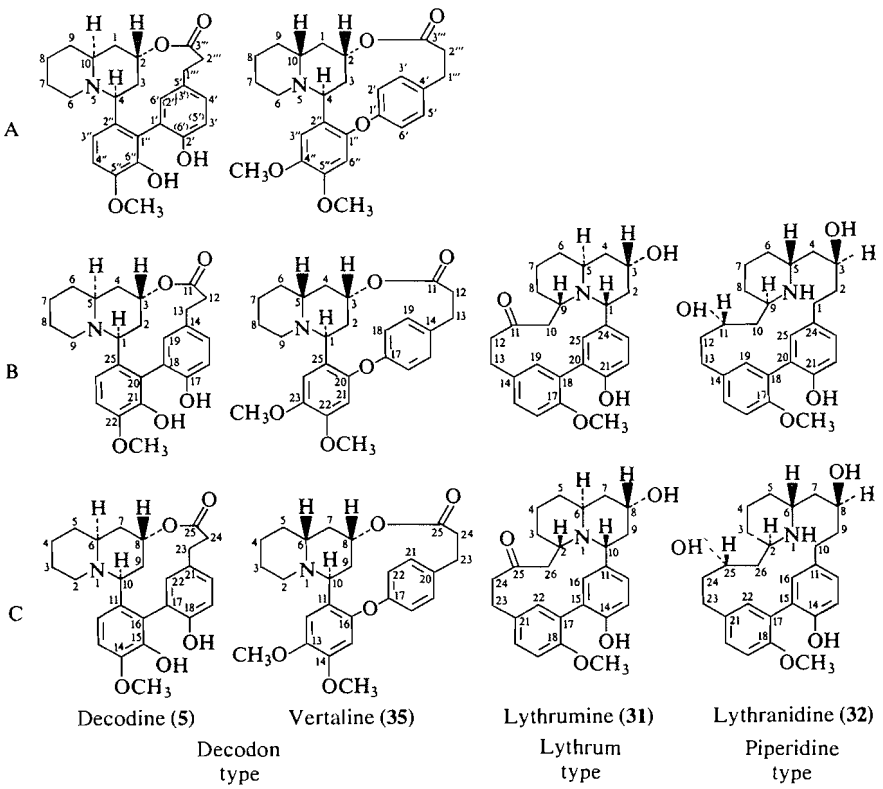

SCHEME 7. Numbering of the Lythraceae alkaloids.

the piperidine-type alkaloids (group 3) (e.g., lythranidine (**32**)).

The numbering system A, in common use for the *Decodon*-type alkaloids, was introduced by Ferris and co-workers (29, 39, 40) and adopted and extended by Rother and Schwarting (3). The quinolizidine nucleus is numbered as recommended by *The Ring Index* (ref. 41, RRI 1687) but primed and multiply primed numbers are employed for other C-atoms and the system is thus not rationally adaptable to use with the alkaloid skeletons of groups 2 and 3.

Numbering system B for the latter two groups of alkaloids was introduced by Fujita and co-workers (42, 43) and is generally used for these alkaloids. This system is readily adaptable to the alkaloids of group 1. Extrusion of C-10 of the group 2 skeleton, and union of C-11 with the O-atom at C-3, formally yields a group 1 skeleton.

The numbering system of the group 1 alkaloids which is generated in this manner is attractive for several reasons: (i) carbon atoms which correspond in biogenetic origin in the three structural groups maintain corresponding numbers; (ii) the numbering of the quinolizidine ring system, even though different from that recommended by *The Ring Index* (41) which, with a minor change is also used by Chemical Abstracts, is not new but corresponds to that originally employed by Schöpf *et al.* (44); and (iii) the numbering of only one of the three structural groups of alkaloids is changed, while currently used numbering is maintained for the other two groups.

An entirely new numbering system[6] for all three groups of alkaloids which is chemically as well as biogenetically rational, is system C, in which the quinolizidine ring is numbered as in the lupine alkaloids.

We have employed system B, since it shows common biogenetic origin while minimizing changes in current practice.

[6]We are indebted to Dr. V. Snieckus, University of Waterloo, for this suggestion.

The total synthesis of (±)-luciduline[1]

JERZY SZYCHOWSKI[2] AND DAVID B. MACLEAN
Department of Chemistry, McMaster University, Hamilton, Ont., Canada L8S 4M1

Received December 14, 1978

JERZY SZYCHOWSKI and DAVID B. MACLEAN. Can. J. Chem. 57, 1631 (1979).

(±)-Luciduline has been synthesised in seven steps from 2-(2-cyanoethyl)-5-methylcyclohex-2-en-1-one. The synthetic approach is adaptable to the synthesis of intermediates of interest in biosynthetic studies of the Lycopodium alkaloids.

JERZY SZYCHOWSKI et DAVID B. MACLEAN. Can. J. Chem. 57, 1631 (1979).

On a synthétisé la (±)-luciduline en sept étapes à partir de la (cyano-2 éthyl)-2 méthyl-5 cyclohexène-2 one-1. On pourrait adapter cette approche à la synthèse d'intermédiaires intéressants dans des études biosynthétiques des alcaloïdes du lycopodium.

[Traduit par le journal]

Luciduline (**1**) (originally designated L21) was first described by Manske and Marion (1) who isolated the alkaloid from *Lycopodium lucidulum* Michx. Its structure was elucidated by Ayer *et al.* (2) by chemical degradation and by an X-ray study. Luciduline is the only representative of this ring system that has been isolated from the Lycopodiaceae.

Two syntheses of luciduline have already been reported, the first by Scott and Evans (3) and the second by Oppolzer and Petrzilka (4). Both syntheses lead in straightforward steps to the stereochemically desired intermediates and eventually to the product. Neither however is related to the biosynthesis of the alkaloid in the plant. The synthetic approach reported here is not biomimetic but leads to an intermediate that may however be involved in the biosynthesis, not only of luciduline itself but also of other ring systems in this family of alkaloids (5).

In a recent paper Nyembo *et al.* (6) have proposed that the amino acid **2** and compounds of general structure **3**, the phlegmarines, both of unspecified stereochemistry, may be biosynthetic intermediates on the pathway to many of the Lycopodium alkaloids. It was the purpose of the present study, not only to develop a general method for the synthesis of compounds of type **2** and **3** so that they might be eventually tested as biosynthetic precursors but also to develop a synthesis of (±)-luciduline and of the phlegmarines. A part of this work has been completed and we report here a synthesis of **4**, the ethyl ester of the lactam of **2**, and its conversion to luciduline.

The compound used as starting material in the synthesis was 2-(2-cyanoethyl)-5-methylcyclohex-2-en-1-one (**5**). This compound has recently been used by Heathcock *et al.*[3] in their synthesis of lycopodine. We have prepared it from 5-methyl-1,3-cyclohexanedione (6) using Clark and Heathcock's procedure (7) with slight modification.

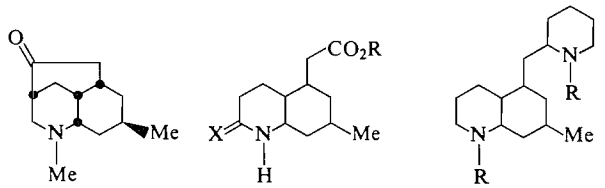

1 Luciduline

2 X = H_2; R = H
4 X = O; R = C_2H_5

3 R = H or CH_3

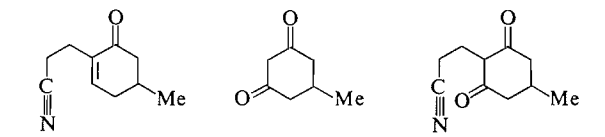

5

6

7

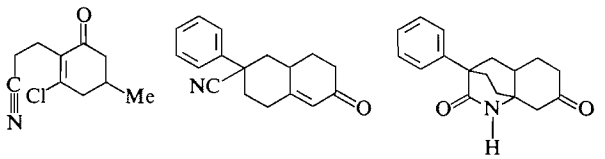

8

9

10

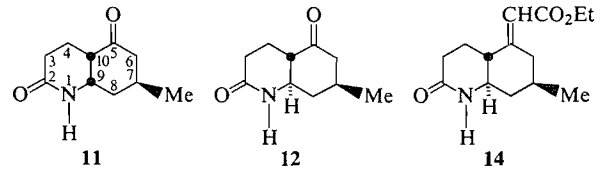

11

12

14

[1] This paper is dedicated to the memory of R. H. F. Manske who was associated with the discovery of luciduline and many other alkaloids of the Lycopodium family.

[2]Present address: Institute of Fundamental Problems of Chemistry, University, Pasteura 1, 02-093 Warsaw, Poland.

[3]C. H. Heathcock. Personal communication.

0008-4042/79/131631-07$01.00/0

The dione **6** was prepared by the method of Crossley and Renouf (8), a method that has been used with varying success by others (9, 10). We have found that the key to acceptable and reproducible results in this procedure rests in the manner of hydrolysis of the intermediate keto ester. The dione **6** was treated with acrylonitrile yielding 2-(2-cyanoethyl)-5-methyl-1,3-cyclohexanedione (**7**) according to the method of Reinshagen (11). Compound **7** was converted to 2-(2-cyanoethyl)-5-methyl-3-chlorocyclohex-2-en-1-one (**8**) by treatment with oxalyl chloride and that in turn to **5** by reduction with Zn activated by Ag (7). We found that our product was contaminated with variable quantities of some fully reduced material contrary to the earlier study (7).

Compound **5** was converted to a mixture of bicyclic keto lactams making use of a little known annelation reaction. Some years ago it was reported that compound **9** cyclized to the lactam **10** upon treatment with alkali (12). We found that a similar cyclization occurred when **5** was treated with methanolic NaOH. Two lactams, **11** and **12**, were separated from the reaction mixture by chromatography on alumina and separated from one another for analytical purposes by careful chromatography on silica gel. They were assigned the structures shown on the basis of nmr examination. The spectra were remarkably different, especially in the signals at H-9 which are clearly separated from the other signals in the two spectra. In isomer **11**, in which the bridgehead protons were deduced to be *cis*, the signal for H-9 was a nearly regular quartet, δ 4.12, J = 3.5 Hz, whereas in isomer **12**, in which the bridgehead protons are considered *trans*, this signal appeared as a triplet, split into doublets, δ 3.30, J = 11.0 and 4.0 Hz. In the *cis*-isomer **11** this implies coupling with three protons with nearly equivalent dihedral angles to H-9, namely H-10, H-8a, and H-8e, while for the *trans*-isomer **12** there are probably two equal *trans*-diaxial couplings of H-9, with H-10 and H-8a, and one axial–equatorial coupling between H-9 and H-8e. On these grounds isomer **11** was assigned conformation **11***a* (it may exist in equilibrium with a small amount of **11***b*) and compound **12** was assigned stereostructure **12***a*. The dihedral angles observed from molecular models of the *cis*- and *trans*-isomers conform with these deductions.

A detailed examination of the spectrum of **11** was carried out at 220 MHz in chloroform and benzene and in mixtures of the two. Through these studies it was possible to assign tentatively all the protons of **11** and to confirm some of the assignments by decoupling studies as reported in the experimental section. The change in chemical shift in changing solvent from chloroform to benzene was in the same direction (upfield) and of the same magnitude for H-9, H-10, H-8a, and H-6a, namely 0.75, 0.96, 0.62, and 0.75 ppm, respectively. The *C*-methyl group was shifted upfield by 0.3 ppm but H-7a by only 0.2 ppm. These results imply a *cis* relationship among H-9, H-10, H-8a, H-6a, and the *C*-methyl group since benzene might be expected to coordinate with only one face of the molecule.

Both broadband and off-resonance ^{13}C spectra of **11** were also recorded. The assignments that were made are shown in Fig. 1 where they are compared with those of 3-methylcyclohexanone (13) chosen as a model in this study. The upfield shift of C-7 relative to the model is ascribed to the γ-gauche interaction with the axial substituent at C-9. The ^{13}C spectrum is compatible with the structure deduced from the ^{1}H nmr data.

The relative stereochemistry, especially at the *C*-methyl group, deduced from nmr, was not definitely established however until the synthesis of luciduline was complete.

The mechanism of cyclization of **5** seems to involve the attack of OH^- on the carbon atom of the C≡N group with subsequent attack of the negatively charged nitrogen on the enone system (12). Protonation of the resulting enol then leads to the amides **11** and **12** (Fig. 2).

The predominance of **11** in the reaction product shows that nitrogen attack occurs mainly on the side of the enone system *trans* to the methyl group. A similar directive influence of a methyl group in a conjugate addition to a cyclohexenone was observed by Stork (14) in his synthesis of lycopodine. Allinger and Riew (15) have provided an analysis of the stereochemistry of the copper-catalysed Michael additions of Grignard reagents to methylcyclohexenone which is in accord with the present observations. The enol resulting from attack of negatively charged nitrogen on the side opposite to the methyl group protonates to give **11***a* in which the carbon–carbon bonds at C-7 and C-10 are equatorial in the carbocyclic ring. This isomer seems relatively stable to isomerization and none of its epimer at C-10 has been detected. The ratio, **11**–**12**, usually greater than 5:1, does however vary with

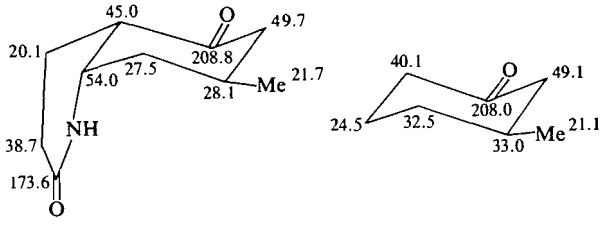

FIG. 1. ^{13}C nmr spectra of **11** and 3-methylcyclohexanone.

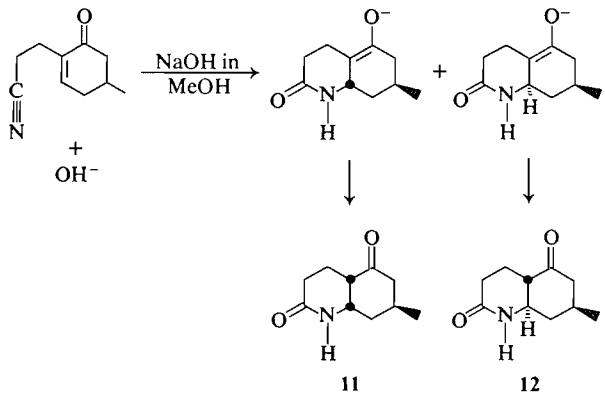

FIG. 2. The cyclization of 2-(2-cyanoethyl)-5-methylcyclohex-2-en-1-one (**5**).

reaction time and this suggests that isomerization may occur but it must take place at C-9 rather than at C-10, for an interconversion of **11** to **12**. Isomerization at C-9 may result from a reverse Michael reaction followed by ring closure but that has not been established. Nevertheless it is apparent that the isomerization of **11** to its epimer at C-10 is by no means facile, contrary to the generally held belief that compounds with a ketone α to a bridgehead isomerize readily from the *cis* to the *trans* configuration.

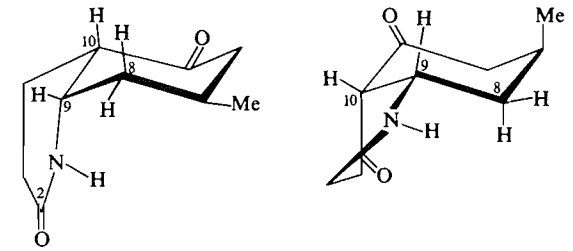

11*a* **11***b*

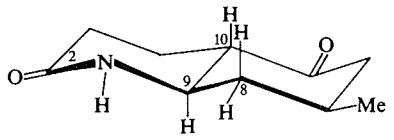

12*a*

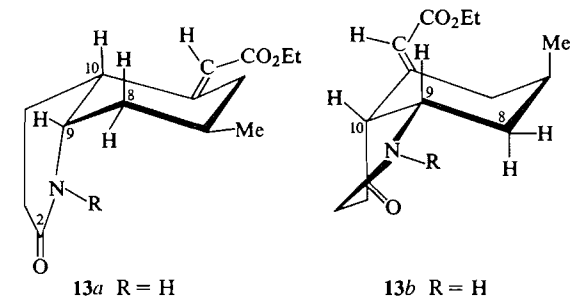

13*a* R = H
17*a* R = Me

13*b* R = H
17*b* R = Me

Compound **12** is derived from an enol resulting from attack by nitrogen on the enone system *cis* to the methyl group. This enol also protonates to give an equatorial bond at C-10 resulting in an all equatorial array of substituents in the carbocyclic ring as shown in stereo formula **12***a*.

It was now necessary to add to C-5 the two carbon atoms required to complete the skeleton of luciduline. Initial studies in which **11** was treated with ethyl triethylphosphonoacetate in base did not give satisfactory results. Although some of the desired **13** was present, the product proved to be a mixture of isomers in which those isomers with an endocyclic double bond predominated. However **13** was obtained in good yield in the Peterson reaction (16) with ethyl trimethylsilyl acetate (17). The reaction was normally carried out on the mixture of *cis*- and *trans*-lactams obtained from the cyclization step. The *trans*-isomer was found to react faster than the *cis* and to give a mixture of isomers about the newly formed double bond, one of which, **14**, was obtained crystalline. The *cis*-isomer **11** gave however only a single isomer **13** to which the *E* configuration has been assigned on the following grounds. In the nmr spectrum of **13** there is a signal at 3.18 δ that is absent in the dihydro compounds **15** and **16** (*vide infra*). Accordingly this signal can be assigned only to H-10 or to one of the two protons at C-6. Its low field position is attributed not only to its allylic position but also to deshielding by the ester function. Because the signal at 3.18 δ is a doublet of doublets (J = 15.0 and 4.0 Hz) it has been assigned to H-6e. The 15 Hz coupling is attributed to a geminal coupling to H-6a and the 4.0 Hz coupling to a vicinal coupling to H-7a. The signal for H-10 would be expected to be more complex and was excluded from consideration on these grounds. The conformation of the product represented in formula **13***a*, is favoured because the signal at H-9 still appears as a near quartet at 3.83 δ. The conformation **13***b* is also shown and a small amount of it may exist in equilibrium with **13***a*.

Hydrogenation of **13***a* might have been expected to yield only a single isomer. Instead, two products **15** and **16** (in a ratio of 2:1) that are epimeric at C-5 were isolated from reaction of **13** with hydrogen over an Adams' catalyst. The isomers **15** and **16** have been assigned the configurations and conformations shown from examination of the signal at H-9. In **15**, the desired isomer, this signal appears at 3.62 δ as a quintet formed by overlap of two triplets. In this conformation the protons at H-10 and H-8e will have approximately the same coupling constant, J = 6 Hz, to H-9 forming the triplet and this will be split by coupling with H-8a, J = 12 Hz. The methyl group at C-7 is axial and the carboethoxymethyl group at

C-5 is equatorial under these circumstances. On the other hand isomer **16** appears to have a conformation similar to **13***a* because the signal at H-9 appears as a quartet at 3.71 δ. Both the methyl and carboethoxymethyl groups will therefore adopt equatorial positions in the carbocyclic ring of **16**. The chemical shifts of the methyl groups in the two isomers reflect their axial–equatorial relationship.

The *N*-methylation of **15** was not attempted because we considered that cyclization at nitrogen might occur under the conditions required to introduce the *N*-methyl group. We therefore decided to introduce the *N*-methyl before hydrogenation and accordingly treated **13** with dimethyl sulfate in the presence of base; the reaction proceeded normally yielding **17**. Examination of **17** by nmr showed that conformation **17***b* was favoured over **17***a*. The signal for H-9 now appeared at 3.55 δ as a doublet of triplets in a manner similar to **15**. The *C*-methyl group of **17***b* must adopt an axial position but the *N*-methyl group occupies a position where its interactions with the carbocyclic ring are minimized relative to **17***a*.

Examination of models indicated that hydrogenation of **17** might now be less favoured from the top face of the molecule. This indeed proved to be the case and when **17** was treated with hydrogen over Adams' catalyst it yielded a 1 : 1 mixture of **18** and **19**. The conformations of **18** and **19** follow from examination of the signal at H-9 in the two compounds. In **18** this signal appears as a doublet of triplets centred at 3.44 δ, J = 5 and 12 Hz, and the molecule is assigned conformation **18***a* while in **19** it appears as a near quartet at 3.58 δ, J = 3 Hz, and the molecule assumes the conformation shown. The difference in chemical shift of the methyl group in the two isomers also reflects the difference in configuration and conformation.

Cyclization of **18** to luciduline lactam requires that it adopt conformation **18***b* with the methyl group equatorial at C-7 and the carboethoxymethyl axial at C-5. It is apparent that the barrier to interconversion is not high because **18** was successfully converted to **20**, (±)-luciduline lactam, in good yield on treatment with base. The spectroscopic properties in solution of (±)-luciduline lactam were identical within experimental error with those reported previously (2). It seems likely however that the assignments of H-3 and H-6 should be reversed. The chemical shift and coupling constant for H-6 are very similar to those of the corresponding proton in the bicyclic intermediates of similar conformation discussed previously. Moreover H-3 might be expected to be a multiplet with long range 'W' couplings to H-1 and H-5.

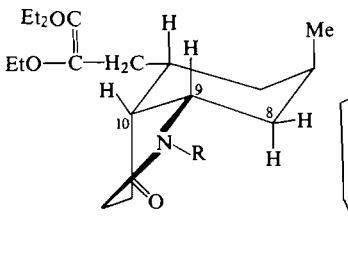

15*a* R = H
18*a* R = Me

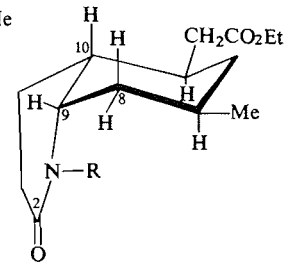

16 R = H
19 R = Me

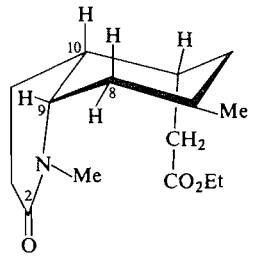

18*b*

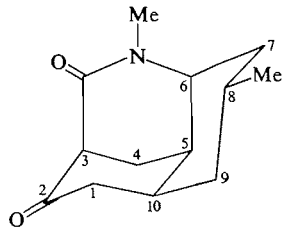

20
(±)-Luciduline lactam

The reduction of **20** with lithium aluminum hydride gave (±)-dihydroluciduline with spectroscopic properties in solution identical with a sample of dihydroluciduline **21** prepared by reduction of natural luciduline with sodium borohydride. (±)-Luciduline, with spectroscopic properties in solution identical with those of natural luciduline, was obtained on Jones' oxidation of **21**.

The completion of the synthesis places on a firm foundation the configurational assignments made for the intermediates on the basis of nmr examination. In particular we can now proceed to prepare labelled **15** and **18** for biosynthetic studies knowing that their stereochemistry is secure. Moreover it is now possible to proceed from **11** and **12** to prepare compounds of the phlegmarine structure and in this way arrive at the stereochemistry of the naturally occurring bases.

Experimental

Apparatus, Methods, and Materials

The infrared spectra were determined on a Perkin Elmer 383 spectrophotometer in chloroform solution. The nmr spectra were run at 90 MHz on a Varian EM 390 spectrometer or Bruker WH 90 spectrometer. The 220 MHz proton spectra were obtained at the Canadian 220 MHz NMR Centre, University of Toronto, Toronto, Ont. Chemical shifts are reported in ppm (δ) from tetramethylsilane. The symbols s (singlet), d (doublet), t (triplet), q (quartet), and m (multiplet) are used to report the multiplicity of signals. Coupling constants are accurate within ±0.5 Hz. Mass spectra were recorded on a CEC 21-110B mass spectrometer at an ionizing voltage of 80 eV and a source temperature of 150–200°C. High resolution measurements were performed by the method already de-

scribed (18). Natural abundance ^{13}C nuclear magnetic resonance spectra were recorded on a Bruker WH-90 Fourier transform spectrometer at 22.62 MHz and a probe temperature of +35.0°C. Samples were 0.08–0.15 *M* in $CDCl_3$; TMS was used as an internal reference.

Melting points and boiling points are uncorrected. Microanalyses were performed by Microanalysis Laboratories Ltd., Toronto, Ont.

The purity of all samples was checked by thin-layer chromatography in several solvent systems. Silica gel 60F-254 (Merck) was used for tlc and for column chromatography. Mixtures of methanol (3–10%) in ether were used in most cases to develop tlc silica plates. Tetrahydrofuran was always distilled before use over lithium aluminum hydride.

*5-Methyl-1,3-cyclohexanedione (**6**)*

Sodium (20.2 g) was dissolved in absolute ethanol (240 mL) and ethyl acetoacetate (120 g) and ethyl crotonate (100 g, 96%) were added. The mixture was heated on a steam bath for 6–7 h (after 0.5 h the mixture partly solidified) and the alcohol was then removed under reduced pressure. The residue was dissolved in H_2O (1 L) and treated with aqueous KOH (100 g in 400 mL) in two portions, the second portion being added at room temperature after 2 h. The reaction mixture was maintained at room temperature for a further 4 h and then boiled for 0.5 h to remove the remaining alcohol. The mixture was cooled to 60°C and acidified with aqueous sulfuric acid. It was then slowly heated and finally boiled for 15–20 min to complete the decarboxylation. 5-Methyl-1,3-cyclohexanedione crystallized from the mixture upon cooling. The crystals were separated by filtration, dried and recrystallized from ethyl acetate. The product melted at 126–127°C, yield 58–68%.

*2-(2-Cyanoethyl)-5-methyl-1,3-cyclohexanedione (**7**)*

This compound was prepared from **6** by the method of Reinshagen (11) in a yield of 50%. It melted at 148–152°C after one recrystallization from ethyl acetate and was used as such in the next step.

*2-(2-Cyanoethyl)-3-chloro-5-methylcyclohex-2-en-1-one (**8**)*

This compound was obtained by the method of Clark and Heathcock (7) from **7** as a colorless liquid in 77% yield. It boiled at 123–125°C/0.2 Torr.

*2-(2-Cyanoethyl)-5-methylcyclohex-2-en-1-one (**5**)*

This compound was prepared by the method of Clark and Heathcock (7) from the chloro derivative above in 77% yield as a colorless oil boiling at 95–97°C/0.6 Torr. The oil solidified on standing in the refrigerator and melted at 22–23°C. This product always contained variable amounts of 2-(2-cyanoethyl)-5-methylcyclohexanone which could be removed by allowing compound **5** to crystallize from methanol at −78°C. Optimum yields of **5** (ca. 95%) were obtained if the progress of the reaction was monitored by gc (3% OV-17, 110–120 mesh Anakrom ABS, 4 mm id × 2 m, 170°C) and stopped when all the starting material was consumed.

*Preparation of the Lactams (**11** and **12**)*

2-(2-Cyanoethyl)-5-methylcyclohex-2-en-1-one **5** (5 g), was dissolved in a mixture of methanol (100 mL) and sodium hydroxide (2.4 g). The solution was heated under reflux for 44 h under an atmosphere of argon. The solution was then cooled, neutralized with glacial acetic acid (3.6 mL), and the solvent removed on a rotary evaporator. The residue was dissolved in chloroform (100 mL) and washed with water (20 mL). Evaporation of the chloroform yielded a residue that showed two major spots on tlc on alumina, one of which was the starting material. By column chromatography on alumina (Al_2O_3 neutral, Fischer Scientific Company, 250 g, activity III) the starting material (1.4 g) was eluted with benzene and the product (2.4 g) with chloroform. The solid residue from the chloroform (mp 153–166°C) showed two components of very similar R_f value on tlc on silica. A portion was separated on a silica column (20 g) with ether–methanol, 10:1 on a 200 mg scale into the *trans*- and *cis*-isomers in a ratio of 1:5, respectively.

The *trans*-isomer **12** after recrystallization from ether–benzene melted at 225–227°C (with sublimation); ir ν_{max} ($CHCl_3$): 3400 (NH), 1720 (carbonyl), 1670, 1660 cm^{-1} (lactam); ^1H nmr, 90 MHz ($CDCl_3$) δ: 1.10 (3H, d, J = 6 Hz, —CH—CH_3), 3.30 (1H, t, split into doublets, J = 11.0 and 4 Hz, H-9), ~ 7.0 (1H, br s, —NH, disappears after D_2O exchange). *Mol. Wt.* calcd. for $C_{10}H_{15}NO_2$: 181.110; found (ms): 181.114.

The *cis*-isomer **11** was recrystallized from benzene and melted at 168–169°C; ir ν_{max}($CHCl_3$): 3400 (NH), 1720 (carbonyl), 1660 cm^{-1} (lactam); ^1H nmr, 220 MHz ($CDCl_3$) δ: 1.05 (3H, d, J = 6 Hz, CH—CH_3), 4.12 (1H, q, J = 3.5 Hz, H-9); *Mol. Wt.* calcd. for $C_{10}H_{15}NO_2$: 181.110; found (ms): 181.111.

The ^1H nmr spectrum measured in $CHCl_3$–benzene 4:3 (data given below) gave the best separation of signals. From an examination of this spectrum and comparison of it with the spectra from pure chloroform, pure benzene, and $CHCl_3$–C_6H_6 4:1 and 2:1 it was possible to make the following assignments of chemical shift and coupling constant for each proton. An asterisk indicates a decoupling experiment was performed; δ: 2.49 (H-3a, $J_{3a,3e}$ = 18.5 Hz, $J_{3a,4a}$ = 12 Hz, $J_{3a,4e}$ = 7 Hz), 2.13 (H-3e, $J_{3e,4a} = J_{3e,4e}$ = 7 Hz), 1.25 (H-4a), 2.1 (H-4e), 1.65 (H-6a, $J_{6e,6a}$ = 13 Hz, $J_{6a,7}$ = 13 Hz), 2.24 (H-6e, $J_{6e,7}$ = 3 Hz), 1.87 (H-7a), 0.85 (CH_3, $^*J_{CH_3,7a}$ = 6.0 Hz), 1.24 (H-8a, $J_{8a,7}$ = 14 Hz, $J_{8a,8e}$ = 14 Hz, $^*J_{8a,9}$ = 3.5 Hz), 1.72 (H-8e, $J_{8e,7}$ = 3 Hz, $^*J_{8e,9}$ = 3.5 Hz), 3.66 (H-9, $^*J_{9,10}$ = 3.5 Hz), 2.01 ppm (H-10, $J_{10,4a} = J_{10,4e}$ ~ 3–4 Hz).

*Reaction of the Lactams (**11** and **12**) with Ethyl Trimethylsilyl Acetate*

N-Isopropylcyclohexylamine (5.6 g, 40 mmol) was treated with 2.42 *M n*-butyllithium (16 mL, 39 mmol) at −60°C under an atmosphere of argon. To this solution after 1 h there was added dropwise ethyl trimethylsilylacetate (6.4 g, 40 mmol) prepared according to the method of Fessenden and Fessenden (17). The mixture was kept at −60°C during the addition and for 20 min thereafter and then the epimeric lactams (*trans–cis* 3:7), 3.26 g (18 mmol) were added. The solution was maintained at −60°C for 1 h, then at −20°C for 2 h, and finally at 0°C for 0.75 h. The whole mixture was then quenched with 160 mL of 0.5 *M* HCl and extracted once with benzene (200 mL) and twice with chloroform (2 × 50 mL). The extracts were worked up separately. The chloroform solution contained a mixture of *N*-isopropylcyclohexylamine and starting lactam (2.05 g) while the benzene extract contained a mixture of starting lactam, silyl ester, and product (5.2 g). A portion of the mixture derived from benzene (4.2 g) was separated by column chromatography on silica (100 g, SiO_2 for tlc) using ether–ethanol 9:1. The reaction product of the ester with the *trans*-lactam (1.1 g) was eluted first. Spectroscopic examination revealed that this was a mixture probably consisting of isomers about the newly generated double bond.

One isomer **14** was separated by crystallization from ether and melted at 193–195°C; ^1H nmr, 90 MHz ($CDCl_3$) δ: 1.06 (3H, d, J = 6 Hz, CHCH_3), 1.30 (3H, t, J = 7 Hz,O—CH_2—CH_3), 3.12 (1H, d of t, J = 3 and 11 Hz, H-9), 4.00 (1H, d with

additional small coupling, J = 11 Hz, probably C-6_{eq}), 4.23 (2H, q, J = 7 Hz, OCH_2—CH_3), 5.65 (1H, s, =CH), 6.95 (1H, br s, disappears after exchange in D_2O, N*H*); *Mol. Wt.* calcd. for $C_{14}H_{21}NO_3$: 251.152; found (ms): 251.149.

The second isomer was not investigated further.

The *cis*-isomer **13** (0.8 g), eluted next, was crystallized from ether and melted at 158–159°C; ir ν_{max}($CHCl_3$): 3400 (NH), 1715 (ester), 1660 cm^{-1} (lactam); ^1H nmr, 90 MHz ($CDCl_3$) δ: 0.97 (3H, d, J = 6 Hz, CH—CH_3), 1.30 (3H, t, J = 7 Hz, —OCH_2—CH_3), 3.18 (1H, d of d, J = 4 and 15 Hz, probably H-6_{eq}), 3.83 (1H, q, better defined after D_2O exchange, J = 5 Hz, H-9), 4.20 (2H, q, J = 7 Hz, O$CH_2$$CH_3$), 5.82 (1H, s, =C*H*), 6.57 (1H, br s, disappeared after D_2O exchange, —N*H*); *Mol. Wt.* calcd. for $C_{14}H_{21}NO_3$: 251.152; found (ms): 251.153. *Anal.* calcd. for $C_{14}H_{21}NO_3$: C 66.91, H 8.42, N 5.57; found: C 66.81, H 8.44, N 5.39.

*Preparation of the 7-Methyl-5-carboethoxymethyloctahydro-2-quinolones (**15** and **16**)*

A solution of 7-methyl-5-carboethoxymethyleneoctahydro-2-quinolone (**13**) (232 mg, 0.92 mmol) in ethanol (15 mL) was treated with hydrogen at atmospheric pressure over Adams' catalyst (50 mg). The reaction was complete in 40 min, (H_2 absorbed: 22.0 mL; calcd: 20.7 mL). The catalyst was separated by decantation and the solvent removed by distillation. The product showed two spots on tlc on silica. Separation of the two components was achieved by column chromatography on silica (silica for tlc, 25 g). The first component (77 mg), designated **16**, was eluted from the column with ether–ethanol 9:1. After recrystallization from hexane it melted at 147–149°C; ir ν_{max}($CHCl_3$): 3400 (NH), 1730 (ester), 1660 cm^{-1} (lactam); ^1H nmr, 90 MHz ($CDCl_3$) δ: 0.90 (3H, d, J = 6 Hz, CHCH_3), 1.26 (3H, t, J = 7 Hz, —O$CH_2$$CH_3$), 3.71 (1H, q (better defined after D_2O exchange), J = 3 Hz, H-9), 4.14 (2H, q, J = 7 Hz, —O$CH_2$$CH_3$), 5.59 (1H, br s, disappears on D_2O exchange, N*H*); *Mol. Wt.* calcd. for $C_{14}H_{23}NO_3$: 253.168; found (ms): 253.168.

The second component (150 mg) designated **15**, melted at 112–113°C after recrystallization from hexane: ir $\nu_{max}CHCl_3$: 3400 (NH), 1730 (ester), 1660 (lactam); ^1H nmr, 90 MHz ($CDCl_3$) δ: 1.04 (3H, d, J = 7 Hz, CH—CH_3), 1.26 (3H, t, J = 7 Hz, —O$CH_2$$CH_3$), 3.62 (1H, m, changes to quintet after D_2O exchange; caused by superposition of two triplets, J = 6 and 12 Hz, H-9), 4.16 (2H, q, J = 7 Hz, O$CH_2$$CH_3$), 6.00 (1H, disappears on D_2O exchange, NH); *Mol. Wt.* calcd. for $C_{16}H_{23}NO_3$: 253.168; found (ms): 253.167.

*Preparation of 1,7-Dimethyl-5-carboethoxymethyleneoctahydro-2-quinolone (**17**)*

N-Isopropylcyclohexylamine (0.423 g, 3 mmol) in THF (50 mL) was treated with butyllithium (2.6 mmol) at −60°C under an atmosphere of argon. The mixture was stirred for 1 h and 7-methyl-5-carboethoxymethyleneoctahydro-2-quinolone (**13**) (625 mg, 2.5 mmol) was added and after another 0.5 h at −40°C, dimethyl sulfate (378 mg, 3 mmol) was added. The mixture was then allowed to warm to room temperature (it became cloudy but cleared again) and was kept at this temperature for an additional 3 h. Water (5 mL) and benzene (50 mL) were then added. The aqueous layer was separated and extracted again with benzene (10 mL). The combined benzene extract was dried, the benzene removed, and the residue subjected to column chromatography on silica with ether–ethanol 9:1 to separate *N*-isopropylcyclohexylamine and starting material from the methylation product. 1,7-Dimethyl-5-carbomethoxymethyleneoctahydro-2-quinolone (**17**) (410 mg, 62%), recrystallized from hexane, melts at 93–94°C; ir ν_{max} ($CHCl_3$): 1715 (unsaturated ester), 1630 cm^{-1} (lactam); ^1H nmr, 90 MHz ($CDCl_3$) δ: 0.94 (3H, d, J = 7 Hz, CHCH_3), 1.28 (3H, t, J = 7 Hz, —O$CH_2$$CH_3$), 2.92 (3H, s, N—$CH_3$), 3.55 (2H, d of t, J = 4 and 12 Hz, H-9 superimposed on another proton, probably H-10), 4.16 (2H, q, J = 7 Hz, O$CH_2$$CH_3$), 5.90 (1H, s, =C*H*); *Mol. Wt.* calcd. for $C_{15}H_{23}NO_3$: 265.168; found (ms): 265.169; *Anal.* calcd. for $C_{15}H_{23}NO_3$: C 67.90, H 8.74, N 5.28; found: C 68.41, H 8.49, N 5.13.

*Preparation of 1,7-Dimethyl-5-carboethoxymethyloctahydro-2-quinolones (**18** and **19**)*

A solution of 1,7-dimethyl-5-carboethoxymethyleneoctahydro-2-quinolone **17** (330 mg, 1.25 mmol) in ethanol (15 mL) was treated with hydrogen at atmospheric pressure over Adams' catalyst (75 mg). The reaction was complete in 0.5 h as judged by the completion of the uptake of hydrogen. The product obtained after removal of catalyst and solvent showed two spots on tlc on silica. The mixture was separated by column chromatography on silica (35 g, SiO_2 for tlc) using first ether and then ether with 5% ethanol as eluants. The first compound to be eluted, designated **19** (157 mg), melted at 61–62°C after recrystallization from hexane; ir ν_{max}($CHCl_3$): 1730 (ester), 1620 cm^{-1} (lactam); ^1H nmr, 90 MHz ($CDCl_3$) δ: 0.91 (3H, d, J = 6 Hz, CHCH_3), 1.26 (3H, t, J = 7 Hz, O$CH_2$$CH_3$), 2.93 (3H, s, N—$CH_3$), 3.58 (1H, apparent q, J = 3 Hz, H-9), 4.14 (2H, q, J = 7 Hz, O$CH_2$$CH_3$); *Mol. Wt.* calcd. for $C_{15}H_{25}NO_3$: 267.183; found (ms): 267.184.

The second isomer, **18** (154 mg) was a colorless oil; ir ν_{max}($CHCl_3$): 1730 (ester), 1620 cm^{-1} (lactam); ^1H nmr, 90 MHz ($CDCl_3$) δ: 1.07 (3H, d, J = 7 Hz, CHCH_3), 1.26 (3H, t, J = 7 Hz, —O$CH_2$$CH_3$), 2.92 (3H, s, N—$CH_3$), 3.44 (1H, d of t, J = 5 and 12 Hz, H-9), 4.15 (2H, q, J = 7 Hz, O$CH_2$$CH_3$); *Mol. Wt.* calcd. for $C_{15}H_{25}NO_3$: 267.183; found (ms): 267.181.

*(±)-Luciduline Lactam (**20**)*

N-Isopropylcyclohexylamine (71 mg, 0.5 mmol) in THF (20 mL) was treated with *n*-butyllithium (0.5 mmol) at −60°C in an atmosphere of argon and the mixture stirred for 0.5 h. 1,7-Dimethyl-5-carboethoxyethyloctahydro-2-quinolone **18** (135 mg, 0.5 mmol) in THF (10 mL) was then added. The solution was stirred for 0.5 h at −60°C, then allowed to warm to room temperature, and stirred for an additional 3 h. A few drops of acetic acid were then added and the solvent removed on the rotary evaporator. The residue was dissolved in benzene (50 mL) and washed with 5% hydrochloric acid (5 mL). The benzene extract was evaporated yielding luciduline lactam (100 mg, 90%) which melted at 97–99°C after crystallization from hexane; ir ν_{max}($CHCl_3$): 1730 (ketone), 1640 cm^{-1} (lactam); ^1H nmr, 90 MHz ($CDCl_3$) δ: 0.97 (3H, d, J = 6 Hz, CHCH_3), 2.99 (3H, s, N—CH_3), 3.33 (1H, m, H-3), 3.67 (1H, q, J = 3 Hz, H-6). *Mol. Wt.* calcd. for $C_{13}H_{19}NO_2$: 221.142; found (ms): 221.142.

(±)-Dihydroluciduline

Luciduline lactam (57 mg) was added to a suspension of lithium aluminum hydride (50 mg) in ether (20 mL) and the mixture boiled for 1 h. The excess lithium aluminum hydride was then decomposed with wet ether, the ether layer separated, and the residue extracted with benzene (5 mL). The combined organic extract was taken to dryness leaving a colorless oil that slowly solidified (49 mg). The crude solid residue was dissolved in ether and purified by filtration through alumina (5 g, activity III). Evaporation of the ether gave (±)-dihydroluciduline (30 mg, 63%) melting at 70–73°C. The ir (in $CHCl_3$), nmr (in benzene), the mass spectra of the synthetic sample and the tlc behaviour were identical with those of an authentic sample of dihydroluciduline prepared from luciduline by reduction with $NaBH_4$ (2).

(±)-Luciduline (1)

(±)-Dihydroluciduline (17 mg) in acetone (0.5 mL) was added to Jones' reagent (0.8 mL). The latter was prepared by dissolving CrO_3 (0.7 g) in 5 mL of H_2O and 1.2 mL 98% H_2SO_4 and adding this solution to 100 mL of acetone just before use. The reaction mixture was quenched with water (10 mL) after a period of 10 min, the solution was basified with sodium hydroxide and extracted with benzene (3 × 5 mL). The extract was taken to dryness and showed on tlc examination two spots corresponding to starting material and luciduline. Separation by chromatography on alumina yielded 13.6 mg of (±)-luciduline which had spectroscopic properties (ir in $CHCl_3$, nmr in benzene, and ms) and tlc behaviour identical with those of natural luciduline.

The hydrochloride of (±)-luciduline was prepared in acetone and after recrystallization melted at 238–239°C in a sealed capillary. Scott and Evans (3) report a melting point of 171–172°C and Oppolzer and Petrzilka (4) a melting point of 238–240°C.

Acknowledgements

We wish to thank Dr. A. A. Grey for providing the 220 MHz spectra and giving advice on their interpretation and Pierre Degré for assistance in the preparation of starting materials for this synthesis. We thank the National Research Council of Canada for financial support.

1. R. H. F. MANSKE and L. MARION. Can. J. Res. B, **24**, 57 (1946).
2. W. A. AYER, N. MASAKI, and D. S. NKUNIKA. Can. J. Chem. **46**, 3631 (1968).
3. W. L. SCOTT and D. A. EVANS. J. Am. Chem. Soc. **94**, 4779 (1972).
4. W. OPPOLZER and M. PETRZILKA. J. Am. Chem. Soc. **98**, 6722 (1976).
5. D. B. MACLEAN. *In* The alkaloids. *Edited by* R. H. F. Manske. Academic Press, New York. 1973. Vol. XIV, p. 348; 1968. Vol. X, p. 305.
6. L. NYEMBO, A. GOFFIN, C. HOOTELÉ, and J.-C. BRAEKMAN. Can. J. Chem. **56**, 851 (1978).
7. R. D. CLARK and C. H. HEATHCOCK. Synthesis, 74 (1974); J. Org. Chem. **41**, 636 (1976).
8. A. W. CROSSLEY and N. RENOUF. J. Chem. Soc. **107**, 602 (1915).
9. J. P. BLANCHARD and H. L. GOERING. J. Am. Chem. Soc. **73**, 5863 (1951).
10. H. O. HOUSE and W. F. FISCHER, JR. J. Org. Chem. **33**, 949 (1968).
11. H. REINSHAGEN. Justus Liebigs Ann. Chem. **681**, 84 (1965).
12. K. NOMURA, J. ADACHI, M. HANAI, S. NAKAYAMA, and K. MITSUHASHI. Chem. Pharm. Bull. **22**, 1386 (1974).
13. J. B. STOTHERS. Carbon-13 NMR spectroscopy. Academic Press, New York, NY. 1972. p. 173.
14. G. STORK. Pure Appl. Chem. **17**, 383 (1968).
15. N. L. ALLINGER and C. K. RIEW. Tetrahedron Lett. 1269 (1966).
16. D. J. PETERSON. J. Org. Chem. **33**, 780 (1968).
17. R. F. FESSENDEN and J. S. FESSENDEN. J. Org. Chem. **32**, 3535 (1967).
18. C. K. YU and D. B. MACLEAN. Can. J. Chem. **49**, 3025 (1971).

Isolation of ergovaline, ergoptine, and ergonine, new alkaloids of the peptide type, from ergot sclerotia[1,2]

RUDOLF BRUNNER, PETER LEOPOLD STÜTZ, HANS TSCHERTER, AND PAUL ALBERT STADLER

Chemical Research, Pharmaceutical Department, SANDOZ Ltd., CH-4002 Basle, Switzerland

Received December 6, 1978

RUDOLF BRUNNER, PETER LEOPOLD STÜTZ, HANS TSCHERTER, and PAUL ALBERT STADLER. Can. J. Chem. 57, 1638 (1979).

The isolation of three new ergot alkaloids of the peptide type from sclerotia of *Claviceps purpurea* and from mother liquors of rye ergot alkaloid extraction processes is described. The constitution of the new alkaloids ergovaline, ergoptine, and ergonine has been established by comparison with compounds previously obtained by total synthesis.

RUDOLF BRUNNER, PETER LEOPOLD STÜTZ, HANS TSCHERTER et PAUL ALBERT STADLER. Can. J. Chem. 57, 1638 (1979).

Trois nouveaux alcaloides de l'ergot de type peptidique ont pu être isolés à partir de sclérotes de *Claviceps purpurea* et à partir d'eaux mères accumulées après l'extraction d'autres alcaloides de l'ergot. La structure de ces nouveaux alcaloides ergovaline, ergoptine et ergonine a été etablie par comparaison à des produits obtenus auparavant par synthèse totale.

Genuine ergot alkaloids of the peptide type are found as pairs of diastereomers in nature. Their relative amounts depend strongly on the method of isolation, owing to an easy and reversible isomerization in position 8 of the lysergic acid moiety (1). Up to now seven pairs of alkaloids of the peptide type have been isolated from ergot sclerotia and also partly from mycelia of *Claviceps purpurea* fermentations (2–7). Systematically, ergot peptide alkaloids can be divided into three natural groups by their differing substituents (R) at position 2′ of the peptide moiety (Table 1) (see general structure **1**).

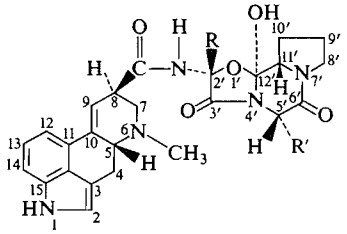

1

Of the ergotoxine group, with an isopropyl group at C-2′, four natural alkaloid pairs have been isolated from natural sources: ergocristine–ergocristinine (4), α-ergokryptine–α-ergokryptinine (5), β-ergokryptine–β-ergokryptinine (7), and ergocornine–ergocorninine (5).

Hitherto, in the ergotamine group only two alkaloid pairs have been isolated, ergotamine–ergotaminine (2) and ergosine–ergosinine (3). The ergoxine group has as yet been represented only by the pair ergostine–ergostinine (6).

The total synthesis of ergotamine, achieved some 15 years ago (8), may be regarded as a breakthrough for the total synthesis of new ergot alkaloids of the peptide type. All 12 alkaloid pairs listed in Table 1 have been synthesized following more or less the successful approach employed in the ergotamine total synthesis (6, 9–12).

The availability of synthetic samples of ergot peptide alkaloids also expected to occur in nature somewhat simplified the hunt for the missing links. In a systematic search crude alkaloid extracts of field harvests of new *Claviceps* strains, on the one hand, and mother liquors of the current peptide alkaloid extraction processes, on the other, were tested by paper chromatography for new alkaloids.

Ergovaline **2**

In 1967, an experimental field harvest of our *Claviceps purpurea* strain 235, grown on Swiss rye, produced a mixture of α- and β-ergokryptine, ergocornine, ergosine, and ergometrine as the main alkaloids; the presence of ergovaline in an amount of about 4% of the total alkaloid content was verified by chromatography.

Following the usual procedure, a combined crude alkaloid yield of 0.85% was obtained by extraction of the sclerotia. The main alkaloids mentioned above were separated by chromatography on alumina; some middle fractions probably contained ergovaline: analysis by paper chromatography revealed the presence of about 70% of ergosine and about 20%

[1]Dedicated to the memory of R. H. F. Manske.

[2]88th communication on ergot alkaloids. For part 87, see ref. 14.

0008-4042/79/131638-04$01.00/0

TABLE 1. Natural groups of ergot peptide alkaloids

R′	Ergotamine group R = CH_3	Ergoxine group R = C_2H_5	Ergotoxine group R = $CH(CH_3)_2$
$CH_2—C_6H_5$	Ergotamine	Ergostine	Ergocristine
$CH_2—CH(CH_3)_2$	Ergosine	Ergoptine†	α-Ergokryptine
$CHCH_3—C_2H_5$	β-Ergosine*	β-Ergoptine*	β-Ergokryptine
$CH(CH_3)_2$	Ergovaline†	Ergonine†	Ergocornine

NOTE: All names listed above correspond to those isomers with an equatorial carboxylic acid amide function at C-8 of the lysergic acid moiety; the 8-epimeric isomers derived from isolysergic acid, characterized by the ending -inine, are omitted here for the sake of simplicity.
*Not yet found in nature.
†Isolation reported in this paper.

of a new alkaloid with the same R_f values as synthetic ergovaline.

The isolation of ergovaline **2** on a preparative scale from this fraction proved to be a tedious task owing to its structural similarity to ergosine. Comparison of all chemical and physical properties of synthetic ergovaline with ergosine revealed practically no differences in solubilities, pK values, partition coefficients, and chromatographic behavior on silica gel thin-layer plates.

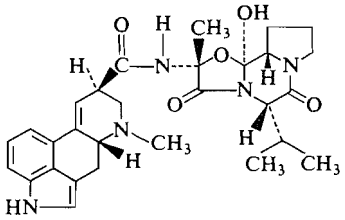

Ergovaline, **2**

After testing several chromatographic systems on alumina thin-layer plates, it was found that the two alkaloids showed a slight R_f difference of 0.06 in a solvent mixture of ethyl acetate – n-butanol 9:1. Column chromatography on alumina using this mixture permitted sufficient enrichment of the new alkaloid for further purification to be effected by crystallization.

Natural ergovaline **2** melted at 207–208°C (dec.) in contrast to the reported (9) melting point of synthetic ergovaline (177–178°C, dec.). Yet after a few recrystallizations of an original sample of synthetic ergovaline from ethyl acetate, its melting point could be raised to a constant 209–210°C (dec.). This phenomenon can be attributed to dimorphism, often observed with ergot alkaloids. Otherwise the specimen of ergovaline isolated from *Claviceps purpurea* sclerotia was completely identical with a sample originating from total synthesis.

Ergoptine 3, Ergonine 4

Ergoptine **3** and ergonine **4** are members of the ergoxine group of ergot peptide alkaloids, hitherto represented only by ergostine, sometimes accompanying ergotamine as a minor constituent (≦0.5%) in nature (6). As a working hypothesis it was therefore assumed that these alkaloids might occur in ergokryptine–ergocornine-producing strains. Indeed, after thorough analysis of all types of mother liquors derived from technical ergokryptine–ergocornine extraction plants, a few revealed the presence of ergoptine and ergonine, previously obtained by synthesis (11), in the alkaloid mixture.

For example, in the isolation of ergoptine **3** a

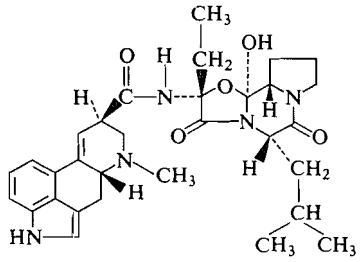

Ergoptine, **3**

mother liquor with an estimated content of about 10% served as starting material. Its main constituent, about 40%, was ergocornine which could be partially separated by two consecutive chromatographic steps. Synthetic ergoptine gives a well crystallizing and more sparingly soluble salt with di-*p*-toluyl-L-tartaric acid than ergocornine. Thus, a fraction containing about 80% ergoptine, could be further purified as the above mentioned salt. Subsequent chromatography of the base on a silica gel column followed by crystallization from acetone–water gave pure natural ergoptine **3**, identical in all respects with a synthetic specimen.

For the isolation of ergonine **4** a mother liquor consisting of almost 90% ergosine and about 10% ergonine was at hand. Again, the different solubilities of the di-*p*-toluyl-L-tartrates of ergosine and ergonine in methanol could be exploited for their separation,

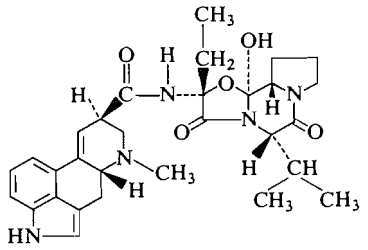

Ergonine, **4**

the salt of the latter being more soluble. Therefore, most of the ergosine present could be removed in pure form. The mother liquors, enriched in ergonine, were subjected to further purification as free base by column chromatography on alumina. Crystallization from ethanol – diisopropyl ether finally led, with great losses, to pure, natural ergonine **4**, identical with a synthetic specimen.

The separatory procedures described above do not, of course, provide a basis for accurate estimation of the relative amounts of **3** and **4** occurring in raw alkaloid extracts obtained from ergokryptine–ergocornine-producing strains. Very approximately, the concentration of ergoptine may be assumed not to exceed 0.5% of the total alkaloids present, whereas the ergonine concentration is even lower, probably in the region of 0.1%. The occurrence of ergovaline **2** in certain strains of *Claviceps purpurea* appears to be only sporadic.

Experimental

Owing to decomposition, melting points of ergot alkaloids were determined on a Tottoli apparatus in high vacuum and are uncorrected. Ultraviolet (uv) spectra were recorded on a Beckman spectrophotometer, model DK 2, in dichloromethane solution. The wavelengths of absorption maxima are reported in nanometers (nm) with log ε values in parentheses. Infrared (ir) spectra were measured on a Perkin Elmer model 21 spectrophotometer. The absorption maxima are reported in wavenumbers (cm^{-1}). Proton magnetic resonance (^{1}Hmr) spectra were measured on a Varian high resolution spectrometer. Chemical shift values are given in the δ (ppm) scale relative to tetramethylsilane (TMS) used as internal standard. The integrated peak areas, signal multiplicities, and eventual proton assignments are given in parentheses. Low resolution mass spectra (ms) were determined on an AEI-MS-30 spectrometer, high resolution ms on a CEC-21-110B apparatus.

Ergovaline **2**

Sclerotia (1.4 kg) of *Claviceps purpurea* (strain No. 235, grown in the summer of 1967 on rye in an experimental field in the outskirts of Basle were ground and consequently defatted by extraction with petrol ether (2 × 5 L). The dark violet residue was extracted with a mixture of 70% acetone and 30% water containing 5% tartaric acid (4 × 5 L). The extracts were concentrated *in vacuo* at 50°C to a volume of 5 L, removing practically all acetone. The acidic solution was rendered alkaline by addition of Na_2CO_3, extracted with ethyl acetate (3 × 5 L), washed with water, dried (Na_2SO_4), and evaporated at 50°C *in vacuo*. The raw residue (12 g) showed a total alkaloid content of 40% on colorimetric determination (reagent of Van Urk (15)); semiquantitative determination of the alkaloids by paper chromatography gave ergometrine (7%), ergometrinine (1%), ergosine (14%), ergosinine (3%), ergocristine (5%), α- and β-ergokryptine (26%), ergocornine (26%), mixture of ergotoxinine (12%), and a new alkaloid (4%) with the same R_f values as synthetic ergovaline.

Chromatography of the raw extract (12 g) on alumina (600 g, activity II) afforded fraction 1 (chloroform – 0.5% methanol, 5 g, ergotoxine alkaloids, discarded), fraction 2 (chloroform – 1.5% methanol, 1.5 g, ergosine and new alkaloid), and fraction 3 (chloroform – 3% methanol, 0.6 g, ergometrine, discarded). Chromatography of fraction 2 (1.5 g) on alumina (100 g) gave a purified fraction 2 (chloroform – 1.5% methanol, 0.7 g, colorimetric alkaloid content 80%, paper chromatography: ergosine, 70%, and the new alkaloid, 30%). Chromatography of purified fraction 2 (0.7 g) on alumina (420 g, DS-O Camag, activity I, elution with ethyl acetate – *n*-butanol 9:1, fractions of 20 mL) gave the following fractions. Fraction 6 (15 mg), rest of ergokryptine and ergocornine, discarded. Fractions 7–10 (382 mg) primarily ergosine, discarded. Fractions 11–13 (199 mg), containing the new alkaloid, were combined and purified by crystallization: natural ergovaline **2** (60 mg); mp 207–208°C (ethyl acetate), mixture mp 207–208°C (synthetic ergovaline mp 207–208°C (ethyl acetate)); $[\alpha]_D^{20}$ −172° (*c* 0.5, chloroform); uv λ_{max}: 237 (4.3), 307 (3.95); ir (dichloromethane) ν_{max}: 3466, 1727, 1666 (sh), 1650; ^{1}Hmr (DMSO) δ: 10.8 (1H, s, N1-H), 9.37 (1H, s, CONH), 7.0–7.3 (4H, m, aromatic H), 6.75 (1H, d, J = 2 Hz, OH), 6.33 (1H, s, C9-H), 4.31 (1H, d, J = 5 Hz, C5′-H), 2.53 (3H, s, N6-CH_3), 1.7–3.9 (~14H, m), 1.58 (3H, s, C2′-CH_3), 1.08 (6H, d, J = 7 Hz, $CH(CH_3)_2$). *Exact Mass* calcd. for $C_{29}H_{35}N_5O_5$: 533.2638; found (ms): 533.2602.

Ergoptine **3**

A mother liquor (251 g) of the ergokryptine–ergocornine production with a total alkaloid content of about 80% (determined colorimetrically with the reagent of Van Urk) was chromatographed on alumina (8 kg, activity II). Elution with chloroform and 0.3% methanol led to a first fraction (110 g) which consisted primarily of ergokryptine and ergocornine and was not further considered. A second fraction (95 g) was obtained on elution with chloroform and 0.6% methanol which contained on analysis by paper chromatography about 25% ergoptine. This fraction was chromatographed again on alumina (3 kg, activity II). A first fraction obtained on elution with chloroform and 0.3% methanol again contained ergokryptine and ergocornine and was discarded. Elution with chloroform and 0.6% methanol gave a second fraction (23 g). Its analysis by paper chromatography revealed a content of about 80% ergoptine **3**, 5% ergonine **4**, and 15% ergotoxine alkaloids. For the isolation of ergoptine this fraction was converted into the salt with di-*p*-toluyl-L-tartaric acid. The fraction (23 g, ~40 mmol) was dissolved in methanol (230 mL), a solution of di-*p*-toluyl-L-tartaric acid (17 g, 44 mmol) in methanol (170 mL) was added whereupon the salt (30 g, 31.6 mmol) crystallized. Being too poorly soluble to be recrystallized in a reasonable amount of solvent, the salt (30 g) was cleaved by partition between chloroform – 2 *N* Na_2CO_3 giving an amorphous resin (17.2 g, 30.6 mmol) which was again converted into the salt with di-*p*-toluyl-L-tartaric acid by the same procedure. The salt (27.3 g, 28.8 mmol) thus obtained, mp 177–178°C, was cleaved by partition in chloroform – 2 *N* Na_2CO_3 and afforded 15.2 g (27 mmol) base, purity about 95%. Further purification of that base by chromatography on a column of silica gel (700 g, Merck, 70–230 mesh, ASTM) followed by crystallization from acetone–water 7:3 yielded homogeneous ergoptine **3** (7.8 g); mp 198–199°C, mixture mp 199–200°C (synthetic ergoptine mp 199–200°C);

$[\alpha]_D^{20}$ −188° (*c* 0.8, chloroform); uv λ_{max}: 238 (4.34), 308 (3.98); ir (dichloromethane) ν_{max}: 3470, 3150–3300, 1732, 1671 (sh), 1653; ^{1}Hmr ($CDCl_3$) δ: 9.58 (1H, s, N1-H), 8.17 (1H, s, CONH), 7.1–7.3 (3 + 1H, m aromatic H, OH), 6.99 (1H, s, C2-H), 6.34–6.5 (1H, m, C9-H), 4.58 (1H, t, J = 6 Hz, C5′-H), 2.8–4 (~9H, m, C4-H, C5-H, C7-H, C8-H, C8′-H, C11′-H), 2.68 (3H, s, C6-CH_3), 1.7–2.4 (~9H, m, C2′-CH_2, C5′-CH_2, C9′-CH_2, C10′-CH_2, side-chain CH), 1.9–2.2 (9H, m, side-chain CH_3). *Exact Mass* calcd. for $C_{31}H_{39}N_5O_5$: 561.2951; found (ms): 561.2875.

Ergonine 4

A mother liquor (2.9 g, ~5.3 mmol) of an ergokryptine–ergocornine-producing strain of *Claviceps purpurea* was shown by paper chromatography to consist of almost 90% ergosine and 10% ergonine. For the removal of ergosine the mother liquor was dissolved in a mixture of dichloromethane (15 mL) and methanol (15 mL) and a solution of di-*p*-toluyl-L-tartaric acid (1.87 g, 4.84 mmol) in methanol (20 mL) was added. The resulting salt of di-*p*-toluyl-L-tartaric acid with ergosine crystallized on concentration of the solution *in vacuo*. Recrystallization of the salt from dichloromethane–methanol yielded ergosine di-*p*-toluyl-L-tartrate (2.47 g, 2.65 mmol), mp 184–185°C, chromatographic purity 99%. The mother liquors were recrystallized several times from dichloromethane–methanol giving additional ergosine di-*p*-toluyl-L-tartrate (0.94 g, 1 mmol), mp 181–182°C. The combined mother liquors of the salt were cleaved by partition between dichloromethane and 2 *N* Na_2CO_3 and the resulting base (670 mg) chromatographed on alumina (67 g, activity II). With dichloromethane and 0.3% methanol the ergonine containing fractions were eluted from the column. Further purification was performed by crystallization from a little ethanol and diisopropylether and yielded natural ergonine **4** (20 mg), chromatographic purity 99%; mp 206–207°C, mixture mp 206–207°C (synthetic ergonine mp 207–208°C); uv λ_{max}: 238 (4.31), 307.5 (3.95); ir (dichloromethane) ν_{max}: 3460, 1728, 1668 (sh), 1649; ^{1}Hmr ($CDCl_3$) δ: 9.05 (1H, s, N1-H), 8.2 (1H, s, CONH), 7.0–7.3 (3 + 1H, m, aromatic H, OH), 6.9 (1H, s, C2-H), 6.2–6.5 (1H, m, C9-H), 4.4 (1H, d, J = 5 Hz, C5′-H), 1.5–4.0 (~16H, m), 2.6 (3H, s, N6-CH_3), 1.15 (3 + 3H, d, J = 7 Hz, $CH(CH_3)_2$), 0.91 (3H, t, J = 7 Hz, CH_2—CH_3). *Mol. wt.* calcd. for $C_{30}H_{37}N_5O_5$: 547; found (field desorption): 547.

1. A. Stoll, A. Hofmann, and F. Troxler. Helv. Chim. Acta, **32**, 506 (1949).
2. A. Stoll. Swiss Patent No. 79879 (Apr. 1918); Helv. Chim. Acta, **28**, 1283 (1945).
3. S. Smith and G. M. Timmis. J. Chem. Soc. 396 (1937).
4. A. Stoll and E. Burckhardt. Hoppe-Seyler's Z. Physiol. Chem. **250**, 1 (1937).
5. A. Stoll and A. Hofmann. Helv. Chim. Acta, **26**, 1570 (1943).
6. W. Schlientz, R. Brunner, P. A. Stadler, A. J. Frey, H. Ott, and A. Hofmann. Helv. Chim. Acta, **47**, 1921 (1964).
7. W. Schlientz, R. Brunner, A. Rüegger, B. Berde, E. Stürmer, and A. Hofmann. Experientia, **23**, 991 (1967).
8. A. Hofmann, A. J. Frey, and H. Ott. Experientia, **17**, 206 (1961); P. A. Stadler, A. J. Frey, and A. Hofmann. Helv. Chim. Acta, **46**, 2300 (1963); A. Hofmann, H. Ott, R. Griot, P. A. Stadler, and A. J. Frey. Helv. Chim. Acta, **46**, 2306 (1963).
9. P. A. Stadler, A. J. Frey, H. Ott, and A. Hofmann. Helv. Chim. Acta, **47**, 1911 (1964).
10. P. A. Stadler, S. Guttmann, H. Hauth, R. L. Huguenin, E. Sandrin, G. Wersin, H. Willems, and A. Hofmann. Helv. Chim. Acta, **52**, 1549 (1969).
11. P. Stütz, P. A. Stadler, and A. Hofmann. Helv. Chim. Acta, **53**, 1278 (1970).
12. P. A. Stadler, P. Stütz, and E. Stürmer. Experientia, **33**, 1552 (1977).
13. A. Stoll and A. Hofmann. Helv. Chim. Acta, **26**, 922 (1943).
14. P. L. Stütz, P. A. Stadler, J.-M. Vigouret, and A. Jaton. J. Med. Chem. **21**, 754 (1978).
15. H. W. Van Urk. Pharm. Weekblad, **66**, 473 (1929).

Splendidine, a new oxoaporphine alkaloid from *Abuta rufescens* Aublet[1]

JERRY W. SKILES, JOSE M. SAA, AND MICHAEL P. CAVA
Department of Chemistry, University of Pennsylvania, Philadelphia, PA 19104, U.S.A.

Received October 30, 1978

JERRY W. SKILES, JOSE M. SAA, and MICHAEL P. CAVA. Can. J. Chem. 57, 1642 (1979).

The oxoaporphine alkaloids lysicamine, homomoschatoline, imenine, and splendidine have been isolated from *Abuta rufescens* Aublet (=*Abuta splendida* Krukoff and Moldenke). Splendidine has been shown to be 1,2,4-trimethoxy-7*H*-dibenzo[*de*,*g*]quinolin-7-one (**1**) by total synthesis.

JERRY W. SKILES, JOSE M. SAA et MICHAEL P. CAVA. Can. J. Chem. 57, 1642 (1979).

On a isolé les alcaloïdes oxoaporphines, lysicamine, homomoschatoline, imenine et splendidine à partir du *Abuta rufescens* Aublet (=*Abuta splendida* Krukoff et Moldenke). On a démontré, par synthèse, que la structure de la splendidine est la triméthoxy-1,2,4 7*H*-dibenzo-[*de*,*g*]quinoléinone-7 (**1**).

[Traduit par le journal]

As part of a broad search for anticancer agents in the South American *Menispermaceae*, we recently described the isolation of several bisbenzylisoquinoline alkaloids from the Amazonian species, *Abuta rufescens* (=*Abuta splendida* (1))[2]. We now report the isolation of several oxoaporphines from this plant, including the new alkaloid splendidine, and the proof of structure **1** for splendidine by total synthesis.

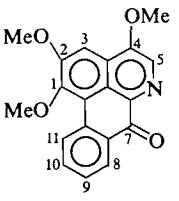

1

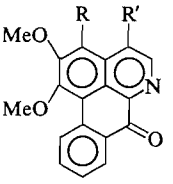

2 R = R′ = H
3 R = OMe; R′ = H
4 R = R′ = OMe

Isolation of Splendidine

The most weakly basic alkaloidal fraction from *Abuta rufescens* (=*A. splendida*) contained a complex mixture of highly colored compounds, the four major components of which were separated by dry-column silica chromatography. Three of these compounds proved to be the known oxoaporphine alkaloids lysicamine (**2**), homomoschatoline (**3**), and imenine (**4**) (3). The fourth compound was the new yellow crystalline alkaloid splendidine, mp 235°C, for which structure **1** was proposed on the basis of spectroscopic data (*vide infra*).

The high-resolution mass spectrum of splendidine established its composition as $C_{19}H_{15}NO_4$. Its ultraviolet spectrum in ethanol (λ_{max} 237, 270, 290sh, and 415 nm), which showed no alkaline bathochromic shift, was characteristic of a typical nonphenolic 7-oxoaporphine (4), as was its infrared carbonyl band at 1665 cm^{-1}.

The nmr spectrum of splendidine showed its three noncarbonyl oxygens to be present in the form of well-resolved methoxyls at δ 4.01, 4.10, and 4.21. Of the six aromatic protons present, only the two at δ 7.56 and 8.47 were singlets; the remaining four formed a multiplet characteristic of an oxoaporphine unsubstituted on the lower ring (i.e., compounds **2**–**4**). Significantly, the typical AB quartet (J = 5.5–6.0 Hz) due to the C(4)—C(5) protons of an oxoaporphine was not present, suggesting that splendidine might be the second example (after imenine) of a 4-oxygenated 7-oxoaporphine. Since all naturally-occurring aporphines are oxygenated at C(1) and C(2), structure **1** seemed appropriate for splendidine and its confirmation was sought by total synthesis.

Synthesis of Splendidine

The key intermediate for the synthesis of splendidine was the hitherto unreported 4-hydroxy-6,7-dimethoxyisoquinoline (**6**), which was prepared in two fundamentally different ways from the readily available 4-hydroxy-6,7-dimethoxy-1,2,3,4-tetrahydroisoquinoline (**5**) (5). The first method illustrates a basically new synthesis of 4-hydroxyisoquinolines. Thus, amino alcohol **5** was selectively tosylated by 1 equiv. of tosyl chloride in pyridine solution to give,

[1]Dedicated to the memory of Dr. R. H. F. Manske.

[2]*Abuta splendida* has been very recently reduced to synonymy of *Abuta rufescens* (2). According to B. A. Krukoff (private communication), the identification of the plant previously examined by us phytochemically and cited as *A. rufescens* (3) cannot be verified as apparently no voucher was deposited by a Brazilian collector anywhere.

0008-4042/79/131642-05$01.00/0

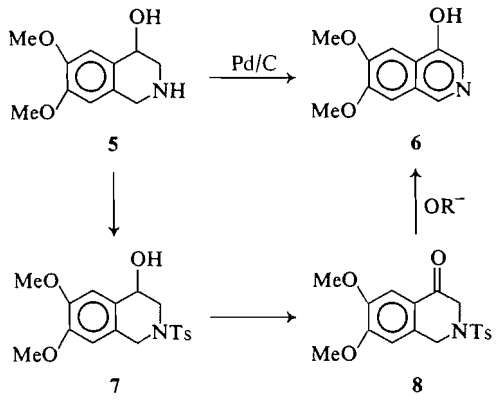

in high yield (92%), the *N*-tosyl alcohol **7**. Oxidation of the latter by Collins' reagent gave (63%) the *N*-tosyl ketone **8**, which underwent elimination of *p*-toluenesulfinic acid on treatment with potassium *tert*-butoxide to give the desired phenol **6** in 76% yield. The second method of converting alcohol **5** to phenol **6** involved direct catalytic dehydrogenation, using 10% palladium-on-charcoal catalyst. When this reaction was carried out under conditions reported earlier for a closely related alcohol (*p*-cymene at 140–145°C) (6), the yield of phenol **6** was poor (10–12%); when dimethylformamide was used as the solvent, however, the yield of **6** rose to 57%.

Reaction of phenol **6** with diazomethane afforded 4,6,7-trimethoxyisoquinoline (**9**), which was converted by potassium cyanide and benzoyl chloride into 2-benzoyl-1,2-dihydro-4,6,7-trimethoxyisoquinaldonitrile (**10**). Alkylation of Reissert compound **10** by *o*-nitrobenzyl chloride under phase-transfer conditions (7) gave 2-benzoyl-1,2-dihydro-1-(*o*-nitrobenzyl)-4,6,7-trimethoxyisoquinaldonitrile (**11**) in good yield (61%), in addition to a lesser amount (20%) of the difficultly separated 1-cyano-4,6,7-trimethoxyisoquinoline (**12**). Reaction of the alkylated Reissert compound **11** with Triton B in dimethylformamide (8) gave a mixture of nitrile **12** (>33%) and 1-(*o*-nitrobenzyl)-4,6,7-trimethoxyisoquinoline (**13**, ca. 58%). The latter nitro compound, which could not be separated completely from nitrile **12**, was reduced by Adams' catalyst in methanol. The resulting oily amine (**14**) was directly diazotized and subjected to Pschorr cyclization under conditions favorable to 7-oxoaporphine formation (3). Chromatographic purification gave, in 19% yield, yellow needles of 1,2,4-trimethoxy-7*H*-dibenzo[*de*,*g*]quinolin-7-one (**1**), which proved to be identical with splendidine from *Abuta rufescens* (=*Abuta splendida*).

Experimental

Melting points are uncorrected. Elemental analyses were carried out by Midwest Microlabs, Indianapolis, IN. Nuclear magnetic resonance spectra were determined in $CDCl_3$ solution with Me_4Si as internal standard using Varian A-60A, HA-100D, and HA-220 instruments. Infrared (KBr), ultraviolet (ethanol), and low-resolution mass spectra were determined using Perkin-Elmer Models 137, 202, and 270B instruments, respectively. *Abuta rufescens* (=*Abuta splendida*) (*Schunke 1971/38*) was collected by J. Schunke in Mariscal

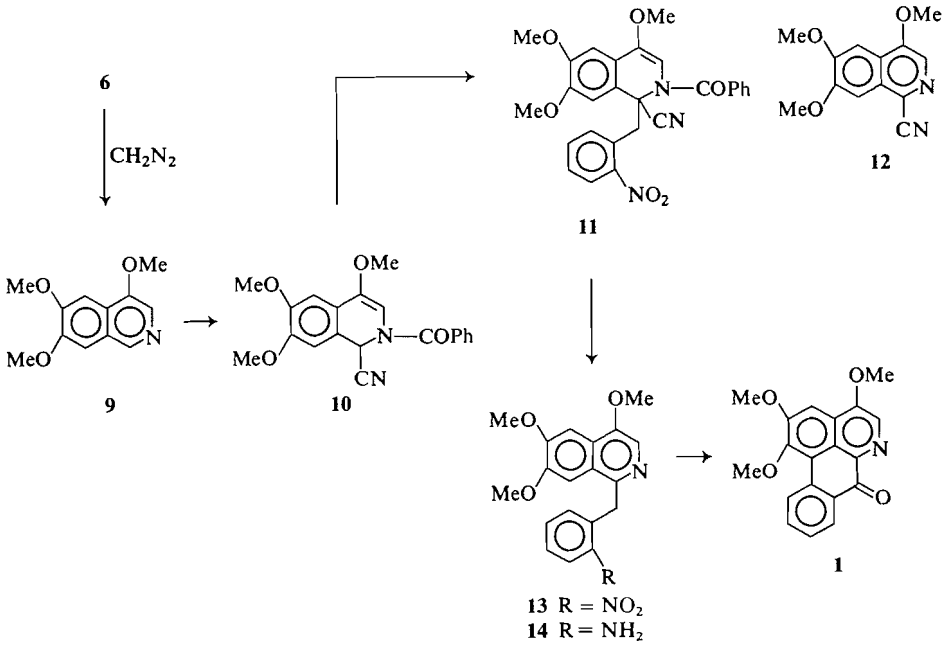

Caceres, Tocache Nuevo, Department of San Martin, Peru, and identified by B. A. Krukoff. A voucher specimen has been deposited at the New York Botanical Garden and other institutions.

Isolation of Lysicamine (2), Homomoschatoline (3), Imenine (4), and Splendidine (1) from Abuta rufescens *(=*Abuta splendida*)*

The extraction and countercurrent distribution (200 transfers) of the total alkaloidal material used here has been described earlier. In the presently reported study, the highly colored and weakly basic alkaloids of tube fractions 171 and 175 were combined and 2.4 g of the mixture was subjected to dry-column silica chromatography, using ethyl acetate as the developer solvent. Good band separation resulted only after running the developer through the column for several hours. The column was then cut into bands A–E, which were individually extracted with chloroform–methanol.

Bands A and B contained the same major constituent, homomoschatoline (**3**, 1.0 g), which crystallized from ethyl acetate as orange prisms, mp 181–182°C, identical (mp, ir, nmr) with synthetic material (3).

Band C afforded an orange mixture of bases (0.130 g) which were not identified.

Band D was a mixture (0.780 g) of two components which could not be separated by repeated chromatography. The components were separated readily, however, by partitioning the mixture between chloroform and 5% aqueous sulfuric acid. The chloroform phase, on evaporation and crystallization of the residue from acetone, gave yellow needles of imenine (**4**), mp 205–206°C, identical (mp, ir, uv, nmr) with authentic material (3, 6). The aqueous acid phase was made basic and extracted with chloroform. Evaporation of the solvent and crystallization from acetone–chloroform gave yellow crystals of lysicamine (**2**), mp 207–208°C, identical (mp, ir, uv, mass spectrum) with authentic material (9).

Band E formed the purple-green segment at the top of the silica column. The extract of this band was rechromatographed (silica, ethyl acetate developer) to give, after crystallization from methanol–chloroform, bright yellow needles of splendidine (**1**, 0.100 g), mp 235°C; ir (KBr) 1665 cm^{-1}; uv (EtOH) λ_{max} (log ε): 237 (4.36), 270 (4.34), 290sh (4.15), 415 nm (4.05); nmr δ: 4.01 (s, 3H, OCH_3), 4.10 (s, 3H, OCH_3), 4.21 (s, 3H, OCH_3), 7.51 (t, 1H, $J_{8,9} = J_{9,10} = 8.75$ Hz, C(9)-H), 7.56 (s, 1H, C(3)-H), 7.69 (t, 1H, $J_{9,10} = J_{10,11} = 8.75$ Hz, C(10)-H), 8.47 (s, 1H, C(5)-H), 8.54 (d, 1H, $J_{8,9} = 8.75$ Hz, C(8)-H), 9.13 (d, 1H, $J_{10,11} = 8.75$ Hz, C(11)-H); ms *m/e* (relative intensity): 321 (M^+, 100), 306 (14), 291 (6), 278 (65), 263 (29), 248 (8), 235 (14), 220 (28), 207 (11), 192 (11), 164 (22), 160.5 (5), 150 (10); high-resolution mass spectrum *m/e* calcd. for $C_{19}H_{15}NO_4$: 321.1001; found: 321.1021.

1,2,3,4-Tetrahydro-6,7-dimethoxy-2-(p-*toluenesulfonyl)-4-isoquinolinol (7)*

4-Hydroxy-6,7-dimethoxyisoquinoline (**5**, 3.28 g, 15.6 mmol) was dissolved in dry pyridine (25 mL) and the resulting solution was cooled in an ice bath. Freshly recrystallized tosyl chloride (3.43 g, 18.0 mmol) was added portionwise and the mixture was stirred at 5 to 10°C for 2 h and then placed in a refrigerator overnight. Most of the solvent was evaporated and the residue was diluted with water. The product was extracted several times into chloroform. The extract was washed with 5% HCl, 5% $NaHCO_3$, and water. The solvent was dried ($MgSO_4$) and evaporated to yield a colorless solid which was recrystallized from ether to afford colorless needles of **7** (5.2 g, 92%), mp 132–134°C; nmr δ: 2.39 (s, 3H, CH_3), 2.96–3.55 (m, 3H), 3.77 (s, 6H, 2 × OCH_3), 4.05 (br s, 1H), 4.24 (br s, 1H), 4.69 (br s, 1H, OH), 6.53 (s, 1H), 6.93 (s, 1H), 7.32 (d, 2H, $J = 8.5$ Hz), 7.74 (d, 2H, $J = 8.5$ Hz). *Anal.* calcd. for $C_{18}H_{21}NO_5S$: C 59.50, H 5.79, N 3.86, S 8.82; found: C 59.74, H 5.65, N 3.85, S 8.74.

2,3-Dihydro-6,7-dimethoxy-2-(p-*toluenesulfonyl)-4(1H)-isoquinolone (8)*

Chromium trioxide (9.42 g, 0.0942 mol) was added to a magnetically stirred solution of freshly distilled dry pyridine (14.7 mL, 0.188 mol) in pure methylene chloride (240 mL). The flask was stoppered with a drying tube containing Drierite and the deep burgundy solution was stirred for 15 min at room temperature. At the end of this period a solution of alcohol **7** (4.351 g, 0.012 mol) in a small volume of methylene chloride was added in one portion. A black deposit separated immediately. After stirring an additional 15 to 20 min at room temperature, the solution was decanted from the residue and the residue was washed with methylene chloride (200 mL). The combined organic solution was washed with 100 mL of 5% aqueous NaOH, 100 mL of 5% aqueous HCl, 100 mL of 5% aqueous $NaHCO_3$, 100 mL of saturated NaCl, and dried ($MgSO_4$). Evaporation of the solvent gave a colorless solid which was recrystallized from methanol to afford colorless cubes of **8** (2.7 g, 62.4%), mp 153–154°C; ir (KBr): 1686 (C=O), 1342 (SO_2), 1167 cm^{-1} (SO_2); nmr δ: 2.39 (s, 3H, CH_3), 3.88 (s, 3H, OCH_3), 3.96 (s, 5H, OCH_3 and CH_2), 4.51 (s, 2H, CH_2), 6.79 (s, 1H), 7.33 (d, 2H, $J = 8.0$ Hz), 7.38 (s, 1H), 7.74 (d, 1H, $J = 8.0$ Hz). *Anal.* calcd. for $C_{18}H_{19}NO_5S$: C 59.81, H 5.31, N 3.88, S 8.87; found: C 59.88, H 5.66, N 3.72, S 8.76.

4-Hydroxy-6,7-dimethoxyisoquinoline (6)

Ketone **8** (477 mg, 1.30 mmol) was dissolved in dry *tert*-butyl alcohol (25 mL). The solution was heated to reflux and potassium *tert*-butoxide (0.310 g) was added in one portion. The resulting mixture was placed under nitrogen and heated at reflux for 4 h. The solution was cooled, water (10 mL) was added, the organic solvent was evaporated, and additional water (25 mL) was added. The solution was neutralized (NH_4Cl) and the product was extracted into chloroform. The extract was washed (water), dried ($MgSO_4$), and evaporated to give a residue which crystallized from methanol to give prisms of **6** (206 mg, 76%), 243–245°C; nmr δ: 4.01 (s, 3H, OCH_3), 4.03 (s, 3H, OCH_3), 7.52 (s, 1H), 7.60 (s, 1H), 8.16 (s, 1H, C(1)-H), 8.79 (s, 1H, C(3)-H). *Anal.* calcd. for $C_{11}H_{11}NO_3$: C 64.39, H 5.37, N 6.83; found: C 64.45, H 5.40, N 6.75.

The phenol **6** was also prepared directly from the tetrahydroisoquinoline **5**. Alcohol **5** (10.0 g, 0.0478 mol) was dissolved in dimethylformamide (200 mL) and 10% palladium-on-carbon (2.0 g) was added. The mixture was heated for 5 h at reflux under argon. The catalyst was filtered off and the solvent was evaporated to give a dark gummy residue. On scratching under methanol the product crystallized as slightly green prisms, which were recrystallized from methanol (Soxhlet) to give light colored prisms (5.12 g, 52%), mp 243–245°C.

4,6,7-Trimethoxyisoquinoline (9)

A distilled solution of diazomethane in ether (85 mL) was prepared in the usual way from *N*-methyl-*N*-nitroso-*p*-toluenesulfonamide (Diazald, 8.0 g, 0.0372 mol) and added to a cold solution of phenol **6** (2.05 g, 0.010 mol) in 1:1 methanol–dioxane (50 mL).

The resulting mixture was lightly corked and allowed to stand overnight in the dark at room temperature. Excess diazomethane was destroyed with a few drops of glacial acetic acid and the solvent was evaporated. The residue was basified to pH 8 to 9 with 10% ammonium hydroxide and the product was extracted into chloroform. The extract was washed

successively with 10% NaOH and water. The solvent was dried over magnesium sulfate, filtered, and evaporated to give light colored needles which were filtered and washed with a small amount of cold ether to give **9** (2.14 g, 98%). The product was recrystallized from methanol to give needles, mp 166–167°C; nmr δ: 3.98 (s, 3H, OCH_3), 4.01 (s, 3H, OCH_3), 4.03 (s, 3H, OCH_3), 7.17 (s, 1H), 7.43 (s, 1H), 8.77 (s, 1H). *Anal.* calcd. for $C_{12}H_{13}NO_3$: C 65.75, H 5.94, N 6.39; found: C 65.80, H 5.93, N 6.34.

*2-Benzoyl-1,2-dihydro-4,6,7-trimethoxyisoquinaldonitrile (**10**)*

To 4,6,7-trimethoxyisoquinoline (**9**, 2.204 g, 0.010 mol) in methylene chloride (25 mL) was added potassium cyanide (1.95 g, 0.030 mol) in water (10 mL). The resulting mixture was cooled in an ice bath and benzoyl chloride (2.82 g, 0.020 mol) in methylene chloride (15 mL) was added dropwise over 15 min. The resulting mixture was stirred at ice temperature for 1 h and then at room temperature for an additional 4 h. Water (50 mL) was added and the layers were separated. The organic layer was washed with water, 10% HCl, 10% NaOH, again with water, and dried (Na_2SO_4). Filtration followed by removal of the solvent gave a brown gum which on scratching under methanol afforded the Reissert compound **10** as colorless needles (1.84 g, 52.1%). The analytical sample was crystallized from ethanol to give colorless needles, mp 150–151°C; nmr δ: 3.72 (s, 3H, C(4)-OCH_3), 3.92 (s, 3H, OCH_3), 3.95 (s, 3H, OCH_3), 6.14 (br s, 1H, C(3)-H), 6.63 (br s, 1H, C(1)-H), 6.98 (s, 1H), 7.22 (s, 1H), 7.38–7.86 (m, 5H, OCOPh). *Anal.* calcd. for $C_{20}H_{18}N_2O_4$: C 68.57, H 5.14, N 8.00; found: C 68.53, H 5.11, N 7.71.

*2-Benzoyl-1,2-dihydro-4,6,7-trimethoxy-1-(o-nitrobenzyl)isoquinaldonitrile (**11**)*

In a 100-mL three-necked flask, fitted with a serum cap and a gas inlet adapter extending to the bottom of the flask, were placed 2-benzoyl-1,2-dihydro-4,6,7-trimethoxyisoquinaldonitrile (**10**, 1.203 g, 3.44 mmol), *o*-nitrobenzyl chloride (0.600 g, 3.50 mmol), and 50 mg of phase-transfer catalyst (cetrimonium bromide). Benzene (50 mL) was added and argon was bubbled through the solvent for 10 min. Sodium hydroxide (10 mL of a 50% by weight aqueous solution) was added in one portion and the resulting mixture was stirred at room temperature for 1.5 h. Argon was bubbled through the solvent throughout the reaction period. The contents of the flask were cooled in an ice bath and acidified to pH 6 with 5% sulfuric acid. The product was extracted several times into benzene and the extract was washed with water and dried (Na_2SO_4). Evaporation of the solvent gave a gum which was chromatographed on silica, eluting with benzene. Two components were isolated. Fraction A, the least polar fraction, crystallized from ether to give 1-cyano-4,6,7-trimethoxyisoquinoline (**12**, 160 mg, 20%) as colorless needles, mp 196–197°C; ir (KBr): 2237 cm^{-1} (CN); nmr δ: 4.04 (s, 6H, 2 × OCH_3), 4.13 (s, 3H, OCH_3), 7.29 (s, 1H), 7.38 (s, 1H), 8.04 (s, 1H, C(3)-H). *Anal.* calcd. for $C_{13}H_{12}N_2O_3$: C 63.92, H 4.96, N 11.47; found: C 63.66, H 5.14, N 11.76.

Fraction B, the more polar fraction, crystallized from ethanol to give 2-benzoyl-1,2-dihydro-4,6,7-trimethoxy-1-(*o*-nitrobenzyl)isoquinaldonitrile (**11**, 1.017 g, 61%) as bright yellow prisms, mp 170–171°C; ir (KBr): 1681 (amide carbonyl), 1658 (amide carbonyl), 1527 (NO_2), 1325 cm^{-1} (NO_2). The ion corresponding to M − HCN was the species observed at highest mass in its high resolution mass spectrum; high-resolution mass spectrum *m/e* calcd. for M − HCN, $C_{26}H_{22}N_2O_6$: 458.14778; found: 458.14541; nmr δ: 3.47 (s, 3H, OCH_3), 3.65 (s, 3H, OCH_3), 3.88 (s, 3H, OCH_3), 4.14 (dd, 2H, J_{gem} = 13.0 Hz, $\Delta_{A,B}$ = 29 Hz, δ_A = 3.90, δ_B = 4.38, benzylic protons), 5.76 (s, 1H, C(3)-H), 6.58 (s, 1H), 6.97 (s, 1H), 7.17–7.92 (m, 9H).

*1-(o-Nitrobenzyl)-4,6,7-trimethoxyisoquinoline (**13**)*

2-Benzoyl-1,2-dihydro-4,6,7-trimethoxy-1-(*o*-nitrobenzyl)-isoquinaldonitrile (**11**, 400 mg, 0.825 mmol) was dissolved in dry dimethylformamide (20 mL) and the system was flushed with argon for 10 min. Triton B (0.20 mL, 40% methanolic benzyltrimethylammonium hydroxide) was syringed in, when an intense blue color resulted. The system was stirred at room temperature under argon for 45 min. The reaction flask contents were diluted with water, the product was extracted into chloroform, and the extract was washed with water and dried (Na_2SO_4). Evaporation of the solvent gave a gum which was chromatographed on silica, eluting with benzene. Fraction A, the less polar fraction, crystallized from ether to give 1-cyano-4,6,7-trimethoxyisoquinoline (**12**, 66 mg, 33%) as colorless needles, mp 196–197°C. Fraction B, obtained from the polar zone, gave 1-(*o*-nitrobenzyl)-4,6,7-trimethoxyisoquinoline (**13**) as a pale yellow oil which by nmr analysis proved to be contaminated with approximately 10% of nitrile **12**. All attempts to remove the contaminant failed. The yield of **13**, after compensation for contaminant **12**, was 58% (169 mg); nmr δ: 3.92 (s, 3H, OCH_3), 4.00 (s, 6H, 2 × OCH_3), 4.81 (s, 2H, CH_2), 7.17–7.50 (m, 6H), 7.90 (s, 1H, C(3)-H).

*1-(o-Aminobenzyl)-4,6,7-trimethoxyisoquinoline (**14**)*

Crude **13** (125 mg, 0.353 mmol) was dissolved in methanol (50 mL) and potassium carbonate (50 mg) was added. Adams' catalyst (50 mg) in methanol (25 mL) was added. The resulting mixture was hydrogenated at an initial pressure of 45 psi for 4 h. The catalyst was filtered off and the solvent was evaporated. Water (50 mL) was added to the residue and the product was extracted into chloroform. The extract was washed with water, dried (Na_2SO_4), and evaporated to give a gum which was chromatographed over silica, eluting initially with benzene followed by chloroform–methanol, to give two components. Fraction A, the less polar fraction, afforded nitrile **12** (8 mg, 6.5%), mp 195–197°C. Fraction B, the more polar fraction, afforded 1-(*o*-aminobenzyl)-4,6,7-trimethoxyisoquinoline (**14**) as a pale yellow oil (93 mg, 82%) which was used in the Pschorr reaction without further purification; nmr δ: 3.95 (s, 3H, OCH_3), 3.98 (s, 6H, 2 × OCH_3), 4.37 (br s, 2H, concentration-dependent NH_2), 4.38 (s, 2H, CH_2), 6.67–7.55 (m, 6H), 7.86 (s, 1H, C(3)-H).

*1,2,4-Trimethoxy-7H-dibenzo[de,g]quinolin-7-one (**1**)*

1-(*o*-Aminobenzyl)-4,6,7-trimethoxyisoquinoline (**14**, 70 mg, 0.216 mmol) was dissolved in 30 ml of methanol and 2 *N* sulfuric acid (2 mL) was added. The resulting solution was cooled to 0 to 5°C and a solution of $NaNO_2$ (83 mg, 1.203 mmol) in a small amount of water was added dropwise. The resulting mixture was stirred for 30 min at 0 to 10°C. Sulfamic acid (83 mg) dissolved in a small amount of water, was added to destroy excess nitrous acid. One minute after adding the sulfamic acid, excess copper–bronze was added. A rapid evolution of nitrogen resulted. The reaction was stirred for 30 min at room temperature followed by 1.5 h at 45 to 50°C. Copper was filtered off and most of the solvent was evaporated. Water was added to the residue and the solution was basified to pH 8 to 9 with concentrated ammonium hydroxide. The precipitate was extracted several times into chloroform and the extract was washed with water, twice with 5% NaOH, again with water, and dried (Na_2SO_4). Evaporation of the solvent gave dark gum which was chromatographed on silica plc plates, developing with chloroform–methanol. A yellow band was isolated from the polar zone which was rechromatographed on silica by dry column chromatography, eluting with purified ethyl acetate. A

bright yellow polar band appeared which was isolated and crystallized from acetone to afford **1** as bright yellow needles (13 mg, 19%), mp 231–235°C. Its tlc, nmr spectrum, mass spectrum, and infrared spectrum were all identical to those of natural splendidine, and a mixture melting point determination of the two samples showed no melting point depression.

Acknowledgments

We thank the National Institutes of Health for a grant (CA-22337-01) in partial support of this work, and also the Fundación Juan March for the supporting fellowship to one of us (J. M. Saá). We also thank the following individuals for their invaluable assistance: B. A. Krukoff (Honorary Curator of the New York Botanical Garden and Consulting Botanist of the Merck Sharp and Dohme Research Laboratories) for the supply of plant material, identification of the vouchers, and botanical consultation; Dr. C. Costello (Massachusetts Institute of Technology) for the determination of high-resolution mass spectra.

1. J. M. Saa, M. V. Lakshmikantham, M. J. Mitchell, and M. P. Cava. J. Org. Chem. **41**, 317 (1976).
2. B. A. Krukoff and R. C. Barneby. Phytologia, **39**, 283 (1978).
3. M. P. Cava, K. T. Buck, I. Noguchi, M. Srinivasan, M. G. Rao, and A. I. DaRocha. Tetrahedron, **31**, 1667 (1975).
4. M. Shamma. The isoquinoline alkaloids: chemistry and pharmacology. Academic Press, New York. 1972.
5. M. Sainsbury, D. W. Brown, S. F. Dyke, and G. Hardy. Tetrahedron, **25**, 1881 (1969).
6. M. P. Cava and I. Noguchi. J. Org. Chem. **38**, 60 (1973).
7. J. W. Skiles and M. P. Cava. Heterocycles, **9**, 653 (1978).
8. M. P. Cava and M. V. Lakshmikantham. J. Org. Chem. **35**, 1867 (1970).
9. M. P. Cava, A. Venkateswarlu, M. Srinivasan, and D. L. Edie. Tetrahedron, **28**, 4299 (1972).

Berberidic acid[1]

P. CHINNASAMY AND M. SHAMMA

Department of Chemistry, The Pennsylvania State University, University Park, PA 16802, U.S.A.

Received September 15, 1978

P. CHINNASAMY and M. SHAMMA. Can. J. Chem. 57, 1647 (1979).

Berberidic acid (**2**), obtained by nitric acid oxidation of berberine (**1**), can be esterified to diester **3**, or to monoesters **4** and **5**. Sodium borohydride reduction of **4** provides γ-lactone **6** which can be oxidized with iodine to pyridinium salt **7**. In like fashion, monoester **5** leads to γ-lactone **8** which is oxidized by mercuric acetate to salt **9**. Berberidic acid dimethyl ester (**3**) is hydrogenated to *allo* hexahydro diester **10** from which normal diester **11** can be derived by base isomerization. Hydrogenation of lactone **6** produces *allo* lactone **14** whose further reduction with lithium aluminum hydride gives diol **15**. This same diol can also be obtained from the lithium aluminum hydride reduction of hexahydro diester **10**. Alternatively, lithium aluminum hydride reduction of diester **11** gives rise to diol **16**, diastereomeric with **15**. Catalytic hydrogenation of lactone **8** provides normal lactone **18** which is transformed to diol **16** by lithium aluminum hydride.

P. CHINNASAMY et M. SHAMMA. Can. J. Chem. 57, 1647 (1979).

L'acide berbéridique (**2**), que l'on obtient par oxydation avec de l'acide nitrique de la berbérine (**1**), peut être estérifié en diester **3** ou en monoester **4** et **5**. La réduction de **4** par le borohydrure de sodium fournit la γ-lactone **6** qui peut être oxydée par l'iode pour donner le sel de pyridinium **7**. De la même manière, le monoester **5** conduit à la γ-lactone **8** qui peut être oxydée par l'acétate mercurique pour donner le sel **9**. L'hydrogénation de l'ester diméthylique de l'acide berbéridique (**3**) conduit à l'hexahydro diester *allo* (**10**) à partir duquel on peut obtenir l'isomère normal (**11**) par isomérisation en milieu basique. L'hydrogénation de la lactone **6** fournit la lactone *allo* (**14**) qui par réduction subséquente par l'hydrure de lithium et d'aluminium fournit le diol **15**. On peut aussi obtenir le même diol par réduction de l'hexahydro diester **10** par $LiAlH_4$. Par ailleurs, la réduction de **11** par $LiAlH_4$ fournit le diol **16** diastéréoisomère de **15**. L'hydrogénation catalytique de la lactone **8** fournit la lactone normale **18** qui peut être transformée en diol **16** sous l'influence de $LiAlH_4$.

[Traduit par le journal]

In a short communication in 1958, Resplandy reported (1) the oxidation of berberine (**1**) using hot dilute nitric acid to the betaine berberidic acid, which was assigned structure **2**. However, the exact experimental conditions as well as the yield and the full details of the structural elucidation were not described.

As part of an effort to study the varied aspects of the chemistry of berberine, it was decided to re-investigate this transformation and also to explore the chemistry of berberidic acid.

In our hands, the optimum conditions for the oxidation of berberine chloride were found to involve the use of 15% nitric acid together with gentle heating on a steam bath for 16 h. The maximum yield obtained was 53%. The Resplandy structure for berberidic acid (**2**) was confirmed by a study of the ^{1}Hmr spectrum of this product in TFA as described in expression **2**.

Esterification of berberidic acid (**2**) with methanol in the presence of hydrogen chloride gave berberidic acid dimethyl ester (**3**). On the other hand, the use of concentrated sulfuric acid as a catalyst during esterification yielded a mixture of diester **3** and monoesters **4** and **5** in 10, 65, and 15% yields, respectively.

The relative positions of the carbomethoxyl groups in **4** and **5** were established as follows. On reduction with excess sodium borohydride in ethanol, **4** provided the unsaturated lactone **6** which upon iodine oxidation generated the pyridinium salt **7**. The ^{1}Hmr spectrum of **7** in TFA is summarized in expression **7**. Noteworthy is the downfield aromatic singlet at δ 9.20 assigned to H-4 which is in a *peri* relationship to the carbonyl oxygen. In like fashion, sodium borohydride reduction of monoester **5** led to the γ-lactone **8**. Since iodine oxidation of **8** proved to be unsuccessful, mercuric acetate in acetic acid was used to furnish the pyridinium salt **9**. The ^{1}Hmr spectrum of **9** in TFA is summarized in expression **9**. Significantly, the lactone methylene protons appear as multiplets, whereas H-4 is also a multiplet between δ 8.73 and 8.92.

Berberidic acid dimethyl ester (**3**) could be hydrogenated quantitatively to the hexahydro diester **10** using Adams' catalyst. Even though three asymmetric centers are formed in this reduction, only one racemate, assigned the all-*cis allo* stereochemistry, was

[1]This paper is dedicated to the memory of R. H. F. Manske.

0008-4042/79/131647-05$01.00/0

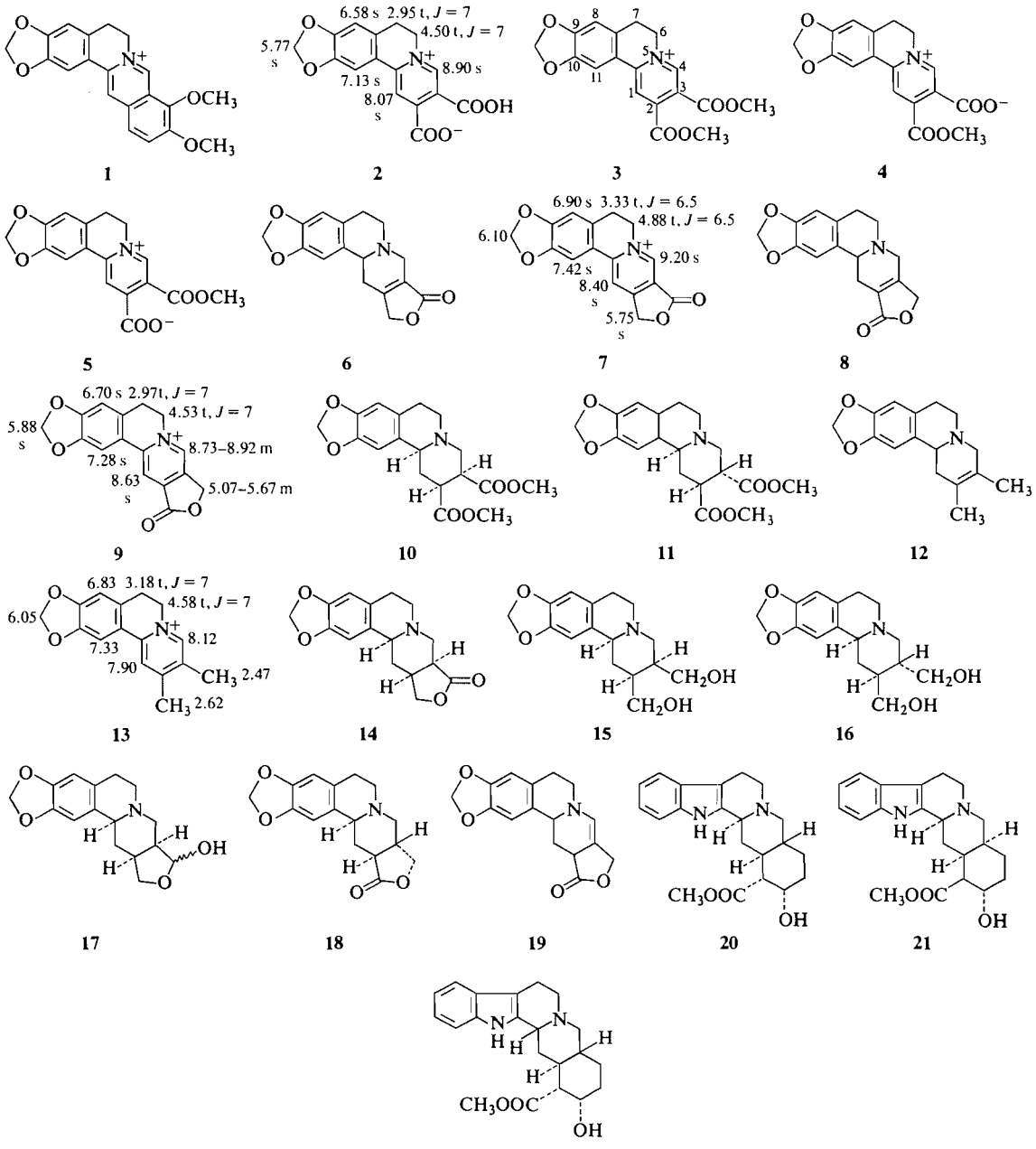

obtained. Compound **10** could be isomerized to its normal diastereomer **11** using sodium methoxide in methanol, indicating that **10** is the thermodynamically less stable isomer.

Reduction of berberidic acid dimethyl ester (**3**) with zinc in hot concentrated hydrochloric acid took an unexpected course to supply the dimethyl compound **12**, albeit in low yield. Oxidation of this piperidine derivative with mercuric acetate in acetic acid furnished the pyridinium salt **13** whose ^{1}Hmr spectrum (TFA) exhibits two aromatic methyls, one methylenedioxy group, and four aromatic protons. Significantly, H-4 appeared relatively upfield at δ 8.12. Reduction of salt **13** with sodium borohydride in methanol regenerated the dimethyl compound **12**.

Hydrogenation of the unsaturated lactone **6** over Adams' catalyst produced the saturated *allo* γ-lactone **14** which could be further reduced with lithium aluminum hydride to the diol **15**. The same diol was also obtained upon lithium aluminum

hydride reduction of the hexahydro diester **10**. Alternatively, lithium aluminum hydride reduction of the normal diester **11** supplied the diol **16** which is diastereomeric with **15**.

Turning again to the α,β-unsaturated lactone **6**, its lithium aluminum hydride reduction gave rise to the hemiacetal **17** and the *allo* diol **15** in 28 and 30% yields, respectively.

Finally, catalytic hydrogenation of the unsaturated lactone **8** gave the normal lactone **18**. In turn, lithium aluminum hydride reduction of this lactone led to the normal diol **16** rather than to the *allo* diol **15**.

Stereochemical Considerations

The Wenkert–Bohlmann bands and the rates of methiodide formation were the primary tools used in solving the stereochemical problems. All the tertiary bases prepared in the present study were found to contain Wenkert–Bohlmann bands in their infrared spectra between 2650 and 2800 cm^{-1}, thus suggesting the ubiquitous presence of a *trans*-quinolizidine system (2).

The small amounts (≈3 mg) of alkaloids or nitrogenous bases required for following the pseudo-first-order kinetics of quaternization of tertiary amines in acetonitrile make this method a particularly attractive one (3). The pseudo-first-order rate constants observed are listed in Table 1.

To interpret the data in Table 1, it is necessary to consider first the particularly apposite examples of the rates of methiodide formation for yohimbine (**20**), α-yohimbine (**21**), and pseudoyohimbine (**22**). Yohimbine (**20**), which possesses the normal configuration, shows a moderate rate of *N*-methylation, 48×10^{-4} s^{-1}. α-Yohimbine (**21**), which is *allo* and has a hindered nitrogen, exhibits an appreciably slower rate of 1×10^{-4} s^{-1}. Pseudoyohimbine (**22**) has a very fast rate of quaternization, 7×10^{-2} s^{-1}, reflecting the presence of an unhindered nitrogen.

All the bases in the present study assigned the *allo* configuration, namely species **10**, **14**, **15**, and **17**, were found to have slow rates between 5 and 10×10^{-4} s^{-1}, whereas those compounds of the normal configuration such as **11**, **16**, and **18**, understandably exhibited faster rates between 19 and 21×10^{-4} s^{-1}.

TABLE 1. Pseudo-first-order rates of methiodide formation

Compound	Rate × 10^{-4} (s^{-1})
6	9
8	14
10	5
11	21
12	125
14	5
15	10
16	19
17	9
18	19

The dimethyl compound **12** which possesses a 2,3-double bond and is thus unhindered to attack by methyl iodide showed a very fast rate, 125×10^{-4} s^{-1}. However, similar unsaturation in γ-lactones **6** and **8** resulted in slower rates of 9 and 14×10^{-4} s^{-1}, respectively, owing to the presence of the carbonyl electron withdrawing group.

The stereochemical results of the catalytic hydrogenation studies are interesting and worthy of note. Reduction of pyridinium salt **3** leads to the all-*cis* diester **10**. In like fashion, reduction of unsaturated γ-lactone **6** produces *allo* γ-lactone **14**. In contrast, the structurally isomeric unsaturated γ-lactone **8** furnishes upon catalytic reduction the normal γ-lactone **18**. A possible rationalization for these results is that it may be relatively easy for compound **8** to isomerize during the reductive process to the enamine **19** which could then suffer reduction to generate the product **18**.

Experimental

General Procedures

Melting points are uncorrected. ^1H nuclear magnetic resonance spectra were recorded on a Varian A-60A spectrometer. Where elemental analyses indicated that solvent (methanol) was present, the sample was dissolved in TFA, the solvent evaporated, and fresh TFA added by which time ^1Hmr spectroscopy indicated that the original solvent (methanol) had completely evaporated. The pseudo-first-order rates of methiodide formation in acetonitrile were followed by conductivity measurements using a conductivity cell with black platinized electrodes, an audiooscillator to generate a 1000 Hz current, a Leeds and Northrup Maxwell bridge No. 1553, a condenser to balance the capacitance, and an oscilloscope as a galvanometer to measure the null point (3). Thin layer chromatography was done on Merck 254 silica gel plates. Spots were visualized under short and long uv light and spraying was with chloroplatinate or chromatropic acid reagent.

The numbering system adopted for berberidic acid and its derivatives is analogous with that used in the emetine series.

Berberidic Acid (2)

A mixture of berberine chloride (5 g, 0.013 mmol) in 5 mL concentrated HNO_3 and 18 mL water was heated gently on a steam bath for 16 h. The precipitate was filtered and washed with water and then triturated with MeOH to provide yellow crystals of **2** (2.2 g, 53%); mp 230–235°C (dec.) (MeOH); λ_{max} (EtOH): 230sh, 295, and 385 nm (log ε 3.64, 3.61, and 3.56).

Berberidic Acid Dimethyl Ester Chloride (3)

Berberidic acid (**2**) (1 g, 3.2 mmol) was mixed with dry MeOH (25 mL) and the mixture saturated with dry HCl gas. The solution was refluxed for 16 h. Work-up provided diester **3** (1.1 g, 90%); mp 195–198°C (dec.) (MeOH); λ_{max} (EtOH): 277, 303, and 405 nm (log ε 4.28, 4.43, and 4.47); ^1Hmr (TFA) δ: 3.40 (2H, m, H-7), 4.20 (3H, s, $COOCH_3$), 4.25 (3H, s,

$COOCH_3$), 4.90 (2H, m, H-6), 6.23 (2H, s, OCH_2O), 7.03 (1H, s, H-8), 7.57 (1H, s, H-11), 8.47 (1H, s, H-1), and 9.27 (1H, s, H-4). *Anal.* calcd. for $C_{18}H_{16}NO_6Cl{\cdot}CH_3OH$: C 55.68, H 4.88, N 3.42; found: C 55.77, H 4.89, N 3.55.

*Berberidic Acid Monomethyl Esters **4** and **5***

Berberidic acid (1 g, 3.2 mmol) was refluxed for 16 h in 25 mL MeOH and 10 drops concentrated H_2SO_4. The products were separated by tlc using 40% MeOH in $CHCl_3$ as eluent. The band with R_f 0.56 was the diester **3** (120 mg, 10%). The band with R_f 0.23 furnished monoester **5** (157 mg, 15%); mp 203–206°C (MeOH); λ_{max} (EtOH): 232, 252, 271, 292, and 380 nm (log ε 4.03, 3.99, 4.02, 4.05 and 4.12); ^{1}Hmr (TFA) δ: 3.33 (2H, m, H-7), 4.13 (3H, s, $COOCH_3$), 4.87 (2H, m, H-6), 6.12 (2H, s, OCH_2O), 6.90 (1H, s, H-8), 7.43 (1H, s, H-11), 8.28 (1H, s, H-1), and 9.22 (1H, s, H-4). *Anal.* calcd. for $C_{17}H_{13}NO_6{\cdot}\frac{1}{2}CH_3OH$: C 61.22, H 4.37, N 4.08; found: C 61.49, H 4.08, N 4.28.

The band with R_f 0.19 gave monoester **4** (680 mg, 65%); mp 210–215°C (dec.) (MeOH); λ_{max} (EtOH): 290 and 373 nm (log ε 3.49 and 3.38); ^{1}Hmr (TFA) δ: 3.30 (2H, m, H-7), 4.10 (3H, s, $COOCH_3$), 4.83 (2H, m, H-6), 6.08 (2H, s, OCH_2O), 6.88 (1H, s, H-8), 7.40 (1H, s, H-11), 8.23 (1H, s, H-1), and 9.13 (1H, s, H-4). *Anal.* calcd. for $C_{17}H_{13}NO_6{\cdot}\frac{1}{2}CH_3OH$: C 61.22, H 4.37, N 4.08; found: C 61.27, H 4.23, N 4.16.

*Lactone **6***

Monoester **4** (400 mg, 1.2 mmol) was dissolved in 200 mL EtOH and $NaBH_4$ (2 g, 53 mmol) was added with stirring. Work-up gave colorless needles of **6** (280 mg, 81%); mp 224–226°C (MeOH); λ_{max} (EtOH): 292 nm (log ε 3.70); ^{1}Hmr ($CDCl_3$) δ: 4.77 (2H, br s, CH_2OCO), 5.92 (2H, s, OCH_2O), 6.60 (1H, s, H-8), and 6.62 (1H, s, H-11). *Exact mass* calcd. for $C_{16}H_{15}NO_4$: 285.1001; found (high resolution ms): 285.1001.

*Lactone **7***

Lactone **6** (100 mg, 0.4 mmol), I_2 (270 mg, 1.1 mmol), and EtOH (25 mL) were refluxed for 4 h. Excess I_2 was destroyed with $NaHSO_3$ solution. The EtOH was removed and the aqueous solution extracted with $CHCl_3$. Drying and evaporation of the solvent left a residue which was purified by tlc using 40% MeOH in $CHCl_3$. The major yellow band, R_f 0.21, consisted of **7** as the iodide (57 mg, 40%); λ_{max} (EtOH): 280 and 375 nm (log ε 3.97 and 3.91).

*Lactone **8***

Monoester **5** was reduced with $NaBH_4$ in the manner described above for **4**. When 400 mg (1.2 mmol) of **5** was used, 280 mg (81%) of **8** was obtained; mp 211–215°C (MeOH); λ_{max} (EtOH): 290 nm (log ε 3.53); ^{1}Hmr ($CDCl_3$) δ: 4.85 (2H, m, CH_2OCO), 5.97 (2H, s, OCH_2O), 6.62 (1H, s, H-8), and 6.72 (1H, s, H-11). *Exact Mass* calcd. for $C_{16}H_{15}NO_4$: 285.1001; found (high resolution ms): 285.0992.

*Lactone **9***

Lactone **8** (50 mg, 0.2 mmol) was mixed with 20% HOAc and $Hg(OAc)_2$ (270 mg, 0.8 mmol) and the mixture heated for 16 h on a steam bath. The product was filtered and the filtrate treated with $(NH_4)_2S$ solution. The resulting black suspension was heated on a steam bath for 1 h and the precipitate filtered through Celite. The resulting solution was mixed with a saturated KI solution and extracted with $CHCl_3$. The organic layer was dried and evaporated. The residue was purified by tlc (40% MeOH in $CHCl_3$). The major band, R_f 0.18, was collected and proved to be salt **9** as the iodide (29 mg, 40%); λ_{max} (EtOH): 235, 283, and 375 nm (log ε 3.95, 4.00, and 3.79).

*Hexahydro Diester **10***

Berberidic acid dimethyl ester chloride (**3**) (100 mg, 0.26 mmol) in 25 mL EtOH was hydrogenated over Adams' catalyst for 8 h. Work-up furnished 91 mg (100%); mp 200–202°C (MeOH); λ_{max} (EtOH): 292 nm (log ε 3.62); ^{1}Hmr ($CDCl_3$) δ: 3.67 (3H, s, $COOCH_3$), 3.72 (3H, s, $COOCH_3$), 5.88 (2H, s, OCH_2O), 6.52 (1H, s, H-8) and 6.73 (1H, s, H-11). *Anal.* calcd. for $C_{18}H_{21}NO_6$: 347.1368, C 62.25, H 6.05; found (high resolution ms): 347.1366, C 62.43, H 6.09.

*Hexahydro Diester **11***

Freshly cut Na (0.5 g) was added to dry MeOH (25 mL) under N_2. Diester **10** (100 mg) was added to the cooled solution and the mixture stirred for 1 h at room temperature under N_2. Two millilitres of water was added and the solvent evaporated. The residue was taken up in water and $CHCl_3$. Evaporation of the organic layer provided **11**, ν_{max} ($CHCl_3$): 1740 and 2760 cm^{-1}; ^{1}Hmr ($CDCl_3$) δ: 3.72 (6H, s, $COOCH_3$), 5.87 (2H, s, OCH_2O), 6.53 (1H, s, H-8), and 6.63 (1H, s, H-11). *Exact Mass* calcd. for $C_{18}H_{21}NO_6$: 347.1368; found (high resolution ms): 347.1382.

Zinc Reduction of Berberidic Acid Dimethyl Ester

Diester chloride **3** (500 mg, 1.3 mmol) was dissolved in concentrated HCl (10 mL) and warmed to 60°C. Zinc dust (2 g) was added slowly and the mixture stirred for 2 h around 60°C. The product was cooled and basified with cold NH_4OH. Extraction with $CHCl_3$ left a dark residue which was purified by tlc using 4% MeOH in $CHCl_3$, R_f 0.37, to provide **12** as an oil; λ_{max} (EtOH): 292 nm (log ε 3.51); ^{1}Hmr ($CDCl_3$) δ: 1.62 (6H, s, CH_3), 5.75 (2H, s, OCH_2O), 6.42 (1H, s, H-8) and 6.53 (1H, s, H-11). *Exact Mass* calcd. for $C_{16}H_{19}NO_2$: 257.1415; found (high resolution ms): 257.1415.

*Salt **13***

A mixture of amine **12** (50 mg, 0.2 mmol), 20% HOAc (10 mL), and $Hg(OAc)_2$ (270 mg, 0.8 mmol) was heated for 16 h on a steam bath. The mixture was filtered while hot and then treated with $(NH_4)_2S$ solution. The suspension was heated on a steam bath for 1 h and the precipitate filtered off through Celite. The resulting solution was treated with KI solution and extracted with $CHCl_3$. Evaporation of the solvent and tlc using 40% MeOH in $CHCl_3$ provided a major band, R_f 0.41, which furnished amorphous salt **13** as the iodide (30 mg, 40%); λ_{max} (EtOH): 267 and 355 nm (log ε 3.54 and 3.42).

Three milligrams of **13** was reduced with excess $NaBH_4$ in MeOH to afford **12** in near quantitative yield.

*Lactone **14***

Lactone **6** (500 mg, 1.8 mmol) was dissolved in methanolic HCl and the solution evaporated to dryness. The residue was dissolved in EtOH and hydrogenated over Adams' catalyst for 8 h. Work-up supplied lactone **14** (500 mg, ≈100%); mp 216°C (MeOH); λ_{max} (EtOH): 290 nm (log ε 3.61); ^{1}Hmr ($CDCl_3$) δ: 3.88–4.37 (2H, m, CH_2OCO), 5.87 (2H, s, OCH_2O), 6.52 (1H, s, H-8) and 6.60 (1H, s, H-11). *Exact Mass* calcd. for $C_{16}H_{17}NO_4$: 287.1157; found (high resolution ms): 287.1149.

*$LiAlH_4$ Reduction of **6***

Lactone **6** (150 mg, 0.5 mmol) was refluxed in dry THF (30 mL) containing $LiAlH_4$ (40 mg, 1.1 mmol) for 1 h under N_2. Thin-layer chromatography of the product mixture showed two major spots (10% MeOH in $CHCl_3$). The band with R_f 0.58 furnished hemiacetal **17** (43 mg, 28%); mp 156–158°C (MeOH); λ_{max} (EtOH): 290 nm (log ε 3.72); ^{1}Hmr

($CDCl_3$) δ: 3.82 (2H, m, CH_2OCHOH), 5.42 (1H, d, J = 6 Hz, $OCHOH$), 5.87 (2H, s, OCH_2O), 6.50 (1H, s, H-8), and 6.60 (1H, s, H-11). *Exact Mass* calcd. for $C_{16}H_{19}NO_4$: 289.1313; found (high resolution ms): 289.1319.

The band with R_f 0.33 yielded diol **15** (46 mg, 30%), mp 173–176°C (MeOH); λ_{max} (EtOH): 290 nm (log ε 3.85); ν_{max} ($CHCl_3$): 2775, 2820 and 3330 cm^{-1}. *Exact Mass* calcd. for $C_{16}H_{21}NO_4$: 291.1470; found (high resolution ms): 291.1450.

*$LiAlH_4$ Reduction of Lactone **14***

Compound **14** (100 mg, 0.35 mmol) was reduced with $LiAlH_4$ (26 mg, 0.7 mmol) in THF. Work-up supplied diol **15** (61 mg, 60%).

*$LiAlH_4$ Reduction of Diester **10***

Compound **10** (100 mg, 0.29 mmol) was reduced with $LiAlH_4$ (22 mg, 0.58 mmol) in THF to supply diol **15** (65 mg, 77%).

*Diol **16***

A few milligrams of diester **11** were reduced with excess $LiAlH_4$ in THF. Work-up provided colorless crystals of **16**, R_f 0.1 (10% MeOH in $CHCl_3$); mp 248–251°C (MeOH); ms *m/e*: 291 (30) $(M)^+$, 290 (60) $(M - H)^+$, 260 (50), 232 (30), and 175 (base). *Exact Mass* calcd. for $C_{16}H_{21}NO_4$: 291.1470; found (high resolution ms): 291.1461.

*Lactone **18***

Unsaturated lactone **8** (100 mg, 0.35 mmol) was hydrogenated with Adams' catalyst in EtOH. Work-up provided **18** (100 mg, ≈100%); mp 217–218°C (MeOH); λ_{max} (EtOH): 292 (log ε 3.53); ^{1}Hmr ($CDCl_3$) δ 3.88–4.38 (2H, m, CH_2OCO), 5.90 (2H, s, OCH_2O), 6.54 (1H, s, H-8), and 6.77 (1H, s, H-11). *Exact Mass* calcd. for $C_{16}H_{17}NO_4$: 287.1156; found (high resolution ms): 287.1108.

*$LiAlH_4$ Reduction of Lactones **8** and **18***

Ten milligrams of each of lactones **8** and **18** were reduced separately using excess $LiAlH_4$ in THF. The product was purified by tlc using 10% MeOH in $CHCl_3$ to provide in each case a major band (R_f 0.1) which proved to be diol **16**.

Acknowledgments

This project was supported by NIH research grant CA-11450, awarded by the National Cancer Institute, PHS/DHEW.

1. A. Resplandy. C. R. Acad. Sci. Ser. C, **247**, 2428 (1958).
2. F. Bohlmann. Angew. Chem. **69**, 641 (1957); Chem. Ber. **91**, 2157 (1958); E. Wenkert, C.-J. Chang, H. P. S. Chawla, D. W. Cochran, E. W. Hagaman, J. C. King, and K. Orito. J. Am. Chem. Soc. **98**, 3645 (1976).
3. M. Shamma and J. M. Richey. J. Am. Chem. Soc. **84**, 1739 (1962); **85**, 2507 (1963); M. Shamma, C. D. Jones, and J. A. Weiss. Tetrahedron, **25**, 4347 (1969).

^{13}C nuclear magnetic resonance spectra of some C_{19}-diterpenoid alkaloids and their derivatives[1]

S. William Pelletier, Naresh V. Mody, and Rajinder S. Sawhney

Institute for Natural Products Research and the Department of Chemistry, University of Georgia, Athens, GA 30602, U.S.A.

Received December 15, 1978

S. William Pelletier, Naresh V. Mody, and Rajinder S. Sawhney. Can. J. Chem. **57**, 1652 (1979).

The natural abundance carbon-13 nuclear magnetic resonance spectra of some C_{19}-diterpenoid alkaloids and their alkamines (lappaconitine, lappaconine, lapaconidine, ranaconine, 14-dehydrobrowniine, aconine, pseudoaconine, deoxyaconine, and hypaconine) have been determined at 15.03 MHz. With the aid of proton decoupling techniques, additivity relationships, and comparison with spectra of related alkaloids, self-consistent and unambiguous assignments of nearly all carbon resonances for these alkaloids have been made. Some important chemical shift trends have been observed, which are useful for identifying the basic C_{19}-diterpenoid alkaloid skeleton and the hydroxy and methoxy group substitution patterns in these alkaloids. On the basis of ^{13}C nmr spectra of lappaconitine and lappaconine, the anthranoyl ester moiety is assigned to the C-4 position in lappaconitine. The ^{13}C nmr spectra of lapaconidine, aconine, and pseudoaconine taken in pyridine and chloroform have been compared to determine the conformational changes of the ring A hydroxy groups in these alkaloids.

S. William Pelletier, Naresh V. Mody et Rajinder S. Sawhney. Can. J. Chem. **57**, 1652 (1979).

Opérant à 15.03 MHz, on a déterminé les spectres rmn du ^{13}C en abondance naturelle de quelques alcaloïdes diterpènoïdes en C_{19} et de leurs alkylamines (lappaconitine, lappaconine, lapaconidine, ranaconine, déhydro-14 browniine, aconine, pseudoaconine, déoxyaconine et hypaconine). Faisant appel aux techniques de découplage des protons, à des règles d'addition et à des comparaisons avec les spectres d'alcaloïdes apparentés, on a pu proposer des attributions autocohérentes et non ambigües de pratiquement toutes les résonances de carbones de ces alcaloïdes. On a observé quelques tendances importantes des déplacements chimiques qui sont utiles pour identifier le squelette fondamental des alcaloïdes diterpénoïdes en C_{19} ainsi que la disposition des groupes hydroxyles et méthoxyles attachés à ce squelette. En se basant sur les spectres rmn du ^{13}C de la lappaconitine et de la lappaconine, on attribue la position ester anthranoyle à la position C-4 de la lappaconitine. On a comparé les spectres rmn du ^{13}C de la lapaconidine, de l'aconine et de la pseudoaconine, déterminées en solution dans la pyridine et le chloroforme, pour évaluer les changements conformationnels du groupe hydroxyle attaché au cycle A de ces alcaloïdes.

[Traduit par le journal]

Introduction

During the last 10 years, investigators have made extensive use of carbon-13 nmr spectroscopy in the structure elucidation of natural products. This technique has played an important role in solving problems which otherwise would be very difficult, e.g., determination of the existence of C-20 epimers in atisine and related alkaloids (1). Carbon-13 nmr spectra provide detailed information about the degree and sites of oxygen substitution in the basic skeleton of diterpenoid alkaloids.

Jones and Benn (2) were the first to apply carbon-13 nmr spectroscopy to a study of the C_{19}-diterpenoid alkaloids. Later we reported a comprehensive ^{13}C nmr study of more than 50 aconitine- and lycoctonine-type alkaloids and their derivatives (3, 4). Using these data, we have revised and elucidated the structures of several complex C_{19}-diterpenoid alkaloids (3–5). We present here an analysis of the ^{13}C nmr spectra of additional alkaloids and alkamines. We anticipate that these data will be of use in the structure elucidation of newly isolated alkaloids from various *Aconitum*, *Consolida*, and *Delphinium* species.

Results and Discussion

The general procedure for ^{13}C nmr data acquisition and assignment of the carbon resonances for the compounds reported here involved determination of the noise-decoupled and the single-frequency off-resonance decoupled (SFORD) spectra. The carbon resonances were assigned with the aid of the single-frequency proton off-resonance decoupling techniques, direct analysis of nonprotonated carbon centers, application of known chemical shift rules

[1]Dedicated to the memory of R. H. F. Manske.

0008-4042/79/131652-04$01.00/0

TABLE 1. Carbon-13 chemical shifts and assignments for C_{19}-diterpenoid alkaloids and their derivatives[a]

Carbon	1[b]	2	3	3[c]	4	5	6	7	7[c]	8	8[c]	9	10
1	84.2	85.2	72.5	73.0	84.9	85.5	85.2	84.1	84.4	84.5	85.3	85.4	85.2
2	26.2	26.6	29.8	30.7	27.1	25.5	25.5	35.5	38.3	35.9	38.1	26.5	26.5
3	31.9	36.3	33.5	34.6	36.8	32.5	32.5	71.9	69.3	72.2	69.0	35.3	34.9
4	84.7	71.1	70.7	70.0	71.1	38.5	38.4	43.2	44.3	43.5	44.6	39.1	39.3
5	48.6	50.8	48.2	48.3	51.1	46.1	45.1	49.0	48.9	49.3	49.5	49.3	49.2
6	26.8	26.9	27.4	27.9	32.4	89.8	90.1	83.0	83.6	82.4	83.5	83.7	83.6
7	47.6	47.8	47.0	47.6	78.0	88.9	89.1	51.3	48.9	52.2	53.6	49.3	50.0
8	75.6	75.7	76.3	75.5	86.5	85.5	76.3	76.4	77.2	72.9	73.5	76.5	75.7
9	78.6	78.8	77.6	78.2	78.7	53.8	49.6	50.1	50.3	50.4	51.0	48.2	48.1
10	36.4	37.4	36.3	37.1	37.5	43.9	36.4	42.4	42.6	42.0	42.7	41.8	42.0
11	51.0	51.0	50.4	51.0	51.4	49.0	48.2	50.5	50.3	50.2	50.4	48.9	50.1
12	24.2	23.7	23.1	24.0	26.3	29.7	27.5	37.4	39.1	33.8	35.8	38.0	35.3
13	49.0	49.0	48.4	47.9	51.1	49.5	46.1	78.8	78.9	76.9	77.3	79.2	76.4
14	90.2	90.3	90.4	90.8	90.2	216.3	75.3	80.6	81.3	79.6	80.0	80.6	79.0
15	44.9	44.7	45.1	44.2	38.1	33.1	33.1	78.5	79.6	40.1	42.1	78.8	78.9
16	82.9	83.1	83.0	83.9	83.0	85.5	81.7	91.8	93.4	83.2	83.7	91.1	91.2
17	61.5	61.7	63.1	62.9	63.2	65.9	65.4	60.8	61.5	62.4	62.6	61.4	62.4
18	—	—	—	—	—	77.9	78.0	77.4	77.1	77.5	80.0	81.5	80.4
19	55.5	58.0	60.4	61.5	56.8	52.7	52.7	48.3	47.9	48.7	48.0	53.8	56.1
N—CH_2	49.9	49.9	46.5	50.2	50.0	51.4	51.3	46.2	47.1	47.4	47.8	48.9	42.8
CH_3	13.5	13.5	13.1	13.2	14.5	14.3	14.3	13.4	13.8	13.7	13.9	13.5	—
1′[d]	56.5	56.5	—	—	56.3	56.1	56.0	55.7	55.6	56.3	55.8	56.2	56.5
6′	—	—	—	—	—	57.6	57.5	58.0	57.8	57.4	57.5	58.0	57.9
14′	57.9	58.0	58.1	57.6	57.9	—	—	—	—	—	—	—	—
16′	56.1	56.1	56.3	56.0	56.3	56.3	56.5	61.9	61.3	57.9	58.3	61.4	61.5
18′	—	—	—	—	—	59.2	59.1	59.1	58.8	59.4	58.9	59.1	59.0

[a]Chemical shifts in ppm downfield from TMS; solvent is deuteriochloroform unless otherwise mentioned.
[b]The ^{13}C chemical shifts and assignments of the anthranoyl ester group in lappaconitine are shown separately on structure **1**.
[c]Spectra were taken in pyridine-d_5.
[d]Values given for primed carbons refer to chemical shifts for methoxyls.

for hydroxyl substitution, esterification shifts, steric effects, and from comparisons of spectra from compound to compound (6).

Assignments for Lappaconitine (1), Lappaconine (2), Lapaconidine (3), and Ranaconine (4)

During a reinvestigation of the alkaloids present in the roots of *Aconitum septentrionale* Koelle, we isolated the previously reported alkaloids lappaconitine (**1**) and lapaconidine (**3**). Basic hydrolysis of lappaconitine afforded the parent alkamine, lappaconine (**2**), and *N*-acetylanthranilic acid. On the basis of extensive chemical studies, Marion and co-workers (7) assigned structure **2** for lappaconine, which was confirmed by an X-ray analysis of lappaconine hydrobromide (8). Subsequently Soviet workers assigned the *N*-acetylanthranilic ester moiety to the C-4 position in lappaconitine (9). We have confirmed this assignment by the ^{13}C nmr spectral analyses of lappaconitine and lappaconine as discussed below.

The ^{13}C chemical shifts and assignments for lappaconitine (**1**), lappaconine (**2**), lapaconidine (**3**), and ranaconine (**4**) are reported in Table 1. The chemical shift assignments for these alkaloids were made by correlation with previously published ^{13}C nmr spectra of a variety of model *Aconitum* and *Delphinium* alkaloids (3, 4). The presence of the *N*-acetylanthranilic acid moiety in lappaconitine was confirmed by a comparison of observed resonances in **1** with the values observed for methyl anthranilate. The chemical shifts of compounds **1** and **2** are in agreement with their respective structures. Comparison of the spectrum of lappaconine (**2**) with that of lappaconitine (**1**) revealed the absence in lappaconine of chemical shifts due to the *N*-acetylanthranoyl ester group, a major change in the chemical shift of C-4, and some minor changes in the chemical shifts of C-3, C-5, and C-19. These results lead to the conclusion that the ester group is present at the C-4 position in lappaconitine. The spectrum of lapaconidine (**3**), when compared with lappaconine (**2**), reveals the presence of a hydroxyl group at C-1 in the α-configuration (see discussion on conformation of ring A). The ^{13}C chemical shifts of lapaconidine are in agreement with the structure (**3**) reported by Yunusov and his co-workers (10).

Recently, we have elucidated the structure of the highly oxygenated alkaloid, ranaconitine, by the help of ^{13}C nmr spectroscopy (11). We report here the

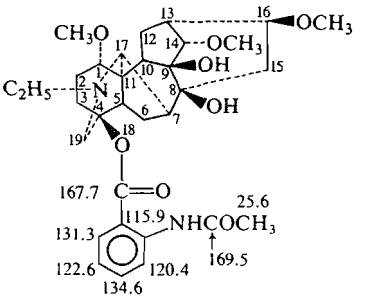

1 Lappaconitine

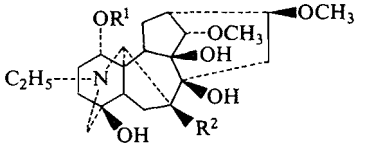

2 $R^1 = CH_3$; $R^2 = H$ Lappaconine
3 $R^1 = R^2 = H$ Lapaconidine
4 $R^1 = CH_3$; $R^2 = OH$ Ranaconine

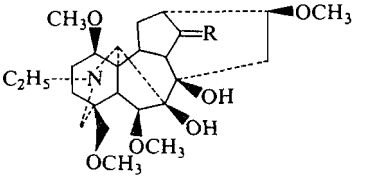

5 R = O 14-Dehydrobrowniine
6 R =  Browniine

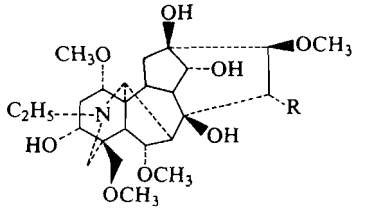

7 R = OH Aconine
8 R = H Pseudoaconine

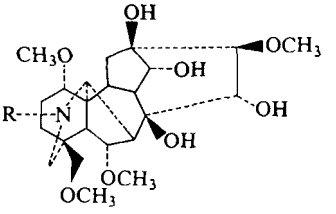

9 $R = C_2H_5$ Deoxyaconine
10 $R = CH_3$ Hypaconine

chemical shifts of ranaconine (**4**), the parent alkamine of ranaconitine. Comparison of the spectrum of ranaconine with that of lappaconine (**2**) revealed the presence of an additional quaternary carbon singlet at 78 ppm and the absence of a methine carbon doublet, results which indicate the presence of an extra tertiary hydroxyl group in ranaconine. The downfield shift of the C-6, C-8, and C-17 carbon resonances in ranaconine in comparison with lappaconine indicated the presence of an extra tertiary hydroxyl group at C-7. The ^{13}C nmr data of bases **1–4** indicate the structural similarity within this group of alkaloids. These examples demonstrate the usefulness of ^{13}C nmr spectroscopy in determining the structures of newly isolated alkaloids without tedious chemical work.

Assignments for 14-Dehydrobrowniine (5)

In 1966 Benn (12) isolated a known derivative of browniine, 14-dehydrobrowniine (**5**), as a natural product from *Delphinium cardinale*. We have prepared alkaloid **5** from browniine (**6**) to examine its ^{13}C nmr spectrum and to make a comparison with browniine. A downfield singlet at 216.3 ppm in alkaloid **5** indicates the presence of the carbonyl group at the C-14 position. The presence of the C-14 carbonyl group in **5** moved the chemical shifts of C-8, C-9, C-10, C-11, C-12, C-13, and C-16 significantly downfield in comparison with browniine. These shifts are a result of the disappearance of the 1,3-diaxial interactions of the C-14 α-hydroxyl with the C-16 β-methoxyl and the C-8 hydroxyl when browniine is transformed to ketone **5**.

Assignments for Aconine (7), Pseudoaconine (8), Deoxyaconine (9), and Hypaconine (10)

Alkamines **7** to **10** were prepared by published procedures (13). The chemical shift assignments for alkamines **7** to **10** were made by correlation with previously published ^{13}C nmr spectra of the corresponding naturally occurring alkaloids (3). The absence of C-3 and C-15 secondary hydroxyl groups in deoxyaconine (**9**) and pseudoaconine (**8**), respectively, greatly facilitated the unambiguous assignments of ^{13}C chemical shifts in aconine (**7**). The patterns of ^{13}C chemical shifts in these alkamines are very similar. Comparison of the spectra of the alkamines revealed precise information for identifying the basic C_{19}-diterpenoid alkaloid skeleton and the hydroxy and methoxy groups substitution pattern in these alkaloids.

Thus, the presence of a hydroxyl group at C-15 in

aconine (**7**) deoxyaconine (**9**), and hypaconine (**10**) was detected by observing the downfield shift of the C-8 (~3.5 ppm) and C-16 (~8 ppm) resonances in comparison with pseudoaconine (**8**). A doublet at ~91 ppm in the SFORD spectra of the alkamines of the aconitine-type alkaloids is characteristic of the presence of a hydroxy group in the α-configuration at the C-15 position when the methoxyl group is present at C-16 in the β-configuration. A secondary hydroxy group at C-3 can be easily detected in aconine (**7**) and pseudoaconine (**8**) by observing the presence of a doublet at ~72 ppm and a downfield singlet of C-4 at ~43 ppm in comparison with alkamines without a C-3 hydroxy group, e.g., deoxyaconine (**9**) and hypaconine (**10**). Alkaloids with a $-CH_2OCH_3$ group at C-4 and with H at C-3, are characterized by a singlet between 38–39 ppm, e.g., 14-dehydrobrowniine (**5**), browniine (**6**), and deoxyaconine (**9**).

Conformation of Ring A in Lapaconidine, Aconine, and Pseudoaconine

It is known that in C_{19}-diterpenoid alkaloids containing $-CH_2OCH_3$ at C-4, ring A bearing a C-1 α-hydroxy *or* a C-3 α-hydroxy group exists in a boat conformation (3). Ring A is in the chair conformation in the cases where the C-1 α-substituent is acetoxyl *or* methoxyl, *or* in the case where the C-1 substituent is in the β-configuration (3). On the basis of ^{13}C nmr data from several alkaloids containing C-1 α- and β-hydroxyl groups, we observed that the resonance of C-1 bearing an α-hydroxyl group appears at ~72 ppm (e.g., neoline, neoline 8-acetate, delphisine, condelphine, isotalatizidine), whereas the resonance of C-1 bearing a β-hydroxyl group appears at ~69 ppm (1-*epi*-delphisine, 1-*epi*-neoline). The orientation of the C-1 hydroxyl also affected the chemical shifts of other carbons in ring A.

From these observations, we postulated that the C-1 α-hydroxyl group forms a hydrogen bond with the lone-pair electrons of the nitrogen and thus stabilizes ring A in a boat form (3). However, when the C-1 hydroxyl is in the β-configuration, the hydroxyl group is not available to form a hydrogen bond with the lone-pair electrons of nitrogen and thus ring A remains in a chair conformation. This idea prompted us to investigate the behavior in chloroform and pyridine of ring A in lapaconidine (**3**), aconine (**7**), and pseudoaconine (**8**), bases which contain the C-1 or C-3 α-hydroxyl group.

The spectra of lapaconidine (**3**) taken in chloroform and pyridine were almost identical. No significant differences in their chemical shifts other than normal solvent effects were observed. But it is interesting to note that the ^{13}C nmr spectra of aconine (**7**) and pseudoaconine (**8**) taken in chloroform and pyridine were significantly different in the chemical shifts at C-2, C-3, and C-4 (Table 1). This observation suggests that in pyridine the C-3 α-hydroxyl group forms a hydrogen bond with the solvent instead of with the lone-pair electrons of nitrogen and thus hydrogen bond formation between the C-3 α-hydroxyl group and pyridine stabilizes ring A in a chair conformation. In contrast, in chloroform solution, ring A exists in the boat conformation.

Experimental

Carbon-13 nmr spectra were determined at 15.03 MHz in the Fourier mode using an FX-60 spectrometer in conjunction with a JEC-980 computer. The spectra were determined at 30°C in deuteriochloroform solutions (which also provided the lock signal) with 5% tetramethylsilane as internal reference. Samples were contained in precision ground 5 mm o.d. tubes. The spectrometer was used in the crosscoil configuration. On the average a 5μs pulse, corresponding to an approximate tilt angle of 45°, was employed. For the average spectral width of 4000 Hz, the delay between pulses was 2 s. Acquisition times averaged 1–2 h over 8 K data points for concentrations of the order of 0.4–1.0 *M*. For off-resonance spectra this time was 5–10 h.

The alkaloids and their derivatives used here were isolated and/or synthesized by procedures given in the literature cited.

Acknowledgement

The authors thank Dr. Arne Jørgen Aasen of the University of Oslo for a sample of lappaconitine.

1. N. V. Mody and S. W. Pelletier. Tetrahedron, **34**, 2421 (1978).
2. A. J. Jones and M. H. Benn. Can. J. Chem. **51**, 486 (1973).
3. S. W. Pelletier and Z. Djarmati. J. Am. Chem. Soc. **98**, 2626 (1976).
4. S. W. Pelletier, N. V. Mody, R. S. Sawhney, and J. Bhattacharyya. Heterocycles, **7**, 327 (1977).
5. S. W. Pelletier, N. V. Mody, A. J. Jones, and M. H. Benn. Tetrahedron Lett. 3025 (1977).
6. J. B. Stothers. Carbon-13 NMR spectroscopy. Academic Press, New York, NY. 1972.
7. N. Mollow, M. Tada, and L. Marion. Tetrahedron Lett. 2189 (1969).
8. G. I. Birnbaum. Tetrahedron Lett. 2193 (1969).
9. V. A. Tel'nov, M. S. Yunusov, and S. Yu. Yunusov. Khim. Prir. Soedin. **6**, 583 (1970).
10. V. A. Tel'nov, M. S. Yunusov, Ya. V. Rashkes, and S. Yu. Yunusov. Khim. Prir. Soedin. **7**, 622 (1971).
11. S. W. Pelletier, N. V. Mody, A. P. Venkov, and N. M. Mollov. Tetrahedron Lett. 5045 (1978).
12. M. H. Benn. Can. J. Chem. **44**, 1 (1966).
13. S. W. Pelletier and N. V. Mody. *In* The alkaloids. Vol. 17. *Edited by* R. H. F. Manske and R. Rodrigo. Academic Press, New York. 1979. Chapt. 1.

Aliphatic diazo compounds. XII. The synthesis of 5-*endo*-hetero-atom-substituted 3-diazo-2-norbornanones and the proton magnetic resonance spectra of these diazo ketones and their precursors[1,2]

PETER YATES AND GORDON F. HAMBLY[3]

Lash Miller Chemical Laboratories, Department of Chemistry, University of Toronto, Toronto, Ont., Canada M5S 1A1

Received November 30, 1978

PETER YATES and GORDON F. HAMBLY. Can. J. Chem. 57, 1656 (1979).

Treatment of 6-*endo*-acetoxy-5,5-dimethyl-2,3-norbornanedione (**6**) with tosylhydrazine gives the 2-tosylhydrazone (**7**), which is converted to 5-*endo*-acetoxy-3-diazo-6,6-dimethyl-2-norbornanone (**1**) by basic alumina; the exclusive formation of the 2-tosylhydrazone is ascribed to the smaller steric effect of the *endo* C-6 acetoxyl relative to the *endo* C-5 methyl group. The 6-*endo*-methoxy analogue of **6**, **17**, and the related 6-*endo*-chloro- and 6-*endo*-bromo-1,5,5-trimethyl-2,3-norbornanediones (**23** and **26**) are similarly converted to the corresponding α-diazo ketones **2–4**. The ^{1}H nmr spectra of the diazo ketones **1–4** have their C-1 bridgehead proton signals shifted to higher field relative to the corresponding bridgehead proton signals of the related α-diketones, whereas the C-4 bridgehead proton signals of **1** and **2** are shifted to lower field in relation to the corresponding α-diketone signals. The ^{1}H nmr spectra of the α-diketones show an unusual long range coupling ($^4J \geq 1$ Hz) between the C-4 bridgehead protons and the *exo* C-6 protons that is significantly smaller or absent in the spectra of the related diazo ketones and monoketones. In all of these types of compound an *endo*-methoxyl or -acetoxyl group at C-5(6) shifts the *exo* and *endo* C-6(5) methyl signals to lower and higher field, respectively, whereas an *endo*-halo substituent at C-5(6) shifts both the *exo* and *endo* C-6(5) methyl signals to lower field.

PETER YATES et GORDON F. HAMBLY. Can. J. Chem. 57, 1656 (1979).

La réaction de l'acétoxy-6-*endo* diméthyl-5,5 norbornanedione-2,3 (**6**) avec de la tosylhydrazine conduit à la tosylhydrazone-2 (**7**) qui est transformée en acétoxy-5-*endo* diazo-3 diméthyl-6,6 norbornanone-2 (**1**) par de l'alumine basique; la formation exclusive de la tosylhydrazone-2 est attribuée à l'effet stérique plus faible de l'acétoxyle *endo* en C-6 par rapport au groupe méthyle *endo* en C-5. L'analogue méthoxy-6-*endo* de **6**, **17**, et les chloro-6-*endo* et bromo-6-*endo* triméthyl-1,5,5 norbornanediones-2,3 (**23** et **26**) qui leur sont apparentées sont transformées d'une manière semblable en α-diazo cétones correspondantes (**2–4**). Dans les spectres rmn du ^{1}H, les signaux des protons portés par le carbone de pont C-1 des diazo cétones **1–4** sont déplacés à des champs plus élevés par rapport aux signaux des protons correspondants des α-dicétones auxquelles elles sont reliées; toutefois les signaux des protons portés par le carbone de pont C-4 de **1** et de **2** sont déplacés vers un champ plus bas par rapport aux signaux des α-dicétones correspondantes. Dans le spectre rmn du ^{1}H des α-dicétones, on observe une constante de couplage à longue distance ($^4J \geq 1$ Hz) entre les protons portés par l'atome de pont C-4 et les protons *exo* en C-6 qui est inhabituelle et qui est beaucoup plus faible ou absente dans le spectre des diazo cétones et monocétones apparentées. Dans tous ces types de composés les groupes méthoxyle ou acétoxyle *endo* en C-5(6) déplacent les signaux des groupes méthyles *exo* et *endo* en C-6(5) respectivement vers des champs plus faibles et plus élevés alors qu'un halogène *endo* en C-5(6) déplace les signaux des méthyles *exo* et *endo* en C-6(5) vers des champs plus faibles.

[Traduit par le journal]

In connection with our studies on the copper-catalyzed decomposition of α-diazo ketones (1–5), we wished to examine the copper-catalyzed decomposition of 3-diazo-2-norbornanones that possess an *endo* carbon – hetero atom bond at C-5. We describe here the synthesis of the diazo ketones **1–4**, prepared for this purpose, and discuss the ^{1}H nmr spectra of the diazo ketones and their precursors, which showed features of intrinsic interest in addition to providing evidence for the structural assignments. The investigation of the copper-catalyzed decomposition of the diazo ketones is described in the following paper (6).

Synthesis of the α-Diazo Ketones

Some years ago Meinwald *et al.* (7) reported the synthesis by the route shown in Scheme 1 of an α-diazo ketone that was either **1** or **5**. For their

[1]Dedicated to the memory of R. H. F. Manske.

[2]For Part XI, see ref. 1.

[3]Present address: Chemistry Department, John Abbott College, Ste. Anne de Bellevue, P.Q., Canada H9X 3L9.

0008-4042/79/131656-12$01.00/0

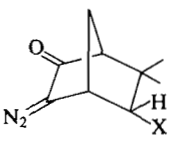

1 X = OAc
2 X = OMe

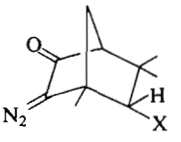

3 X = Cl
4 X = Br

purpose, which was its photochemical Wolff rearrangement, it was immaterial which of these two structures the diazo ketone possessed. For our purpose it was necessary that it be **1**, which seemed to us to be the more likely structure, and we have now established this to be the case. The basis of our optimism was the knowledge that the conformational free energy difference for an axial and an equatorial methyl group on a cyclohexane ring is ca. 1.0 kcal/mol greater than that in the case of an acetoxyl group (8). Thus the steric crowding between the *endo*-hydroxyl group and the *endo*-methyl group in **10** should be appreciably more severe than that between the *endo*-hydroxyl group and the *endo* acetoxyl group in **9**. The known high propensity for 2-norbornanones lacking a 7-*syn*-methyl substituent to undergo *exo* nucleophilic attack at the carbonyl group (9) and the circumstance that the rate-determining step in hydrazone formation under acidic conditions is the formation of the intermediate adduct (10) makes it likely that **9** and **10** will be the intermediates for the formation of **7** and **8**, respectively, and that their relative rates of formation will determine the relative rates of formation of the latter. Thus the single monotosylhydrazone reported to be formed from **6** may be anticipated to be **7** and the derived diazo ketone to be **1**.[4,5]

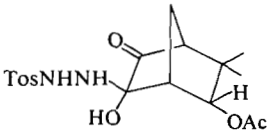

9 10

The dione **6** was prepared from *dl*-camphenilone (**11**) as previously reported (7) (Scheme 2). The product isolated from the chromic acid oxidation of **13** was earlier tentatively formulated as the 5-acetoxy-2-norbornanone **14** on the reasonable grounds of analogy with the similar oxidation of bornyl acetate to the corresponding acetoxy ketone (12). The fact that the oxidation product of **13** shows in its ^{1}H nmr

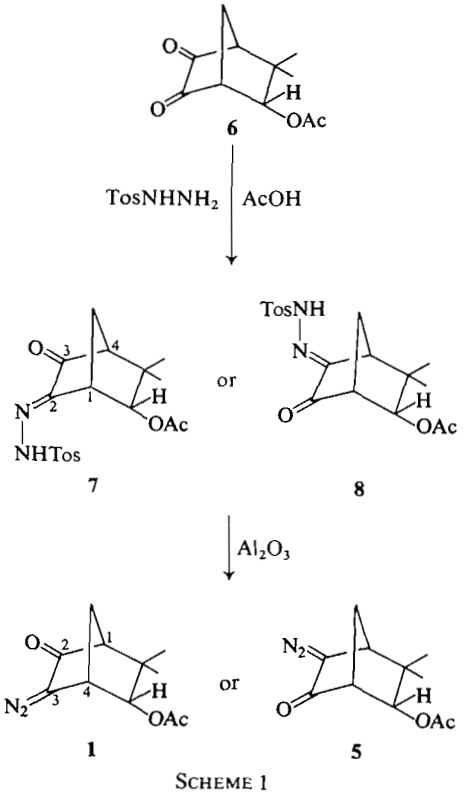

SCHEME 1

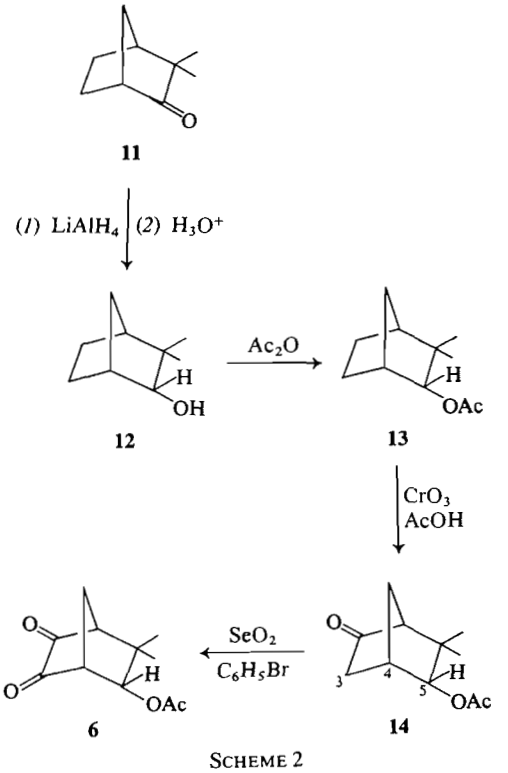

SCHEME 2

[4]For a related difference in reactivity, see ref. 11.

[5]Polar and hydrogen-bonding effects, to the extent that they are operative, would also be expected to favor formation of **7**.

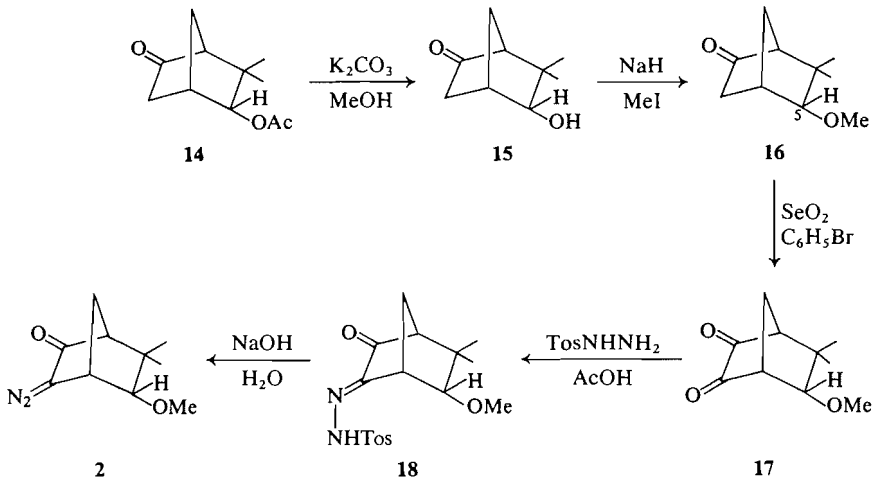

SCHEME 3

spectrum a doublet of doublets at δ 4.89 (J = 4.2, 1.0 Hz), demonstrating that the *exo* C-5 proton is coupled both with the C-4 proton and the *exo* C-3 proton (*vide infra*), excludes the alternative 6-acetoxy-2-norbornanone structure and confirms the assignment to it of structure **14**. Selenium dioxide oxidation of **14** to **6** was found to give considerably better yields when carried out in bromobenzene rather than the acetic anhydride used as solvent previously.

Treatment of **6** with slightly more than 1 equiv. of tosylhydrazine in acetic acid gave a single monotosylhydrazone that is assigned structure **7** rather than **8**, on the following grounds. Although the acetoxyl methyl proton chemical shifts in the ^{1}H nmr spectra of **6**, **13**, and **14** are normal (δ 2.02–2.07), that of the monotosylhydrazone is at abnormally high field (δ 1.79). This can be attributed to shielding of the acetoxyl methyl group by the aromatic ring of the tosylhydrazone residue, which must therefore be located at C-2 as in **7**. This assignment was confirmed and also the structure of the diazo ketone formed by chromatography of the monotosylhydrazone on basic alumina was established as **1** rather than **5** by the observation that in the ^{1}H nmr spectrum of the diazo ketone the signal of the bridgehead proton adjacent to the diazo group is shifted downfield by 0.3 ppm relative to the corresponding signal in the spectrum of the dione **6**, whereas the signal of the bridgehead proton adjacent to the carbonyl group is shifted upfield by 0.4 ppm relative to the corresponding signal for **6**. We have found that in the spectra of 3-diazo-2-norbornanones in general the signal due to the bridgehead proton at C-4 is shifted downfield and that of the bridgehead proton at C-1 upfield relative to their respective chemical shifts in the corresponding 2,3-norbornanediones (*vide infra*). The bridgehead protons adjacent to the acetoxyl group and the *gem*-dimethyl group in the diazo ketone derived from **6** must therefore be adjacent to the diazo and carbonyl groups, respectively, establishing its structure as **1**.

The diazo ketone **2** was also prepared from the acetoxy ketone **14** by the route shown in Scheme 3. Hydrolysis with methanolic aqueous potassium carbonate gave the hydroxy ketone **15**. Methylation of **15** gave the methyl ether **16**, which like **14** and **15** showed the C-5 proton signal in its ^{1}H nmr spectrum as a doublet of doublets with $J \sim 4$ and 1 Hz.

The selenium dioxide oxidation of **16** to **17** proved to be unexpectedly difficult. Initial experiments were carried out with crude methoxy ketone **16** that contained hydroxy ketone **15** as the major impurity. When treatment with selenium dioxide was carried out in boiling acetic anhydride, no reaction other than acetylation of **15** to **14** occurred. But subsequent treatment of the reaction mixture, after removal of the acetic anhydride, in bromobenzene with selenium dioxide gave **17** in 70% yield based on the amount of **16** in the mixture. However, repetition of the oxidation with pure **16** in bromobenzene failed to give **17**. Deliberate addition of **14** did result in oxidation of **16** to **17** by selenium dioxide in bromobenzene, albeit in low yield. It is possible that the active species responsible for the oxidation of **16** is a Se(II) compound generated in the oxidation of **14**.

Conversion of **17** to the monotosylhydrazone **18**, followed by treatment with 0.3 N aqueous sodium hydroxide (13) gave the diazo ketone **2**. The structure of **2** was established by the correspondence in the relationship between its ^{1}H nmr spectrum and that of its α-diketone precursor **17** with that between the spectra of **1** and **6** (*vide supra*). Corroboration for the

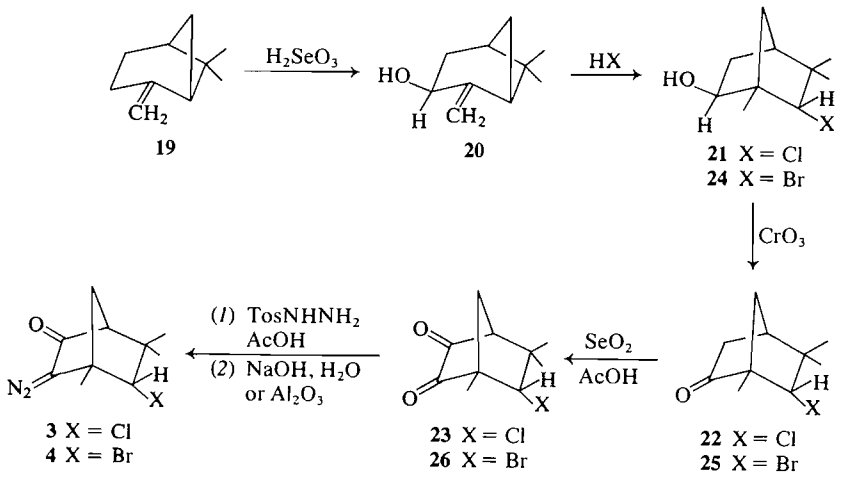

SCHEME 4

structural assignment derives from an alternative, but less efficient, synthesis of **2** from **16** via hydroxymethylenation followed by treatment with *p*-carboxybenzenesulfonyl azide and triethylamine (14, 15). It was expected that the monotosylhydrazone formed from **17** would be **18**, and thus that the diazo ketone would be **2**, on the basis of the considerations discussed earlier and the fact that the conformational free energy difference between an axial and an equatorial methoxyl group on a cyclohexane ring is, like that of an acetoxyl group, ca. 1 kcal/mol less than that of a methyl group (8).

The chloro diazo ketone **3** was prepared from (−)-β-pinene (**19**) by the route shown in Scheme 4. Oxidation of **19** with selenous acid gave *trans*-pinocarveol (**20**) (16), which on treatment with hydrogen chloride gave **21**. Although a different structure was originally assigned to this product (16), it is clear from subsequent work on the action of hydrogen bromide on **20** (17, 18) that the hydrogen chloride adduct has structure **21**. This structural assignment is confirmed by the ^{1}H nmr spectra of the hydrogen chloride adduct and its chromic acid oxidation product **22** and by the ir spectrum of the latter (see Experimental). Selenium dioxide oxidation of **22** in acetic acid gave **23** in modest yield, which could probably be improved by the use of bromobenzene as solvent. Conversion of **23** to a monotosylhydrazone followed by treatment with aqueous sodium hydroxide gave the diazo ketone **3**, whose structure was again established by the correspondence in the relationship between its ^{1}H nmr spectrum and that of its α-diketone precursor **23** with that between the spectra of **1** and **6**.

The bromo diazo ketone **4** was prepared from (−)-β-pinene (**19**) via **24**–**26** in analogous fashion. Treatment of the monotosylhydrazone with aqueous sodium hydroxide gave impure **4** in low yield, perhaps because bromide ion is a better leaving group than chloride ion in S_N2 reactions. Under the milder conditions of chromatography of the tosylhydrazone on basic alumina (7), **4** was produced in good yield.

Spectra of the α-Diazo Ketones and their Precursors

Salient ir bands and the ^{1}H nmr signals of the 5- and 6-hetero-atom-substituted 2-norbornanones are given in Tables 1 and 2, together with corresponding data (19) for the parent 6,6-dimethyl-2-norbornanone (**27**) and isofenchone (**28**).

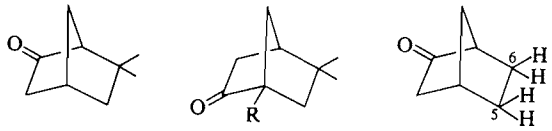

27 **28** R = Me, **30** R = H **29**

It is well known that in the ^{1}H nmr spectra of both norbornane and norbornene the *endo* protons are shielded relative to the *exo* protons (20, 21), and in an exhaustive study of the ^{1}H nmr spectrum of 2-norbornanone (**29**) Marshall and Walter (22) have shown that the same is true of the *endo* and *exo* protons at each of C-5 and C-6. Furthermore, the methyl signals of 6-*endo*-methyl-2-norbornanone and 6-*exo*-methyl-2-norbornanone occur at δ 0.93 (23) and 1.04 (24), respectively. It is thus reasonable to assign the methyl signals at δ 1.02 and 1.12 in the spectrum of **27** to the *endo* and *exo* methyl groups, respectively. Introduction of an *endo* C-5 oxygen substituent in **15**, **16**, and **14** leads to a greater separation of the methyl signals, which can be interpreted as resulting from an upfield shift of the *endo* methyl signals in all cases and a downfield shift of

TABLE 1. Infrared and ^{1}H nmr spectra of 6,6-dimethyl-2-norbornanone (**27**) and 5-*endo*-oxygen-substituted 6,6-dimethyl-2-norbornanones

Spectrum	Assignment	**27** (X = H)	**15** (X = OH)	**16** (X = OMe)	**14** (X = OAc)
$\lambda_{max}(CCl_4)$ (μm)	OH, OMe		2.82, 2.95	3.53	
	C=O	5.75	5.74	5.74	5.74[a]
	CH_2CO		7.11	7.11	7.10
	C—O			9.00	8.10
δ_H ($CDCl_3$)[b]	*endo*-Me	1.02(s)	0.88(s)	0.88(s)	0.83(s)
	exo-Me	1.12(s)	1.12(s)	1.14(s)	1.23(s)
	1, 3, 7	1.3–2.3(m)[c]	1.3–2.4(m)	1.3–2.2(m)	1.6–2.3(m)
	4	2.6(m)	2.7(m)	2.8(m)	2.83(m)
	5		3.98(dd, J = 4.0, 1.0 Hz)	3.44(dd, J = 4.0, 1.1 Hz)	4.89(dd, J = 4.2, 1.0 Hz)
	OH, OMe, OAc		3.02(s)[d]	3.34(s)	2.07(s)

[a]Superimposed ketone and acetate C=O stretching bands.
[b]The relative intensities of the ^{1}H nmr signals are in accord with the assignments.
[c]Also includes H5 signals.
[d]Concentration dependent.

TABLE 2. Infrared and ^{1}H nmr spectra of isofenchone (**28**) and 6-*endo*-halo-substituted 1,5,5-trimethyl-2-norbornanones

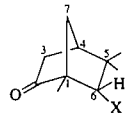

Spectrum	Assignment	**28** (X = H)	**22** (X = Cl)	**25** (X = Br)
$\lambda_{max}(CCl_4)$ (μm)	C=O	5.73	5.71	5.71
	CH_2CO	7.10	7.10	7.12
δ_H ($CDCl_3$)[a]	*endo*-5-Me	1.03(s)	1.12(s)	1.15(s)[b]
	exo-5-Me	1.12(s)	1.30(s)	1.28(s)
	1-Me	1.17(s)	1.20(s)	1.15(s)[b]
	3, 4, 7	1.3–2.5(m)[c]	1.3–2.9(m)	1.3–2.7(m)
	6		3.81(s)	3.93(s)

[a]The relative intensities of the ^{1}H nmr signals are in accord with the assignments.
[b]Superimposed signals.
[c]Also includes H-6 signals.

the *exo* methyl signals in the case of the methoxy and acetoxy compounds. Related effects of hydroxy (25) and acetoxy (26) substitution in the norbornane series have been observed previously; the effect of hydroxy substitution has been attributed to the anisotropic effect of the C—O bond (25). The methyl signals at δ 1.03, 1.12, and 1.17 in the spectrum of **28** can be assigned to the *endo* C-5, *exo* C-5, and C-1 methyl groups, respectively, on the basis of comparison with the methyl signals at δ 1.03 and 1.12 in the spectrum of 5,5-dimethyl-2-norbornanone (**30**) (19) and of the relationship of the *endo* and *exo* C-5 proton signals in the spectrum of **29** referred to above. Introduction of the C-6 chlorine atom in **22** shifts the methyl signals to δ 1.12, 1.20, and 1.30. Comparison of the chemical shifts of the methyl protons in the spectra of the four stereoisomeric 5-chloro-6-methylnorbornenes (27) with those of the methyl protons in the spectra of 5-*exo*-methyl- and 5-*endo*-methylnorbornene (28) shows that the introduction of either a *cis* or *trans* chlorine atom adjacent to the methyl groups of the latter compounds results in a downfield shift, which is greater in the *trans* case. On this basis the signals of **22** at δ 1.12, 1.20, and 1.30 are assigned to the *endo* C-5, C-1, and *exo* C-5 methyl groups, respectively. The methyl signals of the corresponding bromo compound **25**, are assigned as in Table 2 by analogy.

TABLE 3. Infrared and ^1H nmr spectra of 5,5-dimethyl-2,3-norbornanedione (**31**) and 6-*endo*-oxygen-substituted 5,5-dimethyl-2,3-norbornanediones

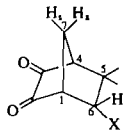

Spectrum	Assignment	**31** (X = H)	**17** (X = OMe)	**6** (X = OAc)
$\lambda_{max}(CCl_4)$ (μm)	C=O	5.65, 5.71	5.64, 5.70	5.61, 5.68, 5.72
	C—O		9.08	8.12
δ_H ($CDCl_3$)[a]	*endo*-Me	1.07(s)	0.94(s)	0.91(s)
	exo-Me	1.27(s)	1.32(s)	1.41(s)
	anti-7	1.4–2.6(m)[b]	1.93(dt, J = 13, 1.5 Hz)	2.03(dt, J = 12, 1.5 Hz)
	syn-7		2.40(dt, J = 13, 1.5 Hz)	2.60(dt, J = 12, 1.5 Hz)
	4	2.62(m)	2.65(m)	2.71(m)
	1	3.05(m)	3.4(m)[c]	3.33(m)
	6		3.72(dd, J = 4.8, 1.0 Hz)	5.14(dd, J = 5.2, 1.0 Hz)
	OMe, OAc		3.38(s)[c]	2.06(s)

[a]The relative intensities of the ^1H nmr signals are in accord with the assignments.
[b]Also includes H-6 signals.
[c]Overlapping signals.

The interesting observation has been made (22, 29) that the C-4 proton signal of **29** (δ 2.61) appears at lower field than the C-1 signal (δ 2.41). The spectra of compounds **27**, **15**, **16**, and **14** all show a one-proton multiplet in the region δ 2.6–2.8 and this is therefore assigned to the C-4 proton in each case. The downfield shift of this signal in the spectra of the last three compounds relative to its position in the spectra of **27** and **29** is attributable to the presence of the electron-withdrawing *endo* C-5 oxygen substituents. No individual signals could be assigned to the C-1 protons of compounds **27**, **15**, **16**, and **14** because of overlap with signals arising from the C-3 and/or C-7 protons (and C-5 protons in the case of **27**).

It remains to discuss the signals of the *exo* C-5 and *exo* C-6 protons in the spectra of **15**, **16**, and **14** and of **22** and **25**, respectively. As expected these are the lowest-field signals in each spectrum, occurring at δ 3.4–4.9. In the former group of compounds these signals appear as doublets of doublets. First-order analysis in terms of an AMX system gives values of $J \sim 4$ and 1 Hz for the coupling constants.[6] These can be ascribed to coupling of the C-5 proton with the C-4 and *exo* C-3 protons, respectively (25, 30–34). As expected in terms of this interpretation of the coupling of the C-5 protons in **15**, **16**, and **14**, the *exo* C-6 proton signals of **22** and **25** appear as singlets.

The strong ir bands and the ^1H nmr signals of the C-6 hetero-atom-substituted 2,3-norbornanediones are given in Tables 3 and 4, together with corresponding data (19) for the parent 5,5-dimethyl-2,3-norbornanedione (**31**) and isofenchoquinone (**32**).

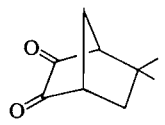

31

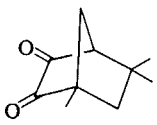

32

The methyl signals in the ^1H nmr spectrum of **31** at δ 1.07 and 1.27 can be assigned to the *endo* and *exo* methyl groups, respectively, on the basis of considerations similar to those invoked in the assignment of the methyl signals for **27**. As in the case of the latter, introduction of an *endo* methoxy or *endo* acetoxy substituent on the methylene carbon adjacent to the carbon bearing the geminal methyl groups, as in **17** and **6**, leads to an increase in the chemical shift difference between the geminal-methyl protons that can be interpreted as resulting from an upfield shift of the *endo* methyl signal and a downfield shift of the *exo* methyl signal. Similarly, the signals of **32**, at δ 1.03 (3H) and 1.28 (6H) can be assigned to the *endo* C-5 methyl group and a combination of the *exo* C-5 and the C-1 methyl groups, respectively, and again in analogy with the monoketone series, the effect of *endo* halogen substitution as in **23** and **26** can be interpreted in terms of down-

[6]The justification of the applicability of such a first-order analysis derives from the observation in analogous systems that none of the *exo* C-3, C-4, and *exo* C-5 protons are strongly coupled with one another and from the fact that in the present cases the lack of further splitting of the *exo* C-5 proton signal indicates that this proton is not virtually coupled with other protons; cf. refs. 30 and 31.

TABLE 4. Infrared and ^{1}H nmr spectra of isofenchoquinone (**32**) and 6-*endo*-halo-substituted 1,5,5-trimethyl-2,3-norbornanediones

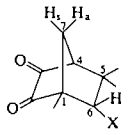

Spectrum	Assignment	**32** (X = H)	**23** (X = Cl)	**26** (X = Br)
$\lambda_{max}(CCl_4)$ (μm)	C=O	5.65, 5.70	5.64, 5.71	5.63, 5.69
δ_H ($CDCl_3$)[a]	*endo*-5-Me	1.03(s)	1.07(s)	1.11(s)
	exo-5-Me	1.28(s)[b]	1.36(s)	1.37(s)
	1-Me	1.28(s)[b]	1.33(s)	1.30(s)
	anti-7	1.4–2.6(m)[c]	1.91(dd, J = 13, 1.5 Hz)	2.01(dd, J = 12.5, 1.5 Hz)
	syn-7		2.43(dd, J = 13, 1.5 Hz)	2.54(dd, J = 12.5, 1.5 Hz)
	4	2.58(m)	2.73(m)	2.78(m)
	6		3.96(d, J = 1.2 Hz)	4.07(d, J = 1.25 Hz)

[a]The relative intensities of the ^{1}H nmr signals are in accord with the assignments.
[b]Superimposed signals.
[c]Also includes H-6 signals.

field shifts of the signals of both the adjacent *exo* and *endo* methyl protons, with the former effect having the greater magnitude.

The signals of the C-7 protons of **17** and **6** each appear as doublets of triplets with approximate values of $J_{7s,7a}$ of 12–13 Hz and $J_{1,7s}$ ($\sim J_{1,7a} J_{4,7s} \sim J_{4,7a}$) of 1.5 Hz. The lower-field signal in each case (δ 2.40 and 2.60, respectively) is assigned to the *syn* proton and the higher-field signal (δ 1.93 and 2.03, respectively) to the *anti* proton, in analogy with the relationship between the chemical shifts of the *syn* and *anti* C-7 proton signals of **29** (22). The assignment is corroborated by the observation that the signal of the *anti* C-7 proton of the α-dione **33** appears at δ 2.26;[7] it would be expected that this would be downfield from the signal of the *anti* C-7 protons of **17** and **6** because of deshielding by the C-7 methyl group in **33**. The C-7 proton signals of **23** and **26** each appear as doublets of doublets with $J \approx 13$ and 1.5 Hz, and again the lower-field signals are assigned to the *syn* proton and the higher-field signals to the *anti*-protons.

Multiplets at δ 3.4 and 3.33 in the spectra of **17** and **6**, respectively, are assigned to the C-1 protons; the latter has $w_{1/2} \sim 10$ Hz as expected to result from coupling J = 1–2 Hz with *syn* and *anti* C-7 and C-4 protons and $J \sim 5$ Hz with the *exo* C-6 proton (*vide infra*); in the case of **17** the multiplet is partially obscured by the methoxyl signal at δ 3.38. The chemical shifts of these multiplets may be compared with the chemical shift of the signal assigned to the C-1 proton (δ 3.05) in the parent compound **31**. This assignment is made in the expectation that, of the two bridgehead protons, the C-1 proton will give rise to a signal at lower field because of shielding of the C-4 proton by the C—C bond of the *exo* C-5 methyl group (35). The downfield bridgehead proton multiplet has a considerably greater band width, reflecting the additional coupling of the C-1 proton with the *exo* C-6 proton. The downfield shift of this signal in the spectra of **17** and **6** is attributable to the electron-withdrawing effect of the *endo* C-6 oxygen substituents. In accord with these interpretations, no signals appear in the δ 3.0–3.5 region of the spectra of compounds **32**, **23**, and **26**.

The *exo* C-6 signals in the spectra of **17** and **6** appear as doublets of doublets with $J \sim 5$ and 1 Hz. The larger splitting is expected as a result of coupling with the C-1 proton but the smaller is unusual in that it does not correspond to any of the common 'W pattern' long-range proton couplings in the norbornane system (33). That it involves long-range coupling with the C-4 proton was demonstrated by irradiation at the frequency of the C-4 proton signal (*vide infra*) in each case, which led to the collapse of the C-6 proton signals to doublets with J = 4.8 and 5 Hz, respectively. Analogous long-range coupling is also observed in the spectra of **23** and **26**, where the *exo* C-6 protons give rise to doublets with J = 1.2 and 1.25 Hz, respectively. Similar, unusual long-range couplings have been observed in the spectra of the α-diketones **34** and **35**

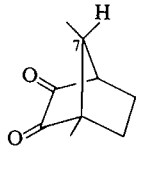

33

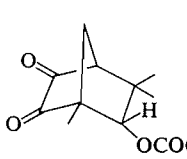

34

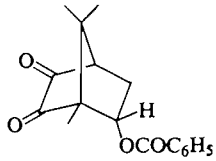

35

[7]P. Yates and D. G. B. Boocock. Unpublished results.

TABLE 5. Infrared and ^{1}H nmr spectra of 3-diazo-6,6-dimethyl-2-norbornanone (**36**) and 5-*endo*-oxygen-substituted 3-diazo-6,6-dimethyl-2-norbornanones

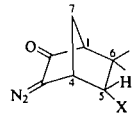

Spectrum	Assignment	**36** (X = H)	**2** (X = OMe)	**1** (X = OAc)
$\lambda_{max}(CCl_4)$ (μm)	C=$\overset{+}{N}$=$\overset{-}{N}$	4.85	4.82	4.82
	C=O	5.90	5.90	5.77, 5.90
	C=$\overset{+}{N}$=$\overset{-}{N}$	7.35	7.35	7.32
	C—O		9.05	8.09
δ_H ($CDCl_3$)[a]	*endo*-6-Me	1.10(s)	0.99(s)	0.94(s)
	exo-6-Me	1.17(s)	1.19(s)	1.27(s)
	7	1.90(m)	1.79(t, J = 1.8 Hz)	1.91(m)
	1	2.22(m)	2.18(m)	2.27(m)
	4	3.47(m)	3.65(m)[b]	3.63(m)
	5	1.5–1.9(m)	3.60(d, J = 3.4 Hz)[b]	5.03(d, J = 3.6 Hz)
	OMe, OAc		3.36(s)	2.06(s)

[a]The relative intensities of the ^{1}H nmr signals are in accord with the assignments.
[b]Overlapping signals.

TABLE 6. Infrared and ^{1}H nmr spectra of 3-diazoepiisofenchone (**37**) and 5-*endo*-halo-substituted 3-diazo-6,6-dimethyl-2-norbornanones

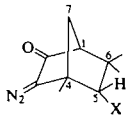

Spectrum	Assignment	**37** (X = H)	**3** (X = Cl)	**4** (X = Br)
$\lambda_{max}(CCl_4)$ (μm)	C=$\overset{+}{N}$=$\overset{-}{N}$	4.85	4.82	4.82
	C=O	5.90	5.90	5.90
	C=$\overset{+}{N}$=$\overset{-}{N}$	7.40	7.41, 7.51	7.42, 7.62
δ_H ($CDCl_3$)[a]	*endo*-6-Me	1.10(s)	1.12(s)	1.18(s)
	exo-6-Me	1.17(s)	1.25(s)	1.22(s)
	4-Me	1.43(s)	1.51(s)	1.50(s)
	7	1.60(br s)	1.90(d, J = 1.7 Hz)	1.98(d, J = 1.5 Hz)
	1	2.20(m)	2.30(t, J = 1.7 Hz)	2.33(t, J = 1.5 Hz)
	5	1.7–2.1(m)	3.92(s)	4.08(s)

[a]The relative intensities of the ^{1}H nmr signals are in accord with the assignments.

(36), and we have discussed the origin of such couplings elsewhere (37). Although such couplings with $J \geq 1$ Hz have only been observed for α-diketones, it should be pointed out, that analogous, albeit smaller, couplings have been observed in the case of 2-norbornanone (**29**), where $J_{1,5x} = 0.15$ Hz and $J_{4,6x} = 0.65$ Hz, although $J_{1,3x} = 0.0$ Hz (22).

Multiplets at δ 2.6–2.8 in the spectra of all the compounds in Tables 3 and 4 are assigned to the C-4 protons, as discussed earlier for the case of **31**. In the case of **17** and **6** these signals have a considerably narrower bandwidth than the signals assigned to the C-1 protons, as for **31**, and appear as quintuplets with peak separations of ~1.5 Hz, in accord with previously assigned couplings of this order of magnitude between the C-4 and C-1, *exo* C-6, C-7_a, and C-7_s protons.

The strong bands in the ir spectra and the ^{1}H nmr signals of the *endo* C-5 hetero-atom-substituted 3-diazo-2-norbornanones are given in Tables 5 and 6, together with corresponding data (19) for the parent 3-diazo-6,6-dimethyl-2-norbornanone (**36**) and 3-diazoepiisofenchone (**37**).

Assignments of the ^{1}H nmr signals to the methyl protons are made on the basis of considerations analogous to those discussed previously. The effects

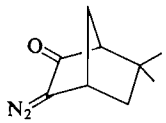

36

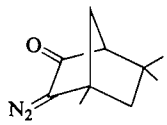

37

of the introduction of the *endo* C-5 hetero-atom substituents on the positions of the methyl signals are entirely analogous to those found for the corresponding mono- and α-diketones. It is noteworthy that in the cases of all pairs of similarly substituted α-diazo ketones and diketones, the *endo* C-6 methyl signal is shifted downfield in the diazo ketone spectrum whereas the *exo* C-6 methyl signal is shifted upfield. Comparison of the chemical shifts of the bridgehead methyl protons in **3**, **4**, and **37** with those in the corresponding diketones shows that replacement of the 3-keto group with a 3-diazo group leads to a downfield shift of this signal (Δδ 0.15–0.2).

The *syn* and *anti* C-7 protons in the spectra of the diazo ketones **1–4** are approximately chemically equivalent, unlike the C-7 protons in the corresponding diketones, and give rise to signals whose chemical shifts are similar to those of the *anti* C-7 protons in these diketones but appreciably upfield of the *syn* C-7 proton signals.

The signals of the bridgehead protons of diazo compounds **1**, **2**, and **36** appear as multiplets in the ranges δ 2.2–2.3 and 3.5–3.65. The former are assigned to the C-1 and the latter to the C-4 protons on the basis of comparison with the C-1 proton signals of the diazo ketones **3**, **4**, and **37**, which appear in the range δ 2.2–2.3 and of comparisons of the chemical shifts of the bridgehead protons of 3-diazoapocamphor (**38**) (δ 2.06, 2.92) with that of the bridgehead proton of 3-diazocamphor (**39**) (δ 2.92) (38) and those of the bridgehead protons of 3-diazo-2-norbornanone (**40**) (δ 2.62, 3.50) (39) with that of 3-diazo-β-santenone (**41**) (δ 3.15).[7] When account is taken of anisotropic shielding (Δδ ~ 0.3 per methyl group) of the bridgehead protons in **38**, **39**, and **41** by the C—CH_3 bonds of the C-7 methyl

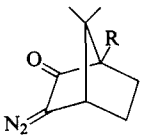

38 R = H
39 R = Me

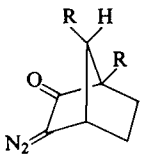

40 R = H
41 R = Me

groups, it can be seen that the C-4 proton signals of 3-diazo-2-norbornanones occur at considerably lower field than the C-1 proton signals. Comparison with the corresponding α-diketones shows that the C-4 proton signals are shifted downfield whereas the C-1 proton signals are shifted upfield. In accord with the above differentiation between the chemical shifts of the C-1 and C-4 protons the single C-1 bridgehead proton signals of **3**, **4**, and **37** occur in the range δ 2.2–2.3. The bandwidths and multiplicities of the signals assigned to the bridgehead protons of the diazo ketones are in accord with the attributions. Thus in the spectra of **1** and **2** the multiplets at δ 2.27 and 2.18, respectively, assigned to the C-1 protons are much narrower than the multiplets at δ 3.63 and 3.65, respectively, assigned to the C-4 protons. In each case the bridgehead proton is coupled with the other bridgehead proton and the C-7 protons but the C-4 protons are in addition coupled with the *exo* C-5 protons, accounting for the greater width of their signals. The multiplicities of the C-5 proton signals of **1–4** are of particular interest. In the case of **1** the signal is a doublet with $J = 3.6$ Hz, arising from coupling with the C-4 proton; in that of **2**, an analogous doublet can be discerned although here it overlaps with the signal due to the C-4 proton. In the cases of **3** and **4** the C-5 proton signals appear as singlets. These observations show that the coupling in these diazo ketones between the *exo* C-5 and C-1 protons, if any, is significantly less than in the case of the corresponding diketones. Possible interpretations of the enhanced coupling of this type in the diketone spectra have been discussed previously (37).

Experimental

Melting points and boiling points are uncorrected. Infrared spectra were recorded with carbon tetrachloride as solvent unless otherwise specified. Proton magnetic resonance spectra were recorded with deuteriochloroform as solvent. Solutions in organic solvents were dried over anhydrous magnesium sulfate and evaporated with a rotary evaporator unless otherwise specified.

*Camphenilone (**11**)*

Camphenilone was prepared by ozonolysis of *dl*-camphene (Aldrich; 80%, remainder tricyclene) (40) or by conversion of camphene to ω-nitrocamphene with nitrogen dioxide followed by treatment of this with aqueous sodium hydroxide (41); bp 78–83°C/18 Torr (lit. (42) bp 70–80°C/11 Torr); λ_{max}: 5.75 μm; δ_H: 1.2–2.6 (m, 8H), 1.02 (s), and 1.00 (s) (6H).

endo-*Camphenilol (**12**)*

A solution of camphenilone (**11**, 55.3 g) in anhydrous ether (100 mL) was added dropwise with stirring at a rate that maintained gentle refluxing to lithium aluminum hydride (9.0 g) in anhydrous ether (100 mL). After the addition was complete, the reaction mixture was stirred and boiled under reflux for 1 h. The excess lithium aluminum hydride was decomposed by cautious dropwise addition of water to the ice-cooled, stirred slurry. The aqueous layer was made homogeneous by addition of 5% sulfuric acid and the ethereal layer was separated. The aqueous layer was extracted with ether (4 × 100 mL) and the combined ethereal extracts were dried and filtered. The ether was removed and the residue was recrystallized from hexane to give **12** (34.5 g). Slow evaporation of hexane from the filtrate gave further **12** (16.0 g; total

yield, 50.5 g, 90%), mp 71–73°C (lit. (7) mp 66–69°C); λ_{max}: 2.75 μm; δ_H: 3.66 (br d, J = 4 Hz, 1H), 2.2 (m, 1H), 2.0 (s, shifts on dilution, 1H), 1.2–1.9 (m, 7H), 0.99 (s, 3H), 0.85 (s, 3H).

endo-*Camphenilyl Acetate (**13**)*

A solution of *endo*-camphenilol (**12**, 78.7 g) in acetic anhydride (280 mL) and pyridine (400 mL) was boiled under reflux with stirring for 3 h, cooled, and poured into a large amount of ice water. The mixture was extracted four times with ether. The combined ethereal extracts were washed with 10% hydrochloric acid, aqueous sodium bicarbonate, and water and dried. Distillation gave **13** (91.3 g, 89%), bp 98–99°C/17 Torr (lit. (7) bp 97–99°C/14 Torr); λ_{max}: 5.80, 8.09 μm; δ_H: 4.58 (br d, J = 4.0 Hz, 1H), 2.2 (m, 1H), 2.02 (s, 3H), 1.2–1.9 (m, 7H), 1.06 (s, 3H), 0.82 (s, 3H).

5-endo-*Acetoxy-6,6-dimethylbicyclo[2.2.1]heptan-2-one (**14**)*

A slurry of pulverized chromium trioxide (50 g) in glacial acetic acid (100 mL) was carefully added in small portions over 1 h to a stirred solution of *endo*-camphenilyl acetate (**13**, 25.0 g) in glacial acetic acid (35 mL) at a rate such that the reaction mixture temperature was maintained below 100°C. After the addition was complete, the solution was boiled under reflux and stirred for 30 min, cooled, and transferred to a separatory funnel with water (1200 mL). The green solution was extracted with ether (7 × 100 mL), and the combined ethereal extracts were washed with water (3 × 200 mL) and with saturated aqueous sodium bicarbonate (100 mL) and were dried. Distillation gave **13** (7.2 g), bp 42–50°C/25 × 10^{-3} Torr, and **14** (6.76 g, 35%), bp 70–71°C/25 × 10^{-3} Torr (lit. (7) bp 91–100°C/1.2 Torr); the product solidified slowly on standing at −20°C. One recrystallization from hexane gave a white solid, mp 61.0–63.0°C (lit. (7) mp 65.0–65.5°C); λ_{max}: 5.74, 7.10, 8.10 μm; δ_H: 4.89 (dd, J = 4.2 and 1.0 Hz, 1H), 2.83 (m, 1H), 2.07 (s, 3H), 2.1–2.3 and 1.6–2.0 (m, 5H), 1.23 (s, 3H), 0.83 (s, 3H).

6-endo-*Acetoxy-5,5-dimethylbicyclo[2.2.1]heptane-2,3-dione (**6**)*

A mixture of **14** (1.0 g), selenium dioxide (Alfa, 1.0 g), and bromobenzene (15 mL) was boiled under reflux with stirring for 9 h. The reaction was conveniently followed by examining the ^{1}H nmr spectra of aliquots that showed, when the reaction was complete, signal patterns identical with those in the ^{1}H nmr spectrum of **6** in benzene. The yellow solution was cooled and chromatographed on Florisil (100 g). Elution with benzene (750 mL) gave bromobenzene. Elution with 50% ether–benzene (450 mL) gave **6** as a yellow solid (0.75 g, 70%), mp 120.5–122.0°C (lit. (7) mp 121–122°C); λ_{max}: 5.61, 5.68, 5.72, 8.12 μm; δ_H: 5.14 (dd, J = 5.2 and 1.0 Hz, 1H), 3.33 (m, 1H), 2.71 (m, 1H), 2.60 (dt, J = 12 and 1.5 Hz, 1H), 2.03 (dt, J = 12 and 1.5 Hz, 1H), 2.06 (s, 3H), 1.41 (s, 3H), 0.91 (s, 3H).

6-endo-*Acetoxy-5,5-dimethylbicyclo[2.2.1]heptane-2,3-dione 2*-p-*Toluenesulfonylhydrazone (**7**)*

A warm solution of tosylhydrazine (0.96 g, 5.15 mmol) in glacial acetic acid (2.7 mL) was added to a warm solution of **6** (1.00 g, 4.75 mmol) in glacial acetic acid (1.6 mL). After standing at room temperature for 0.5 h the yellow solution was added dropwise to ice (100 g), forming a white precipitate that was filtered, washed thoroughly with water, and air dried overnight to give **7** (1.60 g, 88%), mp 159.5–162.0°C (lit. (7) mp 161–162°C); λ_{max}: ($CHCl_3$) 5.78, 6.11, 6.26 μm; δ_H: 7.7–8.0 (m, 2H), 7.2–7.5 (m, 2H), 4.90 (d, J = 4 Hz, 1H), 3.25 (m, 1H), 1.7–2.6 (m, 10H) with singlets at 2.40 (3H) and 1.79 (3H), 1.28 (s, 3H), 0.78 (s, 3H).

5-endo-*Acetoxy-3-diazo-6,6-dimethylbicyclo[2.2.1]heptan-2-one (**1**)*

A slurry of tosylhydrazone **7** (0.72 g) in benzene was placed on a 2.5 × 0.5 in. column of basic alumina (Merck 71707, 2.5 × 0.5 in.) packed in benzene. The reaction mixture was eluted with benzene. The first 600 mL of eluate contained most of the product. Any solid tosylhydrazone that remained on top of the column was mixed with the alumina by means of a long rod and elution with benzene was continued. Evaporation of the benzene from the eluate, and recrystallization of the residual solid from a small amount of hexane afforded **1** as yellow crystals (0.295 g, 70%), mp 69.0–71.0°C (lit. (7) mp 70–71°C); λ_{max}: 4.82, 5.77, 5.90, 7.32, 8.09 μm; δ_H: 5.03 (d, J = 3.6 Hz, 1H), 3.63 (m, 1H), 2.27 (m, 1H), 2.06 (s, 3H), 1.91 (m, 2H), 1.27 (s, 3H), 0.94 (s, 3H).

5-endo-*Hydroxy-6,6-dimethylbicyclo[2.2.1]heptan-2-one (**15**)*

A solution of **14** (2.0 g) in 50% methanol–water (24 mL) and potassium carbonate (5.0 g) was boiled under reflux with stirring for 2.5 h. After cooling the red solution was extracted with ether (70 and 35 mL) and the combined ethereal extracts were dried and filtered. Evaporation of the ether afforded the hygroscopic keto alcohol **15** (1.25 g, 80%), which was a semi-solid at room temperature; λ_{max}: 2.82, 2.95, 5.74, 7.11 μm; δ_H: 3.98 (dd, J = 4.0 and 1.0 Hz, 1H), 3.02 (s, shifts on dilution, 1H), 2.7 (m, 1H), 1.3–2.4 (m, 5H), 1.12 (s, 3H), 0.88 (s, 3H).

5-endo-*Methoxy-6,6-dimethylbicyclo[2.2.1]heptane-2-one (**16**)*

To a stirred mixture of **15** (1.25 g), methyl iodide (1.4 mL), 1,2-dimethoxyethane (10 mL), and anhydrous sodium sulfate (ca. 0.2 g) was added over 0.5 h pure sodium hydride obtained by washing a 53% dispersion of sodium hydride (0.440 g) in oil three times with ether and drying under a stream of nitrogen. After an additional 0.5 h of stirring, further methyl iodide (0.5 mL) was added and the mixture was stirred overnight. The mixture was filtered, and the ether and excess methyl iodide were evaporated. The product was treated with warm hexane (40 mL) and the hexane-soluble fraction was decanted. Evaporation of the hexane gave **16** (88% pure as determined by vpc; 0.95 g, 69%). The impure **16** (100 mg) was chromatographed on Florisil (10 g). After elution with benzene (175 mL) and 5% ether–benzene (40 mL), pure **16** (24 mg) was obtained from the next 20 mL of 5% ether–benzene eluate; bp 56°C/50 × 10^{-3} Torr); λ_{max}: 3.53, 5.74, 7.11, 9.00 μm; δ_H: 3.44 (dd, J = 4.0 and 1.1 Hz, 1H), 3.34 (s, 3H), 2.8 (m, 1H), 1.3–2.2 (m, 5H), 1.14 (s, 3H), 0.88 (s, 3H). *Anal.* calcd. for $C_{10}H_{16}O_2$: C 71.39, H 9.59; found: C 71.65, H 9.55.

6-endo-*Methoxy-5,5-dimethylbicyclo[2.2.1]heptane-2,3-dione (**17**)*

A mixture of **16** (0.99 g), **14** (0.20 g), selenium dioxide (Alfa, 0.99 g), and bromobenzene (6.6 mL) was stirred and heated in an oil bath at 150°C for ca. 4 h. As the reaction proceeded, the ^{1}H nmr spectra of aliquots showed a new signal, assigned to the methoxyl protons of **17**, at slightly lower field than the signal attributed to the methoxyl protons of **16**. The red solution was cooled and chromatographed on Florisil (150 g). Elution with benzene (600 mL) gave bromobenzene and elution with a further 50 mL of benzene gave **14**. Elution with a further 250 mL of benzene gave crude **17** (193 mg), which was recrystallized from hexane to give **17** (148 mg, 14%) as yellow crystals, mp 54.5–55.5°C; λ_{max}: 5.64, 5.70, 9.08 μm; δ_H: 3.72 (dd, J = 4.8 and 1.0 Hz, 1H), 3.4 (m) and 3.38 (s) (4H), 2.65 (m, 1H), 2.40 (dt, J = 13 and 1.5 Hz, 1H), 1.93 (dt,

J = 13 and 1.5 Hz, 1H), 1.32 (s, 3H), 0.94 (s, 3H). *Anal.* calcd. for $C_{10}H_{14}O_3$: C 65.91, H 7.74; found: C 65.81, H 7.89.

*3-Diazo-5-*endo*-methoxy-6,6-dimethylbicyclo[2.2.1]heptan-2-one (2)*

A warm solution of tosylhydrazine (75 mg, 0.40 mmol) in glacial acetic acid (0.2 mL) was added to a warm solution of **17** (65 mg, 0.36 mmol) in glacial acetic acid (0.2 mL). After standing for 2.5 h at room temperature the yellow solution was added dropwise to ice (10 g), forming a light yellow precipitate of tosylhydrazone **18** that was collected and washed thoroughly with water. Five millilitres of 0.3 *M* aqueous sodium hydroxide was added to the tosylhydrazone and the yellow solution that formed after a few minutes of stirring was stirred vigorously with hexane (20 mL) for 0.5 h. The hexane layer was removed, ether (25 mL) was added, and the mixture was stirred vigorously for 2 h. The ethereal layer was removed, fresh ether (25 mL) was added, and the mixture was again stirred vigorously for 2 h. This process was repeated until the ethereal layer was colorless (ca. 8 h). The combined organic extracts were dried over anhydrous sodium sulfate for 4 h and filtered. Evaporation of the solvent gave **2** (39 mg, 57%) as a yellow oil that solidified on standing, mp 57–59°C; λ_{max}: 4.82, 5.90, 7.35, 9.05 μm; δ_H: 3.65 (m, 1H), 3.60 (d, J = 3.4 Hz, 1H), 3.36 (s, 3H), 2.18 (m, 1H), 1.79 (t, J = 1.8 Hz, 2H), 1.19 (s, 3H), 0.99 (s, 3H). *Mol. Wt.* calcd. for $C_{10}H_{14}N_2O_2$: 194.1055; found (ms): 194.1050.

*6-*endo*-Chloro-1,5,5-trimethylbicyclo[2.2.1]heptan-2-*exo*-ol (21)*

An ice-cooled solution of *trans*-pinocarveol (**20**, 5.0 g) (42) in anhydrous ether (25 mL) was saturated with hydrogen chloride. The light brown solution was kept at 0°C for 20 h and poured onto ice (80 g). Ether (50 mL) was added and the ethereal extract was washed with water (4 × 50 mL), dried, and filtered. Evaporation of the ether afforded **21** (5.89 g, 92%) as a volatile solid, mp 84–91°C (lit. (16) mp 99.5°C); δ_H: 4.02 (ddd, J = 7.0, 3.5, and 1.3 Hz, 1H), 3.69 (s, 1H), 1.3–2.8 (m, including a singlet at 2.2 that shifts on dilution, 6H), 1.15 (s, 3H), 1.06 (s, 3H), 0.95 (s, 3H).

*6-*endo*-Chloro-1,5,5-trimethylbicyclo[2.2.1]heptan-2-one (22)*

To an ice-cooled, stirred solution of **21** (4.9 g) in glacial acetic acid (12 mL) was added dropwise a solution of chromium trioxide (4.0 g) in a small amount of water and glacial acetic acid (18 mL). After 22 h standing the dark green solution was poured into water (100 mL) and extracted with ether (2 × 75 mL). The ethereal extracts were washed with saturated aqueous sodium bicarbonate and dried. Distillation afforded **22** (1.77 g, 37%), bp 93–97°C/2 Torr (lit. (15) bp 132–122°C/15 Torr); λ_{max}: 5.71, 7.10 μm; δ_H: 3.81 (s, 1H), 1.3–2.9 (m, 5H), 1.30 (s, 3H), 1.20 (s, 3H). 1.12 (s, 3H).

*6-*endo*-Chloro-1,5,5-trimethylbicyclo[2.2.1]heptane-2,3-dione (23)*

A mixture of **22** (100 mg), glacial acetic acid (2 mL), and selenium dioxide (150 mg) was boiled under reflux with stirring for 19 h, cooled, poured into water, and extracted with ether (2 × 20 mL). The ethereal extracts were washed with saturated aqueous sodium bicarbonate, dried, and filtered. Evaporation of the ether and recrystallization of the residue from hexane afforded **23** (33 mg, 31%) as yellow needles, mp 108–114°C; further recrystallizations gave yellow needles, mp 115.0–116.2°C; λ_{max}: 5.64, 5.71 μm; δ_H: 3.96 (d, J = 1.2 Hz, 1H), 2.73 (m, 1H), 2.43 (dd, J = 13 and 1.5 Hz, 1H), 1.91 (dd, J = 13 and 1.5 Hz, 1H), 1.36 (s) and 1.33 (s) (6H), 1.07 (s, 3H). *Anal.* calcd. for $C_{10}H_{13}O_2Cl$: C 59.87, H 6.53, Cl 17.67; found: C 59.69, H 6.40, Cl 17.44.

*5-*endo*-Chloro-3-diazo-4,6,6-trimethylbicyclo[2.2.1]heptan-2-one (3)*

A warm solution of tosylhydrazine (152 mg, 0.82 mmol) in glacial acetic acid (1.4 mL) was added to a warm solution of **23** (148 mg, 0.74 mmol) in glacial acetic acid (0.7 mL). After standing for 1.25 h at room temperature the yellow solution was added dropwise to ice (14 g) forming a light yellow precipitate, which was collected and washed with water. Five millilitres of 0.3 *M* aqueous sodium hydroxide was added to the solid and the mixture was stirred for a few minutes until a yellow solution formed. Hexane (5 mL) was added, and the mixture was stirred vigorously for 1 h. The yellow hexane layer was removed, further hexane (5 mL) was added, the mixture was stirred vigorously for a further 2.5 h, and the faintly yellow hexane layer was removed. The combined hexane extracts were dried and filtered. Evaporation of the ether and recrystallization of the residue from hexane afforded **3** (95 mg, 62%) as yellow needles, mp 77–79°C; λ_{max}: 4.82, 5.90, 7.41, 7.51 μm; δ_H: 3.92 (s, 1H), 2.30 (t, J = 1.7 Hz, 1H), 1.90 (d, J = 1.7 Hz, 2H), 1.51 (s, 3H), 1.25 (s, 3H), 1.12 (s, 3H). *Anal.* calcd. for $C_{10}H_{13}N_2OCl$: C 56.48, H 6.16, Cl 16.67; found: C 56.32, H 6.19, Cl 16.28.

*6-*endo*-Bromo-1,5,5-trimethylbicyclo[2.2.1]heptan-2-*exo*-ol (24)*

An ice-cooled solution of *trans*-pinocarveol (**20**, 19.3 g) (46) in anhydrous ether (90 mL) was saturated with hydrogen bromide and kept at 0°C for 20 h. Evaporation of the ether and excess hydrogen bromide followed by air drying for 0.5 h gave **24** (26.0 g, 88%). After one recrystallization from petroleum ether (bp 60–70°C) **24** was obtained as fluffy white needles, mp 111–114°C (lit. (17) 118–119°C); λ_{max}: 2.79, 9.45 μm; δ_H: 3.97 (ddd, J = 7.4, 3.5, and 0.8 Hz, 1H), 3.85 (s, 1H), 1.3–2.8 (m, including a singlet at 2.2 that shifts on dilution, 6H), 1.18 (s, 3H), 1.08 (s, 3H), 1.02 (s, 3H).

*6-*endo*-Bromo-1,5,5-trimethylbicyclo[2.2.1]heptan-2-one (25)*

The method used was similar to that previously described (17). To the complex formed from chromium trioxide (8.3 g) and pyridine (125 mL) was added a solution of **24** (5.0 g) in pyridine (8 mL), and the mixture was stirred at room temperature for 44 h. The reaction mixture was poured into a separatory funnel, and ether (400 mL) and a solution of concentrated hydrochloric acid (137 mL) in water (250 mL) was added. The emulsion that formed on shaking this mixture was filtered to separate a brown sludge. The ethereal layer from the filtrate was washed with 10% hydrochloric acid (2 × 50 mL) and saturated aqueous sodium bicarbonate (2 × 50 mL), dried, and filtered. Evaporation of the ether afforded **25** (3.73 g, 75%); λ_{max}: 5.71, 7.12 μm; δ_H: 3.93 (s, 1H), 1.3–2.7 (m, 5H), 1.28 (s, 3H), 1.15 (s, 6H).

*6-*endo*-Bromo-1,5,5-trimethylbicyclo[2.2.1]heptane-2,3-dione (26)*

A mixture of **25** (0.50 g), selenium dioxide (0.75 g), and acetic acid (10 mL) was boiled under reflux with stirring for 3.5 h. The mixture was cooled and ether (150 mL) was added. The ethereal solution was washed with saturated aqueous sodium bicarbonate until the evolution of carbon dioxide ceased, dried, and filtered. Evaporation of the ether afforded a red oil. Hexane (20 mL) was added to the oil, the mixture was heated, and the hexane-soluble fraction was decanted and cooled to −20°C, affording orange crystals (190 mg). Sublimation at 80°C/50 × 10^{-3} Torr gave **26** (161 mg, 31%) as a yellow solid, mp 120–123°C; recrystallizations from hexane raised the melting point to 131.5–132.5°C; λ_{max}: 5.63, 5.69 μm; δ_H: 4.07 (d, J = 1.25 Hz, 1H), 2.78 (m, 1H), 2.54 (dd, J = 12.5 and 1.5 Hz, 1H), 2.01 (dd, J = 12.5 and 1.5 Hz, 1H), 1.37 (s,

3H), 1.30 (s, 3H), 1.11 (s, 3H). *Anal.* calcd. for $C_{10}H_{13}O_2Br$: C 49.00, H 5.35, Br 32.60; found: C 48.97, H 5.49, Br 32.48.

5-endo-Bromo-3-diazo-4,6,6-trimethylbicyclo[2.2.1]heptan-2-one (4)

A warm solution of tosylhydrazine (250 mg, 1.34 mmol) in glacial acetic acid (2.4 mL) was added to a warm solution of **26** (290 mg, 1.18 mmol) in glacial acetic acid (1.2 mL). After standing for 2.0 h in an oil bath at 50°C the yellow solution was added dropwise to ice (15 g) forming a light yellow precipitate that was collected on a sintered glass funnel, washed thoroughly with water, and dried in a desiccator *in vacuo* overnight. The tosylhydrazone (mp 136–139°C; 510 mg, 86%) was dissolved in benzene and placed on a column of basic alumina (Merck 71707, 3.0 × 0.5 in.), and the product was eluted with benzene (200 mL). Evaporation of the benzene, and recrystallization of the residual yellow solid from hexane afforded **4** (194 mg, 64% based on **26**) as yellow needles, mp 95.0–96.5°C; further recrystallizations raised the melting point to 99.0–100.0°C; λ_{max}: 4.82, 5.90, 7.42, 7.62 μm; δ_H: 4.08 (s, 1H), 2.33 (t, J = 1.5 Hz, 1H), 1.98 (d, J = 1.5 Hz, 2H), 1.50 (s, 3H), 1.22 (s) and 1.18 (s) (6H). *Anal.* calcd. for $C_{10}H_{13}N_2OBr$: C 46.71, H 5.10, N 10.89, Br 31.08; found: C 46.85, H 5.23, N 10.52, Br 30.81.

Acknowledgement

We thank the National Research Council of Canada for support of this work.

1. P. YATES, F. X. GARNEAU, and G. F. HAMBLY. Polish J. Chem. In press.
2. P. YATES. J. Am. Chem. Soc. **74**, 5376 (1952).
3. P. YATES and J. FUGGER. Chem. Ind. (London), 1511 (1957).
4. P. YATES and S. DANISHEFSKY. J. Am. Chem. Soc. **84**, 879 (1962).
5. P. YATES and R. J. CRAWFORD. J. Am. Chem. Soc. **88**, 1562 (1966).
6. P. YATES and G. F. HAMBLY. Can. J. Chem. This issue.
7. J. MEINWALD, P. G. GASSMAN, and J. J. HURST. J. Am. Chem. Soc. **84**, 3722 (1962).
8. F. R. JENSEN and C. H. BUSHWELLER. Adv. Alicyclic Chem. **3**, 139 (1971); H. BOOTH and J. R. EVERETT. J. Chem. Soc. Chem. Commun. 278 (1976).
9. H. C. BROWN and J. MUZZIO. J. Am. Chem. Soc. **88**, 2811 (1966).
10. W. P. JENCKS. J. Am. Chem. Soc. **81**, 475 (1959); R. L. REEVES. *In* The chemistry of the carbonyl group. Vol. 1. *Edited by* S. Patai. Wiley-International, London. 1966. p. 567.
11. D. E. MCGREER. Can. J. Chem. **40**, 1554 (1962).
12. J. BREDT and A. GOEB. J. Prakt. Chem. [2] **101**, 273 (1921); cf. E. HEINÄNEN. Suom. Kemistil. B, **42**, 53 (1969).
13. K. B. WIBERG, B. R. LOWRY, and T. H. COLBY. J. Am. Chem. Soc. **83**, 3998 (1961).
14. J. B. HENDRICKSON and W. A. WOLF. J. Org. Chem. **33**, 3610 (1968).
15. M. ROSENBERGER, P. YATES, J. B. HENDRICKSON, and W. WOLF. Tetrahedron Lett. 2285 (1964).
16. W. TREIBS, M. MÜLHLSTÄDT, R. MEGGES, and I. KLOTZ-HERDMANN. Justus Liebigs Ann. Chem. **634**, 118 (1960).
17. M. P. HARTSHORN and A. F. A. WALLIS. J. Chem. Soc. 5254 (1954).
18. P. P. WILLIAMS. Chem. Ind. (London), 1583 (1964).
19. R. A. BLATTEL. Ph.D. Thesis, University of Toronto, Toronto. 1971.
20. A. P. MARCHAND and N. W. MARCHAND. Tetrahedron Lett. 1365 (1971).
21. R. R. FRASER. Can. J. Chem. **40**, 78 (1962).
22. J. L. MARSHALL and S. R. WALTER. J. Am. Chem. Soc. **96**, 6358 (1974).
23. D. E. GWYNN and L. SKILLERN. Chem. Commun. 490 (1968).
24. W. C. AGOSTA and A. B. SMITH III. J. Am. Chem. Soc. **93**, 5513 (1971).
25. K. T. LIU. J. Chin. Chem. Soc. (Taipei), **23**, 1 (1976).
26. J. B. STOTHERS and K. C. TEO. Can. J. Chem. **54**, 1222 (1976).
27. L. A. HULL and P. D. BARTLETT. J. Org. Chem. **40**, 824 (1975).
28. E. PRETSCH, H. IMMER, C. PASCUAL, K. SCHAFFNER, and W. SIMON. Helv. Chim. Acta, **50**, 105 (1967); W. L. DILLING, R. D. KROENING, and J. C. LITTLE. J. Am. Chem. Soc. **92**, 928 (1970); R. V. MOEN and H. S. MAKOWSKI. Anal. Chem. **43**, 1629 (1971).
29. D. G. FARNUM and G. MEHTA. J. Am. Chem. Soc. **91**, 3256 (1969).
30. J. I. MUSHER. Mol. Phys. **6**, 93 (1963); F. A. L. ANET. Can. J. Chem. **39**, 789 (1961).
31. T. J. FLAUTT and W. F. ERMAN. J. Am. Chem. Soc. **85**, 3212 (1963).
32. A. RASSAT, C. W. JEFFORD, J. M. LEHN, and B. WAEGELL. Tetrahedron Lett. 233 (1964).
33. L. M. JACKMAN and S. STERNHELL. Applications of nuclear magnetic resonance spectroscopy in organic chemistry. 2nd ed. Pergamon Press, Oxford. 1969. pp. 289, 334.
34. M. BARFIELD and B. CHAKRABARTI. Chem. Rev. **69**, 757 (1969).
35. J. W. APSIMON, W. G. CRAIG, P. V. DEMARCO, D. W. MATHIESON, L. SAUNDERS, and W. B. WHALLEY. Chem. Commun. 359 (1966); K. C. RAMEY, D. C. LINI, R. M. MORIARTY, H. GOPAL, and H. G. WELSH. J. Am. Chem. Soc. **89**, 2401 (1967); R. G. FOSTER and M. C. MCIVOR. Chem. Commun. 280 (1967); P. YATES and D. G. B. BOOCOCK. J. Org. Chem. **38**, 3651 (1973).
36. G. CHALIER, A. RASSAT, and A. ROUSSEAU. Bull. Soc. Chim. Fr. 428 (1966); G. CHALIER, D. GAGNAIRE, and A. RASSAT. Bull. Soc. Chim. Fr. 387 (1969).
37. G. F. HAMBLY, J. LEITCH, P. YATES, and S. C. NYBURG. Can. J. Chem. **51**, 4076 (1973).
38. J. D. FENWICK. Ph.D. Thesis, University of Toronto, Toronto. 1970.
39. R. J. CRAWFORD. Ph.D. Thesis, University of Toronto, Toronto. 1965.
40. P. S. BAILEY. Chem. Ber. **88**, 795 (1965).
41. S. V. HINTIKKA and G. KOMPPA. Justus Liebigs Ann. Chem. **383**, 293 (1912); M. HANACK and H. EGGENSPERGER. Justus Liebigs Ann. Chem. **648**, 3 (1961).
42. L. M. JOSHEL and S. PALKIN. J. Am. Chem. Soc. **64**, 1008 (1942).

Aliphatic diazo compounds. XIII. The copper-catalyzed decomposition of 5-*endo*-hetero-atom-substituted 3-diazo-2-norbornanones[1,2]

PETER YATES AND GORDON F. HAMBLY[3]

Lash Miller Chemical Laboratories, Department of Chemistry, University of Toronto, Toronto, Ont., Canada M5S 1A1

Received November 29, 1978

PETER YATES and GORDON F. HAMBLY. Can. J. Chem. 57, 1668 (1979).

The copper-catalyzed decomposition of 5-*endo*-acetoxy-3-diazo-6,6-dimethyl-2-norbornanone (**4**) in dilute solution in benzene gives as the major product 2-acetoxy-5,5-dimethyltricyclo[2.2.1.$0^{2,6}$]heptan-3-one (**12**) together with 5-*endo*-acetoxy-6,6-dimethyl-2-norbornanone (**8**), 6-*endo*-acetoxy-5,5-dimethyl-2,3-norbornanedione (**9**), and 5-*endo*-acetoxy-3-*endo*-hydroxy-6,6-dimethyl-2-norbornanone (**10**). The structure of **12** was established by its independent synthesis from 5-*endo*-bromo-7,7-dimethyl-2,3-norbornanedione (**19**) by treatment with lithium followed by acetic anhydride. Copper-catalyzed decomposition of **4** labelled with ^{18}O in the acetoxyl carbonyl shows that the major pathway for the formation of **12** involves bonding of the carbenoid center at C-3 to the carbonyl oxygen of the acetoxyl group and not insertion into the *endo* C-5–oxygen bond. Similar copper-catalyzed decomposition of **5**, the methoxy analogue of **4**, gives only 9,9-dimethyl-5-oxatricyclo[4.2.1.$0^{3,7}$]nonan-2-one (**31**), the product of carbenoid insertion into a C—H bond of the methoxyl methyl group. Copper-catalyzed decomposition of 5-*endo*-chloro-3-diazo-4,6,6-trimethyl-2-norbornanone (**6**) and of **7**, its bromo analogue, gives as major products the corresponding α-diketones and azines; if insertion into the *endo* C-5–halogen bond occurs at all it can only represent a minor pathway. Thus although very ready carbenoid insertion into an *endo* C-5–hydrogen bond occurs in the copper-catalyzed decomposition of 3-diazo-2-norbornanones, such insertion into an *endo* C-5 – hetero atom bond occurs with difficulty, if at all.

PETER YATES et GORDON F. HAMBLY. Can. J. Chem. 57, 1668 (1979).

La décomposition catalysée par le cuivre de l'acétoxy-5-*endo* diazo-3 diméthyl-6,6 norbornanone-2 (**4**) en solution diluée dans le benzène fournit l'acétoxy-2 diméthyl-5,5 tricyclo-[2.2.1.$0^{2,6}$]heptanone-3 (**12**) comme produit principal aux côtés d'acétoxy-5-*endo* diméthyl-6,6 norbornanone-2 (**8**), d'acétoxy-6-*endo* diméthyl-5,5 norbornanedione-2,3 (**9**) et d'acétoxy-5-*endo* hydroxy-3-*endo* diméthyl-6,6 norbornanone-2 (**10**). On a déterminé la structure de **12** en effectuant sa synthèse à partir de la bromo-5-*endo* diméthyl-7,7 norbornanedione-2,3 (**19**) par une réaction avec du lithium suivie par de l'anhydride acétique. La décomposition catalysée par le cuivre de **4** dont le carbonyle de l'acétoxyle est marqué au ^{18}O démontre que la voie principale conduisant à la formation de **12** implique la liaison du centre carbénoïde en C-3 à l'oxygène du carbonyle du groupe acétoxyle et non pas l'insertion dans la liaison C-5–oxygène *endo*. Une décomposition semblable, catalysée par le cuivre, de **5**, l'analogue méthoxylé de **4**, ne fournit que la diméthyl-9,9 oxa-5 tricyclo[4.2.1.$0^{3,7}$]nonanone-2 (**31**), le produit provenant de l'insertion d'un carbénoïde dans une liaison C—H du groupe méthyle du méthoxyle. Les compositions catalysées par le cuivre de la chloro-5-*endo* diazo-3 triméthyl-4,6,6 norbornanone (**6**) et de **7**, son analogue bromé, conduisent aux α-dicétones et aux azines correspondants comme produits principaux; s'il se produit la moindre insertion dans la liaison C-5–halogène *endo* elle ne représente qu'une voie de réaction mineure. Donc, même s'il se produit des insertions faciles de carbénoïdes dans une liaison C-5–hydrogène lors de la décomposition catalysée par le cuivre de diazo-3 norbornanones-2, de telles insertions dans une liaison C-5 – hétéro atome *endo* ne se produisent, au mieux, qu'avec difficulté.

[Traduit par le journal]

It has long been known that thermal or copper-catalyzed decomposition of 3-diazocamphor (**1**) gives cyclocamphanone (**2**) (2). Several other 3-diazobicyclo[2.2.1]heptan-2-ones (3-diazo-2-norbornanones) have been found to undergo analogous reactions (3, 4) and it has become generally accepted (5) that such reactions involve loss of nitrogen from the α-diazo ketone to give an α-oxocarbene (e.g., **3**) or α-oxocarbene–copper complex that undergoes intramolecular C—H insertion to give the tricyclic

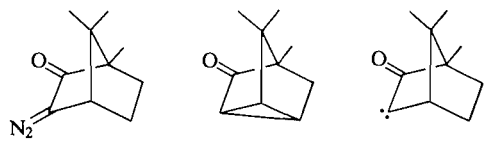

1 **2** **3**

[1]Dedicated to the memory of R. H. F. Manske.

[2]For paper XII, see ref. 1.

[3]Present address: Chemistry Department, John Abbott College, Ste. Anne de Bellevue, P.Q., Canada H9X 3L9.

0008-4042/79/131668-11$01.00/0

ketone.[4] In accord with such a mechanism, all of the 3-diazo-2-norbornanones that have been reported to undergo the reaction possess an *endo* C—H bond at C-5. We thought it of interest to study the course of the copper-catalyzed decomposition of 3-diazo-2 norbornanones, that possess an *endo* carbon–hetero atom bond at C-5 and to this end have examined the copper-catalyzed decomposition of the α-diazo ketones **4**–**7** (1).

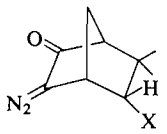

4 X = OAc
5 X = OMe

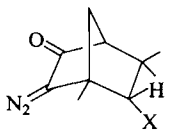

6 X = Cl
7 X = Br

Products from the Copper-catalyzed Decomposition of the Diazo Ketones

The diazo ketone **4** was decomposed in the presence of an excess of copper in benzene under high dilution conditions to minimize the occurrence of bimolecular reactions. The product distribution from such decomposition of **4** was found to be remarkably dependent on the provenance of the copper used as catalyst. In general four products were obtained. Two of these were **8** and **9**, compounds which were

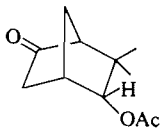

8

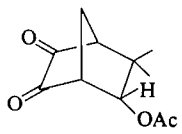

9

readily identified since they had been prepared as intermediates in the synthesis of **4** (1).

Another product is assigned structure **10** on the following basis. Its mass spectrum showed that it is a compound $C_{11}H_{16}O_4$ and its ir spectrum (λ_{max} 2.95, 5.74 μm) indicated that it is a hydroxy ketone. Its ^{1}H nmr spectrum indicated that it retains the CHOAc grouping (δ 2.08 (s, 3H), 5.07 (br d, J = 4 Hz, 1H)) and has another proton on a carbon bearing an oxygen atom (δ 4.03 (br d, J = 4 Hz)). This structural assignment was confirmed by hydrogenation of the dione **9**, which gave a mixture whose major component is identical with the hydroxy ketone obtained from the copper-induced decomposition of **4**, as indicated by its vpc retention time and ^{1}H nmr spectrum. The minor product is considered to be **11** on the basis of its ^{1}H nmr spectrum (δ 2.04 (s), 4.22 (d, J = 4 Hz), 4.92 (d, J = 4 Hz)). The formation of the *endo* hydroxy isomers **10** and **11** on

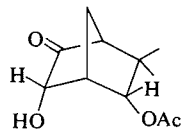

10

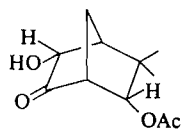

11

hydrogenation of **9** is expected since it involves addition of hydrogen from the least hindered *exo* face (7).

The fourth product from the copper-induced decomposition of **4** was the most volatile product and was the major product (74%) when the most active copper catalysts were used. Its elemental composition and mass spectrum showed that it corresponds in composition to loss of nitrogen from **4**. Its ir spectrum includes strong bands of equal intensity at 5.60 and 5.65 μm suggesting the retention of two carbonyl groups. Its ^{1}H nmr spectrum shows a sharp three-proton singlet at δ 2.11 and no signals at lower field than δ 2.35, indicating the presence of a tertiary acetate and the absence of vinylic protons; it also shows two three-proton singlets at δ 1.05 and 1.27, indicating the retention of the geminal methyl groups, and an apparent one-proton quintuplet (J = 1.5 Hz) at δ 1.65 (*vide infra*). On the basis of these data and its origin, it was concluded that this product has structure **12**. Thus the position of its ir

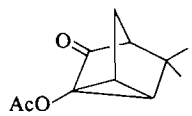

12

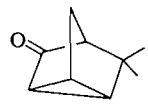

13

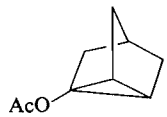

14

carbonyl stretching bands relative to those of cyclocamphanone (**2**) and cycloapocamphanone (**13**) (5.70 μm)[5] and of 1-acetoxynortricyclene (**14**) (5.68 μm (8)) can be interpreted in terms of the well-known shift to lower wavelength of both carbonyl stretching bands of α-acetoxy ketones relative to the bands in the corresponding ketones and acetates (9*a*). It is noteworthy that the C—O stretching band of the acetate group in **12** is at unusually long wavelength (8.28 μm) relative to simple acetates (8.0–8.1 μm (9*b*)), in accord with the observation of Jones and Herling (10) that the wavelengths of the C—O bands of a number of steroid acetates are inversely related

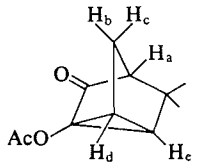

12′

[4]In the case of **1** and its 4-methyl derivative, the reaction has also been shown to be catalyzed by silver salts (6).

[5]Cycloapocamphanone (**13**) was prepared by the copper-catalyzed decomposition of 3-diazoapocamphor (4).

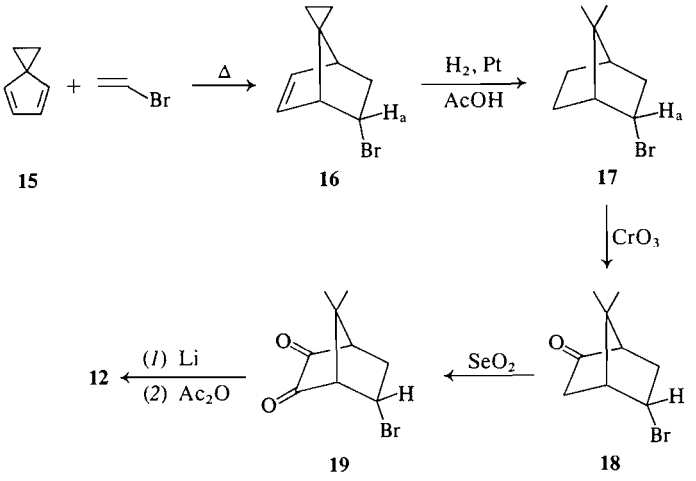

SCHEME 1

to the wavelengths of their C=O bands. The geminal methyl signals in the ^{1}H nmr spectrum of **12** are more widely separated ($\Delta\delta$ 0.22) than they are in the spectrum of **13** (δ 1.04 and 1.08 (4)), a circumstance that can be attributed to deshielding of one of the methyl groups in **12** by the acetoxyl group. The one-proton quintuplet at δ 1.65 is assigned to H_a (see **12'**); its high-field position is attributed to shielding by the cyclopropane ring and its multiplicity to approximately equivalent vicinal coupling with H_b and H_c and long range (^4J) coupling with H_d and H_e ($J \sim 1.5$ Hz). Analogous long-range coupling has been observed in the spectrum of **13** (4) and corresponds to the well-known 'W-pattern' couplings of the C-1 and C-4 protons in 2-norbornanones (11).

The assignment of structure **12** to the major product from the copper-catalyzed decomposition of **4** was confirmed by an independent synthesis of **12** by the route shown in Scheme 1.

The spiro diene **15** (12)[6] and vinyl bromide at 170°C gave the Diels–Alder adduct **16** in good yield. The ^{1}H nmr spectrum of **16** shows a doublet of triplets at δ 4.47 (J = 8.0, 3.5 Hz, 1H), assigned to H_a; comparison with the spectra of *endo*- and *exo*-5-bromonorbornene (**20** and **21**, respectively) (13) leaves no doubt that the adduct has the *endo* configuration as in **16**. Hydrogenation of **16** proceeded with the uptake of 2 molar equiv. of hydrogen (14) to give apobornyl bromide (**17**) in high yield; this shows a very broad multiplet in its ^{1}H nmr spectrum at δ 4.62 ($w_{1/2}$ = 21 Hz), assigned to H_a, again demonstrating the *endo* configuration (1, 15).

An alternative route to **17** was investigated, based on the report that addition of hydrogen bromide to apopinene (**22**) in chloroform gave a mixture of bromides that upon treatment with silver acetate in acetic acid, hydride reduction, and oxidation gave apocamphor (**23**) (16), since it appeared likely that this mixture of bromides contained **17**. Apopinene (**22**) on treatment as described gave in high yield a

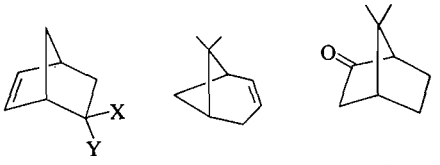

20 X = H, Y = Br
21 X = Br, Y = H
22
23

mixture of three compounds; ^{1}H nmr spectroscopy showed that the major product was **17** (~53%) and that this was accompanied by its *exo* isomer **24**

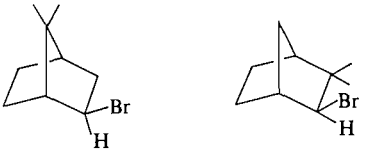

24 **25**

(~39%) (δ 4.00 (dd, J = 8.5, 5.0 Hz)) and compound **25** (8%) (δ 3.71 (d, J = 2.0 Hz)) (1.15). It was anticipated that in the next step of the synthesis of **12** from **17**, which involves the chromic acid oxidation of the latter, the *exo* bromides **24** and **25** would undergo solvolysis and therefore **17** would not have to be separated from the mixture of bromides. Although this proved to be the case, it was found to be preferable to synthesize **17** by the route of Scheme 1.

Chromic acid oxidation of apobornyl bromide (**17**) gave the ketone **18** in analogy with the similar oxidation of other bornyl derivatives (17). Its ir spectrum shows a strong band at 5.71 μm and its ^{1}H nmr spectrum shows a very broad multiplet

[6]We thank Dr. John D. Fenwick for providing us with a sample of **15**.

($w_{1/2}$ = 21 Hz) at δ 4.78 analogous to that due to H_a in the spectrum of **17**. Selenium dioxide oxidation of **15** in bromobenzene gave the α-diketone **19**, whose ir spectrum exhibits bands at 5.61 and 5.70 μm assigned to the coupled C=O stretching vibrations (18), similar to those at 5.63 and 5.69 μm in the spectrum of compound **26**, an intermediate in the preparation of the diazo ketone **7** (1). The ^{1}H nmr spectrum of **19** shows two methyl-proton singlets at δ 1.15 and 1.21 and five one-proton signals at 2.13, 2.75, 2.94, 3.18, and 4.75, assigned, respectively, to H_c, H_e, H_a, H_b, and H_d (see **19′**). The multiplicities

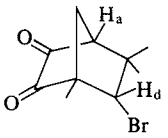

26

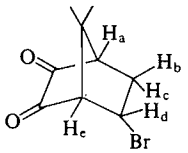

19′

of these signals could readily be interpreted in a first-order manner in terms of the following coupling constants: J_{ab} = 5.0 Hz, J_{ad} = 1.5 Hz, J_{bc} = 15 Hz, J_{bd} = 10 Hz, J_{be} = 0.8 Hz, J_{cd} = 4.0 Hz, J_{de} = 5 Hz. These values are in general in accord with expectation (11, 15), with the exception of the unusually large long range J_{ad}. However, several other examples of such unusually large J_{ad} values have been observed in the case of closely related 2,3-norbornanediones (1, 19), e.g., in the case of **26**, J_{ad} = 1.25 Hz.

The final step in Scheme 1, the conversion of **19** to **12** by treatment with lithium followed by acetic anhydride was conceived on the basis of the report by Hamon and Sinclair (20) that **27** is converted to

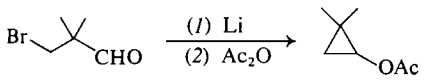

27 **28**

28 by similar treatment. Because of the crucial nature of this final step in the synthetic scheme and the considerable difference between the substrates **19** and **17**, its feasibility was tested on the α-diketone **26**, which is much more closely related to **19**, before the synthetic scheme was embarked upon. Compound **26** in ether was stirred with lithium for 2 days and the resulting solution was treated with acetic anhydride to give a product in 52% yield that is assigned structure **29**. The close relationship of this structure to **12** is most readily seen from its representation as its enantiomorph, **29*a***. Its ir spectrum is very similar to that of **12**, exhibiting strong bands at 5.61, 5.65, and 8.30 μm. Its ^{1}H nmr spectrum shows four three-proton signals at δ 1.05, 1.21, 1.33, and 2.13 (cf. the three three-proton signals of **12** at δ 1.05, 1.27, and

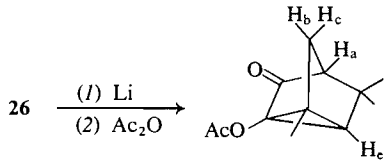

29

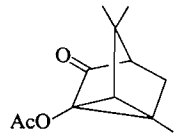

29*a*

2.11). A one-proton signal at δ 1.66 appears as a distorted quartet ($J \sim$ 1.5 Hz) and is assigned to H_a (cf. the quintuplet ($J \sim$ 1.5 Hz) at δ 1.65 assigned to H_a of **12**). A doublet (J = 1.7 Hz) at δ 1.82 is assigned to H_e, coupled with H_a. The acetoxyl methyl singlet at δ 2.13 is superimposed on a doublet at δ 2.10 (J = 1.5 Hz), the total intensity corresponding to five protons; this doublet is considered to arise from H_b and H_c, which are accidentally chemically equivalent and coupled with H_a.

The successful conversion of **26** to **29** encouraged us to pursue the synthesis of **12** via **19**. Treatment of **19** in ether with lithium followed by acetic anhydride gave a product in 50% yield that is identical with the most volatile product obtained in the copper-catalyzed decomposition of **4**, thus firmly establishing its structure as **12**.

Preparatory to examining the copper-catalyzed decomposition of diazo ketone **5**, the methoxy analogue of the acetoxy diazo ketone **4**, we sought to synthesize **30**, the analogue of **12**, so that it could be readily recognized if it were a product from the decomposition of **5**. Treatment of the bromo α-diketone **19** with lithium, followed by methyl iodide, gave no **30**, but treatment with lithium followed by dimethyl sulfate afforded the volatile methoxy ketone in low yield.[7] The ir spectrum of **30** shows a strong C=O stretching band at 5.68 μm. Its ^{1}H nmr spectrum is closely related to that of **12**, exhibiting two C—CH_3 singlets at δ 1.00 and 1.17, a quintuplet at δ 1.51 ($J \sim$ 1.5 Hz) assigned to H_a, a multiplet at δ 2.0–2.3 assigned to the other ring protons, and a methoxyl singlet at δ 3.47.

Copper-catalyzed decomposition of **5** in benzene in the same manner as for **4** gave a single volatile product in 90% yield: this is considerably less volatile than **30**. It was shown by high resolution mass spectrometry to have an elemental composition corresponding to the loss of nitrogen from **5**, i.e., to be isomeric with **30**. It is assigned structure **31** on the

[7]These results presumably reflect the greater reactivity of dimethyl sulfate as an alkylating agent (21).

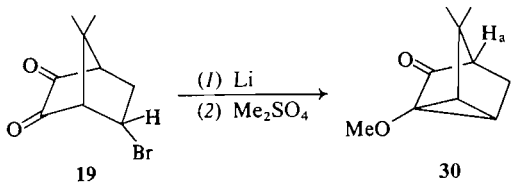

19 30

basis of the following considerations. Its ir spectrum possesses a strong C=O stretching band at 5.73 μm. Its ^1H nmr spectrum lacks a three-proton singlet in the δ 3–4 region, demonstrating that the methoxyl group is no longer present. Three-proton singlets at δ 0.84 and 1.02 indicated the retention of the geminal methyl groups. A broad doublet (J = 4.8 Hz, 1H) at δ 4.04 is assigned to H_d, coupled with H_e (see **31***a*);

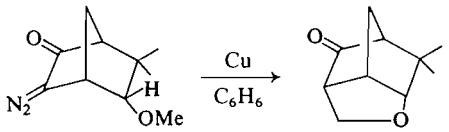

5 31

a two-proton multiplet at δ 3.75–3.95 is assigned to H_i and H_j, which form the AB part of an ABX system, with H_f acting as X. A doublet of triplets (J = 12, 1.5 Hz, 1H) at δ 1.82 is assigned to one of H_g and H_h; the other of these gives rise to a signal at δ 2.03 that is a doublet (J ~ 12 Hz) with further small splittings but is partially obscured by a multiplet at δ 2.09, assigned to H_a. Broad multiplets at δ 2.5 (1H) and 3.0 (1H) are assigned to H_e and H_f. The pattern of the multiplet assigned to H_i and H_j is very similar to that reported for the corresponding protons in **32** and **33** (22); in addition, the chemical shifts of H_d, H_i, and H_j in **31***a* relate well with those reported for the corresponding protons in **32** and **33**.

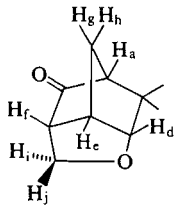

31*a*

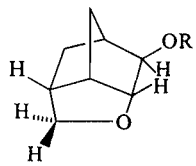

32 R = Ac
33 R = Tos

A preliminary investigation of the copper-catalyzed decomposition of **6** in benzene in the same manner as for **4** and **5** gave two major products. One of these (48%) was readily identified as the α-diketone **34**, which had been prepared as an intermediate in the synthesis of **6** (1). The other (32%) is considered to be a mixture of stereoisomeric azines **35**, as indicated by its mass, ir, and ^1H nmr spectra. In an attempt to eliminate azine formation the copper-catalyzed decomposition of **6** was carried out at very high dilution (0.02% in benzene). The reaction required 10 days for completion and still gave **35** (24%); **34** was again the major product (40%). There was only one minor component (~5%) that was sufficiently volatile to be **36**, the analogue of **12**. Fractions enriched in this product showed an ir band at 5.67 μm, but insufficient material was available for purification and

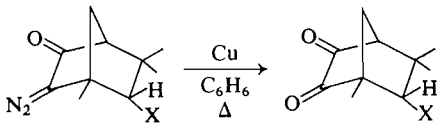

6 X = Cl
7 X = Br

34 X = Cl
37 X = Br

+

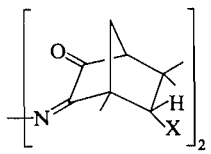

35 X = Cl
38 X = Br

identification. Decomposition of **7** under similar high dilution conditions required 4 days and gave the α-diketone **37** (42%) and the azine **38** (28%). A third product (22%) that was considerably more volatile

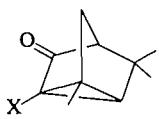

36 X = Cl
39 X = Br

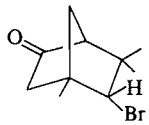

40

than **37** was formed. It had a band in its ir spectrum at 5.67 μm, and included peaks in its mass spectrum at *m/e* 228 (9) and 230 (11), corresponding to the elemental composition of **39**. But again insufficient material was available for purification and identification. A minor product (ir bands at 5.72 and 7.12 (w) μm) is considered to be **40**, the analogue of **8**. Although we have not firmly established that the

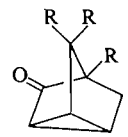

2 R = Me
41 R = H

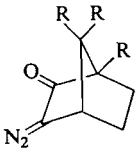

1 R = Me
42 R = H

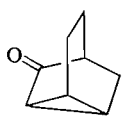

43

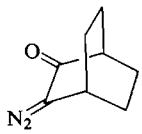

44

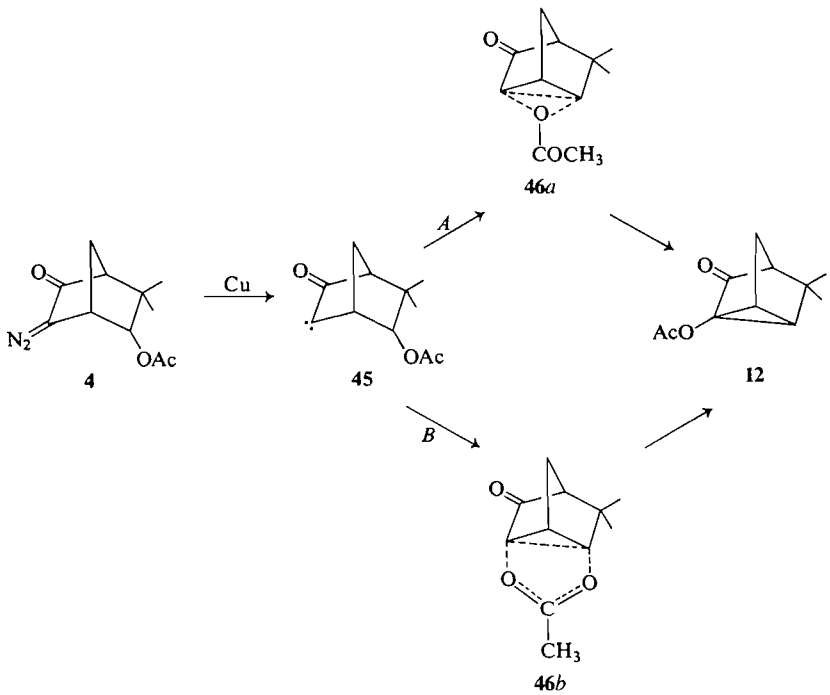

SCHEME 2

tricyclic compounds **36** and **39** are formed from **6** and **7**, respectively, our preliminary investigation has clearly shown that if these compounds are in fact formed it is with considerable reluctance.

Mechanisms of the Decomposition Reactions of the Diazo Ketones

The high yields of cyclocamphanone (**2**) and nortricyclanone (**41**) obtained in the copper-catalyzed decomposition of 3-diazocamphor (**1**) and 3-diazo-2-norbornanone (**42**), respectively, in benzene (2, 3) contrast sharply with the very low yield of the tricyclic ketone **43** obtained in the similar decomposition of 3-diazobicyclo[2.2.2]octan-2-one (**44**) (3). This suggests that the geometry of the 2-norbornanone system is particularly favorable for the insertion of a carbenoid center at C-3 into the *endo* C—H bond at C-5 and that *endo* carbon – hetero atom bonds might undergo such insertion. The formation of the acetoxynortricyclanone derivative **12** from the diazo ketone **4** could be accounted for in this way (route *A* in Scheme 2). However, there is an alternative pathway that must be considered, wherein the carbonyl oxygen of the original acetoxyl group bonds with the carbenoid center (route *B* in Scheme 2). Two qualifications apply to each of the routes depicted in Scheme 2. First, the representation of the common intermediate as the free oxocarbene **45** may be an oversimplification; the copper-catalyzed decomposition of α-diazo ketones most probably gives an oxocarbene–copper complex (5, 23) which could be the species in which acetoxyl migration occurs (although it is not excluded that the reactive species is the free oxocarbene **45**, which is in equilibrium with its copper complex). Second, although the representation of the transition states as **46***a* and **46***b* implies that the acetoxyl migration is concerted with carbon–carbon bond formation, this need not be the case.

In order to distinguish between routes of type *A* and *B* the synthesis of **4***a*, labelled in the acetoxyl carbonyl with oxygen-18 was undertaken. The label was introduced by acetylation of the hydroxy ketone **47**, which had previously been prepared in the synthesis of **5** (1), with ^{18}O-labelled acetic anhydride to give **8***a*.[8] The ir spectrum of **8***a* shows bands at 5.74 and 5.86 μm in contrast to the single band at 5.74 μm in the ir spectrum of unlabelled **8**. The band at 5.86 μm is ascribed to the acetoxyl C=^{18}O stretching vibration.[9] Oxidation of **8***a* with selenium dioxide in bromobenzene as in the preparation of **1** (1) gave the labelled α-diketone **9***a*. The ir spectrum of **9***a* shows,

[8] ^{18}O-labelled acetic anhydride was prepared by the method of Gerrard and Thrush (24). Although two-thirds of the ^{18}O label is lost with this acetylating agent, it was found to be preferable to acetyl chloride because of losses in the preparation of the latter due to its high volatility.

[9] Substitution of ^{16}O by ^{18}O in ketones has been reported to cause an increase of ~0.10 μm (calcd. 0.13 μm) in the wavelength of the C=O stretching vibration (25).

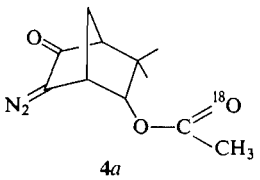

4*a*

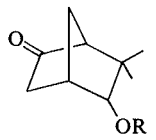

47 R = H
8*a* R = C(=^{18}O)CH$_3$

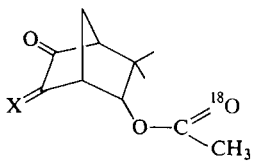

9*a* X = O
48 X = NNHTos

in addition to bands associated with unlabelled **9**, a broad band at 5.82 μm ascribed to the acetoxyl C=^{18}O stretching vibration (cf. the corresponding C=^{16}O band at 5.72 μm). Mass spectral analysis of **9***a* showed that it contained ~32% of ^{18}O label (see Experimental). The tosylhydrazone of **9***a*, **48**, was prepared in the usual way (1) and was shown by mass spectrometry to contain ~32% of ^{18}O label. It was converted to the diazo ketone **4***a* by chromatography on basic alumina (1, 26). The ir spectrum of **4***a* shows a close similarity to that of unlabelled **4** with the exception that the band at 5.90 μm is much stronger than the 5.77 μm band. The former band in the spectrum of **4***a* is ascribed to overlap of the diazo ketone C=^{16}O and acetoxyl C=^{18}O bands. Mass spectral analysis again indicated the presence of ~32% of ^{18}O label. The copper-catalyzed decomposition of **4***a* in the usual manner afforded a mixture (1.9 mg) of labelled tricyclic acetoxy ketone **12** (70%) and **8** (30%), as determined by vpc. The latter must be labelled as in **8***a*. The ir spectrum of the mixture included bands due to labelled **12** of equal intensity at 5.60 and 5.65 μm. This indicates that the labelled tricyclic acetoxy ketone consists largely of **12***b* rather than **12***a*, since if the latter had been present in major amount the diminution of the band due to the CH$_3$C=^{16}O carbonyl stretching vibration would have been expected to result in a significant difference in the intensities of the 5.60 and 5.65 μm bands. The mass spectrum of the mixture included peaks at *m/e* 43 (100) and 45 (18), indicating that 15% of the components of the mixture contained an acetoxyl group labelled with C=^{18}O. Clearly much of the peak at *m/e* 45 arises from the ~30% of **8***a* present in the mixture, and the ratio of **12***b* to **12***a* is calculated to be ~4:1 (see Experimental); thus it can be concluded that the major pathway for formation of **12** from **4** involves route *B* in Scheme 2.

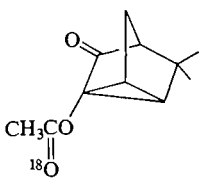

12*a*

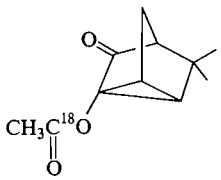

12*b*

The failure of **4** to follow route *A* as a major pathway is matched by the results with diazo ketones **5–7**. In these cases no equivalent to route *B* is available and the formation of tricyclanyl derivatives occurs not at all or at most as a minor pathway. Thus in the case of **5** the formation of the carbon–hydrogen insertion product **31** is the sole process observed, although insertion into the C—O bond would have been expected to be more facile in this case than in that of **4**. The preliminary results with **6** and **7** also show that insertion into the carbon–halogen bond is not a facile reaction and indeed is so slow that bimolecular reaction occurs more readily, even at high dilution. Thus in spite of the presumed favorable geometry C-3 carbenoid insertion into an *endo* C-5 carbon – hetero atom bond occurs with difficulty, if at all.[10]

We conclude by discussing briefly the putative origin of the other types of products formed from **4**, **6**, and **7**. The formation of the reduction products **8** and **40** is considered to involve hydrogen atom abstraction by the oxocarbene or carbenoid intermediate, perhaps after intersystem crossing from the singlet to triplet state. The oxidation products **9**, **34**, and **37** are thought to result from reaction of the same intermediate with adventitious oxygen, perhaps again after intersystem crossing. The hydroxy ketone **10** is considered to arise from **4** via the intervention of adventitious water. The formation of the azines **35** and **38**, which finds precedent in the copper-catalyzed decomposition of other α-diazo ketones (see for example refs. 3 and 27), can be interpreted in terms of reaction of the oxocarbene or carbenoid intermediate with undecomposed diazo ketone. The formation of these various other types of product again reflects the reluctance of the oxocarbene or carbenoid intermediate to insert into a carbon – hetero atom bond; only in the case of the formation of the carbon–hydrogen insertion product **31** from **5** is there no appreciable competition from intermolecular reactions.

Experimental

Melting points and boiling points are uncorrected. Infrared

[10]This result is in striking contrast to the report by one of us that such insertion can occur into a carbon–carbon bond (27); see, however, ref. 5.

spectra were recorded with carbon tetrachloride as solvent unless otherwise specified. Proton magnetic resonance spectra were recorded with deuteriochloroform as solvent. Solutions in organic solvents were dried over anhydrous magnesium sulfate and evaporated with a rotary evaporator, unless otherwise specified. Vapor phase chromatography was carried out on 10% SE 30 on Chromosorb P columns with a Perkin Elmer model 11 chromatograph.

Copper-catalyzed Decomposition of 5-endo-*Acetoxy-3-diazo-6,6-dimethyl-bicyclo[2.2.1]heptan-2-one (**4**). Formation of **8**, **9**, **10**, and **12***

Anhydrous benzene (dried by boiling under reflux for several days over lithium aluminum hydride and distillation immediately before use; ca. 500 mL); copper powder (Fisher, electrolytic metal, washed with ether and hexane, and vacuum dried prior to use; 6 g), and **4** (100 mg) were placed in a flame-dried, two-necked, 1-L flask containing a magnetic stirring bar and fitted with a nitrogen inlet tube, a double-surface condenser, and an outlet tube that directed the exit gases through a pool of mercury (a nitrogen bubbler with the inlet tube stoppered was used). Oxygen-free nitrogen[11] was passed through the solution for 0.5 h. The mixture was boiled under reflux with vigorous stirring under a stream of nitrogen for 40 h, cooled, and filtered. Evaporation of the light yellow solution afforded a viscous oil (104 mg). The volatile products in the residue were **12** (74%), **8** (5.5%), **9** (13%), and **10** (7.5%), as determined by vpc. The residue was digested for a short time with boiling hexane (ca. 10 mL). The hexane solution was cooled to −20°C, and the hexane soluble fraction was decanted from the precipitated **9** and **10**. Evaporation of the hexane soluble fraction afforded a viscous oil (62 mg) containing **12** (89.5%), **8** (7.5%), and **9** (3%). The isolated yield of **12** was 64%; it was purified by preparative vpc or chromatography on Florisil with elution with benzene (some decomposition was observed); it slowly solidified on standing. Recrystallization from hexane afforded chunky crystals of **12**, mp 47.5–48.5°C; λ_{max}: 5.60, 5.65, 8.28 μm; δ_H: 2.0–2.4 (m, with a sharp singlet at δ 2.11, 7H), 1.65 (m, 1H), 1.27 (s, 3H), 1.05 (s, 3H). *Anal.* calcd. for $C_{11}H_{14}O_3$: C 68.02, H 7.27; found: C 68.00, H 7.33.

The keto acetate **8** was identified by comparison of its vpc retention time, ir spectrum, and mass spectrum with those of authentic **8** (1).

The dione **9** and the ketol **10** were separated by preparative vpc or fractional recrystallization from hexane at 2°C. The dione **9** was identified by a mixture melting point determination and comparison of its vpc retention time and ir spectrum with those of authentic **9** (1). The ketol **10** is a white solid, mp 60–63°C; λ_{max}: 2.95, 5.74 μm; δ_H: 5.07, (br d, J = 4 Hz), 4.0 (m), 3.0 (m), 2.08 (s), 1.27 (s), 0.89 (s); *m/e* 212. It was identified by independent synthesis (*vide infra*).

5-endo-*Acetoxy-3-*endo-*hydroxy-6,6-dimethylbicyclo[2.2.1]-heptan-2-one (**10**) and* 6-endo-*Acetoxy-3-*endo-*hydroxy-5,5-dimethylbicyclo[2.2.1]heptan-2-one (**11**)*

A mixture of **9** (91.5 mg), anhydrous ether (10 mL), and platinum (10 mg) was stirred vigorously under a hydrogen atmosphere until the ethereal solution was colorless (ca. 45 min). Filtration of the mixture and evaporation of the ether afforded a mixture of the ketols **10** and **11** (92 mg, 100%); λ_{max}: 2.95, 5.74 μm; δ_H: 5.07 (br d, J = 4 Hz), 4.03 (br d, J = 4 Hz), 3.0 (m), 2.3 (m), 1.5–2.0 (m), 2.08 (s), 1.27 (s), 0.89 (s), 4.92 (br d, J = 4 Hz), 4.22 (br d, J = 4 Hz), 2.04 (s), 1.06 (s).

*2-Acetoxy-1,5,5-trimethyltricyclo[2.2.1.0^{2,6}]heptan-3-one (**29**)*

A mixture of **26** (49 mg) (1), anhydrous ether (6 mL), and lithium (washed twice with hexane, once with ether, and cut into small pieces; 40 mg) was vigorously stirred under nitrogen for 40 h. A grey precipitate of lithium bromide formed. The excess lithium was removed and destroyed in methanol. Addition of acetic anhydride (0.4 mL) to the stirred reaction mixture produced an immediate white precipitate of lithium acetate. Ether (15 mL) was added to the mixture and the ethereal layer was washed with water (5 × 20 mL), dried, and filtered. Distillation afforded **29** (22 mg, 52%), bp 80°C/18 Torr; λ_{max}: 5.61, 5.65 μm; δ_H: 2.13 (s) and 2.10 (d, J = 1.5 Hz) (5H), 1.82 (d, J = 1.7 Hz, 1H), 1.66 (m, J = 1.5 Hz, 1H), 1.33 (s, 3H), 1.21 (s, 3H), 1.05 (s, 3H). *Mol. Wt.* calcd. for $C_{12}H_{16}O_3$: 208.1099; found (ms): 208.1105.

5′-endo-*Bromospiro(cyclopropane-1,7′-norborn-2′-ene) (**16**)*

Vinyl bromide (4.30 g), a small amount of hydroquinone, and a mixture (3.34 g) of 60% of the diene **15**[6] and 40% of 1,2-dibromoethane (12) were heated in a sealed glass tube at ca. 170°C for 13.5 h. After cooling to room temperature the sealed tube was further cooled in a Dry Ice – acetone bath and opened. Distillation of the orange solution afforded 1,2-dibromoethane, bp 37–42°C/22 Torr, and **16** (2.66 g, 62%), bp 95–98°C/22 Torr; λ_{max}: 3.30, 6.08 μm; δ_H: 6.38 (m, 1H), 6.18 (m, 1H), 4.47 (dt, J = 8.0, 3.5 Hz, 1H), 2.0–2.7 (m, 3H), 1.39 (dd, J = 12.5, 3.5 Hz, 1H), 0.42 (m, 4H). *Anal.* calcd. for $C_9H_{11}Br$: C 54.30, H 5.57, Br 40.14; found: C 54.08, H 5.72, Br 39.90.

*Apobornyl Bromide (**17**)*

A mixture of **16** (1.99 g, 10.0 mmol), glacial acetic acid (15 mL), and a small amount of platinum catalyst was stirred at 80°C under an atmosphere of hydrogen until the absorption of hydrogen ceased (18.4 mmol was absorbed); 8.5 h reaction time was required. To the cooled reaction mixture was added ether (300 mL), and the ethereal solution was decanted from the platinum, washed with water (5 × 100 mL), and saturated aqueous sodium bicarbonate (2 × 100 mL), dried, and filtered. Evaporation of ether afforded apobornyl bromide (**17**; 1.80 g, 89%), bp 83–86°C/10 Torr; δ_H: 4.62 (m, 1H), 1.15–2.9 (m, 8H), 1.11 (s) and 1.06 (s) (6H). *Anal.* calcd. for $C_9H_{15}Br$: C 53.22, H 7.44, Br 39.34; found: C 53.29, H 7.54, Br 39.34.

6-endo-*Bromoapocamphor (**18**)*

A slurry of pulverized chromium trioxide (35 g) in glacial acetic acid (100 mL) was added in small portions over 0.6 h to a stirred solution of apobornyl bromide (**17**, 11.86 g) in glacial acetic acid (10 mL) at a rate such that the reaction mixture temperature was maintained near 75°C. After the addition was complete, the green solution was stirred at 75°C for 1 h, cooled, and diluted with water (350 mL). The solution was extracted with ether (10 × 50 mL), and the combined ethereal extracts were washed with water (2 × 300 mL) and saturated aqueous sodium bicarbonate (100 mL), dried, and filtered. Distillation afforded **18** (5.40 g, 43%) as an unstable colorless oil, bp 73–80°C (50 μm); λ_{max}: 5.71, 7.09 μm; δ_H: 4.78 (m, 1H), 1.3–3.0 (m, 6H), 1.14 (s, 6H). *Anal.* calcd. for $C_9H_{13}BrO$: C 49.79, H 6.04, Br 36.81; found: C 50.52, H 6.03, Br 36.16. *Mol. Wt.* calcd. for $C_9H_{13}BrO$: 216.0134, 218.0110; found (ms): 216.0150, 218.0130.

5-endo-*Bromoapocamphorquinone (**19**)*

A mixture of **18** (5.31 g), selenium dioxide (7.0 g), and bromobenzene (35 mL) was stirred at 150°C for 24 h and then cooled. The red bromobenzene solution was decanted from the

[11]Nitrogen was passed twice through Fieser's solution (28), and once through acid, sodium hydroxide, and silica gel desiccant, to remove oxygen and water.

selenium. The selenium was washed with small amounts of ether until the ethereal extracts were colorless. Distillation of the combined bromobenzene and ether solutions afforded an orange oil, bp 50°C/15 Torr, which was mainly bromobenzene. The undistilled residue was chromatographed on Florisil (120 g) with elution with benzene. After a light yellow forerun, **19** was eluted with 10% ether–benzene. Recrystallization from hexane (100 mL) afforded **19** (1.89 g, 33.5%) as a very unstable yellow solid, mp 86–89°C. Sublimation and recrystallization raised the melting point to 92.0–93.5°C; λ_{max}: 5.61, 5.70 μm; δ_H: 4.75 (m, 1H), 3.18 (m, 1H), 2.94 (dd, J = 5.0, 1.5 Hz, 1H), 2.75 (br d, J = 5 Hz, 1H), 2.13 (dd, J = 15, 4.0 Hz), 1.21 (s, 3H), 1.15 (s, 3H). *Mol. Wt.* calcd. for $C_9H_{11}BrO_2$: 229.9942, 231.9915; found (ms): 229.9943, 231.9923.

*Treatment of **19** with Lithium and Acetic Anhydride. Formation of **12***

A mixture of **19** (freshly recrystallized; 50 mg) anhydrous ether (7 mL), and lithium (washed twice with hexane, once with ether, and cut into small pieces; 100 mg) was vigorously stirred under nitrogen for 24 h. A grey precipitate of lithium bromide formed. The excess lithium was removed. Acetic anhydride (100 mg) was added to the stirred reaction mixture and produced an immediate white precipitate of lithium acetate. Ether (20 mL) was added to the mixture and the ethereal layer was washed with water (5 × 10 mL), dried, and filtered. The ether was evaporated, and the residue was digested in boiling hexane (2 mL) for a short time; the mixture was then cooled to −20°C, and the hexane-soluble fraction was decanted. Evaporation of the hexane afforded **12** (21 mg, 50%) as a colorless oil that crystallized slowly on standing. Preparative vpc gave material with a melting point of 45.0–48.0°C. A mixture of this material with pure **12**, mp 47.5–48.5°C, obtained in the copper-catalyzed decomposition of **4**, had mp 46.0–48.0°C.

*Apopinene (**22**)*

Apopinene (**22**) was prepared by the method of Eschinazi and Pines (29) by oxidation of α-pinene to myrtenal with selenium dioxide (30) and decarbonylation of this with palladium hydroxide on barium sulfate (31); bp 84–88°C/118 Torr (lit. (30) 47–48°C/30 Torr); λ_{max}: 3.32, 6.15 μm; δ_H: 6.12 (m, 1H), 5.55 (m, 1H), 1.9–2.7 (m, 6H), 1.29 (s, 3H), 0.90 (s, 3H).

*Addition of Hydrogen Bromide to Apopinene (**22**). Formation of **17**, **24**, and **25***

Hydrogen bromide was bubbled into an ice-cold solution of **22** (13.95 g, 0.115 mol) in chloroform (16 mL) until at least 9.3 g (0.115 mmol) of hydrogen bromide had been absorbed. After standing at 2°C overnight the purple solution was distilled, producing a mixture of bromides (18.50 g, 80%); bp 68–72°C/1.2 Torr (lit. (16) bp 43°C/0.15 Torr). The mixture contained **17** (53%), **24** (39%), and **25** (8%), as determined by ^{1}H nmr spectroscopy; δ_H: 4.62 (m), 4.00 (dd, J = 8.5, 5.0 Hz), 3.71 (d, J = 2.0 Hz).

*2-Methoxy-5,5-dimethyltricyclo[2.2.1.0^{2,6}]heptan-3-one (**30**)*

A mixture of **19** (321 mg), lithium (washed twice with hexane, once with ether, and cut into small pieces; 400 mg), and anhydrous ether (16 mL) was vigorously stirred under nitrogen for 44 h. The excess lithium was removed with tweezers from the brown mixture, washed with ether, and destroyed in methanol; the ethereal washings were combined with the reaction mixture. Dimethyl sulfate (0.2 mL) was added to the stirred mixture. The white solid that formed was filtered, and the ether in the filtrate was evaporated. The residue was digested in boiling hexane (30 mL) and the solution was cooled to −20°C; the hexane-soluble layer was separated from the hexane-insoluble layer by decantation and heated with water (20 mL) on a steam bath for 0.5 h to destroy the remaining dimethyl sulfate. The solution was cooled and extracted three times with ether. The ethereal extracts were dried and filtered. Distillation gave **30** (26 mg, 15% based on unrecovered **19**), bp ca. 75°C/15 Torr. Preparative vpc afforded a sample, mp 41.8–43.0°C; λ_{max}: 5.68 μm; δ_H: 3.47 (s, 3H), 2.0–2.3 (m, 4H), 1.51 (m, 1H), 1.17 (s, 3H), 1.00 (s, 3H). *Mol. Wt.* calcd. for $C_{10}H_{14}O_2$: 166.0994; found (ms): 166.0995.

The hexane-insoluble layer was worked up in the same way as the hexane-soluble layer. Recrystallization of the residue from hexane (20 mL) afforded **19** (86 mg).

*Copper-catalyzed Decomposition of the Methoxy Diazo Ketone (**5**). Formation of 9,9-Dimethyl-5-oxatricyclo[4.2.1.0^{3,7}]nonan-2-one (**31**)*

The conditions described for the copper-catalyzed decomposition of **4** were employed. A mixture of **5** (38 mg), benzene (distilled from lithium aluminum hydride; 190 mL) and copper (Pfaltz and Bauer; washed twice with hexane, once with ether, and dried at water-aspirator pressure; 1.6 g), was boiled under reflux with vigorous stirring under a stream of oxygen-free nitrogen. After 16 h the solution was almost colorless. The mixture was cooled and filtered; evaporation of the filtrate left an orange oil (39 mg). Distillation afforded **31** (29 mg, 90%) as a semisolid (decomposes on standing at room temperature), bp ca. 80°C/20 Torr; λ_{max}: 5.73 μm; δ_H: 4.04 (br d, J = 4.8 Hz, 1H), 3.75–3.95 (m, 2H), 3.0 (m, 1H), 2.5 (m, 1H), 2.09 (m, 1H), 2.03 (d, J ~ 12 Hz, 1H), 1.82 (dt, J = 12, 1.5 Hz, 1H), 1.02 (s, 3H), 0.84 (s, 3H). *Mol. Wt.* calcd. for $C_{10}H_{14}O_2$: 166.0994; found (ms): 166.0993.

*Copper-catalyzed Decomposition of the Chloro Diazo Ketone **6**. Formation of **34** and **35***

All the precautions described for the copper-catalyzed decomposition of **4** were employed. A mixture of **6** (49 mg), benzene (distilled from lithium aluminum hydride; 250 mL) and copper powder (Fisher electrolytic metal powder, washed with ether and hexane, and dried at water-aspirator pressure; 1.0 g) was boiled under reflux with vigorous stirring under a stream of oxygen-free nitrogen for 10 days. The mixture was cooled and filtered. Evaporation of the filtrate afforded a brown semisolid (46 mg), which was digested in boiling hexane (1 mL) for a few min. The hexane solution was decanted from the yellow residue of the azine **35** (11 mg, 24%), mp ca. 310°C (dec.); λ_{max}: ($CHCl_3$): 5.76, 6.19 μm; δ_H: 3.92 (br s), 0.8–2.4 (m); ms m/e: 396 (16), 398 (10), 400 (3).

The dione **34**, which precipitated on cooling the hexane solution was identified by comparison of its ir spectrum and vpc retention time with those of an authentic sample and accounted for 40% of the products, as determined by vpc. The remaining solution was evaporated and the residue was chromatographed on a column of Florisil (1.0 g) with elution with 2% ether–benzene. The first fraction (8 mL) contained a product with an ir band at 5.67 μm; its vpc retention time was compatible with its being **36**, but insufficient material was available for purification and identification. It composed ~5% of the total product mixture. Subsequent fractions contained **34** and **6**.

*Copper-catalyzed Decomposition of the Bromo Diazo Ketone (**7**)*

All the precautions described for the copper catalyzed decomposition of **4** were employed. A mixture of **7** (40 mg), benzene (distilled from lithium aluminum hydride; 200 mL), and

copper (Pfaltz and Bauer, washed twice with hexane, once with ether and dried at water-aspirator pressure; 0.90 g) was boiled under reflux with vigorous stirring under a stream of oxygen-free nitrogen. After 96 h the decomposition was almost complete as determined by the ir spectrum of an aliquot. The mixture was cooled and filtered; evaporation of the filtrate left an orange semisolid (34 mg). This residue was digested in boiling hexane (13 mL) for a few min; the yellow hexane solution was separated by decantation from **38** which was obtained as a yellow solid (9.8 mg, 28%), mp ca. 310°C (dec.); λ_{max} ($CHCl_3$): 5.76, 6.19 μm; ms *m/e*: 406 (M − HBr).

The hexane solution contained three other products in yields of greater than 3%. The hexane was evaporated, and the residue was chromatographed (preparative thin layer) on silica gel with elution with ethyl acetate followed by extraction of the yellow band with an R_f of 0.72 with methanol. The methanol was evaporated and the residue was dissolved in hexane, and the solution was cooled to −20°C; the hexane solution was decanted from the yellow precipitate of dione **37**, identified by comparison of its ir spectrum and vpc retention time with those of an authentic sample. The dione accounted for 42% of the products as determined by vpc of the crude reaction residue. Evaporation of the hexane-soluble layer decanted from **37** afforded a volatile product mixture, containing a single major product (70%, as estimated by vpc) which is tentatively considered to be **39**. This compound accounted for 22% of the products as determined by vpc; λ_{max}: 5.67 μm; ms *m/e* 228 (9), 230 (11).

Preparative vpc of a sample of the crude reaction residue, after removal of **38**, afforded a small amount of a compound assigned structure **40**; λ_{max}: 5.72, 7.12 μm; ms *m/e*: 230 (11), 232 (11).

6-endo-*(Acetoxycarbonyl-^{18}O)-5,5-dimethylbicyclo*[*2.2.1*.]-*heptane-2,3-dione (**9**a)*

Acetyl chloride was added dropwise to $H_2{}^{18}O$ (136 mg, 6.80 mmol)[12] until the weight increased to 424 mg (6.80 mmol of acetic acid-^{18}O). The acetic acid was allowed to stand at room temperature for *ca.* 16 h to scramble the label; λ_{max}: 5.86, 5.91 μm. To a stirred solution of this (202 mg, 3.26 mmol) and pyridine (259 mg, 3.26 mmol) in anhydrous ether (2 mL), cooled in an ice–salt bath, was added thionyl chloride (195 mg, 1.63 mmol) in anhydrous ether (1 mL). The mixture was stirred for 10 min and the precipitate was filtered and washed with anhydrous ether (5 mL). The filtrate and washings were concentrated on a water bath at ca. 40°C, giving a yellow liquid (401 mg) that was 75% ether and 25% by weight of labelled acetic anhydride (58% yield), as determined by ^{1}H nmr spectroscopy; λ_{max}: 5.50, 5.58, 5.70, 5.79 μm.

A mixture of this labelled acetic anhydride, **47** (220 mg, 1.42 mmol), and pyridine (5 mL) was boiled under reflux with stirring for 3.5 h. The solution was cooled, and ether (60 mL) was added. The ethereal solution was washed with saturated aqueous sodium bicarbonate (20 mL) and aqueous 10% hydrochloric acid (3 × 20 mL), dried, and filtered. Evaporation of the ether afforded **8***a* (220 mg, 63%) of 80% purity, as determined by ^{1}H nmr spectroscopy, as an oil; λ_{max}: 5.74, 5.86, 7.10, 8.10 μm.

A mixture of **8***a* (80%; 220 mg), selenium dioxide (220 mg), and bromobenzene (3 mL) was heated at 150°C with stirring for 5 h. The mixture was cooled and chromatographed on Florisil (50 g). Elution with benzene gave bromobenzene. Elution with 50% ether–benzene (250 mL) gave **9***a* as a yellow solid (95 mg, 50%); λ_{max}: 5.61, 5.68, 5.72, 5.82 (br), 8.12 μm; ms *m/e*: 43 (100), 45 (44), indicating ca. 32% labelling when account is taken of the fact that 4% of the *m/e* 43 peak in the spectrum of **9** arises from $C_3H_7^+$, as determined by high resolution mass spectrometry.[13]

5-endo-*(Acetoxycarbonyl-^{18}O)-3-diazo-6,6-dimethylbicyclo-*[*2.2.1*]*heptan-2-one (**4**a)*

A warm solution of tosylhydrazine (90 mg, 0.48 mmol) in glacial acetic acid (0.4 mL) was added to a warm solution of **9***a* (93 mg, 0.44 mmol) in glacial acetic acid (0.2 mL). After standing at room temperature for 1 h the yellow solution was added to ice (ca. 25 g), forming a white precipitate that was collected, washed thoroughly with water, and air dried to give **48** (145 mg, 88%); ms *m/e* 43 (100), 45 (54), indicating ca. 32% labelling when account is taken of a small peak at *m/e* 45 in the spectrum of the unlabelled tosylhydrazone.[13]

Tosylhydrazone **48** (140 mg) was placed on a column of basic alumina (Merck: 1.5 × 0.3 in.). Elution with benzene (100 mL) and ether (100 mL) followed by evaporation of the eluate and recrystallization from hexane afforded **4***a* (45 mg, 55%) as a chunky yellow solid; λ_{max}: 4.82, 5.77, 5.90, 7.32, 8.02 μm; ms *m/e*: 43 (100), 45 (47), indicating ca. 32% labelling.[13]

*Copper-catalyzed Decomposition of **4**a. Formation of 2-(Acetoxyalkoxyl-^{18}O)-5,5-dimethyltricyclo*[*2.2.1.0^{2,6}*]-*heptan-3-one (**12**b)*

All the precautions described for the copper-catalyzed decomposition of **4** were employed. A mixture of the labelled diazo ketone **4***a* (5.0 mg), benzene (distilled from lithium aluminum hydride), and copper (Pfaltz and Bauer, washed twice with hexane, once with ether, and dried at water-aspirator pressure: 0.50 g) was boiled under reflux with vigorous stirring under a stream of oxygen-free nitrogen for 40 h. The mixture was cooled and filtered. The filtrate was evaporated and the residue was dissolved in warm hexane (1 mL), and the solution was cooled to −20°C. The hexane-soluble layer was separated by decantation and evaporated affording an oil (1.9 mg) consisting of labelled **12** (70%) and **8** (30%) as determined by vpc; 5.60, 5.65, 5.7–5.85 (sh) μm; *m/e* 43 (100), 45 (18), indicating that when account is taken of the presence of **8***a* the ratio **12***b*–**12***a* is ~4:1.[13]

Acknowledgement

We thank the National Research Council of Canada for support of this work.

1. P. YATES and G. F. HAMBLY. Can. J. Chem. This issue.
2. J. BREDT and W. HOLZ. J. Prakt. Chem. **95**, 133 (1917); R. SCHIFF. Chem. Ber. **14**, 1375 (1881); A. ANGELI. Gazz. Chim. Ital. **24**, Part II, 317 (1874).
3. P. YATES and R. J. CRAWFORD. J. Am. Chem. Soc. **88**, 1562 (1966).
4. J. D. FENWICK. Ph.D. Thesis, University of Toronto, Toronto, Ont. 1970.
5. P. YATES, F. X. GARNEAU, and G. F. HAMBLY. Polish J. Chem. In press.

[12]Labelled water, 98.76% ^{18}O, was obtained from the Yeda Research and Development Co. Ltd., the Weizmann Institute of Science, Rehovoth, Israel.

[13]The extent of the labelling was calculated on the basis of comparison of the mass spectrum of the reaction product with the mass spectra of unlabelled compounds recorded under identical conditions with a Bell and Howell CEC 21-490 single focussing spectrometer.

6. F. C. BROWN, D. G. MORRIS, and A. M. MURRAY. Synth. Commun. **5**, 477 (1975).
7. H. RUPE and F. MÜLLER. Helv. Chim. Acta, **24**, 265E (1941); B. PFRUNDER and C. TAMM. Helv. Chim. Acta, **52**, 1630 (1969); S. J. ANGYAL and R. J. YOUNG. J. Am. Chem. Soc. **81**, 5467 (1959).
8. H. HART and R. A. MARTIN. J. Am. Chem. Soc. **82**, 6362 (1960).
9. R. N. JONES. *In* Chemical applications of spectroscopy. *Edited by* W. West. *In* Technique of organic chemistry. Vol. IX. *Edited by* A. Weissberger. Interscience Publishers, Inc., New York, NY. 1956. (*a*) pp. 480–481. (*b*) p. 503.
10. R. N. JONES and F. HERLING. J. Am. Chem. Soc. **78**, 1152 (1956).
11. A. RASSAT, C. W. JEFFORD, J. M. LEHN, and B. WAEGELL. Tetrahedron Lett. 233 (1964); M. BARFIELD and B. CHAKRABARTI. Chem. Rev. **69**, 757 (1969).
12. K. ALDER, H. J. ACHE, and F. H. FLOCK. Chem. Ber. **93**, 1888 (1960).
13. J. PAASIVIRTA. Suomen Kemi. **38** B, 130 (1965); P. LASZLO and P. VON R. SCHLEYER. J. Am. Chem. Soc. **85**, 2709 (1963).
14. P. VON R. SCHLEYER and V. BUSS. J. Am. Chem. Soc. **91**, 5880 (1969); C. W. WOODWORTH, V. BUSS, and P. VON R. SCHLEYER. Chem. Commun. 569 (1968).
15. J. I. MUSHER. Mol. Phys. **6**, 93 (1963); T. J. FLAUTT and W. F. ERMAN. J. Am. Chem. Soc. **85**, 3212 (1963); L. M. JACKMAN and S. STERNHELL. Applications of nuclear magnetic resonance spectroscopy in organic chemistry. 2nd ed. Pergamon Press, Oxford. 1969. pp. 289, 334; J. R. MARSHALL and S. L. WALTER. J. Am. Chem. Soc. **96**, 6358 (1974).
16. Y. CHRÉTIEN-BESSIÈRE and J. MONTHÉARD. C.R. Acad. Sci., Paris, **258**, 937 (1964).
17. K. B. WIBERG. Oxidation in organic chemistry. Academic Press, New York, NY. 1965. pp. 109–124.
18. K. ALDER, H. K. SCHÄFER, H. ESSER, H. KRIEGER, and R. REUBKE. Justus Liebigs Ann. Chem. **593**, 23 (1955).
19. G. F. HAMBLY, J. LEITCH, P. YATES, and S. C. NYBURG. Can. J. Chem. **51**, 4076 (1973).
20. D. G. G. HAMON and R. W. SINCLAIR. Chem. Commun. 890 (1968).
21. J. M. CONIA. Bull. Soc. Chim. Fr. 533 (1950).
22. H. C. RAMEY, D. C. LINI, R. M. MORIARITY, H. GOPAL, and H. G. WELSH. J. Am. Chem. Soc. **89**, 2401 (1967).
23. D. S. WULFMAN. Tetrahedron, **32**, 1231 (1976).
24. W. GERRARD and A. M. THRUSH. J. Chem. Soc. 741 (1952).
25. M. HALMANN and B. PINCHAS. J. Chem. Soc. 1703 (1958); E. A. BRAUDE and D. W. TURNER. Chem. Ind. (London), 1223 (1955).
26. J. MEINWALD, P. G. GASSMAN, and J. J. HURST. J. Am. Chem. Soc. **84**, 3722 (1962).
27. P. YATES and S. DANISHEFSKY. J. Am. Chem. Soc. **84**, 879 (1962).
28. L. F. FIESER. J. Am. Chem. Soc. **46**, 2639 (1924).
29. H. E. ESCHINAZI and H. PINES. J. Org. Chem. **24**, 1369 (1959).
30. V. IPATIEFF, G. J. CZAJKOWSKI, and H. PINES. J. Am. Chem. Soc. **73**, 4098 (1951).
31. H. E. ESCHINAZI and E. D. BERGMANN. J. Am. Chem. Soc. **72**, 5651 (1950).

Studies on the syntheses of heterocyclic compounds. Part 782. Another total synthesis of (±)-tubulosine and (±)-deoxytubulosine[1,2]

TETSUJI KAMETANI, YUKIO SUZUKI, AND MASATAKA IHARA
Pharmaceutical Institute, Tohoku University, Aobayama, Sendai 980, Japan

Received December 13, 1978

TETSUJI KAMETANI, YUKIO SUZUKI, and MASATAKA IHARA. Can. J. Chem. 57, 1679 (1979).

(±)-Tubulosine (**1**) and (±)-deoxytubulosine (**3**) were totally synthesized by the Pictet–Spengler reaction of (±)-4-oxoprotoemetine (**7**) with serotonin (**8**) or tryptamine (**9**) followed by reduction with sodium bis(2-methoxyethoxy)aluminum hydride in pyridine.

TETSUJI KAMETANI, YUKIO SUZUKI et MASATAKA IHARA. Can. J. Chem. 57, 1679 (1979).

On a effectué des synthèses totales de la (±)-tubulosine (**1**) et de la (±)-désoxytubulosine (**3**) par la réaction de Pictet–Spengler de la (±)-oxo-4 protoemétine (**7**) avec la sérotonine (**8**) ou la tryptamine (**9**) suivie par une réduction à l'aide du $Na(CH_3OCH_2CH_2O)_2AlH_2$.

[Traduit par le journal]

Tubulosine (**1**), isotubulosine (**2**), and deoxytubulosine (**3**) were isolated as levorotatory forms from the same plant, *Alangium lamarckii* (2). Tubulosine derivatives are known to inhibit the protein synthesis and expected to be potential antineoplastic agents (3). Recently we have developed a short synthetic route to emetine through (±)-4-oxoprotoemetine (**7**) which was stereoselectively prepared by the condensation of 3,4-dihydro-6,7-dimethoxy-1-methylisoquinoline (**4**) with dimethyl 3-methoxyallylidenemalonate (**5**) in several steps via the intermediate enamide **6** (Scheme 1). The total yield from **4** was 60% (4). Thus, we have examined the synthesis of tubulosine and related compounds from aldehyde **7**, and we wish to report here the total synthesis of the above alkaloids, during whose reaction a new method of reducing the amide group was also revealed.

Serotonin (**8**) is commercially available as a complex with creatinine sulfate and was liberated from the complex using Amberlite XAD-4 column chromatography. Condensation of **8** with (±)-4-oxoprotoemetine (**7**) was carried out by stirring an equimolecular mixture in acetic acid at room temperature for 2 days. The Mannich base, *m/e* 489 (M^+), obtained in high yield, consisted of (±)-4-oxotubulosine (**10**) and its C-1′ epimer (**11**) in a 4:1 ratio; the identities of **10** and **11** were verified by tlc and nmr (DMSO-d_6) analysis. The ratio did not change appreciably even when the reaction was carried out under more acidic conditions or at a higher temperature. The product was very insoluble in ordinary solvents and a separation of the diastereoisomeric mixture could not be achieved. Mainly because of its slight solubility, reduction of a mixture of **10** and **11** with lithium aluminum hydride in hot dioxane gave none of the desired product. Eventually the reduction was carried out by treatment of a mixture of **10** and **11** with sodium bis(2-methoxyethoxy)aluminum hydride in pyridine at room temperature for 1 h. The reduction product was purified by column chromatography and recrystallization from methanol to afford (±)-tubulosine (**1**), mp 249–250°C, whose nmr (DMSO-d_6) and mass spectra and chromatographic behavior (tlc and hplc) were identical with those of natural tubulosine donated by Prof. Szántay (4). (±)-Isotubulosine (**2**) was obtained as a minor product but could not be separated from **1** completely. However the structure of **2** was supported by the nmr spectrum (DMSO-d_6), which exhibited one of the methoxyl groups at high field (3.49 ppm) (**6**), and tlc behavior on silica gel, which showed the compound to have a lower R_f value than that of tubulosine (5–7). The preferential formation of tubulosine (**1**) over isotubulosine (**2**) in the Pictet–Spengler reaction using (−)-protoemetine and serotonin (**8**) was also observed by Szántay and Kalaus (5).

Stirring a mixture of aldehyde **7** and tryptamine (**9**) hydrochloride in acetic acid at room temperature for 2 days yielded a mixture of (±)-4-oxodeoxytubulosine (**12**) and its epimer (**13**) in a 4:1 ratio. The former (**12**) was obtained in pure form after preparative thin-layer chromatography and was reduced with sodium bis(2-methoxyethoxy)aluminum hydride in pyridine under the same condition as above to furnish (±)-deoxytubulosine (**3**), mp 156–158°C. The nmr spectrum ($CDCl_3$) of this product was superimposable upon that of an authentic sample of compound **3** given to us by Prof. Battersby. Since lactam **12** was soluble in hot dioxane, reduction with

[1]Dedicated to the memory of R. H. F. Manske.
[2]For Part 781, see ref. 1.

0008-4042/79/131679-03$01.00/0

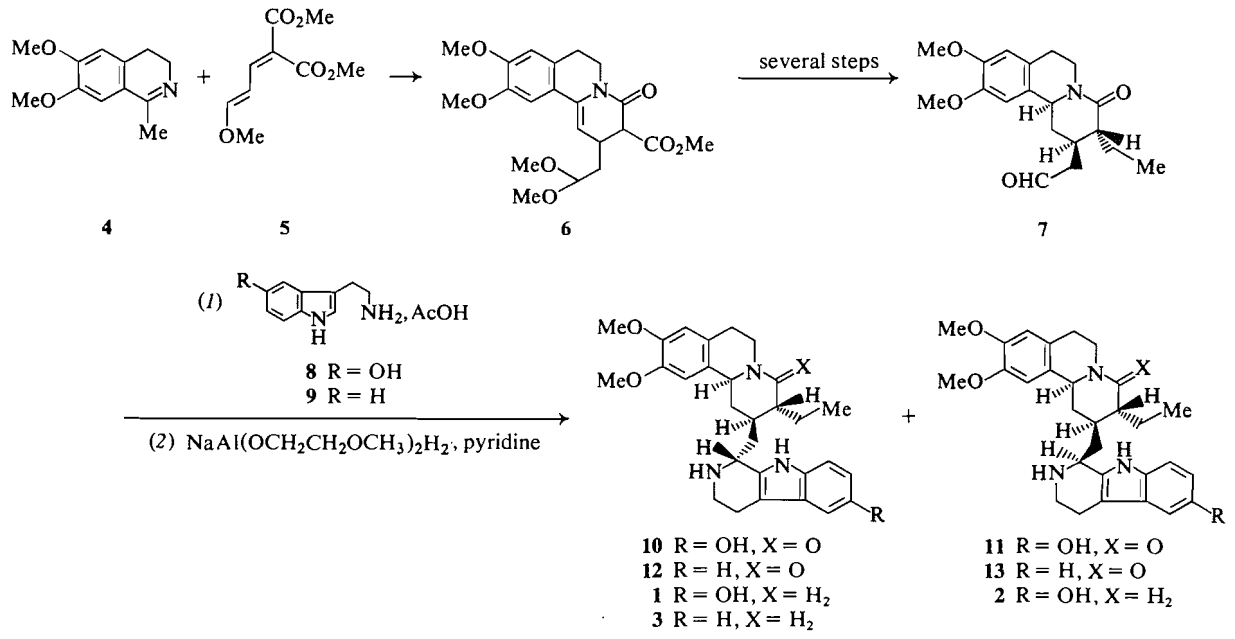

SCHEME 1[3]

lithium aluminum hydride under reflux was examined but **3** was obtained in very poor yield. Sodium bis(2-methoxyethoxy)aluminum hydride reduced the tertiary amides under mild condition in pyridine and the limit and the scope of this reduction is under investigation.

Experimental

Melting points were determined with a Yanaco micro-melting point apparatus and are uncorrected. Infrared spectra were taken with a Hitachi 215 spectrophotometer. Nuclear magnetic resonance spectra were measured with a JNM-PMX-60 instrument with tetramethylsilane as an internal standard. Mass spectra were taken with Hitachi M-52 spectrometer.

(±)-Tubulosine (1)

A solution of serotonin (**8**) – creatinine sulfate complex (300 mg) in water (50 mL) was subjected to Amberlite XAD-4 (80 mL) column chromatography. After elution with water (100 mL), an eluate of methanol–water (1:1 v/v) gave serotonin (124 mg), which was judged free from creatinine sulfate on the basis of its nmr analysis.

A mixture of serotonin (**8**) (124 mg) and (±)-4-oxoprotoemetine (**7**) (217 mg) in AcOH (30 mL) was stirred for 2 days at room temperature. The solvent was evaporated to give a caramel which was dried under reduced pressure. To a stirred 70% solution of $NaAl(OCH_2CH_2OCH_3)_2H_2$ in toluene (2 mL) was added a solution of the above material in pyridine (2 mL) and the resulting solution was stirred for 1 h at room temperature. The solvents were evaporated and excess reagent was decomposed and neutralized by the addition, under ice-cooling, of a saturated NH_4Cl solution. The resulting mixture was extracted several times with $CHCl_3$. The $CHCl_3$ extract was washed with a saturated NaCl solution, dried (Na_2SO_4), and evaporated to give a reddish viscous material which was purified by column chromatography on silica gel. Elution with $CHCl_3$–MeOH (20:1 v/v), followed by concentration of the solvent, gave a solid, which was recrystallized from MeOH to afford (±)-tubulosine (**1**) (65 mg, 21%) as fine colorless needles, mp 249–250°C, the mass and nmr (DMSO-d_6) spectra and hplc and tlc behavior of which were identical with those of natural tubulosine. *Anal.* calcd. for $C_{29}H_{37}N_3O_3 \cdot 2H_2O$: C 68.08, H 8.08; found: C 67.86, H 7.79.

Further elution with the same solvent gave a fraction which mainly consisted of (±)-isotubulosine (**2**) and a small amount of (±)-tubulosine which were not separable by recrystallization.

(±)-4-Oxodeoxytubulosine (12)

A mixture of (±)-4-oxoprotoemetine (**7**) (150 mg) and tryptamine (**9**) hydrochloride (90 mg) in AcOH (5 mL) was stirred for 2 days at room temperature. After evaporation of the solvent, the residue was basified with a saturated $NaHCO_3$ solution and extracted with $CHCl_3$. The $CHCl_3$ extract was washed with a saturated NaCl solution, dried (Na_2SO_4), and evaporated to give a syrup, which was purified by ptlc on silica gel to afford (±)-4-oxodeoxytubulosine (**12**) (128 mg, 59.8%) as a syrup; ir ν_{max} ($CHCl_3$): 1620 cm^{-1} (C=O); nmr ($CDCl_3$) δ: 1.00 (3H, m, CH_2CH_3), 3.93 (6H, s, 2 × OMe), 6.67 and 6.87 (2H, each s, 2 × ArH); ms *m/e* 473 (M^+).

(±)-Deoxytubulosine (3)

To a stirred 70% solution of $NaAl(OCH_2CH_2OCH_3)_2H_2$ in toluene (2 mL) was added (±)-4-oxodeoxytubulosine (**12**) (128 mg) in pyridine (2 mL) and the solution was stirred for 1 h at room temperature. The solvents were removed and excess reagent was decomposed and neutralized by the addition, with ice cooling, of a saturated NH_4Cl solution. The resulting mixture was extracted with $CHCl_3$. The extract was washed with a saturated NaCl solution, dried (Na_2SO_4), and evaporated to give a reddish viscous material which was dissolved in 2% HCl (5 mL). The resulting solution was washed with Et_2O. The aqueous layer was basified with solid $NaHCO_3$ and extracted with $CHCl_3$. The extract was washed with a

[3]All compounds having chiral centers are racemates.

saturated NaCl solution, dried (Na_2SO_4), and evaporated to give a reddish solid. Recrystallization from $CHCl_3$–MeOH gave (±)-deoxytubulosine (**3**) (51 mg, 41%) as colorless needles, mp 156–158°C; the nmr spectrum ($CDCl_3$) was identical with that of the authentic sample (**3**); ms *m/e* 459 (M^+). *Anal.* calcd. for $C_{29}H_{37}N_3O_2 \cdot H_2O$: C 72.86, H 8.23, N 8.80; found: C 72.65, H 8.18, N 8.75.

Acknowledgments

We thank Prof. C. Szántay and Prof. A. R. Battersby for their kind gifts of (−)-tubulosine and of an nmr spectrum of deoxytubulosine, respectively. We also thank Mr. K. Kawamura, Mrs. C. Koyanagi, Miss K. Mushiake, Mrs. R. Kobayashi, Miss M. Tanno, Miss K. Katsuma, Miss K. Kikuchi, Miss. Y. Katoh, and Miss J. Okazaki for microanalyses and spectral measurements and for the preparation of this manuscript.

1. T. Kametani, Y. Kigawa, H. Nemoto, M. Ihara, and K. Fukumoto. Heterocycles, **12**, 685 (1979).
2. T. Kametani. The chemistry of the isoquinoline alkaloids. Vol. I. Elsevier Publishing Co., New York. 1969. p. 163; Vol. II. Kinkodo Publishing Co., Sendai, Japan. 1974. pp. 266–267.
3. R. S. Gupta and L. Siminovitch. Biochemistry, **16**, 3209 (1977); C. Pareyre and G. Deysson. Cell Tissue Kinet. **8**, 67 (1975); C. Pareyre. Bull. Soc. Bot. Fr. **121**, 3 (1974); R. K. Johnson and W. R. Washington. Biochem. J. **140**, 87 (1974); C. Pareyre and G. Deysson. C. R. Acad. Sci. Ser. D. **277**, 2689 (1973).
4. T. Kametani, Y. Suzuki, H. Terasawa, M. Ihara, and K. Fukumoto. Heterocycles, **8**, 119 (1977); T. Kametani, Y. Suzuki, H. Terasawa, and M. Ihara. J. Chem. Soc. Perkin Trans. I. In press.
5. C. Szántay and G. Kalaus. Chem. Ber. **102**, 2270 (1969).
6. A. Popelak, E. Haack, and H. Spingler. Tetrahedron Lett. 5077 (1969).
7. H. T. Openshaw and N. Whittaker. J. Chem. Soc. C, 91 (1969).
8. A. R. Battersby, J. R. Merchant, E. A. Ruveda, and S. S. Salgar. Chem. Commun. 315 (1965); A. R. Battersby, R. S. Kapil, D. S. Bhakuni, S. P. Popli, J. R. Merchant, and S. S. Salgar. Tetrahedron Lett. 4965 (1966).

Total synthesis of indole and dihydroindole alkaloids. XVII. The total synthesis of catharine and vinamidine (catharinine)[1–3]

JAMES P. KUTNEY, JOHN BALSEVICH, AND BRIAN R. WORTH

Department of Chemistry, University of British Columbia, 2075 Wesbrook Place, Vancouver, B.C., Canada V6T 1W5

Received December 8, 1978

JAMES P. KUTNEY, JOHN BALSEVICH, and BRIAN R. WORTH. Can. J. Chem. 57, 1682 (1979).

Oxidation of 16,18-dicarbomethoxycleavamine gave the epoxide (**6**) and the enamide (**9**). Similar oxidation of 3′,4′-dehydrovinblastine (**8**) or leurosine (**7**) gave the natural product catharine (**3**). Potassium permanganate oxidation of **7** or **8** gave 3*R*-hydroxyvinamidine (**19**) whereas similar oxidation of 4′-deoxyleurosidine (**29**) gave the alkaloid vinamidine (**4**).

JAMES P. KUTNEY, JOHN BALSEVICH et BRIAN R. WORTH. Can. J. Chem. 57, 1682 (1979).

L'oxydation de la dicarbométhoxy-16,18 cléavamine conduit à l'époxyde (**6**) et à l'énamide (**9**). Une oxydation semblable de la déhydro-3′,4′ vinblastine (**8**) ou de la leurosine (**7**) fournit le produit naturel catharine (**3**). L'oxydation de **7** ou **8** par le permanganate de potassium fournit l'hydroxy-3*R* vinamidine (**19**) alors qu'une oxydation semblable de la déoxy-4′ leurosidine (**29**) conduit à l'alcaloïde vinamidine (**4**).

[Traduit par le journal]

The important oncolytic action of many of the members of the vinblastine (**1**) – vincristine (**2**) family initiated innumerable investigations into the chemistry and biochemistry of these 'dimeric' alkaloids. Indeed efforts from several laboratories led to syntheses of some of the natural products as well as many derivatives while more recent work enabled unambiguous structure identification of two interesting ring cleaved compounds catharine (**3**) (4) and vinamidine (catharinine) (**4**) (5, 6). This report describes total syntheses of both **3** and **4**, and several related compounds.

In the early stages of our investigation of totally synthetic routes to 'bisindole' alkaloids, considerable emphasis was placed on selective functionalisation of model systems of the cleavamine type, particularly the protected indole derivative (**5**) (8). In this regard, aerial or hydroperoxide oxidation of (**5**) (7, 8) provided the 3*R*,4*S*-epoxide (**6**) and later adaption of this transformation allowed the first of several syntheses of the natural product leurosine (**7**) from synthetic 3′,4′-dehydrovinblastine (**8**) (7, 8).

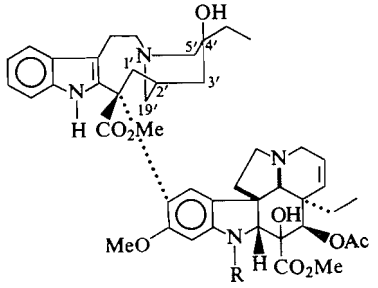

1 R = CH_3
2 R = CHO

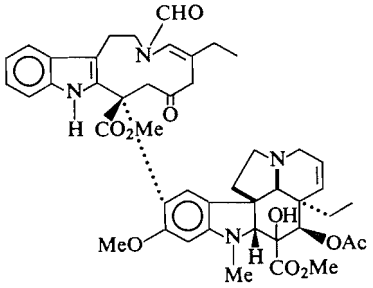

3

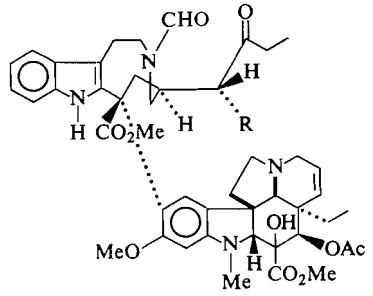

4 R = H **20** R = OAc
19 R = OH **28** R = $OCSC_6H_5$

In an attempt to optimise conditions for the formation of the epoxide **6**, the aerial oxidation of **5** in peroxide-free tetrahydrofuran (THF) containing a small amount of aqueous trifluoroacetic acid (TFA) was studied, the course of the reaction being monitored by thin-layer chromatography (tlc) after 3, 5,

[1]Dedicated to the memory of R. H. F. Manske.
[2]For part XVI, see ref. 1.
[3]For preliminary reports on this work see refs. 2 and 3.

0008-4042/79/131682-09$01.00/0

and 8 days. At ambient temperature, no reaction was apparent after 3 days, whereas both **5** and **6** were detected after 5 days. The starting material (**5**) had been consumed after 8 days but the epoxide **6** (isolated in only 10% yield) had undergone further transformation to **9** which was isolated in 52% yield. Based on an assumption that the cleavamine skeleton was intact, this latter product was originally assigned as the 5-oxo derivative **10** (8). The revised assignment (**9**) followed further analysis of spectral properties and results of a chemical transformation. Thus the ^{1}Hmr spectrum of **9** exhibited absorbances at δ 8.13 (N_b-CHO), 5.23 (C5-H), and 1.90 ppm (—CH_2CH_3) in accord with the proposed structure. The duplication of various resonances as observed in this spectrum has also been noted in a number of alkaloids exhibiting rotomers of a formamide group (9). The infrared spectrum showed strong absorbance at 1680 and 1650 cm^{-1} in support of the enamide assignment. The presence of a ketone carbonyl function was substantiated by sodium borohydride reduction to the corresponding secondary alcohol

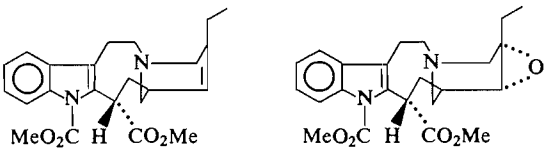

5 **6**

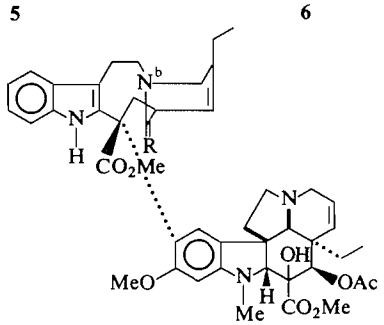

8 R = H_2
16 R = H_2, N_b-oxide
18 R = O

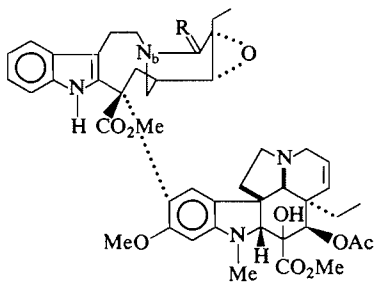

7 R = H_2
15 R = O
17 R = H_2, N_b-oxide

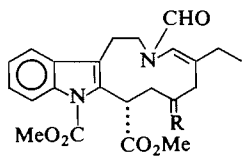

9 R = O
11 R = H, OH

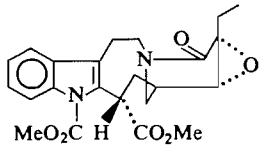

10

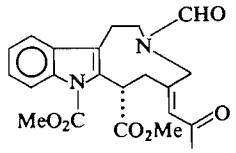

12

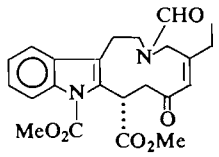

13

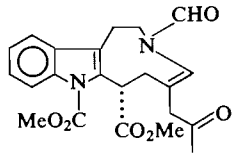

14

(**11**), thus ruling out structure **10**. Infrared absorption at 1669 and 1651 cm^{-1} for **11** corroborated the enamide assignment (**9**) and eliminated the alternate cleavage possibilities **12** and **13**. The alternative enamide structure (**14**) was incompatible with the ^{1}Hmr quartet resonance at δ 1.90 ppm due to the methylene of the ethyl group.

Subsequently, the apparent existence of an induction period for the oxidation led to an observation that when THF, which had already undergone some aerial oxidation, was used the alkene **5** was converted to **6** in 4 h and that after 22-h work up afforded **6** (32%) and **9** (25%). Reproducible conditions were found using peroxide-free THF containing a small amount of 1% TFA and added *tert*-butylhydroperoxide. In this manner, a 76% yield of **6** was attained and in fact these conditions were later used for the synthesis of the alkaloid leurosine (**7**). In this regard, similar protection of the indole nitrogen of **8** was neither possible nor necessary and leurosine was obtained directly from **8** without observable oxidation at the β-position of the indole system. Examination of the reaction mixture by tlc indicated that on prolonged treatment leurosine also underwent further oxidation to yield a product readily detected on tlc by its distinct green colouration after spraying with ceric sulphate reagent. Again this product was initially assigned the 5′-oxo structure **15** (8, 10). Later comparison of this product with naturally occurring catharine (**3**)[4], a structure derived

[4]The authors are very grateful to Dr. Gordon Svoboda, Eli Lilly and Company, Indianapolis, IN, for providing samples of catharine and vinamidine.

TABLE 1. Aerial and *tert*-butyl hydroperoxide oxidations

Entry	Substrate	Reaction conditions	Products
1	**8**	*t*BuOOH, THF, 1% TFA(aq), 22 h	**7, 3, 16, 17**
2	**8**	*t*BuOOH, THF, 1% TFA(aq), 5 days	**3, 7, 16, 17**
3	**8**	*t*BuOOH, THF, H_2O, 22 h	**7, 3, 16, 17**
4	**8**	*t*BuOOH, THF, 22 h	**3, 7, 8, 16, 17**, others
5	**8**	*t*BuOOH, THF, 1% TFA(aq), MeOH, 22 h	**8, 7, 16, 17**
6	**8**	*t*BuOOH, THF, 1% TFA(aq), inhibitor*	**8, 16**
7	**16**	*t*BuOOH, THF, 1% TFA(aq), 22 h	No reaction
8	**8**	*t*BuOOH, THF, 5% TFA(aq), 22 h	No reaction
9	**7**	*t*BuOOH, THF, 5% TFA(aq), 22 h	No reaction
10	**7**	*t*BuOOH, THF, 1% TFA(aq), 22 h	**7, 3, 17**
11	**7**	Air, THF, 1% TFA(aq), 11 days	**7, 3**, others
12	**8**	Air, THF, 1% TFA(aq), 11 days	**8, 3**, others
13	**7**	*t*BuOOH, CH_2Cl_2	**3**, others
14	**7**	*t*BuOOH, THF, 1% TFA(aq), dark, inhibitor,* 22 h	**7, 17**
15	**7**	*t*BuOOH, THF, 1% TFA(aq), dark, inhibitor,* 44 h	**17**
16	**17**	*t*BuOOH, THF, 1% TFA(aq), 22 h	No reaction
17	7	Air, CH_2Cl_2, 22 h	No reaction

*The radical inhibitor used was 3-*tert*-butyl-4-hydroxy-5-methylphenyl sulphide.

by X-ray analysis (4), showed its identity; mp (acetone) 213–215°C (lit. (4) mp 213–215°C); mp (ethanol) 162–166°C (lit. (11) mp 171–175°C),[5] undepressed on admixture with an authentic sample; $[\alpha]_D$ −49° (*c* 0.7, $CHCl_3$), (lit. (11) $[\alpha]_D$ −51°). Again duplication of ^{1}Hmr signals was consistent with a formamide function (9) and the spectrum of **3** was superimposable on that of authentic catharine.

Under the conditions employed for the formation of **3**, an acid-catalysed or radical mechanism was possible and a further examination of the reaction was needed to distinguish the pathway involved. Aerial or *tert*-butylhydroperoxide oxidation of **8** in THF containing a small amount of 1% aqueous TFA gave catharine (**3**) (ca. 30% yield) after 11 or 5 days, respectively, and monitoring the course of the reaction by tlc implicated leurosine (**7**) as a precursor of **3**. Accordingly aerial or *tert*-butylhydroperoxide oxidation of leurosine (**7**) also afforded catharine (Table 1, entries 10, 11). Alternatively, reaction of **7** or **8** with *tert*-butylhydroperoxide could be inhibited or the course of reaction changed on addition of a radical inhibitor (entries 6, 14, 15). The role of aqueous acid in the transformation of **8** to **7** was obscure, since although leurosine was formed in small amounts in the absence of acid, the product mixture was very complex. On the other hand, formation of catharine did not require acid or water (entries 4, 13). Indeed optimum conditions for the transformation of **7** to **3** (48% yield) were found using *tert*-butylhydroperoxide in dichloromethane. Finally, the possible intermediacy of the corresponding N_b-oxides **16** and **17** was eliminated since these substrates did not react under the original experimental conditions (entries 7, 16).

[5]In our hands, an authentic sample had mp 164–168°C.

Thus the alkene **8** could be converted to the alkaloid leurosine (**7**), via a radical mechanism. Aqueous acid was necessary for a synthetically useful transformation possibly owing to inhibition of unwanted side reactions at N_b. Catharine (**3**) was in turn formed from leurosine via a radical pathway possibly as shown in Scheme 1. Notably, recent work from these laboratories has shown the biosynthetic intermediacy of leurosine in the natural formation of catharine (12).

Although hydroperoxide oxidation of cleavamine systems led to C19′—C2′ cleavage products, potassium permanganate oxidation allowed an alternative mode of ring cleavage. Here oxidation of **8** with $KMnO_4$ in acetone gave two products (3). The minor component of the mixture was identical with the known 19′-oxo derivative (**18**) (8). The major product

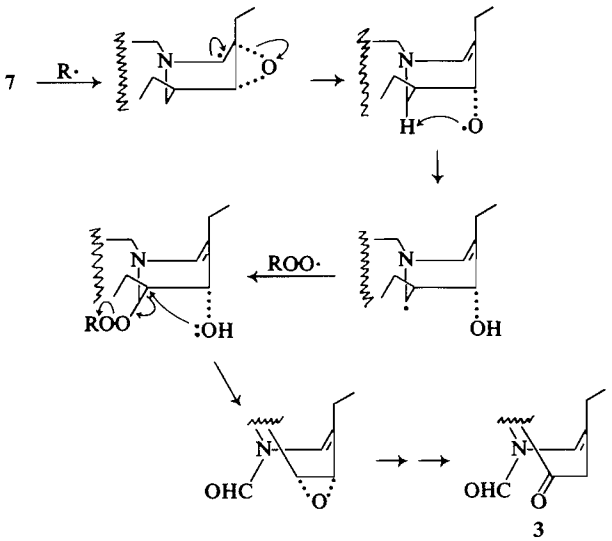

SCHEME 1

was identified, *ex post facto*, as 3*R*-hydroxyvinamidine (**19**). The identity of this product was established by spectral analysis and by chemical transformations. High resolution mass spectrometry gave the molecular formula $C_{46}H_{56}N_4O_{11}$ while infrared absorbance at 1660 cm^{-1} suggested the presence of an

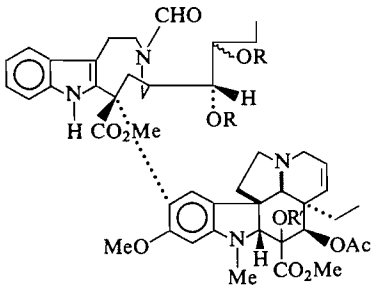

21 R = R′ = H
22 R = R′ = Ac
23 R = Ac, R′ = H

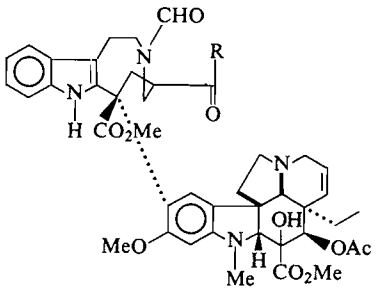

24 R = $COCH_2CH_3$
26 R = H

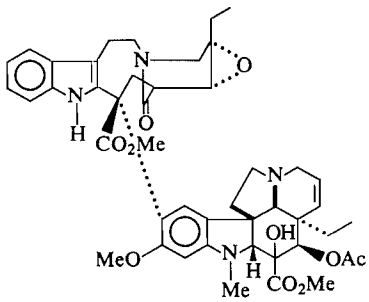

27

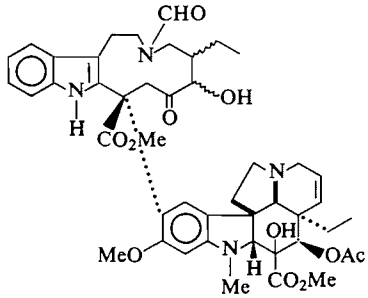

25

N_b-formyl function, further evidenced by ^{1}Hmr singlet resonance at δ 7.30 ppm. Acetylation in the usual manner gave the keto acetate **20** with ^{1}Hmr signals at δ 4.80 (bs, C3′-H) and 2.10 (s, —$OCOCH_3$) indicating a secondary alcohol group in **19**. Alternatively reduction of **19** with sodium borohydride gave the triol **21** which on acetylation gave a mixture of the tetraacetate **22** and the triacetate **23**. Oxidation of **19** with cupric acetate (14) in hot methanol gave the α-diketone (ν_{max} 1713 cm^{-1}) **24** thus confirming the α-ketol function in **19**. The possible cleavage structure **25** was eliminated as periodate cleavage of either **19** or **21** gave only the aldehyde **26** exhibiting singlet absorbances at δ 7.61 (N_b-CHO) and 9.20 ppm (—CHO). High resolution mass spectrometry gave the molecular formula $C_{43}H_{50}N_4O_{10}$ thus confirming the loss of a three-carbon fragment. The formation of an aldehyde by periodate cleavage of **19** also supported the ketol orientation as shown. The stereochemistry at C3′ in **19** was assigned *R* on the basis of the permanganate cleavage of leurosine (**7**) to **19** (27% yield) with the assumption that the stereochemical integrity at C3′ had been maintained. The lactam **27** was also isolated from this oxidation.

At this time the structure of the alkaloid vinamidine (catharinine) (**4**) was reported (5) and we sought a method to convert the hydroxy derivative **19** to the natural product. However attempted reductive cleavage of the derived acetate **20** was unsuccessful under a variety of conditions as were efforts to form the corresponding thionobenzoate **28**.

Therefore an alternative route to **4** was considered. The plausible mechanism (outlined in Scheme 2) for the oxidative cleavage of **7** or **8** to give **19** suggested that a substrate of lower oxidation state might similarly lead to vinamidine (**4**). In the event oxidation of 4′-deoxyleurosidine (**29**) with $KMnO_4$ in acetone gave the lactam **30** together with vinamidine (**4**). The cleavage product was identical with an authentic sample[4] of the alkaloid and the specific rotation of the sodium borohydride reduction product was in agreement with the literature value (5).

Thus propitious use of potassium permanganate oxidant enabled preparation of several unusual seco-4′,5′ derivatives including the natural product vinamidine (catharinine) (**4**). Alternatively, hydroperoxide oxidation of leurosine **7** or **8** afforded the seco-2′,19′ compound catharine (**3**).

Experimental

Melting points were determined on a Kofler block and are uncorrected. Ultraviolet (uv) spectra were recorded on a Cary 15 spectrophotometer in ethanol solution. The wavelengths of absorption maxima are reported in nanometers (nm) with log ε values in parentheses. Infrared (ir) spectra were measured on a Perkin Elmer model 710 or 457 spectrophotometer in chloroform solution. The absorption maxima are reported in

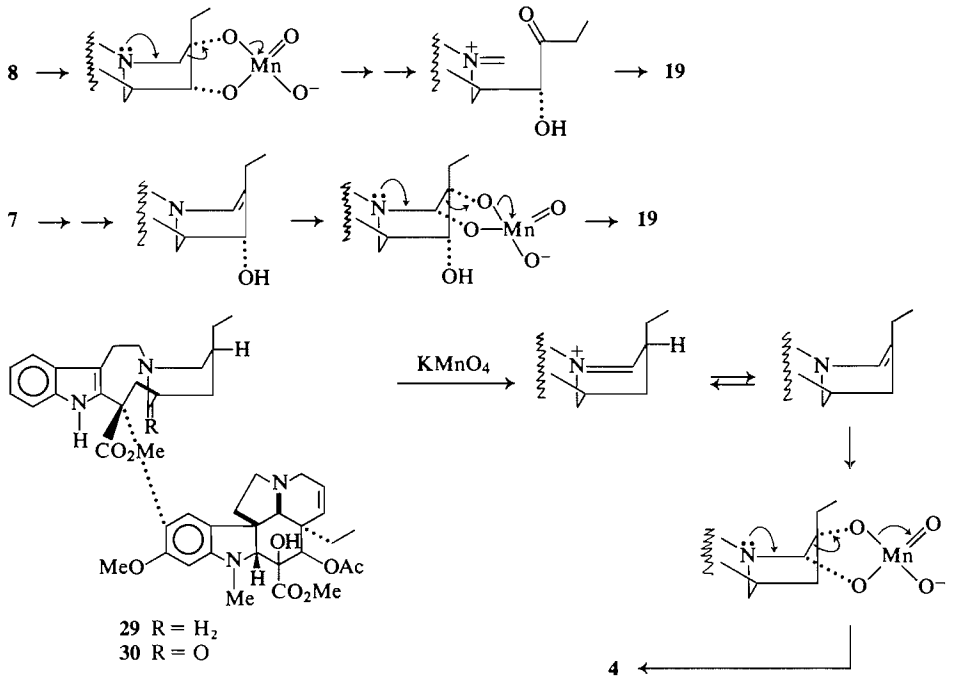

SCHEME 2

wavenumbers (cm^{-1}), calibrated with respect to the absorption band of polystyrene at 1601 cm^{-1}. Proton magnetic resonance (^{1}Hmr) spectra were measured in deuteriochloroform ($CDCl_3$) solution at ambient temperature on either a Varian HA-100 or XL-100 spectrometer. Chemical shift values are given in the δ (ppm) scale relative to tetramethylsilane (TMS) used as internal standard. The integrated peak areas, signal multiplicities, and proton assignments are given in parentheses. Low resolution mass spectra (ms) were determined on either an AEI-MS-902 or an Atlas CH-4B spectrometer. High resolution mass spectra were measured on an AEI-MS-902 instrument. Microanalyses were carried out by Mr. P. Borda of the Microanalytical Laboratory, University of British Columbia.

Thin-layer chromatography (tlc) utilized Merck silica gel G (according to Stahl) containing 2% fluorescent indicator. For preparative-layer chromatography (plc), plates (20 × 20 or 20 × 60 cm) of 1-mm thickness were used. Visualization was effected by viewing under ultraviolet light and/or by colour reaction with ceric sulphate spray reagent. Column chromatography utilized Merck silica gel 60 (70–230 mesh) or Merck aluminum oxide 90 (neutral).

As a matter of routine, all reagents and solvents were recrystallized or distilled before use.

Autoxidation of 16,18-Dicarbomethoxycleavamine

A solution of 16,18-dicarbomethoxycleavamine (**5**) (400 mg, 1 mmol) in peroxide-free tetrahydrofuran (10 mL) containing aqueous 1% trifluoroacetic acid (1 mL) was stirred at ambient temperature in the presence of air for a period of 8 days. After drying (K_2CO_3), the solvent was removed *in vacuo*. Chromatography of the residue on alumina (activity III, benzene) afforded the epoxide **6** (40 mg, 10%) and the keto enamide **9** (230 mg, 54%).

16,18-Dicarbomethoxy-3*R*,4*S*-epoxydihydrocleavamine **6**, mp 131–132°C (ether); uv λ_{max}: 294 (3.66), 283 sh (3.76), 268 (4.08), 262 (4.09), 227 (4.32); ir ν_{max}: 1728; ^{1}Hmr δ: 8.1 (1H, m, C14-H), 7.3 (3H, m, C11–C13-H's), 5.84 (1H, d, J = 6 Hz, C18-H), 3.91 (3H, s, —OCH_3), 3.57 (3H, s, —OCH_3), 1.00 (3H, t, J = 7.5 Hz, —CH_2CH_3); ms *m/e*: 412 (M^+), 224 (base peak), 152, 138; ^{13}Cmr δ: 173.4 (—CO_2CH_3), 152.0 (—CO_2CH_3), 137.1 (C17), 136.0 (C15), 129.8 (C10), 124.5 (C12), 122.9 (C11), 119.5 (C9), 118.2 (C13), 115.9 (C14), 62.7 (C4), 60.6 (C3), 53.4 (C7 and —OCH_3), 52.7 (C5), 51.9 (—OCH_3), 50.6 (C19), 39.5 (C18), 33.6 (C8 and C2), 30.0 (—CH_2CH_3), 26.3 (C1), 8.9 (—CH_2CH_3). *Mol. Wt.* calcd. for $C_{23}H_{28}N_2O_5$: 412.1997; found (high resolution ms): 412.2027. *Anal.* calcd. for $C_{23}H_{28}N_2O_5$: C 66.97, H 6.84, N 6.79; found: C 66.81, H 6.87, N 6.71.

Keto enamide **9** (as a foam); uv λ_{max}: 293 (3.67), 281 sh (3.78), 265 (4.05), 259 (4.06), 227 (4.38); ir ν_{max}: 1732, 1680, 1650; ^{1}Hmr δ: 8.13 (1H, s, N_b-C*H*O), 8.10 (1H, m, C14-H), 7.3 (3H, m, C11–C13-H's), 5.23 (1H, bs, C5-H), 4.00 (3H, bs, —OCH_3), 3.66 (3H, s, —OCH_3), 1.90 (2H, q, J = 7 Hz, —CH_2CH$_3$), 0.79 (3H, t, J = 7 Hz, —CH$_2$CH_3); ms *m/e*: 426 (M^+, base peak), 394, 228; ^{13}Cmr δ: 188.8 (N_b-*C*HO), 163.0 (—*C*O_2CH_3), 160.7 (—*C*O_2CH_3), 135.9 (C17), 132.3 (C15), 128.8 (C10), 126.9 (C5), 125.1 (C12), 123.3 (C11), 122.7 (C4), 119.9 (C9), 118.9 (C13), 116.0 (C14), 53.6 (—O*C*H$_3$), 52.5 (—O*C*H$_3$), 48.7 (C7), 44.9 (C3), 44.3 (C2), 40.0 (C18), 30.3 (C8), 24.5 (—*C*H$_2$CH$_3$), 12.3 (—CH$_2$*C*H$_3$). *Mol. Wt.* calcd. for $C_{23}H_{26}N_2O_6$: 426.1791; found (high resolution ms): 426.1795. *Anal.* calcd. for $C_{23}H_{26}N_2O_6 \cdot \frac{1}{2}CH_3OH$: C 63.80, H 6.33, N 6.33; found: C 64.08, H 6.11, N 6.31.

Oxidation of 16,18-Dicarbomethoxycleavamine (5) in 'Preoxidized' Tetrahydrofuran[6]

A solution of **5** (900 mg, 2.27 mmol) in 'preoxidized' tetrahydrofuran (20 mL) containing aqueous 1% trifluoroacetic acid (2 mL) was stirred at ambient temperature for 20 h. The

[6]'Preoxidized' tetrahydrofuran refers to tetrahydrofuran which had undergone aerial oxidation and contained an unspecified amount of peroxides.

reaction mixture was poured into a saturated solution of sodium bicarbonate (20 mL) and extracted with ethyl acetate (2 × 40 mL). The combined organic portion was washed with water (3 × 15 mL) and brine (1 × 20 mL). After drying (Na_2SO_4) the solvent was removed *in vacuo* and the residue was chromatographed on alumina (activity III, benzene) to afford the epoxide **6** (306 mg, 33%) and the keto enamide **9** (250 mg, 26%). These compounds were identical with the respective products obtained above.

Oxidation of 16,18-Dicarbomethoxycleavamine (5) using tert-*Butyl Hydroperoxide*

A solution of **5** (1.76 g, 4.4 mmol) in freshly distilled tetrahydrofuran (50 mL) containing aqueous 1% trifluoroacetic acid (10 mL) and *tert*-butyl hydroperoxide (9 mL) was stirred at ambient temperature for 21 h. The reaction mixture was poured into a saturated solution of sodium bicarbonate (40 mL) and extracted with ethyl acetate (2 × 30 mL). The combined organic portion was washed with 5% sodium hydroxide solution (1 × 20 mL), water (1 × 20 mL), and brine (1 × 20 mL). After drying (Na_2SO_4) the solvent was removed *in vacuo* to give a viscous oil. Chromatography on alumina (activity III, benzene) afforded the epoxide **6** (1.22 g, 67%) identical with that obtained above.

Hydroxy Enamide (11)

A solution of the keto enamide (**9**) (10 mg, 0.023 mmol) in 95% ethanol (2 mL) was treated with sodium borohydride (4 mg, 0.1 mmol). The reaction mixture was stirred at ambient temperature for 20 min, taken up in water (10 mL), and extracted with methylene chloride (3 × 5 mL). After drying (Na_2SO_4), the solvent was removed *in vacuo* and the residue chromatographed on silica gel (ether) to afford the hydroxy enamide **11** (6 mg, 60%) as a film; uv λ_{max}: 293 (3.50), 281 sh (3.68), 262 (4.03), 224 (4.32); ir ν_{max}: 3530, 3420, 1730, 1669, 1651; ^{1}Hmr δ: 8.05 (1H, m, C14-H), 8.02 (1H, s, N_b-C*H*O), 7.6–7.2 (3H, m, C11–C13-H's), 5.48 (1H, bs, C5-H), 4.00 (3H, s, —OCH_3), 3.66 (3H, s, —OCH_3), 0.98 (3H, t, J = 7.5 Hz, —CH_2CH_3); ms *m/e*: 428 (M^+), 315, 201, 126 (base peak). *Mol. Wt.* calcd. for $C_{23}H_{28}N_2O_6$: 428.1947; found (high resolution ms): 428.1928.

Leurosine (7)

This compound was prepared as described earlier (8).

Catharine (3)

(*A*) A solution of leurosine (7) (30 mg, 0.037 mmol) in tetrahydrofuran (2 mL) containing aqueous 1% trifluoroacetic acid (0.2 mL) was stirred in the presence of air for 11 days. The reaction mixture was diluted with a saturated solution of sodium bicarbonate (5 mL) and extracted with methylene chloride (3 × 5 mL). The combined organic portion was dried (Na_2SO_4) and the solvent was removed *in vacuo*. Chromatography of the residue on silica gel (ethyl acetate – 12% methanol) afforded leurosine (7) (4 mg) and catharine (**3**) (4 mg, 15%). The synthetic catharine had mp 213–215°C (acetone) (lit. (4) mp 213–215°C); mp 162–166°C (ethanol) (lit. (11) mp 171–175°C),[5] undepressed on admixture with an authentic sample; $[\alpha]_D$ −49° (*c* 0.7, $CHCl_3$) (lit. (11) $[\alpha]_D$ −51°). The ^{1}Hmr, uv, ir, and mass spectra were superimposable with those of authentic material.

(*B*) Oxidation of 3′,4′-dehydrovinblastine (**8**) as above afforded catharine in 34% yield.

(*C*) A solution of leurosine (**7**) (45 mg, 0.56 mmol) in methylene chloride containing *tert*-butyl hydroperoxide (0.06 mL) was stirred at ambient temperature for 24 h. The solvent was removed *in vacuo* and the residue chromatographed on silica gel (methylene chloride – 5% methanol) to afford catharine (22 mg, 48%).

Comparative Oxidations of 3′,4′-Dehydrovinblastine (8), Leurosine (7), and Derivatives, Utilizing tert-*Butyl Hydroperoxide*

All reactions were carried out utilizing 10 mg of substrate dissolved in 0.5 mL tetrahydrofuran containing 0.05 mL of *tert*-butyl hydroperoxide. To these solutions were added any further reagents used. The product composition of the reactions was ascertained via tlc. Authentic samples of 3′,4′-dehydrovinblastine (**8**), leurosine (**7**), catharine (**3**), pleurosine (**17**) (14), and 3′,4′-dehydrovinblastine N_b-oxide (**16**) (8) were used for comparison purposes. The solvent systems used for the chromatographic analysis were ethyl acetate – 20% methanol and methylene chloride – 6% methanol. Visualization was achieved by spraying with ceric sulfate spray reagent and heating at 100°C for 1 h. The relative amounts of products formed were *estimated* from the visualized chromatograms.

Reaction of 3′,4′-Dehydrovinblastine (8) with Potassium Permanganate

A solution of 3′,4′-dehydrovinblastine (**8**) (250 mg, 0.316 mmol) in methylene chloride (2 mL) and acetone (5 mL) was treated at 0°C with a solution of potassium permanganate (105 mg, 0.665 mmol) in acetone (5 mL). The reaction mixture was stirred at 0°C for 5 min and the solvent was removed *in vacuo*. The residue was triturated with methylene chloride (5 mL) and filtered through silica gel (ethyl acetate – 25% methanol). Removal of the solvent *in vacuo* followed by chromatography of the residue on silica gel (ethyl acetate – 15% methanol) afforded the ketol **19** (111 mg, 42%) as the major product (R_f 0.4). 19′-Oxo-3′,4′-dehydrovinblastine (**18**) (25 mg, 9.8%) identical with an authentic sample (8) (tlc, ms, ^{1}Hmr) was obtained as the minor product (R_f 0.75).

Ketol **19**, mp 198–202°C (ethanol); uv λ_{max}: 310 (3.80), 294 (4.08), 284 (4.14), 268 (4.19), 212 (4.72); ir ν_{max}: 3475, 1734, 1660, 1612; ^{1}Hmr δ: 7.88 (1H, bs, N*H*), 7.51 (1H, m, C14′-H), 7.32 (1H, s, NC*H*O), 7.14 (3H, m, C11′–C13′-H's), 6.71 (1H, s, C14-H), 6.00 (1H, s, C17-H), 5.86 (1H, dd, J = 10 and 4 Hz, C7-H), 5.49 (1H, s, C4-H), 5.30 (1H, d, J = 10 Hz, C6-H), 3.97 (1H, bs, C3′-H), 3.79 (3H, s, —OCH_3), 3.73 (3H, s, —OCH_3), 3.51 (3H, s, —OCH_3), 2.69 (3H, s, —NCH_3), 2.12 (3H, s, —OCOCH_3), 0.79 (3H, t, J = 7 Hz, —CH_2CH_3), 0.70 (3H, t, J = 7 Hz, —CH_2CH_3); ms *m/e*: 840 (M^+), 781, 680, 573, 135 (base peak). *Mol. Wt.* calcd. for $C_{46}H_{56}N_4O_{11}$: 840.3945; found (high resolution ms): 840.3966.

Reaction of Leurosine (7) with Potassium Permanganate

A solution of leurosine (**7**) (105 mg, 0.13 mmol) in acetone (1 mL) and methylene chloride (0.5 mL) was treated with a solution of potassium permanganate (40 mg, 0.25 mmol) in acetone (4 mL). The reaction mixture was stirred at ambient temperature for 3 min and the solvent was removed *in vacuo*. The residue was treated as above to afford the ketol **19** (30 mg, 27%), identical with that obtained above, and 19′-oxoleurosine (**27**) (20 mg, 19%) as a colorless film.

19′-Oxoleurosine (**27**); uv λ_{max}: 309 sh (3.74), 294 (4.00), 284 (4.05), 262 (4.13), 214 (4.66); ir ν_{max}: 3470, 1738, 1644; ^{1}Hmr δ: 8.06 (1H, bs, N*H*), 7.57 (1H, m, C14′-H), 7.18 (3H, m, C11′–C13′-H's), 6.65 (1H, s, C14-H), 6.19 (1H, s, C17-H), 5.90 (1H, dd, J = 10.5 and 3.5 Hz, C7-H), 5.51 (1H, s, C4-H), 5.33 (1H, d, J = 10.5 Hz, C6-H), 4.76 (1H, m, C2′-H), 3.85 (3H, s, —OCH_3), 3.83 (3H, s, —OCH_3), 3,63 (3H, s, —OCH_3), 2.76 (3H, s, NCH_3), 2.12 (3H, s, —OCOCH_3), 1.01 (3H, t, J = 7.5 Hz, —CH_2CH_3), 0.84 (3H, t, J = 7 Hz, —CH_2CH_3); ms *m/e*: 822 (M^+), 763, 282, 135 (base peak); ^{13}Cmr δ: 163.0 (C19′), 61.6 (C3′), 59.8 (C4′), 8.9 (—CH_2CH_3), 8.5 (—CH_2CH_3). *Mol. Wt.* calcd. for $C_{46}H_{54}N_4O_{10}$: 822.3839; found (high resolution ms): 822.3806.

TABLE 2. Comparative oxidations of 3′,4′-dehydrovinblastine (**8**), leurosine (**7**), and derivatives using *tert*-butyl hydroperoxide

Reaction conditions			Products (%, approximate)				
Substrate	Time	Additive	**3**	**7**	**8**	**16** or **17**	Others
8	22 h	0.05 mL 1% trifluoroacetic acid	5	95	—	5	—
8	5 days	0.05 mL 1% trifluoroacetic acid	40	25	—	5	30
8	22 h	0.05 mL water	5	30	—	5	60
8	22 h	—	30	10	5	10	45
8	22 h	0.05 mL 1% trifluoroacetic acid 0.1 mL methanol	—	50	45	5	—
8	22 h	0.05 mL 1% trifluoroacetic acid 5 mg radical inhibitor*	—	25	70	5	—
16	22 h	0.05 mL 1% trifluoroacetic acid	—	—	—	100	—
8	22 h	0.05 mL 5% trifluoroacetic acid	—	—	100	—	—
7	22 h	0.05 mL 5% trifluoroacetic acid	—	100	—	—	—
7	22 h	0.05 mL 1% trifluoroacetic acid	20	65	—	15	—
7	22 h	0.05 mL 1% trifluoroacetic acid 5 mg radical inhibitor*	5	90	—	5	—
7	44 h	0.05 mL 1% trifluoroacetic acid 10 mg radical inhibitor*	—	—	—	100	—
17	22 h	0.05 mL 1% trifluoroacetic acid	—	—	—	100	—

*3-*tert*-Butyl-4-hydroxy-5-methylphenyl sulphide.

*Keto Acetate **20***

A solution of the ketol **19** (22 mg, 0.026 mmol) in pyridine (2 mL) at ambient temperature under a nitrogen atmosphere was treated with acetic anhydride (4 drops). The reaction mixture was stirred for 30 h. Methanol (1 mL) and toluene (10 mL) were added and the solvent was removed *in vacuo*. Chromatography of the residue on silica gel (ethyl acetate – 10% methanol) afforded the keto acetate **20** (15 mg, 65%) as a white amorphous solid; uv λ_{max}: 310 (3.81), 294 (4.10), 285 (4.17), 270 (4.21), 213 (4.73); ir ν_{max}: 3470, 1738, 1660, 1612; ^{1}Hmr δ: 7.90 (1H, bs, N*H*), 7.51 (1H, m, C14′-H), 7.32 (1H, s, NC*H*O), 7.12 (3H, m, C11′–C13′-H's), 6.64 (1H, s, C14-H), 6.00 (1H, s, C17-H), 5.86 (1H, dd, J = 10 and 4 Hz, C7-H), 5.48 (1H, s, C4-H), 5.31 (1H, d, J = 10 Hz, C6-H), 4.80 (1H, bs, C3′-H), 3.79 (3H, s, —OC*H*$_3$), 3.76 (3H, s, —OC*H*$_3$), 3.72 (1H, s, C2-H), 3.62 (3H, s, —OC*H*$_3$), 2.69 (3H, s, NC*H*$_3$), 2.14 (3H, s, —OCOC*H*$_3$), 2.10 (3H, s, —OCOC*H*$_3$), 0.77 (3H, t, J = 7 Hz, —CH$_2$C*H*$_3$), 0.70 (3H, t, J = 7 Hz, —CH$_2$C*H*$_3$); ms *m/e*: 882 (M^+), 822, 762, 720, 613, 555, 354, 181, 169, 135, 131, 119 (base peak). *Mol. Wt.* calcd. for $C_{48}H_{58}N_4O_{12}$: 882.4050; found (high resolution ms): 882.4046.

*Triol **21***

A solution of the ketol **19** (50 mg, 0.06 mmol) in 95% ethanol (3 mL) was treated with sodium borohydride (6 mg, 0.16 mmol). The reaction mixture was stirred at ambient temperature for 30 min and treated with acetone (1 mL). The solvent was removed *in vacuo* and the residue was triturated with methylene chloride (20 mL) and filtered through Celite. Removal of the solvent *in vacuo* followed by chromatography of the residue on silica gel (methylene chloride – 5% methanol) afforded the triol **21** (33 mg, 66%) as a colorless film; uv λ_{max}: 310 (3.65), 295 (4.00), 284 (4.06), 267 (4.11), 212 (4.65); ir ν_{max}: 3585, 3472, 1738, 1660, 1613; ^{1}Hmr δ: 7.98 (1H, s, N*H*), 7.53 (1H, m, C14′-H), 7.45 (1H, s, NC*H*O), 7.15 (3H, m, C11′–C13′-H's), 6.76 (1H, s, C14-H), 6.12 (1H, s, C17-H), 5.90 (1H, dd, J = 10 and 4 Hz, C7-H), 5.46 (1H, s, C4-H), 5.35 (1H, d, J = 10 Hz, C6-H), 3.82 (3H, s, —OC*H*$_3$), 3.80 (3H, s, —OC*H*$_3$), 3.76 (1H, s, C2-H), 3.55 (3H, s, —OC*H*$_3$), 2.71 (3H, s, NC*H*$_3$), 2.10 (3H, s, —OCOC*H*$_3$), 0.84 (3H, t, J = 7.5 Hz, —CH$_2$CH$_3$), 0.79 (3H, t, J = 7 Hz, —CH$_2$C*H*$_3$); ms *m/e*: 842 (M^+), 783, 681, 574, 516, 135 (base peak). *Mol. Wt.* calcd. for $C_{46}H_{58}N_4O_{11}$: 842.4102; found (high resolution ms): 842.4060.

*Acetylation of Triol **21***

A solution of the triol **21** (32 mg, 0.38 mmol) in pyridine (2 mL) at ambient temperature under a nitrogen atmosphere

was treated with acetic anhydride (0.1 mL). The reaction mixture was stirred for 22 h at which point methanol (0.5 mL) and toluene (10 mL) were added. The solvent was removed *in vacuo* and the residue was chromatographed on silica gel (methylene chloride – 5% methanol) to yield the tetraacetate **22** (9 mg, 24%, R_f 0.4) and the triacetate **23** (9 mg, 26%, R_f 0.35). Both compounds were obtained as colorless films.

Tetraacetate **22**; uv λ_{max}: 310 (3.73), 294 (4.06), 284 (4.11), 267 (4.15), 212 (4.70); ir ν_{max}: 3468, 1732, 1666, 1618; ^{1}Hmr δ: 8.06 (1H, bs, N*H*), 7.50 (H, m, C14′-H), 7.36 (1H, s, NC*H*O), 7.14 (3H, m, C11′–C13′-H's), 6.53 (1H, s, C14-H), 6.13 (1H, s, C17-H), 5.89 (1H, dd, J = 10 and 5 Hz, C7-H), 5.52 (1H, s, C4-H), 5.30 (1H, d, J = 10 Hz, C6-H), 4.90 (1H, m, C4′-H), 4.54 (1H, t, J = 6 Hz, C3′-H), 4.03 (1H, s, C2-H), 4.82 (3H, s, —OCH_3), 4.77 (3H, s, —OCH_3), 4.59 (3H, s, —OCH_3), 2.85 (3H, s, NCH_3), 2.08 (6H, s, 2 × —OCOCH_3), 1.98 (6H, s, 2 × —OCOCH_3), 0.75 (3H, t, J = 7 Hz, —CH_2CH_3), 0.48 (3H, t, J = 7 Hz, —CH_2CH_3); ms *m/e*: 968 (M^+), 765, 659, 600, 135 (base peak). *Mol. Wt.* calcd. for $C_{52}H_{64}N_4O_{14}$: 968.4419; found (high resolution ms): 968.4395.

Triacetate **23**; uv λ_{max}: 309 (3.70), 294 (4.03), 284 (4.08), 269 (4.10), 212 (4.67); ir ν_{max}: 3480, 1732, 1664, 1617; ^{1}Hmr δ: 7.95 (1H, bs, N*H*), 7.54 (1H, m, C14′-H), 7.38 (1H, s, NC*H*O), 7.15 (3H, m, C11′–C13′-H's), 6.54 (1H, s, C14-H), 6.17 (1H, s, C17-H), 5.88 (1H, dd, J = 10 and 4 Hz, C7-H), 5.55 (1H, s, C4-H), 5.30 (1H, d, J = 10 Hz, C6-H), 4.89 (1H, m, C4′-H), 4.41 (1H, t, J = 6 Hz, C3′-H), 3.84 (3H, s, —OCH_3), 3.82 (3H, s, —OCH_3), 3.75 (1H, s, C2-H), 3.58 (3H, s, —OCH_3), 2.73 (3H, s, NCH_3), 2.12 (3H, s, —OCOCH_3), 2.08 (3H, s, —OCOCH_3), 1.97 (3H, s, —OCOCH_3), 0.76 (6H, t, J = 7 Hz, 2 × —CH_2CH_3); ms *m/e*: 926 (M^+), 867, 765, 659, 600, 135 (base peak). *Mol. Wt.* calcd. for $C_{50}H_{62}N_4O_{13}$: 926.4313; found (high resolution ms): 926.4331.

*Diketone **24***

A solution of the ketol **19** (30 mg, 0.036 mmol) and cupric acetate (monohydrate) (20 mg, 0.11 mmol) in methanol (3 mL) was heated at reflux for 25 min. The solvent was removed *in vacuo* and the residue was triturated with methylene chloride (2 mL) and filtered through Celite. Removal of the solvent *in vacuo* followed by chromatography of the residue on silica gel (methylene chloride – 5% methanol) afforded the diketone **24** (16 mg, 53%) as a pale yellow film; uv λ_{max}: 308 (3.70), 293 (4.03), 277 (4.11), 260 (4.20), 207 (4.70); ir ν_{max}: 3450, 1739, 1713, 1662, 1615; ^{1}Hmr δ: 7.94 (2H, bs, N*H*, NC*H*O), 7.52 (1H, m, C14′-H), 7.18 (3H, m, C11′–C13′-H's), 6.77 (1H, s, C14-H), 6.10 (1H, s, C17-H), 5.91 (1H, dd, J = 10 and 4 Hz, C7-H), 5.51 (1H, s, C4-H), 5.34 (1H, d, J = 10 Hz, C6-H), 3.82 (3H, s, —OCH_3), 3.74 (3H, bs, —OCH_3), 3.62 (3H, s, —OCH_3), 2.74 (3H, s, NCH_3), 2.12 (3H, s, —OCOCH_3), 1.04 (3H, t, J = 7.5 Hz, —CH_2CH_3), 0.79 (3H, t, J = 7 Hz, —CH_2CH_3); ms *m/e*: 838 (M^+), 779, 678 (base peak), 570, 135. *Mol. Wt.* calcd. for $C_{46}H_{54}N_4O_{11}$: 838.3789; found (high resolution ms): 838.3770.

*Periodic Acid Cleavage of **21***

A solution of **21** (25 mg, 0.030 mmol) in tetrahydrofuran (2 mL) at ambient temperature under a nitrogen atmosphere was treated with a solution of periodic acid (8.5 mg, 0.066 mmol) in tetrahydrofuran (0.5 mL). The reaction mixture was stirred for 2 min and concentrated *in vacuo*. Chromatography of the residue on silica gel (methylene chloride – 5% methanol – 0.1% ammonium hydroxide) afforded the N_b-formyl aldehyde **26** (15 mg, 65%) as a colorless film; uv λ_{max}: 310 (3.67), 294 (4.00), 284 (4.08), 268 (4.15), 213 (4.66); ir ν_{max}: 3464, 1732, 1661, 1612; ^{1}Hmr δ: 9.20 (1H, s, —C*H*O), 7.96 (1H, bs, N*H*), 7.61 (1H, s, NC*H*O), 7.56 (1H, m, C14′-H), 7.18 (3H, m, C11′–C13′-H's), 6.64 (1H, s, C14-H), 6.11 (1H, s, C17-H), 5.88 (1H, dd, J = 10 and 4 Hz, C7-H), 5.49 (1H, s, C4-H), 5.29 (1H, d, J = 10 Hz, C6-H), 3.80 (6H, s, 2 × —OCH_3), 3.62 (3H, s, —OCH_3), 3.50 (1H, s, C2-H), 2.71 (3H, s, NCH_3), 2.11 (3H, s, —OCOCH_3), 0.74 (3H, t, J = 7 Hz, —CH_2CH_3); ms *m/e*: 782 (M^+), 723, 621, 514, 135 (base peak). *Mol. Wt.* calcd. for $C_{43}H_{50}N_4O_{10}$: 782.3515; found (high resolution ms): 782.3484.

*Periodic Acid Cleavage of the Ketol **19***

A solution of the ketol **19** (40 mg, 0.048 mmol) in tetrahydrofuran (2 mL) at ambient temperature under a nitrogen atmosphere was treated with a solution of periodic acid (15 mg, 0.117 mmol) in tetrahydrofuran (1 mL). The reaction mixture was stirred for 4 h and the solvent was removed *in vacuo*. Chromatography of the residue on silica gel (methylene chloride – 5% methanol – 0.1% ammonium hydroxide) afforded the N_b-formyl aldehyde **26** (20 mg, 54%) identical with that obtained above.

*Reaction of 4′-Deoxyleurosidine (**29**) with Potassium Permanganate*

A solution of 4′-deoxyleurosidine (**29**) (260 mg, 0.33 mmol) in acetone (5 mL) and methylene chloride (2 mL) at ambient temperature under a nitrogen atmosphere was treated with a solution of potassium permanganate (158 mg, 1 mmol) in acetone (3 mL). The reaction mixture was stirred for 20 min and the solvent was removed *in vacuo*. The residue was triturated with methylene chloride (10 mL) and filtered through silica gel (ethyl acetate – 25% methylene chloride – 15% methanol). Removal of the solvent *in vacuo* followed by chromatography of the residue on silica gel (ethyl acetate – 13% methanol) afforded vinamidine (**4**) (60 mg, 22%) and 19′-oxo-4′-deoxyleurosidine (**30**) (30 mg, 11%). The synthetic vinamidine had $[\alpha]_D$ −35° (*c* 1.1, $CHCl_3$) (lit. (5) $[\alpha]_D$ −33°). The ^{1}Hmr and mass spectra as well as the tlc properties of the synthetic material were in accord with those exhibited by an authentic sample.

19′-Oxo-4′-deoxyleurosidine (**30**); uv λ_{max}: 311 (3.92), 294 (4.03), 284 (4.08), 263 (4.13), 212 (4.72); ir ν_{max}: 3476, 1736, 1640, 1615; ^{1}Hmr δ: 8.05 (1H, bs, N*H*), 7.58 (1H, m, C14′-H), 7.17 (3H, m, C11′–C13′-H's), 6.65 (1H, s, C14-H), 6.16 (1H, s, C17-H), 5.88 (1H, dd, J = 10.5 and 4 Hz, C7-H), 5.51 (1H, s, C4-H), 5.31 (1H, d, J = 10 Hz, C6-H), 4.84 (1H, m, C2′-H), 3.82 (6H, s, 2 × —OCH_3), 3.78 (1H, s, C2-H), 3.61 (3H, s, —OCH_3), 2.74 (3H, s, NCH_3), 2.12 (3H, s, —OCOCH_3), 0.92 (3H, t, J = 7 Hz, —CH_2CH_3), 0.84 (3H, t, J = 7 Hz, —CH_2CH_3); ms *m/e*: 808 (M^+), 749, 690, 646 (base peak), 589, 540, 135. *Mol. Wt.* calcd. for $C_{46}H_{56}N_4O_9$: 808.4079; found (high resolution ms): 808.4046.

Catharininol

Catharininol was prepared from the synthetic vinamidine (catharinine) via the literature procedure (5). This material had $[\alpha]_D$ −78° (*c* 0.42, $CHCl_3$) (lit. (5) $[\alpha]_D$ −80°).

Acknowledgements

Financial aid from the National Research Council of Canada and from contract NO1-CM-23223, National Cancer Institute, National Institutes of Health, Bethesda, Maryland, is gratefully acknowledged. The authors also wish to thank the Lilly Research Laboratories, Indianapolis for samples of various alkaloids.

1. J. P. KUTNEY, J. BALSEVICH, T. HONDA, P-H. LIAO, H. P. M. THIELLIER, and B. R. WORTH. Can. J. Chem. **56**, 2560 (1978).
2. J. P. KUTNEY, J. BALSEVICH, and B. R. WORTH. Heterocycles, **9**, 493 (1978).

3. J. P. KUTNEY, J. BALSEVICH, and B. R. WORTH. Heterocycles. In press.
4. P. RASOANAIVO, A. AHOND, J. P. COSSON, N. LANGLOIS, P. POTIER, J. GUILHEM, A. DUCRUIX, C. RICHE, C. PASCARD, and M. M. JANOT. C. R. Acad. Sci. Ser. C, **279**, 75 (1974).
5. R. Z. ANDRIAMIALISOA, N. LANGLOIS, P. POTIER, A. CHIARONI, and C. RICHE. Tetrahedron, **34**, 677 (1978).
6. S. TAFUR, W. E. JONES, D. E. DORMAN, E. E. LOGSDON, and G. H. SVOBODA. J. Pharm. Sci. **64**, 1953 (1975).
7. J. P. KUTNEY, J. BALSEVICH, G. H. BOKELMAN, T. HIBINO, I. ITOH, and A. H. RATCLIFFE. Heterocycles, **4**, 997 (1976).
8. J. P. KUTNEY, J. BALSEVICH, G. H. BOKELMAN, T. HIBINO, T. HONDA, I. ITOH, A. H. RATCLIFFE, and B. R. WORTH. Can. J. Chem. **56**, 62 (1978).
9. D. J. ABRAHAM, N. R. FARNSWORTH, R. N. BLOMSTER, and A. G. SHARKEY. Tetrahedron Lett. 317 (1965); J. R. HYMON and H. SCHMID. Helv. Chim. Acta, **49**, 2067 (1966); C. HOOTELE and J. C. BRAEKMAN. Bull. Soc. Chim. Belg. **78**, 271 (1969).
10. J. P. KUTNEY, J. BALSEVICH, and G. H. BOKELMAN. Heterocycles, **4**, 1377 (1976).
11. G. H. SVOBODA, M. GORMAN, N. NEUSS, and A. J. BARNES. J. Pharm. Sci. **50**, 409 (1961).
12. K. L. STUART, J. P. KUTNEY, T. HONDA, and B. R. WORTH. Heterocycles, **9**, 1391 (1978).
13. N. L. WENDLER, D. TAUB, and R. P. GRABER. Tetrahedron, **7**, 173 (1959).
14. N. NEUSS, M. GORMAN, N. J. CONE, and L. L. HUCKSTEP. Tetrahedron Lett. 783 (1968).

Megastachine, a new alkaloid from *Lycopodium megastachyum*[1]

JEAN-CLAUDE BRAEKMAN, CLAUDE HOOTELE, AND NOAH MILLER
Service de Chimie Organique, Faculté des Sciences, Université Libre de Bruxelles, 1050 Bruxelles, Belgium
AND
JEAN-PAUL DECLERCQ, GABRIEL GERMAIN, AND MAURICE VAN MEERSSCHE
Laboratoire de Chimie Physique et de Cristallographie, Université de Louvain, Louvain-la-Neuve, Belgium

Received November 2, 1978

JEAN-CLAUDE BRAEKMAN, CLAUDE HOOTELE, NOAH MILLER, JEAN-PAUL DECLERCQ, GABRIEL GERMAIN, and MAURICE VAN MEERSSCHE. Can. J. Chem. **57**, 1691 (1979).

The isolation of the novel pentacyclic base megastachine (**1**), representative of a new type of *Lycopodium* alkaloid, is reported. Its structure has been determined by X-ray diffraction analysis.

JEAN-CLAUDE BRAEKMAN, CLAUDE HOOTELE, NOAH MILLER, JEAN-PAUL DECLERCQ, GABRIEL GERMAIN et MAURICE VAN MEERSSCHE. Can. J. Chem. **57**, 1691 (1979).

Dans le présent travail, nous décrivons l'isolement d'une base pentacyclique nouvelle, la megastachine (**1**), représentative d'un type nouveau d'alcaloïdes des *Lycopodium*. Sa structure est établie par l'analyse du diagramme de diffraction des rayons-X.

In the course of our systematic search for new *Lycopodium* alkaloids of possible biogenetic significance (1), we have examined the basic extract of the African species *Lycopodium megastachyum* Baker (syn. *Huperzia megastachia* (Bak.) Tard) collected in the Ifody forest (Madagascar). This species is actively sought by the natives as a substitute for hashish.

In a previous communication, we reported the isolation from the light petroleum extract of this plant of eight triterpenes of the serratane type (2). We wish to describe now the isolation and the structure determination of megastachine, a new base isolated from the methanol extract.

The molecular formula of megastachine (**1**, $C_{20}H_{29}NO_3$) was established through high resolution mass spectrometry on the free base. One of the oxygen atoms is clearly involved in a secondary alcohol function (ν_{OH} at 3140 cm^{-1}; broad signal of 1H at δ 2.54, disappearing on treatment with D_2O; double quartet of 1H (J = 6.5 and 3 Hz) at δ 4.28). Acetylation of (**1**) afforded a monoacetate (**2**) confirming the presence of only one hydroxyl group and implying that the nitrogen atom of the molecule is tertiary.

The ^1H nmr spectrum of megastachine shows a 1H doublet (J = 4 Hz) at δ 5.63 and two 3H doublets (J = 7 Hz) at δ 1.29 and 1.02, attributed to a trisubstituted double bond and to two CH—CH_3 groups respectively. Moreover, the slightly deshielded signal observed for one of these doublets suggests that one of the methyl groups is geminal to an oxygen atom.

Mass spectra of both **1** and **2** show a base peak at

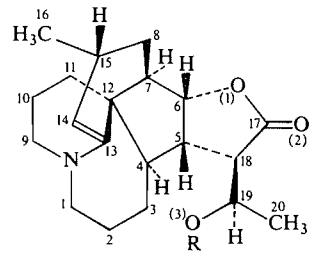

1 R = H
2 R = $COCH_3$

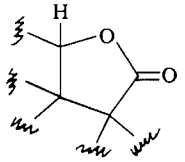

3

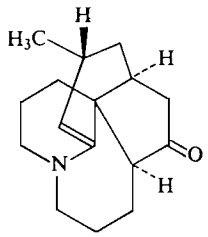

4

m/e 286 ($C_{18}H_{24}NO_2$ by high resolution ms) corresponding to the loss from the molecular ion of 45 and 87 mass units, respectively (metastable ions at *m/e* 247 for **1** and at *m/e* 220 for **2**). This suggests the presence in the molecule of a CH_3—CHOH group. Moreover, the multiplicity of the proton geminal to the hydroxyl group led us to extend this part structure to CH_3—CH(OH)—CH—.

The presence of only one double bond in megastachine was substantiated by the obtention of a dihydro derivative on catalytic hydrogenation.

[1]Dedicated to the memory of R. H. F. Manske.

0008-4042/79/131691-03$01.00/0

The two last oxygen atoms of **1** are probably involved in a γ-lactone ring such as **3** ($\nu_{C=O}$ at 1760 cm^{-1}; double doublet of 1H at δ 4.65). On lithium aluminium hydride reduction, megastachine afforded a diol (arising, most probably, from the partial reduction of the γ-lactone to the corresponding hemiacetal) which could be converted to the corresponding diacetate.

None of the known *Lycopodium* alkaloid skeletons (3, 4) fits the data obtained for **1** and, consequently, megastachine must have an original structure. As the available quantities of **1** were insufficient to permit a complete structure determination by chemical methods, the problem was solved using X-ray diffraction performed on the methiodide. The computer drawing of this salt is reproduced in Fig. 1 and the atomic parameters are given in Table 1.

Thus megastachine represents a new structural type amongst the *Lycopodium* alkaloids. Its formal relationship to the other *Lycopodium* alkaloids is implicit in the numbering system shown in formula **1**. It is closely related to fawcettidine (**4**) and its congeners (4).

Biogenetically, megastachine can formally be obtained by substitution, from the less hindered side of the molecule, of the C-5 hydroxyl group of a precursor such as **5**, by an acetoacetic unit (see Scheme 1).

Experimental

The plant material was collected in the Ifody forest near Sabotsy-Anjiro (Madagascar) by P. Boiteau.

TABLE 1. Atomic parameters of megastachine methiodide

C-1	4269(7)	234(9)	8 158(13)
C-2	4984(9)	−325(11)	7 694(16)
C-3	5822(7)	136(9)	7 859(12)
C-4	5810(6)	1 126(7)	8 456(12)
C-5	6636(7)	1 561(8)	8 368(12)
C-6	6902(6)	1 710(7)	10 030(15)
C-7	6324(6)	1 256(9)	11 026(12)
C-8	6679(8)	305(8)	11 336(14)
C-9	3742(7)	1 192(9)	10 218(13)
C-10	4200(6)	2 046(8)	9 754(14)
C-11	5046(7)	2 068(8)	10 408(12)
C-12	5519(5)	11 083(6)	10 057(15)
C-13	5034(6)	373(8)	10 560(11)
C-14	5267(9)	255(8)	11 478(14)
C-15	6092(8)	301(8)	12 143(14)
C-16	6049(9)	72(10)	13 826(14)
C-17	6772(6)	3 119(7)	8 929(15)
C-18	6675(6)	2 484(8)	7 667(13)
C-19	7344(7)	2 646(9)	6 591(14)
C-20	7242(9)	2 049(10)	5 180(14)
C-21	3699(8)	−414(11)	10 365(18)
O-1	6866(5)	2 691(5)	10 213(9)
O-2	6741(5)	3 919(5)	8 899(10)
O-3	8070(5)	2 393(5)	7 345(9)
N	4211(5)	363(6)	9 839(11)
I	5318(0)	−2 767(1)	9 992(1)

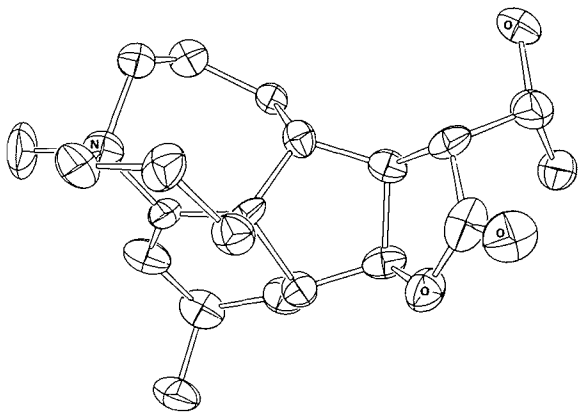

FIG. 1. Computer drawing of megastachine methiodide.

The defatted dry powder of *Lycopodium megastachyum* (4.5 kg) was continuously extracted in glass Soxhlets with MeOH. The extract was evaporated to dryness under reduced pressure and the residue was treated several times with an aqueous solution of 2% HCl. After filtration the aqueous acid solution was made basic by addition of ammonia and extracted with $CHCl_3$. The chloroform phases were combined and evaporated to dryness under reduced pressure, yielding 2.84 g of crude alkaloids. This fraction was then submitted to a countercurrent distribution ($CHCl_3$ – McIlvaine buffer pH 5.8, 23 transferts) and fractionized into three subfractions: A (0.3 g, $K = 0$), B (0.22 g, $K = 1$), and C (1.99 g, $K = 20$). Fraction A gave negative Aebisch and Reichstein tests and was discarded. Fraction C was found to be a complex mixture of high molecular weight basic compounds. Fraction B was chromatographed on alumina (eluent: (*i*) C_6H_6; (*ii*) AcOEt); this led to the isolation of 34 mg of megastachine homogeneous on tlc,

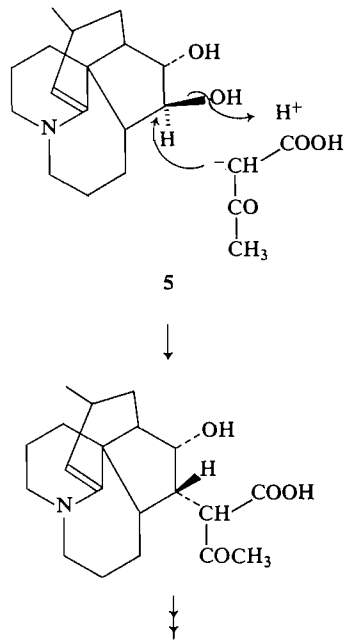

SCHEME 1

mp 167–169°C (from acetone); high resolution ms: M^+ (80%) calcd. for $C_{20}H_{29}NO_3$: 331.2147; found: 331.2153; $M^+ - 45$ (100%) calcd. for $C_{18}H_{24}NO_2$: 286.181; found: 286.183; ms: characteristic peaks at *m/e* 331 (M^+, 80), 316 ($M^+ - 15$, 65), 286 ($M^+ - 45$, 100), 242 (40), 231 (25), 176 (81), 160 (40), 152 (40), 150 (35); ir (KBr): ν_{OH} at 3140, $\nu_{C=C}$ at 1660, 1180, 1110, 1030, 920 cm^{-1}; ^1H nmr ($CDCl_3$, TMS, 60 MHz) δ: 1.02 (3H, d, J = 7 Hz), 1.29 (3H, d, J = 6.5 Hz), 2.54 (1H, broad signal disappearing on treatment with D_2O), 4.28 (1H, double q, J = 6.5 and 3 Hz), 4.65 (1H, dd, J = 6 and 2 Hz), 5.63 (1H, d, J = 4 Hz).

O-*Acetylmegastachine*

Treatment of megastachine (4 mg) with the mixture (1 mL) pyridine – acetic anhydride (2:1) at room temperature for 12 h yielded, after the usual work up, crude *O*-acetylmegastachine (4 mg) which was purified by filtration on alumina, mp 140–142°C; ir (KBr): $\nu_{C=O}$ at 1760 and 1740 cm^{-1}, $\nu_{C=C}$ at 1660 and 1237 cm^{-1}; ms intense ions *m/e*: 373 (M^+, 25), 372 (95), 358 ($M^+ - 15$, 55), 286 ($M^+ - 87$, 100), 270 (25), 242 (37), 176 (66).

H_4LiAl Reduction of Megastachyne

To 50 mg of H_4LiAl dissolved in 3 mL of anhydrous THF was added 5 mg of megastachyne dissolved in 10 mL of THF. The mixture was stirred at room temperature for 24 h. After the usual work-up, 4 mg of an oil was obtained; ir: ν_{OH} at 3400 cm^{-1} and $\nu_{C=C}$ at 1660 cm^{-1}; ms: M^+ at *m/e* 333 (95), 318 (42), 290 (80), 246 (50), 176 (100), 163 (77); the spectrum also showed the presence of a small quantity of a triol (M^+ at 335). After acetylation a diacetate was obtained ir ($CHCl_3$): $\nu_{C=O}$ at 1735 cm^{-1} and $\nu_{C=C}$ at 1660 cm^{-1}; ms: M^+ at *m/e* 417 (64), 402 (52), 186 (100), 168 (90), 148 (67); the spectrum also showed the presence of a small quantiy of a triacetate (M^+ at 461).

Dihydromegastachine

Catalytic hydrogenation of megastachine (6 mg) in MeOH (8 mL) at atmospheric pressure for 120 h yielded, after filtration and evaporation of the solvent under reduced pressure, 5 mg of dihydromegastachine which could not be induced to crystallize; ir (KBr): ν_{OH} at 3350 cm^{-1}, $\nu_{C=O}$ at 1760, 1460, and 1180 cm^{-1}; ms: intense ions at *m/e* 333 (M^+, 100), 318 ($M^+ - 15$, 22), 290 (16), 288 (19), 286 (17), 164 (90), 158 (27), 149 (35).

X-ray Diffraction Data

The X-ray diffraction analysis was performed on the methiodide of megastachine (mp 215–220°C (dec.); $C_{21}H_{32}INO_3$) using a Syntex diffractometer. Space group $P2_12_12_1$ with a = 16.708, b = 14.967, c = 9.150 Å, Z = 4. Radiation MoKα; $2\theta_{max}$ = 47°; number of independent reflections measured, 1493; number of reflections observed, 1493. The structure was solved by direct methods, using the random approach described by Baggio *et al.* (5). The refinements were realized using the XRAY 72 programs (6). R final: 0.048.

Acknowledgements

The authors are indebted to Professor P. Potier who generously furnished the plant material. The F.R.F.C. is gratefully acknowledged for the purchase of the diffractometer.

1. L. NYEMBO, A. GOFFIN, C. HOOTELE, and J. C. BRAEKMAN. Can. J. Chem. **56**, 851 (1978).
2. N. MILLER, C. HOOTELE, and J. C. BRAEKMAN. Phytochemistry, **12**, 1759 (1973).
3. D. B. MACLEAN. *In* The alkaloids. Vol. X. *Edited by* R. H. F. Manske. Academic Press. 1968. p. 305.
4. D. B. MACLEAN. *In* The alkaloids. Vol. XIV. *Edited by* R. H. F. Manske. Academic Press. 1973. p. 347.
5. A. BAGGIO, M. M. WOOLFSON, J. P. DECLERCQ, and G. GERMAIN. Acta Crystallogr. In press.
6. J. M. STEWART, G. J. KRUGER, H. L. AMMON, C. DICKINSON, and S. R. HALL. X-Ray System, Technical Report TR-192, Computer Science Center, University of Maryland, U.S.A. 1972.

An approach to the synthesis of quadrigemine-A[1]

P. K. BATTEY, D. L. CROOKES, AND G. F. SMITH
Department of Chemistry, The University, Manchester, England M13 9PL

Received December 28, 1978

P. K. BATTEY, D. L. CROOKES, and G. F. SMITH. Can. J. Chem. 57, 1694 (1979).

Two syntheses of *N*-{2-[1′-benzyl-3′-(indole-7′′-yl)oxindol-3′-yl]ethyl}-*N*-methylacetamide (**6**), a possible intermediate in a synthesis of quadrigemine-A, are described. The more efficient of the two syntheses gives an overall yield of 12% in 11 steps from tryptamine.

P. K. BATTEY, D. L. CROOKES et G. F. SMITH. Can. J. Chem. 57, 1694 (1979).

On décrit deux synthèse du *N*-{benzyl-1′ (indolyl-7′′)-3′ oxindolyl-3′]-2 éthyl} *N*-méthyl-acétamide (**6**), un intermédiaire possible dans la synthèse de la quadrigémine-A. La meilleure des deux synthèses conduit au produit désiré en 11 étapes à partir de la tryptamine avec un rendement global de 12%.

[Traduit par le journal]

The alkaloid quadrigemine-A is a minor constituent of the leaves of the East Australian shrub *Hodgkinsonia frutescens* F. Muell. (Rubiaceae). The alkaloids of this species were first investigated by Anet *et al.* (1) who isolated the main crystalline alkaloid, hodgkinsine (**1**), the structure of which was elucidated by degradation (2) and was confirmed by X-ray structure determination (3). The minor alkaloids, quadrigemine-A (**2**) and quadrigemine-B (**3**) were more recently isolated by a long countercurrent separation process and the gross structures, excluding stereochemistry, elucidated by degradation (4). These two alkaloids were obtained in small quantity and are as yet inseparable mixtures of diastereoisomers. Synthesis will, we hope, open the way to the preparation of the set of diastereoisomers and to a complete solution of the stereochemical problem.

These alkaloids belong to the small calycanthaceous group, of which the prototypes are (−)- and *meso*-chimonanthine (**4** and **5**). The chimonanthines have been synthesized by four distinct routes by three different groups of workers, Hendrickson *et al.* (5), Scott *et al.* (6), and Hino *et al.* (7, 8), all involving a β–β′ dimerisation of indole or oxindole units. This approach can in principle be applied to a synthesis of quadrigemine-A and our work in this direction has had as objective a synthesis of the 3-(7′-indolyl)-oxindole system, for which there is no precedent.

This paper describes the synthesis of *N*-{2-[1′-benzyl-3′-(indole-7′′-yl)oxindol-3′-yl]ethyl}-*N*-methylacetamide (**6**).

The first approach started with *N*-benzyloxindole and involved the introduction at C3 of a hydroxycyclohexyl group and a cyanomethyl group: the former was then converted into the 7′-indolyl substituent and the latter into the ethanamine side chain.

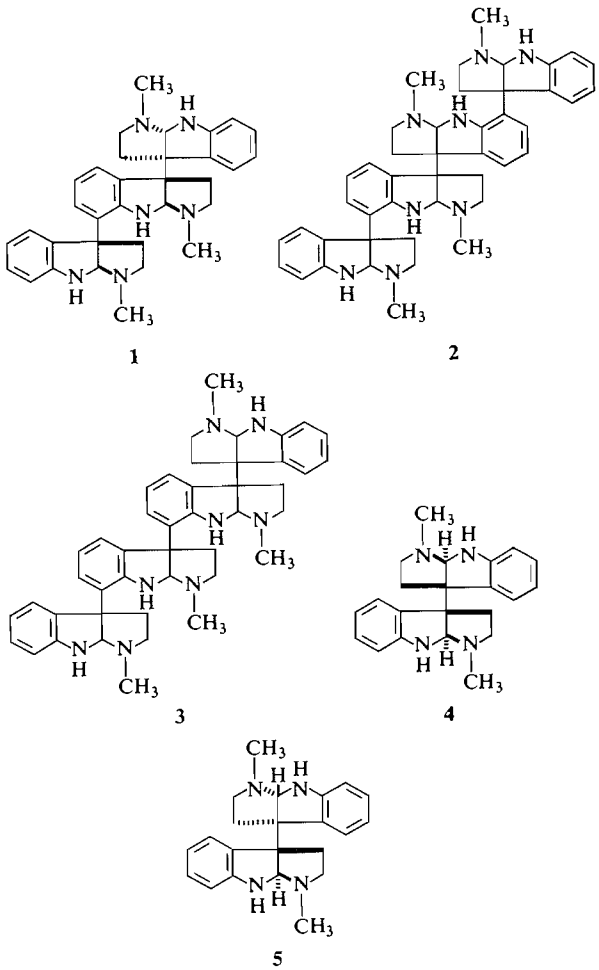

1 **2** **3** **4** **5**

[1]Dedicated to the memory of R. H. F. Manske.

0008-4042/79/131694-13$01.00/0

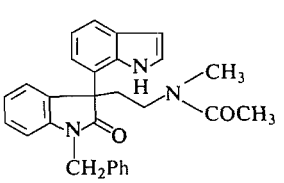

6

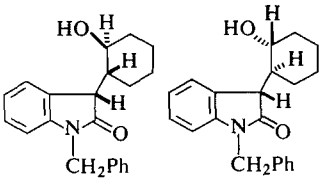

7

The introduction of a β-hydroxyalkyl function at the oxindole C3 position has a precedent in the reaction of 1,3-dimethyl-5-methoxyoxindole sodium enolate with ethylene oxide (9) to give 3-(2′-hydroxyethyl)-1,3-dimethyl-5-methoxyoxindole in 21% yield: in our hands, repetition of this reaction with 1,3-dimethyloxindole in the absence of air yielded 3-(2′-hydroxyethyl)-1,3-dimethyloxindole in 42% yield. The reaction of the lithium enolate of *N*-benzyloxindole with cyclohexene oxide in anisole under nitrogen proceeded very much more efficiently and gave a 90% yield of an approximately 1:1 mixture of the two diastereoisomers **7**. This makes the plausible assumption that the reaction leads to *trans*-disubstituted cyclohexanes. Column chromatography allowed the isolation of the diastereoisomers as pure compounds but unfortunately spectral and other data in this case, and in all subsequent cases of diastereoisomerism in this series, did not allow a clear assignment of relative stereochemistry. This failure however is not very serious, since the diastereoisomerism disappears in the product **6**.

The introduction of a cyanomethyl group at C3 was effected at this point. The hydroxyl group in **7** was protected by acetylation and the corresponding sodium oxindole enolate treated with chloroacetonitrile in THF, which gave an excellent yield of 3-(2′-acetoxycyclohexyl)-1-benzyl-3-cyanomethyloxindole (**8**) as a mixture of diastereoisomers. These were isolated, one as a pure compound and the other contaminated with a small percentage of a product of further cyanomethylation.

The next step was the reduction of the nitrile function which had to be effected without reduction of the oxindole carbonyl or hydrogenolysis of the *N*-benzyl group. Catalytic hydrogenation proved to be surprisingly difficult, but was eventually achieved with W5 Raney nickel in acetic anhydride – NaOH at 85°C and 6.5 atm (10). This led to *N*-{2-[1′-benzyl-3′-(2″-acetoxycyclohexyl)oxindol-3′-yl]ethyl}acetamide (**9**), in almost quantitative yield as a mixture consisting mainly of two easily separable diastereoisomers. However, even these hydrogenation conditions led to problems of reproducibility and of scaling up, and eventually to the search for an alternative approach.

Direct *N*-methylation of the secondary acetamide **9** under a range of conditions led to mixtures, the major by-product being that derived from *O*-deacetylation and subsequent *O*-methylation, so protection of the hydroxyl function as a THP ether had to be resorted to. This was achieved in high overall yield by hydrolysis with aqueous alcoholic Na_2CO_3 followed by treatment with dihydropyran-HCl in

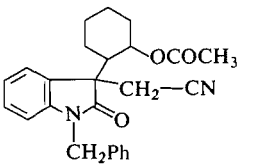

8

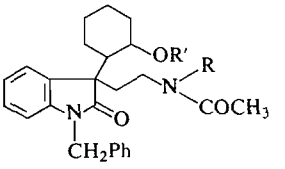

9 (R = H, R′ = $COCH_3$)
10 (R = CH_3, R′ = H)

DMF (significantly lower yields of THP ether were obtained in THF or HMPA as solvents). *N*-Methylation by KOBu*t*–THF–MeI then led to a quantitative yield of pure mixed diastereoisomers moving as one spot on tlc, smoothly hydrolysed by dilute HCl to *N*-{2-[1′-benzyl-3′-(2″-hydroxycyclohexyl)oxindol-3′-yl]ethyl}-*N*-methylacetamide **10**. The two diastereoisomers in this case were separable by preparative tlc, and spectral data, which only differed slightly between the two compounds, were entirely compatible with the gross structure **10**. The nmr spectra (at 25°C) show doubling of *N*-methyl and acetyl methyl signals due to hindered rotation of the ethanamine side chain: single signals were, however, observed at 85°C. Similar effects were observed with most of the following compounds and will not be discussed again. Oxidation of the mixture of alcohols with chromic acid in acetone led to a 70% yield of two separable diastereoisomeric ketones (**11**) each of

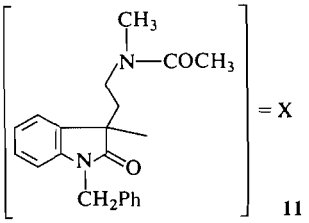

= X

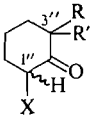

11 R = R′ = H
12 R = H, R′ = CHO
13 R = $CH_2CH{=}CH_2$, R′ = CHO
14 R = $CH_2CH{=}CH_2$, R′ = H

which was the sole product of analogous oxidation of the separated diastereoisomeric alcohols **7**.

The plan now was to build up a pyrrole ring by the introduction of —CH_2CHO at C3″, then dehydrogenate to the indole system. To ensure specific alkylation at C3″, and not at the alternative C1″

position, formylation at C3'' followed by alkylation and deformylation was undertaken.

Formylation was achieved in nearly 90% yield by the action of a large excess of ethyl formate and NaOEt in dry C_6H_6 (20): the formyl compound (**12**) was then allylated with allyl iodide in the presence of lithium carbonate in aqueous acetone to give a high yield of **13**, nearly quantitative deformylation of which to *N*-{2-[1'-benzyl-3'-(2''-keto-3''-allylcyclohexyl)oxindol-3'-yl]ethyl}-*N*-methylacetamide (**14**) occurred in 2.5% aqueous alcoholic KOH at room temperature. It may be noted that allylation of **12** with allyl bromide in the presence of sodium carbonate in aqueous acetone gave a 3:2 mixture of **13** and the corresponding *O*-allyl compound.[2] Ozonolysis in dry methanol at −30°C and reductive work-up with Me_2S (21) gave the keto aldehyde **15** in up to 91% yield. The reproducibility of this step was poor and the factors leading to failure were not discovered. Compounds **12–15** all ran on tlc as oval

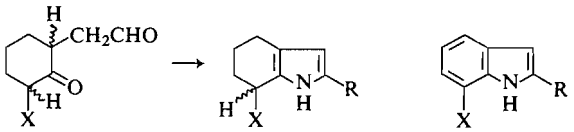

15

16 R = H
17 R = $COCCl_3$
18 R = CO_2CH_3
19 R = $CO_2CH_2CH_3$

6 R = H
20 R = CO_2CH_3
21 R = CO_2H
43 R = $CO_2CH_2CH_3$

spots, probably indicative of diastereoisomeric mixtures; in no case, however, was a mixture resolved.

Keto aldehyde **15** was most satisfactorily converted into the pyrrole **16** on treatment with $(NH_4)_2CO_3$ in dry ethanol (cf. ref. 22). The yield was somewhat variable, generally around 50% of product being obtained by preparative tlc which allowed partial resolution of the two diastereoisomers, produced in about equal amounts. This pyrrole is very susceptible to autoxidation and has to be stored under N_2 at low temperatures. All attempts to dehydrogenate **16** to the indole **6** either failed or gave unacceptably low yields. The best results, which gave about 20% of a mixture of **16** and **6**, were obtained with palladium-on-charcoal. Also tried were other Pd catalysts under a wide range of conditions, DDQ, chloranil, MnO_2, Raney nickel, potassium hexacyanoferrate(III), and tristriphenylphosphine rhodium(I) chloride.

It was eventually decided to reduce the reactivity of the pyrrole ring by the introduction of an ester function at the α-position. This was achieved in the low overall yield of 30% by trichloroacetylation followed by treatment of the intermediate trichloroacetyl derivative with sodium methoxide in methanol (17). Dehydrogenation in this case proceeded satisfactorily, DDQ in refluxing benzene affording a 69% yield of the indole ester **20**. Now that the molecule contains only one asymmetric atom, it runs cleanly as a round spot on tlc. Saponification of this ester under mild conditions yielded the corresponding acid, which was decarboxylated smoothly in refluxing quinoline in the presence of copper(II) acetate (17) to give a 71% yield of *N*-{2-[1'-benzyl-3'-(indol-7''-yl)oxindol-3'-yl]ethyl}-*N*-methylacetamide (**6**).

The weak points in this synthesis are the difficulties in reproducing the high yield hydrogenation of the nitrile **8** and the ozonolysis of the allyl compound **14**. Furthermore, the aromatisation of the pyrrole **16** to the indole **6** contains too many unsatisfactory reactions, the overall yield of 14% in five steps being poor.

The reduction of a nitrile function half-way through the synthesis could be avoided by starting with a tryptamine derivative. The very convenient and high yield oxidation of indoles to oxindoles by DMSO and HCl (18), which appeared at about this point in our deliberations, made this approach viable. *N*-[2-(1'-Benzylindol-3'-yl)ethyl]-*N*-methylacetamide (**22**) was oxidised by DMSO concentrated HCl in AcOH to the corresponding oxindole **23** in 84% yield. Numerous attempts to introduce the 2-hydroxycyclohexyl group at C3 in oxindole **23** by the interaction of epoxycyclohexane with the enolate anion failed. This may be due to steric hindrance by the ethanamine side chain to approach of the epoxycyclohexane, cyclohexane compounds being well known as being sterically more demanding in S_N2 type reactions.

It was then found that, in complete contrast, the oxindole enolate anion derived from **23** reacted very smoothly with 6-bromo-1-methoxycyclohexene (19) to give a 78% yield of *N*-{2-[1'-benzyl-3'-(1''-me-

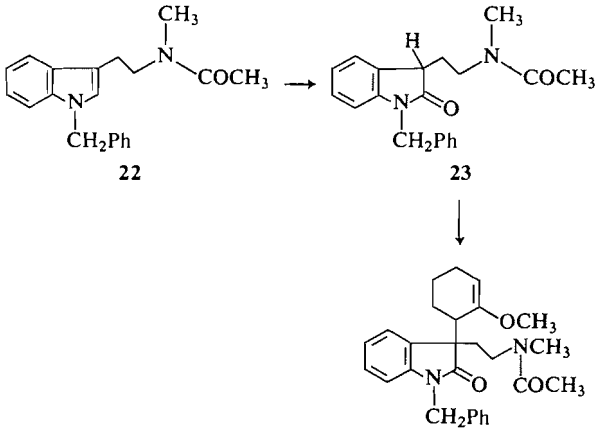

22 **23** **24**

[2]See ref. 16, Chapt. 9, pp. 521–530, for an excellent review of the question of *C* vs. *O* alkylation.

thoxycyclohex-1''-en-6''-yl)oxindol-3'-yl]ethyl}-*N*-methylacetamide (**24**). This great ease of reaction may well reflect the allyl halide nature of the reactant which gives a greater S_N1 character to the displacement reaction. Two aspects of the spectral properties of this compound are not satisfactory: the first concerns the mass spectrum, in which three significant peaks at *m/e*: 269, 267, and 254 cannot be rationalised and the second concerns the nmr spectrum, in which the signal intensities in the enol ether CH and CH_3 are too low. The latter anomaly may be due to large upfield shifts into the general CH envelope above τ7 caused by shielding effects of the oxindole benzene ring in certain conformations. That the structure **24** must be correct, however, is indicated by mild acidic hydrolysis, which gave an 89% yield of the mixed diastereoisomers of ketone **11**. This represents an overall yield of 37% in six steps from tryptamine, a considerable improvement over the earlier approach from isatin, which gave a 28% yield in 10 steps.

When it was found that the simple pyrrole **16** could not be satisfactorily dehydrogenated and had to be converted into the ester **18**, the exploration of the Fischer–Fink synthesis, which leads directly from the keto aldehyde **12** to the ester **18**, was undertaken. The low yields reported for simple cases of this synthesis, together with the possible formation of isomeric or other pyrrole esters as by-products, had deterred us from exploring this route in the first instance. As it turns out, it affords a satisfactory route to the indole ester **20**, giving a 47% yield in two steps but the isolation necessitated preparative tlc. However, by saponifying the total crude dehydrogenation product and isolating the acid fraction, the pure acid **21** could be obtained in 41% overall yield from the keto aldehyde **12** in three steps without the isolation of intermediates, which is a great improvement on the earlier route, which gave 8% overall yield in eight steps.

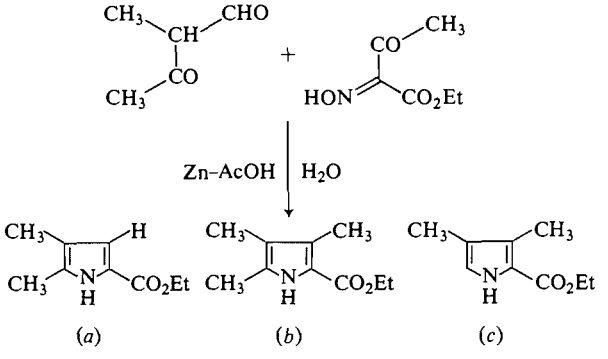

The Fischer–Fink synthesis involves the condensation of a β-ketoaldehyde with 2-aminoacetoacetic ester and might be expected to yield three pyrroles; thus 3-formylbutan-2-one and aminoacetoacetic ester (produced *in situ*) gave the pyrrole esters shown in a 10:2:1 (*a*:*b*:*c*) ratio (11). This was not promising for our purposes. In the event, however, when this reaction was applied to our keto aldehyde **12**, the desired ester **19** was produced in 70% nonisolated yield completely free from the isomer **25** and containing about 1% of the homologue **26**, as far as could be judged from spectral and chromatographic observations. It is noteworthy that at the stage of indole **6**, the +14 homologue peak is totally absent. The absence of the isomer **25** is easily explained in steric terms, since the ester function would interact very strongly with the very bulky oxindole residue X. The fortunately very low percentage production of homologue **26** is not obviously rationalisable.

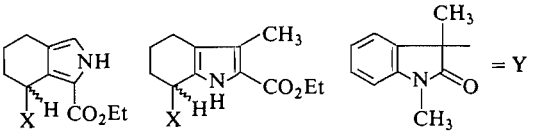

25 **26**

In the course of this work, the exploration of most of the reactions involved was carried out on model compounds based on the 1,3-dimethyloxindole system Y. The synthesis and spectral properties of the following are described in the Experimental section: the Y analogues of **6**, **9**, **11**, **12**, **13**, **14**, **15**, **16**, **18**, and **20** (i.e., **27**, **28**, **29**, **30**, **31**, **32**, **33**, **34**, **36**, and **37**, respectively). Also described in the Experimental section are Y – Z, where Z = CH_2CH_2OH (**39**), **40**, **41**, **42**, and **45**.

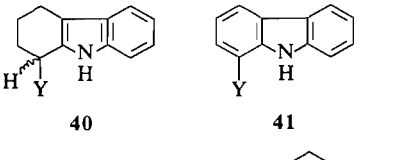

40 **41**

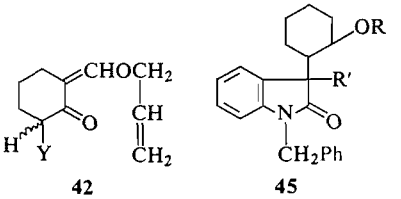

42 **45**

Experimental

Thin-layer chromatography: adsorbent: S, silica gel F 254 (Merck); solvent systems: *A*, chloroform–methanol (9:1); *B*, benzene–ether (1:1); *C*, benzene–ether (4:1); *D*, ethyl acetate – ethanol (10:1); *E*, toluene – ethyl acetate – methanol (2:2:1). Preparative-layer chromatography: adsorbent S', silica gel (Merck analytical precoated plates).

1-Benzyl-3-(2'-hydroxycyclohexyl)oxindole (7)

A solution of 1-benzyloxindole (4.46 g, 0.02 mol) in dry anisole (25 mL) was purged with N_2 for 30 min, then *n*-butyllithium in hexane (10.25 mL, 0.024 mol) was added from a

syringe through a septum cap to the well stirred solution. After 10 min, 1,2-epoxycyclohexane (2.94 g, 0.03 mol) was added with stirring from a syringe and the reaction solution heated to 90°C for 2 h. Glacial acetic acid (1.23 g, 0.024 mol) was then added to the cooled reaction, the anisole distilled off at the water pump, and the residue partitioned between ether and water. The ether-soluble product (6.5 g) (shown by tlc to be made up mainly of the two diastereoisomers of **7**) was chromatographed on silica gel (500 g): elution with ethyl acetate – 60–80 petrol – ether, 3:7:7 with gradually increasing proportions of Et_2O. The eluates were monitored by tlc and combined into four fractions: (*i*) 40 mg unidentified material; (*ii*) 225 mg of pure diastereoisomer A: (*iii*) 6.15 g of mixed diastereoisomers A and B; (*iv*) 25 mg of pure diastereoisomer B. The overall yield was 90%.

Diastereoisomer A—R_f 0.45 (S/*B*) was a white crystalline solid, mp 126.5–128°C, and crystallised well from petrol – ethyl acetate; ν_{max} ($CHCl_3$): 3540 (w), 3450–3200 (w), 1700 cm^{-1} (s); λ_{max} (EtOH): 253 (τ 8150); λ_{infl} 280 nm (ε 1650); τ ($CDCl_3$): 2.70–3.50 (m, 9H), 5.05 (d, 1H, J = 15.6 Hz), 5.23 (d, 1H, J = 15.6 Hz), 5.80–6.30 (m, 2H), 7.34 (br s, 1H, exchange with D_2O), 7.50–9.20 (br m, 9H); *m/e*: 321 (M^+, 29), 304 (7), 303 (46), 249 (6), 237 (6), 236 (27), 235 (18), 224 (18), 223 (100), 158 (7), 145 (17), 132 (7), 118 (5), 91 (100). *Anal.* calcd. for $C_{21}H_{23}NO_2$: C 78.50, H 7.17, N 4.36; found: C 78.6, H 7.5, N 4.4.

Diastereoisomer B—R_f 0.36 (S/*B*) recrystallized from petrol – ethyl acetate, mp 129–132°C; ν_{max} ($CHCl_3$): 3510 (w), 3450–3150 (w), 1700 cm^{-1} (s); λ_{max} (EtOH): 253 (ε 8100), λ_{infl} 280 nm (ε 1030); τ ($CDCl_3$): 2.50–3.52 (m, 9H), 5.00 (d, J = 15.6 Hz, 1H), 5.21 (d, J = 15.6 Hz, 1H), 5.85 (d, J = 3.0 Hz, 1H), 6.00–6.40 (br m, 1H), 7.50–9.00 (br m, 10H); *m/e*: 321(M^+, 29), 304 (8), 303 (32), 237 (5), 236 (20), 235 (12), 224 (18), 223 (100), 158 (5), 145 (16), 132 (6), 91 (87). *Anal.* calcd. for $C_{21}H_{23}NO_2$: C 78.50, H 7.17, N 4.36; found: C 78.0, H 7.1, N 4.8.

3-(2′-Acetoxycyclohexyl)-1-benzyloxindole

A solution of **7** (1.0 g) in acetic anhydride (2.5 mL) was refluxed under N_2 for 10 min. The reaction mixture was poured into water and stirred with addition of small quantities of Na_2CO_3 until the excess Ac_2O had been hydrolysed. Ether extraction yielded a pale brown viscous liquid (1.005 g, 89%) which crystallised on standing. Thin-layer chromatography (S/*B*) showed one spot only, at R_f 0.79. Even after three recrystallisations from petrol the melting point had the wide range of 105–125°C, thus indicating that the product is a mixture of the two diastereoisomers of 3-(2′-acetoxycyclohexyl)-1-benzyloxindole; ν_{max} ($CHCl_3$): 1720(s), 1705 cm^{-1} (s); λ_{max} (EtOH): 252.5 (ε 8060), λ_{infl} 279 nm (ε 1370); τ ($CDCl_3$): 2.25–3.50 (m, 9H), 4.60–5.50 (m, 3H), 6.27 (d, J = 3 Hz) and 6.37 (d, J = 3 Hz) together 1H, 8.00 (s) and 8.12 (s) together 3H, 7.20–9.00 (br m, 9H); *m/e*: 363 (M^+, 24), 304 (25), 303 (100), 262 (6), 260 (5), 249 (9), 237 (6), 236 (30), 235 (23), 223 (13), 212 (8), 158 (6), 132 (6), 91 (55). *Anal.* calcd. for $C_{23}H_{25}NO_3$: C 76.03, H 6.89, N 3.86; found: C 75.8, H 6.9, N 4.2.

*3-(2′-Acetoxycyclohexyl)-1-benzyl-3-cyanomethyloxindole (**8**)*

A solution of 3-(2′-acetoxycyclohexyl)-1-benzyloxindole (12 g, 0.033 mol) in dry THF (20 mL) was added to mineral oil free sodium hydride (1.68 g, 0.07 mol) under N_2, when vigorous evolution of H_2 occurred over 15 min. Freshly distilled chloroacetonitrile (3.02 g, 0.04 mol) was added with stirring. After standing for 10 min, water (10 mL) was added, the THF boiled off at room temperature at the water pump, and the residue partitioned between ether and water. This yielded a pale yellow foam (13.2 g, 99%), tlc analysis of which showed it to consist exclusively of the two diastereoisomers described below. An earlier procedure which used anisole as solvent yielded a less pure product, 3.6 g of which was chromatographed on a column of silica gel (300 g). Elution with ethyl acetate – 60–80°C petrol – ether (3:7:1) yielded (after combining the appropriate fractions) diastereoisomer A (0.836 g) contaminated with a small amount of dicyanomethylated product, mixed diastereoisomers A and B likewise contaminated (0.412 g), pure mixed A and B (1.146 g), and pure diastereoisomer B (0.567 g).

Diastereoisomer A—A colourless glass, R_f 0.41 (S/*C*); ν_{max} ($CHCl_3$): 2240 (w), 1720 (s), 1710 cm^{-1} (s); λ_{max} (EtOH): 254, λ_{infl} 283 nm; τ ($CDCl_3$): 2.05–3.45 (m, 9H), 4.98 (d, J = 15.6 Hz), 5.21 (d, J = 15.6 Hz) both superimposed on 4.60–5.40 (broad absorption) together 3H, 6.94 (d, 1H, J = 15.0 Hz), 7.28 (d, 1H, J = 15.0 Hz), 7.35–9.20 (broad absorption, 13H) including 8.31 (s, 3H); *m/e*: 441 (M^+ + CHCN, 3), 402 (M^+, 13.5), 342 (5), 303 (5), 302 (8), 263 (9), 262 (35), 261 (6), 260 (10), 236 (5), 235 (13.5), 184 (6), 171 (6), 141 (6), 99 (6), 92 (11), 91 (100), 81 (21), 65 (11), 43 (44). *Exact Mass* calcd. for $C_{25}H_{26}N_2O_3$: 402.194340; found: 402.190315.

Diastereoisomer B—A white crystalline solid, mp 139–140°C; R_f 0.34 (S/*C*); ν_{max} ($CHCl_3$): 2240 (w), 1720 (s), 1710 cm^{-1} (s); λ_{max}: 254 (ε 7210), λ_{infl} 283 nm (ε 780); τ ($CDCl_3$): 2.40–3.30 (m, 9H), 4.78 (d, J = 15.6 Hz), 5.39 (d, J = 15.6 Hz) both superimposed on 5.00–5.60 (broad absorption) together 3H, 7.03 (d, 1H, J = 15.0 Hz), 7.38 (d, 1H, J = 15.0 Hz), 7.50–9.00 (broad absorption, 13.5H) including 8.09 (s, 3H); *m/e* 402 (M^+, 19), 342 (2), 302 (5), 263 (10), 262 (57), 261 (7), 260 (21), 235 (14), 184 (4), 171 (3), 141 (3), 99 (4), 91 (100), 81 (16), 65 (6), 43 (36). *Anal.* calcd. for $C_{25}H_{26}N_2O_3$: C 74.63, H 6.47, N 6.97; found: C 74.8, H 6.8, N 6.8.

N-{2-[*1′-Benzyl-3′-(2″-acetoxycyclohexyl)oxindol-3′-yl*]-*ethyl*}*acetamide (**9**)*

A solution of the diastereoisomers **8** (760 mg) in acetic anhydride (50 mL) was hydrogenated in a Parr hydrogenator in the presence of W5 Raney nickel (1 g) and powdered A.R. sodium hydroxide (2.5 g) for 6 h at 85°C and 6.5 atm. The catalyst was filtered off and the acetic anhydride was boiled off at the water pump. The residue was suspended in water and treated with Na_2CO_3 until permanent neutrality was reached. Shaking with ether dissolved some of the product, but left a white powder suspended in the aqueous phase, which was extracted by chloroform. The ether soluble fraction (545 mg) was a mixture of diastereoisomers running as one spot on tlc, R_f 0.72 (S/*A*); the chloroform soluble fraction (279 mg) was pure diastereoisomer A, R_f 0.72 (S/*A*). The combined yield was almost quantitative. It is noteworthy that this very high yield was obtained in several runs (P.K.B), where two years later it could not be reproduced at all, H_2 uptake being very slow and reduction incomplete (D.L.C.).

Diastereoisomer A (low ether solubility)—This crystallised from 80–100 petrol as white crystals, mp 190.5–192°C; ν_{max} ($CHCl_3$): 3375 (w), 1720 (s), 1702 (s), 1665 (s); λ_{max} (EtOH): 253.5 (ε 7000), λ_{infl} 281 nm (ε 1300); τ ($CDCl_3$): 2.50–3.30 (m, 9H), 4.67 (d, J = 15.6 Hz), 5.63 (d, J = 15.6 Hz), 4.40–4.90 (broad hump), 5.40–6.05 (broad hump) last four signals adding up to 4H, 6.75–7.25 (br m, 2H), 7.30–9.00 (broad absorption, about 18H) including sharp 3H singlets at 8.18 and 8.40; *m/e*: 448 (M^+, 20), 389 (7), 388 (14), 364 (6), 363 (16), 345 (5), 316 (5), 309 (8), 308 (22), 307 (17), 306 (23), 305 (5), 304 (17), 303 (57), 302 (9), 250 (6), 249 (20), 248 (20), 247 (18), 238 (5), 237 (12), 236 (46), 235 (14), 234 (10), 223 (6), 158 (17), 141 (7), 92 (11), 91 (100), 81 (16). *Anal.* calcd. for $C_{27}H_{32}N_2O_4$: C 72.32, H 7.15, N 6.25; found: C 72.1, H 7.0, N 6.0.

Diastereoisomer B (high ether solubility)—Repeated ether extraction from the solid mixture gave the pure compound as white crystals from 60–80 petrol – ethyl acetate, mp 163–164°C; ν_{max} identical with A; λ_{max} (EtOH): 255 (ε 6850), λ_{infl} 282 nm (ε 1350); τ ($CDCl_3$): 2.70–3.50 (m, 9H), 4.25–4.70 (br s, 1H), 5.05 (d, J = 15.6 Hz), 5.27 (d, J = 15.6 Hz), 5.0–5.3 (br s), the last three signals adding up to 3H, 6.75–7.25 (br m, 2H), 7.40–9.00 (broad absorption, about 18H) including sharp 3H singlets at 8.20 and 8.30; *m/e*: 448 (M^+, 33), 389 (6), 388 (12), 376 (7), 364 (11), 363 (34), 316 (7), 309 (8), 308 (26), 307 (16), 306 (18), 305 (6), 304 (26), 303 (100), 302 (11), 260 (6), 259 (22), 258 (24), 257 (16), 237 (14), 236 (59), 235 (16), 234 (10), 223 (8), 158 (19), 141 (8), 99 (7), 92 (10), 91 (100), 81 (18). *Anal.* calcd. for $C_{27}H_{32}N_2O_4$: C 72.32, H 7.15, N 6.25; found: C 71.9, H 7.1, N 6.1.

N-{2-[*1′-Benzyl-3′-(2′′-hydroxycyclohexyl)oxindol-3′-yl*]-*ethyl*}*acetamide*

A solution of **9** (115 mg) in a mixture of ethanol (5 mL) and 10% aqueous sodium carbonate (10 mL) was refluxed for 17 h. The reaction mixture was then boiled down to dryness at the water pump and the residue partitioned between ether and water to yield a colourless foam (97 mg, 93%). Preparative tlc (S/*A*) of this product (70 mg) cleanly separated the two diastereoisomers.

Diastereoisomer A—R_f 0.57 (31.2 mg), crystallised from 60–80 petrol – ethyl acetate as white crystals, mp 197–198°C; ν_{max}: 3520 (w), 3400 (m), 3480–3200 (m), 1700 (s), 1665 cm^{-1} (m); λ_{max} (EtOH): 253 (ε 7700), λ_{infl} 281 nm (ε 890); τ ($CDCl_3$): 2.00–3.40 (m, 9H), 4.20–4.60 (br s, 1H, exchanges slowly with D_2O), 5.02 (d, 1H, J = 15.6 Hz), 5.27 (d, 1H, J = 15.6 Hz), 6.89 (d, J = 5.4 Hz), 7.09 (d, J = 5.4 Hz) overlying ~6.8 (m) together 3H, 7.50–9.05 (broad absorption, 17H) including 8.32 (s, 3H) and ~8.50 (br s exchanges with D_2O); *m/e*: 406 (M^+, 21), 334 (5), 322 (16), 321 (66), 320 (5), 319 (5), 309 (14), 308 (47), 307 (7), 306 (7), 304 (11), 303 (28), 302 (5), 266 (6), 263 (5), 262 (13), 250 (7), 249 (26), 248 (13), 247 (11), 238 (16), 237 (7), 236 (14), 235 (7), 225 (9), 220 (5), 217 (6), 159 (6), 158 (25), 146 (7), 130 (7), 92 (11), 91 (100), 81 (8). *Anal.* calcd. for $C_{25}H_{30}N_2O_3$: C 73.90, H 7.39, N 6.90; found: C 73.8, H 7.4, N 7.0.

Diastereoisomer B—R_f 0.44, crystallised from 60–80 petrol – ethyl acetate, mp 176–179°C; ν_{max} identical with A; λ_{max} (EtOH): 253.5 (ε 6900), λ_{infl} 280 nm (ε 1040); τ ($CDCl_3$): 2.00–3.40 (m, 9H), 3.87–4.23 (br s, 1H), 5.01 (d, 1H, J = 15.6 Hz), 5.25 (d, 1H, J = 15.6 Hz), 6.05–6.60 (br m, 1H), 6.60–9.00 (broad absorption, ~17H) including 8.25 (s, 3H); *m/e*: 406 (M^+, 12), 388 (3), 334 (5), 322 (14), 321 (47), 310 (5), 309 (16), 304 (10), 303 (35), 262 (7), 249 (16), 248 (10), 237 (10), 236 (48), 235 (10), 223 (5), 158 (17), 146 (5), 130 (5), 92 (10), 91 (100), 78 (50). *Anal.* calcd. for $C_{25}H_{30}N_2O_3$: C 73.90, H 7.39, N 6.90; found: C 73.5, H 7.3, N 7.2.

N-[2-{*1′-Benzyl-3′-[2″-(2‴-tetrahydropyranyloxy)cyclohexyl*]-*oxindol-3′-yl*}*ethyl*]*acetamide*

A solution of the above alcohol, as the mixture of diastereoisomers (4.2 g), 2,3-dihydropyran (20 mL), freshly purified DMF (30 mL), and concentrated HCl (1 drop) was left at room temperature for 40 h. The reaction solution was dissolved in ether (200 mL) and washed several times with 10% aqueous sodium carbonate. Removal of volatiles under reduced pressure yielded an orange liquid from an ether solution of which the product was precipitated with 40–60 petrol. It was obtained as a foam which eventually crystallised (4.77 g, 94%). This was homogeneous on tlc (S/*A*, R_f 0.63). Four recrystallisations from 60–80°C petrol – ethyl acetate yielded a product with mp 163.5–165°C; ν_{max} ($CHCl_3$): 3440 (w), 1680 cm^{-1} (s); λ_{max}: 254.5 (ε 9540), λ_{infl} 280 nm (ε 2190); τ ($CDCl_3$): 2.50–3.50 (m, 9H), 3.85–4.45 (broad signal, 1H), 4.45–5.72 (m, 3H), 5.80–8.80 (broad absorption, ~27H) including sharp 3H singlets at 8.26 and 8.35; *m/e*: 490 (M^+, 1), 407 (3), 406 (11), 389 (8), 387 (4), 347 (3), 345 (6), 322 (8), 321 (42), 309 (12), 308 (64), 303 (16), 249 (18), 248 (6), 237 (8), 236 (50), 235 (5), 223 (3), 158 (10), 92 (6), 91 (100). *Anal.* calcd. for $C_{30}H_{38}N_2O_4$ (490.2831): C 73.50, H 7.75, N 5.73; found (490.2846): C 73.7, H 7.8, N 5.3.

N-[2-{*1′-Benzyl-3′-[2″-(2‴-tetrahydropyranyloxy)-cyclohexyl*]*oxindol-3′-yl*}*ethyl*]-N-*methylacetamide*

A solution of the above acetylethanamino compound (4.7 g of unrecrystallised material) in dry THF (50 mL) was added to a solution of freshly sublimed potassium tertiary butoxide (4.7 g) in THF (100 mL) and the resultant solution left at room temperature for 30 min. A solution of methyl iodide (20 mL) in THF (25 mL) was then added dropwise over about 20 min. The reaction mixture was then boiled down to a thick slurry under water pump vacuum, and the residue partitioned between ether and water to give the product as a pale yellow foam (4.85 g, 99%) running as a single oval spot on tlc (S/*A*, R_f 0.68); ν_{max} ($CHCl_3$): 1710 cm^{-1} (s); λ_{max} (EtOH): 254 (ε 6350), λ_{infl} 280 nm (ε 1370); τ ($CDCl_3$): 2.00–3.30 (m, 9H), 4.30–8.75 (broad complex absorption, ~32H) including N—CH_3 at 7.22 and 7.26 (restricted rotation); *m/e*: 504 (M^+, 1), 421 (3), 420 (9), 419 (4), 403 (7), 346 (3), 335 (8), 323 (8), 322 (58), 321 (100), 304 (6), 303 (25), 286 (4), 262 (3), 250 (3), 249 (14), 248 (4), 237 (7), 236 (24), 235 (6), 223 (4), 158 (5), 100 (4), 92 (6), 91 (92), 86 (12), 85 (32). *Anal.* calcd. for $C_{31}H_{40}N_2O_4$ (504.2988): C 73.79, H 7.95, N 5.56; found (504.2998): C 73.9, H 8.2, N 5.2.

N-{2-[*1′-Benzyl-3′-(2′′-hydroxycyclohexyl)oxindol-3′-yl*]*ethyl*}-N-*methylacetamide* (***10***)

A solution of the above tetrahydropyranyl ether (4.7 g) in ether (60 mL) was stirred vigorously with 2.5 *M* hydrochloric acid (60 mL) at room temperature for 2 h. The ether soluble product, **10**, was obtained as a foam (3.64 g, 93%) pure by tlc, running as two clean spots (R_f 0.65, 0.54; S/A) corresponding to the two diastereoisomers A and B respectively. These were separated by preparative tlc.

Diastereoisomer A—This compound did not crystallise; ν_{max} ($CHCl_3$): 3570 (m), 3400 (broad, w), 1700 cm^{-1} (s); λ_{max} (EtOH): 253.5 (ε 10 000), λ_{infl} 280 nm (ε 1630); τ ($CDCl_3$) 2.60–3.40 (m, 9H), two overlapping AB systems, together = 2H, 5.11 (d, J = 16 Hz), 5.38 (d, J = 16 Hz), 5.12 (d, J = 15 Hz), 5.32 (d, J = 15 Hz), changing at 85°C to 5.12 (d, J = 15 Hz, 1H) and 5.32 (d, J = 15 Hz, 1H), 6.60–9.10 (broad complex absorption, 21H) including sharp singlets at 7.28, 7.33, 8.15, and 8.23, changing at 85°C to a sharp singlet at 7.30 and a broad singlet at 8.23; *m/e*: 420 (M^+, 2), 335 (7), 322 (9), 321 (17), 304 (9), 303 (24), 264 (6), 249 (11), 236 (17), 223 (7), 91 (100). *Exact Mass* calcd. for $C_{26}H_{32}N_2O_3$: 420.2413; found: 420.2410.

Diastereoisomer B—This compound likewise did not crystallise; ν_{max} ($CHCl_3$): 3570 (w), 3400 (m), 1700 cm^{-1} (s); λ_{max} (EtOH): 253.5 (ε 8250), λ_{infl} 280 nm (ε 1615); τ ($CDCl_3$): 2.50–3.40 (m, 9H), overlapping singlet and AB system, together = 2H, 5.18 (s), 5.09 (d, J = 16 Hz), 5.30 (d, J = 16 Hz), changing at 85°C to a broad singlet at 5.17 (2H), 6.10–9.00 (broad complex absorption, 21H) including sharp singlets at 7.23, 7.30, 8.12, and 8.24 changing at 85°C to a sharp singlet at 7.28, and a broad singlet at 8.20; *m/e*: 420 (M^+, 6), 335 (8), 322 (12), 321 (36), 304 (12), 303 (40), 264 (6), 249 (12), 248 (6), 237 (8), 236 (24), 235 (12), 223 (8), 91 (100). *Exact Mass* calcd. for $C_{26}H_{32}N_2O_3$: 420.2413; found: 420.2410.

N-{2-[1′-*Benzyl-3′-(2″-ketocyclohexyl)oxindol-3′-yl]ethyl*}-N-*methylacetamide* (**11**)

A solution of the mixed diastereoisomers of alcohol **10** (3.0 g) in pure acetone (45 mL) was treated with a solution of sodium dichromate (3.0 g) and concentrated H_2SO_4 (4.5 g) in water (30 mL). After 30 min at room temperature the reaction solution was neutralised with solid $NaHCO_3$, the acetone distilled off at the water pump and the aqueous residue extracted with ethyl acetate (4 × 50 mL). The extracts were washed with aqueous 1*M* HCl, water, and dried. The solvent was boiled off, and the product obtained as a yellow foam (2.1 g, 70%) which gave one spot at R_f 0.66 (S/*A*) and was thus pure mixed diastereoisomers of the ketone. Similar oxidation of the separated diastereoisomers of alcohol **10** gave the corresponding pure diastereoisomers of ketone **11**.

Diastereoisomer A—This was obtained as a colourless gum; ν_{max} ($CHCl_3$): 1710 (s), 1640 cm^{-1} (s); λ_{max} (EtOH): 254 (ε 9530), λ_{infl} 280 nm (ε 1830); τ ($CDCl_3$): 2.50–3.40 (m, 9H), 5.01 (br s, 2H), 6.20–8.50 (complex absorption, 19H) including sharp singlets at 7.22, 7.26, 8.06, and 8.24 changing at 60°C to a broad singlet at 7.26 and broad humps at 8.06 and 8.24; *m/e*: 418 (M^+, 5), 320 (8), 319 (35), 291 (22), 262 (6), 248 (7), 223 (5), 158 (5), 154 (12), 126 (10), 100 (5), 98 (12), 97 (5), 95 (7), 91 (100). *Exact Mass* calcd. for $C_{26}H_{30}N_2O_3$: 418.2256; found: 418.2266.

Diastereoisomer B—This was likewise obtained as a colourless gum; ν_{max}: same as A; λ_{max} (EtOH): 254 (ε 9530), λ_{infl} 280 nm (ε 1820); τ ($CDCl_3$): 2.20–3.40 (m, 9H), 5.08 (br s, 2H), 6.70–9.00 (complex absorption, 19H) including sharp singlets at 7.27, 8.15, and 8.22; the last two coalesce at 60°C to a broad singlet at 8.19; *m/e*: 418 (M^+, 9), 320 (12), 319 (55), 318 (5), 292 (5), 291 (22), 262 (5), 248 (10), 100 (8), 92 (8), 91 (100). *Exact Mass* calcd. for $C_{26}H_{30}N_2O_3$: 418.2256; found: 418.2261.

N-{2-[1′-*Benzyl-3′-(2″-keto-3″-formylcyclohexyl)oxindol-3′-yl]ethyl*}-N-*methylacetamide* (**12**)

A mixture of sodium ethoxide (1.73 g, 25 mmol) and freshly purified ethyl formate (2.81 g, 38 mmol) in dry benzene (25 mL) was left at room temperature under N_2 for 2.5 h. A solution of the ketone **11** (418 mg, 1 mmol) in dry benzene (20 mL) was then added, the mixture left for 10 h at room temperature, acidified with dilute aqueous HCl, and extracted with ethyl acetate (3 × 25 mL). The combined extracts were then extracted with 10% aqueous sodium carbonate (3 × 30 mL). The combined carbonate extracts were washed with ether (2 × 20 mL), acidified with 6 *M* aqueous HCl, keeping the temperature below 10°C, and then extracted with ethyl acetate (3 × 50 mL). This yielded a pale brown foam (403 mg) which after charcoaling in benzene became a very pale yellow foam of the formyl compound **9** (390 mg, 87%). The product runs as a streaking spot on tlc at R_f 0.65 (S/*A*); ν_{max}: 3400 (w), 1710 (s), 1640 cm^{-1} (s); λ_{max} (EtOH): 258 (ε 13 390), 285 nm (ε 11 550); λ_{max} (EtOH–NaOH): 253.5 (ε 11 000), 322 nm (ε 19 500); τ ($CDCl_3$): −4.95 (br s) and −4.21 (br s) together = 1H and exchange with D_2O, 1.58 (br s) and 2.01 (br s) together = 1H, sharpen on addition of D_2O, 2.20–3.50 (m, 9H), 5.10 (compact m, 2H), 6.30–8.50 (complex absorption, 17H) including close-packed sharp signals centred at 7.18, and sharp singlets at 8.06, 8.09, 8.12, and 8.22; *m/e*: 446 (M^+, 3), 347 (6), 322 (6), 249 (4), 248 (6), 223 (9), 91 (100). *Anal.* calcd. for $C_{27}H_{30}N_2O_4$ (446.2204): C 72.67, H 6.73, N 6.28; found (446.2206): C 72.4, H 6.8, N 6.0.

N-{2-[1′-*Benzyl-3′-(2″-keto-3″-allyl-3″-formylcyclohexyl)-oxindol-3′-yl]ethyl*}-N-*methylacetamide* (**13**)

This allylation was carried out in a darkroom because of the high light sensitivity of allyl iodide. A large excess of allyl iodide (8 mL) was added to a stirred solution of the lithium salt of formyl ketone **12**, prepared by stirring a suspension of **12** (835 mg, 1.87 mmol) and lithium carbonate (244 mg, 3.3 mmol) in water (12 mL). Pure acetone (100 mL) was added to render the reaction mixture homogeneous and the solution was left at room temperature for 1 h. The acetone and allyl iodide were then removed under water pump vacuum at 30°C and the residue partitioned between 5% aqueous Na_2CO_3 (25 mL) and ethyl acetate (25 mL). The aqueous phase was further extracted with ethyl acetate (3 × 25 mL) and the combined organic extracts washed with aqueous Na_2CO_3, then with water. Removal of the solvent yielded a pale yellow foam of essentially pure allyl formyl compound **13** (758 mg, 83%) which ran as a slightly elongated spot at R_f 0.70 (S/*A*). (The acidic (Na_2CO_3 soluble) portion of the reaction mixture (109 mg) contained at least seven components.) ν_{max}: 3000 (m), 1710 (s), 1640 cm^{-1} (s); λ_{max} (EtOH): 255 (ε 8220), λ_{infl} 280 (ε 2100); τ ($CDCl_3$): 0.22 (s), 0.45 (s) together = 1H, 2.20–3.50 (m, 9H), 4.10–5.90 (complex absorption, 5H), 6.30–8.60 (complex absorption, 20H) including sharp singlets at 7.26, 7.27, 8.09, 8.17, 8.25, 8.26; *m/e*: 486 (M^+, 1), 458 (0.3), 445 (2), 387 (9), 346 (9), 322 (5), 263 (4), 236 (9), 223 (2), 176 (8), 158 (5), 134 (5), 117 (5), 105 (5), 104 (4), 91 (100). *Anal.* calcd. for $C_{30}H_{34}N_2O_4$ (486.2518): C 74.06, H 7.00, N 5.76; found (486.2493): C 71.8, H 6.9, N 5.4.

N-{2-[1′-*Benzyl-3′-(2″-keto-3″-allylcyclohexyl)oxindol-3′-yl]ethyl*}-N-*methylacetamide* (**14**)

A solution of the allyl formyl compound **13** in 2.5% aqueous alcoholic KOH (40 mL) was left at room temperature under N_2 for 1 h. The solvent was nearly completely removed by distillation under reduced pressure. Partition of the residue between water (10 mL) and ethyl acetate (25 mL), followed by further extraction of the aqueous phase with ethyl acetate (3 × 30 mL) gave the allyl compound **14** as a pale yellow foam (700 mg, 98%) which ran as a single oval spot on tlc (R_f 0.70, S/*A*); ν_{max} ($CHCl_3$): 3400 (w), 1705 (s), 1640 cm^{-1} (s); λ_{max} (EtOH): 255 (ε 7150), λ_{infl} 280 nm (ε 1790); τ ($CDCl_3$): 2.10–3.33 (m, 9H), 3.40–5.30 (complex absorption, 5H), 6.60–9.10 (complex absorption, 20H) including sharp singlets at 7.28, 8.10, 8.18, 8.23, 8.39; *m/e*: 458 (M^+, 21), 360 (13), 359 (49), 358 (9), 322 (7), 318 (10), 278 (6), 262 (6), 250 (6), 249 (13), 248 (16), 235 (24), 234 (6), 223 (25), 158 (7), 100 (18), 91 (100). *Exact Mass* calcd. for $C_{29}H_{34}N_2O_3$: 458.2569; found: 458.2577.

N-{2-[1′-*Benzyl-3′-(2″-keto-3″-ethanalylcyclohexyl)oxindol-3′-yl]ethyl*}-N-*methylacetamide* (**15**)

A stream of ozonised oxygen was passed through a solution of the allyl compound **14** (350 mg) in dry methanol (8 mL) at −30°C for 45 min. The solution was then cooled to −60°C, purged with nitrogen for 15 min, and treated with dimethyl sulphide (3 mL). After 1 h at room temperature, the reaction solution was boiled down at the water pump, and the residual colourless oil partitioned between ethyl acetate (25 mL) and 5% aqueous Na_2CO_3 (25 mL). The aqueous phase was extracted with ethyl acetate (3 × 30 mL) and normal work-up of the nonacidic and acidic organic products gave the aldehyde **15** (318 mg, 91%) as an off-white foam and the corresponding carboxylic acid (30 mg, 8%) as a colourless gum. This good experimental result was reproduced several times, but on a number of occasions was not. These failures could not be accounted for.

The aldehyde **15** ran as a single elongated spot on tlc (R_f 0.57, S/*A*); ν_{max} ($CHCl_3$): 2740 (w), 1710 (s), 1640 cm^{-1} (s); λ_{max} (EtOH); 253.5 (ε 8080), λ_{infl} 280 nm (ε 1840); τ ($CDCl_3$): 0.20 (br s), 0.34 (br s) together = 1H, 2.10–3.35 (m, 9H), 5.06 (br s) overlapping 5.0–5.40 (br m) together = 2H, 6.50–8.70

(complex absorption, 21H) including 7.24 (br s) and sharp singlets at 8.06, 8.14, 8.20, 8.25; *m/e*: 460 (M^+, 7), 361 (27), 343 (36), 333 (14), 322 (18), 249 (14), 248 (14), 236 (20), 223 (27), 168 (14), 150 (11), 149 (14), 106 (23), 105 (18), 91 (100). *Exact Mass* calcd. for $C_{28}H_{32}N_2O_4$: 460.2362; found: 460.2382.

N-{2-[*1'-Benzyl-3'-(2''-keto-3''-carboxycyclohexyl)oxindol-3'-yl]ethyl*}-N-*methylacetamide*

The acidic fraction from the above ozonolysis gave analytical and spectral data consistent with the structure proposed. It ran on tlc as a streaking spot at variable R_f around 0.27 (S/*A*); ν_{max} ($CHCl_3$): 3300–2600 (broad, w), 1715 (s), 1640 cm^{-1} (s); λ_{max} (EtOH): 254 (ε 8500), λ_{infl} 280 nm (ε 1730); τ ($CDCl_3$): 0.80–1.80 (very broad s, 1H, exchange with D_2O), 2.20–3.50 (m, 9H), 5.08 (br s) overlying a broad hump 4.75–5.50, together = 2H, 6.20–9.20 (complex absorption, 22H), including broad singlet at 7.24; *m/e*: 476 (M^+, 2), 377 (4), 361 (5), 359 (5), 322 (17), 249 (17), 237 (9), 236 (22), 223 (17), 165 (7), 158 (20), 149 (17), 91 (100). *Exact Mass* calcd. for $C_{28}H_{32}N_2O_5$: 476.2311; found: 476.2307.

N-{2-[*1'-Benzyl-3'-(4'',5'',6'',7''-tetrahydroindol-7''-yl)-oxindol-3'-yl]ethyl*}-N-*methylacetamide* (***16***)

The keto aldehyde **15** (180 mg) was added to a suspension of ammonium carbonate (0.5 g) in absolute ethanol (15 mL) under nitrogen. After a further 2 g of ammonium carbonate had been added, the stirred mixture was refluxed for 2 h, during which time further ammonium carbonate was added (5 × ~0.5 g). The ethanol was then boiled off under reduced pressure and the pale brown solid residue partitioned between ethyl acetate (10 mL) and water (10 mL); the aqueous phase was reextracted with ethyl acetate (3 × 10 mL). The combined organic extracts yielded an orange-brown foam (180 mg). This product ran as two main spots on tlc, at R_f 0.70 and 0.64, together with three faint lower-running components and much baseline material. Preparative tlc (S′/*A*) of 25 mg on four plates (S′/*A*) under a N_2 atmosphere gave diastereoisomer A (3.3 mg), mixed diastereoisomers A and B (7.0 mg), and diastereoisomer B (3.5 mg) as colourless oils. The yield of A + B is thus 54%.

Diastereoisomer A—This ran as a round spot on tlc at R_f 0.70 (S/*A*); ν_{max} ($CHCl_3$): 3280 (m), 1700 (s), 1640 cm^{-1} (s); λ_{max} (EtOH): 257, λ_{infl} 281 nm; τ ($CDCl_3$): −0.80 to −0.30 (broad hump, 1H, did not exchange with D_2O), 2.60–3.60 (m, 9H), 3.66 (m, 1H), 4.04 (m, 1H), 4.98 (d, 1H, *J* = 14 Hz), 5.21 (d, 1H, *J* = 14 Hz), 5.70–8.50 (complex absorption, ~17H) including sharp singlets at 7.04 and 7.93; *m/e*: 441 (M^+, 1), 322 (6), 236 (5), 121 (20), 120 (100), 119 (5), 118 (13), 103 (5), 91 (64). *Exact Mass* calcd. for $C_{28}H_{31}N_3O_2$: 441.2416; found: 441.2399.

Diastereoisomer B—This ran as a round spot on tlc at R_f 0.64 (S/*A*); ν_{max} ($CHCl_3$): 3430 (m), 1700 (s), 1640 cm^{-1} (s); λ_{max} (EtOH): 257, λ_{infl} 281 nm; nmr spectrum not satisfactory (sample too small) but pyrrole CH's and benzyl CH_2 visible, and NMe and $COCH_3$ each split into two signals (sharp singlets 7.18, 7.23, and 8.04, 8.22) by restricted rotation; *m/e*: 441 (M^+, 1), 342 (6), 322 (4), 249 (4), 236 (8), 167 (4), 158 (4), 121 (9), 120 (98), 118 (16), 103 (4), 92 (6), 91 (100). *Exact Mass* calcd. for $C_{28}H_{31}N_3O_2$: 441.2416; found: 441.2420.

Palladium-on-charcoal Dehydrogenation of ***16***

A solution of **16** (6.5 mg) in decalin (1.5 mL) containing suspended 10% Pd/C (2 mg) was heated for 1 h at 165°C under N_2. Thin-layer chromatographic assay showed total consumption of the diastereoisomer B of **16** and just one main running spot at R_f 0.70 (S/*A*) coincident with diastereoisomer A of **16**. The mass spectrum of this fraction (1.3 mg after preparative tlc) showed it to be a mixture of the diastereoisomer A of **16** and the desired indole **6**; *m/e*: 441 (M^+), 437 (M^+), 338, 247, 120, 100, 91. *Exact Mass* calcd. for $C_{28}H_{31}N_3O_2$: 441.2416; found: 441.2402. *Exact Mass* calcd. for $C_{28}H_{27}N_3O_2$: 437.2103; found: 437.2107.

N-{2-[*1'-Benzyl-3'-(2''-methoxycarbonyl-4'',5'',6'',7''-tetrahydroindol-7''-yl)oxindol-3'-yl]ethyl*}-N-*methylacetamide* (***18***)

A solution of the tetrahydroindole **16** (88.2 mg, 0.2 mmol) in dry, ethanol-free chloroform (2 mL) was added over a period of 20 min to a solution of trichloroacetyl chloride (91 mg, 0.5 mmol) in pure chloroform (3 mL) containing a suspension of anhydrous potassium carbonate (276 mg, 2 mmol). After a further 25 min, the solids were filtered off and washed with chloroform (2 × 5 mL). The combined chloroform solutions were washed with saturated aqueous $NaHCO_3$ solution (2 × 5 mL) and then with water (2 × 10 mL) to give an orange yellow solution. This yielded a brown foam (104 mg) which ran as one major spot (R_f 0.7, S/*A*) together with baseline material. This crude product (100 mg) was dissolved in methanol (2 mL) and treated with a solution of sodium methoxide in methanol (made from Na, 11.5 mg, and MeOH, 3 mL). After 5 min, the methanol was boiled off at the water pump and the residue partitioned between ethyl acetate (10 mL) and water (10 mL). The aqueous phase was further extracted with ethyl acetate (2 × 5 mL) and the combined extracts boiled down to yield a brown liquid (70 mg) which ran as several spots on tlc (S/*A*), one of which, at R_f 0.6, was dominant. Preparative tlc (S′/*A*, six plates) of 60 mg of the product mixture gave the ester **18** as a pale orange foam (22 mg, 30% yield from **16**), which ran as a round spot on tlc at R_f 0.6 (S/*A*); ν_{max} ($CHCl_3$): 3430 (m), 3240 (m), 1700 (s), 1635 cm^{-1} (s); λ_{max} (EtOH): 284.5 nm (ε 16 480); *m/e*: 499 (M^+, 2), 468 (2), 323 (7), 322 (23), 249 (8), 236 (11), 223 (3), 178 (100), 146 (48), 91 (71); τ ($CDCl_3$): −0.95 (br s) and −0.15 (br s) neither is exchangeable with D_2O and both together = 1H, 2.30–3.70 (m, 10H), 4.50–5.40 (m, 2H), 6.25 (s) and 6.31 (s) together = 3H, 6.40–8.70 (complex absorption, 18H) including sharp singlets at 7.11, 7.22, 8.00, and 8.22. *Exact Mass* calcd. for $C_{30}H_{33}N_3O_4$: 499.2471; found: 499.2492.

N-{2-[*1'-Benzyl-3'-(2''-methoxycarbonylindol-7''-yl)oxindol-3'-yl]ethyl*}-N-*methylacetamide* (***20***)

A solution of the tetrahydroindole **18** (17 mg, 0.034 mmol) and DDQ (15.5 mg, 0.068 mmol) in benzene (5 mL) was refluxed for 1.25 h. Ethyl acetate (10 mL) was added to the cooled reaction mixture and the solution extracted with aqueous sodium bicarbonate (3 × 5 mL) and water (2 × 5 mL). The ethyl acetate solution yielded the indole **20** as a pale greenish brown viscous liquid (11.7 mg, 69%), which ran as a single round spot on tlc at R_f 0.62 (S/*A*); ν_{max} ($CHCl_3$) 3300 (m), 1705 (s), 1690 (s), 1640 cm^{-1} (s); λ_{max} (EtOH): 258 (ε 11 180), 293 (ε 18 500), λ_{infl} 230 nm (ε 27 850); τ ($CDCl_3$): −1.1 (br s, 1H, not exchangeable with D_2O), 2.00–3.20 (m, 11.5H, 1.5H too high), 5.05 (br s, 2H), 6.04 (s, 3H), 6.50–8.90 (complex absorption, 11H, 1.0H too high) including broad singlets at 7.20 and 8.15; *m/e*: 495 (M^+, 7), 409 (4), 397 (7), 396 (23), 365 (4), 364 (17), 363 (4), 305 (4), 273 (6), 207 (7), 178 (9), 149 (17), 100 (44), 91 (100). *Exact Mass* calcd. for $C_{30}H_{29}N_3O_4$: 495.2157; found: 495.2163.

N-{2-[*1'-Benzyl-3'-(2''-carboxyindol-7''-yl)oxindol-3'-yl]ethyl*}-N-*methylacetamide* (***21***)

A solution of the above ester **20** (7 mg) in a mixture of 95% ethanol (1.5 mL) and 0.1 *M* aqueous NaOH (1.5 mL) was left at room temperature for 18 h, then boiled down at 20°C at the water pump to remove the ethanol, and the aqueous residue

partitioned between 5% aqueous Na_2CO_3 (5 mL) and ethyl acetate (5 mL). The aqueous phase was then acidified with concentrated HCl and extracted with ethyl acetate (3 × 5 mL). This yielded the indole carboxylic acid **21** as a pale brown foam (6.3 mg, 93%) running as a streaking spot on tlc with a variable R_f (S/*A*). This product crystallised; recrystallisation from ethyl acetate gave colourless crystals, mp 139.5–141°C: ν_{max} ($CHCl_3$): 3550–2600 (broad m), 3300 (m), 1690 (s), 1640 cm^{-1} (s); λ_{max} (EtOH): 258 (ε 12 000), 269 (ε 12 000), 292 nm (ε 16 250); τ ($CDCl_3$): −1.15 (s) and −1.10 (s) not exchangeable with D_2O, together = 1H, changing at 85°C to 0.9 (br s, 1H); 1.25 (broad hump, 1H) exchange with D_2O, shifting at 85°C to 0.68; 2.30–3.40 (m, 13H), 5.10 (s, 2H), 5.60–7.75 (m, 7H) including sharp singlets at 7.20 and 7.24 (changing at 85°C to 7.24); 8.12 (s) and 8.15 (s) together = 3H (changing at 85°C to 8.15); *m/e*: 481 (M^+, 9), 438 (8), 437 (18), 395 (1), 383 (15), 382 (44), 381 (8), 364 (14), 363 (8), 351 (8), 339 (13), 338 (38), 337 (15), 291 (11), 273 (11), 248 (8), 247 (25), 245 (10), 218 (9), 203 (8), 130 (8), 100 (93), 91 (100). *Exact Mass* calcd. for $C_{29}H_{25}N_3O_4$: 481.2002; found: 481.2003.

N-{2-[*1′-Benzyl-3′-(indol-7″-yl)oxindol-3′-yl*]*ethyl*}-N-*methylacetamide* (**6**)

A solution of the indolecarboxylic acid **21** (594 mg) in pure quinoline (30 mL) containing cupric acetate monohydrate (120 mg) was heated at 200°C for 8 h under nitrogen, the cooled reaction mixture poured into ethyl acetate (100 mL) and extracted with aqueous 1 *M* hydrochloric acid (5 × 40 mL) and water (2 × 10 mL). The ethyl acetate soluble product, which produced one major spot at R_f 0.7 and a small spot of less polar compound, in addition to baseline material (S/*A*), was dissolved in the minimum volume of chloroform and transferred onto an alumina column (8 × 2 cm). Elution with carbon tetrachloride removed the less polar impurity; elution with methanol then gave the pure indole **6** as a pale orange foam (380 mg, 70.5%), which ran as a round spot at R_f 0.7 (S/*A*) and 0.65 (S/*E*); ν_{max} ($CHCl_3$); 3470 (w), 3350 (m), 1700 (s), 1680 cm^{-1} (s); λ_{max} (EtOH): 259 (ε 11 990), 285 (ε 9680), 290 nm (ε 8290); τ ($CDCl_3$): —0.52 (broad hump) and −0.41 (broad hump) together = 1H, not exchangeable with D_2O, changing at 85°C to −0.24 (broad hump, 1H); 2.40–3.40 (m, 13H); 5.18 (s, 2H); 6.70–8.00 (complex absorption, 7H) including sharp singlets at 7.31 and 7.36 (changing at 85°C to a sharp singlet at 7.36, ~3H); 8.21 (s) and 8.30 (s) together = 3H (changing at 85°C to a singlet at 8.26, 3H); *m/e*: 437 (M^+, 60), 364 (5), 351 (18), 339 (32), 338 (100), 337 (41), 310 (5), 273 (14), 260 (5), 248 (14), 247 (50), 246 (9), 245 (14), 231 (14), 230 (9), 218 (18), 204 (14), 130 (14), 100 (95), 91 (91). *Exact Mass* calcd. for $C_{28}H_{27}N_3O_2$: 437.2104; found: 437.2103.

N-[2-(*1′-Benzylindol-3′-yl*)*ethyl*]-N-*methylacetamide* (**22**)

(1-Benzyltryptamine was prepared for the first time by *N*-benzylation of tryptamine. Of the several methods available for the specific 1-alkylation of tryptamine, that reported by Potts and Saxton (12) for 1-methylation gave by far the best results; the *N*-methylacetamide **22** had been previously prepared from 1-benzylindole-3-carboxaldehyde (13) and also by a Fischer synthesis from 1-phenyl-1-benzylhydrazine (14).)

A solution of *N*-[2-(1′-benzylindol-3-yl)ethyl]acetamide (960 mg, 3.2 mmol) in dry THF (5 mL) was added to a stirred solution of freshly sublimed potassium *tert*-butoxide (1.08 g, 9.6 mmol) in dry THF (20 mL) under N_2. After 30 min at room temperature a solution of methyl iodide (4.6 g, 32 mmol) in dry THF (5 mL) was added dropwise with stirring. After a further period of 30 min at room temperature, the reaction mixture was boiled down at the water pump and partitioned between water (50 mL) and ether (50 mL). The aqueous phase was further extracted with ether (2 × 50 mL). The combined dried ether extracts then yielded the *N*-methyl compound **22** as a white crystalline product (980 mg). Crystallisation from toluene gave pure **22**, mp 98–98.5°C (821 mg, 82%); moves as a round spot at R_f 0.63 (S/*A*) and at 0.40 (S/*D*); ν_{max} ($CHCl_3$): 1635 cm^{-1} (s); λ_{max} (EtOH): 289 (ε 5450), λ_{infl} 281 (ε 5000), 299 nm (ε 4900); τ ($CDCl_3$): 2.90–3.05 (m, 9H), 3.12 (d, *J* = 2.5 Hz, 1H), 4.82 (s, 2H), 6.39–6.58 (m, 2H), 6.95–7.21 (m, 5H) including sharp singlets at 7.08 and 7.19, 8.00 (s, 1.5H), 8.16 (s, 1.5H); *m/e*: 306 (M^+, 5), 289 (1), 288 (1), 233 (45), 220 (17), 129 (3), 91 (100). *Anal.* calcd. for $C_{20}H_{22}N_2O$ (306.1732): C 78.43, H 7.19, N 9.15; found (306.1736): C 78.9, H 7.2, N 9.2.

N-[2-(*1′-Benzyloxindol-3′-yl*)*ethyl*]-N-*methylacetamide* (**23**)

A solution of the indole **22** (5 g) in glacial acetic acid (50 mL) containing dimethyl sulphoxide (5 mL) and concentrated HCl (2.5 mL) was left overnight at room temperature under nitrogen. The reaction solution was added to water (200 mL) and extracted with ether (4 × 75 mL). The combined ether extracts were carefully neutralised with solid $NaHCO_3$ at 0°C, washed with saturated aqueous $NaHCO_3$ (2 × 100 mL), then with water. The extracts yielded a colourless viscous liquid (4.9 g) part of which (61.7 mg) yielded the pure oxindole (55.4 mg, 90%) by preparative tlc (S/*D*). The yield for the reaction is 84%, allowing for the 90% purity of the isolated product. The *purified* compound failed to crystallise and was used in the following analytical and spectral measurements; moves as a round spot at R_f 0.58 (S/*A*) and 0.32 (S/*D*); ν_{max} ($CHCl_3$): 1706 (s), 1635 cm^{-1} (s); λ_{max} (EtOH): 256 (ε 7150), λ_{infl} 280 (ε 1380); τ ($CDCl_3$): 2.5–3.5 (m, 9H), 5.13 (s, 2H), 6.09–6.85 (m, 3H), 7.05 (s, 1.6H), 7.10 (s, 1.4H), 7.55–8.10 (m, 5H), including a sharp singlet at 8.0 (~3H); *m/e*: 322 (M^+, 17), 280 (0.5), 279 (0.5), 249 (6), 236 (18), 223 (2), 158 (5), 130 (4), 117 (4), 103 (2), 91 (100). *Exact Mass* calcd. for $C_{20}H_{22}N_2O_2$: 322.1681; found: 322.1684.

N-{2-[*1′-Benzyl-3′-(1″-methoxycyclohex-1″-en-6″-yl)oxindol-3′-yl*]*ethyl*}-N-*methylacetamide* (**24**)

A solution of the crude oxindole (**23**) (1.29 g, 4 mmol) in dry THF (5 mL) was added dropwise under N_2 to a stirred solution of freshly sublimed potassium *tert*-butoxide (492 mg, 4.4 mmol) in dry THF (5 mL). After 30 min at room temperature, a solution of 6-bromo-1-methoxycyclohex-1-ene (840 mg, 4.4 mmol) in THF (5 mL) was added dropwise with stirring. After a further period of 30 min at room temperature, water (25 mL) and then saturated aqueous NaCl (150 mL) were added, and the whole extracted with ethyl acetate (3 × 50 mL). The extracts yielded a colourless liquid (1.60 g). Preparative tlc of 61.1 mg of this product (S/*E*) yielded the pure product (**24**) as mixed diastereoisomers (45.6 mg, corresponding to a 78% yield, allowing for the 90% purity of crude **20** used); the mixed diastereoisomers ran as one spot on tlc at R_f 0.38 (S/*D*) and at 0.54 (S/*E*); ν_{max} ($CHCl_3$): 1702 (s), 1630 cm^{-1} (s); λ_{max} (EtOH): 257 (ε 7450), λ_{infl} 280 nm (ε 2420); τ ($CDCl_3$): 2.50–3.40 (m, 9H), 5.08 (m, 0.75H), 5.12 (s, 0.5H), 5.21 (m, 0.75H), 5.60 (m, 0.6H), 6.41 (s, 0.7H), 6.44 (s, 0.3H), 6.60–8.40 (m, 19H), including sharp singlets at 7.21, 7.25, 7.30, 7.34, 8.07, 8.13, and 8.22; *m/e*: 432 (M^+, 0.4), 417 (1.8), 357 (0.8), 340 (2), 332 (1), 322 (18), 318 (5), 305 (1), 291 (2), 269 (8), 267 (22), 254 (10), 249 (10), 236 (12), 223 (2), 158 (3), 129 (3), 111 (10), 91 (100), 87 (14). *Exact Mass* calcd. for $C_{27}H_{32}N_2O_3$: 432.2413; found: 432.2406.

Hydrolysis of **24** *to the Ketone* **11** *and Formylation to the Formylketone* (**12**)

A solution of the crude enol ether **24** as obtained above, in aqueous methanolic HCl (from 27 mL MeOH and 3 mL 3 *M*

aqueous HCl) was left at room temperature under N_2 for 2.5 h; solid $NaHCO_3$ (3 g) was then added and the methanol boiled off at the water pump. The residue was partitioned between ethyl acetate (100 mL) and water (50 mL). The organic phase yielded a yellow viscous liquid (1.33 g) shown to contain 72.5% of ketone **11** by preparative tlc. This corresponds to a yield of 89% for the hydrolysis step and an overall 58% in three steps based on the indole **22**. The purified ketone **11** was found to run as two spots corresponding to the two diastereoisomers at R_f 0.36 and 0.26 (S/*D*), and at 0.52 and 0.47 (S/*E*); ketone prepared by the earlier method (oxidation of the corresponding alcohol) showed identical behaviour.

The crude product (containing 72.5% of **11**) was used directly in the formylation step, which was carried out as described earlier in this experimental (toluene was used instead of benzene): the acidic fraction of the reaction proved to be pure **12** and was formed in 83% yield (overall 48% yield in the four steps from the indole **22**).

N-{2-[*1′-Benzyl-3′-[2″-ethoxycarbonyl-4″,5″,6″,7″-tetrahydroindol-7″-yl)oxindol-3-yl*]*ethyl*}-N-*methylacetamide (**19**)*

A solution of the formyl ketone **12** (3.6 g, 8 mmol) in THF (4 mL) was added to a refluxing solution of sodium acetate (1.45 g, 17.8 mmol) in water (24 mL) and glacial acetic acid (25 mL) under N_2. A solution of ethyl 2-amino-3-oxobutanoate hydrochloride (15) (the literature procedure was simplified by the use of concentrated HCl instead of dry HCl and by the use of a 10:1 ratio of oxime to catalyst; 1.46 g, 8.1 mmol) in aqueous acetic acid (4 mL) was then added dropwise with stirring and refluxing. After about 15 min, a second equivalent of the amine hydrochloride was gradually added, and the refluxing continued for a further 15 min. After cooling in an ice–salt bath, a cold solution of 10% aqueous Na_2CO_3 (200 mL) was added and the whole extracted with ethyl acetate (4 × 100 mL). The combined extracts were then washed with 5% aqueous Na_2CO_3 (4 × 100 mL), dried, and boiled down to yield a brown product, which after charcoal treatment was obtained as a pale red oil (3.89 g). Preparative tlc showed this to contain 70% of the ethyl ester (**19**) as a mixture of two diastereoisomers. The purified **19** runs as two spots at R_f 0.39 and 0.35 (S/*D*), and as one spot at 0.52 (S/*E*); ν_{max} ($CHCl_3$): 3440 (w), 3250 (w), 1697 (s), 1635 cm^{-1} (s); λ_{max} (EtOH): 286 nm (ε 19 700); τ($CDCl_3$): 0.25 (hump, 0.5H), 1.01 (hump), and 1.35 (hump) together = 0.5H, 2.55–3.62 (m, 10H), 4.92 (d, J = 13.8 Hz), 5.26 (d, J = 13.8 Hz), 4.91 (d, J = 10.8 Hz), 5.43 (d, J = 10.8 Hz) all four doublets = 2H, 5.7–6.1 (two sharp closely overlapping quartets, 2H), 6.4–6.9 (m, 2H), 7.05–8.95 (complex absorption, 20H) including sharp singlets at 7.13, 7.21, 7.23, 8.01, 8.05, 8.22, and two sharp closely overlapping triplets 8.68–8.86; *m/e*: 513 (M^+, 0.2), 468 (1), 322 (20), 249 (9), 236(14), 192 (100), 146 (35), 91 (35). *Exact Mass* calcd. for $C_{31}H_{35}N_3O_4$: 513.2627; found: 513.2627.

N-{2-[*1′-Benzyl-3′-(2″-ethoxycarbonylindol-7″-yl)oxindol-3′-yl*]*ethyl*}-N-*methylacetamide (**43**)*

A solution of DDQ (3.04 g, 13.4 mmol) in dry toluene was added under nitrogen over 5 min to a solution of the crude pyrrole ester **19** (3.416 g, 6.7 mmol) in dry toluene (40 mL) at 80°C and the reaction solution kept at that temperature for 75 min. Ethyl acetate (100 mL) was then added and the whole extracted with 0.5 *M* $NaHCO_3$ (4 × 75 mL). The dried organic phase yielded, after charcoaling, a dark brown oil (3.125 g) preparative tlc of which (56.5 mg, S/*E*) gave 29.8 mg of pure indole ester **43** (53%). This compound moves as a single spot at R_f 0.50 (S/*D*) and at 0.58 (S/*E*); ν_{max} ($CHCl_3$): 3440 (w), 3310 (m), 1705 (s), 1639 cm^{-1} (s); λ_{max} (EtOH): 293.5 nm (ε 18 300); τ ($CDCl_3$): −0.83 (broad s, 1H, no exchange with D_2O), 2.26–3.40 (m, 14H), 5.08 (s, 2H), 5.63 (q, J = 7.5 Hz, 2H), 6.60–7.15 (multiplet, 8H) including a sharp singlet at 7.21, 8.13 (s), and 8.15 (s) together = 3H, 8.60 (t, J = 7.5 Hz, 3H); *m/e*: 509 (M^+, 7), 464 (1), 423 (3), 410 (30), 364 (25), 273 (6), 100 (65), 91 (100). *Exact Mass* calcd. for $C_{31}H_{31}N_3O_4$: 509.2314; found: 509.2323.

*Hydrolysis of Crude Ethyl Ester **43** to Pure Indole Carboxylic Acid **21***

The total reaction product mixture as obtained above (2.8 g) was saponified as described for the methyl ester (**20**). The total acidic fraction was obtained as a pale brown crystalline solid (1.49 g) recrystallisation of which from ethyl acetate gave the pure indole carboxylic acid **21** as colourless crystals, mp 139.5–141°C (1.21 g, which represents an 86% yield based on the 53% content of ester in the crude starting material).

*3-(2′-Hydroxyethyl)-1,3-dimethyloxindole (**39**)*

A 15% solution of *n*-butyl lithium in hexane (4.3 mL, 0.01 mol) was added dropwise over 5 min to a stirred solution of 1,3-dimethyloxindole (1.61 g, 0.01 mol) in dry anisole (25 mL) under N_2 at 0°C. The solution was left at 10°C for 15 min, then cooled to 0°C and treated dropwise with stirring over 2 min with a solution of ethylene oxide (0.88 g, 0.02 mol) in dry anisole (4 mL). The reaction solution was left under N_2 at room temperature for 19 h. Glacial acetic acid (0.6 g, 0.01 mol) was then added and, after a period of 15 min, the anisole distilled off at the water pump. The residue was thoroughly extracted with ether. Distillation of the product yielded a viscous yellow liquid (1.2 g, bp 160°C/0.6 Torr). Preparative tlc (S/*B*) of 86 mg gave two products: (*a*) at R_f 0.28 3-(2′-hydroxyethyl)-1,3-dimethyloxindole (**39**) as white crystals, mp 75.5–77.5°C (60.2 mg, 42% yield); ν_{max} ($CHCl_3$): 3570 (m), 3500–3150 (m), 1700 (s); λ_{max} (EtOH): 252.5 (ε 8630), λ_{infl} 281 (ε 1670); τ ($CDCl_3$): 2.50–3.20 (m, 4H), 6.10–6.60 (m, 2H), 6.78 (s, 3H), 7.50–7.70 (br s, 1H), exchange with D_2O), 7.60–8.30 (m, 2H), 8.60 (s, 3H); *m/e*: 205 (M^+, 30), 175 (5), 174 (17), 162 (13), 161 (100), 160 (72), 159 (9), 130 (13), 117 (10), 103 (5), 91 (10), 77 (10). *Anal.* calcd. for $C_{12}H_{15}NO_2$: C 70.22, H 7.37, N 6.83; found: C 70.0; H 7.3, N 6.7. (*b*) at R_f 0.40: 1,3-dimethyldioxindole as a white solid, mp 151–153°C (lit. (23) mp 148–149°C) (17 mg, 13% yield); *m/e*: 177 (M^+, 100); τ ($CDCl_3$): 2.45–3.25 (m, 4H), 6.10–6.50 (br s, 1H), exchange with D_2O) 6.79 (s, 3H), 8.39 (s, 3H).

*1,3-Dimethyl-3-(2′-hydroxycyclohexyl)oxindole (**28**)*

A 15% solution of *n*-butyl lithium in hexane (4.7 mL, 11 mmol) was added dropwise over 5 min under N_2 to a well stirred solution of 1,3-dimethyloxindole (1.61 g, 10 mmol) in anisole (20 mL) at 0°C. The solution was warmed to room temperature and a solution of 1,2-epoxycyclohexane (1.47 g, 15 mmol) in anisole (4 mL) was added dropwise over 5 min. The reaction solution was then left at room temperature for 20 h under N_2, then 2 h at 100°C. Glacial acetic acid (0.66 g, 11 mmol) was then added to the cooled mixture, the solvents boiled off at the water pump, and the residue partitioned between ethyl acetate (100 mL) and water (50 mL). The organic phase gave a white crystalline product (2.36 g), recrystallisation of which from 60–80 petrol – ethyl acetate yielded pure **28**, mp 169.5–170.5°C, R_f 0.1 (S/*B*) (1.51 g, 58%); ν_{max} ($CHCl_3$): 3520 (m), 3500–3250 (broad, w), 1698 cm^{-1} (s); λ_{max} (EtOH): 252.5 (ε 8580), λ_{infl} 280.5 nm (ε 1650); τ ($CDCl_3$): 2.60–3.25 (m, 4H), 6.83 (s, 3H), 6.95–9.00 (complex absorption, 14.5 H) including a sharp doublet 8.57 (J = 10 Hz, exchange with D_2O, about 1H) and a sharp singlet at 8.72, ~3H; *m/e*: 259 (M^+, 18), 175 (4), 174 (30), 162 (15), 161 (100), 160 (25), 159 (5), 158 (4), 146 (4), 144 (4), 130 (5), 118 (4), 117 (4), 91 (4),

81 (6). *Anal.* calcd. for $C_{16}H_{21}NO_2$: C 74.10, H 8.16, N 5.40; found: C 74.5, H 8.1, N 5.2.

*1,3-Dimethyl-3-(2'-ketocyclohexyl)oxindole (**29**)*

A solution of sodium dichromate dihydrate (77.6 mg, 0.26 mmol) and 98% H_2SO_4 (101.4 mg, 1.1 mmol) in water (0.7 mL) was added dropwise over 15 min at room temperature to a vigorously stirred suspension of the alcohol **28** (100 mg, 0.39 mmol) in ether (10 mL). After being stirred for 5 h the aqueous phase was separated and extracted with ether (5 × 5 mL), the combined extracts were washed with 10% aqueous Na_2CO_3 (3 × 5 mL) and then water. The dried solution yielded a pale yellow solid (67 mg). Preparative tlc (S/*B*) of the product (48.5 mg) led to the isolation of the pure ketone **29** as a mixture of diastereoisomers, mp 137–140°C (80–100 petrol – ether acetate) (35.9 mg, 50% yield); ν_{max} ($CHCl_3$): 1705 (s), 1695 cm^{-1} (s); λ_{max} (EtOH): 252 (ε 9050), λ_{infl} 280 nm (ε 1730); τ ($CDCl_3$): 2.30–3.30 (m, 4H), 6.75 (s) and 6.79 (s) together = 3H, 6.80–8.90 (complex absorption 12H) including sharp singlets at 8.57 and at 8.72 together ~3H; *m/e*: 257 (M^+, 14), 223 (4), 205 (3), 180 (3), 174 (4), 161 (20), 160 (32), 149 (4), 130 (4), 128 (4), 117 (4), 91 (4), 75 (5), 74 (75), 73 (11), 71 (6), 59 (100), 45 (62). *Anal.* calcd. for $C_{16}H_{19}NO_2$: C 74.70, H 7.46, N 5.45; found: C 74.4, H 7.5, N 5.5.

*1,3-Dimethyl-3(1',2',3',4'-tetrahydrocarbazol-1'-yl)oxindole (**40**)*

A solution of the ketone **29** (139 mg, 0.54 mmol) in glacial acetic acid (1.5 mL) was heated to 100°C. Pure phenylhydrazine (58.4 mg, 0.54 mmol) in glacial acetic acid (1 mL) was added dropwise with stirring to the solution at 100°C. After 30 min the acetic acid was boiled off at the water pump and the residue partitioned between ether and water. The aqueous phase was further extracted with ether (3 × 10 mL), the combined extracts washed with saturated aqueous $NaHCO_3$ (3 × 10 mL), then with water. This yielded a yellow solid (161.3 mg) which crystallised from 80–100 petrol – ethyl acetate and gave the tetrahydrocarbazole **40** as colourless crystals, mp 192–194°C; the compound moves as one spot on tlc at R_f 0.52 (S/*B*); ν_{max} ($CHCl_3$): 3380 (m), 1690 cm^{-1}(s); λ_{max} (EtOH): 228 (ε 34 950), 256 (ε 10 390), 286 (ε 9770), 293 (ε 7880); τ ($CDCl_3$): 2.10 (br s, 1H, no exchange with D_2O), 2.50–3.40 (m, 8H), 6.10–6.60 (m, 1H), 6.72 (s, 3H), 7.10–8.40 (complex absorption, 6H), 8.48 (s, 3H); *m/e*: 330 (M^+, 3), 171 (20), 170 (100), 169 (16), 168 (41), 167 (30), 166 (7), 161 (9), 160 (9), 154 (9), 143 (25), 130 (20), 128 (11), 118 (20), 117 (16), 115 (16), 81 (16), 77 (16). *Anal.* calcd. for $C_{22}H_{22}N_2O_2$: C 80.00, H 6.66, N 8.49; found: C 79.8, H 6.7, N 8.1.

*3-(1'-Carbazolyl)-1,3-dimethyloxindole (**41**)*

o-Chloranil (37.5 mg, 0.15 mmol) was added portionwise to a stirred solution of the tetrahydrocarbazole **40** in decalin (3 mL) at 120°C. After completion of the addition, the reaction was left at 120°C for 10 min, the decalin then distilled off under reduced pressure and the residue subjected to preparative tlc (S/*B*). The main band at R_f 0.68 was the carbazole **41** (18 mg) which after three crystallisations from 60–80 petrol – ethyl acetate was obtained as colourless crystals, mp 171–173°C; ν_{max} ($CHCl_3$): 3280 (m), 1690 cm^{-1} (s); λ_{max} (EtOH): 236 (ε 36 200), 245 (ε 26 620), 258.5 (ε 15 100), 282.5 (ε 10 210), 292.5 (ε 13 350), 323.5 (ε 3560), 336.5 nm (ε 3080); τ ($CDCl_3$): −0.35 (br s, 1H), no exchange with D_2O), 1.80–2.20 (m, 2H), 2.30–3.20 (m, 10H), 6.80 (s, 3H), 8.02 (s, 3H); *m/e*: 326 (M^+, 84), 325 (6), 312 (26), 311 (100), 309 (5), 295 (6), 294 (8), 283 (15), 282 (8), 281 (8), 280 (6), 279 (5), 268 (15), 267 (9), 266 (8), 265 (5), 255 (5), 254 (13), 253 (6), 252 (5), 241 (5), 167 (8), 163 (8), 155 (11), 149 (9), 116 (7), 110 (6). *Anal.* calcd. for $C_{22}H_{18}N_2O$ (326.1419): C 80.98, H 5.52, N 8.59; found (326.1427): C 79.8, 79.6; H 5.9, 5.7; N 7.9, 8.2.

*1,3-Dimethyl-3-(3'-formyl-2'-ketocyclohexyl)oxindole (**30**)*

Ethanol-free sodium ethoxide (from sodium, 0.67 g, 0.029 g-at.) was treated with pure ethyl formate (3.2 g, 44 mmol) in benzene (30 mL) under N_2. After 2 h at room temperature, the ketone **29** (3.5 g, 14 mmol) was added and the reaction solution left for a further 2.5 h. The benzene was then boiled off at the water pump and the orange solid residue partitioned between 10% aqueous Na_2CO_3 (50 mL) and ether (50 mL). Further extraction of the ether phase with aqueous Na_2CO_3 (2 × 25 mL) and washing of the combined aqueous phases with ether was followed by careful acidification with concentrated HCl, the temperature being kept at 0°C. The acidified mixture was extracted with ether (3 × 50 mL) which yielded a white solid (3.32 g, 84%). Four recrystallisations from 60–80 petrol – ethyl acetate gave pure formyl ketone **30** as colourless crystals, mp 122–123°C. It ran as an elongated spot on tlc, R_f 0.37 (S/*B*); ν_{max} ($CHCl_3$): 3600–2600 (w), 1705 (s), 1640 cm^{-1} (m); λ_{max} (EtOH): 253.5 (ε 11 170), 282 nm (ε 8330); τ ($CDCl_3$): −4.20 (br d, J = 5.4 Hz, 1H, exchange with D_2O), 1.95 (d, J = 5.4 Hz, 1H) changing to singlet with D_2O, 2.50–3.27 (m, 4H), 6.40–8.90 (complex absorption, 13H) including sharp singlets ~3H at 6.75 and 8.67; *m/e*: 285 (M^+, 21), 174 (9), 162 (17), 161 (93), 160 (100), 159 (9), 158 (7), 145 (9), 144 (10), 132 (21), 131 (10), 130 (19), 128 (7), 118 (10), 117 (21), 115 (7), 103 (9), 91 (12), 77 (12). *Anal.* calcd. for $C_{17}H_{19}NO_3$: C 71.57, H 6.67, N 4.91; found: C 72.0, H 7.0, N 5.1.

*3-(3'-Allyl-3'-formyl-2'-ketocyclohexyl)-1,3-dimethyloxindole (**31**) and 3-(3'-Allyloxymethylene-2'-ketocyclohexyl)-1,3-dimethyloxindole (**42**)*

The formyl ketone **30** (2.5 g, 8.8 mmol) was dissolved in sodium carbonate (1.06 g, 10 mmol) and water (1 mL) and allyl bromide (60 g, 500 mmol) were then added, followed by sufficient acetone to form a homogeneous solution (100 mL). After 12 h at room temperature, the acetone and excess allyl bromide were distilled off at the water pump and the residue partitioned between ether (50 mL) and aqueous Na_2CO_3 (50 mL). The aqueous phase was further extracted with ether (3 × 20 mL). The combined extracts yielded a colourless liquid (3 g) which was chromatographed on silica gel (300 g). Elution was started with a 7:3 mixture of 60–80 petrol – ethyl acetate, proceeding with an increasing proportion of ether: the *C*-allyl compound **31** was eluted with 5–10% ether (2.42 g, 85% yield), and the *O*-allyl compound **42** came off as a quite distinct band with 15–60% ether (0.38 g, 13.5%).

*The C-allyl compound (**31**)*—This formed colourless crystals, mp 117.5–119°C, after three recrystallisations from 60–80 petrol – ethyl acetate. It runs as a round spot on tlc at R_f 0.47 (S/*B*); ν_{max} ($CHCl_3$): 1710 (s), 1645 cm^{-1} (w); λ_{max} (EtOH): 252.5 (ε 9000), λ_{infl} 280 (ε 1980); τ ($CDCl_3$): 0.44 (s, 0.4H), 2.50–3.30 (m, 4H), 4.00–5.10 (m, 3H), 6.50–8.90 (complex absorption, 13H) including sharp singlets ~3H each at 6.74 and 8.71; *m/e*: 325 (M^+, 73), 187 (24), 186 (16), 174 (30), 162 (48), 161 (100), 160 (98), 137 (46), 132 (20), 130 (26), 117 (28), 109 (13), 91 (24), 77 (25), 67 (22). *Anal.* calcd. for $C_{20}H_{23}NO_3$: C 73.85, H 7.09, N 4.31; found: C 74.1, H 7.25, N 4.3.

*The O-allyl compound (**42**)*—This could not be induced to crystallise. It runs at R_f 0.33 (S/*B*); ν_{max} ($CHCl_3$): 1705 (s), 1685 cm^{-1} (sh, s); λ_{max} (EtOH): 253.5 (ε 12 530), 280 nm (ε 4900); τ ($CDCl_3$): 2.45–3.25 (m, 5H), 3.90–5.10 (m, 3H), 5.65 (d, J = 6 Hz, 2H), 5.95–8.90 (complex absorption, 16H) including sharp singlets, each ~3H at 6.70 and at 8.71; *m/e*: 325 (M^+, 13), 285 (9), 284 (36), 257 (10), 176 (6), 162 (32), 161 (43), 160 (100), 145 (5), 144 (6), 132 (9), 130 (9), 117 (10),

109 (5), 108 (6), 91 (5), 77 (5). *Exact Mass* calcd. for $C_{20}H_{23}NO_3$: 325.1678; found: 325.1668.

3-(3'-Allyl-2'-ketocyclohexyl)-1,3-dimethyloxindole (32)

A solution of the formyl compound **31** (500 mg) in 2.5% aqueous alcoholic potassium hydroxide was heated to 50°C for 6 h under nitrogen. The aqueous alcohol was boiled off at the pump and the residue neutralised with dilute hydrochloric acid before being extracted with ether (3 × 25 mL). This yielded a diastereoisomeric mixture of **32** in the form of a colourless oil (480 mg), running as two round spots on tlc (S/*B*). Separation by preparative tlc (55 mg, S/*B*) gave diastereoisomers A and B.

Diastereoisomer A—R_f 0.5 (24.9 mg) colourless crystals, mp 83.5–84.5°C, after recrystallisation twice from 60–80°C petrol and twice from cyclohexane; ν_{max} ($CHCl_3$): 1710 (s), 1700 (s), 1645 cm^{-1} (m); λ_{max} (EtOH): 253 (ε 8390); λ_{infl} 279 (ε 1925); τ ($CDCl_3$): 2.30–3.40 (m, 4H), 3.82–5.75 (m, 3H), 6.60–9.00 (complex absorption, 16H) including sharp singlets, each 3H, at 6.77 and 8.58; *m/e*: 297 (M^+), 48), 187 (5), 174 (17), 173 (5), 162 (12), 161 (80), 160 (100), 159 (6), 158 (5), 146 (23), 145 (10), 144 (12), 137 (6), 132 (8), 131 (6), 130 (12), 129 (6), 128 (7), 118 (7), 117 (13), 116 (7), 115 (12), 103 (7), 91 (13), 77 (10). *Anal.* calcd. for $C_{19}H_{23}NO_2$: C 76.76, H 7.74, N 4.71; found: C 76.8, H 7.8, N 4.7.

Diastereoisomer B—R_f 0.47 (24.7 mg) a colourless oil which failed to crystallise; ν_{max} ($CHCl_3$): identical with A; λ_{max} (EtOH): 253; λ_{infl} 280; τ ($CDCl_3$): 2.50–3.60 (m, 4H), 3.88–5.67 (m, 3H), 6.60–9.00 (complex absorption, 16H) including sharp singlets, each 3H at 6.74 and 8.73; *m/e*: 297 (M^+, 14), 174 (20), 173 (3), 162 (8), 161 (88), 160 (100), 144 (9), 132 (7), 130 (11), 117 (13), 91 (9), 77 (13). *Exact Mass* calcd. for $C_{19}H_{23}NO_2$: 297.1729; found: 297.1728.

1,3-Dimethyl-3-(2'-keto-3'-ethanalylcyclohexyl)oxindole (33)

The diastereoisomeric mixture of compound **32** (1.2 g) was dissolved in dry methanol (15 mL) and an ozone–oxygen mixture bubbled through the solution at −30°C for 40 min. The reaction mixture was cooled to −60°C and the system purged with nitrogen for 15 min before addition of dimethyl sulphide (6 mL). The colourless solution was allowed to warm to room temperature gradually over a period of 2 h before distillation of the solvent at the pump. The residual yellow oil was partitioned between water (25 mL) and ether (4 × 25 mL). The combined ethereal solutions were extracted first with water (10 mL) and then with 5% sodium bicarbonate solution (3 × 10 mL). The basic extracts were acidified with concentrated hydrochloric acid at 0°C and ether extracted (3 × 25 mL). The two ethereal solutions gave *a* and *b* respectively.

(*a*) Nonacidic material (898 mg) identified as being a diastereoisomeric mixture of **33** (75%). Preparative tlc (S/*B*) on the mixture (105 mg) gave the following.

Diastereoisomer A—R_f 0.30 (49.6 mg), a pale yellow oil; ν_{max} ($CHCl_3$): 3410 (w), 2730 (m), 1720 (s), 1705 (s), 1695 cm^{-1} (s); λ_{max} (EtOH); 253.5, λ_{infl} 279; τ ($CDCl_3$): 0.25 (s, 0.85H) 2.35–3.30 (m, 4H), 6.60–8.70 (complex absorption, 18H) including sharp singlets, each 3H, at 6.76 and 8.58; *m/e*: 299 (M^+, 21), 271 (<1), 174 (12), 162 (12), 161 (100), 160 (99), 146 (5), 132 (8), 130 (7), 121 (23), 118 (5), 117 (8), 111 (7), 91 (8), 77 (8). *Exact Mass* calcd. for $C_{18}H_{21}NO_3$: 299.1521; found: 299.1554.

Diastereoisomer B—R_f 0.17 (42.5 mg) a pale yellow foam; ν_{max} ($CHCl_3$) identical with A with the exception of 3410 (m), 2730 cm^{-1} (w); λ_{max} (EtOH): 252.5 (ε 9310), λ_{infl} 278.5 (ε 1830); τ ($CDCl_3$): 0.39 (br s, 0.6H), 2.60–3.30 (m, 4H), 6.65–8.90 (complex absorption, 18H) including sharp singlets, each 3H, at 6.78 and 8.72; *m/e*: 299 (M^+, 25), 271 (<1), 174 (15), 162 (7), 161 (68), 160 (100), 117 (5), 85 (5), 83 (8). *Exact Mass* calcd. for $C_{18}H_{21}NO_3$: 299.1521; found: 299.1557.

(*b*) The carboxylic acid corresponding to **33** (136.7 mg, 11%) and running as two spots on tlc R_f 0.21 and 0.32, S/*B*); *m/e*: 315 (M^+, 8), 300 (4), 299 (8), 177 (12), 174 (17), 162 (12), 161 (83), 160 (100), 132 (21), 130(17), 118 (12), 117 (21), 91 (38), 77 (29). *Exact Mass* calcd. for $C_{18}H_{21}NO_4$: 315.1521; found: 315.1522.

1,3-Dimethyl-3-(4',5',6',7'-tetrahydroindol-7'-yl)oxindole (34)

The keto aldehyde **33** (105 mg) was dissolved in 95% ethanol (5 mL) and saturated aqueous ammonium carbonate solution (5 mL) added. The mixture was refluxed under nitrogen with periodic addition of solid ammonium carbonate (200 mg) over 1 h. The aqueous ethanol was distilled off at the pump and the residue partitioned between water (10 mL) and ethyl acetate (4 × 10 mL). The combined organic extracts gave a pale yellow foam which was identified as being predominantly a diastereoisomeric mixture of **34** (91% yield). Preparative tlc (S/*B*) of 25 mg of the mixture under nitrogen atmosphere gave diastereoisomers A and B.

Diastereoisomer A—R_f 0.5 (1.7 mg), colourless crystals, mp 157.5–158.5°C; ν_{max} ($CHCl_3$): 3440 (w), 3300 (m), 1690 cm^{-1} (s); λ_{max} (EtOH): 253 (ε 7010), λ_{infl} 279 (ε 1590); τ ($CDCl_3$): 0.25–0.85 (br s, 1H) fails to exchange with D_2O, 2.50–3.35 (m, 4H), 3.34 (t, J = 2.4 Hz, 1H), 4.02 (t, J = 2.4 Hz, 1H), 6.60–7.40 (m, 4H) including 3H singlet at 6.79, 7.40–7.90 (6m, 2H), 7.90–8.80 (6m, 7H) including a 3H singlet at 8.65; *m/e*: 280 (M^+, 4), 161 (14), 160 (5), 146 (7), 121 (11), 120 (100), 119 (5), 118 (20), 117 (5), 103 (8), 91 (7), 77 (5). *Anal.* calcd. for $C_{18}H_{20}N_2O$ (280.1576): C 77.2, H 7.2, N 10.0; found (280.1574): C 77.7, H 7.2, N 9.7.

Diastereoisomer B—R_f 0.45 (4.0 mg), a colourless oil; ν_{max} ($CHCl_3$) identical with that of A, with the exception of 3440 cm^{-1} (m) and the absence of 3300 cm^{-1}; λ_{max} (EtOH): 254: λ_{infl}: 280; τ ($CDCl_3$): 1.91–2.41 (br s, 1H) fails to exchange with D_2O, 2.00–3.35 (m, 4H), 3.55 (t, J = 2.4 Hz,1H), 4.20 (t, J = 2.4 Hz, 1H), 6.78 (s, 3H), 7.35–8.40 (complex absorption, 6H), 8.52 (s, 3H); *m/e*: 280 (M^+, 4) 161 (3), 160 (6), 121 (11), 120(100), 119 (3), 118 (10), 117 (4), 105 (3), 103 (6), 93 (3), 91 (4), 77 (4). *Exact Mass* calcd. for $C_{18}H_{20}N_2O$: 280.1576; found: 280.1560.

1,3-Dimethyl-3-(2'-carbomethoxy-4',5',6',7'-tetrahydro-7'-indolyl)oxindole (36)

The tetrahydroindole **34** (56 mg, 0.2 mmol) was dissolved in dry ethanol-free chloroform (2 mL) and added to a mixture of trichloroacetyl chloride (46 mg, 0.25 mmol) and anhydrous potassium carbonate (138 mg, 1.0 mmol) in similarly purified chloroform (2 mL) over 20 min. After stirring for a further 25 min, the solid was filtered from the deep red suspension and the filter cake washed with chloroform (2 × 5 mL) and water (2 × 10 mL) and the solvent removed at the pump to give an orange brown foam (72.4 mg). This was dissolved in methanol (5 mL) and added to a methanolic solution of sodium methoxide (from sodium (5.5 mg) and methanol (1.2 mL)) and stirred for 5 min. The methanol was removed at the pump and the orange-red residual oil partitioned between water (10 mL) and ethyl acetate (1 × 10 mL, 2 × 5 mL). The organic phase gave an orange-red oil (57.6 mg) which after dissolving in benzene and treating with charcoal to remove polar material resulted in an orange oil (44.4 mg). Isolation of the material running at R_f 0.4 (S/*B*) by preparative tlc afforded the ester **36** as a white foam (21.8 mg, 38% yield); λ_{max} (EtOH): 255, 282,5; τ ($CDCl_3$): −0.20 (br s, 0.5H), 2.40–3.5 (m, 5H), 6.18 (s, 3H), 6.30–8.75 (complex absorption, 10H) including 3H singlets at 6.80 and 8.60; *m/e*: 338 (M^+, 2) 307 (2), 279 (2), 178 (100), 160 (11), 146 (49), 130 (7), 118 (20), 117 (14), 91 (38).

1,3-Dimethyl-3-(2′-carbomethoxy-7′-indolyl)oxindole (37)

The tetrahydroindole ester **36** (3.1 mg, 9.2×10^{-3} mmol) was dissolved in benzene (1 mL) and heated to reflux under nitrogen. A solution of DDQ (4.2 mg, 1.84×10^{-2} mmol) in benzene was added dropwise over 5 min and the yellow solution refluxed for 1.5 h during which time a brown precipitate formed and the solution became virtually colourless. Ethyl acetate (10 mL) was added to the cooled reaction mixture and the solution extracted with dilute aqueous sodium bicarbonate solution (3×5 mL) and water (2×5 mL). The organic phase (an orange oil) (4.6 mg), on charcoal treatment in benzene solution, afforded a colourless oil (2.7 mg). Isolation of the material running at R_f 0.58 (S/*B*) by preparative tlc gave the pure indole ester **37** (2.5 mg, 81% yield) as a colourless oil; λ_{max} (EtOH): 232, 252.5, 292; *m/e*: 334 (M^+, 100), 320 (20), 319 (84), 288 (11), 287 (50), 259 (29), 160 (13), 91 (18). *Anal.* calcd. for $C_{20}H_{18}N_2O_3$: 334.1317; found: 334.1308.

Methylation of 3-(2′-Hydroxycyclohexyl)-1-benzyloxindole (7)

A solution of **7** (100 mg, 0.031 mmol) in anisole (0.75 mL) under N_2 was treated with a solution of *n*BuLi (40 mg, 0.0625 mmol) in hexane (0.55 mL). After stirring at 20°C for 10 min, a large excess of methyl iodide (3 mL) was added and the mixture refluxed for 30 min and left at 20°C for 62 h. The anisole was distilled off under reduced pressure and the residue partitioned between ether and water. The extract gave a yellowish brown viscous liquid (83 mg). Preparative-layer chromatography of 75 mg (S′/*B*) gave two products.

(a) 3-(2′-Methoxycyclohexyl)-1-benzyl-3-methyloxindole (45, R = R′ = CH_3)

This compound, R_f 0.61 (22 mg), was isolated as white crystals, mp 120.5–122.5°C after three crystallisations from 60–80°C petrol; τ ($CDCl_3$): 2.5–3.5 (m, 9H), 4.89 (d, J = 15 Hz, 0.9H), 5.48 (d, J = 15 Hz, 0.9H), 7.55 (s, 3H, the high-field shift for this methoxyl is due to shielding by the oxindole benzene ring), 7.5–9.2 (complex absorption, 16H) including a 3H singlet at 8.75; *m/e* 349 (M^+, 3), 237 (77), 113 (14), 91 (100).

(b) 3-(2′-Hydroxycyclohexyl)-1-benzyl-3-methyloxindole (45, R = H, R′ = CH_3)

This compound, R_f 0.37 (24 mg), was isolated as white crystals, mp 146–149°C after crystallisation from 60–80 petrol; τ ($CDCl_3$): 2.5–3.5 (m, 9H), 5.02 (d, J = 16 Hz, 1H), 5.24 (d, J = 16 Hz, 1H), 6.7–9.0 (complex absorption, 26H) including a 3H singlet at 8.65; *m/e*: 335 (M^+, 43), 250 (30), 237 (100), 159 (13), 146 (10), 91 (100). *Anal.* calcd. for $C_{22}H_{25}NO_2$: C 78.82, H 7.45, N 4.18; found: C 79.0, H 7.6, N 4.1.

Acknowledgement

We thank the S.R.C. for maintenance grants (P.K.B. and D.L.C.).

1. E. F. L. J. Anet. Ph.D. Thesis, Sydney. 1949; E. F. L. J. Anet, G. K. Hughes, and E. Ritchie. Aust. J. Chem. **14**, 173 (1961).
2. R. Atitullah. Ph.D. Thesis, Manchester. 1966; 4th Int. Symp. Chem. Nat. Products, Stockholm. 1966. p. 84.
3. J. Fridrichson, M. F. Mackay, and A. McL. Mathieson. Tetrahedron Lett. 3521 (1967); Tetrahedron, **30**, 85 (1974).
4. K. P. Parry. Ph.D. Thesis, Manchester. 1968; K. P. Parry and G. F. Smith. J. Chem. Soc. Perkin I, 1671 (1978).
5. J. B. Hendrickson, R. Goschke, and R. Rees. Proc. Chem. Soc. 383 (1962); Tetrahedron, **20**, 565 (1964).
6. A. I. Scott, F. McCapra, and E. S. Hall. J. Am. Chem. Soc. **86**, 302 (1964); Tetrahedron, **23**, 4131 (1967).
7. T. Hino and S. Yamada. Tetrahedron Lett. 1757 (1963).
8. T. Hino, S. Kodato, K. Takahashi, H. Yamaguchi, and M. Nakagawa. Tetrahedron Lett. 4913 (1978).
9. R. B. Longmore and B. Robinson. Coll. Czech. Chem. Commun. **32**, 2184 (1967).
10. A. A. Paulic and H. Adkins. J. Am. Chem. Soc. **68**, 1471 (1946).
11. H. Falk, O. Hofer, and H. Lehner. Monatsh. Chem. **104**, 925 (1973).
12. K. T. Potts and J. E. Saxton. J. Chem. Soc. 2641 (1954).
13. G. L. Papayan and L. S. Galstyan. Arm. Khim. Zh. **27**, 963 (1972).
14. R. Duschinsky. U.S. Patent No. 2,642,438 (June 16, 1953); Chem. Abstr. **48**, 5230c (1954).
15. T. Kato and K. Sato. Chem. Abstr. **68**, 95285n (1968).
16. H. O. House. Modern synthetic reactions. 2nd ed. W. A. Benjamin Inc., Menlo Park, CA. 1972.
17. E. Piers and R. K. Brown. Can. J. Chem. **40**, 559 (1962).
18. W. E. Savigi and A. Fontana. J. Chem. Soc. Chem. Commun. 599 (1976).
19. E. W. Garbisch, Jr. J. Org. Chem. **30**, 2109 (1965); K. Shank and W. Pack. Chem. Ber. **102**, 1892 (1969).
20. W. S. Johnson and H. Posvic. J. Am. Chem. Soc. **69**, 1361 (1947); S. M. Mukherji and N. K. Bhattacharyya. J. Org. Chem. **17**, 1202 (1952).
21. J. J. Pappas, W. P. Keaveney, E. Gaucher, and M. Berger. Tetrahedron Lett. 4273 (1966).
22. P. Bruni. Ann. Chim. (Rome), **57**, 376 (1967).
23. E. Giovannini and J. Rosales. Helv. Chim. Acta, **46**, 1332 (1963).

Pseudozoanthoxanthins from gold coral[1]

ROBERT E. SCHWARTZ, MARK B. YUNKER,[2] AND PAUL J. SCHEUER
Department of Chemistry, University of Hawaii at Manoa, Honolulu, HI 96822, U.S.A.
AND
TOR OTTERSEN
Department of Chemistry, University of Oslo, Blindern, Oslo 3, Norway

Received December 28, 1978

ROBERT E. SCHWARTZ, MARK B. YUNKER, PAUL J. SCHEUER, and TOR OTTERSEN. Can. J. Chem. **57**, 1707 (1979).

From a deep water Pacific zoanthid, *Gerardia* sp., we have isolated two new fluorescent nitrogenous pigments, derivatives of tetrazacyclopentazulene. The first was characterized by uv, ^1H and ^{13}C nmr data, and by X-ray diffraction; the second by interconversion.

ROBERT E. SCHWARTZ, MARK B. YUNKER, PAUL J. SCHEUER et TOR OTTERSEN. Can. J. Chem. **57**, 1707 (1979).

On a isolé, d'un zoanthide provenant des profondeurs du Pacifique, *Gerardia* sp., deux nouveaux pigments fluorescents contenant de l'azote et dérivés du tétrazacyclopentazulène. On en a caractérisé un par uv, par rmn du ^1H et du ^{13}C et par diffraction de rayon-x; la structure du second a été établie par interconversion.

[Traduit par le journal]

A spectacular feature of tropical coral reefs is the brilliant coloration of its fauna. Yet surprisingly, aside from a number of novel carotenoids (1) and quinones (2, 3), and the unconventional chlorin bonellin (4), so far only one group of pigments belonging to an entirely new structural type has been reported. These pigments are tetrazacyclopentazulenes or zoanthoxanthins which were first isolated in 1973 from Mediterranean zoanthids (Coelenterata, Anthozoa, Zoantharia ≡ Hexacorallia) by Prota and co-workers (*5a–e*), and subsequently by a Japanese group from the Sagami Bay coelenterate *Parazoanthus gracilis* (6). Discovery of the linear zoanthoxanthin (**1**) and the angular pseudozoanthoxanthin (**2**) skeletons led Prota and co-workers to speculate (*5d*) that the biogenesis of these pigments might involve dimerization of two arginine-derived C_5N_3 units. Büchi and co-workers (*7a, b*) based their ingenious biomimetic synthesis of the two ring systems (**1**, **2**, R,R′ = H) on an oxidative coupling reaction of two suitably functionalized C_5N_3 moieties.

Inspection of formulas **1** and **2** shows that the angular skeleton may lead to a third structural type, **3**. In a preliminary communication (8) we reported isolation of the first member of this new series from gold coral, which is a deep water (−350 m) *Gerardia* sp.[3] The structure of this metabolite is entirely consistent with the suggested C_5N_3 biogenetic building blocks of these pigments. In this paper we present the details of this investigation, including the structure of a second member having skeletal type **3**.

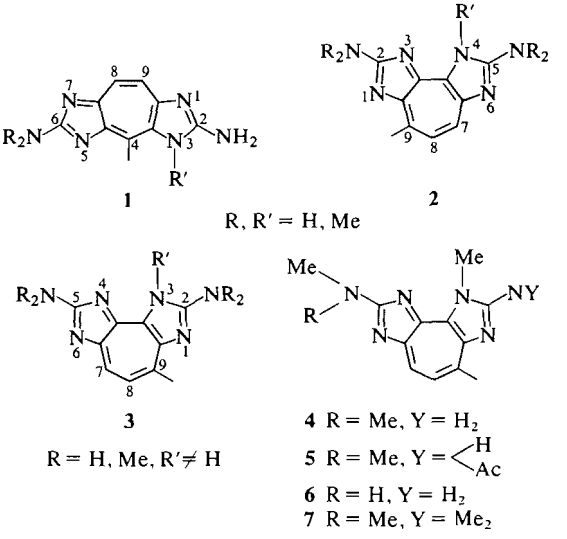

1 **2**

R, R′ = H, Me

3

R = H, Me, R′ ≠ H

4 R = Me, Y = H_2
5 R = Me, Y = <H/Ac
6 R = H, Y = H_2
7 R = Me, Y = Me_2

In Hawaii, a precious coral fishery is maintained in part by a minisubmarine operating at depths ranging to −350 m. We first became interested in the organic constituents of one of these corals, *Gerardia*

[1]Dedicated to the memory of R. H. F. Manske.

[2]NRCC Postdoctoral Fellow, 1975–1977. Present address: Department of Chemistry, University of Victoria, Victoria, B.C., Canada V8W 2Y2.

[3]In our preliminary communication (8) the animal was erroneously referred to as *Parazoanthus* sp. These corals are currently being examined at the U.S. National Museum by K. Muzik.

0008-4042/79/131707-05$01.00/0

5	MeOH	425(4.12)	306(4.22)	289(4.22)	259(4.31)	224(4.21)
5	MeOH—H^+	419(4.23)	291(4.35)		257(4.18)	226(4.18)

TABLE 1. Ultraviolet data of the 3*H* pseudozoanthoxanthins and derivatives

Compound	Solvent	Wavelength, nm (log ε)					
4	MeOH	416(4.18)	377(4.00)	317 sh (4.49)	306(4.59)	261(4.02)	226(4.02)
4	MeOH–H^+	414(4.32)	359(3.74)		298(4.61)	249(4.07)	241(4.02)
5	MeOH	414(4.14)			306(4.56)	261(4.04)	226(3.96)
5	MeOH–H^+	415(4.26)			298(4.53)	248(3.98)	216(4.02)
6	MeOH	409(4.07)	371(4.00)	310 sh (4.59)	300(4.65)	256(4.03)	224(4.12)
6	MeOH–H^+	407(4.24)	363(3.85)		302(4.72)	247(3.96)	221(4.09)
7	MeOH	420(3.75)	373(3.45)		314(4.07)	262(3.48)	218(3.82)

TABLE 2. Proton magnetic resonance data of 3*H* pseudozoanthoxanthins

Compound	Aromatic protons	NH_2	Nuclear N—Me	NHMe	NMe_2	C—Me	O ‖ C—Me
4[a]	8.29 1Hd, 8.04 1Hd J = 10 Hz		4.63 3Hs	3.42 3Hs	3.55 6H bs	2.96 3Hs	
4[b]	7.74 1Hd, 7.36 1Hd J = 11 Hz	7.29 2H bs[c]	4.30 3Hs		3.27 6Hs	2.69 3Hs	
5[b]	7.62 bs		4.26 3Hs		3.32 6Hs	2.82 3Hs	2.26 3Hs
6[a]	8.30 1Hd, 8.03 1Hd J = 11 Hz		4.62 3Hs	3.42 3Hs		2.99 3Hs	
7[a]	8.22 1Hd, 8.02 1Hd J = 11 Hz		4.60 3Hs		3.62 6Hs, 3.54 6Hs[d]	2.96 3Hs	

[a]In CF_3CO_2D δ = 0 ppm.
[b]In DMSO-d_6 δ = 0 ppm.
[c]D_2O exchangeable.
[d]Overlapping singlets.

sp., trivially named gold coral, because of the golden luster of its polished endoskeleton, since this coral was causing adverse reactions to the skin and mucous membranes of the workers who handled the freshly harvested coral with bare hands. We did not succeed in finding a suitable laboratory bioassay which would trace the bioactive constituent(s). We were, however, prompted by the strong fluorescence of the ethanolic extract of the animals to pursue research into the nature of the fluorescent compounds.

Purification of the fluorescent ethanolic extract by ion exchange, adsorption, and gel permeation chromatography yielded as the major constituent (**4**) an amorphous yellow powder, $C_{13}H_{16}N_6$, which decomposed at approximately 200°C, characterized further as an orange monoacetate (**5**), $C_{15}H_{18}N_6O$, mp 125–129°C. The minor component (**6**), also an amorphous yellow solid, $C_{12}H_{14}N_6$, decomposing at approximately 180°C could be converted into the major constituent (**4**) by reaction with methyl iodide in sodium – liquid ammonia.

The strong fluorescence and the biological origin of these compounds from *Gerardia* sp. led us to suspect that we might be dealing with zoanthoxanthin pigments (*vide supra*). Comparison of the uv spectra of our compounds (Table 1) with those reported for zoanthoxanthin (**1**) and pseudozoanthoxanthin (**2**) derivatives (8) convinced us that we were dealing with a new skeletal type.[4] The complexity of the spectra suggested that our compounds belonged to the angular (pseudo) series. The composition of the major constituent (**4**), $C_{13}H_{16}N_6$, indicated the presence of three additional carbons, shown by ^1H nmr data (Table 2) to be present as a

[4]The trivial nomenclature of these pigments has become unnecessarily complex. We should like to suggest simplification by omitting prefixes (*para*, *epi*) which denote methylation patterns and/or biological origin. Instead, we propose to call the linear system zoanthoxanthin (**1**) and the angular system pseudozoanthoxanthin (**2**) with numbering as shown. The position number of saturated nuclear nitrogen followed by *H* will distinguish among the major groups of zoanthoxanthins. Zoanthoxanthin (**1**, R, R′ = Me) becomes a 3*H* zoanthoxanthin, norpseudozoanthoxanthin (**2**, R = H, R′ = Me) becomes a 4*H* pseudozoanthoxanthin, and compounds of structural type **3** become 3*H* pseudozoanthoxanthins.

nuclear *N*-methyl singlet at δ 4.63 and two side-chain *N*-methyls appearing as a broad six-proton singlet at δ 3.55. A three-proton singlet at δ 2.96 and AB quartet for two aromatic protons, plus the ^{13}C nmr data (see Experimental) were equally compatible for a number of structures. X-ray diffraction of crystalline **4** monohydrate defined the structure as 2-amino-3,9-dimethyl-5-dimethylamino-3*H*-1,3,4,6-tetrazacyclopent[*e*]azulene and confirmed that we were dealing with a new series of angular zoanthoxanthins, i.e. pseudozoanthoxanthins.

The minor component (**6**), $C_{12}H_{14}N_6$, differed from **4** by a methyl group. ^1H nmr data, chiefly a three proton singlet at δ 3.42, were evidence for a methylamino substituent at C-2 or C-5. Methylation of **6** yielded three products. The major component was identical with **4** thereby proving unequivocally structure **6**, 2-amino-3,9-dimethyl-5-methylamino-3*H*-1,3,4,6-tetrazacyclopent[*e*]azulene. A second component was isolated as a yellow solid, $C_{15}H_{20}N_6$, decomposing at approximately 155°C, which was a trimethyl-**6** and is formulated as **7**, 2,5-bisdimethylamino-3,9-dimethyl-3*H*-1,3,4,6-tetracyclopent[*e*]azulene. A small amount of a third compound was not characterized.

An interesting aspect of this work relates to the longstanding question whether organic metabolites of marine coelenterates are synthesized by the animals or by the symbiotic zooxanthellae (9). Clearly, in our case, these nitrogenous pigments must be the products of the animals which live at a depth of −350 m, where no photosynthesis takes place.

Experimental

Apparatus, Methods, and Materials

Natural abundance ^{13}C nmr spectra were recorded on a Varian XL-100 Fourier transform spectrometer at 25.2 MHz. Field–frequency locking was provided by the deuterium signals of CF_3CO_2D and D_2O. ^1H nmr spectra were recorded on a Varian XL-100 nmr spectrometer at 100 MHz; TMS was used as an internal reference. Mass spectra were determined on a MAT 311 mass spectrometer at an ionizing voltage of 70 eV. A Beckman ACTA CIII spectrophotometer was used for the uv spectra. Melting points were taken on a Fisher-Johns apparatus. New England Nuclear silica gel OF 250 μ plates were used for all tlc examinations.

Isolation

Fresh animals (320 g) were soaked in 95% ethanol overnight and concentrated to a water layer of about 100 mL, which was diluted to approximately 350 mL, acidified to pH 1, and continuously extracted with CH_2Cl_2 overnight. This CH_2Cl_2 extract was discarded.

The resulting aqueous acidic layer was again diluted, to 1.5 L and passed through a Dowex 50W-4X cation exchange column. The column was then washed with 7 L of 1*N* HCl, followed by water until the eluant reached pH 6.

The top quarter of the column was removed and slurried with aqueous NH_3, to about 2 *N*. This suspension was then extracted twice with *n*BuOH and four times with $CHCl_3$–MeOH (4:3). All six extracts were combined and concentrated to yield 1.2 g dry residue.

This solid was chromatographed on silica gel with $CHCl_3$–MeOH – 25% aqueous NH_3 (80:20:2), which was followed by chromatography on Sephadex LH-20 with $CHCl_3$–MeOH (4:3) yielding about 900 mg of **4** and 60 mg of **6**.

2-Amino-3,9-dimethyl-5-dimethylamino-3H-1,3,4,6-tetraza-cyclopent[e]azulene (**4**)

Compound **4** was isolated as an amorphous yellow powder decomposing at ~200°C, R_f 0.61, $CHCl_3$–MeOH – 25% aqueous NH_3 (80:20:2); ^{13}C nmr (CF_3CO_2D): 153.67 (s), 150.68 (s), 149.09 (s), 139.06 (s), 137.47 (d), 136.85 (s), 130.16 (s), 121.88 (d), 39.37 (2q), 35.14 (q), and 23.51 (q) ppm. The ninth sp^2 carbon, which was obscured by the solvent absorbances in the CF_3CO_2D spectrum, was found at 160.57 (s) ppm in the D_2O spectrum of the dihydrochloride salt of **4**. Mass spectrum *m/e* 256 (67%, M^+), 241 (100%, $M^+ - CH_3$), 227 (70%, $M^+ - NCH_3$), 212 (17%, $M^+ - NMe_2$). *Exact Mass* calcd. for $C_{13}H_{16}N_6$: 256.143647; found: 256.14353. Compound **4** was crystallized from EtOH–H_2O (80:20) by adding a minimum amount of hot solvent and allowing it to stand overnight. Crystalline **4** also decomposed at approximately 200°C.

2-Acetylamino-3,9-dimethyl-5-dimethylamino-3H-1,3,4,6-tetrazacyclopent[e]azulene (**5**)

Acetylation of 20 mg of **4** with Ac_2O–pyridine yielded 10 mg of cyclopent[*e*]azulene (**5**) as an orange amorphous solid, mp 125–129°C, R_f 0.81, $CHCl_3$–MeOH – 25% aqueous NH_3 (80:20:2); *m/e*: 298 (58%, M^+), 283 (39%, $M^+ - CH_3$), 269 (36%, $M^+ - NCH_3$), 255 (22%, $M^+ - COCH_3$), 241 (100%), 227 (44%). *Exact Mass* calcd. for $C_{15}H_{18}N_6O$: 298.15423; found: 298.1523.

2-Amino-3,9-dimethyl-5-methylamino-3H-1,3,4,6-tetraza-cyclopent[e]azulene (**6**)

Compound **6** was isolated as an amorphous yellow solid decomposing at ~180°C, R_f 0.30, $CHCl_3$–MeOH – 25% aqueous NH_3 (80:20:2); *m/e* 242 (100%, M^+), 214 (43%, $M^+ - CNH_2$), 186 (36%). *Exact Mass* calcd. for $C_{12}H_{14}N_6$: 242.127997; found: 242.127770.

Methylation of 6

In 20 mL of liquid NH_3 and 45 mg of Na, 15.4 mg **6** was reacted with 1.5 mL of MeI to give 4.8 mg of a compound identical with **4** (uv, ms, nmr), 4.0 mg of **7**, and 2.6 mg of a compound not further characterized.

2,5-Bisdimethylamino-3,9-dimethyl-3H-1,3,4,6-tetraza-cyclopent[e]azulene (**7**)

Compound **7** was isolated as an oily yellow solid decomposing at ~115°C, R_f 0.71, $CHCl_3$–MeOH – 25% aqueous NH_3 (80:20:2); *m/e* 284 (100%, M^+), 269 (78%, $M^+ - CH_3$), 255 (42%, $M^+ - NCH_3$). *Exact Mass* calcd. for $C_{15}H_{20}N_6$: 284.174948; found: 284.17469.

X-ray Diffraction

Oscillation and Weissenberg diagrams indicated monoclinic symmetry, and the systematic absences were those characteristic of the space group $P2_1/c$. (Most of the crystals were twinned leading to a doubling of the *c* axis and orthorhombic symmetry.) A crystal of approximate dimensions 0.2 × 0.1 × 0.05 mm was used for the crystallographic work. A computer controlled Syntex $P\bar{1}$ diffractometer with graphite-monochromatized Mo K_α radiation was utilized in the determination of cell parameters and the collection of intensity data. Cell dimensions were determined by a least-squares treatment of the angular coordinates of 15 reflections with 2θ-values between 14° and 32°.

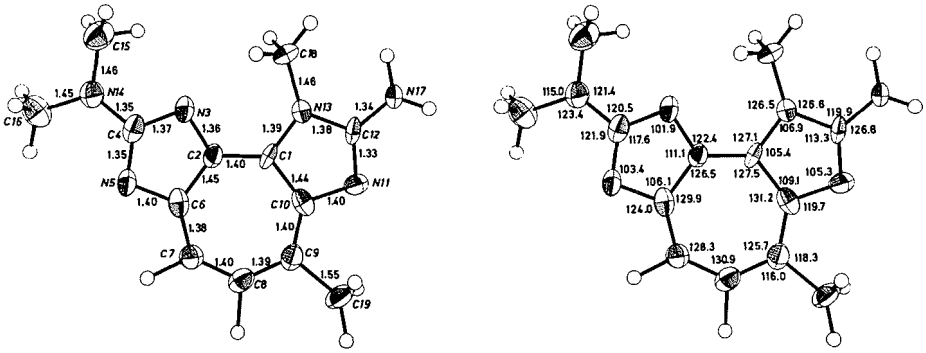

FIG. 1. Bond lengths (Å) and bond angles (°). The estimated standard deviations in bond lengths are 0.01 Å and in angles 0.8–0.10°. The ellipsoids are given for 50% probability, the hydrogens are drawn artificially small.

Three-dimensional intensity data were recorded using the θ-2θ scanning mode with scan speed (2θ) variable from 2 to 8° min^{-1} depending on the intensity of the reflection. Background counting time was equal to 0.35 × scan time on each side of the scan range, which was from $2\theta(\alpha_1) - 0.9°$ to $2\theta(\alpha_2) + 0.9°$. The temperature was maintained within 1° at 19°C. The intensities of three standard reflections which were remeasured regularly showed no significant variations.

The estimated standard deviations in the net intensities, I, were calculated as:

$$\sigma(I) = \left(I_{scan} + (B_1 + B_2)\left(\frac{\text{scan time}}{2 \times \text{background time}}\right)^2 + (0.02 \times I)^2\right)^{1/2}$$

where

$$I = I_s - (B_1 + B_2)\frac{\text{scan time}}{2 \times \text{background time}}$$

The factor 0.02 × I is an addition for experimental uncertainties. Of the 1271 reflections measured ($2\theta_{max} = 40°$) 757 had intensities larger than twice their standard deviations. These were regarded as observed, and the remaining were excluded from the refinements. The intensities were corrected for Lorentz and polarization effects. The computer program used, as well as programs subsequently employed, is part of a local assembly of programs for CYBER-77 which is described in ref. 10.

Atomic scattering factors used were those of Doyle and Turner (11) for carbon, nitrogen, and oxygen and of Stewart *et al.* (12) for hydrogen. The phase problem was solved by the MULTAN 77 program package (13). The structure model was refined to a conventional R of 0.24. Owing to this relatively high R-factor a difference Fourier synthesis was calculated and this revealed the position of an oxygen atom (H_2O). The water molecule was situated such that it participated in three hydrogen bonds. The introduction of anisotropic temperature factors for all 20 nonhydrogen atoms and least-squares refinements lowered R to 0.096. The positions of the 18 hydrogens were found in a difference Fourier synthesis. These were included with estimated isotropic thermal parameters in the structure factor calculations. Full-matrix least-squares refinement of all nonhydrogen parameters converged to an R of 0.075 and an R_w of 0.058. Final atomic parameters are given in Table 3.[5] A list of observed and calculated structure factors may be obtained from the authors upon request.

Crystal Data for 2-amino-3,9-dimethyl-5-dimethylamino-3*H*-1,3,4,6-tetracyclopent[*e*]azulene monohydrate.

$C_{13}H_{16}N_6 \cdot H_2O$ $M = 274.33$ amu

Space group $P2_1/c$, $a = 11.111(5)$ Å, $b = 16.567(12)$ Å, $c = 7.368(2)$ Å, $\beta = 98.32°(3)$, $V = 1342.0(12)$ Å^3, $Z = 4$, $D_{calcd} = 1.357$ g cm^{-3}, $F(000) = 584$.

Description of the Structure

The molecular structure and atomic numbering is shown in Fig. 1, where bond lengths and bond angles are also listed. The molecule is planar; deviations from a least-squares plane through all nonhydrogen atoms are given in Table 4.[5] The maximum deviation is only 0.1 Å for N17. The bond lengths and the planarity of the system imply a totally aromatic molecule. The double bond character varies from 0.33(6) to 0.76(6). (Double bond character is calculated in the standard way as p from bond length = single bond length − 0.18 p.)

The water molecule participates in three hydrogen bonds, which leads to a three-dimensional net of hydrogen bonding in the crystal. Hydrogen bond parameters are as follows: 020-H202-N5 (in position: $1 - x$, $0.5 + y$, $1.5 - z$), 020-N5: 2.89(1) Å; 020-H201-N5 ($1 - x$, $1 - y$, $1 - z$), 020-N5: 3.01(1) Å; N17-H172-020 ($1 + x$, $0.5 - y$, $0.5 + z$), N17-020: 2.99(1) Å.

[5]Photocopies of Tables 3 and 4 may be obtained, at a nominal charge, upon request from the Depository of Unpublished Data, CISTI, National Research Council of Canada, Ottawa, Ont., Canada K1A 0S2.

Acknowledgments

We thank Bo Bartko and Maui Divers Inc. for collecting samples of gold coral; Richard W. Grigg and Katy Muzik for identifying the animal; and the National Science Foundation for financial support.

1. S. LIAAEN-JENSEN. *In* Marine natural products: chemical and biological perspectives. Vol. 2. *Edited by* P. J. Scheuer. Academic Press, New York, NY. 1978.
2. G. PROTA, M. D'AGOSTINO, and G. MISURACA. J. Chem. Soc. Perkin Trans. 1, 1614 (1972).
3. R. T. LUIBRAND, T. R. ERDMAN, J. J. VOLLMER, P. J. SCHEUER, J. FINER, and J. CLARDY. Tetrahedron. In press.
4. A. PELTER, J. A. BALLANTINE, V. FERRITO, V. JACCARINI, A. F. PSAILA, and P. J. SCHEMBRI. J. Chem. Soc. Chem. Commun. 999 (1976).
5. (*a*) L. CARIELLO, S. CRESCENZI, G. PROTA, F. GIORDANO, and L. MAZZARELLA. J. Chem. Soc. Chem. Commun. 99

(1973); (*b*) L. CARIELLO, S. CRESCENZI, G. PROTA, S. CAPASSO, F. GIORDANO, and L. MAZZARELLA. Tetrahedron, **30**, 3281 (1974); (*c*) L. CARIELLO, S. CRESCENZI, G. PROTA, and L. ZANETTI. Tetrahedron, **30**, 6611 (1974); (*d*) L. CARIELLO, S. CRESCENZI, G. PROTA, and L. ZANETTI. Experientia, **30**, 849 (1974); (*e*) L. CARIELLO, S. CRESCENZI, G. PROTA, and L. ZANETTI. Tetrahedron, **30**, 4191 (1974).

6. Y. KOMODA, S. KANEKO, M. YAMAMOTO, M. ISHIKAWA, A. ITAI, and I. ITAKE. Chem. Pharm. Bull. **23**, 2464 (1975).
7. (*a*) M. BRAUN and G. BÜCHI. J. Am. Chem. Soc. **98**, 3049 (1976); (*b*) M. BRAUN, G. BÜCHI, and D. F. BUSHLEY. J. Am. Chem. Soc. **100**, 4208 (1978).
8. R. E. SCHWARTZ, M. B. YUNKER, P. J. SCHEUER, and T. OTTERSEN. Tetrahedron Lett. 2235 (1978).
9. L. S. CIERESZKO and T. B. K. KARNS. *In* Biology and geology of coral reefs. Vol. 2. Biology 1. *Edited by* O. A. Jones and R. Endean. Academic Press, New York, NY. 1973.
10. P. GROTH. Acta Chem. Scand. **27**, 1837 (1973).
11. P. A. DOYLE and P. S. TURNER. Acta Crystallogr, Sect. A, **24**, 390 (1968).
12. R. F. STEWART, E. R. DAVIDSON, and W. T. SIMPSON. J. Chem. Phys. **42**, 3175 (1965).
13. G. GERMAIN, P. MAIN, and M. M. WOOLFSON. Acta Crystallogr. Sect. A, **27**, 368 (1971).

The formation and interconversion of oxazines and dioxazines from the reaction of nitrosocarbonyl compounds with cyclopentadienes[1]

LÊ H. DAO,[2] JULIAN M. DUST,[3] DONALD MACKAY, AND KENNETH N. WATSON

The Guelph–Waterloo Centre for Graduate Work in Chemistry, Waterloo Campus, Department of Chemistry, University of Waterloo, Waterloo, Ont., Canada N2L 3G1

Received October 5, 1978

LÊ H. DAO, JULIAN M. DUST, DONALD MACKAY, and KENNETH N. WATSON. Can. J. Chem. **57**, 1712 (1979).

The nitrosocarbonyl arenes or -alkanes, obtained by oxidation of hydroxamic acids, behave as dienophiles towards cyclopentadiene to give the bridged oxazines **1**. In the case of pivalohydroxamic acid, however, the nitrosocarbonyl compound also reacts as a heterodiene, giving, as well as the oxazine **1***d*, the 1,4,2-dioxazine **2***d*; **1***d* is not converted into **2***d* under the conditions of the oxidation reaction.

Extended heating of compounds **1** slowly converts them into **2** and other more complex reaction products. This contrasts with the rapid and quantitative isomerization of the analogous azodicarbonyl adducts, and probably reflects the lesser crowding of the reacting NCOR group by an adjacent oxygen than by an adjacent NCOR group.

1,4-Dimethyl-2,3-diphenylcyclopentadiene traps the nitroso compounds to form the labile oxazines **8**, which rapidly isomerize to the dioxazines **9** on brief heating or in polar solvents. In the case of the benzoyl compound **8***a* the isomerization to **9***a* is reversible in benzene at 80°C, favouring the latter isomer by a factor of about 9:1.

LÊ H. DAO, JULIAN M. DUST, DONALD MACKAY et KENNETH N. WATSON. Can. J. Chem. **57**, 1712 (1979).

Les nitrosocarbonyl-arènes ou -alcanes, obtenus par oxydation d'acides hydroxamiques, se comportent comme des diénophiles vis-à-vis le cyclopentadiène et conduisent aux oxazines pontées **1**. Toutefois dans le cas de l'acide pivalohydroxamique, le composé nitrosocarbonyle réagit aussi comme une hétérodiène fournissant en plus de l'oxazine **1***d*, l'oxadiazine-1,4,2 (**2***d*); on ne peut pas transformer **1***d* en **2***d* dans les conditions utilisées pour la réaction d'oxydation.

Par chauffage prolongé, **1** se transforme lentement en **2** et d'autres produits de réaction plus complexes. Ceci est en opposition avec l'isomérisation rapide et quantitative des adduits azidocarbonyle analogues et reflète probablement un encombrement moindre du groupe NCOR qui réagit par un oxygène voisin plutôt que par un groupe NCOR.

Le diméthyl-1,4 diphényl-2,3 cyclopentadiène piège les composés nitroso pour former des oxazine labiles **8** qui s'isomérisent rapidement en dioxazines **9** lorsqu'on les chauffe brièvement ou lorsqu'on les place dans des solvants polaires. Dans le cas du composé benzoyle **8***a*, l'isomérisation en **9***a* est reversible dans le benzène à 80°C favorisant le dernier isomère par un facteur d'envirion 9:1.

[Traduit par le journal]

The formation of *C*-nitrosocarbonyl compounds (RCONO) as intermediates in the oxidation of hydroxamic acids (RCONHOH) has for some time been suspected (1) and has now been confirmed (2, 3) by their addition reactions with thebaine and other dienes. The analogous *O*-nitrosocarbonyl compounds (ROCONO) can also be produced, by oxidation of *N*-hydroxyurethanes (ROCONHOH), and behave similarly (4). These intermediates form in part the subject of a recent review by Kirby (5).

In principle two kinds of Diels–Alder adducts with a diene are possible, as illustrated for cyclopentadiene and a *C*-nitrosocarbonyl compound. In path *i*, RCONO acts as a heterodienophile to give a bridged bicyclic 1,2-oxazine **1** (4 + 2 mode) and in path *ii* it acts as a heterodiene to give a fused bicyclic 1,4,2-dioxazine **2** (2 + 4 mode); in the latter reaction a regioisomer is of course possible. Normally only the product of path *i* is produced. However from the reaction of nitrosocarbonylbenzene with ergosteryl acetate both types of B-ring adduct were isolated but it was shown that the dioxazine arose, not by path *ii* but by partial isomerization of the oxazine formed in path *i* (3).

The isomerization of the oxazine to the dioxazine, formally a [3,3]-sigmatropic rearrangement, has analogies in other heterocyclic systems. A clear general example is the conversion of the adducts **3** of

[1]This paper is dedicated to the memory of Dr. R. H. F. Manske.

[2]Present address: Department of Chemistry, York University, Downsview, Ont., Canada M3J 1P3.

[3]Present address: Department of Chemistry, Mount Allison University, Sackville, N.B., Canada E0A 3C0.

0008-4042/79/131712-08$01.00/0

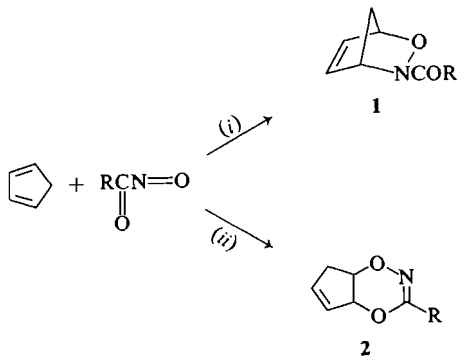

a R = Ph
b R = *p*BrC$_6$H$_4$
c R = *p*NO$_2$C$_6$H$_4$
d R = C(CH$_3$)$_3$

azodicarbonyl compounds into the 1,3,4-oxadiazines **4**, which we have studied in some detail (6). This process is especially favourable with the adducts of cyclopentadiene, **5** → **6**, and prompted us to prepare and to examine the stability of a number of adducts of nitrosocarbonyl arenes and -alkanes with cyclopentadiene and with 1,4-dimethyl-2,3-diphenylcyclopentadiene.

In a preliminary report we showed that generally oxazines only are formed from cyclopentadiene and dioxazines only from dimethyldiphenylcyclopentadiene (7). A notable exception was the oxidation of pivalohydroxamic acid in the presence of cyclopentadiene from which reaction both types of adduct were isolated and we concluded that in this case *both* paths were being utilized.

The synthesis and properties of these and related adducts are now described in more detail. Firm proof is provided of the independent occurrence of path *ii* in the oxidation of pivalohydroxamic acid in the presence of cyclopentadiene. It is confirmed that the thermal isomerization of the oxazine to the dioxazine (3) does occur, in general, for the adducts of cyclo-

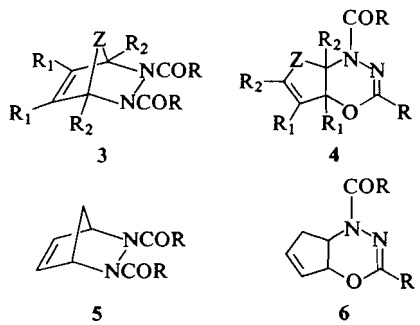

a R = Ph
b R = *p*BrC$_6$H$_4$
c R = *p*NO$_2$C$_6$H$_4$
d R = C(CH$_3$)$_3$

TABLE 1. Properties of 3-acyl-2,3-oxazabicyclo[2.2.1]hept-5-enes (**1** and **8**)

Compound	Melting point (°C)*	ν(CCl$_4$) (cm^{-1}) C=O	τ (ppm)† $H_{5,6}$	$H_{1,4}$ or $Me_{1,4}$	H_7	Aryl or other	Formula	Analysis C Calcd.	C Found	H Calcd.	H Found	N Calcd.	N Found
1*a*	73–75.5(a)	1658	3.30, 3.68	4.63, 4.78	7.91, 8.22d	2.0–2.3(2H), 2.4–2.8(3H)(f)	$C_{12}H_{11}NO_2$	71.63	71.74	5.51	5.65	6.96	7.02
1*b*	83–83.5(b)	1654	3.46, 3.58	4.65(2H)	7.90, 8.14	2.18, 2.35, 2.38	$C_{12}H_{10}BrNO$	51.45	51.62	3.60	3.65	5.00	5.11
1*c*‡	119.5–121(c)	1660	3.33, 3.57	4.57(2H)	7.85, 8.05d	2.55(q, 4H)(g) 1.66, 1.83, 1.98	$C_{12}H_{10}N_2O_4$	58.54	58.62	4.09	4.17	11.38	11.11
1*d*	37–38(d)	1643	3.43, 3.73	4.77(2H)	8.06, 8.28	2.15(q, 4H)(g) 8.93(s, 9H, CMe_3) (f)	$C_{10}H_{15}NO_2$	66.27	65.97	8.34	8.35	7.73	7.95
			3.96, 4.42	5.05, 5.62	8.60, 9.06 (ABq)	8.95(s, 9H, CMe_3) (h)							
8*a*	96.5–97(e)	1653		8.00, 8.40	7.73, 7.83 (ABq)	2.0–2.5(2H), 2.5–3.2(8H), 2.78 (s, 5H)(g)	$C_{26}H_{23}NO_2$	81.86	81.53	6.08	6.40	3.67	3.71
				7.88, 8.64	7.99, 8.30 (ABq)	1.7–2.0(2H), 2.2–2.5(2H), 2.6–3.2(6H), 3.07 (s, 5H)(h)							

*Crystallization from: (a) hexane; (b) acetone–isooctane; (c) benzene–isooctane; (d) pentane; (e) ether–hexane.
†τ values separated by a dash are at the extremes of the absorption. All absorptions are multiplets unless otherwise stated. *J* values for the C7-methylene are all 9 Hz. Solvents: (f) CCl_4; (g) $CDCl_3$; (h) C_6D_6.
‡λ_{max} (EtOH): 264 nm (ε 12 000).

TABLE 2. Rate constants of reaction (k) at 80°C of adducts of cyclopentadiene with nitrosocarbonylarenes (**1**) and with azodiaroyls (**5**), and yields of isomerization products **2** and **6***

Adduct	10^6k (s^{-1})			Yield of isomer **2** or **6** (%)
	Benzene	Isooctane	Ethanol	
1*a*	2.3			45
1*b*	2.1			44
1*c*	4.4			68
1*d*	2.9			10
5*a*		242	325	100
5*b*			867	100
5*c*			2250	100
5*d*		9700	9800	100

*The kinetic analysis on compounds **1***a–d* was carried out by integration of appropriate peaks in the ^{1}Hmr spectrum in C_6D_6. The probable limits of error are ± 15%. The values for **5***a–d* are from refs. 6 and 12, and were obtained spectrophotometrically, with a probable error of ± 5%.

pentadiene; however, it does so slowly and only in competition with pathways to much more complex products. It is also shown that the dioxazines isolated from the reaction with dimethyldiphenylcyclopentadiene are probably formed exclusively by isomerization of a labile oxazine.

In the hydroxamic acid oxidations silver oxide or lead dioxide were found to be excellent alternatives to the more common reagents tetraethylammonium periodate (8) and *N*-bromosuccinimide (6).

With cyclopentadiene as substrate, the yields of isolated adducts (Table 1), all crystalline solids, varied from 40 to 70%. Their identity as compounds **1** followed from their spectra. The ^{1}Hmr spectra resembled those of adducts from cyclopentadiene and unsymmetrical azodicarbonyl derivatives, both in chemical shifts and in couplings (9). The carbonyl stretching frequencies (1640–1660 cm^{-1}) were in the range expected for *O,N*-dialkyl-*N*-acylhydroxylamines (10).

The purification of compounds **1***a–c* was readily achieved by crystallization techniques but the low melting pivaloyl adduct **1***d* required column chromatography. The elution of **1***d* was always preceded by fractions containing small amounts of an oil. This was readily recognized as the isomer **2***d* by the absence of OH, NH, and C=O stretching frequencies in the ir spectrum, in which a medium intensity band at 1621 cm^{-1}, attributable to C=N, was the most significant feature. The ^{1}Hmr spectrum supported structure **2***d*, showing a large downfield shift of its methylene protons and an upfield shift of one tertiary proton relative to those of **1***d* (parallel changes are observed in the spectra of **6** relative to **5** (9)).

On the basis of the known lability of the azodipivaloyl adduct **5***d* (9) it was first assumed that **2***d* was a secondary reaction product, generated by the isomerization of **1***d* under the reaction conditions or during work-up. To monitor small amounts of **2***d* we used ^{1}Hmr spectroscopy in benzene-d_6, taking particular advantage of the coincidence of its vinylic peaks as a sharp singlet at 4.73 τ, unobscured by peaks from **1***d* or other reaction products. This enabled **2***d* to be detected in the presence of **1***d* in amounts as small as 1%. A wide range of gas–liquid chromatography columns failed to give a clean separation.

It was confirmed that **2***d* was present before chromatography by directly analyzing the hexane extracts from the crude reaction product. The measured yields varied from 2 to 10% of the total isomeric mixture, depending on the oxidizing agent. It was also shown not to be an artifact of the reaction conditions, since **1***d* did not isomerize in the presence of *N*-bromosuccinimide–pyridine in methylene chloride. Compound **1***d*, and presumably all the adducts **1**, showed considerable stability to polar solvents, to bases, and in marked contrast with the azodicarbonyl adducts **3** (11), to strong acids.

The occurrence of path *ii* is thus established. Nitrosocarbonylisobutane at least can function as a heterodiene as well as a heterodienophile. Whether this is true for most nitrosocarbonyl compounds in their reaction with cyclopentadiene has not been established. In the case of benzohydroxamic acid a rigorous search was made for the dioxazine by chromatography of the total oxidation products but it could not be conclusively detected.

We have now reexamined the effect of heat on the oxazines **1**. On prolonged refluxing in benzene the solutions darkened and the adducts slowly decomposed. The ^{1}Hmr spectra became complex but the dioxazines **2** could be detected among the products. Analysis of the relative amounts of **1**, **2**, and by-products, by integration of the spectra, led to approximate values for the yields of **2** and the first-order rate constants of decomposition of **1**. These are shown in Table 2, along with the first-order rate

constants of the (quantitative) isomerization of the azodicarbonyl adducts **5***a–d* taken from earlier work (6, 12).

Work-up of the benzene solutions led to the isolation of the *p*-bromo and *p*-nitro adducts, **2***b* and **2***c*, which were crystalline (Table 3). Efforts to purify **2***a* failed and the isolation of the small amount of the product **2***d* (10% yield) was not attempted. The isomerization to **2***d* is highly unfavourable relative to other pathways; the complex by-products are derived solely from **1***d* and not from **2***d*, since the latter was unaffected after 4 days in refluxing benzene.

^{1}Hmr and ir spectra of compounds **2***a–c* were in line with those of **2***d*, described above. The *p*-nitrobenzimidoyl group in **2***c* absorbs at 307 nm, compared with 264 nm for the *p*-nitrobenzoyl group in **1***c*; a similar red shift was noted in the product of isomerization of **5***c*.

There are two features of note in Table 2: (*a*) The nitrosocarbonyl adducts **1** are much more stable than the azodicarbonyl adducts **5**. In particular the pivaloyl adduct **5***d* isomerizes 3000 times faster than **1***d* (a difference in free energy of activation, $\Delta\Delta G^{\ddagger}$, of 5.7 kcal mol^{-1} at 80°C) and the rate of formation of **6***d* is 30 000 times faster than that of **2***d* ($\Delta\Delta G^{\ddagger} = 7.3$ kcal mol^{-1}). (*b*) The nitrosocarbonyl adducts show little substituent steric effect compared with the azodicarbonyl adducts. The small spread in *k* values for **1***a–d* is in marked contrast with the large value for **5***d*, relative to those for **5***a–c*.

The lesser reactivity of **1** compared with **5** is itself probably steric in origin, reflecting the more severe crowding of the reacting NCOR group by the adjacent NCOR group in **5** than by the adjacent oxygen atom in **1**. Such crowding is relieved if the reacting nitrogen adopts a pyramidal geometry, which is also the geometry necessary for the transition state to product, if the reaction is concerted. This is known to be the case for the isomerization **5** → **6** but it has not been established for **1** → **2**.

One factor militating against a pyramidal geometry at nitrogen for the adduct **1** is that the conformational arrangement then produced around the N—O bond is likely one of very high energy. In this conformation the N—C and O—C ring bonds are eclipsed, or nearly so, and the nitrogen atom is pyramidal, with a localized electron pair and an electron-withdrawing substituent (RCO). Theoretical calculations predict that this geometry is very near the potential energy maximum for the internal rotation of the N—O bond (13, 14) and this seems to be supported by spectroscopic evidence (15–17).

An alternative nonconcerted route from **1** to **2**, which avoids this interaction, involves the open dipole **7**, stabilized by local resonance in each of its charged moieties. The intermediate **7** is consistent

TABLE 3. Properties of *cis*-3-aryl (or alkyl)-4a,7a-dihydro-7*H*-cyclopenta-1,4,2-dioxazines (**2** and **9**)

Compound	Mp(°C)*	ν(CCl$_4$) (cm^{-1}) C=O	τ (ppm)†					Analysis					
			$H_{5,6}$ or Me_6	H_{4a}	H_{7a} or Me_{7a}	H_7	Aryl or other	Formula	C		H		N	
									Calcd.	Found	Calcd.	Found	Calcd.	Found
2*a*	Oil		4.02	4.68	5.63	7.33(2H)	1.7–2.3(2H), 2.3–3.0(3H) (a)							
2*b*	82.5–83	1620	3.98	4.65	5.62q	7.30(2H)	2.15, 2.30, 2.40, 2.55(q, 4H) (a)	$C_{12}H_{10}BrNO$	51.45	51.71	3.60	3.70	5.00	4.98
2*c*‡	151–152	1621	3.95(2H)	4.58	5.56q	7.28(2H)	1.67, 1.83, 1.92, 2.08(q, 4H) (a)	$C_{12}H_{10}N_2O_4$	58.54	58.73	4.09	4.38	11.38	11.18
2*d*	Oil	1621	4.05(2H)	4.92	5.85q	7.40(2H)	8.89(s, 9H, CMe_3) (b)							
9*a*	144–146	1617	4.73(2H) 8.33	5.62	6.40 8.97	7.85, 8.22 7.27, 7.70	9.07(s, 9H, CMe_3) (c) 1.6–2.1(2H), 2.4–3.2(13H) (c)	$C_{26}H_{23}NO_2$	81.86	82.18	6.08	6.38	3.67	3.69
9*b*	159–160	1620	8.32		9.00	7.31, 7.71	2.15, 2.28, 2.80 2.93(q, 4H) 2.4–3.2(10H) (c)	$C_{26}H_{22}BrNO_2$	67.83	67.35	4.82	5.24	3.04	3.08
9*c*	164.5–166	1620	7.92		8.98	7.28(2H)	1.73, 1.88, 2.93, 2.18(q, 4H); 2.63 (s, 5H); 2.87(s, 5H) (a)	$C_{26}H_{22}N_2O_4$	73.23	73.28	5.20	5.22	6.57	6.61

*Compound **2***b* recrystallized from acetone–isooctane; all other solids from acetone–methanol. Compounds **9***a–c* decompose near the melting points, which were taken by inserting the capillary tube a few degrees below.
†τ values separated by a dash are at the extremes of the absorption. All absorptions are multiplets unless otherwise stated. *J* values for the C_7 methylene in **9***a* and *b* are 17 Hz. Solvents: (a) $CDCl_3$; (b) CCl_4; (c) C_6D_6.
‡λ_{max} (EtOH): 307 nm (ε 9500).

with the higher rate and yield observed in the formation of **2***c*, since a *p*-nitro group would further stabilize the negative charge in **7** (R = $pC_6H_4NO_2$).

In our first experiments (7) using 1,4-dimethyl-2,3-diphenylcyclopentadiene as a trapping agent, the oxidation of benzo-, *p*-bromobenzo-, and *p*-nitrobenzohydroxamic acids in ethyl acetate at room temperature proceeded smoothly to give, not the oxazines **8***a–c*, but the crystalline dioxazines **9***a–c* (Table 3). They were isolated in yields of 45–70% by treatment of the crude reaction residues[4] with cold methanol. The structures were inferred from their spectra. Typically **9***c* had widely separated methyl singlets at 7.92 and 8.98, and a broad allylic methylene absorption at 7.28 τ in its ^{1}Hmr spectrum ($CDCl_3$); its ir spectrum (CCl_4) had a low intensity absorption at 1620 cm^{-1} (C=N) and no carbonyl absorption.

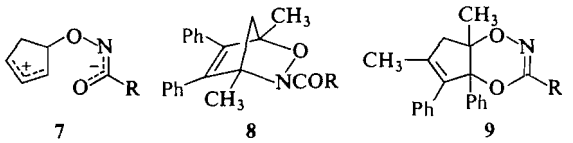

7 **8** **9**

a R = Ph *c* R = $pNO_2C_6H_4$
b R = $pBrC_6H_4$ *d* R = $C(CH_3)_3$

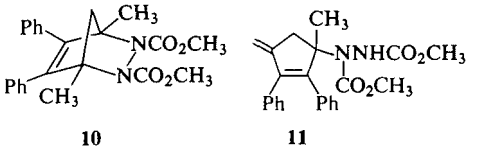

10 **11**

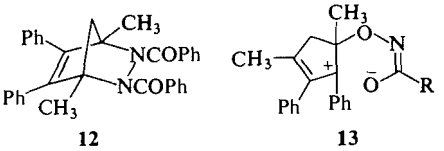

12 **13**

Compounds **9** were extremely sensitive to acids. The ^{1}Hmr spectrum of **9***b* in $CDCl_3$ containing trifluoroacetic acid was degraded completely in less than 1 min, becoming very complex. The rapid disappearance of the methyl peaks suggests that protonation of the heterocyclic ring is followed by deprotonation of a methyl group, similarly to the acid catalyzed isomerization of the corresponding azo ester adduct **10** in which the isomer **11** was produced (18). If the analogous diene is formed here it is evidently unstable.

The failure to isolate **8** was surprising since the known (9) accelerating effect on isomerization of the ring substituents would not have been predicted to prevent its survival at room temperature. Thus **12** is only 70–80 times as labile as **5***a* at 25°C in isooctane, with a half life of ca. 12 h.[5] The stability of **8** should be at least that great in view of the retarding effect found for the ring oxygen in **1**.

It was thought that the isomerization of **8** might have been promoted by the use of the polar solvent ethyl acetate in the oxidation reaction, since the azo adduct **12** had been shown to be rather sensitive to solvent polarity in its isomerization (thus $k_{aq\ EtOH}/k_{isooctane} = 25$ at 25°C).[5]

Accordingly, the oxidations were repeated in benzene. Direct ^{1}Hmr analysis of the filtered and concentrated solution from the oxidation with benzohydroxamic acid showed a new product, recognizable by a pair of methyl singlets at 7.99 and 8.30 τ. Its yield could be brought to 80% by carrying out the oxidation at 4°C. The methyl singlets slowly diminished at the expense of those of **9***a*. The new product was clearly **8***a*. Careful work-up in the cold led to the isolation of the crystalline adduct, which was fully characterized. It melted at 96.5–97°C and immediately solidified to crystals which then had the melting point of pure **9***a*.

The half-life of **8***a* at 25°C was about 9 h in chloroform-*d* and 28 h in benzene-d_6. At 80°C in the latter solvent it was 7 min but continued heating led to a levelling off in the production of **9***a* to an equilibrium concentration of 11% of **8***a* (ΔG = 1.5 kcal mol^{-1} at 80°C). This was identical with the value reached when a similar solution of pure **9***a* was heated at 80°C. At 110°C in benzene the equilibrium value was 14%. The formal [3,3]-sigmatropic rearrangement of **8***a* to **9***a* is thus detectably reversible, a feature which has been observed in at least one example in the related isomerization of an *N*-acylpyridazine to a 1,3,4-oxadiazine (19). A dipolar species, analogous to **7**, seems a particularly likely intermediate between **8** and **9**; thus the resonance form **13** is highly stabilised by the positive charge at benzylic carbon.

Formation of a benzene solution rich in **8***b* could be achieved similarly; the *p*-nitro compound **8***c* was at best only a minor product. The ^{1}Hmr spectrum of **8***b* was analogous to that of **8***a*. No effort was made to isolate it.

The amounts of dioxazine **9***a* (~20%), detected in the oxidation in benzene at 4°C, must be reconciled with the observation that pure **8***a* is <2% isomerized (the detection limit) in benzene at the same temperature. This might suggest the possibility that some **9***a* is formed directly (path *ii*). It is more likely, however, that other ingredients in the oxidation reaction catalyze the isomerization of **8***a*, e.g., H_2O, $PhCO_2H$

[4]Retrospective examination of the spectra of these residues showed small amounts of Me singlets due to unisomerized oxazines.

[5]By extrapolation of rate data from ref. 6.

(a common trace product in the oxidation of the hydroxamic acid), colloidal Ag, or Ag^+ (perhaps complexed with the alkene bond in **8***a*).

The mode of regioisomeric fusion and the *cis* stereochemistry in the dioxazines **2** and **9** have been tacitly assumed. In fact their spectroscopic properties do not unequivocally justify these choices. Either a concerted mechanism or a dipolar intermediate like **7** or **13** requires the regioisomers given (the alternative dipole formed on opening the oxazine would lead to a fused 2-acyloxazetidine). Only the concerted mechanism requires the *cis* stereochemistry.[6]

Experimental

The following spectrometers were used: for ir, a Beckman IR 10; for uv, a Unicam SP .800 B; for ^{1}Hmr, a Varian T-60 or Perkin Elmer R12B. Melting points are uncorrected.

Reagents

Benzo-, *p*-bromobenzo-, and *p*-nitrobenzohydroxamic acids were prepared from their methyl or ethyl esters by the standard method (20). Pivalohydroxamic acid was best prepared by dropwise addition at room temperature of the acid chloride to a threefold excess of hydroxylamine hydrochloride in an eightfold excess of pyridine, followed by evaporation to dryness and leaching out of the product with hot ethyl acetate. Recrystallization from ethyl acetate gave needles (45%), mp 170–171°C (lit. (21*a*) mp 163.6–164.1°C (dec.) lit. (21*b*) mp 169°C).

The following oxidizing agents were used in the hydroxamic acid reactions: silver oxide, lead dioxide, tetraethylammonium periodate (8), *N*-bromosuccinimide–pyridine; the potassium salts of the hydroxamic acids could also be oxidized directly with *N*-bromosuccinimide.

*3-Acyl-2,3-oxazabicyclo[2.2.1]hept-5-enes (**1**) (Table 1)*

*The Benzoyl Compound **1**a*

To a stirred suspension of benzohydroxamic acid (2.74 g, 0.02 mol) in methylene chloride (40 mL), containing pyridine (1.58 g, 0.02 mol) and cyclopentadiene (7 mL), was added, in portions, *N*-bromosuccinimide (3.56 g, 0.02 mol). When the reaction mixture had become clear the solution was washed once with water, twice with saturated aqueous sodium hydrogen carbonate, then with water again and dried. Evaporation gave an oil which was extracted thoroughly with several portions of hot hexane. The hexane solution gave a crystalline residue (2.8 g, 70%) whose ^{1}Hmr spectrum showed it to be substantially pure **1***a*. Recrystallization from hexane gave prisms, mp 73–75.5°C.

*Alternative Syntheses of **1**a*

Yields of at least 50% were consistently obtained when the oxidation was carried out by oxidizing (*a*) the benzohydroxamic acid in ethyl acetate with aqueous acetic acid containing sodium acetate and tetraethylammonium periodate or (*b*) the potassium salt of the hydroxamic acid in methylene chloride with *N*-bromosuccinimide.

The p*-Bromobenzoyl Compound **1**b*

A suspension of *p*-bromobenzohydroxamic acid (1.08 g, 5.0 mmol), silver oxide (2.0 g, 8.6 mmol), and sodium sulfate (2 g) was stirred for 1 h at room temperature in ethanol (50 mL) containing cyclopentadiene (1 mL). The mixture was filtered, evaporated to dryness, and the residue treated with ether (50 mL). Filtration from traces of silver followed by evaporation gave an oily residue (0.61 g) whose ^{1}Hmr spectrum showed it to be about 80% **1***b* (about 45% yield). This oil was extracted with hot hexane (100 mL) which was allowed to evaporate at room temperature and deposited crystals of the product. A recrystallization from acetone–isooctane gave **1***b* as large prisms, mp 83–83.5°C.

The p*-Nitrobenzoyl Compound **1**c*

The potassium salt of *p*-nitrobenzohydroxamic acid (2.20 g, 10 mmol), *N*-bromosuccinimide (1.6 g, 9 mmol), and anhydrous sodium sulfate (1 g) were added to a stirred solution of cyclopentadiene (5 mL) in methylene chloride (50 mL). The reaction was at first exothermic. Stirring was continued for 20 h, the solution was filtered from potassium and sodium salts, and then shaken out with water (100 mL). It was dried and evaporated to a semisolid residue which on trituration with pentane containing a little ether gave crystalline **1***c* (1.40 g, 63%). It was recrystallized from benzene–isooctane as small yellow prisms, mp 119.5–121°C.

The synthesis of **1***c* could also be achieved using *N*-bromosuccinimide and pyridine, as described for **1***a*.

*The Pivaloyl Compound **1**d*

Silver oxide or lead dioxide (7.9 or 8.2 g, 0.034 mol) was added to a stirred solution of pivalohydroxamic acid (4.0 g, 0.034 mol) and cyclopentadiene (8 mL) in ethyl acetate (100 mL) containing suspended sodium sulfate (1 g). After 4 h the solution was filtered and washed with water, aqueous sodium hydrogen carbonate and water again. It was then dried and evaporated to an orange-brown gum, which was refluxed for 1 h with hexane (100 mL). The hexane solution furnished a pale yellow syrup (3.7 g) whose ^{1}Hmr spectrum showed it to contain about 85% (51% yield, routinely 50–55%) of the expected adduct.

(*N*-Bromosuccinimide and pyridine in methylene chloride gave overall yields of 40–45%.)

Column chromatography of the hexane extract was done on neutral alumina (1 g/100 g) from benzene solution, using increasing amounts of ether as eluant. In a typical run from 3.3 g of extract from the above reaction 1% ether caused the elution of 0.078 g of the isomer **2***d*, followed by 0.520 g of a mixture of **2***d* and **1***d*; 2% ether gave 0.408 g of **1***d*. The separation was somewhat more efficient on Florisil. ^{1}Hmr analysis of the mixed fractions showed that a total of 0.235 g of **2***d* and 0.771 g of **1***d* were recovered from the column.

The total of 1.0 g compared with the expected amount of 2.8 g reflects the considerable loss of these volatile adducts during the evaporation of chromatographic fractions. Furthermore the proportions of the adducts are at variance, being biased towards **2***d*, with the true values obtained directly from the extracts before chromatography (see below).

Repeated crystallization from pentane gave **1***d* as prisms, mp 37–38°C (earlier value (7) 36–37.5°C).

*Control Experiment: Exposure of **1**d to Reaction Conditions of its Synthesis*

The adduct (150 mg), *N*-bromosuccinimide (148 mg), and pyridine (66 mg) (8.3 mmol in each case) were stirred for 0.5 h in methylene chloride (25 mL). The work-up was as described in the synthesis of **1***a*. The ^{1}Hmr spectrum of the reisolated adduct showed none of the isomer **2***d*.

*Stability of **1**d*

Polar Solvent

The adduct **1***d* (100 mg) was completely unchanged on refluxing in methanol (10 mL) for 2 h.

[6]NOTE ADDED IN PROOF: An X-ray analysis has confirmed the structure of the bromo compound **9***b*. It has the *cis* stereochemistry.

Acid Catalyzed

The adduct (70 mg, 0.39 mmol) and trifluoracetic acid (4.5 mg 0.04 mmol) were heated at the boiling point in benzene-d_6 (0.3 mL). After 26 h the solution had darkened considerably. The ^{1}Hmr spectrum showed that only about 30% of the starting material had decomposed, but there was no evidence of the presence of **2***d*.

Base Catalyzed

A solution of **1***d* (150 mg) in pyridine-d_5 (0.5 mL) was heated at 80°C; there was little change after 20 h.

The adduct (100 mg) was likewise unaffected by refluxing it for 3 h in 0.2 *M* NaOMe in MeOH (10 mL); the solution was evaporated and the residue extracted with carbon tetrachloride for ^{1}Hmr analysis.

Analysis of Product Ratio in Oxidation Reactions of Pivalohydroxamic Acid with Cyclopentadiene

Gas–liquid chromatography gave poor separations of **1***d* and **2***d* using a wide range of columns.

^{1}Hmr analysis in CCl_4 or $CDCl_3$ was unsuitable for the determination of small amounts of **2***d* which had no peak that was clearly distinguishable from peaks of **1***d* or of by-products. With C_6D_6 as solvent an excellent analytical technique was available using the intensity of the broad singlet of the two vinylic hydrogens of **2***d* at 4.73 τ, which was unobscured by any other absorptions. A detection limit of 0.6% of **2***d* in 50 mg of mixture was determined using authentic samples of the purified isomers.

Measurements of the proportions of each isomer originally produced in the oxidation, involved removing the hexane from the extracts (see synthesis of **1***d*) through a fractionating column to minimize losses of the volatile isomers. Analysis of the residue in C_6D_6 revealed the percentages of **2***d* in the total isomeric mixture for the following oxidizing agent to be: silver oxide, 4%; lead dioxide, 2%; *N*-bromosuccinimide, 7–10% (several runs).

cis-*3-Aryl(or Alkyl)-4a,7a-dihydro-*7H-*cyclopenta-1,4,2-dioxazine (2) (Table 3)*

Solutions of the adducts **1** were refluxed in benzene (ca. 1%). Aliquots were periodically removed, evaporated, and the residue analyzed by ^{1}Hmr spectroscopy in $CDCl_3$. Integration of all peaks in the aliphatic region (> 3 τ) allowed the proportions of **1**, **2**, and by-products to be determined. The yields of **2** are shown in Table 2. When the reaction was nearly complete, the solution was cooled, filtered from the dark precipitate (< 5%) present, and evaporated to a dark sticky residue which was worked up as described.

For the adduct **1***d* the isomerization was monitored directly by ^{1}Hmr analysis using a solution containing 0.1 g in 0.5 mL C_6D_6. No effort was made to scale up the reaction to isolate **2***d*. Its isolation as a co-product with **1***d* is described above.

In a control reaction the pure isomer **2***d* was heated under identical conditions for 80 h without any change in its spectrum.

Approximate rate constants of decomposition of compounds **1** are shown in Table 2.

The phenyl and the *tert*-butyl compounds, **2***a* and **2***d*, were oils; the purification of **2***d* is described above; the *p*-bromo- and *p*-nitrophenyl compounds, **2***b* and **2***c*, had melting points of 144–146 and 151–152°C.

3-Acyl-1,4-dimethyl-5,6-diphenyl-2,3-oxazabicyclo[2.2.1]hept-5-enes (8) (Table 1)

The Benzoyl Compound **8**a

To a solution of 1,4-dimethyl-2,3-diphenylcyclopentadiene (1.04 g, 4.1 mmol) in benzene (50 mL, spectroscopic grade from J. T. Baker Chemical Co.), kept at 4°C by a benzene – solid carbon dioxide bath, were added benzohydroxamic acid (0.56 g, 4.1 mmol), silver oxide (2.0 g, 8.6 mmol), and sodium sulfate (2 g). The whole was stirred for 4 h, filtered through Celite, and evaporated below room temperature. The ^{1}Hmr spectrum of the concentrated residue showed about 80% of the isomeric mixture to be **8***a*. Evaporation to dryness and addition of ether caused the precipitation of further silver residues. Filtration, concentration to a small volume, and dropwise addition of hexane caused precipitation of **8***a*. The whole was chilled to −10°C and filtered giving product of high purity (0.48 g, 31%). Recrystallization was effected by dissolving it at room temperature in ether, adding hexane till crystallization just began, filtering, and storing at −10°C for 1 h. It formed prisms which melted sharply at 96.5–97°C. The melt solidified almost immediately to give pure **9***a*, the crystals melting again at 144–146°C.

At 25°C a 0.3 *M* solution of **8***a* had a half-life of 9 h in chloroform-*d* and 28 h in benzene-d_6. At 4°C no isomerization could be detected after 20 h in a 0.3 *M* solution in benzene-d_6 (the detection limit is ca. 2% of **9***a*).

Reversible Isomerization of **8**a

A sample of **8***a* (50 mg) in benzene-d_6 (0.5 mL, 0.26 *M*) was heated in an nmr tube at 80°C and periodically monitored by measuring peak heights of the upfield Me group in **8***a* and **9***a* (a control reaction on a freshly prepared equimolar mixture of the two isomers showed the heights of the peaks to be identical). The half-life of **8***a* was 7 min but in the later stages of the reaction the kinetics drifted from first order, the decay of **8***a* becoming increasingly slow. An equilibrium value of 11% **8***a* remained. The identical value was reached when a solution of **9***a* was similarly heated. At 110°C the equilibrium concentration of **8***a* was 14%. In the reaction at 80°C no compounds were detected other than **8***a* and **9***a* but at 110°C there was slight decomposition.

Other Oxazines **9**

Similar oxidation at room temperature of *p*-bromobenzohydroxamic acid gave a benzene solution of **8***b* and **9***b*, in a ratio of 1.6:1. The former was easily characterized by its Me absorptions at 8.19 and 8.87 τ.

The oxidation of *p*-nitrobenzohydroxamic acid was more complex and peaks due to **8***c* could not be recognized with certainty in the spectrum.

cis-*3-Aryl-4a,5-diphenyl-6,7a-dimethyl-4a,7a-dihydro-*7H-*cyclopenta-1,4,2-dioxazine (9) (Table 3)*

Typically a solution of the diene (1.0 g, 4.1 mmol) was stirred for 12 h with the hydroxamic acid (4.6 mmol), silver oxide (1.6 g, 7.0 mmol), and sodium sulfate (2 g) in ethyl acetate (40 mL, washed with aqueous sodium bicarbonate and dried). The solution was filtered through Celite and evaporated to dryness. Methanol (5 mL) was added to the stickly residue which crystallized. The isolated yields were: **9***a*, 46%; **9***b*, 67%; **9***c*, 65%.

Instability of Dioxazine **9**b *to Acid*

A solution of **9***b* (50 mg, 0.11 *M*) in $CDCl_3$ (0.5 mL) in an nmr sample tube was treated with 5 μL (0.13 *M*) of trifluoracetic acid. The solution became deep yellow at once, then darkened, and finally became purple. In less than 1 min the methyl peaks of **9***b* had completely disappeared in the ^{1}Hmr spectrum. The spectrum of the purple solution was complex. An ether – aqueous sodium hydrogen carbonate work-up led only to an intractable solid.

Acknowledgements

We thank the National Research Council of Canada for financial assistance.

1. B. SKLARZ and A. F. AL-SAYYAB. J. Chem. Soc. 131 (1964); D. F. MINOR, W. A. WATERS, and J. V. RAMSBOTTOM. J. Chem. Soc. B, 180 (1967); J. E. ROWE and A. D. WARD. Aust. J. Chem. **21**, 2761 (1968); U. LERCH and J. G. MOFFAT. J. Org. Chem. **36**, 3391 (1971); T. R. OLIVER and W. A. WATERS. J. Chem. Soc. B, 677 (1971).
2. G. W. KIRBY and J. G. SWEENY. J. Chem. Soc. Chem. Commun. 704 (1973); G. JUST and L. CUTRONE. Can. J. Chem. **54**, 867 (1976).
3. G. W. KIRBY and J. W. M. MACKINNON. J. Chem. Soc. Chem. Commun. 23 (1977).
4. G. W. KIRBY, J. W. M. MACKINNON, and R. P. SHARMA. Tetrahedron Lett. 215 (1977).
5. G. W. KIRBY. Chem. Soc. Rev. **6**, 1 (1977).
6. J. A. CAMPBELL, I. HARRIS, D. MACKAY, and T. D. SAUER. Can. J. Chem. **53**, 535 (1975).
7. D. MACKAY, K. N. WATSON, and L. H. DAO. J. Chem. Soc. Chem. Commun. 702 (1977).
8. A. K. QURESHI and B. SKLARZ. J. Chem. Soc. C, 412 (1966).
9. J. A. CAMPBELL, D. MACKAY, and T. D. SAUER. Can. J. Chem. **50**, 371 (1972).
10. P. M. PEART and A. D. WARD. Aust. J. Chem. **27**, 1341 (1974).
11. C. Y-J. CHEUNG, D. MACKAY, and T. D. SAUER. Can. J. Chem. **50**, 1568 (1972).
12. T. D. SAUER. M.Sc. Thesis, University of Waterloo, Waterloo, Ont. 1971.
13. L. RADOM, W. J. HEHRE, and J. A. POPLE. J. Am. Chem. Soc. **94**, 2371 (1972).
14. E. LOMBARDINI, G. TARANTINI, L. PIROLA, and P. TORSELLINI. J. Chem. Phys. **64**, 5229 (1976).
15. P. A. GIGUÈRE and I. D. LIU. Can. J. Chem. **30**, 948 (1952).
16. S. TSUNEKAWA. J. Phys. Soc. Jpn. **33**, 167 (1972).
17. K. TAMAGAKE, Y. HAMADA, J. YAMAGUCHI, A. Y. HIRAKAWA, and M. TSUBOI. J. Mol. Spectrosc. **49**, 232 (1974).
18. L. H. DAO and D. MACKAY. Can. J. Chem. **56**, 1724 (1978).
19. C. Y-J. CHEUNG, D. MACKAY, and T. D. SAUER. Can. J. Chem. **50**, 3315 (1972).
20. A. H. BLATT (*Editor*). Organic synthesis. Coll. Vol. II. John Wiley and Sons Inc., New York. 1943. p. 67.
21. D. C. BERNDT and H. SHECHTER. (*a*) J. Org. Chem. **29**, 916 (1964); (*b*) Br. Patent No. 894,119 (Apr. 1962); Chem. Abstr. **57**, 8445b (1962).

Selective *O*-demethylation of isoquinoline alkaloids: Preparation of hydrocotarnoline from hydrocotarnine and conversion of *S*-(+)-laureline into *S*-(+)-roemerine via *S*-(+)-mecambroline[1]

JUN-ICHI MINAMIKAWA AND ARNOLD BROSSI

Medicinal Chemistry Section, Laboratory of Chemistry, NIAMDD, National Institutes of Health, Bethesda, MD 20014, U.S.A.

Received December 13, 1978

JUN-ICHI MINAMIKAWA and ARNOLD BROSSI. Can. J. Chem. 57, 1720 (1979).

The methoxy group in the simple isoquinoline alkaloid hydrocotarnine and in the aporphine alkaloid *S*-(+)-laureline can be cleaved selectively with trimethylsilyl iodide in boiling *o*-dichlorobenzene in the presence of DABCO, affording hydrocotarnoline and *S*-(+)-mecambroline, respectively. Deoxygenation of *S*-(+)-mecambroline afforded *S*-(+)-roemerine.

JUN-ICHI MINAMIKAWA et ARNOLD BROSSI. Can. J. Chem. 57, 1720 (1979).

On peut éliminer sélectivement le groupe méthoxy d'un alcaloïde simple de l'isoquinoléine, l'hydrocotarnine et d'un alcaloïde de l'aporphine, la *S*-(+)-lauréline, en faisant appel à l'iodure de triméthylsilyle dans le *o*-dichlorobenzène au reflux en présence de DABCO; il y a formation d'hydrocotarnoline et de *S*-(+)-mécambroline. La désoxygénation de la *S*-(+)-mécambroline fournit la *S*-(+)-roemérine.

[Traduit par le journal]

The selective cleavage of an aromatic methoxy group in the presence of an aromatic methylenedioxy group (1) has now been studied with isoquinolines. Hydrocotarnine (**1**), readily prepared from cotarnine (2), afforded a rather complex mixture of reaction products when heated with trimethylsilyl iodide (Me_3SiI) in quinoline (1).

Quaternization of **1** and initially formed hydrocotarnoline trimethylsilyl ether (**2**, $OSiMe_3$ instead of OH) with simultaneously generated methyl iodide offered a reasonable explanation for the formation of by-products. Replacement of quinoline with a much stronger base therefore seemed to be indicated and supported by the following observations: Ether cleavage took place when hydrocotarnine (**1**) was heated with Me_3SiI in *o*-dichlorobenzene in the presence of 1,4-diazabicyclo[2.2.2]octane (DABCO), or similarly, when **1** was heated in *o*-dichlorobenzene with a preformed DABCO–Me_3SiI complex (1:1) and excess DABCO. Heating of a hydrocotarnine–Me_3SiI complex (1:1) to 190°C for 2.5 h gave no reaction and heating this complex with excess amounts of DABCO in *o*-dichlorobenzene gave only very little hydrocotarnoline (**2**).

Cleavage of the methyl ether function in **1**, affording **2**, is probably initiated by the iodide anion of a DABCO–Me_3SiI complex. Methyl iodide formed simultaneously, is trapped by DABCO. Thus it was possible to obtain by either of the two variations (heating **1** with Me_3SiI and DABCO or heating **1** with a preformed DABCO–Me_3SiI complex (1:1) and DABCO) after methanolysis and the usual work-up, about 30% of chemically pure hydrocotarnoline (**2**) taking recovered starting material into account.

Simple conversion of abundantly available polyoxygenated alkaloids into less oxygenated congeners is important for chemical correlation, for determining absolute structures and for biological evaluation (3, 4). With the methodology elaborated with the isoquinoline **1**, the conversion of more complicated methoxymethylenedioxy-substituted aporphines into hydroxymethylenedioxy- and demethoxymethylenedioxy-substituted congeners seemed feasible. *S*-(+)-Laureline (**4**), prepared from *S*-(+)-bulbocapnine (**3**) by catalytic deoxygenation of its phenyltetrazolyl ether derivative (4), was for this purpose an attractive alkaloid to study. Heating *S*-(+)-laureline (**4**) with Me_3SiI and DABCO in *o*-dichlorobenzene afforded chemically and optically pure *S*-(+)-mecambroline (**5**) in 60% overall yield. The physical data of **5** are in good agreement with those reported for mecambroline (**5**) from *Meconopsis cambrica* species (5, 6) and *O*-methylation of **5** with diazomethane afforded optically pure *S*-(+)-laureline (**4**). Conversion of **5** into *S*-(+)-roemerine (**7**) (7) by catalytic deoxygenation of the phenyltetrazolyl ether derivative **6** was accompanied by partial racemization, as **7** was obtained as an oil and with a specific rotation about 20% lower than that reported for crystalline *S*-(+)-roemerine (**7**) (7). Purification was possible by converting optically impure material into the sparingly soluble (ethanol) tartrate with (−)-tartaric acid. From the tartrate crystalline and optically pure **7** could readily be obtained, thus chemically corre-

[1]Dedicated to the memory of Dr. R. H. F. Manske.

0008-4042/79/131720-03$01.00/0

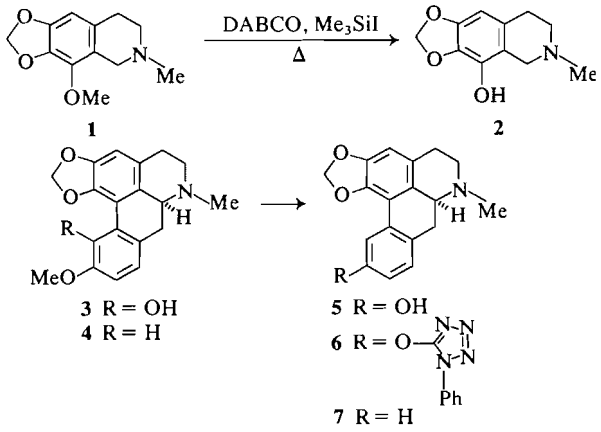

SCHEME 1

lating the following aporphine alkaloids directly with each other: *S*-(+)-bulbocapnine (**3**), *S*-(+)-laureline (**4**), *S*-(+)-mercambroline (**5**), *S*-(+)-roemerine (**7**). Accumulated data show that racemization during catalytic deoxygenation of phenyltetrazolyl ether derivatives probably occurs with the deoxygenated aporphines and is more likely with compounds lacking oxygen functions in one or both aromatic rings: *R*-(−)-aporphine (4), *S*-(+)-10,11-dimethoxyaporphine (3), and *S*-(+)-roemerine. To avoid racemization it seems at this time prudent to perform the catalytic deoxygenation of optically active phenyltetrazolyl ether derivatives under conditions which are as mild as possible (room temperature, same amount of active catalyst as substrate).

Experimental

Melting points were determined in open capillary tubes on a Thomas-Hoover melting point apparatus and are corrected. Elemental analyses were performed by the Section on Microanalytical Services and Instrumentation of this laboratory. Infrared (ir) spectra were obtained on a Beckman IR 4230 (absorption maxima ν_{max} in cm^{-1}), ultraviolet (uv) spectra on Beckman DB-G (wavelength of λ_{max} reported in nm with ε values) and mass spectra on a Hitachi Perkin-Elmer RMU-6E (70 eV) spectrometer. Optical rotations were measured with a Perkin-Elmer model 141. Thin-layer chromatography (tlc) utilized silica gel plates from Analtech (Newark, Delaware). Organic extracts were dried using Na_2SO_4.

Purification of Hydrocotarnine (1)

Cotarnine, prepared from narcotine (2) by published procedures, was reduced with sodium borohydride in methanol and crude **1**, after evaporation of solvent, extracted with ether and converted with 48% hydrobromic acid into the crystalline hydrobromide salt. Crystallization from 25% aqueous sodium bromide solution afforded **1**·HBr of mp 237–238°C (lit. (8) mp 237°C); methiodide mp 205–206°C (lit. (8) mp 206°C).

Hydrocotarnoline (2) from 1

Hydrocotarnine (**1**) (1.7 g) prepared from the HBr salt in the usual way and 2.5 g DABCO in 10 mL *o*-dichlorobenzene were mixed with 2.0 mL Me_3SiI. This reaction mixture was heated for 2 h at 170–180°C (bath) in a sealed system. The reaction mixture was cooled, acidified with 20% HCl, and the aqueous solution washed with ether, basified with $NaHCO_3$, and extracted with chloroform (4 × 100 mL). The combined chloroform extracts were evaporated and the residue obtained chromatographed on silica gel with ether–methanol (9:1). The first eluates (monitored with tlc), afforded 827 mg (49.8%) of hydrocotarnine (**1**) (HBr salt mp 233–235°C). Further elution afforded 334 mg of hydrocotarnoline (**2**) which was purified by sublimation (180–190°C/1 Torr) and crystallization from ether to give 252 mg (16.2%) hydrocotarnoline (**2**); mp 196–198°C (lit. (9) mp 198°C); ir ($CHCl_3$): 3590; ms *m/e*: 207 M^+. *Anal.* calcd. for $C_{11}H_{13}NO_3$: C 63.75, H 6.32, N 6.72; found: C 63.34, H 6.42, N 7.01.

Methylation of hydrocotarnoline (**2**) with ethereal diazomethane solution in methanol afforded hydrocotarnine (**1**) (tlc, HBr salt mp 237°C).

S-(+)-Mecambroline (5) from S-(+)-Laureline (4)

Me_3SiI (2.0 mL) was added to a solution of *S*-(+)-laureline (1.1 g) and DABCO (1.2 g) in 10 mL *o*-dichlorobenzene. The reaction mixture was treated as above. The cooled solution was diluted with methanol (30 mL), acidified with concentrated HCl, and after standing for 1.5 h, diluted with ether (100 mL) and extracted with 1 *N* NaOH (5 × 50 mL). From the organic phase 167 mg (15.1%) of starting material **4** (tlc, mp 113–115°C) was recovered.

The combined NaOH extracts afforded after acidification with concentrated HCl, filtration, basification with NH_4OH, and extraction with chloroform (5 × 50 mL) an oil, which was chromatographed on silica gel (ether; ether–methanol (9:1) and (7:3)). The material obtained was crystallized from ether to afford 559 mg (54.1%) of pure *S*-(+)-mecambroline (**5**); mp 254–255°C (lit. (5) mp 252–253°C); $[\alpha]_D^{23}$ +74° (*c* 0.5, $CHCl_3$) (lit. (5) $[\alpha]_D^{23}$ +76° (*c* 0.48, $CHCl_3$)); uv (95% EtOH): 266 (15 800), 276 (17 000), and 312 (10 000); after addition of 0.1 *N* NaOH: 236, 255 (sh), and 318 (ref. 10); ms *m/e*: 295 M^+. *Anal.* calcd. for $C_{18}H_{17}NO_3$ (295.30): C 73.20, H 5.80, N 4.74; found: C 72.84, H 5.77, N 4.62.

S-(+)-Mecambroline O-Phenyltetrazolyl Ether (6)

Mecambroline (**5**) (561 mg) was reacted with 5-chloro-1-phenyl-1*H*-tetrazole (1.03 g) and sodium hydride (250 mg of 50% oily dispersion) in dry DMF (20 mL) under nitrogen for 1 h at 100°C. The cooled reaction mixture was diluted with water (50 mL) and extracted with chloroform (5 × 50 mL). The oily residue obtained from the combined extracts was purified by filtration through silica gel (1.5 g, ether–methanol (9:1)) and the crude product crystallized from hexane–methylene chloride (10:1) to afford 709 mg (84.7%) of the ether derivative **6**; mp 187–188°C; $[\alpha]_D^{20}$ +35.9° (*c* 0.55, $CHCl_3$); ir ($CHCl_3$): 1600; ms *m/e*: 439 M^+. *Anal.* calcd. for $C_{25}H_{21}N_5O_3$ (439.49): N 15.94; found: N 15.71.

S-(+)-Roemerine (7) from 6

Mecambroline tetrazolyl ether (180 mg) was hydrogenated in acetic acid (30 mL) over 10% Pd/C catalyst (200 mg) at 50 psi for 22 h at room temperature. Usual work-up afforded an oily base which was filtered through a 10-fold amount of silica gel (ether–methanol (9:1)) to afford 81 mg of roemerine (**7**, 71%); oil; $[\alpha]_D^{20}$ +62.4° (*c* 0.54, EtOH). For further purification this oil was dissolved in ethanol (25 mL) and combined with a hot solution of (−)-tartaric acid in ethanol (50 mg, 10 mL). The precipitate was crystallized from ethanol to give 112 mg of roemerine tartrate; mp 263–264°C (lit. (7) mp 264.5°C). Optically pure roemerine (**7**) was prepared from the

tartrate (80 mg) by treatment with NH_4OH, extraction with ether, and crystallization from ether (40 mg, 77%); mp 87–88°C (lit. (7) mp 87 and 102°C); $[\alpha]_D^{21}$ +81.3° (*c* 0.6, EtOH), (lit. (7) $[\alpha]_D$ +80.2° (*c* 0.18, EtOH)); uv (95% EtOH): 272 (22 400), 292 (sh, 9100), and 315 (5000); ms *m/e*: 279 M^+. Roemerine methiodide mp 225–226°C (lit. (7) mp 224.5°C). Methylation of **5** with ethereal diazomethane in methanol afforded after 48 h *S*-(+)-laureline (**4**), mp 115–117°C, $[\alpha]_D^{22}$ +97.3 (*c* 1, EtOH), identical with an authentic sample.

Acknowledgement

We would like to thank Dr. Max Gerecke, Pharmaforschung C, F. Hoffmann-La Roche & Co., AG., Basle, Switzerland, for a most valuable gift of *S*-(+)-laureline.

1. J. MINAMIKAWA and A. BROSSI. Tetrahedron Lett. 3085 (1978).
2. M. SHAMMA. The isoquinolines. II. Alkaloids. Academic Press, New York. 1972. p. 361.
3. S. TEITEL and J. O'BRIEN. Heterocycles, **5**, 85 (1976).
4. A. BROSSI, M. F. RAHMAN, K. C. RICE, M. GERECKE, R. BORER, J. O'BRIEN, and S. TEITEL. Heterocycles, **7**, 277 (1977).
5. J. SLAVIK and S. SLAVIKOVA. Collect. Czech. Chem. Commun. **28**, 1720 (1963).
6. D. H. R. BARTON, D. S. BHAKUNI, G. M. CHAPMAN, and G. W. KIRBY. Chem. Commun. 259 (1966).
7. L. MARION and V. GRASSIE. J. Am. Chem. Soc. **66**, 1290 (1944).
8. L. F. SMALL. Chemistry of opium alkaloids. Public Health Report No. 103, U.S. Government Printing Office, Washington, DC. 1932. p. 95; M. WINDHOLZ (*Editor*). The Merck index. 9th ed. Merck and Co., Inc., Rathway, NJ. 1976. p. 630.
9. B. GOBER and S. PFEIFER. Arch. Pharm. **299**, 196 (1966).
10. M. SHAMMA, S. Y. YAO, B. R. PAI, and R. CHARUBALA. J. Org. Chem. **36**, 3253 (1971).

Perturbed normal-mode analysis of induction times, relaxation times, and reaction rates in unimolecular reactions

ANDREW W. YAU[1] AND HUW O. PRITCHARD

Centre for Research in Experimental Space Science, York University, Downsview, Ont., Canada M3J 1P3

Received October 16, 1978

ANDREW W. YAU and HUW O. PRITCHARD. Can. J. Chem. 57, 1723 (1979).

A perturbed normal-mode analysis is presented of the induction (or incubation) time, the relaxation rate, and the reaction rate of a diluted unimolecular system. At high temperature, the unimolecular rate approaches the Lindemann behaviour and the low-pressure rate is related to the normal modes of relaxation of the reactive states in a simple manner. In a step-ladder model system, the network relationship between the normal modes and the microscopic transition probabilities leads to explicit theoretical correlations between the respective experimental quantities. Illustrative calculations of such correlations are presented for the decomposition reactions of N_2O and CO_2 diluted in Ar at shock wave temperatures, and are compared with experiment.

ANDREW W. YAU et HUW O. PRITCHARD. Can. J. Chem. 57, 1723 (1979).

On présente une analyse en mode normal perturbé pour le temps d'induction (ou d'incubation), le taux de relaxation et la vitesse de réaction d'un système unimoléculaire dilué. A température élevée, la vitesse unimoléculaire approche le comportement de Lindemann et la vitesse à basse pression est reliée aux modes normaux de relaxation des états réactifs d'une manière simple. Dans un système modèle à échelons, la relation de réseau entre les modes normaux et les probabilités de transition microscopique conduit à des corrélations théoriques explicitées entre les quantités expérimentales respectives. On présente des calculs illustrant de telles corrélations pour les réactions de décomposition du N_2O et du CO_2 dilués dans Ar à des températures d'onde de choc et on les compare avec les résultats expérimentaux.

[Traduit par le journal]

I. Introduction

A master-equation formulation is required for a realistic treatment of thermal unimolecular reactions in the low and fall-off pressure regions (1–3). At the low pressure limit where collisional energy transfer is rate-determining, analytic solutions of the master equation have been obtained (2, 4) for several collisional transition probability models, and the possibility of extracting information on collisional energy transfer from these solutions has been the subject of much discussion (2, 5). In the fall-off pressure region where the intermolecular energy transfer and intramolecular reaction rates are comparable, the master equation is less amenable to analytic solutions, and little attention has so far been directed to the implications of the master-equation solution in this pressure region for collisional energy transfer studies.

Using the perturbed normal-mode approach (6–9), we have recently presented a master-equation formulation of thermal unimolecular reactions (3): the microscopic reaction processes were treated explicitly as dissipative perturbations to the normal modes of collisional relaxation of the reactant; and the solution for the unimolecular reaction rate was derived analytically at all pressures in terms of the relevant microscopic reaction probabilities and relaxation elements (8). The solution relates the various experimental quantities (the unimolecular reaction rate, the relaxation rate, etc.) directly to the collisional transition probability functions of the reactant system. Where sufficient experimental data are available, it is possible to undertake a semi-quantitative analysis of the experimental data using the analytic properties of the solution, and to study the energy transfer properties of the reactant molecule. Such analyses are useful in small polyatomic systems where reliable theoretical information on collisional energy transfer properties in the reactive energy range is virtually non-existent (10). The aim of this paper is to present such analyses for the decomposition reactions of N_2O and CO_2 diluted in Ar at high temperature.

II. The Relaxation and Unimolecular Reaction Rates

Following earlier works (3, 9), we envisage the reactant molecule to possess a set of n discrete states, and define $\eta_i(t)$ as the population of state i at time t, $\tilde{n}_i$ the equilibrium population of state i *in the absence*

[1]Present address: Herzberg Institute of Astrophysics, National Research Council of Canada, Ottawa, Ont., Canada K1A 0R6.

0008-4042/79/131723-08$01.00/0

of reaction, k_i the microscopic reaction probability of state i, and q_{ij} the transition rate constant from state i to state j via collisions with heat-bath molecules M. The master equation for the evolution of the population vector $\boldsymbol{\eta}(t)$ is

$$[1] \qquad \mathrm{d}\boldsymbol{\eta}(t)/\mathrm{d}t = \mathbf{J}\cdot\boldsymbol{\eta}(t) = (\mathbf{A} + \mathbf{D})\cdot\boldsymbol{\eta}(t)$$

where $a_{ij} = q_{ji}[\mathrm{M}]$, $a_{ii} = -\sum_{j\neq i} a_{ji}$, and $\mathrm{d}_{ij} = \delta_{ij}\mathrm{d}_i = -\delta_{ij}k_i$. The evolution eq. [1] may be transformed (3) to

$$[2] \qquad \mathrm{d}\boldsymbol{\chi}(t)/\mathrm{d}t = \mathbf{R}\cdot\boldsymbol{\chi}(t)$$

where

$$[3] \qquad \boldsymbol{\chi}(t) = \mathbf{E}^{-1/2}\cdot\boldsymbol{\eta}(t)$$

and

$$[4] \qquad \mathbf{R} = \mathbf{E}^{-1/2}\cdot\mathbf{J}\cdot\mathbf{E}^{1/2} = \mathbf{B} + \mathbf{D}$$

with

$$[5] \qquad \mathbf{B} = \mathbf{E}^{-1/2}\cdot\mathbf{A}\cdot\mathbf{E}^{1/2}$$

and $e_{ij} = \tilde{n}_i\delta_{ij}$. Both **B** and **R** are symmetric, and may be diagonalised (3) to

$$[6] \qquad \mathbf{B} = \mathbf{S}\cdot\boldsymbol{\Lambda}\cdot\mathbf{S}^{t}$$

and

$$[7] \qquad \mathbf{R} = \boldsymbol{\Psi}\cdot\boldsymbol{\Gamma}\cdot\boldsymbol{\Psi}^{t}$$

with the respective eigenvalues λ_j and γ_j being non-positive, as follows

$$[8] \qquad 0 = \lambda_{n-1} > \lambda_{n-2} \geq \lambda_{n-3} \geq \ldots \geq \lambda_0$$

and

$$[9] \qquad 0 > \gamma_{n-1} \gg \gamma_{n-2} \geq \gamma_{n-3} \geq \ldots \geq \gamma_0$$

Formally, the solution for the population evolution eq. [1] is

$$[10] \qquad \boldsymbol{\eta}(t) = \mathbf{E}^{1/2}\cdot\boldsymbol{\Psi}\cdot\exp(\boldsymbol{\Gamma}t)\cdot\boldsymbol{\Psi}^{t}\cdot\mathbf{E}^{-1/2}\cdot\boldsymbol{\eta}(0)$$

or equivalently,

$$[10a] \qquad \eta_i(t) = \tilde{n}_i^{1/2}\sum_j \exp(\gamma_j t)\psi_{ij}\sum_k \psi_{kj}\eta_k(0)\tilde{n}_k^{-1/2}$$

At short time ($t \ll |\gamma_{n-1}|^{-1}$), the system goes through a transient phase during which the initial distribution of the reactant molecules relaxes to a new distribution via collision (VR-T) energy transfer with the heat-bath molecules; it is convenient to treat this "vibrational relaxation" phase using the approach of normal modes of relaxation (refs. 11, 12; see, however, ref. 4*b* for the implications at very high temperature), and relate the experimental energy relaxation rate to the characteristic time constant of the slowest relaxation mode. Explicitly (12),

$$[11] \qquad k_{\mathrm{rel}} = \lim_{t\to\infty} -\mathrm{d}\ln[E(t) - \tilde{E}]/\mathrm{d}t \simeq -\lambda_{n-2}$$

$E(t)$ and $\tilde{E}$ being the average internal energy of the reactant at time t and at equilibrium, respectively.

At long time ($t > |\gamma_{n-1}|^{-1}$), the term associated with γ_{n-1} in the j-summation of eq. [10*a*] will dominate, and the total population of the reactant molecule becomes

$$[12] \qquad \eta(t) = \sum_i \eta_i(t) \rightarrow \left(\sum_i \tilde{n}_i^{1/2}\psi_{i,n-1}\right) \times \left[\sum_k \psi_{k,n-1}\eta_k(0)\tilde{n}_k^{1/2}\right]\exp(\gamma_{n-1}t)$$

This compares with

$$[13] \qquad \eta(t) = \eta(0)\exp[-k_{\mathrm{uni}}(t - \tau_{\mathrm{ind}})]$$

whence the unimolecular reaction rate and the induction (or incubation) time are respectively

$$[14] \qquad k_{\mathrm{uni}} = -\gamma_{n-1}$$

and

$$[15] \qquad \tau_{\mathrm{ind}} = -\gamma_{n-1}^{-1}\left[\ln\left(\sum_i \tilde{n}_i^{1/2}\psi_{i,n-1}\right) + \ln\left(\sum_i \psi_{i,n-1}\eta_i(0)\tilde{n}_i^{-1/2}/\eta(0)\right)\right]$$

The induction time τ_{ind} comprises two parts: the first depends only upon the transition probabilities at the temperature of the reaction; the second, as shown by Brau, Keck, and Carrier (13), depends on the initial population also.

The solution of the master equation predicts (9) that, at least for weak-collision systems, the unimolecular rate expression approaches the simple Lindemann form at high temperature; viz.

$$[16] \qquad k_{\mathrm{uni}} = k_\infty/\{1 + k_\infty/k_0[\mathrm{M}]\}$$

where k_∞ and k_0 are respectively the infinite-pressure unimolecular and low-pressure bimolecular rate constants. This prediction has indeed been confirmed for the decomposition reactions of diluted N_2O, CO_2, NO_2, and N_2H_4 at shock-wave temperatures (9).

The conformity of a reaction to the Lindemann behaviour has the interesting implication that the bimolecular rate constant k_0 is related to the relaxation elements associated with the reactive states (9), which, for a step-ladder model system ($q_{ij} = 0$ for $|i - j| > 1$), are related to the detailed transition rate constants $q_{i,i+1}$ in a network-like manner (7, 8). Explicitly,

[17] $$k_0 = \left(\sum_{j=0}^{n-2} t_j\right)^{-1}$$

where

$$t_j = \left(\sum_{i=0}^{j} \tilde{n}_i\right)^2 \Big/ \tilde{n}_j q_{j,j+1}$$

Notice that the bimolecular rate constant k_0 is independent of the microscopic reaction probabilities k_i, since collisional energy transfer is rate-determining at the low pressure limit.

III. Calculations

Under these conditions, the overall reaction rate depends principally on the average energy transfer $\langle \Delta E \rangle$ and is only weakly dependent on the detailed functional form of the collisional transition probabilities (2, 5, 7, 8, 14); moreover, it has been shown (5, 8), particularly when the relevant energy states are grouped into pseudo-levels in the actual calculation, that the step-ladder model gives a reasonable (but coarsely averaged) description of the collisional energy-transfer properties of the reactant system. Hence, it is a simple matter to calculate the bimolecular rate constant k_0 using eq. [17] given the transition rate constants $q_{i,i+1}$; also, once k_0 is determined, the eigenvector Ψ_{n-1} and hence the induction time τ_{ind} in eq. [15] may be calculated non-iteratively. Our method of calculation is then to (*i*) grain the energy states of the reactant molecule into pseudo-levels; (*ii*) characterise the transition rate constants in the form of

[18] $$q_{i,i+1} = q_{01} f_i$$

with q_{01} so chosen that the relaxation eigenvalue λ_{n-2} coincides with (minus) the experimental relaxation rate (cf. eqs. [5], [6], and [11]); and (*iii*) examine the dependence of the calculated bimolecular reaction rate and induction time on the respective functional forms f_i.

A. Graining of Energy States

The colossal number of vibration–rotation states in the interesting energy region ($\sim 10^7$ and $\sim 10^8$ for N_2O and CO_2, respectively, below the bond dissociation energy) necessitates the grouping of near-degenerate states into pseudo-levels — an approximation justified by the relatively large collisional energy transfer rates between levels of similar energies. The grained system then contains $\bar{n}$ pseudo-levels, with energies $\bar{\varepsilon}_i$ and degeneracies $\bar{g}_i$ ($i = 0, 1, 2, \ldots, \bar{n}-1$) where

[19] $$\bar{\varepsilon}_i = i\bar{\varepsilon}$$

and

[20] $$\bar{g}_i = G\left(\frac{2i+1}{2}\bar{\varepsilon}\right) - G\left(\frac{2i-1}{2}\bar{\varepsilon}\right)$$

the sum of states $G(\varepsilon)$ up to energy ε being computed by direct count (15) for $\varepsilon \leq 4000$ cm^{-1} and by steepest-descent (16) for $\varepsilon > 4000$ cm^{-1}. Notice that the graining scheme covers energy states from $\varepsilon_{min} = 0$ to $\varepsilon_{max} = (\bar{n} + \frac{1}{2})\bar{\varepsilon}$.

The state sum $G(\varepsilon)$ depends upon the chosen model for the reactant molecule. Both in diatomic and in polyatomic systems, rotation has often been ignored altogether in the enumeration of the state-sum. Yet, as we have shown (8), rotational effects are important in diatomic dissociation; rotational dissociation is believed to be important in polyatomic molecules also. In addition, there are no arbitrary reasons to exclude rotation in collisional energy transfer. Hence, we examine the effect of inclusion of rotation in the state-sum using two series of calculations: one including both vibration and rotation (VR) in the state-count and the other including vibration only (V), with the vibrations treated as independent oscillators in both cases.

In N_2O, the two stretching modes are well represented by two independent Morse oscillators (17); the two degenerate bending modes are treated as harmonic. For CO_2, all four vibrations are treated as harmonic. The relevant spectroscopic parameters are listed in Table 1.

The grain size $\bar{\varepsilon}$ is chosen to be one vibrational quantum for the bending mode (600 and 700 cm^{-1} for N_2O and CO_2, respectively); other grain sizes have also been used in test calculations to examine the sensitivities of the calculated quantities with variations in $\bar{\varepsilon}$, see below. The topmost pseudo-level, $\bar{n}$, is chosen so that $\bar{\varepsilon}_{\bar{n}}$ lies above the critical energy of reaction, ε_{crit}. The latter quantity is actually uncertain; it corresponds to the crossing point of the singlet and triplet adiabatic potentials, and is placed at ~ 64 and ~ 125 kcal/mol for N_2O and CO_2 respectively, by experiments (18, 19) and by theoretical calculations (20). Thus, we set $\bar{n} = 39$ for N_2O, corresponding to $\bar{\varepsilon}_{\bar{n}-1} = 63.5$ and $\bar{\varepsilon}_{\bar{n}} = 65.2$ kcal/mol. (For CO_2, $\bar{n} = 64$, $\bar{\varepsilon}_{\bar{n}-1} = 124.1$, and $\bar{\varepsilon}_{\bar{n}} = 126.1$ kcal/mol.) Again, the value of $\bar{\varepsilon}_{\bar{n}}$ was varied in test calculations; the calculated rates are not sensitive to the uncertainties in $\bar{\varepsilon}_{\bar{n}}$ since they depend primarily on the transition probabilities associated with levels below the reactive energy region.

B. Transition Probability Models

Within the framework of the step-ladder model, two functional forms of f_i (cf. eq. [18]) were examined: the constant f_i model (CF), with

TABLE 1. Spectroscopic parameters in reactant molecule

Molecule	$\omega_e(x_e)^a$				B_x (cm^{-1})	Reference
N_2O	1298.4 (0.0048)	599.4	599.4	2283.1 (0.0066)	0.41901	35, 36
CO_2	1388.2	667.4	667.4	2349.2	0.39021	36

$^a\varepsilon_v = \omega_e[(1 - x_e)v - v^2x_e]$, ω_e in cm^{-1}.

[21a] $$q_{i,i+1} = q_{01}$$

for all i; and the Landau–Teller model (LT), with

[21b] $$q_{i,i+1} = (i + 1)q_{01}$$

For each model, q_{01} is related through eqs. [5], [6], and [11] to the experimental relaxation time,[2] the latter being given by

[22] $$\log_{10} p\tau_{rel}\,(\text{atm}\ \mu\text{s}) = -1.36 + 13.6T^{-1/3} \qquad (800 < T < 2370\ \text{K})$$

for N_2O in Ar (21) and

[23] $$\log_{10} p\tau_{rel}\,(\text{atm}\ \mu\text{s}) = -1.56 + 21.3T^{-1/3} \qquad (450 < T < 3000\ \text{K})$$

for CO_2 in Ar (22, 23).

C. The Reaction Rate

It should be reiterated that eq. [17] is valid only when the unimolecular fall-off is Lindemann-like, i.e., when eq. [16] is obeyed. Hence, we shall restrict our calculations in this Section to $T > 2000$ K for N_2O and $T > 3000$ K for CO_2, where the experimental rates have been found to conform to eq. [16] (9).

N_2O

The low-pressure dissociation rates of N_2O diluted in Ar have been measured by several authors. The high temperature data (2160–3590 K) of Dove *et al.* (21) are in good agreement with those of Olschewski *et al.* (25) at lower temperatures (1400–2500 K); the data of Gutman *et al.* (26) are in good agreement with both Dove *et al.* (21) and Olschewski *et al.* (25) near 2000 K, but are systematically lower at higher temperatures. Figure 1 compares these experiments with three calculations. The first one, labelled VR-LT, includes rotation in the state-count and assumes the LT transition probability model for the transition rates between the *grained* levels (eq. [21b]).

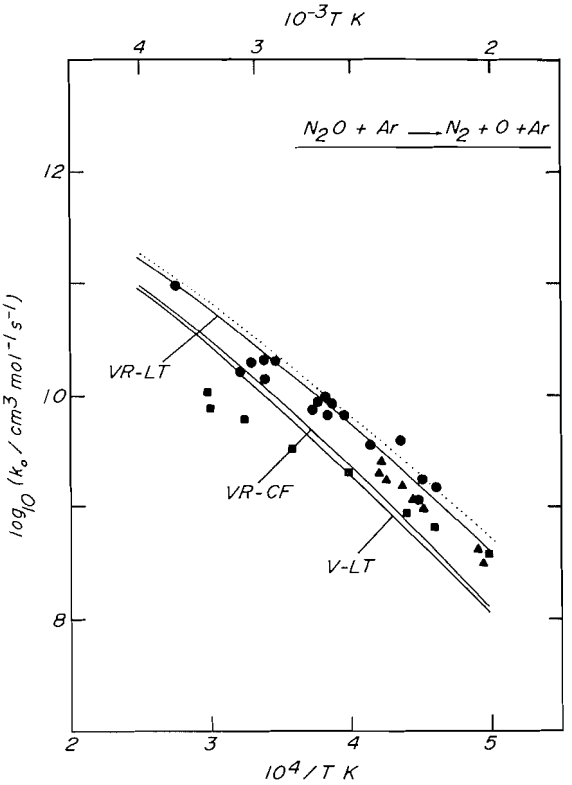

FIG. 1. Low-pressure rate constant for dissociation of N_2O diluted in Ar. Experiments: ●, Dove *et al.* (21); ▲, Olschewski *et al.* (25) with 0.2% N_2O in argon; ■, representative data points of Gutman *et al.* (26). Calculations — solid curves: VR-LT, vibration-rotational state-count and Landau–Teller transition probability model, eq. [21b]; VR-CF, vibration-rotational state-count and constant f_i model, eq. [21a]; V-LT, vibrational state-count, and Landau–Teller model. Calculations — dotted curve: VR-LT calculation with a step-size of 1200 cm^{-1} in LT model (see text).

The second, labelled VR-CF, differs from the first one in that it assumes the constant f_i model (eq. [21a]) instead. The third calculation, labelled V-LT, excludes rotation in the state-count and assumes the LT model. Notice that the absolute magnitude of the transition probabilities in the three models are chosen to yield the same (experimental) relaxation rate (see previous subsection). Yet, they predict appreciably different reaction rates. This is not unexpected since relaxation and reaction rates are in general related to the collisional energy transfer

[2]The expression $q_{01} = k_{rel}/[\exp((\varepsilon_1 - \varepsilon_0)/kT) - 1]$, which is used extensively (8, 24) to relate q_{01} to the experimental relaxation rate in diatomic systems, is not applicable to polyatomic systems. Hence, we compute the eigenvalue λ_{n-2}' for the reduced transition matrix A′ (A′ being constructed with $q_{i,i+1}' = f_i$) and relate q_{01} to the experimental relaxation rate using the relationship $q_{01} = -k_{rel}/\lambda_{n-2}'$. For the transition probability patterns that we examined, this latter expression can differ from the former one by as much as a factor of ten.

properties of the reactant molecule at different energy regions. It is now well recognized (14) that they are the consequences of a network of microscopic processes, and it is generally not possible to associate them with a particular transition (27). The energy region of importance to the reaction rate is characterised by the bottleneck (7, 8), which shifts to lower energy as temperature increases. The corresponding region for the relaxation rate is associated with levels carrying the largest energy fluxes; it is more subtle and a normal-mode analysis is needed for a detailed understanding (11).

That the VR-CF rates are smaller than the experimental rates (of Dove *et al.* (21) and Olschewski *et al.* (25)) by a factor of two to three is not surprising, since the transition rates are expected to increase at higher energy, rather than being constant at all energies. Hence, eq. [21*a*] represents an underestimate for the transition rates in the reactive energy region; and this underestimate is reflected in the calculated reaction rates.

Likewise, the V-LT rates are expected to be smaller than the experimental data, since the exclusion of rotation in the state-count underestimates the state-density (and population) of the reactive energy levels.

Note, however, that the VR calculations are likely to be (slight) overestimates, since in the graining procedure, we have grouped all energy states above the critical energy for reaction into reactive pseudo-levels, whereas in reality some of these states (those in very high rotational states) are non-reactive. We believe it is this overestimate that compensates for the underestimate in the LT transition rate constants, yielding the good agreement between the VR-LT rates and experiment; while the present calculations suggest the LT model to be much more realistic than the CF model, we would hesitate to attach any physical interpretation or justification to the model.

The activation energies of the three calculated rates are compared in Table 2. (*i*) The inclusion of rotation in the state-count lowers the activation energy (difference between VR-LT and V-LT) by 5 kcal/mol at 2100 K and more at higher temperatures; the reasons for this lowering have been discussed earlier in diatomic dissociation (8). (*ii*) The lower activation energies of the VR-LT rates, compared with the corresponding VR-CF data, arise from the faster energy transfer rates at high energy in the LT model and hence more drastic population disequilibrium at high temperature: the reasons for this have also been discussed before (8).

To examine the effect of the grain size $\bar{\varepsilon}$ on the calculated reaction rate, the VR-LT calculation was repeated using $\bar{\varepsilon} = 1200\ cm^{-1}$ (instead of $600\ cm^{-1}$); the calculated rates increase by less than 30% (dotted curve in Fig. 1), showing that the calculation is indeed not sensitive to the grain size chosen.

TABLE 2. Activation energy for the dissociation of N_2O in Ar at low pressure

		$\varepsilon_{act,0}$[a]		
T_1	T_2	VR-LT	V-LT	VR-CF
4000	3500	42.1	48.0	45.4
3500	3250	43.5	49.6	47.4
3250	3000	44.9	50.9	49.2
3000	2750	46.5	52.5	51.2
2750	2500	48.5	54.3	53.5
2500	2300	50.5	56.0	55.7
2300	2100	52.4	57.5	57.6

[a] $\varepsilon_{act,0} = -k \ln [k_0(T_1)/k_0(T_2)]/[1/T_1 - 1/T_2]$, in kcal/mol.

CO_2

The dissociation of diluted CO_2 at shock wave temperatures has received much experimental attention in the last two decades; nevertheless, data of various workers were not always concordant, see ref. 28. The experimental activation energy at low pressure is significantly lower than the bond dissociation energy ($\varepsilon_{act,0} \sim 105$ kcal/mol at 3300 K (29) compared with D(O—CO): 125.75 kcal/mol). Theoretically, Gilbert (30) obtained from model calculations an activation energy of 98 kcal/mol at 4000 K. However, his calculations assume energy-independent collision cross sections, and it is not clear if these cross sections are in fact consistent with the temperature dependence of the relaxation rate. Since the activation energy for reaction is related to that of the relaxation rate, it is not possible to assess the calculated activation energies with respect to experiment. More recently, Tardy (31) obtained $\varepsilon_{act,0} \simeq 100$ kcal/mol at 3500 K by applying corrections to the strong-collision rate constants and using his "universal function" for collision efficiency. Again, the consistency between the experimental relaxation rate and the transition probabilities assumed in this calculation is not at all clear. Both of these calculations ignore rotation; inclusion of rotation would lower the calculated activation energies substantially.

In this section, we calculate the reaction rate by synthesising the transition probabilites from eq. [21] (*a* and *b*) and experimental relaxation rate data. Figure 2 compares our calculations with the experimental data of Dean (32), Vasatko (33), Davies (34), and Wagner and Zabel (29). The data of Dean and Vasatko are in good agreement; those of Wagner and Zabel (29) are systematically lower. Again, the

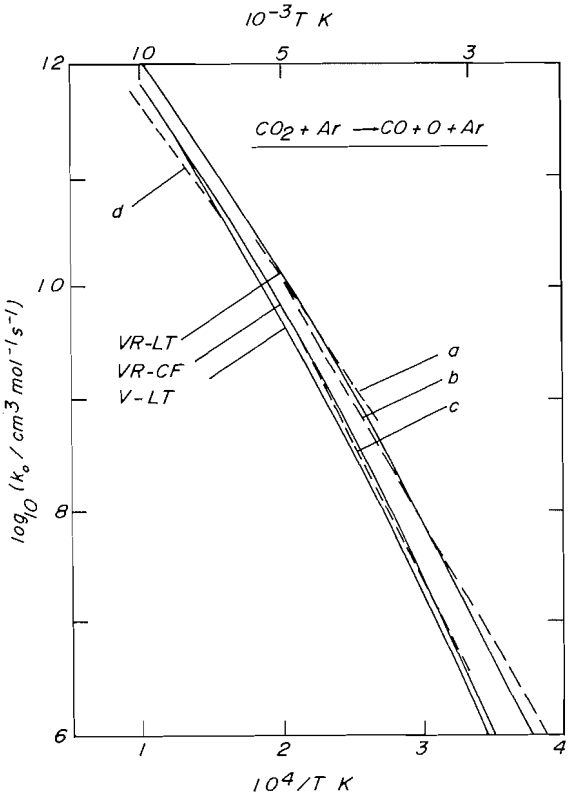

FIG. 2. Low-pressure rate constant for dissociation of CO_2 diluted in Ar. Experiments: *a*, Dean (32); *b*, Vasatko (33); *c*, Wagner and Zabel (29); *d*, Davies (34). Calculations: see caption in Fig. 1 for details.

VR-LT rates, which are in good agreement with the experiments of Dean (32) and Vasatko (33), are a factor of 2–4 larger than the V-LT and VR-CF rates.

Table 3 compares the activation energies of the respective rates. (*i*) Again, rotation leads to a noticeable reduction in the activation energy: from 7 kcal/mol at 3500 K to 10 kcal/mol at 10 000 K. (*ii*) Note also the dependence of the activation energy on the transition probability model, which becomes more appreciable at high temperature; cf. the VR-LT vs. VR-CF data. (*iii*) The activation energies of the VR-LT rates are in good accord with experimental estimates: the calculated value of $\varepsilon_{act,0} = 109.3$ kcal/mol between 3000 and 3500 K compares favourably with the experimental value (29) of 105 kcal/mol at 3300 K. Clearly, the low activation energies at very high temperatures are not anomalous at all.

D. The Induction Time

In the relaxation experiment of Dove *et al.* (21), the induction time for the N_2O reaction was measured and reported in terms of its ratio to the vibrational relaxation time, τ_{ind}/τ_{rel}. The ratio ranges between 4 and 7 at 2160–3590 K. To our knowledge, no measurements exist for the CO_2 reaction.

TABLE 3. Activation energy for the dissociation of CO_2 in Ar at low pressure

		$\varepsilon_{act,0}$[a]		
T_1	T_2	VR-LT	V-LT	VR-CF
10000	7500	79.1	89.4	82.9
7500	6000	83.2	94.6	89.2
6000	5000	89.8	101.2	97.3
5000	4500	98.1	108.2	106.6
4000	3500	104.9	113.2	113.4
3500	3000	109.3	116.3	117.4

[a]See footnote in Table 2.

TABLE 4. Induction to relaxation time ratio of the N_2O–Ar system

	τ_{ind}/τ_{rel}		
T(K)	VR-LT	V-LT	VR-CF
4000	2.13	2.05	1.47
3000	2.37	2.31	1.78
2500	2.56	2.48	2.10
2100	2.72	2.58	2.58

TABLE 5. Induction to relaxation time ratio of the CO_2–Ar system

	τ_{ind}/τ_{rel}		
T(K)	VR-LT	V-LT	VR-CF
10000	2.08	2.00	1.33
6000	2.42	2.43	1.73
4000	2.94	2.83	2.42
3500	3.03	2.71	1.74

From eq. [15], τ_{ind} is proportional to the reaction time $\tau_{react}(= -1/\gamma_{n-1})$. Hence, it is in general more convenient to characterise the induction time in terms of the ratio τ_{ind}/τ_{react}. Nevertheless, in the low-pressure limit, τ_{react} is directly proportional to τ_{rel}, and it is equally convenient to characterise τ_{ind} in terms of τ_{ind}/τ_{rel}; to facilitate comparison with experiment, we present our results in this section in this form.

Tables 4 and 5 list the ratios τ_{ind}/τ_{rel} for the N_2O and CO_2 reactions, respectively, for the three sets of calculations.[3] Notice that τ_{ind} is dependent upon the initial population distribution, $\eta(0)$; nevertheless, as for relaxation time, the dependence is not significant

[3]Kiefer and Hajduk (24) have recently cautioned against the numerical difficulties associated with the use of eq. [15]. We did not encounter any difficulties in our calculations. However, the alleged difficulties may well arise in calculations at lower temperatures.

for polyatomic systems in experimental shock conditions: in all calculations, an initial temperature of 300 K was assumed to mimic the experiment. For both reactions, the ratio decreases slightly with increasing temperature, in accord with the experiment of Dove *et al.* (21); the calculated ratios of 2–3 are in reasonable agreement with the experimental ratios of 4–7, considering the simplicity of the theoretical model and the difficulty of the experiment. Note the similar patterns between the corresponding data in the two reactions: the VR-LT and V-LT induction times are very similar; on the other hand, the difference between the VR-LT and VR-CF induction times is quite appreciable, especially at high temperature. This is because the induction time is related predominantly to the transition probability pattern, and less so to the energy level structure of the reactant molecule.

IV. Discussions

The present master-equation analysis of the relaxation and reaction behaviour of the N_2O–Ar and CO_2–Ar systems provides interesting insights into the energy transfer properties of small polyatomics ("weak collision systems") at high temperature.

In the master-equation formulation, the reaction rate at low pressure is explicitly related to the internal (collisional) relaxation behaviour of the reactant. It is important to note that the relaxation rate has, in general, no direct connection with the "strong" collision rate. (Indeed, the transition rate constant q_{01} is not related to the Lennard–Jones collision number at all!) Nor is there any similar relationship between the (non-equilibrium) reaction rate and the strong collision number. Thus, to relate these last two quantities using a collisional efficiency parameter has, at best, operational meaning only.[4] For meaningful interpretations of a reaction at high temperature and the energy transfer properties of the reactant, the collisional relaxation behaviour of the molecular system must be explicitly considered. Note also that it is in general not possible to relate the reaction rate to the collision (or energy transfer) rate from a particular energy state or group of states in the reactant molecule; rather, the overall rate represents a co-operative effect of a network of microscopic transition processes.

The treatment of the microscopic reaction processes in unimolecular systems as dissipative perturbations to the internal (collisional) relaxation of the reactant molecule is attractive for several reasons. The algebra involved in the treatment bears close resemblance to perturbation formalisms in quantum mechanics; this facilitates not only the analytic solution for the unimolecular reaction rate at all pressures, but also the physical interpretations of the relevant theoretical results. Thus, the theoretical origin of the Lindemann behaviour is now well understood: it occurs *either* when the molecule has only one reactive state, in which case the internal relaxation amongst its various states has the overall effect of grouping all the non-reactive states into one (3); *or* when the relaxation modes associated with the respective reaction states (as characterised by the respective relaxation elements (8)) are identical, in which case the reaction-relaxation behaviour of all the reactive states is similar. The latter follows from the fact that the reaction bottleneck lies in the non-reactive energy region, and that the reaction behaviour does not depend at all on the microscopic processes associated with the reactive states (9).

This latter point is important since it leads to the prediction of the Lindemann fall-off behaviour at high temperature and, in turn, the direct association of the low-pressure reaction rate at high temperature with the relaxation elements of the reactive states. Within the step-ladder model, the justification of which for a grained system we have discussed earlier, this direct identification facilitates a straightforward semiquantitative analysis of the collisional energy transfer properties of a reactant system, from the experimental relaxation and reaction rate data.

The present master-equation analysis of the various experimental data (the relaxation rate, the reaction rate, and the induction time) of the N_2O and CO_2 systems demonstrates that (*i*) rotation should be taken into account in rate calculations; (*ii*) both "vibrational" population disequilibrium and rotation are important contributors to the lowering of the low pressure activation energy at high temperature; and (*iii*) an (initial-) state-independent energy transfer model is inadequate, even for the description of thermal systems; in the model we have used, the initial state is characterised only by its total energy (and not by its rotational and vibrational components), but within this framework of coarsely-grained pseudo-levels, a Landau–Teller transition probability model seems to give semi-quantitatively reasonable results. As we have noted before (8) it is not rotational energy transfer nor rotational disequilibrium that are of vital importance in determining the reaction rate at these temperatures, or its Arrhenius temperature coefficient: it is simply the proper accounting for the rotational states taken

[4]The "strong collision" rate constants for the two reactions have recently been calculated by Troe (2), using slightly different spectroscopic data. For N_2O, the collisional efficiency decreases from 0.09 at 900 K to 0.02 at 2500 K; for CO_2 it increases from 0.005 at 1000 K to 0.03 at 3000 K.

together with the fact that at high temperatures, rotational energy and vibrational energy seem to be roughly equally effective in promoting dissociation (8).

Acknowledgment

This work was supported by the National Research Council of Canada.

1. H. O. PRITCHARD. Can. J. Chem. **55**, 284 (1977).
2. J. TROE. J. Chem. Phys. **66**, 4745 (1977); **66**, 4758 (1977).
3. A. W. YAU and H. O. PRITCHARD. Can. J. Chem. **56**, 1389 (1978).
4. A. P. PENNER and W. FORST. (*a*) J. Chem. Phys. **67**, 5296 (1977); (*b*) Chem. Phys. Lett. **56**, 117 (1978).
5. D. C. TARDY and B. S. RABINOVITCH. Chem. Rev. 77, 369 (1977).
6. A. W. YAU. Ph.D. Thesis, York University, Downsview, Ont. 1978.
7. A. W. YAU and H. O. PRITCHARD. Proc. R. Soc. London A, **362**, 113 (1978).
8. A. W. YAU and H. O. PRITCHARD. J. Phys. Chem. **83**, 134 (1979).
9. A. W. YAU and H. O. PRITCHARD. Chem. Phys. Lett. **60**, 140 (1978).
10. H. H. SUZUKAWA, JR., M. WOLFSBERG, and D. L. THOMPSON. J. Chem. Phys. **68**, 455 (1978).
11. H. O. PRITCHARD and N. I. LABIB. Can. J. Chem. **54**, 329 (1976).
12. A. W. YAU and H. O. PRITCHARD. Can. J. Chem. **55**, 737 (1977).
13. C. A. BRAU, J. C. KECK, and G. F. CARRIER. Phys. Fluids, **9**, 1885 (1966).
14. H. O. PRITCHARD. Spec. Period. Rep. React. Kinet. **1**, 243 (1975).
15. S. E. STEIN and B. S. RABINOVITCH. J. Chem. Phys. **58**, 2438 (1973).
16. A. W. YAU and H. O. PRITCHARD. Can. J. Chem. **55**, 992 (1977).
17. I. SUZUKI. J. Mol. Spectrosc. **32**, 54 (1969).
18. J. TROE. *In* Modern developments in shock tube research. *Edited by* G. Kamimoto. Shock Tube Research Society, Kyoto, Japan. 1975. p. 29.
19. J. TROE and H. GG. WAGNER. *In* Physical chemistry of fast reactions. Vol. 1. *Edited by* B. P. Levitt. Plenum, London. 1973. p. 1.
20. A. W. YAU and H. O. PRITCHARD. Can. J. Chem. This issue.
21. J. E. DOVE, W. S. NIP, and H. TEITELBAUM. Fifteenth symposium (international) on combustion. The Combustion Institute, Pittsburgh, PA. 1974. p. 903.
22. C. J. S. M. SIMPSON, T. R. D. CHANDLER, and A. C. STRAWSON. J. Chem. Phys. **51**, 2214 (1969).
23. C. J. S. M. SIMPSON and T. R. D. CHANDLER. Proc. R. Soc. London A, **317**, 265 (1970).
24. J. H. KIEFER and J. C. HAJDUK. Chem. Phys. Lett. **52**, 174 (1977).
25. H. A. OLSCHEWSKI, J. TROE, and H. GG. WAGNER. Ber. Bunsenges. Phys. Chem. **70**, 450 (1966).
26. D. GUTMAN, R. L. BELFORD, A. J. HAY, and R. J. PANCIROV. J. Phys. Chem. **70**, 1793 (1966).
27. N. C. BLAIS and D. G. TRUHLAR. J. Chem. Phys. **69**, 846 (1978).
28. D. L. BAULCH, D. D. DRYSDALE, J. DUXBURY, and S. GRANT. Evaluated kinetic data for high temperature reactions. Vol. 3. Butterworths, London. 1976. p. 309.
29. H. GG. WAGNER and F. ZABEL. Ber. Bunsenges. Phys. Chem. **78**, 705 (1974).
30. R. GILBERT. Chem. Phys. Lett. **11**, 146 (1971).
31. D. C. TARDY. Chem. Phys. Lett. **17**, 431 (1972).
32. A. M. DEAN. J. Chem. Phys. **58**, 5202 (1973).
33. H. VASATKO. Ph.D. Thesis, University of Göttingen, Göttingen, Germany. 1970.
34. W. O. DAVIES. J. Chem. Phys. **41**, 1846 (1964).
35. A. CHEDIN, C. AMIOT, and Z. CIHLA. J. Mol. Spectrosc. **63**, 348 (1976).
36. G. HERZBERG. Electronic spectra of polyatomic molecules. Van Nostrand, New York, NY. 1966. p. 596.

Unimolecular reactions of N_2O and CO_2 at high pressure

ANDREW W. YAU[1] AND HUW O. PRITCHARD

Centre for Research in Experimental Space Science, York University, Downsview, Ont., Canada M3J 1P3

Received December 6, 1978

ANDREW W. YAU and HUW O. PRITCHARD. Can. J. Chem. 57, 1731 (1979).

An *a priori* calculation in the framework of the theory of radiationless transitions is presented for the non-adiabatic spin-forbidden reactions of N_2O and CO_2. The calculation is two-dimensional, incorporating the two stretching degrees of freedom, and the microscopic reaction process is formulated using the relative coordinate system of Rosen as modified by Beswick and Jortner. All microscopic parameters required for the calculation are derived from spectroscopic data; no adjustable parameter is included. For each reaction, a purely theoretical reaction probability function $k(E)$ is synthesised and used to derive a theoretical Arrhenius expression for the infinite-pressure reaction rate. The calculated high-pressure unimolecular dissociation rates for both reactions are in reasonable agreement with experiment. High-pressure recombination rate coefficients are also presented for CO_2; they exhibit positive activation energies which increase from 0.5 kcal/mol at room temperature to 8 kcal/mol at 5000 K.

ANDREW W. YAU et HUW O. PRITCHARD. Can. J. Chem. 57, 1731 (1979).

On présente un calcul *a priori*, dans le cadre de la théorie des transitions sans radiation, pour les réactions non adiabatiques interdites d'après les spin, du N_2O et du CO_2. On présente le calcul bidimensionnel incorporant les deux degrés de liberté d'élongation et le procédé de réaction microscopique en faisant appel au système de coordonnées relatives de Rosen, modifié par Beswick et Jortner. On a déduit tous les paramètres microscopiques requis pour les calculs à partir de données spectroscopiques; on n'a ajouté aucun paramètre ajustable. Pour chaque réaction, on a synthétisé une fonction de probabilité de réaction purement théorique $k(E)$ et on l'a utilisée pour déduire une expression d'Arrhénius théorique pour des vitesses de réaction à pression infinie. Les vitesses de dissociation unimoléculaires à haute pression, calculées pour les deux réactions, sont en bon accord avec les valeurs expérimentales. On rapporte aussi, pour le CO_2, les coefficients de vitesse de recombinaison à haute pression; ils comportent des énergies d'activation positives qui augmentent de 0.5 kcal/mol à température ambiante à 8 kcal/mol à 5000 K.

[Traduit par le journal]

I. Introduction

Since the pioneering paper of Rice on the quantal treatment of radiationless transitions in 1929 (1), time-dependent perturbation theory has found itself applied to various types of physical/chemical processes in the last 50 years — autoionisation (2), diatomic predissociation (3), radiationless electronic relaxation (4), and unimolecular reaction (5) — in the framework of the theory of configuration interactions (2, 6, 7). Indeed, time-dependent perturbation treatments of unimolecular reaction kinetics date back to the remarkable model calculations of Rosen (8) in 1933 on the predissociation of a vibrationally excited metastable molecule. To the extent that the distinction between vibrational predissociation (involving nuclear motion along only one potential surface) and electronic predissociation (involving two electronic configurations) is not well defined, and that the theoretical frameworks of the two kinds of reactions are not dissimilar within the configuration-interaction approach, the calculations of Stearn and Eyring (9), Olschewski *et al.* (10), and Gilbert and Ross (11) for the non-adiabatic spin-forbidden reaction of N_2O represent natural developments from the work of Rosen (8).

These practical calculations were not without inherent difficulties. Required spectroscopic information was often approximate and incomplete, and had to be supplemented by informed guesswork. The required numerical computations were not trivial, even with drastic simplifications and analytic approximations. In the calculation of Stearn and Eyring (9), an empirical potential surface was constructed for the ground electronic state from experimental vibrational frequencies; an inverted Morse function with arbitrarily chosen range parameters was assumed for the repulsive upper-state potential. The semi-classical expression of Zener (12) for the non-adiabatic crossing of energy levels was used for calculating the microscopic decomposition probabilities. The Zener expression is inadequate (13); also, the value adopted in the calculation (50 kcal/

[1]Present address: Herzberg Institute of Astrophysics, National Research Council of Canada, Ottawa, Ont., Canada K1A 0R6.

0008-4042/79/131731-12$01.00/0

mol) for the energy of curve crossing is a gross underestimate and the calculated infinite-pressure activation energy (52 kcal/mol) differs substantially from the experimental value (60 kcal/mol) (10). Nevertheless, some of the empirical estimates for the relevant molecular parameters in the calculation are remarkably realistic; indeed, the theoretical implications of these estimates have served as useful guides for the later works (10, 11).

A different approach was adopted in Olschewski *et al.* (10): a theoretical analysis was undertaken for the infinite-pressure rate constant in terms of spectroscopic parameters of the two electronic states; the theoretical results were then compared with experimental rate data, and "experimental" values were deduced for the relevant molecular parameters. The calculation was similar to that of Stearn and Eyring (9) in some regards: as in Stearn and Eyring (9), the overlap integral in the microscopic reaction probability term was evaluated one-dimensionally (along the N—O coordinate), and was related to the potential surfaces only through their slope along the coordinate at the curve-crossing point; also, the values for the two slopes were chosen empirically. Unlike Stearn and Eyring (9), however, the semi-classical expression of Rice (14), which is more accurate (3) than that of Zener near the curve-crossing region, was used for the overlap integral. Three calculations were performed to examine semi-quantitatively the consequence of allowing energy from other vibrational modes for reaction (within the one-dimensional formalism). By comparison between computational and experimental data, the energy of curve crossing was placed at 63 ± 1 kcal/mol — 3.5 kcal/mol above the experimental activation energy. Also, a value of 39 cm^{-1} was obtained for the spin–orbit coupling constant, with an uncertainty of a factor of two.

The calculation of Gilbert and Ross (11) is different from the two earlier works (9, 10) in two regards: it was two dimensional; also, the relevant wavefunction overlaps were evaluated numerically, rather than being approximated by semi-classical expressions. The incorporation of the second degree of freedom (N—N stretch) and the evaluation of the two-dimensional overlap integrals substantially compounded the required computational elaboration, even with drastic approximations such as the neglect of anharmonicity in the ground-state potential. The calculation was exploratory in nature: the upper-state potential was defined in terms of adjustable parameters, which were chosen to effect agreement between the calculated and experimental activation energies; a factor of four agreement was obtained between the calculated and experimental rates. Comparable agreement was also obtained in another rather similar calculation by Gebelein and Jortner (15); they employed instead an anharmonic (Morse) function for the ground-state N—O potential and adjusted the upper-state repulsive potential, assuming it to obey an inverse power dependence.

These reasonable agreements between the calculated and experimental rates point to a purely theoretical calculation which allows no arbitrarily adjustable parameters. Comparison between such a calculation and experiment would then provide realistic assessment of the validity of the various simplifications in the theoretical framework. The aim of this paper is to present such a calculation for the spin-forbidden reactions of N_2O and CO_2:

[1] $$N_2O(\tilde{X}^1\Sigma^+) \rightarrow N_2(X^1\Sigma_g^+) + O(^3P)$$

[2a] $$CO_2(\tilde{X}^1\Sigma_g^+) \rightarrow CO(X^1\Sigma^+) + O(^3P)$$

Our objectives are three-fold. First, we synthesize a purely theoretical $k(E)$ function from the microscopic reaction probabilities for the two reactions: the calculation is two-dimensional; however, our theoretical approach obviates the formidable amount of numerical computation involved in the work of Gilbert and Ross (11). Second, we derive from the $k(E)$ function a 'theoretical' Arrhenius rate expression for the high-pressure reaction rates of both reactions; in a future publication, we will use the latter to examine the sensitivity of the Slater–Forst inversion procedure (16, 17) of high-pressure rate laws — a question of some interest in thermal unimolecular reaction theory. Third, we study the low-temperature behaviour of the reverse (recombination) reaction of [2a];

[2b] $$CO(X^1\Sigma^+) + O(^3P) \rightarrow CO_2(\tilde{X}^1\Sigma_g^+)$$

in the high-pressure region. The current knowledge, both experimental and theoretical, of the kinetics of [2b] is uncertain (18); our aim here is to examine the theoretical temperature dependence of the reaction in the high-pressure limit.

II. Formulation

The microscopic dissociation process is described by a bound vibrational state of a Born–Oppenheimer electronic state $|b\rangle$ coupled by intramolecular non-adiabatic coupling H_{int} to a set of vibrational continua belonging to another Born–Oppenheimer unbound electronic state $|u\rangle$. For a linear triatomic molecule ABX restricted to linear motion, the total wavefunctions for the two electronic states are

[3a] $$|b\rangle = |\Psi_b\rangle|b,v_{b1},v_{b2}\rangle$$

[3b] $$|u\rangle = |\Psi_u\rangle|u,\varepsilon_{u1},v_{u2}\rangle$$

where $|\Psi_s\rangle$, $s \equiv b, u$, are the electronic wavefunctions, v_{b1},v_{b2} the vibrational quantum numbers in the bound electronic state, v_{u2} the vibrational quantum number of the diatomic fragment AB, and ε_{u1} the relative kinetic energy of the AB—X pair.

Following the Beswick–Jortner modification (19) of Rosen's relative coordinate system (8), we characterise the nuclear dynamics in terms of the centre of mass coordinate of the entire system, the separation r_1 between X and the centre of mass of AB, and the internuclear separation r_2 of AB. Note that

$$[4] \qquad r_1 = \theta r_2 + r_{BX}$$

where $\theta = m_A/(m_A + m_B)$. In this representation, the motion of the centre of mass of the entire system is factored out, and the nuclear Hamiltonian for the internal motion assumes the form

$$[5] \quad H = -(\hbar^2/2\mu_1)(\partial^2/\partial r_1^2) - (\hbar^2/2\mu_2)(\partial^2/\partial r_2^2) + V_s$$

where μ_1 is the reduced mass of AB and X ($\mu_1 = (m_A + m_B)m_X/(m_A + m_B + m_X)$) and μ_2 the reduced mass of AB ($\mu_2 = m_A m_B/(m_A + m_B)$); V_s denotes the potential of electronic state s.

We now assume that the potentials in both electronic states can each be written as the sum of component potentials between neighbouring nuclei, viz.

$$[6] \qquad V_s = V_{s1}(r_{BX}) + V_{s2}(r_{AB})$$

$s \equiv b, u$, and partition the nuclear Hamiltonian H into the zero-order Hamiltonian H^0 and the residual perturbation H^1, with

$$[7a] \quad H^0 = -(\hbar^2/2\mu_1)(\partial^2/\partial r_1^2) + V_{s1}(r_1 - \theta\bar{r}_{AB,s}) - (\hbar^2/2\mu_2)(\partial^2/\partial r_2^2) + V_{s2}(r_2)$$

and

$$[7b] \quad H^1 = V_{s1}(r_1 - \theta r_2) - V_{s1}(r_1 - \theta\bar{r}_{AB,s})$$

The zero-order Hamiltonian then corresponds to the motion of the diatomic fragment AB and the motion of X relative to the centre of mass of AB which is 'frozen' at its equilibrium separation $\bar{r}_{AB,s}$. Its 'diabatic' wavefunctions are[2]

$$[8a] \qquad |b,v_{b1},v_{b2}\rangle = \phi_{v_{b1}}(r_1)\,\chi_{v_{b2}}(r_2)$$

for the bound state $|b\rangle$ and

$$[8b] \qquad |u,\varepsilon_{u1},v_{u2}\rangle = \phi_{\varepsilon_{u1}}(r_1)\chi_{v_{u2}}(r_2)$$

for the unbound state $|u\rangle$.

[2]Notice that the diabatic states $|b\rangle$ are *not* separable in the conventional normal-mode coordinates; the use of the latter is valid only for low-lying vibrational levels and is inadequate for the dissociating states.

These zero-order nuclear-diabatic states are coupled: the intrastate (discrete–discrete and continuum–continuum) couplings by the residual perturbation H^1 have been discussed by Atabek *et al.* (20) and by Beswick and Jortner (19);[3] our interest here is the interstate coupling by the intramolecular non-adiabatic terms in the Hamiltonian between the discrete levels in $|b\rangle$ and the continuum states in $|u\rangle$:

$$[9] \qquad H^{u,\varepsilon_{u1},v_{u2}}_{b,v_{b1},v_{b2}} = \langle u|H_{int}|b\rangle$$

which, invoking the Condon approximation, reduces to

$$[10] \quad H^{u,\varepsilon_{u1},v_{u2}}_{b,v_{b1},v_{b2}} = \langle\Psi_u|H_{int}|\Psi_b\rangle\langle u,\varepsilon_{u1},v_{u2}|b,v_{b1},v_{b2}\rangle$$

The synthesis of the microscopic reaction probability k_{i-j} from level i ($i \equiv v_{b1},v_{b2}$) in the 'reactant' to level j ($j \equiv \varepsilon_{u1},v_{u2}$) in the 'product' centres upon the nuclear factor $\langle u,\varepsilon_{u1},v_{u2}|b,v_{b1},v_{b2}\rangle$ and the electronic factor $\langle\Psi_u|H_{int}|\Psi_b\rangle$ in eq. [10]. Explicitly,

$$[11] \quad k_{i-j} \equiv k^{u,\varepsilon_{u1},v_{u2}}_{b,v_{b1},v_{b2}} = (2\pi/\hbar)|H^{u,\varepsilon_{u1},v_{u2}}_{b,v_{b1},v_{b2}}|^2 = (2\pi/\hbar)R_{ub}{}^2 q_{\varepsilon_{u1}v_{u2}v_{b1}v_{b2}}$$

where $R_{ub} = \langle\Psi_u|H_{int}|\Psi_b\rangle$ is the electronic transition moment between $|u\rangle$ and $|b\rangle$;

$$q_{\varepsilon_{u1}v_{u2}v_{b1}v_{b2}} = |\langle u,\varepsilon_{u1},v_{u2}|b,v_{b1},v_{b2}\rangle|^2$$

is the Franck–Condon density of the ($\varepsilon_{u1},v_{u2} - v_{b1},v_{b2}$) transition, and factorises into

$$[12] \qquad q_{\varepsilon_{u1}v_{u2}v_{b1}v_{b2}} = q_{\varepsilon_{u1}v_{b1}}q_{v_{u2}v_{b2}}$$

with

$$q_{\varepsilon_{u1}v_{b1}} = |\langle\phi_{\varepsilon_{u1}}|\phi_{v_{b1}}\rangle|^2$$

and

$$q_{v_{u2}v_{b2}} = |\langle\chi_{v_{u2}}|\chi_{v_{b2}}\rangle|^2$$

For the bound state $|b\rangle$, we assume a harmonic potential for the AB bond and a Morse potential for the BX bond,

$$[13a] \quad V_{b1}(r_{BX}) = D_e\{1 - \exp[-\alpha(r_{BX} - \bar{r}_{BX,b})]\}^2$$

$$[13b] \qquad V_{b2}(r_{AB}) = \tfrac{1}{2}k_b(r_{AB} - \bar{r}_{AB})^2$$

For the unbound state $|u\rangle$, we assume a harmonic potential for the diatomic fragment AB,

$$[14a] \qquad V_{u2}(r_{AB}) = \tfrac{1}{2}k_u(r_{AB} - \bar{r}_{AB,u})^2$$

and an exponential repulsive potential along the BX

[3]The discrete–discrete couplings in van der Waals molecules have been shown (19) to be negligible; the couplings between the high-lying states in conventional molecules are likely to be similar. The continuum–continuum couplings are important in modifying the final product state distribution.

coordinate,

$$[14b] \quad V_{u1}(r_{BX}) = A \exp(-a\bar{r}_{BX}) = \tilde{A} \exp[-a(r_{BX} - \bar{r}_{BX,b})]$$

The eigenfunctions corresponding to these potentials are (21–23):

$$[15] \quad \phi_{v_{b1}}(r_1) = [(2\kappa - 2v_{b1} - 1)\alpha/(v_{b1}!\Gamma(2\kappa - v_{b1}))]^{1/2} z^{-1/2} W_{\kappa,\kappa-v_{b2}-1/2}(z)$$

$$[16] \quad \phi_{\varepsilon_{u1}}(r_1) = 2/\pi[\mu_1/a \sinh(2\pi k/a)]^{1/2} K_{2ik/a}(\eta)$$

$$[17] \quad \chi_{v_{s2}}(r_2) = (\alpha_{s2}/\pi)^{1/4}(2^{v_{s2}}v_{s2}!)^{-1/2} \times \exp(-\alpha_{s2}x_s^2) H_{v_{s2}}(\alpha_{s2}^{1/2}x_s)$$

where

$$\kappa = (2\mu_1 D_e)^{1/2}/(\alpha\hbar)$$

$$z = (8\mu_1)^{1/2}/(\alpha\hbar) \exp[-\alpha(r_1 - \bar{r}_{BX,b} - \theta\bar{r}_{AB,b})]$$

$$k = (2\mu_1\varepsilon)^{1/2}/\hbar$$

$$\eta = (8\mu_1 A)^{1/2} \exp[-\tfrac{1}{2}a(r_1 - \theta\bar{r}_{AB,u})]/(a\hbar)$$

$$x_s = r_2 - \bar{r}_{AB,s}$$

$$\alpha_{s2} = (\mu_2 k_s/\hbar^2)^{1/2}$$

$$s \equiv b \text{ or } u$$

$W_{\lambda,\mu}(x)$ is the Whittaker function, $K_\lambda(x)$ the Bessel function, $H_n(x)$ the Hermite polynomial, and $\Gamma(x)$ the Gamma function (24). Notice that $\phi_{\varepsilon_{u1}}$ is normalised to the delta-function with respect to energy. The bound states are characterised by energies

$$E(b,v_{b1},v_{b2}) = E_{b0} + E_{v_{b1}} + E_{v_{b2}}$$

where E_{b0} is the electronic origin of $|b\rangle$,

$$E_{v_{b1}} = \omega_{b1}(v_{b1} + \tfrac{1}{2}) - \omega_{b1}x_{b1}(v_{b1} + \tfrac{1}{2})^2$$

$$E_{v_{b2}} = \omega_{b2}(v_{b2} + \tfrac{1}{2})$$

Likewise, the continuum states have energies

$$E(u,\varepsilon_{u1},v_{u2}) = E_{u0} + \varepsilon_{u1} + E_{v_{b2}}$$

with

$$E_{v_{u2}} = \omega_{u2}(v_{u2} + \tfrac{1}{2})$$

Note that

$$\omega_{b1} = \hbar\alpha(2D_e/\mu_1)^{1/2}$$

$$\omega_{b1}x_{b1} = \hbar^2\alpha^2/(2\mu_1)$$

$$\omega_{s2} = \hbar(k_s/\mu_2)^{1/2} \qquad (s \equiv u, b)$$

The overlap of the wavefunctions $\chi_{v_{u2}}$ and $\chi_{v_{b2}}$ is approximated by the analytic expression

$$[18] \quad q_{v_{u2}v_{b2}} = |\langle\chi_{v_{u2}}|\chi_{v_{b2}}\rangle|^2 \simeq (m!/n!)\eta^{n-m}[L_m^{n-m}(\eta)]^2 \exp(-\eta)$$

where

$$m = \min(v_{u2}, v_{b2})$$

$$n = \max(v_{u2}, v_{b2})$$

$$\eta = \tfrac{1}{2}(\alpha_{u2}\alpha_{b2})^{1/2}(\bar{r}_{AB,u} - \bar{r}_{AB,b})^2$$

and $L_m^n(x)$ is the generalised Laguerre polynomial (24). The expression [18] is exact when $\alpha_{u2} = \alpha_{b2}$, and is an excellent approximation in real physical systems where α_{u2} is close to α_{b2}; the derivation of [18] is straightforward by approximating α_{u2} and α_{b2} by $(\alpha_{u2}\alpha_{b2})^{1/2}$ in [17].

For the overlap of the wavefunctions $\phi_{\varepsilon_{u1}}$ and $\phi_{v_{b1}}$, the dominant contribution is localised in the curve-crossing region. Hence, one may employ the semi-classical approximation by linearising the respective potentials at their turning points and approximating the wavefunctions by Airy functions. One then obtains

$$[19] \quad q_{\varepsilon_{u1}v_{b1}} = |\langle\phi_{\varepsilon_{u1}}|\phi_{v_{b1}}\rangle|^2 \simeq \{4\mu^2/[\hbar^4 F_u F_b(F_u - F_b)^2]\}^{1/3}\alpha \times [(2D_e/\mu_1)^{1/2} - (2v_{b1} + 1)\alpha/(2\mu_1)] \times \mathrm{Ai}^2[(2\mu_1 F_u F_b/(\hbar^2(F_u - F_b)))]^{1/3}\Delta r]$$

where

$$\Delta r = r_{tu} - t_{tb} = \alpha^{-1} \ln[1 - (E_{v_{b1}}/D_e)^{1/2}] - a^{-1} \ln(\varepsilon/\tilde{A}) + \theta(\bar{r}_{AB,u} - \bar{r}_{AB,b})$$

$$F_u = -\partial V_{u1}/\partial r_1|_{r_{tu}} = \varepsilon b$$

$$F_b = -\partial V_{b1}/\partial r_1|_{r_{tb}} = -2\alpha E_{v_{b1}}^{1/2}(D_e^{1/2} - E_{v_{b1}}^{1/2})$$

The derivation of [19] is given in the Appendix.

In spin-forbidden reactions, the intramolecular non-adiabatic coupling H_{int} is the spin–orbit coupling between states of different spin. Hence, one may identify the electronic transition moment R_{ub} with the spin–orbit coupling constant between the two spin states, H_{ub}^{so},

$$[20] \quad R_{ub} = \langle\Psi_u|H_{int}|\Psi_b\rangle = H_{ub}^{so}$$

Given the relevant spectroscopic parameters, the microscopic reaction probabilities $k_{i\to j}$ may be computed using eqs. [11], [12], [18], [19], and [20].

III. Spectroscopic Data

The relevant parameters in the model potentials are derived from spectroscopic data: they are summarised in Table 1.

For the harmonic potential in the dissociative state, V_{u2}, the force constant k_u is related to the vibrational frequency of the diatomic molecule by

$$k_u = \mu_2\omega_{AB,u}^2/\hbar^2$$

TABLE 1. Spectroscopic parameters for model potentials[a]

Potential	Parameter (AB—X)	Value N$_2$—O	Value OC—O
V_{b1}	α (Å^{-1})	2.8510(25)	2.5583[b]
	$\bar{r}_{BX,b}$ (Å)	1.1856(25)	1.1621(26)
	D_e (cm^{-1})[c]	30560.2[d]	61447.0[d]
	$zpe_{BX,b}$ (cm^{-1})	648.4 (27)	994.3[e]
V_{b2}	$\omega_{AB,b}$ (cm^{-1})	2252.8(27)	1988.6[f]
	$\bar{r}_{AB,b}$ (Å)	1.1266(25)	1.1621(26)
	k_b (au)	1.3447[g]	1.0261(28)
	$zpe_{AB,b}$ (cm^{-1})	1137.8(27)	994.3[e]
V_{u1}	$\tilde{A}$ (cm^{-1})[h]	20400.2[i]	21797.1[j]
	a (au)	0.65[k]	6.0[k]
V_{u2}	$\omega_{AB,u}$ (cm^{-1})	2330.7(29)	2143.3(29)
	$\bar{r}_{AB,u}$ (Å)	1.0975(25)	1.1282(29)
	k_u (au)[l]	1.4393	1.2016
	$zpe_{AB,u}$ (cm^{-1})	1176.2(29)	1071.6(29)
	Additional parameters		
	ω_{bend} (cm^{-1})	599.4(27)	677.2(28)
	B_e (cm^{-1})	0.41901(26)	0.39021(26)
	D_0(AB—X) (kcal/mol)	38.55(30)	125.75(30)
	$E_{u0} - E_{b0}$ (cm^{-1})[m]	14692.5	45576.3
	zpe_{ABX} (cm^{-1})[n]	2385.5	2665.9
	μ_1 (amu)	10.1806	10.1791
	μ_2 (amu)	7.0015	6.8562

[a]Conversion factor for energy: 1 au = 219 474.7 cm^{-1}; 1 kcal/mol = 349.758 cm^{-1}; for mass: 1 amu = 1822.853 au; for length: 1 au = 0.529177 Å.
[b]$\alpha = (k_b/2D_e)^{1/2}$.
[c]$D_e = D_0$(AB—X) + $zpe_{ABX} - zpe_{AB,u} + E(X^*)$; $E(X^*)$ being the energy of X in the excited product state.
[d]$E(X^*) = E(O^1D) = 15\,867.7$ cm^{-1} (31).
[e]Approximated by $\frac{1}{2}\hbar(k_b/\mu_2)^{1/2}$.
[f]$\omega_{AB,b} = \hbar(k_b/\mu_2)^{1/2}$.
[g]$k_b = \mu_2\omega_{AB,b}^2/\hbar^2$.
[h]See eq. [21] in text.
[i]$\Delta E_{vert} = 34\,482.8$ cm^{-1} from Sponer and Bonner (32).
[j]$\Delta E_{vert} = 66\,459.4$ cm^{-1} from Winter *et al.* (33).
[k]See text.
[l]$k_u = \mu_2\omega_{AB,u}^2/\hbar^2$.
[m]$E_{u0} - E_{b0} = D_0$(AB—X) + $zpe_{ABX} - zpe_{AB,u}$.
[n]$zpe_{ABX} = zpe_{AB,b} + zpe_{BX,b} + \omega_{bend}$.

ω_{AB} being the vibrational frequency of the diatomic molecule AB; $\bar{r}_{AB,u}$ is simply the equilibrium separation of the diatomic AB.

The potentials V_{b1} and V_{b2} are derived from the ground-state potential surface of the triatomic. For N_2O, Morse type functions have been found (25) to be very good approximations in describing the stretching potentials for the two bonds. Following Suzuki (25), V_{b1} is identified with the stretching potential in the NO bond, and V_{b2} with that in the N_2 bond: the use of a harmonic potential for the latter is justified here since the dissociation energy is higher (for the N_2 bond) and the important reactive states are associated with low excitation in this bond. For CO_2, the model potential surfaces assumed here do not, in fact, have the proper symmetry in the Franck–Condon region, where either oxygen atom may dissociate: to circumvent this deficiency, a symmetry number of 2 is incorporated into the microscopic dissociation probability. The bound state potentials V_{b1} and V_{b2} are constructed from the potential energy function of Cihla and Chedin (28) along the CO coordinate: for V_{b2}, $k_b = 1.0261$ au ($=2f_1r_{12}^{0\,2}$, in the notation of ref. 28) and $\bar{r}_{AB,b} = 1.1621$ Å; for V_{b1}, the range parameter α is obtained using the relationship $\alpha = (k_b/2D_e)^{1/2}$.

Spectroscopic data for the repulsive potential V_{u1} are less complete. Indeed, there is no a priori justification for representing the potential by a pure exponential repulsive form, aside from its associated analytic tractability, and the fact that only two parameters are necessary to characterise the geometry of the potential. The strength parameter $\tilde{A}$ may be deduced from the vertical transition energy between the two electronic states at the ground-state equilibrium nuclear configuration. Explicitly,

$$[21]\quad \tilde{A} \equiv Ae^{-a\bar{r}_{BX,b}} = \Delta E_{vert} + zpe_{ABX} - zpe_{AB,u} - \omega_{bend} - (E_{u0} - E_{b0})$$

where $(E_{u0} - E_{b0}) = D_0(\text{AB—X}) + zpe_{\text{ABX}} - zpe_{\text{AB},u}$ is the difference of the two electronic origins; D_0(AB—X) the thermochemical dissociation energy of ABX; zpe_x the zero-point-energy of species x, and ω_{bend} the bending frequency. The spectroscopic values of the vertical transition energies for both N_2O and CO_2 are in fact uncertain. Nor are the state assignments unambiguous. Two dissociative triplet states correlate with the ground dissociation limit: $^3\Sigma^-$ and $^3\Pi$. The two states lie close to one another. In CO_2, the $^3\Sigma^-$ state is 1 eV below the $^3\Pi$ state; the corresponding separation in N_2O is unknown. We assume for the purpose of this work the $^3\Sigma^-$ state to be the upper repulsive state; it is clear that insofar as the present rate calculation is concerned, the state assignment is not important. For N_2O, Hall *et al.* (34) concluded from their electron loss spectrum that the $^3\Sigma^-$ state lies within 6.2 eV above the ground $^1\Sigma^+$ state. This conclusion is not inconsistent with the weak absorption maximum at 2900 Å in the continuous N_2O spectrum of Sponer and Bonner (32), which corresponds to a vertical energy of 4.27 eV, and, using eq. [21], a value of 20 400.2 cm^{-1} for $\tilde{A}$. For CO_2, Winter *et al.* obtained a value of 8.24 eV for the vertical energy of the $^3\Sigma_u^-$ state from configuration interaction calculations. No experimental data exist for this state to assess the accuracy of the theoretical value. Nevertheless, the theoretical results for the higher states compare favourably with the experimental data of Hall *et al.* (35). Using $\Delta E_{\text{vert}} = 8.24$ eV and eq. [21], we obtain $\tilde{A} = 21\,797.1$ cm^{-1}.

Spectroscopic data relevant for the shape parameter a in V_{u1} are not available for the N_2O $^3\Sigma^-$ and CO_2 $^3\Sigma_u^-$ states; the corresponding data for their neighbouring states do, however, exist. Thus, for the N_2O $^1\Sigma$ state (that correlates with $N_2(X^1\Sigma_g^+) + O(^1S)$) Shapiro (36) obtained from photodissociation data a fit to the repulsive potential in the bi-exponential form, viz. $V = A_1 \exp(-a_1 r) + A_2 \exp(-a_2 r)$, with $a_1 = 0.62$ au and $a_2 = 0.68$ au. Now, there is no a priori reason for the shape parameter of different repulsive electronic states of a molecule to be the same, but they are not expected to be appreciably different. For lack of precise data, it is reasonable to assume for the purpose of our calculation the same value of a for the $^3\Sigma^-$ state, whence we have $a = 0.65$ au for N_2O. Likewise, for CO_2, the value of 6.0 au for the dissociative state correlated with $CO(a'^3\Sigma^+) + O(^3P)$ (37) (obtained from photodissociation data (38)) is used in the present calculation.

No theoretical calculations have yet been reported for the spin–orbit interactions in the N_2O and CO_2 systems, although procedures are available for relating the values in the two molecular systems to those of the component atoms. The spin–orbit interaction between $O(^1D_2)$ and $O(^3P_2)$ is 106 cm^{-1}; the values for both N_2O and CO_2 may be expected to be similar (9).[4] We assume $H_{ub}^{so} = 106$ cm^{-1} in our calculations.

IV. Microscopic Reaction Probability

Using the spectroscopic data in Table 1 and the theoretical results in Section II, we have computed the microscopic reaction probabilities k_{i-j} for reactive states i up to 100 and 180 kcal/mol (relative to the electronic origin) for N_2O and CO_2, respectively.

The potential surface geometries (in the important energy region) for the two reactions are qualitatively different, and this is reflected in the behaviour of the respective probabilities. Figure 1 *a* and *b* shows the assumed model potentials for N_2O and CO_2 respectively, along their 'reaction co-ordinates'. In N_2O, the repulsive potential spans a relatively wide range (the range parameter $a = 0.65$ is small) and the curve-crossing point lies about 24 kcal/mol above the dissociation limit. In contrast, the repulsive potential in CO_2 is much steeper (the range parameter $a = 6.0$ is large) and the curve crossing lies only barely above the dissociation limit. Now for reactive channels below the curve-crossing point [i.e. $\Delta = \varepsilon_{u1} - (E_c - E_0) < 0$], the Franck–Condon density $q_{\varepsilon_{u1} v_{b1}}$ in eq. [19] decreases exponentially with $|\Delta|$. The implication of this is that in N_2O, k_{i-j} is extremely small (compared with the maximum value of $\sim 10^{12}$ s^{-1}) for states lying within 20 kcal/mol above the reaction threshold E_0. In CO_2 on the other hand, where the curve-crossing point lies close to the threshold, the first maximum of k_{i-j} is reached within 5 kcal/mol above the threshold.

Note that in the present collinear model, the reaction probability k_{i-j} is a function of three quantities: v_{b1}, v_{b2}, and one of ε_{u1} and v_{u2} (the four being related to one another by $E_{b0} + E_{v_{b1}} + E_{v_{b2}} = E_{u0} + \varepsilon_{u1} + E_{v_{u2}}$) and it is not feasible to discuss in detail the results for all of the thousands of reaction channels. Rather, it is more instructive to highlight the qualitative features of the k_{i-j} function in terms of the calculated results for representative groups of reaction channels. Figure 2 gives the logarithmic plots of k_{i-j} versus the energy of the reactive states for four groups of reaction channels in the N_2O reaction: ($v_{b2} = 0 \rightarrow v_{u2} = 0$), ($v_{b2} = 0 \rightarrow v_{u2} = 1$), ($v_{b2} = 4 \rightarrow v_{u2} = 3$), and ($v_{b2} = 4 \rightarrow v_{u2} = 2$): only reactive channels for which $k_{i-j} > 10^7$ s^{-1} are shown.

[4] $H_{ub}^{so} \simeq 100$ cm^{-1} for O_2 $B^3\Sigma_u^-$ and $^3\Pi_u$ (39), and $\simeq 70$ cm^{-1} for NO $^4\Sigma^-$ and $^2\Pi$ (29). Also, the coupling constants for N_2O^+ $X^2\Pi_g$ and CO_2^+ $X^2\Pi_g$ are 133 cm^{-1} and 160 cm^{-1}, respectively (40).

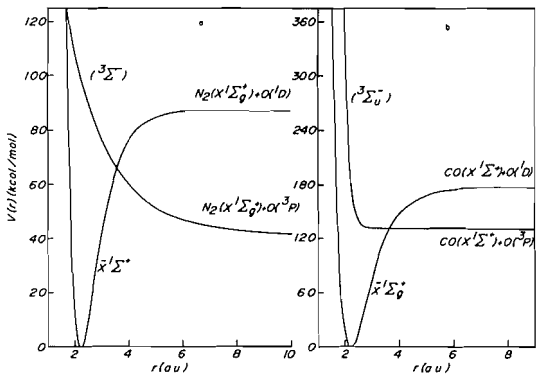

FIG. 1. (*a*) Potential energy curve for N_2O along the N_2—O coordinate; r is the internuclear separation between N and O. The triplet state assignment is uncertain. The two curves cross at 66.2 kcal/mol (64.3 kcal/mol above the zero point energy). (*b*) Potential energy curve for CO_2 along the OC—O coordinate; r is the internuclear separation between C and O. The triplet state assignment is uncertain. The two curves cross at 130.3 kcal/mol (127.5 kcal/mol above the zero point energy).

Note that the energy is relative to the zero point energy *zpe* ($= \frac{1}{2}\omega_{b1} - \frac{1}{4}\omega_{b1}x_{b1} + \frac{1}{2}\omega_{b2}$) and the reaction threshold corresponds to $D_0(N_2—O) =$ 38.55 kcal/mol in the scale of the diagram. (*i*) Above the curve-crossing point, the reaction probability k_{i-j} exhibits quasi-periodic fluctuations within each (v_{b2},v_{u2}) series; the increase in fluctuation frequency with energy is related in part to the increased steepness of the repulsive potential at high energy. (*ii*) Between the two $v_{b2} = 0$ series, the first one ($v_{u2} = 0$) has larger reaction probabilities than the second ($v_{u2} = 1$); this is not surprising in view of the respective wavefunction overlaps $q_{v_{u2}v_{b2}}$ (eq. [18]). Indeed, the corresponding probabilities for the ($v_{b2} = 0 \rightarrow v_{u2} = 2$) series are even smaller. (*iii*) On the other hand, between the two $v_{b2} = 4$ series, the one corresponding to $\Delta v = v_{b2} - v_{u2} = 2$ has *larger* reaction probabilities than the other ($\Delta v = 1$) near 80 kcal/mol. This is because the wavefunction overlap $q_{\varepsilon_{u1}v_{b1}}$ is now overwhelmingly more favourable for the former series. (*iv*) The reaction probabilities in these two series are much smaller than the $v_{b2} = 0$ series in magnitude. Nevertheless, these reactive channels become important above 85 kcal/mol where there are fewer and fewer bound states belonging to the low v_{b2} groups. (*v*) The maximum value of k_{i-j} is about 10^{12} s^{-1}; this compares with the classical vibrational frequency of the order 10^{14} s^{-1} along the v_{b1} (NO) coordinate, and corresponds to a curve-crossing probability of the order of 0.01. (*vi*) The successive maxima in the $v_{b2} = v_{u2} = 0$ series are similar in magnitude. This contrasts the corresponding behaviour in CO_2.

Figure 3 gives the k_{i-j} versus energy plots for the

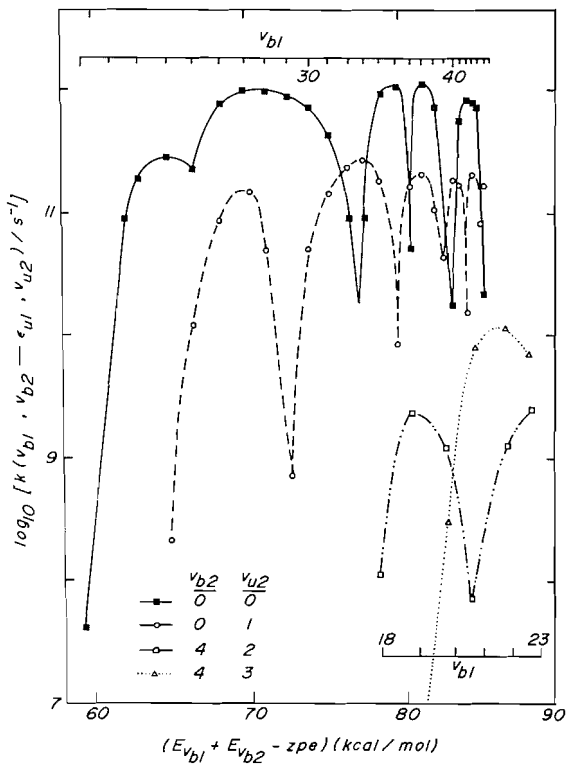

FIG. 2. Microscopic reaction probability for the dissociation of N_2O. $k(v_{b1},v_{b2} - \varepsilon_{u1},v_{u2})$ is the probability between discrete state (v_{b1},v_{b2}) in electronic state $|b\rangle$ and continuum state $(\varepsilon_{u1},v_{u2})$ in electronic state $|u\rangle$. The energy is relative to the zero point energy; the reaction threshold is 38.55 kcal/mol in the scale of the diagram.

($v_{b2} = v_{u2} = 0$) and the ($v_{b2} = 0 \rightarrow v_{u2} = 1$) series in CO_2. (*i*) There is now a systematic decrease in the magnitude of the k_{i-j} maxima with increasing energy. (*ii*) The fluctuation of the magnitude of k_{i-j} with energy is more frequent. (*iii*) The solid triangles correspond to reactive channels above 150 kcal/mol, in which $v_{b2} > 0$ and for which $k_{i-j} > 2 \times 10^{11}$ s^{-1}. These triangles indicate that in this energy region reaction channels in excited v_{b2} states are more important than those in the ground v_{b2} states. (*iv*) The first maximum of k_{i-j} is at 131 kcal/mol, only 4 kcal/mol above the reaction threshold. These features, compared with those in N_2O, are the direct consequences of the relative steepness of the repulsive potential and the closeness between the curve crossing and the reaction threshold energies.

Within the framework of the collinear model, one may in principle determine from k_{i-j} the product distribution of a reaction, given the reactant state distribution; of course, it should be kept in mind that the continuum–continuum (intrastate) coupling by

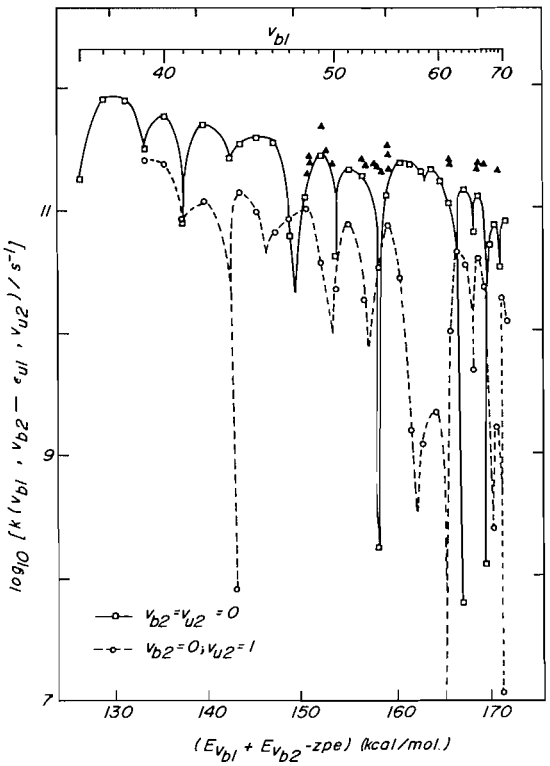

FIG. 3. Microscopic reaction probability for the dissociation of CO_2. $k(v_{b1},v_{b2} - \varepsilon_{u1},v_{u2})$ is the probability between discrete state (v_{b1},v_{b2}) in $|b\rangle$ and continuum state $(\varepsilon_{u1},v_{u2})$ in $|u\rangle$. The energy is relative to the zero point energy; the reaction threshold is 125.75 kcal/mol in the scale of the diagram. The solid triangles refer to reactive states above 150 kcal/mol relative to the zero point energy and with reaction probabilities greater than 2×10^{11} s^{-1}; see text.

the residual perturbation may modify the "nascent" product distribution.[3]

V. High-pressure Unimolecular Reaction Rate

In the high-pressure limit, the unimolecular reaction rate is (17)

$$[22] \qquad k_\infty = \sum \tilde{n}_i k_i$$

where $\tilde{n}_i$ is the equilibrium fractional population, k_i is the reaction probability from reactive state i, and the summation is over all reactive states. Explicitly

$$[23] \qquad \tilde{n}_i = g_i \exp(-\beta E_i)/Q(\beta)$$

and

$$[24] \qquad k_i = \sum_j k_{i-j}$$

where $\beta = 1/kT$ is the inverse temperature, $Q(\beta)$ is the partition function, g_i is the state-degeneracy of i, and the j-summation in eq. [24] is over all accessible product channels.

A full *ab-initio* calculation of the microscopic reaction probability for linear triatomics should incorporate not only the two stretching modes, but also the two bending modes and the rotation of the reactant molecule. However, the increase of elaboration in incorporating the bending and rotational motions into the theoretical treatment is formidable (41) and the current knowledge of the potential surfaces does not justify any such calculations. In the present work, we make the assumption that the microscopic reaction probability from a state $(v_{b1}, v_{b2}, v_{\text{bend}}, J, M_J)$ is independent of v_{bend}, J, and M_J, where v_{bend}, J, and M_J are respectively the bending and rotational quantum numbers. Explicitly, we have

$$[25] \qquad k_{v_{b1},v_{b2},v_{\text{bend}},J,M_J} = k_{v_{b1},v_{b2},0,0,0}$$

where

$$[25a] \qquad k_{v_{b1},v_{b2},0,0,0} \equiv k_{v_{b1}v_{b2}} = \sum_{v_{u2}} k^{u,\varepsilon_{u1},v_{u2}}_{b,v_{b1},v_{b2}}$$

$$[26] \qquad E_{v_{b1},v_{b2},v_{\text{bend}},J,M_J} = E_{v_{b1},v_{b2},0,0,0} + (v_{\text{bend}} + 1)\omega_{\text{bend}} + J(J+1)B_e$$

where

$$[26a] \qquad E_{v_{b1},v_{b2},0,0,0} \equiv E_{v_{b1},v_{b2}} = E_{v_{b1}} + E_{v_{b2}}$$

The high-pressure rate expression [22] then reduces to

$$[27] \qquad k_\infty = \frac{\sum_{v_{b1}} \sum_{v_{b2}} k_{v_{b1},v_{b2}} \exp(-\beta E_{v_{b1},v_{b2}})}{\sum_{v_{b1}} \sum_{v_{b2}} \exp(-\beta E_{v_{b1},v_{b2}})}$$

The activation energy E_∞ and pre-exponential factor A_∞ in the Arrhenius expression are respectively

$$[28] \qquad E_\infty = \frac{\left\{\sum_{v_{b1}} \sum_{v_{b2}} k_{v_{b1},v_{b2}} E_{v_{b1},v_{b2}} \exp(-\beta E_{v_{b1},v_{b2}})\right\}}{\left\{\sum_{v_{b1}} \sum_{v_{b2}} k_{v_{b1},v_{b2}} \exp(-\beta E_{v_{b1},v_{b2}})\right\}} - \frac{\sum_{v_{b1}} \sum_{v_{b2}} E_{v_{b1},v_{b2}} \exp(-\beta E_{v_{b1},v_{b2}})}{\sum_{v_{b1}} \sum_{v_{b2}} \exp(-\beta E_{v_{b1},v_{b2}})}$$

and

$$[29] \qquad A_\infty = k_\infty \exp(\beta E_\infty)$$

Given the reaction probabilities $k_{v_{b1},v_{b2}}$ and the energy levels $E_{v_{b1},v_{b2}}$, it is straightforward to calculate k_∞, E_∞, and A_∞ using eqs. [27]–[29]. In the following calculations, we have excluded reactive states for which the reaction probabilities are less than 10^5 s^{-1} since their contributions to k_∞ are negligible (except for temperatures below 200 K in N_2O). There are 527 (v_{b1},v_{b2}) states in N_2O for which $k_{v_{b1},v_{b2}}$ exceeds 10^5 s^{-1}; 949 states in CO_2.

A. N_2O Dissociation

The decomposition of N_2O represents one of the most extensively studied unimolecular reactions; a thorough evaluation of the relevant kinetic data has recently been presented by Baulch *et al.* (42). Nevertheless, data at high pressure (first order region) are limited. Figure 4 compares the data of Olschewski *et al.* (10) between 1400 and 2100 K and those of Johnston (43) at 888 K with calculation above 800 K. The calculated curve is in good agreement with experiments, both in the activation energy and actual magnitude, except above 1700 K, where there is a gradual departure. The departure is more apparent in the inset, where the actual experimental data points of Olschewski *et al.* (10) are shown. The origin of this seemingly divergent departure is not clear, though it could well be due to the inadequacy of the theoretical model; for example, rotation might lower the activation energy at high temperature, as is the case in diatomic dissociation (44, 45). The assumed potential surface is fairly realistic, possessing the various qualitative features that are important to the reaction process, and it is unlikely that within the framework of the present collinear model, improved spectroscopic data will significantly modify the calculated rates.

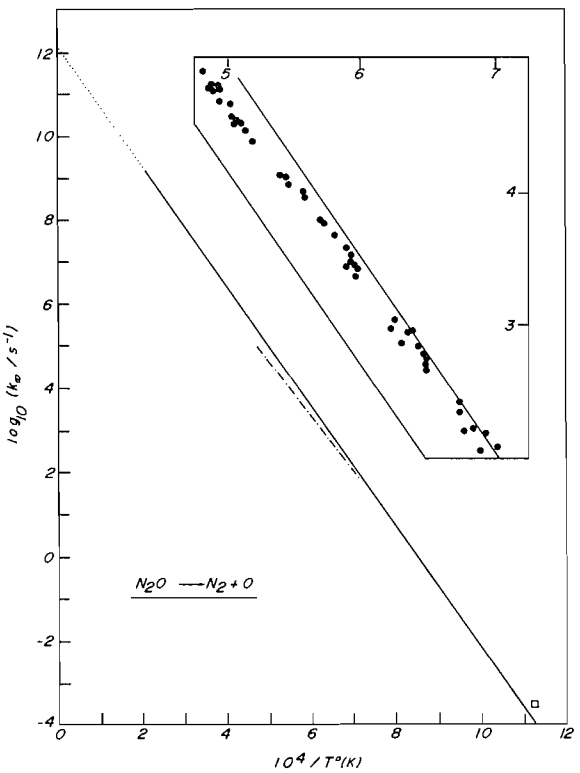

FIG. 4. Arrhenius plot for the infinite-pressure rate constant for the dissociation of N_2O. Experiments: ·····, Olschewski *et al.* (10), □, Johnston (43). Theory: —, eq. [27]; · · ·, Arrhenius rate law with $A_{\infty,\text{calcd}} = 1.41 \times 10^{12}\ s^{-1}$, and $E_{\infty,\text{calcd}} = 65.1$ kcal/mol. Inset: ●, data of Olschewski *et al.* (10); —, calculated rates from eq. [27].

Table 2 lists the Arrhenius parameters A_∞ and E_∞ between 5000 and 300 K. Despite the strong variation of the reaction probabilities with energy near the threshold in N_2O, the activation energy E_∞ varies only by about 10% over the temperature range covered in the table, and by about 5% in the temperature range of experimental interest (1000–2500 K). The pre-exponential factor A_∞ varies by less than a factor of two above 1000 K, and it is only below 750 K that it falls rapidly with temperature. The moderate variations in both A_∞ and E_∞ with temperature mean that the calculated rates may be *very well approximated* by a strict Arrhenius rate expression, viz. $k_\infty = A_{\infty,\text{calcd}} \exp(-E_{\infty,\text{calcd}}/RT)$, with $A_{\infty,\text{calcd}} = 1.41 \times 10^{12}\ s^{-1}$ and $E_{\infty,\text{calcd}} = 65.1$ kcal/mol, as is shown by the dotted line in Fig. 2. The implications of this on the Slater–Forst inversion procedure (16–17) of high-pressure experimental rate data will be examined in detail in a future publication.

B. CO_2 Dissociation

Compared with the N_2O reaction, the decomposition of CO_2 is less well understood. A variety of explanatory mechanisms have been proposed to account for the observed behaviour of the reaction rate (see ref. 18). In particular, an attractive triplet state ($^3B_2$) that correlates with ground state $CO(^1\Sigma^+)$ and $O(^3P)$ has been proposed by Lin and Bauer (46) and by Clyne and Thrush (47) to account for the "anomalous" activation energy of the reaction rate at low pressure. We have shown in the accompanying paper (48) that the low activation energy of the low-pressure reaction rate at high temperature is due, in fact, to the severe population disequilibrium in the reactant; the postulation of an attractive triplet potential does not seem necessary for the interpretation of rate data at low pressure and high temperature. The high-pressure reaction rate is not influenced

TABLE 2. Arrhenius parameters for the dissociation of N_2O

T (K)	A_∞ (s^{-1})	E_∞ (kcal/mol)
5000	8.24(11)[a]	61.2
4000	1.12(12)	64.0
3000	1.44(12)	65.8
2000	1.53(12)	66.1
1000	8.93(11)	64.7
750	5.94(11)	64.0
500	3.05(11)	63.2
300	7.15(10)	62.1

[a]8.24(11) = 8.24×10^{11}.

TABLE 3. Arrhenius parameters for the dissociation and recombination of CO_2

T (K)	A_∞[a] (s^{-1})	E_∞[a] (kcal/mol)	K_c[b] (mol/cm^3)	$k_{\infty,rec}$[b] (cm^3/mol s)	$E_{\infty,rec}$[c] (kcal/mol)
6000	1.07(12)[d]	121.4	2.926(−3)	1.39(10)	8.9
5000	1.31(12)	123.6	4.351(−4)	1.20(10)	8.0
4000	1.60(12)	125.4	2.316(−5)	9.79(9)	6.7
3000	1.96(12)	126.8	1.544(−7)	7.40(9)	5.0
2000	2.43(12)	127.8	5.384(−12)	4.86(9)	3.1
1000	2.72(12)	128.2	1.148(−25)	2.24(9)	1.8
700	2.25(12)	127.9	1.701(−37)	1.53(9)	1.1
500	1.61(12)	127.5	2.614(−53)	1.12(9)	0.71
400	1.24(11)	127.3	3.734(−67)	9.34(8)	0.50
300	8.75(11)	127.1	3.190(−90)	7.58(8)	0.42
250	7.20(11)	127.0	1.152(−108)	6.58(8)	0.42
200	5.89(11)	126.9	2.632(−136)	5.33(8)	

[a]Equation [29].
[b]Equation [30].
[c]$E_{\infty,rec} = -R \ln [k_{\infty,rec}(T_1)/k_{\infty,rec}(T_2)]/(T_1^{-1} - T_2^{-1})$.
[d]1.07(12) = 1.07×10^{12}.

by the collisional energy transfer (and non-equilibrium effects) of the reactant; rather, it is related to the $k(E)$ function which depends on the reactant potential surface. The present calculation assumes a purely repulsive rather than attractive triplet state potential and comparison with experimental data should throw further light on this point.

The high-pressure decomposition rate has been measured by Olschewski *et al.* (49) to be

$$k_{\infty,expt} = 2.5 \times 10^{11} \exp(-110/RT)\ s^{-1} \quad (2800\text{–}3700\ K)$$

and by Wagner and Zabel (50) to be

$$k_{\infty,expt} = 9.0 \times 10^{12} \exp(-129.7/RT)\ s^{-1} \quad (3000\text{–}3700\ K)$$

The two experiments are in good mutual agreement, despite the apparently large discrepancy between the two activation energies. Figure 5 compares these data with the calculated rates, and Table 3 lists the Arrhenius parameters A_∞ and E_∞ for the reaction from 6000 to 200 K. As discussed in Section III, a symmetry number of two has been incorporated into the calculation of $k(E)$ to take into account the symmetry of the potential surface. The good accord between the theoretical and experimental activation energies indicates that a purely repulsive triplet state is not inconsistent with experimental observations at high temperature and pressure. Notice that the variation of the activation energy with temperature is more moderate in this reaction (than in the N_2O reaction), being 5% between 200 and 6000 K and 1% in the experimental temperature range of 2000–4000 K. This smaller variation here is attributed to the less drastic variation of the $k(E)$ function with energy near the reaction threshold (cf. Fig. 3).

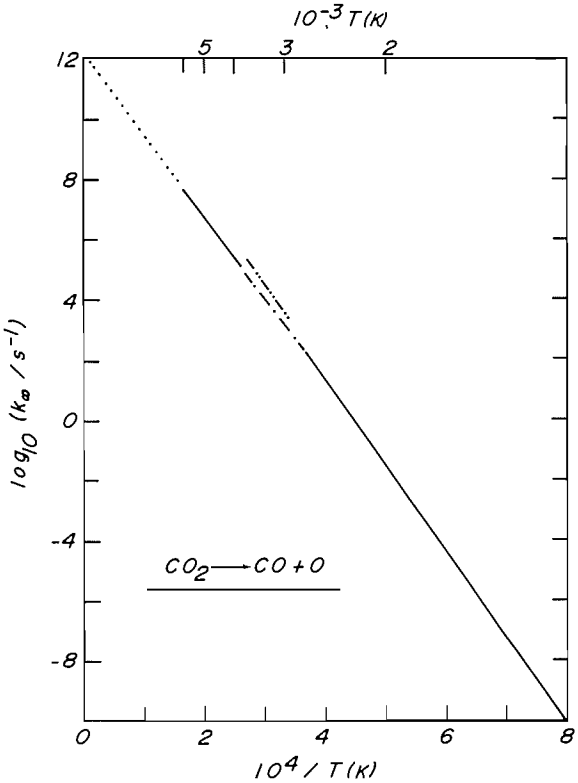

FIG. 5. Arrhenius plot for the infinite-pressure rate constant for the dissociation of CO_2. Experiments: ·····, Olschewski *et al.* (49); –·–·–, Wagner and Zabel (50). Theory: —, eq. [27]; · · ·, Arrhenius rate law with $A_{\infty,calcd} = 1.80 \times 10^{12}\ s^{-1}$ and $E_{\infty,calcd} = 127.3$ kcal/mol. The theoretical (solid) curve overlaps with the experimental (dash-dot) curve of Olschewski *et al.* (49).

Likewise, the pre-exponential factor varies only moderately, by about a factor of two between 1000 and 6000 K. Also, the dramatic drop at low temperature in N_2O is absent here. Again, the calculated

rates are well approximated by a strict Arrhenius rate expression, with $A_{\infty,\text{calcd}} = 1.80 \times 10^{12}\ \text{s}^{-1}$ and $E_{\infty,\text{calcd}} = 127.3$ kcal/mol.

C. CO_2 Recombination

The room temperature recombination rate of CO and O in the second order region has been determined on two occasions. Gaedtke *et al.* (51) studied the photolysis of NO_2 in the presence of CO and obtained an upper limit of 3×10^8 cm^3/mol s for the recombination rate coefficient $k_{\infty,\text{rec}}$. Their value is to be compared with the work of DeMore (52), who measured the relative recombination rates of CO + O and O_2 + O, and obtained (using the O_2 + O recombination rate data of Sauer (53) and of Hippler and Troe (54)) $k_{\infty,\text{rec}} \simeq 5 \times 10^8$ cm^3/mol s. The calculation of the recombination rate coefficient k_{rec} is straightforward from eq. [27] and the rate quotient law:

$$[30] \qquad k_{\infty,\text{rec}} = k_{\infty,\text{diss}}/K_c$$

Table 3 lists the recombination rate coefficient and activation energy, as well as the equilibrium constant K_c for the reaction between 200 and 6000 K. The calculated value of 7.6×10^8 cm^3/mol s at 300 K is in satisfactory agreement with the experimental values.

The temperature dependence of the high-pressure reaction rate is of some interest, even though no experimental data yet exist. Table 3 shows that the recombination reaction has a positive activation energy at high pressure. This activation energy actually varies moderately with temperature: it increases from 0.4 kcal/mol at 250 K to 9 kcal/mol at 6000 K. Experimental studies of the activation energy for the reaction should provide a stringent test on the quality of the calculated rates.

Acknowledgments

This work was supported by the National Research Council of Canada. We would also like to thank Philippe Baille for stimulating discussions concerning the theory of radiationless transitions.

1. O.K. Rice. Phys. Rev. **33**, 748 (1929).
2. U. Fano. Phys. Rev. **124**, 1866 (1961).
3. M. S. Child. Spec. Period. Rep. Mol. Spectrosc. **2**, 466 (1974).
4. M. Bixon and J. Jortner. J. Chem. Phys. **48**, 715 (1968).
5. F. H. Mies and M. Krauss. J. Chem. Phys. **45**, 4455 (1966).
6. H. Feshbach. Ann. Phys. **5**, 357 (1958).
7. R. A. Van Santen. Physica, **62**, 51 (1972).
8. N. Rosen. J. Chem. Phys. **1**, 319 (1933).
9. A. E. Stearn and H. Eyring. J. Chem. Phys. **3**, 778 (1935).
10. H. A. Olschewski, J. Troe, and H. Gg. Wagner. Ber. Bunsenges. Phys. Chem. **70**, 450 (1966).
11. R. G. Gilbert and I. G. Ross. Aust. J. Chem. **24**, 1541 (1971).
12. C. Zener. Proc. R. Soc. London A, **137**, 696 (1932).
13. J. N. Murrell and J. M. Taylor. Mol. Phys. **16**, 609 (1969).
14. O. K. Rice. J. Chem. Phys. **1**, 375 (1933).
15. H. Gebelein and J. Jortner. Theor. Chim. Acta, **25**, 143 (1972).
16. W. Forst. J. Phys. Chem. **76**, 342 (1972).
17. A. W. Yau and H. O. Pritchard. Can. J. Chem. **56**, 1389 (1978).
18. D. L. Baulch, D. D. Drysdale, J. Duxbury, and S. Grant. Evaluated kinetic data for high temperature reactions. Vol. 3. Butterworths, London. 1976.
19. J. A. Beswick and J. Jortner. J. Chem. Phys. **68**, 2277 (1978).
20. O. Atabek, J. A. Beswick, R. Lefebvre, S. Mukamel, and J. Jortner. J. Chem. Phys. **65**, 4035 (1976).
21. P. M. Morse. Phys. Rev. **34**, 57 (1929).
22. J. M. Jackson and N. F. Mott. Proc. R. Soc. London A, **137**, 703 (1932).
23. L. C. Pauling and E. B. Wilson, Jr. Introduction to quantum mechanics. McGraw Hill, New York, NY, 1935.
24. M. Abramowitz and I. A. Stegun. Handbook of mathematical functions. NBS-AMS 55 (1964).
25. I. Suzuki. J. Mol. Spectrosc. **32**, 54 (1969).
26. G. Herzberg. Electronic spectra of polyatomic molecules. Van Nostrand, New York, NY. 1966.
27. A. Chedin, C. Amiot, and Z. Cihla. J. Mol. Spectrosc. **63**, 348 (1976).
28. Z. Cihla and A. Chedin. J. Mol. Spectrosc. **40**, 337 (1971).
29. G. Herzberg. Spectra of diatomic molecules. Van Nostrand, New York, NY. 1950.
30. D. R. Stull and H. Prophet. JANAF thermochemical tables. 2nd ed. NSRDS-NBS 37 (1971).
31. C. E. Moore. Atomic energy levels. Vol. I. NSRDS-NBS 35 (1971).
32. H. Sponer and L. G. Bonner. J. Chem. Phys. **8**, 33 (1940).
33. N. W. Winter, C. F. Bender, and W. A. Goddard III. Chem. Phys. Lett. **20**, 489 (1973).
34. R. I. Hall, A. Chutjian, and S. Trajmar. J. Phys. B, **6**, L365 (1977).
35. R. I. Hall, A. Chutjian, and S. Trajmar. J. Phys. B, **6**, L264 (1977).
36. M. Shapiro. Chem. Phys. Lett. **46**, 442 (1977).
37. M. D. Morse, K. F. Freed, and Y. B. Band. Chem. Phys. Lett. **49**, 399 (1977).
38. L. C. Lee and D. L. Judge. Can. J. Phys. **51**, 378 (1973).
39. H. F. Schaefer III and W. H. Miller. J. Chem. Phys. **55**, 4107 (1971).
40. J. A. Horsley and J. A. Hall. Mol. Phys. **25**, 483 (1973).
41. M. D. Morse, K. F. Freed, and Y. B. Band. Chem. Phys. Lett. **44**, 125 (1976).
42. D. L. Baulch, D. D. Drysdale, D. G. Horne, and A. C. Lloyd. Evaluated kinetic data for high temperature reactions. Vol. 2. Butterworths, London. 1973.
43. H. S. Johnston. J. Chem. Phys. **19**, 663 (1951).
44. A. W. Yau and H. O. Pritchard. J. Phys. Chem. **83**, 134 (1979).
45. H. O. Pritchard. Acc. Chem. Res. **9**, 99 (1976).
46. M. C. Lin and S. H. Bauer. J. Chem. Phys. **50**, 3377 (1969).
47. M. A. A. Clyne and B. A. Thrush. Proc. R. Soc. London A, **269**, 404 (1962).
48. A. W. Yau and H. O. Pritchard. Can. J. Chem. This issue.
49. H. A. Olschewski, J. Troe, and H. Gg. Wagner. Ber. Bunsenges. Phys. Chem. **70**, 1060 (1966).
50. H. Gg. Wagner and F. Zabel. Ber. Bunsenges. Phys. Chem. **78**, 705 (1974).

51. H. GAEDTKE, K. GLANZER, H. HIPPLER, K. LUTHER, and J. TROE. Fourteenth Symposium (International) on Combustion, Pittsburgh, PA. 1972. p. 295.
52. W. B. DEMORE. J. Phys. Chem. **76**, 3527 (1972).
53. M. C. SAUER, JR. J. Phys. Chem. **71**, 3311 (1967).
54. H. HIPPLER and J. TROE. Ber. Bunsenges. Phys. Chem. **75**, 27 (1971).

Appendix

The wavefunction $|\phi_{v_{b1}}\rangle$ is approximated by (3)

[A1] $$\phi_{v_{b1}}(r_1) \simeq N_b \,\mathrm{Ai}\,[-c_b(r_1 - r_{tb})]$$

where

$$N_b = [2\mu_1/(F_b^{1/2}\hbar^2)]^{1/3}\rho_b^{1/2}$$
$$c_b = (2\mu_1 F_b/\hbar^2)^{1/3}$$
$$F_b = -\partial V_{b1}/\partial r_1|_{r_{tb}}$$

ρ_b the state density and r_{tb} the outer turning point. Explicitly,

$$r_{tb} = \bar{r}_{\mathrm{BX},b} + \theta\bar{r}_{\mathrm{AB},b} - \alpha^{-1}\ln(1 - E_{v_{b1}}^{1/2}/D_e^{1/2})$$

$$\rho_b = \alpha[(2D_e/\mu_1)^{1/2} - (2v_{b1} + 1)\alpha/(2\mu_1)]$$

and

$$F_b = -2\alpha\, E_{v_{b1}}^{1/2}(D_e^{1/2} - E_{v_{b1}}^{1/2})$$

Likewise, the wavefunction $|\phi_{\varepsilon_{u1}}\rangle$ is approximated by

[A2] $$\phi_{\varepsilon_{u1}}(r_1) = N_u \,\mathrm{Ai}\,[-c_u(r_1 - r_{tu})]$$

where

$$N_u = [2\mu_1/(F_u^{1/2}\hbar^2)]^{1/3}$$
$$c_u = (2\mu_1 F_u/\hbar^2)^{1/3}$$
$$F_u = -\partial V_{u1}/\partial r_1|_{r_{tu}}$$

and

$$r_{tu} = \bar{r}_{\mathrm{BX},b} + \theta\bar{r}_{\mathrm{AB},u} - a^{-1}\ln(\varepsilon/\tilde{A})$$
$$F_u = b\varepsilon$$

Substitution of the respective expressions into [A1] and [A2] and integration of the two Airy functions lead to [19].

The generation of *C*-glycosides through the enolate Claisen rearrangement[1]

ROBERT E. IRELAND, CRAIG S. WILCOX, SUVIT THAISRIVONGS, AND NOEL R. VANIER
Division of Chemistry and Chemical Engineering, California Institute of Technology, Pasedena, CA 91125, U.S.A.

Received January 25, 1979

ROBERT E. IRELAND, CRAIG S. WILCOX, SUVIT THAISRIVONGS, and NOEL R. VANIER. Can. J. Chem. **57**, 1743 (1979).

The [3,3]-sigmatropic rearrangements of silyl ketene acetals obtained from aliphatic esters of furanoid and pyranoid glycals is described. The heterocyclic γ,δ-unsaturated carboxylic acids **II** are produced in good yields. A new preparation of furanoid and pyranoid glycals is described.

ROBERT E. IRELAND, CRAIG S. WILCOX, SUVIT THAISRIVONGS et NOEL R. VANIER. Can. J. Chem. **57**, 1743 (1979).

On décrit les transpositions sigmatropiques [3,3] de silylcétènes acétals obtenus à partir d'esters aliphatiques de glycals furannoïdes et pyrannoïdes. On obtient les acides carbocycliques γ,δ non saturés hétérocycliques II avec de bons rendements. On décrit une nouvelle préparation des glycals furannoïdes et pyrannoïdes.

[Traduit par le journal]

The application of the ester enolate Claisen rearrangement (1, 2) to aliphatic esters derived from β-hydroxy enol ethers was recently reported from this laboratory (3). This rearrangement provides a means for the stereoselective synthesis of either of two diasteromeric α-alkyl-β-alkoxycarboxylic acids without regard to their relative thermodynamic stabilities. Application of this procedure to furanoid and pyranoid enol ethers of type **I***a* or **I***b* provides a valuable route to oxygen heterocycles of type **II***a,b*

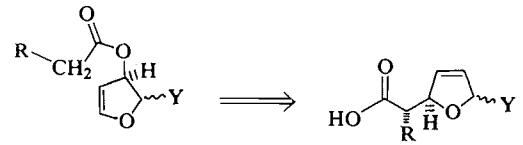

I*a* **II***a*

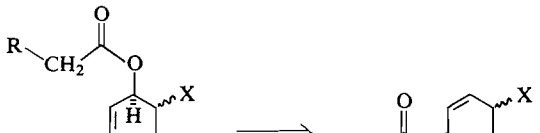

I*b* **II***b*

in which the chirality of the side chain may be preselected. Such an approach was envisioned as a key component of a convergent, general approach to the polyether class of ionophoric antibiotics, and the initial investigation that demonstrates the viability of this concept is presented here.

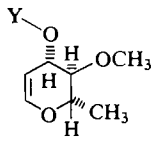

1

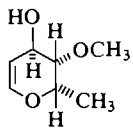

2

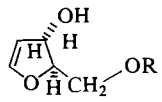

3*a* (R = —CH_3)
3*b* (R = —CH_2OCH_3)

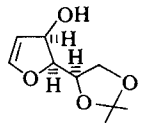

4

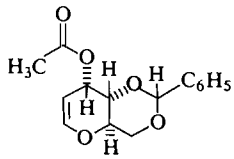

5

The preparation of the glycals **1** (Y = H), **2**, and **3***a* by an efficient new technique developed in this laboratory has already been described (4). For the synthesis of the glycal **3***b*, the lactol **6***a* (evaporative distillation 80–90°C/0.005 Torr; $[\alpha]_D^{25} = +0.9°$ (*c* 0.89, $HCCl_3$))[2] was prepared in 95% overall yield from 2,3-*O*-isopropylidene-D-(+)-ribonicacid γ-lactone by 5-*O*-methoxymethylation ($[(CH_3)_2CH]_2NC_2H_5$, CH_2Cl_2, $ClCH_2OCH_3$), and then partial reduction (DIBAL, Et_2O, −78°C). Treatment of the lactol **6***a* with CCl_4–$P(NMe_2)_3$ in tetrahydrofuran solution, and then reduction of the crude chloride with lithium in liquid ammonia (4) afforded the glycal **3***b* (evaporative distillation, 70–80°C/0.005 Torr; $[\alpha]_D^{24}$ +259° (*c* 0.91, $HCCl_3$)) in 80% overall yield,

[1]Dedicated to the memory of R. H. F. Manske.

[2]Satisfactory combustion analyses were obtained on all new substances.

0008-4042/79/131743-03$01.00/0

TABLE 1. Direct esterification–rearrangement of furanoid and pyranoid glycals

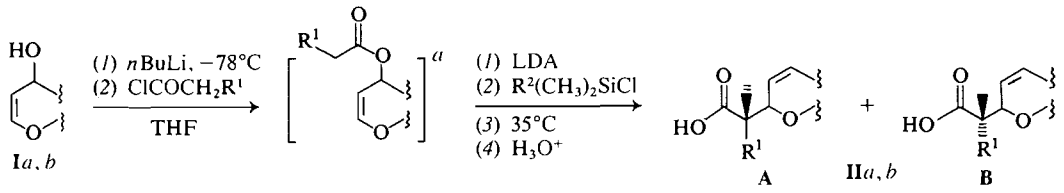

Ia, b IIa, b

Entry	Starting material	—R¹	Solvent[b]	—R²	Overall yield (%)	Products isolated	Ratio A:B[c]	$t_{1/2}$ (min)[d]
1	**1** (Y = —H)	$-CH_3$	100% THF	$-tC_4H_9$	79	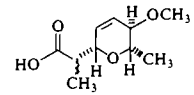	18:82	30±5
2	**2**	$-CH_3$	100% THF	$-tC_4H_9$	69		80:20	
3	**2**	$-CH_3$	23% HMPA–THF	$-tC_4H_9$	74	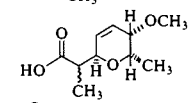	17:83	30±5
4	**3***a*	$-C_2H_5$	100% THF	$-CH_3$	75		21:79	
5	**3***a*	$-C_2H_5$	23% HMPA–THF	$-CH_3$	62	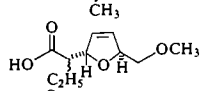	91:9	≤3
6	**3***b*	$-C_2H_5$	100% THF	$-CH_3$	73		19:81	
7	**3***b*	$-C_2H_5$	23% HMPA–THF	$-CH_3$	60	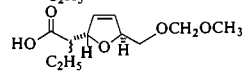	79:21	≤3
8	**4**	$-CH_3$	100% THF	$-CH_3$	52		82:18	
9	**4**	$-CH_3$	23% HMPA–THF	$-CH_3$	52	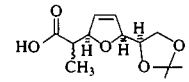	46:54[e]	≤3

[a]Intermediate ester not isolated.
[b]Solvent employed during enolization.
[c]Ratio of diastereomers obtained as determined by nmr or gc analysis.
[d]Approximate half-life for the rearrangement of silyl ketene acetal to silyl ester at 35°C.
[e]The low stereocontrol in this experiment can be attributed to an unfavorable interaction of the intermediate ketene acetal with the dioxolane side chain.

together with 13% of the simple reduction product **6***b*.[2] The glycal **4** (evaporative distillation 70–110°C/0.06 Torr; $[\alpha]_D^{23}$ −100° (*c* 1.0, $HCCl_3$)), previously prepared in 11% yield by reduction of the bromide **7***c* with sodium sand in toluene (5), was available in 75% yield, together with a 9% yield of the bisacetonide **7***b*,[3] by lithium – liquid ammonia reduction of the chloride **7***a* (6), followed by chromatography of the reduction product on silica gel. The glycal acetate **5** was generously provided by Professor B. Fraser-Reid (University of Waterloo, Ontario).

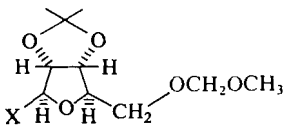

6*a* (X = —OH)
6*b* (X = —H)

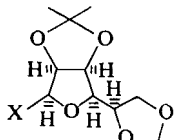

7*a* (X = —Cl)
7*b* (X = —H)
7*c* (X = —Br)

Acylation of the pyranoid glycal **1** (Y = H) with propionyl chloride and pyridine in dichloromethane solution at 0°C provided the propionate **1** (Y = $COCH_2CH_3$) (evaporative distillation 90–95°C/0.7 Torr; $[\alpha]_D^{22}$ +125° (*c* 1.1, $HCCl_3$)). Treatment of this ester under the standard conditions for ester enolate Claisen rearrangement afforded a mixture of diastereomeric acids **A** and **B** in good yield. As expected, the relative ratios of these two products was dependent upon the solvent used in the enolization step (1–3). The stereochemistry proposed for the side chain in this example and in the examples below is based upon (*i*) the control of enolate geometry previously demonstrated (2) for propionate esters and (*ii*) the assumption of a boat-like transition state for the [3,3]-sigmatropic rearrangement.

The esters derived from the pyranoid glycal **2** and especially the esters of the furanoid glycals **3***a*, **3***b*, and **4** were too unstable to allow isolation in acceptable yields. Therefore, with these substrates the technique described earlier (3) for direct acylation and rearrangement without isolation of the intermediate esters was used. Table 1 presents these results.

The enolate of the acetate **5** was best prepared with potassium hexamethyldisilazide in tetrahydrofuran at −78°C and in contrast to the ketene acetals of the monocyclic esters described above, this ketene acetal rearranged very slowly at 35°C. The half-life for the rearrangement was 8 ± 1 h at 80°C and the best yield (61%) of the rearranged product **8** (mp 95–95.5°C, $[\alpha]_D^{23}$ +67.1° (*c* 1.24, $HCCl_3$)) was obtained

[3]The production of small amounts of **6***b* and **7***b* in these reactions is in accordance with our previous experience with furanosyl chloride reductions. (See ref. 4.)

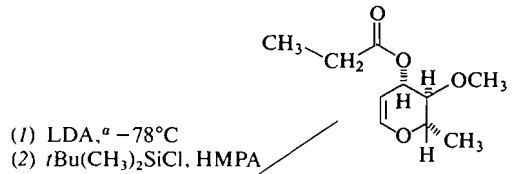

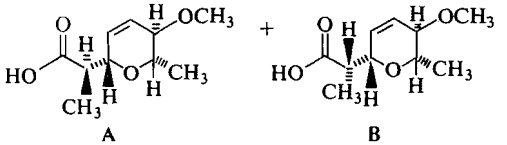

A **B**

Solvent[b]	Overall yield (%)	A:B[c]
100% THF	73	19:81
23% HMPA–THF	71	82:18

[a]LDA, lithium diisopropylamide.
[b]Solvent employed during enolization.
[c]Ratio of diastereomers as determined by nmr analysis.

by heating the isolated ketene acetal in toluene at 100°C for 23 h.

The above examples illustrate the yields and products available by application of the ester enolate Claisen rearrangement to esters derived from furanoid and pyranoid glycals. The use of these procedures and products in the enantiospecific total syntheses of several natural products is under active investigation in these laboratories.

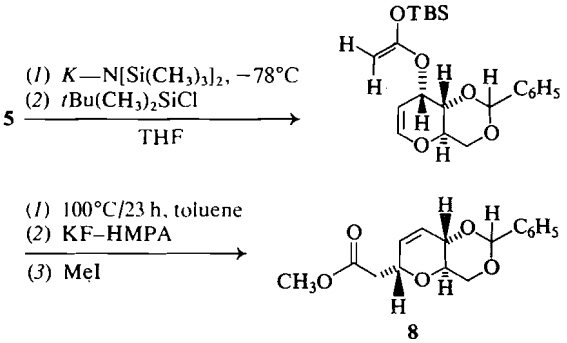

8

Acknowledgments

This work was made possible by a grant from the National Institutes of Health, Grant No. HL 21367-01.

1. R. E. IRELAND and R. H. MUELLER. J. Am. Chem. Soc. **94**, 5897 (1972).
2. R. E. IRELAND, R. H. MUELLER, and A. K. WILLARD. J. Am. Chem. Soc. **98**, 2868 (1976).
3. R. E. IRELAND and C. S. WILCOX. Tetrahedron Lett. 2839 (1977).
4. R. E. IRELAND, C. S. WILCOX, and S. THAISRIVONGS. J. Org. Chem. **43**, 786 (1978).
5. S. J. EITELMAN and A. JORDAAN. J. Chem. Soc. Chem. Commun. 552 (1977).
6. K. FREUDENBERG and A. WOLF. Chem. Ber. **60**, 232 (1927).

Stereoselective routes to some unsaturated α- and β-*C*-glycopyranosides[1]

BERT FRASER-REID, ROBERT DAVID DAWE,[2] AND DEEN BHANDU TULSHIAN
Guelph–Waterloo Centre for Graduate Work in Chemistry, University of Waterloo, Waterloo, Ont., Canada N2L 3G1

BERT FRASER-REID, ROBERT DAVID DAWE, and DEEN BHANDU TULSHIAN. Can. J. Chem. **57**, 1746 (1979).

4,6-*O*-Benzylidene-D-allal, **1***a*, undergoes the Eschenmoser–Claisen rearrangement giving the unsaturated α-*C*-hex-2-enopyranoside, **4** (3,7-anhydro-6,7-*O*-benzylidene-4,5-dideoxy-D-*lyxo*-oct-4-*N*,*N*-dimethyl amide) in 85% yield. The corresponding β-anomer **13***a* (methyl 3,7-anhydro-6,7-*O*-benzylidene-4,5-dideoxy-D-*ribo*-oct-4-enonate) is prepared by reductive elimination of the β-*C*-glucopyranoside **11**. The latter is obtained as the sole product from 4,6-*O*-ethylidene-D-glucose in two steps involving Wittig addition of carboxymethylene followed by cyclization of the resulting α,β-unsaturated ester under thermodynamic conditions.

BERT FRASER-REID, ROBERT DAVID DAWE et DEEN BHANDU TULSHIAN. Can. J. Chem. **57**, 1746 (1979).

Le *O*-benzylidène-4,6 D-allal, **1***a*, subit une transposition de Eschenmoser–Claisen conduisant à l'α-*C*-hexèno-2 pyrannoside insaturé, **4** (anhydro-3,7 *O*-benzylidène-6,7 didéoxy-4,5 D-*lyxo*-octéno-4 *N*,*N*-diméthylamide), avec un rendement de 85%. On a préparé l'anomère β correspondant, **13***a* (anhydro-3,7 *O*-benzylidène-6,7 didéoxy-4,5 D-*ribo*-octène-4 onate de méthyle), par une élimination réductrice du β-*C*-glucopyrannoside **11**. On a obtenu ce dernier comme seul produit, à partir du *O*-éthylidène-4,6 D-glucose, en deux étapes impliquant une addition de Wittig de carboxyméthylène suivie d'une cyclisation de l'ester α,β non saturé qui en résulte à l'aide de conditions thermodynamiques.

[Traduit par le journal]

Tetrahydropyranoid rings bearing alkyl substituents at positions 2 and 6 are frequently encountered as components of natural products. Chiral representations of these segments are readily conceived from carbohydrate *C*-glycopyranoses, a class of compounds which are of interest in their own right in view of their relationship to the *C*-nucleosides (1). Some of the latter display pronounced antitumor and antiviral activity (2) but in all of these instances the sugar rings are furanoid and synthetic developments reflect this circumstance (1*a*, 3–7). Thus *C*-glycofuranoses bearing the C-1 and C-4 substituents in either *cis* or *trans* relationship may be prepared with a high degree of stereoselectivity (7). However the same does not hold for the pyranose analogues (8–10), routes to the 1,5-*trans*- (e.g. α-D) *C*-glycopyranoses being particularly elusive (11). The latter are required by us for certain synthetic projects and in the course of our investigations we have developed stereospecific routes to both α-D- and β-D-*C*-glycopyranoses. We report on these studies in this communication.

The most incontrovertible approach to the desired α-*C*-glycoside envisages a Claisen rearrangement[3] on the glycal **1***a* (12) (Scheme 1). Attempts to apply the classical procedure to the vinyl ether **1***b* were plagued by incompleteness of the conversion **1***a* → **1***b* (cf. refs. 13–15), an obstacle which made it unacceptable for our purposes.[4] Of the recently modified versions of the Claisen rearrangement, the Johnson process is experimentally the simplest but when applied to **1***a* a quantitative 1:1 mixture of the propionate esters **2** and **3**[5] was obtained. On the other hand, the Eschenmoser modification (17) was found to afford an 85% yield of the amide **4**.[6,7] The Ireland variation as applied to the propionate of **1***c* is described in the adjoining communication (18).

With regard to a functionalized one-carbon substituent at the anomeric centre, the [2,3]-sigmatropic rearrangement developed recently by Still and Mitra (19) seemed promising particularly since the intermediate stanylmethyl ether **5***a* could be prepared in 80% yield. Unfortunately metalation of **5***a* (−78°C → room temperature, 12 h) afforded only 25% yields of

[1]Dedicated to the memory of R. H. F. Manske.

[2]Holder of an R. H. F. Manske Fellowship.

[3]The first application of the Claisen rearrangement to unsaturated sugars was carried out by Ferrier and Vethaviryasar (13). For more recent applications see refs. 15 and 16.

[4]In a recently reported investigation the vinyl ether of 3-epi-**1***a* was prepared in a 44% yield (52% recovery of starting material) and the yield in the subsequent thermal rearrangement step was 52% (15).

[5]This compound gave satisfactory 220 MHz, ^{1}Hmr, ir, and mass spectral analyses.

[6]This compound gave satisfactory elemental and spectroscopic analysis.

[7]3,7-Anhydro-6,7-*O*-benzylidene-4,5-dideoxy-D-*lyxo*-oct-4-eno-*N*,*N*-dimethylamide.

0008-4042/79/131746-04$01.00/0

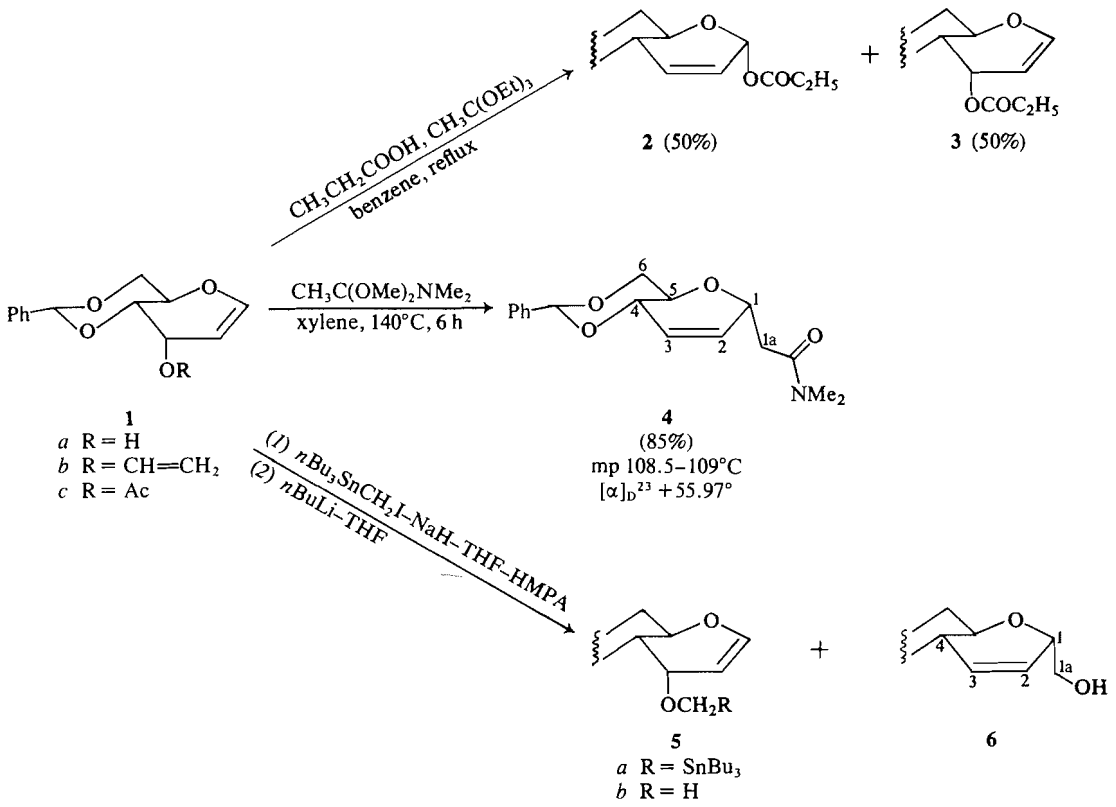

SCHEME 1

6,[5] the methyl ether **5***b* being one of the major products.

In view of developments in the use of the Wittig reaction for the synthesis of *C*-glyco*furanosides* (7, 20) we examined the addition of the phosphorane **8** to 4,6-*O*-ethylidene-D-glucopyranose, **7** (Scheme 2). Initially, cyclization of the adduct **9**[6] was followed by tlc and the resulting product was isolated and converted into an alkene (21) so as to enable ^{1}Hmr (Table 1) and ^{13}Cmr spectroscopic comparisons with

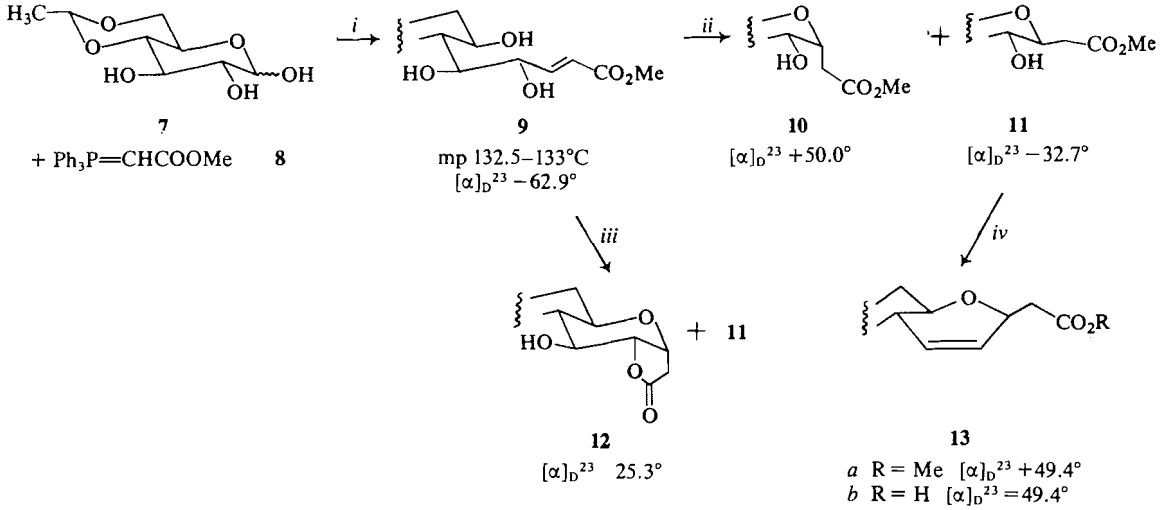

SCHEME 2. (*i*) CH_3CN, reflux, 60 h; (*ii*) 5×10^{-3} *M* KOH in MeOH; (*iii*) 0.7% imidazole in water; (*iv*) see ref. 19.

TABLE 1. 220 MHz ^{1}Hmr parameters for some *C*-glycopyranosides

Compound	H-1a′	H-1a″	H-1	H-2	H-3
4	2.52(dd) J = 14.5, 5.5 Hz	2.82(dd) J = 14.5, 7.5 Hz	4.40(m)	6.03(m)	5.85(m)
6	3.45(m)		4.32(m)	6.13(m)	5.80(m)
9 (60 MHz)	6.10(dd) J = 16.0, 1.3 Hz		7.00(dd) J = 1.3, 5.7 Hz	NA*	NA
11	2.50(dd) J = 16.0, 8.5 Hz	2.86(dd) J = 16.0, 4.0 Hz		NA	NA
12		2.81(dd) J = 18.0, 10.0 Hz	4.86(dt) J = 7.5, 7.5, 10.0 Hz	NA	NA
13 (100 MHz)	2.55(d) J = 6.0 Hz		4.68(m)	5.92(d) J = 11.0 Hz	5.69(d) J = 11.0 Hz

*NA, not assigned.

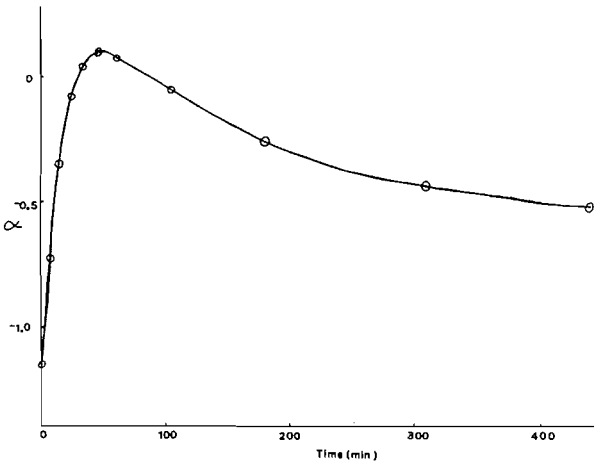

FIG. 1. Plot of change in observed rotation (α) vs. time for the reaction of **9** with 5.0 × 10^{-3} *M* potassium hydroxide in methanol.

the Eschenmoser–Claisen product **4**. In the ^{13}Cmr spectra, carbon-5 of **4** was found to resonate at 65.824 ppm while with the new alkene, the signal occurred at 70.912 ppm. This trend, in accordance with the γ-effect (22), indicated β-D-orientation for the alkene **13***a*[6,8] and pointed to **11** as the product of the Wittig–Michael sequence.

However, to eliminate the possibility that epimerisation at carbon-1 was occurring during the reductive elimination of **11** to give **13**, it was decided to monitor the ring closure of **9** by a technique more discriminating than tlc. Since *C*-glycopyranosides usually obey Hudson's rule of isorotation[9] (8*a*, 10, 11, 20) polarimetry was the technique of choice and our study is recorded in Fig. 1. The substance at equilibrium, isolated in 70% yield, and examined by 220 MHz ^{1}Hmr, was entirely consistent with the pure β-D-ester **11**.[5] On the other hand, the substance at maximum rotation was isolated in 80% yield as an inseparable 1:1 mixture of **10** and **11**.

In an attempt to bias the cyclization in favour of the α-*C*-glycoside, compound **9** was treated with an aqueous solution of imidazole. Our objective was in fact realized since the product proved to be a 3:2 mixture of the β-ester **11** and the α-lactone **12**. On the other hand the stability of the β-D-anomer could be gauged by the fact that the optical rotation of a solution of **13***a* in potassium hydroxide remained constant over a 5-h period. Consistent with this observation, the product isolated in quantitative yield was the carboxylic acid **13***b*.[6]

[8]Methyl 3,7-anhydro-6,7-*O*-benzylidene-4,5-dideoxy-D-*ribo*-oct-4-enonate.

[9]Briefly, the rule states that the α-D-anomer is more dextrorotatory than the corresponding β-D-anomer.

Acknowledgments

We thank the National Research Council of Canada, Bristol Laboratories (Syracuse), and Merck, Sharpe, and Dohme (Rahway) for financial support. We are indebted to the Canadian 220 MHz Centre and to Professor J. B. Stothers for ^{1}Hmr and ^{13}Cmr spectra, and to Professor R. E. Ireland for informing us of his results before publication.

1. (*a*) S. HANESSIAN and A. G. PERNET. Adv. Carbohydr. Chem. Biochem. **33**, 111 (1976); (*b*) K. GERZON, D. C. DELONG, and J. C. KLINE. Pure Appl. Chem. **28**, 489 (1971); (*c*) R. J. SUHADOLNIK. Nucleoside antibiotics. Wiley-Interscience, New York. 1970; (*d*) J. J. FOX, K. A. WATANABE, and A. BLOCH. Prog. Nucl. Acid Res. Mol. Biol. **5**, 251 (1966).
2. (*a*) K. SASAKI, Y. KASAKABE, and S. ESUMI. J. Antibiot. (Jpn.), **25**, 151 (1972); (*b*) G. KOYAMA and H. UMEZAWA.J. Antibiot. (Jpn.), **18**A, 175 (1965); (*c*) M. E. HORI. T. ITO, G. TAKIDA, G. KOYAMA, T. TAKEUCHI, and H. UMEZAWA. J. Antibiot. Ser. A, **17**, 96 (1964); (*d*) N. NISHIMURA, M. MAYMA, Y. KOMATSU, H. KATO, N. SHIMAOKA, and Y. TANAKA. J. Antibiot. Ser. A, **17**, 148 (1964).
3. R. NOYORI, T. SATO, and Y. HAYAKAWA. J. Am. Chem. Soc. **100**, 2561 (1978).

4. G. JUST and A. MARTEL. Tetrahedron Lett. 1517 (1973).
5. L. KALVODA, J. FARKAS, and F. SORM. Tetrahedron Lett. 2297 (1970).
6. J. G. BUCHANAN, A. R. EDGAR, M. J. POWER, and P. D. THEAKER. Carbohydr. Res. **38**, C22 (1974); J. G. BUCHANAN, A. D. DUNN, and A. R. EDGAR. J. Chem. Soc. Perkin Trans. I, 68 (1976) and papers cited therein.
7. H. OHRUI, G. H. JONES, J. G. MOFFATT, M. L. MADOX, A. T. CHRISTENSEN, and S. K. BYRAM. J. Am. Chem. Soc. **97**, 4602 (1975).
8. (*a*) S. HANESSIAN and A. G. PERNET. Can. J. Chem. **52**, 1266 (1974); (*b*) B. HELFERICH and K. L. BELLIN. Chem. Ber. **94**, 1158 (1961).
9. A. ROSENTHAL and A. ZALUNGO. Can. J. Chem. **50**, 1192 (1972).
10. D. L. WALKER, B. FRASER-REID, and J. K. SAUNDERS. J. Chem. Soc. Chem. Commun. 319 (1974).
11. A. ROSENTHAL and M. RATCLIFFE. Can. J. Chem. **54**, 91 (1976).
12. R. U. LEMIEUX, E. FRAGA, and K. A. WATANABE. Can. J. Chem. **46**, 61 (1968).
13. R. J. FERRIER and N. VETHAVIRYASAR. J. Chem. Soc. Trans. I, 1791 (1973).
14. W. H. WATANABE and L. E. CONLON. J. Am. Chem. Soc. **79**, 2828 (1957).
15. K. HEYNS and R. HOHLWEG. Chem. Ber. **111**, 1632 (1978).
16. E. J. COREY, M. SHIBASAKI, and J. KNOLLE. Tetrahedron Lett. 1625 (1977); O. HERNANDEZ. Tetrahedron Lett. 219 (1978).
17. A. E. WICK, D. FELIX, K. STEEN, and A. ESCHENMOSER. Helv. Chim. Acta, **47**, 2425 (1964).
18. R. E. IRELAND, C. A. WILCOX, S. THAISRIVONGS, and N. R. VANIER. Can. J. Chem. This issue.
19. W. C. STILL and A. MITRA. J. Am. Chem. Soc. **100**, 1927 (1978).
20. YU. A. ZHDANOV, YU. E. ALEXEEV, and V. G. ALEXEEVA. Adv. Carbohydr. Chem. Biochem. **27**, 227 (1972).
21. B. FRASER-REID and B. BOCTOR. Can. J. Chem. **47**, 393 (1969); R. S. TIPSON and A. COHEN. Carbohydr. Res. **1**, 338 (1965).
22. J. B. STOTHERS. Carbon-13 nmr spectroscopy. Academic Press, New York. 1972. Chapt. 3.

Canadian Journal of Chemistry
Published by
THE NATIONAL RESEARCH COUNCIL OF CANADA

Journal canadien de chimie
Publié par
LE CONSEIL NATIONAL DE RECHERCHES DU CANADA

Volume 57 Number 14 July 15, 1979 Volume 57 numéro 14 15 juillet 1979

An *ab initio* and ion cyclotron resonance study of the protonation of borazine

C. E. DOIRON, F. GREIN, T. B. MCMAHON, AND K. VASUDEVAN
Department of Chemistry, University of New Brunswick, P.O. Box 4400, Fredericton, N.B., Canada E3B 5A3

Received December 28, 1978

C. E. DOIRON, F. GREIN, T. B. MCMAHON, and K. VASUDEVAN. Can. J. Chem. **57**, 1751, (1979).

The gas phase ion–molecule reactions and proton affinity of borazine have been investigated by both theoretical *ab initio* and ion cyclotron resonance techniques. The experimental proton affinity has been determined from competitive proton transfer equilibria with standard reference bases and found to be 196.4 ± 0.2 kcal/mol. Ion–molecule reaction schemes for reaction of borazine molecular ions have been proposed. *Ab initio* calculations find the proton affinity of borazine to be 203.4 kcal/mol and the most energetically favorable structure of the borazinium ion is one in which very little structural change occurs relative to neutral borazine with the exception of the geometry about the protonated nitrogen atom. Charge distributions and bond lengths are used to explain bonding changes upon protonation.

C. E. DOIRON, F. GREIN, T. B. MCMAHON et K. VASUDEVAN. Can. J. Chem. **57**, 1751 (1979).

On a étudié les réactions ion–molécule en phase gazeuse et l'affinité protonique du borazine par des calculs théoriques *ab initio* et des techniques de résonance ionique dans des cyclotrons. On a déterminé l'affinité protonique expérimentale à partir d'équilibres compétitifs de transferts de proton avec des bases de référence et on l'évalue à 196.4 ± 0.2 kcal/mol. On propose des schémas de réaction ion–molécule pour la réaction d'ions moléculaires du borazine. Par calculs *ab initio*, on trouve que l'affinité protonique du borazine est de 203.4 kcal/mol et on trouve que la structure de l'ion borazinium qui est la plus favorisée sur une base énergétique est celle dans laquelle il ne se produit que de faibles changements structuraux par rapport au borazine neutre à l'exception de la géométrie autour de l'atome d'azote protoné. On utilise les distributions de charge et les longueurs de liaisons pour expliquer les changements de liaison lors de la protonation.

[Traduit par le journal]

Introduction

The similarity of borazine in structure and physical properties to its important organic analogue, benzene, has engendered considerable experimental and theoretical interest in the electronic structure of this boron–nitrogen heterocycle (1–14). Since protonated benzenes and borazines are frequently implicated in reactions in acidic media (15) and under radiolysis conditions (16) an accurate determination of the energetics and structure of these species becomes highly desirable. A knowledge of geometry changes which occur upon protonation provides valuable clues to the mechanisms of reactions of protonated species and offers insight into the nature of bonding in both neutral and protonated molecules.

Very recently highly accurate determinations of the proton affinity of benzene have been made by both high pressure mass spectrometry (17) and ion cyclotron resonance spectroscopy (18). In addition Hehre and Pople have carried out *ab initio* calculations to examine the energetics and geometry of protonated benzene (19). The agreement between theoretically calculated and experimentally determined proton affinities is found to be very good and the optimized geometry is in good agreement with spectroscopic, nmr, and X-ray crystallographic studies of other protonated benzenoid aromatics (20).

Study of the gas phase protonation of borazine has been considerably less extensive, however. Porter has conducted several photo-ionization high pressure

0008-4042/79/141751-07$01.00/0

mass spectrometric studies of borazine and substituted borazines and suggested limits for the proton affinity of borazine of 203 ± 7 kcal/mol. Semi-empirical CNDO calculations (11) to determine the approximate structure of protonated borazine were also carried out leading to the conclusion that the most favorable site of protonation is either at nitrogen or above the boron–nitrogen bond at a point near the nitrogen atom. No experimental determination of the structure of protonated borazine is available for comparison.

In the present work we wish to report an accurate determination of the proton affinity of borazine using the ion cyclotron resonance (ICR) trapped-ion equilibrium technique (22, 23). In addition several ion–molecule reactions of borazine ions with borazine and other molecules are reported. In conjunction with the experimental work an *ab initio* study of the energetics and structure of protonated borazine has also been done. The experimental and theoretical results have been found to be complementary, giving proton affinity values in good agreement.

Experimental

The ion cyclotron resonance spectrometer used in the present work was of basic Varian design but extensively modified to permit trapped-ion experiments according to the method of McMahon and Beauchamp (24). Switching of cell voltages from trapping to detect modes was accomplished using timing circuitry similar to that described previously (25), interfaced to an analog dual DPST switch (26). The transient output of the marginal oscillator was amplified with a PAR Model 113 Low Noise Pre Amp and this signal subsequently integrated using a PAR Model CW-1 Boxcar Integrator (26). All other techniques of ICR used were identical to those described in detail elsewhere. Pressures were monitored by ion pump current and ionization gauge readings calibrated against a MKS Model 170 M Baratron Capacitance Manometer.

Borazine was synthesized according to the method of Hohnstedt and Haworth (27) by reaction of B-trichloroborazine (Alfa Inorganics) with sodium borohydride in triethylene glycol dimethyl ether solvent at 0°C. Impurities of diborane and hydrogen were removed by flowing the gaseous products of reaction through a series of cold traps of decreasing temperature. The final borazine product was routinely degassed by several freeze, pump, thaw cycles before use.

Ammonia was obtained from Matheson of Canada, Ltd. All other chemicals from commercial sources were reagent grade purity and were used without further purification.

All equilibrium constant and rate constant determinations are the average of at least three independent determinations. In the case of proton affinity experiments relative pressures of borazine and reference bases were varied by at least a factor of 10.

Quantum Mechanical Method

Ab initio molecular orbital calculations were carried out on borazine and protonated borazine using the Gaussian 70 (27) program system on the UNB IBM 370/158 computer. Geometry optimizations were performed with the STO-3G basis set while final total energies and proton affinity values were determined from the 4-31G basis.

Results

(a) Experimental

At 12 eV electron energy the only ion observed in the low pressure borazine mass spectrum is the borazine molecule ion. The observed intensities of *m/e* 78–81 in the low pressure ICR spectrum are in excellent agreement with those calculated from the natural abundances of boron isotopes for a species containing three boron atoms. The variation of relative ionic abundances with time in pure borazine at 12 eV and 1.0×10^{-6} Torr is shown in Fig. 1. The only ion–molecule reaction products observed are protonated borazine (reaction [1]) and a dimer species containing six borons and six nitrogens (reaction [2]).

[1] $B_3N_3H_6^+ + B_3N_3H_6 \rightarrow B_3N_3H_7^+ + B_3N_3H_5$

[2] $B_3N_3H_6^+ + B_3N_3H_6 \rightarrow B_6N_6H_{11}^+ + H$

[3] $B_6N_6H_{11}^+ + B_3N_3H_6 \rightarrow B_3N_3H_7^+ + B_6N_6H_{10}$

The dimeric species, $B_6N_6H_{11}^+$, is observed to subsequently react via proton transfer (reaction [3]) to

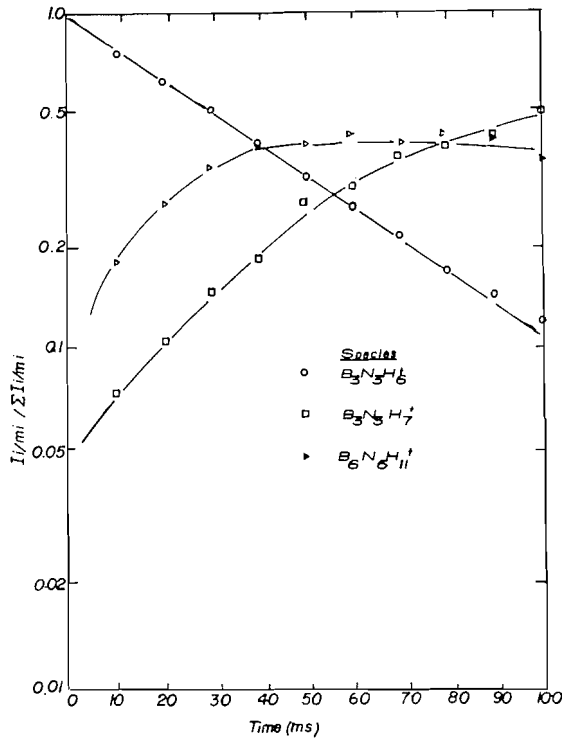

FIG. 1. Variation of relative ionic abundances with reaction time in borazine at 1.6×10^{-6} Torr and an electron energy of 12 eV.

produce the borazinium ion. The identity of $B_6N_6H_{11}^+$ was confirmed by the correct distribution of intensities in the mass range *m/e* 155–161 for a species containing six boron atoms.

Porter has previously suggested that $B_6N_6H_{11}^+$ results exclusively from reaction of protonated borazine (reaction [4]). However, the fact that the

[4] $$B_3N_3H_7^+ + B_3N_3H_6 \rightarrow B_6N_6H_{11}^+ + H_2$$

$B_6N_6H_{11}^+$ abundance is greater than that of $B_3N_3H_{11}^+$ at short reaction times in the present study and at low pressures in Porter's study preclude this possibility. In addition, in proton affinity experiments where the borazinium ion was produced in the absence of the borazine molecule ion no dimeric $B_6N_6H_{11}^+$ was observed.

The rate constants for reactions [1] and [2] obtained from the overall rate of disappearance of $B_3N_3H_6^+$ and the ratio of $B_3N_3H_7^+$ to $B_6N_6H_{11}^+$ at short times are $k_1 = 1.2 \times 10^{-10}$ cm^3 molecule^{-1} s^{-1} and $k_2 = 3.0 \times 10^{-10}$ cm^3 molecule^{-1} s^{-1}. The overall disappearance rate constant for $B_3N_3H_6^+$ is in poor agreement with Porter's value of 1.3×10^{-9} cm^3 molecule^{-1} s^{-1}.

The proton affinity of borazine was experimentally determined using a series of bimolecular proton transfer equilibria (17, 18). Porter previously assigned a proton affinity of 203 ± 7 kcal/mol to borazine based on occurrence of proton transfer from $B_3N_3H_7^+$ to ammonia and failure to observe proton transfer to 2-butyne (21). Initial ICR trapped-ion experiments involving borazine–ammonia mixtures revealed the proton affinity of borazine to be sufficiently less than that of ammonia to prevent establishment of equilibrium. Reaction [5] was observed to occur which is analogous to reaction [2] for the pure borazine system.

[5] $$NH_3^+ + B_3N_3H_6 \rightarrow B_3N_3H_6{-}NH_2^+ + H$$

Mixtures of borazine and compounds of successively lower proton affinity were examined until bases were found for which equilibrium could be attained. The variation of intensities of protonated borazine and a protonated ethyl formate with reaction time is shown in Fig. 2 and that for protonated borazine and protonated 1,4-dioxane is shown in Fig. 3. The equilibrium constant data and thermochemical information derived are summarized in Table 1. The results obtained for the two proton transfer equilibria show excellent agreement, allowing an assignment of 196.4 ± 0.2 kcal/mol for the proton affinity of borazine.[1] The heat of formation of the borazinium

[1]The proton affinity scale summarized in ref. 28 has been used, corrected to a proton affinity for ammonia of 207 kcal/mol.

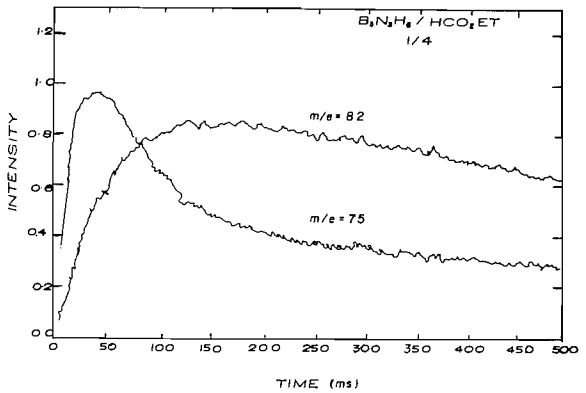

FIG. 2. Experimental temporal variation of intensities of protonated ethyl formate and protonated borazine ions in a 4:1 borazine:ethyl formate mixture at a total pressure of 2.6×10^{-6} Torr and an electron energy of 70 eV.

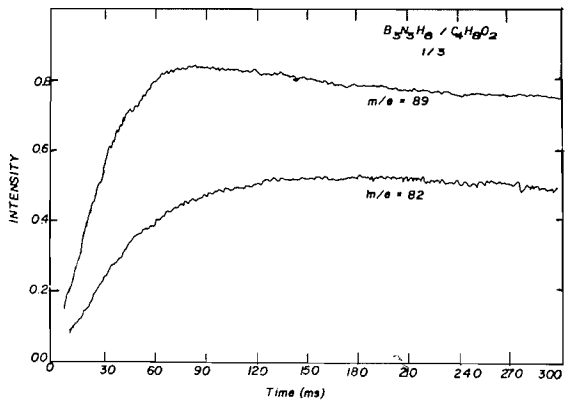

FIG. 3. Experimental temporal variation of intensities of protonated dioxane and protonated borazine in a 3:1 borazine:dioxane mixture at a total pressure of 2.0×10^{-6} Torr and an electron energy of 70 eV.

cation may then be calculated as 46 ± 3 kcal/mol using $\Delta H_f^0(B_3N_3H_6) = -124 \pm 3$ kcal/mol.

(b) Theoretical

A preliminary CNDO study of protonated borazine established the most energetically favorable site of protonation as a nitrogen lone pair rather than face protonation of the ring or B—N bond protonation. A more detailed study of the geometry of the protonated species was then undertaken by *ab initio* molecular orbital calculations using a STO-3G basis set. For protonated borazine two separate approaches to the geometry optimization were used. The first of these, resulting in structure I, was modelled on the study of Hehre and Pople (19), in which the geometry of the ring other than about the protonated site is held fixed while the distance from the center of the ring to N_1 is varied. Varying this distance causes a simultaneous change in the N_1B_2 and N_1B_6 dis-

TABLE 1. Equilibrium and thermodynamic data relevant to the proton affinity of borazine

Reaction	K_{eq}[a]	ΔG^0 (kcal/mol)	ΔS^{0}[b] (cal/K)	ΔH^0 (kcal/mol)	PA(borazine)[c] (kcal/mol)
$(HCO_2C_2H_5)H^+ + B_3N_3H_6 \rightleftharpoons B_3N_2H_7^+ + HCO_2C_2H_5$	5.3	−1.0	2.2	−0.4	196.3
$c(C_4H_8O_2)H^+ + B_3N_6H_6 \rightleftharpoons B_3N_3H_7^+ + cC_4H_8O_2$	3.3	−0.7	0.8	−0.5	196.5

[a]Average of at least three independent determinations.
[b]Entropy changes are estimated simply on the basis of changes in symmetry of products and reactants.
[c]All data relative to $PA(NH_3) = 207$ kcal/mol.[1] Relative proton affinities of reference bases are well established by work of Yamdagni and Kebarle (17) and Wolf *et al.* (18).

tances and the $N_5B_6N_1$, $B_6N_1B_2$, and $N_1B_2N_3$ bond angles. In addition the H_7N_1 and H_1N_1 bond distances and $H_1N_1H_7$ bond angles were then optimized.

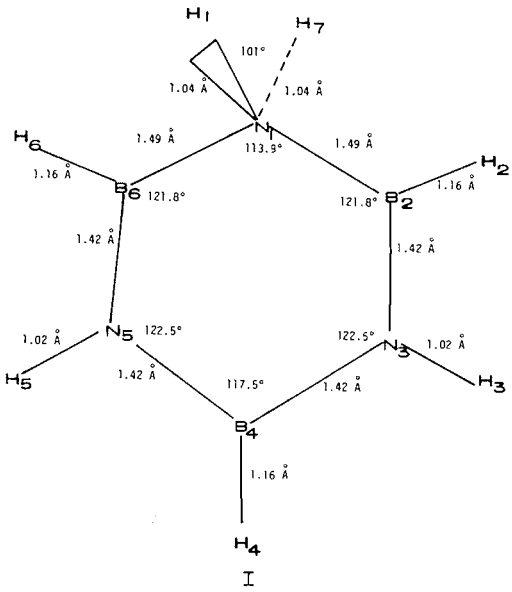

I

A second more complete geometry optimization was also carried out in which the structure of the entire ring system is relaxed. Beginning with a ring geometry identical to that of neutral borazine and N_1H_1 and N_1H_7 bond distances and an $H_1N_1H_7$ bond angle equal to those of structure I the final geometry shown in structure II was arrived at by the sequence of coordinate variations described below.

1. Optimize all N—H and B—H bond distances and the $N_1N_1H_7$ bond angle.

2. Optimize the B_6N_1 and B_2N_1 bond distances while holding the N_3, B_4, and N_5 coordinates fixed. As this variation takes place the $N_5B_6N_1$, $N_1B_2N_3$, $B_2N_3B_4$, and $B_6N_5B_4$ bond angles also vary.

3. Optimize the B_2N_3 and B_6N_5 bond distances while holding the $N_5B_4N_3$ angle fixed. During this optimization the $B_2N_3B_4$, $B_6N_5B_4$, $N_1B_2N_3$, and $N_1B_6N_5$ bond angles vary.

4. Optimize the B_4N_5 and N_3B_4 bond distances holding the $N_5B_4N_3$ angle fixed. The same four ring angles again vary.

5. Optimize the $B_6N_1B_2$ bond angle by moving N_1 along the ring C_2 axis holding the N_1B_6 and N_1B_2 distances fixed. The same four ring angles again vary.

6. Optimize the $N_5B_4N_3$ bond angle by moving B_4 along the ring C_2 axis. The same four ring angles again vary.

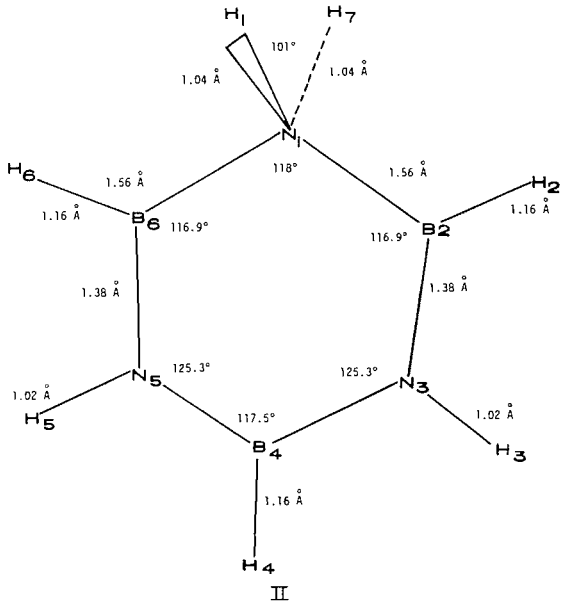

II

Effects of ring puckering were separately examined by moving N_1 out of the ring plane. All such structures led to an increase in total energy.

In addition to the borazinium ion the geometry of the neutral borazine molecule was also optimized. Experimental studies (29) and previous semi-empirical calculations (30) support a structure of D_{3h} symmetry with unequal BNB and NBN angles. The STO-3G optimization of BN bond distances, NBN and BNB bond angles, and NH and BH bond distances lead to structure III.

Proton affinities for borazine were calculated by taking the differences in STO-3G total energies of structures II and III and I and III. In addition calculations using the 4-31G basis were also carried out on I, II, and III and the corresponding proton affinities also calculated. Total energies and derived proton

TABLE 2. Total energies of borazine and borazinium ions

Species	Total energy (au)		Proton affinity (kcal/mol)	
	STO-3G	4-31G	STO-3G	4-31G
$B_3N_3H_7^+$ (I)	−238.521493	−241.127126	234.3	193.9
$B_3N_3H_7^+$ (II)	−238.545125	−241.14225	249.0	203.4
$B_3N_3H_6$ (III)	−238.147696	−240.818175		

affinities are summarized in Table 2. These data show a significant lowering of the proton affinity using the 4-31G basis and also reveal structure II as the more stable borazinium ion.

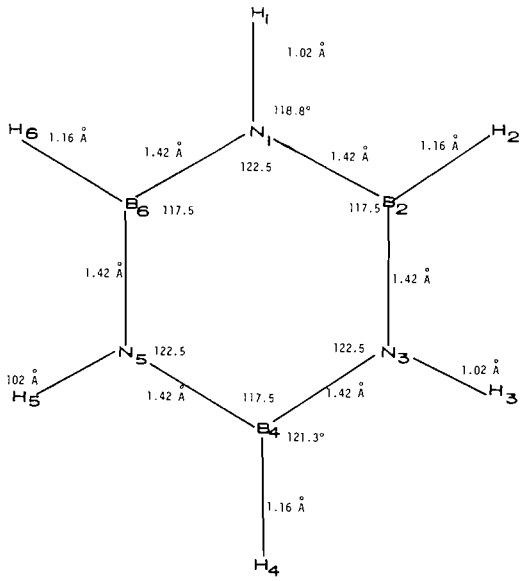

III

Changes in charge density for protonation of borazine may be seen from the Mulliken population analyses for II and III shown in Table 3. Most evident from these total electron population analyses is the rather small change in charge density at individual atoms with total loss of 0.05 to 0.1 electron occurring at each site. More dramatic, however, is the

TABLE 3. STO-3G total atom charges

Atom(s)	Borazine (III)	Borazinium ion (II)
N_1	−0.511	−0.460
B_2, B_6	+0.417	+0.480
N_3, N_5	−0.512	−0.499
B_4	+0.416	+0.482
H_1 (H_7)	+0.184	+0.285
H_2, H_6	−0.089	+0.014
H_3, H_5	+0.184	+0.250
H_4	−0.089	−0.026

TABLE 4. STO-3G ring π charges

Atom(s)	Borazine (III)	Borazinium ion (II)
N_1	+0.393	+0.798
B_2, B_6	−0.393	−0.333
N_3, N_5	+0.393	+0.456
B_4	−0.393	−0.285

shift in π electron density which may be seen from the comparison of ring π charges summarized in Table 4. The large increase in positive charge at N_1 due to donation of the lone pair to the approaching proton is accompanied by a decrease in π electron density throughout the ring giving rise to the several bond length changes described below.

Discussion

The magnitude of the proton affinity of borazine is of interest relative to that for other amino compounds. Unlike ordinary alkyl amines the nitrogen lone pair in borazine participates in partial π bond formation with the adjacent electron deficient borons. From the π ring charges given by the Mulliken population analysis donation of approximately 0.4 electron from a nitrogen lone pair to an empty boron $2p$ orbital occurs. This partial π bond formation thus lowers the availability of the nitrogen lone pair for coordination with the approaching proton and upon protonation the partial π bond is broken. This thus results in an overall lowering of the proton affinity of borazine relative to ammonia. Also, as a consequence of the electron deficient nature of boron, the borons in the ring system may be expected to exert an electron withdrawing inductive effect thus destabilizing the positive charge center. Inductive effects of boron substituents have not been extensively characterized to date for comparison purposes. In this light the borazine proton affinity of 196.4 kcal/mol is quite reasonable compared to an ammonia proton affinity of 207 kcal/mol.[1]

Bond lengths obtained for the borazinium ion are quite similar to those found in analogous boron–nitrogen compounds. For example the N_1B_2 and N_1B_6 bond distances of 1.56 Å are quite close to those of other boron–nitrogen single bonds such as

in $B_2H_5NH_2$ (1.56 Å) (31) and $B_2H_5N(CH_3)_2$ (1.54 Å) (32). They are also seen to be slightly shorter than bond lengths representative of boron–nitrogen coordination compounds such as $(CH_3)_3NBH_3$ (1.64 Å) (33), $NH_3B(CH_3)_3$ (1.61 Å) (30), and NH_3BH_3 (1.59 Å) (30) and somewhat longer than B—N bond lengths where partial π bond formation may occur such as $B_3N_3H_6$ (1.44 Å) (9); $B(N(CH_3)_2)_3$ (1.45 Å) (30); $(CH_3)_2NB(CH_3)_2$ (1.42 Å) (30). The slight decrease in B_2N_3 and B_6N_5 bond distances in the borazinium ion (1.38 Å relative to 1.42 Å) is a reflection of the increased electron demand of B_2 and B_6 caused by the protonation of N_1 which increases π electron density in these two B—N bonds relative to neutral borazine. Similarly the slight increase in the N_3B_4 and N_5B_4 distances is caused by the overall shift in electron density toward N_1 to compensate for the effect of addition of the positively charged proton.

The ring bond angles are observed to remain relatively invariant upon protonation, with the largest changes being the $B_6N_1B_2$ angle which contracts by 4.5° and the $B_2N_3B_4$ and $B_6N_5B_4$ angles which expand by 2.8°. All of the remaining ring angles change by less than 1° from their corresponding values in the neutral borazine molecule. Hehre and Pople (19) have found that upon protonation of benzene the benzenium ion achieves a nearly tetrahedral geometry at the protonated site, although only an incomplete geometry optimization was carried out. Similarly in borazine it might be expected that the protonated nitrogen of the borazinium ion would achieve a tetrahedral geometry analogously to ammonium ions. This expectation is not borne out as can be seen from the final borazinium ion geometry which bears close resemblance to the borazine structure (9). This rigidity of the ring structure is due to the π system which maintains the ring structure close to its most energetically favored geometry for sp^2 nitrogen and boron atoms.

This argument leads to the suggestion that a complete geometry optimization for benzene might yield a more energetically favorable structure with less drastic changes in ring angles. This possibility is currently under investigation by us.

Conclusions

We have determined the proton affinity of borazine both by experimental and theoretical *ab initio* techniques and found the two methods to be in good agreement. In addition, the theoretical calculations have provided a geometry for the borazinium ion which is not available from any previous experimental determination. The proton affinity values for borazine and calculated geometry of the borazinium ion are seen to be reasonable when compared to analogous data for model compounds. Studies such as the present one in which both experimental gas phase measurements and *ab initio* calculations are used to provide complementary data for ionic systems can thus be seen to be a valuable means for providing energetic and structural information for chemically interesting species. Further studies of this nature are currently in progress in these laboratories.

Acknowledgements

The financial assistance of the Natural Sciences and Engineering Research Council of Canada is gratefully acknowledged. We also thank Dr. M. E. MacBeath for advice and assistance in the synthesis of borazine.

1. B. L. Crawford, Jr. and J. T. Edsall. J. Chem. Phys. **7**, 223 (1939).
2. J. R. Platt, H. B. Klevens, and G. W. Schaeffer. J. Chem. Phys. **15**, 598 (1947).
3. L. E. Jacobs, J. R. Platt, and G. W. Schaeffer. J. Chem. Phys. **16**, 116 (1948).
4. C. C. J. Roothaan and R. S. Mulliken. J. Chem. Phys. **16**, 118 (1948).
5. D. W. Davies. Trans. Faraday Soc. **56**, 1713 (1960).
6. O. Chalvet, R. Daudel, and J. J. Kaufman. J. Am. Chem. Soc. **87**, 399 (1965).
7. P. G. Perkins and D. H. Wall. J. Chem. Soc. A, 235 (1966).
8. P. M. Kuznesof and D. F. Shriver. J. Am. Chem. Soc. **90**, 1683 (1968).
9. W. Harshbarger, G. Lee, R. F. Porter, and S. H. Bauer. Inorg. Chem. **8**, 1683 (1969).
10. S. D. Peyerimhoff and R. J. Buenker. Theor. Chim. Acta Berlin, **19**, 1 (1970).
11. A. Kaldor and R. F. Porter. Inorg. Chem. **10**, 775 (1971).
12. A. Kaldor. J. Chem. Phys. **55**, 4641 (1971).
13. W. F. Young, F. Grein, J. Passmore, and I. Unger. Can. J. Chem. **49**, 233 (1971).
14. E. R. Bernstein and P. Reilly. J. Chem. Phys. **57**, 3960 (1972).
15. G. H. Dahl and R. Schaeffer. J. Am. Chem. Soc. **83**, 3034 (1961).
16. A. Stefano and R. F. Porter. Inorg. Chem. **14**, 2882 (1975).
17. R. Yamdagni and P. Kebarle. J. Am. Chem. Soc. **98**, 1320 (1976).
18. J. F. Wolf, R. H. Staley, I. Koppel, M. Taagepera, R. T. McIver, Jr., J. L. Beauchamp, and R. W. Taft. J. Am. Chem. Soc. **99**, 5417 (1977).
19. W. J. Hehre and J. A. Pople. J. Am. Chem. Soc. **94**, 6901 (1972).
20. G. A. Olah, R. H. Schlosberg, D. P. Kelly, and G. D. Mateescu. J. Am. Chem. Soc. **94**, 2034 (1972), and references therein.
21. L. D. Betowski, J. J. Solomon, and R. F. Porter. Inorg. Chem. **11**, 424 (1972).
22. R. T. McIver, Jr. and J. R. Eyler. J. Am. Chem. Soc. **93**, 6334 (1971).

23. T. B. McMAHON, R. J. BLINT, D. P. RIDGE, and J. L. BEAUCHAMP. J. Am. Chem. Soc. **94**, 5934 (1972).
24. T. B. McMAHON and J. L. BEAUCHAMP. Rev. Sci. Instrum. **43**, 509 (1972).
25. T. B. McMAHON. Ph.D. Thesis, California Institute of Technology, 1973.
26. T. B. McMAHON. To be published.
27. L. F. HOHNSTEDT and D. T. HAWORTH. J. Am. Chem. Soc. **82**, 89 (1960).
28. P. KEBARLE. Ann. Rev. Phys. Chem. **28**, 445 (1977).
29. M. V. KILDAY, W. H. JOHNSON, and E. J. PROSEN. J. Res. Natl. Bur. Stand. **65A**, 101 (1961).
30. M. J. S. DEWAR and M. L. McKEE. J. Am. Chem. Soc. **99**, 5231 (1977).
31. J. BLOCK and W. FUSS. Angew. Chem. Int. Ed. Engl. **10**, 182 (1971).
32. P. CASSOUX, R. L. KUSZKOWSKI, P. S. BRYAN, and R. C. TAYLOR. Inorg. Chem. **14**, 126 (1975).
33. J. E. DE MOOR and G. P. VAN DER KELEN. J. Organomet. Chem. **9**, 23 (1967).

Partial deconvolution of the absorption spectrum of trapped electrons in 15 *M* LiCl aqueous glasses at 77 K

TUAN QUOC NGUYEN

Chemistry Department, The University of British Columbia, Vancouver, B.C., Canada V6T 1W5

Received September 6, 1978

TUAN QUOC NGUYEN. Can. J. Chem. 57, 1758 (1979).

Evidence is presented for the composite nature of the solvated (or trapped) electron absorption band in LiCl aqueous glass at 77 K. It is shown that the overall visible absorption spectrum can be deconvoluted into a homogeneously-bleachable 'green' band and a heterogeneously-bleachable 'red' band, whose relative magnitude and absorption band-maxima change with the concentration of electrolyte. From the combined results of time-resolved and steady-state photobleaching experiments, it is concluded that at least two unstable bands are formed during photobleaching (with smaller lifetimes for the band lying further towards the infrared) which then reconverted into the 'green' band with over 40% efficiency.

TUAN QUOC NGUYEN. Can. J. Chem. 57, 1758 (1979).

Les résultats montrent que le spectre d'absorption de l'électron solvaté (ou piégé) dans les verres aqueux contenant du LiCl à 77 K est la résultante de plusieurs bandes d'absorption distinctes. Par photoblanchiment fractionné, il a été possible de déconvolutionner partiellement cette bande d'absorption en deux composants: une bande "verte" qui se comporte de manière homogène sous photoblanchiment, et une bande "rouge" non-homogène. Le rapport des intensités et la position de chacun des deux pics d'absorption changent avec la concentration en électrolyte. Les résultats obtenus par photoblanchiment résolu dans le temps et ceux par photoblanchiment stationnaire ont permis de conclure qu'au moins deux bandes instables sont ainsi formées par photoblanchiment (avec une durée de vie d'autant plus courte que leur absorption se trouve loin dans l'infrarouge), qui se retransforment ensuite en bande "verte" avec un rendement supérieur à 40%.

Introduction

It seems to be well documented that the optical absorption spectrum of the equilibrated solvated electron (e_{vis}^-) in aqueous glasses at 77 K is the result of overlapping of narrower bands, each of which may originate from a distinct species of electron traps (1–4). The problem remains unsettled, however, whether there is a continuous distribution of substructures or only a small number of discrete overlapping bands contributing to the overall absorption band (5, 6). A related question concerns itself with how much narrower is each individual band than the overall band (7, 8).

Many of the conclusions reached so far rely solely upon the results of steady-state bleaching (2, 9) and this has been shown to introduce ambiguities (10). In the hope of resolving these issues more conclusively, both steady-state and time-resolved photobleaching experiments have been conducted on the same system, and this is the topic of this paper.

Frozen aqueous LiCl glass was chosen as the medium for this study because its radiation chemistry has been thoroughly investigated (11), it accommodates the infrared-absorbing electron state (e_{ir}^-) (12, 13), a range of electrolyte concentrations can be used (10, 12), and its steady-state (14) and time-resolved (10, 15) bleaching has been examined previously.

Experimental

The experimental set-up for time-resolved photobleaching experiments is a modified version of the one used previously (10, 13) and is indicated in Fig. 1. One particular improvement is the use of a metallic Dewar (D) provided with four Suprasil windows. The liquid nitrogen is contained in a separate compartment in good thermal contact with the sample but without interfering with the optical path. This solves the problem of bubbling and the consequent scattering of laser light by liquid nitrogen. L_1 and L_2 are two Q-switched lasers which provide single 15 ns pulses at 530 nm and 694 nm. Optical attenuators A_1 and A_2 are used to limit the energy of the laser pulse reaching the sample, they are made from solutions of $CoSO_4$ for 530 nm and $CuSO_4$ for 694 nm laser light. W_1 is a 150 W tungsten lamp powered with a regulated power-supply (Sorensen DCR40-20A), and used conjointly with 10 nm bandwidth interference filter combinations F_1 and F_2. It was used either as a bleaching or as a monitoring light source. To get the baseline for absorbance measurements, the irradiated sample was bleached with a white light source (W_2). E_1 is a mechanical shutter employed to prevent bleaching by the monitoring light and to trigger the laser and the oscilloscope through pulse delay units (C). V is a digital voltmeter connected in parallel with the oscilloscope (O) to measure the change in absorbance during steady-state experiments. P is a photomultiplier (1P28, R213, or R446) which was replaced by an InAs photodiode for measurements in the infrared at 970 nm and 1850 nm. Various interference filters, Corning color glass cut-off filters, and neutral density filters (placed at

0008-4042/79/141758-07$01.00/0

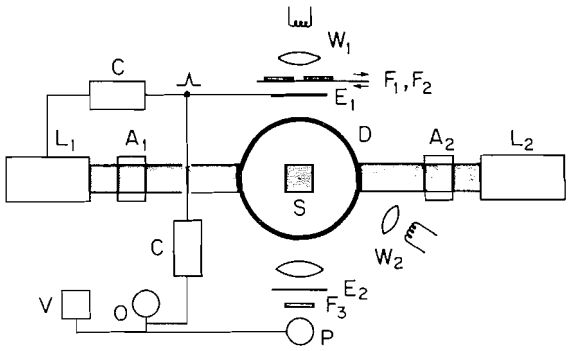

FIG. 1. Schematic representation of the apparatus used to measure the steady-state and time-resolved photobleaching. S is the sample γ-irradiated at 77 K; D the liquid N_2 Dewar vessel with four windows; L_1 and L_2, a frequency-doubled neodynium laser and a ruby laser with the corresponding light attenuators A_1 and A_2; E_1 and E_2 are mechanical shutters; F_1 to F_3 light filters; W_1 is the monitoring and bleaching light source; W_2 an auxiliary bleaching lamp; O an oscilloscope; V a digital voltmeter; P either a photomultiplier or a photodiode.

F_3) were used to block scattered laser-light, and to reduce the light level reaching the photomultiplier so that the drain current was always less than 1 mA. Even so, non-linearity corrections from a calibration curve were necessary to ensure good accuracy. To prevent fatigue of the photomultiplier during steady-state bleaching, the shutter E_2 was opened only for < 2 s during the time of the measurement.

The incident flux from the tungsten lamp was measured with a Spectra Physics power meter (Model 402B) and calibrated at 420 nm, 450 nm, and 480 nm with 0.15 *M* solutions of ferrioxalate, for which Φ_{Fe3+} was taken as 1.05 at 420 nm, 1.00 at 450 nm, and 0.94 at 480 nm (16). The incident intensity was typically 1×10^{15} to 9×10^{15} photons s^{-1} cm^{-2} depending on the wavelength. Each experiment lasted up to 30 min. For laser pulses, a Korad power meter (Model 102C) was used to determine the intensity and the number of absorbed photons. The equilibrated trapped electron state (e_t^-) was produced at the desired absorbance by γ-irradiation in the dark at 77 K at a dose-rate of 35 rad s^{-1}. The anhydrous LiCl used was of the highest purity available (99.999%) from Spex and recrystallized once from D_2O. D_2O was from Merck, Sharp and Dohme with a quoted isotopic purity of 99.7%.

Results and Discussion

Steady-state Bleaching

A γ-irradiated sample of 15 *M* $LiCl/D_2O$ glass when bleached with light at longer wavelength than the absorption band maximum (i.e. with $\lambda > 580$ nm) selectively lost the red component (the 'red' band) of its absorption spectrum. Subsequent bleaching with red light (>620 nm) did not change the position and shape of the remaining part of the absorption band which will be referred to as the 'green' band. However, when light of wavelength shorter than λ_{max} was used, the band shifted to the red, in accord with the previous findings of photoshuffling in other aqueous glasses (2, 17).

In Fig. 2, the change in absorbance due to bleaching is shown as a function of the monitoring wavelength for various extents of bleaching. This kind of plot clearly indicates the heterogeneous nature of the absorption band.

Bleaching with light at 646 nm initially removes mainly the 'red' band but also some of the 'green' band. Extended bleaching depletes the 'red' band so that only the 'green' band is available for bleaching at the end.

Bleaching with 750 nm light revealed that the 'red' band is itself a composite spectrum consisting of at least two overlapping absorbing species, as shown by the initial removal of its red edge (Fig. 2).

After the entire 'red' band and about 20% of the 'green' band were removed with light at 646 nm, the remaining 'green' band was bleached at different wavelengths and the results are given in Fig. 3. It is possible to see from this figure that if the monitoring wavelength is on the blue side of the bleaching wavelength, the observed rate of bleaching was identical to that at the bleaching wavelength itself, whereas it was always less from the red side. This behaviour can be understood if the 'red' band is reformed by photoshuffling during bleaching of the 'green' band. At any wavelength, the net observed rate of steady-state bleaching is equal to the rate of bleaching of the 'green' band minus the rate of formation of the 'red' band, where the last term itself is the difference between the rate of photoshuffling and the rate of

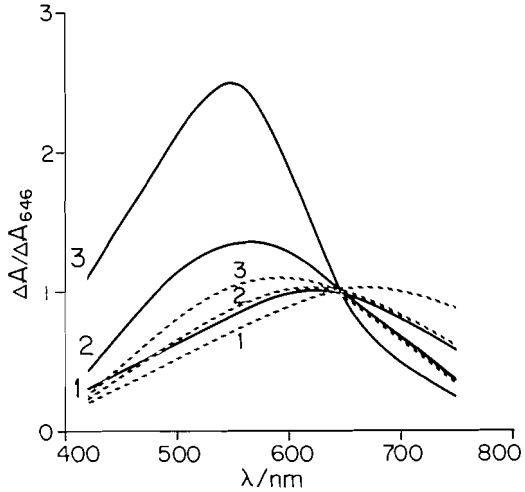

FIG. 2. Differential bleaching spectra normalized to 646 nm. The ordinates represent the loss of absorbance, normalized to the loss at 646 nm, between two different bleaching times. The dotted lines are for bleaching with 750 nm light and the full lines at 646 nm. The extent of bleaching is used as a parameter: curves (*1*) from 0–15% of bleaching, curves (*2*) from 45–55%, and curves (*3*) from 75–80%.

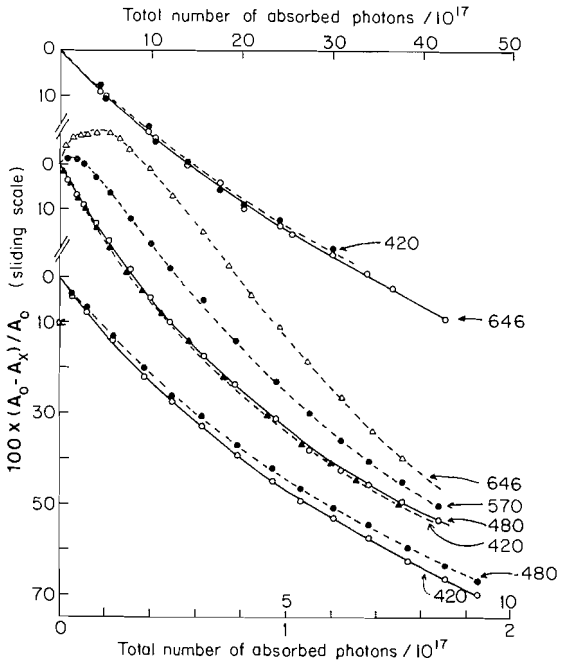

FIG. 3. Bleaching of the 'green' band as a function of accumulated number of absorbed photons. A_0: initial absorbance of the γ-irradiated sample. A_x: absorbance after the sample was bleached with x absorbed photons (x being the number on the abscissa). The monitoring wavelengths are given next to each line. The bleaching wavelength was 420 nm for the bottom two curves, 480 nm for the middle four curves, and 646 nm for the top two. A solid line is drawn when the monitoring and bleaching wavelengths are the same. The horizontal scales, starting from the bottom, refer respectively to the curves with λ_b = 420 nm, λ_b = 480 nm, and λ_b = 646 nm.

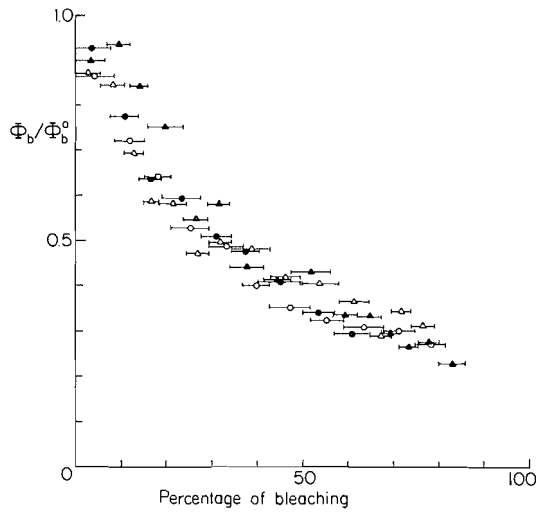

FIG. 4. Variation of the quantum yield for bleaching of the 'green' band with the extent of bleaching (Φ_b^0 is the initial value). The horizontal bars denote the range of bleaching over which the quantum yield was computed. △ is for λ_b = 420 nm, ▲ for λ_b = 450 nm, ○ for λ_b = 480 nm, and ● for λ_b = 521 nm.

bleaching of the 'red' band. With the gradual decrease in the contribution of the 'red' band when one goes towards shorter wavelengths, the rate of formation of the 'red' band relative to the rate of bleaching of the 'green' band diminishes appropriately. In any case, the rate of bleaching on the blue side of the bleaching wavelength was smaller than the rate at the bleaching wavelength itself, even when both were far apart (for example: λ_b at 646 nm and λ_m = 420 nm in Fig. 3), and this again supports the homogeneous nature of the 'green' band over more than 1 eV. If the quantum yield for bleaching is independent of the percentage of bleaching of the band, then the plots of Fig. 3 should give straight lines. Actually, the quantum yield decreases with the fraction of bleaching as observed in other aqueous glasses (2, 18) and this fact is emphasized by the use of Fig. 4 for four bleaching wavelengths, 521, 480, 450, and 420 nm. (Contrary to Fig. 3, only the 'red' band was bleached with light at 750 nm and the 'green' band remained untouched on Fig. 4.) The dependence of Φ_b on the percentage of bleaching is identical for the four wavelengths within experimental errors; this shows that the quasi-free electron (e_{qf}^-) formed has the same fate even if it may have different kinetic energy upon being released from the trap.

The dependence of Φ_b on the bleaching wavelength is depicted in Fig. 5. All the values refer to the initial quantum yield, when less than 10% of the band was bleached. (The same wavelength was used for bleaching and for monitoring the absorbance.) The most interesting feature of Fig. 5 is the sharp increase in Φ_b by going from 480 nm to 420 nm. This is common to most aqueous glasses (19, 20) except that the sharp rise occurs at shorter wavelengths and is sharper than previously reported. For example, Rice and Kevan (21) found the threshold for conductivity at ~600 nm in 10 *M* LiCl glass at 85 K, right at the maximum of the absorption band, compared to our value of ~500 nm which is 40 nm to the blue of λ_{max} for the 'green' band in 15 *M* LiCl at 77 K. This discrepancy, however, arises from the heterogeneous nature of the overall e_t^- absorption band which was not previously taken into account. (In the extreme case, if there is a broad distribution of overlapping bands, one may expect to obtain a flat or smooth curve like the one observed in 10 *M* NaOH glass (3, 21), even though each individual band may have a sharp threshold for bleaching or for photoconductivity.)

In Table 1 are reported the position of the λ_{max} and the *G* values for the overall, 'green' and 'red' band

TABLE 1. Position of the band maximum and G values for the overall, 'green' and 'red' bands in $LiCl/D_2O$ glasses at 77 K

	Overall band			'Green' band			'Red' band		
[LiCl]/M	λ_{max}/nm	G	$W_{1/2}$/eV	λ_{max}/nm	G	$W_{1/2}$/eV	λ_{max}/nm	G	$W_{1/2}$/eV
6.5	600	0.10	1.04	590	0.065	1.01	680	0.036	0.80
7.5	590	0.27	1.02	580	0.16	0.98	670	0.11	0.72
9.5	590	0.63	0.99	570	0.37	0.82	660	0.26	0.73
12	580	1.17	1.02	550	0.65	0.91	650	0.52	0.75
15	580	1.65	1.13	540	0.86	1.03	640	0.79	0.77

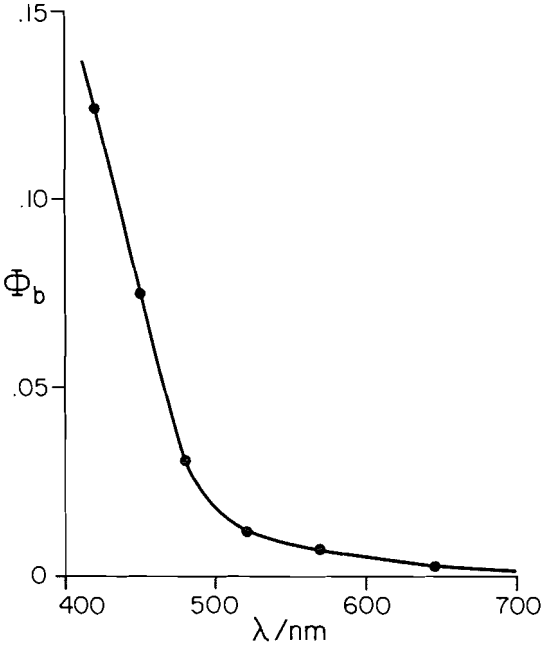

FIG. 5. Dependence of the initial quantum yield for bleaching of the 'green' band on the bleaching wavelength (the dose used was 15 krads for all samples).

(by taking $\varepsilon_{max} = 1.8 \times 10^4\ M^{-1}\ cm^{-1}$ (22) for the overall band) at different concentrations of LiCl. There is a gradual blue shift of both bands with increasing content of electrolyte as observed in the liquid state (22) and in BeF_2 glasses (23), and an enhancement of the ratio of intensities of 'red' band/'green' band which may be peculiar to LiCl glasses since this ratio was found to be constant in BeF_2 glasses (23).

Time-resolved Bleaching

The heterogeneity of the e_t^- absorption band in 15 M $LiCl/D_2O$ glass is best illustrated with pulsed-photobleaching experiments. The 'green' band has a small absorbance and a very low bleaching quantum yield at 694 nm. Therefore, only the 'red' band is bleached significantly with ruby laser light. With the doubled frequency of the Nd laser (530 nm), both bands are bleached. However, by selectively bleaching-off the 'red' band first, the 'green' band can be studied independently.

Figure 6(*a*) depicts schematically the observed behaviour of the absorbance at several monitoring wavelengths when the solvated electron band is bleached with 694 nm light. At 480 nm, after a sharp decrease immediately after the laser pulse, the absorbance is almost independent of time. The spike (during and just after the pulse) is due to luminescence stemming from e_{ir}^- (13, 24), as shown by firing the laser without the monitoring light. At 646 nm, in addition to the initial bleaching, some post-pulse bleaching occurred between 10^{-3} and 1 s, as mentioned previously by Walker and May (15). In lower concentrations of LiCl (7.5 M and 9.5 M), partial recovery of the original absorbance was observed as well (10). At 750 nm, there was a slight increase in absorbance immediately after the pulse followed by post-pulse bleaching which happened on the same time-scale as at 646 nm. At 1850 nm, some immediate increase in absorbance was observed which then decayed on a microsecond time-scale. The species responsible for the infrared absorption at >1500 nm was identified before as a second type of trapped electron (11, 13) and its yield and decay rate depend strongly on the concentration of LiCl (10, 20). The loss of absorbance at 480 nm, compared to the immediate loss at 646 nm, is entirely consistent with the 'red' band being bleached by 694 nm light and with there being no photoshuffling, even transiently, from the 'red' band to the 'green' band. By contrast, the reverse takes place readily in accord with the results of steady-state photobleaching experiments.

Figure 6(*b*) is analogous to Fig. 6(*a*), except that the bleaching wavelength is 530 nm. At 480 nm (and 570 nm), an immediate bleaching was observed followed by a post-pulse recovery. The sharp spike during the pulse was both scattered light from the laser and luminescence of the aqueous glass. When the absorbance was monitored at 646 nm, no bleaching was seen during the pulse but a post-pulse decay

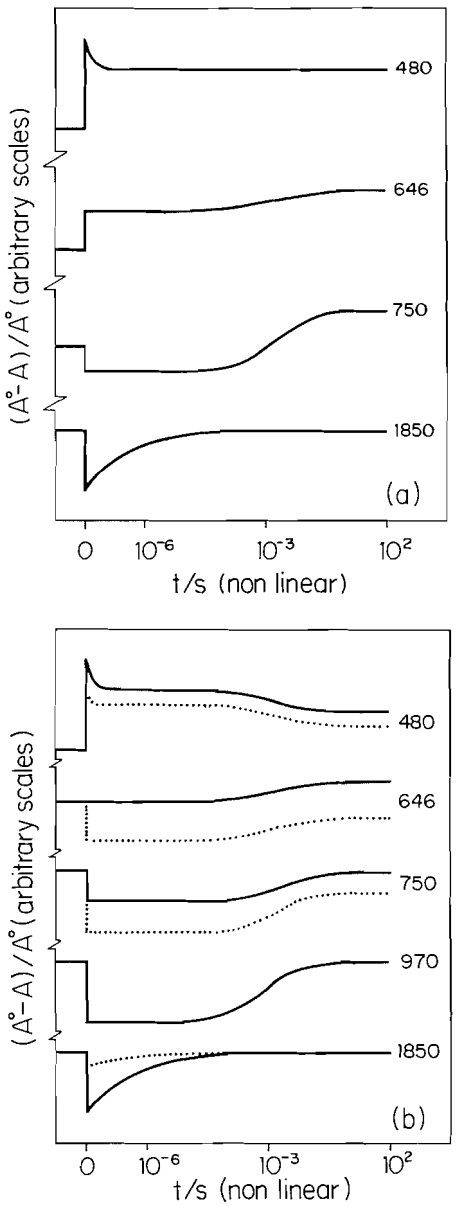

FIG. 6. Schematic representation of the approximate time scales involved for various types of bleaching observed in 15 *M* $LiCl/D_2O$ glass at different wavelengths: (*a*) is for bleaching with laser light at 694 nm and (*b*), at 530 nm. The full curves are for fresh samples, and the dotted curves for samples previously bleached with red light at 750 nm. *A* is the absorbance at times after a laser pulse and A^0 the initial absorbance.

occurred on the millisecond time-scale. In contrast, an irradiated sample pre-bleached with red light at 750 nm showed an immediate increase in absorbance. This was followed by a post-pulse bleaching which is identical to the temporal behaviour observed at 750 nm (dotted line in Fig. 6(*b*)). Pre-bleaching with red light again increased the absorbance at 750 nm without affecting the general shape of the decay.

Experimental evidence indicates the formation of unstable species during photobleaching which absorb in the near infrared, in addition to the infrared electron. This is analogous to the 'red wing' found in pulse-radiolysis (23, 25). The decay of the 'red wing' is linear over five decades of time when the absorbance is plotted against log (time) as in Fig. 7. This is in accord with a geminate tunnelling mechanism (26) for the decay of the 'red wing'. Therefore, it resembles the disappearance of e_{ir}^-, except it occurs on a much longer time-scale (initial half-life ~ 8 ms for the $e^-_{\text{red wing}}$ compared to < 1 μs for the e_{ir}^-). Moreover, the fractional decay is identical whether monitored at 646 nm or 750 nm, consistent with the possibility that it is homogeneous over this entire range of wavelengths. At 970 nm, the decay curve can be broken down into two components: one with a fast decay (5–8 μs for the half-lifetime) and accounts for 30–35% of the initial absorbance; the other 65–70% has a half-lifetime of ~ 8 ms and is identical with the decay observed at 646 nm and 750 nm. The recovery at 480 nm was also found to be

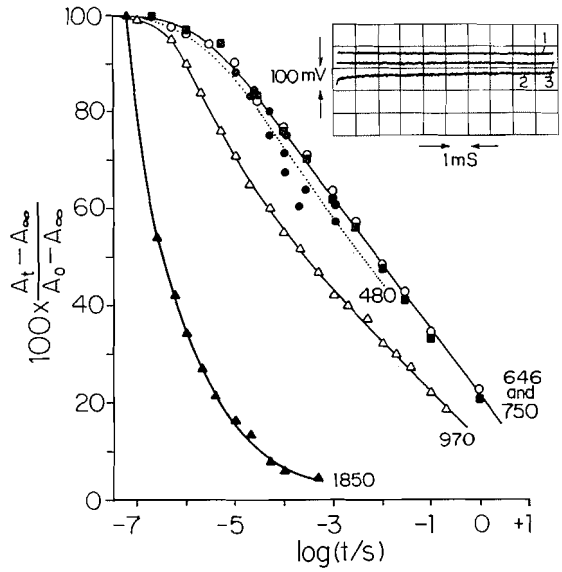

FIG. 7. Decay kinetics of the 'red wing' at 646 nm, 750 nm, and 970 nm and the recovery of the 'green' band at 480 nm on a log (time) scale, after bleaching with a 530 nm laser pulse. The decay of the 'infrared' band at 1850 nm is for the unbleached sample. Insert shows a typical oscilloscope trace as observed at 750 nm: (*1*) is the baseline, (*2*) the trace following the laser pulse, and (*3*) some 100 s later (I_0 = 1000 mV). A_0 on the ordinates is the absorbance at time zero (immediately after the pulse) limited by the response-time of the detectors used: ~ 60 ns for the InAs detector (11) and ~ 100 ns for the photomultiplier (load resistance 1 kΩ). A_∞ is the absorbance measured 100 s after the laser pulse.

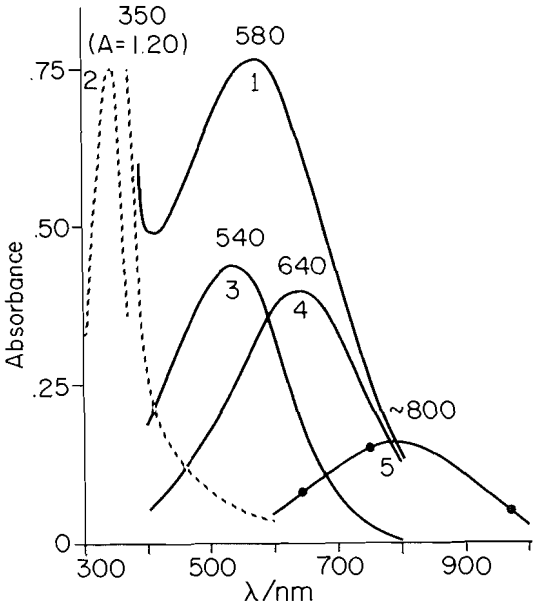

FIG. 8. Partial deconvolution of the absorption spectrum of e_{vis}^- in 15 *M* $LiCl/D_2O$ glass at 77 K into different bands: (*1*) is the overall equilibrated e_{vis}^- absorption spectrum, (*2*) the Cl_2^- band, (*3*) the 'green' band, (*4*) the 'red' band, and (*5*) the 'red wing'. The numbers indicate the position of the absorption maxima.

linear on a log (time) plot, as shown in Fig. 7 and has a half-lifetime of 2–5 ms (a precise determination is rendered difficult by the luminescence from the aqueous glass at that wavelength). The similarity between the decay rate of the 'red wing' and the recovery of absorbance at 480 nm suggests that photoshuffled electrons from the 'red wing' can tunnel back to the 'green' band. The observed recovery of the 'red' band in 7.5 *M* and 9.5 *M* LiCl glasses (10, 15) may have the same origin. If this is true, then this reversed photoshuffling provides a direct observation of a trap-to-trap tunnelling proposed previously by Buxton and Kemsley (27) (although they excluded 10 *M* LiCl glasses in their conclusions).

By comparing the amounts of bleaching and recovery, and assuming the same oscillator strength for the different bands, it is found that ~70% of the bleached electrons from the 'green' band photoshuffled to the 'red wing' and some 40–50% of the decay of the 'red wing' gave back the 'green' band; the overall recovery is one third of the initial bleaching of the 'green' band.

The shape of the 'red wing' is sketched in Fig. 8 (not on scale with the other bands), together with the Cl_2^-, the 'green' and the 'red' bands. It is obtained by plotting the absorbance due to the 'red wing' at 646, 750, and 970 nm (subtracted from the fast component at this later wavelength) and normalized for the same number of absorbed photons of the laser.

The maximum γ-irradiation dose used was 17 krads. This is far from the e_t^--saturation dose which is >100 krads for 15 *M* $LiCl/D_2O$ glass and should be of the order of several Mrads as found in high concentration alkaline glasses (28).[1] Even so, prebleaching with 750 nm light increased the amount of photoshuffling to the 'red' band by more than a factor of two, without influencing the photoshuffling to the 'red wing' (Fig. 6(*b*)). This has two important implications: (*i*) a substantial fraction of the occupied 'green' and 'red' traps are close together, probably within the same spur; (*ii*) the quasi-free electrons ejected from the 'green' trap have limited travelling distances and disappear by chemical reactions if no empty sites are immediately available for retrapping.

Another inference from Fig. 6(*b*) is the difference in fate of the photo-released electron, depending on if it came from the 'green' band or the 'red' band: the main process for a bleached electron from the 'green' band is photoshuffling with a very small yield for formation of the e_{ir}^-, whereas the contrary is true for an electron photobleached from the 'red' band.

Conclusions

These observations can be rationalized if the 'red' traps are closer to the positive charge than are the 'green' traps, and if photo-released electrons from the 'green' or 'red' traps have to move towards this positive charge and can only get retrapped along this path. The 'red wing' and the 'infrared' traps should be even closer to the positive hole and this may explain why these bands are unstable. This is reminiscent of the coulombic distortion model proposed by Albrecht (29). The absence of photoshuffling from 'red' to 'green' fits satisfactorily this coulombic picture as each e_{qf}^- can only move 'downhill'. Spontaneous shift from 'red' to 'green', however, is possible and indeed observed (this paper and ref. 23) if the trapped electron can tunnel to a site of lower energy or digs its own hole. In these situations it is not mobile enough to drift to a positive charge. It is worth noting at this point the recent model of ion pairs formation, proposed by Kroh and Polevoi (5), as the origin of the 'red' band in concentrated aqueous alkaline glasses. It is not clear at the present if the results from alkaline glasses can be extrapolated to other neutral aqueous glasses.

The different processes mentioned above are summarized in Scheme 1.

[1]T. Q. Nguyen and D. C. Walker. Unpublished results.

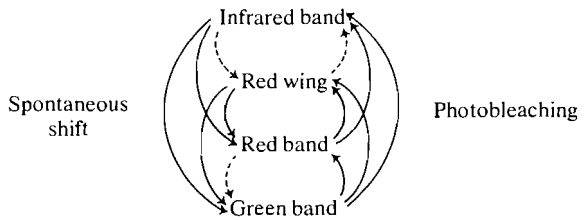

SCHEME 1

Spontaneous shifts from 'infrared' to 'red' band and/or 'red wing' are observed in BeF_2 aqueous glasses (23) but not in 15 *M* $LiCl/D_2O$ glass; also shifts from 'red wing' to 'red' band seemed to occur in low concentration LiCl glasses (10, 15). The broken arrows are processes not observed so far; however, there is no experimental evidence to exclude them. The relative importance of the different mechanisms changes, depending on which part of the spectrum one is looking at. In fact, it is possible to reproduce the five types of bleaching observed by Walker and May (15) in a variety of glasses simply by using 15 *M* $LiCl/D_2O$ and changing the monitoring wavelength (Fig. 6). The processes involved are complex and the fact that bleaching is observed at 570 nm and not at 646 nm does not necessarily imply that the absorption band is narrower than this spectral range. The 'red wing' and the 'infrared band' are not without similarity. Both can be formed either by pulse-radiolysis or by photobleaching. Both are unstable and decay with the same kinetics, albeit with more than four orders of magnitude difference in the lifetimes. There are some indications that the yield and lifetime of the 'red wing' change with the amount of electrolyte added to the glass (23) and a study of this dependence, as was done with the 'infrared band' (12, 23), should provide some insight into the nature of this trap.

Acknowledgements

I would like to thank Dr. Josh van Houten for providing the actinometry solutions and the Physics Division of the National Research Council of Canada in Ottawa for loan of the InAs detector.

I would also like to thank Professor David C. Walker for his suggestions and his contributions in effort and time to this paper which could never have been completed otherwise.

1. B. G. ERSHOV and A. K. PIKAEV. Radiat. Res. Rev. **2**, 1 (1969).
2. G. V. BUXTON, F. S. DAINTON, T. E. LANTZ, and F. P. SARGENT. Trans. Faraday Soc. I, **66**, 2962 (1970).
3. H. HASE and L. KEVAN. J. Chem. Phys. **54**, 908 (1971).
4. L. KEVAN. *In* Radiation chemistry of aqueous systems. *Edited by* G. Stein. Interscience, New York. 1968.
5. J. KROH and P. POLEVOI. Radiat. Phys. Chem. **11**, 111 (1978).
6. H. B. STEEN. *In* Electron–solvent and anion–solvent interactions. *Edited by* L. Kevan and B. Webster. Elsevier, Amsterdam, Holland. 1976.
7. D. C. WALKER. Can. J. Chem. **55**, 1987 (1977).
8. K. K. HO and L. KEVAN. Int. J. Radiat. Phys. Chem. **3**, 193 (1971).
9. S. NODA and L. KEVAN. J. Phys. Chem. **78**, 2454 (1974).
10. T. Q. NGUYEN and D. C. WALKER. J. Chem. Phys. **67**, 2399 (1977).
11. G. V. BUXTON, H. A. GILLIS, and N. V. KLASSEN. Can. J. Chem. **54**, 367 (1976).
12. H. A. GILLIS, G. G. TEATHER, and G. V. BUXTON. Can. J. Chem. **56**, 1889 (1978).
13. H. A. GILLIS and D. C. WALKER. J. Chem. Phys. **65**, 4590 (1976).
14. G. V. BUXTON and K. G. KEMSLEY. J. Chem. Soc. Faraday Trans. **71**, 568 (1975).
15. D. C. WALKER and R. MAY. Int. J. Radiat. Phys. Chem. **6**, 345 (1974).
16. J. G. CALVERT and J. N. PITTS. *In* Photochemistry. Wiley, New York. 1966.
17. A. HABERSBERGEROVA, L. JOSIMOVIC, and J. TEPLY. Trans. Faraday Soc. I, **66**, 656 (1970).
18. T. SHIDA and M. IMAMURA. J. Phys. Chem. **78**, 232 (1974).
19. H. B. STEEN and J. MOAN. J. Phys. Chem. **76**, 3366 (1972).
20. K. KAWABATA. J. Chem. Phys. **55**, 3672 (1971).
21. S. A. RICE and L. KEVAN. J. Phys. Chem. **81**, 847 (1977).
22. (*a*) M. ANBAR and E. J. HART. J. Phys. Chem. **69**, 1244 (1964); (*b*) T. P. ZHESTKOVA and A. K. PIKAEV. High Energy Chem. **9**, 138 (1975).
23. T. Q. NGUYEN, D. C. WALKER, and H. A. GILLIS. J. Chem. Phys. **69**, 1038 (1978).
24. T. Q. NGUYEN and D. C. WALKER. J. Chem. Soc. Faraday Trans. **73**, 1958 (1977).
25. J. MOAN and B. HØVIK. Chem. Phys. Lett. **36**, 120 (1975).
26. M. TACHIYA and A. MOZUMDER. Chem. Phys. Lett. **34**, 77 (1975).
27. G. V. BUXTON and K. G. KEMSLEY. J. Chem. Soc. Faraday Trans. **72**, 466 (1976).
28. A. M. RAITSIMRING, R. I. SAMOILOVA, and YU. D. TSVETKOV. Radiat. Phys. Chem. **10**, 171 (1977).
29. A. C. ALBRECHT. Acc. Chem. Res. **3**, 328 (1970).

Substituent effects in electron transfer reactions. II. The chromium(II) reduction of 2-acetylbutane-1,3-dionatobis(ethylenediamine)cobalt(III) and 3-acetylpentane-2,4-dionatobis(ethylenediamine)cobalt(III)

ROBERT J. BALAHURA[1] AND NITA A. LEWIS[2]

The Guelph–Waterloo Centre for Graduate Work in Chemistry, Department of Chemistry, University of Guelph, Guelph, Ont., Canada N1G 2W1

Received December 28, 1978

ROBERT J. BALAHURA and NITA A. LEWIS. Can. J. Chem. **57**, 1765 (1979).

The chromium(II) reduction of the complexes en_2Co(3-acetyl-ptdn)$^{2+}$ (**1**) and en_2Co(2-acetyl-btdn)$^{2+}$ (**2**) has been studied. Both complexes obey the rate law

$$-\mathrm{d}\ln[\mathrm{Co(III)}]/\mathrm{d}t = k[\mathrm{Cr(II)}]$$

At 25°C, $I = 1.0\ M$ ($LiClO_4$), $k = (4.5 \pm 0.2) \times 10^{-4}\ M^{-1}\ s^{-1}$, $\Delta H^{\ddagger} = 13.0 \pm 0.7$ kcal mol^{-1}, $\Delta S^{\ddagger} = -30 \pm 2$ eu for complex **1** and $k = (5.6 \pm 0.4) \times 10^{-3}\ M^{-1}\ s^{-1}$, $\Delta H^{\ddagger} = 11 \pm 1$ kcal mol^{-1}, $\Delta S^{\ddagger} = -30 \pm 4$ eu for complex **2**. Product studies indicate attack at the uncoordinated acetyl functions in both complexes. The results are compared to those obtained for reduction of en_2Co(3-formyl-ptdn)$^{2+}$ and en_2Co(ptdn)$^{2+}$ by chromium(II).

ROBERT J. BALAHURA et NITA A. LEWIS. Can. J. Chem. **57**, 1765 (1979).

On a étudié la réduction du chrome(II) des complexes en_2Co(acétyl-3 ptdn)$^{2+}$ (**1**) et en_2Co(acétyl-2 btdn)$^{2+}$ (**2**). Les lois de vitesse pour chacun des complexes sont exprimées par l'équation

$$-\mathrm{d}\ln[\mathrm{Co(III)}]/\mathrm{d}t = k[\mathrm{Cr(II)}]$$

A 25°C $I = 1.0\ M$ ($LiClO_4$), $k = (4.5 \pm 0.2) \times 10^{-4}\ M^{-1}\ s^{-1}$, $\Delta H^{\ddagger} = 13.0 \pm 0.7$ kcal mol^{-1} et $\Delta S^{\ddagger} = -30 \pm 2$ eu pour le complexe **1** et $k = (5.6 \pm 0.4) \times 10^{-3}\ M^{-1}\ s^{-1}$, $\Delta H^{\ddagger} = 11 \pm 1$ kcal mol^{-1} et $\Delta S^{\ddagger} = -30 \pm 4$ eu pour le complexe **2**. Une étude des produits indique que l'attaque est initiée dans chacun des complexes, au niveau des fonctions acétyles qui ne sont pas coordonnées. On compare ces résultats à ceux obtenus lors de la réduction des complexes en_2Co(formyl-3 ptdn)$^{2+}$ et en_2Co(ptdn)$^{2+}$ par le chrome(II).

[Traduit par le journal]

Introduction

As part of our continuing studies (1) on electron transfer through the pseudo-aromatic chelate ring pentane-2,4-dione (ptdn)[3] and its analogues, we would like to report the Cr(II) reduction studies on en_2Co(3-acetyl-ptdn)$^{2+}$ (**1**) and en_2Co(2-acetyl-btdn)$^{2+}$ (**2**).[4] We have previously reported the details

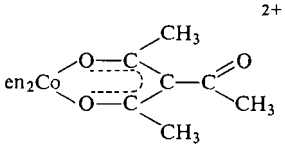

1

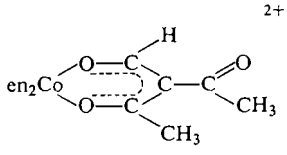

2

of the chromium(II) reduction of the linkage isomer of **2**, that is, en_2Co(3-formyl-ptdn)$^{2+}$ (**3**) (1), and of the parent compound $en_2Co(ptdn)^{2+}$ (**4**) (2). Our

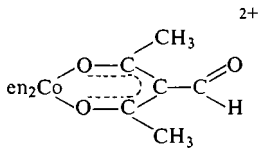

3

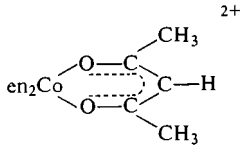

4

interest lies in determining the effect of changes in substituent at the C-3 position of the ptdn ring on the electron transfer rate and mechanism. It was anticipated that ptdn may have unusual electron mediating ability due to its pseudo-aromatic character. Furthermore, we hoped to determine the effect of small structural changes in the chelate skeleton.

In this paper we explore the result of substitution of the acetyl function at C-3 in complex **1** and the effect of replacing the coordinated acetyl function in **1** with a formyl group in the ring skeleton in complex **2**.

Experimental

Reagents

All reagent solutions were prepared in water which was deionised, distilled, and then redistilled from alkaline perman-

[1]To whom all correspondence should be addressed.

[2]Present address: Department of Chemistry, Stanford University, Stanford, CA 94305, U.S.A.

[3]Pentane-2,4-dione is commonly called acetylacetone (acac).

[4]btdn = butane-1,3-dione.

0008-4042/79/141765-07$01.00/0

ganate in an all-glass apparatus. Lithium perchlorate solutions were made as previously described (3). Chromium(II) perchlorate solutions were prepared by reduction of chromium(III) perchlorate (G. Frederick Smith Chemical Co.) in aqueous perchloric acid solution using zinc–mercury amalgam. The solutions were standardised as reported earlier (3) and were stored and handled using standard syringe techniques, in an atmosphere of high purity argon.

Complexes

The preparation of $[en_2Co(2\text{-acetyl-btdn})](PF_6)_2$ has been described (1).

Preparation of $[en_2Co(3\text{-acetyl-ptdn})](PF_6)_2$

Triethylphosphate (150 mL, BDH Chemicals Ltd.) was dried over molecular sieves before adding $NOBF_4$ (4.11 g, Alfa Products). The resulting solution was allowed to stir over molecular sieves for a further 2 h.

The complex *cis*-$[en_2Co(N_3)_2]ClO_4$ (4) (7.76 g) was added in several portions and after further stirring to allow for evolution of gases, the ligand triacetylmethane (3-acetylpentane-2,4-dione, 2.50 mL, Aldrich Chemical Company, Inc.) was introduced into the reaction mixture. The solution was stirred for two weeks at room temperature and the complex was then precipitated by adding the reaction mixture slowly to diethyl ether. The resulting precipitate was dissolved in water and ion-exchanged on Rexyn 102 (H) weak acid cation exchange resin (Fisher Scientific Co.) in the sodium ion form (5). The desired red band was physically removed from the column and was placed on a smaller column. The complex was then removed from the resin by passing a saturated solution of NaCl through the small column and the red product was precipitated by the addition of solid NH_4PF_6. *Anal.* calcd. for $[Co(C_2H_8N_2)_2(C_7H_9O_3)](PF_6)_2$: C 24.37, H 4.65, N 10.33; found: C 24.70, H 4.59, N 10.85.

Kinetic Measurements

The rate of reduction of the $[en_2Co(3\text{-acetyl-ptdn})]^{2+}$ and $[en_2Co(2\text{-acetyl-btdn})]^{2+}$ compounds was followed by observing the change in absorbance of the longest wavelength maximum of the cobalt(III) complex. The kinetic runs were performed on a Beckman Acta CIII spectrophotometer with the temperature controls described previously (6). All reactions were carried out in cylindrical cells sealed with rubber serum caps in the absence of oxygen. The reactions were run under pseudo first-order conditions (reductant in a 20–160 fold excess over oxidant).

Product Analyses

Reactions were carried out at Cr(II):Co(III) ratios between 1:1 and 4:1 and subjected to cation exchange chromatography on Dowex 50W-X8, 200 mesh resin. Elution was carried out using a standard 0.5 *M* $NaClO_4$, 0.1 *M* $HClO_4$ solution. The eluting solution was added in one-quarter strength and the concentration gradually increased as separation was achieved. Generally the 2+ ions were removed from higher charged species with the one-quarter strength solution and eluted from the column with half-strength solution. The total time spent on the ion exchange column was about 2 h. The products were characterized by their uv–visible spectra. The extinction coefficients were calculated on the basis of the chromium concentration which was determined spectrophotometrically as chromate ($\varepsilon_{372\,nm} = 4.815 \times 10^3\ M^{-1}\ cm^{-1}$).

Physical Measurements

The proton magnetic resonance spectra were obtained on a Varian A60 spectrometer. The ultraviolet and visible spectra were measured on a Beckman Acta CIII spectrophotometer. The infrared spectra were recorded on a Beckman IR 12 spectrophotometer.

Results and Discussion

Preparation of $[Co(en)_2(3\text{-acetyl-ptdn})](PF_6)_2$

Friedel–Crafts acetylations of tris(pentane-2,4-dionato) complexes were found by earlier investigators (7) to proceed much more slowly than other electrophilic substitutions such as nitrations, halogenations, and thiocyanogenations. This was thought to be the result of the considerable steric bulk at the reaction site for the acetylation reaction. Nevertheless, for the chelates of chromium, cobalt, and rhodium, it was possible to acetylate all three rings in dichloromethane using acetic anhydride and boron trifluoride etherate (8).

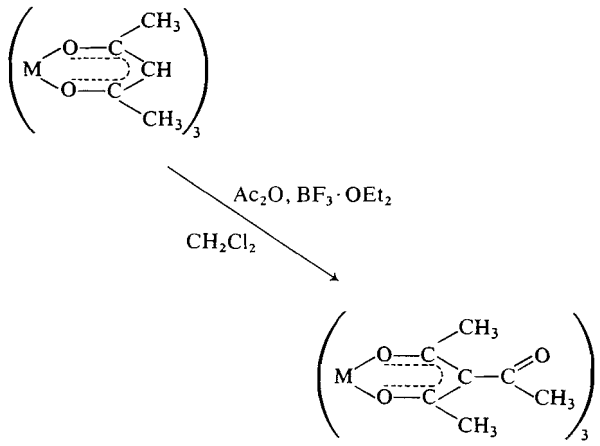

M = Co(III), Cr(III), Rh(III)

We were not able to use this technique to acetylate $[Co(en)_2(acac)]^{2+}$, which is a charged species, since it was not sufficiently soluble in CH_2Cl_2 or other slightly polar solvents. Attempts to perform this reaction in more polar solvents were unsuccessful.

The complex $[Co(en)_2(3\text{-acetyl-ptdn})](PF_6)_2$ was prepared by adaptation of a technique developed by Taube and co-workers (9) for preparation of pentaamminecobalt(III) complexes. The starting material, *cis*-$[Co(en)_2(N_3)_2]^+$, was dissolved in the weakly coordinating solvent triethylphosphate (TEP). The azide ligands were liberated as gaseous products by the addition of nitrosyl tetrafluoroborate. The desired ligand, in this case 3-acetylpentane-2,4-dione, was then added to replace the weakly bound solvent molecules. By optimising the temperature, reaction time, and amount of free ligand used, the substituted complex could be obtained as the sole product.

Physical Studies

There is a large body of literature on the infrared spectra of β-diketone complexes (10, 11). Two bands appear in the region $1515 \pm 10\ cm^{-1}$ (*B* band) and $1575 \pm 30\ cm^{-1}$ (*A* band) for unsubstituted chelate rings (e.g. structure **4**). Although the two modes are coupled slightly to each other, the *A* band is pre-

dominantly a C=C stretching mode and the *B* band is mostly a C=O stretch.

Dryden and Winston (12) developed an empirical rule for chelates of pentane-2,4-dione which are substituted at the 3-position. The rule states that metal complexes of pentane-2,4-dione possessing a hydrogen on the central carbon of the chelate ring exhibit two strong infrared bands in the 1500–1600 cm^{-1} region, whereas complexes with a group other than hydrogen in this position show a singlet in this region. The rule appears to be valid for single atom substituents such as halogen but, as pointed out earlier, for double-bonded species such as formyl or acetyl functions the rule may be violated. It also appears that the medium used to run the spectrum is important since the number and position of the peaks in the 1500–1600 cm^{-1} region may be different depending on whether the spectrum is run in Nujol or as a KBr disc. The $[Co(en)_2(3\text{-acetyl-ptdn})](PF_6)_2$ complex (**1**), however, showed only a singlet in this region, at 1576 cm^{-1} as a KBr disc and at 1566 cm^{-1} in Nujol. This complex apparently obeys Dryden's rule, in sharp contrast to complexes **2** and **3**, both of which showed two peaks in the 1500–1600 cm^{-1} region when run as Nujol mulls. Thus, it appears that the number of peaks exhibited by substituted β-diketones is not subject to prediction.

The ^1H nmr spectrum (Fig. 1) shows two methyl peaks in a 2:1 ratio as predicted for $[Co(en)_2(3\text{-acetyl-ptdn})]^{2+}$. The peak at 2.14 δ corresponds to the methyl groups of the cobalt substituted acetyl functions. That this peak is a singlet implies that rotation about the $C_3—C_{acetyl}$ bond is fast. The peak for the free acetyl protons occurs at 2.50 δ and $—CH_2—$ protons of the ethylenediamine appear at 2.74 δ.

The positions of the absorption bands in the visible and ultraviolet regions of the spectrum for various substituted pentane-2,4-dione complexes are given in Table 1. The lowest energy band in the visible spectrum can be assigned to the $d \rightarrow d$ transition $^1A_{1g} \rightarrow {}^1T_{1g}$ (based on pseudo-octahedral symmetry). The expected $^1A_{1g} \rightarrow {}^1T_{2g}$ transition is observed as a shoulder at 376 nm in $[Co(en)_2(ptdn)]^{2+}$ but is obscured by ligand transitions in the substituted complexes. The bonds in the ultraviolet spectrum are due to ligand and charge transfer transitions and are assigned following Boucher and Bailar (13).

Collman (14) suggested that the lowest energy $\pi \rightarrow \pi^*$ ligand transition would provide evidence for steric inhibition of resonance for substituted β-diketones. A shift of the band at 237 nm in the parent complex $[Co(en)_2(ptdn)]^{2+}$ to lower energy upon substitution at the 3-position would imply that the substituent was conjugated with the pseudo-aromatic chelate ring. For $[Co(en)_2(3\text{-formyl-ptdn}]^{2+}$ and

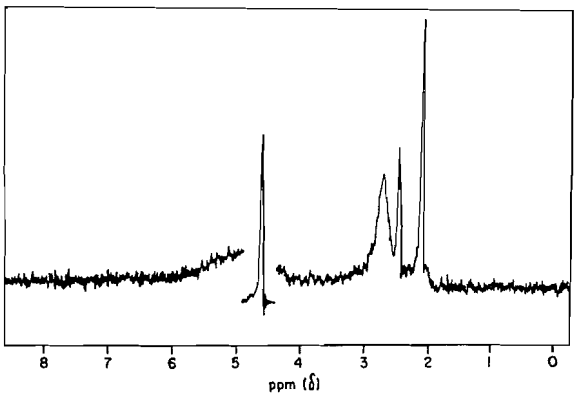

FIG. 1. Proton magnetic resonance spectrum of 3-acetylpentane-2,4-dionatobis(ethylenediamine)cobalt(III) in D_2O. Peaks are relative to DOH peak at 4.61 δ.

$[Co(en)_2(2\text{-acetyl-btdn})]^{2+}$, a shift of 15 and 10 nm, respectively, to lower energy was observed (Table 1). This implies that the formyl and acetyl functions are conjugated with the ring in complexes **3** and **2**, respectively, and hence are coplanar with the pseudo-aromatic chelate. For $[Co(en)_2(3\text{-acetyl-ptdn})]^{2+}$, however, the band is shifted only 2 nm to lower energy, suggesting that there may be some interference of the 'flanking' methyl groups with the methyl of the free acetyl group. Thus, it may be more difficult for the free acetyl function to become coplanar with the ring and this might be expected to influence the rate of electron transfer through the ligand.

Kinetic Studies

Reductions of $[Co(en)_2(2\text{-acetyl-btdn})]^{2+}$ and $[Co(en)_2(3\text{-acetyl-ptdn})]^{2+}$ by Cr(II) both follow the rate law

$$-d[[Co(III)\ complex]/dt = k[Cr(II)][Co(III)\ complex]$$

Summaries of the kinetic data for these reactions are given in Tables 2 and 3. The progress of the reaction of the complex $[Co(en)_2(2\text{-acetyl-btdn})]^{2+}$ with Cr(II) was also followed by scanning the range 300–700 nm with varying ratios of Cr(II) and Co(III) and with different hydrogen ion concentrations. A typical scan is shown in Fig. 2. Good isosbestic behaviour was observed in all cases with isosbestic points at 397, 423, 544, and 646 nm. The final spectrum in each reaction indicated that the product of the reduction was not $Cr(OH_2)_6^{3+}$ and that, therefore, an inner-sphere pathway was implicated.

Product studies on the reaction of Cr(II) with $[Co(en)_2(2\text{-acetyl-btdn})]^{2+}$ showed that a single product was formed, with 78 ± 3% of the ligand being transferred. It was the symmetrical linkage isomer of Cr(III) and was identical to the product formed by

TABLE 1. Position of the electronic spectral bands of cobalt β-diketone complexes in aqueous solution

Complex	No.	$\lambda_{max}(\varepsilon_{max})$, nm ($M^{-1}$ cm^{-1})[a]		
		$^1A_{1g} \rightarrow {}^1T_{1g}$	$d\varepsilon \rightarrow \pi^*$	$\pi \rightarrow \pi^*$
$[Co(en)_2(3\text{-acetyl-ptdn})](PF_6)_2$	1	493(155 ± 2)	324((36.4 ± 0.5) × 10^2)	239((192 ± 3) × 10^2) 211((218 ± 3) × 10^2)
$[Co(en)_2(2\text{-acetyl-btdn})](PF_6)_2$	2	489(149 ± 5)	316((25.0 ± 0.5) × 10^2)	248((308 ± 5) × 10^2) 211((209 ± 3) × 10^2)
$[Co(en)_2(3\text{-formyl-ptdn})](PF_6)_2$	3	488(144 ± 2)	298((30.9 ± 0.5) × 10^2)	252((270 ± 3) × 10^2) 209((217 ± 1) × 10^2)
$[Co(en)_2(ptdn)](PF_6)_2$	4	499(147 ± 1)	324((44.0 ± 0.3) × 10^2)	237((171 ± 1) × 10^2) 217((255 ± 5) × 10^2)

[a]The errors shown on the extinction coefficients are actual deviations from the average value obtained from at least three separate determinations using different samples.

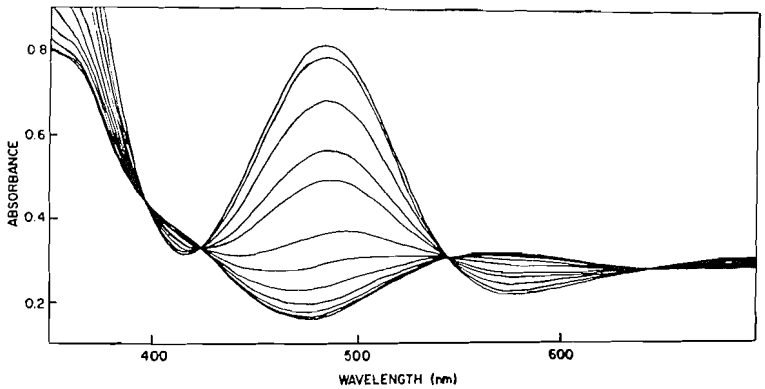

FIG. 2. Typical scan run for the chromium(II) reduction of 2 - acetylbutane - 1,3 - dionatobis(ethylenediamine)cobalt(III). Initial concentrations of reacting species were $[en_2Co(2\text{-acetyl-btdn})^{2+}] = 1.26 \times 10^{-3}$, $[Cr^{2+}] = 1.00 \times 10^{-2}$, $[H^+] = 0.10$. Temperature = 25°C, $I = 1.0$ M ($LiClO_4$). The spectral scans were started at 5, 15, 65, 145, 205, 355, 495, 679, 850, 1022, 1193, and 1365 min after mixing. The last two show essentially no change. (The peak at 489 nm decreases with increasing time while an increase in absorbance with increasing time is observed at 410 and 570 nm.)

TABLE 2. Kinetic data for the reduction of 2-acetylbutane-1,3-dionatobis(ethylenediamine)cobalt(III) by chromium(II)[a]

Temp.[c] (°C)	[Oxidant][b] × 10^3	[Reductant][b] × 10^2	$[H^+]$[b]	$k \times 10^3$ (M^{-1} s^{-1})
25.0	1.25	0.250	0.10	5.39
	1.25	2.59	0.20	5.48
	1.25	2.59	0.80	5.22
	1.25	13.3	0.10	5.92
		$k(25°C) = (5.6 \pm 0.4) \times 10^{-3}$ M^{-1} s^{-1}		
35.0	1.25	2.51	0.80	11.5
	2.50	11.9	0.10	11.0
	1.25	12.4	0.10	11.8
	2.98	12.8	0.10	11.1
45.0	1.25	1.95	0.80	19.5
	1.25	2.59	0.10	20.6
	1.25	6.18	0.10	20.9
	1.25	12.4	0.10	19.5

[a]For all runs, ionic strength, $I = 1.0$ M ($LiClO_4$).
[b]Concentrations are initial values in molar units.
[c]The temperature was accurate to ±0.1°C.

substitution of the free ligand on $[Cr(OH_2)_6]^{3+}$ (1) (see Scheme 1 and Table 4). As noted earlier (1), these products adhere fairly strongly to the ion-exchange resin used in separating the reaction mixtures and it is difficult to effect complete removal. Also, our scan runs imply quantitative ligand transfer.

Substitution on $Cr(OH_2)_6^{3+}$ by 3-formyl-ptdn gives an equilibrium mixture of mono-, di-, and trisubstituted products which are readily separated by cation exchange chromatography (1). If substitution is allowed to continue for more than 10 h some 3-formyl-ptdn decomposes to ptdn which also substitutes on $Cr(OH_2)_6^{3+}$. The fact that only a single product is obtained from the electron transfer reaction (reaction time 20 h) thus tends to rule out an outer-sphere pathway followed by substitution on $Cr(OH_2)_6^{3+}$. These results and those discussed above are consistent with an inner-sphere mechanism for the electron transfer as outlined in Scheme 1.

TABLE 3. Kinetic data for the reduction of 3-acetylpentane-2,4-dionatobis(ethylenediamine)cobalt(III) by chromium(II)[a]

Temp.[b] (°C)	[Oxidant][c] × 10^4	[Reductant][c] × 10	$[H^+]$	$k \times 10^4$ (M^{-1} s^{-1})
25.0	6.4	1.82	0.10	4.41
	6.0	1.81	0.10	4.60
	6.4	1.82	0.10	4.41
		$k(25°C) = (4.5 \pm 0.2) \times 10^{-4}$ M^{-1} s^{-1}		
35.0	5.5	1.83	0.10	9.15
	5.5	1.83	0.10	9.47
	5.5	1.83	0.10	9.37
45.0	5.5	0.884	0.50	19.0
	5.5	0.888	0.10	18.1
	5.5	0.444	0.10	19.9
	5.5	0.177	0.10	18.4
	5.5	0.884	0.05	19.6

[a]For all runs, $I = 1.0$ M ($LiClO_4$).
[b]The temperature was accurate to ± 0.1°C.
[c]Concentrations are initial values in molar units.

We infer from these results that the Cr(II) attacked at the oxygen of the free acetyl function of $[Co(en)_2(2\text{-acetyl-btdn})]^{2+}$ followed by rapid ring closure over the other acetyl group. It seems clear that the Cr(II) did *not* attack at the co-ordinated aldehyde function since the expected product of this reaction (**5**) is known to be stable (1). If attack occurred at the co-ordinated acetyl function, the reaction would be expected to be at least 100 times slower, i.e. it should occur on the same time scale as the reduction of the

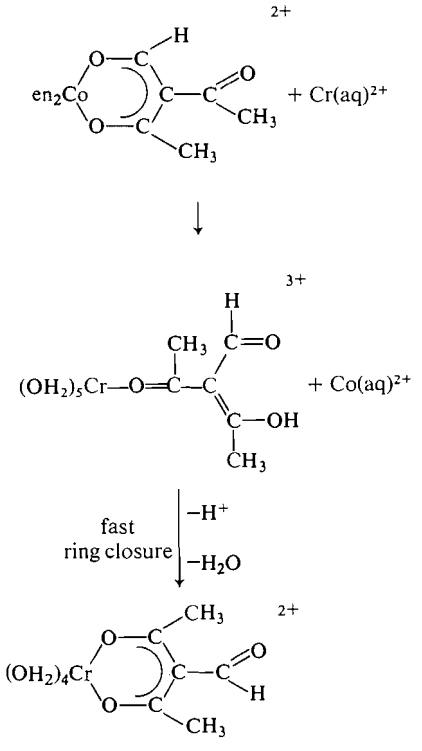

SCHEME 1

TABLE 4. Position of the electronic spectral bands for chromium(III) linkage isomers of 3-formylpentane-2,4-dione in aqueous solution

Complex	Preparation[a]	$\lambda_{max}(\varepsilon_{max})$, nm ($M^{-1}$ cm^{-1}) $^4T_2 \leftarrow {}^4A_2$	$^4T_1(^4F) \leftarrow {}^4A_2$	$d\varepsilon \rightarrow \pi^*$	$\pi \rightarrow \pi^*$	Reference
$[Cr(OH_2)_4(3\text{-formyl-ptdn})]^{2+}$	SUB	557(30.4 ± 0.2)	Obscured	315((46.4 ± 0.5) × 10^2)	244((116 ± 2) × 10^2) 231((141 ± 2) × 10^2)	1, 17
$[Cr(OH_2)_4(3\text{-formyl-ptdn})]^{2+}$	ET[b]	554[c](31.0 ± 0.3)	Obscured	314((46.5 ± 0.3) × 10^2)	245((116 ± 1) × 10^2) 231((138 ± 3) × 10^2)	This work
$[Cr(OH_2)_4(2\text{-acetyl-btdn})]^{2+}$	ET[d]	547(34.9 ± 0.5)	408(48 ± 2)	309((51.0 ± 0.3) × 10^2)	246((131 ± 5) × 10^2) 238((127 ± 5) × 10^2)	1, 17

[a]SUB = substitution of 3-formylpentane-2,4-dione on $[Cr(OH_2)_6]^{3+}$. ET = electron transfer preparation via reduction of appropriate cobalt(III) complex by chromium(II).
[b]Chromium(II) reduction of $[Co(en_2)(2\text{-acetyl-btdn})]^{2+}$ (2).
[c]Shift due to presence of Co(II) as a result of isolation procedure.
[d]Chromium(II) reduction of $[Co(en_2)(3\text{-formyl-ptdn})]^{2+}$ (3).

TABLE 5. Summary of rate constants and activation parameters for the chromium(II) reductions of substituted β-diketone complexes of cobalt(III)

No.	Complex	Temperature (°C)	$k^{a,b}$ (M^{-1} s^{-1})	$\Delta H^{\ddagger a}$ (kcal mol^{-1})	$\Delta S^{\ddagger a}$ (eu)	Ref.
1	$[Co(en)_2(3\text{-acetyl-ptdn})]^{2+}$	25.0	$(4.5\pm0.2)\times10^{-4}$	13.0 ± 0.7	-30 ± 2	This work
2	$[Co(en)_2(2\text{-acetyl-btdn})]^{2+}$	25.0	$(5.6\pm0.4)\times10^{-3}$	11 ± 1	-30 ± 4	This work
3	$[Co(en)_2(3\text{-formyl-ptdn})]^{2+}$	25.0	$(8.7\pm0.4)\times10^{-2}$	9.9 ± 0.8	-30 ± 3	1
4	$[Co(en)_2(ptdn)]^{2+}$	50.0	$(5.7\pm0.5)\times10^{-5}$	—	—	2

[a]Errors shown are standard deviations.
[b]Rate constants are calculated from the transition state equation when the activation parameters are known.

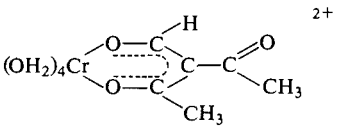

5

unsubstituted (parent) complex, $[Co(en)_2(ptdn)]^{2+}$. We have argued elsewhere (2) that at least part of the reduction of the parent complex goes by the inner-sphere pathway with $k(50°C) = 5.7 \times 10^{-5}$ M^{-1} s^{-1}. Thus, the results are more consistent with reductant attack at the free acetyl group of the complex $[Co(en)_2(2\text{-acetyl-btdn})]^{2+}$.

Reduction of the acetyl-substituted complex $[Co(en)_2(3\text{-acetyl-ptdn})]^{2+}$ was surprisingly slow, but it was still 1–2 orders of magnitude faster than the parent compound (see Table 5). The slowness of this reaction precluded doing scan runs or product studies to determine the mechanism of reduction since substitution reactions interfere with electron transfer before the latter reaction is complete. Therefore, although an outer-sphere reaction cannot be ruled out, it seems unlikely to predominate in view of the number of potential bridging groups present. Since there was a definite rate enhancement over the parent compound, it seems likely that attack again occurred at the remote acetyl function.

It is interesting to note that linkage isomer **2** is reduced some 15 times more slowly than isomer **3** (Table 5). This rate ratio for attack of Cr(II) at a free aldehyde function over a free acetyl function is typical; the rate of reduction in the former case is usually 10 to 270 times faster than in the latter case (15–17). This may be due to the presence of lower energy empty π-antibonding orbitals on the formyl substituent relative to the acetyl group (18). The ability of the formyl group to achieve coplanarity with the aromatic ring more readily than does the acetyl group (19) may also contribute to the increased rate.

The twelve-fold difference in rates observed for reduction of complexes **1** and **2** may be due to a steric effect. The only difference between these two species is that complex **2** has an aldehyde function coordinated to cobalt(III) whereas complex **1** has an acetyl group in this position. We have argued, in both cases, that reduction occurs by attack of the reductant at the uncoordinated acetyl group at C-3 of the chelate skeleton. Thus it may be more difficult to form the precursor complex in the case of complex **1** and this could account for the decreased rate with respect to the 2-acetyl-btdn complex (**2**). It is also possible that the activation step for electron transfer is less favourable for the chelate skeleton of the 3-acetyl-ptdn complex than for that of the 2-acetyl-btdn complex due to the weaker ordination of the aldehyde oxygen. Effects of this type have been referred to before (20) but no systematic data are available.

Acknowledgements

The authors wish to thank the National Research Council of Canada for financial support and for a post-graduate scholarship to N.A.L. We are also grateful to Professor H. Taube for allowing one of us (N.A.L.) to prepare a sample of $[Co(en)_2(2\text{-acetyl-btdn})](PF_6)_2$ in his laboratories.

1. R. J. BALAHURA and N. A. LEWIS. Can. J. Chem. **53**, 1154 (1975).
2. R. J. BALAHURA and N. A. LEWIS. J. Am. Chem. Soc. **99**, 4716 (1977).
3. R. J. BALAHURA and R. B. JORDAN. J. Am. Chem. Soc. **93**, 625 (1971).
4. P. J. STAPLES and M. L. TOBE. J. Chem. Soc. 4812 (1960).
5. R. J. BALAHURA and N. A. LEWIS. J. Chem. Educ. **53**, 324 (1976).
6. R. J. BALAHURA and L. HUTLEY. Can. J. Chem. **51**, 3712 (1973).
7. J. P. COLLMAN. Adv. Chem. Ser. **37**, 78 (1963).
8. J. P. COLLMAN, R. L. MARSHALL, W. L. YOUNG III, and C. T. SEARS, JR. J. Org. Chem. **28**, 1449 (1963).
9. R. B. JORDAN, A. M. SARGESON, and H. TAUBE. Inorg. Chem. **5**, 1091 (1966).
10. K. NAKAMOTO. Infrared spectra of inorganic and coordination compounds. 3rd ed. Wiley-Interscience, New York, NY. 1978. pp. 249–258.
11. K. NAKAMOTO and P. MCCARTHY. Spectroscopy and structure of metal chelate compounds. Wiley, New York, NY. 1968. p. 250.
12. R. P. DRYDEN and A. WINSTON. J. Phys. Chem. **62**, 635 (1958).

13. L. J. BOUCHER and J. C. BAILAR, JR. Inorg. Chem. **3**, 589 (1964).
14. J. P. COLLMAN. Angew. Chem. Int. Ed. **4**, 132 (1965).
15. (*a*) R. G. LINCK and J. C. SULLIVAN. Inorg. Chem. **6**, 171 (1967); (*b*) R. SNELLGROVE and E. L. KING. J. Am. Chem. Soc. **84**, 4609 (1962).
16. (*a*) J. C. M. TSIBRIS and R. W. WOODY. Coord. Chem. Rev. **5**, 417 (1970); (*b*) M. GILROY, F. A. SEDOR, and L. E. BENNETT. J. Chem. Soc. Chem. Commun. 181 (1972).
17. N. A. LEWIS. Ph.D. Thesis, University of Guelph, Guelph, Ont., Canada. 1977.
18. R. J. BALAHURA and W. L. PURCELL. J. Am. Chem. Soc. **98**, 4457 (1976).
19. R. J. BALAHURA and W. L. PURCELL. Inorg. Chem. **14**, 1469 (1975).
20. F. A. SEDOR. Ph.D. Thesis, The University of Florida, Gainesville, Florida. 1971.

Charge distributions and chemical effects. XIX. Analysis of 'bonded' and 'non-bonded' energy contributions in saturated hydrocarbons

SÁNDOR FLISZÁR AND MARIE-THÉRÈSE BÉRALDIN

Département de Chimie, Université de Montréal, Montréal (Qué.), Canada H3C 3V1

Received December 21, 1978

SÁNDOR FLISZÁR and MARIE-THÉRÈSE BÉRALDIN. Can. J. Chem. **57**, 1772 (1979).

Total Coulomb interactions between non-bonded atoms behave in general in a 'quasi-additive' fashion, not only in simple linear and branched paraffins, but also in polycyclic hydrocarbons constructed from chair and boat cyclohexane rings. Because of their relative insensitivity to structural features, they cannot be regarded as being the leading terms in the explanation of energetic effects related to structural changes. The prime factors governing molecular stabilities, as well as the explanation of the structural effects which are at their origin, are found in the behavior of the charge dependent energy contributions associated with bonded atoms, i.e., in the chemical bonds themselves.

SÁNDOR FLISZÁR et MARIE-THÉRÈSE BÉRALDIN. Can. J. Chem. **57**, 1772 (1979).

Les sommes des interactions Coulombiennes entre atomes non liés se comportent en général de manière "quasi additive", tout aussi bien dans les paraffines linéaires et ramifiées que dans les hydrocarbures polycycliques constitués d'anneaux cyclohexaniques en forme chaise ou bateau. En raison de leur faible sensibilité aux modifications structurales, ces interactions ne peuvent jouer de rôle prépondérant dans leur interprétation. Les principaux facteurs déterminant les stabilités moléculaires, ainsi que l'explication des effets structuraux qui sont à leur origine, se retrouvent dans le comportement des contributions énergétiques associées aux charges des atomes liés, c'est-à-dire dans les liaisons chimiques elles-mêmes.

The molecular energy of isolated molecules in their hypothetical vibrationless state is the quantity of choice for the study of energy partitioning. This is particularly true if one wishes to extract information about possible additive contributions. Indeed, at this level the problem is not obscured by other forms of molecular energies, namely zero-point (ZPE) and thermal ($H_T - H_0$) energies, which cannot be regarded as truly additive properties (1).

This particular choice is not restrictive because atomization energies (ΔE_a*) of vibrationless molecules can be derived from the corresponding standard enthalpies of formation ΔH_f^0 (gas, 298.16 K) and appropriate spectroscopic data (eq. [1]; $\sum n_i$ = total number of atoms in the molecule, T = 298.16 K).

$$[1]\quad \Delta E_a^* = \sum \Delta H_f^0(\text{atoms}) - \Delta H_f^0 + \text{ZPE} + H_T - H_0 - 5\sum n_i RT/2$$

Here we investigate saturated hydrocarbons $C_nH_{2n+2-2m}$ considering both simple paraffins and six-membered cyclic compounds, including polycyclic hydrocarbons (m = number of cycles) such as adamantane, bicyclo[2.2.2]octane, iceane, etc. Attention is focussed on energy partitioning and additivity rules involving ΔE_a*.

Formulation of Additivity

Because of our central interest in additivity, a few preliminary remarks about its formulation are in order. Let X be a molecular property and $X(2)$, $X(1)$ the corresponding values for ethane and methane. If X is exactly additive, then

$$[2]\quad X = (1 - m)X(2) + (n - 2 + 2m) \times [X(2) - X(1)]$$

where $X(2) - X(1)$ is the change in X going from methane to ethane, i.e., the contribution of one CH_2 group. The meaning of eq. [2] is obvious for noncyclic compounds (m = 0). For cyclohexane (m = 1), which consists of $n - 2 + 2m = 6$ CH_2 groups, the $(1 - m)X(2)$ term of eq. [2] cancels. Decalin is constructed from two cyclohexane units. In this case $n - 2 + 2m$ accounts for 12 CH_2 groups, but one additional ethane $X(2)$ contribution (i.e., that of two CH_2 and two H atoms) is subtracted with respect to cyclohexane, i.e., a total of $2X(2)$ contributions with respect to noncyclic alkanes. Similar arguments applied to other polycyclic saturated hydrocarbons

Bicyclo[3.3.1]nonane

Adamantane

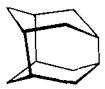

Iceane

Bicyclo[2.2.2]octane

0008-4042/79/141772-07$01.00/0

verify the validity of eq. [2] as a test for exact additivity.

Energy Partitioning

The ΔE_a^* energy is the amount of energy which must be given to vibrationless molecules (1 mol) at 0 K in order to break them up entirely. If a molecule is viewed as an assembly of 'chemical bonds' possessing energies of their own and, moreover, if it is also considered that non-bonded atoms do interact, then ΔE_a^* is clearly made up from that part required to break all bonds, ΔE_a^*(bonds), plus the contribution required to annihilate all non-bonded interaction energies, E_{nb}^*, i.e.,[1]

$$[3] \qquad \Delta E_a^* = \Delta E_a^*(\text{bonds}) - E_{nb}^*$$

Molecular quantum mechanics, of course, does not allow for such a distinction since the chemical bonds themselves are not defined quantum mechanically. The concept of chemical bond can, however, be translated into a wave-mechanical language. Indeed, the energy of a Slater determinant for a closed-shell ground state consisting of doubly occupied molecular orbitals is invariant under a unitary transformation of the spin orbitals with which the corresponding Slater determinant has been constructed. Therefore, we can always assume that the σ molecules under study consist only of localized bonds which are described by orthogonal two-centre bonding molecular orbitals. In this type of analysis, Del Re (2) has shown that a valid approximation for non-bonded interactions in σ systems is Coulombic in nature, i.e.,

$$[4] \qquad E_{nb}^* = \tfrac{1}{2} \sum_{k,l}^{n.b.} \frac{q_k q_l}{r_{kl}}$$

where q_k, q_l are the net (= nuclear minus total electronic) atomic charges of non-bonded atom pairs, at a distance r_{kl}.

Equation [4] may represent a severe simplification. To begin with, let us proceed with the calculation of the Coulombic term of eq. [4] for a number of molecules. The validity of this approach for describing E_{nb}^*, at least as a first approximation, is a point to be dealt with after examination of the results derived in this manner, in comparison with experiment.

Coulomb Interactions

Interatomic distances were derived from standard geometries, with all angles set at 109.47°, r_{CC} = 1.54 Å and r_{CH} = 1.09 Å and/or from optimized geometries given by the STO-3G *ab initio* method (3). The results do not differ significantly.

Atomic net charges are of STO-3G quality, involving full optimization of all variational parameters (*3b*), and correspond to a population analysis which does not imply halving of all overlap population terms, as is the case in the familiar Mulliken scheme (4). They are recalculated from the latter using eqs. [5] and [6],

$$[5] \qquad q_C = q_C(\text{Mulliken}) + Np$$

$$[6] \qquad q_H = q_H(\text{Mulliken}) - p$$

where N = number of H atoms attached to C and $p = 30.12 \times 10^{-3}$ electron is the departure from the usual halving of the CH overlap population, for one C—H bond. (The reasons leading to this type of analysis are given in detail elsewhere (5, 6).) The same carbon atomic charges are also obtained from C-13 nmr shifts (6) (eq. [7]), in ppm from TMS

$$[7] \qquad \delta_C = -237.1 q_C / 69.40 \times 10^{-3} + 242.64$$

where the q_C's are expressed in electron units and 69.40×10^{-3} e is the net charge of the carbon atoms in ethane. Of course, one can do without eq. [7] and use only optimized STO-3G results. There is, however, no real point in not taking advantage of this relationship, just for the sake of 'theoretical purity', since the charges obtained from the two methods agree within ~0.15% for the class of compounds investigated here.

The total Coulomb interactions between non-bonded centers calculated under these premises are presented in Table 1.

Attractive (i.e., stabilizing) interactions are negative. Butane appears to be 0.14 kcal/mol more stable than isobutane in Coulombic energy. Now, the corresponding *experimental* atomization energies (7) ΔE_a^* are 1298.15 and 1299.70 kcal/mol respectively, which makes isobutane 1.55 kcal/mol more stable than its normal isomer. Similarly, the *experimental* ΔE_a^*'s of neopentane and normal pentane are (7) in that order, 1595.94 and 1592.20 kcal/mol, thus indicating that the branched isomer is 3.74 kcal/mol more stable. In non-bonded Coulombic energy, however, the reverse order is found, by 0.44 kcal/mol. Clearly, Coulombic interaction energies between non-bonded atoms cannot be invoked to explain the major differences between isomers.

Of course, it is not surprising that branching increases repulsive contributions, but the effect does not appear to be large. Let us examine the situation

[1]Energy differences (Δ) are defined as 'sum of atomic values less the molecular value'. For non-bonded interaction energies, it follows that $\Delta E_{nb}^* = -E_{nb}^*$, hence the negative sign in eq. [3].

TABLE 1. Non-bonded Coulomb interaction energies

Molecule	$\frac{1}{2}\sum_{k,l}^{n.b.} q_k q_l / r_{kl}$ (kcal/mol)
1 CH_4	0.36
2 C_2H_6	−0.28
3 C_3H_8	−0.78
4 C_4H_{10}	−1.25
5 2-MeC_3H_7	−1.11
6 C_5H_{12}	−1.70
7 2-MeC_4H_9	−1.51
8 2,2-$Me_2C_3H_6$	−1.26
9 2,2-$Me_2C_4H_8$	−1.66
10 2,3-$Me_2C_4H_8$	−1.53[a]
11 2,2,3-$Me_3C_4H_7$	−1.82
12 2,2,3,3-$Me_4C_4H_6$	−1.73
13 Cyclohexane	−2.86
14 Bicyclo[2.2.2]octane	−4.05
15 Bicyclo[3.3.1]nonane	−4.42
16 *trans*-Decalin	−4.95
17 *cis*-Decalin	−4.82
18 Adamantane	−5.08
19 Iceane	−6.30

[a]Calculated for the statistical average (8) of one *anti* (−1.55) and two *gauche* (−1.52) forms.

which would result from a neglect of non-bonded Coulomb energy differences between isomers.

In this approximation, we can ask whether Coulomb interactions behave, at least to some extent, as if they were additive. This is simply done with the aid of eq. [2] which expresses exact additivity. This equation, applied to the energies given in Table 1, yields the result presented in Fig. 1.

This result is self-explanatory. Coulomb interactions behave in general in a 'quasi-additive' manner if we agree upon accepting an uncertainty of ~0.2 kcal/mol due to the neglect of differences between isomers. Branching causes a systematic trend toward higher energies (repulsive destabilization) but situations of extreme steric crowding are required, such as those encountered in 2,2,3,3-tetramethylbutane and, to a lesser extent, in 2,2,3-trimethylbutane, in order to produce sizeable departures from 'quasi-additivity'. This result strongly suggests that non-bonded Coulomb interactions cannot be primely responsible for the bulk of the energy differences between isomers. Let us now examine the energy associated with the bonded atoms.

Analysis of the Atomization Energy ΔE_a^*

The partitioning of ΔE_a^* into energy terms ε_{ij} referring to the individual bonds ij, i.e.,

$$[8] \qquad \Delta E_a^* = \sum \varepsilon_{ij}$$

has been studied recently (7) without explicit consideration of non-bonded interactions, thus including

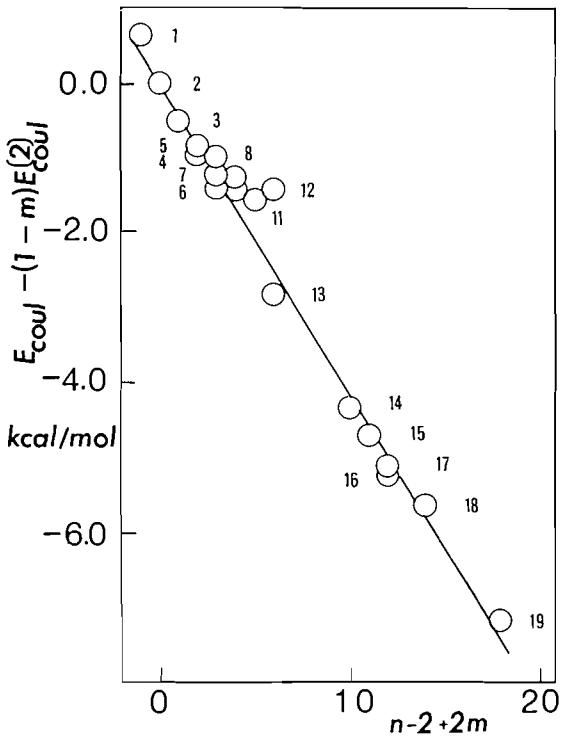

FIG. 1. Additivity test for Coulomb energies by means of eq. [2]. The radii of the circles represent an uncertainty of 0.125 kcal/mol.

them as 'quasi-additive' contributions in the ε_{ij} terms. Postulating that the individual bond-energy terms are some function

$$[9] \qquad \varepsilon_{ij} = \varepsilon_{ij}(Q_i, Q_j)$$

of the total electron populations Q_i and Q_j of the bond-forming atoms, the following expression was derived for saturated hydrocarbons (7).

$$[10] \quad \Delta E_a^* = (1 - m)\Delta E_a^*(2) + (n - 2 + 2m) \times [\Delta E_a^*(2) - \Delta E_a^*(1)] + \lambda_1 \sum N_{CC}\delta + \lambda_2[(n - 2 + 2m)\delta(1) + \sum\delta]$$

Comparing eq. [10] with eq. [2] one recognizes the first two terms of eq. [10] as an additive part, in which $\Delta E_a^*(2)$ and $\Delta E_a^*(1)$ are the ΔE_a^*'s of ethane and methane, i.e., a description of the result corresponding to invariant CC and CH bond contributions. The last two terms of eq. [10] measure the departure from simple additivity attributed to the fact that the charges of the bond-forming atoms are not exactly the same in the various environments because of some charge transfer from neighboring bonds. Here, this charge dependence is expressed conveniently in terms of C-13 nmr shifts, δ, relative to ethane (δ(1) ≡ methane-C shift), using eq. [7].

TABLE 2. Experimental and calculated enthalpies of formation, and data required for their calculation (kcal/mol, viz. ppm from ethane)[a]

Molecule	$\Sigma N_{CC}\delta$	$\Sigma\delta$	ΔE_a^{*bond}	ZPE + $H_T - H_0$	$-\Delta H_f^0$ Eqs.[1,3,4,13]	Exp.	Eqs.[1,10]
CH_4	0	−8.0	419.64	29.5	17.93	17.89	17.92
C_2H_6	0	0	710.28	48.02	20.06	20.04	20.04
C_3H_8	39.8	29.6	1003.57	65.94	25.30	25.02	25.29
C_4H_{10}	91.0	52.8	1296.96	84.38	30.09	30.03	30.02
2-MeC_3H_7	113.4	74.8	1298.96	83.89	32.44	32.07	32.50
C_5H_{12}	139.6	77.6	1590.33	102.83	34.83	35.00	34.76
2-MeC_4H_9	161.6	87.7	1591.69	102.14	36.69	36.82	36.74
2,2-$Me_2C_3H_6$	190.4	124.4	1594.72	101.30	40.31	40.27	40.61
2,2-$Me_2C_4H_8$	233.4	128.3	1886.78	119.51	43.93	44.35	44.21
2,3-$Me_2C_4H_8$	222.8	110.0	1885.41	119.65	42.29	42.49	42.67
2,2,3-$Me_3C_4H_7$	290.1	145.7	2180.07	137.31	48.95	48.96	49.43
2,2,3,3-$Me_4C_4H_6$	351.0	176.4	2474.22	155.08	54.61	53.99	55.57
Cyclohexane	261.6	130.8	1758.14	107.54	29.68	29.50	29.54
Bicyclo[2.2.2]octane	363.7	163.1	2214.32	130.83	23.72	23.75	24.09
trans-Decalin	630.8	277.1	2810.91	166.90	43.88	43.52	43.58
Adamantane	662.3	285.4	2682.70	153.54	30.38	30.65	30.75

[a]The ^{13}C nmr shifts are extracted from literature: C_1–C_6 (10), 2,2,3-Me_3C_4 (11), cyclohexane (12), bicyclo[2.2.2]octane (13), *trans*-decalin (14), adamantane (15). Zero-point energies were derived (7) from experimental and calculated frequencies (16), except those of methane (1), 2-methylbutane (17), 2,3-dimethylbutane (17), and bicyclo[2.2.2]octane (18). Heat-content ($H_T - H_0$) values are from ref. 19, except for *trans*-decalin, adamantane (7), and bicyclo[2.2.2]octane (18). Enthalpies of formation are from ref. 19, except for ethane, propane, butane, isobutane (20), neopentane (21), cyclohexane, *trans*-decalin (22), bicyclo[2.2.2]octane, and adamantane (18).

The parameters λ_1 and λ_2, constructed from the derivatives $\partial\varepsilon_{ij}/\partial Q_i$ of Taylor expansions of eq. [9] for the CC and CH bonds, are empirically adjusted. N_{CC} is the number of CC bonds formed by the C atom whose shift is δ.

Dividing now the total ΔE_a^* energy of the molecule into intra-bond and non-bonded contribution (eq. [3]), the inclusion of the effects of the environment on any specific bond term ε_{ij}^{bond} is evaluated in terms of charges allocated to the bond-forming atoms, i.e.,

$$\varepsilon_{ij}^{bond} = \varepsilon_{ij}^{bond}(Q_i, Q_j) \quad [11]$$

The sum

$$\Delta E_a^{*bond} = \sum\varepsilon_{ij}^{bond} \quad [12]$$

is obtained by following the same sequence of calculations (7) which led to eq. [10] from eqs. [8] and [9], with the result

$$\Delta E_a^{*bond} = (1 - m)\Delta E_a^{*bond}(2) + (n - 2 + 2m)[\Delta E_a^{*bond}(2) - \Delta E_a^{*bond}(1)] + \lambda_1\sum N_{CC}\delta + \lambda_2[(n - 2 + 2m)\delta(1) + \sum\delta] \quad [13]$$

To the extent that non-bonded interactions behave, at least approximately, in an additive manner, i.e.,

$$E_{nb}^* \simeq (1 - m)E_{nb}^*(2) + (n - 2 + 2m) \times [E_{nb}^*(2) - E_{nb}^*(1)] \quad [14]$$

it is clear that the total atomization energies obtained from eqs. [3], [13], and [14] equal those given by eq. [10]. The quality of this approximation is best discussed by comparing with experimental results.

Experimental Verifications

The ΔE_a^{*bond} energies (eq. [13]) were calculated with $\lambda_1 = 0.0380$ and $\lambda_2 = 0.0526$, as determined by least-squares analysis. Then, assuming that eq. [4] is approximately valid, we have deduced the corresponding ΔE_a^* energies by means of eq. [3] and the results given in Table 1. Finally, using experimental ZPE + $H_T - H_0$ energies, as well as (9) $\Delta H_f^0(C) = 170.89$ and $\Delta H_f^0(H) = 52.09$ kcal/mol at $T = 298.16$ K, we have calculated the enthalpies of formation (eq. [1]) indicated in Table 2. On the other hand, similar calculations were performed using instead ΔE_a^* values derived directly from eq. [10], implying exact additivity of non-bonded interactions. Not surprisingly, in this model the parameters ($\lambda_1 = 0.03244$ and $\lambda_2 = 0.05728$) differ slightly from the previous ones.

The results obtained from eq. [10] are in general good agreement with their experimental counterparts, virtually within experimental uncertainty. While this is not a new aspect of this type of analysis (7), the point made here is that such an agreement points to a quasi-additive behavior of non-bonded interaction energies. The obvious exception, 2,2,3,3-tetramethylbutane, is discussed further below.

It is difficult to evaluate how well Coulomb energies represent total interactions between non-

bonded pairs. Present results indicate that, individually, both E_{nb}* and $\frac{1}{2}\sum q_k q_l / r_{kl}$ energies behave, within narrow limits, essentially in an additive manner. Consequently, to the extent that eq. [4] can be regarded as a reasonable first approximation, we find here a justification for the observed approximate validity of eq. [10].

It also appears that ΔH_f^0 calculations involving explicitly non-bonded contributions described by eq. [4] are no better, in a statistical sense, than those using simply eq. [10]. Indeed, the average deviations from the experimental values are in both cases 0.18 kcal/mol,[2] excluding 2,2,3,3-tetramethylbutane. This means that, within experimental precision, eq. [10] largely recovers the error introduced in assuming exact additivity of non-bonded contributions as long as the latter behave in a quasi-additive manner. As an important corollary, the prime factors governing molecular stabilities, as well as the explanation of the structural effects which are at their origin, are found in the behavior of the charge dependent bonded contributions. For example, neopentane appears to be more stable than *n*-pentane in $\Delta E_a{}^{*bond}$ energy by 4.39 kcal/mol (Table 2), but also 0.44 kcal/mol less stable in Coulomb energy (Table 1), for a net difference in atomization energy ΔE_a* of 3.95 kcal/mol (experimental, from eq. [1], 3.74 kcal/mol). The dominant role of the energy terms associated with the chemical bonds can be expressed as a rule of thumb 'in comparisons between isomers, the more stable compound is that whose carbon skeleton best approaches electroneutrality, which is reflected in eq. [10] by larger (downfield) δ values'. Again, it should be stressed that these considerations apply to molecules in their hypothetical vibrationless state. The enthalpy values given in Table 2 indicate, however, that the same general trends are followed by molecules in their real states at $T = 298.16$ K.

These results should not be used to minimize the importance of non-bonded interactions, which is particularly well revealed by the properties of 2,2,3,3-tetramethylbutane. For this alkane, the error in ΔH_f^0 accompanying its calculation using eq. [10] is exceptionally large, and there seems to be little doubt concerning the experimental value (25). Moreover, the difficulties associated with the evaluation of its ZPE energy[3] can hardly be invoked to justify such a large discrepancy. The published ^{13}C nmr spectrum (11) has also been duplicated. Turning now to the detailed calculation of ΔH_f^0 by means of eqs. [3], [4], and [13], the Coulomb term is seen to significantly reduce the error. While the residual discrepancy remains important, possibly pointing to an imperfection when assimilating Coulomb with total non-bonded interactions, it would also be difficult to draw definite conclusions in that matter. It is important, however, to recognize that in cases involving extreme steric crowding any significant deviation from 'quasi-additivity' is a warning against the straightforward use of eq. [10].

Conclusions

In saturated hydrocarbons, total Coulomb interaction energies between non-bonded atoms behave in general in a 'quasi-additive' fashion as they are little affected by structural features, even major ones, except for situations of extreme steric crowding. As a consequence, they cannot be primarily responsible for the bulk of the energy differences between isomers or conformers.

The atomization energies of molecules in their hypothetical vibrationless state are, on the contrary, not simply additive, the departures being attributed to the charges of the bond-forming atoms which are not exactly the same in the various environments because of some transfer from (or to) neighboring bonds. The prime factors governing molecular stabilities are found in the behavior of the charge dependent bonded contributions. The corresponding eq. [10] can be used with confidence in a wide variety of cases, unless non-bonded Coulomb terms depart markedly from 'quasi-additivity'.

[2]We have also examined the possibility of describing E_{nb}* by the Coulomb energies of Table 1 multiplied by k^2, on the grounds that the net charges are perhaps in error by a factor k. This is a definite possibility. Indeed, the C and H charges derived from optimized STO-3G, Hoylands' bond-order (23), 7*s*3*p*/3*s* (24), and 6-31G *ab initio* calculations are in all cases in a ratio (k) of 1: 1.3: 0.86: 0.84, after readjustment through eqs. [5] and [6], evidently without any change in their relative ordering (5). Here, the search for the best k yields $k = 0.7$–0.95 (depending upon whether or not one or another compound is left out of the correlation), with an insignificant improvement in the calculations of the ΔH_f^0's, the average deviation being now 0.15 kcal/mol. Hence, within the precision of this type of analysis, there is no point in trying to improve the description of the E_{nb}* interactions simply by taking some multiple of the Coulomb energies given in Table 1. There is an indication, however, that Coulomb terms are even closer to 'quasi-additivity' than is shown in Fig. 1. Indeed, because of this 'shrinking' of the Coulomb term, the differences (e.g., those between isomers) must now also be multiplied by k^2, which is less than 1.

[3]Because of the significantly larger than usual deviations (1.83%) between calculated and observed frequencies (16) and the fact that only 17 of the 48 fundamentals were observed, our present estimate of the ZPE enegy of 2,2,3,3-Me_4C_4 (147.60 kcal/mol) is based on the regular progression of the increments in ZPE in going from 2-MeC_3 to 2,2-Me_2C_3 (16.66), from 2-MeC_4 to 2,2-Me_2C_4 (16.76), and from 2,3-Me_2C_4 to 2,2,3-Me_3C_4 (16.88) and on the value (130.61 kcal/mol) for 2,2,3-Me_3C_4. Though open to criticism, this estimate is more consistent in comparisons with other molecules than the sum $h\Sigma\nu_l/2 = 146.97$ kcal/mol derived from calculated frequencies (16), which represents an increment of only 16.36 kcal/mol with respect to 2,2,3-Me_3C_4, rather than the 16.99 increment suggested by the progression.

Of course, under usual working conditions one also has to take into account the zero-point and thermal energies for evaluating the various aspects of molecular energies at, say, 298.16 K in a realistic manner. This now seems to be the real problem arising in the discussion of molecular energies.

Acknowledgments

The most generous support by the Centre de Calcul de l'Université de Montréal and the financial aid from the National Research Council of Canada are gratefully acknowledged. We also thank Dr. P. Ausloos and the National Bureau of Standards, Washington, DC, for a sample of pure 2,2,3,3-tetramethylbutane.

1. T. L. COTTRELL. J. Chem. Soc. 1448 (1948).
2. G. DEL RE. Gazz. Chim. Ital. **102**, 929 (1972).
3. (*a*) W. J. HEHRE, R. F. STEWART, and J. A. POPLE. J. Chem. Phys. **51**, 2657 (1969); (*b*) G. KEAN and S. FLISZÁR. Can. J. Chem. **52**, 2772 (1974).
4. R. S. MULLIKEN. J. Chem. Phys. **23**, 1833 (1955); **23**, 1841 (1955); **23**, 2338 (1955); **23**, 2343 (1955).
5. S. FLISZÁR, G. KEAN, and R. MACAULAY. J. Am. Chem. Soc. **96**, 4353 (1974).
6. S. FLISZÁR, A. GOURSOT, and H. DUGAS. J. Am. Chem. Soc. **96**, 4358 (1974); S. FLISZÁR. Can. J. Chem. **54**, 2839 (1976).
7. H. HENRY, G. KEAN, and S. FLISZÁR. J. Am. Chem. Soc. **99**, 5889 (1977).
8. L. LUNAZZI, D. MACCIANTELLI, F. BERNARDI, and K. U. INGOLD. J. Am. Chem. Soc. **99**, 4573 (1977).
9. D. R. STULL and G. C. SINKE. Adv. Chem. Ser. No. 18 (1956).
10. D. M. GRANT and E. G. PAUL. J. Am. Chem. Soc. **86**, 2984 (1964).
11. L. P. LINDEMAN and J. A. ADAMS. Anal. Chem. **43**, 1245 (1971).
12. J. B. STOTHERS. Carbon-13 NMR spectroscopy. Academic Press, New York, NY. 1972.
13. G. E. MACIEL and H. C. DORN. J. Am. Chem. Soc. **93**, 1268 (1971).
14. K. DALLING, D. M. GRANT, and E. G. PAUL. J. Am. Chem. Soc. **95**, 3718 (1973).
15. G. E. MACIEL, H. C. DORN, R. L. GREEN, W. A. KLESCHICK, M. R. PETERSON, and G. H. WAHL. J. Org. Magn. Reson. **6**, 178 (1974).
16. R. G. SNYDER and J. H. SCHACHTSCHNEIDER. Spectrochim. Acta, **21**, 169 (1965).
17. S. CHANG, D. MCNALLY, S. SHARY-TEHRANY, M. J. HICKEY, and R. H. BOYD. J. Am. Chem. Soc. **92**, 3109 (1970).
18. R. H. BOYD, S. N. SANWAL, S. SHARY-TEHRANY, and D. M. MCNALLY. J. Phys. Chem. **75**, 1264 (1971).
19. F. D. ROSSINI. Selected values of physical and thermodynamic properties of hydrocarbons and related compounds. Carnegie Press, Pittsburgh, PA. 1952.
20. D. A. PITTNAM and G. PILCHER. J. Chem. Soc. Faraday Trans. I, **68**, 2221 (1972).
21. G. PILCHER and J. D. M. CHADWICK. Trans. Faraday Soc. **63**, 2357 (1967).
22. J. D. COX and G. PILCHER. Thermochemistry of organic and organometallic compounds. Academic Press, New York, NY. 1970.
23. J. R. HOYLAND. J. Chem. Phys. **50**, 473 (1969).
24. J. M. ANDRÉ, P. DEGAND, and G. LEROY. Bull. Soc. Chim. Belg. **80**, 585 (1971).
25. W. D. GOOD. J. Chem. Thermodyn. **4**, 709 (1972).
26. R. ROBERGE and S. FLISZÁR. Can. J. Chem. **53**, 2400 (1975).
27. G. KEAN, D. GRAVEL, and S. FLISZÁR. J. Am. Chem. Soc. **98**, 4749 (1976).
28. H. HENRY and S. FLISZÁR. Can. J. Chem. **52**, 3799 (1974).
29. R. W. TAFT. *In* Steric effects in organic chemistry. *Edited by* M. S. Newman. Wiley, New York, NY. 1956; J. Am. Chem. Soc. **75**, 4231 (1953).

Appendix

The atomic charges of methane, ethane, propane, butane, isobutane, and neopentane were extracted from the literature (3*b*, 5), as well as those of cyclohexane (26) and adamantane (27), and correspond to the population analysis described by eqs. [5] and [6]. For the other molecules, carbon atomic charges were derived from ^{13}C nmr shifts, using eq. [7].

The appropriateness of the population analysis employed here has been verified in the following manner. Equation [10] was written in its original form (7) in terms of atomic charges instead of ^{13}C nmr shifts, whereby the charge dependent part takes the form $\lambda_1'\sum N_{CC}\Delta q_C + \lambda_2'\sum\Delta q_C$. The Δq_C's are the differences in C charges with respect to the ethane-C atom, i.e., $\Delta q_C = q_C - q_C(\text{ethane})$. The q_C's were then expressed as in eq. [5] using Mulliken populations as input and leaving p as the unknown to be determined. The $\Delta E_a{}^*$'s constructed in this fashion were compared with their experimental counterparts calculated from eq. [1] and p was determined by least-squares analysis. This procedure amounts to an experimental partitioning of Mulliken overlap populations. The result, $p = (30.3 \pm 0.3) \times 10^{-3}$ electron equals, within experimental uncertainty, that found by similar procedures for ^{13}C resonance shifts (6, 26, 27) and adiabatic ionization potentials (28), i.e., $p = 30.12 \times 10^{-3}$ electron. Consequently, the charges derived from eqs. [5] and [6] are appropriate for the problem at hand and are adequately represented by ^{13}C resonance shifts, through eq. [7], as was done in eqs. [10] and [13].

When fully optimized STO-3G calculations were not feasible, we have deduced the H net charges from the C charges derived from chemical shifts by carrying out a renormalization reflecting the detailed trends revealed by standard STO-3G results. In the case of 2-methylbutane, 2,2-dimethylbutane, and 2,2,3-trimethylbutane, additional verifications were made by means of the "inductive" approach (5) which has been shown to be in excellent agreement with fully optimized STO-3G results. In R—CH_3 compounds the net charge of the CH_3 group is given by the equation $q(CH_3) = a\sigma_R{}^*$ in which $\sigma_R{}^*$ is the Taft polar constant (29) of R and for R—R′ structures we have calculated $q(R') = a(\sigma_R{}^* - \sigma_{R'}{}^*)$,

TABLE 3. Atomic charges, 10^{-3} electron units[a]

Molecule	Atomic charge							
	C_1	C_2	C_3	C_4	$H(C_1)$	$H(C_2)$	$H(C_3)$	$H(C_4)$
C_2H_6	69.40				−23.13			
C_5H_{12}	66.95	64.41	60.92		−26.05	−27.00	−29.69	
2-MeC_4H_9	64.69	62.35	61.85	67.74	−25.23	−35.61	−29.91	−24.83
2,2-$Me_2C_4H_8$	62.59	62.12	60.31	68.50	−26.60		−31.44	−25.47
2,3-$Me_2C_4H_8$	65.40	61.07			−29.50	−36.50		
2,2,3-$Me_3C_4H_7$	63.12	61.45	59.93	65.84	−28.48		−37.0	−26.69
2,2,3,3-$Me_4C_4H_6$	63.63	60.88			−27.97			
Bicyclo[2.2.2]octane	63.79	63.17			−36.19	−36.19		
Bicyclo[3.3.1]nonane	62.86	61.77	64.44	60.75	−41.16	−39.09	−52.89	−38.21 (e)
						−37.00	+3.19	(a)
trans-Decalin	60.85	63.07		58.08	−33.21	−31.42		−40.95 (e)
					−34.75	−33.12		(a)
cis-Decalin	62.30	63.82		60.21	−34.72	−33.17		−43.37 (e)
					−35.77	−30.71		(a)
Iceane	62.63		61.75		−48.87		−34.76	(e)
							−40.75	(a)

[a]The conventional atom numbering is used, except for the decalins and bicyclo[3.3.1]nonane, where C-4 corresponds to the position 9. For *cis*-decali one also finds the following H charges (in the usual atom numbering): −32.32 (e), −33.21 (a) at C-3 and −37.22 (e), −31.96 (a) at C-4.

where the constant a takes the value 52.43×10^{-3} e appropriate for reproducing the fully optimized STO-3G results. Taking 2-methylbutane as an example, which can be considered as isoC_3H_7—C_2H_5, isoC_4H_9—CH_3, and s-C_4H_9—CH_3, we find (in 10^{-3} electron units) $q(C_2H_5) = -4.72$, $q(CH_3) = -6.76$ (C-4 atom), and $q(CH_3) = -11.01$ (C-1). The charges of the various molecular fragments being determined in this way, those of the H atoms are deduced using the carbon charges derived from eq. [7]. The hydrogen atomic charges were required only for deriving Coulomb energies. It has been verified that possible minor uncertainties associated with these charges do not affect the calculated Coulomb energies to any significant extent. The results are given in Table 3.

On the planarity of the NSi_3 skeleton in the trisilylamine molecule. A normal coordinate analysis involving complex symmetry coordinates

H. F. SHURVELL AND A. DUNHAM

Department of Chemistry, Queen's University, Kingston, Ont., Canada K7L 3N6

AND

S. J. CYVIN AND J. BRUNVOLL

Department of Physical Chemistry, University of Trondheim, N 7034 Trondheim NTH, Norway

Received January 4, 1979

H. F. SHURVELL, A. DUNHAM, S. J. CYVIN, and J. BRUNVOLL. Can. J. Chem. **57**, 1779 (1979).

Normal coordinate calculations have been carried out for the $N(SiH_3)_3$ molecule. A model with C_{3h} symmetry was used, which is based on a planar NSi_3 skeleton. The presence of complex numbers for the characters of degenerate irreducible representations of the point group C_{3h} leads to an unusual problem when factoring the **G** and **F** matrices. A set of real degenerate symmetry coordinates for the E' and E'' species can be constructed, but these are not true symmetry coordinates under the C_{3h} point group. However, they can be obtained from the genuine (complex) symmetry coordinates by a unitary transformation. For a degenerate species, this procedure leads to *a* and *b* blocks of the factored **G** and **F** matrices, which contain interaction terms. Consequently both blocks must be taken together when forming the secular equation, and subsequently the calculated frequencies appear as pairs of identical numbers.

A valence force field that includes all reasonable interactions has been obtained and used to predict the wavenumbers of the ^{15}N and d_9 isotopic molecules. Details of the normal vibrations in the three molecules have been obtained from potential energy distributions. The results show reasonable agreement with the limited experimental data available for the isotopic molecules.

H. F. SHURVELL, A. DUNHAM, S. J. CYVIN et J. BRUNVOLL. Can. J. Chem. **57**, 1779 (1979).

On a effectué des calculs de coordonnées normales pour la molécule de $N(SiH_3)_3$. On a utilisé un modèle avec une symétrie C_{3h} qui est basée sur un squelette NSi_3 plan. La présence de nombres complexes pour les caractères de représentations irréductibles dégénérées du groupe ponctuel C_{3h} conduit à un problème exceptionnel lorsqu'on veut factoriser les matrices **G** et **F**. On a construit un ensemble de coordonnées de symétrie dégénérées réelles pour les espèces E' et E'', mais elles ne sont pas des coordonnées de symétrie vraies pour le groupe ponctuel C_{3h}. Toutefois, on peut les obtenir à partir de coordonnées de symétrie véritables (complexes) par une transformation unitaire. Dans le cas des espèces dégénérées, cette façon d'agir conduit à des chocs *a* et *b* des matrices **G** et **F** factorisées qui contiennent des termes d'interaction. Il en résulte que l'on doit considérer les deux blocs comme un ensemble lorsque l'on forme l'équation séculaire et les fréquences calculées apparaissent donc sous forme de paires de nombres identiques.

On a obtenu un champ de force de valence qui comprend toutes les interactions vraisemblables et on l'a utilisé pour prédire les nombres d'onde de molécules contenant des isotopes ^{15}N et d_9. On a obtenu les détails des vibrations normales de trois molécules à partir de distributions d'énergies potentielles. Les résultats présentent un bon accord avec les valeurs expérimentales restreintes disponibles pour des molécules marquées.

[Traduit par le journal]

Introduction

On the basis of infrared and Raman spectra of trisilylamine $N(SiH_3)_3$, Ebsworth *et al.* (1) and Robinson (2) concluded that the NSi_3 skeleton was planar in this compound and that the point group of the molecule was C_{3h}. Electron diffraction studies (3, 4) support these conclusions. A later paper (5) reported infrared spectra of trisilylamine in gas and solid states and in an argon matrix. It was concluded that the infrared spectra of the matrix isolated sample fits C_{3v} selection rules better than C_{3h}. Miller *et al.* (6) recently reported careful measurements of Raman wavenumbers of the totally symmetric NSi_3 stretching modes of $^{14}N(SiH_3)_3$ and $^{15}N(SiH_3)_3$. In the gas phase the isotopic shift was found to be zero within experimental error, indicating that the NSi_3 skeleton is planar.

Previous vibrational calculations (1, 6) were based on planar or pyramidal XY_3 models for $N(SiH_3)_3$ and made use of the valence force field equations from Herzberg's book (7). Ebsworth *et al.* (1) obtained a value of 4.1 mdyn $Å^{-1}$ for the N—Si

0008-4042/79/141779-06$01.00/0

stretching force constant and 0.2 mdyn $Å^{-1}$ for the stretch–stretch interaction constant of the planar C_{3h} structure. Miller *et al.* (6) in considering the possible ^{14}N–^{15}N isotopic shift of the NSi_3 symmetric stretching mode in a pyramidal C_{3v} structure used the force constants reported by Ebsworth *et al.* (1) together with bending and bend–bend interaction constants. Neither group of workers made calculations of isotopic shifts of vibrational modes of the C_{3h} model, although wavenumbers for some bands in ^{15}N and ^{2}H isotopic molecules were reported.

In this article we report a normal coordinate calculation on the $^{14}N(SiH_3)_3$ molecule using a general valence force field. It was intended that the refined force field could be used to predict the wavenumbers of the $^{15}N(SiH_3)_3$ and $^{14}N(SiD_3)_3$ molecules for comparison with observed wavenumbers. Potential energy distributions (P.E.D.) have also been obtained. The P.E.D. gives the contribution of every force constant of the refined force field to each calculated normal frequency and, from this, qualitative descriptions of the fundamentals can be given.

Structure and Calculations

The structure of trisilylamine (Fig. 1) was taken from the electron diffraction study of ref. 4 where the Si—N and Si—H bond lengths were reported as 1.734 Å and 1.485 Å respectively. The SiNSi angle was reported as $119.7 \pm 0.1°$. However, this apparent slight deviation from planarity is associated with a shrinkage effect (8) on the Si—Si distance. We have used 120.0° for the SiNSi angle and the SiH_3 groups were assumed to be tetrahedral with HSiN and HSiH angles of 109.5°. The electron diffraction results [4] indicate that the HSiN angle is in fact slightly less and the HSiH angle slightly greater than the exact tetrahedral value.

The normal vibrations of the $N(SiH_3)_3$ molecule can be divided into $6A' + 5A'' + 7E' + 4E''$ modes according to the point group C_{3h}. The A' and E'' modes are Raman active, the A'' modes are infrared active, and the E' modes are both infrared and Raman active. From the recorded spectra, wavenumbers can be assigned to 31 of the 33 fundamentals. Only the N—(SiH_3) torsions have not been observed.

The Wilson **FG** matrix method (9) was used for the calculations. An iterative procedure for refining an initial set of force constants was employed. A modified (10) version of the Fortran program written by Schachtschneider (11) was used for these calculations, which were carried out on a Burroughs 6700 computer.

Internal Coordinates and Symmetry Coordinates

A set of 37 internal coordinates was chosen. These

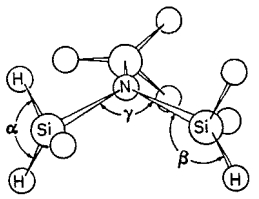

FIG. 1. The structure of the $N(SiH_3)_3$ molecule showing typical internal coordinates.

comprise three N—Si stretches (R_1–R_3), nine Si—H stretches (R_4–R_{12}), three Si—N—Si bends (γ_1–γ_3), nine H—Si—H bends (α_1–α_9), nine N—Si—H bends (β_1–β_9), one NSi_2 out-of-plane wag (ω_1), and three N—SiH_3 torsions (τ_1–τ_3). This set of internal coordinates, which contains four redundancies, involving bending of the angles around the N and Si atoms, was used to calculate the **G** matrix. The corresponding **F** matrix was set up algebraically using the usual **Z** matrix formulation (10, 11). The valence force field contains seven diagonal force constants corresponding to N—Si and Si—H stretching, Si—N—Si, H—Si—H, and N—Si—H bending, NSi_2 wagging, and N—SiH_3 torsion. To take account of all reasonable interactions, 21 independent interaction constants were added. Interactions involving N—SiH_3 torsion and NSi_2 wagging with stretching or bending were omitted, but a wag–torsion interaction was included. These force constants with their final refined values are listed in Table 1.

Non-degenerate symmetry coordinates for the A' and A'' species can be obtained by the usual methods (9, 12). However, these methods cannot be applied to the degenerate species E' and E'', because the character table of the C_{3h} point group contains complex numbers for the degenerate irreducible representations. A similar situation was encountered previously for the cyclic $(HF)_6$ molecule (point group C_{6h}) (13) and for boric acid $B(OH)_3$ (point group C_{3h}) (14). The solution to the problem has been given by Cyvin *et al.* (13). It was noted that the character table for the point group C_{3h} contains two rows for each degenerate species and that these rows contain complex numbers. If the corresponding characters in the two rows are added, one obtains a set of real numbers. Using an analogous procedure, pairs of complex symmetry coordinates can be combined by addition or subtraction to give real degenerate pairs of symmetry coordinates. Although these are not true symmetry coordinates under the C_{3h} point group, they can be used to factor the secular equation in the usual way. As an example, consider the degenerate N—Si_3 stretching mode (E'). The genuine (complex) degenerate symmetry coordinates are:

$$S_{1a} = (1/\sqrt{3})(R_1 + \varepsilon R_2 + \varepsilon^* R_3)$$

$$\varepsilon = \exp(2\pi i/3)$$

$$S_{1b} = (1/\sqrt{3})(R_1 + \varepsilon^* R_2 + \varepsilon R_3)$$

These can be combined to give the pair of real degenerate symmetry coordinates:

$$\mathfrak{S}_{1a}(E') = (1/\sqrt{6})(2R_1 - R_2 - R_3)$$

$$\mathfrak{S}_{1b}(E') = (1/\sqrt{2})(-R_2 + R_3)$$

In this way, the set of real degenerate symmetry coordinates listed in Table 2 was obtained. Table 2 also contains the non-degenerate symmetry coordinates and the four redundant coordinates ($2A' + E'$). A group theoretical justification for this treatment has been given in ref. 13, where it is shown that real degenerate symmetry coordinates such as those of Table 2 are connected with the genuine complex degenerate symmetry coordinates through a unitary transformation.

It should be emphasized that because these real coordinates are not true symmetry coordinates they do not give the usual complete factoring of the **G** and **F** matrices. These normally appear as block diagonalized matrices with pairs of identical blocks for doubly degenerate species. In the present case a single block of twice the normal dimensions is obtained for each degenerate species. The form of these blocks has been discussed in ref. 13. Both **F** and **G** matrices obtained using the $\mathfrak{S}$ coordinates of Table 2 have the same form. These double sized blocks must be used in the solution of the secular equation $(\mathbf{FG} - \mathbf{I}\lambda) = 0$. This leads to calculated frequencies which appear as pairs of identical numbers for each degenerate mode.

TABLE 1. Valence force constants for trisilylamine

Number	Description*	Final refined value†
1	N—Si stretch	3.04
2	Si—H stretch	2.67
3	Si—N—Si bend	0.57731
4	H—Si—H bend	0.42375
5	N—Si—H bend	0.69
6	N—Si_2 wag	0.32
7	N—(SiH_3) torsion	0.023
8	N—Si stretch/N—Si stretch	0.71
9	N—Si stretch/Si—H stretch	0.0
10	N—Si stretch/Si—N—Si bend[a]	0.0
11	N—Si stretch/Si—N—Si bend[b]	−0.298
12	N—Si stretch/H—Si—H bend	0.1741
13	N—Si stretch/N—Si—H bend	0.2947
14	Si—H stretch/Si—H stretch	0.04
15	Si—H stretch/Si—N—Si bend	0.0
16	Si—H stretch/H—Si—H bend[a]	0.0
17	Si—H stretch/H—Si—H bend[b]	0.05444
18	Si—H stretch/N—Si—H bend[b]	−0.02386
19	Si—H stretch/N—Si—H bend[a]	0.0
20	Si—N—Si bend/Si—N—Si bend	−0.08489
21	Si—N—Si bend/H—Si—H bend	0.0
22	Si—N—Si bend/N—Si—H bend[a]	0.0
23	Si—N—Si bend/N—Si—H bend[b]	0.07281
24	H—Si—H bend/H—Si—H bend	0.031
25	H—Si—H bend/N—Si—H bend[a]	0.0
26	H—Si—H bend/N—Si—H bend[b]	0.006
27	N—Si—H bend/N—Si—H bend	0.04
28	Wag/torsion interaction	0.001

*a and b refer to interactions between stretches and bends having no common bond and a common bond respectively.

†Units for force constants are: stretches and stretch/stretch interactions, mdyn Å^{-1}; bends and bend/bend interactions, mdyn Å; stretch-bend interactions, mdyn.

Results and Discussion

Initial values for the diagonal force constants were obtained from previous calculations on the NSi_3 skeleton (1, 6, 15) and SiH_3 groups (16, 17). Refinement of the force field was made by the introduction of various interaction constants and eventually an acceptable fit between observed and calculated wavenumbers was obtained for the $N(SiH_3)_3$ molecule. These wavenumbers are listed in the first two columns of Tables 3 and 4. The set of force constants that give the calculated values is listed in Table 1. Of course no claim for uniqueness is made for this force field and the large number of significant figures associated with some force constants are shown only because they produce the wavenumbers given in Tables 3 and 4.

G matrices were calculated for the $N(SiD_3)_3$ and $^{15}N(SiH_3)_3$ isotopic molecules. After factorization using the symmetry coordinates of Table 2, wavenumbers were calculated for these molecules using the force field of Table 1. Calculated values for $N(SiD_3)_3$ are listed in Tables 3 and 4 and values for $^{15}N(SiH_3)_3$ are given in column 3 of Table 4 for the A'' and E' modes. These are the only vibrations of C_{3h} structure which involve motion of the nitrogen atom. For several of these fundamentals, significant wavenumber shifts are predicted for the ^{15}N isotopic molecule. The largest shifts are for the two E' fundamentals ν_{15} and ν_{16}, both of which involve N—Si—H bending and N—Si stretching. These modes also involve H—Si—H bending and undergo large shifts in the deuterated molecule.

Assignments

Several previous workers (1, 2, 5, 6) have made assignments of the observed infrared and Raman bands to the fundamentals of trisilylamine. These assignments will be discussed in the light of the present calculations. Two different numbering sequences have been employed previously for the E' and A'' modes. If the latter are numbered ν_7–ν_{11}, then the E' modes will be ν_{12}–ν_{18}. This was the scheme used in refs. 1, 5, 6 and it has been adopted

TABLE 2. Symmetry coordinates for an $X(YZ_3)_3$ molecule of symmetry C_{3h}

Species	Symmetry coordinate	Description
A'	$S_1 = (1/\sqrt{3})(R_1 + R_2 + R_3)$	XY stretch
	$S_2 = (1/\sqrt{3})(R_4 + R_7 + R_{10})$	YZ stretch
	$S_3 = (1/\sqrt{6})(R_5 + R_6 + R_8 + R_9 + R_{11} + R_{12})$	YZ stretch
	$S_4 = (1/\sqrt{6})(\alpha_1 + \alpha_2 + \alpha_4 + \alpha_5 + \alpha_7 + \alpha_8)$	ZYZ bend
	$S_5 = (1/\sqrt{3})(\alpha_3 + \alpha_6 + \alpha_9)$	ZYZ bend
	$S_6 = (1/\sqrt{3})(\beta_1 + \beta_4 + \beta_7)$	XYZ bend
	$S_7 = (1/\sqrt{3})(\gamma_1 + \gamma_2 + \gamma_3)$	Redundancy
	$S_8 = (1/\sqrt{6})(\beta_2 + \beta_3 + \beta_5 + \beta_6 + \beta_8 + \beta_9)$	Redundancy
E_a'	$\mathcal{S}_{1a} = (1/\sqrt{6})(2R_1 - R_2 - R_3)$	XY stretch
	$\mathcal{S}_{2a} = (1/\sqrt{6})(2R_4 - R_7 - R_{10})$	YZ stretch
	$\mathcal{S}_{3a} = (1/\sqrt{12})(2R_5 + 2R_6 - R_8 - R_9 - R_{11} - R_{12})$	YZ stretch
	$\mathcal{S}_{4a} = (1/\sqrt{12})(2\alpha_1 + 2\alpha_2 - \alpha_4 - \alpha_5 - \alpha_7 - \alpha_8)$	ZYZ bend
	$\mathcal{S}_{5a} = (1/\sqrt{6})(2\alpha_3 - \alpha_6 - \alpha_9)$	ZYZ bend
	$\mathcal{S}_{6a} = (1/\sqrt{6})(2\beta_1 - \beta_4 - \beta_7)$	XYZ bend
	$\mathcal{S}_{7a} = (1/\sqrt{6})(2\gamma_1 - \gamma_2 - \gamma_3)$	YXY bend
	$\mathcal{S}_{8a} = (1/\sqrt{12})(2\beta_2 + 2\beta_3 - \beta_5 - \beta_6 - \beta_8 - \beta_9)$	Redundancy
E_b'	$\mathcal{S}_{1b} = (1/\sqrt{2})(-R_2 + R_3)$	XY stretch
	$\mathcal{S}_{2b} = (1/\sqrt{2})(-R_7 + R_{10})$	YZ stretch
	$\mathcal{S}_{3b} = (1/2)(-R_8 - R_9 + R_{11} + R_{12})$	YZ stretch
	$\mathcal{S}_{4b} = (1/2)(-\alpha_4 - \alpha_5 + \alpha_7 + \alpha_8)$	ZYZ bend
	$\mathcal{S}_{5b} = (1/\sqrt{2})(-\alpha_6 + \alpha_9)$	ZYZ bend
	$\mathcal{S}_{6b} = (1/\sqrt{2})(-\beta_4 + \beta_7)$	XYZ bend
	$\mathcal{S}_{7b} = (1/\sqrt{2})(-\gamma_2 + \gamma_3)$	YXY bend
	$\mathcal{S}_{8b} = (1/2)(-\beta_5 - \beta_6 + \beta_8 + \beta_9)$	Redundancy
A''	$S_1 = (1/\sqrt{6})(R_5 - R_6 + R_8 - R_9 + R_{11} - R_{12})$	YZ stretch
	$S_2 = (1/\sqrt{6})(\alpha_1 - \alpha_2 + \alpha_4 - \alpha_5 + \alpha_7 - \alpha_8)$	ZYZ bend
	$S_3 = (1/\sqrt{6})(\beta_2 - \beta_3 + \beta_5 - \beta_6 + \beta_8 - \beta_9)$	XYZ bend
	$S_4 = \omega_1$	XY_2 wag
	$S_5 = (1/\sqrt{3})(\tau_1 + \tau_2 + \tau_3)$	X—(YZ_3) torsion
E_a''	$\mathcal{S}_{1a} = (1/\sqrt{12})(2R_5 - 2R_6 - R_8 + R_9 - R_{11} + R_{12})$	YZ stretch
	$\mathcal{S}_{2a} = (1/\sqrt{12})(2\alpha_1 - 2\alpha_2 - \alpha_4 + \alpha_5 - \alpha_7 + \alpha_8)$	ZYZ bend
	$\mathcal{S}_{3a} = (1/\sqrt{12})(2\beta_2 - 2\beta_3 - \beta_5 + \beta_6 - \beta_8 + \beta_9)$	XYZ bend
	$\mathcal{S}_{4a} = (1/\sqrt{6})(2\tau_1 - \tau_2 - \tau_3)$	X—(YZ_3) torsion
E_b''	$\mathcal{S}_{1b} = (1/2)(-R_8 + R_9 + R_{11} - R_{12})$	YZ stretch
	$\mathcal{S}_{2b} = (1/2)(-\alpha_4 + \alpha_5 + \alpha_7 - \alpha_8)$	ZYZ bend
	$\mathcal{S}_{3b} = (1/2)(-\beta_5 + \beta_6 + \beta_8 - \beta_9)$	XYZ bend
	$\mathcal{S}_{4b} = (1/\sqrt{2})(\tau_2 - \tau_3)$	X—(YZ_3) torsion

here. Robinson (2) used the alternative notation with the E' modes numbered ν_7–ν_{13} and the A'' modes ν_{14}–ν_{18}. The A' modes (ν_1–ν_6) and E'' modes (ν_{19}–ν_{22}) are the same in both systems of numbering.

SiH Stretching Modes

For the normal molecule the calculations indicate two groups of SiH stretching frequencies with $\nu_1(A')$ and $\nu_{12}(E')$ near 2160 cm^{-1} and $\nu_2(A')$, $\nu_{13}(E')$, $\nu_7(A'')$, and $\nu_{19}(E'')$ about 8 cm^{-1} lower. No separation is observed in gas or liquid phase spectra. However, Miller *et al.* (6) reported eight frequencies between 2180 and 2138 cm^{-1} in the Raman spectrum of the solid. This is the number of components that would be expected, for the Raman active modes, if the E' and E'' degeneracies were removed by a low site symmetry. Five features were also reported in the infrared spectrum of the solid between 2185 and 2146 cm^{-1} (6). Again this is the expected number if the E' degeneracies are lifted by the site symmetry. The predicted Si—D stretching frequencies in the d_9 isotopic molecule are very close to the values reported by Robinson (2) and Ebsworth *et al.* (1).

N—Si Stretching Modes

These two vibrations $\nu_6(A')$ and $\nu_{14}(E')$ are characterized by small deuterium isotope shifts and in the case of ν_{14} an ^{15}N isotope shift. The observed wavenumber for the A' mode in $N(SiD_3)_3$ is very close to the calculated value (Table 3). However, the

TABLE 3. Observed and calculated wavenumbers (cm^{-1}) for the A' and E'' modes of $N(SiH_3)_3$ and predicted values for $N(SiD_3)_3$

	$N(SiH_3)_3$		$N(SiD_3)_3$		
	Obsd (ref. 6)	Calcd	Calcd	Obsd (refs. 1, 2)	Assignment[a]
A' modes					
ν_1	2170	2163	1560	1568	SiH stretch
ν_2	2138	2155	1538	—	SiH stretch
ν_3	1011	990	749	—	N—Si—H bend + H—Si—H bend
ν_4	919	924	656	—	H—Si—H bend
ν_5	697	683	508	—	N—Si—H bend
ν_6	493	490	456	459	N—Si stretch
E'' modes					
ν_{19}	2152	2155	1560	1563	SiH stretch
ν_{20}	921	924	657	—	H—Si—H bend
ν_{21}	697	683	509	—	N—Si—H bend
ν_{22}	—	30	22	—	N—(SiH_3) torsion

[a]Based on the potential energy distribution.

TABLE 4. Observed and calculated wavenumbers (cm^{-1}) for the A'' and E' modes of $^{14}N(SiH_3)_3$ and predicted values for $^{15}N(SiH_3)_3$ and $^{14}N(SiD_3)_3$

	$^{14}N(SiH_3)_3$		$^{15}N(SiH_3)_3$		$^{14}N(SiD_3)_3$		
	Obsd (ref. 6)	Calcd	Calcd	$\Delta\nu$	Calcd	Obsd (refs. 1, 2)	Assignment[a]
A'' modes							
ν_7	2166	2155.3	2155.3	0.0	1561	1563	Si—H stretch
ν_8	945	939.2	937.5	1.7	696	698	H—Si—H bend + N—Si—H bend
ν_9	748	773.8	769.4	4.4	627	587	N—Si—H bend + H—Si—H bend
ν_{10}	312	303.7	300.2	3.5	260	—	NSi_2 wag (NSi_3 deformation)
ν_{11}	—	29.0	28.7	0.3	20	—	N—(SiH_3) torsion
E' modes							
ν_{12}	2163	2163.8	2162.8	0.0	1561	1563	Si—H stretch
ν_{13}	2146	2155.6	2155.6	0.0	1537	—	Si—H stretch
ν_{14}	997	996.7	992.1	4.6	931	964	N—Si stretch + N—Si—H bend
ν_{15}	946	961.3	952.0	9.3	715	—	N—Si—H bend + H—Si—H bend
ν_{16}	898	894.2	884.5	9.7	655	—	H—Si—H bend
ν_{17}	661	635.2	632.9	2.3	485	—	N—Si—H bend + N—Si stretch
ν_{18}	195	194.7	194.5	0.2	180	—	Si—N—Si bend + N—Si stretch

[a]Based on the potential energy distribution.

agreement is not so good for the E' mode (Table 4). In the latter case it is noted that the potential energy distribution indicates a much greater contribution from the N—Si stretching force constant in the heavy isotopic molecule than in the light molecule.

Other Modes

The modes usually described as SiH_3 deformation and SiH_3 rocking are found between 1000 and 650 cm^{-1}. The P.E.D. shows that these modes all involve N—Si—H and H—Si—H bending and in the case of the E' vibrations, there is a considerable contribution from the N—Si stretching force constant.

The out-of-plane NSi_2 wagging mode $\nu_{10}(A'')$ can also be described as an NSi_3 deformation. A small ^{15}N isotopic shift (3.5 cm^{-1}) is predicted for this mode. The two torsional modes $\nu_{11}(A'')$ and $\nu_{22}(E'')$ have not been observed experimentally, although complete Raman spectra and infrared spectra as low as 35 cm^{-1} have been recorded (6). The SiH_3 groups are expected to rotate almost freely if the NSi_3 skeleton is planar and the calculated wavenumbers for the torsions in Tables 3 and 4 are not unreasonable.

Comments on Previous Assignments

A Raman line at 1011 cm^{-1} was assigned to $\nu_3(A')$ by Ebsworth *et al.* (1), while Robinson (2) assigned an infrared band at 944 cm^{-1} to this mode, as well as to $\nu_8(A'')$, $\nu_{15}(E')$, and $\nu_{20}(E'')$. The present calculation supports the former assignment and in any case ν_3 is not infrared active. Robinson (2) also

assigned an infrared band at 748 cm^{-1} to $\nu_5(A')$, $\nu_9(A'')$, $\nu_{17}(E')$, and $\nu_{21}(E'')$. Again the A' assignment is unlikely to be correct on symmetry grounds, but the A'' assignment is supported by the calculation. The assignment of Ebsworth *et al.* of a Raman line at 697 cm^{-1} to ν_5 is in agreement with the calculation. However, these authors, like Robinson, also assigned this band to ν_{17} and ν_{21}. The more recent work of Miller *et al.* (6) has provided a separate wavenumber (661 cm^{-1}) for ν_{17}. The calculation supports this, but confirms the accidental degeneracy between ν_5 and ν_{21}.

It is suggested, on the basis of our calculations, that $\nu_4(A')$ and $\nu_{20}(E'')$ be assigned to the very strong doublet 919/921 cm^{-1} reported in ref. 6 from the Raman spectrum of solid trisilylamine. The calculated wavenumber is 924 cm^{-1} for both modes again confirming the expected accidental degeneracy.

Conclusions

A reasonable valence force field has been obtained for trisilylamine and this has been used to predict wavenumbers for the normal modes of the fully deuterated and the ^{15}N isotopic molecules. The results are in reasonable agreement with the limited experimental data available. It is unfortunate that more complete spectra of $^{15}N(SiH_3)_3$ and $N(SiD_3)_3$ are not available for comparison with the present predictions.

Potential energy distributions indicate that the qualitative assignments made by previous workers (1, 2, 5) are essentially correct. A few changes suggested by the present calculations have been noted in the discussion.

While the present calculation does little to support the planar structure of the NSi_3 skeleton, it does provide predicted sets of vibrational wavenumbers for isotopic species with structures based on the C_{3h} model. The calculation has also provided a further example of a method for dealing with complex symmetry coordinates.

Acknowledgements

This work has been supported by grants from the National Research Council of Canada.

1. E. A. V. Ebsworth, J. R. Hall, M. J. MacKillop, D. C. McKean, N. Sheppard, and L. A. Woodward. Spectrochim. Acta, **13**, 202 (1958).
2. D. W. Robinson. J. Am. Chem. Soc. **80**, 5924 (1958).
3. K. Hedberg. J. Am. Chem. Soc. **77**, 6491 (1955).
4. B. Beagley and A. R. Conrad. Trans. Faraday Soc. **66**, 2740 (1970).
5. T. D. Goldfarb and B. N. Khare. J. Chem. Phys. **46**, 3379 (1967).
6. F. A. Miller, J. Perkins, G. A. Gibbon, and B. A. Swisshelm. J. Raman Spectrosc. **2**, 93 (1974).
7. G. Herzberg. Infrared and Raman spectra of polyatomic molecules. Van Nostrand, Princeton, NJ. 1945.
8. A. Almenningen, O. Bastionsen, and T. Munthe-Kaas. Acta Chem. Scand. **10**, 261 (1956).
9. E. B. Wilson, Jr., J. C. Decius, and P. C. Cross. Molecular vibrations. McGraw-Hill, New York. 1955.
10. W. V. F. Brooks. Private communication.
11. J. H. Schachtschneider. Technical Report No. 57-65, Shell Development Co. 1965.
12. S. J. Cyvin. Molecular vibrations and mean square amplitudes. Elsevier, Amsterdam. 1968.
13. S. J. Cyvin, V. Devarajan, J. Brunvoll, and Ø. Ra. Z. Naturforsch. **28A**, 1787 (1973).
14. R. W. Mooney, S. J. Cyvin, J. Brunvoll, and L. K. Kristiansen. J. Chem. Phys. **42**, 3741 (1965).
15. H. Kriegsmann and W. Forster. Z. Anorg. Allgem. Chem. **298**, 212 (1959).
16. K. Ramaswamy and S. Rangarajan. Acta Chim. Acad. Sci. Hung. **69**, 87 (1971).
17. J. L. Duncan. Spectrochim. Acta, **20**, 1807 (1964).

Reactions of triethylenetetramine with protons and bivalent zinc, cadmium, and lead in aqueous solution and aqueous dioxane (50% v/v)

W. A. E. McBRYDE AND H. K. J. POWELL[1]

Guelph–Waterloo Centre for Graduate Work, University of Waterloo, Waterloo, Ont., Canada N2L 3G1

Received November 17, 1978

W. A. E. McBRYDE and H. K. J. POWELL. Can. J. Chem. 57, 1785 (1979).

The reactions of triethylenetetramine with protons and with bivalent Zn, Cd, and Pb have been studied in aqueous solution and in 50% (v/v) aqueous 1,4-dioxane, 25°C, $I = 0.10$ M KNO_3. log K (potentiometric) and ΔH (calorimetric) data are interpreted in terms of electrostatic effects and solvation effects operative in the two solvents.

Protonation constants are higher by 0.2–0.6 log units in aqueous solution. Stepwise enthalpies of protonation $-\Delta H_n$ ($n = 2, 3, 4$) are significantly higher, and the corresponding entropies lower, in aqueous solution. The complexes $[ML]^{2+}$ are of similar stability in the two solvents but $-\Delta H$ is ca. 10–20% lower in aqueous dioxane.

W. A. E. McBRYDE et H. K. J. POWELL. Can. J. Chem. 57, 1785 (1979).

On a étudié les réactions de la triéthylènetétramine avec des protons et des ions Zn, Cd et Pb bivalents en solutions aqueuses et en solutions dioxanne–eau (50% v/v), à 25°C et $I = 0.10$ M KNO_3. On a interprété les données de log K (potentiométrique) et de ΔH (calorimétrique) en termes des effets électrostatique et de solvatation présents dans les deux solvants.

Les constantes de protonation sont de 0.2 à 0.6 unités logarithmiques plus élevées en solution aqueuse. En solution aqueuse, les enthalpies progressives de protonation, $-\Delta H_n$ ($n = 2, 3, 4$) sont beaucoup plus élevées et les entropies correspondantes sont plus faibles. Les stabilités des complexes $[ML]^{2+}$ dans les deux solvants sont semblables mais le $-\Delta H$ est environ 10 à 20% plus faible dans le dioxanne–eau.

[Traduit par le journal]

Introduction

The stabilities of metal complexes are determined by an interplay of many factors including metal ion size and electronic configuration, ligand basicity and ring size, and donor atom orbital energies. The distinctive patterns of affinity which class A and class B metal ions have for different types of donor atoms relate to the factors which enhance either ionic or covalent (σ and π) bond formation, and to the contribution which metal ion and ligand solvation make to the enthalpy and entropy changes.

Some understanding of the role of solvation can be achieved by comparing series of reactions in water and in a non-aqueous solvent. Ahrland *et al.* (1, 2) have studied the reactions of bivalent Zn and Cd with Cl^-, Br^-, and I^- in dimethylsulfoxide and in water. The class A character of the metal ion is enhanced in the solvent of lower dielectric constant, i.e. there is an enhanced relative affinity for the smallest anion. The effect of solvent dielectric on electrostatic interactions was not emphasized, but from ΔH and ΔS values it was deduced that (*i*) the stronger solvation of small (hydrogen bonding) anions such as Cl^- in water, and (*ii*) the larger gain in entropy associated with desolvating a metal ion in the less structured solvent DMSO made important contributions to the change in stability.

This work describes a thermodynamic study of the reactions of triethylenetetramine with protons and with bivalent Zn, Cd, and Pb in water and in 50% (v/v) aqueous dioxane. The choice of a non-ionic ligand minimizes the effect of electrostatic contributions to ΔH and ΔS for metal complex formation, avoids the complication of ion-pairing in a solvent of low dielectric constant, and focuses attention on solvation effects. Aqueous dioxane is less structured than water, the density being greater than that for an ideal mixture at all compositions (3, 4). The basicities of amines are lower in aqueous dioxane than in water and for ethylenediamine basicity is at a minimum at compositions close to 50% (v/v) (5, 6). Free energies and enthalpies of transfer from water into aqueous dioxane establish that cations (and the proton) are more strongly solvated in the mixed solvent. Parker and co-workers (6, 7) noted the effect which the structure of solvent water has in reducing hydration energies. Bennetto and Feakins (8) have emphasized the enhanced basicity of aqueous dioxane over water; this results from the transfer of negative charge from the dioxane oxygen to water oxygen via a hydrogen bond.

Aqueous dioxane (50% (v/v)) has a dielectric constant of 35.7 at 25°C (6) and is 17.3 mol% dioxane.

[1]On leave from University of Canterbury, Christchurch, New Zealand.

0008-4042/79/141785-07$01.00/0

TABLE 1. Thermodynamic data for protonation of triethylenetetramine (L) in aqueous solution and in 50% (v/v) aqueous 1,4-dioxane; 25°C, $I = 0.10\ M\ KNO_3$ (values for aqueous dioxane, k_n*, ΔX_n*, in parentheses)

Reaction	n	$\log k_n$[a,b]	$-\Delta G_n$ / kJ mol^{-1}	$-\Delta H_n$[a] / kJ mol^{-1}	ΔS_n / J K^{-1} mol^{-1}
$L + H^+ \rightleftharpoons LH^+$	1	9.88±0.01 (9.63±0.02)	56.4 (54.9)	44.3±0.6 (48.3±1.2)	40.5±2.0 (22±4)
$LH^+ + H^+ \rightleftharpoons LH_2^{2+}$	2	9.15±0.01 (8.75±0.02)	52.2 (50.0)	47.9±0.5 (42.9±1.0)	14.4±1.7 (24±4)
$LH_2^{2+} + H^+ \rightleftharpoons LH_3^{3+}$	3	6.88±0.01 (6.11±0.05)	38.1 (35.1)	39.7±0.3 (30.4±0.8)	−5.3±1.1 (16±4)
$LH_3^{3+} + H^+ \rightleftharpoons LH_4^{4+}$	4	3.40±0.01 (2.80±0.05)	19.4 (15.9)	31.3±0.6 (16.4±9)	−40.0±2.0 (−2±7)

[a]Values for aqueous 0.1 M KCl: $\log k_n = 9.78, 9.06, 6.55$, and 3.24, and $-\Delta H_n = 46.1, 47.1, 39.9$, and 28.6 kJ mol^{-1} for $n = 1$ to 4 respectively, ref. 16. Values for aqueous 0.1 M $NaClO_4$: $\log k_n = 9.80, 9.08, 6.55, 3.25$, ref. 17.
[b]Values for aqueous 0.1 M $NaNO_3$: $\log k_n = 9.89, 9.21, 6.71, 3.45$, $n = 1$ to 4 respectively (T. B. Field and W. A. E. McBryde, to be published).

The dioxane molecule has a gas phase dipole moment of zero, while the low dielectric constant of liquid dioxane (2.2) is consistent with a dominant chair conformation. However, Grunwald *et al.*'s (9) evidence for specific dioxane interactions with univalent cations in aqueous dioxane and the anomalous dependence of K_A for ion pairing upon the bulk dielectric constant for aqueous dioxane solvents (10) have led to postulates that existence of the boat conformation is enhanced by the electrostatic fields about cations.

Experimental and Results

Triethylenetetramine Tetrahydronitrate

Triethylenetetramine (Baker Analyzed Reagent, 15 cm^3) was stirred in ethanol (150 cm^3) in an ice bath. Nitric acid (25 cm^3) in ethanol (100 cm^3) was added dropwise, and the precipitated salt was collected and washed with ethanol. The product was recrystallized as colorless platelets from hot water, washed on the filter crucible with absolute ethanol and ether, then dried at 85°C for 60 min. Molar mass by pH titration (end points determined by Gran's analysis) was 395.5; calculated 398.2 g mol^{-1}.

Solvents and Solutions

All aqueous solutions were prepared with CO_2-free distilled water. The preparation and analysis of the metal salt solutions have been described (11). Dioxane (Baker Analyzed Reagent) was refluxed with sodium and distilled through a 35 cm Vigreaux column in a nitrogen atmosphere; distillation was essential to remove the preservative sodium diethyldithiocarbamate (0.001%). Solvent purity was checked by ultraviolet spectroscopy and by pH titration to determine dissolved CO_2.

pH Measurements

For work in aqueous solution pH^+ measurements were made with the equipment and procedure described previously (11). In aqueous dioxane pH measurements were made with a Beckman E-2 glass electrode and EIL calomel electrode (utilizing a filling solution of 0.1 M KCl in 1.25 M KNO_3) coupled with a Radiometer PHM52 Digital pH meter. The electrode pair was calibrated as a hydrogen-ion concentration probe by titration of (*i*) HNO_3 into KNO_3 solution and into KNO_3/HNO_3 solution (pH^+ 1.6–2.7), and (*ii*) KOH into KNO_3 solution (pOH^- 2.9–2.0), all solutions and titrants being in 50% (v/v) aqueous dioxane, 25°C, $I = 0.10$ M (KNO_3).

Ligand protonation was studied by titration of standard KOH from a Gilmont micrometer syringe into solutions (40 cm^3) of ligand salt (ca. 2×10^{-3} M) and KNO_3 ($I = 0.10\ M$) in the appropriate solvent. The stepwise (amino) protonation constants in Table 1 were computed from derived $\bar{n}_H$(obsd) – pH data by use of the least-squares procedures detailed elsewhere (12) ($\bar{n}_H$ average number of protons bound per ligand molecule). A typical titration involved 50 data points in the range $\bar{n}_H$ = 0.2–3.6 (aqueous solution) or 0.4–3.35 (aqueous dioxan). R factors (13) of 0.3% (1% for aqueous dioxan) were achieved and there were no systematic trends in the residuals $\bar{n}_H$(obsd) − $\bar{n}_H$(calcd).

The formation of complexes $[ML]^{2+}$ and $[M(HL)]^{3+}$ was studied by titration of KOH into solutions of metal nitrate (ca. 1×10^{-3} M), ligand salt (ca. $1.2–1.6 \times 10^{-3}$ M), and KNO_3 ($I = 0.10\ M$) in the appropriate solvent. The titration curves for Zn, Cd, and Pb showed an end point at pH^+ 3.9–4.9 (after addition of 1 mol of OH^- per mole of ligand) followed by a buffer region (at pH^+ 4.8–5.6, 5.0–6.1, and 5.2–6.1, respectively) and a second end point corresponding to completion of the reaction

$$M(aq)^{2+} + LH_3^{3+} + 3OH^- \rightarrow [ML]^{2+} + 3H_2O$$

TABLE 2. Thermodynamic data for the formation of triethylenetetramine complexes $[ML]^{2+}$ and $[M(HL)]^{3+}$, (M = Mn, Zn, Cd, Pb) in aqueous solution and 50% (v/v) aqueous dioxane, 25°C, I = 0.10 M KNO_3 (values in parentheses for aqueous dioxane)

Metal	log K_1	$-\Delta H_1$ / kJ mol^{-1}	ΔS_1 / J K^{-1} mol^{-1}	log K_2	ΔH_2 / kJ mol^{-1}	Reference
Mn	4.91	9.6±2.1	63	—	—	27[a]
	(5.61±0.10)	—	—	—	—	This work[b]
Zn	12.02±0.05	37.2±0.6	105±2	—	—	27[a]
	(12.05±0.02)	(29.7±0.5)	(131±2)	(6.90±0.04)	(30±4)	This work[b]
Cd	10.83±0.01	—	—	6.09±0.04	—	27[a]
	(11.11±0.01)	—	—	(6.95±0.04)	—	This work[b]
Pb	10.50±0.02	48.2±0.5	39±2	5.94±0.05	25.2±5.0	This work[b]
	(10.35±0.02)	(43.3±1.2)	(53±4)	(6.07±0.08)	(15.8±7.8)	This work[b]

[a]0.1 M KCl.
[b]0.10 M KNO_3.

plus one mole of OH^- per mole of excess ligand. (The end point for the reaction $LH_3^{3+} + OH^- \rightarrow LH_2^{2+} + H_2O$ is at ca. pH^+ 8.0.) For Zn, Cd, and Pb the data in the buffer region were analysed in terms of the equilibria [1] and [2] by use of the computer program SCOGS (14).

$$[1] \qquad M(aq)^{2+} + L \overset{K_1}{\rightleftharpoons} [ML]^{2+}$$

$$[2] \qquad M(aq)^{2+} + HL^+ \overset{K_2}{\rightleftharpoons} [M(HL)]^{3+}$$

The standard deviation in titer ($V_{calcd} - V_{obsd}$) was typically 3.5 × 10^{-4} cm^3 and there were no systematic trends in the residuals. For Mn the titration curve showed much less distinct inflections and a poorly defined buffer region at pH^+ 7.7–8.7; these solutions were very oxygen-sensitive. The data in the buffer region were best analysed in terms of the single equilibrium reaction [1]. All solutions were swept with N_2 during titration; this was essential for Mn solutions (both solvents) and for aqueous dioxane which rapidly absorbs atmospheric CO_2.

Calorimetric Measurements

The calorimeter has been described (11). For the protonation of triethylenetetramine in aqueous solution buffered solutions of the ligand (C_L ca. 3 × 10^{-3} M, $\bar{n}_H$ 0.4, I = 0.10 M KNO_3) were titrated in the calorimeter with HNO_3 (1 M). ΔH_i values were determined from the measured heat changes (2–8 J) as outlined previously (11). The least-squares fit gave an R factor of 1.2% and a standard deviation of 0.08 J in $Q_{obsd} - Q_{calcd}$. The ΔH_i values in Table 1 result from 14 data points (2 titrations). For the protonation of triethylenetetramine in aqueous dioxane buffered solutions of the ligand (C_L 1.7 × 10^{-3} M, $\bar{n}_H$ 0.35) were titrated with HNO_3 (0.5 M; 50% aqueous dioxane). The measured heat changes were corrected for the heat of dilution of the titrant acid (determined from the average of 8 measurements as 1.4 ± 2 kJ mol^{-1} for a 625-fold dilution of titrant), and for the neutralization of OH^- produced by the reaction $L + H_2O \rightleftharpoons LH^+ + OH^-$ (ΔH = −57.82 kJ mol^{-1}) (15). The ΔH_i values in Table 1 result from 17 data points (3 titrations); R factor 3.0%, standard deviation 0.12 J.

For the complexes $[M(HL)]^{3+}$ and $[ML]^{2+}$ calorimetric measurements involved titration of HNO_3 into solutions of metal nitrate (1 × 10^{-3} M) and ligand salt (1.6 × 10^{-3} M), starting at pH^+ ca. 5.9 (Pb) or 5.4 (Zn) (cf. titration curves); i.e. the enthalpy changes for dissociation of the complex and protonation of the ligand were determined:

$$[ML]^{2+} + nH^+ \rightarrow M(aq)^{2+} + LH_n^{n+}$$

$$[M(HL)]^{3+} + (n-1)H^+ \rightarrow M(aq)^{2+} + LH_n^{n+}$$

The composition of the calorimeter solution at each titration point was calculated as described previously (11). The enthalpy changes for reactions [1] and [2] (ΔH_1 and ΔH_2) were calculated from a least-squares fit to the equation $Q_{corr} = a_1\Delta H_1 + a_2\Delta H_2$ where a_1 and a_2 are the changes in the number of moles of $[ML]^{2+}$ and $[M(HL)]^{3+}$ respectively between successive titration points. Q_{corr} is the observed heat change corrected as above and for protonation of ligand displaced from the metal. The ΔH_2 values (Table 2) carry significant uncertainties. The distribution curves for $[ML]^{2+}$ and $[M(HL)]^{3+}$ as a function of pH^+ show that the concentration of $[M(HL)]^{3+}$ varies less with pH than does the concentration of $[ML]^{2+}$; e.g. for a 1 × 10^{-3} M zinc solution (C_L = 1.18 × 10^{-3} M) the concentration of $[ML]^{2+}$ increases from 3.2 × 10^{-4} to 6.6 × 10^{-4} M between pH^+ 5.12 and 5.44, whereas in this pH range the concentration of $[M(HL)]^{3+}$ increases from 6.4 × 10^{-5} to 6.9 × 10^{-5} M at pH^+ 5.27 then decreases to 6.3 × 10^{-5} M. Thus in the calorimetric titration $a_2 \ll a_1$ for each data point and ΔH_2 carries a larger error than ΔH_1.

Discussion

Ligand Protonation in Aqueous Solution

The log k_n and ΔH_n data reported here for protonation of triethylenetetramine (L) in 0.1 *M* KNO_3 are in satisfactory agreement with those reported for 0.1 *M* KCl (16) and 0.1 *M* $NaClO_4$ (17). The observed trend $-\Delta H_1 < -\Delta H_2 > \Delta H_3 > \Delta H_4$ is typical for protonation of linear polyamines in aqueous solution. It has been postulated that the first protonation of a polyamine gives a tautomeric mixture in which the proton has added predominantly to the slightly more basic secondary amino center(s) (18). For a secondary alkylamine $-\Delta H$ is smaller and ΔS is larger (typically ca. 43 J K^{-1} mol^{-1}) (19) than for protonation of a primary amine. The second step involves predominantly the (more exothermic) protonation of primary amino groups and is characterized by a larger $-\Delta H$ value (when the protonation sites are sufficiently separated) and a smaller ΔS value (typically ca. 23 J K^{-1} mol^{-1}) for a primary alkylamine. The dominant tautomeric form of the dication LH_2^{2+} is postulated to be that having both terminal amino groups protonated.

The enthalpy changes ΔH_n result from several effects: (*i*) the difference in solvation enthalpy for a polar amino group, an alkylammonium group, and a hydronium ion, (*ii*) the relative donor strengths of the amino group and the solvent towards the proton, and (*iii*) intramolecular electrostatic interactions between an ammonium group and adjacent ionic or polar sites. Solvation effects encompass hydrogen bonding, formation of primary and secondary spheres of ion- or dipole-oriented solvent molecules (interactions which relate to the polarity, polarizability, and dielectric constant of the solvent), and charging effects associated with placing a charge site in a medium of given dielectric. It is only when some of these effects are approximately constant for a series of structurally related ligands in a given solvent, or for a given ligand in a series of solvents, that clear deductions can be made from series of thermodynamic values.

Ligand Protonation in Aqueous Dioxane

The data in Table 1 indicate that for each protonation step the free energy change is more negative in water (ΔG_n) than in aqueous dioxane (ΔG_n^*). This is in accord with the results for ethylenediamine (5). As expected on the basis of intramolecular inductive effects and electrostatic interactions between ionic sites, ΔG_n becomes less negative with increasing n. Further, the difference $-(\Delta G_n - \Delta G_n^*)$ increases from 0.25 for $n = 1$ to 0.62 for $n = 4$. This trend indicates a contribution from 'through solvent' intra-ionic interactions.

The sites of addition for the first two protons might be inferred if ΔH and ΔS data were available for model compounds in this solvent, as is discussed above for aqueous solution. The order of alkylamine basicities, secondary > primary > tertiary, has been established for aqueous solution (20) and for 1,4-dioxane (21), and it could be assumed for the mixed solvents. For both solvents it is expected that the dominant tautomeric form for the diammonium cation LH_2^{2+} will have both terminal groups protonated; it follows that in both solvents the addition of the third (and fourth) proton will be predominantly to secondary amino groups.

The stepwise protonations can be divided into two groups. The addition of the first proton to give LH^+ is characterized by $-\Delta H_1^* > -\Delta H_1$ and $\Delta S_1 > \Delta S_1^*$. These relationships may indicate a difference in solvation energies for reactants and product in the two solvents. For addition of the second, third, and fourth protons, reactions in which intramolecular electrostatic interactions will also contribute, $-\Delta H_n$ is greater than $-\Delta H_n^*$, and $\Delta S_n^* > \Delta S_n$. ΔH_n^* values are significantly less exothermic (by 5.0, 9.3, and 14.9 kJ mol^{-1}) and ΔS_n^* values significantly more favorable (by 9, 21, and 38 J K^{-1} mol^{-1}, $n =$ 2, 3, 4 respectively) than the corresponding values for reaction in aqueous solution.

Effect of Dielectric on Ion–Ion Interactions

The more positive values for ΔH_n^* and ΔS_n^* ($n =$ 2, 3, 4) are consistent with the effects of ion–ion interactions in media with different dielectric properties. For the approach of spherical ions of charge ν and γ to separation a_n in a structureless homogeneous medium of fixed macroscopic dielectric constant ε, the free energy, enthalpy, and entropy changes are given by eqs. [3]–[5]

$$\Delta G = -T\Delta S_t - A \qquad [3]$$

$$\Delta H = -A\left(1 + \frac{T}{\varepsilon}\cdot\frac{\partial E}{\partial T}\right) \qquad [4]$$

$$\Delta S = \Delta S_t - A\left(\frac{1}{\varepsilon}\cdot\frac{\partial \varepsilon}{\partial T}\right) \qquad [5]$$

where ΔS_t is the difference in translational entropy of product and reactants and A is the electrostatic work involved in the process, $A = Ne^2\lambda\nu/a_n\varepsilon$ (22). The partition of ΔG between ΔH and ΔS depends on the solvent, viz. on $\partial\varepsilon/\partial T$, this term being non-zero for both solvents. The polar H_2O molecules in solvent water ($\partial\varepsilon/\partial T = -0.36$ at 25°C) (22) have a larger capacity to release (or absorb) enthalpy in a solvent orientation (or release) process than do dioxane molecules ($\partial\varepsilon/\partial T = -0.21$ for 45% w/w

dioxane–water) (23); $\partial\varepsilon/\partial T$ measures the extent to which thermal motion can offset the alignment of solvent dipoles. Substituting macroscopic values of ε and $\partial\varepsilon/\partial T$ into eqs. [3]–[5] we obtain

$$\Delta H_n - \Delta H_n^* = -A_n'\,(0.016)$$

and

$$\Delta S_n - \Delta S_n^* = -A_n'\,(0.001)$$

where A_n' ($= Ne^2\lambda v/a_n$) is positive. Thus ΔS_n^* will be greater than ΔS_n and $-\Delta H_n > -\Delta H_n^*$. These predictions are consistent with the experimental data. They indicate that formation of multiple cationic center in LH_n^{n+} ions causes greater net solvent orientation in water than in aqueous dioxane.

It can be approximated that for addition of the second proton, $LH^+ + H^+ \rightarrow LH_2^{2+}$, $a_n = 3d$ where d is the mean distance between adjacent amino groups in triethylenetetramine. For the third proton the new ammonium site is at distances d and $2d$ from charge centers, while for the fourth proton the distances are d, d, and $2d$. One can write

$$\Delta H_n = -A''\cdot f(d)\cdot f(\varepsilon)$$

or

$$\Delta H_n - \Delta H_n^* = -A''\cdot f(d)\cdot f(\varepsilon,\varepsilon^*)$$

where $A'' = Ne^2v$ and $f(d) = 1/3$, $3/2$, and $5/2$ for $n = 2$, 3, 4 respectively. Plots of $\Delta H_n - \Delta H_n^*$, ΔH_n, and $\Delta S_n - \Delta S_n^*$ against $f(d)$ are linear within experimental error (Fig. 1). These plots support the model assumed for stepwise protonation.

The reaction $L + H^+ \rightarrow LH^+$ differs from those discussed above in that no ion–ion repulsions are involved. Desolvation of an amino group and a proton, and solvation of a newly formed ammonium group will contribute to the solvation enthalpy and entropy. The reaction involves a larger net increase in entropy in aqueous solution than in aqueous dioxane. The polar amino group will contribute to the observed trend: an amino group can hydrogen bond to a water molecule via the nitrogen lone pair, and we infer that it will have a lower partial molal entropy in water than in aqueous dioxane in which hydrogen bonding between dioxane and water is considered to decrease the charge density on the hydrogen atoms in the water molecules (8). The positive transfer enthalpies for halide ions from water to aqueous dioxane are consistent with this concept (24).

The proton is more strongly solvated than an alkylammonium group ($-\Delta H_{soln} = 1129$ kJ mol^{-1}; cf. $C_2H_5NH_3^+$ 314 kJ mol^{-1} in water) (20) and desolvation of a proton and solvation of an ammonium ion is expected to involve a net release of solvent. At 25°C the density of 50% (v/v) aqueous dioxane is greater than that of an ideal solution (3)

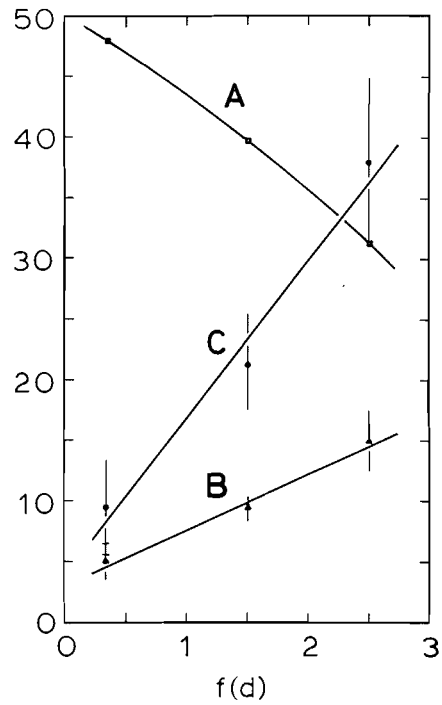

FIG. 1. Plots of thermodynamic functions vs. $f(d)$. Curve A, $-\Delta H_n$/kJ mol^{-1}; curve B, $(\Delta H_n^* - \Delta H_n)$/kJ mol^{-1}; curve C, $(\Delta S_n^* - \Delta S_n)$/J K^{-1} mol^{-1}.

implying a less ordered solvent structure than in water, as also indicated by X-ray diffraction (25). Thus release of solvent molecules from cations and their incorporation in the bulk solvent is expected to involve a more positive entropy change in aqueous dioxane. Thus solvation reactions of the polar amino group and the cations are expected to make opposing contributions to the entropy change. From the observed ΔS_1 values it is inferred that solvation of the polar amino group is the dominant factor in determining relative basicity in the two solvents.

Metal–Triethylenetetramine Complexes

Schwarzenbach (26) reported log K values for the formation of complexes $[MnL]^{2+}$, $[FeL]^{2+}$, and $[ML]^{2+}$, $[M(HL)]^{3+}$ ($M = Co^{2+}$, Ni^{2+}, Cu^{2+}, Zn^{2+}, Cd^{2+}, Hg^{2+}, Ag^+) at 20°C. Sacconi *et al.* (27) corrected the values for Mn, Fe, Co, Ni, Cu, Zn to 25°C by use of their calorimetrically determined ΔH values. Values of log K for the Pb^{2+} complex (25°C) have been reported from polarographic studies (9.9, 1 M KNO_3) (28) and pH measurement (10.4, 0.1 M) (29).

Sacconi *et al.* (27) measured ΔH for formation of $[ML]^{2+}$ complexes by titrating metal ion solution into a buffered solution of the ligand. Under the conditions used the concentration of $[M(HL)]^{3+}$ in

solution was immeasurably small and only ΔH_1 (reaction [1]) was determined. A similar approach was used by Wright *et al.* (30) for divalent Ni, Cu, Zn, and Cd. In the present work enthalpy changes have been determined by titration of HNO_3 into a buffered solution of the metal and ligand, i.e. the decomposition reactions of $[ML]^{2+}$ and $[M(HL)]^{3+}$ have been studied. However, for reasons noted under Experimental, the ΔH_2 values (reaction [2]) are subject to a very large uncertainty; values are reported in Table 2 but are not discussed further.

The entropy change for formation of $[ZnL]^{2+}$ in aqueous solution is ca. 42 J K^{-1} mol^{-1} greater than that for formation of complexes $[ML]^{2+}$, M = Mn, Co, Fe, Ni (27). It was deduced that the zinc complex has a lower coordination number (probably 4) than do the other complexes (probably $[ML(H_2O)_2]^{2+}$). No ΔH or ΔS data have been reported previously for the Pb–triethylenetetramine system in aqueous solution.

The data in Table 2 establish that the stability of each complex is similar in the two solvent systems. This result is consistent with those observed for many metal-ion hydrolysis reactions in water and aqueous dioxane (31). The similar log K values conceal significant differences in ΔH and ΔS values. For Zn^{2+} and Pb^{2+}, $-\Delta H_1$ is greater than $-\Delta H_1$* (by 7.5 and 5 kJ mol^{-1} respectively) and ΔS_1 is less than ΔS_1* (by 26 and 14 J K^{-1} mol^{-1}). These compensating ΔH and ΔS values indicate that solvation effects are different in the two solvents.

From Raman studies on zinc nitrate solutions (32) it has been deduced that there is no significant solvation of zinc ions by dioxane molecules in aqueous dioxane. Aqueous dioxane is a less structured solvent (fewer hydrogen bonds) than water. Thus for a given metal ion, if n' (reaction [6])

$$[6] \quad M(H_2O)_6^{2+} + L(nH_2O) \rightarrow [ML]^{2+} + n'H_2O$$

is the same in both solvents, the binding properties of the bulk solvent toward the released water molecules will lead to a higher $-\Delta H$ and lower ΔS in solvent water. This is consistent with the results recorded in Table 2.

It has been postulated (*loc. cit.*) that the polar amino centers of the ligand will be more strongly solvated in aqueous solution. Thus desolvation of L will be more endothermic in water but this apparently does not offset the effect of n' water molecules binding into the water lattice.

Although there is no evidence for specific Zn^{2+}–dioxane interactions in aqueous dioxane, such interactions (involving the boat conformation of dioxane) have been postulated for solutions of alkali metal ions (9) and tetraalkylammonium ions (10). These results are not contradictory if it is noted that the average binding energy of a water molecule to a bivalent cation is strongly dependent on the polarizability of the water molecule. For example, for $Fe(H_2O)_6^{2+}$ the permanent and induced dipoles in the water molecule contribute 217 and 138 kJ mol^{-1} respectively to the average bond energy (33). In contrast, for $K(aq)^+$ the figures are 71 and 17 kJ mol^{-1} and under these circumstances the less polarizable dioxane molecule can compete with the water molecule in the metal-ion coordination sphere.

1. S. Ahrland and N. O. Björk. Acta Chem. Scand. A**30**, 257 (1976).
2. S. Ahrland, N. O. Björk, and R. Portanova. Acta Chem. Scand. A**30**, 270 (1976).
3. P. F. Waters and S. Jaffer. J. Chem. Soc. Chem. Commun. 529 (1975).
4. V. S. Griffiths. J. Chem. Soc. 1326 (1952).
5. K. Mui, W. A. E. McBryde, and E. Nieboer. Can. J. Chem. **52**, 1821 (1974).
6. G. R. Hedwig, D. A. Owensby, and A. J. Parker. J. Am. Chem. Soc. **97**, 3888 (1975).
7. G. R. Hedwig and A. J. Parker. J. Am. Chem. Soc. **96**, 6589 (1974).
8. H. P. Bennetto and D. Feakins. *In* Hydrogen bonded solvent systems. *Edited by* A. J. Covington and P. Jones. Taylor and Francis, London. 1968. p. 235.
9. E. Grunwald, G. Baughman, and G. Kohnstam. J. Am. Chem. Soc. **82**, 5801 (1960).
10. J. B. Hyne. J. Am. Chem. Soc. **85**, 304 (1963).
11. R. J. Gualtieri, W. A. E. McBryde, and H. K. J. Powell. Can. J. Chem. **57**, 113 (1979).
12. G. R. Hedwig and H. K. J. Powell. Anal. Chem. **43**, 1206 (1971).
13. A. Vacca, A. Sabatini, and M. A. Gristina. Coord. Chem. Rev. **8**, 45 (1972).
14. I. G. Sayce. Talanta, **15**, 1397 (1968); **18**, 653 (1970).
15. G. Gutnikov and H. Freiser. Anal. Chem. **40**, 39 (1968).
16. P. Paoletti, M. Ciampolini, and A. Vacca. J. Phys. Chem. **67**, 1065 (1963).
17. D. W. Margerum, D. B. Rorabacher, and J. F. G. Clarke. Inorg. Chem. **2**, 667 (1963).
18. G. R. Hedwig and H. K. J. Powell. J. Chem. Soc. Dalton Trans. 793 (1973).
19. A. G. Evans and S. D. Hamann. Trans. Faraday Soc. **47**, 34 (1951).
20. D. H. Aue, H. M. Webb, and M. T. Bowers. J. Am. Chem. Soc. **98**, 318 (1976).
21. R. G. Pearson and D. C. Vogelsong. J. Am. Chem. Soc. **80**, 1038 (1958).
22. G. Schwarzenbach. Electrostatic and non-electrostatic contributions to ion association in solution. 13th International Conference on Co-ordination Chemistry, Sydney. 1969. Plenary lectures.
23. H. S. Harned and B. B. Owen. Physical chemistry of electrolyte solutions. 3rd ed. Reinhold, New York. 1958. p. 713.
24. O. N. Bhatnagar. Can. J. Chem. **54**, 3487 (1976).

25. F. FRANKS. Water, a comprehensive treatise. Vol. 2. Plenum Press, New York. 1973. p. 22.
26. G. SCHWARZENBACH. Helv. Chim. Acta, **33**, 974 (1950).
27. L. SACCONI, P. PAOLETTI, and M. CIAMPOLINI. J. Chem. Soc. 5115 (1961).
28. T.-T. LAI and J.-Y. CHEN. J. Electroanal. Chem. **16**, 413 (1968).
29. L. G. SILLEN and A. E. MARTELL. Stability constants. Chem. Soc. London. Spec. Publ. No. 17. 1964.
30. D. L. WRIGHT, J. H. HOLLOWAY, and C. N. REILLEY. Anal. Chem. **37**, 884 (1965).
31. M. MATSUI and H. OHTAKI. Bull. Chem. Soc. Jpn. **50**, 1472 (1977).
32. Y. K. SZE and D. E. IRISH. Personal communication.
33. F. BASOLO and R. G. PEARSON. Mechanisms of inorganic reactions. 2nd ed. J. Wiley and Sons, New York. 1958. p. 62.

Flash photolysis of alkali metal anions in tetrahydrofuran and dimethoxyethane[1]

W. A. SEDDON, J. W. FLETCHER, F. C. SOPCHYSHYN, AND E. B. SELKIRK

Physical Chemistry Branch, Atomic Energy of Canada Limited, Chalk River Nuclear Laboratories, Chalk River, Ont., Canada K0J 1J0

Received November 17, 1978

W. A. SEDDON, J. W. FLETCHER, F. C. SOPCHYSHYN, and E. B. SELKIRK. Can. J. Chem. **57,** 1792 (1979).

Flash photolysis of K^-, Rb^-, and Cs^- in tetrahydrofuran (THF) produces the corresponding ion-pairs (K^+, e_s^-), (Rb^+, e_s^-), and (Cs^+, e_s^-), followed by the regeneration of the parent metal anion, M^-. In mixed-metal solutions containing Na and M where M is K, Rb, or Cs, photolysis of Na^- also forms the (M^+, e_s^-) ion-pair and M^-, but with the latter then reforming Na^- on an extended time scale. Similar results were obtained in dimethoxyethane (DME) at 213 K, but in this case with the initial formation of a loose ion-pair, $(M^+, e_s^-)_{loose}$.

Based on a Gaussian–Lorenztian shape function, the 'best-fit' optical bands for the (M^+, e_s^-) and M^- species were used to simulate the experimental spectra and deduce the corresponding extinction coefficients in both solvents.

The overall mechanism is complex but is in good agreement with previous interpretations deduced by pulse radiolysis.

W. A. SEDDON, J. W. FLETCHER, F. C. SOPCHYSHYN et E. B. SELKIRK. Can. J. Chem. **57,** 1792 (1979).

La photolyse éclair de K^-, Rb^- et Cs^- dans le tétrahydrofuranne (THF) conduit aux paires d'ions correspondantes (K^+, e_s^-), (Rb^+, e_s^-) et (Cs^+, e_s^-) qui sont suivies par une regénération de l'anion métallique apparenté, M^-. Dans des solutions de métaux mixtes contenant du Na et du M où M est égal à K, Rb et Cs, la photolyse de Na^- conduit aussi à la formation de la paire d'ions (M^+, e_s^-) et de M^-; ce dernier conduit à la reformation de Na^- sur une échelle de temps prolongée. On a obtenu des résultats semblables dans le diméthoxyéthane (DME) à 213 K; toutefois, dans ce cas, il y a une formation initiale d'une paire d'ions lâche, $(M^+, e_s^-)_{lâche}$.

Sur la base d'une fonction de forme Gaussienne–Lorenztienne, on a utilisé les bandes optiques qui concordent le mieux pour les espèces (M^+, e_s^-) et M^- pour simuler le spectre expérimental et pour en déduire les coefficients d'extinction correspondants dans les deux solvants.

Le mécanisme global est complexe mais il est en bon accord avec les interprétations antérieures déduites d'études par radiolyse pulsée.

[Traduit par le journal]

Introduction

Steady state photolysis and flash photolysis of alkali metal anions, M^-, in ethers have been investigated previously (1–3). The primary photolysis step is considered to be reaction [1] involving the formation of solvated electrons, e_s^-, and a species of stoichiometry M, best regarded as an ion-pair (M^+, e_s^-) (4, 5).

$$[1] \qquad M^- \xrightarrow{h\nu} (M^+, e_s^-) + e_s^-$$

However, because of Na^+ contamination and, what are now known to be incorrect spectral assignments, the early work (1) on the flash photolysis of potassium in tetrahydrofuran (THF) and dimethoxyethane (DME) requires reinterpretation. Furthermore, a more recent study (4) has indicated a basic inconsistency in the spectra attributed to the species (Na^+, e_s^-), as generated by flash photolysis (3), and pulse radiolysis (4).

This paper describes the flash photolysis of potassium rubidium, and cesium solutions in THF and DME together with similar studies on mixed metal solutions containing sodium/potassium, sodium/rubidium, and sodium/cesium. The results clearly substantiate the conclusions reached earlier by pulse radiolysis (4, 6).

Experimental

A detailed description of the flash photolysis apparatus has been given elsewhere (7). Briefly, solutions were photolyzed with a 60 J, 1 μs flash from two quartz arc lamps (iLC Sunnyvale Inc., California, #L378-008) connected in series. The flash was filtered by surrounding each lamp with the solvent under investigation. The analyzing light was filtered at the source with a Corning glass filter #2-62 and at the monochromator with either a 7-56 or a 1400 nm "cut-on" interference filter at the appropriate wavelengths. Quartz flow systems containing 2 cm × 1 cm diameter reaction cells were otherwise identical to those described previously (8, 9). Methods of sample preparation, solvent purification, and optical detection are also well documented (8, 10). However, it is worth noting that dissolution of the alkali metals to form

[1]AECL No. 6550.

0008-4042/79/141792-09$01.00/0

M^- is greatly facilitated by immersion of the container in an ultrasonic bath. Initial M^- spectra were measured on a Cary 17 Recording Spectrophotometer. Simulation of the experimental spectra was accomplished using a Hewlett Packard 9830 calculator, 9864A digitizer, and 9862 plotter, to store and compute the ratio of component species produced after the flash.

Results and Discussion

In THF (and DME) alkali metal solutions the equilibrium optical spectra are predominantly due to the formation of M^- (11), with only small concentrations of (M^+, e_s^-) and e_s^- detectable by electron spin resonance (12). The reported optical spectra (13–16) show good agreement in the position of the band maxima but often significant differences in band width and intensity, particularly on the high energy side of the spectrum. Utilizing the most reliable data (free of Na^+ contamination) (15, 16) in comparison with our own initial spectra, the overall band envelope for each M^- species was established by a Gaussian–Lorenztian (G–L) shape function analogous to the method used for e_s^- (17–19). Since sodium is insoluble in THF (and DME) our Na^- spectra were obtained either by the addition of dicyclohexano-18-crown-6 (16) or from Na/Cs solutions in which the final equilibrium spectrum is due to Na^-.

Figure 1 shows the best-fit G–L spectra for the species Na^-, K^-, Rb^-, and Cs^- in THF observed by conventional steady state techniques. The experimental data only begin to diverge from these curves at a point corresponding to about half the peak intensity on the high energy Lorenztian tail of the spectrum. This may be due to light scattering by finely distributed metal particles or, in the absence of added sodium, due to contamination by Na^-. Representative experimental points are shown for Na^- and K^- to illustrate the region of discrepancy.

A similar fitting procedure was adopted for the ion-pair species (Na^+, e_s^-), (K^+, e_s^-), and (Cs^+, e_s^-) (10, 20). The (Rb^+, e_s^-) spectrum was deduced by the flash photolysis of Rb^- solutions (see Fig. 4 and discussion below). In general the G–L fits are even better than observed for the M^- species and are given in Fig. 2 along with a few representative experimental points where differences occur.

Although empirical the G–L band shapes, particularly with respect to M^-, were chosen for the purposes of simulation (see below) because these gave the closest fit to the bleached M^- photolysis bands. For the purposes of this paper the precise shape in this region is of relatively minor importance. However, because they are observed as a difference in optical properties before and after the flash, the photolysis spectra do suggest that the high energy "wing" is adequately described by the Lorenztian function. The alternative involves a somewhat arbitrary choice between the broader (15, 16) or narrower (3, 13) bands reported previously. In all other respects equally good fits to the data were obtained using the experimentally observed equilibrium spectra. This simply reflects how

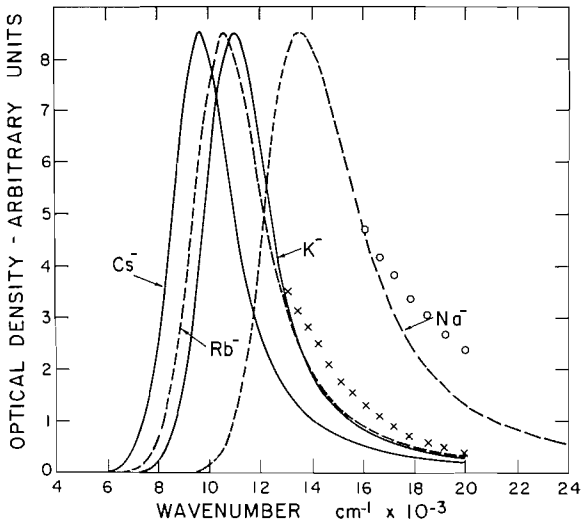

FIG. 1. Gaussian–Lorenztian shape functions describing the optical absorption spectra of alkali metal anions in THF. ○, ×, representative experimental points for Na^- and K^- to illustrate divergences on the high energy sides of the spectra.

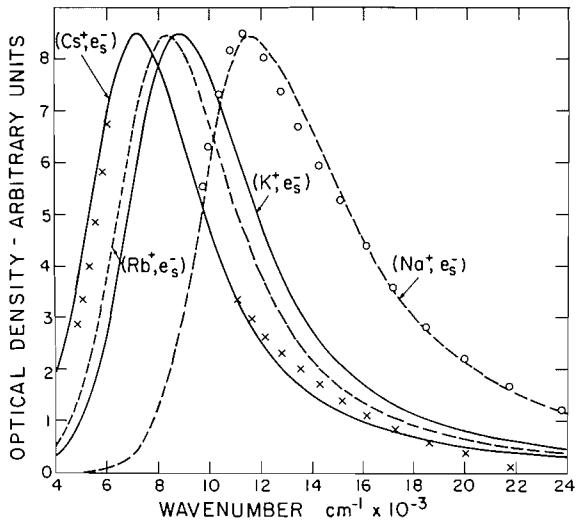

FIG. 2. Gaussian–Lorenztian shape functions describing the optical absorption spectra of alkali metal ion-pairs in THF. ○, ×, representative experimental points for (Na^+, e_s^-) and (Cs^+, e_s^-) to illustrate agreement with G–L spectra.

well the G–L shapes otherwise describe the overall (M^+, e_s^-) and M^- absorption bands.

Flash Photolysis of M^- Solutions in THF-spectra

Figures 3, 4, and 5 (open circles) show the spectra observed at the end of the flash (~6 μs) in ~2.5 μ*M* K^-, ~8 μ*M* Rb^- (saturated solutions) and ~10 μ*M* Cs^- solutions in THF at 294 K. In essence each spectrum represents the bleaching of the respective M^- species together with the concurrent formation of an infrared absorption band which shifts to longer wavelengths on progressing from K^- to Cs^- solutions. For K^- and Cs^- solutions such absorption bands correspond to those expected for the appropriate ion-pairs (K^+, e_s^-) and (Cs^+, e_s^-), respectively (10). Likewise we suggest that the corresponding band observed from Rb^- solutions represents the formation of (Rb^+, e_s^-). Its band maximum is intermediate to that of (K^+, e_s^-) and (Cs^+, e_s^-) and entirely consistent with established trends for the M^- and (M^+, e_s^-) series from Na to Cs (21).

However, the experimental spectra in Figs. 3–5 cannot be duplicated entirely on the basis of the spectra given in Figs. 1 and 2. In each case the bleached band contains a small, but significant, contribution from Na^-, presumably formed from spurious Na^+ contamination. Furthermore, the infrared absorption observed from the photolysis of K^- is, at wavelengths >1300 nm, significantly greater than anticipated from (K^+, e_s^-) alone suggesting, in addition, a small contribution from e_s^-.

Assuming $[K^+] \sim [K^-] = 2.5$ μ*M*, the presence

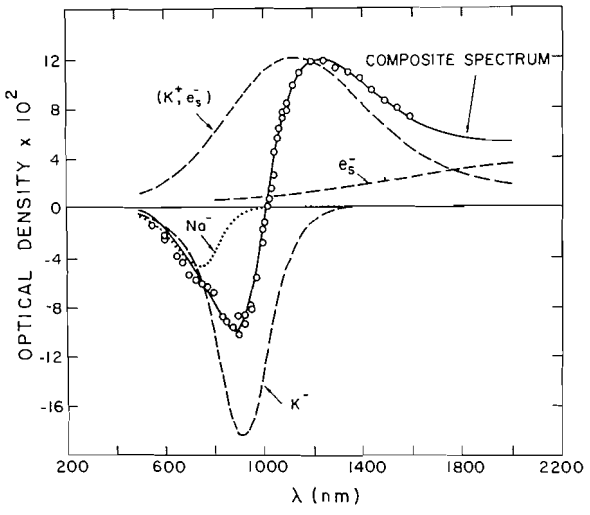

FIG. 3. Optical spectrum (open circles) observed at the end of the flash in ~2.5 μ*M* K^- solutions in THF. The solid line represents the composite spectrum simulated from the component species, Na^-, K^-, (K^+, e_s^-), and e_s^-.

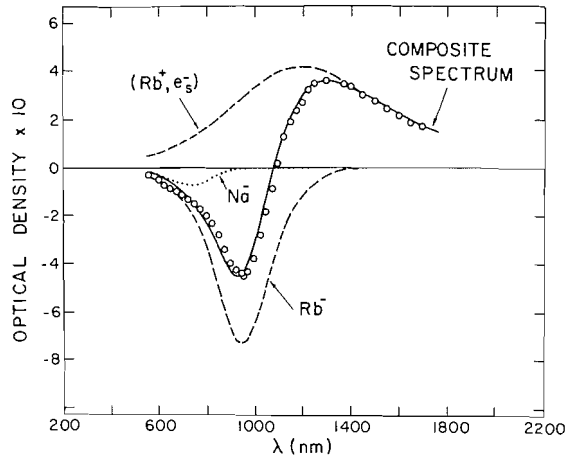

FIG. 4. Optical spectrum (open circles) observed at the end of the flash in ~8 μ*M* Rb^- solutions in THF. The solid line represents the composite spectrum simulated from the component species Na^-, Rb^-, and (Rb^+, e_s^-).

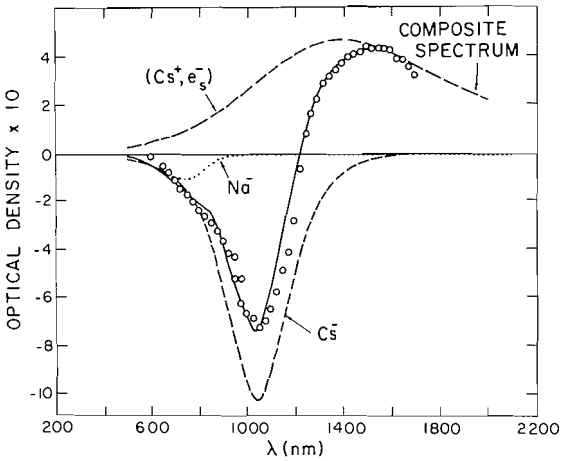

FIG. 5. Optical spectrum (open circles) observed at the end of the flash in ~10 μ*M* Cs^- solutions in THF. The solid line represents the composite spectrum simulated from the component species Na^-, Cs^-, and (Cs^+, e_s^-).

of e_s^- is consistent with the dissociation constant $1/K_2 = 4 \pm 2 \times 10^{-7}$ *M* (10).

[2] $$K^+ + e_s^- \rightleftharpoons (K^+, e_s^-)$$

Since $k_2 = 4.6 \pm 0.6 \times 10^{11}$ L mol^{-1} s^{-1} (10) reaction [2] will be essentially complete at the end of the flash and hence $[e_s^-]/[(K^+, e_s^-)] = 0.16 \pm 0.08$. The solid line drawn through the experimental points in Fig. 3 represents the simulated spectrum deduced by adding the appropriate optical densities for the component species Na^-, K^-, and (K^+, e_s^-) (Figs. 1 and 2) and e_s^- (10). Taking the extinction coefficients $\varepsilon_{e_s^-}$ and $\varepsilon_{(K^+, e_s^-)} = 5 \pm 0.5 \times 10^4$ and $2.9 \pm 0.2 \times 10^4$ L mol^{-1} cm^{-1}, respectively (10),

TABLE 1. Optical parameters for alkali metal anions and ion-pairs in THF

Species	ν_{max}	$\omega_{1/2}{}^{G}$*	$\omega_{1/2}{}^{L}$*	$\varepsilon_{max} \times 10^{-4}$ L mol^{-1} cm^{-1}	
				Flash photolysis	Calcd. from [3]
Na^-	13.5	1.5	2.85	8.2±0.3†	7.6
K^-	11.1	1.4	1.6	10.0±1.3	11.6
Rb^-	10.64	1.44	1.76	10.8	10.8
Cs^-	9.60	1.2	1.65	12.5±1.0	12.0
(Na^+, e_s^-)	11.5	2.05	4.80	2.4±0.2‡	2.4
(K^+, e_s^-)	8.80	2.20	3.75	2.9±0.2‡	3.2_5
(Rb^+, e_s^-)	8.33	2.16	3.32	2.7±0.2	3.1
(Cs^+, e_s^-)	7.20	2.15	3.20	2.5±0.2‡	3.1_5

*In $cm^{-1} \times 10^{-3}$.
†Reference 24 and this work (see later).
‡Reference 10.

then $[e_s^-]/[(K^+, e_s^-)] = 0.17 \pm 0.02$, in excellent agreement with the above $1/K_2$.

It is worth noting that using the experimentally observed component spectra to simulate the composite spectrum in Fig. 3 gives, within experimental error, the same result.

Interpretation of the Rb^- and Cs^- photolysis spectra was accomplished in a similar manner. However, in both cases the infrared band appears to be due entirely to (Rb^+, e_s^-) or (Cs^+, e_s^-), respectively. Hence, the dissociation constant for both ion-pairs must be $< 1/K_2$. Again this is consistent with recognized trends for equilibrium constants in alkali metal solutions (22) and with the decreasing dissociation constants, from Na to Cs, for alkali metal salts of tetraphenylboron in THF (23).

Extinction Coefficients

Having established that the flash photolysis spectra are essentially composed of M^- (bleached) and (M^+, e_s^-) then, based on the material balance inherent in [1] and [2], one can deduce their relative extinction coefficients. Taking ε_{Na^-}, $\varepsilon_{(K^+, e_s^-)}$, and $\varepsilon_{(Cs^+, e_s^-)} = 8.2 \pm 0.3$, 2.9 ± 0.2, and $2.5 \pm 0.2 \times 10^4$ L mol^{-1} cm^{-1}, respectively (10, 24), the absolute values for ε_{K^-} and ε_{Cs^-} can be determined experimentally. Furthermore, the oscillator strength, f, for a Gaussian–Lorenztian absorption band is given by [3] (18).

$$[3] \quad f = 4.32 \times 10^{-9} (1.065\omega_{1/2}{}^{G} + 1.571\omega_{1/2}{}^{L})\varepsilon$$

where $\omega_{1/2}{}^{G}$ and $\omega_{1/2}{}^{L}$ represent the width at half height on the Gaussian and Lorenztian sides, respectively. Since $f = 1$ for (M^+, e_s^-) (20) and $f = 2$ for M^- (24), it is also possible to calculate $\varepsilon_{(M^+, e_s^-)}$ and ε_{M^-} from the spectra given in Figs. 1 and 2. In this way both the experimental and calculated values can be compared for self-consistency.

With respect to the experimental value for ε_{Na^-} (24) it should be noted that this was determined in ethylenediamine (EDA). Although the absorption maximum in EDA occurs at higher energy (15 000 cm^{-1}) the overall band shape is very close to that given for THF in Fig. 1 ($\nu_{max} = 13\,500\ cm^{-1}$). Consequently, it seems reasonable to assume the same extinction coefficient in THF.

Table 1 summarizes the optical parameters and extinction coefficients deduced by experiment and calculation from the results given in Figs. 1–5. The calculated value for ε_{Rb^-} was used to deduce $\varepsilon_{(Rb^+, e_s^-)}$ from Fig. 4. It can be seen that the agreement between both sets of data is well within experimental error and hence substantiates the overall mass balance and validity of the G–L spectra in Figs. 1 and 2.

Kinetics

The decay of the infrared absorption and concomitant recovery of the bleached M^- band follow neither good first nor second order kinetics. In potassium solutions the decay at 1450 nm appears to be a better second order process with $k/\varepsilon = 4.3 \times 10^5$ cm s^{-1} at 1450 nm. From the known spectrum and $\varepsilon_{(K^+, e_s^-)}$ we calculate $\varepsilon_{1450} = 1.8 \times 10^4$ L mol^{-1} cm^{-1} and hence $k = 7.7 \times 10^9$ L mol^{-1} s^{-1} at 294 K. Similar kinetic analysis between 213 and 270 K gives for the decay process, an energy of activation, $E_a = 20 - 30$ kJ mol^{-1}. This is consistent with the reformation of M^- by either reaction [4f] or [5f] or, some combination of both.

$$[4] \quad (M^+, e_s^-) + e_s^- \overset{f}{\rightleftharpoons} M^-$$

$$[5] \quad (M^+, e_s^-) + (M^+, e_s^-) \overset{f}{\rightleftharpoons} M^- + M^+$$

However, we are unable to differentiate between these alternatives because of the equilibrium nature of the overall system.

In cesium solutions and rubidium solutions a much better first order fit is obtained. This is not under-

stood and a detailed study of the overall kinetics is in progress.

Pure Metals in DME

Compared to THF the M^- solutions are considerably less stable and require low temperatures to minimize autodecomposition. Because of this inherent difficulty we were unable to obtain reliable spectra from the photolysis of Rb^- or Cs^- in DME.

Figure 6 shows the spectrum observed after the flash in $\sim 5\ \mu M\ K^-$ solutions in DME at 213 K. Whereas the bleached band is similar to that obtained in THF the infrared absorption is significantly different. Previous investigators (3) have assigned this band to e_s^-. However, attempts to simulate the experimental spectra using the known spectrum for e_s^- at 213 K (4) were not entirely satisfactory (see Fig. 6) and gave a very poor material balance. On the other hand good agreement is obtained when the infrared band is assigned to the formation of a loose ion-pair $(K^+, e_s^-)_{loose}$. The absorption spectrum of the latter (shown in Fig. 6) was obtained from the pulse radiolysis of 10^{-2} *M* potassium tetraphenylboron in DME at 213 K. Its spectrum is very similar to that reported previously for $(Na^+, e_s^-)_{loose}$ (4) and is significantly narrower than e_s^- at wavelengths below the band maximum.

The solid line drawn through the experimental points in Fig. 6 represents the composite spectrum produced by the bleaching of K^-, and a small amount of Na^-, together with the formation of $(K^+, e_s^-)_{loose}$. The band shapes taken for Na^- and K^- were as shown in Fig. 1 but with the maxima

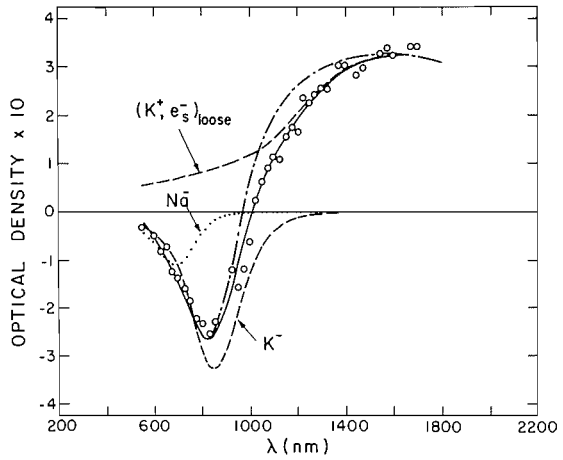

FIG. 6. Optical spectrum (open circles) observed at the end of the flash in $\sim 5\ \mu M\ K^-$ solutions in DME at 213 K. The solid line represents the composite spectrum simulated from the component species, Na^-, K^-, and $(K^+, e_s^-)_{loose}$. The broken line ----- shows a corresponding simulation using e_s^- instead of $(K^+, e_s^-)_{loose}$.

shifted to 14 280 cm^{-1} and 11 575 cm^{-1}, respectively, to compensate for effects of temperature (15, 16). As in the case of K/THF solutions the Na^- must arise from inadvertent Na^+ contamination. Excluding Na^- from the simulation gives a narrower bleached band and a significant absorption at wavelengths <600 nm. The latter is not observed experimentally.

Extinction Coefficients

Taking the experimental extinction coefficients in Table 1 for ε_{Na^-} and ε_{K^-}, and the component optical densities in Fig. 6, then $\varepsilon_{(K^+, e_s^-)_{loose}}$ at 213 K = $3.6 \pm 0.5 \times 10^4$ L mol^{-1} cm^{-1}. This is in reasonable agreement with the value of $2.8 \pm 0.4 \times 10^4$ L mol^{-1} cm^{-1} estimated by pulse radiolysis (4).

Kinetics

Both the decay of the infrared band and concomitant recovery of K^- appear to follow second order kinetics. Taking $\varepsilon_{(K^+, e_s^-)_{loose}} = 3.6 \times 10^4$ L mol^{-1} cm^{-1} to be independent of temperature, then k/ε_{1600} ranges from 3.8×10^9 L mol^{-1} s^{-1} at 270 K to 3.7×10^8 L mol^{-1} s^{-1} at 213 K with $E_a = 20$ kJ mol^{-1}.

Mixed Metal Solutions in THF-spectra

Figures 7, 8, and 9 show the spectra obtained as a function of time in Na/K, Na/Rb, and Na/Cs solutions, respectively. In each case two distinct time resolved processes can be observed. The decay of the infrared absorption, and partial recovery of the bleached band, occurs on a μs time scale to produce a long-lived intermediate absorption which then decays over a period of ~ 50 ms to re-establish the pre-photolysis equilibrium. These observations parallel those reported previously in both amine and ether solutions. A variety of explanations have been offered (1, 3, 25), the most recent of which (3) attributes the intermediate absorption to the formation of the (Na^+, e_s^-) ion-pair. As the ensuing discussion will show, the former interpretations are incorrect, but instead reflect a complexity, namely, the formation of Na^- in a mixed-metal solution.

From the earlier discussion concerning 'pure' M^- solutions it is evident from Figs. 7–9 that, qualitatively, the spectra observed immediately after the flash correspond to the bleaching of Na^- with the associated formation of (K^+, e_s^-), (Rb^+, e_s^-), and (Cs^+, e_s^-), respectively. The long-lived spectra clearly show a remaining contribution from Na^- along with the production of K^-, Rb^-, and Cs^-, respectively.

Quantitatively, the situation is more complex. In Na/K alloy solutions we have noted (10) that the M^- band is in fact composed of both Na^- and K^-.

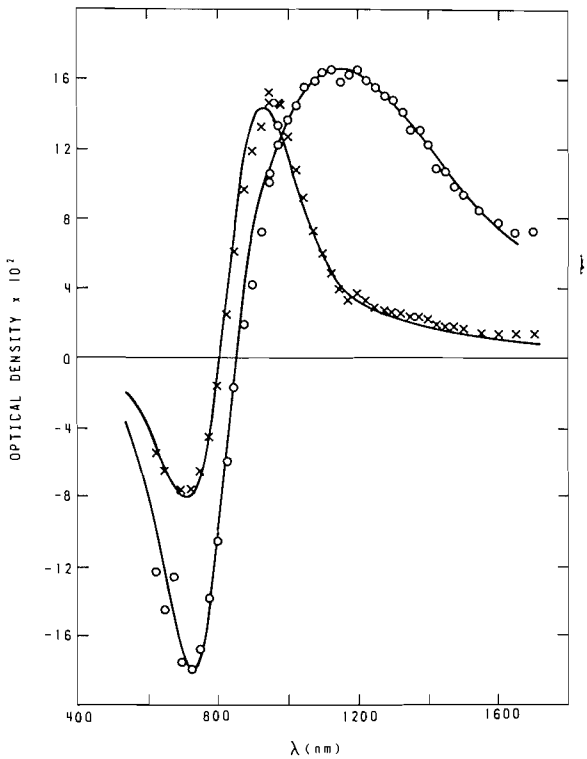

FIG. 7. Optical spectra observed following the flash photolysis of Na/K alloy solutions in THF: ○, immediately after the flash; ×, ~80 μs after the flash. The solid lines represent the composite spectra simulated from the component species with the following peak optical densities; ○, Na^-, −0.233; K^-, −0.023; e_s^-, 0.017; (K^+, e_s^-), 0.163; ×, Na^-, −0.124; K^-, 0.136; (K^+, e_s^-), 0.025.

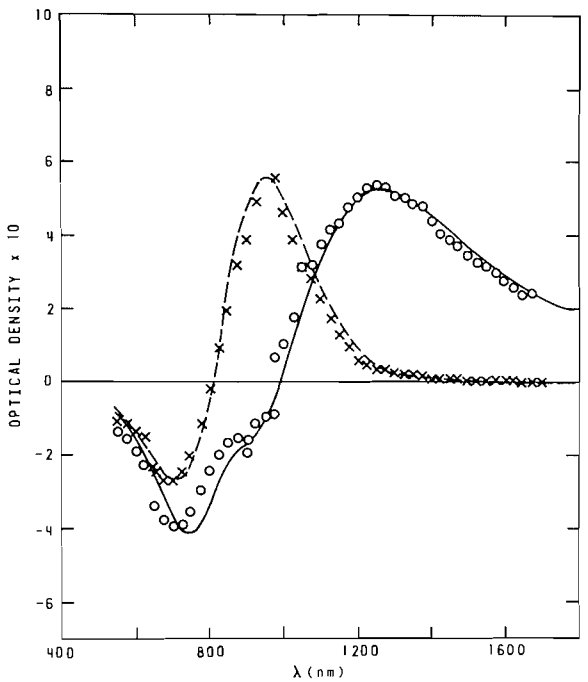

FIG. 8. Optical spectra observed following the flash photolysis of Na/Rb solutions in THF: ○, immediately after the flash; ×, ~180 μs after the flash. The solid and dashed lines represent the composite spectra simulated from the component species with the following peak optical densities; ○, Na^-, −0.45; Rb^-, −0.47; (Rb^+, e_s^-), 0.564; ×, Na^-, −0.404; Rb^-, 0.572.

Utilizing the spectra in Fig. 1, and the experimental extinction coefficients in Table 1, the relative concentrations correspond to 3.3×10^{-6} and 0.67×10^{-6} *M*, for Na^- and K^-, respectively. Consequently, the photolysis of both species is involved in the overall mechanism. This can be demonstrated more graphically for Na/Rb and Na/Cs solutions. In both cases the ultimate formation of Na^- occurs over a period of a week or more such that photolysis of a mixed M^- solution can be investigated. Representative examples are shown in Figs. 8 and 10, illustrating the simultaneous bleaching of both Na^-/Rb^- and Na^-/Cs^- solutions.

Extinction Coefficients

The solid line drawn through the experimental points represents, in all cases, the composite spectrum simulated from the individual species in Figs. 1 and 2. Relative optical densities of the latter are given in the caption. Taking $\varepsilon_{Na^-} = 8.2 \times 10^4$ L mol^{-1} cm^{-1}, the extinction coefficients for both M^- and (M^+, e_s^-) can then be determined. Based on a series of independent experiments we find $\varepsilon_{(K^+, e_s^-)}$, $\varepsilon_{(Rb^+, e_s^-)}$, and $\varepsilon_{(Cs^+, e_s^-)} = 2.8 \pm 0.2$, $\varepsilon_{K^-} = 12.3 \pm 1.0$, $\varepsilon_{Rb^-} = 11.1 \pm 1.0$, and $\varepsilon_{Cs^-} = 13.5 \pm 1.5$ all $\times 10^4$ L mol^{-1} cm^{-1}. All are in excellent agreement with the values deduced earlier and at the same time the material balance in the Na/K solution (Fig. 7) confirms the value for $\varepsilon_{Na^-} = 8.4 \pm 0.8 \times 10^4$ L mol^{-1} cm^{-1}. Further evidence of their self-consistency is illustrated by the fact that the disappearance of the (M^+, e_s^-) absorption corresponds in concentration to the intermediate M^- formation and partial recovery of Na^-.

Kinetics

The overall kinetics are complex and will be discussed in detail elsewhere. Qualitatively the results are consistent with the following mechanism

[1] $M^- \xrightarrow{h\nu} (M^+, e_s^-) + e_s^-$

[4] $(M^+, e_s^-) + e_s^- \rightleftharpoons M^-$

[5] $(M^+, e_s^-) + (M^+, e_s^-) \rightleftharpoons M^- + M^+$

[6] $M^+ + e_s^- \rightleftharpoons (M^+, e_s^-)$

[7] $Na^- \xrightarrow{h\nu} (Na^+, e_s^-) + e_s^-$

[8] $(Na^+, e_s^-) + e_s^- \rightleftharpoons Na^-$

[9] $(Na^+, e_s^-) + (Na^+, e_s^-) \rightleftharpoons Na^- + Na^+$

[10] $Na^+ + e_s^- \rightleftharpoons (Na^+, e_s^-)$

[11] $(Na^+, e_s^-) + M^+ \rightleftharpoons (M^+, e_s^-) + Na^+$

[12] $(Na^+, e_s^-) + (M^+, e_s^-) \rightleftharpoons Na^- + M^+$

[13] $M^- + Na^+ \rightleftharpoons (Na^+, e_s^-) + (M^+, e_s^-)$

At the end of the flash reactions [1] and [7], followed by [6], [10], and [11], are essentially complete to form (M^+, e_s^-). Some Na^- is reformed on a μs time scale by a combination of reactions [8], [9], and [12] with [9] predominating. As mentioned earlier, reactions [4] and [5] produce M^- also on a μs time scale. The slow rate determining step for the regeneration of Na^- is considered to be reaction [13]. This process appears to be pseudo first order with, for the three Na/M solutions investigated, $k_{13} \sim 50\ s^{-1}$.

These observations are entirely consistent with the mechanism deduced by pulse radiolysis for solutions in ethylamine (6). Regardless of the detailed kinetics it is clear that dominant reactions are [11] and [13] with the long-lived intermediate species being M^-.

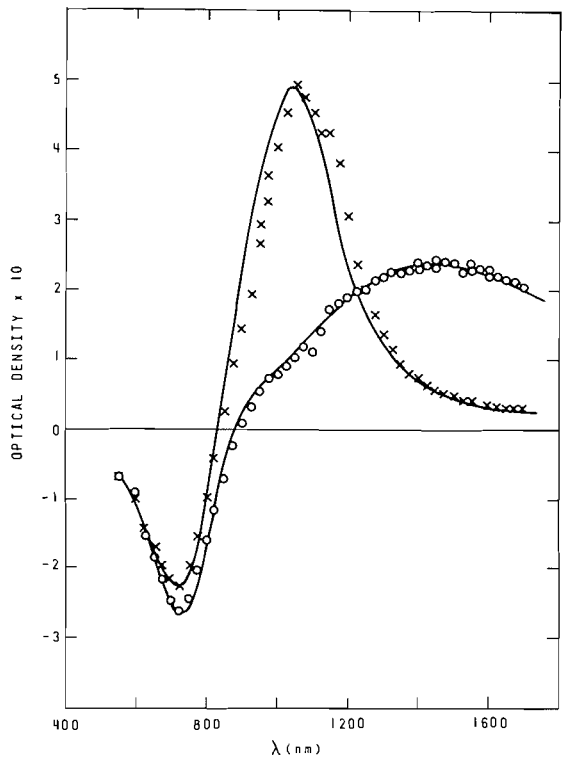

FIG. 9. Optical spectra observed following the flash photolysis of Na/Cs solutions in THF: ○, immediately after the flash; ×, ~90 μs after the flash. The solid lines represent the composite spectra simulated from the component species with the following peak optical densities: ○, Na^-, −0.302; Cs^-, −0.046; (Cs^+, e_s^-), 0.225; e_s^-, 0.033; ×, Na^-, −0.299; Cs^-, 0.468; (Cs^+, e_s^-), 0.034.

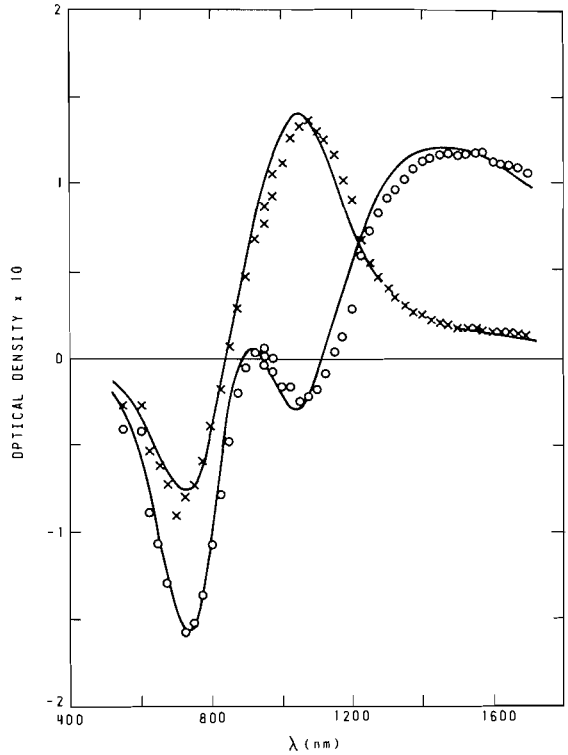

FIG. 10. Optical spectra observed following the flash photolysis of Na/Cs solutions in THF containing appreciable concentrations of both Na^- and Cs^-. ○, Immediately after the flash; ×, ~85 μs after the flash. The solid lines represent the composite spectra simulated from the component species with the following peak optical densities: ○, Na^-, −0.213; Cs^-, −0.144; (Cs^+, e_s^-), 0.128; (Na^+, e_s^-), 0.063; ×, Na^-, −0.098; Cs^-, 0.132; (Cs^+, e_s^-), 0.014.

It is interesting to note that in the original work (1), the absorption spectrum of potassium in THF, is significantly broader on the high energy side than is the long-lived photolysis intermediate which has the same absorption maximum. The latter very closely corresponds to the K^- spectrum given in Fig. 1 whereas the former clearly indicates the presence of Na^-, presumably due to the leaching of Na^+ from the Pyrex containers. Inadvertently, the results stem not from the photolysis of K^- but rather from a mixed metal solution.

Mixed Metal Solutions in DME-spectra

Figures 11 and 12 show the spectra observed from Na/K and Na/Cs alloy solutions in DME at 213 K. Although there is more scatter in the experimental points it is clear that the infrared absorption is distinctly different from that observed in comparable THF solutions. As in K/DME solutions, we attribute this absorption to the formation of $(K^+, e_s^-)_{loose}$ or

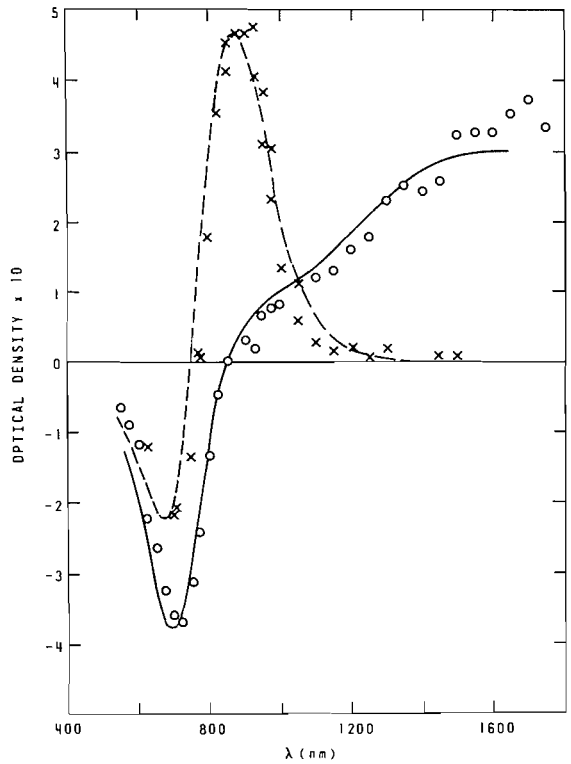

FIG. 11. Optical spectra observed immediately following the flash photolysis of Na/K solutions in DME at 213 K. ○, Immediately after the flash; ×, ~1.8 ms after the flash. The solid and dashed lines represent the composite spectra simulated from the component spceies with the following peak optical densities: ○, Na^-, −0.437; $(K^+, e_s^-)_{loose}$, 0.301; ×, Na^-, −0.369; K^-, 0.522.

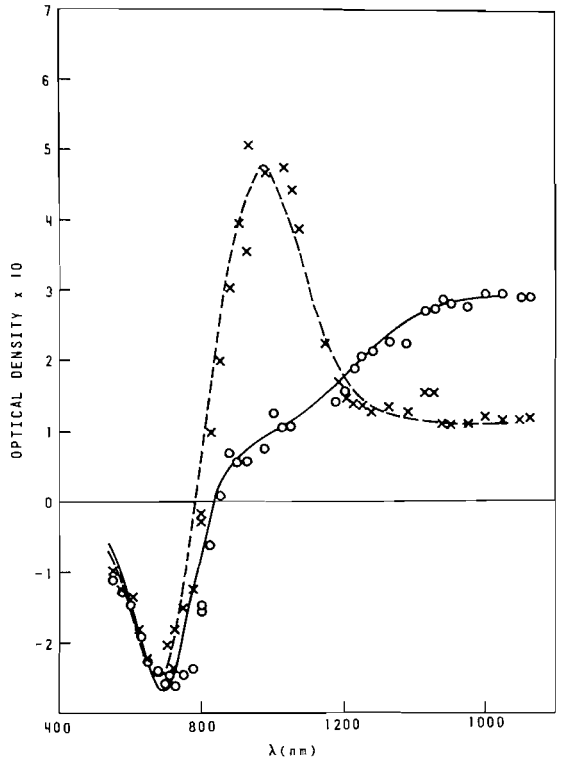

FIG. 12. Optical spectra observed immediately following the flash photolysis of Na/Cs solutions in DME at 213 K. ○, Immediately after the flash; ×, ~1.0 ms after the flash. The solid and dashed lines represent the composite spectra simulated from the component species with the following peak optical densities. ○, Na^-, −0.328; $(Cs^+, e_s^-)_{loose}$, 0.294; ×, Na^-, −0.349; $(Cs^+, e_s^-)_{loose}$, 0.111; Cs^-, 0.444. It is assumed that the $(Cs^+, e_s^-)_{loose}$ spectrum is the same as $(K^+, e_s^-)_{loose}$.

$(Cs^+, e_s^-)_{loose}$, respectively. However, since the absorption spectra of the $(K^+, e_s^-)_{loose}$ and $(Na^+, e_s^-)_{loose}$ are virtually the same at 213 K the distinction between the potassium and cesium ion-pairs is made by analogy with THF solutions.

The long-lived absorption spectra correspond to those expected for K^- and Cs^- after correcting the band maxima to slightly higher energies, 11 575 and 10 350 cm^{-1}, respectively, at 213 K. The solid and dashed lines in both figures represent the simulated spectra derived from the appropriate M^- species and $(K^+, e_s^-)_{loose}$. The corresponding optical densities are given in the caption.

Allowing therefore for the effect of temperature and solvent (4), the results in DME are entirely analogous to those observed in THF. The long-lived intermediate absorption is due to M^-, and not (Na^+, e_s^-), as originally suggested (3).

Extinction Coefficients

Quantitatively the results in DME are not as reproducible as in THF mainly because of experimental difficulties associated with the low temperature experiments, instability of the initial solutions, and photolysis of the much longer lived M^- intermediate by the analyzing light. Taking $\varepsilon_{(K^+, e_s^-)_{loose}} = 2.8 \pm 0.4 \times 10^4$ L mol^{-1} cm^{-1} (4), then from the results in Fig. 11 we obtain $\varepsilon_{Na^-} = 8.1 \pm 1.1 \times 10^4$ L mol^{-1} cm^{-1}, a value in very good agreement with that deduced earlier in THF and measured in EDA (24). Based on this value then $\varepsilon_{K^-} = 11.5 \pm 1.0$, again in good agreement with that given in Table 1 for THF. Similarly from the results in Fig. 2 we find $\varepsilon_{(Cs^+, e_s^-)_{loose}} = 3.7 \pm 0.3$ and $\varepsilon_{Cs^-} = 16.0 \pm 1.0 \times 10^4$ L mol^{-1} cm^{-1}, in reasonable agreement with the values obtained in THF.

Kinetics

The overall kinetics are explicable on the same basis as proposed for THF. However, the conversion of M^- to Na^- is significantly slower at 213 K, requiring ≥0.1 s to return to the pre-flash equili-

brium condition. This could not be measured with any precision on our apparatus but is consistent with previous observations (3).

Summary

The flash photolysis of alkali metal anions M^- proceeds via the formation of the intermediate ion-pair species (M^+, e_s^-) which, in turn, ultimately decays to reform M^-. In mixed-metal solutions containing Na^- and M^+ the photolysis again proceeds via (M^+, e_s^-) and M^- with, in this case, regeneration of Na^- occurring via M^-. Extinction coefficients deduced by experiment for both (M^+, e_s^-) and M^- are in good agreement with those calculated on the basis of Gaussian–Lorenztian shape functions for the individual optical spectra.

1. J. ELORANTA and H. LINSCHITZ. J. Chem. Phys. **38**, 2214 (1963).
2. S. H. GLARUM and J. H. MARSHALL. J. Chem. Phys. **52**, 5555 (1969).
3. J. G. KLOOSTERBOER, L. J. GILING, R. P. H. RETTSCHNICK, and J. D. W. VAN VOORST. Chem. Phys. Lett. **8**, 462 (1971).
4. W. A. SEDDON, J. W. FLETCHER, F. C. SOPCHYSHYN, and R. CATTERALL. Can. J. Chem. **55**, 3356 (1977).
5. J. L. DYE. Pure Appl. Chem. **49**, 3 (1977).
6. W. A. SEDDON, J. W. FLETCHER, and F. C. SOPCHYSHYN. Can. J. Chem. **54**, 3672 (1976).
7. W. A. SEDDON and E. B. SELKIRK. Atomic Energy of Canada Limited, Internal Report CRNL-1717, November 1977.
8. J. W. FLETCHER, W. A. SEDDON, and F. C. SOPCHYSHYN. Can. J. Chem. **51**, 2975 (1973).
9. W. A. SEDDON, J. W. FLETCHER, J. JEVCAK, and F. C. SOPCHYSHYN. Can. J. Chem. **51**, 3653 (1973).
10. G. A. SALMON, W. A. SEDDON, and J. W. FLETCHER. Can. J. Chem. **52**, 3259 (1974).
11. J. L. DYE. Electrons in fluids. *Edited by* J. Jortner and N. R. KESTNER. Springer-Verlag, West Berlin. 1973. p. 77.
12. R. CATTERALL, J. SLATER, and M. C. R. SYMONS. Metal–ammonia solutions, Colloque Weyl II, Int. Union Pure Appl. Chem. *Edited by* J. J. Lagowski and M. J. Sienko. Butterworth and Co., London. 1970. p. 329.
13. F. CAFASSO and B. R. SUNDHEIM. J. Chem. Phys. **31**, 809 (1959).
14. J. ELORANTA and H. LINSCHITZ. J. Chem. Phys. **38**, 2214 (1963).
15. I. HURLEY, T. R. TUTTLE, JR., and S. GOLDEN. Metal–ammonia solutions, Colloque Weyl II, Int. Union Pure Appl. Chem. *Edited by* J. J. Lagowski and M. J. Sienko. Butterworth and Co., London. 1970. p. 449.
16. M. T. LOK, F. J. TEHAN, and J. L. DYE. J. Phys. Chem. **76**, 2975 (1972).
17. K. S. SESHADRI and R. N. JONES. Spectrochim. Acta, **19**, 1013 (1963).
18. F. Y. JOU and L. M. DORFMAN. J. Chem. Phys. **58**, 4715 (1973).
19. F. Y. JOU and G. R. FREEMAN. Can. J. Chem. **54**, 3693 (1976).
20. B. BOCKRATH and L. M. DORFMAN. J. Phys. Chem. 77, 1002 (1973).
21. W. A. SEDDON, J. W. FLETCHER, and R. CATTERALL. Can. J. Chem. **55**, 2017 (1977).
22. J. L. DYE, C. W. ANDREWS, and S. E. MATHEWS. J. Phys. Chem. **79**, 3065 (1975).
23. D. N. BHATTACHARYYA, C. L. LEE, J. SMID, and M. SZWARC. J. Phys. Chem. **69**, 608 (1965).
24. M. G. DEBACKER and J. L. DYE. J. Phys. Chem. **75**, 3092 (1971).
25. M. OTTOLENGHI, K. BAR-ELI, and H. LINSCHITZ. J. Chem. Phys. **43**, 206 (1965).

Electrochemical studies of the $Pb^{2+}/Pb(Hg)$ system in aqueous and aqueous ethylene glycol solutions

TIBOR RABOCKAI

Instituto de Química, Universidade de São Paulo, Caixa Postal 20.780, São Paulo, SP, Brasil

Received November 23, 1978

TIBOR RABOCKAI. Can. J. Chem. 57, 1801 (1979).

The electrochemical behavior of the $Pb^{2+}/Pb(Hg)$ system in aqueous and aqueous ethylene glycol solutions is studied in the temperature range of 20.0 to 50.0°C by means of current reversal chronopotentiometry. It is shown that the reduction of Pb^{2+} ion is reversible and that kinetic or catalytic complications are not present. The value of $dE_{1/2}/dT$ is -0.6 mV/deg in the aqueous solution and -0.5 mV/deg in the solution with 56% (w/w) or higher concentrations of the organic solvent. In the above concentration range of ethylene glycol the activation energies of diffusion and viscosity vary from 4.3×10^3 to 7.2×10^3 cal mol^{-1} and from 3.7×10^3 to 6.7×10^3 cal mol^{-1}, respectively. For all solutions the solvodynamic mean radius of the diffusing species remains constant within the experimental error, suggesting that the diffusing species is always the hydrated Pb^{2+} ion.

TIBOR RABOCKAI. Can. J. Chem. 57, 1801 (1979).

On a étudié le comportement électrochimique du système $Pb^{2+}/Pb(Hg)$ en solutions aqueuses et en solutions eau–éthylèneglycol à des températures de 20.0 à 50.0°C à l'aide de la technique de chronopotentiométrie de renversement de courant. On montre que la réduction de l'ion Pb^{2+} et réversible et qu'il n'y a pas de complications cinétique ou catalytique. En solution aqueuse, la valeur de $dE_{1/2}/dT$ est de -0.6 mV/deg alors qu'elle est de -0.5 mV/deg dans des solutions contenant au moins 56% (p/p) de solvant organique. Aux concentrations d'éthylène glycol mentionnées plus haut, les énergies d'activation de diffusion et de viscosité varient respectivement de 4.3×10^3 à 7.2×10^3 cal mol^{-1} et de 3.7×10^3 à 6.7×10^3 cal mol^{-1}. Pour toutes les solutions, le rayon solvodynamique moyen des espèces qui diffusent reste constant à l'intérieur des erreurs expérimentales. Ceci suggère que l'espèce qui diffuse est toujours un ion Pb^{2+} hydraté.

[Traduit par le journal]

Introduction

Ethylene glycol, hereafter called EG, is a good solvent for inorganic and organic substances. In comparison with water, EG has a lower freezing point, a higher boiling point, and a higher viscosity. In electrochemistry, EG has been used in reference electrodes for low temperature pH measurements (1); in polarographic studies of various inorganic substances (2, 3); in some practical applications, such as the electrochemical refining of germanium (4) and the electrodeposition of silver (5). Mn(II) ion (6) and Tl_2SO_4 (7) were studied in EG–water mixtures.

In this paper we describe the study of the $Pb^{2+}/Pb(Hg)$ system in aqueous and aqueous ethylene glycol solutions using chronopotentiometry with current reversal in the temperature range of 20.0 to 50.0°C. Since the organic solvent can affect the charge transfer reaction as well as the transport properties of the species in solution, information on these properties was, therefore, included in our study.

Experimental

The electrochemical cell employed has been described previously (8). The working electrode was a shielded mercury pool with an area of 3.51 cm^2. A commercial sce was used as reference electrode. The junction potentials between the sce and the mixed-solvent electrolyte were negligible. The temperature of the cell was maintained within 0.1°C. Dissolved oxygen was removed from the electrolyte by bubbling purified nitrogen. An Electroscan™ 30 was used as both constant current source and recorder for potential/time curves. Solutions of $Pb(NO_3)_2$ (10^{-3} to 10^{-2} *M*) containing the appropriate amount of ethylene glycol were investigated and 0.1 *M* KNO_3 was used as supporting electrolyte. All solutions were prepared from stock solutions of analytical grade $Pb(NO_3)_2$ and KNO_3. Ethylene glycol (Carlo Erba, p.a) was purified according to the procedure described by Dzaparidze *et al.* (9). The water content of the purified ethylene glycol was determined by the Karl Fisher method. The viscosity of the solutions was measured with an Ostwald viscosimeter, and the density of the solutions with a 5 mL picnometer.

The constant current was within the range of 0.05 mA to 2 mA. Chronopotentiometric transition times were measured according to the procedure described by Adams (10). The potentials at time $t = \tau/4$ (τ = transition time) were measured by the empirical method shown in Fig. 1.

Results and Discussion

(a) Diffusion Coefficients

The current reversal chronopotentiometry of the solutions containing Pb^{2+} displays well defined cathodic and anodic transition times (τ_c and τ_a,

0008-4042/79/141801-03$01.00/0

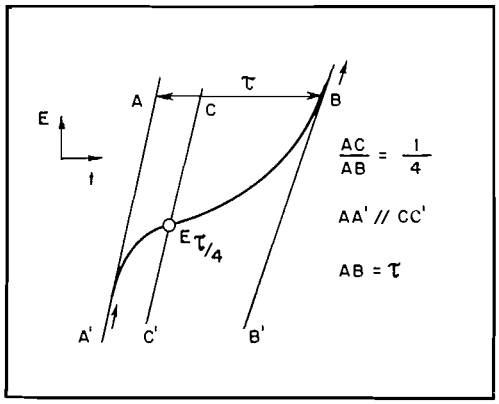

FIG. 1. Determination of transition times and $E_{\tau/4}$ potentials.

respectively). Within the investigated concentration and current ranges the $i\tau_c^{1/2}/C_0^0$ ratio (i = current density, $C_0^0 = Pb^{2+}$ concentration) is independent of C_0^0 and i, for a given ethylene glycol concentration and temperature. Thus, for each ethylene glycol concentration and temperature, the average value of the $i\tau_c^{1/2}/C_0^0$ ratio was calculated. From the average values, the diffusion coefficients D_0 of Pb^{2+} were calculated by means of the well-known Sand's equation. The diffusion coefficients are shown in Table 1. Assuming that the solvated electroactive species is a spherical particle with an average radius r, the latter was estimated from D_0 and viscosity data by means of the Stokes–Einstein equation, $D_0 = RT/(6\pi\eta rN)$. The experimental value of r was 2.7 ± 0.1 Å, independently of temperature and EG content. Thus the increase of diffusion coefficient with increasing temperature and water content, as shown in Table 1, is due to changes of viscosity. Taking into account that the mean ionic radius of Pb^{2+}, water, and ethylene glycol are, respectively, 1.32 (11), 1.9 (8), and 4 Å (this latter estimate is based on a molecular model from Framework Molecular Model, Prentice-Hall, NJ), one may conclude, from the value of solvodynamic radius, that the diffusing species is always the hydrated Pb^{2+} ion.

(b) Variation of Potential with the Electrolysis Time

For all the investigated temperature range and ethylene glycol concentration range the plots of the potential vs. log $[(\tau^{1/2} - t^{1/2})/t^{1/2}]$ are linear. The slopes calculated are in good agreement with the theoretical value of $2.303(RT/nF)$, which is observed in the case of a reversible charge transfer (12).

TABLE 1. Diffusion coefficient data of Pb^{2+} in ethylene glycol aqueous solutions

Temperature (°C)	$D_0 \times 10^6$ (cm² s⁻¹) for % ethylene glycol w/w = 0	20	39	56	73	94
20.0	8.1	5.4	3.0	1.7	1.0	0.5
30.0	10.4	6.5	4.0	2.5	1.6	0.7
40.0	13.0	8.7	5.3	3.4	2.2	1.0
50.0	16.1	10.8	6.8	4.5	2.9	1.1

(c) Ratio between Direct and Reverse Transition Times

The ratios between direct and reverse transition times present a value of 0.33, which is independent of EG content, temperature, and the values of direct transition times. The constancy of τ_a/τ_c and $i\tau_c^{1/2}/C_0^0$ indicates the absence of any kinetic or catalytic process interfering with the electrode reaction, according to the criteria already reported in the literature (12, 13).

(d) Half-wave Potentials

The observed $E_{\tau/4}$ values are independent of the electroactive species concentration and current density. It was found that direct and reverse chronopotentiograms exhibit the same values for $E_{\tau/4}$ after correction for the ohmic drop. The equality of direct and reverse $E_{\tau/4}$ values and their independence relative to electroactive species concentration and current density agrees with the previous conclusion that the reaction

$$Pb(II) + 2e = Pb(Hg)$$

is reversible in ethylene glycol–water mixtures (12). It is known that in the case of a reversible charge transfer which takes place on a mercury electrode we have $E_{\tau/4} = E_{1/2}$ where $E_{1/2}$ is the same as the corresponding polarographic half-wave potential (12). The change of the sce potential with temperature is given by (14)

$$[1] \qquad E = 0.2415 - 7.6 \times 10^{-4}(t - 25)$$

so that, the half-wave potentials may be referred to the value of E at 25.0°C. The results are illustrated in Fig. 2, for solutions containing 0% and 56% (w/w) of EG. From the straight lines of Fig. 2, the values of $dE_{1/2}/dT$ are −0.6 mV/deg and −0.5 mV/deg, respectively. The latter value does not change with increasing EG concentration.

(e) Diffusion and Viscosity Activation Energies

According to Eyring and co-workers (15) the phenomena of diffusion and viscosity may be described by the absolute rate theory. Thus the influence of temperature on diffusion coefficient and on viscosity is given by an equation of the form

$$[2] \qquad Z = A \exp[-E^*/(RT)]$$

where Z means either diffusion coefficient or viscosity, and E^* is the diffusion or viscosity activation energy, respectively.

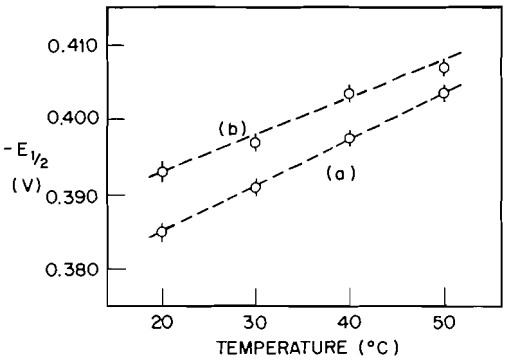

FIG. 2. Variation of half-wave potentials with temperature in solutions with (*a*) 0% (w/w) and (*b*) 56% (w/w) of ethylene glycol.

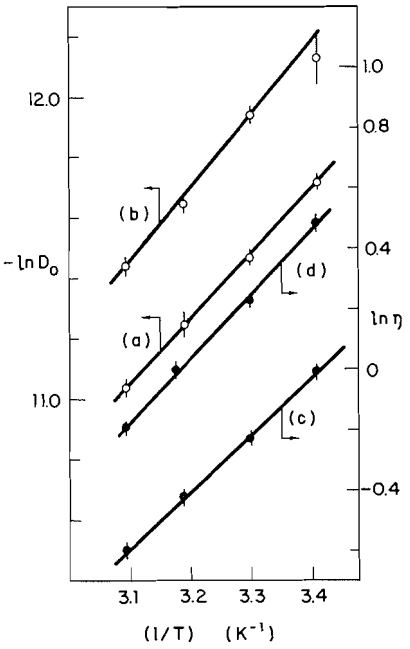

FIG. 3. Plot of ln D_0 and ln η vs. $1/T$ for the calculation of the activation energies; lines (*a*), (*c*) refer to 0% (w/w) and lines (*b*), (*d*) to 20% (w/w) of ethylene glycol.

As eq. [2] shows, the activation energies may be calculated from the slope of the straight line representing ln Z vs. $(1/T)$. These plots are illustrated in Fig. 3. Table 2 assembles the activation energies obtained. These data reveal that diffusion and viscosity are affected to the same extent by ethylene glycol: an increase of the order of 50% in the value of the activation energies when going from zero to about 80% of non-aqueous solvent is observed. The values of the diffusion activation energy, E_D*, are slightly higher than those of the viscosity energy of activation, E_V*.

TABLE 2. Activation energies for diffusion and viscosity

% Ethylene glycol (w/w)	$10^{-3} \times E_D$* (cal/mol)	$10^{-3} \times E_V$* (cal/mol)
0	4.3±0.4	3.7±0.1
20	4.8±0.4	4.3±0.1
39	5.2±0.4	4.8±0.1
56	5.8±1.0	5.2±0.1
73	6.6±0.7	5.8±0.1
94	7.2±0.7	6.7±0.1

1. L. VAN DEN BERG. Anal. Chem. **32**, 628 (1960).
2. C. H. R. GENTRY. Nature, **157**, 479 (1946).
3. D. B. BRUSS and T. DE VRIES. J. Am. Chem. Soc. **75**, 4205 (1953).
4. G. SZEKELY. J. Electrochem. Soc. **98**, 318 (1955).
5. S. TAJIMA, S. KOMATSU, and N. BABA. Electrochim. Acta, **19**, 921 (1974).
6. J. K. GUPTA and C. M. GUPTA. Monatash. Chem. **100**, 2019 (1969).
7. S. LAL and S. N. SRIVASTAVA. Indian J. Appl. Chem. **32**, 227 (1969).
8. T. RABOCKAI and I. JORDAN. Anal. Lett. **7**, 647 (1974).
9. D. I. DZAPARIDZE, G. A. TEODORADZE, and SH. S. DZEPARIDZE. Elektrokhimiya, **5**, 894 (1969) (Engl. Transl.).
10. R. N. ADAMS. Electrochemistry at solid electrodes. Marcel Dekker, Inc., New York. 1969. p. 184.
11. T. MOELLER. Química Inorgânica. Editorial Reverté. 3rd ed. S. A., Barcelona. 1954. p. 129.
12. P. DELAHAY and T. BERZINS. J. Am. Chem. Soc. **75**, 2486 (1953).
13. C. FURLANI and G. MORPURGO. J. Electroanal. Chem. **1**, 351 (1959/1960).
14. S. GLASSTONE. An introduction to electrochemistry. D. Van Nostrand Company, Inc., New York. 1942. p. 232.
15. S. GLASSTONE, K. J. LAIDLER, and H. EYRING. The theory of rate processes. McGraw-Hill Book Company, Inc., New York. 1941.

Five-coordinate iron(II) porphyrins derived from *meso*-α,β,γ,δ tetraphenylporphin: synthesis, characterization, and coordinating properties

MICHEL MOMENTEAU,[1] BERNARD LOOCK, AND EMILE BISAGNI

Institut Curie, Section de Biologie, FRA no 25 de l'Inserm, Centre Universitaire, Bâtiment 112, 91405 Orsay, France

AND

MICHEL ROUGEE

Laboratoire de Biophysique du Muséum National d'Histoire Naturelle, 61, Rue Buffon, 75005 Paris, France

Received November 28, 1978

MICHEL MOMENTEAU, BERNARD LOOCK, EMILE BISAGNI, and MICHEL ROUGEE. Can. J. Chem. **57**, 1804 (1979).

Meso-α,β,γ,δ,tetraphenylporphin derivatives bearing acrylic (*cis* and *trans* isomers) and propionic side chains with a terminal imidazole group have been synthesized. Intermediate compounds obtained during their preparation were characterized by visible spectroscopy and nmr. In non-coordinating solvents (benzene or toluene), the iron(III) complexes of these compounds do not show intramolecular coordination of the terminal base on the metal ion. The reduced forms of the compounds have been obtained from ferric forms by heterogeneous reduction with aqueous dithionite and exhibit optical spectra characteristic of five-coordinate ferrous complexes. The nitrogenous bases and carbon monoxide affinities of the latter have been measured and the results indicate that the '*trans influence*' exerted by the terminal imidazole does not depend greatly on the nature and the structure of the covalent side chain. In contrast the stability of the five-coordinate compounds depends on the side chain (*trans* acrylic < propionic < *cis* acrylic) as suggested by the values reported for the replacement constants of the terminal imidazole by 4-cyanopyridine in unsymmetrical six-coordinate derivatives. The stability of these compounds towards oxidation is also reported.

MICHEL MOMENTEAU, BERNARD LOOCK, EMILE BISAGNI et MICHEL ROUGEE. Can. J. Chem. **57**, 1804 (1979).

La synthèse de composés dérivés de la *meso*-α,β,γ,δ,tétraphenylporphine possédant une chaîne acrylique (isomères *cis* et *trans*) ou une chaîne propionique et substituée par un groupe imidazole terminal est décrite. Les composés intermédiaires obtenus au cours de cette synthèse sont caractérisés par spectrophotométrie visible et par rmn. Dans les solvants non-coordinants (benzène ou toluène), les complexes ferriques de ces composés ne montrent pas de coordination intramoléculaire de la base terminale sur l'ion métallique. Les formes réduites obtenues par réduction hétérogène des complexes ferriques présentent des spectres d'absorption caractéristiques des complexes ferreux pentacoordonnés. Les constantes d'affinité de ces composés pour les bases azotées et le monoxyde de carbone ont été mesurées. Elles indiquent que l'"*effet trans*" exercé par l'imidazole terminal ne dépend ni de la nature ni de la structure de la chaîne. Au contraire, la stabilité des composés pentacoordonnés en dépend (*trans* acrylique < propionique < *cis* acrylique) comme le suggèrent les valeurs des constantes de remplacement de l'imidazole par la 4-cyanopyridine dans les dérivés hexacoordonnés. La stabilité de ces composés vis-à-vis de l'oxydation est également décrite.

Introduction

For some years, several studies have been made in order to understand the factors controlling the binding of oxygen in oxygen carriers, such as hemoglobin and myoglobin, or in oxygen activating hemoproteins. Synthesis of models for the active sites in these proteins has demonstrated the role of the hydrophobic environment and of the *trans* coordinating base upon the fixation of oxygen and the stabilization of the resulting oxygen complexes. In these models, the pentacoordination of iron(II) arises from an axial ligand covalently linked either to the vinyl side chains of protoheme via a thioether linkage (1–3) or to the propionic acid side chain of the heme IX molecules (4–7). More recently, Molinaro *et al.* (8) developed a synthetic route to monosubstituted tetraarylporphyrins in which the axial base is covalently linked to one of the four mesoaryl substituents.

As a part of our continuing study of the preparation and reactivity of new synthetic five-coordinate iron porphyrins, we wish to report in this paper the synthesis of new derivatives of *meso*-α,β,γ,δ,tetraphenylporphin (TPP) functionalized by either an acrylic acid side chain (*cis* or *trans* substituted isomers) or a propionic one on which a ligand group (imidazole or pyridine) was linked. The synthesis of

[1]Author to whom all correspondence should be addressed.

0008-4042/79/141804-10$01.00/0

porphyrins carrying a peptide acrylic side chain has been reported recently by Callot *et al.* (9) in an independent work. We have followed the same route to prepare our models, but used other metallo TPP compounds as starting materials. Thus, aside from better yields of intermediate derivatives, we have isolated several new compounds which have been characterized by their spectroscopic properties. We also describe comparative chemical properties of their iron(II) derivatives towards external ligands such as nitrogenous bases or neutral small molecules (carbon monoxide or oxygen).

Results and Discussion

1. Preparation of Substituted meso-α,β,γ,δ,*Tetraphenylporphins*[2]

The synthesis of porphyrins bearing an acrylic acid side chain was performed following the method described by Callot (10, 11) from Cu-TPP (**1***b*). In a first step, a formyl group was introduced into a pyrrolic position using Vilsmeier formylation; after hydrolysis, the Cu-monoformyl compound **2***b* was obtained in a good yield (>95%), but demetallation of **2***b* under various sulfuric acid conditions did not yield the corresponding free-base. Thin layer chromatography on silica gel showed that several compounds were formed, suggesting direct attack of the formyl group and/or sulfonation of the porphyrin ring. These results are different from those obtained in the sulfuric acid treatment required for the demetallation of formylated Cu-etioporphyrin I and Cu-octaethylporphyrin (12).

An alternative route to the formylporphyrin free-base was then considered using the iron(III)TPP as starting material, but under the same formylating conditions as for Cu-TPP, iron(III)TPP appeared considerably less reactive (10% yield). This difference in reactivity probably lies in the electronegativity of the central metal ion. The presence of electron donor metals leads to a greater reactivity of the porphyrin ring by increasing the electron density especially on the pyrrolic carbon (13). Despite the low yield of formylated iron(III)TPP, this method allowed us to obtain the formyl-TPP free-base since, in this case, removal of iron is easily performed by treatment with iron(II) sulfate in dilute acids at room temperature (14). Silica gel column chromatography afforded two compounds: TPP starting material **1***a* and formyl-TPP **2***a*. The latter showed a

[2]Abbreviations: TPP: *meso*-α,β,γ,δ,tetraphenylporphin; Im: imidazole; Py: pyridine; *N*MeIm: *N*-methylimidazole; *N*buIm: *N*-butylimidazole; 4-PyCN: 4-cyanopyridine; nmr: nuclear magnetic resonance.

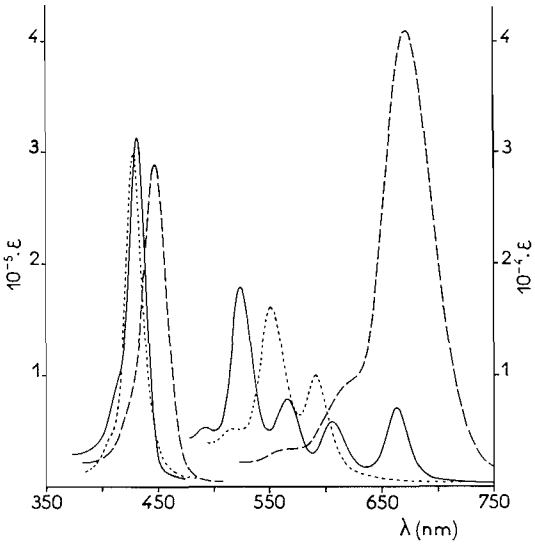

FIG. 1. Optical absorption spectra (optical path, visible 1 cm, Soret 1 mm) of formyl-*meso*-tetraphenylporphin **2***a* (—); formyl-*meso*-tetraphenylporphin dicationic form (– – –); copperformyl-*meso*-tetraphenylporphin **2***b* (---) in benzene.

typical porphyrin spectrum (Fig. 1) in which a bathochromic shift of the absorption maxima was caused by the aldehyde group substitution. Furthermore some noticeable differences were observed: the visible spectrum was of a type which had not been observed previously in the porphyrins bearing a single carbonyl group in the β or *meso* position (15). These strongly electron-withdrawing groups caused a 'Rhodo' type spectrum. The extinction coefficient of band I (663 nm) in the formyl-TPP spectrum is more intense than that of band II (605 nm). The new type of spectrum (band IV > III > I > II) could result from the strong asymmetric delocalization of the π electron cloud, due to the formyl substituent group.

As in Callot's work, the acrylic derivatives were directly obtained by condensation of carbethoxyethyl-methenyl-triphenylphosphorane with Cu-formyl-TPP according to the Wittig reaction (12). *Cis–trans* isomers (**3***b* and **4***b* respectively) were isolated as red crystals in 28.9 and 47.1% yields respectively. These compounds were rapidly transformed into free-base derivatives **3***a* and **4***a* under mild conditions with gaseous hydrogen-chloride and identified by their nmr spectra. The preparation of the propionic derivative **5***a* was achieved in good yield by catalytic hydrogenation of compounds **3***a* or **4***a* on palladium charcoal in formic acid.

Reaction of triethylphosphonoacetate with Cu-formyl-TPP was an alternative method (16) for the

TABLE 1. Structures of substituted *meso*-tetraphenylporphins and their metal complexes*

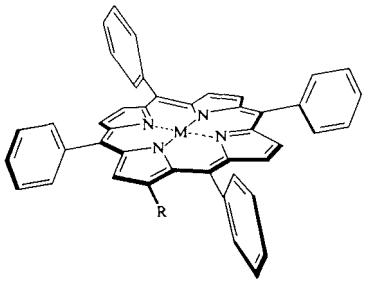

Compound	R	
1	H	
2	CHO	
3	CH=CH—$CO_2C_2H_5$	(*cis*)
4	CH=CH—$CO_2C_2H_5$	(*trans*)
5	CH_2—CH_2—$CO_2C_2H_5$	
6	CH=CH—CO—NH—$(CH_2)_3$—N⟨imidazole⟩	(*cis*)
7	CH=CH—CO—NH—$(CH_2)_3$—N⟨imidazole⟩	(*trans*)
8	CH_2—CH_2—CO—NH—$(CH_2)_3$—N⟨imidazole⟩	
9	CH_2—CH_2—CO_2—$(CH_2)_3$—⟨pyridine⟩	

*a, M = 2H; *b*, M = Cu(II); *c*, M = Fe(III)Cl^-; *d*, M = Fe(II).

preparation of acrylic derivatives **3***b* and **4***b* in yields of 4.5 and 85.5%, respectively. This method appeared more suitable for the preparation of **5***a* because isolation of the mixed *cis–trans* isomers was easier and hydrogenation could then be performed directly, without purification of acrylic acid intermediates.

When **3***a*, **4***a*, and **5***a* were saponified with alcoholic potassium hydroxide, acidification afforded free acid compounds in 95% yield. After treatment with oxalyl chloride (17), acid chloride derivatives were then condensed with 1-(3-aminopropyl)imidazole (18) giving compounds **6***a*, **7***a*, and **8***a* in 70% yield. Their iron(III) complexes have been prepared by treatment of free-bases with an excess of ferrous acetate in hot acetic acid under argon (19). In the same way, acylation of 3-(3-pyridyl)-1-propanol with the acid chloride of compound **5***a* in methylene chloride gave the derivative **9***a* which was converted into the iron complex **9***c*.

All acrylic and propionic TPP derivatives **3***a*, **4***a*, **5***a*, **6***a*, **7***a*, **8***a*, and **9***a* showed 'etio' type absorption spectra but the presence of a double bond in the side chain of the acrylic compounds caused a bathochromic shift of the absorption bands in comparison with the spectrum of propionic acid derivatives. This shift is greater in the *trans* isomer (10 nm) than in the *cis* one (5 nm).

All nmr spectra are characterized by the non-equivalence of the seven pyrrolic protons in contrast to *meso*-tetraphenylporphin (20) (Table 3). In the *cis* derivatives, the α and β vinyl protons are shifted upfield relative to the equivalent *trans* ones. The coupling constants $J_{\alpha\beta}$ = 12 Hz and 16 Hz for the *cis* and *trans* ethylenic configurations respectively are similar to those observed by Callot in Ni-vinyl-TPP (10). A more important effect is observed in the resonance of the ethyl ester protons of compounds **3***a*, **4***a*, and **5***a* and the imidazole ring protons of compounds **6***a*, **7***a*, and **8***a*. In the *cis* acrylic derivatives **3***a* and **6***a*, the proton resonances of the ethyl ester group and imidazole ring appear upfield. Those in the *trans* acrylic isomers **4***a* and **7***a* are shifted downfield relative to the normal values for the ethyl ester and imidazole protons, as a result of the ring current of the macrocycle. These resonances may be due to different stereochemical configurations of *cis* and *trans* acrylic isomers, in which the ethyl ester groups and imidazole rings are positioned over the conjugated macrocycle in the former compounds and outside the macrocycle plane in the latter.

2. Physico-chemical Properties of Iron(II) Derivatives

The porphyrins **6***a*, **7***a*, **8***a* and their related iron(III) and iron(II) derivatives have side chains of different geometry. Molecular models show that the terminal imidazole lies close to the center of the porphyrin ring in the *cis* acrylic isomer and in the saturated propionic derivatives **6***a* and **8***a*, but far from this center in the case of the *trans* acrylic isomer **7***a*, in agreement with the nmr results. In this connection, Fuhrhop *et al.* (21) have noted an observation on sterically fixed porphyrins having rigid axial ligands through the central ion. The phenyl group of the benzyl ester of [2,2-bis(benzyloxycarbonyl)vinyl]porphyrin lying '*cis*' to the porphyrin occurs in position exactly above the center of the macrocycle. Such a conformation is also observed in our '*cis*' compounds.

In toluene solution, the optical spectra of the ferric derivatives **6***c*, **7***c*, and **8***c* are quite similar to that of Fe(III)Cl-TPP **1***c*, except for a bathochromic shift observed with the two '*cis* and *trans*' acrylic compounds as observed for the related free-bases. This similarity indicates that the imidazole group is not coordinated to the sixth coordination position of the iron ion, even in the '*cis*' acrylic derivative. Also, the similarity between the spectra of the same isomer in which the side chain bears ethyl ester or imidazole shows that in the imidazole compounds the ferric complexes are in the high spin state, without an

imidazole on the iron ion. The low affinity constant of Fe(III)Cl-TPP for the first imidazole derivative as reported by Walker *et al.* (22) is in good agreement with the coordination state of iron(III) in our compounds suggested from the absorption spectra. A similar observation has been found with deuterohemin 6(7) methyl ester, 7(6) histidine methyl ester, in which the histidine methyl ester attached to the side chain was not firmly bound to the iron(III) (7).

The reduction of hemins **6***c*, **7***c*, and **8***c* with aqueous sodium dithionite, under anaerobic conditions, in a two-phased system ($C_6H_5CH_3/H_2O$) (23) gives orange compounds **6***d*, **7***d*, and **8***d* which are stable in the absence of oxygen. Their absorption spectra are characterized by one broad visible band (near 540 nm) with two shoulders (615 and 570 nm) and a Soret band at 440 nm (Fig. 2). These spectra are clearly distinct from both that of bare Fe(II)TPP (24) and four-coordinate iron(II) compounds **3***d*, **4***d*, and **5***d* and that of typical six-coordinate TPP (24). However, they are quite similar to that obtained with the well-identified five-coordinate species, mono(2-methylimidazole) TPP, except for the increase of absorbance at 540 nm (25, 26). These results unambiguously show that in non-coordinating solvents at room temperature, typical five-coordinate complexes with imidazole bound in the fifth axial coordination position of iron(II) are obtained. However the Soret band of the *trans* acrylic isomer is less sharpened than those of the *cis* acrylic isomer and propionic derivative. This could reflect the constraint exerted by the side chain in the coordination of the terminal imidazole.

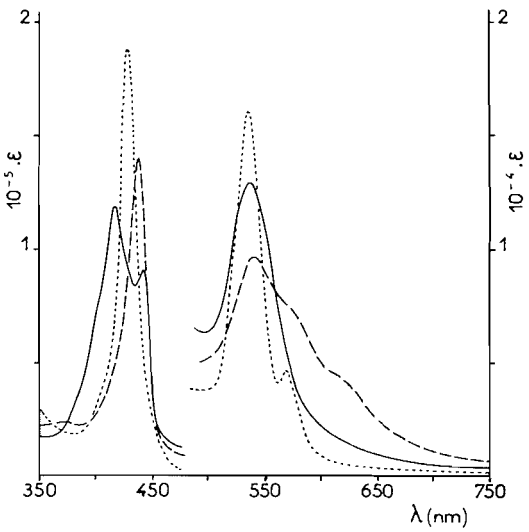

FIG. 2. Optical absorption spectra (optical path, visible 1 cm, Soret 1 mm) of Fe(II) *meso*-tetraphenylporphin **1***d* (—), Fe(II) *meso*-tetraphenyl-1-[3-(*N*-imidazolyl propyl)propionamido]porphin **8***d* (– – –), *N*-methylimidazole-Fe(II) *meso*-tetraphenyl-1-[3-(*N*-imidazolyl propyl)propionamido]porphin (---) in benzene.

Progressive addition of *N*-methylimidazole to the five-coordinate compounds **6***d*, **7***d*, and **8***d* in benzene at 20°C progressively leads to species whose absorption spectra are similar to that of the symmetrical six-coordinate complexes (hemochromes) resulting from the binding of two imidazole or *N*-methylimidazole molecules to Fe(II)TPP **1***d* and to the four-coordinate species **3***d*, **4***d*, **5***d*. The bathochromic shift of the absorption maxima noted for the bare *cis* and *trans* acrylic isomers **3***d*, **4***d*, compared to the propionic related compound **5***d*, is also observed for the corresponding symmetrical (**3***d*, **4***d* + 2 *N*-methylimidazole) and unsymmetrical (**6***d*, **7***d* + *N*-methylimidazole) complexes.

Titrations of ca. 2×10^{-5} *M* (= $[P_0]$) of all three five-coordinate species by L = *N*-methylimidazole appears almost quantitative. Full hemochrome spectra are obtained for $[P_0] < L_t \ll 2[P_0]$ (L_t standing for the total added ligand concentration) thus indicating that only one external L ligand is required to get the unsymmetrical six-coordinate hemochrome. As noted by Antonini and Brunori (27) this means that $K_{Im}^{L}[P_0] \gg 1$. The values reported in Table 5 obtained assuming $K_{Im}^{L}[P_0] > 10$, are probably slightly higher than the second affinity constant K_L^L measured in the case of Fe(II)TPP ($1.4 \times 10^5\ M^{-1}$). Unfortunately, because of these very high values, it has not been possible to detect experimentally any influence of the structure of the covalent chain upon the *trans influence* exerted by the terminal imidazole. Moreover, attempts to determine the exchange constants $K_L^{Im,L}$ by increasing the *N*-methylimidazole concentration have been unsuccessful either because this constant is too low or because of the great similarity of the symmetrical and unsymmetrical hemochrome spectra (further complications arise upon dilution when adding an excess of *N*-methylimidazole to the initial solution).

On the contrary, titrations of the five-coordinate species **6***d*, **7***d*, **8***d* by L′ = 4-cyanopyridine occurs in two distinct steps. In the first, one 4-cyanopyridine molecule binds to the sixth coordination site with a high affinity, $K_{Im}^{L'} = \sim 2.5 \times 10^5\ M^{-1}$, which is rather insensitive to the structure of the side chain linking the terminal imidazole and comparable to, but slightly lower, than other K_{Im}^{L} values. Hemochrome type spectra are obtained at the end of this step. Further modifications of these intermediate spectra are observed in the red when the 4-cyanopyridine concentration is greatly increased, and the spectra obtained at the end of this second step (Fig.

TABLE 2. Absorption, in nm, and molecular absorption coefficients (in parentheses), in mL mol^{-1} cm^{-1}, of substituted *meso*-tetraphenylporphins in toluene

Compound	Data				
1*a*	418.5 (468)	515 (19)	548 (7.9)	592 (5.3)	648.5 (3.4)
2*a*	430.5 (309)	523.5 (17.8)	566 (7.7)	605 (5.7)	663 (7)
3*a*	424 (300.2)	519 (16.3)	553 (5.6)	595 (4.8)	651 (2.9)
4*a*	429 (252.2)	522 (15.7)	559 (6.4)	600 (4.8)	657 (2.3)
5*a*	420 (420.5)	515 (18.8)	548 (6.0)	591 (5.4)	646 (2.8)
1*b*	416.5 (443)	539 (21.2)	570 shoulder (2.8)		
2*b*	429.5 (302)	551 (16)	590 (9.9)		
3*b*	422 (314.6)	544 (19.8)	580 shoulder (3.8)		
4*b*	427 (267)	547 (18.6)	686 (7.4)		

3) are almost identical to those of the symmetrical hemochromes resulting from the coordination of two 4-cyanopyridine molecules to the corresponding four-coordinate species **3***d*, **4***d*, **5***d* (the slight differences observed can be related to the fact that a very high 4-cyanopyridine concentration is needed to get the pure symmetrical hemochromes). The measured affinity constants, $K_{L'}^{Im,L'} = 1$, 30, and 1.2 M^{-1} for **6***d*, **7***d*, **8***d* respectively, show that the terminal imidazole is more easily replaced by a 4-cyanopyridine molecule in the case of the *trans* acrylic isomer **7***d*, than in the case of the *cis* isomer **6***d* and the saturated propionic derivative **8***d*.

In order to get further information about the role of the covalent attachment of the axial chain upon the affinities for externally added ligands, we have also studied the coordination of Fe(II)TPP **1***d* and of the four-coordinate compounds **3***d*, **4***d* and **5***d*.

1*d* and **5***d* bind L = *N*-methylimidazole in two overlapping steps, as previously observed for the titration of Fe(II)TPP by imidazole and pyridine (24, 26). (The values reported in Table 5 have been redetermined at 20°C.) However, the affinity constants for *N*-methylimidazole are significantly higher than the values obtained for imidazole, in agreement with the more basic character of *N*-methylimidazole ($pK_a = 7.33$) with respect to Im ($pK_a = 6.65$). Only the overall affinity constant $K^L K_L^L$ can be estimated for **3***d* and **4***d*. Comparison of the values reported in Table 5 shows that the reactivity at the iron center is not greatly influenced by the nature of the noncoordinating side chain.

Spectrophotometric titrations of **1***d*, **3***d*, **4***d*, and **5***d* by L′ = 4-cyanopyridine indicate a two-base fixation in a single step, with affinity constants $K^{L'} K_{L'}^{L'} = 5$, 2.9, 2.5, and 1.3×10^8 M^{-2}, respectively, which are again little affected by the presence of the side chain.

Defining Im-P ⇄ P(Im), (K = [P(Im)]/[Im-P]) the equilibrium between the four and five-coordinate forms of species **6***d*, **7***d*, **8***d* and assuming that the affinities of the former for L′ are the same as that of species **3***d*, **4***d*, **5***d* respectively, we obtain $K^{L'} K_{L'}^{L'}$ (for **3***d*, **4***d*, **5***d*) = $K\, K_{Im}^{L'}\, K_{L'}^{Im,L'}$ (for **6***d*, **7***d*, **8***d*). From the values reported in Table 5, we obtain K = 950, 65, and 430 for **6***d*, **7***d*, **8***d* respectively, which corroborates the strong predominance of the five-coordinate versus the four-coordinate form of these three models. A significant decrease of the equilibrium constant is observed for the *trans* acrylic isomer **7***d*, whereas the values for models **6***d* and **8***d* are comparable to the value K = 800 obtained by Geibel *et al.* (28) for their five-coordinate model derived from mesoporphyrin IX.

The particular features of the hemochrome spectra obtained with L′ = 4-cyanopyridine together with

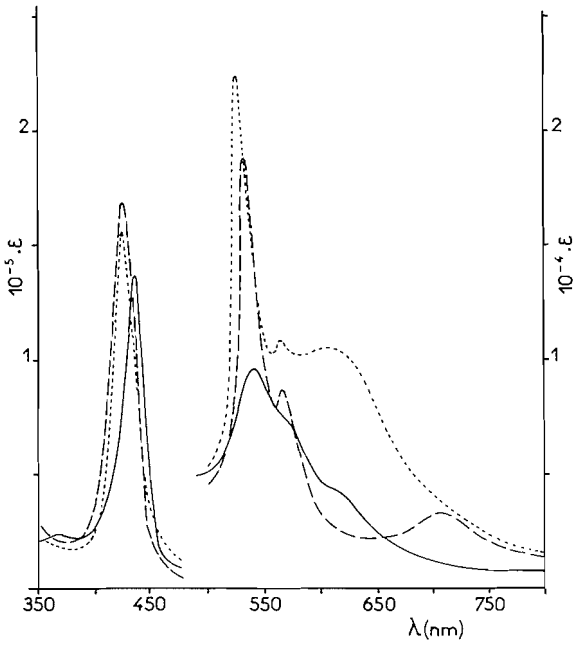

FIG. 3. Optical absorption spectra (optical path, visible 1 cm, Soret 1 mm) of Fe(II) *meso*-tetraphenyl-1-[3-imidazolyl propyl)propionamido]porphin **8***d* (—); 4-cyanopyridine-Fe(II) *meso*-tetraphenyl-1-[3-(*N*-imidazolyl propyl)propionamido]-porphin (– – –); (4-cyanopyridine)$_2$-Fe(II) *meso*-tetraphenyl-1-[3-(*N*-imidazolyl propyl)propionamido]porphin (---) in benzene.

TABLE 3. The nmr signals of substituted *meso*-tetraphenylporphins in deuterochloroform at 34°C (in ppm)

	—H_{Pyr}	—$H_{Phe(o.m.p.)}$	—NH_{Pyr}	—CHO	⩾—CH=	=CH—	⩾—CH_2—	—CH_2—CO_2Et		
1*a*	8.84	8.22 7.78 7.72	−2.76							
2*a*	9.26–8.77	8.20 7.80 7.77	−2.52	9.41					—CO_2—CH_2—CH_3	—CO_2—CH_2—CH_3
3*a*	8.83–8.77	8.19 7.78 7.74	−2.70		6.95 6.83	5.69 5.57			3.97	0.83
4*a*	8.96–8.79	8.15 7.78 7.78	−2.67		7.51 7.35	6.63 6.47			4.25	1.40
5*a*	8.84–8.59	8.16 7.78 7.76	−2.75				3.21	2.78	4.10	1.20
									—$(CH_2)_3$—	—Im
6*a*	8.80–8.75	8.16 7.77 7.77	−2.76		6.88 6.76	5.71 5.59			3.15 2.81 1.25	6.90 6.49 5.89
7*a*	8.91–8.80	8.17 7.76 7.76	−2.64		7.22 7.06	6.61 6.46			3.4 3.4 1.70	7.88 7.58 7.19
8*a*	8.84–8.57	8.17 7.75 7.75	−2.76				3.21	2.58	3.76 3.01 1.77	7.37 6.95 6.69
NH_2—$(CH_2)_3$Im									4.02 2.69 1.86	7.44 7.03 6.89

TABLE 4. Absorption maxima, in nm, and molecular absorption coefficients (in parentheses), in mL mol^{-1} cm^{-1}, of iron(III) and iron(II) substituted *meso*-tetraphenylporphins in benzene or toluene

Compound	Data				
1*c*	372 (56)	418 (121)	507 (14.1)	572 (4.0)	686 (3.5)
2*c*	374 (56.5)	421 (116)	508 (14.0)	573 (4.2)	687 (3.4)
3*c*	376 (58)	423 (116)	511 (14)	575 (4.8)	682 (3.1)
4*c*	375 (49)	430 (116)	513 (13.9)	575 (5.4)	685 (3.5)
5*c*	377 (60)	420 (115)	508 (13.4)	575 (3.8)	682 (3.0)
6*c*	380 (55)	424 (119)	512 (13.1)	575 (4.0)	690 (3.0)
7*c*	380 (49)	430 (138)	515 (13.2)	575 (5.2)	680 (3.0)
8*c*	385 (45)	421 (110)	508 (11)	570 (5.4)	680 (25)
9*c*	378 (56)	420 (110)	508 (12)	575 (3.8)	683 (2.9)
1*d*	418 (120)	443 (93)	539 (12.8)		
2*d*	420 (116)	444 (90)	541 (12.4)		
3*d*	423 (110)	445 (90)	544 (12.8)		
4*d*	428 (106)	450 (93)	545 (12.0)		
5*d*	420 (106)	446 (76)	540 (10.0)		
6*d*	440 (197)	538 (9.5)	570 shoulder (7.8)	615 shoulder (3.3)	
7*d*	445 (121)	545 (9.7)	575 shoulder (7.8)	620 shoulder (3.2)	
8*d*	440 (141)	540 (9.6)	570 shoulder (7.8)	615 shoulder (4.5)	
9*d*	436 (175)	535 (9.8)	565 shoulder (7)	612 shoulder (3.1)	

the great difference of the affinity constants of Fe(II)TPP **1***d* for L′ and L = *N*-methylimidazole allowed us to study the stepwise replacement of L by L′ (and vice-versa) in the case of Fe(II)TPP. Values of $K_L^{L,L'} = 1$ and $K_{L'}^{L,L'} = 0.06$ agree with the overall affinity constants $K^L K_L^L = 0.85 \times 10^{10}\ M^{-2}$ and $K^{L'} K_{L'}^{L'} = 5 \times 10^8\ M^{-2}$ measured in separate experiments (see Experimental section). Besides, knowledge of $K_L^L = 1.4 \times 10^5\ M^{-1}$ gives $K_L^{L'} = 1.4 \times 10^5\ M^{-1}$, which compares well with the affinity constant of the five-coordinate models **6***d*, **7***d*, **8***d* for 4-cyanopyridine, $K_{Im}^{L'} \sim 2.5 \times 10^5\ M^{-1}$. In other words, the *trans influence* exerted by the covalently linked imidazole, irrespective of the nature of the covalent chain, is not very different from that exerted by the free base *N*-methylimidazole in solution.

Compounds **6***d*, **7***d*, **8***d* strongly bind CO, leading to the well characterized monocarbonyl hemochromes. Affinity constants $K_{Im}^{CO} \sim 1 \times 10^8\ M^{-1}$ are obtained which are comparable to the value obtained by Geibel *et al.* (28) on their mesoheme derivative (**1**, $K = 6 \times 10^8\ M^{-1}$, determined by kinetic methods).

Replacement of L = *N*-methylimidazole by CO in the symmetrical hemochromes of **3***d*, **4***d*, **5***d* gives constants $K_L^{L,CO} = 1.05$, 1.2, and 1.6×10^3, respectively. Knowledge of $K_L^L = 1.3 \times 10^5\ M^{-1}$ for **5***d* gives $K_L^{CO} = 2.1 \times 10^8\ M^{-1}$, which is again comparable with the above K_{Im}^{CO} value.

On exposure to oxygen at room temperature, compounds **6***d*, **7***d*, and **8***d* are immediately and irreversibly oxidized to iron(III) complexes. However admission of oxygen to a toluene solution of these compounds at low temperature (−45°C) immediately gives new species which are characterized by a visible band near 545 nm with a shoulder at 583 nm, and a Soret band at 432 nm. These oxygenations at low temperature are fully reversible, and bubbling argon restores the initial spectra.

Conclusions

In non-coordinating solvents such as benzene or toluene, the physico-chemical properties of iron substituted *meso*-tetraphenylporphins with imidazole covalently attached to either an acrylic (*cis–trans* isomers) or a propionic side chain show that the internal coordination is only observed in the reduced form.

Quantitative titration of the three iron(II) compounds by 4-cyanopyridine shows that internal fifth coordination is much less favourable in the *trans* acrylic derivative than in the *cis* propionic derivatives. This conclusion may be related to the stereochemistry of their free-bases observed in nmr studies.

However, the '*trans influence*' exerted by imidazole upon external fifth ligands is not particularly marked either by the nature or by the structure of the side chain.

The affinity of these compounds derived from the synthetic H_2TPP porphyrin ring is comparable to that of other five-coordinate models derived from meso- (5) and deuteroporphyrin IX rings (7), and related hemoproteins such as isolated α and β chains of human hemoglobin containing protoporphyrin IX as prosthetic group, indicating that porphyrin substituent effects are weak. As quoted by James *et al.* (29), porphyrin substituent effects with 2,4 substituted deuteroporphyrins (proto, meso) and H_2TPP

seem small compared with those observed on changing to octamethyltetrabenzoporphyrin and phthalocyanine. On the contrary, the reactivity of iron(II) model compounds seems more dependent on the length of the chain bearing the terminal base and on the nature of the base (28).

Our own results show that iron(II) derivatives of TPP are as valuable as those derived from naturally occurring porphyrins to mimic the active site of hemoproteins.

Experimental

meso-α,β,γ,δ,Tetraphenylporphin (H_2TPP) and its metal complexes (Cu and Fe) were synthesized as described by Adler *et al.* (30) and Rothemund and Menotti (31) respectively. All chemicals used were of reagent grade. Silica gel was purchased from Merck Company. *N*-Methylimidazole, 4-cyanopyridin, and 3-(3 pyridyl)-1-propanol were purchased from Aldrich. Prediluted CO in nitrogen, grade U (1.08×10^{-4} *M* in volume) was especially supplied by Air Liquide.

Optical spectra in the Soret and visible regions were recorded using a Beckman DKU or a Varian-Techtron 635 spectrophotometer. Proton magnetic resonance spectra in deuterochloroform (CEA, France) were recorded at 100 MHz in the Fourier transform mode using 4K data points in the frequency domain. Chemical shifts were referenced to internal tetramethylsilane (TMS).

The spectrophotometric titrations of the four- and five-coordinate Fe(II) compounds by externally added ligands (including CO) have been performed as previously described (23, 24, 32). The solubility of CO in benzene at 20°C is assumed to be 6.7×10^{-3} *M* atm^{-1} (19). The abbreviations and notations used throughout are the same as in ref. 32 for the four-coordinate species, and are derived from them for the five-coordinate species, as briefly summarized below.

Titration of four-coordinate species, P = **1***d*, **3***d*, **4***d*, **5***d*, by ligands L, L′:

$$P + L \rightleftharpoons PL \qquad (K^L, M^{-1})$$

$$PL + L \rightleftharpoons PL_2 \qquad (K_L^L, M^{-1})$$

$$PL + L' \rightleftharpoons PLL' \qquad (K_L^{L'}, M^{-1})$$

$$PL_2 + L' \rightleftharpoons PLL' + L$$

$$K_L^{L,L'} = [PLL'][L]/[PL_2][L']$$

$$PLL' + L' \rightleftharpoons PL'_2 + L$$

$$K_{L'}^{L,L'} = [PL'_2][L]/[PLL'][L']$$

leading to the obvious relationship

$$K_L^{L'} = K_L^L \times K_L^{L,L'}$$

$$K^L K_L^L \times K_L^{L,L'} \times K_{L'}^{L,L'} = K^{L'} K_{L'}^{L'}$$

and any combination between them.

Titration of five-coordinate species P(Im) = **6***d*, **7***d*, **8***d*, by a ligand L:

$$P(Im) + L \rightleftarrows P(Im)L \qquad (K_{Im}^L, M^{-1})$$

$$P(Im)L + L \rightleftarrows Im—PL_2 \qquad (K_L^{Im,L}, M^{-1})$$

All the constants were obtained at 20°C ± 0.1°C in benzene. Each value was calculated as an average of at least three determinations, with an estimated error of ±30%.

Formylation of Transition Metal Complexes of meso-α,β,γ,δ,-*Tetraphenylporphin*

(1) Cu-TPP. To a mixture of phosphoryl chloride (40 mL) in dimethylformamide (40 mL) was added a solution of metal complex (5 g) in 1,2-dichloroethane (550 mL). The mixture was heated under reflux for 18 h. Saturated sodium acetate solution (600 mL) was added and the mixture was warmed under stirring for a further 2 h. The product was extracted with chloroform. The chloroformic solution was washed with water (× 3), dried over sodium sulfate, and evaporated to dryness. The desired product was crystallized from methylene chloride:methanol (1:5) giving Cu-*meso*-tetraphenyl-1(formyl)porphin **2***b* (4.8 g; 92%). *Anal.* calcd. for $C_{45}H_{28}N_4OCu$: C 76.74, H 4.01, N 7.96; found: C 76.22, H 4.19, N 7.85.

(2) Fe-TPP. Phosphoryl chloride (17 mL) was added to dry dimethylformamide (17 mL) cooled in an ice-bath and the solution was kept at room temperature for 1 h with vigorous stirring. A solution of Fe(III)Cl·TPP (2 g) in 1,2-dichloroethane (100 mL) was added and heated under reflux for 24 h. Following the foregoing treatment, we obtained a residue which was then dissolved in a mixture of pyridine (15 mL), acetic acid (600 mL), and chloroform (250 mL). A saturated solution of iron(II) sulfate in hydrochloric acid (12 *N*, 40 mL) was added under nitrogen. After 5 min, the mixture was poured into a saturated sodium acetate solution. The products were extracted with chloroform. The chloroformic solution was washed with water (× 3) and dried over sodium sulfate. The organic solvent was removed under reduced pressure and the residue dissolved in benzene–cyclohexane (4:1) and chromatographed on a silica gel column. The first compound eluted with the same solvent corresponded to *meso*-tetraphenylporphin **1***a* (1.432 g, 82%). The second one eluted with pure benzene was identified by nmr as formyl-*meso*-tetraphenylporphin **2***a* (231 mg, 12.7%). *Anal.* calcd. for $C_{45}H_{30}N_4O$: C 84.09, H 4.70, N 8.72; found: C 83.79, H 4.80, N 8.64.

Cu-meso-*Tetraphenyl-1-[2-ethoxycarbonylvinyl]porphin (*Cis *and* Trans *Isomers)* **3**b *and* **4**b

Method 1

To a toluene solution of Cu-*meso*-tetraphenyl-1(formyl)porphin **2***b* (2.11 g) was added carbethoxyethyl-methenyl-triphenylphosphorane (15 g). The mixture was refluxed overnight. The solution was evaporated under reduced pressure, and the residue was chromatographed on a silica gel column (3.5 × 100 cm). Elution with toluene gave two successive bands. The first band contained *cis*-Cu-*meso*-tetraphenyl-1-[2-ethoxycarbonylvinyl]porphin **3***b* (0.670 g from chloroform–methanol, 2:7; 28.9%). *Anal.* calcd. for $C_{49}H_{34}N_4O_2Cu$: C 76.00, H 4.43, N 7.24; found: C 75.77, H 4.42, N 7.48. The second one yielded *trans*-Cu-*meso*-tetraphenyl-1-[2-ethoxycarbonylvinyl]porphin **4***b* (1.093 g from chloroform–methanol, 2:7; 47.1%). *Anal.* calcd. for $C_{49}H_{34}N_4O_2Cu$: C 76.00, H 4.43, N 7.24; found: C 75.08, H 4.40, N 7.57.

Method 2

Triethyl phosphonoacetate (10.08 g) was added dropwise under stirring to a slurry of sodium hydride (2.16 g of 50% dispersion in mineral oil) in 90 mL of dry 1,2-dimethoxyethane at 10°C. The solution was then stirred until gas evolution had ceased. Cu-formyl-TPP **2***b* (2.11 g) in 1,2-dimethoxyethane (25 mL) was added and the mixture stirred for 4 h. The reaction mixture was poured in water (500 mL) and the compounds were extracted with chloroform. The organic layer was washed with water (× 2), dried over sodium sulfate, and evaporated under reduced pressure. The residue was dissolved in toluene and chromatographed on a silica gel column in the same solvent to give two isomers as described above.

TABLE 5. Absorption maxima of hemochromes and affinity constants in benzene at 20°C

Species	Ligands		λ in nm (ε in mL mol^{-1} cm^{-1})				Affinity constants
1*d*	Im						1.3 $\times 10^4$ M^{-1} [a]
1*d*	Im	Im	427 (215)	533.5 (17)	565 (4.5)		1.2 $\times 10^5$ M^{-1} [b]
1*d*	NBuIm						2 $\times 10^4$ M^{-1} [a]
1*d*	NBuIm	NBuIm	429 (230)	534 (19.0)	566 (5.7)		1.1 $\times 10^5$ M^{-1} [b]
1*d*	NMeIm						6 $\times 10^4$ M^{-1} [a]
1*d*	NMeIm	NMeIm	429 (280)	535 (21.5)	567 (6.4)		1.4 $\times 10^5$ M^{-1} [b]
1*d*	Py						2.2 $\times 10^3$ M^{-1} [a]
1*d*	Py	Py	424 (190)	530 (19.5)	562 (4.5)		3 $\times 10^4$ M^{-1} [b]
1*d*	4PyCN	4PyCN	423 (195)	529 (25)	563 (11.8)	610 (11)	5 $\times 10^8$ M^{-2} [c]
3*d*	NMeIm	NMeIm	437 (175)	540 (19.3)	572 (6.5)		$>10^{10}$ M^{-2} [c]
4*d*	NMeIm	NMeIm	447 (180)	543 (14.8)	580 (10.9)		$>10^{10}$ M^{-2} [c]
5*d*	NMeIm						3 $\times 10^4$ M^{-1} [a]
5*d*	NMeIm	NMeIm	430 (195)	536 (15.7)	567 (5.6)		1.3 $\times 10^5$ M^{-1} [b]
3*d*	4PyCN	4PyCN	430 (185)	534 (23.8)	568 (12.8)	610 sh. (10)	2.9 $\times 10^8$ M^{-2} [c]
4*d*	4PyCN	4PyCN	436 (185)	537 (21.7)	572 (17.3)	620 sh. (8.0)	2.5 $\times 10^8$ M^{-2} [c]
5*d*	4PyCN	4PyCN	426 (146)	530 (17.7)	565 (8.9)	610 sh. (7.6)	1.3 $\times 10^8$ M^{-2} [c]
3*d*	NMeIm	CO	430 (250)	548 (13.4)	590 sh. (5.3)		1.05 $\times 10^3$ [d]
4*d*	NMeIm	CO	439 (200)	552 (12.0)	585 sh. (8.1)		1.2 $\times 10^3$ [d]
5*d*	NMeIm	CO	426 (260)	545 (10.1)	580 sh. (5.2)		1.6 $\times 10^3$ [d]
3*d*	4PyCN	CO	426 (235)	543 (12.8)	590 sh. (4.6)		0.65 $\times 10^3$ [d]
4*d*	4PyCN	CO	434 (180)	550 (12.0)	585 sh. (9.3)		0.7 $\times 10^3$ [d]
5*d*	4PyCN	CO	424 (230)	541 (9.8)	580 sh. (5.2)		0.9 $\times 10^3$ [d]
6*d*	[Im]	NMeIm	434 (190)	538 (16.5)	572 (6.5)		$>5\times 10^5$ M^{-1} [e]
7*d*	[Im]	NMeIm	444 (150)	544 (13.0)	580 (8.4)		$>5\times 10^5$ M^{-1} [e]
8*d*	[Im]	NMeIm	431 (188)	538 (16)	570 (4.6)		$>5\times 10^5$ M^{-1} [e]
6*d*	[Im]	4PyCN	430 (170)	537 (19.2)	570 (10)	710 (3.2)	3 $\times 10^5$ M^{-1} [e]
6*d*	4PyCN	4PyCN					1 M^{-1} [f]
7*d*	[Im]	4PyCN	437 (150)	540 (15.7)	575 (11.9)		2.5 $\times 10^5$ M^{-1} [e]
7*d*	4PyCN	4PyCN	435 (185)	536 (21.3)	572 (16.0)	620 sh. (8.5)	30 M^{-1} [f]
8*d*	[Im]	4PyCN	430 (170)	537 (19)	567 (8.8)	705 (3.2)	2.5 $\times 10^5$ M^{-1} [e]
8*d*	4PyCN	4PyCN	427 (160)	532 (22.5)	567 (11.2)	610 (10.8)	1.2 M^{-1} [f]
6*d*	[Im]	CO	428 (290)	547 (11.1)	585 sh. (5.4)		1.3 $\times 10^8$ M^{-1} [e]
7*d*	[Im]	CO	435 (160)	550 (8.4)			1 $\times 10^8$ M^{-1} [e]
8*d*	[Im]	CO	428 (310)	547 (12)	583 sh. (5.4)		1.3 $\times 10^8$ M^{-1} [e]
1*d*	NMeIm	4PyCN					1.0 [g]
1*d*	4PyCN	4PyCN	423 (188)	529 (24.5)	563 (11)	610 (10.5)	0.06 [h]

NOTE: [a] K^{L}; [b] $K_{L}{}^{L}$; [c] $K^{L}K_{L}{}^{L}$; [d] $K_{L}{}^{L,CO}$; [e] $K_{Im}{}^{L}$; [f] $K_{L}{}^{Im,L}$; [g] $K_{NMeIm}{}^{NMeIm,4PyCN}$; [h] $K_{4PyCN}{}^{NMeIm,4PyCN}$.

Cis-Cu-*meso*-tetraphenyl-1-[2-ethoxycarbonylvinyl]porphin, **3***b* (0.104 g; 4.5%).

Trans-Cu-*meso*-tetraphenyl-1-[2-ethoxycarbonylvinyl]porphin, **4***b* (1.980 g; 85.5%).

meso-*Tetraphenyl-1-[2-ethoxycarbonylvinyl]porphin (*Cis *and* Trans *Isomers)* **3**a *and* **4**a

To a solution of Cu-porphin **3***b* (or **4***b*) (1.35 g) in chloroform (250 mL), containing 1% water, gaseous hydrochloric acid was bubbled. Demetallation of metalloporphins was followed by changes in the absorption spectra of the reaction mixture. After completion of the reaction, the solution was successively washed with water, aqueous 0.2 *N* ammonium hydroxide and water, then dried over sodium sulfate and evaporated to dryness. The residue crystallized from methylene chloride–methanol (2:7).

Cis-isomer **3***a*; 1.038 g, 83.5%. *Anal.* calcd. for $C_{49}H_{36}N_4O_2$: C 82.56, H 5.09, N 7.86; found: C 82.79, H 4.98, N 7.64.

Trans-isomer **4***a*; 1.056 g, 85%. *Anal.* calcd. for $C_{49}H_{36}N_4O_2$: C 82.56, H 5.09, N 7.86; found: C 82.98, H 5.05, N 7.72.

meso-*Tetraphenyl-1-[2-ethoxycarbonylethyl]porphin* **5**a

Porphin-*trans*-isomer **4***a* (0.932 g) was dissolved in formic acid (100 mL) and hydrogenated over 30% palladium on charcoal (250 mg) at 40–50°C. Hydrogenation was followed by spectrophotometry. At the end of the reaction the catalyst was removed by filtration and the filtrate evaporated to dryness under reduced pressure. The residue was dissolved in chloroform. The chloroformic solution was successively washed with water, aqueous sodium bicarbonate and water, then dried over sodium sulfate. The crude compound was chromatographed on a silica gel column (3.5 × 45 cm) with benzene as eluting solvent. The porphin fraction was evaporated to dryness and crystallized from methylene chloride–methanol (1:6) to give *meso*-tetraphenyl-1-[2-ethoxycarbonylethyl]porphin **5***a* (735 mg, 80%).

Anal. calcd. for $C_{49}H_{38}N_4O_2$: C 82.33, H 5.36, N 7.84; found: C 82.09, H 5.48, N 7.96.

meso-*Tetraphenyl-1-[3-acrylic acid]porphin (*Cis *and* Trans *Isomers)*

A solution of *meso*-tetraphenyl-1-[2-ethoxycarbonylvinyl] porphin **3***a* (or **4***a*) (1.038 g) dissolved in a mixture of tetrahydrofuran (150 mL) and 80% hydroalcoholic solution of potassium hydroxyde (2 *N*, 75 mL) was shaken for 2 h. The formation of

acid porphin was controlled by analytical thin layer chromatography. The solution was evaporated to dryness. The residue was dissolved in water and acidified by hydrochloric acid giving a compound which was extracted with chloroform (100 mL). The organic solvent was washed with water (× 3) and dried over sodium sulfate. The product was precipitated from methylene chloride by addition of light petroleum.

Cis-isomer: 956 mg, 96%.

Trans-isomer: 936 mg, 94%.

meso-*Tetraphenyl-1-[3-propionic acid]porphin*

This compound was obtained from *meso*-tetraphenyl-1-[2-ethoxycarbonylethyl]porphin **5***a* (735 mg) by the foregoing procedure (671 mg, 95%).

meso-*Tetraphenyl-1-[3-(*N-*imidazolyl propyl)acrylamido]porphin (*Cis *and* Trans *Isomers)* **6**a *and* **7**a

The free acid compounds (154 mg) in benzene (50 mL) were treated with an excess of oxalyl chloride (120 μL) at 50°C until gas evolution has ceased. The solvent was evaporated to dryness. The residue is taken up in methylene chloride and mixed with a solution of *N*-(3-aminopropyl)imidazole in the same solvent. The mixture was stirred for 2 h, then washed successively with water, aqueous sodium bicarbonate, and water, then dried over sodium sulfate. After evaporation, the residue was chromatographed on a silica gel column (1 × 20 cm) (eluting solvent: methylene chloride – methanol, 100:5) and was precipitated with heptane.

Cis-isomer **6***a*: 120 mg, 67%. *Anal.* calcd. for $C_{53}H_{41}N_7O$: C 80.37, H 5.22, N 12.38; found: C 79.98, H 5.26, N 12.43.

Trans-isomer **7***a*: 118 mg, 66%. *Anal.* calcd. for $C_{53}H_{41}N_7O$: C 80.37, H 5.22, N 12.38; found: C 80.03, H 5.31, N 12.41.

meso-*Tetraphenyl-1-[3-(*N-*imidazolyl propyl)propionamido]porphin* **8**a

The foregoing procedure was used. 128 mg, 71%. *Anal.* calcd. for $C_{53}H_{43}N_7O$: C 80.18, H 5.46, N 12.35; found: C 80.36, H 5.29, N 12.31.

meso-*Tetraphenyl-1-[2-(3'pyridyl-*n *propyloxy)carbonylethyl]porphin* **9**a

The acid chloride obtained from 160 mg of free acid of **5***a* by the foregoing procedure and an excess of 3-(3-pyridyl)-1-propanol at 0°C in methylene chloride were stirred for 3 h, and washed successively with water, aqueous sodium bicarbonate, and water, then dried over sodium sulfate. The solvent was removed under reduced pressure and the residue purified by chromatography on a silica gel column (1 × 20 cm) (eluting solvent, chloroform–methanol, 100:2) and precipitated with heptane (112 mg, 60%).

Anal. calcd. for $C_{55}H_{43}N_5O_2$: C 81.96, H 5.38, N 8.69; found: C 81.58, H 5.24, N 8.61.

Iron Complexes

The insertion of iron in the substituted nitrogenous base porphyrins **6***a*, **7***a*, **8***a*, and **9***a* was carried out in a solution of ferrous acetate in acetic acid according to the method of Alben *et al.* (19).

The iron(III) complexes were chromatographed on a silica gel column (1 × 20 cm), eluted with methylene chloride – methanol (100:10), washed with saturated aqueous sodium chloride, and then precipitated with heptane as chloro derivatives (**6***c*, **7***c*, **8***c*, and **9***c*).

Acknowledgement

This work was supported by the Institut National de la Santé et de la Recherche Médicale (CRL No. 77.4.091.3).

1. W. LAUTSCH. Kolloid Z. **161**, 1 (1958).
2. S. SANO, K. IKEDA, and S. SAKAKIBARA. Biochem. Biophys. Res. Commun. **15**, 284 (1964).
3. M. MOMENTEAU and B. LOOCK. Biochim. Biophys. Acta, **343**, 535 (1974).
4. K. WARME and H. P. HAGER. Biochemistry, **9**, 1599 (1970).
5. C. K. CHANG and T. G. TRAYLOR. Proc. Natl. Acad. Sci. U.S.A. **70**, 2647 (1973).
6. C. E. CASTRO. Bioinorg. Chem. **4**, 45 (1974).
7. M. MOMENTEAU, M. ROUGEE, and B. LOOCK. Eur. J. Biochem. **71**, 63 (1976).
8. F. S. MOLINARO, R. G. LITTLE, and J. A. IBERS. J. Am. Chem. Soc. **99**, 5628 (1977).
9. H. J. CALLOT, B. CASTRO, and C. SELVE. Tetrahedron Lett. 2877 (1978).
10. H. J. CALLOT. Tetrahedron, 899 (1973).
11. H. J. CALLOT. Bull. Soc. Chim. **12**, 3413 (1973).
12. H. H. INHOFFEN, J. H. FUHRHOP, H. VOIGT, and H. BROCKMAN. Liebigs Ann. **695**, 133 (1966).
13. J. H. FUHRHOP. Angew. Chem. **13**, 321 (1974).
14. R. LEMBERG, B. BLOOMFIELD, P. CAIGER, and W. LOCKWOOD. Aust. J. Exp. Biol. **33**, 435 (1955).
15. K. M. SMITH. *In* Porphyrins and metalloporphyrins. Elsevier. 1975. p. 21.
16. G. R. GRIFFITHS, G. W. KENNER, S. W. MACCOMBIC, K. M. SMITH, and M. J. SUTTON. Tetrahedron, **32**, 275 (1976).
17. L. F. FIESER and M. FIESER. *In* Advanced organic chemistry. Reinshold Publishing Corporation. 1961. p. 383.
18. T. J. SCHWAN. J. Heterocycl. Chem. **4**, 633 (1967).
19. J. O. ALBEN, W. H. FUSCHSMAN, C. A. BEAUDREAU, and W. S. CAUGHEY. Biochemistry, **7**, 624 (1968).
20. C. B. STORM, Y. TEKLU, and E. A. SOKOLSKI. Ann. N.Y. Acad. Sci. **206**, 631 (1973).
21. J. H. FUHRHOP, L. WITTE, and W. S. SHELDRICK. Liebigs Ann. Chem. 1537 (1976).
22. F. A. WALKER, M. W. LO, and M. T. REE. J. Am. Chem. Soc. **98**, 5552 (1976).
23. M. MOMENTEAU. Biochim. Biophys. Acta, **304**, 814 (1973).
24. D. BRAULT and M. ROUGEE. Biochemistry, **13**, 4591 (1974).
25. J. P. COLLMAN and C. A. REED. J. Am. Chem. Soc. **95**, 2048 (1973).
26. D. BRAULT and M. ROUGEE. Biochem. Biophys. Res. Commun. **57**, 654 (1974).
27. E. ANTONINI and M. BRUNORI. *In* Hemoglobin and myoglobin in their reactions with ligands. Amsterdam, Holland. 1971. p. 167.
28. J. GEIBEL, J. CANNON, D. CAMPBELL, and T. G. TRAYLOR. J. Am. Chem. Soc. **100**, 3575 (1978).
29. B. R. JAMES, K. J. REIMER, and T. C. T. WONG. J. Am. Chem. Soc. **99**, 4815 (1977).
30. A. D. ADLER, F. R. LONGO, J. D. FINARELLI, J. ASSOUR, and L. KORSAKOFF. J. Org. Chem. **32**, 476 (1967).
31. P. ROTHEMUND and A. R. MENOTTI. J. Am. Chem. Soc. **70**, 1808 (1948).
32. M. ROUGEE and D. BRAULT. Biochemistry, **14**, 4100 (1975).

Vibrations de réseau de quelques dérivés dihalogénés du benzène

J. SERRIER, F. BREHAT, B. WYNCKE ET A. HADNI[1]

Laboratoire Infrarouge Lointain, Université de Nancy I, C.O. no 140, 54037, Nancy Cedex, France

Reçu le 2 janvier 1979

J. SERRIER, F. BREHAT, B. WYNCKE et A. HADNI. Can. J. Chem. 57, 1814 (1979).

Les modes de vibration de réseau actifs en absorption infrarouge sont mis en évidence dans le cas des *p*-$C_6H_4X_2$ (X = Cl, Br, I), *m*-$C_6H_4I_2$ et *o*-$C_6H_4I_2$. Le spectre de diffusion Raman est également présenté dans le cas du *m*-$C_6H_4I_2$. Dans le cas des *p*-$C_6H_4X_2$, la position des atomes dans la maille cristalline est connue et les fréquences de vibration externes sont calculées par la méthode de la matrice **GF**. La comparaison avec les valeurs obtenues par les spectres d'absorption infrarouge est acceptable bien qu'on ait négligé toutes les forces multipolaires à grand rayon d'action.

J. SERRIER, F. BREHAT, B. WYNCKE, and A. HADNI. Can. J. Chem. 57, 1814 (1979).

Low frequency lattice modes of *p*-$C_6H_4X_2$ (X = Cl, Br, I), *m*-$C_6H_4I_2$, and *o*-$C_6H_4I_2$ were observed by infrared absorption. Raman scattering spectra were recorded in the case of *m*-$C_6H_4I_2$.

When atomic positions were known in the unit cell (*p*-$C_6H_4X_2$), the lattice mode frequencies were computed by the **GF** matrix method.

The agreement between calculated and experimental values is reasonable although we did not consider the multipole–multipole long range interactions.

I. Introduction

Ce travail fait suite à celui que nous avons publié (1) sur les dérivés dihalogénés du benzène qui sont liquides à température ambiante. A 300 K les composés étudiés ici se présentent sous forme de cristaux moléculaires dont la formule brute est $C_6H_4X_2$ (X = Cl, Br, I). Les halogènes sont substitués aux hydrogènes en position *ortho*, *méta* et *para*. A cette étude nous avons ajouté celle des spectres infrarouge lointain des *p*-chloroiodo- et *p*-bromoiodobenzène.

II. Expérimentation

Les monocristaux utilisés sont fabriqués au laboratoire par la méthode de Bridgmann. Nous les avons taillés et orientés suivant les axes cristallographiques. Les lingots sont orientés à l'aide des rayons X par la méthode de Laue en retour. La tête goniométrique, sur laquelle sont disposés les cristaux, est placée sur une scie à fil. Les lames obtenues ont une épaisseur variant entre 0.5 et 1 mm. Pour obtenir des lames de 100 μm d'épaisseur nous avons collé les plaquettes de 16 × 16 mm^2 sur des cales de verre à l'aide de paraffine. L'épaisseur désirée est obtenue par usure des lames sur du papier abrasif (Norton 600 A). Suivant le domaine spectral étudié l'épaisseur des échantillons est comprise entre 100 μm et 1 mm. Les échantillons sont facilement sublimables et il est nécessaire de les enfermer dans une cuve étanche à fenêtres de quartz.

Les spectres d'absorption dans l'infrarouge lointain (15–250 cm^{-1}) sont enregistrés en lumière polarisée à 80 et 300 K, à l'aide d'un spectromètre Cameca SI 36 équipé d'un cryostat et d'un polariseur. La limite de résolution est de l'ordre de 1 à 2 cm^{-1}.

Nous avons vérifié le spectre de diffusion Raman de ces composés, en particulier celui du *m*-diiodobenzène. Le spectrophotomètre utilisé est un appareil Coderg T 800 équipé d'un laser Spectra Physics 165 à argon (488 nm). La limite de résolution spectrale est de l'ordre de 1 cm^{-1}.

III. Résultats expérimentaux

Le *p*-dichlorobenzène (PDC) dans la phase α cristallise dans le système monoclinique et possède le groupe d'espace $C_{2h}^5(P_{2_1/a})$ et deux molécules par maille. Il suffit donc pour l'étude de l'absorption infrarouge d'orienter le champ électrique ***E*** de l'onde excitatrice suivant l'axe binaire ***b*** et normalement à celui-ci. Il en est de même pour le *p*-dibromobenzène (PDB) dont la structure est isomorphe à celle du PDC α. Sur la fig. 1 nous avons représenté la variation de l'indice d'absorption *k* du PDB en fonction de la fréquence spatiale $\bar{\nu}$ (cm^{-1}). Le spectre du PDC a déjà été publié antérieurement (2). La structure des *p*-chloroiodo- (PCI) et *p*-bromoiodobenzène (PBI) n'est pas connue avec exactitude mais nous supposerons avec Prasad et coll. (3) qu'ils cristallisent dans le système monoclinique. L'axe binaire étant désigné par ***b***, nous présentons sur la fig. 1 le spectre d'absorption dans l'infrarouge lointain de ces deux composés.

Selon Hendricks et coll. (4) l'*o*-diiodobenzène (ODI) possède une structure monoclinique et très probablement le groupe d'espace $C_{2h}^1(P_{2/m})$ ou $C_{2h}^2(P_{2_1/m})$, il y aurait quatre molécules par maille. Sur la fig. 1, nous avons porté la variation de l'indice d'absorption *k* d'une lame polycristalline d'ODI. Il ne nous a pas été possible de faire une étude en lumière polarisée d'un monocristal d'ODI par suite de son point de fusion peu élevé (pf = 23°C). Nous avons dû nous contenter de solidifier le liquide entre

[1]Equipe de Recherche Associée au CNRS no 14.

0008-4042/79/141814-09$01.00/0

deux lames de quartz. Il peut y avoir une orientation partielle des cristallites. Toutefois nous avons enregistré le spectre infrarouge lointain plusieurs fois dans des conditions de cristallisation différentes. Nous observons toujours huit maximums d'absorption sur les neuf possibles et il est probable que deux ou plusieurs maximums de types différents soient superposés.

Les *m*- et *p*-diiodobenzène (MDI et PDI) cristallisent dans le système orthorhombique (4). Sur la fig. 2 nous présentons les variations de l'indice d'absorption $k = f(\dot{\nu})$ lorsque le champ électrique $\boldsymbol{E}$ de l'onde excitatrice est orienté suivant chacun des axes cristallographiques. Les résultats de cette étude sont rassemblés dans les tableaux 1 à 7.

IV. Discussion

IV.1. Attribution des maximums d'absorption observés

Les structures monocliniques de PDC, PDB, PCI et PBI possèdent le groupe d'espace $C_{2h}^5(P_{2_1/a})$. Les deux molécules de la cellule élémentaire occupent le site C_i. En conséquence l'analyse du groupe facteur C_{2h} permet de prévoir la répartition des modes de réseau: trois modes de translation de type $u(2a_u + 1b_u)$ actifs en absorption infrarouge et six modes de type $g(3a_g + 3b_g)$ qui correspondent aux librations actives en diffusion Raman.

Dans le cas de l'ODI les quatre molécules de la maille sont en position générale et il n'est plus possible de distinguer les translations des rotations. Les modes de réseau se répartissent en $6a_g + 6b_g + 5a_u + 4b_u$. La maille à faces *C* centrées du MDI est multiple, et peut être réduite en une maille élémentaire contenant seulement deux molécules. Dans le groupe facteur C_{2v}, les neuf modes de réseau du MDI se répartissent en $2a_1 + 3a_2 + 2b_1 + 2b_2$. Ces modes sont actifs en absorption et en diffusion à l'exception des modes a_2 qui ne se manifestent qu'en Raman. Les modes de réseau du PDI se séparent en translations actives en infrarouge $(2b_{1u} + 2b_{2u} + 2b_{3u})$ et en librations $(3a_g + 3b_{1g} + 3b_{2g} + 3b_{3g})$ actives en diffusion puisque le groupe d'espace est D_{2h}^{15} et que la maille élémentaire comporte quatre molécules occupant des sites C_i. Le PDI présente une transition de phase à 326 K (12). Nous n'avons pas observé de modifications importantes dans le spectre. Il y a seulement un élargissement des bandes ce qui réduit considérablement la précision de la position des maximums d'absorption.

Récemment Clayman et coll. (13) ont publié le spectre infrarouge lointain du PDI. Nos résultats sont en bon accord avec les leurs. Toutefois nous avons observé un maximum d'absorption supplémentaire à 15.5 cm^{-1} qui passe à 16 cm^{-1} lorsqu'on abaisse la température à 80 K. Ce mode est attribué à une vibration de réseau (tableau 7).

Ces quelques remarques nous permettent de proposer une attribution pour les maximums d'absorption que nous avons observés. Nous avons rassemblé tous ces résultats dans les tableaux 1 à 7. Dans le tableau 6 nous avons porté les modes que nous avons observés en diffusion Raman dans le cas du MDI. Pour les autres composés les résultats obtenus (5–7) sont identiques à ceux publiés par d'autres auteurs.

Le spectre de ces composés dissous dans le tétrachlorure de carbone nous permet de séparer les vibrations internes des molécules des vibrations de réseau. Les résultats que nous obtenons sont en bon accord avec ceux publiés par Green (8). Dans les tableaux nous avons indiqué l'attribution proposée par cet auteur.

Seul l'ODI présente un maximum d'absorption dans les basses fréquences lorsqu'il est dissout dans le tétrachlorure de carbone. Ce maximum d'intensité s'explique par le caractère fortement polaire de la molécule d'ODI.

Afin d'étayer l'attribution précédente des modes de réseau à tel ou tel mouvement de translation ou de pivotement, nous avons calculé la valeur des fréquences des vibrations de réseau en utilisant la méthode de la matrice **GF** (14) (**G** représente l'inverse de l'énergie cinétique dans le système des coordonnées internes et **F** l'énergie potentielle).

IV.2. Calcul des fréquences de vibration du réseau

Le calcul des fréquences de vibration de réseau par la méthode de la matrice **GF** nécessite la connaissance exacte de la position des atomes dans la maille élémentaire.

Les données structurales du PDC (15), du PDB (16) et du PDI (4) sont connues et nous avons effectué le calcul des fréquences des modes de réseau de ces trois composés. La cohésion de la structure de ces cristaux moléculaires est assurée par des liaisons de type Van der Waals et nous considérons en première approximation que les molécules sont rigides. Lors des mouvements de réseau la distance r_{ij} qui sépare deux atomes de molécules différentes varie. Si k_{ij} désigne la constante de force correspondante nous pouvons évaluer l'expression du potentiel. Nous choisirons un potentiel transférable comme celui de Buckingham:

$$V_{ij}(r_{ij}) = A_{ij} \exp(-B_{ij}r_{ij}) - C_{ij}r_{ij}^{-6}$$

La constante de force de la liaison *i–j* est donnée par la dérivée seconde par rapport à r_{ij} de l'expres-

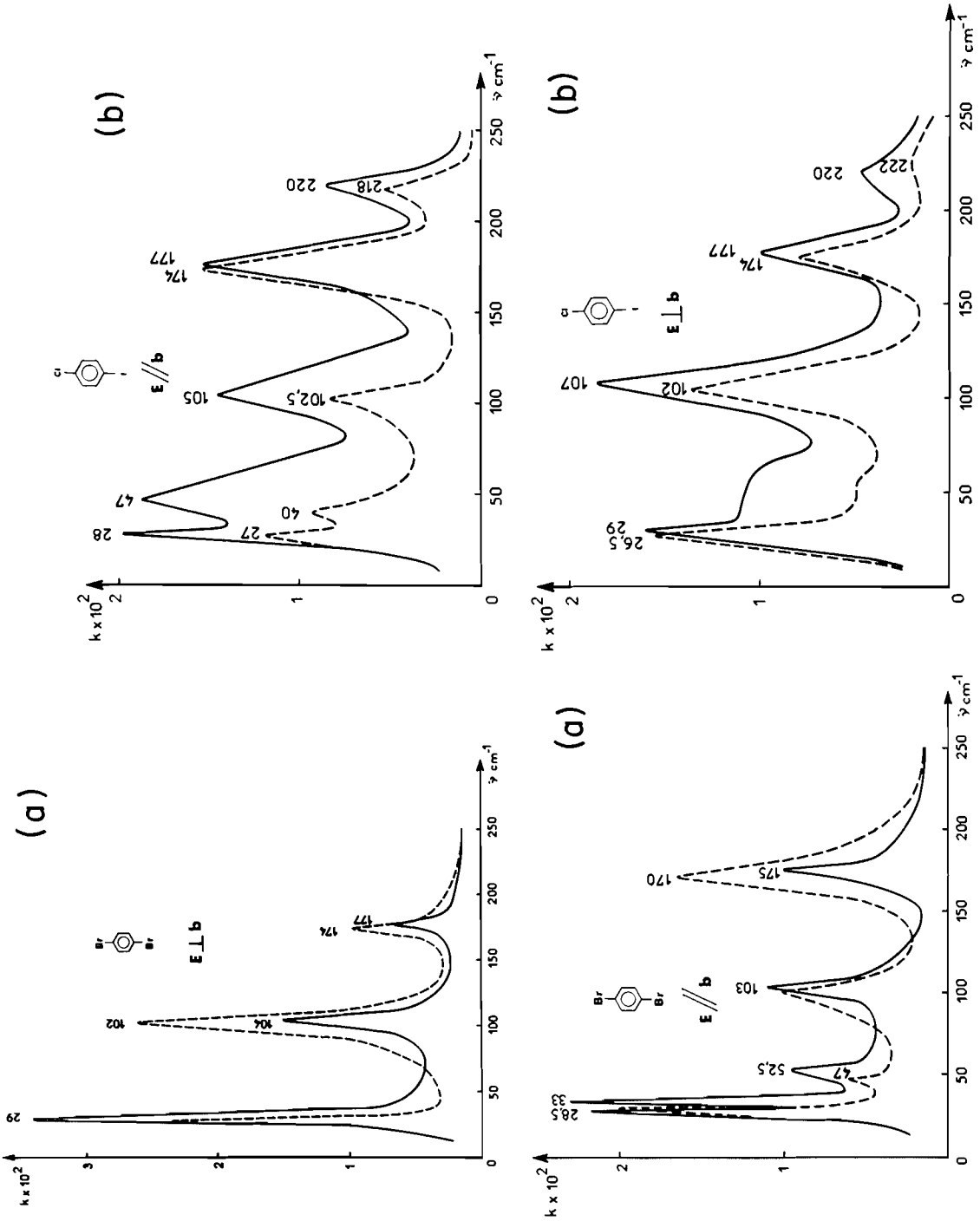

FIG. 1 (Part 1).

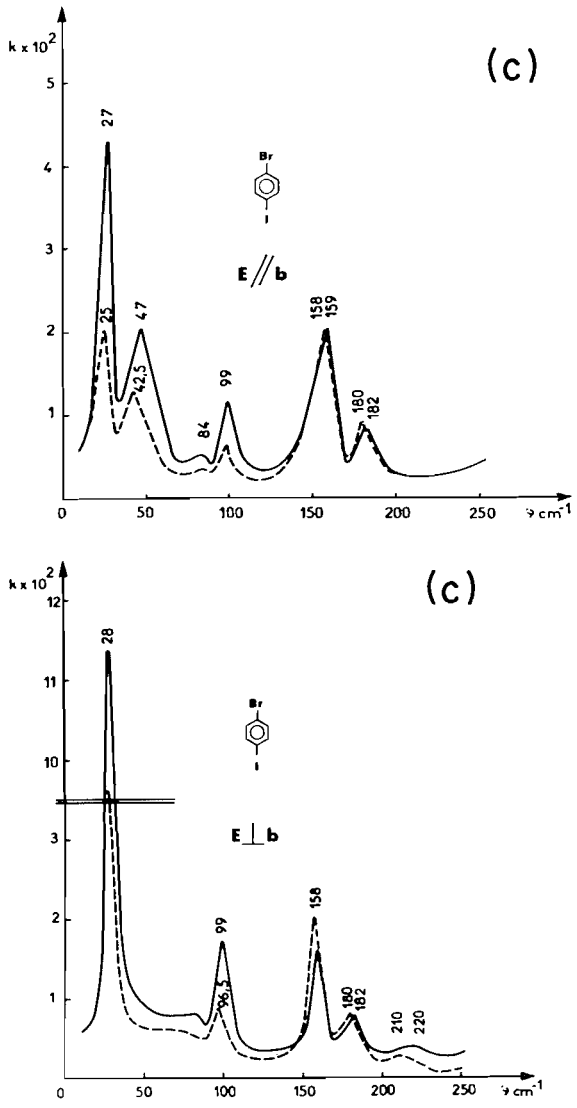

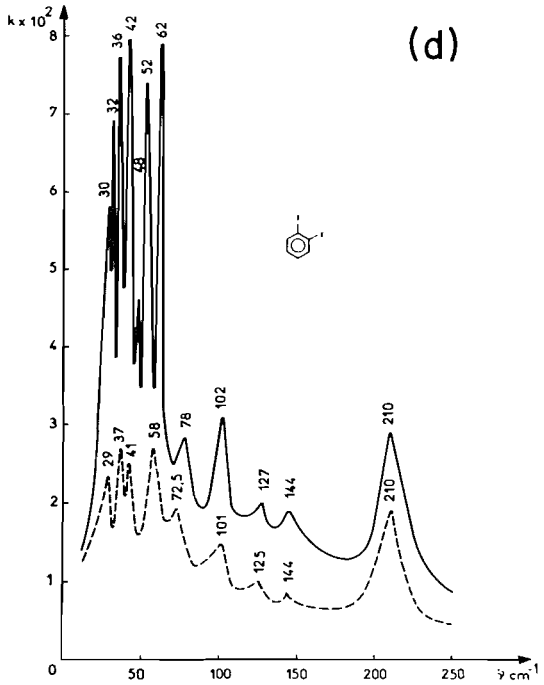

FIG. 1 (Part 2) (*Concluded*). Variation de l'indice d'absorption k en fonction de la fréquence spatiale $\bar{\nu}$ (cm^{-1}) à 80 (—) et 300 K(---): (*a*) du *p*-dibromobenzène; (*b*) du *p*-chloroiodobenzène; (*c*) du *p*-bromoiodobenzène; le champ électrique ***E*** est orienté suivant l'axe binaire ***b*** et normalement à celui-ci; (*d*) de l'*o*-diiodobenzène polycristallin.

sion du potentiel:

$$k_{ij}(r_{ij}) = A_{ij}B_{ij}^{2} \exp(-B_{ij}r_{ij}) - 42C_{ij}r_{ij}^{-8}$$

Les coefficients empiriques A_{ij}, B_{ij} et C_{ij} dépendent uniquement de la nature des atomes i et j. L'interaction moléculaire totale s'obtient par sommation sur chacune des paires d'atomes présentes dans le cristal. L'énergie du réseau est égale à la somme de tous ces potentiels s'il n'y a pas d'interactions dipolaires ou quadrupolaires électriques et si les liaisons sont purement covalentes:

$$E = \tfrac{1}{2}\sum_{ij}\{A_{ij}\exp(-B_{ij}r_{ij}) - C_{ij}r_{ij}^{-6}\}$$

Les coefficients A, B, C doivent être choisis de façon à retrouver l'énergie de sublimation, les paramètres de la maille, la vitesse du son et les fréquences de vibration du réseau. Dashevsky et coll. (17) proposent une sérié de valeurs obtenue à partir d'une étude structurale de dérivés aromatiques. Il en est de même de Williams (18) qui considère une série de composés aromatiques (benzène, naphtalène, ... ovalène). Kitaigorodskii et coll. (19) proposent une autre série de valeurs obtenue en évaluant l'énergie de réseau du benzène cristallisé. Nous avons également utilisé une autre série due à Bartell-Crowell cité par Ozora et coll. (20). Pour les liaisons entre atomes d'halogènes identiques nous avons suivi les indications de Hill (21) pour calculer la valeur des coefficients A, B, C. Il faut reconnaître que les valeurs empiriques des coefficients A, B et C du même potentiel de Buckingham varient beaucoup suivant les auteurs. Par exemple, $A_{CC} = 26.19$ (Dashevsky) et $A_{CC} = 51.76$ (Kitaigorodskii); $A_{CH} = 11.17$ (Bartell-Crowell) et $A_{CH} = 28.19$ (Kitaigorodskii). Pour des liaisons entre atomes différents (C—H, C—Cl, H—Cl) nous avons appliqué les relations:

$$A_{ij} = (A_{ii}B_{jj})^{1/2}$$

$$B_{ij} = \tfrac{1}{2}(B_{ii} + B_{jj})$$

$$C_{ij} = (C_{ii}C_{jj})^{1/2}$$

Dans le calcul des modes de réseau du PDC, du

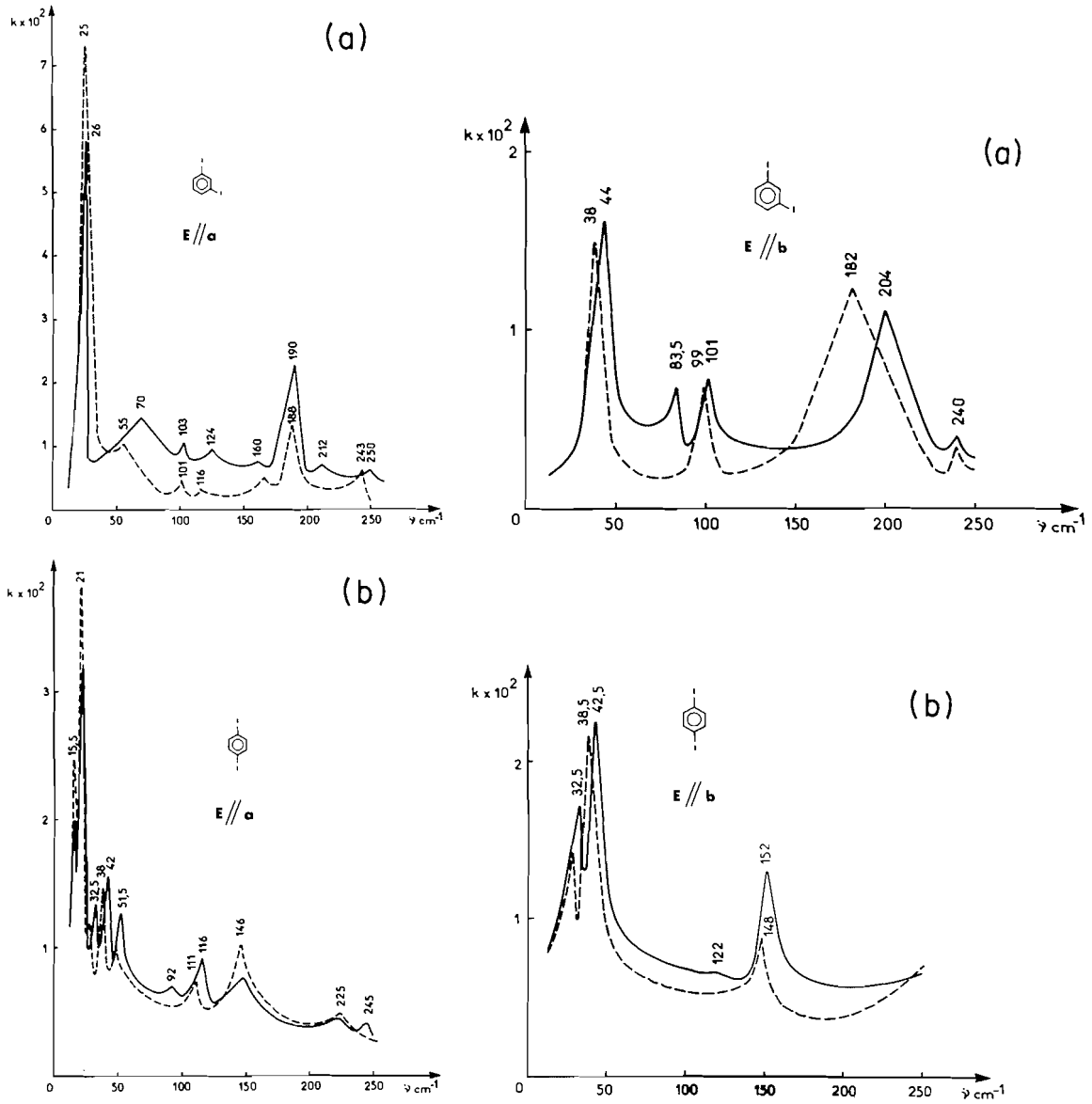

FIG. 2 (Part 1).

PDB et du PDI nous n'avons retenu que les liaisons dont les constantes de force sont supérieures à 8×10^{-3} mdyn/Å. Les constantes de force k_{ij} sont les éléments diagonaux de la matrice **F** représentative de l'énergie potentielle d'interaction rapportée à la maille élémentaire et exprimée dans un système de coordonnées internes.

On montre (22) que la matrice **G** représentative de l'énergie cinétique, exprimée dans un système de coordonnées normales, est égale à la matrice identité **E**. L'équation séculaire $|\mathbf{GF} - \mathbf{E}\Lambda| = 0$, se simplifie suivant $|\mathbf{F} - \mathbf{E}\Lambda| = 0$, où **Λ** est la matrice diagonale des valeurs propres λ de la matrice **F**. L'équation séculaire est résolue simplement dans le système des coordonnées de symétrie (23).

IV.3. Comparaison des fréquences calculées aux fréquences observées expérimentalement

Le calcul des fréquences a été effectué avec les séries de paramètres proposés par les auteurs cités ci-dessus (17–20).

Nous remarquons que le meilleur accord entre les fréquences calculées et observées est obtenu avec le système des coefficients proposés par Williams.

Dans ce cas, le calcul de PED (potential energy distribution) permet d'évaluer le pourcentage des

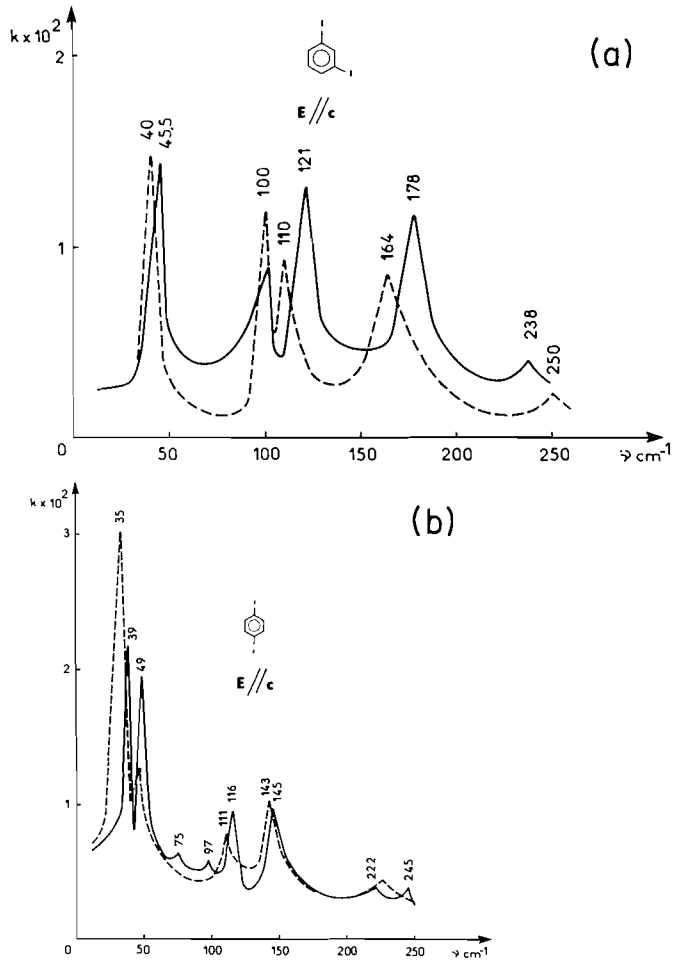

FIG. 2 (Part 2) (*Concluded*). Variation de l'indice d'absorption k en fonction de la fréquence spatiale $\tilde{\nu}$ (cm^{-1}) à 80 (—) et 300 K (---): (*a*) du *m*-diiodobenzène; (*b*) du *p*-diiodobenzène. Le champ électrique $\boldsymbol{E}$ est orienté suivant les axes cristallographiques ***a***, ***b***, ***c***.

TABLEAU 1. Fréquences en cm^{-1} des modes de réseau observés et calculés du *p*-dichlorobenzène (T'_b translation des molécules suivant l'axe binaire ***b***; T'_{ac} translation des molécules dans le plan normal à l'axe binaire; R_U, R_V, R_W libration des molécules autour de ses axes d'inertie ***OU***, ***OV***, ***OW***)

	Infrarouge (obs.)			Raman (obs.) (90 K) (réfs. 6, 7)	Calc.			
	Solution CCl_4	$E \perp b$ (80 K)	$E \parallel b$ (80 K)	Attribution		PED (%)	Réf. 24 (77 K)	Réf. 25
		27		$T'_b(b_u)$		$42T_b + 58T_{ac}$	39	25
				$R_W(b_g)$	32.5	$39R_U + 27R_V + 34R_W$	30	28
			44	$T'_{ac}(a_u)$		$6T_b + 94T_{ac}$	39	32
				$R_W(a_g)$	57.5	$13R_U + 17R_V + 70R_W$	52	48
				$R_V(a_g)$		$54R_U + 15R_V + 31R_W$	56	45
Cl Cl			64	$T'_{ac}(a_u)$		$20T_b + 80T_{ac}$	59	46
				$R_V(b_g)$	64	$10R_U + 28R_V + 62R_W$	60	50
				$R_U(a_g)$	107	$14R_U + 86R_V$	119	102
				$R_U(b_g)$	114	$95R_V$	124	105
				Réf. 8				
		124	124	122 $\nu_{30}(b_{3u})$				
	115			Internes				
		235	230	226 $\nu_{27}(b_{2u})$				

TABLEAU 2. Fréquences en cm^{-1} des modes de réseau observés et calculés du *para*-dibromobenzène

Infrarouge (obs.) Solution CCl_4	Infrarouge (obs.) $E \perp b$ (300 K)	Infrarouge (obs.) $E \parallel b$ (300 K)	Attribution	Raman (obs.) (300 K) (réfs. 6, 7)	Calc. PED (%)		Calc. Réf. 26
			$R_W(b_g)$	20	36	$88R_W$	22.4
	27		$T'_b(b_u)$		37	$42T_b + 58T_{ac}$	36.3
		29	$T'_{ac}(a_u)$		39	$3T_b + 97T_{ac}$	31.4
			$R_W(a_g)$	37.5	23	$75R_U + 13R_V + 12R_W$	33.2
			$R_V(b_g)$	39	52.4	$17R_U + 18R_V + 65R_W$	46.1
			$R_V(a_g)$	40.5	57.1	$89R_W$	40.0
		47	$T'_{ac}(a_u)$		62	$100T_{ac}$	50.4
			$R_U(a_g)$	93	104	$15R_U + 85R_V$	93.9
			$R_U(b_g)$	96	101	$99R_W$	96.1
			Réf. 8				
94	102	100	103 $\nu_{30}(b_{3u})$				
			Internes				
171	174	170	171 $\nu_{27}(b_{2u})$				

TABLEAU 3. Fréquences en cm^{-1} des maximums d'absorption observés dans le *para*-chloroiodobenzène

Infrarouge (obs.) Solution CCl_4	Infrarouge (obs.) $E \perp b$ (80 K)	Infrarouge (obs.) $E \parallel b$ (80 K)	Attribution	Réf. 8
		28	$T'_{ac}(a_u)$	
	29		$T'_b(b_u)$	
		47	$T'_{ac}(a_u)$	
	58			
98	107	105		103 $\nu_{20}b_1$
170	177	177	Internes	173 $\nu_{30}b_2$
	220	220		220 $\nu_{11}a_1$

TABLEAU 4. Fréquences en cm^{-1} des maximums d'absorption observés dans le *para*-bromoiodobenzène

Infrarouge (obs.) Solution CCl_4	Infrarouge (obs.) $E \perp b$ (80 K)	Infrarouge (obs.) $E \parallel b$ (80 K)	Attribution	Réf. 8
		27	$T'_{ac}(a_u)$	
	28		$T'_b(b_u)$	
		47	$T'_{ac}(a_u)$	
	84	84		97 $\nu_{20}b_1$
90	99	99		
160	159	159	Internes	155 $\nu_{30}b_2$
	182	182		180 $\nu_{11}a_1$
	220			

TABLEAU 5. Fréquences en cm^{-1} des maximums d'absorption observés dans l'*ortho*-diiodobenzène (R = rotations; T = translations)

Infrarouge (obs.) Solution CCl_4	Infrarouge (obs.) Solide polycristallin (80 K)	Attribution	Réf. 8
	30	R	
	32	R	
	36		
50	42	T	
	48	T	
	52	T	
	62		
	78	R	
97	102		98 $\nu_{11}A_1$
125	127	Internes	124 $\nu_{16}A_2$
143	144		200 $\nu_{20}B_1$
200	210		206 $\nu_{30}B_2$

mouvements élémentaires (translations–rotations) dans les modes de vibration. Le désaccord le plus important concerne la fréquence observée à 57.5 cm^{-1} (a_g) que l'on fait correspondre à la fréquence 12 cm^{-1} (tableau 1). Signalons d'autre part que l'on attribue la fréquence 57.5 cm^{-1} à deux vibrations de même type a_g. En effet au cours d'une étude en lumière polarisée, Rousset (11) a montré que deux modes a_g étaient superposés vers 57 cm^{-1}. Pour les autres attributions, l'accord est relativement bon, surtout si l'on remarque que nous avons négligé l'action des moments dipolaires électriques locaux dus aux halogènes comme l'avaient fait Ozora et coll. (20).

Dans les tableaux 1 et 2 nous avons indiqué les fréquences calculées par Reynolds et coll. (24), par Bonadeo et coll. (25) ainsi que celles de Burgos et Bonadeo (26).

V. Conclusion

Nous avons mis en évidence les modes de réseau de basse fréquence par l'étude de l'absorption dans l'infrarouge lointain d'une série de dérivés *p*-dihalogénés du benzène. Le calcul des fréquences des

TABLEAU 6. Fréquences en cm^{-1} des maximums d'absorption infrarouge et des raies de diffusion Raman observés dans le *meta*-diiodobenzène

Infrarouge (obs.)					Raman (obs.)			
					Lumière naturelle		Réf. 10	Réf. 10
Solution CCl_4	$E \parallel a$ (80 K)	$E \parallel b$ (80 K)	$E \parallel c$ (80 K)	Attribution	300 K	100 K	(300 K)	(300 K)
	26			R_U, R_W	25	28	24	24
		44		R_V, T	40	44	38	
			45.5	R_V, T			46	
	70			R_U, R_W	55 67		67	
		83.5		R_V, T	80	86	79	79
				R_U	102	103	101	101
				Réf. 8				
98	103	101	101	98 $\nu_{20}B_1$	112	121	110	
	124		121	109 $\nu_{11}A_1$	116		116	
142	160		178	164 $\nu_{30}B_2$				
183	190			186 $\nu_{14}A_2$				
		204		201 $\nu_{10}A_1$				
226	212							
	250	240	250	238 $\nu_{29}B_2$				

TABLEAU 7. Fréquences en cm^{-1} des modes de réseau observés et calculés du *para*-diiodobenzène (T_a, T_b, T_c translation des molécules suivant les axes *a*, *b* et *c* de la maille orthorhombique R_U, R_V, R_W libration des molécules autour de ses axes d'inertie *OU*, *OV*, *OW*)

Infrarouge (obs.)					Raman (obs.)		Calc.	
Solution CCl_4	$E \parallel a$ (300 K)	$E \parallel b$ (300 K)	$E \parallel c$ (300 K)	Attribution	Réf. 11 (300 K)	Réf. 12 (2 K)		PED (%)
				b_{3g}	11	21.4	27.5	$98R_W$
				a_u			13.5	$31T_a + 53T_b + 15T_c$
				b_{1g}	15	29.8	27.5	$98R_W$
	15.5			b_{3u}			14.9	$27T_a + 11T_b + 62T_c$
	21			b_{3u}				
				a_g	24	31.4	27.5	$98R_W$
				b_{2g}	27	31.4	27.5	$98R_W$
	27.5			b_{3u}				
				a_u			28.7	$72T_a + 7T_b + 21T_c$
		28		b_{2u}			37	$27T_a + 73T_b$
			35	b_{1u}			37.8	$27T_a + 11T_b + 62T_c$
				b_{1g}		35.7	33.4	$100R_W$
				b_{3g}	37	38	33.4	$100R_W$
	38			b_{3u}			47.7	$90T_a + 4T_b + 6T_c$
		38.5		b_{2u}			51.1	$2T_a + 87T_b + 11T_c$
				a_g		43.6	33.4	$100R_W$
				b_{2g}		46.9	33.4	$100R_W$
			45.5	b_{1u}			53.9	$2T_a + 87T_b + 11T_c$
				a_u			45.8	$27T_a + 12T_b + 61T_c$
	48			b_{3u}	49			
				Réf. 8	90			
	111		111	105 $\nu_{30}b_{3u}$	115			
				a_g		135.3	90.6	$100R_V$
				b_{3g}		141.1	90.6	$100R_V$
144	146	148	143	144 $\nu_{27}b_{2u}$				
				b_{1g}		142.9	90.6	$100R_V$
200 225	225		225	b_{2g}		158.2	90.6	$100R_V$

modes de vibration de réseau effectué dans le cas du PDC, PDB et PDI permet de préciser la nature des modes observés par absorption infrarouge et par diffusion Raman. L'accord entre la valeur des fréquences calculées et observées est acceptable dans la mesure où nous nous sommes limités à un nombre réduit d'interactions entre atomes.

Mis à part le PDC dont les transitions de phase sont connues nous n'avons pas mis en évidence de transition de phase entre 300 et 80 K, dans la série de composés étudiés, contrairement à ce que nous avons observé lors du refroidissement des structures solides des dérivés dihalogénés du benzène liquide à température ambiante (1).

1. B. WYNCKE, F. BREHAT, A. HADNI, J. SERRIER et M. BAVEREZ. Can. J. Chem. **56**, 1638 (1978).
2. B. WYNCKE, A. HADNI et X. GERBAUX. J. Phys. **31**, 893 (1970).
3. P. N. PRASAD et E. D. STEVENS. J. Chem. Phys. **66**, 862 (1977).
4. S. B. HENDRICKS, L. R. MAXWELL, V. L. MOSLEY et M. E. JEFFERSON. J. Chem. Phys. **1**, 549 (1933).
5. A. K. RAY. Indian J. Phys. **25**, 459 (1951).
6. B. PASQUIER, D. BOUGEARD, N. LE CALVE et R. ROMAIN. Mol. Cryst. Liq. Cryst. **32**, 17 (1976).
7. N. LE CALVE, S. PARENT et B. PASQUIER. J. Raman Spectrosc. **2**, 431 (1974).
8. J. H. S. GREEN. Spectrochim. Acta, **26**A, 1503 (1970); **26**A, 1523 (1970); **26**A, 1913 (1970).
9. A. ROUSSET et R. LOCHET. J. Phys. Rad. **3**, 146 (1942).
10. D. A. DOWS. J. Chem. Phys. **32**, 1342 (1960); **35**, 282 (1961); **36**, 2836 (1962).
11. A. ROUSSET. Conferences Rapports. Vol. 3. Editions CNRS. 1947.
12. S. P. CRAMER, B. HUDSON et D. M. BURLAND. J. Chem. Phys. **64**, 1140 (1976).
13. B. P. CLAYMAN, B. FARNWORTH et R. W. WARD. J. Chem. Phys. **68**, 4930 (1978).
14. T. SHIMANOUCHI, M. TSUBOI et T. MIYAZAWA. J. Chem. Phys. **35**, 1597 (1961).
15. G. L. WHEELER et S. D. COLSON. J. Chem. Phys. **65**, 1227 (1976).
16. R. W. G. WYCKOFF. Crystal structure. Vol. VI. Interscience Publishers, NY. 1969.
17. P. G. DASHEVSKY, U. T. STERNCHUKOF et S. A. AKAPPAYAN. J. Struct. Chem. USSR, **7**, 594 (1966).
18. D. E. WILLIAMS. Acta Crystallogr. A**30**, 71 (1974).
19. A. I. KITAIGORODSKII, K. V. MIRSKAYA et A. B. TOVBIS. Sov. Phys. Crystallogr. **13**, 176 (1968).
20. A. OZORA, T. NAKAGAWA et M. ITO. Bull. Chem. Soc. Jpn. **45**, 95 (1972).
21. T. L. HILL. J. Chem. Phys. **16**, 399 (1948).
22. S. D. ROSS. Inorganic infrared and Raman spectra. McGraw-Hill, NY. 1972.
23. J. SERRIER. Thèse de 3ème cycle, Nancy. 1978.
24. P. A. REYNOLDS, J. K. KJEMS et J. W. WHITE. J. Chem. Phys. **60**, 824 (1974).
25. H. BONADEO, E. D'ALESSIO, E. HALAC et E. BURGOS. J. Chem. Phys. **68**, 4714 (1978).
26. E. BURGOS et H. BONADEO. Chem. Phys. Lett. **49**, 475 (1977).

Crystal and molecular structure of bis[methyltris(1-pyrazolyl)gallato]nickel(II)

STEVEN J. RETTIG, ALAN STORR, AND JAMES TROTTER

Department of Chemistry, University of British Columbia, 2075 Wesbrook Mall, Vancouver, B.C., Canada V6T 1W5

Received February 2, 1979

STEVEN J. RETTIG, ALAN STORR, and JAMES TROTTER. Can. J. Chem. **57**, 1823 (1979).

Crystals of bis[methyltris(1-pyrazolyl)gallato]nickel(II) are rhombohedral, $a = 9.6670(5)$, $c = 23.893(1)$ Å, $Z = 3$, space group $R\bar{3}$. The structure was solved by direct methods and was refined by full-matrix least-squares procedures to a final R of 0.030 and $R_w = 0.035$ for 925 reflections with $I \geq 3\sigma(I)$. The crystal structure consists of well separated molecules of $[MeGa(N_2C_3H_3)_3]_2Ni$ having exact $\bar{3}$ (S_6) symmetry and approximate D_{3d} symmetry. The coordination geometry about the nickel atom is octahedral with Ni—N = 2.109(2) Å, N—Ni—N = 90.65(6) and 89.35(6)°. The gallium atom has distorted tetrahedral coordination geometry with Ga—N = 1.939(2), Ga—C = 1.940(4) Å, N—Ga—N = 99.55(6), and N—Ga—C = 118.16(5)°.

STEVEN J. RETTIG, ALAN STORR et JAMES TROTTER. Can. J. Chem. **57**, 1823 (1979).

Les cristaux du bis[méthyltris(pyrazolyl-1) gallato] nickel(II) sont rhomboédriques, $a = 9.6670(5)$, $c = 23.893(1)$ Å, $Z = 3$, groupe d'espace $R\bar{3}$. On a résolu la structure par des méthodes directes et on l'a affinée par la méthode des moindres carrés (matrice complète) jusqu'à une valeur finale de $R = 0.030$ et $R_w = 0.035$ pour 925 réflexions avec $I \geq 3\sigma(I)$. La structure cristalline est composée de molécules séparées de $[MeGa(N_2C_3H_3)_3]_2Ni$ de symétrie exacte $\bar{3}$ (S_6) et de symétrie approximative D_{3d}. La géométrie de coordination autour du nickel est octaédrique avec Ni—N = 2.109(2) Å, N—Ni—N = 90.65(6) et 89.35(6)°. La géométrie de coordination autour de l'atome de gallium est tétraédrique (déformée) avec Ga—N = 1.939(2), Ga—C = 1.940(4) Å, N—Ga—N = 99.55(6) et N—Ga—C = 118.16(5)°.

[Traduit par le journal]

Introduction

A series of complexes incorporating the anionic tridentate chelating ligand $[MeGa(N_2C_3H_3)_3]^-$ has been reported (1). An X-ray structural study on a molybdenum complex containing one of these ligands confirmed the denticity and chelating nature of the pyrazolyl gallate moiety (1). In that initial report a number of L_2M (where L = $MeGa(N_2C_3H_3)_3$, M = Mn → Zn) complexes were also characterized and the evidence collected at the time suggested an octahedral MN_6 core with incorporation of both the ligands as tridentate chelating moieties. The present account details the X-ray structure determination of one of these complexes, namely, $[MeGa(N_2C_3H_3)_3]_2Ni$.

Experimental

The title compound was prepared as previously described (1). The lilac crystals were indefinitely stable in air. A spherical crystal with a radius of 0.17 mm was mounted in a general orientation. Unit-cell parameters were refined by least squares on 2 sin θ/λ values for 30 reflections measured on a diffractometer with Mo K_α radiation (λ = 0.71073 Å). Crystal data (at 22°C) are:

$C_{20}H_{24}Ga_2N_{12}Ni$ fw = 630.64

Rhombohedral, $a = 9.6670(5)$, $c = 23.893(1)$ Å, $V = 1933.7(2)$ Å^3, $Z = 3$, $\rho_c = 1.625$ g cm^{-3}, $F(000) = 954$, μ(Mo K_α) = 29.4 cm^{-1}. Absent reflections: hkl, $-h + k + l \neq 3n$. Space group $R\bar{3}$ (C_{3i}^2, No. 148) from structure analysis.

Intensities were measured with graphite monochromatized Mo K_α radiation on an Enraf-Nonius CAD4-F diffractometer. An ω–θ scan at 0.72–6.71° min^{-1} over a range of (0.45 + 0.35 tan θ) degrees in ω (extended by 25% on both sides for background measurement) was employed. Data were measured to $2\theta = 60°$. The intensities of three check reflections, measured every 3600 s throughout the data collection, remained constant to within 2%. After data reduction, an absorption correction was applied (spherical crystal, $\mu R = 0.5$). Of the 1250 independent reflections measured, 925 (74%) had intensities greater than $3\sigma(I)$ above background where $\sigma^2(I) = S + 2B + (0.04(S - B))^2$ with S = scan count and B = background count.

Laue symmetry $\bar{3}$ limits the possible space groups to $R3$ and $R\bar{3}$, the latter being assumed on the basis of the E-statistics. The structure was solved by direct methods, an E-map calculated from the best set of phases giving positions for all of the non-hydrogen atoms. After full-matrix least-squares refinement of the non-hydrogen atoms with anisotropic thermal parameters to $R = 0.064$, a difference map gave the positions of the four unique hydrogen atoms which were included in all subsequent cycles of refinement with isotropic thermal parameters. The scattering factors of ref. 2 were used for non-hydrogen atoms and those of ref. 3 for hydrogen atoms. Anomalous scattering factors from ref. 4 were used for the Ga and Ni atoms. The weighting scheme, $w = 1/\sigma^2(F)$ where $\sigma^2(F)$ is derived from the previously defined $\sigma^2(I)$, gave uniform average values of $w(|F_o| - |F_c|)^2$ over ranges of $|F_o|$ and was employed in the final stages of refinement. Convergence was reached at $R = 0.030$ and $R_w = 0.035$ for 925 reflections with $I \geq 3\sigma(I)$. For all 1250 reflections $R = 0.050$ and $R_w = 0.038$.

On the final cycle of refinement the mean and maximum parameter shifts corresponded to 0.009 and 0.15σ, respectively. The mean error in an observation of unit weight was 1.0158. A final difference map showed maximum fluctuations of ±0.4 e Å^{-3} in the vicinity of the Ga and Ni atoms and

0008-4042/79/141823-03$01.00/0

TABLE 1. Final positional parameters (fractional × 10^5, H × 10^3) with estimated standard deviations in parentheses

Atom	x	y	z
Ga	0	0	14538(1)
Ni	0	0	0
N(1)	15099(19)	19795(19)	5038(7)
N(2)	15772(18)	19112(18)	10709(7)
C(1)	26055(26)	34520(24)	3523(10)
C(2)	33959(26)	43591(26)	8197(10)
C(3)	27162(25)	33506(26)	12600(10)
C(4)	0	0	22659(17)
H(1)	276(3)	376(3)	−2(1)
H(2)	418(3)	546(3)	84(1)
H(3)	284(3)	349(3)	159(1)
H(4)	84(3)	72(3)	238(1)

± 0.2 e Å^{-3} elsewhere. The final positional and thermal parameters appear in Tables 1 and 2 respectively.[1] Measured and calculated structure factors have been placed in the Depository of Unpublished Data.[1] Bond lengths and angles are listed in Tables 3 and 4 respectively and intra-annular torsion angles are given in Table 5.

Results and Discussion

The crystal structure consists of discrete molecules of $[MeGa(N_2C_3H_3)_3]_2Ni$ separated by normal van der Waals distances. The molecule (Fig. 1) possesses crystallographic $\bar{3}$ (S_6) symmetry and approximate D_{3d} symmetry, the distortion from D_{3d} symmetry being a twist of the pyrazolyl rings with respect to the threefold axis (the angle between the c axis and the pyrazolyl mean plane, ideally 0°, is 4.8°). The nickel atom is bonded to six nitrogen atoms, three from each of the tridentate $MeGa(N_2C_3H_3)_3^-$ ligands. The coordination geometry about the nickel atom shows only a very small trigonal distortion from ideal octahedral geometry. The unique Ni—N distance is 2.109(2) Å and the intra- and interligand N—Ni—N angles are slightly, but significantly, different (90.65(6) and 89.35(6)° respectively). The gallium atom has trigonally distorted tetrahedral coordination geometry with Ga—N = 1.939(2), Ga—C = 1.940(4) Å, N—Ga—N = 99.55(6) and N—Ga—C = 118.16(5)°.

The related molecule $[HB(N_2C_3H_3)_3]_2Co$ (5) also has approximate D_{3d} symmetry, but has no crystallographically imposed symmetry. The trigonal distortion of the Co coordination sphere is more pronounced than in the present compound, with mean intra- and interligand N—Co—N angles of 85.5(6) and 94.5(21)° respectively. Although the M—N distances are similar in these two complexes (mean Co—N = 2.129(7) Å), the potential for steric crowding about the central metal is greater in the gallium complex (Ni...C(1) = 3.128(2) Å while the corresponding mean distance is 3.207 Å in $[HB(N_2C_3H_3)_3]_2Co$). This result is to be expected on the basis of previous spectroscopic (6) and structural (1) studies. The variation in the M...C(1) distances observed arises primarily from the different sizes of Ga and B atoms. The pyrazolyl N—N bonds are canted towards the boron atom in $[HB(N_2C_3H_3)_3]_2Co$ whereas they are nearly parallel to the threefold axis in $[MeGa(N_2C_3H_3)_3]_2Ni$, resulting in the closer approach of C(1) to the metal atom for the gallate ligand. In this regard it is possible to prepare 3,5-dimethyl substituted $[HB(N_2C_5H_7)_3]_2M$ compounds (7) whereas attempts to prepare $[MeGa(N_2C_5H_7)_3]_2M$ have so far failed.

TABLE 3. Bond lengths (Å) with estimated standard deviations in parentheses*

Bond	Distance	Bond	Distance
Ga —N(2)	1.939(2)	C(1) —C(2)	1.389(3)
Ga —C(4)	1.940(4)	C(2) —C(3)	1.359(3)
Ni —N(1)	2.109(2)	C(1) —H(1)	0.93(3)
N(1) —N(2)	1.360(2)	C(2) —H(2)	0.95(3)
N(1) —C(1)	1.331(3)	C(3) —H(3)	0.81(3)
N(2) —C(3)	1.349(3)	C(4) —H(4)	0.81(2)

*Here and in Tables 4 and 5 primed atoms have coordinates $-y, x-y, z$ and double primed atoms $y, y-x, -z$.

The Ni—N distance (2.109(2) Å) is similar to the Ni—N(pyrazolyl) distances of 2.085(3) and 2.097(6) Å observed for the *sym-fac-* and *mer* isomers of $[Me_2Ga(OCH_2CH_2NH_2)(N_2C_3H_3)]_2Ni$ (8) but is much longer than the mean Ni—N distance of 1.895(4) Å in the square planar complex $[Me_2Ga(N_2C_3H_3)_2]_2Ni$ (9). This has also been observed for the complexes $[HB(N_2C_3H_3)_3]_2Co$ (5), Co—N = 2.129(7) Å, and tetrahedral $[H_2B(N_2C_3H_3)_2]_2Co$ (10), Co—N = 1.967(12) Å. As pointed out in ref. 10, these differences in M—N bond lengths are probably due to changes in coordination number and steric requirements of the different ligands. The Ga—N distance in the tridentate gallate ligand (1.939(2) Å) is much shorter than the mean Ga—N distance of 1.977(1) Å in $[Me_2Ga(N_2C_3H_3)_2]_2Ni$ (9).

The relative strengths of the Ga—N and Ni—N bonds affect the internal geometry of the pyrazolyl ligand, resulting in significant differences between the pairs of C—C and C—N bonds (see Table 3). The pyrazolyl ring is planar to within ± 0.0007 Å (χ^2 = 0.26) with both Ni and Ga significantly displaced from the mean plane (by 0.0998(6) and −0.1800(5) Å respectively). The geometry of the ligand is very similar to that found for $[MeGa(N_2C_3H_3)_3]Mo$-

[1]The structure factor table and Table 2 (thermal parameters) are available, at a nominal charge, from the Depository of Unpublished Data, CISTI, National Research Council of Canada, Ottawa, Ont., Canada K1A 0S2.

TABLE 4. Bond angles (deg) with estimated standard deviations in parentheses

(*a*) Non-hydrogen atoms

Bonds	Angle (deg)	Bonds	Angle (deg)
N(2)—Ga —N(2′)	99.55(6)	Ga —N(2)—N(1)	118.9(1)
N(2)—Ga —C(4)	118.16(5)	Ga —N(2)—C(3)	132.2(1)
N(1)—Ni —N(1′)	90.65(6)	N(1)—N(2)—C(3)	108.5(2)
N(1)—Ni —N(1″)	89.35(6)	N(1)—C(1)—C(2)	110.4(2)
Ni —N(1)—N(2)	123.6(1)	C(1)—C(2)—C(3)	104.7(2)
Ni —N(1)—C(1)	129.4(1)	N(2)—C(3)—C(2)	109.5(2)
N(2)—N(1)—C(1)	106.9(2)		

(*b*) Angles involving hydrogen atoms

Bonds	Angle (deg)	Bonds	Angle (deg)
N(1)—C(1)—H(1)	121(2)	N(2)—C(3)—H(3)	119(2)
C(2)—C(1)—H(1)	128(2)	C(2)—C(3)—H(3)	132(2)
C(1)—C(2)—H(2)	128(2)	Ga —C(4)—H(4)	111(2)
C(3)—C(2)—H(2)	127(2)	H(4)—C(4)—H(4′)	108(2)

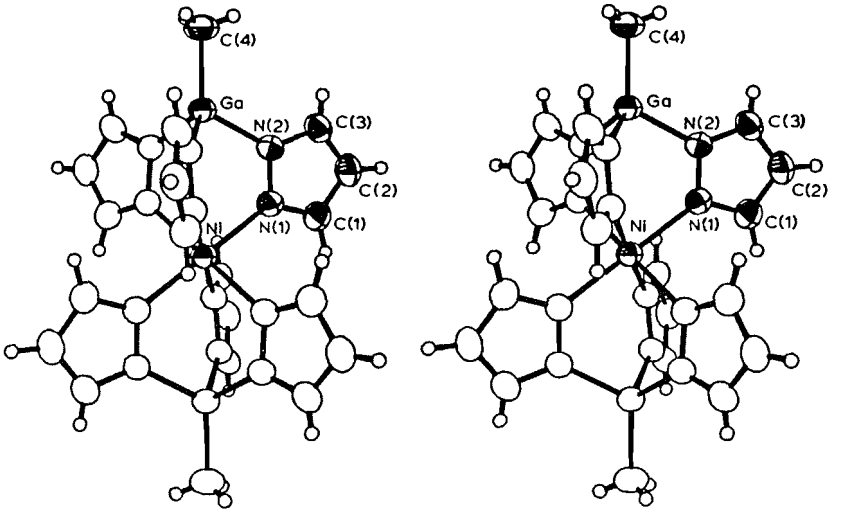

FIG. 1. Stereo view of the bis[methyltris(1-pyrazolyl)gallato]nickel(II) molecule, 50% ellipsoids are shown for the non-hydrogen atoms.

TABLE 5. Intra-annular torsion angles (deg) chelate ring

Ga—N(2)—N(1)—Ni—N(1′)—N(2′)

Bond	Obs.	Bond	Obs.
Ga —N(2)	−45.3(1)	Ni —N(1′)	−39.7(1)
N(2)—N(1)	−9.4(1)	N(1′)—N(2′)	−9.4(1)
N(1)—Ni	50.9(1)	N(2′)—Ga	56.1(1)

$(CO)_2(\eta^3\text{-}C_3H_5)$ (1). The Ga—(N—N)$_2$—Ni chelate rings have slightly twisted boat conformations (see Table 5).

Acknowledgments

We thank the National Research Council of Canada for financial support and the University of British Columbia Computing Centre for assistance.

1. K. R. BREAKELL, S. J. RETTIG, D. L. SINGBEIL, A. STORR, and J. TROTTER. Can. J. Chem. **56**, 2099 (1978).
2. D. T. CROMER and J. B. MANN. Acta Crystallogr. Sect. A, **24**, 321 (1968).
3. R. F. STEWART, E. R. DAVIDSON, and W. T. SIMPSON. J. Chem. Phys. **42**, 3175 (1965).
4. D. T. CROMER and D. LIBERMAN. J. Chem. Phys. **53**, 1891 (1970).
5. M. R. CHURCHILL, K. GOLD, and C. E. MAW, JR. Inorg. Chem. **9**, 1597 (1970).
6. F. G. HERRING, D. J. PATMORE, and A. STORR. J. Chem. Soc. Dalton Trans. 711 (1975).
7. S. TROFIMENKO. J. Am. Chem. Soc. **89**, 6288 (1967).
8. K. S. CHONG, S. J. RETTIG, A. STORR, and J. TROTTER. Can. J. Chem. **56**, 1212 (1978).
9. D. F. RENDLE, A. STORR, and J. TROTTER. J. Chem. Soc. Dalton Trans. 176 (1975).
10. L. J. GUGGENBERGER, C. T. PREWITT, P. MEAKIN, S. TROFIMENKO, and J. P. JESSON. Inorg. Chem. **12**, 508 (1973).

Use of XαSW calculations for parametrising the CNDO method for the heavier elements. II. Tests for the elements aluminium to sulphur

J. D. HEAD AND K. A. R. MITCHELL

Department of Chemistry, University of British Columbia, Vancouver, B.C., Canada V6T 1W5

Received December 12, 1978

J. D. HEAD and K. A. R. MITCHELL. Can. J. Chem. 57, 1826 (1979).

In Part I (Mol. Phys. **35**, 1681 (1978)) we used results from the Xα scattered wave (XαSW) method for guiding the parametrisation of the complete neglect of differential overlap (CNDO) method for clusters of silver, and we proposed the extension of this approach to other heavier elements for which CNDO schemes are not well developed. The main purpose of the present paper is to test this approach for the elements aluminium to sulphur for which more information is available. XαSW calculations have been made for the molecular clusters Al_7, Si_5H_{12}, and P_4, and comparisons made with experiment and with other calculations where possible. The charge distributions and transition-state energies, along with information obtained previously for S_8 by Salahub *et al.*, have been used to derive new parameters (designated CNDO/HM) for the elements aluminium to sulphur essentially following the procedure in Part I. Calculations using these parameters have then been tested against an XαSW calculation made here for an Al_{10} cluster (which simulates the (111) surface of aluminium), and against other calculations made previously for P_8, P_4S_3, SiH_4, PH_3, H_2S, and SO_2. Comparisons are also made with results from the CNDO/2 scheme. Generally the CNDO/HM procedure seems at least as successful as CNDO/2.

J. D. HEAD et K. A. R. MITCHELL. Can. J. Chem. **57**, 1826 (1979).

Dans le travail précédent 1 ère partie (Mol. Phys. **35**, 1681 (1978)) on a utilisé les résultats obtenus par la méthode des ondes diffractées Xα (ODXα) comme guide pour la paramétrisation de la méthode CNDO pour les agrégats d'argent et on a proposé une extension de cette approche à des éléments plus lourds pour lesquels aucun schéma CNDO n'a été développé. Le but du présent travail est de vérifier cette approche pour les éléments de l'aluminium au soufre pour lesquels plus d'informations sont disponibles. On a fait des calculs ODXα pour les agrégats Al_7, Si_5H_{12} et P_4 et l'on a effectué des comparaisons avec les données expérimentales et, si possible, avec d'autres calculs. On a utilisé les distributions de charge et les énergies des états de transition de même que les informations obtenues antérieurement pour le S_8 par Salahub et ses collaborateurs afin de dériver de nouveaux paramètres (désignés comme CNDO/HM) pour les éléments de l'aluminium au soufre en suivant essentiellement la méthode décrite dans le travail antérieur. On a évalué les calculs effectués à l'aide de ces paramètres par rapport aux calculs ODXα faits ici pour un agrégat de Al_{10} (qui simule la surface (111) de l'aluminium) et par rapport à d'autres calculs faits antérieurement pour P_8, P_4S_3, SiH_4, PH_3, H_2S et SO_2. On a aussi fait des comparaisons avec des résultats obtenus par le schéma CNDO/2. D'une façon générale, les calculs CNDO/HM semblent au moins aussi bons que les calculs CNDO/2.

[Traduit par le journal]

1. Introduction

Although the complete neglect of differential overlap (CNDO) method has been used for a number of years for making routine, and reasonably reliable, calculations of wave functions for molecules formed by the lighter elements (1), this method has so far been less successful in general for the heavier elements, particularly for metals. Nevertheless, for the latter, there are continuing needs for computational methods that can give helpful assessments of molecular orbital levels, charge distributions, and energetics for large molecular systems and for clusters, such as those involved in catalytic and nucleation processes and those which model aspects of solids and solid surfaces (2). Satisfactory developments of the CNDO method for the heavier elements have been hindered by a scarcity of accurate non-empirical calculations for comparison; moreover those that are available are frequently restricted to diatomic species. An earlier study (3), which deduced improved CNDO parameters for Li and F for the purpose of investigating ionic LiF systems, used a near-Hartree–Fock wave function of diatomic LiF for comparison, but in general larger reference molecules appear advantageous for guiding the parametrisations. This is because polyatomic molecules both give more data for comparing with the CNDO calculations and they are more likely to contain atoms which manifest typical local stereochemical arrangements. On the other hand, the larger the reference molecule the less likely there will be calculations of near-Hartree–Fock quality with which to compare the CNDO results.

0008-4042/79/141826-13$01.00/0

Such considerations encouraged us earlier to use the Xα scattered wave (XαSW) method (4) for deducing CNDO parameters appropriate to silver (5). The XαSW method appears to offer a helpful compromise between successful calculations and computational tractability (6).

A potential advantage of the approach of deriving CNDO parameters from comparisons with results from the XαSW method is that it can be extended systematically and consistently to a wide range of elements including the transition elements. Part I of this series describes the determination of new CNDO parameters for some clusters of silver (5). However, before extending to other transition metal systems, it seemed prudent to assess the reliability of this approach by comparing for some elements for which CNDO schemes are better developed. The main purpose of the present paper therefore is to assess the use of XαSW calculations for deducing CNDO parameters for the elements aluminium to sulphur; a number of these second-row elements have already been investigated by CNDO schemes to a fair degree (7–10). This experience should be valuable in extending the basic approach used in Part I to other elements where CNDO procedures are at best poorly developed. An area of immediate importance is for clusters of transition metal atoms where, for investigating properties such as reaction profiles or for comparing different adsorption sites, the computational expense of the XαSW method can be appreciable, especially for systems of low symmetry. For such cases there would be great advantages in having faster and cheaper procedures which are useful for exploratory purposes, and in this category we include the CNDO method.

The four elements considered here range from a free-electron metal, through a semi-conductor to molecular solids in the cases of phosphorus and sulphur, and these differences in basic characteristics influence the particular molecular clusters considered for the purpose of parametrising the CNDO method. For phosphorus and sulphur, the molecular forms P_4 and S_8 seem natural choices. Silicon is represented by the molecule Si_5H_{12} since the local environment around the central silicon atom corresponds to that in the silicon lattice; also the presence of the hydrogen atoms limits effects associated with broken covalent bonds. For aluminium, we consider the clusters Al_7 and Al_{10} which have been chosen to provide relatively simple simulations of the (111) surface. For the parametrisations, it seems preferable that all the XαSW calculations are at corresponding levels of refinement. A problem here is that many XαSW calculations in the literature have been made only in the non-overlapping-spheres scheme, as in the earliest formulation of the method, although, at the present time, the XαSW approach has probably been most successful with the overlapping-spheres version (11). For this reason we have made new XαSW calculations for the Al_7 and Al_{10} clusters, and we have repeated and refined some earlier calculations made for Si_5H_{12} and P_4; for S_8 we have used results produced by Salahub *et al.* (12).

2. Calculational Methods

The XαSW calculations reported here for Al_7, Al_{10}, Si_5H_{12}, and P_4 involved standard procedures for solving the scattered wave equations (13) and for calculating transition-state energies (14). All these calculations used exchange-correlation parameters given by Schwartz (15) (except $\alpha = 0.77725$ for hydrogen (6)), and basis sets through to $l = 1$ for each atomic sphere of the second-row atom ($l = 0$ only for hydrogen) and to $l = 3$ for the outersphere. Generally the atomic spheres have been allowed to overlap as extensively as possible without introducing unrealistic features such as negative intersphere charges in some molecular orbitals. The actual degree of sphere overlap is specified below for each particular system, as well as the corresponding virial ratio since close satisfaction of the virial theorem has often been used for guiding the choice of absolute values of sphere overlap (11).

In the first instance, the CNDO calculations made here for the elements aluminium to sulphur use only *s* and *p* functions in the basis sets, although the extension to include *d* functions is considered later (section 6). We followed the basic scheme detailed by Santry and Segal (7) for this basis set, but for one minor difference. This concerns the expression for the resonance parameter

$$[1] \qquad \beta_{AB} = \tfrac{1}{2}K(\beta_A + \beta_B)$$

where the constant K is now kept equal to unity, whereas previously it had been taken as 0.75 if either A or B is an atom of the second row. Our initial choice of CNDO parameters is restricted to four for each element: (*i*) the exponents $\xi_s = \xi_p$ in the Slater-type orbitals which are used for evaluating the overlap and Coulomb integrals; (*ii*) the average of the ionisation energy and electron affinity for each member of the basis set, i.e. $\frac{1}{2}(I_s + A_s)$ and $\frac{1}{2}(I_p + A_p)$ which are used in the diagonal elements of the Fock matrix; and (*iii*) the bonding parameters $\beta_s = \beta_p$ which correspond to the terms on the right-hand-side of eq. [1] and which are used in the off-diagonal elements of the Fock matrix.

3. Selection of CNDO Parameters

Earlier we obtained new CNDO parameters for silver by comparing one-electron energies and charge distributions from CNDO calculations on silver clusters with the corresponding quantities calculated with the XαSW method (5). The one-electron energies were compared visually through total density of states (DOS) curves, and the charge distributions were compared by inspection of atomic populations and local DOS curves. In principle these comparisons would be easier to make, and perhaps less subjective, with the provision of a numerical index which measures the correspondence of one-electron energy levels and charge distributions from the two types of calculation. Previously we found new CNDO parameters for diatomic LiF (3) by minimizing a function of the type

$$[2] \quad R = \sum_i (\varepsilon_i^{\text{CNDO}} - \varepsilon_i^{\text{ref}})^2 + \sum_i (\mu_i^{\text{CNDO}} - \mu_i^{\text{ref}})^2$$

where the ε_i and μ_i represent one-electron energies and dipole moments from either the CNDO or reference calculations for the ith molecular orbital. Such a function seemed satisfactory for LiF, where the two types of properties compared make similar contributions to the value of R, but further experience has indicated that considerable care is needed for larger molecules since, with this type of function, either the charge distributions or the energies can be preferentially emphasized in the comparison.

In the present work, the one-electron charge distributions and the one-electron energy levels from the two sets of calculations are compared separately, and attempts have been made to assess those CNDO parameters which offer the best overall agreement. A simple function for the charge distributions is

$$[3] \quad R_q = \sum_i \eta_i \sum_j \omega_j (q_{ij}^{\text{CNDO}} - q_{ij}^{\text{X}\alpha\text{SW}})^2$$

where q_{ij}^{CNDO} and $q_{ij}^{\text{X}\alpha\text{SW}}$ represent populations (either total or alternatively the individual partial-wave populations) on the jth atom for the ith molecular orbital from the CNDO and XαSW calculations respectively. The populations from the CNDO calculations are derived using the analysis of Mulliken (16), and those from the XαSW calculations are obtained by allocating the intersphere and outersphere charges in the ratios of the component atomic sphere charges for each molecular orbital. In eq. [3], the η_i and ω_j are appropriate weight factors; in this study η_i has been taken as the occupation number of the ith molecular orbital, but, as discussed further below, the ω_j have been treated in various ways depending on the particular molecular system. That the two sets of populations are defined differently represents an unsatisfactory feature of this part of the comparison of XαSW and CNDO calculations; nevertheless some support for the use of [3] is provided by observations for P_4S_3 (17) where the CNDO/2 and XαSW calculations gave similar trends in charge distributions for corresponding molecular orbitals even though the ordering of the energy levels differed in some cases. The simplest index for comparing the distribution of energy levels is

$$[4] \quad R_\varepsilon = \sum_i \eta_i (\varepsilon_i^{\text{CNDO}} - \varepsilon_i^{\text{X}\alpha\text{SW}})^2$$

with an analogous notation to those used above. Our previous experience with the silver clusters (5) indicated that variations in some CNDO parameters (e.g. the values of $(I + A)/2$) cause primarily a shift in energy levels, whereas changes in other parameters (e.g. the values of β) cause mainly a change in scale. Such observations were confirmed in the present work, and as a result we found it convenient in practice to use a modified form of the function in eq. [4], namely

$$[5] \quad R_\varepsilon' = \sum_i \eta_i [R(\varepsilon_i^{\text{CNDO}} - S) - \varepsilon_i^{\text{X}\alpha\text{SW}}]^2$$

For a set of CNDO parameters that give a perfect match to the XαSW energy levels, it is clear that R_ε' is zero, the scale factor R is unity, and the energy shift S is zero. For matching the CNDO and XαSW energy levels our objective has been to find CNDO parameters that allowed the closest approach to these limiting values. Except for S_8, the values of $\varepsilon_i^{\text{X}\alpha\text{SW}}$ used in these analyses are transition state energies; then both $\varepsilon_i^{\text{CNDO}}$ and $\varepsilon_i^{\text{X}\alpha\text{SW}}$ represent approximations to ionisation energies.

The determination of new CNDO parameters for the elements aluminium to sulphur involved searching for minima of the correspondence functions, such as [3] and [5], by calculating these functions for many combinations of CNDO input parameters. The basic approach started with the parameters given for s and p basis functions by Santry and Segal (7). We considered first the effect of varying ξ over the range covered by the values given by Slater (18), Burns (19), and Clementi and Raimondi (20); this gave an improved value for the exponent. With this new value of ξ, β was then varied to minimize the correspondence functions, and the approach continued by varying ξ and β iteratively. Next $(I_s + A_s)/2$ was varied, and if the modification from the original CNDO value was substantial the values of ξ and β were reinvestigated. The value of $(I_p + A_p)/2$ was kept equal to the value used by Santry and Segal. By this means it was hoped that the parameters derived here for the second-row atoms should maintain a broad consistency with the

conventional parameters given for atoms of the first row in the CNDO/2 scheme (1). In cases where a range of CNDO parameters gave comparable overall levels of correspondence to the XαSW results, the final selection was completed by comparing calculated bond lengths with experimental values for some simple molecules. The values found from this procedure for the elements aluminium to sulphur are listed in Table 1; these parameters and the calculations made with them are designated in the following discussions by the label CNDO/HM. Further information for each reference molecular system is given in the next section, where comparisons are detailed between the XαSW, CNDO/2, and CNDO/HM calculations.

4. Particular Molecular Systems

4.1 Al_7 and Al_{10}

Results of the XαSW calculations for these two clusters are given here, although only those for Al_7 have actually been used for deriving the CNDO/HM parameters for aluminium in Table 1; results for Al_{10} are used for testing the CNDO/HM scheme in section 5. The clusters Al_7 and Al_{10} both have C_{3v} symmetry and they correspond to fragments of the bulk structure: Al_7 is composed of two layers of three atoms arranged around the C_3 symmetry axis and a lower atom on the C_3 axis as detailed previously for the corresponding cluster of silver (21). In Al_{10}, one plane involves seven atoms so that six are close packed around a central atom; the second plane has three atoms which occupy alternate three-fold sites below the first plane. The XαSW calculations were made with internuclear distances equal to the bulk value of 2.86 Å (22). For Al_7, the atomic spheres had radii 15% greater than those that just touch, and an outersphere of radius 4.51 Å was centred at the intersection of the C_3 axis with the plane containing the three atoms designated B in Table 3. For the XαSW calculation on Al_{10}, some negative intersphere charges required the sphere radii to be reduced to a 6% increase over the contact radius; the outersphere was centred on the central atom of the 7-atom layer and had a radius of 4.38 Å. The exchange parameter α was fixed at 0.72853 through all regions of both clusters.

TABLE 1. CNDO/HM parameters for aluminium, silicon, phosphorus, and sulphur

Parameter	Value			
	Al	Si	P	S
ξ	1.23	1.59	1.80	2.04
$\frac{1}{2}(I_s + A_s)$/eV	7.77	10.03	13.24	19.07
$\frac{1}{2}(I_p + A_p)$/eV	3.00	4.13	5.46	6.99
β/eV	−5.00	−5.25	−11.30	−13.61

TABLE 2. Valence-shell energies* (in eV) calculated for Al_7 and Al_{10}

Al_7			Al_{10}	
Level†	$-\varepsilon_{X\alpha SW}$	$-\varepsilon_{TS}$	Level†	$-\varepsilon_{X\alpha SW}$
$5a_1$	4.83	6.76	$6a_1$	4.74
$3e$	5.27	7.16	$4e$	5.34
$4a_1$	5.32	7.15	$5a_1$	5.45
$2e$	6.99	8.96	$4a_1$	6.02
$3a_1$	7.46	9.49	$1a_2$	6.71
$1e$	9.39	11.43	$3e$	7.84
$2a_1$	10.49	12.55	$3a_1$	8.05
$1a_1$	13.22	15.39	$2e$	8.63
			$2a_1$	10.38
			$1e$	11.16
			$1a_1$	13.54

*$\varepsilon_{X\alpha SW}$ designates the XαSW one-electron energies and ε_{TS} the transition-state energies.
†The numbering scheme is for the valence orbitals only.

TABLE 3. Total *s,p* populations* for the valence shells of Al_7 and Al_{10}

Cluster	Calculation	q_A^s	q_A^p	q_B^s	q_B^p	q_C^s	q_C^p
Al_7	CNDO/2	1.17	1.85	1.21	1.77	1.35	1.66
	XαSW	1.60	1.51	1.66	1.38	1.64	0.94
	CNDO/HM	1.64	1.42	1.74	1.23	1.81	1.12
Al_{10}	CNDO/2	0.74	2.18	1.16	1.77	1.37	1.69
	XαSW	1.59	2.20	1.76	1.41	1.74	1.04
	CNDO/HM	1.11	2.08	1.68	1.34	1.74	1.22

*The atoms are designated A, B, C in order of decreasing coordination number; for Al_7 they correspond to atoms with coordination numbers 5, 4, and 3 respectively, and for Al_{10} they are for coordination numbers 9, 5, and 4 respectively.

The valence-shell one-electron energies ($\varepsilon_{X\alpha SW}$) are reported in Table 2 for Al_7 and Al_{10} where all orbitals, including those of the core, have been determined self-consistently. For Al_7, the highest-occupied level ($5a_1$) is singly occupied; in Al_{10} the highest-occupied level ($6a_1$) has a one-electron energy which is very close to that (−4.70 eV) of the first unoccupied level ($5e$). Transition state energies (ε_{TS}) for the occupied levels of Al_7 are also reported in Table 2, and charge distributions calculated for Al_7 and Al_{10} are included in Table 3. Local and total DOS from the XαSW calculation on Al_{10} are shown in Fig. 1. The virial ratio $-2T/V$ is 1.000354 for Al_7 and 1.000864 for Al_{10}.

Previous XαSW calculations for aluminium have been made for clusters with O_h symmetry to represent bulk atoms (23), and for clusters with C_{4v} symmetry for investigating the (100) surface and its adsorption of oxygen (24, 25). Salahub and Messmer (23) noted for some large clusters, e.g. Al_{25} and Al_{43}, a rough correspondence with the $E^{1/2}$ dependence expected for a free-electron metal, where E is measured from

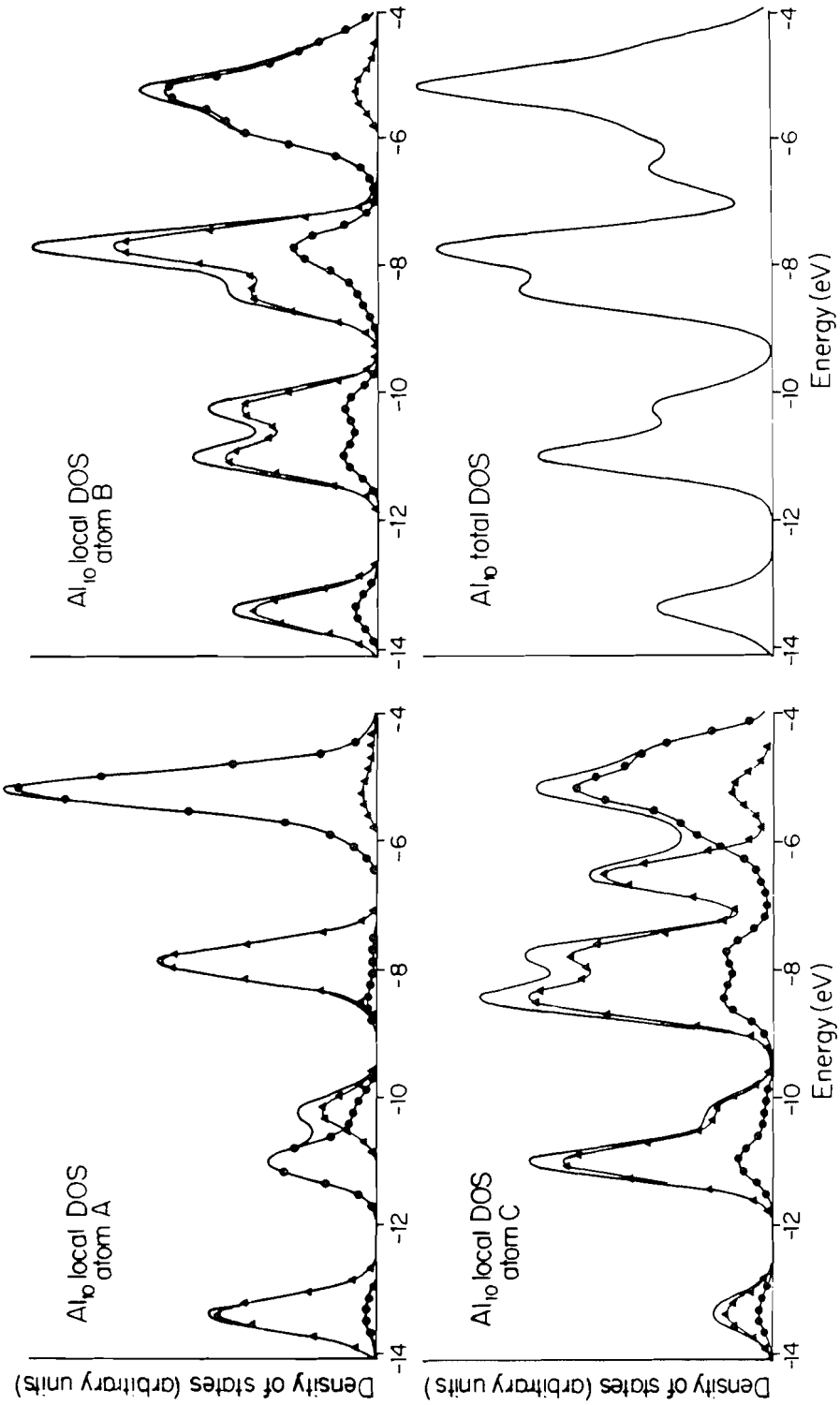

FIG. 1. Local and total DOS calculated with the XαSW method for Al_{10}. The curves designated by triangles and circles correspond to s and p components respectively.

the bottom of the valence band. We certainly find an increase in the total DOS with energy for both Al_7 and Al_{10}, but, as expected for small clusters, our results also bring out a substantial dependence on the local environment; this is apparent both in the local DOS for Al_{10} (see Fig. 1) and in the charge distributions (Table 3). Total sphere charges increase with coordination number, and the variations are associated especially with the populations of the *p*-functions. Indeed *s* to *p* promotion appears important for the bonding of the high-coordinate atoms in clusters of aluminium, and this relates to analogous effects in the corresponding clusters of silver (26). A dominant feature in the electronic structures of the silver clusters is the substantial localisation of the *d*-functions on those atoms of high coordination which are adjacent to atoms with appreciably lower coordination numbers. This depends on the reduced potential energy around the high-coordination atoms, and the small nearest-neighbour overlap for the relevant *d*-functions. This localisation is less marked for aluminium, in part because of the greater diffuseness of the atomic orbital functions of the valence shell.

In using the XαSW results of Al_7 for deriving CNDO/HM parameters of aluminium, the ω_j have been equated to the number of atoms in each unique set. Energy levels from the CNDO/2, XαSW, and CNDO/HM calculations are plotted in Fig. 2 and the separation between the lowest and highest occupied levels from each calculation is 26.54, 8.63, and 16.35 eV respectively. The separation between the $1a_1$ and $5a_1$ levels for CNDO/2 is therefore 3.07 times greater than that for the XαSW calculation; the corresponding ratio with the CNDO/HM parameters is reduced to 1.89. In choosing the final CNDO/HM parameters, the aim was to make the spread of levels as comparable as possible with that from the XαSW method while preserving the same ordering of the levels. The wide spread of the CNDO/2 levels relative to that from the XαSW calculation highlights the problem of defining a suitable numerical index for measuring overall improvements in the correspondence between the energy levels from the two sets of calculations. Thus, it is clear that in directly using eq. [4], starting with the CNDO/2 parameters, the comparisons would be overdominated by the differences for the $1a_1$ levels, and to a lesser extent from the $2a_1$ levels. These difficulties are reduced by including the scaling parameter *R* in the function defined by eq. [5].

Analysis of the *s* and *p* atomic populations for each valence orbital from the different calculations on Al_7 shows that the CNDO/HM calculation agrees with XαSW in that the lower levels essentially involve *s*

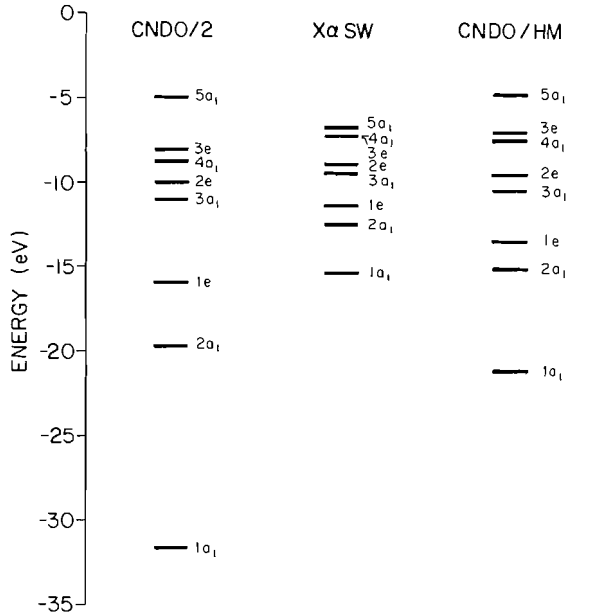

FIG. 2. Comparison by Al_7 of one-electron energies calculated with the CNDO/2 and CNDO/HM schemes and transition-state energies calculated with the XαSW method.

functions while the higher levels $4a_1$, $3e$, and $5a_1$ are largely associated with *p* functions. By contrast the CNDO/2 calculation indicates a high degree of *s* and *p* mixing; this has the effect of increasing the *p* populations at the expense of the *s* populations. Table 3 indicates that the CNDO/HM and XαSW calculations are in good agreement for the distribution of the total populations in Al_7.

4.2 Si_5H_{12}

The XαSW calculations made here for Si_5H_{12} have a number of features in common with those made previously by Cartling *et al.* (27). The main differences are that we use: (*i*) realistic Si—H distances; (*ii*) the overlapping-spheres version of the XαSW method; and (*iii*) exchange-correlation parameters appropriate to the H spheres. Our calculations were made for a model in which the central Si atom is surrounded tetrahedrally by the other four Si atoms, and the twelve H atoms are directed from the outergroup of four Si atoms towards where the next group of Si atoms would be in the actual silicon lattice. This molecule has T_d symmetry, and all Si—Si and Si—H distances are fixed equal to 2.35 and 1.47 Å respectively. The atomic sphere radii used are 1.29 Å for Si and 0.80 Å for H; these values were determined by Norman's procedure (11) for a 10% increase in radius for spheres which just touch in the silicon lattice. The outersphere was centred on the central Si atom with a radius equal to 3.96 Å (so making it just touch each of the H spheres).

Cartling *et al.* included vacancy spheres in their calculations, and it seemed worthwhile to investigate their value in this case, particularly in view of some recent discussion about their validity for this type of calculation (28). Vacancy spheres enable some of the intersphere potential to be spherically averaged rather than be reduced to a constant value. In these calculations the vacancy spheres were given the same radii as the Si spheres and were positioned tetrahedrally around the central Si atom so that their centres, and the centres of the four surrounding Si spheres, mark the corners of a cube. The exchange-correlation parameter for silicon ($\alpha = 0.72751$) is also used in the vacancy sphere, the outersphere, and the intersphere regions. Valence shell energies and charge distributions calculated with the XαSW method for Si_5H_{12} are shown in Tables 4 and 5 respectively; all orbitals, including those of the core, have been determined self-consistently. It is clear that the vacancy spheres have a negligible effect for this molecule; the population of the vacancy sphere comes almost entirely from the intersphere region. The virial ratios are 1.000436 and 1.000439 when the vacancy spheres are included and neglected respectively.

Some significant differences have been found from the results of Cartling *et al.* (27), and these are presumably associated with the differences noted above between the two sets of calculations. Surprisingly, Cartling *et al.* report the central Si sphere to contain 0.9 electron more than that in the neighbouring Si spheres; our XαSW calculations indicate a difference of 0.15 electron. Also the energy level structure is different from the two calculations; Cartling *et al.* report the $3t_2$ level to be just below $1e$ whereas we find $1t_1$, $1e$, and $2t_2$ to be close together and the $3t_2$ level nearly 3 eV higher in energy. According to our XαSW calculations, the lowest level $1a_1$ largely involves interactions between *s*-orbitals on the central and outer-Si atoms; $2a_1$ is concentrated especially on the *s*-orbital of the central-Si atom, and $1t_2$ corresponds to strong interactions between outer-Si *s*-orbitals and the neighbouring hydrogen 1*s*-orbitals. The band of levels $2t_2$, $1e$, and $1t_1$ involves basically Si3*p*–H1*s* interactions, while $3t_2$ corresponds to interactions between the central-Si 3*p* orbitals and those on the outer-Si atoms.

Although $Si(SiH_3)_4$ is known (29), its photoelectron spectrum does not seem to have been measured so far. The trends in structure (and their assignments) for photoelectron spectra of linear silanes (30) and permethylated silanes, including $Si[Si(CH_3)_3]_4$ (31), seem broadly consistent with the calculated transition state energies in Table 4. These latter values should be helpful for interpreting data from photoelectron spectroscopy for $Si(SiH_3)_4$.

TABLE 4. Valence-shell energies* (in eV) for Si_5H_{12}

Level†	Vacancy spheres included $-\varepsilon_{X\alpha SW}$	Vacancy spheres neglected $-\varepsilon_{X\alpha SW}$	Vacancy spheres neglected $-\varepsilon_{TS}$
$3t_2$	5.70	5.78	7.92
$1t_1$	8.52	8.56	10.52
$1e$	8.78	8.78	10.72
$2t_2$	8.94	8.99	10.88
$2a_1$	10.80	10.87	13.05
$1t_2$	13.42	13.46	15.56
$1a_1$	14.43	14.49	16.53

*$\varepsilon_{X\alpha SW}$ designates the XαSW one-electron energies and ε_{TS} the transition-state energies.
†The numbering scheme is for the valence orbitals only.

TABLE 5. Total *s*,*p* populations* for the valence shell of Si_5H_{12}

Method	q_{Sic}^s	q_{Sic}^p	q_{Sio}^s	q_{Sio}^p	q_H^s
CNDO/2	1.05	3.09	1.05	2.54	1.12
XαSW	1.41	2.74	1.23	2.43	1.10
CNDO/HM	1.58	2.50	1.23	2.38	1.12

*Sic = central, Sio = outer Si atom.

In determining CNDO/HM parameters for silicon, we wished to minimize the possibility of the hydrogen charge distribution dominating the correspondence functions such as R_q; accordingly for this molecule the weight factors ω_j were taken equal to unity for each set of symmetrically equivalent atoms. The valence shell energy levels from the various calculations are plotted in Fig. 3. Although the highest-occupied to lowest-occupied separation is greater from the CNDO/HM calculation, compared with that from the XαSW calculation, by a factor of 1.31, this does represent an improvement over the CNDO/2 calculation for which the corresponding factor is 1.85. The CNDO/HM calculation reproduces the XαSW result that the orbitals $2t_2$, $1e$, and $1t_1$ are associated with Si3*p* orbitals bonding with the hydrogen atoms, but the CNDO/2 calculation also includes the $2a_1$ orbital in this category. The overall atomic populations from the XαSW calculation are reproduced fairly well with the CNDO/HM procedure (Table 5).

4.3 P_4

This molecular cluster has T_d symmetry, with all P—P distances equal to 2.21 Å. The XαSW calculations were made with atomic sphere radii equal to to 1.38 Å (corresponding to a 25% increase over the radii which just touch). The outersphere, with a radius of 2.73 Å, was centred at the centre of the

TABLE 6. Calculated energies (in eV) for P_4 and ionisation energies from photoelectron spectroscopy

Level	This work $-\varepsilon_{X\alpha SW}$	This work $-\varepsilon_{TS}$	Ionisation energies*	Ref. 32 $-\varepsilon_{TS}$	Ref. 33 $-0.92\varepsilon_{SCF}$
$2e$	6.09	8.93	9.5, 9.9	10.44	9.63
$6t_2$	7.14	10.05	10.4, 10.6	11.42	10.26
$5a_1$	8.54	11.47	11.87	12.27	11.46
$5t_2$	12.89	15.90	15.2, 16.3, ~17.5	17.58	19.32
$4a_1$	20.70	24.17	22.3		28.98

*From ref. 33 except $4a_1$ which is from ref. 34; the multiple entries relate to Jahn–Teller splittings of the ionic states.

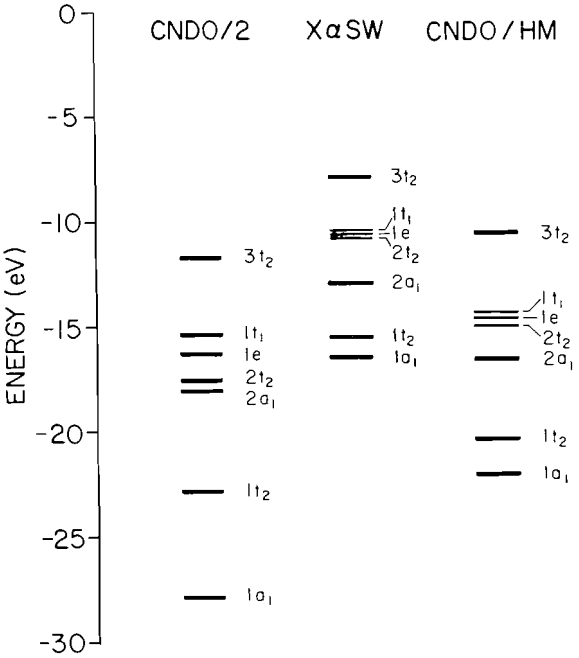

FIG. 3. Comparison for Si_5H_{12} of one-electron energies calculated with the CNDO/2 and CNDO/HM schemes and transition-state energies calculated with the XαSW method.

tetrahedron. The exchange correlation parameter was fixed equal to 0.72620 in all regions. On taking the calculations to the self-consistent limit, the calculated valence shell charges are 1.68 of *s* type and 2.80 of *p* type in each P sphere; the outersphere and intersphere charges being 0.99 and 1.11 respectively. The virial ratio was 1.000158.

Valence shell energies from this XαSW calculation are reported in Table 6, and comparisons are made with experimental ionisation energies and with previous calculations. Specifically for the latter we report transition state energies calculated in the non-overlapping sphere version of the XαSW method (32) and values using Koopmans' theorem (but reduced by a factor 0.92) from a non-empirical molecular orbital calculation with an *s,p* Gaussian basis set (33). The present XαSW calculations appear to provide a satisfactory level of agreement with the experimental ionisation energies.

The high symmetry and the smallness of this molecule combine to make it somewhat less than ideal for parametrising the CNDO method since all the atoms are equivalent and the number of different energy levels is restricted. A consequence of the high symmetry for the function R_q is that all the unique information is contained in the *s*-orbital populations. Minima in the functions R_q and R_ε' (eqs. [3] and [5]) could not be found simultaneously for a single combination of values of β and $(I_s + A_s)/2$; this type of problem was encountered previously by Santry (8). From the possible combinations of β and $(I_s + A_s)/2$, the final selection (Table 1) was made by ensuring that the calculated P—P distance was as close as possible to the experimental value.

The CNDO/HM and CNDO/2 level structures shown in Fig. 4 are in good agreement with those from the XαSW calculation, although the valence band is broader in both cases: by factors of 1.24 and 1.54 for the CNDO/HM and CNDO/2 calculations respectively. Information on the charge distributions from the different calculations is given in Table 7.

4.4 S_8

Overlapping-spheres XαSW calculations have been reported recently for this molecule (12); the D_{4d} symmetry ensures all sulphur atoms are equivalent. As for P_4, this restricts the amount of information for making the parametrisations, although for S_8 the number of different energy levels is greater. Again to make the final selection of CNDO/HM parameters for sulphur (Table 1), it was necessary to check the calculated values of the S—S bond length against the experimental value.

The energy levels from the different calculations are plotted in Fig. 5. The CNDO/HM calculation gives a good account of the separation of *s*-type and *p*-type molecular orbitals found with the XαSW

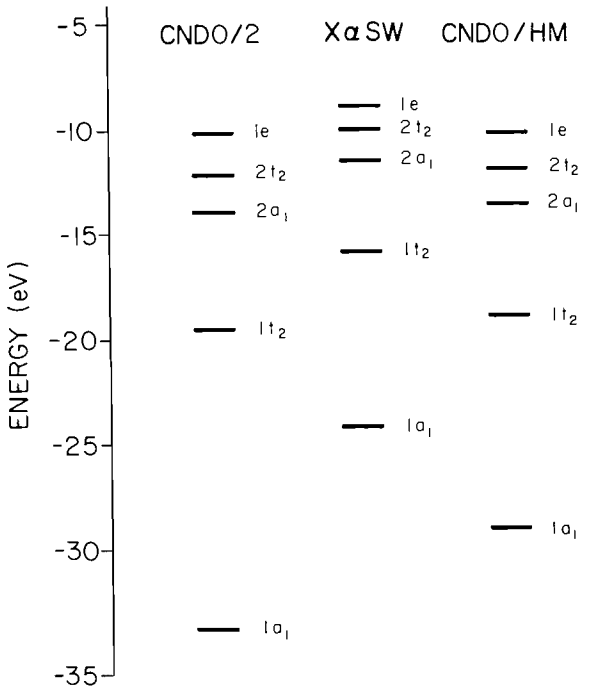

FIG. 4. Comparison for P_4 of one-electron energies calculated with the CNDO/2 and CNDO/HM schemes and transition-state energies calculated with the XαSW method.

TABLE 7. Individual and total *s* populations for the valence shell of P_4

Method	Population					Total
	$1a_1$	$2a_1$	$1e$	$1t_2$	$2t_2$	
CNDO/2	0.19	0.06	0	0.17	0.04	1.77
XαSW	0.17	0.04	0	0.20	0.02	1.73
CNDO/HM	0.20	0.05	0	0.20	0.02	1.83

method (i.e. the levels $1a_1$ to $1b_2$ are predominantly *s*-type while the upper levels are predominantly *p*-type), whereas the CNDO/2 calculation shows a degree of overlap between the *s* and *p* regions. Some differences in ordering of the levels in the *p* regions are found with both the CNDO/2 and CNDO/HM calculations compared with the XαSW calculation. These differences can be associated in part with the high density of states. Some errors within the CNDO procedures are inevitable; thus the approximations required for rotational invariance tend to blur some differences between orbitals with σ and π characteristics. The total atomic populations for *s* functions are 1.82, 1.95, and 1.91 for the CNDO/2, XαSW, and CNDO/HM calculations respectively.

5. Applications to Other Molecules

In this section CNDO/HM calculations, using the parameters of Table 1, are applied to a number of

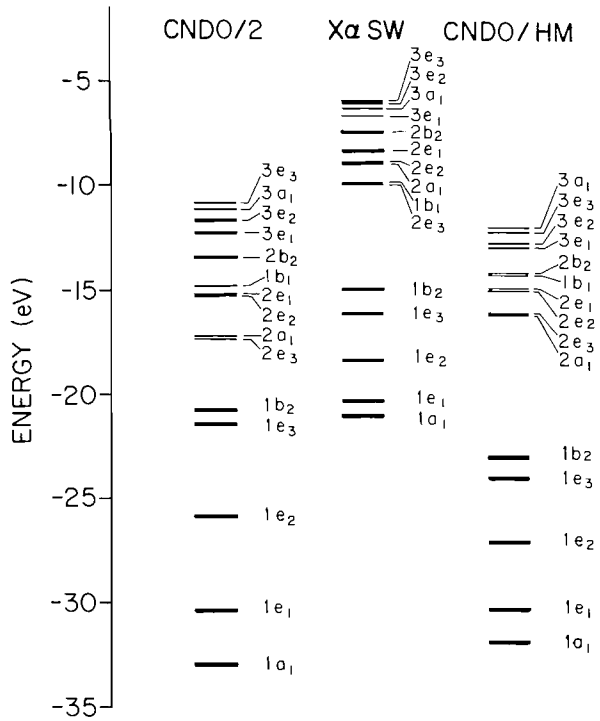

FIG. 5. Comparison for S_8 of one-electron energies calculated with the CNDO/2, CNDO/HM, and XαSW methods. The XαSW results are from ref. 12.

other molecules and molecular clusters formed by the elements aluminium to sulphur; the objective is to assess how the parameters derived for the particular reference molecules transfer to other molecules. First we check for some homonuclear clusters which are larger than those used in deriving the CNDO/HM parameters. Figure 6 compares valence-shell energy levels from the three types of calculation on Al_{10}. The separation between the highest- and lowest-occupied levels is much greater from CNDO/2 than from the XαSW calculation, and there are some differences in the ordering of the higher levels. The total energy separation from the CNDO/HM calculation is intermediate, but the ordering and relative positions of the levels are in better agreement with those from the XαSW method; the $5a_1$ and $4e$ levels are reversed but these two levels have very similar energies from both calculations. The charge distributions in each molecular orbital from CNDO/HM agree better with the XαSW distributions than do those from the CNDO/2 calculation; the total populations over the occupied levels are included in Table 3. Figure 7 compares valence-shell energy levels from the various calculations for the hypothetical P_8 molecule; again the CNDO/HM scheme appears to give a better account of the XαSW level structure (32) than does the CNDO/2 method.

Next an assessment is made of the applicability of

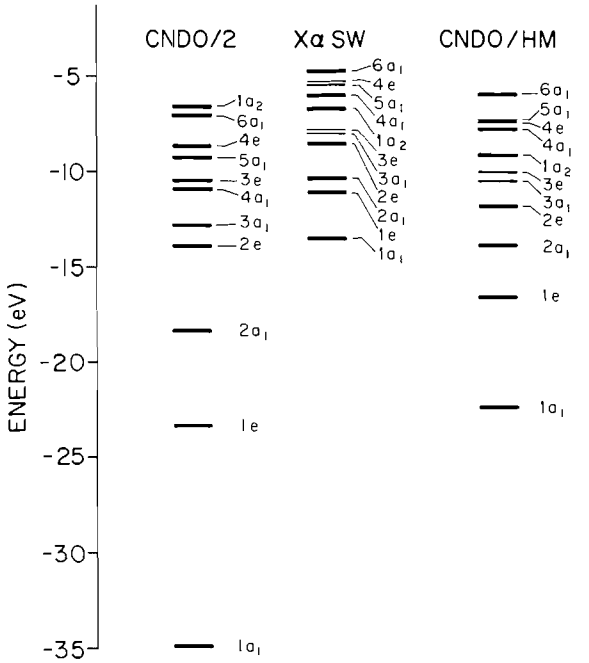

FIG. 6. Comparison for Al_{10} of one-electron energies calculated with the CNDO/2, CNDO/HM, and XαSW methods. The transition-state energies should be about 2 eV lower than the one-electron energies from the XαSW method.

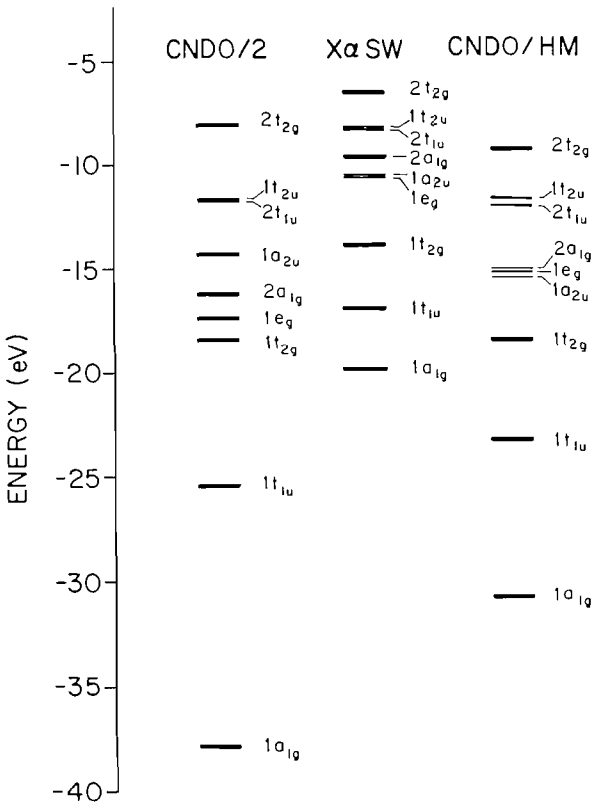

FIG. 7. Comparison for P_8 of one-electron energies calculated with the CNDO/2, CNDO/HM, and XαSW methods. The transition-state energies should be about 3 eV lower than the one-electron energies from the XαSW method (from ref. 32).

the CNDO/HM parameters for the hydrides SiH_4, PH_3, and H_2S. The calculated energy levels are given in Table 8. Compared with the XαSW calculations, the CNDO calculations show rather greater separations between the lowest and highest occupied levels. In the CNDO/HM calculation for H_2S the separation between $1b_2$ and $2a_1$ seems too small, but overall the CNDO/HM calculations show reasonable levels of agreement for the energy levels of these hydrides. The charge distributions from the CNDO/HM scheme correspond very closely to those from CNDO/2; it is satisfying that the atomic charges vary smoothly over the series of molecules, for example according to CNDO/HM the net charges on the H atoms are -0.134, -0.047, and $+0.036$ for SiH_4, PH_3, and H_2S respectively. The overall similarity in the results from CNDO/HM and CNDO/2 for these hydrides may perhaps suggest that there is a certain flexibility in choosing the CNDO parameters, particularly for molecules containing just a single second-row atom. However, our experience with the larger clusters suggests this flexibility is reduced for molecules containing several second-row atoms.

Valence-shell energies for P_4S_3 from six different calculations encompassing the XαSW, CNDO/2, and CNDO/HM procedures are given in Fig. 8 and information on the atomic charges is in Table 9. The XαSW calculation (designated *A*) includes *d* waves in the atomic spheres; some consideration of an extension of the basis set to include *d* functions for the CNDO-type calculations is given below. The entries in Fig. 8 and Table 9 designated *B* and *D* to correspond respectively to the CNDO/2 and CNDO/HM calculations for an *s,p* basis. It is immediately apparent that the CNDO/HM scheme accounts better

TABLE 8. Comparison of ionisation energies (in eV) calculated with the CNDO/2, CNDO/HM, and XαSW procedures for SiH_4, PH_3, and H_2S

Molecule	Orbital	CNDO/2	CNDO/HM	XαSW
SiH_4	$1t_2$	15.90	14.63	11.97*
	$1a_1$	22.77	21.11	17.70
PH_3	$2a_1$	13.62	13.99	10.61†
	$1e$	15.90	15.62	13.42
	$1a_1$	25.54	24.86	20.55
H_2S	$1b_1$	13.13	13.85	11.7‡
	$2a_1$	15.85	16.04	13.8
	$1b_2$	17.02	16.51	15.7
	$1a_1$	27.50	28.59	24.2

*Reference 35.
†Reference 11.
‡Reference 36. This calculation for H_2S uses the discrete variational method.

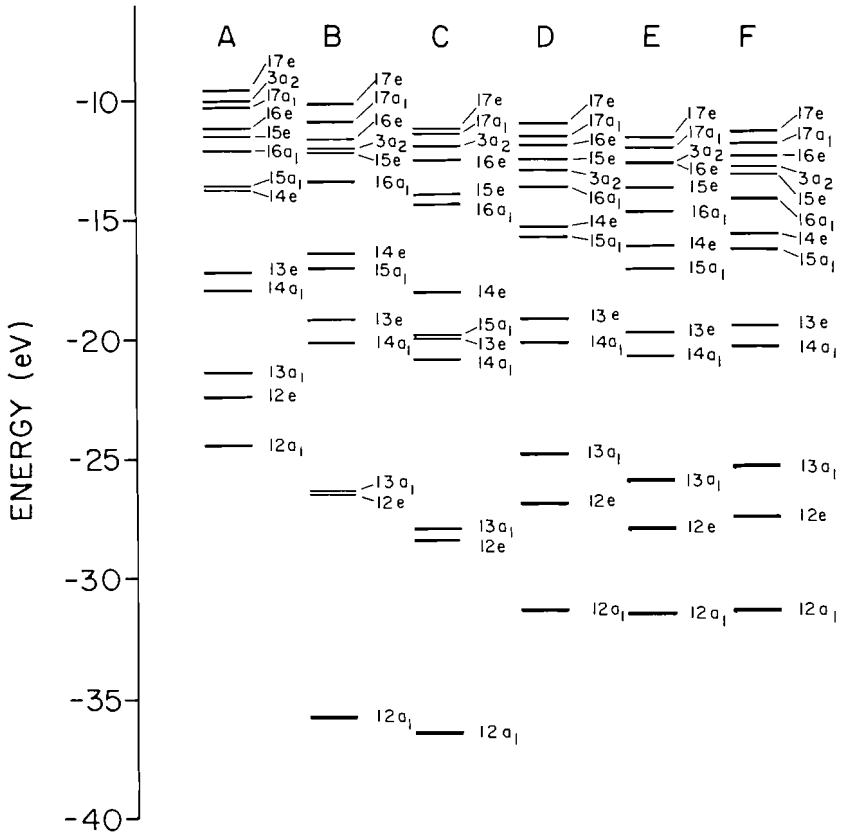

FIG. 8. Comparison of valence-shell energy levels for P_4S_3. The designations are: *A*, transition state energies from XαSW calculation including *d* waves (17); *B*, one-electron energies from CNDO/2 calculation with *s,p* basis: *C*, as *B* but *s,p,d* basis; *D*, one-electron energies from CNDO/HM calculation with *s,p* basis; *E*, as *D* but *s,p,d* basis with $\beta_d = \beta_s = \beta_p$; *F*, as *E* except the β_d values are -5 eV for P and -9 eV for S.

than the CNDO/2 procedure for the energy separation between the highest and lowest occupied valence levels given by the XαSW calculation, although both CNDO calculations interchange the closely-spaced levels $14e$ and $15a_1$, and they depress the $3a_2$ level compared with the XαSW calculation. The charge distributions in the individual molecular orbitals show that the CNDO/HM calculations, unlike the CNDO/2 calculations, follow the XαSW calculation in characterizing the orbitals as predominantly *s*-type and predominantly *p*-type (17). Associated with this is an observation from Table 9 that the CNDO/HM calculations indicate slightly higher *s* populations than do the CNDO/2 calculations. The experience here for P_4S_3 and the hydrides suggests that the CNDO/HM parameters extend satisfactorily to some molecules involving different types of atoms, even though these parameters were deduced primarily for homonuclear molecules.

6. Inclusion of *d* Orbitals

For many years there have been frequent discussions about the extent of the involvement of *d* orbitals in the bonding of molecules containing second-row atoms (37, 38). Generally this involvement seems greatest for atoms in high valence states, but even for the low valence states (e.g. divalent S, trivalent P) *d* orbitals can be needed in computational schemes either as polarisation functions or to take up deficiencies associated with other aspects of the calculations. In extending the CNDO/2 method to the second row, Santry and Segal (7) considered three basis sets: a simple *s,p* basis, an *s,p,d* basis where the *d* functions are included in an analogous way to the *s* and *p* functions, and a basis corresponding to an intermediate involvement of the *d* functions. In extending the basis set to include *d* orbitals in the present work, consideration was given to various values for the parameters ξ_d, $(I_d + A_d)/2$ and β_d. However, this examination indicated that a satisfactory approach involved the *d* exponent being given the same value as used for the corresponding *s* and *p* orbitals with $\frac{1}{2}(I_d + A_d)$ kept at the value used by Santry and Segal. The final parameter to be fixed is then the bonding parameter β_d. In the calculations for P_4S_3 designated *C* and *E* (Fig. 8 and Table 9), β_d

TABLE 9. Total s,p,d populations* for the valence shell of P_4S_3

Calculation†	$q_{Pa}{}^s$	$q_{Pa}{}^p$	$q_{Pa}{}^d$	$q_{Pb}{}^s$	$q_{Pb}{}^p$	$q_{Pb}{}^d$	$q_S{}^s$	$q_S{}^p$	$q_S{}^d$
A	1.76	2.71	0.34	1.81	2.76	0.24	2.00	4.07	0.19
B	1.68	3.02	—	1.72	3.20	—	1.79	4.39	—
C	1.61	2.39	0.95	1.65	2.62	0.71	1.75	3.93	0.36
D	1.75	3.02	—	1.78	3.14	—	1.88	4.27	—
E	1.72	2.48	0.64	1.74	2.68	0.52	1.85	4.03	0.23
F	1.72	2.72	0.36	1.76	2.91	0.27	1.86	4.12	0.14

*Pa = apical, Pb = basal P atom.
†*A* = XαSW calculation where *d* waves are included in the atomic spheres (17); *B* = CNDO/2 calculation with *s,p* basis; *C* = CNDO/2 calculation with *s,p,d* basis; *D* = CNDO/HM calculation with *s,p* basis; *E* = CNDO/HM calculation with *s,p,d* basis where $\beta_d = \beta_s = \beta_p$; *F* = CNDO/HM calculation where the β_d values are reduced, namely −5 eV for P and −9 eV for S.

has been given the same value as for the *s* and *p* functions; *C* corresponds to the CNDO/2 calculation and it is apparent from the atomic populations that the *d* populations are too large. These are reduced somewhat in the CNDO/HM scheme, although the *d* populations are still about twice those from the XαSW calculation. We find a similar situation for other molecules referred to in sections 4 and 5; thus usually the orderings of the energy levels are essentially unchanged when *d* functions are included within the CNDO/HM procedure, but the *d* populations can be as large as 0.5 electron per atom. (Inclusion of *d* orbitals in the CNDO/HM scheme does change the orbital orderings in the *p* region for S_8, but this is not surprising in view of the relatively high density of states.) Santry and Segal (7) proposed that the *d* populations should be reduced to more plausible values by reducing the β_d value. Table 9 shows that the CNDO/HM calculation for P_4S_3 gives a rather good account of the XαSW populations when the β_d values are reduced to −5 eV for P and −9 eV for S (entry *F*), although the corresponding energy level structure (Fig. 8) is seen to be changed only marginally from those for the calculations designated by *D* and *E*.

Figure 9 compares the valence level structures for SO_2 from a number of different calculations. The XαSW calculation included *d* waves in the sulphur sphere (39), and it is clear that the inclusion of *d* orbitals in the CNDO calculations affects the ordering of the upper levels. Again the CNDO/HM calculations appear somewhat more successful than the CNDO/2 calculations at matching up the orderings and relative spacings found from the XαSW calculation; the two CNDO/HM calculations which include *d* orbitals (designated *E* and *F* in Fig. 9) seem equally successful in this regard although, compared with the XαSW results, the $3a_1$ level seems too low and the $2b_2$ level too high.

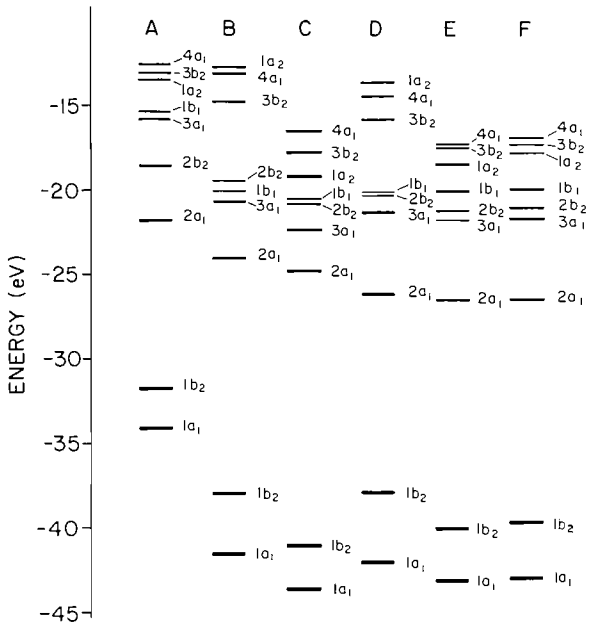

FIG. 9. Comparison of valence-shell energy levels for SO_2. The designations are: *A*, transition-state energies from XαSW calculation including *d* waves (39); *B*, one-electron energies from CNDO/2 calculation with *s,p* basis; *C*, as *B* but *s,p,d* basis for S; *D*, one-electron energies from CNDO/HM calculation with *s,p* basis; *E*, as *D* but *s,p,d* basis for S with $\beta_d = \beta_s = \beta_p$; *F*, as *E* except $\beta_d = -9$ eV.

7. Concluding Remarks

The new XαSW calculations reported here relate to three neighbouring atoms in the second row, and as expected the populations of the valence shell *p*-functions increase with atomic number through the clusters considered. For P_4, the occupied levels show a clear separation into *s*-type orbitals ($4a_1$ and $5t_2$) and *p*-type orbitals ($5a_1$ to $2e$), and this has been reported previously from molecular orbital calculations on P_4 (33) and from XαSW calculations on P_4S_3 (17) and S_8 (12). For Al_7 and Al_{10}, on the other hand, there is a greater mixing of *s*- and *p*-characteristics in the individual molecular orbitals; a somewhat intermediate situation is indicated for the silicon atoms in Si_5H_{12}. The calculated XαSW one-electron energies reported in this paper for Al_7, Si_5H_{12}, and P_4 show closely linear relationships to the corresponding transition state energies. Indeed we assumed this relationship extends to S_8 since only one-electron

energies were available for deducing CNDO/HM parameters from the XαSW calculation on this molecule (12).

Within the limits of our present experience, the CNDO/HM parameters given in Table 1 for the elements aluminium to sulphur seem at least as sucessful as the conventional CNDO/2 parameters for simple molecules containing a single second-row atom, and these parameters appear more successful for molecules containing a number of second-row atoms. The main objective here has been to check that the CNDO/HM procedure can give broadly consistent results in relation to the basic CNDO/2 scheme. At present we have not addressed ourselves to comparing CNDO/HM calculations with the several variations of CNDO that have been used previously for these second-row elements, nor do we claim that the parameters in Table 1 are optimal for all situations for these elements. Although the band widths are generally better with the CNDO/HM procedure than with the CNDO/2 procedure, it is clear that the former are still often too large compared with those from the XαSW calculations. The band widths calculated with CNDO/HM could no doubt be improved with a double-zeta basis set; that is one refinement that may be needed in making systematic extensions to transition metal systems. The approach used here attempts to find a balance between matching band widths and matching orderings of levels. Both of course are important, and ultimately the suitability or otherwise of this CNDO scheme must be judged by its ability to guide interpretations of experimental measurements. For the present, we feel that the observations made in this paper do not discourage the possibility of the CNDO/HM approach providing a helpful route for getting CNDO parameters for systems of the heavier elements for which alternative procedures are hindered by the unavailability or sparsity of both near-Hartree–Fock calculations and suitable experimental data.

Acknowledgements

We are grateful for support by the National Research Council of Canada, and for helpful guidance on the XαSW method by Dr. L. Noodleman. We also thank Dr. D. R. Salahub for providing detailed results for the XαSW calculations on S_8 in ref. 12.

1. J. A. POPLE and D. L. BEVERIDGE. Approximate molecular orbital theory. McGraw-Hill, New York, NY. 1970.
2. R. P. MESSMER. Semiempirical methods of electronic structure calculation. Part B: applications. *Edited by* G. A. Segal. Plenum, New York, NY. 1977. p. 215.
3. J. D. HEAD, K. A. R. MITCHELL, and M. L. WILLIAMS. Mol. Phys. **29**, 1929 (1975).
4. J. C. SLATER and K. H. JOHNSON. Phys. Rev. B, **5**, 844 (1972).
5. J. D. HEAD and K. A. R. MITCHELL. Mol. Phys. **35**, 1681 (1978).
6. J. C. SLATER. The self consistent field for molecules and solids. McGraw-Hill, New York, NY. 1974.
7. D. P. SANTRY and G. A. SEGAL. J. Chem. Phys. **47**, 158 (1967).
8. D. P. SANTRY. J. Am. Chem. Soc. **90**, 3309 (1968).
9. D. T. CLARK. Tetrahedron, **24**, 2663 (1968).
10. R. J. BOYD and M. A. WHITEHEAD. J. Chem. Soc. Dalton Trans. 73 (1972).
11. J. G. NORMAN. J. Chem. Phys. **61**, 4630 (1974).
12. D. R. SALAHUB, A. E. FOTI, and V. H. SMITH. J. Am. Chem. Soc. **99**, 8067 (1977).
13. K. H. JOHNSON. Adv. Quantum Chem. **7**, 143 (1973).
14. J. C. SLATER. Adv. Quantum Chem. **6**, 1 (1972).
15. K. SCHWARTZ. Phys. Rev. B, **5**, 2466 (1972).
16. R. S. MULLIKEN. J. Chem. Phys. **23**, 1833 (1955).
17. J. D. HEAD, K. A. R. MITCHELL, L. NOODLEMAN, and N. L. PADDOCK. Can. J. Chem. **55**, 669 (1977).
18. J. C. SLATER. Phys. Rev. **36**, 57 (1930).
19. G. BURNS. J. Chem. Phys. **41**, 1521 (1964).
20. E. CLEMENTI and D. L. RAIMONDI. J. Chem. Phys. **38**, 2686 (1963).
21. J. D. HEAD, K. A. R. MITCHELL, and L. NOODLEMAN. Surface Sci. **61**, 661 (1976).
22. W. B. PEARSON. A handbook of lattice spacings and structures of metals and alloys. Pergamon, New York, NY. 1958.
23. D. R. SALAHUB and R. P. MESSMER. Phys. Rev. B, **16**, 2526 (1977).
24. J. HARRIS and G. S. PAINTER. Phys. Rev. Lett. **36**, 151 (1976).
25. R. P. MESSMER and D. R. SALAHUB. Phys. Rev. B, **16**, 3415 (1977).
26. J. D. HEAD, K. A. R. MITCHELL, and L. NOODLEMAN. Surface Sci. **69**, 714 (1977).
27. B. CARTLING, B. ROOS, and U. WAHLGREN. Chem. Phys. Lett. **21**, 380 (1973).
28. F. HERMAN. Electrons in finite and infinite structures. *Edited by* P. Phariseau and L. Scheire. Plenum, New York, NY. 1976. p. 382.
29. F. FEHER and R. FREUND. Inorg. Nucl. Chem. Lett. **9**, 937 (1973).
30. H. BOCK, W. ENSSLIN, F. FEHER, and R. FREUND. J. Am. Chem. Soc. **98**, 668 (1976).
31. H. BOCK and W. ENSSLIN. Angew. Chem. Int. Ed. Engl. **10**, 401 (1971).
32. J. G. NORMAN. Unpublished calculations.
33. C. R. BRUNDLE, N. A. KUEBLER, M. B. ROBIN, and H. BASCH. Inorg. Chem. **11**, 20 (1972).
34. M. S. BANNA, D. C. FROST, C. A. MCDOWELL, and B. WALLBANK. J. Chem. Phys. **66**, 3509 (1977).
35. M. L. SINK and G. E. JURAS. Chem. Phys. Lett. **20**, 474 (1973).
36. A. ROSEN and D. E. ELLIS. J. Chem. Phys. **62**, 3039 (1975).
37. C. A. COULSON. Nature, **221**, 1106 (1969).
38. K. A. R. MITCHELL. Chem. Rev. **69**, 157 (1969).
39. L. NOODLEMAN and K. A. R. MITCHELL. Inorg. Chem. **17**, 2709 (1978).

Ab initio SCF and CI calculations for ground and low-lying valence and Rydberg excited states of HOCl and HClO in linear and bent nuclear conformations

PABLO J. BRUNA, GERHARD HIRSCH, AND SIGRID D. PEYERIMHOFF
Lehrstuhl für Theoretische Chemie der Universität Bonn, Wegelerstraße 12, D-5300 Bonn, West Germany
AND
ROBERT J. BUENKER
Lehrstuhl für Theoretische Chemie der Gesamthochschule Wuppertal, Gaußstraße 20, D-5600 Wuppertal, West Germany
Received December 28, 1978

PABLO J. BRUNA, GERHARD HIRSCH, SIGRID D. PEYERIMHOFF, and ROBERT J. BUENKER. Can. J. Chem. 57, 1839 (1979).

Potential curves are reported for the ground and various valence and Rydberg excited states of HOCl and HClO using *ab initio* SCF and CI methods. The states of HOCl are found to be generally favored over their counterparts in HClO, but the calculations indicate that small barriers nevertheless exist for angular interconversion between at least some pairs of such states; they also show that dissociation processes involving ClO bond breaking are universally favored for both HOCl and HClO. Additional calculations for the ions have also been carried out, from which the heat of formation of $HOCl^+$ is calculated to be 237 kcal/mol and it is pointed out that a previous estimate for the corresponding HOCl quantity has subsequently been substantiated by experiment; the relative energies of the first four states of $HOCl^+$ are found to be in good agreement with experiment as well.

PABLO J. BRUNA, GERHARD HIRSCH, SIGRID D. PEYERIMHOFF et ROBERT J. BUENKER. Can. J. Chem. 57, 1839 (1979).

On rapporte les courbes de potentiel pour les états fondamentaux, divers états de valence et pour des états excités Rydberg du HOCl et du HClO évaluées par des méthodes SCF et CI. On a trouvé que les états de HOCl sont généralement favorisés par rapport à leurs contreparties de HClO mais les calculs indiquent toutefois qu'il existe de faibles barrières à l'interconversion angulaire entre au moins quelques-uns de ces états; ils montrent aussi que le processus de dissociation impliquant le bris de la liaison ClO est universellement favorisé pour HOCl et HClO. On a effectué des calculs additionnels sur ces molécules et l'on peut en déduire que la chaleur de formation de $HOCl^+$ est égale à 237 kcal/mol et l'on signale que l'évaluation antérieure de la quantité correspondante pour HOCl a depuis été confirmée expérimentalement; on a trouvé que les énergies relatives des quatre premiers états du $HOCl^+$ sont aussi en bon accord avec les valeurs expérimentales.

[Traduit par le journal]

1. Introduction

In a previous study[1] (1) the relative stability of the HOCl molecule with respect to the HClO nuclear arrangement and the various fragments H + ClO, OH + Cl, O + HCl, and H + Cl + O has been investigated by means of *ab initio* configuration interaction treatments. The first four low-lying excited states of HOCl were also studied in I, and it has been found, as confirmed in a similar study by Jaffe and Langhoff (2), that population of all these species promotes dissociation of the molecule into OH and Cl.

Interest in the HOCl molecule has increased considerably in the past few years because of its possible role as an intermediate in the chlorine chemistry of the troposphere and stratosphere (3, 4). Furthermore, in view of the large stability difference found between HClO in I additional interest of a more theoretical nature has arisen, especially since isomerization energies for HAB systems composed exclusively of first-row atoms have quite generally been found to be much smaller. It thus becomes important to understand what differences in electronic structure cause the HOCl arrangement to be so preferred in nature and furthermore to establish whether a similar situation exists for the excited states of these systems.

For part of the present work only the SCF level of treatment is employed since potential energy curves obtained for ground and pertinent low-lying excited states in this approximation are often satisfactory for gaining information on the general structural behavior of the system under various nuclear displacements. These calculations are supplemented by CI treatments at various key points along the potential energy surfaces when necessary in

[1]Hereafter referred to as I.

0008-4042/79/141839-13$01.00/0

order to obtain information of quantitative significance. At the same time the original study (I) is extended in order to predict the location of additional excited states of valence and Rydberg character and their possible role in photochemical reactions of this system.

2. Technical Details

The HOCl system is placed in the xy plane for the present investigations. The AO basis set chosen is of double-zeta plus polarization quality and for the majority of calculations consists of 48 contracted cartesian gaussian functions (basis A of I). The (4, 2) oxygen contraction is thereby taken from Dunning (5) and a (6,4) chlorine set is adopted from the work of Veillard (6), while a (2,1) set with scaling factor $\eta^2 = 2.0$ is centered at the hydrogen site (1). Polarization is taken into account by bond functions of s, p, and d type centered in the ClO bond and an s species located between hydrogen and the respective heavier atom. Long-range functions of s and p_x, p_y, p_z type ($\alpha = 0.015$) are also located at the center of the ClO bond in order to represent the first members of corresponding Rydberg series. In addition for a few cases which are critical for destruction of the Cl—O bond the d bond functions are replaced by a set of d functions centered at each of the heavy atoms O and Cl.

The CI procedure employed is of the multi-reference double-excitation (MRD-CI) type with configuration selection and energy extrapolation (7); it is wholly analogous to the treatment in I and maintains a core of 12 electrons (corresponding to the K and L shells in chlorine and the K shell in oxygen) uncorrelated.

3. Comparison of the HOCl Structures

A. Orbital Characteristics

The experimental (8) structural data for HOCl are: OH = $1.83a_0$, ClO = $3.194a_0$, and $\angle$HOCl = 102.4° while those determined by calculations in I for HOCl are: OH = $1.876a_0$, ClO = $3.220a_0$, and $\angle$HOCl = 104.0°, and for HClO: HCl = $2.48a_0$, ClO = $3.10a_0$, and $\angle$HClO = 104.4°. The orbital energies obtained for both isomers in the same basis are contained in Table 1 and these data show that the charge distribution around the respective oxygen and chlorine atoms in the two species are markedly different from one another; the distinctly higher inner-shell orbital energy for chlorine ($1a'$) in HOCl compared to HClO reflects the larger negative charge around the chlorine atom when it is in the terminal position than what is found when it is located in the middle; similarly the lower $2a'$ energy in HOCl indicates that oxygen is less negative in HOCl than in HClO. Both observations taken together show that the more negatively charged atom is preferred at the terminal position in each case, a finding which is quite consistent with what has been observed generally in other triatomic systems, including molecules of A_3 type (9).

TABLE 1. Orbital energies (in hartree) for HOCl and HClO in their equilibrium nuclear arrangements (basis A of I)

ε	HOCl	HClO
$1a'$	−104.9041	−104.9785
$2a'$	−20.6489	−20.5593
$3a'$	−10.6045	−10.6797
$4a'$	−8.08093	−8.15586
$5a'$	−8.07827	−8.15428
$6a'$	−1.41331	−1.32464
$7a'$	−1.05870	−1.10042
$8a'(\pi)$	−0.71491	−0.70503
$9a'(\sigma)$	−0.59538	−0.56702
$10a'(\pi^*)$	−0.46619	−0.45642
$1a''$	−8.07805	−8.15371
$2a''(\pi)$	−0.61110	−0.59456
$3a''(\pi^*)$	−0.44231	−0.42776

Similarly large differences in the valence orbital energies are obvious from the results of Table 1. A comparison of the various charge density contour diagrams shows that the $6a'$ is to a large extent the $\sigma_g(2s + 3s)$ type MO in both systems, while the $7a'$ is the antibonding $\sigma_u(2s - 3s)$ counterpart and the $9a'$ can be looked upon as the $\sigma_g(p\sigma)$ bonding orbital (Fig. 1). The $8a'$ and $10a'$ species correspond to π and π^* respectively with a typical hydrogen admixture. It is interesting that in the bent equilibrium geometry the σ-type orbital $9a'$ lies between the π and π^* species (for both in-plane and out-of-plane components), in contrast to the situation for the linear HOCl geometry, for which the energy order is $\sigma(\varepsilon = -0.695$ hartree), $\pi(\varepsilon = -0.577)$, and $\pi^*(\varepsilon = -0.430)$.

The lowest unoccupied MO ($11a'$) is of σ^* type, as can also be seen from Fig. 1. It is strongly Cl—O antibonding and shows a definite preference for the linear nuclear arrangement, as will become clear from consideration of the geometrical characteristics of electronic states which occupy this species. Finally the out-of-plane MO's (Fig. 2) exhibit clear differences in charge distribution; in HOCl oxygen character is dominant in the $2a''$ (π-type MO) and that of chlorine is more important in the antibonding $3a''$ MO while the situation is reversed in HClO.

A localized MO representation (10) indicates quite clearly that the ClO bond is stronger in the more stable HOCl species (Fig. 3), since the charge distribution is much more evenly distributed between

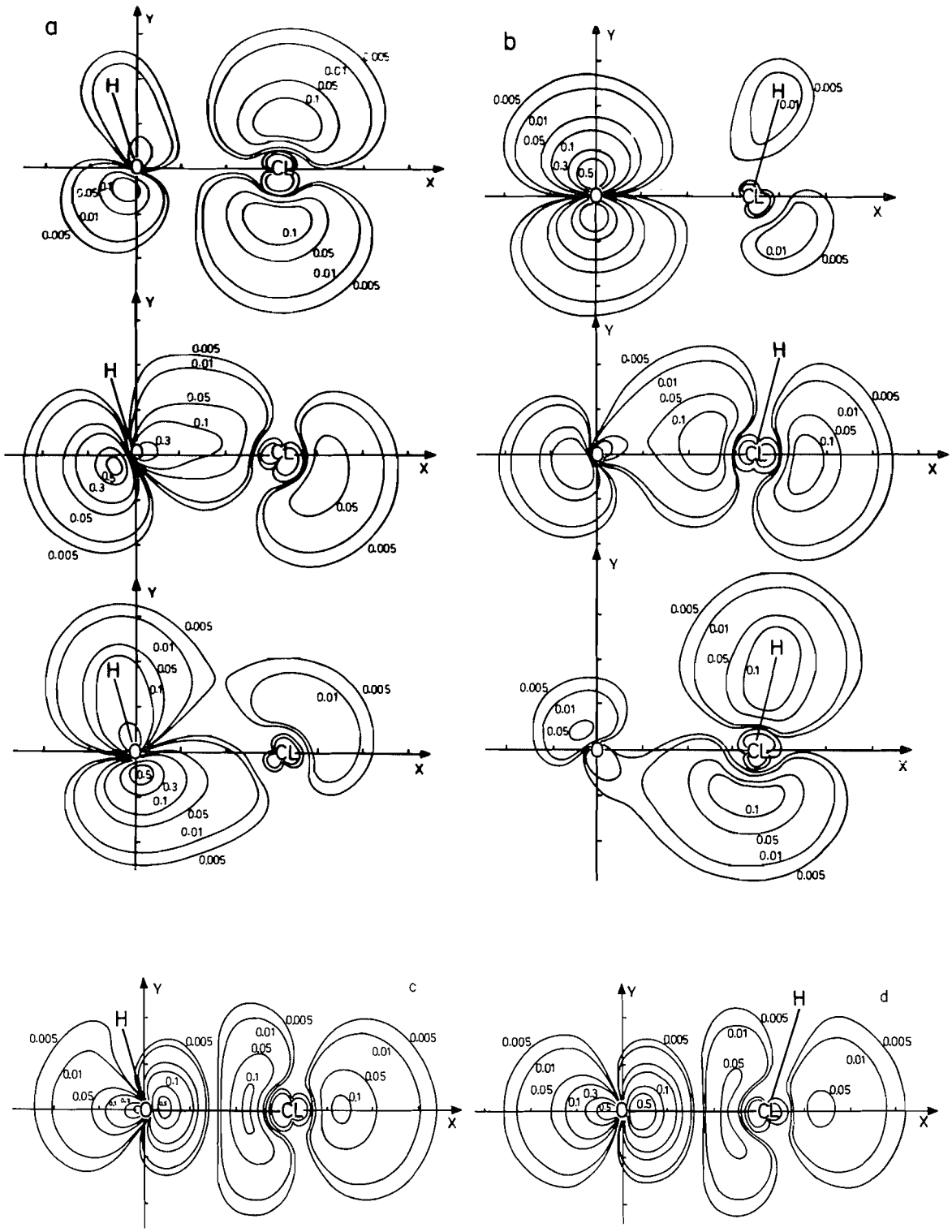

FIG. 1. Canonical orbital charge density contours for the three highest occupied a' MO's ($8a'$ to $10a'$ from bottom to top) of (*a*) HOCl and (*b*) HClO in their respective ground state equilibrium geometries, and for the lowest unoccupied (σ^*) MO in the same systems, (*c*) and (*d*).

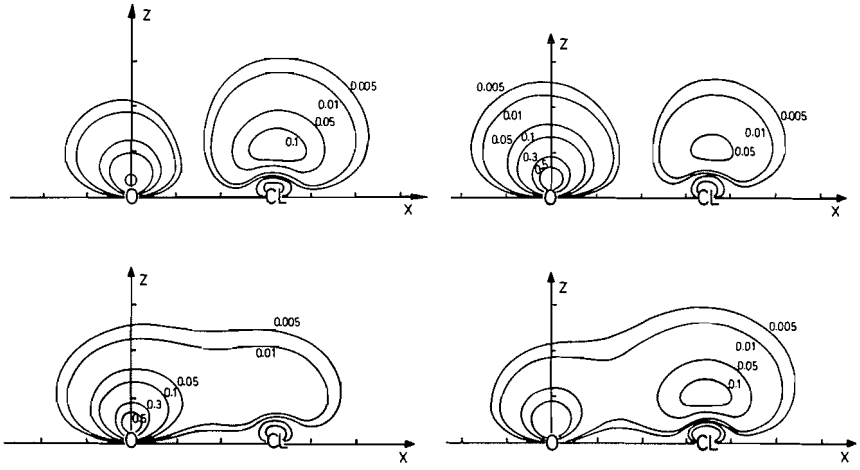

FIG. 2. Canonical orbital charge density contours for the π and π^* MO's of HOCl (left) and HClO (right) respectively.

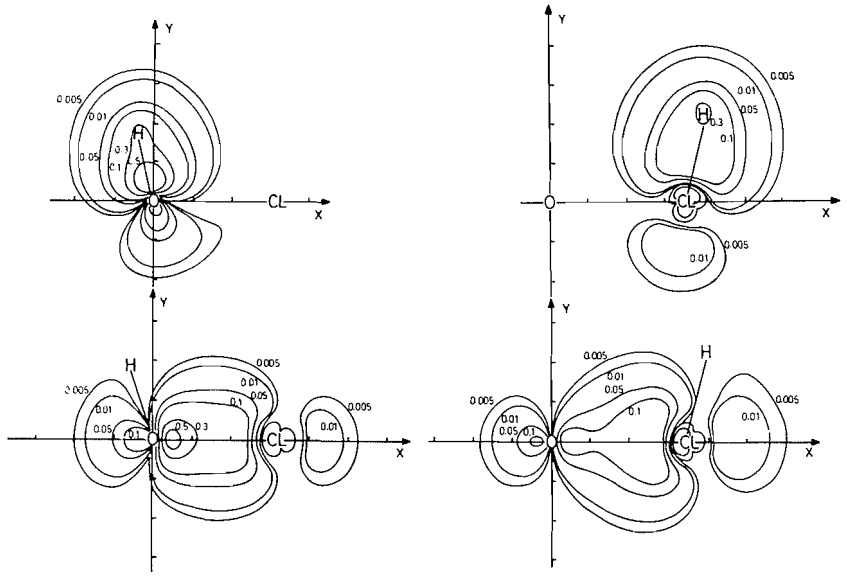

FIG. 3. Localized orbital charge density contours for the OH and ClO bonds in HOCl (left) and for the HCl and ClO bonds of HClO (right).

the two nuclei in the corresponding orbital than in its HClO counterpart. Since the respective dissociation products (OH + Cl and HCl + O) are known (11, 12) to be nearly isoenergetic, the difference in ClO bond strengths is essentially equal to the stability difference of the two systems, which has been calculated to be 60 kcal/mol in I. The localized OH and ClH bonding orbitals (also in Fig. 3) show quite normal behavior; their relation to the canonical MO's is given in Table 2 and shows that there are always four MO's which contribute to the localized bonds. The σ_g-type species $6a'$ and $9a'$ (Fig. 1) contribute in the main to the ClO bond, while the OH species gains its dominant character from the $6a'$ and $8a'$ canonical MO's and the $7a'$ and $8a'$ MO's predominate in forming the HCl bond.

B. Angular Potential Energy Curves

A series of SCF calculations is carried out at various internuclear angles for all low-lying electronic states of HClO and HOCl which are accessible via the Roothaan procedure, and the results are summarized in Fig. 4; the various bond lengths are held constant thereby at their optimal values in the respective equilibrium conformations.

The correlation between the various states is obvious for the ground and those states resulting from $\pi^* \rightarrow \sigma^*$ ($11a'$) excitation; the relation between

TABLE 2. Expansion coefficients for the localized orbitals representing the H—X and Cl—O bonds in the basis of the canonical MO's

	Bond	$6a'$	$7a'$	$8a'$	$9a'$	$10a'$
HOCl	O—H	0.56	0.36	0.71	—	−0.21
	Cl—O	0.55	−0.30	−0.33	−0.69	—
HClO	Cl—O	−0.52	−0.11	+0.30	−0.79	—
	Cl—H	0.36	0.52	0.76	—	−0.10

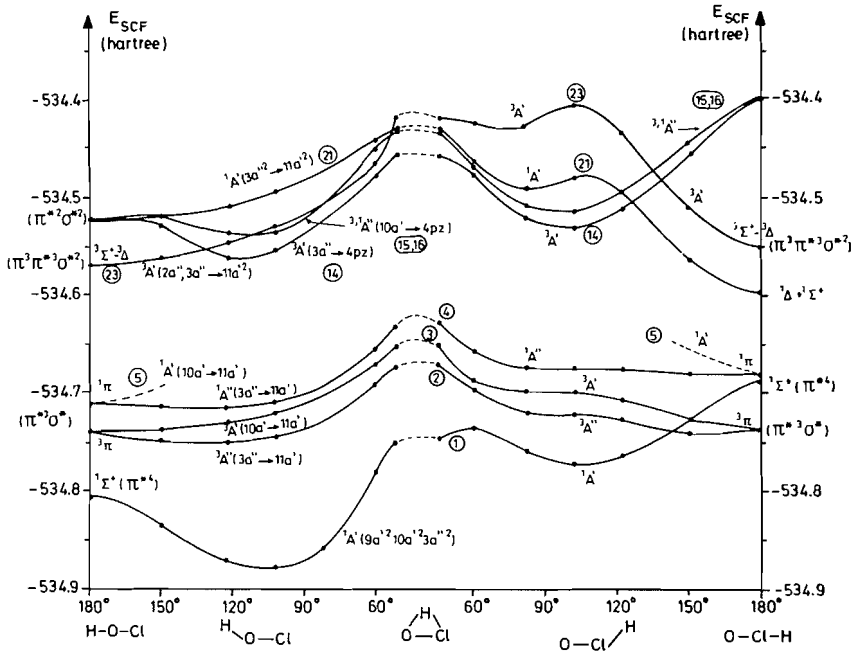

FIG. 4. SCF potential curves for the angular interconversion of HOCl and HClO in ground and various excited states (OH = $1.83a_0$ and ClO = $3.194a_0$ for HOCl and HCl = $2.48a_0$ and ClO = $3.10a_0$ for HClO). The enumeration of the potential curves is made according to the notation of Table 3. The $10a' \rightarrow 11a'\,^1A'$ state has not been treated in the SCF calculations but an estimate of the nature of its potential curve (as indicated with a dashed line) is given, based on subsequent CI calculations.

the various species in different symmetry and the abbreviations used in the figure are indicated in Table 3, along with details of the corresponding CI calculations. The SCF potential energy curves show that all the states under discussion are higher in energy in the less stable HClO form than in HOCl, and CI calculations (Fig. 5) carried out for the four representative points, linear HOCl, equilibrium HOCl, equilibrium HClO, and linear HClO, demonstrate that the relative spacing and form of the SCF curves is not unrealistic in this case (HOCl and HClO vertical transition energies are given in Table 4). A barrier for interconversion from HClO to HOCl is indicated for each state, however, but optimization of the various structural parameters is expected to reduce these quantities relative to Fig. 4 and probably eradicate them entirely in some instances. On the other hand, in states such as the $^{3,1}A'$ $(10a' \rightarrow 11a')$ pair (curves *4* and *5*) which strongly prefer the linear nuclear arrangement in HClO it is quite unlikely that the corresponding barriers disappear upon optimization of the internuclear distances at each bond angle. Nonetheless since the HClO ground state is considerably more stable in the bent geometry it is possible that no barrier to angular interconversion is actually present in this important case. In this connection it is interesting that a substantial barrier for HNC → HCN interconversion (of the order of 35 kcal (13)) and also for $HOC^+ \rightarrow HCO^+$ (14) is found in calculations, while only a very small barrier results for the related HSiN → HNSi process (of the order of 4 kcal (15))

TABLE 3. Characterization of HOCl states treated and technical details of the CI calculations. The corresponding HClO states are treated in a similar manner

State	Label	Excitation[a]	Treatment[b] (nM/mR)	Secular equation generated/solved	Corresponding $C_{\infty v}$ symmetry
$X\,^1A'$	1	—	2/1	17181/2353	$\sigma^2\pi^4\pi^{*4}\sigma^{*0}$
$^3A''$	2	$3a'' \rightarrow 11a'$	2/1	63498/2829	
$^1A''$	4		2/1	38160/2785	$\pi^* \rightarrow \sigma^*$
$^3A'$	3	$10a' \rightarrow 11a'$	2/1	53264/2804	
$^1A'$	5		3/1	39933/2789	
$^3A''$	6	$2a'' \rightarrow 11a'$	6/2	119127/4739	$\pi \rightarrow \sigma^*$
$^1A''$	7		6/2	72168/4795	
$^1A''$	8	$3a'' \rightarrow 4s$	3/1	79690/2733	$\pi^* \rightarrow 4s$
$^3A'$	9	$9a' \rightarrow 11a'$	5/1	114121/2581	$\sigma \rightarrow \sigma^*$
$^1A'$	10		9/1	84563/2540	
$^1A'$	11	$10a' \rightarrow 4s$	5/1	108781/2773	$\pi^* \rightarrow 4s$
$^1A''$	12	$3a'' \rightarrow 4p(a')$	5/2	130204/5061	
$^1A''$	13	$3a'' \rightarrow 4p(a')$			
$^1A'$	14	$3a'' \rightarrow 4p(a'')$	1/1	19446/2781	$\pi^* \rightarrow 4p\sigma$
$^3A''$	15	$10a' \rightarrow 4p(a'')$	5/1	113668/2877	$\pi^* \rightarrow 4p\pi$
$^1A''$	16		5/1	68644/2679	
$^1A'$	17	$10a' \rightarrow 4p(a')$	9/2	210619/3537	
$^1A'$	18	$10a' \rightarrow 4p(a')$			
$^3A''$	19	$3a''10a' \rightarrow 11a'^2$	5/2	109662/5232	
$^1A''$	20		5/2	66288/5227	$\pi^{*2} \rightarrow \sigma^{*2}$
$^1A'$	21	$3a''^2 \rightarrow 11a'^2$	2/1	17775/2566	
$^3A'$	22	$10a'^2 \rightarrow 11a'^2$	Estimated from a less extensive calculation		
$^3A'$	23	$2a''3a'' \rightarrow 11a'^2$	1/1	33891/2542	$\pi\pi^* \rightarrow \sigma^{*2}$
$^2A''$	30	$3a'' \rightarrow \infty$	4/2	120670/3950	$\pi^* \rightarrow \infty$
$^2A'$	31	$10a' \rightarrow \infty$	4/2	90181/4053	
$^2A''$	32	$2a'' \rightarrow \infty$	4/2	120670/3950	$\pi \rightarrow \infty$
$^2A'$	33	$9a' \rightarrow \infty$	4/2	90181/4053	$\sigma \rightarrow \infty$

[a]Excitation is always taken relative to the ground state electronic configuration $8a'^2 2a''^2 9a'^2 10a'^2 3a''^2 11a'^0$.
[b]Selection of configurations is made for m roots while n main (or reference) species are employed for the configuration generation.

TABLE 4. Calculated vertical excitation energies in eV for low-lying states of HOCl and HClO

State	Label[a]	ΔE_e HOCl	ΔE_e HClO	State	Label	ΔE_e HOCl	ΔE_e HClO
$X\,^1A'$	1	0.0	0.0	$^3A'$	—	Not calc.[b]	—
$^3A''$	2	3.50	1.87	$^1A'$	11	8.34	7.25
$^1A''$	4	4.54	3.20	$^1A''$	12	8.36	—
$^3A'$	3	4.73	2.52	$^1A''$	13	8.55	—
$^1A'$	5	5.75	3.92				
$^3A''$	6	7.49	8.64	$^1A'$	14	8.60	7.00
$^1A''$	7	8.19	9.20	$^3A''$	15	9.45	—
$^3A''$	—	Not calc.[b]	—	$^1A''$	16	9.53	7.62
$^1A''$	8	7.16	5.73	$^1A'$	17	9.33	—
$^3A'$	9	7.92	(7.30)	$^1A'$	18	9.40	—
$^1A'$	10	9.97	—				
$^3A''$	19	9.42	6.57	$^2A''$	30	10.93	10.05
$^1A''$	20	9.93	8.46	$^2A'$	31	11.95	10.77
$^1A'$	21	9.92[c]	7.78	$^2A''$	32	14.55	15.30
$^1A'$	22	11.30	—	$^2A'$	33	15.48	15.42
$^3A'$	23	11.24	10.32				

[a]The numbering refers to the states given in Table 3.
[b]Since the singlet–triplet splitting is very small in Rydberg states, generally only one multiplet is calculated explicitly.
[c]This value is misprinted in I (8.92 instead of 9.92).

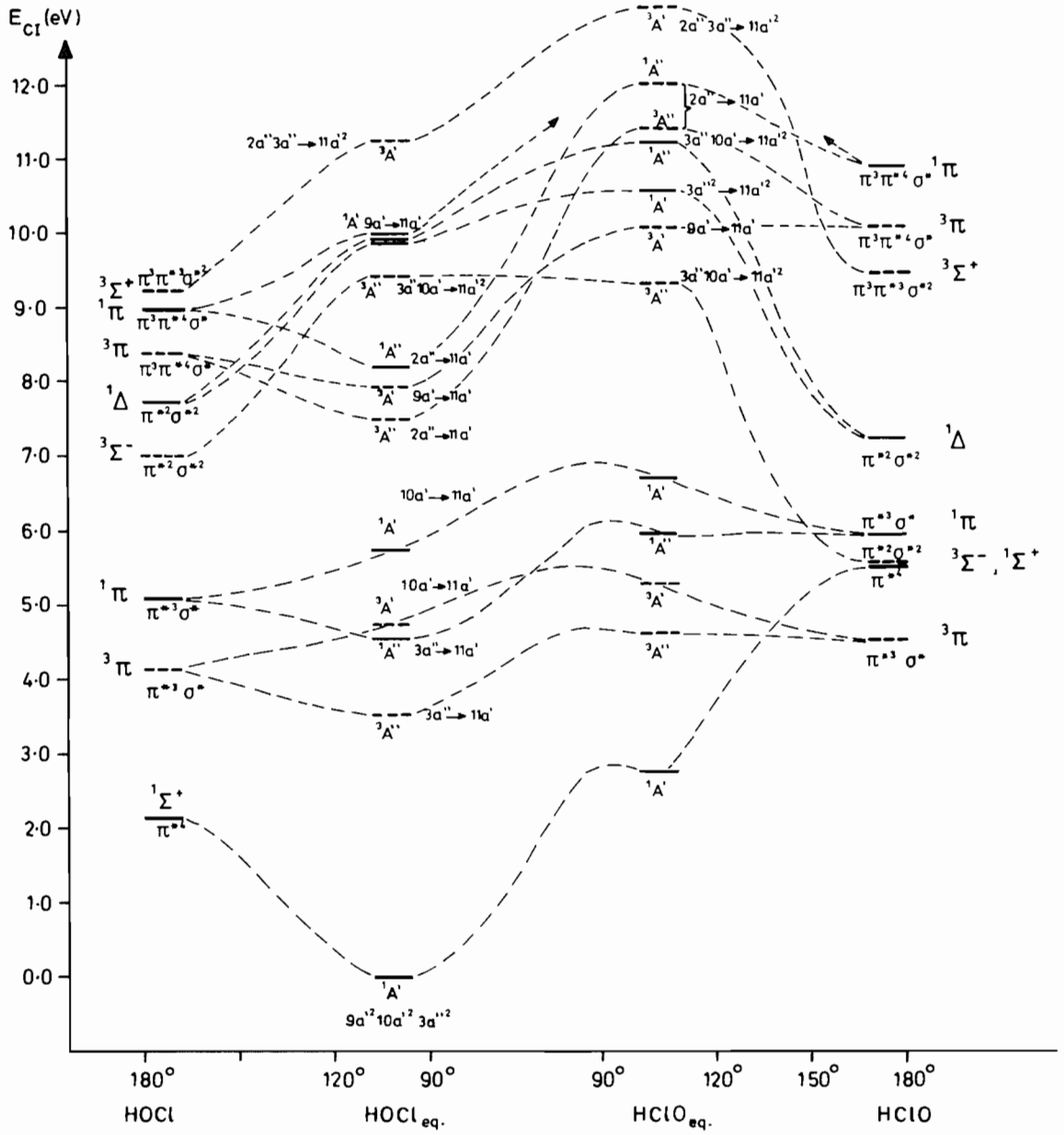

FIG. 5. Comparison of calculated CI energy levels for the ground and lowest-lying valence excited states of bent and linear HOCl and HClO. The dashed lines connect states of equivalent electronic configuration in each case (avoided crossings are not taken into account).

and no barrier at all for the HCS^+–HSC^+ pair (16), whereby HCS^+ is calculated to be the more stable by 110 kcal/mol.

One further observation (Figs. 4 and 5) is the finding that for linear HClO it is the $^3\Pi$ state which has the lowest energy and not the $^1\Sigma^+$; in addition there is another low-energy state $^3\Sigma^-$ ($\pi^{*2}\sigma^{*2}$) in close proximity to the $^1\Sigma^+$. This result can be traced back to the decidedly less stable σ MO in HClO[2] compared to HOCl (Fig. 1, *a* and *b*) and consequently its less antibonding (more stable) σ*

[2]The orbital energies of the π MO's are very similar: $\varepsilon(\pi) = -0.5764$, $\varepsilon(\pi^*) = -0.4303$ in the $^1\Sigma^+$ state of linear HOCl and $\varepsilon(\pi) = -0.5893$, $\varepsilon(\pi^*) = -0.4453$ in linear HClO, while the σ energies are −0.6946 and −0.6621 hartree respectively for $^1\Sigma^+$ of linear HOCl and HClO.

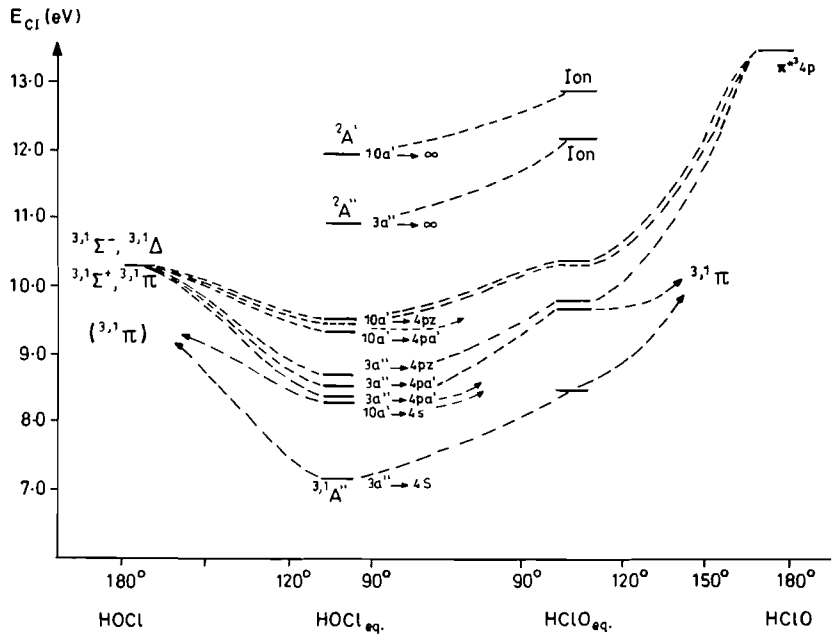

FIG. 6. Comparison of calculated CI energy levels for the lowest-lying Rydberg states and ions of bent and linear HOCl and HClO (fixed bond lengths of the same magnitudes as in Fig. 4). Estimated appearance of the corresponding angular potential curves is indicated in the figure with dashed lines; note that fewer states have actually been treated for the less stable HClO conformer.

species (Fig. 1*c*), whereby the π and π^* MO's exhibit very similar stability in both linear conformers. This situation, on the other hand, is not unusual since similar observations have been made in related molecule pairs such as HNO–HON (17, 18) or HCO^+–HOC^+ (14), for example, in which an exchange of singlet and triplet ground states or the reverse ordering of (π,π^*) and (σ,π^*) states in the respective pairs of isomeric forms has also been noted.

The end result of the various changes in relative orbital stability in the two systems is that the vertical transition energies of stable HOCl are generally much higher than for HClO, as can be seen in Table 4 as well as in Fig. 5. A similar but even more extreme example of this phenomenon has been found in the study of the HNSi–HSiN pair (15, 19), for which the lowest excited state becomes nearly isoenergetic with the closed shell ground state in the less stable (HSiN) form. Since as mentioned above there is at most a small barrier for angular interconversion of the HClO ground state to the much more stable HOCl species it is doubtful whether this clear distinction between these two systems can be observed experimentally. In this connection it should be noted, however, that there is still an open question concerning the HOCl spectrum, as observed by Fergusson *et al.* (20, 2). Although the first strong experimental band at 5.64 eV is quite plausibly assigned as the $2^1A'$–$^1A'$ transition of HOCl (calculated at 5.75 eV; Table 4), a second weaker system with an absorption maximum at 3.87 eV does not fit in well at all with any other dipole-allowed species for this system. The analogous ($2^1A'$–$^1A'$) transition in HClO does lie in the proper range (3.92 eV; Table 4), as does the $^3A''$–$^1A'$ HOCl species (3.50 eV), but it is certainly unclear whether either of these transitions is in any way related to the above experimental findings.

The analysis of the more highly excited states involving the π MO or double substitutions from π and π^* is more difficult since a number of states lying in the same energy region are mixed (in the CI or already at the SCF level of treatment) because of the lower C_s symmetry of the bent molecule. There is also the additional complication that although σ ($8a'$) and π ($9a'$,$2a''$) are energetically well separated in the linear nuclear framework, the in-plane $8a'$ and $9a'$ components can mix so that for the equilibrium bent structure (see Fig. 1, *a* and *b*) it is the $9a'$ MO which possesses σ character in both isomers while the $8a'$ is predominantly an in-plane π orbital; hence identification of the dominant configuration in a given state must be coupled with the knowledge of the specific character of the MO's in order to allow for a proper microscopic description of the state.

A relatively clear pattern is present for the lowest members of the Rydberg states (Fig. 6). All first

singlet members for the most stable equilibrium form of HOCl are treated by CI calculations ($3a'' \rightarrow 4s$, $4p_x$, $4p_y$, and $4p_z$ and $10a' \rightarrow 4s$, $4p_x$, $4p_y$, $4p_z$), while calculation of the corresponding triplet species (with the exception of the $10a' \rightarrow 4p_z$) is not undertaken because of the well-known small triplet–singlet separation for such Rydberg states. The typical features of Rydberg states are obvious: the $4s$ state is found well below the $4p$ species, of which all spatial components lie very close in energy; furthermore the energy difference between the series originating from the $3a''$ and the $10a'$ MO and their respective ionic limits is very similar (approximately 30 000 cm^{-1} for the s series). The pattern of Rydberg levels for the other arrangements of nuclei is equivalent (even though not all states have been treated explicitly in CI calculations), especially once it is realized that $3a''$ and $10a'$ become degenerate in the linear molecular geometry.

The Rydberg states lying in the energy range between 7 and 13 eV might possibly mix with valence states (21) of the proper symmetry and energy (Fig. 5), although this feature has not been explicitly treated in the present work. On the other hand, such mixing is already partially accounted for in the SCF data of Fig. 4, and as a result the corresponding potential curves exhibit a rather unconventional form with several minima in some areas.

The valence-shell states involving higher than $\pi^* \rightarrow \sigma^*$ transitions are also calculated for HOCl and HClO in the CI treatment and the results are collected in Fig. 5 and Table 4. Correlation with corresponding states in the four nuclear conformations is shown, while crossing of states is only indicated; details concerning the various states are contained in Table 3. It is generally seen that the higher valence-shell states prefer a linear structure, while the Rydberg states (Fig. 6) are generally more stable in the bent nuclear arrangement (as are the corresponding ions), leading to the interactions of various states mentioned above.

4. The Molecules HOCl and HClO and their Fragments

In order to investigate the possible destruction of HOCl into its various components or formation therefrom, potential energy curves connecting the different partners in a number of electronic states are calculated and will be discussed in what follows.

A. HOCl and its Components HO + Cl

The calculated SCF curves for separation of HOCl into OH and a Cl atom are contained in Fig. 7 while the CI values for the pertinent end points are given in Fig. 8. It is obvious that the first valence states

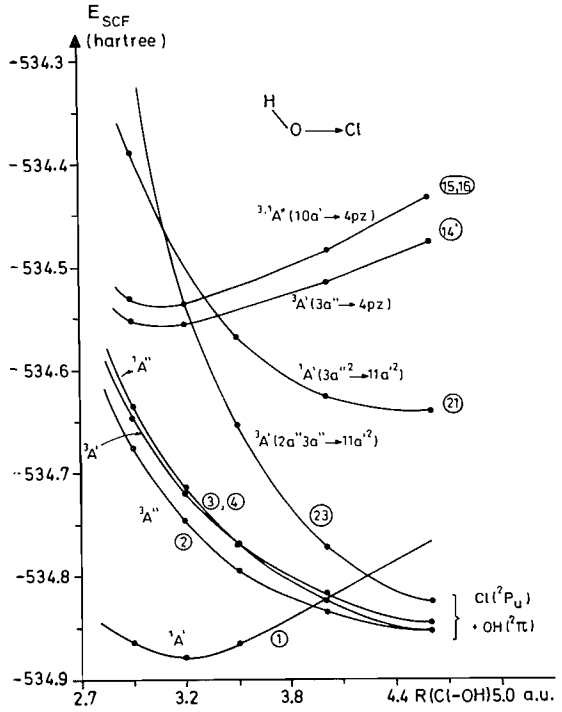

FIG. 7. SCF potential curves for Cl—O stretch in ground and various excited states of HOCl.

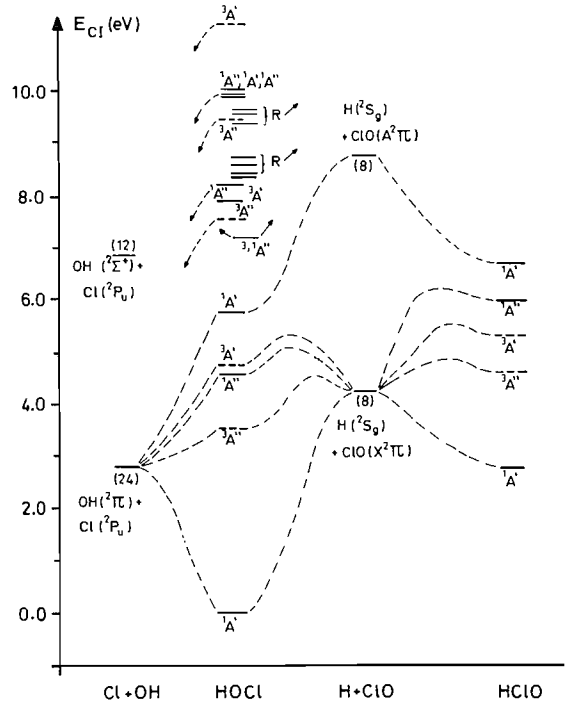

FIG. 8. Comparison of calculated CI energy levels of HOCl and HClO in ground and various excited states with those of the dissociation products H + ClO and OH + Cl respectively. (The degeneracies of the various fragment energy levels are given in parentheses in each case.)

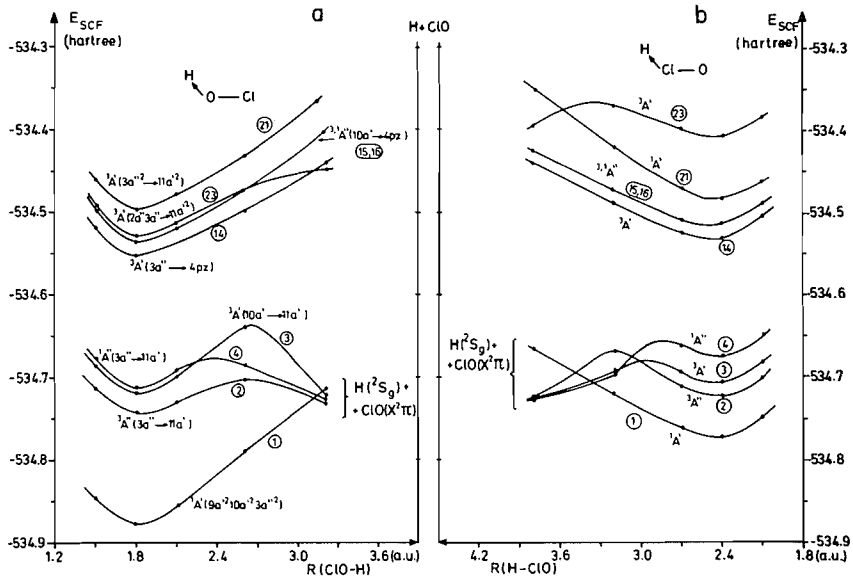

FIG. 9. SCF potential curves for hydrogen removal of (*a*) HOCl and (*b*) HClO in ground and various excited states (calculated equilibrium values for the ClO bond length and corresponding bond angle are used in each case).

$^{3,1}A'$ and $^{3,1}A''$ arising from $\pi^* \rightarrow \sigma^*$ excitations promote immediate decomposition into $OH(^2\Pi)$ and $Cl(^2P_u)$ as a consequence of populating the strongly ClO antibonding σ^* orbital, as has been pointed out earlier in I, as well as by Jaffe and Langhoff (2). The Rydberg states (Figs. 7 and 8) are not repulsive and show potential curves similar to that of the positive ion, i.e. they prefer a somewhat smaller Cl—O bond length than does the ground state, which is also stable with respect to Cl + OH separation. Various high-energy states (Figs. 7 and 8) populating the antibonding σ^* twice are strongly repulsive and furnish the remaining curves leading to the ground state products (Fig. 8). The conclusion from these results is that any excitation of HOCl below the first Rydberg species (7 eV) will immediately lead to fragmentation into OH and Cl (calculated fragment total energies are given in Table 5 of I for comparison with the HOCl vertical excitation energies in Table 4).

B. Hydrogen Removal Processes

The calculated SCF potential energy curves for hydrogen removal HOCl → H + ClO and HClO → H + ClO are contained in Fig. 9, *a* and *b*; the corresponding CI data are also presented in Fig. 8. Both ground state curves show the typical behavior of a bound state with one minimum[3], and approximately 95 kcal/mol must be added to the system in order to remove the hydrogen atom from HOCl in its ground state (Table 5 of I).[4] All excited states in Fig. 9 *a* and *b* with minima in the same general energy range as the ground state fragments H (^2S_g) + ClO ($^2\Pi$) exhibit a potential barrier for larger hydrogen distances. Although the calculated barriers in Fig. 9 *a* and *b* will most probably be reduced considerably when relaxation of the ClO bond is taken into account in the process, it is still likely that a small barrier remains in each case in analogy to what is found for similar states in HCO, HN_2, or HNO (for example see ref. 24). All potential energy curves involving HOCl or HClO Rydberg states correlate with electronically excited fragments and the SCF calculations of Fig. 9 again suggest that substantial energy is required before dissociation into H + ClO can take place via these states.

Finally consideration of Fig. 8, which shows the realistic relative positions of the various energy levels, makes it clear that loss of hydrogen in any of the HOCl states treated is extremely unlikely, especially since in the excited states dissociation into $OH(^2\Pi)$ + $Cl(^2P_u)$ can take place so easily instead. Similarly formation of the molecule in its ground state from $H(^2S_g)$ + $ClO(^2\Pi)$ is probably not

[3]The long-range SCF part must be corrected in the standard way to obtain a realistic description of the bond-breaking process involving the open-shell fragments.

[4]The measurement of a heat of formation for HOCl of −18 kcal/mol by Molina and Molina (22) and of −19 kcal/mol by Timmons (private communication, value of R. Timmons transferred to authors by D. Phillips (NASA)) as compared to the predicted value for this quantity in I of −19.2 ± 3.9 kcal, gives at least some indication of the overall reliability of the present *ab initio* results.

favored since the excess energy of this reaction would readily promote dissociation into OH and Cl. Furthermore although the OH + Cl destruction channel is not directly open to the HClO isomer, consideration of Fig. 5 suggests that a small supply of energy in the bending vibrational mode might favor interconversion from the HClO excited states into HOCl (not even considering the HCl + O pathway), which again would be followed by fragmentation into OH + Cl rather than dissociation from the excited HClO states into H + ClO.

C. HClO and the Components O + HCl

The SCF potential energy curves connecting the fragments O and HCl with the system HClO are given for various states in Fig. 10 (whereby the internuclear angle of 102.4° is held constant) while the complementary CI data are contained in Fig. 11. In this case the adiabatic correlation of states is especially simple since all low-lying triplet HClO states correlate with $O(^3P_g)$ + $HCl(^1\Sigma^+)$, while the corresponding singlet species must be connected with $O(^1D_g)$ + $HCl(^1\Sigma^+)$. It is seen that except for that of the ground state the low-energy curves are all

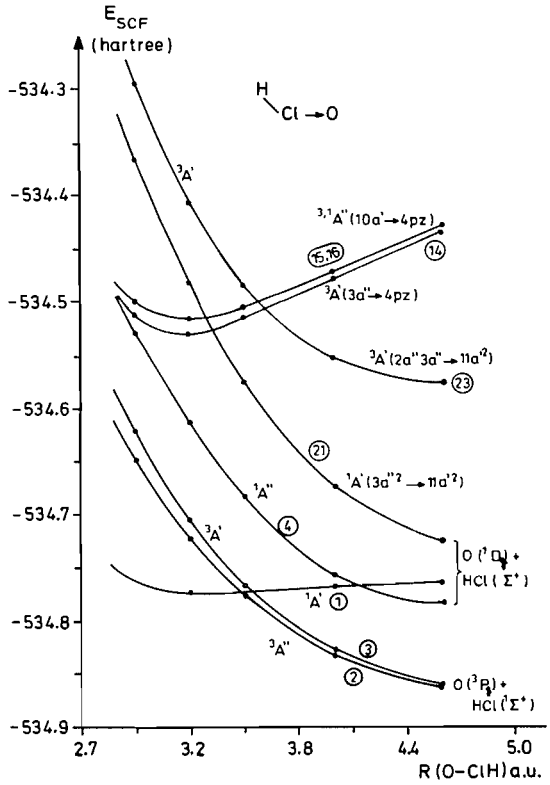

FIG. 10. SCF potential curves for Cl—O stretch in ground and various excited states of the HClO system (calculated equilibrium values for the H—Cl bond length and HClO bond angle are assumed throughout).

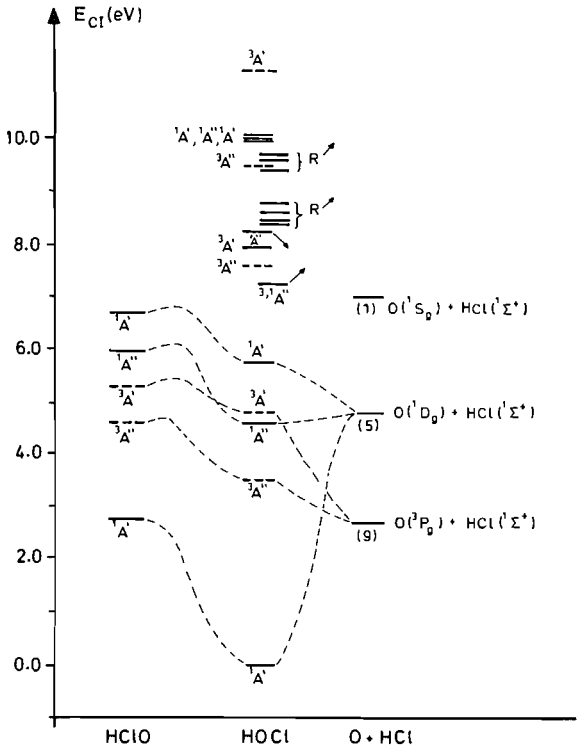

FIG. 11. Comparison of calculated CI energy levels of HOCl and HClO with those of various O + HCl dissociation products. (The degeneracies of the various fragment energy levels are given in parentheses in each case.)

repulsive, favoring dissociation into O + HCl in a manner quite similar to the HOCl dissociation (Fig. 7) into OH + Cl.

The reaction $O(^1D_g)$ + HCl has been studied experimentally (25) and it has been found to yield the products OH + Cl rather than ClO + H. According to the present study this reaction could proceed with very little activation energy (if any) in a favorable geometrical position via the lowest excited $^1A''$ state (which is essentially isoenergetic with $O(^1D_g)$ + HCl $(^1\Sigma^+)$ if the oxygen inserts to give the HOCl arrangement; see Fig. 11), which has been shown to be strongly repulsive with respect to the OH + Cl fragments. Reaction via the ground state HClO–HOCl surface could lead to an HOCl entity provided the high excess energy of this reaction can be set free appropriately. Again, as discussed earlier (Fig. 8), dissociation into OH + Cl is preferred over that in H + ClO in any of the low-energy HOCl states, in accordance with experimental observation (2, 25).

The rate of the corresponding triplet reaction $O(^3P_g)$ + $HCl(^1\Sigma^+)$ → $OH(^2\Pi)$ + $Cl(^2P_u)$ has been investigated by various experimental techniques (11, 26–29) and an activation barrier of approximately 0.25 eV (11, 25) has been estimated. From

the overall experimental evidence there is an indication (25, 30), although not conclusive (11), that this reaction proceeds via a non-adiabatic transition from the triplet to the lowest-lying singlet surface, as discussed by Nikitin and co-workers (30, 31). Furthermore the absence of vibrational to translational and rotational energy transfer is taken as an indication (28) that the representative pathway cuts the corner of the potential energy surface and does not penetrate into the deep HOCl equilibrium well.

According to the present potential energy curves a pathway involving the $^3A''$ state is only conceivable with a low activation energy of a few kcal/mol if the hydrogen migration occurs for large O—Cl distances and requires very little energy for such structures; since the corresponding potential energy surfaces (Figs. 4 and 5) are only calculated for structures close to equilibrium, the present study cannot support or discard this possibility. Because of the strongly repulsive nature of the $^3A''$ curve an intersection with the corresponding singlet to yield a stable HOCl molecule via a spin–orbit curve crossing must also occur at quite large O—Cl distances, unless (as in the previous case) the repulsive nature changes considerably with the angle of approach of oxygen to HCl, a situation which is unlikely to occur. A curve crossing is found in CI calculations for $\angle HClO = 140°$, $HCl—O = 3.45a_0$, for example, but this point is already 1.0 eV above the initial products, so that a study of this phenomenon must involve larger HCl—O separations.

5. Vertical Ionization of HOCl and HClO

The ground state for both the $HOCl^+$ and $HClO^+$ isomers is a $^2A''$ species, arising from the loss of an electron from the corresponding $3a''$ MO in the respective neutral system. Because of the nodal characteristics of the latter orbital it can be predicted from Walsh's rules that little change in equilibrium geometry accompanies ionization in this instance. Hence it is expected that the values for the vertical minimum IP for both HOCl and HClO will be only slightly higher than for the corresponding adiabatic quantities. The lowest ionization potential of HOCl has recently been measured experimentally to be 11.22 eV (32), in good agreement with the present calculated value of 10.90 eV (Table 4), as well as with another theoretical result given in the literature (33). Furthermore because of the above geometrical considerations for such ions it is possible to identify the energy difference between lowest and higher vertical IP's with the vertical transition energies of the ion itself. In the case of $HOCl^+$ the results obtained in this manner (1.08, 3.62, and 4.55 eV) correspond to transitions into the $3a''$ MO from the $10a'$, $2a''$, and $9a'$ orbitals respectively and are found to be in good agreement with experimental values for these quantities (32).

If the lowest adiabatic IP is taken to be 11.1 eV (32) the heat of formation of $HOCl^+$ can thus be estimated to be in the order of 237 kcal/mol, based on the ΔH_f^0 value for HOCl of -19 kcal/mol discussed earlier (1, 22). The $HOCl^+$ heat of formation can then be combined with known ΔH_f^0 values for possible dissociation fragments of this system to obtain predictions of its bond strengths. For example, heats of reaction of the order of 100 kcal/mol each are thereby indicated for decomposition into both $Cl^+(^3P_g) + OH(^2\Pi)$ and $Cl(^2P_u) + OH^+(^3\Sigma^-)$. Comparison of these results with the corresponding value for the neutral reaction, $HOCl \rightarrow Cl(^2P_u) + OH(^2\Pi)$, of 57 kcal/mol leads to the conclusion that the ClO bond is some 43 kcal/mol stronger in $HOCl^+$ than in neutral HOCl; such a finding is clearly consistent with the ClO antibonding characteristics of the $3a''$ (π^*) species from which ionization takes place. On the other hand, similar calculations indicate that the OH bond strength is very nearly the same (95 kcal/mol) before and after the $3a''$ ionization, as again seems quite reasonable based on the lack of H-atom character in this molecular orbital.

Analogous calculations can be made for the $HClO^+$ system, for which a ΔH_f^0 value of 260 ± 5 kcal/mol results. Taking the difference between these two ΔH_f^0 values leads to an estimate for the isomerization energies of $HOCl^+$ and $HClO^+$ of 22 ± 5 kcal/mol, markedly less than for the corresponding neutral systems. By comparison the isomerization energy for the HSO–SOH pair of the same number of electrons as the ions has been calculated at a similar level of CI treatment (23) to be 12 kcal/mol, again with the system containing the second-row atom in the terminal position indicated to be the more stable. Finally it is found that the Cl—O bond of $HClO^+$ should be 75 kcal/mol stronger than in HClO, while its H—Cl counterpart should be about 35 kcal/mol stronger than in the neutral system.

6. Conclusion

The present study has investigated various points of the potential energy surface of the HOCl–HClO system in ground and a number of excited states in connection with interconversion of the two isomeric forms and their fragmentation into (or formation from) OH, Cl, H, ClO, HCl, $O(^3P_g)$, and $O(^1D_g)$. It is found that the ground state and the four lowest singlet and triplet states occupying the σ^* MO can be followed very easily from products to various fragments, while higher excited species, including the

Rydberg states, will generally change their energy ordering among one another upon structural deformations so that no definite reaction channels will be preferred in the higher-energy range of fragments and products.

The calculations indicate further that isomer conversion into the more stable HOCl form is likely in the ground state without substantial activation barrier, but that in at least some of its excited states HClO prefers a linear nuclear arrangement and should not be easily converted into HOCl in these cases. In general the antibonding π^* and σ^* MO's in these systems are found to be relatively more stable in HClO than in HOCl, while the opposite is true for the corresponding bonding orbitals. As a result the vertical transition energies in the less stable HClO conformer are often markedly smaller than for the corresponding excitations in HOCl.

All four first excited states $^{3,1}A''$ and $^{3,1}A'$ (and also higher species) exhibit strongly repulsive potential energy curves and hence decidedly favor dissociation into $OH(^2\Pi) + Cl(^2P_u)$ as soon as one of these excited states is populated. Since furthermore this fragment energy is considerably lower than that of $H(^2S_g) + ClO(X^2\Pi)$, decomposition into OH + Cl is preferred over hydrogen removal; in addition it is found that barriers towards hydrogen removal are present even in the excited states, as has been observed in related systems, and this eventuality makes such processes even less likely. Dissociation of HOCl in its first two triplet excited states also seems possible via repulsive energy curves into $O(^3P_g) + HCl(^1\Sigma^+)$, i.e. fragments which are practically isoenergetic with $OH(^2\Pi) + Cl(^2P_u)$; on the other hand, crossing with the ground state singlet curve might introduce (via spin–orbit coupling) some complications. Decomposition of HOCl in its first two singlet states into $O(^1D_g) + HCl(^1\Sigma^+)$ via repulsive potential energy surfaces is also conceivable, although the energetically more favorable channel OH + Cl is probably preferred in this case.

Acknowledgements

One of us (G.H.) wishes to thank the Studienstiftung des Deutschen Volkes for a stipend to work on the present problem. The services and computer time made available by the Computer Center (RHRZ) of the University of Bonn are hereby gratefully acknowledged.

1. G. Hirsch, P. J. Bruna, S. D. Peyerimhoff, and R. J. Buenker. Chem. Phys. Lett. **52**, 442 (1977).
2. R. L. Jaffe and S. R. Langhoff. J. Chem. Phys. **68**, 1638 (1978).
3. F. C. Fehsenfeld, P. J. Crutzen, A. L. Schmeltekopf, C. J. Howard, D. L. Albritton, and E. E. Ferguson. J. Geophys. Res. **81**, 4454 (1976).
4. P. Warneck. Z. Naturforsch. **32a**, 1254 (1977).
5. T. H. Dunning. J. Chem. Phys. **53**, 2823 (1970).
6. A. Veillard. Theor. Chim. Acta, **12**, 405 (1968).
7. R. J. Buenker, S. D. Peyerimhoff, and W. Butscher. Mol. Phys. **35**, 771 (1978).
8. A. M. Mirri, F. Scappini, and G. Cazzoli. J. Mol. Spectrosc. **38**, 218 (1971).
9. S. D. Peyerimhoff and R. J. Buenker. J. Chem. Phys. **47**, 1953 (1967).
10. S. F. Boys. Theory of atoms, molecules and solids. *Edited by* P. O. Löwdin. Academic Press, New York, NY. 1966.
11. R. D. H. Brown and I. W. M. Smith. Int. J. Chem. Kinet. **7**, 301 (1975).
12. J. Wolfrum. Ber. Bunsenges. Phys. Chem. **81**, 114 (1977).
13. P. K. Pearson, H. F. Schaefer III, and U. Wahlgren. J. Chem. Phys. **62**, 350 (1975).
14. P. J. Bruna, S. D. Peyerimhoff, and R. J. Buenker. Chem. Phys. **10**, 323 (1975).
15. R. Preuß, R. J. Buenker, and S. D. Peyerimhoff. J. Mol. Struct. **49**, 171 (1978).
16. P. J. Bruna, S. D. Peyerimhoff, and R. J. Buenker. Chem. Phys. **27**, 33 (1978).
17. P. J. Bruna and C. M. Marian. Results of this laboratory.
18. G. A. Gallup. Inorg. Chem. **14**, 563 (1975).
19. R. Preuß, R. J. Buenker, and S. D. Peyerimhoff. Chem. Phys. Lett. **62**, 21 (1979).
20. W. C. Ferguson, L. Slotin, and D. W. G. Style. Trans. Faraday Soc. **32**, 956 (1936).
21. R. J. Buenker and S. D. Peyerimhoff. Chem. Phys. Lett. **36**, 415 (1975); S. D. Peyerimhoff. Gazz. Chim. Ital. **108**, 411 (1978).
22. L. T. Molina and M. J. Molina. J. Phys. Chem. **82**, 2410 (1978).
23. A. B. Sannigrahi, S. D. Peyerimhoff, and R. J. Buenker. Chem. Phys. **20**, 381 (1977); R. J. Buenker, P. J. Bruna, and S. D. Peyerimhoff. Isr. J. Chem. To be published.
24. S. D. Peyerimhoff. Ber. Bunsenges. Phys. Chem. **78**, 119 (1974); K. Vasudevan, S. D. Peyerimhoff, and R. J. Buenker. J. Mol. Struct. **29**, 285 (1975); P. J. Bruna, R. J. Buenker, and S. D. Peyerimhoff. J. Mol. Struct. **32**, 217 (1976); A. A. Wu, S. D. Peyerimhoff, and R. J. Buenker. Chem. Phys. Lett. **35**, 316 (1977).
25. M. C. Addison, R. J. Donovan, and H. M. Gillespie. Chem. Phys. Lett. **44**, 602 (1976).
26. W. Hack, G. Mex, and H. G. Wagner. Ber. Bunsenges. **81**, 677 (1977).
27. A. R. Raviskankara, G. Smith, R. T. Watson, and D. D. Davis. J. Phys. Chem. **81**, 2220 (1977).
28. B. A. Blackwell, J. C. Polanyi, and J. J. Sloan. Chem. Phys. **24**, 25 (1977).
29. J. E. Butler, J. W. Hudgens, M. C. Lin, and G. K. Smith. Chem. Phys. Lett. **58**, 216 (1978).
30. E. E. Nikitin and A. V. N. Konrat'ev. Translation from Dokl. Akad. Nauk SSSR, **212**, 149 (1973).
31. E. E. Nikitin and S. Ya. Umanskii. Discuss. Faraday Soc. **53**, 7 (1972).
32. D. Colbourne, D. C. Frost, C. A. McDowell, and N. P. C. Westwood. J. Chem. Phys. **68**, 3574 (1978).
33. D. P. Chong, F. G. Herring, and Y. Takahata. J. Electron Spectrosc. Relat. Phenom. **13**, 39 (1978).

9-Oxobenzomorphans. I. General syntheses of dihydrobenz[*e*]indolines as key intermediates

GERRY KAVADIAS,[1] STEPHAN VELKOF, AND BERNARD BELLEAU

Bristol Laboratories of Canada, 100 Industrial Boulevard, Candiac, P.Q., Canada J5R 1J1

Received December 20, 1978

GERRY KAVADIAS, STEPHAN VELKOF, and BERNARD BELLEAU. Can. J. Chem. **57**, 1852 (1979).

Various 5,9b-dihydrobenz[*e*]indolines were synthesized by three general methods: (*a*) by alkylation with the appropriate alkyl halide of 1,2,4,5-tetrahydro-1*H*-benz[*e*]indoles, themselves obtained by alkylation with bromochloroethane of enamines derived from 7-alkoxy-2-tetralones; (*b*) from 1-alkylaminoethyl-2,2-ethylenedioxy-1,2,3,4-tetrahydronaphthalenes by acid hydrolysis, and (*c*) by reduction of 2-oxo-2,3,5,9b-tetrahydro-1*H*-benz[*e*]indoles which in turn were obtained from ethyl 2-oxo-1,2,3,4-tetrahydro-1-naphthalene acetates by reaction with methylamine followed by dehydration. These substances are key intermediates in the synthesis of 9-oxobenzomorphans.

GERRY KAVADIAS, STEPHAN VELKOF et BERNARD BELLEAU. Can. J. Chem. **57**, 1852 (1979).

On a synthétisé diverses dihydro-5,9b benz[*e*] indolines par trois méthodes générales: (*a*) par alkylation, à l'aide d'un halogénure d'alkyle approprié, de tétrahydro-1,2,4,5 1*H*-benz[*e*] indoles, eux mêmes obtenus par alkylation avec du bromochloroéthane des ènamines provenant d'alkoxy-7 tétralones-2; (*b*) par hydrolyse acide d'alkylaminoéthyl-1 éthylènedioxy-2,2 tétrahydro-1,2,3,4 naphtalènes et (*c*) par réduction des oxo-2 tétrahydro-2,3,5,9b 1*H*-benz[*e*] indoles qui sont obtenus à partir des oxo-2 tétrahydro-1,2,3,4 naphtalènes acétates d'éthyle-1 par réduction avec de la méthylamine suivie par une déshydratation. Ces substances sont des intermédiaires clés dans la synthèse des oxo-9 benzomorphanes.

[Traduit par le journal]

As part of our continuing search for medicinally useful analgesics, it became necessary to have ready access to variously substituted 9-oxobenzomorphans. The best known method for their synthesis is the one described by Murphy *et al.* (1) more than 20 years ago. This process involves as the ultimate step the pyrolysis of a quaternary salt such as the methiodide of 2′-methoxy-2,5-dimethyl-9-oxo-6,7-benzomorphan and accordingly its applicability is limited to compounds that can survive the vigorous pyrolytic conditions. A new general process for the synthesis of 9-oxo-benzomorphans was therefore developed and after our work was completed, Takeda *et al.* (2) described an approach which is conceptually similar. However, in our hands, the process described by these authors was not generally applicable and led to low yields of product. In this paper we wish to describe three general methodologies (Schemes 1–3) which provide for ready accessibility to 5,9b-dihydrobenz[*e*]indolines **5***a–h* (Fig. 1) as key intermediates in the synthesis of the desired 9-oxobenzomorphans (see accompanying papers).

Treatment of the 2-tetralones **1***a,b* with the appropriate amines according to published procedures (3, 4) afforded the enamines **2***a–d* in 96–99% yields (Scheme 1).

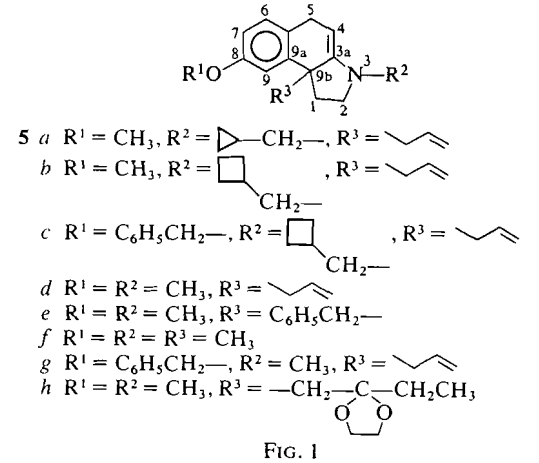

FIG. 1

Applying a procedure similar to that previously described by Evans *et al.* (4) for the synthesis of 3-methyl-1,2,4,5-tetrahydro-3*H*-benz[*e*]indole, the enamines **2***a–d*, after conversion to 'bidendate' nucleophiles with isopropyl magnesium chloride, were reacted with bromochloroethane to give **3***a–d* in 95–99% yields. The nmr spectra of these products lacked any olefinic proton resonances in the region δ 3.3–6.3, thus ruling out the formation of the isomeric enamines with the double bond unconjugated with the benzene ring (5). The benz[*e*]indolines **3***a–d* were alkylated with the appropriate alkyl halides to

[1]To whom correspondence may be addressed.

0008-4042/79/141852-09$01.00/0

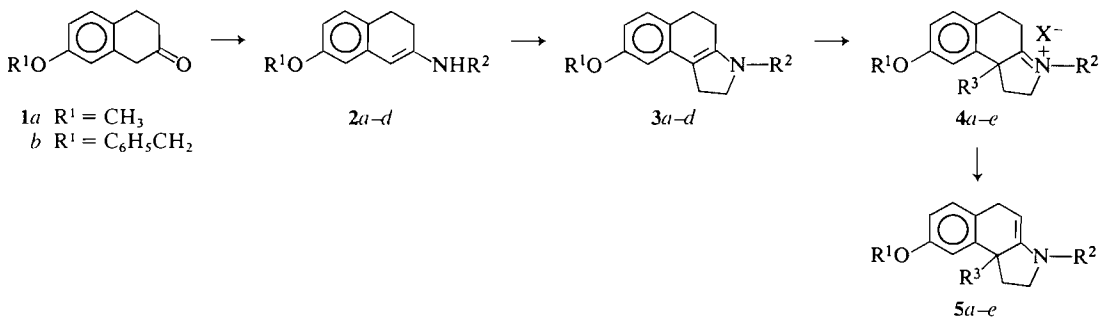

		R¹	R²	R³	X
2 and 3	a	CH_3		—	—
	b	CH_3		—	—
	c	$C_6H_5CH_2$		—	—
	d	CH_3	CH_3	—	—
4	a	CH_3			Br
	b	CH_3			Br
	c	$C_6H_5CH_2$			Br
	d	CH_3	CH_3		Picrate ion
	e	CH_3	CH_3	$C_6H_5CH_2$	Picrate ion

SCHEME 1

produce **4***a–e*. To some extent *N*-alkylation was a competing reaction and the ratio of the desired *C*-alkylated products to *N*-alkylated compounds varied with the alkylating agent and the solvent (6). Thus, alkylation of **3***a–c* with allyl bromide in acetonitrile proceeded mainly to give *C*-alkylation. The expected products **4***a–c* (X = Br) were thus obtained in 60–63% yields in pure crystalline form. Alkylation of **3***d* with allyl bromide in the same solvent produced the *C*-alkylated product, isolated as the picrate salt **4***d*, in 76% yield. The yields of **4***a–d* were approximately 10% lower when benzene was used as the solvent in place of acetonitrile. The effect of solvent was more pronounced when benzyl chloride was employed as the alkylating agent. For instance, reaction of **3***d* with benzyl chloride in solvents such as benzene, dioxane, or acetonitrile produced the *C*-alkylated product **4***e*, isolated as the picrate salt in yields of 10, 39, and 46%, respectively. Alkylation of **3***d* with methyl iodide in benzene or acetonitrile provided the methiodide of **3***d* as the major product (82–92%). The salts **4***a–e* were stable and could be conveniently stored at room temperature for several months. When treated with base they were quantitatively converted to the oxygen-sensitive benz[*e*]indolines **5***a–e*.

An alternative synthesis of **5***a* and **5***b* is outlined in Scheme 2. Alkylation of the sodium enolate of **6***a* with chloroacetonitrile in DMF afforded **7** in good yield (76%). The conversion of **7** into **8** was carried out without difficulty. Reduction of the ketal nitrile **8** with lithium aluminium hydride in ether produced the ketal amine **9** in quantitative yield. Acylation of **9** with the appropriate acyl halides gave the amides **10***a,b* which after reduction with lithium aluminium hydride afforded the ketal amines **11***a,b*. Acid hydro-

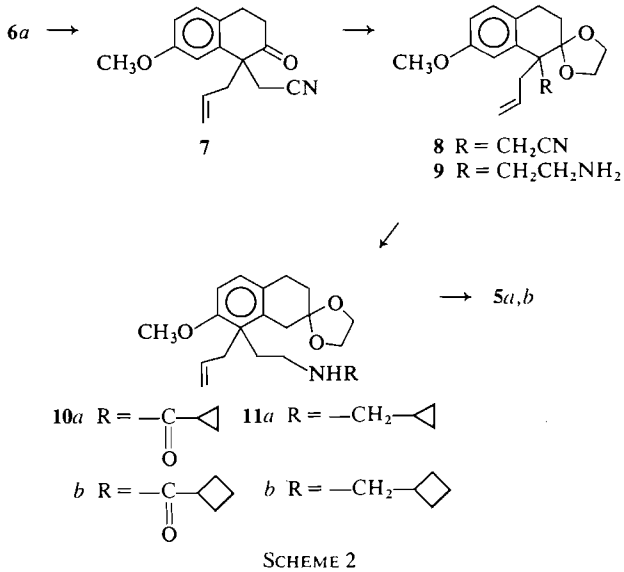

SCHEME 2

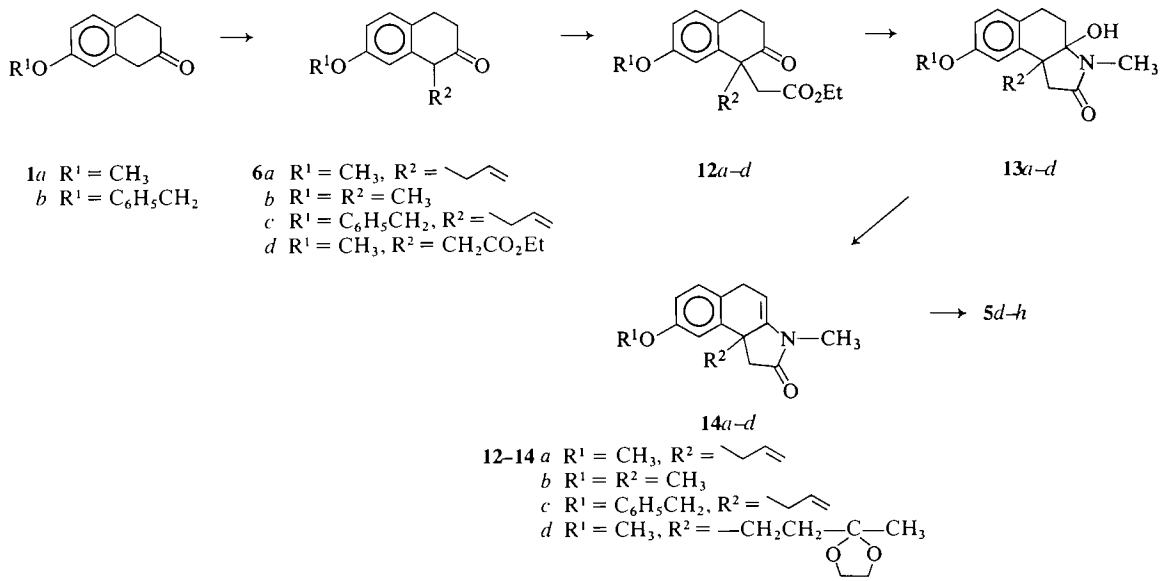

SCHEME 3

lysis of **11***a* produced the dihydrobenz[*e*]indoline **5***a* in 92% yield which was identical in every respect with the product obtained according to Scheme 1. Analogously, the ketal amine **11***b* was converted to **5***b* (98%) which was also identical to the product obtained above by Scheme 1.

A third process for the synthesis of 5,9b-dihydrobenz[*e*]indolines is shown in Scheme 3 and was applied to the preparations of **5***d–h*. Alkylation of the 2-tetralones **1***a,b* with the appropriate alkyl halides by Stork's enamine procedure (1*a*, 3), produced **6***a–d* in 67–94% yields. The subsequent alkylation of the sodium enolates of **6***a–d* with ethyl bromoacetate in dimethylformamide afforded the 1,1-disubstituted products **12***a–d* in good yields (66–88%). Treatment of **12***a–d* with excess methyl amine in ethanol produced the hydroxy lactams **13***a–d* (80–86% yields) in crystalline form, except for **13***d* which was a syrup. Evidence for their assigned structures was provided by elemental analysis and ir spectroscopy. The ir spectra of **13***a–d* showed absorption bands for hydroxyl (3300–3500 cm^{-1}) and lactam-carbonyl groups (1670–1690 cm^{-1}), but no absorption bands for ketone-carbonyl. The hydroxy lactams **13***a–d* are relatively stable in crystalline forms and in solution at temperatures below 40°C. At higher temperatures, water is eliminated and they are quantitatively converted to the unsaturated lactams **14***a–d*. The conversion to **14***a–d* was preferably carried out by heating a solution of **13***a–d* in benzene or toluene with a catalytic amount of *p*-toluenesulfonic acid. Reduction of the unsaturated lactams **14***a–d* with lithium aluminium hydride in ether provided the corresponding dihydrobenz[*e*]-indolines **5***d–h* in 90–95% yield as air-sensitive oils.

The structures assigned to the products **5***a–h* are supported by ir and nmr spectroscopy. The ir spectra showed strong C=C absorption at 1670 cm^{-1}. The nmr spectra showed a one proton band in the area of δ 4.4 either as a doublet of doublets (X part of ABX system, J_1 = 5.5, and J_2 = 2.5 Hz) for **5***d–f* or as an unresolved band for **5***a–c*.

In view of the air sensitivity of the products **5***a–h* and of the intermediate enamines **2** and **3**, it was clearly advantageous to carry out the reactions and all other operations (such as extractions, filtrations, and evaporations) under an atmosphere of nitrogen. This precaution minimized air oxidation of the unstable products and led to comparatively good yields. Storage of **5***a–h* required conversion to stable salts such as hydrobromides and picrates from which they were quantitatively regenerated by treatment with base.

Experimental

The melting points were determined on a Mel-Temp melting point apparatus and are uncorrected. The ir spectra were recorded on a Unicam Sp-200G grating ir spectrometer. The nmr spectra were recorded on a Varian A-60A spectrometer using deuteriochloroform as the solvent. The chemical shifts are expressed in δ values using tetramethylsilane as internal reference. Microanalyses were performed by Micro-Tech Laboratories Inc., Skokie, IL, U.S.A. All experiments involving enamines, and work-up processes such as filtration, extraction, and release of vacuum after evaporation, were performed under a nitrogen atmosphere.

2-N-Cyclopropylmethylamino-7-methoxy-3,4-dihydronaphthalene (2a)

Into a three-neck round-bottomed flask fitted with mechanical stirrer, a Soxhlet extractor packed with molecular sieves (50 g, type 3A), a condenser, and a nitrogen inlet tube, was added 10.75 g (100 mmol) cyclopropylmethylamine hydrochloride, 0.75 mL water (to solubilize the salt), and 10.1 g (100 mmol) triethylamine. After stirring for 10–15 min to liberate the cyclopropylmethylamine, a solution of 12.30 g (70 mmol) of 7-methoxy-2-tetralone (**1***a*) in 100 mL benzene was added and the mixture (under nitrogen) was heated under reflux while stirring for 5 h. After cooling to room temperature, the solids (triethylamine hydrochloride) were filtered off quickly and washed with ether (50 mL). The combined filtrates and washings were evaporated to dryness to give 15.8 g (99%) of **2***a* as a pale yellow air-sensitive liquid; ir (neat): 3420 (NH), 1635 cm^{-1} (C=C—N); nmr δ: 0.15–1.15 (m, 5H, cyclopropyl), 2.15 (m, benzylic), 2.63–2.95 (m, 4H, allylic and N-CH_2), 3.40 (broad, 1H, NH), 3.75 (s, 3H, OCH_3), 5.18 (s, 1H, C-1H), 6.63–7.0 (m, 3H, ArH). *Anal.* calcd. for $C_{15}H_{19}NO$: C 78.57, H 8.35, N 6.11; found: C 78.93, H 8.41, N 6.03.

2-N-Cyclobutylmethylamino-7-methoxy-3,4-dihydronaphthalene (2b)

Employing the procedure described above for the synthesis of **2***a*, 7-methoxy-2-tetralone (70.4 g, 400 mmol) was reacted with cyclobutylmethylamine (generated *in situ* from 62.7 g (516 mmol) of its hydrochloride by treatment with an equimolar amount of triethylamine and 4.0 mL of water) in benzene (300 mL) to provide 93.4 g (96.5%) of **2***b* as a pale yellow air-sensitive syrup; ir (neat): 3420 (NH), 1635 cm^{-1} (C=C—N); nmr δ: 3.70 (s, 3H, OCH_3), 5.15 (s, 1H, C-1H), 6.25–6.90 (m, 3H, ArH). *Anal.* calcd. for $C_{16}H_{21}NO$: C 78.97, H 8.69, N 5.75; found: C 79.26, H 8.73, N 5.65.

7-Benzyloxy-2-N-cyclobutylmethylamino-3,4-dihydronaphthalene (2c)

In a manner analogous to that given for **2***a*, 7-benzyloxy-2-tetralone (36.5 g, 145 mmol) was reacted with cyclobutylmethylamine (generated *in situ* from 22.7 g (187 mmol) of its hydrochloride by treatment with an equimolar amount of triethylamine and 1.5 mL water) in benzene (110 mL) and the product isolated as above to yield 46.28 g (99%) of **2***c* as a pale yellow, air-sensitive syrup; ir (neat): 3420 (NH), 1635 cm^{-1} (C=C—N); nmr δ: 4.98 (s, 2H, $ArCH_2O$), 5.15 (s, 1H, C-1H), 6.35–7.40 (m, 8H, ArH). *Anal.* calcd. for $C_{22}H_{25}NO$: C 82.83, H 7.89, N 4.38; found: C 82.87, H 7.79, N 4.23.

7-Methoxy-2-N-methylamino-3,4-dihydronaphthalene (2d)

This compound was prepared according to the procedure described by Evans *et al.* (4) for the synthesis of 2-*N*-methylamino-3,4-dihydronaphthalene. Thus, into a dry, nitrogen-purged, 500 mL three-neck flask fitted with mechanical stirrer, dropping funnel, and nitrogen inlet tube was added a solution of 14.3 g (460 mmol) methylamine in anhydrous ether (100 mL) and a solution of 20.0 g (113.5 mmol) of 7-methoxy-2-tetralone in the same solvent (100 mL), and the solution was blanketed with nitrogen and cooled to −18°C (ice–methanol). A solution of 11.56 g (61 mmol) titanium tetrachloride in pentane (50 mL) was added dropwise while stirring over a 30 min period. After the addition was completed, the reaction mixture was stirred at room temperature for 1 h and then rapidly filtered. The solid residue was washed with ether (50 mL) and the filtrate and washings were combined. Removal of the solvent *in vacuo* gave 20.6 g (96%) of **2***d* as an oxygen-sensitive oil which crystallized on standing; ir (neat): 3430 (NH), 1630 cm^{-1} (C=C—N); nmr δ: 2.15 (m, 2H, benzylic), 2.55 (m, 2H, allylic), 2.70 (s, 3H, NCH_3), 3.15 (broad, NH), 3.70 (s, 3H, OCH_3), 5.13 (s, 1H, C-1H), 6.25–6.90 (m, 3H, ArH). *Anal.* calcd. for $C_{12}H_{15}NO$: C 76.15, H 7.99, N 7.40; found: C 75.44, H 7.92, N 7.19.

3-Cyclopropylmethyl-8-methoxy-1,2,4,5-tetrahydro-3H-benz[e]indole (3a)

This compound was prepared according to the procedure described by Evans *et al.* (4) for the synthesis of 3-methyl-1,2,4,5-tetrahydro-3*H*-benz[*e*]indole as follows. Into a dry, nitrogen-filled, 1 L three-neck flask fitted with reflux condenser, septum cap, dropping funnel, and magnetic stirrer, was added a solution of 38.55 g (167.9 mmol) of **2***a* in dry tetrahydrofuran (50 mL) under nitrogen. A 2.20 *M* solution of isopropylmagnesium chloride in THF (96.1 mL, 211.7 mmol) was added slowly with a syringe at such a rate as to maintain gentle reflux. After the addition was completed (15 min), 30.72 g (214.2 mmol) of bromochloroethane was added to the warm reaction mixture at a rate sufficient to maintain gentle reflux. After addition of the alkyl halide was completed, an additional 52.3 mL (115 mmol) of the Grignard reagent was added at a controlled rate. The reaction mixture was cooled in an ice-bath and 270 mL of 1 *M* aqueous solution of ethylenediaminetetraacetic acid tetrasodium salt was added slowly (with stirring) followed by 600 mL 1:1 ether–benzene. The organic layer was separated and the aqueous phase was extracted with ether. The combined extracts were washed with water (2 × 100 mL), dried ($MgSO_4$), and the solvent evaporated to yield 43.0 g (99%) of **3***a* as a pale yellow oxygen-sensitive oil; ir (neat): 1635 cm^{-1} (C=C—N). *Anal.* calcd. for $C_{17}H_{21}NO$: C 79.96, H 8.29, N 5.48; found: C 79.86, H 8.35, N 5.41.

3-Cyclobutylmethyl-8-methoxy-1,2,4,5-tetrahydro-1H-benz[e]indole (3b)

Employing the procedure described above for the preparation of **3***a*, compound **2***b* (93.4 g) was converted to **3***b* (98.0 g, 94.5%), a pale brown oxygen-sensitive oil; ir (neat): 1635 cm^{-1} (C=C—N). *Anal.* calcd. for $C_{18}H_{23}NO$: C 80.25, H 8.60, N 5.19; found: C 80.15, H 8.71, N 5.09.

8-Benzyloxy-3-cyclobutylmethyl-1,2,4,5-tetrahydro-1H-benz[e]indole (3c)

Employing the procedure described above for the preparation of **3***a*, compound **2***c* (46.0 g) was converted to **3***c*; yield 48.0 g (98%); ir ($CHCl_3$): 1635 cm^{-1} (C=C—N). *Anal.* calcd. for $C_{24}H_{26}NO$: C 83.43, H 7.87, N 4.06; found: C 83.72, H 7.77, N 3.96.

3-Methyl-8-methoxy-1,2,4,5-tetrahydro-1H-benz[e]indole (3d)

In a manner analogous to that given for **3***a*, compound **2***d* (19.0 g) was converted to **3***d* in 96% yield; ir (neat): 1635 cm^{-1} (C=C—N); nmr δ: 2.62 (s, 3H, NCH_3), 3.75 (s, 3H, OCH_3), 6.6–7.1 (m, 3H, ArH). A sample was converted to the picrate salt; mp 108.5–110°C (acetone–ether). *Anal.* calcd. for $C_{20}H_{21}N_4O_8$: C 53.93, H 4.75, N 12.58; found: C 53.79, H 4.65, N 12.68.

9b-Allyl-3-cyclopropylmethyl-8-methoxy-5,9b-dihydrobenz[e]indole (5a) and Its Hydrobromide Salt 4a

(a) Preparation from 3-Cyclopropylmethyl-8-methoxy-1,2,4,5-tetrahydro-3H-benz[e]indole (3a)

A solution of 43.0 g (167.9 mmol) of **3***a* and 25.0 g (206 mmol) of allyl bromide in dry benzene (120 mL) was heated under reflux while stirring under a nitrogen atmosphere for 10 h. An oily precipitate formed. After cooling to room temperature, the supernatant was decanted and the residue

treated with acetone (50 mL) to give a crystalline precipitate which was collected to give 36.3 g (57.5%) of **4***a* (X = Br), mp 160–165°C. An analytical sample was obtained by recrystallization from acetone–ether, mp 172–174°C. *Anal.* calcd. for $C_{20}H_{26}BrNO$: C 63.84, H 6.94, Br 21.24; found: C 63.94, H 6.94, Br 21.13.

The yield of crystalline **4***a* was 67% when acetonitrile was used as the solvent in place of benzene in the above procedure.

Benz[*e*]indoline **5***a* was quantitatively obtained from the hydrobromide **4***a* by treatment with 10% aqueous sodium hydroxide and extraction with ether; ir (neat): 1670 cm^{-1} (C=C—N); nmr δ: 3.77 (s, 3H, OCH_3), 4.35 (broad, 1H, NC=CH), 4.75–5.91 (m, 3H, olefinic), 6.5–7.1 (m, 3H, ArH).

(b) Preparation from **11***a*

To a solution of 30.4 g (85 mmol) of **11***a* in ethanol (125 mL) was added a solution of 4% hydrochloric acid (125 mL). The reaction mixture was stirred at room temperature overnight (16 h) and then concentrated under vacuum to about half its volume. It was made basic with 10% sodium hydroxide and extracted with ether (2 × 100 mL). The combined extracts were washed with water (2 × 80 mL), dried ($MgSO_4$), and the solvent evaporated *in vacuo* to give 23.0 g (92%) of **5***a*, which was identical to the material prepared in part (*a*) above.

9b-Allyl-3-cyclobutylmethyl-8-methoxy-5,9b-dihydrobenz[e]*indoline (***5***b) and Its Hydrobromide Salt* **4**b

(a) Preparation from 3-Cyclobutylmethyl-8-methoxy-1,2,4,5-tetrahydro-1H-benz[e]*indole (***3***b)*

A solution of 18.0 g (67 mmol) of **3***b* and 10.5 g (87 mmol) of allyl bromide in dry acetonitrile (60 mL) was heated under reflux under nitrogen for 16 h. After removal of the solvent *in vacuo*, the residue was treated with acetone (50 mL) and the crystalline product collected to give 15.5 g (59%) of **4***b*, mp 168–170°C. *Anal.* calcd. for $C_{21}H_{28}BrNO$: C 64.61, H 7.23, Br 20.47; found: C 64.38, H 7.25, Br 20.35.

The yield of crystalline **4***b* was 49% when benzene was used as the solvent in place of acetonitrile in the above procedure.

Benz[*e*]indoline **5***b* was quantitatively obtained from the hydrobromide **4***b* by treatment with sodium hydroxide and extraction with ether; ir (neat): 1670 cm^{-1} (C=C—N); nmr δ: 3.75 (s, 3H, OCH_3), 4.36 (broad, 1H, NC=CH), 4.75–5.9 (m, 3H, olefinic), 6.5–7.1 (m, 3H, ArH).

(b) Preparation from the Ketal Amine **11**b

Compound **11***b* (33.7 g) was treated with hydrochloric acid in aqueous ethanol and the product isolated as in the case of **5***a* (part (*b*)) to give 27.5 g (98%) of **5***b*, identical with the material obtained in part (*a*) above.

9-Allyl-8-benzyloxy-3-cyclobutylmethyl-5,9b-dihydrobenz[e]*indoline (***5***c) and Its Hydrobromide Salt* **4**c

A mixture of 48.0 g (139 mmol) **3***c* and 21.9 g (181 mmol) of allyl bromide in dry acetonitrile (140 mL) was heated under reflux under nitrogen for 16 h. After removal of the solvent by evaporation, the residue was treated with acetone (150 mL) and the crystalline material collected to give 40.0 g (63%) of **4***c* (X = Br), mp 181–183.5°C. An analytical sample was obtained by recrystallization from ethanol; mp 183–184°C. *Anal.* calcd. for $C_{27}H_{32}BrNO$: C 69.52, H 6.91, N 3.00, Br 17.13; found: C 69.56, H 6.92, N 2.90, Br 16.96.

The benz[*e*]indoline **5***c* was quantitatively obtained from the hydrobromide **4***c* by treatment with sodium hydroxide and extraction with ether; ir (neat): 1670 cm^{-1} (C=C—N); nmr δ: 4.40 (broad, 1H, NC=CH), 5.07 (s, 2H, $ArCH_2O$), 4.73–5.90 (m, 3H, olefinic), 6.75–7.5 (m, 8H, ArH).

9b-Allyl-8-methoxy-3-methyl-5,9b-dihydrobenz[e]*indoline (***5***d) and Its Picrate Salt* **4**d

(a) Preparation from **3**d

A solution of 5.04 g (23.4 mmol) **3***d* and 3.70 g (30.5 mmol) of allyl bromide in dry acetonitrile (20 mL) was heated under reflux for 16 h under nitrogen. Removal of the solvent *in vacuo* left a sticky residue of **4***d* (X = Br) which was purified by conversion to the picrate salt as follows: The hydrobromide **4***d* (X = Br) was dissolved in water (100 mL) and extracted with ether (2 × 50 mL) to remove neutral material. The aqueous phase was made alkaline with 10% sodium hydroxide (30 mL) and extracted with ether (2 × 70 mL). The ethereal solution was washed with water (3 × 30 mL), dried ($MgSO_4$), and the solvent removed *in vacuo*. The liquid residue (5.1 g) was dissolved in ethanol (20 mL) and added to a solution of 6.8 g picric acid in hot ethanol (50 mL) and allowed to crystallize at room temperature. The crystalline product was filtered to give 8.6 g (76%) of **4***d* (X = picrate ion), mp 143–147°C. An analytical sample was obtained by recrystallization from ethanol–acetone (1:15), mp 147–148°C. *Anal.* calcd. for $C_{23}H_{24}N_4O_8$: C 57.02, H 5.00, N 11.56; found: C 57.15, H 5.35, N 11.61.

The yield of the picrate **4***d* was 66% when benzene was used in place of acetonitrile in the above procedure.

The benz[*e*]indoline **5***d* was regenerated from the picrate **4***d* as follows: A mixture of finely powdered **4***d* (10 mmol), 1 *N* aqueous lithium hydroxide (50 mL), ethanol (20 mL), and ether (100 mL) in a separatory funnel was shaken until all the picrate had dissolved. The ether phase was washed with water and, after drying, was evaporated to dryness to give **5***d* in quantitative yield as a pale yellow and air-sensitive liquid; ir (neat): 1670 cm^{-1} (N—C=C); nmr δ: 2.60 (s, 3H, NCH_3), 3.68 (s, 3H, OCH_3), 4.60 (d of d, 1H, NC=CH, J_1 = 5.5, J_2 = 2.5 Hz), 4.63–5.98 (m, 3H, olefinic), 6.43–7.0 (m, 3H, ArH).

(b) Preparation from **14**a

To a suspension of 5.8 g (155 mmol) of lithium aluminium hydride in 190 mL dry ether was added dropwise under a slow stream of nitrogen and while stirring a solution of 28.19 g (104.8 mmol) of **14***a* in 190 mL dry ether at such a rate as to maintain gentle refluxing. Following the addition (20 min), stirring at room temperature was continued for 2 h. The reaction mixture was cooled in an ice-bath and treated successively with 5.9 mL water, 4.4 mL 20% aqueous sodium hydroxide, and 20.6 mL water (7) to provide a granular precipitate which was filtered under nitrogen and rinsed with ether. The combined filtrate and washings were evaporated to dryness under reduced pressure. After removal of the solvent was complete, the flask containing the product was filled with nitrogen. The compound **5***d* thus obtained was a pale yellow syrup, 26.2 g (98%), and was identical to that obtained in part (*a*) above. A sample was converted to picrate **4***d*, mp 147–148°C.

9b-Benzyl-8-methoxy-3-methyl-5,9b-dihydrobenz[e]*indoline (***5***e) and Its Picrate Salt* **4**e

A solution of 27.3 g (127 mmol) of **3***d* and 25.0 g (197 mmol) of benzyl chloride in 130 mL dry acetonitrile was heated under reflux under nitrogen for 18 h. Removal of the solvent *in vacuo* left a residue (**4***e*, X = Br) which resisted crystallization. The residue was dissolved in water (150 mL), extracted with ether (2 × 100 mL) to remove neutral material, and the aqueous phase treated with 10% sodium bicarbonate (200 mL) and extracted with ether (3 × 100 mL). The combined ethereal extracts were washed with water (2 × 100 mL), dried, and the solvent removed *in vacuo* to give 30 g (78%) of **5***e* as a light brown syrup. The purity of this material was approximately 90% as estimated by nmr. The crude benz[*e*]indoline **5***e* was treated with picric acid as in the case of **5***d* above to give 28.5 g (42% based on **3***d*) of the picric acid salt **4***e*, mp 123–126°C (ethanol–acetone, 1:4). *Anal.* calcd. for $C_{27}H_{26}N_4O_8$: C 60.66, H 4.90, N 10.48; found: C 59.99, H 4.93, N 10.52.

The benz[*e*]indoline **5***e* was quantitatively regenerated from

the picrate **4***e* by the procedure described above for **5***d*; ir (neat): 1670 cm^{-1} (C=C—N); nmr δ: 2.65 (s, 3H, NCH_3), 2.80 (s, 2H, $ArCH_2$), 3.72 (s, 3H, OCH_3), 4.37 (d of d, 1H, NC=CH, J_1 = 5.5, J_2 = 2.5 Hz), 6.50–7.35 (m, 8H, ArH).

In another experiment, where dioxane was used as the reaction solvent instead of acetonitrile, the yield of the crude **5***e* was 60% and the yield of the picrate salt was 39%.

The yield of crude **5***e* was 10%, where benzene was used as the reaction solvent in the above procedure.

3,9b-Dimethyl-8-methoxy-5,9b-dihydrobenz[e]*indoline (***5***f)*

To a stirred suspension of 3.40 g (89.4 mmol) of lithium aluminium hydride in 110 mL dry ether under a slow stream of nitrogen was added dropwise a solution of 14.65 g (60.2 mmol) of crude **14***b* in 500 mL of dry ether and at such a rate as to maintain gentle refluxing. After the addition was completed (25 min) stirring was continued at room temperature for 1.5 h. The product was isolated as in the case of **5***d* (part (*b*)) above to give 13.42 g (98%) of the air-sensitive **5***f* as a pale brown liquid; ir (neat): 1670 cm^{-1} (N—C=CH); nmr δ: 1.20 (s, 3H, CH_3), 2.67 (s, 3H, NCH_3), 3.74 (s, 3H, OCH_3), 4.30 (d of d, 1H, NC=CH, J_1 = 5.5, J_2 = 2.5 Hz). *Anal.* calcd. for $C_{15}H_{19}NO$: C 78.56, H 8.35, N 6.10; found: C 78.06, H 8.24, C 5.93.

When the reduction of **14***b* was carried out in ether–THF, a sticky product was obtained which contained very little **5***f* as evidenced by nmr.

9b-Allyl-8-benzyloxy-3-methyl-5,9b-dihydrobenz[e]*indoline (***5***g)*

This compound was prepared by reduction of the crude **14***c* with lithium aluminium hydride in ether by the method described above for **5***d* (part (*a*)); yield, 95%; ir (neat): 1670 cm^{-1} (NC=C); nmr δ: 2.70 (s, 3H, NCH_3), 4.36 (d of d, 1H, NC=CH, J_1 = 5.5, J_2 = 2.5 Hz), 4.73–5.90 (m, 3H, olefinic), 5.08 (s, 2H, $PhCH_2O$), 6.25–7.53 (m, 8H, ArH).

9b-(3-Ethylenedioxy)butyl-8-methoxy-3-methyl-5,9b-dihydrobenz[e]*indoline (***5***h)*

To a suspension of 0.5 g (13 mmol) lithium aluminium hydride in 50 mL dry ether was added portionwise, under nitrogen and while stirring, 3.43 g (10 mmol) of crystalline **14***d*. After the addition was completed (15 min), the mixture was heated under reflux under nitrogen for 45 min; 30 mL ether was added and heating continued while stirring for a total of 2.5 h under nitrogen. The reaction mixture was cooled in an ice-bath and the excess lithium aluminium hydride decomposed by the dropwise addition of water (0.6 mL). After stirring for 45 min the mixture was filtered under nitrogen and the solids washed with ether. The ether solution was dried and evaporated to dryness to give 3.1 g (94%) of **5***h* as a pale yellow syrup; ir (neat): 1670 cm^{-1}; nmr δ: 1.20 (s, 3H, CH_3), 2.65 (s, 3H, NCH_3), 3.80 (s, 7H, OCH_2CH_2O and OCH_3), 4.41 (d of d, 1H, NC=CH, J_1 = 5.5, J_2 = 2.5 Hz).

*1-Allyl-3,4-dihydro-7-methoxy-2(1*H*)-naphthalenone (***6***a)*

To a solution of 104.1 g (0.59 mol) of **1***a* in 110 mL dry benzene was added 62.5 g of pyrrolidine (0.88 mol) dropwise under nitrogen while stirring at room temperature. After the addition was completed (10–15 min), the reaction mixture was heated under reflux for 2.5 h with azeotropic removal of water and then cooled to room temperature. The enamine solution was added dropwise to 143.8 g (1.19 mol) of allyl bromide while stirring at a rate sufficient to maintain gentle refluxing. A heavy precipitate formed. Benzene (50 mL) was added to facilitate stirring and heating continued for 4 h; 700 mL of water was then added and heating resumed. After 2 h, the reaction mixture was cooled to room temperature and diluted with 100 mL benzene. The benzene layer was separated and the aqueous phase extracted with benzene (2 × 100 mL). The combined extracts were washed with water (2 × 100 mL) and dried (Na_2SO_4). After evaporation of the solvent, the residue was distilled to give 113.5 g (89%) of **6***a*, bp 114–118°C/0.1–0.05 Torr (lit. (8) bp 118–120°C/0.05 Torr); ir (neat): 1715 cm^{-1}; nmr δ: 2.40–3.10 (m, 6H, allylic and alicyclic), 3.45 (t, 1H, C-1H, J = 6.5 Hz), 3.75 (s, 3H, OCH_3), 4.8–6.1 (m, 3H, olefinic), 6.7–7.2 (m, 3H, ArH).

*3,4-Dihydro-7-methoxy-1-methyl-2(1*H*)naphthalenone (***6***b)*

This compound was prepared in 84% yield by the method described in the literature (1*a*); bp 110–112°C/0.3–0.4 Torr (lit. (1*a*) bp 110–115°C/0.3–0.4 Torr); nmr δ: 1.43 (d, 3H, CH_3, J = 7.0 Hz), 3.68 (s, 3H, OCH_3), 6.65–7.20 (m, 3H, ArH).

*1-Allyl-7-benzyloxy-3,4-dihydro-2(1*H*)-naphthalenone (***6***c)*

To a mixture of 22.7 g (90 mmol) **1***b* and 50 mL of dry benzene was added dropwise at room temperature a solution of 9.6 g (135 mmol) of pyrrolidine in 50 mL benzene while stirring under nitrogen. After the addition was completed (10 min), the reaction mixture was heated under reflux with azeotropic removal of water for 3 h and then cooled to room temperature. A solution of 22.0 g (181 mmol) of allyl bromide in 25 mL benzene was added dropwise (10 min) and then heating under reflux continued. Benzene (100 mL) was added to facilitate stirring and heating continued for 4 h. Water (200 mL) was added and reflux continued for another 2 h. After the reaction mixture had cooled to room temperature, the benzene phase was separated and the aqueous phase was extracted first with benzene (50 mL) and then with ether (100 mL). The combined extracts were washed with water (100 mL), dried (Na_2SO_4), and evaporated to dryness to give 24.8 g (94%) of liquid **6***c*; ir ($CHCl_3$): 1715 cm^{-1}; nmr δ: 5.15 (s, 2H, $PhCH_2O$), 4.8–6.1 (m, 5H, olefinic and $PhCH_2O$), 6.80–7.50 (m, 8H, ArH). *Anal.* calcd. for $C_{20}H_{20}O_2$: C 82.14, H 6.89; found: C 80.72, H 6.75.

This material was used in the next step without further purification.

*Ethyl-7-methoxy-2-oxo-1,2,3,4-tetrahydro-1-naphthaleneacetate (***6***d)*

This compound was prepared in 78% yield according to a described procedure (9).

*1-Allyl-7-methoxy-2-oxo-1,2,3,4-tetrahydro-1-naphthaleneacetonitrile (***7***)*

Compound **6***a*, (256.5 g or 1.186 mol) in 250 mL dry DMF was added dropwise to a stirred, cold (ice-bath) suspension of 24.86 g (1.186 mol) of sodium hydride (or 49.92 g of a 57% dispersion in oil washed with benzene) in 350 mL DMF under nitrogen. After the addition was completed (1 h), the reaction mixture was stirred at room temperature for 2 h and then cooled in an ice-bath. A solution of 89.54 g (1.186 mol) of chloroacetonitrile in 300 mL dry DMF was added over a period of 1 h, then the cooling bath removed, and stirring continued at room temperature overnight. Water (1500 mL) and ether (300 mL) were added and while stirring a crystalline material precipitated. It was collected to give 210 g of **7**. The organic phase of the filtrate was separated and the aqueous phase was extracted with benzene (4 × 200 mL). The combined extracts were washed with water (3 × 150 mL), dried, and evaporated to dryness. The syrupy residue was triturated with ether (200 mL) and on cooling it crystallized to give an additional 40.0 g of product **7**. The two crystalline crops were combined (250 g) and recrystallized from 1:1 ethanol–ether to give 231.0 g (76%) of **7**, mp 90–96°C. A sample was distilled at 150–160°C/0.1 Torr and the distillate was crystallized from EtOH to give an analytical sample, mp 94–96°C; ir ($CHCl_3$): 2250 (CN), 1715 cm^{-1} (CO); nmr δ: 3.77 (s, 3H, OCH_3), 4.75–5.65 (m, 3H, $CH=CH_2$), 6.65–7.15 (m, 3H, ArH). *Anal.*

calcd. for $C_{16}H_{17}NO_2$: C 75.26, H 6.71, N 5.48; found: C 74.85, H 6.97, N 5.54.

*1-Allyl-2,2-ethylenedioxy-7-methoxy-1,2,3,4-tetrahydro-1-naphthaleneacetonitrile (**8**)*

A round bottomed flask fitted with a Soxhlet extractor packed with molecular sieves 3A (80 g), a condenser, and magnetic stirrer was charged with 71.5 g (200 mmol) of crude 7 (mp 90–96°C), 90 mL ethylene glycol, 1.0 g *p*-toluenesulfonic acid and 250 mL of dry toluene. The mixture was heated under reflux while stirring and at intervals (8–10 h) the sieves were replaced with fresh ones. After refluxing for 48 h, the reaction mixture was cooled to room temperature and diluted with 10% aqueous sodium bicarbonate (100 mL). The organic phase was separated and the aqueous phase extracted with benzene (2 × 50 mL). The combined extracts were washed with water, dried, and the solvent evaporated. Trituration of the residue with ethanol (60 mL) gave 64.0 g (76%) of compound **8**, mp 82–85°C. A sample recrystallized twice from the same solvent melted at 85–86°C; ir ($CHCl_3$): 2250, 1615, 1505 cm^{-1}; nmr δ: 3.75 (s, 3H, OCH_3), 4.06 (s, 4H, OCH_2CH_2O), 4.85–6.0 (m, 3H, olefinic), 6.6–7.15 (m, 3H, ArH). *Anal.* calcd. for $C_{18}H_{21}NO_3$: C 72.21, H 7.07, N 4.68; found: C 72.23, H 7.10, N 4.50.

*1-Allyl-2,2-ethylenedioxy-7-methoxy-1-(2-aminoethyl)-1,2,3,4-tetrahydronaphthalene (**9**)*

A solution of 33.2 g (111 mmol) of **8** in 480 mL of dry ether was added dropwise under nitrogen and while stirring to a suspension of 8.43 g (222 mmol) of lithium aluminium hydride in 210 mL dry ether. After the addition was completed (30 min), stirring at room temperature was continued for 48 h. The reaction mixture was cooled in an ice-bath and the excess hydride and salts decomposed by the dropwise consecutive addition of 8.5 mL water, 6.4 mL 20% sodium hydroxide, and 29.5 mL water (7). The granular inorganic precipitate was collected, rinsed with ether (100 mL), and the ether solution dried ($MgSO_4$). Removal of the solvent *in vacuo* afforded 33.5 g (100%) of **9** as a syrup. The ir spectrum of the reduction product and tlc (alumina, CH_2Cl_2) established the absence of any unreduced nitrile. A sample was purified by chromatography on aluminium oxide; elution with methylene chloride at first removed some impurities; subsequent elution with ethanol removed the product; nmr δ: 1.05 (s, 2H, NH_2), 3.70 (s, 3H, OCH_3), 3.91 (s, 4H, OCH_2CH_2O), 4.73–6.0 (m, 3H, olefinic), 6.5–7.0 (m, 3H, ArH). *Anal.* calcd. for $C_{18}H_{25}NO_3$: C 71.25, H 8.30, N 4.61; found: C 70.74, H 8.35, N 4.50.

*1-Allyl-1-(2-cyclopropanecarboxamidoethyl)-2,2-ethylenedioxy-7-methoxy-1,2,3,4-tetrahydronaphthalene (**10**a)*

To an ice cold solution of 10.8 g (35.7 mmol) of **9** and 8.3 mL (60 mmol) triethylamine in 25 mL methylene chloride was added dropwise while stirring a solution of 4.18 g (40 mmol) of cyclopropanecarbonyl chloride in 15 mL of methylene chloride. After stirring for 1 h in the cold and 2 h at room temperature, it was washed with water and 10% aqueous sodium bicarbonate and dried (Na_2SO_4). Evaporation of the solvent and trituration of residue with ether (50 mL) gave 10.5 g (79.5%) of crystalline **10***a*, mp 94–95°C, solidified and remelted at 114–115°C; ir ($CHCl_3$): 3320 (NH), 1650, and 1555 (CO) cm^{-1}; nmr δ: 0.3–0.8 (m, 5H, cyclopropyl), 3.75 (s, 3H, OCH_3), 4.0 (s, 4H, OCH_2CH_2O), 4.75–6.0 (m, 3H, olefinic), 6.50–7.10 (m, 3H, ArH). *Anal.* calcd. for $C_{22}H_{29}NO_4$: C 71.13, H 7.87, N 3.77; found: C 71.10, H 8.03, N 3.67.

*1-Allyl-1-(2-cyclobutanecarboxamidoethyl)-2,2-ethylenedioxy-7-methoxy-1,2,3,4-tetrahydronaphthalene (**10**b)*

Reaction of **9** with cyclobutanecarbonyl chloride as described above for the preparation of **10***a* provided an 83% yield of **10***b*, mp 99–101°C (benzene–ligroin); nmr δ; 3.81 (s, 3H, OCH_3), 4.06 (s, 4H, OCH_2CH_2O), 4.86–6.05 (m, 3H, olefinic), 6.6–7.1 (m, 3H, ArH). *Anal.* calcd. for $C_{23}H_{31}NO_4$: C 71.66, H 8.10, N 3.63; found: C 71.60, H 8.21, N 3.42.

*1-Allyl-1-[2-(N-cyclopropylmethylamino)ethyl]-2,2-ethylenedioxy-7-methoxy-1,2,3,4-tetrahydronaphthalene (**11**a)*

To a suspension of 3.0 g (81 mmol) lithium aluminium hydride in dry ether (160 mL) was added dropwise while stirring a solution of 14.8 g (40 mmol) of **10***a* in dry THF (160 mL) at a rate such as to maintain gentle refluxing. After stirring at room temperature for 48 h, the reaction mixture was cooled in an ice-bath and the excess hydride and complexes were decomposed (7) by the consecutive dropwise addition of water (3.0 mL), 20% sodium hydroxide (2.25 mL), and water (10.5 mL). The inorganic precipitate was collected and rinsed with ether (50 mL). The combined filtrate and washings were dried ($MgSO_4$) and evaporated to dryness to give 14.0 g (98%) of **11***a* as a syrup; nmr δ: 3.71 (s, 3H, OCH_3), 3.95 (s, 4H, OCH_2CH_2O), 4.7–6.0 (m, 3H, olefinic), 6.5–7.0 (m, 3H, ArH). *Anal.* calcd. for $C_{22}H_{31}NO_3$: C 73.91, H 8.74, N 3.91; found: C 73.38, H 8.89, N 3.76.

*1-Allyl-1-[2-(N-cyclobutylmethylamino)ethyl]-2,2-ethylenedioxy-7-methoxy-1,2,3,4-tetrahydronaphthalene (**11**b)*

Compound **11***b* was obtained in 95% yield by reduction of **10***b* according to the above procedure for the preparation of **11***a*; nmr δ: 3.76 (s, 3H, OCH_3), 4.0 (s, 4H, OCH_2CH_2O), 4.8–6.0 (m, 3H, olefinic), 6.60–7.10 (m, 3H, ArH). *Anal.* calcd. for $C_{23}H_{33}NO_3$: C 74.35, H 8.95, N 3.77; found: C 74.36, H 9.13, N 3.56.

*Ethyl-1-allyl-7-methoxy-2-oxo-1,2,3,4-tetrahydro-1-naphthaleneacetate (**12**a)*

Into a flame-dried, 500 mL three-neck flask equipped with a mechanical stirrer, a dropping funnel, and a nitrogen inlet tube was placed 4.21 g of sodium hydride (55% dispersion in oil, 100 mmol) while maintaining a nitrogen atmosphere. The mineral oil was washed out with benzene (3 × 30 mL), then 40 mL of dry DMF was added, and the suspension stirred while cooling in an ice-bath. A solution of 21.6 g (100 mmol) **6***a* in 10 mL DMF was added dropwise (10 min), the cooling bath removed, and stirring at room temperature continued until the evolution of gas ceased (2 h). The brown-colored reaction mixture was cooled (ice-bath) and a solution of 16.7 g (100 mmol) of ethyl bromoacetate in 40 mL DMF was added dropwise while keeping the reaction temperature below 25°C. After the addition was completed (15–20 min), stirring in the cold was continued for 1 h and then overnight at room temperature. Water (300 mL) was added and the mixture extracted with ether (3 × 100 mL). The combined ether extracts were washed with water (2 × 100 mL), dried ($MgSO_4$), the solvent removed by evaporation, and the residue distilled to give 26.0 g (86%) of **12***a*, bp 145–150°C/0.05–0.01 Torr; ir (neat): 1740, 1715 cm^{-1}; nmr δ: 1.05 and 3.92 (triplet and quartet for OCH_2CH_3), 3.75 (s, 3H, OCH_3), 4.65–6.0 (m, 3H, $CH{=}CH_2$), 6.55–7.15 (m, 3H, ArH). *Anal.* calcd. for $C_{18}H_{22}O_4$: C 71.50, H 7.33; found: C 71.27, H 7.28.

*Ethyl-7-methoxy-1-methyl-2-oxo-1,2,3,4-tetrahydro-1-naphthaleneacetate (**12**b)*

Compound **6***b* (28.23 g, 148 mmol) was reacted with ethyl bromoacetate by the above method to yield 36.0 g (88%) **12***b*, bp 138–140°C/0.1 Torr; ir (neat): 1740 cm^{-1} (unresolved ketone and ester bands); nmr δ: 1.05 and 3.93 (triplet and quartet for $CO_2CH_2CH_3$), 1.37 (s, 3H, CH_3), 3.80 (s, 3H, OCH_3), 6.6–7.3 (m, 3H, ArH). The distillate crystallized on

standing. A sample recrystallized from ethanol melted at 55–55.5°C. *Anal.* calcd. for $C_{16}H_{20}O_4$: C 69.54, H 7.29; found: C 69.75, H 7.33. The distilled product was used as such in the next step.

*Ethyl-1-allyl-7-benzyloxy-2-oxo-1,2,3,4-tetrahydro-1-naphthaleneacetate (**12**c)*

Compound **6c** (22.9 g, 78.5 mmol) was reacted with ethyl bromoacetate by the method described above for the preparation of **12***a* to yield 25.5 g (87%) crystalline **12***c*. Recrystallization from ethanol gave 19.5 g (66%), mp 83–85°C; ir ($CHCl_3$): 1725, 1710 (ketone and ester) cm^{-1}; nmr δ: 1.05 and 3.96 (triplet and quartet for OCH_2CH_3), 4.8–5.8 (m, 5H, olefinic and $PhCH_2O$), 5.15 (s, 2H, $PhCH_2O$), 6.80–7.55 (m, 8H, ArH). *Anal.* calcd. for $C_{24}H_{26}O_4$: C 76.16, H 6.92; found: C 76.09, H 6.96.

*Ethyl-1-(3-ethylenedioxy)butyl-7-methoxy-2-oxo-1,2,3,4-tetrahydro-1-naphthaleneacetate (**12**d)*

This compound was prepared in 87% yield from **6***d* according to a described procedure (9) and was used without purification in the next step.

*9b-Allyl-3a-hydroxy-8-methoxy-3-methyl-2-oxo-2,3,3a,4,5,9b-hexahydro-1H-benz[e]indole (**13**a)*

Methylamine (gas) (6.80 g, 220 mmol) was dissolved in ethanol (25 mL) and the solution added to 21.2 g (70 mmol) of **12***a*. After standing at room temperature for 24 h a crystalline product formed and was collected to give 12.5 g (62%) of **13***a*, mp 146–149°C. After evaporation of the filtrate (35°C) and treatment of the residue with ether (50 mL), an additional 3.8 g of **13***a*, mp 147–150°C, was obtained, increasing the yield to 81.5%; ir ($CHCl_3$): 3500, 1690, 1615, 1505 cm^{-1}; nmr δ: 2.88 (s, 3H, N—CH_3), 3.92 (s, 3H, OCH_3), 4.62 (broad singlet, OH), 4.9–6.1 (m, 3H, olefinic), 6.8–7.3 (m, 3H, ArH). *Anal.* calcd. for $C_{17}H_{21}NO_3$: C 71.05, H 7.37, N 4.87; found: C 70.90, H 7.38, N 4.67.

*3,9b-Dimethyl-3a-hydroxy-8-methoxy-2-oxo-2,3,3a,4,5,9b-hexahydro-1H-benz[e]indole (**13**b)*

A solution of 22.0 g (79.7 mmol) of **12***b* and 7.5 g (240 mmol) of methylamine in 25 mL of ethanol was left at room temperature for 24 h. The crystalline precipitate which formed was collected to give 15.5 g (74.5%) of **13***b*, mp 182–186°C. After evaporation (35°C) of the filtrate and treatment of the residue with ether, another 1.0 g of **13***b* was obtained to give a total yield of 79.5%; ir (Nujol): 3300 (OH), 1670 (lactam) cm^{-1}; nmr ($CDCl_3$–DMSO) δ: 1.48 (s, 3H, CH_3), 2.82 (s, 3H, N—CH_3), 3.78 (s, 3H, OCH_3), 6.6–7.1 (m, 3H, ArH). *Anal.* calcd. for $C_{15}H_{19}NO_3$: C 68.94, H 7.32, N 5.36; found: C 68.74, H 7.30, N 5.53.

*9b-Allyl-8-benzyloxy-3a-hydroxy-3-methyl-2-oxo-2,3,3a,4,5,9b-hexahydro-1H-benz[e]indole (**13**c)*

A mixture of 63.0 g (167 mmol) of **12***c*, 31.0 g of methylamine, and 200 mL of 1:1 ethanol–dioxane was stirred at room temperature for 3 days. The reaction mixture was concentrated by evaporation (35–40°C) to half its volume and diluted with 200 mL of ether to give **13***c* as a crystalline product weighing 51.0 g (86%); mp 188–190°C; ir (Nujol): 3250, 1665, 1615, 1505 cm^{-1}. *Anal.* calcd. for $C_{23}H_{25}NO_3$: C 76.00, H 6.93, N 3.85; found: C 75.89, H 6.87, N 3.90.

*9b-Allyl-8-methoxy-3-methyl-2-oxo-2,3,5,9b-tetrahydro-1H-benz[e]indole **14**a*

A solution of 14.0 g (48.7 mmol) of **13***a* and 24 mg *p*-toluenesulfonic acid in 100 mL benzene was heated under reflux for 2 h with azeotropic distillation of water. After cooling to room temperature, the solution was washed with water and dried. Evaporation of the solvent gave 13.0 g (100%) of **14***a* as a pale yellow syrup;[2] ir (neat): 1725, 1685, 1615, 1505 cm^{-1}; nmr δ: 2.24 (d, 2H, allylic, J = 7.0 Hz), 2.75 (s, 2H, CH_2CO), 2.94 (s, 3H, NCH_3), 3.34 (m, 2H, benzylic), 3.75 (s, 3H, OCH_3), 4.75–5.85 (m, 4H, olefinic), 6.5–7.2 (m, 3H, ArH). *Anal.* calcd. for $C_{17}H_{19}NO_2$: C 75.80, H 7.11, N 5.20; found: C 75.93, H 7.10, N 5.19.

*3,9b-Dimethyl-8-methoxy-2-oxo-2,3,5,9b-tetrahydro-1H-benz[e]indole (**14**b)*

A solution of 11.25 g (43.2 mmol) of **13***b* and 25 mg *p*-toluenesulfonic acid in 100 mL toluene was heated under reflux for 2 h with azeotropic removal of water. After cooling to room temperature, the solution was washed with water and dried (Na_2SO_4). Removal of the solvent *in vacuo* and trituration of the residue with ether (20 mL) gave 9.5 g (90%) of crystalline **14***b*, mp 106–108°C; ir ($CHCl_3$): 1725, 1685 cm^{-1}; nmr δ: 1.27 (s, 3H, CH_3), 2.72 and 2.76 (s, 2H, CH_2CO), 2.95 (s, 3H, NCH_3), 3.34 (m, 2H, benzylic), 3.78 (s, 3H, OCH_3), 5.14 (d of d, 1H, NC=CH, J_1 = 5.0, J_2 = 3.5 Hz), 6.7–7.3 (m, 3H, ArH). *Anal.* calcd. for $C_{15}H_{17}NO_2$: C 74.04, H 7.04, N 5.75; found: C 74.28, H 7.06, N 5.89.

*9b-Allyl-8-benzyloxy-3-methyl-2-oxo-2,3,5,9b-tetrahydro-1H-benz[e]indole (**14**c)*

This compound was obtained quantitatively from **13***c* by the procedure described in the preparation of **14***a* and was used in the next step without further purification; ir (neat): 1725, 1685, 1610, 1505 cm^{-1}; nmr δ: 2.26 (d, 2H, allylic, J = 7.0 Hz), 2.78 (s, 2H, CH_2CO), 3.0 (s, 3H, HCH_3) 3.41 (m, 2H, benzylic), 4.8–5.8 (m, 5H, olefinic, $PhCH_2O$), 6.7–7.6 (m, 8H, ArH).

*9b-(3-Ethylenedioxy)butyl-8-methoxy-3-methyl-2-oxo-2,3,5,9b-tetrahydro-1H-benz[e]indole (**14**d)*

To a solution of 15.0 g (0.5 mol) of methylamine in 50 mL of ethanol was added 30.0 g (80 mmol) of **12***d* and the solution allowed to stand at room temperature for 49 h. Evaporation of the solvent, addition of benzene, and re-evaporation left **13***d* as a dark brown syrup. The crude product was dissolved in toluene, 50 mg *p*-toluenesulfonic acid was added, and the mixture heated under reflux for 1 h with azeotropic removal of water. The solvent was evaporated and the residue dissolved in ethanol (25 mL), the solution diluted with ether (120 mL), and the product allowed to crystallize at room temperature. The crystalline **14***d* was collected and weighed, 7.0 g. Evaporation of the filtrate left a residue which was dissolved in a small amount of methylene chloride and the solution passed through a sintered glass funnel packed with silica (6 cm long × 9.5 cm id). After washing with 4% ethanol – methylene chloride and evaporation of the eluate, the dark brown residue (14.0 g) was dissolved in ether (50 mL) and the product allowed to crystallize at room temperature. The crystalline precipitate was collected to give an additional 5.0 g of **14***d*. The mother liquor, after cooling to 0°C overnight, deposited an additional 1.0 g of **14***d*. The above crystalline crops were combined to provide a total of 13.0 g (48%) of **14***d*. Thin layer chromatography on silica (4% EtOH–CH_2Cl_2) showed one major spot and a trace of another with lower R_f value. Recrystallization from ethanol (35 mL) – ether (20 mL) gave 10.0 g of analytically pure **14***d*, mp 143–145°C; ir ($CHCl_3$): 1725, 1680, 1610, 1505 cm^{-1}; nmr δ: 1.18 (s, 3H, CH_3), 2.80 (s, 2H, CH_2CO), 3.0 (s, 3H, NCH_3), 3.80 (s, 7H, OCH_2CH_2O and

[2]On several occasions, this product developed a dark brown color on standing at room temperature. This could be prevented by washing an organic solution of the product with 3% aqueous HCl, an operation which led to discoloration.

OCH_3), 5.25 (d of d, 1H, NC=CH, J_1 = 3.5 and J_2 = 5.0 Hz), 6.70–7.35 (m, ArH). *Anal.* calcd. for $C_{20}H_{25}NO_4$: C 69.94, H 7.33, N 4.07; found: C 69.45, H 7.67, N 4.29.

1. (*a*) J. G. MURPHY, J. H. AGER, and E. L. MAY. J. Org. Chem. **25**, 1386 (1960); (*b*) E. L. MAY and J. G. MURPHY. J. Org. Chem. **20**, 257 (1955).
2. M. TAKEDA, M. KONDA, H. INOUE, S. SAITO, and H. KUGITA. J. Org. Chem. **37**, 2677 (1972).
3. S. STORK, A. BRIZZOLARA, H. LANDESMAN, J. SZMUSZKOVICZ, and R. TERRELL. J. Am. Chem. Soc. **85**, 217 (1963).
4. D. A. EVANS, C. A. BRYAN, and G. M. WAHL. J. Org. Chem. **35**, 4122 (1970).
5. M. G. REINECKE and L. R. KRAY. J. Org. Chem. **31**, 4215 (1966).
6. G. H. HALT. Electrophilic substitution and addition to enamines. *In* The enamines. *Edited by* A. G. Cook. M. Dekker, New York and London. 1969.
7. L. F. FIESER and M. FIESER. Reagents for organic synthesis. Vol. 1. John Wiley and Sons, Inc., New York, NY. 1967. p. 584 and references therein.
8. K. WIESNER. Experientia, **26**, 1030 (1970).
9. K. WIESNER, J. G. MCCLUSKEY, J. K. CHANG, and V. SMULA. Can. J. Chem. **49**, 1092 (1971).

9-Oxobenzomorphans. II. A versatile process for the synthesis of 9-oxo-6,7-benzomorphans

GERRY KAVADIAS,[1] STEPHAN VELKOF, AND BERNARD BELLEAU

Bristol Laboratories of Canada, 100 Industrial Boulevard, Candiac, P.Q., Canada J5R 1J1

Received December 20, 1978

GERRY KAVADIAS, STEPHAN VELKOF, and BERNARD BELLEAU. Can. J. Chem. **57**, 1861 (1979).

The synthesis of 5-allyl-2′-methoxy-2-methyl-9-oxo-, 2′-methoxy-2,5-dimethyl-9-oxo-, 5-allyl-2-cyclopropylmethyl-2′-methoxy-9-oxo-, and 5-(3-ethylenedioxy)butyl-2′-methoxy-3-methyl-9-oxo-6,7-benzomorphans (**5***a–d*) by an improved process is described. It involves bromination of the 5,9b-dihydrobenz[*e*]indolines to the bromoiminium bromides, followed by hydrolysis with ammonium bicarbonate which converted them to 4-bromo-5,9b-dihydrobenz[*e*]indolines (in a fast step). These underwent hydration (in a slow step) followed by rearrangement to **5***a–d*. The course of these reactions was different when sodium, potassium, and ammonium hydroxides were substituted for ammonium bicarbonate.

GERRY KAVADIAS, STEPHAN VELKOF et BERNARD BELLEAU. Can. J. Chem. **57**, 1861 (1979).

On décrit la synthèse, par un procédé amélioré, des allyl-5 méthoxy-2′ méthyl-2 oxo-9, méthoxy-2′ diméthyl-2,5 oxo-9, allyl-5 cyclopropylméthyl-2 méthoxy-2′ oxo-9 et (éthylènedioxy-3)-butyl-5 méthoxy-2′ méthyl-3 oxo-9 benzo-6,7 morphanes (**5***a–d*). Le procédé implique la bromation des dihydro-5,9b benz[*e*] indolines en bromures des bromoiminium, suivie par une hydrolyse à l'aide du bicarbonate d'ammonium qui les transforme en bromo-4 dihydro-5,9b benz[*e*] indolines (étape rapide). Celles-ci subissent une hydratation (étape lente) qui est suivie par une transposition en **5***a–d*. La nature des produits de ces réactions varie si l'on remplace le bicarbonate d'ammonium par des hydroxydes de sodium, de potassium ou d'ammonium.

[Traduit par le journal]

In the course of our studies on the synthesis of new analgesics structurally related to benzomorphans and morphinans, 9-oxo-6,7-benzomorphans with various substituents at 2-, 2′-, and 5-positions were needed. At the inception of this work, the best known method for the synthesis of such compounds was that developed by Murphy *et al.* (1, 2) as applied to the synthesis of 2′-methoxy-2,5-dimethyl-9-oxo-6,7-benzomorphan (**5***b*). This process involves in the ultimate step the pyrolysis of a quaternary salt such as the methobromide of **5***b*, and therefore the process is limited to the synthesis of substances that can survive the vigorous pyrolytic conditions. Furthermore, the method is limited to the synthesis of *N*-methyl substituted-9-oxobenzomorphans, and the substitution of *N*-methyl by other groups is a tedious task. The procedures employed in the benzomorphan series for the conversion of *N*-methyl benzomorphans to other *N*-substituted analogs involve demethylation of the parent compound by a variety of methods (3) followed by acylation and reduction (4, 5). This methodology cannot readily be applied to 9-oxocompounds.

Our need for 9-oxobenzomorphans carrying such substituents as allyl, benzyl, 3-ethylenedioxybutyl at the 5-position, as well as *N*-substituents such as methyl, cyclopropylmethyl, and cyclobutylmethyl, prompted us to develop a new synthetic methodology. The present report describes the synthesis of the desired compounds **5***a–d* by a process involving bromination of the indolines **1***a–d* to bromoiminium bromides **2***a–d*, followed by hydrolysis (Scheme 1).

After the completion of this work (in 1972), Takeda *et al.* (6) described a parallel approach to the synthesis of 9-oxobenzomorphans. However, in our hands, the process described by these authors was not generally applicable and led to low yields of products.

The 5,9b-dihydrobenz[*e*]indolines (enamines) **1***a–d* were prepared by our previously published methods (see Part I of this series (7)) and used immediately after their preparation. As expected on the basis of literature precedents (8), bromination of **1***a–d* yielded the bromoiminium bromides **2***a–d*. However, the yields and purity of the products were influenced by such factors as solvent, reaction temperature, and mode of mixing of the reagents. Thus, bromination of **1***a* in ether at −40°C by a described procedure (9) yielded a mixture of **2***a* and the hydrobromide salt of **1***a*, as evidenced by elemental analysis (low bromine content) and by the fact that the corresponding free base (after bicarbonate treatment) exhibited nmr absorption at δ 4.3 which is attributed to the proton at position-4 of **1***a*. Chlorinated solvents such as

[1]To whom correspondence may be addressed.

0008-4042/79/141861-05$01.00/0

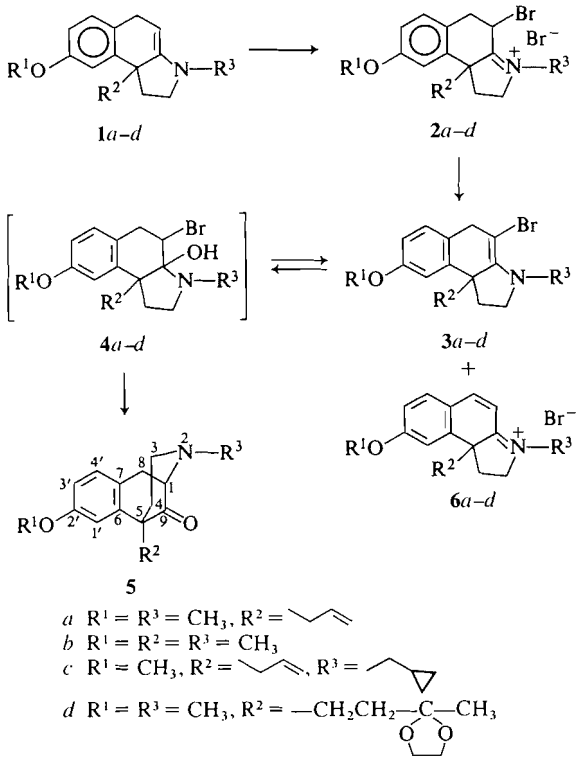

SCHEME 1

carbon tetrachloride and chloroform gave good results but methylene chloride proved to be the solvent of choice for this bromination reaction. The best results were obtained when a solution of **1***a* in methylene chloride was rapidly added (in one portion) to a solution of bromine in the same solvent at −60°C. This procedure was followed for the bromination of **1***a–d*. Fast reversed mixing of the reagents at −60°C also gave good results. But if the bromine solution in methylene chloride was added dropwise to a solution of **1***a* in the same solvent the product was contaminated with the hydrobromide of **1***a*. Bromination of **1***b* in methylene chloride, by the above recommended procedure for the preparation of **2***a*, afforded crystalline **2***b* in quantitative yield. In an analogous manner, **1***c* was brominated to give crystalline **2***c* in 98% yield; under the same conditions, **1***d* afforded **2***d* as a syrup in 97% yield.

The structures of **2***a–d* which can be deduced from simple mechanistic considerations were confirmed by elemental analysis, and by nmr and ir spectroscopy. The parent enamines **1***a–d* exhibited nmr resonances at δ 4.3 for the proton at the 4-positions; these bands were eliminated after bromination. The ir spectra of **2***a–d* showed double bond absorption at 1660 cm^{-1} which was more intense and at a lower frequency than for the parent enamines **1***a–d* (1670 cm^{-1}), in agreement with previous observations with analogous compounds (10). There are two possible isomeric forms for each compound of the **2***a–d* series and apparently both are formed. Since both isomers can be converted to the corresponding 9-oxobenzomorphan (see mechanism below), no attempt was made to fractionate the mixtures although this was possible in certain cases.

The conversion of the bromoiminium salts **2***a–d* to 9-oxobenzomorphans **5***a–d* will now be discussed. It was anticipated that basic hydrolysis of **2***a–d* would initially form the carbinolamine A (Fig. 1) which could rearrange directly to **5***a–d* or rearrange via an intermediate bromoketone B (Fig. 1) followed by ring closure. The reported (11) conversion of α-bromoiminium bromides to α-aminoketals and α-aminoaminals by reaction with alkoxides and secondary amines respectively (eq. [1]) favors the first mechanistic possibility.

Treatment of **2***a* in aqueous ethanol with sodium, potassium, or ammonium hydroxide gave a product which contained only traces of **5***a* as evidenced by tlc and ir spectroscopy. When sodium or ammonium bicarbonate were used, **5***a* was produced in 35–65%

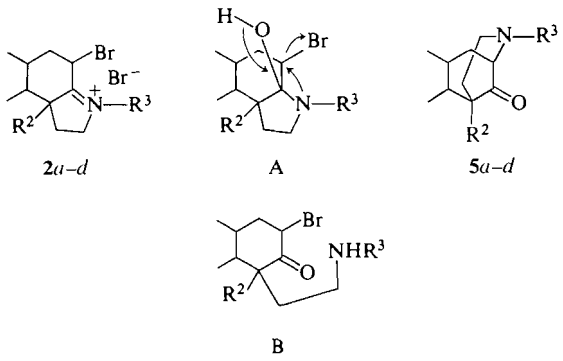

FIG. 1

yields. A thorough investigation of the reaction conditions for maximum yields of **5***a* was therefore undertaken. The following variables were examined: the nature of the base (alkali hydroxides, carbonates, and bicarbonates), the mode of addition of the base,

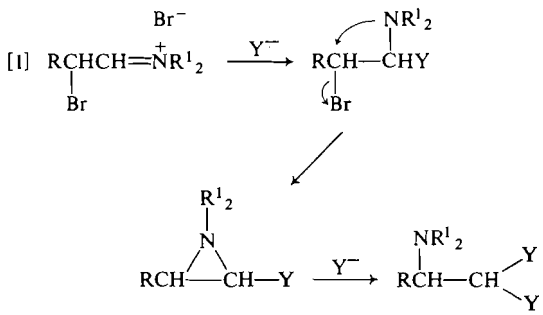

the nature of the solvent, and finally the effects of temperature. The best yields (~64%) of **5***a* were obtained when an aqueous solution of 1 equiv. of ammonium bicarbonate was added slowly (1.5 h) to a solution of **2***a* in 95% ethanol at −10°C followed by stirring at room temperature for 24 h. This procedure was adopted for the conversion of compounds **2***a–d* to **5***a–d*. Thus, treatment of **2***b* with ammonium bicarbonate by this procedure produced **5***b*, isolated as the oxalate salt, in 58% yield. Similar treatment of **2***c* gave **5***c* (as the oxalate salt) in 50% yield. In an analogous manner, **2***d* was converted to **5***d* in 35.5% yield.

In the early stage of the basic hydrolysis reaction of **2***a–d* the bromoenamines **3***a–d* precipitated out, but gradually dissolved as the reaction progressed. The bromoenamine **3***a* was a crystalline solid and on one occasion it was isolated in 47% yield by rapid filtration under nitrogen. Compound **3***a* was very sensitive to air oxidation but could be stored under nitrogen for 2–3 days at room temperature before decomposing. The structural assignment for bromoenamine **3***a* was based on its solubility properties, its nmr and ir spectra, and its chemical behavior. It was soluble in ether and insoluble in water, unlike **2***a*. Its nmr spectrum lacked the band at δ 4.3 which is characteristic of the proton at the 4-position of enamine **1***a*; the ir spectrum showed strong C=C absorption at 1670 cm^{-1}. Furthermore, it gave rise to **5***a* when in contact with aqueous solvents.

Treatment of **2***a* with excess aqueous sodium bicarbonate gave **3***a* (55%) as an ether-soluble fraction together with a water-soluble compound extractable with chloroform. This latter fraction gave a positive test for bromide ion and showed strong C=C absorption in the ir at 1650 cm^{-1}. Treatment of this material with aqueous solvents did not produce **5***a*. On that basis, it would appear that **6***a* represents the structure of the secondary product. Accordingly, base treatment of **2***a–d* not only produces the bromoenamines **3***a–d*, which are the precursors of **5***a–d*, but also leads to dehydrohalogenation products **6***a–d* which are not convertible to **5***a–d*. The proportions of the two types of products depend on the nature of the base, strong ones yielding **6***a–d* as the major products. This may explain the low yields of **5***a* from **2***a* following treatment with sodium, potassium, or ammonium hydroxides.

It should be pointed out at this point that the results of Takeda *et al.* (6) on the conversion of **2***b* to **5***b* by treatment with ammonium hydroxide are at variance with our own observations. We therefore repeated this reaction under the exact conditions reported by these authors, but in our hands the yield of **5***b* was only 21% and isolation required chromatographic procedures. In the case of **5***a* the yield was vanishingly small.

In summary then, we have shown that the bromoiminium bromides **2***a–d* upon treatment with an appropriate weak base are rapidly converted to the expected bromoenamines **3***a–d* which react more slowly with water to give via intermediates **4***a–d* the desired and difficultly accessible 9-oxobenzomorphans **5***a–d* in fair to good yields.

Experimental

The melting points were determined on a Mel-Temp melting point apparatus and are uncorrected. The ir spectra were recorded on a Unicam Sp-200G grating spectrometer. The nmr spectra were recorded on a Varian A-60A spectrometer using deuteriochloroform as the solvent. The chemical shifts are expressed in δ values using tetramethylsilane as internal reference. Microanalyses were performed by Micro-Tech Laboratories Inc., Skokie, IL, U.S.A.

*9b-Allyl-4-bromo-8-methoxy-2,4,5,9b-tetrahydro-1*H*-benz*[e]*indole Methobromide (***2***a)*

To a stirred solution of 5.84 g (36.4 mmol) of bromine in 360 mL methylene chloride, previously cooled to −60°C (acetone – dry ice bath) under nitrogen, was added all at once a solution of 9.28 g (36.4 mmol) of the enamine **1***a* in 40 mL methylene chloride. After stirring at −60°C for 5 min, the cooling bath was removed and stirring continued for 20 min. Evaporation of the solvent gave 15.0 g (99%) of **2***a* as a sticky syrup which resisted crystallization; ir (Nujol): 1660 cm^{-1}. *Anal.* calcd. for $C_{17}H_{21}Br_2NO$: C 49.18, H 5.10, N 3.37, Br 38.49; found: C 51.79, H 5.53, N 3.69, Br 36.74.

This product was unstable at room temperature and was used without delay.

A sample of **2***a* was dissolved in water, sodium bicarbonate was added, and the solution extracted with ether. After drying and evaporation of the extract to dryness, **3***a* was obtained as a syrup; its nmr spectrum showed it to be free of the enamine **1***a* (no absorption at δ 4.3), thus showing that **2***a* was free of the hydrobromide salt of **1***a*.

Reverse rapid mixing of the reagents (bromine added in methylene chloride to the enamine solution in the same solvent at −60°C) also produced **2***a* uncontaminated by **1***a* hydrobromide.

In another experiment a 1 *M* solution of bromine in methylene chloride was added dropwise over a 20 min period to a 0.1 *M* solution of **1***a* in the same solvent at −60°C. After stirring at −60°C for 10 min and at room temperature for 15–20 min, the solvent was removed *in vacuo* to give **2***a*. Treatment of the crude **2***a* with sodium bicarbonate and extraction with ether gave **3***a* as a syrup contaminated to the extent of 15–20% with **1***a* as evidenced by nmr spectroscopy (small band at δ 4.3). This shows that **2***a* as obtained by this procedure was contaminated by **1***a* hydrobromide.

In another experiment, a 1 *M* solution of bromine in ether was added dropwise over a 5–10 min period to a 0.1 *M* solution of **1***a* in the same solvent at −40°C. The product thus obtained was an approximately 1:1 mixture of **2***a* and **1***a* hydrobromide as evidenced by elemental analysis (low bromine content) and by nmr spectroscopy (band at δ 4.3 for enamine **1***a*).

*4-Bromo-9b-methyl-8-methoxy-2,4,5,9b-tetrahydro-1*H*-benz*[e]*-indole Methobromide (***2***b)*

To a stirred solution of 9.4 g (58.6 mmol) of bromine in

600 mL methylene chloride at −60°C under nitrogen was added all at once a solution of 13.4 g (58.6 mmol) of the enamine **1***b* in 60 mL methylene chloride. After stirring at −60°C for 10 min the cooling bath was removed and stirring continued for another 20 min. Removal of the solvent by evaporation and trituration of the syrupy residue with ether gave 22.8 g (100%) of **2***b* as a crystalline mass. The analytical sample was prepared by recrystallization from ethanol; mp 125–127°C (lit. (6) mp 124–125°C); ir (Nujol): 1660 cm^{-1}. *Anal.* calcd. for $C_{15}H_{19}Br_2NO \cdot \frac{1}{2}H_2O$: C 45.24, H 5.06, Br 40.13, N 3.54; found: C 45.37, H 5.10, Br 39.15, N 3.51.

*9b-Allyl-4-bromo-8-methoxy-2,4,5,9b-tetrahydro-1*H*-benz*[e]*indole Cyclopropylmethobromide (2*c*)*

To a stirred solution of 11.9 g (74.5 mmol) of bromine in 750 mL methylene chloride at −60°C under nitrogen was added all at once a solution of 22.06 g (74.5 mmol) of the enamine **1***c* in 50 mL of the same solvent and the mixture stirred at −60°C for 10 min and at room temperature for 20 min. Removal of the solvent by evaporation left a solid residue which was triturated with ether (100 mL) and collected to give 33.0 g (98.5%) of **2***c*, mp 112–117°C; ir (Nujol): 1660 cm^{-1}. *Anal.* calcd. for $C_{20}H_{25}Br_2NO$: C 52.76, H 5.53, Br 35.10; found: C 52.65, H 5.48, Br 34.96.

This material was used as such in the next step.

An analytical sample was obtained by recrystallization from ethanol, mp 133–134°C. *Anal.* found: C 52.68, H 5.79, Br 35.05.

*9b-(3-Ethylenedioxy)butyl-4-bromo-8-methoxy-2,4,5,9b-tetrahydro-1*H*-benz*[e]*indole Methobromide (2*d*)*

Following the above procedure for **2***c*, treatment of the enamine **1***d* (3 g, 9.1 mmol) with bromine (1.46 g, 9.1 mmol) in methylene chloride gave 3.6 g (97%) of **2***d* as a solid which turned sticky when exposed to air; ir (Nujol): 1660 cm^{-1}. This material was used as such in the next step.

9b-Allyl-4-bromo-8-methoxy-3-methyl-5,9b-dihydrobenz[e]*indoline (3*a*) and Compound 6*a

To a stirred solution of 3.75 g (9.05 mmol) of **2***a* in 55 mL of 95% ethanol at −10°C under nitrogen was added dropwise 20 mL of a 0.5 *M* aqueous ammonium bicarbonate solution. After addition of the ammonium bicarbonate solution was completed (45 min), stirring at −10°C was continued for 30 min. The crystalline precipitate was collected by rapid filtration under a blanket of nitrogen, placed in a flask previously dried under high vacuum, and filled with nitrogen. The yellowish crystalline **3***a* thus obtained weighed 1.4 g (47%) and had mp 50–60°C (dec.); ir ($CHCl_3$): 1670 cm^{-1} (strong N—C=C); nmr ($CDCl_3$) δ: 1.85–2.35 (m, 4H, allylic and CH_2), 3.14 (s, 3H, NCH_3), 3.76 (s, 3H, OCH_3), 3.14–3.76 (m, 4H, benzylic and NCH_2—), 4.70–5.80 (m, 3H, olefinic), 6.50–7.15 (m, 3H, ArH).

Compound **3***a* was very sensitive to air oxidation and had to be kept under nitrogen. It was stable at room temperature for 2–3 days.

In another experiment, 3.4 g (8.2 mmol) of **2***a* was treated with 30 mL of 10% aqueous sodium bicarbonate and the mixture extracted with ether (5 × 40 mL). The ether extracts were dried and were evaporated to give 1.5 g (55%) of **3***a*, identical (ir and nmr) to the material obtained above.

The dark brown aqueous phase was extracted with chloroform (4 × 40 mL), the extracts dried and evaporated to give 1.0 g of a sticky dark brown residue; ir ($CHCl_3$): 1650 cm^{-1}. A test for bromine was positive.

*5-Allyl-2′-methoxy-2-methyl-9-oxo-6,7-benzomorphan (5*a*)*

A 250 mL three-neck flask fitted with mechanical stirrer, dropping funnel, and nitrogen inlet and outlet tubes, was charged with a solution of 8.05 g (19.4 mmol) of **2***a* in 170 mL of 95% ethanol, placed under a slow stream of nitrogen, and cooled to −10°C. To this stirred solution was added dropwise over a period of 1.5 h a solution of 1.58 g (20 mmol) of ammonium bicarbonate in 42 mL of water. A pale yellow crystalline precipitate (**3***a*) formed and after the addition of the ammonium bicarbonate solution was completed, the mixture was stirred in the cold for 2 h and at room temperature for 24 h under nitrogen. The dark brown mixture was concentrated *in vacuo* to about 50 mL, basified with 10% aqueous sodium bicarbonate (50 mL), and extracted with ether (3 × 50 mL). The combined extracts were washed with water (3 × 50 mL), dried, and evaporated to give 4.2 g of **5***a* as a syrup. It exhibited strong carbonyl absorption at 1730 cm^{-1} and a small band at 1670 cm^{-1} (enamine). The crude syrup **5***a* was dissolved in 20 mL dry acetone and added to a solution of 2.0 g anhydrous oxalic acid in 20 mL dry ether and the solution allowed to deposit crystals first at room temperature and then at 0°C overnight. The product was collected to give 4.12 g (58.5%) of **5***a* oxalate, mp 156–159°C. Recrystallization from 94% ethanol gave an analytical sample of the oxalate monohydrate, mp 115–120°C, resolidified and melted at 160–161°C (lit. (12) mp 160–161°C). *Anal.* calcd. for $C_{19}H_{23}NO_6H_2O$: C 60.15, H 6.64, N 3.69; found: C 60.09, H 6.68, N 3.56.

The yield of **5***a* was 64% after purification by chromatography on alumina (activity II) (methylene chloride as eluent).

The free base **5***a* was regenerated from its oxalate salt by base treatment and extraction with ether; ir (neat): 1730 cm^{-1}; nmr ($CDCl_3$) δ: 2.42 (s, 3H, NCH_3), 3.75 (s, 3H, OCH_3), 4.70–6.15 (m, 3H, olefinic), 6.60–7.15 (m, 3H, ArH).

The yield of **5***a* was not lowered appreciably when sodium bicarbonate or ammonium carbonate were used.

In other experiments the solution of sodium or ammonium bicarbonate was added all at once to the solution of **2***a*. This caused the yield of **5***a* to drop to 30–35%.

In DMSO–H_2O or DMF–H_2O as the solvents and ammonium bicarbonate as the base, the yields of **5***a* were 40–45%.

When sodium hydroxide was used as the base and aqueous ethanol as solvent **5***a* was formed in only trace amounts.

With ammonium hydroxide as the base using conditions described in the literature (6) for the preparation of **5***b*, the yield of **5***a* was negligible.

*2′-Methoxy-2,5-dimethyl-9-oxo-6,7-benzomorphan (5*b*)*

*(*a*) Using the Procedure Described Above for the Preparation of 5*a

A solution of 7.78 g (20 mmol) of **2***b* in 175 mL of 95% ethanol was treated with a solution of 1.64 g (20.6 mmol) of ammonium bicarbonate in 42 mL water. After stirring at room temperature for 24 h, the mixture was concentrated *in vacuo* to a small volume (~50 mL), treated with 10% aqueous sodium bicarbonate (50 mL), and extracted with ether (5 × 50 mL). The combined extracts were washed with water (2 × 50 mL), dried, and evaporated to give a syrupy residue (3.46 g) which was dissolved in 10 mL dry acetone and the solution added to a solution of 2.0 g anhydrous oxalic acid in 10 mL acetone. Crystals separated first at room temperature and then at 0°C overnight. The product was collected, washed with acetone (20 mL), and dried to give 3.91 g (58%) of the oxalate salt of **5***b*, mp 140–142°C. The free base **5***b* was quantitatively regenerated from its oxalate salt by treatment with ammonium hydroxide followed by extraction with chloroform; ir (neat): 1730 cm^{-1}; nmr ($CDCl_3$) δ: 1.36 (s, 3H, CH_3), 2.32 (s, 3H, NCH_3), 3.65 (s, 3H, OCH_3), 6.5–7.1 (m, 3H, ArH).

A sample of **5***b* in ether was treated with an ethereal solution of hydrogen chloride to give the hydrochloride salt of **5***b*. Recrystallization from 95% ethanol gave the hydrochloride of

the ethanol hemiacetal adduct of **5***b* (no C=O absorption in the ir; ethoxy absorption in the nmr spectrum); mp 122°C; resolidified and melted at 186–188°C. When the hydrochloride of **5***b* was recrystallized from aqueous acetone it gave the hydrochloride monohydrate, mp 130–132°C (lit. (6) 130–132°C).

(b) By the Process Described in the Literature (6)

Following the procedure given by Takeda *et al.* (6), 3.89 g (10 mmol) of **2***b* in methylene chloride was treated with aqueous ammonium hydroxide and the product isolated as described and purified by chromatography on alumina to give 0.51 g (21%) of **5***b*.

5-Allyl-2-cyclopropylmethyl-2'-methoxy-9-oxo-6,7-benzomorphan (5c)

The procedure described above for the preparation of **5***a* was used. Thus, a solution of 9.1 g (20 mmol) of **2***c* in 95% ethanol (170 mL) was treated with a solution of 1.7 g (21.5 mmol) ammonium bicarbonate in 21 mL of water. Initially, **3***c* precipitated as an oil. After stirring at room temperature for 48 h the oil had dissolved and the reaction mixture was concentrated *in vacuo* to a small volume (~50 mL), basified with 10% aqueous sodium bicarbonate (50 mL), and extracted with ether (4 × 50 mL). The combined extracts were washed with water, dried, and evaporated to give 4.6 g of **5***c* as a syrup. Thin layer chromatography on alumina (ether) showed one major spot with R_f 0.78 (**5***c*) and a minor one with R_f 0. The syrup **5***c* was dissolved in acetone (10 mL) and treated with a solution of 2.0 g anhydrous oxalic acid in acetone (10 mL) and the resulting solution diluted with dry ether (10 mL). The crystalline product was collected to give 4.0 g (50%) of the oxalate salt of **5***c*, mp 148.5–150°C. *Anal.* calcd. for $C_{22}H_{27}NO_6$: C 65.82, H 6.78, N 3.48; found: C 65.57, H 7.08, N 3.40.

The free base **5***c* was quantitatively regenerated from its oxalate salt by treatment with sodium hydroxide and extraction with ether; ir (neat): 1730 cm^{-1}.

The yield of **5***c* was reduced to 30% when the ammonium bicarbonate solution was added all at once to the solution of **2***c*.

5-(3-Ethylenedioxy)butyl-2'-methoxy-3-methyl-9-oxo-6,7-benzomorphan (5d)

The procedure described above for the preparation of **5***a* was followed. The bromoiminium bromide **2***d* (9.1 mmol) was treated with ammonium bicarbonate in 95% ethanol and after stirring at room temperature for 30 h the product was isolated as described above and purified by chromatography on silica using ether as the eluent to give 1.1 g (35.5%) of **5***d* as an oil; ir (neat): 1730 cm^{-1}; nmr ($CDCl_3$) δ: 1.40 (s, 3H, CH_3), 2.47 (s, 3H, NCH_3), 3.84 (s, 3H, OCH_3), 3.98 (s, 4H, OCH_2CH_2O), 6.7–7.2 (m, 3H, ArH). *Anal.* calcd. for $C_{20}H_{27}NO_4$: C 69.54, H 7.88, N 4.05; found: C 69.02, H 7.63, N 4.03.

1. J. G. MURPHY, J. H. AGER, and E. L. MAY. J. Org. Chem. **25**, 1386 (1960).
2. E. L. MAY and J. G. MURPHY. J. Org. Chem. **20**, 257 (1955).
3. K. C. RISE. J. Org. Chem. **40**, 1850 (1975).
4. N. B. EDDY and E. L. MAY. Synthetic analgesics, Part B. Pergamon Press, Oxford, London. 1966.
5. D. C. PALMER and M. J. STRAUSS. Chem. Rev. **77**, 1 (1977) and references therein.
6. M. TAKEDA, M. KONDA, H. INOUE, S. SAITO, and H. KUGITA. J. Org. Chem. **37**, 2677 (1972).
7. G. KAVADIAS, S. VELKOF, and B. BELLEAU. Can. J. Chem. This issue.
8. A. G. COOK. Enamines: synthesis, structure and reactions. Marcel Dekker, New York and London. 1969.
9. M. E. KUEHNE. J. Am. Chem. Soc. **83**, 1492 (1961).
10. R. L. PEDERSON, J. L. JOHNSON, R. P. HOLYSZ, and A. C. OTT. J. Am. Chem. Soc. **79**, 1115 (1957).
11. P. DUHAMEL, L. DUHAMEL, C. COLLET, and A. HAIDER. C. R. Acad. Sci. Ser. C, **273**, 1461 (1971).
12. F. R. AHMED, M. SAUCIER, and I. MONKOVIC. Can. J. Chem. **53**, 3276 (1975).

9-Oxobenzomorphans. III. Synthesis of derivatives with various substituents at 2-, 2′-, and 5-positions

GERRY KAVADIAS,[1] STEPHAN VELKOF, AND BERNARD BELLEAU

Bristol Laboratories of Canada, 100 Industrial Boulevard, Candiac, P.Q., Canada J5R 1J1

Received December 20, 1978

GERRY KAVADIAS, STEPHAN VELKOF, and BERNARD BELLEAU. Can. J. Chem. 57, 1866 (1979).

5-Allyl-2-cyclobutylmethyl-2′-methoxy-, 5-allyl-2′-benzyloxy-2-methyl-, 5-benzyl-2′-methoxy-2-methyl-, and 5-allyl-2′-benzyloxy-2-cyclobutylmethyl-9-oxo-6,7-benzomorphans were prepared by a previously described process. The process involves bromination of the 5,9b-dihydrobenz[*e*]indolines to β-bromoiminium bromides followed by treatment with a weak base in aqueous organic solvents. Ammonium bicarbonate and aluminium oxide are effective bases for the conversions of the β-bromoiminium salts to 9-oxobenzomorphans **5***a–g*. The mechanism of the reaction involves formation of the bromoenamines (fast step) followed by hydration of the latter (slow step) and rearrangement to **5***a–g*.

GERRY KAVADIAS, STEPHAN VELKOF et BERNARD BELLEAU. Can. J. Chem. 57, 1866 (1979).

On a préparé par un procédé décrit antérieurement, les allyl-5 cyclobutylméthyl-2 méthoxy-2′, allyl-5 benzyloxy-2′ méthyl-2, benzyl-5 méthoxy-2′ méthyl-2 et allyl-5 benzyloxy-2′ cyclobutylméthyl-2 oxo-9 benzo-6,7 morphanes. Le procédé implique la bromation des dihydro-5,9b benz[*e*] indolines en bromures des β-bromoiminium suivie par une réaction avec une base faible dans des solvants organiques aqueux. Le bicarbonate d'ammonium et l'oxyde d'aluminium sont des bases efficaces pour la transformation des sels des β-bromoiminium en oxo-9 benzomorphanes **5***a–g*. Le mécanisme de la réaction implique la formation des bromoènamines (étape rapide) suivie par une hydratation de ces dernières (étape lente) et une transposition en **5***a–g*.

[Traduit par le journal]

The preceding papers of this series (1, 2) described the preparation of 9-oxo-6,7-benzomorphans by a process which involves bromination of the indolines **1** to bromoiminium bromides **2** followed by hydrolysis with aqueous ammonium bicarbonate (Scheme 1). The present paper is an extension of that work and describes the synthesis of the new 9-oxo-benzomorphans **5***a–d* by the same process. It also describes a novel and efficient way of converting the bromoiminium salts **2** to 9-oxobenzomorphans **5**, namely, by treatment with aluminium oxide.

The 5,9b-dihydrobenz[*e*]indolines (cyclic enamines) **1***a–g* were prepared as previously described (see Part I of this series (1)) and used without delay.

Bromination of the enamines **1***a–d* to the bromoiminium salts **2***a–d* was performed by the procedure previously developed (see Part II of this series (2)) and involves rapid mixing of a solution of the enamine in methylene chloride with a solution of an equimolar amount of bromine in the same solvent at −60°C. Thus, bromination of **1***a* produced crystalline **2***a* in 91% yield (Scheme 1). Bromination of **1***b* afforded **2***b* in quantitative yield as a syrup. Bromination of **1***c* and **1***d* gave **2***c* and **2***d* as crystalline products in 93% and 90% yields respectively. The structures of **2***a–d* as β-bromoiminium salts were confirmed by elemental analyses and by ir and nmr spectroscopy. The ir spectra of **2***a–d* showed strong C=C absorption at 1660 cm^{-1}, a frequency which is lower than that of the analogous absorption (1670 cm^{-1}) of the parent enamines **1***a–d* as would be expected (2, 3). The nmr spectra showed an absence of the signal at δ 4.3 which is characteristic for the proton at C-4 in the parent enamines **1***a–d*.

The conversion of the bromoiminium salts **2***a–c* to **5***a–c* was accomplished by the procedure described earlier (2) and involved treatment of **2***a–e* with ammonium bicarbonate in aqueous ethanol. More specifically, treatment of a solution of **2***a* in 95% ethanol with an aqueous solution of ammonium bicarbonate, first at −5 to 0°C for 2 h and then at room temperature for 48 h (method *A*), produced the 9-oxobenzomorphan **5***a* isolated in 55% yield as the oxalate salt. In an analogous manner, **2***b* was converted to **5***b* which was similarly isolated in 42% yield. Intermediate **2***c* was also converted to **5***c* which was separated by chromatography on alumina and obtained in 30% yield. As previously observed (2) in the early stage of the conversion of **2***a–c* to **5***a–c*, the bromoenamines **3***a–c* initially precipitated followed by slow dissolution as the hydration progressed to give **5***a–c*.

An effective alternative procedure for the conversion of the bromoiminium salts **2***a–g* to 9-oxoben-

[1]To whom correspondence may be addressed.

0008-4042/79/141866-04$01.00/0

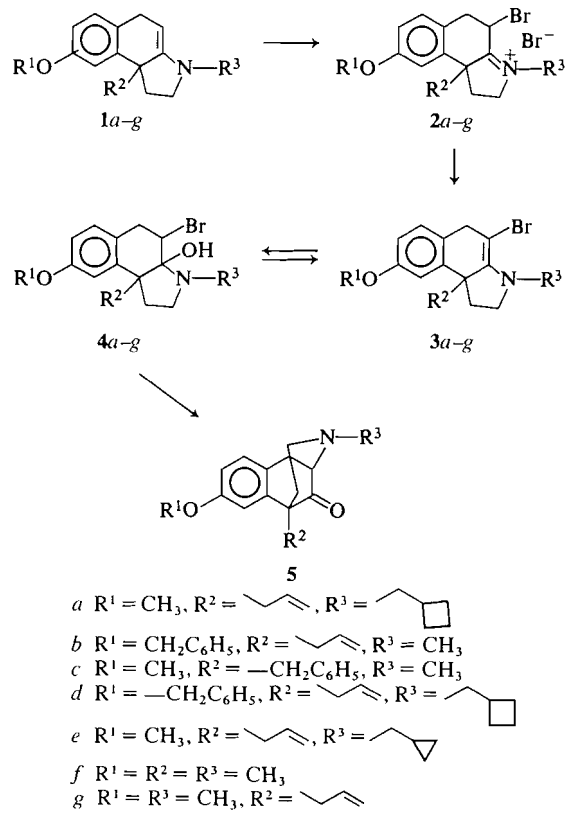

SCHEME 1

zomorphans **5***a–g* involved treatment of the salts with alumina in aqueous organic solvents at room temperatures for 24–48 h (method *B*). For instance, stirring a mixture of **2***e* and alumina (Merck, type E) (5 g Al_2O_3/g of **2***e*) in DMSO–water (3:1) for 24 h at room temperature produced **5***e* isolated in 66% yield as the oxalate salt. The yields at **5***e* were sensitive to solvent volume and the proportion of alumina. Similar treatment of the bromoiminium salts **2***c–g* with alumina under the same conditions gave the 9-oxobenzomorphans **5***c–g* in fair to good yields that were comparable to those obtained by the ammonium bicarbonate method (Table 1). The role of the aluminium oxide in this process is to convert the bromoiminium salts **2***a–g* to the bromoenamines **3***a–g* which then react with a mole of water to give ketones **5***a–g* via intermediates **4***a–g*. In fact, when a solution of **2***e* in chloroform was stirred with aluminium oxide for 5 min followed by rapid filtration under nitrogen, the intermediate bromoenamine **3***e* was produced in 80% yield as an air-sensitive oil. The same product was obtained when **2***e* was treated with sodium bicarbonate followed by extraction with ether. In the ir, compound **3***e* showed strong C=C absorption at 1670 cm^{-1} and when dissolved in DMSO–water was converted to **5***e*.

TABLE 1. Yields obtained by methods *A* and *B*

9-Oxobenzomorphan	Yield	
	Method *A*	Method *B*
5*a*	55[a]	
5*b*	42[a]	
5*c*	30[b]	25[b]
5*d*		51[a]
5*e*	50[a]	66[a]
5*f*	58[a]	58.5[a]
5*g*	58.5[a]	55[a]

[a]Isolated as the oxalate salt.
[b]Purified by chromatography.

Experimental

The melting points were determined on a Mel-Temp melting point apparatus and are uncorrected. The ir spectra were recorded on a Unicam Sp-200G grating ir spectrometer. The nmr spectra were recorded on a Varian A-60A spectrometer using deuteriochloroform as the solvent. The chemical shifts are expressed in δ values using tetramethylsilane as internal reference. Microanalyses were performed by Micro-Tech Laboratories Inc., Skokie, IL, U.S.A. All experiments with enamines (work-up, filtration, extraction, release of vacuum after evaporation, etc.) were carried out under a nitrogen atmosphere.

*9b-Allyl-4-bromo-8-methoxy-2,4,5,9b-tetrahydro-1H-benz[e]indole Cyclobutylmethobromide (***2a***)*

To a stirred solution of 5.18 g (32.4 mmol) of bromine in 325 mL of methylene chloride at −60°C under nitrogen was added all at once a solution of 10 g (32.4 mmol) of the enamine **1***a* in 40 mL methylene chloride. After stirring at −60°C for 5 min, the cooling bath was removed and the reaction mixture stirred for an additional 20 min. The solvent was evaporated and the solid residue recrystallized from acetone–ether (1:2, 75 mL) to give 13.8 g (91%) of **2***a*, mp 117–120°C; ir (Nujol): 1660 cm^{-1}. *Anal.* calcd. for $C_{21}H_{26}Br_2NO$: C 53.86, H 5.59, Br 34.12, N 2.99; found: C 53.88, H 5.85, Br 34.24, N 2.86.

*9b-Allyl-8-benzyloxy-4-bromo-2,4,5,9b-tetrahydro-1H-benz[e]indole Methobromide (***2b***)*

Following the above procedure for the preparation of **2***a*, the enamine **1***b* (51.2 g, 154 mmol) was reacted with bromine in methylene chloride to give 75.5 g (100%) of crude **2***b* as a syrup. The crude **2***b* was used in the next step without delay.

*9b-Benzyl-4-bromo-8-methoxy-2,4,5,9b-tetrahydro-1H-benz[e]indole Methobromide (***2c***)*

Following the preceding method for the preparation of **2***a*, the enamine **1***c* (14.0 g, 46.8 mmol) was reacted with bromine (7.4 g, 46 mmol) in methylene chloride (500 mL) at −60°C. Evaporation of the solvent and trituration of the residue with acetone–ether (60 mL, 1:1) gave 19.2 g (93%) of **2***c*, mp 103–106°C; ir (Nujol): 1660 cm^{-1}. *Anal.* calcd. for $C_{21}H_{23}Br_2NO$: C 54.21, H 4.98, Br 34.35; found: C 54.46, H 5.01, Br 34.08.

*9b-Allyl-8-benzyloxy-4-bromo-2,4,5,9b-tetrahydro-1H-benz[e]indole Cyclobutylmethobromide (***2d***)*

The enamine **1***d* (30.1 g, 78.2 mmol) was reacted with bromine (12.5 g, 160 mmol) in methylene chloride (850 mL) at

−60°C by the procedure described for **2***a*. Evaporation of the solvent left a solid residue which was triturated with acetone–ether (100 mL, 1:1) and collected to give 37 g (90%) of **2***d*, mp 109–112°C. A sample recrystallized twice from ethanol–ether (1:8) had mp 114–115°C; ir (Nujol): 1660 cm^{-1}. *Anal.* calcd. for $C_{27}H_{31}Br_2NO$: C 59.46, H 5.72, Br 29.30, N 2.56; found: C 59.64, H 5.88, Br 29.12, N 2.57.

*5-Allyl-2-cyclobutylmethyl-2′-methoxy-9-oxo-6,7-benzomorphan (***5***a). Method* A

5*a* was obtained from **2***a* by treatment with ammonium bicarbonate according to the previously described procedure (see Part II). To a stirred solution of 46.9 g (100 mmol) of **2***a* in 1 L 95% ethanol at −5° to 0°C under nitrogen was added dropwise over a 90 min period a solution of 8.5 g (108 mmol) of ammonium bicarbonate in 100 mL of water. After the addition was complete the reaction mixture was stirred in the cold for 2 h and then at room temperature for 48 h under nitrogen. In the early stage of the reaction, the bromoenamine **3***a* precipitated as an oil which slowly dissolved as the reaction progressed. The solvent was evaporated, the residue treated with 8% aqueous sodium bicarbonate (300 mL), and the mixture extracted with ether (4 × 200 mL). The combined extracts were washed with water, dried, and evaporated to give a residue which after chromatography on alumina (activity II) using methylene chloride as the eluent gave 20 g of **5***a* as an oil. It was dissolved in 60 mL dry acetone and the solution added to a solution of 10 g anhydrous oxalic acid in the same solvent (50 mL) and diluted with 40 mL of anhydrous ether. The crystalline product was collected, washed with acetone, and dried to give 23 g (55%) of the oxalate salt of **5***a*, mp 182–182.5°C. *Anal.* calcd. for $C_{23}H_{29}NO_6$: C 66.48, H 7.03, N 3.37; found: C 66.72, H 6.99, N 3.25.

The free base was regenerated from the oxalate salt by treatment with sodium hydroxide and extraction with ether; ir (neat): 1730 cm^{-1}; nmr ($CDCl_3$) δ: 3.75 (s, 3H, OCH_3), 4.85–6.15 (m, 3H, olefinic).

*5-Allyl-2′-benzyloxy-2-methyl-9-oxo-6,7-benzomorphan (***5***b)*

Following the procedure described above for the preparation of **5***a* (method *A*), crude **2***b* (17.2 g, 35 mmol) was treated with ammonium bicarbonate in aqueous ethanol and the product isolated as above to yield **5***b* (10.7 g) as an oil. This crude material was dissolved in anhydrous ether and treated with a solution of anhydrous oxalic acid in the same solvent. The oxalate salt thus obtained was recrystallized from ethanol (10 mL) – acetone (40 mL) to yield 6.7 g (42%) of the oxalate monohydride salt of **5***b*, mp 104–107°C. *Anal.* calcd. for $C_{25}H_{27}NO_6 \cdot H_2O$: C 65.91, H 6.41, N 3.07; found: C 65.15, H 6.41, N 2.89.

The free base **5***b* was regenerated from its oxalate salt by treatment with sodium hydroxide and extraction with ether; ir (neat): 1730 cm^{-1}; nmr ($CDCl_3$) δ: 2.40 (s, 3H, NCH_3), 4.90 (s, 2H, $PhCH_2O$), 4.85–6.15 (m, 3H, olefinic), 6.60–7.30 (m, 8H, ArH).

*5-Allyl-2-cyclopropylmethyl-2′-methoxy-9-oxo-6,7-benzomorphan (***5***e). Method* B

5*e* was obtained from **2***e* by treatment with aluminium oxide. To a solution of 5 g (11 mmol) of **2***e* in DMSO–water (3:1) (50 mL) was added 25 g aluminium oxide G (Merck, type E), the mixture blanketed with nitrogen, and stirred at room temperature. After 24 h the mixture was filtered and the alumina washed first with ethanol (2 × 15 mL) and then with water (2 × 20 mL). The filtrate and washings were combined, diluted with water (50 mL), treated with 8% aqueous sodium bicarbonate (50 mL), and extracted with ether (4 × 50 mL). The combined extracts were washed with water (3 × 50 mL) dried, and evaporated to give 2.7 g of **5***e* as a syrup. It was dissolved in 20 mL dry acetone, treated with a solution of 1.2 g anhydrous oxalic acid in 5 mL of the same solvent, and the solution diluted with 15 mL dry ether. The crystalline precipitate was collected to give 2.72 g (62%) of the oxalate salt of **5***e*, mp and mixture mp with an authentic sample (Part II of this series) 148–150°C.

On a larger scale experiment (43 g of **2***e*) the above procedure led to the oxalate salt of **5***e* in 58% yield.

When the amount of aluminium oxide was reduced (2 g of Al_2O_3/g of **2***e*) the yield of the oxalate salt of **5***e* was 53%, whereas an increase in solvent volume to 20 mL/g of **2***e* raised the yield to 66%.

The free base of **5***e* was quantitatively regenerated from its oxalate salt (sodium hydroxide – ether) and was identical in all respects to an authentic sample (Part II of this series).

*5-Benzyl-2′-methoxy-2-methyl-9-oxo-6,7-benzomorphan (***5***c)*

(a) From **2***c by Treatment with Ammonium Bicarbonate (Method* A*)*

Following the above method for the preparation of **5***a* (method *A*), a solution of 6.97 g (15 mmol) of **2***c* in 200 mL of 95% ethanol was treated with a solution of 1.28 g (16.2 mmol) of ammonium bicarbonate in 20 mL water and the reaction mixture stirred at room temperature for 72 h. At first, the bromoenamine **3***c* precipitated and gradually dissolved as the reaction progressed. Work-up of the mixture as described for **5***a* gave 2.4 g of crude **5***c* as a syrup, which after chromatography on alumina (activity II) using 1% ethanol in methylene chloride as the eluent gave 1.4 g (30%) of **5***c*, mp 136.5–137.5°C (ethanol); ir ($CHCl_3$): 1730 cm^{-1}; nmr ($CDCl_3$) δ: 2.40 (s, 3H, NCH_3), 3.35 (s, 2H, $ArCH_2$), 3.65 (s, 3H, OCH_3), 6.6–7.2 (m, 3H, ArH). *Anal.* calcd. for $C_{21}H_{23}NO_2$: C 78.47, H 7.21, N 4.36; found: C 78.42, H 7.28, N 4.30.

(b) From **2***c by Treatment with Aluminium Oxide (Method* B*)*

Following method *B* above for the preparation of **5***e*, a mixture of 4.65 g (10 mmol) of **2***c* and 23 g aluminium oxide in 90 mL 85% DMSO–water was stirred at room temperature for 48 h. The crude product (2.7 g) was chromatographed on alumina (as in part *a* above) to give 0.8 g (25%) of **5***c* identical in every respect with the product obtained above (Method *A*).

*5-Allyl-2′-benzyloxy-2-cyclobutylmethyl-9-oxo-6,7-benzomorphan (***5***d). Method* B *Above*

To a solution of 5.45 g (10 mmol) of **2***d* in 115 mL of DMSO–water (3:1) was added 25 g aluminium oxide and the mixture stirred under nitrogen at room temperature for 72 h. The mixture was filtered and the solids washed with ethanol (2 × 15 mL) and with water (2 × 20 mL). The combined filtrate and washings were diluted with 250 mL of water, the solution basified with 8% aqueous sodium bicarbonate (50 mL), and extracted with ether (5 × 60 mL). The combined extracts were washed with water (3 × 60 mL), dried, and evaporated to give 3.0 g of **5***d* as a syrup. It was dissolved in dry acetone (10 mL), a solution of 1.2 g anhydrous oxalic acid in the same solvent (20 mL) was added, and the solution diluted with dry ether (30 mL). The crystalline product was collected to give 2.5 g (51%) of the oxalate salt of **5***d*, mp 165–167°C.

The free base **5***d* was quantitatively regenerated from its oxalate salt by treatment with sodium hydroxide and extraction with ether; ir (neat): 1730 cm^{-1}; nmr ($CDCl_3$) δ: 5.05 (s, 2H, $ArCH_2O$), 5.85–6.15 (m, 3H, olefinic), 6.85–7.50 (m, 8H, ArH).

The hydrobromide salt of **5***d* had mp 198–199°C (ethanol–ether). *Anal.* calcd. for $C_{27}H_{31}NO_2 \cdot HBr$: C 67.21, H 6.68, N 2.90; found: C 67.07, H 6.83, N 3.01.

2′-Methoxy-2,5-dimethyl-9-oxo-6,7-benzomorphan (5f). (Method B for 5e)

A mixture of 3.89 g (10 mmol) of **2***f* and 23 g aluminium oxide in 90 mL DMSO–water (3:1) was stirred under nitrogen for 24 h, filtered, the solids washed with ethanol (2 × 15 mL) and then water (2 × 20 mL). The combined filtrate and washings were diluted with water (250 mL), basified with 8% aqueous sodium bicarbonate (50 mL), and extracted with ether (7 × 50 mL). The combined extracts were washed with water (2 × 50 mL), dried, and evaporated to give a liquid residue (1.74 g) which was dissolved in 5 mL dry acetone and a solution of 1.0 g anhydrous oxalic acid in 5 mL acetone added. The crystalline product was collected to give 1.97 g (58.5%) of the oxalate salt of **5***f*, mp and mixture mp with an authentic sample (Part II of this series), 130–132°C.

5-Allyl-2′-methoxy-2-methyl-9-oxo-6,7-benzomorphan (5g). (Method B for 5e)

A mixture of 3.78 g (9.08 mmol) of **2***g* and 20 g of aluminium oxide in 40 mL DMSO–water (3:1) was stirred at room temperature under nitrogen for 24 h. Work-up as in **5***e* gave 1.7 g of **5***g* as a syrup which was dissolved in 10 mL dry acetone and a solution of 1.0 g anhydrous oxalic acid in 10 mL dry ether added. The crystalline precipitate was collected to give 1.8 g (55%) of the oxalate salt of **5***g*, mp and mixture mp with an authentic sample (2) 156–159°C.

9b-Allyl-4-bromo-8-methoxy-3-cyclopropylmethyl-5,9b-dihydrobenz[e]indoline (3e)

(a) From 2e by Treatment with Ammonium Bicarbonate

To a solution of 1.0 g (2.2 mmol) of **2***e* in 15 mL water was added 10 mL of 8% aqueous sodium bicarbonate and the solution extracted quickly with ether (3 × 20 mL) under nitrogen. Removal of the solvent *in vacuo* gave 0.5 g (61%) of the air-sensitive **3***e*; ir (neat): 1670 cm^{-1}.

(b) From 2e by Treatment with Alumina

To a solution of 1.0 g (2.2 mmol) of **2***e* in 50 mL chloroform was added 10 g of alumina (activity II) and the mixture stirred for 5 min under nitrogen followed by filtration under a blanket of nitrogen. Evaporation of the solvent left 0.65 g (80%) of **3***e* as an air-sensitive light brown liquid; ir (neat): 1670 cm^{-1}. When left in DMSO–water (3:1) or 95% ethanol at room temperature for 24 h, **3***e* was converted to 9-oxobenzomorphan **5***e*.

1. G. KAVADIAS, S. VELKOF, and B. BELLEAU. Can. J. Chem. This issue.
2. G. KAVADIAS, S. VELKOF, and B. BELLEAU. Can. J. Chem. This issue.
3. R. L. PEDERSON, J. L. JOHNSON, R. P. HOLYSZ, and A. C. OTT. J. Am. Chem. Soc. **79**, 1115 (1957).

Aminocyclitols. III. Synthesis of diaminocyclohexanediols

GERRY KAVADIAS[1] AND ROBERT DROGHINI

Bristol Laboratories of Canada, 100 Industrial Boulevard, Candiac, P.Q., Canada J5R 1J1

Received December 1, 1978

GERRY KAVADIAS and ROBERT DROGHINI. Can. J. Chem. **57**, 1870 (1979).

Reaction of *N,N'*-diethoxycarbonyl-2,5-dideoxystreptamine (**1***b*) with thionyl chloride produced the iminoether dihydrochloride **8** which, upon simple treatment with water gave the di-*N,O*-carbonyl compound **9**. Acidic hydrolysis of **9** yielded the aminocyclitol **2***a*. Alternatively, **2***a* was prepared from *N,N'*-dibenzoyl-2,5-dideoxystreptamine (**1***c*) via the oxazoline **10** followed by acidic hydrolysis. Treatment of **1***c* with triethyl orthoacetate in the presence of boron trifluoride etherate produced the oxazoline **11** and the latter product was hydrolyzed to give **3***a*. By the same reaction sequence, **1***e* and **1***h* were converted to the oxazolines **12** and **13** which upon acidic hydrolysis provided the enantiomeric aminocyclitols **4** and **5**. Ring-opening reactions of *cis*- and *trans*-1,4-diepoxycyclohexanes (**14** and **16**) with sodium azide to the diazido compounds **15** and **17**, followed by reduction, afforded the aminocyclitols **6** and **7**.

GERRY KAVADIAS et ROBERT DROGHINI. Can. J. Chem. **57**, 1870 (1979).

La réaction de la *N,N'*-diéthoxycarbonyldidéoxy-2,5 streptamine (**1***b*) avec le chlorure de thionyle fournit le dichlorure de l'iminoéther (**8**) qui, par un traitement simple avec de l'eau, conduit au composé di-*N,O*-carbonyle **9**. Une hydrolyse acide de **9** fournit l'aminocyclitol **2***a*. On peut préparer **2***a* par une autre voie à partir de la *N,N'*-dibenzoyl didéoxy-2,5 streptamine (**1***c*) par l'intermédiaire de l'oxazoline **10** après une hydrolyse acide. Si l'on traite **1***c* par de l'orthoacétate de triéthyle en présence de l'éthérate de trifluorure de bore on obtient l'oxazoline **11** qui, par hydrolyse, conduit à **3***a*. Par la même suite de réaction, on a pu transformer **1***e* et **1***h* en oxazolines **12** et **13**, qui, par hydrolyse acide, donnent respectivement naissance aux aminocyclitols énantiomères **4** et **5**. Les réactions d'ouverture de cycle des diépoxy-1,4 cyclohexanes *cis* et *trans* (**14** et **16**) par l'azoture de sodium fournissent les diazotures **15** et **17** qui, par réduction, conduisent aux aminocyclitols **6** et **7**.

[Traduit par le journal]

In the previous papers of this series (1, 2) we have reported the syntheses of several aminocyclitols and their derivatives to be used as substrates in chemical and biochemical studies related to the synthesis of novel aminocyclitol antibiotics.

The present paper describes the syntheses of the aminocyclitols **2**–**7** (Fig. 1) and their derivatives and provides evidence for their assigned structures.

The readily available 2,5-dideoxystreptamine (**1***a*) (1) served as the starting material for the preparations of the aminocyclitols **2**–**5**. Thus, treatment of **1***a* with ethyl chloroformate in aqueous methanol, in the presence of sodium bicarbonate, gave *N,N'*-diethoxycarbonyl-2,5-dideoxystreptamine (**1***b*) in high yield. Reaction of **1***b* with an excess of thionyl chloride at the reflux temperature for 2 h produced the iminoether dihydrochloride **8** which on simple treatment with water gave a 74% yield of di-*N,O*-carbonyl-(1,3,4,6/0)-4,6-diamino-1,3-cyclohexanediol (**9**). Acidic hydrolysis (acetic acid – hydrochloric acid) of **9** afforded the dihydrochloride salt of (1,3,4,6/0)-4,6-diamino-1,3-cyclohexanediol (**2***a*) in 90% yield (Scheme 1). Alternatively, **2***a* was prepared from *N,N'*-dibenzoyl-2,5-dideoxystreptamine (**1***c*) via the oxazoline **10** and acidic hydrolysis. Thus, treatment of **1***c* with thionyl chloride by our previously described procedure (2), afforded a 72% yield of the oxazoline **10**. When **10** was treated with a dilute acid solution for a short period of time and the product neutralized with base, (1,3,4,6/0)-4,6-dibenzamido-1,3-cyclohexanediol (**2***b*) was obtained in 90% yield. Treatment of **10** with a concentrated acid solution (acetic acid – hydrochloric acid 1:1) at the reflux temperature, afforded a 49% yield of **2***a* dihydrochloride. Structural assignment to **2***a* was based on mechanistic considerations (two independent syntheses) and was further confirmed by ^{1}Hmr spectroscopy. The ^{1}Hmr spectrum of **2***a* dihydrochloride exhibited a two-proton eight-line multiplet at δ 3.60 with coupling constants of 10.5, 6, and 3 Hz which were ascribed to the magnetically equivalent N—C—H protons. The coupling pattern and the coupling constant magnitudes show that the two N—C—H protons are axially oriented and each one coupled with a neighboring axial and two neighboring equatorial protons. It also showed a two-proton five-line multiplet at δ 4.20 with coupling constants of 6, 6, and 3 Hz, assigned to the magnetically equivalent O—C—H protons, thus indicating that these protons are equatorially oriented and each coupled with

[1]To whom correspondence should be addressed.

0008-4042/79/141870-07$01.00/0

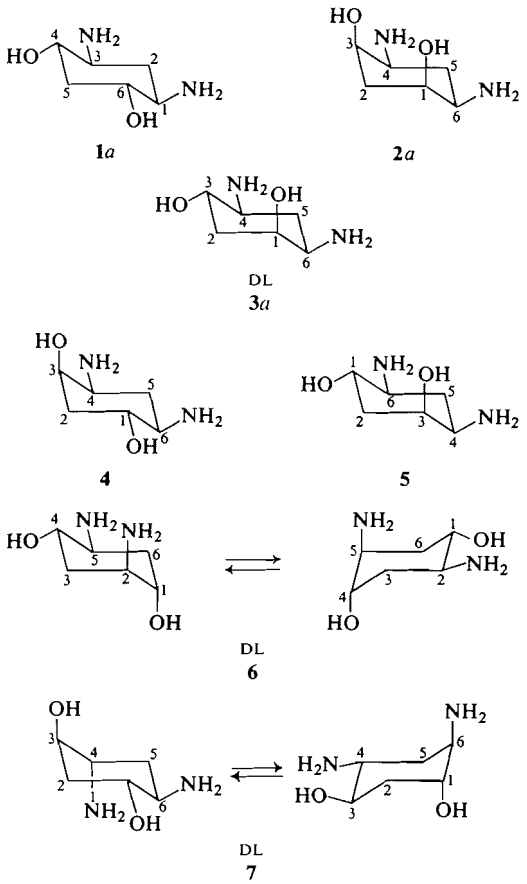

FIG. 1

two axial and one equatorial adjacent protons. This spectral data confirms the all-*cis*-configuration for **2***a* dihydrochloride and further indicates that the preferred conformation of the molecule is the one where the two amino groups are in equatorial and the two hydroxyls in axial orientations, with little or no ring inversion.

DL-(1,4,6/3)-4,6-Diamino-1,3-cyclohexanediol (**3***a*) and the enantiomers **4** and **5** were prepared by the reaction sequences outlined in Scheme 2. Treatment of *N*,*N*′-dibenzoyl-2,5-dideoxystreptamine (**1***c*) with triethyl orthoacetate in dimethylformamide in the presence of boron trifluoride etherate by the procedure we have previously described (2) produced the oxazoline **11** in 75% yield. Upon mild acidic hydrolysis, the oxazoline **11** was converted to DL-(1,4,6/3)-4,6-dibenzamido-1,3-cyclohexanediol (**3***b*) in 90% yield. When **11** was refluxed in a concentrated acid solution (AcOH–HCl), an 85% yield of **3***a* dihydrochloride was obtained. The stereochemical assignment to **3***a* was supported by ^{1}Hmr spectroscopy. The ^{1}Hmr spectrum of **3***a* dihydrochloride exhibited signals due to the four nonequivalent ring methine protons which were interpretable by a first-order method. Thus, a double triplet at δ 3.26 having coupling constants of 11, 11, and 4 Hz was ascribed to the axial H-4 proton (N—C—H) indicating that this proton was coupled with two axial and one equatorial adjacent protons. An eight-line multiplet at δ 3.57 with coupling constants of 12, 5, and 3 Hz was ascribed to the axial H-6 proton (N—C—H), coupled with one axial and two equatorial neighboring protons. The spectrum also showed a double triplet at δ 4.06 ($J_{2a,3} = J_{3,4} = 11$ Hz, $J_{2e,3} = 5$ Hz) due to the axial H-3 (O—C—H) and a five-line multiplet at δ 4.26 ($J_{1,2a} = J_{1,6} = 5$ Hz, $J_{1,2e} = 3$ Hz) due to the equatorial H-1 proton. This spectral data is in complete accord with the 1,4*N*,6*N*/3 stereochemistry of **3***a*. Attempts to resolve racemic **3***a* were unsuccessful.

The optical isomers **4** and **5** were prepared as follows. 1-*N*-Ethoxycarbonyl-2,5-dideoxystreptamine (**1***d*) of known absolute configuration (1), was *N*-benzoylated to produce 3-*N*-benzoyl-1-*N*-ethoxycarbonyl-2,5-dideoxystreptamine (**1***e*). Treatment of **1***e* with triethyl orthoacetate in DMF containing boron trifluoride etherate gave a 78.5% yield of the oxazoline **12** (2) which, on acidic hydrolysis, produced (1*R*,3*R*,4*S*,6*R*)-4,6-diamino-1,3-cyclohexanediol (**4**) dihydrochloride in 72% yield. In a similar manner, 3-*N*-ethoxycarbonyl-2,5-dideoxystreptamine (**1***f*) (1) (the enantiomer of **1***d*) was *N*-benzoylated and the product **1***h* was treated with triethyl orthoacetate in DMF in the presence of boron trifluoride etherate to produce the oxazoline **13** (88%). Acidic hydrolysis of **13** gave a 75% yield of (1*S*,3*S*,4*R*,6*S*)-4,6-diamino-1,3-cyclohexanediol (**5**) dihydrochloride, identical with **4** dihydrochloride in all respects except optical activity. The ^{1}Hmr spectra of **4** and **5** were identical to that of the racemic products **3***a* discussed above, thus confirming the stereochemical assignments to these products.

The preparation of the aminocyclitols **6** and **7** was carried out via ring-opening of the diepoxides **14** and **16** with sodium azide to the diazido compounds **15** and **17**, followed by reduction (Scheme 3). Thus, treatment of *cis*-1,4-diepoxycyclohexane **14** with an excess of sodium azide in a DMSO–water mixture in the presence of *p*-toluenesulfonic acid at 70°C for 22 h, gave a 67% yield of (1,4/2,5)-2,5-diazido-1,4-cyclohexanediol (**15**). Catalytic hydrogenation of **15** with palladium on carbon afforded (1,4/2,5)-2,5-diamino-1,4-cyclohexanediol (**6**) in 84% yield. The assignment of the 1,4/2*N*,5*N* stereochemistry to **6**, was based upon the mechanism of the reactions involved in its synthesis and the ^{1}Hmr spectrum of this material. Since *trans* opening of the epoxide rings by

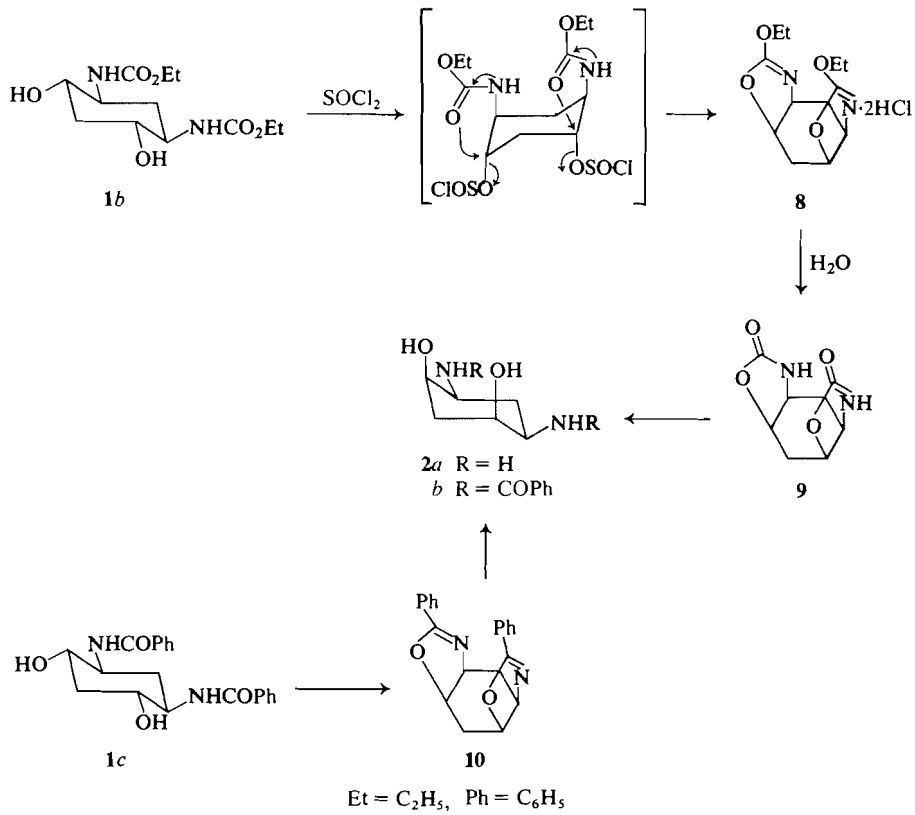

SCHEME 1

nucleophiles is assumed, the *cis* diepoxide **14** should produce (via respective diazido compounds) the isomeric aminocyclitols **6** and (or) the known product **1***a*. The physical and spectral properties exhibited by **6** were different from those of **1***a* and therefore its structure could be deduced by elimination. The ^{1}Hmr spectrum of **6** exhibited a two-proton quartet at δ 2.93 with a coupling constant of 6 Hz assigned to the two equivalent N—C—H protons. It also showed a two-proton quartet at δ 3.66 with a coupling constant of 6 Hz assigned to the two equivalent O—C—H protons. The appearance of both the N—C—H and O—C—H signals as quartets was taken as evidence for time averaging of the axial and equatorial protons in these positions by ring inversion and confirmed the assigned structure to this product. Treatment of *trans*-1,4-diepoxycyclohexane (**16**) with sodium azide, as described above for the preparation of **15**, gave a 70% yield of (1,4/3,6)-4,6-diazido-1,3-cyclohexanediol (**17**) which upon catalytic reduction afforded (1,4/3,6)-4,6-diamino-1,3-cyclohexanediol (**7**) in 82% yield. The ^{1}Hmr spectrum of **7** revealed a two-proton quartet at δ 3.71 for the O—C—H protons, both with coupling constants of 6 Hz. These spectral data indicate a time averaging of the axial and equatorial protons in these positions as a result of rapid ring inversion and confirms the 1,4*N*/3,6*N* stereochemistry for **7**.

The ring-opening reactions of the *cis*- and *trans*-diepoxides **14** and **15** with sodium azide to the diazido products **15** and **17**, respectively, are in accord with previous reports on the stereochemical course of the ring-opening reactions of these compounds with other nucleophiles and confirm the *trans* and diaxial opening (3, 4).

Experimental

The melting points were determined on a Mel-Temp melting point apparatus and are not corrected. The ir spectra were recorded on a Unicam SP-200G grating ir spectrometer. The ^{1}Hmr spectra were taken with a Varian EM-360A 60 MHz spectrometer. The chemical shifts are expressed in δ values using tetramethylsilane (for solutions other than deuterium oxide) and sodium 4,4-dimethyl-4-silapentane-1-sulfonate (for solutions of deuterium oxide) as internal standards. Thin-layer chromatography (tlc) was carried out on microscope slides coated with silica gel. Optical rotations were measured with a Perkin-Elmer model 141 polarimeter. The analyses were performed by Micro-Tech Laboratories, Skokie, IL.

N,N′-*Diethoxycarbonyl-2,5-dideoxystreptamine* (*1b*)

A solution of 24.6 g (150 mmol) of 2,5-dideoxystreptamine monohydrate (**1***a*) (1) and 46 g (0.55 mol) of sodium bicar-

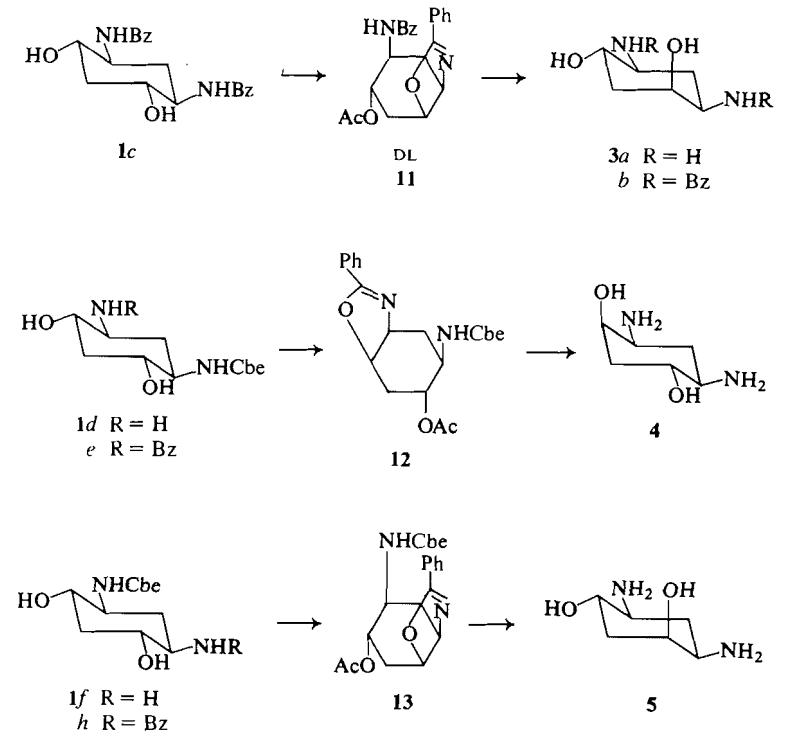

Ac = $COCH_3$, Bz = COC_6H_5, Cbe = $CO_2C_2H_5$, Ph = C_6H_5,

SCHEME 2

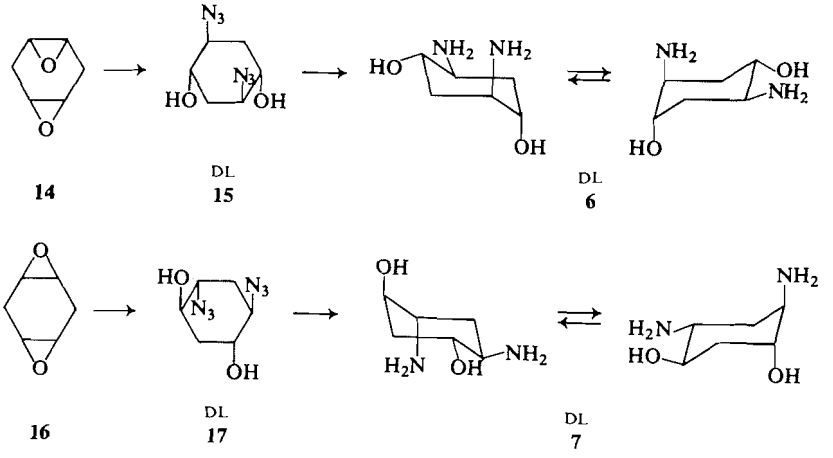

SCHEME 3

bonate in 500 mL of water was diluted with 30 mL of methanol and cooled in an ice-bath while stirring. Ethyl chloroformate (54 g or 0.5 mol) was added dropwise and at a rate to maintain the solution temperature below 20°C. After completion of the addition (5 min), stirring was continued at 4–6°C for 30 min and then at room temperature for 3 h. The reaction mixture was evaporated and the residue was dissolved in water (400 mL) and extracted continuously with ethyl acetate until all the product **1***b* was extracted (48 h). Compound **1***b* crystallized in the ethyl acetate extract and was collected by filtration to give 40.9 g (94%), mp 197–199°C. The analytical sample was obtained by recrystallization from ethanol, mp 204–205°C; ir (Nujol): 3320, 1695, 1545 cm^{-1}. *Anal.* calcd. for $C_{12}H_{22}N_2O_6$: C 49.64, H 7.64, N 9.65; found: C 49.58, H 7.70, N 9.61.

N,N′-*Dibenzoyl-2,5-dideoxystreptamine (1c)*

To an ice-cold solution of 17.8 g (122 mmol) of 2,5-dideoxystreptamine (**1***a*) and 35 g (330 mmol) of sodium carbonate in 210 mL water and 70 mL methanol was added dropwise

(15 min), with stirring, a solution of 44.4 g (305 mmol) of benzoyl chloride in 70 mL of dry acetone. After stirring at 0°C for 30 min and at room temperature for 1 h, the reaction mixture was diluted with water (400 mL). The resulting precipitate was collected by filtration, washed successively with water (2 × 130 mL), ethanol (100 mL), and ether (2 × 130 mL), and dried to give 40.8 g of **1***c*, mp 278–282°C. This product was stirred in boiling ethanol and filtered to give 39.0 g (90%) of **1***c*, mp 280–282°C (dec.). This material was used in the next reaction. The analytical sample was prepared by recrystallization from DMF–EtOH (1:1); mp 283–285°C, resolidified and melted at 294–295°C; ir (Nujol): 3400, 3300, 1625, 1615, 1575, 1565 cm^{-1}. *Anal.* calcd. for $C_{20}H_{22}N_2O_4$: C 67.78, H 6.25, N 7.90; found: C 67.70, H 6.26, N 8.03.

*3-N-Benzoyl-1-N-ethoxycarbonyl-2,5-dideoxystreptamine (**1**e)*

To a solution of 7.81 g (35.6 mmol) of 1-*N*-ethoxycarbonyl-2,5-dideoxystreptamine (**1***d*) and 5.04 g (60 mmol) of sodium bicarbonate in 40 mL water was added 40 mL of acetone and 5 mL of methanol and the mixture was cooled in an ice-bath while stirring. A solution of 7.03 g (50 mmol) of benzoyl chloride in 15 mL of dry acetone was added dropwise. After the addition (15 min), the reaction mixture was stirred at room temperature for 1.5 h and then evaporated *in vacuo*. The residue was treated with water (50 mL) and the solid product collected by filtration, washed with water (2 × 30 mL) and ether (50 mL), and dried first at room temperature, then at 100°C, to give 8.90 g of **1***e*, mp 254–256°C. The aqueous filtrate was extracted continuously with ethyl acetate to give 2.2 g of **1***e*, mp 254–256°C. The two crops were combined to a total of 11.1 g (96.5%). A sample was recrystallized from ethanol–ether (1:3), mp 240–245°C, resolidified and melted at 254–256°C; $[\alpha]_D^{25}$ −18.6 (*c* 0.8, EtOH); ir (Nujol): 3350, 1700, 1650, 1550 cm^{-1}. *Anal.* calcd. for $C_{16}H_{22}N_2O_5 \cdot \frac{1}{2}H_2O$: C 57.99, H 6.99, N 8.45; found: C 57.66, H 6.90, N 8.19.

*1-N-Benzoyl-3-N-ethoxycarbonyl-2,5-dideoxystreptamine (**1**h)*

3-*N*-Ethoxycarbonyl-2,5-dideoxystreptamine (**1***f*) was *N*-benzoylated by the procedure described above for the synthesis of **1***e* to give a 91% yield of **1***h*, mp 244°C; resolidified and melted at 254–256°C; $[\alpha]_D^{25}$ +17.6 (*c* 0.8, EtOH); ir (Nujol): 3350, 1700, 1650, 1550 cm^{-1}. *Anal.* calcd. for $C_{16}H_{22}N_2O_5$: C 59.61, H 6.88, N 8.69; found: C 59.65, H 7.01, N 8.70.

*Di-N,O-carbonyl-(1,3,4,6/0)-4,6-diamino-1,3-cyclohexanediol (**9**)*

To 35 g (120 mmol) of powdered *N,N'*-diethoxycarbonyl-2,5-dideoxystreptamine (**1***b*) in a 1 L round-bottomed flask was added portionwise 120 mL of thionyl chloride. After the reaction had subsided, the reaction mixture was refluxed until the evolution of gasses ceased (2 h) and then evaporated to dryness. The residue was evaporated with toluene to remove traces of thionyl chloride and the product was cooled in an ice-bath. Water (100 mL) was slowly added to it and after the material had dissolved 100 mL of ether was added. The crystalline precipitate that was formed was collected by filtration, washed with ether, and dried to give 12.7 g of **9**, mp 254–256°C (dec.). The aqueous phase of the filtrate was separated, neutralized with an anion exchange resin (Rexyn 201, in the OH form, from Fisher Scientific Co.), and evaporated to dryness. The solid residue was treated with ethanol (15 mL) and filtered to give 4.8 g of **9**, mp 255–257°C (dec.). The two fractions were combined to give a total of 17.5 g (73.5%) of **9**; ir (Nujol): 3300, 1750 cm^{-1}; ^{1}Hmr (DMSO-d_6): 1.46–2.25 (m, 4H, CH_2), 3.85 (m, 2H, N—C—H), 4.70 (octet, 2H, O—C—H, J_1 = 10 Hz, J_2 = 8 Hz, J_3 = 5.5 Hz), 7.4 (s, 2H, NH). *Anal.* calcd. for $C_8H_{10}N_2O_4$: C 48.48, H 5.08, N 14.23; found: C 48.21, H 5.07, N 14.08.

*Bisoxazoline (**10**)*

Powdered *N,N'*-dibenzoyl-2,5-dideoxystreptamine (**1***c*) (20.0 g, 56.4 mmol) was added to 100 mL of thionyl chloride and the mixture was stirred at room temperature for 3 min and then heated on a steambath for 3 min. The solution was cooled in an ice-bath and then evaporated to dryness at 30°C. The residue, on trituration with ether (150 mL), solidified. The ether phase was decanted and the crystalline oxazoline dihydrochloride was treated with 6% aqueous sodium hydroxide (250 mL) and extracted with chloroform (250 mL). The chloroform solution, after drying, was evaporated to dryness to give 15.3 g of crude **10**. Thin-layer chromatography (10% ethanol–chloroform) showed, under uv, one major spot of R_f 0.23 (**10**) and four minor spots of R_f 0, 0.37, 0.43, and 0.50. The crude product was boiled and stirred with 70 mL acetone (5–10 min) and then cooled in an ice-bath and filtered to give 12.8 g (72%) of the bisoxazoline **10**, mp 191–195°C. Thin-layer chromatography showed one major spot (R_f 0.23) and a trace of the spot with R_f 0.37. This material was used in the next reaction. The analytical sample was obtained by recrystallization from ethanol (twice); mp 196–198°C; ir ($CHCl_3$): 1650, 1585, 1500 cm^{-1}. *Anal.* calcd. for $C_{20}H_{18}N_2O_2$: C 75.45, H 5.70, N 8.80; found: C 75.68, H 5.75, N 8.69.

*(1,3,4,6/0)-4,6-Diamino-1,3-cyclohexanediol (**2**a)*

Method A

2*a* was obtained from the dicarbamate **9** by acidic hydrolysis. A solution of 6.0 g (30.3 mmol) of the dicarbamate **9** in 15 mL of 20% hydrochloric acid was heated under reflux for 24 h. The solution was filtered and the filtrate evaporated to dryness. The solid residue was stirred with cold ethanol (50 mL), collected by filtration, washed with ethanol (2 × 20 mL), and dried to give 5.5 g of the dihydrochloride salt of **2***a*, mp 315°C (decomposition starts at 290°C). The filtrate and washings were combined, evaporated to dryness, and the residue was crystallized from ethanol (30 mL) to give 0.4 g more of the dihydrochloride salt of **2***a*. The two fractions were combined to a total of 5.9 g (89.5%). Thin-layer chromatography on silica plates with H_2O–NH_4OH–MeOH–$CHCl_3$ (1:1:4:1) as eluent showed a single spot of R_f 0.18; ^{1}Hmr (D_2O): 1.63–2.53 (m, 4H, two CH_2), 3.60 (octet, 2H, H-4 and H-6, $J_{4,5a}$ = $J_{5a,6}$ = 10.5 Hz, $J_{3,4}$ = $J_{1,6}$ = 6 Hz, $J_{4,5e}$ = $J_{5e,6}$ = 3 Hz), 4.20 (five-line multiplet, 2H, H-1 and H-3, $J_{1,2a}$ = $J_{2a,3}$ = $J_{3,4}$ = $J_{1,6}$ = 6 Hz, $J_{1,2e}$ = $J_{2e,3}$ = 3 Hz). *Anal.* calcd. for $C_6H_{14}N_2O_2 \cdot 2HCl$: C 32.89, H 7.36, Cl 32.36, N 12.79; found: C 32.85, H 7.44, Cl 32.34, N 12.95.

The free base **2***a* was quantitatively regenerated from its dihydrochloride salt by treatment with an anion exchange resin (Rexyn 201, OH form); mp 119–121°C.

Method B

2*a* was obtained from the bis-oxazoline **10** by acidic hydrolysis. A solution of 0.4 g (1.26 mmol) of the bis-oxazoline **10** in 20 mL of acetic acid – concentrated hydrochloric acid mixture (1:1) was heated under reflux for 36 h. After removal of the solvent by evaporation, the residue was dissolved in water and the solution extracted with ether (to remove benzoic acid). The aqueous phase was evaporated. The solid residue was boiled with ethanol (5 mL) and after cooling to room temperature, the crystalline product was collected to give 0.136 g (49%) of the dihydrochloride of **2***a* identical in all respects with the product above.

*(1,3,4,6/0)-3,6-Dibenzamido-1,3-cyclohexanediol (**2**b)*

To a solution of the bis-oxazoline **10** (0.5 g or 1.57 mmol) in 90% ethanol (15 mL) was added concentrated hydrochloric acid (0.5 mL) and the reaction mixture was heated under reflux for 15 min and then evaporated. The residue was dissolved

in 25 mL of 1 *N* sodium hydroxide solution in aqueous ethanol (1:1) and the solution stirred at room temperature for 1 h. Removal of the solvent *in vacuo* left a residue to which 20 mL of water was added, stirred for 5 min, and then the aqueous phase decanted. The residue, on trituration with ether, solidified. The solid product was suspended in water (20 mL) and the mixture was stirred for a few minutes. The crystalline product was collected by filtration, washed with water and ether, and dried to give 500 mg (90%) of **2***b*, mp 224–228°C. Recrystallization from ethanol–ether gave an analytical sample, mp 227–228°C. *Anal.* calcd. for $C_{20}H_{22}N_2O_4$: C 67.78, H 6.25, N 7.90; found: C 67.72, H 6.24, N 7.90.

Oxazoline ***11***

To a suspension of 14.2 g (40 mmol) of *N,N'*-dibenzoyl-2 2,5-dideoxystreptamine (**1***c*) in 80 mL dry DMF was added 30 mL of triethyl orthoacetate and 10 mL of boron trifluoride etherate and the mixture, protected from moisture, was stirred at room temperature for 24 h. The reaction mixture was poured into a cold solution of 8% sodium bicarbonate (500 mL) and the precipitate was collected and washed with water (3 × 100 mL). After drying, the crystalline product was dissolved in chloroform (200 mL), filtered to remove some insoluble matter, and the filtrate evaporated to dryness. The solid residue was treated with a 1:1 ether – petroleum ether solution (60 mL) and filtered to give 12.1 g, mp 186–189°C. Recrystallization from ethanol (200 mL) gave 10.2 g of **11**, mp 189–190°C. A further 1.1 g of **11** were recovered from the mother liquor after evaporation and recrystallization from ethanol (30 mL). The two crops were combined to a total of 11.3 g (75%); ir (Nujol): 3350, 1740, 1660, 1530 cm^{-1}. *Anal.* calcd. for $C_{22}H_{22}N_2O_4$: C 69.83, H 5.85, N 7.40; found: C 69.80, H 5.86, N 7.34.

DL-*(1,4,6/3)-4,6-Diamino-1,3-cyclohexanediol (3*a*) Dihydrochloride*

A solution of 2 g (5.3 mmol) of the oxazoline **11** (racemic) in 20 mL of a 1:1 acetic acid – concentrated hydrochloric acid mixture was heated under reflux for 16 h. The reaction mixture was evaporated, the residue dissolved in water (50 mL), and the solution extracted with ether (3 × 20 mL) to remove benzoic acid. The aqueous solution was evaporated and the residue was refluxed with 20 mL of ethanol. After cooling to room temperature, the solid precipitate was collected to give 0.99 g (85.5%) of **3***a* dihydrochloride. Thin-layer chromatography on silica plates with H_2O–NH_4OH–MeOH–$CHCl_3$ (1:1:4:1) as eluent showed a single spot of R_f 0.25. Recrystallization from water (1 mL) – ethanol (5 mL) gave the analytical sample, mp 305–307°C; ^{1}Hmr (D_2O): 1.42–2.49 (m, 4H, two CH_2), 3.26 (dt, 1H, H-4, $J_{3,4} = J_{4,5a} = 11$ Hz, $J_{4,5e} = 4$ Hz) 3.57 (octet, 1H, H-6, $J_{5a,6} = 12$ Hz, $J_{5e,6} = 3$ Hz, $J_{1,6} = 5$ Hz), 4.06 (dt, 1H, H-3, $J_{2a,3} = J_{3,4} = 11$ Hz, $J_{2e,3} = 5$ Hz), 4.26 (five-line multiplet, 1H, H-1, $J_{1,2a} = J_{1,6} = 5$ Hz, $J_{1,2e} = 3$ Hz). *Anal.* calcd. for $C_6H_{14}N_2O_2 \cdot 2HCl$: C 32.89, H 7.36, N 12.78; found: C 32.81, H 7.29, N 12.79.

DL-*(1,4,6/3)-4,6-Dibenzamido-1,3-cyclohexanediol (3*b*)*

A mixture of 1.14 g (3 mmol) of the oxazoline **11** with 15 mL of 90% ethanol and 0.5 mL of concentrated hydrochloric acid was heated under reflux for 15 min while stirring. The reaction mixture was evaporated and the residue dissolved in a 1 *N* sodium hydroxide solution in aqueous ethanol (1:1, 25 mL) and the resulting solution stirred at room temperature for 1 h. The solvent was removed by evaporation and replaced with 20 mL of water. The mixture was stirred for 5 min and the crystalline precipitate that was formed was collected by filtration, washed with water and with ether, and dried to give 0.95 g (90%) of **3***b*, mp 232–233°C; ir (Nujol): 3350, 1650, 1560 cm^{-1}. *Anal.* calcd. for $C_{20}H_{22}N_2O_4$: C 67.78, H 6.25, N 7.90; found: C 67.95, H 6.32, N 7.97.

Oxazoline ***12***

To a solution of 37.1 g (112 mmol) of **1***e* in dry DMF (110 mL) was added 50 mL triethyl orthoacetate and 15 mL boron trifluoride etherate and the solution, protected from moisture, was stirred at room temperature for 20 h. The mixture was then poured into a cold solution of 8% sodium bicarbonate (1 L) and extracted with ether (4 × 350 mL). The ether solution was washed with water (2 × 250 mL), dried, and evaporated to dryness to yield a syrup which crystallized on trituration with ether to give 31.2 g (78.5%) of **12**, mp 108–112°C. Thin-layer chromatography with 5% ethanol–ether showed, under uv, a major spot of R_f 0.54 (**12**) and a minor one of R_f 0.85. This material was used in the next experiment without further purification. A small sample was recrystallized from ethyl acetate – petroleum ether (1:3), mp 111–113°C; $[\alpha]_D^{25}$ −64.2 (*c* 1.0, EtOH); ir (Nujol): 3350, 1730, 1690, 1660, 1640, 1540 cm^{-1}. *Anal.* calcd. for $C_{18}H_{22}N_2O_5$: C 62.41, H 6.40, N 8.09; found: C 62.54, H 6.43, N 7.95.

Oxazoline ***13***

Compound **1***h*, (6.0 g, 18.2 mmol) was reacted with triethyl orthoacetate (9 mL) and boron trifluoride etherate (2.0 mL) in dry DMF (19 mL), as described in the preparation of **12**, to give 5.5 g (88%) crude **13** as a solid. Thin-layer chromatography with 5% ethanol–ether showed one major spot of R_f 0.53 and a minor one of R_f 0.90. This material was used in the next reaction. The analytical sample was obtained after three recrystallizations from ethyl acetate (1.5 mL/g) – petroleum ether (6 mL/g), mp 111–113°C; one spot on tlc: $[\alpha]_D^{25}$ +63.7 (*c* 1.0, EtOH); ir (Nujol): 3350, 1745, 1700, 1655, 1550 cm^{-1}. *Anal.* calcd. for $C_{18}H_{22}N_2O_5$: C 62.41, H 6.40, N 8.09; found: C 62.35, H 6.43, N 8.09.

*(1*R*,3*R*,4*S*,6*R*)-4,6-Diamino-1,3-cyclohexanediol (4) Dihydrochloride*

A mixture of 2.23 g of the oxazoline **12** and 20 mL of 1:1 acetic acid – concentrated hydrochloric acid solution was refluxed for 18 h and the reaction mixture was then evaporated. The residue was dissolved in water (20 mL) and extracted with ether (3 × 20 mL) to remove benzoic acid. The aqueous solution was evaporated and the solid residue (1.43 g) was recrystallized from 90% ethanol (20 mL) – ether (7 mL) to give 1.0 g (71.5%) of **4** dihydrochloride, mp 312–314°C (dec.). Thin-layer chromatography on silica with H_2O–NH_4OH–MeOH–$CHCl_3$ (1:1:4:1) showed a single spot of R_f 0.31; $[\alpha]_D^{25}$ −44.4 (*c* 1.0, H_2O); ^{1}Hmr (D_2O) was identical to that of the racemic product **3***a* dihydrochloride. *Anal.* calcd. for $C_6H_{14}N_2O_2 \cdot 2HCl$: C 32.89, H 7.36, N 12.79; found: C 32.82, H 7.13, N 12.75.

*(1*S*,3*S*,4*R*,6*S*)-4,6-Diamino-1,3-cyclohexanediol (5) Dihydrochloride*

In a manner analogous to that given above for the preparation of **4**, acidic hydrolysis of 1.73 g of **13** gave 1.07 g of crude product. Recrystallization from 90% ethanol (20 mL) – ether (7 mL) afforded 0.82 g (75%) of **5** dihydrochloride, mp 312–314°C (dec.); $[\alpha]_D^{25}$ +44.0 (*c* 1.0, H_2O); tlc on silica with H_2O–NH_4OH–MeOH–$CHCl_3$ (1:1:4:1) showed a single spot of R_f 0.31; ^{1}Hmr (D_2O) was identical to that of the racemic product **3***a* dihydrochloride. *Anal.* calcd. for $C_6H_{14}N_2O_2 \cdot 2HCl$: C 32.89, H 7.36, N 12.79; found: C 32.85, H 7.32, N 12.72.

(1,4/2,5)-2,5-Diazido-1,4-cyclohexanediol (15)

cis-1,4-Diepoxycyclohexane (**14**) (6.7 g or 60 mmol) was reacted with hydrazoic acid (generated *in situ* from 14.6 g sodium azide and 30.4 g *p*-toluenesulfonic acid in DMSO–

water) as in the procedure given below for the preparation of **17**. After the reaction was complete (22 h) the reaction mixture was diluted with water (100 mL) and continuously extracted with ether (5 h). The ethereal extract, after drying ($MgSO_4$), was evaporated to dryness. The solid residue was recrystallized from acetone (15 mL) – benzene (50 mL) mixture to give 6.0 g of **15**, mp 138–141°C. The mother liquor was evaporated to dryness, the residue was triturated with benzene (25 mL), and the crystalline product was collected by filtration to give 3.0 g of **15**, mp 137–140°C, which was combined with the above fraction to give a total of 9.0 g product. Recrystallization from acetone – petroleum ether (1 : 1, 50 mL) gave 8.0 g (67%) of **15**, mp 142–143°C; ir (Nujol): 3350 (OH), 2110 (N_3) cm^{-1}. *Anal.* calcd. for $C_6H_{10}N_6O_2$: C 36.36, H 5.08, N 42.41; found: C 36.32, H 4.99, N 42.66.

*(1,4/3,6)-4,6-Diazido-1,3-cyclohexanediol (**17**)*

To a solution of 14.6 g (220 mmol) of sodium azide in 60 mL 1 : 1 DMSO–water mixture was added 30.4 g (160 mmol) *p*-toluenesulfonic acid monohydrate and the solution was stirred at room temperature for 30 min, *trans*-1,4-diepoxycyclohexane (**16**) (6.70 g or 60 mmol) was added, and the reaction mixture was heated at 75°C with stirring for 22 h. After cooling to room temperature, the reaction mixture was diluted with water (100 mL) and extracted with ether (6 × 60 mL). The ethereal solution, after drying over magnesium sulfate, was evaporated to dryness to give 9.0 g of crystalline product. Recrystallization from benzene (45 mL) afforded 8.0 g of **17**, mp 93–95°C. The aqueous phase was extracted continuously with ether, and the ethereal extract was evaporated to dryness. The residue was recrystallized from benzene to give an additional 0.5 g of **17**, mp 93–95°C, which was combined with the first fraction to give a total of 8.5 g (70%) of product. A sample was recrystallized from benzene–ether mixture (1 : 1) to give the analytical sample, mp 96–97°C; ir (Nujol): 3350 (OH), 2110 (N_3) cm^{-1}. *Anal.* calcd. for $C_6H_{10}N_6O_2$: C 36.36, H 5.08, N 42.41; found: C 36.44, H 5.07, N 42.57.

*(1,4/2,5)-2,5-Diamino-1,4-cyclohexanediol (**6**)*

Reduction of the azide **15** (5 g, 25.2 mmol) by the procedure described below for the preparation of **7** gave 3.1 g (84%) of **6**, mp 212–213.5°C (dec.); ^{1}Hmr (D_2O) δ: 1.6–1.9 (m, H, CH_2), 2.93 (q, 2H, N—C—H, J = 6 Hz, band intensities ratio 1 : 3 : 3 : 1), 3.66 (q, 2H, O—C—H, J = 6 Hz, band intensities ratio 1 : 3 : 3 : 1). *Anal.* calcd. for $C_6H_{14}N_2O_2$: C 49.30, H 9.65, N 19.16; found: C 49.25, H 9.61, N 19.06.

*(1,4/3,6)-4,6-Diamino-1,3-cyclohexanediol (**7**)*

A solution of 1.98 g (10 mmol) of **17** in 50 mL of ethanol and 0.1 g of 10% Pd/C was shaken under hydrogen in a Paar apparatus at room temperature and an initial pressure of 50 psi for 4 h. The catalyst was removed by filtration and the filtrate was evaporated to dryness. The solid residue (1.42 g) was recrystallized from ethanol–ether (14 mL, 1 : 1) to give 1.2 g (82%) of **7**, mp 155–157°C; ^{1}Hmr (D_2O) δ: 1.61–1.96 (m, 4H, CH_2), 2.88 (q, 2H, N—C—H, J = 6 Hz, band intensities ratio 1 : 3 : 3 : 1), 3.71 (q, 2H, O—C—H, J = 6 Hz, band intensities ratio 1 : 3 : 3 : 1). *Anal.* calcd. for $C_6H_{14}N_2O_2$: C 49.30, H 9.65, N 19.16; found: C 49.24, H 9.63, N 18.98.

1. G. KAVADIAS, S. VELKOF, and B. BELLEAU. Can. J. Chem. **56**, 404 (1978).
2. G. KAVADIAS and R. DROGHINI. Can. J. Chem. **56**, 2743 (1978).
3. T. W. CRAIG, G. R. HARVEY, and G. A. BERCHTOLD. J. Org. Chem. **32**, 3743 (1967).
4. G. E. MCCASLAND, A. K. M. ANISUZZAMAN, S. R. NAIK, and L. J. DURHAM. J. Org. Chem. **37**, 1201 (1972).

Solvent-induced changes in ^2J(H, F) for fluoroform via van der Waals interactions. Non-contact contributions to spin–spin coupling constants involving a proton?

TED SCHAEFER, HAROLD M. HUTTON, AND SALMAN R. SALMAN[1]

Department of Chemistry, University of Manitoba, Winnipeg, Man., Canada R3T 2N2

Received December 6, 1978

TED SCHAEFER, HAROLD M. HUTTON, and SALMAN R. SALMAN. Can. J. Chem. 57, 1877 (1979).

The spin–spin coupling between the proton and the fluorine nuclei, ^2J, in fluoroform varies by 1% in a range of solvents. It is argued that ^2J decreases algebraically as the van der Waals solute–solvent interactions increase in magnitude. Such a decrease is also observed for coupling constants which likely contain a substantial positive orbital contribution. If the van der Waals interactions perturb the spin–orbital term in J, then ^2J in fluoroform may well contain orbital contributions, as recently calculated for ^2J in methyl fluoride. In that event, the large discrepancies between observed ^2J(H,F) values and those calculated by semiempirical theories of the contact term may be partially attributed to the neglect of orbital terms.

TED SCHAEFER, HAROLD M. HUTTON et SALMAN R. SALMAN. Can. J. Chem. 57, 1877 (1979).

Le couplage spin–spin entre le proton et le fluor, ^2J, du fluoroforme varie par 1% dans divers solvants. On suggère que ^2J diminue d'une façon algébrique au fur et à mesure d'une augmentation des interactions de van der Waals soluté-solvant. On observe aussi une telle diminution des constantes de couplage qui contiennent probablement une contribution orbitalaire positive importante. Si les interactions de van der Waals perturbent le terme orbitalaire du spin de J, il est possible que la valeur ^2J du fluoroforme puisse contenir des contributions orbitalaires semblables à celles calculées récemment pour le ^2J du fluorure de méthyle. Alors, on pourrait attribuer en partie les grandes différences observées entre les valeurs de ^2J(H,F) observées et calculées par des théories semi-empiriques au fait que des termes orbitalaires ont été omis.

[Traduit par le journal]

Introduction

The theory of Barfield and Johnston (1) accounts rather well for the medium dependence (2, 3) of a variety of spin–spin coupling constants, J. It is a one-electron theory, based on an INDO MO FPT formulation (4), and implies that solvent effects on coupling constants involving a proton arise from electrostatic (polarization) perturbations of the contact interaction. It has usually been accepted (5) that couplings involving at least one proton are adequately described in terms of the contact term in Ramsey's formulation of J (6).

Barfield and Johnston recognize (1) that dispersion (van der Waals) effects on coupling constants could be important if orbital contributions to J were to exist. There exists experimental evidence that couplings involving heavier nuclei than protons are sensitive to dispersion interactions with neighbouring molecules (7–10). Furthermore, recent *ab initio* MO calculations (11–13) indicate the presence of sizeable orbital contributions to couplings between nuclei, one or both of which are protons.

The purpose of the measurements reported here is to present evidence for a van der Waals dependence of a coupling to a proton in a molecule in which the coupled nuclei are contained in atoms on the periphery of the molecule. For this purpose, CHF_3 was chosen. The one-electron theory has been used to calculate the solvent dependence of $^1J(^{13}C,H)$, $^1J(^{13}C,F)$, and ^2J(H,F) in this molecule, reasonable agreement with experiment being found for the one-bond couplings (1). On the other hand, the predicted increase of ^2J(H,F) as the solvent polarity (or dielectric constant) increases (1) apparently disagrees with experiment (14, 15), which finds ^2J(H,F) as largely solvent independent.

Again, the extensive work on solvent effects on the proton chemical shift of methane (16–18) has allowed Rummens and co-workers to establish reliable shift parameters characterizing its van der Waals interactions with a variety of solvents. The site factors (16, 17) for methane and fluoroform are rather similar so that these solvent parameters can possibly be used to establish a correlation between ^2J(H,F) and van der Waals fields (perhaps attractive and (or) repulsive[2]) from dipole–dipole interactions.

[1]On sabbatical leave from the Department of Chemistry, University of Baghdad, Iraq.

[2]Short-range, repulsive interactions dominate the local arrangements of molecules in simple liquids (19). Thus, the local structures of liquid CH_3CN and CS_2 resemble one another (19) because the molecular shapes are very similar. The molecular shapes of CH_4 and CHF_3 are also similar, as are their polarizabilities (2.6 and 2.8 $\times$ 10^{-24} cm^3, respectively) but, of course, not their dipole moments.

0008-4042/79/141877-04$01.00/0

TABLE 1. Proton–fluorine spin–spin coupling constant in Hz and proton chemical shift in ppm for fluoroform in various solvents

Solvent	^2J(H,F)	δ_H	ε^c	Solvent	^2J(H,F)	δ_H	ε
1. CHF_3	79.70[e]	6.322	—	11. CBr_2F_2	79.41	6.365	—
	79.68*[a]	6.303	—	12. C_6F_6	79.64	6.550	—
	79.69[b]	6.253	—	13. *s*-$C_6H_3F_3$	79.41	6.408	—
2. $CHCl_3$*[a]	79.27	6.477	4.8	14. C_6H_6*[a]	79.29	5.260	2.3
3. $CHBr_3$	79.08	6.588	4.4	15. *c*-C_6H_{12}*[a]	79.28	6.255	2.0
4. CH_2Cl_2*[a]	79.28	6.523	8.9	16. CS_2	79.14	6.372	2.6
5. CH_2Br_2	79.12	6.577	7.5	17. CH_3CN*[a]	79.38	6.753	37.5
6. CH_2I_2	78.90	6.698	5.3	18. $(CH_3)_2C{=}O$*[a]	79.47	7.038	20.7
7. CCl_4*[a]	79.18	6.463	2.2	19. DMF*[a]	79.30	7.317	36.7
8. $CFCl_3$	79.41	6.357	—	20. DMSO*[a]	79.12	7.257	46.7
9. $CBrCl_3$	79.20	6.491	—	21. CH_3NO_2[d]	79.38	6.74	35.9
10. CCl_2F_2	79.46	6.307	—				

[a]Starred solvents at a probe temperature of 301 K, unstarred solvents at 305 K.
[b]At 313 K, i.e., above critical temperature.
[c]Dielectric constant.
[d]Data taken from ref. 15.
[e]At 295 K.

Furthermore, if van der Waals interactions perturb the orbital contribution to J, it is intuitive that short-range solvent molecule interactions with fluorine atom orbitals should perturb the orbital terms in J more than would solvent interactions with the hydrogen orbitals. The high ratio of fluorine to hydrogen in fluoroform is therefore an advantage if perturbations of orbital contributions are sought; although, of course, fluoroform is not very polarizable and observed changes in ^2J(H,F) may therefore be small.

Experimental

Using a vacuum line, CHF_3 (Matheson) was transferred to thick-walled 5 mm od sample tubes containing solvent and enough TMS to provide an internal lock. As little as 0.4 mol% and as much as 3 mol% of CHF_3 was present in different solutions, as judged by a comparison of appropriate peak intensities from solute and solvent protons. Sample tubes were flame-sealed on a vacuum rack. ^{1}H nmr spectra were recorded on DA60I and HA100 spectrometers at probe temperatures of 301 and 305 K, respectively. Calibrations were performed in the frequency-sweep mode, at sweep rates of 0.02 Hz/s and a dispersion of 1 Hz/cm, by reading sweep and manual oscillator frequencies of calibration lines placed about each peak. The values of ^2J(H,F) in these first-order spectra are thought to be accurate to at least 0.05 Hz, about twice the standard deviations of the measured peak frequencies. Some samples were examined in both spectrometers. For example, in DMSO solution ^2J(H,F) was 79.12 ± 0.02 Hz at 60 MHz and was 79.09 ± 0.03 Hz at 100 MHz.

Results and Discussion

Table 1 presents the values of ^2J(H,F) in CHF_3 for 21 solvents, the last datum being taken from ref. 15. Included are the proton chemical shifts relative to internal TMS, δ_H, and the approximate dielectric constant of the solvent, when known. ^2J(H,F) varies by 1%, from 79.68 Hz in neat CHF_3 to 78.90 Hz in CH_2I_2 solution (~0.4 mol% in CHF_3).

Dependence of ^2J(H,F) on van der Waals Interactions

Perusal of the data in Table 1 leads to the following observations.

(*i*) The polar properties of the solute and solvent are not the main determinants of the variation in ^2J(H,F). For example, ^2J(H,F) is 79.68 Hz in neat CHF_3 and is 79.64 Hz in C_6F_6 solution. CHF_3 has a dipole moment of 1.65 D (20), whereas the dipole moment of C_6F_6 is probably insignificant (its quadrupole moment is nonzero, of course). Again, the dielectric constants of CH_3CN and of 1,3,5-trifluorobenzene (*s*-$C_6H_3F_3$) differ by about 35, yet ^2J(H,F) is the same in the two solutions.

(*ii*) The variation in ^2J(H,F) is apparently more closely related to the polarizability of the solvent molecules than to the dielectric constant of the solvent. For example, the dielectric constants of $CHCl_3$ and $CHBr_3$ are almost the same, yet ^2J(H,F) differs by 0.2 Hz (25% of its variation) in the two solutions. Again, ^2J(H,F) is smallest in CH_2I_2 solution and largest in neat CHF_3. The polarizabilities of these two molecules span those of the molecules in Table 1, being 2.8×10^{-24} cm^3 for CHF_3 (21) and 12.9×10^{-24} cm^3 for CH_2I_2 (17). These observations suggest that van der Waals interactions dominate the medium dependence of ^2J(H,F).

(*iii*) Rummens finds parameters which measure the van der Waals term in the solvent-induced proton chemical shifts of methane. This term can be written as a product of two factors, one characterizing the solute molecule[3] and the other characteristic

[3]The similar molecular radii of CH_4 and CHF_3 (17, 22) and the fact that in liquid CHF_3 the reorientational motion of the CHF_3 molecule is effectively isotropic (23) suggest that the cavity radii and possibly also the site factors of the two molecules will be closely related, so that the solvent parameters, derived by Rummens (17) and possibly model dependent, can still be sensibly used in the manner proposed here.

of the solvent (see eq. [2] in refs. 16, 17). In Fig. 1, ^2J(H,F) is plotted versus the medium shifts of methane, σ_m, as measured in ref. 18 at 303 K and corrected for bulk susceptibility by Rummens (16). A similar plot of ^2J(H,F) versus σ_w, as determined in (17) for a set of solvents somewhat different from that in Fig. 1, agrees with Fig. 1 in indicating that the medium dependence of ^2J(H,F) is indeed related to the van der Waals interactions of CHF_3 with the solvent and is not strongly influenced, for example, by dipole–dipole interactions between solute and solvent. Thus, ^2J(H,F) is essentially the same in CS_2 and DMSO solutions, and is large in acetone and smallest in CH_2I_2 solutions (see points 6, 16, 18 in Fig. 1).

(*iv*) The solvent effects on ^2J(H,F) in CHF_3 are reminiscent of those found for ^1J(F,Si) in SiF_4 (24). Raynes (25) shows that the solvent dependence of ^1J(F,Si) in halomethane solvents is reproduced by the following bond parameters assigned to the solvents: j(C—F) = 0.18, j(C—H) = 1.23, j(C—Cl) = 1.98 Hz. The small value for C—F bonds is striking, particularly as ^1J(F,Si) varies by as much as 8 Hz. Comparison of ^2J(H,F) magnitudes in Table 1 for CHF_3, C_6H_6, *s*-$C_6H_3F_3$, and C_6F_6 solvents, for example, emphasizes the similarity of the behaviour of solvent C—F bonds in perturbing J in the two solute molecules. In fact, because the variation of ^2J(H,F) in CHF_3 is so small, the value of ^2J(H,F) in the gas phase at low pressure is probably very close to the 79.69 Hz measured in the gas phase at 313 K (Table 1), just above the critical temperature of 306 K (the critical pressure is 47 atm).

The Coupling Mechanism for ^{2}J(H,F) in CHF_3

Polarization (electrostatic) models predict an algebraic *increase* in ^2J(H,F) in CHF_3 when dissolved in a polar solvent (1), arising from an increase in the magnitude of the contact contribution. Now, it is interesting that coupling constants for which the presence of orbital components are not disputed display an algebraic *decrease* as the solute molecule is subjected to van der Waals interactions. For example, ^1J(F,Cl) in FCl is +840 Hz in the gas phase (26) and is 770 Hz in the liquid phase (27). Again, ^1J(F,P) is very likely negative in PF_3 (28), and its magnitude is 1404 Hz in the gas phase and 1423 Hz in CCl_4 solution (29). Similar remarks apply to ^1J(F,Si) in SiF_4 (7, 24, 25).

Furthermore, ^2J(F,F) in 1,1-difluoroethene also decreases algebraically as the polarizability of the solvent increases (9). Again, in cyclopropane derivatives (30), ^2J(F,F) decreases algebraically as the intramolecular mean square fields increase in magnitude. ^2J(F,F) is calculated to contain a large positive orbital component (12).

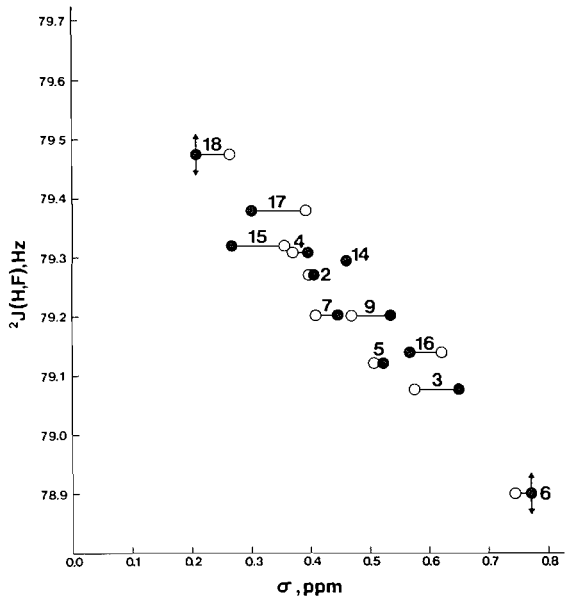

FIG. 1. The coupling constant, ^2J(H,F), in fluoroform is plotted versus the gas-to-medium proton shift, σ_m, of methane from ref. 18, as corrected for bulk susceptibility in ref. 16. The open circles refer to the van der Waals shift, σ_w, as calculated in ref. 16. Point 14 refers to benzene (numbering of solvents as in Table 1) and only σ_w is plotted because σ_m undoubtedly contains a large anisotropy contribution.

If van der Waals interactions act to decrease the magnitude of orbital contributions, as might be anticipated if intermolecular mean square electric fields interfere with spin-induced orbital currents in the solute molecule, and if the orbital components are positive as calculated for ^1J(H,F) in HF (11), for ^2J(H,F) in CH_3F (13), and for ^2J(F,F) in $CF_2{=}CH_2$ (12), then it seems reasonable to attribute the observed algebraic decrease in ^2J(H,F) in CHF_3 to a solvent-induced reduction in the magnitude of its orbital component. Of course, an increase in ^2J(H,F) from the contact term cannot be excluded on the basis of the data in Table 1. However, such an increase must be masked by other interactions.

It is also of interest that INDO MO FPT calculations of ^2J(H,F), although remarkably successful for many coupling constants, disagree badly with observation (4). Such calculations take only the contact term into account.

For all the molecules discussed in this section, at least one of the heavy atoms containing a coupled nucleus lies on the periphery of the molecule. In tetramethyltin, ^2J(H,Sn) *increases* algebraically as the van der Waals interactions with the solvent molecules become larger (8). Tetramethyltin differs from the molecules above in that the heavy atom lies at the center of the molecule and therefore it is the hydrogen atom orbitals which are primarily exposed to buffeting by the solvent molecules, suggesting

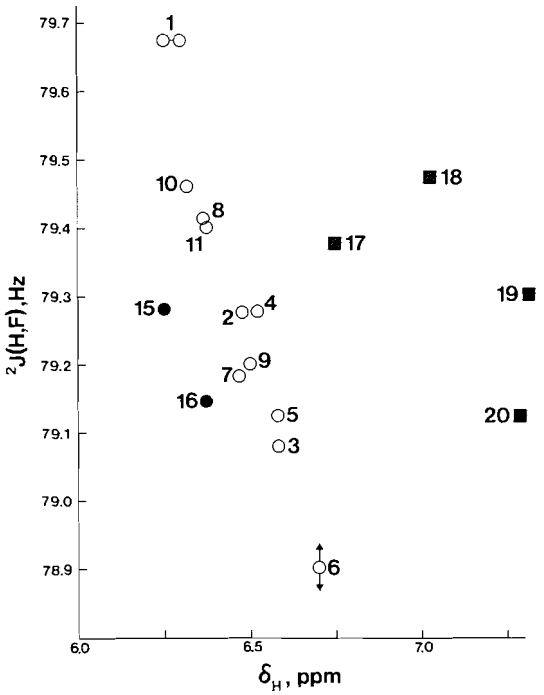

FIG. 2. ^2J(H,F) is plotted versus δ_H from Table 1. Open circles refer to halomethane solvents. Solid squares refer to solvents with which specific (hydrogen bonding) solute–solvent interactions are thought to occur.

perhaps that the electrostatic theory (1) is applicable here.

The Proton Chemical Shift of CHF_3

The proton and fluorine chemical shifts of CHF_3 in 11 solvents have been discussed (15). Fig. 2 displays a plot of ^2J(H,F) versus δ_H, the shift to low field from internal TMS for many of the solvents in Table 1. Referencing to internal TMS removes only some of the van der Waals contributions to δ_H. In the figure, open circles refer to halomethane solvents. If changes in ^2J(H,F) are indeed determined mainly by van der Waals interactions, it appears that δ_H in these solvents is also dominated by such interactions. On the other hand, solvents like DMSO or acetone, for which specific interactions of the polar C—H bond in CHF_3 with the carbonyl or sulfoxide bond may well occur, do not display a correlation between δ_H and ^2J(H,F), the latter being dominated by van der Waals effects (Fig. 1). In particular, δ_H in benzene solution is 5.26 ppm and does not fall on the figure scale at all. In such respects, CHF_3 behaves like $CHCl_3$, for which hydrogen bonding to acetone or to the π electrons of the benzene molecules apparently occurs (31).

Acknowledgments

We are grateful to the National Research Council of Canada for financial assistance.

1. M. BARFIELD and M. D. JOHNSTON. Chem. Rev. **73**, 53 (1973).
2. P. LASZLO. Prog. Nucl. Magn. Reson. Spectrosc. **3**, 231 (1968).
3. S. L. SMITH. Top. Cur. Chem. **27**, 117 (1972).
4. J. A. POPLE, J. W. MCIVER, and N. S. OSTLUND. J. Chem. Phys. **49**, 2960 (1968); **49**, 2965 (1968).
5. J. KOWALEWSKI. Prog. Nucl. Magn. Reson. Spectrosc. **11**, 78 (1977).
6. N. F. RAMSEY. Phys. Rev. **91**, 303 (1953).
7. H. M. HUTTON, E. BOCK, and T. SCHAEFER. Can. J. Chem. **44**, 2772 (1966).
8. P. LASZLO and A. SPEERT. J. Magn. Reson. **1**, 291 (1969).
9. C. J. MACDONALD and T. SCHAEFER. Can. J. Chem. **45**, 3157 (1967).
10. A. M. IHRIG and S. L. SMITH. J. Am. Chem. Soc. **94**, 34 (1972).
11. M. F. GUEST, V. R. SAUNDERS, and R. E. OVERILL. Mol. Phys. **35**, 427 (1978).
12. A. C. BLIZZARD and D. P. SANTRY. J. Chem. Phys. **55**, 950 (1971); **58**, 4714 (1973).
13. R. DITCHFIELD and L. C. SNYDER. J. Chem. Phys. **56**, 5823 (1972).
14. R. H. COX and S. L. SMITH. J. Magn. Reson. **1**, 432 (1969).
15. W. B. SMITH and A. M. IHRIG. J. Phys. Chem. **75**, 497 (1971).
16. F. H. A. RUMMENS. Can. J. Chem. **54**, 254 (1976).
17. F. H. A. RUMMENS and F. M. MOURITS. Can. J. Chem. **55**, 3021 (1977).
18. A. D. BUCKINGHAM, T. SCHAEFER, and W. G. SCHNEIDER. J. Chem. Phys. **32**, 1227 (1960).
19. C. S. HSU and D. CHANDLER. Mol. Phys. **36**, 215 (1978).
20. J. N. SHOOLERY and A. H. SHARBAUGH. Phys. Rev. **82**, 95 (1951).
21. J. APPLEQUIST. Acc. Chem. Res. **10**, 79 (1977).
22. J. H. CHAFFIN and P. S. HUBBARD. J. Chem. Phys. **46**, 1511 (1967).
23. J. W. HARRELL. J. Magn. Reson. **23**, 335 (1976).
24. R. B. JOHANNESEN, F. E. BRINCKMAN, and T. D. COYLE. J. Phys. Chem. **72**, 660 (1968).
25. W. T. RAYNES. Mol. Phys. **15**, 435 (1968).
26. B. FABRICANT and J. S. MUENTER. J. Chem. Phys. **66**, 5274 (1977).
27. K. T. GILLEN, D. C. DOUGLAS, and J. E. GRIFFITHS. J. Chem. Phys. **69**, 461 (1978).
28. R. R. DEAN and W. MCFARLANE. J. Chem. Soc. Chem. Commun. 840 (1967).
29. W. T. RAYNES, T. A. SUTHERLEY, H. J. BUTTERY, and C. M. FENTON. Mol. Phys. **14**, 599 (1968).
30. M. G. BARLOW, R. FIELDS, and F. P. TEMME. Spectrochim. Acta, Part A, **34**, 613 (1978).
31. R. L. LICHTER and J. D. ROBERTS. J. Phys. Chem. **74**, 912 (1970).

Derivatives of diphenylmethane. Preferred conformations and barriers to internal rotation by the *J* method

TED SCHAEFER, WALTER NIEMCZURA, WERNER DANCHURA, AND TIMOTHY A. WILDMAN

Department of Chemistry, University of Manitoba, Winnipeg, Man., Canada R3T 2N2

Received December 4, 1978

TED SCHAEFER, WALTER NIEMCZURA, WERNER DANCHURA, and TIMOTHY A. WILDMAN. Can. J. Chem. **57**, 1881 (1979).

The long-range spin–spin coupling constants over six bonds, $^6J_p^{H,CH}$ and $^6J_p^{F,CH}$, in 3,5-dibromodiphenylmethane and 4,4′-difluorodiphenylmethane, respectively, imply that the ground state conformations of these molecules have C_{2v} symmetry (gable conformations). In terms of a hindered rotor model which assumes a twofold barrier to internal rotation about the exocyclic carbon–carbon bond, the barrier in the dibromo derivatives is 1.1 ± 0.3 kcal/mol. A satisfactory fit to the temperature dependence of $^6J_p^{F,CH}$ is found for a gable conformation. If the conformational properties of these molecules and of diphenylmethane are determined mainly by steric interactions between *ortho* C—H bonds on neighbouring phenyl groups, it seems likely that the results above are a first approximation to the conformational behaviour of diphenylmethane. Some molecular orbital calculations are in semiquantitative agreement with the conclusions based on coupling constants.

TED SCHAEFER, WALTER NIEMCZURA, WERNER DANCHURA et TIMOTHY A. WILDMAN. Can. J. Chem. **57**, 1881 (1979).

Les constantes de couplage spin–spin à longue distance à travers six liaisons, $^6J_p^{H,CH}$ et $^6J_p^{F,CH}$, dans les dibromo-3,5 diphénylméthane et difluoro-4,4′ diphénylméthane, impliquent respectivement que la symétrie des conformations, dans l'état fondamental, de ces molécules est C_{2v} (conformations gables). Si l'on utilise comme modèle un rotor empêché qui implique une barrière binaire à la rotation interne autour de la liaison carbone–carbone exocyclique, la barrière dans les dérivés dibromés est de 1.1 ± 0.3 kcal/mol. On trouve une corrélation satisfaisante pour la relation entre la température et la valeur de $^6J_p^{F,CH}$ dans le cas d'une conformation "gables". Si les propriétés conformationnelles de ces molécules et du diphénylméthane sont principalement déterminés par des interactions stériques entre les liaisons C—H *ortho* des groupes phényles voisins, il semble que les résultats rapportés ci-dessus correspondent à une première approximation du comportement conformationnel du diphénylméthane. Quelques calculs d'orbitales moléculaires sont en accord semi-quantitatif avec des conclusions basées sur les constantes de couplage.

[Traduit par le journal]

Introduction

The most stable conformation of and the barrier to internal rotation in diphenylmethane are uncertain. Kerr constants in CCl_4 solution (1) at 298 K suggest a structure in which both benzene planes are rotated by 41° out of a planar conformation, **1**. Because of steric hindrance between *ortho* C—H bonds on neighbouring phenyl groups, it is assumed here[1] that these rotations correspond to $\psi = -\psi' = 41°$. Such a conformation would be chiral.

In the crystal, the conformation of 3,3′-dichloro-4,4′-dihydroxydiphenylmethane (2) is defined by $\psi = -\psi' = 52°$. Intermolecular hydrogen bonding forces a layered arrangement of molecules and the C—C_7—C angle is apparently as large as 120°.

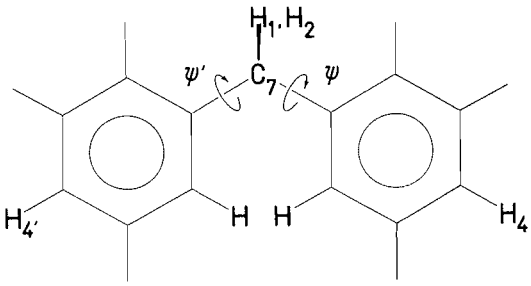

1

Raman scattering data (3) demonstrate that the reorientation of the phenyl groups in diphenylmethane is slower than in toluene.

In this paper, the conformational properties of some diphenylmethane derivatives are discussed in terms of **1** ($\psi = \psi' = 0°$), **2** ($\psi = \psi' = 90°$), **3** ($\psi = 0°$, $\psi' = 90°$), **4** ($\psi = \psi' = 60°$), and of **5** ($\psi = -\psi' = 60°$). Conformation **1** is unstable, of

[1]In **1**, positive ψ values correspond to clockwise rotation viewed along the H_4—C_7 direction, whereas a positive ψ' value corresponds to anticlockwise rotation viewed along the $H_{4'}$—C_7 direction. $\psi = \psi' = 0°$ means that the phenyl groups are coplanar.

0008-4042/79/141881-06$01.00/0

course, because of strong nonbonded repulsions between *ortho* C—H bonds on neighbouring phenyl groups and will not be significantly populated at the temperatures involved in the present set of experiments.

Conformation **2**, here called the gable conformation and of C_{2v} symmetry, can be represented as shown (viewed along the C_7—H_4 axis of one phenyl group while projecting the sidechain into a plane perpendicular to this phenyl group). Distances between *ortho* hydrogen atoms on neighbouring phenyl groups in **2** are well beyond the sum of their van der Waals radii, so that **2** is a candidate for a low-energy conformer.

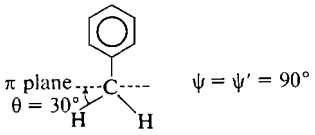

2

Conformer **3** can be derived from **2** by rotation by 90° of the explicitly depicted phenyl group in **2**, yielding C_s symmetry. It is unlikely that **3** is of low energy, because one *ortho* hydrogen must penetrate the π cloud of the neighbouring ring, and will not be discussed further.

Conformation **4** has C_s symmetry also and one methylene C—H bond lies in a plane with each phenyl group. Again, because of strong repulsion between one set of *ortho* C—H bonds on neighbouring rings, **4** is considered to have relatively high energy.

Finally, **5** has a skew conformation of C_2 symmetry in which one methylene C—H bond is in the plane of one phenyl group and the second methylene C—H bond lies in the plane of the other phenyl group. This conformer has a structure rather similar to that found for a derivative in the solid state (3). **5** does not possess a rotation–reflection axis and is chiral.

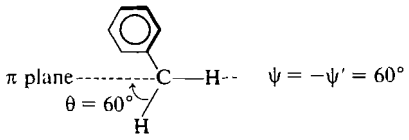

5

It seems that **2** and **5** are candidates for the most stable conformation of diphenylmethane. Note that their structural formulae are here depicted on the assumption that the methylene carbon is sp^3 hybridized. The one-bond spin–spin coupling constant, $^1J(^{13}C,H)$, in diphenylmethane is 126.0 Hz (4, 5), very close to its value in methane (6) and in toluene (4, 6). In the absence of polar substituents (7–11) on the methylene carbon atom, this result strongly suggests minor deviations from tetrahedral geometry at the methylene carbon.

As recently discussed in considerable detail (12), the long-range spin–spin coupling constant over six bonds, $^6J_p^{H,CH}$, between a sidechain proton and a ring proton in the *para* position can be written as

$$[1] \qquad {}^6J_p^{H,CH} = -1.24\langle\sin^2\theta\rangle \text{ Hz}$$

Equation [1] holds in benzyl-X, for example, if the electronegativity of the substituent X is not high (CH_3 or SH groups). The angle θ measures the deviation from coplanarity of the sidechain C—H bond and the benzene ring. Thus, θ is 30° for both methylene C—H bonds in **2** and is 60° and 0° for the C—H bonds in **5**. Again, $\langle\sin^2\theta\rangle$ is the value of $\sin^2\theta$ averaged over the motion about the exocyclic C—C bond. For a twofold barrier, V_2, a hindered rotor treatment yields $\langle\sin^2\theta\rangle$ as a function of temperature, of the magnitude of V_2, and of the reduced moment of inertia about the internal rotation axis. Such a treatment has been successful in the determination of the stable conformations and of internal rotational barriers in molecules such as ethylbenzene (13), phenylcyclopropane (14), phenylcyclohexane (12), and benzyldimethylarsine (12).

Determination of $^6J_p^{H,CH}$ in diphenylmethane is beyond the applicability of current high-resolution nmr techniques. However, $^6J_p^{H,CH}$ can be reliably determined for the substituted ring in 3,5-dibromodiphenylmethane, **6**. If, as seems very likely, the stable conformation and the internal rotational barrier in diphenylmethane are primarily determined by interactions between *ortho* C—H bonds on neighbouring phenyl groups, then substitution at the *meta* positions may well represent a minor perturbation. Certainly, the stable conformation and the barrier about the sp^2–sp^3 carbon–carbon bond in 3,5-dibromophenylethane measured by means of [1] agree exactly with recent low-resolution microwave (15) and heat capacity data (16) on phenylethane.

Cross-conjugation in 4,4′-difluorodiphenylmethane, **7**, is apparently slight (17). In addition, it seems that $^6J_p^{F,CH}$ (fluorine on the ring) can be used in a way similar to $^6J_p^{H,CH}$ by writing (18)

$$[2] \qquad {}^6J_p^{F,CH} = 2.24\langle\sin^2\theta\rangle$$

Because $|^6J_p^{F,CH}| \sim 2|^6J_p^{H,CH}|$, the possibility arises that the temperature dependence of $^6J_p^{F,CH}$, and therefore of $\langle\sin^2\theta\rangle$, is experimentally accessible (at least for a favorable magnitude of V_2) and that some of the deductions based on $^6J^{H,CH}$ in **6** can be verified by a study of $^6J^{F,CH}$ in **7**. A comparison (18) of barrier magnitudes deduced from $^6J^{H,CH}$ and $^6J^{F,CH}$ for a

TABLE 1. Spectral data for 4-aminodiphenylmethane, 3,5-dibromodiphenylmethane (**6**), and 4,4′-difluorodiphenylmethane (**7**)

4-Aminodiphenylmethane[a]		3,5-Dibromodiphenylmethane[a]		4,4′-Difluorodiphenylmethane[c]	
Parameter[b]	Value	Parameter	Value	$^6J_p^{F,CH_2}$	T(K) ± 1.0
ν_2	679.690(3)	ν_2	698.904(7)	0.80_8	250
ν_3	623.269(3)	ν_4	730.117(8)	0.82_5	296
ν_{CH_2}	368.7	ν_{CH_2}	339.9	0.85_4	343
ν_{NH_2}	287.5	$^4J_{24}$	1.775(8)	0.87_9	370
$^3J_{23}$	7.887(4)	$^4J_o^{H,CH_2}$	−0.636(10)		
$^4J_{22}$	2.571(4)	$^6J_p^{H,CH_2}$	−0.498(11)		
$^4J_{33}$	2.163(4)	Error (rms)	0.025		
$^5J_{23}$	0.426(5)				
$^4J_o^{H,CH_2}$	−0.612(4)				
$^5J_m^{H,CH_2}$	0.283(4)				
Error (rms)	0.009				

[a]Concentration 5 mol% in toluene-d_8.
[b]Chemical shifts in Hz at 100 MHz to low field of internal TMS, coupling constants, J, in Hz; numbers in parentheses give the standard deviation in the last place.
[c]Concentration 10 mol% in toluene-d_8; reproducibility of J is about 0.01 Hz.

number of benzyl-X compounds (X = CN, Cl, Br), suggests that V_2 values derived from $^6J^{F,CH}$ data are somewhat higher than those derived from $^6J^{H,CH}$ data, although the correct preferred conformations are given by both types of coupling constants. In view of the extensive discussion in (18), it appears that $^6J^{H,CH}$ data are more reliable indicators of V_2. Nevertheless, the temperature dependence of $^6J^{F,CH}$ may provide valuable confirmation of conformational conclusions based on $^6J_p^{H,CH}$.

Experimental

A 5 mol% solution of 4-aminodiphenylmethane (K&K) in toluene-d_8, a 5 mol% solution of 3,5-dibromodiphenylmethane (prepared from the amino compound by a standard procedure) in toluene-d_8, and a 10 mol% solution of 4,4′-difluorodiphenylmethane (Aldrich) in toluene-d_8 were degassed by the freeze–pump–thaw technique and flame-sealed into 5 mm od sample tubes containing small amounts of tetramethylsilane (TMS).

The ^{1}H nmr spectra of the substituted phenyl groups in the first two compounds were calibrated on an HA100 spectrometer at a probe temperature of 305 K. Calibrations were performed in the frequency-sweep mode by repeated measurements of sweep and manual oscillator frequencies of markers placed at ca. 5 Hz intervals, at sweep rates of 0.02 Hz/s and a spectral dispersion of 1 Hz/cm.

The ^{19}F nmr spectra of 4,4′-difluorodiphenylmethane were recorded on a WH-90 spectrometer in the FT mode at 84.69 MHz and at probe temperatures as measured by the thermocouple supplied with the spectrometer. The ring proton internal chemical shifts are very small, so that the ^{19}F nmr spectrum is complex. However, decoupling of the ring protons (coherent mode) yielded a 1:2:1 triplet for the ^{19}F nmr spectrum, the splitting arising from $^6J_p^{CH_2,F}$. This triplet was recorded at four temperatures between 250 and 370 K. In these experiments, the pulse width was 2.8 μs (tip angle ~40°), the spectral width was 500 Hz, the acquisition time was ca. 32 s, and 32 K of data storage was employed. The ring proton spectrum spreads over 10 Hz only, so that the amplitude of the decoupling field could be kept small enough to prevent off-resonance decoupling of the methylene protons, resonating 2.7 ppm to high field of the ring protons. The amplitude of the decoupling field was kept well below a value at which off-resonance perturbations of the methylene proton transitions were noticeable in the ^{19}F nmr spectrum.

Results and Discussions

Spectral Analysis

The computer program LAME (19, 20) gave the results in Table 1. The analysis of the ^{1}H nmr spectrum of the substituted ring in 4-aminodiphenylmethane as a six-spin system (four ring and two methylene protons) demonstrated insignificant cross-ring coupling constants. Iterations could be carried out only on ring proton transition frequencies because the methylene protons are coupled to all ring protons. The ^{1}H nmr spectrum of **6** was treated as part of a five-spin system, the presence of the bromine substituents ensuring sufficient dispersion of the chemical shifts of the protons in different phenyl groups.

Figure 1 displays the ^{19}F spectrum of **7** at 370 K under conditions in which the ring protons are decoupled.

The Model for Internal Rotation

Because of the structure of diphenylmethane and of **6** and **7**, it is reasonable to assume that the main component of the barrier to internal rotation about the exocyclic C—C bond will be twofold in character. In terms of the hindered rotor model (21, 22), a vanishing barrier implies that $\langle \sin^2 \theta \rangle = 0.5$ and, from [1], that $^6J_p^{H,CH}$ is 0.5×-1.24 or -0.62 Hz. If **2** is of lowest energy, a relatively large barrier implies $\langle \sin^2 \theta \rangle \sim 0.25$ because $\theta \sim 30°$, so that $^6J_p^{H,CH}$ becomes -0.31 Hz, as observed, for example, in 2,6-dichlorophenylethane (23). A small barrier entails $0.3 < |^6J_p^{H,CH}| < 0.6$. Similarly, from [2], $0.56 < |^6J_p^{F,CH}| < 1.12$ in **7**. The other plausible

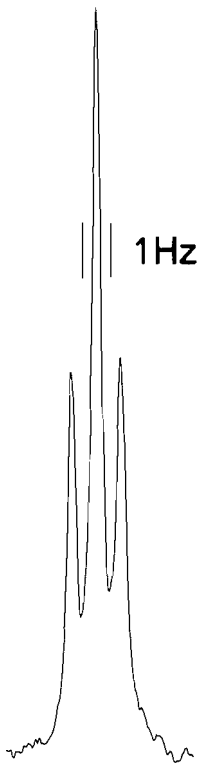

FIG. 1. The ^{19}F spectrum of 4,4′-difluorodiphenylmethane as a ca. 10 mol% solution in toluene-d_8 recorded at 84.69 MHz at 370 K under conditions in which the ring protons are decoupled. The spectral dispersion is 0.975 Hz/cm. The triplet spacings are both 0.87_9 Hz, as determined from cursor readings for a 32 K transform of a region corresponding to 500 Hz. Some of the peak width may be caused by incomplete decoupling and (or) by nonambient temperature conditions.

low-energy conformation, **5**, implies that $^6J_p^{H,CH}$ and $^6J_p^{F,CH}$ lie between 0.375 and 0.5 of -1.24 Hz and 2.24 Hz, respectively.

It is a simple matter to compute (21, 22) $\langle \sin^2 \theta \rangle$ for a range of reduced moments of inertia, of V_2 values, and of temperatures. A grid of V_2 and T values can be chosen such that linear interpolations between $\langle \sin^2 \theta \rangle$ values are valid for a given reduced moment of inertia about the assumed internal rotation axis. Observed J values are then matched to this grid.

Conformation and Barrier in **6** *Based on* $^6J_p^{H,CH}$

$^6J_p^{H,CH}$ is -0.49_8 Hz in **6**, yielding $\langle \sin^2 \theta \rangle$ as $0.49_8/1.24 = 0.40_2$. For a reduced moment of inertia of 2×10^{-38} g cm^2 ($\langle \sin^2 \theta \rangle$ versus V_2 curves are insensitive to changes by a factor of two in the reduced moment of inertia, thereby obviating complications caused by variations introduced by the rotational motion), the assumption of **2** as the low-energy form implies a V_2 of 1.1_1 kcal/mol. Allowance for errors in ^6J suggests that $V_2 = 1.1 \pm 0.3$ kcal/mol is a reasonable estimate.

If **5** were the low-energy conformer, then a ^6J of $-1.24(\sin^2 60° + \sin^2 0°)/2 = -0.46_5$ Hz should be observed for a 'rigid' conformer, that is, for a V_2 of greater than about 4 kcal/mol. The observed ^6J of -0.49_8 Hz is compatible with a situation in which the barrier is then about 3 kcal/mol. However, models of phenylethane, where V_2 is 1.2 kcal/mol (13, 16) and of diphenylmethane suggest that a large V_2 in the latter molecule is unrealistic.

Barrier and Conformation Based on $^6J_p^{F,CH}$

$^6J_p^{F,CH}$ in **7** is 0.80_8 Hz at 250 K, rising to 0.87_9 Hz at 370 K. In Fig. 2 calculated and observed ^6J values are plotted versus temperature for an assumed ground-state conformation **2** and a V_2 of 1.5_5 kcal/mol, using [2]. A realistic error estimate suggests $V_2 = 1.5_5 \pm 0.25$ kcal/mol. Again, $^6J_p^{F,CH}$ at room temperature is compatible with a large V_2 and a stable conformer **5**. However, a large V_2 would not lead to the temperature dependence plotted for ^6J in Fig. 2.

It may be noted that the value of V_2 is one for which a maximum dJ/dT is expected for a hindered rotor model at practical temperatures and that, even here, a 120° temperature range leads to only a 0.07 Hz change in J, i.e., $dJ/dT \sim 7 \times 10^{-4}$ Hz/K.

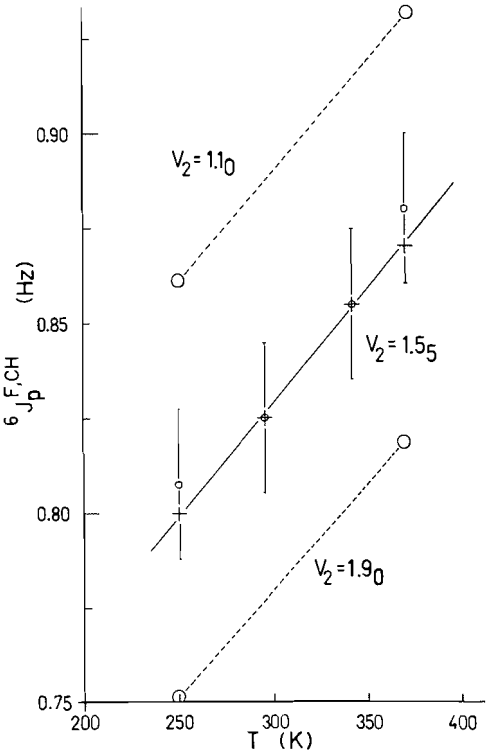

FIG. 2. The calculated (crosses) and observed (circles) values of $^6J_p^{F,CH}$ in 4,4′-difluorodiphenylmethane are plotted versus temperature for an assumed twofold internal rotational barrier of 1.55 kcal/mol, and a ground state conformer **2**.

As noted above, V_2 values for benzyl derivatives derived from $^6J_p^{H,CH}$ are somewhat lower than those based on $^6J_p^{F,CH}$, while the deductions about the low energy conformations are the same. Because of the factors which may influence $^6J^{F,CH}$ (18), the barrier based on $^6J_p^{H,CH}$ is the more reliable one. However, the combined experimental error overlaps both values. It is clear from Fig. 2 that the temperature dependence of $^6J_p^{F,CH}$ is compatible also with the barrier based on $^6J_p^{H,CH}$. The observed temperature dependence supports the gable conformation as the stable form. Of course, the present results do not prove that diphenylmethane behaves in the same manner. If, however, the ground state conformation and the origins of V_2 of all three molecules are determined by steric interactions between *ortho* C—H bonds, the results for **6** and **7** are compatible and do perhaps imply very similar conformational properties in diphenylmethane.

Long-range Couplings over Four and Five Bonds

It is fairly certain that $^4J_o^{H,CH_2}$ and $^5J_m^{H,CH_2}$ in 4-amino- and in 3,5-dibromophenylmethane contain both σ and σ–π electron contributions (24). Their conformational dependence is not as simple as that of $^6J_p^{H,CH_2}$. However, a rough empirical correlation between V_2 and $^4J_o^{H,CH_2}$ apparently occurs for some benzyl derivatives (25). In such a correlation, the $^4J_o^{H,CH_2}$ values in Table 1 agree with the derived V_2 value for 3,5-dibromodiphenylmethane to within experimental error.

Theoretical Calculations

Diphenylmethane is too large for *ab initio* calculations at the STO 3G level of molecular orbital theory, at least as used in this laboratory. However, INDO MO computations (26), using a standard geometry (27) and a 370/168 IBM system, gave **3** and **5** respectively as 1.99 and 1.07 kcal/mol less stable than **2**, in qualitative agreement with the conclusions above.

Molecular mechanics calculations on diphenylmethane are not feasible because of an unknown crucial torsional potential.[2]

Conclusions

It seems probable that the gable conformation, **2**, of diphenylmethane is the stable conformer in solution and that the twofold barrier to rotation about the exocyclic C—C bond is 1.3 ± 0.4 kcal/mol. Confirmation of this likelihood by other means is desirable.

Manipulation of models and considerations of the molecular symmetry emphasize, of course, that the actual motion about the C—C bond is more complex than would be inferred from a simple twofold potential and, therefore, that higher terms in a Fourier series expansion of the potential barrier may be significant. The present data allow no estimate of such terms. However, the strong indication of **2** as the ground state may be of help in future attempts to characterize the internal rotation more fully by vibrational and (or) rotational spectroscopies (28). The present implication, that the methyl and phenyl groups are similar in their steric demands during rotation in phenylethane and diphenylmethane, has its counterpart in other compounds (29).

[2]N. L. Allinger. Private communication.

Acknowledgments

We are grateful to Dr. N. L. Allinger for a discussion of molecular mechanics calculations, to Dr. A. A. Bothner-By for very helpful comments on the use of coupling constants in conformational analysis, to Rudolf Sebastian and Bert Krawchuk for experimental help, and to the National Research Council of Canada for financial assistance.

1. M. J. Aroney, R. J. W. Le Fèvre, G. L. D. Ritchie, and A. N. Singh. J. Chem. Soc. London, 5810 (1965).
2. E. J. W. Whittaker. Acta Crystallogr. **6**, 714 (1953).
3. H. Nomura, Y. Miyahara, and S. Koda. Bull. Chem. Soc. Jpn. **49**, 811 (1976).
4. R. Waack, M. A. Doran, E. B. Baker, and G. A. Olah. J. Am. Chem. Soc. **88**, 1272 (1966).
5. K. L. Servis, W. P. Weber, and A. K. Willard. J. Phys. Chem. **74**, 3960 (1970).
6. N. Muller and D. E. Pritchard. J. Chem. Phys. **31**, 768 (1959); **31**, 1471 (1959).
7. N. Muller and P. I. Rose. J. Am. Chem. Soc. **84**, 3973 (1962).
8. C. Juan and H. S. Gutowsky. J. Chem. Phys. **37**, 2198 (1962).
9. R. D. Bertrand, D. M. Grant, E. L. Allred, J. C. Hinshaw, and A. B. Strong. J. Am. Chem. Soc. **94**, 997 (1972).
10. D. M. Grant and W. M. Litchman. J. Am. Chem. Soc. **87**, 3994 (1965).
11. F. J. Weigert and J. D. Roberts. J. Am. Chem. Soc. **89**, 5962 (1967).
12. T. Schaefer, W. Niemczura, and W. Danchura. Can. J. Chem. **56**, 2229 (1978); **57**, 355 (1979).
13. T. Schaefer, L. Kruczynski, and W. Niemczura. Chem. Phys. Lett. **38**, 498 (1976).
14. W. J. E. Parr and T. Schaefer. J. Am. Chem. Soc. **99**, 1033 (1977).
15. M. S. Farag. Diss. Abstr. Int. B, **35**, 1594 (1974).
16. A. Miller and D. W. Scott. J. Chem. Phys. **68**, 1317 (1978).
17. P. J. Mitchell, L. Phillips, S. J. Roberts, and V. Wray. Org. Magn. Reson. **6**, 126 (1974).
18. T. Schaefer, W. Danchura, W. Niemczura, and J. Peeling. Can. J. Chem. **56**, 2442 (1978).
19. S. Castellano and A. A. Bothner-By. J. Chem. Phys. **41**, 3863 (1964).
20. C. W. Haigh and J. M. Williams. J. Mol. Spectrosc. **32**, 398 (1969).
21. P. B. Ayscough, M. C. Brice, and R. E. D. McClung. Mol. Phys. **20**, 41 (1971).

22. T. SCHAEFER, J. B. ROWBOTHAM, W. J. E. PARR, K. MARAT, and A. F. JANZEN. Can. J. Chem. **54**, 1322 (1976).
23. A. F. JANZEN and T. SCHAEFER. Can. J. Chem. **49**, 1818 (1971).
24. R. WASYLISHEN and T. SCHAEFER. Can. J. Chem. **50**, 1852 (1972).
25. T. SCHAEFER, L. J. KRUCZYNSKI, and W. J. E. PARR. Can. J. Chem. **54**, 3210 (1976).
26. J. A. POPLE, J. M. MCIVER, and N. S. OSTLUND. J. Chem. Phys. **49**, 2960 (1968); **49**, 2965 (1968).
27. J. A. POPLE and M. S. GORDON. J. Am. Chem. Soc. **89**, 4253 (1967).
28. D. G. LISTER, J. N. MACDONALD, and N. L. OWEN. Internal rotation and vibration. Academic Press, London, Engl. 1978.
29. W. H. LAARHOVEN, W. H. M. PETERS, and A. H. A. TINNEMANS. Tetrahedron, **34**, 769 (1978).

Fluoride ion promoted synthesis of alkyl phenyl ethers

JACK M. MILLER[1] AND K. H. SO
Department of Chemistry, Brock University, St. Catharines, Ont., Canada L2S 3A1
AND
JAMES H. CLARK
Department of Chemistry, University of York, York Y01 5DD, England

Received November 14, 1978

JACK M. MILLER, K. H. SO, and JAMES H. CLARK. Can. J. Chem. 57, 1887 (1979).

Tetraethylammonium fluoride in dimethylformamide promotes the alkylation of phenols with alkyl iodides and benzyl chloride to provide good yields of alkyl phenyl ethers. A number of phenols have been investigated including examples of sterically hindered phenols, phenols containing anion stabilising groups, and intramolecularly hydrogen bonded phenols, the majority of which react smoothly and efficiently in the fluoride system.

JACK M. MILLER, K. H. SO et JAMES H. CLARK. Can. J. Chem. 57, 1887 (1979).

Le fluorure de tétraéthylammonium dans le diméthylformamide favorise l'alkylation des phénols par les iodures d'alkyles et le chlorure de benzyle conduisant à des phénoxyalcanes. On a étudié un certain nombre de phénols, y compris des phénols stériquement empêchés, des phénols contenant des groupes stabilisant l'anion et des phénols comportant des liaisons hydrogène; ces composés réagissent généralement facilement et d'une manière efficace dans le système au fluorure.

[Traduit par le journal]

Introduction

The preparation of alkyl phenyl ethers is an important synthetic reaction which is usually accomplished by the alkylation of the phenoxide ion although numerous modifications of the familiar Williamson synthesis have been developed (1) including those employing diazomethane (for methylations) (2), phase-transfer catalysis (3), tetraalkylammonium phenoxides (4), sodium hydride (5), and anion-exchange resins (6).

We now wish to report results on the use of fluoride ion as the base in the alkylation of a variety of phenols with alkyl halides. The simplicity and efficiency of the fluoride ion method has been demonstrated for many typically base-assisted reactions (7–13) and it is desirable to test its effectiveness in the synthesis of alkyl phenyl ethers. Furthermore, the role of the fluoride ion has been shown to often depend on its ability to behave as a powerful hydrogen bond electron donor (7–9) and the importance of hydrogen bonding in controlling the course of phenol alkylations is well established (14, 15).

Experimental

^{1}H nmr spectra were recorded in $CDCl_3$ with a Varian A60 (60 MHz) spectrometer ($SiMe_4$ standard). Mass spectra were determined with an AEI MS-30 double beam mass spectrometer. Infrared spectra were recorded on Perkin Elmer 237B and 735 spectrophotometers.

A solution of tetraethylammonium fluoride was prepared by neutralisation of 20% aqueous tetraethylammonium hydroxide with 48% aqueous hydrofluoric acid. The phenols and alkyl halides were commercial grade samples used without further purification.

Reactions

The technique used in each reaction was the same. Most of the reactions were carried out at room temperature (see Table 1). All products are known compounds and gave ^{1}H nmr, ir, and mass spectra consistent with their structure and, where reported data is available, consistent with those reported in the literature. Details of a representative preparation are given below.

Preparation of Benzyl 2-Nitro Phenyl Ether

An aqueous solution of tetraethylammonium fluoride (0.02 molar equiv.) was placed in a round-bottomed flask immersed in a boiling water-bath and connected via a splash-head, tap, and trap to an efficient water pump. The system was maintained at 10–20 Torr for ca. 0.5 h or until a white solid hydrate formed and no further ebullition was evident. 2-Nitrophenol (0.01 mol in 10 cm^3 dimethylformamide) was added and the mixture was returned to the boiling water bath and kept under reduced pressure (10–20 Torr) for a further 10 min. Benzyl chloride (0.01 mol in 20 cm^3 dimethylformamide) was added and the resulting solution stirred in a closed flask for approximately 3 h at room temperature (ca. 20°C) at which point sampling and ^{1}H nmr analysis showed no starting material remaining. Diethyl ether (200 cm^3) and water (100 cm^3) were added to the reaction mixture and after vigorous shaking, the aqueous layer was washed with ether (2 × 100 cm^3) and the combined ethereal layers were then washed with equal volumes of water (3 ×) so as to remove the dimethylformamide, dried over anhydrous $MgSO_4$ and

[1]To whom all correspondence should be addressed.

0008-4042/79/141887-03$01.00/0

evaporated on a rotary evaporator to give a yellow liquid. Purification on a basic alumina column using pentane as eluent gave benzyl 2-nitrophenyl ether (1.9 g, 0.0083 mol, 83%) oil; (lit. (16) mp 25°C); ^{1}H nmr δ: ~7.5 (4H, m, ring CH), 7.45 (5H, m, Ph), and 5.25 ppm (2H, s, CH_2); ir ν_s: 1520, 1350 (NO_2), 1250 (Ar—O—C asym.) and 1010 cm^{-1} (Ar—O—C sym.); ms *m/e* 229 (M^+).

Results and Discussion

The ability of the fluoride anion to behave as a powerful hydrogen bond electron donor is well known and its strong association with a variety of H-bond electron acceptors including HF (17), carboxylic acids (18, 19), amines (7), and thiols (7) has been described. In a recent article (7) it was shown that phenol and fluoride formed a strong H-bond together resulting in a large shift of the hydroxyl stretching band in the ir ($\Delta\nu_s$(OH) ~ 1000 cm^{-1}). The strongly H-bonded fluoride-carboxylic acid systems have been shown to behave as powerful sources of the carboxylate anion (20) and it seemed reasonable to assume that fluoride-phenol systems might behave in a similar manner. On treating phenol-tetraethylammonium fluoride with methyl iodide, ethyl iodide, or benzyl chloride in dimethylformamide solution, reaction occurs generally at room temperature to produce the corresponding alkyl phenyl ether. Yields are generally good (Table 1) and compare favourably with those obtained by classical and more recent methods. There is no evidence for the formation of any side products in the listed reactions and the isolation of pure products is simple and straightforward. The tetraethylammonium iodide or chloride, bifluoride and any unreacted fluoride may be recovered in aqueous solution and the whole regenerated into the fluoride form by passing through an ion-exchange column.

It was of interest to extend the utility of the present method to the etherification of isomeric nitrophenols and of highly hindered phenols.

Alkylation methods involving initial formation of the phenoxide ion may prove unsatisfactory in the cases of 2- and 4-nitrophenols because of resonance stabilisation in the nitrophenoxide anions effectively lowering the nucleophilicity of those ions. The direct alkylation of phenols by the use of phase-transfer catalysis does not suffer from this drawback (3). We have found that the times required for alkylation of these nitrophenols using tetraethylammonium fluoride are comparable or less than those required for alkylation of unsubstituted or methyl substituted phenols. The results of the alkylation of 2- and 4-nitrophenols using Et_4NF/DMF (ca. 3 h, 70–83%) would seem to be comparable to those using $NaOH/R_4NBr/CH_2Cl_2/H_2O$ (2–12 h, 79–83%—only methylations reported) (3).

TABLE 1. Preparation of alkyl phenyl ethers (ArOR)[a]

Phenol	Alkylating agent	Ether yield[b] (%)
C_6H_5OH	CH_3I	70
$2\text{-}CH_3C_6H_4OH$	CH_3I	75
$2\text{-}O_2NC_6H_4OH$	CH_3I	72
$4\text{-}O_2NC_6H_4OH$	CH_3I	76
$4\text{-}FC_6H_4OH$	CH_3I	80
$2\text{-}MeCOC_6H_4OH$	CH_3I	85
$2,6\text{-}(CH_3)_2C_6H_3OH$[c]	CH_3I	82
$2,4,6\text{-}(CH_3)_3C_6H_2OH$[c]	CH_3I	70
$2,4\text{-}(tC_4H_9)_2C_6H_3OH$[c]	CH_3I	60
$4\text{-}(CH_3)\text{-}2,6\text{-}(tC_4H_9)_2C_6H_2OH$[c]	CH_3I	72
C_6H_5OH	CH_3CH_2I	75
$2\text{-}CH_3C_6H_4OH$	CH_3CH_2I	65
$2\text{-}O_2NC_6H_4OH$	CH_3CH_2I	72
$4\text{-}O_2NC_6H_4OH$	CH_3CH_2I	70
$4\text{-}FC_6H_4OH$	CH_3CH_2I	65
$2\text{-}MeCOC_6H_4OH$	CH_3CH_2I	78
$2,6\text{-}(CH_3)_2C_6H_3OH$[c]	CH_3CH_2I	40
$2,6\text{-}(CH_3)_2C_6H_3OH$[c]	$(CH_3)_2CHI$	65
C_6H_5OH	$PhCH_2Cl$	68
$2\text{-}CH_3C_6H_4OH$	$PhCH_2Cl$	60
$2\text{-}O_2NC_6H_4OH$	$PhCH_2Cl$	83
$4\text{-}O_2NC_6H_4OH$	$PhCH_2Cl$	75
$4\text{-}FC_6H_4OH$	$PhCH_2Cl$	80
$2,6\text{-}(CH_3)_2C_6H_3OH$[c]	$PhCH_2Cl$	80
$2,4,6\text{-}(CH_3)_3C_6H_2OH$[c]	$PhCH_2Cl$	68
$2,4\text{-}(tC_4H_9)_2C_6H_3OH$[c]	$PhCH_2Cl$	70
2-Naphthol	$PhCH_2Cl$	85

[a]All of the reactions were carried out in dimethylformamide using ca. 0.01 molar equiv. of phenol, 0.01 molar equiv. alkyl halide, and 0.02 molar equiv. tetraethylammonium fluoride at room temperature (unless otherwise noted) and were complete in 2–24 h.
[b]Isolated yield.
[c]At 100°C.

The esterification of 2-hydroxyacetophenone was also found to proceed rapidly in the fluoride system. Indeed the reactions with methyl and ethyl iodide were complete in less than 2 h, precipitation of tetraethylammonium iodide being evident on addition of the alkyl iodide to the DMF–phenol-fluoride solution. This phenol fails to react with the powerful methylating agent, diazomethane (21), and this has been explained as being due to intramolecular H-bonding between the hydroxyl and carbonyl groups (22). The fluoride anion is a considerably more powerful H-bond electron donor than the carbonyl group and should readily break the intramolecular H-bond (23) enabling rapid alkylation.

Attempted alkylation of the 2,6-disubstituted sterically hindered phenols shown in Table 1 failed to give satisfactory yields at room temperature; however, on raising the temperature of the reaction mixture, good yields were obtained.

As with 2- and 4-nitrophenols, attempted alkylation of such sterically hindered phenols by initial generation of the phenoxide ion may provide less

than satisfactory results and more direct methods such as phase-transfer catalysis are preferred (3). Our method would again appear to offer a reasonable alternative.

In the reactions of 2,6-di-*tert*-butylphenol with alkyl halides in the presence of fluoride, products resulting from *O*-alkylation, *C*-alkylation, and phenol oxidation were recovered. Kornblum and Seltzer observed comparable mixtures in their investigations of the alkylation of the potassium salt of this phenol (24). These were the only reactions that we investigated where other than *O*-alkylation occurred. Further work on the nature of these reactions, in particular with special reference to the autoxidations, is underway and will be discussed elsewhere.

Acknowledgements

The Imperial Oil Co. Ltd., is thanked for financial support. The authors are also grateful to N.A.T.O. for a collaborative research grant (to J.M.M. and J.H.C.).

1. C. A. BUEKLER and D. E. PEARSON. Survey of organic synthesis. Wiley-Interscience, New York, NY. 1970. pp. 285–302; H. FEUER and J. HOOZ. *In* The chemistry of the ether linkage. *Edited by* S. Patai. John Wiley and Son, New York, NY. 1967. pp. 445–498.
2. J. BLAIR and G. T. NEWBOLD. J. Chem. Soc. 2871 (1955); T. A. GEISSMAN and E. HINREINER. J. Am. Chem. Soc. **73**, 782 (1951); F. A. HOCHSTEIN and R. PASTERNAK. J. Am. Chem. Soc. **73**, 5008 (1951).
3. A. MCKILLOP, J.-C. FIAUD, and R. P. HUG. Tetrahedron, **30**, 1379 (1974).
4. J. UGELSTAD, T. ELLINGSEN, and A. BERGE. Acta Chem. Scand. **20**, 1593 (1966).
5. B. A. STOOCHNOFF and N. L. BENOITON. Tetrahedron Lett. 21 (1973).
6. G. GELBARD and S. COLONNA. Synthesis, 113 (1977).
7. J. H. CLARK and J. M. MILLER. J. Am. Chem. Soc. **99**, 498 (1977).
8. J. H. CLARK and J. M. MILLER. J. Chem. Soc. Perkin Trans. I, 1743 (1977); 2063 (1977).
9. J. H. CLARK and J. M. MILLER. Can. J. Chem. **56**, 141 (1978).
10. S. HOZ, M. ALBECK, and Z. RAPPOPORT. Synthesis, 162 (1975).
11. Y. S. KLAUSNER and M. CHOREV. J. Chem. Soc. Perkin Trans. I, 627 (1977).
12. J. PLESS. J. Org. Chem. **39**, 2644 (1974).
13. K. HORIKI, K. IGANO, and K. INOUYE. Chem. Lett. 165 (1978).
14. H. O. HOUSE. Modern synthetic reactions. 2nd ed. W. A. Benjamin, Menlo Park, CA. 1972.
15. N. KORNBLUM, P. J. BERRIGAN, and W. J. LENOBLE. J. Am. Chem. Soc. **85**, 1141 (1963); N. KORNBLUM, R. SELTZER, and P. HABERFIELD. J. Am. Chem. Soc. **85**, 1148 (1963).
16. R. HIGGINBOTTOM and H. SUSCHITZKY. J. Chem. Soc. 2367 (1962).
17. D. G. TUCK. *In* Progress in inorganic chemistry. Vol. 9. *Edited by* F. A. Cotton. Interscience, New York, NY. 1968. p. 161.
18. J. EMSLEY. J. Chem. Soc. A, 2511 (1971); 2702 (1971).
19. J. H. CLARK and J. EMSLEY. J. Chem. Soc. Dalton Trans. 2154 (1973); 1125 (1974).
20. J. H. CLARK and J. EMSLEY. J. Chem. Soc. Dalton Trans. 2129 (1975).
21. A. SCHONBERG and A. MUSTAFA. J. Chem. Soc. 746 (1946).
22. I. D. SADEKOV, V. I. MINKIN, and A. E. LUTSKII. Russ. Chem. Rev. **39**, 179 (1970).
23. J. H. CLARK. J. Chem. Soc. Perkin Trans. II, 1326 (1978).
24. N. KORNBLUM and R. SELTZER. J. Am. Chem. Soc. **83**, 3668 (1961).

Application of photoelectron spectroscopy to substituent effects. Conformational analysis of some flexible allylic ethers and alcohols

R. S. BROWN, R. W. MARCINKO, AND A. TSE

Department of Chemistry, University of Alberta, Edmonton, Alta., Canada T6G 2G2

Received January 22, 1979

R. S. BROWN, R. W. MARCINKO, and A. TSE. Can. J. Chem. **57**, 1890 (1979).

He(I) photoelectron (pe) spectroscopy is applied to determine the preferred gas phase conformations of a limited number of flexible allylic ethers and alcohols. Based on earlier observations that the π-ionization energy is increased more when the allylic C—O bond is coplanar (with the π-system) than when it is perpendicular, the pe spectrum of *cis* and *trans*-4-*tert*-butyl-2-cyclohexanol and their corresponding ethers, and 5α-hydroxy(and methoxy)-10α-Δ^3-octalin have been determined. The results indicate that when a coplanar arrangement of the allylic C—O bond can be attained, it is preferred, leading to a favored conformation of the allylic alcohol or ether.

R. S. BROWN, R. W. MARCINKO et A. TSE. Can. J. Chem. **57**, 1890 (1979).

On a appliqué la spectroscopie photoélectronique (pe) He(I) pour déterminer les conformations privilégiées en phase gazeuse d'un nombre limité d'alcools et d'éthers allyliques flexibles. On a déterminé les spectres pe des *tert*-butyl-4 cyclohexène-2 ols *cis* et *trans* et de leurs éthers correspondants ainsi que ceux des hydroxy (et méthoxy)-5α 10α-octaline-Δ^3. Des observations antérieures permettant de prédire que l'énergie d'ionisation π est plus élevée lorsque la liaison C—O allylique est coplanaire (avec le système π) que lorsqu'elle est perpendiculaire, on peut déduire de nos résultats que s'il est possible, l'arrangement coplanaire est préféré et qu'il en résulte une conformation privilégiée pour l'alcool ou de l'éther.

[Traduit par le journal]

Introduction

For some time we have been interested in applying the techniques of photoelectron spectroscopy (pes) to substituent effects (1). Prompted by calculations (2) which suggest that molecules of the type X—CH_2—Y (**1**) are stabilized by a bond – no bond resonance form

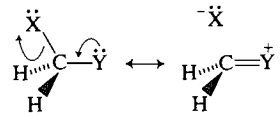

1

when X and Y are electronegative groups such as OR, OH, NH_2, F, and Cl, we set out to determine whether this phenomenon was experimentally observable by pes. Two important consequences of structures such as **1** require that (*a*) the 'lone pair' and the C—X bond be coplanar for maximum effect and (*b*) the pair of electrons on Ÿ should be more difficult to ionize when coplanarity is achieved than when the C—X bond is orthogonal. We first sought to probe the ionization energy (ip) of a π-bond (group Ÿ) as a function of the orientation of a single electronegative allylic group (X).

From the models in which the allylic substituent is orthogonal (or nearly so) to the π-bond (**2** and **3**) changing from *a* to *b* or *c* within a series stabilized[1] the π-bond considerably less than in the models in which the allylic C—X bond was coplanar with the π-system (**4** and **5**) (1*a*). Because there seemed to be a

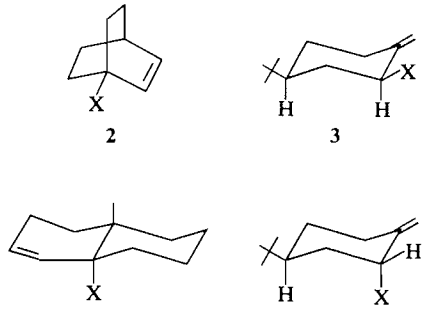

2 **3**

4 **5**

a X = H, *b* X = OH, *c* X = OCH_3

clear orientational effect it appeared possible that one might be able to use the technique to determine the orientations of similar substituents in systems which were not as conformationally rigid as **2**–**5** provided suitable model compounds were available. Compounds **6** and **7** which contain an anchored cyclohexene with an allylic pseudo-axial and pseudo-equatorial (*vide infra*) substituent and octalin **8** which can potentially exist in two conformations having the allylic C—X bond coplanar with (**8**) and orthogonal to (**8′**) the π-bond came to mind. The following reports the findings of this study.

[1]In this context the term 'stabilized' means an increase in ionization energy (3).

0008-4042/79/141890-07$01.00/0

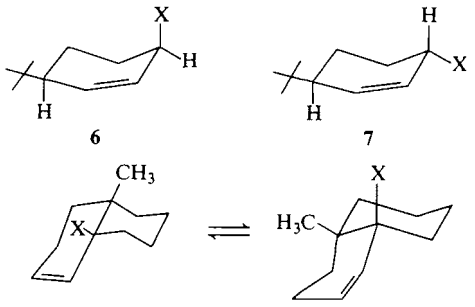

6 7

8 8′

a X = H, *b* X = OH, *c* X = OCH_3

Results

Compounds **6** and **7** can be prepared in routine fashion (see Experimental) and are easily characterized. An attempt to establish the dihedral angle between the allylic methine hydrogen and adjacent vinyl hydrogen in **6***b*,*c* and **7***b*,*c*, and by inference the dihedral angle between the π-bond and C—OR by ^{1}H nmr coupling constants, proved fruitless and no solution or gas phase data on this problem appear available.

Octalin **8***a* (X = H) is to our knowledge an unreported material, and since it serves as a key parent compound with which to compare **8***b* and **8***c*, it is important that its structure be on firm ground. Its method of synthesis via a Clemmensen reduction (4) of the corresponding α,β-unsaturated ketone (**9**) (5) could potentially have given **8***a*, **10** (*cis* or *trans*), **11**, and **4***a* (which was produced in 10% yield and identified by comparison with an authentic sample prepared by an independent route (1*a*)) (Scheme 1).

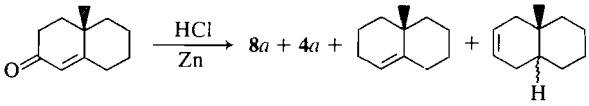

9 **11** **10**

SCHEME 1

^{1}H nmr data for the major olefinic fraction showed two vinyl hydrogens centred at δ 5.52 (inconsistent with **11**) and ambiguously supported **8***a*. ^{13}C nmr spectroscopy indicated that the two vinyl carbons were separated by about 7 ppm (132.09 and 125.34 ppm respectively in $CDCl_3$) and appeared as doublets when proton coupled, again inconsistent with **11**. The large chemical shift difference for the vinyl carbons is more appropriate for **8***a* than **10** (6) but independent proof was sought by chemical degradation according to Scheme 2.

Ozonolysis of **8***a* (7) followed by Jones oxidation of the presumed dialdehyde intermediate **12** and finally treatment with diazomethane gave, after chromatography over silica gel, diester **13** in good yield. Integration of the α-hydrogens in **13** (which are well separated from the aliphatic resonances) relative to the methoxyl singlets clearly indicated a ratio of 1:2 as expected if the starting olefin had been **8***a*.[2]

The vertical ionization energies as well as the appropriate assignments for compounds **6**–**8** and for comparison purposes **3**–**5** (1*a*) are presented in Tables 1 and 2. Table 3 lists the same data for the saturated counterparts which were prepared as an aid to assignment. Photoelectron spectra of selected examples **3***c* and **5***c* and **6***c* and **7***c* are displayed in Figs. 1 and 2, while Fig. 3 illustrates the observations

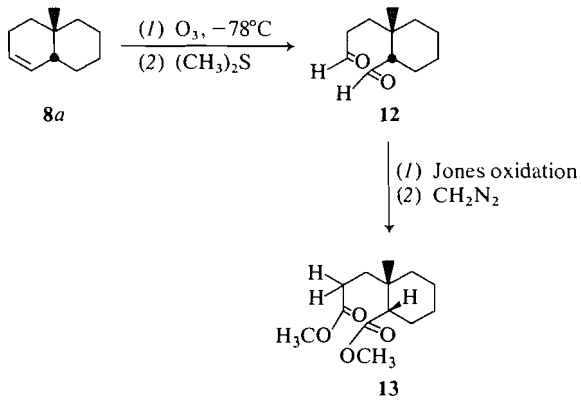

8*a* **12** **13**

SCHEME 2

for **8***a*–*c*. The assignments for **3**–**5** have been described (1*a*) and those for **6**–**8** were made analogously. Assignment of the $n_{\ddot{O}R}$ peaks in the allylic alcohols and ethers were made on the basis of which band moved markedly to lower binding energy on substitution of a CH_3 for H; the remaining band was assigned to the π-ionization. Comparison of the spectra of the saturated and unsaturated analogues confirmed the assignments.

A *general*[3] observation in these and related systems (8) is that two electronegative groups have increased ip's when they are together than when they are inde-

[2]A small sample of a mixture of **4***a* and **8***a* when ozonolized according to the route in Scheme 2 gave two isomeric diesters, one the same as **13** and one very slightly different in terms of its 200 MHz ^{1}H nmr spectrum.

[3]Conjugative and inductive effects operate simultaneously to produce the observed spectra. For a system of two interacting non-degenerate orbitals centred on electronegative groups, the lower lying orbital experiences reinforcing conjugative and inductive effects, while the upper orbital may be stabilized inductively but destabilized conjugatively by through-space or bond mechanisms. The $n_{\ddot{O}R}$ orbitals of **4***c* and **8***c* are cases in point when compared with their saturated analogues in Table 3.

TABLE 1. Vertical ionization energies (ip) and assignments for compounds **3**, **5**, **6**, and **7**

Compound		Vertical ionization energies (eV) $n_{\ddot{O}R}$	π	$\Delta ip^{a,b}$
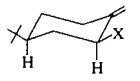 **3**[c]	*a* X = H		9.09	0.0
	b X = OH	10.15[d]	9.18	0.09
	c X = OCH_3	9.55	8.97	−0.12
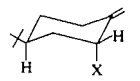 **5**[c]	*b* X = OH	9.97[d]	9.37	0.28
	c X = OCH_3	9.54	9.30	0.21
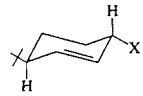 **6**	*a* X = H		8.94	0.0
	b X = OH	10.21[d]	9.18	0.24
	c X = OCH_3	9.61	8.97	0.03
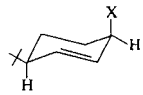 **7**	*b* X = OH	10.07[d]	9.33	0.39
	c X = OCH_3	9.53	9.29[e]	0.35

[a]All values are the averages of at least three runs and have a precision of ±0.02 eV unless otherwise noted.
[b]Calibrated against argon; Δip = ipπ(compound) − ipπ(parent olefin).
[c]Reference *1a*.
[d]Tentatively assigned; appears as a well-defined shoulder on the edge of the σ-envelope.
[e]Precision of ±0.03 eV.

TABLE 2. The vertical ionization energies and assignments for some 1-methyl-5-substituted Δ^3-octalins (**4** and **8**)

Compound		Vertical ionization energies (eV)[a,b] $n_{\ddot{O}R}$	π	Δip
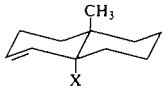 **4**[c]	*a* X = H		8.92	0.0
	b X = OH	9.58	9.35	0.43
	c X = OCH_3	9.00	9.34	0.42
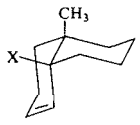 **8(8′)**	*a* X = H		8.92	0.0
	b X = OH	9.64	9.26	0.34
	c X = OCH_3	9.00	9.34	0.42

[a]Values are reported to a precision of ±0.02 eV and are averages of at least three runs.
[b]Δip = ipπ(compound) − ipπ(parent olefin).
[c]Reference *1a*.

pendent; each group apparently stabilizes the other but not necessarily by equivalent amounts.

Discussion

It has been determined that for 3-substituted cyclohexenes in the half-chair conformation (**14**)

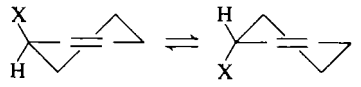

14

electronegative groups such as OH and OAc (9) (for a different interpretation see ref. 10), Cl (11), and Br (11, 12) tend to favor a pseudo-axial form in contrast to their well-known equatorial preference in the cyclohexane series (13). A similar preference for axial over equatorial orientations exists in cases where an electronegative group occupies the 2-position of a tetrahydropyran and has been termed the anomeric effect (14). Explanations for the effect in terms of dipole–dipole interactions (14*a*,*g*) and more recently electron-delocalization of n (or π) electrons into the adjacent electronegative X—C σ*-orbital

TABLE 3. Vertical ionization energies for the $n_{\ddot{O}R}$ orbitals of saturated analogues of compounds **4**, **6**, **7**, and **8**

Compound		Vertical ip $n_{\ddot{O}R}$[a] (eV)
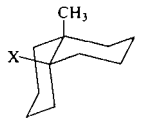	X = OH	9.45
	X = OCH_3	9.08
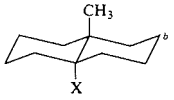	X = OH	9.41
	X = OCH_3	9.10
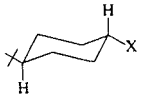	X = OH	9.91
	X = OCH_3	9.32
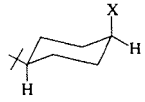	X = OH	9.82
	X = OCH_3	9.36

[a]Average of at least three runs. Precision of ± 0.02 eV or better.
[b]Reference 1*a*.

(2*b*,*c*, 12, 15) have been advanced. Recently Lessard *et al.* (12) have determined a preference for a pseudo-axial conformation of the electronegative substituent in some cyclohexenes and methylene cyclohexanes and interpreted their data in terms of a double bond – no bond resonance form as illustrated in **15**.

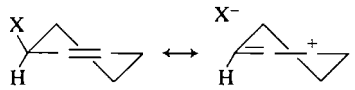

15

Model compounds **3***c* and **5***c* are anchored in a single chair conformation (16) and orient the allylic OCH_3 group so it is nearly[4] orthogonal to (in **3***c*) and coplanar with (in **5***c*) the π-bond. Correspondingly the pe spectra (Fig. 1) and data (Table 1) indicate the π-bond in the *trans* isomers (**5***b*,*c*) is markedly stabilized[1] relative to the parent (**3***a*) while that in the *cis* isomers (**3***b*,*c*) shows only a small stabilization (**3***b*) and net destabilization (**3***c*). Analogously, cyclohexenes **6** and **7** (Fig. 2) show similar trends in that the pseudo-axial substituent in **7***b*,*c* stabilizes the π-bond far more than it does when it is pseudo-equatorial (**6***b*,*c*). Although the term 'pseudo' does not allow a quantitative measure of the dihedral angles (θ and φ in **16** and **17**), molecular models seem to indicate that θ is likely to be smaller than φ,

[4]From Dreiding models the C—OR bond in **3** is some 10° from orthogonality while in **5** it is roughly 20–30° from coplanarity with the π-bond. Conjugative interactions are proportional to the overlap $S_{\pi-\sigma*}$ which is itself dependent on the cosine of the dihedral angle. A 30° distortion from coplanarity still leads to 87% of the maximum conjugation (17).

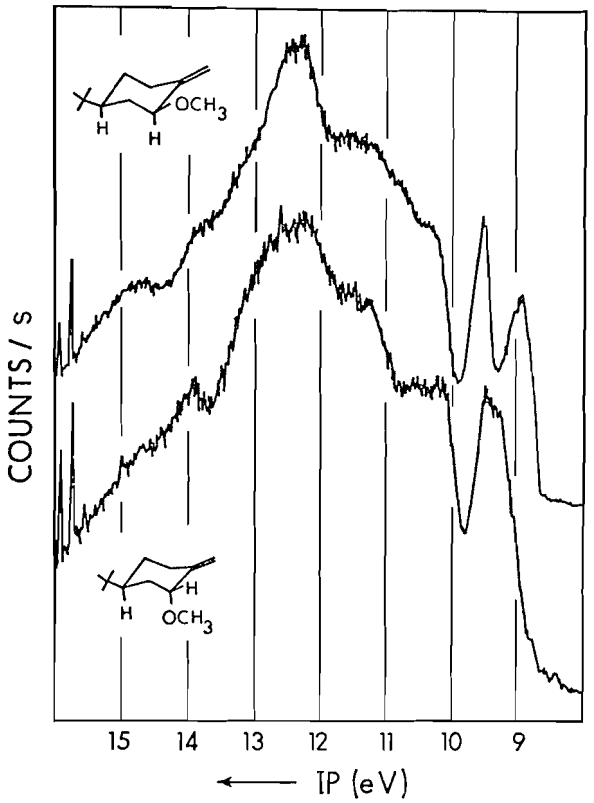

FIG. 1. The pe spectra of *cis*- and *trans*-2-methoxy-4-*tert*-butylmethylenecyclohexane (**3***c* and **5***c*) using argon as an internal calibrant.

allowing a better overlap between the C—OR σ*-orbital and π in **16**. The models clearly cannot account for torsional and subtle non-bonded effects but the similarity of the pe spectral data between the anchored models (**3** and **5**) and flexible systems (**6** and

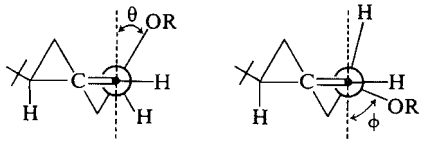

16 **17**

7) to us indicates that the dihedral angles must be similar in the two comparison series.

A more interesting example comes to light in the examination of the pe spectra of **8***a*–*c* shown in Fig. 3. Temperature dependent ^{13}C nmr spectra of **8***a* reveal a roughly 1:1 ratio of **8***a* and **8***a*′ (18) and the observed gas phase pe spectrum is probably a resultant of some equilibrium distribution of the two. The sharpness of the π-ionization for **8***a*, however, suggests that even if both conformations are present, their pe spectra must be very similar. The quoted value in Table 2 for the π-ionization energy of the *trans*

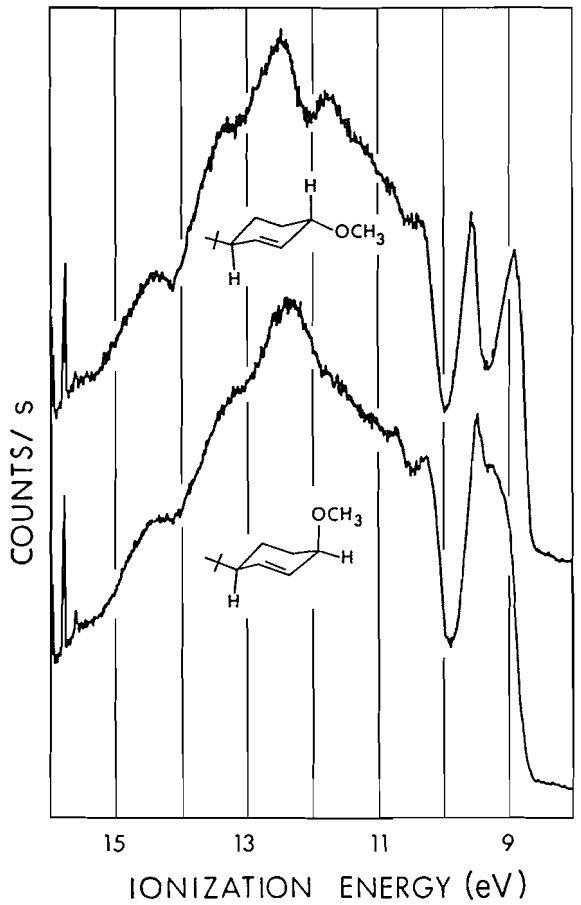

FIG. 2. The pe spectra of *cis*- and *trans*-3-methoxy-6-*tert*-butylcyclohexene (**7***c* and **6***c*) using argon as an internal calibrant.

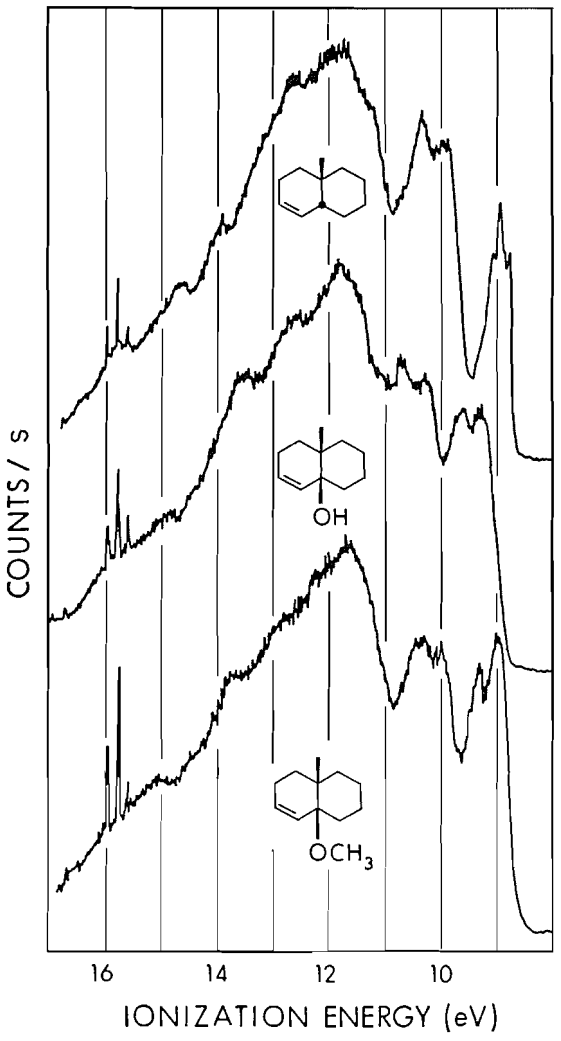

FIG. 3. The pe spectra of 5α-substituted-10α-methyl-Δ^3-octalins (**8***a–c*) using argon as an internal calibrant.

isomer **4***a* is identical to that of the *cis* isomer and indicates that the π-ionization energy is not very sensitive to the orientation of an allylic H, or alkyl substituent.

On the other hand solution phase ^{13}C nmr data reveal that the ratio of **8***b*:**8**′*b* and **8***c*:**8**′*c* is 5:1 and 6:1 respectively (18); in other words when the electronegative substituent is present, the conformation adopted is the one which aligns the π- and C—OR bonds. The large stabilization of the π-bond in **8***b* and **8***c* of 0.34 and 0.42 eV respectively (relative to **8***a*) is reminiscent of that observed in the rigid colinear *trans* series **4***a* → **4***b* → **4***c* and supports a dominant colinear conformation in the gas phase. Were the dominant conformation really **8**′*b* (**8**′*c*), a much smaller π-stabilization (or perhaps even destabilization) would have been observed (1*a*).

The present examples seem to indicate that in cases where one has an allylic alcohol or ether, interaction between π and σ* (C—OR) is sufficient to stabilize one of the possible conformations, perhaps due to a hyperconjugative interaction which requires coplanarity of the orbitals (12, 15). For example, according to models, the pseudo-axial and equatorial orientations (**16** and **17**) can attain similar dihedral angles with little effort,[5] and yet a stabilizing π–σ* interaction in **16** could favor a 'more' axial orientation leading to the observed pe spectrum. In order for the pseudo-equatorial isomer (**17**) to maximize the stabilizing π–σ* interaction, the molecule is forced to assume an unfavorable twist boat conformation.

Several literature examples seem to indicate that the pe observations may be general. For example, when compared with propene (π_{ip} = 9.88 eV (19)),

[5]Dreiding models obviously cannot assess torsional and nonbonded interactions which contribute to the stability of the adopted conformation.

allyl fluoride, chloride, and bromide show π_{ip}'s of 10.56, 10.34, and 10.18 eV respectively (19). Allyl fluoride and chloride have been said to exist preferentially in conformations which align the C—X bond with the π-system (20), although conflicting data for the fluoride have been reported (21). The pe observations are consistent both with electronegativity arguments and a hyperconjugative π–σ^* interaction, but only the latter explanation requires coplanarity.

Allyl alcohol also adopts a preferred conformation in which the C—OH bond is nearly coplanar with the π-system (22). Photoelectron data show the π_{ip} (10.22 eV (23)) to be 0.34 eV greater than the parent propene (19), close to the stabilization found for the coplanar alcohols found in Tables 1 and 2.

Conclusions

For these selected flexible allylic alcohols and ethers, pe spectroscopy indicates that in the gas phase the molecules prefer to adopt a conformation which aligns the π and adjacent C—OR σ-bond.

Experimental

Photoelectron spectra were determined using a MacPherson 36 ESCA spectrometer and were calibrated using argon or nitrogen as an internal calibrant. The resolution on the argon $2P_{1/2}$–$2P_{3/2}$ lines was commonly 25–35 meV during operation. Linearity of the spectrometer for electron kinetic energies between 17 and 7 eV was ensured by independent runs using argon and methyl iodide and was found to vary no more than 0.01 eV. Spectra are computer stored in 1006 channels for a 10 eV scan and peak positions were determined from an intensity vs. channel number listing. Each value reported is an average of at least three independent runs, and has a precision of ±0.02 eV unless otherwise noted. Routine ir and ^{1}H nmr spectra were recorded on a Nicolet 7199 FT-IR spectrophotometer and a Varian Associates HA-100 spectrometer. Melting and boiling points are uncorrected.

cis *and* trans-*4*-tert-*Butyl-2-cyclohexen-1-ol (7*b *and* 6*b)*

Seven grams of a 3:7 mixture of **7***b* and **6***b* (24) were chromatographed over 350 g of grade III alumina as published (25) to give 0.9 g of pure **7***b*, mp 51–54°C (from petroleum ether) (lit. (21) mp 44–49°C) and 6 g of mixture. The *trans* isomer (**6***b*) was obtained by a published procedure (26) from 9 g of a 3:7 mixture of **7***b* and **6***b* to give 2.5 g of **6***b*, mp 32–34°C (lit. (26) mp 31–32°C).

cis-*2-Methoxy-6-*tert-*butylcyclohexene (7*c*)*

Alcohol **7***b* (0.25 g, 1.49 × 10^{-3} mol) was methylated (27) to give after final microdistillation (70–80°C/14 Torr) 0.170 g (63%) of **7***c*; ^{1}H nmr ($CDCl_3$) δ: 0.89 (s, 9H), 1.20–2.20 (m, 5H), 3.32 (s, 3H), 3.44–3.70 (m, 1H), 5.78 (s, 2H). *Anal.* calcd. for $C_{11}H_{20}O$: C 78.57, H 11.90; found: C 78.43, H 11.99.

trans-*3-Methoxy-6-*tert-*butylcyclohexene (6*c*)*

Methylation (27) of 0.5 g (2.98 × 10^{-3} mol) **6***b* gave after microdistillation (80°C/12 Torr) 0.40 g (74%) of **6***c*; ^{1}H nmr ($CDCl_3$) δ: 0.88 (s, 9H), 1.12–2.40 (m, 5H), 3.36 (s, 3H), 3.60–4.00 (m, 1H), 5.78 (b s, 2H). *Anal.* calcd. for $C_{11}H_{20}O$: C 78.57, H 11.90; found: C 78.51, H 12.11.

*10-Methyl-*cis*-3-octalin (8*a*)*

Five grams (0.03 mol) of 10-methyl-4-octalin-3-one (**9**) (5) was added to amalgamated zinc (prepared from 6.1 g (0.03 mol) of granular zinc) in a solution of water (6.1 mL) and concentrated hydrochloric acid (6.4 mL) according to the procedure of Davis and Woodgate (4). After refluxing for 3.5 h, the mixture was cooled and extracted with ether which was subsequently dried ($MgSO_4$), filtered, and evaporated to yield 4.0 g (88% crude yield) of viscous brown oil which proved to be a mixture of **8***a* and its *trans* isomer **4***a* in a 10:1 ratio. Preparative glpc (16 ft × 3/8 in. – 20% DEGS on Chrom. WAW-DMCS (80–100 mesh)) gave first the major isomer (**8***a*) which was collected and microdistilled (50°C, 5.0 Torr) to give a clear liquid; ^{1}H nmr ($CDCl_3$) δ: 0.94 (s, 3H, 10-CH_3); Fourier transform ir (Ftir) (cast film): 3005, 2920, 2850, 1450, 1378, and 775 cm^{-1}. *Exact Mass* calcd. for $C_{11}H_{18}$: 150.1409; found: 150.1405.

*Degradation of 8*a *to Diester 13*

Twenty-five milligrams (1.67 × 10^{-4} mol) of olefin **8***a* was collected by preparative glpc as described above and ozonized (7) in 25 mL dry CH_2Cl_2 at −78°C until the solution turned blue. After flushing the solution with O_2 to remove excess ozone, 1 mL of dimethyl sulfide was added and the mixture stirred 2 h at 25°C. The mixture was then extracted with H_2O, dried over Na_2SO_4, and evaporated. The residue in 5 mL acetone was oxidized by the addition of Jones reagent, worked up by the addition of H_2O, and extracted with CH_2Cl_2 which was subsequently dried over Na_2SO_4. Evaporation produced a second residue which was methylated with CH_2N_2 in ether, and after ether removal, the residue was chromatographed over silica gel using 19:1 petroleum ether – ether to yield 11.4 mg of diester; 200 MHz, ^{1}H nmr ($CDCl_3$) δ: 0.95 (s, 3H), 2.12–2.40 (m, 3H, (α-H's)), 3.64 (s, OCH_3), 3.66 (s, OCH_3); Ftir (cast film): 1739 cm^{-1}. *Exact Mass* calcd. for $C_{13}H_{22}O_4$: 242.1518; found: 242.1511.

*5α-Hydroxy-10α-methyl-3-octalin (8*b*)*

A mixture of **8***b* and its *trans* isomer **4***b* was prepared as described (1*a*) and separated by preparative tlc (silica gel (1 mm), pentane–ether, 4:1) and the band of higher R_f value collected. Microdistillation (90°C/1 Torr) gave a clear liquid; ^{1}H nmr ($CDCl_3$) δ: 1.00 (s, 3H, 10-CH_3) 5.6 (m, 2H, olefinic H); Ftir (cast film): 3445, 3010, 2920, 2850, and 1445 cm^{-1}. *Exact Mass* calcd. for $C_{11}H_{18}O$: 166.1358; found: 166.1356.

5α-Hydroxy-10α-methyldecalin

Hydrogenation of 115 mg of **8***b* (50 mL dry ether, 5 drops triethylamine, 400 mg 5% Pd–C) at 50 psi for 120 h followed by work-up (as described for its *trans* isomer (1*a*)) yielded after microdistillation (100°C/3 Torr) 97 mg (83%) of a clear liquid; ^{1}H nmr ($CDCl_3$) δ: 0.97 (s, 3H, 10-CH_3), 1.4 (m, 17H); Ftir (cast film): 2930, 2860, and 1449.7 cm^{-1}. *Exact Mass* calcd. for $C_{11}H_{20}O$: 168.1509; found: 168.1514.

*5α-Methoxy-10α-methyl-3-octalin (8*c*)*

Methylation (27) of a mixture (1.0 g, 9 × 10^{-3} mol) of **8***b* and its *trans* isomer (**4***b*) yielded after work-up 0.95 g (88%) of a viscous yellow oil containing both allylic ethers. Preparative glpc (16 ft × 3/8 in., 10% polyphenyl ether on Chrom. WAW-DMCS (80–100 mesh)) gave as a major component having a longer retention time **8***c* which was collected and microdistilled (95°C/7 Torr) to give a clear liquid; ^{1}H nmr ($CDCl_3$) δ: 0.97 (s, 3H, 10-CH_3), 3.19 (s, 3H, 5-OCH_3), 5.7 (m, 2H, vinyl H); Ftir (cast film): 2930, 1377, 1277, 1085 cm^{-1}. *Exact Mass* calcd. for $C_{12}H_{20}O$: 180.1515; found: 180.1513.

5α-Methoxy-10α-methyldecalin

Hydrogenation of **8***c* (100 mg, 5.5 × 10^{-4} mol) in 40 mL

dry ether containing 6 drops of triethylamine and 400 mg of 5% Pd–C was carried out at 50 psi over a period of 5 days. Work-up (similar to that reported for the *trans* isomer (1*a*)) and microdistillation (80°C/5 Torr) gave 95 mg (94%) of liquid; ^{1}H nmr ($CDCl_3$) δ: 0.94 (s, 3H, 10-CH_3), 1.5 (s, 16H, methylene protons), 3.09 (s, 3H, 5-OCH_3). *Exact Mass* calcd. for $C_{12}H_{22}O$: 182.1672; found: 182.1671.

3-tert-*Butylcyclohexene (7a)*

Prepared by the published procedure (28).

cis *and* trans-*4*-tert-*Butylcyclohexanol*

Seven grams of commercially available material (4:1, *trans*:*cis*) was separated as reported (29) to give 1.2 g *cis*, mp 82–83°C (lit. (29) mp 81–82°C) and 2.6 g *trans*, mp 81–82°C (lit. (29) mp 80–81°C) as well as 3 g of mixture.

Acknowledgements

The authors thank the University of Alberta and the National Research Council of Canada for support of this work, and Prof. J. B. Stothers for a preprint of his results (ref. 18).

1. (*a*) R. S. Brown and R. W. Marcinko. J. Am. Chem. Soc. **100**, 5721 (1978); (*b*) R. S. Brown and R. W. Marcinko. J. Am. Chem. Soc. **100**, 5584 (1978); (*c*) R. S. Brown. Can. J. Chem. **54**, 1521 (1976); (*d*) R. S. Brown. Can. J. Chem. **54**, 805 (1976).
2. (*a*) J. A. Pople. Abstracts of the 172nd ACS National Meeting, San Francisco, CA, Phys. O. 79 (1976); (*b*) L. Radom, W. J. Hehre, and J. A. Pople. J. Am. Chem. Soc. **94**, 2371 (1972); (*c*) L. Radom, W. J. Hehre, and J. A. Pople. J. Am. Chem. Soc. **93**, 289 (1971).
3. T. Koopmans. Physica, **1**, 104 (1934).
4. B. R. Davis and P. D. Woodgate. J. Chem. Soc. 5943 (1965).
5. B. Branchaud, T. Maestrone, and P. A. Zoretic. Tetrahedron Lett. 527 (1975).
6. H. Beierbeck, J. K. Saunders, and J. W. ApSimon. Can. J. Chem. **55**, 2813 (1977).
7. J. J. Pappas and W. P. Keaveney. Tetrahedron Lett. 4273 (1966).
8. (*a*) B. J. M. Neizen, R. F. Schmitz, G. W. Klumpp, and C. A. de Lange. Tetrahedron, **31**, 873 (1975); (*b*) D. Chadwick, D. C. Frost, and L. Weiler. J. Am. Chem. Soc. **93**, 4320 (1971); 4962 (1971). (*c*) G. Worrell, J. W. Verhoeven, and W. N. Speckamp. Tetrahedron, 3525 (1974); (*d*) E. J. McAlduff, P. Caramella, and K. N. Houk. J. Am. Chem. Soc. **100**, 105 (1978).
9. Y. Senda and S. Imaizumi. Tetrahedron, **30**, 3813 (1974).
10. R. J. Ferrier and N. Prasad. J. Chem. Soc. C, 1417 (1967).
11. K. Sakashita. J. Chem. Soc. Jpn. **81**, 49 (1966).
12. J. Lessard, P. V. M. Tan, R. Martino, and J. K. Saunders. Can. J. Chem. **55**, 1015 (1977).
13. E. L. Eliel, N. L. Allinger, S. J. Angyal, and G. A. Morrison. Conformational analysis. John Wiley and Sons, New York, NY. 1965.
14. (*a*) R. U. Lemieux. *In* Molecular rearrangements. Vol. II. *Edited by* P. de Mayo. Interscience, New York, NY. 1964. p. 709; (*b*) R. U. Lemieux. Pure Appl. Chem. **25**, 527 (1971); (*c*) H. Booth and R. U. Lemieux. Can. J. Chem. **49**, 777 (1971); (*d*) E. L. Eliel. Acc. Chem. Res. **3**, 1 (1970); (*e*) E. L. Eliel. Angew. Chem. Int. Ed. Engl. **11**, 739 (1972); (*f*) S. J. Angyal. Angew. Chem. Int. Ed. Engl. **8**, 157 (1969); (*g*) J. T. Edward. Chem. Ind. (London), 1102 (1955).
15. (*a*) C. Romers, C. Altona, H. R. Buys, and E. Havinga. Top. Stereochem. **4**, 39 (1969); (*b*) S. David, O. Eisenstein, W. J. Hehre, L. Salem, and R. Hoffmann. J. Am. Chem. Soc. **95**, 3806 (1973); (*c*) O. Eisenstein, N. T. Anh, Y. Jean, A. Devaquet, J. Cantacuzène, and L. Salem. Tetrahedron, **30**, 1717 (1974); (*d*) C. Baddeley. Tetrahedron Lett. 1645 (1973).
16. (*a*) B. Cross and G. H. Whitham. J. Chem. Soc. 3892 (1960); (*b*) B. Cross and G. H. Whitham. J. Chem. Soc. 1650 (1961).
17. A. Streitweiser. Molecular orbital theory for organic chemists. John Wiley and Sons, New York, NY. 1961. p. 15.
18. L. M. Browne, R. E. Klinck, and J. B. Stothers. Org. Magn. Reson. In press.
19. H. Schmidt and A. Schweig. Angew. Chem. Int. Ed. Engl. **12**, 307 (1973).
20. (*a*) R. E. Rondeau and L. A. Harrah. J. Mol. Spectrosc. **21**, 332 (1966); (*b*) C. Sourisseau and B. Pasquier. J. Mol. Struct. **12**, 1 (1972); (*c*) E. Hirota. J. Mol. Spectrosc. **35**, 9 (1970).
21. E. Hirota. J. Chem. Phys. **42**, 2071 (1965).
22. (*a*) A. N. Murty and R. F. Curl. J. Chem. Phys. **46**, 4176 (1967); (*b*) C. O. Kadzhar, A. A. Abbasov, and L. M. Imanov. Izv. Akad. Nauk Az. SSR, Ser. Fiz-Tekh, Mat. Nauk, 85 (1968); Chem. Abstr. **71**, 118121r (1968).
23. G. W. Mines and H. W. Thompson. Spectrochim. Acta, **29**, 1377 (1973).
24. E. W. Garbisch. J. Org. Chem. **30**, 2109 (1965).
25. P. L. Barili, G. Bellucci, G. Berti, M. Golfarini, F. Marioni, and V. Scartone. Gazz. Chim. Ital. **104**, 107 (1974).
26. E. Dunkelblum, R. Levene, and J. Klein. Tetrahedron, **28**, 1009 (1972).
27. R. K. Brown, U. E. Diner, and F. Sweet. Can. J. Chem. **44**, 1591 (1966).
28. H. L. Goering, R. L. Reeves, and H. H. Espy. J. Am. Chem. Soc. **78**, 4926 (1956).
29. S. Winstein and N. J. Holness. J. Am. Chem. Soc. **77**, 5562 (1955).

Polymerisation of the 3-halogenomethyl-5-methyl(or 5-phenyl)-3′(5′)-methyl-1,5′(3′)-dipyrazolylmethane. Synthesis of new macrocyclic systems

ALAIN FRUCHIER, ABDELKRIM RAMDANI, AND GEORGES TARRAGO[1]

Laboratoire de Synthèse et d'Etudes Physicochimiques d'Hétérocycles Azotés, Université des Sciences et Techniques du Languedoc, Place Eugène Bataillon, 34060 Montpellier Cedex, France

Received December 22, 1978

ALAIN FRUCHIER, ABDELKRIM RAMDANI, and GEORGES TARRAGO. Can. J. Chem. **57**, 1897 (1979).

The study of the polymerisation of the 3-halogenomethyl-5-methyl(or 5-phenyl)-3′(5′)-methyl-1,5′(3′)-dipyrazolylmethane allowed the isolation of five new macrocyclic compounds with four or six pyrazole rings. Their structures have been determined by mass spectrometry and proton nmr spectroscopy.

A scheme is proposed which takes into account the different possible orientations of this reaction.

ALAIN FRUCHIER, ABDELKRIM RAMDANI et GEORGES TARRAGO. Can. J. Chem. **57**, 1897 (1979).

L'étude de la polymérisation de l'halogénomethyl-3-méthyl (ou phényl)-5-méthyl-3′(5′)-dipyrazolyl-1,5′(3′)-méthane nous a permis d'isoler cinq nouveaux composés macrocycliques comportant 4 ou 6 noyaux pyrazoliques. Leurs structures ont été déterminées par spectrométrie de masse et de rmn protonique.

Un schéma réactionnel, rendant compte des différentes orientations possibles de cette réaction, est proposé.

Introduction

We described in a preceding paper (1) the synthesis of a new macrocyclic compound of the 1,6,11,16-tetraazaporphyrinogen type by polymerization of a halogenomethyldipyrazolylmethane.

Nevertheless, the poor yield (about 15%) with which we obtained the first compound led us to study the other products formed during this reaction.

Experimental

The polymerisation has been effected by heating for 2 h at 100°C the 3-halogenomethyl-3′,5′-dimethyl-1,5′-dipyrazolylmethane, **1***a*, and the 3-halogenomethyl-3′-methyl-5-phenyl-1,5′-dipyrazolylmethane, **1***b*, in dimethylformamide in the presence of potassium iodide. After solvent concentration, the residue was chromatographed on alumina. Physical properties of isolated compounds are given in Table 1. Their structures have been determined essentially by 100 MHz proton nmr analysis.

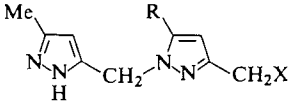

1*a* R = methyl
1*b* R = phenyl

Mass spectra were recorded by M. Guiraud on the JEOL JMS-D-100 spectrometer of the Laboratoire de Mesures Physiques of U.S.T.L. in Montpellier.

Proton nmr spectra were obtained in the same laboratory using a Varian HA-100 spectrometer. Concentrations were about 10% by weight in deuteriochloroform and the chemical shifts are expressed in δ units from TMS. When they have been measured, coupling constants are given, in hertz, in parentheses.

Results

In the polymerisation of each of **1***a* and **1***b*, the compound with the largest R_f has an *m/e* value corresponding to a macrocyclic ring with six pyrazole rings (Table 1). Theoretically, four isomers of this type can be obtained but only two of them were isolated.

The first compound, when R = methyl, shows two methyl signals of equal intensities which indicate a symmetric structure. The signal at 2.10 ppm belongs to a 5-methyl group of a pyrazole ring (2) coupled (J = 0.6 Hz) with the close H_4 whose signal appears at 5.82 ppm. The other methyl signal at 2.17 ppm shows no measurable coupling and is characteristic of a 3-methyl pyrazolic group, the corresponding H_4 signal being at 5.79 ppm. Two methylene signals are also observed (5.23 and 5.34 ppm) but their assignment is not possible. This spectrum is only compatible with the symmetric structure **2***a*.

When R = phenyl, only one methyl signal is observed at 2.14 ppm which belongs to 3-methylpyrazolic groups (no measurable coupling but the signal is broadened), with the corresponding H_4 signal at 5.58 ppm. The signal of the H_4 close to 5-phenyl groups (narrow multiplet at 7.36 ppm) appears at 6.14 ppm and those of methylenes at 5.35 and 5.46 ppm. Thus it is clear that this spectrum corresponds to structure **2***b*.

[1]To whom all correspondence should be addressed.

0008-4042/79/141897-04$01.00/0

TABLE 1. Products isolated from the polymerisation of **1***a* and **1***b**

Product	R_f	Melting point (°C)	*m/e*	Yield (%)	Product	R_f	Melting point (°C)	*m/e*	Yield (%)
2*a*	0.58	263–265	564	10	**2***b*	0.48	277–280	750	12
3*a*	0.47	232–235	564	13	**3***b*	0.24	158–160	750	14
4*a*	0.41	276–277	376	13	**4***b*	0.51	210–212	500	13
5*a*	0.27	229–230	376	13	**5***b*	0.45	243–245	500	14
6*a*	0.09	298–302	376	15	**6***b*	0.17	295–297	500	16

*The residues are formed by non-identified polymers for which the yields are under 4%.

The second type of macrocycle with six pyrazole rings which has been isolated has a spectrum indicating a non-symmetric structure.

When R = methyl, four methyl signals (1.78 (0.5), 2.01 (0.5), 2.11, 2.24 ppm, the last two being twice as intense as the others), five methylene signals (4.71, 4.95, 5.10 (4H), 5.14, 5.26 ppm), and five H_4 pyrazolic signals (5.30 (2H), 5.39, 5.76, 5.87, 6.09 ppm) are observed. When three drops of deuteriobenzene are added to this solution, six methyl signals become clearly visible, four of which bear a coupling constant of 0.6 Hz while two are broadened.

This spectrum can be attributed to the structure **3***a* which has two pyrazole rings with 3-methyl groups and four with 5-methyl groups.

These results are confirmed by the compound **3***b* (R = phenyl). Its spectrum has three methyl signals (2.00 (0.6), 2.12 (broadened), 2.20 (broadened)) but only the first one belongs to a 5-methyl group. Six methylene signals (4.93, 4.96, 5.00, 5.20, 5.25, 5.34 ppm) and six 4-pyrazolic protons (5.31 and 5.86 (pyrazole with a 3-methyl group), 5.76 (pyrazole with a 5-methyl group), 5.72, 5.99, 6.03 (pyrazole with 5-phenyl group)) are also observed.

Also isolated are three further types of macrocycles showing *m/e* corresponding to four pyrazole rings (Table 1) which is the same number of isomers as predicted. The results of their nmr analysis are collected in Table 2. To facilitate comparisons between them, we have adopted for **4** and **5** a numerotation similar to the conventional one used for compound **6** (Fig. 1).

When R = methyl, the identification of compounds **4***a*, **5***a*, and **6***a* presents no difficulty. One of them has a very simple spectrum with three signals of relative intensities 3:2:1. Only the structure **6***a* has a symmetry compatible with this spectrum. On the contrary, structure **5***a* has no symmetry and its spectrum bears four signals of each type (methyl, methylene, and pyrazolic protons). The signals at 5.00 and 5.02 ppm can be assigned to the 10- and 15-methylene groups which have an environment similar to the methylenes in **6***a* (signal at 4.98 ppm). Likewise, the 5- and 20-methylenes in **5***a* can be compared to the 5,15- and 10,20-methylenes in **4***a* respectively. The structure **4***a* has a C_2 axis which leads the 2,12- and the 7,17-methyl groups, the 3,13- and the 8,18-protons, the 5,15- and the 10,20-methylene groups being equivalent respectively. The coupling constant (0.7 Hz) between the 7,17-methyl groups and the 8,18-protons allows the assignment of their signals.

When R = phenyl, the structure **6** loses its C_4 axis which is replaced by a C_2 axis. Then **6***b* and **4***b* should have similar spectra. Effectively, spectra are of the same type and, at first sight, the major difference is the appearance of the phenyl signal. Again, the identification is made on the basis of the coupling constant between the methyl group and the adjacent pyrazolic proton. The value is 0.7 Hz in **6***b* (methyl in position 5 of a pyrazole ring) and is not measurable in **4***b* (methyl in position 3).

Discussion

Some comments can be made about these results.

(*1*) In structure **1**, the pyrazole ring unsubstituted on nitrogen presents, owing to the well known prototropy in such systems, two nucleophilic centers localised on the nitrogens.

(*2*) Generally, the *N*-alkylation site of a pyrazole ring is directed by steric factors involving the substituents close to the nitrogens (3). This is observed when the substituents are alkyl or aryl, but not if one of them contains a lone electronic pair adequately situated (as in structure **1**). In this case, we have shown (4) that the lone pair play a great part in the orientation of the reaction: the alkylation of the β site is then favoured even against an eventual steric hindrance of this site.

(*3*) When the final macrocycle is not (or only

FIG. 1. Polymerisation reaction scheme (percentages indicated are theoretical ones based on final experimental yields). *a*, R = methyl; *b*, R = phenyl. P = non-isolated degradation and polymerisation products. None of them should have yield over 3%. Q = products which could be obtained from the cyclisation of the intermediate compound **D**. Nevertheless, the global yield of **D** cannot be over 6%. Thus the yield of each Q product is under 3% and explains why they have not been isolated.

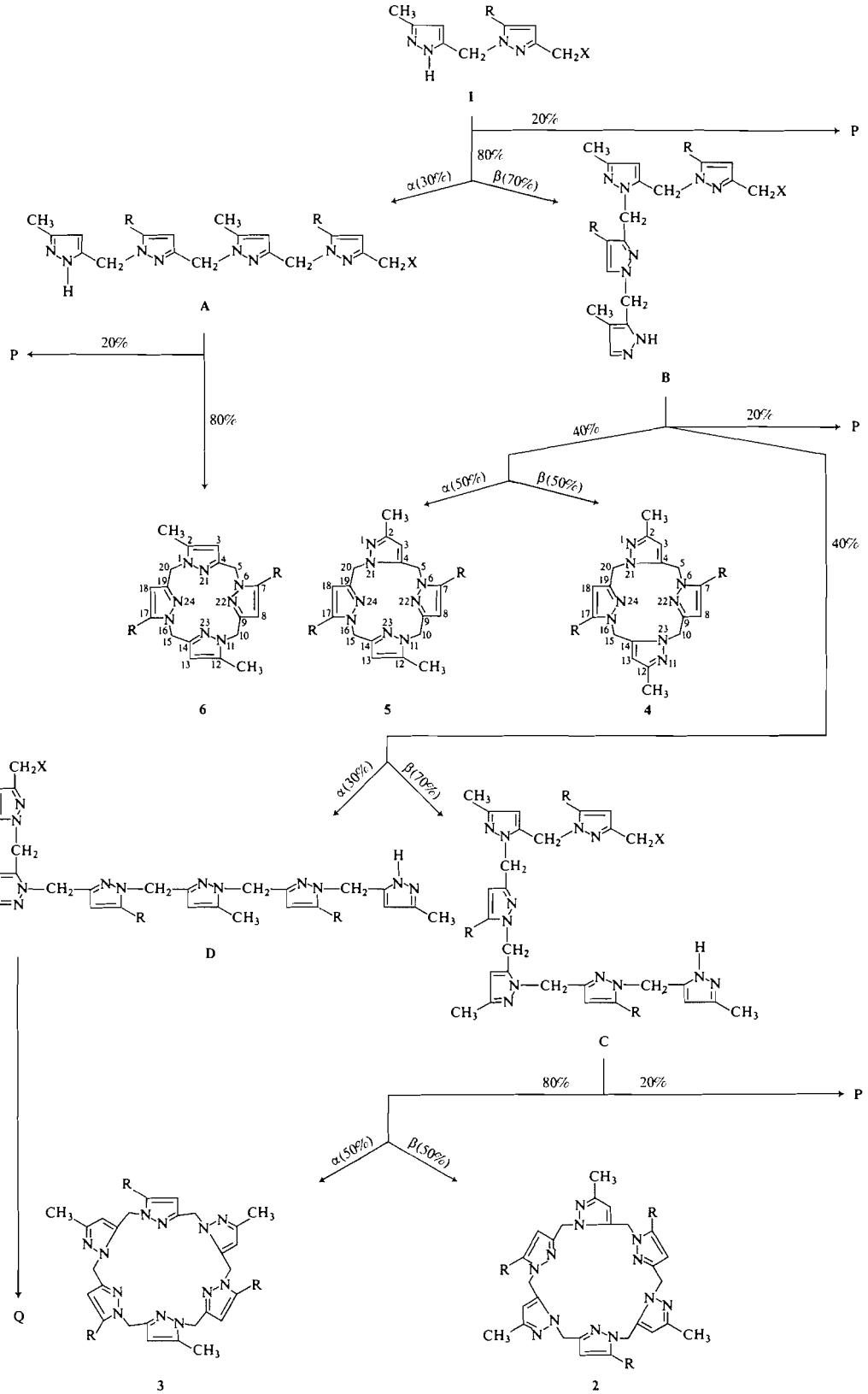

TABLE 2. Proton nmr spectra of some analogs of azaporphyrinogen

Compound		δ
	$2,12\text{-}CH_3$	2.25 (a)
	$7,17\text{-}CH_3$	1.88 (0.7)
4a	$5,15\text{-}CH_2$	5.35 (b)
	$10,20\text{-}CH_2$	5.20 (b)
	3,13-CH	6.08 (a)
	8,18-CH	4.95 (0.7)
	$2\text{-}CH_3$	2.21 (a)
	$7\text{-}CH_3$	2.11 (0.7)(c)
	$12\text{-}CH_3$	2.18 (0.7)(c)
	$17\text{-}CH_3$	2.26 (0.7)(c)
	$5\text{-}CH_2$	5.33 (d)
	$10\text{-}CH_2$	5.02 (e)
5a	$15\text{-}CH_2$	5.00 (e)
	$20\text{-}CH_2$	5.18 (d)
	3-CH	5.98 (a)
	8-CH	5.75 (0.7)(f)
	13-CH	5.80 (0.7)(f)
	18-CH	5.94 (0.7)(f)
	$2,7,12,17\text{-}CH_3$	2.26 (0.7)
6a	$5,10,15,20\text{-}CH_2$	4.98
	3,8,13,18-CH	5.81 (0.7)
	$2,12\text{-}CH_3$	2.06 (a)
	$5,15\text{-}CH_2$	5.43 (g)
	$10,20\text{-}CH_2$	5.32 (g)
4b	3,13-CH	5.19 (a)
	8,18-CH	5.45
	$7,17\text{-}C_6H_5$	7.08 (2H) 7.32 (3H)
	$2\text{-}CH_3$	2.04 (0.3)
	$12\text{-}CH_3$	2.12 (0.7)
	$5\text{-}CH_2$	5.35 (h)
	$10\text{-}CH_2$	5.10 (i)
	$15\text{-}CH_2$	5.18 (i)
	$20\text{-}CH_2$	5.37 (h)
5b	3-CH	5.09 (a)
	8-CH	6.06 (j)
	13-CH	5.63 (0.7)
	18-CH	6.31 (j)
	$7,17\text{-}C_6H_5$	7.40
	$2,12\text{-}CH_3$	2.26 (0.7)
	$5,15\text{-}CH_2$	5.09 (k)
6b	$10,20\text{-}CH_2$	5.11 (k)
	3,13-CH	5.63 (0.7)
	8,18-CH	6.14
	$7,17\text{-}C_6H_5$	7.45

NOTES: (a) = these signals are broadened; (b), (c), (d), (e), (f), (g), (h), (i), (j), (k) = assignments can be reversed.

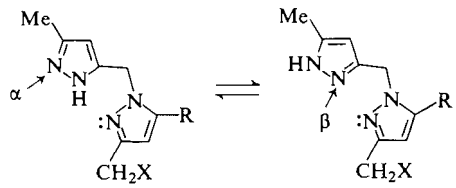

1

slightly) strained, the intramolecular cyclisation occurs more rapidly than the intermolecular substitution. This is observed when the compound **A** (Fig. 1) gives the macrocycle **6** only, by cyclisation. We demonstrated this point in a preceding paper (1) where we described the isolation, with a good yield, of a compound of type **6** from the cyclisation of an analog of **A** (all pyrazole rings having one phenyl substituent) unequivocally synthesised. In the case of the intermediate compound **B** (Fig. 1), a competition exists between the cyclisation which gives **4** and **5** and the intermolecular reaction giving the intermediate compounds **C** and **D**.

1. J. FIFANI, A. RAMDANI, and G. TARRAGO. Nouv. J. Chim. **1**, 521 (1977).
2. J. ELGUERO and R. JACQUIER. J. Chim. Phys. 1242 (1966).
3. J. ELGUERO and R. JACQUIER. Bull. Soc. Chim. Fr. 2832 (1966).
4. G. TARRAGO, A. RAMDANI, J. ELGUERO, and M. ESPADA. J. Heterocycl. Chem. In press.

Dihydroxy-4′,5 tétraméthoxy-2′,3,7,8 flavone, et hydroxy-5 pentaméthoxy-2′,3,4′,7,8 flavone, deux nouveaux composés naturels isolés de *Notholaena affinis* (Ptéridophytes)

MAURICE JAY ET JEAN FAVRE-BONVIN

Département de Biologie Végétale, Service de Phytochimie, Université Claude Bernard, Lyon I, 43 boulevard du 11 novembre, 69621 Villeurbanne, France

ET

ECKHARD WOLLENWEBER

Botanisches Institut der TH, Schnittspahnstr. 3, D-61 Darmstadt, Allemagne

Reçu le 22 novembre 1978

MAURICE JAY, JEAN FAVRE-BONVIN et ECKHARD WOLLENWEBER. Can. J. Chem. **57**, 1901 (1979).

Les structures dihydroxy-4′,5 tétraméthoxy-2′,3,7,8 flavone et hydroxy-5 pentaméthoxy-2′,3,4′,7,8 flavone ont été attribuées à deux flavonoïdes nouveaux isolés d'un exsudat farineux de *Notholaena affinis*; ce résultat découle de l'analyse des spectres uv, sm et rmn des produits naturels et de leurs dérivés.

MAURICE JAY, JEAN FAVRE-BONVIN, and ECKHARD WOLLENWEBER. Can. J. Chem. **57**, 1901 (1979).

The structures 4′,5-dihydroxy-2′,3,7,8-tetramethoxyflavone and 5-hydroxy-2′,3,4′,7,8-pentamethoxyflavone have been attributed to two new compounds isolated from a farinose exudate of *Notholaena affinis*; this result is derived from uv, ms, and nmr spectra of the natural products and their derivatives.

Introduction

Dans le cadre de nos recherches biochimiques sur les processus d'excrétion chez les végétaux vasculaires et plus particulièrement ici chez les Fougères (1), nous venons d'isoler d'un exsudat farineux de fronde de *Notholaena affinis* (Mett.) Moore deux méthyl-3 flavonols dont les structures ont été établies après analyse spectrale comme dihydroxy-4′,5 tétraméthoxy-2′,3,7,8 flavone **1** et hydroxy-5 pentaméthoxy-2′,3,4′,7,8 flavone **2**. Il s'agit de constituants mineurs au sein du pool flavonique de cette farine et d'espèces moléculaires nouvelles pour la littérature flavonique.

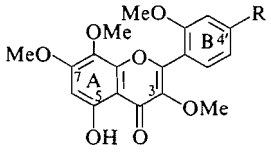

1 R = OH
2 R = OMe

Résultats et discussion

Les spectres uv dans le MeOH laissent supposer une parenté structurale entre les deux composés qui montrent en effet les mêmes λ_{max} (I = 264 nm, II = 354 nm) et le même profil original des spectres avec une dissymétrie très accusée entre les bandes I et II (30% et 100% respectivement). En outre, au vu du λ_{max} de la bande I et de la fluorescence violette en chromatographie sur papier, l'hypothèse d'un flavonol méthylé en position 3 peut être retenue. Les réactifs classiques en spectrophotométrie de flavonoïdes (2) conduisent aux conclusions structurales suivantes: les deux composés ont des OH bloqués en position 7 (pas de déplacement bathochrome de la bande II en présence de NaOAc), des OH libres en position 5 (+55 nm sur la bande I en présence de $AlCl_3$ + HCl par rapport au MeOH); ils ne possèdent sur leur squelette aucun groupement *ortho*-dihydroxylé (pas de déplacement hypsochrome entre $AlCl_3$ et $AlCl_3$ + HCl sur la bande I); en position 4′, la substitution est de type hydroxyle pour le composé **1** (+30 nm sur la bande I en présence de NaOH par rapport au MeOH, sans diminution d'intensité du pic), et de type méthoxyle pour le composé **2** (très faible déplacement bathochrome sur la bande I avec diminution d'intensité du pic).

La formule chimique brute obtenue par mesure de masse à haute résolution permet de reconnaitre en **1** ($C_{19}H_{18}O_8$) une tétraméthoxy, dihydroxy-flavone, et en **2** ($C_{20}H_{20}O_8$) une pentaméthoxy, monohydroxy-flavone. L'étude des fragments selon le mécanisme proposé par Audier (3) permet de préciser la distribution des substituants entre les noyaux A et B du squelette flavone: pour les deux composés un ion-fragment apparait à 197 ($C_9H_9O_5$) témoignant d'un noyau A diméthoxylé et monohydroxylé; un second ion-fragment donne pour le composé **1** un pic *m/e* 151 ($C_8H_7O_3$) caractéristique d'un noyau

0008-4042/79/141901-02$01.00/0

B monométhoxylé et monohydroxylé, pour le composé **2** un pic *m/e* 165 ($C_9H_9O_3$) typique d'un noyau B diméthoxylé.

En première conclusion, il apparait que ces deux composés flavoniques ont le même noyau A, le même hétérocycle et des noyaux B qui diffèrent par la nature de leurs substituants. La position relative de ces derniers est déterminée par rmn de ^1H; en effet, la figure de résonance observée dans la région des protons aromatiques est très significative: pour le composé **2**, nous notons deux protons couplés en *ortho* (H-6′ et H-5′), le plus blindé des deux (H-5′) étant lui-même couplé en *méta* avec un troisième proton (H-3′); les deux substituants du noyau B sont donc portés par les carbones 2′ et 4′ (soit diméthoxy-2′,4′); les attributions ont été faites en tenant compte des δ, les protons H-2′ et H-6′ étant toujours les plus déblindés chez les composés flavoniques, ce qui dans ce cas exclut une substitution de type 2′,5′. Pour le composé **1** où la figure de résonance est voisine, le noyau B est monométhoxylé en 2′ et monohydroxylé en 4′ (voir uv).

En ce qui concerne le noyau A commun aux deux composés, la spectrophotométrie uv a permis de localiser un hydroxyle en 5 et un méthoxyle en 7; il ne reste à placer que le second groupement méthoxyle pour lequel deux hypothèses se présentent: OMe-6 ou OMe-8. Le spectre de rmn ne permet pas de trancher entre les deux termes de l'alternative, car le signal singulet relatif au proton libre résonne à une valeur de champ qui peut être le fait aussi bien d'un H-6 que d'un H-8 (2). Le spectre de masse des produits naturels dans lequel nous relevons un pic de base correspondant à l'ion $M - 15$, oriente vers une structure méthoxy-8 flavonoïde (4); cette hypothèse est d'ailleurs confirmée après méthylation du groupement OH-5, le spectre de masse montrant alors un M^+ pic de base (5); il a en effet été démontré (4, 5) que les spectres de masse des OH-5 diOMe-7,8 flavones, flavonols et méthyl-3 flavonols présentent un pic moléculaire inférieur au pic $M - 15$ (pic de base), et que cette figure spectrale s'inverse pour les dérivés triOMe-5,7,8.

Conclusions

Les deux composés flavoniques isolés de *Notholaena affinis* se voient attribuer les structures suivantes: dihydroxy-4′,5 tétraméthoxy-2′,3,7,8 flavone (**1**), monohydroxy-5 pentaméthoxy-2′,3,4′,7,8 flavone (**2**). Ces deux flavonoïdes naturels nouveaux sont proches au plan structural de quatre autres composés précédemment isolés de la farine de *Notholaena affinis*; ces derniers montraient en effet un noyau B disubstitué en 2′ et 4′, mais possédaient un noyau A tétrasubstitué en 5, 6, 7 et 8 (6).

Partie expérimentale

Matériel végétal

Les frondes de *Notholaena affinis* ont été récoltées au Costa Rica (Prov. Gabacaste, Dec. 1976); un échantillon d'herbier est conservé au Museo nacional de Costa Rica à San José (LDG 4725).

Isolement des flavonoïdes

L'exsudat foliaire de 98 g de frondes est dissous par lavage avec Me_2CO et C_6H_6; il représente environ 6% du poids sec. Après élimination par filtration des cristaux du flavonol majeur (environ 2 g) (7), 1.2 g d'extrait initial est adsorbé sur poudre de polyamide MN SC6; le fractionnement est réalisé sur colonne (3 × 30 cm) du même adsorbant élué avec du C_6H_6 enrichi progressivement en MeCOEt et MeOH (8). Les fractions alors collectées, ici 3 (15 mg) et 7 (26 mg) sont purifiées en CCM préparative de polyamide MN DC 11 dans les systèmes solvants: C_6H_6: petrol 100–140: MeCOEt: MeOH 60:26:7:7, 60:60:7:7 et 30:60:5:5. Finalement 2.5 mg du composé **1** et 4.5 mg du composé **2** sont récupérés.

Dihydroxy-4′,5 tétraméthoxy-2′,3,7,8 flavone (1)—uv λ_{max} nm: MeOH (254), 264, 354; NaOAc (254), 264, 380; NaOAc + H_3BO_3 (256), 266, 356; $AlCl_3$ 272, 306, 346, 412; $AlCl_3$ + HCl 272, 340, 418; NaOMe 264, 384 stable; sm (70 eV) *m/e*: 374 (M^+, 75%, 374.0997, calculé pour $C_{19}H_{18}O_8$ 374.1002), 359 ($M - 15$, 100%), 346 ($M - CO$, 7%), 343 ($M -$ OMe, 6%), 197 (ion D selon Audier, 5%, 197.0441, calculé pour $C_9H_9O_5$ 197.0450), 151 (ion C selon Audier, 10%, 151.0393, calculé pour $C_8H_7O_3$ 151.0397); rmn, 100 MHz (DMSO) (δ en ppm/TMS): 3.71 (3H, s, OMe), 3.73 (3H, s, OMe), 3.79 (3H, s, OMe), 3.93 (3H, s, OMe), 6.57 (3H, m, H-3′, H-5′, H-6), 7.35 (1H, d, $J = 8.5$ Hz, H-6′).

Hydroxy-5 pentaméthoxy-2′,3,4′,7,8 flavone (2)—uv λ_{max} nm: MeOH 264, 352; NaOAc 266, 350; NaOAc + H_3BO_3 264, 350; $AlCl_3$ 272, 340, 412; $AlCl_3$ + HCl 270, 340, 408; NaOMe 268, 360 stable avec diminution d'intensité de BI; sm (70 eV) *m/e*: 388 (M^+, 71%, 388.1151, calculé pour $C_{20}H_{20}O_8$ 388.1158), 373 ($M - 15$, 100%), 357 ($M -$ OMe, 6%), 197 (ion D selon Audier, 5%, 197.0442, calculé pour $C_9H_9O_5$ 197.0450), 165 (ion C selon Audier, 10%, 165.0553, calculé pour $C_9H_9O_3$ 165.0552); rmn, 100 MHz (DMSO) (δ en ppm/TMS): 3.73 (6H, s, deux OMe), 3.85 (3H, s, OMe), 3.89 (3H, s, OMe), 3.93 (3H, s, OMe), 6.64 (1H, s, H-6), 6.72 (1H, dd, $J = 2.5$ et 8.5 Hz, H-5′), 6.78 (1H, s, H-3′), 7.48 (1H, d, $J = 8.5$ Hz, H-6′); sm après méthylation au diazométhane de **2**: 402 (M^+, 100%), 387 ($M - 15$, 50%).

Remerciements

Nous remercions Monsieur L. D. Gomez, directeur du Museo Nacional de Costa Rica, pour la fourniture du matériel végétal.

1. E. Wollenweber. Am. Fern J. **68**, 13 (1978).
2. T. J. Mabry, K. R. Markham et M. B. Thomas. The systematic identification of flavonoids. Springer, Berlin. 1970.
3. H. Audier. Bull. Soc. Chim. Fr. 2892 (1966).
4. M. Goudard, J. Favre-Bonvin, P. Lebreton et J. Chopin. Phytochemistry, **17**, 145 (1978).
5. M. Goudard, J. Strelisky, J. Favre-Bonvin et J. Chopin. Phytochemistry, **18**, 153 (1979).
6. M. Jay, E. Wollenweber et J. Favre-Bonvin. Phytochemistry. Sous presse.
7. E. Wollenweber, J. Favre-Bonvin et P. Lebreton. Phytochemistry. **17**, 1684 (1978).
8. M. Jay, J. F. Gonnet, E. Wollenweber et B. Voirin. Phytochemistry, **14**, 1605 (1975).

Synthesis of some alkoxyfluorophosphoranes and alkoxyfluorophosphines and characterization by ^{1}H, ^{19}F, and ^{31}P nuclear magnetic resonance spectroscopy[1]

ALEXANDER F. JANZEN AND LEONARD J. KRUCZYNSKI

Department of Chemistry, University of Manitoba, Winnipeg, Man., Canada R3T 2N2

Received December 27, 1978

ALEXANDER F. JANZEN and LEONARD J. KRUCZYNSKI. Can. J. Chem. **57**, 1903 (1979).

The preparation of phosphoranes $C_6H_5PF_2HOR$ by the oxidative addition of alcohols to $C_6H_5PF_2$, followed by elimination of HF to give phosphines C_6H_5PFOR (R = CH_3, CH_2CH_3, CH_2CF_3, $CH(CF_3)_2$, $CH(CF_3)C_6H_5$, $C(CH_3)_3$), is described. All products were characterized by ^{1}H, ^{19}F, and ^{31}P nmr spectroscopy. The ^{31}P nmr spectrum of $C_6H_5PFOCH(CF_3)C_6H_5$ confirms the presence of diastereomers. Rapid ligand exchange in phosphoranes $C_6H_5PF_2HOR$ occurs upon addition of a base such as pyridine.

ALEXANDER F. JANZEN et LEONARD J. KRUCZYNSKI. Can. J. Chem. **57**, 1903 (1979).

L'addition oxydante d'alcools à du $C_6H_5PF_2$ conduit aux phosphoranes $C_6H_5PF_2HOR$ qui par élimination de HF conduisent aux phosphines C_6H_5PFOR(R = CH_3, CH_2CH_3, CH_2CF_3, $CH(CF_3)_2$, $CH(CF_3)C_6H_5$, $C(CH_3)_3$). On a caractérisé tous les produits par spectroscopie rmn ^{1}H, ^{19}F et ^{31}P. Le spectre rmn ^{31}P du $C_6H_5PFOCH(CF_3)C_6H_5$ confirme la présence de diastéréoisomères. L'échange rapide du ligand des phosphoranes $C_6H_5PF_2HOR$ se produit par addition d'une base comme la pyridine.

[Traduit par le journal]

Phosphines undergo oxidative addition reactions with alcohols, amines, thiols, hydrogen halides, or halogens to give five-coordinate phosphoranes (see, for example, ref. 1). We have prepared a variety of phosphoranes $C_6H_5PF_2HOR$ by the oxidative addition reaction of $C_6H_5PF_2$ with alcohols and studied their conversion to phosphines C_6H_5PFOR by the elimination of HF.

The reaction of $C_6H_5PF_2$ with alcohols occurred under mild conditions, typically at -10 to $+10$°C within 5 to 30 min in an nmr tube (eq. [1]).

[1] $$C_6H_5PF_2 + HOR \longrightarrow C_6H_5P(F)(H)(OR)(F)$$

1–6

1 R = CH_3
2 R = CH_2CH_3
3 R = CH_2CF_3
4 R = $CH(CF_3)_2$
5 R = $CH(CF_3)C_6H_5$
6 R = $C(CH_3)_3$

The products were characterized by ^{1}H, ^{19}F, and ^{31}P nmr (Table 1) and the nmr data are in agreement with trigonal bipyramidal phosphoranes in which fluorines occupy axial sites. The phosphoranes were stable at temperatures below $+10$°C in the absence of pyridine or excess $C_6H_5PF_2$.

The synthesis of $C_6H_5PF_2HOC(CH_3)_3$ (**6**) was carried out at $+5$°C in the presence of a small amount of pyridine; attempts to prepare **6** at $+25$°C resulted in the formation of $(CH_3)_3CF$ (85%), $(CH_3)_2C{=}CH_2$ (15%), $C_6H_5P(O)HF$, and HF.

Conversion of $C_6H_5PF_2HOR$ to C_6H_5PFOR

At temperatures above $+10$°C, HF elimination occurred and the phosphoranes were converted to phosphines C_6H_5PFOR **7–12** which were characterized by ^{1}H, ^{19}F, and ^{31}P nmr (Table 2). The presence of $C_6H_5PF_2$ favours the conversion to C_6H_5PFOR because HF is then removed as $C_6H_5PF_3H$.

Reaction [2] must be taken into account when

[2] $$C_6H_5P(F)(H)(OR)(F) \longrightarrow HF + C_6H_5P(F)(OR)$$

7–12

$C_6H_5PF_2$ ↓

$C_6H_5PF_3H$

7 R = CH_3
8 R = CH_2CH_3
9 R = CH_2CF_3
10 R = $CH(CF_3)_2$
11 R = $CH(CF_3)C_6H_5$
12 R = $C(CH_3)_3$

choosing the appropriate conditions for the synthesis of $C_6H_5PF_2HOR$ because, for those alcohols that

[1]Presented at the EUCHEM Conference, Menton, France, June 27–30, 1976.

0008-4042/79/141903-03$01.00/0

TABLE 1. Proton, fluorine, and phosphorus nmr chemical shifts and coupling constants of some phosphoranes[a]

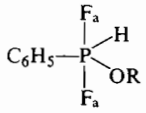

	Chemical shift (ppm)			Coupling constant (Hz)			
	δ_P	δ_{F_a}	δ_H	$^1J_{F_aP}$	$^1J_{HP}$	$^2J_{HPF_a}$	$^3J_{HCOP}$
1 R = CH_3	−44.8	−38.2	7.42	733	842	123	14.8
2 R = CH_2CH_3	−46.6	−37.8	7.43	735	834	122	10.0
3 R = CH_2CF_3	−44.9	−35.9	7.19	764	850	122	8.8
4 R = $CH(CF_3)_2$	−44.3	−38.9	7.49	794	865	122	15.3
5 R = $CH(CF_3)C_6H_5$	−45.5	−36.8	7.41	768	853	122	11
6 R = $C(CH_3)_3$	−45.9	−26.7	7.19	728	777	122	—

[a]Chemical shifts are negative if upfield from TMS, $CFCl_3$, and 85% H_3PO_4.

TABLE 2. Fluorine and phosphorus nmr chemical shifts and coupling constants of some phosphines[a]

Compound	δ_P	δ_F	$^1J_{PF}$
7	185	−111	1076
8	184		1076
9	189	−109	1099
10[b]	199	−102	1126
11[c]	190.2		1105
	189.8		1107
12	171	−98.1	1073

[a]Chemical shifts are negative if upfield from TMS, $CFCl_3$, and 85% H_3PO_4.
[b]Previous nmr data in ref. 2.
[c]See Fig. 1.

react slowly with $C_6H_5PF_2$, any unreacted $C_6H_5PF_2$ will favour the conversion of $C_6H_5PF_2HOR$ to C_6H_5PFOR; on the other hand, for reactive alcohols such as CH_3OH or C_2H_5OH, $C_6H_5PF_2$ is consumed before it seriously affects the conversion to C_6H_5PFOR.

The phosphines **7**–**12** have a chiral center at phosphorus which leads to magnetically nonequivalent CF_3 groups in **10** (2). An additional chiral center at carbon is found in **11** and the ^{31}P nmr spectrum of **11** clearly shows the presence of diastereomers with the coupling constant $^4J_{POCCF}$ differing by a factor of 2 in the isomers (Fig. 1).

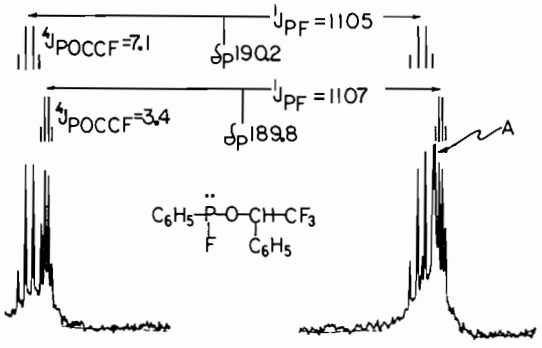

FIG. 1. The ^{31}P nmr spectrum (proton decoupled) of $C_6H_5PFOCH(CF_3)C_6H_5$ (**11**) showing the presence of diastereomers. Peak A is due to unreacted $C_6H_5PF_2$.

HF, H_2O, Base Catalysts, and Ligand Exchange

As a continuation of previous work (3, 4), we briefly investigated the effect of HF, H_2O, and base catalysts on exchange processes. It was found that addition of a small amount of H_2O to $C_6H_5PF_2$ resulted in an instantaneous reaction to give, mainly, $C_6H_5P(O)HF$ and $C_6H_5PF_3H$ (eq. [3]).

[3] $C_6H_5PF_2 + H_2O \longrightarrow C_6H_5P(O)HF + HF$

$C_6H_5PF_2$ ↓

$C_6H_5PF_3H$

Addition of HF to $C_6H_5PF_3H$ produced only very slow fluorine exchange, on the nmr time scale,[2] unlike the situation in the $CH_3SiF_4^-$–HF system (4). Unreacted alcohols gave separate nmr peaks in the presence of phosphoranes $C_6H_5PF_2HOR$; however, addition of a base such as pyridine produced rapid ligand exchange in the $C_6H_5PF_2HOR$–HOR system. Presumably, the function of the base catalyst is to produce a six-coordinate phosphorus

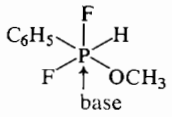

species as the first step towards rapid ligand exchange and chemical reaction, as suggested previously for analogous phosphorus and silicon compounds (3, 4). A more detailed study of intra- and intermolecular ligand exchange in $C_6H_5PF_3H$ and $C_6H_5PF_2HOCH_3$ is in progress.[2]

Experimental

General

Tetramethylene sulfone (Aldrich), $C_6H_5PCl_2$ (Aldrich), and SbF_3 (Fisher) were used without further purification. DL-Phenyltrifluoromethyl carbinol (Burdick and Jackson Laboratories) and $(CF_3)_2CHOH$ (Aldrich) were stored over molecular

[2]R. K. Marat and A. F. Janzen. Unpublished results.

sieve. CH_3OH, C_2H_5OH, CF_3CH_2OH, and $(CH_3)_3COH$ were distilled from sodium prior to use. Conventional vacuum line techniques were used for handling volatile materials.

Fluorine and proton nmr spectra were recorded on a Varian A-56/60A spectrometer at 56.4 and 60 MHz for fluorine and proton, respectively; phosphorus nmr spectra were recorded on a Bruker WH90 spectrometer at 36.44 MHz. ^{31}P chemical shifts are reported with respect to external 85% H_3PO_4. Temperatures were calibrated by the method of Van Geet (6).

$C_6H_5PF_2$ was prepared most conveniently from $C_6H_5PCl_2$ and NaF in tetramethylene sulfone according to the method of Schmutzler (7). It was also prepared from SbF_3 (27 g, 0.15 mol) in tetramethylene sulfone (200 mL) by adding $C_6H_5PCl_2$ dropwise at room temperature (8). A slightly exothermic reaction occurred immediately and volatile $C_6H_5PF_2$, along with about 5–10% $C_6H_5PF_4$, was condensed into the vacuum line. Enough pyridine was added to complex out $C_6H_5PF_4$:py and the volatile $C_6H_5PF_2$ was condensed into a reaction flask at 22°C and 10^{-3} Torr. $C_6H_5PF_2$ was prepared in yields of 80–90% (lit. yield 14% (8)). On standing for several weeks, $C_6H_5PF_2$ decomposed to $(C_6H_5P)_5$ and $C_6H_5PF_4$ (5, 8), therefore samples of $C_6H_5PF_2$ were used within several days of redistillation.

Preparation of Phosphoranes $C_6H_5PF_2HOR$

In a typical reaction, $C_6H_5PF_2$ (5.0 mmol) and ROH (5.0 mmol) were condensed into a 5 mm nmr tube containing C_6D_6 (1 mL). The reactions were generally very slow below −10°C, as monitored by nmr, but proceeded at a reasonable rate between 0 and +20°C. For example, $C_6H_5PF_2HOCH_3$ was formed in 90% yield at 0°C for 30 min and in quantitative yield at +10°C for 10 min. $C_6H_5PF_2HOCH_2CH_3$ was formed quantitatively within 2 h at +18°C and $C_6H_5PF_2HOCH(CF_3)C_6H_5$ was formed within 5 min at 0°C. All phosphoranes $C_6H_5PF_2HOR$ were stable indefinitely at temperatures below +10°C; above this temperature decomposition occurred; for example, only 30% of $C_6H_5PF_2HOCH_3$ remained after 2 days at +22°C.

Preparation of $C_6H_5PF_2HOC(CH_3)_3$

Initial attempts to prepare $C_6H_5PF_2HOC(CH_3)_3$ were unsuccessful. Reaction of $C_6H_5PF_2$ with $(CH_3)_3COH$ is very slow below +10°C; however, attempts to increase the rate of reaction by increasing the temperature to +25°C resulted in complete decomposition to give $(CH_3)_3CF$ (85%), $(CH_3)_2C{=}CH_2$ (15%) and $C_6H_5P(O)HF$. Eventually, it was observed that pyridine catalyzed the formation of phosphorane; hence, $C_6H_5PF_2HOC(CH_3)_3$ was prepared from $C_6H_5PF_2$ (5.0 mmol) and $(CH_3)_3COH$ (5.0 mmol) plus pyridine (0.4 mmol) in C_6D_6 (1 mL) at +5°C.

Conversion of Phosphorane $C_6H_5PF_2HOR$ to Phosphine C_6H_5PFOR

The presence of excess $C_6H_5PF_2$ resulted in the conversion of phosphorane $C_6H_5PF_2HOR$ to phosphine C_6H_5PFOR plus $C_6H_5PF_3H$. The phosphines C_6H_5PFOR could therefore be produced in two ways: either by adding $C_6H_5PF_2$ to $C_6H_5PF_2HOR$, or by mixing $C_6H_5PF_2$ and alcohol in a 2:1 molar ratio. In a typical reaction, $C_6H_5PF_2$ (5.0 mmol) and CF_3CH_2OH (2.5 mmol) in C_6D_6 (1 mL) were mixed at +25°C. After several hours, nmr examination showed an equilibrium mixture of $C_6H_5PF_2HOCH_2CF_3$, $C_6H_5PF_2$, $C_6H_5PFOCH_2CF_3$, and $C_6H_5PF_3H$. The ^1H, ^{19}F, and ^{31}P nmr spectra of phosphines C_6H_5PFOR are shown in Table 2.

Acknowledgements

This research was supported by an operating grant from the National Research Council of Canada. We thank the NRCC, the University of Manitoba, and its Faculty of Graduate Studies for capital grants for the purchase of a Bruker WH-90 spectrometer.

1. R. SCHMUTZLER. *In* Halogen chemistry. Vol. 2. *Edited by* V. Gutmann. Academic Press, London, Engl. 1967. p. 31; D. HELLWINKEL. *In* Organic phosphorus compounds. Vol. 3. *Edited by* G. M. Kosolapoff and L. Maier. Wiley-Interscience, New York, NY. 1972. p. 185; G. I. DROZD, S. Z. IVIN, V. V. SHELUCHENKO, and M. A. LANDAU. Zh. Obshch. Khim. **38**, 1653 (1968); Chem. Abstr. **70**, 11754v (1969); G. I. DROZD, S. Z. IVIN, and V. V. SHELUCHENKO. Zh. Obshch. Khim. **38**, 1655 (1968); Chem. Abstr. **69**, 96831v (1968); F. SEEL and K.-D. VELLEMAN. Chem. Ber. **105**, 406 (1972); L. F. CENTOFANTI and R. W. PARRY. Inorg. Chem. **12**, 1456 (1973).
2. D. DAKTERNIEKS, G.-V. RÖSCHENTHALER, and R. SCHMUTZLER. Z. Naturforsch. **33b**, 507 (1978).
3. J. A. GIBSON, D. G. IBBOTT, and A. F. JANZEN. Can. J. Chem. **51**, 3203 (1973); R. E. WASYLISHEN, G. S. BIRDI, and A. F. JANZEN. Inorg. Chem. **15**, 3054 (1976); R. K. MARAT and A. F. JANZEN. Can. J. Chem. **55**, 3845 (1977).
4. R. K. MARAT and A. F. JANZEN. Can. J. Chem. **55**, 1167 (1977).
5. H. G. ANG and R. SCHMUTZLER. J. Chem. Soc. A, 702 (1969).
6. A. L. VAN GEET. Anal. Chem. **42**, 679 (1970).
7. R. SCHMUTZLER. Chem. Ber. **98**, 552 (1965).
8. V. N. KULAKOVA, YU. M. ZINOV'EV, and L. Z. SOBOROVSKII. Zh. Obshch. Khim. **29**, 3957 (1959); Chem. Abstr. **54**, 20846e (1960).

COMMUNICATION

Interaction of the unusual bonds in cyclopropane with an extra electron in the dense fluid[1]

NORMAN GEE AND GORDON R. FREEMAN

Chemistry Department, University of Alberta, Edmonton, Alta., Canada T6G 2G2

Received April 9, 1979

NORMAN GEE and GORDON R. FREEMAN. Can. J. Chem. **57**, 1906 (1979).

An unexpectedly strong interaction between electrons and closely packed cyclopropane molecules has been discovered through measurement of electron mobilities in the liquid and gas phases. In the low density vapors the mobilities fell in the expected order cyclopropane > propane > propene; at STP they were 9000, 6000, and 2040 cm^2/V s, respectively. In the liquids the order was propane > propene > cyclopropane; at 273 K the mobilities were 1.4, 0.12, and 0.017 cm^2/V s, respectively. The abnormally low mobility in liquid cyclopropane is attributed to the formation of transient dimeric anions. The reaction is only significant at densities greater than about 0.4 times the critical density.

NORMAN GEE et GORDON R. FREEMAN. Can. J. Chem. **57**, 1906 (1979).

A la suite de mesures de mobilités électroniques en phases liquide et vapeur, on a découvert une interaction particulièrement forte entre des électrons et des molécules de cyclopropane bien tassées. A des densités de vapeur faibles, les mobilités diminuent dans l'ordre attendu: cyclopropane > propane > propène; aux conditions NTP, elles sont respectivement 9000, 6000 et 2040 cm^2/V s. Dans les liquides, l'ordre est: propane > propène > cyclopropane; à 273 K, les mobilités sont respectivement 1.4, 0.12 et 0.017 cm^2/V s. On attribue la mobilité anormalement faible dans le cyclopropane liquide à la formation d'anions dimères transitoires. La réaction n'est toutefois significative qu'à des densités qui sont plus grandes que 0.4 fois la densité critique.

[Traduit par le journal]

The magnitude of the diffusion coefficient (cm^2/s) or mobility (cm^2/V s) of thermal electrons in a fluid is an indicator of the interactions between the electrons and the fluid. In a low density gas an electron interacts with one molecule at a time, in which case the mobility provides a measure of the electron–molecule scattering cross section (1). If the density of the gas is increased along the vapor/liquid coexistence curve, van der Waals clusters of molecules become an important component of the gas (2–5). At densities greater than about 10% of that of the normal liquid, electron interactions with the clusters are detectable (6, 7). In the liquid phase, the electron interacts continuously with several molecules at once, which can either enhance (6) or diminish (6, 7) the scattering, depending on the nature of the molecules and the density of the fluid. Molecules that possess a permanent dipole moment or an anisotropic polarizability, such as methanol (8) or ethane (9), provide sufficiently large potential fluctuations in the liquid that an extra electron can become localized in a potential minimum. Molecules that are nearly spherical in shape and are isotropically polarizable, such as methane and neopentane, present a relatively constant potential to the electron throughout the liquid; electrons do not form localized states in these liquids to a large extent (9–13).

For the low density gas phase of the C_3 hydrocarbons, considerations of molecular dipole moment (14) and size (reflected in the mean polarizability (15), see Table 1) lead one to expect that electron mobilities would fall in the order cyclopropane > propane > propene. This order has been observed (1). For the liquid phase, the relative anisotropies of polarizability (Table 1) lead one to expect (16) that the mobilities would fall in the order propane > cyclopropane > propene. However, the observed order was propane > propene > cyclopropane (9).

TABLE 1. Molecular properties in the dilute gases

Molecule	D* (Debye)	$\bar{\alpha}$† (10^{-24} cm^3)	α^a‡ (10^{-24} cm^3)
$(CH_2)_3$	0.00	5.5	1.45
$CH_3CH_2CH_3$	0.084	6.2	0.9
CH_3CHCH_2	0.366	5.8	2.1

*Electric dipole moment (14).
†Mean polarizability (15).
‡Anisotropy of polarizability (15).

[1]Assisted financially by NSERC.

0008-4042/79/141906-03$01.00/0

The mobility in liquid cyclopropane was anomalously low. To learn more about the behavior of electrons in these fluids we have measured mobilities in each of the three compounds over a 100-fold range of densities.

As expected from theory, in each dilute gas the mobility was inversely proportional to the gas density. At STP the values of the mobilities in cyclopropane, propane, and propene were respectively 9000, 6000, and 2040 cm^2/V s. In the liquids at 273 K the respective mobilities were 0.017, 1.4, and 0.12 cm^2/V s. The mobility in liquid cyclopropane is two orders of magnitude lower than that in liquid propane, and at least one order of magnitude lower than expected on the basis of the relative anisotropies of polarizability. The low mobility means that a localized state of electrons is especially stable in liquid cyclopropane.

The localized state could be either a solvated electron or an anion. One might suggest that the solvation energy of electrons is greater in cyclopropane than in propene, due to the greater density of the former liquid.[2] However, the permanent dipole moment and anisotropy of polarizability are larger for propene (Table 1), which would tend to make the solvation energy greater in that liquid. We therefore suggest that anions are formed.

Monomeric anions would be expected to form more readily in propene than in cyclopropane, by addition to the double bond, producing a lower mobility for the negative charge in the former liquid.

The high degree of symmetry of the molecular orbitals in cyclopropane (17–19), and the relatively small amount of steric hindrance to packing the molecules together,[2] lead one to suggest that transient dimeric anions are formed in the liquid. The extra electron would occupy the lowest unoccupied molecular orbitals of adjacent molecules. The shared orbitals probably occur along edges of the molecules (17–19), but the detailed configuration is difficult to predict.

[1] $$e_s^- + 2(CH_2)_3 \rightarrow [(CH_2)_3]_{2,s}^-$$

The subscripts s in reaction [1] indicate solvation. The possibility of trimeric anions would depend upon attainment of a favorable geometry and cannot be excluded.

At 294 K the mobility of electrons in liquid cyclopropane, $\mu = 0.04$ cm^2/V s, is even smaller than that in benzene, $\mu = 0.12$ cm^2/V s (20). Transient anion formation was postulated to explain the relatively high temperature coefficient of mobility in benzene (20).

[2] $$e_s^- + C_6H_6 \rightleftarrows C_{6,s}H_6^-$$

The temperature dependence of the mobility in liquid cyclopropane indicates that the binding energy of the electron in the ion would be ~ 0.1 eV greater than that in a solvation site. Ion formation is apparent only in the high density fluid, so the electron affinity of an isolated pair of cyclopropane molecules (van der Waals dimer) would be negative. The slight stability of the anion in the dense fluid would be gained through polarization of the surrounding solvent.

The crossover of the electron mobilities in propane and cyclopropane occurs in the saturated vapors at 1.3×10^{21} molecules/cm^3, which is 0.4 of the critical density. This can be taken to be near the lower limit of the density at which the special nature of cyclopropane need be considered. The mobilities at this density are 95 cm^2/V s, in the regime of gas phase transport modified by interaction with van der Waals clusters.

[2]The density of liquid cyclopropane at 250–300 K is 16% greater than that of propene and 20% greater than that of propane. The densities inversely reflect the relative amounts of steric hindrance to packing the molecules together.

Acknowledgements

We would like to thank the staff of the Radiation Research Center for aid with the electronics, and colleagues in the Chemistry Department for discussions of the bonding and possible crystal structures of cyclopropane.

1. C. W. Duncan and I. C. Walker. J. Chem. Soc. Faraday Trans. II, **70**, 577 (1974), and references therein.
2. J. H. Halloway. Noble-gas chemistry. Methuen, London. 1968. pp. 41–48.
3. M. Rigby. Q. Rev. **24**, 416 (1970).
4. G. C. Maitland and E. B. Smith. Chem. Soc. Rev. **2**, 181 (1973).
5. G. E. Ewing. Acc. Chem. Res. **8**, 185 (1975).
6. (*a*) J.-P. Dodelet and G. R. Freeman. J. Chem. Phys. **65**, 3376 (1976); (*b*) S. S.-S. Huang and G. R. Freeman. Can. J. Chem. **56**, 2388 (1978).
7. S. S.-S. Huang and G. R. Freeman. J. Chem. Phys. **68**, 1355 (1978).
8. I. A. Taub, D. A. Harter, M. C. Sauer, Jr., and L. M. Dorfman. J. Chem. Phys. **41**, 979 (1964).
9. M. G. Robinson and G. R. Freeman. Can. J. Chem. **52**, 440 (1974).
10. H. Schnyders, S. A. Rice, and L. Meyer. Phys. Rev. **150**, 127 (1966).
11. P. H. Tewari and G. R. Freeman. J. Chem. Phys. **51**, 1276 (1969).
12. W. F. Schmidt and A. O. Allen. J. Chem. Phys. **52**, 4788 (1970).
13. R. M. Minday, L. D. Schmidt, and H. T. Davis. J. Chem. Phys. **76**, 442 (1972).
14. R. D. Nelson, Jr., D. R. Lide, Jr., and A. A. Maryott. Selected values of electric dipole moments for molecules in

the gas phase. NSRDS-NBS 10, U.S. Government Printing Office, Washington, DC. 1967.
15. (*a*) M. J. AVOEY, R. J. W. LEFÈVRE, W. LUTTKE, G. L. D. RITCHIE, and P. J. STILLS. Aust. J. Chem. **21**, 2551 (1968); (*b*) R. J. W. LEFÈVRE. Rev. Pure Appl. Chem. **20**, 67 (1970).
16. J.-P. DODELET and G. R. FREEMAN. Can. J. Chem. **50**, 2667 (1972).
17. A. D. WALSH. Trans. Faraday Soc. **45**, 179 (1949).
18. R. HOFFMAN and R. B. DAVIDSON. J. Am. Chem. Soc. **93**, 5699 (1971).
19. W. L. JORGENSEN and L. SALEM. The organic chemists' handbook of orbitals. Academic Press, New York. 1973. p. 153 *ff*.
20. K. SHINSAKA and G. R. FREEMAN. Can. J. Chem. **52**, 3495 (1974).

Canadian Journal of Chemistry
Published by
THE NATIONAL RESEARCH COUNCIL OF CANADA

Journal canadien de chimie
Publié par
LE CONSEIL NATIONAL DE RECHERCHES DU CANADA

Volume 57 Number 15 August 1, 1979 Volume 57 numéro 15 1 août 1979

The crystal and molecular structure of the molybdenum tetracarbonyl complex of 1,4-diphenyl-2,2′,3,3′,5,5′6,6′-octamethylcyclo-1,4-diphospha-2,3,5,6-tetrasilahexane

JOSEPH C. CALABRESE, RICHARD T. OAKLEY,[1] AND ROBERT WEST
Department of Chemistry, University of Wisconsin, Madison, WI 53706, U.S.A.

Received January 25, 1979

JOSEPH C. CALABRESE, RICHARD T. OAKLEY, and ROBERT WEST. Can. J. Chem. **57**, 1909 (1979).

The crystal and molecular structure of the molybdenum tetracarbonyl complex of 1,4-diphenyl-2,2′,3,3′,5,5′,6,6′-octamethylcyclo-1,4-diphospha-2,3,5,6-tetrasilahexane, $(PhPSi_2Me_4)_2Mo(CO)_4$, has been determined by single crystal X-ray diffraction. The crystals are monoclinic, space group $P2_1/n$, with $a = 15.983(5)$, $b = 19.316(6)$, $c = 10.580(3)$ Å, $\beta = 99.99(2)°$, $V = 3217(2)$ Å^3, $Z = 4$, and $\rho_{calcd} = 1.356$ g/cm^3. The structure was solved by Patterson heavy atom methods and was refined by full-matrix least-squares procedures to a final R_1 of 3.3% and R_2 of 4.3%, for 6342 reflections with intensities greater than 2σ. The coordination of the boat-shaped $(PhPSi_2Me_4)_2$ ligand to molybdenum tetracarbonyl produces a distorted octahedral environment about the metal. The mean Si—Si (2.358(14) Å) and P—Si (2.275(19) Å) distances are not greatly altered from the values found for them in the free ligand. The structural consequences of P → Si π-bonding in the latter are therefore minimal. The relatively long P—Mo (mean length 2.592(13) Å) distances are interpreted as the result of reduced back-bonding from the metal, caused by the presence of the relatively electropositive silyl groups on phosphorus. Consistently, the equatorial Mo—C bonds, which are *trans* to the diphosphine ligand, are shorter (mean length 1.968(19) Å) than the corresponding bonds to the axial carbonyl groups (mean length 2.021(15) Å).

JOSEPH C. CALABRESE, RICHARD T. OAKLEY et ROBERT WEST. Can. J. Chem. **57**, 1909 (1979).

On a déterminé la structure cristalline et moléculaire du complexe tétracarbonylmolybdène du diphényl-1,4 octaméthyl-2,2′,3,3′,5,5′,6,6′ cyclodiphospha-1,4 tétrasila-2,3,5,6 hexane, $(PhPSi_2Me_4)_2Mo(CO)_4$, par diffraction de rayons-X de monocristaux. Les cristaux sont monocliniques, groupe d'espace $P2_1/n$, avec $a = 15.983(5)$, $b = 19.316(6)$, $c = 10.580(3)$ Å, $\beta = 99.99(2)°$, $V = 3217(2)$ Å^3, $Z = 4$ et $\rho_{calculé} = 1.356$ g/cm^3. On a résolu la structure par les méthodes de Patterson appliquées aux atomes lourds et on l'a affinée par la méthode des moindres carrés (matrice complète) jusqu'à une valeur finale de R_1 de 3.3% et de R_2 de 4.3% pour 6342 réflexions avec des intensités plus grandes que 2σ. Le ligand $(PhPSi_2Me_4)_2$ qui est en forme bateau subit, par sa coordination au tétracarbonyle molybdène, une déformation autour du métal qui a un environnement octaédrique. Les distances Si—Si (2.358(14) Å) et P—Si(2.275(19) Å) moyennes ne diffèrent pas beaucoup de celles observées dans le ligand libre. Les conséquences structurales de la liaison P → Si dans ce dernier sont donc minimales. On interprète la distance P—Mo relativement longue (valeur moyenne de 2.592(13) Å) comme résultant d'une réduction de la reformation d'une liaison à partir du métal qui proviendrait de la présence de groupes silyles relativement électropositifs sur le phosphore. En conséquence, les liaisons Mo—C équatoriales qui sont *trans* par rapport au ligand diphosphine sont plus courtes (longueur moyenne de 1.968(19) Å) que les liaisons correspondantes qui sont axiales par rapport aux groupes carbonyles (longueur moyenne de 2.021(15) Å).

[Traduit par le journal]

[1]To whom all correspondence should be addressed. Present address: Department of Chemistry, University of Calgary, Calgary, Alta., Canada T2N 1N4.

0008-4042/79/151909-06$01.00/0

Introduction

The influence of the size (1) and electronegativity (2) of the substituents X on the coordination properties of phosphine ligands PX_3 is well known. However, the chemical and structural importance of such effects for phosphines possessing group IV substituents (X = Si≡, Ge≡, Sn≡) has not been greatly explored, and, for example, there has been only one structural report of a transition metal complex of such a compound (3). As a part of our studies on the properties of cyclic phosphasilanes we have determined the crystal and molecular structure of **II**,[2] the molybdenum tetracarbonyl complex of the

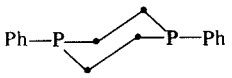

I

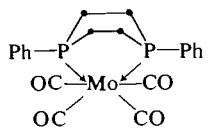

II

 = $SiMe_2$

cyclophosphasilane **I**. We have recently reported the preparation (5) and crystal structure (6) of the neutral ligand, and we now describe the structural changes which occur upon its coordination to a metal centre, and also the effect on the ligand–metal interaction brought about the polarity of the silicon–phosphorus bond.

Experimental

Crystals suitable for X-ray work were obtained by crystallization from warm chloroform; the one chosen for study had approximate dimensions of 0.33 × 0.35 × 0.55 mm. Crystal data (at 22°C) are:

$MoP_2Si_4O_4C_{24}H_{34}$

Monoclinic, $a = 15.983(5)$, $b = 19.316(6)$, $c = 10.580(3)$ Å, $\beta = 99.99(2)°$, $V = 3217(2)$ Å^3 (based on 15 reflections).

Data were collected on a Syntex P$\bar{1}$ diffractometer, using monochromated MoK_α radiation. Systematic absences of $0k0$ (k odd) and $h0l$ ($h + l$ odd) indicate the space group $P2_1/n$: $\pm[x, y, z]$; $\frac{1}{2} + x, \frac{1}{2} - y, \frac{1}{2} + z$; $Z = 4$; $\rho_{calcd} = 1.356$ g/cm^3; $\mu = 6.67$ cm^{-1}. Data collection (at 22°C): variable scan speed 2° to 24°/min, scan range 2°, scan method θ–2θ fixed background with background:scan time ratio 0.67, standards 2/50, 1% variation; data limits $3° < 2\theta < 50°$; total data 6342; unique data 5677; non-zero data 4581 ($I > 2\sigma(I)$); $q = 0.055$; uncorrected for absorption. The structure was solved by Patterson heavy atom methods;[3] isotropic least-squares[4] convergence at $R_1 = 6.9\%$, $R_2 = 9.2\%$;[5] anisotropic least-squares convergence $R_1 = 3.3\%$ and $R_2 = 4.3\%$; esd of an observation of unit weight, 1.14;[6] data parameter ratio 14.5. Hydrogen atoms were included as fixed atom contributers with a C—H bond length of 0.95 Å and $\beta_{iso} = 5.0$ Å^2. No attempt was made to refine the hydrogen atom parameters. The full-matrix refinement was converged to completion. The final positional parameters of the non-hydrogen atoms are given in Table 1*a*; those of the hydrogen atoms are deposited in Table 1*b*.[7] The thermal parameters of the non-hydrogen atoms are deposited in Table 2.[7] The derived bond distance and valence angle information (with esd's from the full inverse variance–covariance refinement) are given in Tables 3 and 4.

Results and Discussion

The crystal structure of the title compound consists of discrete molecules of **II**. All intermolecular contacts correspond to normal van der Waals' interactions. A general view of the molecule with the crystallographic numering scheme is shown in Fig. 1. Figure 2 gives an alternative view, and illustrates the boat conformation of the six-membered P_2Si_4 ring. The cyclic $(PhPSi_2Me_4)_2$ ligand (**I**), which exists in a chair conformation with equatorial phenyl groups when uncoordinated (6), is forced to adopt the boat conformation upon coordination to molybdenum. As a consequence, there are several angular changes. The dihedral angle between the $P_1Si_1Si_2$ and $P_2Si_3Si_4$ planes and the central $Si_1Si_2Si_3Si_4$ plane (111.4° and 108.5°, respectively) are reduced from the corresponding angles (mean value 114.8(1)°) found in the free ligand, and the endocyclic angles at phosphorus (mean value 107.3(1)°)[8] and silicon (mean value 101.5(4)°) are altered slightly in opposite senses from the values found for them (104.4(1)° and 104.9(2)°, respectively) in the uncomplexed ring.

[2]The preparation of this complex has recently been reported (4). In the present work, the compound was prepared by the displacement of norbornadiene from $C_7H_8Mo(CO)_4$ by the phosphasilane **I** in hexane (yield 84%). The product was recrystallized from benzene as pale yellow air stable prisms, dec. > 190°C. *Anal.* calcd. for $C_{24}H_{34}O_4P_2Si_4Mo$: C 43.9, H 5.2, P 9.4; found: C 44.1, H 5.2, P 9.9.

[3]All crystallographic programs used in the structural determination and least-squares refinement were written by one of us (J.C.C.). Plots were made using the ORTEP program of C. K. Johnson.

[4]The least-squares refinement was based on the minimization of $\Sigma w_i||F_o| - |F_c||^2$ with individual weights $w_i = 1/\sigma(F_o)^2$. Atomic scattering factors used for all non-hydrogen atoms are from ref. 7 and those for the hydrogen atoms are from ref. 8.

[5]$R_1 = \Sigma||F_o| - |F_c||/\Sigma|F_o| \times 100\%$. $R_2 = [\Sigma w_i||F_o| - |F_c||^2/\Sigma w_i|F_o|^2]^{1/2} \times 100\%$.

[6]The standard deviation of an observation of unit weight is defined as $[\Sigma w_i||F_o| - |F_c||^2/(m - n)]^{1/2}$, where m is the number of observations and n is the number of parameters fitted to the data set.

[7]A copy of the observed and calculated structure factor table, Table 1*b*, and Table 2 is available, at a nominal charge, from the Depository of Unpublished Data, CISTI, National Research Council of Canada, Ottawa, Ont., Canada K1A 0S2.

[8]Here and elsewhere in this report, integers quoted in parentheses refer to esd's for single-valued parameters, and indicate ranges of results for the averages of chemically equivalent parameters.

TABLE 1*a*. Final atomic coordinates ($\times 10^4$) for non-hydrogen atoms, with estimated standard deviations in parentheses

Atom	*x*	*y*	*z*
Mo	1888.4(2)	1025.6(1)	980.3(2)
P(1)	1178.4(5)	1489.1(4)	2842.8(8)
P(2)	3195.8(5)	1312.1(4)	2705.4(8)
Si(1)	1618.5(6)	833.9(6)	4616.3(9)
Si(2)	1701.9(6)	2577.4(5)	3255.3(10)
Si(3)	3084.2(6)	771.9(5)	4590.1(9)
Si(4)	3149.8(6)	2466.1(5)	3074.8(9)
O(1)	2006(2)	−588(1)	1508(3)
O(2)	209(2)	711(2)	−929(3)
O(3)	1746(3)	2392(2)	−672(3)
O(4)	2943(2)	614(2)	−1113(3)
C(1)	1098(3)	−37(3)	4304(4)
C(2)	1313(3)	1193(3)	6113(4)
C(3)	1095(3)	3156(2)	2025(5)
C(4)	1632(3)	2940(3)	4878(5)
C(5)	3751(3)	1165(2)	6026(4)
C(6)	3430(3)	−141(2)	4442(4)
C(7)	3444(3)	2918(2)	1650(4)
C(8)	3852(2)	2807(2)	4540(4)
C(9)	23(2)	1498(2)	2758(3)
C(10)	−446(2)	944(2)	2177(4)
C(11)	−1314(3)	910(3)	2161(4)
C(12)	−1719(3)	1428(3)	2695(5)
C(13)	−1280(3)	1979(3)	3237(4)
C(14)	−400(2)	2023(3)	3299(4)
C(15)	4264(2)	1072(2)	2433(3)
C(16)	4376(2)	446(2)	1837(3)
C(17)	5182(2)	248(2)	1632(4)
C(18)	5864(2)	669(2)	2023(4)
C(19)	5761(2)	1279(2)	2603(5)
C(20)	4969(2)	1485(2)	2825(4)
C(21)	1944(2)	4(2)	1435(4)
C(22)	819(2)	825(2)	−211(3)
C(23)	1812(3)	1935(2)	36(4)
C(24)	2559(2)	764(2)	−329(3)

TABLE 3. Bond lengths (Å) between non-hydrogen atoms, with esd's in parentheses

Bonds	Bond length (Å)
Mo—P(1)	2.598(1)
Mo—P(2)	2.585(1)
Mo—C(21)	2.029(4)
Mo—C(22)	1.978(4)
Mo—C(23)	2.014(4)
Mo—C(24)	1.959(4)
P(1)—C(9)	1.834(3)
P(2)—C(15)	1.839(3)
Si(1)—P(1)	2.271(1)
Si(2)—P(1)	2.277(1)
Si(3)—P(2)	2.285(1)
Si(4)—P(2)	2.266(1)
Si(3)—Si(1)	2.351(2)
Si(4)—Si(2)	2.365(2)
Si(1)—C(1)	1.881(5)
Si(1)—C(2)	1.869(5)
Si(2)—C(3)	1.856(5)
Si(2)—C(4)	1.875(5)
Si(3)—C(5)	1.860(4)
Si(3)—C(6)	1.863(4)
Si(4)—C(7)	1.871(4)
Si(4)—C(8)	1.869(4)
C(21)—O(1)	1.149(4)
C(22)—O(2)	1.149(4)
C(23)—O(3)	1.151(5)
C(24)—O(4)	1.152(4)
C(9)—C(10)	1.388(5)
C(10)—C(11)	1.386(5)
C(12)—C(11)	1.365(7)
C(13)—C(12)	1.347(7)
C(14)—C(13)	1.400(6)
C(9)—C(14)	1.394(5)
C(16)—C(15)	1.391(5)
C(16)—C(17)	1.396(5)
C(18)—C(17)	1.364(6)
C(18)—C(19)	1.352(6)
C(20)—C(19)	1.386(5)
C(20)—C(15)	1.384(5)

The Si—Si—C_{ax} angles (range 108.8(1)–115.9(2)°, mean 112.3°) are similar to the Si—Si—C_{eq} angles (range 111.1(1)–114.1(1)°, mean 112.5°) but the P—Si—C_{eq} angles (range 106.8(1)–107.5(1)°, mean 107.0°) differ significantly from the P—Si—C_{ax} (range 113.8(2)–117.2(1)°, mean 115.3°). The difference here is probably the result of the cross-ring repulsions of the axial methyl groups (C_5—C_8 = 3.556 Å, C_2—C_4 = 3.686 Å), which causes a mutual rotation of the Si—C_{ax} bonds away from each other, thus widening the P—Si—C_{ax} angles. Despite these changes, the C—Si—C angles (mean 108.1(8)°) are very close to those found in the free ligand (mean 108.0(2)°), and the equivalent axial and equatorial Si—C bonds (mean 1.868(25) Å) are essentially unaltered from the uncomplexed molecule (mean 1.867(3) Å). As in the free ligand, the orientation of the phenyl groups is slightly distorted, and the Si—P—C angles fall into two classes ((*i*) mean 109.5(1)° and (*ii*) mean 103.0(15)°). Nonetheless, the mean P—C (1.837(5) Å) and C—C(phenyl) (1.379(53) Å) distances and the mean C—C—C angles (120.0(26)°) are all normal.

The mean silicon–silicon distance (2.358(14) Å) is slightly longer than in the complexed molecule (2.345(3) Å) and $(SiMe_2)_6$ (2.338(6) Å) (9), the steady decrease in length along the series possibly arising from σ-hybridization changes at silicon. The mean P—Si distance (2.275(19) Å) is longer than in the uncomplexed structure (2.252(4) Å), and, even though hybridization changes would tend to accentuate the difference, the lengthening is too small to be definitely ascribed to a $p\pi$–$d\pi$ contraction in the latter. There have been several recent structural reports (3, 6, 10, 11–13) of compounds containing silicon–phos-

TABLE 4. Interbond angles (deg.) between non-hydrogen atoms, with esd's in parentheses

Bonds	Bond angles (deg)
P(2)—Mo—P(1)	78.27(3)
P(1)—Mo—C(21)	99.3(1)
P(1)—Mo—C(22)	96.2(1)
P(1)—Mo—C(23)	94.5(1)
P(1)—Mo—C(24)	171.8(1)
P(2)—Mo—C(21)	92.5(1)
P(2)—Mo—C(22)	174.4(1)
P(2)—Mo—C(23)	97.8(1)
P(2)—Mo—C(24)	94.6(1)
C(21)—Mo—C(23)	164.2(2)
C(21)—Mo—C(24)	84.9(2)
C(22)—Mo—C(21)	87.6(1)
C(22)—Mo—C(23)	83.3(2)
C(22)—Mo—C(24)	91.0(1)
C(23)—Mo—C(24)	82.4(2)
Mo—P(1)—Si(1)	108.73(5)
Mo—P(1)—Si(2)	105.62(4)
Mo—P(2)—Si(3)	110.03(4)
Mo—P(2)—Si(4)	106.61(4)
Si(2)—P(1)—Si(1)	107.77(5)
Si(4)—P(2)—Si(3)	106.79(5)
P(1)—Si(1)—Si(3)	100.67(5)
Si(4)—Si(2)—P(1)	103.46(5)
P(2)—Si(3)—Si(1)	102.46(5)
P(2)—Si(4)—Si(2)	99.49(5)
Mo—C(21)—O(1)	169.4(4)
Mo—C(22)—O(2)	178.2(3)
Mo—C(23)—O(3)	169.4(4)
Mo—C(24)—O(4)	178.9(3)
C(1)—Si(1)—C(2)	107.9(2)
C(3)—Si(2)—C(4)	108.1(2)
C(5)—Si(3)—C(6)	108.6(2)
C(8)—Si(4)—C(7)	107.8(2)
Si(3)—Si(1)—C(1)	111.3(2)
P(1)—Si(1)—C(1)	106.8(1)
Si(3)—Si(1)—C(2)	115.9(2)
P(1)—Si(1)—C(2)	113.8(2)
P(1)—Si(2)—C(3)	106.9(2)
Si(4)—Si(2)—C(3)	113.5(2)
Si(4)—Si(2)—C(4)	108.8(1)
P(1)—Si(2)—C(4)	116.2(2)
Si(1)—Si(3)—C(5)	113.6(2)
P(2)—Si(3)—C(5)	113.9(1)
P(2)—Si(3)—C(6)	106.9(1)
Si(1)—Si(3)—C(6)	111.1(1)
Si(2)—Si(4)—C(7)	114.1(1)
P(2)—Si(4)—C(7)	107.5(1)
P(2)—Si(4)—C(8)	117.2(1)
Si(2)—Si(4)—C(8)	110.9(1)
Mo—P(1)—C(9)	122.4(1)
Si(2)—P(1)—C(9)	109.5(1)
Si(1)—P(1)—C(9)	102.2(1)
Mo—P(2)—C(15)	119.6(1)
Si(4)—P(2)—C(15)	109.5(1)
Si(3)—P(2)—C(15)	103.7(1)
P(1)—C(9)—C(10)	118.4(3)
P(1)—C(9)—C(14)	122.9(3)
P(2)—C(15)—C(16)	119.1(2)
P(2)—C(15)—C(20)	122.5(3)
C(14)—C(9)—C(10)	118.7(3)
C(9)—C(10)—C(11)	120.2(4)
C(10)—C(11)—C(12)	120.4(4)
C(13)—C(12)—C(11)	120.4(4)
C(14)—C(13)—C(12)	120.8(5)
C(9)—C(14)—C(13)	119.4(4)
C(20)—C(15)—C(16)	118.4(3)
C(15)—C(16)—C(17)	120.2(3)
C(16)—C(17)—C(18)	120.0(3)
C(17)—C(18)—C(19)	120.2(3)
C(20)—C(19)—C(18)	121.0(4)
C(15)—C(20)—C(19)	120.2(3)

TABLE 4 (*Concluded*)

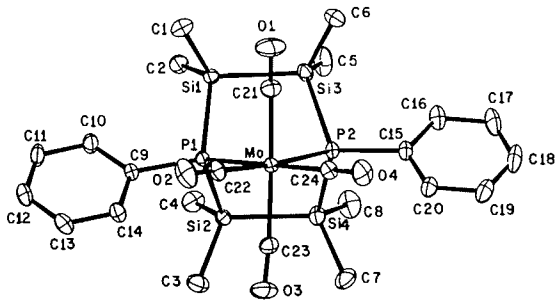

FIG. 1. An ORTEP drawing of the $(PhPSi_2Me_4)_2Mo(CO)_4$ molecule, showing the crystallographic numbering scheme used. For purposes of clarity, the hydrogen atoms have been omitted from the diagram.

TABLE 5. Mean P—Si distances observed in molecules containing silicon–phosphorus bonds

Compound	L(P—Si) (Å)	Reference
$(SiH_3)PH_2$[a]	2.249(3)	14
$(SiH_3)PHMe$[a]	2.248(3)	14
$(SiH_3)PMe_2$[a]	2.245(3)	14
$(SiH_3)_3P$[a]	2.248(3)	15
$((SiMe_3)_2PMe_2)^+(Co(CO)_4)^-$	2.292(5)	10
$(PPhHSi_2Me_4PPhH)Mo(CO)_4$	2.266(1)	3
$P_7(SiMe_3)_3$	2.288(16)	11
$P_4(SiMe_2)_3$	2.283(1)[b]	11
	2.247(1)[c]	
$(Me_2Si)_3P_4(CMe_3)_2$	2.259(2)[d]	12
	2.291(1)[e]	
$(Me_2Si)_6P_4$	2.249(1)	13
$(PhPSi_2Me_4)_2$	2.252(4)	6
$(PhPSi_2Me_4)_2Mo(CO)_4$	2.275(19)	This work

[a]By electron diffraction.
[b]Basal P—Si bonds.
[c]Apical P—Si bonds.
[d]From bridging phosphorus atoms.
[e]From non-bridging phosphorus atoms.

phorus bonds, as well as electron diffraction studies on simple silylphosphines (14, 15), and the range of P—Si bond lengths in all these molecules (see Table 5) provides no clearcut difference between the molecules containing three- and four-coordinate phosphorus atoms. The discrepancy between the apical and basal P—Si bonds in $P_4(SiMe_2)_3$ (11) and between the bonds to the bridging and non-bridging phosphorus atoms in $(Me_2Si)_3P_4(CMe_3)_2$ (12) sug-

TABLE 6. Mean P—Mo, Mo—C_{axial}, and Mo—$C_{equatorial}$ distances,[a] and carbonyl stretching frequencies[b] of some diphosphine molybdenum tetracarbonyls $L_2Mo(CO)_4$

L	L(P—Mo)	L(Mo—C_{ax})	L(Mo—C_{eq})	ν(CO) solvent	Reference
$PMe_2P(t\text{-}Bu)PMe_2$	2.497(3)	2.024(18)	1.986(62)	2023, 1934, 1908 *n*-Hexane	17
$PMe_2P_2Me_4PMe_2$	2.489(6)	2.05(2)	2.02(2)	2021, 1933, 1914, 1908 *n*-Hexane	18
$PMe_2As_2Me_4PMe_4$	2.453(7)	1.96(4)	1.94(3)	2021, 1932, 1910 *n*-Hexane	19
$PPhHSi_2Me_4PPhH$	2.550(1)	2.008(4)	1.994(4)	2016, 1934, 1912 *n*-Hexane	3, 4
$(PhPSi_2Me_4)_2$	2.598(1)[d] 2.585(1)	2.021(15)	1.959(4)[d] 1.978(4)	2016, 1909, 1888 Carbon disulphide[c]	This work
$(EtP)_5$	2.523(5)	2.012(15)	1.931(18)	2018, 1930, 1917, 1906 Cyclohexane	20
$Ph_2PCH_2PPh_2$	2.518(34)	2.04(5)	1.93(2)	2020, 1920, 1907, 1879 Dichloroethane	21

[a]In Å.
[b]In cm^{-1}.
[c]2005, 1914, and 1894 cm^{-1} in *n*-hexane (4).
[d]Mo—P and Mo—C_{eq} bond distances are given for the two *trans* pairs.

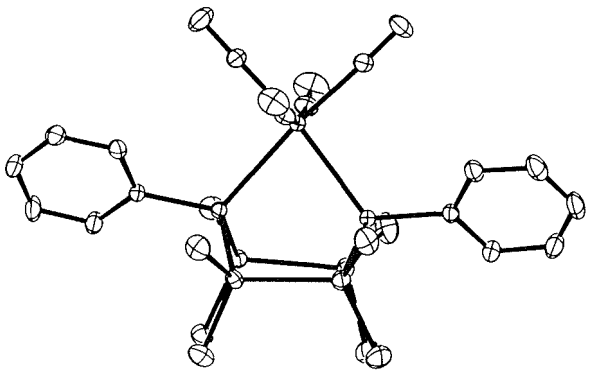

FIG. 2. An alternative view of the $(PhPSi_2Me_4)_2Mo(CO)_4$ molecule, illustrating the boat conformation of the P_2Si_4 ring. Hydrogen atoms are not shown.

gests that other factors, such as hybridization effects or non-nearest neighbour bonding, as in P_4S_3 (16), may be as important in causing bond length variations as π-donation from phosphorus to silicon.

The coordination of the $(PhPSi_2Me_4)_2$ ligand to molybdenum tetracarbonyl produces a distorted octahedral environment about the metal. The axial carbonyl groups are bent away from the perpendicular (C_{21}—Mo—C_{24} = 164.2(2)°), presumably to relieve possible steric crowding from the bulky phosphasilane ligand. Similar distortions, of varying magnitude, are observed in other diphosphine molybdenum tetracarbonyls (6, 17–21). Again as elsewhere, the axial and equatorial Mo—C bonds are of unequal length (Table 6), the shorter equatorial bonds reflecting the increased π-back-donation from the metal to the carbonyl groups *trans* to the phosphine ligand. In the case of the C—O bonds, whose lengths are less sensitive to changes in back-bonding (22), the axial and equatorial bonds are equal within experimental error.

The P—Mo bonds (mean length 2.592(15) Å)[9] are significantly longer than in other phosphine molybdenum carbonyls (2.37–2.53 Å) (6, 17–21, 23), and we believe that the lengthening, which is observed to a lesser extent in $(PhPHSi_2Me_4PPhH)Mo(CO)_4$ (3), is the result of a cumulative reduction in π-back-bonding from molybdenum to phosphorus caused by the low electronegativity of silicon and the consequent polarity of the P—Si bonds. Consistently, the carbonyl stretching frequencies of **II** are slightly but significantly lower than in related compounds (Table 6). The poorer acceptor ability of the phosphasilane ligand causes a shift of electron density from the metal into the π* levels of the carbonyl groups (2, 5).

Coordination of the $(PhPSi_2Me_4)_2$ ligand to molybdenum effectively freezes the six-membered P_2Si_4 ring into a boat conformation and, in contrast to the free ligand, whose ^1H nmr spectrum displays only averaged signals at ambient temperatures (5), the proton resonances of the axial and equatorial methyl groups are easily distinguished (Fig. 3). Both signals appear as $X_6AA'X'_6$ coupling patterns (24), and although the resolution is insufficient to allow the determination of the value of $J_{PP'}$, the appearance of the multiplets indicates that ^{31}P—^{31}P coupling in the complex **II** is considerably greater than in the ligand **I** (5).[10] As expected, electronic interactions via molybdenum are greater than through the —(Si_2Me_4)— units. The difference Δ in the ^{31}P

[9]The difference in the two Mo—P bonds (2.598(1), 2.585(1) Å) correlates well with the Mo—C_{eq} bonds *trans* to them (1.989(4), 1.978(4) Å respectively); i.e., the longer Mo—P bond is found opposite the shorter Mo—C bond, and vice versa.

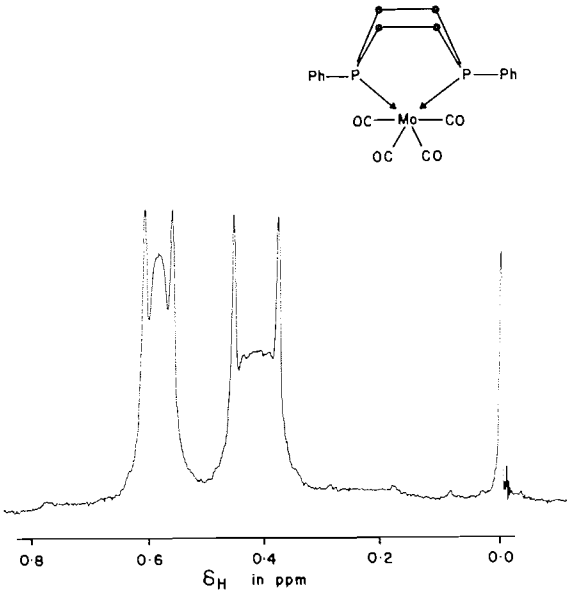

FIG. 3. The 100 MHz ^{1}H nmr spectrum $(PhPSi_2Me_4)_2Mo(CO)_4$ (phenyl region not included), illustrating the $X_6AA'X'_6$ coupling pattern of the axial and equatorial methyl groups.

chemical shifts of the free and complexed ligand[10] ($\Delta = \delta_P(\mathbf{I}) - \delta_P(\mathbf{II}) = -139.4 + 95.6 = -43.8$ ppm) is smaller than for diphos and diphos·$Mo(CO)_4$ (−67.2 ppm) (25), and is consistent with the smaller Δ values found for the more electropositive elements in the series of compounds $(Me_3E)_3PMo(CO)_5$ (E = C, Si, Ge, Sn) (26).

Acknowledgements

This work was supported by the U.S. Air Force Office of Scientific Research, (NC)-OAR, USAF Grant No. AF-AFOSR 74-2644. We thank the Natural Sciences and Engineering Research Council of Canada for a fellowship to R.T.O.

1. C. A. TOLMAN. Chem. Rev. **77**, 313 (1977).
2. (*a*) F. A. COTTON and G. WILKINSON. Advanced inorganic chemistry. 3rd ed. Interscience. 1972. p. 720; (*b*) W. D. HORROCKS, JR. and R. C. TAYLOR. Inorg. Chem. **2**, 723 (1963); (*c*) F. A. COTTON. Inorg. Chem. **3**, 702 (1964); (*d*) W. STROHMEIER and F. J. MULLER. Chem. Ber. **100**, 2812 (1967).
3. W. S. SHELDRICK and A. BORKENSTEIN. Acta Crystallogr. B**33**, 2916 (1977).
4. G. JOHANNSEN and O. STELZER. Chem. Ber. **110**, 3438 (1977).
5. R. T. OAKLEY, D. A. STANISLAWSKI, and R. WEST. J. Organomet. Chem. **157**, 389 (1978).
6. A. W. CORDES, P. F. SCHUBERT, and R. T. OAKLEY. Can. J. Chem. **57**, 174 (1979).
7. P. HANSON, F. HERMAN, J. D. LEA, and S. SKILLMAN. Acta Crystallogr. **17**, 1040 (1964).
8. F. STEWART, E. R. DAVIDSON, and W. T. SIMPSON. J. Chem. Phys. **42**, 3175 (1975).
9. H. L. CARRELL and J. DONOHUE. Acta Crystallogr. B**28**, 1566 (1972).
10. H. SCHAFER and A. G. MACDIARMID. Inorg. Chem. **15**, 848 (1976).
11. VON W. HONLE and H. G. v. SCHNEERING. Z. Anorg. Allg. Chem. **440**, 168 (1978).
12. VON W. HONLE and H. G. v. SCHNEERING. Z. Anorg. Allg. Chem. **442**, 107 (1978).
13. VON W. HONLE and H. G. v. SCHNEERING. Z. Anorg. Allg. Chem. **442**, 91 (1978).
14. C. GLIDEWELL, P. M. PINDER, A. G. ROBIETTE, and G. M. SHELDRICK. J. Chem. Soc. Dalton, 1403 (1972).
15. B. BEAGLEY, A. G. ROBIETTE, and G. M. SHELDRICK. J. Chem. Soc. A, 3002 (1968).
16. J. D. HEAD, K. A. R. MITCHELL, L. NOODLEMAN, and N. L. PADDOCK. Can. J. Chem. **55**, 669 (1977).
17. W. S. SHELDRICK. Acta Crystallogr. B**32**, 308 (1976).
18. W. S. SHELDRICK. Chem. Ber. **108**, 2242 (1975).
19. W. S. SHELDRICK. Acta Crystallogr. B**31**, 1789 (1975).
20. M. A. BUSH and P. WOODWARD. J. Chem. Soc. A, 1221 (1968).
21. K. K. CHEUNG, T. F. LAI, and K. S. MOK. J. Chem. Soc. A, 1644 (1971).
22. F. A. COTTON and R. M. WING. Inorg. Chem. **4**, 314 (1965).
23. (*a*) D. M. BRIDGES, G. C. HOLYWELL, D. W. H. RANKIN, and J. M. FREEMAN. J. Organometal. Chem. **32**, 87 (1971); (*b*) A. W. CORDES, R. D. JOYNER, R. D. SHORES, and E. D. DILL. Inorg. Chem. **13**, 132 (1974); (*c*) J. R. DELERNO, L. M. TREFONAS, M. Y. DARENSBOURG, and R. J. MAJESTE. Inorg. Chem. **15**, 816 (1976); (*d*) R. J. DOEDENS and L. F. DAHL. J. Am. Chem. Soc. **87**, 2576 (1965); (*e*) M. R. CHURCHILL and J. P. FENESSEY. Inorg. Chem. **7**, 953 (1968); (*f*) A. T. MCPHAIL, G. R. KNOX, C. G. ROBERTSON, and G. A. SIM. J. Chem. Soc. A, 205 (1971); (*g*) D. S. PAYNE, J. A. A. MOKULU, and J. C. SPEAKMAN. Chem. Commun. 599 (1965); (*h*) H. LUTH, M. R. TRUTER, and A. ROBSON. J. Chem. Soc. A, 28 (1969).
24. R. K. HARRIS. Can. J. Chem. **42**, 2275 (1964).
25. P. E. GARROU. Inorg. Chem. **14**, 1435 (1975).
26. (*a*) H. SCHUMANN, L. ROSCH, H.-J. KROTH, J. PICKARDT, H. NEUMANN, and B. NEUDERT. Z. Anorg. Allg. Chem. **430**, 51 (1977); (*b*) B. E. MANN, C. MASTERS, and B. L. SHAW. J. Chem. Soc. A, 1105 (1971).

[10] ^{1}H nmr spectrum of **II** (100 MHz, δ, $CDCl_3$, internal TMS) 0.59 (12H, multiplet (see text), separation of outermost lines = 4.6 Hz) (lit. (4), 0.50 (J_{PH} = 5.4 Hz)); 0.42 (12H, multiplet (see text), separation of outermost lines = 7.6 Hz) (lit. (4) 0.30 (J_{PH} = 8.3 Hz)). ^{31}P nmr spectrum (40.5 MHz, δ, $CDCl_3$, external H_3PO_4) −95.6 (singlet, with doublet satellites from ^{29}Si coupling, $^1J_{PSi}$ = 19.4 Hz, $^2J_{PSi}$ = 5.4 Hz) (lit. (4) δ_P = −95.6 ppm).

Excess volumes for binary liquid mixtures of butylamine with aromatic and aliphatic hydrocarbons

ABBURI KRISHNAIAH, MARIPURI SREENIVASULU, AND PULIGUNDLA R. NAIDU[1]

Department of Chemistry, College of Engineering, Sri Venkateswara University, Tirupati 517 502, India

Received December 24, 1978

ABBURI KRISHNAIAH, MARIPURI SREENIVASULU, and PULIGUNDLA R. NAIDU. Can. J. Chem. 57, 1915 (1979).

Excess volume data for binary liquid mixtures of butylamine with aromatic and aliphatic hydrocarbons were measured as a function of composition dilatometrically at 303.15 and 313.15 K. The hydrocarbons include: benzene, toluene, three isomeric xylenes, hexane, heptane, and octane. The values of V^E were found to be positive over the entire range of composition in all the eight systems at both the temperatures. The positive values were ascribed to the break-up of hydrogen bonds in the aggregates of amine by the hydrocarbons.

ABBURI KRISHNAIAH, MARIPURI SREENIVASULU et PULIGUNDLA R. NAIDU. Can. J. Chem. 57, 1915 (1979).

Faisant appel à la dilatométrie et opérant à 303.15 et à 313.15 K, on a mesuré les volumes d'excès de mélanges liquides binaires de butylamine avec des hydrocarbures aromatiques et aliphatiques. Les hydrocarbures sont: le benzène, le toluène, les trois xylènes, l'hexane, l'heptane et l'octane. On a trouvé que les valeurs V^E sont positives à toutes les compositions des huit systèmes et aux deux températures. On attribue les valuers positives au bris des liaisons hydrogène des agrégats d'amine par les hydrocarbures.

[Traduit par le journal]

Introduction

A survey of the literature has shown that few attempts have been made to study systematically the excess thermodynamic properties of binary liquid mixtures of an alkylamine with aromatic and aliphatic hydrocarbons. Excess thermodynamic properties of these binary liquid mixtures give an insight into self-association of the amine and the structure-breaking effect of hydrocarbons. Hence excess volumes of mixtures of butylamine with aromatic and aliphatic hydrocarbons have been determined at 303.15 and 313.15 K. Aromatic hydrocarbons, benzene, toluene α, and the three isomeric xylenes, form a homologous series. Hexane, heptane, and octane constitute the homologous series of aliphatic hydrocarbons. Butylamine has been chosen as a common component as it is less volatile than the lower homologues.

Experimental

Materials

Butylamine was dried over potassium hydroxide for 3 days, then refluxed for 2 h and fractionally distilled (1). The aromatic hydrocarbons were made thiophene-free as described by Vogel (2), dried over anhydrous calcium chloride, and finally fractionally distilled over metallic sodium. The column used contained 12 theoretical plates. The aliphatic hydrocarbons were purified using the methods described by Riddick and Bunger (1). The purity of the samples was checked by comparing the measured densities with those reported in literature (3, 4). The densities were determined with a bicapillary pycnometer described by Rao (5). The data are given in Table 1.

Excess Volumes

Excess volumes were determined at 303.15 and 313.15 K using a single composition per loading type dilatometer described by Rao and Naidu (6). The mixing cell contained two bulbs of different capacities and connected through a U-tube using mercury to separate the two components. The end of one bulb was fitted with a ground glass stopper and the end of another bulb was fitted with a capillary having a detachable Teflon cap with a small orifice at the top. The composition was determined directly by weighing. Four dilatometers with different capacities were used to cover the entire mole fraction range. The dilatometers were kept in a thermostat maintained at ±0.01 K. Excess volumes were accurate to ±0.003 $cm^3\ mol^{-1}$. This accuracy offered by the dilatometer was checked by comparing the measured data for the system cyclohexane + benzene with those reported in literature (7).

TABLE 1. Densities of pure component liquids

Component	T/K	Density ρ/g cm^{-3} Experimental	Literature
Butylamine	298.15	0.73452	0.73460
Benzene	303.15	0.86835	0.86836
Toluene	303.15	0.85762	0.85766
o-Xylene	303.15	0.87157	0.87161
m-Xylene	303.15	0.85566	0.85565
p-Xylene	303.15	0.85224	0.85232
Hexane	303.15	0.65018	0.65020
Heptane	303.15	0.67519	0.67520
Octane	303.15	0.69440	0.69450

[1]To whom all correspondence should be addressed.

0008-4042/79/151915-04$01.00/0

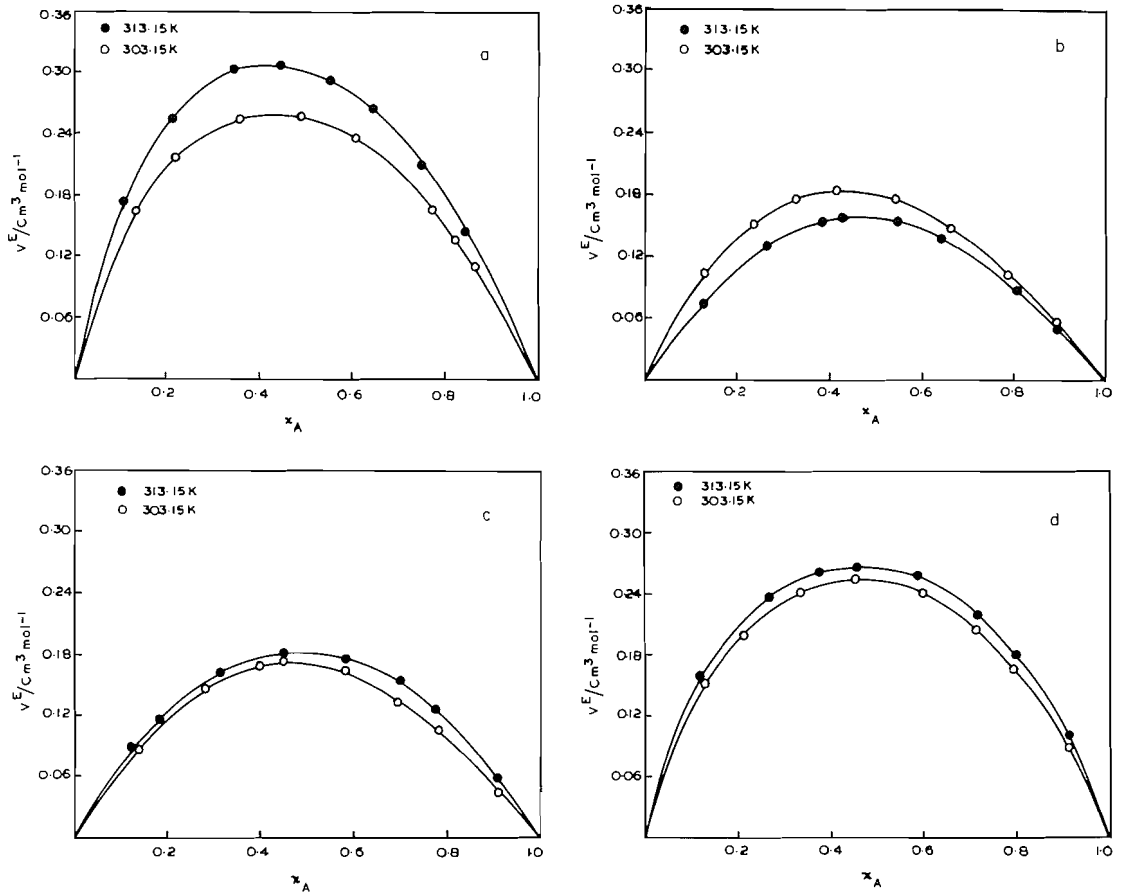

FIG. 1. The values of V^E plotted against the mole fraction x_A of butylamine for (*a*) butylamine + benzene, (*b*) butylamine + toluene, (*c*) butylamine + *o*-xylene, (*d*) butylamine + *m*-xylene.

TABLE 2. Values of the parameters of [1] for the various mixtures at 303.15 and 313.15 K along with standard deviation $\sigma(V^E)$

Mixture	T/K	a_0	a_1	a_2	$\sigma(V^E)$ / cm^3 mol^{-1}
Butylamine + benzene	303.15	1.0242	−0.3190	0.2725	0.003
Butylamine + toluene	303.15	0.7187	−0.2266	0.0057	0.002
Butylamine + *o*-xylene	303.15	0.6857	−0.1220	−0.0679	0.002
Butylamine + *m*-xylene	303.15	1.0012	−0.1680	0.3329	0.004
Butylamine + *p*-xylene	303.15	0.8074	−0.1717	0.1160	0.006
Butylamine + hexane	303.15	2.0849	−0.1431	−0.0493	0.005
Butylamine + heptane	303.15	2.3372	−0.1302	−0.4584	0.004
Butylamine + octane	303.15	3.2155	−0.4057	0.4632	0.004
Butylamine + benzene	313.15	1.2130	−0.3447	0.3270	0.003
Butylamine + toluene	313.15	0.6452	−0.0901	−0.1221	0.004
Butylamine + *o*-xylene	313.15	0.7256	−0.0246	0.0596	0.001
Butylamine + *m*-xylene	313.15	1.0527	−0.0937	0.4935	0.005
Butylamine + *p*-xylene	313.15	0.8381	−0.2108	0.1101	0.001
Butylamine + hexane	313.15	2.5930	0.1097	1.3614	0.005
Butylamine + heptane	313.15	2.6679	0.0099	1.3402	0.005
Butylamine + octane	313.15	3.7577	−0.1218	0.7592	0.005

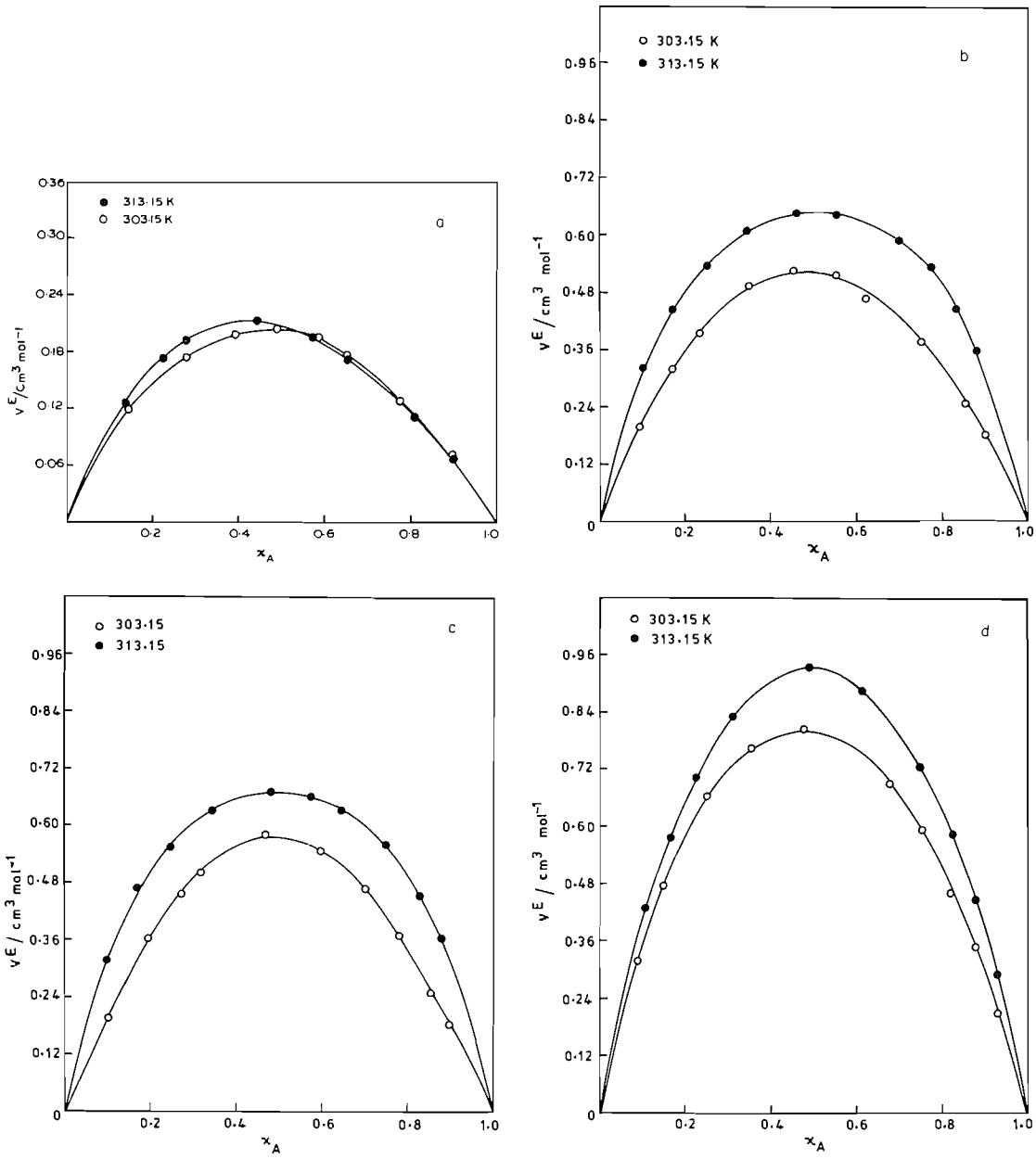

FIG. 2. The values of V^E plotted against the mole fraction x_A of butylamine for (*a*) butylamine + *p*-xylene, (*b*) butylamine + hexane, (*c*) butylamine + heptane, (*d*) butylamine + octane.

Results

Values of V^E determined for the eight systems at 303.15 and 313.15 K are graphically represented in Figs. 1 and 2. The results are fitted to the equation

$$[1] \quad V^E/\text{cm}^3\ \text{mol}^{-1} = x_A x_B[a_0 + a_1(x_A - x_B) + a_2(x_A - x_B)^2]$$

where a_0, a_1, and a_2 are adjustable parameters and x_A and x_B are the mole fractions of butylamine and hydrocarbons respectively. The parameters were evaluated by the method of least-squares. The values of the parameters along with the standard deviation $\sigma(V^E)$ are given in Table 2. Tables 3 and 4, which record the molar excess volumes of mixtures of butylamine with aromatic and aliphatic hydrocarbons at 303.15 and 313.15 K, respectively, are placed in the Depository of Unpublished Data.[2]

[2]Complete set of data may be obtained, at a nominal charge, from the Depository of Unpublished Data, CISTI, National Research Council of Canada, Ottawa, Ont., Canada K1A 0S2.

Discussion

Values of V^E are positive over the whole range of composition in the eight mixtures. The positive values may be ascribed to break-up of hydrogen bonds in hydrogen bonded aggregates of butylamine by the aromatic and aliphatic hydrocarbons. According to Schug and Chang (8), self-association of butylamine through hydrogen bonding leads to the formation of linear trimers. The addition of hydrocarbons would, therefore, be expected to depolymerize the amine trimers. This would contribute to expansion in volume. The observed values of V^E are therefore in order.

The positive excess volumes of butylamine with benzene and toluene at 298.15 K, reported by Letcher and Bayles (9) and Letcher (10) also support the contention that the self-associated amine is depolymerized by the hydrocarbons. However, the method used by these workers offered an accuracy of 0.02 $cm^3\ mol^{-1}$. Hence the data of these workers are out of line with those presented here.

Excess volumes for mixtures of butylamine with aliphatic hydrocarbons are larger than those with aromatic hydrocarbons. This may be attributed to the presence of π-electrons in the aromatic hydrocarbons. π-Electrons in the aromatic hydrocarbons may lend themselves for the formation of weak NH---π complexes. This interaction may mitigate the expansion in volume resulting due to depolymerization.

There is no regular trend between excess volume and temperature in the mixtures of butylamine with aromatic hydrocarbons. The temperature coefficient of V^E is positive in the mixtures of amine with benzene, and the three xylenes. The coefficient is negative in mixtures of butylamine with toluene. However, the trend between V^E and temperature is regular in the mixtures of amine with aliphatic hydrocarbons. The three mixtures have a positive temperature coefficient for V^E.

1. J. A. RIDDICK and W. B. BUNGER. Organic solvents. Wiley-Interscience, New York. 1970.
2. A. VOGEL. Practical organic chemistry. Longman Green and Co., London. 1968.
3. J. TIMMERMAN. Physico-chemical constants of pure-organic compounds. Elsevier, New York. 1950.
4. A. WEISSBERGER, E. S. PROKSAUER, J. A. REDDICK, and E. E. TROOPS, JR. Techniques of organic chemistry. Vol. VII. Interscience, New York. 1957.
5. M. V. P. RAO and P. R. NAIDU. Can. J. Chem. **52**, 788 (1974).
6. M. V. P. RAO. Ph.D. Thesis. Sri Venkateswara University, India. 1974.
7. R. L. STOKES, B. J. LEVIEN, and K. N. MARSH. J. Chem. Thermodyn. **2**, 43 (1970).
8. J. C. SCHUG and W. E. CHANG. J. Phys. Chem. **75**, 938 (1971).
9. T. M. LETCHER and J. W. BAYLES. J. Chem. Eng. Data, **16**, 266 (1970).
10. T. M. LETCHER. J. Chem. Thermodyn. **4**, 159 (1972).

Determination of solubility products of hydroxylapatite, chlorapatite, and their solid solutions

T. S. B. NARASARAJU, K. K. RAO, AND U. S. RAI

Department of Chemistry, Banaras Hindu University, Varanasi-221005, India

Received November 28, 1978

T. S. B. NARASARAJU, K. K. RAO, and U. S. RAI. Can. J. Chem. 57, 1919 (1979).

Solubility equilibria of hydroxylapatite, chlorapatite, and a series of their solid solutions were investigated at 37°C in the pH range 4.25 to 7.40 and their solubility products evaluated. Proof could be obtained for their stoichiometric dissolution.

T. S. B. NARASARAJU, K. K. RAO et U. S. RAI. Can. J. Chem. 57, 1919 (1979).

Opérant à 37°C et à des pH allant de 4.25 à 7.40, on a étudié les équilibres de solubilité de l'hydroxylapatite, de la chloroapatite et d'une série de leurs solutions solides et on a déterminé leurs produits de solubilité. On a pu obtenir une preuve concernant leur dissolution stoechiométrique.

[Traduit par le journal]

Introduction

It is well known that hydroxylapatite (OHAp), $Ca_{10}(PO_4)_6(OH)_2$, a constituent (1) of human bones and teeth, and chlorapatite (ClAp), $Ca_{10}(PO_4)_6Cl_2$, belong to an isomorphous series (2, 3) of compounds and are therefore capable of forming solid solutions. The presence of a large excess of chloride ions in the body fluids enables the formation of such solid solutions at the bone/body-fluid interface. An investigation of the dependence of the solubility product of such samples on their chloride content is of extensive biological significance from the point of view of calcification and resorption and hence the present studies were undertaken.

Experimental

While OHAp was obtained by a wet method (4) the rest of the samples were prepared by an appropriate solid state reaction (5) using OHAp and $CaCl_2$ as starting materials. The samples were characterized through chemical, X-ray, electron microscopic, infrared, and thermal analyses as reported earlier (4–6). The solubility product of each sample was determined at the biologically significant temperature of 37°C by analyses of their saturated solutions, the pH of the dissolving medium being varied in the pH range 4.25 to 7.40 using suitable buffer combinations. The experimental details for the equilibration of the samples to prepare their saturated solutions and to separate them from the likely colloidal component of the solute were reported elsewhere (7–9). From the saturated solutions so prepared calcium was determined complexometrically (10) while phosphate and chloride were estimated spectrophotometrically (11, 12), separate aliquots being taken each time.

Results and Discussion

In Table 1 are included a few representative sets of results on the determination of the solubility products of OHAp, ClAp, and nine of their solid solutions. For each sample at a given pH, from which the OH^- ion concentration was calculated and given in column 6, the experimentally determined concentrations of calcium, phosphorus, and chloride are given in columns 3 to 5. In order to scrutinize the stoichiometric dissolution of the samples, the g atom ratios, Ca/P, are reported in column 8 of the table. Adopting a method of calculation reported earlier (9), the total phosphorus, given in column 4, was subdivided into undissociated orthophosphoric acid and its dissociation products, using its three dissociation constants (13–15) and the final pH of the saturated solution given in column 2 of the table. For the sake of brevity all these subdivided values are not included in the table. However, the concentrations of PO_4^{3-} needed to calculate the ionic product, K_{ip}, of the samples are reported in column 7 while the values of the pK_{ip}'s, $(-\log K_{ip})$ and their averages are given in columns 9 and 10 respectively. Based on a series of determinations of each of these values, it could be concluded that the error limits involved did not exceed $\pm 1\%$.

The medium of dissolution adopted in the present investigations consisted of buffer (9) combinations of desired pH maintained at a molarity of 0.165 with respect to sodium nitrate in order to keep the ionic strength during dissolution virtually constant. To overcome the inaccuracy involved in the evaluation of the activity coefficients of the dissolved ionic species of these systems, La Mer (16) suggested that an aqueous solution of 0.165 *M* sodium chloride, a solvent of biological importance, may be considered as a standard solvent of reference in which all the activity coefficients may be assigned a value of unity. Since the use of sodium chloride is not permissible

0008-4042/79/151919-04$01.00/0

TABLE 1. Solubility product of hydroxylapatite, chlorapatite, and their solid solutions

S. No.	Final pH	Measured conc. (g atoms/L) [Ca] ($\times 10^3$)	[P] ($\times 10^3$)	[Cl] ($\times 10^4$)	Calculated conc. (g ions/L) $[OH^-]$ ($\times 10^7$)	$[PO_4^{3-}]$ ($\times 10^{11}$)	g atom ratio Ca/P	pK_{ip}*	Average pK_{ip}
				Solute: $Ca_{10}(PO_4)_6(OH)_2$					
1	4.92	8.42	4.830	—	0.0083	0.099	1.74	110.9	
2	5.00	6.59	3.910	—	0.0100	0.166	1.68	111.4	
3	5.15	5.49	3.350	—	0.0141	0.198	1.64	110.5	
4	5.35	5.37	1.950	—	0.0223	0.287	1.73	111.3	
5	5.57	2.15	1.300	—	0.0371	0.523	1.65	111.2	110.6
6	5.95	1.30	0.810	—	0.0891	1.810	1.61	109.4	
7	6.15	0.81	0.490	—	0.1410	2.650	1.67	110.1	
8	7.20	0.12	0.070	—	1.5800	24.400	1.80	110.5	
9	7.45	0.08	0.044	—	2.8200	37.200	1.80	110.7	
				Solute: $Ca_{10}(PO_4)_6(OH)_{1.8}Cl_{0.2}$					
10	4.90	7.21	4.28	1.41	0.0079	0.080	1.68	111.1	
11	5.05	5.34	3.18	1.12	0.0112	0.119	1.68	111.2	
12	5.25	3.82	2.39	0.78	0.0178	0.223	1.60	110.6	
13	5.45	2.32	1.46	0.51	0.0282	0.341	1.60	111.4	111.0
14	5.58	1.87	1.13	0.26	0.0380	0.477	1.64	111.3	
15	5.95	1.02	0.62	0.20	0.0891	1.389	1.65	110.5	
16	6.20	0.61	0.37	0.14	0.1580	2.440	1.66	110.8	
				Solute: $Ca_{10}(PO_4)_6(OH)_{1.6}Cl_{0.4}$					
17	4.85	6.86	4.06	2.88	0.0071	0.061	1.69	111.0	
18	5.05	5.19	3.13	2.27	0.0112	0.117	1.65	110.2	
19	5.15	3.70	2.23	1.52	0.0141	0.132	1.66	111.3	
20	5.40	2.22	1.36	0.92	0.0251	0.253	1.63	111.5	111.3
21	5.55	1.75	1.11	0.76	0.0355	0.410	1.58	111.1	
22	5.80	0.96	0.55	0.40	0.0631	0.630	1.75	112.3	
23	6.10	0.55	0.32	0.23	0.1260	1.420	1.70	112.2	
				Solute: $Ca_{10}(PO_4)_6(OH)_{1.4}Cl_{0.6}$					
24	4.88	4.990	3.010	2.99	0.0076	0.052	1.66	111.6	
25	5.00	3.590	2.200	2.42	0.0160	0.065	1.64	112.5	
26	5.40	2.150	1.270	1.35	0.0251	0.236	1.69	110.8	
27	5.50	1.680	1.040	0.99	0.0316	0.304	1.62	111.2	111.6
28	5.75	0.920	0.550	0.56	0.0562	0.501	1.67	112.3	
29	6.10	0.550	0.307	0.31	0.1260	1.350	1.79	111.6	
30	7.25	0.078	0.046	0.04	1.7800	20.400	1.69	111.9	
				Solute: $Ca_{10}(PO_4)_6(OH)_{1.2}Cl_{0.8}$					
31	4.70	4.89	2.89	3.85	0.0050	0.022	1.69	113.0	
32	4.90	3.49	2.08	2.78	0.0079	0.039	1.68	113.0	
33	5.20	2.12	1.25	1.68	0.0158	0.093	1.69	112.5	
34	5.45	1.60	0.91	1.27	0.0282	0.120	1.76	111.4	112.3
35	5.75	0.85	0.53	0.67	0.0562	0.487	1.60	111.8	
36	6.10	0.54	0.29	0.43	0.1260	1.270	1.84	111.1	
37	7.15	0.08	0.04	0.06	1.4100	13.400	1.81	112.7	
38	7.40	0.05	0.03	0.04	2.5100	21.200	1.71	113.3	
				Solute: $Ca_{10}(PO_4)_6(OH)_{1.0}Cl_{1.0}$					
39	4.65	4.74	2.84	4.62	0.0045	0.017	1.67	112.6	
40	4.83	3.37	2.00	3.52	0.0068	0.027	1.68	112.9	
41	5.15	2.00	1.19	1.98	0.0141	0.070	1.68	112.5	
42	5.30	1.50	0.87	1.43	0.0199	0.162	1.72	111.5	112.3
43	5.70	0.83	0.52	0.78	0.0501	0.376	1.64	111.8	
44	6.00	0.52	0.31	0.49	0.1000	0.863	1.68	111.6	
45	7.10	0.07	0.04	0.08	1.2600	11.100	1.72	113.2	

TABLE 1 (*Concluded*)

S. No.	Final pH	Measured conc. (g atoms/L) [Ca] ($\times 10^3$)	[P] ($\times 10^3$)	[Cl] ($\times 10^4$)	Calculated conc. (g ions/L) [OH^-] ($\times 10^7$)	[PO_4^{3-}] ($\times 10^{11}$)	g atom ratio Ca/P	pK_{ip}*	Average pK_{ip}
				Solute: $Ca_{10}(PO_4)_6(OH)_{0.8}Cl_{1.2}$					
46	4.55	4.64	2.73	5.80	0.0035	0.010	1.70	112.7	
47	4.75	3.34	1.92	3.92	0.0056	0.018	1.74	112.7	
48	5.10	1.90	1.12	2.30	0.0126	0.053	1.69	112.4	
49	5.30	1.40	0.79	1.60	0.0199	0.093	1.77	112.2	112.5
50	5.65	0.87	0.50	1.03	0.0446	0.293	1.73	111.3	
51	5.90	0.54	0.32	0.59	0.0794	0.581	1.68	111.6	
52	7.30	0.047	0.03	0.048	1.9900	14.500	1.72	114.0	
				Solute: $Ca_{10}(PO_4)_6(OH)_{0.6}Cl_{1.4}$					
53	4.40	4.490	2.650	6.00	0.0025	0.005	1.69	113.6	
54	4.55	3.220	1.810	4.52	0.0035	0.007	1.77	114.3	
55	5.05	1.850	1.100	2.31	0.0112	0.041	1.68	112.1	
56	5.25	1.350	0.760	1.69	0.0178	0.071	1.77	112.1	112.8
57	5.60	0.820	0.480	1.10	0.0398	0.224	1.69	111.3	
58	5.90	0.470	0.290	0.62	0.0794	0.523	1.63	111.7	
59	6.95	0.071	0.043	0.096	0.8910	6.480	1.67	113.9	
60	7.30	0.047	0.028	0.056	1.9900	14.500	1.72	113.7	
				Solute: $Ca_{10}(PO_4)_6(OH)_{0.4}Cl_{1.6}$					
61	4.25	4.370	2.59	6.62	0.0018	0.0024	1.68	114.3	
62	4.50	3.070	1.76	4.52	0.0032	0.0052	1.75	113.9	
63	4.90	1.700	1.03	2.44	0.0079	0.0194	1.64	113.4	
64	5.20	1.300	0.77	1.89	0.0158	0.0571	1.69	111.8	113.5
65	5.80	0.450	0.27	0.70	0.0631	0.3140	1.64	112.4	
66	6.90	0.070	0.04	0.10	0.7940	5.8600	1.73	114.2	
67	7.22	0.045	0.03	0.07	1.6600	10.4000	1.73	114.3	
				Solute: $Ca_{10}(PO_4)_6(OH)_{0.2}Cl_{1.8}$					
68	4.25	4.20	2.47	6.82	0.0018	0.0023	1.70	113.2	
69	4.50	2.99	1.71	5.01	0.0032	0.0051	1.75	112.8	
70	4.80	1.65	0.98	2.85	0.0063	0.0116	1.68	113.7	
71	5.06	1.25	0.71	1.78	0.0115	0.0279	1.75	112.9	113.3
72	5.40	0.70	0.41	1.18	0.0251	0.0756	1.72	113.1	
73	5.70	0.46	0.27	0.76	0.0501	0.2000	1.68	112.7	
74	6.90	0.07	0.04	0.10	0.7940	4.9500	1.65	114.2	
75	7.20	0.05	0.03	0.06	1.5800	9.8100	1.81	114.1	
				Solute: $Ca_{10}(PO_4)_6Cl_{2.0}$					
76	4.30	2.70	1.55	5.08	0.0020	0.0018	1.74	114.7	
77	4.50	1.50	0.94	2.84	0.0032	0.0028	1.60	116.7	
78	5.10	0.75	0.50	1.46	0.0126	0.0233	1.57	114.7	
79	5.40	0.45	0.27	0.93	0.0251	0.0510	1.64	115.3	115.4
80	5.55	0.37	0.21	0.71	0.0355	0.0774	1.78	115.2	
81	6.10	0.17	0.11	0.37	0.1260	0.4960	1.50	115.0	
82	7.10	0.04	0.03	0.09	1.2600	6.5500	1.71	115.0	
83	7.40	0.03	0.02	0.05	2.5700	10.6000	1.71	116.5	

*$pK_{ip} = -\log [Ca^{2+}]^{10}[PO_4^{3-}]^6[X^-]^2$ where $[X^-] = [Cl^-] + [OH^-]$.

in these systems sodium nitrate was made use of and the ionic product of the samples calculated were taken as the solubility products.

The solubilities of the samples were characterized by a marked increase with increasing hydrogen ion concentration of the medium of dissolution. It is evident that in a saturated aqueous solution of OHAp the following equilibrium is established:

[1] $Ca_{10}(PO_4)_6(OH)_2 \rightleftharpoons 10Ca^{2+} + 6PO_4^{3-} + 20H^-$

Among the products of dissolution PO_4^{3-} and OH^- are capable of participating in a few more simultaneous pH-dependent equilibria as shown below:

[2] $PO_4^{3-} + H_3O^+ \rightleftharpoons HPO_4^{2-} + H_2O$

[3] $HPO_4^{2-} + H_3O^+ \rightleftharpoons H_2PO_4^- + H_2O$

[4] $H_2PO_4^- + H_3O^+ \rightleftharpoons H_3PO_4 + H_2O$

[5] $OH^- + H_3O^+ \rightleftharpoons 2H_2O$

A shift from left to right occurs in all the above

equilibria when H_3O^+ ion concentration is increased. While all these equilibria are collectively responsible for influencing equilibrium [1], those in which PO_4^{3-} (reaction [2]) and OH^- ions (reaction [5]) participate are naturally more dominant. Analogous to the equilibria operative in the case of OHAp as mentioned above, a saturated solution of ClAp is characterized by the following equilibrium in addition to those given in reactions [2] to [4]:

[6] $Ca_{10}(PO_4)_6(Cl_2) \rightleftharpoons 10Ca^{2+} + 6PO_4^{3-} + 2Cl^-$

The above arguments are substantiated by the observed fact that the calculated proportions of PO_4^{3-} ions, given in column 7 of Table 1, decreased with an increase in the hydrogen ion concentration of the medium of dissolution. The marked pH-dependence of the solubilities of OHAp and its solid solutions with ClAp can thus be accounted for.

It could be shown (17) that the free energy of dissolution of an ionic crystal is dependent on ionic replacement since the latter brings about a change in the lattice energy. The lattice energy of ClAp being higher than that of OHAp can account for the diminution in the solubility of the former over that of the latter and also for the observed systematic reduction in the solubility of the solid solutions with an increase in the Cl^- content. In addition, the non-availability of OH^- ions as products of dissolution in the case of ClAp indicates that equilibrium [5] has no effect on its dissolution. Further, Cl^- ions produced due to dissolution of ClAp remain unaffected due to the absence of their tendency to associate with H_3O^+ ions consequent upon the high dissociation of hydrochloric acid. Such an additional consideration could be advanced to account for the low solubilities of ClAp and their solid solutions.

An explanation which can be applied exclusively to the lower solubilities of the solid solutions over that of OHAp is based on the structural considerations as was shown by Young *et al.* (18). According to them an important feature of the structure of apatite, $Ca_{10}(PO_4)_6X_2$, is the occurrence of the X^- ions in columns or linear chains, coincident with its six-fold screw (6_3) axis, where X can be, among others, F^-, Cl^-, and OH^- or a combination of them. It could be established (19, 20) through infrared spectral studies that the OH^- and Cl^- ions, constituting the lattice of a solid solution of OHAp and ClAp, are linked through hydrogen bonding. The hindrance caused to the diffusion of the OH^- ions through the X^- ion column can be a factor in reducing the solubility of the solid solutions since the X^- ion column offers itself as the most vulnerable point (21, 22) for the diffusion of the ions located in the column into the medium of dissolution.

It is evident that the pK_{ip} values and the g atom ratio, Ca/P, of the samples, reported in Table 1 provide unambiguous evidence for the stoichiometric dissolution of the samples. Arguments in favour of such a theoretically favoured stoichiometric dissolution were advanced independently by Clark (23), Moreno *et al.* (24), and Wier *et al.* (25). Based on the fundamental thermodynamic concepts (17) applicable to the dissolution of ionic crystals, it could be concluded from the present investigations that the free energy of solution of the compounds is a linear function of the Cl content.

Acknowledgements

The authors thank Professor O. P. Malhotra, former Head, Chemistry Department, Banaras Hindu University, for encouragement and provision of facilities. Financial assistance given to one of us (U.S.R.) by UGC (India) is also gratefully acknowledged.

1. A. S. Posner. *In* Phosphorus and its compounds. Vol. II. *Edited by* J. R. Van Wazer. Interscience Publishers, Inc., New York, NY. 1961. p. 1429.
2. H. Bourne Geoffrey. The biochemistry and physiology of bone. Academic Press Inc., New York, NY. 1956. p. 161.
3. Gmelin's Handbuch Der Anorganischem Chemie 8. Auflaga Calcium: Teil B-Lieferung 3, Verlag Chemie, GMBH Germany. 1961. p. 1146.
4. T. S. B. Narasaraju, R. P. Singh, and V. L. N. Rao. J. Inorg. Nucl. Chem. **34**, 2072 (1972).
5. D. C. Oshea, M. L. Bartlett, and R. A. Young. Arch. Oral Biol. **19**, 995 (1974).
6. T. S. B. Narasaraju, R. P. Singh, K. K. Rao, and B. K. Kapoor. Indian J. Chem. **14A**, 904 (1976).
7. T. S. B. Narasaraju, N. S. Chickerur, and R. P. Singh. J. Inorg. Nucl. Chem. **33**, 3194 (1971).
8. N. S. Chickerur, R. P. Singh, and T. S. B. Narasaraju. Naturwissenschaften, **56**, 282 (1969).
9. T. S. B. Narasaraju, K. K. Rao, U. S. Rai, and B. K. Kapoor. Indian J. Chem. **14A**, 1014 (1977).
10. R. P. Singh, N. S. Chickerur, and T. S. B. Narasaraju. Z. Anal. Chem. **237**, 117 (1968).
11. T. S. B. Narasaraju and V. L. N. Rao. Z. Anal. Chem. **258**, 365 (1972).
12. J. S. Swain. Chem. Ind. May 26, 418 (1956).
13. L. F. Nims. J. Am. Chem. Soc. **56**, 1110 (1934).
14. L. F. Nims. J. Am. Chem. Soc. **55**, 1946 (1933).
15. C. E. Vanderzee and A. S. Quist. J. Phys. Chem. Ithaca, **65**, 118 (1961).
16. V. K. La Mer. J. Phys. Chem. **66**, 973 (1962).
17. D. L. Leussing. *In* Treatise on analytical chemistry. Part I. *Edited by* I. M. Kolthoff, P. J. Elving, and E. B. Sandell. The Interscience Encyclopaedia Inc., New York, NY. 1959. p. 675.
18. R. A. Young, W. Vander Lugt, and J. C. Elliot. Nature, **223**, 739 (1969).
19. R. A. Young. J. Dent. Res. **53**, 193 (1974).
20. E. Dykes and J. C. Elliot. Celcif. Tissue Res. **7**, 241 (1971).
21. G. Montel. C.R. Acad. Sci. Paris, **253**, 468 (1961).
22. G. Montel. Bull. Soc. Chim. Fr. 1693 (1968).
23. J. S. Clark. Can. J. Chem. **33**, 1696 (1955).
24. E. C. Moreno, T. M. Gregorry, and W. E. Brown. J. Res. Natl. Bur. Stand. Sect. A, **72**, 773 (1968).
25. D. R. Wier, S. H. Chien, and C. A. Black. Soil Sci. **111**, 107 (1971).

Photolysis of diarylcadmium compounds in benzene

A. M. OSMAN, AHMED I. KHODAIR,[1] A. A. ABDEL-WAHAB, AND A. M. EL-KHAWAGA

Chemistry Department, Assiut University, Assiut, Egypt

Received January 11, 1979

A. M. OSMAN, AHMED I. KHODAIR, A. A. ABDEL-WAHAB, and A. M. EL-KHAWAGA. Can. J. Chem. 57, 1923 (1979).

Photochemical decomposition of selected diarylcadmium compounds in dilute benzene solutions was investigated. This reaction was found to involve initial cleavage of the aryl–cadmium bonds followed by coupling of the aryl radicals to give symmetrical biaryls in good yields. Arylation products were obtained in only 5–25% yields, in contrast with the photolysis of iodoaromatic compounds in benzene which gives arylation products in high yields. Diarylcadmium compounds derived from polynuclear aromatic compounds, e.g. di(*p*-biphenyl)-cadmium and di(α-naphthyl)cadmium gave, under the same conditions, predominantly hydrogen transfer products. In carbon tetrachloride, photolysis of diarylcadmium compounds gave chloroarenes in high yields.

A. M. OSMAN, AHMED I. KHODAIR, A. A. ABDEL-WAHAB et A. M. EL-KHAWAGA. Can. J. Chem. 57, 1923 (1979).

On a étudié la décomposition photochimique, en solutions benzéniques diluées, de composés diarylcadmium choisis. On a trouvé que cette réaction implique une rupture initiale des liaisons aryl–cadmium suivie par un couplage des radicaux aryles qui conduit aux byaryles symétriques avec de bons rendements. On a obtenu des produits d'arylation qu'avec des rendements de 5 à 25% alors que la photolyse de composés iodo aromatiques dans le benzène conduit aux produits d'arylation avec de bons rendements. Soumis aux mêmes conditions, les composés diaryl-cadmium issus de composés aromatiques polycondensés comme le di(*p*-biphényl) cadmium et le di(α-naphthyl) cadmium fournissent principalement des produits de transfert d'hydrogène. Dans le tétrachlorure de carbone, la photolyse de composés diaryl-cadmium conduit à des chloroarènes avec de bons rendements.

[Traduit par le journal]

Introduction

Although photolytic studies on organometallic compounds received considerable attention (1), apparently photolysis of organocadmium compounds has not been investigated yet. Recent research from our laboratories (2) explored the potentialities of these compounds as useful synthetic intermediates. In extension of these studies we investigated the photolytic decomposition of selected diarylcadmium. compounds in dilute solutions.

Results and Discussion

The required cadmium reagents were prepared from the corresponding Grignard reagents and dilute solutions (2 m*M*) were photolysed in a Vycor glass cell using a Mineralight low pressure mercury arc. The solutions were irradiated for 100 h with continuous stirring and the products were identified by direct comparison with authentic samples and estimated by quantitative gas–liquid chromatography. The results are shown in Table 1.

Photolysis of diphenylcadmium in dilute benzene solution gave only biphenyl in 75% yield. No other products could be detected by glc, similar photolysis of dibenzylcadmium gave dibenzyl in 80% yield along with small amounts of diphenylmethane (5%). Di(*p*-tolyl)cadmium afforded *p*,*p*′-bitolyl in 60% yield together with *p*-methylbiphenyl in 15% yield. Photolysis of di(*p*-anisyl)cadmium behaved similarly, but no appreciable amount of the arylation product (*p*-methoxybiphenyl) could be detected.

The results presented above may be accounted for by a sequence involving initial cleavage of the aryl–cadmium bonds followed by dimerisation of the aryl radical with side reaction involving arylation as follows:

$$\mathrm{Ar{-}Cd{-}Ar} \longrightarrow 2\mathrm{Ar}^{\cdot} + \mathrm{Cd}$$

$$2\mathrm{Ar}^{\cdot} \longrightarrow \mathrm{Ar{-}Ar} \qquad \text{Major reaction}$$

$$\mathrm{Ar}^{\cdot} + \bigcirc \xrightarrow{-\mathrm{H}^{\cdot}} \mathrm{Ar{-}}\bigcirc \qquad \text{Minor reaction}$$

That the initial step involves formation of an aryl free radical is supported by trapping this radical via halogen or hydrogen abstraction. Thus photolysis of dilute solutions of the above mentioned compounds in carbon tetrachloride gave chloroarenes in high yield (cf. Exps. 7–10, Table 1). Only small amounts of the coupling products were observed. Similar photolysis in chloroform afforded predominantly

[1]Present address: Department of Chemistry, Faculty of Science, Suez Canal University, Ismailia, Egypt.

0008-4042/79/151923-03$01.00/0

TABLE 1. Photolysis of diarylcadmium in benzene, carbon tetrachloride, and chloroform

			Products					
Exp.	Diarylcadmium	Solvent	Coupling products	%yield*	Arylation products	%yield	Abstraction products	%yield
1	Diphenylcadmium	Benzene	Biphenyl	75	—	—	—	—
2	Di(*p*-tolyl)cadmium	Benzene	*p*-Ditolyl	65	*p*-Methylbiphenyl	15	Toluene	Trace
3	Dibenzylcadmium	Benzene	Dibenzyl	80	Diphenylmethane	5	—	—
4	Di(*p*-anisyl)cadmium	Benzene	*p*-Dianisyl	55	—	—	Anisole	Trace
5	Di(α-naphthyl)cadmium	Benzene	—	—	—	—	Naphthalene	50
6	Di(*p*-biphenyl)cadmium	Benzene	—	—	Terphenyl	25	Biphenyl	65
7	Diphenylcadmium	CCl_4	Diphenyl	15	—	—	Chlorobenzene benzene	73.3 Trace
8	Di(*p*-tolyl)cadmium	CCl_4	*p,p'*-Ditolyl	19	—	—	*p*-Chlorotoluene toluene	70.0 Trace
9	Di(α-naphthyl)cadmium	CCl_4	—	—	—	—	α-Chloronaphthalene Naphthalene	66.0 16.0
10	Dibenzylcadmium	CCl_4	Dibenzyl	10	—	—	Benzyl chloride	70.0
11	Diphenylcadmium	$CHCl_3$	Diphenyl	11	—	—	Benzene Chlorobenzene	70.0 2.0
12	Di(*p*-tolyl)cadmium	$CHCl_3$	*p,p'*-Ditolyl	10	—	—	Toluene	74.0
13	Di(*p*-anisyl)cadmium	$CHCl_3$	—	—	—	—	Anisole	80.0
14	Di(*p*-chlorophenyl)-cadmium	$CHCl_3$	—	—	—	—	Chlorobenzene	70.0
15	Di(B-phenylethyl)-cadmium	$CHCl_3$	—	—	—	—	Ethylbenzene	80.0
16	Di(*p*-biphenyl)cadmium	$CHCl_3$	—	—	—	—	Diphenyl	80.0

*All yields shown above are overall yields calculated on the basis of 1 mol bromoarene yielding ½ mol of coupling product or 1 mol of either arylation or abstraction products.

hydrogen abstraction products (cf. Exps. 11–16, Table 1).

It is of interest to note that no rearrangement of the initially formed radical occurred as coupling and chlorine abstraction took place at the position where the cadmium atom was originally linked to the aromatic nucleus.

Photolysis of diarylcadmium derived from polynuclear aromatic compounds behaved somewhat differently. Irradiation of di(*p*-biphenyl)cadmium in dilute benzene solutions under the usual conditions gave biphenyl in 65% yield together with *p*-terphenyl (25% yield). The coupling product *p*-tetraphenyl could not be detected by glc or tlc. The preference of hydrogen abstraction over arylation of benzene by the biphenyl radical in spite of the fact that the concentration factor could be attributed to the relative stability of the biphenyl radical which permits it to live long enough to find the hydrogen donor. Similar results were reported earlier (3). Similar photolysis of di(α-naphthyl)cadmium yielded only naphthalene and no coupling or arylation products were formed. These results complement those reported earlier by Razuvaev and Petukhov (4) on the photolysis of di(α-naphthyl)mercury who attributed the formation of naphthalene to disproportionation of the initially formed naphthyl radical. In our case, however, the fact that some of the ether inevitably remained in solution during the preparation of the organocadmium compounds may be responsible for at least some of the hydrogen transfer to the aryl radicals.

These results demonstrate the high potential of this procedure as a synthetic tool for synthesis of symmetrical biaryls.

Experimental

Physical Measurements

Distillations were done through a 2-ft simple Podbielniak-type column, and gas chromatography was done with an Aerograph (Hi-Fi) model 600 D equipped with a flame ionisation detector and an integrating recorder. Photolyses were carried out in a cell made of Vycor glass and irradiated with a Mineralight low pressure cold cathode mercury arc. Melting points were determined on a Kofler melting point apparatus and are uncorrected.

Photolysis of Diarylcadmium Compounds (General Procedure)

Diarylcadmium compounds were prepared from the corresponding Grignard reagents according to the published procedure (5). In a typical run, 0.006 g-atom of magnesium turnings were placed in a three-necked flask and a solution of 0.006 mol of the bromoarene in 50 mL dry ether was added dropwise while stirring. After the complete dissolution of magnesium, the contents of the flask were refluxed for 10 min, cooled, and 0.65 g (0.003 mol) of anhydrous cadmium chloride was added. The reaction mixture was refluxed till it gave a negative Gilman test (5). The ether was evaporated by distillation on a water bath maintained at 60°C till dryness and the produced cadmium compound was dissolved in the required solvent (benzene, carbon tetrachloride, or chloroform) and diluted to the proper concentration (2 m*M* solution).

A 100 mL of this solution was placed in the photolysis cell which was equipped with reflux condenser protected with a drying tube. This solution was irradiated, with continuous stirring, for 100 h, at the end of which the content of the cell was quantitatively transferred after filtration into a 100 mL flask. The products were then identified and estimated by gas liquid chromatography (using 8 ft × 1/8 in. SE 30 column at 100°C or 160°C). The results are presented in Table 1.

In case of photolysis of di(*p*-anisyl)cadmium in benzene, evaporation of the solvent left a solid residue which, when chromatographed using a 60 × 1 cm column packed with basic alumina, gave 0.2 g (50% yield) of *p,p'*-dianisyl from 60–80°C petroleum ether – benzene mixture (3:2), mp 170°C, lit. (6) mp 171–172°C.

Preparation of Authentic Samples

Diphenylmethane

From benzyl chloride and benzene, in the presence of amalgamated aluminium turnings (7), diphenylmethane was obtained in 50% yield, mp 25°C, lit. (7) mp 25–26°C.

Ethylbenzene

Acetophenone was converted to ethylbenzene according to the published procedure (7) in 60% yield, bp and reported bp 135–136°C.

p-*Chlorotoluene*

p-Chlorotoluene was prepared from *p*-toluidine via Sandmeyer's reaction (8) in 83% yield, bp 160°C, lit. (8) bp 158°C.

α-*Chloronaphthalene*

Starting with α-naphthylamine and with applying Sandmeyer's reaction (8), α-chloronaphthalene was collected (65% yield) at 106°C/13 mm Hg, lit. (6) bp 105°C/13 mm Hg.

1. (*a*) N. Prileshajeva and A. Terinin. Trans. Faraday Soc. **31**, 1483 (1953); (*b*) G. A. Razuvaev and Yu. A. Ol'dekop. Akad. Nauk SSSR, **2**, 981 (1955); (*c*) G. A. Razuvaev and Yu. A. Ol'dekop. Dokl. Akad. Nauk SSSR, **64**, 77 (1949); (*d*) W. H. Glaze and A. C. Ranade. J. Org. Chem. **36**, 3331 (1971).
2. (*a*) A. I. Khodair, A. A. Abdel-Wahab, and A. M. El-Khawaga. Z. Naturforsch. **33b**, 403 (1975); (*b*) A. I. Khodair, A. A. Swelim, and A. A. Abdel-Wahab. J. Phosphorous Sulfur, **2**, 165 (1976); (*c*) **2**, 169 (1976).
3. A. I. Khodair. Ind. J. Chem. **14B**, 552 (1975).
4. (*a*) G. A. Razuvaev and G. G. Petukhov. Zh. Obshch. Khim. 38 (1), (1968); (*b*) G. A. Razuvaev. Dokl. Akad. Nauk. SSSR, **64**, 77 (1949).
5. J. Cason and H. Rapoport. Laboratory text in organic chemistry. 2nd ed. Prentice-Hall, Inc., Englewood Cliffs, NJ. 1962. p. 465.
6. I. Helbron and H. M. Bunbury. Dictionary of organic compounds. Vol. 1. Eyre and Spottiswodde, London. 1943.
7. A. I. Vogel. A textbook of organic chemistry. 3rd ed. Lowe and Brydone, London. 1965.
8. C. S. Marvell and S. M. McElvain. Organic synthesis. Coll. Vol. 2. 1940. p. 170.

Thermochemical measurement of the ligand field splitting energies for hexaaquocopper(II) and hexaamminecopper(II) ions[1]

MUHAMMAD BADRI AND JAMES W. S. JAMIESON

Department of Chemistry, Universiti Pertanian Malaysia, Serdang, Selangor, Malaysia

Received March 30, 1978[2]

MUHAMMAD BADRI and JAMES W. S. JAMIESON. Can. J. Chem. 57, 1926 (1979).

The vacuum dehydration of copper(II) sulphate pentahydrate has been shown to pass through the transitory trihydrate state before proceeding to the monohydrate composition. Based on this, the heat of solution data for the high-energy modification hydrates have been reinterpreted and the low-energy crystalline hydrates of various compositions have been prepared and their heats of solution measured. From the heat of solution data the maximum energy difference expressed in kcal/mol heptahydrate appears to be of the right order of magnitude to be regarded as the ligand field splitting energy for the hexaaquocopper(II) ion. Similar measurement for the ammine complexes of copper(II) sulphate has also been done and the maximum energy difference was found to agree well with the value of LFSE obtained by spectroscopic method.

MUHAMMAD BADRI et JAMES W. S. JAMIESON. Can. J. Chem. 57, 1926 (1979).

On a montré que la déshydratation sous vide du pentahydrate du sulfate de cuivre(II) procède par l'intermédiaire d'un état trihydraté avant d'atteindre la composition monohydraté. En ce basant sur cette observation, on a interprété les données relatives à la chaleur de solution des modifications des hydrates d'énergie élevée; on a de plus préparé des hydrates cristallins de basse énergie et de compositions diverses et on a mesuré leurs chaleurs de solution. Sur la base de ces chaleurs de solution, il semble que l'amplitude de la différence d'énergie maximale, exprimée en kcal/mol d'heptahydrate, soit telle qu'on peut la considérer comme égale à l'énergie de dissociation de champ de ligand (EDCL) pour l'ion hexaquocuivre(II). On a aussi effectué des mesures semblables pour les complexes aminés du sulfate de cuivre(II) et la différence maximale d'énergie est en bon accord avec la valeur de EDCL évaluée par une méthode spectroscopique.

[Traduit par le journal]

Introduction

In the previous publications on the thermochemical measurement of the ligand field splitting energies of the hexaaquo and hexaammine complexes of some transition metal(II) ions (1–4) the values for the complexes of copper(II) ion were not included. By spectroscopic measurement, however, the $10Dq$'s for the hexaaquocopper(II) and hexaamminecopper(II) ions have been found to be 16×10^3 cm^{-1} and 12×10^3 cm^{-1} respectively (5, 6). Later work (7–10) has shown that the values are actually lower and, furthermore, are of the same order of magnitude as has been found for similar complexes of other transition metal(II) ions of the same series, i.e. about 10×10^3 cm^{-1}.

The heat of solution data for various hydrates of copper(II) sulphate have also been published and are reproduced in Fig. 1. Frost, Moon, and Tompkins (11) found that the crystalline hydrates, which were prepared by heating the pentahydrate in an oven, have their heats of solution falling along the lines BF and FX in Fig. 1 where X, F, and B are at the pentahydrate, trihydrate, and monohydrate compositions respectively. The line FX in Fig. 1 has been extrapolated to C where C is at the heptahydrate composition. The high-energy modification hydrates, which were prepared by heating the pentahydrate *in vacuo*, have higher heats of solution compared to their corresponding low-energy hydrates. Frost *et al.* also showed that the high-energy hydrates with water contents less than that of the monohydrate have their heats of solution along the line FGH, where G and H are at the monohydrate and the anhydrous salt compositions respectively. The line CDE has been drawn parallel to the line FGH to represent the maximum possible heat of solution line for the high-energy modification hydrates originating from the heptahydrate. However, the lines FGH and CDE are not parallel to the heat of solution line BA which was obtained earlier (12, 13) for the crystalline hydrates of compositions less than that of the monohydrate. This does not concur with what has been found in other cases (1–4) even though by thermochemical method the energy difference at the monohydrate composition, BD, or at the anhydrous salt composition, AE, would give a value of an

[1]Part of the experimental work was done while the author was at Dalhousie University, Halifax, Nova Scotia.

[2]Revision received February 26, 1979.

0008-4042/79/151926-06$01.00/0

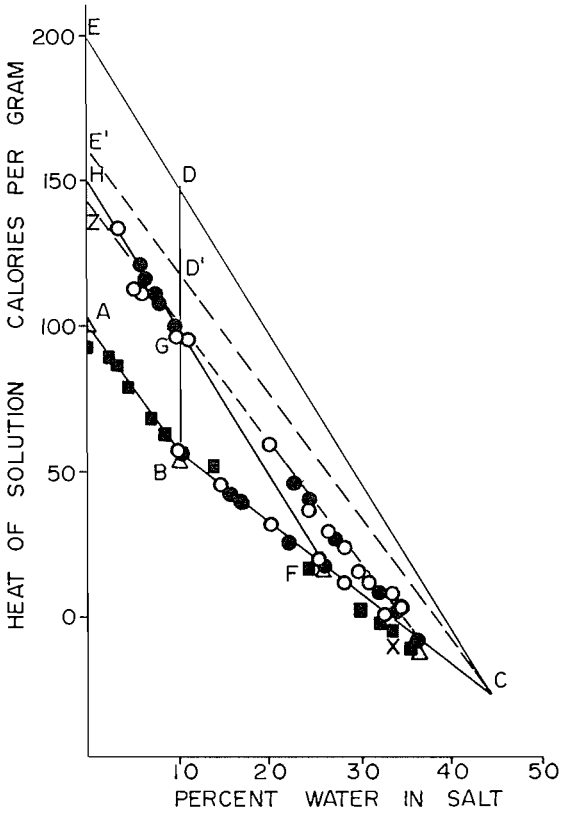

FIG. 1. Heats of solution for hydrates of copper(II) sulphate: ●, from ref. 11; ■, from ref. 13; △, from ref. 12; ○, present data.

acceptable magnitude for $10Dq$ for the complex hexaaquocopper(II) ion.

On the other hand, if all the heat of solution data for the products of vacuum dehydration of copper(II) sulphate pentahydrate were considered, a line XYZ can be drawn to pass through all the points representing them in Fig. 1, where Y and Z are at the monohydrate and the anhydrous salt compositions respectively. This line is parallel to the line BA which is in accord with all the systems that have been studied. However, if the line CD′E′ is similarly drawn to represent the heat of solution line for the high-energy modification hydrates originating from the pentahydrate, the estimation of the heat of transition from B to D′ at the monohydrate composition or from A to E′ at the anhydrous salt composition would give a value of 17 kcal/mol heptahydrate only. This value is too small to be considered as $10Dq$ for the hexaaquocopper(II) ion even compared to a low value given by Roos (28). Thus the present work is done to explain this anomaly and to help to establish the general applicability of the calorimetric technique for the measurement of the ligand field splitting energy.

Experimental

1. $CuSO_4 \cdot 5H_2O$

$CuSO_4 \cdot 5H_2O$ of Baker analysed reagent grade was used for the preparation of some lower hydrates of copper(II) sulphate. The samples, each of about 0.7 g, were ground slightly before dehydration. The methods of dehydration were similar to those described for the hydrates of other metal sulphates (1, 2).

Some small crystals of the pentahydrate were also prepared. These were obtained by adding absolute ethanol slowly to a concentrated solution of copper(II) sulphate in distilled water (14). The small crystals formed were collected and dried over a stream of air at room temperature. Thermogravimetric analysis showed that in each case the water content was in good agreement with the calculated value.

The heats of solution were measured by dissolving the samples in a calorimeter containing 1 L of distilled water.

2. $CuSO_4 \cdot 3H_2O$

$CuSO_4 \cdot 3H_2O$ was prepared by crystallizing the salt from a solution of $CuSO_4 \cdot 5H_2O$ in absolute methanol (15). The pentahydrate was added slowly, while stirring, into a beaker containing warm methanol. The solution was cooled to room temperature. When crystals of the trihydrate appeared, they were collected and dried over a stream of air. Trihydrate composition was confirmed by thermogravimetric analysis.

This salt was used to prepare other hydrates of copper(II) sulphate also. To prepare the higher hydrates, the trihydrate was rehydrated by exposing it to water vapour. To prepare the lower hydrates, the trihydrate was heated in an oven. When the lower hydrates of desired composition were obtained, the heat of solution measurements were done immediately. Samples with the monohydrate composition or less were heated in sealed glass tubes at various temperatures for various time intervals.

For the preparation of the high-energy modification hydrates, the trihydrate was dehydrated under vacuum at a pressure of 1×10^{-4} Torr or less. In each case the composition of the product obtained was determined by the loss in weight. The heat of solution was measured immediately by dissolving the salt in 1 L of distilled water.

3. $CuSO_4 \cdot 3H_2O \cdot 2D_2O$

About 1 g sample of copper(II) sulphate pentahydrate was dehydrated over concentrated H_2SO_4 to obtain the trihydrate. The sample was then exposed to $CuSO_4 \cdot 5D_2O$ (prepared by crystallizing a saturated solution of $CuSO_4$ in 99% D_2O). The completeness of rehydration was checked by measuring the gain in weight due to the absorption of D_2O.

For the ir study, the crystalline $CuSO_4 \cdot 3H_2O$ was again obtained by dehydrating $CuSO_4 \cdot 3H_2O \cdot 2D_2O$ over concentrated H_2SO_4 for a period of 3 weeks. About 0.1 g samples were used for the preparation of the high-energy modification lower hydrates under vacuum at a pressure of 1×10^{-4} Torr or less. The spectra were obtained from Nujol mulls of the samples on Beckman Acculab 3 IR Spectrophotometer.

4. Ammines of Copper(II) Sulphate

The starting material used was anhydrous copper(II) sulphate. This salt was obtained by heating $CuSO_4 \cdot 5H_2O$ (supplied by Fisher Scientific Co.) at 250°C (16) for a period of 2 days. The anhydrous salt was then reacted with anhydrous ammonia (supplied by Matheson of Canada Ltd.) in a manner previously described (17). The composition of the product

was analysed by the gain in weight as well as by gravimetric sulphate analysis. The ammonia content in the sample was found to be 34.79% which is close to the pentaammine composition. Since this salt is not stable, it was stored in a desiccator under an ammonia atmosphere.

Deammoniation of the salt was done under vacuum or in an oven at various temperatures previously determined (18–20). After partial loss of ammonia, the products were sealed in glass tubes to prevent water vapour in the air from reacting with the lower ammines. It has been pointed out (21) that the monoammine of copper(II) sulphate prepared by heating higher ammines in an oven is noncrystalline. Some lower ammines were also heated in sealed glass tubes at various temperatures and for various time intervals to ensure crystallization. The heats of solution were measured by dissolving about 0.3 g of the salt in 1 L of 0.3 *M* aqueous ammonia.

5. Calorimetry

The calorimeter used consists of a silvered Dewar flask equipped with a mechanical stirrer and a Beckmann thermometer. One litre of solvent was used in each experiment. The heat capacity of the calorimeter was determined from the change in temperature caused by a known quantity of electrical energy from a heater made of chromel A wire. Throughout the period of heating, the voltage and the current were quite steady at 4.00 ± 0.02 V and 6.00 ± 0.02 A. Time was measured with a stop watch to about 240.0 ± 0.1 s. Determination of the temperature change due to either the energy input or solution of the sample appeared to be accurate to ± 0.002°C. The average heat capacity of the calorimeter for each solvent was used in all calculations. The error in heat of solution was about ± 2.1 cal.

Results

1. $CuSO_4 \cdot 5H_2O$

The heat of solution measurements for the hydrates of copper(II) sulphate prepared by dehydrating the pentahydrate were done to reproduce the data given earlier in the literature. The values[3] have been corrected for the dilution effect by applying the experimental results obtained by Lang *et al.* (22). Some of the results are plotted in Fig. 1. The agreement with the previous data is very good except that there is no change in the slope of the line BC at the trihydrate composition.

2. $CuSO_4 \cdot 3H_2O$

The heats of solution for the hydrates of copper(II) sulphate prepared from $CuSO_4 \cdot 3H_2O$ are plotted in Fig. 2. The linear relations calculated by the method of least squares are

$$y_{BC} = 62.2 - 1.95x$$

for the low-energy hydrates, and

$$y_{FH} = 144 - 5.17x$$

for the high-energy hydrates where x is the percentage of water in that salt and y is its heat of solution. The heat of solution for the crystalline monohydrate, at B, has been estimated as 42.4 cal/g and that of the heptahydrate, at C, as -23.6 cal/g. Using the slope of the line FH as -5.17, the equation for the line CE, parallel to the lines AB and FH and passing through point C, the heptahydrate composition, on the line BC, has been calculated to be

$$y_{CE} = 205 - 5.17x$$

The heat of solution for the high-energy monohydrate, point D in Fig. 2, could then be estimated as 153 cal/g. Therefore the energy difference between points D and B is 110 cal/g monohydrate or 31.3 kcal/mol of heptahydrate. Expressed in wavenumbers, this energy is equivalent to 11.0×10^3 cm^{-1}.

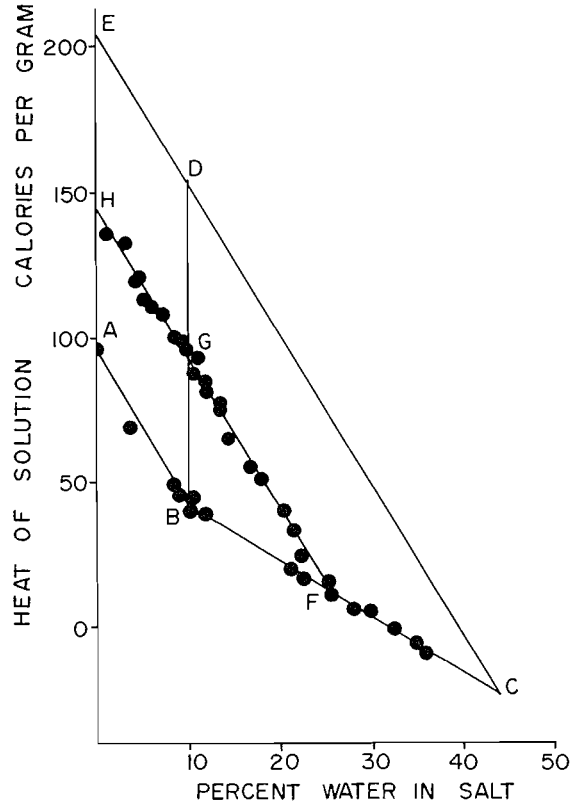

FIG. 2. Heats of solution for hydrates of copper(II) sulphate prepared from the trihydrate.

3. $CuSO_4 \cdot 3H_2O \cdot 2D_2O$

The ir spectrum from $CuSO_4 \cdot 3H_2O \cdot 2D_2O$ shows absorptions at about 3300 cm^{-1} and 2400 cm^{-1} (spectrum *A*, Fig. 3). When the salt is dehydrated over concentrated sulphuric acid, the product, $CuSO_4 \cdot 3H_2O$, shows only the absorption at 3300 cm^{-1} (spectrum *B*).

Spectra *C*, *D*, and *E* are for the salts obtained by vacuum dehydration of $CuSO_4 \cdot 3H_2O \cdot 2D_2O$. Spec-

[3]Complete set of tabular data is available, at a nominal charge, from the Depository of Unpublished Data, CISTI, National Research Council of Canada, Ottawa, Ont., Canada K1A 0S2.

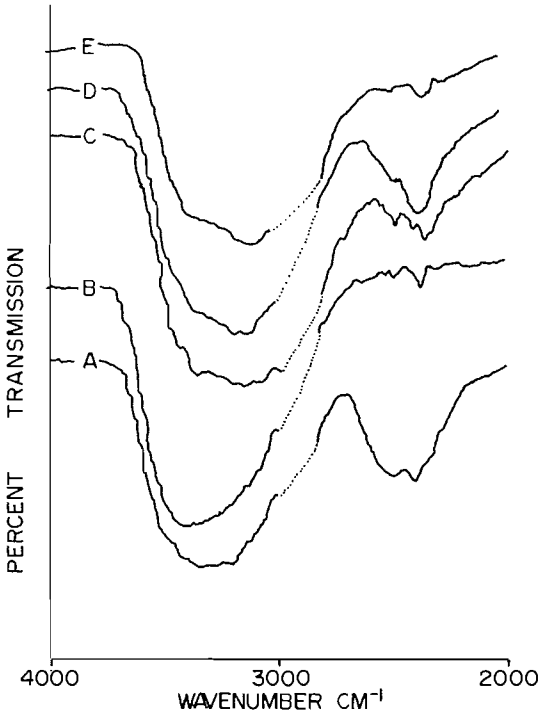

FIG. 3. Infrared spectra for hydrates of copper(II) sulphate. *A*, $CuSO_4 \cdot 3H_2O \cdot 2D_2O$; *B*, $CuSO_4 \cdot 3H_2O$; *C*, $CuSO_4 \cdot xH_2O \cdot yD_2O$ ($x + y \approx 3$); *D*, $CuSO_4 \cdot xH_2O \cdot yD_2O$ ($x + y \approx 2$); *E*, $CuSO_4 \cdot xH_2O \cdot yD_2O$ ($x + y \approx 1$).

trum *C* is that given by a hydrate of high-energy modification of composition $CuSO_4 \cdot xH_2O \cdot yD_2O$ where $x + y \approx 3$ (about the trihydrate composition). The amount of $H_2O + D_2O$ left in the sample is about 29.3%. Spectrum *C* gives both maxima at 3300 cm^{-1} and 2400 cm^{-1}. Though the intensity of the latter is comparatively less, it clearly indicates the presence of D_2O in the product. Spectrum *D* is that of $CuSO_4 \cdot xH_2O \cdot yD_2O$ with $x + y \approx 2$. The amount of $H_2O + D_2O$ left in the sample is about 18.7%. Both absorption maxima still persist and they do so even at a lower composition (spectrum *E*). Spectrum *E* is that of $CuSO_4 \cdot xH_2O \cdot yD_2O$ with $x + y \approx 1$. The amount of $H_2O + D_2O$ left in the sample is 13.4%.

4. Ammines of Copper(II) Sulphate

The heats of solution for the ammines of copper(II) sulphate are plotted as a function of percent ammonia in Fig. 4. In the figure, B, F, and C are at the monoammine, pentaammine, and heptaammine compositions respectively. The heats of solution for the low-energy ammines fall on the lines FB and BA whereas those for the high-energy modification ammines fall on the line FH. The lines AB, BC, and FH are drawn with the slopes calculated by using the method of least squares. The linear relations are

$$y_{AB} = 61.5 - 7.57x$$

$$y_{BC} = 90.6 - 3.68x$$

and

$$y_{FH} = 218 - 7.52x$$

where x is the percent ammonia in the sample and y is its solution. The heat of solution for the heptaammine of copper(II) sulphate which is probably hexaamminecopper(II) sulphate monoammine, $Cu(NH_3)_6SO_4 \cdot NH_3$, at point C, was estimated by extrapolating the line BC. It is found to be −74.5 cal/g. Using the slope of the line FH as −7.52, the line CE has been drawn to pass through the point C. This line allows the estimation of the heat of solution for the high-energy modification $CuSO_4 \cdot NH_3$ at point D as 174.7 cal/g. By using the equation for the line BC, the heat of solution for low-energy modification $CuSO_4 \cdot NH_3$ at point B is estimated to be 53.4 cal/g. Thus the heat of transition, Q_{DB}, is 121.3 cal/g monoammine which is equivalent to 11.8 × 10^3 cm^{-1} per mole heptaammine.

Discussion

The heats of solution for the crystalline hydrates of copper sulphate that are now reported in Fig. 2 give only a single straight line BC joining all the

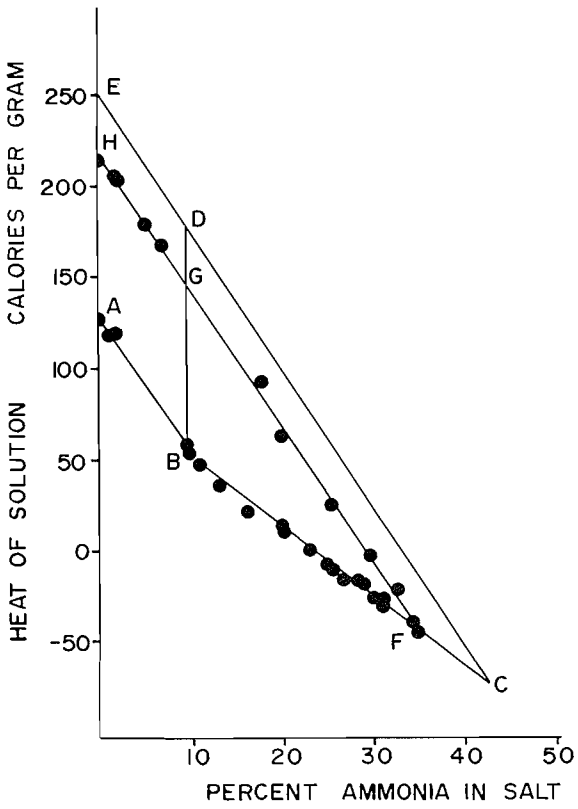

FIG. 4. Heats of solution for various ammines of $CuSO_4$.

points on the heat of solution curve. Furthermore, the gradient of the line CB in Fig. 2 is smaller than those given by Frost *et al.* (11) for the lines FB and CF in Fig. 1.

This could be explained on the assumption that the present technique for the preparation of the lower hydrates of low-energy modification yields completely crystalline products. It has been a common practice to prepare the lower hydrates by heating the pentahydrate in an oven. For example, when $CuSO_4 \cdot 5H_2O$ is heated at 101°C the trihydrate is formed (26). However, this trihydrate may contain a very small quantity of noncrystalline trihydrate (27). The quantity may be so small that the heat of solution would not give any detectable difference from that of the completely crystalline sample. Further dehydration may yield the monohydrates with a greater proportion of noncrystalline material so that the heat of solution would be considerably higher than that of the completely crystalline form.

Frost *et al.* (11) gave an equation to describe the heat of solution data for the high-energy modification hydrates of composition less than that of the monohydrate as

$$y_{FH} = 149.0 - 5.098x$$

The line FH intercepts the line BC at approximately the trihydrate composition. The equation for the line FH agrees quite well with the present results (Fig. 2) for the heats of solution for the hydrates of high-energy modification obtained by the dehydration of the crystalline trihydrate under vacuum. Therefore, it seems possible to conclude that all those hydrates that have their heats of solution described by the line FH must originally come from the trihydrate of copper(II) sulphate.

Since the line XZ in Fig. 1 intercepts the line FH at about the monohydrate composition, it seems likely that the products of vacuum dehydration of the pentahydrate which have water content higher than that of the monohydrate are really mixtures. These mixtures consist of the initial pentahydrate and high-energy modification monohydrate originating from the crystalline trihydrate. It seems that during vacuum dehydration when a molecule of $CuSO_4 \cdot 5H_2O$ loses its two molecules of ligand water, further loss of two more is enhanced. Thus that molecule will be dehydrated further to the monohydrate regardless whether other molecules adjacent to it have been dehydrated or not. If this is so, a product with an intermediate composition between the monohydrate and the pentahydrate is really a mixture of these two salts. Its heat of solution would fall on a line joining the values for the pentahydrate and the high-energy monohydrate, following a rule given by Donnan and Hope (13).

Thus it appears that the decomposition of the pentahydrate of copper(II) sulphate under vacuum to form the trihydrate would be accompanied by lattice rearrangement. The trihydrate stage is transitory (29). At the moment of its formation dehydration would proceed to the monohydrate stage with the formation of the corresponding high energy form. Garner and Tanner (30) arrived at a similar conclusion although in a less definitive way. Kohlschütter and Nitschmann (31) have studied the X-ray diffraction pattern of the products of vacuum dehydration of the pentahydrate of copper(II) sulphate and arrived at a similar conclusion.

The ir study that was done clearly shows this phenomenon. The ir spectra of free H_2O and D_2O in the gas phase show absorption maxima at about 3756 cm^{-1} and 2789 cm^{-1} respectively (23, 24) due to O—H and O—D assymetric stretchings. When the compound $CuSO_4 \cdot 3H_2O \cdot 2D_2O$ was formed from the trihydrate, it is assumed that D_2O absorbed has filled the vacant coordination positions in the $[Cu(H_2O)_2]^{2+}$ ion to form the $[Cu(H_2O)_2(D_2O)_2]^{2+}$ ion. Due to coordination, the corresponding vibrations in the salt are lowered (25). When the salt was dehydrated over concentrated H_2SO_4, it seems that all the D_2O originally present in the salt was lost, leaving the crystalline trihydrate again as the product (spectrum *B*, Fig. 3). Since the trihydrate has no D_2O, the spectrum would only show absorption at 3400 cm^{-1}. From the spectra *C*, *D*, and *E*, it is clear that under vacuum the D_2O are not completely removed even when the composition of the product is close to that of the monohydrate. This could mean one of two things: (*a*) the ligands are evolved at random, non-stepwise, regardless of the coordination positions, or (*b*) for every molecule, once D_2O is evolved, H_2O immediately follows. It is stepwise but fast in sequence to the extent that some molecules have only the anionic water left while the others still have all the ligands bonded. Since the second mechanism agrees well with the heat of solution data, it seems that it is the more likely one.

With these assumptions, it seems that the present results on the heat of solution measurements give better values than those given by earlier workers. Furthermore the value of $10Dq$ obtained by the thermochemical technique for the hexaaquocopper(II) ion as 11.0×10^3 cm^{-1} is comparable to that obtained by Pappalardo (8) as 11.2×10^3 cm^{-1} for a truely octahedral hexaaquocopper(II) ion in $CuSiF_6 \cdot 6H_2O$.

Eliott and Hathaway (10) have studied the reflectance spectra of the *d–d* transitions for the hexaamminecopper(II) halides and pentaamminecopper(II) sulphate. From their studies, they have assigned the value of $10Dq$ ranging from 10.4 ×

10^3 cm^{-1} to 10.6 × 10^3 cm^{-1} for the halides and 10 × 10^3 cm^{-1} for the sulphates. Roos (28) has calculated the energy levels for the $[Cu(NH_3)_5]^{2+}$ ion to confirm the experimental measurements of Bjerrum *et al.* (32). He assigned a value of 9.75 × 10^3 cm^{-1} to the $10Dq$ for this complex. From the present work we obtained a value of 11.8 × 10^3 cm^{-1} for the hexaamminecopper(II) ion. Even though it is slightly higher than those values quoted above it is still smaller than that originally proposed (5, 6). Compared to the value for the hexaaquocomplex it is very encouraging. Going back to the earlier paper (4) and substituting the present values in the figure showing the relative magnitudes of $10Dq$ for the complexes, the high values for that of hexaammine and hexaaquocopper(II) ions are removed. Thus the present results lend more support to the validity of the thermochemical measurement of the ligand field splitting energy.

1. J. W. S. Jamieson, G. R. Brown, D. W. Gruener, R. Peiluck, and R. A. La Montagne. Can. J. Chem. **43**, 2148 (1965).
2. J. W. S. Jamieson, R. A. La Montagne, B. S. Pattern, and G. R. Brown. Can. J. Chem. **43**, 3129 (1965).
3. B. Muhammad and J. W. S. Jamieson. Can. J. Chem. **48**, 2177 (1970).
4. M. Badri and J. W. S. Jamieson. Can. J. Chem. **55**, 3530 (1977).
5. C. K. Jørgenson. Acta Chem. Scand. **9**, 1362 (1955).
6. L. E. Orgel. An introduction to transition metal chemistry, ligand field theory. Methuen, London. 1960. p. 46.
7. O. G. Holmes and D. S. McClure. J. Chem. Phys. **26**, 1685 (1957).
8. R. Pappalardo. J. Mol. Spectrosc. **6**, 554 (1961).
9. N. S. Hush and R. J. M. Hobbs. Prog. Inorg. Chem. **10**, 259 (1968).
10. H. Eliott and B. J. Hathaway. Inorg. Chem. **5**, 885 (1965).
11. G. B. Frost, K. A. Moon, and E. H. Tompkins. Can. J. Chem. **29**, 604 (1951).
12. F. R. Bichowsky and F. D. Rossini. The thermochemistry of the chemical substances. Reinhold, New York, NY. 1936.
13. F. G. Donnan and G. D. Hope. Trans. Faraday Soc. **5**, 244 (1909).
14. S. Skramousky, R. Forster, and G. F. Huttig. Z. Phys. Chem. B**25**, 1 (1934).
15. J. Hume and J. Colvin. Trans. Faraday Soc. **34**, 969 (1938).
16. H. J. Borchardt and F. Daniels. J. Phys. Chem. **61**, 917 (1957).
17. J. W. Mellor. A comprehensive treatise on inorganic and theoretical chemistry. Vol. III. Longmans, Green & Co., Inc., London. 1936. p. 251.
18. E. Rencker and P. Vallet. C. R. Acad. Sci. Paris, **204**, 1337 (1937).
19. M. M. T. Anous. Recl. Trav. Chem. **78**, 97 (1962).
20. W. W. Wendlandt and J. P. Smith. The thermal properties of transition metal ammine complexes. Elsevier, Amsterdam. 1967. p. 137.
21. V. Kohlschütter and H. Nitschmann. Z. Phys. Chem. 503 (1931).
22. E. Lang, J. Monheim, and A. L. Robinson. J. Am. Chem. Soc. **55**, 4732 (1933).
23. G. Herzberg. Molecular spectra and molecular structure. Vol. III. IR and Raman spectra of polyatomic molecules. Van Nostrand, Princeton. 1964. pp. 197, 282.
24. E. F. Baker and W. W. Slater. J. Chem. Phys. **3**, 660 (1935).
25. C. Rocchiccioli. C. R. Acad. Sci. Paris, **257**, 3851 (1963).
26. W. W. Wendlandt. Thermochim. Acta, **1**, 11 (1970).
27. J. R. Partington. J. Chem. Soc. **99**, 475 (1911).
28. B. Roos. Acta Chem. Scand. **20**, 1673 (1966).
29. J. Hume and J. Colvin. Trans. Faraday Soc. **29**, 576 (1933).
30. W. G. Garner and M. G. Tanner. J. Chem. Soc. 47 (1930).
31. V. Kohlschütter and H. Nitschmann. Z. Phys. Chem. (Bodenstein Band), 494 (1932).
32. J. Bjerrum, C. J. Ballhausen, and C. K. Jørgensen. Acta Chem. Scand. **8**, 1275 (1954).

β-Lactams. V. The synthesis of D,L-4-hydroxymethylnocardicin A (17*N*), D,L-4-hydroxymethyl-*N*-phenylacetylnocardicinic acid (8*N*-*f*), and their α-epimers 17*U* and 8*U*-*f*

GHOLAM HOSEIN HAKIMELAHI AND GEORGE JUST

Department of Chemistry, McGill University, Montreal, P.Q., Canada H3A 2K6

Received October 10, 1978

GHOLAM HOSEIN HAKIMELAHI and GEORGE JUST. Can. J. Chem. **57,** 1932 (1979).

The synthesis of title compounds and some aromatic ring substituted analogues is described.

GHOLAM HOSEIN HAKIMELAHI et GEORGE JUST. Can. J. Chem. **57,** 1932 (1979).

On décrit la synthèse des composés sus-mentionnés ainsi d'analogues substitués sur le noyau aromatique.

Nocardicin A (1), the first 'monocyclic' β-lactam antibiotic described, is remarkably active against Gram-negative organisms in vivo (2) although it displays but little activity in vitro (3, 4). It differs from all hitherto described β-lactam antibiotics, 1770–1780 cm^{-1}, in having a relatively unstrained (1725 cm^{-1}) β-lactam ring, and therefore being quite stable towards nucleophilic attack. It occurred to us that the in vivo activation may well be linked to an oxidation of nocardicin A to the corresponding quinonemethine, in which the β-lactam frequency should be considerably augmented, thus leading to a chemically and therefore perhaps biologically reactive lactam.

Since the nocardicin A sidechain is relatively complex, nocardicinic acid derivatives carrying a phenylacetamide sidechain, a group known to confer antibiotic activity to classical β-lactam antibiotics, were prepared as model compounds, and the experience gathered applied to the synthesis of nocardicin A.

Because of the difficulties in preparing quinonemethines (5) it was decided to prepare, in addition to **8***N*-*f*, catechol derivatives of type **8***N*-*g*, in which an in vivo and (or) in vitro oxidation to *o*-quinones may be more easily achieved, and which may perhaps exist in part as the *p*-quinonemethine tautomer. Since several total syntheses of nocardicin have already been reported (6), it was decided to prepare 4-hydroxymethylnocardicinic acid, which would allow the synthesis of fused nocardicins. This will be described in the following paper.

Because of lack of substantial in vivo antibacterial activity of hydroxymethylnocardicin A (**17***N*), due presumably to the hydroxymethyl group, the corresponding catechol (**17***N*-*g*) was not synthesized.

As a model, methyl D,L-phenylglycinate (**3***a*) was converted to its cinnamylidine Schiff base **4***a*. Reaction with azidoacetyl chloride (7) using the methods described by Doyle *et al.* (8), gave β-lactam **5***a* as a mixture of epimers at the carboxyl bearing carbon. All the β-lactams obtained by this method were *cis*-fused (8), as could be determined by nmr (J = 5 Hz) of all derivatives in which the relevant protons did not overlap with other signals. The azide function in **5***a* was reduced with hydrogen sulfide – triethyl amine (8), and the resulting amine directly acylated with phenylacetyl chloride in pyridine to give **6***a*. This method was used throughout to convert the azide group to a phenylacetamide function and proceeded in approximately 70% overall yield. When methyl D-phenylglycinate (D-**3***a*) was transformed to **5***a*, the product was optically inactive, indicating that racemization took place as observed previously (9) in a similar reaction in which D-serine had been used as a starting material.

Next, *p*-benzyloxybenzaldehyde (**1***b*), piperonal (**1***c*), 3,4-dibenzyloxybenzaldehyde (**1***d*), and 4-carboxybenzaldehyde (**1***h*) were transformed to the corresponding cyanoamines **2***b*–*d* and **2***h* by means of $NaCN$–NH_4Cl–NH_3 in methanol, or methanol–tetrahydrofuran in the case of **1***b* and **1***d*. The cyanoamines **2** were methanolysed to the aminoester **3**, the overall yield for the transformation **1** → **3** being approximately 65% except in the case of **3***d*, in which the cyanoamine formation **1***d* → **2***d* proceeded in 5% yield only, and the methanolysis in 40%. Schiff base formation **3** → **4** proceeded in general quantitatively, and β-lactam formation **4** → **5** in approximately 70% yield. **5***b*–*e* were transformed to **6***b*–*e* as described above.

Since, at this point, it was not known whether the methyl ester group could be hydrolysed in the presence of a β-lactam group, β-lactams **6***a*, *b*, *d*, *e* were treated with 1 equiv. of sodium hydroxide in methanol as a 1% solution at room temperature.

0008-4042/79/151932-07$01.00/0

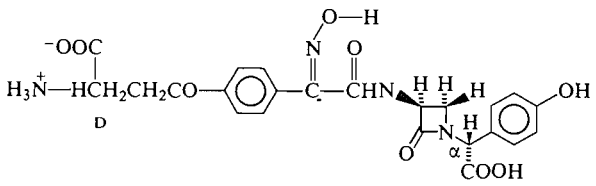

D

Nocardicin A

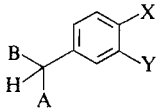

1 A, B = O
2 A = CN, B = NH_2
3 A = COOMe, B = NH_2
4 A = COOMe, B = N=CH—CH=CHPh

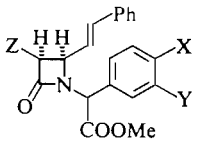

5 Z = N_3
6 Z = $NHCOCH_2Ph$

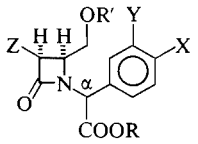

7 R = Me, Z = $NHCOCH_2Ph$, R′ = H
8 R = H, Z = $NHCOCH_2Ph$, R′ = H
9 R = CH_2Ph, Z = N_3, R′ = H
10 R = CH_3, Z = N_3, R′ = H
11 R = CH_3, Z = NH_2, R′ = H
12 R = CH_3, Z = NH_2, R′ = $SiMe_3$

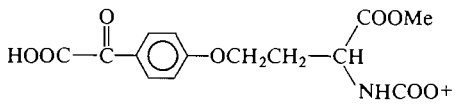

D,L-**13**

a X = Y = H, *b* X = OCH_2Ph, Y = H, *c* X = Y = —O—CH_2—O—, *d* X = Y = OCH_2Ph,
e X = COOMe, Y = H, *f* X = OH, Y = H, *g* X = Y = OH, *h* X = COOH, Y = H, *i* X = $OSiMe_3$, Y = H
N: having the nocardicin A configuration at α
U: α-epimer of *N*

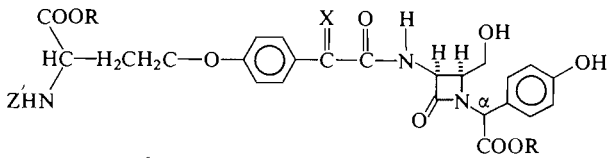

14 R = Me, X = O, Z = $COOCMe_3$
15 R = H, X = O, Z = $COOCMe_3$
16 R = H, X = O, Z = H
17 R = H, X = NOH(*syn*), Z = H

Esters **6***a*,*b*,*d* were transformed to the corresponding acids in 60–65% yield, and were characterized by remethylation. In the case of carbomethoxyphenyl derivative **6***e*, the β-lactam function was hydrolysed more rapidly than either ester function.

Styryl-β-lactam **6***c* derived from piperonal was ozonised in methanol at −78°C, and the crude product reduced with sodium borohydride at −40°C. Although it was possible to isolate **7***c* by preparative tlc, the yield was very low, and it seemed that the methylene-dioxy bridge was attacked during ozonolysis. Moreover, the methylene bridge could not be cleaved in the presence of the β-lactams with boron trichloride – methylene chloride (10) or boron tribromide (11), so that no further work was done in this series.

Ozonolysis of the *p*-benzyloxy-β-lactam **6***b* using standard ozonolysis conditions, followed by sodium borohydride reduction at −40°C, gave the expected diols **7***b* in 20% yield only. However, when ozone and nitrogen were introduced simultaneously (12), and the reaction mixture then reduced with sodium borohydride, **7***b* was obtained in over 80% yield. Similar results were obtained in the dibenzyloxy series **7***d*. The diastereomeric mixtures **7***a*,*b*,*d* were separated into their constituents by column chromatography.

The less polar products were assigned the stereochemistry of the 'natural' nocardicin **7***N* based on the fact that the ester function absorbed in the infrared at 1740 cm^{-1} (hydrogen-bonded carbomethoxy group) and the hydroxyl function at 3300–3500 cm^{-1} (hydrogen-bonded hydroxyl), with a concomitant lowering of the chemical shift of the proton α to the carbomethoxy group to 5.8 ppm. The corresponding numbers for the more polar isomer **7***U* were 1750 cm^{-1}, 3400–3600 cm^{-1} and 5.5 ppm. Model studies indicated that hydrogen bonding of the ester and hydroxyl group resulted in the phenyl group being placed away from the β-lactam ring in the case of **7***N*, whereas in isomer **7***U*, hydrogen bonding would place the phenyl group very close to the β-lactam ring. Equilibration of two related isomers by heating either **9***U-a* or **9***N-a* (13) for a day at 80°C in pyridine gave a 30:70 ratio of **9***U-a* and **9***N-a* indicating that the hydrogen bond made **9***N-a* slightly more stable than **9***U-a*. When the hydroxy group in **9***U-a* or **9***N-a* was blocked by mesylation or acetylation, equilibration gave a 50:50 mixture of the corresponding mesylates or acetates of **9***U-a* and **9***N-a*, as established by nmr.

Catalytic hydrogenation of **7***U-b*, **7***U-d*, **7***N-b*, and **7***N-d* over Pd/C, followed by hydrolysis of the ester group with 1% aqueous sodium hydroxide, gave **8***U-f*, **8***U-g*, **8***N-f*, and **8***N-g* respectively.

In order to attach the nocardicin A sidechain to the β-lactam moiety, a mixture of diastereomeric styryl azides **5***b* were ozonised and reduced to a mixture of **10***b*, which could be separated into their constituents **10***U-b* and **10***N-b* as described for **7***U* and **7***N*.

D,L-Azido-β-lactam **10***N-b* was reduced with Pd/C in methanol, and the resulting phenolic aminoalcohol **11***N-f* obtained in nearly quantitative yield, was silylated *in situ* to give **12***N-i*. Coupling of **12***N-i* with glyoxylic acid DL-**13** using *N*-ethoxycarbonyl-2-ethoxy-1,2-dihydroquinoline (EEDQ) (14) in methylene chloride for 16 h, gave, after washing and chromatography on silica gel, 80% of amide **14***N* as a mixture of inseparable diastereomeric racemates. Hydrolysis with 2 equiv. of sodium hydroxide in aqueous methanol, followed by removal of the *t*-BOC group by means of trifluoroacetic acid, gave **16***N* in 56% overall yield. Oximation was carried out using $NH_2OH{\cdot}HCl$ in water at pH 7 (15). Purification by ion exchange gave **17***N* in 60% yield. The ir, nmr, and uv spectra at pH 7 and 12 of **17***N* (two racemic diastereomers) were virtually indistinguishable from those of nocardicin A, except for the presence of the CH_2OH group, which was clearly visible in the nmr spectrum. The same sequence could also be applied to the epimer **10***U-b*, giving **17***U*.

Biological Tests

Phenylacetimidonocardicinic acids **8***N-f*, **8***N-g*, **8***U-f*, and **8***U-g* and nocardicin A analog **17**-*U* were tested against 32 strains of *Ps. aeruginosa*, *K. pneumoniae*, *E. aerogenes*, *E. cloacae*, *P. mirabilis*, *P. vulgaris*, *P. morganii*, *S. aureus*, and *S. lutea* and found to be inactive at a level of 256 μg/mL.

The diastereomeric mixture of racemates **17***N* was found to be active at the level of 32 μg/mL versus *S. lutea*, as compared to nocardicin A which had a mic of 6.25 μg/mL against the same organism. However, **17***N* exhibited no in vivo activity.

Experimental

Solvents were of reagent grade unless otherwise specified. Infrared spectra were run on Unicam SP1000 and P.E. 257 spectrophotometers. Nuclear magnetic resonance spectra were run on Varian T-60A or HA-100 spectrometers. Mass spectra were taken on an AEI-MS-902 mass spectrometer using the direct sample inlet system with a 70 eV ionization energy or on a LKB-9000 mass spectrometer.

Melting points were determined on a Gallenkamp block in open capillary tubes and are uncorrected.

Merck S160 silica gel was used for column chromatography. Merck silica gel HF 254 was used for thin layer chromatography (1 mm) on glass plates (20 × 20 cm). Elemental analyses were performed by Heterocyclic Chemical Corporation or Midwest Microlab. Ltd.

Aminonitriles **2**b,c,d,h

Benzaldehydes **1** (0.02 mol) were dissolved in solvent *A*. Ammonium chloride (2.6 g, 0.05 mol) and sodium cyanide (1.25 g, 0.025 mol) were added, and the solution was saturated with ammonia at 0°C (10 min), and stirred in a pressure bottle at 25–30°C for 15 h. After evaporation, solvent *B* was added, and the product either filtered and recrystallized from solvent *C* or extracted with ethyl acetate. The nmr (DMSO-d_6) showed a 2H broad singlet at *D* ppm, exchangeable with D_2O (NH_2), a 1H singlet at δ*E* ppm (CH), aromatic proton at *F* ppm, and other appropriate signals. All compounds absorbed in the infrared at 3300–3500 cm^{-1} (NH_2) and 2200 cm^{-1} (CN). Yield *G*%.

Compound **2***b*: *A* 100 mL methanol, 30 mL THF; *B* water; *C* methanol; mp 93–95°C; *D* 2.8–3.4; *E* 4.83; *F* 6.8–7.5 (9H); 5.1 ppm (2H, s, CH_2Ph); ms *m/e*: 238 (M^+); *G* 90.

Compound **2***c*: *A* 100 mL methanol; *B* water, extracted with ethyl acetate; *D* 2.0; *E* 4.80; *F* 6.8–7.2 (3H); 6.0 ppm (2H, s, O—CH_2—O); *G* 80.

Compound **2***d*: *A* 100 mL methanol, 30 mL THF; *B* water; the precipitate consisted of methanol insoluble **2***d*, and large amounts of soluble cyanohydrin; mp 49–50°C; *D* 1.63–1.82; *E* 4.90; *F* 7.0–7.7 (13H); 5.2 ppm (4H, s, $(CH_2Ph)_2$); ms *m/e*: 344 (M^+); *G* 5.

Compound **2***h*: *A* 100 mL methanol; *B* acetic acid; filtration; water; filtration. mp >250°C (dec.); *D* 4.8 (3H); *E* 5.4; *F* 7.6–8.2 (4H); *G* 80.

Amino Acid **3**b,c,d,e

Cyanoamines **2***b,c,d,h* (0.018 mol) were dissolved in 250 mL methanol–water (95:5), and HCl gas was bubbled in at room temperature without cooling for 10 min. The solution was gently refluxed for 3 h, the solvent then evaporated and a mixture of 20 mL acetone – 60 mL ether was added. The colourless precipitate was washed with ether, and **3***b,c,e*·HCl obtained in approximately 80% yield, except for **3***d*·HCl which was obtained in 50% yield. All compounds obtained had nmr

spectra similar to those described for the cyanoamines except for additional methyl ester peaks.

Compound **3***b*·HCl: *Anal.* calcd. for $C_{16}H_{18}O_3NCl$: C 62.44, H 5.85, N 4.55; found: C 62.22, H 5.95, N 4.53.

Compound **3***d*·HCl: *Anal.* calcd. for $C_{23}H_{24}O_4NCl$: C 66.75, H 5.80, N 3.38; found: C 66.35, H 5.50, N 3.30.

All hydrochlorides were converted to the parent amine **3** according to the following procedure:

Compound **3***b*·HCl (4.6 g, 0.015 mol) was mixed with 50 mL of 10% aqueous $NaHCO_3$, and the resulting amine **3***b* extracted into 50 mL of ether. After evaporation, 3.25 g of **3***b* (80% yield) was obtained as an oil; nmr ($CDCl_3$) δ: 1.8 (s, 2H, NH_2, exchanged with D_2O); 3.5 (s, 3H, OCH_3), 4.4 (s, 1H, CH), 4.9 (s, 2H, CH_2O), 6.65–7.4 ppm (m, 9H, aromatic); ir (CH_2Cl_2): 3300–3400 (NH_2), 1740 (ester) cm^{-1}.

Schiff Base **4**a–e

All the Schiff bases were prepared in a similar manner and used without purification. The following is a representative procedure:

To a solution of **3***b* (2.71 g, 0.01 mol) in 100 mL dry CH_2Cl_2 was added cinnamaldehyde (1.32 g, 0.01 mol). The solution was brought to reflux and the CH_2Cl_2 distilled slowly with the constant addition of dry CH_2Cl_2 so as to maintain the same volume of liquid in the reaction vessel. After the water of reaction was all removed (~7 h), the solution was cooled and $MgSO_4$ was added. After 2.5 h, it was filtered and evaporated to yield 3.85 g (100%) Schiff base **4***b* as an oil; nmr ($CDCl_3$) δ: 3.8 (s, 3H, CH_3), 5.1 (s, 2H, CH_2), 5.3 (s, 1H, CH), 6.8 (m, 2H, CH=CH), 7–7.6 (m, 14H, Ph), 8.0 (m, 1H, N=CH); ir (CH_2Cl_2): 1735 (ester), 1635 (HC=N) cm^{-1}. In the case of **4***d*, the yield seemed to be somewhat lower (85%) as ascertained by nmr.

Azido-β-*lactams* **5**a–e

All β-lactams were prepared in an identical manner and obtained in approximately 80% yield. Their spectra were similar except for variations due to aromatic substituents. All their mass spectra showed $M^+ - N_2$ or, in the case of **5***a*, M^+.

The following is a representative procedure:

β-*Lactam* **5**b

To the freshly prepared Schiff base (3.85 g, 0.01 mol) in 100 mL dry CH_2Cl_2 was added at −20°C (dry ice – CCl_4) triethylamine (1.01 g, 0.01 mol). A solution of azidoacetyl chloride (1.2 g, 0.01 mol) in 30 mL dry CH_2Cl_2 was added dropwise over 10 min. The solution was stirred for 1 h and evaporated to dryness. The residue was dissolved in ether, treated with charcoal, filtered, and evaporated to give 3.7 g (80%) **5***b* as an oily mixture of diastereomers; nmr ($CDCl_3$) δ: 3.8 (d, 3H, CH_3) 4.2–4.4 (m, 1H, β-lactam) 4.7–4.9 (m, 1H, β-lactam), 5.1 (s, 2H, CH_2), 5.5–5.6 (d, 1H, CH), 6.5 (m, 2H, CH=CH), 6.8–7.6 (m, 14H, Ph). Chromatography over silica gel using CH_2Cl_2 as eluent separated one of the diastereomers, which was obtained in 30% yield as an oil; nmr ($CDCl_3$) δ: 3.75 (s, 3H, CH_3), 4.2–4.4 (m, 1H, β-lactam), 4.8 (d, 1H, J = 5 Hz, β-lactam), 5.1 (s, 2H, CH_2), 5.5 (s, 1H, CH), 6.5 (m, 2H, CH=CH), 6.8–7.5 (m, 14H, Ph); ir (CH_2Cl_2): 2100 (N_3), 1760 (β-lactam), 1740 (ester) cm^{-1}, identical to that of the diastereomeric mixture; ms *m/e*: 440 ($M^+ - N_2$).

Phenylacetamido-β-*lactams* **6**a–e

All transformations were performed in an identical manner, and the mixture of diastereomers **6** obtained in 70% yield after purification. Their spectra were similar except for variations due to aromatic substituents. All their mass spectra showed M^+, $M^+ - (Ph—CH_2CONHCH=C=O)$, $M^+ - (Ph—CH=CH—CH=CH—NHCOCH_2Ph)$, except for the dibenzyloxy derivative which showed no molecular ion but $M^+ - (Ph—CH_2CONHCH=C=O)$, $M^+ - (Ph—CH=CH—CH=CH—NHCOCH_2Ph)$.

The following is a representative procedure:

To a solution of a diastereomeric mixture of azido β-lactam **5***b* (4.68 g, 0.01 mol) in 100 mL dry CH_2Cl_2 at 0°C was added triethylamine (1.2 g, 0.012 mol). A stream of H_2S gas was bubbled in for 45 min. The solution was allowed to stand for 2 h at room temperature. Evolution of nitrogen gas was observed. A stream of nitrogen gas was bubbled in for 30 min, then was added 2.3 g (0.03 mol) pyridine, followed by dropwise addition of 1.8 g (0.012 mol) phenylacetyl chloride in 20 mL CH_2Cl_2. The solution was stirred for 2 h at 25°C, then was washed with 10% HCl solution, 10% $NaHCO_3$ solution, and brine. It was then dried over Na_2SO_4, and evaporated to give 5 g (89%) of impure amide **6***b* which was chromatographed on silica gel. Methylene chloride eluted impurities, and chloroform gave 4 g (70%) of β-lactam **6***b*, mp 100–106°C, as a mixture of diastereomers; nmr ($CDCl_3$) δ: 3.4 (s, 2H, amide CH_2), 3.6–3.8 (2s, 3H, CH_3), 4.2–4.4 (m, 1H, β-lactam), 4.8–5.1 (2s, 2H, CH_2), 5.4–5.7 (m, 2H, CH and β-lactam), 6.2–6.5 (m, 2H, CH=CH), 7–7.6 (m, 20H, Ph and NH). Two recrystallizations from absolute ethanol separated one of the diastereomers; mp 168–169°C; nmr ($CDCl_3$) δ: 3.42 (s, 2H, CH_2), 3.7 (s, 3H, CH_3), 4.2–4.4 (m, 1H, β-lactam), 5.1 (s, 2H, CH_2), 5.3–5.6 (s, 1H, C*H*COOMe and m, 1H, β-lactam, J_1 = 5 Hz and J_2 = 8 Hz), 6.2–6.6 (m, 2H, CH=CH), 6.2–7.6 (m, 20H, Ph and NH); ir (CH_2Cl_2): 3390 (NH), 1756 (β-lactam), 1740 (ester), 1680 (amide) cm^{-1}, identical to that of the mixture of diastereomers; ms *m/e*: 560 (M^+).

Compound **6***U-b* or **6***N-b*: *Anal.* calcd. for $C_{35}H_{32}O_5N_2$: C 74.98, H 5.75, N 5.00; found: C 74.63, H 5.98, N 4.88.

Compound **6***c*: *Anal.* calcd. for $C_{29}H_{26}O_6N_2$: C 69.87, H 5.22, N 5.62; found: C 69.69, H 5.27, N 5.37; mp 69–70°C (ethanol).

Compound **6***d*: *Anal.* calcd. for $C_{42}H_{38}O_6N_2$: C 75.67, H 5.70, N 4.20; found: C 75.33, H 5.79, N 3.88; mp 130–131°C (ethanol).

4-Hydroxymethyl-β-*lactams* **7**U-b, **7**U-d, **7**N-b, *and* **7**N-d

Both mixtures of diastereomeric monobenzyloxylactam **6***b* and dibenzyloxylactam **6***d* were submitted to identical reaction conditions and separation procedures, which will be described for **6***b* only.

β-Lactam **6***b* (2 g, 0.0035 mol) in a mixture of 50 mL CH_2Cl_2 and 100 mL dry methanol was saturated with nitrogen gas at −78°C (3 min). Then a mixture of O_3–N_2 gas was bubbled in until the KI starch paper showed excess ozone (30 min). The excess ozone was removed by passing a stream of N_2 for 10 min. The temperature was allowed to rise to −40°C, at which time was added $NaBH_4$ (0.2 g, 0.005 mol). The temperature of the solution was permitted to rise to 25°C over 2 h, following which 5 mL 10% HCl was added. The solution was evaporated to 50 mL, diluted with H_2O, and was extracted with ethyl acetate, washed with water, dried over Na_2SO_4, and evaporated to give crude product in quantitative yield.

A wash with a mixture of ether–hexane (1:14) removed benzyl alcohol, and a 1:1 mixture of diastereomers (1.5 g, 85%) of **7***b*, mp 50–54°C, was obtained, as evidenced by nmr.

Chromatography on silica gel and elution with $CHCl_3$ separated completely the diastereomers **7***N-b* and **7***U-b*. The less polar diastereomer **7***N-b* was obtained in 40% yield, and melted at 84–85°C after crystallization from diethyl ether; nmr ($CDCl_3$) δ: 3.4 (b, 2H, CH_2O), 3.6 (s, 2H, CH_2CO), 3.8 (s, 3H, CH_3), 4.2–4.6 (m, 1H, C*H*—CH_2OH), 5.18 (s, 2H, CH_2Ph), 5.4–5.7 (q, 1H, C*H*—NHCO, J_1 = 5 Hz and J_2 = 10 Hz, after D_2O exchange: d, J = 5 Hz), 5.8 (s, 1H, CH), 7–7.6 (m, 15H, Ph and NH); ir (CH_2Cl_2): 3380–3440 (NH and OH), 1760 (β-lactam), 1740 (ester), 1670 (amide) cm^{-1}.

Compound **7***U-b* was obtained in 40% yield and was crystallized from diethyl ether, mp 59–60°C; nmr ($CDCl_3$) δ:

2.8–3.2 (b, 2H, CH_2O), 3.5 (s, 2H, CH_2CO), 3.7 (s, 3H, CH_3), 4–4.1 (m, 1H, C*H*–CH_2OH), 5.1 (s, 2H, CH_2Ph), 5.4–5.7 (m, 1H, C*H*—NHCO, J_1 = 5 Hz and J_2 = 10 Hz, and 1H, s, CH), 6.8–7.8 (m, 15H, Ph and NH); ir (CH_2Cl_2): 3380–3440 (NH and OH), 1760 (β-lactam), 1750 (ester), 1670 (amide) cm^{-1}; ms *m/e*: 429 (M^+ − COOMe), 297 (M^+ − $HOCH_2$-CH=CHNHCOCH_2Ph), identical to that of the other diastereomer. *Anal.* calcd. for $C_{28}H_{28}O_6N_2$: C 68.84, H 5.87, N 5.73; found: C 68.62, H 6.05, N 5.47.

Compound **7***N-d* was obtained by the same purification method in 40% yield and melted at 85–87°C (Et_2O); nmr ($CDCl_3$) δ: 3–3.3 (b, 2H, CH_2O), 3.6 (s, 2H, CH_2CO), 3.8 (s, 3H, CH_3), 4.2–4.4 (m, 1H, C*H*—CH_2OH), 5.2 (s, 4H, $2CH_2Ph$), 5.3–5.6 (q, 1H, C*H*—NHCO, J_1 = 5 Hz and J_2 = 10 Hz), 5.7 (s, 1H, CH), 6.7–7.6 (m, 19H, Ph, NH). Its ir was identical to that of **7***N-b*.

Compound **7***U-d* was obtained by the same purification method in 40% yield; mp 70–72°C; nmr ($CDCl_3$) δ: 2.6–2.7 (b, 1H, OH exchanged with D_2O), 3.0–3.2 (b, 2H, CH_2O), 3.6 (s, 2H, CH_2CO), 3.7 (s, 3H, CH_3), 3.9–4.0 (m, 1H, C*H*—CH_2OH), 5.2 (s, 4H, $2CH_2Ph$), 5.4–5.72 (m, 1H, C*H*—NHCO, J_1 = 5 Hz and J_2 = 10 Hz and 1H, s, CH), 6.8–7.6 (m, 19H, Ph, NH); ir was identical to that of **7***U-b*; ms *m/e*: 594 (M^+) identical to that of the other diastereomer. *Anal.* calcd. for $C_{35}H_{34}O_7N_2$: C 70.71, H 5.72, N 4.71; found: C 70.69, H 5.70, N 4.69.

β-*Lactam* **7**U-f *and* **7**N-f

To β-lactam **7***N*-b (1.5 g, 0.003 mol) in 60 mL methanol was added 10% Pd/C (0.2 g), and the mixture was hydrogenated at room temperature and 40 psi for 1 h. (The pressure dropped to 37 psi.) The solution was then filtered and evaporated to give 1 g (83%) of **7***N-f*; mp 76–78°C (Et_2O); nmr ($CDCl_3$) δ: 3.4–3.6 (b, 2H, CH_2O), 3.7 (s, 2H, CH_2CO), 3.8 (s, 3H, CH_3), 4.2–4.6 (b, 2H, OH and C*H*—CH_2OH), 5.4–5.67 (q, 1H, C*H*—NHCOR, J_1 = 5 Hz and J_2 = 10 Hz), 5.7 (s, 1H, CH), 6.8–7.5 (m, 10H, Ph and NH), 8.3 (b, 1H, phenolic OH); ir (CH_2Cl_2): 3350 (OH and NH), 1760 (β-lactam), 1725 (ester), 1660 (amide) cm^{-1}; **7***U-f* was obtained by the same method in 80% yield; mp 68–69°C (Et_2O); nmr ($CDCl_3$) δ: 3.2 (b, 2H, CH_2O), 3.6 (s, 2H, CH_2CO), 3.79 (s, 3H, CH_3), 4.2 (b, 2H, OH and C*H*—CH_2OH), 5.4–5.7 (m, 2H, CH and C*H*NHCOR, J_1 = 5 Hz and J_2 = 10 Hz), 6.8–7.6 (m, 11H, Ph, NH and phenolic OH); ir (CH_2Cl_2): 3350 (OH and NH), 1760 (β-lactam), 1735 (ester), 1660 (amide) cm^{-1}; ms *m/e*: 339 (M^+ − COOMe), 148(M^+ − COOMe + $HOCH_2CH$=CHNH-$COCH_2Ph$) identical to that of the diastereomer **7***N-f*.

β-*Lactam* **8**U-f *and* **8**N-f

β-Lactam **7***N-f* (1 g, 0.0025 mol) was dissolved in 30 mL methanol. One percent aqueous NaOH (10 mL) was added dropwise over a period of 10 min. It was then stirred for 15 min and acidified with HCl to pH 3. The methanol was evaporated and the aqueous solution was extracted with ethyl acetate. Drying (Na_2SO_4) and evaporation gave 0.8 g (84%) **8***N-f*; mp 160–162°C, after dissolving in 5% aqueous $NaHCO_3$, and acidifying to pH 3; nmr ($CDCl_3$–DMSO-d_6) δ: 3.4–3.7 (b, 5H, CH_2O, CH_2CO, C*H*—CH_2OH), 5.2–5.4 (q, 1H, C*H*—NHCOR, J_1 = 5 Hz and J_2 = 10 Hz), 5.6 (s, 1H, CH), 6.8–7.4 (m, 11H, Ph, COOH, OH), 8.0 (b, 1H, NH). Addition of D_2O resulted in exchange of four protons and considerable sharpening of spectrum. Infrared (KBr): 3250–3350 (OH, NH, COOH), 1735 (β-lactam), 1710 (acid), 1625 (amide) cm^{-1}. Treatment of **8***N-f* with diazomethane resulted in quantitative formation of **7***N-f*. Compound **8***U-f* was obtained from **7***U-f* by the same method in 80% yield; mp 117–120°C; nmr was identical to that of the other diastereomer; ir (KBr): 3300–3400 (NH, OH, COOH), 1740–1730 (β-lactam and acid), 1660 (amide) cm^{-1}. Treatment of **8***U-f* with diazomethane gave **7***U-f* quantitatively.

β-*Lactam* **8**U-d *and* **8**N-d

Compounds **7***U-d* and **7***N-d* were hydrolysed to **8***U-d* and **8***N-d* in about 80% yield using the method described for the formation of **8***N-f*.

Compound **8***N-d*: mp 122–125°C; nmr ($CDCl_3$, DMSO-d_6, D_2O) δ: 3.3–3.7 (m, 5H, CH_2O, CH_2CO, C*H*—CH_2OD), 5.2 (s, 4H, $2CH_2O$), 5.3–5.5 (d, 1H, C*H*—NDCOR), 5.63 (s, 1H, CH), 6.8–7.4 (m, 18H, Ph); ir (KBr): 3200–3400 (NH, OH, COOH), 1750–1730 (β-lactam and acid), 1640 (amide) cm^{-1}; treatment of **8***N-d* with CH_2N_2 gave **7***N-d* quantitatively.

Compound **8***U-d*: mp 95–98°C; nmr was identical to that of the **8***N-d*; ir (KBr): 3200–3400 (NH, OH, COOH), 1750–1740 (β-lactam and acid), 1680 (amide) cm^{-1}; treatment of **8***N-d* with CH_2N_2 gave **7***U-d*.

β-*Lactams* **7**U-g, **7**N-g, **8**U-g, *and* **8**N-g

The **8***U-d* and **8***N-d* were debenzylated to **8***U-g* and **8***N-g* in 80% yield by catalytic hydrogenation as described for the preparation of **7***N-f*.

Compound **8***N-g*: mp 116–119°C (dec.); nmr (acetone-d_6, D_2O) δ: 3.5–3.8 (b, 5H, CH_2O, CH_2CO, C*H*—CH_2O), 5.3–5.5 (d, 1H, CH—ND—COR, J = 5 Hz), 5.6 (s, 1H, CH), 6.8–7.4 (m, 8H, Ph); ir (KBr): 2800–3500 (OH, COOH), 1750 (β-lactam), 1730 (acid), 1640 (amide) cm^{-1}. Treatment of **8***N-g* with CH_2N_2 gave **7***N-g* quantitatively.

Compound **7***N-g*: mp 84–87°C; nmr ($CDCl_3$–D_2O) δ: 3.4–3.8 (m, 8H, CH_2O, CH_2CO, CH_3, C*H*—CH_2O), 5.2–5.4 (d, 1H, C*H*—NDCOCH_2Ph, J = 5 Hz), 5.7 (s, 1H, CH), 6.5–7.4 (m, 8H, Ph); ir ($CHCl_3$): 3100–3500 (OH, NH), 1770 (β-lactam), 1740 (ester), 1680 (amide) cm^{-1}; ms *m/e*: 414 (M^+).

Compound **8***U-g*: mp 95–98°C; its nmr was identical to that of **8***N-g*; ir (KBr): 2800–3500 (OH, COOH), 1750–1740 (β-lactam, acid), 1670 (amide) cm^{-1}. It was treated with CH_2N_2 to give the corresponding methyl ester **7***U-g*; ms *m/e*: 414 (M^+).

Azido Alcohol **10**N-b *and* **10**U-b

β-Lactam **5***b* (4.68 g, 0.01 mol) in a mixture of 61 mL CH_2Cl_2 and 100 mL dry methanol was saturated with nitrogen gas at −78°C (3 min). Then a mixture of O_3 and N_2 gas was bubbled in until the KI starch paper showed excess ozone (60 min). The excess ozone was removed by passing a stream of N_2 for 10 min. The temperature was allowed to rise to −40°C, at which time was added $NaBH_4$ (0.38 g, 0.01 mol). The temperature of the solution was permitted to rise to 25°C over 2 h, following which 10 mL 10% aqueous HCl was added. The solution was evaporated to 50 mL, diluted with water, and extracted with ethyl acetate, washed with water, dried over Na_2SO_4, and evaporated to give crude product in quantitative yield.

A wash with a mixture of ether–hexane (1:14) removed benzyl alcohol, and an oily 1:1 mixture of diastereomers (3 g, 70%) of **10***N-b*/**10***U-b* was obtained as evidenced by nmr.

Chromatography on silica gel and elution with CH_2Cl_2 separated one of the diastereomers **10***N-b* in 30% yield as a foam; **10***U-b* was eluted with $CHCl_3$ in 30% yield as a foam.

Less polar diastereomer **10***N-b*: nmr ($CDCl_3$) δ: 3.4–3.8 (b, 4H, C*H*—C*H*$_2$O*H*), 3.7 (s, 1H, CH_3), 4.4–4.6 (d, 1H, C*H*—N_3, J = 5 Hz) 5.1 (s, 2H, CH_2), 5.78 (s, 1H, CH), 6.9–7.55 (m, 9H, Ph); ir (CH_2Cl_2): 3300–3500 (OH), 2100 (N_3), 1770 (β-lactam), 1740 (ester) cm^{-1}.

More polar diastereomer **10***U-b*: nmr ($CDCl_3$) δ: 2.2–2.4 (b, 1H, OH exchanged with D_2O), 3.2–3.4 (b, 2H, CH_2O), 3.6 (s, 3H, CH_3), 4.0–4.3 (m, 1H, C*H*—CH_2O), 4.75–4.9 (d, 1H,

CH—N_3, J = 5 Hz), 5.3 (s, 2H, CH_2), 5.5 (s, 1H, CH), 6.9–7.5 (m, 9H, Ph); ir (CH_2Cl_2): 3400–3600 (OH), 2100 (N_3), 1770 (β-lactam), 1750 (ester) cm^{-1}. Mass spectra showed M^+, $M^+ - COOMe$, $M^+ - (N_3CH{=}CH{-}CH_2OH)$, and $M^+ - (N_3{-}CH{=}C{=}O)$ identical to that of the **10***N-b*.

β-*Lactam* ***11***N-f

β-lactam **10***N-b* (3.8 g, 0.01 mol) was dissolved in 60 mL methanol. Pd/C (0.4 g) was added, and the mixture was hydrogenated at room temperature and 40 psi for 1.5 h. The solution was then filtered and evaporated to give 2.6 g (90%) β-lactam **11***N-f*, mp 110–113°C; nmr (DMSO-d_6) δ: 3.2 (b, 2H, NH_2), 3.6 (s, 3H, CH_3), 3.8-4.1 (m, 4H, CH_2O and *CH*—CH_2OH), 4.6 (m, 1H, *CH*—NH_2), 5.40 (s, 1*H*, CH), 6.6–7.4 (q, 5H, Ph and phenolic OH); ir (Nujol): 3000–3400 (OH, NH_2), 1760–1750 (β-lactam, ester).

Compound **11***U-f* was obtained by the same method in 90% yield, mp 100–103°C; nmr (DMSO-d_6) δ: 3.2 (b, 2H, NH_2), 3.6 (s, 3H, CH_3), 3.8–4.1 (m, 4H, CH_2O and *CH*—CH_2OH), 4.4–4.6 (m, 1H, *CH*—NH_2), 5.38 (s, 1H, CH), 6.6–7.4 (q, 5H, Ph and phenolic OH); ir was identical to that of **11***N-f*.

β-*Lactam* ***12***N-i

To a suspension of β-lactam **11***N-f* (2.6 g, 0.009 mol) in 50 mL dry CH_2Cl_2 containing triethylamine (1.01 g, 0.01 mol) was added dropwise within 5 min trimethyl silyl chloride (1.09 g, 0.01 mol) dissolved in 15 mL dry CH_2Cl_2. The solution was stirred for 30 min at room temperature, evaporated to dryness, and diethyl ether added. Filtration, and evaporation of the filtrate gave 3.4 g (88%) of **12***N-i* as an oil; nmr ($CDCl_3$) δ: 0.1–0.3 (d, 18H, 2(OSi(Me)$_3$)), 2.2–2.6 (b, 2H, NH_2), 3.8 (s, 3H, CH_3), 4.0–4.6 (m, 4H, *CH*—*CH*—CH_2—OSi), 5.4 (s, 1H, CH), 6.8–7.4 (q, 4H, Ph); ir (CH_2Cl_2): 3300–3400 (NH_2), 1750 (ester), 1770 (β-lactam) cm^{-1}.

Compound **12***U-i* was obtained by the same method in 85% yield. Its ir and nmr spectra were identical to those of **12***N-i*.

β-*Lactam* ***14***N

β-Lactam **12***N-i* (0.21 g, 0.49 mmol) and acid DL-**13** (0.2 g, 0.52 mmol) were dissolved in 40 mL dry CH_2Cl_2. EEDQ (0.13 g, 0.52 mmol) was added and the reaction mixture was stirred for 16 h at room temperature. The solution was washed with 10% aqueous HCl and 10% aqueous $NaHCO_3$, dried over $MgSO_4$, filtered, and evaporated to give 0.3 g (94%) crude product, which was chromatographed on silica gel using CH_2Cl_2 to remove all impurities. Elution with $CHCl_3$ gave 0.25 g (77.5%) of **14***N* as a foam; nmr ($CDCl_3$) δ: 1.4 (s, 9H, —CMe_3), 2.1–2.4 (m, 2H, CH_2), 3.7 (d, 6H, $2CH_3$), 4.0 (m, 5H, *CH*—CH_2OH and MeOOCC*H*—NHR), 4.5 (t, 2H, CH_2OPh), 5.4–5.6 (m, 1H, *CH*–NHCOR, after D_2O exchange, J = 5 Hz), 5.65 (s, 1H, CH), 6.8–7.1 (m, 9H, Ph, NH, phenolic OH), 8.2–8.4 (d, 2H, aromatic, J = 8 Hz); ir ($CHCl_3$): 3200–3450 (OH, NH), 1750–1760 (ester, β-lactam), 1715 (*t*-BOC), 1670–1680 (amide, ketone) cm^{-1}.

Compound **14***U* was obtained by the same method in 80% yield; ir was identical to that of diastereomer **14***N*; nmr was identical to that of **14***N* except for benzylic methine proton which showed at δ 5.5 ppm.

β-*Lactam* ***15***N

β-Lactam **14***N* (0.25 g, 0.38 mmol) was dissolved in 20 mL methanol. One percent NaOH (10 mL) was added dropwise over a period of 10 min. It was then stirred for 13 min and acidified with HCl to pH 3. The methanol was evaporated and the aqueous solution was extracted with ethyl acetate. Drying ($MgSO_4$) and evaporation gave 0.2 g (80%) crude product as foam, which was dissolved in 5% aqueous $NaHCO_3$ and after filtration was acidified with HCl to pH 3 to give 0.15 g (63%) **15***N*; mp 165–167°C (dec.); nmr (acetone-d_6–D_2O) δ: 1.4 (s, 9H, —CMe_3), 2.18–2.4 (m, 2H, CH_2), 3.6–3.9 (m, 3H, —CH_2—OD and DOOCC*H*—NDR), 4.2–4.5 (m, 3H, *CH*—CH_2OD and CH_2OPh), 5.4 (d, 1H, *CH*—NDCOR, J = 5 Hz), 5.6 (s, 1H, CH), 6.9–7.3 (m, 6H, Ph), 8.2–8.4 (d, 2H, aromatic, J = 8 Hz); ir (Nujol): 3100–3300 (OH, NH), 1740–1720 (β-lactam, acid, *t*-BOC), 1660 (amide, ketone).

Compound **15***U* was obtained by the same method in 67% yield; mp 158–160°C (dec.); ir and nmr were identical to those of **15***N*.

β-*Lactam* ***16***N

A solution of β-lactam **15***N* (0.2 g, 0.32 mmol) in 5 mL trifluoroacetic acid was stirred at room temperature for 2 h, then diethyl ether was added to give a white precipitate, which was filtered and washed three times with ether to give 0.15 g (90%) of **16***N*, becoming brown at 185°C; mp 226–220°C (dec); nmr (D_2O–$NaHCO_3$) δ: 2.0–2.4 (m, 2H, CH_2), 3.6–3.9 (b, 3H, CH_2OD and $^-OOCCH\overset{+}{N}D_3$), 4.0–4.2 (m, 1H, *CH*—CH_2OD), 4.3–4.5 (t, 2H, —CH_2OPh), 5.4–5.5 (d, 1H, *CH*ND—COR), 5.6 (s, 1H, CH), 6.9–7.4 (m, 6H, Ph), 8.2–8.4 (d, 2H, aromatic, J = 8 Hz); ir (Nujol): 3450 ~ 3100 and 2500 ~ 2700 (OH, NH_2, COOH), 1750–1730 (β-lactam, acid), 1660 (amide and ketone) cm^{-1}; λ_{max} ($EtOH–H_2O$): 226 (ε 18 500), 299 (15 800) nm .

Compound **16***U* was obtained by the same method in 92% yield; mp 185°C (brown), 215–218°C (dec); ir, nmr, and uv were identical to those of **16***N*.

β-*Lactam* ***17***N

β-Lactam **16***N* (0.15 g, 0.29 mmol) was suspended in 10 mL water. Hydroxylamine hydrochloride (0.1 g, 1.4 mmol) was added, then a saturated aqueous solution of $NaHCO_3$ was added dropwise until pH 7 was reached. The solution was heated at 50°C for 2 h. Then it was cooled and acidified to pH 3 with HCl (the volume of solution was about 20 mL). The solution was poured into a column containing Resin XAD4. All inorganic salts were removed by water, and the compound was eluted with methanol to give 0.1 g (62%) **17***N*; mp 184°C (brown), 217–220°C (dec.); nmr (D_2O–$NaHCO_3$) δ: 2.2–2.42 (2H, CH_2, m), 3.5–3.77 (b, 3H, *CH*—CH_2OD), 3.8–4.0 (t, 1H, DOOCC*H*ND_2, J = 6 Hz), 4.2–4.5 (t, 2H, CH_2O, J = 6 Hz), 5.3–5.5 (d, 1H, *CH*—NDCOR, J = 5 Hz), 5.6 (s, 1H, CH), 6.95–7.5 (m, 8H, Ph); ir (Nujol): 3400–3100 and 2500 ~ 2700 (OH, NH, COOH), 1740–1730 (β-lactam, acid), 1660 (amide), 1610 cm^{-1}; λ_{max} ($EtOH–H_2O$): 220 (ε 20 500), 273 (14 000) nm; λ_{max} (EtOH–0.1 *N* NaOH): 245 (ε 23 000), 286 (11 500) nm.

Compound **17***U* was obtained by the same method in 65% yield; mp 180°C (brown), 200–204°C (dec.); ir, nmr, and uv were identical to those of **17***N*.

Acknowledgements

We wish to thank the National Research Council of Canada and Lederle Laboratories for financial support, Drs. W. C. Curran, M. Sassiver, J. H. Boothe, and Ms. A. Ross for a generous gift of the nocardicin A sidechains (unpublished results) and Ms. N. Kuck for biological tests. One of us (G.H.H.) wishes to thank the Ministry of Science and Higher Education of Iran and University of Shiraz, for a scholarship.

1. H. Aoki, H. Sakai, M. Kohsaka, T. Konomi, J. Hosoda, T. Kubochi, E. Iguchi, and H. Imanaka. J. Antibiot. **29**, 492 (1976).
2. Y. Mine, S. Nonoyama, H. Kojo, S. Fukada, M.

NISHIDA, S. GOTO, and S. KUWAHARA. J. Antibiot. **30**, 932 (1977).
3. Y. MINE, S. NONOYAMA, H. KOJO, S. FUKADA, M. NISHIDA, S. GOTO, and S. KUWAHARA. J. Antibiot. **30**, 917 (1977).
4. H. KOJO, Y. MINE, M. NISHIDA, and T. YOKOTA. J. Antibiot. **30**, 926 (1977).
5. D. J. HART, P. A. CAIN, and D. A. EVANS. J. Am. Chem. Soc. **100**, 1548 (1978).
6. T. KAMIYA *et al. In* Recent advances in the chemistry of β-lactam antibiotics. No. 28. *Edited by* J. Elks. The Chemical Society, London, Engl. 1977. p. 290.
7. A. K. BOSE, M. S. MANHAS, J. S. CHIB, J. P. S. CHAWLA, and B. DAYAL. J. Org. Chem. **39**, 2877 (1974).
8. T. W. DOYLE, B. BELLEAU, B. YULUH, C. F. FERRARI, and M. P. CUNNINGHAM. Can. J. Chem. **55**, 468 (1977).
9. G. JUST and T. J. LIAK. Can. J. Chem. **56**, 211 (1978).
10. S. TEITEL, J. O'BRIEN, and A. BROSSI. J. Org. Chem. **37**, 3368 (1972).
11. A. M. FELIX. J. Org. Chem. **39**, 1427 (1974).
12. J. K. STILLE and R. T. FOSTER. J. Org. Chem. **28**, 2703 (1963).
13. G. H. HAKIMELAHI and G. JUST. Can. J. Chem. This issue.
14. B. BELLEAU and G. MALEK. J. Am. Chem. Soc. **90**, 1651 (1968).
15. Ger. Patent No. 2,714,628.

β-Lactams. VI. The synthesis of homocycloanalogues of nocardicin A

GHOLAM HOSEIN HAKIMELAHI AND GEORGE JUST

Department of Chemistry, McGill University, Montreal, P.Q., Canada H3A 2K6

Received October 10, 1978

GHOLAM HOSEIN HAKIMELAHI and GEORGE JUST. Can. J. Chem. **57**, 1939 (1979).

The synthesis of the title compounds is reported. It is shown that, in contrast to benzylic ketones, benzylic oximes are stable to hydrogenolysis conditions necessary for the removal of benzyl protecting groups of carboxylic acids and phenols.

GHOLAM HOSEIN HAKIMELAHI et GEORGE JUST. Can. J. Chem. **57**, 1939 (1979).

On rapporte la synthèse des composés sus-mentionnés. On a montré que, contrairement aux cétones benzyliques, les oximes benzyliques sont stables vis-à-vis les conditions d'hydrogénolyse nécessaires à l'enlèvement des groupes benzyliques utilisés pour la protection des acides carboxyliques et des phénols.

[Traduit par le journal]

We have recently described the synthesis of 4-hydroxymethylnocardicinic acid derivatives (1). In this paper, we wish to report on the cyclization of these compounds to homocyclo nocardicinic acid derivatives. Most reactions described were carried out initially on the known methyl esters of substituted phenylglycine **1***a–c*. However, β-lactam **24** could not be hydrolysed without destruction of the β-lactam ring, so that the reaction sequence was carried out on benzylesters **3***a–c*. Their reactions followed those developed for the methyl esters (1), and will be described in more detail.

Methyl glycinates **1***a–c* (1) were hydrolysed with 4% aqueous sodium hydroxide, and the amino acids **2***a–c* benzylated with thionyl chloride and benzyl alcohol (2). The resulting benzyl esters **3***a–c* were transformed to their cinnamylidene Schiff bases, **4***a–c*, and treated with azidoacetyl chloride–triethylamine in dry methylene chloride at −20°C for 1 h. An inseparable mixture of β-lactams **6***a–c* was obtained. Ozonolysis, in methylene chloride–methanol in the presence of a nitrogen stream (3), followed by sodium borohydride reduction, gave a mixture of diastereomeric alcohols **8***a–c* and **15***a–c* contaminated by some methyl ester **7***a–c* and **14***a–c*, presumably arising by transesterification. Chromatography separated isomers **8** and **15**, and their structures were assigned as described previously (1). Alcohols **8***a* and **15***a* were transformed to their respective mesylates **9***a* and **16***a*. Attempts to cyclize these mesylates in benzene containing triethylamine failed. Attempted conversion of the mesylates to their respective iodides using sodium iodide in acetone or tetra-*n*-butylammonium iodide in refluxing benzene failed, presumably because of steric hindrance (4). Successful cyclization could be achieved when alcohol **15***a* was treated with 2 equiv. of thionyl chloride and 3 equiv. of pyridine in dry benzene at 70–73°C for 7 h, in which case 70% of cyclization product **23***a* and 20% of chloro compound **11**/**18***a* were obtained. In boiling benzene, the ratio of products was reversed and 70% of the chloro compounds **11**/**18***a* were obtained, whereas at lower temperatures, little conversion took place. In the case of **15***b–c*, 80–85% of the cyclization product was obtained using the same conditions, whereas isomers **8***a–c* gave an approximately 1:1 mixture of cyclization and chloro compounds **23***a–c* and **11**/**18***a–c*. The latter compounds could be converted to the former ones in low yield by means of silver acetate refluxing in acetonitrile.

Since both diastereoisomers **8** and **15** gave one cyclization product only, we next attempted to effect cyclization without isomerisation of the benzylic proton. Alcohol **15***a* was treated with 3 equiv. of $SOCl_2$ in boiling benzene for 90 min. The resulting chlorosulfite, the structure of which was established by nmr and hydrolysis to starting alcohol **15***a*, was treated with 3 equiv. of AgOAc in boiling benzene for 2 h. Chromatographic separation gave acetate **20***a* and cyclization product **21** in 75 and 4% yield, respectively. The structure of **20***a* was deduced by comparison with **20***a*, obtained by treatment of **15***a* with boiling Ac_2O. The nmr spectrum of **21** was very similar to that of **23***a*, except for the position of the benzylic CH_2-group adjacent to the β-lactam ring, which appeared approximately 0.5 ppm downfield from the corresponding protons in **23***a*. Upon treatment of **21** with pyridine in refluxing benzene for 7 h, it was converted quantitatively to **23***a*.

The protons α to the carbobenzyloxy group and the protons of the mesylate group were clearly different in **9***a*, δ 5.6 (*CH*COOBn) and 2.85 ppm (SO_2CH_3) and **16***a*, δ 5.51 and 2.65 ppm. There was

0008-4042/79/151939-06$01.00/0

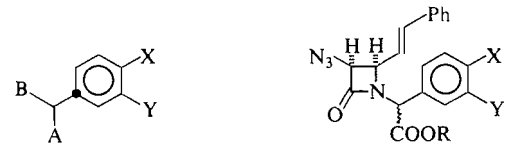

1 A = COOMe, B = NH_2
2 A = COO^-, B = NH_3^+
3 A = COOBn, B = NH_2
4 A = COOBn, B = N=CH—CH=CHPh

5 R = CH_3
6 R = Bn

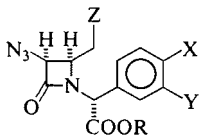

7 R = CH_3, Z = OH
8 R = Bn, Z = OH
9 R = Bn, Z = OMS
10 R = CH_3, Z = Cl
11 R = Bn, Z = Cl
12 R = Bn, Z = OSOCl
13 R = Bn, Z = OAc

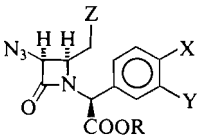

14 R = CH_3, Z = OH
15 R = Bn, Z = OH
16 R = Bn, Z = OMS
17 R = CH_3, Z = Cl
18 R = Bn, Z = Cl
19 R = Bn, Z = OSOCl
20 R = Bn, Z = OAc

(Bn = benzyl)

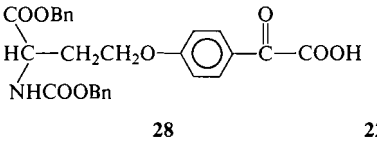

28

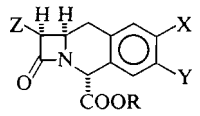

22 R = Me, Z = N_3
23 R = Bn, Z = N_3
24 R = Me, Z = $NHCOCH_2Ph$
25 R = Bn, Z = $NHCOCH_2Ph$
26 R = H, Z = $NHCOCH_2Ph$
27 R = Bn, Z = NH_2

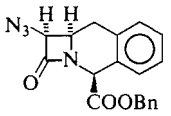

21

a X = Y = H
b X = OBn, Y = H
c X = Y = OBn
d X = OH, Y = H
e X = Y = OH

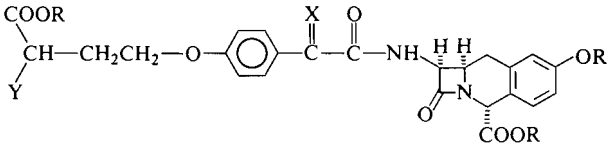

29 R = Bn, X = O, Y = NHCOOBn
30 R = H, X = H, OH, Y = NH_2
31 R = Bn, X = NOH(*syn*), Y = NHCOOBn
32 R = H, X = NOH(*syn*), Y = NH_2

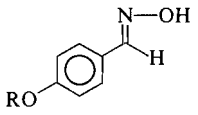

33 R = Bn
34 R = H

equally no major problem in distinguishing acetate **13***a*, δ 5.65 (CHCOOBn) and 2.1 ppm (OAc), and **20***a*, δ 5.60 and 1.98 ppm. In chlorosulfites **12***a* and **19***a*, the benzylic methine protons appeared much closer at 5.60 and 5.59 ppm. For chloro compounds **11***a* and **18***a*, all nmr signals were identical in $CDCl_3$ and C_6D_6. In order to prove that a mixture of chloro compounds **11***a*/**18***a* was obtained during the cyclization reactions using $SOCl_2$–pyridine in benzene, **11***a* and **18***a* were treated with 3 equiv. $AgNO_3$ in boiling acetonitrile for 2 h. A 30% yield of a 1:1 mixture of products of cyclization **21** and **23***a* was obtained, as established by nmr only. The two isomers could not be separated by tlc. Epimerization using pyridine in boiling benzene converted the mixture of cyclization products to the more stable **23***a* having the 'natural' nocardicin stereochemistry. In related bicyclic nocardicin precursors, Cooper *et al.* (5) have observed a similar epimerization.

Reduction of azides **22***b*,*c* and **23***b*,*c* with H_2S–Et_3N (6), followed by acylation with phenylacetylchloride in the presence of pyridine, gave **24***b*,*c* and **25***b*,*c*. Selective hydrolysis of the methyl ester function in **24***b*,*c* failed. However, catalytic debenzylation of **25***b*,*c*, using 10% Pd/C in methanol at 40 psi, gave **26***d*,*e* in good yield. Having established that the ring system was stable to reaction conditions necessary to convert the azide function to an amide bond, and to hydrogenolysis necessary to remove the benzylic blocking groups, DL-azido-β-lactam **23***b* was converted to **27***b* by means of hydrogen sulfide – triethylamine (6). Column chromatography gave pure amine, which was coupled with DL-dibenzylglyoxylic acid **28**, using EEDQ in methylene chloride. After purification an 80% yield of **29** was obtained. Catalytic hydrogenation in methanol, using Pd/C as catalyst, resulted in complete debenzylation and reduction of the keto-function to alcohol **30**, as evidenced by nmr and uv spectra, and inability to form an oxime. We next investigated if debenzylation by catalytic hydrogenation would be achieved in the presence of an oxime. We chose as a model *p*-benzyloxybenzaldehyde oxime **33**. We found that catalytic reduction in ethanol using 10% Pd/C at 35 psi for 15–30 min removed selectively the benzyl group, and that only a mixture of **33** and **34** was isolated.

Ketone **29** was converted to *syn*-oxime **31**, using hydroxylamine hydrochloride in pyridine–ethanol. Catalytic hydrogenation in ethanol for 40 min, using 10% Pd/C as catalyst, converted oxime **31** to the deblocked oxime **32** in 81% yield. Its spectral characteristics were very similar to those of nocardicin A, except for the presence of an extra CH_2-group in the nmr.

Further reduction of **32** by the method described by Hashimoto *et al.* (7), using Pd/C in water on the sodium salt of **32**, resulted in reduction of the oxime function, as evidenced by a change in uv spectrum similar to the one described (7), and presumably gave the corresponding amine. However, no attempt was made to characterize this compound because of lack of material. It should be noted that **32** was also obtained as a mixture of two racemic diastereomers.

Because of the variability of catalyst activity, it is recommended that the reduction be carried out first on model compound **33**, and the results obtained on **33** be transposed to the nocardicin derivative. It is also imperative that the sample to be debenzylated be completely sulphur free, as judged by absence of odor.

Biological Tests

None of the nocardicin A analogs prepared showed notable activity against 32 strains of pathogenic microorganisms (1).

Experimental

For general procedures, see ref. 1.

Amino Acids **2**b,c

Amino esters **1***b,c* (0.036 mol) were stirred in 4% aqueous NaOH (40 mL) for 10 min and acidified with HCl to pH 3. The colourless precipitate was filtered, washed with water, and dried. Compounds **2***b,c* were obtained in about 90% yield; **2***b* mp 270–273°C (dec.); nmr (DMSO-d_6) δ: 5.05 (s, 1H, CH), 5.1 (s, 2H, CH_2), 7.05–7.61 (m, 9H, Ph), 11.4–11.6 (b, 3H, NH_3^+); **2***c* mp 259–261°C (dec.); its nmr spectra was similar to that of the **2***b* except for variations due to aromatic substituents.

Amino Esters **3**a–c

Amino acids **2***a–c* (0.027 mol) were suspended in benzyl alcohol (200 mL) at 0–5°C. Thionyl chloride (30 mL) was added slowly, over a period of 20 min. Then the reaction mixture was heated at 90°C while stirring for 5 h. Then it was cooled and dry diethyl ether added. The white precipitate was filtered and washed three times with ether. Compounds **3***a–c*·HCl were obtained in approximately 65% yield, except for **3***c*·HCl which was obtained in 40% yield; **3***a*, mp 235–236°C; **3***b*, 225–226°C; **3***c*, 210–212°C. All compounds obtained had nmr spectra similar to those described for the amino acids except for additional benzyl ester peaks. All hydrochlorides were converted to the parent amine **3** according to the following procedure: Compound **3***b*·HCl (6.8 g, 0.017 mol) was mixed with 50 mL of saturated aqueous $NaHCO_3$ and the resulting amine **3***b* extracted into 50 mL of ether. After evaporation 5 g of **3***b* (82% yield) was obtained as an oil; nmr ($CDCl_3$) δ: 2.0–2.1 (b, 2H, NH_2 exchanged with D_2O), 4.6 (s, 1H, CH), 5.0–5.02 (d, 4H, $2CH_2$), 6.8–7.6 (m, 14H, Ph); ir (CH_2Cl_2): 3300–3400 (NH_2), 1740 (ester) cm^{-1}.

Schiff Base **4**a–c

All the Schiff bases were prepared in a similar manner and used without purification. The following is a representative procedure: To a solution of **3***b* (5 g, 0.014 mol) in 100 mL dry CH_2Cl_2 was added cinnamaldehyde (1.9 g, 0.014 mol). The solution was brought to reflux and the CH_2Cl_2 distilled slowly with the constant addition of dry CH_2Cl_2. After ~10 h the solution was cooled and $MgSO_4$ was added. After 3 h, it was filtered and evaporated to yield 6.9 g Schiff base **4***b* as an oil; nmr ($CDCl_3$) δ: 5.15–5.27 (m, 5H, $2CH_2$ and CH), 7.0–7.6 (m, 21H, Ph and CH=CH), 8.0–8.2 (m, 1H, CH=N); ir (CH_2Cl_2): 1735 (ester), 1635 cm^{-1} (HC=N). In the case of **4***c*, the yield seemed to be somewhat lower (80%) as ascertained by nmr.

Azido-β-lactams **5**/**6**a–c

For preparation of these β-lactams, see ref. 1. Their spectra were similar to those described in the previous paper except for ester variations and variations due to aromatic substituents. All their mass spectra showed $M^+ - N_2$.

4-Hydroxymethyl-β-lactams **7**a, ***14***a, **7**b, ***14***b, **7**c, ***14***c, ***8***a, ***15***a, ***8***b, ***15***b, ***8***c, *and* ***15***c

The mixtures of diastereomeric β-lactams **5***a*, **5***b*, **5***c*, **6***a*, **6***b*, and **6***c* were submitted to identical reaction conditions and separation procedures which will be described for **6***b* only. All their mass spectra showed M^+, $M^+ - COOR$, $M^+ - (N_3CH{=}CH{-}CH_2OH)$, and $M^+ - (N_3{-}CH{=}C{=}O)$ except for **8***b*, **15***b*, **8***c*, and **15***c* which showed no molecular ion but $M^+ - (N_3CH{=}CHCH_2OH)$ and $M^+ - (N_3{-}CH{=}C{=}O)$.

β-Lactam **6***b* (5.44 g, 0.01 mol) in a mixture of 60 mL CH_2Cl_2 and 100 mL dry methanol was saturated with nitrogen gas at −78°C (3 min). Then a mixture of O_3 and N_2 gas was bubbled in until the KI starch paper showed excess ozone (60 min). The excess ozone was removed by passing a stream of N_2 for 10 min. The temperature was allowed to rise to −40°C, at which time was added $NaBH_4$ (0.38 g, 0.01 mol). The temperature of the solution was permitted to rise to 25°C over 2 h, following which 10 mL 10% aqueous HCl was added. The solution was evaporated to 50 mL, diluted with water, extracted with ethyl acetate, washed with water, dried over Na_2SO_4, and evaporated to give crude product in quantitative yield.

A wash with a mixture of ether–hexane (1:14) removed benzyl alcohol, and an oily 1:1 mixture of diastereomers (3 g, 63%) of **8**/**15***b* contaminated with approximately 5% **7**/**14***b* was obtained, as evidenced by nmr.

Chromatography on silica gel and elution with CH_2Cl_2 separated one of the diastereomers **8***b* in 30% yield as a foam. Compound **15***b* was eluted with $CHCl_3$ in 30% yield as a foam.

Less polar diastereomer **8***b*: nmr ($CDCl_3$) δ: 3.4–3.8 (b, 4H, *CH—CH*$_2$*OH*), 4.4–4.6 (d, 1H, *CH*—N_3, J = 5 Hz), 5.0–5.2 (d, 4H, $2CH_2$), 5.78 (s, 1H, CH), 6.9–7.55 (m, 14H, Ph); ir (CH_2Cl_2): 3300–3500 (OH), 2100 (N_3), 1770 (β-lactam), 1740 (ester) cm^{-1}. More polar diastereomer **15***b*: nmr ($CDCl_3$) δ: 2.2–2.4 (b, 1H, OH exchanged with D_2O), 3.2–3.4 (b, 2H, CH_2O), 4.0–4.3 (m, 1H, *CH*—CH_2O), 4.75–4.9 (d, 1H, *CH*—N_3, J = 5 Hz), 5.01–5.3 (d, 4H, $2CH_2$), 5.5 (s, 1H, CH), 6.9–7.5 (m, 14H, Ph); ir (CH_2Cl_2): 3400–3600 (OH), 2100 (N_3), 1770 (β-lactam), 1750 (ester) cm^{-1}.

Compound **8***c* was obtained by the same purification method as **8***b* in 35% yield; nmr ($CDCl_3$) δ: 3.4–3.8 (b, 4H, *CH—CH*$_2$*OH*, exchanged with D_2O), 4.3–4.5 (d, 1H, *CH*—N_3,

J = 5 Hz), 5.0–5.2 (m, 6H, $3CH_2$), 5.71 (s, 1H, CH), 6.8–7.6 (m, 18H, Ph); ir was identical to that of **8***b*.

Compound **15***c* was obtained by the same purification method as **15***b* in 35% yield; nmr ($CDCl_3$) δ: 2.2–2.4 (b, 1H, OH exchanged with D_2O), 3.1–3.25 (d, 2H, CH_2O, J = 6 Hz), 3.8–4.2 (m, 1H, C*H*—CH_2O), 4.8–4.98 (d, 1H, CH—N_3, J = 5 Hz), 5.1–5.3 (m, 6H, $3CH_2$), 5.7 (s, 1H, CH), 7.0–7.7 (m, 18H, Ph); ir was identical to that of **15***b*.

Compound **8***d* was obtained by the same purification method as **8***b* in 40% yield; nmr ($CDCl_3$) δ: 3.4–3.8 (b, 4H, C*H*—C*H*$_2$ O*H* exchanged with D_2O), 4.4–4.6 (d, 1H, CH—N_3, J = 5 Hz), 5.8 (s, 1H, CH), 7.4 (d, 10H, Ph); ir was identical to that of **8***b*.

Compound **15***a* was obtained by the same purification method as **15***b* in 40% yield; nmr ($CDCl_3$) δ: 2.2–2.4 (b, 1H, OH exchanged with D_2O), 3.2–3.37 (d, 2H, CH_2O, J = 6 Hz), 4.0–4.3 (m, 1H, C*H*—CH_2O), 4.75–4.9 (d, 1H, C*H*—N_3, J = 5 Hz), 5.5 (s, 1H, CH), 7.4 (d, 10H, Ph); ir was identical to that of **15***b*.

Compounds 7*a*, **7***b*, and **7***c* were obtained by the same purification method as **8***b* in 50% yield. Their nmr were similar to that of **8***b* except for their ester variation and variations due to aromatic substituents. Their ir spectra were identical to that of **8***b*.

Compounds **14***a*, **14***b*, and **14***c* were obtained by the same purification method as **15***b* in 40% yield. Their nmr were similar to that of the **15***b* except for their ester variation and variations due to aromatic substituents. Their ir spectra were identical to that of **15***b*.

Mesylates **9**a *and* ***16***a

To β-lactam **15***a* (0.366 g, 1 mmol) and NEt_3 (0.101 g, 1 mmol) in 50 mL dry CH_2Cl_2 was added dropwise at −20°C (dry ice – CCl_4) a solution of mesyl chloride (0.115 g, 1 mmol) in 10 mL dry CH_2Cl_2 over a period of 5 min. The solution was stirred for 30 min and evaporated to dryness. The residue was dissolved in ether, filtered, and evaporated to give 0.4 g (90%) of crude product. Chromatography on silica gel using $CHCl_3$ as eluent gave **16***a* as an oil in 80% yield, nmr ($CDCl_3$) δ: 2.65 (s, 3H, CH_3), 3.62–3.82 (t, 2H, CH_2O, J_1 = 6 Hz, J_2 = 11 Hz), 4.2–4.5 (m, 1H, C*H*—CH_2O), 4.8–4.96 (d, 1H, C*H*—N_3, J = 5 Hz), 5.2 (s, 2H, CH_2), 5.51 (s, 1H, CH), 7.38 (d, 10H, Ph); ir (CH_2Cl_2): 2100 (N_3), 1780 (β-lactam), 1750 (ester) cm^{-1}.

Compound **9***a* was obtained by the same method in 80% yield; nmr ($CDCl_3$) δ: 2.85 (s, 3H, CH_3), 3.62–3.82 (t, 2H, CH_2O, J_1 = 6 Hz, J_2 = 11 Hz), 4.25–4.5 (m, 1H, C*H*—CH_2O), 4.6–4.78 (d, 1H, *CH*—N_3, J = 5 Hz), 5.19 (s, 2H, CH_2), 5.6 (s, 1H, CH), 7.4 (d, 10H, Ph); ir was identical to that of **16***a*.

Isomerization of Mesylates **9**a *and* ***16***a

Compound **9***a* or **16***a* was refluxed with 3 equiv. pyridine in dry benzene and gave **9***a*/**16***a* (1:1) quantitatively, as determined by nmr.

Chlorosulfites ***12***a/***19***a

To a mixture of β-lactams **8***a*/**15***a* (0.183 g, 0.5 mmol) in 40 mL dry benzene was added thionyl chloride (0.36 g, 3 mmol). The solution was refluxed for 90 min and evaporated to dryness to give **12***a*/**19***a* quantitatively; nmr ($CDCl_3$) δ: 3.8 (m, 2H, CH_2O), 4.4–4.8 (m, 2H, C*H*—C*H*—N_3), 5.2 (s, 2H, CH_2), 5.59–5.60 (d, 1H, CH), 7.38 (d, 10H, Ph).

Compounds **12***a*/**19***a* were treated with water and extracted with ether to give quantitatively **8***a*/**15***a*.

Chloroesters ***10***b,c/***17***b,c *and* ***11***a–c/***18***a–c

All β-lactams were obtained in an identical manner in approximately 70% yield. Their spectra were similar except for the ester variations and variations due to aromatic substituents. All their mass spectra showed M^+.

The following is a representative procedure.

To β-lactams **8***b*/**15***b* (1 g, 0.002 mol) in 60 mL dry benzene was added pyridine (0.474 g, 0.006 mol). The solution was brought to reflux and thionylchloride (0.6 g, 0.004 mol) was added. After 2 h it was cooled and 50 mL of ether was added. The solution was washed with water, dried over $MgSO_4$, and evaporated to give 0.8 g (85%) of **11***b*/**18***b* as an oil; nmr ($CDCl_3$) δ: 3.8–4.1 (b, 3H, C*H*—*CH*$_2$Cl), 4.7 (d, 1H, C*H*N_3, J = 5 Hz), 5.13–5.23 (d, 4H, $2CH_2$), 5.6 (s, 1H, CH), 7.0–7.6 (m, 14H, Ph); ir (CH_2Cl_2): 2100 (N_3), 1760 (β-lactam), 1750 (ester) cm^{-1}; ms *m*/*e*: 490–492 (M^+). By this method about 10% **23***b* was obtained as ascertained by nmr.

β-*Lactams* ***22***a–c *and* ***23***a–c

All β-lactams were obtained in an identical manner in approximately 70–80% yield using method I and 50% yield using method II. Their spectra were similar except for the ester variations and variations due to aromatic substituents. All their mass spectra showed $M^+ - (N_3CH{=}C{=}O)$, except for **23***c* in which case no good mass spectrum was obtained.

The following is a representative procedure.

Method I

To β-lactam **15***b* (1 g, 0.002 mol) in 60 mL dry benzene was added pyridine (0.474 g, 0.006 mol). Thionylchloride (0.6 g, 0.004 mol) was added. The solution was kept at 70–73°C (bath temperature) for 7 h. Then it was cooled, diluted with 50 mL of ether, and washed with water, 5% aqueous HCl, dried over $MgSO_4$, and evaporated to give 90% of crude product. Chromatography on silica gel and elution with CH_2Cl_2 gave first 15% of **11***b*/**18***b*, as ascertained by nmr, and then 0.75 g (80%) **23***b* as an oil; nmr ($CDCl_3$) δ: 2.7–3.4 (m, 2H, CH—*CH*$_2$Ph), 4.3–4.6 (m, 1H, *CH*—CH_2Ph), 4.81–5.0 (d, 1H, *CH*N_3, J = 5 Hz), 5.1–5.3 (d, 4H, $2CH_2$), 6.8–7.5 (m, 13H, Ph); ir (CH_2Cl_2): 2100 (N_3), 1775 (β-lactam), 1750 (ester) cm^{-1}; ms *m*/*e*: 371 ($M^+ - N_3CH{=}C{=}O$).

Method II

Chloro compounds **11***b*/**18***b* (0.8 g, 0.0016 mol) and AgOAc (4 equiv.) in 60 mL dry CH_3CN were refluxed for 2 h. Then it was filtered and evaporated to dryness. The residue was dissolved in 50 mL ether and after filtration was evaporated to give 0.7 g product containing ~50% **23***b* and ~50% starting material as ascertained by nmr. These compounds have about the same polarity and could be separated with difficulty only by column chromatography using silica gel and eluted with CH_2Cl_2.

β-*Lactams* ***20***a, ***21***, ***13***a, *and* ***23***a

β-Lactam **15***a* (0.366 g, 0.001 mol) in 60 mL dry benzene containing thionylchloride (0.36 g, 0.003 mol) was refluxed for 90 min. Silver acetate (4 equiv.) was then added and refluxing continued for 2 h. Then it was filtered and evaporated to dryness. The residue was dissolved in 40 mL ether and after filtration was evaporated to give 0.3 g product containing ~80% **20***a* and ~10% **21** as ascertained by nmr; purification by column chromatography using silica gel and elution with CH_2Cl_2 gave ~4% of **21** contaminated with a trace of **20***a* as an oil, and ~75% of **20***a* contaminated with a trace of **21** as an oil.

Compound **20***a*: nmr ($CDCl_3$) δ: 1.98 (s, 3H, CH_3), 3.78 (d, 2H, CH_2O), 4.4 (m, 1H, *CH*—CH_2O), 4.8–4.91 (d, 1H, *CH*—N_3, J = 5 Hz), 5.23 (s, 2H, CH_2), 5.6 (s, 1H, CH), 7.4 (s, 10H, Ph); ir (CH_2Cl_2): 2100 (N_3), 1760 (β-lactam), 1740–1750 (ester) cm^{-1}.

Compound **21**: nmr ($CDCl_3$) δ: 3.2–3.9 (m, 2H, CH—*CH*$_2$-Ph), 4.4 (m, 1H, *CH*CH_2Ph), 4.83–4.97 (d, 1H, C*H*—N_3,

J = 5 Hz), 5.23 (s, 2H, CH_2), 5.58 (s, 1H, CH), 7.4 (s, 9H, Ph); ir (CH_2Cl_2): 2100 (N_3), 1770 (β-lactam), 1750 (ester) cm^{-1}; ms *m/e*: 348 (M^+).

Boiling **21**, which contained approximately 5% **20***a*, and 2 equiv. pyridine in benzene for 7 h gave quantitatively **23***a* and a trace of an isomeric mixture of **20***a*/**13***a* as ascertained by nmr.

β-*Lactams* ***24***b,c *and* ***25***b,c

All transformations were performed in an identical manner in approximately 75% yield. Their spectra were similar except for the ester variations and variations due to aromatic substituents. All their mass spectra showed $M^+ - (PhCH_2CONHCH{=}C{=}O)$, except for **25***c* which gave a poor mass spectrum but satisfactory microanalysis results.

The following is a representative procedure.

To a solution of β-lactam **23***c* (1.5 g, 2.4 mmol) in 60 mL dry CH_2Cl_2 at 0°C was added triethylamine (0.24 g, 2.4 mmol). A stream of H_2S gas was bubbled in for 20 min. The solution was stirred for 2 h at room temperature. Evolution of nitrogen gas was observed. A stream of nitrogen gas was bubbled in for 20 min, then 0.46 g (0.006 mol) pyridine was added, followed by dropwise addition of 0.36 g (0.0024 mol) phenyl acetyl-chloride in 15 mL CH_2Cl_2. The solution was stirred for 2 h at 0–10°C, washed with 5% aqueous HCl, 5% aqueous $NaHCO_3$, and brine. It was then dried over $MgSO_4$, and evaporated to give quantitatively impure amide **25***c*, which was chromatographed on silica gel. Methylene chloride eluted impurities, and chloroform gave 1 g (90%) of β-lactam **25***c* as a foam. Recrystallization from absolute ethanol gave 0.88 g (80%) of **25***c*; mp 140–142°C; nmr ($CDCl_3$) δ: 2.9–3.1 (m, 2H, CH—CH_2 Ph), 3.6 (s, 2H, CH_2CO), 4.2–4.41 (m, 1H, *CH*—CH_2Ph), 5.1–5.2 (d, 6H, $3CH_2$), 5.21–5.59 (q, 1H, *CH*—*NHCOCH*$_2$Ph, J_1 = 5 Hz, J_2 = 10 Hz), 5.6 (s, 1H, CH), 6.4–6.6 (d, 1H, NH), 6.9–7.6 (m, 22H, Ph); ir (CH_2Cl_2): 3350–3400 (NH), 1770 (β-lactam), 1750 (ester), 1670 (amide) cm^{-1}. *Anal.* calcd. for $C_{41}H_{36}N_2O_6$: C 75.44, H 5.56, N 4.29; found: C 75.45, H 5.56, N 4.17.

β-*Lactams* ***26***d *and* ***26***e

Both β-lactams **25***b* and **25***c* were submitted to identical hydrogenolysis procedures, and gave **26***d* and **26***e* in about 70% yield. Their spectra were similar except for variations due to aromatic substituents. Their mass spectra showed no M^+ but $M^+ - (PhCH_2CONHCH{=}C{=}O)$ while their corresponding methyl esters **24***d* and **24***e* showed M^+.

The following is a representative procedure.

To β-lactam **25***b* (1 g, 0.0018 mol), in 50 mL methanol was added 10% Pd/C (0.5 g), and the mixture was hydrogenated at room temperature and 40 psi for 1.5 h. The solution was filtered and evaporated to give 0.5 g (72%) of **26***d*; mp 147–150°C (dec.); nmr ($CDCl_3$:DMSO-d_6:D_2O), 1:1:3 drops) δ: 2.7–3.4 (m, 2H, CH—*CH*$_2$Ph), 3.61 (s, 2H, CH_2CO), 4.3 (m, 1H, *CH*—CH_2Ph), 5.3–5.38 (d, 1H, *CH*—*NDCOCH*$_2$Ph J = 5 Hz in the absence of D_2O, q, 1H, J_1 = 5 Hz and J_2 = 10 Hz), 5.45 (s, 1H, CH), 6.9–7.4 (m, 8H, Ph); ir (KBr): 3600 ~ 2700 (NH, OH, COOH), 1760 (β-lactam), 1720 (acid), 1660 (amide) cm^{-1}; ms *m/e*: 191 ($M^+ - PhCH_2CONHCH{=}C{=}O$). Treatment of **26***d* with CH_2N_2 gave **24***d* quantitatively as a foam; ms *m/e*: 380 (M^+).

β-*Lactam* ***27***b

β-Lactam **23***b* (0.5 g, 1 mmol) was dissolved in 50 mL dry CH_2Cl_2. Triethyl amine (0.12 g, 1.2 mmol) was added at 0°C. A stream of hydrogen sulfide gas was bubbled in for 15 min. The solution was stirred at room temperature for 2 h. Evolution of nitrogen gas was observed. A stream of nitrogen gas was bubbled in for 15 min. The mixture was washed with water (two times), dried, and evaporated. The oily product was purified by column chromatography using silica gel, all impurities were eluted with CH_2Cl_2 and compound **27***b* (0.4 g, 90%) was eluted with $CHCl_3$ as an oil; nmr ($CDCl_3$) δ: 1.8–2 (b, 2H, NH_2, exchangeable with D_2O), 3.1 (d, 2H, CH_2, J = 6 Hz), 4.0–4.5 (m, 2H, —*CH*—*CH*—NH_2), 5.1–5.3 (d, 4H, $2CH_2Ph$), 5.6 (s, 1H, CH), 6.83–7.6 (m, 13H, Ph); ir (CH_2Cl_2): 3300–3350 (NH_2), 1750 (ester), 1770 (β-lactam) cm^{-1}.

β-*Lactam* ***29***

β-Lactam **27***b* (0.4 g, 0.9 mmol) and acid **28** (0.491 g, 1 mmol) were dissolved in 50 mL CH_2Cl_2. EEDQ (0.247 g, 1 mmol) was added and stirred for 16 h at room temperature. The solution was washed with 5% aqueous HCl and 5% aqueous $NaHCO_3$, dried over $MgSO_4$, filtered, and evaporated to give 0.9 g (99%) of crude **29** which was chromatographed on silica gel using CH_2Cl_2 to remove impurities. Elution with $CHCl_3$ gave 0.7 g (85%) of **29** as a foam; nmr ($CDCl_3$) δ: 2.39 (m, 2H, CH_2), 3.1 (m, 2H, $PhCH_2$—CH), 3.9–4.15 (t, 2H, *CH*—CH_2 and BnOOC—*CH*—NHR, J = 6 Hz), 4.4–4.6 (t, 2H, CH_2OPh, J = 6 Hz, 5.1–5.3 (q, 8H, $4CH_2Ph$), 5.38–5.6 (q, 1H, *CH*—NHCOR, J = 5 Hz), 5.62 (s, 1H, CH), 6.8–8.4 (q, 4H, Ph, J = 8 Hz), 7.0–7.4 (m, 25H, Ph, NH); ir (CH_2Cl_2): 3400 (NH), 1770 (β-lactam), 1745 (ester), 1725 (BnOCO), 1665 (amide, ketone) cm^{-1}.

β-*Lactam* ***30***

β-Lactam **29** (0.2 g, 0.22 mmol) was dissolved in 30 mL methanol; 10% Pd/C (0.1 g) was added, and the mixture was hydrogenated at room temperature and 40 psi for 40 min. The solution was then filtered and evaporated to give 0.09 g (81%) of **30**; mp 181°C (brown), 200–205°C (dec.); nmr (D_2O–$NaHCO_3$) δ: 2.38 (m, 2H, CH_2), 3.2 (m, 2H, Ph—CH_2CH), 3.6 (m, 1H, *CH*—CH_2), 3.8 (t, 1H, $^-OOCCHND_3^+$, J = 6 Hz), 4.2 (m, 2H, CH_2OPh), 5.3 (d, 1H, CH—NDCOR, J = 5 Hz), 5.4 (s, 1H, CH), 5.5–5.8 (d, 1H, CH—OD), 6.9–7.5 (m, 7H, Ph); ir (Nujol): 3400–3100 and 2500 ~ 2700 (OH, NH, COOH), 1760 (β-lactam), 1720 (acid), 1660 (amide), 1610 cm^{-1}; λ_{max} (EtOH–H_2O): 225 (ε 18 000), 272 (2000) nm.

β-*Lactam* ***31***

β-Lactam **29** (0.2 g, 0.22 mmol) was dissolved in a mixture of 5 mL ethanol and 5 mL pyridine. Hydroxylamine hydrochloride (0.2 g, 2.8 mmol) was added. The solution was warmed at 70°C for 2 h. Then 50 mL chloroform was added and solution washed with 5% aqueous HCl. Then it was dried over Na_2SO_4, filtered, and evaporated to give 0.2 g (90%) crude **31** which was purified by column chromatography using silica gel. Elution with $CHCl_3$–EtOAc (1:1) gave 0.15 g (71%) **31** as a foam; nmr ($CDCl_3$) δ: 2.2 (b, 2H, CH_2), 3.1 (m, 2H, $PhCH_2CH$), 3.8–4.0 (b, 3H, *CH*—CH_2, *BnOOCCHNHCOR*, OH), 4.3–4.6 (m, 2H, CH_2OPh), 5.0–5.2 (q, 8H, $4CH_2Ph$), 5.3–5.5 (q, 1H, *CH*—NHR, J = 5 Hz), 5.6 (s, 1H, CH), 6.6–7.4 (m, 29H, Ph and 2NH); ir (CH_2Cl_2): 3300–3450 (OH, NH), 1775 (β-lactam), 1750–1730 (ester and BnOCO), 1680 (amide), 1520 (oxime) cm^{-1}; λ_{max}(EtOH): 273 (ε 15 000) nm.

β-*Lactam* ***32***

β-Lactam **31** (0.15 g, 0.16 mmol) was dissolved in 30 mL absolute ethanol; 10% Pd/C (0.075 g) was added, and the mixture was hydrogenated at room temperature and 35 psi for 40 min. The solution was then filtered and evaporated to give 0.07 g (81%) of **32**; mp 160°C (brown), 186–189°C (dec.); nmr (D_2O–$NaHCO_3$) δ: 2.4 (m, 2H, CH_2), 3.1 (m, 2H, $PhCH_2CH$), 3.6 (m, 1H, *CH*—CH_2), 4.0 (t, 1H, $^-OOCCHND_3^+$), 4.4 (t, 2H, CH_2OPh, J = 6 Hz), 5.3 (d, CH—NDR, J = 5 Hz), 5.5 (s, 1H, CH), 6.9–7.5 (m, 7H, Ph); ir (Nujol):

3400–3100 and 2500 ~ 2700 (OH, COOH, NH), 1755 (β-lactam), 1720 (acid), 1660 (amide), 1610 cm^{-1}; λ_{max} (EtOH–H_2O): 221 (ε 20 800), 272 (14 500) nm; λ_{max} (EtOH – 0.1 *N* NaOH): 246 (ε 23 500), 286 (12 000) nm.

Acknowledgements

We wish to thank the National Research Council of Canada and Lederle Laboratories for financial support, Drs. W. C. Curran, M. Sassiver, and H. A. Boothe and Ms. A. Ross for a generous gift of the nocardicin A sidechains (unpublished results) and Ms. N. Kuck for biological tests. One of us (G.H.H.) wishes to thank the Ministry of Science and Higher Education of Iran and University of Shiraz for a scholarship.

1. G. H. HAKIMELAHI and G. JUST. Can. J. Chem. This issue.
2. R. P. PATEL and S. PRICE. J. Org. Chem. **30**, 3575 (1965).
3. J. K. STILLE and R. T. FOSTER. J. Org. Chem. **28**, 2703 (1963).
4. T. W. DOYLE, B. YULUH, D. T. WUCHU, and B. BELLEAU. Can. J. Chem. **55**, 2719 (1977).
5. G. A. KOPPEL, L. MCSHANE, F. JOSE, and R. D. G. COOPER. J. Am. Chem. Soc. **100**, 3933 (1978).
6. T. W. DOYLE, B. BELLEAU, B.-Y. LUH, C. F. FERRARI, and M. P. CUNNINGHAM. Can. J. Chem. **55**, 468 (1977).
7. M. HASHIMOTO, T. KOMORI, and T. KAMIYA. J. Antibiot. **29**, 890 (1975).

β-Lactams. VII.[1] The synthesis of 3-vinyl and 3-isopropenyl 4-substituted azetidinones

ROBERT ZAMBONI[2] AND GEORGE JUST

Department of Chemistry, McGill University, Montreal, P.Q., Canada H3A 2K6

Received November 21, 1978

ROBERT ZAMBONI and GEORGE JUST. Can. J. Chem. **57**, 1945 (1979).

The reaction of crotonyl and dimethylacryloyl chloride with various Schiff bases is described. The resulting β-lactams derived from aliphatic amines all have a *cis* stereochemistry.

ROBERT ZAMBONI et GEORGE JUST. Can. J. Chem. **57**, 1945 (1979).

On décrit la réaction des chlorures de crotonyle et de dimethyl acrylyl avec des bases de Schiff. Ces β-lactames dérivés d'amines aliphatiques ont tous la stéréochemie *cis*.

The addition of azidoacetyl chloride to imines, as developed by Bose and used by several groups (1–4), has proven to be a powerful method for preparing β-lactam antibiotics. We wished to know if a similar methodology using crotonyl chloride (CC) or dimethylacryloyl chloride (DAC) could lead to the formation of β-lactams **1** which could be transformed to thienamycins **2***a*,*b*.

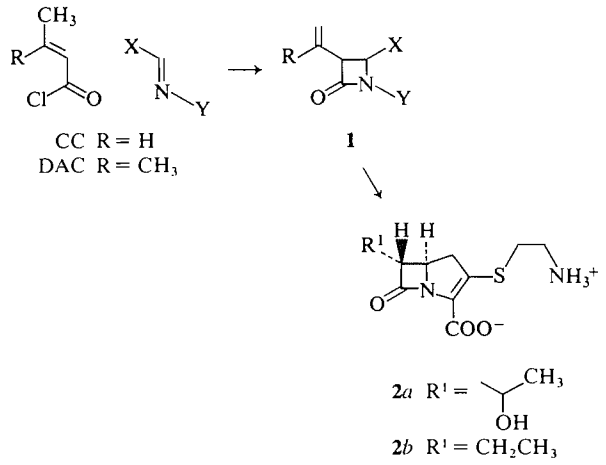

In this paper, we describe the addition of CC or DAC chloride to some Schiff bases derived from aromatic and aliphatic amines and cinnamaldehyde, furfural, or methyl glyoxylate (3).

Bose briefly reported that reaction of benzylidene aniline **3***a* and CC gave the corresponding *trans*-β-lactam **4***a* exclusively in fair yield (5), and we have confirmed this result, carrying out the reaction in methylene chloride both at room temperature and at reflux.

Much to our surprise, reaction of cinnamylidene aniline **3***b* with CC containing triethylamine in methylene chloride, conditions which were used throughout the paper, gave at room temperature a 5:1 mixture of *cis* and *trans* β-lactams **5***b* and **4***b* in approximately 30% yield. In boiling methylene chloride, this ratio was inverted, and the yield increased to 40–45%. Separation could be effected with considerable losses by flash chromatography (6). The *cis* isomer **5***b* showed a coupling constant $J_{3,4} = 6$ Hz, while *trans* isomer **4***b* showed $J_{3,4} = 2.5$ Hz. The coupling constants were typical for all the β-lactams obtained and the yields reported are based on the integration of the appropriate ^{1}Hmr signals. When furfurylidene Schiff base **3***d* was treated with either CC or DAC, an approximately 70% yield of *trans* lactams **4***d* or **4***e* was obtained. As was found out in the course of many reactions, CC or DAC could be used interchangeably with little variation in yield or stereochemistry of product obtained.

When ethyl benzylidene glycinate (**6***a*, R=Ph) was heated with DAC–triethylamine at 20°C or reflux,

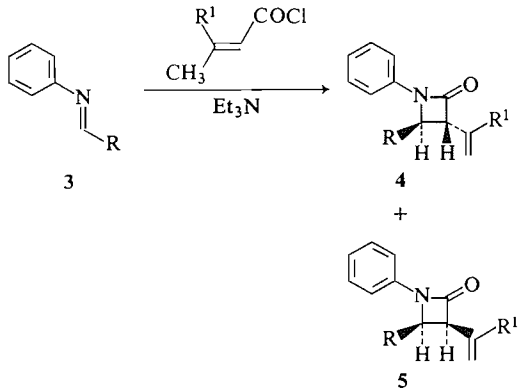

		Temp. (°C)	Yield *trans* (%)	Yield *cis* (%)
a	R = Ph, R^1 = H	20–39	40	
b	R = CH=CH—Ph, R^1 = H	20	5	25
c	R = CH=CH—Ph, R^1 = H	39	35	7
d	R = furfuryl, R^1 = H	39	70	
e	R = furfuryl, R^1 = CH$_3$	39	70	

[1]For preceding papers, see papers published by Just in this journal in the years 1977–1978.

[2]Holder of a NRCC Postgraduate Scholarship, 1974–1978.

0008-4042/79/151945-04$01.00/0

little if any β-lactam could be detected in the reaction product. However, the cinnamylidene Schiff bases of either ethyl glycinate **6***a* or serine derivative **6***b* (2) give a good yield of adduct **7***a* or **7***b* having *cis* configuration. Similarly, the furfurylidene derivative of serine **6***c* gave exclusively *cis* β-lactam **7***c*, albeit in a more modest yield.

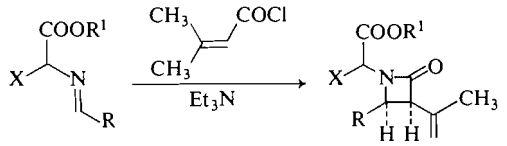

6 **7**

a R = CH=CHPh, X = H, R¹ = CH_2CH_3
b R = CH=CHPh, X = $CH_2OTBDMS$, R¹ = CH_3
c R = furfuryl, X = $CH_2OTBDMS$, R¹ = CH_3

Similar results were obtained with the cinnamylidene Schiff base of diethylaminomethyl phosphonate **8***a* (7) and its corresponding furyl derivative **8***b* (synthesized from furfuraldehydediazine using the procedure of Rachon and Wasielewski (8)), which both gave the corresponding *cis* β-lactams **9***a* and **9***b* in good yield. Glyoxylic ester derivative **10** (3) also afforded *cis* β-lactams **11** and **12** with CC and DAC respectively.

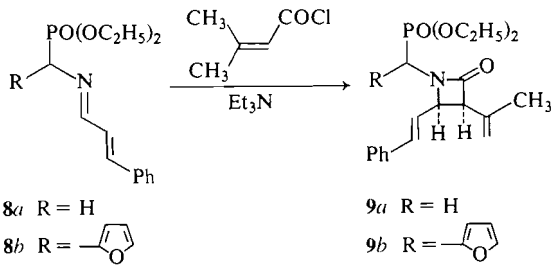

8*a* R = H
8*b* R =

9*a* R = H
9*b* R =

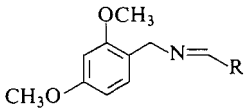

10 R = $COOCH_3$

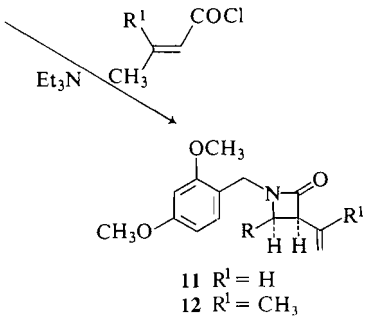

11 R^1 = H
12 R^1 = CH_3

The behaviour of DMAC and CC is similar to that of azidoacetyl chloride, in that its addition to cinnamylidene and glyoxylic ester Schiff bases of aliphatic amines gave exclusively *cis* adducts. With cinnamylidine aniline one obtains mixtures. It may be recalled that with azidoacetyl chloride one obtains *cis* β-lactams with cinnamylidene Schiff bases derived from aromatic amines with pk_a's $\geq$ 2.4, while one obtains mixtures or pure *trans* β-lactams with imines derived from aromatic amines with pk_a's < 2.4 (9).

These results can be rationalized by postulating the existence of two pathways for the reaction of Schiff bases with azidoacetyl chloride, DMAC and CC. Nucleophilic imines react with these acid chlorides to give *cis* β-lactams by the mechanism proposed by Doyle *et al.* (1) and supported by Sullivan *et al.* (10). They proposed the formation of an immonium ion followed by cyclization, in which the *cis* stereochemistry is ensured by electrostatic interaction between the two 'sidechains.' With a lowering either of the nucleophilicity of the Schiff base nitrogen, or of the electrophilicity of the acid chloride, or of the acidity of the proton to be removed to effect ring closure, one could expect the rate of this reaction to slow down. A competing side reaction, perhaps involving azido ketene, may then give *trans*-lactam.

The formation of mixtures in the reaction of cinnamylidene aniline with CC can therefore be explained by the lower electrophilicity of CC versus azidoacetyl chloride, thus requiring a more nucleophilic Schiff base to give an immonium ion, and a lower acidity of the proton to be removed to effect ring closure. The effect of temperature on the *cis*–*trans* ratio in the formation of **4***a* and **5***a* probably reflects the different temperature dependence of the two reaction pathways.

Experimental

Solvents are of reagent grade unless otherwise specified. Infrared measurements were run on Unicam SP1000 and P.E. 257 spectrophotometers. Nuclear magnetic resonances were done on Varian T-60, T-60A, or Brucker FT-90 spectrophotometers. Mass spectra were taken on an AEI MS-902 or on a LKB 9000 mass spectrophotometer using the direct sample inlet system with a 70 eV ionization energy. Melting points were determined on a Gallenkamp block in open capillary tubes and were uncorrected. Merck SI60 silica gel was used for thick layer chromatography. Merck silica gel HF 254 was used for thick layer chromatography (1 mm) on glass plates (20 × 20 cm). Elemental analyses were performed by Midwest Microlab Ltd., IN.

Schiff Base **3**b, **3**d

The aldehyde (20 mmol) and aniline (1.86 g, 20 mmol), in benzene (50 mL) were refluxed for 4 h using a Dean Stark trap to remove the water formed. Evaporation of the benzene afforded the Schiff base in quantitative yield.

Schiff Base **3**b

^{1}H nmr ($CDCl_3$) δ: 7–7.6 (m, 12H, C_6H_5 + CH=CH), 8.3 ppm (t, 1H, CH=N); ir ($CDCl_3$) ν_{max}: 1630 cm^{-1} (C=N).

Schiff Base **3**d

^{1}H nmr ($CDCl_3$) δ: 6.1 (m, 1H, furan), 6.6 (m, 1H, furan),

6.8–7.2 (m, 5H, C_6H_5), 7.3 (m, 1H, furan), 7.9 ppm (s, 1H, CH=N); ir ($CDCl_3$) ν_{max}: 1630 cm^{-1} (C=N).

Schiff Base **6**a

Cinnamaldehyde (2.64 g, 20 mmol) in CH_2Cl_2 (5 mL) was added dropwise to a solution of ethyl glycinate (2.0 g, 20 mmol) in CH_2Cl_2 (40 mL) at 0°C containing $MgSO_4$ (~1–2 g). After stirring for 2 h at 0°C, the solution was filtered through Celite. Evaporation of the methylene chloride afforded Schiff base **6***a* approximately 85–90% pure by ^1H nmr; ^1H nmr (CCl_4) δ: 1.2 (t, 3H, CH_3), 4.0–4.5 (m, 4H, OCH_2CH_3, CH_2), 7.0 (d, 2H, *CH*=*CH*—Ph), 7.2–7.6 (m, 5H, C_6H_5), 7.8–8.0 ppm (m, 1H, C*H*=N).

Schiff Base **6**c

A solution of furfuraldehyde (0.96 g, 10 mmol) and amine **6***c* (2.33 g, 10 mmol) in CH_2Cl_2 (50 mL) was refluxed overnight using a Dean Stark trap filled with 4A molecular sieves. Evaporation afforded Schiff base **6***c* in approximately 90% yield by ^1H nmr; ^1H nmr (CCl_4) δ: 0.05 (s, 6H, $Si(CH_3)_2$), 0.90 (s, 9H, SiBu^t), 3.7 (s, 3H, OCH_3), 3.7–4.2 (m, 3H, $CHCH_2O$), 6.4 (s, 1H, furan), 6.8 (d, 1H, furan), 7.5 (m, 1H, furan), 8.0 ppm (s, 1H, CH=N); ir (film) ν_{max}: 2950, 1740 (ester), 1640 cm^{-1} (C=N).

β-*Lactam* **5**b

Crotonyl chloride (1.0 g, 10 mmol) in methylene chloride (20 mL) was added dropwise over 30 min to a solution of Schiff base **3***b* (2 g, 10 mmol) in methylene chloride at room temperature. After stirring for 1 more hour, the dark solution was washed with water (2 × 25 mL), dried ($MgSO_4$), and evaporated. ^1H nmr showed that the product contained approximately 25% **5***b*. Flash chromatography of the residue afforded 500 mg (15%) of pure *cis* β-lactam **5***b*; ^1H nmr (C_6D_6) δ: 4.2 (t, 1H, *CH*CH=CH_2, J = 6 Hz), 4.8 (q, 1H, *CH*CH=CHPh, $J_{3,4}$ = 6 Hz, $J_{4,5}$ = 7 Hz), 5.2–6.0 (m, 3H, —CH=CH_2), 6.2 (q, 1H, *CH*=CHPh, $J_{4,5}$ = 7 Hz, $J_{5,6}$ = 16 Hz), 6.8 (d, 1H, CH=*CH*Ph, J = 16 Hz), 7.0–7.7 ppm (m, 10H, C_6H_5); ir (film) ν_{max}: 2950, 1750 (C=O), 1600 cm^{-1} (C=C); ms *m/e*: 275 (13.70), 207 (38), 206 (100), 156 (92.9).

Preparation of Schiff Bases **8**a *and* **8**b

The aldehyde (10 mmol) was added to a solution of the amino phosphonate (10 mmol) in methylene chloride (25–30 mL) containing magnesium sulphate, at room temperature. The mixture was stirred at room temperature for 2–5 h, until the ir spectrum of the reaction mixture did not change. The solution was filtered. Evaporation of the filtrate afforded the Schiff base in 85–95% yield by ^1H nmr. All Schiff bases were used without further purification for the cycloaddition. The ^1H nmr spectrum showed a multiplet at approximately 7.8 ppm for the Schiff base proton, along with all other appropriate signals. The ir spectrum of the Schiff bases showed absorption at approximately 1650 cm^{-1} for the C=N bond.

Preparation of β-*Lactams* **4**a, **4**b, **4**d, **4**e, **7**a, **7**b, **7**c, **9**a, **9**b, ***11***, *and* ***12***

To the appropriate Schiff base (10 mmol) and triethylamine (1.0 g, 10 mmol) in methylene chloride (50 mL) at reflux under nitrogen was added dropwise over 45 minutes a solution of the acid chloride (10 mmol) in methylene chloride (25 mL). The reaction mixture was refluxed for 1 more hour and then washed with H_2O (2 × 50 mL). The methylene chloride layer was dried ($MgSO_4$) and evaporated. Recrystallization or chromatography of the residue afforded the β-lactam in the indicated yield.

β-*Lactam* **4**a

The yield was 40%, mp 100–102°C; ^1H nmr ($CHCl_3$) δ: 4.2 (bd, 1H, *CH*—CH=CH_2), 4.9 (d, 1H, *CH*—Ph, J = 2.5 Hz), 5.2–6.5 (m, 3H, CH=CH_2), 7.2–7.5 ppm (m, 10H, C_6H_5); ir ($CHCl_3$) ν_{max}: 2950, 1750 (C=O), 1600 cm^{-1} (C=C).

β-*Lactam* **4**b

The yield by ^1H nmr was ~40%, isolated yield 20%; ^1H nmr (C_6D_6) δ: 3.6 (bq, 1H, *CH*CH=CH_2), 4.3 (q, 1H, *CH*CH=CHPh, $J_{3,4}$ = 2.5 Hz, $J_{4,5}$ = 7 Hz), 5.0–6.0 (m, 3H, CH=CH_2), 6.2 (q, 1H, *CH*=CHPh, $J_{5,6}$ = 16 Hz, $J_{4,5}$ = 7 Hz), 6.6 (d, 1H, CH=*CH*Ph, J = 16 Hz), 6.8–7.4 ppm (m, 10H, C_6H_5); ir (film) ν_{max}: 2950, 1750 (C=O), 1600 cm^{-1} (C=C); ms *m/e*: 275 (12.2), 208 (21.7), 207 (57.11), 156 (100).

β-*Lactam* **4**d

The yield was 50%, mp 98–99°C; ^1H nmr ($CDCl_3$) δ: 4.05 (bq, 1H, *CH*CH=CH_2), 4.8 (d, 1H, J = 2.5 Hz, *CH*-furyl), 5.7–6.2 (m, 3H, CH=CH_2), 6.3–6.5 (m, 2H, furan), 7.0–7.5 ppm (m, 6H, C_6H_5, furan); ir (CH_2Cl_2) ν_{max}: 1750 (C=O), 1600 cm^{-1} (C=C); ms *m/e*: 239 (M^+), 120, 119.

β-*Lactam* **4**e

The yield was 30% upon recrystallization, greater than 70% by ^1H nmr, mp 84–86°C; ^1H nmr ($CDCl_3$) δ: 1.85 (s, 3H, CH_3—C=CH_2), 4.1 (bd, 1H, *CH*—C(CH_3)=CH_2), 4.9 (d, 1H, *CH*—furyl, J = 2.5 Hz), 4.9–5.1 (m, 2H, C(CH_3)=CH_2), 6.2–6.4 (m, 2H, furan), 6.8–7.4 ppm (m, 6H, C_6H_5 and furan); ir (CH_2Cl_2) ν_{max}: 1750 (C=O), 1600 cm^{-1} (C=C); ms *m/e*: 253 (M^+), 171, 134, 119.

β-*Lactam* **7**a

The yield was 50%; ^1H nmr ($CDCl_3$) δ: 1.3 (t, 3H, OCH_2CH_3), 1.7 (s, 3H, CH_2=C—CH_3), 4.2 (AB quartet, 2H, J = 18 Hz, CH_2CO_2Et), 4.0–4.4 (m, 3H, OCH_2CH_3 and $CHC(CH_3)$=CH_2), 4.5 (q, 1H, *CH*CH=CHPh, J_1 = 5 Hz, J_2 = 7 Hz), 5.1 (bd, 2H, C(CH_3)=CH_2), 6.1 (q, 1H, *CH*=CHPh, J_1 = 7 Hz, J_2 = 16 Hz), 6.7 (d, 1H, CH=*CH*Ph, J = 16 Hz), 7.2–7.5 ppm (m, 5H, C_6H_5); ir (film) ν_{max}: 3000, 1755 cm^{-1} (C=O); ms *m/e*: 299 (M^+), 282, 170, 82.

β-*Lactam* **7**b

The yield was 70%: nmr ($CDCl_3$) δ: 0.05 (d, 6H, Bu^{t}Si-(CH_3)$_2$), 0.95 (s, 9H, Bu^{t}Si(CH_3)$_2$), 1.8 (s, 3H, CHC(CH_3)=CH_2), 3.5 (s, 3H, OCH_3), 3.8–4.0 (m, 3H, CH_2O, *CH*C(CH_3)=CH_2), 4.3 (t, 1H, *CH*CH_2O), 4.4 (q, 1H, *CH*CH=CHPh, $J_{3,4}$ = 5 Hz, $J_{4,5}$ = 7 Hz), 4.8 (bd, 2H, CHC(CH_3)=CH_2), 5.8 (q, 1H, *CH*=CHPh, $J_{4,5}$ = 7 Hz, $J_{5,6}$ = 16 Hz), 6.4 (d, 1H, CH=*CH*Ph, J = 16 Hz), 6.8–7.0 ppm (m, 5H, C_6H_5); ir (film) ν_{max}: 2900, 1760 (β-lactam), 1740 cm^{-1} (ester).

β-*Lactam* **7**c

The yield was 30% by ^1H nmr, 10% upon recrystallization, mp 79–80°C; ^1H nmr ($CDCl_3$) δ: −0.1 (d, 6H, Bu^{t}Si (CH_3)$_2$), 0.80 (s, 9H, Bu^{t}Si(CH_3)$_2$), 1.3 (bs, 3H, C(CH_3)=CH_2), 3.7 (s, 3H, OCH_3), 3.8 (t, 2H, CH_2O), 4.2 (bd, 1H, *CH*C(CH_3)=CH_2), 4.4 (t, 1H, *CH*CH_2O), 4.9 (bd, 2H, C=CH_2), 5.1 (d 1H, CH—furyl, J = 2.5 Hz), 6.2 (m, 2H, furyl), 7.2 ppm (m, 1H, furyl); ir ($CHCl_3$) ν_{max}: 2900, 1760 (β-lactam), 1740 cm^{-1} (ester); ms *m/e*: 336 (M^+ − 57).

β-*Lactam* **9**a

The yield was 60%; ^1H nmr ($CDCl_3$) δ: 1.4 (d of t, 6H, OCH_2CH_3), 1.7 (s, 3H, CH_2=CCH_3), 3.4 (d of AB quartet, 2H, J_1 = 18 Hz, J_2 = 10 Hz, $CH_2PO(OEt)_2$), 4.2 (m, 5H, OCH_2CH_3, *CH*C(CH_3)=CH_2), 4.5 (d of q, 1H, *CH*CH=CHPh, J_1 = 1 Hz, J_2 = 5 Hz, J_3 = 7 Hz), 5.1 (bd, 2H, CH_2=CCH_3), 6.0 (q, 1H, J_1 = 7 Hz, J_2 = 16 Hz, *CH*=CHPh), 6.8 (d, 1H, CH=*CH*Ph, J = 16 Hz), 7.3 ppm (m, 5H, C_6H_5); ir (film) ν_{max}: 3000, 1760 (C=O), 1000 cm^{-1}; ms *m/e*: 363 (M^+), 282, 170, 82.

β-*Lactam* ***11***

The yield was 40%, mp 68–69°C; ^1H nmr (C_6D_6) δ: 3.4 (s, 6H, OCH_3), 3.5 (s, 3H, OCH_3), 3.7 (bd, 1H, *CH*CH=CH_2), 4.0 (d, 1H, J = 5 Hz, $CHCO_2CH_3$), 4.5 (2H, AB quartet, CH_2), 4.9–6.0 (m, 3H, CH=CH_2), 6.2–7.2 ppm (m, 3H,

C_6H_3); ir (KBr) ν_{max}: 2950, 1750 (C=O), 1610 cm^{-1}; ms *m/e*: 305 (M^+), 193, 151.

β-*Lactam* ***12***

The yield was 30%, mp 72–72.5°C; ^1H nmr (C_6D_6) δ: 1.6 (s, 3H, $CH_2=CCH_3$), 3.3 (s, 6H, OCH_3), 3.4 (s, 3H, OCH_3), 3.6 (bd, 1H, $CHC(CH_3)=CH_2$), 3.9 (d, 1H, J = 5 Hz, $CHCO_2CH_3$), 4.5 (AB quartet, 2H, CH_2), 5.0 (bd, 2H, $CH_2=CCH_3$), 6.0–7.0 ppm (m, 3H, C_6H_3); ir (KBr) ν_{max}: 2950, 1750 (C=O), 1610 cm^{-1}; ms *m/e*: 319 (M^+), 193, 151.

β-*Lactam* ***9***b

The yield was 60%; ^1H nmr ($CDCl_3$) δ: 1.2–1.6 (m, 6H, OCH_2CH_3), 1.6 (bs, 3H, $C(CH_3)=CH_2$), 4.0–4.8 (m, 5H, OCH_2CH_3, $CHC(CH_3)=CH_2$), 4.9 (d of q, 1H, $CHCH=$CHPh, J_1 = 2 Hz, J_2 = 5 Hz, J_3 = 7 Hz), 5.2 (bd, 2H, $CH_2=CCH_3$), 5.3 (d, $CHPO(OEt)_2$ of one diastereomer, J = 20 Hz), 5.5 (d, $CHPO(OEt)_2$ of other diastereomer, J = 20 Hz), 5.4–7.6 ppm (m, 10H, CH=CHPh, furan); ir ($CHCl_3$) ν_{max}: 1760 cm^{-1} (C=O).

Acknowledgements

We wish to thank the National Research Council of Canada and Lederle Laboratories for financial support.

1. T. M. Doyle, B. Belleau, C. F. Ferrari, M. Menard, J. L. Douglas, D. T.-W. Chu, G. Linn, L. R. Morris, D. Rivest, and M. Casey. Can. J. Chem. **55**, 484 (1977).
2. G. Just and T. J. Liak. Can. J. Chem. **56**, 211 (1978).
3. W. F. Huffman, K. G. Holden, T. F. Buckley III, J. G. Gleason, and L. Wu. J. Am. Chem. Soc. **99**, 2352 (1977).
4. B. C. Christensen. Annual reports in medicinal chemistry. *Edited by* F. H. Clarke. Academic Press, New York, NY. 1976. p. 271.
5. A. K. Bose, G. Spiegelman, and M. S. Manhas. Tetrahedron Lett. 3167 (1971).
6. W. Still, M. Kahn, and A. Mitra. J. Org. Chem. **43**, 2923 (1978).
7. R. W. Ratcliffe and B. G. Christensen. Tetrahedron Lett. 4649 (1973).
8. J. Rachon and C. Wasielewski. Z. Chem. 254 (1974).
9. G. Just, R. Zamboni, and A. Ugolini. Synth. Commun. 117 (1979).
10. D. F. Sullivan, D. I. Scopes, A. F. Kluge, and J. A. Edward. J. Org. Chem. **41**, 1112 (1976).

Carbon-13 nuclear magnetic resonance spectral study of some isomeric derivatives of 2-methoxytropone. Troponoid-II[1]

J. F. BAGLI, T. BOGRI, AND B. PALAMETA

Department of Chemistry, Ayerst Research Laboratories, Montreal, P.Q., Canada H3C 3J1

AND

M. ST-JACQUES[2]

Département de chimie, Université de Montréal, Montréal (Qué.), Canada H3C 3V1

Received January 25, 1979

J. F. BAGLI, T. BOGRI, B. PALAMETA, and M. ST-JACQUES. Can. J. Chem. **57**, 1949 (1979).

The ^{13}C nmr spectra of several isomeric monosubstituted derivatives of 2-methoxytropone together with some dibromo derivatives have been obtained and analysed. Substituent parameters were defined and shown to exhibit additivity. Differences with corresponding parameters for monosubstituted benzene analogs suggest proximity interactions between the 3-substituents and the 2-OCH_3 group as well as between 7-substituents and the adjacent carbonyl group. The data indicates that the OCH_3 group is a convenient probe to investigate the orientation of mesomeric electronic charge transfer to the various carbons of the tropone seven-membered ring. Finally, it is demonstrated that ^{13}C nmr is quite useful to distinguish between the various substituted 2-methoxytropones.

J. F. BAGLI, T. BOGRI, B. PALAMETA et M. ST-JACQUES. Can. J. Chem. **57**, 1949 (1979).

On a déterminé et analysé les spectres rmn du ^{13}C de plusieurs dérivés monosubstitués isomères de la méthoxy-2 tropone de même que quelques dérivés dibromés. On a défini les paramètres des substituants et on a montré leur additivité. Les différences entre ces paramètres et ceux qui leur correspondent dans des benzènes monosubstitués suggèrent l'existence d'interactions de proximité entre les substituants en 3 et le groupe OCH_3 en 2 de même qu'entre les substituants en 7 et le groupe carbonyle voisin. Les données indiquent que le groupe OCH_3 est une sonde appropriée pour étudier l'orientation du transfert de charge électronique mésomère à divers carbones du cycle à sept chaînons de la tropone. Enfin on a démontré que la rmn du ^{13}C est très utile pour distinguer diverses méthoxy-2 tropones substituées.

[Traduit par le journal]

Tropone derivatives constitute a class of non-benzenoid aromatic substances (1) some of which are biologically active as antibacterial and antifungal agents (2). Consequently, we have been interested in the synthesis of various substituted tropones and concomitantly in establishing the value of several methods of isomer identification applicable to this family of organic compounds.

Whereas proton magnetic resonance (^1H nmr) has been used with some success in the determination of substituent position for some disubstituted derivatives of 2-methoxytropone (3), we have found that isomer identification is less straightforward for monosubstituted derivatives owing to strong coupling between the four remaining ring protons. Although shift reagents can be useful in certain cases (4), recent results (5) suggest that carbon-13 magnetic resonance (^{13}C nmr) spectroscopy should be a powerful and possibly more general technique.

Accordingly we wish to report the results of a ^{13}C nmr spectral study of several isomeric monosubstituted derivatives of 2-methoxytropone together with some dibromo derivatives. The data obtained contribute to our understanding of the complex and subtle substituent effects on the tropone skeleton in addition to further defining the scope and limitation of ^{13}C nmr spectroscopy as a characterization technique in this area of organic chemistry.

[1]Dedicated to Professor K. Wiesner on his 60th anniversary.

[2]To whom all correspondence should be addressed.

Results

Synthesis

Several methods for the preparation of isomeric mono- and dibrominated tropolones have been reported (6). We have modified the procedure described by Toda *et al.* (6*c*) to improve the yield of monobromotropolone in the resulting mixture from which the regioisomeric methyl ethers **1***a* and **1***b* were obtained. Methylation of the residual bromination mixture led to the isolation of methyl ethers **2**, **3**, and **4***b* of 5-bromotropolone, 3,7-dibromotropolone, and 5,7-dibromotropolone respectively. No unequivocal structural assignment of compound **4***b* had previously been reported (6*e*). The ^{13}C nmr analysis given herein has provided one.

0008-4042/79/151949-09$01.00/0

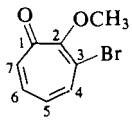

1*a*

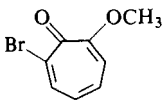

1*b*

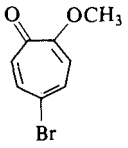

2

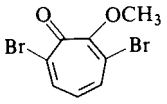

3

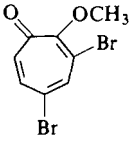

4*a*

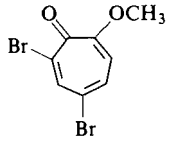

4*b*

Compound **6**, prepared from 5-aminotropolone (**5**), was methylated with dimethyl sulfate to yield the methyl ether 7 (7, 8).

Tropolone acetic acid **8** and 3-methyltropolone[3] (**10**) (9) were each methylated to give the pairs of regioisomers **9***a*, **9***b* and **11***a*, **11***b*.

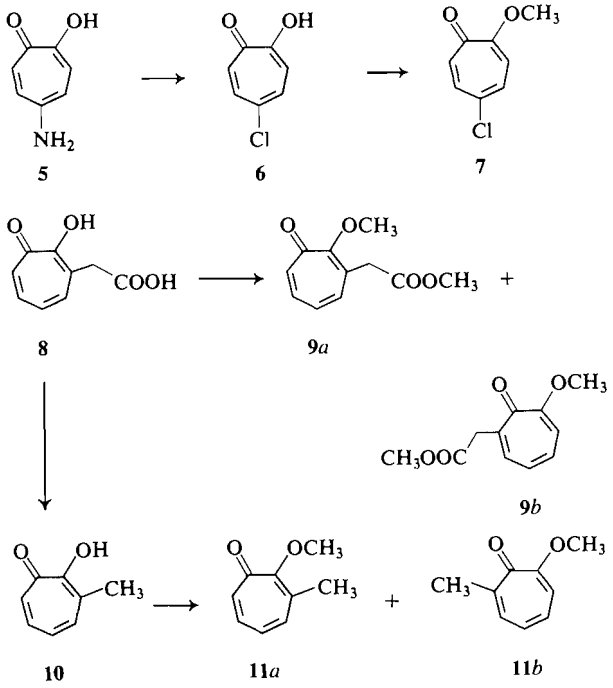

[3]The nomenclature of 3-substituted tropolone used here is for convenience. Monosubstituted tropolone derivatives exist as a mixture of undetermined proportion of 3- and 7-substituted regioisomers.

A mixture of the methoxytropolone derivatives **12** and **13** (10) was methylated and careful chromatographic separation led to the isolation of 2,3-, 2,7-, and 2,6-dimethoxytropones (**14***a*, **14***b*, and **15** respectively). The presence of a fourth compound (2,4-dimethoxytropone) was detected but it was not possible to isolate it in the pure state. Finally 2,5-dimethoxytropone (**16**) was prepared from 5-hydroxytropolone (7, 11).

^{13}C Nuclear Magnetic Resonance Spectral Assignment

The assignment of the various carbon signals for the compounds investigated in this work was achieved through a consideration of relaxation effects in the proton decoupled ^{13}C nmr spectra, signal multiplicity in the coupled spectra, ^{1}H selectively decoupled spectra, and the analysis of substituent effects on the tropone ring (12).

The ^{13}C spectral data for 2-methoxytropone recently published (5) is reported in Table 1 because these parameters will be used as reference data later on. Derivatives of this parent compound are designated by the symbol *x*-S where S is the substituent and *x* is its position on the ring.

Let us begin with the assignment of the signals for **2** (5-Br) and **7** (5-Cl) which contain a single substituent at position 5. The C-1, C-2, and C-5 lines were readily identified by their lower intensity and assigned by comparison with 2-methoxytropone. The analysis of the coupled spectrum permitted the identification of the C-3 and C-7 signals from the observed absence of splitting due to $^{3}J_{CH}$ coupling (5) and thus confirming the position of the substituent. The signal between 110 and 115 ppm was attributed to C-3 by analogy with the chemical shift of C-3 (δ 112.2) for 2-methoxytropone. The C-4 and C-6 signals of these two compounds have not been assigned unequivocally at this point; the chemical shifts given in Table 1 will be shown to be correct later from arguments involving the additivity of substituent effects.

The C-5 signal of **3** was also assigned directly from the coupled spectrum because it alone showed no splitting due to $^{3}J_{CH}$ (5).

The position of the bromine atom in the remaining two monobromo derivatives (**1***a* and **1***b*) can easily be determined from the observation (or absence) of a signal in the range 110–115 ppm attributed to protonated C-3. Consequently, the compound with a substituent on C-3 does not give a signal in that range and is labelled *a*. The C-7 substituted isomer which contains a signal between 110 and 115 ppm is labelled *b*. This labelling scheme is adopted throughout this work for other pairs of 3- and 7-substituted isomers.

TABLE 1. Carbon-13 chemical shifts of several derivatives of 2-methoxytropone in $CDCl_3$ solution[a]

Compound	C-1	C-2	C-3	C-4	C-5	C-6	C-7	C-8
H[b]	180.1	165.0	112.2	132.4	127.6	136.3	136.3	55.9
3-Br(**1***a*)	179.2	162.9	127.9[c]	137.9	128.1	134.7	138.0	59.1
7-Br(**1***b*)	173.6	162.6	112.2	132.8	125.1	139.6	137.5[c]	56.5
5-Br(**2**)	179.2	164.6	111.2	134.0	122.2[c]	139.6	135.7	56.2
3,7-Br_2(**3**)	173.1	159.8	127.6[c]	137.7[d]	125.2	138.1[d]	139.1[e]	59.5
5,7-Br_2(**4***b*)	173.2	161.8	111.5	134.5	119.3[c]	142.6	136.9[e]	56.8
5-Cl(**7**)	178.8	164.0	110.6	130.4	133.2[c]	137.2	135.6	56.0
3-$CH_2CO_2CH_3$(**9***a*)	181.4	164.4	132.0[c]	135.5	129.4	136.8[d]	138.6[d]	58.7[e]
7-$CH_2CO_2CH_3$(**9***b*)	178.7	164.1	112.2	132.2	126.6	137.5	142.2[e]	56.1[e]
3-CH_3(**11***a*)	181.1	163.7	136.2[c]	134.8	129.0	137.5[d]	136.2[d]	58.0
7-CH_3(**11***b*)	179.1	162.6	111.7	130.3	126.4	135.5	145.6[c]	55.6
3-OCH_3(**14***a*)	180.7	154.5	158.6[c]	127.8[d]	129.7[d]	133.2[g]	140.5[g]	(58.6, 59.4)[f]
7-OCH_3(**14***b*)	173.7	161.7	114.1	125.7	125.7	114.1	161.7[c]	56.2
6-OCH_3(**15**)	177.8	165.4[c]	108.2	129.9	124.0	163.2[c]	113.2	(55.0, 55.5)[f]
5-OCH_3(**16**)	178.6	159.0[d]	112.9	107.1	158.5[c,d]	132.1	136.2	(54.9, 55.3)[f]

[a]The chemical shifts of the substituent carbons other than OCH_3 are not shown in this table.
[b]The chemical shifts of the parent 2-methoxytropone are listed here. The nature of the substituents for each derivative of 2-methoxytropone is shown below for clarity together with the compound identification number.
[c]Less intense lines observed in the proton decoupled spectra other than those originating from C-1 and C-2.
[d]The assignment of the two closely spaced lines could be reversed.
[e]The substituent OCH_3 groups absorbed nearby, at 52.0 and 51.8 ppm for **9***a* and **9***b* respectively.
[f]Assignment not made for each of the two methoxy groups whose chemical shifts are given in parentheses.
[g]The assignment of these two lines is assumed.

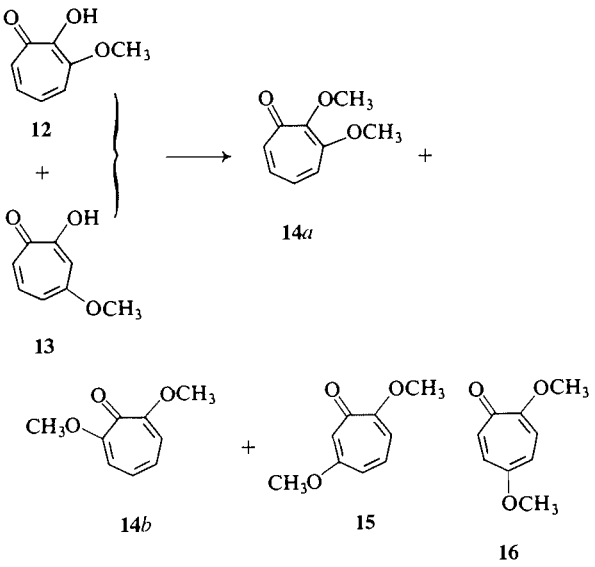

The examination of the ^{13}C nmr spectra of the two dibromo derivatives prepared revealed that of the three possible structures (**3**, **4***a*, and **4***b*), **4***a* (3,5-Br_2) was not obtained. Thus compound **3** (3,7-Br_2) was readily identified from the analysis of the coupled ^{13}C nmr spectrum while a signal at 111.5 ppm for the other isomer is compatible only with **4***b* (5,7-Br_2).

Knowing the structure of all five bromo derivatives and having assigned the signals of **2** and **3** (C-4 assumed upfield from C-6 initially) it is possible to complete the assignment for **1***a*, **1***b*, and **4***b* and confirm the assignment for **2** and **3** from a consideration of additivity of chemical shifts (*vide infra*). Thus the line assignment given in Table 1 for the bromo compound is the only one for which additivity is observed.

Of the two carbomethoxy derivatives **9***a* and **9***b*, that with a signal at 112.2 ppm is confirmed as **9***b*. Their spectral assignment is relatively straightforward and is summarized in Table 1. The spectral assignments for **11***a* and **11***b* were carried out by analogy with those of **9***a* and **9***b* because of their similar features. Here also uncertainty persists in the assignment of the C-6 and C-7 signals of **11***a* as reported in Table 1.

The different symmetry properties of **14***a* (3-OCH_3) and **14***b* (7-OCH_3) allow ready identification of these isomers and the chemical shift data characterizing **14***b* is reported in Table 1.

While the absence of a signal near 112 ppm is compatible with C-3 substitution for **14***a* the line assignment for this compound is more complex than **14***b* owing to the large shifts produced by the second methoxy group. Because **15** and **16** provide useful data on the magnitude of the substituent effect of OCH_3 on adjacent carbons, the spectral analysis of **14***a* will be deferred until later.

The identity of **16** (5-OCH_3) is clearly established from the ^{13}C nmr coupled spectrum in which the characteristic C-5 triplet (5) is absent. The three non-protonated carbon signals were readily identified from their lower intensity but the signals of C-2 and C-5 were too close for reliable assignment. The four intense lines between 105 and 140 ppm were assigned from the analysis of the coupled spectrum and ^1H selectively decoupled carbon-13 spectra (5) as described next.

The 100 MHz ^1H nmr spectrum of **16** showed two

methoxy singlets at 3.77 and 3.86 ppm, a broad A_2 singlet centered at 7.10 ppm and an AB quartet with doublet components at 6.78 and 6.39 ppm (J_{AB} = 10.8 Hz). Because H-7 is expected to be at lowest field (2, 4, 13), then the A_2 pattern must arise from both H-6 and H-7 which consequently have very similar chemical shifts. The upfield doublet component of the AB pattern is much broader owing to $^4J_{HH}$ coupling (3) with H-6; consequently it belongs to H-4 while the downfield doublet belongs to H-3. Selective irradiation of each identified ^1H frequency together with the analysis of the coupled ^{13}C nmr spectrum gave the results reported in Table 1.

Substituent shifts arising from the 5-OCH_3 group can now be determined relative to 2-methoxytropone used as reference. Thus it was calculated that the 5-OCH_3 group shifts C-4 upfield by 25.3 ppm and C-6 upfield by only 4.2 ppm.

The derivative assigned structure **15** (6-OCH_3) was identified from the observed pair of triplets for the protonated C-5 at 124.0 ppm in the coupled ^{13}C spectrum which suggested that the second methoxy group must be at either C-4 or C-6. The calculated substituent effect of −3.6 ppm for C-5 relative to 2-methoxytropone produced by the second methoxy group suggests that this group must be located on C-6 because if it had been on C-4 a much larger upfield shift (greater than 20 ppm) would have been observed for C-5 (*vide infra*).

The three weak signals from C-1, C-2, and C-6 of **15** were easily identified but a distinction between the signals of C-2 and C-6 is not made in Table 1. Of the three intense signals remaining, only the C-4 signal was identified in the coupled ^{13}C spectrum as a doublet centered at 129.9 ppm owing to the absence of $^3J_{CH}$ coupling.

The 100 MHz ^1H nmr spectrum of **15** consists of an ABC pattern with the easily recognizable H-7 signal (6.65 ppm) at the centre of the complex multiplet. Consequently, selective decoupling at the centre of the ^1H multiplet, the lower field side (+15 Hz) and the upfield side (−25 Hz) gave the complete assignment reported in Table 1.

Returning to the ^{13}C nmr spectrum of **14***a* we can easily recognize the C-1, C-2, and C-3 lines from their smaller intensity and assign the least intense of the three lines at 154.5 ppm to C-2 from arguments based on relaxation effects (13). The 3-OCH_3 group is expected to shift C-2 upfield more than C-4 although the electron donating properties of the two OCH_3 groups are modified by mutual steric interaction (*vide infra*). Thus the C-2 line is shifted upfield by 10.5 ppm, whereas either lines at 127.8 or 129.7 ppm could account for the small (4.6 or 2.5 ppm) upfield shift expected for C-4. It is therefore not possible to assign the C-4 signal on this basis. Analysis of the multiplicity in the coupled spectrum is not expected to resolve this problem and the fact that the 100 MHz ^1H nmr spectrum shows a tightly coupled multiplet for the four ring protons suggests that ^1H selective decoupling experiments will not be successful. Furthermore it is difficult to predict which of C-6 or C-7 ought to be most affected by the 3-OCH_3 and it was not possible to assign the lines at 133.2 and 140.5 ppm confidently to these carbons. The assignment given in Table 1 then appears most probable.

Discussion

A description of the chemical shift changes caused by replacing a hydrogen atom by various substituents in terms of characteristic substituent effects constitutes a useful approach to rationalize chemical shift data for many classes of compounds (14). The task of identifying the origin of the various substituent effects, whether they be the α, β, γ, and δ effects for saturated systems (15, 16) or the X, *o*, *m*, and *p* effects for benzene derivatives (17), has not been totally successful. Even though the accumulated knowledge has not provided a quantitative evaluation of the various contributions to chemical shift changes, it frequently allows one to describe the major contributing factor for a given substituent.

It is significant that the characteristic substituent effects generally are additive (14, 18) and empirical correlations based on additivity have proven to be very useful in practical applications to spectral and structural analyses. The examination of the data given in Table 1 for the bromo derivatives **1***a*, **1***b*, **2**, **3**, and **4***b* reveals that additivity exists for only one of the possible chemical shift assignment schemes. It is this combination of chemical shifts which has been retained as the correct assignment in Table 1 for these compounds. For example it can be verified that the chemical shifts of the two dibromo derivatives can be predicted from the appropriate monobromo compounds (i.e., **3** from **1***a* and **1***b*, and **4***b* from **1***b* and **2**). The exchange of any two chemical shifts for one or more compounds leads to a non-additive assignment.

Substituent Effects

It has been shown that substituent perturbation of the tropone ring electronic distribution bears some resemblance to that observed for benzene derivatives (5). Consequently, our discussion of the data from Table 1 will deal in part with a comparison of substituent effects of groups located at positions 3, 5, and 7 of 2-methoxytropone with those from suitable aromatic models.

At the outset it is useful to describe the structural

TABLE 2. Chemical shift changes produced on various ring carbons by substituents on carbon-5[a]

Substituent	C-2(δ)	C-3(γ)	C-4(β)	C-5(α)	C-6(β′)	C-7(γ′)	C-X[b]	C-*o*	C-*m*	C-*p*
Br	−0.4	−1.0	+1.6	−5.4	+3.3	−0.6	−5.5	+3.4	+1.7	−1.6
Cl	−1.0	−1.6	−2.0	+5.6	+0.9	−0.7	+6.2	+0.4	+1.3	−1.9
OCH_3	−6.0	+0.7	−25.3	+30.9	−4.2	−0.1	+31.4	−14.4	+1.0	−7.7

[a]Substituent effects are relative to 2-methoxytropone taken as reference. A + sign indicates a downfield shift.
[b]The symbols represent the following positions for monosubstituted benzene derivatives: X = substituted carbon, *o* = ortho carbon, *m* = meta carbon and *p* = para carbon. These values are taken from ref. 18.

features which characterize the three substituent positions of interest. Only position 5 is free of adjacent groups and it is here that substituent effects are expected to best reflect on the particular electronic structure of the seven-membered ring. For substituents at position 3, it will be necessary to consider the possible consequences of a steric interaction between the various substituents and the 2-methoxy group. Similarly the proximity of substituents on carbon-7 and the adjacent carbonyl group will have to be considered. Substituent effects characteristic of groups at each of the three positions will now be examined in succession.

Substituents on Carbon-5

The data summarized in Table 2 consist of substituent effects on the chemical shifts of various ring carbons calculated for a few substituents located at position 5 of the seven-membered ring relative to the corresponding chemical shifts for 2-methoxytropone taken as reference (5).

It is useful to label the carbons on the side of the double bond as β, γ, δ, etc. and those on the side of the single bond as β′, γ′, δ′, etc. Carbon-5 is therefore labelled α in Table 2, C-4 is β, and C-6 is β′, etc.

It is instructive to compare these effects with those known for the same substituents on benzene; for this purpose the C-X, C-*o*, C-*m*, and C-*p* values are also listed in Table 2. It is thus seen that C-5(α) and C-X values have very similar magnitudes whereas differences exist between either C-4(β) or C-6(β′) values and C-*o* values. For these adjacent carbon atoms, however, it is seen that similar trends are observed. In fact plots of C-4(β) and C-6(β′) values vs. C-*o* values reveal two essentially linear relationships with different slopes, the larger one belonging to C-4(β). But because only three substituents are available this observation can only be considered qualitatively. The values for C-3(γ), C-7(γ′), and C-*m* are all small as well as those for C-2(δ) and C-*p*, except for 5-OCH_3 which reveals comparable and larger shifts on these latter carbons. It is furthermore interesting to note that although the C-5(α) and C-4(β) substituent effects follow the same trend as observed for the same substituents in 1-substituted ethylenes (14), the actual values differ for each carbon atom. It may be significant to note that the substituent effect for C-2 of 1-methoxyethylene is −37.3 and therefore that the value for C-4(β) falls between this value and −14.4 observed for C-*o* (Table 2).

The relationship between ^{13}C chemical shifts and electronic structure has been reviewed recently (18) and among the various classes of compounds accounted for, aromatic compounds have received the most attention. It is now well known that the chemical shift changes observed for the ring carbon nuclei of monosubstituted benzene derivatives are primarily related to a redistribution of electron density. Furthermore, the mechanisms responsible for this redistribution are varied and dependent on the nature of the substituent, so that it has not been easy (19, 20) to assess their relative importance quantitatively for all groups. The following mechanisms need ordinarily to be considered: σ-inductive, π-inductive, mesomeric, and field effects, as well as steric interactions and bond-order changes.

It has been amply reported that iodine and to some extent bromine exert effects not related to their electronegativity and mesomeric abilities in 1-substituted ethylene and monosubstituted aromatic compounds whereas chlorine is better behaved (17). The 'heavy halogen effect' has been used historically to single out this observation. The idea that spin–orbit interaction (21) on a heavy atom can give rise to spin polarization that may be propagated along a molecule has been used lately as a rationale. Whatever the origin of the phenomenon, it is clear that the effects of bromine and chlorine arise from different origins and that mesomeric contribution is relatively more important for the latter. On the other hand, all evidence indicates that the mesomeric contribution is dominant when an OCH_3 group is bonded to an unsaturated carbon.

In addition to the above general considerations, the alternance of single and double bond character in tropone (22, 23) imparts a distinct electronic feature which could affect the mode of transmission of substituent effects to the various ring carbon atoms. In this respect Table 2 shows that C-4(β) and C-6(β′) are indeed very differently affected by the substituents on C-5. It is seen that both OCH_3 and Cl

shift C-4(β) more than C-6(β′) whereas for Br it is the opposite. This behaviour is qualitatively in accord with a dominant contribution of mesomeric effects for Cl and OCH_3 (especially strong for the latter) which can be illustrated with the resonance forms **17** to **20**. Such a model seems to adequately account for the large upfield C-4(β) shift produced by the 5-OCH_3 group, in addition to the significant upfield shift of C-2(δ) which is comparable to that observed for *para*-carbons in aromatic compounds for which it is known that resonance plays a dominant role for this substituent.

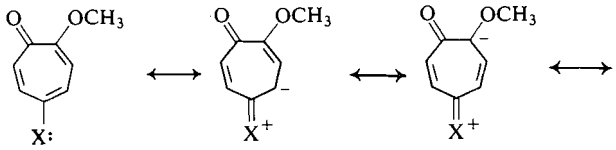

17 **18** **19**

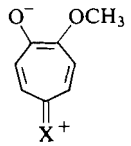

20

Since no resonance form with accrued negative charge on C-6 can be drawn, it is reasonable to assume that the mesomeric contribution will not be very important here in agreement with the relatively small upfield shift observed. The difference in the magnitudes of C-4(β) and C-6(β′) substituent effects for Cl are also consistent with accrued electron density on C-4 through a mesomeric contribution involving **18**.

As for the perturbations of C-4 and C-6 by the 5-Br substituent, the data in Table 2 reveal that they are of the same order of magnitude as for C-*o*. Although the C-4 (β) shift cannot be accounted for adequately by a mesomeric effect involving **18**, the fact that this carbon is less shifted downfield than C-6 suggests that some charge transfer through **18** might cancel part of the downfield shift caused by the field effect of the Br atom.

Substituents on Carbon-7

A summary of the chemical shift changes produced by several substituents located at position 7 is given in Table 3. The C-7(α) substituent effects for Br and OCH_3 are somewhat dissimilar to the corresponding C-5(α) effects in Table 2. Because significant differences between C-7(α) and C-X values also exist, some interaction between the 7-substituents and the adjacent carbonyl group is indicated.

Substituent effects published for 2-substituted tropones (5) undoubtedly provide the best indication of the importance of the above interaction and its consequence on the chemical shifts of atoms adjacent to the carbonyl group. Because in tropone both C-2 and C-7 are equivalent by symmetry, it is of interest to find out whether the C-7(α) values given in Table 3 differ significantly from the C-2(α) effects reported earlier (5). For example the values of CH_3 are +9.3 and +10.3 respectively; for OCH_3 they are +25.4 and +23.3 while for Br they are +1.2 and about −0.5.[4] Furthermore, the C-1(β′) substituent effects for CH_3 and OCH_3 in Table 3 are very similar to those reported for the corresponding 2-substituted tropones (5). In fact such a comparison is valid for all subsequent carbons whose effects are given in Table 3. Consequently, it is apparent that the suggested substituent–carbonyl proximity interaction leads to very similar chemical shift changes for both classes of compounds in agreement with expectations from the additivity of substituent effects.

It is also interesting to point out that the C-6(β) effect for OCH_3 is −22.2 and comparable to the −25.3 value for C-4(β) of Table 2.

The slight differences between the shifts produced by the CH_3 and the $CH_2CO_2CH_3$ groups in aromatic systems are best explained in terms of a π-inductive effect (19, 20) whereby the largest effect is noted for C-X whose values are +8.9 and +5.9 respectively.[5] The difference of 3.4 ppm for the C-7(α) substituent effects given in Table 3 is compatible with the above explanation.

Substituent on Carbon-3

Chemical shift changes produced by several substituents on C-3 are summarized in Table 4. Because of uncertainties in the assignment of the C-6 and C-7 signals for some of the compounds listed, these two carbons have been omitted from the table.

The proximity of the C-3 substituent and the C-2 methoxy group suggests that it is important to evaluate possible shifts resulting from the existence of a steric interaction between these two groups. Such a steric interaction has previously been suggested to explain observations for *ortho*-substituted anisoles (24).

Table 4 reveals that the C-3(α) substituent effects are much larger than the corresponding C-X effect

[4]This value for Br has been obtained by extrapolation from Fig. 2 of ref. 5 using the line characterizing the substituent effects for CH_3, Cl, and NH_2. The error is probably ±1.

[5]The C-X, C-*o*, C-*m* and C-*p* effects of the $CH_2CO_2CH_3$ group were calculated to be +5.9, +0.1, +0.9, and −1.4 ppm respectively. The actual chemical shifts are given in spectrum 40 of 'The Sadtler standard carbon-13 nmr spectra' and the substituent effects were obtained relative to benzene (δ_c = 128.6).

TABLE 3. Chemical shift changes produced by substituents on carbon-7[a]

Substituent	C-1(β′)	C-7(α)	C-6(β)	C-5(γ)	C-4(δ)
Br	−6.5	+1.2	+3.3	−2.5	+0.4
$CH_2CO_2CH_3$	−1.4	+5.9	+1.2	−1.0	−0.2
CH_3	−1.0	+9.3	−0.8	−1.2	−2.1
OCH_3	−6.4	+25.4	−22.2	−1.9	−6.7

[a]Substituent effects are relative to 2-methoxytropone taken as reference. A + sign indicates a downfield shift.

TABLE 4. Chemical shift changes produced by substituents on carbon-3[a]

Substituent	C-1(γ)	C-2(β)	C-3(α)	C-4(β′)	C-5(γ′)
Br	−0.9	−2.1	+15.7	+5.5	+0.5
$CH_2CO_2CH_3$	+1.3	−0.6	+19.8	+3.1	+1.8
CH_3	+1.0	−1.3	+24.0	+2.4	+1.4
OCH_3	+0.6	−10.5	+46.4	−4.6	+2.1

[a]Substituent effects are relative to 2-methoxytropone taken as reference. A + sign indicates a downfield shift.

for analogous benzene derivatives. It is also seen that the C-3 signals have been shifted downfield by at least 15 ppm in excess of predictions based on α-effects for C-5(α) given in Table 2. An observation of similar magnitude for 2,6-disubstituted anisoles (24) was interpreted in terms of the inhibition of resonance of the methoxy group as a consequence of steric interaction with the *ortho*-substituents. Similar reasoning applied to the 2-OCH_3 group is able to explain the greater downfield shift observed for C-3(α) in Table 4. Thus the normal upfield β-effect of 2-OCH_3 is reduced by interaction with the 3-substituents and the overall downfield shift of C-3 produced by 3-substitution is effectively larger than predicted from the 'normal' α-effect obtained from Table 2.

The β-effects determined for C-2(β) in Table 4 are significantly different from the 'normal' β-effects given in Table 2 for each of Br and OCH_3. Thus C-2 next to 3-Br is shifted more upfield than expected whereas C-2 next to OCH_3 appears less upfield than expected from the data in Table 2. The magnitude of the perturbations is much larger for 3-OCH_3 than 3-Br, however.

Assuming that the α-effect is predominantly determined by inductive effects and essentially independent of the conformation of the OCH_3 groups and furthermore that the C-2(β) shift should arise predominantly from mesomeric contributions of the 3-OCH_3 group, it then appears that a reduction in mesomeric charge transfer from the 3-OCH_3 group to C-2 could rationalize the lesser upfield shift of C-2. Thus it is suggested that the steric interaction between the 2-OCH_3 and the 3-OCH_3 groups alters the conformation of the 3-OCH_3 group relative to the C(3)—C(2) double bond from that which would exist in the absence of interaction as is the case for the 5-OCH_3 group.

The observation that C-4(β′) values for Br and OCH_3 from Table 4 are close to those for C-6(β′) from Table 2 suggests that the inhibition of resonance suggested above does not perturb C-4 significantly in agreement with very little mesomeric charge transfer across the formal single bond of the tropone ring.

The examination of Table 1 further reveals that the presence of a substituent at position 3 produces a downfield shift (2–3 ppm) of the 2-methoxy carbon. This observation is similar to the 3.9 ppm downfield shift reported for 2,6-dimethylanisole (24).

Finally it is significant to note that the difference between the C-3(α) effects of CH_3 and $CH_2CO_2CH_3$ is 4.2 ppm and of the same magnitude as that observed for C-X values; it can be accounted for by the π-inductive effect (19, 20).

Conclusions

The chemical shift changes produced by substituents located at positions 3, 5, and 7 of 2-methoxytropone given in Tables 2, 3, and 4 reveal that mesomeric effects play a very important role, especially for the methoxy group which exhibits the largest effects. The observation that such resonance is effective only for the β, γ, and δ side of each substituted carbon is particularly significant. Thus we see that the OCH_3 group is a convenient probe to investigate the orientation of mesomeric electronic charge transfer to the various carbons of the tropone seven-membered ring.

The chemical shift data for **15** (6-OCH_3) given in Table 1 yields the following substituent effects: C-6(α) = +26.9, C-7(β) = −23.1, and C-5(β′) =

−3.6. These values are very similar to those reported for 5-OCH_3 (**16**) in Table 2. Since no proximity interactions exist for **15** and **16** these substituent effects then ought to reflect the actual electronic structure of the ring and their similarity is compatible with an alternating π-electronic distribution involving single-like and double-like bonds (23). The fact that the 'normal' β-substituent effect of OCH_3 is about mid-way between those found for methylvinyl ether and anisole (i.e., −23 to −26 compared to −37.3 and −14.4 ppm respectively) might be taken as an indication of the extent of delocalization in the tropone ring.

The chemical shift changes for substituents located at positions 3 and 7 revealed proximity interactions and their consequences on chemical shifts. In addition the data has been very useful to distinguish unambiguously between pairs of regioisomers such as those identified by *a* and *b* throughout the text. The presence of a signal near 110–112 ppm indicates a protonated C-3 and hence substitution at C-7. Because several reactions of tropolone and other tropone derivatives can give similar mixtures of regioisomers, ^{13}C nmr could be an extremely valuable tool of identification.

On the other hand it is seen that, even for the relatively simple compounds investigated in this work, complete spectral assignment is often tedious. Consequently structure identification of other substituted tropones might often not be a simple task and for this purpose ^{13}C and ^{1}H nmr are shown to provide complementary information. The carbon-13 substituent effects determined in this work then provide initial basic parameters which should be useful in solving such practical problems.

Experimental

The ir spectra were taken on a Perkin Elmer diffraction grating spectrometer. Routine ^{1}H nmr spectra were recorded on a Varian A-60A spectrometer located at Ayerst Laboratories. The mass spectra were obtained on a Hitachi NMR-60 spectrometer. The melting points were determined on a Thomas Hoover apparatus and are uncorrected. Organic extracts were dried over anhydrous magnesium sulfate and all solvents were removed under vacuum. Merck silica gel 60 (70–230 mesh) was used for column chromatography.

The 100 MHz ^{1}H nmr (CW) spectra and the 22.63 MHz ^{13}C nmr (pulse FT) spectra were recorded respectively on a JEOL JNM-4H-100 and a Bruker WH-90 spectrometer located at the Université de Montréal. Heteronuclear ^{1}H–^{13}C double resonance experiments were carried out using the standard proton decoupler of the WH-90 instrument. The decoupler power was calibrated by proton off-resonance decoupling of a methanol sample (12). In the selective double resonance experiments the magnitude of irradiating field was set at about 850 Hz.

All ^{13}C nmr spectra were recorded at ambiant temperature using 10 mm tubes for solutions of the compounds in $CDCl_3$ which also acted as internal reference with δ = 76.9. The pulse duration was 6 μs (12 μs corresponds to a 90° pulse) and the number of accumulations depended on the concentration of the sample which varied with the amount available (30 to 200 mg). The coupled spectra were obtained through the gated decoupling technique (12) using the standard procedure for WH-90 spectrometers equipped with the Nicolet model 293 I/O Controller.

All spectra were recorded with 8K data points using a spectral width of 6024 Hz for ^{1}H decoupled spectra and 3012 Hz for the coupled spectra.

5-Chlorotropolone (6)

To a suspension of 5-aminotropolone (**5**) (25 g) in water (170 mL) was added hydrochloric acid (650 mL) at room temperature. The mixture was stirred and cooled to −10°C. After 15 min of stirring a solution of sodium nitrite (12.6 g) in water (36 mL) was added while maintaining the temperature at −10°C. The mixture was stirred at that temperature for 1.25 h. It was then warmed to room temperature and heated to 80°C for 2.5 h. The mixture was then cooled to room temperature, poured on to crushed ice (ca. 900 g) and the precipitate filtered to yield the crude product (20 g). The filtrate was extracted with chloroform, dried, and the solvent was removed. The residue was triturated with ether and filtered to yield 1.7 g more of solid. Total yield was 75%. The product had mp 180–182°C (lit. (7) mp 181–183°C).

2-Methoxy-5-chlorotropone (7)

5-Chlorotropolone (3.13 g, 1 equiv.) was suspended in methyl ethyl ketone (40 mL). Potassium carbonate (3.04 g, 2.2 equiv.) was added and the mixture was heated to 70°C (bath temperature) for about 10 min. Dimethyl sulfate (4.16 mL, 2.2 equiv.) was then added and the mixture kept at 80°C for 1.5 h. When the reaction was complete (indicated by tlc) the mixture was cooled and filtered. The filtrate was evaporated to dryness under vacuum, and the residue was suspended in ether and filtered to give the crude product (2.9 g). Crystallization from methanol–ether gave the pure product (2 g), mp 123–124°C (lit. (8) mp 123°C).

Bromomethoxytropones

3-Bromo- and 7-Bromo-2-methoxytropone (1a) and (1b)

Bromotropolone was methylated with dimethyl sulfate as described above to give a less polar product, mp 69–70°C (mp reported for 3-bromo-2-methoxytropone 76.5–77°C (6*d*)), and a more polar isomer, mp 87–88°C (mp reported for 7-bromo-2-methoxytropone 90–91°C (6*d*)).

3,7-Dibromo-2-methoxytropone (3)

This product was obtained from the corresponding 3,7-dibromotropolone, using the above procedure; mp 130–131°C (lit. (6*b*) mp 132–132.5°C).

5-Bromo-2-methoxytropone (2)

This compound was isolated from the methylation experiment and had mp 132–134°C (lit. (6*b*) mp 135–136°C).

5,7-Dibromo-2-methoxytropone (4b)

This compound had mp 208–210°C (lit. (6*e*) mp 207–209°C).

2-Methoxytropone-3-acetic Acetic Acid Methyl Ester (9a) and 2-Methoxytropone-7-acetic Acid Methyl Ester (9b)

These compounds were obtained from the methylation of tropolone acetic acid **8** with diazomethane. Chromatography of the mixture on silica gel yielded a more polar solid, mp 106–108°C; ir (Nujol): 1725 cm^{-1}; ^{1}H nmr ($CDCl_3$) δ: 7.45 (1H, m, aromatic), 6.9 (3H, m, aromatic), 3.9 (3H, s, —OCH_3), 3.65 (5H, s, OCH_3; CH_2—CO); and a less polar oily product, ir (Nujol): 1725 cm^{-1}; ^{1}H nmr ($CDCl_3$) δ: 7.02 (4H, m, aromatic), 3.90 (3H, s, OCH_3), 3.67 (5H, d, OCH_3, CH_2—CO). The solid was tentatively assigned structure **9***a* and the oil **9***b*.

*2-Methoxymethyltropones (**11**a and **11**b)*

A solution of tropolone-2-acetic acid **8** (ca. 1 g) in pyridine (5 mL) was heated to reflux for 1.5 h. The solvent was removed under vacuum to yield a residue (0.57 g) which was mixed with an ethereal solution of diazomethane and stirred for 1.5 h. The solvent was evaporated and the product was purified by chromatography on silica gel (30 g) using 30% ethyl acetate – benzene. Earlier fractions yielded an oily product (0.06 g); ^{1}H nmr ($CDCl_3$) δ: 7.1 (4H, m, aromatic), 3.92 (3H, s, OCH_3), 2.35 (3H, s, =C—CH_3). This compound was tentatively assigned structure **11***a*. Further elution gave another isomer; mp 37–39°C; ^{1}H nmr δ: 7.5 (1H, m, aromatic), 6.85 (3H, m, aromatic), 3.92 (3H, s, OCH_3), and 2.36 (3H, s, C—CH_3). The structure **11***b* followed from the above assignment. These structures were later confirmed by ^{13}C nmr.

*2,3-, 2,7-, and 2,6-Dimethoxytropone (**14**a, **14**b, **15**)*

These compounds were prepared by methylation of a mixture of isomeric methoxytropolone obtained using a described procedure (10).

Methylation using dimethyl sulfate gave a mixture of isomers that were separated by chromatography. A less polar oily isomer which showed in its ^{1}H nmr ($CDCl_3$) δ: 7.1 (4H, m, aromatic), 3.89 (3H, s, OCH_3), and 3.72 (3H, s, OCH_3), was tentatively assigned structure **14***a*. Another more polar component was obtained from chromatography; after recrystallization from methanol–ether it gave a mp 106–108.5°C. The ^{1}H nmr spectrum of this compound showed only one singlet at δ 3.78 (6H, s) indicating two equivalent OCH_3 groups and structure **14***b* was assigned to it. A third isomer was purified with difficulty by rechromatography and was obtained as an oil. A mass spectrum showed the following ions: M^+ (*m/e* 166, 100%); $M^+ - 15$ (*m/e* 151, 5%). Its ^{1}H nmr spectrum showed two singlets arising from two OCH_3 groups at δ 4.17 and 4.27. The structure was confirmed using ^{13}C nmr spectroscopy to be 2,6-dimethoxytropone (**15**).

*2,5-Dimethoxytropone (**16**)*

The title compound was prepared from 2,5-dihydroxytropone (7) as described above. The compound is reported as an oil (11). We were able to get it as a crystalline solid; mp 77–80°C; M^+ (*m/e* 166, 100%). The structure of the compound was confirmed by ^{13}C nmr.

Acknowledgements

We wish to acknowledge the technical (nmr) contribution of M. Robert Mayer from the Université de Montréal and the financial contribution of the National Research Council of Canada for the purchase of the Bruker WH-90 NMR spectrometer.

1. D. Lloyd. Carbocyclic non-benzenoid aromatic compounds. Elsevier Publishing Co., New York, NY. 1966. p. 118.
2. P. L. Pauson. Chem. Rev. **55**, 9 (1955).
3. S. Seto, K. Ogura, H. Toda, Y. Ikegami, and T. Ikenoue. Bull. Chem. Soc. Jpn. **41**, 2696 (1968).
4. H. Tanida, T. Tsushima, and Y. Terui. Tetrahedron Lett. 399 (1972).
5. J. F. Bagli and M. St-Jacques. Can. J. Chem. **56**, 578 (1978).
6. (*a*) T. Nozoe, S. Seto, T. Mukai, K. Yamane, and A. Matsukuma. Proc. Jpn. Acad. **27**, 224 (1951); (*b*) T. Nozoe, S. Seto, T. Kemi, and T. Arai. Proc. Jpn. Acad. **27**, 102 (1951); (*c*) T. Toda, H. Kubata, and T. Nozoe. Nippon Kagaku Zasshi, **88**, 1234 (1967); Chem. Abstr. **68**, 101342X (1968); (*d*) T. Nozoe, S. Seto, H. Takeda, S. Morosawa, and T. Matsumoto. Sci. Rep. Tohoku Univ. **36**, 126 (1952); (*e*) G. Sunagawa, N. Soma, H. Nakano, and Y. Matsumoto. Yakugaku Zasshi, **81**, 1799 (1961); Chem. Abstr. **57**, 16533g (1962).
7. T. Nozoe, S. Seto, S. Ito, and M. Sato. Proc. Jpn. Acad. **27**, 426 (1951).
8. T. Sato. Nippon Kagaku Zasshi, **80**, 1171 (1950); Chem. Abstr. 4389 (1961).
9. K. Takase. Bull. Chem. Soc. Jpn. **37**, 1460 (1964).
10. T. Yametani, M. Yasunami, and K. Takase. Tetrahedron Lett. 1725 (1970).
11. T. Nozoe, S. Seto, S. Ito, M. Sato, and T. Katono. Proc. Jpn. Acad. **28**, 488 (1952).
12. F. W. Wehrli and T. Wirthlin. Interpretation of carbon-13 nmr spectra. Heyden, New York, NY. 1976.
13. A. J. Jones, D. M. Grant, and K. F. Kuhlmann. J. Am. Chem. Soc. **91**, 5013 (1969).
14. G. E. Maciel. *In* Topics in carbon-13 nmr spectroscopy. Vol. 1. *Edited by* G. C. Levy. Wiley-Interscience, New York, NY. 1974. p. 53.
15. H. Beierbeck and J. K. Saunders. Can. J. Chem. **53**, 1307 (1975).
16. D. G. Gorenstein. J. Am. Chem. Soc. **99**, 2254 (1977).
17. J. B. Stothers. Carbon-13 nmr spectroscopy. Academic Press, New York, NY. 1972.
18. G. L. Nelson and E. A. Williams. *In* Progress in physical organic chemistry. Vol. 12. *Edited by* R. W. Taft. Interscience, New York, NY. 1976. p. 229.
19. W. F. Reynolds, I. R. Peats, M. H. Freedman, and J. R. Lyerla, Jr. Can. J. Chem. **51**, 1857 (1973).
20. W. F. Reynolds, and G. H. Hamer. J. Am. Chem. Soc. **98**, 7296 (1976).
21. (*a*) I. Morishima, K. Endo, and T. Yonezawa. J. Chem. Phys. **59**, 3356 (1973); (*b*) Y. Nomura, Y. Takeuchi, and N. Nahagawa. Tetrahedron Lett. **8**, 638 (1969).
22. D. J. Bertelli, T. A. Andrews, Jr., and P. O. Crews. J. Am. Chem. Soc. **91**, 5286 (1969).
23. H. Kuroda and T. Kunii. Theor. Chim. Acta, **7**, 220 (1967).
24. K. S. Dhami and J. B. Stothers. Can. J. Chem. **44**, 2855 (1966).

Synthèse et réactivité des halogéno-2 sulfonyl-2 aziridines

JEAN-MARC GAILLOT, YVONNE GELAS-MIALHE ET ROGER VESSIERE

Groupe de Recherche de Chimie Organique 2, U.E.R. des Sciences Exactes et Naturelles, Université de Clermont-Ferrand, B.P. 45, 63170 Aubiere, France et Ecole Nationale Supérieure de Chimie, 71 Boulevard Côte Blatin, 63000 Clermont-Ferrand, France

Reçu le 3 janvier 1979

JEAN-MARC GAILLOT, YVONNE GELAS-MIALHE et ROGER VESSIERE. Can. J. Chem. **57,** 1958 (1979).

Les halogéno-2 phénylsulfonyl-2 aziridines sont obtenues par action du tétrahalogénure de carbone, en présence de potasse, sur les phénylsulfonyl-2 aziridines.

A partir des isopropylsulfonyl-2 aziridines, on obtient une monochloro et une dichloro-aziridine; la réaction de Ramberg–Bäcklund n'est pas observée.

Ces composés halogénés se décomposent, soit thermiquement, soit en milieu acide, pour conduire aux α-halogénoacétamides et α-phénylsulfonylacétamides *N*-substitués. Les halogéno-2 phénylsulfonyl-2 aziridines ne réagissent pas avec le cyanure de potassium ou le benzènethiolate de sodium. Elles sont réduites par le méthylate, l'éthylate et l'éthanethiolate de sodium, on obtient alors les phénylsulfonyl-2 aziridines; le rôle du solvant est précisé.

JEAN-MARC GAILLOT, YVONNE GELAS-MIALHE, and ROGER VESSIERE. Can. J. Chem. **57,** 1958 (1979).

Carbon tetrahalide reacts rapidly with 2-phenylsulfonyl aziridines in the presence of KOH, leading to 2-phenylsulfonyl 2-haloaziridines.

Starting with 2-isopropylsulfonyl aziridines, a monochloro and a dichloroaziridine are produced; the Ramberg–Bäcklund reaction is not observed.

These halo compounds decompose either thermally or in acidic medium leading to *N*-substituted α-haloacetamides and α-phenylsulfonylacetamides. 2-Phenylsulfonyl 2-haloaziridines are unreactive toward potassium cyanide or sodium thiophenoxide. Sodium methoxide, sodium ethoxide, or sodium thioethoxide reduce them to 2-phenylsulfonyl aziridines; the reaction depends upon the solvent.

Dans un précédent mémoire (1) nous avons décrit la préparation des phénylsulfonyl-2 aziridines **1**, **2** et **3** par action, dans le diméthylsulfoxyde, d'une amine primaire sur une sulfone α-bromée α,β-éthylénique. Par la suite, nous avons fait appel à ce procédé pour accéder aux alkylsulfonyl-2 aziridines **4** et **5**:

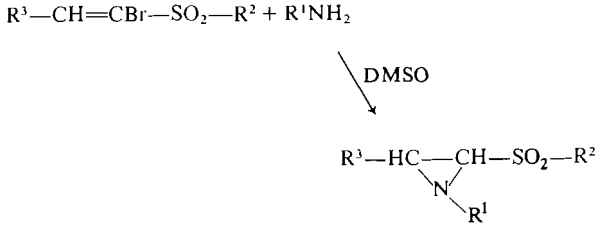

1 $R^3 = H$; $R^2 = Ph$
2 $R^3 = CH_3$; $R^2 = Ph$
3 $R^3 = Ph$; $R^2 = Ph$
4 $R^3 = H$; $R^2 = CH_3$
5 $R^3 = H$; $R^2 = CH(CH_3)_2$

Dans le présent mémoire, nous nous proposons de décrire le comportement de cette nouvelle classe d'aziridines dans des réactions d'halogénation, au cours desquelles nous avons obtenu des halogéno-2 sulfonyl-2 aziridines, composés jusqu'alors inconnus. Certains de ces produits, généralement solides, abandonnés à température ambiante, deviennent déliquescents et présentent au bout de quelques jours un spectre de rmn considérablement perturbé. Ceci nous a conduit à étudier leur stabilité thermique et leur hydrolyse. Nous avons, par ailleurs, examiné leur comportement vis-à-vis de quelques nucléophiles.

Halogénation des sulfonyl-2 aziridines

Parmi les nombreux procédés permettant l'introduction d'un halogène en α d'une fonction sulfonyle, nous avons utilisé celui mis au point par Meyers *et al.* (2).

Les phénylsulfonyl-2 aziridines **1***b*, **1***c*, **2***b*, **2***d* et **3***a* traitées par le tétrachlorure ou le tétrabromure de carbone en présence de potasse en poudre et d'alcool *tert*-butylique, conduisent, avec de bons rendements, aux halogéno-2 phénylsulfonyl-2 aziridines **6***b*, **6***c*, **7***b*, **7***d*, **8***a*, **9***b*, **9***c*, **10***b*, **10***d* et **11***a* identifiées par leur analyse élémentaire et leur spectre de rmn (voir partie expérimentale):

0008-4042/79/151958-09$01.00/0

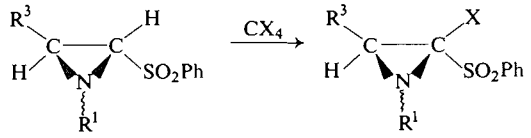

1 $R^3 = H$ — *a* $R^1 = CH_2CH_3$ — **6** $R^3 = H$; X = Cl
2 $R^3 = CH_3$ — *b* $R^1 = CH(CH_3)_2$ — **7** $R^3 = CH_3$; X = Cl
3 $R^3 = Ph$ — *c* $R^1 = C(CH_3)_3$ — **8** $R^3 = Ph$; X = Cl
d $R^1 = CH_2Ph$ — **9** $R^3 = H$; X = Br
10 $R^3 = CH_3$; X = Br
11 $R^3 = Ph$; X = Br

Ces réactions se déroulent par l'intermédiaire d'un α-sulfonylcarbanion (2). Nous avons montré dans un précédent mémoire (1) que l'α-phénylsulfonyl carbanion formé à partir des phénylsulfonyl-2 aziridines possédait très probablement une géométrie pyramidale avec une haute barrière d'inversion. En effet, traitée par l'éthylate de sodium dans l'éthanol deutérié l'aziridine **2***d* incorpore le deutérium en position 2; par ailleurs sa stéréochimie n'est pas modifiée par traitement pendant 17 h à température ambiante par une solution d'éthylate de sodium dans l'éthanol. En conséquence, les halogéno-2 phénylsulfonyl-2 aziridines **7**, **8**, **10** et **11** ont la même configuration que les dérivés **2** et **3** à partir desquels elles sont formées. Nous avons précisé par ailleurs (1) que les atomes de carbone C-2 et C-3 des composés **2** et **3** sont de configurations *R*R**. Ces mêmes atomes ont donc la configuration *R*S** chez les produits **7**, **8**, **10** et **11**.

Les isopropylsulfonyl-2 aziridines **5** possèdent en α et en α′ de la fonction sulfone deux atomes d'hydrogène mobiles. La réaction d'halogénation pourrait donc évoluer vers la formation d'un composé éthylénique du type méthylèneaziridine (réaction de Ramberg–Bäcklund) (2, 3). Du produit brut de chloration par le tétrachlorure de carbone en milieu basique de chacune des aziridines **5***b* et **5***d* nous avons isolé deux composés que nous avons identifiés aux aziridines monochlorées **12***b* et **12***d* d'une part et aux aziridines dichlorées **13***b* et **13***d* d'autre part:

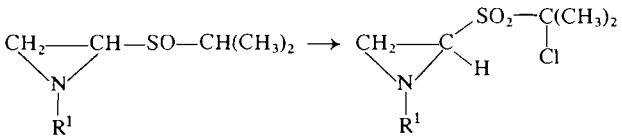

5*b* $R^1 = CH(CH_3)_2$ — **12***b* $R^1 = CH(CH_3)_2$
5*d* $R^1 = CH_2Ph$ — **12***d* $R^1 = CH_2Ph$

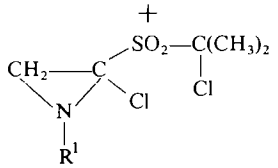

13*b* $R^1 = CH(CH_3)_2$
13*d* $R^1 = CH_2Ph$

Si l'on arrête la réaction d'halogénation de l'aziridine **5***d* avant son terme, les composés mono- et dihalogénés sont présents dans le mélange réactionnel à côté du produit de départ, le dérivé dihalogéné étant largement prépondérant (**13***d*/**12***d* = 43/7, déterminé par rmn). La dihalogénation est donc plus rapide que la monohalogénation et qu'une éventuelle élimination 1,3 ayant pour siège le composé monohalogéné. L'aziridine monohalogénée **12***b*, mise en solution dans le THF et traitée par *t*BuOK pendant 5 h à 0°C est retrouvée inchangée. Ce mélange, chauffé à reflux pendant 5 h, conduit au produit d'élimination 1,2 **14***b*:

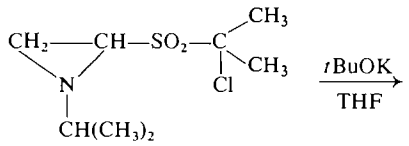

12*b*

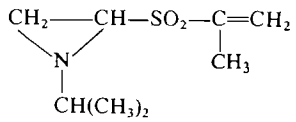

14*b*

On n'observe pas la formation du produit éthylénique provenant d'une réaction type Ramberg–Bäcklund; ceci peut être attribué à l'importante contrainte à laquelle serait soumise l'épisulfone spirannique intermédiaire:

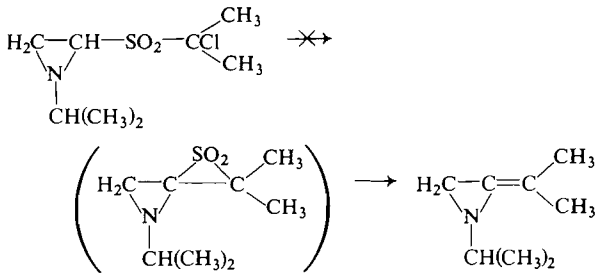

Stabilité thermique et hydrolyse des halogéno-2 sulfonyl-2 aziridines

Afin de déterminer la nature des produits de décomposition spontanée des halogéno-2 sulfonyl-2 aziridines, nous avons chauffé ces composés pendant des temps variables à 60°C (température inférieure à leur température de fusion). Les durées de thermolyse et le pourcentage de transformation sont indiqués dans la partie expérimentale. On peut noter que les bromo-2 aziridines se décomposent plus facilement que les chloro-2 aziridines et que les composés possèdant un groupe méthyle en position 3 apparaissent plus stables.

Au départ des aziridines **6***b* et **9***b* on sépare, par

chromatographie sur colonne, deux produits. L'un d'eux est identifié à l'aide de ses spectres ir et de rmn et par comparaison à un échantillon authentique au *N*-isopropyl α-halogénoacétamide. Le deuxième constitue le benzènethiosulfonate de phényle:

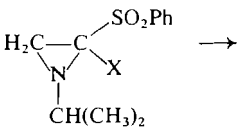

6*b* X = Cl
9*b* X = Br

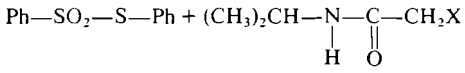

Chauffés en présence d'eau, les composés **6***b* et **9***b* se décomposent plus lentement (la réaction est totale après 6 jours de chauffage à 60°C dans le cas de **6***b*, 4 jours à 60°C pour **9***b*). Trois produits sont alors formés; le *N*-isopropyl α-halogénoacétamide, le benzènethiosulfonate de phényle et le *N*-isopropyl α-phénylsulfonylacétamide; ce dernier est identifié par ses spectres ir et de rmn et par comparaison à un échantillon authentique.

Ces résultats sont tout à fait comparables à ceux que l'on observe avec les *gem*-dihalogénoaziridines (4), les nitro-2 aziridines (5) ou les *gem*-dihalogénocyclopropanes (6). Un mécanisme analogue à ceux invoqués peut rendre compte de nos résultats (Schéma 1):

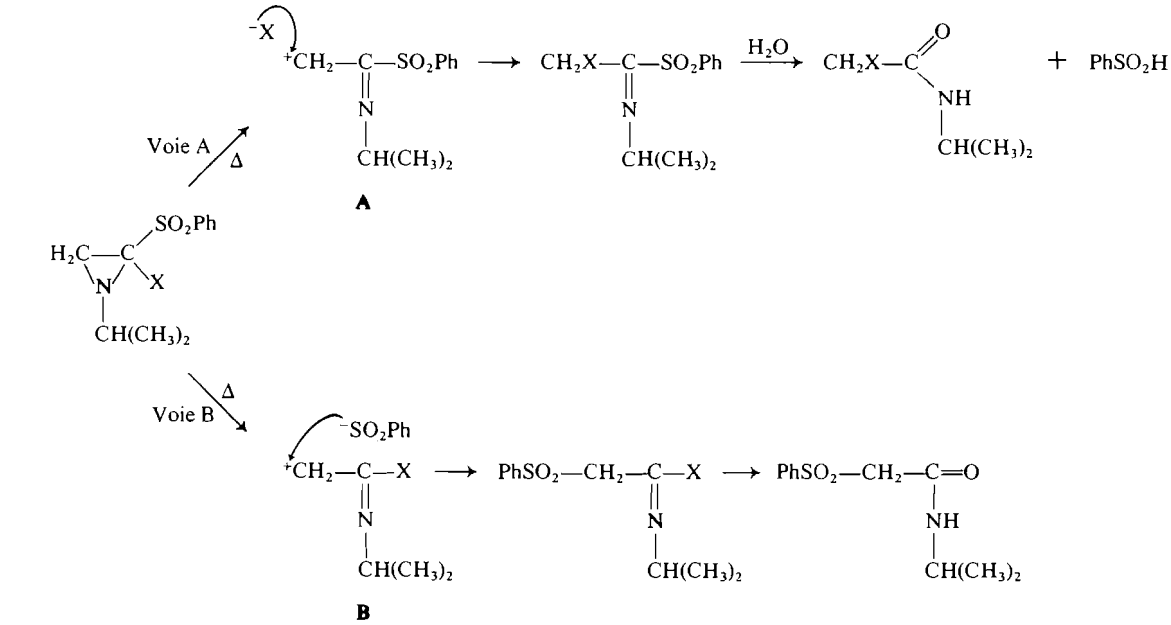

SCHÉMA 1

Selon la voie A (Schéma 1) l'hétérolyse de la liaison carbone–halogène et la rupture simultanée de la liaison C^3—N conduisent, par l'intermédiaire du cation A à la formation d'une sulfonylimine dont l'hydrolyse donne l'α-halogénoacétamide. Quant à l'acide sulfinique, il se décomposerait suivant [1] (7):

[1] $3PhSO_2H \rightarrow PhSO_2SPh + PhSO_3H + H_2O$

On pourrait également envisager un mécanisme non concerté faisant intervenir le cation cyclique A′; une telle voie est toutefois peu probable en raison de l'effet déstabilisant exercé par le groupe sulfonyle porté par le carbone positif (Schéma 2):

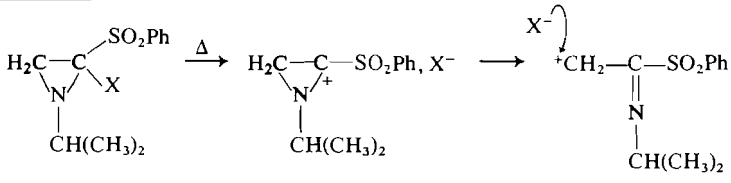

A′ A

SCHÉMA 2

Par ailleurs, l'hétérolyse de la liaison carbone–soufre (voie B, Schéma 1) peut être compétitive avec celle de la liaison carbone–halogène. L'iminosulfone formée par l'intermédiaire du cation B est ensuite hydrolysée en *N*-isopropyl α-phénylsulfonylacétamide.

La plus grande réactivité des dérivés bromés par rapport aux dérivés chlorés est justifiée par une vitesse d'hétérolyse supérieure de la liaison C—Br par rapport à la liaison C—Cl.

Une réaction en tous points analogue est observée avec les aziridines dihalogénées **13***b* et **13***d*. En effet chacune d'elles, abandonnée quelques jours à température ambiante, est totalement décomposée en deux produits que nous avons identifiés au chloro-1 méthyl-1 éthylthiosulfonate de chloro-1 méthyl-1 éthyle et au *N*-alkyl α-chloroacétamide:

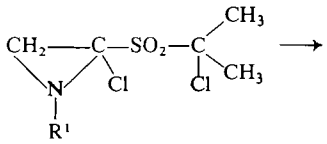

13*b* $R^1 = CH(CH_3)_2$
13*d* $R^1 = CH_2Ph$

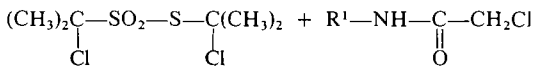

L'hydrolyse acide en milieu homogène (HCl dans un mélange éthanol–eau) conduit à un résultat comparable; au départ de la *tert*-butyl-1 chloro-2 phénylsulfonyl-2 aziridine **6***c* on isole, à côté du benzènethiosulfonate de phényle, un composé identifié au *N-tert*-butyl α-chloroacétamide; à partir de la bromo-2 aziridine **10***b* on obtient également du benzènethiosulfonate de phényle et un mélange de deux composés que nous n'avons pas pu séparer et que nous avons identifiés au *N*-isopropyl α-chloropropionamide (55%) et au *N*-isopropyl α-bromopropionamide (45%) (pourcentage déterminé sur le spectre de rmn).

Un mécanisme identique à celui précédemment proposé permet d'interpréter ces résultats, notamment la formation d'un mélange d'amides α-bromée et α-chlorée à partir de l'aziridine bromée **10***b*. En effet, selon le Schéma 1, voie A, l'hétérolyse de la liaison carbone–halogène de l'aziridine libère le cation A qui peut alors être soumis à une attaque compétitive de la part des ions Cl^- et Br^- présents dans le milieu.

Bien que les produits obtenus dans ces réactions aient une structure analogue à ceux qui proviennent de la solvolyse de la diphényl-1,2 dichloro-3,3 aziridine (4*a*), il semble que les mécanismes de formation de ces composés soient différents. En effet, Brooks *et al.* (4*a*) ont montré dans le cas précédent que la réaction procédait, de façon prédominante, par migration intramoléculaire de chlore; la présence d'un amide α-chloré comme produit d'hydrolyse de l'aziridine bromée **10***b* prouve dans notre cas la participation des ions présents dans le milieu réactionnel.

Action des nucléophiles sur les halogéno-2 arylsulfonyl-2 aziridines

Contrairement aux chlorocyclopropanes, dérivés généralement inertes vis-à-vis des agents nucléophiles, les monochloroaziridines conduisent, sous l'action de ces réactifs, aux produits de substitution normalement attendus (8). D'autre part, divers travaux (9) ont montré la très faible réactivité des α-halogénosulfones vis-à-vis des nucléophiles, lesquels provoquent quelquefois uniquement une réduction de la sulfone au niveau de l'halogène (9*c*). Compte tenu de ces résultats, il pouvait être intéressant d'étudier le comportement des halogéno-2 sulfonyl-2 aziridines vis-à-vis de divers nucléophiles.

Le benzènethiolate de sodium et le cyanure de potassium ne donnent aucune réaction avec les aziridines **6***b* et **9***b* qui sont, par contre, réduites au niveau de l'atome d'halogène, par le méthylate, l'éthylate ou l'éthanethiolate de sodium; la réaction conduit alors à l'isopropyl-1 phénylsulfonyl-2 aziridine **1***b*. L'aziridine bromée **9***b* est plus facilement réduite que l'aziridine chlorée **6***b*. On observe, par ailleurs, un accroissement de vitesse considérable lorsque la réaction est effectuée dans le diméthylsulfoxyde, par rapport aux réactions réalisées en utilisant comme solvant un alcool ou le diméthylformamide.

Les éqs [2], [3] et [4] rendent compte de nos résultats expérimentaux:

[2] 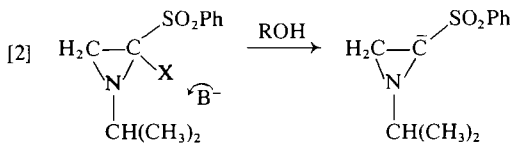

6*b* X = Cl
9*b* X = Br
$B^- = RO^-$ ou EtS^-

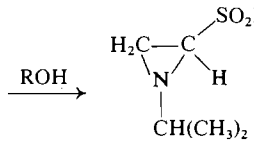

1*b*

En présence d'alcoolate ou d'éthanetiolate de sodium dans l'alcool, le nucléophile attaque directement l'halogène en créant un carbanion dont la vitesse de formation détermine la vitesse de réaction (éq. [2]). Dans le diméthylsulfoxyde, le nucléophile attaque le solvant dont la base conjuguée constitue

[3] $C_2H_5ONa + CH_3—SO—CH_3 \rightarrow C_2H_5OH + {}^-CH_2—SO—CH_3, Na^+$

[4] 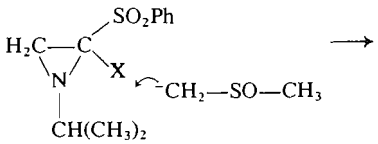

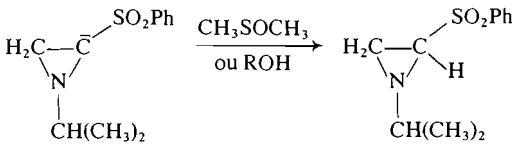

alors le véritable agent réducteur (éqs [3] et [4]), ce qui justifie l'accroissement de vitesse observé. Un mécanisme analogue a été proposé pour la réduction de *gem*-dibromocyclopropanes (10). La protonation du carbanion pourrait être réalisée, soit par le solvant, soit à l'hydrolyse. Cette deuxième hypothèse doit être écartée. En effet, l'hydrolyse par l'eau lourde du mélange réactionnel provenant de l'action de l'éthylate de sodium dans le diméthylsulfoxyde sur l'aziridine **9***b*, conduit au produit de réduction **1***b* sans incorporation de deutérium en position 2. Le composé deutérié en 2 est, par contre, obtenu lorsque la réaction est effectuée dans le diméthylsulfoxyde deutérié, après hydrolyse par H_2O, ce qui prouve l'intervention du solvant lors de la protonation du carbanion.

Partie expérimentale

Les spectres de résonance magnétique nucléaire ont été enregistrés à l'aide d'un appareil Varian A 60 ou Varian T 60 en utilisant le tétraméthylsilane comme référence interne; les déplacements chimiques sont exprimés en ppm et les constantes de couplage en hertz. Les spectres infrarouge ont été effectués sur un spectrophotomètre Perkin-Elmer 157. Les chromatographies sur colonne ont été réalisées sur gel de silice (7734 Merck).

*Synthèse des alkylsulfonyl-2 aziridines **4** et **5***

Préparation de la méthyl α-bromovinylsulfone et de l'isopropyl α-bromovinylsulfone

Le schéma réactionnel utilisé pour accéder à ces deux composés est le même, il est résumé ci-dessous:

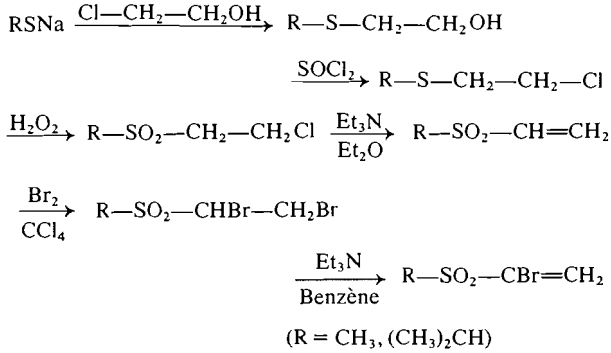

(R = CH_3, $(CH_3)_2CH$)

(a) *(Hydroxy-2 éthyl)alkylsulfure*—Il est préparé selon un mode opératoire décrit (11).

(Hydroxy-2 éthyl)méthylsulfure: rdt 70%; pé 75°C/25 Torr; n_D^{20} 1.487 (lit. (14) pé 80.5–81°C/30 Torr; n_D^{30} 1.4867); ir: 3350 cm^{-1}; rmn: 3.72 (2H, t, J = 6 Hz), 3.48 (1H, s), 2.65 (2H, t, J = 6 Hz), 2.10 (3H, s).

(Hydroxy-2 éthyl)isopropylsulfure: rdt 83%; pé 88°C/25 Torr; n_D^{20} 1.466 (lit. (15) pé 82–83°C (12 Torr.); rmn: 3.70 (2H, t, J = 6 Hz), 2.6 à 2.9 (2H, m), 2.5 à 3.2 (1H, m), 2.75 (1H, s), 1.25 (6H, d).

(b) *(Chloro-2 éthyl)alkylsulfure*—Ce composé est préparé selon une méthode décrite (12).

(Chloro-2 éthyl)méthylsulfure: rdt 80%; pé 56°C/40 Torr; n_D^{20} 1.486 (lit. (14) pé 44°C/20 Torr; n_D^{20} 1.4902); rmn: 2.6 à 3.9 (4H, m), 2.18 (3H, s).

(Chloro-2 éthyl)isopropylsulfure: rdt 95%; pé 74–76°C/35 Torr; n_D^{20} 1.471 (lit. (16) pé 60–62°C/17 Torr); rmn: 3.5 à 3.8 (2H, m), 2.7 à 3.3 (3H, m), 1.28 (6H, d).

(c) *Alkylvinylsulfone*—L'alkyl(chloro-2 éthyl)sulfure est oxydé par l'eau oxygénée en milieu acétique, selon un mode opératoire connu (13). Il est utilisé brut pour la réaction suivante, également décrite (13).

Méthylvinylsulfone: rdt 60%; pé 78°C/1 Torr (lit. (13) pé 115–117°C/19 Torr); rmn: 6.1 à 7.2 (3H, m), 2.98 (3H, s).

Isopropylvinylsulfone: rdt 75%; $pé_{0.5}$ = 82°C; rmn: 6.1 à 6.7 (3H, m), 2.8 à 3.4 (1H, m), 1.82 (6H, d, J = 7 Hz). *Anal.* calc.: C 44.78, H 7.46, S 23.88; trouvée: C 44.50, H 7.42, S 24.01.

(d) *Dibromo-1,2 alkylsulfone*—Le mode opératoire utilisé a été précédemment décrit (1).

Dibromo-1,2 méthylsulfone: rdt 80%; pf = 70°C; rmn: 5.05 (1H, dd, J = 3.5 Hz, J = 8.5 Hz), 4.25 (1H, dd, J = 11.5 Hz, J = 3.5 Hz), 3.78 (1H, dd, J = 11.5 Hz, J = 8.5 Hz), 3.20 (3H, s).

Dibromo-1,2 isopropylsulfone: rdt 98%; rmn: 5.05 (1H, dd, J = 3.5 Hz, J = 10 Hz), 4.35 (1H, dd, J = 11.5 Hz, J = 3.5 Hz), 3.75 (1H, dd, J = 10 Hz, J = 11.5 Hz), 3.6 à 4.2 (1H, m), 1.42 (3H, d, J = 6.5 Hz), 1.45 (3H, d, J = 6.5 Hz).

(e) *(Bromo-1 vinyl)alkylsulfone*—Ce composé est préparé selon une méthode décrite (1).

TABLEAU 1. Description des alkylsulfonyl-2 aziridines **4** et **5**

N°	Rdt (%)	F (°C)	Analyse
4*b*	65	40[b]	Calc.: C 44.17, H 7.98, N 8.59, S 19.63 Trouvée: C 44.33, H 7.95, N 8.75, S 19.32
4*c*	60	66[b]	Calc.: C 47.46, H 8.47, N 7.91, S 18.08 Trouvée: C 47.27, H 8.45, N 7.72, S 18.22
4*d*	60	138[c]	Calc.: C 56.87, H 6.16, N 6.64, S 15.17 Trouvée: C 56.82, H 6.14, N 6.58, S 15.02
5*a*[a]	70	—	Calc.: C 47.46, H 8.47, N 7.91, S 18.08 Trouvée: C 47.50, H 8.43, N 7.81, S 18.18
5*b*[a]	71	—	Calc.: C 50.26, H 8.90, N 7.33, S 16.75 Trouvée: C 50.14, H 8.80, N 7.36, S 16.43
5*c*	75	59[b]	Calc.: C 52.68, H 9.27, N 6.83, S 15.61 Trouvée: C 52.50, H 9.16, N 6.90, S 15.38
5*d*	75	71[b]	Calc.: C 60.25, H 7.11, N 5.86, S 13.39 Trouvée: C 60.15, H 7.21, N 5.75, S 13.48

[a]Purifiée par chromatographie sur colonne: (éther de pétrole 7 – acétate d'éthyle 3).
[b]Recristallisée dans éthanol – éther de pétrole.
[c]Recristallisée dans l'éthanol.

TABLEAU 2. Spectres de rmn ($CDCl_3$) des alkylsulfonyl-2 aziridines **4** et **5**:

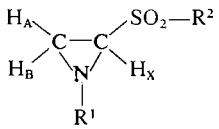

N°	R^1	R^2	δ H_X	δ H_A	δ H_B	δ H_{R1}	δ H_{R2}	*J* AX	*J* BX	*J* AB	*J* HR^1	*J* HR^2
4*b*	$CH(CH_3)_2$	CH_3	2.98 dd	2.48 d	1.87 d	1.20 d 1.29 d 1.5–2 m	2.98 s	2.5	6	0	6	—
4*c*	$C(CH_3)_3$	CH_3	3.14 dd	2.32 d	2.04 d	1.06 s	2.95 s	2.5	6	0	—	—
4*d*	CH_2Ph	CH_3	3.00 dd	2.65 d	2.02 d	7.37 s 3.35 (AB)	2.47 s	2.5	6	0	12.5	—
5*a*	C_2H_5	$CH(CH_3)_2$	2.99 dd	2.50 d	1.80 d	1.21 t 2.48 q	1.45 d 1.52 d 3.1–3.6 m	3	6	0	7	7
5*b*	$CH(CH_3)_2$	$CH(CH_3)_2$	3.00 dd	2.51 d	1.81 d	1.20 d 1.28 d 1.6–2 m	1.45 d 1.50 d 3.1–3.6 m	3	6	0	6	7
5*c*	$C(CH_3)_3$	$CH(CH_3)_2$	3.20 dd	2.35 d	2.0 d	1.05 s	1.38 d 1.40 d 3–3.5 m	3	6	0	—	7
5*d*	CH_2Ph	$CH(CH_3)_2$	3.08 dd	2.60 d	1.92 d	7.5 s 3.60 (AB)	1.00 d 1.25 d 3.1–3.6 m	3	6	0	13	7

(Bromo-1 vinyl)méthylsulfone: rdt 80%; pé 67–68°C/0.5 Torr (lit. (17) pé 63–64°C/0.4 Torr); rmn: 7.0 (1H, d, J = 3.5 Hz), 6.38 (1H, d), 3.07 (3H, s).

(Bromo-1 vinyl)isopropylsulfone: rdt 90%; rmn: 7.02 (1H, d, J = 3.5 Hz), 6.50 (1H, d), 3.2 à 3.8 (1H, m), 1.36 (6H, d, J = 6.8 Hz).

Préparation des aziridines 4 et 5

Le mode opératoire utilisé a été précédemment décrit (1). On relève sur le spectre ir de chaque composé deux bandes, l'une à 1330 cm^{-1}, l'autre à 1150 cm^{-1}, caractéristiques de la fonction sulfone. Les rendements, constantes physiques, analyses et spectres de rmn des produits préparés sont donnés dans les Tableaux 1 et 2.

Chloration des sulfonyl-2 aziridines

Elle est réalisée selon une méthode mise au point par Meyers *et al.* (2).

On porte à reflux pendant une heure un mélange de 0.01 mol de sulfonylaziridine, 20 mL de CCl_4, 20 mL de *tert*-butanol et 11.2 g de potasse finement pulvérisée. Les solvants sont évaporés et on reprend par l'eau. Les sulfonylaziridines chlorées brutes sont filtrées ou extraites à l'éther, lavées à l'eau, séchées et recristallisées (benzène 3 – acétate d'éthyle 1). Leurs spectres ir présentent deux raies larges et intenses à 1160 et 1320 cm^{-1} caractéristiques de la fonction sulfone. Leurs rendements, points de fusion, analyses et spectres de rmn sont donnés dans les Tableaux 3 et 4.

Le produit brut de chloration de l'aziridine **5***b* d'une part, de l'aziridine **5***d* d'autre part, est purifié par chromatographie sur colonne (éther de pétrole 7 – acétate d'éthyle 3). Dans chaque cas, on isole en premier l'aziridine dichlorée, l'aziridine monochlorée est éluée ensuite.

Isopropyl-1 chloro-2 ((chloro-1 méthyl-1 éthyl)sulfonyl)-2 aziridine **13***b*: ir: 1120, 1340 cm^{-1}; rmn: 1.25 et 1.35 (6H, 2d, J = 7 Hz, $(CH_3)_2C$), 2.02 et 2.10 (6H, 2s, $(CH_3)_2C$), 1.90 (1H, s, proton du cycle), 2.95 (1H, s, proton du cycle), 2.60 (1H, m, N—CH). *Anal.* calc.: C 36.92, H 5.77, N 5.38, S 12.31; trouvée: C 37.01, H 5.72, N 5.41, S 12.27.

TABLEAU 3. Description des halogéno-2 phénylsulfonyl-2 aziridines

N°	Rdt (%)	F (°C)	Analyse
6*b*	70	110	Calc.: C 50.87, H 5.39, N 5.39, O 12.33 Trouvée: C 50.65, H 5.47, N 5.32, O 12.40
6*c*	70	67	Calc.: C 52.65, H 5.85, N 5.12, O 11.70 Trouvée: C 52.62, H 5.98, N 5.11, O 11.63
7*b*	79	109	Calc.: C 52.65, H 5.85, N 5.12, O 11.70 Trouvée: C 52.30, H 5.88, N 5.04, O 11.71
7*d*	73	71	Calc.: C 59.72, H 4.98, N 4.36, O 9.95 Trouvée: C 59.50, H 4.92, N 4.48, O 9.90
8*a*	71	76	Calc.: C 59.72, H 4.98, N 4.36, O 9.95 Trouvée: C 59.61, H 4.88, N 4.28, O 10.02
9*b*	74	103	Calc.: C 43.42, H 4.61, N 4.61, O 10.53 Trouvée: C 43.69, H 4.57, N 4.68, O 10.28
9*c*	75	87	Calc.: C 45.28, H 5.03, N 4.40, O 10.06 Trouvée: C 45.46, H 5.13, N 4.51, O 10.16
10*b*	75	120	Calc:. C 45.28, H 5.03, N 4.40, O 10.06 Trouvée: C 45.34, H 4.97, N 4.42, O 10.09
10*d*	41[a]	70	Calc.: C 52.46, H 4.37, N 3.83, O 8.74 Trouvée: C 52.46, H 4.45, N 3.85, O 8.71
11*a*	75	80	Calc.: C 52.46, H 4.37, N 3.83, O 8.74 Trouvée: C 52.47, H 4.34, N 3.61, O 8.70

[a]On obtient d'autre part 40% de l'aziridine mise en réaction.

TABLEAU 4. Spectres de rmn ($CDCl_3$) des halogéno-2 phénylsulfonyl-2 aziridines

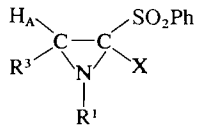

				δ				J	
N°	R^1	R^3	X	H_A	H_{R3}	H_{R1}	H_{Ph}	H_A—R^3	H_{R1}
6*b*	$CH(CH_3)_2$	H	Cl	2.91 s	1.91 s	0.68 d 1.20 d 2.1–2.6 m	7.5–8.2 m	0	6.5
6*c*	$C(CH_3)_3$	H	Cl	2.60 d	2.25 d	1.02 s	7.5–8.2 m	2.5	
7*b*	$CH(CH_3)_2$	CH_3	Cl	3.11 q	1.30 d	0.61 d 1.12 d 2.4–3 m	7.5–8.2 m	6	6.5
7*d*	CH_2Ph	CH_3	Cl	3.20 q	1.30 d	8.2 s 3.68 (AB)	7.3–8 m	6	13
8*a*	C_2H_5	Ph	Cl	4.08 s	7.35 s	3.42 dq 1.25 t	7.5–8.2 m	—	7.5
9*b*	$CH(CH_3)_2$	H	Br	2.90 d	1.92 d	0.68 d 1.20 d 1.9–2.4 m	7.5–8.2 m	1	6.5
9*c*	$C(CH_3)_3$	H	Br	2.53 d	2.23 d	1.02 s	7.5–8.2 m	3	—
10*b*	$CH(CH_3)_2$	CH_3	Br	2.98 q	1.32 d	0.61 d 1.12 d 2.2–2.8 m	7.5–8.2 m	6	6.5
10*d*	CH_2Ph	CH_3	Br	3.08 q	1.32 d	7.2 s 3.61 (AB)	7.3–8 m	6	13
11*a*	C_2H_5	Ph	Br	4.0 s	7.30 s	1.27 t 3.45 dq	7.5–8.2 m	—	7.5

Benzyl-1 chloro-2 ((chloro-1 méthyl-1 éthyl)sulfonyl)-2 aziridine **13***d*: ir: 1150, 1320 cm^{-1}; rmn: 1.95 et 2 (7H, 2s, $(CH_3)_2C$ et un proton du cycle), 2.92 (1H, s, proton du cycle), 3.95 (2H, AB, J = 13.5 Hz, N—CH_2), 7.35 (5H, s, C_6H_5). *Anal.* calc.: C 46.75, H 4.87, N 4.55, S 10.39; trouvée: C 46.40, H 4.82, N 4.58, S 10.44.

Isopropyl-1 ((chloro-1 méthyl-1 éthyl)sulfonyl)-2 aziridine **12***b*: ir: 1120, 1150, 1180, 1320, 1335 cm^{-1}; rmn: 1.20 (3H, d, J = 6.5 Hz), 1.30 (3H, d, J = 6.5 Hz), 1.92 (3H, s), 2.02 (3H, s), 1.78 (1H, d, J = 6 Hz), 2.41 (1H, d, J = 2.8 Hz), 3.40 (1H, dd, J = 6 Hz et J = 2.8 Hz), 1.80 (1H, m). *Anal.* calc.: C 42.57, H 7.10, N 6.21, S 14.19; trouvée: C 42.68, H 7.08, N 6.23, S 14.30.

Benzyl-1 (chloro-1 méthyl-1 éthyl)sulfonyl-2 aziridine **12***d*: ir: 1120, 1330 cm^{-1}; rmn: 1.80 (3H, s), 1.86 (3H, s), 1.90 (1H, d, J = 6.2 Hz), 2.50 (1H, d, J = 2.8 Hz), 3.50 (1H, dd, J = 2.8 Hz, J = 6.2 Hz), 3.68 (2H, AB, J = 13 Hz), 7.4 (5H, s). *Anal.* calc.: C 52.65, H 5.85, N 5.12, S 11.70; trouvée: C 52.32, H 5.81, N 5.21, S 11.62.

Une solution de 4.4 mmol du composé **12***b* dans 50 mL de THF est agitée pendant 5 h à 0°C en présence de 13 mmol de *t*BuOK. On ajoute de l'eau, extrait à l'éther, lave le phase éthérée, sèche et évapore le solvant. Le résidu est d'après son spectre rmn constitué de la seule aziridine mise en réaction.

Un mélange de 4.4 mmol de l'aziridine **12***b*, 13 mmol de *t*BuOK et 50 mL de THF est chauffé à reflux sous agitation pendant 5 h. Après les traitements classiques, le spectre rmn de produit brut montre qu'il est constitué de 60% de l'aziridine mise en réaction et de 40% du dérivé **14***b*. Ces deux composés sont séparés par chromatographie sur colonne (éther de pétrole – acétate d'éthyle 30).

Isopropyl-1 (méthyl-1 vinyl)sulfonyl-2 aziridine **14***b*: ir: 1130, 1310, 1640 cm^{-1}; rmn: 1.15 (6H, d, J = 6 Hz), 1.75 (1H, d, J = 6 Hz), 2.20 (3H, s large), 2.45 (1H, d, J = 2 Hz), 2.80 (1H, dd, J = 2 Hz, J = 6 Hz), 5.80 (1H, s large), 6.15 (1H, s). *Anal.* calc.: C 50.79, H 7.94, N 7.41, S 16.93; trouvée: C 50.52, H 7.89, N 7.45, S 16.78.

TABLEAU 5. Thermolyse des halogéno-2 sulfonyl-2 aziridines

Aziridine N°	Durée de thermolyse (h)	Pourcentage de décomposition[a]
6*b*	8	100
6*c*	10	100
7*b*	170	45
7*d*	48	10
8*a*	3	70
9*b*	2.5	100
9*c*	5	100
10*b*	170	70
10*d*	3.5	35
11*a*	1	50

[a]Déterminé sur les spectres de rmn.

TABLEAU 6. Action des réactifs nucléophiles sur les chloro-2 et bromo-2 aziridines **6***b* et **9***b*

Aziridine N°	Solvant	CH_3O^-; $C_2H_5O^-$	$C_2H_5S^-$	$C_6H_5S^-$	CN^-
6*b*	ROH	10 jours; 80°C; aucune réaction	10 jours; 80°C; aucune réaction	—	—
6*b*	DMF	10 jours; 80°C; aucune réaction	10 jours; 80°C; aucune réaction	—	—
6*b*	DMSO	1 h; 20°C; R[a]	24 h; 20°C; R	—	—
9*b*	ROH	72 h; 80°C; R	72 h; 80°C; R	8 h; 80°C; aucune réaction	8 h; 80°C; aucune réaction
9*b*	DMF	8 h; 80°C; R	—	—	—
9*b*	DMSO	1 min; 20°C; R	10 min; 20°C; R	10 jours; 80°C; aucune réaction	10 jours; 80°C; aucune réaction

[a]R = réaction de réduction.

Bromation des phénylsulfonyl-2 aziridines

Selon le mode opératoire décrit (2), on porte à reflux pendant une heure un mélange de 0.01 mol d'aziridine, 10 g de tétrabromure de carbone, 10 mL de *tert*-butanol, 15 mL de benzène et 11.2 g de potasse pulvérisée. Les solvants sont évaporés. On reprend le résidu à l'eau, extrait à l'éther, lave les extraits éthérés, sèche et évapore l'éther. Le résidu est purifié par chromatographie sur colonne. On sépare d'abord l'excès de CBr_4 (éluant: éther de pétrole) puis l'aziridine bromée (éluant: éther de pétrole 9 – acétate d'éthyle 1). Les aziridines bromées présentent en ir deux bandes larges et intenses à 1160 et 1320 cm^{-1}; leurs rendements, points de fusion, analyses et spectres de rmn sont donnés dans les Tableaux 3 et 4.

Thermolyse des halogéno-2 sulfonyl-2 aziridines

L'aziridine (0.01 mol) est portée à 60°C en tube scellé. Après un temps variable, le produit déliquescent obtenu est analysé par rmn. Les dérivés de thermolyse et le pourcentage de décomposition sont donnés dans le Tableau 5.

Le produit brut de thermolyse des composés **6***b* et **9***b* est chromatographié sur colonne. On sépare ainsi:

Le benzènethiosulfonate de phényle: eluant: éther de pétrole 9 – acétate d'éthyle 1; pf 44°C (lit. (18) pf 42–44°C); ir: 1150 et 1320 cm^{-1}; rmn: 7.2 à 7.6 (m). *Anal.* calc.: C 57.60, H 4.00, O 12.80, S 25.60; trouvée: C 57.72, H 3.94, O 12.75, S 25.56.

Le *N*-isopropyl α-halogénoacétamide: eluant: éther de pétrole 7 – acétate d'éthyle 3: *N*-isopropyl α-chloroacétamide: pf 60°C (lit. (19) pf 62–62.5°C); rmn: 1.20 (6H, d, J = 6.5 Hz), 4.0 (2H, s), 4.10 (1H, m). *N*-isopropyl α-bromoacétamide: pf 70°C (lit. (20) pf 66–67°C); ir: 3300, 1660 cm^{-1}; rmn: 1.20 (6H, d, J = 7 Hz), 3.85 (2H, s), 4.05 (1H, m).

Thermolyse avec apport d'eau

L'halogénoaziridine (0.01 mol) est portée à 60°C en tube scellé avec 0.10 mol d'eau. Après 6 jours de chauffage pour **6***b*, 4 jours pour **9***b*, on reprend au chlorure de méthylène, décante, sèche et évapore le solvant. Par chromatographie sur colonne on sépare, à côté des composés précédemment décrits, le *N*-isopropyl α-phénylsulfonylacétamide (éluant: éther de pétrole 2 – acétate d'éthyle 8): ir: 1160, 1360, 1700 cm^{-1}; rmn: 1.15 (6H, d, J = 6.5 Hz), 4.05 (1H, s), 3.7 à 4.3 (1H, m), 7.5 à 8.1 (5H, m), 6.7 (1H, pic large). *Anal.* calc.: C 54.77, H 6.22, N 5.81, O 19.92, S 13.28; trouvée: C 54.93, H 6.18, N 6.04, O 19.75, S 13.24.

Synthèse du N-*isopropyl α-phenylsulfonylacétamide*

Une solution de 1.35 g (0.01 mol) de *N*-isopropyl α-chloroacétamide dans 10 mL d'alcool est ajoutée à 1.64 g (0.01 mol) de benzènesulfinate de sodium dans 20 mL d'alcool. Le mélange est porté à reflux pendant 4 h. La solution est évaporée, reprise par le chlorure de méthylène, lavée à l'eau et séchée. Après évaporation du solvant, l'amide cristallise; pf 118°C.

Décomposition des aziridines dichlorées ***13***b *et* ***13***d

Les aziridines **13***b* et **13***d*, abandonnées quelques jours à température ambiante, se décomposent. Par chromatographie sur colonne (éther de pétrole 70 – acétate d'éthyle 30), on sépare le chloro-1 méthyl-1 éthylthiosulfonate de chloro-1 méthyl-1 éthyle et le *N*-alkyl α-chloroacétamide.

Chloro-1 méthyl-1 éthylthiosulfonate de chloro-1 méthyl-1 éthyle: rmn: 1.75 (s). *Anal.* calc.: C 28.69, H 4.78, S 25.50; trouvée: C 28.50, H 4.72, S 25.65.

N-Benzyl-α-chloroacétamide: pf 92–93°C (lit. (21) pf 93–93.6°C); ir: 1700 (C=O); rmn: 7.4 (5H, s), 4.50 (2H, s), 4.20 (2H, s).

Hydrolyse acide

On chauffe à reflux pendant 1 h 0.01 mol d'aziridine dans 34 mL d'acide chlorhydrique 2*N* en solution hydroalcoolique. On évapore l'alcool et le résidu, après extraction au chlorure de méthylène, est chromatographié sur colonne. On sépare d'abord le benzènethiosulfonate de phényle déjà décrit (éluant: éther de pétrole 9 – acétate d'éthyle 1). On obtient ensuite, à partir de l'aziridine **6***c*, le *N-tert*-butyl α-chloroacétamide (éther de pétrole 7 – acétate d'éthyle 3); pf 80°C (lit. (19) pf 82–83°C); rmn: 1.40 (10H, s, $C(CH_3)_3$ et N—H), 3.95 (2H, s large).

A partir de l'aziridine **10***b*, on obtient un mélange de 55% de *N*-isopropyl α-chloropropionamide et 45% de *N*-isopropyl α-bromopropionamide (éther de pétrole 7 – acétate d'éthyle 3); rmn: 6.50 (1H, pic large), 4.40 (1H, q, J = 7 Hz), 3.70 à 4.40 (1H, m), 1.85 (0.45H, d, J = 7 Hz), 1.70 (0.55H, d, J = 7 Hz), 1.18 (6H, d, J = 6.8 Hz).

Action des nucléophiles

A une solution de 0.01 mol d'aziridine dans 50 mL de solvant, on ajoute 0.05 mol de réactif nucléophile. Les temps et températures de réaction sont indiqués dans le Tableau 6. On ajoute 200 mL d'eau et extrait à l'éther. Après évaporation du solvant, le produit brut est analysé en rmn.

1. P. CARLIER, Y. GELAS-MIALHE et R. VESSIERE. Can. J. Chem. **55**, 3190 (1977).
2. C. Y. MEYERS, A. M. MALTE et W. S. MATTHEWS. J. Am.

Chem. Soc. **91**, 7510 (1969); C. Y. MEYERS et W. S. MATTHEWS. Brevet U.S. No 3.830.862 (août, 1974).
3. (*a*) L. RAMBERG et B. BACKLUND. Chem. Abstr. **34**, 4725 (1940); (*b*) F. G. BORDWELL. Organosulfur chemistry. *Edited by* M. J. Janssen. John Wiley, Inc., New York, NY. (1968); (*c*) L. A. PAQUETTE. Acc. Chem. Res. **1**, 209 (1968); (*d*) L. A. PAQUETTE. Org. React. **25**, 1 (1977).
4. (*a*) R. E. BROOKS, J. O. EDWARDS, G. LEVEY et F. SMITH. Tetrahedron, **22**, 1279 (1966); (*b*) E. K. FIELDS et J. M. SANDRI. Chem. Ind. (London), 1216 (1959); (*c*) A. G. COOK et E. K. FIELDS. J. Org. Chem. **27**, 3686 (1962); (*d*) H. W. HEINE et A. B. SMITH III. Angew. Chem. Int. Ed. Engl. **2**, 400 (1963); (*e*) K. ICHIMURA et M. OHTA. Tetrahedron Lett. 807 (1966); (*f*) D. J. ANDERSON, T. L. GILCHRIST, D. C. HORWELL et C. N. REES. J. Chem. Soc. C, 576 (1970); (*g*) M. K. MEILAHN, L. L. AUGENSTEIN et J. L. MCMANAMAN. J. Org. Chem. **36**, 3627 (1971); (*h*) M. SENO, S. SHIRAISHI, Y. SUZUKI et T. ASAHARA. Bull. Chem. Soc. Jpn. **49**, 1893 (1976).
5. H. PERSON et A. FOUCAUD. Bull. Soc. Chim. 1119 (1976).
6. (*a*) J. SONNENBERG et S. WINSTEIN. J. Org. Chem. **27**, 748 (1962); (*b*) M. S. BAIRD, D. G. LINDSAY et C. B. REESE. J. Chem. Soc. C, 1173 (1969).
7. C. J. M. STIRLING. Int. J. Sulfur Chem. B, **6**, 277 (1971).
8. (*a*) J. A. DEYRUP et R. B. GREENWALD. J. Am. Chem. Soc. **87**, 4538 (1965); (*b*) A. HASSNER, S. S. BURKE et J. CHENG-FANI. J. Am. Chem. Soc. **97**, 4692 (1975).
9. (*a*) F. G. BORDWELL et G. D. COOPER. J. Am. Chem. Soc. **73**, 5184 (1951); (*b*) L. A. PAQUETTE. J. Am. Chem. Soc. **86**, 4085 (1964); (*c*) W. M. ZIEGLER et R. CONNOR. J. Am. Chem. Soc. **62**, 2596 (1940).
10. (*a*) C. G. CARDENAS, A. N. KHAFAJI, C. L. OSBORN et P. D. GARDNER. Chem. Ind. (London), 345 (1965); (*b*) C. L. OSBORN, T. C. SHIELDS, B. A. SHOULDERS, C. G. CARDENAS et P. D. GARDNER. Chem. Ind. (London), 766 (1965).
11. W. WINDUS et P. R. SHILDNECK. Org. Synth. **14**, 54 (1934).
12. W. R. KIRNER et W. WINDUS. Org. Synth. **14**, 18 (1934).
13. G. D. BUCKLEY, J. L. CHARLISH et J. D. ROSE. J. Chem. Soc. 1514 (1947).
14. W. R. KIRNER. J. Am. Chem. Soc. **50**, 2446 (1928).
15. Z. J. VEJDELEK, V. TRCKA, H. CHYBOVA et L. TUMA. Chem. Listy, **47**, 49 (1953); Chem. Abstr. **49**, 337b (1955).
16. A. G. BAYER. Brevet Brit. No 733.123 (juillet, 1955); Chem. Abstr. **50**, 10799g (1956).
17. J. C. PHILIPS et M. OKU. J. Am. Chem. Soc. **94**, 1012 (1972).
18. H. F. WHALEN et L. W. JONES. J. Am. Chem. Soc. **47**, 1353 (1925).
19. A. J. SPEZIALE et P. C. HAMN. J. Am. Chem. Soc. **78**, 2556 (1956).
20. W. E. WEAVER et W. M. WHALEY. J. Am. Chem. Soc. **69**, 515 (1947).
21. C. A. BUEHLER et C. A. MACKENZIE. J. Am. Chem. Soc. **59**, 421 (1937).

An investigation of the photodecomposition of *N*-bromosuccinimide; the generation and reactivity of succinimidyl radical[1]

FU-LUNG LU, YOUSRY M. A. NAGUIB, MASAYUKI KITADANI, AND YUAN L. CHOW

Department of Chemistry, Simon Fraser University, Burnaby, B.C., Canada V5A 1S6

Received July 19, 1978[2]

FU-LUNG LU, YOUSRY M. A. NAGUIB, MASAYUKI KITADANI, and YUAN L. CHOW. Can. J. Chem. **57**, 1967 (1979).

The photolysis of acetonitrile solutions of *N*-bromosuccinimide (NBS) in the presence of ethylene oxide and an excess of olefins or benzene in the $-30 \sim 20°C$ range was shown to generate the succinimidyl radical in competition with the bromine atom reactions. The succinimidyl radical preferentially attacked a π bond to give 1-succinimidyl-2-bromoalkanes, rather than abstracting alkyl hydrogens. Allylic bromination also occurred and competed with the 1,2-addition. Formation of 3-bromocyclohexene in the presence of cyclohexene at 10–20°C could be effectively reduced at lower temperatures or in the presence of a high concentration of ethylene oxide; the 1,2-addition process was favored at low temperature but surprisingly not facilitated significantly in the presence of ethylene oxide. The primary adducts from benzene readily eliminate HBr to give *N*-phenylsuccinimide. The attack of a bromine atom on a carbon–carbon double bond may become an important step in the $0 \sim -30°C$ range. The ease of the addition reaction suggests that this succinimidyl radical may have a Σ electronic configuration.

FU-LUNG LU, YOUSRY M. A. NAGUIB, MASAYUKI KITADANI et YUAN L. CHOW. Can. J. Chem. **57**, 1967 (1979).

On a montré que la photolyse de solutions de *N*-bromosuccinimide (NBS) dans l'acétonitrile en présence d'oxyde d'éthylène et d'oléfines en excès ou de benzène à des températures allant de -30 à $+20°$ donne lieu à la formation de radicaux succinimidyles en compétition avec les réactions des atomes de brome. Le radical succinimidyle attaque de préférence une liaison π pour conduire à des succinimidyl-1 bromo-2 alcanes plutôt que d'arracher les hydrogènes des groupes alkyles. La bromation allylique se produit aussi et elle est en compétition avec l'addition-1,2. On peut réduire d'une façon efficace la formation du bromo-3 cyclohexène en présence de cyclohexène à 10–20°C en abaissant la température ou en présence de concentrations élevées d'oxyde d'éthylène; la réaction d'addition-1,2 est favorisée à basse température mais elle n'est toutefois pas rendue beaucoup plus facile en présence d'oxyde d'éthylène. Les adduits primaires avec le benzène éliminent facilement du HBr et donnent lieu à la *N*-phénylsuccinimide. L'attaque d'un atome de brome sur la liaison double carbone–carbone peut devenir une étape importante à des températures de 0 à $-30°C$. La facilité avec laquelle le radical succinimidyle s'additionne suggère qu'il peut avoir une configuration électronique Σ.

[Traduit par le journal]

Introduction

Ziegler *et al* (1) have demonstrated that the decomposition of *N*-bromosuccinimide (NBS) in the presence of olefins selectively brominates allylic positions under the appropriate conditions, i.e., thermolysis and (or) photolysis of NBS in boiling carbon tetrachloride. This allylic bromination has been shown to occur by a radical chain mechanism (2–7) and has been extensively utilized in synthesis primarily because of its simplicity and good yield (2–5). The original Ziegler reaction conditions have been used for allylic bromination without much modification until recently, when it was recognized that conditions affect the NBS decomposition pathways significantly (11–14). Interest in this allylic bromination was heightened when the bromine radical chain mechanism proposed earlier by Goldfinger and co-workers (9) was confirmed in 1963 (8); a straightforward succinimidyl radical chain mechanism proposed by Bloomfield (10) was shown to be not operating *at least under Ziegler's conditions* (11).

The Goldfinger Mechanism

[1] $Br_2 \overset{\Delta \text{ or } h\nu}{\rightleftharpoons} 2Br^{\bullet}$

[2] $CH_2{=}CHCH_2{-} + Br^{\bullet} \rightleftharpoons CH_2{=}C\dot{H}CH{-} + HBr$

[3] $(CH_2CO)_2NBr + HBr \rightarrow (CH_2CO)_2NH + Br_2$

[4] $CH_2{=}C\dot{H}CH{-} + Br_2 \rightarrow CH_2{=}CHCHBr{-} + Br^{\bullet}$

[1]Some of these results have been presented at the 52nd annual meeting of the Chemical Institute of Canada at Winnipeg; June 4–7, 1978. A communication of this work submitted to the Journal of American Chemical Society in September 28, 1977 was not accepted.

[2]Revision received January 25, 1979.

0008-4042/79/151967-10$01.00/0

The Bloomfield Mechanism

$$[5]\quad (CH_2CO)_2NBr \xrightarrow{\Delta \text{ or } h\nu} (CH_2CO)N^{\cdot} + Br^{\cdot}$$

$$[6]\quad (CH_2CO)_2N^{\cdot} + CH_2{=}CHCH_2{-} \rightarrow (CH_2CO)_2NH + CH_2{=}C\dot{H}CH{-}$$

$$[7]\quad CH_2{=}C\dot{H}CH{-} + (CH_2CO)_2NBr \rightarrow CH_2{=}CHCHBr{-} + (CH_2CO)_2N^{\cdot}$$

$$[8]\quad Br^{\cdot} + {-}CH{=}CHCH_2 \rightleftharpoons {-}CHBr\dot{C}HCH_2{-}$$

There have been numerous contributions to our knowledge of the mechanism of the NBS decomposition; these have been summarized in a review by Thaler (6). The major credit should go to Goldfinger who has suggested that NBS reacts rapidly with HBr to generate a low concentration of bromine, i.e., a concentration high enough to maintain the propagation step [4] but low enough to avoid ionic addition to olefins as an integral part of the chain processes; in other words, NBS serves as a reservoir of bromine. This proposal has been nicely substantiated recently (8*a*, 11).

In recent years, decompositions of NBS have been studied in bromination reactions of less active substrates (e.g., haloalkanes and alkanes) under a variety of conditions (e.g., uses of methylene chloride or acetonitrile as solvent to effect a homogenous reaction) much different from Ziegler's heterogeneous conditions (11–15). These studies that related to controversies over the anchimeric assistance of a neighboring bromine atom (12–15) led to the discovery that product patterns obtained in the comparative bromination of these alkanes with bromine and with NBS under homogeneous conditions are different (12, 13). This has led to the recognition of the succinimidyl radical as the possible chain carrier in the NBS decomposition (12, 13).

Although esr studies have not succeeded in identifying the succinimidyl radical directly, its presence in NBS decompositions has been indicated in the formation of β-bromopropionyl isocyanate (16) and in the esr determination of the stable nitroxide resulting from 2-nitroso-2-methyl-propane trapping (17). Oxidation of 1-phenylethanol in the decomposition of *N*-iodosuccinimide has been claimed to involve the succinimidyl radical as the chain carrier (18). It is noteworthy that the decomposition of NBS in the presence of benzyl ethers has been reported to give α-succinimidyl benzyl ethers (19); these results offer a new facet to the mechanism of NBS decomposition.

Theoretical calculations by simple molecular orbital theory carried out by Hedaya *et al.* (20) suggested that a succinimidyl radical may have Σ electronic configuration in the ground state, as in **A**, because of the electronegativity of the acyl groups attached to the nitrogen radical center; they have also predicted that a Σ radical should be more reactive and less selective. This prediction seems to be borne out by the recent works of Traynham and Lee (13) and Skell and co-workers (12) who have concluded that the succinimidyl radical is as reactive and unselective as the chlorine atom. Recent INDO calculations have shown that the ground state of the succinimidyl radical may have a Π (or Σ_0) configuration, as in **C**, and that the Σ_N configuration **A** (excited state) correlates with the electronic ground state of the acyl isocyanate radical in the β-scission (21).

Our interests in radical species at amino centers have led us to recognize the peculiar reactivities of these radicals. In particular, the aminyl (22, 23) and *N*-alkylamidyl (RCONR) (24, 25) radicals exclusively abstract allylic hydrogen atoms from olefins, while aminium radicals exclusively add to carbon–carbon double bonds (23, 26). In general, it may be expected that amine centered radicals with electron deficiency preferentially add to olefins (25). This expectation has been supported by Lessard and co-workers (27, 28) who have demonstrated that halogen substituted amidyl radicals ($XCH_2CO\dot{N}H$) add more efficiently as both the electronegativity and number of halogen atoms X increase. As the nitrogen center of the succinimidyl radical carries two electron-withdrawing acyl groups which could enter into delocalization with the lone pair electrons if it has Σ configuration as in **B**, one might expect the succinimidyl radical to have electrophilic character.

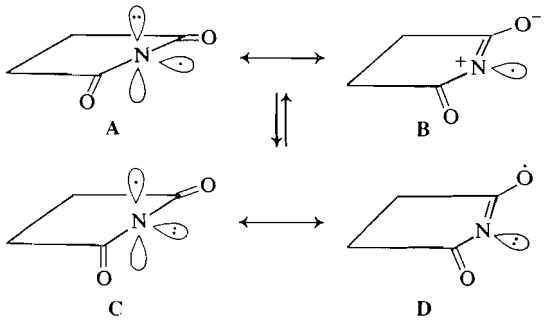

There is scattered evidence that the decomposition of NBS in the presence of olefins does give rise to addition products, although in poor yields (29–34); in some cases the adducts have been implied to arise by ionic addition pathways because of the observed orientations (32–34). However, others may have involved a direct attack of succinimidyl radical on the double bonds, particularly if substrates carry *unreactive hydrogens* (1, 29–32), e.g., $CH_2{=}CH_2$-

CH_2CN. These considerations have led us to reinvestigate the decomposition of NBS hoping to shed some light on the generation and reactivity of the succinimidyl radical. Recent communications by Skell and co-workers (35) on the addition of NBS to olefins and aromatic compounds when decomposed in the presence of these substrates prompts us to publish our results.

The complexity of the reaction pattern of NBS in the presence of an olefin has been discussed in detail by Thaler (6). Some of the complications arise from a reversible bromine atom addition to olefins as in reaction [8], the reversibility of reaction [2], and the instability of some allylic bromides. A general strategy of generating the succinimidyl radical would be to suppress the bromine atom chain mechanism (reactions [2]–[4]) so that NBS decomposition and propagation involving NBS as in reactions [5] and [7] can be encouraged. In practice, the $HBr–Br_2$ cycle has to be efficiently interrupted, and direct or indirect succinimidyl radical generation as in reactions [5] and [7] has to be accelerated. Our plan was to use ethylene oxide to scavenge HBr, and a high concentration of an olefin to scavenge molecular bromine (11); the latter was also the substrate in the present scheme. Epoxides have been used to scavenge HBr in bromination of ketones and aralkanes (36, 37). Acetonitrile was the choice as the solvent owing to its small tendency to donate hydrogen to electrophilic radicals and its reasonably good solubilizing power for NBS (15).

Results

In acetonitrile NBS exhibits an absorption maximum (shoulder) at 245 nm (ε 317) which tails above the 300 nm region (ε_{300} 13). This allowed us to carry out the decomposition of NBS by photolysis in a Pyrex apparatus with temperature controls. However, since there were no reliable kinetic data on reactions [1]–[8], an a priori prediction of temperature effects on the reaction pattern was not possible. Acetonitrile solution containing NBS (0.047 *M*) and ethylene oxide (0.35 *M*) reacted instantaneously at −10°C with HBr to show a pale yellow color and a weak absorption of bromine at 405 nm. A good amount of ethylene bromohydrin was also obtained from this reaction, indicating that HBr reacted rapidly with both substrates. Qualitatively, it was shown that HBr reacted with ethylene oxide with the order of decreasing efficiency in acetonitrile > methylene chloride > benzene ≈ carbon tetrachloride.

Photolysis of NBS in acetonitrile in the presence of 3,3-dimethyl-1-butene (neohexene, **1***a*) and ethylene oxide under nitrogen was carried out in a Pyrex apparatus immersed in a cooling bath. Generally the concentration of NBS was 0.016–0.02 *M* and the molar ratio of NBS, olefins, and the oxide was 1:10:8. The reaction mixture was vigorously stirred with a magnetic stirrer and its progress was monitored with potassium iodide – starch paper test and (or) iodimetry. For each experiment, a dark reaction was run simultaneously to confirm that thermal reactions occurred to only a small extent (<5%) or not at all. The photolysate was evaporated to give a crude product which, in this case, exhibited a clean nmr spectrum essentially similar to that of 1-succinimidyl-2-bromo-3,3-dimethylbutane (**2***a*, 85% yield by vpc). The gc–ms analysis of the crude product showed that it contained trace amounts of four minor products; the minor components had no succinimido moiety (no peak at *m/e* 100) and were not likely to be $BrCH_2C(CH_3)_2CH{=}CH_2$. Recrystallization of the crude product afforded **2***a* in a 65% yield which showed physical constants and analysis in agreement with an addition product. Reduction of **2***a* with zinc powder and sodium iodide gave **3***a*. The nmr spectrum of the latter exhibited, in addition to two singlets, symmetrical multiplets of type A_2B_2 at τ 8.54 and 6.48; the latter chemical shift is commonly found for a methylene attached to a succinimido group.

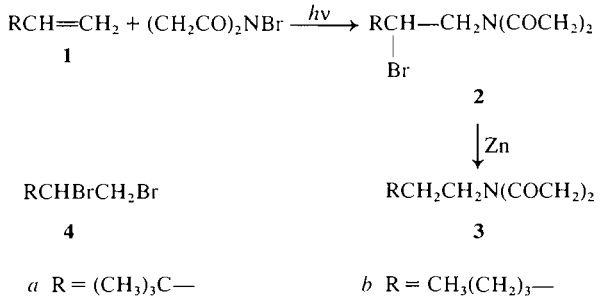

Under similar photolysis conditions, the photodecomposition of NBS in the presence of 1-hexene (**1***b*) gave a 60% yield of 1-succinimidyl-2-bromohexane (**2***b*) and a small amount of 1,2-dibromohexane (**4***b*). Reduction of **2***b* with zinc powder and sodium iodide gave *N*-hexylsuccinimide (**3***b*) synthesised from hexylamine and succinic anhydride (38). Both photoadditions indicated that the succinimido group attached itself to the less substituted carbon, and the bromine to the more substituted carbon of the double bond.

The photoaddition of NBS to cyclohexene under similar conditions gave complex product patterns (as shown by vpc analysis) which varied noticeably with a slight change of the conditions. The crude product showed an ir absorption at 2260 cm^{-1} typical of an isocyanate group and gave reproducible vpc analyses.

The photodecomposition of NBS at $-10°C$ gave the *trans*-1-bromo-2-succinimidylcyclohexane (**5**, ca. 30%) as the major product in addition to *trans*-1,2-dibromocyclohexane (**6**), *trans*-1-bromo-2(2′-bromoethoxy)cyclohexane (**7**), and 3-bromocyclohexene (**8**). By vpc analysis, several components in lesser amounts were detected, two of which were shown by gc–ms analysis and comparison with authentic mass spectra to be 2-cyclohexenol and 2-cyclohexenone. Varying amounts of succinimide were also isolated. By careful chromatography, a small amount of what appeared to be a mixture of 1- and 3-succinimidylcyclohexene was also isolated in the tail fractions; the postulate was based on the presence of succinimidyl and cyclohexene moieties in the fraction as judged from nmr, ir, and mass spectra.

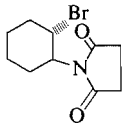

5

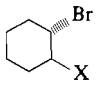

6 X = Br
7 X = OCH_2CH_2Br

Both **6** and **7** were prepared by the addition of bromine to cyclohexene in the presence of ethylene oxide. Adduct **5** showed ir absorptions at 1770, 1700, and 1170 cm^{-1} and a strong *m/e* peak at 100 (for $C_4H_6NO_2^+$) common to compounds containing a succinimido moiety. Zinc powder reduction of **5** gave the known *N*-cyclohexylsuccinimide independently synthesised by another route (38). The *trans* configuration in **5**, **6**, and **7** was decided by typical doublets of a triplet arising from the diaxial orientation of the 1,2-protons. A similar photolysis at $-20°C$ gave a lighter colored crude product and a better yield of adduct **5** (38%).

Photolysis of NBS in benzene in the presence of ethylene oxide was run in a similar manner at 10°C to give an isomeric mixture of **10** as the major product and a small amount of *N*-phenylsuccinimide. The isomeric mixture (40% yield) could not be separated by chromatography; these chromatographic fractions showed similar mass spectral patterns but drastically different nmr patterns, and gave good analyses for $C_{10}H_{10}Br_3NO_2$ arising from the addition of NBS and Br_2 to benzene. These fractions contained structural and stereochemical isomers of **10**. By extensive chromatography and recrystallization, small amounts of pure isomers having mp 204–207°C and mp 153–157°C were isolated; the complexity of their nmr spectra did not permit determination of structures. The structure of **11** was readily decided by direct comparison with an authentic sample prepared by the reaction of succinic anhydride and aniline. It was assumed that

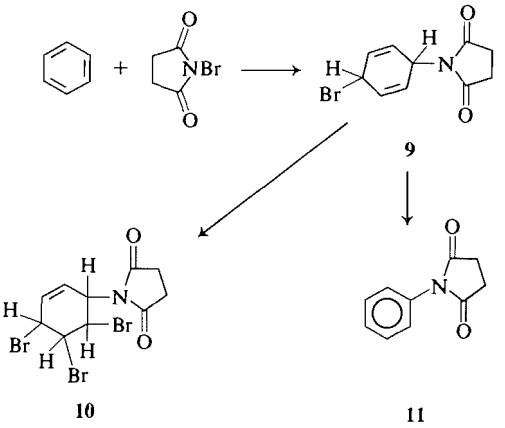

9

10 **11**

both **10** and **11** were formed from the primary adducts, such as **9** or its isomer, by bromine addition and HBr elimination, respectively.

The photolysis of NBS in acetonitrile containing benzene and ethylene oxide was carried out with a 450 W Hanovia lamp through a Corex filter in the presence of neohexene (neohexene–benzene, ca. 1/15) to scavenge bromine. In this case the reaction was very rapid and a good yield of **11** (54%) was obtained. In cases where the ratio of neohexene to benzene was higher, small amounts of adduct **2***a* were also formed but the ir absorption at 2260 cm^{-1} was not present in the crude products. When a lamp with less power or a Pyrex filter was used, the time for completion of the NBS decomposition was longer and the yields of **11** were much lower. Vapor phase chromatographic analysis indicated that a considerable amount of succinimide was formed and the yields of dibromide **4***a* were at least as much as those of **11** and that no other peak, such as that of bromobenzene, was present in the spectra.

In view of the extensive formation of bromine, as witnessed by the isolation of **10**, in spite of the presence of ethylene oxide, photolysis of bromine in the presence of ethylene oxide and NBS in benzene was examined using a filter to cut off the light source below 334 nm. NBS decreased slowly owing partially to the interference from the precipitated succinimide, but no reaction of NBS and bromine was observed in the dark. From the photolysate, in addition to a nearly quantitative yield of succinimide, a large amount of a mixture of polybrominated benzene derivatives was obtained without a trace of benzene derivatives containing the succinimido moiety. Photobromination of benzene has been reported to yield hexabromocyclohexane slowly through the bromine radical addition (39, 40).

More detailed studies on the NBS decomposition in the presence of cyclohexene were carried out in order to explore the effects of changes in the con-

TABLE 1. Product patterns of NBS decompositions in the presence of cyclohexene and ethylene oxide in acetonitrile[a]

Exp. No.	Time (h)	Temp. (°C)	Percentage of products[b] 5	8	6	7	$(CH_2CO)_2NH$	Remark
1	2.5	20	18	17	24	0	16	[c]
2	2.5	20	22	13	14	3.5	6	
3	4	10	28	9	12	5	9	
4	10	0	29	8	24	6	25	
5	14	−10	31	8	25	7	—	
6	21	−20	35	7	19	7	24	
7	26	−30	42	3	16	8	32	
8	1.5	19	6	14	30	5	71	[d]
9	18	−30	25	7	14	6	58	[d]
10	1.5	20	18	1	25	9	42	[e]
11	0.5	−10	36	<1	20	10	30	[f]

[a]Unless specified otherwise, solutions of 0.0113 mol of NBS in 240 mL of acetonitrile were photolysed with a 100 W Hanovia lamp in a Pyrex apparatus and the mole ratio of NBS:cyclohexene:ethylene oxide was 1:10:8.
[b]The % yields were based on NBS. 8 is 3-bromocyclohexene.
[c]No ethylene oxide added.
[d]Air leaked in inadvertently.
[e]The mole ratio of NBS:cyclohexene:ethylene oxide was 1:10:20.
[f]Photolysed with a 450 W Hanovia lamp in Corex filter.

ditions. For this purpose a series of photolyses in acetonitrile was carried out at various temperatures under a set of standardized conditions, e.g., apparatus, reagents, and procedures of operation and vpc analyses, as described in the Experimental. The vpc peaks of **5–8** did not change significantly (e.g., ±1%) within experimental error, but the peak of succinimide was partially superimposed on an unknown peak which increased with time; the percentage yields of succinimide were therefore less reliable (Table 1). As the temperature decreased from 20 to −30°C, the yields of adduct **5** increased and those of 3-bromocyclohexene (**8**) decreased but the yields of ionic products **6** and **7** remained substantial regardless of the conditions. Ethylene oxide had no effects on the yield of **5** but at higher concentrations it almost suppressed the formation of **8**. The presence of trace amounts of air caused erratic changes in the yields as well as photolysis times. The material balance based on the bromine was better than 90% except for a few cases which were at the 70% range. The material balance based on the succinimidyl moiety (30–80%) was better at higher concentrations of ethylene oxide and increased as the temperature was lowered. The time required for complete photolysis increased as the temperature was lowered, but particularly sharply in the range −10 to −30°C.

Photodecomposition of NBS in the presence of ethylene oxide alone in acetonitrile was shown to induce the formation of bromine, the light yellow color of which persisted even when all the NBS was decomposed. Under these conditions, ethylene bromohydrin, succinimide, and β-bromopropionamide were identified as the major products in addition to a small amount of bromoacetaldehyde and many other minor components.

Discussion

Both the failure of the dark reaction and the orientation of the NBS addition to neohexene and 1-hexene as found in **2** are straightforward indications that the succinimidyl radical has been generated in the photolysis and initiates the attack on the π-bond followed by attack of bromine atom donors as in reactions [9] and [10]. In the photolysis, radical halogenation processes probably involving allylic hydrogen abstraction also occur in competition with the 1,2-radical addition. Indeed the yields of 1,2-addition, **2** and **5**, at 0° to −10°C increase as the number of allylic hydrogens decrease as in cyclohexene < 1-hexene < neohexene; substantial amounts of 3-bromocyclohexene **8** under the comparable conditions might indicate relatively facile allylic hydrogen abstraction from cyclohexene. As shown in Table 1, the 1,2-addition product **5** increases and **8** decreases as the temperature is lowered. Such temperature effects have been observed by Touchard and Lessard (27) in the photochemical reaction of *N*-bromoacetamides with cyclohexene. The succinimidyl radical also attacks benzene efficiently under the photolysis conditions to give the 1,4-adduct **9** (or 1,2-adduct) as the primary product.

[9] $CH_2{=}CHCH_2{-} + (CH_2CO)_2N^{\cdot} \rightarrow (CH_2CO)_2NCH_2\dot{C}HCH_2{-}$

[10] $(CH_2CO)_2NCH_2\dot{C}HCH_2{-} + (CH_2CO)_2NBr(\text{or } B\dot{r}) \rightarrow (CH_2CO)_2NCH_2CHBrCH_2{-} + (CH_2CO)_2N^{\cdot}$

Judging from the excellent yield of adduct **2***a*, the abstraction of hydrogens by the succinimidyl radical from the *tertiary* butyl group does not compete to any significant extent with its addition to the π-bond of neohexene in spite of the conclusion reached by Traynham and Lee (13) and Skell and co-workers (12) that the succinimidyl radical is a voracious (and indiscriminate) hydrogen abstractor. In view of the complex product patterns observed in the detailed studies in the presence of cyclohexene, 3-bromocyclohexene **8** might be formed by both bromine and succinimidyl radical processes. While the strongly reactive succinimidyl radical (12, 13) requires only low activation energies in hydrogen abstraction or addition, the bromine atom, being a moderate (and selective) hydrogen abstractor needs a relatively higher energy (13). This implies that hydrogen abstraction by a bromine atom (reaction [2]) is retarded more than the succinimidyl radical reactions [6] and [9]) as the temperature is lowered. Therefore at −30°C succinimidyl radical reactions should be the major pathways in which addition reaction [6] occurs overwhelmingly over abstraction reaction [9]. Since the mode of the succinimidyl radical reactions is not expected to change significantly over a small temperature range, the increased yields of **8** in the −10–20°C range are most likely derived from the operation of bromine radical reaction [2]. An extrapolation of this trend (experiments 2–7) predicts that this process would probably operate more extensively at temperatures higher than 20°C; this may explain the lack of the formation of **5** in a similar experiment (in the absence of ethylene oxide) communicated by Skell and co-workers (12). However, it must be noted that at 20°C, even in the absence of ethylene oxide, a reasonable amount of adduct **5** can be formed (experiment 1) indicating that the presence of ethylene oxide is advantageous but not very effective in promoting the succinimidyl radical addition.

Epoxides have been known to scavenge HBr efficiently in the photobromination of ketones in carbon tetrachloride (36). In the present cases, ethylene oxide in polar solvents such as acetonitrile appears to scavenge HBr efficiently as shown by the formation of ethylene bromohydrin. Unfortunately, as shown in Table 1, it surprisingly exerts no effect on the yield of the 1,2-addition process but appears to retard the halogenation process only if the ethylene oxide/NBS molar ratio is of the order of 20:1. Its effects on the NBS decomposition are probably much more complex than expected as shown by the unpredictable variations of the yields of **6** and **7** as the concentrations of ethylene oxide increase (experiments 1, 2, and 10).

The uneven variation of the yields of dibromide **6** in contrast to the monotonic change of those of **7** might suggest that **6** is formed by dual pathways of ionic addition as well as bromine radical addition, while **7** is formed by the single ionic pathway. The reversibility of reaction [8] has been suggested independently by generation of β-bromocarbon radicals which preferentially undergo elimination with a small activation energy (~5 kcal/mol) (41). At −30°C, reaction [8] may not revert efficiently and constitutes the major pathway for formation of **6**. At temperatures higher than 20°C, reaction [8] reverts efficiently as demonstrated (41) and regenerates the bromine atoms for allylic bromination by Goldfinger's mechanism (9).

The persistent formation of the bromination products **6** and **7** under various conditions in spite of fairly efficient scavenging of HBr by ethylene oxide leads us to suspect there might be another pathway for bromine formation since the bromine generated by reaction [3] is expected to be a relatively minor amount under the conditions. Skell and co-workers (35) have recently suggested that reaction [11] occurs

$$[11]\quad (CH_2CO)_2NBr + Br^{\cdot} \rightarrow (CH_2CO)_2N^{\cdot} + Br_2$$

in the NBS photodecomposition in neopentane and methylene chloride, both of which are unreactive substrates. Further, they have proposed that the succinimidyl radical generated in reaction [11] is a Π-radical, different from that generated in reactions [5], [7], and [10] (a Σ radical). The formation of bromine from NBS by a radical pathway is hinted from two experiments: (*i*) photolysis of NBS in acetonitrile with ethylene oxide in the absence of an olefin to scavenge radicals efficiently and (*ii*) photolysis of bromine in the presence of NBS in benzene in which only bromination of benzene by a radical pathway can occur slowly (39, 40). Although the complexity of the reaction pattern does not allow us to pin-point the reaction for the bromine formation, reaction [11] is a straightforward possibility provided the failure of the succinimidyl radical reaction with benzene can be satisfactorily explained. However, possible mechanisms other than reaction [11] and, indeed, other pathways to account for the decomposition of NBS, cannot be excluded at this stage.

The overwhelming addition reactivity of the succinimidyl radical generated from reactions [5], [7], and [10] to olefinic and benzene π-bonds suggests that this radical is highly electrophilic and, in turn, hints that it has the Σ rather than the Π electronic configuration. It is known that a carbon radical having the unpaired electron in an sp^2 orbital is generally more electrophilic than that in

a p or sp^3 orbital (42). In analogy to this general correlation and also owing to a polar resonance contribution as in **B**, the Σ electronic configuration of the succinimidyl radical is expected to be more electrophilic than its Π electronic configuration. In view of some theoretical calculations (21) assigning the Σ configuration to a higher energy (excited) state species, it would be a challenge to identify Σ as well as Π radicals and to correlate their electronic configurations with their reactivities by quantitative means.

The addition of NBS to benzene has been observed previously (43) in a decomposition using benzene as the solvent. The comparable yields of **11** obtained under present conditions (54%) and by Skell and co-workers (45%) in the absence of ethylene oxide (35) seem to indicate, in agreement with the above conclusion, that ethylene oxide has very limited influence on the generation of the succinimidyl radical. The surprisingly good yield of tribromo adducts **10** (40%) in benzene in the presence of ethylene oxide might also be taken as an indication that bromine is formed by alternative pathways such as reaction [11]. The coupling products of the cyclohexadienyl radical, such as those obtained in homolytic additions of phenyl radicals to arenes (42), have not been isolated, probably owing to a rapid reaction of this radical with bromine donors to give **9** (or the 1,2-isomer).

It is expected that not only the *trans*-adduct **5** but also the corresponding *cis*-adduct is formed in the NBS photoaddition to cyclohexene as is generally observed in radical addition to cyclohexene (26). The probable presence of a mixture of 1- and 3-succinimidylcyclohexene suggests that these compounds might be formed by dehydrobromination of the *cis*-adduct during work-up since in this compound the C—Br bond can readily take the *axial* orientation favorable to *anti*-elimination. In conclusion, we can say that the photodecomposition of NBS in the presence of olefins and benzene containing no allylic hydrogen occurs by the succinimidyl radical addition to give straightforward addition products, but that in the presence of olefins containing readily abstractable allylic hydrogen it is complicated by various side reactions involving the bromine atom and bromine.

Experimental

Unless otherwise specified, the following conditions are used. Nuclear magnetic resonance spectra were recorded with a Varian A56/60 or XL-100 equipped with a Nicolet 1080 computer in $CDCl_3$ using TMS as the internal standard. Infrared spectra were recorded as Nujol mulls or neat liquids with a Perkin Elmer model 457 grating spectrophotometer and mass spectra with a Hitachi–Perkin-Elmer RMU-6E instrument at 80 eV. Melting points were recorded with a Fisher Johns hot stage and are uncorrected. The vpc analyses were carried out with a Varian Aerograph series 1200 with a flame ionization detector. Elemental analyses were performed by Mr. M. K. Yang, Department of Biosciences, Simon Fraser University, using a Perkin Elmer 240 microanalyser. Nitrogen was scrubbed through a Fieser solution, followed by concentrated sulfuric acid and potassium hydroxide pellets. *N*-Bromosuccinimide was recrystallized from water to give white crystals, mp 181–183°C, and was kept in a dark desiccator.

Preparations of Authentic Compounds

N-phenylsuccinimide (**11**), *N*-cyclohexylsuccinimide, and *N*-hexylsuccinimide **3***b* were prepared by the method described by Cava *et al.* (38) using succinic anhydride and the respective amines as the reactants. **11** was recrystallized from cyclohexane to give white needles; mp 154–155°C (lit. mp (43) 155.2–155.7°C); ir: 1780(w), 1710(s), 1595(w), 1500(w), 1445(m), 1395(m), 1190(s), 700(m), and 600(m) cm^{-1}; nmr τ: 2.65 (m, 5H) and 7.15 (s, 4H); ^{13}C nmr 175.9(s), 131.6(s), 128.7(d), 128.1(d), 126.1(d) and 27.9(t); ms *m/e* (%): 175(100), 120(34), 119(45), and 93(28).

N-Cyclohexylsuccinimide was sublimed to give crystals; mp 44.5–46°C (lit. (44) mp 41–42°C); ir: 1765(m), 1690(s, b), 1399(s), 1378(s), 1190(s) cm^{-1}; nmr τ: 6.03 (tt, J = 12 and 4 Hz, 1H), 7.35 (s, 4H), 7.7–8.8 (m, 10H); ^{13}C nmr: 176.6(s), 51.2(d), 28.3(t), 27.7(t), 25.5(t), 24.6(t); ms *m/e* (%): 181 (2.5, M^+), 138(10), 101(20), 100(100), and 55(28). **3***b* was distilled as an oil; ir: 1770(m), 1700(s), 1400(m), 1172(m), 1130 and 825(m) cm^{-1}; nmr τ: 6.50 (t, J = 7 Hz, 2H), 7.32 (s, 4H), ~8.7(m) and 9.11 (t, J = 5.5 Hz, 3H); ^{13}C nmr 177.0(s), 38.6(t), 31.0(t), 27.9(t), 27.4(t), 26.2(t), 22.2(t), and 13.7(q) ppm; ms *m/e* (%): 183 (54, M^+), 168(9), 140(14), 113(80), 100(100), and 84(35).

Addition of bromine to neohexene gave a colorless 1,2-dibromo-3,3-dimethylbutane (**4***b*) which darkens on storage. The distilled oil showed ir: 1380(s), 1320(m), 1260(m), 1230(m), 900(m), and 875(m) cm^{-1}; nmr τ: 5.90 (m, 2H), 6.45 (dd, J = 11 and 9.5 Hz, 1H), 8.85 (s, 9H); ms *m/e* (%): 246(0.2), 244(0.6), 242(0.3), 231(1.8), 229(3.4), 227(1.8), 165(29), 163(31), 147(9.3), 149(9.7), and 83(32).

3-Bromocyclohexene was prepared according to Ziegler *et al.*'s method (1) and was distilled at 64°C/14 Torr; ir: 3040(m), 1640(w), 1188(s), 862(s), and 732(s) cm^{-1}; nmr τ: 3.96 (m, 2H), 5.16 (m, $W_{1/2}$ = 9, 1H), 7.1–8.1 (m, 8H); ms *m/e*: 162, 160, and 81 (100%).

Photodecomposition of NBS

In the Presence of 3,3-Dimethyl-1-butene

A solution of NBS (2 g), the olefins (10 g), and ethylene oxide (2 mL) in acetonitrile (70 mL) was purged with nitrogen for a few minutes and was irradiated with a Hanovia lamp (100 W) at −10°C for 3.5 h. At intervals, small samples were withdrawn for iodimetric tests or titrations to follow the progress of the reaction. The zero hour sample kept at −10°C in the dark showed no decomposition after 4 h as shown by titration. The photolysate was evaporated to afford a white solid (2.72 g). The oil showed a nmr spectrum which was essentially that of adduct **2***a* in addition to small signals at τ 6.77, 7.74, and 9.00, and a vpc trace which contained one major and four minor peaks (2 ~ 3%). By quantitative peak matching the major peak was shown to correspond to **2***a* (85% yield); gc–ms analysis showed that the first two minor components contained no bromine atom and showed strong *m/e* at 57 and 56. The fourth peak showed a very strong peak at *m/e* 126 which was probably derived from $(CH_3)_3CCH(OCH_2CH_2Br)CH_2Br$. Recrystallization of the solid (1.56 g) from

petroleum ether gave white solid of 1-succinimido-2-bromo-3,3-dimethylbutane (**2***a*, 65%); mp 85–87°C; ir: 1700 and 1150 cm^{-1}; nmr τ: 8.85 (s, 9H), 7.25 (s, 4H), and 5.6–6.5 (m, an ABC system, 3H); ^{13}C nmr in ppm: 176.2(s), 63.9(t), 41.5(t), 34.6(s), 27.6(t), 26.9(q); ms *m/e* (%): 263(25), 261(25), 248(10), 246(10), 207(92), 205(93), 183(17), 182(100), 166(38), 149(6), 127(11), 126(90), 112(65), 100(92), 84(49), 83(78), 82(18). *Anal.* calcd. for $C_{10}H_{16}NO_2Br$: C 45.81, H 6.15, N 5.34; found: C 46.04, H 6.16, N 5.26.

Adduct **2***a* (156 mg) was stirred in 80% acetic acid (3 mL) with sodium iodide and zinc powder (900 mg) for 48 h (45). A usual work-up gave a solid (59 mg) which was recrystallized from cyclohexane to afford white crystals; mp 96–99°C; ir: 1760(w), 1695(s), 1405(s), 1355(s), 1305(w), 1235(s), and 1150(s) cm^{-1}; nmr τ: 9.08 (s, 9H), 7.32 (s, 4H), 8.54 and 6.48 (A_2B_2, multiplets, 2H each); ^{13}C nmr: 176.4(s), 40.2(t), 34.7(t), 29.1(s), 28.4(q), and 27.5(t).

In the Presence of 1-Hexene

A solution of NBS (2 g), 1-hexene (10 mL), and ethylene oxide (2 mL) in acetonitrile (70 mL) was irradiated under nitrogen for 2.5 h at 0°C until iodimetric tests were negative. A similar mixture kept in the dark at 0°C was iodimetrically titrated after 3 h to give the same amount of the titrant as the zero hour sample. The photolysate was evaporated to give a residue (2.53 g) which showed an ir absorption at 2260 cm^{-1}. This residue taken up in methylene chloride was extracted with water; the methylene chloride was dried and evaporated to give an oil (2.18 g); nmr τ: 8.5 (m, 9H), 7.25 (s, 4H), 6.2 (m, 2H), and 5.7 (m, 1H); ir: 1705, 1770, 1400, 1160, 820, and 735 cm^{-1}. Chromatography of the oil taken up in methylene chloride on silicic acid gave a forerun (128 mg) containing several minor and one major component. This oil was separated by preparative tlc to give 1,2-dibromohexane (**4***b*); ir: 2960, 2930, 2860, 1460, 1430, 1220, 1150, 965; nmr τ: 5.7–6.7 (m, 3H), 8.0 (m, 2H), 8.5 (m, 4H), 9.1 (m, 3H); ms *m/e*: 185, 187, 189, 163, and 165. The next nine fractions (1.83 g) contained 1-succinimidyl-2-bromohexane **2***b* with a trace of impurities. A portion was further chromatographed to give pure **2***b* as an oil; ir: 1775, 1702, 1400, 1160, and 819 cm^{-1}; nmr τ: 5.49 (m, 1H), 5.8–6.5 (m, 2H), 7.24 (s, 4H), 7.9–8.8 (m, 6H), and 903 (t, 3H); ^{13}C nmr ppm: 177.1(s), 51.0(d), 44.9(t), 35.4(t), 29.1(t), 27.8(t), 21.8(t), 13.4(q); ms *m/e* (%): 263 (5, M^+), 261(5), 182(74), 164(3), 162(3), 138(13), 112(47), 100(100), 99(20), 86(41), 84(68), 83(46), and 82(31).

Adduct **2***b* (156 mg), sodium iodide (150 mg), and zinc powder (900 mg) in 80% acetic acid (3 mL) were stirred for 24 h. The filtrate was evaporated and the residue was diluted with water. The aqueous phase was extracted with carbon tetrachloride. The latter phase was washed with dilute sodium thiosulfate solution and was worked up to give an oil (80 mg) of *N*-hexylsuccinimide; the ir, nmr, and mass spectra were superimposable with those of the authentic sample.

In the Presence of Cyclohexene

(*1*) A solution of NBS (2 g), cyclohexene (12 mL), and ethylene oxide (2 mL) in acetonitrile (70 mL) was kept under nitrogen at −10°C and was photolysed for 3 h until the KI–starch test showed negative. The photolysate was evaporated and the residue taken up in methylene chloride (3 ~ 4 mL) was filtered. The solid (544 mg) was identified as succinimide by ir and nmr spectroscopy and by mixture mp 121–122°C. The methylene chloride solution (containing 2.5 g of the residue) was chromatographed on a silica gel column to afford 12 fractions.

Fraction 2 (378 mg) decomposed to tar on attempted microdistillation at 10 Torr. A portion of this oil (150 mg) was subjected to preparative tlc on silicic acid using 10% CH_2Cl_2 in petroleum ether as eluent to give *trans*-1,2-dibromocyclohexane **6** (56 mg) and ether **7** (28 mg). These products showed spectra identical with those of authentic samples.

Fractions 4–7 (917 mg) showed one spot on tlc with a trace of impurity and decomposed on distillation at 120°C. A portion of this oil was subjected to preparative tlc to give an oil of *trans*-1-succinimidyl-2-bromocyclohexane (**5**); ir: 1770(m), 1700(s), 1450(m), 1176(s), 966, 820 cm^{-1}; nmr τ: 5.14 (dt, J = 11 and 4 Hz, 1H), 5.88 (dt, J = 11 and 4 Hz, 1H), 7.30 (s, 4H), 8.30(m); ^{13}C nmr ppm: 176(s), 57.1(d), 50.3(d), 37.1(t), 29.1(t), 27.5(t), 26.2(t), 24.5(t); ms *m/e* (%): 262 (47, M^+), 260(47), 180(100), 162(89), 160(89), 138(100), 110(55), 100(100), 96(60), 84(63), 82(100), and 81(100). *Anal.* calcd. for $C_{10}H_{14}NO_2Br$: C 46.17, H 5.42, N 5.40; found: C 46.35, H 5.46, N 5.31.

Fractions 8–10 (85 mg) were rechromatographed to give the adduct **5** (60 mg) and an oily fraction (15 mg). The total yield of the adduct **5** (977 mg) was 32%.

Fraction 11 (22 mg) showed one major spot and four minor spots on tlc and the following physical constants; ir: 3025, 1760(m), 1700(s), 1380(s), 1170(s) cm^{-1}; nmr τ: 4.15(m), 6.2(m), 6.8(m), 7.35(s); ms *m/e* (%): 179(100), 151(75), 150(70), 122(120), 121(100), 100(280), 81(175), and 80(290).

Adduct **5** (120 mg) was stirred with zinc powder and sodium iodide in 80% aqueous acetic acid to afford a crude product (62 mg). The oil was chromatographed to afford *N*-cyclohexylsuccinimide; the ir, nmr, and mass spectra and the vpc retention time were identical with the sample prepared by other routes (38).

(*2*) In a separate experiment, a mixture of the same composition was photolysed at −20°C for 5 h. The photolysate was worked up as before to afford a light brown oil (2.72 g) and succinimide (444 mg). The ir spectrum of the oil exhibited a weak absorption at 2260 cm^{-1}. The vpc spectrum of the oil showed the peaks matching with succinimide, 3-bromocyclohexene (**8**), *trans*-1,2-dibromocyclohexane (**6**), ether **7**, and adduct **5** in addition to four trace amount peaks. The peak of **5** was the major and others were about 1/6 to 1/7 in area of the peak of **5**. The oil was chromatographed on a silica gel column to afford adduct **5** (1.14 g, 38%). By gc–ms analysis, the first two trace amount peaks following the solvent peak were shown to possess the mass spectral patterns of 2-cyclohexenenone and 2-cyclohexenol (46).

(*3*) A solution of NBS (2 g), cyclohexene (12 mL), and ethylene oxide (4 mL) in acetonitrile (240 mL) at 0°C was purged with nitrogen and was irradiated with a Hanovia lamp (100 W). Samples were withdrawn at every hour and iodimetrically titrated. The solution was kept under a slight positive pressure of nitrogen at all times. The zero hour sample kept at 0°C in the dark for 15 h gave a titration volume the same as that at the zero hour. The same experiment was repeated at −10°C.

Photolysis of NBS in the Presence of Benzene

(1) In the Absence of Neohexene

A benzene (350 mL) solution containing NBS (1.5 g) and ethylene oxide (5 mL) was irradiated with a Hanovia lamp (200 W) in a Pyrex vessel under nitrogen at 5–10°C for 12 h until the photolysate gave a negative KI–starch test. The residue (2.2 g) obtained after evaporation of the solvent was chromatographed on a silicic acid column using methylene chloride containing 0–5% methanol as eluent. The first four fractions (455 mg) gave very similar ms and ir but different nmr patterns. The semi-solids showed major mass spectral peaks at *m/e* 338, 336, 334, 257, 256, 254, 238, 236, 234, 176, 175, 158, 156, 120, 119, 100, and 93, and major ir absorptions at about 1710(s, b), 1150, 1180, 770 cm^{-1}. Recrystallizations

of these fractions from methanol or methylene chloride gave crystalline compounds with wide melting ranges. The fifth and sixth fractions were rechromatographed to afford a similar semi-solid (81 mg) as above and a crystalline compound (120 mg) identified as *N*-phenylsuccinimide (**11**) by comparisons of ir, nmr, and mass spectra with those of the authentic sample. Elution with 5% MeOH–CH_2Cl_2 gave succinimide.

The semi-solid fractions were combined and chromatographed on an alumina column to afford many fractions, one of which (60 mg) was recrystallized from MeOH–CH_2Cl_2 to afford white crystals; mp 204–207°C; ir: 1700, 1185, 1165, and 780 cm^{-1}; nmr τ: 7.14 (s, 4H), 5.2–4.83 (m, 3H), 4.66–4.38 (m, 1H), and 4.00 (m, 2H); ms *m/e* (%): 419(0.2), 417(0.5), 415(0.5), 413(0.2), and 100(100). *Anal.* calcd. for $C_{10}H_{10}NBr_3O_2$: C 28.85, H 2.40, N 3.37; found: C 29.20, H 2.45, N 3.15.

(2) In the Presence of Neohexene

A solution of NBS (599 mg, 3.3 mmol), benzene (2.6 mL, 29 mmol), ethylene oxide (1.5 mL, 23 mmol), and neohexene (0.3 mL, 2 mmol) in acetonitrile (100 mL) was irradiated with a 450 W Hanovia lamp through a Corex filter for 20 min at 0°C under nitrogen. The solution was evaporated to afford a brown oil (769 mg), The oil (384 mg) was chromatographed on silica gel using MeOH–CH_2Cl_2 as eluent. The first fraction (53 mg) was polybrominated compounds and was not investigated further. The fractions (144 mg) collected with 0.1–0.2% MeOH–CH_2Cl_2 were mixtures containing some **11**. The fractions (191 mg) eluted with 0.5 ~ 1% MeOH were crystallized from cyclohexane to give **11**; the ir, nmr, and mass spectra were superimposable with those of the authentic compound.

In a separate experiment, a solution of benzene (10 mL), NBS (893 mg), neohexene (0.3 mL), and ethylene oxide (2 mL) in acetonitrile was irradiated in a Pyrex vessel with a 100 W Hanovia lamp at 0°C for 25 h. Half of the solution was treated with triethylamine (1 mL) for 8 h at room temperature. The solution was worked up in the usual manner to afford an oil. Analysis by the vpc peak matching method gave three peaks corresponding to dibromide **4***a* (3%), succinimide (31%), and **11** (13.6%).

The other half of the photolysate was evaporated and the residue was analysed by vpc as above to give dibromide **4***a* (4.6%), succinimide (40%), and **11** (8.6%). In both cases neither adduct **2***b* nor bromobenzene were detected.

Photolysis of Bromine in the Presence of NBS

A solution containing NBS (3.55 g), bromine (880 mg), and ethylene oxide (6 mL) in benzene (130 mL) was photolysed through a G.W.C. filter[3] (cut off at 334 nm) at about 10°C. Aliquots withdrawn at intervals were treated with a drop of cyclohexene and tested with KI–starch paper. The zero hour sample kept for 40 hours in the dark was similarly treated with cyclohexene and titrated iodimetrically to show no decomposition. It took 35 h for NBS to disappear during which white solids precipitated. The solid (1.13 g) was shown to be succinimide by an ir spectral comparison. The filtrate was evaporated to give an oil. The oil was chromatographed on silica gel to give a mixture of polybromobenzenes (1.93 g) and a small amount of succinimide. Rechromatography of the former gave five fractions that were mixtures, in various proportions, of brominated benzenes. By gc–ms analysis of each fraction, bromobenzene, dibromobenzene, tribromobenzenes, tetrabromobiphenyl, and tetrabromocyclohexadiene were identified in addition to minor amounts of other brominated benzenes. These fractions showed no ir absorption or nmr signals typical of the succinimido moiety.

Reaction of HBr with NBS and Ethylene Oxide

To a solution of NBS (167 mg) and ethylene oxide (0.35 mL, 0.007 mol) in acetonitrile (20 mL) was added an acetonitrile solution of HBr (0.01 *M*, 1.5 mL) at −10°C. The solution became pH 6–8 immediately. The uv spectrum of this pale yellow solution showed a weak absorption at 404 nm for bromine. This solution was evaporated and the residue was worked up in the usual manner to give ethylene bromohydrin as an oil; nmr τ: 7.22(s, D_2O exchangeable, 1H), 6.09(t, J = 5.2 Hz), 6.48(t, J = 5.2 Hz).

Reaction of Bromine Cyclohexene and Ethylene Oxide

To a solution of cyclohexene (14 mL) and ethylene oxide (2.3 mL) in methylene chloride (100 mL), bromine (3.2 mL) was added dropwise at 0°C. The solvents were evaporated to give an oil (14.6 g). The oil was distilled to afford a fraction at bp 112–113°C/14 Torr which showed nmr and ir spectra identical to those of **6** (46). The vpc analysis of the forerun showed no peak corresponding to 3-bromocyclohexene. The residue (1.5 g) was chromatographed on silica gel using petroleum ether as eluent to afford an oil (916 mg) which showed one peak on vpc analysis. Preparative tlc of a portion of this oil gave 1-bromo-2-(2′-bromoethoxy)cyclohexane (**7**); ir: 2930, 2860, 1445, 1190, and 1100 (s, b); nmr τ: 6.10 (t, J = 5.5 Hz, 2H), 6.60 (t, J = 5.5 Hz, 2H), 6.00 (dt, J = 8 and 3 Hz, 1H), 6.54 (dt, J = 6 and 1.5 Hz, 1H); ms *m/e* (%): 288(6), 286(11), 284(6), 165(28), 163(31), 109(41), 107(44), 97(60), and 81(100). *Anal.* calcd. for $C_8H_{14}Br_2O$: C 33.59, H 4.93; found: C 34.07, H 4.96.

Photodecomposition of NBS in the Presence of Ethylene Oxide

A solution of NBS (1.17 g) and ethylene oxide (20 mL) in acetonitrile (140 mL) was irradiated with a 450 W Hanovia lamp at 0–5°C under nitrogen. During irradiation, a yellow color developed. A sample treated with a drop of cyclohexene gave a colorless solution; potassium iodide starch test with this solution was used to follow the progress of the reaction. After 5 h, the solution remained yellowish but NBS was consumed. The zero hour sample kept in the dark showed no decomposition by iodimetry. The crude product was analysed by gc–ms to give many peaks. Most of them showed mass spectral patterns indicative of one or two bromines. Among them, the major peaks corresponding to ethylene bromohydrin, succinimide, and β-bromopropionamide and a minor peak of bromoacetaldehyde were identified by their mass spectral patterns and (or) peak matchings. The mass spectrum of β-bromopropionamide showed prominent peaks at *m/e* 153, 151, 109, 107, 72 (100%), and 44.

Photoreaction of NBS in the Presence of Cyclohexene

In a conventional Pyrex photocell, acetonitrile (240 mL), NBS (2.017 g, 0.011 mol), cyclohexene (12 mL, 9.72 g), and ethylene oxide (4 mL, 3.56 g) were placed at 0°C. The mole ratio of NBS, cyclohexene, and ethylene oxide was 1:10:8. The solution was purged with nitrogen for 5 min and brought to the desired temperature. While the solution was kept under a small positive pressure of nitrogen, it was irradiated with a 100 W medium pressure Hanovia lamp. Irradiation was continued until the photolysate responded negative to KI–starch tests.

On completion of irradiation, the photolysate (50 mL) was evaporated in a rotary evaporator. A portion of the crude oil and biphenyl were weighed into a 5 mL volumetric flask and diluted with acetonitrile to the mark. This solution was analysed with a 10% SE 30 on Chromosorb Q 100/120, 1/8 in.

[3]We are grateful to Dr. G. Pfundt, Max-Plank-Institut für Kohlenforschung, Mülheim a.d. Ruhr, who provided the filter.

× 6 ft stainless steel column with oven temperature 100–200°C (4°C/min programming, the flow rate 33 mL/min at 26 psi). Under these conditions the retention times (in brackets, in minutes) are 3-bromocyclohexene (**8**, 2.75), succinimide (3.5), *trans*-dibromocyclohexane (**6**, 5.0), ether **7** (10.5), adduct **5** (16.3), 2-cyclohexenone (2.0), 2-cyclohexenol (2.3), unknown **1** (6.3), and biphenyl (7.8). Experiments at different temperatures were repeated to ascertain the reproducibility.

For known compounds, correction factors were first established by injecting the known concentrations of biphenyl and a pure sample to be analysed. The measured areas and concentration gave the correction factors. For each sample injected, the peak areas were measured and the absolute contents of each component calculated from these correction factors. The percentage yields of each compound are summarised in Table 1.

An acetonitrile solution of 3-bromocyclohexene always gave two peaks at 0.5 and 2.5 min, even when an analytically pure compound was used. The correction factor was calculated on the second peak. The peak area corresponding to succinimide increased gradually as the time elapsed on storage of the crude product; typically, area ratios of succinimide to biphenyl changed from 0.0776 at 5 h to 0.32 at 50 h after isolation.

Acknowledgement

We are grateful to the National Research Council of Canada for its financial support of this project.

1. K. Ziegler, A. Späth, E. Schaaf, W. Schumann, and E. Winkelmann. Justus Liebigs Ann. Chem. **551**, 80 (1942).
2. C. Djerassi. Chem. Rev. **43**, 271 (1948).
3. G. Sosnovsky. Free radical reaction in preparative organic chemistry. MacMillan, New York. 1964. Chapt. 8.
4. N. P. Buu-Hoi. Rec. Chem. Progr. **13**, 30 (1952).
5. L. Horner and E. H. Winkelmann. Angew. Chem. **71**, 349 (1959).
6. W. A. Thaler. Methods Free-Radical Chem. **2**, 121 (1969).
7. M. L. Poutsma. Free radicals. Vol. 2. *Edited by* J. K. Kochi. John Wiley and Sons, New York, NY. 1973. p. 159.
8. (*a*) R. E. Pearson and J. C. Martin. J. Am. Chem. Soc. **85**, 354 (1963); (*b*) G. A. Russel, C. DeBoer, and K. M. Desmond. J. Am. Chem. Soc. **85**, 365 (1963); (*c*) C. Walling, A. L. Rieger, and D. D. Tanner. J. Am. Chem. Soc. **85**, 3129 (1963).
9. (*a*) J. Adam, P. A. Gosselain, and P. Goldfinger. Nature, **171**, 704 (1953); (*b*) P. A. Gosselain, J. Adam, and P. Goldfinger. Bull. Soc. Chim. Belg. **65**, 533 (1956).
10. G. F. Bloomfield. J. Chem. Soc. 114 (1944).
11. K. J. Shea, D. C. Lewis, and P. S. Skell. J. Am. Chem. Soc. **95**, 7770 (1973).
12. J. C. Day, M. J. Lindstron, and P. S. Skell. J. Am. Chem. Soc. **96**, 5616 (1974).
13. J. G. Traynham and Y. S. Lee. J. Am. Chem. Soc. **96**, 3590 (1974).
14. D. D. Tanner, D. Darwish, M. W. Mosher, and N. J. Bunce. J. Am. Chem. Soc. **91**, 7398 (1969).
15. (*a*) D. D. Tanner, M. W. Mosher, N. C. Das, and E. V. Blackburn. J. Am. Chem. Soc. **93**, 5846 (1971); (*b*) D. D. Tanner, J. E. Rowe, T. Pace, and Y. Kosugi. J. Am. Chem. Soc. **95**, 4705 (1973).
16. (*a*) H. W. Johnson and D. E. Bublitz. J. Am. Chem. Soc. **80**, 3150 (1958); (*b*) J. C. Martin and P. D. Bartlett. J. Am. Chem. Soc. **79**, 2553 (1957).
17. (*a*) C. Lagerkrantz and E. Forshult. Acta Chem. Scand. **23**, 708 (1969); (*b*) O. E. Edwards, D. H. Paskovich, and A. H. Redoch. Can. J. Chem. **51**, 978 (1973).
18. T. R. Beebe and F. M. Howard. J. Am. Chem. Soc. **91**, 3379 (1969).
19. (*a*) D. G. Markers. J. Org. Chem. **23**, 1490 (1958); (*b*) L. L. Braun and J. H. Looker. J. Org. Chem. **26**, 574 (1961).
20. E. Hedaya, R. L. Hinman, V. Schomaker, S. Theodoropulos, and L. M. Kyle. J. Am. Chem. Soc. **89**, 4875 (1967).
21. T. Koenig and R. A. Wielsek. Tetrahedron Lett. 2007 (1975).
22. R. W. Lockhart, R. W. Snyder, and Y. L. Chow. J. Chem. Soc. Chem. Commun. 51 (1976).
23. L. J. Magdzinski and Y. L. Chow. J. Am. Chem. Soc. **100**, 2444 (1978).
24. J. N. S. Tam, R. W. Yip, and Y. L. Chow. J. Am. Chem. Soc. **96**, 4543 (1974).
25. R. S. Neale, N. L. Marcus, and R. S. Schepers. J. Am. Chem. Soc. **88**, 3051 (1966).
26. Y. L. Chow. Acc. Chem. Res. **6**, 354 (1973).
27. D. Touchard and J. Lessard. Tetrahedron Lett. 4425 (1971); 3827 (1973).
28. D. Touchard. Ph.D. Thesis, University of Sherbrooke, Sherbrooke, P.Q. 1975.
29. L. H. Zalkow and C. D. Kennedy. J. Org. Chem. **29**, 1290 (1964).
30. W. J. Bailey and J. Bello. J. Org. Chem. **20**, 525 (1955).
31. K. Sakai, N. Koga, and J.-P. Anselme. Tetrahedron Lett. 4543 (1970).
32. J. M. Landesber and M. Siegel. J. Org. Chem. **35**, 1074 (1970).
33. A. Guillemonat, G. Peiffer, J. C. Traynard, and A. Leger. Bull. Soc. Chim. Fr. 1192 (1964).
34. J. R. Shelton and C. Cialdella. J. Org. Chem. **23**, 1128 (1958).
35. (*a*) J. C. Days, M. G. Katsaros, W. D. Kocher, A. E. Scott, and P. S. Skell. J. Am. Chem. Soc. **100**, 1950 (1978); (*b*) P. S. Skell and J. C. Day. J. Am. Chem. Soc. **100**, 1951 (1978).
36. V. Calo, L. Lopez, and G. Pesce. J. Chem. Soc. Perkin Trans. 1, 501 (1977).
37. D. D. Tanner and N. Wada. J. Am. Chem. Soc. **97**, 2190 (1975).
38. M. P. Cava, A. A. Deana, K. Muth, and M. J. Mitchell. Org. Synthesis. Coll. Vol. **V**, 944 (1973).
39. W. Weindinger. Z. Phys. Chem. **B5**, 29 (1929); E. Rabinowitch. Z. Phys. Chem. **B19**, 190 (1932).
40. F. R. Mayo and W. B. Hardy. J. Am. Chem. Soc. **74**, 911 (1952).
41. J. W. Wilt. *In* Free radicals. Vol. 1. *Edited by* J. K. Kochi. John Wiley and Sons, New York, NY. 1973. Chapt. 8; D. D. Tanner, E. V. Blackburn, Y. Kosugi, and T. C. S. Ruo. J. Am. Chem. Soc. **99**, 2714 (1977).
42. M. J. Perkins. *In* Free radicals. Vol. 2. *Edited by* J. K. Kochi. John Wiley and Sons, New York, NY. 1973. p. 231.
43. E. R. Buchman and D. R. Howton. J. Am. Chem. Soc. **70**, 2517 (1948).
44. G. Losse, E. Wottgen, and H. Just. J. Prakt. Chem. **7**, 28 (1958).
45. O. Schneider, J. P. Bourquin, and A. Grüssner. Helv. Chim. Acta, **28**, 510 (1945).
46. Sadtler Spectral Catalogue. No. K28910, Sadtler Research Laboratory, Philadelphia, PA.

Pyrrolidine- and piperidine-alkanoic acid hydrochlorides. Synthesis by hydrogenation of pyrrolyl ester and pyridine-alkanoic acid hydrochlorides

SOOI-KAY TSUI AND JAMES DOUGLAS WOOD

Department of Biochemistry, University of Saskatchewan, Saskatoon, Sask., Canada S7N 0W0

Received January 23, 1979

SOOI-KAY TSUI and JAMES DOUGLAS WOOD. Can. J. Chem. **57**, 1977 (1979).

2-Pyrrolidylacetic acid and β-(2-pyrrolidyl)propionic acid hydrochloride have been prepared by hydrogenation of ethyl 2-pyrrolylacetate and diethyl 2-pyrrolylmethylenemalonate respectively, over rhodium on alumina in HCl solution, followed by acidic hydrolysis. Similarly, 1-methylnipecotic acid, 1-methylisonipecotic acid, 2- and 3-piperidine-acetic acid, and 3-piperidine-propionic acid hydrochlorides have been prepared by hydrogenation of the corresponding pyridine-alkanoic acid hydrochlorides over platinum oxide, rhodium on alumina, or palladium on carbon in water.

SOOI-KAY TSUI et JAMES DOUGLAS WOOD. Can. J. Chem. **57**, 1977 (1979).

On a préparé les chlorhydrates des acides pyrrolidyl-2 acétique et β(pyrollidyl-2) propionique par hydrogénation respectivement du pyrrolyl-2 acétate d'éthyle et du pyrrolyl-2 méthylènemalonate de diéthyle sur du rhodium sur l'alumine en solution HCl, suivie par une hydrolyse acide. De la même manière, on a préparé les chlorhydrates des acides méthyl-1 nipécotique, méthyl-1 isonipécotique, pipéridine-2 (et -3) acétique et pipéridine-3 propionique par hydrogénation des chlorhydrates des acides pyridine alcanoïques correspondants sur de l'oxyde de platine, du rhodium sur l'alumine ou du palladium sur du charbon dans l'eau.

[Traduit par le journal]

Introduction

It is well established that γ-aminobutyric acid (GABA) is an important neurotransmitter in the mammalian central nervous system (1). Various structural analogues of this substance have been isolated or synthesized which affect its metabolism and function (2). Such compounds are of pharmacological interest as potential antiepileptics.

Recently, nipecotic acid **6***d* has been reported as a potent inhibitor of the uptake of GABA by slices of rat cerebral cortex (3) and we have found that 1-methylnipecotic acid **4***a* has similar effects (manuscript in preparation). As a result we became interested in the possibility of a rapid high-yield preparation of easily purifiable, water soluble, hydrochloride salts of related piperidine- and pyrroline-alkanoic acids by hydrogenation of the corresponding pyrrolyl ester and pyridine alkanoic acid hydrochlorides at medium to low pressure.

Discussion

Hydrogenation was complete at 2.5 atm and at room temperature for all pyridines regardless of the catalyst used (platinum oxide, 5% rhodium on alumina, or 10% palladium on carbon); for pyrrolines, shorter times were required and less tar was found using 5% rhodium on alumina. Completeness of hydrogenation was more correctly assessed from the absence of any olefinic hydrogen in the ^{1}Hmr spectra of the products rather than from hydrogen uptake which may stop prematurely due to catalyst poisoning.

Compounds **2***a* and **2***b* were prepared by reduction of the esters **1***a* and **1***b* followed by hydrolysis, since hydrolysis of the starting pyrrolyl esters led to in-

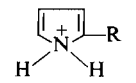

1

a R = CH_2CO_2Et
b R = $CH{=}C(CO_2Et)_2$

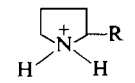

2

a R = CH_2COOH
b R = CH_2CH_2COOH

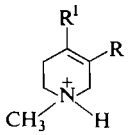

3

a R^1 = H, R = COOH
b R^1 = COOH, R = H

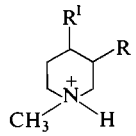

4

a R^1 = H, R = COOH
b R^1 = COOH, R = H

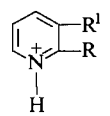

5

a R^1 = H, R = CH_2COOH
b R^1 = CH_2COOH, R = H
c R^1 = CH=CHCOOH, R = H
d R^1 = COOH, R = H

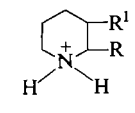

6

a R^1 = H, R = CH_2COOH
b R^1 = CH_2COOH, R = H
c R^1 = CH_2CH_2COOH, R = H
d R^1 = COOH, R = H

(In all cases the anion was chloride)

0008-4042/79/151977-03$01.00/0

tractable tar formation. Hydrogenation was carried out in dilute HCl (0.05 *M*), the acid added being sufficient to promote hydrogenation but not enough to cause tar formation. Solution of starting material was incomplete at the beginning of the reaction but complete at the end. This route to **2***b* is simpler than the previous 2-step procedure (4).

Compounds **4***a* and **4***b* were obtained in high yields by direct hydrogenation of **3***a* and **3***b* respectively. Compound **4***a* had previously been prepared in good yield by the hydrogenation of the corresponding 1-methylnicotinic betaine with platinum but hydrogen pressure and temperature were not specified (5). Direct hydrogenation of **5***d* over PtO_2 has provided **6***d* in high yield (6).

Piperidines **6***a* and **6***b* were obtained in high yield from **5***a* and **5***b* respectively. Compound **6***a* had previously been assumed to be unstable under these hydrogenation conditions (7). Compound **6***c* was obtained, also in high yield, from **5***c*.

Attempts to use acetic acid in place of hydrochloric acid led to longer hydrogenation times and acetate salts which were difficult to purify. The direct reduction of the hydrochloride salts of the appropriate pyridine compound avoids the need for ester hydrolysis which is frequently accompanied by decarboxylation (8). In most cases the starting hydrochloride salt is commercially available or readily obtained by hydrolysis of the corresponding ester.

Experimental

Nuclear magnetic resonance spectra were measured on a Varian T60 spectrometer in D_2O with sodium 2,2-dimethyl-2-silapentane-5-sulfonate (DSS) as internal standard. Infrared spectra were recorded with KBr on Perkin Elmer or Beckman infrared spectrophotometers. Melting points were determined on a Mel-Temp hot stage apparatus. Elemental analyses were conducted by Mr. R. G. Teed, Department of Chemistry and Chemical Engineering, University of Saskatchewan.

Hydrogenation of Pyrrolyl Esters with 5% Rhodium on Alumina

General Procedure

A mixture of 1.0 g of freshly prepared pyrrolyl ester in 20 mL of 0.05 *M* HCl solution was hydrogenated with 0.4 g of 5% rhodium on alumina. After a period of 20 h, the mixture was filtered. The clear solution was added to 10 mL of 37% HCl and refluxed for 4 h. The solution was then treated with charcoal and dried *in vacuo*. The residue was recrystallized from ether–ethanol. The ^{1}Hmr spectrum of the crude products after acid hydrolysis showed that the hydrogenation was complete for both the following pyrrolyl esters **1***a* (9), **1***b* (10).

2-Pyrrolidylacetic Acid Hydrochloride **2**a

The yield was 45%; mp 170–171°C; ir ν_{max}: 3170–2400, 1730, 1400, and 1180 cm^{-1}; ^{1}Hmr δ: 1.40–2.52 (m, 4H), 2.75–3.10 (m, 2H), 3.15–3.57 (m, 2H), 3.80–4.15 (s b, 1H). *Anal.* calcd. for $C_6H_{12}ClNO_2$: C 43.51, H 7.31, N 8.46; found: C 43.62, H 7.36, N 8.33.

β-*(2-Pyrrolidyl)propionic Acid Hydrochloride* **2**b

The yield was 40%; mp 115–117°C (lit. (4) mp 115–118°C); ir ν_{max}: 3100–2450, 1700, 1420, and 1200 cm^{-1}; ^{1}Hmr δ: 1.50–2.18 (m, 6H), 2.30–2.85 (m, 2H), 3.20–3.95 (m, 3H). *Anal.* calcd. for $C_7H_{14}ClNO_2$: C 46.80, H 7.85, N 7.79; found: C 46.79, H 7.88, N 7.66.

Hydrogenation of Pyridine Alkanoic Acid Hydrochloride with Different Catalysts: Platinum Oxide, Rhodium on Alumina, or Palladium on Carbon

General Procedure

A solution of 0.55 g of pyridine alkanoic acid hydrochloride in 20 mL of water was hydrogenated with 0.05 g of platinum oxide (or 0.35 g of 5% rhodium on alumina, or 10% palladium on carbon). After a period of 10 h the solution was filtered and dried in a freezer–dryer at 0.01 Torr. Except where noted, purification of product was unnecessary. The ^{1}Hmr spectra of the crude products indicated that only in the case of hydrogenation of 2-pyridineacetic acid hydrochloride **5***a* with palladium on carbon was a reduction time in excess of 10 h required, the 10-h reduction period being sufficient to complete the hydrogenation of **3***a*, **3***b* (11), **5***b*, and **5***c* to form their respective products. The compounds synthesized by these hydrogenations follow.

1-Methylnipecotic Acid Hydrochloride **4**a

The yield was 75–85%; mp 173–174°C (ether–ethanol) (lit. (5) mp 174–175°C); ir ν_{max}: 3200–2500, 1730, 1470, and 1200 cm^{-1}; ^{1}Hmr δ: 1.38–2.40 (m, 4H), 2.55–3.85 (m, 5H), 2.90 (s, 3H). *Anal.* calcd. for $C_7H_{14}ClNO_2$: C 46.80, H 7.85, N 7.79; found: C 46.80, H 8.13, N 7.77.

1-Methylisonipecotic Acid Hydrochloride **4**b

The yield was 74–86%; mp 230–232°C (ether–ethanol); ir ν_{max}: 3070–2470, 1720, 1450, 1200 cm^{-1}; ^{1}Hmr δ: 1.45–2.55 (m, 4H), 2.6–3.85 (m, 5H), 2.9 (s, 3H). *Anal.* calcd. for $C_7H_{14}ClNO_2$: C 46.80, H 7.85, N 7.79; found: C 46.46, H 7.86, N 7.54.

2-Piperidineacetic Acid Hydrochloride **6**a

The yield was 60–70%; mp 180–182°C (ether–ethanol) (lit. (12) mp 180–182°C); ir ν_{max}: 3200–2770, 1730, 1380, and 1175 cm^{-1}; ^{1}Hmr δ: 1.22–2.20 (m, 6H), 2.80–3.82 (m, 3H), 2.80 (d, 2H). *Anal.* calcd. for $C_7H_{14}ClNO_2$: C 46.80, H 7.86, N 7.79; found: C 47.16, H 7.97, N 7.51.

3-Piperidineacetic Acid Hydrochloride **6**b

The yield was 85–90%; mp 202–204°C; ir ν_{max}: 3120–2750, 1720, 1400, and 1180 cm^{-1}; ^{1}Hmr δ: 1.20–2.21 (m, 4H), 2.52–3.62 (m, 5H), 2.39 (s b, 2H). *Anal.* calcd. for $C_7H_{14}ClNO_2$: C 46.80, H 7.85, N 7.79; found: C 46.21, H 7.93, N 7.63.

β-*(3-Piperidine)propionic Acid Hydrochloride* **6**c

The yield was 86–91%; mp 224–226°C; ir ν_{max}: 3170–2730, 1730, 1395, and 1180 cm^{-1}; ^{1}Hmr δ: 1.35–2.15 (m, 7H), 2.32–2.62 (t, 2H), 2.62–3.62 (m, 4H). *Anal.* calcd. for $C_8H_{16}ClNO_2$: C 49.61, H 8.33, N 7.23; found: C 49.53, H 8.30, N 7.19.

Acknowledgements

The authors thank Dr. R. O. Martin for his help in the preparation of the manuscript and the Medical Research Council of Canada for financial support.

1. K. KRNJEVIC. Physiol. Rev. **54**, 419 (1974).
2. G. A. R. JOHNSTON. Ann. Rev. Pharmacol. Toxicol. **18**, 269 (1978).
3. P. KROGSGAARD-LARSEN and G. A. R. JOHNSTON. J. Neurochem. **25**, 797 (1975).

4. C. CORONELLI, A. VIGEVANI, B. CAVALLERI, and G. G. GALLO. J. Antibiot. **24**, 497 (1971).
5. P. H. LIST and K. TERLINDEN. Pharm. Ind. **30**, 219 (1968).
6. S. M. MCELVAIN and R. ADAMS. J. Am. Chem. Soc. **45**, 2738 (1923).
7. M. FREIFELDER. Practical catalytic hydrogenation. John Wiley and Sons, Toronto, Ont. 1971. p. 588.
8. M. FREIFELDER. J. Org. Chem. **28**, 602 (1963).
9. L. MANDELL and E. C. ROBERTS. J. Heterocycl. Chem. **2**, 479 (1965).
10. G. R. CLEMO, N. FLETCHER, G. R. FULTON, and R. RAPER. J. Chem. Soc. 1140 (1950).
11. R. E. LYLE, E. F. PERLOWSKI, H. J. TROSCIANIEC, and G. G. LYLE. J. Org. Chem. **20**, 1761 (1955).
12. W. D. MARSHALL, T. T. NGUYEN, D. B. MACLEAN, and I. D. SPENSER. Can. J. Chem. **53**, 41 (1975).

Acidity function 'failure.' I. 2-Thiohydantoins

JOHN T. EDWARD AND SIN CHEONG WONG

Department of Chemistry, McGill University, Montreal, P.Q., Canada H3A 2K6

Received November 6, 1978

JOHN T. EDWARD and SIN CHEONG WONG. Can. J. Chem. **57,** 1980 (1979).

The protonation of 2-thiohydantoin and of eight derivatives variously substituted at the 1-, 3-, and 5-positions with alkyl groups or a single phenyl followed h_0 (Cox–Yates $m^* \sim 1.1$); however, the protonation of 3,5-diphenyl-2-thiohydantoin followed h_T ($m^* = 1.50$), and of 5,5-diphenyl-2-thiohydantoin an acidity function intermediate between h_0 and h_T ($m^* = 1.24$). Results were analyzed also in terms of the Cox–Yates X function to obtain pK_{BH^+} values, which were compared with those obtained by alternative analyses of the data.

JOHN T. EDWARD et SIN CHEONG WONG. Can. J. Chem. **57,** 1980 (1979).

La protonation de la thio-2 hydantoine et de huit de ses dérivés, substitués en positions -1, -3 et -5 par des groupes alkyles ou un simple phényle, se fait suivant h_0 (Cox–Yates $m^* \sim 1.1$); toutefois la protonation de la diphényl-3,5 thio-2 hydantoine suit h_T ($m^* = 1.50$) alors que celle de la diphényl-5,5 thio-2 hydantoine suit une fonction d'acidité intermédiaire entre h_0 et h_T ($m^* = 1.24$). On a aussi analysé les résultats en termes de la fonction X de Cox–Yates pour obtenir des valeurs de pK_{BH^+} que l'on compare à celles obtenues par une autre analyse des données.

[Traduit par le journal]

Introduction

Forty-seven years ago Hammett and Deyrup (1) introduced the concept of the acidity function, H_0, with the expectation that it would furnish a general measure of the acidity of concentrated aqueous acid solutions, in the way that pH furnishes a general measure of the acidity of very dilute aqueous acid solutions. However, after much experimental work it became apparent that H_0 was not a unique measure of acidity, but only one of a series of acidity functions H_B, defined by

$$[1] \quad -H_B \equiv \log a_{H^+} f_B / f_{BH^+} = \log C_{BH^+}/C_B - pK_{BH^+}$$

where a = activity, C = molarity, and f = molarity activity coefficient. Each separate H_B applies to a set of closely related Brønsted bases B: H_A for amides (2), H_I for indoles (3), H_T for thiocarbonyl compounds (4), and so on. This loss of generality was characterized by Arnett (5) as 'acidity function failure.'

For a particular function H_B to be valid for the protonation of a series of bases B_1, B_2, ... , it is necessary that in all concentrations of acid

$$[2] \quad f_{B_1}/f_{B_1H^+} = f_{B_2}/f_{B_2H^+} = \ldots.$$

(the 'cancellation assumption' (6)). It is the frequent failure of the cancellation assumption to apply when bases B and C belong to different classes of compounds which leads to acidity function failure and the need for two functions H_B and H_C. It has been found, however, that the various acidity functions are approximately linear with respect to each other for concentrations of acid such that $H_0 < 0$:

$$[3] \quad H_C = mH_B$$

Hence pK_{CH^+} values are often obtained (7) in the absence of an appropriate acidity function H_C for bases C_1, C_2, ... , by the equation

$$[4] \quad \log I = -mH_B + pK_{CH^+}$$

where I ($\equiv C_{CH^+}/C_C$) is the ionization ratio. This equation yields pK_{CH^+} values not greatly different from those obtained by other treatments (8, 9), but can only be approximate: in particular, [3] must fail for more dilute solutions when all acidity functions H_B, H_C, ... are becoming equal to pH, and m is changing towards unity.

The empirical relation of Bunnett and Olsen (10, 11),

$$[5] \quad H_C + \log C_{H^+} = (1 - \phi)(H_0 + \log C_{H^+})$$

ϕ being a parameter characteristic of bases of type C, is free from this objection, applying equally to dilute and concentrated acid solutions. It leads to the additional two relations

$$[6] \quad \log \frac{f_C f_{H^+}}{f_{CH^+}} = (1 - \phi) \log \frac{f_B f_{H^+}}{f_{BH^+}}$$

$$[7] \quad \log I + H_0 = \phi(H_0 + \log C_{H^+}) + pK_{CH^+}$$

where B and BH^+ now represent the conjugate aniline–anilinium ion pairs on which the H_0 scale is

0008-4042/79/151980-06$01.00/0

now based (12). The pK_{CH^+} value of *C* may be obtained by application of [7] using H_0, and without the necessity of knowing the acidity function H_C.

On the basis of the linearity of activity coefficient terms shown in [6], Marziano, Passerini, and their co-workers (13) and more recently Cox and Yates (6) have developed alternative functions for measuring the acidity of concentrated acid solutions. Cox and Yates define their 'excess acidity' function *X* by

$$[8] \qquad \log \frac{f_C f_{H^+}}{f_{CH^+}} = m^* \log \frac{f_B f_{H^+}}{f_{BH^+}} \equiv m^* X$$

where B* is a hypothetical standard base. From [8] it follows that

$$[9] \qquad \log I - \log C_{H^+} = m^* X + pK_{CH^+}$$

Cox and Yates report *X* values for 0–99.5% aqueous sulfuric acid, based on ionization ratio data reported for 165 weak bases, and *X* values for 0–78% perchloric acid, based on ionization data for 76 weak bases. The *X* function has the advantage of being a single function for a given acid–water mixture covering *all* classes of bases, and hence replacing the multiplicity of functions H_0, H_0''', H_A, H_T, etc., as well as being applicable to compounds for which no acidity function has yet been developed. On the other hand, this generality has been obtained at the expense of introducing another parameter, the scaling factors m_B^*, m_C^*, ..., characteristic of the different classes of bases B, C, ... To a reasonable approximation $m^* \simeq 1 - \phi$, and hence the variation in m^* for various classes of bases, like the variation in Bunnett and Olsen's ϕ (10), can be explained very plausibly in terms of the 'solvation hypothesis' of Scorrano and his co-workers (14).

While these developments may remedy the 'acidity function failure' of the type noted by Arnett, in this series of papers we shall be concerned with a more serious type of failure: that of compounds within a single class B to follow a single acidity function H_B or, equivalently, to have constant values of ϕ or m_B^*. The problem of carbonyl compounds has already been noted by Scorrano *et al.* (14) and by us (9), and will be discussed in a future paper. In the present paper we consider the case of 2-thiohydantoins **1** which are (as we show below) protonated on

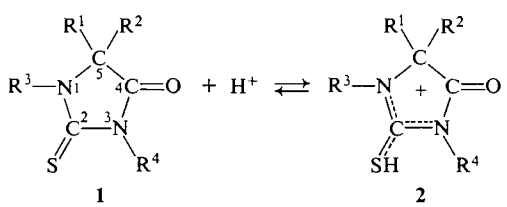

1 **2**

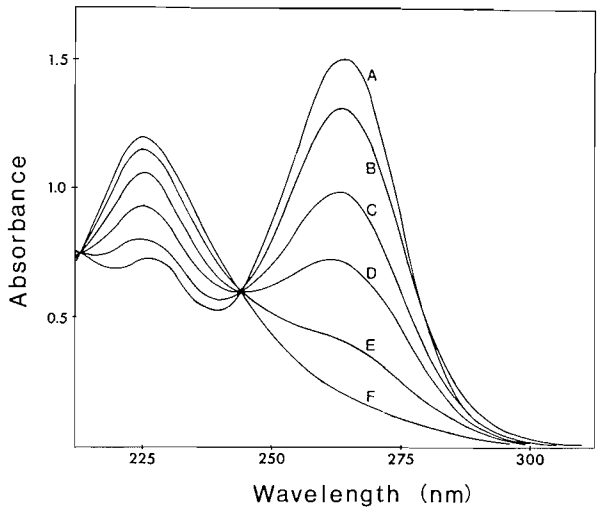

FIG. 1. Spectral curves of 5-benzyl-2-thiohydantoin in aqueous sulfuric acid: (*A*) 36.4%; (*B*) 59.7%; (*C*) 64.7%; (*D*) 67.1%; (*E*) 70.1%; (*F*) 80.5%.

sulfur to give the cation **2**. 2-Thiohydantoins are cyclic *N*-acylthioureas, and hence their protonation would be expected to follow h_T, as does the protonation of acyclic *N*-acylthioureas (15), and of the closely related 2,4-dithiohydantoins (**1**; S in place of O) (4, 16). Instead, the present (admittedly limited) data indicate the protonation of 2-thiohydantoins and of 1-acyl-2-thiohydantoins to follow h_0 (17). This requires that the cancellation assumptions ([2] or [6], [8])[1] do not apply when 2-thiohydantoins are included with other thioureas. In an attempt to understand this anomaly we have studied the activity coefficient and protonation behaviour of variously substituted 2-thiohydantoins.

Results and Discussion

Site of Protonation

In Fig. 1 are shown the uv spectra of 5-benzyl-2-thiohydantoin in 36–80% sulfuric acid. The other 2-thiohydantoins, with the exception of the 1,3-diphenyl compound (discussed below), show similar spectral changes.

The disappearance in concentrated acid of the type II band (λ_{max} 260 nm) due to the $\pi \rightarrow \pi^*$ transition of the thioamide function suggests protonation

[1]It has been pointed out by a referee, and already pointed out by us (4), that the extrathermodynamic assumption ([2]) underlying pK_{BH^+} values obtained by the original acidity function approach is not the same as that ([6] or [8]) underlying the Bunnett–Olsen or Cox–Yates approaches, except for the special case when $\phi = 0$ or $m^* = 1$. For the same reason, the explanation of variations in ϕ in terms of differing solvation of B and BH^+ (but not H^+) by Scorrano *et al.* (14) must be regarded as a convenient simplification.

on sulfur (16), as in **3** → **4**. This is confirmed by the similarity in the spectra of 1-methyl-5,5-pentamethylene-2-thiohydantoin (**3**) in 80% acid ($\lambda\lambda_{max}$ 223, 238 nm; $\varepsilon\varepsilon_{max}$ 10 200, 7400 (shoulder)), and of 2-methylthio-1-methyl-5,5-pentamethylene-4-imidazol-4-one hydrochloride (**5**) in 10% acid ($\lambda\lambda_{max}$ 228, 245 nm; $\varepsilon\varepsilon_{max}$ 15 200, 9500). This would be expected from the similarity in structure of **4** and **5** when the

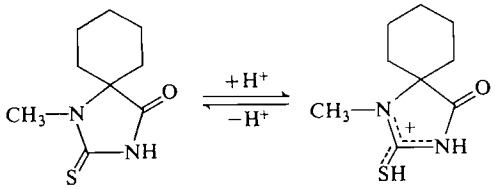

3 4

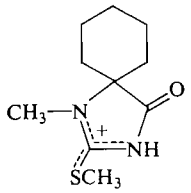

5

bathochromic effect of the S-methyl group is taken into consideration (16) and points to S-protonation. The 2-thiohydantoins accordingly resemble the acyclic acylthioureas in protonating first on sulfur rather than on oxygen (15).

The curves of Fig. 1 almost pass through an isosbestic point, so that ionization ratios[2] may be calculated by the usual procedure (1) without making corrections for medium effects (9).

The character of the spectral changes attending the protonation of 1,3-diphenyl-2-thiohydantoin is completely different (Fig. 2). Protonation results in a bathochromic, not a hypsochromic shift, and medium effects are large, like those for amides (15) and carbonyl compounds generally (9). This indicates a switchover from S-protonation to O-protonation. The pK's of S- and O-basic sites in acylthioureas are almost identical (15), and evidently flanking the S-site with two base-weakening phenyl groups (18) tilts the scales from S- to O-protonation.

Protonation Constants

The protonation constants pK_{BH^+} of the 2-thiohydantoins have been calculated from their ionization ratios by the acidity function relation [4], the Bunnett–Olsen linear free energy relation [7],

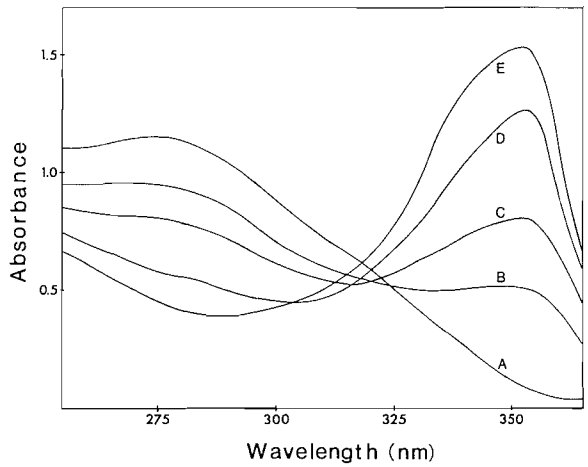

FIG. 2. Spectral curves of 1,3-diphenyl-2-thiohydantoin in sulfuric acid – water – ethanol mixture: (*A*) 56.6% acid, 10% ethanol; (*B*) 66.9% acid, 10% ethanol; (*C*) 69.2% acid, 5% ethanol; (*D*) 72.1% acid, 5% ethanol; (*E*) 76.5% acid, 5% ethanol.

and the Cox–Yates excess acidity relation [9] using H_0 (19), H_T (4), C_{H^+} (6), and X values (6) in the literature. Because of the low solubilities of the diphenyl-substituted 2-thiohydantoins in pure aqueous acid, ionization ratios of 3,5- and 5,5-diphenyl-2-thiohydantoins were determined in acid solutions containing 2% ethanol (by volume). Replacement of water by this small amount of ethanol should not significantly affect the protonation power of the acid, and the corresponding values of acidity functions or excess acidity for pure aqueous acid were used in the calculations.[3] The pK_{BH^+} values obtained from these equations are given in Table 1 along with slope parameters m (for [4] using H_0 as H_B), m' ([4] using H_T), ϕ, and m^*.[4]

It is evident that previous results (17) were not misleading: the majority of 2-thiohydantoins follow the H_0 acidity function reasonably well ($m \sim 1.0$, $\phi \sim 0$, and $m^* \sim 1.1$). Furthermore, the m, ϕ, and m^* values are (within limits) independent of the extent to which the hydrogen atoms attached to the 1- and 3-nitrogen atoms are replaced by alkyl or aryl groups. The 2-thiohydantoins differ in this respect from anilines (5) and benzamides (2), perhaps because the positive charge is so delocalized that hydration by hydrogen-bonding to acidic protons is less important. However, while the presence of a

[2]Experimental data for the thiohydantoins of Table 1 are available, at a nominal charge, from the Depository of Unpublished Data, CISTI, National Research Council of Canada, Ottawa, Ont., Canada K1A 0S2.

[3]1,3-Diphenyl-2-thiohydantoin could be dissolved only in 10% ethanol – 90% aqueous acid solutions, and its pK_{BH^+} value was not calculated.

[4]Standard deviations associated with the evaluation of pK_{BH^+} by the four procedures were calculated and are available as supplementary material. The goodness of fit was usually very slightly better with the Cox–Yates analysis, but the differences for the four procedures were not significant.

single phenyl substituent is without effect, the presence of two phenyls causes a change in behaviour: 3,5-diphenyl-2-thiohydantoin follows the h_T acidity function ($m = 1.35$, $m' = 1.03$)[5]; and 5,5-diphenyl-2-thiohydantoin follows neither h_0 nor h_T but an intermediate acidity function ($m = 1.12$, $m' = 0.86$). (The switchover to O-protonation with 1,3-diphenyl-2-thiohydantoin has been discussed above.) The pK_{BH^+} values obtained by [1] (H_0 for H_B) and by the Bunnett–Olsen relation [7] agree remarkably well, but in many cases differ considerably from the values afforded by the Cox–Yates relation [9]. This might be considered an argument against the validity of the last-named, but we think not. The accuracy of pK_{BH^+} values derived from both [1] and [7] depends on the accuracy of H_0 values, which are based on a limited number of indicators and are subject to cumulative error at higher acidities because of the overlap procedure involved, and because the parallelism of log I for different indicators in changing acid concentration is not always perfect. The excess acidity function X, on the other hand, does not depend on the parallelism of a series of indicators, but on the diverse ionization behaviour of a very large number of indicators; the only assumption is the linearity of activity coefficient terms exhibited in [6] and [8] (not the same as [2] (4)), and this seems to be well supported by the satisfactory correlations reported by Cox and Yates (6). We accordingly follow these authors in believing that the numerical values given by application of [9] are the closest approach to true thermodynamic pK_{BH^+} values available at present.[6]

The trends in pK_{BH^+} values resulting from alkyl and phenyl substitution are in very general agreement with those expected from earlier related work (16, 18, 20), but the data are not complete enough to justify a quantitative analysis such as was done by Janssen for the basicity of thioureas (18). However, the pronounced base-weakening effect of the 5-phenyl group of 3,5-diphenyl-2-thiohydantoin (**1**; $R^1 = R^4 =$ Ph; $R^2 = R^3 =$ H) (compare with 1-methyl-3-phenyl-2-thiohydantoin (**1**: $R^1 = R^2 =$ H, $R^3 =$ Me, $R^4 =$ Ph)) which is found no matter which method is used to analyze the experimental data is remarkable and is not easily explained.

Effect of Acid Concentration on f_B

The protonation behaviour of 2-thiohydantoins indicates that their activity coefficient ratios f_B/f_{BH^+} do not change with increasing acid concentration in the same way as do the activity coefficient ratios of acyclic acylthioureas and 2,4-dithiohydantoins (21, 22). We have accordingly studied the activity coefficients f_B of as many as possible of the free bases[7] in varying concentrations of acid by observing the changes in partition coefficient between chloroform and aqueous acid (22). The results are available as supplementary material,[1] and are shown graphically in Fig. 3; they include data for 5,5-pentamethylene-4-thiohydantoin (**1**; $R^1R^2 = (CH_2)_5$; $R^3 = R^4 =$ H; S and O interchanged) and 5,5-pentamethylene-2,4-dithiohydantoin (**1**; $R^1R^2 = (CH_2)_5$; $R^3 = R^4 =$ H; S in place of O), as well as for eight 2-thiohydantoins. All of the bases show similar behaviour, being first salted-out (increasing f_B) with increasing acid concentration, and then being salted-in (decreasing f_B). This is an almost universal pattern (22). The differences in f_B of 2-thiohydantoins and of 5,5-pentamethylene-2,4-dithiohydantoin are not great enough to explain why the protonation of 2-thiohydantoins follows h_0 and the protonation of the

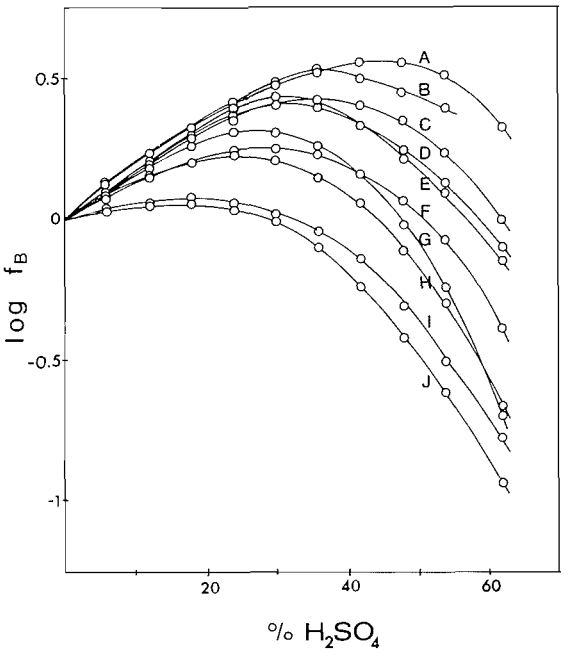

FIG. 3. Activity coefficients f_B in 0–60% sulfuric acid of 5,5-pentamethylene-2,4-dithiohydantoin (*B*), 5,5-pentamethylene-4-thiohydantoin (*G*), and the following substituted 2-thiohydantoins: 5,5-diphenyl- (*A*); 5-benzyl- (*C*); 5,5-pentamethylene- (*D*); 3,5-diphenyl: (*E*); 3,5,5-trimethyl- (*F*); 1-methyl-5,5-pentamethylene- (*H*); 1-methyl-3-phenyl- (*I*); and 1,3-dimethyl- (*J*).

[5] ϕ and m^* values are equally indicative.

[6] A referee has pointed out that "the X-function approach gives pretty good agreement with the H_T approach, which is after all based on thio compounds, even if the present compounds do not follow H_T as a class."

[7] 2-Thiohydantoin itself was insufficiently extracted by chloroform from aqueous acid for a partition coefficient to be obtained.

TABLE 1. Ionization constants of 2-thiohydantoin and of substituted 2-thiohydantoins

Substituents	Log I vs. H_0		Log I vs. H_T		Bunnett–Olsen		Cox–Yates	
	m	pK_{BH+}	m'	pK_{BH+}	ϕ	pK_{BH+}	m^*	pK_{BH+}
None	0.96	−4.85	0.76	−5.17	0.04	−4.88	1.10	−5.25
5,5-Pentamethylene-	1.01	−4.70	0.77	−4.90	−0.01	−4.70	1.16	−5.10
5-Benzyl-	0.97	−5.02	0.76	−5.34	0.03	−5.04	1.12	−5.42
3,5,5-Trimethyl-	0.94	−4.84	0.73	−5.14	0.06	−4.88	1.07	−5.25
1-Methyl-5,5-pentamethylene-	1.00	−5.04	0.78	−5.35	0.00	−5.04	1.15	−5.46
1,3-Dimethyl-	1.04	−6.03	0.76	−6.01	−0.04	−6.01	1.08	−5.98
3-Phenyl-	1.01	−5.18	0.80	−5.61	−0.01	−5.18	1.16	−5.60
3-Ethyl-1-phenyl-	1.00	−5.55	0.76	−5.72	0.00	−5.55	1.10	−5.76
1-Methyl-3-phenyl-	0.96	−5.63	0.70	−5.61	0.04	−5.66	1.00	−5.65
5,5-Diphenyl-	1.11	−5.90	0.86	−6.16	−0.12	−5.81	1.24	−6.08
3,5-Diphenyl-	1.35	−7.57	1.03	−7.79	−0.37	−7.29	1.50	−7.53

2,4-dithiohydantoins follows h_T. (In contrast, the protonation of amides in 0–40% sulfuric acid follows h_A and the protonation of thioamides h_T, largely because of the different responses of f_A and f_T to changing acid concentration (4).)

Accordingly, the different protonation behaviour of 2-thiohydantoins and of 2,4-dithiohydantoins must result chiefly from the differing reponse of f_{BH+} of the two classes of compounds to changing acid concentration. This can be seen in Fig. 4, which shows f_B and $f_{BH+}{}^*$ for 5,5-pentamethylene-2-thiohydantoin and 5,5-pentamethylene-2,4-dithiohydantoin, as well as for 5,5-pentamethylene-4-thiohydantoin (which protonates on the carbonyl oxygen and follows h_A (16)). The $f_{BH+}{}^*$ values (21, 22) were calculated by the equation

$$[10] \quad \log f_{BH+}{}^* = -m_B{}^* X - \log C_{H+} + \log a_{H+}{}^* + \log f_B$$

where the asterisks of $f_{BH+}{}^*$ and $a_{H+}{}^*$ indicate activity coefficients and activities *relative* to the tetraethylammonium ion (21, 22). (This equation follows from [1] and [9].) It is immediately apparent that the protonation of the 4-thiohydantoin follows h_A because the O-protonated compound (probably strongly hydrated (14)) is strongly salted-out (destabilized) as the sulfuric acid concentration goes up and the water activity goes down. This is general for protonated oxygen bases (14, 22). Both the 2-thio- and 2,4-dithiohydantoin are protonated on the sulfur at the 2-position, and protonated sulfur bases in general are weakly hydrated and hence are little salted-out as the acid concentration goes up (23). This remains true for the protonated form of 5,5-pentamethylene-2,4-dithiohydantoin, which accordingly behaves like most thiocarbonyl compounds in following h_T. The reason why the replacement of sulfur by oxygen at the 4-position should lead to a marked increase in the rate of salting-out, as the acid concentration goes up, is not readily apparent in terms of the usual hypotheses (22), and may indicate that other (e.g., counterion (24)) effects are also important. The differing behaviour of 1-acyl-2-thioureas, which follow h_T, and whose conjugate acids can assume a coiled, hydrogen-bonded conformation as in **6** (15), and 2-thiohydantoins, whose

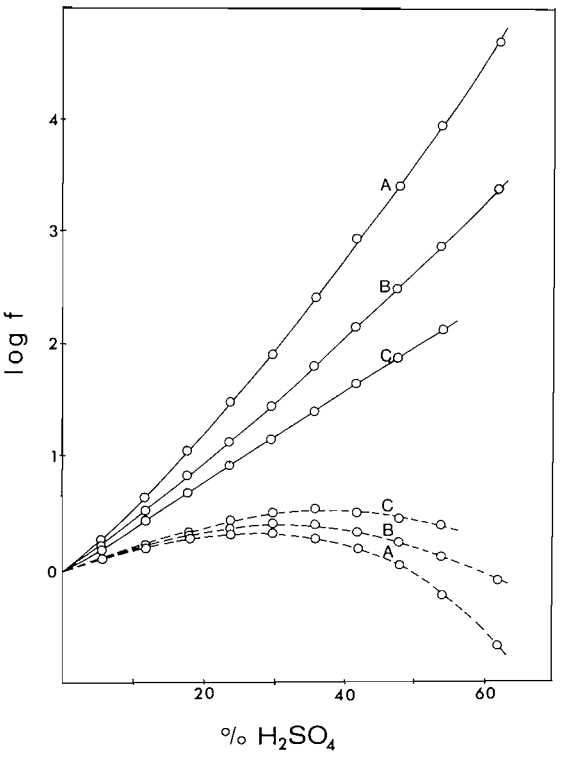

FIG. 4. Change with sulfuric acid concentration in log f_B (broken lines) and log f_{BH+} (solid lines) of (*A*) 5,5-pentamethylene-4-thiohydantoin, (*B*) 5,5-pentamethylene-2-thiohydantoin, and (*C*) 5,5-pentamethylene-2,4-dithiohydantoin.

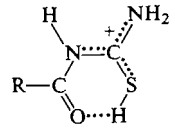

6

carbonyl groups are prevented by the ring structure from participating in such hydrogen-bonding, would seem to indicate that the interaction of the carbonyl group with some component of the acid solution is important. The desirability of further studies of thioureas containing carbonyl groups is indicated.

Experimental

Materials

The 2-thiohydantoins (20), 5,5-pentamethylene-4-thiohydantoin (25) and 5-5-pentamethylene-2,4-dithiohydantoin (25) were all prepared by the methods described in the literature and purified to constant melting points.

Sulfuric acid solutions were prepared by diluting reagent grade concentrated acid (96%) with distilled water or with distilled water and ethanol. The final acid concentrations were determined by titration.

pK_{BH^+} Measurements

Stock solutions of the 2-thiohydantoins were prepared by dissolving weighed samples in tetrahydrofuran. Aliquots of 5 μL of stock solutions were introduced by a Hamilton syringe into 5 mL volumetric flasks and diluted with sulfuric acid of appropriate concentrations. Ultraviolet spectra of the solutions were then recorded by a Unicam SP.800 spectrophotometer with a cell block thermostatted at 25.0 ± 0.1°C. Spectral curves were analyzed by conventional methods (26) at the λ_{max} of the neutral species. (Medium effects (9) were small, except for 1,3-diphenyl-2-thiohydantoin, and were neglected.) Results are given in Table 1.

Activity Coefficient Determinations

Stock solutions of the 2-thiohydantoins in chloroform (~0.025 *M*) were prepared. Aliquots (5 mL) of the solutions were shaken with 10 mL of distilled water or with 10 mL of sulfuric acid of the appropriate concentration at 25.0 ± 0.1°C. Optical densities of the aqueous and chloroform layers were then recorded by a spectrophotometer. The ratios of distribution coefficient in pure water to that of the acid solutions, corrected for protonation, gave the activity coefficients of the 2-thiohydantoins in the acid solutions (22).

Acknowledgments

We are grateful to Professors K. Yates and R. A. Cox for discussions, suggestions, and access to unpublished manuscripts, and to the National Research Council of Canada for financial support.

1. L. P. Hammett and A. J. Deyrup. J. Am. Chem. Soc. **54**, 2721 (1932).
2. K. Yates, J. B. Stevens, and A. R. Katritzky. Can. J. Chem. **42**, 1957 (1964); K. Yates and J. B. Stevens. Can. J. Chem. **43**, 529 (1965).
3. R. L. Hinman and J. Lang. J. Am. Chem. Soc. **86**, 3796 (1964).
4. J. T. Edward, I. Lantos, G. D. Derdall, and S. C. Wong. Can. J. Chem. **55**, 812 (1977).
5. E. M. Arnett and G. W. Mach. J. Am. Chem. Soc. **88**, 1177 (1966).
6. R. A. Cox and K. Yates. J. Am. Chem. Soc. **100**, 3861 (1978).
7. K. Yates and R. A. McClelland. J. Am. Chem. Soc. **89**, 2686 (1967).
8. G. C. Greig and C. D. Johnson. J. Am. Chem. Soc. **90**, 6453 (1968).
9. J. T. Edward and S. C. Wong. J. Am. Chem. Soc. **99**, 4229 (1977).
10. J. F. Bunnett and F. P. Olsen. Can. J. Chem. **44**, 1899 (1966).
11. L. P. Hammett. Physical organic chemistry. 2nd ed. McGraw-Hill, New York, NY. 1970. p. 276.
12. M. J. Jorgenson and D. R. Hartter. J. Am. Chem. Soc. **85**, 878 (1963).
13. N. C. Marziano, G. M. Cimino, and R. C. Passerini. J. Chem. Soc. Perkin Trans. II, 1915 (1973); R. Passerini, N. C. Marziano, and P. G. Traverso. Gazz. Chim. Ital. **105**, 901 (1975); N. C. Marziano, P. G. Traverso, and R. Passerini. J. Chem. Soc. Perkin Trans. II, 306 (1977); N. C. Marziano, P. G. Traverso, A. Tomasin, and R. C. Passerini. J. Chem. Soc. Perkin Trans. II, 309 (1977).
14. A. Levi, G. Modena, and G. Scorrano. J. Am. Chem. Soc. **96**, 6505 (1974).
15. W. I. Congdon and J. T. Edward. J. Am. Chem. Soc. **94**, 6096 (1972).
16. J. T. Edward and J. K. Liu. Can. J. Chem. **47**, 1117 (1969).
17. W. I. Congdon and J. T. Edward. Can. J. Chem. **50**, 3767 (1972).
18. M. J. Janssen. Recl. Trav. Chim. **79**, 464 (1960).
19. C. D. Johnson, A. R. Katritzky, and S. A. Shapiro. J. Am. Chem. Soc. **91**, 6654 (1969).
20. J. T. Edward and S. Nielsen. J. Chem. Soc. 5075 (1957), and references therein.
21. R. K. Boyd. J. Am. Chem. Soc. **85**, 1555 (1963).
22. K. Yates and R. A. McClelland. Progress in physical organic chemistry. Vol. XI. *Edited by* A. Streitwieser and R. W. Taft. John Wiley, New York, NY. 1974. p. 323.
23. P. Bonvicini, A. Levi, V. Lucchini, G. Modena, and G. Scorrano. J. Am. Chem. Soc. **95**, 5960 (1973).
24. J. T. Edward, G. Welch, and S. C. Wong. Can. J. Chem. **56**, 935 (1978).
25. H. C. Carrington and W. S. Waring. J. Chem. Soc. 354 (1950).
26. L. A. Flexser, L. P. Hammett, and A. Dingwall. J. Am. Chem. Soc. **57**, 2103 (1935).

The self-association of naturally occurring purine nucleoside 5′-monophosphates in aqueous solution[1]

KLAUS J. NEUROHR AND HENRY H. MANTSCH
Division of Chemistry, National Research Council of Canada, Ottawa, Ont., Canada K1A 0R6

Received January 26, 1979

KLAUS J. NEUROHR and HENRY H. MANTSCH. Can. J. Chem. 57, 1986 (1979).

The parameters characterizing the base-stacking self-association of adenosine, inosine, and guanosine 5′-monophosphate have been obtained from ^{1}H nmr dilution studies. The thermodynamic parameters for the formation of adenosine 5′-monophosphate stacks are $\Delta H^0 = -14.5$ kJ mol^{-1} and $\Delta S^0 = -42.3$ J K^{-1} mol^{-1}, with an apparent equilibrium constant of $K_c = 1.92\ M^{-1}$ at 30°C. The corresponding equilibrium constants for the self-association of inosine and guanosine 5′-monophosphate are 1.36 M^{-1} and 1.29 M^{-1}, respectively. The negative enthalpy and entropy changes cannot be explained by the concept of classical hydrophobic interactions; however, they strongly support the conclusion that dipole induced dipole forces play a major role for base-stacking in aqueous solution. The sequence of the equilibrium constants for the purine nucleoside 5′-monophosphates can be well explained by the concept of mutual polarization. The stacking geometries for adenosine and inosine 5′-monophosphate are presented as obtained from fitting the experimental shift data to refined isoshielding contours. It is concluded that the stacking pattern is not restricted to a unique geometry.

KLAUS J. NEUROHR et HENRY H. MANTSCH. Can. J. Chem. 57, 1986 (1979).

Faisant appel à des études de rmn ^{1}H à diverses dilutions on a pu déterminer les paramètres caractérisant l'auto-association par superposition des bases du monophosphate-5′ de l'adénosine, de l'inosine et de la guanosine. Les paramètres thermodynamiques pour l'empilement du monophosphate-5′ d'adénosine sont $\Delta H^0 = -14.5$ kJ mol^{-1} et $\Delta S^0 = -42.3$ J K^{-1} mol^{-1}; la constante d'équilibre apparente $K_c = 1.92\ M^{-1}$ à 30°C. Les constantes d'équilibre correspondantes pour les monophosphates-5′ d'inosine et de guanosine sont respectivement 1.46 M^{-1} et 1.29 M^{-1}. On ne peut pas expliquer les changements négatifs d'enthalpie et d'entropie à l'aide du concept d'interactions hydrophobes classiques; toutefois elles supportent fortement la conclusion que les forces dipolaires induites par des dipoles jouent un rôle important dans l'empilement des bases en solution aqueuse. L'ordre des constantes d'équilibre de monophosphates-5′ des nucléosides de bases purines peut facilement être expliqué par le concept de la polarisation mutuelle. On présente les géométries d'empilement des monophosphates-5′ d'adénosine et d'inosine telles qu'on les a obtenues en ajustant les données concernant les déplacements expérimentaux avec les contours affinés d'isoblindage. On en conclut que les empilements ne sont pas restreints à une seule géométrie.

[Traduit par le journal]

Introduction

The association of naturally occurring nucleobases, nucleosides, and nucleotides in aqueous solution has been the subject of numerous investigations by various experimental techniques such as vapour pressure osmometry, microcalorimetry, equilibrium sedimentation, ultrasound and uv, cd, ir, and nmr spectroscopy (1–38). The field has been reviewed by Ts'o (8, 15). It is generally agreed that the self-association of these compounds is of the stacking type and that it proceeds beyond the dimer stage (2, 6, 19). It is also well established that the stacking affinity of the nucleobases, and not hydrogen bonding, represents the major contribution to the free energy sustaining the nucleic acid secondary structure (39, 40). Interactions involving base-stacking also play an important role in the selective recognition of individual nucleotides by macromolecules such as proteins and enzymes (41, 42).

Despite many studies devoted to the solution conformation of purine nucleotides and in particular to the stacking geometry of adenosine 5′-monophosphate (11, 12, 19, 33, 43–46), so far no attempts have been made to obtain thermodynamic parameters characterizing the self-association of purine mononucleotides. In the present study we describe the parameters characterizing the self-association, in aqueous solution, of the naturally occurring purine nucleotides adenosine 5′-monophosphate (5′-AMP), inosine 5′-monophosphate (5′-IMP), and guanosine 5′-monophosphate (5′-GMP). Apparent equilibrium constants, dimer shifts, and the corresponding Gibbs

[1]NRCC No. 17446.

0008-4042/79/151986-09$01.00/0

energy changes are obtained from the concentration dependence of individual proton nmr shifts.

Experimental

Sample Preparation

All biochemicals were commercial products of the highest available purity. Adenosine 5′-monophosphate, inosine 5′-monophosphate, and guanosine 5′-monophosphate (sodium salts) were from Boehringer Mannheim. Nuclear magnetic resonance samples were prepared in 99.8% D_2O at pD 7.4 (meter reading), containing 10 mM phosphate buffer, 1 mM NaCl, 50 μM EDTA, and 1 mM *tert*-butanol. Individual nucleotide concentrations were accurately determined from the ultraviolet absorption, using $\varepsilon_{mM}^{260} = 15.4$ for 5′-AMP, $\varepsilon_{mM}^{249} = 12.7$ for 5′-IMP, and $\varepsilon_{mM}^{252} = 13.7$ for 5′-GMP, respectively.

Nuclear Magnetic Resonance Measurements

The ^1H nmr spectra were taken at 100 MHz with a Varian XL 100/12 spectrometer operating under a Varian 620/L data system. The digital resolution was 0.0025 ppm, the 90° pulse-time 20 μs. The temperature of the probe was regulated with the Varian temperature controller and monitored with a special thermometer in the probe. Unless specified otherwise, the probe temperature was 30°C. Typically three, but at least two, independent measurements were made for each sample. All proton chemical shifts were measured with respect to *tert*-butanol as internal reference. For the evaluation of association parameters and all other calculations a PDP 8/I computer was used.

Results and Discussion

The Self-association of Adenosine 5′-Monophosphate

As a probe for studying the concentration-dependent intermolecular association of this adenine nucleotide, we used the ^1H nmr resonances of the base protons in position 8 (A8) and 2 (A2) and that of the ribose proton in position 1′ (A1′) (see inset in Fig. 1), which are well separated from the resonances of the other strongly coupled ribose protons and have been assigned unequivocally in the literature (7, 47, 48). The resonances of these three protons undergo remarkable upfield shifts (increased shielding) with increasing 5′-AMP concentration, as displayed in Fig. 1. The differences in the magnitude of the shifts observed for individual protons is used in deriving the stacking geometry for 5′-AMP aggregates, as will be shown later. From the concentration-dependence of these ^1H chemical shifts, we have obtained the equilibrium constants characterizing this association, by applying the isodesmic model of Dimicoli and Hélène (49, 50). Figure 2 shows a typical plot, according to this model, of $(\delta\sigma/C)^{1/2}$ versus $\delta\sigma$ at 16°C, with similar plots for other temperatures ($\delta\sigma$ is the difference between the chemical shift of a particular 5′-AMP proton at concentration C and that at infinite dilution). From the slope of the linear traces in this plot, apparent microscopic equilibrium constants were obtained for the individual protons, while the x_0-intercepts yielded the corresponding dimer shifts.

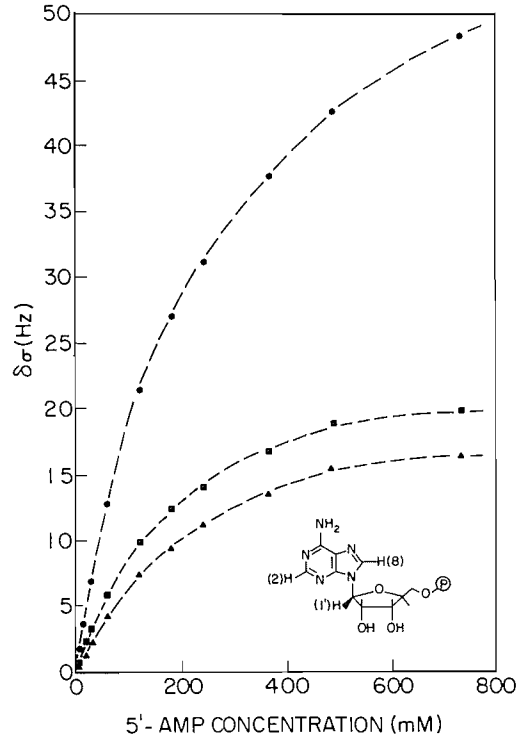

FIG. 1. ^1H nmr chemical shift differences ($\delta\sigma$) for the 5′-AMP protons A2 (●), A8 (■), and A1′ (▲) (see inset), as a function of 5′-AMP concentration, at 16°C and pH 7.4; $\delta\sigma$ is defined as $\sigma - \sigma_0$, where σ is the observed chemical shift at a given concentration, C, and σ_0 is the extrapolated chemical shift for infinite dilution.

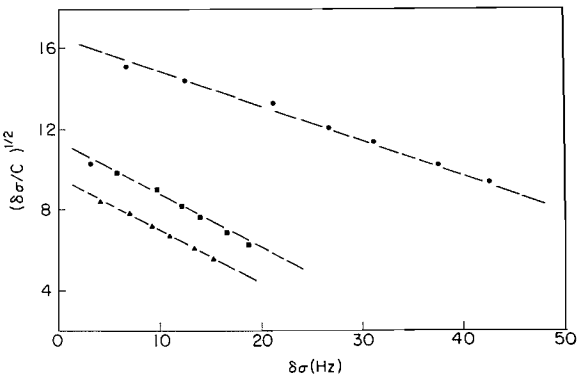

FIG. 2. Graphical evaluation of the apparent equilibrium constant for the self-association of 5′-AMP at 16°C and pH 7.4 according to the isodesmic model (49), determined from the concentration dependent chemical shift differences of the A2 (●), A8 (■), and A1′ (▲) protons.

In order to derive thermodynamic parameters,

TABLE 1. Effect of temperature on the apparent equilibrium constant (K_c), the corresponding Gibbs energy change (ΔG^0), and the dimer shift ($\delta\sigma_{A_2}$) for the self-association of 5′-AMP according to the isodesmic model at pH 7.4

t (°C)	K_c (M^{-1})[a]			$\bar{K}_c$ (M^{-1})[b]	ΔG^0 (kJ mol^{-1})[c]	$\delta\sigma_{A_2}$ (Hz)[d]		
	H8	H2	H1′			H8	H2	H1′
16	3.00	2.60	2.32	2.64	−2.33	21.3	51.0	19.2
30	1.91	1.96	1.88	1.92	−1.64	18.0	44.6	13.3
45	1.90	1.50	1.77	1.72	−1.44	13.2	39.2	9.8
60	1.82	1.17	1.50	1.50	−1.11	8.8	30.2	3.9

[a]Estimated errors for these microscopic equilibrium constants are 6–10%.
[b]Proton averaged equilibrium constant.
[c]Standard Gibbs energy changes were obtained from the proton averaged equilibrium constants.
[d]Estimated errors for the dimer shifts are 1–3%.

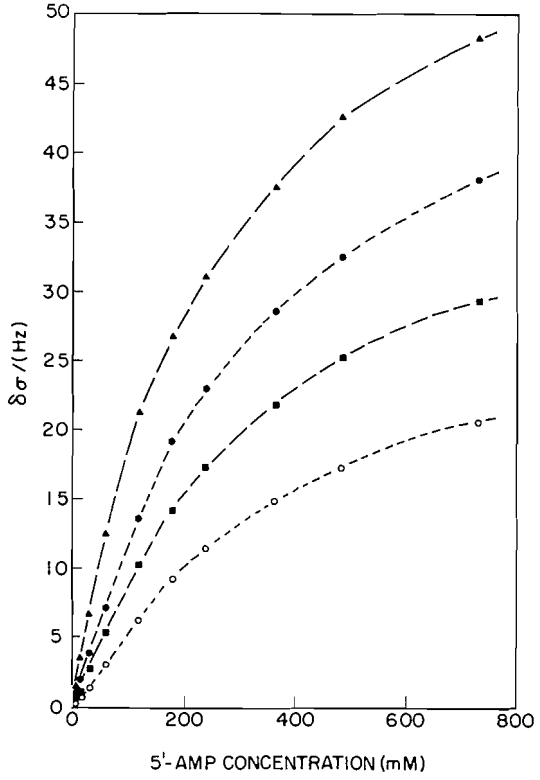

FIG. 3. Effect of temperature on the base-stacking association of 5′-AMP. Chemical shift differences are displayed for the A2 base proton as a function of 5′-AMP concentration at 16°C (▲), 30°C (●), 45°C (■), and 60°C (○).

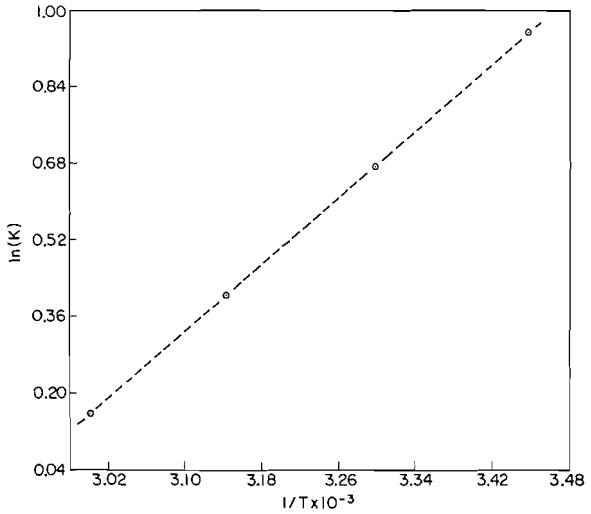

FIG. 4. van't Hoff plot representing the variation of the logarithm of the apparent equilibrium constant K_c (obtained from the A2 base proton of 5′-AMP) with reciprocal temperature.

we also investigated the concentration dependence of these ^{1}H chemical shifts at various temperatures. With increasing temperature, downfield shifts were observed, indicating a breakdown of the stacking aggregates. Displayed in Fig. 3 is the temperature effect on the chemical shift of the A2 proton of 5′-AMP. A similar temperature dependence is obtained for the A8 and A1′ protons. The corresponding equilibrium constants, dimer shifts, and Gibbs energy changes are given in Table 1. Both the equilibrium constants and standard Gibbs energy changes reported here are based on concentrations, as recommended by the ICSU Commission on Biothermodynamics (51). The magnitude of the equilibrium constant decreases with increasing temperature; the Gibbs energy changes reveal that the tendency of self-association at 16°C is about twice that at 60°C.

The thermodynamic parameters characterizing the association phenomenon have been computed from the equilibrium constants of the A2 proton obtained at different temperatures. Figure 4 shows a van't Hoff plot for this proton. From the temperature dependence of the apparent equilibrium constant K_c, we obtained an enthalpy change of −14.5 kJ mol^{-1} with an entropy change of −42.3 J K^{-1} mol^{-1} for the self-association of 5′-AMP. These

TABLE 2. Thermodynamic parameters characterizing the association through base-stacking of adenine derivatives in aqueous solution[a]

Compound	ΔH^0 (kJ mol^{-1})	ΔG^0 (kJ mol^{-1})	ΔS^0 (J K^{-1} mol^{-1})	K_c (M^{-1})	Ref.
5′-AMP	−14.5	−1.6	−42.3	1.9[b]	[c]
Adenosine	[d]	−3.7	[d]	4.5[b]	4
Deoxyadenosine	−27.2	−4.8	−75.3	6.8[e]	8
N(6,6)-Dimethyladenosine	−26.8	−7.7	−58.7	24.0[f,g]	34
	−25.9	−7.6	−61.1	21.7[b]	24
N(6,6)-Dimethyladenine	−39.3	−9.0	−102.1	38.0[b]	24
	−38.1	−10.2	−94.1	61.7[f]	13

[a]Apparent equilibrium constants for 25°C, unless otherwise specified.
[b]From nmr.
[c]This study; K_c for 30°C.
[d]No temperature studies available.
[e]From osmometry.
[f]From microcalorimetry.
[g]K_c for 20°C.

thermodynamic parameters are compared in Table 2 with literature values for other adenine derivatives which also undergo self-association via base-stacking; the sign and order of magnitude of ΔH^0 and ΔS° for 5′-AMP compares well with these data. There is an obvious decrease in the equilibrium constant in the sequence: nucleobase, nucleoside, nucleotide. Methyl substitution at the 6-amino group increases the tendency for self-association of the adenine base moiety (9, 15, 23, 24).

The Stacking Geometry of Adenosine 5′-Monophosphate Aggregates

Several studies have been devoted already to the geometry of 5′-AMP stacking aggregates (11, 12, 19, 33). This geometry was derived from experimental ^{1}H nmr shifts which were fitted to the theoretically computed isoshielding contours for the adenine base moiety (52). It is, however, not possible to derive a unique stacking geometry from only these data; thus, two different geometries have been proposed, leading to different placements of the ribosyl substituents relative to each other. While Ts'o and co-workers (4, 8, 15) and Evans and Sarma (19) have proposed a head-to-head arrangement, which places the ribosyl moieties on the same side of the stack, more recent results (11, 12, 33), based mainly on nuclear Overhauser effect studies and ^{1}H spin–lattice relaxation time measurements, favoured the head-to-tail arrangement, where the ribosyl moieties are placed on opposite sides of the stack. The older calculations of isoshielding contours were based on the ring current effect only. Recently, these calculations were refined by Giessner-Prettre and Pullman by including the anisotropy of atomic diamagnetic susceptibility (53). Inspection of the new isoshielding contours reveals that the introduction of the atomic contribution leads to an increase in shielding, which for adenine amounts to about 25%. The head-to-head and head-to-tail base-stacking patterns obtained for 5′-AMP by fitting the experimental dimer shifts from Table 1 to the new isoshielding contours are displayed in Figs. 5*a* and 5*b*, respectively. It is interesting to note that both models are in agreement with the experimental nmr shift data and it is not possible to favour one of these geometries over the other. These stacking patterns have been constructed according to the isodesmic model of Dimicoli and Hélène (49) which takes into account the magnetic anisotropy of nearest neighbours only, and assumes that these effects are additive. Shielding effects at twice the intermolecular distance are very small. The change in chemical shift of a molecule located inside an *n*-mer, relative to the free molecule, is therefore assumed to be twice that observed in the dimer. The stacking patterns in Figs. 5*a* and 5*b* show dimers; however, they also apply to *n*-mers where 5′-AMP molecules are added to both sides of the initial stack, leading to a perpetual head-to-head or head-to-tail stacking pattern. Sarma and co-workers (54–56) have determined the molecular topology of 3′,5′-, and 2′,5′-pApAp dinucleotides in aqueous solution. In the first case the two adenine bases show a preference for a head-to-head stacking while the arrangement in the latter case is neither head-to-head nor head-to-tail. It was further shown by one of us (36), that the *N*(1)-oxide analog of 5′-AMP undergoes an anomalous base-stacking in aqueous solutions where only the imidazole moieties overlap, while the pyrimidine moieties are not involved in the stacking.

The results in this study, along with the above observations, lead to the conclusion that the exact geometry of interacting adenine nucleotides can be different. Individual nucleotide molecules are in rapid motion and base-stacking is a very fast process; ultrasonic studies of the self-association of *N*(6,6)-dimethyl-

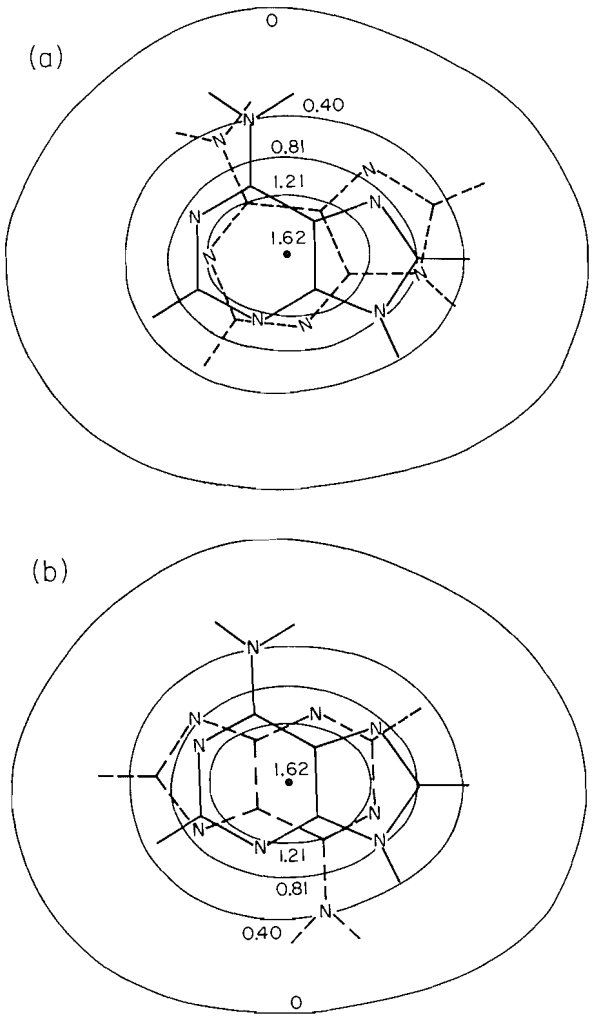

FIG. 5. Display of the head-to-head (*a*) and head-to-tail (*b*) base-stacking patterns of 5′-AMP. The ellipsoidal-shaped shielding contours represent the shielding (in ppm) experienced by the adenine base protons of the top 5′-AMP molecule (broken lines) due to the sum of the ring current effect and the anisotropy of atomic diamagnetic susceptibility of the adenine moiety of the bottom 5′-AMP molecule (solid lines). Both models have been constructed by fitting the 5′-AMP dimer shifts $\delta\sigma_{A_2}$ at 16°C from Table 1 to the recently revised isoshielding values for protons located 3.4 Å above the adenine base (53).

adenosine (38) and of similar adenine derivatives (9, 21, 27) have led to rate constants of the magnitude of 10^9 s^{-1} M^{-1}, indicating that base-stacking is a diffusion-controlled process. The dielectric properties of aqueous solutions of nucleobases and nucleosides were recently investigated by Shepherd and Schwarz (57). According to the single relaxation times found for the individual solute dispersions, an aggregation model had been suggested, where each monomer can rotate freely in the plane of stacking. From the rate constant for dissociation of *N*(6,6)-dimethyladenine (6.6×10^7 s^{-1}), the mean time for which two neighbouring bases are associated has been calculated to be 1.5×10^{-8} s (57). This value has to be compared with the dielectric relaxation time measured for *N*(6,6)-dimethyladenine at the same temperature, approximately 2×10^{-10} s (57). The comparison indicates that there is ample time for the rotation of individual molecules relative to each other within an aggregate of n monomers, before it dissociates at any of the $(n - 1)$ possible sites. Recent proton nmr data (33) yielded a reorientational correlation time for 5′-AMP of 1.1×10^{-10} s at 30°C, which again is much shorter than the mean time for which two neighbouring bases are associated.

The above studies show that the bases in the plane of stacking are very mobile and that the stacking interaction is not restricted to a unique geometry. It is thus most likely that both head-to-head and head-to-tail stacking geometries are formed when 5′-AMP molecules interact via base-stacking in aqueous solution. Also, due to the flexibility about the glycosidic bond, 5′-AMP should be able to assume any geometry, which optimizes both in-plane hydrogen bonding and out-of-plane base-stacking interactions with a given receptor macromolecule.

The Self-association and Stacking Geometry of Inosine 5′-Monophosphate

This purine nucleotide is the immediate precursor in the pathway for the biosynthesis of 5′-AMP (58). It is found in the anticodon loop of many *t*-RNAs (59); besides other unusual bases, such as the Y-base or the ψ-base, the hypoxanthine base of this nucleotide seems to play an important role in establishing the characteristic tertiary structure of *t*-RNA and is essential for its biological activity. Therefore, it becomes important to gain some information regarding the stacking capability of this base at the nucleotide level, particularly in comparison with that of the other naturally occurring purine nucleotides 5′-AMP and 5′-GMP.

We have measured the concentration dependence of the ^{1}H nmr chemical shifts of inosine 5′-monophosphate and monitored the resonances of the non-exchangeable inosine protons I2, I8, and I1′ (see Fig. 6, inset). The chemical shift differences for these protons are shown in Fig. 6 as a function of 5′-IMP concentration. All three protons show upfield shifts with increasing concentration. The shifts of the individual protons are very similar in magnitude, in contrast to 5′-AMP, where the proton in position 2 showed a much larger shift compared to those in

TABLE 3. Equilibrium constants, standard Gibbs energy changes, and dimer shifts characterizing the self-association of naturally occurring purine nucleoside 5′-monophosphates in aqueous solution[a]

Nucleotide	K_c (M^{-1}) H8	K_c (M^{-1}) H2	K_c (M^{-1}) H1′	$\bar{K}_c$ (M^{-1})[b]	ΔG^0 (kJ mol^{-1})[c]	$\delta\sigma_{A_2}$ (Hz) H8	$\delta\sigma_{A_2}$ (Hz) H2	$\delta\sigma_{A_2}$ (Hz) H1′
5′-AMP	1.91	1.96	1.88	1.92	−1.6	18.0	44.6	13.3
5′-IMP	1.07	1.79	1.22	1.36	−0.8	14.4	12.0	12.7
5′-GMP	1.06	—	1.52	1.29	−0.6	11.9	—	7.1

[a]All parameters refer to 30°C and pH 7.4.
[b]Proton averaged apparent equilibrium constant.
[c]Standard Gibbs energy changes were obtained from the proton averaged constants.

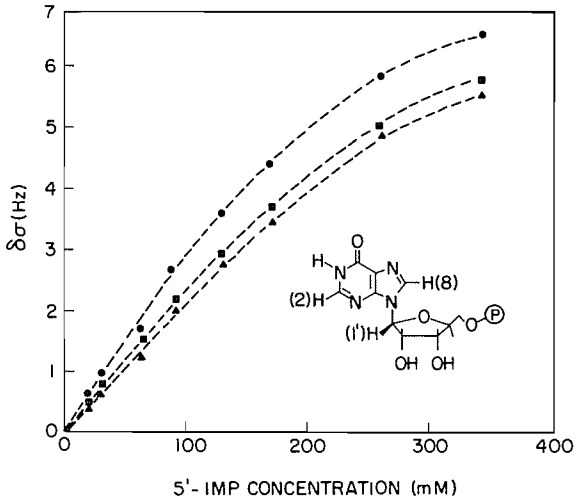

FIG. 6. Dependence of ^{1}H nmr chemical shifts for the inosine protons I2 (●), I8 (■), and I1′ (▲) on 5′-IMP concentration at 30°C and pH 7.4; δσ is defined as in Fig. 1.

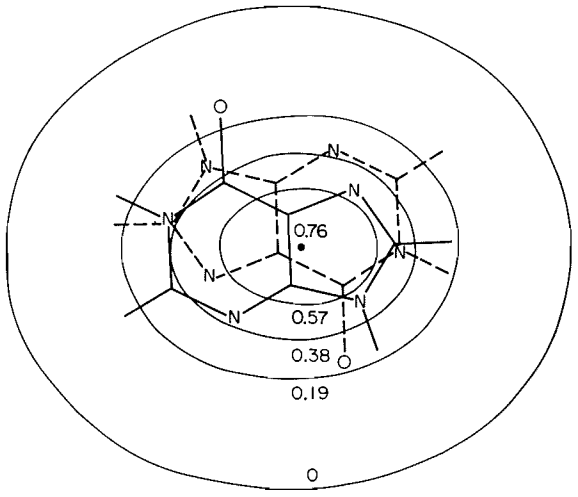

FIG. 7. Display of the head-to-tail stacking pattern of 5′-IMP. The contours show the shieldings (in ppm) experienced by the base protons of the top 5′-IMP molecule (broken lines) due to the ring current effect of the hypoxanthine base of the bottom 5′-IMP molecule (solid lines). The model was constructed from the 5′-IMP dimer shifts and the isoshielding contours calculated for a plane 3.4 Å above the hypoxanthine base (C. Giessner-Prettre. Private communication).

position 8 and 1′. We also performed an analysis of the chemical shift differences for 5′-IMP according to the isodesmic model; the corresponding microscopic equilibrium constants and dimer shifts, along with the proton averaged apparent equilibrium constant and the Gibbs energy change, are summarized in Table 3. Although K_c is smaller for 5′-IMP and ΔG^0 is about half that for 5′-AMP, this nucleotide also can engage in base-stacking interactions via its hypoxanthine base.

As in the case of 5′-AMP, the dimer shifts for the three protons investigated can be used to derive a model for the 5-IMP stacking aggregates. The theoretical isoshielding contours for the hypoxanthine base were sent to us by Dr. Giessner-Prettre prior to publication. In the calculation based on the ring current effect, the centre of shielding with a value of 0.76 ppm is located in the five-membered imidazole ring, unlike the situation with adenine where it has a considerably higher value and is localized in the six-membered pyrimidine ring. The second zone of shielding in 5′-IMP, with a value of 0.38 ppm, extends over both the five- and six-membered rings of the hypoxanthine base, while the third shielding contour covers the periphery of the two rings, where the two aromatic protons are located, and has a value of only 0.19 ppm. The shielding values for the hypoxanthine base are thus remarkably smaller than the corresponding values for the adenine base. This explains the much smaller upfield shifts observed for the 5′-IMP protons with increasing concentration, compared to the shifts for the corresponding 5′-AMP protons. Figure 7 illustrates a head-to-tail model for two stacked 5′-IMP molecules as obtained from fitting the dimer shifts in Table 3 to the isoshielding contours of Giessner-Prettre. Again, it has to be pointed out that this model represents only one of the possible stacking geometries and, as in the case of 5′-AMP, a head-to-head model would also be in agreement with the chemical shift data.

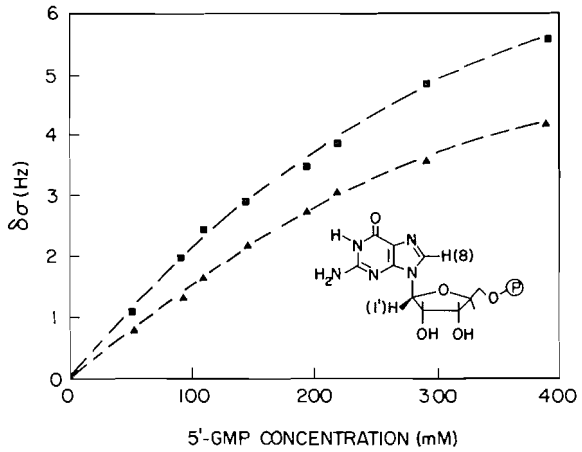

FIG. 8. ^{1}H nmr chemical shift differences for the guanosine protons G8 (■) and G1′ (▲) as a function of 5′-GMP concentration at 30°C and pH 7.4; δσ is defined as in Fig. 1.

The Self-association of Guanosine 5′-Monophosphate

Guanosine 5′-monophosphate has been shown to possess a unique ability to undergo spontaneous formation of a regular, ordered structure in aqueous solution. Guschlbauer and co-workers (60, 61) demonstrated that guanosine derivatives, in contrast to all other bases, have a strong tendency towards gel formation. The guanine base moieties first associate via hydrogen bonding to form a planar tetramer; two such tetramers then form octamers, which stack up to form highly viscous pseudopolymers. Pinnavaia *et al.* (28) investigated the 220 MHz proton nmr spectra of neutral 5′-GMP in aqueous solutions at fairly high concentrations. With increasing concentration and (or) decreasing temperature, the sharp G8 resonance broadens and two, later three, new G8 lines occur due to formation of a new regular structure in slow chemical exchange with unassociated monomers or stacked aggregates.

In order to compare the association parameters for 5′-GMP with those obtained for 5′-AMP and 5′-IMP, we also measured the concentration dependence of the ^{1}H chemical shifts of the non-exchangeable 5′-GMP protons G8 and G1′ at fairly low concentrations (up to 390 mM). As demonstrated by the concentration-dependent upfield shifts in Fig. 8, this concentration range is dominated by the formation of stacking aggregates, similar to those observed with 5′-AMP and 5′-IMP, which are in rapid chemical exchange with monomers and give time-averaged nmr spectra. The chemical shift differences were analyzed according to the isodesmic model; the apparent equilibrium constants, the Gibbs energy change, and the dimer shifts obtained from the two observable 5′-GMP protons are compared in Table 3 with the corresponding association parameters for the other two purine nucleotides. As can be seen from this table, due to the large diamagnetic ring current of the adenine base, 5′-AMP shows the highest tendency for self-association among the naturally occurring purine nucleotides. 5′-IMP and 5′-GMP have a similar, but considerably smaller tendency to form such aggregates in aqueous solutions. In the case of 5′-GMP, at concentrations above 400 mM, the self-association through base-stacking of 5′-GMP monomers is in competition with the formation of hydrogen bonded pseudopolymers (28).

Concluding Remarks

In spite of numerous publications dealing with the stacking properties of nucleobases, the nature of this interaction is still not fully understood. As base-stacking occurs only in water, the hydrophobic nature of this phenomenon has been strongly emphasized. Classical hydrophobic interactions are characterized by positive enthalpy and positive entropy changes (62). The base-stacking self-association of nucleobases, however, is accompanied by negative enthalpy and entropy changes, as has been directly obtained from calorimetric measurements of several systems (3, 5, 13), and is shown here for the 5′-AMP nucleotide. Moreover, the hydrophobic interaction is a rather unspecific phenomenon, which cannot account for the observed high specificity of the base-stacking interaction. Although the involvement of classical hydrophobic interactions in the stabilization of stacking complexes of alkylated uracils has been demonstrated (29), there is little doubt that in the case of highly polarizable purine derivatives, dipole induced dipole forces play a major role in this type of interaction (9, 22, 30). This conclusion is also supported by X-ray data (63); stacking patterns of purine bases in the crystal reveal base–base interactions with only partial overlap between neighbouring bases and with polar substituents of one base located over the ring system of an adjacent base (63). From this, the concept of mutual polarization of adjacent base moieties by partial bond moments was put forward (22). According to this concept, the stacking affinity between two adjacent bases is dependent on the degree of mutual polarization, where polarization depends both on polarizability and polarizing power.

The polarizability of an aromatic or heteroaromatic ring system, such as that of the purine bases, arises from the total electron density above and below the molecular plane. The polarizing strength is related to the bond moments of the nucleobases, due to the sp^2 nitrogen atoms and the polar keto and amino substituents. Since all nucleobases are rela-

TABLE 4. Correlation between the intermolecular shielding values of purine bases and the apparent equilibrium constants for the corresponding nucleoside 5′-monophosphates

	Adenine	Hypoxanthine	Guanine
Intermolecular shielding values[a]	1.62	1.13	1.05
K_c for corresponding nucleoside 5′-monophosphates[b]	1.92	1.36	1.29

[a]Largest shielding (in ppm), due to the sum of the ring current and the anisotropy of atomic diamagnetic susceptibility in a plane 3.4 Å from the molecular surface (ref. 53 and G. Giessner-Prettre. Private communication).
[b]Proton averaged equilibrium constants (in M^{-1}) obtained at 30°C and pH 7.4, from the isodesmic model.

tively polar compounds, the polarizing power is not the limiting factor and the free energy for self-association should be governed by the polarizability of the nucleobases. In Table 4 we compare the intermolecular shielding values for the purine bases which, at least to a first approximation, should parallel the polarizability of the bases, with the proton averaged equilibrium constants for the corresponding nucleotides, which should be representative for the degree of association. The data in Table 4 show that the magnitude of the intermolecular shielding values, and thus the polarizability, decreases in the order adenine, hypoxanthine, guanine. It is interesting that not only do the equilibrium constants follow these isoshielding values, but the larger difference between adenine and hypoxanthine and the smaller difference between hypoxanthine and guanine are closely paralleled in both sequences. Therefore we may conclude that the concept of mutual polarization is very useful in explaining the stacking affinities between nucleobases.

Acknowledgments

We express our thanks to Dr. I. C. P. Smith for helpful criticism and to Drs. Giessner-Prettre and Pullman for providing us with the isoshielding contours for the hypoxanthine base prior to publication. We are also grateful to the Deutsche Akademische Austauschdienst, Bonn, for a research fellowship to K.J.N.

1. P. O. P. Ts'o, I. S. Melvin, and A. C. Olson. J. Am. Chem. Soc. **85**, 1289 (1963).
2. G. P. Rosetti and K. E. van Holde. Biochem. Biophys. Res. Commun. **26**, 717 (1967).
3. S. J. Gill, M. Downing, and G. F. Sheats. Biochemistry, **6**, 272 (1967).
4. A. D. Broom, M. P. Schweizer, and P. O. P. Ts'o. J. Am. Chem. Soc. **89**, 3612 (1967).
5. E. L. Farquhar, M. Downing, and S. J. Gill. Biochemistry, 7, 1224 (1968).
6. M. P. Schweizer, A. D. Broom, P. O. P. Ts'o, and D. P. Hollis. J. Am. Chem. Soc. **90**, 1042 (1968).
7. P. O. P. Ts'o, N. S. Kondo, M. P. Schweizer, and D. P. Hollis. Biochemistry, **8**, 997 (1969).
8. P. O. P. Ts'o. *In* Fine structure of proteins and nucleic acids. *Edited by* G. D. Fasman and T. N. Timasheff. Marcel Dekker, New York, NY. 1970. p. 49.
9. D. Poerschke and F. Eggers. Eur. J. Biochem. **26**, 490 (1972).
10. H. T. Miles and J. Frazier. Biochem. Biophys. Res. Commun. **49**, 199 (1972).
11. M. Gueron, C. Chachaty, and T. D. Son. Ann. N.Y. Acad. Sci. **222**, 307 (1973).
12. T. D. Son and C. Chachaty. Biochim. Biophys. Acta, **335**, 1 (1973).
13. M. G. Marenchic and J. M. Sturtevant. J. Phys. Chem. 77, 544 (1973).
14. V. L. Antonovsky, A. S. Gukovskaja, G. V. Nekrasova, B. J. Sukhorukov, and I. I. Tchervin. Biochim. Biophys. Acta, **331**, 9 (1973).
15. P. O. P. Ts'o. *In* Basic principles in nucleic acid chemistry. Vol. 1. *Edited by* P. O. P. Ts'o. Academic Press, New York, NY. 1974. p. 526.
16. G. R. Kelly and T. Kurucsev. Biopolymers, **13**, 769 (1974).
17. R. Bretz, A. Lustig, and G. Schwarz. Biophys. Chem. **1**, 237 (1974).
18. D. J. Patel. Biochemistry, **13**, 1476 (1974).
19. F. E. Evans and R. H. Sarma. Biopolymers, **13**, 2117 (1974).
20. F. E. Evans and R. H. Sarma. J. Biol. Chem. **249**, 4757 (1974).
21. F. Garland and R. C. Patel. J. Phys. Chem. **78**, 848 (1974).
22. R. Lawaczeck and K. G. Wagner. Biopolymers, **13**, 2003 (1974).
23. W. Schimmack, H. Sapper, and W. Lohmann. Biophys. Struct. Mechanism, **1**, 113 (1975).
24. W. Schimmack, H. Sapper, and W. Lohmann. Biophys. Struct. Mechanism, **1**, 311 (1975).
25. M. P. Heyn and R. Bretz. Biophys. Chem. **3**, 35 (1975).
26. T. R. Krugh and Y. C. Chen. Biochemistry, **14**, 4912 (1975).
27. F. Garland and S. D. Christian. J. Phys. Chem. **79**, 1247 (1975).
28. T. J. Pinnavaia, H. T. Miles, and E. D. Becker. J. Am. Chem. Soc. **97**, 7198 (1975).
29. E. Plesiewicz, E. Stepien, K. Bolewska, and K. L. Wierzchowski. Biophys. Chem. **4**, 131 (1976).
30. E. Plesiewicz, E. Stepien, K. Bolewska, and K. L. Wierzchowski. Nucleic Acids Res. **3**, 1295 (1976).
31. T. J. Gilligan and G. Schwarz. Biophys. Chem. **4**, 55 (1976).
32. W. Egan. J. Am. Chem. Soc. **98**, 4091 (1976).
33. A. P. Zens, T. A. Bryson, R. B. Dunlap, R. R. Fisher, and P. D. Ellis. J. Am. Chem. Soc. **98**, 7559 (1976).
34. L. P. Vickers and G. K. Ackers. Arch. Biochem. Biophys. **174**, 747 (1976).
35. Y. F. Lam and G. Kotowycz. Can. J. Chem. **55**, 3620 (1977).
36. H. H. Mantsch and O. Barzu. Z. Naturforsch. **32c**, 901 (1977).

37. M. MATTHIES and G. ZUNDEL. J. Chem. Soc. Perkin Trans. 2, **14**, 1824 (1977).
38. M. P. HEYN, C. U. NICOLA, and G. SCHWARZ. J. Phys. Chem. **81**, 1611 (1977).
39. G. FELSENFELD and H. T. MILES. Ann. Rev. Biochem. **36**, 407 (1967).
40. R. H. SARMA and S. S. DANYLUK. Int. J. Quantum Chem. **4**, 269 (1977).
41. I. LASCU, T. BARZU, N. G. TY, L. D. NGOC, O. BARZU, and H. H. MANTSCH. Biochim. Biophys. Acta, **482**, 251 (1977).
42. O. BARZU, R. TILINCA, D. PORUTIU, V. GORUN, G. JEBELEANU, L. G. NGOC, M. KEZDI, I. GOIA, and H. H. MANTSCH. Arch. Biochem. Biophys. **182**, 42 (1977).
43. C. CHACHATY and G. LANGLET. FEBS Lett. **68**, 181 (1976).
44. C. CHACHATY, T. ZEMB, G. LANGLET, and T. D. SON. Eur. J. Biochem. **62**, 45 (1976).
45. T. IMOTO, S. SHIBATA, K. AKASAKA, and H. HATANO. Biopolymers, **16**, 2705 (1977).
46. C. F. G. C. GERALDES and R. J. P. WILLIAMS. Eur. J. Biochem. **85**, 463 (1978).
47. C. D. JARDETZKY and O. JARDETZKY. J. Am. Chem. Soc. **82**, 222 (1960).
48. I. FELDMAN and R. P. AGARWAL. J. Am. Chem. Soc. **90**, 7329 (1968).
49. J. L. DIMICOLI and C. HÉLÈNE. J. Am. Chem. Soc. **95**, 1036 (1973).
50. K. J. NEUROHR. M.Sc. Thesis, Justus Liebig University, Giessen, West Germany. 1978.
51. B. DREYFUS. Recommendations for measurement and presentation of biochemical equilibrium data. CODATA Bulletin 20, Paris. 1976.
52. C. GIESSNER-PRETTRE and B. PULLMAN. J. Theor. Biol. **27**, 87 (1970).
53. C. GIESSNER-PRETTRE and B. PULLMAN. Biochem. Biophys. Res. Commun. **70**, 578 (1976).
54. M. M. DHINGRA and R. H. SARMA. Nature (London), **272**, 798 (1978).
55. D. M. CHENG and R. H. SARMA. J. Am. Chem. Soc. **99**, 7333 (1977).
56. C. H. LEE, F. S. EZRA, N. S. KONDO, R. H. SARMA, and S. S. DANYLUK. Biochemistry, **15**, 3627 (1976).
57. J. C. W. SHEPHERD and G. SCHWARZ. Biophys. Chem. **7**, 193 (1977).
58. A. L. LEHNINGER. *In* Biochemistry. 2nd ed. Worth Publishers, New York, NY. 1976. p. 729.
59. S. MANDELES. Nucleic acid sequence analysis. Columbia University Press, New York, NY. 1972.
60. P. TOUGARD, J. F. CHANTOT, and W. GUSCHLBAUER. Biochim. Biophys. Acta, **308**, 9 (1973).
61. W. GUSCHLBAUER. *In* Nucleic acid structure. Springer Verlag, Berlin. 1976. p. 91.
62. G. NEMETHY and H. A. SCHERAGA. J. Phys. Chem. **66**, 1773 (1962).
63. C. E. BUGG. *In* The purines—theory and experiment. The Jerusalem Symposia on Quantum Chemistry and Biochemistry, IV, Israel Academy of Sciences and Humanities, Jerusalem. 1972. p. 178.

Mass spectrometry of some furanocoumarins

SHENG-YUH TANG, JOHN C. MCGOWAN, MARSHA SINGH, PAUL GALATSIS, BRIAN E. ELLIS, AND ROBERT K. BOYD

Guelph–Waterloo Centre for Graduate Work in Chemistry (Guelph Campus), Guelph, Ont., Canada N1G 2W1

AND

STEWART A. BROWN

Department of Chemistry, Trent University, Peterborough, Ont., Canada K9J 7B8

Received October 27, 1978

SHENG-YUH TANG, JOHN C. MCGOWAN, MARSHA SINGH, PAUL GALATSIS, BRIAN E. ELLIS, ROBERT K. BOYD, and STEWART A. BROWN. Can. J. Chem. 57, 1995 (1979).

The mass spectra of two isomeric methoxyfuranocoumarins have been investigated using electron-impact ionisation. Unambiguous distinction between the two isomers is possible through a combination of conventional mass spectra with collision-induced dissociations of the molecular ions and of selected fragment ions. The fragmentation mechanisms of these and related molecular systems were investigated in an attempt to identify the fate of each oxygen atom under electron-impact conditions. To this end, 2-pyrone, benzpyrone (coumarin), benzofuran, and some of its structural isomers were synthesised and studied via metastable spectra, collisionally activated spectra, appearance potentials, and kinetic energy release. Only partial success was achieved in this investigation, but it was possible to write a mechanistic scheme consistent with the present findings and literature data. If valid, this scheme permits identification of two of the four oxygen atoms in the methoxyfuranocoumarins.

SHENG-YUH TANG, JOHN C. MCGOWAN, MARSHA SINGH, PAUL GALATSIS, BRIAN E. ELLIS, ROBERT K. BOYD et STEWART A. BROWN. Can. J. Chem. 57, 1995 (1979).

On a étudié la spectroscopie de masse de deux méthoxyfurannocoumarines isomères sous impact électronique. On peut distinguer les deux isomères sans ambiguité grâce à une combinaison de la spectroscopie de masse conventionnelle avec des dissociations induites par des collisions d'ions moléculaires et d'ions fragmentés sélectionnés. On a étudié les mécanismes de fragmentation de ces systèmes moléculaires et d'autres qui leur sont apparentés afin d'identifier le sort de chacun des atomes d'oxygène sous des conditions d'impact électronique. A cette fin, on a synthétisé la pyrone-2, la benzpyrone (coumarine), le benzofuranne et quelques-uns de ses isomères de structure et on les a étudiés grâce à des spectres métastables, à des spectres activés par collision, à leur potentiels d'apparition et par leur habilité à perdre de l'énergie cinétique. On n'a obtenu que des succès partiels au cours de cette étude; il est toutefois possible de proposer un schéma mécanistique en accord avec nos données et celles de la littérature. Si ce schéma est valable il permet l'identification de deux des quatre atomes d'oxygène des méthoxyfurannocoumarines.

[Traduit par le journal]

Introduction

The furanocoumarins are a group of plant products of special interest for their dermal photosensitizing properties (1). Recent studies on their biogenesis (2) have outlined the route of formation of the linear furanocoumarin carbon skeleton but the source of the aromatic ring hydroxyls remains to be established. As an approach to this question we have studied the mass spectrometric fragmentation pattern of substituted furanocoumarins in hopes of identifying specific oxygen-containing fragments uniquely derived from each oxygenated portion of the furanocoumarin molecule. This information would then allow the crucial $^{18}O_2$ biogenesis experiments to be carried out.

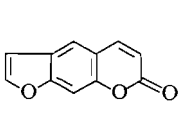

1

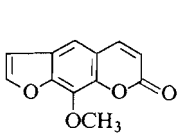

2

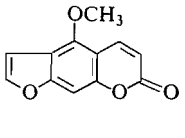

3

The furanocoumarins studied in the present work were psoralen (**1**), xanthotoxin (**2**), and bergapten (**3**). A comprehensive review of the mass spectrometry of these and related compounds is available (3). In addition to the mechanistic studies, it was of interest to develop a mass spectrometric technique capable of distinguishing between **2** and **3**. The conventional electron-impact (EI) mass spectra of **2** and **3** are very similar. The approach adopted in the present work

0008-4042/79/151995-09$01.00/0

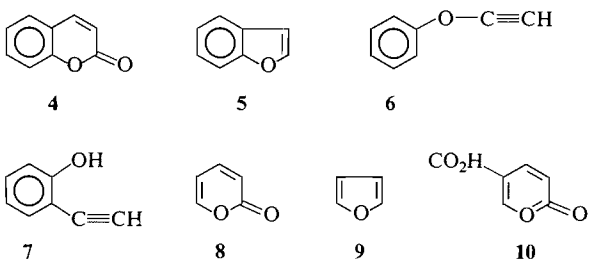

has been to use the fragmentation patterns of metastable and collisionally activated ions, decomposing in the first field region of a double-focussing mass spectrometer. The diagnostic capabilities of such techniques have been well documented (4).

In addition, the identity of the oxygen atoms contained in neutral fragments expelled in various reactions was of interest from the biochemical viewpoint. The most unambiguous method of investigating this question would require synthesis of specific ^{18}O-labelled versions of **1–3**. However, these were not available, and metastable ion (MI) and collisionally activated (CA) spectra of unlabelled **1–3** were used to investigate how far the oxygen atoms in **1–3** could be identified. To this end, the EI, MI, and CA spectra of coumarin (**4**), benzofuran (**5**), phenoxyacetylene (**6**), 2-ethynylphenol (**7**), α-pyrone (**8**), and furan (**9**) were investigated.

Experimental

Apparatus

All mass spectrometric measurements were made on a VG Organic 7070F double focussing mass spectrometer, equipped with a VG 2025 data system, a collision cell in the first field-free region, and a Hall-effect probe with associated circuitry to permit linked-scans of both the B/E (daughter-ion spectra) and B^2/E (parent-ion spectra) types. Helium and nitrogen were used as collision gases, at pressures sufficient to reduce the main beam intensity to 30% of its original value. Appearance potentials were measured using an accurate 10-turn potentiometer controlling the accelerating voltage for the ionising electron beam. The peak of interest was tuned to occupy the centre two-thirds of the monitoring screen, and the integrated signal (1 s scans) fed from the integrating ion monitor to a strip-chart recorder.

Materials

The substances **1–9** were obtained as follows.

*Psoralen (**1**)*, of natural origin, was a gift of Dr. S. K. Mukerjee, Indian Agricultural Research Institute, New Delhi. It was purified by vacuum sublimation before use.

*Xanthotoxin (**2**)* was obtained from Schwarz/Mann, Orangeburg, NY.

*Bergapten (**3**)* was synthesised from isoimperatorin prepared using a published procedure (2). One gram of this isoimperatorin was dissolved in 10 mL of glacial acetic acid, with stirring at room temperature. Stirring was continued after the addition of 4 drops of concentrated sulphuric acid. Bergaptol began to separate almost immediately. After 45 min, the product (505 mg) was filtered, washed, dried, and dissolved in methylene chloride without further purification. Treatment with a substantial excess of diazomethane in ether converted the phenol to **3** in good yield.

*Coumarin (**4**)* was obtained from British Drug Houses, Ltd.

*2,3-Benzofuran (**5**)* was obtained from Aldrich Chemical Co.

*Phenoxyacetylene (**6**)* was prepared by a literature method (26, 27). The infrared spectrum (Beckman IR5A) was characterised by bands at 3310 cm^{-1} (≡C—H), 2170 cm^{-1} (C≡C), and 1240 cm^{-1} (aromatic C—O); the nmr spectrum (Varian A60 spectrometery) showed a distinctive absorption at δ = 2.32 ppm, characteristic of an acetylenic proton. The integrated nmr intensities gave a ratio very close to 5:1 for the total aromatic proton to acetylenic proton intensities, as expected.

2-Ethynylphenyl (**7**) was also prepared by a literature method (28). The infrared spectrum showed bands at 3510 cm^{-1} (aromatic O—H), 3290 cm^{-1} (≡C—H), 2140 cm^{-1} (C≡C), and 1220 cm^{-1} (aromatic C—O). The nmr spectrum had characteristic lines at δ = 2.15 ppm (≡C—H) and a broad band at δ = 5.85 ppm, typical of a phenolic proton. The integrated intensities were very close to 4:1:1, for aromatic:acetylenic:phenolic protons, as required.

2-Pyrone (**8**) was prepared by an adaptation of a literature method (29), whereby the mercury salt of coumalic acid (**10**) was heated in a stream of dry nitrogen (rather than hydrogen (29)) to give **8** in low yield. The ir spectrum showed a broad absorption in the region 1600–1750 cm^{-1}, with a distinguishable band at 1700 cm^{-1}; the latter probably corresponds to the (C=O) stretch, superimposed upon the ring vibration frequencies. Bands at 1090 and 1045 cm^{-1} correspond to C—O frequencies. The nmr spectrum was consistent with the structure of 2-pyrone but showed some evidence of impurities, also apparent from the mass spectrum.

Furan (**9**) was obtained from Aldrich Chemical Co., and was purified by fractional freezing before use.

Results and Discussion

Mass Spectrometric Distinction between Isomeric Methoxy-furanocoumarins

The EI spectra of **2** and **3** were found to be very similar, though not identical (Table 1). The most clear-cut differences lie in the lower mass range (m/e < 90), and are thus most susceptible to interference from background ions from impurities, solvent, etc. However, the $63^+/51^+$ ratio does offer a fairly clear-cut distinction between the two isomers, in the absence of such interferences.

A mass spectrometric technique which circumvents such problems involves selecting for study just one ion (typically through not necessarily the molecular ion), and generating a daughter-ion spectrum of this preselected parent ion. In the present work, the B/E linked-scan technique (5) was used to generate CA spectra of the molecular ions of **2** and **3**, and also of the corresponding M—CH_3 (m/e = 201) ions. The results obtained are summarised in Table 2; the CA spectra obtained for the molecular ions are shown in Fig. 1. Viewed simply as fingerprints, these spectra can be used to distinguish between **2** and **3**. The most clear-cut difference appears at m/e = 199 in the daughter-ion spectra of the two

TABLE 1. Major peaks in EI spectra (70 eV, 200°C) of furanocourmarins

	Relative intensity		
m/e	Psoralen (**1**)	Xanthotoxin (**2**)	Bergapten (**3**)
217	—	11	10
216	—	100	100
201	—	27	30
188	—	8	9
187	11	—	—
186	100	—	—
173	—	42	48
158	56	—	—
145	—	15	22
130	12	—	—
102	19	—	—
89	—	19	9
83	—	5	7
79	5	—	—
76	8	—	—
75	6	—	—
63	—	13	5
51	16	7	10
50	7	—	—

TABLE 2. Collisionally activated spectra of ions from furanocoumarins

	Xanthotoxin (**2**)			Bergapten (**3**)	
m/e					
216	Parent			Parent	
215	20			2	
202	8			9	
201	100	Parent		100	Parent
200	0	0		0	0
199	5	0		0	0
189	2	0		4	0
188	14	0		29	0
187	8	0		4	0
186	1	0		0	0
185	1	0		2	0
175	0	0		1	0
174	1	14		5	27
173	9	100		9	100
146	0	0		0	7
145	0	4	Parent	0	34
144	0	2		0	5
117	0		10	0	0
89	0		100	0	0

molecular ions. While this peak is not very intense in the case of **2**, it is completely absent from the spectrum of **3**; repeated attempts to find this peak in the case of **3**, using various pressures of both N_2 and He as collision gases, failed completely. Other differences between the CA spectra of the isomeric molecular ions occur at m/e = 215, 188, and 174, although these are no more striking than the differences in the EI spectra (Table 1). They are, however, much less susceptible to interferences from impurities. If the $(M—CH_3)^+$ ions (m/e = 201) are used as parent ions for the CA spectra, striking differences (Table 2) are found in the relative intensities of fragment ions at mass 145. A combination of EI and CA spectra can thus unambiguously distinguish between the two isomers.

Fragmentation Mechanisms of Pyrone and Coumarin

The problem of trying to identify by mass spectrometry which oxygen atom in **1–3** is expelled in a specified fragmentation reaction involves the question of the fragmentation mechanisms responsible for the observed mass spectra. Considerable literature exists on the related systems **4**, **5**, **8**, and **9**. Most of this information has been extensively discussed previously (6) and will be briefly summarised here.

The mass spectrum (6) of 2-pyrone (**8**) is characterised by expulsion of CO followed by further fragmentations of the M—CO ion, which are closely similar to those of the molecular ion of furan (**9**). Accordingly, the $C_4H_4O^{+\cdot}$ ion (M—CO ion) from **8** has frequently been assigned a furan-like structure, even though no positive evidence exists supporting a closed-ring structure for the $C_4H_4O^{+\cdot}$ ions from either **8** or **9**. A study of the EI mass spectra of the four monodeuterio-2-pyrones (8) appears to rule out any structure for the $C_4H_4O^{+\cdot}$ ion from **8** in which the H (or D) atom, originally at the 6-position of 2-pyrone, is not unique. This experimentally observed uniqueness of the 6-position in **8** rules out a furan-like structure for the M—CO ion from **8**, even if the molecular ion of **8** does not retain the intact pyrone structure (6). A number of possible structures for this ion are consistent with these findings (6), but the objections raised (9) to exclusion of a furan-like structure, based upon earlier labelling experiments (7), appear to have been convincingly answered (6).

Studies of the shapes of metastable peaks arising from expulsion of CO from the molecular ions of substituted 2-pyrones (10) indicated no substituent effect upon the kinetic energy release in these reactions. This was considered (10) to demonstrate the existence of non-furan-like structures for the M—CO ions arising from 2-pyrones. Finally, the MI spectra of the $C_4H_4O^{+\cdot}$ ions arising from **8** and **9** have been compared (11) to demonstrate that these ions are not identical in both structure and internal energy.

In the present work, both MI and CA spectra of $C_4H_4O^{+\cdot}$ ions from **8** and **9** were obtained using the B/E linked scan technique (5); the results obtained are summarised in Table 3. Since only the $C_4H_4O^{+\cdot}$

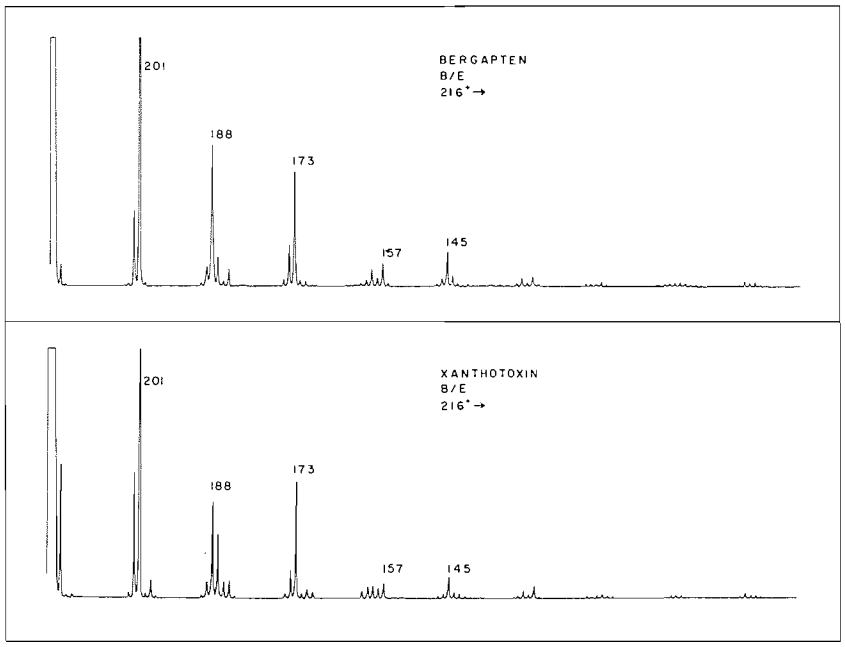

FIG. 1. Collisonally activated spectra of molecular ions of xanthotoxin (**2**) and bergapten (**3**).

ions were selected for study, the minor impurities present in our sample were of little importance. The MI spectra confirm that these ions differ in one or both of structure and internal energy, but differ somewhat from earlier results (11). In this regard, it must be emphasised that the B/E linked scan (5) picks out only those ions corresponding to the centre of a metastable peak. This accounts for the higher mass resolution of such spectra, relative to those obtained by the accelerating-voltage scans used previously (11); this could account, in part, for the larger number of peaks observed in the MI spectra. For the same reason, the intensities (peak heights) reported here are not directly comparable with the areas under the full metastable peaks (11). In addition, it is clear (12, 13) that the B/E linked-scan technique is liable to produce artifact peaks, particularly weak peaks corresponding to fragment ions arising from precursors differing by one mass unit from that actually preselected. Accordingly, the significance of some of the weaker peaks should be approached with some reserve, although the intensities of precursor ions at $m/e = 69$ and 67 are not large in the present case, and such artifacts seem unlikely to be important here. Collisionally activated (CA) spectra of ions are known (14) to be much less sensitive to internal energies of the precursor ions, so that differences observed are more likely to be ascribable to differences in structures. For purposes of such structural comparisons, it is best (14) to exclude those peaks also observed in the MI spectra, since the probabilities of the low-energy reactions responsible for such peaks will be strongly dependent upon the internal energies of the precursor ions. The most significant difference

TABLE 3. Metastable ion (in parentheses) and CA spectra of $C_4H_4O^{+\cdot}$ ions obtained by the B/E linked scan

m/e	2-pyrone (**8**)		Furan (**9**)	
68	Parent		Parent	
67	56	(15)	83	(100)
66	12		10	(5)
65	0		5	(2)
54	7		2	
53	2		10	
52	0		2	
51	4		7	
50	10		10	
49	5		2	
43	2	(9)	10	
42	8	(7)	17	(3)
41	12	(100)	110	(46)
40	32	(85)	42	(3)
39	100		100	
38	40		34	
37	27		17	
29	20		15	
28	1		5	
27	2		15	
26	10		12	
25	2		2	

TABLE 4. Metastable ion (in parentheses) and CA spectra of $C_8H_6O^{+\cdot}$ ions

m/e	Coumarin (**4**)		Benzofuran (**5**)		Phenoxyacetylene (**6**)		2-Ethynylphenol (**7**)	
118	Parent		Parent		Parent		Parent	
117	40	(3)	330	(2)	20		70	(4)
116	17	(2)	33	(1)	5		10	
105	0		0		0		20	
101	0		0		0		20	
93	0		0		5		10	
92	8	(3)	10	(1)	32	(3)	10	
91	50	(14)	75	(12)	470	(70)	70	(14)
90	540	(100)	610	(100)	660	(100)	650	(100)
89	430	(5)	410	(2)	125		430	(4)
88	17		22		5		20	
87	17		22		5		20	
86	8		10		5		20	
78	0		0		60		0	
77	5		10		*100*		10	
76	17		20		26		10	
75	20		20		20		30	
74	17		20		16		30	
65	5		10		20		20	
64	33		33		10		40	
63	*100*		*100*		32		*100*	
62	40		50		10		50	
61	5		10		5		20	
51	33		25		25		30	
50	33		33		20		30	

between the two CA spectra involves the relative intensities of the peaks at $m/e = 54$ and 53 (loss of CH_2 and CH_3, respectively); the differing intensities at $m/e = 27$ and 26 also appear to be significant, and were observed consistently. These differences probably reflect different structures, or mixtures of structures, for the $C_4H_4O^{+\cdot}$ ions sampled in the CA experiments. These results alone do not, of course, permit structures to be assigned to $C_4H_4O^{+\cdot}$ ions arising from either **8** or **9**.

This question was not pursued further in this work. A thorough investigation of $C_4H_4O^{+\cdot}$ ions generated from various precursors has been undertaken (J. L. Holmes, private communication). Using information derived from CA spectra and heats of formation of ions, non-fragmenting $C_4H_4O^{+\cdot}$ ions generated by CO loss from the molecular ions of 2- and 4-pyrone were shown to have predominantly a furanoid structure, with some contribution from a vinyl ketene structure. Clearly, the structures to be assigned to $C_4H_4O^{+\cdot}$ ions depend markedly on the internal energies of the ions.

The presence of the aromatic ring fused to the pyrone ring in the compounds of interest here (**1–3**) could have a sufficiently large effect to make inapplicable these conclusions concerning the fragmentation of 2-pyrone. Accordingly, the fragmentation of coumarin (**9**) was studied in the same fashion. A vast literature exists (3) concerning the mass spectrometry of coumarins, and only the more relevant work will be mentioned here. The principal fragmentation reactions of the molecular ion of **4** involves successive expulsion of neutral CO fragments. Experiments with ^{13}C labels have shown (15, 16) that expulsion of that CO moiety which is present as the carbonyl group in the pyrone ring occurs first. This was true (15, 16) in cases where several other possibilities existed for the origins of the first CO fragment. By analogy with the case of 2-pyrone, it has been widely surmised (3) that the $C_8H_6O^{+\cdot}$ ion, formed by loss of CO from the molecular ion of **4**, has the closed-ring structure of benzofuran (**5**). This suggestion has been challenged on energetic grounds (17); it was suggested (17) that the $C_8H_6O^{+\cdot}$ ion from **4** has a structure corresponding to that of *o*-ethynylphenol (**7**).

In the present work, the three compounds **5–7** were synthesised, and their mass spectra investigated. These isomers correspond to possible stable structures arising from expulsion of the carbonyl group from **4**. The 70 eV EI mass spectra of **5–7** were very similar to one another and to that of coumarin (**4**) below $m/e = 118$. Accordingly, the MI and CA spectra of ions of $m/e = 118$, from **4–7**, were obtained, and are summarised in Table 4.

TABLE 5. Heats of formation of $C_8H_6O^{+\cdot}$ ions (kJ mol^{-1})

Precursor (H_f^0/kJ mol^{-1})[a]	AP/eV	Neutral fragment	ε/eV	$\Delta H_f^0(C_8H_6O^{+\cdot})$	References
Coumarin (**4**)	10.8	CO	1.50[b]	851	Present work
(−156.9)	10.84[d]	CO	0.26[c]	974	(17, 18)
Benzofuran (**5**)	8.8	—	—	837	Present work
(−12.1)	8.42	—	—	801	(19)
	8.29	—	—	788	(20)
	8.6	—	—	818	(17)
Phenoxyacetylene (**6**)					
(+199.6)	8.7	—	—	1040	Present work
2-Ethynylphenol (**7**)	8.5	—	—	973	Present work
(+153.1)	8.71	—	—	993	(17)
Benzocyclobutenone					
(+161)	8.99	—	—	1028	(21)

[a]ΔH_f^0 of all neutral precursors estimated by group contribution method of Benson (22).
[b]ε is sum of ε_i^0 plus kinetic shift appropriate to first field-free region reaction of metastable ions.
[c]Determined (17) from width of 'metastable plateau' using single-focussing instrument.
[d]Most recent value (18) obtained using critical-slope method.

If, for the purposes of comparing ion structures, those peaks in the CA spectrum which appear also in the MI spectrum are again ignored (14), the results of Table 4 *cannot* distinguish between the $C_8H_6O^{+\cdot}$ ions arising from **4** and **5**. On the other hand, significant differences exist in the CA spectra of **6** and **7**. In the case of **6**, the strong peak at $m/e = 77$ corresponds to loss of the (O—C≡CH) group, which thus appears to remain intact in the molecular ion of **6**. The peak at $m/e = 78$ is more difficult to interpret, but is characteristic of **6** in the same way. The main distinctive features in the CA spectrum of **7** are the fragment ions of masses 105 and 101; these are weak peaks, whose significance was confirmed by several independent scans. The fragment ion of mass 101 corresponds to M—OH, which is not unexpected; however, that at mass 105 corresponds to M—CH. Since this peak is absent from all other spectra in Table 4, it must be characteristic of the ethynyl group attached directly to the benzene ring. Its origins are not known.

Thus, in contrast with the case of 2-pyrone, the CA spectra of benzofuran (**5**) molecular ion and of the M—CO ion from coumarin (**4**) are indistinguishable. As a further check upon the relationship between these ions, their heats of formation were estimated. The values obtained in the present work are compared with literature data in Table 5. Experimental heats of formation appear to be available for *none* of the neutral percursors used (**4**–**7**). Accordingly, these were estimated using group-contribution methods (22), of unknown accuracy for the compounds of interest.

The most striking discrepancy between the present work and literature data concerns the value of the kinetic energy release derived from the width of the metastable peak corresponding to loss of CO from the molecular ion of **4**. Figure 2 shows the peak shape obtained in the present work, using a high-voltage scan. At the low-energy side, a weaker peak corresponding to formation of a fragment ion of mass 118 from a parent ion of mass less than 146 can be seen. The maximum of this second peak is not clearly defined. The high-energy side is free from such interference, however, and was used to establish the peak width. Several measures of the peak width were converted to values for kinetic-energy release T, using the simple one-dimensional formula (4) (corresponding to scattering angles for the fragment ion of 0 and π only). The values obtained for T were as follows: T(horns) = 0.27 eV; T(half-height) = 0.56 eV; T(max) = 1.50 eV. The simple formula is exact for T(max).

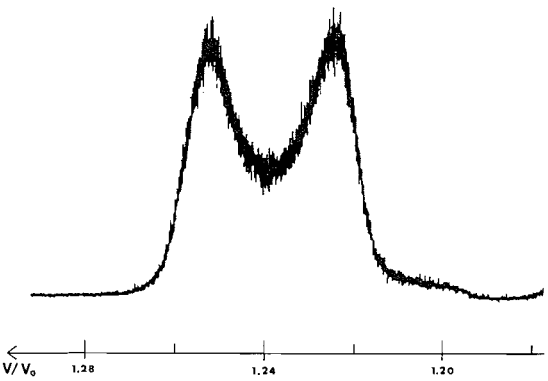

FIG. 2. Metastable peak for reaction $146^+ \rightarrow 118^+$ in coumarin (**4**), obtained by scan of accelerating voltage. Entrance and exit slits set for mass resolution of 3000, and beta slit closed until no further improvement in kinetic energy resolution obtained.

Previous measurements of this quantity yielded values of 0.26 eV (17) and 0.17 eV (10). These earlier values (19, 17) were obtained from observations of

'flat-topped' metastable peaks using single-focussing instruments; no precise information was given concerning the actual peak width parameter measured. Such a technique, involving a shorter distance travelled by the fragment ions before collection, inherently involves less *z*-axis discrimination, and thus less dishing, than does the present technique utilising the first field-free region of a double-focussing instrument (4). Thus, the present dished metastable peak (Fig. 2) could correspond to a flat-topped peak in a single-focussing instrument, with a plateau width corresponding approximately to the present separation between the horns. This is, indeed, observed, though the precise relationship depends upon details of the instrumental geometry.

In the present work the appropriate value of kinetic energy release, used to correct the appearance potential to yield ΔH_f^0 of the fragment ion, was taken to be T_{max}, corresponding to the peak width at the base. T_{max} must correspond (23) to a *lower* limit to the quantity $(\varepsilon_{MI}^{\ddagger} + \varepsilon_r^0)$, where ε_r^0 is the energy barrier for the reverse reaction and $\varepsilon_{MI}^{\ddagger}$ is the kinetic shift pertinent to the metastable ions in the instrument actually used. The correction actually desired is $(\varepsilon_{AP}^{\ddagger} + \varepsilon_r^0)$, where $\varepsilon_{AP}^{\ddagger}$ is the kinetic shift pertinent to the fragment ions formed in the ion source in the threshold region of the appearance potential measurements. In general, the longer timescale characteristic of the metastable ion experiment will tend to make $\varepsilon_{MI}^{\ddagger} < \varepsilon_{AP}^{\ddagger}$, but this trend will be at least partly compensated by the greater sensitivity available in the usual experimental procedure for measurement of appearance potentials. This procedure accounts for the discrepancy between the present and earlier values for $\Delta H_f^0(C_8H_6O^{+\cdot})$ (Table 5). This discrepancy is extremely important, since the use of T(max) as the correction gives a value for $\Delta H_f^0(C_8H_6O^{+\cdot})$, from **4** as precursor, in reasonable agreement with that from **5**, to within the experimental uncertainties. The heats of formation, thus calculated, are in agreement with the CA spectra (Table 4) in that the $C_8H_6O^{+\cdot}$ ion from coumarin (**4**) is not distinguishable from the molecular ion of benzofuran (**5**), while those arising from **6** and **7** are clearly different.

Fragmentation of Furanocoumarins

The three furanocoumarins studied here (**1**–**3**) yield intense molecular ions in their 70 eV EI spectra (Table 1). In the case of the parent compound psoralen (**1**) the only important fragmentation mechanism involves successive expulsion of 3 molecules of CO. By analogy with earlier ^{13}C labelling work on related systems (15, 16), it seems likely that the first CO moiety expelled is that originally present as the carbonyl in the pyrone ring. No further conclusion seems possible. Indeed, if formation of the M—CO ion of **1** does indeed involve closure of the furan ring, this ion would be symmetrical and no distinction between the two remaining oxygens would be possible. There is no evidence for or against ring closure in this case, though it is clear (Tables 4 and 5) that the M—CO ion from **4** is thus far indistinguishable from the molecular ion of **5**. This is in contrast with the analogous result of comparing **8** and **9**, and probably reflects a stabilising effect of the fused aromatic ring.

The two isomeric methoxy derivatives **2** and **3**, however, show at least two competing fragmentation pathways. One of these involves initial expulsion of CO (presumably that originally present as carbonyl), while the more important has as an initial step the loss of $CH_3^{\cdot}$, followed by expulsion of CO. While all three oxygen atoms are fairly readily expelled from **1** (Table 1), the situation is more complicated in the cases of **2** and **3**. Thus, loss of $(CH_3)(CO)_2$, in various permutations of three steps, occurs fairly readily with the mechanism involving initial loss of CH_3 as the main contributor. However, the ion of $m/e = 117$ (corresponding to loss of $(CH_3)(CO)_3$) is of very low intensity ($\sim 3\%$) in the EI spectra of **2** and **3**, and is completely absent from the CA spectra (Table 2). On the other hand, the ion of $m/e = 89$, which corresponds to loss of $(CH_3)(CO)_4$, is reasonably intense (Table 1). Similar trends have been noted previously (24), and can be rationalised on the basis of work (25) on the EI spectra of aromatic-methyl ethers.

Figure 3 illustrates such a speculative rationalisation for the case of xanthotoxin (**2**); a similar scheme can be written for **3**. For aromatic-methyl ethers with substituents placed in the aromatic ring such that it is possible to write quinonoid structures for the M—CH_3 ion, fission of the aromatic-ether bond is suppressed in favour of expulsion of $CH_3^{\cdot}$ (25). Otherwise, loss of CH_2O (presumably formaldehyde) is favoured. In the case of **2** and **3**, a very weak peak ($< 1\%$) at $m/e = 185$ was observed in the EI spectrum with no signal at 186. Three independent attempts to measure the accurate mass of these ions resulted in an average value of 185.024 $\pm$ 0.010. This very poor precision was due to the low intensity of the peak, but is sufficient to identify these ions as M—CH_3O rather than M—C_2H_7, from **2** and **3**. The complete absence of a peak at $m/e = 186$, corresponding to M—CH_2O, confirms that **2** and **3** follow the general pattern established previously (25) for aromatic ethers, readily rationalised in terms of structure **2***c* (Fig. 3) for the ion of $m/e = 201$. Such an ion could readily lose one or two molecules of CO, or alternatively C_2H_3 (2CO + H), etc. (Table 2).

The molecular ion of **2** has been written as in **2***a*,

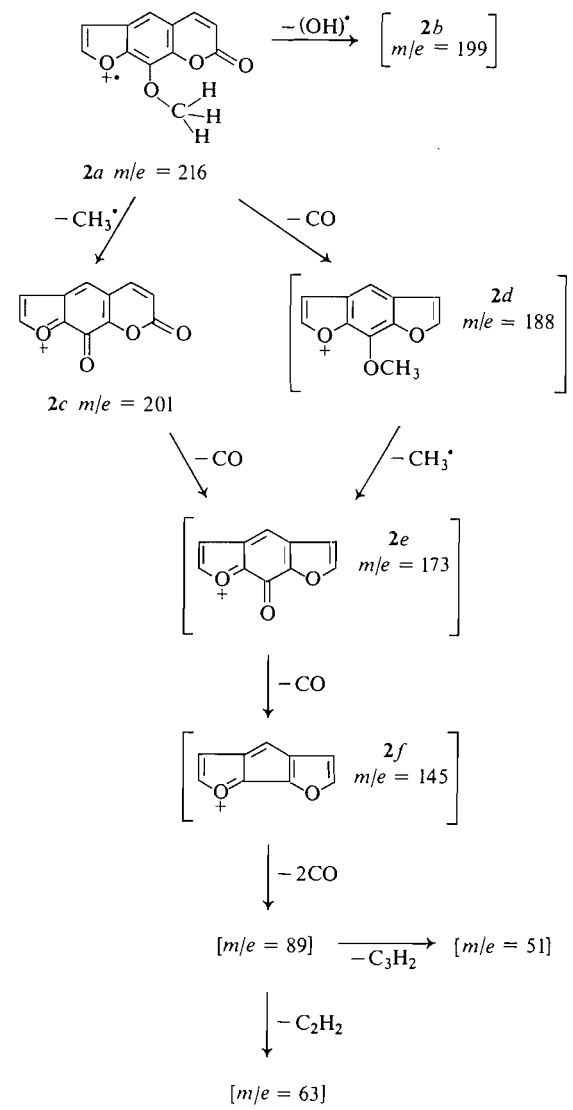

FIG. 3. Proposed rationalisation of fragmentation mechanism of xanthotoxin (**2**) under EI conditions. Ions of unknown or particularly uncertain structures are written in square brackets (see text).

with a conceivable six-membered ring intermediate leading to expulsion of HO•, (m/e = 199, Table 2). The analogous structure **3***a* could not be written in this way, thus rationalising the total absence of m/e = 199 as a daughter ion for this isomer.

Ions formed by expulsion of the carbonyl CO from the pyrone ring have been written with benzofuran-like structures **2***d* and **2***e*, i.e., with ring closure subsequent to CO loss. There is no real evidence for this assumption. The apparent identity of the $C_8H_6O^{+\bullet}$ ions from **4** and **5**, described above, does not necessarily require such closed-ring structures for either ion, but merely rules out ion structures derived from **6** and **8**.

The molecule of CO expelled from **2***e* is assumed to be the carbonyl group (i.e., that derived from the original methoxy group), again by analogy with the results of ^{13}C labelling experiments on related systems (15, 16). The resulting ion at m/e = 145 is of even more uncertain structure, and structure **2***f* written in Fig. 3 was so written merely to emphasise that this ion must have either a highly strained fused ring structure (**2***f*) or else a highly unsaturated, and thus high energy, open chain structure. The rapid expulsion of two molecules of CO from this ion is thus not unexpected, and is confirmed by the appropriate CA spectrum for the case of m/e = 145 from **2** (Table 2). It is not necessary to postulate expulsion of a single neutral fragment C_2O_2, as was done previously (16). In this regard, it is perhaps worthwhile to point out that, in the context of MI and CA spectra, the term 'simultaneous' applied to the expulsion of two molecules of CO as in the present example, means 'within the time period during which the ions are in the appropriate field-free region.'

Acknowledgements

We are indebted to Dr. S. K. Mukerjee, of the Indian Agricultural Research Institute, New Delhi, for the gift of psoralen. Financial support of this work by the National Research Council of Canada is gratefully acknowledged.

1. T. O. SOINE. J. Pharm. Sci. **53**, 231 (1964).
2. S. A. BROWN and S. SAMPATHKUMAR. Can. J. Biochem. **55**, 686 (1977).
3. S. E. DREWES. Chroman and related compounds. *In* Progress in mass spectrometry. Vol. II. *Edited by* H. Budzikiewicz. Verlag Chemie. 1974.
4. R. G. COOKS, J. H. BEYNON, R. M. CAPRIOLI, and G. R. LESTER. Metastable ions. Elsevier, Amsterdam. 1973.
5. R. K. BOYD and J. H. BEYNON. Org. Mass Spectrom. **12**, 163 (1977).
6. W. H. PIRKLE and M. DINES. J. Am. Chem. Soc. **90**, 2318 (1968).
7. P. BROWN and M. M. GREEN. J. Org. Chem. **32**, 1681 (1967).
8. W. H. PIRKLE. J. Am. Chem. Soc. **87**, 3022 (1965).
9. H. NAKATA and A. TATEMATSU. Tetrahedron Lett. 4101 (1967).
10. M. M. BURSEY and L. R. DUSOLD. Chem. Commun. 712 (1967).
11. W. T. PIKE and F. W. MCLAFFERTY. J. Am. Chem. Soc. **89**, 5954 (1967).
12. A. P. BRUINS, K. R. JENNINGS, and S. EVANS. Int. J. Mass Spectrom. Ion Phys. **26**, 395 (1978).
13. R. P. MORGAN, C. J. PORTER, and J. H. BEYNON. Org. Mass Spectrom. **12**, 735 (1977).
14. F. W. MCLAFFERTY. *In* High performance mass spectrometry: chemical applications. *Edited by* M. L. Gross. American Chemical Society Symposium Series. 1978.

15. R. A. W. JOHNSTONE, B. J. MILLARD, F. M. DEAN, and A. W. HILL. J. Chem. Soc. C, 1712 (1966).
16. F. M. DEAN, J. GOODCHILD, R. A. W. JOHNSTONE, and B. J. MILLARD, J. Chem. Soc. C, 2232 (1967).
17. J. L. OCCOLOWITZ and G. L. WHITE. Aust. J. Chem. **21**, 997 (1968).
18. J. L. OCCOLOWITZ, B. J. CERIMELE, and P. BROWN. Org. Mass Spectrom. **8**, 61 (1974).
19. M. J. S. DEWAR, A. J. HARGET, N. TRINAJSTIC, and S. D. WORLEY. Tetrahedron, **26**, 4505 (1970).
20. J. H. D. ELAND. Int. J. Mass Spectrom. Ion Phys. **2**, 457 (1969).
21. O. A. MAMER, F. P. LOSSING, E. HEDAYA, and M. E. KENT. Can. J. Chem. **48**, 3606 (1970).
22. S. W. BENSON. Thermochemical kinetics. 2nd ed. Wiley-Interscience, New York. 1976.
23. R. K. BOYD and J. H. BEYNON. Int. J. Mass Spectrom. Ion Phys. **23**, 163 (1977).
24. C. S. BARNES and J. L. OCCOLOWITZ. Aust. J. Chem. **17**, 975 (1964).
25. C. S. BARNES and J. L. OCCOLOWITZ. Aust. J. Chem. **16**, 219 (1963).
26. T. L. JACOBS, R. CRAMER, and F. T. WEISS. J. Am. Chem. Soc. **62**, 1852 (1950).
27. L. F. HATCH and H. O. WEISS. J. Am. Chem. Soc. **77**, 1798 (1955).
28. Y. ODAIRA. Bull. Chem. Soc. Jpn. **29**, 470 (1956).
29. A. VON PECHMAN. Justus Liebigs Ann. Chem. **264**, 305 (1891).

Erratum: Infrared spectra of the ammonium ion in crystals. Part VI. Hydrogen bonding in simple and complex ammonium halides

OSVALD KNOP AND IAN A. OXTON
Department of Chemistry, Dalhousie University, Halifax, N.S., Canada B3H 4J3
AND
MICHAEL FALK
Atlantic Regional Laboratory, National Research Council of Canada, Halifax, N.S., Canada B3H 3Z1

(Ref.: Can. J. Chem. **57**, 404 (1979))
Received May 14, 1979

On p. 412, line 12 of the main paragraph of the left-hand column, should read **1–17** instead of **2–17**.

The correct caption of Fig. 7 (p. 413) should read: The $\nu_2 + \nu_6$ and $\nu_4 + \nu_6$ region of the spectrum of NH_4^+ in $(NH_4)_2SnCl_6$ (**23**) at 298 and 22 K.

On p. 423, lines 5 and 6 of the right-hand column, the chemical formulae should read $(NH_4)_3AlF_6$ and $(NH_4)_3FeF_6$.

In the first paragraph of the right-hand column on p. 413 and in the second paragraph of the left-hand column on p. 417 the discussion of NH_4SnF_3 is based, erroneously, on the assumption that the axial N—H vector points away from the Sn atom of the nearest SnF_3^- ion on the threefold axis and consequently, that the three equivalent nonaxial hydrogen bonds are to the F atoms of that SnF_3^- ion. In fact, even though the H atoms have not been located, the conclusion from the evidence presented in ref. 39 must be that the axial N—H vector points in the *opposite* direction, i.e., to the Sn atom. H–H repulsion cannot therefore be the cause of the high value of $\nu_1(a)$. This matter will be discussed more fully, together with additional ir results for NH_4SnF_3, in Part VIII of this series. The H...X and NHX* entries for **36** in Table 4 are correct.

On p. 419, right-hand column, line 20 from top, read "The displacement" instead of "This displacement".

On p. 422, the subgroup sequence on line 20 of the right-hand column should read $D_{4h}^6 \supset D_{2h}^{12} \supset C_{2h}^5$.

Thermodynamics of transfer of Ph_4C; scaled-particle theory and the Ph_4As^+/Ph_4B^- assumption for single ions

MICHAEL H. ABRAHAM AND ASADOLLAH NASEHZADEH
Chemistry Department, University of Surrey, Guildford, Surrey, England

Received November 1, 1978

MICHAEL H. ABRAHAM and ASADOLLAH NASEHZADEH. Can. J. Chem. 57, 2004 (1979).

Free energies of transfer of Ph_4C from acetonitrile to 20 other solvents have been calculated from literature data. The contribution of the cavity term to the total free energy has been obtained from scaled-particle theory and Sinanoglu – Reisse – Moura Ramos theory. It is shown that there is little connection between the cavity term and the total free energy of transfer, and that there must be, in general, a large interaction term. If the latter is important for transfer of Ph_4C, we argue that it must also be important for transfer of the ions Ph_4As^+ and Ph_4B^-. Previous suggestions that the interaction term is zero for transfer of these two ions are thus seen to be unreasonable. We also show, for six solvents, that the interaction term for Ph_4C is very large in terms of enthalpy and entropy, and that scaled-particle theory seems not to apply to transfers of Ph_4C between pure organic solvents.

The free energy, enthalpy, and entropy of transfer of $Ph_4As^+ = Ph_4B^-$ have been calculated by dividing the total transfer values into neutral and electrostatic contributions; reasonable agreement is obtained between calculated and observed values.

MICHAEL H. ABRAHAM et ASADOLLAH NASEHZADEH. Can. J. Chem. 57, 2004 (1979).

On a calculé, à partir de données de la littérature, les énergies libres de transfert du Ph_4C de l'acétonitrile à 20 autres solvants. On a déduit la contribution du terme de cavité à l'énergie libre totale à partir de la théorie des particules graduées et de la théorie de Sinanoglu – Reisse – Moura Ramos. On a montré qu'il n'existe que peu de corrélation entre le terme de cavité et l'énergie libre totale de transfert et qu'il doit exister d'une façon générale un terme d'interaction important. Si ce dernier est important pour le transfert de Ph_4C, on suggère qu'il doit aussi être important pour le transfert des ions Ph_4As^+ et PhB^-. Des suggestions antérieures à l'effet que le terme d'interaction est égal à zéro pour ces deux ions ne semblent donc pas raisonnables. On montre aussi, pour six solvants, que le terme d'interaction pour le Ph_4C est important en termes d'enthalpie et d'entropie et qu'il ne semble pas que la théorie des particules graduées puisse s'appliquer aux transferts du Ph_4C entre des solvants organiques purs.

On a calculé l'énergie libre, l'enthalpie et l'entropie de transfert de $Ph_4As^+ = Ph_4B^-$ en divisant les valeurs totales de transfert en contributions neutre et électrostatique; on a obtenu une corrélation vraisemblable entre les valeurs calculées et observées.

[Traduit par le journal]

Introduction

The free energy of transfer of a solute from one solvent to another, ΔG_t^0, is often broken down into a cavity term and an interaction term:

$$[1] \qquad \Delta G_t^0 = \Delta G_t^0(\text{cavity}) + \Delta G_t^0(\text{int})$$

The former term represents the contribution due to the work required to make a cavity in the solvents (in the scaled-particle theory, this term includes also a correction term $RT \log (V_1/V_2)$ where V_1 and V_2 are the molar volumes of the two solvents), and the latter term arises from the interaction of the solute with the solvent molecules surrounding the cavity. Treiner (1) has applied eq. [1] to test the Ph_4As^+/Ph_4B^- assumption for single-ion free energies of transfer.[1] In the method used by Treiner, an additional hypothesis was introduced, namely that $\Delta G_t^0(\text{int}) = 0$ for Ph_4As^+ and Ph_4B^-. We later advanced a number of reasons why this hypothesis could not be correct (2), but since there is always an arbitrary element in single-ion quantities we felt it would be more satisfactory to investigate the thermodynamics of transfer of a suitable nonelectrolyte. In connection with the ions Ph_4As^+ and Ph_4B^-, the tetraphenyl derivatives of the Group IV elements are obvious choices as nonelectrolytes. Since Ph_4C has been studied more extensively than the other tetraphenyl compounds, we selected this particular compound, although results for the other tetraphenyls are almost identical. Our method is simply to use literature data in order to obtain ΔG_t^0 values for Ph_4C, to calculate ΔG_t^0(cavity) by both the scaled-particle theory and the Sinanoglu – Reisse – Moura Ramos (SRMR) theory, and thus to determine via eq. [1] whether or not ΔG_t^0(int) can be taken as zero

[1]This assumption is simply that ΔG_t^0 for $Ph_4As^+ = \Delta G_t^0$ for Ph_4B^-.

0008-4042/79/152004-06$01.00/0

TABLE 1. Free energies of transfer from acetonitrile of the solute Ph_4C, and calculated cavity terms, in kcal mol^{-1} at 298 K on the mole fraction scale

Solvent	σ[a]	ΔG_t^0[b]	ΔG_t^0(cavity)	
			Scaled-particle theory[c]	SRMR theory
Water	2.76	6.9	7.4	18.6
Methanol	3.59	0.8	−1.1	−1.5
Ethanol	4.36	0.5	0.8	−2.0
Formamide	3.63	1.2	0.1	12.5
N-Methylformamide		0.5		
Propylene carbonate	5.40	−0.3	7.7	7.0
Dimethylsulphoxide	5.05	−0.2	9.0	5.4
Sulpholane	5.76	−0.9(8)	13.4	1.2
Dimethylacetamide	5.57[d]	−1.4	7.4	1.1
Nitromethane	4.66[d]	0.2(6)	16.7	2.6
Dimethylformamide	4.98	−1.2	2.0	2.0
Acetonitrile	4.12	0	0	0
N-Methylpyrrolidone	5.69	−2.0	8.7	3.0
HMPT	6.86[d]	−1.9	0.3	−0.8
Acetone	4.86[d]	−0.8	1.4	−3.2
1,2-Dichloroethane	5.08[d]	−2.2[e]	3.1	−0.8
1,1-Dichloroethane	5.07[d]	−2.4[e]	0.1	−3.4
Diethyl ether	5.30[d]	−1.1 (3)[f]	−3.3	−6.3
Benzene	5.25[d]	−2.5 (3)[f]	1.3	−2.2
Dioxan	5.44[d]	−2.4 (3)[f]	9.2	−0.2
Carbon tetrachloride	5.17[d]	−2.2 (3)[f]	−2.8	−3.1
Hexane	5.88[d]	−0.6 (3)[g]	−3.1	−6.0

[a]Solvent diameter from ref. 1 unless shown otherwise.
[b]From ref. 9 unless shown otherwise.
[c]This is the combined term (2), ΔG_t^0(cavity) + $RT \log (V_1/V_2)$.
[d]Calculated from solvent heats of vaporisation, see text. We also carried out calculations using σ values derived from log K^H values (see text), viz. nitromethane (4.31), acetone (4.76), benzene (5.26), carbon tetrachloride (5.37), and hexane (5.92). Only in the case of nitromethane are results very different.
[e]Estimated values.
[f]From data at 293 K.
[g]From data (3) for Ph_4Si, Ph_4Ge, Ph_4Sn, and Ph_4Pb.

for Ph_4C. If ΔG_t^0(int) is indeed zero (within a certain experimental error), then Treiner's hypothesis for Ph_4As^+ and Ph_4B^- must be considered reasonable. If, however, ΔG_t^0(int) is definitely not zero for Ph_4C, we can rigorously conclude that Treiner's hypothesis does not hold for Ph_4C, and hence by implication that it does not hold for the ions Ph_4As^+ and Ph_4B^-.

At the same time, we thought it useful to investigate also the corresponding hypotheses in terms of enthalpy and entropy and to consider an alternative method of calculating the thermodynamic parameters for transfer of Ph_4As^+ and Ph_4B^-.

Calculations on Ph_4C

Several workers (3–8) have determined the solubility of Ph_4C in various solvents; from these measurements the standard free energy of transfer of Ph_4C from a given reference solvent may be obtained. Quite recently, Kim (9) has redetermined many of these solubilities and has given a set of mean values of ΔG_t^0 for Ph_4C from the best data. In Table 1 are ΔG_t^0 values, mostly taken from Kim's work and converted to the mole fraction scale with acetonitrile as a reference solvent. We also give in Table 1 ΔG_t^0 values for transfer to a number of solvents not considered by Kim, so that we have a range of solvents from highly polar (water, formamide, DMSO, etc.) to quite nonpolar (carbon tetrachloride, hexane, etc.) molecules.

The ΔG_t^0(cavity) terms were calculated as before (2) using the scaled-particle theory outlined by Pierotti (10) for a solute of diameter 8.04 Å, the value suggested (11) for Ph_4C. In addition to the solute diameter, it is necessary also to estimate the values of the solvent diameters, σ. For consistency, we took, where available, values used by Treiner (1) and by ourselves (2) previously. In the case of the remaining solvents we estimated σ values from solvent heats of vaporisation, as outlined by Pierotti. Although we feel that the alternative method of estimating σ values from log K^H values of rare gases (10) is rather better, lack of data in many solvents prevented us from applying this method to all the remaining solvents;

we thought it more consistent to use just one method and so we chose only the heat of vaporisation method. The estimated solvent σ values (and hence the calculated cavity terms) are not always the same for the two methods of estimation, but our general conclusions are in no way affected by the actual method chosen. Details of the cavity term calculation by scaled-particle theory are in Table 1, together with cavity terms calculated by SRMR theory (12, 13) for a solute of molar volume 282 mL mol^{-1}. In all cases acetonitrile was chosen as the arbitrary reference solvent. It is quite clear that the ΔG_t^0(cavity) term cannot in general be equated with the overall ΔG_t^0 values for Ph_4C; the two terms differ by over 4 kcal mol^{-1} for 10 out of the 20 solvents listed. These inequalities persist, no matter which solvent is chosen as the reference solvent. We conclude that if the cavity terms are calculated by scaled-particle theory, then the interaction term in eq. [1] is generally not zero for Ph_4C in pure solvents, and we can reasonably deduce that it will not be zero for the solutes Ph_4As^+ and Ph_4B^-. As we have shown before (2), the Ph_4As^+/Ph_4B^- assumption does not itself involve any hypothesis about the interaction term other than if the cavity terms for Ph_4As^+ and Ph_4B^- are equal, then the interaction terms will also be equal in magnitude for Ph_4As^+ and Ph_4B^-. Treiner (1), however, argues that where ΔG_t^0(int) is calculated to be not zero for Ph_4As^+ or Ph_4B^-, then the Ph_4As^+/Ph_4B^- assumption is not valid. However, the large values of ΔG_t^0(int) for Ph_4C bear no relation to the Ph_4As^+/Ph_4B^- assumption, and we can argue as follows. If the scaled-particle cavity calculations are realistic, then the ΔG_t^0(int) terms can be large for Ph_4C, Ph_4As^+, and Ph_4B^-, the interaction term for Ph_4As^+ can equal that for Ph_4B^-, and the Ph_4As^+/Ph_4B^- assumption can still be valid. On the other hand, if the scaled-particle calculations are not realistic, nothing can be deduced about the Ph_4As^+/Ph_4B^- assumption, which, therefore, can still be valid. It therefore seems quite clear that the scaled-particle cavity calculations, together with the additional hypothesis that ΔG_t^0(int) is zero, cannot be used to disprove the Ph_4As^+/Ph_4B^- assumption and cannot be used to account for or to predict the total free energy of transfer of Ph_4C between pure solvents.

A few enthalpies of transfer of Ph_4C are available from the work of Cox and Parker (8), and in Table 2 are given the observed ΔH_t^0 values and the calculated ΔH_t^0(cavity) terms; the latter include also the correction terms (1, 2) $\alpha p_2 RT^2 - \alpha p_1 RT^2$. There is almost no connection between the observed transfer enthalpies and the calculated cavity terms, so that clearly the ΔH_t^0(int) term must be very large for transfers of Ph_4C between pure solvents. Again we

TABLE 2. Enthalpies and entropies of transfer from acetonitrile of the solute Ph_4C, and calculated cavity terms, at 298 K on the mole fraction scale

		ΔH_t^0(cavity)/kcal mol^{-1}	
Solvent	ΔH_t^{0a}	Scaled-particle theory[b]	SRMR theory
Methanol	2.3	−4.6	−2.8
Propylene carbonate	−1.3[c]	29.5	2.8
Dimethyl sulphoxide	−0.1	10.7	8.3
Sulpholane	−0.2	10.6	−1.7
Dimethylformamide	−0.8	−5.1	11.2
Acetonitrile	0.0	0.0	0.0

		ΔS_t^0(cavity)/cal K^{-1} mol^{-1}	
Solvent	ΔS_t^0	Scaled-particle theory	SRMR theory
Methanol	5	−12	−4
Propylene carbonate	−3[c]	73	−14
Dimethyl sulphoxide	0	6	10
Sulpholane	2	−10	−10
Dimethylformamide	1	−24	31
Acetonitrile	0	0	0

[a]All values from ref. 8.
[b]This is the term (ΔH_t^0(cavity) + $\alpha p_2 RT^2 - \alpha p_1 RT^2$), see ref. 2.
[c]These are from the original values of Cox and Parker (8) for solution of Ph_4C in propylene carbonate, $\Delta G_s^0 = 4.2$ and $\Delta H_s^0 = 7.2$ kcal mol^{-1}. Krishnan and Friedman (19) have analysed Cox and Parker's data to obtain $\Delta G_s^0 = 4.5$ and $\Delta H_s^0 = 9.8$ in propylene carbonate, but our own least-squares analysis yields values of $\Delta G_s^0 = 4.2$ and $\Delta H_s^0 = 7.8$ that are quite close to the original values.

can deduce that the interaction term must also be large for Ph_4As^+ and Ph_4B^-, when the cavity term is calculated by scaled-particle theory. It should be pointed out that the calculations and results given in Tables 1 and 2 do not by themselves indicate any failure of scaled-particle theory itself; they merely show that for Ph_4C the interaction terms ΔG_t^0(int) and ΔH_t^0(int) are in general quite large, and cannot be disregarded.

The situation is quite different in terms of entropies of transfer, because on the scaled-particle theory as used by Pierotti (10) the term ΔS_t^0(int) is indeed taken as zero. Thus if Pierotti's version of the scaled-particle theory applies to Ph_4C, the calculated cavity terms, ΔS_t^0(cavity), must equal the observed ΔS_t^0 values, at least within a reasonable error. Details of the observed (8) and calculated entropy values are in Table 2; the discrepances are so large that we are forced to conclude that the scaled-particle theory cannot be applied usefully to solutes such as Ph_4C in pure organic solvents.

We also give in Tables 1 and 2 the various cavity terms for Ph_4C calculated by the Sinanoglu – Reisse – Moura Ramos (SRMR) theory (12, 13) assuming

a solute molar volume of 282 mL mol^{-1}. For transfers between many of the solvents there are rather large discrepancies between the calculations based on SRMR theory and scaled-particle theory. For a solute such as Ph_4C there is no possibility of deciding in favour of one or other method of calculation because there is no way of independently obtaining estimates of the interaction terms. The present calculations, however, indicate that considerable caution is advisable in making deductions based on the calculation of cavity terms for large solutes in pure solvents.

Application to Ph_4As^+ and Ph_4B^-

There have been suggested a number of assumptions that may be used to obtain free energies, enthalpies, and entropies of transfer of single ions. Several workers have compared assumptions and have concluded that the Ph_4As^+/Ph_4B^- assumption, eq. [2] with P = G, yields realistic single ion free energies of transfer (6, 8, 14–17),

$$[2] \qquad \Delta P_t^0 \text{ for } Ph_4As^+ = \Delta P_t^0 \text{ for } Ph_4B^-$$

although other assumptions have sometimes been preferred (18). Indeed, it has been pointed out that there is spectroscopic and other evidence to show that in several solvents there are differences in the solvation properties of Ph_4As^+ and Ph_4B^- (19). It does seem, however, that whatever causes these solvation differences, they are not manifested in the free energy of transfer of Ph_4As^+ and Ph_4B^-. The situation is not the same for enthalpies (and hence entropies) of transfer; Krishnan and Friedman (20) have suggested on the basis of experimental data on enthalpies of transfer from methanol to propylene carbonate that solvation of Ph_4B^- is very different from that of Ph_4As^+ in methanol. In this connection, it is perhaps significant that single ion entropies of transfer obtained by the correspondence plot method (21) are usually in quite good agreement with those obtained from the Ph_4As^+/Ph_4B^- assumption, eq. [2] with P = S, for transfers involving water and aprotic solvents, yet differ in the case of transfers to or from methanol (22) and ethanol (23). Inasmuch as the differences can be ascribed to any one ion, the effects do seem to be due to the Ph_4B^- ion. Even in the transfers to or from methanol and ethanol, however, the differences between the cation and anion assignments on the two methods are only about 7 cal K^{-1} mol^{-1}, i.e. equivalent to 2 kcal mol^{-1} in free energy.

In the previous section, we have shown that for transfers of Ph_4C, and presumably of Ph_4As^+ and Ph_4B^-, the interaction term is usually quite large. Since at the present time it is not feasible to calculate the term ΔG_t^0(int) in eq. [1] for species such as Ph_4As^+ and Ph_4B^-, it follows that the total free energy of transfer, ΔG_t^0, cannot be obtained by scaled-particle theory or SRMR theory. A calculation of the thermodynamics of transfer of Ph_4As^+ and Ph_4B^- would certainly be of relevance to the Ph_4As^+/Ph_4B^- assumption, and so we have attempted such calculations using another approach.

Several workers (7, 9, 24–26) have suggested that parameters for the transfer of a charged solute can be represented by eq. [3], in which P = G, H, or S, and

$$[3] \qquad \Delta P_t^0 = \Delta P_c^0 + \Delta P_n^0$$

where ΔP_c^0 and ΔP_n^0 indicate the electrostatic and neutral contributions to the total; the neutral contribution is normally taken as the observed transfer value for a suitable nonpolar solute of the same shape and size as the charged ion. Berne and Popovych (7) first used eq. [3] to calculate ΔG_t^0 values for the ions Ph_4As^+ and Ph_4B^-. They took ΔG_n^0 as the average transfer value for Ph_4C, Ph_4Si, and Ph_4Sn and calculated ΔG_c^0 by the simple Born equation. For transfer from acetonitrile to the pure solvents methanol and ethanol, the calculated values of ΔG_t^0 for Ph_4As^+ or Ph_4B^- were too small by 1.4 and 1.8 kcal mol^{-1}, respectively. Kim (9) later used a much more elaborate procedure in which Ph_4Ge and Ph_4C were used as the neutral solutes to obtain ΔG_n^0 for Ph_4As^+ and Ph_4B^-, and in which allowance was made for ion–dipole interactions as well as for the Born charging energy. For the three pure solvents studied by Berne and Popovych, however, the results of Kim (9) were no better than those of the earlier workers, calculated ΔG_t^0 values now being too large by 1.9 and 1.5 kcal mol^{-1} for the above transfers. We therefore felt that a detailed calculation was not justified and took the solute Ph_4C as the neutral counterpart of Ph_4As^+ or Ph_4B^- and then calculated the electrostatic term by the improved theory of Abraham and Liszi (27). In Table 3 are given the calculated free energies, together with the observed values for Ph_4As^+ and Ph_4B^- (9, 22, 23, 28–30). Most of the observed values are those suggested by Kim (9); in some cases they differ slightly from those used by us before (2). Our present simple method of calculation yields results that are comparable to those obtained by Kim; for the 12 common solvents agreement with experiment averages 1.1 kcal mol^{-1} on both methods of calculation.[2]

[2]The largest disagreement between our calculated values and the observed values arises for the transfer to water. The value of ΔG_n^0 we used for this transfer is derived from the solubility of Ph_4C in water reported by Cox and Parker (5). Recent work of Kim (9) on Ph_4Ge agrees well with Cox and Parker's values, the derived ΔG_t^0 values for transfer from methanol to water

TABLE 3. Calculation of free energies of transfer from acetonitrile of Ph_4As^+ and Ph_4B^-, in kcal mol^{-1} at 298 K on the mole fraction scale

Solvent	ΔG_e^{0a}	ΔG_n^{0b}	ΔG_t^0 Calcd	ΔG_t^0 Obsd[c]	Calcd − obsd value: This work	Calcd − obsd value: Kim (9)[d]
Water	−1.9	6.9	5.0	8.3	−3.3	0.8
Methanol	−0.3	0.8	0.5	2.2	−1.7	1.9
Ethanol	0.5	0.5	1.0	2.7	−1.7	1.5
1-Propanol	1.0	0.3[e]	1.3	1.5(2)	−0.2	—
Formamide	−0.9	1.2	0.3	2.3	−2.0	−1.5
N-Methylformamide	0.0	0.5	0.5	0.0	0.5	1.2
Propylene carbonate	0.4	−0.3	0.1	−0.8	0.9	0.0
Dimethylsulphoxide	0.3	−0.2	0.1	−1.1	1.2	1.6
Sulpholane	0.4	−0.9	−0.5	−1.5(2)	1.0	—
Dimethylacetamide	0.8	−1.4	−0.6	−1.4	0.8	1.5
Dimethylformamide	0.5	−1.2	−0.7	−1.4	0.7	1.2
Acetonitrile	0	0	0	0	0	0
N-Methylpyrrolidone	0.9	−2.0	−1.1	−1.8	0.7	—
HMPT	1.9	−1.9	0.0	−1.7	−1.7	0.8
Acetone	1.0	−0.8	0.2	0.0	0.2	1.3
1,2-Dichloroethane	2.3	−2.2	0.1	−0.3(2)	0.4	—
1,1-Dichloroethane	2.5	−2.4	0.1	1.0(2)	−0.9	—

[a]Calculated by the method of Abraham and Liszi (27).
[b]From the values for Ph_4C, Table 1.
[c]From ref. 9 unless shown otherwise, assuming that ΔG_t^0 for Ph_4As^+ equals ΔG_t^0 for Ph_4B^-.
[d]These are the differences for ($Ph_4As^+ + Ph_4B^-$), found by Kim (9), divided by two.
[e]Estimated value.

Our objective, however, is not to compare our results with those of Kim, but firstly to show that both of these calculations via eq. [3] lead to very much better agreement with experimental ΔG_t^0 values than does the alternative method of calculation using only the cavity term in the scaled-particle theory (compare the results in Table 3 with those in Table 1), and secondly to calculate the corresponding enthalpy and entropy terms using eq. [3]. There are only six solvents for which the necessary ΔH_t^0 and ΔS_t^0 values are known for the neutral solute Ph_4C, Table 2, and so we have mainly restricted our calculations to these solvents. The electrostatic terms were again calculated by the method of Abraham and Liszi (27), and the results for the six solvents are given in Table 4. There is good agreement with experiment, both in the case of the enthalpy data (where there is an average deviation of 0.8 kcal mol^{-1} between calculated and observed values) and the entropy data (where the deviation is 3 cal K^{-1} mol^{-1} for the same six solvents). Since ΔS_t^0 for Ph_4C is numerically very small for transfers from acetonitrile to other aprotic solvents, we have taken this value as zero for transfers to the solvents acetone, 1,2-dichloroethane, and 1,1-dichloroethane and have thus been able to calculate also ΔS_t^0 for Ph_4As^+ or Ph_4B^- for transfer to the three additional solvents. Agreement with the observed values is again very good (Table 4).

Thus very simple calculations using eq. [3] yield free energies, enthalpies, and entropies of transfer of Ph_4As^+ or Ph_4B^- from acetonitrile to other pure organic solvents that are in substantial agreement with the experimental values obtained via the Ph_4As^+/Ph_4B^- assumption, eq. [2]. However, we wish to point out that although our calculations and those of Kim (9) indicate that the Ph_4As^+/Ph_4B^- assumption is reasonable, the calculations do not and cannot prove the assumption to be correct. For example, the calculated and observed value for ΔS_t^0 of $Ph_4As^+ = Ph_4B^-$ is 2 cal K^{-1} mol^{-1} for transfer from acetonitrile to dimethylsulphoxide, yet it is logically possible for the 'correct' division to be, say, +6 for Ph_4As^+ and −2 for Ph_4B^- and for our calculations to be wrong. A more cogent example is the entropy of transfer from acetonitrile to methanol, where there is disagreement over the cation and anion division using the Ph_4As^+/Ph_4B^- assumption or the correspondence plot method (22, 29). On the Ph_4As^+/Ph_4B^- assumption, the observed entropies of transfer are −2 for Ph_4As^+ and −2 for Ph_4B^-; the calculated values are +4 in each case, but we could argue that the Ph_4As^+/Ph_4B^- division is correct and that our calculations are in error by 6 cal K^{-1} mol^{-1}

being (in kcal mol^{-1} on the mole fraction scale) 6.1 for Ph_4C and 6.3 for Ph_4Ge. However, both these values seem very small when compared to ΔG_t^0 values for other aromatic compounds, viz. 3.4 for benzene and 5.7 for biphenyl, and we would expect the ΔG_t^0 values for the Ph_4M compounds to be not less than 10 kcal mol^{-1} for the methanol to water transfer, rather than the observed values of 6.1–6.3 kcal mol^{-1}.

TABLE 4. Calculation of enthalpies and entropies of transfer from acetonitrile of Ph_4As^+ or Ph_4B^-, at 298 K on the mole fraction scale[a]

Solvent	ΔH_e^{0b}	ΔH_n^{0c}	ΔH_t^0(calcd)	ΔH_t^0(obsd)[d]
Methanol	−0.7	2.3	1.6	1.9
Propylene carbonate	0.7	−1.3	−0.6	−1.2
Dimethylsulphoxide	0.7	−0.1	0.6	−0.5
Sulpholane	0.7	−0.2	0.5	−0.2
Dimethylformamide	0.4	−0.8	−0.4	−2.4
Acetonitrile	0.0	0.0	0.0	0.0
Solvent	ΔS_e^{0b}	ΔS_n^{0c}	ΔS_t^0(calcd)	ΔS_t^0(obsd)[d]
Methanol	−1	5	4	−2
Propylene carbonate	1	−3	−2	−1
Dimethylsulphoxide	2	0	2	2
Sulpholane	1	2	−1	4
Dimethylformamide	0	1	1	−3
Acetonitrile	0	0	0	0
Acetone	−3	0[e]	−3	−4
1,2-Dichloroethane	−10	0[e]	−10	−9
1,1-Dichloroethane	−9	0[e]	−9	−10

[a]Enthalpies in kcal mol^{-1}, entropies in cal K^{-1} mol^{-1}.
[b]Calculated by the method of Abraham and Liszi (27).
[c]Values for Ph_4C, Table 2.
[d]Values for $Ph_4As^+ = Ph_4B^-$ from refs. 22, 23, 28–30.
[e]Estimated values, see text.

in each ion. Using the correspondence plot method, the observed values are +5 for Ph_4As^+ and −9 for Ph_4B^-; we could now argue that the correspondence method is correct, our calculation for Ph_4As^+ is correct, but that some additional interaction between Ph_4B^- and methanol has led to a discrepancy of 13 cal K^{-1} mol^{-1} between the observed and calculated value. Unfortunately, the present method of analysis is not refined enough to decide in favour of either the Ph_4As^+/Ph_4B^- assumption or the correspondence plot method for entropies of transfer to or from methanol.

1. C. TREINER. Can. J. Chem. **55**, 682 (1977).
2. M. H. ABRAHAM and A. NASEHZADAH. Can. J. Chem. **57**, 71 (1979).
3. W. STROHMEIER and K. MILTENBERGER. Chem. Ber. **91**, 1357 (1958).
4. A. J. PARKER and R. ALEXANDER. J. Am. Chem. Soc. **90**, 3313 (1968).
5. B. G. COX and A. J. PARKER. J. Am. Chem. Soc. **94**, 3674 (1972).
6. R. ALEXANDER, A. J. PARKER, J. H. SHARP, and W. E. WAGHORNE. J. Am. Chem. Soc. **94**, 1148 (1972).
7. D. H. BERNE and O. POPOVYCH. Anal. Chem. **44**, 817 (1972).
8. B. G. COX and A. J. PARKER. J. Am. Chem. Soc. **95**, 402 (1973).
9. J. I. KIM. J. Phys. Chem. **82**, 191 (1978).
10. R. A. PIEROTTI. Chem. Rev. **76**, 717 (1976).
11. E. GRUNWALD, G. BAUGHMAN, and G. KOHNSTAM. J. Am. Chem. Soc. **82**, 5801 (1960).
12. T. HALICIOGLU and O. SINANOGLU. Ann. N. Y. Acad. Sci. **158**, 308 (1969).
13. J. J. MOURA RAMOS, M. LEMMERS, R. OTTINGER, M.-L. STEIN, and J. REISSE. J. Chem. Res. (S) 56 (1977); (M) 0658–0667 (1977).
14. I. M. KOLTHOFF and M. K. CHANTOONI. J. Am. Chem. Soc. **76**, 2024 (1972).
15. J. W. DIGGLE and A. J. PARKER. Electrochim. Acta, **18**, 975 (1973).
16. D. A. OWENSBY, A. J. PARKER, and J. W. DIGGLE. J. Am. Chem. Soc. **96**, 2682 (1974).
17. G. GRITZNER. Inorg. Chim. Acta, **24**, 5 (1977).
18. O. POPOVYCH. Crit. Rev. Anal. Chem. **1**, 73 (1970).
19. C. V. KRISHNAN and H. L. FRIEDMAN. *In* Solute–solvent interactions Vol. 2. *Edited by* J. F. Coetzee and C. D. Ritchie. Marcel Dekker, New York. 1976.
20. C. V. KRISHNAN and H. L. FRIEDMAN. J. Phys. Chem. **75**, 388 (1971); **75**, 3606 (1971).
21. C. M. CRISS, R. P. HELD, and E. LUKSHA. J. Phys. Chem. **72**, 2970 (1968).
22. M. H. ABRAHAM. J. Chem. Soc. Faraday Trans. I, **69**, 1375 (1973).
23. M. H. ABRAHAM and A. F. DANIL DE NAMOR. J. Chem. Soc. Faraday Trans. I, **74**, 2101 (1978).
24. N. BJERRUM and E. JÓZEFOWICZ. Z. Phys. Chem. **159A**, 194 (1932).
25. M. ALFENAAR and C. L. DE LIGNY. Recl. Trav. Chim. **86**, 929 (1967).
26. M. H. ABRAHAM and G. F. JOHNSTON. J. Chem. Soc. A, 1610 (1971).
27. M. H. ABRAHAM and J. LISZI. J. Chem. Soc. Faraday Trans. I, **74**, 1604 (1978); **74**, 2858 (1978).
28. B. G. COX, G. R. HEDWIG, A. J. PARKER, and D. W. WATTS. Aust. J. Chem. **27**, 477 (1974).
29. M. H. ABRAHAM and A. F. DANIL DE NAMOR. J. Chem. Soc. Faraday Trans. I, **72**, 955 (1976).
30. M. H. ABRAHAM, A. F. DANIL DE NAMOR, and R. A. SCHULZ. J. Solution Chem. **5**, 529 (1976).

Relation entre pression interne et température de fusion. L'entropie volumique de fusion

GIANFRANCESCO BERCHIESI, MARIA A. BERCHIESI, GIOVANNI VITALI ET VENANZIO VALENTI

Istituto Chimico dell'Università, 62032 Camerino, Italie

Reçu le 7 novembre 1978

GIANFRANCESCO BERCHIESI, MARIA A. BERCHIESI, GIOVANNI VITALI ET VENANZIO VALENTI. Can. J. Chem. **57**, 2010 (1979).

La relation pression interne – température est discutée pour des nombreuses substances organiques et pour des sels à la température de fusion.

GIANFRANCESCO BERCHIESI, MARIA A. BERCHIESI, GIOVANNI VITALI, and VENANZIO VALENTI. Can. J. Chem. **57**, 2010 (1979).

The relation between the internal pressure and the temperature at the melting point is discussed for several organic substances and for some salts.

Introduction

Malgré les nombreux efforts, soit théoriques soit expérimentaux, dédiés jusque à maintenant à l'étude de l'énergétique de la fusion et de l'état liquide (1, 2), un remarquable interêt est adressé encore à cette problématique à cause des points obscurs. Dans cette note nous rapportons des mesures expérimentales de pression interne dans des liquides organiques et nous comparons les résultats obtenus avec ceux obtenus précédemment.

Méthodes expérimentales

La pression interne P_i d'un liquide est obtenue à l'aide des données ultrasoniques, densimétriques et calorimétriques selon les formules suivantes:

$$[1] \quad \beta_s = (u^2\rho)^{-1}$$

$$[2] \quad \beta_T = \beta_s + \alpha^2 TV/c_p$$

$$[3] \quad P_i = \alpha T/\beta_T$$

où β_s, β_T, α, T, V représentent respectivement la compressibilité adiabatique, la compressibilité isotherme, le coefficient d'expansion thermique, la température et le volume. La densité, ρ, a été obtenue par pycnométrie comme précédemment décrit (5); la thermostatation à des températures plus basses que celle ambiante a été possible au moyen d'un ultracryostat Lauda, employé comme réfrigérant d'un bain de 100 L agitée et thermorégulé; une thermostatation de ± 0.01°C était obtenue. La chaleur spécifique à pression constante c_p a été deduite de la bibliographie (6, 7). La vitesse ultrasonore, u, a été mésurée à l'aide d'un interféromètre ultrasonore IPPT (Warszawa) précédemment décrit (3, 4), en employant comme indicateur de l'impulsion le même oscilloscope de l'appareillage au lieu d'un oscilloscope externe. La precision des mésures est 1 m/s pour la vitesse et 2 bars pour la pression interne. Ce niveau de précision est suffisant pour obtenir P_i/T_f (T_f represente la température de fusion) à une précision de 0.005 cal/K mL. 1,2-Dibrométhane et 1,4-diméthylbenzène sont produits Fluka (purété > 99%).

TABLEAU 1. Valeurs des paramètres des équations expérimentales [4]–[8] et déviationsstandard pour les éqs [4], [5], [7]

Paramètre	Valeur	
	C_8H_{10}	$C_2H_4Br_2$
a (g/mL)	0.8665	2.1985
b (g/mL K)	8.45×10^{-4}	20.24×10^{-4}
c (m/s)	1364	1033
d (m/s K)	4.20	2.39
e (bar^{-1})	81.3×10^{-6}	57.8×10^{-6}
f (bar K)$^{-1}$	5.99×10^{-7}	3.49×10^{-7}
g (bar)	3420	4510
h (bar/K)	7.68	6.10
i (cal/K mol)	30.8	23.9
l (cal/K^2 mol)	0.0983	0.0041
T_{max}	313.0	300.0

Déviations standard concernant les équations de u, ρ, P_i

	u	ρ	P_i
$C_2H_4Br_2$	0.3	0.00023	4.9
C_8H_{10}	1.2	0.00020	6.0

Résultats et discussion

Intéressés à la valeur de la pression interne à la température de fusion nous avons exécuté des mésures à différentes températures à partir de 1 ou 2 degrés au dessus de T_f jusqu'à une température T_{max}, indiqué dans le tableau. En général l'intervalle de température exploré est de 15 ou 20°C. Les résultats obtenus ont été exprimés sous forme d'équations derivées par la méthode des moindres carrés:

$$[4] \quad \rho = a - b(T - T_f)$$

$$[5] \quad u = c - d(T - T_f)$$

0008-4042/79/152010-03$01.00/0

TABLEAU 2. Valeurs P_{iL}, P_{iL}/T_f, c_p/c_v au point de fusion, V_{dis}, V_{dis}/n_t pour les substances étudiées dans cette note et d'autres composés étudiés précédemment

Composé	P_{iL} (bar)	T_f (K)	P_{iL}/T_f (cal/K mL)	$(c_p/c_v)_{T_f}$	V_{dis} (mL/mol)	V_{dis}/n_t (mL/mol)	Réf.
Tétradécane	2890	279.1	0.24	1.17	158	3.6	10
Acide stéarique	3379	339.3	0.24	1.17	161	2.9	3
Acide palmitique	3401	334.6	0.24	1.16	137	2.7	3
Acide laurique	3244	316.0	0.24	1.16	102	2.7	3
1,4-Dimethylbenzène	3420	286.5	0.28	1.31	51	2.8	Ce trav.
Cyclohexane	3390	279.8	0.28	1.40	8	0.4	10
CCl_4	3190	250.2	0.30	1.31	8	1.6	10
Acide oléique	3656	289.5	0.30	1.19	154	2.7	4
Benzène	3952	278.7	0.33	1.45	26	2.2	4
Benzothiophène	4530	305.2	0.35	1.27	27	1.8	10
1,2-Dibrométhane	4510	283.0	0.38	1.36	25	3.1	Ce trav.
Etanediole	4250	262.0	0.38	1.10	28	2.8	10
1,4-Dioxane	4590	285.0	0.38	1.39	27	1.9	10
Nitrobenzène	4780	278.9	0.40	1.28	24	1.7	10
LiCl			0.39			14	11
NaCl			0.28			22	11
KCl			0.23			26	11
CsCl			0.22			24	11
LiBr			0.31			17	11
NaBr			0.22			28	11
KBr			0.21			29	11
CsBr			0.18			34	12
NaI			0.22			27	11
KI			0.18			33	11
$NaNO_3$			0.45			14	11

et les déviations standard ont été données dans le tableau 1, avec les paramètres empiriques de ces équations. La compressibilité β_T, la pression interne P_i, déduites à l'aide des éqs [1]–[3] et la chaleur spécifique à volume constant $c_v = c_p\beta_s/\beta_T$, ont été exprimées de la façon suivante:

$$[6] \quad \beta_T = e + f(T - T_f)$$

$$[7] \quad P_i = g - h(T - T_f)$$

$$[8] \quad c_v = i + l(T - T_f)$$

La valeur g de pression interne du liquide extrapolée à la température de fusion ($P_{i,L}$) est employée pour le calcul de P_{iL}/T_f, qui est donné en tableau 2 avec les valeurs concernant les autres substances étudiées précédemment. Il a été déjà montré (4) que le paramètre P_{iL}/T_f n'est pas un paramètre empirique, au contraire il a une signification thermodynamique précise parce qu'il représente dS/dV (où S représente l'entropie) calculé à l'extrémité de l'intervalle de fusion où le crystal est pratiquement transformé en liquide (côté liquide) selon la formule suivante:

$$[9] \quad dS/dV = P_i/T_f$$

dS/dV dans le côté crystal du processus de fusion est plus grande que dans le côté liquide parce que $P_{ic} > P_{iL}$ à T_f, comme montré (4), même si en général l'équation $P_{ic} \sim P_{iL}$ (1, 8) est acceptée comme simple approximation (P_{ic} représente la pression interne du crystal au point de fusion).

A ce moment, nous nous intéressons au paramètre P_{iL}/T_f, à cause de la difficulté d'avoir des valeurs de pression interne des solides. Ils sont donnés au tableau 2 et montrent que malgré le caractère hétérogène des composés, soit ioniques soit moléculaires à structure paraffinique ou aromatique, avec ou sans des hétéroatomes la valeur de l'entropie volumique de fusion est comprise entre 0.21 et 0.45 cal/K mL. L'équation [9] peut être écrite de la façon suivante:

$$[10] \quad \Delta S = \int_c^L dS = \int_c^L P_i/T_f \, dV$$

$$\simeq P_{iL}/T_f \int_c^L dV = (P_{iL}/T_f)V_{dis}$$

où V_{dis} n'est pas nécessairement égale au volume de fusion à cause de l'approximation de l'intégration et comme discuté précédemment (3). Les valeurs V_{dis} sont rapportées aussi au tableau 2. L'entropie de fusion peut être séparée en deux paramètres: P_{iL}/T_f, intensif et indépendant de l'extension des molécules: V_{dis} extensif et dépendant de la dimension des molécules.

Le terme P_{iL}/T_f présente une variation regulière, dans le cas des produits ioniques, avec les rayons ioniques et sauf le cas de $NaNO_3$ (pour lequel la présence d'un ion planaire produit probablement un mecanisme de fusion différent) une équation $P_{iL}/T_f = 0.42_5 - 0.080r^+r^-$ ($\sigma = 0.03$) est suffisante à rendre compte de cette variation (r^+, r^- rayons cathioniques et anioniques respectivement). Dans le cas des produits organiques la relation entre P_{iL}/T_f et la nature chimique du composé est moins évidente: ce que l'on peut remarquer est la suivante échelle de variation de P_{iL}/T_f:

Alcane, acides aliphatiques < composés aromatiques ou cycliques apolaires < composés polaires.

La présence de groupes polaires élève la valeur de P_{iL}/T_f, sauf le cas des acides aliphatiques; il faut chercher probablement la raison de cette exception dans la structure dimèrique de ces acides (9) qui "ferme" la polarité dans le dimère et qui, par conséquence, rend l'intéraction dimère–dimère semblable à celle molécule–molécule dans les alcanes. Etant donné que pour le rapport c_p/c_v, calculé au point de fusion, une échelle pareille à celle relative à P_{iL}/T_f peut être écrite (excéption: acide oléique, ethanediole) il est raisonable penser que P_{iL}/T_f (comme c_p/c_v) soit aussi affecté par l'activation de dégrés internes d'énergie. Sur cette base, probablement, il faudrait chercher l'explication de la différence de P_{iL}/T_f entre composés linéaires (alcanes et acides aliphatiques) et composés cycliques ou aromatiques.

V_{dis} (tableau 2) est dépendant de la dimension moléculaire, tandis que V_{dis}/n_t (où n_t représente le nombre total d'atomes dans la molécule) semble dépendre plutôt de la rigidité des liaisons chimiques. Dans le cas des alogénures de métaux alcalins une grossière dépendance V_{dis} contre r^+ peut être remarquée.

En outre, il est intéressant de remarquer que pour les substances examinées et dans l'intervalle de T examiné, les grandeurs P_i, V, T sont reliées par la simple équation:

$$[11] \quad P_iV = RT + A/V$$

les valeurs du paramètre A sont: 31.0 et 48.1 L^2 atm mol^{-2} pour 1,2-dibrométhane et 1,4-diméthylbenzène respectivement.

Remerciements

Nous savons gré au CNR (Rome) pour l'aide financière et à M. le Docteur Z. Kozłowski, chef du département d'acoustique physique de IPPT (Académie Polonaise des Sciences, Varsovie) pour nous avoir mis à disposition des transducteurs prévus pour les basses températures.

1. A. BONDI. Chem. Rev. **67**, 565 (1967).
2. A. R. UBBELOHDE. Melting and crystal structure. Clarendon Press, Oxford. 1965.
3. G. BERCHIESI, G. VITALI et M. A. BERCHIESI. J. Thermal Anal. **13**, 105 (1978).
4. G. BERCHIESI, G. VITALI, M. A. BERCHIESI et V. VALENTI. Gazz. Chim. **108**, 483 (1978).
5. M. A. BERCHIESI, G. BERCHIESI et G. GIOIA LOBBIA. J. Chem. Eng. Data, **19**, 326 (1974).
6. J. W. WILLIAMS et F. DANIELS. J. Am. Chem. Soc. **46**, 903 (1924).
7. K. S. PITZER. J. Am. Chem. Soc. **62**, 331 (1940).
8. R. A. ORIANI. J. Chem. Phys. **19**, 93 (1951).
9. M. R. BARR, B. A. DUNNEL et R. F. GRANT. Can. J. Chem. **41**, 1188 (1963); G. BERCHIESI, A. CINGOLANI et D. LEONESI. J. Thermal Anal. **6**, 91 (1974); G. BERCHIESI, D. LEONESI et A. CINGOLANI. J. Thermal Anal. **7**, 659 (1975).
10. G. VITALI, G. BERCHIESI, M. A. BERCHIESI et V. VALENTI. Gazz. Chim. En presse.
11. J. O'M. BOCKRIS et N. E. RICHARDS. Proc. R. Soc. A, **241**, 44 (1957).
12. G. J. JANZ. Molten salts handbook. Academic Press, London. 1967. pp. 249, 255.

Primary mechanisms in the radiolysis of amines: pulse and γ-radiolysis of neutral and acidic ethylamine, *n*-propylamine and ethylenediamine

J. A. DELAIRE AND J. R. BAZOUIN

Laboratoire de Physico-Chimie des Rayonnements (Associé au CNRS), Université de Paris-Sud, Centre d'Orsay, 91405 Orsay, France

Received December 19, 1978

J. A. DELAIRE and J. R. BAZOUIN. Can. J. Chem. **57**, 2013 (1979).

The transient spectra in pure ethylamine (EA), *n*-propylamine (*n*PA), and ethylenediamine (EDA) show, besides the visible and infrared band associated with the solvated electron, e^-_s, a small ultraviolet band attributed to oxidizing radicals. Upper limits for the recombination rate constants k of e^-_s with the acidic cation are 1.5×10^{12} and 3.5×10^{12} L mol^{-1} s^{-1} in EA and *n*PA respectively, and $k = 2 \times 10^{10}$ L mol^{-1} s^{-1} in EDA. The yield of e^-_s at 3 ns ($G(e^-_s)_{3ns}$ = 1.5, 1.2, and 3.1 molecules/100 eV in EA, *n*PA, and EDA respectively) has been deduced by biphenyl scavenging. The yield of molecular hydrogen after γ-radiolysis $G_0(H_2)$ = 5.7 and 3.6 in pure *n*PA and EDA respectively. The effect of solutes, such as biphenyl, alkylammonium chloride, and allyl alcohol, on $G(H_2)$ is interpreted in terms of scavenging of e^-_s and/or H atoms. From the pulse-radiolysis determination of $G(e^-_s)$, we deduce $G_H \simeq 0$ and $G_{H_2} \simeq 2.0$ in *n*PA.

Finally, the decay of solvated electrons seems to occur only via recombination with the cation in EA and *n*PA, but in EDA there is a competition between this reaction and reaction with oxidizing radicals.

J. A. DELAIRE et J. R. BAZOUIN. Can. J. Chem. **57**, 2013 (1979).

Les spectres d'absorption transitoire dans l'ethylamine (EA), la *n*-propylamine (*n*PA) et l'éthylènediamine (EDA) pures montrent, en plus de la bande visible et infra-rouge associée à l'électron solvaté, e^-_s, une petite bande ultra-violette attribuée aux radicaux oxydants. Les constantes de vitesse de recombinaison k de l'électron solvaté avec le cation acide sont inférieures à 1.5×10^{12} et 3.5×10^{12} L mol^{-1} s^{-1} respectivement dans EA et *n*PA, et $k = 2.0 \times 10^{10}$ L mol^{-1} s^{-1} dans EDA. Les rendements de e^-_s à 3 ns ($G(e^-_s)_{3ns}$ = 1.5, 1.2 et 3.1 molecules/100 eV respectivement dans EA, *n*PA et EDA) ont été déterminés par capture par le biphényle. Le rendement d'hydrogène moléculaire après radiolyse γ $G_0(H_2)$ = 5.7 et 3.6 respectivement dans *n*PA et EDA pures. L'effet des solutés tels que le biphényle, le chlorure d'alkylammonium et l'alcool allylique sur le rendement en hydrogène est interprété en terme de capture de e^-_s et/ou des atomes H. Compte-tenu de la valeur déterminée pour $G(e^-_s)$ en radiolyse pulsée, nous déduisons $G_H \simeq 0$ et $G_{H_2} \simeq 2$ dans *n*PA. Enfin, la recombinaison des électrons solvatés semble se faire uniquement par réaction avec le cation dans EA et *n*PA, mais dans EDA, il y a compétition entre cette réaction et la capture par des radicaux oxydants.

Introduction

Amines belong to that class of solvents which have the property of dissolving alkali metals to give metastable solutions. The nature of the so-called blue solutions has been extensively studied (1). Solvated electrons (e^-_s), alkali metal cation – electron pairs (M^+,e^-_s), and anions (M^-) are present in these solutions. Pulse radiolysis has been used in the past to study absorption spectra and reactions of these species, mostly in amines (2). Yields of the solvated electron $G(e^-_s)$ have been determined in methylamine (MA) (3), ethylamine (EA) (3), and isopropylamine (*i*PA) (3) at different temperatures, but the precise mechanism of its disappearance is unknown. Attempts to determine primary yields other than that of e^-_s — essentially yields of atomic and molecular hydrogen — have been made by γ-radiolysis in MA (4) and EA (5). Furthermore, studies in ammonia (6, 7) and hydrazine (7, 8) have shown that there exists a large similarity in the primary mechanisms of the radiolysis of both solvents: the main recombining reaction of the solvated electron seems to occur with radicals and not with the counter cation. At the same time, $G(e^-_s)$ is found to be high (~3) in both solvents (7). Therefore, it seems interesting to check whether the correlation between the high G-value and the low recombination rate constant established in NH_3 (static dielectric constant ε_s = 17) and N_2H_4 (ε_s = 54) is valid for weakly polar amines as EA (ε_s = 7 (9)), *n*-propylamine (*n*PA) (ε_s = 5.5 (10)) and ethylenediamine (EDA) (ε_s = 14 (9)).

In addition to the fate of e^-_s, this paper deals with the behavior of radicals formed in the radiolysis of amines. Pulse radiolysis has been used to determine $G(e^-_s)$ and the reactivity of e^-_s with the counter

0008-4042/79/152013-09$01.00/0

cation and/or with radicals. Determination of molecular hydrogen yields after γ-radiolysis of amines with different scavengers gives information on a possible mechanism.

Experimental

The experimental set-up has been described earlier (11, 12). A 600 keV Febetron 706 accelerator with a pulse width of 3 ns was used as the electron source. Dosimetry was established from the end-of-pulse absorption of the hydrated electron taking $G_{e^-_{aq}} = 3.3$ (13) and $\varepsilon_{e^-_{aq}} = 1.3 \times 10^4$ dm^3 mol^{-1} cm^{-1} (14) at 600 nm, and corrected for the differences in density, taking $\rho(C_2H_5NH_2) = 0.68$ g cm^{-3}, $\rho(n\text{-}C_3H_7NH_2) = 0.71$ g cm^{-3}, and $\rho(NH_2C_2H_4NH_2) = 0.9$ g cm^{-3} at 20°C. As previously shown (15), the optical detection has been improved in the near infrared (ir) up to 1400 nm, the limit being due to solvent absorption. A germanium photodiode (Judson J 18) ir detector was used in the photovoltaic mode, and the photocurrent preamplified using the circuit shown in Fig. 1. Two cascade amplifiers and a line driver circuit amplify the current and match the output impedance to a 50 Ω coaxial line. The dark current was adjusted to zero using the offset on the first stage of the amplifier. The diode-preamplifier system has a rise-time (10–90%) of about 20 ns, and the gain is about 200. Signals from 50 mV to 1 V were found to be linear with the incident photon flux.

A high resolution grating monochromator (Jobin Yvon, type HRS) was used with different gratings. The bandwidth changed from 2 nm in the uv and the visible to 7.5 nm in the infrared.

The silica cell for pulse radiolysis and the purification of *n*-propylamine have been described previously (15). Ethylamine and ethylenediamine were prepared in the same way. Biphenyl (Merck, Zone refined) and acidic salts (ethylamine·HCl from Schuchardt, *n*-propylamine·HCl from Fluka, and ethylenediamine·2HCl from Merck) were used as received.

For γ-radiolysis studies, purified solvents were distilled under vacuum into Pyrex cells containing, if necessary, the needed quantities of solutes and then sealed off. The method for analysis of gases after γ-irradiation has already been described (16). The dose rate of the cobalt source was about 10^{19} eV cm^{-3} h^{-1}.

Results

1. Pure Solvents

The end-of-pulse (10 ns) spectra are shown in Fig. 2. For wavelengths greater than 1000 nm, the spectra were measured 50 ns after the beginning of the pulse and normalized to the 10 ns spectra at 1000 nm. In our detection range, only EDA exhibits a maximum

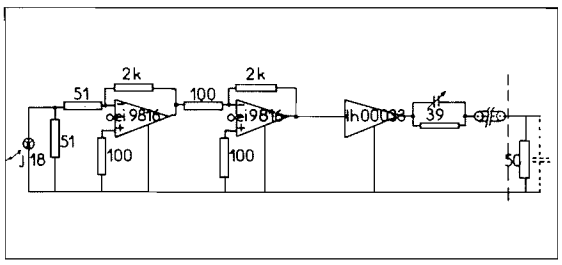

FIG. 1. Circuit diagram for the preamplifier used with germanium photodiode.

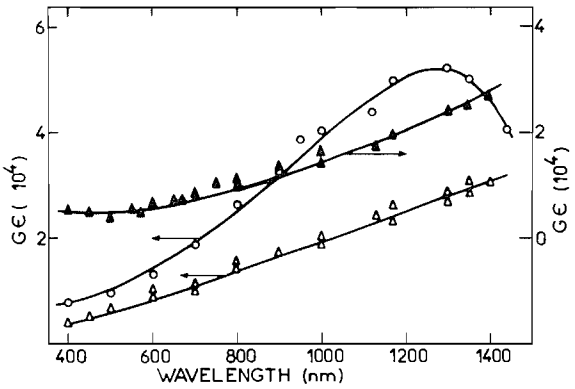

FIG. 2. End-of-pulse (10 ns) absorption spectra of solvated electron in △ ethylamine, ▲ *n*-propylamine, ○ ethylenediamine. The spectrum of *n*-propylamine has been shifted vertically for clarity.

for the ir absorption band associated with the solvated electron. This maximum is located near 1300 nm, in agreement with previous studies by pulse radiolysis (17) or dilute cesium solutions (18). For EA the maximum has been estimated to be near 1950 nm (3*b*), but λ_{max} in *n*PA is not known.

In addition to the ir and visible bands, the transient absorption spectra in each amine also exhibit a ultraviolet (uv) band which increases in intensity up to the solvent cut-off (250 nm for EA, 255 nm for *n*PA, and 290 nm for EDA). These uv bands are clearly shown in Figs. 3, 4, and 5 for EA, *n*PA, and EDA respectively.

Because the time behavior of the uv and ir absorbances are different, the former cannot be due to e^-_s. Under our experimental conditions, the decay time of e^-_s is shorter in EA and *n*PA ($\simeq 1$ μs) than in EDA ($\simeq 8$ μs) and uv absorbance decays more slowly without noticeable change in its spectrum (see curves with full circles in Figs. 3, 4, and 5). By analogy with uv absorptions in the radiolysis of ammonia (6, 12), hydrazine (8), or alcohols (19, 20), these bands are attributed to primary radicals of the radiolysis of amines. Evidence for $CH_3\dot{N}H$ radicals absorbing below 500 nm has been obtained in the pulse radiolysis of aqueous solutions of MA (21). Pulse radiolysis of pure triethylamine leads to a similar uv absorption (22).

The decay of e^-_s was found to obey second order kinetics for EA and *n*PA, as shown in Fig. 6. For EDA, the kinetics do not seem to obey any simple order, as is usually the case for e^-_s decay in pure liquids. From the slopes in Fig. 6 and the extinction coefficients of e^-_s (see section 3), upper limits for second order recombination rate constants can be given as $(1.5 \pm 0.5) \times 10^{12}$, $(3.5 \pm 1) \times 10^{12}$ L mol^{-1} s^{-1} for EA and *n*PA respectively. Each value

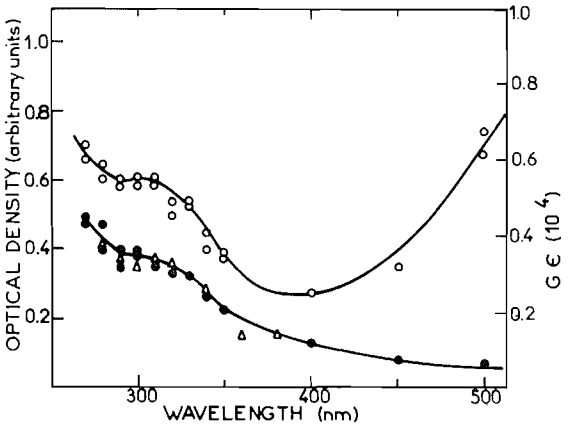

FIG. 3. Ultraviolet absorption spectra in pure ethylamine: ○ end of pulse, ● t = 400 ns; and in a solution containing ethylammonium chloride: (0.17 mol L^{-1}) △ t = 400 ns.

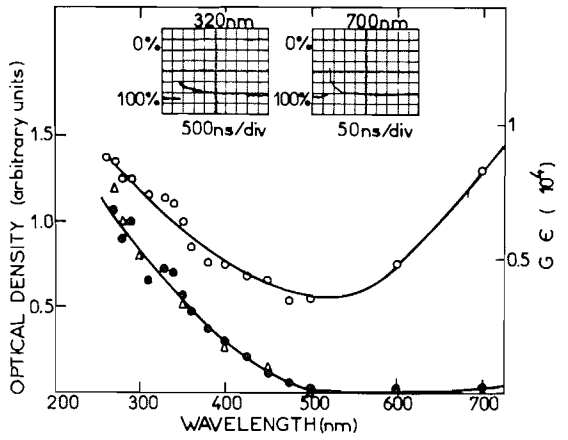

FIG. 4. Ultraviolet absorption spectra in pure n-propylamine: ○ end of pulse, ● t = 100 ns; and in a solution containing 100 ns n-propylammonium chloride (0.1 mol L^{-1}) △ t = 100 ns. Inserts: oscilloscope traces in pure n-propylamine, at 700 nm (50 ns/division) and at 320 nm (500 ns/division).

is a mean of about ten determinations, made at different wavelengths.

In the uv, the decays generally fit second order kinetics for each solvent. This is a further argument for assigning these absorbances to radicals, which are known to dimerize. Nevertheless, in order to obtain a satisfactory second order plot in the case of EDA, it is necessary to consider that the radicals dimerize to give a longer lived transient absorbing at the same wavelength (see Fig. 5). The slopes of the second order plots give the values $k/\varepsilon = 8.0 \times 10^6$, 6.7×10^6, and 3×10^6 cm s^{-1} for EA, nPA, and EDA (after correction) respectively at 300 nm.

2. Acidic Solutions

These solutions contain the 'acidic' cation RNH_3^+

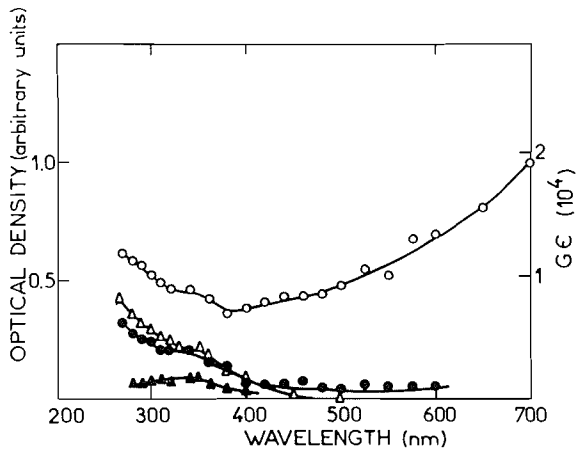

FIG. 5. Ultraviolet absorption spectra in pure ethylenediamine: ○ end of pulse, ● t = 2 μs, ▲ t = 14 μs and in a solution containing ethylenediammonium chloride (0.5 mol L^{-1}) △ t = 2 μs.

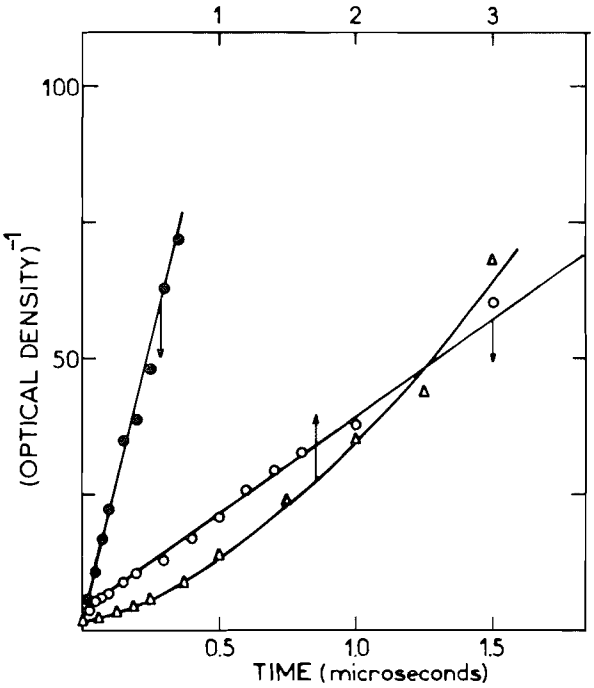

FIG. 6. Tests of second order plots for the decrease of e^-_s in pure ethylamine at 1300 nm (○), n-propylamine 900 nm (●), and ethylenediamine 800 nm (△).

of the amine RNH_2. In fact, this cation is the main cation of the radiolysis of amines (7), and a measure of its reactivity with e^-_s is useful. However, the state of association (pairs and higher associated species) of the amine hydrochlorides dissolved in their respective amines is generally unknown and a whole conductimetric study of some of these solutions is needed (10).

We shall present here the values of the rate constant k_2 for the reaction of e^-_s with the acidic salt, irrespective of its state of dissociation. Results are shown in Fig. 7, for EA and *n*PA. In both solvents, concentrations of acidic salts higher than 10^{-2} mol L^{-1} are necessary to accelerate the decay of e^-_s. At concentrations higher than 10^{-1} mol L^{-1}, experimental points deviate from linearity. From the slopes in Fig. 7 we obtain values for the second order rate constants $k_2 = 5.7 \times 10^8$ and 6.0×10^8 L mol^{-1} s^{-1} for EA and *n*PA respectively. In this concentration range (10^{-2}–10^{-1} mol L^{-1}) ions are considered to exist mainly as pairs (10) so we shall consider that both rate constants refer to the reactivity of e^-_s towards a cation paired with a chloride ion. In a previous paper (7) we considered, to a first approximation, that the rate constant between free ions had to be multiplied by a factor of ten, giving a value of $k_{e^-_s + RNH_3^+} = 7 \times 10^9$ L mol^{-1} s^{-1} for *n*PA (7). However, the decay kinetics of e^-_s in the pure solvent allow one to obtain an upper value for $k_{e^-_s + RNH_3^+}$. In fact, it will be shown in the discussion that e^-_s decays mainly by recombination with the cation in both solvents. So we may conclude from the high values measured here for the recombination rate constants in the pure solvents that the amplification factor suggested previously (7) may be as high as 10^3.

By dissolving ethylene diammonium dichloride in EDA, the monoacid $EDAH^+$ ($NH_3^+CH_2CH_2NH_2$) conjugated with the base EDA is thought to be formed, at a concentration twice that of the added salt. First order experimental rate constants are plotted in Fig. 8 versus the logarithm of the concentration of the monoacid. The main feature is the plateau value reached by the experimental rate constant for concentrations of reactant higher than 10^{-1} mol L^{-1}. Thus, it appears again that the reactivity of e^-_s towards the cation is greatly reduced when the latter is associated with the anion: a more detailed study of this reactivity in connection with conductimetric measurements gives the value of the recombination rate constant at zero ionic strength for isolated ions $k_{e^-_s + RNH_3^+} = 2 \times 10^{10}$ L mol^{-1} s^{-1} (10). This value is higher by a factor of 10^3 than that obtained in previous work using a stopped flow method (23). However, the latter results were not corrected for ionic association and ionic strength effects, which largely explains the above discrepancy.

We also investigated the influence of the acidic cation on the decay of the uv absorbance in each amine for a concentration such that e^-_s disappears in a few nanoseconds. At the end of the pulse, the spectra were found to be identical to those in pure solvents. At longer times the influence of the acidic cation differs according to the nature of the amine. As shown in Figs. 3 and 4, the decay is exactly the same as in the pure solvent for EA and *n*PA, but is slowed down in EDA. In fact, for molar concentration of $EDAH^+$ in EDA, the decay remains second order, but the rate constant is three times lower than in pure solvent.

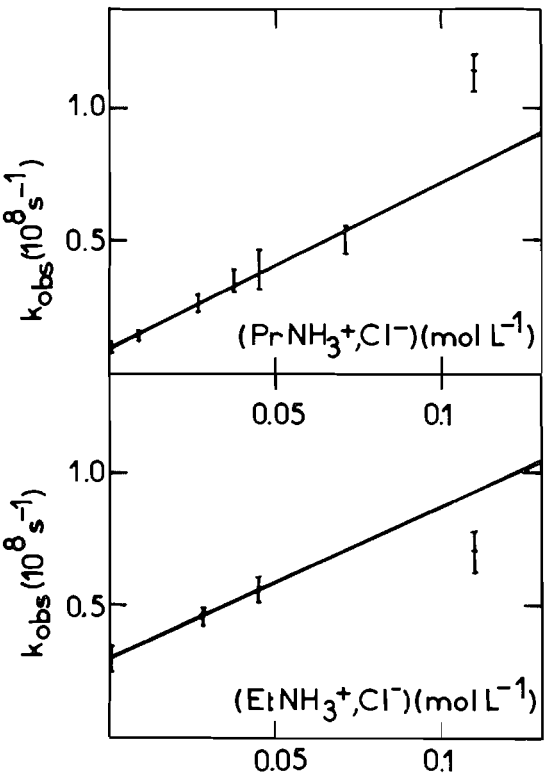

FIG. 7. Observed first order rate constant for the decay of e^-_s as a function of the amine hydrochloride concentration. Upper curve: *n*-propylamine. Lower curve: ethylamine.

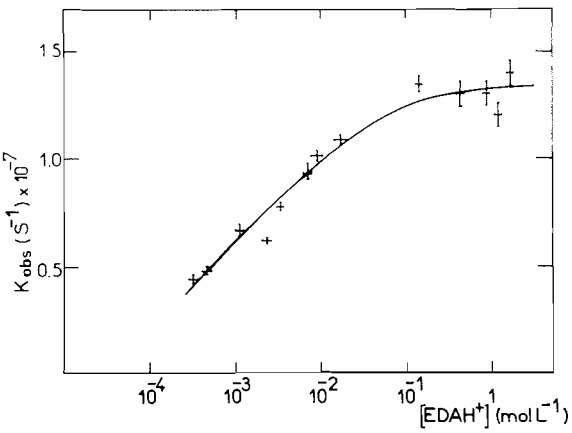

FIG. 8. Observed first order rate constant for the decay of e^-_s in ethylenediamine as a function of concentration of monoacidic ion, plotted on a logarithmic scale.

3. *Extinction Coefficient and Yield of Solvated Electron*

Yields $G(e^-_s)$ and extinction coefficients $\varepsilon_{e^-_s}$ were determined using biphenyl (Ph_2) as a scavenger. The method uses the known extinction coefficients of biphenyl anion (Ph_2^-) determined in tetrahydrofuran at 410 nm and 640 nm (24, 25) and assumes that these coefficients are independent of the solvent. Although there is no direct evidence of this hypothesis, the invariance of the Ph_2^- spectrum shape also suggests invariance of $\varepsilon_{Ph_2^-}$. Furthermore, it has been shown that the above method applied to ammonia (26) gives the same G-value (3.2) as the direct determination of the yield, knowing the deposited dose and extinction coefficient $\varepsilon_{e^-_s}$.

For concentrations of Ph_2 lower than 10^{-2} mol L^{-1}, the decrease of e^-_s absorbance was observed simultaneously with the associated increase of Ph_2^- absorbance. The absorbance of Ph_2^- was measured after a time corresponding to the end of its formation, or the end of the decay of e^-_s.

Figure 9 shows the anion yields as a function of solute concentrations, assuming $\varepsilon_{Ph_2^-} = 1.21 \times 10^4$ L mol^{-1} cm^{-1} at 640 nm (24, 25). The measured yield $G(Ph_2^-)$ depends on the scavenger concentration, a consequence of the competition between the scavenging reaction and the non-homogeneous (spur) and homogeneous (bulk) reactions of e^-_s. This solute dependence has been described according to an empirical equation originally proposed for hydrocarbons (27) and adapted to our problem (see Discussion). The calculated dependence of $G(Ph_2^-)$ on solute concentration is shown in Fig. 9 (full lines). However, the quantity of interest is $G(e^-_s)$ at a time t, $G(e^-_s)_t$. It has been shown that this quantity is exactly the inverse Laplace transform of $G(Ph_2^-)$ (28). As a first approximation, we shall consider that for a Ph_2 concentration such that the halftime of reaction is $t_{1/2} = 3$ ns (half-height duration of the triangular pulse), the yield of electrons which is scavenged is $G(e^-_s)_{3\,ns}$. This approximation is justified because the decay rate of e^-_s in the pure solvent at the end of the pulse is much slower than in the presence of the above Ph_2 concentration.

Extinction coefficients for e^-_s were also determined by comparing the optical density of e^-_s, $OD(e^-_s)$, at the end of the pulse (10 ns) with that of Ph_2^- at 640 nm, $OD(Ph_2^-)$, for a Ph_2 concentration such that the reaction half time is 10 ns. If, under such conditions, we consider that all the solvated electrons present at the end of the pulse, and only these electrons, are scavenged, eq. [1] applies:

$$[1] \quad OD(e^-_s)/OD(Ph_2^-) = \varepsilon_{e^-_s}/\varepsilon_{Ph_2^-}$$

$\varepsilon_{e^-_s}$ was also determined in another way: in the 500–700 nm region, the absorption spectra of both e^-_s and Ph_2^- have two isobestic points. These points were determined by looking for flat absorbance on oscillograms, and it was verified that they were independent of biphenyl concentration. The values obtained for $\varepsilon_{e^-_s}$ were the same as above within the limit of experimental error. The last method gives further support to the derivation of $G(e^-_s)_{3ns}$.

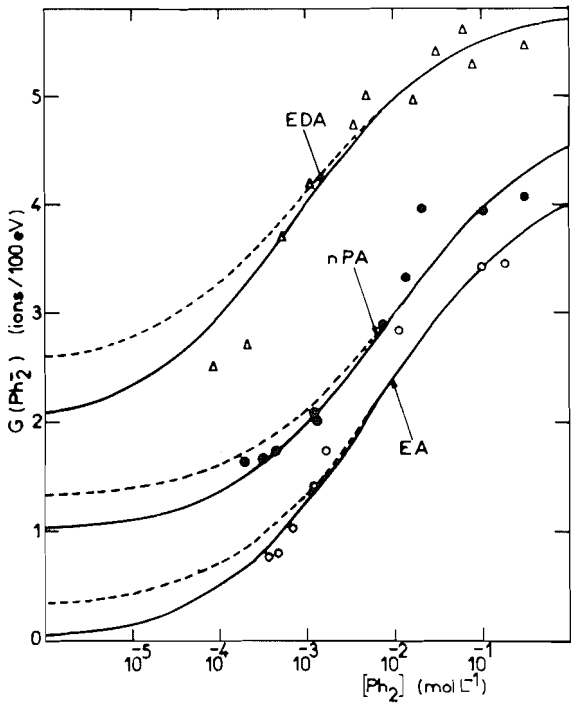

FIG. 9. Biphenyl anion yields as a function of biphenyl concentration, in ethylamine (○), *n*-propylamine (●), and ethylenediamine (△). Dashed curve: equation of ref. 27. Solid curve: eq. [4]. For sake of clarity the curves of *n*-propylamine and ethylenediamine are shifted vertically by 1 and 2 units of G respectively.

The values of $G(e^-_s)_{3ns}$ and $\varepsilon_{e^-_s}$ are given in Table 1, and compared with literature data (see Discussion).

In spite of the short lifetime of e^-_s in EA and *n*PA, it was possible to find a range of biphenyl concentrations (from 2×10^{-4} to 2×10^{-3} mol L^{-1}) from which the rate constant k_s for the reaction of e^-_s with biphenyl could be determined. Values equal to $(1.45 \pm 0.1) \times 10^{11}$, $(1.35 \pm 0.1) \times 10^{11}$, and $(1.8 \pm 0.1) \times 10^{10}$ L mol^{-1} s^{-1} were obtained in EA, *n*PA, and EDA respectively.

4. *Hydrogen Yields in the γ-Radiolysis of* n*PA and EDA*

Molecular hydrogen yields were measured for pure solvents, and for solvents containing an electron scavenger (biphenyl), electron, and H atom scaven-

TABLE 1. Properties of e^-_s in amines ($T \simeq 293$ K)

Solvent	λ_{max} (nm)	$\varepsilon \times 10^{-4}$ (L mol^{-1} cm^{-1})	μ_e[e] (cm^2 V^{-1} s^{-1})	$G(e^-_s)_{3ns}$
EA	1950[b]	3.2±0.5 (λ_{max})[b]	1.5×10^{-2}	1.2[f]
		3.8±0.2 (1400 nm)[a]		1.5[a]
*n*PA		3.4±0.2 (1400 nm)[a]	1.5×10^{-2}	1.2[a]
*i*PA	2100[c]	3.2±0.5 (λ_{max})[c]		1.0[f]
EDA	1300[a]	1.9±0.2 λ_{max}) [a]	1.8×10^{-3}	3.1[a]
	1280[d]	2.0±0.3 (λ_{max})[d]		
MA	1900[b]	3.3±0.2 (λ_{max})[b]		2.25[f]

[a]Our work.
[b]Reference 3*b*.
[c]Reference 29.
[d]Reference 17.
[e]This work, eq. [2].
[f]From scavenging curves of ref. 3*b*, applying the same method as the one explained in the text to determine $G(e^-_s)_{3\ ns}$ and using our values for $k_{e^-_s + Ph_2}$.

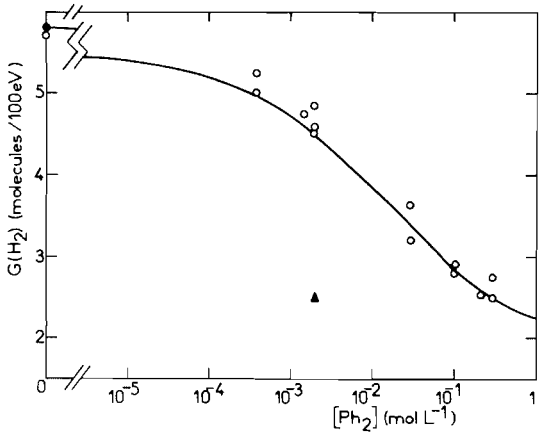

FIG. 10. Molecular hydrogen yield as a function of biphenyl concentration in pure *n*-propylamine (○) or in solutions containing propylamine hydrochloride (1 mol L^{-1}) (●) or allyl alcohol (1 mol L^{-1}) (△) solid curve: eq. [13].

gers (biphenyl + allyl alcohol) or acidic cation. The yield of hydrogen was found to be independent of dose in the range used (0.2 to 1 × 10^{19} eV mL^{-1}). In both amines, hydrogen was the main gas produced by radiolysis.

The yield of hydrogen $G_0(H_2)$ in pure *n*PA is 5.7 ± 0.3. For biphenyl concentrations higher than 10^{-1} mol L^{-1}, the yield of hydrogen drops to 2.5 ± 0.3. The same decrease is observed in a solution containing biphenyl 2 × 10^{-3} mol L^{-1} and allyl alcohol 1 mol L^{-1}. Addition of 1 *M* propylamine hydrochloride (*n*PAH$^+$Cl$^-$) has practically no effect on the yield of hydrogen ($G(H_2) = 5.8 \pm 0.3$) (see Fig. 10).

$G_0(H_2)$ in pure EDA is 3.5 ± 0.1 and rises to 4.3 ± 0.1 when the acidic salt is added at concentrations of 1.4 × 10^{-2} or 3.1 × 10^{-2} mol L^{-1}.

Discussion

1. Properties of Solvated Electrons in Amines

Table 1 summarizes some properties of e^-_s in several amines. Our values of $\varepsilon_{e^-_s}$ and those from the literature are in good agreement for EDA. Assuming that the shape of the spectrum is the same as that given in ref. 3*b* for EA, our determination of $\varepsilon_{e^-_s}$ at 1400 nm would lead to $\varepsilon_{max} = (4.5 \pm 0.5) \times 10^4$ L mol^{-1} cm^{-1}. This value is slightly higher than that given in ref. 3*b*. We interpret this discrepancy as a consequence of too high a value determined in the above reference for $G(e^-_s)$.[1]

Another physical property of interest is the mobility (μ_e) of e^-_s. Due to the instability of metal solutions in amines (1), conductance studies of such solutions have been limited to MA (30) and EDA (31). Furthermore, the limiting value of the equivalent conductance depends on the nature of the metal (30, 31). In addition there are some experiments on the conductivity of excess electrons in amines in the microsecond range (32). However, the mobilities found for these solvents of low dielectric constant may involve an associated form of the electron which may be formed in a fast process (15).

In contrast with direct methods which, due to their long response time, are unable to give mobilities of isolated solvated electrons, the calculation of mobility from the diffusion-controlled rate constant with effective scavengers is, as already suggested (33), of more general use for these solvents. Actually, the reduced Smoluchowski–Debye equation applies:

$$[2] \quad k_s = 4\pi k T \rho_s \mu_e / e$$

where k is the Boltzmann constant, T the temperature, k_s the scavenging rate constant, e the electron charge, and ρ_s the effective reaction radius. If one admits that the scavenging of e^-_s by biphenyl is diffusion controlled, use of eq. [2] with $\rho_s = 5$ Å

[1]After a 0.3 μs pulse in EA and *i*PA, as in the work by Seddon *et al.* (3*b*), the true solvated electron yield is indeed lower than the yield of escaped electrons determined from the scavenging curve, since in the pure solvent, a fraction of the latter will recombine during the pulse.

gives the mobilities listed in Table 1. In EDA, the mobility is lower by a factor of ten than in EA and *n*PA, and higher than those given in ref. 32.

2. Efficiency of e^-_s–Cation Reaction

In preceding papers (6–8) we emphasized the role of the efficiency factor for the e^-_s–cation recombination on the survival probability of e^-_s. For this purpose, diffusion-controlled rate constants are estimated from the Smoluchowski–Debye equation:

$$[3] \quad k_{diff} = 4\pi\rho_s Dx/(1 - \exp(-x))$$

where D is the mutual diffusion coefficient and x is the ratio $e^2/\varepsilon_s\rho_s kT$. As the diffusion coefficient for e^-_s, $D_{e^-_s}$, is larger than the diffusion coefficient for the cation, one can consider as a first approximation that $D \simeq D_{e^-_s} \cdot D_{e^-_s}$ is obtained from the above data on conductivity, and ρ_s is the sum of the cavity radius of e^-_s, estimated to be 2 Å, and of the crystal radius of alkylammonium ion, estimated from partial ionic molar volumes in water to be 2.7, 2.9, and 3.0 Å for EA, *n*PA, and EDA respectively (34). The diffusion-controlled rate constants k_{diff} are found to be equal to 4.7×10^{12}, 5.9×10^{12}, and 2.9×10^{11} L mol^{-1} s^{-1} in EA, *n*PA, and EDA respectively. As explained earlier, the only accurate experimental measurement of the recombination rate constant k_{exp} is for EDA: $k_{exp} = 2 \times 10^{10}$ L mol^{-1} s^{-1}. So, in this solvent, the efficiency factor f, defined as the ratio k_{exp}/k_{diff}, is only 7×10^{-2}. In EA and *n*PA, because of the arguments developed above, we think that the second order rate constants determined from analysis of the decay in the pure solvent can be used as upper limits for k_{exp}. The efficiency factors estimated with such limits are equal to 0.3 and 0.6 in EA and *n*PA respectively. So, contrary to EDA, rate constants of recombining reactions in EA and *n*PA may be almost diffusion controlled.

3. Solvated Electron, H Atom- and H_2-yields

In the three solvents, the yield of biphenyl anion formed by electron capture shows a marked dependence on biphenyl concentration (Fig. 9). In order to analyse such a dependence, we used the empirical equation proposed in the case of hydrocarbons (27), corrected to take account of homogeneous competition between the decay of free ions and their scavenging by Ph_2 (35).

$$[4] \quad G(Ph_2^-) = G(e^-_s)_f[\delta S/(1 + \delta S)] + G(e^-_s)_g[(\alpha S)^{1/2}/(1 + (\alpha S)^{1/2})]$$

where $G(e^-_s)_f$ and $G(e^-_s)_g$ represent the yields of the solvated electrons, free and geminate respectively, S is the concentration of the scavenger, α is a parameter which represents the competition between recombination of *geminate* electrons with cations or radicals in the spur and reaction towards the solute, δ is the ratio k_s/k_d where k_d is the first order rate constant for the decay of *free* electrons. This constant has been estimated from [5]

$$[5] \quad k_d = k_{e^-_s + RNH_3^+}[RNH_3^+]$$

where $[RNH_3^+]$ is the concentration of cations at the end of geminate recombination in the presence of a solute at concentration S. From the charge balance, we can write

$$[6] \quad [RNH_3^+] = 10DN_A G(e^-_s)_g \times [(\alpha S)^{1/2}/(1 + (\alpha S)^{1/2})]$$

where D is the deposited dose (eV × cm^{-3}) and N_A is Avogadro's number. The solid curves drawn in Fig. 9 represent the best fit of eq. [4] using for EA, *n*PA, and EDA, respectively: $G(e^-_s)_g = 4.0$, 3.55, and 3.3, $G(e^-_s)_f = 0.3, 0.3$, and 0.5, and $\alpha = 125$, 90, and 900. For the sake of comparison the broken curves represent values of $G(Ph_2^-)$ from the original scavenging equation (27) without corrections, using the same parameters as above. In spite of the correction expressed in eq. [4], experimental yields for concentrations of the scavenger lower than 10^{-3} mol L^{-1} are smaller than those calculated in EDA due to the decay of Ph_2^- during its formation. For this reason, the values given for $G(e^-_s)_f$ are to be considered as lowest limits.

More certain are the values of the total scavengeable yields $G_{e^-_s}$ found to be equal to 4.3, 3.85, and 3.8 for EA, *n*PA, and EDA respectively. These values are higher than those given previously for MA, EA, or *i*PA (3*b*). The discrepancy may be a consequence of the fact that, during the electron pulse (0.3 μs) used in ref. 3*b*, the biphenyl anions partly recombine.

These yields are to be compared with those deduced from molecular hydrogen yields after the γ-radiolysis of amines in the absence and presence of various scavengers. In addition to primary unscavengeable molecular hydrogen, H atoms and solvated electrons may form molecular H_2:

$$[7] \quad e^-_s + RHN_3^+ \rightarrow (RNH_3) \rightarrow H + RNH_2$$

H atoms are assumed to react with the solvent to give H_2 (36)

$$[8] \quad H + RNH_2 \rightarrow H_2 + R\dot{N}H$$

Therefore, in the pure solvent,

$$[9] \quad G_0(H_2) = G_{H_2} + G_H + \beta G_{e^-_s}$$

where G_{H_2}, G_H, and $G_{e^-_s}$ are the primary yields of H_2, H, and e^-_s, and β is the fraction of e^-_s undergoing recombination with cations (reaction [7]). When an electron scavenger such as biphenyl is added in a

high concentration, then

[10] $G(H_2)_{Ph_2} = G_{H_2} + G_H$

Similarly, in the presence of a high concentration of acidic salt, then

[11] $G(H_2)_{acid} = G_{H_2} + G_H + G_{e^-_s}$

So, if the above hypotheses are correct:

[12] $G(H_2)_{acid} - G(H_2)_{Ph_2} = G_{e^-_s}$

For EA, such a difference obtained from the literature gives $G_{e^-_s} = 2.7 \pm 0.1$ (5) which is to be compared with our limiting value of 4.3. The agreement is better for *n*PA where our results in γ-radiolysis (see Fig. 10) give $G_{e^-_s} \simeq 3.5$, to be compared with $G_{e^-_s} = 3.85$ from the Ph_2 scavenging experiments.

The decrease $\Delta G(H_2)$ of molecular hydrogen yield in the presence of biphenyl, compared to that in the presence of high concentration of acidic salt, can be expressed in the form:

[13] $\Delta G(H_2) = G(e^-_s)_f + G(e^-_s)_g \times (\alpha S)^{1/2}/[1 + (\alpha S)^{1/2}]$

By choosing the same parameters as those given above for *n*PA, one obtains the solid curve in Fig. 10. This fits the experimental data quite well, giving further support to the above values. At concentrations used, biphenyl has been considered not to scavenge H atoms that react efficiently with the solvent by reaction [8]. If H atom scavenging occurred the decrease in $G(H_2)$ would be higher and the difference in eq. [12] would give $G_{e^-_s} + G_H \simeq 3.5$. As $G_{e^-_s} = 3.85$ has been found from pulse radiolysis we deduce $G_H \simeq 0$. The same conclusion is reached when experimental data concerning allyl alcohol solutions are examined. Allyl alcohol is known as an ineffective scavenger of hydrated electrons ($k_{e^-_{aq} + CH_2=CHCH_2OH} < 10^6$ L mol^{-1} s^{-1} (37)), but as an efficient scavenger of H atoms in water such that the main scavenging reaction is

[14] $H + CH_2{=}CHCH_2OH \rightarrow C_3H_6OH$

which does not yield H_2 (37). The rate constant k_{14} is higher than 10^9 L mol^{-1} s^{-1} in water (38). Since a molar solution of allyl alcohol causes the same decrease in $G(H_2)$ as a molar solution of biphenyl, it is concluded that allyl alcohol scavenges only H atoms produced via reaction [7]. Again, the conclusion is $G_H \simeq 0$. As allyl alcohol in molar solutions competes with the solvent molecules to scavenge H atoms, we deduce that $k_8 < 5 \times 10^7$ L mol^{-1} s^{-1}.

Finally, the yield of unscavengeable molecular hydrogen G_{H_2} is deduced from the asymptotic value of $G(H_2)$ at high biphenyl concentrations (see Fig. 10): $G_{H_2} = 2.0 \pm 0.3$.

4. Main Recombination Reactions for Solvated Electrons in Amines

Mass spectrometer studies on gaseous ionic reactions in ammonia (39–41) and methylamine (42) have shown that the initial cation is rapidly replaced through ion–molecule reactions by the protonated molecule ions. Assuming that the same ion–molecule reactions occur in EA, *n*PA, and EDA, then the primary radiolysis species are as follows:

[15] $RNH_2 \rightarrow RNH_3^+, e^-_s, RNH^{\cdot}, (H^{\cdot}, R^{\cdot}, NH_2^{\cdot})$

Radicals like $RNH^{\cdot}$, $R^{\cdot}$, or $NH_2^{\cdot}$ may also be formed in small amounts by decomposition of excited molecules (43).

Because in amines the solvated electron associated with alkali cations is metastable, reactions of e^-_s with the solvent molecule or another e^-_s are relatively unimportant (7). Therefore the main reactions for the disappearance of e^-_s are [7] and [16].

[16] $e^-_s + RNH^{\cdot} \rightarrow RNH^-$

In ammonia and hydrazine, the main reaction of disappearance has been found to be reaction [16], because of the low efficiency of reaction [7] (6, 7). At the same time, $G(e^-_s)$ has been found to be high ($G(e^-_s) = 3.0$ and 3.4 in NH_3 and N_2H_4 respectively).

When acidic cation is added to both EA and *n*PA in order to accelerate the e^-_{solv}–cation recombination, the uv absorption attributed to radicals is unchanged compared with the pure solvent and there is only a slight increase in hydrogen yield ($\Delta G(H_2) = 0.1$) leading to $\beta \simeq 1$ in eq. [9]. Both features suggest that reaction [7] is the main recombination reaction in EA and *n*PA. Consequently, the measured rate constant of the decay in pure solvents has been assumed to be $k_{e^-_s + RNH_3^+}$ (see above) and has been found to be almost diffusion controlled.

The escape probability N at a given time t, $N_t = G(e^-_s)_t/G_{e^-_s}$ is 0.35 and 0.31 at 3 ns for EA and *n*PA respectively. These values are a little higher than the corresponding probability determined in dimethoxyethane ($\varepsilon_s = 5$), in which $N_{3ns} = 0.20$ if we consider that $G(e^-_s)_{3ns} = 0.8$ (7) and $G_{e^-_s} = 4.0$ by analogy with the value determined for tetrahydrofuran (44). These probabilities are low in correlation with the fact that the efficiency factor f is near unity.

The escape probability N_{3ns} equals 0.82 in EDA. This high value can be correlated, as for NH_3 and N_2H_4, with the low value of f. In fact, the mechanism for disappearance of e^-_s in EDA is intermediate between that of polar NH_3 and N_2H_4, in which $f \simeq 0$, and that of weakly polar amines, as EA and *n*PA, in which $f \simeq 1$: reaction [16] takes place in competition with reaction [7]. Indeed, by addition of acidic salts, radicals are protected and $G(H_2)_{acid}$

increases ($\Delta G(H_2) = 0.8$). Considering the initial decay rate of e^-_s and the experimental value for the rate constant of reaction [7], and supposing a radical yield equal to the solvated electron yield, we find that the rate constant of reaction [16] equals 4×10^{10} L mol^{-1} s^{-1}. This value indicates that the efficiency factor for reaction [16] is high, as is the case for NH_3 (8).

In conclusion, pulse- and γ-radiolysis studies of EA, *n*PA, and EDA give evidence for the influence of efficiency factors of the neutralization reaction and recombination with radicals on the yield of escaped solvated electrons. By solving the Smoluchowski equation with a boundary condition expressing the partially reflective character of the reaction sphere (7), we have shown that it is possible to describe qualitatively the influence of f on the escape probability. The approximation method used to solve the equation was "prescribed diffusion" (45). In order to improve the accuracy of the theoretical calculation of N_t and to introduce possible reaction with radicals, numerical solution of the Smoluchowski equation is in progress. In this way, we hope to get some idea of the mean initial thermalisation length for the solvated electron in cases where recombination with the cation is not the only recombination process.

Acknowledgements

The authors wish to thank Drs. J. Belloni, M. O. Delcourt, and P. Cordier for valuable discussions throughout the work. We also thank Mrs. Miñana for technical assistance in sample preparation and gas analysis. This work was performed under contract with the Centre National de la Recherche Scientifique (ATP No. 2215).

1. J. L. Dye. Electrons in fluids. *Edited by* J. Jortner and N. R. Kestner. Colloque Weyl III. Springer Verlag, Berlin. 1973. p. 77.
2. J. W. Fletcher and W. A. Seddon. Colloque Weyl IV. J. Phys. Chem. **79**, 3055 (1975) and references therein.
3. (*a*) J. W. Fletcher and W. A. Seddon. Faraday Discuss. **63**, 18 (1977); (*b*) W. A. Seddon, J. W. Fletcher, and F. C. Sopchyshyn. Can. J. Chem. **56**, 839 (1978).
4. D. Smithies and A. J. Whitworth. J. Chem. Soc. A, 1987 (1969).
5. A. Habersbergerova, I. Janovsky, and J. Teply. Chem. Commun. 1678 (1970).
6. J. Belloni, P. Cordier, and J. A. Delaire. Chem. Phys. Lett. **27**, 241 (1974).
7. J. Belloni, F. Billiau, P. Cordier, J. A. Delaire, M. O. Delcourt, and M. Magat. Faraday Discuss. **63**, 58 (1977).
8. J. A. Delaire, P. Cordier, J. Belloni, F. Billiau, and M. O. Delcourt. J. Phys. Chem. **80**, 1687 (1976).
9. A. A. Maryott and E. R. Smith. Natl. Bur. Stand. Circular 514, U.S. Department of Commerce. 1951.
10. M. O. Delcourt. To be published.
11. J. A. Delaire. Thèse 3è cycle, Orsay. 1973.
12. J. Belloni, F. Billiau, P. Cordier, J. A. Delaire, and M. O. Delcourt. J. Phys. Chem. **82**, 532 (1978).
13. J. K. Thomas and R. V. Bensasson. J. Chem. Phys. **46**, 4147 (1967).
14. E. J. Hart and M. Anbar. The hydrated electron. Wiley-Interscience, New York, NY. 1970. p. 42.
15. J. A. Delaire, J. Belloni, P. Cordier, and M. O. Delcourt. Protons and ions involved in fast dynamic phenomena. Elsevier, Amsterdam. 1978. p. 245.
16. J. Belloni. Int. J. Radiat. Phys. Chem. **1**, 441 (1969).
17. J. L. Dye, M. G. De Backer, and L. M. Dorfman. J. Chem. Phys. **52**, 6251 (1970).
18. R. R. Dewald and J. L. Dye. J. Phys. Chem. **68**, 121 (1964).
19. (*a*) M. Simic, P. Neta, and E. Hayon. J. Phys. Chem. **73**, 3794 (1969); (*b*) J. W. Fletcher, P. J. Richards, and W. A. Seddon. Can. J. Chem. **48**, 3765 (1970).
20. D. W. Johnson and G. A. Salmon. Can. J. Chem. **55**, 2030 (1977).
21. A. Wigger, W. Grünbein, A. Henglein, and E. J. Land. Z. Naturforsh. **24b**, 1262 (1969).
22. F. S. Dainton, G. A. Salmon, and C. Von Sonntag. Proc. R. Soc. London A, **313**, 31 (1969).
23. L. H. Feldman, R. R. Dewald, and J. L. Dye. Adv. Chem. Ser. **50**, 163 (1965).
24. K. H. Buschow, J. Dieleman, and G. I. Hoytinck. Mol. Phys. 7, 1 (1963).
25. D. Gill, J. Jagur-Grodzinski, and M. Szwarc. Trans. Faraday Soc. **60**, 1424 (1964).
26. W. A. Seddon, J. W. Fletcher, F. C. Sopchyshyn, and J. Jevcak. Can. J. Chem. **52**, 3269 (1974).
27. J. M. Warman, K. D. Asmus, and R. H. Schuler. Adv. Chem. Ser. **82**, 25 (1968).
28. L. Monchick. J. Chem. Phys. **24**, 381 (1956).
29. W. A. Seddon, J. W. Fletcher, and F. C. Sopchyshyn. Chem. Phys. **15**, 377 (1976).
30. R. R. Dewald and K. W. Browall. J. Phys. Chem. **74**, 129 (1970).
31. R. R. Dewald and J. L. Dye. J. Phys. Chem. **68**, 128 (1964).
32. A. V. Vannikov, E. I. Mal'tzev, V. I. Zolotarevsky, and A. V. Rudnev. Int. J. Radiat. Phys. Chem. **4**, 135 (1972).
33. T. Wada, K. Shinsaka, H. Namba, and Y. Hatano. Can. J. Chem. **55**, 2144 (1977).
34. D. H. Aue, H. M. Webb, and M. T. Bowers. J. Am. Chem. Soc. **98**, 318 (1976).
35. S. J. Rzad and J. H. Fendler. J. Chem. Phys. **52**, 5395 (1970).
36. N. Getoff and F. Schwoerer. Int. J. Radiat. Phys. Chem. **3**, 429 (1971).
37. G. Scholes and M. Simic. J. Phys. Chem. **68**, 1731 (1964).
38. R. A. Witter and P. Neta. J. Org. Chem. **38**, 484 (1973).
39. F. T. Jones and T. J. Sworsky. Trans. Faraday Soc. **63**, 2411 (1967).
40. G. M. Meaburn and S. Gordon. J. Phys. Chem. **72**, 1592 (1968).
41. M. S. B. Munson. J. Phys. Chem. **70**, 2034 (1966).
42. E. G. Jones and A. G. Harrison. Can. J. Chem. **45**, 3120 (1967).
43. J. V. Michael and W. A. Noyes, Jr. J. Am. Chem. Soc. **85**, 1228 (1963).
44. E. A. Shaede, H. Kurihara, and L. M. Dorfman. Int. J. Radiat. Phys. Chem. **6**, 47 (1974).
45. A. Mozumder. J. Chem. Phys. **48**, 1659 (1968).

Influence de différents catalyseurs à base d'éléments de transition du groupe VIII sur la polymérisation du norbornène

CHARLES TANIÉLIAN, ALAIN KIENNEMANN[1] ET TEMEL OSPARPUCU

Laboratoire de chimie organique appliquée, 1 rue Blaise Pascal, 67008, Strasbourg, France

Reçu le 27 octobre 1978

CHARLES TANIÉLIAN, ALAIN KIENNEMANN et TEMEL OSPARPUCU. Can. J. Chem. **57**, 2022 (1979).

Les deux types de polymérisation du norbornène ont été étudiés en catalyse homogène. Le palladium conduit à une polymérisation de type vinylique alors que pour le rhodium et le ruthénium nous avons ouverture de cycle. Dans le cas de la polymérisation avec le palladium, nous avons pu piéger un intermédiaire réactionnel: $PdCl_2(C_7H_{10})_4$ et étudier son comportement en polymérisation. Avec le ruthénium, nous avons étudié l'influence de deux ligands: le cyclopentadiène qui conduit à un blocage complet de la réaction et la triphénylphosphine dont l'effet varie suivant le rapport $P\phi_3$/Ru. L'utilisation de trois alcools comme solvant: EtOH, *n*-BuOH, *t*-BuOH, montre une variation de la vitesse réactionnelle en passant de EtOH à *t*-BuOH avec $RuCl_3 \cdot 3H_2O$ et aucun changement pour $RuCl_2(P\phi_3)_3$. Ceci indique que le rôle de l'alcool n'est pas limité à celui de solvant mais qu'il doit participer à la réaction elle-même, notamment au niveau de la formation de l'espèce active.

CHARLES TANIÉLIAN, ALAIN KIENNEMANN, and TEMEL OSPARPUCU. Can. J. Chem. **57**, 2022 (1979).

Both types of norbornene polymerisation with homogeneous catalysts have been studied. Palladium leads to vinyl-type polymerisation whereas rhodium and ruthenium lead to ring opening. In the case of palladium-catalysed polymerisation we have been able to trap the reactive intermediate $PdCl_2(C_7H_{10})_4$ and have studied its behaviour during polymerisation. With ruthenium we have studied the effect of two ligands: cyclopentadiene which leads to a complete blocking of the reaction and triphenylphosphine the effect of which varies according to the ratio $P\phi_3$:Ru. Use of the three alcohols, ethanol, *n*-butanol, and *tert*-butanol, as solvent shows a variation in reaction rate on charge using $RuCl_3 \cdot 3H_2O$ but no change for $RuCl_2(P\phi_3)_3$. This indicates that the role of the alcohol is not limited to that of solvent but it must participate in the reaction especially during the formation of the reactive intermediate.

[Journal translation]

Introduction

De nombreux travaux traitent de l'obtention de polymères à partir de cycloléfines et un certain nombre de mises au point ont été publiées (1–5). Certaines cycloléfines dont le norbornène ont la possibilité de se polymériser suivant deux voies: polymérisation de type vinylique ou par ouverture de cycle. Le choix du système catalytique permet de diriger la réaction vers l'une ou l'autre voie: des acides de Lewis (6), des complexes à base de palladium (7, 8), certains catalyseurs Ziegler–Natta (9–12), des peroxydes (13, 14) conduisent à une polymérisation de type vinylique, alors que la polymérisation par ouverture de cycle est obtenue si l'on utilise des catalyseurs Ziegler–Natta (10, 11, 15) des oxydes de chrome, molybdène ou tungstène réduits (16) des sels ou complexes de ruthénium, osmium, iridium en milieu alcool (17, 18) ou benzène (19) ou d'autres éléments de transition (W, Mo, Re) (20, 21). Malgré ces nombreux travaux, l'étude du mécanisme de la réaction reste d'actualité (21, 22).

Nous nous proposons, dans ce travail, d'étudier les deux types de polymérisation en catalyse homogène avec des métaux du groupe VIII: palladium (polymérisation de type vinylique), rhodium et ruthénium (ouverture de cycle). La mise en évidence d'intermédiaires réactionnels pour le palladium et l'étude d'effets de solvants et de ligands pour le ruthénium permettent une approche des schémas réactionnels de la polymérisation.

Partie expérimentale[2]

Toutes les réactions sont effectuées en utilisant l'argon comme gaz protecteur. Les spectres ir ont été obtenus sur spectromètre Beckman IR-12, solution dans CCl_4 pour les résolutions entre 4000 cm^{-1} et 400 cm^{-1} et sur Beckman IR-11, suspension dans le Nujol pour les résolutions jusqu'à 70 cm^{-1} (complexe norbornène–palladium). Les spectres de rmn ont été obtenus selon (17) sur Varian A60 et Brucker WH90 à $T = 70°C$, le monomère et les polymères étant en solution dans le benzène, à T ambiante pour le complexe norbornène–palladium.

Les alcools utilisés (puriss Fluka): MeOH, EtOH, *n*-BuOH

[1]A qui toute correspondance doit être adressée.

[2]Avec la collaboration de Mme S. Libs pour la partie chromatographique.

0008-4042/79/152022-06$01.00/0

TABLEAU 1. Influence du catalyseur sur la polymérisation du norbornène*

Catalyseurs	Conversion norbornène (%)	Rendement en polymère (%)	Type de polymérisation
$PdCl_2(C_6H_5CN)_2$	42	40	Vinyl
$PdCl_2[P(C_6H_5)_3]_2$	20	17	Vinyl
$PdCl_2[P(Bu)_3]_2$	—	—	—
$PdCl_2(C_7H_{10})_4$	40	40	Vinyl
$RhCl_3 \cdot 3H_2O$	15	5	Ouverture de cycle *trans*
$RhCl[P(C_6H_5)_3]_2$	22	7	Ouverture de cycle *trans*
Complexe Rh–norbornène	10	7	Ouverture de cycle *trans*
$RuCl_3 \cdot 3H_2O$	71	65	Ouverture de cycle *trans*
$RuCl_2[P(C_6H_5)_3]_3$	86	80	Ouverture de cycle *trans*
$Ru_3(CO)_{12}$	43	36	Ouverture de cycle *trans*
$RuClCO[P(C_6H_5)_3]_2$	24	21	Ouverture de cycle *trans*

*T = 68°C durée: 21 h solvant EtOH. (cat Rh) = 2.67×10^{-3} mol/L; (monomère) = 2.5 mol/L. (cat Ru) = 1.5×10^{-2} mol/L; (monomère) = 1.5 mol/L. (cat Pd) = 1.1×10^{-2} mol/L; (monomère) = 2.5 mol/L.

et *t*-BuOH ont été séchés et distillés selon la méthode au phtalate (23). Le benzène (puriss Fluka) a été distillé sur potassium et le norbornène (purum Fluka) distillé et contrôlé par chromatographie phase gazeuse et rmn.

Conduite d'une réaction de cinétique: dans un ballon de 100 mL, on dissout le catalyseur $RuCl_3 \cdot 3H_3O$ (4×10^{-5} mol) dans 0.137 mol EtOH (T = 68°C). On ajoute alors 0.04 mol de norbornène dans 0.137 mol EtOH. La consommation de norbornène est mesurée par prélèvements réguliers en chromatographie phase gazeuse par la méthode de l'étalon interne (octane 2.15×10^{-6} mol). Pour chaque catalyseur la courbe de conversion présente initialement une partie linéaire correspondant à une vitesse de polymérisation constante puis une déviation par rapport à la linéarité (t = 1 h 30 min) correspondant à un début de précipitation du polymère formé. La vitesse de polymérisation décroît alors lentement et le système semble devenir progressivement inactif. Le polymère obtenu est soigneusement lavé au méthanol, séché et pesé.

Les conditions chromatographiques sont les suivantes: catharomètre (Varian 202), colonne: SE 30 10% sur Chromosorb W 80/100 mesh, (2 m, 1/8 po, 75°C) He gaz vecteur, octane étalon interne.

Préparation des catalyseurs

$PdCl_2$–norbornène: 190.5 mg de chlorure de palladium dibenzonitrile (6.8×10^{-4} mol) sont dissous dans 5 mL de méthanol ainsi que 568.4 mg de norbornène (6×10^{-3} mol) dans 25 mL de méthanol. Le mélange est refroidi à −2°C pendant 1/2 h. On note l'apparition d'un précipité jaune. Le mélange est laissé à cette température 24 h puis filtré, lavé et séché. Masse de solide obtenu 225.8 mg. Rendement 60%.

Rh–norbornène: une solution de 5.8×10^{-2} mol de norbornène et 3.2×10^{-3} mol de $RhCl_3 \cdot 3H_3O$ dans 0.45 mol d'éthanol est chauffée sous reflux pendant 2 h. Obtention d'un précipité brun-violet qui est lavé et séché. Rendement 50%.

Résultats et discussion

A. Catalyseurs au palladium

a. Activités-rendements

Des essais avec $PdCl_2$ suivant Schultz (7) ne nous ont donné qu'une faible quantité de polymères due au peu de solubilité du catalyseur dans le milieu. Par contre, des catalyseurs au palladium, solubles dans le milieu (benzène, norbornène): chlorure de palladium dibenzonitrile, chlorure de palladium triphénylphosphine et tributylphosphine ainsi 'qu'un complexe norbornène–palladium $PdCl_2(C_7H_{10})_4$ isolé et étudié en polymérisation ont donné les résultats plus significatifs (tableau 1). Ce tableau nous permet de constater:

α—Une bonne corrélation entre conversion du norbornène et rendement en polymère montrant la formation privilégiée de polymères de poids moléculaires élevés. Dans ce travail nous n'avons pas étudié les équilibres monomère–polymère ou oligomère–polymère comme dans le cas du cyclopentène et du cyclooctène (24–26).

β—Une différence d'activité marquée selon le catalyseur: l'activité décroît lorsque la basicité des ligands augmente (pK_a de $P(Bu)_3$ et $P(C_6H_5)_3$ 8.43 et 2.73 rendement en polymère 0 et 17.3%).

γ—Le complexe palladium–norbornène isolé se comporte d'une façon analogue à celle de $PdCl_2(C_6H_5CN)_2$ dont il dérive.

L'étude infrarouge et rmn des polymères obtenus indiquent une polymérisation type vinylique: en ir absence de bandes à 963 cm^{-1} et 742 cm^{-1} caractéristiques d'une ouverture de cycle, en rmn le spectre est composé de trois massifs principaux à 2.1, 1.6 et 1.1 ppm/TMS et l'assignement complet est identique à celui donné par Gaylord et coll. (13).

b. Complexe norbornène–palladium

Le complexe $PdCl_2(norbornène)_4$ préparé à partir de chlorure de palladium dibenzonitrile et norbornène en proportion 1/1 à 0–2°C dans le méthanol et dont la formule a été déterminée à partir de l'analyse élémentaire Pd, Cl, C, H présente les caractéristiques ir et rmn suivantes: en ir: bande Pd—Cl à 340 cm^{-1} et 309 cm^{-1} (27–29) et Pd—C à 480 cm^{-1}. La bande à 480 cm^{-1} suggère une liaison σ entre le palladium et le carbone. La comparaison des spectres rmn du complexe (3.4 ppm/TMS), du norbornène (5.95 ppm/TMS) et du polymère (1.47 et 1.53 ppm/TMS)

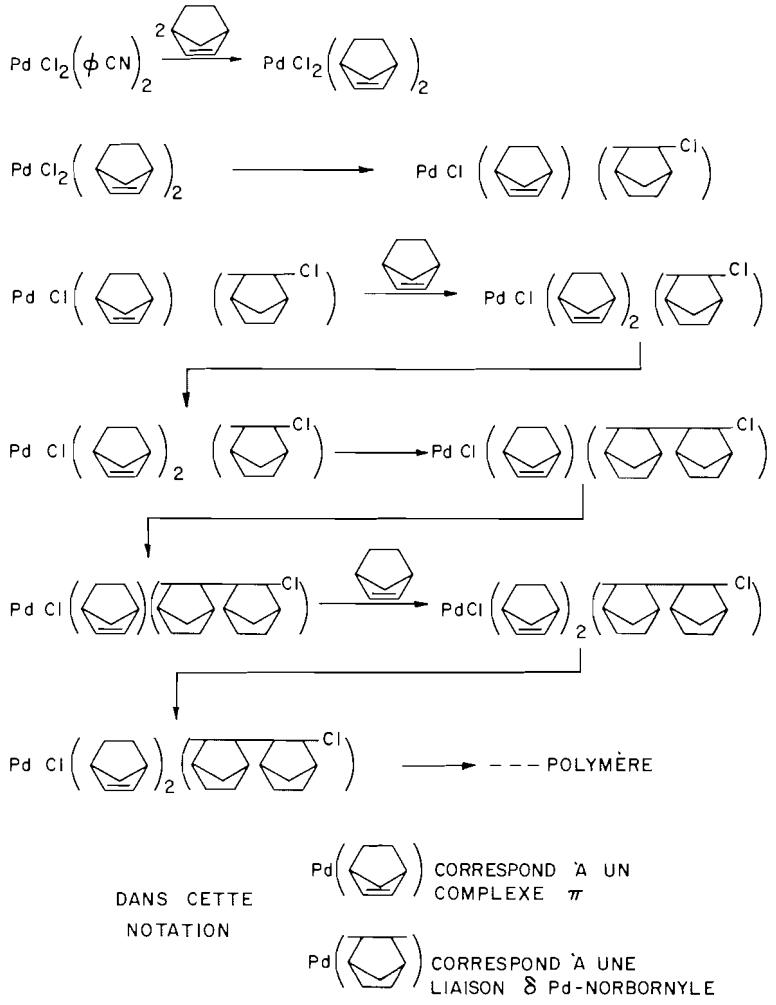

FIG. 1. Polymérisation de type vinylique avec des catalyseurs au palladium.

pour les protons ayant la même position que les protons oléfiniques du norbornène permet de constater une position intermédiaire des protons du complexe entre les protons oléfiniques du norbornène (liaison Π) et ceux du polymère (liaison σ), indiquant la formation d'un complexe Π entre le métal et le norbornène. Comme par ir nous avions déjà mis en évidence une liaison σ Pd—C il faut admettre que *n* motifs norbornène sont liés au métal par des liaisons Π et 4-*n* par des liaisons σ. De plus, la courbe d'intégration permet de préciser la présence d'un proton oléfinique pour dix autres protons. Dans le cas du complexe $PdCl_2$(norbornène)$_4$ ceci nécessite deux motifs monomères liés au métal par une liaison Π, et deux autres l'étant par une liaison σ. Le complexe $PdCl_2$(norbornène)$_4$ ayant donné en polymérisation le même type de polymère avec un rendement identique à celui obtenu avec $PdCl_2(C_6H_5CN)_2$ (tableau 1) ceci laisse prévoir que le complexe isolé est un intermédiaire réactionnel bien qu'il n'ait pu être isolé lors de la polymérisation avec $PdCl_2(C_6H_5CN)_2$ du fait d'une trop grande vitesse de polymérisation.

c. Schéma réactionnel

La polymérisation de type vinylique avec le palladium s'explique par la succession de deux étapes correspondant, l'une à la coordination de la double liaison oléfinique sur le métal, l'autre à une insertion:

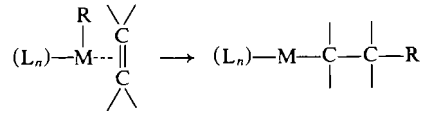

Nos résultats ir et rmn, décrits pour le complexe $PdCl_2$(norbornène)$_4$, indiquent l'existence d'une telle liaison Π et σ entre le palladium et le norbornène. La polymérisation peut alors être schématisée de la manière suivante (fig. 1).

B. Catalyseurs au rhodium

a. Activités-rendements

Nos essais de polymérisation avec $RhCl_3 \cdot 3H_2O$, $RhCl(P\phi_3)_2$ et un complexe Rh–norbornène sont donnés dans le tableau 1.

Le tableau 1 permet les observations suivantes:

α—Nous avons polymérisation par ouverture de cycle avec formation du composé trans mais avec une conversion faible par rapport à celle obtenue dans des conditions identiques avec le ruthénium en accord avec un tableau de réactivité des métaux proposé par Dall'Asta et Motroni (2).

β—Légère augmentation en fin de réaction du taux de conversion, du rendement en polymère et de la vitesse réactionnelle en passant de $RhCl_3 \cdot 3H_2O$ à $RhCl(P\phi_3)_2$ (fig. 2). Ce phénomène, bien que moins prononcé est identique à celui observé pour les catalyseurs au ruthénium.

b. Complexe norbornène-rhodium

Le complexe signalé par Varshavsky et coll. (30): $[Rh(C_7H_9)(C_7H_{10})Cl_2]_2$ a été préparé. Il ne montre pas de variation importante du rendement ou de la vitesse de polymérisation par rapport aux autres complexes étudiés (tableau 1, fig. 2).

C. Catalyseurs au ruthénium

Nous avons repris l'observation de la réaction de polymérisation pour des complexes du ruthénium en solution alcoolique (18) en nous attachant à déterminer le rôle du solvant dans ce type de réaction pour $RuCl_3 \cdot 3H_2O$ et $RuCl_2(P\phi_3)_3$ ainsi que le rôle de ligand que peut jouer la triphénylphosphine ou l'addition d'une nouvelle oléfine tel que le cyclopentadiène.

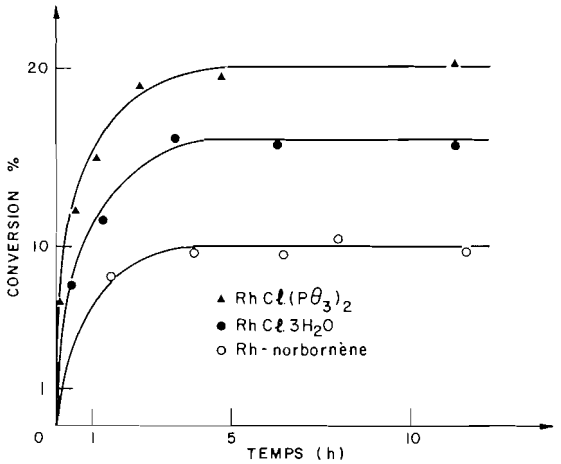

FIG. 2. Influence des catalyseurs au rhodium sur la conversion du norbornène. Solvant EtOH, $T = 68°C$; (catalyseur) $T = 2.6 \times 10^{-3}$ mol/L; (monomère) $T = 2.5$ mol/L.

a. Activités-rendements

Les résultats concernant l'activité du ruthénium en solution alcoolique sont donnés dans le tableau 1. Ce dernier permet de tirer les conclusions suivantes:

α—Polymérisation par ouverture de cycle avec formation privilégiée de polymère.

β—Les catalyseurs au ruthénium utilisés, présentent la particularité d'avoir un degré d'oxydation du métal différent: 0, 1, 2, 3. Les meilleurs résultats sont obtenus avec $Ru_{II}Cl_2(P\phi_3)_3$ alors que $Ru_ICICO(P\phi_3)_2$ donne les plus faibles rendements. Bien qu'il ne semble pas y avoir de corrélation directe entre le degré d'oxydation et le rendement de la polymérisation contrairement à ce que suggère Rinehart et Smith (31) qui proposent une réduction initiale dn métal dans son degré d'oxydation le plus bas, nos résultats ne peuvent l'exclure complètement car cette dernière peut être accompagnée éventuellement d'une variation du nombre de coordination.

b. Etude de l'effet de solvants

Alors que la polymérisation ne se fait pas en milieu dioxane ou tétrahydrofuranne, les solvants alcooliques conviennent bien et leur rôle mérite d'être précisé. Michelotti et Keaveney (17) suggèrent, dans l'étape d'initiation, une attaque nucléophile de l'éthanol sur un complexe Π-métal–oléfine. Rinehart et Smith (31) quant à eux considèrent que l'alcool est un agent réducteur nécessaire. Il faut toutefois remarquer que l'alcool, outre son rôle de solvant peut intervenir comme ligand substituant. Cette possibilité est étayée par les observations suivantes:

α—Le norbornène, en solvant hexane avec $RuCl_3 \cdot 3H_2O$ comme catalyseur ne polymérise pas. Par contre, si on ajoute de l'alcool en quantité stoechiométrique, $|EtOH|/|RuCl_3 \cdot 3H_2O| = 3$, on observe une polymérisation par ouverture de cycle avec un rendement de 48% (température 70°C, EtOH: 1.14 mmol, $RuCl_3 \cdot 3H_2O$: 0.38 mmol, norbornène: 0.05 mol, hexane: 0.15 mol).

β—Les figs 3 et 4 montrent la conversion du norbornène en fonction du temps pour différents alcools: EtOH, *n*-BuOH, *t*-BuOH avec $RuCl_3 \cdot 3H_2O$ et $RuCl_2(P\phi_3)_3$ comme catalyseurs. Les constantes de vitesse calculées sont identiques pour les trois alcools: 1.4×10^{-4} avec $RuCl_2(P\phi_3)_3$ alors qu'elles varient suivant l'alcool pour $RuCl_3 \cdot 3H_2O$ 2.1×10^{-5}, 3.2×10^{-5} et 6.1×10^{-5} pour EtOH, *n*-BuOH et *t*-BuOH respectivement.

L'influence de ligand nous apparaissant primordiale, nous l'avons alors illustrée par deux ligands particuliers: le cyclopentadiène et la triphénylphosphine.

c. Etude de l'effet de ligands

α—*Cyclopentadiène*: Quelques tentatives prélimi-

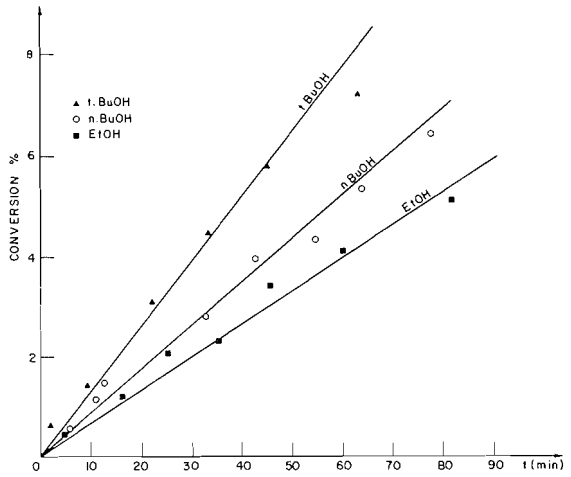

FIG. 3. Influence de l'alcool sur la vitesse de polymérisation; cat: $RuCl_3 \cdot 3H_2O$, $T = 60°C$; ($RuCl_3 \cdot 3H_2O$), $T = 3.94 \times 10^{-3}$ mol/L; (monomère) $T = 3.94$ mol/L.

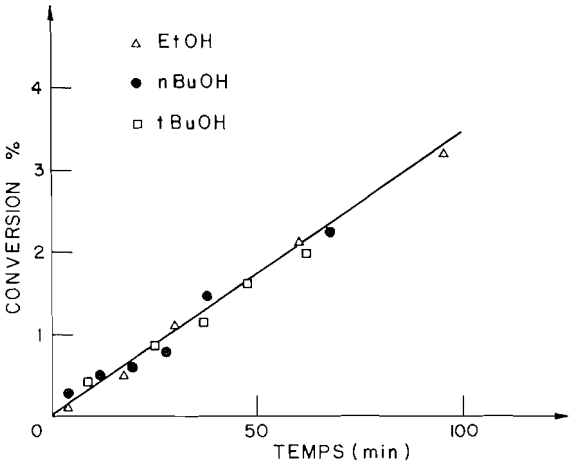

FIG. 4. Influence de l'alcool sur la vitesse de polymérisation; cat; $RuCl_2(P\phi_3)_3$, $T = 68°C$; [$RuCl_2(P\phi_3)_3$], $T = 3.95 \times 10^{-3}$ mol/L; (monomère) $T = 3.94$ mol/L.

naires nous ayant montré que l'addition de cyclopentadiène, avant mise en contact avec le norbornène, conduisait à la désactivation totale, nous avons choisi de suivre la modification de l'évolution de la réaction déjà engagée lorsqu'on ajoute le cyclopentadiène. La fig. 5 montre un blocage presque immédiat de la réaction (conversion 50%) par addition de cyclopentadiène (cyclopentadiène/Ru = 20) après 50 min de polymérisation. De même, le palier de conversion se situe à 20% par addition d'oléfine (cyclopentadiène/Ru = 1) après 20 min de réaction. Dans les deux cas, la conversion aurait dû être de 71% (tableau 1).

β—*Triphénylphosphine*. La fig. 6 montre l'évolution de la réaction par addition de triphénylphosphine. La vitesse de polymérisation varie suivant le

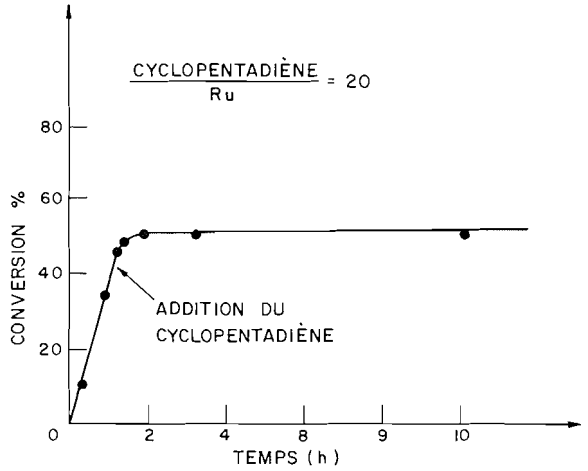

FIG. 5. Influence de l'addition de cyclopentadiène sur le blocage de la réaction; cat: $RuCl_3 \cdot 3H_2O$, $T = 68°C$, solvant EtOH; ($RuCl_3 \cdot 3H_3O$), $T = 2.5 \times 10^{-3}$ mol/L; (monomère) $T = 2.5$ mol/L; (cyclopentadiène) $T = 4.9 \times 10^{-2}$ mol/L.

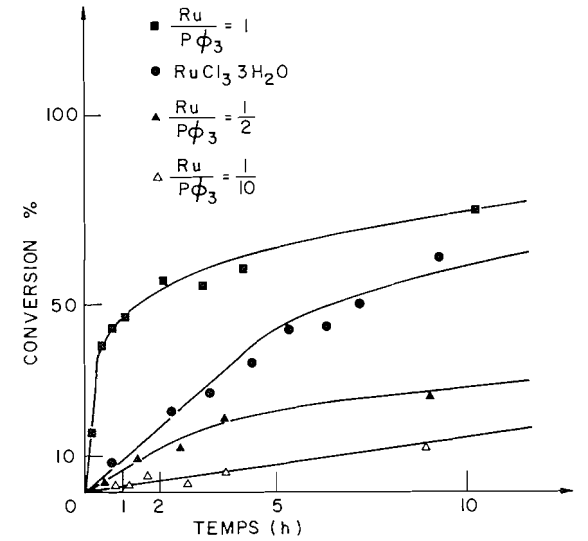

FIG. 6. Influence de la quantité de triphénylphosphine ajoutée sur la vitesse de polymérisation; cat: $RuCl_3 \cdot 3H_2O$, $T = 60°C$, solvant EtOH; ($RuCl_3 \cdot 3H_2O$), $T = 1.9 \times 10^{-3}$ mol/L; (monomère) $T = 1.9$ mol/L.

rapport $P\phi_3$/Ru (fig. 7): maximum d'activité pour le rapport 1/1 (supérieure à $RuCl_3 \cdot 3H_2O$ seul) mais blocage presque complete pour des rapports $P\phi_3$/Ru = 10 (15% de conversion du lieu de 83%).

Discussion

Dans ce travail, nous mettons en évidence l'effet particulier de deux ligands: cyclopentadiène et triphénylphosphine. Le cyclopentadiène est un ligand fort, occupant tous les sites de coordination d'une manière irréversible et empêchant toute poursuite de la réaction, ceci quelque soit le rapport diène/Ru: 1/1 ou 1/20. Ces résultats sont en accord avec ceux

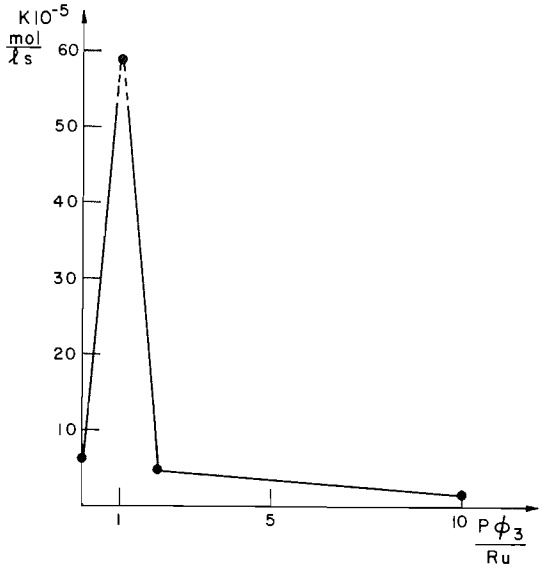

FIG. 7. Influence du rapport $P\phi_3/Ru$ sur la vitesse de polymérisation.

de Porri et coll. (19) sur l'addition d'oléfines aliphatiques. La phosphine, par contre, est un ligand moins fort mais susceptible néanmoins de provoquer la désactivation si elle est en grand excès (fig. 7).

Nous avons également montré le rôle particulier que joue la nature de l'alcool utilisé, indiquant une participation à la réaction puisqu'avec $RuCl_3 \cdot 3H_2O$, la vitesse de polymérisation dépend de l'alcool utilisé contrairement au cas de $RuCl_2(P\phi_3)_3$. L'influence de l'alcool peut s'expliquer en considérant le schéma réactionnel proposé par Laverty et coll. (21), l'alcool jouant un rôle voisin de l'eau dans le schéma proposé. Dans le cas de $RuCl_3 \cdot 3H_2O$, il peut y avoir dissociation du complexe initial $RuX_3L_3 \rightarrow RuX_3L_2 + L$ suivie d'une fixation de l'alcool pour former un nouveau complexe. Ce dernier peut évoluer de manière légèrement différente si EtOH, BuOH ou t-BuOH y sont fixés, notamment dans l'étape suivante de formation de l'hydrure métallique. L'acidité de l'hydrure ainsi formé qui conditionnerait la suite de la réaction, varierait ainsi légèrement d'un alcool à l'autre. Bien que l'eau soit présente avec $RuCl_3 \cdot 3H_2O$, la variation de la constante de vitesse indique plutôt dans notre cas une influence de l'alcool. Dans le cas de $RuCl_2(P\phi_3)_3$, le fait que la nature de l'alcool n'ait pas d'influence sur la vitesse de polymérisation, semble indiquer que l'étape lente de la réaction n'est pas l'échange de ligands mais qu'elle pourrait se situer au niveau de l'étape de métathèse.

Les résultats des effets de solvants et de ligands semblent exclure une interprétation identique pour $RuCl_2(P\phi_3)_3$ et $RuCl_3 \cdot 3H_2O$ tout au moins en ce qui concerne l'étape d'amorçage. Pour ce dernier, l'étape lente de la réaction est l'échange de ligand au niveau du catalyseur. Cette étape ne ferait pas intervenir le monomère mais uniquement le solvant et peut s'effectuer selon un mécanisme associatif ou dissociatif. Pour $RuCl_2(P\phi_3)_3$, l'étape lente de la réaction devrait se situer au niveau de la réaction de métathèse.

Remerciements

Nous remercions madame Pierrette Jutras pour la frappe du manuscrit.

1. K. W. SCOTT, N. CALDERON, E. A. OFSTEAD, W. A. JUDY et J. P. WARD. Rubber Chem. Technol. **44**, 1341 (1971).
2. G. DALL'ASTA et G. MOTRONI. Angew. Makromol. Chem. **16/17**, 51 (1971).
3. N. CALDERON. J. Macromol. Sci. Rev. Macromol. Chem. C7, 105 (1972).
4. G. DALL'ASTA. Rubber Chem. Technol. **47**, 511 (1974).
5. K. W. SCOTT. Polym. Prepr. **13**, 874 (1972).
6. T. TSUJIMO, T. SAEGUSA, S. KOBAYASHI et S. FURAKAWA. J. Chem. Soc. Ind. Chem. Sect. **67**, 1961 (1964).
7. R. G. SCHULTZ. Polym. Lett. **4**, 541 (1966).
8. J. E. MCKEAN et P. S. STARCHER. U.S. Patent No. 3330815 (1967).
9. G. SARTORI, F. CIAMPELLI et N. CAMELI. Chim. Ind. (Milano), **45**, 1478 (1963).
10. T. TSUJIMO, T. SAEGUSA et J. FURUKAWA. Makromol. Chem. **85**, 71 (1965).
11. W. C. TRUETT, D. R. JOHNSON, I. M. ROBINSON et R. A. MONTAGUE. J. Am. Chem. Soc. **82**, 2337 (1960).
12. K. J. IVIN, J. J. ROONEY et C. D. STEWART. Chem. Commun. 603 (1978).
13. N. G. GAYLORD, B. M. MANDOL et H. MARTIN. Polym. Lett. 555 (1976).
14. A. M. POLYAKOVA, A. F. PLATE, M. A. PYRANISHMIKOVO et N. A. LIPALINOV. Neftekhimiya, **1**, 521 (1961); Chem. Abstr. **57**, 10026f (1962).
15. A. W. ANDERSON et N. G. MERCKLING. U.S. Patent No. 2721189 (1955).
16. H. C. EULETERIO. U.S. Patent No. 3074918 (1963).
17. F. W. MICHELOTTI et W. P. KEAVENEY. J. Polym. Sci. Part 1, **3**, 895 (1965).
18. K. HIRAKI et H. HIRAI. J. Polym. Sci. Part A, 2323 (1971).
19. L. PORRI, R. ROSSI, P. DIVERSI et A. LUCHERINI. Polym. Prepr. **13**, 897 (1972).
20. T. OSKIKA et H. TABUCHI. Bull. Soc. Chim. Jpn. **41**, 211 (1968).
21. D. T. LAVERTY, M. A. MCKERVEY, J. J. ROONEY et A. STEWART. Chem. Commun. 193 (1976).
22. K. J. IVIN, J. J. ROONEY, C. D. STEWART, L. H. GREEN et R. MAHTAB. Chem. Commun. 604 (1978).
23. A. I. VOGEL. Practical organic chemistry. 3rd ed. Longman 1970. pp. 168, 170.
24. H. HÖCKER, W. REIMANN, K. REIBEL et Z. SZENTIVANYI. Makromol. Chem. **177**, 1707 (1976).
25. E. A. OFSTEAD et N. CALDERON. Makromol. Chem. **154**, 21 (1972).
26. J. P. SOUFFLET. C.R. Acad. Sci. **276**, 169 (1973).
27. A. D. ALLEN et T. THEOPHANIDES. Can. J. Chem. **42**, 1551 (1964).
28. M. LE POSTOLLEC, J. P. MATHIEU et H. POULET. J. Chem. Phys. **60**, 1319 (1963).
29. G. E. COATEN et C. PARKIN. J. Chem. Soc. 421 (1963).
30. YU. S. VARSHAVSKY, T. G. CHERKASOVA, N. V. BUZINA et V. A. KORMER. J. Organomet. Chem. **77**, 107 (1974).
31. R. E. RINEHART et H. P. SMITH. Polym. Lett. **3**, 1049 (1965).

Temperature and concentration dependence of fluidity of mixed hydrated melts of calcium- and nickel(II)-nitrates

NURUL ISLAM AND ANWAR ALI

Department of Chemistry, Aligarh Muslim University, Aligarh 202001, India

Received January 10, 1979

NURUL ISLAM and ANWAR ALI. Can. J. Chem. 57, 2028 (1979).

The non-Arrhenius temperature dependence of fluidity, ϕ, of molten mixtures of calcium nitrate tetrahydrate and nickel(II) nitrate hexahydrate has been explained in terms of equations based upon the Vogel–Tammann–Fulcher (VTF) and the configurational entropy (CEM) models. The role of the relevant parameters in understanding the successive variations in their behaviour with concentration has been examined. The concentration dependence of fluidity has been explained satisfactorily by an isoenergetic equation. In addition to the linear dependence of the pre-exponential terms of the VTF and the Doolittle equations on the ideal glass-transition temperature, T_0, and the molar intrinsic volume, V_0, respectively, linear interdependence of the two thermodynamic parameters, T_0 on V_0, has been found. Linear dependence of the corrected activation energy, E_{cor}, on the V_0 and the T_0 values have been demonstrated in the system under investigation.

NURUL ISLAM et ANWAR ALI. Can. J. Chem. 57, 2028 (1979).

La fluidité, ϕ, de mélanges fondus du tétrahydrate du nitrate de calcium et de l'hexahydrate du nitrate de nickel(II) n'est pas reliée à la température par une fonction d'Arrhénius; ce fait est expliqué à l'aide d'équations basées sur des modèles de Vogel–Tamman–Fulcher (VTF) et d'entropie configurationnelle. On a examiné le rôle des paramètres appropriés pour comprendre les variations successives de leur comportement avec la configuration. On a expliqué d'une façon satisfaisante le fait que la fluidité varie avec la concentration en faisant appel à une équation isoénergétique. En plus de la relation linéaire des termes pré-exponentiels de VTF et des équations de Doolittle avec la température de transition vitesse idéale, T_0, et le volume molaire intrinsèque, V_0, on a aussi trouvé une relation linéaire entre les deux paramètres thermodynamiques, T_0 et V_0. On a démontré l'existence d'une relation linéaire entre l'énergie d'activation corrigée E_{cor} et les valeurs V_0 et T_0 dans le système étudiée.

[Traduit par le journal]

Introduction

In pursuance of our investigation on the concentration dependence of transport behaviour of mixtures of hydrated melts we attempt to explain such a behaviour quantitatively on the basis of constant T/T_0 $(=c)$ which has the advantage of being isoenergetic and also being independent of the T_0 values of the two constituents in a bicomponent system. The relevant reported (1) expression,

$$[1]\quad \phi = (A_{1(0)} - Q_1N)[(T_{0(0)} - Q_2N)c]^{-1/2} \times \exp\,[-k_1/(T_{0(0)} - Q_2N)(c-1)]$$

assumes the linear dependence of the pre-exponential parameter of the VTF equation, A_1, and that of the ideal glass-transition temperature, T_0, on concentration. Consequently, by combining these latter relations, an interesting linear dependence of A_1 on T_0 has also been obtained earlier (1) as

$$[2]\quad A_1 = [A_{1(0)} \mp T_{0(0)}(Q_1/Q_2)] \pm T_0(Q_1/Q_2)$$

especially in view of the role of A_1 in determining the concentration dependence of viscosities, ϕ^{-1}.

Similarly, in view of the linear concentration dependence of the pre-exponential term of the Doolittle equation and also that of the molar intrinsic volume, V_0, the following two relations obtained earlier (2) are

$$[3]\quad A_2 = [A_{2(0)} \mp V_{0(0)}(Q_3/Q_4)] \pm V_0(Q_3/Q_4)$$

and

$$[4]\quad T_0 = [T_{0(0)} \mp V_{0(0)}(Q_2/Q_4)] \pm V_0(Q_2/Q_4)$$

in which $A_{1(0)}$, $T_{0(0)}$, $A_{2(0)}$, and $V_{0(0)}$ are the corresponding values for the solvent while Q_1, Q_2, Q_3, and Q_4 are the slopes of A_1 vs. N (in mol%), T_0 vs. N, A_2 vs. N, and V_0 vs. N plots, respectively. The signs in these equations signify either increase or decrease in A_1, T_0, A_2, and V_0 with N. Equations [2] to [4] may successfully be applied to any system in which A_1, T_0, A_2, and V_0 vary linearly with concentration.

The present paper is an attempt to test the validity of the recently proposed expressions essentially describing the concentration dependence of the transport properties and to examine further the role

0008-4042/79/152028-04$01.00/0

TABLE 1. Parameters for density equation* for molten $Ca(NO_3)_2 \cdot 3.96H_2O$–$Ni(NO_3)_2 \cdot 6.03H_2O$ system

	Value for $[Ni^{2+}]$ in mol%						
Parameter	0.00	10.19	19.80	29.10	39.83	49.65	60.83
a	2.0009	2.0068	2.0085	2.0072	2.0377	2.0339	2.0539
$b \times 10^{-3}$	0.8317	0.8069	0.8040	0.7670	0.8203	0.7826	0.7990

*The density equation is $\rho(g/cm^3) = a - bT(K)$. The temperature range over which the parameters are valid is 308 to 358 K.

TABLE 3. Computed parameters for the VTF[a] and the CEM[b] equations for the fluidity of molten $Ca(NO_3)_2 \cdot 3.96H_2O$–$Ni(NO_3)_2 \cdot 6.03H_2O$ system

$[Ni^{2+}]$ (mol%)	A_1	k_1 (K)	T_0 (K)	Standard deviation in ln ϕ	A_3	k_3 (K)	T_0 (K)	Standard deviation in ln ϕ
0.00	8443.8	671.00	206.60	0.006	179.5	696.0	206.0	0.008
10.19	8325.3	677.05	204.75	0.006	175.0	697.0	204.7	0.007
19.80	8175.0	671.00	202.00	0.006	170.3	689.2	202.2	0.008
29.10	8025.0	672.00	200.50	0.004	166.5	689.0	201.0	0.005
39.83	7875.0	671.20	199.41	0.009	160.3	687.0	199.2	0.014
49.65	7725.0	671.50	197.00	0.008	157.8	683.0	197.1	0.018
60.83	7600.0	668.70	196.55	0.006	154.0	680.0	196.3	0.016

[a]The VTF equation is $\phi = A_1 T^{-1/2} \exp[-k_1/(T - T_0)]$.
[b]The CEM equation is $\phi = A_3 \exp[-k_3/T \ln T/T_0]$.

of these parameters in understanding the transport behaviour of molten salt systems. Molten $Ca(NO_3)_2 \cdot 3.96H_2O$–$Ni(NO_3)_2 \cdot 6.03H_2O$, being a low melting system, has been chosen for this purpose because of the ease of experimental measurements.

Experimental

Commercial calcium nitrate tetrahydrate (BDH; mp 42.7°C) was used as a solvent in the molten state while nickel(II) nitrate hexahydrate (BDH; mp 56.7°C) as a solute. Samples were prepared in a thermostated paraffin bath at about 60°C in an atmosphere of pure and dry nitrogen. Calcium nitrate tetrahydrate was found to dissolve 60.83 mol% of the solute. The prepared samples were stored in a vacuum desiccator.

Density (±0.3%) and viscosity (±0.1%) measurements were made with a dilatometer (3) of 0.01 mL division, and a Cannon–Ubbelohde type (4) viscometer, respectively, in a thermostated bath of ±0.1° thermal stability.

Results and Discussion

Calcium nitrate tetrahydrate and its mixtures with nickel(II) nitrate hexahydrate have been found to show supercooling tendency to a larger extent. However, as the concentration of the solute increases the supercooling tendency of the successive mixtures keeps decreasing. Therefore one may conclude that the crystallization kinetic constants of nickel(II) nitrate hexahydrate are comparatively more favourable to crystallization than those of calcium nitrate tetrahydrate.

The density and the viscosity of pure calcium nitrate tetrahydrate and those of its mixtures with nickel(II) nitrate hexahydrate measured as functions of temperature and concentration are listed in Tables 1 and 2.[1] The exact water of crystallization was found to be 3.96 (3, 5) and 6.03 (6) in the hydrated nitrates of calcium and nickel(II) respectively. The measured density of the solvent was found to be 0.17 and 0.39% higher when compared with those reported (3, 5) at 25°C. A difference of about 5% was noted in the viscosity at 40°C when compared with those reported by Moynihan (3).

As usual the non-linear ln η vs. $1/T$ plots were linearized by least-squares fitting the data to the VTF and the CEM equations as shown in Figs. 1 and 2.[1] Similarly, the non-linear plots of η versus reciprocal of free-volume were linearized by the Doolittle equation shown in Fig. 3.[1] The computed best fit parameters of these equations are listed in Tables 3 and 4.

The viscosity of the system under study is found to decrease quite markedly with concentration as shown in Fig. 4. Such a trend in viscosity isotherms has been found to be similar to those reported earlier (7, 8). An examination of isotherms *I*, *II*, and *III* reveals that at 10.19 and 39.83 mol%, curves *II* and *III*, in this order, show an increasing tendency for higher viscosities than expected for a smooth variation with concentration. It is apparent from Fig. 4 that as the temperature increases the isotherms tend to be linear,

[1]Complete set of data (Table 2, Figs. 1 to 3) are available, at a nominal charge, from the Depository of Unpublished Data, CISTI, National Research Council of Canada, Ottawa, Ont., Canada K1A 0S2.

TABLE 4. Computed parameters for the Doolittle[a] equation for the fluidity of molten $Ca(NO_3)_2 \cdot 3.96H_2O$–$Ni(NO_3)_2 \cdot 6.03H_2O$ system

$[Ni^{2+}]$ (mol%)	A_2	k_2	V_0 (cm^3 mol^{-1})	Standard deviation in ln ϕ
0.00	271.20	37.11	128.90	0.006
10.19	260.00	36.22	131.15	0.005
19.80	250.00	35.86	133.81	0.005
29.10	240.30	34.22	136.11	0.005
39.83	230.10	36.46	137.84	0.009
49.65	210.00	33.51	140.58	0.007
60.83	200.00	34.14	142.59	0.008

[a]The Doolittle equation is $\phi = A_2 \exp[-k_2/(V - V_0)]$.

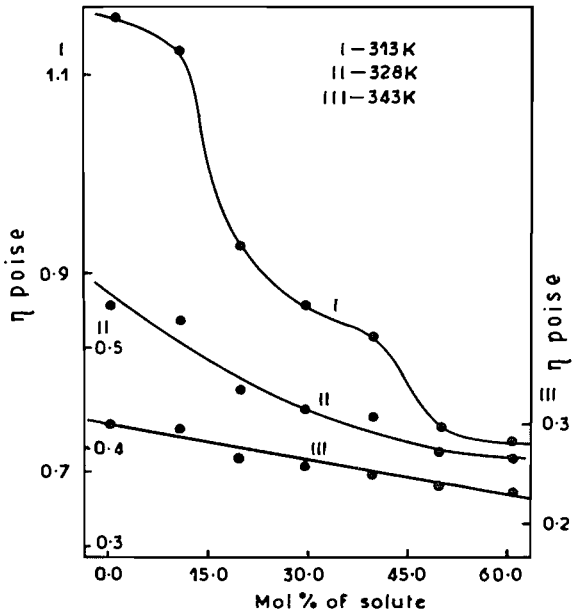

FIG. 4. Viscosity isotherms for molten $Ca(NO_3)_2 \cdot 3.96H_2O$–$Ni(NO_3)_2 \cdot 6.03H_2O$ system.

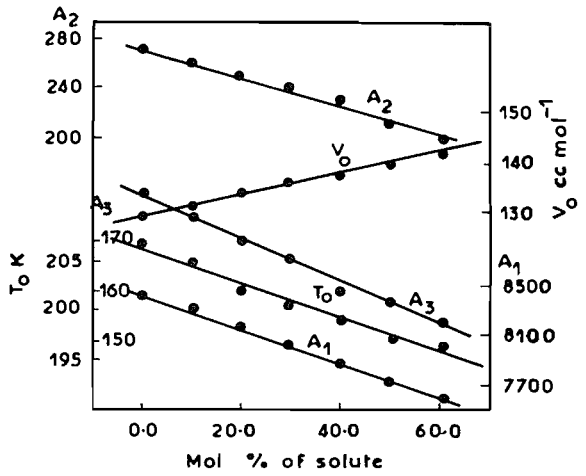

FIG. 5. Variation of A_1, A_2, A_3, T_0, and V_0 with [solute] for molten $Ca(NO_3)_2 \cdot 3.96H_2O$–$Ni(NO_3)_2 \cdot 6.03H_2O$ system.

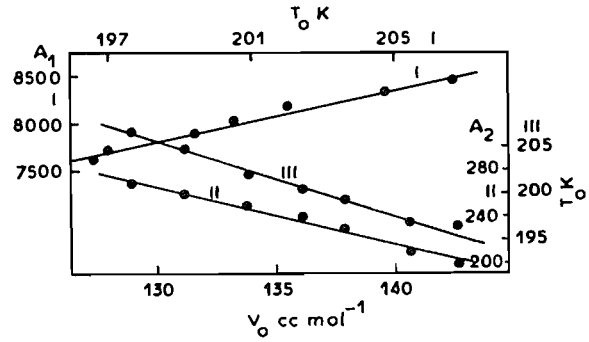

FIG. 6. Variation of (*I*) A_1 with T_0, (*II*) A_2 with V_0, and (*III*) T_0 with V_0 for molten $Ca(NO_3)_2 \cdot 3.96H_2O$–$Ni(NO_3)_2 \cdot 6.03H_2O$ system.

showing the additive nature of viscosity at higher temperatures.

The pre-exponential parameters of the VTF, the CEM, and the Doolittle equations as well as the T_0 and the V_0 values show linear dependence on [solute] as shown in Fig. 5. Thus, a decrease in the T_0 value with increase in [solute] may be due to an increase in the average molecular mass. This is in accordance with the $m^{-1/2}$ dependence relation (9). Such a decrease in T_0 with increase in $[Ni^{2+}]$ may also be due to the additive nature of T_0. The V_0 value, on the other hand, has been found to increase linearly with the [solute], unlike that found in the case of T_0. However, the pre-exponential terms follow the pattern of T_0. The V_0 has been found to be additive in nature as is the case with T_0. The linear dependences expected from [2] to [4] have actually been found in the present system (Fig. 6).

The concentration dependence of fluidities has been explained by least-squares fitting the data to [1] at several values of c corresponding to the experimental temperature, T. The best fit parameters thus obtained are listed in Table 5. The computed parameters, viz., $A_{1(0)}$, Q_1, Q_2, and $T_{0(0)}$ are close to those found from the corresponding plots (Fig. 5).

Finally, the dependence of the corrected activation energy, E_{cor}, on the thermodynamic parameters, V_0 and T_0, has been obtained as

$$[5] \quad E_{cor} = [E_{cor}' \mp V_{0(0)}(Q_5/Q_4)] \pm V_0(Q_5/Q_4)$$

and

$$[6] \quad E_{cor} = [E_{cor}' - T_{0(0)}(Q_5/Q_2)] + T_0(Q_5/Q_2)$$

by combining the linear dependences of E_{cor} vs. N

TABLE 5. Best fit parameters for eq. [1] for the fluidity of molten $Ca(NO_3)_2 \cdot 3.96H_2O$–$Ni(NO_3)_2 \cdot 6.03H_2O$ system

c	$A_{1(0)}$	Q_1	k_1 (K)	$T_{0(0)}$ (K)	Q_2	Standard deviation in ln ϕ
1.6	8443.0	13.87	671.0	206.6	0.19	0.033
1.7	8444.0	13.87	671.2	206.6	0.19	0.028

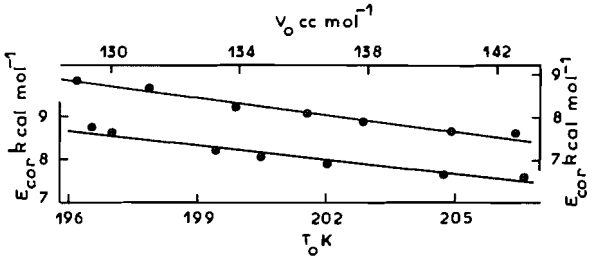

FIG. 7. Variation of E_{cor} with V_0 and T_0 for molten $Ca(NO_3)_2 \cdot 3.96H_2O$–$Ni(NO_3)_2 \cdot 6.03H_2O$ system. $E_{cor} = E_\phi + \frac{1}{2}RT$, in which E_ϕ is obtained by differentiating $\phi = A_\phi T^{-1/2} \times \exp[-k_\phi/(T - T_0)]$ of the VTF equation with respect to the reciprocal of absolute temperature. Adding $\frac{1}{2}RT$ to E_ϕ yields $E_{cor} = Rk_\phi[T/(T - T_0)]^2$.

with V_0 vs. N, and also with T_0 vs. N plots, respectively. E_{cor}' and Q_5 are the intercept and the slope, respectively, of E_{cor} vs. N plot. The expected linear behaviour has actually been found in the present system as shown in Fig. 7.[2] It is interesting to note that increase in the value of E_{cor} with T_0 is physically understandable in view of the successive increase in compactness of the system.

[2]It may be noted further that E_{cor} should also vary linearly with temperature, T, in view of the relation, $T = T_0c$. However, at constant $T/T_0 = c$, E_{cor} turns out to be a temperature independent quantity, viz., $Rk_\phi[c/(c - 1)]^2$. Consequently, this led to the transformation of the VTF equation at constant $T/T_0 = c$ to [1] for the concentration dependence of transport behaviour.

Acknowledgements

The authors thank Professor W. Rahman, Head of the Chemistry Department, for providing the necessary facilities. One of us (A.A.) is thankful to the CSIR (New Delhi) for financial assistance.

1. N. ISLAM, K. P. SINGH, and S. KUMAR. J. Chem. Soc. Faraday Trans. I. In press.
2. N. ISLAM and A. ALI. To be published.
4. C. TANFORD. Physical chemistry of macromolecules. John Wiley and Sons, Inc., New York, NY. 1961. p. 329.
5. W. W. EWING and R. J. MIKOVSKY. J. Am. Chem. Soc. **72**, 1390 (1950).
6. C. N. REILLEY, R. W. SCHMID, and F. S. SADEK. J. Chem. Educ. **36**, 619 (1959).
7. A. J. EASTEAL and I. M. HODGE. J. Phys. Chem. **74**, 730 (1970).
8. H. BLOOM and E. HEYMAN. Proc. R. Soc. (London), **188**, 392 (1947).
9. C. A. ANGELL. J. Am. Ceram. Soc. **51**, 117 (1968).

The solvent extraction of Fe(III) from acidic chloride solutions by open cell polyurethane foam sponge (OCPUFS)

J. J. OREN, K. M. GOUGH, AND H. D. GESSER

Department of Chemistry, University of Manitoba, Winnipeg, Man., Canada R3T 2N2

Received December 1, 1978

J. J. OREN, K. M. GOUGH, and H. D. GESSER. Can. J. Chem. **57**, 2032 (1979).

The extraction of Fe(III) by open cell polyurethane foam sponge was studied as a function of acid, chloride, and iron concentration in the aqueous phase. The results indicate a mixed extraction of $FeCl_3$ and $HFeCl_4$. The results also show a dependence of the metal distribution coefficient on [Fe(III)]aq and indicate a dissociation (in the foam) of the extracted $HFeCl_4$ species. The solid polyurethane is equated to a liquid extractant of a moderate dielectric constant.

J. J. OREN, K. M. GOUGH et H. D. GESSER. Can. J. Chem. **57**, 2032 (1979).

On a étudié l'extraction du Fe(III) par OCPUFS en fonction des concentrations d'acide, d'ion chlorure et de fer dans la phase aqueuse. Les résultats indiquent qu'il se produit une extraction mixte de $FeCl_3$ et $HFeCl_4$. Les résultats démontrent aussi qu'il existe une relation entre le coefficient de distribution du métal et [Fe(III)]aq et ceci indique qu'il se produit une dissociation (dans la mousse) d'espèces $HFeCl_4$ extraites. On considère que le polyuréthane solide ressemble à un extracteur liquide de constante diélectrique moyenne.

[Traduit par le journal]

Introduction

The use of polyurethane foams in the separation of metals from aqueous solutions was first demonstrated by Bowen (1) and the field has been reviewed by Braun and Farag (2, 3). Gesser and co-workers (4, 5) recently studied the extraction of gallium and iron from aqueous acidic chloride solutions into open cell polyurethane foam sponge (OCPUFS) and concluded that metal removal was accomplished by dissolution of the acid tetrahalide complex HMX_4 in the foam. Alternatively, the ether based polyurethane in contact with HX in solution can act as an anion exchanger in the extraction of the MX_4^- species.

The purpose of the present work was to investigate the equilibria involved in systems employing a polyurethane foam sponge as compared to systems using a liquid extractant in the removal of M^{3+} from acidic aqueous solutions. For this purpose iron(III) was chosen as the model metal due to the extensive study that has been made on its liquid extraction by various authors (6–15).

Experimental

Ether based polyurethane, oxypropylene/oxyethylene copolymer polyol, was supplied by Union Carbide. The foam was cut into cylindrical plugs of 2.15 ± 0.05 g, 4 cm diameter and 5.3 cm length. The plugs were cleaned with acetone for several hours in a Soxhlet extractor. An eccentric cam driven by a slow speed motor pushed a glass plunger up and down in a 2.2 cm stroke and at a frequency of 8 strokes per min, squeezing the plug in the test solution at the prescribed temperature. Each plug, before use, was treated three times in this manner for 30 min in 100 mL of 6 *M* HCl and finally washed free of acid with distilled water and air dried. A volume of 50–200 mL of an aqueous test solution was then equilibrated with the sponge in the same fashion for 30 min which was found to be sufficient to establish equilibrium between the two phases. A plug, when used, was cleaned before reuse by slowly flushing with 10 L of 10^{-2} *M* HCl while being squeezed repeatedly. Iron in the initial and in the equilibrium aqueous phase was analyzed by the thiocyanate method, using a Beckman DK-2A spectrophotometer with 1 or 10 cm cells (16). The Fe(III) concentration in the foam was then calculated from the difference between these two values. Proton concentration up to 10^{-1} *M* in the aqueous phase was determined by the procedure suggested by McBryde (17) and Sekine and Dyrssen (18) using a glass–calomel electrode pair and Fisher Accumet Model 520 Digital pH/Ion Meter. Equilibrium $[H^+]$ was equated to initial $[H^+]$ when the latter was > 0.1 *M* (18). The chemicals used were reagent grade.

Results and Discussion

All species in the foam are denoted by the subscript 'o' and those in the aqueous phase by the absence of a subscript. In equations, the charges on the ions are left out for simplicity.

The stability constants of iron(III) species with chloride in the aqueous phase can be represented as follows (12):

$$\mathrm{Fe} + n\mathrm{Cl} \rightleftarrows \mathrm{FeCl}_n^{3-n}$$

$$[1] \quad \beta_n = [\mathrm{FeCl}_n^{3-n}][\mathrm{Fe}]^{-1}[\mathrm{Cl}]^{-n}$$

Since the stability constants of the higher complexes, $FeCl_3$, $FeCl_4^-$, and $HFeCl_4$ are negligibly small (12, 19), the total iron(III) concentration in the aqueous phase can be expressed as follows:

$$[2] \quad [\mathrm{Fe(III)}]_{\mathrm{total}} = [\mathrm{Fe}](1 + \beta_1[\mathrm{Cl}] + \beta_2[\mathrm{Cl}]^2)$$

In the present work the extraction of HCl by the

0008-4042/79/152032-06$01.00/0

foam from an iron(III) free aqueous phase ($[Cl^-] = 4\ M$) was determined in the $10^{-1}\ M$ initial aqueous acidity range and was found to average at $5 \pm 1\%$. Parallel experiments on the extraction of LiCl ($[Li^+] = 4\ M$, $[Cl^-] = 0.1\ M$, $[SO_4] = 1.95\ M$) showed no measurable absorption of the salt by the foam from an iron(III) free aqueous phase. As will be seen, the data were found to be consistent with a mixed extraction of $FeCl_3$ and $HFeCl_4$ species and the ionization of the latter into H_o^+ and $FeCl_4^-{}_o$ in the foams. Under these circumstances the chemical equilibria involved can be presented as follows (12, 15, 20–22):

$$[3] \quad K_{ex_1} = [FeCl_3]_o[Fe]^{-1}[Cl]^{-3}$$

$$[4] \quad K_{ex_2} = [HFeCl_4]_o[Fe]^{-1}[H]^{-1}[Cl]^{-4}$$

$$[5] \quad K_d = [FeCl_4]_o[H]_o[HFeCl_4]_o^{-1} = K_{ex_2}{}^{-1}[FeCl_4]_o[H]_o[Fe]^{-1}[H^{-1}][Cl]^{-4}$$

$$[6] \quad K_{ex_3} = [HCl]_o[H]^{-1}[Cl]^{-1}$$

$$[7] \quad K_d' = [H]_o[Cl]_o[HCl]_o^{-1}$$

The electroneutrality in the organic phase can thus be written as follows:

$$[8] \quad [H]_o = [Cl]_o + [FeCl_4]_o$$

By substituting eqs. [5] through [7] into [8], we can write:

$$[9] \quad [H]_o = [[H][Cl](K_{ex_3}K_d' + K_{ex_2}K_d[Fe][Cl]^3)]^{1/2}$$

The distribution ratio of iron(III) is given by:

$$[10] \quad D = [Fe(III)]_{o,total}[Fe(III)]_{total}^{-1}$$

$$[11] \quad D = \{[FeCl_3]_o + [HFeCl_4]_o + [FeCl_4]_o\} \times \{[Fe](1 + \beta_2[Cl] + \beta_2[Cl]^2)\}^{-1}$$

By substituting eqs. [3] through [5] and [9] into eq. [11], we can write:

$$[12] \quad DY = [Cl]^3\left\{K_{ex_1} + K_{ex_2}[H][Cl] + \frac{K_dK_{ex_2}([H][Cl])^{1/2}}{(K_{ex_3}K_d' + K_{ex_2}K_d[Fe][Cl]^3)^{1/2}}\right\}$$

where $Y = (1 + \beta_1[Cl] + \beta_2[Cl]^2)$. Equation [12] can be simplified into three parts representing the major species in the foam if $K_{ex_3}K_d' \ll K_{ex_2}K_d[Fe][Cl]^3$.

$$[13] \quad DY = [Cl]^3\left\{K_{ex_1} + K_{ex_2}[H][Cl] + \frac{1}{[Cl]}\left(\frac{K_{ex_2}K_d[H]}{[Fe]}\right)^{1/2}\right\}$$

	I	II	III
Principal absorbed species	$FeCl_3$	$HFeCl_4$	$FeCl_4^-$

A summary of the expected properties of eqs. [12] and [13] is shown in Table 1.

Variation of Distribution Ratio with Metal Concentration in the Aqueous Phase

Figure 1, curves *a*, *b*, *c*, *d*, shows the plot of log *D* vs. log iron(III) concentration in the equilibrium aqueous phase at various initial and constant aqueous acid and chloride concentrations. At constant chloride and varying hydrogen ion concentrations, the break in the curve is not appreciably affected by the $[H^+]$ though the plateau value of *D* increases with increase in $[H^+]$. The break in the curve however is shifted to lower $[Fe^{3+}]$ when the $[Cl^-]$ is increased at constant $[H^+]$ (curve *d* vs. curve *b*). This is consistent with the requirements of eq. [13] and shows the overall dependence of *D* on the $[Fe][Cl^-]^3$ term in the denominator of eq. [12]. Though a discussion of the inflection point was given by Saldick (22) and was used (20, 21, 23) to reinterpret Irving and Rossotti's (24) results with $InBr_3$ only a few comparable studies (14, 15) have been reported for the iron(II) chloride – organic solvent system.

The value of *D* was virtually constant when [Fe(III)] was below $\sim 10^{-4}\ M$ but decreased steadily above this concentration with a resulting slope that varied from -0.53 (curve *a*) to about -0.9 (curve *d*) in Fig. 1. Saturation of the foam with iron would lead to a slope of -1.0. This fall-off feature (slope $-\frac{1}{2}$) of complex extraction behavior was reported for Mo(VI) (23); In(III) (24); and for Fe(III) (14, 15), in liquid–liquid extraction systems employing solvents of moderate dielectric constants and was demonstrated to be independent of the level and nature of the acid and supporting salting out electrolyte in the aqueous phase (23, 24).

A detailed study by Friedman (25) of the spectra of iron(III) in acidic chloride aqueous solutions, in diethyl ether extracts from these solutions and in

TABLE 1. Properties of extraction eq. [12]

Dominant term in [13]	Conditions* [H⁺]	[Cl⁻]	[Fe³⁺]	∂(log D)/∂(log [H⁺]) (Fig. 2)	∂(log D)/∂(log [Fe³⁺]) (Fig. 1)	∂(log DY)/∂(log [Cl⁻]) (Fig. 3)
I		−	+	0 (0)†		
	−	−	−		0 (0)	
	−	−	+			3 (2.4)[a]‡
II		+	+	1 (1.1)		
	+	+	−		0 (0)	
	+	+	+		−1 (−0.9)[d]	
	+	+	+			4 (5.3)[c]
						(6.6)[b]
III		−	−	½ (1.2)[b]		
	−	−	+		−½ (−0.53)[a]	
	−	+	−			2 (6.3)[d]
						(4.4)[e]

*+ signifies relatively high concentrations; − signifies relatively low concentrations.
†Values in parentheses are average experimental values obtained in this work or are associated with the lettered curve in the figures indicated at the top of the column.
‡For HCl only.

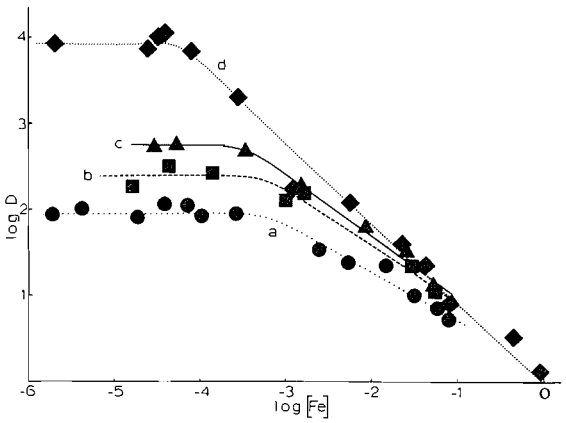

FIG. 1. log D vs. log [Fe] in equilibrium aqueous phase, 22 ± 3°C. Initial [H^+] and [Cl^-] held constant with HCl and LiCl. (*a*) ●, 10^{-2} *M* H^+; 4 *M* Cl^-. (*b*) ■, 1 *M* H^+, 4 *M* Cl^-. (*c*) ▲, 2 *M* H^+, 4 *M* Cl^-. (*d*) ◆, 1 *M* H^+, 7*M* Cl^-.

solid $KFeCl_4$ showed the existence of a $FeCl_4^-$ anion in each case. They also indicated that the proton is not chemically bound to the anion in the organic phase. Conductivity studies by Campbell *et al.* (26) of diisopropyl ether extracts of iron(III) from acidic chloride aqueous media showed that although such ether solutions conduct poorly, the conductivity is much greater than that of HCl solutions of comparable concentrations, indicating that the chloroferric acid is stronger than hydrochloric acid. Diamond and Tuck (20) and Marcus and Kertes (27) concluded that the acid strength of $HFeCl_4$ is comparable to the $HClO_4$.

The Mossbauer spectra (28) of iron in the organic phase of an extraction system of acid iron(III) halide has indicated that the neutral solvated species FeX_3 as well as the ion pair $H^+FeX_4^-$ were being extracted.

In the present work the epr spectra of the iron(III) loaded foam were studied, using a Varian Model E-3 EPR spectrometer, and were found to be identical to those obtained by Hertel and Clark (29), suggesting that $HFeCl_4$ (or the ion pair $H^+FeCl_4^-$) is dissolved in the solid foam.

The experimental slopes obtained from the data under discussion are consistent with the predicted values shown in Table 1; viz. 0 slope for ∂(log D)/∂(log [Fe]) at low concentrations of iron in solution and a slope of $-\frac{1}{2}$ at higher concentrations. At still higher concentrations of iron, the importance of the term III in eq. [12] diminishes and a slope of 0 is again expected. The foam, however, approached saturation with respect to iron before this trend could be realized. Diamond (23), however, has shown such a trend in his work on the liquid–liquid extraction of Mo(IV) from 8 *M* aqueous HCl into his (2 chloroethyl) ether. Similarly, Maddock *et al.* (15*a*), using tracer iron, have obtained the full curve under low extraction conditions, i.e. $D \simeq 10^{-2}$ to 10^{-3}.

Variation of Distribution Ratio with Hydrogen Ion Concentration in the Aqueous Phase

Figure 2, curves *a*, *b*, *c*, *d*, shows the plot of log D vs. log [H^+] concentration in the aqueous phase at constant, 4 *M*, initial chloride concentration and at a constant (1.79×10^{-3} *M* and 4.5×10^{-5} *M*) initial iron(III) concentration. The value of D was found to be practically independent of the hydrogen ion concentration when between 5×10^{-3} *M* to

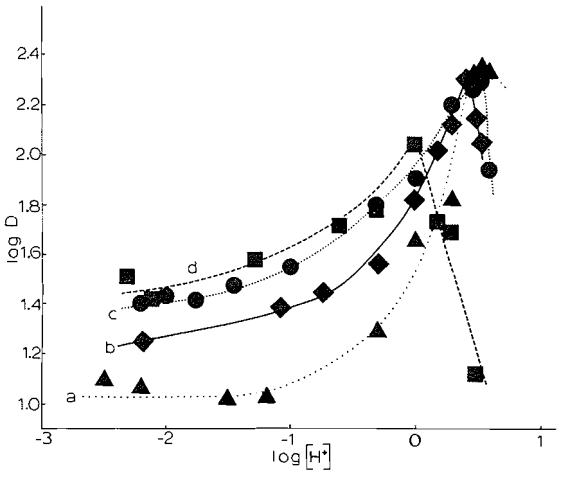

FIG. 2. log D vs. log [H] at constant [Fe] and $[Cl^-] = 4\ M$, in initial aqueous phase. (*a*) ▲, with NaCl, $1.79 \times 10^{-3}\ M$ Fe, 25 ± 1°C. (*b*) ◆, with NaCl, $4.95 \times 10^{-5}\ M$ Fe, 22 ± 3°C. (*c*) ●, with LiCl, $1.79 \times 10^{-3}\ M$ Fe, 22 ± 3°C. (*d*) ■, with LiCl, $1.79 \times 10^{-3}\ M$ Fe, 2.5 ± 1°C.

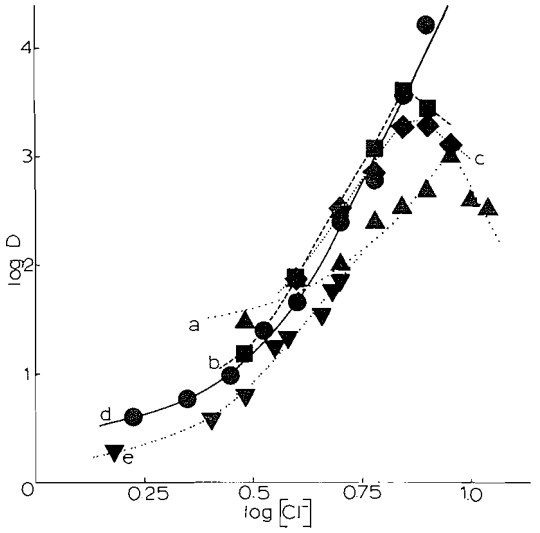

FIG. 3. log D vs. log [Cl] in initial aqueous phase at constant initial [Fe], 22 ± 3°C. Initial $[H^+]$ held constant with HCl except in (*a*). (*a*) ▲, with HCl only, $10^{-3}\ M$ Fe. (*b*) ■, with LiCl, $7.16 \times 10^{-3}\ M$ Fe, $2\ M$ H^+. (*c*) ◆, with LiCl, $7.16 \times 10^{-3}\ M$ Fe, $4\ M$ H^+. (*d*) ●, with LiCl, $10^{-3}\ M$ Fe, $10^{-2}\ M$ H^+. (*e*) ▼, with NaCl, $10^{-3}\ M$ Fe, $10^{-2}\ M$ H^+.

$\sim 10^{-1}\ M$. The distribution ratio, however, increased steadily above this concentration with a resulting slope that varied from 0.72 (curve *c*) to 1.37 (curve *a*) and averaged at 1.1 for the systems investigated at 25 ± 1°C and 22 ± 3°C, curves *a*, *b*, *c*.

Sekine *et al.* (12*a*) studied the distribution of iron(III) between hexane containing trioctylphosphine oxide and acidic chloride aqueous solutions in which $[H^+]$ was varied and $[Cl^-]$ maintained constant, 4 *M*, with NaCl and obtained the slopes of 0 and 1 by a curve fitting method of the experimental data. Similar to the present work an initial constant, $10^{-3}\ M$, [Fe(III)] was employed in these experiments.

The present work confirms most of the predicted slopes shown in Table 1, and leads to the same conclusion arrived at by these authors (12*a*), namely, that the extracted species are mainly $FeCl_3$ and $HFeCl_4$ in the low and high hydrogen ion concentration regions, respectively. Equation [13] predicts that at low concentration of Fe^{3+} and Cl^- in solution, the slope $\partial(\log D)/\partial(\log [H^+])$ should be 1/2. Reducing the concentration of Fe^{3+} from $1.8 \times 10^{-3}\ M$ to $5 \times 10^{-5}\ M$ did not change the slope for $[Cl^-] = 4\ M$. It was not possible to reduce these quantities (Fe^{3+} and Cl^-) further and still see any absorption of iron by the foam.

Variation of Distribution Ratio with Chloride Concentration in the Aqueous Phase

Figure 3, curves *b*, *c*, *d*, *e*, shows the plot of log D vs. log $[Cl^-]$, initial chloride concentration in the aqueous phase, at constant initial $[Fe^{3+}]$ and at constant and various initial $[H^+]$, but not at constant ionic strength. Curve *a* (slope varies from 2.4 to 6.5) is the plot of log D vs. log initial aqueous HCl concentration in the absence of a supporting salt electrolyte. The values of the slopes (curve *b*, 6.6; curve *c*, 5.3; curve *d*, 1.7 to 6.3; curve *e*, 1.5 to 4.4) as computed from the experimental data (Table 1) were found to be higher than those predicted by eq. [12] at the relatively high chloride concentration range. Positive deviations in the values of the slopes were also reported in the foam extraction of Ga(III) from acidic chloride aqueous solutions under similar experimental conditions and were accounted for by the change in ionic strength of the solution and the water activity and the use of concentrations instead of activities in the plots (5).

A fall in the D value was observed at a further increase in $[H^+]$ in each of the four curves in Fig. 2. A similar drop in D value was also noted when the initial [HCl] was changed in the aqueous phase in the absence of Li^+ and Na^+ salts or when the initial [HCl] was kept constant, at 2 *M* and 4 *M*, and the chloride (Li^+) concentration was varied (Fig. 3, curves *a*, *b*, *c*). However, a falloff in log D was absent when the initial $[H^+]$ was kept constant but very low, $10^{-2}\ M$, while the chloride (Li^+,Na^+) concentration was increased (Fig. 3, curves *d* and *e*).

Most recently, Shamus-ud-Zaha and Ejaz (30) recognized a similar decrease in log D when HCl concentration was increased in the absence or pres-

ence of a supporting salting out electrolyte in the extraction of Zn from acidic aqueous solution by 4-(5-nonyl) pyridine in benzene. A similar decrease in D value was also noted in the extraction of $UO_2(NO_3)_2$ into tributyl phosphate from mixed $LiNO_3$–HNO_3 solutions upon increased aqueous acidity (31). The insolubility of the organic phase in acidic chloride aqueous solutions in the above works and in the present work eliminates the possibility that the fall in the distribution ratio is due to a decrease in the aqueous HCl concentration after a volume change caused by the passage of the organic phase into the aqueous, a case that was reported by several authors (6, 10, 32). Also, since the order of hydration for the hydronium and alkali cations is $H_3O^+ \approx Li^+ > Na^+ > K^+ > Cs^+$ (33), an increase rather than a decrease in D value should result as the amount of acid replacing the salt is increased (34). In addition, since no higher chlorocomplex of iron than $FeCl_4^-$ is known (19), a decrease in the distribution ratio with increased acidity cannot be attributed to the formation of more highly charged, nonextracting, iron species. The data of the present work lend support to the suggestion put forward by Diamond (23) that an inflection in log D under these conditions could be accounted for by the extraction of HCl and its coordination with the organic phase so readily as to significantly reduce the 'free' extractant available for the metal complex.

The effect of temperature on the extraction is evident by a comparison of curve *c* (22°C) and curve *d* (2.5°C) in Fig. 2. At the lower temperature, the drop-off in the value of D occurs at a lower initial acid concentration. This premature drop in log D is believed to be due to the lowering of the water activity as the temperature decreases in the presence of a Li^+ cation (35) resulting in an increased activity of HCl in the aqueous phase.

The effect of temperature on the extraction of $FeCl_3$ into trioctylphosphine oxide in CCl_4 has been studied by Maddock and Mederiros (*15b*) who interpret their results in terms of the extraction of $FeCl_3$ as well as the anion complex $FeCl_4^-$.

It is obvious that further work on the extraction of Fe(III) from acidic chloride solution by organic solvents (ethers) and by foam under comparable conditions is required. Organic solvents allow for the analysis of H^+, Fe^{3+} and Cl^- in the organic phase, thereby making possible the determination of the composition of the extracted species. It was not possible to conduct such analysis in the polyurethane foam.

Acknowledgment

Financial support from the National Research Council of Canada is gratefully acknowledged.

1. H. J. M. Bowen. J. Chem. Soc. 1082 (1970).
2. T. Braun and A. B. Farag. Talanta, **22**, 699 (1975).
3. T. Braun and A. B. Farag. Anal. Chim. Acta, **99**, 1 (1978).
4. H. D. Gesser, E. Bock, W. G. Baldwin, A. Chow, D. W. McBride, and W. Lipinsky. Sep. Sci. **11**, 317 (1976).
5. H. D. Gesser and G. A. Horsfall. J. Chim. Phys. **74**, 1072 (1977).
6. R. W. Dodson, G. J. Forney, and E. H. Swift. J. Am. Chem. Soc. **58**, 2573 (1936).
7. J. Axelrod and E. H. Swift. J. Am. Chem. Soc. **62**, 33 (1940).
8. B. V. Nekrasov and V. V. Ovsyankina. J. Gen. Chem. (U.S.S.R.), **11**, 573 (1941); Chem. Abstr. **35**, 7266 (1941).
9. D. E. Metzler and R. J. Myers. J. Am. Chem. Soc. **72**, 3776 (1950).
10. (*a*) N. H. Nachtrieb and J. G. Conway. J. Am. Chem. Soc. **70**, 3547 (1948); (*b*) N. H. Nachtrieb and R. E. Fryxell. J. Am. Chem. Soc. **74**, 897 (1952).
11. D. K. K. Liu, D. T. Shioshita, and R. L. McDonald. J. Phys. Chem. **78**, 2572 (1974).
12. (*a*) T. Sekine, Y. Zenia, and M. Nitsu. Bull. Chem. Soc. Jpn. **49**, 2629 (1976); (*b*) T. Sekine and T. Tetsuka. Bull. Chem. Soc. Jpn. **45**, 1620 (1972).
13. D. E. Chalkley and R. J. P. Williams. J. Chem. Soc. 1920 (1955).
14. R. L. Ericksen and R. L. McDonald. J. Am. Chem. Soc. **88**, 2099 (1966).
15. (*a*) A. G. Maddock, W. Smulek, and A. J. Tench. Trans. Faraday Soc. **58**, 923 (1962); (*b*) A. G. Maddock and L. O. Mederiros. J. Chem. Soc. Dalton, 1088 (1973).
16. A. I. Vogel. Quantitative inorganic analysis. Longmans, London. 1961.
17. W. A. E. McBryde. Analyst, **94**, 337 (1969).
18. T. Sekine and D. Dyrssen. J. Inorg. Nucl. Chem. **26**, 1727 (1964).
19. G. A. Gamlen and D. O. Jordan. J. Chem. Soc. 1435 (1943).
20. R. M. Diamond and D. G. Tuck. *In* Progress in inorganic chemistry. Vol. II. *Edited by* A. F. Cotton. Interscience, New York, NY. 1960. p. 109.
21. R. M. Diamond. J. Phys. Chem. **61**, 69 (1957).
22. J. Saldick. J. Phys. Chem. **60**, 500 (1956).
23. R. M. Diamond. J. Phys. Chem. **61**, 75 (1957).
24. H. Irving and F. J. C. Rossotti. J. Chem. Soc. 1938 (1955).
25. H. L. Friedman. J. Am. Chem. Soc. **74**, 5 (1952).
26. D. E. Campbell, H. M. Clark, and W. H. Bauer. J. Phys. Chem. **62**, 506 (1958).
27. Y. Marcus and A. S. Kertes. Ion exchange and solvent extraction of metal complexes. Wiley-Interscience, London. 1969. p. 575.
28. A. G. Maddock and L. O. Medeiros. J. Chem. Soc. A, 1946 (1969).
29. G. R. Hertel and H. M. Clark. J. Phys. Chem. **65**, 1930 (1961).
30. Shamas-ud-Zuha and M. Ejaz. Anal. Chem. **50**, 740 (1978).
31. E. Hesford and H. A. C. McKay. Trans. Faraday Soc. **54**, 573 (1958).
32. H. Irving and F. J. C. Rossotti. J. Chem. Soc. 1946 (1955).
33. R. A. Robinson. Electrolyte solutions. Butterworths Scientific Publications, London. 1955. Appendices 6.1 and 8.10.
34. R. M. Diamond. J. Phys. Chem. **63**, 659 (1959).
35. R. A. Horne and J. D. Birkett. Electrochim. Acta, **12**, 1153 (1967).

The mass spectra of trifluoroacetyl-2,5-diketopiperazines. I. *cyclo*-(-Gly-X), *cyclo*-(-Ala-X) (X = Gly, Val, Leu, Ile), and *cyclo*-(-Ala-Ala)[1]

GEORGE P. SLATER[2] AND LAWRENCE R. HOGGE

Prairie Regional Laboratory, National Research Council of Canada, Saskatoon, Sask., Canada S7N 0W9

Received November 13, 1978

GEORGE P. SLATER and LAWRENCE R. HOGGE. Can. J. Chem. 57, 2037 (1979).

The trifluoroacetyl derivatives of the 2,5-diketopiperazines *cyclo*-(-Gly-X), *cyclo*-(-Ala-X) (X = Gly, Val, Leu, Ile), and *cyclo*-(-Ala-Ala) were examined by GC–MS. The molecular ion was readily detectable only for TFA-*cyclo*-(-Gly-Gly) (*m/e* 306, 9%). For those compounds containing a valyl or leucyl/isoleucyl residue the ion of highest mass in the spectrum was formed by elimination of C_3H_6 or C_4H_8, respectively, from the molecular ion. In the TFA-*cyclo*-(-Gly-X) series this ion corresponded to the molecular ion of TFA-*cyclo*-(Gly-Gly) (*m/e* 306), and in the TFA-*cyclo*-(-Ala-X) series, to the molecular ion of TFA-*cyclo*-(-Ala-Gly) (*m/e* 320). The fragmentation patterns proposed for these compounds are based on the further degradation of these parent ions so that each compound within a series has a similar mass spectrum. However, sufficient differences were detectable in the various spectra to permit identification of the individual DKP's.

Many of the fragmentation pathways devised to explain the mass spectra were supported by high resolution data and appropriate metastable ions.

GEORGE P. SLATER et LAWRENCE R. HOGGE. Can. J. Chem. 57, 2037 (1979).

On a étudié les dérivés trifluoroacétylés des dicéto-2,5 pipérazines *cyclo*-(-Gly-X), *cyclo*-(-Ala-X) (X = Gly, Val, Leu, Ile) et *cyclo*-(-Ala-Ala) par GC-MS. Seul l'ion moléculaire du TFA-*cyclo*-(-Gly-Gly) a pu être détecté facilement (*m/e* = 306, 9%). Dans le cas des composés contenant un reste valyle ou leucyle/isoleucyle, l'ion dont la masse est la plus élevée se forme par élimination respectivement de C_3H_6 et C_4H_8 à partir de l'ion moléculaire. Dans la série TFA-*cyclo*-(-Gly-X), cet ion correspond à l'ion moléculaire de TFA-*cyclo*-(-Gly-Gly) (*m/e* = 306) et dans la série TFA-*cyclo*-(-Ala-X), à celui de l'ion moléculaire du TFA-*cyclo*-(-Ala-Gly) (*m/e* = 320). Les modèles de fragmentation proposés pour ces composés sont basés sur une dégradation ultérieure des ions parents conduisant à des spectres de masse semblables pour chaque composé. Toutefois on peut détecter suffisamment de différences dans chaque spectre pour distinguer les DCP individuelles.

Plusieurs des voies de fragmentation proposées pour expliquer les spectres de masse sont corroborées par des données à haute résolution et des ions métastables appropriées.

[Traduit par le journal]

Introduction

2,5-Diketopiperazines (DKP's) are produced by fungi (1) and have also been identified as the bitter principles in some food products (2). These compounds also arise from thermal degradation of peptides and application of this transformation has been suggested as an aid to peptide sequencing (3–6).

DKP's can be analyzed directly by gas chromatography (7) or as the trimethylsilyl (TMS) (7) and trifluoroacetyl (TFA) derivatives (8). The TMS-derivatives of some DKP's have been examined by gas chromatography – mass spectroscopy (GC–MS) in relation to peptide sequencing (6) but little information was given about the fragmentation process.

In our experience, the TFA-DKP's are easier to prepare and less susceptible to hydrolysis than the TMS-derivatives. Consequently, a number of TFA-DKP's were examined by GC–MS and the fragmentation pathways are described in this paper.

Results and Discussion

The electron impact – mass spectra of the TFA-DKP's were obtained using a gas chromatograph coupled to a quadrupole mass spectrometer. The fragmentation pathways devised to explain the spectra indicated a number of isobaric ions of relatively high abundance. Where necessary, the TFA-DKP's were subjected to high resolution mass spectroscopy (HRMS) to determine the identity of the various isobars. In addition, several of the compounds were examined by a magnetic sector mass spectrometer to check for metastable ions.

The data from the quadrupole mass spectrometer were automatically normalized relative to the base peak by computer and ions of low relative abun-

[1]NRCC No. 17402.

[2]To whom all correspondence should be addressed.

0008-4042/79/152037-15$01.00/0

dance (<1%) were not readily apparent.[3] When examined by the magnetic sector instrument all of the TFA-DKP's gave molecular ions, those from compounds with a C_3- or C_4-side chain being the weakest, while those with only glycyl and/or alanyl residues being relatively more abundant.

The TFA-DKP's used to collect the present data were synthesized from glycine and/or amino acids of the L-series. A number of DKP's incorporating D-amino acids were also examined but could not be distinguished from their enantiomers by mass spectroscopy.

As might be expected, the ions CF_3CO^+ and CF_3^+ are present in the spectra of all the TFA-DKP's examined (Figs. 1–3), and in some cases the CF_3^+ ion (*m/e* 69) represents the base peak (Figs. 2*a*, 3). Formation of these ions directly from the TFA-DKP's can be represented as in [1] and formation from various ionic fragments in Schemes 1–5 is also possible. Data from HRMS (Tables 7 and 9), indicate that isobaric ions in Schemes 1–4 contribute little to the ion at *m/e* 69.

[1]

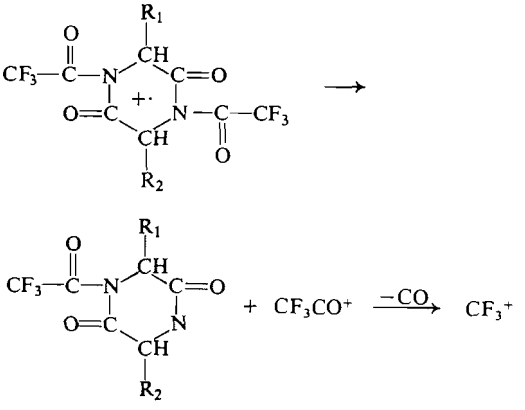

In the mass spectra of all the TFA-DKP's ions are observed corresponding to the ketene $RCH{=}C{=}\overset{+\cdot}{O}$ (R = H, CH_3). The identities of these ions have been confirmed by HRMS and one of several possible methods of formation is shown below in reaction [2].

The mass spectra of the TFA-DKP's synthesized from glycine and another amino acid (i.e. TFA-*cyclo*-(-Gly-X), (X = Val, Leu, Ile)[4]) are quite similar to each other (cf. Fig. 1 *b* and *c*) and to the spectrum of TFA *cyclo*-(-Gly-Gly) (Fig. 1*a*). In each case the ion of highest mass is observed at *m/e* 306

[2]

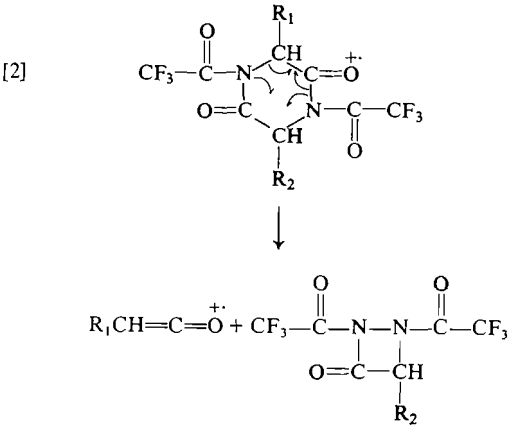

which is equivalent to the molecular ion of TFA-*cyclo*-(-Gly-Gly). This can be explained by elimination of the alkyl side chain in X as olefin [3] to give the enol (**1**, R_1 = H) of the molecular ion of TFA-*cyclo*-(Gly-Gly) which can then revert to the ketonic form and fragment as outlined in Schemes 1–5. Elimination of olefin in this manner has been observed (6, 10) in the fragmentation of underivatized DKP's incorporating valyl and/or leucyl residues. The reactions shown in [3] are supported by metastable ions in the mass spectra of TFA-*cyclo*-(-Gly-Val) (*m/e* 348 → *m/e* 306, *m** = 269.1) and TFA-*cyclo*-(-Ala-Val) (*m/e* 362 → *m/e* 320, *m** = 282.9).

As a result of the fragmentation of the molecular ion of TFA-*cyclo*-(-Gly-X) to give the ion at *m/e* 306 [3] the latter would have a lower energy than the

[3]

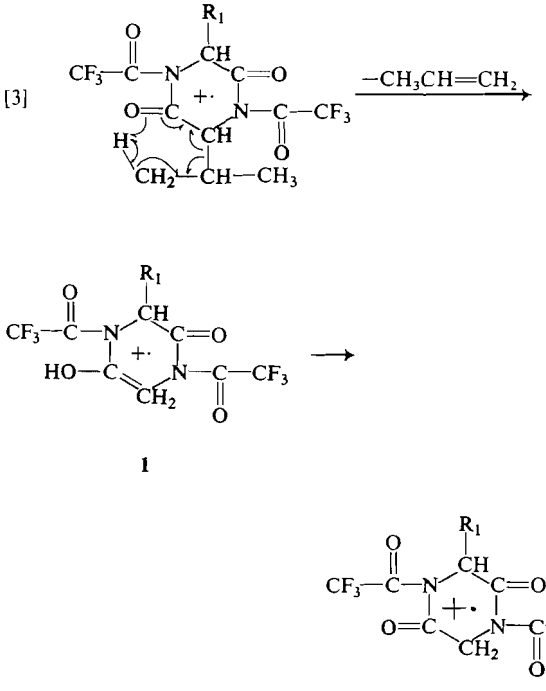

1

[3]The computer printout expresses relative abundances to 0.01% so that lesser values appear as zero. In compiling Tables 1–4 relative abundances less than 0.5% were reported as zero.

[4]The abbreviations used are those recommended by the IUPAC-IUB Commission on Biochemical Nomenclature (9).

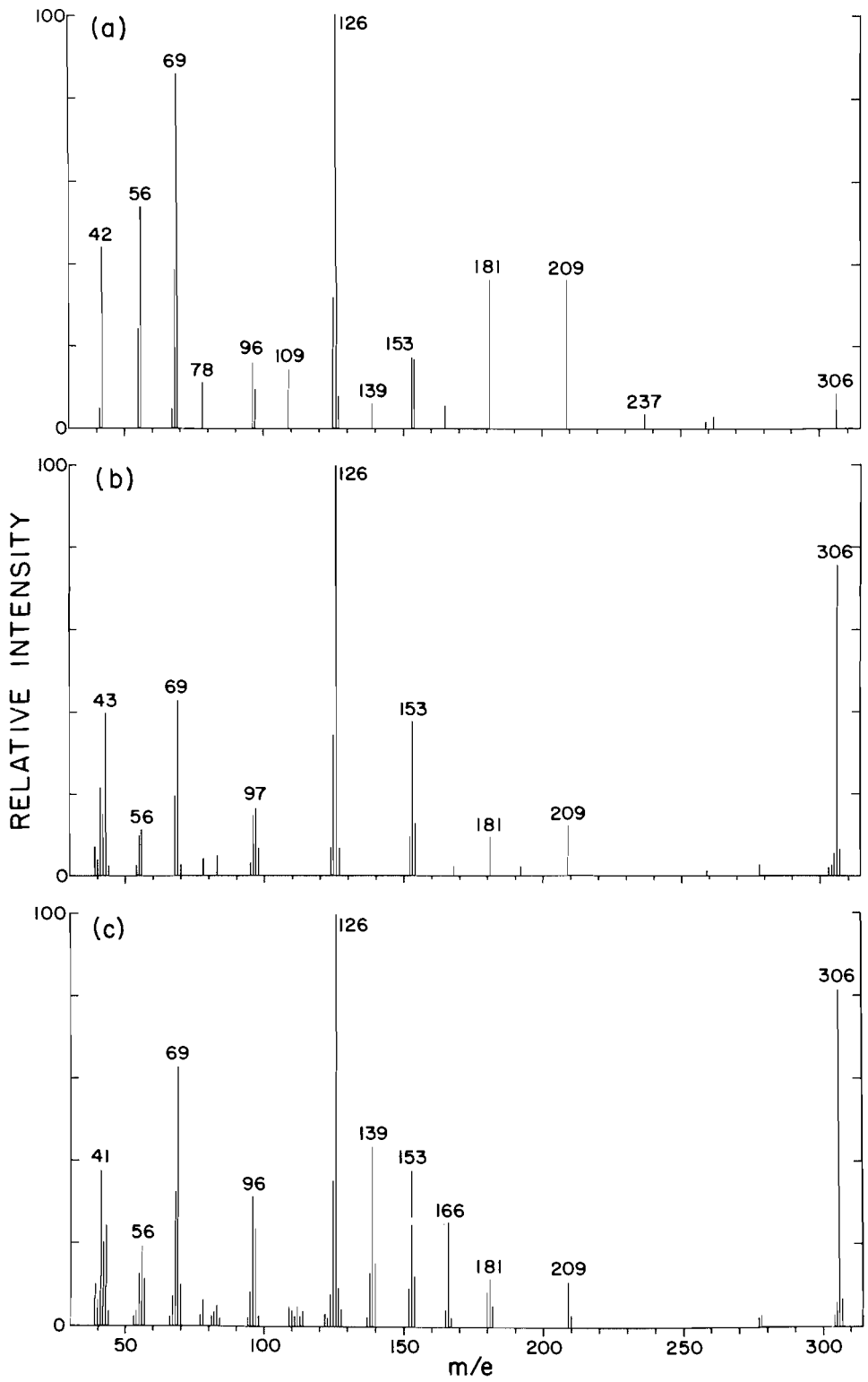

FIG. 1. Mass spectra of (*a*) TFA-*cyclo*-(-Gly-Gly), (*b*) TFA-*cyclo*-(-Gly-L-Val), (*c*) TFA-*cyclo*-(-Gly-L-Leu).

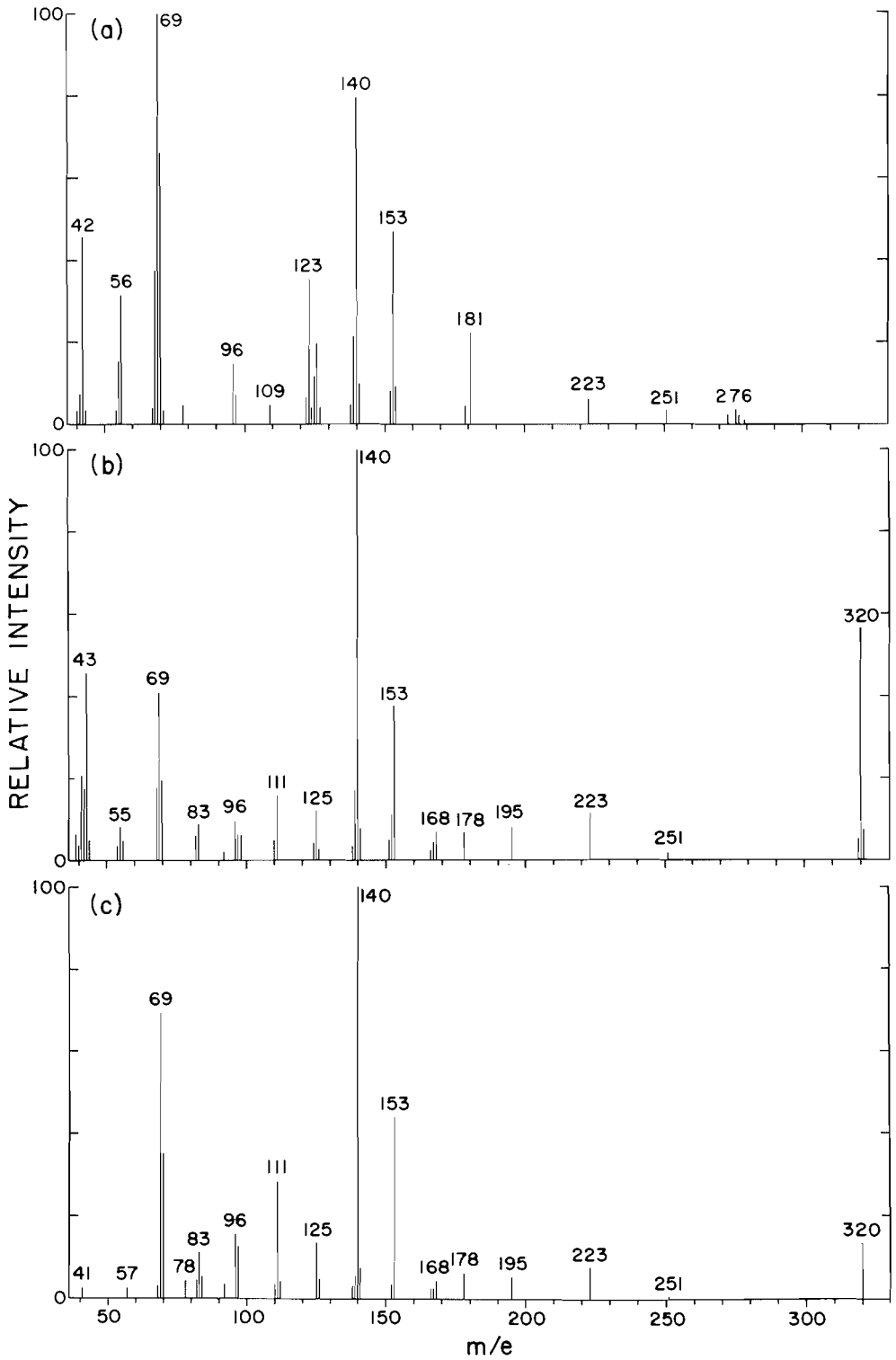

FIG. 2. Mass spectra of (*a*) TFA-*cyclo*-(-L-Ala-Gly), (*b*) TFA-*cyclo*-(-L-Ala-L-Val), (*c*) TFA-*cyclo*-(-L-Ala-L-Ile).

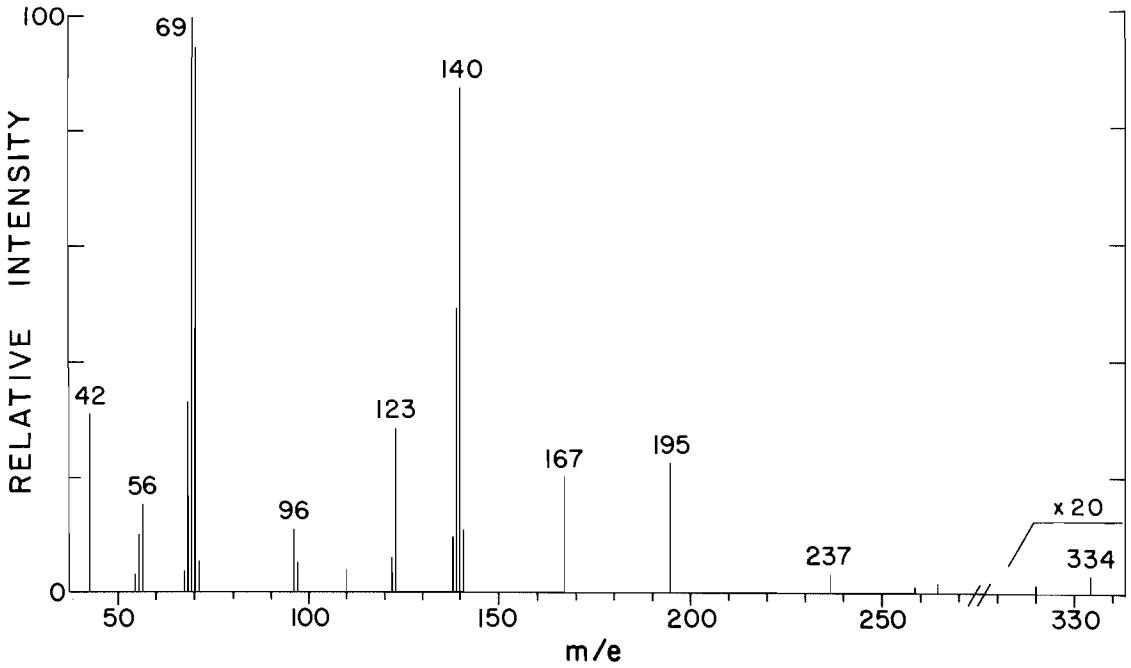

FIG. 3. Mass spectrum of TFA-*cyclo*-(-L-Ala-L-Ala).

molecular ion (*m/e* 306) of TFA-*cyclo*-(-Gly-Gly). This would account for the greater relative abundance of the *m/e* 306 ion in spectra of the former compounds (Table 1). A contributing factor may be the initial formation of the *m/e* 306 ion as the enol **1** [3] for these compounds.

Mass spectral fragmentation pathways for underivatized (10, 11) and *N*-methyl-DKP's (11) have been reported but understandably these do not account for the ions observed in the spectra of the TFA-DKP's. Accordingly, a number of fragmentations are proposed (Schemes 1–5) which are based on the earlier observation (cf. [3]) that the initial step in the ionization of the TFA-DKP's bearing a C_3- or C_4-alkyl side chain is elimination of the latter as olefin. This suggestion is supported by the absence of ions incorporating a C_3H_7 or C_4H_9 group in the spectra of the TFA-DKP's containing a valyl or leucyl/isoleucyl residue. In many cases the proposed fragmentations are supported by appropriate metastable ions (Tables 6 and 8) and HRMS (Tables 7, 9, and 10).

One of the abundant ions in the spectra of the TFA-*cyclo*-(-Gly-X) series (X = Gly, Val, Leu, Ile) occurs at *m/e* 153 (Fig. 1, Table 1) Since the ion of highest mass in these spectra occurs at *m/e* 306 it would appear that symmetrical cleavage of this ion gives the ion at *m/e* 153, and a fragmentation pathway based on this assumption is presented in Scheme 1. Reference to Table 1 indicates that the ions in the scheme contribute significantly to the spectra of the

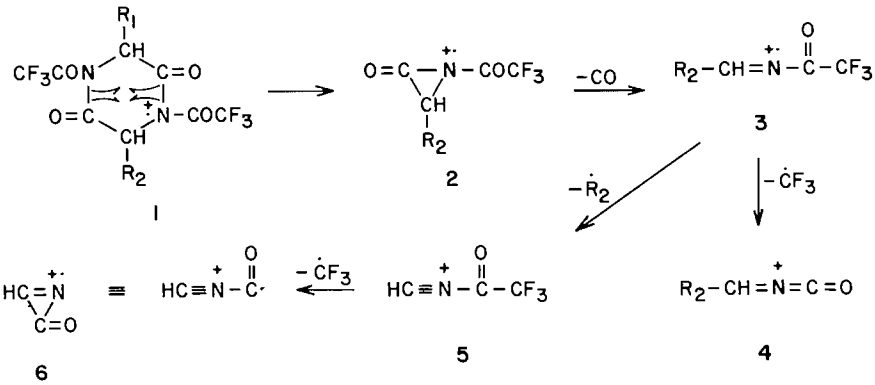

SCHEME 1

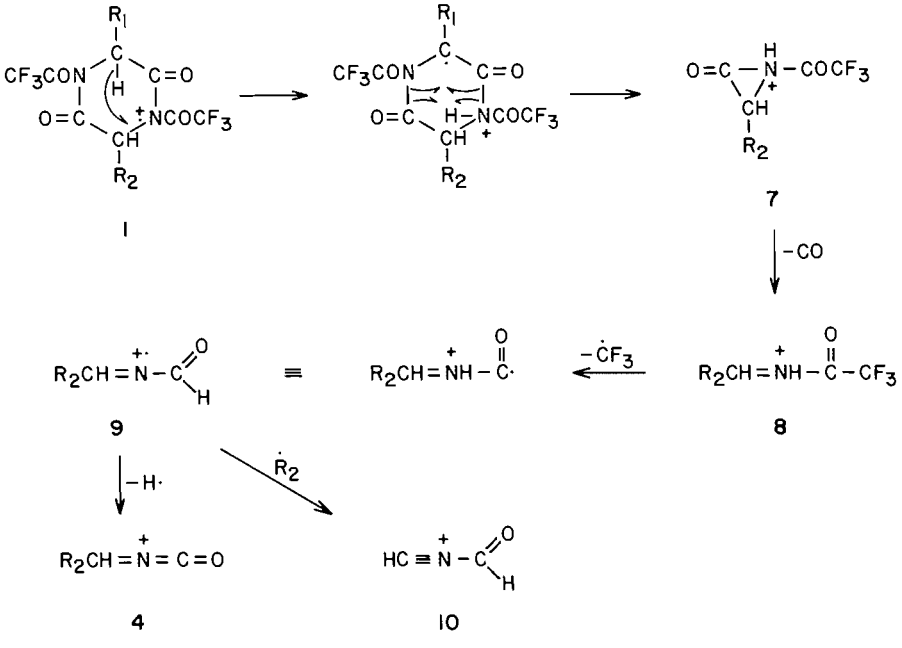

SCHEME 2

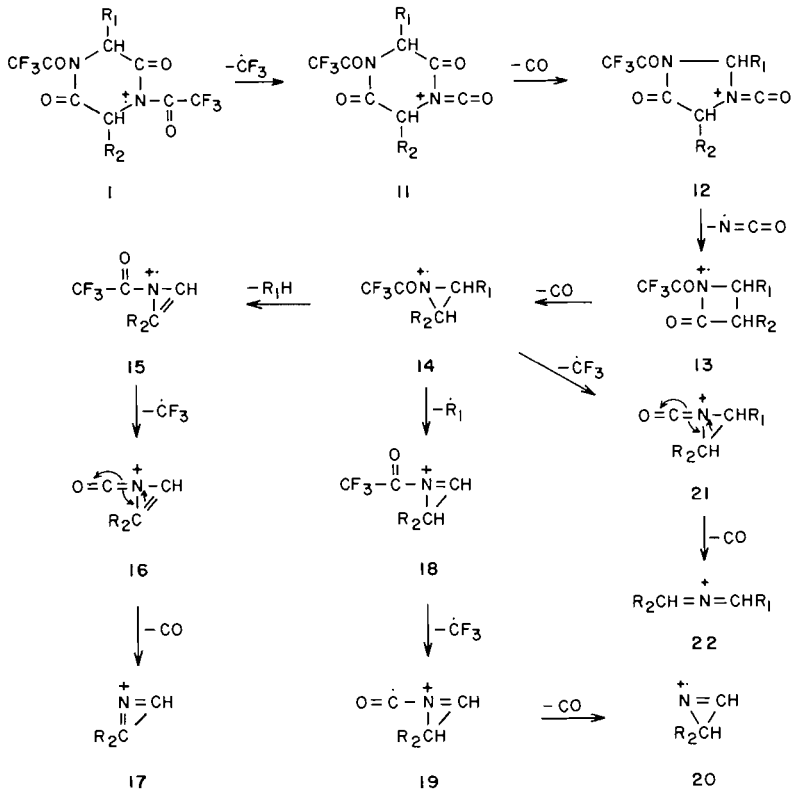

SCHEME 3

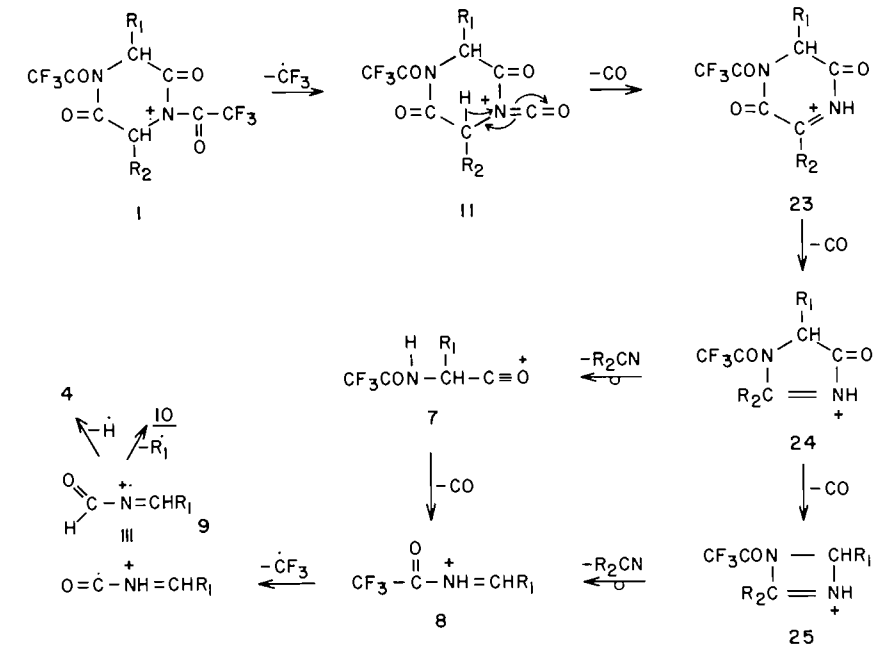

SCHEME 4

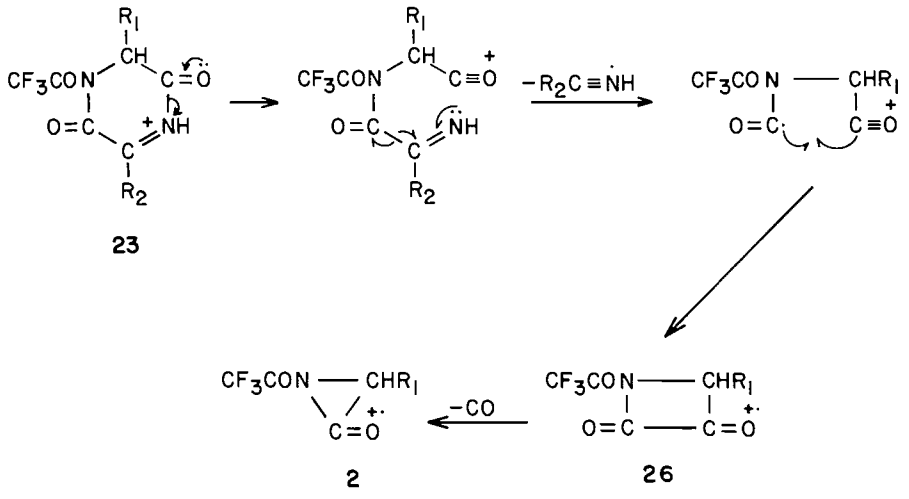

SCHEME 5

TFA-*cyclo*-(-Gly-X) compounds, and the sequence: ion **1** → ion **2** → ion **3** is supported by metastable ions (Table 6) and HRMS (Table 7). In this series, ion **4** (*m/e* 56, R_2 = H) is isomeric with ion **10** (Scheme 2) and these cannot be differentiated by HRMS.

An alternate mode of fragmentation shown in Scheme 2 involves rearrangement of a hydrogen atom prior to cleavage. The relative abundances of the ions (Table 2) indicate that this pathway also represents a major process in the fragmentation of the TFA-*cyclo*-(-Gly-X) series. Formation of the base peak as shown is supported by relevant metastable ions (Table 6). In this scheme the peak at *m/e* 57 is attributed to ion **9**, C_2H_3NO (R_2 = H) and is relatively abundant (11%, 23%) in the spectra of TFA-*cyclo*-(-Gly-Leu/Ile). The high resolution spectrum of TFA-*cyclo*-(-Gly-Ile) indicates that the C_4H_9 ion is the main component (90%) of the peak at *m/e* 57 (Table 7) so that in this case the relative abundance of ion **9** is actually 2% and is similar to that observed for TFA-*cyclo*-(-Gly-Gly/Val) (Table

TABLE 1. Relative abundances (%) of ions in Scheme 1*

			Relative abundance					
			1	**2**	**3**	**4**	**5**	**6**
TFA-DKP	R_1	R_2	*m/e* 306	*m/e* 153	*m/e* 125	*m/e* 56	*m/e* 124	*m/e* 55
c-Gly-Gly	H	H	9	17(16)	32	54	4	24
Gly-Val	H	H	76	38(35)	35	12	7	10
Gly-Leu	H	H	81	38(5)	35	19	8	12
Gly-Ile	H	H	79	42(39)	33	21	6	10
			m/e 320					
c-Ala-Gly	CH_3	H	0	46(12)	12	32(27)	4	16
Ala-Val	CH_3	H	56	38(10)	12	5(4)	4	8
Ala-Leu	CH_3	H	87	36(9)	10	10(9)	4	9
Ala-Ile	CH_3	H	14	44(11)	14	1(1)	3	0
				m/e 167	*m/e* 139	*m/e* 70		
c-Ala-Gly	H	CH_3		0	21	66(66)		
Ala-Val	H	CH_3		4	17	20(20)		
Ala-Leu	H	CH_3		7	59	30(30)		
Ala-Ile	H	CH_3		3	5	35(35)		
			m/e 334					
c-Ala-Ala	CH_3	CH_3	0	22(22)	48(48)	90(80)	3	9

*Numbers in parentheses are relative abundances calculated on the assumption that isobar ratio applies equally to all TFA-DKP's within a series (cf. Tables 7, 9, and 10).

TABLE 2. Relative abundances (%) of ions in Scheme 2*

			Relative abundance					
			1	**7**	**8**	**9**	**10**	**4**
TFA-DKP	R_1	R_2	*m/e* 306	*m/e* 154	*m/e* 126	*m/e* 57	*m/e* 56	*m/e* 56
c-Gly-Gly	H	H	9	18	100	4	54	54
Gly-Val	H	H	76	13	100	1	12	12
Gly-Leu	H	H	81	12	100	11(1)	19	19
Gly-Ile	H	H	79	13	100	23(2)	21	21
			m/e 320					
c-Ala-Gly	CH_3	H	0	10	19	2	32(27)	32(27)
Ala-Val	CH_3	H	56	2	3	1	5(4)	5(4)
Ala-Leu	CH_3	H	87	2	5	7	10(9)	10(9)
Ala-Ile	CH_3	H	14	3	5	3	1(1)	1(1)
				m/e 168	*m/e* 140	*m/e* 71		*m/e* 70
c-Ala-Gly	H	CH_3		0	79	3		66
Ala-Val	H	CH_3		7	100	1		20
Ala-Leu	H	CH_3		4	100	3		30
Ala-Ile	H	CH_3		4	100	2		35
			m/e 334					
c-Ala-Ala	CH_3	CH_3	0	3	88	5	12	90(80)

*See footnote Table 1.

2) which cannot give a C_4H_9 ion. This explanation would also account for the abundance of the ion at *m/e* 57 in the spectrum of TFA-*cyclo*-(-Gly-Leu).

The relatively prominent ion at *m/e* 209 in the spectrum of TFA-*cyclo*-(-Gly-Gly) (Fig. 1*a*) can be explained by consecutive loss of CF_3 and CO from ion **1** as shown in Scheme 3 (ion **1** → ion **11** → ion **12**). Alternatively, this loss could occur as in Scheme 4 (ion **1** → ion **11** → ion **23**), or $CF_3CO^{\cdot}$ could be eliminated from ion **1** to give ion **23** directly. Metastable ions corresponding to the latter fragmentation and to ion **11** → ion **12**/**23** were observed (Table 6). Further degradation of ion **12** (Scheme 3) gives a number of ions of relatively high abundance (Table 3), viz. ion **14** (*m/e* 139), ion **16** (*m/e* 68), ion **19** (*m/e* 69), ion **20** (*m/e* 41), and ion **22** (*m/e* 42). However, ion **19** is isobaric with CF_3^+ and ion **22** with $CH_2{=}C{=}\overset{+\cdot}{O}$ and high resolution data (Table 7) show that ions **19** and **22** are minor components but that ions **14** and **16** are single species. The ion at *m/e*

TABLE 3. Relative abundances (%) of ions in Scheme 3*

			Relative abundance												
TDA-DKP	R_1	R_2	**1** *m/e* 306	**11** *m/e* 237	**12** *m/e* 209	**13** *m/e* 167	**14** *m/e* 139	**15** *m/e* 137	**16** *m/e* 68	**17** *m/e* 40	**18** *m/e* 138	**19** *m/e* 69	**20** *m/e* 41	**21** *m/e* 70	**22** *m/e* 42
c-Gly-Gly	H	H	9	3	36	3	6(6)	3	40	4	1	88(6)	6	4	44(7)
Gly-Val	H	H	76	1	13	1	0(0)	0	20	4	1	43(3)	22(2)	3	15(2)
Gly-Leu	H	H	81	1	10	2	43(43)	2	31	6	13	61(4)	36(3)	9	20(3)
Gly-Ile	H	H	79	2	13	0	1(1)	1	24	6	3	55(4)	43(3)	1	11(2)
			m/e 320	*m/e* 251	*m/e* 223	*m/e* 181	*m/e* 153							*m/e* 84	*m/e* 56
c-Ala-Gly	CH_3	H	0	3	6	22(6)	46(35)	1	38	4	5	100(1)	7	0	32(2)
Ala-Val	CH_3	H	56	2	11	0(0)	38(29)	1	18	4	3	41(0)	21	1	5(0)
Ala-Leu	CH_3	H	87	2	11	2(0)	36(27)	3	23	5	16	54(0)	25	1	10(1)
Ala-Ile	CH_3	H	14	1	8	1(0)	44(33)	1	3	0	3	69(1)	2	5	1(0)
								m/e 151	*m/e* 82	*m/e* 54	*m/e* 152	*m/e* 83	*m/e* 55		
c-Ala-Gly	H	CH_3						2	1	3	8	1	16		
Ala-Val	H	CH_3						5	6	4	11	9	8		
Ala-Leu	H	CH_3						3	4	4	6	4	9		
Ala-Ile	H	CH_3						3	4	0	4	11	0		
			m/e 334	*m/e* 265	*m/e* 237	*m/e* 195	*m/e* 167							*m/e* 98	*m/e* 70
c-Ala-Ala	CH_3	CH_3	0	2	4	24(0)	22(0)	0	1	3	0	1	9	1	90(10)
								m/e 137	*m/e* 68	*m/e* 40					
								1	30	3					

*See footnote Table 1

TABLE 4. Relative abundances (%) of ions in Scheme 4*

			Relative abundance					
			11	**23**	**24**	**25**	**7**	**8**
TFA-DKP	R_1	R_2	*m/e* 237	*m/e* 209	*m/e* 181	*m/e* 153	*m/e* 154	*m/e* 126
c-Gly-Gly	H	H	4	36	36(9)	17(1)	18	100
Gly-Val	H	H	1	13	10(3)	38(3)	13	100
Gly-Leu	H	H	1	11	12(3)	38(3)	12	100
Gly-Ile	H	H	2	13	9(2)	42(3)	13	100
			m/e 251	*m/e* 223	*m/e* 195	*m/e* 167	*m/e* 168	*m/e* 140
c-Ala-Gly	CH_3	H	3	6	1	0	0	79
Ala-Val	CH_3	H	2	11	8	7	0	100
Ala-Leu	CH_3	H	2	11	8	4	0	100
Ala-Ile	CH_3	H	1	8	6	4	0	100
							m/e 154	*m/e* 126
c-Ala-Gly	H	CH_3					9	19
Ala-Val	H	CH_3					2	3
Ala-Leu	H	CH_3					2	5
Ala-Ile	H	CH_3					3	5
			m/e 265	*m/e* 237	*m/e* 209	*m/e* 181	*m/e* 168	*m/e* 140
c-Ala-Ala	CH_3	CH_3	2	4	0	0	3	88

*See footnote Table 1.

41 is of appreciable abundance in the spectra of the valyl-, leucyl-, and isoleucyl-DKP's (Table 3) and for these compounds the ion is mainly due to $C_3H_5^+$ (Table 7).

Scheme 4 shows an alternate fragmentation of ion **11** leading to ions **4**, **7–10** by way of the apparently abundant ions **24** (*m/e* 181) and **25** (*m/e* 153). The latter is isobaric with ion **2** (Scheme 1) and contributes little to the peak at *m/e* 153 (Table 7) whereas ion **24** is isobaric with ion **26** (Scheme 5) and these are present in the ratio 1:3 (Table 7).

Fragmentation of ion **23** as shown in Scheme 5 leads to ion **26** which is the major component of the peak at *m/e* 181 (Table 7) and a metastable ion corresponding to this transition was observed (Table 6). Elimination of CO from ion **26** would provide an alternate pathway to ion **2** (and the remaining ions of Scheme 1); however the corresponding metastable ion was not detected.

The structure of ion **26** is such that alternate fragmentation (loss of ketene and $\cdot CF_3$ or loss of $\cdot CF_3$ and 2CO are possible. In the TFA-*cyclo*-(-Ala-X) series these would lead to isobaric ions of relatively high abundance; however these were eliminated on the basis of HRMS.

Ion **1** (*m/e* 306, $R_1 = R_2 = H$), the starting point for the fragmentations of the TFA-*cyclo*-(-Gly-X) series outlined in Schemes 1–5, is symmetrical so that only one set of ions is possible. For the TFA-*cyclo*-(-Ala-X) compounds (X = Gly, Val, Leu, Ile), however, ion **1** (*m/e* 320, $R_1 = CH_3$; $R_2 = H$; or vice versa) is not symmetrical and two sets of homologous ions are possible depending on the location of the positive charge. Tables 1–5 have been compiled to reflect this possibility and show the occurrence of fragmentation to give ions derived from both the alanyl and glycyl portions of ion **1**. In several instances the ions retaining the methyl group are in greater abundance than their lower homologues which are derived from the glycyl portion of the DKP. Where this occurs (e.g. ions **3**, **4**, **8**; Tables 1

TABLE 5. Relative abundances (%) of ions in Scheme 5*

			Relative abundance	
			23	**26**
TFA-DKP	R_1	R_2	*m/e* 209	*m/e* 181
c-Gly-Gly	H	H	36	36(27)
Gly-Val	H	H	13	10(8)
Gly-Leu	H	H	10	12(9)
Gly-Ile	H	H	13	9(8)
			m/e 223	*m/e* 195
c-Ala-Gly	CH_3	H	6	1
Ala-Val	CH_3	H	11	8
Ala-Leu	CH_3	H	11	8
Ala-Ile	CH_3	H	8	6
				m/e 181
c-Ala-Gly	H	CH_3		22(18)
Ala-Val	H	CH_3		0(0)
Ala-Leu	H	CH_3		2(2)
Ala-Ile	H	CH_3		1(1)
			m/e 237	*m/e* 195
c-Ala-Ala	CH_3	CH_3	4	24(24)

*See footnote Table 1.

TABLE 6. Metastable ions in mass spectra of TFA-*cyclo*-(-Gly-X) (X = Gly, Val, Leu, Ile)

Fragmentation	Metastable ion	
	m/e calculated	*m/e* observed
Ion **1** (*m/e* 306) → ion **2** (*m/e* 153)	76.5	76.3
Ion **2** (*m/e* 153) → ion **3** (*m/e* 125)	102.1	102.5
Ion **1** (*m/e* 306) → ion **7** (*m/e* 154)	77.5	77.5
Ion **7** (*m/e* 154) → ion **8** (*m/e* 126)	103.1	103.3
Ion **14** (*m/e* 139) → ion **21** (*m/e* 70)	35.3	35.3
Ion **1** (*m/e* 306) → ion **12/23** (*m/e* 209)	142.7	142.7
Ion **11** (*m/e* 237) → ion **12/23** (*m/e* 209)	184.3	184.5
Ion **23** (*m/e* 209) → ion **26** (*m/e* 181)	156.8	156.8

and 2) the methyl group is conjugated with the charge site and the ions may be stabilized relative to the lower homologues by hyperconjugation [4]. In

[4] 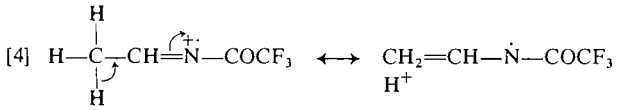

3

other cases (e.g. ions **2**, **7**) the methyl group is not conjugated with the charge site and the relative abundances of the homologous ions are of the same order of magnitude (Tables 1 and 2), except for TFA-*cyclo*-(-Ala-Gly) which may behave differently since its molecular ion has not undergone olefin elimination as have the other DKP's in this group.

The fragmentations suggested in Schemes 1–5 account for the majority of ions in the spectra of the TFA-*cyclo*-(-Ala-X) compounds (Fig. 2). Several of these pathways are supported by the occurrence of relevant metastable ions (Table 8) and the identities of prominent fragments have been confirmed by HRMS (Table 9).

A number of isobaric ions are also indicated for the TFA-*cyclo*-(-Ala-X) series (cf. Tables 1–5) and the more prominent of these were examined by HRMS (Table 9). One of the more interesting groups of isobaric ions occurs at *m/e* 55. This ion was expected to be a mixture of ion **6** (C_2HNO) and ion **20** (C_3H_5N). However, one of the abundant ions was found to correspond to C_3H_3O which could arise by loss of a hydrogen radical from the ketene $CH_3—CH=C=\overset{+\cdot}{O}$. A comparable ion ($C_2HO$, *m/e* 41) was not observed in the TFA-*cyclo*-(-Gly-X) series (Table 7) but was detected at *m/e* 83 ($C_3H_7—CH=C=\overset{+\cdot}{O}$ – [H·]) and *m/e* 97 ($C_4H_9—CH=C=\overset{+\cdot}{O}$ – [H·]) in the spectra of TFA-DKP's synthesized from valine, leucine, and isoleucine (Part II, following paper).

The mass spectra of TFA-*cyclo*-(-Gly-X) (Fig. 1) contain an ion at *m/e* 42 due to ketene [2] and ion **22** (Table 7). By analogy the spectra of TFA-*cyclo*-(-Ala-X) would be expected to show the homologues of these ions and this was confirmed by HRMS (Table 9). However, these spectra also contain an ion at *m/e* 42 which comprises two ions of formula C_2H_2O and C_2H_4N (Table 9) previously found in the spectra of TFA-*cyclo*-(-Gly-X) (Table 7). The C_2H_2O ion results from formation of ketene from the X-position of the DKP [2]. The ion C_2H_4N cannot be accounted for as in the TFA-*cyclo*-(-Gly-X) series, i.e. ion **22**, $R_1CH=\overset{+}{N}=CHR_2$ ($R_1 = R_2 = H$), since in the TFA-*cyclo*-(-Ala-X) DKP's either R_1 or R_2 is a methyl group. Formation of an ion of formula C_2H_4N may result from a process such as the following [5].

[5] 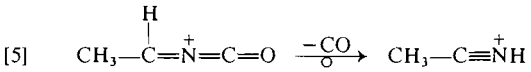

4

The metastable ion corresponding to this fragmentation (*m/e* 70 → *m/e* 42) would be expected at *m/e* 25.2. A metastable ion at this position observed in the spectra of TFA-*cyclo*-(-Ala-X) could also be due to ion **3** (*m/e* 125) → ion **4** (*m/e* 56). However, the same metastable ion occurs in the spectrum of TFA-*cyclo*-(-Ala-Ala) for which the transition ion **3** (*m/e* 125) → ion **4** (*m/e* 56) does not occur (Table 1).

An ion at *m/e* 42 is also quite prominent in the spectrum of TFA-*cyclo*-(-Ala-Ala) (Fig. 3) and was found to contain the same ions as observed in the spectrum of the TFA-*cyclo*-(-Ala-Gly) although the ratio of the C_2H_4N ion to the C_2H_2O ion was much greater (Table 10). The first ion can be accounted for as before [5] but there is no immediate explanation for the second ion.

The mass spectrum of TFA-*cyclo*-(-Ala-Ala) (Fig. 3) is similar to the spectrum of TFA-*cyclo*-(-Ala-Gly)

TABLE 7. High resolution data for TFA-*cyclo*-(-Gly-X) (X = Gly, Val, Leu, Ile)

m/e	Ion	Ion formula	Isobar ratio	TFA-compound examined
41	**20**	C_2H_3N	1	*cyclo*-(-Gly-Leu)
		C_3H_5	12	
42	$CH_2{=}C{=}O^{+\cdot}$	C_2H_2O	5	*cyclo*-(-Gly-Leu)
	22	C_2H_4N	1	
43	$C_3H_7^+$	C_3H_7	3	*cyclo*-(-Gly-Leu)
	$C_2H_3O^+$	C_2H_3O	1	
57	**9**	C_2H_3NO	1	*cyclo*-(-Gly-Ile)
	$C_4H_9^+$	C_4H_9	10	
68	**16**	C_3H_2NO	Single ion	*cyclo*-(-Gly-Gly)
69	CF_3^+	CF_3	13	*cyclo*-(-Gly-Val)
	19	C_3H_3NO	1	
96	$HC{\equiv}N{-}CF_3$	C_2HF_3N	Single ion	*cyclo*-(-Gly-Gly)
97	CF_3CO^+	C_2F_3O	Single ion	*cyclo*-(-Gly-Ile)
109		$C_3H_2F_3N$ [7]	Single ion	*cyclo*-(-Gly-Gly)
139	**14**	$C_4H_4F_3NO$	Single ion	*cyclo*-(-Gly-Leu)
153	**2**	$C_4H_2F_3NO_2$	12	*cyclo*-(-Gly-Gly)
	25	$C_4H_4F_3N_2O$	1	
166		$C_6H_7F_3NO$ [9]	Single ion	*cyclo*-(-Gly-Leu)
181	**24**	$C_5H_4F_3N_2O_2$	1	
	26	$C_5H_2F_3NO_3$	3	*cyclo*-(-Gly-Gly)

TABLE 8. Metastable ions in mass spectra of TFA-*cyclo*-(-Ala-X) (X = Gly, Val, Leu, Ile)

Fragmentation	Metastable ion	
	m/e calculated	*m/e* observed
Ion **2** (*m/e* 153) → ion **3** (*m/e* 125)	102.1	102.3
Ion **3** (*m/e* 125) → ion **4** (*m/e* 56)	25.1	25.2
Ion **1** (*m/e* 320) → ion **7** (*m/e* 168)	88.2	88.2
Ion **7** (*m/e* 168) → ion **8** (*m/e* 140)	116.7	116.5
Ion **10** (*m/e* 181) → ion **2** (*m/e* 153)	129.3	129.5
Ion **12** (*m/e* 84) → ion **4** (*m/e* 56)	37.3	37.2
Ion **15** (*m/e* 251) → ion **16** (*m/e* 223)	198.1	198.4
Ion **4** (*m/e* 70) → C_2H_4N (*m/e* 42) [5]	25.2	25.2

(Fig. 2*a*) except that ions due to the glycine portion of the latter are absent (e.g. *m/e* 125, 126, 153, 154). Metastable ions corresponding to ion **2** → ion **3** → ion **4** were observed and the identities of several ions were established by HRMS (Table 10).

In Scheme 3 ion **14** → ion **15** is shown as occurring by elimination of R_1H. For TFA-*cyclo*-(-Ala-Ala) $R_1 = R_2 = CH_3$ so that elimination of C_2H_6 is possible and the sequence: ion **14** → ion **15** → ion **16** → ion **17** gives ions at *m/e* 137, 68, 40. The ion at *m/e* 68 is relatively abundant (30%) and was found by HRMS (Table 10) to be identical to the *m/e* 68 ion observed in the spectra of the other TFA-DKP's.

The fragmentations outlined in Schemes 1–5 and eqs. [1–3] account for the majority of significant ions in the spectra of the TFA-DKP's. However, one ion (10–30% relative abundance) which is present in the spectrum of each compound and is not indicated by the above schemes occurs at *m/e* 96 (Figs. 1–3). The formula C_2HF_3N ($HC{\equiv}N{-}CF_3$) for this ion was established by HRMS. Formation of the ion could result by rearrangement of ion **3** (Scheme 1) and successive elimination of R_2 and CO [6], or by re-

[6] $R_2CH{=}\overset{+\cdot}{N}{-}\overset{O}{\overset{\|}{C}}{-}CF_3 \longrightarrow R_2CH{=}\overset{+}{N}{-}\overset{CF_3}{\overset{|}{C}}{=}O \xrightarrow{-R_2}$

m/e 125, R_2 = H
m/e 139, R_2 = CH_3

$$HC{=}\overset{+}{N}{<}\begin{matrix}CF_3\\|\\C{=}O\end{matrix} \xrightarrow{-CO} HC{\equiv}\overset{+}{N}{-}CF_3$$

m/e 96

arrangement of the CF_3 group in ion **5** (Scheme 1) followed by elimination of CO. The elimination of CO first rather than R_2 from ion **3** would give an ion at *m/e* 97 (R_2 = H) for the TFA-*cyclo*-(-Gly-X) series and at *m/e* 111 (R_2 = CH_3) for the TFA-*cyclo*-(-Ala-X) compounds. The ion at *m/e* 97 would be isobaric with CF_3CO^+ which was the only ion

TABLE 9. High resolution data for TFA-*cyclo*-(-Ala-X) (X = Gly, Val, Leu, Ile)

m/e	Ion	Ion formula	Isobar ratio	TFA-compound examined
41	**20**	C_2H_3N	1	*cyclo*-(-Ala-Val)
	$C_3H_5^+$	C_3H_5	10	
42	$CH_2{=}C{=}\overset{+\cdot}{O}$	C_2H_2O	2	*cyclo*-(-Ala-Gly)
		C_2H_4N [5]	1	
55	**6**	C_2HNO	8	*cyclo*-(-Ala-Gly)
	20	C_3H_5N	1	
		C_3H_3O	9	
56	**4/10**	C_2H_2NO	11	*cyclo*-(-Ala-Gly)
	$CH_3CH{=}C{=}\overset{+\cdot}{O}$	C_3H_4O	1	
	22	C_3H_6N	1	
69	**19**	C_3H_3NO	1	*cyclo*-(-Ala-Gly)
	CF_3^+	CF_3	99	
70	**4**	C_3H_4NO	Single ion	*cyclo*-(-Ala-Val)
111		$C_5H_5NO_2$ [8]	Single ion	*cyclo*-(-Ala-Ile)
126	**8**	$C_3H_3F_3NO$	Single ion	*cyclo*-(-Ala-Leu)
139	**3**	$C_4H_4F_3NO$	Single ion	*cyclo*-(-Ala-Leu)
153	**2**	$C_4H_2F_3NO_2$	1	*cyclo*-(-Ala-Gly)
	14	$C_5H_6F_3NO$	3	
166		$C_6H_7F_3NO$ [9]	Single ion	*cyclo*-(-Ala-Leu)
181	**26**	$C_5H_2F_3NO_3$	4	*cyclo*-(-Ala-Gly)
	13	$C_6H_6F_3NO_2$	1	

TABLE 10. High resolution data for TFA-*cyclo*-(-Ala-Ala)

m/e	Ion	Ion formula	Isobar ratio
42		C_2H_2O	1
		C_2H_4N[5]	10
68	**16**	C_3H_2NO	Single ion
70	**4**	C_3H_4NO	8
	22	C_4H_8N	1
139	**3**	$C_4H_4F_3NO$	Single ion
167	**2**	$C_5H_4F_3NO_2$	Single ion
	14	$C_6H_8F_3NO$	
195	**26**	$C_6H_4F_3NO_3$	Single ion
	13	$C_7H_8F_3NO_2$	

indicated by HRMS (Table 7). The ion at *m/e* 111 was also eliminated on the basis of high resolution data.

In addition to the ions described so far, several spectra contain ions which are unique to a TFA-DKP containing a particular amino acid residue. These ions and possible fragmentations leading to their formation are listed below. In each case the identity of the ion was confirmed by HRMS.

m/e *43*. This ion is present in the spectra of TFA-*cyclo*-(-Gly-Val/Leu) (40%, 20% relative abundance) and TFA-*cyclo*-(-Ala-Val/Leu) (40%, 17%), but is barely detectable in the normalized spectra of the other TFA-DKP's examined. The ion could be due to $C_3H_7^+$ from the valyl or leucyl portion of the DKP together with a contribution from ^{13}C-ketene. High resolution data (Table 7) show that the ion is in fact due to $C_3H_7^+$ and $C_2H_3O^+$ in the ratio 3:1. The latter ion may be due to protonated ketene $CH_2{=}C{=}\overset{+}{O}H$, which would require rearrangement of a hydrogen atom prior to cleavage as in [2]. The greater abundance of the *m/e* 43 ion in the spectra of the valyl compounds helps to distinguish them from the leucyl-DKP's.

m/e *109(123)*. In the spectrum of TFA-*cyclo*-(-Gly-Gly) the ion at *m/e* 109 is present in 16% relative abundance (Fig. 1*a*). The formula $C_3H_2F_3N$ was indicated by HRMS and an ion of this composition could be formed from ion 14, Scheme 3, as shown below in [7].

[7] 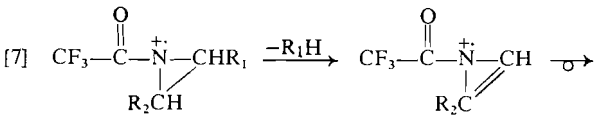

14 (*m/e* 139, $R_1 = R_2 = H$)
(*m/e* 153, $R_1 = H$; $R_2 = CH_3$; or vice versa)
(*m/e* 167, $R_1 = R_2 = CH_3$)

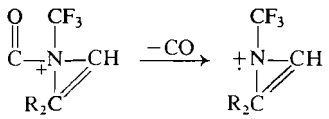

m/e 109 ($R_2 = H$)
m/e 123 ($R_2 = CH_3$)

This mechanism also accounts for the ion at *m/e* 123 in the spectra of TFA-*cyclo*-(-Ala-Gly/Ala) (Figs. 2*a*

and 3) but does not explain why these ions are not as prominent in other relevant spectra.

m/e *111*. The spectra of TFA-*cyclo*-(-Ala-Val/Leu/Ile) contain the ion at *m/e* 111 (16%, 12%, 29%) which is absent in the spectra of the remaining TFA-DKP's. This suggests that the ion is due in part to retention of the alanyl portion of the DKP. High resolution data indicated the formula $C_5H_5NO_2$ and an ion of this composition could arise as follows in [8].

[8]

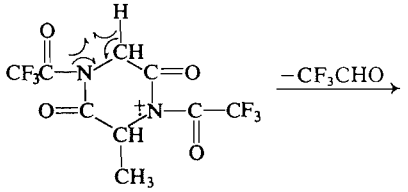

1, *m/e* 320

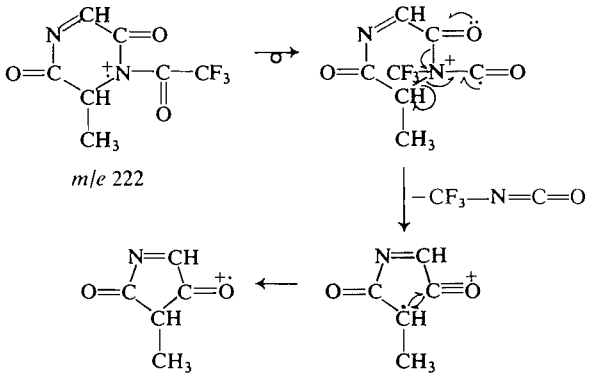

The occurrence of the ion at *m/e* 111 only in the spectra of the alanyl-DKP's containing ion **1** (*m/e* 320) in relatively high abundance lends some support to the proposed fragmentation. In the TFA-*cyclo*-(-Gly-X) series, a similar fragmentation would require formation of a primary radical centre and lead to an ion at *m/e* 97 isobaric with CF_3CO^+, but only the latter was observed (Table 7).

m/e *166*. This ion is abundant (25%, 23%) only in the spectra of TFA-*cyclo*-(-Gly-Leu) and TFA-*cyclo*-(-Ala-Leu) and suggests that the leucyl residue is involved. The formula of this ion $C_6H_7F_3NO$, established by HRMS, has insufficient hydrogen to accommodate the C_4H_9 leucyl side chain. However, if the CF_3CON group is present, the residue C_4H_7 can be accounted for as in eq. [9]. For the isoleucyl-DKP's this fragmentation would require elimination of a primary methyl group which may be energetically less favourable.

One of the objectives of the present study was to determine if the various DKP's could be identified

[9]

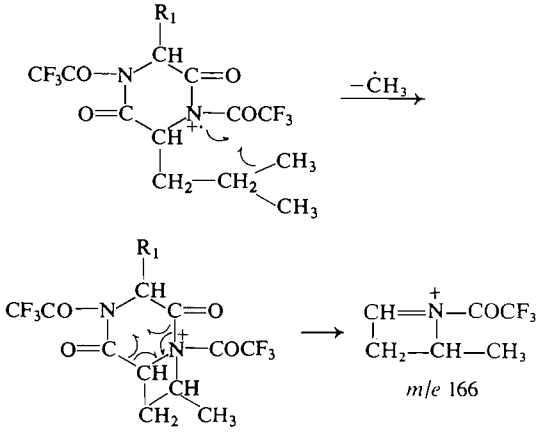

unequivocally by the mass spectra of their TFA-derivatives. On the basis of the fragmentations in Schemes 1–5 and eq. [3] it is possible to assign a DKP to the TFA-*cyclo*-(-Gly-X) or TFA-*cyclo*-(-Ala-X) series (X = Gly, Val, Leu, Ile). TFA-*cyclo*-(-Ala-Ala) can be distinguished from members of the latter series by the absence of ions in its mass spectrum (e.g. *m/e* 125, 126, 153) derived from the glycyl residue (formed by elimination of olefin [3]). Further distinction between compounds within a group is possible using the ions listed above, e.g. the ion at *m/e* 43 is observed only in the spectra of the valyl- and leucyl-DKP's while the ion at *m/e* 166 is found only in spectra of the latter. There are no such special ions in the spectra of TFA-*cyclo*-(-Gly-Gly/Ile) to permit distinguishing between these two compounds. However, the spectrum of TFA-*cyclo*-(-Gly-Ile) contains relatively abundant ions at *m/e* 57 (53%) due to $C_4H_9^+$ (Table 7) and *m/e* 41 (43%) due to $C_3H_5^+$ (Table 7). Although ions at *m/e* 57, 41 are predicted for TFA-*cyclo*-(-Gly-Gly) in Scheme 2 (ion 9) and Scheme 3 (ion 20), respectively, these are barely detectable (Fig. 1*a*). Distinguishing between TFA-*cyclo*-(-Ala-Gly) and TFA-*cyclo*-(-Ala-Ile) is also unpredictable as the spectrum of the latter does not show prominent ions at *m/e* 57, 41 (Fig. 2*c*). Identifying the members of the two pairs of compounds, TFA-*cyclo*-(-Gly-Gly/Ile) and TFA-*cyclo*-(Ala-Ala/Ile), on the basis of mass spectrometry is not unequivocal; however, the GC retention times are sufficiently different to permit a distinction to be made.

The composition of a number of ions in the spectra of the TFA-DKP's have been confirmed by HRMS (Tables 7, 9, and 10). However, this does not indicate the source of the atoms comprising these ions or establish the fragmentations leading to them. Appropriate isotopic labelling can indicate the method of formation of ionic fragments and this will be the subject of a future paper.

Experimental

The mass spectral data in Tables 1–5 were obtained using a Finnigan 3300 GC–MS and 6000 Data System. A glass column, 152 cm (5 ft) long, 6 mm OD, 2 mm ID, packed with 3% OV-1 on Chromosorb W, HP, 80/100 mesh, was used for chromatography of the TFA-DKP's. Helium at 20 cm^3/min was used as carrier gas and the column was programmed from 80 to 250°C at 8°C/min.

High resolution mass spectra were obtained using a MS-902 spectrometer (Associated Electrical Industries) or a CEC 21-110B spectrometer (Du Pont). Metastable ions were determined using a MS-12 instrument (Associated Electrical Industries).

The diketopiperazines were synthesized by hydrogenolysis of appropriate benzyloxycarbonyl dipeptide methyl esters (12). Conversion to the trifluoroacetyl derivatives was achieved by heating (80°C) the DKP's in Reacti-Vials (Pierce Chemical Co.) containing trifluoroacetic anhydride for 10–20 min.

Acknowledgements

High resolution mass spectra were supplied by Dr. D. Durden, Psychiatric Research Division, University Hospital, Saskatoon, and by Dr. D. Jamieson, Atlantic Regional Laboratory, NRCC, Halifax. The metastable ions were recorded by Mr. D. Bain, Chemistry Department, University of Saskatchewan, Saskatoon.

1. J. C. MacDonald. *In* Handbook of microbiology. Vol. III. Microbial products. *Edited by* A. I. Laskin and H. A. Lechevalier. CRC Press, Cleveland, Ohio. 1973. p. 345.
2. T. Shiba and K. Nunami. Tetrahedron Lett. No. 6, 509 (1974); K. Takahashi, M. Tadenuma, and K. Kitamoto. Agric. Biol. Chem. **38**, 927 (1974); W. Pickenhagen, P. Dietrich, and E. Lederer. Helv. Chim. Acta, **58**, 1078 (1975).
3. M. Bodanszky, A. A. Bodanszky, C. A. Ralofsky, R. G. Strong, and R. L. Foltz. J. Antibiot. **24**, 294 (1971).
4. A. B. Mauger. Chem. Biol. Pept. Proc. Am. Pept. Symp. 3rd. 1972. p. 691.
5. R. A. W. Johnstone, T. J. Povall, and J. D. Butz. J. Chem. Soc. Chem. Commun. 392 (1973).
6. R. A. W. Johnstone and T. J. Povall. J. Chem. Soc. Perkin Trans. I, 1297 (1975).
7. A. B. Mauger. J. Chromatogr. **37**, 315 (1968).
8. G. P. Slater. J. Chromatogr. **64**, 166 (1972).
9. IUPAC-IUB Commission on Biochemical Nomenclature. J. Biol. Chem. **247**, 977 (1972).
10. S. Eriksen and I. S. Fagerson. J. Agric. Food Chem. **24**, 1243 (1976).
11. N. S. Vul'fson, V. A. Puchkov, Yu. V. Denisov, B. V. Rozynov, V. N. Bochkarev, M. M. Shemyakin, Yu. A. Ovchinnikov, and V. K. Antonov. Chem. Heterocycl. Compd. **2**, 468 (1966).
12. G. P. Slater. Chem. Ind. 1092 (1969).

The mass spectra of trifluoroacetyl-2,5-diketopiperazines. II. *cyclo*-(-Val-Val/Leu/Ile), *cyclo*-(-Leu-Leu/Ile), and *cyclo*-(-Ile-Ile)[1]

GEORGE P. SLATER[2] AND LAWRENCE R. HOGGE

Prairie Regional Laboratory, National Research Council of Canada, Saskatoon, Sask., Canada S7N 0W9

Received November 13, 1978

GEORGE P. SLATER and LAWRENCE R. HOGGE. Can. J. Chem. **57**, 2052 (1979).

The trifluoroacetyl derivatives of the 2,5-diketopiperazines *cyclo*-(-Val-Val/Leu/Ile), *cyclo*-(-Leu-Leu/Ile), and *cyclo*-(-Ile-Ile) were examined by GC–MS. The fragmentation of these compounds generally follows the same pathways as previously observed for the TFA-*cyclo*-(-Gly-X) series (X = Gly, Val, Leu, Ile). However, the spectra can be interpreted on the basis that the molecular ion fragments prior to, or after, one of the alkyl groups is eliminated as olefin. Some ion fragments indicate that both alkyl groups are eliminated but this does not appear to occur directly from the molecular ion. Support for fragmentation of the molecular ion by the suggested route is indicated by a number of isobaric ions although corresponding metastable ions were not observed.

The spectra enable the compounds in the series TFA-*cyclo*-(-Val-X) (X = Val, Leu, Ile) to be readily identified but this is not the case for TFA-*cyclo*-(-Leu-Leu/Ile) and TFA-*cyclo*-(-Ile-Ile). However, all of these compounds can be distinguished from TFA-*cyclo*-(-Gly-X) and TFA-*cyclo*-(-Ala-X) (X = Gly, Val, Leu, Ile).

GEORGE P. SLATER et LAWRENCE R. HOGGE. Can. J. Chem. **57**, 2052 (1979).

On a étudié les dérivés trifluoroacétylés des dicéto-2,5 pipérazines *cyclo*-(Val-Val/Leu/Ile), *cyclo*-(Leu-Leu/Ile) et *cyclo*-(Ile-Ile) par GC–MS. Les fragmentations de ces composés suivent généralement les mêmes voies que celles observées pour la série TFA-*cyclo*-(-Gly-X) (X = Gly, Val, Leu, Ile). Toutefois on peut interpréter les spectres en faisant l'hypothèse que la fragmentation de l'ion moléculaire se produit avant ou après que l'un des groupes alkyles ait été éliminé sous forme d'oléfine. D'après quelques ions de fragmentation, il semble que les deux groupes alkyles sont éliminés mais il n'apparait pas que ces éliminations se fassent directement à partir de l'ion moléculaire. Les données suggérant le type de fragmentation proposé découlent du nombre d'ions isobares même si l'on n'a pas observé la présence d'ions métastables.

Les spectres permettent d'identifier facilement les composés de la série TFA-*cyclo*-(-Val-X) (X = Val, Leu, Ile) mais tel n'est pas le cas pour les composés TFA-*cyclo*-(-Leu-Leu/Ile) et TFA-*cyclo*-(-Ile-Ile). Toutefois on peut distinguer tous les composés des séries TFA-*cyclo*-(-Gly-X) et TFA-*cyclo*-(-Ala-X) (X = Gly, Val, Leu, Ile).

[Traduit par le journal]

Introduction

In Part I of this series (2) the mass spectra of the trifluoroacetyl derivatives of *cyclo*-(-Gly-X), *cyclo*-(-Ala-X) (X = Gly, Val, Leu, Ile)[3], and *cyclo*-(-Ala-Ala) were described. A number of fragmentation pathways and supporting evidence were presented to account for the mass spectral patterns observed. In general, the spectra could be explained by a series of fragmentations common to all the trifluoroacetyl-2,5-diketopiperazines (TFA-DKP's) examined. Several differences between the various spectra were also noted and these could be used to help characterize the individual DKP's.

The first series of TFA-DKP's examined (2) contained several compounds bearing a C_3-alkyl(valyl) or C_4-alkyl group (leucyl/isoleucyl). The present study is concerned with DKP's synthesized from valine, leucine, and isoleucine only. Thus we have a series of trifluoroacetyl-dialkyl-2,5-diketopiperazines (TFA-DA-DKP's) each of which contains two C_3- or two C_4-alkyl groups, or one of each. This report describes the mass spectra of the TFA-DA-DKP's and indicates apparent differences in the fragmentation of the molecular ions of these compounds and the molecular ions of the TFA-DKP's previously examined (2).

Results and Discussion

The mass spectra of the TFA-DA-DKP's were obtained by gas chromatography – mass spectroscopy (GC–MS) using a quadrupole mass spectrometer, as previously described (2). In addition a number of ions were subjected to high resolution mass spectroscopy (HRMS) and some of the compounds were examined with a magnetic sector instrument to check for metastable ions.

As before (2) the molecular ions of these com-

[1]NRCC No. 17403.

[2]To whom all correspondence should be addressed.

[3]The abbreviations for the amino acids are those recommended by the IUPAC-IUB Commission on Biochemical Nomenclature (1).

0008-4042/79/152052-06$01.00/0

pounds do not appear in the normalized mass spectra (Figs. 1 and 2) produced by the computer. However, these ions are easily seen on the oscillograph trace of maximum sensitivity from the magnetic sector instrument. Several of the remaining ions in the spectra of the TFA-DA-DKP's (Figs. 1 and 2) have the same *m/e* values as ions in the spectra of TFA-*cyclo*-(-Gly-Gly) (2), viz. *m/e* 69, 70, 96, 97, 125, 126, 139, 153, 154, although the relative abundances differ. Examination of these ions by HRMS[4] indicates that the corresponding ions in both sets of spectra are identical, except that several of the above ions for the TFA-DA-DKP's contain isobaric ions which are not possible for TFA-*cyclo*-(-Gly-Gly). The ions at *m/e* 125, 126, 139, 153, 154 in the spectra of the TFA-DA-DKP's imply that these compounds fragment as previously suggested (2) for the TFA-*cyclo*-(-Gly-X) compounds (i.e. both alkyl groups are eliminated as olefin from the molecular ion [1]

[1] 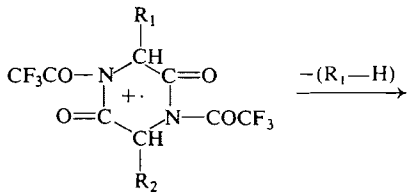

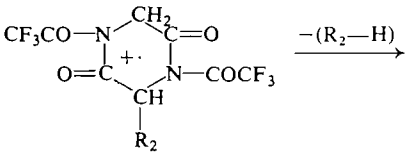

1, *m/e* 348 ($R_2 = C_3H_7$)
m/e 362 ($R_2 = C_4H_9$)

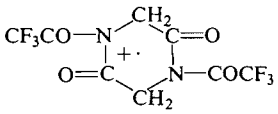

2, *m/e* 306

to give the ions at *m/e* 306 (**2**) corresponding to the molecular ion of TFA-*cyclo*-(-Gly-Gly)). However, the spectra of the valyl-DKP's and the leucyl/isoleucyl-DKP's in the present series contain ions at *m/e* 168 (Fig. 1) and *m/e* 182 (Figs. 1 *b* and *c*, 2) which were found[4] to be the higher homologues of the ion at *m/e* 126 (i.e. ion 8, $R_2CH{=}\overset{+}{N}H{-}COCF_3$; *m/e* 126, $R_2 = H$; *m/e* 168, $R_2 = C_3H_7$; *m/e* 182, $R_2 = C_4H_9$). Since all three ions are present in the spectra of TFA-*cyclo*-(-Val-Leu/Ile) it would appear that the molecular ion fragments to give a mixture of the two higher homologues (*m/e* 168, 182) which could eliminate olefin to produce the ion at *m/e* 126. However, in the spectra of the valyl-DKP's (Fig. 1) and the leucyl/isoleucyl-DKP's (Fig. 2) ions at *m/e* 348, 362 (**1**, [1]) correspond to the loss of C_3H_6 and/or C_4H_8 as previously observed for the TFA-*cyclo*-(-Gly-X) compounds. Fragmentation of ion **1** by pathways proposed for the latter compounds (2) would also account for the ions typical of TFA-*cyclo*-(-Gly-Gly) and the homologous ions at *m/e* 168, 182. Unfortunately, no metastable ions corresponding to these fragmentations of the molecular ion were detected although a metastable ion was observed for *m/e* 153 → *m/e* 125 (*m** 102.1).

To further complicate the issue, the ions at *m/e* 139, 70 have the same formulae ($C_4H_4F_3NO$, C_3H_4NO, respectively) as the corresponding ions in the spectrum of TFA-*cyclo*-(-Gly-Gly), i.e. ions 14, 21 in ref. 2. For these ions to occur their precursor(s) must eliminate both alkyl groups and this could happen by elimination of olefin from ion **1** [1] to give ion **2** (*m/e* 306) which corresponds to the molecular ion of TFA-*cyclo*-(-Gly-Gly). The absence[5] of the ion at *m/e* 306 and low abundances of precursors of ion 14 in which both alkyl groups are absent (viz. ion 11, *m/e* 327; ion 12, *m/e* 204; ion 13, *m/e* 167, cf. Table 3, ref. 2) appear to exclude this possibility. An alternative explanation would require elimination of olefin from ion 14, *m/e* 181 ($R_2 = C_3H_7$) or *m/e* 195 ($R_2 = C_4H_9$). In the absence of relevant metastable ions the present data do not indicate which of the pathways is preferred, however a metastable ion (*m** 35.3) corresponding to elimination [2] of $\cdot CF_3$

[2] 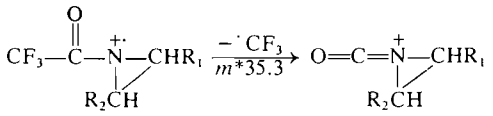

14, *m/e* 181 ($R_2 = C_3H_7$; $R_1 = H$) → **21**, *m/e* 112
m/e 195 ($R_2 = C_4H_9$; $R_1 = H$) → *m/e* 126
m/e 139 ($R_1 = R_2 = H$) → *m/e* 70

from the ion at *m/e* 139 was observed. The presence of one of the higher homologues of ion 21 (viz. *m/e* 126) as an isobar of ion 8 was confirmed by HRMS.[4]

Of the remaining ions in the spectra of the TFA-DA-DKP's which have *m/e* values identical to those in the spectra of the TFA-*cyclo*-(-Gly-X) compounds (2) only the ions at *m/e* 69, 166 (latter for leucyl-

[4]A complete set of these data is available, at a nominal charge, from the Depository of Unpublished Data, CISTI, National Research Council of Canada, Ottawa, Ont., Canada K1A 0S2.

[5]The ion at *m/e* 306 is too small to be seen in the normalized mass spectra produced by computer but is readily apparent in the oscillograph trace for the magnetic sector instrument.

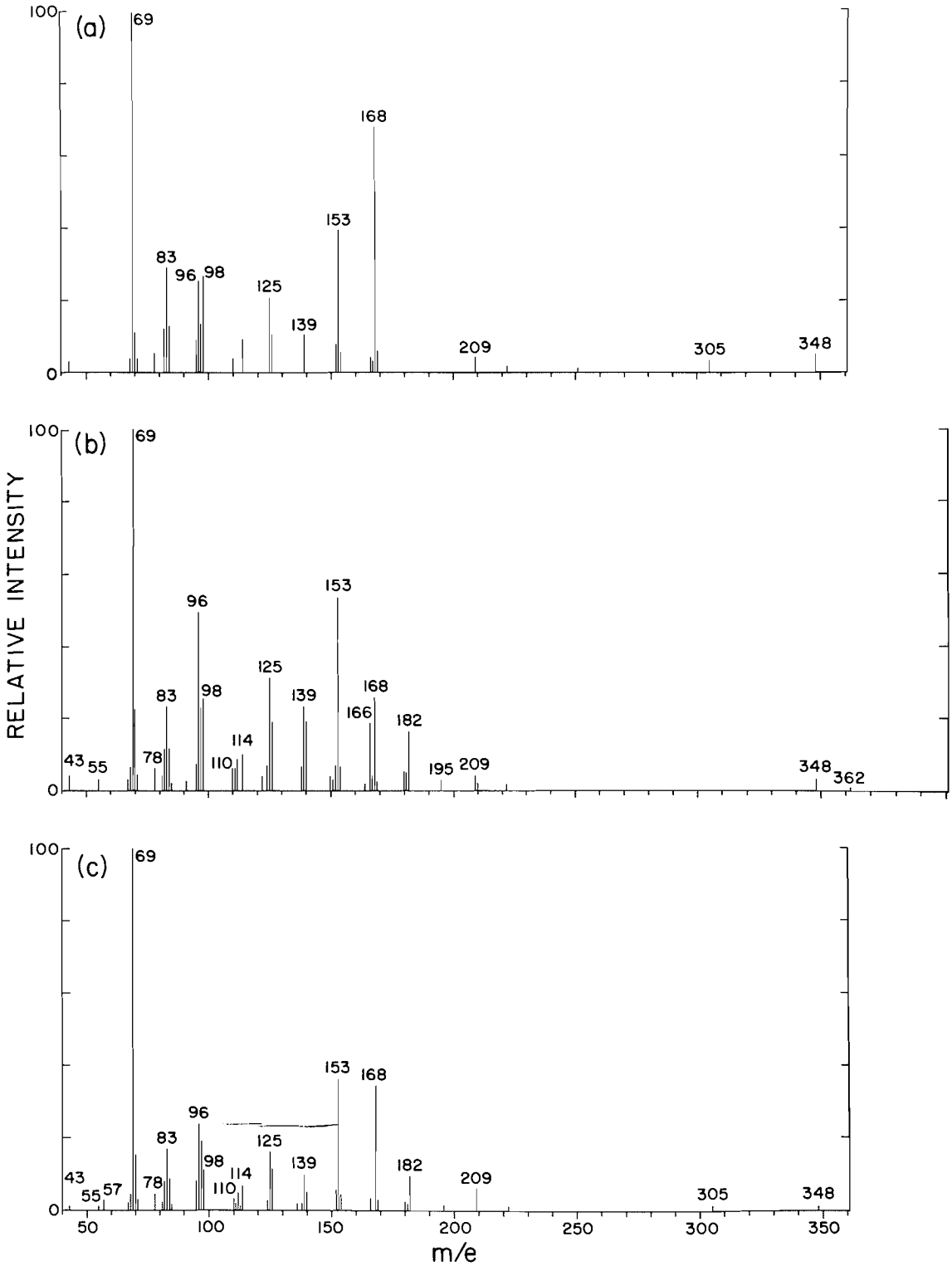

FIG. 1. Mass spectra of (*a*) TFA-*cyclo*-(-Val-Val), (*b*) TFA-*cyclo*-(-Val-Leu), (*c*) TFA-*cyclo*-(-Val-Ile).

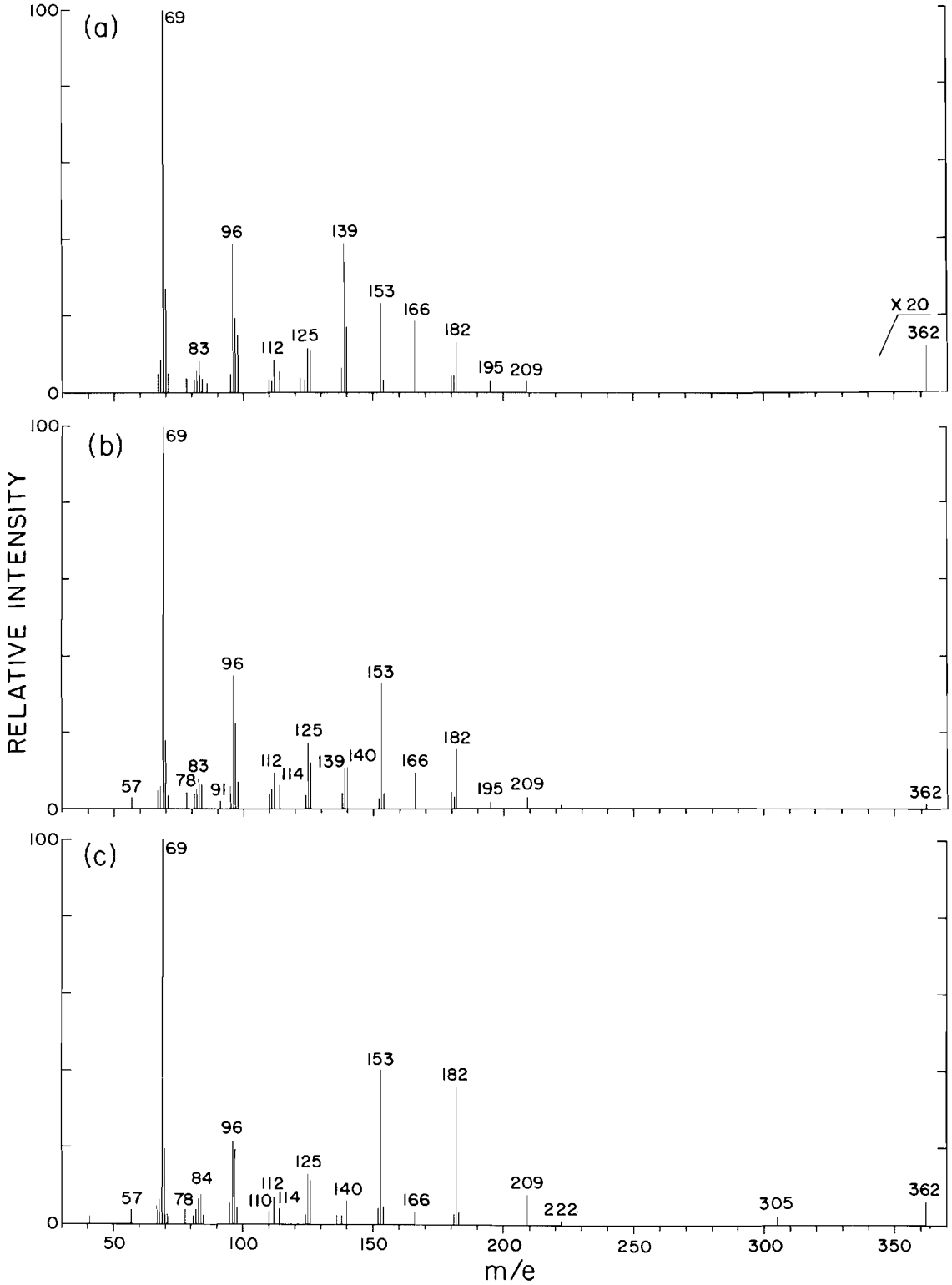

FIG. 2. Mass spectra of (*a*) TFA-*cyclo*-(-Leu-Leu), (*b*) TFA-*cyclo*-(-Leu-Ile), (*c*) TFA-*cyclo*-(-Ile-Ile).

DKP's) were the same for both groups.[4] The ion at *m/e* 96 in the spectra of the leucyl/isoleucyl-DKP's contained three isobars, C_2HF_3N (previously detected, ref. 2), C_4H_9—C_2HN (a homologue of ion 17, ref. 2) and C_6H_8O (C_4H_9—$CH{=}C{=}\overset{+\cdot}{O}$ – $[H_2]$) in the ratio 8:1:8.[4] For TFA-*cyclo*-Val-Val only C_2HF_3N is possible and was the only ion seen. The ion at *m/e* 97 also comprises three isobars for the leucyl/isoleucyl-DKP's, viz. CF_3CO, C_4H_9—C_2H_2N (homologue of ion 20, ref. 2), and C_6H_9O (2:1:3)[4]. The last ion corresponds to loss of H· from the ketene ion C_4H_9—$CH{=}C{=}\overset{+\cdot}{O}$ and the lower homologue at *m/e* 83 (C_3H_7—$CH{=}C{=}\overset{+\cdot}{O}$ – [H·]) was also observed in the spectra of the valyl-DKP's.[4] The ion at *m/e* 83 contained two other isobars, viz. C_3H_7–C_2H_2N (homologue of ion 20, ref. 2) and an ion of formula C_3HNO_2 (possibly $O{=}C{=}CH{-}\overset{+\cdot}{N}{=}C{=}O$ derived from ion **3** [3]).

[3]

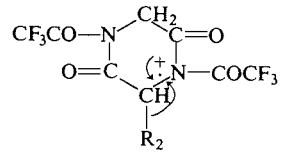

1, *m/e* 348 ($R_2 = C_3H_7$)
m/e 362 ($R_2 = C_4H_9$)

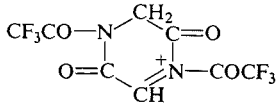

3, *m/e* 305

In the spectra of TFA-*cyclo*-(Val-Val/Ile) (Fig. 1 *a* and *c*) a relatively small ion occurs at *m/e* 305 (cf. footnote 5) which could arise from ion **1** by expulsion of the second alkyl group as a radical [3] and the corresponding metastable ion (*m/e* 267.1) was obtained in the spectrum of TFA-*cyclo*-(-Val-Ile). A metastable ion corresponding to the loss of this radical in the spectrum of underivatized *cyclo*-(-Val-Ile) has been reported previously (3). Several fragmentations of ion **3** involving loss of $\cdot CF_3$, CO, ketene, etc. are possible but none lead to relatively abundant ions.

The spectra of the TFA-DA-DKP's also contain ketene ions, $RCH{=}C{=}\overset{+\cdot}{O}$, at *m/e* 84 (R = C_3H_7) and *m/e* 98 (R = C_4H_9), but none at *m/e* 42 (R = H). The ketene ion, *m/e* 42, was relatively abundant (11–42%) in the spectra of TFA-*cyclo*-(-Gly-X) (X = Gly, Val, Leu, Ile) (2) and its absence in the spectra of the TFA-DA-DKP's (Figs. 1 and 2) suggests that formation of ketene ions in the spectra of the latter compounds occurs preferentially from the molecular ion or from the portion of ion **1** [1] retaining the alkyl group. This is contrary to the results for the TFA-DKP's (2) where ketene ions retaining the valyl- or leucyl/isoleucyl-side chains were not observed.

The ketene ions at *m/e* 84, 98 are isobaric with ions predicted for the TFA-DA-DKP's by Schemes 1 and 3 in the previous paper (2). In the case of TFA-*cyclo*-(-Val-Val) the ion at *m/e* 98 should be due solely to C_3H_7—$CH{=}\overset{+}{N}{=}C{=}O$ (corresponding to ion 4) and this was confirmed by HRMS.[4] For TFA-*cyclo*-(-Val-Leu/Ile) two other isobars are possible, viz. C_4H_9—$CH{=}\overset{+}{N}{=}CH_2$ (ion 22) and the ketene C_4H_9—$CH{=}C{=}\overset{+\cdot}{O}$. All three isobars were found in the high resolution spectrum of TFA-*cyclo*-(-Val-Leu) and is consistent with fragmentation of this compound by way of ion **1** [1] and then Schemes 1–5, or directly by Schemes 1–5. In the case of TFA-*cyclo*-(-Leu-Leu/Ile) and TFA-*cyclo*-(-Ile-Ile) only C_4H_9—$CH{=}\overset{+}{N}{=}CH_2$ and the ketene are possible but only the latter was detected.[4] The high resolution spectrum of TFA-*cyclo*-(-Val-Val) indicated that the ion at *m/e* 84 was due to ketene (C_3H_7—$CH{=}C{=}\overset{+\cdot}{O}$) only.

Identifying the three valyl-DKP's on the basis of the spectra in Fig. 1 is relatively straightforward since the valyl residue gives rise to the characteristic ion at *m/e* 168 and the leucyl/isoleucyl residue to the homologue at *m/e* 182. The ion at *m/e* 166 then allows the leucyl-DKP to be identified. On the other hand, the spectra in Fig. 2 are so similar that it is not possible to identify the individual compounds on this basis. Even the ion at *m/e* 166 occurs in the spectrum of TFA-*cyclo*-(-Ile-Ile) although the relative abundance (3%) is less than that in the spectra of the other two compounds (19%, 10%). The only distinguishing feature appears to be that the ion at *m/e* 139 is quite prominent (39% relative abundance) in the spectrum of TFA-*cyclo*-(-Leu-Leu), much less abundant in the spectra of TFA-*cyclo*-(-Leu-Ile) (11%) and TFA-*cyclo*-(-Ile-Ile) (2%). No reason for the variation in intensity of this ion is apparent since HRMS[4] indicates a single ion of formula $C_4H_4F_3NO$ (ion 14, both alkyl groups removed [2]).

The spectra of TFA-*cyclo*-(-Val-Leu) (Fig. 1*b*) and TFA-*cyclo*-(-Leu-Leu/Ile) (Fig. 2 *a* and *b*) contain an ion at *m/e* 140 which is relatively abundant (18%, 17%, 11%) compared to the other spectra (2–6%). The formula $C_4H_5F_3NO$ was indicated by HRMS[4] and an ion of this composition could be formed from the ion at *m/e* 182 by elimination of propylene [4].

For the isoleucyl-DKP's the analogous fragmentation would result in the loss of ethylene to give an

[4] 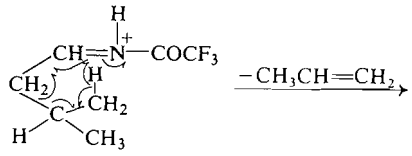

m/e 182

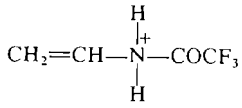

m/e 140

ion at *m/e* 154. This relatively weak ion was in the spectra of all these compounds (Figs. 1 and 2) but was not examined by HRMS. Loss of propylene from leucyl residues in peptides and of ethylene from isoleucyl residues has been noted previously (4), but only the above loss of propylene [4] appears to occur in the fragmentation of the TFA-DA-DKP's.

Comparison of the spectra of the TFA-DA-DKP's (Figs. 1 and 2) with those previously obtained (2) indicates a number of differences. These enable the two groups of compounds to be distinguished but also suggests that the molecular ions of the compounds in the two groups behave differently. When only one alkyl group is present in a TFA-DKP it appears that the molecular ion eliminates the alkyl group as olefin prior to fragmentation since ions containing an alkyl group were not observed in the spectra of these compounds (2). In contrast, when the TFA-DKP's contain two alkyl groups, the spectra (Figs. 1 and 2) indicate the following possibilities: (*1*) the molecular ion fragments (as shown in Schemes 1–5, ref. 2) to give a mixture of ions retaining one or other of the alkyl groups.[4] Some of these ions then partially eliminate the alkyl group as olefin to give fragments identical to those in the spectra of the TFA-glycyl-DKP's (2); (*2*) the molecular ion eliminates one alkyl group to give ion **1** [1] which can then fragment as in (*1*) to give a mixture of ions with and without an alkyl group. Again, some of these ions would have to eliminate olefin to give ions at *m/e* 139, 70, for example; (*3*) concurrent with (*1*) and/or (*2*), ion **1** may eliminate the remaining alkyl group as olefin [1] prior to fragmentation by Schemes 1–5.

The data obtained from the present work do not establish unequivocally all of the proposed fragmentations. In some cases additional information would be available by examination of isotopically labelled compounds and this will be considered in a future communication.

Experimental

The trifluoroacetyl-2,5-diketopiperazines and their mass spectra were obtained as previously described (2).

Acknowledgements

High resolution mass spectra were supplied by Dr. D. Durden, Psychiatric Research Centre, University of Saskatchewan (A.E.I. MS-902), and Dr. D. Jamieson and Mr. D. Embree, Atlantic Regional Laboratory, National Research Council of Canada, Halifax, N.S. (CEC21-110B, DuPont). Metastable ions were determined by Mr. D. Bain, Chemistry Department, University of Saskatchewan (A.E.I. MS-12).

1. IUPAC-IUB Commission on Biochemical Nomenclature. J. Biol. Chem. **247**, 977 (1972).
2. G. P. SLATER and L. R. HOGGE. Can. J. Chem. This issue.
3. S. ERIKSEN and I. S. FAGERSON. J. Agric. Food Chem. **24**, 1243 (1976).
4. P. J. ARPINO and F. W. MCLAFFERTY. *In* Determination of organic structure by physical methods. *Edited by* F. Nachod, J. Zuckerman, and E. W. Randall. Academic Press, New York, NY. 1976.

Fluorosulfates of palladium. Part 2.[1] The hexakis(fluorosulfato)palladate(IV) ion and palladium(II) hexakis(fluorosulfato)metallates(IV)

KEITH C. LEE AND FRIEDHELM AUBKE[2]

Department of Chemistry, The University of British Columbia, Vancouver, B.C., Canada V6T 1W5

Received February 8, 1979

KEITH C. LEE and FRIEDHELM AUBKE. Can. J. Chem. 57, 2058 (1979).

The synthesis of a number of compounds containing the hexakis(fluorosulfato)palladate(IV) anion and the cations Cs^+, Ba^{2+}, NO^+, and ClO_2^+ is reported. All compounds are diamagnetic. Also reported is the synthesis of $Pd[M(SO_3F)_6]$, where M = Pt(IV) and Sn(IV). Here, palladium(II) is found in a regular octahedral environment. Both compounds are paramagnetic, consistent with a $^3A_{2g}$ ground state. Curie–Weiss law behavior is found and ligand field parameters for the Pd(II) derivatives are reported.

Vibrational spectra are reported for all new fluorosulfato complexes.

KEITH C. LEE et FRIEDHELM AUBKE. Can. J. Chem. 57, 2058 (1979).

On rapporte la synthèse d'un certain nombre de composés contenant l'anion hexakis(fluorosulfato)palladate(IV) et les cations Cs^+, Ba^{2+}, NO^+ et ClO_2^+. Tous les composés sont diamagnétiques. On rapporte aussi la synthèse du $Pd[M(SO_3F)_6]$ où M = Pt(IV) et Sn(IV). On a trouvé dans ce cas que le palladium(II) est dans un environnement octaédrique régulier. Les deux composés sont paramagnétiques ce qui est en accord avec un état fondamental $^3A_{2g}$. On a trouvé un comportement qui suit la loi de Curie–Weiss et on rapporte les paramètres de champ de ligand pour les dérivés Pd(II).

On rapporte les spectres vibrationnels de tous les nouveaux complexes fluorosulfato.

[Traduit par le journal]

Introduction

We have recently (1) reported on the syntheses and structural characterization of two binary fluorosulfates of palladium, $Pd(SO_3F)_2$ and '$Pd(SO_3F)_3$'. In contrast to most palladium(II) compounds (2), the fluorosulfates are paramagnetic and for $Pd(SO_3F)_2$ a regular octahedral environment for Pd^{II} is suggested.

In analogy to PdF_3 (3–5), the compound '$Pd(SO_3F)_3$' is best formulated as $Pd^{II}[Pd^{IV}(SO_3F)_6]$, again with Pd^{II} in a regular octahedral environment

In the present study, our work on palladium fluorosulfates is extended in two general directions: (*a*) the synthesis and characterization of Pd^{II} derivatives of the type $Pd^{II}[M^{IV}(SO_3F)_6]$ with M = Pt or Sn; and (*b*) the preparation of complexes containing the $[Pd(SO_3F)_6]^{2-}$ anion, as well as the attempted synthesis of $Pd(SO_3F)_4$.

Magnetic and spectroscopic studies on both sets of compounds are undertaken in support of our earlier structural conclusion.

Experimental

Chemicals

Palladium and platinum powder (both −60 mesh and of 99.95% purity) were obtained from Ventron Corp., and tin (−20 mesh, 99.97% pure) was supplied by BDH. Technical grade fluorosulfuric acid (Allied Chemicals) was doubly distilled at atmospheric pressure as described previously (6). Nitrosylchloride (Matheson) was purified by trap-to-trap distillation and stored over $CaSO_4$ before use. Bis(fluorosulfuryl)peroxide (7), $S_2O_6F_2$, and chlorylfluorosulfate (8), ClO_2SO_3F, were synthesized according to published method. The previously reported fluorosulfates: $Sn(SO_3F)_4$ (9), $Pt(SO_3F)_4$ (10), and '$Pd(SO_3F)_3$' (1) were obtained by an alternative, more convenient method: the oxidation of the metal by $S_2O_6F_2$ in HSO_3F at about +100°C. $Pd(SO_3F)_2$ was obtained by the thermal decomposition of $Pd[Pd(SO_3F)_6]$ at 130°C (1). All other chemicals used in this study were obtained from commercial sources.

Instrumentation

Raman spectra were obtained with either a Cary 81 or a Spex Ramalog 5 spectrophotometer fitted with either a He–Ne (635.5 nm) or an argon ion (514.5 nm) laser respectively. Raman spectra at liquid N_2 temperature were recorded only on the Spex Ramalog 5. The samples were contained in Pyrex melting point tubes. An evacuable two part Pyrex cell, fitted with quartz windows at a 90° angle and a brass sample holder directly cooled with liquid N_2, was employed for the Raman spectra at 80 K.

Infrared spectra were recorded on a Perkin-Elmer 457 spectrophotometer. AgCl, AgBr, and BaF_2 (Harshaw Chemicals) were used as window materials. Spectra were obtained from thin solid films, since the compounds were found to react with the commonly used mulling agents.

Electronic spectra were obtained on powdered samples using a Bausch and Lomb Spectronic 600 spectrophotometer (diffuse reflectance) and on samples mulled in $C_8F_{17}SO_2F$ (perfluoro-octyl sulfuryl-fluoride) using a Cary 14 spectrophotometer. Magnetic susceptibilities were measured using the Gouy apparatus described earlier (12). The coil current of the magnet was regulated to give a field of approximately 4500 G. The temperature of the sample was controlled by the rate of

[1]For Part 1 see ref. 1.

[2]To whom all correspondence should be addressed.

0008-4042/79/152058-07$01.00/0

evaporation of N_2 around the chamber. Calibration was achieved using $HgCo(SCN)_4$ (13). Diamagnetic corrections were made using published Pascals constants (2). For SO_3F^-, a suggested (14) correction of 40×10^{-6} cgs units was used.

All reactions were performed in Pyrex reaction vials of about 40 mL contents fitted with Kontes Teflon stem valves. Volatile materials were handled using vacuum line techniques. Solids were handled in a Vacuum Atmospheres Corp. 'Dri Lab' Model No. HE-43-2 filled with purified dry nitrogen and equipped with a 'Dri-Train' Model No. HE-93-B circulating unit. Filtrations of moisture sensitive materials were carried out in an apparatus described by Shriver (11).

Synthetic Reactions

(a) $Cs_2[Pd(SO_3F)_6]$

A Pyrex reaction vial was charged with 0.104 g (0.977 mmol) of palladium and 0.329 g (1.954 mmol) of CsCl, and approximately 9 g of HSO_3F was added by vacuum distillation. After removal of the HCl *in vacuo*, ~13 g of $S_2O_6F_2$ was distilled onto the mixture *in vacuo*. Reaction occurred at room temperature and the solution turned deep red. The reaction mixture was heated to +120°C for 3 days. After this time all metal powder had been consumed. Removal of all volatiles *in vacuo* with the reaction vial at room temperature yielded a dark red crystalline solid which analysed as $Cs_2[Pd(SO_3F)_6]$. In this reaction, 0.927 g (0.960 mmol) were obtained. $Ba[Pd(SO_3F)_6]$ was prepared in an identical fashion. $BaCl_2 \cdot 2H_2O$ was dried in an oven for 24 h at 150°C. The reaction temperature was 90°C, and the reaction time was 1 week.

(b) $Pd^{II}[Pt^{IV}(SO_3F)_6]$

To a mixture of 0.319 g (1.05 mmol) of $Pd(SO_3F)_2$ and 0.666 g (1.13 mmol) of $Pt(SO_3F)_4$, approximately 5 mL of HSO_3F were added by distillation *in vacuo*. After heating the mixture for 3 days at 80°C, a homogeneous green precipitate had formed. The mixture was filtered and washed with HSO_3F repeatedly. The material was dried by heating to 80°C *in vacuo*.

$Pd^{II}[Sn^{IV}(SO_3F)_6]$ was prepared in an analogous fashion. Reaction time was 1 week and the reaction temperature was +70°C.

(c) $(ClO_2)_2[Pd(SO_3F)_6]$

0.129 g (1.21 mmol) of palladium were allowed to react with a mixture of approximately 0.5 mL of ClO_2SO_3F and 5 mL of $S_2O_6F_2$. After maintaining a reaction temperature of 70°C for 3 days, dark red crystals were formed. Removal of all volatiles yielded 1.013 g (1.21 mmol) of a crystalline material of the composition $(ClO_2)_2[Pd(SO_3F)_6]$.

(d) $(NO)_2[Pd(SO_3F)_6]$

By reaction of 0.110 g (1.03 mmol) palladium with approximately 3 mL of ClNO for 12 h at room temperature, 0.31 g (1.03 mmol) of $(NO)_2PdCl_4$ was formed. This intermediate was allowed to react with a mixture of about 3 mL of HSO_3F and 3 mL of $S_2O_6F_2$ for 1 h at 80°C. Removal of all volatile materials while heating the sample to 70°C yielded a bright red solid analysed as $(NO)_2[Pd(SO_3F)_6]$.

Analysis

Microanalyses on all new compounds were performed by Microanalytical Laboratories, formerly A. Bernhardt, Elbach, West Germany. The nitrogen content of $(NO)_2[Pd(SO_3F)_6]$ was determined by Mr. P. Borda of this department. $Cs_2[Pd(SO_3F)_6]$, dark red hygroscopic crystals, diamagnetic, soluble in HSO_3F, thermally stable up to 200°C. *Anal.* calcd.: Cs 27.50, Pd 11.01, F 11.79; found: Cs 27.25, Pd 10.85, F 11.67. $Ba[Pd(SO_3F)_6]$, orange-red, hygroscopic powder, very sparingly soluble in HSO_3F, thermally stable to approximately 200°C. *Anal.* calcd.: Ba 16.39, Pd 12.70, S 22.95, F 13.60; found: Ba 16.24, Pd 12.64, S 22.89, F 13.82. $(NO)_2[Pd(SO_3F)_6]$, bright red hygroscopic crystals, soluble in HSO_3F, melts with decomposition at about 200°C. *Anal.* calcd.: N 3.68, Pd 13.99, S 25.29, F 14.99; found: N 3.44, Pd 13.81, S 25.11, F 15.17. $(ClO_2)_2[Pd(SO_3F)_6]$, deep red, hygroscopic crystals, soluble in HSO_3F, stable up to ~200°C. *Anal.* calcd.: Cl 8.48, Pd 12.73, F 13.64; found: Cl 8.60, Pd 12.82, F 13.68. $Pd[Pt(SO_3F)_6]$, green powder, hygroscopic, insoluble in HSO_3F at room temperature, thermally stable to about 200°C. *Anal.* calcd.: Pd 11.88, Pt 21.80, F 12.72; found: Pd 11.62, Pt 21.74, F 12.88. $Pd[Sn(SO_3F)_6]$, light blue hygroscopic powder, insoluble in HSO_3F at room temperature, decomposes at around 250°C into a light purple solid. *Anal.* calcd.: Pd 12.98, Sn 14.48, S 23.47, F 13.91; found: Pd 13.06, Sn 14.61, S 23.31, F 13.72.

Results and Discussion

Synthesis

The principal oxidizing and fluorosulfonating agent used in the synthesis of the new hexakis(fluorosulfato)palladates(IV) is a concentrated solution of bis(fluorosulfuryl)peroxide, $S_2O_6F_2$, in fluorosulfuric acid, HSO_3F. This solution combines the excellent oxidizing ability of $S_2O_6F_2$ and the solvating property of HSO_3F rather well and may be effectively used in the syntheses of binary transition metal fluorosulfates, or fluorosulfato complexes (15, 16).

The formation of $Cs_2[Pd(SO_3F)_6]$ via:

$$[1]\quad 2CsSO_3F + Pd + 2S_2O_6F_2 \xrightarrow[3\ \text{days}]{+120^\circ C} Cs_2[Pd(SO_3F)_6]$$

with $CsSO_3F$ formed *in situ* from CsCl and HSO_3F, employs the oxidation of palladium metal to the +4 oxidation state, while the synthesis of $(NO)_2[Pd(SO_3F)_6]$ illustrates the oxidation of palladium from +2 to +4 with the replacement of chloride by fluorosulfate groups:

$$[2]\quad (NO)_2[PdCl_4] + 3S_2O_6F_2 \xrightarrow[1\ \text{h}]{+80^\circ C} (NO)_2[Pd(SO_3F)_6] + 2Cl_2$$

The starting material $(NO)_2[PdCl_4]$ is easily obtained by oxidation of palladium with a large excess of ClNO. The oxidation is followed by weight and the presence of $(NO)_2[PdCl_4]$ is suggested by 2 ir bands at 2150 (νNO) and 332 cm^{-1} ($\nu PdCl_4$). The preceding examples and the syntheses of $Ba[Pd(SO_3F)_6]$ and $(ClO_2)_2[Pd(SO_3F)_6]$ by similar methods suggest that $Pd(SO_3F)_4$ may be obtainable as well and, indeed, solutions containing Pd(IV) in $HSO_3F/S_2O_6F_2$ are obtained by two main routes:

(*a*) The oxidation of palladium yields deep red-brown solutions. The uv spectrum is identical to the one produced by solutions of $(NO)_2[Pd(SO_3F)_6]$ with λ_{max} at 320 nm and an approximate molar absorption coefficient of $1.3 \times 10^4\ M^{-1}\ cm^{-1}$.

(*b*) $Pd[Pd(SO_3F)_6]$ (1) is insoluble in HSO_3F; however, addition of $S_2O_6F_2$ to the suspension produces a dark red-brown solution, but even at elevated reaction temperatures and long reaction times a residue of $Pd[Pd(SO_3F)_6]$ still remains.

Attempts to isolate $Pd(SO_3F)_4$ from solutions after filtration were unsuccessful. Removal of all volatiles *in vacuo* with the solution at room temperature resulted in the gradual precipitation of $Pd[Pd(SO_3F)_6]$. It appears that $Pd(SO_3F)_4$ may not be thermally stable enough to allow its isolation. When the oxidation of palladium in $HSO_3F/S_2O_6F_2$ at temperatures ranging from 25 to 120°C is allowed to go to completion, removal of all volatiles *in vacuo* yields quantitatively pure $Pd[Pd(SO_3F)_6]$ This one step procedure offers a distinct advantage over the originally (1) published method.

In contrast to these findings, the synthetic usefulness of the $HSO_3F/S_2O_6F_2$ mixtures is illustrated by the facile preparation of both $Pt(SO_3F)_4$ and $Sn(SO_3F)_4$ via:

$$[3]\quad M + 2S_2O_6F_2 \xrightarrow[HSO_3F]{} M(SO_3F)_4$$

M = Pt or Sn, where short reaction times, the absence of reaction intermediates, and the use of highly pure metals present additional advantages over the originally reported synthetic routes to both compounds (9, 10).

The subsequent syntheses of the palladium(II) derivatives of $Pd[Sn(SO_3F)_6]$ and $Pd[Pt(SO_3F)_6]$ proceed reasonably fast at +70 to +80°C according to:

$$[4]\quad Pd(SO_3F)_2 + M(SO_3F)_4 \xrightarrow[HSO_3F]{} Pd[M(SO_3F)_6]$$

M = Pt or Sn.

Exactly stoichiometric amounts of both reactants are required to ensure complete reaction.

Compounds containing both the $[Sn(SO_3F)_6]^{2-}$ and the $[Pt(SO_3F)_6]^{2-}$ ions have been reported previously (15, 17, 18) and characterization based on vibrational spectra should be facilitated by these precedents.

The synthesis of $(ClO_2)_2[Pd(SO_3F)_6]$ departs from the general scheme. The presence of a large excess of ClO_2SO_3F, and undercooled liquid at room temperature, makes the addition of HSO_3F unnecessary and the oxidation of palladium by bis(fluorosulfuryl)peroxide proceeds to completion within 3 days.

The hexakis(fluorosulfato)palladates reported here have both heterocations, such as NO^+ and ClO_2^+, or uni- or divalent metal cations, such as Cs^+ and Ba^{2+}, as counter ions. They all are thermally stable up to about 200°C.

Vibrational Spectra

Both infrared and Raman spectra of the fluorosulfato complexes discussed here are not readily obtained for a number of reasons. The oxidizing ability of the hexakis(fluorosulfato)palladates(IV) precludes the use of mulling agents and limits the choice of suitable window materials to BaF_2 with a transmission range to about 800 cm^{-1}. The dark colour of these compounds also interferes with the recording of Raman spectra. When using the 514.5 nm line of the Ar ion laser, well resolved Raman spectra are only obtained when the sample is cooled to ~80 K. At this temperature the colour becomes lighter and higher laser power may be used without risking local thermal decomposition of the sample. Alternatively, Raman spectra at room temperature are obtained for $(NO)_2[Pd(SO_3F)_6]$ and $(ClO_2)_2[Pd(SO_3F)_6]$ on the Cary 81 instrument equipped with a He–Ne laser; however, caused by both low scatter efficiency and low laser power (< 20 mW at the sample), the resolution is rather poor. It can be inferred from the room temperature spectra that the frequency shifts to lower wave numbers for the low temperature spectra are rather small (about 3 to 5 cm^{-1}).

Strong fluorescence of the sample prevented the recording of Raman spectra for $Pd[Sn(SO_3F)_6]$; however, for this compound and for $Pd[Pt(SO_3F)_6]$, infrared spectra down to 450 cm^{-1} are obtainable on solid films pressed between AgCl plates.

A tracing of the Raman spectrum of $Pd[Pt(SO_3F)_6]$ is shown in Fig. 1. The observed vibrational bands together with estimated intensities for all six new compounds and for $Pd[Pd(SO_3F)_6]$ (1) are listed in Table 1. Since generally good agreement between ir and Raman spectra in regard to band position is observed, the Raman shifts are tabulated, because they extend down to about 100 cm^{-1}.

The spectra obtained are typical for monodentate fluorosulfate groups in anionic complexes and agreement with direct precedents, the spectra for $K_2[Sn(SO_3F)_6]$ (17), $Ag[Sn(SO_3F)_6]$ (15), and $Ag[Pt(SO_3F)_6]$ (15), is very good. The Raman spectra for the hexakis(fluorosulfato)palladates(IV) are very similar as well and a common, tentative assignment

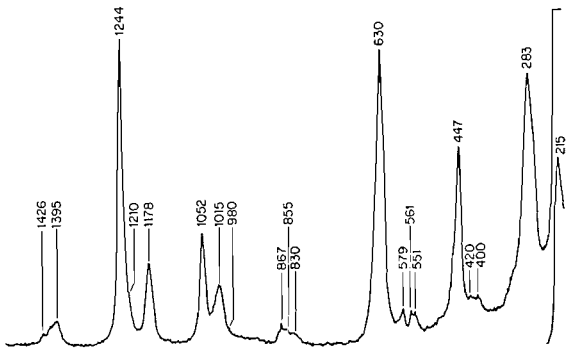

FIG. 1. The Raman spectrum of $Pd^{II}[Pt^{IV}(SO_3F)_6]$.

TABLE 1. Vibrational spectra of $Cs_2[Pd(SO_3F)_6]$, $(NO)_2[Pd(SO_3F)_6]$, $(ClO_2)_2[Pd(SO_3F)_6]$, $Ba[Pd(SO_3F)_6]$, $Pd[Pd(SO_3F)_6]$, $Pd[Pt(SO_3F)_6]$, and $Pd[Sn(SO_3F)_6]$[d]

$Cs_2[Pd(SO_3F)_6]$[a] Raman Δν (cm^{-1}) Int.	$(NO)_2[Pd(SO_3F)_6]$[a] Raman Δν (cm^{-1}) Int.	$(ClO_2)_2[Pd(SO_3F)_6]$[a] Raman Δν (cm^{-1}) Int.	$Ba[Pd(SO_3F)_6]$[a] Raman Δν (cm^{-1}) Int.	$Pd[Pd(SO_3F)_6]$[c] Raman Δν (cm^{-1}) Int.	$Pd[Pt(SO_3F)_6]$ Raman Δν (cm^{-1}) Int.	$Pd[Sn(SO_3F)_6]$ ir ν (cm^{-1}) Int.	Approximate description
1405 w	1407 vw	~1400 vw, b	1399 w, sh	1412 w	1426 w, sh	1425 ms, sh	
1395 vw, sh	1388 mw		1380 m	1396 w	1395 ms	1405 vs	SO_2 asym. stretch
						1385 s	
1300 vw	1290 vs	1293 w[b]		1294 m			
1236 vs	1235 vs	1240 vs	1249 vs	1225 vs	1244 vs	1250 m, sh	SO_2 sym. stretch
1212 m	1209 ms	1215 m	1214 ms	1202 w, sh	~1210 sh	1195 vs, b	
				1172 m	1178 ms		
		1050 m[b]				1105 w	
1020 vs	1024 vs	1020 s	1013 vs	1034 s	1050 ms	1028 vs, b	O—SO_2F stretch
995 ms	1004 ms	1005 w	1001 ms, sh	1001 m	1015 m, b		
975 v, sh	~960 vw, sh	970 m	~980 vw, sh	996 ms	~960 vw		
960 vw, sh							
					867 m	865 m, sh	SF stretch
	852 mw	841 w	857 ms	860 w	855 w	855 vs	
835 vw	835 vw	828 w		822 w	~850 vw		
805 vw	823 w	805 w	830 vw, sh				
785 w							
		623 ms		630 ms	630 vs	648, 632 ms	M—O stretch + M—O—S bend (see text)
618 ms	622 s	607 m	613 vs	612 s			
~585 vw, sh	~590 vw, sh	590 vw	~590 vw	578 w	579 vw	590 s	SO_2 bend
542 w	545 w	545 mw	551 w	538 mw		562, 551 m	SO_2 rock
441 ms	446 ms	444 ms	459 ms	446 ms	447 s	445 ms, sh	M—O stretch + M—OS bend
	420 vw		424 vw	420 m	420 vw		S—O wagging
~400 vw	~400 vw	400 vw	414 w	360 m, sh	~400 w, sh		
270 s	264 s	272 vs	272 vs		283 s		MO deformation
225 ms	~230 ms, sh	~230 m, sh	~230 m, sh		215 ms		SO deformation

[a]Spectrum recorded with sample at ~80 K.
[b]Bands assigned to ClO_2^+.
[c]Reference 1.
[d]Abbreviations: vs = very strong, s = strong, m = medium, w = weak, vw = very weak, sh = shoulder, b = broad.

TABLE 2. Electronic spectra and ligand field parameter of $Pd[Pt(SO_3F)_6]$, $Pd(Sn(SO_3F)_6]$, and $Pd(SO_3F)_2$

Assignment	$Pd[Sn(SO_3F)_6]$[a]		$Pd[Pt(SO_3F)_6]$[a]		$Pd(SO_3F)_2$ (1)	
	nm	kK	nm	kK	nm	kK
$\nu_1\ {}^3A_{2g} \rightarrow {}^3T_{2g}$	905	11.05	880	11.40	850	11.77
$\nu_2\ {}^3A_{2g} \rightarrow {}^3T_{1g}(F)$	590	16.95	590	16.95	575	17.40
$\nu_3\ {}^3A_{2g} \rightarrow {}^3T_{1g}(P)$	372	26.85[b]	378	26.48[b]	370	27.03

Parameter	Value		
	$Pd[Sn(SO_3F)_6]$	$Pd[Pt(SO_3F)_6]$	$Pd(SO_3F)_2$
ν_1/ν_2	1.534	1.492	1.478
Dq (cm^{-1})	1105	1140	1177
B (cm^{-1})	717	642	633
B/B^0	0.864	0.774	0.763

[a]Diffuse reflectance values for ν_2 are 592 nm for $Pd[Sn(SO_3F)_6]$ and 595 nm for $Pd[Pt(SO_3F)_6]$.
[b]Calculated values.

is attempted. In all cases band proliferation, particularly in the SO_3F stretching range, is observed, presumably caused by extensive vibrational coupling and solid state splitting. Interesting intensity differences between ir and Raman spectra point to vibrational coupling resulting in in-phase and out-of-phase vibrations within the anion. For the $[Pd(SO_3F)_6]^{2-}$ derivatives, strong Raman bands at $\sim$1240 (νSO_2 sym) and $\sim$1020 cm^{-1} (νS–O*P*d) have weaker side bands at $\sim$1210 and $\sim$980 cm^{-1} respectively, with the intensities reversed in the infrared spectra.

Bands at $\sim$1170 to 1190 and $\sim$1040 to 1050 cm^{-1} are observed for the three Pd^{II} compounds as well as for the previously reported Ag^{II} complexes, $Ag[Pt(SO_3F)_6]$ and $Ag[Sn(SO_3F)_6]$ (15). Absorptions in this region are generally associated with bidentate bridging fluorosulfate groups (19), and their occurrence here and in the Ag^{II} complexes may be attributed to the polarizing abilities of the two divalent cations and the resulting coordination via oxygen. Hence ionic formulations as $M^{II}[M^{IV}(SO_3F)_6]$, where $M^{II} = Pd^{II}$ and Ag^{II} and $M^{IV} = Pt^{IV}$ and Sn^{IV}, may be somewhat misleading.

Strong Raman bands at $\sim$620 to 640, 440 to 460, and 270 to 280 cm^{-1} are observed for all anionic complexes, with variations in band positions seemingly dependent on the central atoms. These bands, occasionally split into doublets, may be due to M—O vibrations, presumably mixed with SO_3F deformation modes. A similar interpretation has been advanced recently for the $[Au(SO_3F)_4]^-$ ion (16). Strong metal–oxygen bonds are suggested by the vibrational coupling of SO stretching modes discussed earlier.

Absorption bands due to the heterocation NO^+ at 2330 cm^{-1} and for ClO_2^+ at 1293 and 1050 cm^{-1} are consistent with precedents (19, 20); however, the ClO_2 bending mode, usually found at $\sim$520 cm^{-1} (20) is not observed. The NO stretch is found in the ir spectrum only. The band is raised by $\sim$30 cm^{-1} to 2330 cm^{-1} when compared to 2300 for $NOSO_3F$ (21).

In summary, the apparent spectral similarities indicate strong structural similarities. Formulation of '$Pd(SO_3F)_3$' as $Pd[Pd(SO_3F)_6]$ is consistent with the observed vibrational spectrum, when allowance is made for additional coordination of the SO_3F group to Pd^{II}.

Electronic Spectra

Of primary interests are absorption bands due to *d–d* transitions for palladium(II). Previous work (1) had presented evidence for a regular octahedral environment for Pd(II) in $Pd(SO_3F)_2$, implying a tridentate fluorosulfate group, and a ${}^3A_{2g}$ ground state.

The spectra obtained for $Pd[Pt(SO_3F)_6]$ and $Pd[Sn(SO_3F)_6]$, together with values for $Pd(SO_3F)_2$, are listed in Table 2. Of the three expected *d–d* transitions, the two low energy bands ν_1 and ν_2 are obtained from the mull spectra. Diffuse reflectance spectra also yield ν_2 and for $Pd[Sn(SO_3F)_6]$ also a broad band assigned as ν_3. In the platinum compound, ν_3 is not observed because a strong band, presumably due to a charge transfer transition, originates in the ultraviolet and extends well into the visible region.

The good agreement in band positions for all three Pd(II) compounds suggests (*a*) a similar octahedral environment for palladium and (*b*) a ${}^3A_{2g}$ ground state in all instances. The obtained $10Dq$ values are also listed in Table 2 as well as the ligand field parameter B, obtained from the measured ν_2/ν_1 ratio, using Tanabe–Sugano diagrams as suggested by Lever (22). The third band, ν_3, is calculated by using Tanabe–Sugano diagrams as well.

It appears that in the series $Pd(SO_3F)_2$, $Pd[Pt-$

TABLE 3. Magnetic properties of Pd(II) hexakis(fluorosulfato)metallates

$PdSn(SO_3F)_6$				$PdPt(SO_3F)_6$			
T (K)	$\chi_M^{corr} \times 10^3$ (cgsu)	μ_{eff} (BM)	$\mu_{eff,corr}$	T (K)	$\chi_M^{corr} \times 10^3$ (cgsu)	μ_{eff} (BM)	$\mu_{eff,corr}$
306	5.17	3.56	3.61	302	4.57	3.32	3.38
280	5.61	3.54	3.61	278	4.93	3.31	3.37
252	6.12	3.51	3.58	246	5.54	3.30	3.37
229	6.78	3.53	3.60	222	6.12	3.30	3.37
203	7.56	3.50	3.59	193	6.90	3.26	3.35
178	8.52	3.48	3.58	167	7.98	3.26	3.36
154	9.83	3.48	3.59	142	9.35	3.26	3.37
129	11.71	3.48	3.60	119	11.06	3.24	3.38
107	14.07	3.47	3.63	89	14.47	3.21	3.39
80	18.28	3.42	3.62				

$(SO_3F)_6]$, $Pd[Sn(SO_3F)_6]$, the ligand field splitting ($10Dq$) gradually decreases while interelectronic repulsion (B) increases, with the observed B values approaching the free ion value B^0 of 830 cm^{-1} (23). Differences in both $10Dq$ and B may reflect the different coordination of the SO_3F group to Pd(II), tridentate in $Pd(SO_3F)_2$ and presumably monodentate in the two fluorosulfato complexes. In addition, greater free ion character in $Pd[Sn(SO_3F)_6]$ than in $Pd[Pt(SO_3F)_6]$ suggests either structural differences, not apparent from the vibrational spectra, or more likely, a greater ability of Sn(IV) to attract SO_3F groups thus reducing their abilities to produce a ligand field around Pd(II) and to delocalize electron density from it.

Finally, the solution of $(NO)_2[Pd(SO_3F)_6]$ in HSO_3F has been mentioned before. The high intensity of the band at 320 nm is suggestive of a charge transfer spectrum. The observed band extends well into the visible region and seems to obscure any bands due to d–d transitions.

Magnetic Measurements

As expected, the new hexakis(fluorosulfato)palladate(IV) complexes are all diamagnetic, consistent with a d^6 electron configuration and a regular octahedral environment.

The two new Pd(II) derivatives are found to be paramagnetic and, in agreement with expectations for an ion with a $^3A_{2g}$ ground state, the Curie–Weiss law is followed in the range of our measurements (~306 to 80 K). The magnetic susceptibilities and the magnetic moments are listed in Table 3. A $1/\chi$ vs. T plot for all Pd(II) fluorosulfate derivatives is shown in Fig. 2. The two new palladium(II) hexakis(fluorosulfato)metallates have identical Weiss constants of -10 ± 2 K and consequently μ_{eff} for both compounds decreases with temperature. In contrast both $Pd(SO_3F)_2$ and $Pd[Pd(SO_3F)_6]$ have small but positive θ values of $+13 \pm 4$ and $+10 \pm 2$ K respectively. A similar situation is encountered for

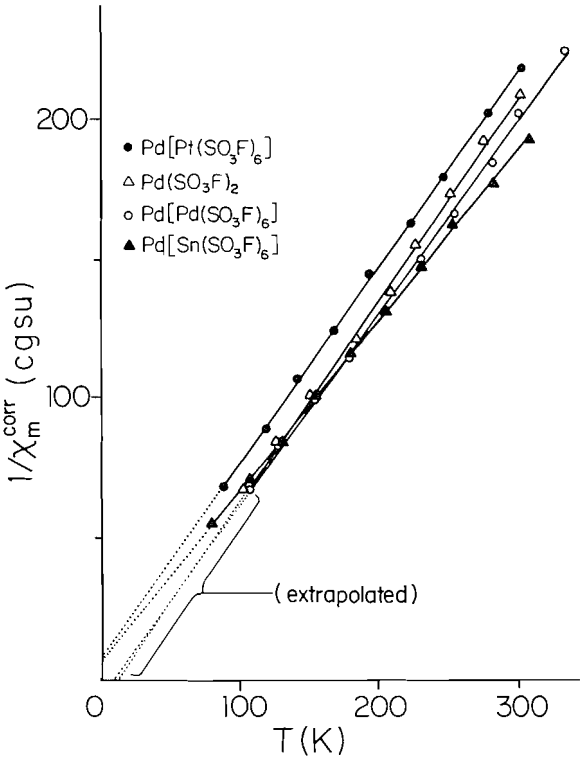

FIG. 2. The temperature dependence of the corrected molar susceptibilities for Pd^{II} fluorosulfate derivatives.

Ag(II) fluorosulfate derivatives where $Ag(SO_3F)_2$ has a positive Weiss constant of +20 K and both $Ag[Sn(SO_3F)_6]$ and $Ag[Pt(SO_3F)_6]$ have small negative Weiss constants. In addition, if the Curie–Weiss law is used in the form: $\chi_M^{corr} = C/(T - \theta)$, negative values for θ are also found for palladium(II) complexes of the type $Pd[MF_6]$ where M = Pt, Pd, Sn, or Ge (4).

Since the Weiss constants are rather small, corrected magnetic moments are calculated for all Pd(II) fluorosulfate compounds by using the relationship: $\mu = 2.828[\chi_M^{corr}(T - \theta)]^{1/2}$, and as seen in Table 3,

TABLE 4. Magnetic properties of some Pd(II) compounds at room temperature

	$\chi_M^{corr} \times 10^3$ (cgsu)	$\mu_{eff,corr}$ (BM)	Temperature dependence (θ = Weiss constant)	Reference
PdF_2	1.28	1.74	Antiferromagnetic coupling	4, 24
$Pd[PdF_6]$	3.31	2.88	$\theta = -28$ K	4, 24
$Pd[SnF_6]$	3.37	2.98	$\theta = -28$ K	4, 24
$Pd[PtF_6]$	3.10	2.72	$\theta = -1$ K	4, 24
$Pd[GeF_6]$	3.34	2.82	$\theta = -31$ K	4, 24
$Pd(SO_3F)_2$	4.77	3.30	$\theta = 13 \pm 4$ K	1
$Pd[Pd(SO_3F)_6]$	4.93	3.37	$\theta = 10 \pm 2$ K	1
$Pd[Sn(SO_3F)_6]$	5.26	3.60	$\theta = -10 \pm 3$ K	This work
$Pd[Pt(SO_3F)_6]$	4.61	3.37	$\theta = -10 \pm 2$ K	This work

the magnetic moments are now independent of temperature in the range of our measurements.

The same corrections are applied for $Pd(SO_3F)_2$ and $Pd[Pd(SO_3F)_6]$. The resulting values and a summary of the magnetic properties for a number of paramagnetic palladium(II) compounds are listed in Table 4.

In contrast to the fluorides, all palladium(II) fluorosulfates are magnetically dilute and the obtained magnetic moments are all substantially higher than the 'spin only' value of 2.83 BM. The corrected magnetic moments increase in the order $Pd(SO_3F)_2 < Pd[Pt(SO_3F)_6] \sim Pd[Pd(SO_3F)_6] < Pd[Sn(SO_3F)_6]$, suggesting an increase in free ion character. The results are consistent with previously discussed trends in Dq and B for $Pd(SO_3F)_2$, $Pd[Pt(SO_3F)_6]$, and $Pd[Sn(SO_3F)_6]$. The complex fluoride derivatives of the type $Pd^{II}[MF_6]$ show a similar trend. The highest magnetic moment, again after correcting for Curie–Weiss law behavior (4, 24), is observed for $Pd[SnF_6]$. However, all magnetic moments for the fluoro complexes fall below 3.00 BM. It seems that orbital contributions to the magnetic susceptibility are more effectively quenched than in the fluorosulfate compounds. Unfortunately, no electronic spectra were reported for the fluoro compounds.

The magnetic moment at room temperature for $Pd[Sn(SO_3F)_6]$ is 3.61 BM. Even though this value is the highest yet observed for Pd^{2+}, values to about 4.0 BM have been reported for divalent Ni^{2+} compounds (2), with Ni^{2+} in an octahedral environment.

Conclusions

Even though $Pd(SO_3F)_4$ could not be obtained, a number of diamagnetic compounds containing the $[Pd(SO_3F)_6]^{2-}$ are obtained and characterized by their vibrational spectra. More extensive spectroscopic and magnetic information on rather unusual octahedral Pd^{2+} complexes are also obtained.

Acknowledgements

Financial support by the Natural Sciences and Engineering Research Council of Canada is gratefully acknowledged. Mrs. B. I. Krizsan is thanked for doing the illustrations.

1. K. C. LEE and F. AUBKE. Can. J. Chem. **55**, 2473 (1977).
2. LANDOLT-BORNSTEIN. Numerical data and functional relationships in science and technology. Vol. 2. Supplement II. Magnetic properties of coordination and organometallic transition metal compounds. Springer Verlag, Berlin. 1966 and 1976.
3. A. G. SHARPE. J. Chem. Soc. 3444 (1950).
4. N. BARTLETT and P. R. RAO. Chem. Soc. Proc. 393 (1964).
5. A. TRESSAUD, M. WINTENBERGER, N. BARTLETT, and P. HAGENMULLER. C. R. Acad. Sci. Ser. C, **282**, 1069 (1976).
6. J. BARR, R. J. GILLESPIE, and R. C. THOMPSON. Inorg. Chem. **3**, 1149 (1964).
7. G. H. CADY and J. M. SHREEVE. Inorg. Synth. **7**, 124 (1963).
8. H. A. CARTER, A. M. QURESHI, and F. AUBKE. Chem. Commun. 1461 (1968).
9. P. A. YEATS, B. L. POH, B. F. E. FORD, J. R. SAMS, and F. AUBKE. J. Chem. Soc. A, 2188 (1970).
10. W. M. JOHNSON, R. DEV, and G. H. CADY. Inorg. Chem. **11**, 2260 (1972).
11. D. R. SHRIVER. The manipulation of air-sensitive compounds. McGraw-Hill, New York, NY. 1969.
12. H. C. CLARK and R. J. O'BRIEN. Can. J. Chem. **39**, 1030 (1961).
13. B. N. FIGGIS and R. S. NYHOLM. J. Chem. Soc. 4190 (1958).
14. J. M. TAYLOR and R. C. THOMPSON. Can. J. Chem. **49**, 511 (1971).
15. P. C. LEUNG and F. AUBKE. Inorg. Chem. **17**, 1765 (1978).
16. K. C. LEE and F. AUBKE. Inorg. Chem. **18**, 389 (1979).
17. P. A. YEATS, J. R. SAMS, and F. AUBKE. Inorg. Chem. **12**, 328 (1973).
18. K. C. LEE and F. AUBKE. To be published.
19. D. W. A. SHARP and J. THORLEY. J. Chem. Soc. 3557 (1963).
20. K. O. CHRISTE and C. J. SCHACK. Adv. Inorg. Chem. Radiochem. **13**, 319 (1976).
21. A. M. QURESHI, H. A. CARTER, and F. AUBKE. Can. J. Chem. **49**, 35 (1971).
22. A. B. P. LEVER. Inorganic electronic spectroscopy. Elsevier Publishing Company Inc., Amsterdam. 1968.
23. B. N. FIGGIS. Introduction to ligand fields. Interscience Publishing Company Inc., New York, NY. 1967.
24. R. P. RAO. Ph.D. thesis, University of British Columbia, Vancouver, B.C. 1965.

Kinetics and mechanism of oxidation of tris-(1,10-phenanthroline)iron(II) by chlorine and bromine and of the reduction of tris-(1,10-phenanthroline)iron(III) by iodide ions

JIDE IGE, J. FOLORUNSO OJO,[1] AND OLUSEGUN OLUBUYIDE

Department of Chemistry, University of Ife, Ile-Ife, Nigeria

Received November 30, 1978

JIDE IGE, J. FOLORUNSO OJO, and OLUSEGUN OLUBUYIDE. Can. J. Chem. 57, 2065 (1979).

The rates of the oxidation of tris-(1,10-phenanthroline)iron(II) by chlorine and bromine, and of the reduction of tris-(1,10-phenanthroline)iron(III) by iodide ions have been measured at ionic strength $I = 1.0$ mol dm^{-3} ($LiClO_4$). All the reactions obey second-order rate law:

$$\text{Rate} = k_{obsd}\,[\text{oxidant}][\text{reductant}]$$

The activation parameters for the reactions are: $Fe(Phen)_3^{2+}/Br_2$: $\Delta H^{\ddagger} = (64.2 \pm 3.2)$ kJ mol^{-1}, $\Delta S^{\ddagger} = -(24.9 \pm 1.5)$ J mol^{-1} K^{-1}. $Fe(Phen)_3^{3+}/I^-$: $\Delta H^{\ddagger} = (39.8 \pm 2.1)$ kJ mol^{-1}, $\Delta S^{\ddagger} = -(19.7 \pm 0.8)$ J mol^{-1} K^{-1}.

The reactions of tris-(1,10-phenanthroline)iron(II) with chlorine and bromine are unaffected by chloride, bromide, and acid. The proposed mechanism for these reactions involves a series of one-electron changes, with the species X_2^- (X = Cl, Br) as reaction intermediates, since good linear free energy correlations for the primary step, resulting in the formation of X_2^-, are obtained. The reduction of tris-(1,10-phenanthroline)iron(III) by iodide ions is catalysed by bromide and chloride ions, whereas the reduction of aquoiron(III) by iodide ions is known to be inhibited by bromide and chloride ions. A mechanistic interpretation of this observation is suggested.

JIDE IGE, J. FOLORUNSO OJO et OLUSEGUN OLUBUYIDE. Can. J. Chem. 57, 2065 (1979).

On a mesuré les vitesses d'oxydation du tris-(phénanthroline-1,10)fer(II) par le chlore et le brome et la réduction du tris-(phénanthroline-1,10)fer(III) par les ions iodures à une force ionique $I = 1.0$ mol dm^{-3} ($LiClO_4$). Toutes les réactions obéissent à une équation de vitesse du deuxième ordre:

$$\text{Vitesse} = k_{obsd}\,[\text{oxydant}][\text{réducteur}]$$

Les paramètres d'activations des réactions sont: $Fe(Phen)_3^{2+}/Br_2$: $\Delta H^{\ddagger} = (64.2 \pm 3.2)$ kJ mol^{-1}, $\Delta S^{\ddagger} = -(24.9 \pm 1.5)$ J mol^{-1} K^{-1}. $Fe(Phen)_3^{3+}/I^-$: $\Delta H^{\ddagger} = (39.8 \pm 2.1)$ kJ mol^{-1}, $\Delta S^{\ddagger} = -(19.7 \pm 0.8)$ J mol^{-1} K^{-1}.

Les réactions du tris-(phénanthroline-1,10)fer(II) avec le brome et le chlore ne sont pas affectées par les ions chlorures et bromures ou par les acides. Le mécanisme proposé pour ces réactions implique une série de changements d'un électron dans laquelle les espèces X_2^- (X = Cl, Br) sont des intermédiaires; ces conclusions reposent sur le fait que l'on obtient de bonnes corrélations linéaires d'énergie libre pour la première étape au cours de laquelle il y a formation de X_2^-. La réduction du tris-(phénanthroline-1,10)fer(III) par les ions iodures est catalysée par les ions chlorure et bromure alors que l'on sait que la réduction de l'aquofer(III) est inhibée par les ions bromure et chlorure. On suggère une interprétation mécanistique de cette observation.

[Traduit par le journal]

Introduction

A study of the oxidation reactions of the halogens, X_2 (X = Cl, Br, I) is interesting because these provide an example of chemically related members of the same group in the periodic table. Their physicochemical behaviour shows the similarities and general gradation in properties often observed from top to bottom within a group (1). They oxidise the metal ions (2–16) at rates which follow the general sequence $k_{Cl_2} > k_{Br_2} > k_{I_2}$ in accordance with their oxidation potentials (17). Also, they are overall two-electron oxidants, and hence their study could provide a means of distinguishing between the two-electron-transfer scheme:

$$[1]\quad \text{Fe(II)} + X_2 \underset{k_{-1}}{\overset{k_1}{\rightleftharpoons}} \text{Fe(IV)} + 2X^-$$

$$[2]\quad \text{Fe(IV)} + \text{Fe(II)} \xrightarrow{k_2} 2\text{Fe(III)}$$

and the series of one-electron changes:

$$[3]\quad \text{Fe(II)} + X_2 \underset{k_{-3}}{\overset{k_3}{\rightleftharpoons}} \text{Fe(III)} + X_2^-$$

$$[4]\quad \text{Fe(II)} + X_2^- \xrightarrow{k_4} \text{Fe(III)} + 2X^-$$

Shakhashiri and Gordon (18) had studied the oxidation of tris-(1,10-phenanthroline)iron(II) by chlorine

[1]To whom all correspondence should be addressed.

0008-4042/79/152065-06$01.00/0

in chloride and nitrate media, with the iron complex in the sulphate form.

The oxidation potential of the couple (19) $Fe(Phen)_3^{2+}/Fe(Phen)_3^{3+}$ (−1.06 V), and those of the halogen (17) systems $X_2/2X^-$ (−1.36 V (Cl_2), −1.06 V (Br_2), and −0.62 V (I_2)) suggest that the reaction represented by eq. [5]

$$[5] \quad 2Fe(Phen)_3^{2+} + X_2 \rightarrow 2Fe(Phen)_3^{3+} + 2X^-$$

is thermodynamically feasible for Cl_2 but less so for Br_2 and I_2.

The reduction of aquoiron(III) by iodide ions (20, 21) had been shown to be inhibited by added bromide and chloride ions. This has been explained in terms of the formation of FeX^{2+} (X = I, Br, Cl) from the complexation of ferric ions with the halide ions, with FeX^{2+} being less reactive than aquoiron(III). In the unlikely event that tris-(1,10-phenanthroline)iron(III) could complex with the halide ions, the effects of bromide and chloride ions on the $Fe(Phen)_3^{3+}/I^-$ system should be of mechanistic interest.

We report here a study of the oxidation of tris-(1,10-phenanthroline)iron(II) by chlorine and bromine and of the reduction of tris-(1,10-phenanthroline)iron(III) by iodide ions in perchlorate medium, bearing in mind the points raised above.

Experimental

Materials

The complexes $Fe(Phen)_3^{2+}$ and $Fe(Phen)_3^{3+}$ were prepared as the perchlorate salts (22, 23) and characterised for purity (24) by their uv–visible spectra. Solutions of $Fe(Phen)_3^{3+}$ in 5 mol dm^{-3} $HClO_4$ were freshly prepared each day and kept in ice before use. Aqueous solutions of chlorine and bromine were prepared and their concentrations determined as recorded in the literature (25). Sodium iodide, sodium bromide, and lithium chloride which were the sources of the anions were Analar grade reagents. Lithium perchlorate, used to maintain the ionic strength at 1.0 mol dm^{-3}, was prepared from Analar lithium carbonate and perchloric acid, and recrystallised thrice, by the usual method (26).

Kinetics

The oxidation of tris-(1,10-phenanthroline)iron(II) by chlorine and bromine was monitored on a Pye Unicam SP 500 spectrophotometer by following the decreasing absorbance (24) of the tris-(1,10-phenanthroline)iron(II) at λ = 510 nm ($\varepsilon = 1.09 \times 10^4$ dm^3 mol^{-1} cm^{-1}). The halogen concentration was always in large excess (≥ tenfold). The fast reduction of tris-(1,10-phenanthroline)iron(III) by iodide ions was monitored on a Durrum-Gibson stopped-flow spectrophotometer at λ = 510 nm, where the tris-(1,10-phenanthroline)iron(II) product has maximum absorption. The iodide concentration was always in large excess. Pseudo first-order behaviour was observed to more than 80% reaction in all cases. The cell compartments were well thermostatted (±1°C) by circulating water from a water-bath regulated to the desired temperature.

Results

The Oxidation of Tris-(1,10-phenanthroline)iron(II) by Chlorine and Bromine

The linearity of the pseudo first-order rate plots for these reactions and the non-dependence of the second-order rate constants on the concentrations of the oxidants (Table 1) suggest that the reactions represented by eq. [5] (X = Cl, Br) obey the rate law:

$$[6] \quad (-1/2)d[Fe(Phen)_3^{2+}]/dt = k_5[Fe(Phen)_3^{2+}][X_2]$$

The rate constants for the reactions of tris-(1,10-phenanthroline)iron(II) with chlorine and bromine are not affected by added chloride and bromide, respectively, and acid (Table 1).

Our results for the oxidation of tris-(1,10-phenanthroline)iron(II) by chlorine agree with those of Shakhashiri and Gordon (18), indicating that sulphate and nitrate ions do not affect the reactions. The reductant self-exchange rate constants (k_{11}), one-electron redox rate constants (k_{12}), and the standard free energy changes (ΔG_{12}^0) for the reduction of chlorine and bromine by some metal ions, including tris-(1,10-phenanthroline)iron(II) are presented in Table 2. The one-electron reduction of a halogen by a metal centre is represented by eq. [7]

$$[7] \quad M_{red} + X_2 \xrightarrow{k_{12}} M_{ox} + X_2^-$$

TABLE 1. Second-order rate constants[a] for the oxidation of tris-(1,10-phenanthroline)iron(II) by chlorine and bromine (I = 1.00 mol dm^{-3} ($LiClO_4$))

(*a*) $Fe(Phen)_3^{2+} + Cl_2$ ($[Fe(Phen)_3^{2+}] = 7.5 \times 10^{-6}$ mol dm^{-3}, t = 25°C)

$10^3[Cl_2]$ (mol dm^{-3})	k_5 (dm^3 mol^{-1} s^{-1})
4.4	2.1[b]
6.8	2.3[b]
12.2	2.2[b]
4.4	2.0[c]

(*b*) $Fe(Phen)_3^{2+} + Br_2$ ($[Fe(Phen)_3^{2+}] = (4.5–8.2) \times 10^{-6}$ mol dm^{-3})

Temperature (°C)	$10^4[Br_2]$ (mol dm^{-3})	k_5 (dm^3 mol^{-1} s^{-1})
25	2.1	1.7[d]
25	4.4	1.6[b]
25	4.4	1.7[e]
25	6.3	1.8[d]
25	10.5	1.5[d]
25	15.7	1.6[d]
20	8.7–11.4	1.2[f]
15	11.4–14.3	0.74[f]
10	11.4–12.3	0.40[f]

[a]All average rate constants are subject to standard error of ≤5%.
[b]Average of k_5 for $[H^+]$ = 0.02–1.00 mol dm^{-3}, with k_5 at each acid concentration being the average of three or four runs.
[c]Average of k_5 for $[Cl^-]$ = 0.10–1.00 mol dm^{-3}.
[d]$[H^+]$ = 0.10 mol dm^{-3}.
[e]Average of k_5 for $[Br^-] = (0.45–13.5) \times 10^{-3}$ mol dm^{-3}.
[f]Average of k_5 for the bromine concentration range given in the table.

TABLE 2. Self-exchange and cross-reaction data used in free energy correlations

Reactant pair	k_{11} (dm^3 mol^{-1} s^{-1})	k_{12} (dm^3 mol^{-1} s^{-1})	$\Delta G_{12}{}^{0a}$ (kJ mol^{-1})	References			
				[b]	[c]	[d]	[e]
V^{3+}, Cl_2	1.0	1.8×10^3	−23.16	44	47	43	[f]
Ti^{3+}, Cl_2	1.0×10^{-2}	1.25×10^2	−48.25	44	47	40	10
V^{2+}, Cl_2	1×10^{-2}	5×10^2	−79.61	44	47	42	15
Pu^{3+}, Cl_2	2×10^2	4.0×10^{-4}	+35.71	44	47	48	48
$Fe(Phen)_3{}^{2+}$, Cl_2	$>3 \times 10^7$	2.4, 2.2	+52.11	19	47	41	18, This work
U^{3+}, Br_2	1.66	7.2×10^5	−110.01	44	45	5	5
V^{3+}, Br_2	1.0	4.57	−14.48	44	45	43	8
Ti^{3+}, Br_2	1×10^{-2}	5×10^2	−39.57	44	45	40	7
V^{2+}, Br_2	1×10^{-2}	2.9×10^4	−70.93	44	45	42	15
$Fe(Phen)_3{}^{2+}$, Br_2	$>3 \times 10^7$	1.6	+60.80	19	45	41	This work

[a]Calculated from E^0's for one-electron change.
[b]Source of E^0 for the metal ion couple $Mn^+/M^{(n+1)+}$.
[c]Sousce of E^0 for the halogen couple $X_2/X_2{}^-$.
[d]Source of k_{11} for reductant.
[e]Source of k_{12} for the reaction between oxidant and reductant.
[f]A. Adegite. Private communication.

and the corresponding self-exchange reactions are represented by eqs. [8] and [9].

[8] $$M_{red} + M_{ox}{}^* \underset{}{\overset{k_{11}}{\rightleftharpoons}} M_{red}{}^* + M_{ox}$$

[9] $$X_2 + {}^*X_2{}^- \underset{}{\overset{k_{22}}{\rightleftharpoons}} X_2{}^- + {}^*X_2$$

Marcus (27) suggested that reactions represented by eqs. [7]–[9] occur by outer-sphere mechanism, if the relationship among the free energies of activation is of the form:

[10] $$\Delta G_{12}{}^{\neq} = 0.5\Delta G_{11}{}^{\neq} + 0.5\Delta G_{22}{}^{\neq} + 0.5\Delta G_{12}{}^0 - 0.5RT \ln f$$

where

[11] $$\ln f = \frac{(-\Delta G_{12}{}^0/RT)^2}{4 \ln \frac{k_{11}k_{22}}{Z^2}}$$

and $Z = 10^{11}$ dm^3 mol^{-1} s^{-1}. Equation [10] implies that if $\Delta G_{12}{}^{\neq} - 0.5(\Delta G_{11}{}^{\neq} - RT \ln f)$ is plotted against $\Delta G_{12}{}^0$, a linear fit should result, with slope 0.5 and intercept $0.5\Delta G_{22}{}^{\neq}$. The free energies of activation were calculated (28) from the familiar eq. [12] where $\bar{K}$ = Boltzmann's constant, h =

[12] $$\Delta G^{\neq} = RT \ln(\bar{K}T/h) - RT \ln k$$

Planck's constant, and T is the absolute temperature. Figures 1 and 2 show the free energy plots obtained, using the data in Table 2. Woodruff and Margerum (29) had obtained k_{22} (eq. [9]) for X = Br and I from the intercepts of such plots by an iterative procedure, using EDTA complexes of iron(II) and cobalt(II) as reductants. The slopes and k_{22} which we obtained from Figs. 1 and 2 are 0.43 ± 0.12, 0.7 dm^3 mol^{-1} s^{-1} (X = Cl) and 0.30 ± 0.10, 84.7 dm^3 mol^{-1} s^{-1} (X = Br), respectively. The

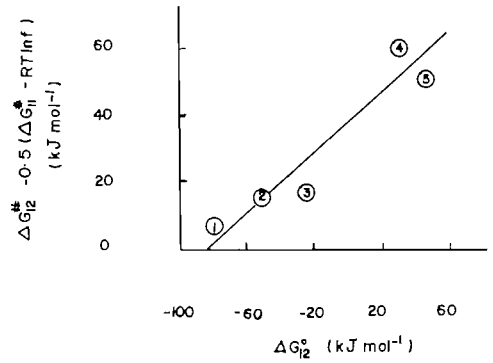

FIG. 1. Marcus plot for the oxidation of some metal ions by chlorine. (*1*) V^{2+}, (*2*) Ti^{3+}, (*3*) V^{3+}, (*4*) Pu^{3+}, (*5*) $Fe(Phen)_3{}^{2+}$.

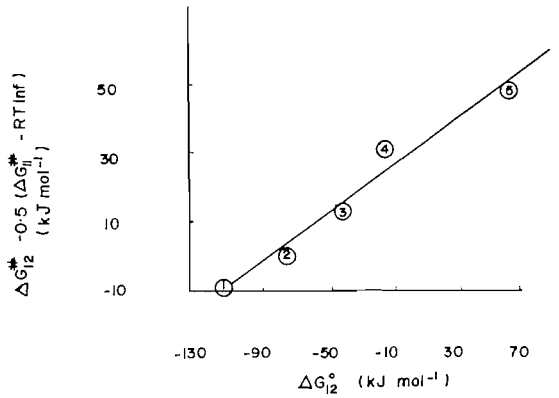

FIG. 2. Marcus plot for the oxidation of some metal ions by bromine. (*1*) U^{3+}, (*2*) V^{2+}, (*3*) Ti^{3+}, (*4*) V^{3+}, (*5*) $Fe(Phen)_3{}^{2+}$.

variation of the second-order rate constants with temperature for the oxidation of tris-(1,10-phenanthroline)iron(II) by bromine was investigated (Table 1). The activation parameters obtained were

TABLE 3. Second-order rate constants[d] for the reduction of tris-(1,10-phenanthroline)-iron(III) by iodide ions (I = 1.00 mol dm^{-3} ($LiClO_4$); [$Fe(Phen)_3^{3+}$] = (2.0–3.0) × 10^{-5} mol dm^{-3})

Temp. (°C)	10^4[I^-] (mol dm^{-3})	[Cl^-] (mol dm^{-3})	[Br^-] (mol dm^{-3})	$10^{-4}k_6$ (dm^3 mol^{-1} s^{-1})
25	3.0	—	—	6.6[a]
25	3.0–7.4	—	—	6.4[b]
25	3.0–9.3	0.10	—	9.0[b]
25	3.0	0.20	—	9.7[c]
25	3.0	0.30	—	11.0[c]
25	3.0	0.40	—	12.8[c]
25	3.0	0.50	—	14.4[c]
25	3.0	0.70	—	18.0[c]
25	3.0	0.90	—	20.2[c]
25	3.0	—	0.010	9.0[c]
25	3.0	—	0.020	9.4[c]
25	3.0	—	0.030	9.9[c]
25	3.0	—	0.040	10.6[c]
25	3.0	—	0.050	10.8[c]
25	3.0	—	0.060	10.9[c]
25	3.0	—	0.070	11.9[c]
25	3.0	—	0.080	12.5[c]
25	3.0	—	0.090	12.6[c]
25	3.0–9.0	—	0.100	13.1[b,c]
20	3.0–4.5	—	—	4.4[b,c]
15	3.0–7.4	—	—	3.4[b,c]
10	7.4–11.5	—	—	2.7[b,c]
5	7.4–15.1	—	—	1.8[b,c]

[a]Average of k_6 for [H^+] = 0.10–1.00 mol dm^{-3}.
[b]Average of k_6 for the iodide concentration given in the table.
[c][H^+] = 0.10 mol dm^{-3}.
[d]All average rate constants are subject to standard error of ≤5%.

$$\Delta H^{\ddagger} = (64.2 \pm 3.2)\ \text{kJ mol}^{-1}$$

$$\Delta S^{\ddagger} = -(24.9 \pm 1.5)\ \text{J mol}^{-1}\ \text{K}^{-1}$$

The Reduction of Tris-(1,10-phenanthroline)iron(III) by Iodide Ions

The data obtained for the reaction (Table 3) fit the rate law:

$$[13] \quad -\mathrm{d}[Fe(Phen)_3^{3+}]/\mathrm{d}t = k_6[Fe(Phen)_3^{3+}][I^-]$$

and the stoichiometry of the reaction was confirmed to be of the form:

$$[14] \quad Fe(Phen)_3^{3+} + I^- \xrightarrow{k_6} Fe(Phen)_3^{2+} + \tfrac{1}{2}I_2$$

The reaction is not affected by added acid, but it is catalysed by added chloride and bromide ions (Table 3), with bromide ions having greater catalysing effect. The observed second-order rate constants (k_{obsd}) vary with the concentrations of the added anion [X^-] according to eq. [15]. Figure 3 shows such

$$[15] \quad k_{obsd} = k_0 + k_x[X^-]$$

variation for X = Br. The values of k_0 and k_x obtained from such variation are:

$$k_0 = 0.85 \times 10^5\ \text{dm}^3\ \text{mol}^{-1}\ \text{s}^{-1}$$

$$k_{Br} = 4.7 \times 10^5\ \text{dm}^6\ \text{mol}^{-2}\ \text{s}^{-1}$$

$$k_0 = 0.68 \times 10^5\ \text{dm}^3\ \text{mol}^{-1}\ \text{s}^{-1}$$

$$k_{Cl} = 1.7 \times 10^5\ \text{dm}^6\ \text{mol}^{-2}\ \text{s}^{-1}$$

The values of the anion-independent rate constants (k_0) agree very well for the two anions (Cl^- and Br^-), and with that (k_6, eq. [13]) obtained in the absence of added anion (Table 3).

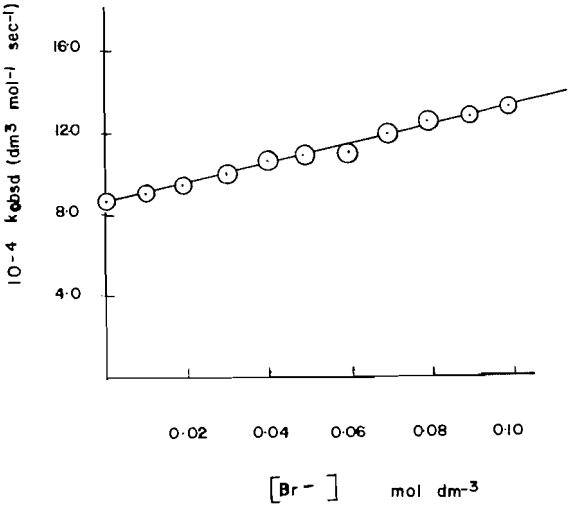

FIG. 3. Effect of added bromide ions on the rate constants for $Fe(Phen)_3^{3+} + I^-$ reaction.

The temperature variation of the rate constant k_6 was investigated, and the activation parameters obtained were

$$\Delta H^{\ddagger} = (39.8 \pm 2.1)\ \text{kJ mol}^{-1}$$

$$\Delta S^{\ddagger} = -(19.7 \pm 0.8)\ \text{J mol}^{-1}\ \text{K}^{-1}$$

Discussion

Application of the steady-state approximation to the concentrations of the transient species (Fe(IV) and X_2^-) involved in the two reaction schemes, eqs. [1] and [2] and eqs. [3] and [4], gives identical second-order rate laws under the likely conditions that $k_{-1} \ll k_2$ and $k_{-3} \ll k_4$. The second-order rate law [6] obtained in this study does not therefore distinguish between these two possibilities. The good linear-free energy correlations obtained (Figs. 1 and 2) suggest that the reactions of chlorine and bromine with tris-(1,10-phenanthroline)iron(II) probably occur by the series of one-electron changes [3] and [4]. The reactions of the other metal ions (5, 8, 10) with the halogens had been shown to occur by these series of one-electron changes. The slopes of the linear-free energy plots are lower than the theoretical value of 0.5, probably as a result of the failure of some of the assumptions of the Marcus theory which has been used to calculate the kinetic parameters from various sources as has been pointed out by various workers (5, 29, 30) and Marcus (31) has suggested some reasons why the slopes of such plots could be less than 0.5 also. Assignment of outer-sphere or inner-sphere mechanism to the reactions cannot be made with certainty on the basis of the linear-free energy correlations obtained, since some inner-sphere redox reactions (32–34) have also shown this Marcus type (26) dependence of reaction rates on ΔG_{12}^{0}. Our main support for suggesting outer-sphere mechanism for the reactions is the substitution — inertness of $Fe(Phen)_3^{2+}$ (35). The formation of $FeCl^{2+}$ as an initial product in the aquoiron(II)–chlorine reaction (25) has been used to support inner-sphere mechanism for this reaction. A similar inner-sphere complex between $Fe(Phen)_3^{2+}$ and X_2 is unlikely, since $Fe(Phen)_3^{2+}$ is inert to substitution.

Inhibition by added ions [X^-] accompanies the oxidation of most metal ions (5, 8–11, 16, 28) as a result of the formation of trihalide ions according to the equilibrium:

[16] $X_2 + X^- \rightleftharpoons X_3^-$

with X_3^- being less reactive than X_2. Our data suggest that Cl_3^- and Br_3^- do not constitute significant reactive species in the oxidation of $Fe(Phen)_3^{2+}$ by chlorine and bromine, since inhibition is not observed.

The form of the rate law for the reduction of tris-(1,10-phenanthroline)iron(III) by iodide ions (eq. [13]) suggests a bimolecular interaction between the reactants. Complicated rate laws have been obtained in the reduction of aquoiron(III) (21, 22) and ferricyanide ions (36, 37) by iodide ions; and inhibition by added chloride and bromide ions (21, 22) observed for the reduction of aquoiron(III). These results have been attributed to inner-sphere complex formation between the oxidant and the added halide ion in the primary step, with FeX^{2+} being less reactive than aquoiron(III). Ford-Smith and Rawsthorne (38) obtained simple second-order rate law in the reduction of octacyanomolybdate(V) by iodide ions and therefore ruled out inner-sphere complexation between the oxidant and the reductant. More recently, Ferranti (39) studied the $Mo(CN)_8^{3-}/I^-$ reaction, but his results are not too different from those of Ford-Smith and Rawsthorne. Inner-sphere coordination of tris-(1,10-phenanthroline)iron(III) to halide ions is also unlikely, since a simple second-order rate law, as observed by Ford-Smith and Rawsthorne (38), is obtained here, and catalysis by chloride and bromide ions rather than inhibition is observed. The added anions could associate with atomic iodine while it is in the process of being formed and since the added anion [X^-] stabilises I, it lowers the energy barrier for the reaction. This implies that in addition to the primary second-order path [17]

[17] $Fe(Phen)_3^{3+} + I^- \rightarrow Fe(Phen)_3^{2+} + I$

there is also the path [18]

[18] $Fe(Phen)_3^{3+} + I^- + X^- \rightarrow Fe(Phen)_3^{2+} + IX^-$

Similar paths have been observed by Wilmarth and Haim (46) in the oxidations of halides and pseudohalides.

Acknowledgement

The authors greatly appreciate financial support from the University of Ife Research Committee.

1. F. A. Cotton and G. Wilkinson. Advanced inorganic chemistry. 3rd ed. Interscience. 1972. Chapt. 16.
2. A. Adegite and M. H. Ford-Smith. J. Chem. Soc. Dalton, 138 (1973).
3. G. Gordon and A. Andrewes. Inorg. Chem. **3**, 1733 (1964).
4. A. Adegite and M. H. Ford-Smith. J. Chem. Soc. Dalton, 134 (1973).
5. A. Adegite, H. Egboh, J. F. Ojo, and R. Olieh. J. Chem. Soc. Dalton, 833 (1977).
6. A. Adegite and H. Egboh. Inorg. Chim. Acta, **21**, 1 (1977).
7. A. Adegite. J. Chem. Soc. Dalton. In press.
8. A. Adegite and M. H. Ford-Smith. J. Chem. Soc. Dalton. 2113 (1972).

9. J. B. RAMSEY and M. J. HELDMAN. J. Am. Chem. Soc. **58**, 1153 (1936).
10. A. ADEGITE and S. EDEOGU. J. Chem. Soc. Dalton, 1203 (1975).
11. C. E. JOHNSON and S. WINSTEIN. J. Am. Chem. Soc. **73**, 2601 (1951).
12. J. H. CRABTREE and W. P. SHOEFOR. Inorg. Chem. **5**, 1348 (1966).
13. D. R. CARTER and H. DAVIDSON. J. Phys. Chem. **56**, 877 (1952).
14. A. V. HERSHEY and W. C. BRAY. J. Am. Chem. Soc. **58**, 1760 (1936).
15. J. M. MALIN and J. H. SWINEHART. Inorg. Chem. **8**, 1407 (1969).
16. A. ADEGITE. J. Chem. Soc. Dalton, 1199 (1975).
17. G. CHARLOT. Selected constants. Supplement to Pure Appl. Chem. IUPAC, Butterworth, London. 1971.
18. B. Z. SHAKHASHIRI and G. GORDON. Inorg. Chem. **7**, 2454 (1968).
19. G. F. SMITH and F. P. RICHTER. Ind. Eng. Chem. Anal. **16**, 580 (1944).
20. A. J. FUDGE and K. W. SYKES. J. Chem. Soc. 119 (1952).
21. K. W. SYKES. J. Chem. Soc. 124 (1952).
22. L. KRUMENACKEN. Ann. Chim. **7**, 425 (1972).
23. A. A. SCHILT and R. C. TAYLOR. J. Inorg. Nucl. Chem. **9**, 211 (1959).
24. R. K. WHARTON, J. F. OJO, and A. G. SYKES. J. Chem. Soc. Dalton, 1526 (1975).
25. T. J. CONOCCHIOLI, E. J. HAMILTON, and N. SUTIN. J. Am. Chem. Soc. **87**, 926 (1965).
26. K. L. SCOTT and A. G. SYKES. J. Chem. Soc. Dalton, 1832 (1972).
27. R. A. MARCUS. Ann. Rev. Phys. Chem. **15**, 115 (1964).
28. S. GLASSTONE, K. J. LAIDLER, and H. EYRING. Theory of rate processes. McGraw-Hill, New York, NY. 1941. p. 195.
29. W. H. WOODRUFF and D. W. MARGERUM. Inorg. Chem. **13**, 2578 (1974).
30. M. CHOU, C. CREUTZ, and N. SUTIN. J. Am. Chem. Soc. **99**, 5615 (1977).
31. R. A. MARCUS. J. Phys. Chem. **72**, 891 (1968).
32. A. HAIM and N. SUTIN. J. Am. Chem. Soc. **88**, 434 (1966).
33. (*a*) K. M. DAVIES and J. E. EARLEY. Inorg. Chem. **15**, 1074 (1976); (*b*) J. E. EARLEY. Prog. Inorg. Chem. **13**, 243 (1970).
34. N. SUTIN and B. M. GORDON. J. Am. Chem. Soc. **83**, 70 (1961).
35. J. E. DICKENS, F. BASOLO, and H. M. NEUMANN. J. Am. Chem. Soc. **79**, 1286 (1957); J. BURGESS, F. M. MEKHAIL, and E. R. GARDNER. J. Chem. Soc. Dalton, 1335 (1973).
36. A. INDELLI and G. C. GUARALDI. J. Chem. Soc. 36 (1964).
37. Y. A. MAJID and K. E. HOWLETT. J. Chem. Soc. A, 679 (1968).
38. M. H. FORD-SMITH and J. H. RAWSTHORNE. J. Chem. Soc. A, 160 (1969).
39. F. FERRANTI. J. Chem. Soc. A, 134 (1970).
40. P. CHALILPOYIL, K. M. DAVIES, and J. E. EARLEY. Inorg. Chem. **16**, 3344 (1977).
41. D. W. LARSEN and A. C. WAHL. J. Chem. Phys. **43**, 3765 (1965).
42. K. V. KRISHNAMURTHY and A. C. WAHL. J. Am. Chem. Soc. **80**, 5921 (1958).
43. A. G. SYKES. Kinetics of inorganic teactions. 1st ed. Pergamon Press Ltd., London. 1966. p. 122.
44. W. M. LATIMER. Oxidation states of the elements and their potentials in aqueous solution. 2nd ed. Prentice-Hall, Inc., New York, NY. 1952.
45. W. H. WOODRUFF and D. W. MARGERUM. Inorg. Chem. **12**, 962 (1973).
46. W. K. WILMARTH and H. HAIM. *In* Peroxide reaction Mechanisms. *Edited by* J. O. Edwards. Wiley-Interscience, New York, NY. 1962. p. 175.
47. S. D. MALONE and J. F. ENDICOTT. J. Phys. Chem. **76**, 2223 (1972).
48. J. H. RAWSTHORNE. Ph.D. Thesis, University of Sussex, Brighton, England. 1967.

Carbon-13 nuclear magnetic resonance spectroscopy of phorbol

M. NEEMAN AND O. D. SIMMONS

Roswell Park Memorial Institute, Buffalo, NY 14263, U.S.A.

Received December 7, 1978

M. NEEMAN and O. D. SIMMONS. Can. J. Chem. 57, 2071 (1979).

The ^{13}C nmr spectrum of the diterpene phorbol has been recorded and the signals of all carbons assigned.

M. NEEMAN et O. D. SIMMONS. Can. J. Chem. 57, 2071 (1979).

On a enregistré le spectre rmn du ^{13}C du diterpène phorbol et on a attribué les signaux de tous les carbones.

[Traduit par le journal]

Phorbol **1**, a pentahydroxy-ketone diterpene from *Croton tiglium* L., and its diesters (for example **2** and **3**) are of continuing interest in oncology: the parent diterpene **1** has leukemogenic action, as well as systemic promoting action in liver, lung, and mammary carcinogenesis in certain rodent strains (1–4). 12,13-Diesters of phorbol (natural products such as **2**, or partially synthetic products such as **3**) have been widely studied as tumor promoters in mouse skin initiation–promotion carcinogenesis (5–9). The phorbol triester **6** is devoid of biological activity.

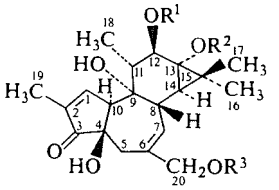

1 $R^1 = R^2 = R^3 = H$
2 $R^1 = CH_3(CH_2)_{12}CO—$, $R^2 = CH_3CO—$, $R^3 = H$
3 $R^1 = R^2 = CH_3(CH_2)_8CO—$, $R^3 = H$
4 $R^1 = CH_3(CH_2)_{12}CO—$, $R^2 = R^3 = H$
5 $R^1 = R^2 = CH_3CO—$, $R^3 = H$
6 $R^1 = R^2 = R^3 = CH_3CO—$
7 $R^1 = R^3 = H$, $R^2 = CH_3CO—$

The determination of the structure and stereochemistry of phorbol and its derivatives utilized ^1H nuclear magnetic resonance (^{1}Hmr) data as evidence for earlier proposed structures (10–12), which were erroneous, and of a later structure **1** (13, 14) which was supported by X-ray crystallographic data for the structure and relative stereochemistry (15, 16), and the absolute configuration (16) of phorbol derivatives.

The present paper reports the ^{13}C nuclear magnetic resonance (^{13}Cmr) spectrum of phorbol. The spectrum was recorded (*a*) without spin decoupling, (*b*) with wide-band noise ^1H decoupling, and (*c*)–(*h*) with selected single frequency ^1H decoupling at 6 frequencies. These frequencies were selected over ranges of 500–600 Hz straddling the decoupling frequency Δν of each protium. The ^{13}C–^1H coupling constants J_0 from (*a*), and residual couplings J_r from (*c*)–(*h*) were utilized to calculate $J_r(J_0^2 - J_r^2)^{1/2}$ for the single frequencies, and Pachler plots were fitted, from which the values of protium decoupling frequency Δν were obtained (17). A ^{1}Hmr spectrum of phorbol was recorded, and the ^1H signals observed were assigned utilizing the ^{1}Hmr analysis of Hecker *et al.* (18). Comparison of the Δν values in the ^{13}Cmr spectrum of phorbol with the chemical shifts of signals in its ^{1}Hmr spectrum made possible the assignment of the ^{13}Cmr signals shown in Table 1, in good accord with the observed J_0 coupling constants and ^{13}Cmr chemical shifts.

The singlets at 212.3 ppm and at 141.3 ppm were assigned, by analogy with the model compound 2-methyl-2-cyclopentenone (19), to carbonyl C-3

TABLE 1. The ^{13}Cmr and ^{1}Hmr spectra of phorbol **1**[a]

C	δ (ppm)[b]	Multiplicity	J_0 (Hz)	Δν (ppm)[b]	δ (ppm)[c]
3	212.3	s			
1	163.5	d	168.2	7.89	8.26
2	141.3	s			
6	134.9	s			
7	130.6	d	155.2	6.80	7.10
12	81.8	d	142.4	4.46	4.57
4[d]	80.0	s			
9[d]	75.3	s			
20	67.8	t	142.0	4.43	4.46
13	63.1	s			
10	58.6	d	126.2	3.51	3.65
11	45.7	d	129.3	2.33	2.24
8	39.8	d	126.8	3.44	3.52
5	37.8	t	125.1	2.97	2.56
14	36.6	d	162.0	1.12	1.34
15	27.1	s			
16	23.9	q	129.5	1.66	1.64[e]
17	17.6	q	126.4	1.43	1.60[e]
18	15.5	q	125.4	1.18	1.51
19	10.6	q	127.2	2.21	2.23

[a]In D_2O (saturated solution).
[b]Relative to TMS external reference in ^{13}Cmr spectrum.
[c]Relative to TMS external reference in ^{1}Hmr spectrum.
[d]Tentative assignments within pair.
[e]These shifts may be reversed.

0008-4042/79/152071-02$01.00/0

TABLE 2. The δ values of C-11, C-12, C-13, and C-14 in phorbol and its esters

	δ (ppm)[a]							
	C-11		C-12		C-13		C-14	
Compound	δ	Δ	δ	Δ	δ	Δ	δ	Δ
1[b]	45.7	0	81.8	0	63.1	0	36.6	0
4[c]	43.2	−2.5	87.4	+5.6	60.9	−2.2	35.3	−1.3
7[d]	45.5	−0.2	76.8	−5.0	67.2	+4.1	35.7	−0.8
5[c]	42.9	−2.8	78.2	−3.6	65.6	+2.5	36.2	−0.4
6[c]	43.0	−2.7	78.0	−3.8	65.5	+2.4	36.1	−0.5

[a]Relative to TMS external standard in D_2O and C_5ND_5–D_2O, and internal standard $CDCl_3$.
[b]In D_2O.
[c]In $CDCl_3$.
[d]In C_5ND_5–D_2O.

and vinyl C-2, respectively. The singlet in the vinyl region at 134.9 ppm was assigned to C-6, and the singlets at 80.0 and 75.3 ppm tentatively to the angular hydroxyl-bearing carbons C-4 and C-9, the more deshielded C-4 being α to conjugate carbonyl C-3. The C-17 methyl group, the axial (13*c*) 11β-H and *pseudo*axial 8β-H in the half chair-ring C (the latter is a 'flagpole' in ring B which has the distorted boat conformation), and the 'flagpole' angular β-OH on C-4 undergo nonbonded interactions, in contrast to the angular 10α-H which does not interact with the remote α-equatorial (13*c*) C-18 methyl group. Carbon C-8 (which is deshielded by one β-OH substituent, and sterically compressed) is 18.8 ppm upfield from C-10 (deshielded by two β-OH substituents). Assignments of the cyclopropyl methyls C-16 and C-17 were made on the basis of the 6.3 ppm difference in shifts between them, which is attributed to steric compression of C-17.

The effects of acylation of 12β-OH or 13α-OH can be compared with those reported for the model compounds *trans*-4-*tert*-butylcyclohexanol and its acetate: acylation effected a downfield shift of the carbinol carbon and an upfield shift of the contiguous carbons (20). The observed shifts given in Table 2 were in the expected directions for C-11, C-12, and C-13 in the mono-acylated phorbol esters **4** and **7**; small upfield shifts were observed for C-14 in **4** as well as **7**. The shifts in the diacetate **5** and in the triacetate **6** were not completely additive in comparison to those in the mono-esters **4** and **7**; the additivity was highest for C-11 and C-13 (Table 2).

Experimental

Phorbol **1** and phorbol 12,13,20-triacetate **6** were purchased from Consolidated Midland Corporation, Brewster, NY, U.S.A., and phorbol 12-myristate **4**, phorbol 12,13-diacetate **5**, and phorbol 13-acetate **7** from Dr. Peter Borchert, Eden Prairie, MI, U.S.A.

The ^{13}Cmr spectra were recorded on a Varian XL-100 nmr spectrometer at 25.2 MHz, and ^{1}Hmr spectra at 100.1 MHz. The undecoupled ^{13}Cmr spectrum of phorbol **1** was run with acquisition time 0.666 s, flip angle 45°, and pulse delay 0.5 s, under conditions of gated decoupling.

Acknowledgements

This study was supported by Research Grant CA 15890-03 and Roswell Park Memorial Core Center Grant CA 16056 of the National Cancer Institute, National Institutes of Health.

1. I. BERENBLUM and V. LONAI. Cancer Res. **30**, 2744 (1970).
2. V. ARMUTH and I. BERENBLUM. Cancer Res. **32**, 2259 (1972).
3. V. ARMUTH and I. BERENBLUM. Cancer Res. **34**, 2704 (1974).
4. V. ARMUTH. Br. J. Cancer, **34**, 516 (1976).
5. E. HECKER. Methods Cancer Res. **6**, 439 (1971).
6. E. HECKER and R. SCHMIDT. Progr. Chem. Org. Nat. Prod. **31**, 377 (1974).
7. B. L. VAN DUUREN. Am. Chem. Soc. Monogr. **173**, 24 (1976).
8. R. K. BOUTWELL. Chemical Rubber Co., Crit. Rev. Toxicol. **2**, 419 (1974).
9. I. BERENBLUM. *In* Cancer, a comprehensive treatise. 1. Etiology: chemical and physical carcinogenesis. *Edited by* F. F. Becker. Plenum Press, New York, NY. 1975. p. 323.
10. E. R. ARROYO and J. HOLCOMB. J. Med. Chem. **8**, 672 (1965).
11. E. HECKER, H. KUBINYI, C. V. SZCZEPANSKI, E. HÄRLE, and H. BRESCH. Tetrahedron Lett. 1837 (1965).
12. E. HECKER, H. KUBINYI, H. BRESCH, and C. V. SZCZEPANSKI. J. Med. Chem. **9**, 246 (1966).
13. (*a*) E. HECKER and H. V. SCHAIRER. Z. Krebsforsch. **70**, 1 (1967); (*b*) E. HECKER. Naturwissenschaften, **54**, 282 (1967); (*c*) E. HECKER, H. BARTSCH, M. GSCHWENDT, E. HÄRLE, G. KREIBICH, H. KUBINYI, H. V. SCHAIRER, C. V. SZCZEPANSKI, and H. W. THIELMANN. Tetrahedron Lett. 3165 (1967).
14. L. CROMBIE, M. L. GAMES, and D. J. POINTER. J. Chem. Soc. C, 1347 (1968).
15. R. C. PETTERSEN, G. FERGUSON, L. CROMBIE, M. L. GAMES, and D. J. POINTER. Chem. Commun. 716 (1967).
16. W. HOPPE, F. BRANDL, I. STRELL, M. RÖHRL, I. GASSMANN, E. HECKER, H. BARTSCH, G. KREIBICH, and C. V. SZCZEPANSKI. Angew. Chem. Int. Ed. Engl. **6**, 809 (1967).
17. K. G. R. PACHLER. J. Magn. Reson. **7**, 442 (1972).
18. E. HECKER, C. V. SZCZEPANSKI, H. KUBINYI, H. BRESCH, E. HÄRLE, H. V. SCHAIRER, and H. BARTSCH. Z. Naturforsch. **21b**, 1204 (1966).
19. D. H. MARR and J. B. STOTHERS. Can. J. Chem. **43**, 596 (1965).
20. H. J. REICH, M. JAUTELAT, M. T. MESSE, F. J. WEIGERT, and J. D. ROBERTS. J. Am. Chem. Soc. **91**, 7445 (1969).

Reaction of alanine-3-sulfinic acid with 2-mercaptoethanol[1]

ALEXANDER J. FINLAYSON AND SAMUEL L. MACKENZIE

National Research Council of Canada, Prairie Regional Laboratory, 110 Gymnasium Road, Saskatoon, Sask., Canada S7N 0W9

AND

JOHN W. FINLEY

Western Regional Research Center, U.S. Department of Agriculture, Berkeley, CA 94710, U.S.A.

Received January 10, 1979

ALEXANDER J. FINLAYSON, SAMUEL L. MACKENZIE, and JOHN W. FINLEY. Can. J. Chem. **57**, 2073 (1979).

The reaction of alanine-3-sulfinic acid with 2-mercaptoethanol (2-ME) was examined at pH 1.5 and pH 4.0 at 110°C. The sulfinic acid is readily reduced at pH 1.5 to cysteine, 2-L-amino-7-hydroxy-4,5-dithiaheptanoic acid, cystine, and three other ninhydrin positive substances. The reduction is much slower at pH 4.0; the major reaction product is the 2-ME/cysteine mixed disulfide. The results show that 2-ME at acid pH does not give quantitative reduction of alanine-3-sulfinic acid to cysteine.

ALEXANDER J. FINLAYSON, SAMUEL L. MACKENZIE et JOHN W. FINLEY. Can. J. Chem. **57**, 2073 (1979).

Opérant à 110°C et à des pH de 1.5 et de 4.0, on a étudié la réaction de l'acide alanine sulfinique-3 avec le mercapto-2 éthanol. A un pH de 1.5, l'acide sulfinique est facilement réduit en cystéine, en acide L-amino-2 hydroxy-7 dithia-4,5 heptanoïque, en cystéine et en trois autres substances qui donnent une réaction positive avec la ninhydrine. La réduction est beaucoup plus lente à un pH de 4.0 et le produit principal est le sulfure mixte de M2E/cystéine. Les résultats démontrent qu'à pH acide, le mercapto-2 éthanol ne conduit pas à une réduction quantitative de l'acide alanine sulfinique-3 en cystéine.

[Traduit par le journal]

Introduction

The oxidations of both protein sulfhydryl and disulfide groups have been shown to be among the contributing factors leading to a wide variety of effects such as enzyme inactivation and reduced protein digestibility. Complete exclusion of oxygen in many reactions involving proteins is not always practical and often small excesses of reducing agents, such as thiols, may be added to protect the sulfur from oxidation.

The reactions between the disulfide reducing agents dithiothreitol (DTT) and 2-mercaptoethanol (2-ME) and cystine have been studied in detail (1, 2) but their reactions with partially oxidized cystine or cysteine derivatives (i.e., alanine-3-sulfinic acid) have not received as much attention. The mechanism for the reduction of a disulfide is generally accepted to be a series of sulfhydryl–disulfide interchange equilibria although the structures of the reactants would influence both the reaction route and the stabilities of the intermediates (2). No doubt, the relative ease of formation of the reducing agent disulfide has an influence on the course of the reaction but since the thiol is nearly always present in excess, its effect on the equilibria is difficult to estimate. The following is one of the accepted mechanisms for disulfide reduction:

$$\left.\begin{matrix} R\text{—}SH + CyS\text{—}SCy \\ R\text{—}S^- + H^+ \end{matrix}\right] \rightleftharpoons RS\text{—}SCy + CyS^-$$

$$RS\text{—}SCy + RS^- \rightleftharpoons CyS^- + RS\text{—}SR$$

$$2CyS^- + 2H^+ \rightleftharpoons 2CySH$$

Because it is possible to have oxidation of the protein disulfide proceed beyond the disulfide stage, it is important to study the reactions of these partially oxidized cystine derivatives with reagents such as DTT and 2-ME. Since 2-ME is widely used in protein chemistry as an anti-oxidant and because the sulfinate state is relatively easily produced by oxidation (3), we have studied the reaction of 2-ME with alanine-3-sulfinic acid at pH 1.5 and 4.0 in an attempt to determine the course of the reduction.

Materials and Methods

Alanine-3-sulfinic acid (Sigma) (1.0 mol) was reduced by 2-ME (Eastman) (1.0 mol to 50 mol excess) at 110°C in a sealed tube for 18 h. A typical experiment was as follows: alanine-3-sulfinic acid (0.013 mmol) in 6 mL 0.05 *M* hydrochloric acid (pH 1.5) containing 0.13 mmol 2-ME was heated at 110°C for 18 h. A series of experiments were also made at pH 4.0, 110°C for 18 h. After reaction, the mixture was evaporated to dryness *in vacuo* at 40°C and stored in a desiccator. A series of reductions at various times from 1 through 18 h at pH 1.5 were made. The reactions of 2-ME at pH 1.5 and 110°C

[1]NRCC No. 17466.

0008-4042/79/152073-05$01.00/0

were also examined to estimate the conditions of formation of the 2-ME disulfide.

The mixed disulfide, 2-L-amino-7-hydroxy-4,5-dithiaheptanoic acid (**1**) was prepared by a modification of the procedure of Abe *et al.* (4). Crystallization of the amino acid (**1**) could not be induced because of the presence of 2-ME side reaction products (i.e., 2-ME disulfide). However, a reasonably pure sample was recovered after chromatography of the reaction mixture on Whatman 3 mm paper using *n*-butanol : ethanol : water (40:11:19) as the solvent. Cystine has an R_f 0.15 while the mixed disulfide had an R_f 0.2. The synthetic **1** had a retention time of 68–69 min on the amino acid analyzer and was distinct from cysteine (62 min) and cystine (90 min). The solid but not crystalline amino acid had a sulfur content of 32.5%; calcd. S content for $C_5H_{11}NO_3S_2$, 32.4%. The mixed disulfide was reduced by 2-ME in 0.05 *M* hydrochloric acid as described above.

Aliquots of all experiments were analyzed by both ion exchange amino acid analysis (Beckman model 120C) and gas–liquid chromatography (gc) (Hewlett-Packard model 7611). Samples for gc were converted to their *N*(*O*)-heptafluorobutyryl (HFB) isobutyl derivatives in the case of amino acids and to their *N*(*O*,*S*)-HFB derivatives for the 2-ME reaction products (5). The column packing and operating temperatures of the gc have been previously described (5). Mass spectra were obtained using a Finnigan model 3300 gas chromatograph – mass spectrometer operated in both the electron impact (ei) mode and the chemical ionization (ci) mode. In the latter mode, methane was used as the carrier gas. All data manipulations were performed using an INCOS data system.

Results and Discussion

The reduction of alanine-3-sulfinic acid at both pH 1.5 and 4.0 produced six ninhydrin positive substances (Fig. 1), three of which appear to represent one of the reduction routes. They are cysteine, the mixed disulfide, 2-L-amino-7-hydroxy-4,5-dithiaheptanoic acid (**1**), and cystine. A number of ninhydrin negative compounds were also produced; two of them are 2,2′-dihydroxydiethyl disulfide and a 'polymer' derived from 2-ME (Fig. 2).

Synthetic **1** was prepared by the method of Abe *et al.* (4); it and the material isolated from the reduction were indistinguishable on both ion exchange and gas–liquid chromatography. The ci mass spectra of **1** from both sources were the same; the major fragmentation peaks are given in Table 1. The molecular weight of the acylated ester of **1** was identified by the ions $M + 1$ (*m/e* 646), $M + 29$ (*m/e* 674), and $M + 41$ (*m/e* 646). The series of ions $M - C_4H_7$ (*m/e* 590), $M - OC_4H_9$ (*m/e* 572), and $M - OCOC_4H_9$ (*m/e* 544) are characteristic of isobutyl esters of a carboxylic acid (6). The mixed disulfide (**1**) was eluted 7 min after cysteine (Fig. 1) on the amino acid analyzer using the protein hydrolyzate buffer system. It was eluted at 27 min on the SE-30 gc column (10 ft × 2 mm id) as its HFB isobutyl derivative (Fig. 2). The recovery of the mixed disulfide corresponds with the results of other work (2) where it has been suggested as an intermediate in the reduction of cystine by 2-ME. The yield of **1** increases until the molar ratio of sulfinic acid:2-ME is about 1:10 but then it declines as the 2-ME concentration increases (Fig. 3).

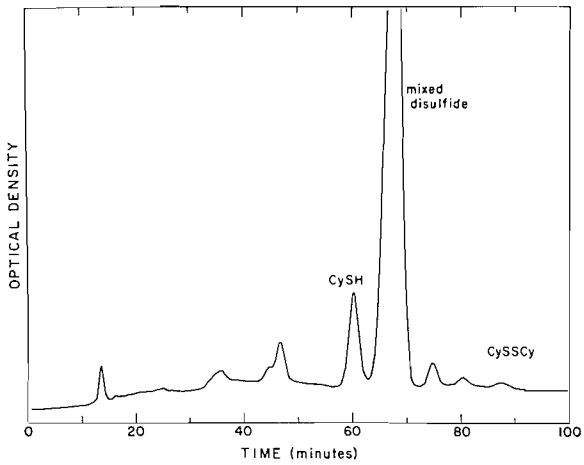

FIG. 1. Reproduction of the amino acid analyzer trace of the reaction products from the reduction of alanine-3-sulfinic acid by 2-mercaptoethanol (1 mol amino acid:20 mol 2-ME) at pH 1.5. The elution times are: cysteine (CySH), 59–61 min; the 2-ME/cysteine mixed disulfide, 68–69 min; cystine (CySSCy) 88–90 min.

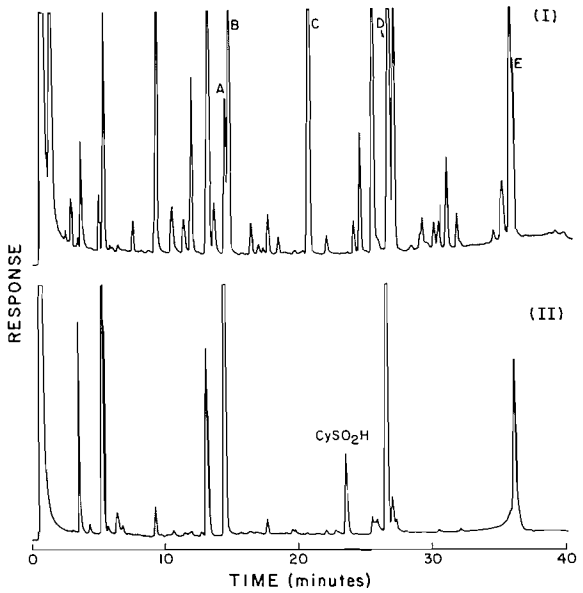

FIG. 2. Chromatographs of *N*(*O*,*S*)-heptafluorobutyryl isobutyl esters of reaction products of alanine-3-sulfinic acid ($CySO_2H$) and 2-mercaptoethanol (2-ME). (I) Reaction mixture of 0.013 mmol $CySO_2H$ and 0.065 mmol 2-ME in 1 *M* HCl at 110°C for 18 h. (II) Reaction mixture of 0.013 mmol $CySO_2H$ and 0.065 mmol 2-ME in water (pH 4.0) at 110°C for 18 h. Peak A denotes the dimer of 2-ME and corresponds to the major peak in II; peak B is cysteine (not present in II); peak C is $(HO—CH_2CH_2—S—CH_2)_2$; peak D is 2-L-amino-7-hydroxy-4,5-dithiaheptanoic acid (present in II); and peak E is cystine.

An analogous reaction between cystine and dithiothreitol (DTT) is considered to involve the mixed

TABLE 1. The 70 eV fragmentation patterns of the *N*(*O*)-HFB, isobutyl ester of the mixed disulfide, 2-L-amino-7-hydroxy-4,5-dithiaheptanoic acid

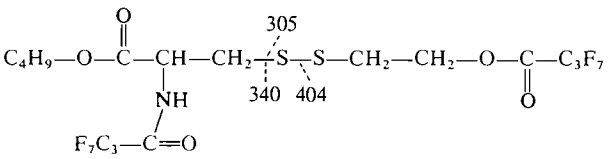

Ion	*m/e*	%
Molecular ion (*M*)	645	—
$M - C_4H_7$	590	1.6
$M - OC_4H_9$	572	0.9
$M - COOC_4H_9$	544	1.5
$M - C_3F_7CONH_2$	432	100.0 base ion
$M - C_3F_7COOCH_2CH_2$	404	6.1
$M - (C_3F_7COONH + C_4H_9)$	376	70.3
$M - (C_3F_7CO_2NH—S—S—)$	340	38.1
$M - (OCOC_4H_9 + C_3F_7CON)$	333	18.7
$M - (C_3F_7CO_2CH_2CH_2—S—S—CH)$	318	18.8
$M - (305 - C_4H_8)$	284	47.3
$M - (305 - C_4H_{10})$	266	6.2

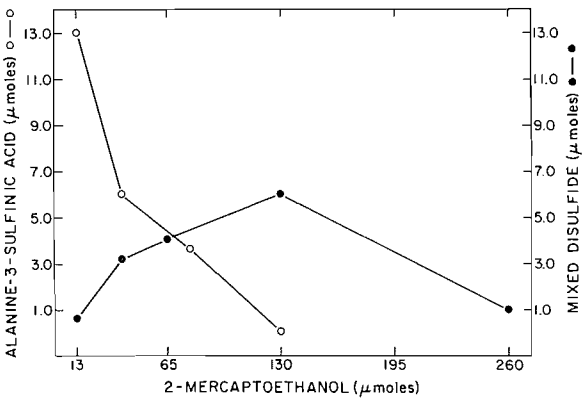

FIG. 3. Yields of the mixed disulfide, 2-L-amino-7-hydroxy-4,5-dithiaheptanoic acid (closed circles), produced from the reduction of alanine-3-sulfinic acid by 2-mercaptoethanol (pH 1.5). Recoveries of unreacted alanine-3-sulfinic acid are shown by the open circles.

disulfide intermediate (**2**) which subsequently reacts with another mole of DTT to yield cysteine.

The release of cysteine from **2** is 10^3–10^4 times faster than it is from the 2-ME/cysteine disulfide and furthermore the rate of reaction between a thiol and the mixed disulfide (DTT/Ellman's reagent) (2) is 10–10^2 times faster than the reaction between a thiol and the 2-ME/Ellman's reagent disulfide. Thus, the recovery of **1** in most of the experiments here is not unusual. It appears then that an excess of 2-ME is required to react with **1** completely although large excesses would certainly enhance the rates of its side reactions (7).

The disulfide, 2,2′-dihydroxydiethyl disulfide is one of the major reaction products (Fig. 2). Its ei mass spectrum (diacylated derivative) is given in Table 2. The molecular ion *m/e* 546 was identified by ei ionization and confirmed by ci. The ions *m/e* 333 ($M - C_3F_7COO$), *m/e* 273 (*M*/2), *m/e* 241 ($C_3F_7COOCH_2CH_2$), *m/e* 169 (C_3F_7), and *m/e* 91 ($CH_2—S—S—CH_2$) were consistent with the structure of the 2,2′-dihydroxydiethyl disulfide. Although a sulfur atom may be hard to distinguish from two oxygen atoms, it is difficult to imagine how such oxygenated derivatives could be products of this reaction. Other compounds from 2-ME are produced in amounts which are related to the acid concentration. The mass spectral data indicate a possible structure for peak C (Fig. 2(I)) is

$$HO—CH_2CH_2—S—(CH_2CH_2—S)_n—CH_2CH_2OH$$

where n = 10–20 accommodates the observed sulfur content. The recovery of this material with about 50% S appears to eliminate the possibility that the 'polymer' is a disulfide. Its production was favored by HCl concentrations of 0.1 *M* and higher. At pH 4, the reaction produced only the dimer of 2-ME (Fig. 2(II)).

Alanine-3-sulfinic acid is readily reduced by 2-ME at acid pH; under the conditions studied here, cysteic acid is not reduced. The sulfinic acid is reduced much more slowly at pH 4.0 than it is at pH 1.5 (Figs. 4, 5) and excess reducing agent is required; 3- to 4-fold excesses do not give complete reduction of the sulfinic acid. For instance, it has completely reacted in 4 h at pH 1.5 but at pH 4.0 about 10% of the sulfinic acid remains after 18 h (Fig. 5). In spite of the slow reaction, the mixed disulfide (**1**) appears to be the initial, stable ninhydrin positive substance produced until the 2-ME concentration in the reaction mixture is about 10 times that of the amino acid. Since at least 10 mol of 2-ME at pH 1.5 are required to react com-

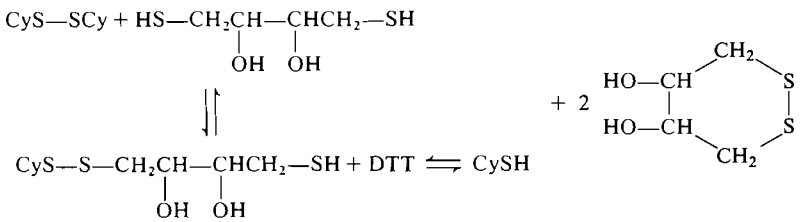

2

TABLE 2. The 70 eV fragmentation patterns of the *N*(*O*)-HFB derivative of 2,2′-dihydroxydiethyl disulfide

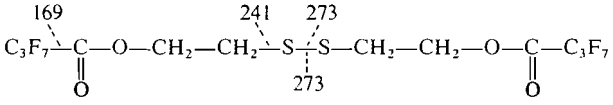

Ion	*m/e*	%
Molecular ion (*M*)	546	—
$M - COOC_3F_7$	333	1.2
$M - SCH_2CH_2COOC_3F_7$	273	2.9
$M - (S—SCH_2CH_2COOC_3F_7)$	241	83.9
$M - CO_2CH_2CH_2SSCH_2CH_2CO_2C_3F_7$	169	100.0

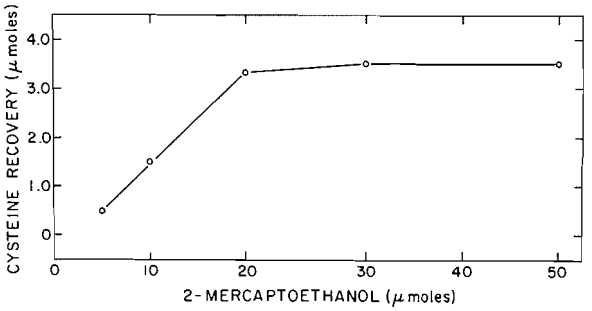

FIG. 4. Yields of cysteine from the reduction of alanine-3-sulfinic acid by 2-mercaptoethanol at pH 1.5.

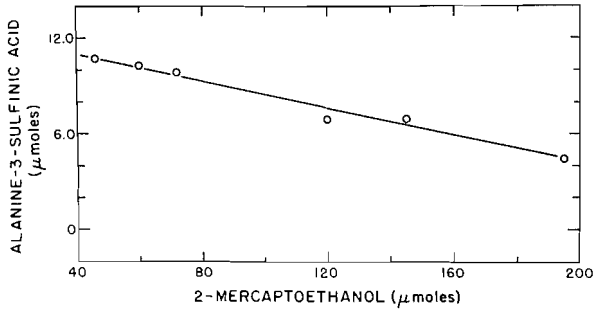

FIG. 5. Amounts of alanine-3-sulfinic acid after reaction with 2-mercaptoethanol for 18 h at 110°C (pH 4.0).

pletely with alanine-3-sulfinic acid, it is obvious the side reactions of 2-ME contribute to the requirement for excess reducing agent. Although the yield of cysteine does not exceed 35% even with a 50-fold excess of 2-ME, a 20-fold excess gives a 30% yield. The yield of cysteine is higher (60%) when alanine-3-sulfinic acid is reduced by DTT in a 1:20 mol ratio; this result agrees with the observation (2) that the cysteine/DDT mixed disulfide is more susceptible to reduction than **1**. Cystine is produced at intermediate concentrations (approximately 20-fold) of 2-ME at pH 4.0 but its recovery is very low at the higher concentrations of reducing agent.

There are three other ninhydrin positive compounds produced in small amounts during the reduction but not all of them have been positively identified. It is not clear where they fit into the reaction scheme. The results we have obtained from the quantitation of **1**, cysteine, and cystine suggest the following as a possible reaction sequence: the initial step is probably the protonation of the sulfinate group analogous to that proposed for the thiosulfinate group (8).

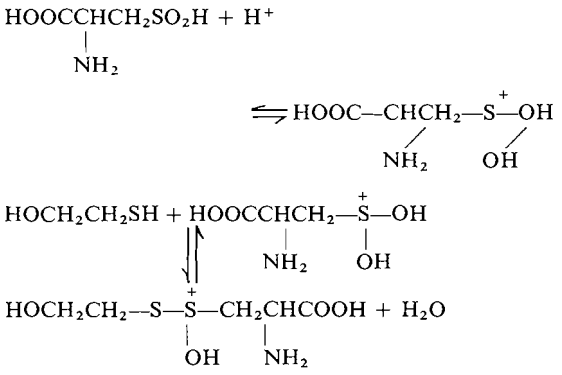

3

Subsequent displacement of the hydroxyl on the sulfur by 2-ME yields the hydroxydisulfide (**3**) which then reacts with a second molecule of 2-ME giving 2,2′-dihydroxydiethyl disulfide and the sulfenic acid, R—SOH.

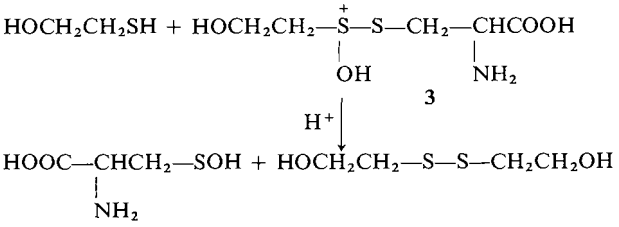

The sulfenic acid, which is apparently too unstable to isolate (9), is then reduced to the mixed disulfide (**1**) by displacement of the hydroxyl on the sulfenic acid by 2-ME.

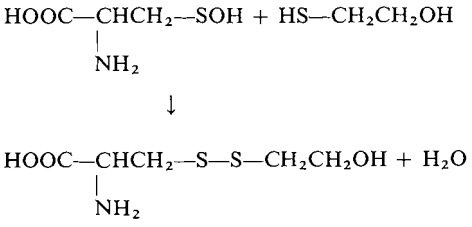

In excess 2-ME, the mixed disulfide is reduced to cysteine although the cysteine yields do not exceed 35% (Fig. 4). The sequence

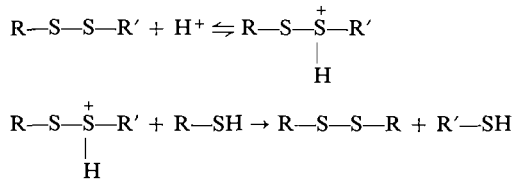

where

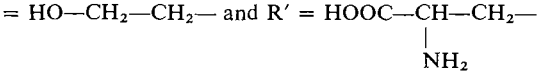

has been suggested (10) to account for disulfide interchange in acid solutions. Presumably, a sulfur atom in the mixed disulfide could be protonated and thus convert a poor leaving group (RS′—) into a better one (10). Subsequent nucleophilic attack by RSH produces the 2-ME disulfide (R—S—S—R) and cysteine (R′—SH). The low yields of cysteine, even when large excesses of thiol are present, may be explained by the stability of the mixed disulfide (**1**) or may result from increases in the rates of side reactions of 2-ME when it is present in high concentrations (2–3 m*M*). For instance, a 3 m*M* solution of 2-ME in 0.5 *M* HCl at 110°C for 18 h gave an 85% yield of the 'polymer'.

The reaction sequence outlined above agrees with the finding that **1** is the initial, stable reaction product and that cysteine and cystine are subsequently derived from it. Because 2-ME itself forms 2,2′-dihydroxydiethyl disulfide under all the conditions examined here, its complete role in the reaction sequences is difficult to assess. High concentrations of it may well inhibit interchange (11) and thus reduce the yields of cysteine but no doubt they also enhance the rates of the other reactions which 2-ME undergoes.

The reduction of alanine-3-sulfinic acid has been postulated to pass through a sulfinic acid intermediate. It has been shown that aryl sulfinic acids and sulfenic acids condense in the following manner (8):

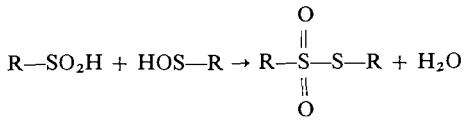

It is not clear if this route occurs in the present case since the cystine dioxide ($CySO_2SCy$) dismutates under acid conditions to alanine-3-sulfinic acid and cystine. The reaction could represent the source of cystine, however.

Some experiments on the reduction by 2-ME of both native and partially oxidized hen's egg white lysozyme showed, after acid hydrolysis, that an amino acid was produced which had chromatographic characteristics the same as **1**. Thus, reductive hydrolysis of a protein using 2-ME at an acid pH would produce some mixed disulfide (**1**); in fact, exposure of the protein to 2-ME at room temperature results in the slow formation of **1**.

To conclude, the results show very clearly that, because of the stability of the cysteine/2-ME mixed disulfide, the reduction at acid pH of alanine-3-sulfinic acid by 2-ME does not give quantitative recoveries of cysteine and that the ratios of the products obtained are pH dependent. Further, the slow release of cysteine from the mixed disulfide is one of the limiting factors in the use of 2-ME for the reduction of either protein cystine residues or their partly oxidized derivatives.

Acknowledgements

The authors wish to thank Mr. C. M. Christ and Mr. D. Tenaschuk for their technical assistance.

1. G. E. Means and R. E. Feeney. Chemical modification of proteins. Holden-Day Inc., San Francisco, CA. 1971. p. 221.
2. G. M. Whitesides, J. E. Lilburn, and R. P. Szajewski. J. Org. Chem. **42**, 332 (1977).
3. J. A. McLaren. Experientia, **17**, 346 (1961).
4. O. Abe, M. F. Lukacovic, and C. Ressler. J. Org. Chem. **38**, 253 (1974).
5. S. L. MacKenzie and D. Tenaschuk. J. Chromatogr. **111**, 413 (1975).
6. S. L. MacKenzie and L. R. Hogge. J. Chromatogr. **132**, 485 (1977).
7. G. I. Brode. U.S. Patent No. 3,824,293; Chem. Abstr. **82**, 44018j (1975).
8. J. L. Kice and G. B. Large. J. Org. Chem. **33**, 1940 (1968).
9. R. E. Penn, E. Block, and L. K. Revelle. J. Am. Chem. Soc. **100**, 3622 (1978).
10. E. Ciuffarin and A. Fava. Prog. Phys. Org. Chem. **6**, 81 (1968).

Canadian Journal of Chemistry
Published by
THE NATIONAL RESEARCH COUNCIL OF CANADA

Journal canadien de chimie
Publié par
LE CONSEIL NATIONAL DE RECHERCHES DU CANADA

Volume 57 Number 16 August 15, 1979 Volume 57 numéro 16 15 août 1979

Ion association and charge-transfer excitation between *N*-heterocyclic cations and cyanoiron complexes

HENRIQUE E. TOMA
Instituto de Química, Universidade de São Paulo, Caixa Postal 20780, São Paulo, Brasil

Received December 13, 1978

HENRIQUE E. TOMA. Can. J. Chem. 57, 2079 (1979).

N-Heterocyclic cations form with substituted pentacyanoferrates a series of outer-sphere complexes of general formula $Fe(CN)_5L//N$-Het, suitable for systematic studies in aqueous solution. The equilibrium constants for the association of dipositive cations (e.g. *N,N'*-dimethyl-4,4-bipyridyl, or paraquat ion) and monopositive cations (e.g. *N*-methylpyrazinium) with the hexacyanoferrate(II) anion are typically in the range of 30–40 M^{-1} and 10–13 M^{-1}. The optical charge-transfer energies depend on the nature of the *N*-heterocyclic acceptor, and on the binding properties of the ligand L as they modify the ionization potentials of the $Fe(CN)_5L^{n-}$ complexes. A linear correlation between the optical charge-transfer energies and ΔE^0 was found, with a slope $(\Delta E_{op}/\Delta G^0)$ of 1.03 ± 0.03. The results were interpreted on the light of Hush's theory for intervalence transitions, with the aid of the equation $E_{op} = 2(\Delta G_{11}^* + \Delta G_{22}^*) + \Delta G_{12}^0$, which correlates the optical energy (E_{op}) for electron-transfer with the intrinsic barriers $(\Delta G_{11}^* + \Delta G_{22}^*)$ of the donor and acceptor ions, and the free energy change (ΔG_{12}^0) for the process.

HENRIQUE E. TOMA. Can. J. Chem. 57, 2079 (1979).

Les cations *N*-hétérocycliques forment avec des pentacyanoferrates substitués une série de complexes de couche externe de formule générale $Fe(CN)_5L//N$-Het, qui sont appropriés pour des études systématiques en solutions aqueuses. Les constantes d'équilibre pour l'association de cations doublement positifs (comme *N,N'*-diméthylbipyridyl-4,4' ou l'ion paraquat) et de cations monopositifs (comme le *N*-méthylpyrazinium) avec l'anion hexacyanoferrate(II) s'échelonnent entre 30–40 M^{-1} et 10–13 M^{-1}. Les énergies de transfert de charge optique dépendent de la nature de l'accepteur *N*-hétérocyclique et des propriétés de liaison du ligand L puisqu'elles modifient les potentiels d'ionisation des complexes $Fe(CN)_5L^{n-}$. On a trouvé une corrélation linéaire entre les énergies de transfert de charge optique et ΔE^0 avec une pente $(\Delta E_{op}/\Delta G^0)$ de 1.03 ± 0.03. On interprète les résultats à la lumière de la théorie de Hush relative aux transitions d'intervalle à l'aide de l'équation $E_{op} = 2(\Delta G_{11}^* + \Delta G_{22}^*) + \Delta G_{12}^0$ qui établit une relation entre l'énergie optique (E_{op}) pour le transfert électronique et les barrières intrinsèques $(\Delta G_{11}^* + \Delta G_{22}^*)$ des ions donneurs et accepteurs et le changement d'énergie libre (ΔG_{12}^0) du processus.

[Traduit par le journal]

Introduction

Aromatic, *N*-heterocyclic cations are of great interest in electron-transfer processes. Due to their high electron affinities, they can act as quenchers of the luminescence of many excited molecules in solution (1, 2), also being able to inhibit the electron-transfer in the cytochrome chain of mitochondria and the electron-transfer chain of chloroplasts.

In the presence of donor species, e.g. iodide (3, 4), MX_4^{2-} ions (5) (M = Cu, Mn, Fe, Co, Zn, Cd, Hg, Pb, Pd, Ag, and Sn; X = Cl, Br, and I) and dianionic dithiolene complexes (6), the aromatic *N*-heterocyclic cations exhibit characteristic charge-transfer bands in the visible and ultraviolet regions, indicative of the occurrence of donor–acceptor interactions.

Generally, the energy of the charge-transfer bands does not depend solely on the nature of the donor and acceptor species, but also, on the properties of

0008-4042/79/162079-06$01.00/0

the solvents. A very useful parameter of solvents (7) has been introduced by Kosower (8) based on the strong solvatochromism exhibited by 1-alkylpyridinium iodides, particularly 1-ethyl-4-methoxycarbonylpyridinium iodide.

Despite the importance of charge-transfer association in aqueous solution the number of systematic studies reported up to the present in the literature is relatively small. It is well known that many pyridine and pyrazine cations can coordinate with π-donor ions such as $Ru(NH_3)_5^{2+}$ and $Fe(CN)_5^{3-}$, forming stable, internal charge-transfer complexes (9, 10). However, the outer-sphere association of the *N*-heterocyclic cations with such donor ions in aqueous solution has never been investigated.

In this paper, a study on the association of a series of substituted cyanoiron complexes and *N*-heterocyclic cations is reported, showing the trends and correlation which exist between the optical electron-transfer energies and the electrochemical properties of the donor and acceptor ions.

Experimental

Compounds

The pentacyanoferrate(II) compounds were prepared from sodium amminepentacyanoferrate(II) trihydrate, as previously described (2, 10–12). The aromatic *N*-heterocyclic cations below were obtained as iodide salts according to the following procedures:

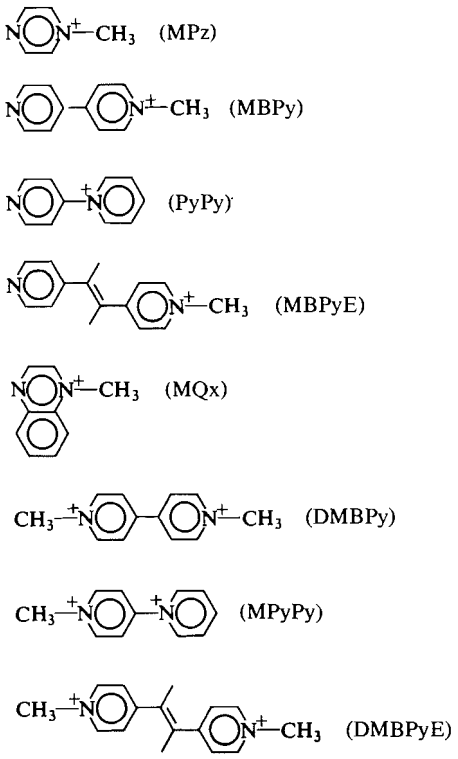

N-Methylpyrazinium Iodide (MPzI) and N-*Methylquinoxalinium Iodide (MQxI)*

Pyrazine (10 g) (Aldrich, gold label) or quinoxaline (Aldrich) was dissolved in 50 mL of methyl iodide and the resulting solution was kept in the dark at room temperature for one week. The hygroscopic yellow (MPzI) or brown (MQxI) crystals formed were recrystallized from ethanol at 60°C and stored under vacuum. *Anal.* calcd. for $C_5N_2H_7I$ (MPzI): C 27.0, N 12.6, H 3.18; found: C 27.1, N 12.8, H 3.22. *Anal.* calcd. for $C_9N_2H_9I$ (MQxI): C 39.7, N 10.9, H 3.33; found: C 40.2, N 10.3, H 3.28.

N-*Methyl-4,4′-bipyridyl Iodide (MBPyI) and* N-*Methyl-1,2-bis(4-pyridyl)ethylene Iodide (MBPyEI)*

4,4′-Bipyridyl (2 g) (Aldrich) or 1,2-bis(4-pyridyl)ethylene (Aldrich) was dissolved in 50 mL of benzene, filtered, and then mixed with 2 mL of methyl iodide. After 3 days in the dark, the yellow solids formed were separated by filtration and recrystallized from ethanol (60°C). *Anal.* calcd. for $C_{11}N_2H_{11}I$ (MBPyI): C 44.3, N 9.39, H 3.72; found: C 44.7, N 9.41, H 3.69. *Anal.* calcd. for $C_{13}N_2H_{13}I$ (MBPyEI): C 48.2, N 8.63, H 4.04; found: C 47.5, N 8.71, H 4.06.

N,N′-*Dimethyl-4,4′-bipyridyl Iodide (DMBPyI$_2$) and* N,N′-*1,2-bis(4-pyridyl)ethylene Iodide (DMBPyEI$_2$)*

4,4′-Bipyridyl (2 g) or 1,2-bis(4-pyridyl)ethylene was dissolved in 50 mL of benzene in the presence of 5 mL of ethanol, and mixed with 20 mL of methyl iodide. The solution was stirred in the dark for one week at room temperature. The red-orange solid formed was separated by filtration and washed with ethanol. The presence of monomethylated products can be easily tested by dissolving a very small amount of the solid in an aqueous solution of the $Na_3Fe(CN)_5NH_3$ complex. A red or violet color indicates the formation of $Fe(CN)_5$(MBPy) or $Fe(CN)_5$(MBPyE) complexes, respectively. When the test was positive, the solid was stirred in a methanolic methyl iodide solution for three days and then filtered and washed with ethanol. The bimethylated cations, in contrast to the monomethylated ones, do not coordinate with the pentacyanoferrate(II) ion. *Anal.* calcd. for $C_{14}N_2H_{16}I_2$ (DMBPyEI$_2$): C 36.1, N 6.00, H 3.46; found: C 36.4, N 6.55, H 3.33. *Anal.* calcd. for $C_{12}N_2H_{14}I_2$ (DMBPyI$_2$): C 32.7, N 6.36, H 3.20; found: C 32.3, N 6.64, H 3.31.

4-Pyridylpyridinium Iodide (PyPyI) and N-*Methyl-4-pyridylpyridinium Iodide (MPyPyI$_2$)*

Pyridylpyridinium hydrochloride (4.5 g) (Aldrich) was dissolved in 100 mL of methanol and then carefully neutralized with 0.85 g of solid lithium hydroxide. The yellowish solution was mixed with 100 mL of ethanol containing 6 g of sodium iodide and then filtered. To this solution, 100 mL of ethyl ether was added in order to precipitate the pyridylpyridinium salt. The solid was dissolved in 200 mL of ethanol at 60°C, and filtered through a sintered glass filter. After one day in the freezer, bright yellow crystals of PyPyI were obtained. The ethanolic solution containing an appreciable amount of dissolved pyridylpyridinium iodide was treated with 20 mL of methyl iodide. After a week in the dark, the orange-brown crystals of the MPyPyI$_2$ salt were separated from the solution and washed with pure ethanol. The product gave a negative test with the pentacyanoferrate(II) ion. *Anal.* calcd. for $C_{10}N_2H_9I$ (PyPyI): C 42.3, N 9.86, H 3.19; found: C 42.1, N 9.28, H 2.90. *Anal.* calcd. for $C_{11}N_2H_{12}I_2$ (MPyPyI$_2$): C 31.0, N 6.57, H 2.83; found: C 31.7, N 6.57, H 2.75.

Spectra

Ultraviolet–visible range spectra were measured on a Cary 14 spectrophotometer at room temperature. Most scans

were made using 10.0 mm quartz cells and solutions containing equimolar amounts of the $Fe(CN)_5L^{n-}$ complexes and of the *N*-heterocyclic ions (usually 10^{-2} *M*). A corresponding solution of the *N*-heterocyclic ion was used as a blank to correct for the absorption of the reactant at the proximity of the ultraviolet region.

Equilibrium Constants

The determination of the association constants of the outer-sphere complexes was made spectrophotometrically, using the 0–0.1 expanded absorbance scale of the Cary 14 spectrophotometer. Potassium nitrate was used to adjust the ionic strength of the 10^{-3} *M* solutions of the donor and acceptor ions. All the manipulations and measurements were carried out in the dark. Solutions of ferrocyanide should be previously stabilized with traces of sodium cyanide; otherwise, the small amounts of $Fe(CN)_5H_2O^{3-}$ which result from the thermal and photochemical dissociation of $Fe(CN)_6^{4-}$ react readily with the monomethylated ions such as MPz and MQx, masking the absorption of the charge-transfer complexes in solution. Such a precaution is not necessary for the dimethylated ions; however, in any case an excess of the CN^- ion should be avoided since this ion was observed to react with most of the *N*-heterocyclic cations. For the $Fe(CN)_5L^{n-}$ complexes, an excess of L was maintained in solution to prevent the dissociation of the coordinated ligand.

The equilibrium constants at 25°C and 0.100 *M* KNO_3 were computed by an iterative procedure, using a Hewlett-Packard, Model 97, calculator. Details concerning the method used to calculate the equilibrium constants are presented in the text.

Results and Discussion

In order to observe the formation of outer-sphere complexes in aqueous solution, a high concentration of the donor and acceptor ions is usually required, since most of the complexes are relatively unstable in ionizing solvents. Moreover, in many cases, the charge-transfer bands of these kind of complexes fall in the ultraviolet region, where they are frequently masked by the absorptions of the donor and acceptor ions. All these difficulties probably explain the small number of systematic studies on charge-transfer interactions in outer-sphere complexes in aqueous solution, reported up to the present in the literature.

By using the highly charged $Fe(CN)_6^{4-}$ ion as a donor, it was possible to detect the occurrence of typical charge-transfer interactions with *N*-heterocyclic cations in aqueous solution. Since $Fe(CN)_6^{4-}$ is very inert to substitution and most of the *N*-heterocyclic cations investigated here cannot coordinate to metal ions, an outer-sphere association process can be postulated, as indicated below.

$$Fe(CN)_6^{4-} + N\text{-Het}^+ \rightleftharpoons Fe(CN)_6^{4-}//N\text{-Het}^+$$

In all the cases, a new, broad band was observed in the visible region, as shown in Fig. 1. The absorption band, not observed in the spectra of the donor and acceptor ions separately, was assigned to the electron-transfer transition, $d(t_{2g}^6)\cdot p(\pi^0)^* \rightarrow d(t_{2g}^5)\cdot p(\pi^1)^*$,

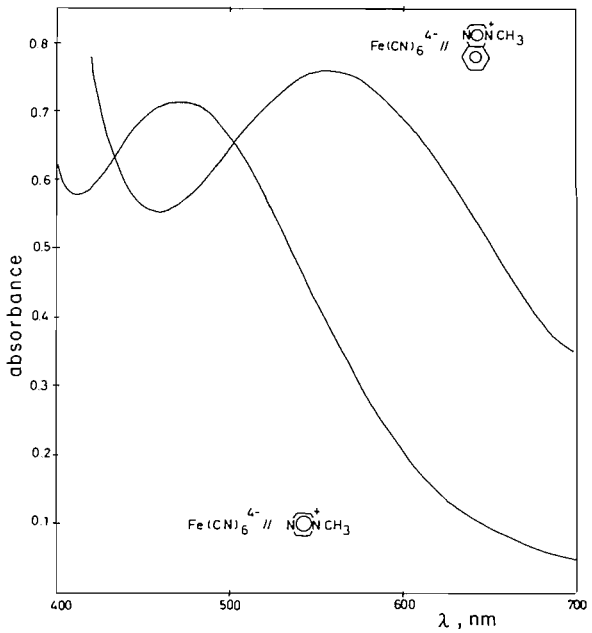

FIG. 1. Absorption spectra of 0.020 *M* solutions of $Fe(CN)_6^{4-}$ and MQx, or MPz ions.

from the occupied metal d_{xz}, d_{yz}, and d_{xy} orbitals to the lowest unoccupied π^* orbitals of the aromatic *N*-heterocyclic cations.

The charge-transfer nature of the $Fe(CN)_6^{4-}//N\text{-Het}^+$ complexes was corroborated by the spectra of acetonitrile solutions of the iodide salts of the *N*-heterocyclic cations, which also exhibited the characteristic charge-transfer bands, although shifted to higher energies. A comparison of the CT energies of the hexacyanoferrate(II) and iodide complexes of the various *N*-heterocyclic cations can be seen in Table 1.

The trends in the energies of the optical electron-transfer can be rationalized according to the simplified equation (13, 14)

$$[1] \quad E_{op} = I_D - E_A + C$$

where I_D is the ionization potential of the donor, E_A is the electron affinity of the acceptor, and C is a coulombic term. For a given donor, D, as the electron affinity of the acceptor A increases, the optical electron-transfer energy is expected to decrease proportionally. Therefore, based on Table 1, the following order of electron affinity can be postulated, MQx > DMBPyE ~ DMBPy > MPyPy > MPz > MBPyE > MBPy ~ PyPy, with the *N*-methylquinoxalinium cation (MQx) as the best electron acceptor of the series.

It is interesting to note that some of the organic

TABLE 1. Charge-transfer energies of some iodide[a] or cyanoiron[b]–*N*-heterocycles, donor–acceptor complexes

Acceptor, A^{n+}	$I^-//A^{n+}$		$Fe(CN)_6^{4-}//A^{n+}$		$Fe(CN)_5A^{2-}$	
	λ_{max} (nm)	$(1/\lambda)$ (kK)[c]	λ_{max} (nm)	$(1/\lambda)$ (kK)[c]	λ_{max} (nm)	$(1/\lambda)$ (kK)[c]
MQx	478	(20.9)	555	(18.0)	785	(12.7)
DMBPyE	436	(22.9)	530	(18.9)	—	—
DMBPy	440	(22.7)	530	(18.9)	—	—
MPyPy	436	(22.9)	520	(19.2)	—	—
MPz	412	(24.2)	470	(21.3)	655	(15.3)
MBPyE	395[d]	(25.3)	460	(21.7)	540	(18.5)
MBPy	375	(26.6)	435	(23.0)	530	(18.9)
PyPy	382	(26.2)	425	(23.5)	485	(20.6)

[a]In acetonitrile solution.
[b]In water.
[c]1 kK = 1000 cm^{-1}.
[d]Shoulder.

acceptors can form stable complexes, by coordinating with the $Fe(CN)_5^{3-}$ ion. Such complexes display very strong charge-transfer bands in the visible, in contrast with the medium-weak intensity observed for most of the outer-sphere complexes. The inner-sphere complexes have been previously investigated by Toma and Malin (10) and are collected in Table 1 for comparison purposes. Although the trends in the electron acceptor properties are practically the same in the three series of complexes (Table 1), it seems that the charge-transfer energies vary more rapidly for the inner-sphere complexes, as compared with the outer-sphere analogs. This may be due to the strong interaction between the metal and the *N*-heterocyclic cation in the inner-sphere complexes, in contrast to the weak interactions in the outer-sphere complexes.

The association constants of the $Fe^{II}(CN)_6//N\text{-Het}^+$ charge-transfer complexes were evaluated from spectrophotometric measurements of equimolar solutions of the donor and acceptor ions (1.0–7.0 × 10^{-3} *M*) using the equation

$$[2]\quad \kappa = \frac{[Fe^{II}(CN)_6^{4-}//N\text{-Het}^+]}{[Fe^{II}(CN)_6^{4-}][N\text{-Het}^+]} = \frac{\varepsilon \cdot A}{\{\varepsilon[Fe(CN)_6^{4-}]_T - A\}\{\varepsilon[N\text{-Het}^+]_T - A\}}$$

where *A* is absorbance, and the subscript T refers to the total concentration of the species. Since the extinction coefficient, ε, for the charge-transfer complex is not known, an iterative procedure was employed in order to obtain the best value of this parameter which minimizes the standard deviation over κ.

For dipositive cations such as DMBPy, association constants of 30–40 M^{-1} were obtained, as compared with 10–13 M^{-1} for monopositive cations such as MPz and MQx. The optimized extinction coefficients were typically 150–200 M^{-1} cm^{-1}, varying slightly with the acceptor properties of the *N*-heterocyclic cation. The association constants agree reasonably well with those predicted for outer-sphere complexes, using the Eigen–Fuoss equation (15) with the crystallographic distance for ferrocyanide (16) (4.4 Å) and approximate radii, previously measured (e.g. DMBPy (17), 6.0 Å; MPz (18), 2.10 Å; MQx (18), 3.12 Å) for some of the *N*-heterocyclic cations.

In order to test for the influence of the donor ion on the charge-transfer energies, the DMBPy ion was used as acceptor (19) in the presence of a series of $Fe(CN)_5L^{n-}$ complexes, where L = CO, dimethylsulfoxide (DMSO), triphenylphosphine, CN^-, pyridine, and imidazole. Some typical charge-transfer spectra obtained for these outer-sphere complexes can be seen in Fig. 2.

The charge-transfer energies of the $Fe(CN)_5L^{n-}//$DMBPy complexes follow approximately the trends of the spectrochemical series for L, in the sequence: 18 000 (imidazole); 18 800 (pyridine); 19 700 (triphenylphosphine); 22 200 (S-bound dimethylsulfoxide); and 25 000 cm^{-1} (CO). The result agrees with the expected behavior from eq. [1], since the stabilization of the metal d_π orbitals through back-bonding interactions with the unsaturated ligands should increase the ionization potentials of the donor ion.

The electronic excitation in the $Fe(CN)_5L^{n-}//N\text{-Het}^+$ complexes can be regarded as an optical

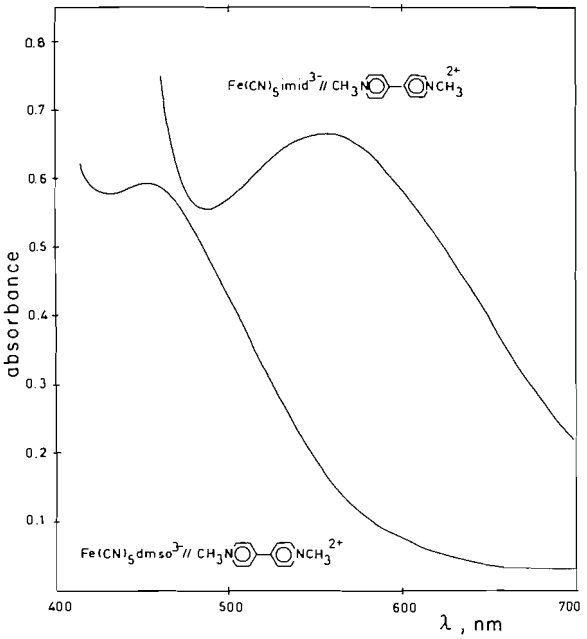

FIG. 2. Absorption spectra of 0.020 *M* solutions of the DMBPy and $Fe(CN)_5(imidazole)^{3-}$ or $Fe(CN)_5(dmso)^{3-}$ ions.

electron-transfer process,

$$Fe^{II}(CN)_5L//N\text{-Het}^+ \xrightarrow{h\nu} Fe^{III}(CN)_5L//N\text{-Het}$$

as in the so-called 'mixed-valence complexes'. Indeed, evidence for radicals has been reported (20), for example, in the photoexcitation of the 4-carbomethoxy-1-ethylpyridinium iodide charge-transfer complex,

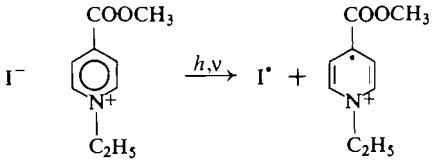

It would be interesting now to compare the optical excitation in those complexes with the thermal electron-transfer process. It is well known that both the $Fe(CN)_5L^{n-}$ complexes and the *N*-heterocyclic species can participate in electron-transfer reactions, acting as reducing and oxidizing agents, respectively. Electron-transfer (1, 2) with excited molecules, e.g. $*Ru(bipy)_3^{2+}$, has proved to be very effective with most of the *N*-heterocyclic cations, proceeding with diffusion controlled rates for DMBPy (1), DMBPyE (1), and MPz (2) cases,

$$*Ru(bipy)_3^{2+} + N\text{-Het}^+ \rightarrow Ru(bipy)_3^{3+} + N\text{-Het}^{\bullet}$$

For a general case of outer-sphere electron-transfer reaction, the following steps have been postulated (21):

$$Ox_1 + Red_2 \rightleftharpoons Ox_1//Red_2$$

$$Ox_1//Red_2 \rightleftharpoons Red_1//Ox_2$$

$$Red_1//Ox_2 \rightleftharpoons Red_1 + Ox_2$$

The activation energies for electron-transfer within the outer-sphere complex, $Ox_1//Red_2$, can be expressed according to the Marcus (22) and Hush (23) equation,

$$[3] \quad \Delta G_{12}^* = (\Delta G_{11}^* + \Delta G_{22}^*)/2 + \Delta G_{12}^0/2$$

provided that $(\Delta G_{12}^0)^2 \ll 8(\Delta G_{11}^* + \Delta G_{22}^*)$. Here, ΔG_{12}^* refers to the activation barrier for electron-transfer from Ox_1 to Red_2, and ΔG_{11}^* and ΔG_{22}^* are the intrinsic barriers associated with the self-exchange reactions, respectively. The ΔG_{12}^0 term expresses the free energy change for the net reaction, and is proportional to the difference of the electrochemical potentials, ΔE_{12}^0, of the reactants.

For an optical electron-transfer process, as shown in Fig. 3, the excitation energy deduced from the harmonic potentials (24) can be expressed by

$$[4] \quad E_{op} = 2(\Delta G_{11}^* + \Delta G_{22}^*) + \Delta G_{12}^0$$

For a symmetrical system, based on eqs. [4] and [3], the energy of the optical Franck–Condon transition is predicted to be four times the activation energy for the thermal electron-transfer. For a non-symmetrical system, as is the case of the complexes reported here, the relationship between E_{op} and E_{th}, the optical and thermal energies, respectively, becomes

$$[5] \quad E_{op} = 4E_{th} - \Delta G_{12}^0$$

Based on eq. [4] one can also expect that the energies of optical electron-transfer in a series of complexes with similar intrinsic barriers should increase linearly with ΔG_{12}^0, with a unit slope. This

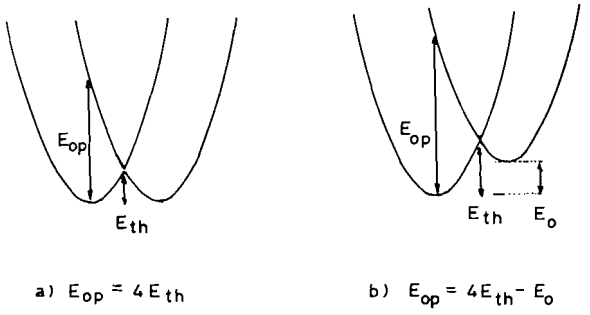

FIG. 3. Reaction coordinate diagrams for electron-transfer: (*a*) $\Delta G^0 = 0$; (*b*) $\Delta G^0 > 0$.

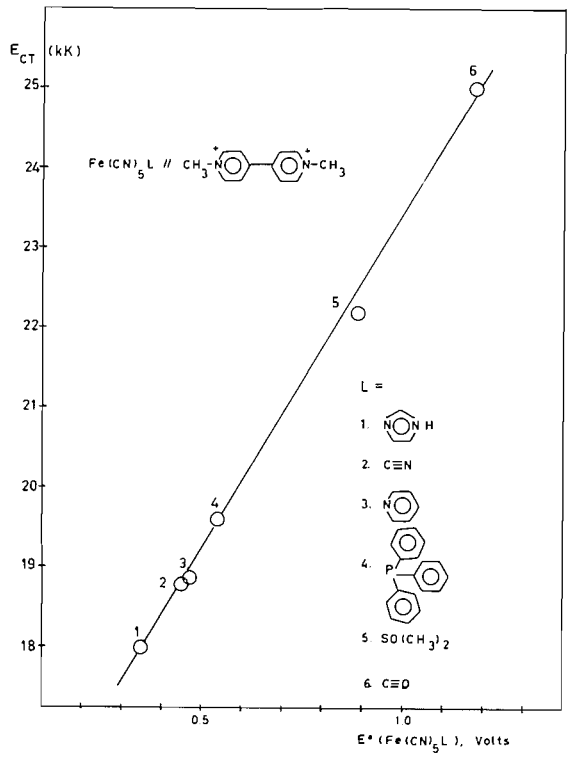

FIG. 4. Correlation of charge-transfer energies with the ΔE^0 values (ref. 2) of the $Fe(CN)_5L$ complexes.

expectation differs from the case of thermal electron-transfer (21), where the theoretical slope of the linear relationship between $\Delta G_{12}{}^*$ and $\Delta G_{12}{}^0$ equals 1/2.

In order to test for the validity of Hush's theory in the outer-sphere complexes reported here, one can estimate the free energy changes from the electrochemical potentials of the free, donor, and acceptor ions, with the assumption that they are not influenced in a significant extent, by the association process. As shown in Fig. 4, a good linear correlation between E_{op} and $\Delta G_{12}{}^0$ (proportional to the E^0 values for the $Fe(CN)_5L$ complexes) results for the several DMBPy//$Fe(CN)_5L$ complexes, with a calculated slope of 1.03 ± 0.03.

A linear correlation between E_{op} and E^0 has also been reported (6) for a series of outer-sphere complexes between pyridinium cations and dianionic, dithiolene complexes, as well as for a series of pyridinium iodides (4). The observed slopes ($\Delta E_{op}/\Delta G_{12}{}^0$) were respectively 1.24 and 1.25 for those series of complexes. A similar behavior has been observed recently for a number of $Ru(NH_3)_6{}^{3+}$//$Fe(CN)_5L^{3-}$ complexes (25, 26).

It is remarkable that the agreement with the theory seems quite reasonable, despite the obvious criticism which arises from the use of harmonic potentials to describe the optical and thermal electron-transfer barriers.

Acknowledgements

A grant from CNPq and helpful and stimulating discussions with Dr. Frank Quina are gratefully acknowledged.

1. C. R. BOCK, T. J. MEYER, and D. G. WHITTEN. J. Am. Chem. Soc. **96**, 4710 (1974).
2. H. E. TOMA and C. CREUTZ. Inorg. Chem. **16**, 545 (1977).
3. E. M. KOSOWER and J. A. SKORCZ. J. Am. Chem. Soc. **82**, 2195 (1960).
4. R. A. MACKAY, J. R. LANDOLPH, and E. J. POZIOMEK. J. Am. Chem. Soc. **93**, 5026 (1971).
5. A. J. MACFARLANE and R. J. P. WILLIAMS. J. Chem. Soc. A, 1517 (1969).
6. I. G. DANCE and P. S. SOLSTAD. J. Am. Chem. Soc. **95**, 7256 (1969).
7. C. REICHARDT. Angew. Chem. Int. Ed. Engl. **4**, 29 (1965).
8. E. M. KOSOWER. J. Am. Chem. Soc. **80**, 3253 (1958); J. Chim. Phys. **61**, 230 (1964).
9. C. CREUTZ and H. TAUBE. J. Am. Chem. Soc. **95**, 1086 (1973); H. E. TOMA and J. M. MALIN. J. Am. Chem. Soc. **94**, 4039 (1972).
10. H. E. TOMA and J. M. MALIN. Inorg. Chem. **12**, 1039 (1973).
11. H. E. TOMA, J. M. MALIN, and E. GIESBRECHT. Inorg. Chem. **12**, 2084 (1973).
12. R. NAST and K. W. KRUGER. Z. Anorg. Allgem. Chem. **341**, 189 (1965).
13. R. L. FLURRY, JR. J. Phys. Chem. **69**, 1927 (1965); **73**, 211 (1969).
14. J. N. MURREL. Q. Rev. London, 191 (1961).
15. G. C. HAMMES and M. L. MORELL. J. Am. Chem. Soc. **86**, 1497 (1964).
16. E. R. NIGHTINGALE, JR. J. Chem. Phys. **63**, 1381 (1959).
17. C. K. PROUT and P. MURRAY-RUST. J. Chem. Soc. A, 1520 (1969).
18. H. E. TOMA and H. C. CHAGAS. An. Acad. Bras. Cienc. **50**, 487 (1978).
19. A. NAKAHARA and J. H. WANG. J. Phys. Chem. **67**, 496 (1963).
20. E. M. KOSOWER and L. LINDQVIST. Tetrahedron Lett. 4481 (1965).
21. N. SUTIN. *In* Inorganic biochemistry. Vol. 2. *Edited by* G. L. Eichhorn. Elsevier Publ., Amsterdam, London, N.Y. 1973. Chapt. 9.
22. R. A. MARCUS. Ann. Rev. Phys. Chem. **15**, 155 (1964); J. Chem. Phys. **43**, 679 (1965).
23. N. S. HUSH. Trans. Faraday Soc. **57**, 557 (1961).
24. N. S. HUSH. Prog. Inorg. Chem. **8**, 391 (1967).
25. J. C. CURTIS and T. J. MEYER. J. Am. Chem. Soc. **100**, 6284 (1978).
26. H. E. TOMA. To be published.

Stannic tetrachloride catalysed glycosylation of 8-ethoxycarbonyloctanol by cellobiose, lactose, and maltose octaacetates; synthesis of α- and β-glycosidic linkages[1]

JOSEPH BANOUB[2] AND DAVID R. BUNDLE

Division of Biological Sciences, National Research Council of Canada, Ottawa, Ont., Canada K1A 0R6

Received December 21, 1978

JOSEPH BANOUB and DAVID R. BUNDLE. Can. J. Chem. 57, 2085 (1979).

The 1,2-*trans*-octaacetates of cellobiose, lactose, and maltose were converted to β-glycosides of 8-ethoxycarbonyloctanol in good yield by a single step reaction. A 1,2-acetoxonium ion generated by stannic tetrachloride in dichloromethane at −10°C leads initially to β-glycosides via 1,2-orthoacetate intermediates. *In situ* anomerisation of the β-maltoside occurred during reaction (4 h) at room temperature and provided a preparative route to this α-glycoside of the disaccharide. The β-lactose and cellobiose glycosides were also anomerised to the respective α-glycosides. The three β- and three α-disaccharide glycosides of the disaccharides have been functionalised for conversion to artificial carbohydrate antigens.

JOSEPH BANOUB et DAVID R. BUNDLE. Can. J. Chem. 57, 2085 (1979).

Les octaacetates *trans*-1,2 du cellobiose, lactose et maltose ont été convertis en glycosides-β du ethoxycarbonyl-8-octanol dans de bon rendements par une reaction en une seule étape.

A −10°C un ion acetoxonium-1,2 est generé par le tétrachlorure d'étain dans le dichloromethane pour conduire initiallement aux glycosides-β via les orthoesters-1,2 comme intérmediaire. L'anomerisation *in situ* du maltoside-β a lieu durant la reaction (4 h) à temperature ambiante et produit ainsi une nouvelle route pour preparer ce glycoside-α du disaccharide.

Les glycosides-β du lactose et cellobiose ont été anomerisés en glycosides-α correspondant.

Les trois disaccharides glycosides-β et les trois disaccharides glycosides-α ont été fonctionalisé afin d'être convertis en antigens artificiels de carbohydrate.

Introduction

The antibody specific for an artificial lactose antigen agglutinates cells of *Neisseria gonorrhaeae* (1), due to the presence of a terminal galactopyranose residue in the cell wall lipopolysaccharide (LPS) (2). In order to investigate further the nature of this cross reaction, related disaccharide antigens have been synthesised, either for subsequent modification at the terminal glycosyl residue prior to conversion to an artificial antigen or for immediate use as antigens, following covalent attachment to protein (3).

A previous preparation of the lactose hapten gave a poor yield of the glycoside **5** (1) but this has been improved by use of silver trifluoromethanesulphonate (triflate) promoted Koenigs–Knorr reactions starting from acetylated glycosyl bromides (4). It has been known for some time that methyl β-D-glucopyranoside may be prepared from penta-*O*-acetyl-β-D-glucopyranose under Lewis acid catalysis (5), and the procedure has been modified recently to provide 1,2-*trans*-linked disaccharides (6, 7). During the preparation of β-glycosides of 8-ethoxycarbonyloctanol by reaction with cellobiose, lactose, and maltose octaacetates in dichloromethane containing 1 mol of stannic tetrachloride, it was observed that extended reaction times and higher temperatures can lead to α-glycosides of disaccharides (Scheme 1).

Results and Discussion

The octaacetates of cellobiose, lactose, and maltose are readily prepared in crystalline form as the β-anomers by standard procedures (8, 9) using sodium acetate and acetic anhydride. When a 1,2-*trans*-sugar per-*O*-acetate is dissolved in dichloromethane containing a molar equivalent of stannic tetrachloride 1,2-acetoxonium ion formation results (10) as is the case with other Lewis acids such as antimony pentachloride (11). Addition of alcohol at −10°C under anhydrous conditions gives *trans*-linked glycosides in excellent yield (6, 7). Under these conditions, −10°C for 4 h, cellobiose **2**, lactose **3**, and maltose **8** octaacetates gave 61–68% yields of the heptaacetyl-β-glycosides of the disaccharides **4**, **5**, and **9** (Scheme 1). Acetylated 8-ethoxycarbonyloctanol, disaccharide hexaacetates, and small amounts of hexaacetyl-disaccharide glycosides are formed as side products in this reaction. This latter product exhibited similar properties to the 2-hydroxy glycoside isolated from Koenigs–Knorr reactions (4). Indeed, if the crude product from the above reaction is de-*O*-acetylated and the 8-methoxycarbonyloctyl-β-glycosides **11**, **12**, and **15** extracted from aqueous solution by chloroform–ethanol (3:2),

[1]NRCC No. 17338.

[2]MDS Health Group Limited, Rexdale, Ontario.

0008-4042/79/162085-06$01.00/0

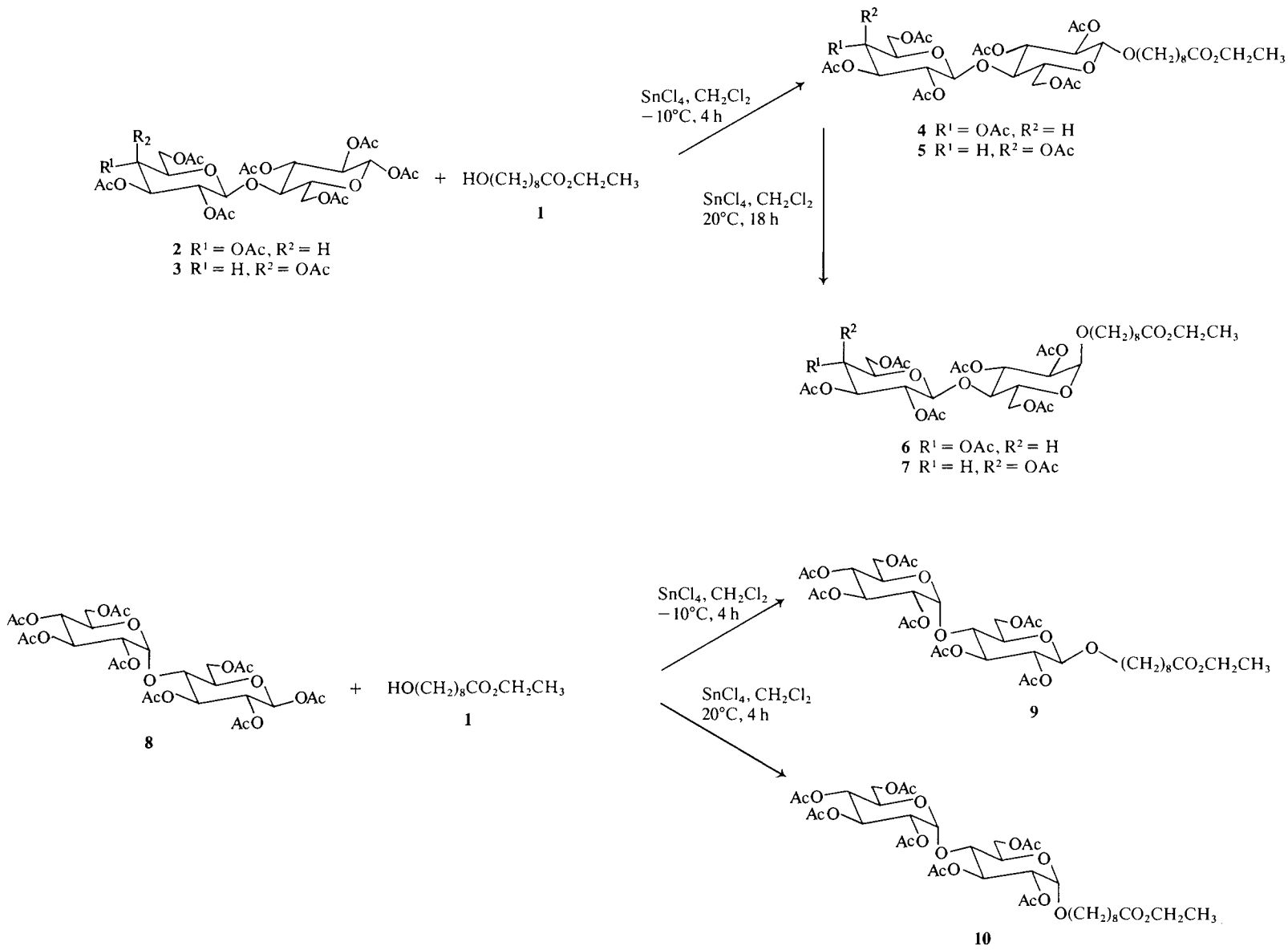

SCHEME 1

the yield of these glycosides is increased by 10–15% over that obtained by de-*O*-acetylation of the purified heptaacetyl glycosides **4**, **5**, and **9**. The increased yield is attributed to the presence in the reaction mixture of significant amounts of 2-hydroxy β-linked glycosides.

Extension of reaction times in conjunction with higher temperatures (20°C) leads to increasing proportions of α-glycosides due to anomerisation. Also observed is a small amount of chloroacetyldisaccharide (7), the yield of which increases if addition of alcohol to the reaction vessel is delayed. Although reaction of maltose octaacetate **8** with 8-ethoxycarbonyloctanol gave optimum yields of the α-glycoside **10** after only 4 h at 20°C, the related glycosides of cellobiose (**6**) and lactose (**7**) were obtained in optimum yields only after work-up and retreatment of the β-glycosides **4** and **5** with stannic tetrachloride in dichloromethane.

Examination of the side-products of this reaction, acetylated aglycon and glycosides lacking a 2-*O*-acetate, supports the conclusion that this reaction proceeds to β-linked glycosides via 1,2-orthoacetate intermediates. The reasoning which leads to this conclusion is similar to that invoked in the accompanying paper (4) which postulates 1,2-orthoacetate intermediates for Koenigs–Knorr reactions. However, in this case it is well documented that suitably oriented polyacetates in the presence of Lewis acid will give 1,2-acetoxonium ions (11). Hanessian and Banoub prepared 1,2-orthoesters via such species, under conditions similar to those used in this work (10). Reaction of cyclic oxocarbonium ions of the type represented in Scheme 2 can lead directly to 1,2-*trans*-glycosides but in the light of the side products of the reaction, probably do so via a 1,2-(8-ethoxycarbonyloctyl orthoacetate) intermediate, which we have demonstrated (4) to rearrange by stannic tetrachloride catalysis. The product distribution seen in this Lewis acid catalysed isomerisation of orthoester is identical to that observed during glycoside synthesis from 1,2-*trans*-octaacetates **2**, **3**, and **8**, ethoxycarbonyloctanol (**1**), and stannic tetrachloride.

The acetylated β- and α-glycosides **4**–**9** were de-*O*-acetylated to provide the corresponding 8-methoxycarbonyloctylglycosides **11**–**16**. Proton nmr (Table 3) in deuterium oxide solution confirmed the anomeric configuration of these glycosides. Conversion to the 8-hydrazinocarbonyloctyl glycosides was performed in ethanol solution with excess hydrazine hydrate. The hydrazides **17**–**22** were analytically pure and gave ^{13}C nmr data in agreement with the assigned structures. The hydrazides are the immediate precursors to artificial antigens and have been coupled

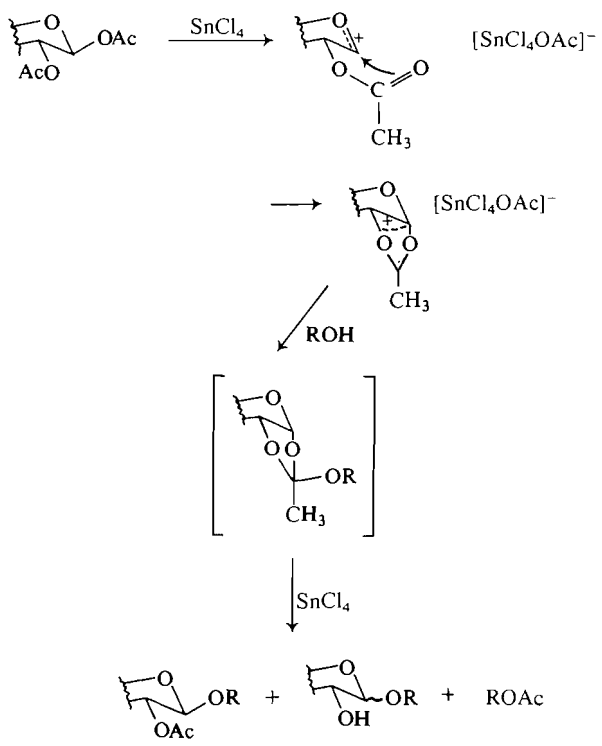

SCHEME 2

to BSA to provide artificial antigens according to a previously published procedure (3, 12).

In addition to the synthesis of the six disaccharide haptens described here, the β-glycoside haptens of

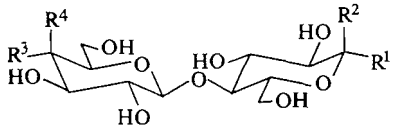

11 $R^1 = O(CH_2)_8CO_2CH_3$, $R^2 = R^4 = H$, $R^3 = OH$
12 $R^1 = O(CH_2)_8CO_2CH_3$, $R^2 = R^3 = H$, $R^4 = OH$
13 $R^1 = R^4 = H$, $R^2 = O(CH_2)_8CO_2CH_3$, $R^3 = OH$
14 $R^1 = R^3 = H$, $R^2 = O(CH_2)_8CO_2CH_3$, $R^4 = OH$
17 $R^1 = O(CH_2)_8CONHNH_2$, $R^2 = R^4 = H$, $R^3 = OH$
18 $R^1 = O(CH_2)_8CONHNH_2$, $R^2 = R^3 = H$, $R^4 = OH$
19 $R^1 = R^4 = H$, $R^2 = O(CH_2)_8CONHNH_2$, $R^3 = OH$
20 $R^1 = R^3 = H$, $R^2 = O(CH_2)_8CONHNH_2$, $R^4 = OH$

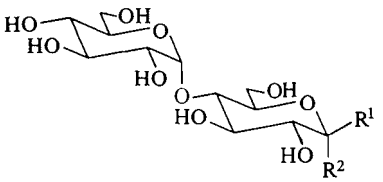

15 $R^1 = O(CH_2)_8CO_2CH_3$, $R^2 = H$
16 $R^1 = H$, $R^2 = O(CH_2)_8CO_2CH_3$
21 $R^1 = O(CH_2)_8CONHNH_2$, $R^2 = H$
22 $R^1 = H$, $R^2 = O(CH_2)_8CONHNH_2$

TABLE 1. Melting point, optical rotation, and analytical data for glycosides **4–22**

Compound	Yield (%)	Melting point (°C)	Specific rotation $[\alpha]_D^{20-23}$	Analytical data
				Anal. calcd. for $C_{37}H_{56}O_{20}$: C 54.13, H 6.89
Acetylated β-cellobioside **4**	68	91–92	−15 (*c* 1.0, $CHCl_3$)	*Anal.* found: C 53.90, H 6.90
Acetylated β-lactoside **5**	61	Syrup	−11.2 (*c* 2.0, $CHCl_3$)	C — , H —
Acetylated β-maltoside **9**	66	Syrup	40.1 (*c* 1.2, $CHCl_3$)	C — , H —
Acetylated α-cellobioside **6**		76–77	39.6 (*c* 1.5, $CHCl_3$)	C 53.84, H 6.93
Acetylated α-lactoside **7**		Syrup	42.8 (*c* 1.0, $CHCl_3$)	C — , H —
Acetylated α-maltoside **10**	59	Syrup	102.8 (*c* 1.9, $CHCl_3$)	C — , H —
				Anal. calcd. for $C_{22}H_{40}O_{13}$: C 51.53, H 7.87
β-Cellobiose, methylester **11**	80	139–140	−18.7 (*c* 1.0, H_2O)	*Anal.* found: C 51.18, H 7.90
β-Lactoside, methylester **12**	86	158–159	3.1 (*c* 1.1, $CHCl_3$)	C 51.50, H 7.88
β-Maltoside, methylester **15**	92	Syrup	43.3 (*c* 2.0, H_2O)	C 51.50, H 8.01
α-Cellobioside, methylester **13**	80	104–106	63.4 (*c* 0.8, H_2O)	C 51.60, H 7.78
α-Lactoside, methylester **14**	79	99–100	68.8 (*c* 1.6, MeOH)	C 51.48, H 7.62
α-Maltoside, methylester **16**	80	Syrup	106.7 (*c* 1.2, MeOH)	C — , H –
				Anal. calcd. for $C_{21}H_{40}N_2O_{12}$: C 49.19, H 7.87, N 5.47
β-Cellobioside, hydrazide **17**		202–204	−16.6 (*c* 1.0, H_2O)	*Anal.* found: C 49.02, H 7.97, N.5.59
β-Lactoside, hydrazide **18**		190–192	−1.9 (*c* 1.0, H_2O)	C 49.00, H 7.83, N 5.67
β-Maltoside, hydrazide **21**		184–185.5	56.4 (*c* 1.0, H_2O)	C 49.02, H 7.97, N 5.57
α-Cellobioside, hydrazide **19**		115–116	58.1 (*c* 1.0, H_2O)	C 48.87, H 7.98, N 5.64
α-Lactoside, hydrazide **20**		117–118	63.2 (*c* 1.0, H_2O)	C 49.33, H 8.08, N 5.78
α-Maltoside, hydrazide **22**		Syrup	109.7 (*c* 1.3, MeOH)	C 49.28, H 8.01, N 5.68

glucose and galactose have been synthesized in approximately 75% yield from the respective penta-*O*-acetyl-β-D-hexopyranoses. Not only is the Lewis acid catalysed glycosylation reaction more rapid than Koenigs–Knorr reactions (1, 4) but the yields of the 8-ethoxycarbonyloctyl glycosides are higher.

Experimental

The general experimental conditions and methods used were as described in the preceding paper (4). Merck silica gel G60 (70–230 mesh) and redistilled solvents were used for column chromatography. Identical but more rapid separations were achieved with a Waters high pressure liquid chromatograph Prep. 500. Proton chemical shifts are expressed relative to 1% tetramethylsilane (TMS) in deuteriochloroform and relative to sodium 3-trimethylsilylpropionate-2,2,3,3-d_4 for deuterium oxide solutions. Carbon-13 shifts are expressed relative to internal TMS in deuteriochloroform and to external TMS for deuterium oxide solutions. Assignments of ^{13}C resonances are based on literature values for monosaccharides and disaccharides (13, 14).

*General Procedure for Preparation of 8-Ethoxycarbonyloctyl 1,2-*trans*-Glycosides*

Stannic tetrachloride (0.98 mL, 9 mmol) was added to a solution of the 1,2-*trans*-disaccharide octaacetate (8, 9) (6.04 g, 9 mmol) in dry dichloromethane (90 mL). After 10 min at room temperature the solution was cooled to −10°C and a white precipitate resulted. A solution of 8-ethoxycarbonyloctanol (3) (2.02 g, 10 mmol) in 10 mL of dichloromethane was added to the reaction mixture and that was then kept at −10°C for 4 h. The reaction mixture was poured into a saturated solution of sodium bicarbonate (60 mL), which was then extracted with chloroform (2 × 100 mL), and the organic phase was washed with water. After solvent removal 10 g of crude syrup was obtained. Column chromatography on silica gel with the solvent ethyl acetate – Skellysolve B 1:1 yielded the pure glycoside **4**, **5**, or **9**. The yields and physical constants for these compounds are reported in Table 1.

Acetylated 8-ethoxycarbonyloctanol was isolated from the reaction mixture together with other side products, which were glycosidic components with tlc mobilities slower than the glycosides **4**, **5**, or **9**. Disaccharide hexaacetates containing no aglycon were also observed. The identification of all three side products was similar to that reported in the accompanying paper (4). Proton spectra for compounds **4**, **5**, and **9** are not reported since this data is not instructive for analytical purposes with the exception that the ratio of polymethylene (—$(CH_2)_6$—, CH_3CH_2) and methyl protons integrate relative to acetate and ring protons in the correct proportion. ^{13}C nmr (Table 2) is much more useful for the identification of the anomeric configuration of the glycosidic linkages.

*8-Ethoxycarbonyloctyl 2,3,6-Tri-*O*-acetyl-4-*O*-(tetra-*O*-acetyl-α-D-glucopyranosyl)-α-D-glucopyranoside (**10**)*

β-Maltose octaacetate (**8**) (17.1 g, 25.5 mmol) was dissolved in dry dichloromethane and stannic tetrachloride (3.5 mL, 25.5 mmol) was added. Immediately after this, 8-ethoxycarbonyloctanol (**1**) (5.1 g, 25 mmol) was added in dichloromethane (10 mL). After 4 h at room temperature the reaction mixture was worked up as described earlier. After purification on silica gel the α-maltose glycoside **10** was obtained as a syrup (12.2 g, 59%). The analytical data and

TABLE 2. Carbon-13 nmr shifts in ppm relative to internal and external TMS for $CDCl_3$ and D_2O solutions of glycosides **4–22**

Compound	Solvent	C-1	C-2	C-3	C-4	C-5	C-6	C-1′	C-2′	C-3′	C-4′	C-5′	C-6′	OCH_2
Acetylated β-cellobioside **4**	$CDCl_3$	100.5	70.2	72.6	76.5	72.6	62.0	100.5	72.0	71.7	67.9	73.0	61.7	71.7
Acetylated β-lactoside **5**	$CDCl_3$	100.5	69.2	71.8	76.3	72.6	62.2	100.9	71.0	71.0	66.8	72.9	61.0	70.6
Acetylated β-maltoside **9**	$CDCl_3$	100.0	69.7	71.9	75.2	73.0	62.8	95.4	68.3	69.7	68.0	69.2	61.4	71.9
Acetylated α-cellobioside **6**	$CDCl_3$	95.6	68.2	68.7	76.9	73.1	61.9	100.8	71.8	72.0	67.9	73.1	61.7	69.8
Acetylated α-lactoside **7**	$CDCl_3$	95.6	68.1	68.6	76.6	70.7	62.0	101.1	70.1	71.1	66.7	71.1	60.9	69.2
Acetylated α-maltoside **10**	$CDCl_3$	95.3	69.2	72.5	73.0	68.3	62.8	95.3	68.4	71.2	67.4	68.0	61.3	69.8
β-Cellobioside hydrazide **17**	D_2O	103.5	74.1	75.9	80.0	75.6	61.8	103.7	74.4	77.2	70.7	76.7	61.3	71.9
β-Lactoside hydrazide **18**	D_2O	103.3	74.1	75.9	79.7	76.7	62.2	104.2	72.2	73.8	69.8	76.5	61.4	71.9
β-Maltoside hydrazide **19**	D_2O	103.3	74.0	75.8	78.1	77.5	61.9	100.8	74.0	74.0	70.5	72.9	61.7	71.8
α-Cellobioside hydrazide **20**	D_2O	99.0	72.3	72.8	79.9	71.6	61.7	103.6	74.2	77.1	70.6	76.7	61.0	69.6
α-Lactoside hydrazide **21**	D_2O	99.0	72.1	72.9	79.6	72.1	62.2	104.0	71.6	73.7	69.9	76.5	61.1	69.7
α-Maltoside **22**	D_2O	99.2	72.4	73.1	78.7	71.6	61.8	101.1	74.8	74.2	70.6	74.0	61.8	69.7

TABLE 3. Proton nmr data* for de-*O*-acetylated glycosides **11–22**

Compound	H-1 (ppm)	$J_{1,2}$ (Hz)	H-1′ (ppm)	$J_{1,'2'}$ (Hz)	OCH_3	CH_2CO	$—(CH_2)_6—$	*T* (°C)
β-Cellobioside, methylester **11**	4.50	7.7	4.59	7.0	3.60	2.33	1.10–1.80	85
β-Lactoside, methylester **12**	4.38	7.8	4.38	7.8	3.60	2.32	1.10–1.80	85
β-Maltoside, methylester **15**	4.44	7.7	5.28	3.4	3.65	2.35	1.10–1.80	85
α-Cellobioside, methylester **13**	4.82	3.4	4.43	7.3	3.60	2.31	1.10–1.80	31
α-Lactoside, methylester **14**	4.89	3.5	4.47	6.7	3.70	2.38	1.10–1.80	85
α-Maltoside, methylester **16**	4.85	3.6	5.33	3.3	3.63	2.31	1.10–1.80	31

*Chemical shifts are expressed relative to internal sodium 3-trimethylsilylpropionate-2,2,3,3-d_4.

^{13}C nmr parameters are recorded in Tables 1 and 2 respectively.

Preparation of 8-Ethoxycarbonyloctyl-α-lactoside 6 and Cellobioside 7

The purified 1,2-*trans*-glycosides **4** or **5** (0.82 g, 1 mmol) were dissolved in dry dichloromethane and stannic tetrachloride (0.12 mL, 1 mmol) was added. After 18 h at room temperature the reaction mixture was worked up in the usual manner. The crude syrup was purified on silica gel to yield **6** or **7** (Tables 1 and 2).

Preparation of 8-Methoxycarbonyloctyl β- and α-Glycosides (11–16)

The acetylated glycosides (**4–10**) (1.6 g, 2 mmol) in 10 mL of dry methanol were transesterified by addition of freshly prepared 0.1 *M* sodium methoxide (0.5 mL). After 18 h the solution was neutralized with Rexyn H^+ resin, filtered, and concentrated to a syrup that could be recrystallised from ethanol (Table 1). Confirmation of the expected structures was obtained by ^{13}C nmr and ^1H nmr which gave the anomeric configuration of glycosidic linkages from the chemical shift and $J_{1,2}$ coupling constants data (Table 3). Physical constants and analytical data are recorded in Table 1.

Preparation of 8-Hydrazinocarbonyloctyl β- and α-Glycosides (17–22)

The de-*O*-acetylated disaccharide glycoside (**11–16**) (518 mg) was suspended in ethanol (4 mL), a solution of 85% hydrazine hydrate (0.5 mL) was added, and the reaction was left at room temperature for 18 h. In some cases the hydrazide crystallised from the reaction mixture and in other cases solvent removal and co-distillation of hydrazine with toluene was necessary prior to crystallisation from ethanol. The physical and analytical data for these compounds are reported in Table 1. Carbon-13 nmr data (Table 2) confirmed the assigned structures.

Acknowledgements

We wish to thank Mr. J. Christ for valuable technical assistance. This work was made possible by a collaborative research project of the National Research Council of Canada and MDS Health Group Ltd. through the Pilot Industry Laboratory Programme.

1. D. R. BUNDLE. Can. J. Biochem. **57**, 367 (1979).
2. M. B. PERRY, V. DAOUST, K. G. JOHNSON, B. B. DIENA, and F. E. ASHTON. Immunobiology of *Neisseria gonorrhoeae*. *Edited by* G. F. Brooks, E. C. Gotschlich, K. K. Holmes, W. D. Sawyer, and F. E. Young. American Society of Microbiology, Washington, DC. 1978.
3. R. U. LEMIEUX, D. R. BUNDLE, and D. A. BAKER. J. Am. Chem. Soc. **97**, 4076 (1975).
4. J. BANOUB and D. R. BUNDLE. Can. J. Chem. This issue.
5. R. U. LEMIEUX and N. P. SHYLUK. Can. J. Chem. **31**, 528 (1953).
6. S. HANESSIAN and J. BANOUB. Am. Chem. Soc. Symp. Ser. **39**, 36 (1976).
7. S. HANESSIAN and J. BANOUB. Carbohydr. Res. **59**, 261 (1977).
8. C. S. HUDSON and J. M. JOHNSON. J. Am. Chem. Soc. **37**, 1270 (1915).
9. C. S. HUDSON and J. M. JOHNSON. J. Am. Chem. Soc. **37**, 1276 (1915).
10. S. HANESSIAN and J. BANOUB. Methods. Carbohydr. Chem. **8**. In press.
11. H. PAULSEN. Methods. Carbohydr. Chem. **6**, 142 (1972).
12. R. U. LEMIEUX, D. A. BAKER, and D. R. BUNDLE. Can. J. Biochem. **55**, 507 (1977).
13. A. S. PERLIN, B. CASU, and H. J. KOCH. Can. J. Chem. **48**, 2596 (1970).
14. D. E. DORMAN and J. D. ROBERTS. J. Am. Chem. Soc. **93**, 4463 (1971).

1,2-Orthoacetate intermediates in silver trifluoromethanesulphonate promoted Koenigs–Knorr synthesis of disaccharide glycosides[1]

JOSEPH BANOUB[2] AND DAVID R. BUNDLE

Division of Biological Sciences, National Research Council of Canada, Ottawa, Ont., Canada K1A 0R6

Received December 21, 1978

JOSEPH BANOUB and DAVID R. BUNDLE. Can. J. Chem. 57, 2091 (1979).

The three disaccharides lactose, cellobiose, and maltose in the form of their acetylated glycosyl bromides have been reacted with 8-ethoxycarbonyloctanol to provide the 1,2-*trans*-glycosides. Conventional Koenigs–Knorr and Helferich conditions provided these glycosides in poor yield but silver trifluoromethanesulphonate, *N,N*-tetramethylurea gave the disaccharide glycosides in 50–60% yield. Use of 2,4,6-trimethylpyridine as proton acceptor provided the corresponding 1,2-orthoacetates in 60–70% yield. These 1,2-orthoesters were rearranged by stannic tetrachloride to the 1,2-*trans*-glycosides. The isolation of acetylated 8-ethoxycarbonyloctanol from Lewis acid catalysed isomerisation of 1,2-orthoesters and from Koenigs–Knorr reactions in which *N,N*-tetramethylurea was the proton acceptor is discussed in terms of a reaction mechanism proceeding from glycosyl halide to glycosidic products via a 1,2-orthoester intermediate. This proposal is supported by ^{1}H nmr evidence for the presence of 1,2-orthoacetate in Koenigs–Knorr reaction mixtures, and by 1,2-orthoacetate isomerisation to glycoside by the conjugate acid of *N,N*-tetramethylurea.

JOSEPH BANOUB et DAVID R. BUNDLE. Can. J. Chem. 57, 2091 (1979).

Les trois disaccharides, lactose, cellobiose et maltose sous forme de bromure de glycosyles peracetylés ont été traités avec le ethoxycarbonyl-8-octanol pour produire les glycosides *trans*-1,2.

Les réactions conventionelles type Koenigs–Knorr et conditions d'Helferich ont produit ces glycosides, dans des pauvres rendements, mais la glycosidation en présence du trifluoromethanesulphonate d'argent et la tetramethyluree-*N,N* conduit aux disaccharides glycosides dans des rendements de 50–60%. L'utilisation de la trimethylpyridine-2,4,6 comme accepteur de proton conduit aux orthoesters-1,2 correspondants dans des rendements de 60–70%. Ces orthoesters-1,2 sont rearrangés par le tétrachlorure d'étain pour former les glycosides *trans*-1,2.

L'isolation de l'acetate du ethoxycarbonyl-8-octanol obtenu à partir de l'isomerisation catalysée par l'acide de Lewis des orthoesters-1,2 et des reactions de Koenigs–Knorr dans lequelles la tetramethylurée-*N,N* est l'accepteur de proton, est discuté en terme de mechanisme de reactions procedant à partir des halogenures de glycosyles pour former les glycosides *trans*-1,2 via les orthoesters-1,2 comme intermediaires. Ceci est verifié par le mise en evidence par rmn de ^{1}H de orthoesters-1,2 dans les mélanges obtenus par les réactions de Koenigs–Knorr et par l'isomérisation de orthoacetates-1,2 en glycosides par l'acide conjugée de la tetramethylurée-*N,N*.

Introduction

Disaccharide glycosides were required in order to investigate serological cross reactions between pathogenic bacteria and antibody prepared against artificial carbohydrate antigens (1, 2). Previous attempts to prepare the 1,2-*trans*-linked glycoside of lactose and the alcohol, 8-ethoxycarbonyloctanol (the alcohol used to prepare artificial antigens, via covalent attachment to proteins (3, 4)) by standard Koenigs–Knorr or Helfrich conditions resulted in very poor yields (2). Following its initial use by Kronzer and Schuerch (5) it has been demonstrated independently in two laboratories (6,7) that silver trifluoromethanesulphonate (triflate), in conjunction with an appropriate proton acceptor, is an excellent promotor of glycosylation reactions between alcohols and glycosyl halides. Consequently it was decided to prepare the disaccharide glycosides in question by this method. In the course of this work it was found that 1,2-orthoacetates are formed exclusively when the acceptor is 2,4,6-trimethylpyridine (collidine), whereas 1,2-*trans*-glycosides are the major product if the proton acceptor is *N,N*-tetramethylurea. ^{1}H nmr and chemical evidence and a consideration of the products of the latter reaction suggest that 1,2-orthoacetates are intermediates in Koenigs–Knorr reactions of acetylated glycosyl halides.

Results

Glycosylation of 8-ethoxycarbonyloctanol in dichloromethane with either acetobromolactose (**2**) or acetobromocellobiose (**1**) (8,9) was accomplished in 60–65% yield by silver triflate, *N,N*-tetramethyl-

[1]NRCC No. 17339.

[2]MDS Health Group Limited, Rexdale, Ontario.

0008-4042/79/162091-07$01.00/0

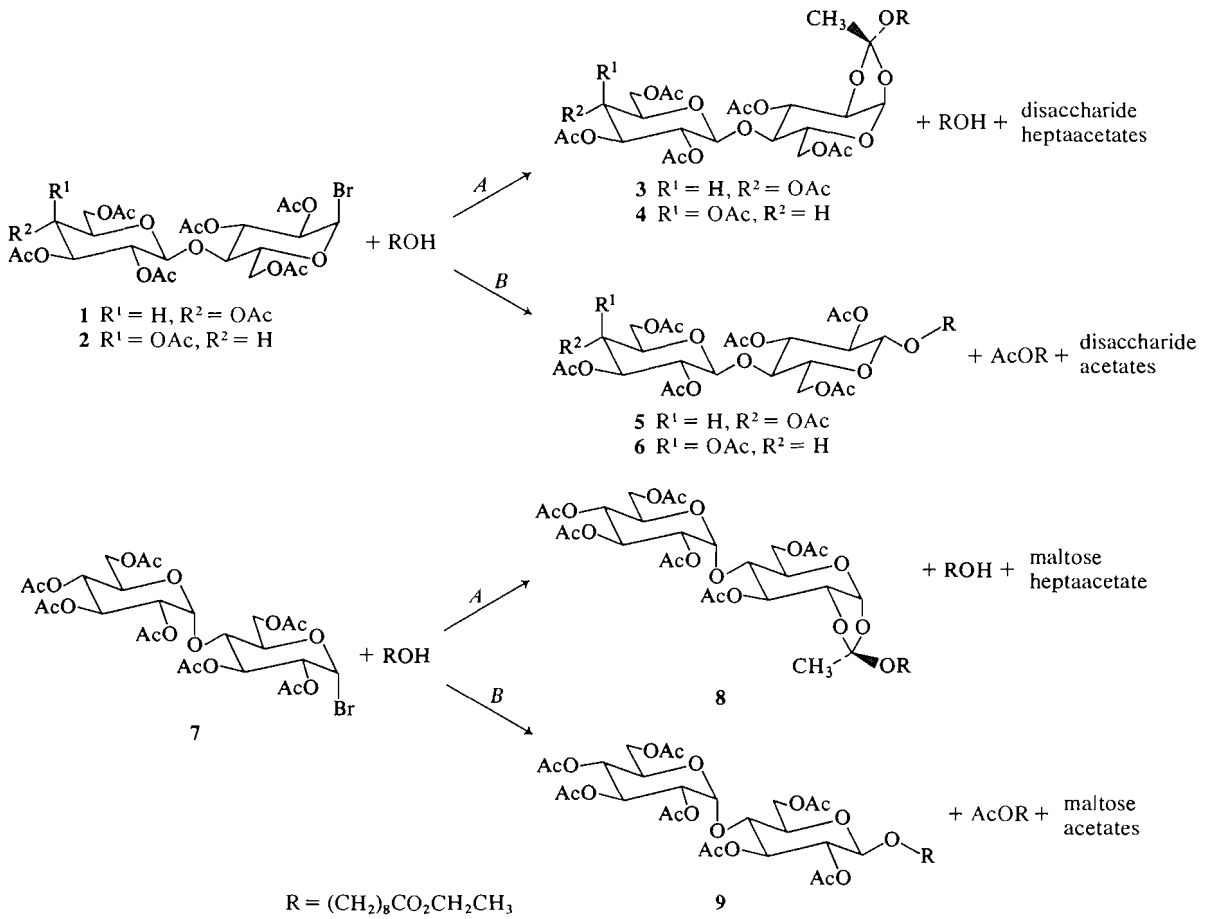

Reaction condition *A*: silver trifluoromethanesulphonate, collidine in CH_2Cl_2
Reaction condition *B*: silver trifluoromethanesulphonate, *N*,*N*-tetramethylurea in CH_2Cl_2

SCHEME 1. Synthesis of cellobiose, lactose, and maltose 1,2-orthoacetates and 8-ethoxycarbonyloctyl glycosides.

urea promoted Koenigs–Knorr reaction (6). Acetobromomaltose (**7**) (8, 9) reacted with 8-ethoxycarbonyloctanol under these conditions to provide glycoside (**9**) in 58% yield. However, when the bromo sugars **1**, **2**, and **7** were reacted with 8-ethoxycarbonyloctanol in the presence of molar quantities of silver triflate and collidine, 60–80% yields of the corresponding 1,2-orthoacetates (**3**, **4**, and **8**) resulted (Scheme 1). Under these latter conditions, which do not use the solvent quantities of hindered pyridines used in standard literature (10, 11) methods of orthoester synthesis, the only side products were unreacted alcohol and a reducing disaccharide heptaacetate. Reaction with silver triflate and *N*,*N*-tetramethylurea (rather than collidine) produced acetylated 8-ethoxycarbonyloctanol, glycoside hexaacetate(s), and reducing disaccharide hexaacetate in addition to the glycoside heptaacetates **5**, **6**, and **9**. The glycoside hexaacetate(s) exhibited tlc mobilities slightly lower than the heptaacetyl glycosides **5**, **6**, and **9**, and integration of ^1H nmr spectra indicated the presence of six acetate groups. The disaccharide hexaacetate contained no aglycon and from ^1H nmr spectra clearly contained no acetate at C-1. Although the product(s) have been assigned the 3,6,2′3′4′6′-hexa-*O*-acetylglycosyl-glucose structure(s) the ^{13}C nmr evidence for this must be considered tentative. Related products were obtained from the glycosylation reactions conducted with acetobromocellobiose (**2**) and acetobromolactose (**1**).

Similar products to those mentioned above were observed when the 1,2-orthoacetates **3**, **4**, and **8** were isomerised by acid. This isomerisation was also performed with stannic tetrachloride (12), which unlike the more general conditions (13) performed at elevated temperatures with Lewis acid or proton catalysis, proceeds at low temperature without additional quantities of alcohol (14) (Scheme 2). Stannic tetrachloride isomerisation of 1,2-orthoacetates **3**, **4**, and **8** to the glycosides **5**, **6**, and **9** gave acetylated

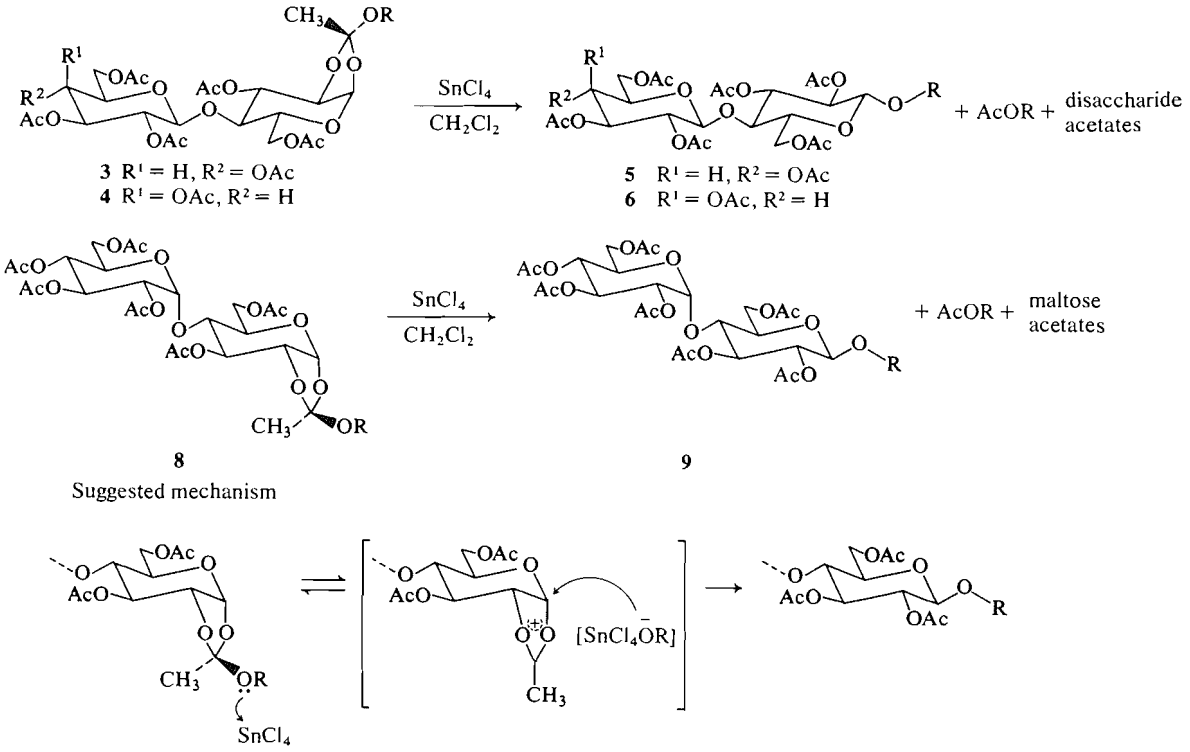

SCHEME 2. Lewis acid catalysed rearrangement of α-D-disaccharide 1,2-orthoacetate to 8-ethoxycarbonyloctyl-β-D-glycosides.

8-ethoxycarbonyloctanol, glycoside hexaacetates, and reducing disaccharide hexaacetates. This product distribution is also reported for the single-step synthesis of the 1,2-*trans*-glycosides **5**, **6**, and **9** from the corresponding 1,2-*trans*-disaccharide octaacetates (15), a process known to occur via a 1,2-acetoxonium intermediate (16).

The presence in Koenigs–Knorr reaction mixtures of acetylated aglycon is consistent with 1,2-orthoacetate intermediates during such reactions and therefore attempts were made to isomerise orthoacetates under these conditions. Glycosylations conducted with silver triflate were observed both in this and other work (17) to give a precipitate of silver halide at temperatures between −40 and −30°C. Since the net result of halide abstraction and attack of alcohol on an acetoxonium ion is formation of the conjugate acid of either *N*,*N*-tetramethylurea or collidine, it was of interest to examine the effect of these acids on 1,2-orthoacetates at low temperatures. A crystalline orthoacetate available from other work (17), 3,4-di-*O*-benzyl-β-L-rhamnose 1,2-(methyl orthoacetate) was particularly suitable for study by ^{1}H nmr, since isomerisation to glycoside would provide new signals uncomplicated by other acetate or ethoxy signals. This would not have been the case for orthoacetates **3**, **4**, or **8**. Isomerisation with *N*,*N*-tetramethylurea – triflic acid (2:1) did not occur at −70°C and only very slowly at −30°C. At −10°C a molar or 0.1 molar equivalent of this acid–base mixture gave a near quantitative yield of methyl 2-*O*-acetyl-3,4-di-*O*-benzyl-α-L-rhamnopyranoside from the 1,2-orthoacetate in 3 h. At 20°C the same isomerisation was complete after 5 min. No isomerisation of 1,2-orthoacetates was observed after several hours when a molar equivalent of triflic acid – collidine 1.02:1.0 was added to the rhamnose 1,2-orthoacetate or the cellobiose 1,2-orthoacetate (3).

When a Koenigs–Knorr reaction between tri-*O*-acetyl rhamnopyranosyl bromide and 8-ethoxycarbonyloctanol in the presence of silver triflate and *N*,*N*-tetramethylurea was quenched at −20°C, it was possible to observe by ^{1}H nmr of the crude mixture the presence of glycoside and 1,2-orthoacetate in approximately equimolar proportions. The complex ^{1}H nmr spectrum was simplified to that of 8-ethoxycarbonyloctyl-tri-*O*-acetyl-α-L-rhamnoside by addition of a catalytic amount of *N*,*N*-tetramethylurea – triflic acid to the contents of the nmr tube. A similar result was obtained when the 1,2-*cis*-glycosyl halide, tetra-*O*-acetyl-α-D-glucopyranosyl bromide was reacted in the same manner.

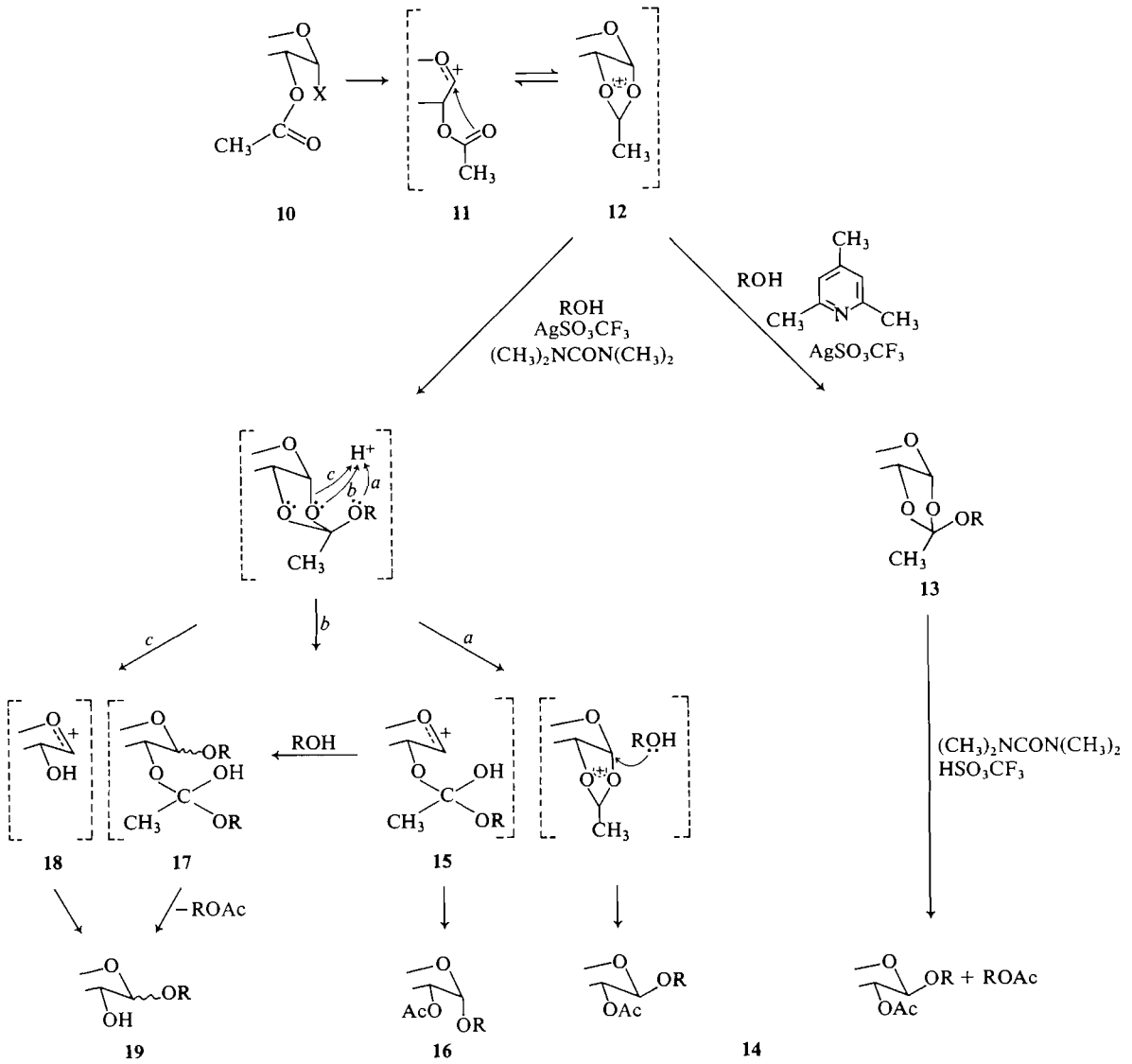

10 11 12 13 14 15 16 17 18 19

SCHEME 3. Possible mechanism for 1,2-orthoacetate intermediates leading to glycosidic products in Koenigs–Knorr reactions.

Discussion

We have demonstrated that whereas silver triflate, *N*,*N*-tetramethylurea promotes reaction between acetobromo sugars and an alcohol to yield 1,2-*trans*-glycosides (route *B*, Scheme 1), silver triflate, collidine yields the isomeric 1,2-orthoacetates (route *A*, Scheme 1). Furthermore, the conjugate acid of the proton acceptor, which results when alcohol reacts with intermediates formed from acetobromo sugars, is capable in the case of *N*,*N*-tetramethylurea, but not collidine, of catalysing the rearrangement of 1,2-orthoacetate to 1,2-*trans*-glycoside.

It is generally accepted (18) that glycosyl halides possessing a participating group at C-2 react under Koenigs–Knorr conditions to yield initially a 1,2-acyloxonium intermediate. The essential elements of these processes have been succinctly summarised by Lemieux (19) and are abbreviated in Scheme 3. The glycosyl halide under the driving force of ring oxygen participation forms an oxocarbonium–halide ion-pair **11**. Participation from an acetate at C-2 leads to an acetoxonium ion **12**. The mechanistic interpretation of the steps leading from **12** or **11** to 1,2-orthoester or glycosidic products are numerous (18, 20, and references cited therein), as are the empirical modifications used to achieve the transformation of

glycosyl halide (**10**) to glycoside (**14**). The results presented in this paper illustrate important aspects of these mechanisms and are interpreted on the basis of a 1,2-orthoester intermediate.

Attack of alcohol on the ambidentate cation **12** may occur at either the dioxolenium carbon atom, leading to 1,2-orthoacetates, or at the anomeric centre, leading to 1,2-*trans*-glycosides. Since the nature of the proton acceptors, *N*,*N*-tetramethylurea or collidine, seems unlikely to influence the site of attack when present directly in only molar ratios, the different products which result in each case are attributed to the ability of protonated *N*,*N*-tetramethylurea to isomerise the initially formed 1,2-orthoacetate. Under kinetic control (−30°C) 1,2-orthoacetates were observed, and isolated, and shown to isomerise when exposed to catalytic amounts of protonated *N*,*N*-tetramethylurea. Protonated collidine was demonstrated to be incapable of catalysing the same isomerisation even when present in molar proportion. The observation of acetylated alcohol (8-ethoxycarbonyloctanol), a frequently observed side product of Koenigs–Knorr reactions (2, 21, 22), is most convincingly explained via a 1,2-orthoacetate intermediate (cf. ref. 18).

We propose, therefore, that acetylated glycosyl halides react under Koenigs–Knorr conditions via 1,2-orthoacetate intermediates, which isomerise under proton or Lewis acid (e.g., in the case of mercuric cyanide promoted glycosylations) catalysis to yield the thermodynamic product, 1,2-*trans*-glycosides. A schematic representation of this argument is presented (Scheme 3) which is based on recent mechanistic proposals of Garegg and Kvanström (14, 23) for proton catalysed 1,2-orthoester isomerisation. In brief, the essentials of the three pathways *a*, *b*, and *c* are as follows. Protonation via pathway *a* leads by way of an acetoxium ion **12** to glycoside **14**. Pathway *b* may result after *intra*molecular rearrangement of **15** in α-glycosides, or alternatively via **17** with loss of acetylated alcohol and either α- or β-glycoside (**19**) formation. The glycosyl cation (**18**) which results from pathway *c* ultimately yields a similar product, the 2-hydroxy α- or β-glycoside (**19**). In the absence of sufficient alcohol, **18** may presumably react to give products during work-up such as the disaccharide hexaacetates observed in these studies (these products appear to be related to products obtained from 1,2-orthoesters in acidic methanol (24)). In polar solvents or at higher temperature (20°C), the direct reaction of **11** or **12** to glycoside cannot be excluded. However, when the Koenigs–Knorr reaction is performed at low temperature (−20–0°C) in weakly polar solvents, the products of kinetic control, 1,2-orthoesters, are formed initially and subsequently isomerise or 'break down' to 1,2-*trans*-glycosides and side products.

The empirical modifications of the Koenigs–Knorr reaction are many and varied (see refs. 18, 20) and several factors affect the stereochemical outcome of the reaction. Consequently an all embracing mechanism which satisfactorily explains all aspects of these reactions is still lacking. However, it has been suggested (25) in the more recent literature that 1,2-orthoester intermediates enjoy at least transient existence in such reactions, and the results reported here support this prediction. Irrespective of mechanistic aspects, silver triflate – *N*,*N*-tetramethylurea provides an excellent route to 1,2-*trans*-linked glycosides especially for alcohols which have been shown to be unreactive in the more conventional Koenigs–Knorr or Helfrich conditions. The use of silver triflate – collidine gives excellent yields of the 1,2-orthoacetates of disaccharides, which are sometimes difficult to prepare by more conventional routes (10, 11).

Experimental

Thin-layer chromatography was performed with Merck precoated silica gel 60 F-254 plates, and the detection of compounds was achieved by quenching of uv fluorescence and by charring after spraying with 5% sulphuric acid in ethanol. Silica gel G60 (70–230 mesh) and redistilled solvents were used for column chromatography. The loading on all columns was 1:50 unless otherwise indicated. Skellysolve B refers to hexane supplied by Getty Refining and Marketing Company, Tulsa, OK. Solvents were purified and dried according to standard procedures (26). Processed solutions were dried over anhydrous sodium sulphate and solvent was removed at bath temperatures 40°C or lower unless otherwise stated. Melting points were determined on a Fisher-Johns apparatus and are uncorrected. Optical rotations were measured at 589 nm in a 1 dm cell at room temperature (20–23°C). Carbon-13 and ^{1}H nmr spectra were recorded at 20 and 79.9 MHz respectively in the pulsed Fourier transform mode on a Varian CFT-20 spectrometer. Proton chemical shifts are expressed relative to 1% tetramethylsilane (TMS) in deuteriochloroform. Carbon-13 shifts are expressed relative to internal TMS in deuteriochloroform.

*3,6-Di-*O*-acetyl-4-*O*-(tetra-*O*-acetyl-*β*-*D*-glucopyranosyl)-*α*-*D*-glucopyranose 1,2-(8-Ethoxycarbonyloctyl Orthoacetate) (3)*

A solution of 8-ethoxycarbonyloctanol (1.61 g, 8 mmol) in 15 mL of dry dichloromethane containing silver triflate (2.57 g, 10 mmol) and collidine (1.21 g, 10 mmol) was cooled to −40°C. Hepta-*O*-acetyl α-D-cellobiosyl bromide (**1**) (6.4 g, 9.15 mmol) (8) in 30 mL of dichloromethane was added dropwise with stirring. After 30 min at −40°C the reaction temperature was allowed to reach 20°C and the reaction was left for 3 h at room temperature. The reaction mixture was filtered through charcoal and Celite and the filtrate was washed with 3% hydrochloric acid, saturated sodium bicarbonate, and water. After evaporation, 7.4 g of crude syrup was obtained and purified by chromatography on silica gel with the solvent mixture, ethyl acetate – Skellysolve B 1:1. Pure orthoester **3** (5.8 g, 78%) crystallised from ether – Skellysolve B, mp 85–86°C, $[\alpha]_D$ +10.3 (*c* 1.1, $CHCl_3$); ^{1}H nmr ($CDCl_3$) δ: 1.15–1.45 (m, 15H, $-(CH_2)_6-$, CH_3-CH_2), 1.69 (s, 3H, CH_3-C

TABLE 1. Lewis acid catalysed rearrangement of 1,2-orthoacetates to 8-ethoxycarbonyloctyl glycosides

1,2-Orthoacetates	1,2-*trans*-Glycosides	Yield (%)	$[\alpha]_D^{23}$ in $CHCl_3$	Melting point (°C)	$AcO(CH_2)_8CO_2Et$ (%)
4	Lactoside **6**	60	−2.4	—	22
3	Cellobioside **5**	68	−15	91–92	20
8	Maltoside **9**	58	55.8	—	20

endo), 1.85–2.13 (m, 18H, CH_3CO—), 2.25 (t, 2H, CH_2CO), 3.64 (t, 2H, CH_2O). 5.59 (d, $J_{1,2}$ = 5.5 Hz, 1H, H-1), 3.3–5.5 (remaining protons). *Anal.* calcd. for $C_{37}H_{56}O_{20}$: C 54.14, H 6.88; found: C 54.01, H 6.90.

*3,6-Di-*O*-acetyl-4-*O*-(tetra-*O*-acetyl-*β*-*D*-galactopyranosyl)-*α*-*D*-glucopyranose 1,2-(8-Ethoxycarbonyloctyl Orthoacetate) (**4**)*

The procedure was similar to that described for **3** except that alcohol (5.05 g, 25 mmol) in 30 mL of dichloromethane containing silver triflate (8.48 g, 32 mmol) and collidine (3.98 mL, 30 mmol) was reacted with hepta-*O*-acetyl-α-D-lactosyl bromide (**2**) (22.7 g, 32 mmol) (9). After chromatography (Skellysolve B – ethyl acetate 1:1), orthoester **4** (12.2 g, 62%) was obtained as a homogeneous syrup, $[\alpha]_D$ = −2.4 (*c* 3.7, $CHCl_3$); R_f 0.62, that contained C—CH_3 *endo* and *exo* isomers in the ratio 11:3; ^{1}H nmr ($CDCl_3$) δ : 1.12–1.42 (m, 15H, —$(CH_2)_6$, CH_3–CH_2), 1.52, 1.69 (S, 3H, *endo* and *exo* CH_3—C), 1.96 (s, 3H, CH_3CO), 2.03 (s, 3H, CH_3CO), 2.09 (s, 6H, CH_3CO), 2.12 (s, 3H, CH_3CO), 2.14 (s, 3H, CH_3CO), 2.25 (t, 2H, CH_2CO), 5.62 (d, $J_{1,2}$ = 5.1 Hz, 1H, H-1), 3.30–5.50 (remaining protons).

Pure **4** (1.2 g) was de-*O*-acetylated in dry methanol (5 mL) containing a catalytic amount of sodium methoxide. After 18 h amorphous crystals (650 mg) were collected; mp 168–170°C (recryst.), $[\alpha]_D$ +14.3 (*c* 3.6, methanol). *Anal.* calcd. for $C_{24}H_{42}O_{14}.H_2O$: C 50.34, H 7.75; found: C 50.65, H 7.79.

*3,6-Di-*O*-acetyl-4-*O*-(tetra-*O*-acetyl-*α*-*D*-glucopyranosyl)-*α*-*D*-glucopyranose 1,2-(8-Ethoxycarbonyloctyl Orthoacetate) (**8**)*

Hepta-*O*-acetyl-α-D-maltosyl bromide **7** (8.8 g, 12.7 mmol) (8) was added to a solution of 8-ethoxycarbonyloctanol (2.02 g, 10 mmol) containing silver triflate (3.34 g, 13 mmol) and collidine (2.5 mL, 12 mmol) under the conditions described for the preparation of orthoester **3**. After chromatography of the crude syrup (9 g) the orthoester **9** (4.9 g) was obtained as a syrup which resisted crystallisation and which by ^{1}H nmr appeared to be a mixture of isomers CH_3—C *endo*:*exo* 9:4, $[\alpha]_D$ +6.8 (*c* 7.5, $CHCl_3$); ^{1}H nmr ($CDCl_3$) δ: 1.12–1.45 (m, 15H, —$(CH_2)_6$—, CH_3CH_2), 1.58, 1.72 (s, 3H, *exo* and *endo* CH_3—C), 1.99–2.15 (m, 18H, CH_3CO), 2.27 (t, 2H, CH_2CO), 5.65 (d, $J_{1,2}$ = 5.0 Hz, 1H, H-1), 3.40–5.60 (remaining protons).

Lewis Acid Rearrangement of 1,2-Orthoacetates **3**, **4**, *and* **9** *to 1,2-*trans*-Glycosides*

General Procedure

Lewis acid, stannic tetrachloride (0.01 mL, 0.1 mmol) was added to a cooled solution of 1,2-orthoacetate (1 mmol) in dry dichloromethane 10 mL. The reaction temperature was maintained at −10°C for 30 min and the mixture was then poured into 10 mL of saturated sodium bicarbonate solution. Extraction with 20 mL of dichloromethane followed by washing of the organic phase provided crude glycosides **5**, **6**, or **9** after the usual work-up. Chromatography on silica gel with the solvent ethyl acetate – Skellysolve B 1:1 yielded pure glycosides and the acetate of 8-ethoxycarbonyloctanol (Table 1). The ^{1}H nmr data for glycosides **5**, **6**, and **9** were exactly as reported later in this section. Acetylated 8-ethoxycarbonyloctanol gave the expected nmr spectrum; ^{1}H nmr ($CDCl_3$) δ: 1.23 (t, 3H, OCH_2CH_3), 0.9–1.60 (b m, 12H, —$(CH_2)_6$—), 2.03 (s, 3H, CH_3CO), 2.26 (t, 2H, CH_2CO), 4.49 (t, 2H, OCH_2), 4.59 (q, 2H, OCH_2CH_3).

Formation of 8-Ethoxycarbonyloctyl Glycosides Using Silver Triflate and N,N*-Tetramethylurea*

*8-Ethoxycarbonyloctyl 2,3,6-Tri-*O*-acetyl-4-*O*-(tetra-*O*-acetyl-*β*-*D*-glucopyranosyl)-*β*-*D*-glucopyranoside (**5**)*

A solution of 8-ethoxycarbonyloctanol (1.01 g, 5 mmol) and *N,N*-tetramethylurea (0.6 mL, 5 mmol) in 10 mL of dry dichloromethane containing silver triflate (1.03 g, 4 mmol) was cooled to −40°C. Hepta-*O*-acetyl-α-D-cellobiosyl, bromide (**1**) (2.8 g, 4 mmol) (8) in dry dichloromethane (20 mL) was added dropwise over 15 min. After 30 min at −40°C the cooling bath was allowed to warm to 20°C and the mixture was left for a further 3 h. The suspension was filtered through a pad of Celite and charcoal and the solids were washed with dichloromethane (50 mL). The filtrate was extracted with saturated sodium bicarbonate and water. After concentration of the dried solution the crude syrup was purified by column chromatography and crystallised from ether, yield 2.23 g, 68%; mp. 91–92°C, $[\alpha]_D$ −15 (*c* 1.0, $CHCl_3$); ^{1}H nmr ($CDCl_3$) δ: 1.1–1.7 (m, 15H, —$(CH_2)_6$—, CH_3CH_2), 2.11 (m, 21H, CH_3CO), 2.24 (t, 2H, CH_2CO), 3.35–5.55 (remaining 18 protons). *Anal.* calcd. for $C_{37}H_{56}O_{20}$: C 54.14, H 6.88; found: C 53.96, H 6.92. Elution of the column after the glycoside was obtained yielded components with ^{1}H and ^{13}C nmr consistent with disaccharide hexaacetates.

*8-Ethoxycarbonyloctyl 2,3,6-Tri-*O*-acetyl-4-*O*-(tetra-*O*-acetyl-*β*-*D*-galactopyranosyl)-*β*-*D*-glucopyranoside (**6**)*

The reaction was carried out on a 4 mmol scale as described for glycoside **5** using hepta-*O*-acetyl-α-D-lactosyl bromide (**2**) (9). Column chromatography gave **6** as a pure syrup (2.03 g), 62%; $[\alpha]_D$ −11.2 (*c* 2.0, $CHCl_3$); ^{1}H nmr ($CDCl_3$) δ: 1.10–1.80 (m, 15H, —$(CH_2)_6$—, CH_3CH_2), 1.93, 2.02, 2.05, 2.07 (s, 21H, CH_3CO), 2.26 (t, 2H, CH_2CO), 3.25–5.55 (remaining 18 protons).

In addition, acetylated 8-ethoxycarbonyloctanol was isolated in 20% yield together with a lactose hexaacetate whose ^{13}C nmr gave C-1(α) 90.0, C-1(β) 95.1, and C-1′(β) 101.0, which is consistent with a reducing disaccharide hexaacetate lacking an acetate at C-2.

*8-Ethoxycarbonyloctyl 2,3,6-Tri-*O*-acetyl-4-*O*-(tetra-*O*-acetyl-*α*-*D*-glucopyranosyl)-*β*-*D*-glucopyranoside (**9**)*

The bromide **7** (4 mmol) (8) was reacted with 8-ethoxycarbonyloctanol in the manner described for glycoside **5**. The glycoside **9** (1.93 g) crystallised from ether and Skellysolve B, mp 63–64°C, $[\alpha]_D$ 39.1 (*c* 1.0, $CHCl_3$); ^{1}H nmr ($CDCl_3$) δ: 1.10–1.80 (m, 15H, —$(CH_2)_6$—, CH_3CH_2), 1.97, 2.00, 2.02, 2.06, 2.10 (s, 21H, CH_3CO), 2.25 (t, 2H, CH_2CO), 3.25–5.55 (remaining 18 protons). *Anal.* calcd. for $C_{37}H_{56}O_{20}$: C 54.14, H 6.88; found: C 53.96, H 6.92.

In addition, a compound with the properties of a hexaacetate was isolated by continued elution after **9** had been eluted from the silica column. The ^{13}C nmr showed no aglycon signals and anomeric signals C-1′(α) 95.5, C-1(β) 94.8, and C-1(α) 89.8 ppm. The intensity of these signals were respec-

tively 8:5:3; ^{1}H nmr gave acetate signals and ring protons only in the ratio 18:16.

Observation of 1,2-Orthoester Intermediates by ^{1}H Nuclear Magnetic Resonance

8-Ethoxycarbonyloctanol (600 mg, 3 mmol) was dissolved in dry dichloromethane (7 mL) containing silver triflate (770 mg, 3 mmol) and *N,N*-tetramethylurea (0.72 mL, 6 mmol). The mixture was cooled to −40°C and 3 mL of a dichloromethane solution containing 2,3,4-tri-*O*-acetyl-α-L-rhamnopyranosyl bromide (1.02 g, 2.89 mmol) (16) was added dropwise over 15 min. The reaction was maintained between −20 and −30°C for 3 h and a mixture of water (1 mL) and triethylamine (1 mL) were added to quench the reaction. The reaction was poured into dichloromethane (10 mL), filtered through a pad of Celite, and then washed with sodium bicarbonate and water. After drying the syrup under high vacuum the ^{1}H nmr was recorded; ^{1}H nmr ($CDCl_3$) δ: 1.08–1.50 (m, $-(CH_2)_6-$, CH_3CH_2, H-6) 1.64 (s, *endo* CH_3C), 1.90 (s, CH_3CO) 1.97 (b s, CH_3CO), 2.03 (b s, CH_3CO).

To the nmr tube containing the crude syrup, one drop of a solution containing *N,N*-tetramethylurea – triflic acid 2:1 (the solution was 1 *M* with respect to acid) was added and the ^{1}H nmr was rerun. The orthoester C—CH_3 peak δ 1.64 was no longer evident and the multiplet complex due to acetate signals had simplified to 3 singlets. The chemical shifts of these signals were identical to those obtained with an authentic sample of 8-ethoxycarbonyloctyl 2,3,4-tri-*O*-acetyl-α-L-rhamnopyranoside (27); ^{1}H nmr ($CDCl_3$) δ: 1.08–1.80 (m, $-(CH_2)_6-$, CH_3CH_2, H-6) 1.94 (s, CH_3CO), 2.00 (s, CH_3CO), 2.10 (s, CH_3CO), 2.25 (t, CH_2CO), 3.30–5.50 (remaining protons).

Reaction of 1,2-Orthoesters with N,N-Tetramethylurea/ Collidine–Triflic Acid

The orthoacetate, 3,4-di-*O*-benzyl-β-L-rhamnose-1,2-(methyl orthoacetate) (1 mmol) in dichloromethane (5 mL) was reacted with 1 mL of *N,N*-tetramethylurea – triflic acid 2:1 (the solution made up in dichloromethane was 1 *M* with respect to triflic acid) at room temperature. After 5 min tlc (Skellysolve B – ethyl acetate 3:1) showed complete reaction to the corresponding glycoside. The reaction was repeated on a small scale in a nmr tube using deuteriochloroform as solvent. The glycoside, methyl 2-*O*-acetyl-3,4-di-*O*-benzyl-α-L-rhamnopyranoside, had ^{1}H nmr ($CDCl_3$) δ: 1.38 (d, $J_{5,6}$ = 6.0 Hz, 3H, H-6), 2.17 (s, 3H, CH_3CO), 3.37 (s, 3H, OCH_3), 3.88 (d d, $J_{2,3}$ = 4 Hz, $J_{3,4}$ = 10 Hz, 1H, H-3), 5.32 (d d, $J_{1,2}$ = 2 Hz, $J_{2,3}$ = 4 Hz, 1H, H-2), 7.34 (b s, 10H, ϕCH_2), 3.35–5.00 (remaining protons). Isomerisation of 1,2-orthoacetate to glycoside was essentially quantitative.

The experiment described above was repeated with 0.1 mmol of *N,N*-tetramethylurea triflic acid with similar results. When this was repeated at −10°C the reaction took 3 h to reach completion. At −70 and −30°C no detectable rearrangement had occurred after 4 h. In these instances reactions were quenched with excess triethylamine.

The rhamnose orthoacetate (1 mmol) was reacted with 1 mmol of collidine – triflic acid 1:1 (1 *M* in dichloromethane) for 4 h at room temperature. After this period tlc showed only starting material, which was confirmed by a similar experiment performed in a nmr tube. The nmr parameters for the 3,4-di-*O*-benzyl-β-L-rhamnose-1,2-(methyl orthoacetate) were ^{1}H nmr ($CDCl_3$) δ: 1.31 (d, $J_{5,6}$ = 5.8 Hz, 3H, H-6), 1.73 (s, 3H, CH_3CO), 3.29 (s, 3H, OCH_3), 3.27–3.79 (m, 3H, H-3, H-4, H-5), 4.40 (d d $J_{2,3}$ = 3.7 Hz, $J_{1,2}$ = 2.4 Hz, 1H, H-2), 4.58–5.02 (m, 4H, ϕCH_2), 5.28 (d, $J_{1,2}$ = 2.4 Hz, 1H, H-1), 7.34 (b s, 10H, ϕCH_2).

The cellobiose 1,2-orthoacetate was treated with *N,N*-tetramethylurea – triflic acid 2:1 and also collidine – triflic acid 1:1.02 in the manner described for the rhamnose orthoacetate. With collidine – triflic acid the two C—CH_3 (*exo* and *endo*) signals at δ 1.61 and δ 1.69 remained unchanged after 4 h. *N,N*-Tetramethylurea – triflic acid caused these signals to disappear after 5 min at room temperature. In addition the H-1 doublet δ $J_{1,2}$ = 5 Hz also disappeared indicating reaction of the orthoester.

Acknowledgements

We wish to thank Mr. J. Christ for technical assistance. The larger portion of this work was made possible by a collaborative research project of the National Research Council of Canada and MDS Health Group Ltd. through the Pilot Industry Laboratory Program. We would like to thank Dr. Klaus Bock for constructive criticism of our original manuscript.

1. D. R. BUNDLE. Abstracts of Papers, IXth International Symposium on Carbohydrate Chemistry, London, England. 1978. p. 373.
2. D. R. BUNDLE. Can. J. Biochem. 57, 367 (1979).
3. R. U. LEMIEUX, D. R. BUNDLE, and D. A. BAKER. J. Am. Chem. Soc. **97**, 4076 (1975).
4. R. U. LEMIEUX, D. A. BAKER, and D. R. BUNDLE. Can. J. Biochem. **55**, 507 (1977).
5. F. J. KRONZER and C. SCHUERCH. Carbohydr. Res. **27**, 379 (1973).
6. S. HANESSIAN and J. BANOUB. Am. Chem. Soc. Symp. Ser. **39**, 36 (1976); Carbohydr. Res. **53**, C13 (1977).
7. R. U. LEMIEUX, T. TAKEDA, and B. Y. CHUNG. Am. Chem. Soc. Symp. Ser. **39**, 90 (1976).
8. J. K. DALE. J. Am. Chem. Soc. **38**, 2187 (1916).
9. C. S. HUDSON and A. KUNZ. J. Am. Chem. Soc. **47**, 2052 (1925).
10. R. U. LEMIEUX and A. R. MORGAN. Can. J. Chem. **43**, 2199 (1965).
11. M. MAZUREK and A. S. PERLIN. Can. J. Chem. **43**, 1918 (1965).
12. S. HANESSIAN and J. BANOUB. Carbohydr. Res. **44**, C14 (1975).
13. N. K. KOCHETKOV, A. J. KHORLIN, and A. F. BOCHKOV. Tetrahedron, **23**, 693 (1967).
14. P. J. GAREGG and I. KVANSTRÖM. Acta Chem. Scand. B, **30**, 655 (1976).
15. J. BANOUB and D. R. BUNDLE. Can. J. Chem. This issue.
16. S. HANESSIAN and J. BANOUB. Methods Carbohydr. Chem. **8**, In press.
17. D. BUNDLE and S. JOSEPHSON. Can. J. Chem. **57**, 662 (1979).
18. G. WULFF and G. RÖHLE. Angew. Chem. **13**, 157 (1974).
19. R. U. LEMIEUX, K. B. HENDRIKS, R. V. STICK, and K. JAMES. J. Am. Chem. Soc. **97**, 4056 (1975).
20. K. IGARASHI. Adv. Carbohydr. Chem. Biochem. **34**, 243 (1977).
21. R. U. LEMIEUX. Chem. Can. **16**, 14 (1964).
22. G. WULFF, G. RÖHLE, and U. SCHMIDT. Chem. Ber. **105**, 1111 (1972).
23. P. J. GAREGG and I. KVANSTRÖM. Acta. Chem. Scand. B, **31**, 509 (1977).
24. A. S. PERLIN. Can. J. Chem. **41**, 555 (1963).
25. R. U. LEMIEUX and T. L. NAGABHUSHAN. Methods Carbohydr. Chem. **6**, 487 (1972).
26. D. D. PERRIN, W. L. ARAMAREGO, and D. R. PERRIN. Purification of laboratory compounds. Pergamon Press, London. 1966.
27. S. JOSEPHSON and D. R. BUNDLE. J. Chem. Soc. Perkin Trans. I. In press.

The oxidation potentials of *cis*- and *trans*-1,2-diphenylcyclopropane and *cis*- and *trans*-2,3-diphenyloxirane[1]

D. R. ARNOLD[2] AND P. C. WONG

Photochemistry Unit, Department of Chemistry, University of Western Ontario, London, Ont., Canada N6A 5B7

Received January 19, 1979

D. R. ARNOLD and P. C. WONG. Can. J. Chem. 57, 2098 (1979).

The oxidation potentials of *cis*- and *trans*-1,2-diphenylcyclopropane (**1**) and *cis*- and *trans*-2,3-diphenyloxirane (**2**) have been determined by cyclic voltammetry, spectroscopically (using an empirical correlation of the long wavelength transition of the charge-transfer complexes with tetracyanoethylene) and by using an empirical correlation based upon the gas phase ionization potentials measured by photoelectron spectroscopy. The values obtained by these three very different techniques agree to within ± 0.15 V. The results are interpreted in terms of the initial formation of the phenyl radical cation with the three-membered ring intact. The higher oxidation potentials of *cis*- and *trans*-**2**, relative to those of *cis*- and *trans*-**1**, are attributed to inductive electron withdrawal from the phenyl group by the oxygen of the oxirane ring. The relevance of these results to the photosensitized (electron transfer) behaviour of these compounds is discussed.

D. R. ARNOLD et P. C. WONG. Can. J. Chem. 57, 2098 (1979).

Faisant appel à de la voltamètrie cyclique, on a déterminé les potentiels d'oxydation des diphényl-1,2 cyclopropanes-*cis* et -*trans* (**1**) et des diphényls-2,3 oxiranne-*cis* et -*trans* (**2**) en utilisant une corrélation empirique de la transition à la grande longueur d'onde des complexes de transfert de charge avec le tétracyanoéthylène et en utilisant une corrélation empirique basée sur les potentiels d'ionisation en phase gazeuse tels que mesurés par spectroscopie photoélectronique. Les valeurs obtenues par ces trois techniques très différentes ne diffèrent que par ± 0.15 V. On interprète les résultats en termes de la formation initiale d'un radical cation phényle avec le cycle à trois chaînons intact. On attribue le fait que les potentiels d'oxydation des produits **2**-*cis* et *trans* sont plus élevés que ceux des produits **1**-*cis* et *trans* à une électro-attraction par l'oxygène du cycle oxiranne qui retire des électrons du phényle. On discute de la relation entre ces résultats et leur comportement photosensibilisé (transfert d'électron).

[Traduit par le journal]

Introduction

We have recently reported the photosensitized (electron transfer) *cis–trans* isomerization of 1,2-diphenylcyclopropane (**1**) (*1a*) and 2,3-diphenyloxirane (**2**) (2). The key step in the mechanism we proposed for these reactions involves electron transfer from the phenyl ring of the cyclopropane or oxirane to the sensitizer singlet excited state. Ring-opened intermediates resulting from cleavage of the cyclopropane or oxirane radical cation, followed by back electron transfer, and subsequent reclosure of the ring allow for the isomerization. We were particularly surprised by the observation that both 1-cyanonaphthalene (**3**) and 1,4-dicyanonaphthalene (**4**) were effective sensitizers for the cyclopropane isomerization; however, while the oxirane isomerization could be sensitized by **4**, **3** was ineffective. Photophysical studies confirmed the involvement of the sensitizer singlet and gave a further indication of the sensitizer–quencher specificity. The fluorescence of **4** was quenched by both *trans*-**1** and *trans*-**2**, while the fluorescence of **3**, which was quenched by *trans*-**1**, was not measurably quenched by *trans*-**2**. The measured fluorescence quenching rate constants are summarized in Table 1.

To account for these results we proposed that the electron transfer step, involving **2** and the excited state of **3**, was uniquely inefficient in this series. We supported this explanation with an estimate of the free-energy (ΔG) for the electron transfer process which was based upon the Weller equation (Table 1); electron transfer from **2** to the singlet excited state of **3** is not favorable. Application of the Weller equation required measurement of the oxidation potentials ($E_{1/2}^{ox}$) of **1** and **2**. These we obtained by cyclic voltammetry. However, analysis of the cyclic voltammagrams clearly indicated that the anodic electron transfer processes were irreversible, and therefore the measured oxidation potentials do not have thermodynamic significance.

[1]Contribution No. 213 from the Photochemistry Unit. This article is dedicated to Professor E. Havinga, on the occasion of his 70th birthday (May 7, 1979).

[2]Address correspondence to this author, Department of Chemistry, Dalhousie University, Halifax, N.S., Canada B3H 4J3.

0008-4042/79/162098-05$01.00/0

TABLE 1. Measured fluorescence quenching rate constants and calculated free energy for the electron transfer processes between the singlet excited states of 1-cyanonaphthalene (**3**) and 1,4-dicyanonaphthalene (**4**) and *trans*-1,2-diphenylcyclopropane (*trans*-**1**) and *trans*-2,3-diphenyloxirane (*trans*-**2**)

Fluorescer	Quencher	k_q (s^{-1} M^{-1})	ΔG (kcal mol^{-1})[a]
3	*trans*-**1**	1.38×10^{10}	−9.3
	trans-**2**	$<3\times10^{7}$[b]	+6.4
4	*trans*-**1**	1.50×10^{10}	−21.5
	trans-**2**	1.16×10^{10}[b]	−6.8

[a]Using the Weller equation $\Delta G = 23.06[E(D/D^+)_V - E(A/A^-)_V - e_0^2/\varepsilon\alpha] - \Delta^1E_{0,0}$ (kcal mol^{-1}), ref. 3. The redox potentials employed are: $E_{1/2}{}^{ox}$ for *trans*-**1** (1.2 V), *trans*-**2** (1.8 V) and $E_{1/2}{}^{red}$ for **3** (−2.33 V) (ref. 4*a*) and **4** (−1.67 V) (ref. 4*a*) vs. $Ag/AgNO_3$ in acetonitrile. The Coulombic attraction term is −1.3 kcal mol^{-1} while the singlet energy of the acceptors are **3** (89.4 kcal mol^{-1}) (ref. 4*a*) and **4** (86.4 kcal mol^{-1}) (ref. 4*a*).
[b]Ref. 2.

Unfortunately, it is not unusual for the interesting electron transfer processes to be irreversible at the electrode; nevertheless, potentials based upon such data have been used and in fact seem to give meaningful correlations (1, 2, 4).

In view of the growing importance of the Weller equation, and similar semi-empirical treatments for the correlation of photophysical and photochemical behaviour which involves electron transfer processes, it is becoming increasingly desirable to have some convenient method for obtaining meaningful oxidation potentials.

We report here the comparison of the oxidation potentials of **1** (*cis*- and *trans*-) and **2** (*cis*- and *trans*-) determined by three very different techniques; (*1*) cyclic voltammetry, where the electron transfer processes are not reversible; (*2*) spectroscopically, using an empirical correlation of the long wavelength transitions of the charge-transfer complexes with tetracyanoethylene (TCNE); and (*3*) using an empirical correlation based upon the gas phase ionization potentials measured by photoelectron spectroscopy. We found acceptable (±0.15 V) agreement between the oxidation potentials of these four compounds using these three methods which, therefore, gives us confidence that the data are meaningful. There are advantages and disadvantages for each of these techniques.

Cyclic voltammetry provides the best in accuracy among these methods; however, complication does arise when the oxidation process is irreversible. Charge-transfer complex measurement provides the simplest method in obtaining reversible oxidation potentials, but the accuracy is hampered by uncertainty in determining the maximum of a broad structureless absorption band and sometimes further complicated in cases of overlapping bands. There has been a dramatic improvement in instrumentation for photoelectron spectroscopy over the past decade; however, on our instrument it is still difficult to get good resolution for large non-volatile molecules. Furthermore, the estimate of oxidation potential is very sensitive to relatively small error in determining the peak position.

Results and Discussion

The cyclic voltammagrams of all four compounds, **1** (*cis* and *trans*) and **2** (*cis* and *trans*), measured in acetonitrile solution using a platinum working electrode and a $Ag/AgNO_3$ (0.1 *M*) reference electrode, were typical of irreversible oxidative electron transfer. No reduction wave was observed upon scanning the voltage from 0 to −2.2 V which is the practical limit of this solvent–electrolyte system. The oxidation potentials ($E_1/_2{}^{ox}$) were estimated as 0.03 V less than the peak position of the voltammagrams using a 100 mV/s sweep rate. These results are summarized in Table 2.

Pysch and Yang have shown that a linear relationship exists between the absorption energy of the charge-transfer complex (ΔE_{CT}) and the oxidation potential ($E_1/_2{}^{ox}$) for a series of aromatic electron donors with 2,4,7-trinitrofluorenone-9 as the electron acceptor (6*a*). They established the empirical relationship

$$E_1/_2{}^{ox} = \Delta E_{CT} + \Delta E_{solv} + \text{constant}$$

where the difference in the solvation term (ΔE_{solv}) is assumed to be constant with a given electron acceptor (6). The absorption energy of the charge-transfer complex (ΔE_{CT}) is taken as the maximum of the long wavelength charge-transfer transition.

The charge-transfer transition of the complex between **2** with trinitrofluorenone would be partially obscured by the long wavelength absorption tail of the acceptor; so tetracyanoethylene was chosen as the acceptor in this study. Solutions (methylene chloride) of all four compounds and the strong electron acceptor tetracyanoethylene were visibly coloured due to the charge-transfer transitions. The visible spectra of these solutions had, in the case of both *cis*- and *trans*-**1**, two obvious, broad, structureless maxima. These overlapping bands were resolved by using a Gaussian–Lorentzian curve fitting computer program. Only one long wavelength maximum was observed in the visible spectra of solutions of both *cis*- and *trans*-**2** under these conditions. The positions of the maximum of these transitions are listed in Table 2. Solutions (methylene chloride) of **1** and **2** with dichloromaleic anhydride (another common acceptor) had absorption at long wavelength due to the charge-transfer complexes, but no distance maximum could be observed. The

TABLE 2. Half-wave oxidation potentials of **1** and **2** determined by various methods

Compound	$E_{1/2}{}^{ox}$ (V)[a]	ΔE_{CT} (kK)[b] (estimated $E_{1/2}{}^{ox}$ (V))	IP (eV)[c] (estimated $E_{1/2}{}^{ox}$ (V))
trans-**1**	1.17[d]	19.58 (1.34)	8.32 (1.31)
cis-**1**	1.41	20.00 (1.39)	8.64 (1.60)
trans-**2**	1.71[e]	26.32 (2.00)	8.90 (1.83)
cis-**2**	1.77[e]	25.45 (1.92)	9.12 (2.03)

[a]Refers to $Ag/AgNO_3$ (0.1 *M*) electrode in acetonitrile.
[b]With TCNE as the acceptor in methylene chloride solution.
[c]First vertical IP.
[d]The reported value is 1.09 V vs. $Ag/AgNO_3$ electrode. See ref. 5.
[e]The previous reported values are 1.9 V and 1.8 V for *trans*-2 and *cis*-2, respectively. See ref. 2.

TABLE 3. Charge-transfer complex absorption of the donors with dichloromaleic anhydride (DCMA)

Compound	Expected λ_{max}[a] (nm)	Onset of absorption[b] (nm)
trans-**1**	373	430
cis-**1**	344	400
trans-**2**	303	370
cis-**2**	295	370

[a]Estimated from values of ΔE_{CT} and $E_{1/2}{}^{ox}$ as given in refs. 8, 9.
[b]Values obtained from uv-visible spectra of the donors (55 m*M*) plus DCMA (18 m*M*) in methylene chloride.

approximate onset of the long wavelength absorptions and the positions (calculated) of the charge-transfer maxima are listed in Table 3.

Fortunately, there has been a sufficient number of maxima for the charge-transfer transitions of various donors complexed with TCNE reported in the literature. We summarize these data, along with the reliable oxidation potentials of the donors, in Table 4. The plot of these data, shown in Fig. 1, has the expected linear relationship represented by [1].

$$[1] \quad E_{1/2}{}^{ox} = 0.095\Delta E_{CT}\,(\text{kK}) - 0.455\ \text{V}$$

From [1] and the observed maximum of the long wavelength transition of the charge-transfer complex between *cis*- and *trans*-**1** and *cis*- and *trans*-**2** with TCNE, estimates of the oxidation potentials were obtained. These are listed in Table 2.

The results from the photoelectron spectra (Fig. 2) of *cis*- and *trans*-**1** and *cis*- and *trans*-**2** are summarized in Table 5. The first (i.e., lowest energy) distinct peak is sharp for all four compounds. This transition can be assigned to the lowest vertical ionization potential (IP) associated with removal of a π-electron of a phenyl ring. Several additional bands are observed below ca. 11 eV which can be attributed to ionization of lower-lying π-electrons. Near 11 eV there is a steep onset of a broad, structured plateau which represents unresolved ionizations from closely spaced σ (and perhaps π) orbitals.

The oxiranes show an additional feature, a doublet peak near 10.4 eV, which we attribute to ionization from the lone pair electrons on oxygen. The comparable transitions are observed near 10.57 eV in the photoelectron spectra of the parent

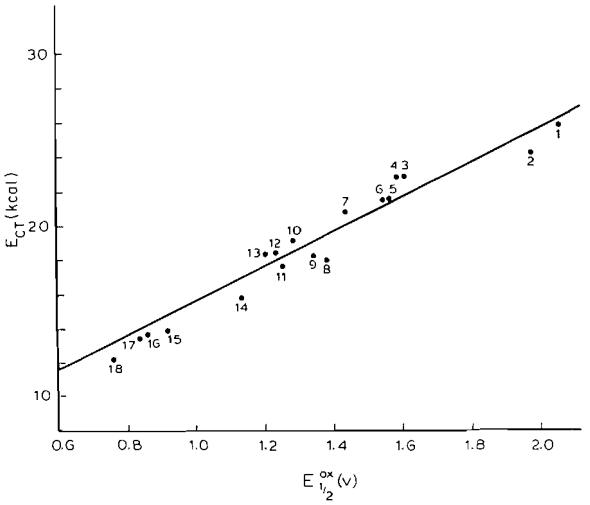

FIG. 1. The absorption energy of the charge-transfer complex (ΔE_{CT}) with TCNE as acceptor vs. the half-wave oxidation potentials of the donors.

TABLE 4. Charge-transfer absorption energy (ΔE_{CT}) with tetracyanoethylene (TCNE) and half-wave oxidation potential ($E_{1/2}{}^{ox}$) of various donors

	Donor	ΔE_{CT} (kK)[a]	$E_{1/2}{}^{ox}$ (V)[b]
1	Benzene	25.8	2.04
2	Toluene	24.2	1.96
3	*m*-Xylene	22.8	1.60
4	*o*-Xylene	22.8	1.58
5	Mesitylene	21.4	1.55
6	*p*-Xylene	21.4	1.54
7	Durene	20.8	1.43
8	Triphenylene	18.0[c]	1.35
9	Naphthalene	18.2	1.34
10	Pentamethylbenzene	19.2	1.28
11	Fluorene	17.7[c]	1.25
12	Phenanthracene	18.5	1.23
13	Hexamethylbenzene	18.4	1.20
14	Chrysene	15.9[c]	1.13
15	Benzo[*a*]anthracene	13.9[d]	0.92
16	Pyrene	13.7	0.86
17	Anthracene	13.2[c]	0.84
18	Benzo[*a*]pyrene	12.2[d]	0.76

[a]The common acceptor is TCNE in methylene chloride solution unless otherwise mentioned. Values taken from ref. 10.
[b]Values taken from ref. 9 refer to $Ag/AgClO_4$ reference electrode in acetonitrile (corrected to the $Ag/AgNO_3$ system by subtracting 0.05 V).
[c]Solvent was carbon tetrachloride.
[d]Solvent was chloroform.

molecule, ethylene oxide (*7a*), and a doublet at ca. 10.5 eV for the phenyloxirane (*7b*).

The expression which relates gas phase ionization potential with the oxidation potential in solution is given in [2] (*6b*). This can be simplified to [3] (6) if all the terms on the right, except the ionization potential, are either relatively small or constant.

$$[2]\quad E_{1/2}^{ox} = \alpha IP + \Delta E_{solv} - \beta EA - \frac{T\Delta S}{F} - \frac{RT}{F} \times \ln \frac{F_0^+ D_R}{F_R D_0^+} + \text{constant}$$

$$[3]\quad E_{1/2}^{ox} = aIP + b$$

The reported values for the constants a and b in [3] vary to some extent depending on the choice of compounds included. The most extensive study has been reported by Miller and co-workers (9) where $a = 0.89$ and $b = -6.04$. When these values are used, along with the first vertical ionization potentials of *cis*- and *trans*-**1** and *cis*- and *trans*-**2**, in [3], the oxidation potentials listed in Table 2 were obtained.

The agreement between the oxidation potentials of *cis*- and *trans*-**1** and *cis*- and *trans*-**2**, obtained by the three techniques (Table 2) is remarkably good considering the experimental limitations and the empirical treatment of the data. We have very little basis for choosing the best values and therefore accept the data from the cyclic voltammetric study.

The larger oxidation potential of *cis*- and *trans*-**2**, relative to *cis*- and *trans*-**1**, can be explained in terms of inductive withdrawal of electrons from the phenyl rings by the more electronegative oxygen of the oxirane ring, relative to the methylene group of the cyclopropane.

It seems likely that, in both cases **1** and **2**, the initially formed radical cations have the ring-closed structure which, from the observed chemical behaviour, must subsequently open to the 1,3-radical cation (1, 2). If the ring cleavage processes were concurrent with oxidation, we would have expected that the greater stability of the α-oxycarbonium ion would have been reflected in a lower oxidation potential for the oxiranes relative to the cyclopropanes.

The oxidation potentials of the *cis*-isomers are (assuming one exceptional determination) slightly (<ca. 0.2 V) greater than those of the *trans*-isomers. This is additional evidence against direct formation of an identical ring-opened radical cation from both configurations, since it is firmly established that the *trans*-isomers are thermodynamically more stable than the *cis*-isomers (11). This is consistent with the results of a photoionization and ion cyclotron resonance study of the parent system ethylene oxide,

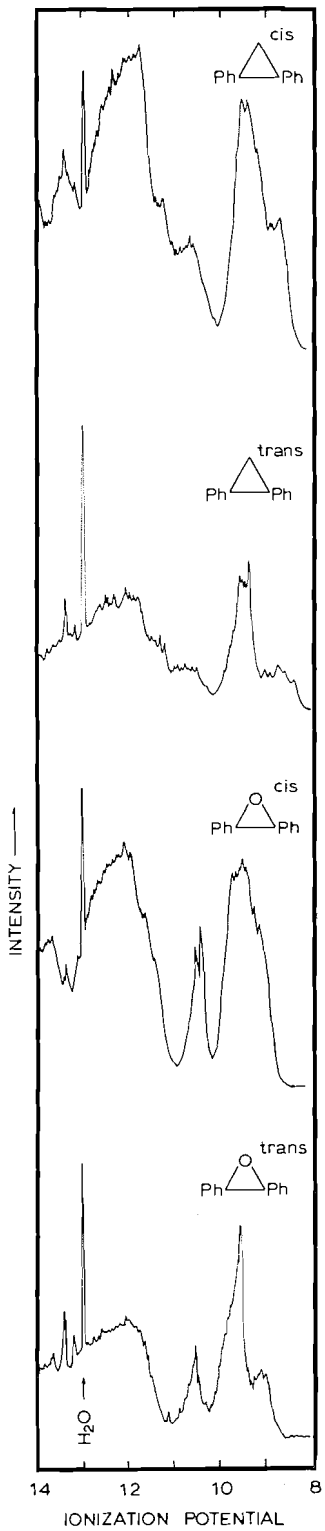

FIG. 2. The photoelectron spectra of *cis*- and *trans*-1,2-diphenylcyclopropane (**1**) and *cis*- and *trans*-2,3-diphenyloxirane (**2**).

TABLE 5. Photoelectron peaks

Compound	Adiabatic (eV)	Vertical (eV)	Assignment
trans-**1**	8.05	8.32	1st IP
	—	8.74	Lower-lying π
	—	9.34	Lower-lying π
	11.60	—	σ or π onset
cis-**1**	8.20	8.64	1st IP
	—	9.37	Lower-lying π
	11.40	—	σ or π onset
trans-**2**	8.60	8.90	1st IP
	—	9.06	Lower-lying π
	—	9.56	Lower-lying π
	10.20	10.50	n of oxygen
	11.20	—	σ or π onset
cis-**2**	8.68	9.12	1st IP
	—	9.46	Lower-lying π
	10.20	10.39	n of oxygen
	11.00	—	σ or π onset

where the parent radical ion is formed by removal of an electron which, in this case, is largely localized on the oxygen atom (12).

Conclusions

The similarity in the oxidation potentials of **1** (*cis* and *trans*) and **2** (*cis* and *trans*) determined by these three different techniques gives us confidence that the values determined by cyclic voltammetry are useful, even though the anodic electron transfer process is irreversible. We must, however, caution against the use of this type of data generally, and we emphasize the utility of analysis of the CT transition and photoelectron spectroscopy as alternative techniques.

We now have additional confidence in the proposed explanation that the inefficiency of the isomerization of *cis*- and *trans*-**2** with **3** as a photosensitizer is the result of the unfavourable electron transfer process.

Experimental

Methylene chloride (Fischer spectroscopic grade) was dried with anhydrous calcium chloride, distilled from phosphorous pentoxide, and stored over a 4A molecular sieve. Acetonitrile (Aldrich Gold Label) was refluxed over calcium hydride under a dry nitrogen atmosphere and distilled. The stilbene oxides were prepared by oxidation of the corresponding stilbene with *m*-chloroperbenzoic acid in chloroform at room temperature (13). The *trans*-isomer was purified by recrystallization, first from methyl alcohol and then twice from cyclohexane. The *cis*-isomer was purified by two recrystallizations from hexanes and was then passed through a column of neutral alumina (Fischer) eluting with cyclohexane and was finally recrystallized once more from hexanes. The isomers were pure as observed by uv and vapour phase chromatography (vpc) (10% SE 30 on on Chromosorb W 60/80, 5 ft at 180°C). The 1,2-diphenylcyclopropanes were prepared following the method described in the literature (14). They were purified by chromatography on a column of silica gel eluting with hexanes and were then separated by preparative vpc (10% DEGS on Chromosorb W 60/80, 6 ft at 180°C). For uv studies, a final purification was performed by passing each isomer through a column of neutral alumina eluting with cyclohexane. Dichloromaleic anhydride was twice vacuum sublimed, recrystallized from methylene chloride, and stored under vacuum. Tetracyanoethylene was recrystallized twice from chlorobenzene and was then twice vacuum sublimed before use.

Spectrophotometric measurements were carried out on a Cary 118 spectrophotometer. All spectra were taken immediately after the solutions were prepared. No reaction between any of the donor–acceptor pairs in methylene chloride was observed (monitoring with vpc and thin layer chromatography). The concentration of dichloromaleic anhydride was 18 m*M* and tetracyanoethylene was 12 m*M*. The concentration of the donors was between 55 and 120 m*M*.

The electrolytic oxidation potential measurements were carried out using a three electrode cyclic voltammetric cell with a Princeton Applied Research Electrochemistry System model 170. The working electrode was a platinum wire. The reference electrode was $Ag/AgNO_3$ (0.1 *M*) with 0.1 *M* tetraethylammonium perchlorate, as the supporting electrolyte, in acetonitrile solution.

Photoelectron spectra were obtained on a McPherson ESCA 36 photoelectron spectrometer. The samples were introduced as vapour at room temperature and 10^{-6} Torr. The He(I) radiation of a He(II) lamp was employed.

Acknowledgements

This work was supported by a grant from the Natural Science and Engineering Research Council (Canada). We gratefully acknowledge the assistance of Mr. B. Lazier in obtaining the photoelectron spectra.

1. (*a*) P. C. WONG and D. R. ARNOLD. Tetrahedron Lett. In press; (*b*) S. S. HIXSON, J. BOYER, and C. GALLUCCI. J. Chem. Soc. Chem. Commun. 540 (1974).
2. A. ALBINI and D. R. ARNOLD. Can. J. Chem. **56**, 2985 (1978).
3. D. REHM and A. WELLER. Isr. J. Chem. **8**, 259 (1970).
4. (*a*) D. R. ARNOLD and A. J. MAROULIS. J. Am. Chem. Soc. **98**, 5931 (1976); (*b*), D. A. LABIANCE, G. N. TAYLOR, and G. S. HAMMOND. J. Am. Chem. Soc. **94**, 3679 (1972).
5. T. SHANO and Y. MATSUMURA. J. Org. Chem. **35**, 4157 (1970).
6. (*a*) E. S. PSYCH and N. C. YANG. J. Am. Chem. Soc. **85**, 2124 (1963); (*b*) W. C. NEIKAM, G. R. DIMELER, and M. M. DESMOND. J. Electrochem. Soc. **111**, 1190 (1964).
7. (*a*) D. W. TURNER, C. BAKER, A. D. BAKER, and C. R. BRUNDLE. Molecular photoelectron spectroscopy. Wiley-Interscience, NY. 1970. p. 207; (*b*) E. J. MCALDUFF and K. N. HOUK. Can. J. Chem. **55**, 318 (1977).
8. (*a*) C. H. J. WELLS. Tetrahedron, **22**, 1985 (1966); (*b*) W. HANSTEIN, H. J. BERWIN, and T. G. TRAYLOR. J. Am. Chem. Soc. **92**, 829 (1970).
9. L. L. MILLER, G. D. NORDBLOM, and E. A. MAYEDA. J. Org. Chem. **37**, 916 (1972).
10. R. FOSTER. Organic charge-transfer complexes. Academic Press, New York. 1969.
11. H. H. J. MACDONALD and R. J. CRAWFORD. Can. J. Chem. **50**, 428 (1972).
12. (*a*) R. R. CODERMAN, P. R. LEBRETON, S. E. BUTTRILL, JR., A. D. WILLIAMSON, and J. L. BEAUCHAMP. J. Chem. Phys. **65**, 4929 (1976); (*b*) W. J. BOUMA, J. K. MACLEOD, and L. RADOM. Nouv. J. Chim. **2**, 439 (1978).
13. D. J. REIF and H. O. HOUSE. Org. Syn. Coll. **IV**, 860 (1963).
14. S. G. BEECH, J. H. TURNBELL, and W. WILSON. J. Chem. Soc. 4686 (1952).

Preparation of two metabolites of isometheptene

WESLEY G. TAYLOR
Agriculture Canada Research Station, Lethbridge, Alta., Canada T1J 4B1
AND
RONALD T. COUTTS
Faculty of Pharmacy and Pharmaceutical Sciences, University of Alberta, Edmonton, Alta., Canada T6G 2N8

Received December 11, 1978

WESLEY G. TAYLOR and RONALD T. COUTTS. Can. J. Chem. 57, 2103 (1979).

trans-(*E*)-2-Methyl-6-methylamino-2-hepten-1-ol (**6**) and *cis*-(*Z*)-2-methyl-6-methylamino-2-hepten-1-ol (**13**), two in vivo metabolites from the antispasmodic agent isometheptene (**2**), ((±)−*N*,1,5-trimethyl-4-hexenylamine) have been synthesized. In the first synthesis of the *trans* isomer, the *N*-trifluoroacetyl derivative of **2** was oxidized with selenium dioxide in ethanol to give *trans*-2-methyl-6-*N*-methyltrifluoroacetamido-2-hepten-1-al (**4**). Aldehyde (**4**) was converted to **6** by reaction with sodium borohydride in ethanol. In the second synthesis, *trans*-2-methyl-6-oxo-2-hepten-1-ol ethylene ketal (**8**) and *cis*-2-methyl-6-oxo-2-hepten-1-ol ethylene ketal (**11**) were hydrolyzed without isomerization to hydroxyketones **9** and **12**. Both **9** and **12** were reductively aminated to the desired metabolites, **6** and **13**.

WESLEY G. TAYLOR et RONALD T. COUTTS. Can. J. Chem. **57**, 2103 (1979).

On a synthétisé les méthyl-2 méthylamino-6 heptène-2 ols-1 *trans*-(*E*) (**6**) et *cis*-(*Z*) (**13**), deux métabolites *in vivo* de l'agent antispasmodique isometheptène (**2**) triméthyl-*N*,1,5 hexenylamine-4 (±). Dans la première synthèse de l'isomère *trans*, on oxyde le dérivé *N*-trifluoroacétyle de **2** par le bioxyde de sélénium dans l'éthanol afin d'obtenir le méthyl-2 *N*-méthyltrifluoro acétamido-6 heptène-2 al-1 *trans* (**4**). On transforme l'aldéhyde **4** en **6** par une réaction avec le borohydrure de sodium dans l'éthanol. Dans la deuxième synthèse, on hydrolyse sans isomération les éthylènecétals des méthyl-2 oxo-6 heptène-2 ol-1 *trans* (**8**) et *cis* (**11**) en hydroxycétones **9** et **12**. La réduction aminante de **9** et **12** conduit aux métabolites désirés **6** et **13**.
[Traduit par le journal]

Isometheptene (**2**), an *N*-methylamine possessing the isobutenyl group, is a drug used in medicine as an antispasmodic agent. After oral administration to male rats, **2** was recently shown (1) to undergo allylic monohydroxylation at each of the methyl carbon atoms of the isobutenyl group. One urinary metabolite was identified as *trans*-2-methyl-6-methylamino-2-hepten-1-ol (**6**); the other was tentatively concluded to be *cis*-2-methyl-6-methylamino-2-hepten-1-ol (**13**). These isomers were detected in rat urinary extracts in an approximate ratio of 80% (*trans*) to 20% (*cis*). An authentic sample of the *trans* isomer (**6**) could not be synthesized for direct comparison with the major rat metabolite of isometheptene. The *N*-acetyl derivative of **6** was synthesized, however, and was identical (by gas chromatography (gc) and mass spectrometry) to the *N*-acetylated metabolite, but numerous attempts to hydrolyze this derivative were unsuccessful. Since it was desirable to compare the properties of metabolites **6** and **13** with those of the parent compound **2**, further attempts were made to prepare these isomers. Synthetic approaches to **6** and **13** are the subject of this paper.

Two routes to the *trans* isomer were explored according to Scheme 1. Both routes utilized selenium dioxide as a key reagent because of its known ability to oxidize isobutenyl groups at one of the methyl carbon atoms with *trans* selectivity (1–4).

In method *A*, the starting material, 6-methyl-5-hepten-2-one (**1**) was converted to **2** using the conditions of Borch (5). The trifluoroacetyl derivative (**3**) was formed in high yield by reacting **2** with trifluoroacetic anhydride in the presence of methylene chloride and pyridine. It was established initially that the *N*-trifluoroacetyl group in **3** could be removed in methanolic ammonia at room temperature and concluded that if **3** could be oxidized at the allylic position, the *N*-protecting group of the expected product **5** could be cleaved under similar mild conditions. This contrasts with the *N*-acetyl derivative of **6** which was stable to *N*-deacetylation even under the influence of boiling barium hydroxide (1).

By reacting **3** with selenium dioxide in refluxing ethanol, the desired trifluoroacetyl aldehyde **4** was obtained as the major product (gc and mass spectral evidence). Crude **4** was reduced with sodium borohydride in ethanol for 1.5 h and, when the reaction mixture was examined by gc, two main components were observed. Both were identified by gc and mass spectrometry; the compound with the longer reten-

0008-4042/79/162103-05$01.00/0

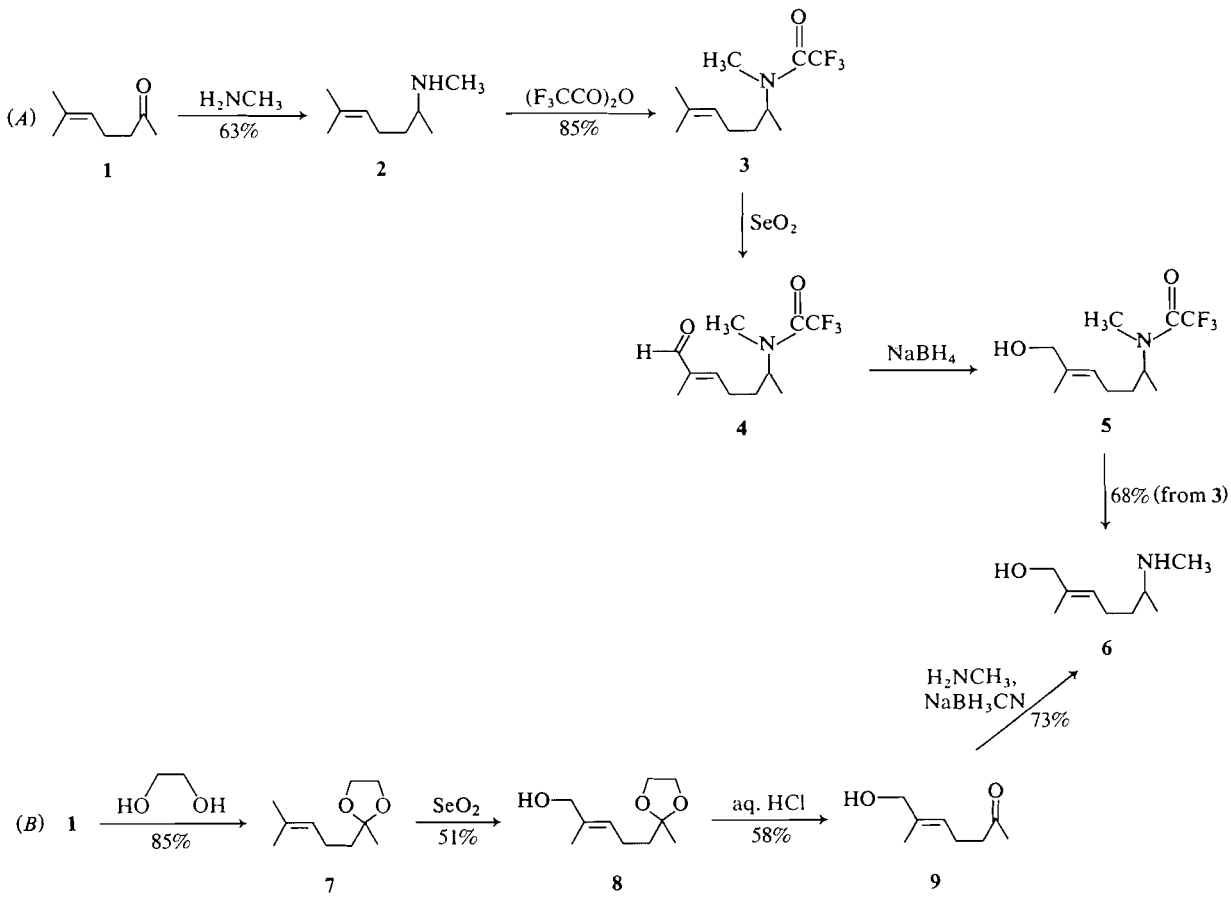

SCHEME 1

tion time was the trifluoroacetyl alcohol, **5**, whereas the more volatile compound was the desired *trans*-2-methyl-6-methylamino-2-hepten-1-ol, **6**. When the reduction reaction was continued for 4–5 h, the quantity of **6** increased at the expense of **5**. Thus, under these conditions, not only was the aldehyde functionality of **4** reduced but also the trifluoroacetyl group of **5** was removed in a gradual and complete manner. The desired product, **6**, was isolated in 68% yield (from **3**).

Molecular ions in the mass spectra of the trifluoroacetyl intermediates were either very weak (**3** and **4**) or absent (**5**). However, the appearance of prominent fragment ions, occurring at *m/e* 154, 110, and 42, were informative and aided in establishing the structures. These three ions have previously been observed in the mass spectra of related trifluoroacetyl compounds (6).

In the synthesis of **6** by method *B*, 6-methyl-5-hepten-2-one ethylene ketal, **7**, was converted to the *trans* olefinic alcohol **8** by reaction with selenium dioxide and then sodium borohydride as outlined previously (3). Deketalization of **8** in an acidified solution of tetrahydrofuran gave hydroxyketone **9** in a moderate yield. The introduction of the methylamino group of **6** was accomplished in 73% yield by the Borch procedure (5), which involved reacting **9** with methylamine and sodium cyanoborohydride in methanol solution.

Although higher yields were generally obtained by method *A*, method *B* was also quite efficient (Scheme 1). Conversion of **3** to **6** did not require purification of **4** and isolation of **5**, thus simplifying the method *A* sequence. Conventional purification methods gave pure compounds (viz. **2**, **3**, **7**, **8**, and **9**) but the final product from both routes was more difficult to purify. Attempts at purification of **6** by salt formation (tartrate, mucate, maleate, or hydrochloride) were unsuccessful because hydroscopic semi-solids or viscous oils formed. The free base was eventually purified by column chromatography on silica gel, followed by fractional distillation. Pure samples of **6** from method *A* and method *B* had identical nmr spectra. The *trans* stereochemistry of **6** was established by *N*-acetylation of **6** with acetic anhydride in methanol. It was found that the *N*-acetyl derivatives

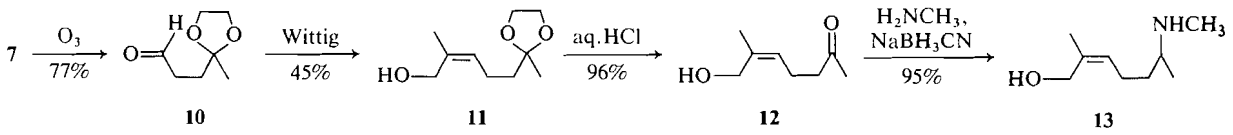

10 11 12 13

SCHEME 2

were identical with the *N*-acetyl derivative of **6** that had been previously characterized (1).

Scheme 2 outlines the synthesis of the *cis* isomer (**13**). Ketal alcohol **11** was obtained from 4-oxo-1-pentanal ethylene ketal (**10**) by a modification of the Wittig reaction that provides *cis* stereoselectivity (7, 8) as previously described (3). Ketal alcohol **11** was converted to aminoalcohol **13** via the hydroxyketone **12** by the same procedures as outlined for the *trans* isomer. The *N*-acetyl derivative of **13** had the same properties as the minor component in the acetylated rat urinary extracts (1).

A verification of *cis* stereochemistry for **13**, and of *trans* stereochemistry for **6**, came from their ^{13}C nmr spectra. Of particular interest were the ^{13}C chemical shifts for the carbon atom bearing the hydroxyl group (C-1). For **13**, C-1 resonated at 61.5 ppm whereas **6** showed a signal for C-1 at 68.2 ppm. These differences in chemical shifts have permitted the assignment of *cis* or *trans* stereochemistry to geometrical isomers of this particular type (1, 2).

The ^1H nmr spectra of the isomers were also informative. When **13** was examined in deuterochloroform solution, the methylene protons at C-1 showed an AB quartet centered at 4.1 ppm. This unexpected nonequivalence contrasted to the appearance of the methylene protons at C-1 in **6**, which resonated as a two-proton singlet near 4 ppm.

Examination of molecular models suggested a plausible explanation for the nonequivalence of the methylene protons at C-1 in the *cis* isomer. As shown by **14**, only the *cis* isomer was capable of adopting an internal hydrogen bonded conformation. The hydrogen bonded conformer **14** imposes a different environment on the C-1 protons because of restricted rotation about the C-1 to oxygen bond. This case is somewhat analogous to the nmr nonequivalence of methylene protons adjacent to the oxygen atom of certain hindered ethers (9).

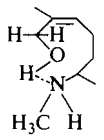

14

The intramolecular hydrogen bonding argument was supported on running the ^1H nmr spectra of **6** and **13** in deuterated dimethylsulfoxide. In this polar solvent, the C-1 methylene protons in both isomers resonated as singlets at 3.8 and 3.9 ppm, respectively.

It is relevant to note that *cis* and *trans* hydroxylation of the isobutenyl group of **2** was species dependent. Although rats gave predominantly **6**, the *cis* isomer **13** was the only isomeric alcohol that was detected in human urine (10). In the case of pentazocine, an analgesic with the isobutenyl group, *cis* hydroxylation was also found to occur in vivo in man (11, 12).

Experimental

Melting points and boiling points are uncorrected. Infrared spectra were taken as liquid films on a Unicam SP 1000 spectrophotometer and on a Perkin Elmer model 137 Infracord instrument. ^1H nmr spectra were recorded at ambient temperature on a Varian EM-360A spectrometer and ^{13}C nmr spectra were measured with a Bruker WP-60 instrument with tetramethylsilane as the internal standard (δ 0). Gas–liquid chromatography was performed on Hewlett-Packard models 5710A and 5838A instruments. The glass column, 1.2 m long and 4 mm id, was packed with 5% OV-101 on acid washed – DMCS treated Chromosorb 750 and the flow rate (nitrogen) was 60 mL/min. Combined gc–ms was performed as described before (1) except for compounds **9** and **12**, whose spectra were recorded (at 70 eV) on a DuPont 21-491 instrument. Elemental analyses were obtained from Galbraith Laboratories, Knoxville, TN, and by Dr. C. Daessle, Montreal, P.Q. Trifluoroacetic anhydride, sodium cyanoborohydride, and 6-methyl-5-hepten-2-one were purchased from the Aldrich Chemical Co. SilicAR cc-7 (200–325 mesh) was obtained from Mallinckrodt Chemical Works, St. Louis, MO.

Isometheptene (2)

This compound was prepared from **1** and isolated as a maleate salt by a known (1) method (45% yield of maleate, mp 109–110°C) or by the method of Borch (5). The latter procedure, using **1** (42.75 g, 0.34 mol), methylamine hydrochloride (30.38 g, 0.45 mol), potassium hydroxide (7.07 g, 0.126 mol), and sodium cyanoborohydride (9.55 g, 0.152 mol) in methanol (350 mL), gave, after adding maleic acid to an ether solution of the crude free base, 54.7 g (63% yield) of **2** maleate, mp 107–108°C. The pure free base was obtained as an oil (gc retention time at 130°C was 1.0 min) by ether extraction of a basified aqueous solution of the maleate salt. The bp of **2** was 43°C at 0.3 Torr.

N-*Trifluoroacetyl*-N-*1,5-trimethyl-4-hexenylamine (3)*

A solution of **2** (18.0 g, 0.128 mol) in dry methylene chloride (400 mL) containing pyridine (20 mL) was cooled to 5°C. Trifluoroacetic anhydride (40 mL) in methylene chloride (100 mL) was added dropwise during 30 min. The mixture was stirred at room temperature (ca. 20°C) for 3 h. After evaporation of the solvent, methanol was added (200 mL). The mixture was stirred and then concentrated on the rotary evaporator. Water (150 mL) was added and the pH was adjusted to 4.5 with 0.1 *N* hydrochloric acid. The aqueous layer was extracted with ether. Evaporation of the dried ($MgSO_4$) organic extract

gave 25.6 g (85%) of **3** as a colorless oil. An analytically pure sample was obtained by distillation: bp 82°C (1.5 Torr); gc retention time (130°C) was 3.1 min; ir: 1695 cm^{-1} (C=O); ms *m/e* (% relative abundance) [identity]: 237 (0.5) [$M^{\ddagger}$], 222 (7) [$M - CH_3$]$^+$, 168(23), 167(11), 154(26) [$CH_3CH{=}\overset{+}{N}(CH_3)COCF_3$], 140(13), 110(90) [$CF_3C{\equiv}\overset{+}{N}(CH_3)$] and [$M - CH_3NHCOCF_3$]‡, 95(100), 85(15), 69(31) [CF_3]$^+$, 67(21), 42(15) [$CH{\equiv}\overset{+}{N}(CH_3)$]. *Anal.* calcd. for $C_{11}H_{18}F_3NO$: C 55.68, H 7.64, N 5.90; found: C 55.89, H 7.64, N 5.65.

The trifluoroacetyl group of **3** was removed (**2** was recovered) by stirring **3** in methanol saturated with ammonia gas for 4 days in a parafilm-sealed flask.

trans-*2-Methyl-6-methylamino-2-hepten-1-ol* (**6**, *Method* A)

To a stirred solution of **3** (23.7 g, 0.1 mol) in 95% ethanol (1000 mL) was added selenium dioxide (26.82 g, 0.24 mol) and the reaction mixture was heated under reflux for 16 h. After leaving overnight at room temperature, the mixture was filtered and the orange filtrate was evaporated to near dryness. The resulting brown oil was dissolved in ether and washed with aqueous sodium bicarbonate solution. The aqueous layer was extracted with ether and the combined organic extracts were dried ($MgSO_4$). A brown, viscous oil (24.85 g) was obtained on evaporation. Gas chromatography at 130°C showed one main peak (gc retention time 10.75 min) which was identified as **4** by ms: *m/e* (% relative abundance) [identity]: 251(0.2) [$M^{\ddagger}$], 236(3) [$M - CH_3$]$^+$, 182(5), 154(100) [$CH_3CH{=}\overset{+}{N}(CH_3)COCF_3$], 124(38) [$M - CH_3NHCOCF_3$]‡, 110(46) [$CF_3{\equiv}\overset{+}{N}CH_3$], 109(15), 95(10), 69(9) [CF_3]$^+$, 42(23) [$CH{\equiv}\overset{+}{N}(CH_3)$].

Aldehyde **4** (12.4 g) was dissolved in 95% ethanol (200 mL) and added dropwise with stirring to a 5°C solution of sodium borohydride (6.2 g) in 95% ethanol (600 mL). The solution was stirred and an aliquot was removed after 1.5 h (see below). After allowing the reaction mixture to approach room temperature during 4.5 h, the ethanol was removed on the rotary evaporator and the resulting yellow semi-solid was dissolved in water (250 mL). The pH was adjusted to 12 with sodium hydroxide. After extracting exhaustively with ether and drying ($MgSO_4$), 5.35 g (68%) of **6** were obtained. This yellow oil was identical with **6** isolated in method *B*.

The aliquot from above was examined by gc and two components were detected in nearly equal amounts. The component with a retention time of 3.2 min (oven temperature 130°C) was identified by ms as **6**. The other component with a retention time of 11.6 min was identified as trifluoroacetyl alcohol **5** by ms: *m/e* (% relative abundance) [identity]: 235(2) [$M - H_2O$]‡, 154(100) [$CH_3CH{=}\overset{+}{N}(CH_3)COCF_3$], 110(50) [$CF_3C{\equiv}\overset{+}{N}CH_3$], 108(32), 93(18), 69(9) [CF_3]$^+$, 42(21) [$CH{\equiv}\overset{+}{N}(CH_3)$].

trans-*2-Methyl-6-oxo-2-hepten-1-ol* (**9**)

Using conditions similar to those of Zoretic and Chiang (13), **8** (14.81 g) was deketalized at room temperature in the presence of tetrahydrofuran (180 mL) and 5.0 *N* hydrochloric acid (60 mL). The mixture was stirred for 11 h, and neutralized to pH 7 with solid sodium bicarbonate. The solvent was removed on the rotary evaporator and the residue was stirred with a saturated solution of sodium chloride. After extracting with ether, drying ($MgSO_4$), and evaporating the solvent, the crude product was distilled under vacuum. There was obtained 6.58 g (58.2%) of **9** as a pale yellow liquid. An analytically pure sample was obtained by column chromatography (silicAR cc-7) eluting with hexane, hexane–ether, and hexane–ethyl acetate mixtures: bp 82°C (0.1 Torr); gc retention time (120°C) was 3.5 min; ir: 3470 (OH) and 1720 cm^{-1} (C=O); ^{1}Hmr ($CDCl_3$) δ: 5.40 (ragged t, 1H, C=C*H*), 4.02 (s, 2H, CH_2OH), 2.17 (s, 3H, CH_3), 2.75–1.30 (m, 5H, CH_2CH_2 and CH_2OH, the latter exchanged with D_2O), 1.68 (s, 3H, C=CCH_3); ms *m/e* (% relative abundance) [identity]: 142(0.1) [$M^{\ddagger}$], 124(24) [$M - H_2O$]‡, 84(24) [$CH_2{=}CHCH_2\overset{+}{C}OCH_3$]‡, 82(14), 81(15), 43(100) [$CH_3C{\equiv}\overset{+}{O}$]. *Anal.* calcd. for $C_8H_{14}O_2$: C 67.57, H 9.92; found: C 67.86, H 10.05.

trans-*2-Methyl-6-methylamino-2-hepten-1-ol* (**6**, *Method* B)

To a solution of methylamine hydrochloride (3.38 g, 0.05 mol) and potassium hydroxide (0.785 g, 0.014 mol) in methanol (100 mL) was added hydroxyketone **9** (5.69 g, 0.04 mol) and the resulting suspension was stirred at room temperature for 30 min. Sodium cyanoborohydride (1.07 g, 0.017 mol) in methanol (30 mL) was added dropwise during 30 min and the reaction mixture was stirred at room temperature for 19 h. Potassium hydroxide (3.0 g) was added and stirring was continued until the pellets dissolved. The suspension was filtered and the KCl cake was washed well with methanol. After evaporating the filtrate under reduced pressure, the resulting oil was stirred with a saturated solution of sodium chloride (75 mL). The mixture was extracted with ether, washed with water, and the organic extract dried ($MgSO_4$). Evaporation of the ether gave 4.6 g (73.1%) of **6**. This oil was further purified by column chromatography on silicAR cc-7. Eluting with hexane–ethyl acetate mixtures and with ethyl acetate removed some brown impurities. Further elution with ethyl acetate – methanol mixtures and finally with methanol gave **6** as a nearly colorless oil. This sample was further purified by distillation: bp 86–88°C (0.2 Torr); gc retention time (130°C) was 3.2 min; ir: 3340 cm^{-1} (OH, NH); ^{1}Hmr ($CDCl_3$) δ: 5.43 (ragged t, 1H, C=C*H*), 4.00 (s, 2H, CH_2OH), 2.40 (s, 3H, NCH_3), 1.70 (s, 3H, C=CCH_3), 2.90–1.20 (m, 5H, CH_2CH_2, $CHCH_3$), 1.07 (d, 3H, J = 6 Hz, $CHCH_3$); ^{13}Cmr ($CDCl_3$) δ: 68.2 ppm (CH_2OH); ms identical to metabolite A in ref. 1. *Anal.* calcd. for $C_9H_{19}NO$: C 68.74, H 12.18, N 8.91; found: C 68.58, H 12.38, N 8.95.

cis-*2-Methyl-6-oxo-2-hepten-1-ol* (**12**)

This alcohol was prepared from **11** (7.0 g) by the same procedure that gave **9** from **8** except that the time of reaction was 4 h. After drying and concentrating the organic extracts, there was obtained 5.13 g (96%) of **12** as a slightly impure yellow oil. An analytically pure sample was obtained by column chromatography on silicAR cc-7, eluting with hexane, hexane–ether, and hexane – ethyl acetate: gc retention time (120°C) was 3.0 min; ir: 3500 (OH) and 1720 cm^{-1} (C=O); ^{1}Hmr ($CDCl_3$) δ: 5.20 (ragged t, 1H, C=C*H*), 4.13 (s, 2H, CH_2OH), 2.13 (s, 3H, CH_3), 2.75–1.30 (m, 5H, CH_2CH_2 and CH_2OH, the latter exchanged with D_2O), 1.79 (s, 3H, C=CCH_3); ms *m/e* (% relative abundance) [identity]: 142(0.2) [$M^{\ddagger}$], 124(22) [$M - H_2O$]‡, 84(24) [$CH_2{=}CHCH_2\overset{+}{C}OCH_3$]‡, 82(15), 81(15), 43(100) [$CH_3C{=}\overset{+}{O}$]. *Anal.* calcd. for $C_8H_{14}O_2$: C 67.57, H 9.92; found: C 67.86, H 10.12.

cis-*2-Methyl-6-methylamino-2-hepten-1-ol* (**13**)

This compound was prepared from **12** (4.98 g, 0.035 mol) by the same procedure used to prepare **6** from **9**. The product, as a brown oil (5.25 g, 95% yield), was purified by silicAR cc-7 chromatography (as described for **6**) and then distilled: bp 85–89°C (0.3 Torr); gc retention time (130°C) was 3.1 min; ir: 3330 cm^{-1} (OH, NH); ^{1}Hmr ($CDCl_3$) δ: 5.25 (ragged t, 1H, C=C*H*), 4.23 and 3.90 (two doublets of an AB quartet, J = 12 Hz, 2H, CH_2OH), 2.33 (s, 3H, NCH_3), 1.80 (s, 3H, C=CCH_3), 3.10–1.20 (m, 5H, CH_2CH_2, $CHCH_3$), 1.03 (d, J = 6 Hz, 3H, $CHCH_3$); ^{13}Cmr ($CDCl_3$) δ: 61.5 ppm

(CH_2OH); ms was the same as obtained for **6**. *Anal.* calcd. for $C_9H_{19}NO$: C 68.74, H 12.18, N 8.91; found: C 68.42, H 11.93, N 8.79.

Acknowledgments

We thank the Medical Research Council of Canada for partial financial assistance. One of us (W.G.T.) thanks Dr. W. O. Haufe, Research Branch, Agriculture Canada, for support in completing this work. We also thank Dr. T. Nakashima, University of Alberta, for useful discussions on the ^1H nmr data and for recording the ^{13}C nmr spectra.

1. W. G. TAYLOR and R. T. COUTTS. Drug. Metab. Dispos. **5**, 564 (1977).
2. U. T. BHALERAO and H. RAPOPORT. J. Am. Chem. Soc. **93**, 4835 (1971).
3. W. G. TAYLOR. J. Org. Chem. **44**, 1020 (1979).
4. M. MATSUI and Y. YAMADA. Agr. Biol. Chem. **29**, 956 (1965).
5. R. F. BORCH. Org. Synth. **52**, 124 (1972).
6. K. K. MIDHA, J. K. COOPER, I. J. MCGILVERAY, R. T. COUTTS, and R. DAWE. Drug Metab. Dispos. **4**, 568 (1976).
7. E. J. COREY and H. YAMAMOTO. J. Am. Chem. Soc. **92**, 226 (1970).
8. E. J. COREY, J. I. SHULMAN, and H. YAMAMOTO. Tetrahedron Lett. 447 (1970).
9. L. M. JACKMAN and S. STERNHELL. *In* Application of nuclear magnetic resonance spectroscopy in organic chemistry. 2nd ed. Pergamon Press, New York, NY. 1969. p. 377.
10. R. T. COUTTS and W. G. TAYLOR. Proc. Can. Fed. Biol. Soc. **20**, 192 (1977).
11. K. A. PITTMAN. Biochem. Pharmacol. **19**, 1833 (1970).
12. N. F. ALBERTSON and F. C. MCKAY. J. Med. Chem. **20**, 602 (1977).
13. P. A. ZORETIC and J. CHIANG. J. Org. Chem. **42**, 2103 (1977).

The application of resonant ion ejection to quadrupole ion storage mass spectrometry: a study of ion/molecule reactions in the QUISTOR

MARY ALISON ARMITAGE, JOHN EDWARD FULFORD, DUONG-NHU-HOA, RICHARD JAMES HUGHES, AND RAYMOND EVANS MARCH

Department of Chemistry, Trent University, Peterborough, Ont., Canada K9J 7B8

Received January 15, 1979

MARY ALISON ARMITAGE, JOHN EDWARD FULFORD, DUONG-NHU-HOA, RICHARD JAMES HUGHES, and RAYMOND EVANS MARCH. Can. J. Chem. **57**, 2108 (1979).

Resonant ejection of ion species from the quadrupole ion store (QUISTOR) is shown to reveal the coupling of reactant ions with product ions in ion/molecule reactions studied with the QUISTOR – quadrupole mass filter combination. The technique involves the use of selective ejection of a chosen ionic precursor and the simultaneous observation of the perturbations in the concentration of product ions. The technique is demonstrated in studies of the ion chemistry and reaction kinetics of two known chemical systems.

MARY ALISON ARMITAGE, JOHN EDWARD FULFORD, DUONG-NHU-HOA, RICHARD JAMES HUGHES et RAYMOND EVANS MARCH. Can. J. Chem. **57**, 2108 (1979).

On a montré que l'éjection résonante d'espèces ioniques par un réservoir d'ions quadrupolaires (QUISTOR) révèle le couplage d'ions réactifs avec des ions produits dans des réactions ion/molécule étudiées à l'aide de la combinaison QUISTOR-filtre de masse quadrupolaire. La technique implique l'utilisation d'une éjection sélective d'un précurseur ionique choisi et l'observation simultanée des perturbations dans la concentration des ions produits. On a démontré la technique dans des études de la chimie ionique et de la cinétique réactionnelle de deux systèmes chimiques connus.

[Traduit par le journal]

Introduction

Much of the available information on ion/molecule reactions has been compiled with non-specific techniques such as high pressure mass spectrometry (1) and the flowing afterglow (2). In complex systems these methods involve the simultaneous reactions of many ion species, analysis of all the products, and interpolation of reaction mechanisms. The same is also true of the first studies with the QUISTOR–quadrupole combination (3–6). Recent interests have been concerned with techniques which permit the selection of one reactant ion and elimination of much of the speculation that was once necessary. Thus tandem mass spectrometers such as the selected ion flow tube (7) are receiving much attention. A recent communication from this laboratory (8) described a selective ion reactor, wherein the QUISTOR–quadrupole combination was operated in a tandem mass spectrometric mode.

Ion cyclotron resonance mass spectrometry has been used widely for the study of ion/molecule reactions. The ion cyclotron double resonance (ICDR) technique can be used to probe specific ion/molecule mechanisms by exciting precursor ions with radiation, and observing perturbations in the product ion distribution (9, 10). In our current investigations of ion motion in the QUISTOR a technique similar to ICDR has been developed and is described as QUISTOR Resonance Ejection (QRE). In both techniques, ions may be selectively excited and ultimately ejected from the ion trap by resonant power absorption. As the resonant excitation is mass dependent, the technique may be applied in a fashion similar to that of ICDR except for the mass analysis which, in the case of the QUISTOR, is carried out with a quadrupole mass filter rather than a marginal oscillator. In this paper we present a demonstration of the use of QRE as a means of elucidating ion/molecule mechanisms and kinetics.

Theory

As has been discussed elsewhere (11, 12), the equations of motion for ions in a three dimensional quadrupole field take the general form of the Mathieu equation

$$[1] \quad d^2u/d\xi^2 + (a_u - 2q_u \cos 2\xi)u = 0$$

where

$$[2] \quad u = r \text{ or } z$$

$$[3] \quad q_z = -2q_r = -4\,eV/mr_0^2\Omega^2$$

$$[4] \quad a_z = -2a_r = -8eU/mr_0^2\Omega^2$$

$$[5] \quad \xi = \Omega t/2$$

U is the dc voltage, V is the o-p RF voltage, m/e is

0008-4042/79/162108-06$01.00/0

the mass-to-charge ratio, r_0 is the radius of the ring electrode, and Ω is the radial frequency of the RF voltage. From the general solution of the Mathieu equation of motion

$$[6] \quad u = \alpha' e^{i\beta\xi} \sum_{n=-\infty}^{\infty} C_{2n} e^{2in\xi} + \alpha'' e^{-i\beta\xi} \sum_{n=-\infty}^{\infty} C_{2n} e^{-2in\xi}$$

The β value is related to the frequency of the ion trajectory and more specifically to the dominant secular frequency, ω_u:

$$[7] \quad \omega_u = \beta_u \Omega/2$$

The oscillation frequency is mass dependent, i.e.

$$[8] \quad \omega_u = \beta_u \Omega/2 = (a_u + q_u^2/2)^{1/2}\Omega/2$$

and in the z direction with $a_z = 0$ (with no dc component)

$$[9] \quad \omega_z = (q_z^2/2)^{1/2}\Omega/2 = \sqrt{2}eV/mr_0^2\Omega$$

The imposition of a low level sinusoidal potential of frequency ω_z will cause the ion oscillating at this frequency to absorb energy and in the limit to be lost from the trapping field. This property permits the selective resonant ejection of a given ion species without disturbance of the other ions being stored under low pressure conditions. The resonant ejection technique can be used as a specific probe for ion/molecule interactions at higher sample pressure. Resonant perturbation of a precursor ion will be transmitted through chemical interactions and change the relative abundance of product ions.

Experimental

The basic apparatus has been described in detail elsewhere (5). In the 2-propanol study, a constant pressure of 5.5×10^{-5} Torr was maintained, while in the argon/carbon dioxide study a 7:1 mixture of argon:carbon dioxide was used at a total pressure of 1×10^{-4} Torr. Pressures were measured using an MKS Baratron gauge. Neutral gas temperatures were estimated to be approximately 320 K. In the 2-propanol study, ion densities within the QUISTOR were estimated from the space charge induced perturbation of the secular frequency, ω_z, from the theoretical value (11). The average ion density after 1 ms of storage was 3.1×10^6 cm^{-3}. The storage times used in this study ranged from 200 μs to 10 ms though the present practical limitation is 100 ms. The resonance oscillator was connected to the repeller endcap (upper end cap electrode in Fig. 1) for application of the resonant signal in the z-direction.

The resonant frequency was applied for continuous ejection of a particular ion mass and in this manner the ion/molecule mechanisms of 2-propanol were probed. The Wavetek Model 134 sweep generator has the capability to provide a burst of a resonant frequency and this technique was used for a kinetic study of the argon:carbon dioxide system. The pulse train is shown in Fig. 2. The Wavetek generator triggered the creation pulse generator which triggered the scan delay generator (Brookdeal Ortec 9425A). The trigger pulse from the scan delay generator triggered simultaneously the ejection pulse generator and the sample-and-hold circuit (Brookdeal Ortec Linear Gate 9415). The argon and carbon dioxide were used as obtained from Matheson of Canada Ltd. The 2-propanol was obtained from Fisher Scientific and degassed by freeze–pump–thaw cycles before use. The spectra were not corrected for the mass discrimination due to the QUISTOR or quadruple mass filter.

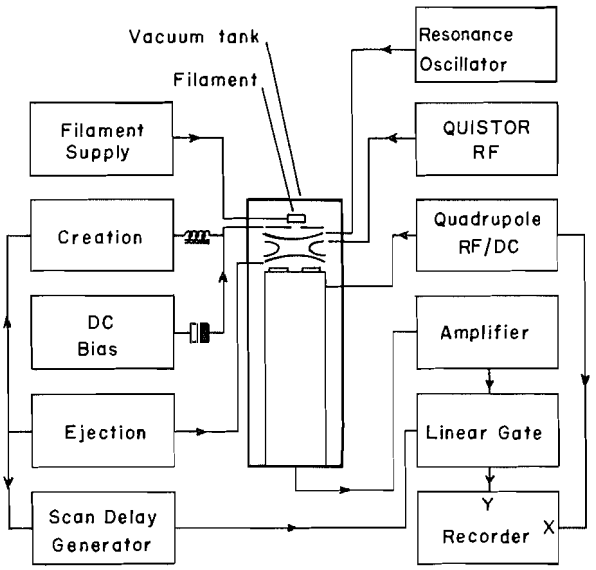

FIG. 1. Schematic diagram of apparatus.

Results and Discussion

The ion chemistry of 2-propanol has been studied by Beauchamp *et al.* (13, 14) using the ion cyclotron double resonance technique (ICDR).

As the 2-propanol system is well documented and falls within the convenient mass range of the quad-

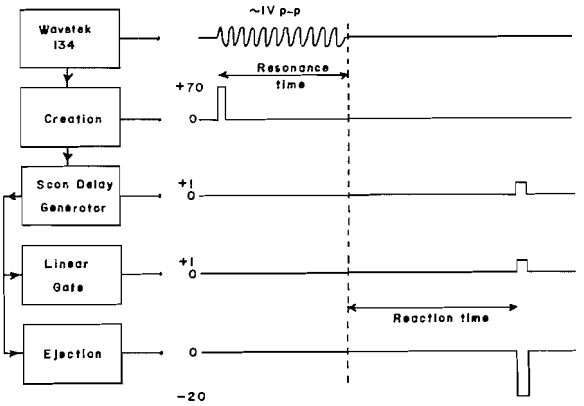

FIG. 2. Pulse train for pulsed resonant ejection.

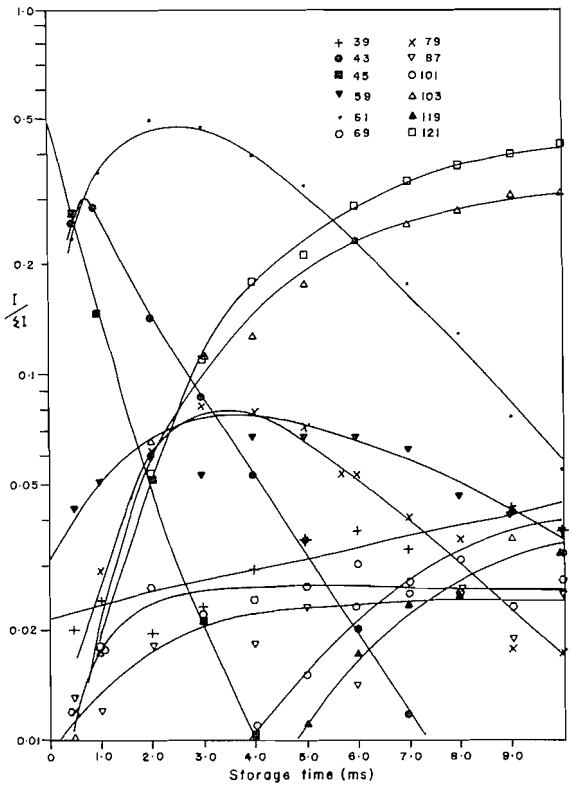

FIG. 3. Variation in the logarithm of normalized ion abundances in 2-propanol; 0–10 ms, 300 Vo-p at 1.6 MHz, 5.5 × 10^{-5} Torr.

rupole mass filter, 2-propanol was chosen as the subject for investigation in the QUISTOR using the resonant ion ejection technique (QRE). The ion profiles of 2-propanol are shown in Fig. 3 and a comparison of observations by ICR and the QUISTOR is shown in Table 1. A comparison of the precursor to product ion dependencies indicated by ICDR and QRE is shown in Table 2. An example of the spectra obtained with and without resonant ion ejection by QRE is shown in Fig. 4. Upon resonant ejection of *m/e* 61, reduction of the ion signal intensities of *m/e* 79, 101, 103, 119, and 121 are readily observed. The data obtained by ICDR and QRE are remarkably similar except for two points: (*i*) *m/e* 39 was observed as a minor component (~4%) in the QRE study but was not reported as a persistent ion in the ICDR studies. (*ii*) *m/e* 59 and its associated product ions were not reported in the ICDR studies. The ICDR work was carried out with ionizing beams of 70 eV and 13.5 eV electrons whereas the QRE study used nominally 70 eV electrons.

The *m/e* 39 ion may originate from a slightly endothermic pathway which becomes available as a result of the small fraction of ions which may be stored with energies in excess of thermal (15). Simi-

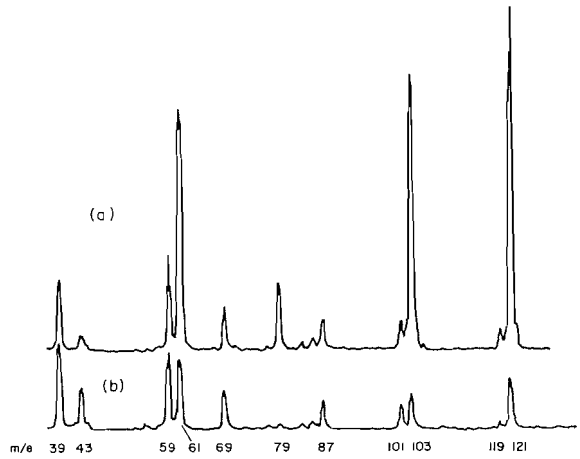

FIG. 4. Spectra of 2-propanol (*a*) without and (*b*) with resonant ejection of *m/e* 61 (ω_z = 86 kHz), RF-254 Vo-p at 1.6 MHz; 4 ms storage time.

larly the observation in the QUISTOR of *m/e* 59 may be explained by dehydrogenation of excited *m/e* 61 according to eq. [10].

$$[10]\quad \left[(CH_3)_2\overset{H}{\underset{|}{C}}-\overset{+}{O}\begin{matrix}H\\H\end{matrix}\right]^* \longrightarrow (CH_3)_2C{=}\overset{+}{O}H + H_2$$

m/e 61 *m/e* 59

ΔH = 12 kcal/mol

The *m/e* 59 ion profile goes through a maximum simultaneously with the *m/e* 61 ion profile; the *m/e* 61 ion being formed from *m/e* 43 (13), *m/e* 45 (a reaction which is exothermic by 11 kcal/mol (14)) and by proton transfer between *m/e* 59 (protonated acetone) and 2-propanol: the proton affinities of acetone and 2-propanol being equal (16).

$$[11]\quad \underset{m/e\ 59}{(CH_3)_2C{=}\overset{+}{O}H} + (CH_3)_2CHOH \rightarrow \underset{m/e\ 61}{(CH_3)_2C\overset{+}{H}OH_2} + (CH_3)_2C{=}O$$

The regeneration of *m/e* 61 through the intermediacy of *m/e* 59 may account for the coupling of both *m/e* 59 and *m/e* 61 with *m/e* 101 and *m/e* 119.

According to the QRE experiments the protonated acetone, *m/e* 59, is coupled to *m/e* 79, 103, and 121. This may be rationalized in the following manner: *m/e* 61, which is coupled with *m/e* 59 through eq. [11], reacts with 2-propanol to form the di-solvated proton, *m/e* 121.

$$[12]\quad \underset{m/e\ 61}{(CH_3)_2C\overset{+}{H}OH_2} + (CH_3)_2CHOH \rightarrow \left[(CH_3)_2CHO\cdots\overset{+}{H}\cdots OCH(CH_3)_2\right]^*$$

m/e 121

TABLE 1. Ions observed in 2-propanol

m/e	Structure	QUISTOR	ICR
39	$[C_3H_3]^+$	Observed	
43	$[C_3H_7]^+$	Observed	Observed
44	$[C_2H_4O]^+$		Observed*
45	$CH_3CH{=}\overset{+}{O}H$	Observed	Observed
59	$(CH_3)_2C{=}\overset{+}{O}H$	Observed	
61	$(CH_3)_2CH{-}\overset{+}{O}H_2$	Observed	Observed
63	$CH_3CH{=}O\cdots\overset{+}{H}\cdots OH_2$		Observed*
69	$[C_5H_9]^+$	Observed	Observed
79	$(CH_3)_2CH{-}\overset{H}{\underset{\vert}{O}}\cdots\overset{+}{H}\cdots OH_2$	Observed	Observed*
87	$CH_3CH{=}\overset{+}{O}{-}CH(CH_3)_2$	Observed	Observed
101	$(CH_3)_2C{=}O\cdots\overset{+}{H}\cdots OH_2$	Observed	
103	$(CH_3)_2C\overset{H}{\underset{\vert}{O}}\cdots\overset{+}{H}\cdots OH_2$	Observed	Observed
105	$(CH_3)_2C\overset{H}{\underset{\vert}{O}}\cdots\overset{+}{H}\cdots O{=}CHCH_3$		Observed*
119	$(CH_3)_2C{=}O\cdots\overset{+}{H}\cdots\overset{H}{\underset{\vert}{O}}CH(CH_3)_2$	Observed	
121	$(CH_3)_2C\overset{H}{\underset{\vert}{O}}\cdots\overset{+}{H}\cdots\overset{H}{\underset{\vert}{O}}CH(CH_3)_2$	Observed	Observed
163	$((CH_3)_2CH)_2O\cdots\overset{+}{H}\cdots\overset{H}{\underset{\vert}{O}}CH(CH_3)_2$	Observed†	Observed*
181	$((CH_3)_2CHOH)_3\overset{+}{H}$		Observed*

*Ions observed with electron energy at 13.5 eV (13).
†Observed as less than 1% of the total ionization.

The excited *m/e* 121 species will yield *m/e* 103 by dehydration or *m/e* 79 by loss of the alkene neutral (13).

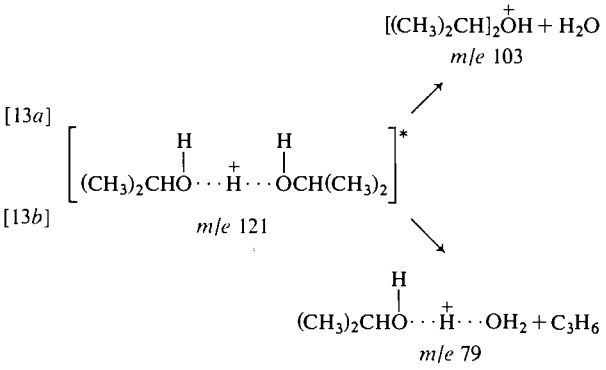

The *m/e* 59 is related also to *m/e* 101 and 119 by a more direct route:

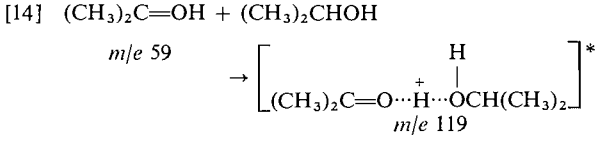

and with stabilization to produce *m/e* 119:

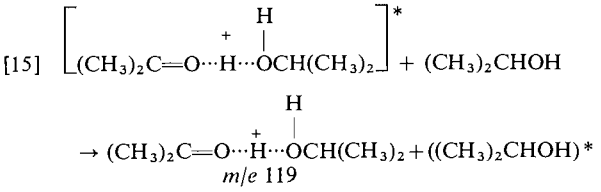

TABLE 2. Reaction sequences observed in 2-propanol. Reactions were identified by the resonance techniques

Precursor ions		Product ions (*m/e*) observed by		
m/e	Structure	ICDR and QRE	QRE	ICDR
43	$[C_3H_7]^+$, $CH_3\overset{+}{C}{=}O$	61, 79, 103, 121, 163	61, 79, 101, 103, 119, 121, 163	61, 79, 103, 121, 163, 181
45	$CH_3CH{=}\overset{+}{O}H$	43, 61, 69, 79, 87, 103, 121, 163	43, 61, 69, 79, 87, 101, 103, 119, 121, 163	43, 61, 63, 69, 79, 87, 103, 105, 121, 163, 181
59	$(CH_3)_2C{=}\overset{+}{O}H$		79, 87, 101, 103, 119, 121, 163	
61	$(CH_3)_2CH\overset{+}{O}H_2$	79, 103, 121, 163	79, 101, 103, 119, 121, 163	79, 103, 121, 163, 181
63	$CH_3CH{=}O\cdots\overset{+}{H}\cdots OH_2$			105
79	$(CH_3)_2CH{-}\overset{H}{\underset{\vert}{O}}\cdots\overset{+}{H}\cdots OH_2$	121	121	121, 181
103	$((CH_3)_2CH)_2\overset{+}{O}H$	163	163	163
105	$CH_3CH{=}O\cdots\overset{+}{H}\cdots\overset{H}{\underset{\vert}{O}}CH(CH_3)_2$			121
121	$(CH_3)_2CH\overset{H}{\underset{\vert}{O}}\cdots\overset{+}{H}\cdots\overset{H}{\underset{\vert}{O}}CH(CH_3)_2$			181

or to lose water and yield *m/e* 101:

[16] $$\left[(CH_3)_2C{=}O\cdots\overset{+}{H}\cdots\overset{H}{\underset{\vert}{O}}CH(CH_3)_2\right]^* \rightarrow \underset{m/e\ 101}{(CH_3)_2C{=}\overset{+}{O}{-}CH(CH_3)_2} + H_2O$$

Studies with low energy electrons were not undertaken with the QUISTOR.

A second application of resonant ejection is the simplification of kinetic studies by the isolation of single reactant ion species. For example, the resonant ejection technique was applied to a 7:1 argon and carbon dioxide mixture for the determination of individual rate constants:

[17] $Ar^+ + CO_2 \rightarrow Ar + CO_2^+$

[18] $Ar^{2+} + CO_2 \rightarrow Ar^+ + CO_2^+$

[19] $Ar^{2+} + Ar \rightarrow 2Ar^+$

Although partial charge transfer reactions of doubly charged ions with neutrals have been investigated intensively in beam experiments (17), relatively few data are available for partial charge transfer reactions, such as reactions [18] and [19], in the thermal energy region. Resonant ejection of Ar^{2+}, formed by electron bombardment, enabled the clear measurement of k_{17} in the absence of contributions to the Ar^+ concentration by reactions [18] and [19]. Pulsed resonant ejection was used to remove Ar^+ during the study of reactions [18] and [19] which enhanced the sensitivity for measurements of the relatively low Ar^{2+} and CO_2^+ signals.

The contribution of reaction [19] to the decay of Ar^{2+} in reaction [18] was calculated from the value obtained for k_{19} and found to be 3%; this is negligible in comparison to the overall uncertainty in k_{18}. The values of rate constants obtained are listed in Table 3 together with values determined by other techniques. The values are in broad agreement except k_{19} which was larger under the conditions of this study in comparison with the flow-drift tube measurement of Howorka (23). Further examination of k_{19} revealed a pressure dependence, implying that more reactive higher electronic states of Ar^{2+} may not be quenched at 1×10^{-4} Torr. This observation is presently under examination and will be reported in a subsequent paper. An extension of the pulsed resonant ejection technique to several ion species in a chemical system could be used for selective storage of a single ion species, thus permitting observation of the reactions of the remaining ion species. This technique would require the superposition of several resonant frequencies and has been demonstrated elsewhere (11).

A present limitation of the pulsed resonant ejection technique is the duration of the irradiation pulse. The pulse must be of sufficient duration to

TABLE 3. Summary of rate constant data for argon:carbon dioxide mixture

Reaction	Rate constant (cm^3 $molecules^{-1}$ s^{-1}) This work[a] (±33%)	Other works
$Ar^+ + CO_2 \rightarrow Ar + CO_2^+$	3.7×10^{-10}	$(6.5,^b 5.3,^c 7.6,^d 4.2,^e 7^f) \times 10^{-10}$
$Ar^{2+} + CO_2 \rightarrow Ar^+ + CO_2^+$	1.1×10^{-9}	$(2.2 \pm 0.77)^b \times 10^{-9}$
$Ar^{2+} + Ar \rightarrow 2Ar^+$	46×10^{-13}	$(4.1 \pm 2.1)^g \times 10^{-13}$

[a]Average of multiple determinations.
[b]Reference 18.
[c]Reference 19.
[d]Reference 20.
[e]Reference 21.
[f]Reference 22.
[g]Reference 23.

eject completely a specific ion species yet at a power which will not perturb the storage conditions for the remaining ions of interest (11). The optimum irradiating power level, applied to an end-cap electrode, varied from 150 mV to 850 mV peak-to-peak depending on the ion intensity. The minimum separation of the end-cap electrodes was 1.414 cm. The irradiating power was applied in tone bursts of up to 1 ms duration; the duration could not be excessively long in comparison to the half-life of the ion/molecule reaction under study. Details of the application of QRE to other systems are given in ref. 11.

Acknowledgements

The authors acknowledge gratefully the financial support of Trent University and the National Research Council of Canada. We also wish to express gratitude to Wayne King and C. J. S. Stewart for equipment construction, to Ed Laughlin and George Wynn for modification of electronics, and to Jim Cashmore and Joan Fowler for the preparation of manuscripts.

1. L. W. SIECK, F. P. ABRAMSON, and J. H. FUTRELL. J. Chem. Phys. **45**, 2859 (1966).
2. E. E. FERGUSON, F. C. FEHSENFELD, and A. L. SCHMELTEKOPF. Advanced atomic molecular physics. Vol. 5. *Edited by* D. R. Bates and I. Estermann. 1969. p. 1.
3. G. LAWSON, R. BONNER, R. E. MATHER, J. F. J. TODD, and R. E. MARCH. J. Chem. Soc. Faraday I, **72**, 545 (1976).
4. G. B. DEBROU, J. E. FULFORD, E. G. LEWARS, and R. E. MARCH. Int. J. Mass Spectrom. Ion Phys. **26**, 155 (1978).
5. J. E. FULFORD, J. W. DUPUIS, and R. E. MARCH. Can. J. Chem. **56**, 2324 (1978).
6. R. F. BONNER, J. W. DUPUIS, J. E. FULFORD, and R. E. MARCH. Unpublished data.
7. N. G. SMITH and D. ADAMS. Int. J. Mass Spectrom. Ion Phys. **21**, 349 (1976).
8. J. E. FULFORD and R. E. MARCH. Int. J. Mass Spectrom. Ion Phys. **26**, 345 (1978).
9. L. R. ANDERS, J. L. BEAUCHAMP, R. C. DUNBAR, and J. D. BALDESCHWIELER. J. Chem. Phys. **45**, 1062 (1966).
10. J. L. BEAUCHAMP, L. R. ANDERS, and J. D. BALDESCHWIELER. J. Am. Chem. Soc. **89**, 4569 (1967).
11. J. E. FULFORD, D. N. HOA, R. J. HUGHES, R. E. MARCH, and G. J. WONG. J. Vac. Sci. Technol. To be published.
12. P. H. DAWSON (*Editor*). Quadrupole mass spectrometry. Elsevier, New York. 1976.
13. J. L. BEAUCHAMP and R. C. DUNBAR. J. Am. Chem. Soc. **92**, 1477 (1970).
14. T. A. LEHMAN, T. A. ELWOOD, J. T. BURSEY, M. M. BURSEY, and J. L. BEAUCHAMP. J. Am. Chem. Soc. **93**, 2108 (1971).
15. R. F. BONNER, R. E. MARCH, and J. DURUP. Int. J. Mass Spectrom. Ion Phys. **22**, 17 (1976).
16. J. L. BEAUCHAMP. *In* Interactions between ions and molecules. *Edited by* P. Ausloos. Plenum Press, New York. 1974. p. 415.
17. J. B. HASTED. Physics of atomic collisions. 2nd ed. Butterworths, London. 1972. p. 12.
18. W. LINDINGER, E. ALGE, H. STÖRI, M. PAHL, and R. N. VARNEY. J. Chem. Phys. **67**, 3495 (1977).
19. I. DOTAN, W. LINDINGER, and D. L. ALBRITON. To be published.
20. F. C. FEHSENFELD, E. E. FERGUSON, and A. L. SCHMELTEKOPF. J. Chem. Phys. **45**, 404 (1966).
21. J. B. LANDENSLAGER, W. T. HUNTRESS, JR., and M. T. BOWERS. J. Chem. Phys. **61**, 4600 (1974).
22. A. WARNECK. J. Chem. Phys. **46**, 513 (1967).
23. F. HOWORKA. J. Chem. Phys. **67**, 2919 (1977).

Regiospecific preparation of 10-allyl-1-ketoquinolizidine and an unexpected disproportionation during its Wolff–Kischner reduction

JOHN M. MCINTOSH

Department of Chemistry, University of Windsor, Windsor, Ont., Canada N9B 3P4

Received March 16, 1979

JOHN M. MCINTOSH. Can. J. Chem. 57, 2114 (1979).

Regiospecific formation of 10-allyl-1-ketoquinolizidine (**7**) is achieved in high yield by a [2.3] sigmatropic rearrangement of *N*-allyl-1-ketoquinolizidinium bromide (**6**). Wolff–Kischner reduction of **7** affords 10-allylquinolizidine (**8**) contaminated by the 10-propyl and 10-ethynyl analogs in amounts which depend on the reaction conditions. The carbon-13 spectrum of **8** indicates a *trans*-fused ring system with an axial substituent at C-10.

JOHN M. MCINTOSH. Can. J. Chem. 57, 2114 (1979).

On a effectué, avec un excellent rendement, la formation régiospécifique de l'allyl-10 céto-1 quinolizidine (**7**) en faisant appel à une transposition sigmatropique du bromure du *N*-allyl céto-1 quinolizidinium (**6**). La réduction selon Wolff–Kischner de **7** conduit à l'allyl-10 quinolizidine (**8**) contaminé par les analogues propyl-10 et éthynyl-10 dont les quantités dépendent des conditions de la réaction. Selon le spectre rmn du ^{13}C de **8** le système cyclique est lié par une jonction *trans* et porte un substituant axial en C-10.

[Traduit par le journal]

In connection with an ongoing research program[1] we required a synthesis of some 10-substituted quinolizidines which contained functionality in the 10-substituent and geminal substitution in one of the heterocyclic rings (e.g., **1***b*). Several examples of **1***a* have been prepared from 5,10-dehydroquinolizidinium perchlorate (**2***a*) (1) or its cyanide adduct and Grignard reagents (2), a reaction pioneered by Leonard and co-workers. However, the syntheses available for **2** at the time we initiated our work were not attractive in terms of yield or applicability to **2***b*. Even less attractive was a route involving cyclization of **4**, since preparation of its precursor **3** appeared complicated and cyclization would be expected to be inhibited by the quaternary centre adjacent to nitrogen. The direct alkylation of **5** (3) at C-10 also appeared to present problems in terms of regiospecificity, but **5** is an attractive starting material since geminally substituted derivatives should be readily prepared.

In this connection, it occurred to us that quaternization of **5** with an allylic halide would provide a product (**6**) in which the hydrogen at C-10 would be greatly labilized and a facile [2.3] sigmatropic rearrangement would be expected (4). Deoxygenation of **7** would provide **8**, which would be capable of functionalization at the double bond by standard methods.

In the event, **5** reacted with allyl bromide quantitatively to give **6** as an extremely hygroscopic solid. Treatment of **6** with potassium *tert*-butoxide in THF/DMSO at −30°C gave a very rapid reaction leading to **7** in 75–80% yield.

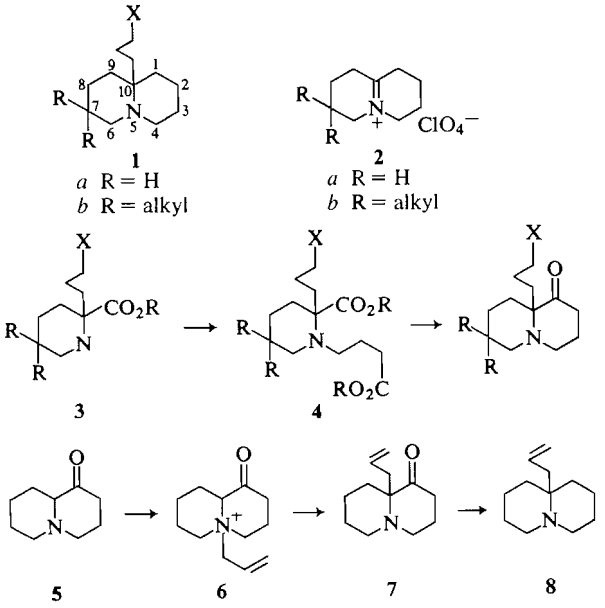

1 *a* R = H, *b* R = alkyl; **2** *a* R = H, *b* R = alkyl; **3**; **4**; **5**; **6**; **7**; **8**

The carbonyl group was now ready for removal. It has been shown that **5** can be reduced using the Wolff–Kischner method, but that acidic conditions (Clemmensen) lead to rearranged products (5). We have been unable to satisfactorily reduce **7** to **8** using a variety of conditions. These failures are *not* due to steric hindrance at the carbonyl group, as a variety of addition reactions at C-1 can be performed successfully. Thus, reduction of **7** using sodium borohydride led to **9***a* as a single diastereomer, and the ethylene ketal (**9***b*), hydrazone **9***c*, and tosylhydrazone **9***d* are all formed in nearly quantitative yield under

0008-4042/79/162114-04$01.00/0

standard conditions. However, attempted preparation of the thioketal **9***e* as a prelude to reductive desulfurization (6) led only to addition at the olefinic double bond.

When the formation of the mesylate of alcohol **9***a* was attempted, only decomposition products could be isolated. This facile decomposition may be initiated by participation of the nitrogen atom in an intramolecular displacement (e.g., **10**) followed by further reactions.

When hydrazone **9***c* was treated with potassium *tert*-butoxide in refluxing xylene, conditions recommended for other α-aminoketones (7), no deoxygenated material was formed. Application of the usual Wolff–Kischner (WK) conditions led to a mixture of products, depending on the reaction conditions. When decomposition of the hydrazone was carried out in refluxing triethylene glycol without distilling out the volatile fraction, two peaks in a ratio of 1 :1 appeared in the gas chromatogram. The proton nmr of the crude mixture was as expected for **8**, except that the integration in the vinyl region was only 0.6 of the expected value and some high field absorption (δ 0.9–1) was evident. No trace of **12** could be detected. Hydrogenation of the WK product led to the uptake of 1.02 equiv. of hydrogen and the formation of a *single* product, identical in all respects with the shorter retention time material formed in the WK reduction. The spectral data and picrate melting point identified this material as 10-propylquinolizidine (**11**) (2). Using refluxing ethylene glycol as the WK solvent and distilling the volatile fraction as it was formed nearly eliminated the formation of **11**, and gave **8** in 52% yield. When **8** was heated with potassium hydroxide in refluxing triethylene glycol, **11** was again formed.

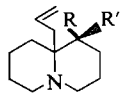

9

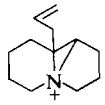

10

a R = H, R′ = OH
b R = R′ = —O—CH_2CH_2—O—
c R = R′ = =N—NH_2
d R = R′ = =NNHTs
e R = R′ = —S—CH_2CH_2—S—

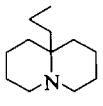

11

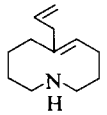

12

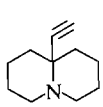

13*a*

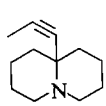

13*b*

In each case where **11** was formed, the longer retention time peak still showed a deficiency in the integration of the vinyl proton region. Whereas the electron-impact mass spectrum of the crude WK reaction mixture showed no molecular ion, field-ionization mass spectrometry (FIMS) showed three strong peaks at m/z = 181, 179, and 177. The first two correspond to the molecular ions of **8** and **11**. The peak at m/z = 177, the formation of **11** from **8**, the reduced vinyl integration, and the formation of *only* **11** when the crude WK product was hydrogenated can only be rationalized by the presence of **13***a* and (or) **13***b* as an inseparable mixture with **8**. Base-catalyzed disproportionation of **8** to **11** and **13** apparently occurs when the temperature exceeds 200°C. Considerable decomposition accompanies the disproportionation as is evidenced by the rapid darkening of the reaction mixture. The absorptions for the acetylenic proton in **13***a* or the methyl group in **13***b* would be obscured by other absorptions in the molecules. It is interesting to note that the same disproportionation apparently occurs when the tosylhydrazone **9***d* is reduced with sodium cyanoborohydride (8) in 1 :1 DMF/sulfolane at 120°C.

Further investigations designed to improve the yield of **8** were abandoned when it was found that the hydroboration–oxidation of **8** led to a mixture of alcohols plus other products. Thus, the goal of preparing **1***a* (X = OH) was frustrated. We hope to report shortly on more successful approaches to this system.

Finally, it is interesting to note that the C-13 spectra of **8** and **11** show only eight lines with chemical shifts which strongly suggest that the C-10 substituent is axially disposed in a *trans*-fused ring system. Extensive investigations on variously methylated quinolizidines (9, 10) have shown a strong preference for *trans*-fused rings, but to our knowledge, this is the first data on the 10-substituted series with a substituent larger than methyl.

Experimental

Proton magnetic resonance spectra were run on a JEOL C60HL spectrometer and C-13 spectra were run on a Bruker CXP 100 spectrometer at 22.64 MHz, using a flip angle of 40°. Spectra are reported in ppm downfield from internal Me_4Si. Gas chromatographic analyses were performed on a Hewlett-Packard model 5750 instrument utilizing a 10 ft × 0.25 in. column packed with 20% SE-30 on Chromosorb W (column A) or a 10 ft × 0.375 in. column packed with 15% Carbowax 20M on Chromosorb W (column B). Mass spectra were run on a Varian MAT CH-5 DF instrument equipped with a field-ionization source. Elemental analyses were performed by Galbraith Laboratories or Canadian Microanalytical Service (Vancouver).

N-Ally-1-ketoquinolizidinium Bromide (6)

1-Ketoquinolizidine (**5**) was prepared from methyl pipecolate by *N*-alkylation with ethyl 4-bromobutyrate in DMF containing excess potassium carbonate at 80°C (62%), followed by cyclization and decarboxylation according to the method

of Leonard (3) (79%). To a solution of 14.0 g (0.09 mol) of **5** in 100 mL of dry acetonitrile was added 14 g (0.115 mol) of allyl bromide. The solution was stirred at ambient temperature for 36 h, the solvent evaporated, and the residue triturated with acetone. Filtration in a dry-box gave 25 g (100%) of a pale brown solid which could be purified by treatment with charcoal in boiling acetonitrile and reprecipitation with acetone to give white crystals, mp 107–110°C (dec.). The material is extremely hygroscopic and normally was not purified before rearrangement. *Anal.* calcd. for $C_{12}H_{20}NOBr$: C 52.56, H 7.35; found: C 52.49, H 7.24.

1-Keto-10-allylquinolizidine (7)

Compound **6** (3 g, 0.011 mol) was dissolved in 20 mL of dry DMSO and 20 mL of dry THF was added. The solution was cooled to −30°C and 1.4 g (1.14 equiv.) of potassium *tert*-butoxide was added all at once. The cooling bath was removed and the mixture stirred under nitrogen at ambient temperature for 1 h. The mixture was diluted with 50 mL of pentane, washed with water (2 × 50 mL), saturated brine (2 × 50 mL), dried over magnesium sulfate, and evaporated to give 1.7 g (80%) of a pale yellow oil. Gas chromatographic analysis (column A, 155°C) indicated a purity of greater than 95% Distillation gave a colorless liquid, bp. 80–83°C (0.4 Torr), which crystallized in the freezer. Compound **7** is a low melting solid which rapidly turns brown on contact with air or chloroform; ir($CHCl_3$): 1710, 1640, 920 cm^{-1}; ^1H nmr (C_6D_6) δ: 5.85–4.71 (bm, 3H), 3.05–1.06 (bm, 16H); ^{13}C nmr (C_6D_6) δ: 208.3, 133.6, 117.2, 67.5, 49.6, 47.8, 37.0, 30.5, 29.2, 25.9, 24.9, 20.3.

The picrate crystallized from ethanol as yellow plates, mp 168–170°C. *Anal.* calcd. for $C_{18}H_{22}N_4O_8$: C 51.18, H 5.25, N 13.26; found: C 51.34, H 5.14, N 13.12.

1-Hydroxy-10-allylquinolizidine (9a)

One gram (5 mmol) of **7** was dissolved in 10 mL of 2-propanol and added dropwise to a mixture of 0.1 g of sodium borohydride (2 equiv.) in 3 mL of 2-propanol and 3 drops of 3 *N* sodium hydroxide. The mixture was stirred at ambient temperature for 3.5 h and then excess hydride was decomposed with 10% HCl. The solution was made basic with 3 *N* hydroxide diluted to 40 mL with water and extracted with ether (3 × 50 mL). The combined ether extracts were washed with water and saturated brine and dried over sodium sulfate. Evaporation of the solvent gave 0.89 g (88%) of white crystals, mp. 74–75°C. This material did not discolor when dissolved in chloroform; ir($CHCl_3$): 3580, 1630, 1110, 1050, 1025, 970, 920 cm^{-1}; ^1H nmr (C_6D_6) δ: 6.52–5.80 (m, 1H), 5.22–4.80 (m, 2H), 3.68–3.05 (m, 1H), 2.50–1.10 (m, 17H); ^{13}C nmr (C_6D_6) δ: 138.2, 115.4, 77.4, 59.5, 49.2, 48.5, 32.8, 29.9, 27.2, 26.3, 24.1, 20.3. *Anal.* calcd. for $C_{12}H_{21}NO$: C 73.80, H 10.84, N 7.17; found: C 73.64, H 10.81, N 6.99.

The sharp melting point and the presence of only 12 signals in the ^{13}C nmr spectrum indicate the presence of only one diastereomer to which we assign the structure ***9a***.

Ethylene Ketal of 7 (9b)

Ketone **7** (0.316 g, 1.6 mmol) was dissolved in 5 mL of ethylene glycol, and 0.4 g triethyl orthoformate and 0.55 g (1.1 equiv.) of tosic acid were added. The flask was flushed with nitrogen and heated at 100°C for 2 h. The cooled solution was diluted with a mixture of 50 mL of water and 10 mL 12 *N* sodium hydroxide and extracted with ether (3 × 25 mL). The ether was washed with water and brine and dried over magnesium sulfate. Evaporation gave 0.34 g (91%) of a pale yellow liquid which gc analysis (column A, 240°C) showed to be 96% pure. Samples for analysis and spectra were collected from glc; ir($CHCl_3$): 1640, 1140, 955, 910 cm^{-1}; ^1H nmr ($CDCl_3$) δ: 6.20–5.50 (m, 1H), 5.03–4.65 (m, 2H), 3.80 (s, 4H), 2.75–1.30 (m, 16H). *Anal.* calcd. for $C_{14}H_{23}NO_2$: C 70.85, H 9.77, N 5.90; found: C 70.55, H 9.76, N 5.71.

Attempted hydroboration–oxidation of ***9b*** using either borane or 9-BBN led to mixtures of products.

Hydrazone of Ketone 7 (9c)

Ketone **7** (0.9 g, 4.7 mmol) dissolved in 4 mL ethylene glycol and 4 mL of 85% hydrazine hydrate was added. The system was purged with nitrogen and heated at 120–130°C for 4 h. The hot solution was poured into 50 mL of water and extracted with ether (3 × 25 mL). The combined ether extracts were dried over sodium sulfate and evaporated to give 0.6 g (62%) of a pale yellow solid, mp 72–74°C; ir($CHCl_3$): 3600–2400, 1640 cm^{-1}.

Attempted Wolff–Kischner reaction of this material using potassium *tert*-butoxide in either hot xylene (7) or DMSO at 50°C (11) failed.

Tosylhydrazone of Ketone 7 (9d)

Ketone **7** (0.425 g, 2.2 mmol) was dissolved in 10 mL of methanol and 0.61 g (1.5 equiv.) of toluenesulfonylhydrazine was added followed by 0.5 g tosic acid. The mixture was sitrred at ambient temperature overnight, evaporated, diluted with 40 mL of water, and made basic with 3 *N* sodium hydroxide. The solution was extracted with chloroform (3 × 25 mL) and the combined organic layers washed with water and dried over sodium sulfate. The filtered solution was evaporated and the residue triturated with ether. The precipitate was filtered and washed with ether to give 0.48 g (60%) of white crystals, mp 122–125°C. Recrystallization from ethanol–water gave a material whose infrared and proton nmr spectra were identical to the above material, but whose melting point was 74–75°C. The analysis and solution spectra of the crude and the recrystallized materials were identical, indicating that two different crystal modifications were being obtained. ir($CHCl_3$): 3250, 1645, 1610, 1170, 1110, 930 cm^{-1}; ^1H nmr ($CDCl_3$) δ: 8.00–7.12 (AB q, 4H), 5.05–4.40 (m, 3H), 2.70–2.26 (m, 7H), 2.00–1.25 (m, 13H). *Anal.* calcd. for $C_{19}H_{27}N_3O_2S$: C 63.13, H 7.53, N 11.62; found: C 62.78, H 7.98, N 11.17.

Reduction of this material using sodium cyanoborohydride in 1 :1 DMF–sulfolane at 120°C (8) gave the same result as the direct Wolff–Kischner reduction described below.

Wolff-Kischner Reduction of Ketone 7

Method A

Ketone **7** (0.795 g, 4.1 mmol) was dissolved in 10 mL triethylene glycol and 5.5 mL hydrazine hydrate was added. The solution was stirred at 120°C for 8 h, cooled, 0.87 g (3 equiv.) of potassium hydroxide was added, and the solution was refluxed for 24 h. The cooled solution was diluted with 50 mL of water and extracted with pentane (3 × 75 mL). The combined organic phases were washed with water, dried over sodium sulfate, and evaporated to give 0.36 g of pale yellow liquid. Gas chromatographic analysis (column B, 145°C) showed two compounds in a 1 :1 ratio. The shorter retention time material was identical to **11** (*vide infra*). The longer retention time material gave the same spectral data as that reported below under method *B* except that the absorptions between δ 6.05 and 4.80 accounted for only two protons. The FIMS of the crude reaction mixture showed strong peaks at m/z = 181, 179, 177, 138, and 137.

Method B

Carrying out the reaction in refluxing ethylene glycol and allowing the volatiles to distill out led to the isolation of a pale yellow liquid which showed the same two peaks in the gas chromatogram, but now in the ratio of ca. 1 :20. The major

product was isolated by glc collection; ir(CCl_4): 2930, 1450, 1300, 1120, 1110, 1000, 910 cm^{-1}; ^1H nmr (C_6D_6) δ: 6.05–5.32 (m, 1H), 5.20–4.80 (m, 2H), 2.75–2.00 (m, 4H), 1.90–0.93 (m, 14H); ^{13}C nmr (C_6D_6) δ: 135.9, 116.5, 55.5, 49.6, 36.1, 26.6, 25.9, 20.5. *Anal.* calcd. for $C_{12}H_{21}N$: C 80.38, H 11.81, N 7.81; found: C 79.88, H 11.52, N 7.43. Refluxing the product of method *B* with potassium hydroxide in triethylene glycol led to the formation of a mixture, identical to that obtained from method *A*.

Hydroboration–oxidation of the product from method *B* afforded a mixture of compounds whose nmr spectrum showed absorptions *inter alia* at δ 3.45 (t) and 3.62 (*m*) suggesting the presence of primary and secondary alcohols.

*10-Propylquinolizidine (**11**)*

The crude reaction mixture from method *A* (0.4 g, 2.23 mmol as $C_{12}H_{21}N$) was dissolved in 5 mL glacial acetic acid and added to a suspension of prereduced platinum oxide in 5 mL of the same solvent. After 30 min, 55.4 mL (99.5%) of hydrogen had been absorbed and the absorption ceased. The solution was filtered and the product **11** (0.395 g, 97%) was isolated as a clear oil. The picrate crystallized from ethanol, mp 177–179°C (lit (2) mp 185–186°C). The ^{13}C spectrum ((C_6D_6) δ: 55.0, 49.4, 36.1, 26.6, 23.7, 20.7, 17.5, 15.3) supports a *trans*-fused quinolizidine bearing an axial 10-substituent. The infrared spectrum, glc retention times, and picrate melting points (separate and mixed) of this material, and the shorter retention time material isolated from method *A* of the Wolff–Kischner reduction indicated the identity of the two substances.

Acknowledgements

Support of this work by the National Science and Engineering Research Council of Canada in the form of operating grants and an equipment grant for the purchase of the Bruker CXP 100 spectrometer is gratefully acknowledged. The author also expresses his appreciation to Dr. G. L. Goe and the Reilly Tar and Chemical Corporation of Indianapolis for a generous gift of pipecolic acid.

1. N. J. Leonard, A. S. Hay, R. W. Fulmer, and V. W. Gash. J. Am. Chem. Soc. **77**, 439 (1955).
2. N. J. Leonard and A. S. Hay. J. Am. Chem. Soc. **78**, 1984 (1956).
3. N. J. Leonard, S. Swann, and J. Figueras. J. Am. Chem. Soc. **74**, 4620 (1952).
4. L. N. Mander and J. V. Turner. J. Org. Chem. **38**, 2915 (1973).
5. G. R. Clemo, T. P. Metcalfe, and R. Raper. J. Chem. Soc. 1429 (1936); N. J. Leonard and W. C. Wildman. J. Am. Chem. Soc. **71**, 3098 (1949).
6. G. R. Pettit and E. E. Van Tameln. Organic reactions. Vol. 12. Wiley, New York, NY. 1962. p. 357.
7. M. F. Grundon, H. B. Henbest, and M. D. Scott. J. Chem. Soc. 1855 (1963).
8. R. O. Hutchins, C. A. Milewski, and B. E. Maryanoff. J. Am. Chem. Soc. **95**, 3662 (1973).
9. T. M. Moynehan, K. Schofield, R. A. Y. Jones, and A. R. Katritzky. J. Chem. Soc. 2637 (1962); C. D. Johnson, R. A. Y. Jones, A. R. Katritzky, C. R. Palmer, K. Schofield, and R. J. Wells. J. Chem. Soc. 6797 (1965).
10. R. T. Lalonde and T. N. Donvito. Can. J. Chem. **52**, 3778 (1974).
11. D. J. Cram, M. R. V. Sahyun, and G. R. Knox. J. Am. Chem. Soc. **84**, 1734 (1962).

A ^{13}C nmr study of metal ion binding to pyridoxine

J. STEPHEN HARTMAN[1] AND ERIC C. KELUSKY

Department of Chemistry, Brock University, St. Catharines, Ont., Canada L2S 3A1

Received October 10, 1978

J. STEPHEN HARTMAN and ERIC C. KELUSKY. Can. J. Chem. **57**, 2118 (1979).

^{13}C nmr confirms that coordination of metal ions by pyridoxine is through the C-3 and C-4′ oxygens in aqueous solution. Nitrogen appears to become more effective as a donor site in water–dimethylsulfoxide mixtures, while with increasing proportions of DMSO some cations are coordinated by DMSO rather than by pyridoxine. Changes in ^{13}C spin–lattice relaxation times on metal ion coordination are more informative about metal binding sites than changes in ^{13}C chemical shift. Some analogous results are reported for pyridoxamine.

J. STEPHEN HARTMAN et ERIC C. KELUSKY. Can. J. Chem. **57**, 2118 (1979).

La rmn du ^{13}C confirme qu'en milieu aqueux la coordination des ions métalliques par la pyridoxine se fait par les oxygènes en C-3 et en C-4′. Il semble que l'azote devient un site donneur plus efficace dans des mélanges eau–diméthylsulfoxyde; si on augmente les proportions de DMSO, quelques cations sont coordonnés par le DMSO plutôt que par la pyridoxine. Les changements dans les temps de relaxation ^{13}C spin–réseau lors de la coordination d'un ion métallique fournissent plus d'informations concernant les sites de complexation métallique que les changements dans les déplacements chimiques ^{13}C. On a obtenu des résultats analogues avec la pyridoxamine,

[Traduit par le journal]

Introduction

Pyridoxine (I) and pyridoxamine (II) are members of the vitamin B6 family of compounds. Enzymic reactions utilizing vitamin B6 can be mimiced by systems containing pyridoxamine or pyridoxal (III),

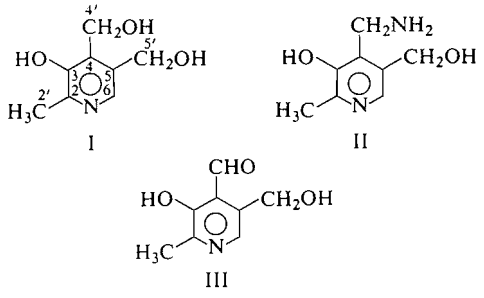

I II III

an amino acid, and a metal ion. Schiff base formation is involved, and the metal ion possibly acts as a template in its formation (1). Thus vitamin B6 – metal complexes have been extensively studied as models of enzymatic behaviour (1). Chaturvedi has reported that in aqueous solution pyridoxine forms 1:1 and 1:2 metal–ligand complexes with Cd^{2+} and Pb^{2+} (2). Similar coordination was found with Cu^{2+} and Ni^{2+}, and because of the similarity of stability constants with 2-picoline, it was proposed that coordination occurred through the ring nitrogen (3). Pyridoxamine's interactions with metals in solution have been studied by a number of workers (4–6) and recently the first crystal structure of a metal complex with pyridoxamine has been determined (7).

^{13}C chemical shifts of the vitamin B6 family of compounds have been reported (8–11). These show pronounced pH-dependence because of protonation and deprotonation reactions (12, 13). For pyridoxine these are:

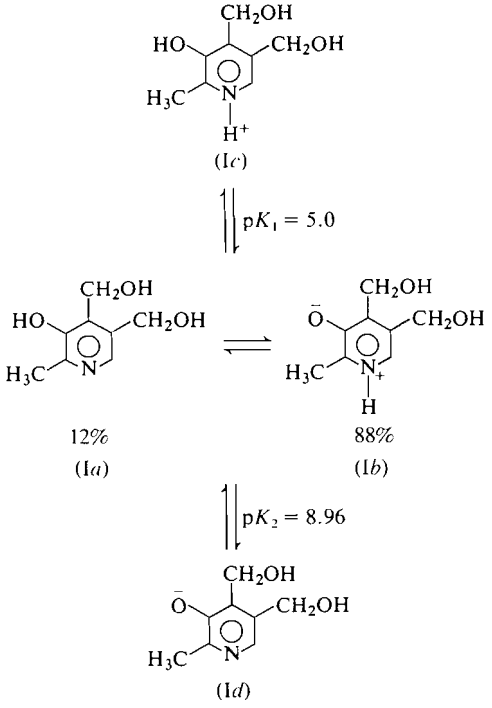

At neutral pH the zwitterionic form I*b* predominates over the non-dipolar form I*a* (12). Similar effects are found in II and III.

[1]To whom all correspondence should be addressed.

0008-4042/79/162118-06$01.00/0

TABLE 1. Metal salt-induced ^{13}C nmr chemical shift changes of pyridoxine[a]

Salt	^{13}C nmr chemical shift							
	C-2	C-3	C-4	C-5	C-6	C-2′	C-4′	C-5′
A. Aqueous solution[b]								
NaCl	0.0	0.2	0.1	0.1	−0.1	0.1	0.1	0.1
NaOAc	0.1	0.2	0.1	0.1	−0.1	−0.1	−0.1	0.0
NaI	0.0	0.2	0.2	0.1	0.1	0.2	0.2	0.2
$MgCl_2$	0.0	0.8	0.6	0.1	−0.7	−0.1	0.1	0.1
$ZnCl_2$	0.8	1.3	1.6	0.2	0.1	−0.2	0.5	0.1
$CdCl_2$[c]	0.4	1.0	0.8	0.4	−0.2	0.1	0.3	0.2
$CdBr_2$	0.7	0.8	0.9	0.2	0.0	0.2	0.4	0.2
CdI_2	0.6	1.0	1.2	0.3	0.3	0.7	0.7	0.4
Pyridoxine chemical shifts[d]	145.4	160.4	139.1	136.1	127.0	16.6	57.1	59.7
B. DMSO-d_6 solution								
$ZnCl_2$	1.2	0.8	0.1	0.1	1.8	1.2	1.2	0.9
$CdCl_2$	0.4	0.4	0.1	0.0	0.7	1.7	0.7	0.4
$HgCl_2$	0.9	0.6	0.0	−0.1	1.3	1.0	1.0	0.7
Pyridoxine chemical shifts	141.2	151.8	140.8	138.8	128.6	14.6	55.5	57.5

[a]0.50 *M* in pyridoxine and in metal salt. Positive values indicate shifts (ppm) to lower applied field.
[b]pH 6.2 for sodium salts, 6.7 for all others.
[c]Reference 17 gives similar values for a 0.050 *M* solution, pH 6.8.
[d]Chemical shifts (pH 6.7) agree closely with those of ref. 17.

There have also been ^{13}C nmr studies of Schiff base formation involving pyridoxal 5′-phosphate and amino acids (14–16). Gallais and co-workers have reported the effects of $CdCl_2$ on ^{13}C chemical shifts of pyridoxine (17); a 1:1 interaction was indicated. However it is known that the presence of salts can cause serious environmental effects on ^{13}C chemical shifts, quite apart from complex formation (18).

With the development of pulse and Fourier transform nmr techniques that have made the measurement of ^{13}C spin–lattice relaxation times (T_1's) a routine, if time-consuming, procedure (19, 20) it has become possible to use T_1 measurements to probe sites of metal ion binding to various molecules, including some which act as ligands for metal ions in biologically important systems (21–23). We report here our initial ^{13}C nmr studies of metal ion – pyridoxine interactions, utilizing changes in chemical shift and in spin–lattice relaxation times in the presence of metal ions.

Results and Discussion

A. Effect of Added Salts on ^{13}C Chemical Shifts

Table 1 summarizes changes in ^{13}C chemical shifts of pyridoxine in H_2O and in DMSO-d_6 on addition of various salts. We note that:

(*i*) The sodium salts have only very small effects; that of sodium iodide is greater than that of the chloride or acetate, especially on the side-chain carbons. However the effects become more pronounced when an excess of the sodium salt is present. Neglect of this, together with the use of sodium chloride to maintain constant ionic strength, has yielded incorrect binding sites in a number of studies of tetracycline, as discussed by Everett and co-workers (24).

(*ii*) The divalent metal halides give much larger shifts than the sodium salts, the most pronounced being at C-3 and C-4, consistent with metal ion chelation at the C-3 and C-4′ oxygens. However, substantial shifts occur at various other carbons as well. The C-4′ shifts are not as great as expected from chelation at C-4′ oxygen, and a steric compression shift might partially counteract the expected low-field shift.

(*iii*) Excess metal halide also has pronounced effects on chemical shifts, as illustrated in Fig. 1 for CdI_2. The break in the curve at 1:1 proportions does indicate a 1:1 complex, consistent with the report of Gallais and co-workers for the pyridoxine–$CdCl_2$ system (17). However, the continuing change in chemical shift past 1:1 proportions must be attributed to the effects of non-complexed CdI_2.

(*iv*) At low pH (2.75), zinc, cadmium, and mercury(II) chlorides have little effect on ^{13}C chemical shifts ($\lesssim$0.2 ppm for most carbons), consistent with the inability of these cations to compete with the proton for donor sites when I*c* is the predominant species.

(*v*) Metal ion-induced shifts in DMSO-d_6 are

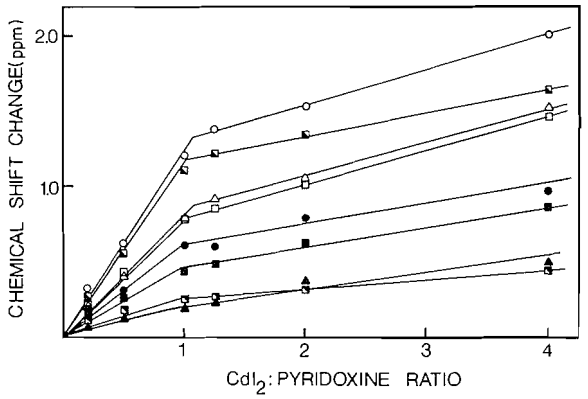

FIG. 1. Plot of ^{13}C chemical shift changes (in ppm) against the CdI_2: pyridoxine ratio. (C-4, ○; C-3, ◪; C-2′, △; C-4′, □; C-2, ●; C-5′, ■; C-6, ▲; C-5, ◪.)

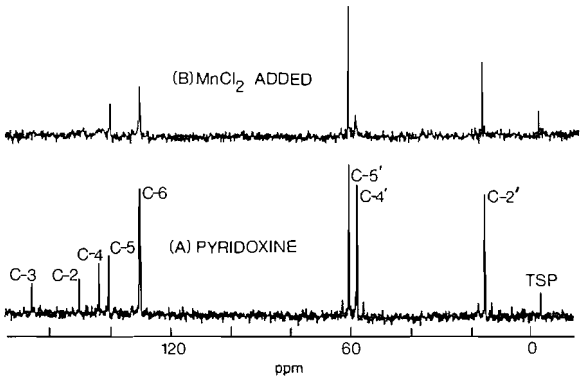

FIG. 2. ^{13}C nmr spectra of (*A*) pyridoxine (0.50 *M*) in D_2O and (*B*) pyridoxine with $MnCl_2$ (1.0×10^{-3} *M*) added.

larger than for the corresponding species in water, and the carbons which are most affected (C-2, C-2′, C-6) are different. This is suggestive of coordination through nitrogen; however, the C-3, C-4′, and C-5′ are also strongly affected. In fact all carbons except C-4 and C-5, which are remote from the periphery and from a possible donor site, are significantly shifted. It is interesting that the effects are greater for $ZnCl_2$ than for $CdCl_2$ or $HgCl_2$. Results discussed below indicate that DMSO displaces pyridoxine from the coordination sphere of some metal ions.

Thus ^{13}C chemical shift changes on adding metal salts can indicate coordination sites but not confirm them. It should be kept in mind that metal ion-induced shifts are small changes superimposed on parameters that are already subject to medium effects such as solvent (Table 1) and pH (17).

B. Effects of Added Mn^{2+}

Figure 2 shows the effect of 0.0010 *M* $MnCl_2$ on the ^{13}C spectrum of pyridoxine in D_2O. The line broadening effect of paramagnetic Mn^{2+} is a result of the shortening of the spin–spin relaxation time T_2, which varies inversely with the line width. If the dipolar relaxation mechanism predominates, T_2 varies directly with the sixth power of the metal to carbon distance (25), and hence line broadening is most pronounced for the carbon atoms nearest to the metal binding sites. The disappearance of the C-2, C-3, C-4, and C-4′ resonances indicates extreme broadening and hence binding of Mn^{2+} to the C-3 and C-4′ oxygens. However, in many cases of line broadening due to Mn^{2+} the dipolar relaxation term is not predominant; scalar coupling can predominate (23, 26). The effects of scalar coupling need not be localized at the donor site but can extend around an aromatic ring. The greater broadening of C-6 compared to C-5 and C-2′ could be due either to scalar coupling or to a small fraction of bonding to the nitrogen. This study does indicate that the principal binding sites are the C-3 and C-4′ oxygens.

A similar study in DMSO-d_6 showed no broadening of pyridoxine resonances, indicating preferential binding of Mn^{2+} to DMSO. This is consistent with the known strong bonding of DMSO to cations of the first transition series (27).

Preliminary studies of pyridoxamine with $MnCl_2$ in D_2O and in DMSO-d_6 gave similar results. Pyridoxamine, in spite of its greater complexing ability compared with pyridoxine (28), is unable to compete with DMSO for Mn^{2+}. In aqueous solution selective broadening removed the C-3 and C-4 peaks, *but not the C-4′ peak*, from the spectrum. This last result is intriguing and merits further investigation. It is known that Cu^{2+} can form a chelate complex with the C-3 oxygen and the C-4′ nitrogen of pyridoxamine (7), and there seems little reason why Mn^{2+} should not do the same. Espersen and Martin (29) have proposed that at high ligand-to-metal-ion ratios the metal ion might be passed from ligand to ligand before proton transfer reactions can occur. Since pyridoxamine is predominantly in the zwitterionic form II*a* (12), with no lone pairs on the C-4′ nitrogen,

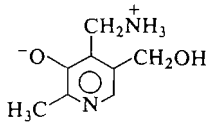

II*a*

insufficient time for proton transfer could account for the lack of broadening of the C-4′ peak. If so, this would illustrate the suggestion (29) that at high ligand-to-metal-ion ratios the predominant complex may not be the same as that existing at more nearly stoichiometric ratios.

C. Spin–Lattice Relaxation Times (T_1's)

^{13}C T_1 values for pyridoxine and pyridoxamine are given in Table 2. These are shorter than typical

TABLE 2. ^{13}C T_1 values (s) at 32°C

a. Protonated carbons

Solute (0.50 *M*)	Solvent	Mol% of DMSO	^{13}C T_1 C-6	C-2′	C-4′	C-5′
Pyridoxine	D_2O(p*D* 5.5)[a]	0	0.78±0.07	2.82±0.12	0.89±0.08	1.16±0.05
Pyridoxine	D_2O/DMSO	13.3	0.39±0.04	1.49±0.11	0.52±0.05	0.46±0.05
Pyridoxine	D_2O/DMSO	26.5	0.34±0.03	1.24±0.12	0.38±0.04	0.39±0.03
Pyridoxine	D_2O/DMSO	33.7	0.38±0.03	1.30±0.15	0.38±0.04	0.41±0.04
Pyridoxine	D_2O/DMSO	50.0	0.40±0.06	1.43±0.12	0.57±0.05	0.57±0.06
Pyridoxine	D_2O/DMSO	81.8	0.74±0.08	2.12±0.11	0.70±0.04	0.69±0.05
Pyridoxine	DMSO	100	0.68±0.05	2.04±0.25	0.73±0.05	0.75±0.06
Pyridoxamine	D_2O(p*D* 6.1)	—	1.37±0.10	3.50±0.25	0.80±0.06	1.25±0.09

b. Non-protonated carbons

Solute (0.50 *M*)	Solvent	^{13}C T_1 C-2	C-3	C-4	C-5
Pyridoxine	D_2O(p*D* 5.5)	6.6±0.7	7.1±1.0	7.60±0.9	13.9±1.2
Pyridoxine + $CuCl_2$ (1×10^{-6} *M*)	D_2O(p*D* 5.5)	5.1±0.6[b]	4.2±1.0[b]	7.1 ±1.3	11.2±1.3

[a]p*D* = pH + 0.41.
[b]Determined by manual plotting.

T_1's for organic liquids (19, 20) since strong solvent–solute hydrogen bonding slows the rotation of solute molecules (19). T_1's of pyridoxine are similar in D_2O and in DMSO solutions, indicating a similar extent of solvent–solute interaction in each solvent. Interestingly, pyridoxine T_1's are much shorter in D_2O/DMSO solvent mixtures. This is in accord with the proposal that water–DMSO association is greater than water–water association, due to a combination of hydrogen bonding and dipolar attraction (30). Such strong association would further restrict the tumbling of solute molecules.

Table 2 includes T_1's for non-protonated carbons in aqueous pyridoxine, with and without added Cu^{2+}. On adding Cu^{2+} there is a pronounced decrease in T_1 for C-3, indicating proximity to a donor site. However the errors are large. Time and instrument stability factors led us to concentrate on protonated carbons for which T_1 data can be accumulated relatively rapidly.

The effect of a paramagnetic metal ion on the relaxation process is given by the relationship

$$[1] \quad 1/T_{1P} = 1/T_{1(obs)} - 1/T_{1,0}$$

where $T_{1(obs)}$ and $T_{1,0}$ are the relaxation times in the presence and absence of the paramagnetic metal, respectively, and T_{1P} is the relaxation time due specifically to the paramagnetic species. T_{1P}, unlike T_{2P}, is dominated by the dipolar relaxation mechanism (23, 29), with only rare exceptions (31). Hence, if a number of simplifying assumptions are made (23), T_{1P}^{-1} can be shown (23, 32) to exhibit reciprocal sixth-power dependence on the metal-to-carbon distance, so that relative T_{1P}^{-1} values can be used to determine metal coordination sites.

In practice the assumptions made, such as isotropic tumbling of molecules, will not be fully valid. In particular, delocalization of unpaired electron density onto ligand carbons is possible. This can be an important perturbing factor even when the extent of such delocalization is very small, because of the reciprocal sixth-power dependence of the dipolar relaxation mechanism (23, 29). In spite of these limitations, Espersen and Martin (29) consider selective T_1 measurements to be useful in estimating metal–carbon and metal–proton distances, and to be certainly far better than the widely used selective line broadening (T_2) method. Led and Grant (31) warn that extreme caution is warranted in drawing *quantitative* conclusions from limited T_1 information.

Table 3 gives T_{1P}^{-1} values for pyridoxine/$CuCl_2$, pyridoxamine/$CuCl_2$, and pyridoxine/$MnCl_2$ solutions. In aqueous solutions, by far the largest T_{1P}^{-1} (corresponding to the greatest metal ion effect in shortening T_1) is found for C-4′, in accord with chelation involving the C-3 oxygen and the C-4′ substituent. The pronounced decrease of pyridoxine/$CuCl_2$ T_{1P}^{-1} values at the higher temperature is indicative of the desired fast exchange conditions (25). The similarity of the effects of Mn^{2+} and Cu^{2+}, when the Mn^{2+} concentration is lower by a factor of five to correct for its five unpaired electrons, indicates a similar mode of interaction of both metal ions with pyridoxine.

TABLE 3. T_{1P}^{-1} values (s^{-1})

Solute (0.50 *M*)	Solvent	Mol% DMSO	T_{1P}^{-1} (s^{-1}) C-6	C-2′	C-4′	C-5′
	A. For addition of 5.0×10^{-6} *M* $CuCl_2$; 32°C					
Pyridoxine	D_2O(p*D* 5.5)	0.0	0.1±0.2	0.2±0.1	0.8±0.2	0.2±0.1
Pyridoxine	D_2O/DMSO	33.7	2.3±0.6	0.1±0.1	0.6±0.3	0.0±0.1
Pyridoxine	D_2O/DMSO	81.8	0.3±0.1	0.1±0.1	0.0±0.1	0.2±0.2
Pyridoxine	DMSO	100.0	0.0±0.1	0.0±0.1	0.0±0.1	0.0±0.1
Pyridoxamine	D_2O(p*D* 6.1)	0.0	0.0±0.1	0.0±0.1	0.6±0.2	0.1±0.1
	B. For addition of 5.0×10^{-6} *M* $CuCl_2$; 70°C					
Pyridoxine	D_2O(p*D* 5.5)	0.0	0.0±0.2	0.0±0.3	0.0±0.2	0.0±0.3
	C. For addition of 1.0×10^{-6} *M* $MnCl_2$; 32°C					
Pyridoxine	D_2O(p*D* 5.5)	0.0	0.0±0.2	0.1±0.1	0.7±0.2	0.0±0.1

Assuming chelation from the C-3 oxygen and the C-4′ substituent in aqueous solution, T_{1P}^{-1} values for the other protonated carbons should be less than 0.1 s^{-1}, based on the geometry of related species (7, 33). Since some T_{1P}^{-1} values for these carbons are somewhat greater than 0.1 s^{-1}, there appears to be either some breakdown of the inverse sixth power dependence, or some interaction of Cu^{2+} with the ring nitrogen or C-5′ oxygen. We can apparently exclude our choice of $T_{1,0}$ value (eq. [1]) as the source of error. $T_{1,0}$ values are only slightly affected by the addition of diamagnetic ions (Mg^{2+} or Zn^{2+}, 5×10^{-6} *M*) to simulate any effects of Cu^{2+} in addition to its paramagnetism. The largest effect of the diamagnetic ions was on C-2′ (T_1 = 2.4 s rather than 2.8 s), and this change had only a small effect on T_{1P}^{-1}.

As noted above, some deviation from the inverse sixth power dependence on distance is to be expected (29, 31), and does not affect our qualitative conclusion of chelation from the C-3 and C-4′ substituents in aqueous solution.

^1H T_{1P}^{-1} values were obtained for the C-H protons of pyridoxine and pyridoxamine in aqueous solution. The C-4′ protons were the most affected by Cu^{2+}, further supporting the C-4′ substituent being a donor to Cu^{2+}. However, there were quite large effects on the other protons as well.

Striking effects occur in the pyridoxine/Cu^{2+} system when the solvent is changed from D_2O to DMSO. In an intermediate solvent mixture T_{1P}^{-1} of C-6 becomes large, but T_{1P}^{-1}'s for both C-6 and C-4′ decrease to small values in a DMSO-rich solution (Table 3). This suggests that the ring nitrogen becomes an important donor site in D_2O/DMSO mixed solvent, but that Cu^{2+} is tied up by DMSO coordination at higher DMSO concentrations.

Donation from ring nitrogen in water–DMSO mixtures is reasonable since neutral pyridoxine, primarily in the zwitterionic form I*b* in aqueous solution, should undergo a shift of the equilibrium to the uncharged form as the dielectric constant of the solvent decreases. Such an effect has indeed been reported in water–dioxane mixtures (12). Large changes in acid–base equilibria are frequently found on transfer from water to dipolar aprotic solvents (34). I*a*, unlike I*b*, has a lone pair on nitrogen, so the nitrogen is much more accessible to metal ions.

Coordination of Cu^{2+} by DMSO in preference to pyridoxine in DMSO-rich solvent mixtures is consistent with our line broadening results with Mn^{2+}, and with the known (27) strong complexing ability of DMSO toward ions of the first transition series; $[Cu(DMSO)_6]^{2+}$, $[Cu(DMSO)_3Cl]^+$, and $[Cu(DMSO)_2Cl_2]$ apparently predominate.

Conclusions

Our evidence is consistent with metal ion coordination through the C-3 and C-4′ oxygens of pyridoxine in aqueous solution, but with a shift to nitrogen coordination on addition of DMSO, and eventual displacement of pyridoxine from the coordination sphere of some metal ions by DMSO. The indications of a shift to coordination by ring nitrogen in D_2O/DMSO solvent mixtures are of particular interest in that this lower dielectric constant medium may mimic enzyme sites more closely than aqueous solutions can.

Experimental

Pyridoxine hydrochloride and pyridoxamine dihydrochloride (Sigma Chemical Co.) were used without further purification for chemical shift measurements in H_2O. For all T_1 measurements and for chemical shifts in DMSO-d_6, pyridoxine was prepared by neutralization of an aqueous solution of the hydrochloride with sodium hydroxide, evaporation to dryness, and separation of pyridoxine from sodium chloride by solution in ethanol. Pyridoxamine monohydrochloride was prepared from the dihydrochloride by a similar procedure. Solutions were made up in deionized distilled water (H_2O or D_2O), or

DMSO or DMSO-d_6, and oxygen was removed by bubbling nitrogen through the solutions for several minutes. Glassware was soaked in EDTA solution prior to use to remove traces of paramagnetic metal ions. Following the addition of metal salts, pH was adjusted to within 0.05 pH units, using a conventional pH meter and glass electrode. For D_2O solutions a correction must be made to the meter reading (35):

$$pD = pH + 0.41$$

pD was adjusted using NaOD or DCl solutions.

Metal salts were reagent grade. Fisher certified reagents were used except for $CuCl_2$ (British Drug Houses), $CdCl_2$ (Research Organic/Inorganic Chemicals), and CdI_2 (AnalaR). All nmr spectra were obtained on a Bruker WP-60 Fourier transform nmr spectrometer. ^{13}C spectra were obtained at 15.08 MHz and 32°C using 10 mm sample tubes. A 3759 Hz sweep width was used, with a 1.09 s acquisition time for an 8K FID. Proton noise decoupling (5 W) was applied. For chemical shift measurements a 30° pulse was used, with the Phase Alternating Pulse Sequence. Between 3000 and 16 000 pulses were accumulated. The FID's were transformed with 0.5 Hz of line broadening. In the H_2O samples used for chemical shift measurements, a concentric 5 mm tube of D_2O containing 5% TSP ($(CH_3)_3SiCD_2CD_2CO_2Na$) was used as the deuterium lock signal; the TSP provided the ^{13}C reference (−1.49 ppm from TMS; values in Table 1 have been converted to ppm to low field of TMS). Internal tetramethylsilane was used as the reference in DMSO-d_6 solutions.

^{13}C T_1 measurements were made using the inversion recovery technique (36, 37) and the Nicolet T_1 Program/II (developed by J. W. Cooper, Nicolet Instrument Corporation). In the pulse sequence $\{180°-\tau-90°-D_2\}_n$ the delay time D_2 was set at 5 times the largest T_1 value and at least eight different τ values between 0.001 and D_2 seconds were used. The 90° pulse varied between 8.8 and 9.2 μs and was checked frequently. Proton noise decoupling (5 W) was applied. Between 100 and 200 scans were accumulated at each τ value. The FID's were transformed with 2.0 Hz of line broadening. All samples were filled to a volume of 2.0 mL.

^1H T_1 measurements were obtained in a similar fashion to the ^{13}C measurements, but at 60 MHz and 29°C using 5 mm tubes, a 500 Hz sweep width, and accumulation of 4 scans. The 90° pulse was 3.8 μs. Spectra were transformed with 0.10 Hz of line broadening.

Acknowledgements

We thank the National Research Council of Canada for an equipment grant, Dr. J. M. Miller and Mr. T. R. B. Jones for assistance with the instrumentation, and Dr. M. F. Richardson, Mr. K. J. Franklin, and Dr. H. L. Holland for helpful discussions and for providing results prior to publication.

1. R. H. Holm. *In* Inorganic biochemistry. Vol. 2. *Edited by* G. L. Eichhorn. Elsevier, New York, NY. 1973. Chapt. 31.
2. D. N. Chaturvedi and C. M. Gupta. J. Inorg. Nucl. Chem. **36**, 2155 (1974).
3. M. S. El-Ezaby and N. Gayed. J. Inorg. Nucl. Chem. **37**, 1065 (1975).
4. M. S. El-Ezaby, M. Rashad, and N. M. Moussa. J. Inorg. Nucl. Chem. **39**, 175 (1977).
5. V. R. Williams and J. B. Neilands. Arch. Biochem. Biophys. **53**, 56 (1954).
6. R. L. Gustafson and A. E. Martell. Arch. Biochem. Biophys. **168**, 485 (1975).
7. K. J. Franklin and M. F. Richardson. J. Chem. Soc. Chem. Commun. 97 (1978).
8. R. D. Lapper, H. H. Mantsch, and I. C. P. Smith. Can. J. Chem. **53**, 2406 (1975).
9. T. H. Witherup and E. H. Abbot. J. Org. Chem. **40**, 2229 (1975).
10. R. C. Haruff and W. T. Jenkins. Org. Magn. Reson. **6**, 298 (1974).
11. R. Haran, F. Nepveu-Juras, and J.-P. Laurent. Org. Magn. Reson. **10**, 203 (1977).
12. D. E. Metzler and E. E. Snell. J. Am. Chem. Soc. **77**, 2431 (1955).
13. O. A. Gansow and R. H. Holm. Tetrahedron, **24**, 4477 (1968).
14. D. K. Dalling, D. M. Grant, and W. J. Horton. J. Biol. Chem. **251**, 7661 (1976).
15. B. H. Jo, V. Nair, and L. Davis. J. Am. Chem. Soc. **99**, 4467 (1977).
16. M. H. O'Leary and J. R. Payne. J. Biol. Chem. **251**, 2248 (1976).
17. F. Gallais, R. Haran, J.-P. Laurent, and F. Nepveu-Juras. Compt. Rend. C. **284**, 29 (1977); A. Mosset, F. Nepveu-Juras, R. Haran, and J. J. Bonnet. J. Inorg. Nucl. Chem. **40**, 1259 (1978).
18. L. G. Marzilli, R. C. Stewart, C. P. Van Vuuren, B. de Castro, and J. P. Caradonna. J. Am. Chem. Soc. **100**, 3967 (1978).
19. J. R. Lyerla and G. C. Levy. Topics in carbon-13 NMR spectroscopy. Vol. 1. *Edited by* G. C. Levy. Wiley-Interscience, New York, NY. 1974. p. 79.
20. E. Breitmaier, K.-H. Spohn, and S. Berger. Angew. Chem. Int. Ed. Engl. **14**, 144 (1975).
21. R. E. Wasylishen and M. R. Graham. Can. J. Chem. **54**, 617 (1976).
22. G. Kotowycz. Can. J. Chem. **52**, 924 (1974).
23. J. J. Led and D. M. Grant. J. Am. Chem. Soc. **97**, 6962 (1975).
24. J. Gulbis, G. W. Everett, and C. W. Frank. J. Am. Chem. Soc. **98**, 1280 (1976).
25. R. A. Dwek, R. J. P. Williams, and A. V. Xavier. *In* Metal ions in biological systems. Vol. 4. *Edited by* H. Sigel. Marcel Dekker, New York, NY. 1974. Chapt. 3.
26. W. G. Espersen and R. B. Martin. J. Phys. Chem. **80**, 161 (1976).
27. V. Gutmann. Coordination chemistry in non-aqueous solutions. Springer-Verlag, New York, NY. 1968. pp. 155–159.
28. M. S. El-Ezaby and F. R. El-Eziri. J. Inorg. Nucl. Chem. **38**, 1901 (1976).
29. W. G. Espersen and R. B. Martin. J. Am. Chem. Soc. **98**, 40 (1976).
30. W. S. MacGregor. Q. Rep. Sulfur Chem. **3**, 149 (1968).
31. J. J. Led and D. M. Grant. J. Am. Chem. Soc. **99**, 5845 (1977).
32. T. T. Swift and R. E. Connick. J. Chem. Phys. **37**, 307 (1962).
33. F. Hanic. Acta Crystallogr. **21**, 332 (1966).
34. B. G. Cox. Ann. Rep. Prog. Chem. Sect. A, **70**, 249 (1973).
35. A. K. Covington, M. Paabo, M. A. Robinson, and R. G. Bates. Anal. Chem. **40**, 700 (1968).
36. R. L. Vold, J. S. Waugh, M. P. Klein, and D. E. Phelps. J. Phys. Chem. **48**, 3831 (1968).
37. R. Freeman and H. D. W. Hill. J. Chem. Phys. **51**, 3140 (1969).

A new synthesis of chasmanine and 13-desoxydelphonine: a preferred route to the aromatic intermediate

THOMAS Y. R. TSAI, KRISHNAN P. NAMBIAR, DIKRAN KRIKORIAN, MAURIZIO BOTTA, RINALDO MARINI-BETTOLO, AND KAREL WIESNER

Natural Products Research Centre, University of New Brunswick, Fredericton, N.B., Canada E3B 5A3

Received February 19, 1979

THOMAS Y. R. TSAI, KRISHNAN P. NAMBIAR, DIKRAN KRIKORIAN, MAURIZIO BOTTA, RINALDO MARINI-BETTOLO, and KAREL WIESNER. Can. J. Chem. 57, 2124 (1979).

An efficient synthesis (stereo- and regiospecific) of compound **I** (Scheme 1) from *o*-cresol is described.

THOMAS Y. R. TSAI, KRISHNAN P. NAMBIAR, DIKRAN KRIKORIAN, MAURIZIO BOTTA, RINALDO MARINI-BETTOLO et KAREL WIESNER. Can. J. Chem. 57, 2124 (1979).

On décrit une synthèse efficace (stéréo- et régiospécifique) du composé I (schéma 1) à partir du *o*-crésol.

[Traduit par le journal]

Introduction

We have described recently a direct fully stereo- and regiospecific synthesis of 13-desoxydelphonine **VII** (1).

The approach which we have used is illustrated in Scheme 1 and it represents the most recent very simple and efficient generation of our systematic studies in this field (2). The starting material **I** was constructed by a fully stereo- and regiospecific process from vanillin (3).

We now wish to disclose the preferred route to the same aromatic intermediate **I** from *o*-cresol.

Discussion

The cresol **1** was simply converted to the indanone **3** via the β-chloropropionyl ester **2** by the procedure of Wagatsuma (4).[1] Methylation of **3** with dimethyl sulfate and potassium carbonate in acetone yielded the methoxy derivative **4**, which was transformed into the enol ether **5**. This last operation was carried out in two steps. The indanone **4** was first converted into the corresponding dimethylacetal in methanol and trimethyl orthoformate in the presence of the acidic ion exchanger Rexyn 101. Pyrolytic elimination of methanol from the dimethylacetal in refluxing *o*-xylene completed the preparation of the enol ether **5**.

Compound **5** was now carboxylated in tetrahydrofuran at −70°C with *n*-butyl lithium and carbon dioxide gas; hydrolysis of the enol ether group on work-up gave the crystalline keto acid **6**. The keto group of **6** was reduced with sodium borohydride and the product **7** was heated under reflux with phosphoric acid in dioxane. The elimination of the hydroxyl was followed by a shift of the double bond and the resulting indene acid was esterified with methanolic hydrogen chloride to the ester **8***a* (Scheme 2).

Compound **8***a* is in a thermal equilibrium with the *o*-quinonoid tautomer **8***b* and as a consequence it adds maleic anhydride quantitatively and yields the adduct **9**. Finally, decarboxylation of this last product by the method of Trost (5) gave the tricyclic olefin **10** in a yield of 85%.

The tricyclic compound **10** was next converted to the acetylaziridine **11** by treatment with trimethyl silyl azide followed by acetic acid and acetic anhydride. The aziridine was not isolated, but it was rearranged *in situ* by several days heating under nitrogen to 85°C. The product of the stereo- and regiospecific aziridine rearrangement **12** was purified by crystallization and it was obtained in a yield of 70%. The mechanism of the rearrangement is portrayed by the arrows in formula **11**. Its complete regiospecificity is due to the aromatic methoxyl, which increases the migratory aptitude of the bond in the *ortho* position and to the ester carbonyl, which makes the competing rearrangement more difficult. This last process is initiated by the opening of the other aziridine carbon–nitrogen bond and it requires the transient development of a positive charge on the carbon α to the carbonyl group—a situation well known to be energetically unfavourable.

In all of our previous work (2) we have used benzenesulfonyl aziridines rather than acetylaziri-

[1]The entire synthesis is in principle similar to our previous work in this field. Consequently to conserve space the Discussion has been abbreviated and the reader is referred to the Experimental for procedures and the characterization of the products.

0008-4042/79/162124-11$01.00/0

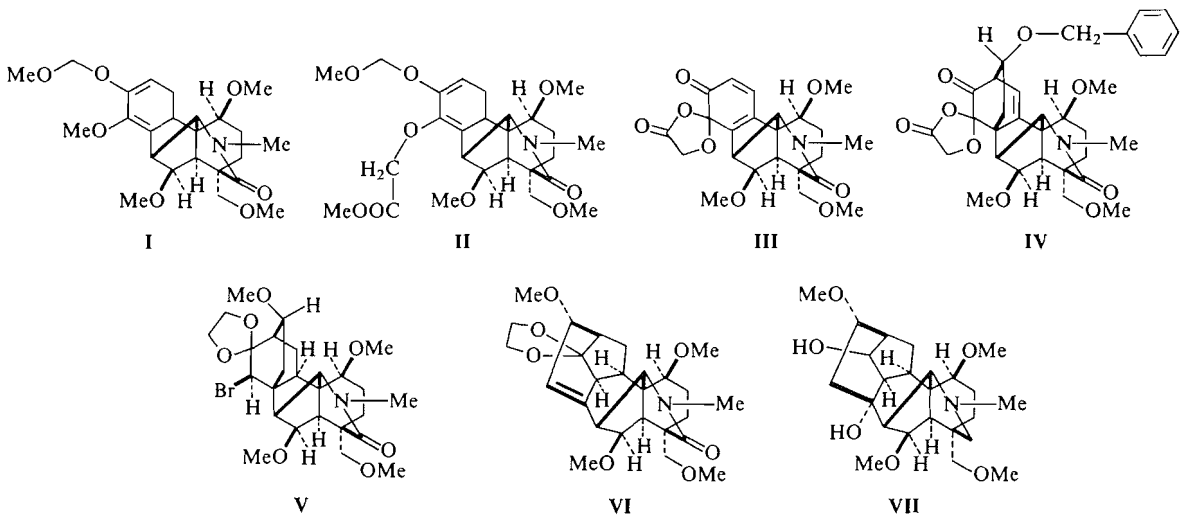

SCHEME 1

dines at a similar stage of the synthesis. This led to some complications and additional steps, but we were unable to prepare efficiently the required acetylaziridines prior to the development of the present trimethyl silyl azide (6) process.

The rearrangement product **12** was oxidized in aqueous acetic acid with ceric ammonium nitrate (7) at room temperature and the aldehyde **13** was obtained in a yield of 75% after crystallization. Methanolysis of **13** in the presence of potassium carbonate yielded the alcohol **14** which was benzylated in dichloromethane with benzyl chloride and potassium carbonate to the benzyl ether **15**.

Finally, the aldehyde group in **15** was degraded with *m*-chloroperbenzoic acid in dichloromethane and the resulting unstable formate ester **16** was immediately methanolyzed in the presence of potassium carbonate to the crystalline phenol **17**. The overall yield of the two steps was 96%.

The high yield of these operations shows clearly that in suitable situations an aromatic methyl group may be used with advantage as a 'stand-in' for a phenol. The purpose of using this device in the present situation is simple. It would have been impossible to conduct the rearrangement of compound **11** in a regiospecific manner in the presence of an electron-releasing substituent in place of the aromatic methyl (cf. ref. 8).

The phenolic group of compound **17** was finally blocked by alkylation with chloromethyl-methyl ether and the product **18** was obtained in a yield of 93%.

It still required the transformation of the carbomethoxyl to an aldehyde group, which was accomplished by reduction with lithium borohydride, followed by reoxidation of the resulting primary alcohol with dimethyl sulfoxide and dicyclohexylcarbodiimide. The overall yield of these transformations was 86% and the synthon **19** was ready for the annelation of the substituted ring A (Scheme 3).

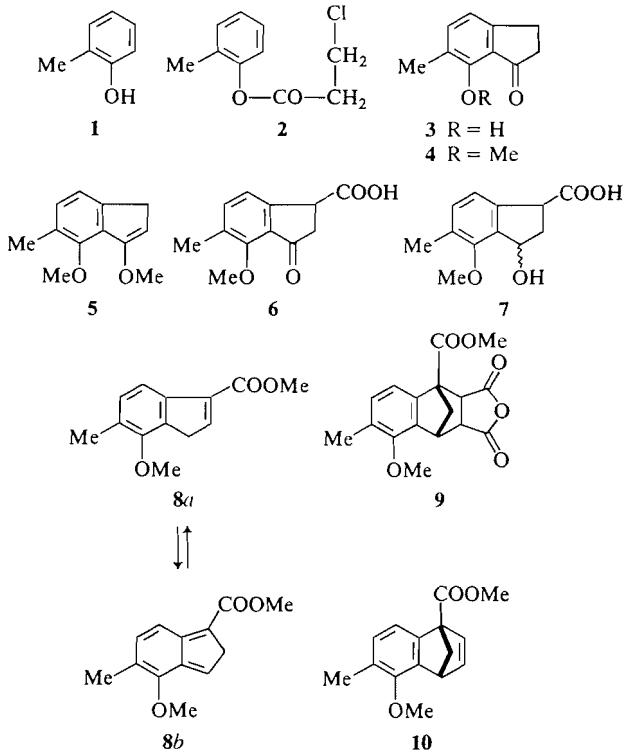

SCHEME 2

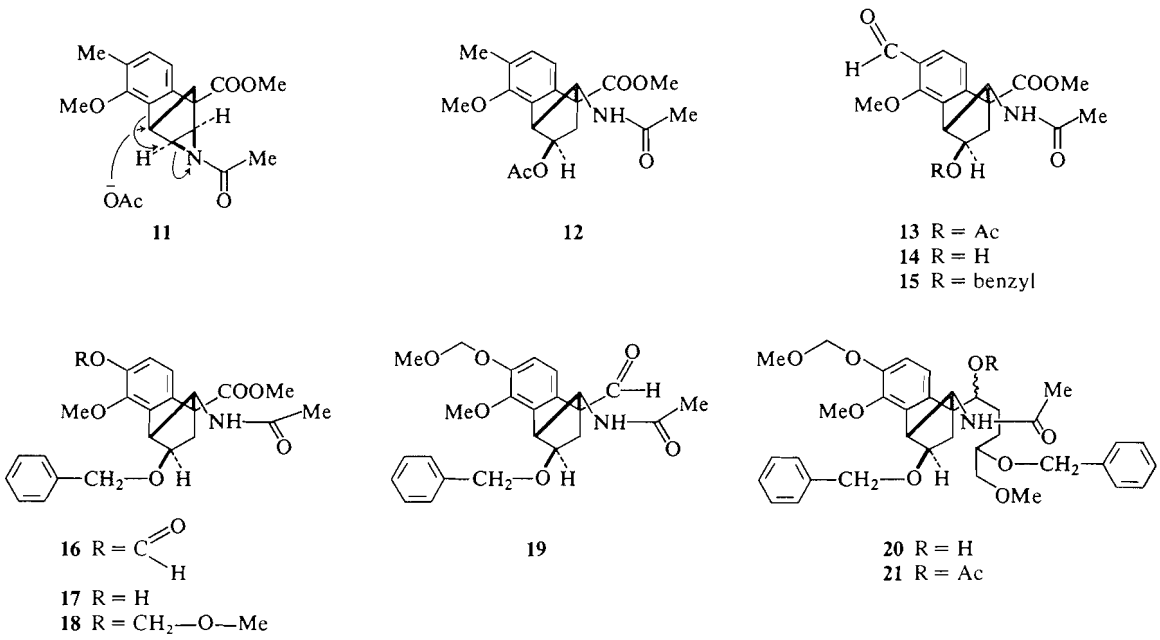

SCHEME 3

The aldehyde **19** was treated with an excess of 3-benzyloxy-4-methoxy-*n*-butyl magnesium bromide (9) and the mixture of the epimeric alcohols **20** was obtained in a yield of 87%. For purposes of characterization and analysis, the subsequent epimeric mixtures were separated by preparative thin layer chromatography (see Experimental). In the main preparative run, however, the epimers were not separated since they finally yielded one single intermediate, the keto lactam **32**.

The alcohols **20** were now quantitatively acetylated to the acetates **21** and this material was hydrogenolyzed over palladium on charcoal to the diols **22**. Oxidation of the two secondary alcoholic groups in this last product with the pyridine – chromium trioxide complex in dichloromethane yielded 85% of the epimeric diketones **23**.

The stage was now set for the closure of ring A. This was accomplished by boiling the diketone **23** under nitrogen with a saturated solution of potassium carbonate in absolute methanol and the α,β-unsaturated ketone **24** was isolated in a yield of 90%.

Photoaddition of vinyl acetate to the conjugated system of compound **24** under our standard conditions is a stereospecific process and the epimers **25** were obtained in a yield of 95% (Scheme 4). While the regiospecificity of the photoaddition is unusual, the stereospecificity is predictable by our addition rule (10) and similar to the observed behaviour of related systems.

Saponification of the acetoxy group by mild treatment with base was accompanied by a retro aldol cleavage and the homo-aldehyde **26** was obtained in a yield of 97%. The configuration of the two newly created chiral centers in compound **26** was deduced (as in similar cases, cf. ref. 1) from the proton magnetic resonance (^{1}Hmr) spectrum of this material. The singlet of the primary methoxyl in the ^{1}Hmr spectrum of compound **26** was shifted upfield to $\tau = 7.27$ as a result of the shielding by the aromatic ring. The only configuration in which the primary methoxyl can find itself in the shielding zone of the aromatic ring is the one portrayed in the formula. It is thus clear that the configuration of the quaternary carbon has been set up correctly, but the configuration of the A/B ring junction was dictated by the greater stability of the cisoid system.

It is now necessary to remove the extra carbon of the homo-aldehyde prior to the closure of the nitrogen ring. Compound **26** was converted into the dimethylacetal **27**, acetylated to **28**, and heated under reflux with dry *o*-xylene and pyridine. Elimination of methanol from the acetal group yielded 92% of the acetylated enol ether **29**. Oxidation of compound **29** with permanganate–periodate followed by esterification with diazomethane gave finally the ester **30** in a yield of 81%. The ^{1}Hmr spectrum of compound **30** (primary methoxyl singlet $\tau = 7.44$) showed clearly that no change has occurred in the A/B *cis* stereochemistry during the various operations to which the material was subjected.

The system **30** is clearly unable to close a lactam

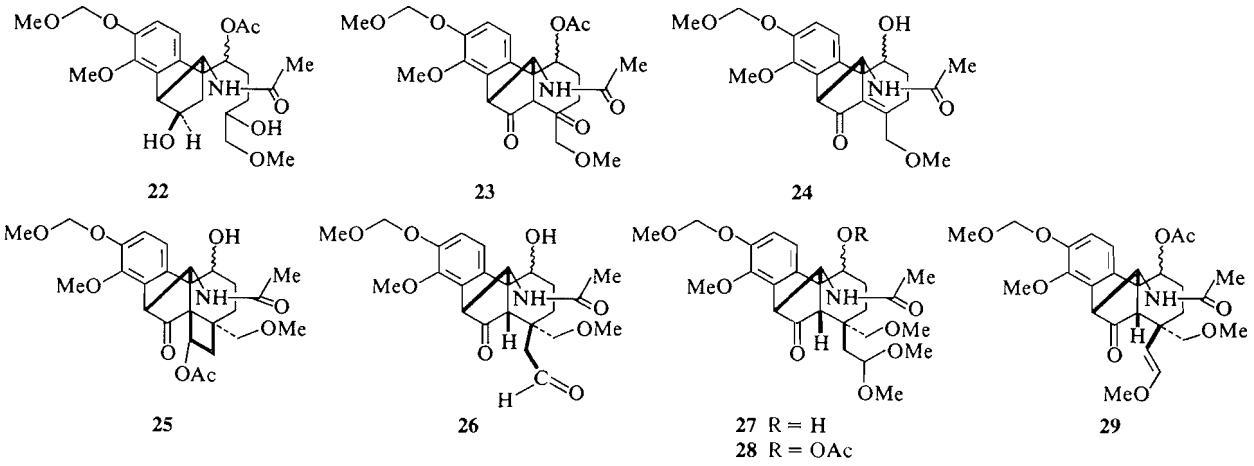

SCHEME 4

ring since the carbomethoxy group can sterically not reach the nitrogen. However, reflux of compound **30** with dilute methanolic sodium methoxide led, as expected, to the formation of the secondary lactam **31** with a simultaneous epimerization of the ring junction in a yield of 85%. The ^{1}Hmr spectrum of compound **31** showed the subject of the primary methoxyl at lower field (τ = 6.63) in agreement with the inverted configuration of the A/B ring junction. Finally, oxidation of the epimeric hydroxylactams **31** with the chromium trioxide – pyridine complex in dichloromethane completed the stereospecific synthesis of the beautifully crystalline diketolactam **32** (mp 178–179°C) in a yield of 90%.

The transformation of the α,β-unsaturated ketone **24** to the keto lactam **31** was carried out in an overall yield of 60%. Nevertheless, we have been attempting for a long time without success to discover a shorter alternative route. Thus, for example, the photoaddition of an acetylenic derivative to compound **24** followed by a direct oxidative cleavage of the resulting cyclobutene was tried in many variations.

Another possibility is the construction of the nitrogen ring by attachment of a suitable side-chain to the nitrogen followed by base-catalysed internal β-addition. The schemes which we developed in this direction offered little advantage over our present process with regard to the number of steps needed and none of them could match our present yields. Nevertheless, we believe that the conversion of the α,β-unsaturated ketone **24** to the keto lactam **31** must be capable of some simplification and of a consequent small improvement in the overall yield.

The diketolactam **32** was next reduced with tri-*tert*-butoxy aluminum hydride and the diol **33** was obtained stereospecifically in a yield of 86% after crystallization. Methylation of this material in dry dioxane with sodium hydride and methyl iodide at reflux temperature gave finally the polymethoxylated *N*-methyl lactam **34**.

Compound **34** was identical in all respects with the same material obtained from vanillin (3) and used as intermediate in our recent synthetic work (1). The correctness of its structure and the configuration of all of its substituents was corroborated, not only by the identity of the final product of the synthesis **VII** with the naturally derived material, but also by an X-ray structural analysis performed recently by Przybylska and Ahmed on the advanced nordenudatine intermediate **VIII** (1) (Fig. 1; Schemes 5, 6).

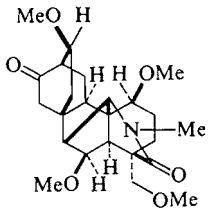

VIII

SCHEME 5

Experimental

Preparation of the Ester 2

A solution of *o*-cresol (103 mL) and 3-chloropropionyl chloride (114.5 mL) in benzene (200 mL) was stirred at room temperature until the evolution of hydrogen chloride ceased. The mixture was heated slowly and finally refluxed for 1 h. The reaction mixture was cooled and the unreacted *o*-cresol was extracted several times with 200 mL of 5% aqueous NaOH. The organic layer was dried over anhydrous magnesium sulfate and distilled to give 157.7 g (79%) of the ester (**2**), bp 104–105°C/2 Torr; *m/e*: 198; ir (CCl_4): 1740 (C=O) cm^{-1}; nmr ($CDCl_3$) τ: 2.9 (m, 4H, aromatic protons), 6.18 (t, 2H, J = 3 Hz, —CH_2—Cl), 7.02 (t, J = 3 Hz, 2H, —OCO—CH_2), 7.85 (s, 3H, aromatic —CH_3).

Preparation of the Ketone 3

Ester **2** (165 g) and $AlCl_3$ (560 g) were mixed with stirring

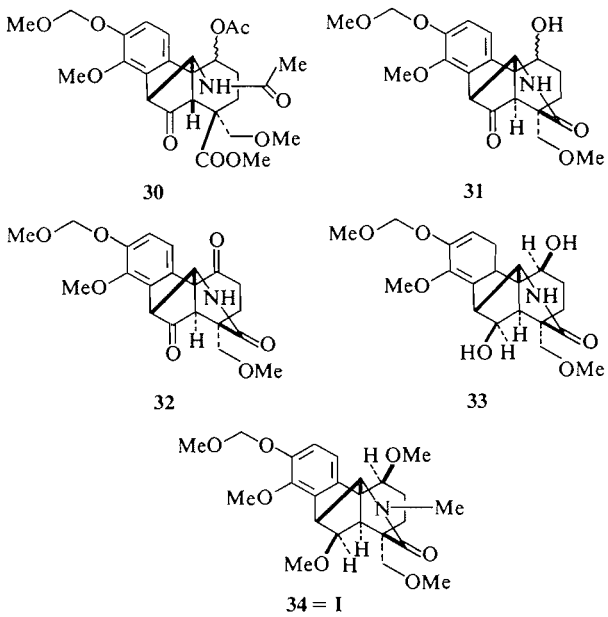

SCHEME 6

and the mixture was heated carefully to 90–100°C for 1 h. After this time the mixture was gradually warmed to 160°C over a period of 2 h and this temperature was maintained for one additional hour. Finally, it was heated to 180°C for 1 h. The cooled reaction mixture was decomposed by cautious addition of ice followed by 200 mL of concentrated HCl. Steam distillation of the decomposed reaction mixture gave 27.4 g (22.6%) of the 6-methyl-7-hydroxy-indan-1-one (**3**) crystallized from petroleum ether to a mp 80–83°C; *m/e*: 162; ir ($CHCl_3$): 3370 (—OH), 1720 (C=O) cm^{-1}; nmr (CCl_4) τ: 7.8 (s, 3H, aromatic —CH_3), 3.3 (AB_q, 2H, J = 7 Hz, $\Delta\nu$ = 15 Hz, aromatic protons), 0.2 (s, 1H, OH). *Anal.* calcd. for $C_{10}H_{10}O_2$: C 74.41, H 6.59; found: C 74.05, H 6.22.

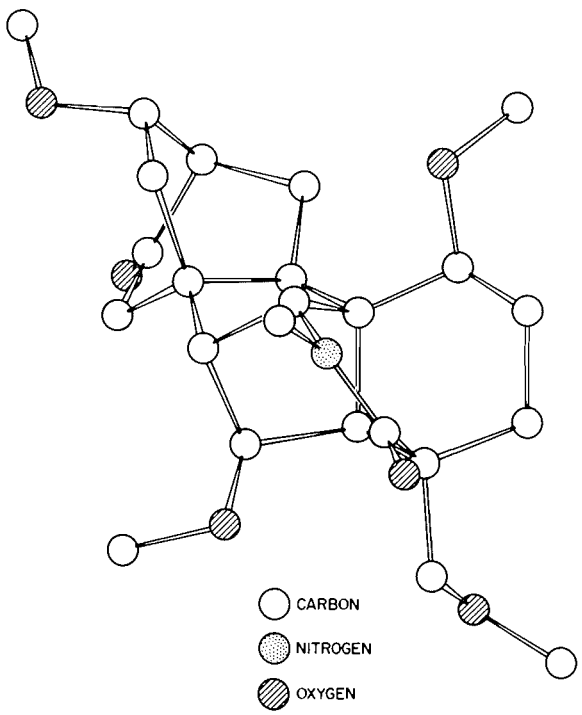

FIG. 1. X-ray structure of Compound **VIII**.

Preparation of Indanone 4

A mixture of 6-methyl-7-hydroxy indan-1-one (**3**) (20 g, 0.17 mol), acetone (508 mL), anhydrous K_2CO_3 (25.8 g, 0.20 mol), and dimethyl sulfate (17.1 mL, 0.18 mol) was refluxed under nitrogen overnight. After cooling, the inorganic salts were removed by filtration, the solvent was evaporated *in vacuo*, and the residue was dissolved in $CHCl_3$. The solution was washed with 2 *N* aqueous hydrochloric acid, water, brine, dried over anhydrous $MgSO_4$, and evaporated to dryness. The crude product was purified by column chromatography on silica gel (30% Et_2O in hexane) affording after crystallization from petroleum ether 27.9 g of indanone (**4**) (94%), mp 54–56°C; *m/e*: 176; ir (CCl_4): 1720 (C=O) cm^{-1}; nmr ($CDCl_3$) τ: 7.8 (s, 3H, aromatic —CH_3), 6.2 (s, 3H, aromatic —OCH_3), 2.8 (AB_q, 2H, J = 7 Hz, aromatic protons). *Anal.* calcd. for $C_{11}H_{12}O_2$: C 74.97, H 6.86; found: C 75.05, H 6.92.

Preparation of the Keto Acid 6

A solution of the indanone (**4**) (50 g) in benzene (200 mL) and absolute methanol (100 mL) was mixed with trimethyl orthoformate (100 mL) and Rexyn 101 (H) (5 g) and the mixture was stirred at room temperature. When the reaction was completed (nmr) the Rexyn was filtered off and the filtrate was basified with triethylamine and evaporated *in vacuo* to give a mixture of the enol ether (**5**) and the corresponding dimethoxyacetal. The mixture was then refluxed for 1 h in dry *o*-xylene (400 mL). The solvent was distilled off and the residue (**5**) was used immediately for the subsequent step.

A solution of the crude enol ether **5** in absolutely anhydrous tetrahydrofuran (1200 mL) was cooled to −70°C (acetone – dry ice) and *n*-butyllithium (225 mL of 2.1 *N* in hexane) was added dropwise with stirring under nitrogen. After the addition was completed, the stirring was continued for 5 h, after which time dry carbon dioxide gas was passed through the solution at a moderate rate overnight. After warming to room temperature, the solution was acidified with 6 *N* aqueous hydrochloric acid.

The aqueous phase was extracted with $CHCl_3$. The combined organic extracts were washed with aqueous solution of $NaHCO_3$, the aqueous extracts were acidified with hydrochloric acid, and the product was taken up in chloroform. The chloroform solution was dried over Na_2SO_4 and evaporated to dryness. The crude residue was crystallized from CCl_4 to give 14.9 g of the pure keto acid **6**, mp 145–146°C; *m/e*: 220; ir ($CHCl_3$): 3300–2800 (—COOH), 1720 (C=O, —COOH) cm^{-1}; nmr (CCl_4) τ: 7.8 (s, 3H, aromatic —CH_3), 6.1 (s, 3H, aromatic —OCH_3), 2.7 (s, 2H, aromatic protons), −0.9 (s, 1H, —COOH). *Anal.* calcd. for $C_{12}H_{12}O_4$: C 65.44, H 5.49; found: C 65.34, H 5.39.

Preparation of the Secondary Alcohol 7

Sodium borohydride (31 g) was added in small portions to a stirred and cooled solution of the keto acid **6** (90 g) in ethyl alcohol (2000 mL). The mixture was stirred at room temperature for 2 h, acidified with 5% aqueous HCl, and the ethanol was evaporated on a rotary evaporator. The residue was taken up in ethyl ether and washed with brine. The ether extracts were dried over anhydrous Na_2SO_4 and evaporated to afford the crude secondary alcohol **7**. The product was purified by recrystallization from ethanol and gave 90 g (98%) of the pure compound, mp 145–146°C; *m/e*: 222; ir ($CHCl_3$): 3550

(—OH), 3200–2800 (—COOH), 1710 (—CO—OH) cm^{-1}; nmr ($CDCl_3$) τ: 7.8 (s, 3H, aromatic —CH_3), 6.1 (s, 3H, aromatic —OCH_3), 4.5 (m, 2H), 2.9 (AB_q, J = 7 Hz, aromatic protons). *Anal.* calcd. for $C_{12}H_{14}O_4$: C 64.85, H 6.35; found: C 64.67, H 6.33.

Preparation of the Indene Ester ***8***a

The alcohol **7** (90 g) was refluxed in dioxane (2000 mL) in presence of 85% *p*-phosphoric acid (200 mL) for 5 h. After cooling to room temperature, the solution was poured into ice – sodium chloride. The mixture was extracted with chloroform and the extract was washed with brine and dried over sodium sulfate. Removal of the solvent gave the indene acid as yellow crystalline compound, 81.4 g (98%); *m/e*: 205; ir ($CHCl_3$): 1600 (olefin), 1690 (—COOH) cm^{-1}; nmr ($CDCl_3$) τ: 7.8 (s, 3H, aromatic —CH_3), 6.4 (d, 2H, J = 2 Hz, —CH_2—), 6.2 (s, 3H, aromatic —OCH_3), 2.8 (AB_q, 2H, J_{AB} = 7 Hz), 2.3 (d, 1H, J = 2 Hz, vinylic H). *Anal.* calcd. for $C_{12}H_{12}O_3$: C 70.57, H 5.92; found: C 70.31, H 5.92.

Saturated methanolic hydrogen chloride (50 mL) was added to a solution of the indene acid (90 g) in dry methanol (2000 mL), and the solution was refluxed overnight. Evaporation of the solvent gave a dark residue which was chromatographed on silica gel with 15% ether in petroleum ether. Recrystallization from petroleum ether afforded the white crystalline indene ester ***8a***, 91 g (95%), mp 57.5–58°C; *m/e*: 218; ir ($CHCl_3$): 1725 (—$COOCH_3$) cm^{-1}; nmr ($CDCl_3$) τ: 7.73 (s, 3H, aromatic —CH_3), 6.5 (d, 2H, J = 2 Hz, benzylic H), 6.2 (s, 6H, aromatic —OCH_3, —$CO{\cdot}OCH_3$), 2.43 (d, 1H, J = 7 Hz, aromatic H), 2.88 (d, 1H, J = 7 Hz, aromatic H), 2.8 (t, 1H, J = 2 Hz, vinylic H). *Anal.* calcd. for $C_{13}H_{14}O_3$: C 71.54, H 6.47; found: C 71.37, H 6.39.

The Adduct ***9***

A solution of the indene ester ***8a*** (26.1 g), maleic anhydride (23.6 g), and hydroquinone (100 mg) in dry *o*-xylene (50 mL) was heated under nitrogen to 185°C (oil bath temperature) for 5 h. After cooling, the excess maleic anhydride and *o*-xylene were removed *in vacuo* at 75°C (bath temperature). The resulting paste was scratched in ether and the crude adduct **9** (33.8 g, 89.3%) crystallized. The crystals and the mother liquors were used in the next reaction without further purification. An analytical sample of the adduct, mp 135–136.5°C, was prepared by crystallization from acetone–ether; *m/e*: 316; ir ($CHCl_3$): 1865, 1785 (anhydride), 1735 (—$COOCH_3$) cm^{-1}; nmr ($CDCl_3$) τ: 7.8 (aromatic —CH_3), 7.78 (d, 2H, J = 3 Hz, apex H), 6.2 (s, 3H, —$COOCH_3$), 6.16 (s, 3H, aromatic —OCH_3), 5.88 (m, 2H, H next to anhydride), 3.05 (s, 2H, aromatic H). *Anal.* calcd. for $C_{17}H_{16}O_6$: C 64.55, H 5.10; found: C 64.52, H 5.11.

Benzobicycloheptene ***10***

A mixture of the adduct **9** (20 g) and bistriphenylphosphine nickel dicarbonyl (81 g) in anhydrous diglyme (990 mL) was heated in a nitrogen atmosphere to vigorous reflux (bath temperature 200°C) for 6 h. After cooling to room temperature, the reaction mixture was filtered through Celite to remove the black nickel precipitate and the solvent was distilled off under reduced pressure. The residue was taken up in ether and filtered. After evaporation of the ether filtrate the residue was subjected to chromatography on silica gel. Elution with 7% ether in *n*-hexane yielded the oily olefin **10** (13.12 g, 85%) homogeneous in tlc; *m/e*: 244; ir ($CHCl_3$): 1735 (—$COOCH_3$) cm^{-1}; nmr ($CDCl_3$) τ: 7.83 (s, 3H, aromatic —CH_3), 7.52 (d, 2H, J = 2 Hz, apex proton), 6.22 (s, 3H, —$COOCH_3$), 6.17 (s, 3H, aromatic —OCH_3), 5.8 (m, 1H, bridgehead H), 3.22 (m, 4H, aromatic H, vinylic H).

Aziridine Rearrangement Product ***12***

The tricyclic olefin **10** (20 g) was dissolved in trimethyl silyl azide (174 mL) and the solution was heated in a nitrogen atmosphere to 85°C for 2 days. The reaction mixture was cooled to room temperature and the excess trimethyl silyl azide was distilled off under reduced pressure. The last traces of trimethyl silyl azide were removed by connecting to a high vacuum pump for 15 min. The residue was dissolved in dry benzene (122 mL) and then cooled in a cold water bath while a mixture of acetic acid (61 mL) and acetic anhydride (61 mL) was added dropwise. After the nitrogen evolution had subsided, the mixture was heated in a nitrogen atmosphere to 85°C for 2 days. The solvent was removed on a rotary evaporator and the last traces were removed by heating to 40°C on the vacuum pump for half an hour. The residue was taken up in chloroform and washed with 5% sodium bicarbonate and saturated sodium chloride. After drying over anhydrous $MgSO_4$ and evaporation of the solvent, 30.5 g crude product was obtained. Column chromatography on silica gel, eluting with 10% ether in chloroform, and recrystallization from ether–petroleum ether yielded the pure crystalline rearrangement product **12** (21 g, 70%), mp 128–130°C. *m/e*: 361; ir ($CHCl_3$): 3450 (N—H), 1735 (—$COOCH_3$ + —O—CO—CH_3), 1685 (—CONH—) cm^{-1}; nmr ($CDCl_3$) τ: 7.98 (s, 3H, —$OCOCH_3$), 7.87 (s, 3H, —$NHCOCH_3$), 7.77 (s, 3H, aromatic —CH_3), 6.19 (s, 3H, —$COOCH_3$), 6.09 (s, 4H, aromatic —OCH_3 and bridgehead H), 5.5 (d, 1H, J = 8 Hz, apex H), 5.08 (m, 1H, $CHCOCH_3$), 3.44 (d, 1H, J = 8 Hz, NH), 3.04 (AB, 2H, J = 8 Hz, $\Delta\nu$ = 9 Hz, aromatic H). *Anal.* calcd. for $C_{19}H_{23}O_6N$: C 63.13, H 6.42, N 3.88; found: C 62.88, H 6.48, N 3.86.

Aromatic Aldehyde ***13***

To a stirred solution of the aziridine rearrangement product **12** (29 g) in 60% aqueous acetic acid (390 mL), a solution of ceric ammonium nitrate (175.36 g) was added dropwise, at room temperature. The mixture was stirred for 4 h at room temperature, extracted several times with ethyl acetate, and the extract was washed several times with aqueous sodium bicarbonate and saturated sodium chloride. After drying over anhydrous $MgSO_4$ and evaporation of the solvent, the crude product was purified by recrystallization from chloroform–ether. The mother liquors were subjected to column chromatography on silica gel, eluting with 10% ether in chloroform. The aromatic aldehyde **13** was obtained (23 g, 75%) as white crystals, mp 162–164°C; *m/e*: 375; ir ($CHCl_3$): 3480 (N—H), 1740 (—OCO—), 1690 (—NHCO, —CHCO) cm^{-1}; nmr ($CDCl_3$) τ: 8.18 (s, 3H, —$OCOCH_3$), 8.06 (s, 3H, NH—CO—CH_3), 6.32 (s, 3H, —$COOCH_3$), 6.08 (s, 3H, aromatic —OCH_3), 5.5 (d, 1H, J = 3 Hz, apex H), 3.44 (d, 1H, J = 8 Hz, NHCO), 3.04 (AB, 2H, J = 8 Hz, aromatic H), −0.2 (aromatic —COH). *Anal.* calcd. for $C_{19}H_{21}O_7N$: C 60.79, H 5.64, N 3.73; found: C 60.61, H 5.52, N 3.44.

Alcohol ***14***

A standard solution of potassium carbonate in methanol was prepared by adding a few drops of 5% aqueous potassium carbonate to methanol until the pH was approximately 9.5–10.0. The aromatic aldehyde **13** (10 g) was dissolved in the standard solution (250 mL) and was stirred at room temperature for 1 h. The reaction mixture was carefully neutralized by the addition of 5% aqueous hydrochloric acid, and the methanol was removed on the rotary evaporator. The residue was taken up in aqueous saturated sodium chloride and extracted 4 times with chloroform. The chloroform extracts were dried over anhydrous magnesium sulfate and evaporated. The product was purified by recrystallization from ether–chloroform and the mother liquors were subjected to

column chromatography on silica gel, eluting with 25% ether in chloroform. The aromatic aldehyde **14** (8.05 g, 93%) was obtained as white crystals melting at 174–175°C; *m/e*: 333; ir ($CHCl_3$): 3615 (OH), 3440 (NHCO), 1740 (—$COOCH_3$), 1690 (—C=OH, $NHCOCH_3$) cm^{-1}; nmr ($CDCl_3$) τ: 8.2 (s, 3H, $NHCOCH_3$), 6.3 (s, 3H, —$COOCH_3$), 6.1 (s, 3H, aromatic —OCH_3), 2.7 (AB_q, 2H, J = 10 Hz, aromatic H), −0.3 (s, 1H, aromatic —C=OH). *Anal.* calcd. for $C_{17}H_{19}O_6N$: C 61.25, H 5.75, N 4.20; found: C 61.27, H 5.57, N 3.91.

Benzyl Ether ***15***

To a solution of the secondary alcohol **14** (10 g) in dry dichloromethane (250 mL), potassium carbonate (20.72 g), benzyl bromide (20.54 g), and crown ether (18-crown-6) (0.015 g) were added. The resulting suspension was refluxed in a nitrogen atmosphere for 2 days. After cooling to room temperature, the carbonate was filtered off and washed with dichloromethane. The solvent was removed *in vacuo* to give an oil which was subjected to column chromatography on silica gel eluting with 10% ether in dichloromethane. Recrystallization from ether afforded the white crystalline compound **15** (10.15 g, 80%), mp 107–109°C; *m/e*: 423; ir ($CHCl_3$): 3420 (NHCO), 1745 ($COOCH_3$), 1680 ($NHCOCH_3$, —C=OH) cm^{-1}; nmr ($CDCl_3$) τ: 8.2 (s, 3H, $NHCOCH_3$), 6.3 (s, 3H, —$COOCH_3$), 6.1 (s, 3H, aromatic —OCH_3), 5.5 (s, 2H, benzylic H), 2.7 (s, 5H, aromatic H of the benzyl), 2.7 (AB_q, 2H, J = 10 Hz, aromatic H), −0.3 (aromatic —C=OH). *Anal.* calcd. for $C_{24}H_{25}O_6N$: C 68.07, H 5.95, N 3.31; found: C 67.87, H 5.87, N 3.07.

Benzyl Phenol ***17***

The aldehyde **15** (10 g) was dissolved in dichloromethane (300 mL) and 85% *m*-chloroperbenzoic acid (5.15 g) was added in portions. The solution was refluxed for 6 h and the progress of the reaction was followed by nmr. After cooling, the solution was washed with aqueous sodium bicarbonate, sodium bisulfite, and saturated sodium chloride and dried over anhydrous $MgSO_4$. Removal of the solvent gave the unstable formate **16** (10 g) which was used in the next reaction without further purification; ir ($CHCl_3$): 3455 (N—H), 1760 (—OCOH), 1735 (—$COOCH_3$), 1675 ($NHCOCH_3$) cm^{-1}; nmr ($CDCl_3$) τ: 8.15 (s, 3H, $NHCOCH_3$), 6.3 (s, 6H, —$COOCH_3$ + aromatic —OCH_3), 5.43 (s, 2H, benzylic H), 3.18 (d, 2H, J = 2 Hz, aromatic H), 2.8 (s, 5H, aromatic H of the benzyl group), 1.9 (s, 1H, —OC=OH).

The formate **16** (10 g) was dissolved in methanol (200 mL) and the pH of the solution was adjusted to 9–10 with 1 *N* aqueous potassium carbonate. The reaction mixture was stirred for 30 min at room temperature. The solution was neutralized with 5% aqueous hydrochloric acid and the methanol was removed on a rotary evaporator. The residue was taken up with ether, washed with saturated sodium chloride, and dried over anhydrous $MgSO_4$. The solvent was removed *in vacuo* to give white crystalline material. Recrystallization from chloroform yielded 9.32 g compound **17** (96%, after two steps), mp 197–199°C; *m/e*: 411; ir ($CHCl_3$): 3600 (—OH), 3450 (NHCO), 1730 ($COOCH_3$), 1690 ($NHCOCH_3$) cm^{-1}; nmr (DMSO, $CDCl_3$) τ: 8.10 (s, 3H, —$NHCOCH_3$), 6.22 (s, 3H, —$COOCH_3$), 6.19 (s, 3H, aromatic —OCH_3), 5.38 (s, 2H, benzylic H), 3.2 (d, 2H, J = 2 Hz, aromatic H), 2.6 (s, 5H, aromatic H of benzyl groups). *Anal.* calcd. for $C_{23}H_{25}O_6N$: C 67.14, H 6.12, N 3.40; found: C 66.96, H 6.07, H 3.34.

Protected Phenol ***18***

A mixture of phenol **17** (10 g), THF/CH_2Cl_2 (1:1) (300 mL), K_2CO_3 (16.4 g), and crown ether (18-crown-6) (0.015 g) was stirred for 30 min at room temperature. Chloromethyl-methyl ether (3.9 g) was added dropwise and the resulting solution was stirred for 10 h at room temperature. The solid was filtered off and the solution was washed with saturated aqueous sodium chloride and dried over anhydrous magnesium sulfate. The solvent was removed *in vacuo* and the oily residue was chromatographed on silica gel eluting with 15% ether in chloroform. Recrystallization from ethyl ether gave 10.3 g (93%) of the protected phenol **18**, mp 95–96°C; *m/e*: 455; ir ($CHCl_3$): 3430 (NHCO), 1730 ($COOCH_3$), 1690 (—$NHCOCH_3$) cm^{-1}; nmr ($CDCl_3$) τ: 8.10 (s, 3H, —$NHCOCH_3$), 6.5 (s, 3H, H_3C—O—CH_2—O—), 6.20 (s, 3H, —$OCOCH_3$), 6.15 (s, 3H, aromatic —OCH_3), 5.38 (s, 2H, benzylic H), 4.8 (s, 2H, H_3C—O—CH_2—O—), 3.0 (s, 2H, aromatic H), 2.6 (s, 5H, aromatic H of benzyl group). *Anal.* calcd. for $C_{25}H_{29}O_7N$: C 65.92, H 6.42, N 3.08; found: C 65.80, H 6.25, N 2.84.

Preparation of Aldehyde ***19***

The protected phenol **18** (4.55 g) was dissolved in absolutely dry THF (80 mL) and lithium borohydride (0.22 g) was added in portions in a nitrogen atmosphere. After stirring for 2 h, the reaction mixture was cooled in an ice bath while water was added to destroy the excess hydride. The resulting solution was evaporated and the residue was extracted several times with chloroform. After washing with saturated aqueous sodium chloride and drying over anhydrous $MgSO_4$, the solvent was removed *in vacuo*. Column chromatography on silica gel, eluting with 20% ether in chloroform, and recrystallization from chloroform–ether yielded the white crystalline primary alcohol (3.84 g, 90%), mp 103–104°C; *m/e*: 427; ir ($CHCl_3$): 3400 (NHCO + OH), 1625 ($NHCOCH_3$) cm^{-1}; nmr ($CDCl_3$) τ: 8.40 (d, 2H, J = 5 Hz, protons β to the benzyloxy), 8.03 (s, 3H, $NHCOCH_3$), 6.5 (s, 3H, CH_3—O—CH_2—O—), 6.1 (s, 3H, aromatic —OCH_3), 5.4 (s, 2H, benzylic H), 4.8 (s, 2H, CH_3—O—CH_2—O—), 3.08 (s, 2H, aromatic H), 2.5 (s, 5H, aromatic H of benzyl). *Anal.* calcd. for $C_{24}H_{29}O_6N$: C 67.42, H 6.83, N 3.28; found: C 67.41, H 6.79, N 3.22.

To a solution of the primary alcohol (35 g) in dry benzene (440 mL), dimethyl sulfoxide (133 mL), dicyclohexyl carbodiimide (47.92 g), pyridine (6.6 mL), and trifluoroacetic acid (3.3 mL) were added in sequence and the mixture was stirred at room temperature for 24 h. The reaction mixture was diluted with ether and filtered. The filtrate was washed with water and aqueous saturated NaCl, dried over anhydrous $MgSO_4$, and evaporated. Chromatography on silica gel and elution with chloroform containing 20% ether and 2% methanol gave the pure aldehyde **19** (33.8 g, 97%) as an amorphous solid, homogeneous in tlc; *m/e*: 425; ir ($CHCl_3$): 3410 (N—H), 2840, 2730 (—C=OH), 1718 (—C=OH), 1675 (NHCO) cm^{-1}; nmr ($CDCl_3$) τ: −0.07 (s, 1H, —C=OH), 2.65 (s, 5H, aromatic H of benzyl), 3.12 (AB_q, J = 8 Hz, Δν = 7.55 Hz, 2H, aromatic H), 4.83 (s, 2H, —O—CH_2—O), 5.37 (s, 2H, benzylic H), 6.12 (s, 3H, aromatic —OCH_3), 6.50 (s, 2H, —O—CH_2—O—CH_3), 8.12 (s, 3H, NHCO—CH_3).

Preparation of the Alcohol ***20***

A small portion (4 mL) of a solution of 3-benzyloxy-4-methoxy-*n*-butyl bromide (9) (89.7 g, sixfold excess) in anhydrous THF (100 mL) was added to a stirred mixture of magnesium turnings (7.8 g) and a crystal of iodine in anhydrous THF (75 mL) under nitrogen at 85°C (oil bath temperature). When the colour of iodine had disappeared, the remaining solution of the bromide was added dropwise with stirring at the same temperature. After the addition was completed, the mixture was stirred for another 2 h. The Grignard reagent was then cooled to 30–35°C and a solution of the aldehyde **19** (23 g) in dry THF (800 mL) was added dropwise with stirring. After the addition was completed, the mixture

was stirred at the same temperature for another hour. The reaction mixture was then cooled in an ice–water bath and the excess Grignard reagent was destroyed by slow addition of saturated aqueous ammonium chloride. The aqueous phase was extracted with ether and the extracts were dried over anhydrous $MgSO_4$ and evaporated. The crude product was chromatographed on silica gel and elution with hexane containing 30% acetone and 2% methanol gave two epimers of **20** in the ratio 11:1 and a yield of 87%.

The Major α-Epimer

Mass spectra *m/e*: 619; ir ($CHCl_3$): 3550–3350 (—OH + N—H), 1655 (NHCO) cm^{-1}; nmr ($CDCl_3$) τ: 2.63 (m, 10H, aromatic H of benzyl), 3.03 (AB_q, J = 8 Hz, Δν = 8.94 Hz, aromatic H), 4.87 (s, 2H, O—CH_2—O), 5.33 (AB_q, J = 12 Hz, Δν = 7.21 Hz, 2H, benzylic H), 5.41 (s, 2H, benzylic H), 6.14 (s, 3H, aromatic —OCH_3), 6.51 (s, 3H, —O—CH_2—O—CH_3), 6.62 (s, 3H, —OCH_3), 8.09 (s, 3H, NHCOCH_3).

The Minor β-Epimer

The mass spectra of both epimers were identical, *m/e*: 619; ir ($CHCl_3$): 3550–3350 (OH + N—H), 1655 (NHCO) cm^{-1}; nmr ($CDCl_3$) τ: 2.61 (m, 1H, aromatic H of benzyl), 3.07 (s, 2H, aromatic H), 4.83 (s, 2H, O—CH_2—O), 5.35 (AB_q, J = 12 Hz, Δν = 7.12 Hz, 2H, benzylic H), 5.38 (s, 2H, benzylic H), 6.14 (s, 3H, aromatic —OCH_3), 6.50 (s, 3H, O—CH_2—O—CH_3), 6.61 (s, 3H, —OCH_3), 8.18 (s, 3H, NH—CO—CH_3).

Preparation of the Acetate ***21***

A solution of the alcohol **20** (35 g) in dry pyridine (70 mL), acetic anhydride (45 mL), and 4-dimethylamino pyridine (0.4 g) were mixed and the mixture was heated to 50–60°C for 24 h. Excess acetic anhydride and pyridine were removed under reduced pressure, and the residue was diluted with ether (300 mL) and washed successively with water, 5% aqueous citric acid, water, saturated $NaHCO_3$, and saturated NaCl. The ether solution was dried over anhydrous $MgSO_4$ and evaporated. Crystallization of the crude product from CH_2Cl_2–hexane gave the pure acetate **21** (35.6 g, 95.3%).

α-Epimer

The melting point was 111–112°C; *m/e*: 661; ir ($CHCl_3$): 3400 (N—H), 1735 (—O—CO—CH_3), 1670 (NH—CO—CH_3) cm^{-1}; nmr ($CDCl_3$) τ: 4.55 (t, J = 6 Hz, 1H, CH—NH—CO), 7.94 (s, 3H, O—CO—CH_3), 8.10 (s, 3H, NH—CO—CH_3). *Anal.* calcd. for $C_{38}H_{47}O_9N$: C 68.98, H 7.18, N 2.11; found: C 68.98, H 7.15, N 2.06.

β-Epimer

The mass spectra of both epimers were identical, *m/e*: 661; ir ($CHCl_3$): 3400 (N—H), 1735 (O—CO—CH_3), 1675 (NH—CO—CH_3) cm^{-1}; nmr ($CDCl_3$) τ: 4.67 (m, 1H, CH—O—CO), 7.90 (s, 3H, —O—CO—CH_3), 8.10 (s, 3H, NH—CO—CH_3).

Preparation of the Diol ***22***

A solution of compound **21** (30.4 g) in absolute methanol (500 mL) was hydrogenated with 10% palladium on charcoal (6 g) at atmospheric pressure and room temperature for 4 h. Catalyst was removed by filtration through Celite and the solvent after neutralization with $(CH_3)_3N$ was evaporated under reduced pressure to give diol **22** (22.1 g, 100%) as an amorphous solid homogeneous in tlc; *m/e*: 481. The mass spectra of both epimers were identical.

α-Epimer

Infrared ($CHCl_3$): 3580 (—OH), 3400 (N—H), 1732 (O—CO—CH_3), 1670 (NH—CO) cm^{-1}; nmr ($CDCl_3$) τ: 2.53 (d, J = 8 Hz, 1H, N—H), 3.12 (s, 2H, aromatic), 4.50 (t, J = 6 Hz, 1H, CH—O—CO—CH_3), 4.83 (s, 2H, O—CH_2—O), 6.15 (s, 3H, —OCH_3), 6.50 (s, 3H, O—CH_2—O—CH_3), 6.63 (s, 3H, —OCH_3), 7.12 (s, 3H, —$OCOCH_3$), 8.01 (s, 3H, NH—CO—CH_3).

β-Epimer

Infrared ($CHCl_3$): 3600 (O—H), 3400 (N—H), 1730 (O—CO—CH_2), 1665 (NH—CO) cm^{-1}; nmr ($CDCl_3$) τ: 2.28 (d, J = 8 Hz, 1H, N—H), 2.9 (AB_q, J = 8 Hz, Δν = 8.94 Hz, 2H, aromatic), 4.82 (s, 2H, O—CH_2—O), 6.13 (s, 3H, aromatic —O—CH_3), 6.47 (s, 3H, —O—CH_2—O—CH_3), 6.62 (s, 3H, —OCH_3), 7.90 (s, 3H, —O—CO—CH_3), 7.97 (s, 3H, NH—CO—CH_3).

Oxidation of the Diol ***22*** *to Diketone* ***23***

A solution of the diol **22** (19 g) in dichloromethane (250 mL) was added to a solution of dipyridine–chromium(VI) oxide complex (122 g) in dichloromethane (2250 mL) with stirring at room temperature. The mixture was stirred at room temperature for 30 min, diluted with ether (1000 mL), and the solid residue was filtered off. The filtrate was washed successively with saturated aqueous sodium bicarbonate, water, 5% aqueous citric acid, and saturated aqueous NaCl, dried over $MgSO_4$, and evaporated. The crude product was purified by filtration through a short column of silica gel to give pure diketone **23** (16 g, 85%) as an amorphous solid, homogeneous in tlc; *m/e*: 477. The mass spectra of both epimers were identical.

α-Epimer

Infrared ($CHCl_3$): 3435 (N—H), 1745 (5-membered C=O), 1735 (C=O and —O—CO—CH_3), 1680 (NH—CO) cm^{-1}; nmr ($CDCl_3$) τ: 2.82 (AB_q, J = 8 Hz, Δν = 8.94 Hz, 2H, aromatic), 3.20 (d, J = 8 Hz, 1H, NH), 4.38 (m, 1H, —CH—O—CO—CH_3), 4.81 (s, 2H, O—CH_2—O), 5.38 (d, J = 8 Hz, CH—N—CO), 5.96 (s, 2H, —CO—CH_2—O), 6.12 (s, 3H, aromatic —OCH_3), 6.47 (s, 3H, —O—CH_2—O—CH_3), 6.55 (s, 3H, side-chain —OCH_3), 7.85 (s, 3H, —O—CO—CH_3), 8.00 (s, 3H, NHCO—CH_3).

β-Epimer

Infrared ($CHCl_3$): 3430 (N—H), 1750 (5-membered C=O), 1735 (—O—CO—CH_3, C=O), 1680 (NH—CO) cm^{-1}; nmr ($CDCl_3$) τ: 2.88 (AB_q, J = 8 Hz, Δν = 11.5 Hz, 2H, aromatic protons), 4.67 (t, J = 6 Hz, 1H, CH—O—CO—CH_3), 4.80 (s, 2H, O—CH_2—O), 5.38 (d, J = 8 Hz, 1H, CH—NH—CO), 5.97 (s, 2H, CO—CH_2—O), 6.13 (s, 3H, aromatic —OCH_3), 6.47 (s, 3H, —O—CH_2—OCH_3), 6.57 (s, 3H, —OCH_3), 7.87 (s, 3H, —O—CO—CH_3), 7.93 (s, 3H, NH—CO—CH_3).

Preparation of the α,β-Unsaturated Ketone ***24***

A solution of the diketone **23** (10 g) in absolute methanol (20 mL) was mixed with a saturated solution of K_2CO_3 in absolute methanol (650 mL) and the mixture was refluxed under nitrogen for 15 h. The mixture was cooled, neutralized with dilute hydrochloric acid (2 *M*), most of the methanol was evaporated *in vacuo*, and the residue was extracted with dichloromethane. The extract was dried over anhydrous $MgSO_4$ and evaporated. The crude product was chromatographed on silica gel eluting with 30% acetone in hexane containing 3% methanol and recrystallization from chloroform–ether gave the pure α,β-unsaturated ketone **24** (7.78 g, 89%).

α-Epimer

Mass spectra *m/e*: 417; mp 90.5–92°C: ir ($CHCl_3$): 3510 (OH), 3410 (N—H), 1720 (CO·C=C<), 1655 (CO·NH + CO·C=C<) cm^{-1}; nmr ($CDCl_3$) τ: 2.90 (AB_q, J = 8 Hz, Δν = 10.24 Hz, 2H, aromatic H), 4.80 (s, 2H, O—CH_2—O), 6.10 (s, 3H, aromatic —OCH_3), 6.47 (s, 3H, O—CH_2—OCH_3), 6.67 (s, 3H, —CH_2—OCH_3), 7.98 (s, 3H, NH—CO—CH_3); uv λ_{max}(EtOH): 230, 258 nm; ε = 15 600, 12 400. *Anal.* calcd.

for $C_{22}H_{27}O_7N$: C 63.30, H 6.52, N 9.43; found: C 63.19, H 6.59, N 9.42.

β-*Epimer*

The mass spectra of both epimers were identical, *m/e*: 417 (oil); ir ($CHCl_3$): 3500–3300 (OH and N—H), 1720 (CO·C=C), 1655 (NH·CO + CO·C=C) cm^{-1}; nmr ($CDCl_3$) τ: 3.08 (AB_q, J = 8 Hz, $\Delta\nu$ = 11.49 Hz, 2H, aromatic H), 4.82 (s, 2H, O—CH_2—O), 6.08 (s, 3H, aromatic —OCH_3), 6.48 (s, 3H, —O—CH_2—O—CH_3), 6.68 (s, 3H, —CH_2—OCH_3), 8.03 (s, 3H, NH—CO—CH_3); uv λ_{max}(EtOH): 232, 260 nm, ε = 16 000, 10 400.

Photoaddition of Vinyl Acetate to the α,β-Unsaturated Ketone ***24***

A solution of the α,β-unsaturated ketone **24** (2 g) and vinyl acetate (60 mL) in freshly distilled tetrahydrofuran (100 mL) was irradiated under nitrogen at −78°C for 3 h with a 200 W Hanovia mercury lamp using a Pyrex filter. Excess vinyl acetate and solvent were removed under reduced pressure and the crude product was crystallized from chloroform–hexane to give the pure photoadduct **25** (2.3 g, 95%).

α-*Epimer*

Melting point 215–216°C; *m/e*: 503; ir ($CHCl_3$): 3500 (OH), 3410 (N—H), 1745 (5-membered C=O), 1730 (—O—CO—CH_3), 1670 (NH—CO) cm^{-1}; nmr ($CDCl_3$) τ: 2.57, 3.00 (2d, J = 8 Hz, 1H for each aromatic H), 4.60 (dd, 1H, C*H*—O—CO—CH_3), 4.80 (s, 2H, O—CH_2—O), 6.12 (s, 3H, aromatic —OCH_3), 6.49 (s, 3H, —O—CH_2—O—CH_3), 7.10 (s, 3H, —CH_2—OCH_3), 7.83 (s, 3H, —$OCOCH_3$), 8.08 (s, 3H, NH—CO—CH_3). *Anal.* calcd. for $C_{26}H_{33}O_9N$: C 62.01, H 6.61, N 2.78; found: C 61.72, H 6.72, N 2.58.

β-*Epimer*

Oil. The mass spectra of both epimers were identical, *m/e*: 503; ir ($CHCl_3$): 3525 (—OH), 3425 (N—H), 1745 (5-membered C=O), 1730 (—$OCOCH_3$), 1655 (NHCO) cm^{-1}; nmr ($CDCl_3$) τ: 3.01 (s, 2H, aromatic H), 4.57 (dd, 1H, C*H*—O—$COCH_3$), 4.80 (s, 2H, —O—CH_2—O), 6.10 (s, 3H, aromatic —OCH_3), 6.48 (s, 3H, —O—CH_2—O—CH_3), 7.11 (s, 3H, —CH_2—O—CH_3), 7.81 (s, 3H, —$OCOCH_3$), 8.08 (s, 3H, NH—CO—CH_3).

Preparation of the Aldehyde ***26***

A solution of the photoadduct **25** (2.8 g) in methanol (150 mL) was mixed with aqueous KOH (19 mL, 0.71 *M*) and the mixture was stirred at room temperature for 30 min. It was then neutralized with dilute HCl (0.7 *M*), the methanol was evaporated *in vacuo*, and the residue was extracted with dichloromethane. The extract was dried over anhydrous $MgSO_4$ and evaporated to give aldehyde **26** (2.5 g, 97%).

α-*Epimer*

Recrystallization from dichloromethane–ether mp 156–157°C; *m/e*: 461; ir ($CHCl_3$): 3500 (OH), 3430 (N—H), 2720 (—C=O·H), 1745 (5-membered C=O), 1712 (—C=O·H), 1665 (CO·NH) cm^{-1}; nmr ($CDCl_3$) τ: 0.23 (t, J = 3 Hz, 1H, —C=O·H), 4.80 (s, 2H, O—CH_2—O), 6.10 (s, 3H, aromatic —OCH_3), 6.50 (s, 3H, —O—CH_2—O—CH_3), 7.27 (s, 3H, —CH_2—OCH_3), 7.93 (s, 3H, NHCO—CH_3).

β-*Epimer*

Oil. The mass spectra of both epimers were identical, *m/e*: 461; ir ($CHCl_3$): 3525–3300 (OH + N—H), 1745 (5-membered CO), 1712 (—C=O·H), 1655 (NHCO) cm^{-1}; nmr ($CDCl_3$) τ: 0.20 (t, J = 3 Hz, —C=O·H), 2.50 (d, J = 4 Hz, 1H, N—H), 3.00 (s, 2H, aromatic H), 4.80 (s, 2H, O—CH_2—O), 6.08 (s, 3H, aromatic —OCH_3), 6.49 (s, 3H, —O—CH_2—O—CH_3), 7.28 (s, 3H, —CH_2—O—CH_3), 7.98 (s, 3H, NHCO—CH_3).

Preparation of the Acetal ***27***

A solution of the aldehyde **26** (2.2 g) in absolute methanol (30 mL) was mixed with trimethyl orthoformate (10 mL) and Rexyn 101 (H) (0.11 g) and the mixture was stirred at room temperature for 1 h. Rexyn was filtered off and the filtrate was evaporated *in vacuo* to give the acetal **27** (2.41 g, 100%) as an amorphous solid, homogeneous in tlc; *m/e*: 507. The mass spectra of both epimers were identical.

α-*Epimer*

Infrared ($CHCl_3$): 3550–3300 (OH and N—H), 1745 (5-membered CO), 1662 (NH·CO) cm^{-1}; nmr ($CDCl_3$) τ: 4.80 (s, 2H, O—CH_2—O), 5.43 (t, J = 5 Hz, 1H, —$CH(OCH_3)_2$), 6.10 (s, 3H, aromatic —OCH_3), 6.50 (s, 3H, —O—CH_2—O—CH_3), 6.67, 6.72 (s, 3H each, —$CH(OCH_3)_2$), 7.47 (s, 3H, —CH_2—OCH_3), 7.93 (s, 3H, NHCO—CH_3).

β-*Epimer*

Infrared ($CHCl_3$): 3550–3250 (OH and N—H), 1745 (5-membered CO), 1655 (NHCO) cm^{-1}; nmr ($CDCl_3$) τ: 3.04 (s, 2H, aromatic H), 4.83 (s, 2H, O—CH_2—O), 5.42 (t, J = 5 Hz, 1H, —$CH(OCH_3)_2$), 6.10 (s, 3H, aromatic —OCH_3), 6.52 (s, 3H, —O—CH_2—OCH_3), 6.68, 6.72 (2s, 3H each, —$CH(OCH_3)_2$), 7.44 (s, 3H, —CH_2—OCH_3), 8.00 (s, 3H, NHCO—CH_3).

Preparation of the Acetal Acetate ***28***

A solution of the acetal alcohol **27** (2.4 g) in dry pyridine (15 mL) was acetylated with acetic anhydride (10 mL) in the presence of 4-dimethylamino pyridine (0.1 g) at room temperature for 10 h. The reaction mixture was evaporated to dryness *in vacuo* and the residue was chromatographed on silica gel. Elution with 30% ether in chloroform containing 5% methanol and 0.01% pyridine gave the pure acetal acetate **28** (2.23 g, 86%) as an amorphous solid homogeneous in tlc; *m/e*: 549. The mass spectra of both epimers were identical.

α-*Epimer*

Infrared ($CHCl_3$): 3400 (N—H), 1745 (5-membered CO), 1725 (—$OCOCH_3$), 1680 (NHCO) cm^{-1}; nmr ($CDCl_3$) τ: 4.80 (s, 2H, O—CH_2—O), 5.08 (t, J = 8 Hz, 1H, C*H*—O·CO·CH_3), 5.45 (t, J = 5 Hz, 1H, —$CH(OCH_3)_2$), 6.16 (s, 3H, aromatic OCH_3), 6.48 (s, 3H, —O—CH_2—O—CH_3), 6.68, 6.72 (2s, 3H each, —$CH(OCH_3)_2$), 7.43 (s, 3H, —CH_2—OCH_3), 7.90 (s, 3H, —O·$COCH_3$), 8.00 (s, 3H, NHCO—CH_3).

β-*Epimer*

Infrared ($CHCl_3$): 3445 (N—H), 1740 (5-membered CO + $OCOCH_3$), 1675 (NH·CO) cm^{-1}; nmr ($CDCl_3$) τ: 4.30 (t, J = 3 Hz, 1H, —C*H*O·$COCH_3$), 4.82 (s, 2H, O—CH_2—O), 5.41 (t, J = 5 Hz, 1H, —$CH(OCH_3)_2$), 6.10 (s, 3H, aromatic —OCH_3), 6.51 (s, 3H, —O—CH_2—O—CH_3), 6.66, 6.70 (2s, 3H each, —$CH(OCH_3)$), 7.43 (s, 3H, —CH_2OCH_3), 7.91 (s, 3H, —O·CO·CH_3), 8.02 (s, 3H, —NHCO—CH_3).

Preparation of the Enol Ether ***29***

A solution of the acetal acetate **28** (2.7 g) in dry *o*-xylene (30 mL) was refluxed with dry pyridine (1.5 mL) under nitrogen for 3 days. The reaction mixture was cooled, the solvent was distilled off under reduced pressure, and the residue was chromatographed on silica gel. Elution with 30% ether in chloroform containing 3% methanol and 0.01% pyridine gave the pure enol ether **29** (2.34 g, 92%) as an amorphous solid, homogeneous on tlc; *m/e*: 517. The mass spectra of both epimers were identical.

α-*Epimer*

Infrared ($CHCl_3$): 3440 (N—H), 1740 (5-membered CO + —$OCOCH_3$), 1680 (NHCO), 1650 (—HC=CH—OCH_3) cm^{-1}; nmr ($CDCl_3$) τ: 3.67, 4.52 (2d, J = 13 Hz, 1H each, vinylic H), 4.78 (s, 2H, O—CH_2—O), 5.05 (t, J = 8 Hz, 1H,

—C*H*—OCOCH$_3$), 6.08 (s, 3H, aromatic —OCH$_3$), 6.43 (s, 3H, —CH=CH—OC*H*$_3$), 6.47 (s, 3H, —O—CH$_2$—O—C*H*$_3$), 7.35 (s, 3H, —CH$_2$—O—C*H*$_3$), 7.89 (s, 3H, —O·CO·CH$_3$), 8.00 (s, 3H, —NH—CO—C*H*$_3$).

β-*Epimer*

Infrared ($CHCl_3$): 3440 (N—H), 1745 (5-membered CO), 1685 (NHCO), 1650 (—CH=CH—OCH$_3$) cm^{-1}; nmr ($CDCl_3$) τ: 3.60, 4.43 (2d, J = 13 Hz, 1H each, vinylic H), 4.83 (s, 2H, O—CH$_2$—O), 6.10 (s, 3H, aromatic —OCH$_3$), 6.43 (s, 3H, —CH=CH—OC*H*$_3$), 6.51 (s, 3H, —O—CH$_2$—O—C*H*$_3$), 7.37 (s, 3H, —CH$_2$—O—C*H*$_3$), 7.92 (s, 3H, —OCO·CH$_3$), 8.02 (s, 3H, —NH—CO—C*H*$_3$).

Preparation of the Keto Ester **30**

A solution of the enol ether **29** (1.2 g) in acetone (25 mL) was added dropwise to a stirred solution of sodium metaperiodate (4.135 g), potassium carbonate (0.78 g), and potassium permanganate (0.124 g) in water (37.2 mL) diluted with acetone (74.4 mL). The reaction mixture was stirred at room temperature for 3 h. The acetone was evaporated under reduced pressure, the residue was diluted with water (50 mL), and the basic aqueous solution was washed with chloroform. The aqueous layer was then acidified with dilute hydrochloric acid (2 *M*) and extracted with chloroform (5 × 50 mL). The combined extracts were washed with saturated aqueous NaCl until neutral, dried over anhydrous $MgSO_4$, and evaporated to dryness *in vacuo* to give the keto acid corresponding to the ester **30** (0.94 g, 80.2%); *m/e*: 505; ir (KBr): 3650–3100 (N—H + —COOH), 1705 (5-membered CO), 1725 (—O·COCH$_3$), 1710 (—COOH), 1650 (NHCO) cm^{-1}; nmr (acetone-d_6) τ: 4.78 (s, 2H, O—CH$_2$—O), 6.13 (s, 3H, aromatic —OCH$_3$), 6.51 (s, 3H, —O—CH$_2$—O—C*H*$_3$), 7.40 (s, 3H, —CH$_2$—OC*H*$_3$), 7.97 (s, 3H, —O·CO·CH$_3$), 8.05 (s, 3H, —NH—CO—C*H*$_3$).

An excess of diazomethane in ether was added to a suspension of the keto acid (0.9 g) in dry dichloromethane (20 mL), and the mixture was stirred at room temperature for 30 min. Excess reagent and solvent were evaporated under reduced pressure and the residue gave the ester **30** on crystallization from dichloromethane–ether (0.924 g, 100%).

α-*Epimer*

Melting point 226–227°C; *m/e*: 519; ir ($CHCl_3$): 3430 (N—H), 1755 (5-membered CO), 1735 (—OCOCH$_3$ + —COOCH$_3$), 1685 (NHCO) cm^{-1}; nmr ($CDCl_3$) τ: 4.80 (s, 2H, O—CH$_2$—O), 4.95 (t, J = 8 Hz, —C*H*·O·CO·CH$_3$), 6.10 (s, 3H, aromatic —OCH$_3$), 6.25 (s, 3H, —COOCH$_3$), 6.47 (s, 3H, —O—CH$_2$—O—C*H*$_3$), 7.44 (s, 3H, —CH$_2$—O—C*H*$_3$), 7.88 (s, 3H, —O·CO·CH$_3$), 8.00 (s, 3H, —NH—CO—C*H*$_3$). *Anal.* calcd. for $C_{26}H_{33}O_{10}N$: C 60.10, H 6.40, N 2.70; found: C 59.73, H 6.30, N 2.41.

β-*Epimer*

The mass spectra of both epimers were identical, *m/e*: 519; ir ($CHCl_3$): 3430 (N—H), 1755 (5-membered CO), 1735 (—O·COCH$_3$ + —COOCH$_3$), 1685 (NHCO) cm^{-1}; nmr ($CDCl_3$) τ: 2.98 (s, 3H, aromatic H), 4.24 (broad s, 1H, —C*H*·O·CO·CH$_3$), 4.82 (s, 2H, O—CH$_2$—O), 6.10 (s, 3H, aromatic —OCH$_3$), 6.22 (s, 3H, —CO·OCH$_3$), 6.51 (s, 3H, —O—CH$_2$—O—C*H*$_3$), 7.43 (s, 3H, —CH$_2$—O—C*H*$_3$), 7.90 (s, 3H, —O·CO·CH$_3$), 8.00 (s, 3H, —NH—CO—C*H*$_3$).

Preparation of the Hydroxy Keto Lactam **31**

A solution of the keto ester **30** (0.8 g) in absolute methanol (30 mL) was added dropwise to a solution of sodium methoxide in methanol (100 mL, 0.26 *M*) and the mixture was refluxed under nitrogen for 15 h. The reaction mixture was then cooled, neutralized with dilute hydrochloric acid (2 *M*), and the methanol was evaporated under reduced pressure. The residue was diluted with water, extracted with chloroform, the extract was dried over anhydrous $MgSO_4$, and evaporated to dryness *in vacuo*. On crystallization from dichloromethane–ether the residue gave colourless crystals of the hydroxy keto lactam **31** (0.52 g, 84%).

α-*Epimer*

Mass spectra *m/e*: 403; mp 169.5–170.5°C; ir ($CHCl_3$): 3550–3300 (OH and N—H), 1750 (5-membered CO), 1665 (NHCO) cm^{-1}; nmr ($CDCl_3$) τ: 2.45, 3.07 (2d, J = 8 Hz, 1H each, aromatic H), 2.67 (d, J = 4 Hz, 1H, N—H), 4.83 (s, 2H, O—CH$_2$—O), 5.58 (m, 2H, >C*H*OH + apex H), 6.15 (s, 3H, aromatic —OCH$_3$), 6.50 (s, 3H, —O—CH$_2$—O—C*H*$_3$), 6.63 (s, 3H, —CH$_2$—O—C*H*$_3$). *Anal.* calcd. for $C_{21}H_{25}O_7N$: C 62.52, H 6.25, N 3.47; found: C 62.37, H 6.05, N 3.19.

β-*Epimer*

Oil. The mass spectra of both epimers were identical, *m/e*: 403; ir ($CHCl_3$): 3600 (OH), 3410 (N—H), 1750 (5-membered C=O), 1665 (NHCO) cm^{-1}; nmr ($CDCl_3$) τ: 3.03 (AB$_q$, J = 8 Hz, Δν = 6 Hz, 2H, aromatic H), 4.83 (s, 2H, O—CH$_2$—O), 6.12 (s, 3H, aromatic —OCH$_3$), 6.50 (s, 3H, —O—CH$_2$—O—C*H*$_3$), 6.63 (s, 3H, —CH$_2$—OC*H*$_3$).

Preparation of Diketo Lactam **32**

A solution of compound **31** (α-epimer) (0.5 g) in dry dichloromethane (10 mL) was added at room temperature to a solution of the chromium trioxide – pyridine complex (1.93 g) in dry dichloromethane (50 mL) with stirring. Stirring was continued at room temperature for 30 min, after which time the mixture was diluted with ether (50 mL) and the solid residue was filtered off. The filtrate was washed successively with saturated aqueous sodium bicarbonate, water, 5% citric acid, and water, dried over anhydrous $MgSO_4$, and evaporated *in vacuo*. The crude product was crystallized from dichloromethane–ether to give fine colourless needles of the diketo lactam **32** (0.446 g, 89%), mp 178–179°C; *m/e*: 401; ir ($CHCl_3$): 3400 (N—H), 1755 (5-membered CO), 1712 (6-membered CO), 1670 (NHCO) cm^{-1}; nmr ($CDCl_3$) τ: 2.45 (d, J = 4 Hz, 1H, N—H), 2.83 (AB$_q$, J = 8 Hz, Δν = 10.24 Hz, 2H, aromatic H), 4.80 (s, 2H, O—CH$_2$—O), 6.12 (s, 3H, aromatic —OCH$_3$), 6.49 (s, 3H, —O—CH$_2$—O—C*H*$_3$), 6.60 (s, 3H, —CH$_2$—O—C*H*$_3$). *Anal.* calcd. for $C_{21}H_{23}O_7N$: C 62.83, H 5.78, N 3.49; found: C 62.89, H 5.74, N 3.23.

Reduction of the Diketo Lactam **23** *to Diol* **33**

Lithium tri-*tert*-butoxy aluminum hydride (2.54 g) was added to a solution of the diketo lactam **32** (0.48 g) in dry tetrahydrofuran (50 mL) under nitrogen and the mixture was heated in an oil bath to 50–55°C for 8 days. The reaction mixture was then cooled and excess reagent was destroyed by dropwise addition of water. The mixture was filtered through Celite and the residue was washed with 10% methanol–chloroform. The filtrate was diluted with chloroform (100 mL) and washed with 5% aqueous citric acid and then with saturated NaCl. The organic layer was dried over anhydrous $MgSO_4$ and evaporated *in vacuo*. The crude product was crystallized from methanol–ether to give the pure diol **33** (0.415 g, 85.7%), mp 190–191°C. The β-hydroxy keto lactam **31** on similar reduction gave the same diol **33**; *m/e*: 405; ir ($CHCl_3$): 3600–3200 (—OH + N—H), 1665 (NH·CO) cm^{-1}; nmr ($CDCl_3$) τ: 3.12 (AB$_q$, J = 8 Hz, Δν = 6 Hz, 2H, aromatic H), 4.85 (s, 2H, O—CH$_2$—O), 5.53 (m, 1H, ring A C*H*OH), 5.58 (t, J = 4 Hz, 1H, ring B C*H*OH), 6.10 (s, 3H, aromatic —OCH$_3$), 6.50 (s, 3H, —O—CH$_2$—O—C*H*$_3$), 6.67 (s, 3H, —CH$_2$—O—C*H*$_3$). *Anal.* calcd. for $C_{21}H_{27}O_7N$: C 62.21, H 6.71, N 3.45; found: C 61.97, H 6.62, N 3.27.

Methylation of Diol ***33***

A solution of diol **33** (415 mg) in dry dioxane (24 mL) was refluxed with sodium hydride (490 mg, 57% oil suspension) under nitrogen for 2 h. The mixture was then cooled, excess methyl iodide (3 mL) was added, and reflux was continued for another 2 h. After cooling, the mixture was filtered through Celite and the residue was washed with dioxane. The solvent was then evaporated under reduced pressure and the crude product was chromatographed on silica gel. Elution with 5% methanol in chloroform gave the pure *N*-methyl lactam **34** (343.5 mg, 75%). A sample after recrystallization from dichloromethane–hexane melted at 163–165°C; *m/e*: 447; ir ($CHCl_3$): 1635 cm^{-1} (⟩NCO); nmr ($CDCl_3$) τ: 3.14 (AB_q, J = 8 Hz, $\Delta\nu$ = 15 Hz, 2H, aromatic H), 4.82 (s, 2H, O—CH_2—O), 6.06 (s, 3H, aromatic —OCH_3), 6.47 (s, 3H, —O—CH_2—O—CH_3), 6.57 (s, 6H, 2 secondary —OCH_3), 6.67 (s, 3H, —CH_2—OCH_3), 7.03 (s, 3H, —N—CH_3). *Anal.* calcd. for $C_{24}H_{33}O_7N$: C 64.41, H 7.43, N 3.13; found: C 64.05, H 7.65, N 2.93.

Acknowledgements

We wish to thank Drs. M. Przybylska and F. R. Ahmed (National Research Council, Ottawa) for the X-ray structure determination of compound **VIII**. We also wish to acknowledge with gratitude the constant financial support of the National Research Council of Canada, Ottawa, and the Hoffmann La Roche Company, Vaudreuil, P.Q. and Nutley, NJ (USA) over many years. Two of us (R.M.B. and M.B.) thank the Centro di studio per la chimica delle sostanze organiche naturali del C.N.R. and the University of Rome (Roma, Italy) for a leave of absence.

1. K. Wiesner, T. Y. R. Tsai, and K. P. Namibar. Can. J. Chem. **56**, 1451 (1978).
2. K. Wiesner. Centenary Lecture 1977. Chem. Soc. Rev. **6**, 413 (1977). K. Wiesner. Plenary Lecture IUPAC, Varna 1978. Pure Appl. Chem. **51**, 689 (1979).
3. K. P. Nambiar. Ph.D. Thesis, University of New Brunswick. 1977.
4. S. Wagatsuma *et al.* Org. Prep. Proced. Int. **5**, 65 (1973).
5. B. M. Trost and F. Chen. Tetrahedron Lett. 2603 (1971).
6. L. Birkofer, A. Ritter, and P. Richter. Chem. Ber. **96**, 2750 (1963).
7. A. McKillop, D. H. Perry, and M. Edwards. J. Org. Chem. **41**, 282 (1976).
8. K. Wiesner, P. T. Ho, R. C. Jain, S. F. Lee, S. Oida, and A. Philipp. Can. J. Chem. **51**, 1448 (1973).
9. S. F. Lee, G. M. Sathe, W. W. Sy, P. T. Ho, and K. Wiesner. Can. J. Chem. **54**, 1039 (1976).
10. K. Wiesner. Tetrahedron, **31**, 1655 (1975).

Conformational preferences of the *syn*-pyridinecarboxaldehyde oximes

WERNER DANCHURA, RODERICK E. WASYLISHEN, JAMES DELIKATNY, AND MOIRA R. GRAHAM

Department of Chemistry, University of Winnipeg, Winnipeg, Man., Canada R3B 2E9

Received March 9, 1979

WERNER DANCHURA, RODERICK E. WASYLISHEN, JAMES DELIKATNY, and MOIRA R. GRAHAM. Can. J. Chem. 57, 2135 (1979).

The results of an ^1H and ^{13}C nmr study of the three *syn*-pyridine aldoximes are reported. Observed $^6J(H_\alpha,H_{para})$ values in the 2- and 3-pyridine aldoximes indicate that the oxime group is twisted approximately 20° out of the pyridine ring plane. Stereospecific $^5J(H_\alpha,H_{meta})$ values measured for acetone solutions of 2-pyridine aldoxime indicate that the ratio of the NCCN *trans* conformation to the NCCN *cis* conformation is 0.86 ± 0.14. The results of similar measurements on 3-pyridine aldoxime give 0.60 ± 0.10 for the ratio of the C_2CCN *trans* and C_2CCN *cis* conformations. *Ab initio* molecular orbital calculations are in good qualitative agreement with experiment. Carbon-13 chemical shifts of the oximes are compared with those previously measured for the parent aldehydes.

WERNER DANCHURA, RODERICK E. WASYLISHEN, JAMES DELIKATNY et MOIRA R. GRAHAM. Can. J. Chem. 57, 2135 (1979).

On rapporte les résultats d'études rmn ^1H et ^{13}C effectuées sur trois aldoximes *syn* de la pyridine. Les valeurs observées pour $^6J(H_\alpha,H_{para})$ des pyridines aldoximes-2 (et -3) indiquent que le groupe oxime est décalé d'approximativement 20° par rapport au plan du cycle de la pyridine. Les valeurs de $^5J(H_\alpha,H_{meta})$ stéréospécifiques mesurées pour des solutions de pyridinealdoxime-2 dans l'acétone indiquent que le rapport des conformations HCCN *trans*:*cis* est de 0.86 ± 0.14. Les résultats de mesures semblables avec le pyridinealdoxime-3 conduisent à un rapport des conformations *trans* et *cis* des C_2CCN de 0.60 ± 10. Des calculs *ab initio* d'orbitales moléculaires sont en bon accord qualitatif avec les expériences. On compare les déplacements chimiques ^{13}C des oximes à ceux mesurés antérieurement pour leurs aldéhydes.

[Traduit par le journal]

Introduction

In recent years several techniques have been used to study the conformation of the CHO group in pyridine aldehydes (1–7). In contrast little attention has been given to the conformation of the oxime moiety in pyridine aldoximes. Here we wish to report the results of an nmr study of the three *syn*-pyridine aldoximes.[1] The principal objective of this study was to estimate the relative stabilities of **1***a* (NCCN *trans*) and **1***b* (NCCN *cis*) and of **2***a* (C_2CCN *trans*) and **2***b* (C_2CCN *cis*) in solution. Experimental results are compared with those obtained using *ab initio* molecular orbital theory with the minimal STO-3G basis set (7–9). The experimental technique used here is based on the stereospecific long-range spin–spin coupling constants over five bonds between the oxime proton, H_α, and the pyridine ring protons (2, 10, 11).

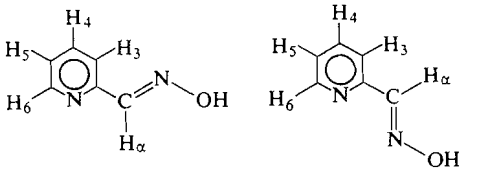

1*a*

1*b*

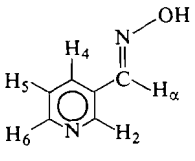

2*a*

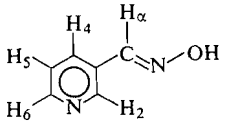

2*b*

As well, the conformational preferences derived for the oximes are compared with those obtained for the pyridine aldehydes. Finally, the influence of the oxime and carbonyl moieties on the ^{13}C nmr chemical shifts of the pyridine ring are compared. The ^{13}C chemical shifts of the pyridine ring carbons are shown to be relatively insensitive to the conformation of the oxime moiety.

Experimental

The pyridine aldoximes were obtained from ICN : K & K Laboratories Inc. The observed melting points of the 2-, 3-, and 4-pyridine aldoximes were 110–112°C, 149–151.5°C, and 130–132°C respectively. The samples used for the proton nmr studies were prepared as degassed solutions in acetone-d_6. The 4-pyridine aldoxime was prepared as a 5 mol% solution whereas the 2- and 3-pyridine aldoximes were prepared as saturated (< 5 mol%) solutions. The samples used for the ^{13}C nmr studies were 1 *M* solutions in DMSO-d_6.

Proton nmr spectra were obtained at 30 ± 2°C using a

[1] In the IUPAC system all *syn*-aldoximes become *E*-aldoximes and all *anti*-aldoximes become *Z*-aldoximes.

0008-4042/79/162135-05$01.00/0

TABLE 1. Observed chemical shifts (ppm) and coupling constants (Hz) of the *syn*-pyridine aldoximes

	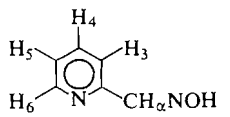	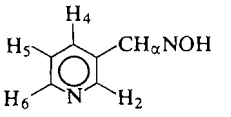	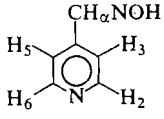
$\delta(H_\alpha)$	8.189	8.215	8.188
$\delta(H_2)$	—	8.794	8.622
$\delta(H_3)$	7.868	—	7.585
$\delta(H_4)$	7.796	8.011	—
$\delta(H_5)$	7.350	7.396	7.585
$\delta(H_6)$	8.594	8.571	8.622
$^3J(H_2,H_3)$	—	—	5.12
$^3J(H_3,H_4)$	8.01	—	—
$^3J(H_4,H_5)$	7.55	7.95	—
$^3J(H_5,H_6)$	4.91	4.83	5.12
$^4J(H_2,H_4)$	—	2.21	—
$^4J(H_3,H_5)$	1.17	—	1.63
$^4J(H_4,H_6)$	1.76	1.71	—
$^4J(H_2,H_6)$	—	0.0	0.0
$^5J(H_2,H_5)$	—	0.90	0.96
$^5J(H_3,H_6)$	1.00	—	0.96
$^4J(H_\alpha,H_o)$	−0.26	−0.43(H_2) −0.45(H_4)	−0.42(H_3) −0.42(H_5)
$^5J(H_\alpha,H_m)$	0.62(H_4) <0.15(H_6)	0.43	0.36
$^6J(H_\alpha,H_p)$	−0.18	−0.16	—

Varian CFT-20 spectrometer operating at 79.54 MHz. Acquisition times of 20.0 s or longer were used to obtain the data reported here. The free induction decay was not weighted. Typically ^1H line widths were less than 0.18 Hz. Proton chemical shifts were measured with respect to the ^1H signal of the residual protons in the solvent. This resonance was found to be 163.08 ± 0.05 Hz down field from internal TMS.

Proton-decoupled ^{13}C nmr spectra were also obtained on the Varian CFT-20 spectrometer at 32 ± 2°C. Chemical shifts were measured with respect to the solvent DMSO-d_6 and converted to the TMS scale by adding 39.56 ppm (12).

The geometry used for all molecular orbital calculations carried out in this study was obtained as follows. The coordinates for the pyridine ring were taken from a microwave study of pyridine (13*a*). The C_α—H_α and O—H bond lengths were 1.08 and 0.96 Å, respectively (14); C_{ring}—C_α (1.469 Å), C_α=N (1.275 Å), and N—O (1.390 Å) were taken from an X-ray diffraction study of *syn*-4-pyridine aldoxime (**3**) (15). In each case the $C_{ring}C_{ring}C_\alpha$ bond angle was taken to be the same as the corresponding CCH bond angles in pyridine (13*a*). The bond angle NOH was taken as 102.77° (13*b*). All other bond angles were taken from the X-ray diffraction study (15): $C_{ring}C_\alpha N$ (120.0°), $C_{ring}C_\alpha H_\alpha$ (122.0°), $H_\alpha C_\alpha N$ (118.0°), and $C_\alpha NO$ (111.1°).

Spin–spin coupling constants were calculated using semi-empirical molecular orbital calculations at the CNDO/2-FPT and INDO-FPT levels of approximation (16, 17). The reliability of these techniques for the calculation of spin–spin coupling constants has recently been reviewed (17*b*).

Results and Discussion

Spectral Analyses

Proton nmr spectra were analyzed using the computer program LAME (18). Results are presented in Table 1. The rms deviations between observed and calculated transition frequencies lie between 0.014 and 0.033 Hz for the various samples. For the 3- and 4-pyridine aldoximes the standard deviations of all spectral parameters are less than 0.01 Hz. For the 2-pyridine aldoxime the largest standard deviation was 0.04 Hz (for $^3J(H_4,H_5)$ and $^4J(H_3,H_5)$).

The coupling constants among the pyridine ring protons are all within 0.25 Hz of those previously observed in the corresponding pyridine aldehydes (2).

Assignment of Isomers

Often it is possible to prepare two different oximes from a given aldehyde, the so-called *syn*- and *anti*-aldoximes (19, 20). Because it is difficult to predict

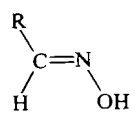

syn

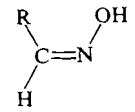

anti

a priori which form will be most stable, a number of techniques have been devised to distinguish between these two isomers (see for example refs. 19–30).

Although both the *syn*- and *anti*-4-pyridine aldoximes are known (15), only one isomer of the 2- and 3-pyridine aldoximes appears to be known (27). On the basis of observed $^2J(^{15}N,H)$ values, Crepaux and Lehn (27) have shown that these latter two compounds exist as the *syn* isomers.

TABLE 2. Calculated spin–spin coupling constants (in Hz)

	1*a*		1*b*		
	CNDO/2	INDO	CNDO/2	INDO	**1**, θ = 90°, INDO
$^4J(H_\alpha,H_3)$	0.15	−0.73	0.02	−0.75	−1.31
$^5J(H_\alpha,H_4)$	0.89	1.64	0.06	0.30	1.17
$^6J(H_\alpha,H_5)$	0.00	−0.45	0.02	−0.40	−1.09
$^5J(H_\alpha,H_6)$	0.12	0.40	0.86	1.61	1.06
	2*a*		**2***b*		
	CNDO/2	INDO	CNDO/2	INDO	**2**, θ = 90°, INDO
$^4J(H_\alpha,H_2)$	0.35	−0.19	0.04	−0.66	−1.15
$^4J(H_\alpha,H_4)$	0.06	−0.84	0.38	−0.16	−1.12
$^5J(H_\alpha,H_5)$	0.80	1.47	0.06	0.27	1.04
$^6J(H_\alpha,H_6)$	−0.01	−0.40	0.04	−0.30	−1.00

	3	
	CNDO/2	INDO
$^5J(H_\alpha,H_2)$	0.06	0.24
$^4J(H_\alpha,H_3)$	0.32	−0.29
$^4J(H_\alpha,H_5)$	0.09	−0.83
$^5J(H_\alpha,H_6)$	0.84	1.52

It is of interest to point out that the ^{1}H chemical shift differences between the O*H* and C*H*$_\alpha$ resonances for 10% DMSO-d_6 solutions of 2-, 3-, and 4-pyridine aldoximes are 3.57, 3.39, and 3.66 ppm respectively, making it difficult to apply the criterion proposed by Kleinspehn *et al.* (21) for distinguishing between *syn*- and *anti*-isomers.

Conformations About The Ring Carbon – Imino Carbon Bond

^{6}J(H_α,H_p) as a Measure of the Planarity of 1 and 2

Previous studies on substituted benzenes indicate that the six-bond coupling between a side chain proton and the proton *para* to the substituent is given by an equation of the form

[1] $^6J(H_\alpha,H_p) = {}^6J_0 + {}^6J_1 \sin^2\theta$

Here $^6J_1 \gg {}^6J_0$ and θ is the $H_\alpha C_\alpha C_1 C_2$ dihedral angle.

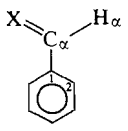

θ = 0°

For the pyridine aldehydes (X = O), $^6J(H_\alpha,H_p) <$ 0.05 Hz and hence $^6J_0 \simeq 0.0$ and $\theta \simeq 0°$. Reliable experimental values of $^6J_1$ are not available. However, on the basis of INDO-MO-FPT calculations (Table 2) we estimate $^6J_1 = -1.05 \pm 0.3$ Hz. This value of $^6J_1$ is similar to the value estimated in toluene (31) and used in a study of 2,6-dichlorobenzaldoxime (32). Thus using [1] with $^6J_0 = 0.0$ and taking $^6J_1 = -1.05 \pm 0.3$ Hz, the observed values of −0.18 Hz and −0.16 Hz in **1** and **2** suggest that the oxime group is twisted out of the pyridine ring plane by 24 ± 6° and 23 ± 6°.

X-ray diffraction data on *syn*-4-pyridine aldoxime (**3**) and *syn*-4-pyrimidine aldoxime (**4**) indicate that

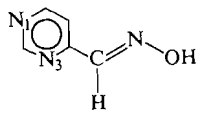

4

the oxime group is twisted out of the ring plane by 13.7° and 5° respectively (15, 33). Early X-ray data on *syn*-4-chlorobenzaldoxime indicated that the oxime moiety lay 19° out of plane (34).

On the basis of the X-ray data above it appears that the nmr estimates of θ are upper limits.

*^{5}J(H_α,H_m) as a Measure of the Relative Populations of 1*a *and 1*b *and of 2*a *and 2*b

In *syn*-4-pyridine aldoxime (**3**) the observed value of $^5J(H_\alpha,H_{2,6})$, 0.36 Hz, is an average of $^5J(H_\alpha,H_2)$ and $^5J(H_\alpha,H_6)$. Previous experimental studies on various aromatic aldehydes (2, 10, 11) indicate that for the conformation of *syn*-4-pyridine aldoxime shown below, $^5J(H_\alpha,H_2)$, must be small (<0.1 Hz), while $^5J(H_\alpha,H_6)$ is approximately 0.7 Hz. This

TABLE 3. Some *ab initio* MO results for the *syn*-pyridine aldoximes

Compound	Conformation	Total energies (au)	Relative energies (kcal/mol)	Dipole moments (D)
1	NCCN *trans*	−409.159664	0.00	2.04
	NCCN *cis*	−409.155882	2.37	1.94
	NCCN 90°	−409.149164	6.59	2.10
2	C(2)CCN *trans*	−409.159442	0.00	2.02
	C(2)CCN *cis*	−409.158820	0.390	1.96
	C(2)CCN 90°	−409.149754	6.08	1.99
3	CCCN planar	−409.158959	0.00	2.08
	CCCN 90°	−409.149516	5.93	1.96

hypothesis is also supported by the CNDO/2-MO-FPT results given in Table 2.

For *syn*-2-pyridine aldoxime, **1**, $^5J(H_\alpha,H_4) = 0.62 \pm 0.02$ Hz while $^5J(H_\alpha,H_6) \leq 0.15$ Hz. Assuming that $^5J_1(H_\alpha,H_4)_{obs} = X_{1a}{}^5J(H_\alpha,H_4)_{1a} + X_{1b}{}^5J(H_\alpha,H_4)_{1b}$ and that $^5J(H_\alpha,H_4)_{1a}$ is 0.72 Hz, or (2 × 0.36) Hz, and that $^5J(H_\alpha,H_4)_{1b}$ is zero, X_{1a}, the fractional population of the *trans* conformation, is 0.62/0.72 = 0.86 ± 0.14. The CNDO/2-MO-FPT calculations support our assumption that for **1***a* $^5J(H_\alpha,H_4)$ will be similar to $^5J(H_\alpha,H_2)$ in **3**.

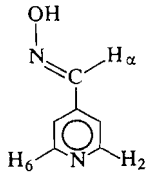

3

For *syn*-3-pyridine aldoxime, **2**, $^5J(H_\alpha,H_5)$ is 0.43 ± 0.02 Hz and using the same procedure as above the fractional population of **2***a* is 0.60 ± 0.10. The CNDO/2-MO-FPT calculations predict almost identical values for $^5J(H_\alpha,H_5)$ in **2***a* and $^5J(H_\alpha,H_6)$ in **3**.

STO-3G ab initio *Molecular Orbital Calculations*

The above estimates for the fractional populations of the *trans* conformations, X_{1a} and X_{2a} for **1** and **2** may be compared with the results of *ab initio* MO calculations presented in Table 3. The calculations predict **1***a* to be 2.38 kcal/mol more stable than **1***b*, hence at 30°C, $X_{1a} = 0.98$. **2***a* is predicted to be only 390 cal/mol more stable than **2***b*, hence at 30°C, $X_{2a} = 0.66$. The relative populations of **1***a* and **1***b* and of **2***a* and **2***b* calculated using the STO-3G basis set are in good qualitative agreement with the values estimated for solutions of **1** and **2** in acetone.

The *ab initio* calculations predict the conformation in which the oxime group is perpendicular to the pyridine ring-plane to be about 6 kcal/mol higher in energy than the completely planar conformations. These values are similar to those calculated (7) and observed (4, 5) for the pyridine aldehydes.

Finally, it is of interest to note that the calculated dipole moments of the pyridine aldoximes are insensitive to the conformation of the oxime group. Consequently, the relative populations of **1***a* and **1***b* and of **2***a* and **2***b* should be relatively insensitive to solvent polarity (2).

Comparison with Related Molecules

It is of interest to compare the results obtained here for the *syn*-pyridine aldoximes with those obtained for the parent aldehydes. In the case of 2-pyridine aldehyde, microwave (3) and nmr data (2, 4, 5) and *ab initio* MO calculations (7) are in agreement that the fractional population of the NCCO *trans* conformation, X_t, is 0.9 ± 0.1.

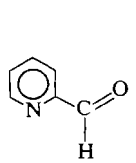

NCCO *trans*

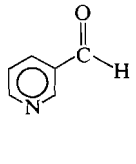

C_2CCO *trans*

For the 3-pyridine aldehyde there is general agreement that the C_2CCO *trans* conformation is slightly favored over the C_2CCO *cis* conformation (X_t = 0.7 ± 0.1). The values obtained for X_t are somewhat dependent on the solvent polarity and temperature (2, 4, 5)

In contrast to the oximes, the aldehydes appear to be planar (2, 3).

Finally it is of interest to mention that in the solid state *syn*-4-pyrimidine aldoxime (**4**) exists entirely in the N_3C_4CN *trans* conformation (33).

Carbon-13 Chemical Shifts

Carbon-13 chemical shifts of the *syn*-pyridine aldoximes are given in Table 4. The influence of the *syn*-CHNOH group on ^{13}C chemical shifts of the pyridine ring is displayed in Table 5. For comparison the analogous literature values for the CHO groups are included in parentheses (35–37). In general the CHNOH group influences the pyridine ring carbon shifts less than does the CHO group. This is particularly true for the carbon *para* to the substitutent; in the 2- and 3-substituted oximes the *para*-substituent effect is 0.1 and 0.0 ppm, respectively, while

TABLE 4. Observed carbon-13 chemical shifts (ppm) of the *syn*-pyridine aldoximes

	1	2	3
C_α	149.0	145.8	146.7
C_2	152.2	147.9	150.2
C_3	119.8	129.1	120.7
C_4	136.8	133.1	140.4
C_5	124.0	123.9	120.7
C_6	149.5	150.1	150.2

TABLE 5. Effect of *syn*-CHNOH and CHO substitution on pyridine ring ^{13}C chemical shifts[a,b] (in ppm)

Substituent at:	C_2	C_3	C_4
C_2	*2.1* (3.2)	−2.2 (1.1)	0.1 (1.4)
C_3	−4.1 (−2.1)	*5.2* (8.4)	−3.2 (−1.1)
C_4	1.0 (1.9)	−2.7 (0.6)	*4.6* (6.1)
C_5	0.1 (4.4)	0.0 (1.1)	−3.2 (−1.1)
C_6	−0.6 (0.4)	0.0 (5.1)	0.1 (1.4)

[a]Values in parentheses are for CHO substitution.
[b]Positive values indicate a downfield shift relative to the value in pyridine.

in the corresponding aldehydes the values are 4.4 and 5.5 ppm. This is also the case when one compares the influence of the CHO and CHNOH moieties on the benzene ring; here the oxime group shifts C_{para} 1.7 ppm downfield while the CHO group induces a 6.0 ppm downfield shift (37, 38).[2]

One might expect the carbon β to the oxime group to be most sensitive to the conformation of the CHNOH moiety (i.e., C_3 in **1**, C_2 and C_4 in **2**, C_3 and C_5 in **3**). In the case of **1**, where the NCCN *trans* conformation is highly favored, the substituent effect on C_3 is −4.1 ppm, not very different from the value of −3.2 ppm observed for C_3 and C_5 in **3**. On the basis of these data it appears that the chemical shifts of the pyridine ring are relatively insensitive to the conformation of the CHNOH group.

Acknowledgements

We wish to thank Professor Ted Schaefer for his encouragement and Dr. Robert Lichter for a preprint of ref. 38. The support of the National Research Council of Canada is gratefully acknowledged.

1. V. GALASSO. Mol. Phys. **26**, 81 (1973).
2. W. DANCHURA, T. SCHAEFER, J. B. ROWBOTHAM, and D. J. WOOD. Can. J. Chem. **52**, 3986 (1974).
3. Y. KAWASHIMA, M. SUZUKI, and K. KOZIMA. Bull. Chem. Soc. Jpn. **48**, 2009 (1975).
4. T. DRAKENBERG. J. Chem. Soc. Perkin Trans. II, 147 (1976).
5. L. LUNAZZI, D. MACCIANTELLI, and G. CERIONI. J. Chem. Soc. Perkin Trans. II, 1792 (1976).
6. L. LUNAZZI, C. ZANNONI, C. A. VERACINI, and A. ZANDANEL. Mol. Phys. **34**, 223 (1977).
7. I. G. JOHN, G. L. D. RITCHIE, and L. RADOM. J. Chem. Soc. Perkin Trans. II, 1601 (1977).

[2]H. J. Jakobsen, M. Hansen, and R. Wasylishen. Unpublished results.

8. W. J. HEHRE, R. F. STEWART, and J. A. POPLE. J. Chem. Phys. **51**, 2657 (1969).
9. W. J. HEHRE, W. A. LATHAN, R. DITCHFIELD, M. D. NEWTON, and J. A. POPLE. Quantum Chemistry Program Exchange, University of Indiana, Bloomington, IN. 1973. Program 236.
10. G. J. KARABATSOS and F. M. VANE. J. Am. Chem. Soc. **85**, 3886 (1963).
11. R. WASYLISHEN and T. SCHAEFER. Can. J. Chem. **49**, 3216 (1971).
12. G. C. LEVY and J. D. CARGIOLI. J. Magn. Reson. **6**, 143 (1972).
13. (*a*) G. O. SORENSEN, L. MAHLER, and N. RASTRUP-ANDERSEN. J. Mol. Struct. **20**, 119 (1974); (*b*) I. N. LEVINE. J. Chem. Phys. **38**, 2326 (1963).
14. J. A. POPLE and M. GORDON. J. Am. Chem. Soc. **89**, 4253 (1967).
15. M. MARTINEZ-RIPOLL and H. P. LORENZ. Acta Crystallogr. Sect. B, **32**, 2322 (1976); **32**, 2325 (1976).
16. J. A. POPLE, J. W. MCIVER, JR., and N. S. OSTLUND. J. Chem. Phys. **49**, 2960 (1968); **49**, 2965 (1968).
17. (*a*) J. A. POPLE and D. L. BEVERIDGE. Approximate molecular orbital theory. McGraw-Hill Book Co., New York. 1970; (*b*) J. KOWALEWSKI. Prog. Nucl. Magn. Reson. Spectrosc. **11**, 1 (1977).
18. C. W. HAIGH. Ann. Rep. NMR Spectrosc. **4**, 311 (1971).
19. C. G. MCCARTY. *In* The chemistry of the carbon–nitrogen double bond. *Edited* by S. Patai. Interscience Publishers, New York. 1970. pp. 383–392.
20. S. R. SANDLER and W. KARO. Organic functional group preparations. Vol. III. Academic Press, New York. 1972. pp. 365–405.
21. G. G. KLEINSPEHN, J. A. JUNG, and S. A. STUDNIARZ. J. Org. Chem. **32**, 460 (1967).
22. G. J. KARABATSOS and R. A. TALLER. Tetrahedron, **24**, 3347 (1968).
23. Z. W. WOLKOWSKI, N. THOAI, and J. WIEMANN. Tetrahedron Lett. 93 (1970).
24. Z. W. WOLKOWSKI. Tetrahedron Lett. 825 (1971).
25. R. L. LICHTER, D. E. DORMAN, and R. WASYLISHEN. J. Am. Chem. Soc. **96**, 930 (1974).
26. G. E. HAWKES, K. HERWIG, and J. D. ROBERTS. J. Org. Chem. **39**, 1017 (1974).
27. D. CREPAUX and J. M. LEHN. Org. Magn. Reson. **7**, 524 (1975).
28. K. D. BERLIN and S. RENGARAJU. J. Org. Chem, **36**, 3912 (1971).
29. G. C. LEVY and G. L. NELSON. J. Am. Chem. Soc. **94**, 4897 (1972).
30. P. GENESTE, R. DURAND, J. M. KAMENKA, H. BEIERBECK, R. MARTINO, and J. K. SAUNDERS. Can. J. Chem. **56**, 1940 (1978).
31. R. WASYLISHEN and T. SCHAEFER. Can. J. Chem. **50**, 1852 (1972), and references therein.
32. T. SCHAEFER and R. WASYLISHEN. Can. J. Chem. **47**, 3707 (1969).
33. M. MARTINEZ-RIPOLL and H. P. LORENZ. Acta Crystallogr. Sect. B, **29**, 2260 (1973).
34. B. JERSLEV. Nature, **180**, 1410 (1957).
35. H. L. RETCOFSKY and R. A. FRIEDEL. J. Phys. Chem. **71**, 3592 (1967); J. Phys. Chem. **72**, 290 (1968); **72**, 2619 (1968).
36. G. MIYAJIMA, Y. SASAKI, and M. SUZUKI. Chem. Pharm. Bull. **20**, 429 (1972).
37. J. B. STOTHERS. Carbon-13 nmr spectroscopy. Academic Press, New York, NY. 1972.
38. A. DANOFF, M. FRANZEN-SIEVEKING, R. L. LICHTER, and S. N. Y. FANSO-FREE. Org. Magn. Reson. In press.

A nuclear magnetic resonance study of pyridinium and *p*-anisidinium carboxylate salts

JOAN A. GOWLAND AND ROBERT A. MCCLELLAND

Department of Chemistry, University of Toronto, Scarborough College, West Hill, Ont., Canada M1C 1A4

Received November 21, 1978

JOAN A. GOWLAND and ROBERT A. MCCLELLAND. Can. J. Chem. 57, 2140 (1979).

The proton nmr chemical shifts for *p*-anisidinium chloride, chloroacetate, dichloroacetate, and trichloroacetate and pyridinium dichloroacetate, trichloroacetate, and trifluoroacetate salts in seven solvents are reported. These shifts are used to estimate the extent of proton transfer between the amine base and carboxylic acid. In non-polar solvents the *p*-anisidinium ion lies intermediate in acidity between monochloroacetic acid and trichloroacetic acid. The pyridinium system is similar; there is also some evidence here for the presence of charge transfer complexes.

JOAN A. GOWLAND et ROBERT A. MCCLELLAND. Can. J. Chem. 57, 2140 (1979).

On rapporte les déplacements chimiques en rmn ^1H pour les chlorure, chloroacétate, dichloroacétate et trichloroacétate de *p*-anisidinium et pour les dichloroacétate, trichloroacétate et trifluoroacétate de pyridinium dans sept solvants. On utilise ces déplacements pour évaluer le taux de transfert protonique entre l'amine basique et l'acide carboxylique. Dans des solvants non polaires, l'acidité de l'ion *p*-anisidinium se situe entre celle des acides monochloro- et trichloro-acétiques. Le système pyridinium est semblable; il existe aussi ici quelques indications relatives à la présence de complexes de transfert de charge.

[Traduit par le journal]

With the recent availabilities of acidities and basicities in the gas phase, it has become increasingly important to evaluate the effects of solvation on acid–base equilibria in solution, since the gas phase measurements underline the importance of this factor in determining the position of equilibria. To date the majority of solution studies have focussed on polar or protic solvents, with few detailed investigations in weakly polar aprotic solvents. In this paper, we report an nmr study of the interaction of two amine bases, *p*-anisidine and pyridine, with chloro-, dichloro-, and trichloroacetic acids in a series of solvents ranging in polarity from water to chloroform. These two bases were chosen since they have similar aqueous solution dissociation constants. The carboxylic acids were chosen since their aqueous pK_a values are such that proton transfer to the two amines is essentially complete in water. Proton nmr was chosen as the tool for the investigation; this technique has been well established to serve as a measure of the electron density of the aromatic system, and as such should serve as a probe for the type of interaction between the aromatic amino base and the added acid (1–8).

Experimental

Chloroacetic acid and trichloroacetic acid were recrystallized from chloroform. *p*-Anisidine was recrystallized from petroleum ether (80–100°C). Dichloroacetic acid was distilled at reduced pressure. Chloroform and pyridine were purified according to standard procedures. Other solvents were Fisher AnalaR or spectral grade, or Merck, Sharp and Dohme deuterated solvents (D_2O, DMSO-d_6, $CDCl_3$, acetone-d_6). Melting points were taken on a Fischer-Johns melting point apparatus and are uncorrected. Infrared spectra were obtained on a Perkin Elmer 237-B Grating IR spectrophotometer. Ultraviolet spectra were obtained on a Unicam SP 800 spectrometer. Analyses were done by A. Gygli, Toronto. Nuclear magnetic resonances were obtained on a Varian T60 nmr spectrometer. Approximately 10% w/w solutions of the salts were used. Chemical shifts are given relative to TMS.

The salts were prepared as follows:

p-*Anisidinium Chloroacetate*

Approximately equimolar amounts of chloroacetic acid and *p*-anisidine were combined in chloroform to give a white precipitate. This was recrystallized from acetone and chloroform to give fluffy white needles, mp 128–119°C. *Anal.* calcd. for $C_9H_{12}ClNO_3$: C 49.61, H 5.57, N 6.29, Cl 16.45; found: C 49.76, H 5.51, N 6.43, Cl 16.29.

p-*Anisidinium Dichloroacetate*

Approximately equimolar amounts of dichloroacetic acid and *p*-anisidine were combined in chloroform. The solution was heated briefly and then cooled to give a white precipitate. This product was recrystallized from acetone and chloroform to give a white powder, mp 133–134°C. *Anal.* calcd. for $C_9H_{11}Cl_2NO_3$: C 42.84, H 4.24, N 5.44, Cl 27.94; found: C 42.68, H 4.36, N 5.55, Cl 28.12.

p-*Anisidinium Trichloroacetate*

Approximately equimolar amounts of trichloroacetic acid and *p*-anisidine were combined in a small amount of chloroform. The solution was heated for two hours and then cooled and scratched to give a white precipitate. The product was recrystallized from chloroform to give white needle-shaped crystals, mp 94–95°C. *Anal.* calcd. for $C_9H_{10}Cl_3NO_3$: C 37.68, H 3.52, N 4.78, Cl 37.09; found: C 37.57, H 3.49, N 4.88, Cl 37.11.

p-*Anisidinium Chloride*

Concentrated hydrochloric acid was added to a solution of *p*-anisidine in benzene to give a white precipitate. This was

0008-4042/79/162140-05$01.00/0

TABLE 1. Chemical shifts for *p*-anisidinium salt ring protons in various solvents (ppm from TMS)[a]

Solvent	*p*-Anisidine	*p*-Anisidinium chloroacetate	*p*-Anisidinium dichloroacetate	*p*-Anisidinium trichloroacetate	*p*-Anisidinium chloride
$CDCl_3$	6.70	6.83	7.30, 6.90	7.38, 6.88	Insoluble
Tetrahydrofuran	6.55	6.58	6.65	7.25, 6.83	Insoluble
Acetone-d_6	6.67	6.78	6.95	7.38, 7.05	7.48, 7.11
Acetonitrile	6.63	6.70	6.80	6.83	Insoluble
Methanol	6.71	6.91	7.28, 6.97	7.30, 7.00	7.37, 7.01
DMSO-d_6	6.57	6.54	6.65	6.67	7.37, 7.00
D_2O	6.80	7.30, 7.00	7.30, 7.00	7.30, 7.00	7.28, 6.97

[a]Where two numbers are given the first refers to protons *ortho* to the methoxy group.

TABLE 2. Chemical shifts for pyridinium ring protons in various solvents (ppm from TMS)

Solvent	Pyridine	Pyridinium dichloroacetate	Pyridinium trichloroacetate	Pyridinium trifluoroacetate
$CDCl_3$	8.63,[a] 7.65, 7.27	8.81, 8.11, 7.80	8.95, 8.33, 7.88	8.89, 8.33, 7.88
Tetrahydrofuran	8.63, 7.65, 7.25	8.58, 7.77, 7.35	8.75, 8.06, 7.62	8.77, 8.15, 7.68
Acetone-d_6	8.58, 7.77, 7.33	8.69, 8.10, 7.65	8.98, 8.47, 7.98	8.98, 8.52, 8.05
Acetonitrile	8.44, 7.57, 7.17	8.70, 8.16, 7.72	8.78, 8.35, 7.88	8.78, 8.35, 7.87
Methanol	8.59, 7.80, 7.42	8.72, 8.28, 7.82	8.83, 8.53, 8.02	8.85, 8.55, 8.05
DMSO-d_6	8.62, 7.75, 7.38	8.61, 7.85, 7.47	8.53, 7.76, 7.38	8.87, 8.41, 7.92
D_2O	8.43, 7.72, 7.35	8.71, 8.53, 8.00	8.73, 8.56, 8.05	8.71, 8.53, 8.03

[a]First number corresponds to H_α, second $-H_\gamma$, third H_β.

recrystallized from ethyl acetate and methanol (cf. ref. 1), mp becomes glossy >186°C. *Anal.* calcd. for $C_7H_{10}ClNO$: C 52.61, H 6.21, N 8.76, Cl 22.2; found: C 52.87, H 6.46, N 8.76, Cl 22.11.

Pyridinium Dichloroacetate

Approximately equimolar amounts of dichloroacetic acid and pyridine were combined in chloroform to give a waxy yellow solid which was very hygroscopic. Recrystallization from anhydrous ether gave colourless needle-shaped crystals, mp 52–54°C (ref. 9 only reports obtaining a hygroscopic salt). Only dry crystals were used for spectral work, but the extremely hygroscopic nature of the salt did not permit satisfactory analysis.

Pyridinium Trichloroacetate

Approximately equimolar amounts of trichloroacetic acid and pyridine were combined in a small amount of chloroform to give shiny white plate-like crystals which were recrystallized from benzene, mp 106–107°C (lit. (10) mp 100–102°C). *Anal.* calcd. for $C_7H_6Cl_3NO_2$: C 34.64, H 2.47, N 5.77, Cl 43.91; found: C 34.44, H 2.43, N 5.71, Cl 43.86.

Pyridinium Trifluoroacetate

Trifluoroacetic acid and pyridine were combined in a small amount of chloroform to give a white precipitate. This was recrystallized from chloroform and ether to give small needle-like crystals, mp 79–81°C (lit. (11) mp 82–83°C).

Results and Discussion

The approach that was employed to prepare the nmr solutions was to synthesize and purify salts of the acid and base, and dissolve these in the solvent in question. With one exception, elemental analysis of the solid salts so prepared corresponds to a 1:1 mixture of acid and base, and their KBr infrared spectra show carboxylate and ammonium bands, and no carboxylic acid band. These are then normal 1:1 salts of an acid and a base. The one exception is the solid which precipitates from concentrated solutions of chloroacetic acid and pyridine; this material appears to be a product of nucleophilic substitution.

In Tables 1 and 2 ring proton chemical shifts for the salts, as well as for the parent bases, are given in ppm relative to TMS. In a small number of cases spectra were obtained without preforming a solid salt, simply with a 1:1 molar solution of acid and base. Spectra of these solutions are identical to those obtained with the salts. The chemical shifts given in the tables are the weighted mean of the set of peaks corresponding to each proton. This is an approximation, since the pyridine spectrum is of the type AA'BB'C, while that of *p*-anisidine is of the type AA'BB'. However, relative shifts at 60 MHz are fairly large, and the shifts of Tables 1 and 2 are probably accurate to ±0.05 ppm. As has been shown previously (6), where a comparison is possible with shifts arrived at by exact analysis, numbers arrived at by this approximate analysis show good agreement.

p-Anisidinium Salts

As anticipated the nmr results obtained in D_2O are consistent with essentially complete proton transfer from acid to base, forming solvent separated ion pairs. This is seen by the fact that all salts have the same ring proton shifts, and is not surprising since

TABLE 3. Percent proton transfer[a] of *p*-anisidinium salts

Solvent	*p*-Anisidinium chloroacetate	*p*-Anisidinium dichloroacetate	*p*-Anisidinium trichloroacetate
DMSO-d_6	0	13	16
Acetonitrile	13	33	38
Tetrahydrofuran	6	20	90[b]
Methanol	12	40	92
Acetone-d_6	16	45	89
$CDCl_3$	30	90	100[b]
D_2O	100	100	100

[a]Numbers are accurate to ± 5–10%.
[b]The chemical shifts for *p*-anisidinium chloride were estimated as 7.4, 7.0.

even with chloroacetic acid the difference in pK_a between the acid and the *p*-anisidinium ion is greater than three. The KBr ir spectra of the solid salts also show full proton transfer.

In the other solvents the general conclusion which emerges is that proton transfer is not as complete. In Table 3 are presented rough estimates of the percent proton transfer, with the solvents arranged in order of increasing ionizing ability. The numbers were arrived at by taking the chemical shift of *p*-anisidine alone for that of a system with no proton transfer, and the chemical shift of *p*-anisidinium chloride for that of a system with full proton transfer. Although no claim can be made that these numbers are very precise (we estimate their accuracy to be at best ±10), several trends emerge.

In acetonitrile and DMSO the acid–base equilibrium is shifted to favor un-ionized species, i.e., there is very little proton transfer. This can be attributed to the very poor solvating capabilities of these two solvents for carboxylate anions (12). In the other four solvents, the trichloroacetate salt is mainly ionized, the chloroacetate salt is mainly un-ionized, and the dichloroacetate takes an intermediate position. Evidence was obtained that the nmr shifts do reflect the position of equilibrium, in that addition of excess acid to a solution of a partially ionized salt causes a downfield chemical shift in the ring protons, i.e., towards that of the ionized form. The general conclusion that emerges is that in these four solvents there is a considerable shift in the *relative* acidities of the *p*-anisidinium ion and the carboxylic acids, such that the former is now somewhere intermediate in acidity between monochloroacetic acid and trichloroacetic acid. This amounts to a change of approximately three log units in the ΔpK_a values, and, what is also somewhat surprising, this change is similar in the four solvents, chloroform, tetrahydrofuran, acetone, and methanol. We can also point out that ir studies have reached a similar conclusion as to the effect of solvent on the ΔpK_a of protonated amines and carboxylic acids (13, 14), indicating that there is consistency between the ir and nmr analyses.

One additional comment should be made regarding this system. It is probably reasonably valid to say that in these non-polar solvents the anilinium carboxylate salt exists in relatively tight ion pairs, so that the counter-ion can have an influence on the exact nmr shift of the *p*-anisidinium group (1). This obviously limits the accuracy of any pK_a value measured using nmr chemical shifts (as in Table 3). For example the difference in *p*-anisidinium chloride and *p*-anisidinium trichloroacetate in acetone can be taken as indicative of less than complete proton transfer for the carboxylate, or more likely can be taken as indicative of different degrees of association within the ion pair.

Pyridinium Salts

In general it can be concluded that the behavior of the pyridinium salts is fairly similar to that of the *p*-anisidinium salts. Both sets are fully ionized in D_2O while in the other solvents significant shifts in acid–base equilibria occur. Pyridine appears to be a weaker base in acetonitrile, as could be expected. The aqueous pK_a values of ions of this type are strongly influenced by hydrogen bonding (15) between N—H and solvent water molecules, but this type of solvation will be far less important in acetonitrile. The *p*-anisidinium ion, which can form three such hydrogen bonds, is stabilized more in water by this type of interaction than the pyridinium ion, where there is only one available hydrogen. The *p*-anisidinium equilibrium therefore suffers more, relatively speaking, on proceeding to the acetonitrile solvent.

A further feature of the pyridinium system which can be commented on is the chemical shift of the α protons, which were found to be very concentration dependent. Typically the H_α chemical shift moved to lower field as the salt concentration increased. The shift, for example, of H_α for pyridinium trichloroacetate varied from 8.70 (5% solution) to 9.21 (saturated solution). In addition to their concentration dependency, the downfield position of these chemical shifts is somewhat unusual. Examination of the litera-

ture reveals that in general H_α of the pyridinium salt appears at 8.8 ± 0.1 (3, 4). The only exceptions to this behavior of which we are aware are the shifts for the α protons of 1,4-diethylpyridinium chloride and iodide, which in $CDCl_3$ appear at 9.81 ppm and 9.45 ppm respectively (7).

We propose that these downfield chemical shifts arise when the pyridinium ion is forming charge-transfer complexes. This is of course a well established feature of pyridinium ions, especially in non-polar solvents (16), but has not been discussed for pyridinium carboxylate salts. In general the presence of a charge transfer interaction is seen in the uv spectrum of a salt by the appearance of additional bands not found in the spectrum of either the cation or anion (16). Neither the pyridinium ion nor the chloroacetate ions show uv absorbance above 300 nm. However absorbance can be seen in this region for the pyridinium chloroacetate salts, particularly with the trichloroacetate (Fig. 1). This long wavelength absorption is consistent with the presence of some charge transfer interaction.

Intuitively one might then expect small upfield nmr shifts for pyridinium protons in a charge transfer complex, since the ion, acting as an acceptor, would have a gain in electron density. However, the following is consistent with downfield shifts for the α protons. Theoretical calculations (17) show that pyridinium chloride in its charge transfer form has the chloride sitting preferentially over C-2 and C-6 of the pyridinium ring. These calculations also suggest that the chlorine–carbon distance in this form is less than the van der Waals radius. Moreover, although there is a net transfer of charge to the pyridinium ring, the charges on C-2 and C-6 become more positive, thus enhancing the electrostatic interaction with the chloride ion (17). Such an interaction would lead to a downfield shift for the α protons while the β and γ protons would remain the same or move somewhat upfield, as we in fact observe. Further evidence for this type of interaction comes from the halide order observed in the 1,4-diethylpyridinium salts (7), where the H_α downfield shifts occur in the order $Cl^- > I^-$. This is opposite to the expected order for charge transfer formation (18, 19). However, the nmr shifts would be a combination of the charge transfer effect and an electrostatic interaction and for the latter, Cl^- would be expected to show the largest effect. (One of the referees suggested that charge transfer complex formation might result in line broadening, due to the production of spin density in the aromatic ring. We find no significant line broadening in our spectra, but this could be obscured because of the complexity of the spectra.)

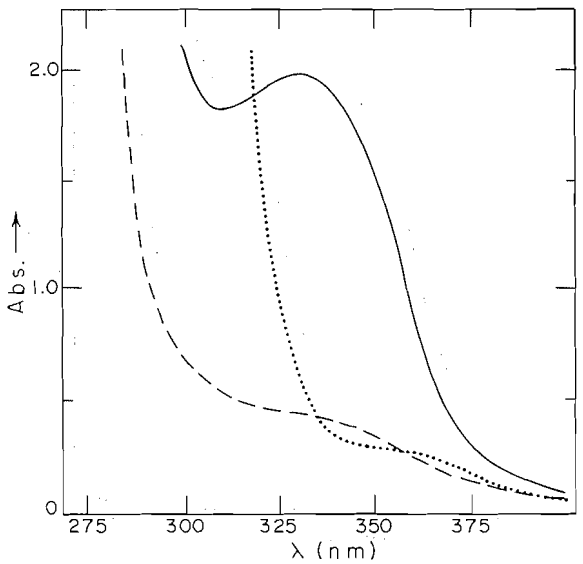

FIG. 1. Ultraviolet spectra of pyridinium solutions in chloroform: (--) saturated pyridinium trichloroacetate salt solution: (—) 0.4 *N* trichloroacetic acid + 0.24 *N* pyridine; (· ·) filtrate of an 0.8 *N* chloroacetic acid + 4 *N* pyridine solution.

For the pyridinium salts in this study the following equilibria can be proposed in non-polar or weakly polar solvents.

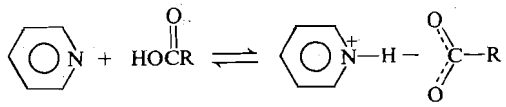

I, ion pairs

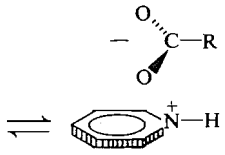

II, charge transfer complexes

Structures I and II differ in the position of the carboxylate group, which is sitting on top of the ring in II, over N, C-2 and C-6. This leads to a similar rearrangement of charge to that observed with the pyridinium halides, and, we propose, accounts for the downfield nmr shifts of H_α and the presence of charge transfer bands in the uv spectra.

Acknowledgement

Financial support from the National Research Council of Canada is gratefully acknowledged.

1. G. FRAENKEL and J. P. KIM. J. Am. Chem. Soc. **88**, 4203 (1966).
2. T. J. BATTERHAM. N.M.R. spectra of simple heterocyclics. Wiley, New York. 1973. Chapt. 1.
3. V. M. S. GIL and J. N. MURRELL. Trans. Faraday Soc. **60**, 248 (1964).

4. G. KOTOWYCZ, T. SCHAEFER, and E. BOCK. Can. J. Chem. **42**, 2541 (1964).
5. G. FRAENKEL, R. E. CARTER, A. M. MCLACHLAN, and J. H. RICHARDS. J. Am. Chem. Soc. **82**, 5846 (1960).
6. W. F. REYNOLDS and T. SCHAEFER. Can. J. Chem. **41**, 2339 (1963).
7. R. J. CHUCK and E. W. RANDELL. Spectrochim. Acta, **22**, 221 (1966).
8. W. F. REYNOLDS and U. R. PRILLER. Can. J. Chem. **46**, 2787 (1968).
9. S. R. GOUGH and A. H. PRICE. J. Phys. Chem. **73**, 459 (1969).
10. S. L. JOHNSON and K. A. RAMON. J. Phys. Chem. **69**, 74 (1965).
11. M. STACEY, J. C. TATLOW, and R. WORRALL. J. Chem. Soc. 2006 (1964).
12. I. M. KOLTOFF, M. K. CHANTOONI, JR., and S. BHOMIK. J. Am. Chem. Soc. **90**, 23 (1967).
13. B. A. DAWA and J. A. GOWLAND. Can. J. Chem. **56**, 2567 (1978).
14. R. LINDEMANN and G. ZUNDEL. J. Chem. Soc. Faraday Trans. II, **73**, 788, 1978.
15. E. M. ARNETT, B. CHAWLA, L. BELL, M. TANGEPERA, W. J. HEHRE, and R. W. TAFT. J. Am. Chem. Soc. **99**, 5729, 1977.
16. E. M. KOSOWER. J. Am. Chem. Soc. **80**, 3253 (1958).
17. F. JORDAN. J. Am. Chem. Soc. **97**, 3330 (1975).
18. A. RAY. J. Am. Chem. Soc. **93**, 7146 (1971).
19. A. RAY and P. MUKERGEE. J. Phys. Chem. **70**, 2138 (1966).

Chemoselectivity in the synthesis of thiocyanates and isothiocyanates: the reaction of alkenes with benzeneselenenyl thiocyanate in methylene chloride

DENNIS G. GARRATT,[1] M. DOMINIC RYAN, AND MARK UJJAINWALLA

Department of Chemistry, University of Ottawa, Ottawa, Ont., Canada K1N 9B4

Received February 7, 1979

DENNIS G. GARRATT, M. DOMINIC RYAN, and MARK UJJAINWALLA. Can. J. Chem. **57**, 2145 (1979).

The reactions of benzeneselenenyl thiocyanate with some simple alkylsubstituted acyclic and cyclic alkenes have been investigated, and the relative distribution of isomeric adducts determined. The relative distribution of β-thiocyanatoalkyl phenyl selenide to β-isothiocyanatoalkyl phenyl selenide is found to be dependent upon the degree of substitution of the initial alkene. Thus mono- and disubstituted alkenes favour formation of the thiocyanato species, whereas tri- and tetrasubstituted alkenes yield isothiocyanato adducts almost exclusively. Stereospecific *anti* addition was established in all cases except that of tricyclo[4.2.2.0^{2,5}]deca-3,9-diene-7,8-dicarboxylic anhydride which gives a 33:67 mixture of *cis* and *trans* adducts.

DENNIS G. GARRATT, M. DOMINIC RYAN et MARK UJJAINWALLA. Can. J. Chem. **57**, 2145 (1979).

On a étudié les réactions du thiocyanate de benzènesélénényle avec quelques alcènes linéaires et cycliques substitués par des groupes alkyles simples et on a déterminé la distribution relative des adduits isomères. On a trouvé que la distribution relative du sélénure de β-thiocyanatoalkyle et de phényle par rapport au sélénure de β-isothiocyanatoalkyle et de phényle dépend du degré de substitution de l'alcène de départ. Les alcènes mono- et disubstituées favorisent la formation d'espèces thiocyanato alors que les alcènes tri- et tétra-substitués conduisent presqu'exclusivement aux adduits isothiocyanato. On a établi que l'addition est stéréospécifiquement *anti* dans tous les cas excepté celui de l'anhydride de l'acide tricyclo[4.2.2.0^{2,5}] décadiène-3,9 dicarboxylique-7,8 qui conduit à un mélange 33:67 des adduits *cis* et *trans*.

[Traduit par le journal]

The isolation of an areneselenenyl thiocyanate was first reported by Foss in 1947 (1) from the reaction of 2-nitrobenzeneselenenyl bromide with potassium thiocyanate in ethyl acetate–methanol solution (eq. [1]). There have been few studies of this class of compounds, with the exception of a brief investigation by Rheinboldt and Perrier on nucleophilic substitution at selenenyl selenium (2).

[1] 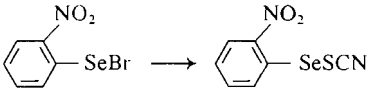

We wish to present the results of an experimental investigation of the addition of benzeneselenenyl thiocyanate to a series of simple alkylsubstituted olefins. In previous papers we have discussed the reactions of the analogous areneselenenyl chlorides with unsaturated substrates of various types and structure, both from the point of view of kinetics and the stereochemical and regiochemical nature of these reactions (3). It was anticipated that areneselenenyl thiocyanates would behave like the analogous chlorides and thus allow one by virtue of the ambident character of the pseudohalide anion, SCN, to draw further mechanistic conclusions with respect to the importance of ion-pairs during these reactions and the subsequent isomerizations of the adducts. Furthermore, it was felt that the use of areneselenenyl thiocyanates might open up a new series of potentially useful synthetic reagents for the introduction, both stereo- and regiospecifically, of sulphur and nitrogen moieties based on the chemistry of alkyl thiocyanates and isothiocyanates. Related studies utilizing iodine thiocyanate have recently been published by Woodgate and co-workers (4).

Benzeneselenenyl thiocyanate, C_6H_5SeSCN, was prepared *in situ* by a modification of the method of Foss from benzeneselenenyl chloride and sodium thiocyanate in methylene chloride as solvent. The presence of a strong sharp peak at 4.65 μm in the infrared spectrum, characteristic of a thiocyanate group, and the absence of an intense, broad band in the 4.67–5.03 μm region indicative of an isothiocyanate group, clearly indicates the reagent to be C_6H_5SeSCN rather than C_6H_5SeNCS. The sodium chloride is removed by filtration and the resultant clear yellow-orange solution used directly for the additions. These solutions should be used within a few hours of preparation. On prolonged standing a

[1]To whom correspondence should be directed.

[2]D. G. Garratt and M. D. Ryan. Unpublished observations. University of Ottawa, Ottawa, Canada.

0008-4042/79/162145-09$01.00/0

deep orange crystalline solid precipitates out of solution. This material is also obtainable directly via evaporation of the solvent and appears to be a form of benzeneselenenyl thiocyanate in a higher state of aggregation. Although this alternate form of the reagent will react with alkenes, we have limited ourselves in this report to a study of the chemistry of the first formed species.

Results and Discussion

Reactions of benzeneselenenyl thiocyanate, **1**, in methylene chloride at ambient temperature with simple alkenes give adducts of the type shown in [2].

[2] $C_6H_5SeSCN + \diagup C{=}C \diagdown \longrightarrow$

1

$C_6H_5Se{-}\overset{|}{\underset{|}{C}}{-}\overset{|}{\underset{|}{C}}{-}SCN$ + $C_6H_5Se{-}\overset{|}{\underset{|}{C}}{-}\overset{|}{\underset{|}{C}}{-}NCS$

A **B**

The relative distribution of β-thiocyanates, **A**, to β-isothiocyanates, **B**, is found to be dependent on the degree of substitution of the initial alkene. For example, the reaction of **1** with ethylene gives under conditions of kinetic control 2-thiocyanatoethyl phenyl selenide **2**, whereas with 2,3-dimethyl-2-butene, one isolates the isothiocyanate adduct **3**.

[3] $C_6H_5SeSCN + H_2C{=}CH_2 \rightarrow C_6H_5SeCH_2CH_2SCN$

2

[4] $C_6H_5SeSCN + (CH_3)_2C{=}C(CH_3)_2 \longrightarrow$

$C_6H_5Se{-}\overset{CH_3}{\underset{CH_3}{C}}{-}\overset{CH_3}{\underset{CH_3}{C}}{-}NCS$

3

When carried out with freshly prepared solutions of **1** these reactions are essentially quantitative: glc yields ≥98%, isolated yields at least 90%, unless otherwise stated. Structural assignments are based on infrared and nmr spectroscopy. Thus the thiocyanato adducts exhibit a sharp absorption between 4.6 and 4.7 μm which is medium to strong in intensity depending upon the surrounding atoms. In contrast the isothiocyanato adducts absorb very strongly, exhibiting a broad band between 4.5 and 5.3 μm with a number of shoulders appearing on either side of the main absorption.

In the assignment of regiochemistry of these and similar species by ^1H nmr it has been observed that protons α to the isothiocyanato group are deshielded relative to those of either the thiocyanato or phenylseleno moieties. In general protons α to the thiocyanato group are *only slightly* deshielded relative to those α to the phenylseleno group. For example, compound **2** exhibits a single sharp resonance at δ 3.16 integrating as four protons (60 MHz, chloroform-*d* solvent). At 100 MHz some fine splitting indicative of a tightly coupled AA'BB' spin system is observed.

In a manner similar to the above, carbon-13 atoms directly bonded to the aforementioned groups are shielded in the order —NCS < —SCN < $—SeC_6H_5$, and therefore allow confirmation of the assignments initially based on ir and ^1H nmr.

The ^1H nmr parameters of the adducts obtained during this investigation are reported in Tables 1, 3, and 4. In every case it was possible to find at least one non-overlapping signal from which the initial (kinetically controlled) isomer distribution could be calculated. The ^{13}C nmr parameters are given in Table 2 and the experimental section. It should be noted that an immediate *in situ* determination of the adduct isomer ratio was necessary because of the observed tendency of many of the adducts to isomerize.

Two types of isomerization are observed. In general, the fastest form of isomerization is the regiospecific conversion of thiocyanate to isothiocyanate and its converse (eq. [5]). Somewhat slower is the

[5] $C_6H_5Se{-}\overset{R'''\ R''}{\underset{R\ \ R'}{C{-}C}}{-}SCN \rightleftharpoons C_6H_5Se{-}\overset{R'''\ R''}{\underset{R\ \ R'}{C{-}C}}{-}NCS$

stereospecific isomerization of regioisomers (eq. [6]). It is not clear in all cases from our data to what degree these secondary isomerizations retain chemical functionality (i.e. RSCN → R'SCN vs. R'NCS).

Exceptions to the above, qualitative observations, have been observed and therefore indicate a note of caution must be applied towards all assignments. For example, the reaction of **1** with propene yields two thiocyanato adducts in the ratio 60:40. It is observed that the subsequent isomerization, **4** ⇌ **5**, which favours formation of the Markownikoff ad-

[6] $C_6H_5Se{-}\overset{R'''\ R''}{\underset{R\ \ R'}{C{-}C}}{-}SCN \rightleftharpoons NCS{-}\overset{R\ R'}{\underset{R'''\ R''}{C{-}C}}{-}SeC_6H_5$

+ $SCN{-}\overset{R\ R'}{\underset{R'''\ R''}{C{-}C}}{-}SeC_6H_5$

TABLE 1. The observed infrared and proton nmr parameters for the products of the addition of benzeneselenenyl thiocyanate to isomeric 1,2-disubstituted ethylenes

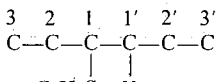

X = SCN, NCS

Initial alkene	Adduct regiochemistry	Infrared (μ, CH_2Cl_2)	Chemical shift assignments (δ, ppm) H3	H2	H1	H1′	H2′	H3′	Coupling constants (Hz) $J_{1,1'}$	$J_{1,2}$	$J_{2,3}$	$J_{1',2'}$	$J_{2',3'}$
Isothiocyanate adducts													
Z-2-Butene		4.76		1.43 d	3.38 dq	3.83 dq	1.42 d		3.9	6.6		7.1	
E-2-Butene		4.74		1.47 d	3.30 dq	3.93 dq	1.40 d		4.8	6.6		7.0	
Z-2-Pentene	M			1.43 d			1.6–2.2 m	0.98 t		7.2			6.4
	*a*M	4.78	1.10 t	1.6–2.2 m	3.10 ddd	4.01 dq	1.41 d		3.6	{5.6 8.8}	6.4	6.4	
E-2-Pentene	M			1.42 d			1.6–2.1 m	1.07 t		7.0			6.2
	*a*M	4.78	1.12 t	1.6–2.1 m	3.27 ddd	3.93 dq	1.40 d		5.6		6.4	6.4	
Z-4-Methyl-2-pentene	M	4.74		1.49 d	2.82 dq	4.13 dd	2.12 m	{1.12 d 1.11 d}	4.0	6.8		5.6	6.4
	*a*M	4.78	{1.13 d 0.97 d}	2.1 m	3.23 dd	3.75 dq	1.55 d		6.4	4.0	{7.0 6.3}	6.8	
E-4-Methyl-2-pentene	*a*M	4.75	{1.01 d 1.17 d}	2.12 m	2.94 dd	4.00 dq	1.52 d		8.8	4.0	{6.8 6.8}	6.8	
Z-4,4-Dimethyl-2-pentene	*a*M	4.77	1.16 s		2.78 d	4.32 dq	1.52 d		1.4			6.8	
E-4,4-Dimethyl-2-pentene	*a*M	4.75	1.04 s		2.92 d	4.47 dq	1.51 d		3.6			6.9	
Thiocyanate adducts													
Z-2-Butene		4.62		1.43 d	3.53 dq	3.67 dq	1.44 d		2.8	6.5		6.5	
E-2-Butene		4.61		1.48 d	3.38 q′	3.48 q′	1.60 d		6.2	6.5		6.5	
Z-2-Pentene	M	4.63		1.46 d	3.67 dq	3.35 ddd	1.9 m	1.00 t	3.0	7.0			6.4
	*a*M	4.62	1.12 t	1.9 m	3.35 ddd	3.78 dq	1.46 d		3.2		6.4	7.0	
E-2-Pentene	M	4.61		1.50 d	3.55 q′	3.22 m	1.9 m	1.03 t	6.5	6.5		{8.6 5.3}	6.3
	*a*M	4.63	1.08 t	1.9 m	3.22 m	3.65 q′	1.58 d		6.7	{8.5 5.5}	6.4	7.0	
Z-4-Methyl-2-pentene	*a*M	4.65	{1.18 d 1.07 d}	2.1 m	3.12 dd	3.78 dq	1.59 d		5.4	4.8	{6.8 6.6}	6.8	
E-4-Methyl-2-pentene	*a*M	4.65	{1.15 d 1.04 d}	2.2 m	3.13 dd	3.63 q′	1.65 d		6.6	1.6	{6.0 7.2}	6.4	
Z-4,4-Dimethyl-2-pentene	*a*M	4.65	1.20 s		3.03 d	4.12 dq	1.51 d		1.6			6.8	
E-4,4-Dimethyl-2-pentene	*a*M	4.63	1.10 s		3.15 d	4.27 dq	1.51 d		3.8			6.8	

TABLE 2. The observed carbon 13 nmr parameters for the products of addition of benzeneselenenyl thiocyanate to isomeric 1,2-disubstituted ethylenes

$R^1\{C^3—C^2—C^1(C_6H_5Se)—C^{1'}(X)—C^{2'}—C^{3'}\}R^2$ or R^3

R^1	R^2	R^3	C-3	C-2	C-1	C-1′	C-2′	C-3′
			Thiocyanate adducts (X = SCN)					
CH_3	CH_3	H		19.1	44.3	51.6	20.5	
CH_3	H	CH_3		15.7	42.8	50.0	15.8	
Et	Et	H	13.2	24.6	53.3	59.4	24.9	12.1
Et	H	Et	12.4	25.9	53.7	59.1	26.6	11.6
*i*Pr	*i*Pr	H	Unknown	----------		adduct too unstable		
*i*Pr	H	*i*Pr	20.9 17.4	28.9	60.6	65.2	30.8	22.3 19.4
CH_3	Et	H		17.1	43.6	59.0	23.6	12.1
CH_3	H	Et		18.3	42.4	59.7	27.5	11.2
CH_3	*i*Pr	H	Unknown	----------		adduct too unstable		
CH_3	H	*i*Pr		21.3	43.3	65.8	31.6	22.9 19.1
Et	CH_3	H	13.2	23.5	53.1	54.0	19.2	
Et	H	CH_3	11.9	26.8	54.2	59.7	18.9	
*i*Pr	CH_3	H	20.9 20.7	31.5	61.5	51.7	22.7	
*i*Pr	H	CH_3	20.8 18.6	31.8	62.0	50.9	21.8	
			Isothiocyanate adducts (X = NCS)					
CH_3	CH_3	H		18.3	44.0	58.1	22.6	
CH_3	H	CH_3		16.8	44.1	58.3	20.1	
Et	Et	H	12.9	26.2	53.0	64.5	27.1	11.1
Et	H	Et	12.4	24.4	52.1	64.4	27.2	10.7
*i*Pr	*i*Pr	H	20.1 18.5	31.9	58.8	68.2	32.4	21.4 20.6
*i*Pr	H	*i*Pr	21.1 15.6	29.4	58.1	68.4	30.9	22.7 17.6
CH_3	Et	H		16.8	43.4	65.3	26.4	11.0
CH_3	H	Et		18.9	42.4	65.0	30.1	10.9
CH_3	*i*Pr	H		19.9	43.0	67.1	30.8	20.9 20.3
CH_3	H	*i*Pr		19.1	43.3	66.0	29.7	21.0 18.6
Et	CH_3	H	12.9	25.3	50.6	57.5	18.8	
Et	H	CH_3	12.6	24.6	54.2	57.8	20.2	
*i*Pr	CH_3	H	20.7 20.6	31.9	62.1	57.1	21.6	
*i*Pr	H	CH_3	21.2 18.6	29.9	62.2	57.5	22.3	

NOTE : Configuration is *erythro* when R^1, R^3 = alkyl; *threo* when R^1, R^2 = alkyl.

duct, **4**, proceeds much faster than the corresponding isomerization(s) to isothiocyanato adducts, in contrast to the normal results for more highly substituted systems.

$C_6H_5SeCH_2CH(SCN)CH_3$ **4** $\qquad$ $NCSCH_2CH(SeC_6H_5)CH_3$ **5**

In the tables we use the designation Markownikoff, M, and *anti*-Markownikoff, *a*M, to distinguish between isomeric adducts. Since such nomenclature is confusing for adducts derived from 1,2-disubstituted or tetrasubstituted ethylenes, we have adopted the convention that when both olefinic carbon atoms contain an identical number of alkyl groups, the Markownikoff isomer is defined as that one in which the pseudohalide is bonded to the carbon whose sum of Taft's inductive substituent constants, $\Sigma\sigma^*$, is the more negative. This method of nomenclature has been previously reported (5).

Reactions with Acyclic Terminal Alkenes

Simple alkenes upon reaction with **1** give only thiocyanato adducts under conditions of kinetic control. For example, 4-methyl-1-pentene yields an 80:20 mixture of *anti*-Markownikoff to Markowni-

TABLE 3. The observed infrared and proton nmr parameters for the Markownikoff adducts from the reaction of benzeneselenenyl thiocyanate with a series of trisubstituted ethylenes

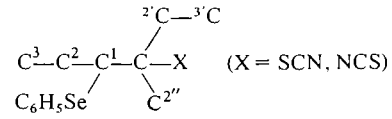

Initial alkene	Infrared (μ, CH_2Cl_2)	Chemical shift assignments (δ, ppm)						Coupling constants (Hz)		
		H3	H2	H1	H2′	H3′	H2′′	$J_{1,2}$	$J_{2,3}$	$J_{2',3'}$
Isothiocyanate adducts										
2-Methyl-2-butene	4.74		1.54d	3.30q	1.55s		1.55s	6.8		
								2.7		
2-Methyl-2-pentene	4.72	1.24t	2.0m	2.94dd	1.55s		1.52s	10.5	6.7	
		1.17d							7.0	
2,4-Dimethyl-2-pentene	4.73	1.09d	1.7m	3.03d	1.63s		1.54s	2.0	6.8	
Z-3-Methyl-2-pentene	4.71		1.58d	3.37q	1.91q	1.01t	1.49s	7.4		7.0
E-3-Methyl-2-pentene	4.73		1.52d	3.34q	1.90q	1.03t	1.49s	6.3		7.1
						1.08d				6.8
Z-3,4-Dimethyl-2-pentene	4.72		1.57d	3.46q	2.2m	1.14d	1.55s	7.1		7.0
						1.04d				7.0
E-3,4-Dimethyl-2-pentene	4.74		1.55d	3.41q	2.3m	1.12d	1.46s	6.7		7.0
Thiocyanate adducts										
2-Methyl-2-butene	4.63		1.48d	3.72q	1.43s		1.38s	6.5		
								3.0		
2-Methyl-2-pentene	4.62	1.10t	2.0m	3.45dd	1.45s		1.39s	10.0	6.8	
		1.00d							7.0	
2,4-Dimethyl-2-pentene	4.62	0.98d	1.7m	3.46d	1.54s		1.46s	<2.0	6.9	
Z-3-Methyl-2-pentene	4.62		1.49d	3.80q	1.73q	0.95t	1.36s	7.0		6.8
E-3-Methyl-2-pentene	4.62		1.50d	3.79q	1.81q	1.10t	1.32s	6.3		7.1
						0.96d				7.0
Z-3,4-Dimethyl-2-pentene	4.63		1.56d	3.47q	2.2m	1.01d	1.46s	7.0		7.0
						0.98d				7.0
E-3,4-Dimethyl-2-pentene	4.62		1.54d	3.52q	2.3m	1.00d	1.35s	6.5		7.0

koff thiocyanato adducts while 3-methyl-1-butene gives the *anti*-Markownikoff species exclusively. These ratios are very similar to those previously reported for the analogous additions of C_6H_5SeCl and C_6H_5SeBr (6). Only in the case of 3,3-dimethyl-1-butene is an anomaly observed in that a 40:60 mixture of thiocyanato to isothiocyanato *anti*-Markownikoff adducts is isolable. These data are indicative of the importance of steric factors towards directing the approach of the SCN anion to the initially formed intermediate at the least hindered primary site, although the importance of nonrepulsive electronic effects cannot be totally ruled out.

1,1-Disubstituted ethylenes, such as methylpropene and 2-methyl-1-butene, give mixtures of all four possible adducts (eq. [7]) with the Markownikoff thiocyanate predominating under conditions of kinetic control. The presence of the *anti*-Markownikoff species was surprising since C_6H_5SeCl had been found to yield the Markownikoff adducts exclusively under equivalent conditions (3*f*, 7). If steric hindrance towards approach of the nucleophile, SCN, to the intermediate were to be important in the product-determining step one would have anticipated the regioselectivity to favour the formation of the *anti*-Markownikoff species as in arenesulphenylation (8).

While a very fast isomerization of the form *anti*-Markownikoff ⇄ Markownikoff might be hypothesized to explain the apparent anomaly between monosubstituted and 1,1-disubstituted ethylenes, it is readily ruled out by the observation that the thermodynamic product distributions often favour the *anti*-Markownikoff adducts in yields greater than those observed under kinetic control.

Reactions with Acyclic Non-terminal Alkenes

The ^1H nmr data (Tables 1, 3, and 4) are consistent with products formed by stereospecific *anti* addition. Symmetrical *E,Z* isomeric alkenes such as the 2-butenes, 3-hexenes, and 2,5-dimethyl-3-hexenes each give only one adduct which differs in its ^1H and ^{13}C nmr spectra in the expected manner. Infrared analysis further indicates that the thiocyanato adducts are the products of kinetic control. It should be noted, however, that the subsequent isomerization to isothiocyanate is quite rapid, usually reaching completion within a few hours at 25°C.

In the case of unsymmetrically 1,2-disubstituted

TABLE 4. The observed infrared and proton nmr parameters for the products of the addition of benzeneselenenyl thiocyanate to a series of tetrasubstituted ethylenes

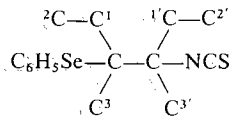

Initial alkene		Infrared (μ, CH_2Cl_2)	Chemical shift assignments (δ, ppm) H3	H2	H1	H1′	H2′	H3′	Coupling constants (Hz)
2,3-Dimethyl-2-butene		4.76 5.02 sh	1.41 s		1.41 s	1.62 s		1.62 s	
2,3-Dimethyl-2-pentene	M	4.73 5.00 sh	1.40 s		1.40 s	1.8 m*	1.08 t	1.72 s	$J_{1',2'}$ 6.8
	*a*M	4.73 5.00 sh	1.40 s	1.16 t	1.8 m*	1.51 s		1.50 s	$J_{1,2}$ 6.9
2,3,4-Trimethyl-2-pentene	M	4.72 5.01 sh	1.43 s		1.52 s	1.6 m*	0.95	1.74 s	$J_{1',2'}$ 7.0 $J_{1,2}$ 6.6
	*a*M	4.72 5.01 sh	1.47 s	0.99 0.91	1.6 m*	1.55 s		1.55 s	6.8 6.7

*Non-resolvable multiplets.

[7] 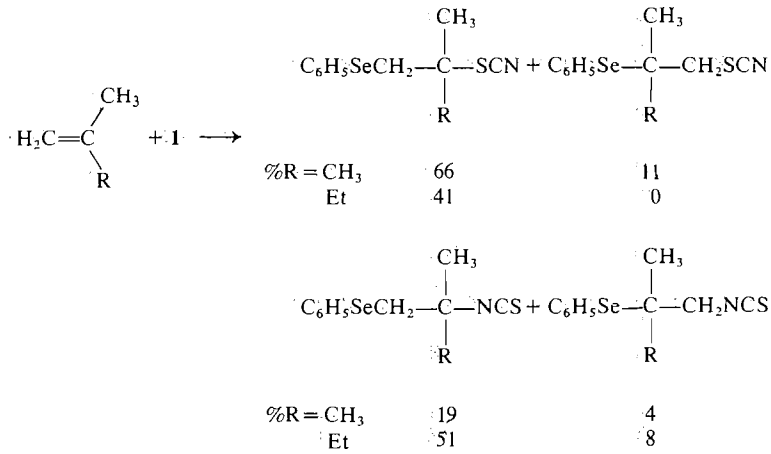

%R = CH_3	66	11
Et	41	0

%R = CH_3	19	4
Et	51	8

ethylenes, such as the 2-pentenes, it is possible to observe the formation of the two possible regioisomers in essentially equal amounts (see Table 5). In contrast, the reaction of **1** with the isomeric 4-methyl-2-pentenes and 4,4-dimethyl-2-pentenes is regiospecific or highly regioselective in the *anti*-Markownikoff sense as shown in [8].

Once again steric hindrance to approach by SCN on the intermediate appears important; the greater steric bulk of the isopropyl and *tert*-butyl groups ensuring regiospecificity or high regioselectivity in the *anti*-Markownikoff sense. These data also differ from those observed for the addition of C_6H_5SeCl to the same series of alkenes where the regioselectivity is much less.

Also of note is the observation that *E*-4,4-dimethyl-2-pentene reacts about 400 times slower than the *Z* isomer in contrast to the normal factor of 10 or less, therefore suggesting a steric barrier to the addition (7). Further comment on this matter must, however, await more quantitative rate studies.

With trisubstituted ethylenes, **1** reacts regiospecifically in the Markownikoff sense, electronic factors apparently overriding steric hindrance to approach

[8] 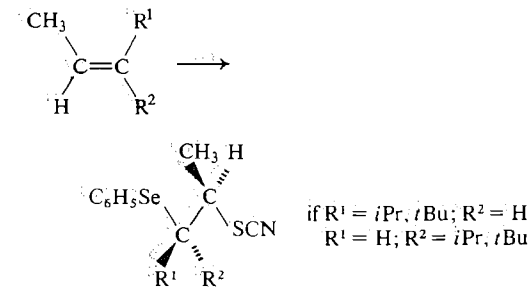

TABLE 5. The kinetically controlled product distributions for the addition of benzeneselenenyl thiocyanate to a series of alkenes in methylene chloride at 20°C

		RSCN		RNCS	
	Alkene	M*	*a*M*	M*	*a*M*
Z	$CH_3CH{=}CHCH_3$	>98		<2	
E		98		2	
Z	EtCH=CHEt	98		2	
E		98		2	
Z	*i*PrCH=CH*i*Pr	95		5	
E		96		4	
Z	$CH_3CH{=}CHEt$	50	50	0	0
E		58	42	0	0
Z	$CH_3CH{=}CHiPr$	0	≥98	0	≤2
E		0	100	0	0
Z	$CH_3CH{=}CHtBu$	0	100	0	0
E		0	100	0	0
	$(CH_3)_2C{=}CHCH_3$	≤5	0	≥95	0
	$(CH_3)_2C{=}CHEt$	15	0	85	0
	$(CH_3)_2C{=}CHiPr$	25	0	75	0
Z	$Et(CH_3)C{=}CHCH_3$	17	0	83	0
E		30	0	70	0
Z	$iPr(CH_3)C{=}CHCH_3$	28	0	72	0
E		33	0	67	0
	$(CH_3)_2C{=}C(CH_3)_2$	0		100	
	$(CH_3)_2C{=}C(CH_3)Et$	0	0	42	58
	$(CH_3)_2C{=}C(CH_3)iPr$	0	0	28	72

*M = Markownikoff; *a*M = *anti*-Markownikoff.

as was observed for the 1,1-disubstituted ethylenes. Furthermore it is observed that the isomer distributions strongly favour the isothiocyanato adduct over the corresponding thiocyanate. In comparison it may be noted that areneselenenyl chlorides show an equivalent regiospecificity, whereas arenesulphenyl chlorides add regioselectively in the opposite, i.e. *anti*-Markownikoff, sense (5, 8).

The reaction of **1** with the isomeric 3-methyl-2-pentenes and 3,4-dimethyl-2-pentenes is stereospecific, presumably *anti* in accord with the stereospecificity observed for simple 1,2-disubstituted ethylenes.

The reaction of **1** with the tetrasubstituted ethylenes (Table 5) is of particular interest since the analogous chloro adducts from the reaction of C_6H_5SeCl proved to be highly unstable under equivalent reaction conditions (3*f*, 7). The isothiocyanates isolated from these reactions are quite stable at room temperature with a shelf life of many months.

Reactions with Cyclic Olefinic Compounds

Bicyclo[2.2.1]hept-2-ene (norbornene) reacts with **1** to yield exclusively the *trans* adduct: *exo*-2-phenylseleno-*endo*-3-isothiocyanatobicyclo[2.2.1]heptane. At 80 MHz the ^1H nmr spectrum has an apparent triplet of a doublet at δ 3.60 ppm and a doublet of doublets at δ 2.78 ppm, each multiplet integrating as one proton. Associating the downfield "dt" with the proton geminal to the isothiocyanato moiety and the "dd" with the proton geminal to the phenylseleno group allows one to make the aforementioned assignment using the observed $^1H...^1H$ coupling constants: $J_{2,3} = 4.9$ Hz, $J_{3,4} = 3.6$ Hz, $J_{2,7-anti} = 2.5$ Hz, and $J_{3,5-exo} = 0.6$ Hz.

[9]

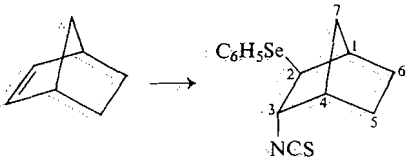

The presence of a very strong broad absorption at 4.75 μm in the infrared confirms the assignment. Attempts to isolate the corresponding thiocyanate or independently synthesize it from the analogous chloride, bromide, or tosylate via attack with sodium thiocyanate in the presence of 18-crown-6, with or without prior ionization using silver hexafluorophosphate, were unsuccessful. Only the isothiocyanate was isolable or observable.

In contrast to the above, the reaction of **1** with tricyclo[4.2.2.0^{2,5}]deca-3,9-diene-7,8-dicarboxylic anhydride is *nonstereospecific*, yielding both *cis* and *trans* thiocyanato adducts in the ratio 33:67 from attack upon the cyclobutene double bond (for related reactions see ref. 9). No evidence for the analogous isothiocyanato species or products of transannular addition was observed. This reaction requires a further comment with respect to the length of time required to reach completion. The aforementioned reactions of **1** with simple alkenes in methylene chloride at 25°C require in general no more than a few minutes. The reaction of **1** with the tricyclic diene above, however, requires approximately 5 h. The value while perhaps slow is much faster than the analogous reaction time of 10 days for C_6H_5SeCl.[2] It should also be noted that C_6H_5SeCl normally reacts much faster than **1** under equivalent conditions. A similar observation has been previously reported for the related sulphenyl derivatives (10). The reason for these anomalous reaction times is not immediately obvious, but suggests a significant change in mechanism for one of the reactants or different transition state geometries in general.

[10]

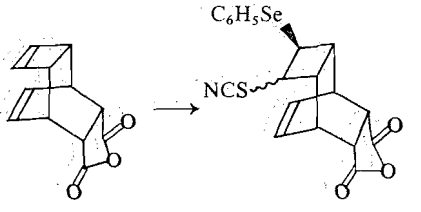

Conclusions

In summary, benzeneselenenyl thiocyanate shows chemical behaviour similar to that of the corresponding halides but with a few marked differences in the regioselectivity as noted in the discussion.

In regard to our initial aim of investigating the potential synthetic utility of this reagent towards the introduction of sulphur and nitrogen synthons, the chemoselectivity, i.e. the distribution of thiocyanato to isothiocyanato adducts under conditions of kinetic control, bears some comment. The relative distribution of these adducts is found to be highly dependent upon the substitution pattern of the substrate olefin. In general, there exists a trend towards a greater reactivity of the nitrogen atom of SCN with increasing electrophilic character of the reaction site on the intermediate. As the electrophilic character of this site increases, the reactivity of the more basic nitrogen atom increases relative to that of the more polarizable sulphur atom. This reagent would therefore appear to hold some promise for selective transformations where synthons of this type are required.

With respect to our alternative aim it is unfortunate that until such time as we or others are able to obtain a more quantitative picture of the rate-determining step, little can be said authoritatively about the effect of types of ion-pairs, etc. on the reaction coordinate.

Experimental

General

Melting points were determined on a Fisher-Johns apparatus and are uncorrected. The ir spectra were recorded as CH_2Cl_2 solutions in matched NaCl cavity cells (0.1071 mm) on a Unicam 1100 spectrophotometer. Only the principal, sharply defined peaks are reported. The ^1H nmr spectra were run on Varian T60, HA100, and (or) HFT 80 spectrometers. The spectra were measured from approximately 30–40% (w/v) solutions in chloroform-*d* with TMS as an internal standard. The ^{13}C nmr spectra were run on a Varian FT 80 spectrometer in 10 mm od amberized tubes as chloroform-*d* solutions. All resonances are referenced to internal TMS. All analytical and preparative tlc separations were performed on Analtech or Macherey-Nagel precoated plates (silica gel GF). Visualization of the spots was accomplished by uv (254 nm) and phosphomolybdic acid/EtOH. Suitable elemental analyses were obtained for all new compounds.

Benzeneselenenyl chloride was a commercial product (Aldrich); recrystallized from CCl_4, mp 64.5°C. Olefins were in general available commercially from Chemical Samples, Inc. Norbornene (Aldrich) was used without further purification.

endo-*Tricyclo[4.2.2.0^{2,5}]deca-3,9-diene-7,8-dicarboxylic Anhydride*

This compound was prepared by the cycloaddition of maleic anhydride with 1,3,5,7-cyclooctatraene (Aldrich) in chlorobenzene under reflux, and crystallized from chlorobenzene; ^1H nmr identical to that reported by Huisgen and co-workers (11).

Benzeneselenenyl Thiocyanate

To 0.192 g (1 mmol) of C_6H_5SeCl in 25 mL of anhydrous CH_2Cl_2 was added 0.082 g (1 mmol) of anhydrous NaSCN. The reaction mixture was stirred for $\simeq$ 1 h until the intense red coloration of the selenenyl chloride had disappeared leaving a bright yellow solution. Filtration followed by evaporation gave an orange oil–platelets from pentane mp > 300°C. This species was normally used without isolation; ^1H nmr ($CDCl_3$) δ:7.82 m (2H), 7.47 m (3H); uv (CH_2Cl_2) λ_{max} (ε):236 (6300), 257 (5600), 352 (445) nm; ir (μ):3.26 w, 3.42 w, 4.65 s, 5.74 m, 6.79 s ~ m, 6.95 s ~ m, 7.30 w, 7.53 w, 7.69 w, 7.90 w, 9.40 w, 9.52 w, 9.80 m, 10.0 w, 14.6 s, 14.9 w, 15.6 m ~ s.

General Procedure for the Reaction of Benzeneselenenyl Thiocyanate with Alkenes

To 0.214 g (1 mmol) of C_6H_5SeSCN in 25 mL of CH_2Cl_2 was added 1 mmol of the respective alkene dissolved previously in 15 mL CH_2Cl_2. The reaction mixture is stirred until the bright yellow coloration of the reagent disappears (formation of RSCN) or is replaced by an intense orange coloration (characteristic of RNCS) usually with a precipitation of the adduct. General reaction times are 2–10 min although exceptions have been noted (see Discussion). Immediate evaporation of the solvent yields colorless to pale yellow oils (RSCN) or deep orange oils (RNCS).

Experimental Data Not Given in Tables

Bicyclo[2.2.1]hept-2-ene gave with **1** after 1.8 h a bright orange oil; ^1H nmr ($CDCl_3$)δ: 3.59 dt (1H), 2.79 dd (1H), 2.53 m (1H), 2.38 m (1H), 1.73 m (2H), 1.56 m (2H), 1.43 m (2H); ir (μ, CH_2Cl_2): 4.75 very broad, intense.

Ethylene gave with **1** a colorless to pale yellow oil; ^1H nmr (60 MHz, $CDCl_3$)δ: singlet, 3.21 ppm (4H) relative to aromatic; tlc silica (80:20 *n*-C_7H_{16}/EtOAc); R_f 0.20–0.34 RSCN, 0.41–0.45 RNCS (sample left a minimum of 5 days from initial formation); ir (μ, CCl_4): 4.67 very sharp RSCN.

Propene gave with **1** a colorless oil shown to be a 60:40 mixture of the M and *a*M adducts, RSCN. M: ^{13}C nmr δ: 34.5 t, 45.0 d, 20.8 q, 110.3 s SCN; ^1H nmr δ: 1.58 d (3H) J = 6.0, 3.0–4.2 ABC spin system; ir (μ, CH_2Cl_2): 4.61 vs sharp. *a*M: ^{13}C nmr δ: 36.7 t, 41.7 d, 19.5 q, 111.9 s SCN; ^1H nmr δ: 1.61 d (3H) J = 6.3, 3.0–4.2 ABC spin system; ir (μ, CH_2Cl_2): 4.59 vs sharp.

3-Methyl-1-butene gave with **1** a single adduct. *a*M, RSCN: ^{13}C nmr δ: 21.7 q, 18.4 q, 30.0 d, 53.6 d, 38.9 t, 134.9 d, 129.5 d, 128.3 d, 129.3 s, 112.0 s SCN; ^1H nmr δ: 0.98 d (3H) J = 6.0, 1.15 d (3H), J = 6.0, 2.2 m (1H), 3.47 m ABC spin system (3H); ir (μ, CCl_4): 4.58 vs sharp. A second species was found upon isomerization (after 2 weeks): M, RSCN: ^{13}C nmr δ: 58.4 d, 31.2 d, 31.0 t, 20.4 q, 17.2 q, 133.4 d, 129.3 d, 127.7 d, 134.6 s; ^1H nmr δ: 0.95 d (3H) J = 6.0, 1.05 d (3H), J = 6.0, 2.1 m (1H), 2.8 m, 3.7 m ABC spin system (3H); ir (μ, CCl_4): 4.73 vs broad.

4-Methyl-1-pentene gave with **1** an 80:20 mixture of the *a*M, RSCN, and M, RSCN adducts as a pale yellow oil. *a*M, RSCN: ^{13}C nmr δ: 22.9 q, 21.3 q, 25.8 d, 34.2 t, 41.9 d, 135.6 d, 129.4 d, 128.6 d, 113.2 SCN; ir (μ, CCl_4): 4.59 vs sharp. M, RSCN: ^{13}C nmr δ: 43.0 t, 49.2 d, 34.0 t, 25.7 d, 22.8 a, 21.2 q, 133.5 d, 129.3 d, 128.9 d; ir (μ, CCl_4): 4.59 vs sharp.

Methylpropene gave with **1** a mixture of all four possible adducts in the ratio 66:11:19:4 for M, RSCN: *a*M, RSCN: M, RNCS: *a*M, RNCS. ^1H nmr: M, RSCN: δ: 1.62 s (6H), 3.42 s (2H); *a*M, RSCN: δ: 1.56 s (6H), 3.32 s (2H); M, RNCS: δ: 1.52 s (6H), 3.20 s (2H); *a*M, RNCS: δ: 1.46 S (6H), 3.53 s (2H). The above ratio changed to 14:0:74:12 after 3 weeks.

2-Methyl-1-butene gave with **1** a mixture of three adducts in the ratio 41:8:51 for M, RSCN: *a*M, RNCS: M, RNCS. M,

RSCN: ^{13}C nmr δ: 40.3 t, 60.8 s, 32.8 t, 25.8 q, 134.7 d, 129.2 d, 127.7 d, 8.9 q, 111.2 s SCN; ^{1}H nmr δ: 1.45 s (3H), 3.17 s (2H), 1.9 m (2H), 0.95 t (3H). M, RNCS: ^{13}C nmr δ: 40.2 t, 65.2 s, 34.2 t, 26.1 q, 8.6 q, 138.3 s NCS, 133.4 d, 129.1 d, 127.5 d; ^{1}H nmr δ: 1.53 s (3H), 3.37 s (2H), 2.1 q (2H), 0.95 t (3H). *a*M, RNCS: ^{1}H nmr δ: 1.33 s (3H), 3.48 s (2H), 2.2 q (2H), 0.95 t (3H).

Acknowledgement

Continued financial support from the National Science and Engineering Research Council of Canada is gratefully acknowledged.

1. O. Foss. J. Am. Chem. Soc. **69**, 2236 (1947).
2. (*a*) H. Rheinboldt and M. Perrier. Bull. Soc. Chim. Fr. 245 (1950); 484 (1953); (*b*) A. M. Giesbrecht. An. Acad. Bras. Cienc. **30**, 115 (1958); (*c*) H. Rheinboldt and E. Giesbrecht. Justus Liebigs. Ann. Chem. **574**, 227 (1951); (*d*) M. Perrier. Sel. Chim. 81 (1957).
3. (*a*) D. G. Garratt and G. H. Schmid. Can. J. Chem. **52**, 3599 (1974); (*b*) G. H. Schmid and D. G. Garratt. Tetrahedron Lett. 3991 (1975); (*c*) G. H. Schmid and D. G. Garratt. Chem. Scr. **10**, 76 (1976); (*d*) D. G. Garratt. Tetrahedron Lett. 1915 (1978); (*e*) D. G. Garratt. Can. J. Chem. **56**, 2184 (1978); (*f*) G. H. Schmid and D. G. Garratt. Tetrahedron, **34**, 2869 (1978); (*g*) D. G. Garratt, P. L. Beaulieu, and M. D. Ryan. Tetrahedron. In press.
4. (*a*) P. D. Woodgate, H. H. Lee, P. S. Rutledge, and R. C. Cambie. Synthesis, **2**, 152 (1978); (*b*) K. E. Klob, D. A. Wilder, and M. A. Taylor. Abstr. 166th Meeting, Am. Chem. Soc. Org. Sect. Paper No. 69 (August 27–31, 1973).
5. G. H. Schmid, C. L. Dean, and D. G. Garratt. Can. J. Chem. **54**, 1253 (1976).
6. (*a*) D. G. Garratt and G. H. Schmid. J. Org. Chem. **42**, 1776 (1977); (*b*) E. G. Kataev, T. G. Mannafov, E. A. Berdinikov, and O. A. Kamarovskaya. Zh. Org. Khim. **9**, 1983 (1973); (*c*) S. Raucher. Tetrahedron Lett. 3909 (1977); (*d*) S. Raucher. J. Org. Chem. **42**, 2950 (1977).
7. D. G. Garratt. Ph.D. thesis, University of Toronto, Toronto, Ont., Canada. 1975.
8. (*a*) M. Oki, W. Nakanishi, M. Fukunaga, G. D. Smith, W. L. Duax, and Y. Osawa. Chem. Lett. 1277 (1975); (*b*) W. H. Mueller and P. E. Butler. J. Am. Chem. Soc. **88**, 2866 (1966); (*c*) W. H. Mueller and P. E. Butler. J. Am. Chem. Soc. **90**, 2075 (1968); (*d*) W. A. Thaler, W. H. Mueller, and P. E. Butler. J. Am. Chem. Soc. **90**, 2069 (1968); (*e*) Y. Kikuzano, T. Yanabe, S. Nagata, H. Kato, and K. Fukui. Tetrahedron, **30**, 2197 (1974); (*f*) W. A. Smit, A. S. Gybin, V. S. Bogdanov, M. S. Krimer, and E. A. Vorobinera. Tetrahedron Lett. 1085 (1978).
9. (*a*) G. Mehta and P. N. Pandey. Tetrahedron Lett. 3567 (1975); (*b*) T. Sasaki, K. Kanematsu, A. Kondo, and Y. Nishitani. J. Org. Chem. **39**, 3569 (1974); (*c*) A. Kondo, T. Yamane, T. Ashida, T. Sasaki, and K. Kanematsu. J. Org. Chem. **43**, 1180 (1978); (*d*) T. Sasaki, K. Kanematsu, and A. Kondo. J. Org. Chem. **39**, 2246 (1974); (*e*) D. G. Farnum and J. P. Snyder. Tetrahedron Lett. 3861 (1965); (*f*) N. S. Zefirov, V. N. Kivin, D. A. Potekhin, A. S. Kozmin, N. D. Sadovaya, E. N. Kuckutova, and I. V. Bodikov. Zh. Org. Khim. **14**, 1224 (1978); Chem. Abstr. **89**, 107841q (1978).
10. (*a*) N. Kharasch, H. L. Wehrmeister, and H. Tigerman. J. Am. Chem. Soc. **69**, 1612 (1947); (*b*) N. Kharasch and A. J. Havlik. J. Am. Chem. Soc. **75**, 3734 (1953); (*c*) N. Kharasch and M. M. Wald. Anal. Chem. **27**, 996 (1955).
11. R. Huisgen, F. Mietzsch, G. Boche, and H. Seidl. Chem. Soc. Spec. Publ. 19. Organic reaction mechanisms. 1965. p. 3.

Crystal structures of medium ring compounds. Part III. The crystal and molecular structure of *trans-anti-trans*-4,5:9,10-biscyclohexano-1,3,6,8-tetraoxecane

ARIS TERZIS[1] AND T. BRUCE GRINDLEY[2]

Department of Chemistry, Dalhousie University, Halifax, N.S., Canada B3H 4J3

Received January 23, 1979

ARIS TERZIS and T. BRUCE GRINDLEY. Can. J. Chem. 57, 2154 (1979).

The crystal structure of *trans-anti-trans*-4,5:9,10-biscyclohexano-1,3,6,8-tetraoxecane (**3**) has been determined by X-ray diffraction. The crystals are monoclinic, $a = 11.919(3)$, $b = 17.330(7)$, $c = 7.019(2)$ Å, $\beta = 98.91(1)°$, $P2_1/c$, with $Z = 4$. The structure was solved by application of the tangent formula and refined by large block least squares to a final R value of 0.060 ($R_w = 0.058$).

The ten-membered ring is present in the crystal in a twist-chair-boat-chair conformation — one which has been calculated to be relatively unstable for cyclodecane. Possible reasons why **3** adopts this conformation are discussed.

ARIS TERZIS et T. BRUCE GRINDLEY. Can. J. Chem. 57, 2154 (1979).

On a déterminé la structure cristalline du biscyclohexano-4,5:9,10 tétraoxécanne-1,3,6,8 *trans-anti-trans* (**3**), par diffraction de rayons-X. Les cristaux sont monocliniques, $a = 11.919(3)$, $b = 17.330(7)$, $c = 7.019(2)$ Å, $\beta = 98.91(1)°$, $P2_1/c$, avec $Z = 4$. On a résolu la structure par l'application de la formule tangente et on l'a raffinée par la méthode des moindres carrés (blocs diagonaux) jusqu'à une valeur finale de R de 0.060 ($R_w = 0.058$).

La conformation, dans le cristal, du cycle à dix chaînons est croisée-chaise-bateau-chaise qui d'après les calculs, serait assez instable dans le cas du cyclodécane. On discute des raisons pour lesquelles **3** adopterait cette conformation.

[Traduit par le journal]

Introduction

Compounds containing seven-membered and medium rings are in one of the few classes of compounds in which non-bonded interactions are very important in the determination of molecular geometry. There has been considerable interest in these systems (1–5), particularly in those molecules which contain ten-membered rings. Virtually all cyclodecane derivatives studied in the solid state contain the ring in one conformation, the boat-chair-boat[3] (BCB) (1), and most force-field calculations performed on cyclodecane (2–4) suggest that this conformation is the most stable, although two of the earlier force fields gave a different result (3). All calculations indicate that there are a number of conformations which are within about 20 kJ/mol of the BCB and there is some experimental evidence in support of this conclusion. For instance, an electron diffraction spectrum (4) of cyclodecane at 130° was analysed as arising from contributions from the BCB (49%), the twist-boat-chair (TBC, 25%), the twist-boat-chair-chair (TBCC, 8%), and the boat-chair-chair (BCC, 8%) conformations. In addition, the substitution pattern of 1,1,5,5-tetramethylcyclodecane is such that the BCB conformation is of high energy and a crystal of this compound contained both the TBC and TBCC conformations (5).

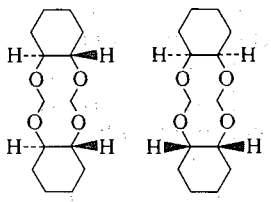

1 **2**

We have shown (6, 7) that two substituted stereoisomeric 1,3,6,8-tetraoxecanes (**1**, **2**) both adopt one BCB conformation in the solid state although the conformational situation for both compounds in solution was more complicated. The BCB conformation observed was considerably narrower than those of cyclodecane derivatives because of relief of some of the transannular non-bonded interactions present in the latter compounds. Surprisingly, another group[4] has observed that *trans*-2,7-diphenyl-2,7-dithieno-1,3,6,8-tetraoxa-2,7-diphosphecane, which has the same arrangement of oxygen atoms as the above molecules and which could accommodate all the substituents on phosphorous in low

[1]Present address: The National Hellenic Research Foundation, 48, Vassileos Constantinou Ave., Athens 501/1, Greece.

[2]To whom all correspondence should be addressed.

[3]The nomenclature used for these conformations was defined by Hendrickson (2*c*).

[4]J. B. Robert. Personal communication.

0008-4042/79/162154-05$01.00/0

energy positions, adopts a twist-chair-chair-chair (TCCC) conformation. We report here the crystal structure of *trans-anti-trans*-4,5:9,10-biscyclohexano-1,3,6,8-tetraoxecane (**3**). In this compound, the stereochemistry of ring fusion makes all BCB conformations unstable. Thus, a study of **3** gives information about the other conformations which are energetically accessible for 1,3,6,8-tetraoxecanes. Accurate structural data for molecules such as **3**, in which nonbonded interactions involving oxygen are important in determining conformation, will be of use for the development of force fields which are parameterized for oxygen.

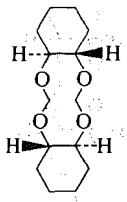

3

Experimental

trans-anti-trans-4,5:9,10-Biscyclohexano-1,3,6,8-tetraoxecane (**3**) was prepared according to the procedure of Brimacombe *et al.* (9). Physical constants of the sample agreed with those recorded in the literature (9). Crystals suitable for study were obtained by recrystallization from ethanol. Crystal data are as follows.

$C_{14}H_{24}O_4$ fw = 256.34

Monoclinic, a = 11.919(3), b = 17.330(7), c = 7.019(2) Å, β = 98.91(1)°, V = 1432.35 Å^3, Z = 4, ρ_c = 1.188 g cm^{-3}, ρ_o = 1.20 g cm^{-3} (18°C $CuK_{\alpha 1}$, λ = 1.54051 Å, μ = 6.16 cm^{-1}). $F(000)$ = 560e.

Preliminary X-ray photographs showed the following systematic absences: $h0l$, $l = 2n + 1$; $0k0$, $k = 2n + 1$. The space group is thus $P2_1/c$. A crystal (0.06 × 0.15 × 0.45 mm) was mounted with the c axis nearly parallel to the ϕ axis of a Picker FACS-1 automated diffractometer with a graphite monochromator. The cell dimensions were refined from 12 general reflections with 2θ between 70–76°. Because the exposed crystal sublimed in the X-ray beam, it was sealed in a capillary tube. Data were collected by the θ–2θ scan technique from 0.95° below the calculated 2θ position for $CuK_{\alpha 1}$ to 0.95° above the calculated position for $CuK_{\alpha 2}$ at 1° min^{-1}. Stationary background counts were taken for 20 s at either end of the scan range. During the course of the data collection, three standard reflections were measured every 58 reflections. Their intensities decreased steadily throughout the data collection by 7%, but could be adjusted to a standard scale by a least-squares fit (σ = 0.035) to a first order decay; from the counting statistics the ratio of esd to reflection for these standards was 0.040. A total of 1919 independent reflections were measured, of which 744 had $I > 3\sigma(I)$. The data were reduced to $|F_o|$ by the routine procedure. Lorentz and polarization but not absorption or extinction corrections were applied. The scattering factors for neutral atoms were taken from Ref. 10; they were corrected for the real part of the anomalous dispersion. Reflections with $|E| > 1.2$ were used to solve the structure by an application of the tangent formula which examined $4096 = 2^{12}$ sets of starting phases and successively eliminated all but the most likely. This program is part of an X-ray system written by Sheldrick (11). The positions of all but the hydrogen atoms were found on the E-map with lowest Karle R factor (12).

The structure was refined by large block least squares ($\Sigma(\Delta|F|)^2$ = min) initially with isotropic temperature factors using only reflections with $I > 3\sigma(I)$. When the conventional R was 0.14, the positions of the hydrogen atoms were calculated from the geometry of the molecule. The subsequent refinement with anisotropic temperature factors on the nonhydrogen atoms converged with R = 0.060 and R_w = 0.058. The least-squares weights were calculated from $w = (\sigma^2|F_o| + 0.000173|F_o|^2)^{-1}$ where σ is the weight for each reflection derived from the diffractometer counting statistics.

Results and Discussion

Atomic positions for **3** are given in Table 1. Tables of observed and calculated structure factor amplitudes, of temperature factors, and of bond angles involving hydrogen were put on deposit.[5] Numbering, bond lengths, torsional angles, and short intramolecular distances of interest are shown in Fig. 1. Table 2 lists the bond angles and Table 3 lists the torsional angles not shown in Fig. 1. Figure 2 is an ORTEP (13) diagram of the crystal structure. This structure determination confirmed the *anti* configuration previously assigned (14) to the relative orientations of the cyclohexane rings on the basis of the ^{1}H nmr spectrum.

The ten-membered ring in **3** adopted a twist-chair-boat-chair (TCBC) conformation which has, within experimental error, the D_2 symmetry expected for such a conformation. Two force-field calculations have been performed on the TCBC conformation of cyclodecane (*2a*, 4). The agreement between the torsional angles found for these two calculations is poor (Table 4). Furthermore the two sets of calculations gave quite different energies (37.5 (4) and 17.0 kJ/mol (*2a*)) relative to the BCB conformation of cyclodecane. However, both results suggest that the TCBC is not an important contributor to the conformational mixture present in cyclodecane.

Several features of the present molecule are particularly favourable for the TCBC conformation. The replacement of methylene groups by oxygens in a cyclodecane ring markedly lowers the transannular non-bonded interactions, since, in the cyclodecane analogue of **3**, the inner hydrogen on a methylene group where O(1) is located would have severe nonbonded interactions with an inner hydrogen on a methylene group in the position of O(4) and to a

[5] A complete set of tabular data is available, at a nominal charge, from the Depository of Unpublished Data, CISTI, National Research Council of Canada, Ottawa, Ont., Canada K1A 0S2.

TABLE 1. Positional parameters (esd's) for *trans-anti-trans*-4,5:9,10-biscyclohexano-1,3,6,8-tetraoxecane*

Atom	*x*	*y*	*z*
O(1)	5560(4)	1913(3)	685(6)
O(2)	6972(4)	1187(3)	2570(6)
O(3)	6054(3)	569(3)	1619(6)
O(4)	7667(4)	1348(3)	−1254(7)
C(1)	4733(5)	1365(4)	−201(10)
C(2)	3604(6)	1782(5)	−595(12)
C(3)	2684(6)	1279(6)	−1700(13)
C(4)	3030(6)	1029(5)	−3606(12)
C(5)	4142(6)	605(5)	−3241(11)
C(6)	5085(5)	1069(4)	−2066(9)
C(7)	6104(6)	1743(5)	2538(10)
C(8)	7026(7)	778(7)	−2356(12)
C(9)	8390(5)	1073(5)	439(9)
C(10)	8055(5)	1472(4)	2205(11)
C(11)	8897(6)	1297(7)	3994(11)
C(12)	10111(7)	1493(9)	3768(16)
C(13)	10434(7)	1056(7)	2025(14)
C(14)	9618(6)	1243(6)	197(12)
H(1)	482(4)	90(2)	69(6)
H(21)	369(7)	225(2)	−143(7)
H(22)	346(6)	196(3)	73(4)
H(31)	194(3)	158(3)	−205(10)
H(32)	258(6)	85(5)	−76(14)
H(41)	244(3)	65(2)	−427(6)
H(42)	307(5)	150(2)	−447(7)
H(51)	448(5)	47(3)	−445(5)
H(52)	409(6)	12(2)	−244(7)
H(6)	533(5)	152(2)	−285(7)
H(71)	645(4)	218(2)	341(6)
H(72)	553(3)	144(2)	318(6)
H(81)	753(6)	32(3)	−256(9)
H(82)	676(5)	104(35)	−364(5)
H(9)	821(5)	52(1)	81(9)
H(10)	795(5)	204(1)	183(9)
H(111)	863(6)	163(2)	505(7)
H(112)	875(6)	73(1)	426(8)
H(121)	1072(6)	140(5)	493(9)
H(122)	1016(8)	205(2)	330(13)
H(131)	1028(4)	49(1)	231(11)
H(132)	1127(2)	113(3)	195(10)
H(141)	957(7)	182(1)	−4(9)
H(142)	980(6)	97(3)	−98(6)

*$\times 10^4$ for non-hydrogen atoms and $\times 10^3$ for hydrogen atoms.

lesser extent with H(10) and H(6) (the O(1)—H(10) and O(1)—H(6) distances in **3** are 2.84 and 2.55 Å respectively). The near D_2 symmetry of **3** requires similar interactions between hydrogens on positions occupied by O(2), O(3), C(9), and C(1). In **3**, the comparable interactions are at distances which are larger than the sum of the van der Waals radii. Moreover, in the TCBC conformation, the two dialkoxymethane fragments can nearly adopt the $+sc$, $+sc$ orientations calculated to be most stable for dimethoxymethane (15, 16), and shown to be present in the gas phase (17) and in crystal structures of carbohydrates (15). The average of the torsional angles in R—O—C—O—R fragments in **3** (80.3°) is somewhat larger than the calculated (60°) (15) to be most stable for dimethoxyethane but the increase in energy required to assume these angles is probably not large (15). However the energy surface has not been mapped in detail. A third factor arises because there are four torsional angles of ~120° in the TCBC conformation which cause eclipsing interactions which considerably destabilize this conformation in the case of cyclodecane itself. Since the comparable torsional angles in **3** are in C—C—O—C fragments, the TCBC conformation for **3** should be considerably stabilized in comparison.

The difference between the O—C bond lengths in O—C—O and O—C—C segments is larger in **3** (0.014 Å) then calculated or observed (15) in the other molecules having R—O—C—O—R segments in a $+sc$, $+sc$ conformation (15). Since the back-donation from oxygen non-bonding *p* orbitals to electronically depleted carbon *p* orbitals which causes this difference in bond lengths (18) is maximized at 90° torsional angles, a structure like **3** with torsional angles closer to 90° than 60° would be expected to show this increase in bond length variation. The ten-membered ring in 1,3,5,7,9-pentaoxecane (**4**) also adopts a TCBC conformation (19) and in it only one R—O—C—O—R group can adopt the $+sc$, $+sc$ conformation. The torsional angles observed were smaller (see Table 4) and, as a result, the short O—C bond lengths were longer (1.411 and 1.408 Å).

It is interesting to note that **3** adopts the TCBC conformation in the solid state, rather than one of the other ten-membered ring conformations which have been calculated (*2a*) to be considerably more stable for the case of cyclodecane. Because of the position, the *anti* relationship and the *trans* fusion of the two cyclohexane rings fused to the tetraoxecane ring, any energetically viable conformation of the tetraoxecane ring must contain two torsional angles which have the same sign and have magnitudes of ~55–80°. Furthermore, these angles must be associated with bonds which are separated by four intervening bonds. Two of the conformations of cyclodecane more stable than the TCBC conformation, namely, the TBC and BCC conformations, fulfil this requirement. The TBC conformation as calculated by Ermer (*2a*) is about 13 kJ/mol more stable than the TCBC. If compound **3** adopted this conformation, it would have ring fusion angles of 60.4° and would have favourable torsional angles in the R—O—C—O—R fragments of +53.5° and +68.4°. Models suggest that a TBC conformation of **3** would be somewhat disfavoured by non-bonded interactions between the hydrogens on one O—CH_2—O group and methylene groups on the two cyclohexane rings. The BCC conformation is

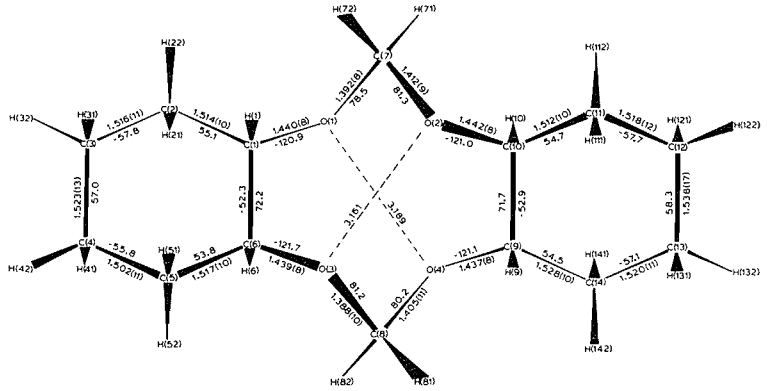

FIG. 1. Numbering and structural parameters from *trans-anti-trans*-4,5:9,10-biscyclohexano-1,3,6,8-tetraoxecane. Bond lengths (Å) with their errors in parentheses (10^3 Å) are shown on the outside of the molecule, torsional angles (deg) between carbon and oxygen atoms are shown on the interior. Intramolecular distances (Å) are indicated by a dashed line. The C(1)—C(6) and C(9)—C(10) bond distances were 1.524(10) and 1.525(10) Å respectively.

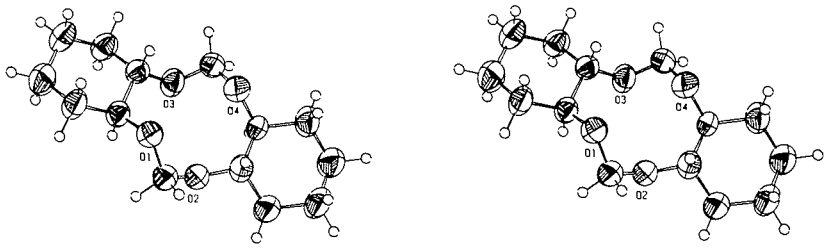

FIG. 2. Stereoscopic view of the solid state structure of *trans-anti-trans*-4,5:9,10-biscyclohexano-1,3,6,8-tetraoxecane.

TABLE 2. Bond angles (esd's) in *trans-anti-trans*-4,5:9,10-biscyclohexano-1,3,6,8-tetraoxecane (**3**)

Bonds	Angle (deg)	Bonds	Angle (deg)
C(6)—C(1)—O(1)	109.4(5)	C(10)—C(9)—O(4)	107.9(6)
C(1)—O(1)—C(7)	116.9(5)	C(9)—O(4)—C(8)	115.3(6)
O(1)—O(7)—O(2)	113.1(6)	O(4)—C(8)—O(3)	113.1(7)
C(7)—O(2)—C(10)	115.9(5)	C(8)—O(3)—C(6)	116.7(6)
O(2)—C(10)—C(9)	110.0(5)	O(3)—C(6)—C(1)	109.5(5)
O(1)—C(1)—C(2)	107.1(6)	O(3)—C(6)—C(5)	107.6(6)
O(2)—C(10)—C(11)	106.3(6)	O(4)—C(9)—C(14)	107.9(6)
C(6)—C(1)—C(2)	111.0(6)	C(9)—C(10)—C(11)	111.1(6)
C(1)—C(2)—C(3)	111.8(7)	C(10)—C(11)—C(12)	112.9(8)
C(2)—C(3)—C(4)	109.9(7)	C(11)—C(12)—C(13)	109.4(9)
C(3)—C(4)—C(5)	109.9(6)	C(12)—C(13)—C(14)	111.1(8)
C(4)—C(5)—C(6)	113.2(7)	C(13)—C(14)—C(9)	111.4(7)
C(5)—C(6)—C(1)	111.5(6)	C(14)—C(9)—C(10)	112.3(6)

calculated to be 8.5 kJ/mol more stable for cyclodecane (2*a*). A BCC conformation of **3** would have favourable fusion angles for the cyclohexane rings (average 60.6°) but would have the unfavourable *sc*, *ap* conformation in its R—O—C—O—R fragments. In comparison the TCBC conformation of cyclodecane has been calculated to have torsional angles of 88.1° (2*a*) or 116° (4) at the position where the cyclohexane rings are fused in **3**; the observed average values were 71.9°. The value observed is somewhat larger than in *trans*-disubstituted cyclohexane derivatives but distorting a cyclohexane ring in this manner is known to be energetically cheap (20). The effect on the interaction between the heteroatoms of slightly opening this torsional angle is probably not unfavourable; for instance, the energy minimum for 1,2-difluoroethane has been calculated to lie at a dihedral angle of 72.7° (21).

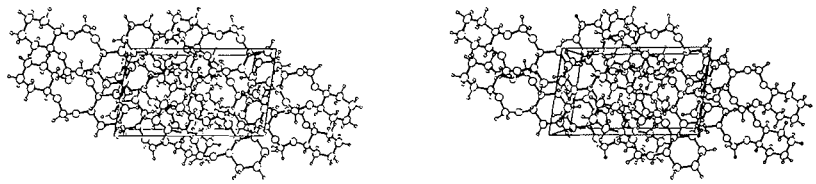

FIG. 3 Stereoscopic view of the molecular packing.

TABLE 3. Torsional angles in **3** not shown in Fig. 1

Atoms	Angle (deg)
C(7)—O(1)—C(1)—C(2)	119.3
C(7)—O(2)—C(10)—C(11)	119.1
C(8)—O(3)—C(6)—C(5)	117.4
C(8)—O(4)—C(9)—C(14)	117.1

TABLE 4. Torsional angles in TCBC conformations

Observed angles		Calculated for cyclodecane	
3[a]	**4**[b]	*A*[c]	*B*[d]
+80.3	+72.9	+58	68.1
−121.2	−118.7	−126	−119.4
+71.9	+84.2	+116	88.1
−121.2	−123.4	−126	−119.4
+80.3	+69.8	+58	68.1

[a]Present values averaged to D_2 symmetry.
[b]For 1,3,5,7,9-pentaoxecane (**4**) (19). The C_2 symmetric structure had the same atoms as the present result for the first torsional angle only.
[c]From ref. 4.
[d]From ref. 2*a*.

The crystal packing is shown in Fig. 3. Very few non-bonded intermolecular interactions at distances significantly shorter than the sum of the van der Waals radii were observed. One H(51)···H(51) distance was 2.264 Å and there were four other interactions at distances slightly less (<1.5%) than the sum of the van der Waals radii. The density of the crystal (1.188 g cm^{-3} calculated) is considerably less than for the two tetraoxecanes (**1**, **2**) previously examined (1.296 and 1.255 g cm^{-3} respectively) (6, 7), both of which adopted BCB conformations. The more efficient packing of the BCB conformation may have an additional factor favouring it in the solid state.

A particularly interesting feature of **3** is that the oxygen atoms in it are ideally oriented for interaction with cations of appropriate size (see ref. 8 for a discussion of the geometric requirements for complex formation). An investigation of the complex-forming ability of **3** is in progress.

Acknowledgements

The authors would like to thank Ms R. Cordes and Dr. J. S. Grossert for discussions and M. J.-F. Guedon for arranging to have the ORTEP diagrams drawn. The authors acknowledge support by the National Research Council of Canada.

1. J. D. DUNITZ. *In* Perspectives in structural chemistry. Vol. 2. *Edited by* J. D. Dunitz and J. A. Ibers. John Wiley and Sons, Inc., New York, NY. 1968. p. 1; G. SAMUEL and R. WEISS. Tetrahedron, **26**, 3005 (1970); O. ERMER, J. D. DUNITZ, and I. BERNAL. Acta Crystallogr. B**29**, 2278 (1973).
2. (*a*) O. ERMER. Struct. Bonding Berlin, **27**, 161 (1976); (*b*) C. ALTONA and D. H. FABER. Fortschr. Chem. Forsch. **45**, 1 (1974); (*c*) J. B. HENDRICKSON. J. Am. Chem. Soc. **89**, 7036 (1967); **89**, 7043 (1967); **89**, 7047 (1967).
3. F. M. ENGLER, J. D. ANDOSE, and P. v. R. SCHLEYER. J. Am. Chem. Soc. **95**, 8005 (1973).
4. R. L. HILDERBRANDT, J. D. WIESER, and L. K. MONTGOMERY. J. Am. Chem. Soc. **95**, 8598 (1973).
5. J. D. DUNITZ, H. ESER, M. BIXON, and S. LIFSON. Helv. Chim. Acta, **50**, 1572 (1967).
6. T. B. GRINDLEY and W. A. SZAREK. Can. J. Chem. **52**, 2566 (1974); A. TERZIS, T. B. GRINDLEY, and J. B. FAUGHT. Can. J. Chem. **55**, 2692 (1977).
7. A. TERZIS, J. B. FAUGHT, and T. B. GRINDLEY. Can. J. Chem. **56**, 1705 (1978).
8. J. M. TIMKO, S. S. MOORE, D. M. WALBA, P. C. HIBERTY, and D. J. CRAM. J. Am. Chem. Soc. **99**, 4207 (1977).
9. J. S. BRIMACOMBE, A. B. FOSTER, B. D. JONES, and J. J. WILLARD. J. Chem. Soc. C, 2404 (1967).
10. International tables for X-ray crystallography. Vol. IV. The Kynoch Press, Birmingham, England. 1974.
11. G. SHELDRICK. X-ray system report. University Chemical Laboratory, Lensfield Rd, Cambridge, England. 1976; J. KARLE and H. HAUPTMAN. Acta Crystallogr. **11**, 264 (1958).
12. J. KARLE and I. L. KARLE. Acta Crystallogr. **21**, 849 (1966).
13. C. K. JOHNSON. ORTEP, Report ORNL-3794, Oak Ridge National Laboratory, Oak Ridge, Tennessee. 1965.
14. T. B. GRINDLEY, J. F. STODDART, and W. A. SZAREK. J. Am. Chem. Soc. **91**, 4722 (1969).
15. G. A. JEFFREY, J. A. POPLE, J. S. BINKLEY, and S. VISHVESHWARA. J. Am. Chem. Soc. **100**, 373 (1978).
16. D. G. GORENSTEIN and D. KAR. J. Am. Chem. Soc. **99**, 672 (1977).
17. E. E. ASTRUP. Acta Chem. Scand. **27**, 3271 (1973).
18. G. A. JEFFREY, J. A. POPLE, and L. RADOM. Carbohydr. Res. **25**, 117 (1972).
19. Y. CHATANI and K. KITAHAMA. Bull. Chem. Soc. Jpn. **46**, 2300 (1973).
20. E. L. ELIEL, N. L. ALLINGER, S. J. ANGYAL, and G. MORRISON. Conformational analysis. Interscience, New York, NY. 1965. p. 77.
21. L. RADOM, W. A. LATHAN, W. J. HEHRE, and J. A. POPLE. J. Am. Chem. Soc. **95**, 693 (1973).

Stabilities of complexes $(N_2)_nH^+$, $(CO)_nH^+$, and $(O_2)_nH^+$ for $n = 1$ to 7 based on gas phase ion-equilibria measurements

K. HIRAOKA,[1] P. P. S. SALUJA, AND P. KEBARLE

Chemistry Department, University of Alberta, Edmonton, Alta., Canada T6G 2G2

Received March 8, 1979

K. HIRAOKA, P. P. S. SALUJA, and P. KEBARLE. Can. J. Chem. 57, 2159 (1979).

The equilibria $B_{n-1}H^+ + B = B_nH^+$ for B = N_2, CO, and O_2 were measured with a pulsed electron beam high ion source pressure mass spectrometer. Equilibria up to $n = 7$ could be observed. van't Hoff plots of the equilibrium constants lead to $\Delta G_{n-1,n}^0$, $\Delta H_{n-1,n}^0$, and $\Delta S_{n-1,n}^0$. While the proton affinities increase in the order $O_2 < N_2 < CO$, the stabilities of the B_2H^+ towards dissociation to $BH^+ + B$ increase in the reverse order, i.e. $CO < N_2 < O_2$. The stabilities towards dissociation of B for B_nH^+ where $n > 2$ are much lower for all three compounds; however for N_2 and CO the stability decreases only very slowly from $n = 3$ to $n = 6$, then there is a large fall off for $n = 7$. The $(O_2)_nH^+$ clusters show large decrease of stabilities as n increases. The B_nH^+ (for $n > 3$) of CO are more stable than those of N_2 or O_2. The above experimental results can be partially explained with the help of results from molecular orbital STO-3G calculations for B, BH^+, and B_2H^+ and general considerations. BH^+ and B_2H^+ for CO and N_2 are found to be linear while those for O_2 are bent. The most stable O_2H^+ is a triplet, while $(O_2)_2H^+$ is a quintuplet.

K. HIRAOKA, P. P. S. SALUJA et P. KEBARLE. Can. J. Chem. 57, 2159 (1979).

On a mesuré l'équilibre $B_{n-1}H^+ + B = B_nH^+$ où B = N_2, CO et O_2 en faisant appel à un spectromètre de masse à pression à source ionique intense avec un faisceau électronique pulsé. On a pu observé l'équilibre jusqu'à $n = 7$. Des courbes de van't Hoff des constantes d'équilibre conduisent à $\Delta G_{n-1,n}^0$, $\Delta H_{n-1,n}^0$ et $\Delta S_{n-1,n}^0$. Alors que les affinités protoniques augmentent dans l'ordre $O_2 < N_2 < CO$, les stabilités de B_2H^+ vis-à-vis la dissociation en $BH^+ + B$ augmente dans l'ordre inverse soit $CO < N_2 < O_2$. Les stabilités vis-à-vis la dissociation de B pour B_nH^+ où $n > 2$ sont beaucoup plus faibles pour les trois composés; toutefois dans le cas de N_2 et de CO, la stabilité ne diminue que très lentement de $n = 3$ à $n = 6$ avant de subir une diminution importante à $n = 7$. Pour les agrégats de $(O_2)_nH^+$, il se produit une diminution rapide des stabilités avec une augmentation de n. Les B_nH^+ (où $n > 3$) de CO sont plus stables que ceux de N_2 ou O_2. Les résultats expérimentaux mentionnés peuvent être expliqués partiellement à l'aide de résultats de calculs d'orbitales moléculaires STO-3G pour B, BH^+ et B_2H^+ et de considérations générales. On a trouvé que BH^+ et B_2H^+ pour CO et N_2 sont linéaires alors que ceux de O_2 sont recourbés. L'état le plus stable pour O_2H^+ est un triplet alors que pour $(O_2)_2H^+$ il s'agit d'un quintuplet.

[Traduit par le journal]

Introduction

The stabilities of gas phase complexes between the proton and a variety of bases B have been examined in previous publications from this and other laboratories (1). The present work deals with proton held complexes: $(B)_nH^+$ of the three diatomic bases: N_2, CO, and O_2. The previously studied bases involved various classes. One group consisted of strong bases containing protic hydrogens which formed strongly hydrogen bonded clusters on protonation. A prime example of this group is the protonated water clusters (2, 3) $H_{2n+1}O_n^+$. Strong bases with blocked hydrogen bonding positions, i.e. dimethyl ether, were another group. In this case, the proton associated strongly with only two of the bases (3). The bonding involving the very weak σ donor bases H_2 and CH_4 was also examined (4). Compared with the above compounds $(N_2)_nH^+$, $(CO)_nH^+$, and $(O_2)_nH^+$ form again a separate class. N_2, CO, and O_2 are weak bases essentially devoid of dipole moment. The formation of large clusters is therefore not expected. On the other hand, since the molecules are small and linear more than two molecules may arrange themselves in close proximity to the proton. If the clusters formed are held largely by physical forces, the absence of dipoles and the similar magnitude of the polarizabilities of N_2, CO, and O_2 should lead to very similar complex stabilities. On the other hand, the operation of specific chemical forces will lead to distinct stability differences.

Carbon monoxide and O_2 are also two important ligands in transition metal ion complexes. The bonding of these molecules to the proton might

[1]Present address: Faculty of Engineering, Yamanashi University, Takeda-4, Kofu, Japan.

0008-4042/79/162159-08$01.00/0

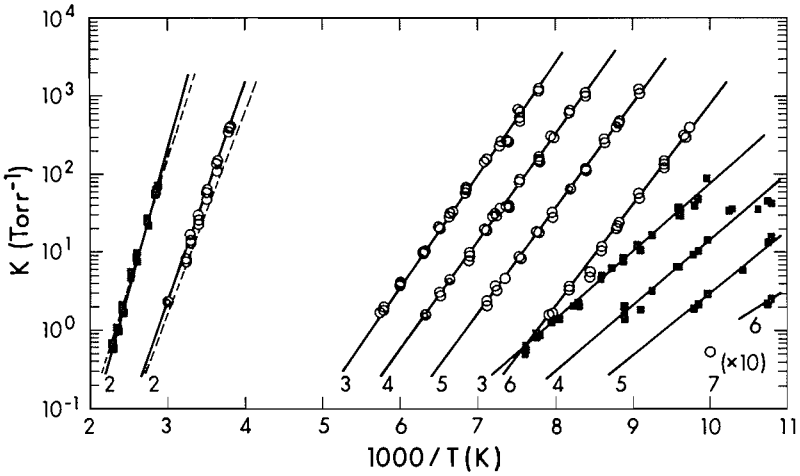

FIG. 1. van't Hoff plots for reactions: $(B)_{n-1}H^+ + B = (B)_nH^+$. ■ B = N_2, ○ B = CO. Numbers below plots give value of n. --- earlier results by Meot-Ner and Field (5). Note stabilities reversal: $D(HN_2^+—N_2) > D(HCO^+—CO)$ but $D(H(N_2)_n^+—N_2) < D(H(CO)_n—CO)$ for $n > 1$. Results also directly indicate large stability changes between $(B)_2H^+$ and $(B)_3H^+$ and $(B)_6H^+$ and $(B)_7H^+$. Latter stability difference based on single point determination of $K_{6,7}(CO)$, see point at lower right of figure.

prove interesting to compare with bonding in the transition metal ion complexes.

Experimental

The measurements of the ion equilibria were made with the pulsed electron beam high pressure ion source mass spectrometer which has been described previously (2).

The ions B_nH^+ where B = CO, N_2, or O_2 were obtained by adding 3–300 mTorr of the gas B to some 4 Torr of hydrogen (carrier) gas. The ions in pure hydrogen are $H_3^+(H_2)_n$ as has been shown by previous studies (4). In the presence of B, which are stronger bases than H_2, the switching reactions shown below occur.

$$(H_2)_nH^+ + B = BH^+ + nH_2$$

These are followed by further clustering of B.

$$B + B_{n-1}H^+ = B_nH^+ \qquad [n-1, n]$$

In some cases the mixed clusters $B_x(H_2)_yH^+$ could also be observed in equilibrium with the B_nH^+ clusters.

The equilibrium constants $K_{n-1,n}$ were found to be essentially independent of the pressure of B for a pressure change by a factor of about 10.

The reaction $HCO^+ + CO + M = (CO_2)_2H^+ + M$ was found to be unusually slow. This equilibrium could be measured only in the presence of relatively large CO partial pressures ($p_{CO} > 0.1$ Torr). This precluded the measurement of the equilibrium constant at lower temperatures since with the relatively large CO pressure, the equilibrium ratio $[(CO)_2H^+]/[HCO^+]$ became too large rapidly at low temperatures. Therefore the temperature range over which this particular equilibrium could be measured was narrower than usual.

In all the above measurements special precautions had to be taken in order to keep the reagent gases and reaction system dry. Even small traces of water interfere with the measurements, since water, being a much stronger base than B, displaces B by the reaction shown below:

$$B_nH^+ + H_2O = (H_2O)B_{n-x}H^+ + xB$$

The traces of water were removed from the H_2 carrier gas by passing it through a trap maintained at 77 K containing molecular sieve 5 Å. The mixed H_2 + reagent gas (N_2, O_2, or CO) at a total pressure of ~4 Torr was then passed through a spiral glass trap maintained at 77 K.

Results and Discussion

(a) Experimental Results

The results for the experimentally measured equilibrium constants for the reactions [1] and [2]

[1] $(CO)_{n-1}H^+ + CO = (CO)_nH^+$

[2] $(N_2)_{n-1}H^+ + N_2 = (N_2)_nH^+$

are summarized in the van't Hoff plots shown in Fig. 1. Also shown in Fig. 1 are the van't Hoff plots obtained earlier by Meot-Ner and Field (5) for reactions [1] and [2] involving [1,2] equilibria. As can be seen from the figure, Field's results are in quite good agreement with the present work.

The spacings between the lines of the van't Hoff plots in Fig. 1 reveal directly the changes of the relative stabilities of the complexes. There is a big gap between the [1,2] and [2,3] equilibria for both $(CO)_nH^+$ and $(N_2)_nH^+$. This shows that the B_2H^+ complexes are very much more stable (towards loss of one ligand) than the B_3H^+ and higher n complexes. These data also reveal that the interactions are not dominated by physical forces, i.e. polarizabilities. For example the greater stability of $(N_2)_2H^+$ would not have been expected on the basis of the polarizabilities of N_2 and CO which are $\alpha_{N_2} = 1.76$ and $\alpha_{CO} = 1.95$ Å^3 (6), i.e. $\alpha_{CO} > \alpha_{N_2}$. Furthermore since N_2 and CO are isoelectronic and of similar size the rather dramatic reversal of relative stabilities ob-

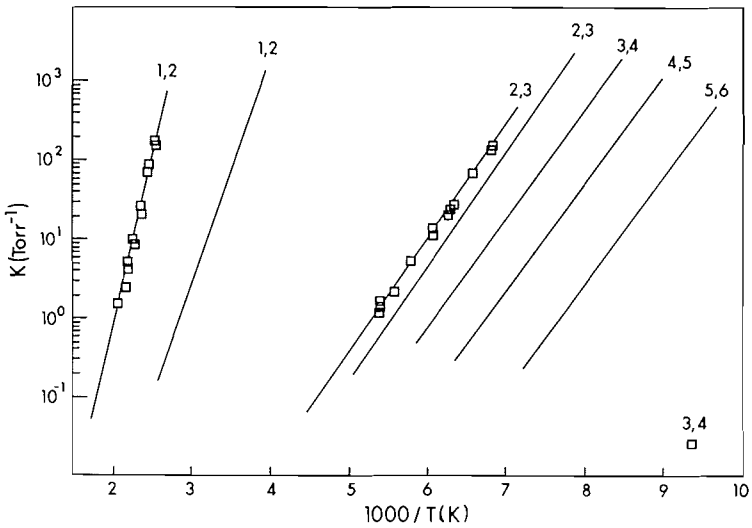

FIG. 2. van't Hoff plots for reactions: $(O_2)_{n-1}H^+ + O_2 = (O_2)_nH^+$. Numbers above plots give $[n-1, n]$. $K_{3,4}$ could be measured at only one temperature. Lines without data points are for equilibria $(CO)_{n-1}H^+ + CO = (CO)_nH^+$, which were displayed in Fig. 1 and are given here for comparison. Note that stability changes for the O_2 system show a very different pattern from those for CO.

served for B_nH^+, $n > 2$ (see Fig. 1), could not have been predicted on the basis of simple considerations.

It is also interesting to note in Fig. 1 that the $(CO)_nH^+$ stabilities decrease very gradually between [2,3], [3,4], [4,5], and [5,6] but then there is a large gap between [5,6] and [6,7]. This means that the $(CO)_7H^+$ is much less stable than $(CO)_6H^+$. We were unable to detect the $(N_2)_7H^+$ ion even at very low temperatures. This means that the $(N_2)_7H^+$ is very much less stable than $(N_2)_6H^+$, i.e. a stability gap occurs also for the $(N_2)_nH^+$ series between $n = 6$ and $n = 7$.

The results for the $(O_2)_nH^+$ equilibria are shown in Fig. 2 together with the $(CO)_nH^+$ equilibria which are included for comparison. It is immediately evident that the $(O_2)_nH^+$ clusters show rather different stability changes when compared to $(CO)_nH^+$ and $(N_2)_nH^+$. The bonding in $(O_2)_2H^+$ is somewhat stronger than that in $(N_2)_2H^+$ and considerably stronger than that in $(CO)_2H^+$. The gap between the [1,2] and [2,3] equilibria is quite large for O_2 and there is an even larger gap between [2,3] and [3,4]. No such gap occurred for the $(CO)_nH^+$ and $(N_2)_nH^+$ equilibria, which showed only small stability decreases from $n = 3$ to $n = 6$.

The $\Delta G_{n-1,n}^0$, $\Delta H_{n-1,n}^0$, and $\Delta S_{n-1,n}^0$ obtained from the van't Hoff plots in Figs. 1 and 2 are summarized in Table 1. The $\Delta H_{n-1,n}^0$ changes with n for the three systems are shown in Fig. 3. These results reflect what was already deduced from the direct examination of the van't Hoff plots.

For CO and N_2 the $\Delta H_{n-1,n}^0$ are found to be almost constant between [3,4] and [5,6], i.e. the stability decreases in that range are indicated to be almost entirely due to entropy decreases. Since the van't Hoff plots were obtained over a rather narrow temperature range, and the presence of some small systematic error cannot be excluded, it may be that the $\Delta H_{n-1,n}$ decreases in this range are actually somewhat larger than the present measurements indicate.

Included in Table 1 are also some results involving equilibria in mixed clusters between H_2 with O_2 or N_2. The corresponding van't Hoff plots are shown in Fig. 4. Results for clusters involving H_2 and HCO^+ were published earlier (7).

(b) Stabilities of $(N_2)_nH^+$, $(CO)_nH^+$, and $(O_2)_nH^+$

In considering the stabilities of the protonated clusters of N_2, CO, and O_2 it is useful first to examine the protonated monomers N_2H^+, OCH^+, and O_2H^+. The proton affinities PA(O_2) = 101, PA(N_2) = 113.7, and PA(CO) = 139.0 kcal/mol have been determined by Bohme and co-workers (8) from measurements of proton transfer equilibria. *Ab initio* theoretical calculations for OCH^+ and N_2H^+ are available in the literature (9, 10). The more extensive and recent calculations of Forsén and Roos (10) lead to PA(N_2) = 118 and PA(CO) = 137 kcal/mol in relatively good agreement with the experimental values given above. The calculated SCF energies for the protonated and unprotonated species were near the Hartree Fock limit; however no corrections for electron correlation were made (10).

TABLE 1. Thermochemical data

Reactions	$-\Delta H^0$ (kcal/mol)	$-\Delta S$ (eu)	$-\Delta G^0$ (kcal/mol)[a]
$(CO)H^+ + CO = (CO)_2H^+$	12.8	24	5.7
$(CO)_2H^+ + CO = (CO)_3H^+$	6.6	24	−0.6
$(CO)_3H^+ + CO = (CO)_4H^+$	6.3	26	−1.4
$(CO)_4H^+ + CO = (CO)_5H^+$	6.2	29	−2.5
$(CO)_5H^+ + CO = (CO)_6H^+$	5.8	32	−3.8
$(N_2)H^+ + N_2 = (N_2)_2H^+$	16.0	24	8.8
$(N_2)_2H^+ + N_2 = (N_2)_3H^+$	4.0	18	−1.4
$(N_2)_3H^+ + N_2 = (N_2)_4H^+$	3.8	20	−2.2
$(N_2)_4H^+ + N_2 = (N_2)_5H^+$	3.5	20	−2.5
$(N_2)_5H^+ + N_2 = (N_2)_6H^+$	3.2[b]		
$(O_2)H^+ + O_2 = (O_2)_2H^+$	20.0	27	11.6
$(O_2)_2H^+ + O_2 = (O_2)_3H^+$	6.6	22	−0.02
$(0_2)_3H^+ + O_2 = (O_2)_4H^+$	3.2[b]		
$(O_2)H^+ + H_2 = (O_2)(H_2)H^+$	12.5	22	6.0
$(O_2)_2H^+ + H_2 = (O_2)(H_2)_2H^+$	4.0	17	−1.1
$H_3^+ + O_2 = (O_2)H^+ + H_2$	0.0	−2.4	0.72
$(N_2)H^+ + H_2 = (N_2)(H_2)H^+$	7.2	22.6	0.4
$(N_2)(H_2)H^+ + H_2 = (N_2)(H_2)_2H^+$	1.8	17	−3.3

[a]At 298 K.
[b]From measured equilibrium constant at one temperature, from which $\Delta G^0 = -RT \ln K$ was evaluated. ΔH^0 was then obtained by assuming that $\Delta S^0 = -20$ eu which is an average value for these reactions as evidenced by measured ΔS^0 for the other reactions given in the table.

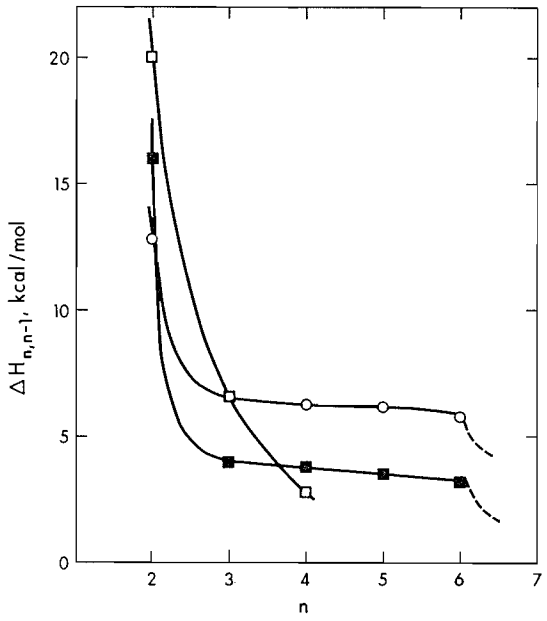

FIG. 3. $\Delta H_{n,n-1} = -\Delta H_{n-1,n}$ values obtained from van't Hoff plots displayed in Figs. 1 and 2. □, $(O_2)_nH^+$; ■, $(N_2)_nH^+$; ○, $(CO)_nH^+$. Note that the B_2H^+ species is of high stability for all three bases. CO and N_2 then build clusters up to B_6H^+ with small ΔH fall offs while $(O_2)_nH^+$ behaves differently showing a large ΔH decrease with every step.

Therefore the relatively good agreement with experiment indicates the near complete cancellation of the correlation error in the protonated and unprotonated species. No theoretical calculations for O_2H^+ and any of the higher protonated clusters of N_2, CO, and O_2 seem to be available in the literature. In order to obtain some theoretical information, we made STO-3G calculations (11) for: N_2, N_2H^+, $(N_2)_2H^+$, O_2, O_2H^+, $(O_2)_2H^+$, CO, COH^+, $(CO)_2H^+$. The proton affinities obtained from the differences of the total energies of the bare and protonated molecule are given in Table 2. The stabilization energies of the dimers obtained from the ΔE(STO-3G) for the reactions $B_2H^+ = BH^+ + B$ are also given in Table 2. The lowest energy structures predicted by STO-3G are shown in Fig. 5. The STO-3G predicted proton affinities and the stabilization energies of the dimers are much larger than the experimental values. Considering Forsén and Roos' (10) calculations, which were in fair agreement with the experimental proton affinities, it is obvious that the minimal basis sets used in STO-3G are at fault. An additional problem occurs for O_2H^+ and $(O_2)_2H^+$. Since the ground state of O_2 is a triplet, if O_2 retains its triplet character O_2H^+ could be a triplet and $(O_2)_2H^+$ a quintuplet. These are in fact the ground states predicted by the STO-3G calculations using open shell unrestricted Hartree Fock. The singlets for these molecules are predicted to be 44 and 95 kcal/mol of higher energy. The STO-3G calculated energy difference between triplet and singlet O_2 is 52 kcal/mol while the spectroscopic value for this separation ($^3\Sigma_g$ to $^1\Delta_g$) is only 22.6 kcal/mol (12). The exaggerated calculated difference is probably largely due to neglect of electron correlation since electron correlation will have a larger stabilizing effect on the singlet state. Differences in cancellation of the correlation error in

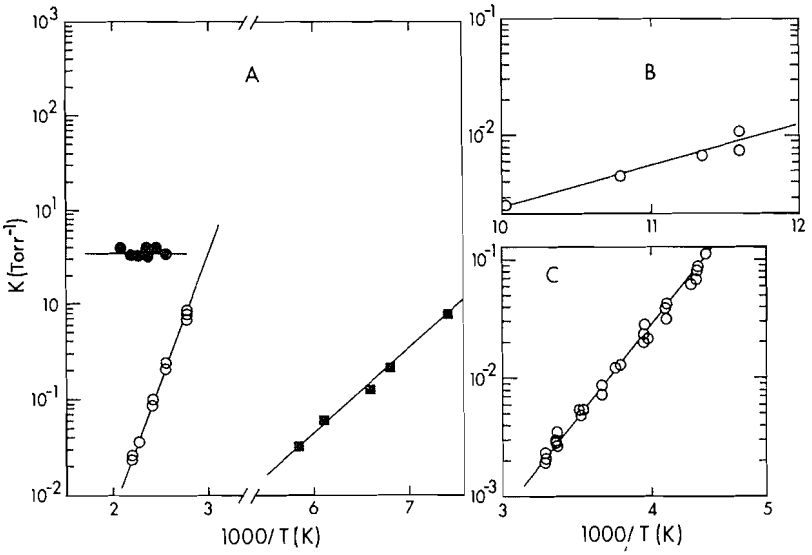

FIG. 4. (*A*) van't Hoff plots for equilibria: $H_3^+ + O_2 = O_2H^+ + H_2$, ●; $O_2H^+ + H_2 = O_2H_2H^+$, ○; $(O_2)_2H^+ + H_2 = (O_2)_2(H_2)H^+$, ■. (*B*) $(N_2)(H_2)H^+ + H_2 = N_2(H_2)_2H^+$. (*C*) $N_2H^+ + H_2 = N_2(H_2)H^+$.

TABLE 2. Energies from STO-3G calculations

ΔE (kcal/mol)[a]		ΔE (kcal/mol)[a]	
N_2H^+	−141.5	$O_2(1)$[c]	51.8
$(N_2)_2H^+$	−176.2[b]	O_2H^+(bent, 3)[c]	−161.4[b]
$D(N_2H^+—N_2)$	34.7[d]	O_2H^+(linear, 3)[c]	−121.2
		O_2H^+(isosceles, 3)[c]	−104.2
OCH^+	−175.6[b]	O_2H^+(isosceles, 1)	−50.0
$(CO)_2H^+$	−207.0	O_2H(bent, 1)[c]	−117.0
$D(OCH^+—CO)$	31.4[d]	$(O_2)_2H^+$(bent, 5)[c]	−199.2
		$(O_2)_2H^+$(bent, 1)[c]	−104.1
		$D(O_2H^+—O_2, 5)$[c]	37.8[d]

[a]ΔE corresponds to energy relative to $E(B) = 0$ where B = N_2, CO, and O_2 (triplet) respectively. For geometries of structures see Fig. 5.
[b]$\Delta E(BH^+) = -PA(B)$.
[c]Number inside parentheses corresponds to multiplicity due to electron spin. Because of differences in cancellation of electron correlation, energies for singlet states are probably ~30 kcal/mol lower than shown in table.
[d]STO-3G predicted bond dissociation energies $D(BH^+ — B) = \Delta E(BH^+) - \Delta E(B_2H^+)$.

the singlets N_2 and N_2H^+ and triplets O_2 and O_2H^+ are probably responsible for the STO-3G predicted proton affinity order $PA(O_2) > PA(N_2)$ which is the reverse of the experimentally observed one.

Evidently the STO-3G closed shell and particularly the open shell calculations are of too low an accuracy to provide relative proton affinities and binding energies. Nevertheless some qualitative information of value is obtained. The COH^+ and N_2H^+ ions are predicted to be linear. This is in agreement with the results of more accurate calculations (9, 10). The bond distances obtained are also very similar to those from the literature (9, 10). The predicted linear geometries and distances in $(CO)_2H^+$ and $(N_2)_2H^+$ are probably also reliable. Of special interest is the predicted bent geometry for O_2H^+ and $(O_2)_2H^+$ (see Fig. 5). The STO-3G calculations for closed shell, singlet, O_2H^+, and $H(O_2)_2^+$ predicted the same bent geometries as those for the multiplets (Fig. 5).

An examination of the electronic changes on formation of the protonated species is of some interest. The approach of the positive field of the proton leads to significant lowering of the energies of all the (formerly diatomic) molecular orbitals. For example in N_2 there is a fairly uniform decrease of about 0.4 au for all orbitals including the core 1*s* orbitals when the proton is brought to its equilibrium position. The spatial changes of the orbitals in N_2 and CO are of three types: hardly any spatial change in the core 1*s* orbitals, polarization of the π orbitals, and polarization and modification through overlap with the 1*s* orbital of the H atom in the 2*s*, 2*p*, σ orbitals. The linearity of the OCH^+ and N_2H^+ species is a consequence of the overlap of the 1*s* of H only with the σ type orbitals. The difference of the proton affinities of the isoelectronic N_2 and CO may be attributed to the electronegativity differences between the N and C atoms. In CO, the orbital with the highest energy is the 5σ which is located on the C atom. It is this orbital which overlaps strongly with the 1*s* of H and experiences the largest energy lowering. In N_2, because of the higher electronegativity of N, the σ orbital that interacts with the 1*s* of H is of lower energy and a weaker interaction and energy lowering occurs on protonation. The proton affinity of CO for protonation on the O atom was calculated by Forsén and Roos (10) to be 19 kcal/mol lower than that for protonation on the carbon atom. This result is also qualitatively in line with electronegativity differences between C and O.

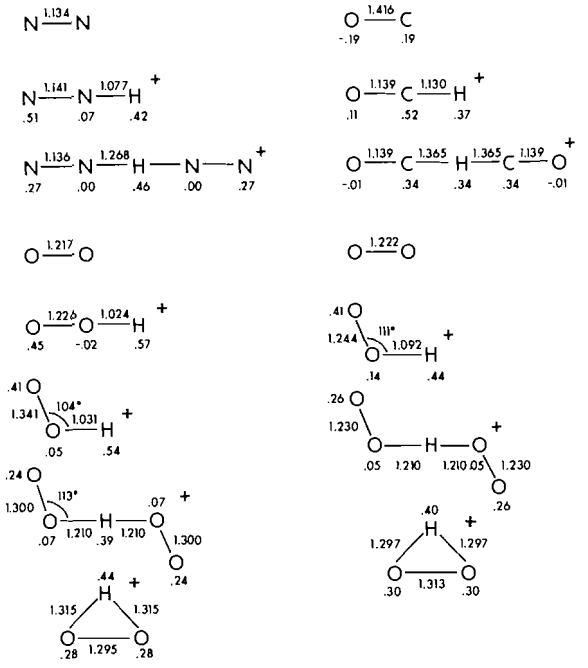

FIG. 5. Structures obtained from STO-3G calculations. Distances in Å. Numbers below atoms correspond to net atomic charges based on Mulliken population analysis. All species except the diatomic molecules are singly charged positive ions. The oxygen containing species involve triplet O_2 on the left side of figure and singlet O_2 on right side of figure. For corresponding energies see Table 2. Most stable oxygen species are bent O_2H^+ (triplet) and bent (*trans*) $(O_2)_2H^+$ (quintuplet).

On the basis of electronegativities a low proton affinity may be expected for O_2. For O_2 the σ type orbitals with which N_2 and CO interacted with the 1*s* of H are of low energy; also they are shielded from the proton by the presence of the unpaired electrons in the antibonding π^* orbital. Therefore quite a different binding occurs. A reorganization somewhat similar to sp^2 hybridization occurs which leads to the bent O_2H^+ molecule. It is interesting to note that the O protonated COH^+ was found (10) to be linear. Thus the sp^2 mixing is found only when the antibonding π^* orbital of the diatomic is occupied.

The changes occurring on formation of the dimers might be thought of as a repetition of the protonation but on a much smaller scale. This view is justified by the geometries for the dimers (Fig. 5). The linear OCH^+ and N_2H^+ are succeeded by linear dimers and the dimer $(O_2)_2H^+$ has a geometry which is like a repetition of the first bond in O_2H^+. As expected the distances between H and the neighbouring atom(s) are considerably larger in the dimers. The optimum geometry for all the three dimers was for H being in the middle between the two neighbouring atoms. A double potential well for motion of H between the two neighbouring atoms was observed only for larger distances between the bases; however these geometries had higher energies.

While the geometries of the dimers were presaged by the geometries of the protonated bases, the experimental binding energies of the dimers do not follow the order of the binding energies of the proton to the bases, i.e. the proton affinities. The STO-3G calculations reproduce the experimental results $D(OC—H^+) > D(N_2—H^+)$ and the reversal $D(OCH^+—CO) < D(N_2H^+—N_2)$ but examination of the orbital energies and changes does not lead to an understanding of the reasons for the reversal of the order in the dimers, since the orbital changes from BH^+ to B_2H^+ are quite numerous. A possible explanation may be contained in the net atomic charges based on the Mulliken population analysis (Fig. 5). While the Mulliken population analysis is strongly basis set dependent and quantitatively unreliable, it may be qualitatively useful. In N_2H^+ and O_2H^+, where two identical atoms are present, electron donation and polarization lead to the development of an appreciable positive charge on the atom which is not directly bonding to the proton, while the directly bonding atom remains almost uncharged. Because of the electronegativity difference between O and C in CO, the situation in OCH^+ is quite different. There is only little electron donation from the O atom and therefore an appreciable positive charge on the C atom. For the same reason we can expect an appreciable positive charge on the C atoms also in the $OCHCO^+$ dimer. Such a distribution is indeed predicted by the calculations (Fig. 5). The repulsion between the partially positive carbons in $OCHCO^+$ is probably responsible for the weak bonding in this dimer. Significantly, the bonding in OCH^+—CO is the one that experiences the greatest lowering relative to the H^+—B bonding in the monomers.

It is interesting to note that in B_2H^+ the bond distances and the charges on the N_2, O_2, and CO change relative to those in BH^+ by moving closer to those present in the unprotonated molecules B (Fig. 5). This is to be expected, of course. Further addition of ligands will promote this return to 'normalcy'. In addition to this change, also the distances to the proton will increase. The observed bonding in the higher clusters $(B)_nH^+$, $n > 2$, may be partially understood on these grounds. CO with the highest polarizability ($\alpha_{CO} = 1.95$, $\alpha_{O_2} = 1.6$, $\alpha_{N_2} = 1.76$ Å^3) (6) may be expected to gradually lead to the strongest bonding. The non-linearity in O_2H^+ and

$(O_2)_2H^+$ may be expected to repeat in the further growth of oxygen clusters. The observed rapid fall off in bonding with increase of n for oxygen is probably due to steric reasons, i.e. rapidly increasing repulsions between the O_2 molecules because of crowding caused by the nonlinear geometry.

The fall off of stability after the $(CO)_6H^+$ and $(N_2)_6H^+$ suggests that these species have octahedral geometry. An interesting question is whether the proton is evenly shared by the six ligands or whether the structure is unsymmetric and one CO interacts strongly with the proton and is solvated by 5 other CO molecules. If this is the case, then of further interest is the height of the six-fold potential barrier for motion of the proton from one CO to the other.

It is interesting to note that a much greater stability of CO as a ligand relative to O_2 and N_2 in the higher clusters parallels the much greater binding power of CO as ligand in transition metal complexes. It is also worthy to note that the bent geometry of O_2H^+ occurs also in some complexes of O_2 with transition metal ions, including the important O_2 complex with porphyrin in myo and hemoglobin (13, 14).

Some transition metal ion complexes with O_2 are π complexes in which the ion interacts equally with the two oxygen atoms such that an isosceles triangle structure results. The O—O distance in such complexes is longer than that in the O_2 molecule and the O_2 is more often in the singlet state (Class I compounds in ref. 14). The STO-3G predicted energies of the singlet and triplet isosceles complexes of O_2 with H^+ are appreciably higher than that of the bent triplet structure. (See Fig. 5 and Table 2.) The triplet isosceles O_2H^+ is some 54 kcal/mol higher than the singlet. Even though the STO-3G calculations exaggerate the stability of the triplets by some 30 kcal/mol, this still means that probably the more stable isosceles O_2H^+ is a triplet. As already mentioned, the STO-3G calculations of the BH^+ and B_2H^+ species are of low accuracy. We believe that the species O_2H^+, $(O_2)_2H^+$, and some of the other protonated bases and dimers are of sufficient interest and therefore merit more accurate calculations by theoretical chemists.

(c) Reactions Involving H_2 as a Base

The last five reactions shown in Table 1 involve H_2. These processes are due to the use of H_2 as carrier gas in the experiments made for the measurements of the B_nH^+ equilibria. Since these reactions are of interest, a brief discussion will be given here.

The proton transfer equilibrium [3], could be measured between the temperatures 120 to 210°C. At lower temperatures clustering interfered, while at higher temperatures the ion signal became weak, because of more rapid diffusion of the ions to the wall and reactions with impurities desorbed from the walls of the apparatus. The van't Hoff plot (Fig. 4) of the available equilibrium constants indicates a zero slope, i.e. $\Delta H_3^0 \approx 0$ although the data are rather scattered. The average equilibrium constant is $K_3 = 3.4 \pm 1$. Assuming $\Delta H_3^0 = 0$, this means that $K_3 \approx 3.4 \pm 1$ also at 25°C. This result is in agreement with the value of 2.3 ± 0.9 by Fehsenfeld *et al.* (15) but in only fair agreement with the value of 0.95 due to Fenelly *et al.* (8). The result $\Delta H_3 \approx 0$ is in agreement with the observation of Fehsenfeld *et al.* (15) that K_3 remained unchanged as the kinetic energy of the participating ions was increased. Assuming $\Delta H_3 = 0$ one obtains $\Delta S_3^0 = 2.4$ eu. Since O_2H^+ is bent and H_3^+ probably has a D_{3h} symmetry (16) a ΔS^0 evaluation, based on rotational symmetry number changes only, gives: $\Delta S_3^0 \approx R \times \ln 6 = 3.5$ eu which is close to the experimental result.

Reactions [4]–[7] represent clustering of H_2 onto O_2H^+ and N_2H^+.

[3] $H_3^+ + O_2 = H_2 + O_2H^+$

[4] $O_2H^+ + H_2 = (O_2)(H_2)H^+$

[5] $(O_2)_2H^+ + H_2 = (O_2)_2(H_2)H^+$

[6] $N_2H^+ + H_2 = (N_2)(H_2)H^+$

[7] $(N_2)(H_2)H^+ + H_2 = (N_2)(H_2)_2H^+$

The ΔH^0 and ΔG^0 results in Table 1 show that H_2 addition leads to clusters of lower stability than the addition of O_2 or N_2. Results for $(H_2)_nH^+$ were reported earlier from this laboratory (4). Weakly held three centre bond structures in which the H—H bond interacts with the partially positive hydrogen in BH^+ were proposed (4) on the basis of theoretical work (16) and the experimental results. In the present reactions [4]–[7] the structures involved are probably of a similar nature.

1. P. KEBARLE. Ann. Rev. Phys. Chem. **28**, 445 (1977).
2. A. J. CUNNINGHAM, J. D. PAYZANT, and P. KEBARLE. J. Am. Chem. Soc. **94**, 7627 (1972).
3. E. P. GRIMSRUD and P. KEBARLE. J. Am. Chem. Soc. **95**, 7939 (1973).
4. K. HIRAOKA and P. KEBARLE. J. Chem. Phys. **62**, 2267 (1975); J. Am. Chem. Soc. **97**, 4179 (1975).
5. M. MEOT-NER and F. H. FIELD. J. Chem. Phys. **61**, 3742 (1974).
6. Landolt-Börnstein-Zahlenwerte und Functionen. Vol. I. Springer. 1951. Part 3, p. 510.
7. K. HIRAOKA and P. KEBARLE. J. Chem. Phys. **63**, 1689 (1975); J. Am. Chem. Soc. **99**, 366 (1977).
8. D. K. BOHME. *In* Interactions between ions and molecules.

Edited by P. Ausloos. Plenum Press, New York, NY. p. 489; P. F. Fennelly, R. S. Hemsworth, H. I. Schiff, and D. K. Bohme. J. Chem. Phys. **59**, 6405 (1973).
9. H. B. JANSEN and P. ROS. Chem. Phys. Lett. **3**, 140 (1969).
10. S. FORSÉN and B. ROOS. Chem. Phys. Lett. **6**, 128 (1970).
11. W. J. HEHRE, R. F. STEWART, and J. A. POPLE. J. Chem. Phys. **51**, 2657 (1969); W. J. HEHRE, W. A. LATHAN, R. DITCHFIELD, M. D. NEWTON, and J. A. POPLE. Gaussian 70 program, Quantum Chemistry Program Exchange, Indiana University, Bloomington, Indiana 47401, U.S.A.
12. G. HERZBERG. Molecular spectra — spectra of diatomic molecules. Van Nostrand. 1950.
13. MASAO KOTANI (*Editor*). Advances in biophysics. Vol. II. Japan Scientific Society Press Tokyo, University Park Press, Baltimore. 1978.
14. J. S. VALENTINE. Chem. Rev. **73**, 235 (1973).
15. F. C. FEHSENFELD, W. LIDINGER, and D. L. ALBRITTON. J. Chem. Phys. **63**, 443 (1975).
16. W. I. SALMON and R. D. POSHUSTA. J. Chem. Phys. **59**, 4867 (1973).

Excited state properties of nitrobenzene derivatives

GIUSEPPE BUEMI, SALVATORE MILLEFIORI, FELICE ZUCCARELLO, AND ARCANGELO MILLEFIORI

Istituto Dipartimentale di Chimica e Chimica Industriale, Università di Catania, Viale A, Doria 8, 95125 Catania, Italy

Received August 17, 1978[1]

GIUSEPPE BUEMI, SALVATORE MILLEFIORI, FELICE ZUCCARELLO, and ARCANGELO MILLEFIORI. Can. J. Chem. 57, 2167 (1979).

Gas-phase and solution spectra of methoxy nitroanilines are reported. MIM and PPP configuration analyses were used to calculate the properties associated with the electronic transitions. The excited state dipole moments associated with the first intense electronic transition were evaluated by the solvent shift method. The spectra of the title compounds are tentatively correlated with those of the corresponding disubstituted benzene derivatives. The effect of the methoxy group on the absorption features of the isomeric nitroanilines is briefly discussed.

GIUSEPPE BUEMI, SALVATORE MILLEFIORI, FELICE ZUCCARELLO et ARCANGELO MILLEFIORI. Can. J. Chem. 57, 2167 (1979).

On rapporte les spectres en solution et en phase gazeuse de méthoxynitroanilines. On a utilisé des analyses configurationnelles MIM et PPP pour calculer les propriétés associées aux transitions électroniques. On a évalué les moments dipolaires de l'état excité associé avec la première transition électronique intense à l'aide de la méthode des déplacements induits par les solvants.

On a établi une corrélation préliminaire entre les spectres des composés mentionnés dans le titre et ceux des dérivés benzéniques disubstitués correspondants. On discute brièvement de l'effet du groupe méthoxy sur les caractéristiques d'absorption des nitroanilines isomères.

[Traduit par le journal]

Introduction

In previous papers (1–3) theoretical (MIM and PPP) and experimental (solvent shift) methods were applied to study the electronic structure of some nitrobenzene derivatives. Extension of this work to some methoxy nitroanilines is here reported with the purpose of correlating the absorption features of methoxy nitroanilines with those of the corresponding disubstituted compounds and to evaluate the effects induced by a third substituent of intermediate donating power (the methoxy group) on the electronic structure of the isomeric nitroanilines. We discuss the nature of the electronic transitions of the studied compounds in terms of locally excited (Λ) and charge transfer configurations. Solvent dependence of the electronic transitions, which is useful for evaluating charge redistribution on excitation and the nature of excited states together with frequency assignment, is obtained by comparing solution spectra with gas-phase spectra.

Experimental

The compounds investigated were commercial products purified by chromatography and crystallization. Gas-phase and solution absorption spectra were obtained as previously described (1). The spectra of methoxy nitroanilines (Fig. 1) resemble the gas-phase spectra of the corresponding nitroanilines (1); the absorption bands in the vapour of the corresponding nitroanisoles are shown in Fig. 2. In every case the gas-phase spectrum appears displaced towards shorter wavelength, thus indicating that all the apparent electronic transitions are of $\pi^* \leftarrow \pi$ type.

Excited-state dipole moments associated with the various electronic transitions can be determined by means of the equation (2)

$$\Delta\nu = \nu_{gas} - \nu_{CE} = \frac{\mu_e^2 - \mu_g^2}{hca^3}\Delta\Phi(D)$$

where CE refers to the solvent cyclohexane, D is the dielectric constant of the solvent, $\Phi(D) = (D - 1)/(D + 2)$ and a is the radius of the cavity, which was evaluated from the molecular volume as previously described (4); a mean value of 3.47 Å was obtained for the three compounds. In the vapour D was taken as unity, $\Phi(D)_{CE} = 0.2543$. Dipole moment changes are reported in Table 1, together with those evaluated by means of Suppan's equation (5)

$$-\Delta\nu = \frac{(\mu_e - \mu_g)\mu_g}{hca^3}\Delta f(D)$$

with $f(D) = 2(D - 1)/(2D + 1)$, in order to compare the present $\Delta\mu$ values with those of the corresponding isomeric nitroanilines obtained by the same method (2, 5). The relation ν versus $f(D)$ is shown in Fig. 3. Both equations give parallel results.

Calculations

Calculations were performed at MIM and PPP levels. The parametrization for MIM calculations on nitroaromatics was previously described in detail (3). It is retained here in order to compare electronic

[1]Revision received March 14, 1979.

0008-4042/79/162167-05$01.00/0

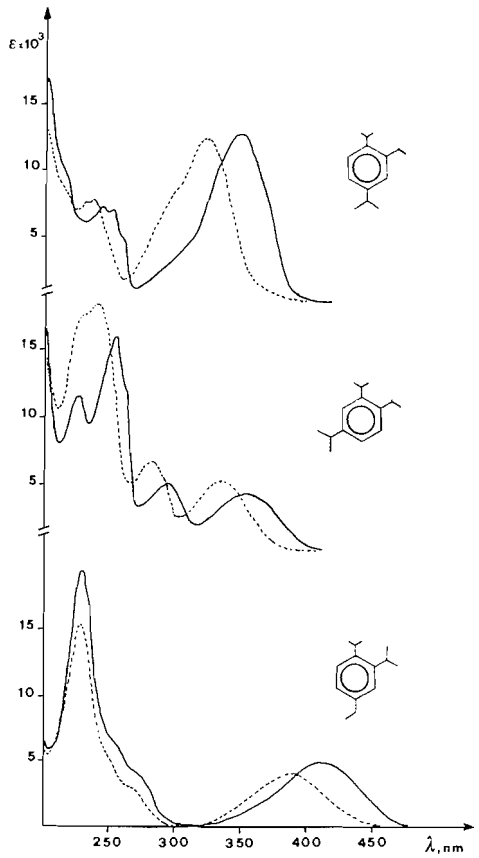

FIG. 1. Gas-phase (---) and solution (cyclohexane) (—) spectra of methoxy nitroanilines. From the top: 2-methoxy-4-nitroaniline, 2-methoxy-5-nitroaniline, 4-methoxy-2-nitroaniline.

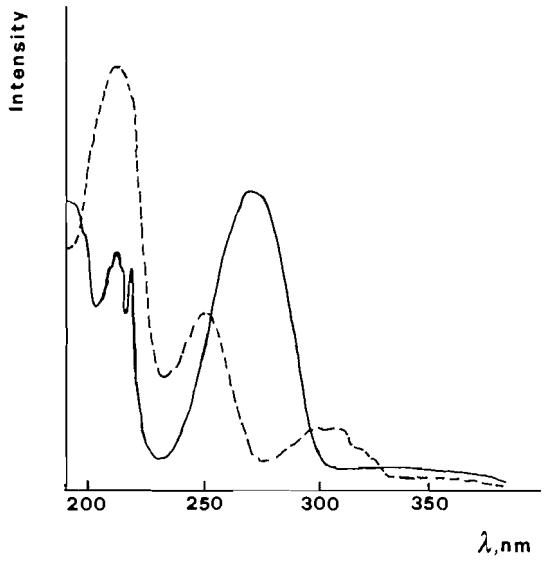

FIG. 2. Gas-phase spectra of *meta*-nitroanisole (---) and *para*-nitroanisole (—).

states of methoxy nitroanilines with those of the corresponding disubstituted benzene derivatives. The MIM calculations have previously applied in the study of nitroaromatics (1, 6, 7). The effect of electron affinity (EA) of the nitro group on the calculated electronic transitions was tested: variation of $EA(NO_2)$ from -0.4 eV to -0.7 eV does not appreciably change the calculated spectroscopic features; a maximum variation of 0.2 eV is observed in the energy of electronic transitions which are charge-transfer in nature, and meaningless variations are observed in the energy of locally excited states.

The PPP calculations were carried out as suggested by Roos and Skancke (8). They optimized integral parameters in order to reproduce ionization potentials and electronic transitions on numerous specimen molecules including nitrobenzene. In particular they introduced in the semiempirical parameter $W\mu$ a dependence on the type of nearest neighbouring atoms. For consistency reasons the geometry of the nitrobenzene framework used by Roos and Skancke was adopted in PPP calculations. The PPP results were interpreted in terms of locally excited and charge-transfer states by means of a configuration analysis (9). The results of the calculations are reported in Table 2.

Results and Discussion

The effect of the methoxy group on the absorption characteristics of nitroanilines can be evaluated by comparing gas-phase spectra and theoretical results on the methoxy nitroanilines with the corresponding experimental (1, 3) and theoretical figures in the isomeric nitroanilines and nitroanisoles. The assignment of the electronic transitions in the *p*-nitroaniline reported in ref. 3 differs from that recently reported by Khalil *et al.* (10), based on CNDO/S-CI calculations. The disagreement is mainly due to the fact that we did not observe in the vapour spectrum of the *p*-nitroaniline a distinct band at 277 nm in hydrocarbon solutions, so that this band was not considered in our calculations.

2-Methoxy-4-nitroaniline

The first low-energy intense absorption band occurs at 3.87 eV; the corresponding band in the *p*-nitroaniline lies at 4.24 eV. This bathochromic shift, as well as the band intensity, is correctly predicted by the calculations. As found in the *p*-nitroaniline, the associated electronic transition is essentially CT (benzene → acceptor) in nature with an appreciable contribution of charge-transfer from the donor (NH_2) to the acceptor (NO_2) group.

However, the CT character is somewhat smaller than in *p*-nitroaniline. These results are in agreement

TABLE 1. Solvent shifts and dipole moment changes, $\mu_e - \mu_g$, in methoxy nitroanilines

Compound	ν_{gas} (cm^{-1})	ν_{CE} (cm^{-1})	μ_g[a] (D)	$\Delta\mu$ (D)
2-Methoxy-4-nitroaniline	31 213	28 955	6.9	4.4, 7.2[b]
p-Nitroaniline				10.1[b,c,d]
2-Methoxy-5-nitroaniline	30 406	28 632	5.4	4.2, 5.4[b]
m-Nitroaniline				6.3[b,c], 7.5[b,d]
4-Methoxy-2-nitroaniline	25 648	24 277	4.3	3.9, 4.3[b]
o-Nitroaniline				5.5[b,d]

[a]Determined in benzene solution by the Halverstadt and Kumler method (J. Am. Chem. Soc. 64, 2988 (1942)).
[b]Evaluated by means of Suppan's equation.
[c]Reference 2.
[d]Reference 5.

with the solvent-shift data and with the relative $\Delta\mu$ values. The second band appears as a shoulder of the first band on the high-energy side at ~4.20 eV. The second transition is calculated at 4.27–4.16 eV (MIM–PPP) and is predicted as less intense than the first transition; it is a benzene locally excited Λ_1 in nature with little contribution of CT_2^A and CT_D^3 states. The composition and intensity of this transition is similar to that found for the first computed transition in *p*-nitroaniline and *p*-nitroanisole (3). The band at 4.20 eV probably includes the first observed band at ~4.08 eV in the *p*-nitroanisole and the first transition at 4.38–4.23 eV in the *p*-nitroaniline. The high energy spectrum shows crowded bands, which are not easily correlated with the corresponding bands in the disubstituted compounds.

2-Methoxy-5-nitroaniline

The first band of 2-methoxy-5-nitroaniline, found at 3.77 eV, corresponds in position and composition to the first band of the *m*-nitroaniline at 3.80 eV, very little bathochromically shifted. The band intensity is higher than in *m*-nitroaniline and this is correctly predicted by the calculations. The corresponding electronic transition is computed at 4.12–3.83 eV (MIM–PPP). The MIM calculations attribute to this band an essentially Λ (benzene) character, while PPP calculations state it to be a mixture of Λ and CT states. A similar result was found for the first electronic transition in *m*-nitroaniline (3). CNDO/S-CI calculations on *m*-nitroaniline (10) indicate a considerable CT nature of this transition. The solvent-shift and $\Delta\mu$ values point to a CT character of the band. The second band shows a maximum at 4.48 eV and a shoulder (not evident in the solution spectrum) at ~4.40 eV. This band could originate from the superposition of the band at 4.57 eV in the *p*-nitroanisole and the band at ~4.96 eV in the *m*-nitroaniline. In this spectral region one transition is computed at 4.45–4.40 eV (MIM–PPP) which is CT_1^A in nature as in the corresponding disubstituted compounds. The two computed transitions at ~5.10 eV and 5.50 eV have a CT_2^A and prevailing Λ (benzene)

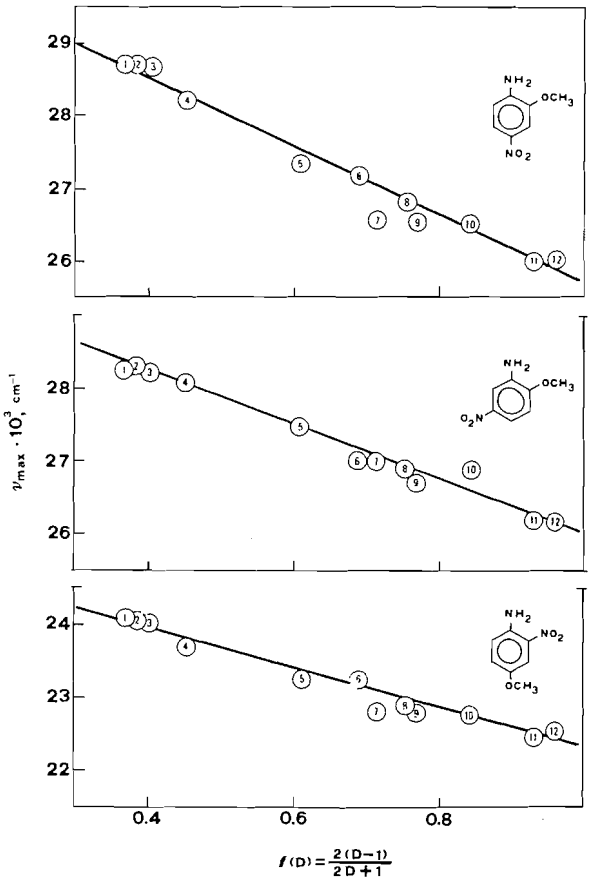

FIG. 3. Solvent shift in methoxy nitroanilines. Solvents: (1) *n*-hexane; (2) isooctane; (3) cyclohexane; (4) carbon tetrachloride; (5) trichloroethylene; (6) ether; (7) chloroform; (8) chlorobenzene; (9) ethylacetate; (10) methylene chloride; (11) methylethylketone; (12) acetonitrile.

character respectively; accordingly the first band at 5.23 eV shows a noticeable solvent shift, while the second band at 5.51 eV is much less solvent dependent. These two bands can be correlated with the CT band at 5.63 eV in *m*-nitroaniline and with the Λ (benzene) band at 5.82 eV in *p*-nitroanisole.

TABLE 2. Electronic transitions in the studied compounds

State	ΔE (eV) MIM	PPP	Exp[a]	*f* MIM	PPP	Exp[b]	Dominating[c] configurations (%)
			2-Methoxy-4-nitroaniline				
Ψ_1	4.44	3.99	3.59–3.87	0.17	0.34	0.23	(10–8)Λ_2, (68–25)T_1^A, (7–9)T_D^A
Ψ_2	4.27	4.16	4.13sh–4.20sh	0.01	0.10	(3.57)	(76–34)Λ_1, (12–6)T_2^A, (4–12)T_D^3
Ψ_3	5.21	5.21	4.96–5.27	0.08	0.24	(3.84)	(14–11)Λ_3, (67–36)T_2^A, (5–12)T_D^3
Ψ_4	5.42	5.62	5.12–5.39	0.03	0.03	(3.86)	(54–26)Λ_2, (14–11)T_1^A, (20–16)T_D^4
			2-Methoxy-5-nitroaniline				
Ψ_1	4.18	3.83	3.55–3.77	0.03	0.12	0.09	(61–19)Λ_1, (19–18)T_2^A, (3–13)T_D^A
Ψ_2	4.55	4.40	4.29–4.48	0.09	0.14	0.10	(15–14)Λ_1, (14–12)Λ_2, (58–29)T_1^A
Ψ_3	5.13	5.11	4.96–5.23	0.07	0.44	0.28	(14–11)Λ_1, (63–18)T_2^A
Ψ_4	5.45	5.51	5.56–5.51sh	0.13	0.13	0.26	(48–20)Λ_2, (17–4)T_1^A, (11–9)T_D^3
			4-Methoxy-2-nitroaniline				
Ψ_1	3.84	3.26	3.01–3.18	0.03	0.16	0.09	(23–8)Λ_1, (40–14)T_2^A, (14–25)T_D^A
Ψ_2	4.62	4.41	4.59sh–4.59sh	0	0.02	0.07	(57–25)Λ_1, (2–10)Λ_2, (9–12)T_1^A (15–3)T_2^A
Ψ_3	5.08	5.15	4.96sh–5.06sh	0.06	0.25	(3.81)	(1–12)Λ_1, (32–5)Λ_2, (35–15)T_1^A (20–19)T_2^A
Ψ_4	5.31	5.32	5.44–5.46	0.45	0.27	0.40	(21–17)Λ_2, (12–4)Λ_3, (30–1)T_1^A (13–16)T_D^3

[a]The first value refers to cyclohexane solution, the second to vapour phase (sh = shoulder).
[b]Values in parentheses are log ε.
[c]Λ = locally excited state; T = charge transfer state (A = NO_2, D = NH_2). (The numbers in parentheses refer to MIM and PPP calculations respectively; PPP figures come from a configuration analysis.)

4-Methoxy-2-nitroaniline

The first computed transition in the 4-methoxy-2-nitroaniline lies at 3.84–3.26 eV (MIM–PPP); it has a CT character with a fair contribution of the Λ_1 (benzene) state. This composition corresponds to that of the first transition in the *o*-nitroaniline computed at 3.87 eV (6). Accordingly the first band at 3.18 eV corresponds to the band at 3.49 eV in the *o*-nitroaniline bathochromically shifted. The solvent shift of this band, 1500 cm^{-1}, is the smallest among those observed in the methoxy nitroanilines, in agreement with the computed composition of the first transition in these compounds.

The second computed transition lies at 4.62–4.41 eV (MIM–PPP) and is a mixture of CT and Λ (benzene) states. The second band is found as a shoulder at ~4.59 eV. The third transition, again a mixture of CT and Λ (benzene) states, is computed to lie at 5.08–5.15 eV (MIM–PPP); it is predicted to be more intense than the previous transition. The third band is found also as a shoulder at ~4.96 eV. The latter two bands correspond to the band at 4.77 eV in *o*-nitroaniline and to the band at 4.92 eV in the *m*-nitroaniline respectively. This correlation is supported by the relative band intensity and composition; however, their relative positions are uncertain. The fourth computed transition at 5.31 eV results from a mixture of Λ (benzene) and CT states and is predicted to be intense (f = 0.45–0.27) (MIM–PPP). This transition can be associated with the intense band (f = 0.40) at 5.46 eV, and correlated to the Ψ_4 in *o*-nitroaniline and *m*-nitroanisole, which show comparable intensity and composition.

Conclusions

The spectra of the studied methoxy nitroanilines can be correlated with the spectra of the corresponding disubstituted compounds by using as a criterion of comparison the nature, energy, and intensity of the electronic transition of the associated experimental band, and the solvent shift of the band. The main effect (inductive) of the methoxy group on the absorption features of the isomeric nitroanilines is related to the lowering of the energy of CT configurations of the nitro group. In particular, as refers to the first absorption band of methoxy nitroanilines, we may summarize the effect of the OCH_3 group as follows.

(*i*) The first band in the spectrum is bathochromically shifted by about 30 nm with respect to the corresponding nitroanilines, with the exception of 2-methoxy-5-nitroaniline where a very small shift is observed. In this compound the enhancement in the band intensity with respect to the *m*-nitroaniline is remarkable.

(*ii*) The $\nu_{gas} - \nu_{CE}$ shift is generally smaller than in the corresponding nitroanilines, suggesting a smaller polarizability of the first excited state in methoxy nitroanilines than in nitroanilines; accordingly the calculated $\Delta\mu$ values in the methoxy nitroanilines are smaller than in the corresponding nitroanilines (Table 1). Moreover, the relative order

of $\Delta\mu$ is the same as in the nitroanilines, where $\Delta\mu$(*p*-nitroaniline) > $\Delta\mu$(*m*-nitroaniline) > $\Delta\mu$(*o*-nitroaniline) (5).

(*iii*) The contributions of CT configurations to the first electronic transition are smaller in methoxy nitroanilines than in the corresponding nitroanilines, in agreement with the above solvent shift results.

By comparing experimental and theoretical results it appears that MIM and PPP calculations correctly predict the observed band shift on passing from the isomeric nitroanilines to the corresponding methoxy nitroanilines; they also correctly predict the relative order of the lowest transition energy in these compounds.

Acknowledgements

This work was partially supported by Consiglio Nazionale delle Ricerche, Italy.

1. S. Millefiori, G. Favini, A. Millefiori, and D. Grasso. Spectrochim. Acta, Part A, **33**, 21 (1977).
2. S. Millefiori, F. Zuccarello, and G. Buemi. J. Chem. Soc. Perkin Trans. II, 849 (1978).
3. F. Zuccarello, S. Millefiori, and G. Buemi. Spectrochim. Acta, Part A, **35**, 223 (1979).
4. G. Favini, A. Gamba, D. Grasso, and S. Millefiori. Trans. Faraday Soc. **67**, 3139 (1971).
5. M. B. Ledger and P. Suppan. Spectrochim. Acta, Part A, **23**, 641 (1967).
6. M. Godfrey and J. N. Murrell. Proc. R. Soc. London, Ser. A, **278**, 71 (1964).
7. G. Favini, A. Gamba, and I. R. Bellobono. Spectrochim. Acta, Part A, **23**, 89 (1967).
8. B. Roos and P. N. Skancke. Acta Chem. Scand. **21**, 233 (1967).
9. H. Baba, S. Suzuki, and T. Takemura. J. Chem. Phys. **50**, 2078 (1969).
10. O. S. Khalil, C. J. Seliskar, and S. P. McGlynn. J. Mol. Spectrosc. **70**, 74 (1978).

Sterically hindered aromatic compounds. IX. Electron spin resonance and product studies of the dediazoniation reaction

L. Ross C. Barclay, Alexander G. Briggs, William E. Briggs, Julian M. Dust, and Jean A. Gray

Department of Chemistry, Mount Allison University, Sackville, N.B., Canada E0A 3C0

Received February 23, 1979

L. Ross C. Barclay, Alexander G. Briggs, William E. Briggs, Julian M. Dust, and Jean A. Gray. Can. J. Chem. 57, 2172 (1979).

An esr study of the dediazoniation of 2,4,6-tri-*tert*-butylaniline with butyl nitrite in methylene chloride indicated the formation of the 2,4,6-tri-*tert*-butylphenyl radical which was spin trapped by the butyl nitrite. The persistent 2,4,6-tri-*tert*-butylphenoxy radical was also formed. Product studies from reactions catalyzed by pivalic acid indicate a novel rearrangement of an *ortho-tert*-butyl group under dediazoniation conditions forming such products as: 3-(3,5-di-*tert*-butylphenyl)-2-methylpropene (**4**), 1-(3,5-di-*tert*-butylphenyl)-2-methylpropene (**5**), 3-(3,5-di-*tert*-butylphenyl)-2-methyl-2-propanol (**6**), 3-(3,5-di-*tert*-butylphenyl)-2-butoxy-2-methylpropane (**7**), 3-(3,5-di-*tert*-butylphenyl)-2-methyl-2-trimethylacetoxypropane (**8**), 2,4,6-tri-*tert*-butylphenyl trimethylacetate (**9**), and 2,4,6-tri-*tert*-butyl-1,4-quinol (**10**). The major products (**4**–**7**) are accounted for by a free radical pathway by rearrangement of the 2,4,6-tri-*tert*-butylphenyl radical. The minor products (esters **8** and **9**) probably form by competing ionic reactions. *N*-Nitroso-2,4,6-tri-*tert*-butylacetanilide decomposes (at least in part) by a radical pathway leading to the rearranged radical $(CH_3)_2\dot{C}CH_2$—Ar which was spin trapped by the nitroso group of the substrate. Spin trapping experiments during the dediazoniation of 2,5-di-*tert*-butylaniline similarly gave evidence for the formation of aryl radicals.

L. Ross C. Barclay, Alexander G. Briggs, William E. Briggs, Julian M. Dust et Jean A. Gray. Can. J. Chem. 57, 2172 (1979).

Une étude rpe de la dédiazotation de la tri-*tert*-butyl-2,4,6 aniline avec le nitrite de butyle en solution dans le chlorure de méthyle indique qu'il y a formation du radical tri-*tert*-butyl-2,4,6 phényle dont le spin est piégé par le nitrile de butyle. Il y a aussi formation du radical tri-*tert*-butyl-2,4,6 phénoxyle. Une étude des produits formés lors de réactions catalysées par l'acide pivalique indique qu'il se produit, dans les conditions de dédiazotation, une nouvelle transposition d'un groupe ortho *tert*-butyle conduisant à la formation des produits suivants: (di-*tert*-butyl-3,5 phényl)-3 méthyl-2 propène (**4**), (di-*tert*-butyl-3,5 phényl)-1 méthyl-2 propène (**5**), (di-*tert*-butyl-3,5 phényl)-3 méthyl-2 propanol-2 (**6**), (di-*tert*-butyl-3,5 phényl)-3 butoxy-2 méthyl-2 propane (**7**), (di-*tert*-butyl-3,5 phényl)-3 méthyl-2 triméthylacétoxy-2 propane (**8**), triméthylacétate de tri-*tert*-butylphényle-2,4,6 (**9**) et tri-*tert*-butyl-2,4,6 quinol-1,4 (**10**). On peut expliquer la formation des produits principaux (**4**–**7**) à l'aide du chemin réactionnel radicalaire impliquant une transposition du radical tri-*tert*-butyl-2,4,6 phényle. Les produits mineurs (esters **8** et **9**) se forment probablement par des réactions ioniques en compétition. Le *N*-nitroso tri-*tert*-butyl-2,4,6 acétanilide se décompose (au moins en partie) par un mécanisme radicalaire conduisant au radical transposé $(CH_3)_2\dot{C}CH_2$—Ar dont le spin est piégé par un groupe nitroso du substrat. Des expériences de piégeage de spin au cours de la dédiazotation de la di-*tert*-butyl-2,5 aniline fournissent des données relatives à la formation de radicaux aryles.

[Traduit par le journal]

Introduction

The aromatic dediazoniation reaction is receiving considerable attention by a number of investigators (1–7). In particular the role of reactive aryl intermediates, aryl cations, aryl radicals, and arynes, is frequently discussed. *Ortho-tert*-butyl-aryldiazonium salts, including the 2,4,6-tri-*tert*-butyldiazonium ion (**1**) (8), are known to be very unstable and this has been attributed to rapid formation of an aryl cation due to steric acceleration (7). There is substantial kinetic evidence for the formation of the aryl cation from benzenediazonium salts (1, 3) and this cation has been the subject of theoretical (9) and some recent experimental (esr) (10) study. On the other hand, aryl dediazoniations are capable of proceeding by either homolytic or heterolytic pathways (6, 7) and small changes in conditions, such as the addition of pyridine (11) or the presence of oxygen (12) appear to cause a changeover in mechanism. We have independently observed the 2,4,6-tri-*tert*-butylphenyl radical (**3**) directly in solution and followed its rearrangement (13). The known properties of this radical should aid in the discrimination between radical and ionic pathways for the reaction of **1**. In addition, formation of an aryne (via **2**) is blocked unless there is extrusion of a *tert*-butyl cation which would be de-

0008-4042/79/162172-08$01.00/0

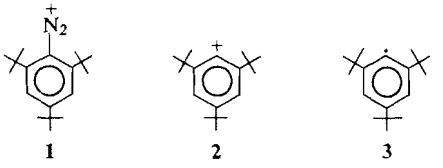

1 2 3

tected by product analysis. Such dealkylations may account for anomalies previously reported in the aqueous acid diazotizations of 2,4,6-tri-*tert*-butylaniline (14). We are investigating the unusual reactivity in dediazoniation of **1** and, with the above features in mind, have undertaken an exploratory study on the esr and product studies from **1**. Some comparative studies are also reported for the 2,5-di-*tert*-butylaryl system.

Results

Dediazoniation of 2,4,6-Tri-tert-*butylphenyldiazo Compounds*

(a) Electron Spin Resonance Studies

Treatment of 2,4,6-tri-*tert*-butylaniline with butyl nitrite and pivalic acid in methylene chloride (aprotic diazotization (15)) in the probe of the esr spectrometer at −40°C generated two sets of esr signals in 30–40 min (see Fig. 1). These became more intense as the temperature was raised through 0°C and the solution quickly became blue in color. The central part of the spectrum consisted of a very persistent 1:2:1 triplet of multiplets ($a^{H}(2H) \simeq 1.6$ G). This proved to be the well-known 2,4,6-tri-*tert*-butylphenoxy radical. The center triplet could be enhanced by injecting a sample of the latter prepared independently by lead dioxide oxidation of the phenol and observing the increase in the superimposed signals. The second radical *appeared* to be a 1:1:1 triplet (the centre portion only partially observed at higher gain due to the more intense signal of the above phenoxy radical) of 1:2:1 triplets ($a_N = 23.86$, $a_{H(2H)} = 2.80$, and $a_{H(2H\ meta)} = 0.75$ G, and $g = 2.00521$). This second radical is assigned to *n*-butoxy-2,4,6-tri-*tert*-butylphenylnitroxide

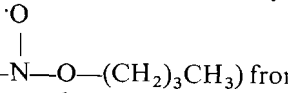

(Ar—N—O—$(CH_2)_3CH_3$) from its close relationship to the analogous ethoxy-2,4,6-tri-*tert*-butylphenylnitroxide radical

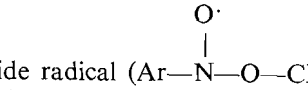

(Ar—N—O—CH_2CH_3, $a_N = 23.98$, $a_{H(2H)} = 2.52$, $a_{H(2H\ meta)} = 0.78$ G, and $g = 2.00528$) generated by spin trapping of ethoxy by photolysis of diethylperoxide in the presence of 2,4,6-tri-*tert*-butylnitrosobenzene. While this work was in progress, the pentoxyphenylnitroxide radical was reported (16) from the reaction of aniline with pentyl nitrite. This radical showed a nitrogen splitting (15.75 G) similar to other simple alkoxyphenylnitroxides (17). The interesting variation in the nitrogen splitting of our substituted alkoxyarylnitroxides ($a_N = 23.86$–23.98 G) contrasted with the $a_N = 15.75$ G for the phenyl case is attributed to the steric hindrance provided by two *ortho-tert*-butyl groups in our hindered nitroxides which force a non-coplanar conformation of the radical so that the a_N approaches the values found for alkylalkoxy nitroxides (17). This effect has been observed before in related aryl nitroxide radicals (18, 19).

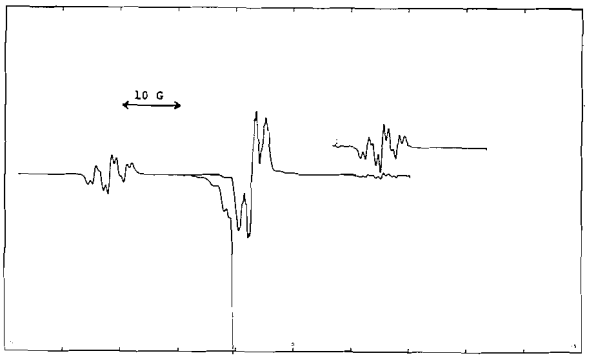

FIG. 1. Electron spin resonance spectrum from diazotization of 2,4,6-tri-*tert*-butylaniline with butyl nitrite and pivalic acid in methylene chloride at 0°C.

It was of interest to study the formation of these free radical species in the *absence* of pivalic acid when the overall reaction proceeded more slowly according to product studies (see (b) below). Under this condition, it was possible to readily observe the consecutive formation of the radicals, as illustrated in Fig. 2*a–d*. The first species observed was the tri-*tert*-butylphenoxy radical (Fig. 2*a*), followed by butoxy-2,4,6-tri-*tert*-butylphenylnitroxide (Fig. 2*b*, when the tri-*tert*-butylphenoxy radical was now hardly observable), then the tri-*tert*-butylphenoxy radical became more prominent as usual (Fig. 2*c*). Finally, on extended reaction time, it was still possible to observe the above two radicals plus a third very persistent species (Fig. 2*d*). This third radical has not been definitely characterized. Assuming that the central portion lies under the prominent tri-*tert*-butylphenoxy, it is estimated that there is a 1:1:1 triplet of 1:2:1 triplets where $a_N = 15.6$ G, $a_{H(2H,meta)} = 1.4$ G, and $g = 2.0058$. This suggests an aromatic nitroxide radical, possibly of the type

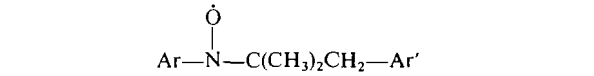

Ar—N—$C(CH_3)_2CH_2$—Ar′

(Ar = 2,4,6-tri-*tert*-butylphenyl, Ar′ = 3,5-di-*tert*-butylphenyl)

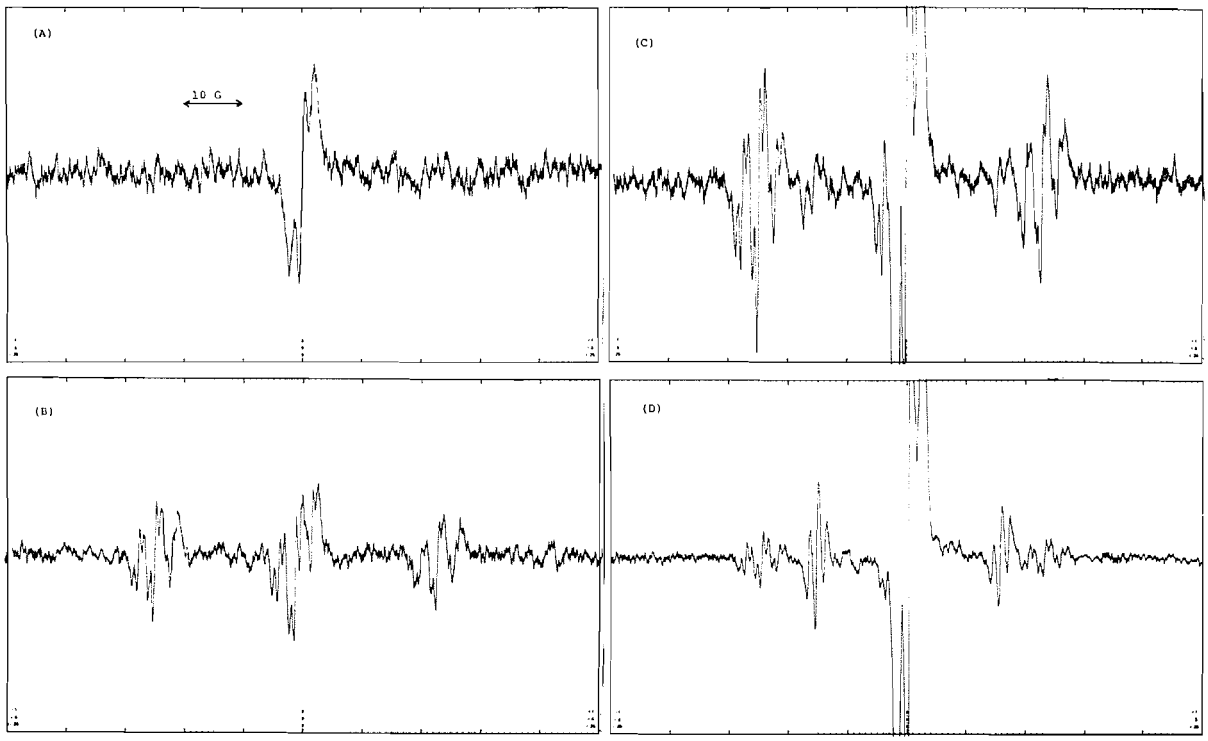

FIG. 2. Electron spin resonance spectra from diazotization of 2,4,6-tri-*tert*-butylaniline with butyl nitrite in methylene chloride at −10°C: (*a*) after 2½ h, appearance of 2,4,6-tri-*tert*-butylphenoxy (**12**); (*b*) after 3½ h, illustrating the butoxy-2,4,6-tri-*tert*-butylphenylnitroxide radical (**11**); (*c*) after 4½ h, showing the mixture of radicals **11** and **12**; (*d*) extended reaction time, showing the appearance of a third radical (triplets) between **11** and **12**.

Decomposition of *N*-nitroso-2,4,6-tri-*tert*-butylacetanilide[1] in methylene chloride in the esr spectrometer at room temperature or above (20–40°C) gave an esr spectrum consisting of a simple 1:1:1 triplet of 1:1:1 triplets without further additional fine structure (a_{N_α} = 13.84 and a_{N_β} = 3.26 G and g = 2.00616). The couplings and g value observed are indicative of a hydrazoxy radical (21) and the lack of additional coupling to hydrogen is suggestive of a radical of the type

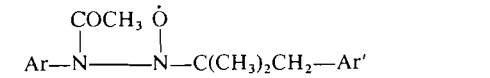

(Ar = 2,4,6-tri-*tert*-butylphenyl, Ar′ = 3,5-di-*tert*-butylphenyl)

formed by spin trapping by the starting nitroso compound of a radical generated in the system (see Discussion). There was no evidence for the tri-*tert*-butylphenoxy radical in this reaction.

(b) Product Studies

Butyl nitrite diazotization of 2,4,6-tri-*tert*-butylaniline, under similar conditions as the esr studies, yielded a complex mixture containing the hydrocarbons 3-(3,5-di-*tert*-butylphenyl)-2-methylpropene (**4**), 1-(3,5-di-*tert*-butylphenyl)-2-methylpropene (**5**), the alcohol 3-(3,5-di-*tert*-butylphenyl)-2-methyl-2-propanol (**6**), the ether 3-(3,5-di-*tert*-butylphenyl)-2-butoxy-2-methylpropane (**7**), the esters 3-(3,5-di-*tert*-butylphenyl)-2-methyl-2-trimethylacetoxypropane (**8**) and 2,4,6-tri-*tert*-butylphenyl trimethylacetate (**9**), and the 2,4,6-tri-*tert*-butyl-1,4-quinol (**10**) (see Table 1).

The hydrocarbons **4** and **5** were identified by their nmr spectra (see Experimental), by the ready acid-catalyzed isomerization of **4** to **5**, and by the oxidation of **5** to the known 3,5-di-*tert*-butylbenzoic acid. The alcohol **6** gave the expected spectroscopic data and it readily underwent dehydration to yield **5**. The ether **7** gave a complex ^{1}Hmr spectrum due to the overlap of the *n*-butyl resonances with those of the other alkyl hydrogens. The structure was determined from its ^{13}C n.m.r. spectrum and the fact that it underwent partial decomposition under glc conditions to yield some **4**, **5**, and *n*-butyl alcohol. The ester **8** was identified from its spectroscopic properties and it also underwent some decomposition on the glc to yield

[1]Such compounds were reported (20) to be too unstable to isolate in pure form. However, we were able to purify this compound by tlc suitable for analytical and spectroscopic data. Product analyses from this decomposition will be reported separately.

TABLE 1. Products from diazotization of 2,4,6-tri-*tert*-butylaniline

Compound	% yields			
	Run 1 (Air)[a]	Run 2 (Air)[b]	Run 3 (N_2)[c]	Run 4 (O_2)[c]
Hydrocarbon **4**	24.3[d]	19.0	22.4	26.6
Hydrocarbon **5**	—	7.4	6.1	7.3
Alcohol **6**	29.2	36.1	32.7	35.6
Ether **7**	21.6	24.6	19.2	16.7
Ester **8**	7.5	8.5	7.8	8.9
Ester **9**	1.6	2.6	—	—
Quinol **10**	2.9	—	2.6	3.4
Totals	87.1	98.2	90.8	98.5

[a]Products were separated by column chromatography on alumina and further purified by tlc.
[b]Relative percentages, determined by glc.
[c]Products were separated by tlc and the percentages of 4 and 5 estimated by nmr.
[d]This value is for 4 and 5.

the hydrocarbons **4** and **5**. The ester **9** gave the expected spectroscopic data and unlike **8** was stable under various glc conditions. A minor product, the quinol **10**, was identified as 2,4,6-tri-*tert*-butyl-4-hydroxy-2,5-cyclohexadien-1-one by its nmr spectrum and by comparison with properties given in the literature. The various compounds **4**–**10** were formed when the reaction was carried out in air, or in a nitrogen or oxygen atmosphere. Furthermore, the percent yields of the various compounds identified remained approximately the same under these conditions (see Table 1). The reaction was also observed directly in the nmr probe whereby the formation of the major components (**4**–**7**) could be observed qualitatively. A comparative small scale (nmr) run was also carried out with triethylsilane added. The latter has been used in methylene chloride as a trap for carbonium ions (22, 23). The same major components were observed (nmr) to form with and without added triethylsilane and the product analyses

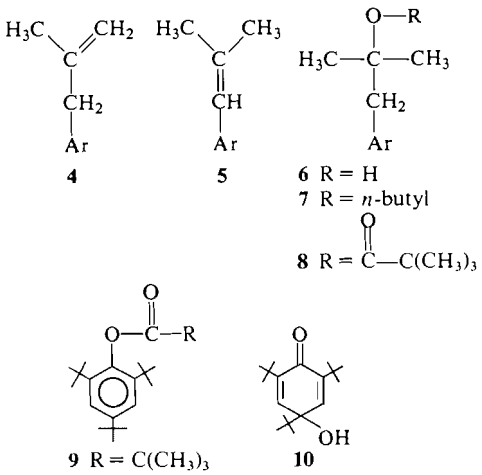

(glc) were also similar. In the absence of pivalic acid, the conversion to these products at temperatures below 0°C was extremely slow and estimated (nmr) to be less than 50% after 6 days. After an additional 2 days at room temperature, this reaction was 82% complete (based on recovered amine). This reaction mixture also contained the hydrocarbons **4** and **5**, the alcohol **6**, the ether **7**, and traces of the quinol **10**.

*Aprotic Diazotization of 2,5-Di-*tert*-butylaniline*

The aprotic diazotization of 2,5-di-*tert*-butylaniline leads to arynoid adducts in the presence of furan (15) and it has been proposed (7, 15) that this is a case of rapid formation of an *ortho-tert*-butylaryl carbonium ion through steric acceleration of dediazoniation. We reinvestigated this reaction to determine if aryl radicals could be trapped. Using 2,5-di-*tert*-butylnitrosobenzene as a trap at room temperature, this reaction did indeed produce a very persistent esr signal consisting of a triplet (1:1:1) of multiplets assigned to the Ar_2N—Ȯ radical (24) (Ar = 2,5-di-*tert*-butylphenyl) (a_N = 11.0 and $a_H \simeq$ 0.5–1 G and g = 2.00579). With tetraphenylcyclopentadienone (tetracyclone) as a trap in this reaction, we observed a very persistent radical (stable for days at room temperature) consisting of a complex 16-line pattern (g = 2.00302) almost superimposable on the radical formed in a similar way by addition of a phenyl radical to position 2 of tetracyclone (g = 2.0032) (2).

Discussion

The following conclusions are derived from these dediazoniations studied to date.

1. The aprotic diazotizations of the aromatic amines, aniline, 2,5-di-*tert*-butylaniline, and 2,4,6-tri-*tert*-butylaniline, with butyl nitrite gave evidence for aryl radicals in solution. With the first two amines, the aryl radicals were trapped with tetracyclone. The 2,5-di-*tert*-butylaryl radical was also spin trapped with 2,5-di-*tert*-butylnitrosobenzene.

In the case of 2,4,6-tri-*tert*-butylaniline, the derived aryl radical (**3**) was trapped by the butyl nitrite used to form the *n*-butoxy-2,4,6-tri-*tert*-butylphenylnitroxide radical (**11**). The formation of the 2,4,6-tri-*tert*-butylphenoxy radical (**12**) in carefully degassed solutions, at the same time or preceding the formation of **11**, can be accounted for by some spin trapping of **3** at the oxygen of butyl nitrite (Scheme 1). Steric effects are known to cause spin trapping at oxygen of a nitroso group, for example, in the case of 2,4,6-tri-*tert*-butylnitrosobenzene (25). Alternatively **12** could form by hydrogen atom transfer from the corresponding phenol. The latter could form from the combination of the aryl radical (**3**) with hydroxy radical (Scheme 2, (*v*)).

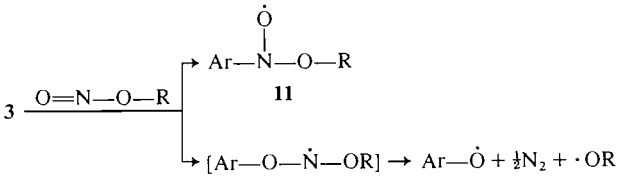

SCHEME 1

2. Decomposition of *N*-nitroso-2,4-6-tri-*tert*-butylacetanilide gave a radical apparently formed by spin trapping of the rearranged radical $Ar'—CH_2—\dot{C}(CH_3)_2$ (**15**, Scheme 2) by the nitroso group of the substrate.

3. The unusual hydrocarbon products **4** and **5** from the butyl nitrite diazotization of 2,4,6-tri-*tert*-butylaniline can be accounted for by a free radical pathway as outlined in Scheme 2. Steps (*i*)–(*iii*) follow the generally accepted (7, 26) Rüchardt mechanism (27) for the formation of aryl radicals by homolytic decomposition of an unstable diazoanhydride intermediate. Although the rather elusive aryl diazotate radical (i.e., **13** in Scheme 2) reported by Cadogan (28) was questioned on the basis of nuclear polarization studies (29), more recent evidence (30) points to its important role in the generation of aryl radicals and related radical reactions. The rearrangements in step (*iv*) (**3** → **14** → **15**) are consistent with the observed behavior of the aryl radical **3** generated independently (13).

4. There are several possibilities for the formation of the oxygenated products. For example, the major oxygen-containing products, the alcohol **6** and the ether **7**, could be formed by free radical combinations of **15** with hydroxy radical and butoxy radical as shown in steps (*v*) and (*vi*). Other speculations include the oxygenation of **15** by **13** (step *vii*) (and analogously of **3** by **13** leading to the stable radical **12**). Furthermore, the trapped radical **11** could be a source of alkoxy radicals via the reported (16) decomposition route $Ar—\overset{\dot{O}}{\underset{|}{N}}—O—R \rightarrow Ar—NO + \cdot OR$. The quinol **10**, a minor product, probably results from hydroxylation of **12** at the *para* position (31) (step (*viii*)), although we cannot rule out oxygenation of **12** by **13** followed by hydrogen abstraction or even air oxidation of **12** during work-up (32).

5. The esters **8** and **9** most probably form in com-

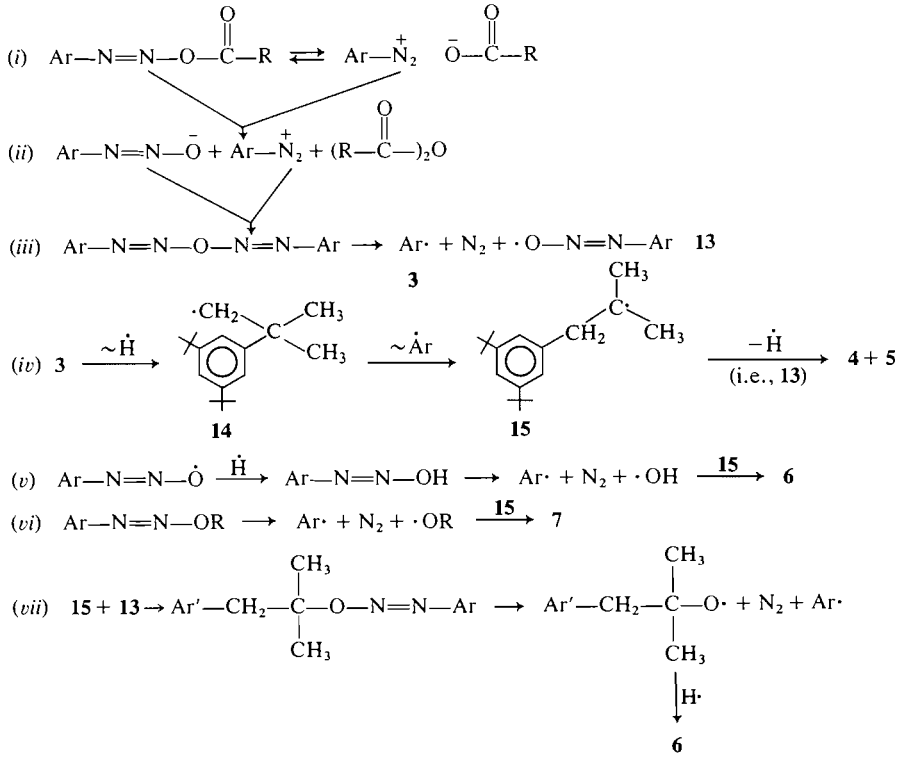

Ar = 2,4,6-tri-*tert*-butylphenyl, Ar′ = 3,5-di-*tert*-butylphenyl

SCHEME 2

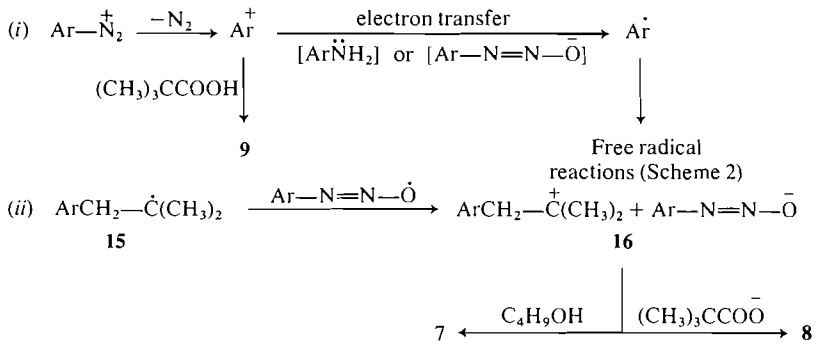

SCHEME 3

peting polar side reactions. The ester **8** is *not* a result of secondary reactions. We found that neither the hydrocarbons (**4** and **5**) nor the alcohol **6** react with pivalic acid or pivalic anhydride under these conditions to give this ester. Thus the formation of **8** and **9** is a strong indication of a competing carbonium ion type reaction. We further speculate that such aryl cationic and free radical reactions may be directly related by electron transfer processes (i.e., step (*i*), Scheme 3). The other oxygen-containing products, such as the alcohol **6** and ether **7**, could also result from ionic reactions on the cation **16** in contrast to the free radical steps (*v*) and (*vi*) suggested in Scheme 3. The cation **16** could result from electron transfer to the aryl diazotate radical (step (*ii*), Scheme 3). A somewhat similar electron transfer from a carbon radical to phenyl diazotate has recently been postulated (30).

6. There was no evidence for the formation of products from a substituted benzyne by the elimination of an *ortho-tert*-butyl from the 2,4,6-tri-*tert*-butylphenyl cation (**2**).

Experimental

The procedures for spectroscopic and chromatographic analyses given earlier (33) were followed unless otherwise stated herein.

Materials

2,4,6-Tri-*tert*-butylaniline was prepared by reduction of the nitro compound with sodium amalgam (34). 2,5-Di-*tert*-butylaniline was best prepared by the catalytic hydrogenation procedure (34). These amines were purified by column chromatography on acidic alumina by elution with petroleum ether–benzene mixtures. The butyl nitrite, pivalic acid, and solvents used were all freshly distilled. The tetracyclone used was commercial material (Eastman). 2,5-Di-*tert*-butylnitroso- and 2,4,6-tri-*tert*-butylnitrosobenzene were described earlier (33). *N*-Nitroso-2,4,6-tri-*tert*-butylacetanilide, prepared by nitrosation of the anilide (mp 273°C) with nitrosyl chloride, was purified by preparative tlc using chloroform solvent, the solvent removed under reduced pressure and the product analyzed without further purification or drying. It melted at 121°C, showed ir (CCl_4) bands at 1750 (C=O) and 1375 (—N=O) cm^{-1}, and nmr bands at δ: 1.12 (s, 18H, 2 × $(CH_3)_3C$—), 1.30 (s, 9H, $(CH_3)_3C$—), 2.80 (s, 3H, CH_3CO), and 7.40 (s, 2H, aryl). *Anal.* calcd. for $C_{20}H_{32}N_2O_2$: C 72.24, H 9.70, N 8.43; found: C 71.63, H 9.75, N 8.56.

Electron Spin Resonance Studies

Electron spin resonance spectra were measured on a Varian E-3 spectrometer or where noted[2] on a Varian E-104A spectrometer. The diazotizations of the amines were carried out in an esr reactor tube equipped with a glass capillary inlet and outlet for purging with dry oxygen-free nitrogen and a third side arm for injecting reactants through a septum. In a typical run, a solution of the amine (0.11 mmol) and pivalic acid (0.14 mmol) in 0.5 mL of methylene chloride was thoroughly purged with nitrogen. The tube was cooled to −40°C in the esr probe, then butyl nitrite (0.11 mmol) in an equal volume of methylene chloride was injected through the septum while the reaction solution was mixed with the inlet nitrogen. The temperature was slowly raised to 0°C while spectra were determined. The same procedure was used in runs without pivalic acid and typical spectra are illustrated in Figs. 1 and 2. Such spectra were also obtained[2] during the diazotization of 2,4,6-tri-*tert*-butylaniline when the solutions were carefully degassed under high vacuum by alternately freezing and thawing. Experiments with radical traps (2,5-di-*tert*-butylnitrosobenzene or tetracyclone) were carried out by mixing equimolar amounts of the amine and the trap before the addition of butyl nitrite as above. The ethoxy-2,4,6-tri-*tert*-butylphenylnitroxide radical was generated by ultraviolet irradiation of a solution of diethylperoxide and 2,4,6-tri-*tert*-butylnitrosobenzene in pentane at −40°C in the esr spectrometer.[2] The *g* values were measured relative to that of tetracene in sulfuric acid, $g = 2.002604$ (35).

Product Analysis

The preparative scale reaction on 2,4,6-tri-*tert*-butylaniline was carried out by adding a solution of the amine (10.6 g, 0.0406 mol) and pivalic acid (5.30 g, 0.0473 mol) in 100 mL of methylene chloride over a 1 h period to a stirred solution of butylnitrite (5.90 g, 0.0573 mol) in 100 mL of methylene chloride kept at 0°C. The solution was kept cold overnight, then allowed to warm to room temperature. The reaction mixture was extracted with aqueous sodium hydroxide, water, dried over sodium sulfate, and the solvent distilled under reduced pressure. The residual oil (11.9 g) was chromatographed on a neutral alumina column by elution with petroleum ether followed by petroleum ether – ethyl ether. The first fraction contained the hydrocarbons **4** and **5**. Fraction 2 contained a mixture of the hydrocarbons with the ether **7** (mainly), fraction 3 contained the ether **7**, fraction 4 the ether mixed with the ester

[2]These studies were made in the laboratory of Dr. K. U. Ingold, Division of Chemistry, National Research Council of Canada, Ottawa, Ont.

8, fraction 5 was a mixture of the esters **8** and **9**, and fraction 6 contained the alcohol **6** mixed with the quinol **10**. The various compounds in the above chromatograph fractions 2–6 were further separated and purified by preparative tlc on silica gel that had been acid treated with 0.1 *m* HCl, with benzene eluent. The compounds eluted on tlc in the order hydrocarbons (**4** and **5**), ether (**7**), esters (**9** then **8**), quinol (**10**), and alcohol (**6**). The percentages of the various compounds are given in Table 1 (run 1).

Gas–liquid chromatographic analysis (8 ft × 1/4 in. column, 20% Carbowax on Chromosorb W at 175°C and helium at 30 cm^3/min) of the products from another run gave the results summarized in Table 1 (run 2). Gas–liquid chromatographic analysis of the purified (tlc) ether **7** showed that it undergoes partial decomposition into hydrocarbons **4** and **5** and *n*-butyl alcohol under these conditions. Similarly the ester **8** yielded some **4** and **5** under these conditions.

Product analyses from smaller scale runs (4 mmol) were carried out by preparative tlc directly after removal of solvent (Table 1, runs 3 and 4). On this scale we failed to detect the ester **9**. Details on the individual products are given below.

*3-(3,5-Di-*tert*-butylphenyl)-2-methylpropene (**4**) and 1-(3,5-Di-*tert*-butylphenyl)-2-methylpropene (**5**)*

The less stable nonconjugated hydrocarbon **4** predominated in the hydrocarbon fraction. Hydrocarbon **4** showed nmr bands at δ: 1.35 (s, 18H, 2 × $(CH_3)_3C$), 1.72 (t, $J \simeq 1$ Hz, 3H, $H_3C-\underset{|}{C}=C$), 3.40 (s, broad, 2H, benzylic—CH_2—), 4.89 (multiplet, 2H, C=CH_2), 7.23 (d, $J \simeq 2$ Hz, 2H, aryl H's 2 and 6), and 7.45 (t, $J \simeq 2$ Hz, 1H, aryl H 4). A sample of this hydrocarbon mixture (270 mg) (mainly **4**) was converted into **5** by refluxing for 30 min in benzene containing 22 mg of *p*-toluenesulfonic acid. Nuclear magnetic resonance analysis of the product showed that it was almost entirely the conjugated alkene **5**. The nmr spectrum of **5** showed bands at δ: 1.35 (s, 18H, 2 × $(CH_3)_3C$), 1.91 (d, $J \simeq 1$ Hz, 6H, $(CH_3)_2C=$), 6.49 (m, 1H, Ar—$\underset{|}{C}=\underset{\diagdown}{\overset{\diagup}{C}}$), 7.29 (d, $J \simeq 2$ Hz, 2H, aryl H's 2 and 6), and 7.46 (t, $J \simeq 2$ Hz, 1H, aryl H 4).

A sample of **5** (1.9 mmol) in 80% pyridine–water was oxidized overnight at room temperature by a mixture of potassium permanganate (37 mg) and periodic acid (4.7 g). One millilitre of this solution was distilled into a solution of 2,4-dinitrophenylhydrazine reagent. The precipitate was collected and chromatographed on neutral alumina by elution with benzene to yield yellow crystals, mp 126°C alone or mixed with authentic acetone 2,4-dinitrophenylhydrazone. The solution from the oxidation was evaporated to dryness, the residue extracted with ethyl ether, which in turn was extracted with aqueous sodium hydroxide. Acidification gave a colorless solid which after sublimation melted at 164°C. This proved to be 3,5-di-*tert*-butylbenzoic acid by mixture melting point and identical infrared spectra with an authentic sample of acid (mp 163–164°C) (36).

*1-(3,5-Di-*tert*-butylphenyl)-2-propanol (**6**)*

The alcohol **6**, purified by sublimation *in vacuo*, gave a mp of 83.5–84°C. It showed a strong band in the infrared at 3400 (—OH) cm^{-1} and nmr bands at δ: 1.15 (s, 6H, $(CH_3)_2\underset{|}{C}-O$), 1.30 (s, 18H, 2 × $(CH_3)_3C$—), 1.43 (s, exchanges with D_2O, 1H, OH), 2.67 (s, 2H, Ar—CH_2—), 6.94 (d, $J \simeq 2$ Hz, 2H, aryl H's 2 and 6), and 7.18 (t, $J \simeq 2$ Hz, 1H, aryl H 4). *Anal.* calcd. for $C_{18}H_{30}O$: C 82.38, H 11.52, Mol. Wt. 262; found: C 82.98, H 11.52, Mol. Wt. (mass spectrum *m/e* 262 M^+).

TABLE 2. The ^{13}Cmr spectrum of ether **7**[a]

Carbon	Chemical shift (decoupled)	Multiplicity (undecoupled)[b]
C-1 × 2	151.3	s
C-2	139.1	s
C-3 × 2	126.4	d
C-4	121.1	d
C-5	76.4	s
C-6	62.6	d
C-7	49.3	t
C-8 × 2	36.2	s
C-9	34.4	—[c]
C-10 × 6	33.5	q
C-11 × 2	26.8	q
C-12	21.0	t
C-13	15.5	q

[a] *Anal.* calcd. for $C_{22}H_{38}O$: C 83.02, H 11.95, Mol. Wt. 318; found: C 82.86, H 11.70, Mol. Wt. (mass spectrum *m/e* 318 M^+).
[b] Abbreviations: s, singlet; d, doublet; t, triplet; q, quartet.
[c] C-9 multiplet obscured under C's at 10.

The alcohol **6** (1.0 mmol) in 6 mL of benzene containing 26 mg of *p*-toluenesulfonic acid was heated under reflux for 2 h in an apparatus fitted with a (Stark) water trap. The solution was washed with aqueous sodium hydroxide, water, and dried over sodium sulfate. Evaporation of the benzene left a product which proved to be better than 96% of the alkene **5** according to glc and nmr analyses.

*1-(3,5-Di-*tert*-butylphenyl)-2-butoxy-2-methylpropane (**7**)*

The ether was isolated as a colorless oil. It gave a strong ir band at 1090 (C—O—C) cm^{-1} and nmr bands at δ: 1.36 (s, 18H, 2 × $(CH_3)_3\underset{|}{C}$—), 1.14 (s, 6H, $(CH_3)_2\underset{|}{C}-O$—), 0.84–1.64 (overlapping above bands) (complex multiplets, 7H, CH_3CH_2-CH_2—), 2.79 (s, 2H, Ar—CH_2—), 3.48 (t, 2H, —CH_2—O—), 7.24 (d, $J \simeq 2$ Hz, 2H, aryl H's 2 and 6), and 7.46 (t, $J \simeq 2$ Hz, 1H, aryl H 4).

The ^{13}Cmr spectrum of **7** measured in $CDCl_3$ on a Varian CFT-20 spectrometer gave a 13-line spectrum. The results are given in Table 2 in order of decreasing chemical shifts and assignments according to the arbitrary numbering of carbons given below:

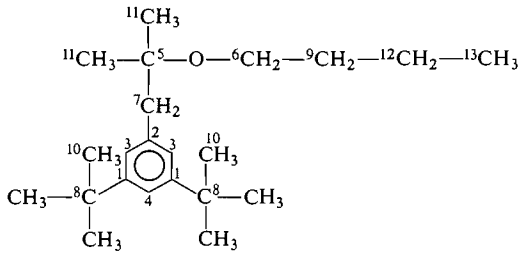

7

*3-(3,5-Di-*tert*-butylphenyl)-2-methyl-2-trimethylacetoxypropane (**8**)*

Sublimed **8** gave a mp of 43–46°C. The nmr spectrum had bands at δ: 1.15 (s, 9H, $(CH_3)_3COO$—), 1.37 (s, 18H, 2 × $(CH_3)_3\underset{|}{C}$—), 1.49 (s, 6H, $(CH_3)_2\underset{|}{C}-O$), 1.73 (s, 2H, Ar—$CH_2$—), 7.23 (d, $J \simeq 2$ Hz, 2H, aryl H's 2 and 6), and

7.49 (t, $J \simeq 2$ Hz, 1H, aryl H 4). A strong band in the ir spectrum appeared at 1735 (ester C=O) cm^{-1}. *Anal.* calcd. for $C_{23}H_{38}O_2$: C 79.71, H 11.05, O 9.23, Mol. Wt. 346; found: C 79.70, H 10.99, O 9.31, Mol. Wt. (mass spectrum *m/e* 346 M^+).

2,4,6-Tri-tert-*butylphenyl Trimethylacetate (**9**)*

Sublimed **9** gave a mp of 108–109°C. The nmr spectrum showed four singlets, δ: 1.38 (9H, *para*-$(CH_3)_3C$—), 1.40 (18H, 2-*ortho*-$(CH_3)_3C$—), 1.49 (9H, $(CH_3)_3C$—C(=O)—O), and 7.64 (2H, aryl H's). A strong band appeared in the ir spectrum at 1755 (ester C=O) cm^{-1}. *Anal.* calcd. for $C_{23}H_{38}O_2$: C 79.71, H 11.05, O 9.23, Mol. Wt. 346; found: C 79.77, H 11.00, O 9.30, Mol. Wt. (mass spectrum *m/e* 346 M^+).

2,4,6-Tri-tert-*butyl-1,4-quinol (**10**)*

Sublimed **10** melted at 132°C. The nmr spectrum had bands at δ: 1.00 (s, 9H, $(CH_3)_3C$—), 1.26 (s, 18H, 2 × $(CH_3)_3C$—), 2.05 (s, exchanges with D_2O, 1H, —OH), and 6.55 (s, 2H, H's at 3 and 5). The ir spectrum was in agreement with that given for **10** (mp 126–127°C) (37). There was not sufficient **10** for an elemental analysis.

Acknowledgements

Research grants provided by the National Research Council of Canada in support of this research are gratefully acknowledged. We are indebted to Drs. K. U. Ingold and D. Griller of the NRCC, Ottawa, for helpful discussions and the use of esr facilities.

1. R. G. Bergstrom, R. G. M. Landells, G. H. Wahl, and H. Zollinger. J. Am. Chem. Soc. **98**, 3301 (1976), and references therein.
2. E. A. Bell, J. I. G. Cadogan, P. W. Milburn, C. D. Murray, R. M. Paton, and J. T. Sharp. J. Chem. Soc. Perkin Trans. II, 558 (1976), and references therein.
3. C. G. Swain *et al.* J. Am. Chem. Soc. **97**, 783 (1975); **97**, 791 (1975); **97**, 796 (1975); **97**, 799 (1975).
4. G. A. Olah and J. Welch. J. Am. Chem. Soc. **97**, 208 (1975).
5. T. J. Broxton and D. L. Roper. J. Org. Chem. **41**, 2157 (1976).
6. H. Zollinger. Angew. Chem. **17**, 141 (1978).
7. J. I. G. Cadogan. Acc. Chem. Res. **4**, 186 (1971).
8. J. Rigaudy and J. C. Vernières. C. R. Acad. Sci. **261**, 5516 (1965).
9. J. D. Dill, P. v. R. Schleyer, and J. A. Pople. J. Am. Chem. Soc. **99**, 1 (1977).
10. A. Cox, T. J. Kemp, D. R. Payne, M. C. R. Symons, and P. P. de Moira. J. Am. Chem. Soc. **100**, 4779 (1978).
11. P. Burri, H. Loewenschuss, H. Zollinger, and G. K. Zowlinski. Helv. Chim. Acta, **57**, 395 (1974).
12. T. J. Broxton, J. F. Bunnett, and C. H. Paik. J. Org. Chem. **42**, 643 (1977).
13. G. Brunton, D. Griller, L. R. C. Barclay, and K. U. Ingold. J. Am. Chem. Soc. **98**, 6803 (1976).
14. A. Rieker and P. Niederer. Chem. Ber. **102**, 3947 (1969).
15. R. W. Franck and K. Yanagi. J. Am. Chem. Soc. **90**, 5814 (1968).
16. R. M. Paton and R. U. Weber. Org. Magn. Reson. **9**, 494 (1977); J. I. G. Cadogan, R. G. M. Landells, R. M. Paton, J. T. Sharp, and R. U. Weber. J. Chem. Res. (S), 108 (1977).
17. A. MacKor, T. A. J. W. Wajer, T. J. DeBoer, and J. D. W. vanVoorst. Tetrahedron Lett. 385 (1967).
18. D. J. Cowley and L. H. Sutcliffe. J. Chem. Soc. 569 (1970).
19. S. Terabe, K. Kuruma, and R. Konaka. J. Chem. Soc. Perkin Trans. II, 1252 (1973).
20. T. Koenig, J. A. Hoobler, C. E. Klopfenstein, G. Hedden, F. Sunderman, and B. R. Russell. J. Am. Chem. Soc. **96**, 4573 (1974).
21. V. Malatesta and K. U. Ingold. Tetrahedron Lett. 3311 (1973).
22. F. A. Carey and H. S. Tremper. J. Am. Chem. Soc. **90**, 2578 (1968).
23. L. R. C. Barclay, H. R. Sonawane, and M. C. MacDonald. Can. J. Chem. **50**, 281 (1972).
24. L. R. C. Barclay, D. L. Carson, J. A. Gray, M. Grossman, P. G. Khazanie, J. R. Milton, and C. E. Scott. Can. J. Chem. **56**, 2665 (1978).
25. S. Terabe and R. Konaka. J. Chem. Soc. Perkin Trans II, 369 (1973).
26. H. Loewenschuss, G. H. Wahl, and H. Zollinger. Helv. Chim. Acta, **59**, 1438 (1976).
27. C. Rüchardt and B. Freudenbert. Tetrahedron Lett. 3623 (1964); C. Rüchardt and C. C. Tan. Chem. Ber. **103**, 1774 (1970).
28. J. I. G. Cadogan, R. M. Paton, and C. Thomson. Chem. Commun. 614 (1969); J. Chem. Soc. B, 583 (1971).
29. E. Lippmaa, T. Pehk, T. Saluvere, and M. Mägi. Org. Magn. Reson. **5**, 441 (1971).
30. J. I. G. Cadogan, J. Cook, R. G. M. Landells, and J. T. Sharp. J. Chem. Soc. Perkin Trans I, 1835 (1977).
31. E. R. Altwicker. Chem. Rev. **67**, 475 (1967).
32. T. Matsuura, K. Watanabe, and A. Nishinaga. Chem. Commun. 163 (1970).
33. L. R. C. Barclay, P. G. Khazanie, K. A. H. Adams, and E. Reid. Can. J. Chem. **55**, 3273 (1977).
34. J. Burgers, M. A. Hoefnagel, P. E. Verkade, H. Visser, and B. M. Wepster. Recl. Trav. Chim. **77**, 491 (1958).
35. B. G. Segal, M. Kaplan, and G. K. Kraenkel. J. Chem. Phys. **43**, 4191 (1965).
36. W. van Hartingsveldt, P. E. Verkade, and B. M. Wepster. Recl. Trav. Chim. **75**, 349 (1956).
37. Sadtler Standard Spectra. Sadtler Research Laboratories, Inc., No. 12085K.

The reaction of benzeneselenenyl thiocyanate with *E*- and *Z*-1-phenylpropene: evidence for anomalous stereospecific *syn* addition

DENNIS G. GARRATT

Department of Chemistry, University of Ottawa, Ottawa, Ont., Canada K1N 9B4

Received February 23, 1979

DENNIS G. GARRATT. Can. J. Chem. 57, 2180 (1979).

The reaction of benzeneselenenyl thiocyanate with *E*- and *Z*-1-phenylpropene has been shown to give products under conditions of kinetic control of *net* stereospecific *syn* addition in the Markownikoff orientation. Furthermore, the reactions were highly specific in that a thiocyanato adduct was formed exclusively from the *Z*-isomer, whereas an isothiocyanato adduct was formed exclusively from the *E*-isomer.

DENNIS G. GARRATT. Can. J. Chem. 57, 2180 (1979).

On a montré que la réaction du thiocyanate de benzènesélénényle avec les phényl-1 propènes *E* et *Z* conduit, dans des conditions de contrôle cinétique, à des produits impliquant une addition stéréospécifique *nette* qui est *syn* dans une orientation Markownikoff. De plus, les réactions sont très spécifiques; en effet il se forme exclusivement un adduit thiocyanate à partir de l'isomère *Z* alors qu'il se forme uniquement un adduit isothiocyanate à partir de l'isomère *E*.

[Traduit par le journal]

The chemistry of organylselenenic acid derivatives, such as areneselenenyl halides and acetates, has been the subject of numerous studies during the last few years. Electrophilic additions of these species to carbon–carbon double and triple bonds have attracted considerable interest (for general reviews see refs. 1*a–c*; 2). Few mechanistic studies have, however, been reported in the literature. In general these additions have been observed to occur in a stereospecific *anti* manner. This observation has been explained by means of a mechanism involving a seleniranium ion intermediate (3). Recently it has been reported that an open cationic species may exist prior to the product determining step in addition to vinyl ethers such as 3,4-dihydro-2*H*-pyran (4). The intermediacy of a bridged species was, however, evident from an analysis of kinetic data, suggesting therefore that a seleniranium ion-like species precedes any cation of the open structure.

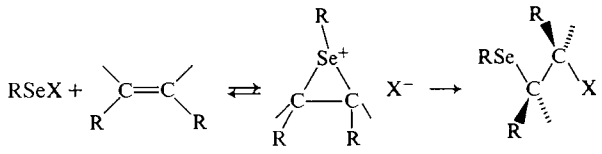

1

In the preceding paper of this series we have extended our studies to areneselenenyl thiocyanates and shown that additions to simple alkyl-substituted alkenes occur in the analogous *anti* stereospecific manner (5). The regiochemistry of these additions and nature of attack by the ambident anion, SCN, is determined by the degree and type of substitution of alkyl groups about the double bond.

Since the stability of an ion such as **1** is determined to some extent by the nature of the counter ion, it was of interest to us to determine to what degree the ion would be stabilized or destabilized by substitution of the thiocyanate ion for a chloride or bromide ion. The 1-phenylpropenes were chosen for this study because the incipient benzylic carbonium ion would be of greater stability than the possible carbonium ions derivable from alkyl-substituted alkenes.

We wish to present studies which have a direct bearing upon the above and which indicate the presence of an alternative mechanistic pathway.

Results

The reaction of a freshly prepared solution of benzeneselenenyl thiocyanate **2** in methylene chloride, with *Z*-1-phenylpropene at 25°C gives, under conditions of kinetic control, a single product **3**. After standing for a few hours the formation of a second product **4** was observed via both ir and ^{1}H nmr. It was further observed that after a period of approximately 5 days two additional products **5** and **6** were also formed, but in relatively low overall yield ($[\mathbf{5} + \mathbf{6}] \leq 8\%$).

The addition of **2** to *E*-1-phenylpropene similarly gives a single product under conditions of kinetic control. This compound was determined to be identical to **5**, above, in all respects. There was no initial observable tendency for **5** to isomerize. After a period of approximately 1 week a small amount of a second

0008-4042/79/162180-05$01.00/0

product identified as **4** was also observed ([**5**]:[**4**] = 95:5). Further isomerization was observed over the next 6 weeks, which gave a mixture of **3–6** with **5** and **6** predominating ([**5**]:[**6**] = 64:36; [**5** + **6**]:[**3** + **4**] = 92:8).

Characterization of compounds **3–6** was initially accomplished by means of infrared and nmr spectroscopy. The infrared spectra of compounds **3** and **6** show strong sharp peaks at 4.63 and 4.60 mμ, respectively, indicative of a thiocyanate group, while compounds **4** and **5** show intense broad bands at 4.84 and 4.75 mμ, indicative of an isothiocyanate group (6).

The Markownikoff orientation of the adducts was established by means of mass spectroscopy. The mass spectra of **3–4** show α-cleavage fragmentation to yield $[C_6H_5SeCHCH_3]^{+\cdot}$ ions (eq. [1]), *m/e* = 185, and $[C_6H_5CHSCN]^{+\cdot}$ ions *m/e* = 148, in accord with the regiochemical specificity shown below.

[1] $$\left[C_6H_5\underset{X}{C}H\underset{SeC_6H_5}{C}HCH_3\right]^{+\cdot} \rightarrow [C_6H_5SeCHCH_3]^{+\cdot} + [C_6H_5CHX]^{\cdot}$$

X = SCN, NCS $\qquad [C_6H_5CHX]^{+\cdot} + [C_6H_5SeCHCH_3]^{\cdot}$

Assignment of stereochemistry was arrived at by two spectroscopic means and an independent synthesis. First of all, it is known that in the proton nmr spectra of a series of racemic *erythro* and *threo* isomers of 1,2-disubstituted 1-arylpropanes, the β-methyl protons of the *threo* isomer always appear at higher field than those of the corresponding *erythro* isomer (7). Secondly, it has been observed that the vicinal proton–proton coupling constant in *erythro* diastereomers is larger than the corresponding coupling in the *threo* isomer (8). Thus it is apparent from an examination of Table 1, if one compares the thiocyanate adducts **3** and **6** or the isothiocyanate adducts **4** and **5**, that compounds **5** and **6** are the *threo* isomers, while **3** and **4** are the *erythro* isomers.

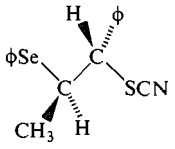

3

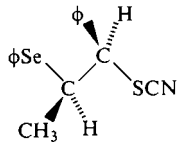

6

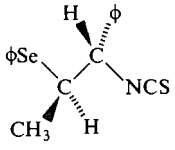

4

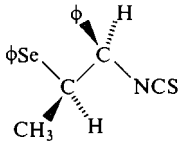

5

These results are very surprising, since they are indicative of a rather anomalous stereospecific *syn* addition under conditions of kinetic control. Furthermore, the stereospecificity of subsequent isomerizations was lost.

In view of the apparent anomalous stereochemistry of the reaction, an independent synthesis of the adducts was carried out. Benzeneselenenyl chloride is known to add across the double bond of *Z*- and *E*-1-phenylpropene in a stereospecific *anti* manner to yield *threo*- and *erythro*-1-chloro-1-phenylpropyl-2 phenyl selenide, **7** and **8**, respectively under conditions of kinetic control (9).

Treatment of the *threo* isomer **7** with 5 equiv. of NaSCN and a catalytic amount of 18-crown-6 in methylene chloride solution gives **5** and **6** stereospecifically in the ratio of 3:7 after approximately 12 h (eq. [2]). Similarly, treatment of the *erythro*

[2]

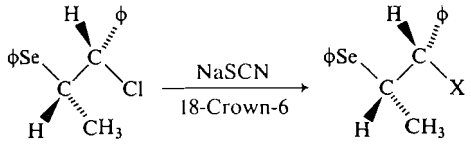

7

isomer **8** yields a 5:3 mixture of **3** and **4**, respectively. In addition to the adducts mentioned above, we isolated smaller amounts (≤20%) of the isomeric chlorides **9** and **10** from the known isomerizations of **7** to **9** and **8** to **10** (eq. [3]).

[3]

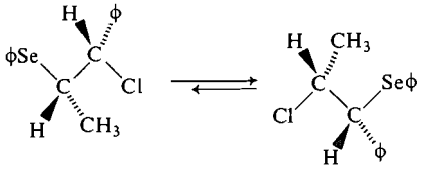

7 **9**

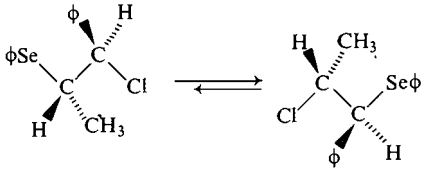

8 **10**

Somewhat surprisingly, we did not isolate or observe under our reaction conditions the formation of the corresponding thiocyanato or isothiocyanato anti-Markownikoff adducts.

We believe that **5** and **6** and **3** and **4** were formed here with retention of configuration at carbon. Control experiments using NaCl instead of NaSCN

TABLE 1. Observed proton magnetic resonance parameters for the adducts of benzeneselenenyl thiocyanate with *Z*- and *E*-1-phenylpropene

Compound $C_6H_5\overset{1}{C}HX\overset{2}{C}HY\overset{3}{C}H_3$	Configuration	Chemical shifts and coupling constants[a] H_1	H_2	H_3	$^3J_{1,2}$	$^3J_{2,3}$
X = SCN Y = SePh	*Threo*	4.80 d	3.60 q′	1.34 d	6.2	7.4
	Erythro	4.49 d	3.68 dq	1.36 d	8.8	7.2
X = NCS Y = SePh	*Threo*	4.95 d	3.59 dq	1.35 d	4.4	7.2
	Erythro	4.47 d	3.79 q′	1.54 d	7.9	6.8
X = Cl Y = SePh	*Threo*	5.11 d	3.80 dq	1.41 d	5.6	7.0
	Erythro	5.02 d	3.73 q′	1.57 d	6.9	7.2
X = PhSe Y = Cl	*Threo*	4.47 d	4.42 dq	1.53 d	3.5	6.5
	Erythro	4.33 d	4.42 q′	1.68 d	6.6	6.4

[a]All chemical shifts are reported δ ppm, downfield from internal TMS. Coupling constants are reported in Hz.

showed no loss of configuration in the presence or absence of 18-crown-6. It seems improbable that retention at carbon would occur in the case of chloride but not for thiocyanate or isothiocyanate. However, as one additional test of this ascertainment we have generated the respective *Z*- and *E*-seleniranium ions (*3a*) by treating, independently, samples of **7** and **8** with a molar equivalent of $AgPF_6$ in anhydrous methylene chloride at 12°C. Filtration of the precipitated AgCl followed by the addition of a molar equivalent of NaSCN to the seleniranium hexafluorophosphates gives the anticipated thiocyanato and isothiocyanato adducts with the latter species predominant in both cases.

Our initial synthesis using simple displacement from the chloro species is therefore in accord with neighbouring group participation of the phenylseleno group during carbon–chlorine bond breaking. Support for anchimeric assistance of this type is found in the stereospecific isomerizations: **7** ⇆ **9**; **8** ⇆ **10**. Furthermore, McManus and Lam have recently shown that the solvolysis of 2-chloroethyl phenyl selenide is an anchimerically assisted reaction in methanol and aqueous ethanol (12).

In summary we believe that these experiments serve to confirm our hypothesis of stereospecific *syn* addition.

Discussion

From the results presented in this paper, it is clear that the addition of benzeneselenenyl thiocyanate to *E*- and *Z*-1-phenylpropene is stereospecifically *syn* within the limits of our ^1H nmr analysis. This result is incompatible with the normal interpretation of a seleniranium ion intermediate. It is difficult to reach any firm mechanistic conclusions in this case because of the absence of kinetic data; particularly the kinetic order of the reaction. However, in analogy with the known second order kinetics of areneselenenyl chlorides to these and related alkenes (*9b*, 10), plus the stereospecificity (*anti*) of benzeneselenenyl thiocyanate additions to alkyl-substituted alkenes, one might also predict an Ad_E2 process to be operating here. In this case a classical open carbonium ion is probably formed, paired with a thiocyanate ion, collapse of the intimate ion-pair occurring with overall *syn* addition. Since different products are obtained from the isomeric alkenes it is concluded that these intimate ion pairs, **11** and **12**, do not equilibrate

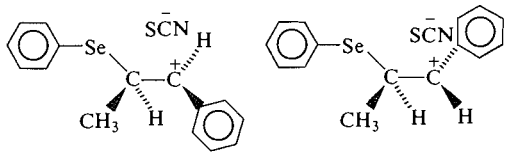

11 **12**

prior to the product forming step. If such a scenario correctly explains these observations one must accept the rationale that the stability of the ionic intermediates is dependant upon the nature of the counter ion. This implies that a seleniranium ion is stable, be its' ring-carbon substituents alkyl or aryl, when the counter ion is, for example, chloride or hexafluorophosphate. A change in stability is, however, observed when the counter ion is thiocyanate. In this case we postulate the existence of a seleniranium ion intermediate only when alkyl ring-carbon substituents are present.

The stereospecific synthesis of compounds **3–6** from seleniranium ions originally coupled to chloride or hexafluorophosphate ions is compatible with the above. When the counter ions exchange, presumably via an ion-pair mechanism, the seleniranium ion will, using the rationale given above, open to a classical carbonium ion. *Anti* attack is still anticipated since the thiocyanate ion would be expected to fill the void in the solvation shell left by the departing counter ion. Our only assumption is that collapse to product must occur faster than reorientation of the thiocyanate ion to the *syn* side which should be retarded in any case because of the bulk of the attached phenylseleno group, as seems reasonable.

Alternatively, an Ad_E3 mechanism might be involved, in accord with the observed third order kinetics, second order in PhSeCl, for benzeneselenenyl chloride additions to both alkenes and alkynes, found in certain solvents such as ethyl acetate (9*b*, 11). A third possibility is the *syn* collapse of an episelenurane species. Unfortunately, until such time as the kinetics may be unambiguously established, our data do not warrant further mechanistic speculation.

Perhaps the most interesting aspect of these experiments is the observation of chemospecific formation of the thiocyanato adduct from the *Z*-isomer and the isothiocyanato adduct from the *E*-isomer. One possible explanation of this observation is based on the theory of hard and soft acids and bases. In general one expects the harder and more basic nitrogen atom of the nucleophile to attack at the more electrophilic site of the resonance stabilized benzylic carbon derived from the *E*-isomer, whereas the softer, more polarizable sulphur atom would prefer to attack the less stabilized benzylic carbonium ion derived from the *Z*-alkene. The reason for the different electrophilicities of the two benzylic carbons is the degree of stabilization one obtains from the phenyl ring. In the *E*-alkene the phenyl ring may easily obtain coplanarity. In the *Z*-alkene coplanarity is essentially impossible because of repulsive interactions with the adjacent methyl group.

Experimental

General

Infrared spectra were recorded on either a Perkin–Elmer 337 or Unicam SP 1100 spectrometer. Proton magnetic resonance samples were run in amberized 5 mm od sample tubes, as chloroform-*d* solutions using Varian T-60 and HA 100 spectrometers. Microanalyses were carried out by Scandinavian Microanalytical Labs, Herlev, Denmark.

Chemicals

Z- and *E*-1-phenylpropene were purchased from Chemical Samples Co. and used without further purification. Methylene chloride was purified as previously reported (9*a*). Benzeneselenenyl chloride was purchased from Aldrich Chemical Co. and recrystallized from petroleum ether 80–90 prior to use. 18-Crown-6 was purchased from Aldrich Chemical Co.

Benzeneselenenyl Thiocyanate, **2**

This compound was prepared as previously described (5).

*1-(*RS*),2-(*SR*)-1-Thiocyanato-1-phenylpropyl-2 Phenyl Selenide*, **3**

To 0.214 g (0.001 mol) of **2** in 25 mL of anhydrous methylene chloride was added 0.118 g (0.001 mol) of *Z*-1-phenylpropene. The reaction mixture was stirred for approximately 3 min until no further color change (yellow to colorless) was observed. Evaporation of the solvent gave a pale yellow oil in 90% yield. Chromatography on silica gel showed no evidence for alternate species under a variety of solvent conditions; ir ($CHCl_3$, mμ): 4.63 vs. sharp *RSCN*; ^{13}C nmr ($CDCl_3$): 52.7 d, 49.8 d, 19.8 q, 130.9 s, 135.8 d, 129.4 d, 128.3 d, 128.7 s, 129.9 d, 129.1 d, 128.9 d, 112.5 s SCN. *Anal.* calcd. for $C_{16}H_{15}SeSN$: C 57.83, H 4.55, S 9.65, N 4.21; found: C 57.80, H 4.48, S 9.69, N 5.08.

*1-(*RS*), 2-(*SR*)-1-Isothiocyanato-1-phenylpropyl-2 Phenyl Selenide*, **4**

From the isomerization of **3** in CH_2Cl_2 or $CHCl_3$ separation was carried out on silica gel eluted with CH_2Cl_2; ir ($CHCl_3$, mμ): 4.84 vs. broad *RNCS*; ^{13}C nmr ($CDCl_3$): 59.7 d, 42.2 d, 19.1 q, 129.9 s, 135.5 d, 129.2 d, 126.9 d, 129.4 d, 128.6 d, 128.4 s, 128.1 d, 137.7 s NCS. *Anal.* calcd. for $C_{26}H_{15}NSSe$: C 57.83, H 4.55, S 9.65, N 4.21; found: C 57.96, H 4.67, S 9.33, N 4.06.

*1-(*RS*), 2-(*RS*)-1-Isothiocyanato-1-phenylpropyl-2 Phenyl Selenide*, **5**

This compound was prepared as for **3** above, but substituting *E*-1-phenylpropene; ir ($CHCl_3$, mμ): 4.75 vs. broad *RNCS*; ^{13}C nmr ($CDCl_3$): 65.2 d, 45.5 d, 15.5 q, 130.9 s, 135.5 d, 129.9 d, 128.2 d, 134.7 d, 129.4 d, 128.4 s, 128.7 d, 137.0 s NCS. *Anal.* calcd. for $C_{16}H_{15}NSSe$: C 57.83, H 4.55, S 9.65, N 4.21; found: C 57.81, H 4.55, S 9.32, N 4.35.

*1-(*RS*), 2-(*RS*)-1-Thiocyanato-1-phenylpropyl-2 Phenyl Selenide*, **6**

This compound was prepared from the isomerization of **5** in CH_2Cl_2; separation was carried out on silica gel eluted with CH_2Cl_2; ir ($CHCl_3$, mμ): 4.60 vs. sharp *RSCN*. *Anal.* calcd. for $C_{16}H_{15}NSSe$: C 57.83, H 4.55, S 9.65, N 4.21; found: C 57.69, H 4.49, S 9.73, N 4.30.

Independent Synthesis and Control Experiments

(i) Synthesis and Reactivity of **7**

To a solution of *Z*-1-phenylpropene (3.42 mmol) in 20 mL of anhydrous methylene chloride was added 3.31 mmol of C_6H_5SeCl, previously dissolved in 5 mL CH_2Cl_2. Upon completion of the reaction this solution was divided into 5 equal parts. In the first case, nothing was done. In the second case was added 5 molar equiv. of NaCl. The third was as above, but with the addition of a catalytic amount of 18-crown-6. The fourth and fifth were as the third and fourth, respectively, but with substitution of NaSCN for NaCl. After 12 h, 1 mL aliquots were worked up (filtration, evaporation of solvent). In samples 1–3 only compounds **7** and **9** were isolated or observed. Samples 4 and 5 gave mixtures of **5**, **6**, **7**, and **9**, although the total amount of **5** + **6** was normally $\leq 5\%$ in experiment 4.

(ii) Synthesis and Reactivity of **8**

A series of experiments were carried out as above with the substitution of *E*-1-phenylpropene for the *Z*-isomer. The work up of subsequent aliquots over a period of 2 weeks showed a gradual isomerization (loss of configurational integrity) between species **3**–**6**. In no case was there observed isomerization between the chlorides except for the known **7** ⇄ **9**; **8** ⇄ **10**.

Synthesis and Reactivity of Z- *and* E-*2-Phenyl-3-methylseleniranium Hexafluorophosphates*

To 0.192 g (1.0 mmol) of benzeneselenenyl chloride in 30 mL CH_2Cl_2 was added 0.118 g of *Z*-1-phenylpropene previously dissolved in 20 mL CH_2Cl_2. To the above was added 0.253 g of $AgPF_6$ (Alfa-Ventron) under nitrogen, followed by filtration under nitrogen to remove the AgCl. The immediate quenching of the filtrate with 0.082 g of NaSCN, previously dried for 24 h, gives the respective adducts in yields of 90% or greater (3*a*).

Acknowledgements

Continued financial support from the Natural Science and Engineering Research Council of Canada is greatly appreciated.

1. (*a*) G. H. SCHMID AND D. G. GARRATT. The chemistry of double bonded functional groups. *Edited by* S. Patai. Wiley and Sons, London. 1977. Supplement A. Part 2. pp. 828–866. (*b*) R. C. FAHEY. *In* Topics in stereochemistry. Vol. 3. *Edited by* E. L. Eliel and N. L. Allinger. Interscience, New York. 1968. p. 237. (*c*) P. B. D. DE LA MARE and R. BOLTON. Electrophilic addition to unsaturated systems. Elsevier, New York. 1966.
2. (*a*) D. G. GARRATT and G. H. SCHMID. J. Org. Chem. **42**, 1776 (1977). (*b*) K. B. SHARPLESS and R. F. LAUER. J. Org. Chem. **39**, 429 (1974). (*c*) H. J. REICH. J. Org. Chem. **39**, 428 (1974). (*d*) F. LAUTENSCHLAEGER. J. Org. Chem. **34**, 4002 (1969).
3. (*a*) G. H. SCHMID and D. G. GARRATT. Tetrahedron Lett. 3991 (1975). (*b*) G. CAPOZZI, O. DELUCCI, V. LUCCHINI, and G. MODENA. Tetrahedron Lett. 2603 (1975). (*c*) W. A. SMIT, M. Z. KRIMER, and E. A. VOROB'EVA. Tetrahedron Lett. 2451 (1975). (*d*) G. H. SCHMID. *In* Topics in sulfur chemistry. *Edited by* A. Senning and P. S. Magee. Georg Thieme Publishers, Stuttgart. 1977. p. 103.
4. D. G. GARRATT. Can. J. Chem. **56**, 2184 (1978).
5. D. G. GARRATT, M. D. RYAN, and M. UJJAINWALLA. Can. J. Chem. This issue.
6. Aldrich library of infrared spectra. 2nd ed. 1975. pp. 463, 464.
7. G. H. SCHMID. Can. J. Chem. **46**, 3415 (1968).
8. (*a*) M. BUZA and E. I. SNYDER. J. Am. Chem. Soc. **88**, 1161 (1966). (*b*) N. L. ALLINGER, H. BLATTES, L. FREIBERG, and F. KARKOWSKI. J. Am. Chem. Soc. **88**, 2999 (1966). (*c*) L. P. KUHN. J. Am. Chem. Soc. **80**, 5950 (1958). (*d*) D. C. BEST, G. UNDERWOOD, and C. A. KINGSBURY. J. Chem. Soc. Chem. Commun. 627 (1969).
9. (*a*) D. G. GARRATT and G. H. SCHMID. Can. J. Chem. **52**, 3599 (1974). (*b*) D. G. GARRATT. Ph.D. Thesis, University of Toronto, Toronto, Ont. 1975.
10. (*a*) D. G. GARRATT. Can. J. Chem. **56**, 2184 (1978). (*b*) G. H. SCHMID and D. G. GARRATT. Tetrahedron, **34**, 2869 (1978).
11. E. G. KATAEV, T. G. MANNOFOV, and M. K. MANNANOV. Kinet. Katal. **9**(5), 1161 (1968).
12. S. P. MCMANUS and D. H. LAM. J. Org. Chem. **43**, 650 (1978).

The consequences of steric effects in the cleavage step of the sulfohaloform reaction

DENIS GEORGE KAY, RICHARD FRANCIS LANGLER,[1] AND JUNE ELLEN TRENHOLM
Department of Chemistry, Dalhousie University, Halifax, N.S., Canada B3H 4J3

Received February 16, 1979

DENIS GEORGE KAY, RICHARD FRANCIS LANGLER, and JUNE ELLEN TRENHOLM. Can. J. Chem. 57, 2185 (1979).

The pathway for the aqueous chlorinolysis of a series of β-sulfonyl-sulfides is elucidated and the S_N2 cleavage step examined. Steric effects in the cleavage of the α-polychloro-oxochlorosulfonium chloride intermediates are held to be responsible for the suppression of the established nucleophilic competition between water molecules and chloride ions with the result that all cleavage products arise from nucleophilic attack by chloride ions. This report details the second known example of successful S_N2 displacement on a carbon atom α to a sulfonyl group.

DENIS GEORGE KAY, RICHARD FRANCIS LANGLER et JUNE ELLEN TRENHOLM. Can. J. Chem. 57, 2185 (1979).

On a étudié les chemins réactionnels impliqués lors de la scission d'une série de β-sulfonyl-sulfures sous l'influence du chlore et on a examiné l'étape de clivage S_N2. On croit que des effets stériques dans le clivage d'intermédiaires chlorure d'α-polychloro-oxo-chlorosulfonium sont responsables de la suppression de la compétition nucléophile bien établie entre les molécules d'eau et les ions chlorures qui donne lieu au fait que tous les produits de clivages proviennent d'une attaque nucléophile par les ions chlorures. Dans ce travail, on donne les détails du deuxième exemple d'une substitution S_N2 réussie sur un atome de carbone en α d'un groupe sulfonyle.

[Traduit par le journal]

Introduction

As a part of our program to study the chlorination of sulfur compounds (1–10), we have recently published details which support a generalized pathway for the conversion of dialkyl sulfides into sulfonyl chlorides (5). The generalized pathway was called the sulfohaloform reaction (*vide* Scheme 1).

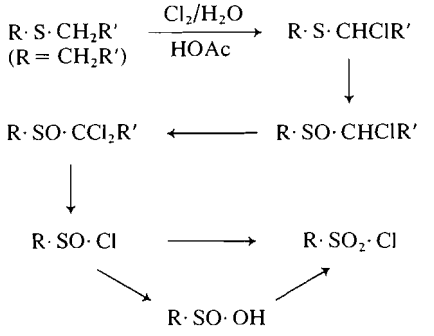

SCHEME 1. The sulfohaloform reaction

The intermediate α-polychloro-oxochlorosulfonium chloride salts were shown (5) to undergo three competing processes, viz. (*i*) cleavage by nucleophilic attack of water molecules on the chlorine-bearing carbon α to the sulfonium sulfur atom, (*ii*) cleavage by nucleophilic attack on the same carbon atom by chloride ions, and (*iii*) Pummerer rearrangement to furnish another α-polychlorosulfoxide. These competing processes are presented for trichloromethyl methyl sulfoxide in Scheme 2.

TABLE 1.* Relative percentages of oxochlorosulfonium chloride cleavage by competing nucleophiles

Sulfoxide precursors	Nucleophile (%)	
	H_2O	Cl^-
$ClCH_2SOCH_3$	0	0
$Cl_2CHSOCH_3$	100	0
Cl_3CSOCH_3	86	14
Cl_3CSOCH_2Cl	71	29
$ClCH_2SOCH_2Cl$	0	0
$Cl_2CHSOCH_2Cl$	84	16
Cl_3CSOCH_2Cl	71	29

*Data calculated from previously published results (5).

Flow charts were detailed (5) defining the balance between the competing processes when the di- and trichlorodimethyl sulfoxides were converted into methane and chloromethane sulfonyl chlorides. Table 1 presents the relative percentages of the cleavage products from the oxochlorosulfonium chloride salts[2] (derived from the sulfoxides listed) induced by nucleophilic attack of water molecules and chloride ions.

[1]To whom all correspondence should be addressed.

[2]Structure **A**, Scheme 2 depicts the structure of an oxochlorosulfonium chloride salt.

0008-4042/79/162185-06$01.00/0

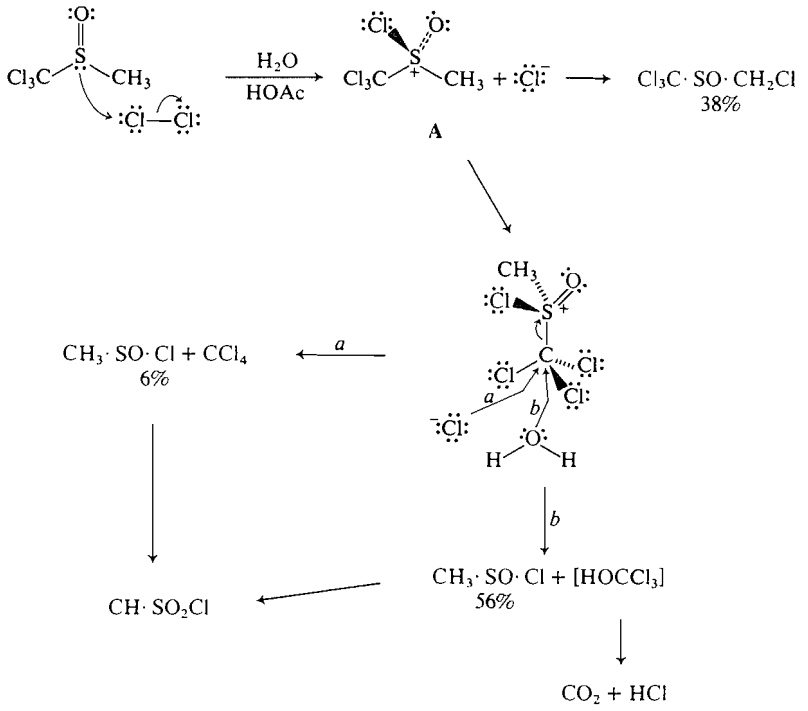

SCHEME 2

From the data in Table 1, we have tentatively inferred that increasing incorporation of bulky chlorine atoms in the oxochlorosulfonium chloride intermediates hinders nucleophilic attack by water molecules substantially more than nucleophilic attack by chloride ions. In order to test this point experimentally, we have undertaken the preparation of systems which would (*i*) provide even more crowded α-polychloro-oxochlorosulfonium chloride intermediates and (*ii*) structurally preclude complicating Pummerer rearrangements. We have chosen to meet these objectives with substrates of the type shown below:

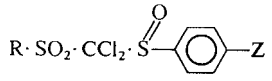

For some time, it was believed that leaving groups attached to a sulfonyl-bearing carbon atom could not be displaced (11–19). The lack of reactivity for these systems was ascribed to "the repulsion of the nucleophilic species by the negative field of the sulfonyl oxygen atoms" (17). An examination of models led to the conclusion that a mesyl group[3] would have "only a small steric effect, unless it is assumed that the partial negative charge on the oxygen atoms would greatly extend their effective radius" (15).

Later, the surprising report of Robson *et al.* (20) documented, without comment, the successful displacement of the chlorine atom of chloromethyl methyl sulfone by mercaptide anions. This reaction was subsequently exploited for synthetic purposes (8, 21) and formed the basis for a more extensive investigation of nucleophilic displacements involving chlorinated sulfones and mercaptide anions (3). Furthermore, an examination of space-filling models convinced us that a mesyl group is very similar in volume to a tertiary butyl group and that the analogy of the mesylmethyl group with the neopentyl group, first suggested and discarded by Bordwell (15), is a very good one. It appeared, at least tentatively, that the assumption of nucleophilic repulsion by sulfonyl oxygen atoms might be unnecessary to account for the known chemistry. In this connection, it is interesting to note that di-*tert*-butyl-methanesulfinyl chloride could not be converted to the corresponding sulfonyl chloride, even under forcing conditions (22). Such an observation might well be a consequence of the crowding necessary to introduce a bulky chlorosulfonyl group into an already crowded molecule.

Results and Discussion

Our previous study (5) established two modes of behaviour for chlorosulfonium chloride salts generated in aqueous media, i.e., (*i*) dialkyl chlorosulfonium chloride salts are very resistant to hydrolysis

[3]Mesyl is an abbreviation of methylsulfonyl.

TABLE 2. Chlorinolysis of 0.1 g $CH_3SO_2CH_2SPh$ (**1***a*)

Volume of Cl_2/H_2O* (mL)	$CH_3SO_2CH_2SPh$ (%)	$CH_3SO_2CH_2SOPh$ (%)	$CH_3SO_2CHClSOPh$ (%)	$CH_3SO_2CCl_2SOPh$ (%)
1.5	90	10	0	0
3	80	15	2	3
6	47	21.2	14.3	17.5
9	21	31	21	26

*H_2O was saturated with Cl_2 at ambient temperature.

and react essentially exclusively by Pummerer rearrangement (1*b*) and (*ii*) α-chlorodialkyl chlorosulfonium chloride salts undergo quantitative hydrolysis with essentially no Pummerer rearrangement as shown in Scheme 1.

A priori, either reaction could be advanced as the first step in the pathway for the aqueous chlorinolyses of the sulfone-sulfides **1***a*–**6***a*, since (*i*) the sulfonyl methyl groups are substantially more electron withdrawing than a chloromethyl group[4] and therefore should enhance the electrophilicity of the sulfonium sulfur atom, thus facilitating hydrolysis of the chlorosulfonium chloride salts derived from **1***a*–**6***a*, and (*ii*) the sulfonyl methyl groups greatly enhance the acidity of the protons adjacent to the sulfonium sulfur atom and consequently might be expected to enhance the rate of the elimination step by which the sulfenium ion (Pummerer intermediate (1*b*)) forms.

The results of a series of controlled chlorinolyses of **1***a* are presented in Table 2. These results establish that the first formed chlorosulfonium chloride salt undergoes hydrolysis preferentially and that further products arise through the intermediacy of the unchlorinated sulfone-sulfoxide. Larger amounts of chlorine furnished the corresponding α,α-dichlorosulfoxide **1***b*. Scheme 3 presents the synthesis and pathway for the reactions which provided the dichlorosulfone-sulfoxides **1***b*–**6***b*. The structure of **1***b* was confirmed by converting a sample into the corresponding dichlorodisulfone (**1***d*). The disulfone **1***d* was shown to be identical to a sample prepared by oxidation of the dichlorosulfone-sulfide **1***c*.

Exhaustive chlorinolysis of the dichlorosulfone-sulfoxides **1***b*–**6***b* furnished an equimolar mixture of the appropriate trichloromethyl sulfone and sulfonyl chloride shown in Table 3. Nucleophilic attack by water molecules at the carbon atom of the dichloromethylene group in the intermediate oxochlorosulfonium chloride would result in the formation of an intermediate hydroxydichloromethyl sulfone. Such a compound would be expected to eliminate

[4]Pauling electronegativities: X_p ($ClCH_2$) = 2.47, X_p ($CH_3SO_2CH_2$) = 2.85, and X_p ($PhSO_2CH_2$) = 2.75 (1*b*, 23).

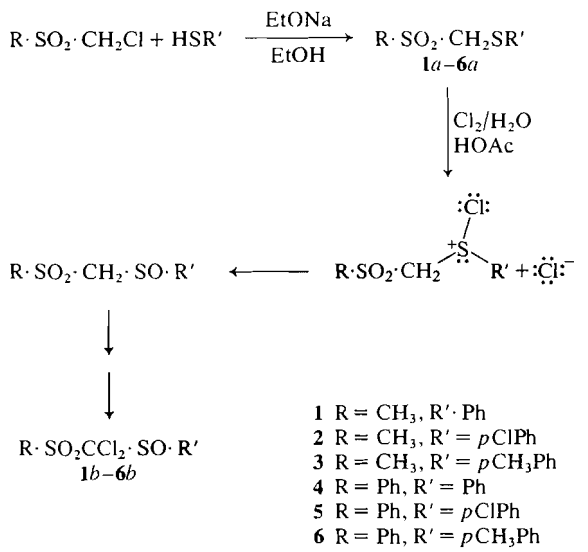

SCHEME 3

HCl, hydrolyze, decarboxylate, and react with molecular chlorine to furnish the appropriate sulfonyl chloride, e.g., this sequence in the case of **1***b* would result in the formation of methanesulfonyl chloride. In no case was there any detectable sulfone-derived sulfonyl chloride present in the product mixture. Consequently the only nucleophiles to attack at the central carbon atom in the oxochlorosulfonium chlorides derived from **1***b*–**6***b* were chloride ions. Scheme 4 presents a rationale for the formation of the observed products.

TABLE 3. Yields* of sulfones and sulfonyl chlorides from exhaustive aqueous chlorinolyses of **1***b*–**6***b*

Substrate	Products: RSO_2Cl (% yield)	Products: $R'SO_2CCl_3$ (% yield)
1*b*	R = Ph (80)	R' = CH_3 (78)
2*b*	R = *p*Cl—Ph (80)	R' = CH_3 (80)
3*b*	R = *p*CH_3Ph (75)	R' = CH_3 (83)
4*b*	R = Ph (86)	R' = Ph (90)
5*b*	R = *p*ClPh (72)	R' = Ph (78)
6*b*	R = *p*CH_3Ph (83)	R' = Ph (81)

*For mechanism see Scheme 4.

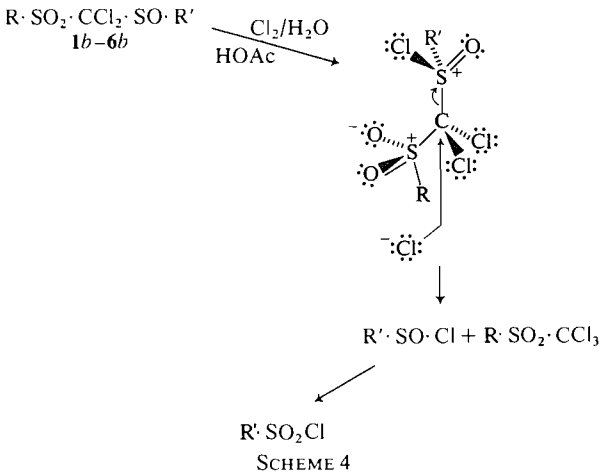

SCHEME 4

We have previously observed (5) a difference in the overall rate of reaction for the aqueous chlorinolysis of chloromethyl phenyl sulfide (product: benzenesulfonyl chloride; relative rate: 1) and the aqueous chlorinolysis of chloromethyl methyl sulfide (product: methanesulfonyl chloride, relative rate: 6.5). The slower reaction for the phenyl sulfide was attributed to an electron-donating effect from the phenyl group which would reduce the electrophilicity of the sulfonium sulfur atom in the oxochlorosulfonium chloride intermediate. However, a comparison of the overall rate of the chlorinolysis of the mesyl dichlorosulfoxide **1***b*, and the rate of chlorinolysis of phenyl trichloromethyl sulfoxide (5) indicates that **1***b* reacts some 22.3 times slower. This difference cannot be attributed to an electronic effect originating with the phenyl group. One might then examine the possible role of the mesyl group in terms of the effect of sulfonyl oxygen atoms on approaching nucleophiles, as outlined earlier. Clearly, if the sulfonyl oxygen atoms offer a 'negative field' they would repel incoming chloride ions much more than incoming water molecules. Since cleavage by nucleophilic attack at the central carbon atom occurs exclusively by the agency of chloride ions we conclude that the effect of the mesyl group is not a special electronic effect but rather a more familiar steric effect.

In order to determine the relative sizes of chloride ions and water molecules, we have made accurate scaled drawings of each species. The somewhat remarkable conclusion was that there is essentially no difference in the cross-sectional area of a chloride ion and a water molecule. The most likely reason for the superior nucleophilicity of chloride ions lies with the greater polarizability of these nucleophiles. An interesting alternative or additional consideration arises from an overview of S_N2 displacements of leaving groups α to sulfonyl groups.

The successful displacement of the sulfinyl chloride group by chloride ions represents the second known case of an S_N2 displacement α to a sulfonyl group. Both nucleophiles, viz. chloride ions and mercaptide ions, which have been effective in accomplishing these displacements involve third-row nucleophiles. An intriguing possibility is that of a complexing interaction between these nucleophiles and the adjacent sulfonyl sulfur atom. We have recently proposed such an interaction in order to rationalize a novel thiolester hydrolysis (1*a*).

The chlorinolyses of the sulfone-sulfoxides **1***b*–**3***b* resulted in the formation of a minor product (ca. 5%) which gave rise to a singlet in the nmr of the crude at δ 3.50. Thin layer chromatography, visualized with NaI–acetone (7), showed the presence of a compound at R_f 0.50. These properties are in accord with the presence of $CH_3SO_2CCl_2SO_2Cl$ (7) which we have characterized previously (8). Furthermore, column chromatography furnished dichloromethyl methyl sulfone which was absent in the crude reaction mixture.

Dichloromethyl methyl sulfone is the known hydrolysis product obtained from $CH_3SO_2CCl_2$-SO_2Cl (3, 8). Chromatography has been shown to furnish substantial hydrolysis of a close structural relative of 7 (7).

It appears that the severe crowding in the oxochlorosulfonium chloride salts derived from **1***b*–**3***b* has succeeded in diverting some nucleophilic attack to the phenyl ring. Attack at the less crowded centre would presumably be carried out by water molecules. A rationale for this process is presented in Scheme 5. The preceding account details the first evidence that nucleophilic attack can be diverted from the chlorine-bearing carbon atom in the cleavage of α-polychloro-oxochlorosulfonium chlorides.

A consequence of the results reported in this paper is that methylsulfonyl groups have potential application in the design of molecules intended for the study of steric effects on chemical reactions. A feature worth noting is the great facility with which they may be introduced into substrates, a feature which they do not share with the ubiquitous tertiary butyl group. A potentially useful property of these groups is their destablization of nearby carbocationic centres (24) which would permit studies of S_N2 cleavages without facilitating S_N1 processes.

In conclusion, a study of sulfonyl substituted α-polychlorosulfoxide chlorinations has shown that the corresponding oxochlorosulfonium chlorides undergo cleavage in which steric factors favor nucleophilic attack by chloride ions and disfavor nucleophilic attack by water molecules. The results obtained are inconsistent with the view that the adjacent sulfonyl groups offer a 'negative field'

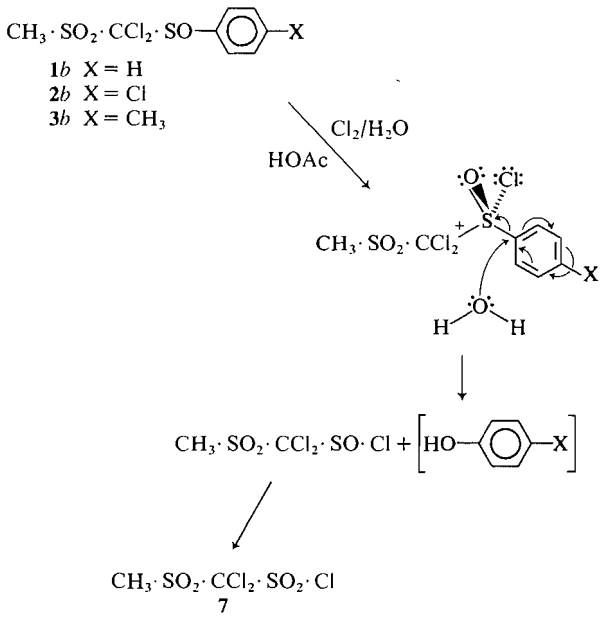

SCHEME 5

which repels nucleophiles. Finally, the substantial crowding achieved in the transition state has shifted a small amount of the nucleophilic attack to the less crowded carbon attached to the sulfonium sulfur atom.

Experimental

General

The ir spectra were recorded on a Perkin Elmer 237B grating spectrophotometer. The nmr spectra were obtained on a Varian T-60 instrument using TMS as the internal standard. The mass spectra were recorded on a Dupont-CEC model 21-104 mass spectrometer. The samples were directly introduced using an all glass probe and the spectra run at 30 eV with a source temperature of 150°C. Melting points were determined on a Fisher-Johns melting point apparatus and are uncorrected.

Preparation of Sulfone-sulfides ***1***a–***6***a

Sodium metal (1 equiv.) was dissolved in absolute ethanol (100 mL) and the appropriate mercaptan (1 equiv.) added. Chloromethyl phenyl sulfone (25) or chloromethyl methyl sulfone (26) (10 g) was added and the reaction mixture refluxed for 24 h. Water (100 mL) was added and the resultant mixture was washed with chloroform (3 × 100 mL aliquots). The organic layers were combined, dried ($MgSO_4$), filtered, concentrated, and the residue recrystallized from 95% ethanol.

$CH_3SO_2CH_2SPh$ **1***a* (9.413 g, mp 47–49°C); ir ($CHCl_3$): 1320 and 1145 cm^{-1}; nmr ($CDCl_3$) δ: 7.36 (5H, m), 4.23 (2H, s), and 2.93 (3H, s); ms *m/e*: 202 (M^+, 4.7%), 123 (86%), and 45 (100%).

p-$ClPhSCH_2SO_2CH_3$ **2***a* (15.88 g, mp 105–106°C); ir ($CHCl_3$): 1320 and 1145 cm^{-1}; nmr ($CDCl_3$) δ: 7.43 (4H, pseudo-quartet), 4.17 (2H, s), and 2.97 (3H, s); ms *m/e*: 238 (1.8%), 236 (M^+, 5.7%), 159 (33.3%), 157 (100%), and 45 (80%).

p-$CH_3PhSCH_2SO_2CH_3$ **3***a* (14.67 g, mp 63.5–65°C); ir ($CHCl_3$): 1320 and 1140 cm^{-1}; nmr ($CDCl_3$) δ: 7.37 (4H, pseudo-quartet), 4.20 (2H, s), 2.90 (3H, s), and 2.33 (3H, s); ms *m/e*: 216 (M^+, 10.3%), 137 (100%), and 45 (41.5%).

$PhSO_2CH_2SPh$ **4***a* (11.00 g, mp 56–58°C); ir ($CHCl_3$): 1320 and 1140 cm^{-1}; nmr ($CDCl_3$) δ: 7.66 (10H, m) and 4.40 (2H, s); ms *m/e*: 264 (M^+, 7.3%), 123 (100%), and 45 (30%).

p-$ClPhSCH_2SO_2Ph$ **5***a* (11.88 g, mp 67–69°C); ir ($CHCl_3$): 1320 and 1145 cm^{-1}; nmr ($CDCl_3$) δ: 7.57 (9H, m) and 4.30 (2H, s); ms *m/e*: 300 (2.2%), 298 (M^+, 6.6%), 159 (33.3%), 157 (100%), and 45 (40%).

p-$CH_3PhSCH_2SO_2Ph$ **6***a* (11.10 g, mp 83–85°C); ir ($CHCl_3$): 1320 and 1145 cm^{-1}; nmr ($CDCl_3$) δ: 7.40 (9H, m), 4.30 (2H, s), and 2.26 (3H, s); ms *m/e*: 141 (58%), 91 (33%), and 77 (100%).

Preparation of $CH_3SO_2CCl_2SPh$ (***1***c)

The sulfone-sulfide **1***a* (1.000 g) was dissolved in carbon tetrachloride (20 mL) and Cl_2 (ca. 200 mL/min) was bubbled into the solution for 20 min. The solvent was evaporated and the residue recrystallized from 95% ethanol affording **1***c* (1.176 g, mp 53–54°C); ir ($CHCl_3$): 1320 and 1145 cm^{-1}; nmr ($CDCl_3$) δ: 7.66 (5H, m) and 3.50 (3H, s); ms *m/e*: 195 (14%), 193 (69%), 191 (100%), 109 (34%), and 77 (44%).

Preparation of $CH_3SO_2CCl_2SO_2Ph$ (***1***d)

The dichlorosulfone-sulfide **1***c* (0.5002 g) was oxidized with chromium trioxide in glacial acetic acid in standard fashion (3). The crude dichlorodisulfone was recrystallized from 95% ethanol (0.276 g, mp 102–105°C); ir: 1355 and 1152 cm^{-1}; nmr ($CDCl_3$) δ: 7.90 (5H, m) and 3.53 (3H, s); ms *m/e*: 141 (73%), 125 (41%), and 77 (100%).

*Preparation of Dichlorosulfone-sulfoxides (****1***b–***6***b)

The desired sulfone-sulfide (**1***a*–**6***a*) (5.00 g) was added to a solution of glacial acetic acid (25 mL) and water (5 mL). Cl_2 (ca. 200 mL/min) was bubbled into the reaction mixture for 0.5 h. During the chlorination the product precipitates from solution. Upon completion of the chlorination water (50 mL) and methylene chloride (100 mL) were added. The layers were separated and the organic layer washed with 2.5% w/v NaOH (2 × 50 mL aliquots), dried ($MgSO_4$), filtered, and the solvent evaporated. The residue was recrystallized from 95% ethanol affording the following compounds.

$CH_3SO_2CCl_2SO·Ph$ **1***b* (5.284 g, mp 149–151°C); ir ($CHCl_3$): 1345, 1150, and 1080 cm^{-1}; nmr ($CDCl_3$) δ: 7.77 (5H, m) and 3.46 (3H, s); ms *m/e*: 290 (0.1%), 288 (0.6%), 286 (M^+, 1%), 125 (100%), 109 (39%), and 77 (43%). *Anal.* calcd. for $C_8H_8Cl_2O_3S_2$: C 33.45, H 2.80; found: C 33.07, H 2.91.

p-$ClPhS(O)CCl_2SO_2CH_3$ **2***b* (5.353 g, mp 84–86°C); ir ($CHCl_3$): 1340, 1145, and 1080 cm^{-1}; nmr ($CDCl_3$) δ: 7.73 (4H, pseudo-quartet) and 3.50 (3H, s); ms *m/e*: 229 (2.2%), 227 (5.7%), 225 (5.7%), 161 (33.3%), and 159 (100%). *Anal.* calcd. for $C_8H_7Cl_3O_3S_2$: C 29.87, H 2.19; found: C 29.95, H 2.15.

p-$CH_3PhS(O)CCl_2SO_2CH_3$ **3***b* (5.150 g, mp 145–147°C); ir ($CHCl_3$): 1345, 1150, and 1085 cm^{-1}; nmr ($CDCl_3$) δ: 7.73 (4H, pseudo-quartet), 3.50 (3H, s), and 2.53 (3H, s); ms *m/e*: 139 (100%), 91 (27.5%), and 45 (12.5%). *Anal.* calcd. for $C_9H_{10}Cl_2O_3S_2$: C 35.88, H 3.34; found: C 35.83, H 3.14.

$PhSO_2CCl_2·SO·Ph$ **4***b* (4.894 g, mp 134–136°C); ir ($CHCl_3$): 1350, 1150, and 1090 cm^{-1}; nmr ($CDCl_3$) δ: 7.80 (m); ms *m/e*: 141 (36%), 125 (64%), 109 (48.6%), and 77 (100%). *Anal.* calcd. for $C_{13}H_{10}Cl_2O_3S_2$: C 44.70, H 2.88; found: C 44.82, H 2.57.

p-$ClPhS(O)CCl_2SO_2Ph$ **5***b* (3.870 g, mp 115–117°C); ir ($CHCl_3$): 1350, 1150, and 1095 cm^{-1}; nmr ($CDCl_3$) δ: 7.83 (m); ms *m/e*: 161 (33.3%), 159 (100%), 141 (43.6%), and 77 (65.9%). *Anal.* calcd. for $C_{13}H_9Cl_3O_3S_2$: C 40.69, H 2.36; found: C 40.47, H 2.42.

p-$CH_3PhS(O)CCl_2SO_2Ph$ **6***b* (4.563 g, mp 140–141°C); ir ($CHCl_3$): 1350, 1150, and 1095 cm^{-1}; nmr ($CDCl_3$) δ: 7.70

(9H, m) and 2.46 (3H, s); ms *m/e*: 139 (100%), 91 (16.6%), and 77 (26.8%). *Anal.* calcd. for $C_{14}H_{12}Cl_2O_3S_2$: C 46.28, H 3.32; found: C 46.01 and H 3.49.

Preparation of $Ph{\cdot}SO{\cdot}CH_2SO_2CH_3$ *1*e

The sulfone-sulfide **1***a* (1.002 g) was dissolved in a solution of 30% H_2O_2 (0.568 g) in dioxane (25 mL). The reaction mixture was refluxed for 0.75 h. The solvent was evaporated and the residue recrystallized from 95% ethanol, (0.815 g, mp 88–90°C); ir ($CHCl_3$): 1320, 1140, and 1045 cm^{-1}; nmr ($CDCl_3$) δ: 7.60 (5H, s), 4.20 (1H, d, J = 3 Hz), 4.13 (1H, d, J = 3 Hz) (26), and 3.23 (3H, s); ms *m/e*: 218 ($M^{\ddagger}$, 10.9%), 125 (100%), 109 (23.1%), and 77 (32.9%). *Anal.* calcd. for $C_8H_{10}O_3S_2$: C 44.01, H 4.61; found: C 43.89, H 4.21.

Controlled Aqueous Chlorinolysis of *1*a

A series of chlorinolyses of **1***a* were conducted and the results are tabulated in Table 2. Details below are provided for the run from which products were isolated.

The sulfone-sulfide **1***a* (0.100 g) was dissolved in glacial acetic acid (75 mL) and distilled water (9 mL). Water (9 mL) which had been saturated with Cl_2 at ambient temperature was added and the reaction mixture stirred at room temperature for 0.5 h. Water (150 mL) was added and the reaction mixture washed with chloroform (300 mL). The organic layer was washed with 2.5% w/v NaOH (3 × 100 mL aliquots), dried, and concentrated. The residue showed four spots on analytical tlc (chloroform development). The nmr of the crude indicated the presence of **1***a* (21%), the corresponding sulfone sulfoxide (**1***e*) (31%), $CH_3SO_2CHClS(=O)Ph$ (21%), and **1***b* (26%). The mixture was run on preparative tlc, developed with $CHCl_3$–Et_2O (1:1). The band at R_f 0.27 was scraped and washed with $CHCl_3$ (60 mL) affording **1***e* which was identical with authentic material by nmr, ir, and tlc. The band at R_f 0.57 was handled in the same way and furnished a mixture of **1***a* and another compound. The identity of **1***a* was confirmed by tlc and addition of authentic material which caused the expected change in the appropriate signals in the nmr of the mixture. Subtraction of the signals due to **1***a* from the nmr of the mixture left the spectrum δ: 7.50 (5H, m), 5.17 (1H, s), and 3.23 (3H, s). On this basis the second compound in the mixture was assigned the monochlorosulfone-sulfoxide structure shown above. The band at R_f 0.81 was processed as described above, and afforded **1***b* which was identical with authentic material by nmr, ir, and tlc.

Oxidation of *1*b

The dichlorosulfone-sulfoxide **1***b* (0.500 g) was oxidized to the dichlorodisulfone **1***d* in the same way described for the oxidation of **1***c*. After recrystallization, the disulfone (0.350 g) was shown to be identical to authentic disulfone by ir, nmr, mp, and mixture mp.

Exhaustive Chlorination of *1*b–*6*b

Exhaustive chlorinations of the dichlorosulfone-sulfoxides **1***b*–**6***b* were carried out as illustrated by the details provided below for the reaction on **2***b*. Results for these systems appear in Table 3.

The sulfone-sulfoxide **2***b* (0.500 g) was dissolved in glacial acetic acid (75 mL) and water (18 mL) added. Cl_2 (ca. 200 mL/min) was bubbled into the reaction mixture for 8 h. Water (150 mL) was added and the resultant mixture washed with methylene chloride (3 × 100 mL aliquots). The combined organic layers were washed with 2.5% w/v NaOH (3 × 100 mL aliquots). The organic layer was dried and concentrated.

The residue was chromatographed on silica gel (50 g) employing carbon tetrachloride elution (50 mL aliquots). Fractions 4–9 were combined and concentrated affording *p*-chlorobenzenesulfonyl chloride (0.262 g) which was identical to authentic material by ir, nmr, ms, and tlc. Fractions 40–60 were combined and concentrated furnishing trichloromethyl methyl sulfone (0.245 g) which was identical to authentic material (27). Fraction 95 contained dichloromethyl methyl sulfone (0.015 g) which was identical to authentic material by ir, nmr, and mp (27).

Acknowledgements

The authors are indebted to Dr. J. H. Kim for running the mass spectra. We are grateful to Dalhousie University for financial support in the form of a grant from the Research Development Fund.

1. (*a*) H. O. Fong, W. R. Hardstaff, D. G. Kay, R. F. Langler, R. H. Morse, and D. N. Sandoval. Can. J. Chem. **57**, 1206 (1979); (*b*) T. P. Ahern, D. G. Kay, and R. F. Langler. Can. J. Chem. **56**, 2422 (1978).
2. R. F. Langler, Z. A. Marini, and J. A. Pincock. Can. J. Chem. **56**, 903 (1978).
3. R. F. Langler and J. A. Pincock. Can. J. Chem. **55**, 2316 (1977).
4. J. S. Grossert, W. R. Hardstaff, and R. F. Langler. Can. J. Chem. **55**, 421 (1977).
5. J. S. Grossert and R. F. Langler. Can. J. Chem. **55**, 407 (1977).
6. R. F. Langler. Can. J. Chem. **54**, 498 (1976).
7. J. R. Jardine and R. F. Langler. J. Chromatogr. **116**, 211 (1976).
8. W. R. Hardstaff, R. F. Langler, J. Leahy, and M. J. Newman. Can. J. Chem. **53**, 2664 (1975).
9. J. S. Grossert, W. R. Hardstaff, and R. F. Langler. Chem. Commun. 50 (1973).
10. J. S. Grossert and R. F. Langler. Chem. Commun. 49 (1973).
11. F. Raschig and W. Prahl. Justus Liebigs Ann. Chem. **448**, 307 (1926).
12. T. Thomson and T. S. Stevens. J. Chem. Soc. 69 (1932).
13. W. M. Ziegler and R. Connor. J. Am. Chem. Soc. **62**, 2596 (1940).
14. T. B. Johnson and I. B. Douglass. J. Am. Chem. Soc. **63**, 1571 (1941).
15. F. G. Bordwell and G. D. Cooper. J. Am. Chem. Soc. **73**, 5184 (1951).
16. F. G. Bordwell and W. T. Brannen. J. Am. Chem. Soc. **86**, 4645 (1964).
17. L. A. Paquette. J. Am. Chem. Soc. **86**, 4085 (1964).
18. F. G. Bordwell and B. Jarvis. J. Org. Chem. **33**, 1182 (1968).
19. M. Cinquini, D. Landini, and A. Maia. Chem. Commun. 734 (1972).
20. P. Robson, P. Speakman, and D. Stewart. J. Chem. Soc. C, 2180 (1968).
21. W. G. Phillips and K. W. Ratts. J. Org. Chem. **36**, 3145 (1971).
22. J. Butler and R. M. Kellogg. J. Org. Chem. **42**, 973 (1977).
23. J. E. Huheey. J. Phys. Chem. **69**, 3284 (1965); **70**, 2086 (1966).
24. T. Durst and F. de Reinach-Hirtzbach. Tetrahedron Lett. 3677 (1976).
25. P. P. Davis, J. S. Grossert, R. F. Langler, and W. S. Mantle. Org. Mass Spectrom. **12**, 659 (1977).
26. W. R. Hardstaff and R. F. Langler. Org. Mass Spectrom. **10**, 215 (1975).
27. W. E. Truce, G. H. Birum, and E. T. McBee. J. Am. Chem. Soc. **74**, 3594 (1952).

^{1}H nuclear magnetic resonance study of 2,2′-anhydro-O^2-β-D-arabinosyluracil. Four- and five-bond coupling constants in the sugar moiety

FRANK E. HRUSKA, JAMES G. DALTON, AND MIECZYSLAW REMIN[1]

Chemistry Department, University of Manitoba, Winnipeg, Man., Canada R3T 2N2

Received February 26, 1979

FRANK E. HRUSKA, JAMES G. DALTON, and MIECZYSLAW REMIN. Can. J. Chem. 57, 2191 (1979).

A high resolution proton magnetic resonance spectrum for 2,2′-anhydro-O^2-β-D-arabinosyluracil in aqueous solution at 80°C is presented. The spectrum provides evidence for the presence of long-range four-bond ($^4J_{1'3'}$, $^4J_{1'4'}$, $^4J_{2'4'}$) and five-bond ($^5J_{1'5'}$, $^5J_{1'5''}$, $^5J_{2'5'}$, $^5J_{2'5''}$) coupling interactions involving the furanose hydrogens. The ^5J data represent the first reported evidence for the presence of coupling interactions involving the anomeric proton and exocyclic $C_{5'}$ protons in a furanose system. The relative signs of the ^4J and ^5J couplings were determined by double resonance methods. The ^4J and ^5J interactions are discussed using crystallographic data and the theory of long-range couplings.

FRANK E. HRUSKA, JAMES G. DALTON et MIECZYSLAW REMIN. Can. J. Chem. 57, 2191 (1979).

On rapporte les spectres de résonance magnétique à haute résolution de l'anhydro-2,2′ O^2-β-D-arabinosyluracile en solution aqueuse à 80°C. Le spectre fournit des preuves de la présence d'interactions de couplage à longue distance à travers quatre liaisons ($^4J_{1'3'}$, $^4J_{1'4'}$, $^4J_{2'4'}$) et cinq liaisons ($^5J_{1'5'}$, $^5J_{1'5''}$, $^5J_{2'5'}$, $^5J_{2'5''}$) impliquant les hydrogènes du furannose. Les données de ^5J représentent les premières preuves rapportées concernant l'existence d'interactions de couplage impliquant un proton anomère et les protons $C_{5'}$ exocycliques dans un système furannose. On a déterminé les signes relatifs des couplages ^4J et ^5J par des méthodes de double résonance. On discute des interactions ^4J et ^5J en faisant appel à des données cristallographiques et à la théorie des couplages à longue distance.

[Traduit par le journal]

Introduction

The appearance of long-range spin–spin coupling interactions involving the hydrogens of a furanose system has been of interest since Hall and coworkers (1) noted that such systems can exhibit an extensive array of ^4J and ^5J H—H couplings which undoubtedly contributed to spectral broadening beyond the 'natural' linewidths. In early 100 MHz studies of the anhydronucleoside, 2,2′-anhydro-O^2-β-D-arabinosyluracil[2] (aU) (Fig. 1), evidence for the presence of the four-bond couplings $^4J_{1'3'}$, $^4J_{1'4'}$, and $^4J_{2'4'}$ was reported for aU in D_2O solution (2–4). Analogous coupling interactions are also apparent in the spectra of several purine nucleosides in liquid ND_3 (5). In more recent 100 and 250 MHz studies on aU in aqueous and DMSO solution (6, 7) long-range coupling interactions were not observed and in fact the presence of these interactions was questioned (6).

In this work we discuss ^{1}H nmr evidence for the appearance of the five-bond ($^5J_{1'5'}$, $^5J_{1'5''}$, $^5J_{2'5'}$, $^5J_{2'5''}$) coupling interactions as well as the four-bond ($^4J_{1'3'}$, $^4J_{1'4'}$, $^4J_{2'4'}$) interactions involving the furanose hydrogens in aU. The five-bond couplings are particularly interesting since they are, to the best of our knowledge, the first reported examples

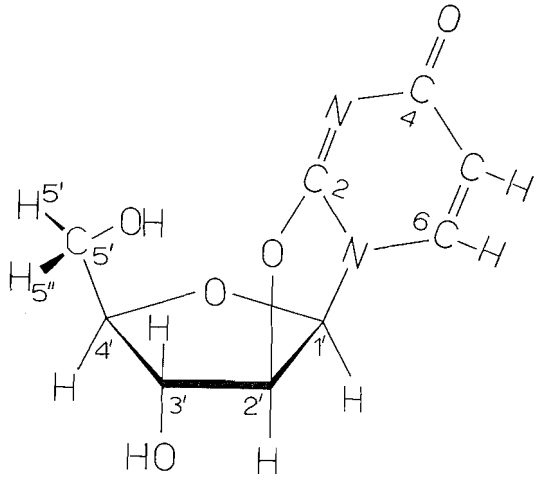

FIG. 1. Structure of 2,2′-anhydro-O^2-β-D-arabinosyluracil (aU).

[1]Permanent address: Department of Biophysics, Institute of Experimental Physics, University of Warsaw, 02-089 Warszawa, Poland.

[2]Abbreviations: aU is 2,2′-anhydro-O^2-β-D-arabinosyluracil; DSS is sodium 2,2-dimethyl-2-silapentane-5-sulfonate.

0008-4042/79/162191-05$01.00/0

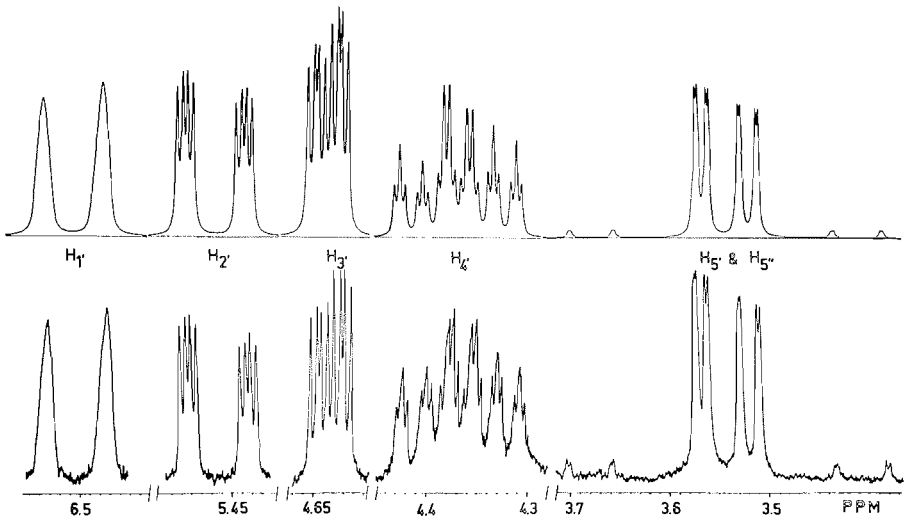

FIG. 2. (*a*) Single scan, continuous wave 100 MHz spectrum of the ribose protons of aU (0.2 *M* in D_2O, pD = 7.0, 80°C). (*b*) Computer simulated spectrum.

of coupling interactions of the anomeric $H_{1'}$ and $H_{2'}$ protons with the exocyclic hydroxymethyl protons in a furanoside. Analogous five-bond coupling between the anomeric hydrogen and the exocyclic methylene hydrogens in pyranoside systems has been suggested by Lemieux *et al.* (8).

Experimental

Samples of aU were obtained from Dr. K. K. Ogilvie and from Terra Marine Bioresearch, California, and used without further purification. The quality of the spectra obtained indicates the absence of significant amounts of paramagnetic impurities (see Fig. 2). DSS was used as an internal nmr reference. Samples were thrice freeze-dried and finally dissolved in 100% D_2O (final concentration ca. 0.2 *M*). The pD of the solution was adjusted to 7.0 ± 0.1 with DCl and NaOD. Spectra were obtained on Bruker WH-90DS and Varian HA-100 spectrometers. The calibration of spectra and double resonance experiments were carried out by standard methods. Spectral analyses were carried out using LAME (9). Computer-stimulated spectra were generated as a test of the chemical shift (δ) and coupling constant (*J*) data. Since our discussion will be restricted to the *J* data, only these are given in Table 1; the δ data have been presented elsewhere (10). Decomposition of aU, presumably by hydrolysis to arabinouridine, was observed at 80°C, but caused no difficulties since the spectra could be accumulated quickly at the concentrations used.

Results and Discussion

Spectra

The 100 MHz spectrum (80°C) of the sugar protons of aU is shown in Fig. 2 accompanied by a computer-generated spectrum. The spectrum is quite unlike nucleoside spectra reported in the literature (those for anhydronucleosides included (6, 7)), showing clearly an extensive array of small splittings which can be attributed to long-range (^4J,^5J) H—H coupling constants. For example, the complex $H_{4'}$ band (4.36 ppm) with 20 discernible lines is completely accounted for by the three vicinal couplings ($^3J_{3'4'}$, $^3J_{4'5'}$, $^3J_{4'5''}$) and a pair of four-bond interactions, $J_{1'4'}$(−0.52 Hz) and $J_{2'4'}$(+0.55 Hz). The sign of $^4J_{2'4'}$ was determined by selective irradiation of the $H_{3'}$ band, while the $H_{2'}$ resonances were being observed. In Fig. 3 are illustrated the results of weak irradiation experiments which demonstrate that $^4J_{1'4'}$ is negative, i.e., of opposite sign to $^4J_{2'4'}$. A series of weak irradiating fields was applied at 0.10 Hz intervals to one, or the other, of the broad $H_{1'}$ bands at 6.53 and 6.47 ppm while the $H_{2'}$ quartets were recorded. As the perturbing field was stepped through the bands towards *high field*, the point of maximum perturbation in the $H_{2'}$

TABLE 1. Proton coupling constants (Hz)[a] for 0.2 *M* 2,2′-anhydro-O^2-β-D-arabinosyluracil in D_2O (pD = 7.0)

J[b]	5°C	30°C	80°C
$^3J_{56}$	7.4	7.4	7.4
$^3J_{1'2'}$	6.0	5.9	5.8
$^3J_{2'3'}$	0.7	0.8	1.0
$^3J_{3'4'}$	1.8	1.9	2.3
$^3J_{4'5'}$	2.9	3.3	4.2
$^3J_{4'5''}$	4.7	4.9	5.1
$^2J_{5'5''}$	(−13.9)[c]	−13.5	−12.6
$^4J_{1'3'}$	−0.81	−0.75	−0.64
$^4J_{1'4'}$	−0.32	−0.36	−0.42
$^4J_{2'4'}$	0.54	0.54	0.55
$^5J_{1'5'}$	[d]	[d]	0.28
$^5J_{1'5''}$	[d]	[d]	0.33
$^5J_{2'5'}$	[d]	[d]	0.05–0.1
$^5J_{2'5''}$	[d]	[d]	0.05–0.1

[a]Estimated error < 0.1 Hz.
[b]Signs were determined at 80°C only.
[c]Not observable since $H_{5'}$ and $H_{5''}$ are isochronous at 5°C. Obtained by extrapolation of 30 and 80°C values.
[d]Not observable.

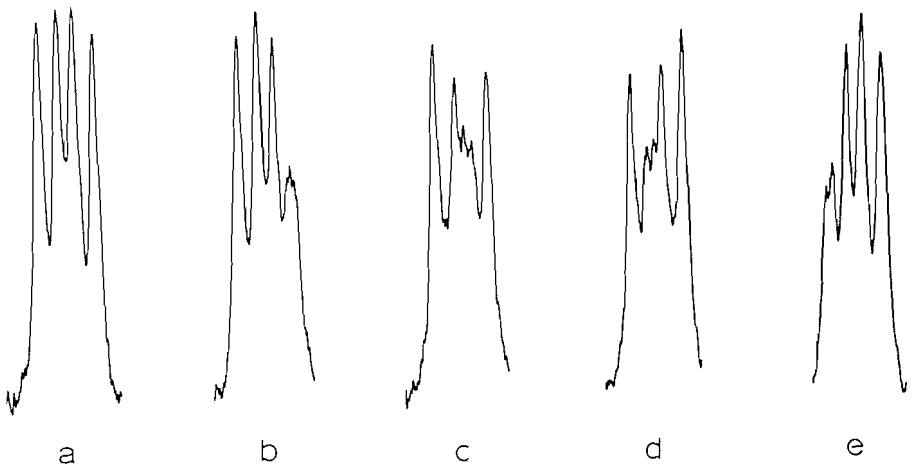

FIG. 3. Low-field $H_{2'}$ quartet (5.04 ppm): (*a*) unperturbed by second irradiating field; (*b–e*) with weak irradiation of the low-field $H_{1'}$ band (6.54 ppm) at 653.68, 653.25, 652.99, and 652.60 Hz respectively. As the perturbing field is stepped towards *high* field, the point of maximum perturbation in the $H_{2'}$ quartet progresses towards *low* field. This pattern of changes indicates that $J_{1'4'}$ and $J_{2'4'}$ have opposite signs, i.e., $J_{1'4'}$ is negative.

quartets progressed uniformly towards *low* field. For example, Fig. 3*a* shows the *unperturbed* low-field $H_{2'}$ quartet at 5.04 ppm while Figs. 3*b*–3*e* show the influence of perturbing fields at 653.68, 653.25, 652.99, 652.60 Hz, respectively. With these careful experiments the progression of the perturbation towards low field is unmistakable. It is a simple matter to show with energy level diagrams that this sequence of changes in the $H_{2'}$ quartets is consistent with opposite signs for $J_{1'4'}$ and $J_{2'4'}$, i.e., $J_{1'4'}$ is negative.

The most interesting of the long-range couplings can be observed in the 5′,5″ spectral band at 80°C (Fig. 2). The four intense lines, as well as the satellite lines, show an additional splitting of about 0.3 Hz. In contrast at 5 and 30°C only two broad bands, with no fine structure, are found in the 5′ region indicating that the 5′,5″ protons are nearly isochronous. The increase in temperature has, therefore, increased the $H_{5'}$,$H_{5''}$ relative shift, and this coupled with the improved resolution at 80°C leads to the appearance of the fine structure.

Strong irradiation of the $H_{1'}$ bands leads to a collapse of the fine splittings in the 5′,5″ region, demonstrating that they are due to $^5J_{1'5'}$ and $^5J_{1'5''}$ interactions. On the other hand, when $H_{2'}$ is irradiated with a strong decoupling field, the linewidths in the 5′,5″ band are noticeably reduced and the fine splittings due to $^5J_{1'5'}$,$^5J_{1'5''}$ interactions become more apparent (Fig. 4). This narrowing provides evidence for the presence of ^5J couplings between $H_{2'}$ and *both* the $H_{5'}$ and $H_{5''}$ protons.

A series of careful selective spin-decoupling and spin-tickling experiments, analogous to those used

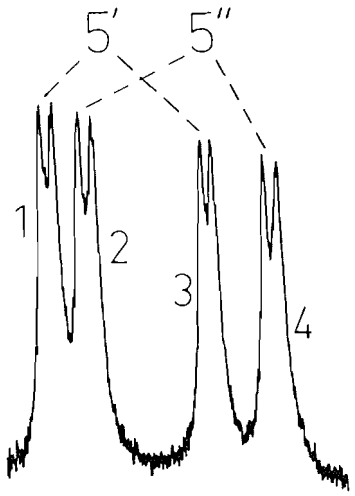

FIG. 4. The strong central resonances of the 5′,5″ band of aU with $H_{2'}$ decoupled (80°C, single scan, 100 MHz).

to determine the signs of $^4J_{2'4'}$ and $^4J_{1'4'}$ (above and Fig. 3), allowed us to determine the signs of the ^5J interactions involving $H_{5'}$, and $H_{5''}$ (all positive). Further details of these experiments are available from the authors upon request.

Double resonance experiments demonstrated that the eight-line $H_{3'}$ band (4.63 ppm) could be attributed to $^3J_{2'3'}$ and $^3J_{3'4'}$ couplings (both positive) and the four-bond interaction $^4J_{1'3'}$ (0.64 Hz and negative). The linewidths in this region are about 0.2 Hz, indicating that ^4J interactions of $H_{3'}$ with $H_{5'}$ and $H_{5''}$ must be less than 0.1 Hz.

Also note (Fig. 2) that the $H_{1'}$ band widths can be reproduced by our spectral simulation which

incorporated the ^4J and ^5J interactions involving $H_{1'}$. Thus, long-range couplings account for the $H_{1'}$ broadening in aU, and undoubtedly contribute to the $H_{1'}$ linewidths for nucleosides in general.

^{3}J *Coupling Constants*

The vicinal couplings $^3J_{1'2'}$, $^3J_{2'3'}$, and $^3J_{3'4'}$ for aU have been discussed elsewhere (2–4, 6, 7, 11) and presented as evidence that the geometry of the furanose ring in solution is similar to that found in the crystal state, i.e., 4′-*endo* (12, 13). Particularly informative are the diminutive *trans* couplings $^3J_{2'3'}$ and $^3J_{3'4'}$ which exhibit, in the 5–80°C interval, ranges of 0.7–1.0 Hz and 1.8–2.3 Hz, respectively, consistent with dihedral angles near 90°. In the crystal two molecules (labelled A and B) are found in the unit cell of aU (12, 13); the observed dihedral angles for $H_{2'}$—$C_{2'}$—$C_{3'}$—$H_{3'}$ and $H_{3'}$—$C_{3'}$—$C_{4'}$—$H_{4'}$ lie in the range 86–96°.

In the crystal state aU assumes the *gauche–trans* conformation about the $C_{4'}$—$C_{5'}$ bond. In solution at 80°C, however, interconversion occurs between the three staggered conformers, with approximately equal populations of each (3, 10).

Not shown in our spectrum is the pair of doublets due to the H_5 and H_6 protons of the base ($^3J_{56}$ = 7.4 Hz). The linewidths in these bands are 0.3 Hz (H_5) and 0.4 Hz (H_6). Hence, long-range interaction $^5J_{1'5}$ and $^5J_{1'6}$ cannot be larger than about 0.1–0.2 Hz. The low value of $^5J_{1'5}$ is consistent with the presence of the *high-syn* conformation about the *N*-glycosyl linkage (12, 13).

^{4}J *Coupling Constants*

^4J H—H couplings in the saturated fragments (I)

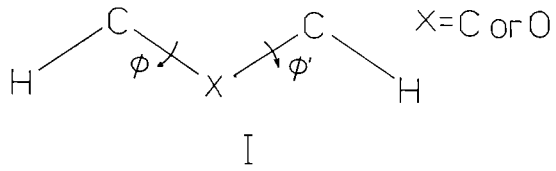

I

are known to depend on the ϕ and ϕ' torsion angles, reaching a maximum (positive) value for the all-*trans* ($\phi = \phi' = 180°$) situation (14, 15). Relevant to our discussion of the $^4J_{1'3'}$, $^4J_{2'4'}$, and $^4J_{1'4'}$ are the fragments $H_{1'}$—$C_{1'}$—$C_{2'}$—$C_{3'}$—$H_{3'}$ (114°, 146°)[3], $H_{2'}$—$C_{2'}$—$C_{3'}$—$C_{4'}$—$H_{4'}$ (148°, 146°), and $H_{1'}$—$C_{1'}$—O—$C_{4'}$—$H_{4'}$ (143°, 146°), respectively. Barfield *et al.* (14) have reported the ϕ,ϕ' dependencies of ^4J in propanic fragments (X = C). Using their plots and assuming the crystallographic angles we estimate $^4J_{2'4'}$ = 0.5–1.0 Hz and $^4J_{1'3'} \simeq 0$ Hz. In the former case, agreement with the experimental value (+0.55 Hz) is reasonable, whereas in the latter case the observed coupling (−0.64 Hz) is somewhat smaller than predicted. However, the predicted stereochemical trend (i.e., $J_{2'4'}$ is more positive than $J_{1'3'}$) agrees with the experimental data.

Though the stereochemistry (ϕ,ϕ') of the four-bond fragments of $^4J_{2'4'}$ and $^4J_{1'4'}$ is virtually identical (see above), these couplings differ markedly (+0.55 Hz and −0.42 Hz, respectively). This difference is probably due to the change in the central atom in the fragments. Barfield and co-workers (14) have studied the effect on ^4J of the change X = C to X = O in fragment I, but unfortunately data for only two conformations were reported: $^4J(cis) = {}^4J(120°, 120°)$ and $^4J(trans) = {}^4J(120°, 240°)$. Their calculations predicted that this substitution should lead to more negative values of $^4J(cis)$ and more positive values of $^4J(trans)$, the changes being 0.5–0.6 Hz in an absolute sense. If we can assume that the $^4J_{2'4'}$ and $^4J_{1'4'}$ fragments, with $\phi \simeq \phi' \approx 145°$, are more *cis*-like than *trans*, then we state that calculations of Barfield *et al.* (14) are in reasonable agreement with the observed trend.

^{5}J *Coupling Constants*

The appearance of the $^5J_{1'5'}$ and $^5J_{1'5''}$ splittings in the 80°C spectrum may be a consequence of several factors, one of which must be the high resolution achievable in water solution at this temperature. Also important must be the fact that, except for $H_{5'}$ and $H_{5''}$, the furanose protons form a loosely coupled spin system, the ratio of relative shift to mutual coupling constant being no less than 11.6 (at 100 MHz) for any pair of protons. Of the many nucleosides examined, aU provides the most loosely coupled system. This means that broadening of the $H_{5'}$,$H_{5''}$ resonances due to virtual coupling to $H_{2'}$ and $H_{3'}$ is minimal.

Another reason, perhaps, why we observe $^5J_{1'5'(5'')}$ interactions in aU, while similar interactions have not been reported in normal nucleosides, i.e., those without the anhydro linkage, could lie in the unique geometry of its sugar *rings*. In aU the ring assumes a 4′-*endo* pucker (12, 13), whereas in solution the furanose ring of normal nucleosides pseudorotates between 2′-*endo* and 3′-*endo* conformations (16, 17). Each of the exocyclic protons in a nucleoside is connected to the anomeric proton by a *single* five-bond path (II) which may be considered a butanic fragment (14, 15) with a single oxygen substitution. Alternate six-bond paths through $C_{2'}$ and $C_{3'}$ also connect these nuclei, but these longer paths should

[3]The angles listed in parentheses will refer respectively to ϕ and ϕ'. For example, in the $H_{1'}$—$C_{1'}$—$C_{2'}$—$C_{3'}$—$H_{3'}$ fragment they refer to the torsion angle about $C_{1'}$—$C_{2'}$ (ϕ) and $C_{2'}$—$C_{3'}$ (ϕ') (see Barfield *et al.* (14)). The values are taken from ref. 13.

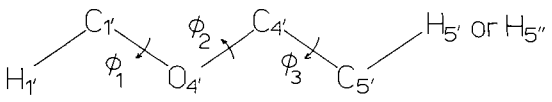

II

be less important than II. In the 4′-*endo* conformation of crystalline aU (12, 13), the dihedral angles ϕ_1 and ϕ_2 are 143 and 96°, respectively. From the Altona–Sundaralingam analysis of nucleoside crystallographic data (16), we estimate that ϕ_1 is approximately 50 and 25° smaller in the 2′-*endo* and 3′-*endo* conformations, respectively. Thus, ϕ_1(2′-*endo*) $\approx$ 95° and ϕ_1(3′-*endo*) $\approx$ 120°. On the other hand ϕ_2 should be larger in the 2′- and 3′-*endo* conformations, i.e., ϕ_2(2′-*endo*) $\approx$ 120° and ϕ_2(3′-*endo*) $\approx$ 145°.

Theoretical calculations, reviewed by Barfield and Chakrabarti (15), indicate that if the indirect mechanism of ^5J coupling predominates in a butanic fragment, then this coupling should be independent of ϕ_2 but should display a Karplus-like dependence on ϕ_1 (as well as ϕ_3, see below). Now, if this theory can be applied to nucleosides, then from the ϕ_1 values we can predict for $^5J_{1'5'(5'')}$ the following trend: ^5J(4′-*endo*) > ^5J(3′-*endo*) > ^5J(2′-*endo*).

The ^5J interactions in fragment II should depend also on ϕ_3 (which can be 180 or 60° depending on whether the $C_{4'}$—$C_{5'}$ bond is oriented *gauche–gauche*, *gauche–trans*, or *trans–gauche*). However, in solution interconversion occurs between the three staggered conformations, making difficult the evaluation of the influence of this conformational feature on the ^5J couplings.

Acknowledgments

This work was supported by grants from the National Research Council of Canada, the Rh Institute of Manitoba, and the Faculty of Graduate Studies of the University of Manitoba. We thank Dr. K. K. Ogilvie (McGill) for a sample of the titled molecule and members of the NMR group in Manitoba for valuable discussions.

1. L. D. Hall, J. F. Manville, and A. Tracey. Carbohydr. Res. **4**, 514 (1967).
2. F. E. Hruska, A. Mak, H. Singh, and D. Shugar. Can. J. Chem. **51**, 1099 (1973).
3. B. P. Cross and T. Schleich. Biopolymers, **12**, 2381 (1973).
4. J. G. Dalton. M.Sc. Thesis, University of Manitoba, Winnipeg, Man. 1971.
5. E. Westhof, O. Roder, I. Croneiss, and H.-D. Lüdemann. Z. Naturforsch. Teil C, **30**, 131 (1975).
6. W. Guschlbauer, T.-D. Son, M. Blandin, and J. C. Catlin. Nucleic Acid Res. **1**, 855 (1974).
7. C.-H. Lee and R. H. Sarma. J. Am. Chem. Soc. **98**, 3541 (1978).
8. R. U. Lemieux, E. Fraga, and K. A. Watanabe. Can. J. Chem. **46**, 61 (1968).
9. C. W. Haigh and J. M. Williams. J. Mol. Spectrosc. **32**, 398 (1969).
10. J. G. Dalton, A. L. George, F. E. Hruska, T. N. McCaig, K. K. Ogilvie, J. Peeling, and D. J. Wood. Biochim. Biophys. Acta, **478**, 261 (1977).
11. F. E. Hruska. *In* Proceedings international symposium on the conformation of biological molecules and polymers, symposia on quantum chemistry and biochemistry. Vol. 5. *Edited by* B. Pullman and E. D. Bergmann. Academic Press, Jerusalem. 1973. p. 345.
12. D. Suck and W. Saenger. Acta Crystallogr. Sect. B, **29**, 1323 (1972).
13. L. T. J. Delbaere and M. N. G. James. Acta Crystallogr. Sect. B, **29**, 2905 (1973).
14. M. Barfield, R. J. Spear, and S. Sternhell. J. Am. Chem. Soc. **93**, 5322 (1971).
15. M. Barfield and B. Chakrabarti. Chem. Rev. **69**, 757 (1969).
16. C. Altona and M. Sundaralingam. J. Am. Chem. Soc. **94**, 8205 (1972).
17. C. Altona and M. Sundaralingam. J. Am. Chem. Soc. **95**, 2333 (1973).

The electrochemical synthesis of some heteronuclear metal carbonyls

JACOB J. HABEEB, DENNIS G. TUCK, AND SAMUEL ZHANDIRE
Department of Chemistry, University of Windsor, Windsor, Ont., Canada N9B 3P4

Received January 22, 1979

JACOB J. HABEEB, DENNIS G. TUCK, and SAMUEL ZHANDIRE. Can. J. Chem. **57**, 2196 (1979).

The electrochemical oxidation of zinc, cadmium, or indium in the presence of $Co_2(CO)_8$ or $Mn_2(CO)_{10}$ in an organic solvent gives rise to the appropriate heteronuclear metal carbonyl $M[M'(CO)_n]_m$ (M = Zn, Cd, In; M′ = Co, Mn; n = 4, 5; m = 2, 3). The advantages of this method are discussed, as is the mechanism of the processes which lead to the reaction products.

JACOB J. HABEEB, DENNIS G. TUCK et SAMUEL ZHANDIRE. Can. J. Chem. **57**, 2196 (1979).

L'oxydation électrochimique du zinc, du cadmium et de l'indium en présence de $Co_2(CO)_8$ ou de $Mn_2(CO)_{10}$ dans un solvant organique conduit au métal carbonyle hétéronucléaire approprié $M[M'(CO)_n]_m$ (M = Zn, Cd, In; M′ = Co, Mn; n = 4, 5; m = 2, 3). On discute des avantages de cette méthode de même que du mécanisme du processus qui conduit aux produits de la réaction.

[Traduit par le journal]

Introduction

The synthesis of heteronuclear metal – metal bonded carbonyls of the general formula $M[M'(CO)_n]_m$ and of the adducts $M[M'(CO)_n]_m \cdot L$ has been a subject of some interest in recent years. One of the reasons for this concern is that such compounds involve the bonding of a transition metal M′ to a main group element (M = Sn, Pb; Ga, In, Tl; Zn, Cd, Hg). The first reported preparation (1) involved the reaction of Zn or Cd with $Co_2(CO)_8$ at high temperatures under high pressures of carbon monoxide. Similar methods, but under milder conditions (refluxing diglyme, 120°C, 10 h), have more recently yielded $M[Mn(CO)_5]_2$ (M = Zn, Cd) (2), and milder conditions again suffice for $M[Co(CO)_4]_4$ (M = Sn, Pb) (3). A different approach, first used in this field by Carey and Noltes (4), involves alkane elimination between a metal alkyl R_2M (M = Zn, Cd) and manganese pentacarbonyl hydride, and similar methods have been employed in the preparation of $M[Re(CO)_5]_2$ (M = Zn, Cd) (5). Another source of the transition metal carbonyl moiety is the carbonylate anion, which reacts with $Hg(CN)_2$ to produce $Hg[Re(CO)_5]_2$ (5), or with RHgOH to give $Hg[Mn(CO)_5]_2$ (6).

We now report electrochemical methods by which zinc, cadmium, or indium can be oxidised in the presence of $Mn_2(CO)_{10}$ or $Co_2(CO)_8$ in non-aqueous media to give the appropriate $M[M'(CO)_n]_m$ species. The compound may be recovered directly, but it is equally convenient to isolate the adduct with some neutral bidentate donor such as 2,2′-bipyridine by adding the latter to the electrochemical cell.

Experimental

Materials

The general experimental set-up was identical to that used previously (7). Cadmium (m4N+) and zinc (m4N5) were used in the form of rods (10 cm long and 1 cm diameter), with the lower part hammered flat to increase the surface area. Tin metal was used in the form of a sheet (5 cm × 5 cm × 0.127 mm) supported by a platinum wire lead, as was the indium electrode, made from indium shot hammered into a thin sheet (2 cm × 2 cm). All metals were supplied by Alfa Inorganics. Platinum wire (10 cm long and 1 mm diameter) was used as the cathode in all experiments.

Methanol (analytical grade) was dried over Linde molecular sieves, and benzene, diethyl ether, and petroleum ether (36–55°C bp) over sodium. Dicobalt octacarbonyl and dimanganese decacarbonyl were used without further purification. 2,2′-Bipyridine (bipy) was used as supplied; *N,N,N′,N′*-tetramethylethylendiamine (TMED) was dried over KOH and then distilled under nitrogen.

Electrochemical Procedures

The electrochemical procedures are very similar to those described earlier (7). The metal to be oxidised formed the anode of a simple cell containing a solution of the metal carbonyl in an organic solvent mixture; this solution also contained any neutral bidentate donor. The details of the solution compositions used are shown in Table 1. The applied voltage was 20–50 V, as dictated by the solution conditions, given that a current of 20–50 mA produced a reasonable rate of reaction without overheating the solution (see Table 1). A Coutant 50/50 power supply provided the applied voltage. Tetraethylammonium perchlorate (ca. 10–15 mg) was generally added to enhance the conductivity of the solution, although in those cases in which more methanol than benzene was present, a sufficient current flowed without any ammonium salt being added.

Infrared and nmr spectra were recorded with Beckman IR-12 and Varian EM-360 spectrometers respectively. Mass spectra were obtained on a Varian CH-5 spectrometer operating in the field desorption mode. Metal analysis was by atomic absorption spectrophotometry.

0008-4042/79/162196-04$01.00/0

TABLE 1. Experimental conditions for the electrochemical preparation of $M[M'(CO)_n]_m$ compounds and their adducts

Product	Vol. of MeOH (cm^3)	Vol. of C_6H_6 (cm^3)	Mass of Co or Mn carbonyl (g)	Mass of ligand (g)	Initial voltage (V)	Initial current (mA)	Time of electrolysis (h)	Mass of metal dissolved (g)	% yield of product on basis of metal dissolved
$Zn[Co(CO)_4]_2$·bipy	40	25	0.6	0.25	6	30	9	0.25	33
$Zn[Mn(CO)_5]_2$·bipy	30	40	1.0	0.5	20	25	26	0.20	55
$Cd[Co(CO)_4]_2$	50	0	0.4	—	8	40	6	0.30	65
$Cd[Co(CO)_4]_2$·TMED	30	30	0.6	0.3	10	25	13	0.25	74
$Cd[Co(CO)_4]_2$·bipy	60	20	1.2	0.56	3	50	8	0.40	64
$Cd[Mn(CO)_5]_2$·bipy	30	40	0.9	0.4	30	20	12	0.50	61
$In[Co(CO)_4]_3$	30	10	0.7	—	8	50	4.5	[a]	82[a]
$In[Co(CO)_4]_3$·bipy	40	10	1.0	0.17	5	60	4	[a]	66[a]
$In[Mn(CO)_5]_3$·bipy	30	20	0.9	0.24	40	30	16	[a]	80[a]

[a]Weight of metal dissolved not measured because metallic indium deposited at the bottom of the cell during experiment; % yield based on $Mn_2(CO)_{10}$ or $Co_2(CO)_8$ added initially.

TABLE 2. Analytical results for $M[M'(CO)_n]_m$ compounds and adducts

Compound	Colour	Analytical results (%)[a] Zn/In/Cd	Mn/Co	C	H	N
$Zn[Co(CO)_4]_2$·bipy	Yellow	11.5 (11.7)	21.2 (21.0)	39.1 (39.0)	1.4 (1.5)	5.0 (5.1)
$Zn[Mn(CO)_5]_2$·bipy	Orange-red	10.4 (10.7)	18.3 (18.0)	39.4 (39.3)	1.3 (1.3)	4.4 (4.6)
$Cd[Co(CO)_4]_2$	Pale yellow	25.3 (25.0)	25.9 (26.2)			
$Cd[Co(CO)_4]_2$·TMED	Pale yellow	19.8 (19.7)	20.8 (20.7)	29.0 (29.5)	2.8 (2.8)	5.3 (4.9)
$Cd[Cd(CO)_4]_2$·bipy	Yellow	18.4 (18.4)	18.9 (19.3)	35.6 (35.4)	1.2 (1.3)	4.5 (4.6)
$Cd[Mn(CO)_5]_2$·bipy	Orange-red	17.1 (17.1)	— —	37.7 (36.5)	1.5 (1.2)	4.4 (4.2)
$In[Co(CO)_4]_3$	Red	18.1 (18.0)	27.8 (28.2)			
$In[Co(CO)_4]_3$·bipy	Red	14.0 (14.7)	23.2 (22.6)			
$In[Mn(CO)_5]_2$·bipy	Violet	13.6 (13.4)	19.0 (19.2)			

[a]Calculated values in parentheses.

Isolation of Products

We describe the electrochemical preparation of two compounds to illustrate the general method used.

$Cd[Co(CO)_4]_2$

A solution of 0.4 g $Co_2(CO)_8$ in 50 cm^3 methanol was electrolysed for 6 h at a current maintained at approximately 40 mA; the initial voltage of 8 V was adjusted occasionally as (presumably) surface contamination of the electrodes occurred. During this period, the brown solution became pale yellow, and some pink material deposited on the cathode. The mixture was filtered under dry nitrogen, and the resulting filtrate evaporated to dryness *in vacuo* to yield pale yellow crystals. This crude product was sublimed at 80°C *in vacuo* yielding 0.35 g of product, a 65% yield on the basis of 0.2 g of Cd dissolved from the previously weighed anode.

$Cd[Co(CO)_4]_2$·TMED

A mixture of 20 mg Et_4NClO_4, 30 cm^3 of methanol, 30 cm^3 of benzene, 0.3 g of TMED, and 0.6 g of $Co_2(CO)_8$ was electrolysed for 13 h at a current of 25 mA (initial voltage 10 V). The voltage was raised as appropriate to maintain this current. At the end of electrolysis, 0.25 g of cadmium was found to have been dissolved from the anode. The mixture of products was filtered, and a (dried) pink residue (0.3 g) was found to contain 52.1% cobalt; insolubility of this product made characterization impossible. The orange-yellow filtrate was reduced in volume *in vacuo* at ambient temperature to give yellow crystals which were filtered off and dried *in vacuo* for 3 h. The total yield of the yellow product was 1.0 g (74%, based on Cd dissolved).

A list of the compounds prepared and the analytical results are given in Table 2. Field desorption mass spectrometry, which has many advantages in inorganic and organometallic chemistry, was also used to identify the products of the electrochemical reactions. In three cases, namely $Cd[Co(CO)_4]_2$, $Cd[Mn(CO)_5]_2$·bipy, and $In[Co(CO)_4]_3$, a molecular ion was observed, and in all other cases ions such as $M[M'(CO)_n]_2^+$, or $LM[M'(CO)_n]^+$ provided clear identification of the reaction products. Further evidence is provided by the infrared spectra in the ν(CO) region (Table 3). The frequencies are in good agreement with the literature values, except in the case of $Zn[Mn(CO)_5]_2$·bipy. For this compound, Mays and Hsieh (8) found only three of the seven predicted absorptions, whereas the spectra of our compounds did in fact show all seven bands for both Zn and $Cd[Mn(CO)_5]$·bipy. The presence of the bidentate ligands bipy and TMED was confirmed in each case by infrared and nmr spectroscopy.

Results and Discussion

The synthetic methods described represent simple and direct routes to these interesting heteronuclear metal carbonyl complexes. The electrochemical

TABLE 3. Infrared vibrations in the ν(CO) region*

Compound	Conditions	ν(CO) (cm^{-1})
$Zn[Co(CO)_4]_2 \cdot bipy$	$CHCl_3$	1970 (vs), 1980 (sh), 2055 (s), 2065 (s)
	Nujol	2043 (s), 1957 (s), 1972 (m), 2055 (vs), 2065 (vs)
$Zn[Mn(CO)_5]_2 \cdot bipy$	Nujol	1924 (s), 1941 (vs), 1960 (s), 1970 (sh), 1990 (m), 2040 (vs), 2060 (s)
$Cd[Co(CO)_4]_2$	$CHCl_3$	1966 (sh), 1970 (b), 2020 (sh), 2054 (vs), 2067 (sh)
	Pentane	1910 (sh), 1970 (m), 2020 (sh), 2060 (m), 2073 (vs)
$Cd[Co(CO)_4]_2 \cdot TMED$	$CHCl_3$	1940 (sh), 1950 (m), 1970 (sh), 1990 (s), 2050 (vs), 2067 (vs)
$Cd[Co(CO)_4]_2 \cdot bipy$	$CHCl_3$	1965 (s), 1983 (sh), 2049 (vs), 2060 (s)
$In[Co(CO)_4]_3$	Nujol	2003 (vs), 2080 (vs), 2090 (sh)

*s = strong, b = broad, m = medium, v = very, sh = shoulder.

synthesis requires simple apparatus, readily available starting materials, and mild conditions (room temperature and pressure). Under the conditions which we have used, the rate of dissolution of the metal typically corresponds to the production of gram quantities of product in a few hours, and it seems likely that larger cells and electrodes, and improved cell design, would allow a substantial increase in the rate of production if required. These factors emphasize the advantages of the method over many of those in the literature (see Introduction), both in the use of ambient conditions, and in the avoidance of the synthesis of intermediates such as carbonyl hydrides, carbonylate anions, or metal alkyls.

Reaction Mechanism

It has been pointed out elsewhere (7, 9) that the current efficiency (E_F) of electrochemical reactions may give an important clue as to the mechanism of the reaction at the anode. We have accordingly measured the mass of anodic metal dissolving at constant current in a number of systems, with the results shown in Table 4.

Any discussion of the interpretation of these E_F values must start with the known polarographic behaviour of $Mn_2(CO)_{10}$ and $Co_2(CO)_8$. Dessy and his co-workers (10, 11) have shown that both compounds undergo 2-electron cathodic reduction to yield two $Mn(CO)_5^-$ and $Co(CO)_4^-$ anions respectively. We assume that these species are the significant current carriers, and that product formation involves reactions during, or subsequent to, the discharge of these anions to radicals at the anode surface. The E_F values for the oxidation of a given metal with either $Mn_2(CO)_{10}$ or $Co_2(CO)_8$ are generally the same, so that we assume that the same mechanism pertains for both anions unless otherwise noted.

Perhaps the simplest system is that involving indium. For $In_{(+)}/Mn_2(CO)_{10}$, the E_F of 1.0 implies that the primary processes at the anode are

[1] $Mn(CO)_5^- \rightarrow Mn(CO)_5 + e^-$

[2] $Mn(CO)_5 + In_{(+)} \rightarrow InMn(CO)_5$

TABLE 4. Current efficiencies (E_F) in the electrochemical preparation of heteronuclear metal carbonyls

System	E_F (mol F^{-1})[a]
$Zn/Co_2(CO)_8/bipy$	0.49
$Zn/Mn_2(CO)_{10}/bipy$	0.49
$Cd/Mn_2(CO)_{10}/bipy$	0.52
$Sn/Mn_2(CO)_{10}/bipy$	0.47
$In/Mn_2(CO)_{10}$	1.01
$In/Co_2(CO)_8$	0.89

[a]At constant currents of approximately 25 mA.

The product is an indium(I) complex, and it is well established (12) that the reaction of indium(I) halides with $Mn_2(CO)_{10}$ yields an indium(III) product by oxidative insertion (13), and the reaction

[3] $In(I)Mn(CO_5) + Mn_2(CO)_{10} \rightarrow In[Mn(CO)_5]_3$

clearly parallels such a process. Reactions [1]–[3] then lead to $E_F = 1.0$ for the production of $In[Mn(CO)_5]_3$ and its adducts. For $In/Co_2(CO)_8$, E_F is significantly below unity (0.89) and we suggest that this reflects a less efficient oxidative insertion process

[4] $InCo(CO)_4 + Co_2(CO)_8 \rightarrow In[Co(CO)_4]_3$

than in the manganese system. In fact products containing indium and cobalt in ratios significantly below 1:3 were obtained on occasions. A yellow insoluble solid containing 40% indium was presumably $InCo(CO)_4$ (calcd. In 40.1%), but the yield was small (~15 mg), and not reproducible. Further work on this topic is planned.

The case of $Sn/Mn_2(CO)_{10}$ is equally interesting. Here the dissolution of Sn in a solution of $Mn_2(CO)_{10}$ in methanol gave $E_F = 0.5$, implying the formation of $Sn[Mn(CO)_5]_2$ by the overall reaction

[5] $Sn_{(+)} + 2Mn(CO)_5^- \rightarrow Sn[Mn(CO)_5]_2$

although we should note immediately that considerable uncertainties exist as to the details of this process (cf. the discussion of zinc and cadmium systems below). We were not able to isolate

$Sn[Mn(CO)_5]_4$ or its adducts from the electrochemical cell. Despite the known (13) reactivity of tin(II) halides towards $Mn_2(CO)_{10}$, it appears that the insertion reaction between $Sn[Mn(CO)_5]_2$ and $Mn_2(CO)_{10}$ does not occur, although a number of uncharacterized products of indeterminate stoichiometry containing Sn, Mn, and CO were in fact isolated. Attempts to find better media for the electrochemical reaction (e.g. acetonitrile, glyme) were unsuccessful.

For zinc and cadmium, the E_F values of 0.5 are readily explicable in terms of the overall reaction stoichiometry

[6] $2Mn(CO)_5^- + Zn_{(+)} \rightarrow Zn[Mn(CO)_5]_2 + 2e^-$

[7] $Zn[Mn(CO)_5]_2 + bipy \rightarrow Zn[Mn(CO)_5]_2 \cdot bipy$

Unfortunately, as in the case of tin, neither the measurement of E_F nor reactions [6] and [7] cast any light on the number or nature of the steps involved in the transformation of $Mn(CO)_5^-$ anions into $—Mn(CO)_5$ ligands. Dessy and his co-workers (10) observed the formation of $Hg[Mn(CO)_5]_2$ when $Mn_2(CO)_{10}$ was reduced at a mercury cathode, and proposed the formation of the radical $Mn(CO)_5^\cdot$ as an intermediate. If this species is generated at the (say) cadmium anode (cf. reaction [1]), an analogy with work on halogens (14) or organic halides (7) leads to the reaction sequence

[8] $Cd + X \rightarrow CdX$

[9] $CdX + X_2 \rightarrow CdX_2 + X$

($X = Mn(CO)_5$), but the regeneration of $Mn(CO)_5$ to perpetuate reactions [8] + [9] would then give current efficiencies in excess of those observed (cf. ref. 14).

A number of possible explanations can be advanced for the E_F values of 0.5. In the first, it is postulated that the reaction sequence involves the discharge of a second $(Mn(CO)_5^-$ anion at a $CdMn(CO)_5$ site before the latter can react with dissolved $Mn(CO)_{10}$. A second approach assumes that the radicals regenerated by reaction [9] at or near the anode migrate and react with $Mn(CO)_5$ anions

[10] $Mn(CO)_5 + Mn(CO)_5^- \rightarrow Mn_2(CO)_{10} + e$

in which case the sum of reactions [1] + [8] + [9] + [10] gives $E_F = 0.5$, but only if reaction [10] accounts for the consumption of each $Mn(CO)_5$ radical formed in [9]. Finally, two $CdMn(CO)_5$ units may dimerise near the electrode surface to give $(CO)_5MnCdCdMn(CO)_5$, which on disproportionation would yield the product plus cadmium metal.

In view of the quantitative uncertainties in these arguments, a detailed comparison of the merits of various schemes does not appear worthwhile at the present time. These problems apart, the main features of the reaction scheme, and the advantages of the electrochemical technique, seem clearly established.

Acknowledgements

This work was supported in part by Operating Grants from the National Research Council of Canada. One of us (S.Z.) acknowledges the receipt of a scholarship from the Canadian International Development Agency.

1. W. Hiebert and U. Teller. Z. Anorg. Allg. Chem. **43**, 249 (1942).
2. J. M. Burlitch. Chem. Commun. 887 (1968).
3. G. Schmidt and G. Etzrodt. J. Organometal. Chem. **131**, 477 (1977).
4. N. A. D. Carey and J. G. Noltes. Chem. Commun. 147 (1968).
5. A. T. T. Hsieh and M. J. Mays. J. Chem. Soc. A, 2648 (1971).
6. W. Hieber and W. Schropp. Chem. Ber. **93**, 455 (1960).
7. J. J. Habeeb and D. G. Tuck. J. Organometal. Chem. **134**, 363 (1977); **146**, 213 (1978).
8. M. J. Mays and A. T. T. Hsieh. J. Chem. Soc. A, 729 (1971).
9. J. J. Habeeb, D. G. Tuck, and F. H. Walters. J. Coord. Chem. **8**, 27 (1978).
10. R. E. Dessy, F. E. Stary, R. B. King, and M. Waldrop. J. Am. Chem. Soc. **88**, 471 (1966).
11. R. E. Dessy, P. M. Weissman, and R. L. Pohl. J. Am. Chem. Soc. **88**, 5117 (1966).
12. H. R. H. Patil and W. A. G. Graham. Inorg. Chem. **5**, 1401 (1966).
13. J. Hoyano, D. J. Patmore, and W. A. G. Graham. Inorg. Nucl. Chem. Lett. **4**, 201 (1968).
14. J. J. Habeeb, L. Neilson, and D. G. Tuck. Inorg. Chem. **17**, 306 (1978).

Canadian Journal of Chemistry
Published by
THE NATIONAL RESEARCH COUNCIL OF CANADA

Journal canadien de chimie
Publié par
LE CONSEIL NATIONAL DE RECHERCHES DU CANADA

Volume 57 Number 17 September 1, 1979

Volume 57 numéro 17 1 septembre 1979

Pyrolysis of trifluoroacetaldehyde, initiated by di-tertiary-butyl peroxide decomposition

LEON F. LOUCKS, MICHAEL T. H. LIU, AND DAVID G. HOOPER
Department of Chemistry, University of Prince Edward Island, Charlottetown, P.E.I., Canada C1A 4P3

Received November 10, 1978

LEON F. LOUCKS, MICHAEL T. H. LIU, and DAVID G. HOOPER. Can. J. Chem. 57, 2201 (1979).

The thermal decomposition of 95:5 mixtures of trifluoroacetaldehyde (TFA) and di-*tert*-butyl peroxide (DTBP) has been studied at 100 Torr over the temperature range of 390 to 440 K. The major decomposition products included CO, CF_3H, CH_3COCH_3, and CH_4 while C_2F_6, $CF_3CHOHCH_3$, CF_3CH_3, CF_3COCH_3, C_2H_6, $(CF_3)_2CHOH$, and H_2 were also found. In addition to the usual reactions for TFA thermal decomposition, reactions of methyl radicals with TFA to form isopropoxyl radicals were found. The alcohol products result from H atom abstraction reactions of the isopropoxyl radicals while CF_3COCH_3 is a decomposition product. Arrhenius parameters for several reactions were determined: for DTBP decomposition, $\log k = 15.82 - 37.73/2.303RT$; for H abstraction from TFA by CH_3, $\log k = 8.30 - 7.37/2.303RT$; for H abstraction from TFA by CF_3, $\log k = 8.98 - 8.61/2.303RT$.[1] Consideration has also been given to several rate constant ratios for the formation and decomposition of isopropoxyl radicals.

A study of the reaction order for the formation of CF_3H, C_2F_6, and CH_4 showed that the orders were 3/2, 1, and 1 respectively for these three products. A reaction mechanism involving 14 individual steps is proposed to explain the reaction products and the observed orders of reaction.

LEON F. LOUCKS, MICHAEL T. H. LIU et DAVID G. HOOPER. Can. J. Chem. 57, 2201 (1979).

Opérant à 100 Torr et à des températures allant de 390 à 440 K, on a étudié la décomposition thermique de mélanges 95:5 de trifluoroacétaldéhyde (TFA) et de peroxyde de di-*tert*-butyle (DTBP). Les produits principaux de la décomposition comprennent CO, CF_3H, CH_3COCH_3, et CH_4 alors que l'on retrouve aussi C_2F_6, $CF_3CHOHCH_3$, CF_3CH_3, CF_3COCH_3, C_2H_6, $(CF_3)_2CHOH$ et H_2. En plus des réactions habituelles pour la décomposition thermique du TFA, on a aussi observé des réactions de radicaux méthyles avec le TFA conduisant à la formation de radicaux isopropoxyles. Les produits hydroxylés proviennent des réactions d'enlèvement d'atomes de H à partir des radicaux isopropoxyles alors que la CF_3COCH_3 est un produit de décomposition. On a déterminé les paramètres d'Arrhénius pour plusieurs réactions: pour la décomposition du (PDTB), $\log K = 15.82 - 37.73/2.303RT$; pour l'enlèvement d'un H du TFA par un CH_3, $\log K = 8.30 - 7.37/2.303RT$; pour l'enlèvement d'un H du TFA par le CF_3, $\log K = 8.98 - 8.61/2.30RT$.[1] On a aussi accordé une certaine considération à plusieurs rapports de constantes de vitesse pour la formation et la décomposition de radicaux isopropoxyles.

Une étude de l'ordre de réaction pour la formation de CF_3H, C_2F_6 et CH_4 a montré que les ordres sont respectivement 3/2, 1 et 1 pour ces trois produits. On propose un mécanisme réactionnel impliquant 14 étapes individuelles pour expliquer la nature des produits réactionnels et les ordres de réaction observés.

[Traduit par le journal]

Introduction

The thermal decomposition of trifluoroacetaldehyde (TFA) has been investigated in detail in several previous studies (1–3) at temperatures near 770 K. The results support a chain mechanism initiated by a first-order process believed to be the cleavage of the C—C bond and terminated by a second-order recombination of CF_3 radicals. In earlier work on the pyrolysis of acetaldehyde (4, 5) at 770 K the

[1]In this paper all energies are in kcal and R is taken to be 0.00199 kcal mol^{-1} K^{-1}.

0008-4042/79/172201-10$01.00/0

formation of acetone as a product was observed and its formation was attributed to the decomposition of isopropoxyl radicals generated by the addition of methyl radicals to acetaldehyde (4). In the pyrolysis of trifluoroacetaldehyde no hexafluoroacetone was observed although the same general mechanism could prevail. The present study was undertaken to determine the differences between the two pyrolyses and to determine whether or not the isopropoxyl radicals and their decomposition products are involved in the trifluoroacetaldehyde system.

Quite a number of previous studies have examined the decomposition of isopropoxyl radicals. Isopropoxyl radicals generated from isopropyl nitrite in the presence of nitric oxide were studied by Ferguson and Phillips (6), Cox, Livermore, and Phillips (7), and Batt and Milne (8). Also, in a nitric oxide system, Yee Quee and Thynne (9) studied the decomposition of isopropoxyl radicals generated from the thermal decomposition of di-isopropyl peroxide. In these systems the acetone formation has been explained by reactions other than the isopropoxyl radical decomposition; the major product for the radical decomposition was observed to be acetaldehyde and a methyl radical. The activation energy for the latter decomposition was reported to be 11.5 to 17.3 kcal mol^{-1} in the various studies (8). In the study by Batt and Milne, acetone formation by disproportionation of isopropoxyl radicals with NO was ruled out and although acetone was observed in amounts about equal to that of acetaldehyde, isopropoxyl radical was discounted as the acetone source because no inhibition by nitric acid oxide was observed. Systems involving no nitric oxide have also been used to generate isopropoxyl radicals. Wijnen (10) studied the gas-phase photolysis of isopropyl propionate and attributed acetaldehyde formation to the decomposition of isopropoxyl radicals by C—C bond scission; although acetone was also observed as a product, its source in this study was believed to be other than the C—H bond scission of the isopropoxyl radical. Yee Quee and Thynne (11) used di-isopropyl peroxide decomposition to generate isopropoxyl radicals. They reported acetaldehyde as the major decomposition product of the radical but also found small amounts of acetone; they estimated the activation energy for this latter decomposition to be about 20 kcal mol^{-1}. Most recently, Hiatt and Rahimi (12) have reported on the decomposition of di-isopropyl peroxide in solution; a reaction mechanism, in part quite different from that proposed by Yee Quee and Thynne for the gas phase, has been invoked to explain their products and product distributions.

To maximize the participation of isopropoxyl radicals in the TFA pyrolysis, the long-chain decomposition of TFA needs to be minimized and this is accomplished at lower temperatures. The appropriate temperature conditions to provide reasonable stability to the isopropoxyl radicals and fairly short-chain decomposition of TFA were obtained with the use of di-*tert*-butyl peroxide as a chain initiating agent. The same general design of experiment was used previously by Morris and Thynne (13) but their emphasis on minor product analysis was much less extensive than in the present work.

Experimental

Trifluoroacetaldehyde (TFA) was prepared by decomposing the ethyl hemiacetal obtained from K & K Laboratories Inc. with concentrated H_2SO_4 (14). The TFA was purified by trap-to-trap distillation from 150 K to 77 K, the initial fraction being discarded. Infrared (ir) and gas chromatography (gc) analyses confirmed the identity and the purity of TFA (99.9%). Di-*tert*-butyl peroxide (DTBP) was obtained from K & K Laboratories and used after degassing. The gc analysis showed no significant impurities in the DTBP.

TFA and DTBP were mixed in a 2 L bulb and stored at 77 K. The reactant was transferred to a 2 L mixing vessel prior to each experiment and mixed with a magnetic stirring device for 45 min. Experiments were conducted in a conventional glass vacuum system with greased stopcocks. The reaction vessel was a 419.6 mL quartz cylinder enclosed in an electrically heated steel cylinder encased in an asbestos board box, packed with glass wool. The temperature of the reaction vessel was controlled to ± 0.3 K by a Thermo Electric Model 400 temperature controller. All experiments were conducted with a reactant mixture containing 5% DTBP and 95% TFA. The reaction vessel was conditioned with about 30 Torr of reactant for 5 min prior to each experiment. Experiments were started by expanding the appropriate amounts of reactant into the reaction vessel and were terminated by freezing the condensable contents of the vessel into two spiral traps at 77 K.

The products were divided into three fractions. Products not condensable in a charcoal trap at 77 K were collected by a Toepler pump and measured in a gas burette. The fraction collected in the charcoal trap was then analyzed by gc on a 2 m molecular sieve column. This fraction contained CO and CH_4. The remaining products were distilled from 150 K to 77 K with pumping for 3 h. The volatile fraction was then analyzed on a 2 m Porapack Q column; this fraction contained CF_3H, C_2F_6, CF_3CH_3, $C_2F_2H_2$, C_2H_6, and the residual TFA. The products which remained nonvolatile at 150 K were analyzed on a 30 cm Porapack Q column; this fraction contained CF_3COCH_3, CH_3COCH_3, $CF_3CHOHCH_3$, and $(CF_3)_2CHOH$. All columns were kept at room temperature and a hot filament detector unit was used.

The compounds used for identification of product peaks were obtained from the following companies: CF_3H, CO, CH_4, C_2F_6, C_2H_6, and CF_3COCF_3 from Matheson; CF_3CH_3 from K & K Laboratories; $CF_3CHOHCH_3$, $CF_3CHOHCF_3$ from Matheson, Coleman and Bell; and CF_3COCH_3 from Aldrich Chemicals.

Results

The decomposition of trifluoroacetaldehyde initiated by the thermal decomposition of di-*tert*-butyl peroxide has been investigated over the temperature

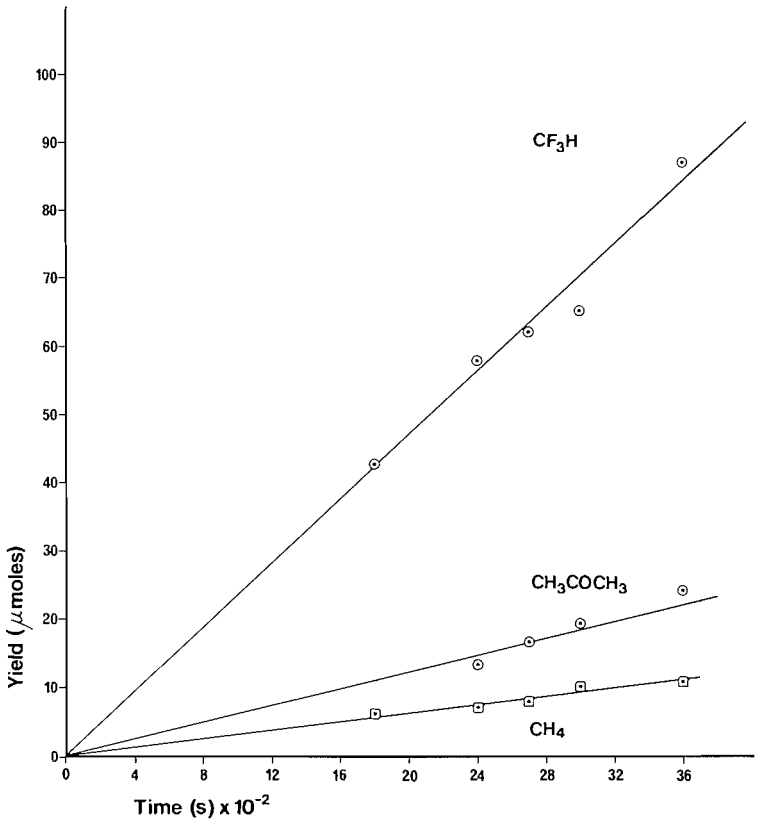

FIG. 1. Major products of the thermal decomposition at 402.2 K. Pressure = 100 Torr (5% DTBP and 95% TFA).

range of 390–440 K at a pressure of 100 Torr. The products observed, in decreasing order of magnitude, were: CO, CF_3H, CH_3COCH_3, CH_4, C_2F_6, $CF_3CHOHCH_3$, CF_3CH_3, CF_3COCH_3, C_2H_6, and H_2. Significant amounts of $(CF_3)_2CHOH$ were detected at the lower temperatures. It was expected that CF_4, $C_2F_2H_2$, and HF might have been observed products but a search for these materials did not reveal their presence. One minor product in the most volatile fraction is known to be none of the above, but remains unidentified.

Typical plots of product yield as a function of time are shown in Figs. 1 and 2. The initial rates given in Table 1 were obtained by extrapolating rates to zero time. For Table 1, all rates were normalized to the rate of formation of acetone set equal to unity; however, as the absolute rate of formation of acetone is given, the absolute rates of formation of all other products can be recalculated.

As part of the overall study, the effect of pressure on the rates of formation of CF_3H and C_2F_6 was investigated in detail at 402.2 K (129°C) over the pressure range of 45 to 271 Torr. The order plots resulting from this study are shown in Fig. 3. It was found that the orders of reaction were 1.49 ± 0.07 and 1.00 ± 0.03 for CF_3H and C_2F_6 respectively.

Discussion

To explain the observed decomposition products and the effects of pressure and temperature on the distribution of products the following mechanism is suggested:

[1] $DTBP \rightarrow 2CH_3 + 2CH_3COCH_3$

[2] $CH_3 + CF_3CHO \rightarrow CH_4 + CF_3CO$

[3] $CH_3 + CF_3CHO \rightarrow CH_3{-}\underset{\displaystyle CF_3}{\overset{\displaystyle O}{\overset{|}{\underset{|}{C}}}}{-}H$

[4] $CH_3{-}\underset{\displaystyle CF_3}{\overset{\displaystyle O}{\overset{|}{\underset{|}{C}}}}{-}H + CF_3CHO \rightarrow CH_3{-}\underset{\displaystyle CF_3}{\overset{\displaystyle OH}{\overset{|}{\underset{|}{C}}}}{-}H + CF_3CO$ (z)

[5] $CH_3{-}\underset{\displaystyle CF_3}{\overset{\displaystyle O}{\overset{|}{\underset{|}{C}}}}{-}H \rightarrow CH_3COCF_3 + H$

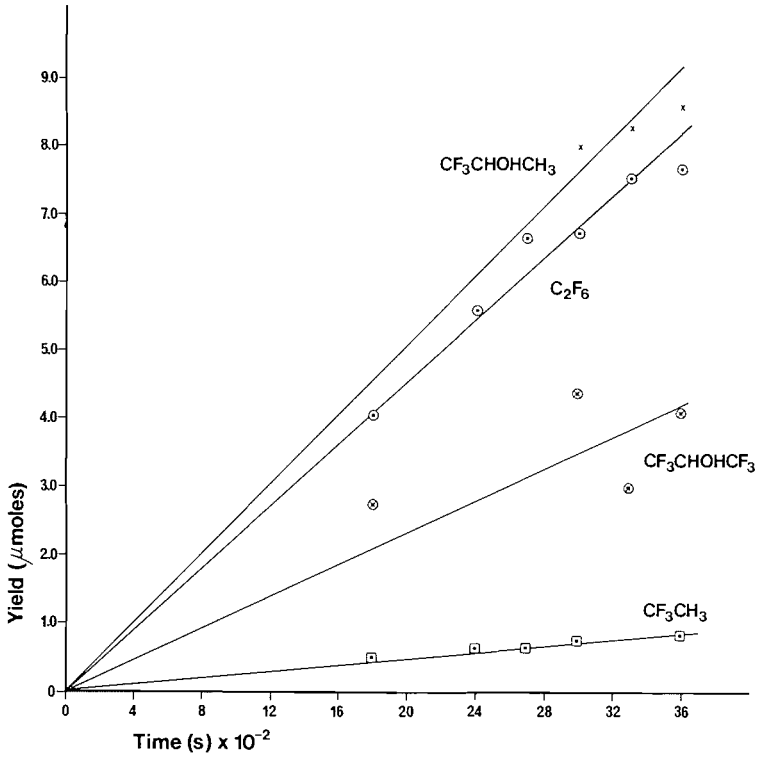

FIG. 2. Minor products of the thermal decomposition at 402.2 K. Pressure = 100 Torr (5% DTBP and 95% TFA).

[6] $CF_3CO \rightarrow CF_3 + CO$

[7] $CF_3 + CF_3CHO \rightarrow CF_3H + CF_3CO$

[8] $CF_3 + CF_3CHO \rightarrow CF_3\text{—}\underset{\displaystyle CF_3}{\overset{\displaystyle O}{\overset{|}{C}}}\text{—}H$

[9] $CF_3\text{—}\underset{\displaystyle CF_3}{\overset{\displaystyle O}{\overset{|}{C}}}\text{—}H + CF_3CHO \rightarrow CF_3\text{—}\underset{\displaystyle CF_3}{\overset{\displaystyle OH}{\overset{|}{C}}}\text{—}H + CF_3CO$

[10] $CF_3 + CF_3 \rightarrow C_2F_6$

[11a] $CF_3 + CH_3 \rightarrow CF_3CH_3^* \xrightarrow{M} CF_3CH_3$

[11b] $CF_3CH_3^* \rightarrow CH_2{=}CF_2 + HF$

[12] $CH_3 + CH_3 \rightarrow C_2H_6$

[13] $H + CF_3CHO \rightarrow H_2 + CF_3CO$

With this mechanism the chain reaction decomposition of TFA is initiated by the methyl radicals arising from the DTBP decomposition; this chain initiation reaction [2] leads to the CH_4 production. The chain carrier reactions are reaction [6], the decomposition of the CF_3CO radical and reaction [7], the abstraction of the aldehyde hydrogen by the CF_3 radical. The chain termination reactions include the various CF_3 and CH_3 combination and disproportionation reactions of reactions [10] to [12]. The reaction products CH_3COCH_3, CH_4, CF_3H, CO, C_2F_6, CF_3CH_3, and C_2H_6 could all be accounted for by a reaction scheme involving only the reactions discussed thus far. However, the fluorinated acetone, fluorinated alcohols, and hydrogen are not explained by a simple mechanism. We believe that these products arise from isopropoxyl radicals formed by the addition of methyl radicals to the reactant molecules. As there are both CH_3 and CF_3 radicals in our system, both an F_3-isopropoxyl and an F_6-isopropoxyl radical can be formed as shown by reactions [3] and [8] respectively. At the temperatures of this study, the isopropoxyl radicals are sufficiently stable to exhibit an abstraction reaction; thus a portion of the isopropoxyl radicals yield F_3-isopropyl alcohol and F_6-isopropyl alcohol as a result of the abstraction of the aldehyde hydrogen from the reactant molecules (reactions [4] and [9], respectively). The decomposition of the isopropoxyl radicals is expected to be facile and one pathway can give acetone and hydrogen atoms. In the present system the F_3-acetone resulting from the F_3-isopropoxyl radical decomposition by reaction [5] was observed but the F_6-acetone was not observed. The fact that the F_6-alcohol was observed in substantially smaller quantities than the F_3-alcohol while the F_3-acetone yield was much smaller than

the F_3-alcohol suggests that the yield of F_6-acetone would be expected to be very small and perhaps it was beyond the limit of collection and detection in our experiments. The hydrogen atoms produced along with the F_3-acetone would be expected to yield H_2 through abstraction by reaction [13]; H_2 was confirmed to be a product. The fact that the $R_{11a}/R_{10}^{1/2}R_{12}^{1/2}$ value observed in this work was only 0.78 suggests that $C_2F_2H_2$ and HF should have been formed in this system. Although a search for these products was conducted, we were unable to detect them and we conclude that they are not significant products. Nevertheless we are including reaction [11*b*] in our scheme, since it is known to occur in related systems (15), where the above ratio was found to be 2.0 at similar pressures.

DTBP Decomposition

The thermal decomposition of DTBP has been thoroughly studied by previous workers and the results of the various studies have been summarized by Shaw and Pritchard (16). An internal check on the consistency of the present work is provided in the measurement of the Arrhenius parameters for DTBP decomposition. The overall rate constant, k_1, for this decomposition can be derived from the rate of formation of acetone. The experimental values for k_1 are shown in Table 2. The Arrhenius plot of Fig. 4 displays the data and the equation of the Arrhenius plot is given by:

$$\log k_1\,(s^{-1}) = 15.82 \pm 0.79 - (37.73 \pm 1.49)/2.303RT$$

where $R = 0.00199$ kcal mol^{-1} K^{-1} and the error limits are standard error estimates. The Arrhenius parameters are in excellent agreement with the values recommended by Shaw and Pritchard (16).

Abstraction Reactions by Methyl Radicals

Under our present experimental conditions, abstraction reactions ([2], [4], [7], [9]) and addition reactions ([3], [8]) are more important than the radical combination reactions ([10], [11*a*], and [12]). The product distribution given in Table 1 shows that the abstraction reaction products CF_3H and CH_4 are more abundant than the predominant radical combination product, C_2F_6; the abstraction reactions become relatively less favored at higher temperatures. With experimental values for the rates of formation of CH_4 and C_2H_6 and upon accepting the literature value for $k_{12} = 10^{10.34}$ L mol^{-1} s^{-1} (17, 18), the rate constant k_2 can be evaluated from:

$$k_2 = R_{CH_4}k_{12}^{1/2}/(R_{C_2H_6})^{1/2}[CF_3CHO]$$

The results shown in Table 2 for k_2 yield the Arrhenius plot shown in Fig. 4; the equation for this

TABLE 1. Relative rates of product formation (acetone rate = 1.0)

Temperature (K)	Relative rate of formation										Absolute rate for CH_3COCH_3 $\times 10^9$ (mol L^{-1} s^{-1})
	CF_3H	CH_3COCH_3	CH_4	C_2F_6	$CF_3\overset{OH}{\overset{\vert}{C}}HCH_3$	CF_3CH_3	CF_3COCH_3	C_2H_6	H_2	$(CF_3)_2\overset{OH}{\overset{\vert}{C}}H$	
390.7	4.30	1.00	0.459	0.263	0.434	0.0195	0.0927	0.0024	0.020	0.156	2.05
402.2	3.82	1.00	0.531	0.368	0.432	0.0403	0.0516	0.0071	*	0.189	6.20
420.7	1.88	1.00	0.467	0.387	0.349	0.0690	0.0384	0.0263	0.0076	0.102	63.2
440.7	1.14	1.00	0.499	0.373	0.121	0.137	0.0262	0.0830	*	n.d.†	406

*Analysis was not attempted.
†n.d., no detectable quantity.

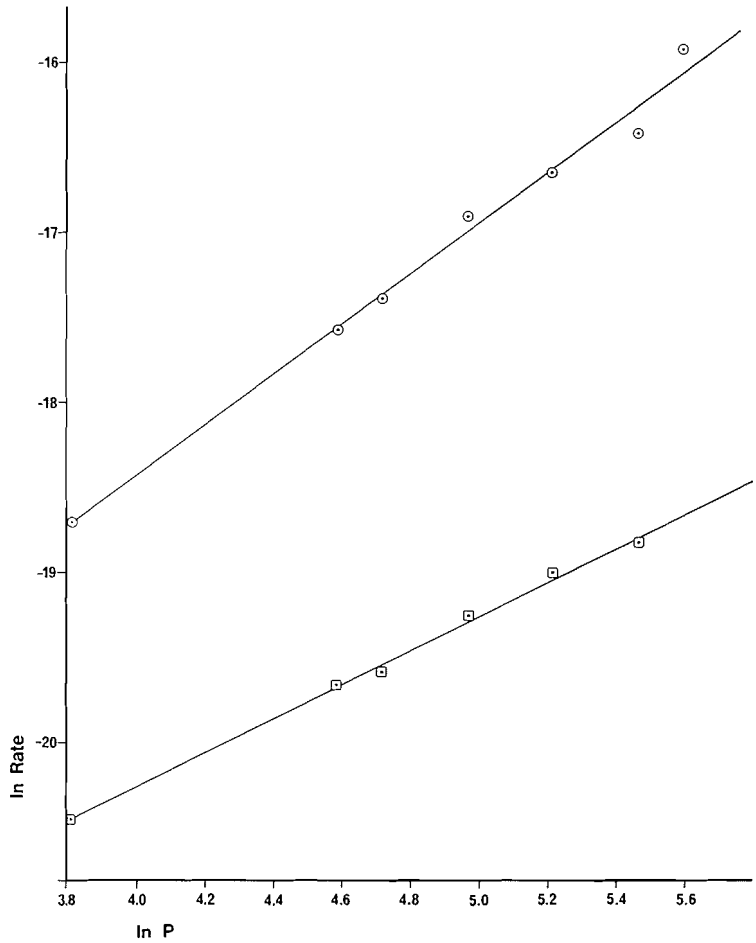

FIG. 3. Order plots for CF_3H formation (indicated by ○) and for C_2F_6 formation (indicated by □) at 402.2 K.

TABLE 2. Rate constant values at four temperatures for reactions [1], [2], and [7], DTBP decomposition, H abstraction by CH_3, and H abstraction by CF_3, respectively

T (K)	k_1 (s^{-1})	k_2 ($L\ mol^{-1}\ s^{-1}$)	k_7 ($L\ mol^{-1}\ s^{-1}$)
390.7	5.55×10^{-6}	1.65×10^{4}	1.48×10^{4}
402.2	1.73×10^{-5}	1.93×10^{4}	1.99×10^{4}
420.7	1.84×10^{-4}	2.95×10^{4}	3.20×10^{4}
440.7	1.24×10^{-3}	4.70×10^{4}	5.22×10^{4}

Arrhenius plot is:

$$\log k_2\ (L\ mol^{-1}\ s^{-1}) = 8.30 \pm 0.41 - \frac{7.37 + 0.77}{2.303RT}$$

The values of activation energy and A-factor compare moderately well with the values 8.7 kcal mol^{-1} and $10^{9.10}$ L mol^{-1} s^{-1} reported by Morris and Thynne (13).

Values of k_7 may be determined by an analogous manner from the rates of formation of CF_3H and C_2F_6 and with Ayscough's value of $k_{10} = 10^{10.36}$ L mol^{-1} s^{-1} (18, 19). The values of k_7 calculated from:

$$k_7 = R_{CF_3H}{k_{10}}^{1/2}/[CF_3CHO](R_{C_2F_6})^{1/2}$$

are shown in Table 2 and the Arrhenius plot is shown in Fig. 4. The equation of the Arrhenius plot is given by:

$$\log k_7\ (L\ mol^{-1}\ s^{-1}) = 8.98 \pm 0.07 - \frac{8.61 \pm 0.14}{2.303RT}$$

The activation energy and A-factor are in good agreement with the values of 8.8, 7.2, 8.2, and 8.44 kcal mol^{-1} and $10^{8.95}$, $10^{8.05}$, $10^{8.65}$, and $10^{8.66}$ L mol^{-1} s^{-1} reported previously by Morris and Thynne (20), Pearce and Whytock (21), Dodd and Smith (18, 22), and the present authors (3), respectively.

It is interesting to note from the data of Table 2 how closely the absolute values of k_2 and k_7 compare with one another in the temperature range of this

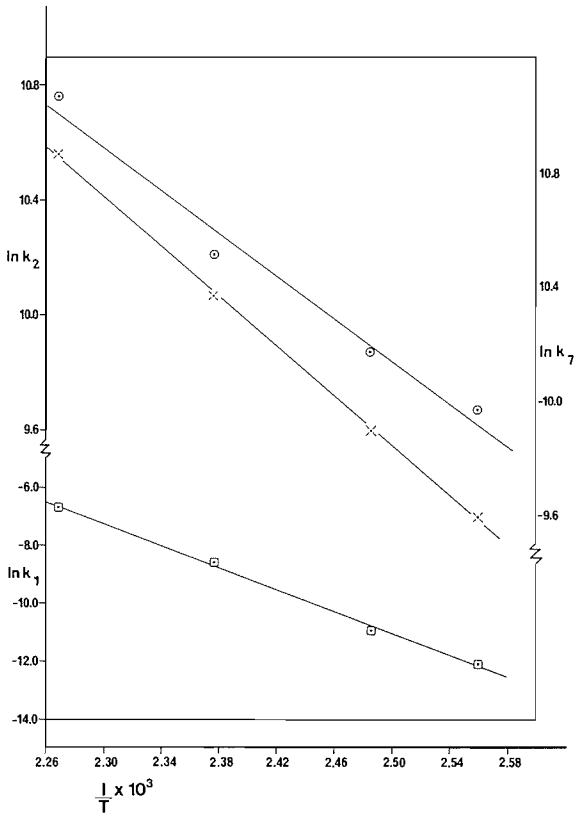

FIG. 4. Arrhenius plots for k_1 (□), k_2 (×), and k_7 (○).

study. Although the abstraction rate constant for CF_3 is usually greater than that for CH_3 (see pp. 279–280 of ref. 18), the present data tend to show that the substrate CF_3CHO may be less anomalous than previous data seemed to indicate. At the same time it should be noted that all values of k_7 would have to be reduced by a factor of $10^{0.32}$ if Hiatt and Benson's value (15) of k_{12} were accepted instead of Ayscough's value.

Methyl Radical Addition to TFA

As seen from the reaction mechanism, the F_3-isopropoxyl radical generated from the addition of CH_3 to TFA leads to the products F_3-isopropanol and F_3-acetone by reactions [4] and [5] respectively. Since these two reaction paths represent the only consumption of the F_3-isopropoxyl radicals the sum of the rates of reactions [4] and [5] must equal the rate of reaction [3] which produces the F_3-isopropoxyl radical. It follows that

$$\frac{k_3}{k_2} = \frac{R_{\text{F}_3\text{-alcohol}} + R_{\text{F}_3\text{-acetone}}}{R_{\text{CH}_4}}$$

An Arrhenius plot for this rate constant ratio is shown in Fig. 5; the data at the three lower temperatures were believed to be more reliable and only these data were used. The activation energy difference $E_2 - E_3$ was evaluated to be 3.4 ± 1.2 kcal mol^{-1}. With $E_2 = 7.37 \pm 0.77$ kcal mol^{-1} from the earlier result of this paper, it follows that E_3, the activation energy for the addition of CH_3 to TFA, is 4.0 ± 2.0 kcal mol^{-1}. This rather low activation energy allows the F_3-isopropoxyl radical to play a major part in the reaction mechanism and results in the experimental observation of significant amounts of F_3-acetone and F_3-alcohol.

The addition of CF_3 to TFA by reaction [8] yields the F_6-isopropoxyl radical. Although its decomposition was expected to yield hexafluoroacetone, none of this product was observed. Thus the rate of formation of the F_6-alcohol may be taken as the rate of formation of the F_6-isopropoxyl radical. From the kinetic expressions it follows that:

$$k_8/k_7 = R_{\text{F}_6\text{-alcohol}}/R_{\text{CF}_3\text{H}}$$

The Arrhenius plot for this rate constant ratio is displayed in Fig. 5; on this occasion data at only the three lower temperatures are available as the F_6-alcohol could not be measured at the highest temperature. The activation energy difference $E_8 - E_7$ was evaluated to be 4.2 ± 1.8 kcal mol^{-1}. With the value of $E_7 = 8.61 \pm 0.14$ kcal mol^{-1} assigned earlier in this paper, it follows that the activation energy for the addition of CF_3 radicals to TFA is 12.8 ± 2.0 kcal mol^{-1}. Notice that whereas the activation energy for addition of CH_3 to TFA was less than the activation energy for the H atom abstraction, in the case of CF_3, the activation energy for addition to TFA is greater than that of the H atom abstraction. The rather low abundance of F_6-isopropoxyl radical reaction products relative to that of F_3-isopropoxyl radical reaction products is the observed experimental consequence of these differences in activation energies.

It is evident from Fig. 5 that a considerable uncertainty exists in the evaluation of these rate constant ratios and this uncertainty is reflected in the standard error estimates in the Arrhenius parameters. While the absolute values for the activation energies show considerable uncertainty, it seems clear that $E_3 < E_2$ while $E_8 > E_7$.

Isopropoxyl Radical Decomposition

The F_3-isopropoxyl radical appears to react only through reactions [4] and [5]. The relative importance of the decomposition pathway relative to the H atom abstraction can be examined from values of the k_5/k_4 ratio evaluated from the rearrangement of rate expressions to the form:

$$k_5/k_4 = R_{\text{F}_3\text{-acetone}}[\text{CF}_3\text{CHO}]/R_{\text{F}_3\text{-alcohol}}$$

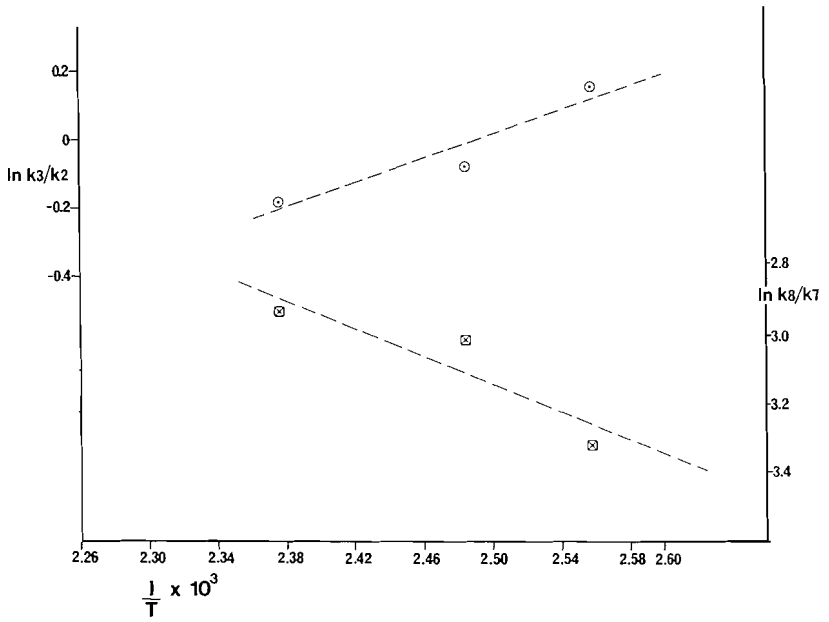

FIG. 5. Arrhenius plots for k_3/k_2 (○) and k_8/k_7 (⊠).

Owing to a significant uncertainty in the F_3-acetone rates, the ratio determined for k_5/k_4 was not entirely reliable. Nevertheless it appeared that the values at higher temperature were greater than those at the lower temperature and hence E_5 for the radical decomposition appears to be greater than E_4 for the abstraction reaction. Although no quantitative evaluation of E_5 is provided here, it should be recalled that Yee Quee and Thynne (11) have suggested an activation energy of 20 kcal mol^{-1} for the decomposition of the unfluorinated analogue to acetone and H atom.

For the decomposition of the F_6-isopropoxyl radical, no F_6-acetone was observed while small but significant amounts of the F_6-alcohol were observed at the lower temperatures. The failure to observe the F_6-acetone while observing the F_6-alcohol suggests that the activation energy for the decomposition of the F_6-isopropoxyl radical according to reaction [14],

$$[14]\quad CF_3{-}\overset{\displaystyle O}{\overset{\|}{C}}{-}H \rightarrow CF_3COCF_3 + H$$

is substantially greater than the activation energy for H atom abstraction from TFA.

As no F_6-acetone is formed, it follows that the only source of H atoms in our system would be from reaction [5]. The H atoms so produced would yield H_2 by reaction [13] and hence the yield of H_2 would be expected to be exactly equal to the yield of F_3-acetone. Such is not the experimental observation as the F_3-acetone is found in amounts several times greater than that of H_2. The excess F_3-acetone may arise from the reactions:

$$[15]\quad CH_3{-}\overset{\displaystyle O}{\overset{\|}{C}}{-}H + R \rightarrow CF_3COCH_3 + RH$$

where $R = CF_3$ or CH_3. The occurrence of these reactions could not be confirmed unequivocally in our system as CF_3H and CH_4 arise in large quantities from other reactions.

Most readers will have noticed our omission of isopropoxyl radical decomposition pathways involving C—C bond scission to give acetaldehydes and methyl radicals. In our experiments this type of reaction occurring as the reverse of reactions [3] and [8] could not be detected as the reaction product would be one of our reactants. We do not dispute the occurrence of the reverse of reactions [3] and [8] and indeed we do expect that they are occurring. There is, however, one C—C bond scission reaction which we expected to see. The decomposition of the F_3-isopropoxyl radical could occur not only by the reverse of reaction [3] but also by a C—C bond scission that would give CF_3 and CH_3CHO. A search for acetaldehyde in the products provided no evidence of that product. However, due to the fact

that the acetaldehyde gc peak occurred at an unfavorable position on the tail of the reactant peak we feel that there is some possibility that the failure to observe acetaldehyde was an analysis problem. Nevertheless, our current evidence indicates no acetaldehyde product and this influences us to believe that the C—C bond scission of isopropoxyl radicals relative to C—H bond scission may not be as strongly favored as earlier work has suggested.

Order of Reaction

As supporting evidence for the reaction mechanism, the order of reaction was experimentally determined at 402.2 K for some of the readily measured products. The orders of formation of CF_3H and C_2F_6 were of special significance to the reaction mechanism.

A steady-state treatment for the reaction mechanism is simplified by the following assumptions which are supported by the experimental observations: (*a*) that production of CF_3CO by reaction [13] is minor; (*b*) that the rates of reactions [8] and [9] are equal, as no other product from the F_6-isopropoxyl radical was observed; (*c*) that reactions [11*a*] and [11*b*] are minor termination steps compared to reaction [10] and may be neglected (at the higher temperatures this is not entirely valid but holds well at the temperature of the order study); (*d*) that CH_3 radical consumption occurs predominantly by reactions [2] and [3] rather than by reactions [11*a*], [11*b*], and [12]; and (*e*) that the rate of reaction [4] is essentially the same as the rate of reaction [3] since $R_5 \ll R_4$.

This simplified steady-state treatment gives the following expressions for the concentrations of CH_3 and CF_3:

$$[16] \quad [CH_3] = \frac{2k_1[DTBP]}{(k_2 + k_3)[CF_3CHO]} = \frac{2k_1}{19(k_2 + k_3)}$$

$$[17] \quad [CF_3] = \left(\frac{k_2 + k_3}{2k_{10}}\right)^{1/2} \times [CF_3CHO]^{1/2}[CH_3]^{1/2} = \left(\frac{k_1}{19k_{10}}\right)^{1/2} [CF_3CHO]^{1/2}$$

In turn these quantities can be used in the rate expressions for the rates of formation of CF_3H, C_2F_6, and CH_4 and one finds that the orders of reaction with respect to CF_3CHO should be 1.5 for CF_3H formation, 1.0 for C_2F_6 formation, and 1.0 for CH_4 formation. The order plots of Fig. 3, already referred to, confirm these orders in the cases of CF_3H and C_2F_6 where experimental orders of 1.49 ± 0.07 and 1.00 ± 0.03, respectively, were observed. A less extensive study involving only four points gave an order of 0.92 ± 0.03 for CH_4, a value rather close to the 1.0 required by the reaction mechanism. Thus the proposed reaction mechanism is consistent with the observed orders of reaction for these individual products.

Additional support for the validity of eqs. [16] and [17] comes from the calculations of the steady-state concentrations of CF_3 and CH_3. Values of k_1 and k_2 were taken from Table 2 while values for k_3/k_2 were obtained from an interpolation of Fig. 5. At 402.2 K the CH_3 concentration was calculated from eq. [16] to be 4.7×10^{-11} mol L^{-1}, a value which is in excellent agreement with a calculation from the observed rate and the rate expression $R_{C_2H_6} = k_{13}[CH_3]^2$. For CF_3 the concentration calculated from eq. [17] was 3.7×10^{-10} mol L^{-1}; again this value showed good agreement with a value calculated from the C_2F_6 rate and rate expression. At 440.7 K the same calculations gave values of 1.6×10^{-9} and 2.5×10^{-9} mol L^{-1} for the concentrations of CH_3 and CF_3 respectively in good agreement with the values calculated from the rate expressions. It should be noted that whereas the $[CF_3]/[CH_3]$ ratio is about 8 at 402.2 K, the temperature at which the order study was conducted, this ratio is reduced to a value of 2 at 440.7 K. All of the above calculations were conducted for a pressure of 100 Torr.

Acknowledgements

We wish to thank the Senate Research Committee of U.P.E.I. and the Natural Sciences and Engineering Research Council of Canada for the financial support which made this work possible.

1. N. L. Arthur and T. N. Bell. Aust. J. Chem. **18**, 1561 (1965).
2. M. T. H. Liu, L. F. Loucks, and R. C. Michaelson. Can. J. Chem. **51**, 2292 (1973).
3. M. T. H. Liu, L. F. Loucks, and D. G. Hooper. Int. J. Chem. Kinet. **9**, 589 (1977).
4. M. T. H. Liu and K. J. Laidler. Can. J. Chem. **46**, 479 (1968).
5. G. N. Côme, M. Dzierzynski, R. Martin, and M. Niclause. Rev. Inst. Franc. Petrole, Ann. Combust. Liquides, **23**, 1365 (1968).
6. J. M. Ferguson and L. Phillips. J. Chem. Soc. 4416 (1965).
7. D. L. Cox, R. A. Livermore, and L. Phillips. J. Chem. Soc. B, 245 (1966).
8. L. Batt and R. T. Milne. Int. J. Chem. Kinet. **9**, 141 (1977).

9. M. J. YEE QUEE and J. C. J. THYNNE. Trans. Faraday Soc. **64**, 1296 (1968).
10. M. J. H. WIJNEN. J. Am. Chem. Soc. **82**, 1847 (1960).
11. M. J. YEE QUEE and J. C. J. THYNNE. J. Phys. Chem. **72**, 2824 (1968).
12. R. HIATT and P. M. RAHIMI. Int. J. Chem. Kinet. **10**, 185 (1978).
13. E. R. MORRIS and J. C. J. THYNNE. Trans. Faraday Soc. **63**, 2470 (1967).
14. D. G. HOOPER, L. F. LOUCKS, and M. T. H. LIU. J. Chem. Educ. **52**, 131 (1975).
15. R. HIATT and S. W. BENSON. Int. J. Chem. Kinet. **4**, 479 (1972).
16. D. H. SHAW and H. O. PRITCHARD. Can. J. Chem. **46**, 2721 (1968).
17. A. SHEPP. J. Chem. Phys. **24**, 939 (1956).
18. P. GRAY, A. A. HEROD, and A. JONES. Chem. Rev. **71**, 247 (1971).
19. P. B. AYSCOUGH. J. Chem. Phys. **24**, 994 (1956).
20. E. R. MORRIS and J. C. J. THYNNE. Trans. Faraday Soc. **64**, 3027 (1968).
21. C. PEARCE and D. A. WHYTOCK. J. Chem. Soc. D, Chem. Commun. 1464 (1971).
22. R. E. DODD and J. W. SMITH. J. Chem. Soc. 1465 (1957).

Thermodynamics of molecular interactions in aniline + benzene mixtures

RAM K. NIGAM,[1] PREM P. SINGH, AND KRISHAN C. SINGH

Department of Chemistry, Maharshi Dayanand University, Rohtak-124 001, Haryana, India

Received November 27, 1978

RAM K. NIGAM, PREM P. SINGH, and KRISHAN C. SINGH. Can. J. Chem. **57**, 2211 (1979).

Heats of mixing, H^E, of aniline + benzene at 298.15 and 308.15 K have been measured over the entire composition range. The results have been analysed in terms of Barker's and ideal associated model theory of non-electrolyte solutions. It has been observed that the ideal associated model approach which assumes the presence of AB, AB_2, A_2B_2, and B molecular species well describes (within ±120 J/mol at the worst) the general behaviour of H^E with x_B (mole fraction of aniline) over the whole composition range for aniline + benzene mixtures. The equilibrium constants for the various association reactions along with the enthalpy of formation of various molecular species have also been calculated.

RAM K. NIGAM, PREM P. SINGH et KRISHAN C. SINGH. Can. J. Chem. **57**, 2211 (1979).

On a mesuré les chaleurs de mélange, H^E, de l'aniline + benzène à 298.15 et à 308.15 K à toutes les compositions. On a analysé les résultats en termes de la théorie de Barker et du modèle associé idéal des solutions non électrolytiques. On a observé que l'approche du modèle associé idéal qui fait l'hypothèse de la présence d'espèces moléculaires AB, AB_2, A_2B_2 et B décrit bien (à ±120 J/mol) le comportement de H^E avec x_B (fraction molaire de l'aniline) à toutes les compositions de mélanges de l'aniline + benzène. On a calculé les constantes d'équilibre des diverses réactions d'association ainsi que l'enthalpie de formation des divers espèces moléculaires.

[Traduit par le journal]

Introduction

Recent trends in the thermodynamics of associated mixtures have been limited to the evaluation of equilibrium constants for 1 : 1 and 1 : 2 molecular complexes only (1, 2). However, Tucker and Christian (3) have made notable contributions by identifying the various associated species in pure alkanols. Aniline molecules are known to be associated (4–7) through hydrogen bonding in the pure state and recent ir spectroscopic studies (8) have indicated that while one of the hydrogens of the $-NH_2$ group of aniline forms a strong hydrogen bond, the second hydrogen in the NH_2 group interacts weakly with the π-electrons of adjacent aniline molecules. It would, therefore, be interesting to study the nature of aniline in its binary mixtures with benzene. The present work describes interactions in aniline + benzene mixtures.

Experimental

Analytical grade aniline and benzene were purified as suggested by Vogel (9) and the purity of the final samples was checked by density determination at 298.15 ± 0.01 K which agreed to within ±0.00005 g/mL with the corresponding literature values (10, 11).

Heats of mixing measurements were made in an adiabatic calorimeter (12) which has been described previously. The time was recorded by an electronic timer (type TO1 SR No. 010, Systronic, Ahemdabad, India) which could read to ±0.0001 s. The temperature fluctuations of the thermostatic bath were found to be within ±0.01 K. The uncertainty in H^E values is about 0.3%.

[1]To whom all correspondence should be addressed.

Results

The heats of mixing at 298.15 and 308.15 K have been fitted by the equation:

$$[1]\quad H^E/x_Ax_B = h_0 + h_1(x_B - x_A) + h_2(x_B - x_A)^2$$

where x_B and x_A are the mole fractions of aniline and benzene respectively. The parameters (h_0, h_1, and h_2) were evaluated by the method of least squares and are recorded together with the standard deviations of molar heats of mixing $\sigma(H^E)$ in Table 1.

Discussion

Deshpande and Pandya (13) have determined H^E for the aniline (B) + benzene (A) system at 298.15 K. Our results are in excellent agreement with those reported by these workers for $0 \leq x_B \leq 0.25$ and $x_B \geq 0.75$. However, in the intermediate range, our results differ from theirs by as much as +80 J mol^{-1} at $x_B = 0.42$. Heats of mixing for aniline + benzene are endothermic throughout the entire concentration range. H^E data at 308.15 K when combined with G^E data (14) at 308.15 K yielded positive TS^E values for all aniline mole fractions. The curve of TS^E against x_B is unsymmetrical about x_B (Fig. 1).

At the simplest qualitative level, the observed H^E data for this mixture may be accounted for if it is

0008-4042/79/172211-06$01.00/0

TABLE 1

(*a*) Measured molar heats, H_{expt}^{E}, of mixing and those calculated according to eq. [1] at different mole fractions x_B of aniline for benzene (A) + aniline (B) at 298.15 and 308.15 K

Temperature 298.15 K			Temperature 308.15 K		
Mole fraction of B	H_{expt}^{E} (J/mol)	H_{calc}^{E} (J/mol)	Mole fraction of B	H_{expt}^{E} (J/mol)	H_{calc}^{E} (J/mol)
0.1802	522.2	529.1	0.2033	521.7	527.3
0.2956	745.7	737.8	0.2711	638.0	641.0
0.4223	835.4	830.1	0.3761	748.1	741.1
0.5711	752.2	760.5	0.4803	744.1	746.9
0.6790	603.7	610.2	0.6588	562.4	566.7
0.7782	428.7	423.4	0.8412	246.8	239.8

(*b*) Parameters of eq. [1] at 298.15 and 308.15 K

Temperature (K)	h_0 (J/mol)	h_1 (J/mol)	h_2 (J/mol)	$\sigma(H^E)$ (J/mol)
298.15	3264.92	−1010.59	−806.12	9.72
308.15	2952.18	−1062.42	−927.87	7.34

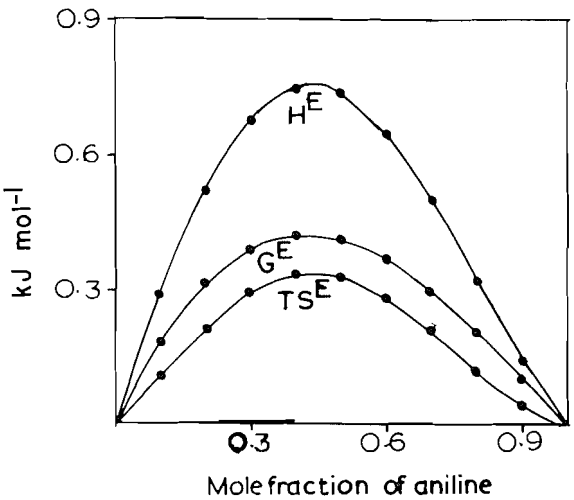

FIG. 1. Properties of the aniline + benzene system at 308.15 K.

assumed that: (*i*) aniline is self-associated and there is a decrease in self-association when it is mixed with benzene, (*ii*) there are weak interactions between aniline and benzene. Consequently, the orientational freedom of unlike molecules would increase due to factor (*i*) so that TS^E should be positive. On the other hand, since the measured H^E is due to the cumulative effects of factors (*i*) and (*ii*), the positive H^E for this mixture may be accounted for if it is assumed that the heat effects due to factor (*i*) outweigh those due to factor (*ii*).

The state of liquid aniline has been a subject of speculation; while some authors favoured self-association in liquid aniline through hydrogen bonding (4–8), Bellamy and Williams (15) suggest that there is no self-association in it. Furthermore, aniline has a permanent dipole moment and its interactions with such simple compounds as benzene should be characterized by dipole-induced dipole interaction. Consequently, it was thought worthwhile to analyse our H^E data for aniline + benzene mixtures in terms of Barker's theory (16) by taking into account the abovementioned views about the nature of aniline.

It was assumed that aniline (B) + benzene (A) have the following geometrical parameters: lattice $Z = 4$, aniline molecule = B, $r_B = 2$, $Q_H^B = 1$, $Q_N^B = 1$, $Q_R^B = 4$, benzene molecule = A, $r_A = 2$, $Q_{R'}^A = 6$ (since molar volumes of aniline + benzene at 298.15 K are nearly the same, it was taken $r_A = r_B = 2$). Three different models were assumed.

Model α

This model assumed that there is no self-association in aniline and that its interaction with benzene is characterized by specific (R...R′) interactions of strength U_2 between the aromatic ring of aniline (R) and the aromatic ring of benzene (R′) and non-specific interactions of strength U_1 for all the remaining contacts. This model was based on the observations of Bellamy and Williams (15) that there is no self-association in aniline.

Model β

This model assumed (*i*) specific (N...H) interactions of strength U_3 between the nitrogen and hydrogen of aniline and (*ii*) an interaction (R...R′) of strength U_2 between the aromatic ring (R) of aniline with the

TABLE 2. Comparison of H^E values calculated according to Barker's theory with the corresponding H^E experimental values at $x_B = 0.3$, 0.5, and 0.7 at 298.15 and 308.15 K for aniline (B) + benzene (A) mixtures

Temperature (K)	H^E (J/mol)	Mole fraction of aniline (x_{B_2})			Interaction energies (J/mol)			
		0.3	0.5	0.7	U_1	U_2	U_3	U_4
298.15	Experimental	743.44	816.23	573.66	—	—	—	—
	From Model α	547.39	742.19	789.42	491.0	−49.08	—	—
	From Model β	618.92	773.64	810.00	491.90	−49.08	−1005.03	—
	From Model γ	660.48	862.83	893.50	491.90	—	−1005.03	−49.08
308.15	Experimental	678.02	738.04	449.54	—	—	—	—
	Model γ	563.60	738.83	762.92	416.35	—	−672.13	−12.78

aromatic ring (R′) of benzene. These interactions correspond to a model that takes into account the self-association of aniline and also dipole-induced dipole interactions (14) between aniline and benzene.

Model γ

Visualized (*i*) specific (N...H) interactions of strength U_3 between aniline–aniline molecules and (*ii*) specific (H...R′) interactions of strength U_4 between the hydrogen of the $—NH_2$ group and aromatic ring (R′) of hydrocarbon. This model is based on the ir spectroscopic studies (8) of aniline by Wolff and Mathias (8).

For the sake of simplicity, non-specific interactions of all the remaining contact sites in these three modes were considered to have the same strength U_1. Excess energy of mixing at constant volume (U_V^E) at x_B = 0.3, 0.5, and 0.7 were then calculated for these three models. Conversion of U_V^E to H^E was performed utilizing the relationship:

$$[2] \qquad U_V^E = H^E - TV^E\alpha_m/(K_T)_m$$

where α_m, $(K_T)_m$, and V^E are the expansivity, isothermal compressibility, and excess volume of the mixture. As $V^E \approx 0$, therefore, $U_V^E \approx H^E$. It is evident from Table 2 that Model α and Model β do not represent adequately the H_{expt}^E values. Model γ provides good agreement at $x_B = 0.3$ and 0.5, but it is poor for $x_B > 0.5$. The probable reason for this failure of Model γ for $x_B > 0.5$ is its simplicity, which does not account for the presence of associated complexes of general formula A_mB_x and B_l.

H_{expt}^E and H_{calc}^E for the three models given above for $x_B = 0.3$, 0.5, and 0.7 at 298.15 and 308.15 K are given in Table 2 along with their interaction energies U_i (i = 1, 2, 3, 4, ...).

The H^E data for this mixture were then analysed in terms of the ideal associated model (17, 18). It is assumed that in a binary solution of aniline + benzene mutual equilibrium of the species A_kB_k, A_mB_x, and B_l occurs. Hereinafter aniline and benzene are designated respectively as B_n and A, the notation B_n indicating that aniline is self-associated. Here:

$$l = 1, 2, 3, ..., l$$
$$m = 1, 2, 3, ..., m$$
$$x = 1, 2, 3, ..., x$$
$$k = 1, 2, 3, ..., k$$
$$n = 1, 2, 3, ..., n$$

The mutual equilibrium is represented by the equation:

$$[3] \qquad A + B_n \rightleftharpoons A_kB_k + A_mB_x + B_l$$

Equilibrium constants for the various association reactions represented by eq. [3] are:

$$[4] \qquad K_{k,k/n} = a_{A_kB_k}/a_A{}^k a_{B_n}{}^{k/n}$$

$$[5] \qquad K_{m,x/n} = a_{A_mB_x}/a_A{}^m a_{B_n}{}^{x/n}$$

and

$$[6] \qquad K_{l/n} = a_{B_l}/a_{B_n}{}^{l/n}$$

where 'a' denotes activities. If the activity coefficients of the various species represented in eq. [3] are assumed to be unity (17), the material balance equation for the system can be written as

$$[7] \quad a_A + a_{B_n} + \sum_k K_{k,k/n} a_A{}^k a_{B_n}{}^{k/n} + \sum_m K_{m,x/n} a_A{}^m a_{B_n}{}^{x/n} + \sum_l K_{l/n} a_{B_n}{}^{l/n} = 1$$

Consider the two simple cases:

Case (*i*)

$$l = m = k = 1; \quad n = 2; \quad x = 2$$

Case (*ii*)

$$l = m = 1; \quad x = n = 2; \quad k = 1, 2$$

The material balance equations for the two cases are then:

$$[8] \quad a_A + a_{B_2} + K_{1,0.5} a_A a_{B_2}{}^{1/2} + K_{1,1} a_A a_{B_2} + K_{0.5} a_{B_2}{}^{1/2} = 1$$

and

$$[9]\quad a_A + a_{B_2} + K_{1,0.5}a_A a_{B_2}^{1/2} + K_{1,1}a_A a_{B_2} + K_{2,1}a_A^2 a_{B_2} + K_{0.5}a_{B_2}^{1/2} = 1$$

Algebraic manipulation of eqs. [8] and [9] yields

$$[10]\quad K_{1,0.5}a_A + K_{1,1}a_A a_{B_2}^{1/2} + K_{0.5} = (1 - a_A - a_{B_2})/a_{B_2}^{1/2}$$

and

$$[11]\quad K_{1,0.5}a_A + K_{1,1}a_A a_{B_2}^{1/2} + K_{2,1}a_A^2 a_{B_2}^{1/2} + K_{0.5} = (1 - a_A - a_{B_2})/a_{B_2}^{1/2}$$

respectively.

Since the observed thermodynamic properties of this mixture would be the cumulative sum of the effects due to (*i*) dispersion forces and (*ii*) equilibria represented by eq. [3], evaluation of the various K's in the eqs. [10] and [11] would require that the observed activities of the components of these binary mixtures be corrected (19–21) for dispersion contributions by expressing

$$a_A = \gamma_A x_A/\gamma_A^*$$

$$a_{B_2} = \gamma_{B_2} x_{B_2}/\gamma_{B_2}^*$$

where γ_A^* and $\gamma_{B_2}^*$ are the activity coefficients of a reference mixture. As cyclohexane is inert and has nearly the same molar volume as that of benzene, cyclohexane (A*) + aniline (B_2*) was taken as the reference system (22) for the present analysis. A series of values were then assumed for the various K's in eqs. [10] and [11] and the process was repeated until a set of K values was obtained which yielded

$$(1 - a_A - a_{B_2})/a_{B_2}^{1/2} = D$$

values that corresponded very closely to those obtained from the experimental a_A and a_{B_2} values. It was observed that eq. [10] with a set of values:

$$K_{1,0.5} = 0.754$$

$$K_{1,1} = 0.076$$

$$K_{0.5} = 0.05$$

and eq. [11] with a set of values:

$$K_{1,0.5} = 0.75$$

$$K_{1,1} = 0.08$$

$$K_{0.5} = 0.08$$

$$K_{2,1} = 0.05$$

yields D values which reproduce well with those obtained from experimental data with this equation. The criterion of effectiveness was the variance of the fit $\sigma^2 D$ defined by

$$[12]\quad \sigma^2 D = \sum_q (D_{calc} - D_{expt})^2/(q - p)$$

where q is the number of points used in the fit and p is the number of adjustable parameters.

Since $\sigma^2 D_{10} = 0.010$ and $\sigma^2 D_{11} = 0.011$ are nearly the same, the analysis of the activity coefficients data described above suggests that these mixtures may be assumed to have either AB, AB_2, and B or AB, AB_2, A_2B_2, and B molecular species in solution.

The experimental H^E data for this mixture were next examined in terms of models that involved consideration of the *First Case* (AB, AB_2, and B) and the *Second Case* (AB, AB_2, A_2B_2, and B) and H^E was expressed as:

$$[13]\quad H^E = (n_{AB}\Delta H_{AB} + n_{AB_2}\Delta H_{AB_2} + n_B\Delta H_B)/(N_A + N_{B_2})$$

$$[14]\quad H^E = (n_{AB}\Delta H_{AB} + n_{AB_2}\Delta H_{AB_2} + n_{A_2B_2}\Delta H_{A_2B_2} + n_B\Delta H_B)/(N_A + N_{B_2})$$

where n_{AB}, n_{AB_2}, $n_{A_2B_2}$, and n_B are the amounts of species AB, AB_2, A_2B_2, and B which are present at equilibrium in solution. N_A and N_{B_2} are the stoichiometric amounts of A and B_2. If the equilibrium mole fractions of A, B_2, AB, AB_2, and B are represented by Z_A, Z_{B_2}, Z_{AB}, Z_{AB_2}, and Z_B then for an ideal associated mixture A + B_2, containing AB, AB_2, and B molecular species, one can write:

$$[15]\quad Z_A + Z_{B_2} + Z_{AB} + Z_{AB_2} + Z_B = 1$$

where

$$Z_{AB} = K_{1,0.5}Z_A Z_{B_2}^{1/2}$$

$$Z_{AB_2} = K_{1,1}Z_A Z_{B_2}$$

$$Z_B = K_{0.5}Z_{B_2}^{1/2}$$

The experimental H^E values were again corrected for dispersion contributions by subtracting from H_{expt}^E the H^E values (21) for the cyclohexane + aniline system at 308.15 K.

Consequently, in eqs. [13] and [14]

$$[15a]\quad H^E = H_{expt}^E - H^E\,(\text{cyclohexane} + \text{aniline})$$

Algebraic manipulation of eqs. [13] and [14] and the material balance equations

$$[16]\quad N_A = n_A + n_{AB} + n_{AB_2}$$

$$[17]\quad N_{B_2} = n_{B_2} + \tfrac{1}{2}n_{AB} + \tfrac{1}{2}n_B + n_{AB_2}$$

TABLE 3. Equilibrium constants K and the enthalpy of formation ΔH for the various molecular species in benzene (A) + aniline (B) mixtures

Property	Value				Reaction
	AB	A_2B_2	AB_2	B	
K	0.754	—	0.076	0.05	$A + B_2 \rightarrow AB + AB_2 + B$
ΔH (kJ/mol)	−3.2	—	−0.50	+2.0	
K	0.75	0.05	0.08	0.08	$A + B_2 \rightarrow AB + A_2B_2 + AB_2 + B$
ΔH (kJ/mol)	−4.5	−1.5	−0.5	+2.1	

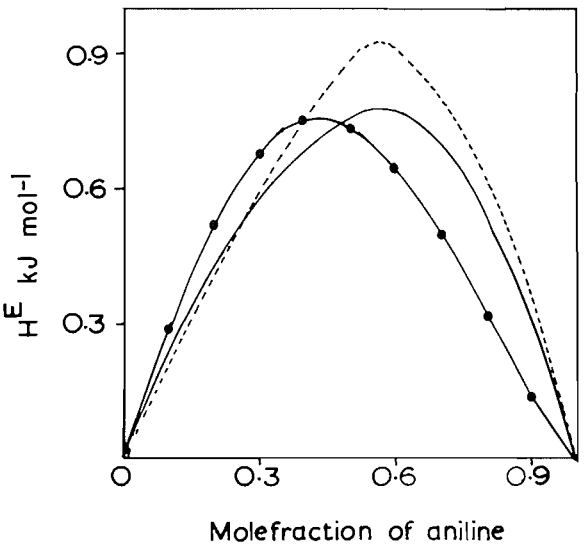

FIG. 2. H^E values of the aniline + benzene system at 308.15 K: ●, experimental; ---, first case; —, second case.

leads to

$$[18] \quad JH^E = K_{1,0.5}Z_A\Delta H_{AB} + K_{1,1}Z_A\Delta H_{AB_2} + K_{0.5}Z_{B_2}{}^{1/2}\Delta H_B$$

where

$$J = (Z_{B_2}{}^{1/2} + 0.5K_{0.5} + 0.5K_{1,0.5}Z_A + K_{1,1}Z_AZ_{B_2}{}^{1/2})/x_{B_2}$$

Further combination of [15]–[17] yields

$$[19] \quad x_{B_2} = \frac{Z_{B_2} + 0.5K_{1,2}Z_{B_2}{}^{1/2} + 0.5K_{1,0.5}Z_AZ_{B_2}{}^{1/2}}{Z_A + Z_{B_2} + 0.5K_{1,1}Z_{B_2}{}^{1/2} + 1.5K_{1,0.5}Z_AZ_{B_2}{}^{1/2}}$$

where

$$Z_A = \frac{1 + Z_{B_2} - K_{0.5}Z_{B_2}{}^{1/2}}{1 + K_{1,0.5}Z_{B_2}{}^{1/2} + K_{1,1}Z_{B_2}}$$

using the various K values described above for a solution containing AB, AB_2, and B molecular species, values of x_{B_2} were calculated from eq. [19] for several values of Z_{B_2}. A number of values was then assigned to ΔH_{AB}, ΔH_{AB_2}, and ΔH_B until they reproduced H^E values (from eqs. [15*a*] and [18]) which compared well with the experimental data. The various ΔH values are presented in Table 3 and calculated H^E values are compared with $H_{expt}{}^E$ values in Fig. 2. It is evident, from Fig. 2, that the predicted H^E values are good for the range $0 \leq x_{B_2} \leq 0.5$. However, for $x_{B_2} > 0.5$ the theoretical H^E values were found to exceed the corresponding $H_{expt}{}^E$ by as much as 140 J/mol.

A similar procedure was applied to the case when the mixture contained AB, AB_2, A_2B_2, and B molecular species. The final expressions are:

$$[20] \quad J'H^E = (K_{1,0.5}Z_A\Delta H_{AB} + K_{1,1}Z_AZ_{B_2}{}^{1/2}\Delta H_{AB_2} + K_{2,1}Z_A{}^2\Delta H_{A_2B_2} + K_{0.5}\Delta H_B)$$

where

$$J' = (Z_{B_2}{}^{1/2} + 0.5K_{0.5} + 0.5K_{1,0.5}Z_A + K_{1,1}Z_AZ_{B_2}{}^{1/2} + K_{2,1}Z_A{}^2)/x_{B_2}$$

and

$$[21] \quad x_{B_2} = \frac{Z_{B_2} + 0.5K_{0.5}Z_{B_2}{}^{1/2} + 0.5K_{1,0.5}Z_AZ_{B_2}{}^{1/2} + K_{1,1}Z_AZ_{B_2} + K_{2,1}Z_A{}^2Z_{B_2}}{Z_A + Z_{B_2} + 0.5K_{0.5}Z_{B_2}{}^{1/2} + 1.5K_{1,0.5}Z_AZ_{B_2}{}^{1/2} + 2K_{1,1}Z_AZ_{B_2} + 3K_{2,1}Z_A{}^2Z_{B_2}}$$

and

$$[22] \quad Z_{B_2} = \frac{-(K_{1,0.5}Z_A + K_{0.5}) \pm \sqrt{(K_{1,0.5}Z_A + K_{0.5})^2 - 4(Z_A - 1)(K_{1,1}Z_A + K_{2,1}Z_A{}^2 + 1)}}{2(K_{1,1}Z_A + K_{2,1}Z_A{}^2 + 1)}$$

where

$$Z_{AB} = K_{1,0.5} Z_A Z_{B_2}^{1/2}$$

$$Z_{AB_2} = K_{1,1} Z_A Z_{B_2}$$

$$Z_{A_2B_2} = K_{2,1} Z_A^2 Z_{B_2}$$

$$Z_B = K_{0.5} Z_{B_2}^{1/2}$$

For different values of Z_A, H^E values were again calculated as already explained. The theoretical H^E curve reproduces reasonably well the corresponding experimental results as is evident from Fig. 2. The various ΔH values are given in Table 3.

The analysis of H^E and activity coefficients data for benzene + aniline mixtures thus suggests that this mixture is characterized by the presence of AB, AB_2, A_2B_2, and B molecular species in the solution.

Acknowledgement

K. C. Singh acknowledges his grateful thanks to the C.S.I.R., New Delhi, for the award of Senior Research Fellowship.

1. G. C. PIMENTAL and A. L. MCCLELLAN. The hydrogen bond. W. H. Freeman, San Francisco, CA. 1960.
2. H. L. LIAO and D. E. MARTIRE. J. Am. Chem. Soc. **96**, 2058 (1974).
3. E. E. TUCKER and S. D. CHRISTIAN. J. Am. Chem. Soc. **97**, 1269 (1975).
4. W. GODRY. J. Chem. Phys. **7**, 600 (1939).
5. C. N. R. RAO and A. S. N. MURTHY. Can. J. Chem. **40**, 963 (1962).
6. I. YAMAGUCHI. Bull. Chem. Soc. Jpn. **34**, 1606 (1961).
7. J. FEENEY and L. H. SUTCLIFFE. J. Chem. Soc. 1123 (1962).
8. H. WOLFF and D. MATHIAS. J. Phys. Chem. **77**, 2081 (1973).
9. A. VOGEL. Practical organic chemistry. 3rd ed. Longman's. 1956.
10. J. C. SMITH, N. J. FOECKING, and W. P. BARBER. Ind. Eng. Chem. **41**, 2289 (1949).
11. A. F. FORZIATI, A. R. GLASGOW, JR., C. B. WILLINGHAM, and F. D. ROSSINI. J. Res. Natl. Bur. Stand. **36**, 120 (1946).
12. R. K. NIGAM and B. S. MAHL. J. Chem. Soc. Faraday Trans. I, **68**, 1508 (1972).
13. D. D. DESHPANDE and M. V. PANDYA. Trans. Faraday Soc. **61**, 1858 (1965).
14. D. D. DESHPANDE and M. V. PANDYA. Trans. Faraday Soc. **63**, 2149 (1967).
15. L. J. BELLAMY and R. L. WILLIAMS. Spectrochim. Acta, **9**, 341 (1957).
16. J. A. BARKER. J. Chem. Phys. **20**, 1526 (1952).
17. M. L. MCGLASHAN and R. P. RASTOGI. Trans. Faraday. Soc. **54**, 496 (1958).
18. D. V. FENBY and L. G. HEPLER. J. Chem. Thermodyn. **6**, 185 (1974).
19. W. J. GAW and F. L. SWINTON. Trans. Faraday Soc. **64**, 2023 (1968).
20. A. G. WILLIAMSON. Trans. Faraday. Soc. **64**, 1763 (1968).
21. D. D. DESHPANDE and S. C. OSWAL. J. Chem. Soc. Faraday Trans. I, **68**, 1059 (1972).
22. R. K. NIGAM, P. P. SINGH, and K. C. SINGH. J. Chem. Soc. Faraday Trans. I. To be published.

Structural studies of steric effects in phosphine complexes. Part VII.[1] Synthesis, crystal and molecular structure of the chloroperchloratotri(*o*-tolyl)phosphinemercury(II) dimer

ELMER C. ALYEA, SHELTON DIAS, GEORGE FERGUSON, AND MASOOD KHAN

Guelph–Waterloo Centre for Graduate Work in Chemistry, Guelph Campus, Department of Chemistry, University of Guelph, Guelph, Ont., Canada N1G 2W1

Received February 23, 1979

ELMER C. ALYEA, SHELTON DIAS, GEORGE FERGUSON, and MASOOD KHAN. Can. J. Chem. 57, 2217 (1979).

The synthesis and crystal and molecular structure of the chloroperchloratotri(*o*-tolyl)phosphinemercury(II) dimer are reported. The compound $[HgP(o\text{-tolyl})_3ClClO_4]_2$ belongs to the orthorhombic space group *Pbca* (D_{2h}^{15}, No. 61) with $a = 12.218(2)$, $b = 13.814(2)$, $c = 26.074(3)$ Å, and $Z = 4$. The structure was refined to a final R of 0.046 for 2584 reflections measured by diffractometer. The crystal structure consists of discrete centrosymmetric dimeric molecules of $[HgP(o\text{-tolyl})_3ClClO_4]_2$ separated by normal van der Waals distances. The unique mercury atom forms two strong bonds (Hg—P 2.395(3), Hg—Cl(1) 2.332(4) Å) which deviate from linearity (P—Hg—Cl 164.1(1)°) and two weak bonds (Hg—O(1) 2.73(2) to the perchlorato group, Hg—Cl(1*) 3.109(4) Å linking the mercury atoms about centers of symmetry). The four-fold coordination geometry about each mercury can be described as trigonal bipyramidal with the phosphorus and Cl(1) axial, and one equatorial site unoccupied. Intramolecular interactions are discussed with the assistance of cone angle calculations and a ligand profile for $P(o\text{-tolyl})_3$ ($\theta = 198°$). Vibrational and ^{31}P nmr spectra data are also presented for $[HgP(o\text{-tolyl})_3ClClO_4]_2$.

ELMER C. ALYEA, SHELTON DIAS, GEORGE FERGUSON et MASOOD KHAN. Can. J. Chem. 57, 2217 (1979).

On rapporte la synthèse et la détermination de la structure cristalline du dimère du chloroperchloratotri(*o*-tolyl)phosphine mercure(II). Le composé $[HgP(o\text{-tolyl})_3ClClO_4]_2$ appartient au groupe d'espace orthorhombique *Pbca* (D_{2h}^{15}, No. 61) avec $a = 12.218(2)$, $b = 13.814(2)$, $c = 26.074(3)$ Å et $Z = 4$. On a raffiné la structure jusqu'à une valeur finale de R de 0.046 pour 2584 réflexions mesurées à l'aide d'un diffractomètre. La structure cristalline est formée de molécules dimères individuelles centro-symétriques de $[HgP(o\text{-tolyl})_3ClClO_4]_2$ séparées les unes des autres par des distances de van der Waals normales. L'atome de mercure unique forme deux liaisons fortes (Hg—P 2.395(3), Hg—Cl(1) 2.332(4) Å) qui ne sont pas linéaires (P—Hg—Cl 164.1(1)° et deux liaisons faibles (Hg—O(1) 2.73(2) avec le groupe perchlorato, Hg—Cl(1*) 3.109(4) Å reliant les atomes de mercure autour des centres de symétrie). On peut décrire la géométrie de coordination quaternaire autour de chaque mercure comme étant trigonale bipyramidale avec le phosphore et le chlore (1) axiaux et un site équatorial inoccupé. On discute des interactions intramoléculaires à l'aide de calculs d'angle conique et un profil de ligand pour le $P(o\text{-tolyl})_3$ ($\theta = 198°$). On présente aussi des données de spectres vibrationnels et rmn ^{31}P pour $[HgP(o\text{-tolyl})_3ClClO_4]_2$.

[Traduit par le journal]

Introduction

Steric effects of phosphorus ligands have been described (1) in terms of cone angles, θ, and estimates of θ from space filling molecular models (1) have been complemented by X-ray analysis (2, 3) of metal complexes of several bulky phosphine ligands.[2] We have also developed the concept of a "ligand profile" (2) which not only yields precise maximum cone angle data based on the X-ray structural results, but also provides quantitative information about the gaps between moieties in a ligand. The steric environments of $P(o\text{-tolyl})_3$ in $[HgP(o\text{-tolyl})_3(OAc)_2]_2$ (4), $Pt[P(o\text{-tolyl})_3]_2I_2$ (5), and $Ir[P(o\text{-tolyl})_3]_2ClCO$ (5, 6) have been previously described. In an attempt to prepare $Hg[P(o\text{-tolyl})_3]_2(ClO_4)_2$ for comparison with $Hg(PCy_3)_2(ClO_4)_2$ (2, 7) we isolated a compound shown by this X-ray analysis to be $[HgP(o\text{-tolyl})_3ClClO_4]_2$. Cone angle data from the single crystal structural determination and spectroscopic results are presented in this paper.

Experimental

Spectroscopic and other physical measurements were performed as previously described (8).

[1]For Part VI, see ref. 3.

[2]Bulky phosphine ligands which have been studied in our laboratories include tri(cyclohexyl)phosphine (PCy_3), tris(*tert*-butyl)phosphine (PBu_3^t), tri(*o*-tolyl)phosphine ($P(o\text{-tolyl})_3$), and trimesitylphosphine ($P(mesityl)_3$).

0008-4042/79/172217-06$01.00/0

Preparation of the Chloroperchloratotri(o-tolyl)phosphinemercury(II) Dimer, $[HgP(o\text{-tolyl})_3ClClO_4]_2$

A solution of mercury(II) chloride (2.72 g, 10.0 mmol) in absolute ethanol (50 mL) was added to a solution of silver perchlorate (4.15 g, 20.0 mmol) in the same solvent (50 mL). The precipitated pale-yellow solid was filtered off and the filtrate diluted to 100 mL in the same solvent. A 20 mL aliquot of this solution was then added to a hot solution of $P(o\text{-tolyl})_3$ (1.30 g, 4.0 mmol) in absolute ethanol (100 mL). The white solid which precipitated was isolated by filtration and washed successively with ethanol and ether. Crystallization from ethanol afforded a white crystalline solid suitable for X-ray analysis; mp 202–204°C (dec). *Anal.* calcd. for $[HgP(o\text{-tolyl})_3ClClO_4]_2$: C 39.42, H 3.31; found: C 39.62, H 3.32.

X-ray Crystallographic Analysis

Weissenberg and precession photographs provided approximate unit cell dimensions; accurate lattice parameters were obtained by a least-squares treatment of the diffractometer setting angles for 12 reflections for which θ_{hkl} (Mo-K_α) was between 10 and 20°. Crystal data (at 21°C) are

$C_{42}H_{42}Cl_4Hg_2O_8P_2$ fw = 1279.7

Orthorhombic, $a = 12.218(2)$, $b = 13.814(2)$, $c = 26.074(3)$, $V = 4400.8$ Å^3, $Z = 4$, $D_c = 1.93$ g cm^{-3}, $F(000) = 2464$, μ(Mo-K_α) = 70.4 cm^{-1}. Absent reflections $hk0$, $h \neq 2n$, $h0l$, $l \neq 2n$ and $0kl$, $k \neq 2n$ determine space group $Pbca$ (D_{2h}^{15}, No. 61) uniquely and require the molecule to be centrosymmetric.

The intensity data for a unique octant within the limits $2 < \theta < 25°$ were collected on a computer-controlled Y290 Hilger and Watts four-circle diffractometer using graphite monochromated Mo-K_α radiation as described previously (9). The crystal turned black during irradiation and the intensities of three standard reflections, monitored every 100 reflections, decreased by 20% during data collection; this was allowed for by appropriate scaling. Data were corrected for Lorentz and polarization factors and a numerical absorption correction was applied. Maximum and minimum values of transmission coefficients are 0.472 and 0.432 respectively. Of the 4075 measured reflections, 2584 reflections with $I > 2\sigma(I)$ were used in the final refinement of the structure parameters.

The structure was solved by Patterson and Fourier methods.[3] The fractional coordinates for the unique mercury atom were obtained from a sharpened three-dimensional Patterson map. A Fourier synthesis phased with the mercury atom contributions revealed the entire structure. Full-matrix least-squares refinement with anisotropic thermal parameters resulted in $R = \Sigma||F_o| - |F_c||/\Sigma(F_o)$ being lowered to 0.055. A difference synthesis at this stage revealed all hydrogen atoms.

In subsequent refinement cycles the hydrogen atoms were constrained to have idealized geometry with C—H 0.95 Å and separate isotropic thermal parameters were refined for phenyl and methyl hydrogens. In three more rounds of calculation, refinement converged with $R = 0.046$ and $R^1 = [\Sigma w\Delta^2/\Sigma wF_o^2]^{1/2} = 0.044$. The weights used were derived from the counting statistics via the expression $w = K/((\sigma^2F_o + gF_o^2)$ where the final values of K and g are 1.885 and 0.0003 respectively. The scattering factors for hydrogen atoms were obtained from ref. 10 and for the non-hydrogen atoms from ref. 11. Anomalous dispersion corrections were applied (12) for Hg, P, and Cl atoms. In the final cycle of refinement the shifts were less than 0.3 esd and a final difference synthesis was featureless.

[3]Calculations were performed on the University of Guelph IBM 370/155 computer using the program system SHELX written by G. M. Sheldrick, University Chemical Laboratory, Cambridge CB2 1EW, England.

TABLE 1. Fractional coordinates (Hg × 10^5, P, Cl, O, and C × 10^4, H × 10^3) for $[HgP(o\text{-tolyl})_3ClClO_4]_2$ with estimated standard deviations in parentheses

Atom	x/a	y/b	z/c
Hg	6901(4)	2381(3)	7055(1)
P	1544(2)	1602(2)	1107(1)
Cl(1)	359(2)	−1192(2)	256(1)
Cl(2)	−1597(3)	−415(3)	1443(1)
O(1)	−470(8)	−298(9)	1552(4)
O(2)	−1795(14)	84(8)	982(4)
O(3)	−1783(11)	−1427(8)	1352(4)
O(4)	−2164(13)	−48(15)	1849(6)
C(11)	1619(8)	2572(7)	639(3)
C(12)	2023(8)	2410(7)	142(3)
C(13)	1927(10)	3184(8)	−200(4)
C(14)	1498(10)	4060(8)	−74(4)
C(15)	1138(10)	4207(8)	425(4)
C(16)	1206(10)	3481(7)	776(4)
C(17)	2568(10)	1499(7)	−26(4)
C(21)	826(9)	2068(7)	1660(3)
C(22)	−239(10)	2337(7)	1654(4)
C(23)	−699(11)	2743(8)	2095(5)
C(24)	−94(11)	2864(8)	2530(5)
C(25)	969(11)	2591(8)	2543(4)
C(26)	1443(10)	2188(7)	2116(4)
C(27)	−955(10)	2271(10)	1183(5)
C(31)	2900(8)	1241(7)	1310(3)
C(32)	3071(9)	434(7)	1624(4)
C(33)	4142(10)	253(8)	1763(5)
C(34)	5007(10)	776(11)	1589(5)
C(35)	4827(12)	1586(9)	1280(4)
C(36)	3780(9)	1825(8)	1141(4)
C(37)	2167(11)	−181(9)	1822(4)
H(131)	217	309	−54
H(141)	145	456	−32
H(151)	84	482	52
H(161)	98	359	112
H(231)	−145	294	209
H(241)	−42	314	283
H(251)	139	268	285
H(261)	219	199	213
H(331)	428	−27	199
H(341)	573	59	168
H(351)	543	197	117
H(361)	365	238	93
H(171)	257	105	25
H(172)	330	164	−13
H(173)	218	123	−31
H(271)	−55	199	91
H(272)	−118	290	109
H(273)	−158	189	126
H(371)	149	5	169
H(372)	215	−15	219
H(373)	228	−83	172

Atomic coordinates and their standard deviations are given in Table 1. Table 2 contains details of molecular geometry. A view of the dimer with our numbering scheme is given in Fig. 1 and the crystal structure is shown in Fig. 2. Lists of calculated and observed structure factors and thermal parameters have been deposited in the Depository of Unpublished Data.[4]

[4]A complete set of tabular data is available, at a nominal charge, from the Depository of Unpublished Data, CISTI, National Research Council of Canada, Ottawa, Ont., Canada K1A 0S2.

TABLE 2. Interatomic distances (Å), angles (deg), and mean plane data for $[HgP(o\text{-tolyl})_3ClClO_4]_2$ with estimated standard deviations in parentheses

(*a*) Intramolecular distances

Bond	Distance	Bond	Distance
Hg—P	2.395(3)	P—C(11)	1.81(1)
Hg—Cl(1)	2.332(4)	P—C(21)	1.81(1)
Hg—Cl(1)*	3.109(4)	P—C(31)	1.81(1)
Hg—O(1)	2.73(2)	Mean phenyl C—C	1.38(2)
Hg—O(2)	3.13(2)	Mean CH_3—C(sp^2)	1.50(2)
Cl(2)—O(1)	1.42(1)		
Cl(2)—O(2)	1.41(1)		
Cl(2)—O(3)	1.44(1)		
Cl(2)—O(4)	1.36(2)		

(*b*) Bond angles

Bonds	Angle	Bonds	Angle
P—Hg—Cl(1)	164.1(1)	O(1)—Cl(2)—O(2)	107(1)
P—Hg—O(1)	95.0(4)	O(1)—Cl(2)—O(3)	107(1)
Cl(1)—Hg—O(1)	94.9(4)	O(1)—Cl(2)—O(4)	107(1)
P—Hg—Cl(1)*	101.5(1)	O(2)—Cl(2)—O(3)	108(1)
Cl(1)—Hg—Cl(1)*	83.2(1)	O(2)—Cl(2)—O(4)	113(1)
O(1)—Hg—Cl(1)*	123.6(4)	O(3)—Cl(2)—O(4)	114(1)
Hg—Cl(1)—Hg*	96.8(1)		
Hg—P—C(11)	108.0(4)	C(11)—C(12)—C(17)	124(1)
Hg—P—C(21)	114.7(5)	C(13)—C(12)—C(17)	120(1)
Hg—P—C(31)	108.0(4)	C(21)—C(22)—C(27)	123(1)
C(11)—P—C(21)	107.4(6)	C(23)—C(22)—C(27)	117(2)
C(11)—P—C(31)	110.7(6)	C(31)—C(32)—C(37)	123(1)
C(21)—P—C(31)	108.0(6)	C(33)—C(32)—C(37)	121(1)
		Mean phenyl C—C—C	120(2)
P—C(11)—C(12)	121(1)		
P—C(11)—C(16)	118(1)		
P—C(21)—C(22)	124(1)		
P—C(21)—C(26)	117(1)		
P—C(31)—C(32)	122(1)		
P—C(31)—C(36)	117(1)		

*The atoms belong to the symmetry related position $-x, -y, -z$.

(*c*) Mean plane equations

(*a*) Plane through atoms C(11)–C(16)
Plane equation: $0.9110X + 0.3128Y + 0.2686Z = 3.3795$
Displacements (Å × 10^3): C(11) −19, C(12) 13, C(13) 1, C(14) −9, C(15) 3, C(16) 11, C(17) 109, P −193

(*b*) Plane through atoms C(21)–C(26)
Plane equation: $0.2720X + 0.9114Y - 0.3089Z = 1.5345$
Displacements (Å × 10^3): C(21) 6, C(22) −3, C(23) −1, C(24) 1, C(25) 2, C(26) −6, C(27) 55, P 104

(*c*) Plane through atoms C(31)–C(36)
Plane equation: $-0.0878X + 0.5812Y + 0.8090Z = 3.4547$
Displacements (Å × 10^3): C(31) −7, C(32) −10, C(33) 23, C(34) −18, C(35) 0, C(36) 12, C(37) 12, P 1

Discussion

Earlier work (8, 13) demonstrated that tri(*o*-tolyl)phosphine forms only 1:1 complexes with mercury(II) halides, thiocyanate, and acetate. In attempts to prepare a 1:2 complex by the reaction of commercially available mercury(II) perchlorate with two or more molar equivalents of tri(*o*-tolyl)-phosphine no products with satisfactory elemental analyses were obtained. Consequently, the presently reported attempt to generate anhydrous mercury(II) perchlorate was carried out, leading to the isolation of a crystalline solid following the reaction with

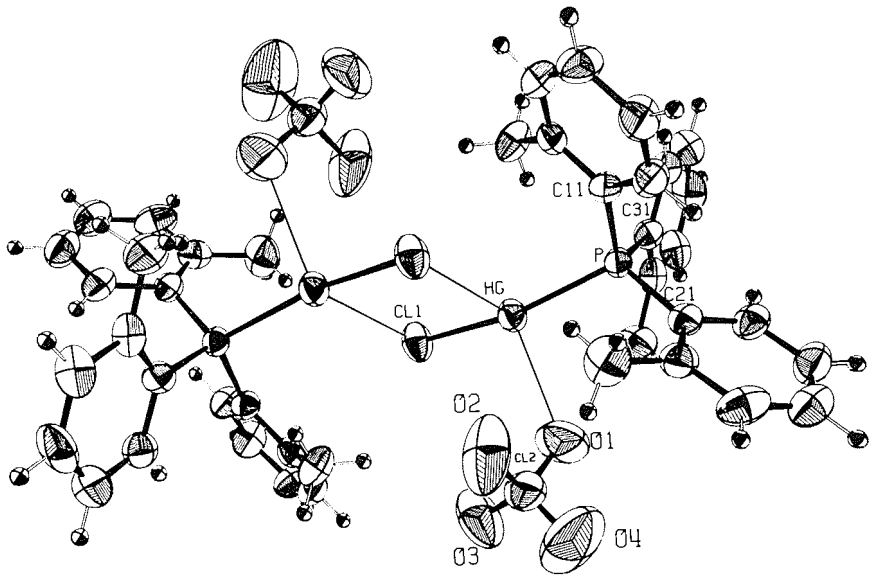

FIG. 1. View of the centrosymmetric $[HgP(o\text{-tolyl})_3ClClO_4]_2$ structure showing our numbering scheme.

tri(*o*-tolyl)phosphine. The stoichiometry of the product was established by the X-ray single crystal determination; subsequent characterization by other physical methods was consistent with the proved structure. $[HgP(o\text{-tolyl})_3ClClO_4]_2$ is a non-electrolyte in dichloroethane (Λ 8.6 ohm^{-1} cm^2 mol^{-1}, 10^{-3} mol dm^{-3}) but becomes a conductor in nitromethane (Λ 133 ohm^{-1} cm^2 mol^{-1}, 10^{-3} mol dm^{-3}). The ^{31}P nmr spectrum for a DMSO-d_6 solution at ambient temperature showed a broad peak at δ 18.0 ppm (downfield from 85% H_3PO_4 as reference) with no satellites due to coupling with mercury -199. The coordination chemical shift of 50.4 ppm is, as expected, comparable to the values found for $HgP(o\text{-tolyl})_3Cl_2$ and $HgP(o\text{-tolyl})_3(OAc)_2$ (14). The low solubility of the complex in non-coordinating solvents did not allow us to obtain meaningful ^{31}P nmr spectral data at lower temperatures or to determine the molecular weight in solution. The infrared spectrum of $[HgP(o\text{-tolyl})_3Cl(ClO_4)]_2$ shows the following bands in the perchlorate region not observed in the spectrum of the free ligand $P(o\text{-tolyl})_3$: 1110 (vs br), 1070 (vs), 1045 (vs), 925 (sh), 917 (m), 686 (w), 666 (w), and 622 (s) cm^{-1}. In the ionic, T_d ClO_4^- ion, the infrared active modes appear at 1119 (s br) cm^{-1} (ν_3) and 625 (m) cm^{-1} (ν_4) (15). Thus the splitting of the ν_3 and ν_4 bands, together with the appearance of ν_1, of ClO_4^- at 917 cm^{-1}, indicates the presence of coordinated perchlorate groups. A weak peak at 190 cm^{-1} observed in the far ir and Raman spectra can tentatively be assigned to the bridging Hg—Cl stretching mode (13). Comparison of the Raman spectrum with those observed previously (8, 13) for similar mercury–phosphine complexes also makes possible the assignment of a medium peak at 158 cm^{-1} to ν(Hg–P).

The crystal structure (Fig. 2) contains discrete centrosymmetric dimeric molecules of $[HgP(o\text{-tolyl})_3ClClO_4]_2$ separated by normal van der Waals distances. The unique mercury atom (Fig. 1) forms two strong bonds (Hg—P 2.395(3), Hg—Cl(1) 2.332(4) Å) which deviate from linearity (P—Hg—Cl 164.1(1)°) because of intramolecular overcrowding (see below). The perchlorate group is weakly bound to mercury (Hg—O(1) 2.73(2) Å) and pairs of $(HgP(o\text{-tolyl})_3ClClO_4)$ moieties are linked about centres of symmetry by weak Hg—Cl(1*) bonds (3.109(4) Å). The four-fold coordination geometry so produced at the mercury can be described as trigonal bipyramidal with the phosphorus and Cl(1) axial, and one equatorial site unoccupied.

The non-linearity of the P—Hg—Cl(1) angle comes about to reduce intramolecular interaction between (*a*) the wedge-like perchlorate group and *o*-tolyl methyl groups (O(2)···H(273) 2.60 Å, O(3)···H(173*) 2.78 Å) and (*b*) atom Cl(1) and *o*-tolyl methyl C(17*) (Cl(1)···H(173*) 3.11 Å). As a consequence of these interactions, C(17) is bent 0.109 Å (Table 2) and the phosphorus atom -0.193 Å, from the C(11)—C(16) plane. Atom C(27) is displaced 0.055 Å and phosphorus 0.104 Å from the C(21)—C(26) plane; the third *o*-tolyl ring (C(31)—C(36)), which is not affected by intramolecular overcrowding, has the methyl group and phosphorus atom coplanar with the ring. The mercury coordination is thus very similar to that found in two of the

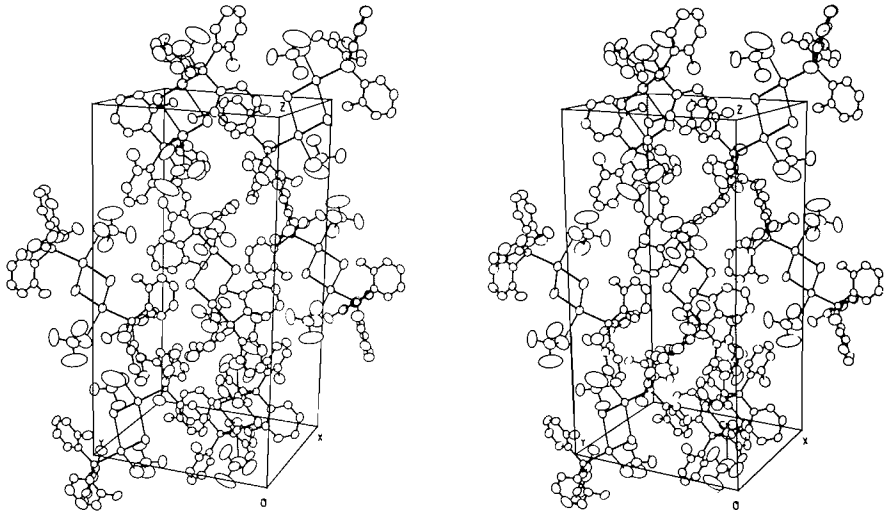

FIG. 2. Stereoview of the crystal structure of $[HgP(o\text{-tolyl})_3ClClO_4]_2$. In this diagram the cell shown runs from $(-\frac{1}{2}, -\frac{1}{2}, -\frac{1}{2})$ to $(\frac{1}{2}, \frac{1}{2}, \frac{1}{2})$; the points labelled '*O*', '*X*', '*Y*', and '*Z*' have crystal coordinates $(-\frac{1}{2}, -\frac{1}{2}, -\frac{1}{2})$, $(\frac{1}{2}, -\frac{1}{2}, -\frac{1}{2})$, $(-\frac{1}{2}, \frac{1}{2}, -\frac{1}{2})$, and $(-\frac{1}{2}, -\frac{1}{2}, \frac{1}{2})$ respectively.

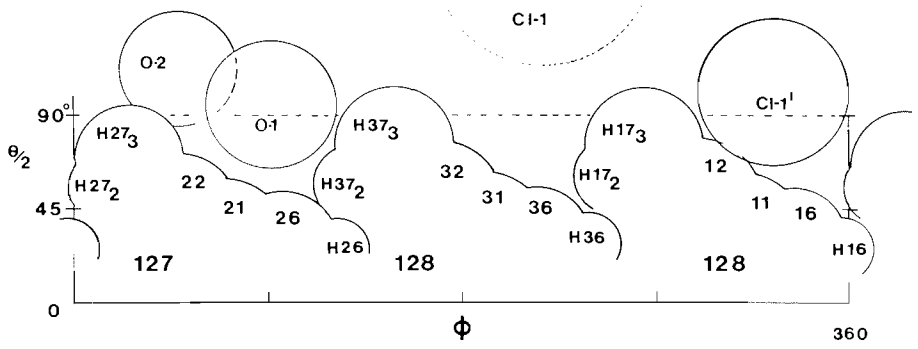

FIG. 3. Ligand profile for $P(o\text{-tolyl})_3$ in $(HgP(o\text{-tolyl})_3ClClO_4]_2$. The ordinate is the maximum semi-cone angle θ/2, the abscissa is the angle φ through which a cone generating vector Hg → X is rotated about the Hg—P bond. For full details see ref. 2. Also included in the profile diagram are the outlines of the encroaching chlorine and perchlorato oxygen atoms. The labels and numbers under the profile curves are the appropriate atom numbers, and values of the Hg—P—C—C(H) torsion angles.

four molecules comprising the asymmetric unit of chloro(diethyl phosphonato)mercury(II) (Cl—Hg—$PO(OC_2H_5)_2$) (16) with dimensions Hg—Cl 2.31–2.38; Hg—P 2.31–2.40; and P—Hg—Cl 173°. Other examples of strong digonal axial phosphorus coordination at mercury with weaker equatorial bonding are found in $Hg(PCy_3)_2(ClO_4)_2$ (7) and $Hg(PCy_3)_2(OAc)_2$ (7).

The $P(o\text{-tolyl})_3$ geometry is unexceptional with mean dimensions Hg—P—C(1) 110.1°, C—P—C 108.8°, and P—C 1.81 Å in agreement with those previously reported in $[HgP(o\text{-tolyl})_3(OAc)_2]_2$ (4), $Pt[P(o\text{-tolyl})_3]_2I_2$ (5), and $Ir[P(o\text{-tolyl})_3]_2ClCO$ (6). The perchlorate ion has the expected tetrahedral geometry with Cl—O 1.36–1.42 Å and O—Cl—O 107–114°. Apart from the weak bond Hg—O(1), the next shortest Hg···O distance (Hg···O(2) 3.13 Å) is just greater than the sum of the van der Waals radii (2.90 Å).

The ligand profile of the *o*-tolyl rings in $[HgP(o\text{-tolyl})_3ClClO_4]_2$ is shown in Fig. 3 (for details of the ligand profile calculations see ref. 2). The *o*-tolyl rings adopt a regular propeller conformation with Hg—P—C—C(H) torsion angles 127, 128, and 128°. The maximum semi-cone angles, θ/2, are 93.6, 101.4, and 102.2° giving a maximum cone angle of 198°, close to the value (194°) predicted by Tolman (1). The ligand profile also shows clearly the gaps between the *o*-tolyl rings whose conformations place steric limitations on the coordination geometry at the mercury atom. With the more strongly bonding acetato anion, the *o*-tolyl phosphine conformation

changes to a non-propeller one, e.g. in $[HgP(o\text{-tolyl})_3(OAc)_2]_2$ (4), with $\theta = 191°$. The flexibility and cog-like nature of the $P(o\text{-tolyl})_3$ ligands is amply demonstrated in the synthesis of *bis* $P(o\text{-tolyl})_3$ metal complexes with bulky anions, e.g. $Pt(P(o\text{-tolyl})_3)_2I_2$ (5), $Ir(P(o\text{-tolyl})_3)_2ClCO$ (6). Ligand profile calculations show that the $P(o\text{-tolyl})_3$ ligand in these complexes adopts a very irregular non-propeller conformation to accommodate ligand intermeshing, with a concomitant decrease in cone angle to 183° (2, 5).

Acknowledgement

We are grateful to the Natural Science and Engineering Research Council for operating grants (to E.C.A. and G.F.).

1. C. A. TOLMAN. Chem. Rev. **77**, 313 (1977).
2. G. FERGUSON, P. J. ROBERTS, E. C. ALYEA, and M. KHAN. Inorg. Chem. **17**, 2965 (1978).
3. E. C. ALYEA, S. A. DIAS, G. FERGUSON, and M. PARVEZ. Abstracts, ACS/CSJ Chemical Congress, Honolulu, Hawaii, Apr. 2–6, 1979. Paper INOR 69; Inorg. Chim. Acta. In press.
4. E. C. ALYEA, S. A. DIAS, G. FERGUSON, M. A. KHAN, and P. J. ROBERTS. Inorg. Chem. In press.
5. E. C. ALYEA, S. A. DIAS, G. FERGUSON, and P. J. ROBERTS. J. Chem. Soc. Dalton Trans. In press.
6. R. BRADY, W. H. DE CAMP, B. R. FLYNN, M. L. SCHNEIDER, J. D. SCOTT, L. VASKA, and M. F. WERNEKE. Inorg. Chem. **14**, 2669 (1975).
7. E. C. ALYEA, S. A. DIAS, G. FERGUSON, and M. KHAN. To be published.
8. E. C. ALYEA and S. A. DIAS. Can. J. Chem. **57**, 83 (1979).
9. R. J. RESTIVO, A. COSTIN, G. FERGUSON, and A. J. CARTY. Can. J. Chem. **53**, 1949 (1975).
10. R. F. STEWART, E. R. DAVIDSON, and W. T. SIMPSON. J. Chem. Phys. **42**, 3178 (1965).
11. D. T. CROMER and J. B. MANN. Acta Crystallogr. A**24**, 321 (1968).
12. D. T. CROMER. Acta Crystallogr. **18**, 17 (1965).
13. E. C. ALYEA, S. A. DIAS, R. G. GOEL, and W. O. OGINI. Can. J. Chem. **55**, 4227 (1977).
14. E. C. ALYEA, S. A. DIAS, R. G. GOEL, W. O. OGINI, P. PILON, and D. W. MEEK. Inorg. Chem. **17**, 1697 (1978).
15. K. NAKAMOTO. I.R. spectra of inorganic and coordination compounds. 2nd ed. Wiley. 1972.
16. J. BENNETT, A. PIDCOCK, C. R. WATERHOUSE, P. COGGON, and A. MCPHAIL. J. Chem. Soc. A, 2094 (1970).

Stereochemistry of six coordinate organotin(IV) compounds with bidentate ligands

J. S. TSE,[1] T. K. SHAM,[2] AND G. M. BANCROFT

Department of Chemistry, University of Western Ontario, London, Ont., Canada N6A 5B7

Received January 31, 1979

J. S. TSE, T. K. SHAM, and G. M. BANCROFT. Can. J. Chem. **57**, 2223 (1979).

Extended ligand–ligand repulsion calculations have been applied to a number of six coordinate organotin complexes of the type $RR'Sn(bidentate)_2$ (R, R′ = Me, Ph, Cl). Qualitatively, the calculations readily predict the decrease in the R—Sn—R′ angle with decrease in bite size of the bidentate ligand. The steric calculations are generally successful in predicting both the *cis–trans* preference of the R groups and the bond angles about the Sn atom. For the Me_2Sn complexes, electronic effects (as expressed by Bent's rule) sometimes have to be used in conjunction with the steric calculations to rationalize the observed stereochemistry.

J. S. TSE, T. K. SHAM et G. M. BANCROFT. Can. J. Chem. **57**, 2223 (1979).

On a appliqué des calculs étendus de répulsion ligand–ligand à un certain nombre de complexes organostanneux hexacoordonnés du type $RR'Sn(bidentate)_2$ (R,R′ = Me, Ph, Cl). Qualitativement, les calculs permettent facilement de prédire une diminution dans la grosseur du ligand bidentate. Les calculs stériques permettent généralement de prédire avec succès la préférence *cis–trans* des groupes R et les angles de liaison autour de l'atome de Sn. Dans le cas des complexes du Me_2Sn, on doit quelquefois faire appel à des effets électroniques (exprimés sous la forme de la règle de Bent) de concert avec des calculs stériques pour rationaliser la stéréochimie observée.

[Traduit par le journal]

Introduction

Recent X-ray structures and ^{119}Sn Mössbauer studies of six coordinate dimethyl and diphenyl tin compounds have shown that the C—Sn—C bond angle varies from close to 90° to 180° (1–4). Nearly all six coordinate dimethyl compounds have the *trans* or distorted *trans* structure, whereas most of the diphenyl analogues have the *cis* structure. The C—Sn—C angle in the dimethyl compounds varies widely, for example from 110° to 136° to 160° to 180° in $Me_2Sn(oxin)_2$, $Me_2Sn(S_2CNMe_2)_2$, $Me_2Sn(Salen)$, and $Me_2Sn(acac)_2$ respectively.

Simple theoretical models based on ligand–ligand repulsion have been proposed to account semiquantitatively for the variation in the C—Sn—C bond angles and the *cis–trans* preference in some organotin compounds (5–7). For example, Kepert (6, 7) has shown that the C—Sn—C angle in $Me_2Sn(bidentate)_2$ compounds decreases from 180° in steric response to a decrease in bite size of the chelating ligand.

In this paper, we incorporate Zahrobsky's concept (5) of steric cone angle into Kepert's ligand–ligand repulsion model, and calculate equilibrium geometries for a number of six coordinate diorganotin compounds. Our calculated angles are usually in good agreement with the observed structural values, although the *cis–trans* preference is sometimes not predicted solely on steric grounds.

Theory

The ligand–ligand repulsion model assumes that the repulsion between donor atoms within a molecule is the predominate factor in determining the equilibrium geometry of that molecule. In Kepert's model (6, 7), donor atoms are assumed to lie on a sphere of unit radius with the metal atom at the centre (i.e. all central atom – donor atom bond distances are equal). However, in reality, bond lengths are seldom equal. In order to apply Kepert's model to obtain bond angles, the concept of steric angle (5) is incorporated into Kepert's model. Thus, in the present model, we suggest that the repulsion between two donor atoms i and j is inversely proportional to their separation r_{ij} and directly proportional to their steric angles θ_i and θ_j subtended at the centre (n_L is the number of ligands):

$$[1] \quad U_{tot} = \frac{1}{2}\sum_{\substack{i}}^{n_L}\sum_{\substack{j \\ i \neq j}}^{n_L} \theta_i\theta_j r_{ij}^{-n} \qquad (n = 1, 2, \ldots)$$

The equilibrium geometry can be calculated by minimizing the total repulsion energy with respect to the donor atom positions.

$$[2] \quad U_{min} = \frac{\delta U_{tot}}{\delta r_{ij}} = \sum_{i=1}^{n_L} \theta_i\theta_j \frac{\delta}{\delta r_{ij}}(r_{ij})^{-n}$$

The steric angles are calculated as by Zahrobsky (5)

[1]To whom all correspondence should be addressed.

[2]Present address: Chemistry Department, Brookhaven National Laboratory, Upton, New York.

0008-4042/79/172223-07$01.00/0

TABLE 1. Van der Waals radii and the range of steric angles used in this work (5)

Element	Van der Waals radius (Å)	Steric angle (deg)†
C	2.00 (methyl)	133–144
	3.40 (phenyl)*	153
N	1.50	83–88
O	1.40	81–83
Cl	1.80	97–100
S	1.85	76–96

*The Van der Waals radius of the phenyl group is taken as the sum of the distance from the centre of the phenyl ring to a carbon atom and the Van der Waals radius of H attached to that carbon.

†The exact steric angle used in the calculation depends of course on the observed Sn—X bond length in the individual compound.

from the known covalent bond lengths and the Van der Waals radii of the ligand atoms. The radii used in calculating the steric angles (mostly taken from Zahrobsky (5)) are given in Table 1. The bond lengths are taken from the literature crystal structures. The minimization of the potential function was carried out using the quasi-Newton Algorithm. All computations were performed using the University of Western Ontario CDC Cyber 73 computer.

The most appropriate value of n in the repulsion energy expression (eq. [1]) cannot be known exactly. As noted previously (7) and again verified through our calculations, variation of n from 1 to 12 does not change our calculated bond angles significantly. Therefore $n = 1$ is used in this paper (as in the previous work (6, 7)), owing to the simplification of the calculations.

For the *trans*-$R_2Sn(bidentate)_2$ compounds, the treatment used is similar to that given by Kepert (6) and the Sn—D (D = O, S, etc.) distances are taken to be equal. For the *cis*-$R_2Sn(bidentate)_2$ compounds, the treatment is more complex. The only symmetry element in such a *cis* compound is a twofold axis, and there are four variables.

We have also done calculations on a number of diorganotin molecules having only unidentate ligands. As suggested by Zahrobsky (5), the minimization problem is simplified by approximating the three dimensional problem into three two dimensional ones. The number of variables is then reduced from nine in the three dimensional case to three variables per plane.

Results and Discussion

(a) The cis–trans *Preference*

Our calculations on diorganotin compounds such as $Me_2SnCl_2(pyO)_2$ (8), $Me_2SnCl_2(DMSO)_2$ (9), and $Ph_2SnCl_2(DMSO)_2$ (10) containing only unidentate ligands confirm Zahrobsky's previous observations (5). Contrary to the *trans*-R_2Sn structure observed

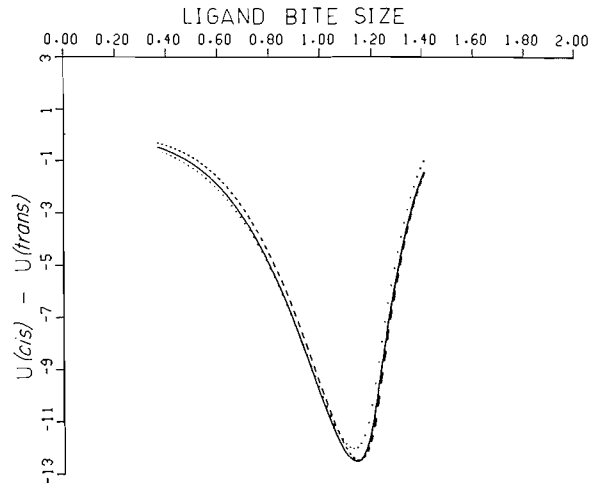

FIG. 1. Stabilization of *cis*-RR′Sn(O—O′)$_2$ relative to *trans*-RR′Sn(O—O′)$_2$ as a function of the ligand normalized bite size; dotted line, R = R′ = Me; full line, R = Me, R′ = Ph; broken line, R = R′ = Ph. The $U_{cis} - U_{trans}$ energy unit is arbitrary. The problem is discussed in ref. 7.

(8–10), the repulsion model predicts the *cis* structure. Electronic effects, as expressed by Bent's rule (11), may outweigh the steric requirements: to maximize Sn 5*s* density in the Sn—C bonds, the strong σ donor R groups prefer the *trans* geometry where they overlap with Sn *sp* hybrids.

For the RR′Sn(bidentate)$_2$ compounds, the repulsion model again sometimes fails to predict the correct stereochemistry (e.g., when R and R′ are *both* Me) at least partially for the electronic reason given above. Plots of $U_{cis} - U_{trans}$ vs. the ligand bite b (7) (Fig. 1) for such compounds show that, except at very large bites, the *cis* structure is always favoured sterically, whereas the Me_2Sn complexes in Table 2 give the *trans* structure. The three plots for Me_2Sn, MePhSn, and Ph_2Sn compounds (Fig. 1) show that there is little change in $U_{cis} - U_{trans}$ with change in steric angle of R. At small bite sizes (e.g. oxin, b = 1.19), $U_{cis} - U_{trans}$ is close to a minimum, and the predicted *cis*-$Me_2Sn(oxin)_2$ structure is observed (12) (Table 3).

In the above discussion we invoked Bent's rule to explain the *trans* preference of the Me_2Sn moiety. To investigate this preference further, we have undertaken Extended-Hückel calculations (13) on different geometries of $Me_2Sn(acac)_2$ and $Cl_2Sn(acac)_2$. The Extended-Hückel method has been evaluated thoroughly and shown to be capable of predicting reasonable geometries for many organometallic compounds (14). We have assumed a 'D_{3d}' symmetry for the R_2SnL_2 complex. We can then vary the R—Sn—R bond angle from 90° to 180° (i.e. *cis* to *trans*) by rotating one plane of the molecule about the 'C_3'

TABLE 2. Bite angles and bond angles of

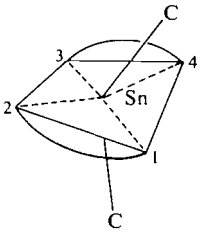

Compound[f]	Bite angle (deg)	Bond angles (deg) 4—Sn—1 Calcd.	4—Sn—1 Observed	C—Sn—C Calcd.	C—Sn—C Observed
trans-$Me_2Sn(NO_3)_2$	54.5	176.6	176.3[a]	120.0	143.6
trans-$Me_2Sn(acac)_2$	86.6	94.0	94.0[b]	180.0	180.0
trans-$Me_2Sn(dtc)_2$	64.3	152.8	149.1[c]	134.0	136.0
trans-$Me_2Sn[ON(Me)COMeO]_2$	71.4	135.0	144.1[d]	148.0	145.8
trans-$Me_2Sn(dedtc)_2$	64.8	151.8	147.7[e]	133.0	142.3

[a]Reference 24.
[b]Reference 25.
[c]Reference 26.
[d]Reference 27.
[e]Reference 18.
[f]Abbreviations: acac, anion of acetylacetone; dtc, anion of bis(*N*,*N*-dimethyldithiocarbamate); dedtc, anion of bis(*N*,*N*-diethyldithiocarbamate).

axis. The parameters used in the calculation are described in the Appendix and Table 4. Figure 2 shows the results of the Extended-Hückel calculation on $Me_2Sn(acac)_2$ and $Cl_2Sn(acac)_2$. The conclusion we obtained from the molecular orbital calculation is puzzling. The calculation predicts the *cis* conformation for both $Me_2Sn(acac)_2$ and $Cl_2Sn(acac)_2$. This is contradicted by the observed *trans*-$Me_2Sn(acac)_2$ and *cis*-$Cl_2Sn(acac)_2$ structures. The calculation also predicts a local minimum at R—Sn—R bond angle of ca. 140°. We think this local minimum is fortuitous. The potential surface of the conformation of a molecule is a function of many variables. Without full optimization of all variables in each geometry, the total valence energy may not be a reliable parameter in predicting the geometry of a molecule. It is also interesting to note that the local minimum occurred when the planes of the molecule are in eclipsed conformation. However, the calculation does show that the main minimum occurs at an R—Sn—R angle of ca. 110°. This bond angle is very close to the 'normal' sp^3 hybridized tetrahedral angle at the tin atom. This observation is in agreement with our argument that the tin atom in a number of R_2SnL_2 complexes is probably sp^3 hybridized having a tetrahedral arrangement of ligands around the metal center (*vide infra*). The differences in Sn—D distances in *trans* compounds (Table 5) may well be a factor in the retention of the *trans* structure. An increase in C—Sn—C angle increases the steric repulsion between the donor ligands and the methyl groups. In order to relieve this repulsion force, one end of the donor bidentate ligand is pushed further away from the Sn atom. Our steric calculations reveal that this distorted *trans* structure is indeed more stable than the undistorted *cis* structure.

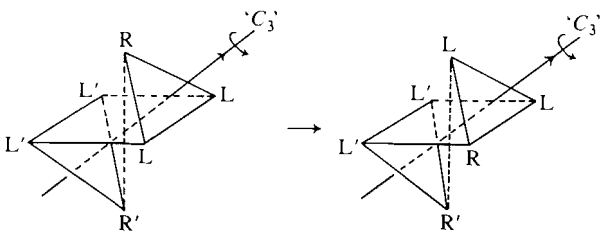

In the *cis* compounds, there is less reason sterically for the Sn—D distances to become different. Also on electronic grounds, the Sn atoms in *cis*-Cl_2Sn and *cis*-Ph_2Sn compounds will be more electronegative than in *trans*-Me_2Sn, and invite better overlap with the bidentate donors. The Sn–donor distances (Table 5) support this argument. Thus, the average Sn—O bond lengths in *trans*-$Me_2Sn(ONR'COMe)_2$ is 2.25 Å, compared to the average of the four Sn—O bond lengths in *cis*-$Cl_2Sn(ONHCOMe)_2$ of 2.09 Å.

It is interesting to note that the energy difference between *cis* and *trans* structures must indeed be very small for large ligand bite size, since *cis*-$Me_2Sn(acac)_2$ has been observed in solution (15), whereas *trans*-$Me_2Sn(acac)_2$ forms in the solid state. Also,

TABLE 3. Calculated/observed bond angles (deg) for

Compound[g]	Bond angle															
	3—Sn—2	4—Sn—1	4—Sn—2	5—Sn—1	5—Sn—2	5—Sn—3	5—Sn—4	6—Sn—1	6—Sn—2	6—Sn—3	6—Sn—4	6—Sn—5				
cis-$Me_2Sn(oxin)_2$[a]	82.3	75.8	160.3	157.0	91.4	83.6	93.2	95.9	164.8	169.3	90.7	88.3	99.5	101.6	99.5	100.7	90.7	86.7	164.8	166.7	93.2	93.0	99.0	110.7
cis-$Ph_2Sn(dtc)_2$[b]	83.0	80.9	154.0	154.9	95.6	95.4	92.8	93.9	155.9	157.5	92.2	88.7	103.6	103.6	103.6	99.5	92.2	94.4	155.9	161.4	92.8	97.2	101.2	101.4
cis-$Cl_2Sn(acac)_2$[c]	85.9	84.5	174.0	172.3	89.0		91.7		175.3	173.5	89.7	94.5	92.4	89.0	92.4		89.7		175.3	186.6	91.7		94.8	97.4
cis-$Cl_2Sn(ONPhCPhO)_2$[d]	89.1	86.0	167.2	167.2	94.5	90.8	91.3	94.6	167.5	166.6	90.2	87.8	97.5	98.5	97.5	94.6	90.2	89.8	167.5	166.5	91.3	90.8	93.2	99.0
cis-$Me_2Sn(ONHCOMe)_2$[e]	77.7	75.8	162.8	147.7	85.1		94.8	94.0	167.4	160.7	90.0	88.3	96.0	104.6	96.0	104.6	90.0	88.3	167.4	160.7	94.8	94.0	102.4	109.1
cis-PhMeSn(oxin)$_2$[f]	80.5		159.1		90.3		93.5		164.2		90.7		99.8		99.8		90.7		164.2		93.5		100.6	
cis-$Ph_2Sn(oxin)_2$[f]	78.5		158.3		89.5		93.9		163.4		90.7		99.6		99.6		90.7		163.4		93.9		102.4	

[a]Reference 12.
[b]Reference 17.
[c]Reference 18.
[d]Reference 19.
[e]Reference 20.
[f]Predicted values.
[g]Abbreviations: oxin, anion of 8-hydroxyquinoline.

TABLE 4. Atom parameters

Orbital	$\zeta(a_0^{-1})$	H_{ii} (eV)
H 1*s*	1.3	−13.6
C 2*s*	1.625	−21.4
C 2*p*	1.625	−11.4
O 2*s*	2.750	−32.3
O 2*p*	2.750	−14.8
Cl 3*s*	2.183	−26.3
Cl 3*p*	2.183	−14.2
Sn 5*s*	2.126	−14.56
Sn 5*p*	2.126	−6.84

FIG. 2. Variation of total valence molecular orbital energy as a function of ∠R—Sn—R in $R_2Sn(acac)_2$ compounds: (*a*) R = methyl, (*b*) R = chloro.

cis-MePhSn compounds form, in contrast to their *trans*-Me_2Sn analogues (16). Thus, *cis*-MePhSn-$(acac)_2$ is obtained rather than *trans*-$Me_2Sn(acac)_2$.

(b) Bond Angles

Within either the *cis* or *trans* structures, the steric model is very successful in predicting the C—Sn—C angle and other bond angles in $RR'Sn(bidentate)_2$ compounds. The predicted variation of C—Sn—C angle with ligand bite size for the *trans*-Me_2Sn, MePhSn, and Ph_2Sn compounds is shown in Fig. 3 (taking all Sn—D distances equal). Qualitatively, as the ligand bite angle increases from 60.5° (*b* = 1)

TABLE 5. Important bond lengths (Å) and angles (deg) in $R_2Sn(bidentate)_2$ complexes with sulphur and oxygen donor ligands

Compound	Bond length Sn—S_1	Sn—S_2	∠S_1—Sn—S_2	Reference
cis-Sn(dedtc)$_4$	2.504(7) 2.534(7)	2.504(7) 2.534(7)	70.63 70.63	28
trans-$Me_2Sn(dtc)_2$	2.497(7) 2.515(8)	2.954(7) 3.061(8)	65.1(2) 63.5(2)	26
trans-$Me_2Sn(dedtc)_2$	2.536 2.518	2.918 2.969	65.0 64.6	18
cis-$Ph_2Sn(dedtc)_2$	2.613(5) 2.548(5)	2.637(5) 2.790(6)	67.6(1) 67.6(2)	17

Compound	Bond length Sn—O_1	Sn—O_2	∠O_1—Sn—O_2	Reference
trans-$Me_2Sn(ONHCOMe)_2$	2.15(1) 2.15(1)	2.35(1) 2.49(1)	72.1(4) 70.7(4)	20
trans-$Me_2Sn(ONHCOMe)_2$	2.17(1) 2.16(2)	2.36(2) 2.43(1)	71.7(5) 71.5(4)	20
trans-$Me_2Sn(ONMeCOMe)_2$	2.107(4) 2.126(4)	2.384(4) 2.374(5)	71.61(14) 71.11(15)	27
cis-$Me_2Sn(ONHCOMe)_2$	2.106(4) 2.106(4)	2.228(4) 2.228(4)	81.5(1) 81.5(1)	20
cis-$Cl_2Sn(ONPhCOMe)_2$	2.054(15) 2.041(16)	2.099(12) 2.180(15)	76.3(5) 76.5(5)	19
trans-$Me_2Sn(acac)_2$	2.20(1) 2.20(1)	2.18(1) 2.18(1)	86 (1) 86 (1)	25
cis-$Cl_2Sn(acac)_2$	2.030 2.030	2.075 2.075	86.6 86.6	18

to 72.5° (b = 1.18), the C—Sn—C angles increase from 126° to 180°, and remain at 180° as the ligand bite size increases. The angle between the bisector of the C—Sn—C angle and the line joining the central atom and a ligand donor atom decreases from 82° (b = 1.0) to 54° (b = 1.18). These observations are consistent with those reported by Kepert (6, 7). As the ligand bite size decreases, the R–ligand repulsion increases. The molecule then tends to distort to a skew-trapezoidal bipyramid structure. This distortion is physically equivalent to a compression of the C—Sn—C angle followed by a twist of the bidentate ligands. The intermediate of such a rotation is the skew-trapazoidal bipyramid structure II. If the ligand bite size decreases further, the *cis*-structure is formed.

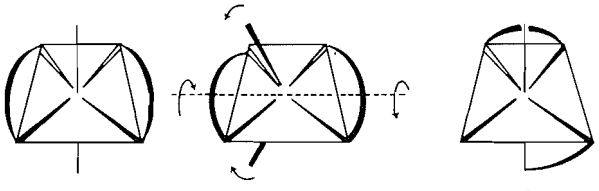

trans II *cis*

On steric grounds alone, for $b < 1.05$, the predicted C—Sn—C angle in *trans* compounds increases in the order $Me_2Sn < MePhSn < Ph_2Sn$; whereas for $b > 1.05$, the C—Sn—C angle increases in the opposite direction (Fig. 3). For *cis* structures, the predicted C—Sn—C angle increases in the order $Me_2Sn < MePhSn < Ph_2Sn$ (Table 3, $Me_2Sn(oxin)_2$, 99.0°; $MePhSn(oxin)_2$, 100.6°, $Ph_2Sn(oxin)_2$, 102.4°). However, at least partially because of Bent's rule, the observed C—Sn—C angle in *cis*-Me_2Sn compounds will tend to increase more than in the other two cases (e.g. $Me_2Sn(oxin)_2$, 110.7°, see below). Figure 3 also indicates that ligand bite size normally plays a much more important role than steric angle of the R groups in determining the C—Sn—C angle in *trans*-RSnR′ compounds (7).

More quantitatively, we have calculated bond angles for the few *trans*-$R_2Sn(bidentate)_2$ compounds known (Table 2). Except for $Me_2Sn(NO_3)_2$, the calculated C—Sn—C angles are in very good agreement with those observed, indicating the considerable power of our simple method for rationalizing and in-

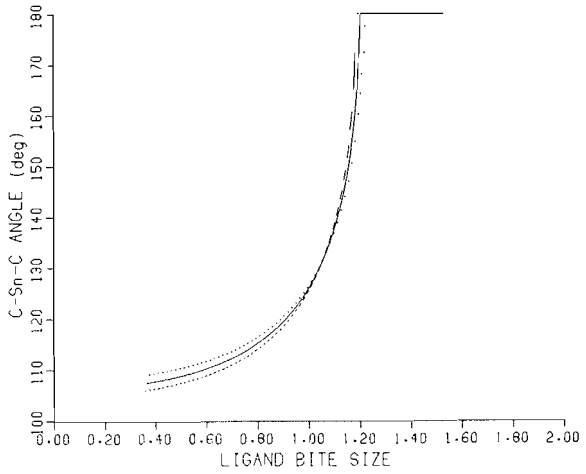

FIG. 3. Variation of C—Sn—C angle (deg) as a function of the ligand normalized bite size; dotted line, R = R′ = Ph; full line, R = Me, R′ = Ph; broken line, R = R′ = Me.

deed predicting bond angles in compounds of this type.

As suggested by Fig. 1, the *cis* configuration is more stable than *trans* on steric grounds, and indeed the *cis* configuration is formed except when R and R′ = Me. Five crystal structures have been determined (12, 17–20) (Table 3) and the experimental bond angles are compared with those observed. Other compounds such as $Ph_2Sn(oxin)_2$, MePhSn-$(oxin)_2$, $MeClSn(acac)_2$, and $PhClSn(acac)_2$ have *cis* structures from Mössbauer and other evidence (16). Predicted bond angles for the two oxin compounds are included in Table 3. In contrast to the *trans* compounds, our calculations for the *cis*-species show that the R—Sn—R (R, R′ = Me, Ph, Cl) angle is not very sensitive to the variation in ligand bite size. Thus the calculated angle is always in the 90°–105° range. Neglecting R, R′ = Me for electronic reasons, the predicted R—Sn—R′ angle for a given ligand bite on steric grounds alone increases in the order Cl—Sn—Cl < Me—Sn—Cl < Ph—Sn—Cl < Me—Sn—Ph < Ph—Sn—Ph.[3] Mössbauer parameters for Ph_2Sn and MePhSn compounds have been previously rationalized using this order (16).

Quantitatively, the agreement between predicted and observed angles is rather good except for Me_2Sn-$(oxin)_2$. For this compound, the observed C—Sn—C angle is 12° higher than that calculated. To maximize the *s* character in the Sn—Me bonds, the C—Sn—C angle increases to approach the tetrahedral value. The C—Sn—C angle in $Me_2Sn(ONHCOMe)_2$ (20) (109.1°) also approaches the tetrahedral value. In these *cis*-Me_2Sn compounds, the Sn atom is probably sp^3 hybridized as proposed by Schlemper (12) and our Extended-Hückel calculations, so that the *s* character is once again maximized in the Sn—Me bonds. The two other Sn hybrid orbitals form two 'three centre' bonds with the chelating ligands. This sp^3 hybridization also gains support from the $^2J_{CH_3-Sn^{119}}$ coupling constants. Thus ^2J is 71.2 Hz for *cis*-$Me_2Sn(oxin)_2$ — almost identical to that for four coordinate compounds such as Me_2SnCl_2 (16).

[3]It is also possible to argue that for a specific orientation of the phenyl group, the steric angle of the phenyl group and chloro group will be smaller than the methyl group, hence the angle will be smaller. We think this explanation is not satisfactory as we have shown that the C—Sn—C angle is not very sensitive to the steric angles in *cis* compounds, and also this cannot explain the apparent constancy of 109.5° for dimethyl compounds.

Conclusions

For RR′Sn(bidentate)$_2$ compounds (R, R′ = Me, Ph, Cl), the ligand–ligand repulsion model is generally successful in predicting both the steric preference of the R groups and the bond angles about the Sn atom. Kepert's work (7) and recent calculations on transition metal complexes (22, 23) also suggest that far more attention should be paid to steric effects when considering the stereochemistry of inorganic and organometallic compounds.

Acknowledgements

We wish to thank Dr. E. O. Schlemper for sending us the structural data on $Cl_2Sn(acac)_2$ and Me_2Sn-$(dedtc)_2$ prior to publication, and the National Research Council of Canada for financial support.

1. B. Y. K. Ho and J. J. Zuckerman. J. Organomet. Chem. **49**, 1 (1973), and references therein.
2. P. J. Smith. A bibliography of organotin X-ray crystal structures. Tin Research Institute, Middlesex, England. 1975.
3. T. K. Sham and G. M. Bancroft. Inorg. Chem. **14**, 2281 (1975), and references therein.
4. B. W. Fitzsimmons, N. J. Seeley, and A. W. Smith. J. Chem. Soc. A, 143 (1969).
5. R. F. Zahrobsky. J. Am. Chem. Soc. **93**, 3313 (1971).
6. D. L. Kepert. J. Organomet. Chem. **107**, 49 (1976).
7. D. L. Kepert. Progress Inorg. Chem. **23**, 1 (1977).
8. E. A. Blom, B. R. Penfold, and W. T. Robinson. J. Chem. Soc. A, 913 (1969).
9. N. W. Isaacs and C. H. L. Kennard. J. Chem. Soc. A, 1251 (1970).
10. L. Coghi, C. Pelizzi, and G. Pelizzi. Gazz. Chim. Ital. **104**, 873 (1974).
11. H. A. Bent. J. Inorg. Nucl. Chem. **19**, 43 (1961).
12. E. O. Schlemper. Inorg. Chem. **6**, 1012 (1967).
13. (*a*) R. Hoffman. J. Chem. Phys. **39**, 1397 (1963); R. Hoffman and W. N. Lipscomb. J. Chem. Phys. **36**, 2179 (1962); **36**, 3489 (1962); **37**, 2872 (1962); (*b*) P. Dibout. QCPE. No. 256 (1976); (*c*) J. Howell, A. Rossi, D. Wallace, K. Haraki, and R. Hoffman. Quantum Chemistry Program Exchange No. 344 (1977).
14. P. K. Mehrotra and R. Hoffman. Theor. Chim. Acta, **48**, 301 (1978).

15. R. B. LEBLANC, JR. and W. H. NELSON. J. Organomet. Chem. **113**, 257 (1976).
16. T. K. SHAM, J. TSE, V. WELLINGTON, and G. M. BANCROFT. Can. J. Chem. **55**, 3487 (1977).
17. P. F. LINDLEY and P. CARR. J. Cryst. Mol. Struct. **4**, 173 (1974).
18. G. A. MILLER and E. O. SCHLEMPER. Inorg. Chim. Acta, **30**, 131 (1978).
19. P. G. HARRISON, T. J. KING, and J. A. RICHARDS. J. Chem. Soc. Dalton, 1414 (1976).
20. P. G. HARRISON, T. J. KING, and R. C. PHILLIPS. J. Chem. Soc. Dalton, 2317 (1976).
21. M. WOLFSBERG and L. HELMHOLZ. J. Chem. Phys. **20**, 837 (1952).
22. B. F. G. JOHNSON. J. Chem. Soc. Chem. Commun. 211 (1976); P. B. HITCHCOCK, R. MASON, and M. TEXTOR. J. Chem. Soc. Chem. Commun. 1047 (1976).
23. H. C. CLARK. Isr. J. Chem. **15**, 210 (1976/77).
24. J. HILTON, E. K. NUNN, and S. C. WALLWORK. J. Chem. Soc. Dalton Trans. 173 (1973).
25. G. A. MILLER and E. O. SCHLEMPER. Inorg. Chem. **12**, 677 (1973).
26. T. KIMURA, N. YASUOKA, N. KASAI, and M. KAKUDO. Bull. Chem. Soc. Jpn. **45**, 1649 (1972).
27. P. G. HARRISON, T. J. KING, and J. A. RICHARDS. J. Chem. Soc. Dalton Trans. 826 (1975).
28. C. S. HARRELD and E. O. SCHLEMPER. Acta Crystallogr. B**27**, 1967 (1971).

Appendix

The calculations were performed using the Extended-Hückel method (13). The geometry of $Me_2Sn(acac)_2$ was taken from its crystal structure (25). For simplicity, the methyl groups on the acetylacetonate ligand were replaced by hydrogen atoms. The Sn—Cl bond distance in $Cl_2Sn(acac)_2$ was taken from ref. 18. Parameters used for the calculation are tabulated in Table 4. All geometrical deformations were examined by extended Hückel calculations without charge iteration. The off diagonal matrix elements were calculated using the Wolfsberg and Helmholz approximation (21):

$$H_{ij} = 0.5KS_{ij}(H_{ii} + H_{jj})$$

with K fixed at 1.75.

The synthesis of oligoribonucleotides. III.[1] The use of silyl protecting groups in nucleoside and nucleotide chemistry. VIII

KELVIN K. OGILVIE, ARIA L. SCHIFMAN, AND CHRISTOPHER L. PENNEY
Department of Chemistry, McGill University, Montreal, P.Q., Canada H3A 2K6

Received December 22, 1978

KELVIN K. OGILVIE, ARIA L. SCHIFMAN, and CHRISTOPHER L. PENNEY, Can. J. Chem. **57**, 2230 (1979).

The synthesis of all isomeric mono- and disilyl derivatives of cytidine, guanosine, and their *N*-benzoyl analogues using the *tert*-butyldimethylsilyl protecting group is described. These compounds and those containing a 5′-monomethoxytrityl group have been condensed via the phosphodichloridite procedure to produce nucleotides rapidly and in good yields. The synthesis of 2′–5′-linked nucleotides is described. A cautionary note is introduced in regard to the preparation of 5′-monomethoxytritylguanosine and a novel methanolysis of certain *N*-benzoylcytidines is mentioned.

KELVIN K. OGILVIE, ARIA L. SCHIFMAN et CHRISTOPHER L. PENNEY, Can. J. Chem. **57**, 2230 (1979).

On décrit une synthèse de tous les dérivés isomères mono- et disylés de la cytidine, de la guanosine et de leurs analogues *N*-benzoylés qui fait appel au groupe protecteur *tert*-butyldiméthylsilyle. On a condensé ces composés et ceux portant un groupe monométhoxytrityl-5′ grâce à la méthode du phosphodichloridite pour obtenir rapidement et avec de bons rendements des nucléotides. On décrit la synthèse de nucléotides reliés par les positions 2′ et 5′. On signale les précautions à prendre lors de la préparation de la monométhoxytrityl-5′ guanosine et on mentionne une nouvelle méthanolyse de cartaines *N*-benzoylcytidines.

[Traduit par le journal]

Introduction

We have recently described the use of alkylsilyl groups, particularly *tert*-butyldimethylsilyl (TBDMS), for protection of hydroxyl groups of deoxynucleosides (1–3), deoxynucleotides (4), ribonucleosides (5, 6), and ribonucleotides (6). The latter work has led to the development of a rapid synthesis of oligoribonucleotides. The previous paper in this series (6) described in detail the synthesis of oligonucleotides of uridine and adenosine using TBDMS and the chlorophosphite triester procedure (7). In this manuscript we wish to describe the extension of these procedures to cytidine and guanosine and their *N*-benzoyl derivatives.

Preparation of Silylated Nucleosides

Two solvent systems have been employed for the silylation of nucleosides (Scheme 1). The DMF–imidazole system usually leads to faster rates of reaction while pyridine as solvent provides higher yields of desired products. These results are summarized in Table 1. Good yields of the desired 2′-protected nucleosides are obtained in all cases. For example the 2′,5′-disilylcytidine (**3***a*) is obtained in 60% yield after a 48 h reaction in pyridine, or in 50% yield after a 2 h reaction in DMF–imidazole (DMF–Im). Similar yields are obtained for 2′,5′-disilyl-N^4-benzoylcytidine (**3***b*; 62% (pyridine), 52% (DMF–Im)). Selective silylation at the 2′-position of 5′-methoxytritylcytidine (**6***a*) and 5′-methoxytrityl-N^4-benzoylcytidine (**6***b*) also proceeds well, particularly in pyridine where yields of **7***a* and **7***b* were 63 and 64% respectively.

With guanosine yields of 2′,5′-protected derivatives are generally lower than for cytidine. For example 2′,5′-disilylguanosine (**3***c*) is obtained in 41% yield while the *N*-benzoyl derivative **3***d* is obtained in 39% yield. Yields for the corresponding 5′-methoxytrityl derivatives are also in the 30–40% range. However, such yields of protected guanosines are quite remarkable especially considering the few steps involved.

The conditions described in Table 1 lead to a minimum of silylation at the bases of cytidine and guanosine. Using larger excesses of silylating agent can lead to silylation at the base particularly in the case of guanosine. We have also noted that the TBDMSCl deteriorates with time and repeated exposure to air such that higher ratios of reagent to nucleoside must be used to obtain the results of Table 1 as the reagent ages.

The position of silylation is easily determined from the ^{13}C spectra. Silylation at a sugar hydroxyl leads to a downfield shift of the sugar carbon to which it is attached. This is true for all of the silylated

[1]For the previous articles in these series, see ref. 6.

0008-4042/79/172230-09$01.00/0

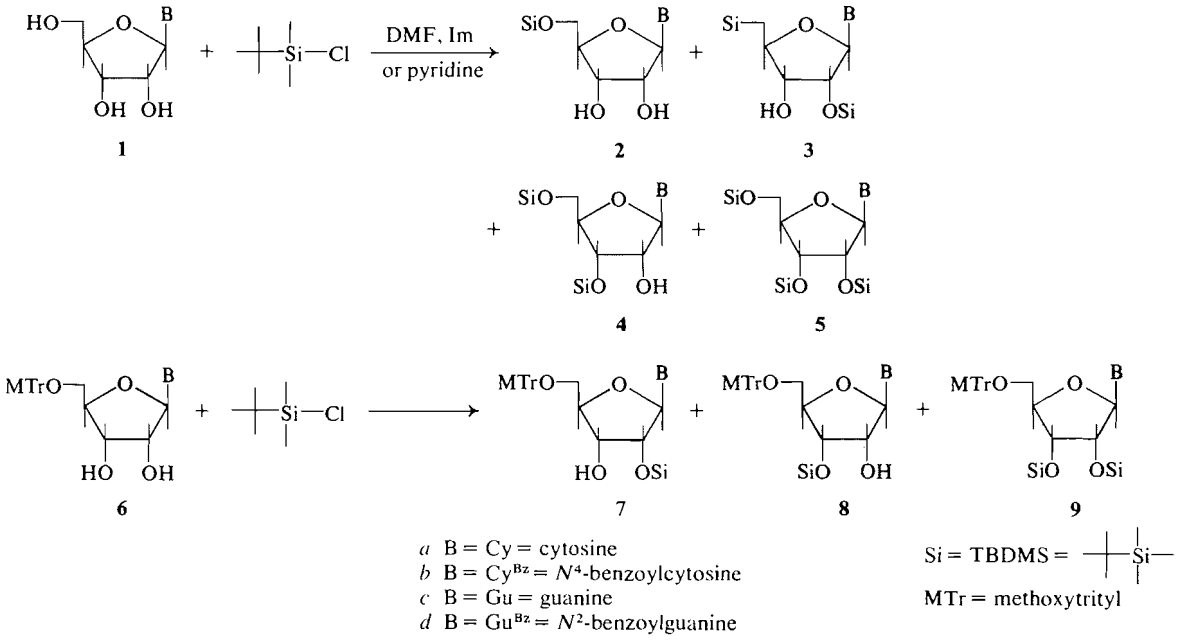

SCHEME I

TABLE 1. Preparation of silylated nucleosides

Starting material	TBDMSCl (mequiv.)	Imidazole (mequiv.)	Solvent*	Time (h)	Isomer yields (%) 5′-	2′,5′-	3′,5′-	2′,3′,5′-
Cytidine	1.25	2.5	DMF	2	75	8	6	—
Cytidine	1.25	0	Pyridine	3	84	7	2	—
Cytidine	2.2	4.4	DMF	2	—	50	36	8
Cytidine	3	0	Pyridine	48	—	60	24	4
Cytidine	7	14	Pyridine	48	—	—	—	98
C^{Bz} (1*b*)	1.25	2.5	DMF	2	65	11	9	—
C^{Bz} (1*b*)	1.25	0	Pyridine (5 mL)	18	90	6	—	—
C^{Bz} (1*b*)	3	0	Pyridine	72	—	62	27	4
C^{Bz} (1*b*)	2.2	4.4	DMF	2	—	52	32	5
C^{Bz} (1*b*)	5	10	DMF	18	—	—	—	98
Guanosine	3	6	DMSO (2 mL)	3	90	—	—	—
Guanosine	3.5	7	DMF (2 mL)	4	—	41	20	8
Guanosine	5	0	Pyridine (6 mL)	72	—	51	19	5
Guanosine	4	10	DMF	48	—	4	4	75
G^{Bz} (1*d*)	1.25	2.5	DMF	2	90	4	4	—
G^{Bz} (1*d*)	1.25	0	Pyridine	2	90	2	2	—
G^{Bz} (1*d*)	2.2	4.4	DMF	2	—	39	41	7
G^{Bz} (1*d*)	5	0	Pyridine	48	11	39	43	5
G^{Bz} (1*d*)	5	10	DMF	48	—	—	—	98
MTr-C (6*a*)	1.6	3.2	DMF	17	—	42	29	9
MTr-C (6*a*)	3	0	Pyridine	48	—	63	23	4
MTr-C^{Bz} (6*b*)	1.25	2.5	DMF	18	—	50	34	9
MTr-C^{Bz} (6*b*)	3	0	Pyridine	72	—	64	21	5
MTr-G (6*c*)	1.25	2.5	DMF	18	—	32	36	4
MTr-G (6*c*)	4.0	0	Pyridine	48	7	43	25	2
MTr-G^{Bz} (6*d*)	1.25	2.5	DMF	18	—	34	39	8
MTr-G^{Bz} (6*d*)	7	0	Pyridine	46	—	36	32	8

*Solutions were 1 mmol of nucleoside per 1 mL of DMF or 2 mL of pyridine except as noted for guanosine and C^{Bz}.

nucleosides[2] including the *N*-benzoyl derivatives. Data for cytidine and guanosine are given below.

Ribose ^{13}C shifts* relative to C-5′ (ppm)

	C-1′	C-4′	C-2′	C-3′	C-5′
Cytidine	30.91	24.30	15.10	9.10	0.00
5′-SiC (**2***a*)	29.21	22.10	13.94	7.16	0.00
2′,5′-DiSiC (**3***a*)	28.83	21.70	15.65	7.02	0.00
3′,5′-DiSiC (**4***a*)	29.80	22.29	13.82	8.92	0.00
5′-SiG (**2***c*)	25.00	21.87	12.39	7.38	0.00
2′,5′-SiG (**3***c*)	24.98	21.85	14.36	7.44	0.00
3′,5′-SiG (**4***c*)	24.09	21.64	10.67	8.66	0.00

*Pyridine-d_5; data collected by F. Hruska and W. G. Niemczura of the University of Manitoba. Similar results have been obtained by Dr. W. Pfleiderer (personal communication).

Additional proof of structure for the *N*-benzoylated compounds (series *b* and *d*) was their direct debenzoylation to the expected (series *a* and *c*) compounds which were prepared directly from the nucleosides as described. Elemental analyses were consistent with the assigned structures.

Compounds **10–12** which have the 5′-position unprotected can be obtained by acetic acid treatment (Scheme 2) of the 5′-silyl nucleosides **3–5** or from the 5′-methoxytrityl compounds **7–9**. In general higher yields are obtained on removal of the methoxytrityl groups (>80% using 80% HOAc at 80–90°C for 20 min) than from removal of a 5′-TBDMS group (50–60% yields). The advantage of using the fully silylated compounds is that they are so readily obtained. The properties of compounds **10–12** are described in Table 2.

We would like to point out a cautionary note in connection with the synthesis of 5′-methoxytritylguanosine (**6***c*). In our attempts to repeat the original Khorana procedure (8) we always obtained very low yields (0–10%). As a result we changed the procedure slightly by using triethylamine as base instead of pyridine. Under these conditions we consistently isolated 43–48% yields of a compound X whose tlc properties were virtually identical to those of authentic 5′-methoxytritylguanosine, **6***c*, prepared by debenzoylation of 5′-methoxytrityl-N^2-benzoylguanosine (**6***d*). However, compound X had a uv spectrum that was definitely different from authentic **6***c* (see Experimental). Further compound X and **6***c* were cleanly separable by high pressure liquid chromatography (hplc). Furthermore, on monosilylation compound X was converted in 80% yield to a new compound (**14**, Scheme 3) which possesses a 5′-TBDMS group since on detritylation it is converted initially to 5′-TBDMS guanosine (**2***c*). These results are in marked contrast to those of authentic **6***c* which is

[2]F. Hruska, W. P. Niemczura, and K. K. Ogilvie. Unpublished results.

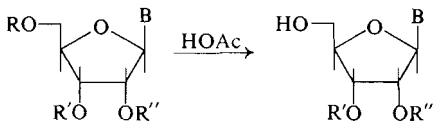

3–5
7–9

10 R′ = H, R″ = Si
11 R′ = Si, R″ = H
12 R′ = R″ = Si
a B = Cy; *b* B = Cy^{Bz};
c B = Gu; *d* B = Gu^{Bz}

SCHEME 2

converted on silylation to a mixture of 2′- and 3′-silyl derivatives, **7***c* and **8***c* (Table 1). These compounds are identical to those obtained by debenzoylation of **7***d* and **8***d*. As a result of these experiments it is obvious that compound X possesses a methoxytrityl group on the guanine ring, most likely at N^2 (compound **13**). The remarkably similar (tlc) chromatographic properties of **13** and **6***c* as well as those of **14** and **7***c* make it necessary to use extreme caution when preparing these compounds. The uv spectrum is critical (8) to interpretation and hplc in determining purity.

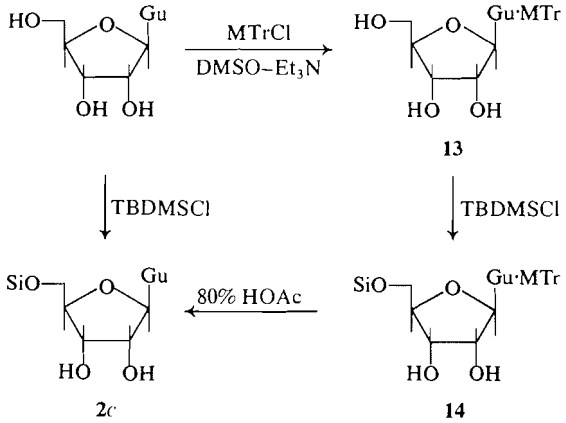

SCHEME 3

Isomerization

As previously reported (6), compounds possessing a silyl group on the 2′- or 3′-position do not isomerize under conditions used for phosphorylation and are stable in most solvents. However, in alcohol solvents isomerization does occur and at rates that are dependent both on the particular nucleoside derivative and on the alcohol employed. For example 2′,5′-disilylcytidine (**3***a*) is converted to a mixture of **3***a* (82%) and the 3′,5′-disilyl isomer (**4***a*, 18%) after 24 h at 30°C in methanol (ratio of **3***a*:**4***a* is 2:1 after 7 days). Compound **8***a* isomerizes most rapidly of all the cytidine derivatives and is converted to a mixture of **8***a* (57%) and **7***a* (42%) after 24 h under the above conditions. However, in ethanol at 30°C only 6%

TABLE 2. Properties of silylated nucleosides

Compound	Melting point* (°C)	λ_{max} (λ_{min})† (nm in 95% EtOH)	R_f (tlc)‡
2*a*(5′-SiC)	160–163	241, 274(229, 255)	0.14[h], 0.24[c]
3*a*(2′,5′-DiSiC)	198–201	241, 274(229, 255)	0.15[a], 0.45[b]
4*a*(3′,5′-DiSiC)	174–178	241, 274(229, 255)	0.07[a], 0.35[b]
5*a*(2′,3′,5′-TriSiC)	103–109	241, 274(229, 255)	0.23[a], 0.53[b]
2*b*(5′-SiC^{Bz})	104–107	262, 304(232, 287)	0.32[a], 0.58[b]
3*b*(2′,5′-DiSiC^{Bz})	67–71	261, 305(232, 287)	0.69[d], 0.45[e]
4*b*(3′,5′-DiSiC^{Bz})	147–151	262, 304(232, 287)	0.17[d], 0.08[e]
5*b*(2′,3′,5′-TriSiC^{Bz})	107–110	262, 305(231, 287)	0.72[d], 0.55[e]
2*c*(5′-SiG)	dec. > 205	254, 270 sh (224)	0.10[b], 0.38[c]
3*c*(2′,5′-DiSiG)	136–140	254, 270 sh (225)	0.20[a], 0.57[b]
4*c*(3′,5′-DiSiG)	144–149	254, 270 sh (224)	0.12[a], 0.48[b]
5*c*(2′,3′,5′(TriSiG)	dec. > 245	254, 270 sh (224)	0.30[a], 0.65[b]
2*d*(5′-SiG^{Bz})	135–138	237, 258, 265, 296 (222, 252, 261, 273)	0.19[a], 0.52[b]
3*d*(2′,5′-DiSiG^{Bz})	141–145	237, 258, 265, 296 (222, 252, 261, 273)	0.80[a], 0.38[d]
4*d*(3′,5′-DiSiG^{Bz})	124–128	237, 258, 265, 296 (222, 252, 261, 273)	0.74[a], 0.28[d]
5*d*(2′,3′,5′-TriSiG^{Bz})	122–126	237, 258, 265, 296 (222, 252, 261, 273)	0.60[d], 0.46[e]
7*a*(MTr-C$^{Si}_{OH}$)	194–198	232, 275(226, 259)	0.16[b], 0.48[c]
8*a*(MTr-C$^{OH}_{Si}$)	227–229	232, 275(226, 258)	0.06[b], 0.36[c]
9*a*(MTr-C$^{Si}_{Si}$)	125–130	232, 275(226, 258)	0.23[b], 0.58[c]
7*b*(MTr-C$^{Bz\,Si}_{OH}$)	112–117	232, 261, 306(225, 248, 290)	0.66[d], 0.42[e]
8*b*(MTr-C$^{Bz\,OH}_{Si}$)	98–103	233, 261, 305(226, 248, 290)	0.19[d], 0.07[e]
9*b*(MTr-C$^{Bz\,Si}_{Si}$)	107–110	233, 261, 305(226, 248, 290)	0.80[d], 0.62[e]
7*c*(MTr-G$^{Si}_{OH}$)	148–153	236, 247 sh, 270 sh(224)	0.24[a], 0.61[b]
8*c*(MTr-G$^{OH}_{Si}$)	141–145	236, 247 sh, 270 sh(224)	0.17[a], 0.54[b]
9*c*(MTr-G$^{Si}_{Si}$)	254–256	236, 247 sh, 270 sh(224)	0.30[a], 0.69[b]
7*d*(MTr-G$^{Bz\,Si}_{OH}$)	128–132	234, 257 sh, 266, 291(224, 262, 273)	0.82[a], 0.39[d]
8*d*(MTr-G$^{Bz\,OH}_{Si}$)	137–141	234, 257 sh, 266, 291(224, 262, 273)	0.75[a], 0.26[d]
9*d*(MTr-G$^{Bz\,Si}_{Si}$)	125–130	234, 257 sh, 266, 291(224, 262, 273)	0.67[d], 0.50[e]
10*a*(2′-SiC)	124–128	241, 274(229, 255)	0.10[b], 0.35[c]
11*a*(3′-SiC)	174–177	241, 274(229, 255)	0.10[b], 0.35[c]
12*a*(2′,3′-DiSiC)	172–176	241, 273(230, 255)	0.06[a], 0.21[b]
10*b*(2′-SiC^{Bz})	92–96	262, 304(232, 287)	0.73[a], 0.39[d]
11*b*(3′-SiC^{Bz})	80–83	262, 304(232, 287)	0.67[a], 0.16[d]
12*b*(2′,3′-DiSiC^{Bz})	67–71	262, 304(232, 287)	0.54[d], 0.45[e]
10*c*(2′-SiG)	dec. > 255	254, 270 sh (224)	0.33[b], 0.60[c]
11*c*(3′-SiG)	dec. > 260	254, 270 sh (224)	0.33[b], 0.60[c]
12*c*(2′,3′-DiSiG)	dec. > 290	254, 270 sh (224)	0.12[a], 0.60[b]
10*d*(2′-SiG^{Bz})	119–123	237, 258, 264, 296(221, 252, 261, 273)	0.16[a], 0.57[b]
11*d*(3′-SiG^{Bz})	125–130	237, 258, 264, 296(221, 252, 261, 273)	0.16[a], 0.57[b]
12*d*(2′,3′-DiSiG^{Bz})	126–130	237, 260, 264, 296(221, 252, 261, 273)	0.40[a], 0.23[d]
6*c*(MTr-G)	198–201	236, 247 sh, 270 sh, 224	0.17[b], 0.55[c]
13(G^{MTr})	dec. > 205	231, 261, 278(229, 247, 274)	0.17[b], 0.55[c]

*Fisher-Johns melting point apparatus, uncorrected.
†Cary 17 spectrophotometer.
‡Brinkman polygram SIL G/UV 254 sheets. Solvents used were (*a*) ethyl acetate; (*b*) chloroform–ethanol (9:1); (*c*) chloroform–ethanol (4:1); (*d*) ethyl ether; (*e*) ether–hexane (4:1).

of **8***a* is isomerized to **7***a*. Guanosine derivatives tend to isomerize at rates similar to those for the cytidine derivatives. A complete study of all the silylated ribonucleosides has been done and will be reported separately (9).

Methanolysis of N-*Benzoylcytidines*

The silylated *N*-benzoylcytidines give rise to a remarkably interesting result in methanol. The 5′-methoxytrityl-2′-TBDMS-N^4-benzoylcytidine **7***b* in methanol (30°C) leads to a mixture of the debenzoy-

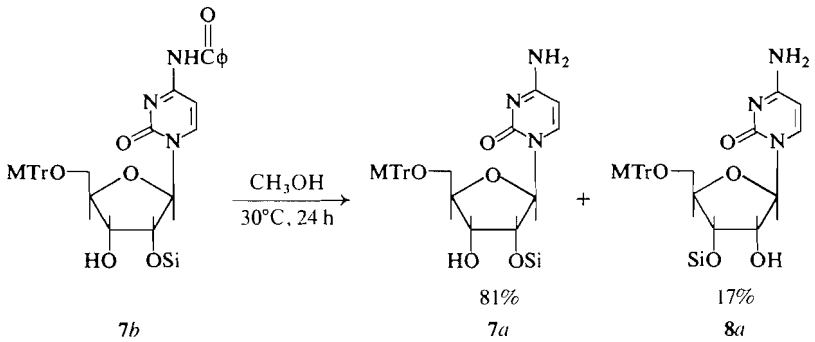

7*b* 7*a* 8*a*

SCHEME 4

lated compound **7***a* (81%) and the isomerized debenzoylated compound **8***a* (17%) after 24 h (Scheme 4). Compound **8***b*, however, is 93% unaffected (neither debenzoylation nor isomerization) after 24 h under the same conditions (0.8% **7***a*, 1.5% **8***a*, 4.6% **7***b*). Both 2′,5′- and 3′,5′-disilyl-N^4-benzoylcytidines (**3***b* and **4***b*) undergo nearly complete debenzoylation after 24 h. Furthermore 5′-TBDMS-N^4-benzoylcytidine is 49% debenzoylated after 24 h. The 2′-TBDMS-C^{Bz} (**10***b*) is 64% debenzoylated after 24 h while the 3′-isomer **11***b* is only 6% debenzoylated and this occurs in the form of **10***a* (3%) and **11***a* (3%) which may result from prior isomerization of **11***b* to **10***b* which may then debenzoylate and isomerize to the observed products. In all cases methyl benzoate is observed and it is obvious that a silyl group on the 2′- or 5′-position is essential. Similar results are obtained with adenosine but not with guanosine. The solvolysis is not observed in ethanol. This very interesting observation is being studied in detail and will be fully discussed (9).

Synthesis of Nucleotides

The silylated derivatives of cytidine and guanosine are easily condensed to form ribonucleotides using the Letsinger phosphorodichloridite procedure (7). This procedure does not require *N*-protection even with cytidine and guanosine. The general procedure is outlined in Scheme 5 and yields for a variety of condensations are recorded in Table 3. These reactions were carried out as described previously (6) at −78°C with total reaction times of about $2\frac{3}{4}$ h. Yields of 3′-5′-linked nucleotides are between 50 and 90%. The reactions described in this report were all worked up using conventional silica gel thick layer chromatography (tlc). The *N*-protected nucleotides of cytidine and guanosine have greater mobilities in less polar solvents than the unbenzoylated analogues. Thus for the synthesis of long chains using tlc separations, the *N*-protected derivatives offer a practical advantage. This feature is not nearly so important if hplc is used to separate products and for such separations the ability to avoid *N*-protection will offer a major advantage.

The general procedure was used (Scheme 6) to prepare the fully protected trinucleotide MTr-$G^{Bz\ Si}_{p}$(TCE)$C^{Bz\ Si}_{p}$(TCE)$C^{Bz\ Si}_{Si}$(**19***a*) and the fully protected tetranucleotide MTr-$G^{Bz\ Si}_{p}$(TCE)$G^{Bz\ Si}_{p}$(TCE)-$C^{Bz\ Si}_{p}$(TCE)$C^{Bz\ Si}_{Si}$(TCE) (**20**). Yields at the tri- and tetranucleotide stages were 56 and 66% respectively. All of the nucleotides described in this report were deprotected as described below to the free nucleotides. The 3′-5′-linked nucleotides were completely degraded by snake venom and spleen phosphodiesterases. Cytidine-containing nucleotides are also completely degradable by pancreatic ribonuclease.

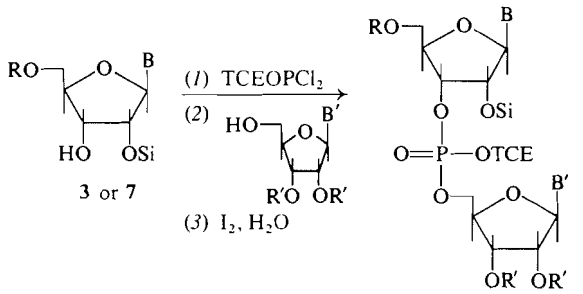

13 B = B′ = Cy, R = MTr, R′ = Si
14 B = B′ = Cy^{Bz}; *a* R = R′ = Si
15 B = B′ = Gu^{Bz}; *b* R = MTr, R′ = Si
16 B = Cy^{Bz}, B′ = Cy, R = MTr, R′ = Si
17 B = Gu^{Bz}, B′ = Ur, R = MTr, R′ = Si
18 B = Gu, B′ = Ur, R = MTr, R′ = Si

SCHEME 5

In order to compare the properties of the 3′-5′-nucleotides with those of the 2′-5′-analogues, some of the latter were prepared. The required starting materials (**4** and **8**) are always obtained as by-products in the preparation of the normally preferred 2′-5′-diprotected nucleosides (**3** and **7**). The fully protected 2′–5′-linked nucleotides of CC (**21**) and GU (**22**) were synthesized by the general procedure. Their chromatographic properties are slightly different from their 3′–5′-linked isomers (Table 5). On

TABLE 3. Summary of nucleotide condensation reactions

Starting material	Second component	Product	Yield (%)
MTr-C^{Si}_{OH}(7*a*)	C^{Si}_{Si}	MTr-C^{Si}_{p}(TCE)C^{Si}_{Si} (**13**)	70
MTr-$C^{Bz\ Si}_{OH}$(7*b*)	C^{Si}_{Si}	MTr-$C^{Bz\ Si}_{p}$(TCE)C^{Si}_{Si} (**16**)	75
Si$C^{Bz\ Si}_{OH}$(3*b*)	C^{BzSi}_{Si}	Si-$C^{Bz\ Si}_{p}$(TCE)C^{Si}_{Si} (**14***a*)	89
MTr-$C^{Bz\ Si}_{OH}$(7*b*)	C^{BzSi}_{Si}	MTr-$C^{Bz\ Si}_{p}$(TCE)$C^{Bz\ Si}_{Si}$ (**14***b*)	83
Si$G^{Bz\ Si}_{OH}$(3*d*)	G^{BzSi}_{Si}	Si-$G^{Bz\ Si}_{p}$(TCE)$G^{Bz\ Si}_{Si}$ (**15***a*)	56
MTr$G^{Bz\ Si}_{OH}$(7*d*)	G^{BzSi}_{Si}	MTr-$G^{Bz\ Si}_{p}$(TCE)$G^{Bz\ Si}_{Si}$ (**15***b*)	54
MTr$G^{Bz\ Si}_{OH}$(7*d*)	U^{Si}_{Si}	MTr-$G^{Bz\ Si}_{p}$(TCE)U^{Si}_{Si} (**17**)	52
MTrG^{Si}_{OH}(7*c*)	U^{Si}_{Si}	MTr-G^{Si}_{p}(TCE)U^{Si}_{Si} (**18**)	63
MTr$C^{Bz\ OH}_{Si}$ (8*d*)	C^{BzSi}	MTr$C^{Bz\ p}_{Si}$(TCE)$C^{Bz\ Si}_{Si}$ (**21**)	67
MTr$G^{Bz\ OH}_{Si}$ (8*d*)	U^{Si}_{Si}	MTr$G^{Bz\ p}_{Si}$(TCE)U^{Si}_{Si} (**22**)	33
MTr$G^{Bz\ Si}_{OH}$(7*d*)	HO$C^{Bz\ Si}_{p}$(TCE)$C^{Bz\ Si}_{Si}$	MTr$G^{Bz\ Si}_{p}$(TCE)$C^{Bz\ Si}_{p}$(TCE)$C^{Bz\ Si}_{Si}$ (**19***a*)	56
MTr$G^{Bz\ Si}_{OH}$(7*d*)	HO$G^{Bz\ Si}_{p}$(TCE)$C^{Bz\ Si}_{p}$(TCE)$C^{Bz\ Si}_{Si}$	MTr$G^{Bz\ Si}_{p}$(TCE)$G^{Bz\ Si}_{p}$(TCE)$C^{Bz\ Si}_{p}$(TCE)$C^{Bz\ Si}_{Si}$ (**20**)	66

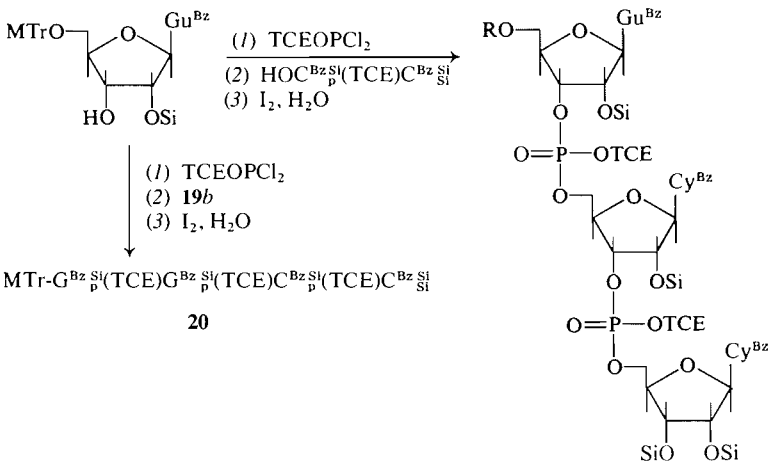

SCHEME 6

complete deprotection, the free 2′-5′-linked nucleotides were identical to authentic samples (Sigma Chemical Co.).

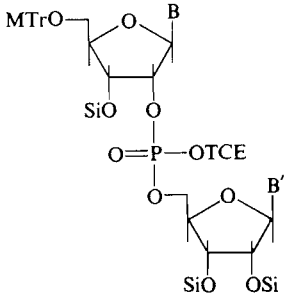

21 B = B′ = Cy^{Bz}
22 B = Gu^{Bz}, B′ = Ur

Deprotection of Protected Nucleotides

For compounds such as **13** which do not contain *N*-protecting groups, acetic acid treatment followed by tetrabutylammonium fluoride (TBAF) gives an 85–90% conversion to the free nucleotide (CpC). Fluoride ion removes both the silyl and trichloroethyl groups in one 30 min step. It also causes ~10% cleavage of the internucleotide linkage as has been noted by others (10). This is a serious limitation in the direct deprotection of longer chains. However, fluoride ion does not cause either degradation or isomerization of phosphodiesters. Consequently all that is necessary is to remove the trichloroethyl group before treatment with TBAF to remove the silyl groups. The whole procedure can be illustrated (Scheme 1) by the deprotection of compound **14***a*

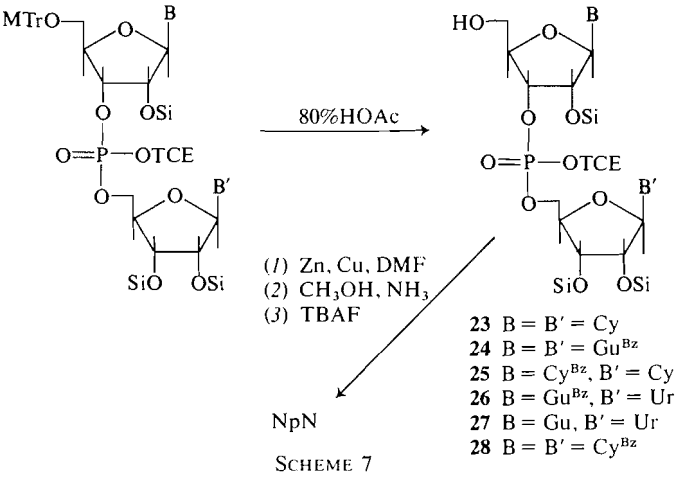

SCHEME 7

($SiC^{Bz\,Si}_{p}(TCE)C^{Bz\,Si}_{Si}$). The trichloroethyl group is removed in 3–20 h using Zn–Cu couple (11) in DMF at 50°C. The time varies from experiment to experiment and may be due to inefficient stirring or variations in quality of the Zn–Cu couple. The progress of the reaction is easily followed by tlc. The resulting diester ($SiC^{Bz\,Si}_{p}(OH)C^{Bz\,Si}_{Si}$) can be isolated on tlc (chloroform–ethanol 9:1) or treated directly with methanolic ammonia to remove the benzoyl groups. We find that for small amounts (< 15 mg) it is best to continue to the end of the ammonia treatment and then isolate the nucleotide (in this case, $SiC^{Si}_{p}C^{Si}_{Si}$) on paper chromatography. Regardless of the manner of isolation we have been consistently obtaining deprotection with *no* other nucleosidic or nucleotidic products arising. Finally the silyl groups are removed in a 30 min treatment with TBAF (6). This step is quantitative with absolutely no chain degradation. However, we find that if isolation after the zinc treatment at either of the two stages mentioned above is omitted then desilylation is incomplete. Apparently the presence of metal ions interferes at this step.

Conclusions

This manuscript, along with the previous article in the series (6), describes the first complete set of protecting groups common to all four normal ribonucleosides. The alkylsilyl groups can be seen to provide a remarkably facile protection of the hydroxyl groups in nucleosides. The silylated nucleosides both with and without *N*-protection are easily coupled to form ribonucleotides using the phosphodichloridite procedure. We are currently using the procedure described in this and the previous article in an attempt to synthesize the sequence of a transfer RNA.

Experimental

General Methods

All general procedures and techniques including chromatography, uv, nmr, mass spectrometry, elemental analyses, melting points, enzyme assays, silylating conditions, phosphorylation procedures and general reagents are as previously described (6) with the following exceptions.

Thin layer chromatographic data (R_f values) are recorded from Brinkman Polygram SIL G/UV 254 analytical sheets. High pressure liquid chromatography experiments were performed using a Spectrophysics SP8000 microprocessor based hplc unit. All results described in this report are based on a Lichrosorb 10 μm RP-8 column (4.6 mm × 25 cm) and the purity of all nucleoside derivatives as well as nucleotides up to and including tetranucleotides can be verified on this column.

Reagents and Chemicals

N^2-Benzoylguanosine (mp 228–231°C dec.) (12, 13), 5′-methoxytrityl-N^2-benzoylguanosine (mp 156–162°C) (14), N^4-benzoylcytidine (mp 218–220°C) (14, 15), 5′-methoxytrityl-N^4-benzoylcytidine (mp 120–125°C) (14), and 5′-methoxytritylcytidine (mp 150–152°C dec.) (8) were all prepared according to literature procedure.

*5′-Methoxytritylguanosine (**6**c)*

Compound **6***d* was treated with an excess of the hydrazine hydrate reagent for 1 h as described by Letsinger (16). On standing the reaction mixture separated into two phases. The top phase was collected and evaporated. The residue was washed with ethanol to leave pure 5′-methoxytritylguanosine (λ_{max}(EtOH)): 236, 250 (sh), and 270 (sh) nm). This compound had identical properties to those reported by Khorana (8). The compound was pure according to the chromatographic techniques used and had a retention time of 164 s (k' 2.6) on hplc (MeOH–H_2O (7:3), 20°C, 2.0 mL/min at 1770 psi).

*N^2-Methoxytritylguanosine (**13**)*

To guanosine (2.83 g, 10 mmol) in DMSO (15 mL) was added triethylamine (4 mL) followed by methoxytrityl chloride (3.3 g, 11 mmol). The mixture was stirred at room temperature for 3 h and poured into 300 mL of 15% NaCl in H_2O. After stirring for a few minutes the residue was collected by filtration (sintered glass) and the gum was washed with ether (300 mL). The residue was then dissolved in methanol (50 mL), the solution was filtered from some insoluble material, and the clear solution was evaporated at reduced pressure. After repeated evaporation of hexane the gum was dried under vacuum, and this usually resulted in a light brown solid. If not, the residue was dissolved in the minimum amount of methanol, and ether was added to induce precipitation. Usually a light brown solid was formed on evaporation of the solvents at re-

TABLE 4. Solvent systems used to develop tlc plates during the isolation of silylated nucleosides

Compound isolated	Solvent used	Number of developments
2*a*, **2***d*, **10***c*, **11***c*	Chloroform–ethanol (9:1)	2
2*b*, **10***a*, **11***a*, **10***d*, **11***d*	Chloroform–ethanol (9:1)	1
3*d*, **4***d*, **7***d*, **8***d*	Chloroform–ether (1:1)	3
2*c*	Chloroform–ethanol (4:1)	1
3*c*, **4***c*, **7***c*, **8***c*	Ethyl acetate – chloroform – ethanol (1:0.9:0.1)	3
5*c*	Ethyl acetate – chloroform – ethanol (1:0.9:0.1)	2
3*a*, **4***a*, **7***a*, **8***a*	Ethyl acetate	2
5*a*	Ethyl acetate	1
5*d*	Ether	1
5*b*	Ether–hexane (1:1)	2
3*b*, **4***b*, **7***b*, **8***b*, **10***b*, **11***b*	Ether–hexane (4:1)	1

TABLE 5. Properties of protected dinucleotides

Compound	Melting point (°C)	λ_{max} (λ_{min}) (nm)	R_f*
$MTrC^{Si}_{p}(TCE)C^{Si}_{Si}$ (**13**)	176–180	231, 273 (226, 261)	0.18[c], 0.42[d]
$HOC^{Si}_{p}(TCE)C^{Si}_{Si}$ (**23**)	185 dec	239, 272 (230, 258)	0.02,[c] 0.27[d]
$SiC^{Bz\ Si}_{p}(TCE)C^{Bz\ Si}_{Si}$ (**14***a*)	128–133	262, 306 (230, 289)	0.95[a], 0.80[b]
$MTrC^{Bz\ Si}_{p}(TCE)C^{Bz\ Si}_{Si}$ (**14***b*)	125–130	235, 262, 305 (229, 243, 291)	0.75[a], 0.55[b]
$HOC^{Bz\ Si}_{p}(TCE)C^{Bz\ Si}_{Si}$ (**28**)	140–146	262, 306 (230, 289)	0.70[a], 0.30[b]
$SiG^{Bz\ Si}_{p}(TCE)G^{Bz\ Si}_{Si}$ (**15***a*)	136–143	238, 258, 265, 298 (221, 252, 261, 273)	0.85[e], 0.78[f]
$MTrG^{Bz\ Si}_{p}(TCE)G^{Bz\ Si}_{Si}$ (**15***b*)	108–113	235, 258, 265, 290 (225, 255, 262, 274)	0.85[e], 0.75[f]
$HOG^{Bz\ Si}_{p}(TCE)G^{Bz\ Si}_{Si}$ (**24**)	122–126	239, 257, 264, 296 (223, 253, 262, 274)	0.58[e], 0.42[e]
$MTrC^{Bz\ Si}_{p}(TCE)C^{Si}_{Si}$ (**16**)	147–151	234, 263, 305 (227, 246, 298)	0.07[a], 0.54[c]
$HOC^{Bz\ Si}_{p}(TCE)C^{Si}_{Si}$ (**25**)	155–159	262, 305 (232, 288)	0.45[c], 0.78[d]
$MTrG^{Si}_{p}(TCE)U^{Si}_{Si}$ (**18**)	152–157	236, 256 (225, 243)	0.75[c], 0.37[e]
$HOG^{Bz\ Si}_{p}(TCE)U^{Si}_{Si}$ (**26**)	138–142	248sh, 258, 264, 295 (225, 261, 291)	0.62[e], 0.30[e]
$MTrG^{Bz\ Si}_{p}(TCE)U^{Si}_{Si}$ (**17**)	129–135	236, 258, 264, 283sh, 296sh (225, 252, 261)	0.83[e], 0.62[f]
$HOG^{Si}_{p}(TCE)U^{Si}_{Si}$ (**27**)	157–161	257 (227)	0.52[e], 0.08[e]
$MTrG^{Bz\ Si}_{p}(TCE)C^{Bz\ Si}_{Si}(TCE)C^{Bz\ Si}_{Si}$ (**19***a*)	155–161	240sh, 262, 303 (228, 290)	0.20[a], 0.70[f]
$HOG^{Bz\ Si}_{p}(TCE)C^{Bz\ Si}_{p}(TCE)C^{Bz\ Si}_{Si}$ (**19***b*)	164–168	263, 303 (230, 289)	0.55[e], 0.36[f]
$MTr\text{-}G^{Bz\ Si}_{p}(TCE)G^{Bz\ Si}_{p}(TCE)C^{Bz\ Si}_{p}(TCE)C^{Bz\ Si}_{Si}$ (**20**)	173–179	240sh, 262, 301 (227, 290)	0.78[e], 0.65[f]
$MTr\text{-}C^{Bz\ p}_{Si}(TCE)C^{Bz\ Si}_{Si}$ (**21**)	121–125	236, 262, 305 (229, 243, 291)	0.45[a], 0.32[b]
$MTrG^{Bz\ p}_{Si}(TCE)U^{Si}_{Si}$ (**22**)	130–134	236, 258, 263sh, 282sh, 296sh (225, 252)	0.83[e], 0.67[f]

*Brinkman polygram SIL G/UV 254 sheets. Solvents used were: (*a*) ethyl ether; (*b*) ether–hexane (4:1); (*c*) chloroform–ethanol (9:1); (*d*) chloroform–ethanol (4:1); (*e*) ethyl acetate; (*f*) ether–chloroform–ethanol (10:3.6:0.4).

duced pressure. The solid obtained at this point was identified as *N*-methoxytritylguanosine, **13**, 2.67 g, 48%, mp dec. < 205°C. This compound was usually 97% pure at this stage as determined by hplc (retention time 225 s, k' 3.6 under same conditions as **7***c* above). Compound **13** showed λ_{max}(EtOH) 231, 261, and 276 nm with λ_{min}(EtOH) 246 and 272 nm.

Compound **13** was treated with TBMSCl under the standard conditions and a compound **14** (mp 140–144°C, R_f(EtOAc) 0.24, R_f($CHCl_3$–EtOH (9:1)) 0.61) was obtained in 80% yield. On treatment with 80% HOAc at room temperature the methoxytrityl group was removed from **14** faster than the TBDMS group such that 5′-TBDMS-guanosine (**2***c*) was produced. On standing in acetic acid for 20 h only guanosine was present.

Silylation of Nucleosides

These procedures were identical to those previously described. The products were isolated from thick layer chromatography and the solvents used to develop the plates are listed in Table 4.

Synthesis of Nucleotides

The procedures used were identical to those previously reported (6). Products were isolated by thick layer chromatography as described. For cytidine we observed very little formation of the 3′–3′-linked by-products (< 5%) and none of the 5′–5′-linked products. This contrasts with the uridine case previously reported (6). For guanosine the amount of 3′–3′-linked products was between 10 and 20% and 5′–5′-linked by-products were also found in 20–30% yields. These products usually have very different chromatographic properties than those of the desired products and are easily separated on chromatography. Properties of isolated products are listed in Table 5. The dinucleotides containing a methoxytrityl group

TABLE 6. Properties of nucleotides

Compound	R_f^A	R_f^F	R_m^{Tp}*	λ_{max} (H_2O) (min) (nm)
CpC	0.11	0.47	0.25	270(250)
CpC(2′–5′)	0.09	0.44	0.25	270(250)
GpU	0.06	0.36	0.32	256(229)
GpU(2′–5′)	0.06	0.40	0.32	256(229)
GpG	0.03	0.23	0.21	253, 270sh(229)
GpCpC	0.02	0.23	0.36	274, 257(272, 233)
GpGpCpC	0.00	0.17	0.42	252, 266sh(243)

*pH 7.5.

were detritylated and the properties of these compounds are also listed in Table 5.

Deprotection of Nucleotides

Fully silylated (or detritylated) nucleotides were treated with Zn–Cu couple in DMF for 3–20 h. Fully silylated compounds were often isolated after this step by tlc chromatography in chloroform–ethanol (9:1). The product at this stage was treated with methanolic ammonia for 48 h as described in the literature (11). If chromatography had not been performed after the Zn–Cu treatment, then the product was chromatographed on Whatman 3MM paper in solvent *A* to remove residual metal ions. The product was then treated with TBAF in THF for 30 min. The products were then passed through a Dowex 50W-X8 (Na^+ form) ion exchange column and applied to Whatman 3MM sheets developed in solvent *A* or *F*. Only single, desired products were obtained from these reactions. The chromatographic and electrophoretic properties of free nucleotides are summarized in Table 6. For dinucleotides reference standards are available from Sigma Chemical Co. Nucleotides were subjected to enzymatic degradation using standard procedures (6) and all 3′–5′-linked nucleotides were completely degraded.

Acknowledgments

We gratefully acknowledge financial support from the National Research Council of Canada, the Quebec Education Ministry, and the Faculty of Graduate Studies of McGill University.

1. K. K. OGILVIE and D. J. IWACHA. Tetrahedron Lett. 317 (1973).
2. K. K. OGILVIE. Can. J. Chem. **51**, 3799 (1973).
3. K. K. OGILVIE, E. A. THOMPSON, M. A. QUILLIAM, and J. B. WESTMORE. Tetrahedron Lett. 2865 (1974).
4. K. K. OGILVIE, S. L. BEAUCAGE, D. W. ENTWISTLE, E. A. THOMPSON, M. A. QUILLIAM, and J. B. WESTMORE. J. Carbohydr. Nucleosides Nucleotides, **3**, 197 (1976).
5. K. K. OGILVIE, K. L. SADANA, E. A. THOMPSON, M. A. QUILLIAM, and J. B. WESTMORE. Tetrahedron Lett. 2861 (1974).
6. K. K. OGILVIE, S. L. BEAUCAGE, A. L. SCHIFMAN, N. Y. THERIAULT, and K. L. SADANA. Can. J. Chem. **56**, 2768 (1978).
7. R. L. LETSINGER and W. B. LUNSFORD. J. Am. Chem. Soc. **98**, 3655 (1976).
8. R. LOHRMANN and H. G. KHORANA. J. Am. Chem. Soc. **86**, 4188 (1964).
9. D. W. ENTWISTLE and K. K. OGILVIE. Manuscript in preparation.
10. C. B. REESE, R. C. TITMAS, and I. YAU. Tetrahedron Lett. 2727 (1978).
11. T. NEILSON and E. S. WERSTIUK. Can. J. Chem. **49**, 3004 (1971).
12. C. B. REESE and R. SAFFHILL. J. Chem. Soc. 2937 (1972).
13. S. CHLADEK and J. SMRT. Collect. Czech. Chem. Commun. **27**, 214 (1964).
14. D. H. RAMMLER and H. G. KHORANA. J. Am. Chem. Soc. **84**, 3112 (1962).
15. T. NEILSON and E. S. WERSTIUK. Can. J. Chem. **49**, 493 (1971).
16. R. L. LETSINGER, P. S. MILLER, and G. W. GRAMS. Tetrahedron Lett. 2621 (1968).

Barriers to rotation about the N—CO bond in N-vinyl amides; a new two-site approximation method

ROBERT R. FRASER AND JEAN-LOUIS A. ROUSTAN
Department of Chemistry, University of Ottawa, Ottawa, Ont., Canada K1N 9B4
AND
JASWANT R. MAHAJAN
Department of Chemistry, University of Brasilia, Brasilia, DF Brazil

Received March 5, 1979

ROBERT R. FRASER, JEAN-LOUIS A. ROUSTAN, and JASWANT R. MAHAJAN. Can. J. Chem. 57, 2239 (1979).

The barriers to rotation about the N—CO bonds in a series of *N*-vinyl amides have been determined by a study of their proton spectra at variable temperatures. A complete LACN 3 analysis of compound **1** gave the parameters used in a complete line shape (CLS) analysis to obtain $\Delta G^{\ddagger}$. A new approximate method was shown to give a value for ΔG that agreed within 0.1 kcal/mol of that obtained by CLS. The approximate method was employed to determine $\Delta G^{\ddagger}$ for other members of the series. The barrier in the *N*-vinyl amide **1** was found to be 2.5 kcal/mol higher than that in its saturated analog. Variations within the series of *N*-vinyl amides amounted to only 1.2 kcal/mol. A steric effect is proposed for the increase in barrier height. The new approximation formula was tested for the general case of unequal singlet coalescence and found to give k's accurate to within 4% for $\Delta\nu > 10$ and to within 10% at lower values of $\Delta\nu$.

ROBERT R. FRASER, JEAN-LOUIS A. ROUSTAN et JASWANT R. MAHAJAN. Can. J. Chem. **57,** 2239 (1979).

On a déterminé les barrières à la rotation autour des liaisons N—CO dans une série de *N*-vinylamides à l'aide d'une étude de leurs spectres protoniques à températures variables. Une analyse LACN 3 complète du composé **1** conduit à des paramètres utilisés dans une analyse complète de la forme des raies (CLS) afin d'en déduire le $\Delta G^{\ddagger}$. On montre qu'une nouvelle méthode approximative conduit à une valeur de ΔG qui est en accord, à 0.1 kcal/mol près, à celle obtenue par CLS. On a employé la méthode approximative pour déterminer le $\Delta G^{\ddagger}$ des autres membres de la série. On a trouvé que la barrière dans le *N*-vinylamide **1** est 2.5 kcal/mol plus élevée que celle de son analogue saturé. Les variations à l'intérieur de la série des *N*-vinylamides ne sont que de 1.2 kcal/mol. On propose un effet stérique pour expliquer l'augmentation dans la hauteur de la barrière. On a vérifié la nouvelle formule approximative dans le cas général de la coalescence en un singulet inégal et on a trouvé qu'elle fournit des valeurs de k qui sont précises à 4% pour un $\Delta\nu >$ et à 10% pour des valeurs de $\Delta\nu$ plus faibles.
[Traduit par le journal]

Measurement of barriers to rotation about the N—CO bond in a wide variety of amides has been achieved through study of their temperature dependent ^{1}H nmr spectra (1–3). Yet the rotational barriers in simple *N*-vinyl amides (acyl enamines) have been reported for only two compounds, *N*-vinyl formamide and *N*-vinyl acetamide (4). In that paper the spectral analysis employed the peak separation method whose inaccuracy has been recognized for some time (5, 6). As a result, the activation parameters reported (E_a and A) for the two amides cannot be considered as accurate and any conclusions based thereon are unreliable. More recently, Grindley *et al.* reported the barrier for the sulfur containing heterocyclic enamide, 4-benzoyl-1-thia-4-azacyclohex-2-ene, to be 14.4 kcal/mol (7). In this paper we wish to describe the determination of barriers to rotation for a series of *N*-acetyl enamines (**1–5**) in order to provide an indication of the effect of the double bond on the rotational barrier. In analysis of the spectra of **1** the accuracy in $\Delta G^{\ddagger}$ at the coalescence temperature using the complete line shape (CLS) method was shown to be comparable to that calculated using a new two-site equation. For the spectra of **2–5** $\Delta G^{\ddagger}$ was obtained by this two-site equation. In addition the use of this approximate

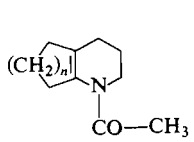

1 $n = 1$
2 $n = 2$
3 $n = 3$
4 $n = 4$
5 $n = 8$

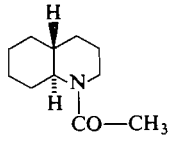

6

0008-4042/79/172239-06$01.00/0

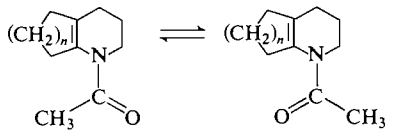

1A (minor) 1B (major)

SCHEME 1

equation as applied to the coalescence of two unequally populated singlets was shown to offer an improvement over previous approximate treatments.

The enamines investigated herein were synthesized by a method described earlier by one of us (8). The ^{1}H spectrum of **1** ($n = 1$) at 0°C exhibited two separate multiplets for the protons at C-2 representing the two diasteroisomers present due to slow rotation about the N—CO bond (see **1A** and **1B** in Scheme 1).[1] Each multiplet represents the AA′ portion of an AA′MM′YY′ system, one which is too large to permit a variable temperature analysis by the CLS method.[2]

We have therefore decided to treat the AA′ absorptions as part of an AA′MM′ system perturbed by first-order coupling with the methyl group (10) and the YY′ nuclei (11). For the CLS analysis these effects are incorporated into the value of T_2^{eff} chosen to best reproduce the observed spectrum at −46°C. The validity of this approximation can be assessed at this temperature where there is no broadening by kinetic exchange. We have conducted exact calculations of the system as an AA′MM′YY′ using LACN3 with the further inclusion of variable first-order long range coupling to the methyl group as well as varied values for T_2. In no case was any better agreement obtained than by incorporating all long range couplings into T_2^{eff}. Figure 1 shows the agreement obtained between the AA′ portion of the calculated spectrum and that measured at −46°C. The parameters employed are given in Table 1. For CLS calculations of the spectra in the region of coalescence, the same parameters were used with the additional inclusion of a small temperature dependence of the chemical shifts AA′ and of the equilibrium constant between conformers, both estimated by extrapolation from measurements between −20 and −46°C as well as by comparison with CLS analysis of spectra at +10°C. The spectra in the region of coalescence are shown in Fig. 2. If we define T_c as the temperature at which only two inflection points remain (*vide infra*), the CLS curve indicates a value for k at T_c of between 38 and 44 s^{-1}. This translates to a barrier to rotation of 14.9_5 kcal/mol.

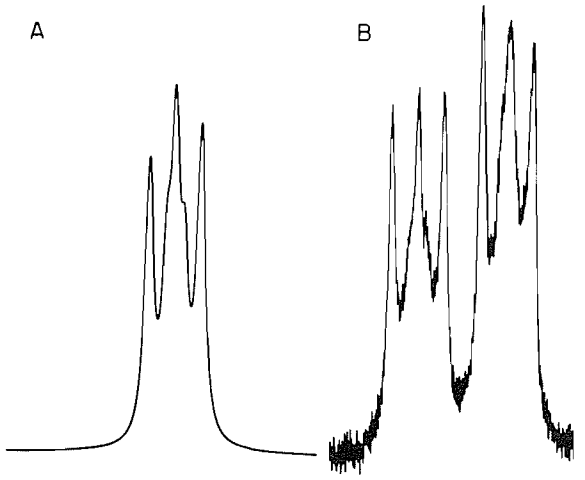

FIG. 1. (A) The absorption due to the C-2 methylene protons of conformer A of **1**, as calculated by LACN 3 using the parameters listed in Table 1, using a line broadening of 2 Hz as determined experimentally and including a first-order perturbation of 0.2 Hz due to long range coupling with the methyl group. (B) The spectrum of the C-2 methylene protons of both conformers of **1** measured at −46°C.

TABLE 1. Parameters used for the LACN 3 calculations in Fig. 1 and, in parentheses where different, for the DNMR 3 calculations in Fig. 2

	Conformer A	Conformer B
$J_{AA'} = J_{MM'}$ (Hz)	−14	−14
$J_{A'M'} = J_{AM}$	3.5	3.13
$J_{AM'} = J_{A'M}$	7.25	6.88
$\delta_A = \delta_{A'}$ (ppm)	3.70 (3.71)[a]	3.52
$\delta_M = \delta_{M'}$	1.84	1.99
ρ	0.46 (0.44)	0.54 (0.56)

[a]Values in parentheses refer to parameters at T_c; others represent values at −46°C.

Accuracy of CLS

While a rigorous error analysis would not be possible due to the number of assumptions made and the variables present, our experience in matching the calculated with the experimental curve indicates the derived k to be little influenced by our choice of T_2^{eff}, in that a 30% change in T_2^{eff} (0.15–0.12) causes no visible change in the curve for a given value of k_A. However, a 2 deg uncertainty in T_c leads to a 0.1 kcal/mol change in $\Delta G^{\ddagger}$ so that k_A would have to change by 15% to produce the same variation in $\Delta G^{\ddagger}$. The very good agreement between the calculated and the experimental spectra around T_c

[1]The major isomer is assigned the *Z* configuration on the basis of the known deshielding effect on the N—CH_2 by an acetyl methyl (13) as observed in the ^{13}C spectrum of 2 at 0°C and correlated with **1–5** by the proton shifts for the N—CH_2 protons.

[2]Our copy of the CLS program (9) has been written to handle up to four spins and each calculated spectrum requires 10 min on our IBM 360/65 computer. Thus, expansion of the program to include six spins in a calculation was deemed too demanding in computer time to be undertaken.

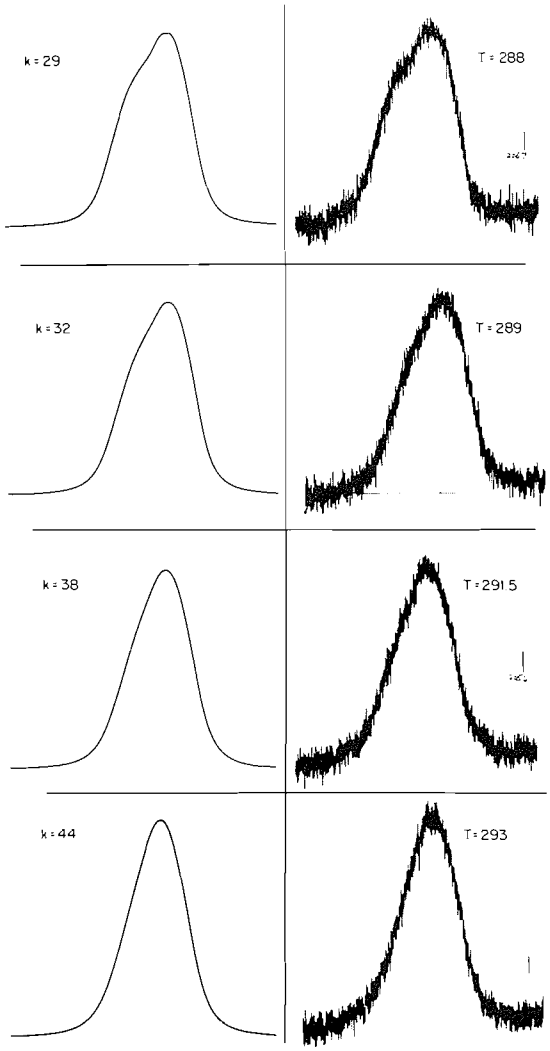

FIG. 2. The proton absorption for the C-2 methylene group of conformer A of **1** as calculated from DNMR 3, using a line broadening of 2.7 Hz for k = 29, 32, 38, and 44 Hz (left side curves) and measured at 288, 289, 291.5, and 293°C (right side curves).

suggest that the error in k_A (due to our choice of T_2^{eff} and our spin system approximation) is less than this amount. This leads to an upper error in $\Delta G^{\ddagger}$ of 1% (i.e., $\Delta G^{\ddagger}$ for **1**A → **1**B = $14.9_5 \pm 0.15$ kcal/mol as estimated using the formula for the linearized relative statistical error (12).

Approximate Methods for Determining k

The complete line shape method of analysis has been a powerful tool for the study of exchange phenomena. In many cases, a careful study of spectral changes over a wide range of temperatures can yield accurate estimates of k throughout the range. Nevertheless, that the accuracy in the measurement of $\Delta G^{\ddagger}$ far exceeds that for $\Delta H^{\ddagger}$ is widely documented (12).

It is because of this limitation in accuracy that approximate methods have been utilized to obtain values for rate constants which are often as reliable as those obtained by the CLS method. The simplest of these, the Gutowsky–Holm eq. [*a*] provides an accurate value for the rate constant k for an exchange between two equally populated sites (each giving rise to singlet absorption) at the coalescence temperature, T_c. Application of this equation to the coalescence of two singlets of unequal intensity has been shown to provide a useful alternate to CLS by Raban and co-workers (14). We wish to examine use of the Gutowsky–Holm equation in a more rigorous way and to assess its applicability to both simple and complex systems undergoing exchange.

In the case of the exchange of an uncoupled proton between two unequally populated sites A and B having $K = \rho_B/\rho_A = 2$, where ρ_B and ρ_A represent the fractional populations of the two sites, Raban (13) found that the larger rate constant $k_{A\to B}$ when calculated from [*a*] is within 20% of the true value (obtained from CLS). The definition proposed for T_c was that temperature at which $\partial^2 G/\partial V^2 = \partial G/\partial V = 0$ (14). Thus, below T_c the spectrum appeared as two maxima separated by a valley (Fig. 4, k = 70) which disappeared at T_c (Fig. 4, k = 98). It can be seen that at this T_c one of the interior inflection points has a tangent of slope zero.

In this treatment the value obtained for the larger of the two rate constants is independent of the value for K. In the present study we have chosen a different definition for T_c, with the result that the values for k_A and k_B will be dependent upon K. In the spectra showing coalescence of equally populated singlets the spectrum below T_c is represented by a curve with four inflection points (Fig. 3) and above T_c one sees a single maximum to a curve containing only two inflection points. At the point of coalescence, which we define as the temperature at which the valley disappears, there are only two inflection points (see Fig. 3). It is this characteristic of T_c which we wish to maintain in defining T_c in the case of unequally populated sites. Specifically one searches for the spectrum possessing the longest "flat spot" (where $\partial G/\partial V$ is constant) as illustrated by the curve for k_A = 145 in Fig. 4.

We have tested the validity of the new approximate formulae [*a*]–[*c*] for the coalescence of two singlets and $K = \rho_B/\rho_A = 2$.

[*a*] $k = (\pi/\sqrt{2})\Delta\nu$

[*b*] $k_A = 2k\rho_B$

[*c*] $k_B = 2k\rho_A$

where k_A represents the process A → B.

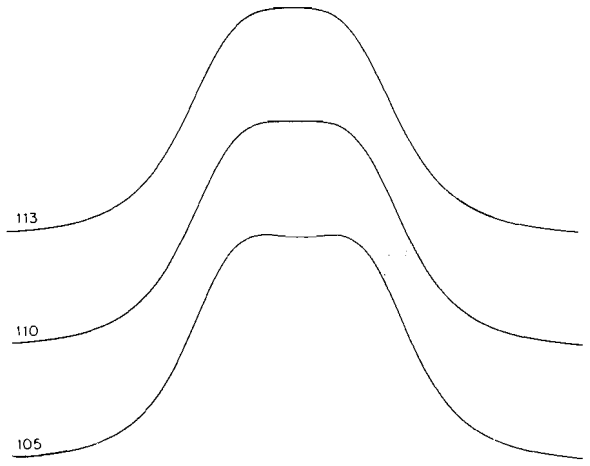

FIG. 3. The curves computed by DNMR 3 to represent a rate of exchange between two equally populated sites which is above, equal to, or below that defined as representing the coalescence temperature.

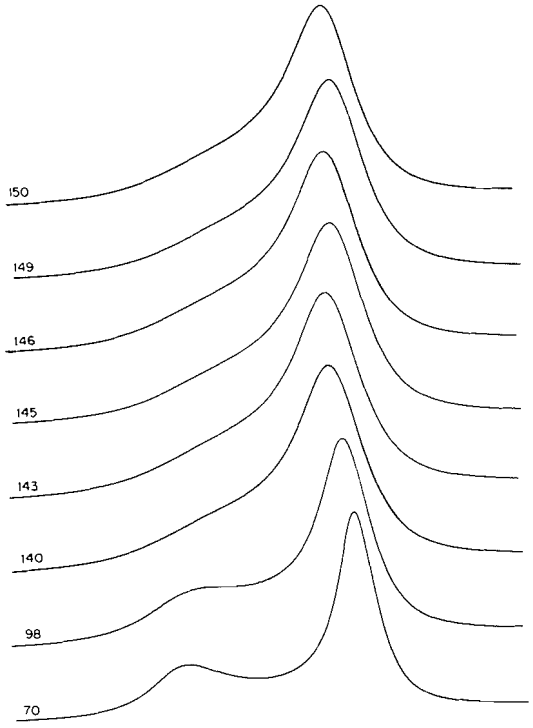

FIG. 4. The curves computed by DNMR 3 to illustrate coalescence of two unequally populated singlets ($K = 2$). The rates chosen represent the following situations: $k = 70$, below coalescence; $k = 98$ represents coalescence as defined by Raban; $k = 140$, 143, rates approaching our definition of coalescence; $k = 145$, 146, 149, rates which could represent the rate at the coalescence temperature; $k = 150$ clearly represents a rate above the coalescence.

Table 2 compares the values for k_A calculated from [*a*] and [*b*] with those obtained by CLS. Examination of the curves computed by DNMR 3 for a range of k's at each value of $\Delta\nu$ revealed surprisingly little uncertainty in the assignment of a curve as that representing T_c. Comparing this curve with a number of those representing rates greater and smaller leaves no doubt as to the choice of k at T_c within the accuracy quoted in Table 2. The curves calculated by CLS for $\Delta\nu = 50$ and a range of k^{CLS} values are illustrated in Fig. 4.

It is thus evident that the two-site approximate equation [*b*] gives an accuracy of better than 5% in k when $\Delta\nu$ is greater than 10. This level of accuracy exceeds that reported by Raban *et al.* and is comparable to that obtained by the more laborious graphical procedure of Shanan-Atidi and Bar-Eli (15*a*).[3] Since it leads to an uncertainty in $\Delta G^{\ddagger}$ of less than that due to an uncertainty in temperature cf ± 2°C (± 0.10 kcal/mol), it is as accurate a method as the CLS for measuring $\Delta G^{\ddagger}$ at T_c.

Application of the Approximate Method to the Exchange Process of ***1***

We next examined the possibility that the approximate two-site equation for unequally populated singlets could be applied with adequate accuracy to the coalescence of the two multiplets representing the AA′ absorptions of the enamide **1**. Equations [*a*] and [*b*] give a value of 47 s^{-1} for k_A from which $\Delta G^{\ddagger}$ is calculated to be 14.8_5 kcal/mol (at 292°C). These values are in good agreement with those obtained by CLS, k (41 s^{-1}) and $\Delta G^{\ddagger}$ (14.9_5 kcal/mol), and thereby justify use of the approximate method to determine k for the closely related acyl enamines **2**–**5**. The rate constants obtained in this way and their associated $\Delta G^{\ddagger}$'s are given in Table 3. Based on a maximum uncertainty in k of 35% and in T_c of 2 deg, the linearized relative statistical error (12) in $\Delta G^{\ddagger}$ is 0.25 kcal/mol.

It can be seen that all the measured barriers fall within the range 13.6 to 14.9 kcal/mol. This activation energy for rotation is lower than that reported for most amides (1). However, an appropriately selected model of similar structure is required to allow the assessment of the effect of a vinyl group on $\Delta G^{\ddagger}$. For this purpose we have prepared *N*-acetyl-*trans*-decahydroquinoline, **6**, (16), and measured its barrier to rotation about the amide bond. This was accomplished by determining the temperature of coalescence of the two equatorial proton absorptions at C-2 to be at -10°C, which by use of our approximate eq. [*c*] with [*a*] gives a $\Delta G^{\ddagger}$ minor → major

[3]For another solution method see ref. 15*b*.

TABLE 2. Comparison of k_A with k^{CLS}

Δν (Hz)	k_A (s^{-1})	k^{CLS} (s^{-1})	Precision[a] (%)
50	149	145–150	3
40	119	115–120	4
30	89	86–90	4
20	59	57–60	4
10	29.8	28.5–30	5
5	14.9	14–15	6
4	11.9	10.8–12	10
3	8.9	8–9	11

[a]The precision is calculated from the range of uncertainty in k^{CLS} as estimated from the average of the independent assessments of two of us.

TABLE 3. Barriers to N—C=O rotation in **1–6**

Compound	T_c	Δν (at T_c)	p_B	k_A	$\Delta G_{A\rightarrow B}$ (±0.25)
1	292	19	0.56	47	14.8_5
			0.56	41	14.9_5 (by CLS)
2	269	16	0.67	47	13.6
3	284	15	0.60	40	14.5
4	270	15	0.56	37	13.8
5	279	9	0.55	22	14.1
6	263	106	0.60	282	12.4

of 12.4 and a $\Delta G^{\ddagger}$ major → minor of 12.6 kcal/mol. Thus, the effect of the double bond in a cyclic vinyl amide is to raise the barrier, whereas previously it was claimed that such barriers would be lower in any vinyl amide (4). One would predict that the resonance interaction of the lone pair on nitrogen with the double bond would lower the barrier to rotation as is clearly the case in *N*-acetyl pyrrole (17) where the barrier is lowered 6 kcal/mol by transition state stabilization. Although the resonance effect may be present and contributing to a lowering of the barrier in **1–5**, it is obvious that in compounds **1–5** other effects must dominate over the resonance effect of the double bond. The observed barrier can be accounted for by steric effects which would be destabilizing and most important in the *ground state* of the saturated amide. Previous studies indicate strong repulsive interaction between the oxygen (or carbon) of the *N*-acetyl group and an equatorial *alpha* substituent, i.e., the proximate methylene group (e.g.; C-8 in **6**). For example, two independent methods of analysis of the ^1H spectral behaviour of *N*-acetyl-2-methylpiperidine assign an exclusive axial orientation to the methyl group (18, 19). Since this conformation possesses 1.9 kcal/mol of strain (19) an equatorial methyl must encounter at least 3.3 kcal/mol of strain when *syn* to either the carbon or oxygen of the acetyl group. In **6**, the *trans* ring junction places the C-8 carbon in just such an equatorial orientation. The fact that the proton spectrum of **6** shows a 4:6 ratio of conformers (with respect to N—CO bond) indicates comparable high strain in either conformer.

With similar and only slightly less strong steric interactions being present in the amides **1–5** it is reasonable that a variation in steric interactions in this series of acetyl enamines could give rise to the observed 1.1 kcal/mol range of barriers. A lack of precise knowledge of the favoured conformations[4] in this series precludes a more accurate interpretation of the barrier data.

It is interesting to note that the raw coalescence data, as opposed to the E_a's used by the authors (4), in the previous paper on acyl enamines reinforces our above interpretation. If one calculates the $\Delta G^{\ddagger}$ for rotation from the measured coalescence temperatures of *N*-vinyl-*N*-methyl formamide and *N*-vinyl-*N*-methyl acetamide, the values obtained are within 1 kcal/mol of the barriers for the corresponding dimethyl amides. The comparative data appears in Table 4. In these simpler amides less severe steric interactions are present and the similarity in $\Delta G^{\ddagger}$ values for amides and enamides indicates the unimportance of a resonance effect of the vinyl substituent.

In summary, we have established that use of the simple two-site formula can be applied to the determination of rates of interconversion of conformations of unequal population whose signals are singlets and also to one case of two multiplets representing the AA′ portions of two AA′MM′ systems. This has allowed determination of the barriers to rotation for a series of acetylenamines all of which were found to be greater than in a model lacking the double bond. The lower barrier in the saturated amide is thought to result from steric destabilization of its ground state.

Experimental

All proton spectra were recorded on a Varian HA-100 spectrometer. Solutions of concentration 0.2 *M* in deuterochloroform were used throughout. The probe temperature was determined before and after the measurement of each spectrum using a thermocouple placed inside a sample tube containing deuterochloroform. This method is thought to provide the temperature to an accuracy of better than ±1°C.[5] Spectra near the coalescence temperature were recorded at sweep widths of 250 Hz using a sweep rate of 0.25 Hz/s. Care was taken to avoid saturation. Coupling constants and chemical shifts have been measured using 250 Hz sweep widths and are accurate to 0.2 Hz.

The ^{13}C spectra of 2 were measured on a 0.2 *M* solution in

[4]The values for J_{cis} (3.5 Hz) and J_{trans} (7 Hz) in **1** are consistent with a normal half-chair conformation for **1**, but do not preclude the presence of up to 30% of one or more boat conformations.

[5]A liberal allowance of ±2°C for the uncertainty in temperature was used in calculating the statistical errors in $\Delta G^{\ddagger}$.

TABLE 4. Barriers to rotation (ΔG^*) calculated from $k = 2.22\Delta\nu$ at T_c

Amide	Solvent	T_c (°C)	$\Delta\nu$ (Hz)	$\Delta G_{T_c}{}^*$ (kcal/mol)	Ref.
$HCON(CH_3)_2$	Neat	386	8.1	20.9	[a]
$HCON(CH_3)CH{=}CH_2$	Neat	372	5.7	20.1	4
$CH_3CON(CH_3)_2$	CCl_4			17.3	10
$CH_3CON(CH_3)CH{=}CH_2$	Neat	309	5.2	16.7	4

[a]Reference 1 lists numerous papers in which the barrier has been measured. The barrier of 20.9 kcal/mol appears to be the most carefully determined one (20).

deuterochloroform using a Varian FT-80 spectrometer. Calculations using the LACN 3 and DNMR 3 programs were carried out on an IBM 360/65. The enamides used in this study were prepared by methods reported in an earlier paper (8).

Acknowledgements

The authors wish to thank the National Research Council of Canada for their financial support.

1. W. E. STEWART and T. H. SIDDALL III. Chem. Rev. **70**, 517 (1970).
2. H. KESSLER. Angew. Chem. **9**, 219 (1970).
3. L. M. JACKMAN. *In* Dynamic nuclear magnetic resonance spectroscopy. *Edited by* L. M. Jackman and F. A. Cotton. Academic Press, Inc., New York. 1975. Chapt. 7.
4. D. G. GEHRING, W. A. MOSHER, and G. S. REDDY. J. Org. Chem. **31**, 3436 (1966).
5. I. O. SUTHERLAND. *In* Annual reports of NMR spectroscopy. Vol. 4. *Edited by* E. F. Mooney. Academic Press, Inc., London. 1971.
6. G. BINSCH. Top. Stereochem. **3**, 97 (1968).
7. T. B. GRINDLEY, B. M. PINTO, and W. A. SZAREK. Can. J. Chem. **55**, 949 (1977).
8. J. R. MAHAJAN, G. A. L. FERREIRA, H. C. ARAUJO, and B. J. NUNES. Synthesis, 313 (1973).
9. D. A. KLEIER and G. BINSCH. DNMR 3. A computer program 165. Quantum Chemistry Program Exchange, Indiana University. 1970; J. Magn. Reson. **3**, 146 (1970).
10. L. W. REEVES, R. C. SHADDICK, and K. N. SHAW. Can. J. Chem. **49**, 3683 (1971).
11. M. BARFIELD. J. Chem. Phys. **41**, 3825 (1964).
12. G. BINSCH. *In* Dynamic nuclear magnetic resonance spectroscopy. *Edited by* L. M. Jackman and F. A. Cotton. Academic Press, Inc., New York. 1975. p. 77.
13. G. C. LEVY and G. L. NELSON. J. Am. Chem. Soc. **94**, 4897 (1972); W. A. TORCHIA, J. R. LYERLA, JR., and C. M. WEBER. J. Am. Chem. Soc. **96**, 5009 (1974).
14. D. KOST, E. H. CARLSON, and M. RABAN. Chem. Commun. 656 (1971); M. RABAN and C. CARLSON. J. Am. Chem. Soc. **93**, 685 (1971); M. RABAN, F. B. JONES, JR., E. H. CARLSON, E. BANUCCI, and N. A. LEBEL. J. Org. Chem. **35**, 1496 (1970).
15. (*a*) H. SHANAN-ATIDI and K. H. BAR-ELI. J. Phys. Chem. **74**, 961 (1970); (*b*) W. EGAN, R. TANG, G. ZON, and K. MISLOW. J. Am. Chem. Soc. **93**, 6205 (1971).
16. H. BOOTH and D. V. GRIFFITHS. J. Chem. Soc. Perkin Trans. II, 111 (1975).
17. K.-I. DAHLQVIST and S. FORSEN. J. Chem. Phys. **73**, 4124 (1969); D. PINDER. J. Chem. Phys. **77**, 567 (1973).
18. Y. L. CHOW, C. J. COLON, and J. N. S. TAM. Can. J. Chem. **46**, 2821 (1968).
19. R. R. FRASER and T. B. GRINDLEY. Tetrahedron Lett. 4169 (1974).
20. M. RABINOVITZ and A. PINES. J. Am. Chem. Soc. **93**, 685 (1971).

Effects of organic cosolvents on enzyme stereospecificity.[1] The enantiomeric specificity of α-chymotrypsin is reduced by high organic solvent concentrations

J. Bryan Jones and Mladen M. Mehes

Department of Chemistry, University of Toronto, Toronto, Ont., Canada M5S 1A1

Received February 27, 1979

J. Bryan Jones and Mladen M. Mehes. Can. J. Chem. **57**, 2245 (1979).

The influence of a range of protic and aprotic solvents of varying polarities on the enantiomeric specificity of α-chymotrypsin has been examined using methyl (2*S*)- and (2*R*)-2-acetamido-2-phenylacetate (**1**) as representative L- and D-substrates. The rates of hydrolysis were determined in solutions containing up to 30% organic solvent. The addition of organic solvent reduced the overall rates of hydrolysis of (2*S*)- and (2*R*)-**1** in each case, with those of the L-enantiomer (2*S*)-**1** being affected more than those of the D-stereoisomer (2*R*)-**1**. However, the enzyme overwhelmingly retains its normal L-enantiomeric preference under all conditions surveyed. It is concluded that α-chymotrypsin, and possibly other strongly stereospecific enzymes, can be used with confidence for asymmetric synthesis or resolution purposes in aqueous solutions to which moderate (up to 40%) proportions of organic cosolvents have been added to increase solubility of hydrophobic organic substrates.

J. Bryan Jones et Mladen M. Mehes. Can. J. Chem. **57**, 2245 (1979).

Faisant appel aux acétamido-2 phényl-2 acétates de méthyle-(2*S*) et -(2*R*) (**1**) comme substrats L et D représentatifs, on a étudié l'influence de divers solvants protiques et aprotiques de polarités variables sur la spécificité énantiomérique de l'α-chymotrypsine. On a déterminé les vitesses d'hydrolyse dans des solutions contenant jusqu'à 30% de solvant organique. L'addition de solvants organiques réduit les vitesses globales d'hydrolyse de chacun des isomères (2*S*) et (2*R*) de **1**; l'énantiomère L, **1**-(2*S*), est plus affecté que l'énantiomère D, **1**-(2*R*). Toutefois l'enzyme retient pratiquement toute sa préférence normale pour l'énantiomère L dans toutes les conditions étudiées. On en conclut que l'α-chymotrypsine, et possiblement d'autres enzymes fortement stéréospécifiques, peuvent être utilisés avec confiance pour des synthèses asymétriques ou pour effectuer des résolutions dans des milieux aqueus auxquels on a ajouté des proportions modérées (jusqu'à 40%) de cosolvants organiques dans le but d'augmenter la solubilité de substrats organiques hydrophobes.

[Traduit par le journal]

The potential of enzymes as practical catalysts for asymmetric synthesis is becoming increasingly recognized. Their advantages derive mainly from the often unique stereospecificity with which they effect their catalyses. A knowledge of all the factors influencing enzymic stereospecificity is therefore of critical synthetic importance.

Up till now, most systematic stereospecificity studies have been carried out in largely aqueous solutions. However, a majority of the substrates of interest to organic chemists are likely to be hydrophobic, requiring the addition of significant proportions of organic cosolvents in order to achieve solubility in the aqueous media preferred for enzyme-catalyzed reactions.

Despite the fact that the effects of organic solvents on various aspects of enzyme catalysis have been quite extensively studied (2–5), virtually no attention has been devoted to their influence on the stereospecificity of enzymes. Accordingly, in view of its obvious importance with respect to asymmetric synthetical applications of enzymes, we have initiated a general study of this topic.

In this paper we report on the effects of some representative protic and aprotic solvents on the enantiomeric specificity of the well documented enzyme α-chymotrypsin. The results obtained show that α-chymotrypsin's capacity to discriminate between the enantiomers of methyl 2-acetamido-2-phenylacetate (**1**) is reduced when the proportion of

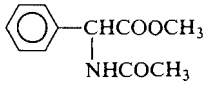

1

each solvent surveyed is increased. However, the effect is not large enough to prevent the enzyme from being used to effect practical-scale resolutions of racemic substrates in solutions containing significant proportions of any of the organic solvents examined.

Results

The enantiomers of methyl 2-acetamido-2-phenylacetate (**1**) were obtained via α-chymotrypsin-cata-

[1]Enzymes in organic synthesis. 15. For Part 14, see ref. 1.

0008-4042/79/172245-04$01.00/0

TABLE 1. Kinetic constants for chymotrypsin-catalyzed hydrolyses of (2*R*)- and (2*S*)-**1** in different aqueous–organic cosolvent solutions[a]

Cosolvent (ε)	Concentration (%)	Substrate	K_m (m*M*)	k_{cat} (s^{-1})	k_{cat}/K_m (s^{-1} M^{-1})	Stereospecificity ratio[b]
Dimethylsulfoxide (48)	5	(2*S*)-**1**	2.1	1.67	795	452
	5	(2*R*)-**1**	6.8	0.012	1.76	
	25	(2*S*)-**1**	3.9	0.51	130	1083
	25	(2*R*)-**1**	58.2	0.007	0.12	
	41.7[c]	(2*S*)-**1**	69.5	0.71	10.3	70.1
	41.7[c]	(2*R*)-**1**	80.0	0.012	0.147	
Acetonitrile (38)	5	(2*S*)-**1**	4.2	1.61	383	239
	5	(2*R*)-**1**	7.5	0.012	1.6	
	15	(2*S*)-**1**	10.4	0.74	71.2	41.6
	15	(2*R*)-**1**	7.6	0.013	1.71	
Dimethylformamide (36.7)	5	(2*S*)-**1**	3.7	1.3	351	362
	5	(2*R*)-**1**	8.2	0.008	0.97	
	25	(2*S*)-**1**	13.5	0.76	56.2	134
	25	(2*R*)-**1**	9.5	0.004	0.42	
Methanol (32)	5	(2*S*)-**1**	2.7	1.11	411	198
	5	(2*R*)-**1**	24.0	0.05	2.08	
	25	(2*S*)-**1**	5.9	0.95	169	108
	25	(2*R*)-**1**	6.4	0.01	1.56	
Acetone (21)	5	(2*S*)-**1**	4.7	1.14	242	341
	5	(2*R*)-**1**	19.7	0.014	0.71	
	30	(2*S*)-**1**	25.1	0.63	25.1	119
	30	(2*R*)-**1**	42.7	0.009	0.21	
2-Propanol (19.9)	5	(2*S*)-**1**	2.4	0.91	379	303
	5	(2*R*)-**1**	8.0	0.01	1.25	
	20	(2*S*)-**1**	17.7	1.35	76.2	191
	20	(2*R*)-**1**	111.0	0.044	0.4	
Dioxan (2.2)	5	(2*S*)-**1**	4.4	0.55	125	463
	5	(2*R*)-**1**	485.0	0.13	0.27	
	20	(2*S*)-**1**	6.9	0.33	47.8	12.4
	20	(2*R*)-**1**	1.3	0.005	3.85	

[a]Kinetics performed at pH 8, 25°C. All data corrected for nonenzymic hydrolysis and enzyme autohydrolysis when necessary.
[b]k_{cat}/K_m for (2*S*)-**1** ÷ k_{cat}/K_m for (2*R*)-**1** under the same conditions.
[c]From ref. 6.

lyzed hydrolysis of the racemate. The *R*-ester (2*R*)-**1** was recovered unchanged from the hydrolysis mixture. The 2*S*-acid isolated was reesterified to give the other enantiomer required, (2*S*)-**1**. This method was found to be much superior to one involving resolution of the racemic acid by recrystallizations of its (+)- and (−)-α-phenethylamine salts.

The kinetics of α-chymotrypsin-catalyzed hydrolysis for each enantiomer were determined at two concentrations of each of the cosolvents dimethylsufoxide, acetonitrile, dimethylformamide, methanol, acetone, isopropanol, and dioxan. The lower concentration was set at 5% for each cosolvent since this conferred sufficient substrate solubility to ensure homogeneous solutions for each kinetic run. The higher concentration used varied for each cosolvent. For all except dimethylsulfoxide, the cosolvent level employed was the maximum for which kinetically significant hydrolysis rates could still be observed. The values determined for the Michaelis constants, K_m, which reflect binding efficiency, and of the overall rate constants, k_{cat}, are recorded in Table 1.

Discussion

Our initial concern over the effects of added organic solvents on enzyme stereospecificity was prompted by the observation that up to 100-fold differences in the specificity constants (k_{cat}/K_m) were manifest for the chymotrypsin-catalyzed hydrolyses of the L- and D-enantiomers of **1** and their homologues in 41.7% aqueous dimethylsulfoxide (6). More disturbing from the asymmetric synthesis viewpoint was the discovery that the enzyme lost all specificity in 100% dimethylsulfoxide (7). With addition of organic solvents being unavoidable in any widespread application of enzymes in organic synthesis, it was clear that more information on this aspect was

required, particularly for the most commonly used water-miscible organic solvents.

α-Chymotrypsin was selected as the enzyme for this initial study since its specificity is well documented and readily rationalized (3*a*) and considerable data are already available on the influence of organic solvents on various aspects of the catalytic process (3, 5, 7, 8–16). The protic and aprotic solvents selected have been used before with α-chymotrypsin (3*a*). They encompass a broad range of polarities, having dielectric constants ranging from 2.2–48. They are also representative of the water-miscible solvents most likely to be employed by organic chemists for increasing the aqueous solubility of any hydrophobic substrate.

The choice of the *S*(L)- and *R*(D)-enantiomers of **1** as the substrates was based on the observation that, although chymotrypsin retained its normal L-enantiomeric specificity preference towards **1**, both enantiomers were kinetically reasonable substrates (6). It was therefore felt that changes in enantiomeric specificity could be readily detected. Also, with potential applications possibilities always in mind, the fact that the acyl group of (2*R*)-**1** is present in ampicillin and amoxycillin did not escape attention.

The kinetics of each enantiomer were determined in aqueous solutions containing 5% of organic cosolvent as a common lower limit and from 15–30% of cosolvent as the upper limit. In each case, the higher limits used (see Table 1) represent the practical maximum for the pH-stat assay procedure employed. The upper cosolvent proportions for dimethylsulfoxide and acetone were restricted by the sluggishness of the electrode response in the partly organic medium. For acetonitrile, dimethylformamide, methanol, 2-propanol, and dioxan, aggregation or precipitation of the enzyme at the higher cosolvent levels became the controlling factor. Furthermore, as the levels of organic solvents are raised, the corresponding reductions in the effective concentration of water contribute towards progressive lowerings of the overall rates of hydrolysis.

A measure of the degree of enantiomeric preference of the enzyme at each solvent concentration is provided by the stereospecificity ratio.[2] As Table 1 shows, the *S*:*R*-stereospecificity ratio is diminished at the higher cosolvent concentration for each of the solvents examined.[3] However, with the exception of dioxan, the reductions in *S*(L):*R*(D) stereospecificity are modest, being in the range 1.6–5.8-fold only. The overall rates of catalysis, as reflected by the specificity constants, of the more efficiently hydrolyzed (2*S*)-**1** enantiomer are affected to a much greater degree then those of the more slowly transformed (2*R*)-**1** stereoisomer under the same conditions. Nevertheless, the enzyme retains an overwhelming L-stereochemical preference throughout, with hydrolysis of the *S*- being favoured over *R*-enantiomer by a large factor under all conditions. With the possible exception of 20% dioxan, α-chymotrypsin could clearly be used with confidence to effect complete resolutions on preparative-scale reactions under each of the aqueous organic solutions listed. The order of decreasing influence of solvent on stereospecificity in the current study is: dimethylsulfoxide < methanol < acetonitrile < 2-propanol < dimethylformamide < acetone < dioxan. This may be used as a guide in selecting the most appropriate solvent for any future resolution experiments.

The introduction of organic solvents to α-chymotryptic-catalyzed hydrolyses of various substrates has generally been found to increase K_m's profoundly while leaving k_{cat}'s relatively unchanged (3*a*, 6, 8, 10*a*, 11). A similar trend is seen for the kinetic constants of (2*S*)-**1**, with K_m generally larger at the higher cosolvent concentration, and k_{cat} much less affected. For (2*R*)-**1**, however, the picture is much more random and no clear patterns of K_m and k_{cat} variations are evident. K_m for (2*R*)-**1** is even reduced at times. This indication of tighter binding is presumably the consequence of increased non-productive binding (3, 8).

The overall influences of the individual cosolvents are complex and the current data do not permit the various contributing factors to be identified. Some of the reasons which have been invoked previously to account for solvent effects, such as nucleophilic participation in the catalytic process by methanol and isopropanol (8–11), and competitive inhibition by acetonitrile, methanol, acetone, and dioxan (8, 10*a*, 12), are undoubtedly important. General solvent effects, including cosolvent-induced dielectric, pK_a, and conformational changes, and denaturation may also be influential (3, 5–8, 10, 13–15, 16*a*). The current data do not show any clear correlation between the stereospecificity ratio and the dielectric constant of the solvent (10*a*, 16*b*).

It is evident that, even with a substrate such as **1** which does not provide an optimum fit at the active site (3*a*), the stereospecificity of α-chymotrypsin is only marginally affected by the presence of 15–25% of several diverse organic solvents. However, from the evidence obtained previously at very high dimethyl-

[2]The stereospecificity ratio is the ratio of the specificity constants, k_{cat}/K_m, for the *S*(L)- and *R*(D)-enantiomers under the same assay conditions.

[3]The 25% dimethylsulfoxide results are the only exception. However, even in this case, the rates of hydrolysis of both enantiomers are much reduced compared with those in 5% dimethylsulfoxide.

sulfoxide concentrations (7), retention of stereospecificity cannot be guaranteed at excessive cosolvent levels even for an enzyme like chymotrypsin,[4] which has such strong enantiomeric preferences. Fortunately, in practice this is unlikely to pose a serious problem for preparative work since loss of catalytic activity will accompany, or even precede, the disappearance of stereospecificity.

On the basis of this quantitative study, and the qualitative data which exist for other enzymes (*3a*), we conclude that in aqueous solutions containing moderate amounts ($\leq$40–50%) of many organic cosolvents, α-chymotrypsin, and probably most other highly specific enzymes, will maintain sufficient stereospecificity to enable them to be used with confidence in asymmetric synthesis applications.

Experimental

All solvents used were reagent grade. They were further purified and redistilled prior to use. α-Chymotrypsin (EC 3.4.-21.1, 3 × crystallized) was purchased from Worthington.

*Preparation of Methyl (2R)- and (2S)-Acetamido-2-phenylacetate (**1**)*

The procedure of Pattabiraman and Lawson (6) was followed. The racemic ester (±)-**1**, mp 76.5–77°C after recrystallization from diisopropyl ether[5] (lit. (6) mp 75.5–76.5°C), was resolved on a 9 g scale using α-chymotrypsin to give (2*R*)-**1** (2.1 g), mp 116–117°C after recrystallization from diisopropyl ether, $[\alpha]_D^{25}$ −176.2° (*c* 0.95, EtOH), (lit. (6) mp 112–113°C, $[\alpha]_D^{25}$ −175.8° (*c* 0.95, EtOH)) and, after esterification of the (2*S*)-acid (3.0 g), the methylester (2*S*)-**1** (0.8 g), mp 117–117.5°C after recrystallization from diisopropyl ether, $[\alpha]_D^{25}$ +178.4° (*c* 1.05, EtOH), (lit. (6) mp 110–112°C, $[\alpha]_D^{25}$ +180.5° (*c* 1.05, EtOH)).

Kinetic Studies

The kinetic studies were carried out at 25°C under nitrogen using Radiometer pH-stat-controlled addition of 10^{-1} to 2.5×10^{-3} *M* aqueous sodium hydroxide to maintain the apparent pH at 8. Stock solutions of the enzyme (in 10^{-3} *M* HCl) and of the (2*R*)- and (2*S*)-**1** substrates (freshly prepared in the appropriate solvent and CO_2-free water) were made up and appropriate aliquots taken to enable 7–10 runs to be performed under steady-state conditions within the substrate concentration range 0.1 to $\leq 5\,K_m$ (depending on solubility factors) and with enzyme concentrations of 3–40 × 10^{-6} *M*. A reaction volume of 10 mL of constant ionic strength (0.1 *M* KCl) was employed throughout. Corrections for spontaneous hydrolysis of (2*R*)- and (2*S*)-**1**, and for enzyme autohydrolysis at high enzyme concentrations, were made when necessary. The enzyme concentration was determined spectrophotometrically (17). The data were analyzed by the Lineweaver–Burk method and were subjected to least-squares regression analysis. The K_m and k_{cat} values obtained at the various solvent concentrations are recorded in Table 1.

[4]However, α-chymotrypsin's substrate binding site seems to be preserved even in 100% dimethylsulfoxide (7).

[5]Caution: explosive peroxides form in air. Only fresh diisopropyl ether, which had been stored over ferrous sulfate crystals for several hours, was used. Mother liquors were discarded immediately. No attempts should be made to recover extra material from them.

Acknowledgment

Support of this work by the National Science and Engineering Research Council is gratefully acknowledged.

1. J. B. Jones and K. P. Lok. Can. J. Chem. **57**, 1025 (1979).
2. M. Dixon and E. C. Webb. Enzymes. 2nd ed. Longmans, London. 1964.
3. (*a*) J. B. Jones and J. F. Beck. Tech. Chem. (NY), **10**, 107 (1976). (*b*) J. B. Jones. Tech. Chem. (NY), **10**, 38 (1976).
4. K. H. Tan and R. Lovrien. J. Biol. Chem. **247**, 3278 (1972).
5. P. Maurel. J. Biol. Chem. **253**, 1677 (1978) and references therein.
6. T. N. Pattabiraman and W. B. Lawson. Biochem. J. **126**, 645 (1972); **126**, 659 (1972).
7. A. A. Klyosov, N. Vanviet, and I. V. Berezin. Eur. J. Biochem. **59**, 3 (1975).
8. C. Niemann. Science, **143**, 1287 (1964).
9. C. E. Macdonald and A. K. Balls. J. Biol. Chem. **221**, 993 (1956).
10. (*a*) G. E. Clement and M. L. Bender. Biochemistry, **2**, 836 (1963). (*b*) M. L. Bender, G. E. Clement, C. R. Gunter, and F. J. Kezdy. J. Am. Chem. Soc. **86**, 3697 (1964). (*c*) M. L. Bender. Chem. Rev. **60**, 53 (1966). (*d*) K. Tanizawa and M. L. Bender. J. Biol. Chem. **249**, 2130 (1974).
11. M. Mares-Guia and F. S. Figureiredo. Biochemistry, **11**, 2091 (1972).
12. J. L. Miles, D. A. Robinson, and W. J. Canady. Fed. Proc. **21**, 231 (1962); J. L. Miles, E. Morey, F. Crain, S. Gross, J. San Julien, and W. J. Canady. J. Biol. Chem. **237**, 1319 (1962).
13. A. L. Fink. Acc. Chem. Res. **10**, 233 (1977); Biochemistry, **13**, 277 (1974).
14. Y. I. Khurgin, V. Y. Roslyakow, Y. M. Azizov, and E. D. Kaverzneva. Izv. Akad. Nauk. SSSR, Ser. Khim. 2840 (1968).
15. E. C. Lucas, M. Caplow, and K. J. Bash. J. Am. Chem. Soc. **95**, 2670 (1973).
16. (*a*) M. L. Barnard and K. J. Laidler. J. Am. Chem. Soc. **74**, 6099 (1952). (*b*) K. J. Laidler and M. C. Ethier. Arch. Biochem. Biophys. **44**, 338 (1953).
17. S. Kumar and G. E. Hein. Anal. Biochem. **30**, 203 (1969).

Intramolecular alkylation of α,β-unsaturated ketones: a total synthesis of (±)-isolongifolene and an approach to the synthesis of zizaane-type sesquiterpenoids

EDWARD PIERS AND MICHAEL ZBOZNY

Department of Chemistry, University of British Columbia, 2075 Wesbrook Mall, Vancouver, B.C., Canada V6T 1W5

Received February 26, 1979

EDWARD PIERS and MICHAEL ZBOZNY. Can. J. Chem. 57, 2249 (1979).

A total synthesis of (±)-isolongifolene **6**, a C_{15} hydrocarbon derived from the acid-catalyzed rearrangement of the sesquiterpenoid longifolene, is described. The known carbomethoxyoctalone **10** was transformed via a 10-step sequence into the unsaturated keto tosylate **9**. The key step of the overall synthesis involved the efficient intramolecular γ alkylation of **9** to produce the tricyclic α,β-unsaturated ketone **5**. The latter compound was converted into the enone **33**, which had previously served as a precursor for the synthesis of (±)-isolongifolene **6**.

EDWARD PIERS et MICHAEL ZBOZNY. Can. J. Chem. 57, 2249 (1979).

On décrit une synthèse totale du (±) isolongifolène **6**, un hydrocarbure en C_{15} qui provient d'une transposition acido-catalysée du sesquiterpène longifolène. Dix étapes sont nécessaires pour transformer la carbométhoxyoctalone connue **10** en tosylate cétonique non saturé **9**. L'étape clé dans la synthèse globale implique l'alkylation intramoléculaire en γ efficace de **9** conduisant à la cétone α,β-non saturée tricyclique **5**. On transforme ce dernier composé en énone **33** qui a servi antérieurement comme précurseur pour la synthèse du (±) isolongifolène **6**.
[Traduit par le journal]

The intramolecular alkylation of α,β-unsaturated ketones has not been employed extensively in organic synthesis. Presumably, one of the main reasons for this lack of use is related to the fact that an alkylation of this type can, in theory, take place at one or more of three different sites: the α′ position, the α position, and the γ position (cf. **1**). Indeed, a perusal of the chemical literature shows that all three modes of cyclization have been observed, the specific site of alkylation depending mainly on the structure of the substrate.[1]

In connection with work related to the synthesis of natural products, we were intrigued by the possibility of forming specifically functionalized tricyclic ring systems by means of intramolecular alkylation of α,β-unsaturated ketones at the γ position. With the exception of those reactions which resulted in the closure of three-membered rings,[2] this type of process apparently has not been employed previously in the area of natural product synthesis.[3] More explicitly, we were interested in the possibility of effecting intramolecular alkylation of the keto tosylate **2**. It is clear that although two different enolate anions (**3** and **4**) could be formed from compound **2**, the only alkylative cyclization reaction possible would involve ring closure of **4** at the γ position to afford **5**. The alternative modes of ring closure involving **3** (α′ alkylation) and **4** (α alkylation) would be precluded by severe strain (bridgehead double bonds) in the (projected) products. On the other hand, successful internal γ alkylation of **4** would produce the intermediate **5**, which would appear to have the potential of serving as an excellent precursor for the synthesis of (±)-isolongifolene (**6**).[4] In addition, it seemed reasonable to propose that **5** could also serve as a convenient precursor for the keto ester **7**. The latter compound had been employed previously by MacSweeney and Ramage (4) as an intermediate in their synthesis of the racemic modification of the sesquiterpenoid zizanoic acid (**8**), which in turn had been transformed into other members of the zizaane class of natural products (4).

In this paper we report (*a*) the preparation of the keto tosylate **9**, (*b*) the efficient intramolecular alkylation of **9** to afford the intermediate **5**, and (*c*) the conversion of **5** into the tricyclic α,β-unsaturated ketone **33**. Since the latter compound had been converted previously into (±)-isolongifolene (**6**) (6), the acquisition of this material completed, in a formal sense, the total synthesis of the sesquiterpene.

[1]For a summary, including specific examples and references, and for a study of the effect of experimental conditions and substrate structure on the site of alkylation, see ref. 1.

[2]For some examples, see ref. 2.

[3]It should be noted that the intramolecular alkylation of substituted phenolic compounds at the *para* position, a type of reaction which is formally analogous to the alkylative cyclization of an α,β-unsaturated ketone at the γ position, has found use in the synthesis of diterpenoids (3).

[4]Isolongifolene is obtained from the acid-catalyzed rearrangement of the well-known sesquiterpenoid longifolene. For the structural elucidation of isolongifolene, see ref. 5. For a previous synthesis of this compound, see ref. 6.

0008-4042/79/172249-07$01.00/0

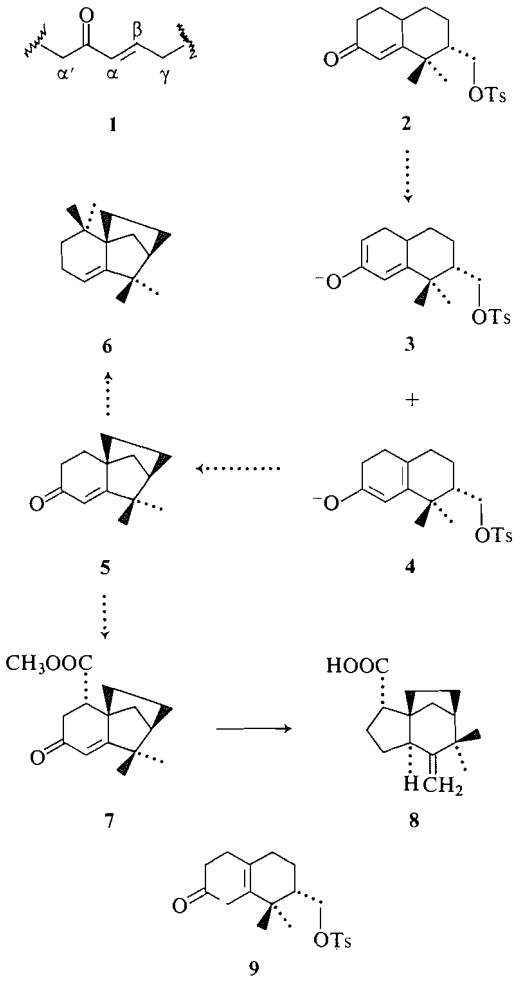

1 2 6 3 5 4 7 8 9

Synthesis and Intramolecular Alkylation of the Keto Tosylate 9 (see Scheme 1)

Alkylation (potassium *tert*-butoxide, *tert*-butyl alcohol) of the known (7) carbomethoxyoctalone **10** with methyl iodide afforded the dimethylated compound **11**, which, when allowed to react with methylenetriphenylphosphorane in dimethylsulfoxide at room temperature, gave the diene **12** (66% from **10**). The latter compound was subjected to hydroboration with disiamylborane in tetrahydrofuran (8) and the intermediate organoborane was oxidized with alkaline hydrogen peroxide. Spectral analysis of the product obtained from this reaction indicated that it consisted of a mixture of the epimeric compounds **13** and **14**. Analysis of this material by gas–liquid chromatography (glc) also indicated the presence of two components, in a ratio of approximately 1:1. However, when a pure sample of each component was obtained by means of preparative glc and subjected to spectral analysis, it became clear that only one of them produced spectra consistent with those expected from a hydroxy ester. This substance was assigned the *trans* structure **14**. Spectral analysis of the second component, a crystalline compound with mp 79–80°C, showed that it was the lactone **15**. It was thus evident that lactonization of the *cis* hydroxy ester **13** had occurred on the glc column.

Treatment of the mixture of hydroxy esters **13** and **14** with acetic anhydride in pyridine produced a mixture of the corresponding diesters **16** and **17**. Allylic oxidation of this material with chromium trioxide – dipyridine complex in dichloromethane (9) proved to be quite sluggish and, therefore, alternative methods to effect this transformation were investigated. Eventually, it was found that the procedure of Finucane and Thomson (10) produced excellent results. Thus, when a solution of compounds **16** and **17** in dioxane was treated with *N*-bromosuccinimide, calcium carbonate, and water, and the resultant mixture was irradiated with visible light, a mixture of the octalones **18** and **19** was obtained in 96% yield.

It is pertinent at this point to comment briefly regarding the stereochemistry of compounds **16–19**, inclusive. Although this point was not crucial in the overall synthetic sequence, it was nevertheless of interest to determine whether or not the stereochemistry of these substances could be assigned. As it turned out, the various configurations could be designated readily on the basis of ^{1}H nmr spectra.

The *trans* hydroxy ester **14** (*vide supra*) showed two 3-proton singlets at δ 1.00 and 1.07, readily assignable to the two tertiary methyl groups. On the other hand, the mixture of **14** and the *cis* epimer **13** exhibited, in addition to the signals at δ 1.00 and 1.07, two singlets at δ 0.82 and 1.22, obviously due to the geminal methyl groups of the *cis* compound **13**. It was thus clear that the chemical shift difference between the two methyl groups of the *cis* compound **13** ($\Delta\delta = 0.40$) was much larger than the corresponding difference in the *trans* isomer **14** ($\Delta\delta = 0.07$). Furthermore, the methyl signals of the latter compound appeared between those of the former substance. This pattern was also present in the diesters **16** and **17** and in the epimeric octalones **18** and **19**.[5] Thus, the diester which exhibited the tertiary methyl signals at δ 0.99 and 1.06 was assigned the *trans* stereochemistry (cf. **17**)[6] while the acetate which showed the comparable singlets at δ 0.80 and 1.19 could be assigned the *cis* configura-

[5]Pure samples of each of the compounds **16–19**, inclusive, were obtained by means of preparative glc.

[6]Mild base hydrolysis of **17** gave a hydroxy ester identical with the *trans* compound **14**, obtained from the hydroboration of **12**.

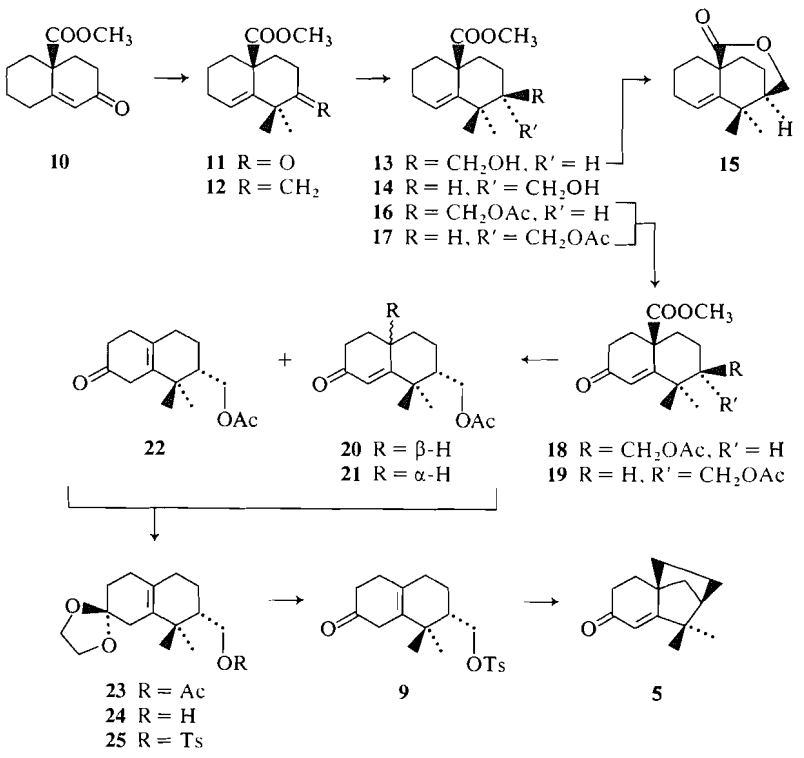

SCHEME I

tion (cf. **16**). In similar fashion, the two octalones **18** and **19** exhibited singlets due to the geminal methyl groups at δ 0.90 and 1.27 and at δ 1.12 and 1.18, respectively.

Decarbomethoxylation of the mixture of octalones **18** and **19** was achieved smoothly by treatment of this material with anhydrous lithium bromide in hot (140–150°C) hexamethylphosphoramide[7] for 4 h. During this time it was necessary to bubble nitrogen through the mixture in order to remove the methyl bromide as it was formed. If this was not done, the enolate anion produced from the decarboxylation step was partially methylated, thus complicating the purification of the final product and lowering the yield of desired material. Appropriate analysis (spectra, glc) of the distilled product of the reaction indicated that it was a mixture of three compounds, presumably the epimeric octalones **20** and **21**, along with the β,γ-unsaturated ketone **22**. Without further purification, this mixture was subjected to standard ketalization conditions (ethylene glycol, *p*-toluenesulfonic acid, benzene), thus affording in 73% overall yield from the octalones **18** and **19** the crystalline ketal acetate **23**, mp 101–102°C. Reduction of this material with lithium aluminum hydride in tetrahydrofuran, followed by tosylation (*p*-toluenesulfonyl chloride in pyridine, room temperature) of the resultant ketal alcohol **24**, produced the ketal tosylate **25**, mp 100–101°C (84% from **23**). Mild hydrolysis (aqueous sulfuric acid in acetone) of **25** gave the β,γ-unsaturated keto tosylate **9** in nearly quantitative yield, thus setting the stage for the key (proposed) intramolecular alkylation reaction.

The alkylative cyclization of compound **9** proved to be a remarkably facile process. Thus, brief treatment of this material with potassium *tert*-butoxide in hexamethylphosphoramide at room temperature afforded, after recrystallization of the distilled product, the tricyclic ketone **5** (mp 63–64°C) in 61% yield. The fact that this product possessed an α,β-unsaturated ketone functionality was shown by its ir (1670, 1640 cm^{-1}) and uv (238 nm, ε = 13 000) spectra. Furthermore, the ^1H nmr spectrum (one-proton singlet at δ 5.70, vinyl proton; six-proton singlet at δ 1.13, tertiary methyl groups) of this material was in full accord with structure **5**.

Conversion of the Tricyclic Endone 5 into the α, β-Unsaturated Ketone 33

The transformation of the tricyclic α,β-unsaturated ketone **5** into enone **33** was accomplished via a straightforward sequence of reactions as outlined in Scheme 2. When **5** was allowed to

[7]This method for ester cleavage is similar to that recorded earlier by McMurry and Wong (11).

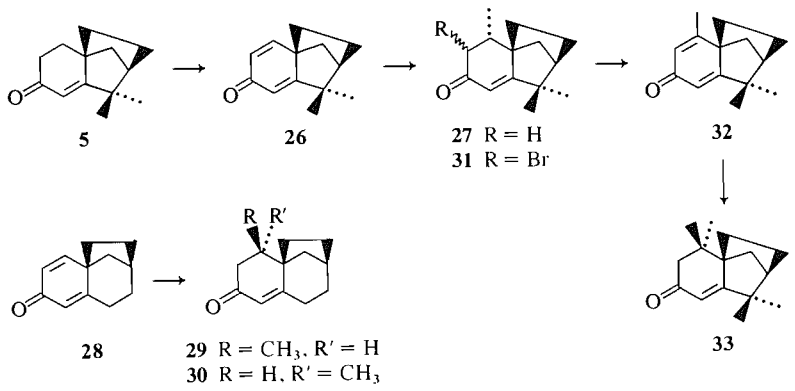

SCHEME 2

react with 2,3-dichloro-5,6-dicyano-1,4-benzoquinone (DDQ) (12) in refluxing dioxane containing acetic acid, the crystalline cross-conjugated dienone **26** was obtained in 60% yield. Conjugate addition of lithium dimethylcuprate (13) to this material was highly site-selective[8] and stereoselective, producing a single enone **27** in 81% yield. The stereochemistry of the newly introduced methyl group was assigned on the basis of steric approach control. The tentative nature of this conclusion should be emphasized, since Marshall and Brady (14) had shown that addition of lithium dimethylcuprate to the structurally similar dienone **28** afforded a mixture of the epimeric enones **29** and **30**, in ratios of 3:1 (reaction done in ether) and 3:2 (reaction done in dioxane–ether), respectively. Nevertheless, molecular models appeared to indicate that the β two-carbon bridge in **26** would offer appreciably greater steric hindrance to approach of the cuprate reagent than the α one-carbon bridge. On the other hand, models indicated that a similar steric preference for approach of the cuprate reagent to the dienone system in **28** was lacking.

Attempted conversion of the enone **27** into the corresponding dienone **32** by treatment of the former compound with DDQ (12) produced very low yields of the desired product. On the other hand, bromination of **27** with pyridinium hydrobromide perbromide in tetrahydrofuran – acetic acid, followed by dehydrobromination (lithium bromide, lithium carbonate, dimethylformamide, reflux) (15) of the resultant crude bromo ketone **31**, afforded the dienone **32** in 40% yield. Addition of lithium dimethylcuprate (13) to this material gave, in mediocre yield, the racemic tetramethyl tricyclic enone **33**. The melting point of this compound, as well as the spectral data (particularly the ^{1}H nmr spectrum) agreed very well with those reported in the literature (5, 6). Since compound **33** had already been converted into (±)-isolongifolene (**6**) (6), the acquisition of the former material formally completed the total synthesis of the sesquiterpene.

The overall conversion of **27** into **33** via the route described above was quite inefficient and it appears highly likely that a more efficient route could be devised. However, lack of sufficient material at this stage of the work precluded the possibility of examining alternatives. Furthermore, investigations into the possibility of converting the tricyclic enone **5** into the keto ester **7** (a precursor for the synthesis of zizaane-type sesquiterpenoids) will also have to await the acquisition of further quantities of **5**.

[8]The chemical literature contains ample precedent for the site-selective addition of cuprate reagents to cross-conjugated dienones possessing structures similar to **26** (see ref. 13).

Experimental

General

Melting points were determined on a Fisher-Johns melting point apparatus and are uncorrected. Infrared spectra were recorded on a Perkin-Elmer model 710 spectrophotometer. Proton magnetic resonance spectra were measured using Varian Associates spectrometers, models T-60 and (or) HA-100 or XL-100. Signal positions are given in δ units, with tetramethylsilane as the internal standard; the multiplicity, integrated peak areas, and proton assignments are indicated in parentheses. High resolution mass spectrometric measurements were recorded on an A.E.I. model MS-50 mass spectrometer. Gas–liquid chromatographic analyses were carried out with a Hewlett-Packard model 5832A gas chromatograph, while preparative gas–liquid chromatography was accomplished with an Aerograph Autoprep, model 700. Microanalyses were performed by Mr. P. Borda, Microanalytical Laboratory, University of British Columbia, Vancouver, B.C.

Preparation of the Keto Ester ***11***

To a warm (35°C), stirred solution of potassium *tert*-butoxide (37 g) in 600 mL of *tert*-butyl alcohol under an atmosphere of nitrogen was added, over a period of 15 min, 34 g (0.16 mol) of the octalone **10** (7). After the resulting solution had been cooled with an ice bath, freshly distilled methyl iodide (140 g, 1 mol) was added and the mixture was heated under reflux for 90 min. Most of the solvent was removed under reduced pressure and the milky residue was

diluted with water, neutralized by addition of dilute hydrochloric acid, and thoroughly extracted with ether. The combined extract was washed successively with water, aqueous sodium thiosulfate, and brine, and then dried over anhydrous magnesium sulfate. Removal of the solvent, followed by distillation (air-bath temperature 118–122°C/0.4 Torr) of the residual oil afforded 31 g (80%) of the keto ester **11**; ir (film): 1730, 1710 cm^{-1}; ^1H nmr ($CDCl_3$) δ: 1.26 (s, 6H, tertiary methyls), 3.66 (s, 3H, —$COOCH_3$), 5.85 (t, 1H, vinyl proton, J = 4 Hz). *Exact mass* calcd. for $C_{14}H_{20}O_3$: 236.1412; found: 236.1408.

Preparation of the Diene ***12***

To a solution of sodium methylsulfinylmethide (20 g, 0.2 mol) in dry dimethyl sulfoxide (250 mL), under an atmosphere of nitrogen, was added a solution of methyltriphenylphosphonium bromide (75 g, 0.21 mol) in 350 mL of dimethyl sulfoxide. After the mixture had been stirred for 15 min, a solution of the keto ester **11** (10 g, 0.042 mol) in 200 mL of dimethyl sulfoxide was added dropwise. The reaction mixture was stirred for 1 h, diluted with 600 mL of water, and then thoroughly extracted with ether – petroleum ether. The combined extract was washed with brine and dried over anhydrous magnesium sulfate. Removal of the solvent, followed by distillation (air-bath temperature 120–125°C/0.4 Torr) of the residual oil, gave 8.0 g (83%) of the pure diene **12**; ir (film) 1735, 1640, 890 cm^{-1}; ^1H nmr ($CDCl_3$) δ: 1.10 (s, 3H, tertiary methyl), 1.24 (s, 3H, tertiary methyl), 3.60 (s, 3H, —$COOCH_3$), 4.58–4.70 (m, 2H, =CH_2), 5.78 (t, 1H, vinyl proton, J = 4 Hz). *Anal.* calcd. for $C_{15}H_{22}O_2$: C 76.88, H 9.46; found: C 76.97, H 9.60.

Hydroboration of the Diene ***12***

To a cold (0°C), stirred solution of disiamylborane (2.0 g, 13 mmol) in 40 mL of dry tetrahydrofuran, under an atmosphere of nitrogen, was added a tetrahydrofuran solution (40 mL) of the diene **12** (2.1 g, 9 mmol). The solution was allowed to warm to room temperature and was stirred at this temperature for 2 h. The solution was cooled and treated (dropwise) successively with 12 mL of 3 *N* sodium hydroxide and 12 mL of 30% hydrogen peroxide. The resulting mixture was stirred at room temperature for 1.5 h and then most of the solvent was removed under reduced pressure. The residue was diluted with water and extracted with ether. The combined extract was washed with brine and dried over anhydrous magnesium sulfate. Removal of the solvent followed by distillation (air-bath temperature 130–140°C/0.3 Torr) of the residual oil afforded 1.9 g (84%) of a clear, colorless oil. The ir and ^1H nmr spectra of this material indicated that it was a mixture of the two diastereomeric alcohols **13** and **14**. The gas–liquid chromatogram of this material showed the presence of two components, in a ratio of about 1:1. A sample of each component was collected by preparative glc. The first compound was the hydroxy ester **14**; ir (film): 3450, 1725 cm^{-1}; ^1H nmr ($CDCl_3$) δ: 1.00 (s, 3H, tertiary methyl), 1.07 (s, 3H, tertiary methyl), 3.36–3.84 (m, 2H, AB part of ABX system, —CH_2OH), 3.66 (s, 3H, —$COOCH_3$), 5.73 (t, 1H, vinyl proton, J = 4 Hz). *Anal.* calcd. for $C_{15}H_{24}O_3$: C 71.39, H 9.59; found: C 71.20, H 9.76.

The second component isolated by preparative glc was the lactone **15**; mp 79–80°C; ir ($CHCl_3$): 1720 cm^{-1}; ^1H nmr ($CDCl_3$) δ: 1.22 (s, 6H, tertiary methyls), 4.04–4.64 (m, 2H, AB part of ABX system, —CH_2O—), 5.80 (t, 1H, vinyl proton, J = 4 Hz). *Anal.* calcd. for $C_{14}H_{20}O_2$: C 76.33, H 9.15; found: C 75.90, H 9.30.

Preparation of the Acetates ***16*** *and* ***17***

A mixture of 10 g (0.04 mol) of the alcohols **13** and **14**, 20 mL of acetic anhydride, and 40 mL of pyridine was heated on a steam bath for 2 min, and the resulting solution was allowed to stand at room temperature for 18 h. The solution was poured into water and the resulting mixture was extracted with ether. The combined ether extract was washed successively with 1 *N* hydrochloric acid, water, aqueous sodium bicarbonate, and brine, and then dried over anhydrous magnesium sulfate. Removal of the solvent, followed by distillation (air-bath temperature 125–130°C/0.5 Torr) of the residual oil, afforded 11.0 g (94%) of a mixture of the acetates **16** and **17**. An analytical sample of each of these compounds was obtained by preparative glc. The *trans* acetate **17** exhibited ir (film): 1730 cm^{-1} (broad); ^1H nmr ($CDCl_3$) δ: 0.99 (s, 3H, tertiary methyl), 1.06 (s, 3H, tertiary methyl), 2.01 (s, 3H, —$OCOCH_3$), 3.63 (s, 3H, —$COOCH_3$), 3.82–4.24 (m, 2H, AB part of ABX system, —CH_2OAc), 5.69 (t, 1H, vinyl proton, J = 4 Hz). *Anal.* calcd. for $C_{17}H_{26}O_4$: C 69.36, H 8.90; found: C 69.10, H 9.10.

The *cis* acetate **16** exhibited ir (film): 1730 cm^{-1} (broad); ^1H nmr ($CDCl_3$) δ: 0.80 (s, 3H, tertiary methyl), 1.19 (s, 3H, tertiary methyl), 2.04 (s, 3H, —$OCOCH_3$), 3.67 (s, 3H, —$COOCH_3$), 3.72–4.20 (m, 2H, AB part of ABX system, —CH_2OAc), 5.87 (t, 1H, vinyl proton, J = 4 Hz). *Anal.* calcd. for $C_{17}H_{26}O_4$: C 69.36, H 8.90; found: C 69.31, H 8.78.

Preparation of the Octalones ***18*** *and* ***19***

To a stirred solution of the mixture of acetates **16** and **17** (4.1 g, 13.9 mmol) in 250 mL of dioxan was added 7.4 g (41.7 mmol) of *N*-bromosuccinimide, 2.8 g (27.8 mmol) of calcium carbonate, and 22 mL of water. The reaction mixture was allowed to stir at room temperature for 20 h while being irradiated with visible light. After the mixture had been filtered through Celite, the filtrate was extracted with ether. The combined ether extract was washed successively with water, aqueous sodium thiosulfate, and brine, and then dried over anhydrous magnesium sulfate. Removal of the solvent, followed by distillation (air-bath temperature 165–170°C/0.25 Torr) of the residual oil, afforded 4.1 g (96%) of a mixture of the two substituted octalones **18** and **19**. An analytical sample of each compound was obtained by preparative glc. The *trans* compound **19** exhibited mp 62–64°C; ir ($CHCl_3$): 1740, 1680, 1610 cm^{-1}; ^1H nmr ($CDCl_3$) δ: 1.12 (s, 3H, tertiary methyl), 1.18 (s, 3H, tertiary methyl), 2.02 (s, 3H, —$OCOCH_3$), 3.71 (s, 3H, —$COOCH_3$), 3.80–4.30 (m, 2H, AB part of ABX system, —CH_2OAc), 6.14 (s, 1H, vinyl proton). *Anal.* calcd. for $C_{17}H_{24}O_5$: C 66.21, H 7.84; found: C 65.96, H 8.00.

The *cis* compound **18** exhibited ir (film): 1730 (broad), 1675, 1610 cm^{-1}; ^1H nmr ($CDCl_3$) δ: 0.90 (s, 3H, tertiary methyl), 1.27 (s, 3H, tertiary methyl), 2.04 (s, 3H, —$OCOCH_3$), 3.70 (s, 3H, —$COOCH_3$), 3.80–4.38 (m, 2H, AB part of ABX system, —CH_2OAc), 6.23 (s, 1H, vinyl proton). *Anal.* calcd for $C_{17}H_{24}O_5$: C 66.21, H 7.84; found: C 66.49, H 7.80.

Preparation of the Ketal Acetate ***23***

To a stirred solution of the mixture of octalones **18** and **19** (5.0 g, 16.2 mmol) in 250 mL of hexamethylphosphoramide was added 18.0 g (0.21 mol) of anhydrous lithium bromide and the resulting mixture was heated to 140–150°C and kept at this temperature for 4 h. During this time, nitrogen was bubbled through the mixture in order to remove the methyl bromide as it was formed. The cooled mixture was diluted with water and then thoroughly extracted with petroleum ether. The combined extract was washed with water and brine and then dried over anhydrous magnesium sulfate. Removal of the solvent, followed by distillation (air-bath temperature 140–150°C/0.35 Torr) of the residual material gave 3.4 g (84%) of decarbomethoxylated material. The latter, which

was shown by glc analysis to be a mixture of three compounds (presumably **20**, **21**, and **22**), was not purified further.

To a solution of the above mixture in benzene (125 mL) was added ethylene glycol (1.3 g, 21 mmol) and a catalytic amount of *p*-toluenesulfonic acid. The solution was refluxed under a Dean-Stark apparatus for 20 h, cooled, washed successively with aqueous sodium bicarbonate and water, and then dried over anhydrous magnesium sulfate. Removal of the solvent, followed by distillation (air-bath temperature 150–160°C/0.3 Torr) of the residual oil, afforded 3.5 g (73% from the octalones **18** and **19**) of the ketal acetate **23**. This material crystallized on standing. Recrystallization of a small amount of this compound from ether – petroleum ether gave an analytical sample; mp 101–102°C; ir ($CHCl_3$): 1730 cm^{-1}; ^1H nmr ($CDCl_3$) δ: 0.87 (s, 3H, tertiary methyl), 1.03 (s, 3H, tertiary methyl), 2.01 (s, 3H, $—OCOCH_3$), 3.74–4.32 (m, 2H, AB part of ABX system, $—CH_2OAc$), 3.95 (s, 4H, ketal protons). *Anal.* calcd. for $C_{17}H_{26}O_4$: C 69.36, H 8.90; found: C 69.19, H 8.83.

Preparation of the Ketal Alcohol ***24***

To a stirred solution of lithium aluminum hydride (1.6 g, 42.1 mmol) in 250 mL of dry tetrahydrofuran was added, dropwise, a solution of 5.0 g (17.0 mmol) of the ketal acetate **23** in 50 mL of dry tetrahydrofuran. The solution was heated under reflux for 1.5 h. The solution was cooled and the excess hydride was destroyed by careful addition of sodium sulfate decahydrate. The resulting mixture was filtered through Celite and the filtrate was evaporated under reduced pressure. The residual material was diluted with ether and the resulting solution was washed with water and brine and dried over anhydrous magnesium sulfate. Removal of the solvent, followed by distillation (air-bath temperature 150–155°C/0.2 Torr) of the residual material, gave 4.0 g (93%) of the ketal alcohol **24**; ir (film): 3400 cm^{-1}; ^1H nmr ($CDCl_3$) δ: 0.83 (s, 3H, tertiary methyl), 1.03 (s, 3H, tertiary methyl), 3.26–3.96 (m, 2H, AB part of ABX system, $—CH_2OH$), 3.92 (s, 4H, ketal protons). *Exact mass.* calcd. for $C_{15}H_{24}O_3$ 252.1725; found: 252.1697.

Preparation of the Ketal Tosylate ***25***

To a solution of the ketal alcohol **24** (4.0 g, 15.8 mmol) in 50 mL of dry pyridine was added 4.5 g (23.7 mmol) of freshly recrystallized *p*-toluenesulfonyl chloride. The solution was stirred at room temperature for 12 h and then poured into 200 mL of ice-water. After the resulting mixture had been stirred for 15 min, it was thoroughly extracted with ether. The combined ether extract was washed successively with ice-cold 1 *N* hydrochloric acid, water, and brine, and then dried over anhydrous magnesium sulfate. Removal of the solvent gave a yellow oil which crystallized on standing. Recrystallization of this material from petroleum ether – acetone gave 5.8 g (90%) of the ketal tosylate **25** as white needles; mp 100–101°C; ir($CHCl_3$): 1600, 1360, 1180 cm^{-1}; ^1H nmr ($CDCl_3$) δ: 0.82 (s, 3H, tertiary methyl), 0.99 (s, 3H, tertiary methyl), 2.46 (s, 3H, aromatic methyl), 3.66–4.32 (m, 2H, AB part of ABX system, $—CH_2OTs$), 3.96 (s, 4H, ketal protons), 7.38, 7.82 (d, d, 2H each, aromatic protons, J = 8.5 Hz). *Anal.* calcd. for $C_{22}H_{30}O_5S$: C 65.01, H 7.44, S 7.88; found: C 65.18, H 7.40, S 7.97.

Preparation of the Keto Tosylate ***9***

To a stirred solution of the ketal tosylate **25** (6.4 g, 15.7 mmol) in a mixture of 125 mL of acetone and 30 mL of water was added, dropwise, 2 mL of sulfuric acid. The solution was warmed to 50°C and stirred at this temperature for 45 min. The cooled solution was poured into ice-cold saturated aqueous sodium bicarbonate and the resulting mixture was extracted with ether. The combined ether extract was washed with water and brine and dried over anhydrous magnesium sulfate. Removal of the solvent yielded 5.6 g (98%) of the keto tosylate **9** as a pale yellow oil which was not purified further; ir (film): 1718, 1360, 1170 cm^{-1}; ^1H nmr ($CDCl_3$) δ: 0.73 (s, 3H, tertiary methyl), 0.93 (s, 3H, tertiary methyl), 2.37 (s, 3H, aromatic methyl), 3.52–4.26 (m, 2H, AB part of ABX system, $—CH_2OTs$), 7.32, 7.73 (d, d, 2H each, aromatic protons, J = 9 Hz).

Preparation of the Tricyclic α,β-*Unsaturated Ketone* ***5***

To a stirred solution of potassium *tert*-butoxide (1.2 g, 15.8 mmol) in 50 mL of dry hexamethylphosphoramide, under an atmosphere of nitrogen, was added, dropwise, a solution of 2.3 g (6.35 mmol) of the crude keto tosylate **9** in 50 mL of dry hexamethylphosphoramide. After the addition was complete, the reaction mixture was allowed to stir for an additional 10 min and was then poured into ice-cold dilute hydrochloric acid. The resulting mixture was extracted thoroughly with petroleum ether. The combined extract was washed several times with water and dried over anhydrous magnesium sulfate. Removal of the solvent, followed by distillation (air-bath temperature 95–110°C/0.2 Torr) gave a colorless oil which crystallized on standing. Recrystallization of this material from ether – petroleum ether afforded 733 mg (61%) of the tricyclic ketone **5**; mp 63–64°C; uv (MeOH): λ_{max} 238 nm (ε = 13 000); ir ($CHCl_3$): 1670, 1640 cm^{-1}; ^1H nmr ($CDCl_3$) δ: 1.13 (s, 6H, tertiary methyls), 5.70 (s, 1H, vinyl proton). *Exact mass* calcd. for $C_{13}H_{18}O$: 190.1361; found: 190.1357.

Preparation of the Dienone ***26***

To a stirred solution of the enone **5** (500 mg, 2.63 mmol) in 70 mL of dioxan was added 3 mL of glacial acetic acid and 890 mg (3.94 mmol) of 2,3-dichloro-5,6-dicyanobenzoquinone. After the resulting mixture had been heated under reflux (nitrogen atmosphere) for 17 h, it was cooled and filtered through a bed of Celite. Most of the solvent was removed (reduced pressure) from the filtrate and the residual material was taken up in ether. The ether solution was washed successively with water, aqueous sodium bicarbonate, and brine, and then dried over anhydrous magnesium sulfate. Removal of the solvent, followed by distillation (air-bath temperature 95–110°C/0.3 Torr) of the residual oil afforded 296 mg (60%) of the cross-conjugated dienone **26** as a colorless oil which crystallized on standing. Recrystallization of a small amount of this material from petroleum ether gave an analytical sample; mp 72–73°C; uv (MeOH): λ_{max} 246 nm (ε = 14 700); ir ($CHCl_3$): 1660, 1630, 1600 cm^{-1}; ^1H nmr ($CDCl_3$) δ: 1.07 (s, 3H, tertiary methyl), 1.13 (s, 3H, tertiary methyl), 6.00 (d, 1H, vinyl proton, J = 1.5 Hz), 6.24 (d of d, 1H, vinyl proton, J = 9.5, 1.5 Hz), 7.00 (d, 1H, vinyl proton, J = 9.5 Hz). *Anal.* calcd. for $C_{13}H_{16}O$: C 82.94, H 8.57; found: C 82.65, H 8.50.

Preparation of the Tricyclic α,β-*Unsaturated Ketone* ***27***

To a cold (0°C), stirred solution of lithium dimethylcuprate (4.5 mmol) in 20 mL of dry ether, under an atmosphere of nitrogen, was added, over a period of 10 min, a solution of the dienone **26** (425 mg, 2.26 mmol) in 15 mL of dry ether. After the solution had been stirred at 0°C for an additional period of 1 h, it was treated with saturated aqueous ammonium chloride and the resultant mixture was stirred for 20 min and then diluted with water and extracted with ether. The combined ether extract was washed with water and brine and then dried over anhydrous magnesium sulfate. Removal of the solvent, followed by distillation (air-bath temperature 105–110°C/0.35 Torr) of the residual oil afforded 375 mg (81%) of the enone **27** as a colorless oil which crystallized on standing. This material exhibited mp 63–64°C; ir ($CHCl_3$): 1655,

1640 cm^{-1}; ^1H nmr ($CDCl_3$) δ: 1.02 (d, 3H, secondary methyl, J = 7 Hz), 1.10 (s, 3H, tertiary methyl), 1.14 (s, 3H, tertiary methyl), 5.71 (s, 1H, vinyl proton). *Anal.* calcd. for $C_{14}H_{20}O$: C 82.30, H 9.87; found: C 81.98, H 10.00.

Preparation of the Dienone 32

To a warm (45°C), stirred solution of the enone **27** (325 mg, 1.59 mmol) in 50 mL of dry tetrahydrofuran and 2 mL of glacial acetic acid, under an atmosphere of nitrogen, was added 530 mg (1.73 mmol) of pyridinium hydrobromide perbromide. After the reaction mixture had been allowed to stir for 1 h, it was cooled and neutralized with sodium bicarbonate. The resulting mixture was extracted thoroughly with ether. The combined extract was washed with water and brine and dried over anhydrous magnesium sulfate. Removal of the solvent gave a crude product which was dissolved in 50 mL of *N,N*-dimethylformamide. To the resulting solution was added 490 mg of lithium bromide and 420 mg of lithium carbonate and the stirred mixture was heated under reflux (nitrogen atmosphere) for 3 h. The reaction mixture was cooled, diluted with water, and extracted with petroleum ether. The combined extract was washed with water and brine and dried over anhydrous magnesium sulfate. Removal of the solvent, followed by distillation (air-bath temperature 125–130°C/0.2 Torr) gave 240 mg of a yellow oil, which was purified further by column chromatography on silica gel. Elution of the column with petroleum ether containing increasing amounts of ether afforded 67 mg of starting material **27** and 100 mg (40%, based on unrecovered starting material) of the pure dienone **32**; ir (film): 1665, 1635 cm^{-1}; ^1H nmr ($CDCl_3$) δ: 1.12 (s, 3H, tertiary methyl), 1.20 (s, 3H, tertiary methyl), 2.02 (d, 3H, vinyl methyl, J = 1.5 Hz), 6.01 (d, 1H, vinyl proton, J = 1.5 Hz), 6.14 (overlapped pair of q, 1H, vinyl proton, J = 1.5 Hz). *Exact mass* calcd. for $C_{14}H_{18}O$: 202.1357; found: 202.1321.

Preparation of the Tricyclic α,β-Unsaturated Ketone 33

To a cold (0°C), stirred solution of lithium dimethylcuprate (0.59 mmol) in 5 mL of dry ether, under an atmosphere of nitrogen, was added, dropwise, a solution of the dienone **32** (30 mg, 0.148 mmol) in 2 mL of ether. After the reaction mixture had been stirred for 5 h at room temperature, it was treated with saturated aqueous ammonium chloride. The resultant mixture was stirred for 20 min, diluted with water, and thoroughly extracted with ether. The combined extract was washed with water and brine and dried over anhydrous magnesium sulfate. Removal of the solvent gave an oil which was subjected to column chromatography on silica gel. Elution of the column with petroleum ether containing increasing amounts of ether gave 14 mg (47%) of starting material **32** and 7 mg (44%, based on unrecovered starting material) of the crystalline enone **33**; mp 53–54°C (lit. (6) mp 54–55.5°C) ir ($CHCl_3$): 1675, 1640 cm^{-1}; ^1H nmr (CCl_4) δ: 1.00, 1.05, 1.10, 1.15 (4 singlets, 3H each, tertiary methyls), 5.66 (s, 1H, vinyl proton). *Exact mass* calcd. for $C_{15}H_{22}O$: 218.1670; found: 218.1692.

Acknowledgement

Financial support for this work from the National Research Council of Canada is gratefully acknowledged.

1. E. Piers, M. Zbozny, and D. C. Wigfield. Can. J. Chem. **57**, 1064 (1979).
2. R. B. Bates, G. Büchi, T. Matsuura, and R. R. Shaffer. J. Am. Chem. Soc. **82**, 2327 (1960); G. Büchi, J. M. Kauffman, and H. J. E. Loewenthal. J. Am. Chem. Soc. **88**, 3403 (1966); G. Büchi, W. Hofheinz, and J. V. Paukstelis. J. Am. Chem. Soc. **91**, 6473 (1969).
3. S. Masamune. J. Am. Chem. Soc. **86**, 288 (1964); **86**, 289 (1964); **86**, 290 (1964); **86**, 291 (1964).
4. D. F. MacSweeney and R. Ramage. Tetrahedron, **27**, 1481 (1971).
5. R. Ranganathan, U. R. Nayak, T. S. Santhanakrishnan, and S. Dev. Tetrahedron, **26**, 621 (1970); J. R. Prahlad and S. Dev. Tetrahedron, **26**, 631 (1970); T. S. Santhanakrishnan, U. R. Nayak, and S. Dev. Tetrahedron, **26**, 641 (1970).
6. R. R. Sobti and S. Dev. Tetrahedron, **26**, 649 (1970).
7. J. A. Marshall and A. E. Greene. J. Org. Chem. **36**, 2035 (1971).
8. H. C. Brown and G. Zweifel. J. Am. Chem. Soc. **83**, 1241 (1961).
9. W. G. Dauben, M. Lorber, and D. S. Fullerton. J. Org. Chem. **34**, 3587 (1969).
10. B. W. Finucane and J. B. Thomson. Chem. Commun. 1220 (1969).
11. J. E. McMurry and G. B. Wong. Synth. Commun. 389 (1972).
12. D. Walker and J. D. Hiebert. Chem. Rev. **67**, 153 (1967).
13. G. H. Posner. Org. React. **19**, 1 (1972).
14. J. A. Marshall and S. F. Brady. J. Org. Chem. **35**, 4068 (1970).
15. E. J. Corey and A. G. Hortmann. J. Am. Chem. Soc. **87**, 5736 (1965).

The ultraviolet photoelectron spectra of C_6F_5X compounds, X = (F, Cl, Br, I, H, CH_3)

BARRY C. TRUDELL AND S. JAMES W. PRICE[1]

Department of Chemistry, University of Windsor, Windsor, Ont., Canada N9B 3P4

Received February 15, 1979

BARRY C. TRUDELL and S. JAMES W. PRICE. Can. J. Chem. 57, 2256 (1979).

This work provides a study of the $1a_{2u}\pi$, $2e_{2g}\sigma$, and $1e_{1g}\pi$ levels of a series of C_6F_5X compounds (X = F, Cl, Br, I, H, CH_3) using ultraviolet photoelectron spectroscopy or more simply PES. The three levels are assigned from the PES spectra using the perfluoro effect. A correlation between the energies of these levels and the energies predicted by CNDO/2 and INDO is presented.

BARRY C. TRUDELL et S. JAMES W. PRICE. Can. J. Chem. 57, 2256 (1979).

Dans ce travail, on rapporte une étude des niveaux $1a_{2u}\pi$, $2e_{2g}\sigma$ et $1e_{1g}\pi$ d'une série de composés C_6F_5X (X = F, Cl, Br, I, H, CH_3) basée sur la spectroscopie photoélectronique ultraviolette ou plus simplement la spectroscopie EP. En se basant sur l'effet perfluoro on peut attribuer les trois niveaux des spectres PE. On présente une corrélation entre les énergies de ces niveaux et les énergies prédites par des calculs CNDO/2 et INDO.

[Traduit par le journal]

Introduction

In two previous works (1, 2) the X-ray photoelectron spectra of the core levels of some C_6F_5X compounds were studied. This is a report furthering the ESCA investigation of six of these molecules. The study utilizes the technique of ultraviolet photoelectron spectroscopy, or more simply PES, to obtain information about the valence levels in C_6F_6, C_6F_5Cl, C_6F_5Br, C_6F_5I, C_6F_5H, and $C_6F_5CH_3$ in the gaseous phase. The ultraviolet spectra of benzene and substituted benzenes have been the topic of study for many workers (3–8). A PES study on the abovementioned perfluoroaromatic compounds has been reported by Turner and co-workers (8), but these spectra were not calibrated with an internal standard and the theoretical discussion is limited.

In the present work, semi-empirical molecular orbital calculations are used as an aid in the interpretation of the spectra obtained.

Experimental

All of the molecules of which ultraviolet photoelectron spectra were taken, i.e. C_6F_5X (X = F, Cl, Br, I, H, CH_3), were obtained from the Imperial Smelting Corporation. They were purified by distillation with only the middle fraction being used in the experimental work.

The spectra were taken from a MacPherson Esca 36 spectrometer employing HeI type radiation at 21.21 eV and gaseous samples. The combined pressure of the sample and internal standard (argon) was always 7×10^{-5} Torr. The argon $3p^3/2$ level (15.81 eV) (9) was used as a calibration. The ionization potentials (binding energies) reported are for the highest peak positions (most number of points) for the particular band, i.e. the vertical ionization potential.

Eigenvalues were calculated using the CNDO and INDO approximations from QCPE No. 290, GEOMO.[2]

Results and Discussion

The spectra for each of the molecules are shown in Fig. 1. The bands in the 14 to 21 eV region represent σ bonding in the ring system, as well as 'π' levels in the fluorine species which are always incorporated to some extent into the σ bonding of the ring system and are of little interest here. The primary consideration in the interpretation of the spectra is the assignment of the levels up to and including the $1a_{2u}\pi$. The assignment of these bands was done using the concept of the perfluoro effect (5, 10, 11). This effect states that on perfluoronation of a particular species, e.g. C_6H_5X to C_6F_5X, the σ molecular orbitals become stabilized by 2 to 3 eV, the π orbitals from about 0 to 1 eV, and the non-bonding orbitals around 1 eV. The assignments of the corresponding C_6H_5X compounds have been well established by various authors (3–8). Figure 2 shows the assignments for the C_6H_5X compounds, as well as their corresponding C_6F_5X partner. Knowing the correct assignments for the C_6H_5X compounds allows for the prediction of the levels in a similar series of C_6F_5X molecules, using the established effect of perfluoronation.

The compounds C_6H_6 and C_6F_5H will be used to demonstrate the procedure for the administration of the perfluoro effect on the assignment of the $1a_{2u}\pi$, $2e_{2g}\sigma$, and $1e_{1g}\pi$ levels. The first three levels

[1]To whom all correspondence should be addressed.

[2]Developed by D. Rinaldi, Université de Nancy. Available through the Quantum Chemistry Program Exchange, University of Indiana.

0008-4042/79/172256-04$01.00/0

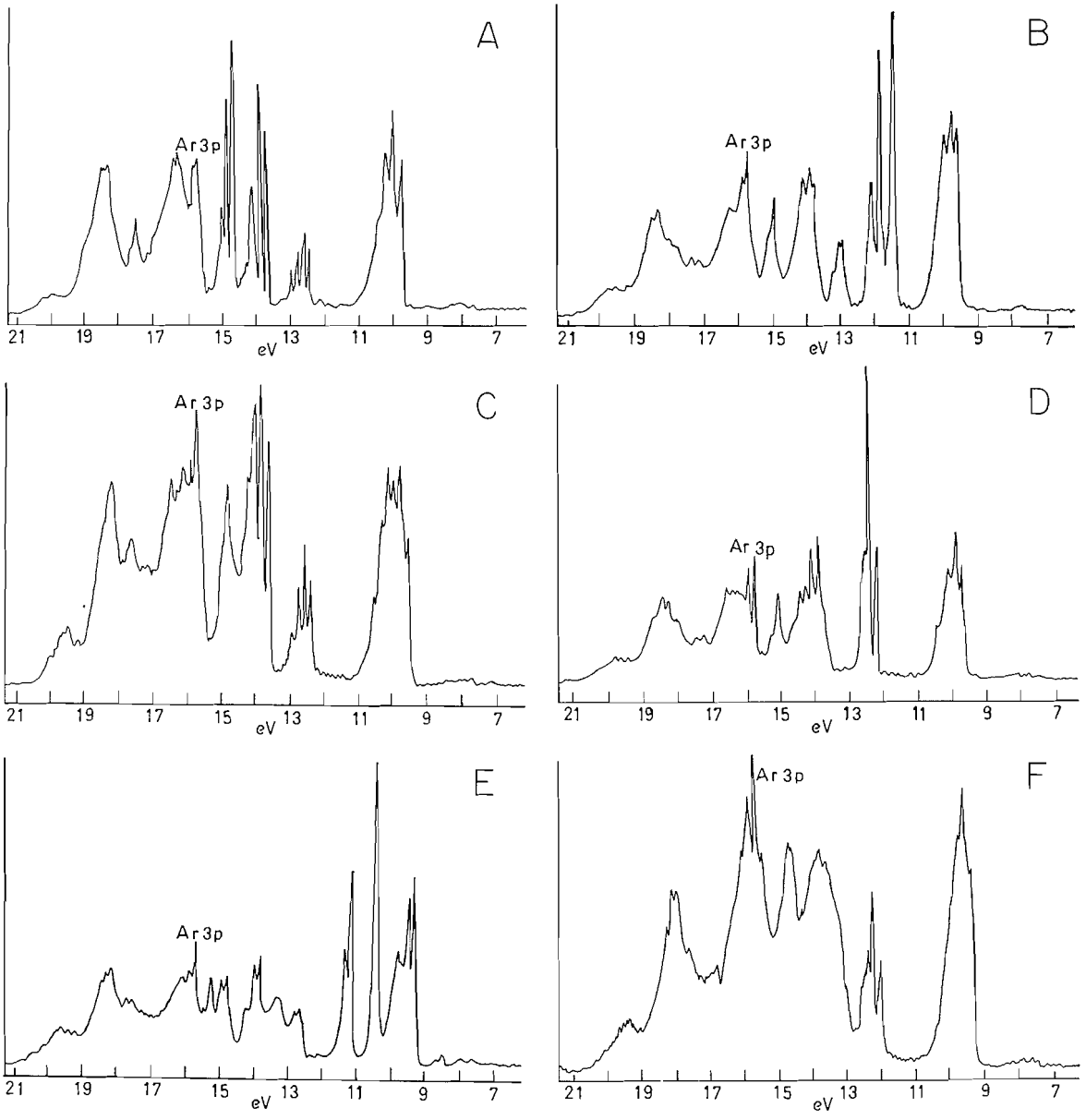

FIG. 1. The photoelectron spectra of (*A*) C_6F_6, (*B*) C_6F_5Br, (*C*) C_6F_5H, (*D*) C_6F_5Cl, (*E*) C_6F_5I, (*F*) $C_6F_5CH_3$.

in C_6H_6 are the $1e_{1g}\pi$ at 9.3 eV, the $2e_{2g}\sigma$ at 11.6 eV, and finally the $1a_{2u}\pi$ band with a binding energy of 12.3 eV. The first three bands in the C_6F_5H spectra have ionization potentials of 9.90, 12.74, and 13.94 eV respectively. A comparison made of the first band in each spectra produces a shift of 0.60 eV which is typical for a π band. Therefore, the first band in C_6F_5H is assigned to the $1e_{1g}\pi$ orbital. The second band in the C_6H_6 spectra appears at 11.6 eV and is labelled $2e_{2g}\sigma$. The perfluoro effect suggests a shift from the σ level of 2 to 3 eV. In the C_6F_5H spectra, there is a band at 13.94 eV which gives a shift of 2.3 eV. This band is then labelled $2e_{2g}\sigma$. The one remaining band in each of the molecules is then matched as the $1a_{2u}\pi$ level and gives a shift of approximately 0.4 eV, which is reasonable for a π band.

Various lone pair or non-bonding levels which lie within the three levels of interest here have also been assigned where applicable. (Diagrams of the assign-

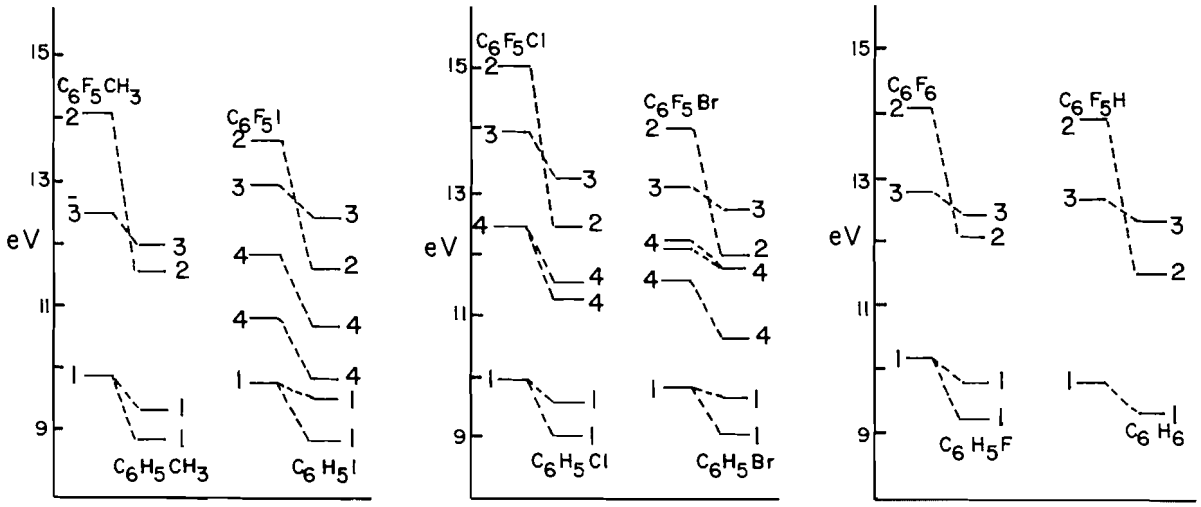

FIG. 2. Correlation of the energy levels using the perfluoro effect. (*1*) $1e_{1g}\pi$, (*2*) $2e_{2g}\sigma$, (*3*) $1a_{2u}\pi$, (*4*) lone pair.

ments for all of the compounds are shown in Fig. 2.)

Since the assignments have been made, some comparisons may be made. First of all, as in the XPS work, all of the binding energies of the various levels in the perfluorinated compounds are higher than in the unfluorinated species. Also, in all cases, the splitting of the $1e_{1g}\pi$ level is smaller or non-existent in the perfluorosystems. It is interesting to compare the ionization potential of the $1e_{1g}\pi$ level in this series of molecules. If the value of ionization potential for the $1e_{1g}\pi$ level in C_6F_5H is taken as a reference level, i.e. the hydrogen substituent has not altered the ionization potential of the $1e_{1g}\pi$ level, it is found that the other binding energies for the same level in the other compounds fall on either side of the reference level, depending on the strength of the inductive and mesomeric effects of the substituent. The first four, C_6F_5X (X = F, Cl, Br, I), follow a decreasing trend due to electronegativity. However, the Br and I substituting species have binding energies less than that of C_6F_5H, indicating that the mesomeric effect is predominant in these cases. The CH_3 group donates charge, both inductively and mesomerically, but very weakly and accordingly has a slightly lower ionization potential than C_6F_5H.

Although the assignments for the $1a_{2u}\pi$, $2e_{2g}\sigma$, and $1e_{1g}\pi$ levels have been made via the perfluoro effect, it was decided to try and correlate the experimental binding energies with the calculated eigenvalues, using CNDO/2 and INDO approximations and Koopmans' (12) theorem. A comparison between the experimental and theoretical values is shown in Table 1. Although the INDO results predict slightly better (lower) energies, both the CNDO/2 and INDO fail to take into account re-

TABLE 1. The CNDO/2, INDO, and experimental values for the ionization potentials of the $1a_{2u}\pi$, $2e_{2g}\sigma$, and $1e_{1g}\pi$ levels in C_6F_5X (X = F, Cl, Br, I, H, CH_3)

		Ionization potential		
Compound	Level	CNDO/2	INDO	Experimental
C_6F_6	$1e_{1g}\pi$	13.48	13.01	10.14
	$1a_{2u}\pi$	17.98	17.14	12.81
	$2e_{2g}\sigma$	17.24	16.60	14.08
C_6F_5Cl	$1e_{1g}\pi$	13.00	12.72	9.94
	$1a_{2u}\pi$	18.96	18.18	13.98
	$2e_{2g}\sigma$	17.98	16.05	15.14
C_6F_5Br[a,b]	$1e_{1g}\pi$			9.57
	$1a_{2u}\pi$	—	—	13.14
	$2e_{2g}\sigma$			14.01
C_6F_5I[b]	$1e_{1g}\pi$	13.32		9.54
	$1a_{2u}\pi$	18.16	—	12.85
	$2e_{2g}\sigma$	15.17		13.48
C_6F_5H	$1e_{1g}\pi$	13.43	12.95	9.90
	$1a_{2u}\pi$	18.23	17.38	12.74
	$2e_{2g}\sigma$	16.53	16.01	13.94
$C_6F_5CH_3$	$1e_{1g}\pi$	12.89	12.47	9.81
	$1a_{2u}\pi$	17.30	16.61	12.44
	$2e_{2g}\sigma$	16.58	16.11	14.04

[a]CNDO/2 eigenvalues predicted for C_6F_5Br could not be assigned to specific levels.
[b]INDO calculations for Br and I were not possible.

organization and correlation effects and, mainly for these reasons, all of the eigenvalues are about 4 to 5 eV too high. Another difficulty in these molecular orbital calculations noted by other authors (13–16) is that in most cases the σ and π levels are not predicted in their correct order. In order to correct this, a 20% reduction in the eigenvalues for the π levels only seems to solve the problem. After the compensation, ordering in agreement with that

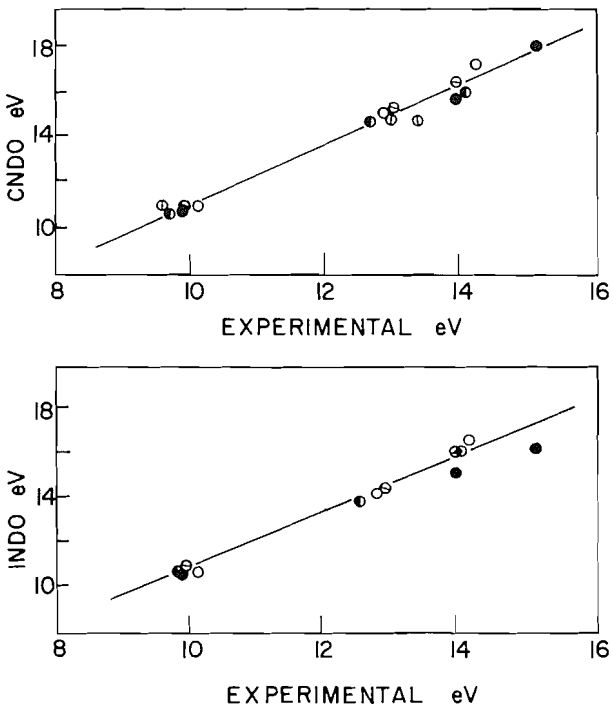

FIG. 3. Plots of CNDO and INDO eigenvalues versus the experimental ionization potentials for the $1e_{1g}\pi$, $1a_{2u}\pi$, and $2e_{2g}\sigma$ levels. ○ C_6F_6, ● C_6F_5Cl, ◫ C_6F_5I, ⊖ C_6F_5H, ◐ $C_6F_5CH_3$.

predicted by the perfluoro effect is obtained in all cases. Plots of experimentally determined binding energies versus theoretical results are shown in Fig. 3. The correlation in both cases is quite reasonable.

Acknowledgements

The authors would like to thank Mr. R. Lazier for his assistance in running the spectra, Mr. R. M. Baillargeon for his cooperation in setting up the programmes used in this paper, and Dr. C. S. Lin for many fruitful discussions. This work was supported by a grant from the National Research Council of Canada.

1. B. C. TRUDELL and S. J. PRICE. Can. J. Chem. **55**, 1275 (1977).
2. B. C. TRUDELL and S. J. PRICE. Can. J. Chem. **56**, 538 (1978).
3. I. D. CLARK and D. C. FROST. J. Am. Chem. Soc. **89**, 244 (1967).
4. A. O. BAKER, D. P. MAY, and D. W. TURNER. J. Chem. Soc. 22 (1968).
5. C. R. BRUNDLE, M. B. ROBIN, and N. A. KUEBLER. J. Am. Chem. Soc. **94**, 1466 (1972).
6. T. P. DEBIES and J. W. RABALAIS. J. Electron Spectrosc. Relat. Phenom. **1**, 355 (1972/73).
7. T. KOBAYASHI and S. NAGAKURA. Bull. Chem. Soc. Jpn. **47**, 2563 (1974).
8. D. W. TURNER, C. BAKER, A. D. BAKER, and C. R. BRUNDLE. *In* Molecular photoelectron spectroscopy. John Wiley and Sons Ltd. 1970.
9. K. SIEGBAHN. J. Electron Spectrosc. Relat. Phenom. **2**, 295 (1973).
10. C. R. BRUNDLE and M. B. ROBIN. J. Am. Chem. Soc. **92**, 5550 (1970).
11. C. R. BRUNDLE, M. B. ROBIN, N. A. KEUBLER, and H. BOSCH. J. Am. Chem. Soc. **94**, 1451 (1972).
12. T. KOOPMANS. Physica, **1**, 104 (1933).
13. D. W. DAVIES. Chem. Phys. Lett. **2**, 173 (1968).
14. J. E. BLOOR and D. L. BREEN. J. Phys. Chem. **72**, 716 (1968).
15. D. C. FROST, F. G. HERRING, C. A. MCDOWELL, M. R. MUSTAFA, and J. S. SANDHU. Chem. Phys. Lett. **2**, 663 (1968).
16. G. R. BRANTON, D. C. FROST, F. G. HERRING, C. A. MCDOWELL, and J. A. STENHOUSE. Chem. Phys. Lett. **3**, 581 (1969).

The hydrolysis of coumarin diethyl acetal and the lactonization of coumarinic acid ethyl ester. The partitioning of tetrahedral intermediates generated from independent sources

R. A. McClelland, R. Somani, and A. J. Kresge

Department of Chemistry, University of Toronto, Scarborough College, West Hill, Ont., Canada M1C 1A4

Received February 19, 1979

R. A. McClelland, R. Somani, and A. J. Kresge. Can. J. Chem. 57, 2260 (1979).

The hydrolysis of coumarin diethyl acetal to coumarin proceeds via two detectable intermediates. A short-lived transient is observed in strongly acidic solutions (pH < 2.5); this is the oxocarbonium ion intermediate of the hydrolysis. That this cation can be detected suggests unusual stability, a fact which can be explained in terms of its pyrilium ion nature. A long-lived intermediate is also observed; kinetic and spectral evidence suggest that this is coumarinic acid ethyl ester. The lactonization of this ester shows a change in rate-determining step as the pH is varied. A corresponding change in products is found in the acetal hydrolysis, the coumarinic acid ester being the major product at high pH, with coumarin the major product at low pH. Both observations can be explained in terms of different modes of partitioning of cationic and neutral tetrahedral intermediates. Analysis in quantitative terms shows that the same tetrahedral intermediate is generated in the two different cases.

R. A. McClelland, R. Somani et A. J. Kresge. Can. J. Chem. 57, 2260 (1979).

L'hydrolyse du diéthylacétal de la coumarine en coumarine se produit via deux intermédiaires que l'on a pu détecter. En solutions fortement acides (pH < 2.5) on observe une espèce provisoire de courte existence; il s'agit de l'ion oxocarbonium intermédiaire dans l'hydrolyse. Le fait que ce cation peut être détecté suggère qu'il est d'une stabilité exceptionnelle qui serait due à sa nature liée à l'ion pyrilium. On observe aussi un intermédiaire de vie plus longue; les données cinétique et spectrale suggèrent qu'il s'agit de l'ester éthylique de l'acide de coumarinique. Si l'on fait varier le pH, il se produit un changement dans l'étape qui détermine la vitesse de lactonisation de cet ester. On note un changement correspondant dans la nature des produits d'hydrolyse de l'acétal; l'ester de l'acide coumarinique est le produit majoritaire à pH élevé alors que la coumarine prédomine à des pH plus faibles. On peut expliquer les deux observations en termes de modes différents de bris des intermédiaires tétraédriques cationique et neutre. Une analyse en termes quantitatifs démontre que le même intermédiaire tétraédrique est généré dans les deux cas différents.

[Traduit par le journal]

The lactonization of coumarinic acids has now seen considerable kinetic investigation. This is in part due to the fact that certain substituted coumarinic acids lactonize with a remarkably enhanced rate (1). This reaction also shows an interesting change in rate-determining step, attributed to the different modes of partitioning of the various protonic forms of the tetrahedral intermediate (2–4).

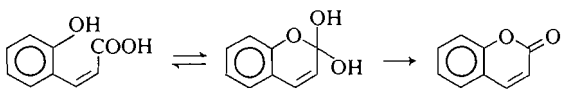

Our interest in this system was prompted by an earlier report (5) that the hydrolysis of 3-phenylcoumarin dimethyl acetal[1] to 3-phenylcoumarin proceeds via an observable intermediate, this intermediate being assigned a hemiacetal[1] structure. This is the tetrahedral intermediate of the lactonization of a

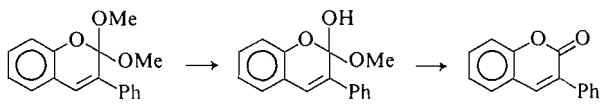

coumarinic acid ester, and bears a close resemblance to the tetrahedral intermediates of the lactonization of the coumarinic acids themselves. Molecules containing the functional group $R'C(OR)_2OH$ have in general been implicated as intermediates in a number of important reactions: ester hydrolysis and alcoholysis, lactonization, ortho ester hydrolysis. However, such a grouping is found in stable species only under special circumstances (6–9), and there are few reports, other than that of the coumarin study (5), of their observation as transient intermediates (10–15). With our involvement in this latter area (11–15), we felt a reinvestigation of the coumarin system was in order, and we report here the results of our study.

Experimental

2-Ethoxy-5,6-benzopyrilium Fluoroborate

Coumarin (0.01 mol) and triethyloxonium fluoroborate

[1]Coumarin acetals are in fact ortho esters. Similarly the hemiacetals are also hemiortho esters or hydrogen ortho esters.

0008-4042/79/172260-08$01.00/0

(0.01 mol) were dissolved in dry methylene chloride (30 mL) and stirred overnight. Dry ether (50 mL) was added, and the resultant white solid filtered in a glove box with exclusion of moisture. The salt was washed with dry ether and the remaining solvent removed in a vacuum desiccator. The salt had mp 90–92°C; nmr (100% H_2SO_4, ext. $(Me)_4Si$) δ: 8.43 (d, 1H, J = 9 Hz), 7.5 (broad s, 4H), 6.87 (d, 1H, J = 9 Hz), 4.77 (q, 2H, J = 7 Hz), 1.33 (t, 3H, J = 7 Hz).

Coumarin Diethyl Acetal

The above salt was dissolved in a minimum amount of dry methylene chloride and added to a stirred solution of sodium ethoxide (excess) in ethanol at 0°C. After 1 h of additional stirring, most of the solvent was removed on a rotary evaporator. Ether and water were added, the ether was dried (K_2CO_3), and distilled. Coumarin diethyl acetal had bp 104°C (0.5 Torr); nmr ($CDCl_3$, $(Me)_4Si$) δ: 6.9–7.2 (m, 4H), 6.75 (d, 1H, J = 10 Hz), 5.72 (d, 1H, J = 10 Hz), 3.67 (q, 4H, J = 7 Hz), 1.18 (t, 6H, J = 7 Hz). *Anal.* calcd. for $C_{13}H_{16}O_3$: C 70.89, H 7.32; found: C 71.12, H 7.37.

Kinetics

(a) Coumarin Diethyl Acetal to Coumarin (pH > 6)

The absorbance increase at λ = 281 nm was monitored. First-order kinetic plots were excellently linear over several half-lives. Rate constants were evaluated as the slopes of plots of ln $(A_\infty - A)$ versus time.

(b) Pyrilium Ion Formation and Decomposition

Coumarin diethyl acetal dissolved in 0.001 M NaOH was mixed in a Durrum–Gibson stopped-flow apparatus with excess HCl, and the oscilloscope trace corresponding to the change in absorbance at λ = 325 nm recorded. This wavelength corresponds to a maximum absorbance of the 2-ethoxy-5,6-benzopyrilium ion. In strongly acidic solutions there is a rapid increase in absorbance at this wavelength, followed by a slower decrease. Rate constants representing the formation of the ion were obtained from the increase in absorbance using the Guggenheim approach over the first three to four half-lives of the reaction. Rate constants for the decay of the ion were obtained from the absorbance decrease from a plot of ln $(A - A_\infty)$ versus time. The initial absorbance readings used in constructing this plot were obtained only after a time corresponding to six to eight half-lives for the formation reaction. Rate constants were obtained only in acids where the formation process is at least 10 times as fast as the decomposition process.

(c) Coumarinic Acid Ethyl Ester to Coumarin

Coumarin diethyl acetal was dissolved in 0.0005 M HCl. After waiting 25 s this solution was mixed with an equal volume of an aqueous HCl solution or an aqueous buffer. The absorbance decrease at 240 nm was monitored; rate constants were obtained as the slopes of plots of ln $(A - A_\infty)$ versus time.

Partitioning of Hemiacetal in Acetal Hydrolysis

A stock solution of coumarin diethyl acetal (0.22 mol L^{-1}) in dry acetonitrile was prepared, and used throughout. A sample of this solution (10 μL) was added to aqueous HCl or aqueous buffer in a 10 mL volumetric flask. After waiting a time corresponding to six half-lives of $k_1[H^+]$ (see Results and Discussion) the absorbance reading at 240 nm was recorded. A second absorbance reading was obtained in several cases by allowing this solution to stand until any coumarinic acid ester was converted to coumarin. This reading was the same, within experimental error, in each case.

Results and Discussion

In solutions with pH > 6 coumarin diethyl acetal **1** is cleanly converted to coumarin **2** with no detectable build-up of any intermediate. This reaction is first order; observed first-order rate constants follow the equation (see also Fig. 1)

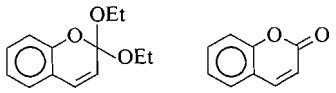

1 **2**

$$k_{obsd}(pH > 6) = k_{H^+}{}^1[H^+] + k_0{}^1 + k_{HA}{}^1[HA]$$

with $k_{H^+}{}^1 = 6.63 \times 10^3\ M^{-1}\ s^{-1}$ and $k_0{}^1 = 1.6 \times 10^{-4}\ s^{-1}$ (25°C, μ = 1.0). The term in HA represents general acid catalysis, which is weak (phosphate buffer) but detectable.

In solutions more acidic than pH 6, there can be detected two intermediates in the overall hydrolysis of coumarin diethyl acetal to coumarin, a short-lived species to which we assign the pyrilium ion structure **3**, and a long-lived species to which we assign the structure of the coumarinic acid ester **4**. The hemiacetal **5** is not observed, although it must be formed during the course of the reaction. In the following

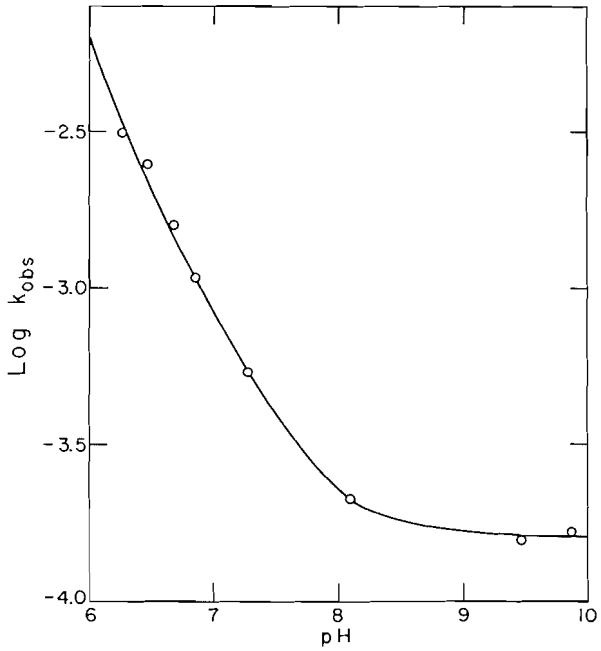

FIG. 1. First-order rate constants for the conversion of coumarin diethyl acetal to coumarin (25°C, μ = 1.0). The points are experimental, and have been obtained after extrapolation to zero buffer concentration. The curve is calculated from $k_{obsd} = 6.63 \times 10^3[H^+] + 1.6 \times 10^{-4}$.

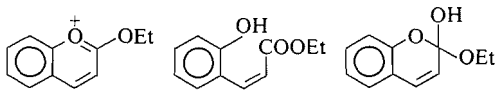

3 4 5

discussion we will present our evidence that structures **3** and **4** do represent the two intermediates. The formation of the ester **4** is particularly significant. The hemiacetal **5** can break down in two directions, forming ester **4** by ring opening or forming coumarin **2** by loss of the ethoxy group. As we will describe, this partitioning is pH dependent, and we have been able to place a quantitative measure on the partitioning, based on the ratio of **4**/**2**. The ester **4**, once formed, lactonizes to coumarin. This process is very rapid at pH > 6, but is relatively slow in more acidic solutions, and we have constructed the rate–pH profile. This lactonization, like that of the coumarinic acids (2–4), shows a change in rate-determining step, attributable to a change in the partitioning of the hemiacetal **5** which must be an intermediate. With an appropriate kinetic analysis, we have again obtained a quantitative measure of the partitioning. This means that there are available two independent measures of the partitioning of the same intermediate.

Pyrilium Ion Intermediate

When coumarin diethyl acetal dissolved in dilute NaOH is mixed with HCl solutions in a stopped-flow spectrophotometer, a short-lived transient is observed. The uv spectrum of this species was constructed in 0.5 *M* HCl (Fig. 2), where its rate of formation is much greater than its rate of decay. We propose that this transient is the ion **3**, the oxocar-

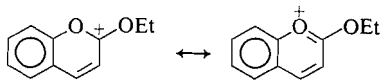

3

bonium ion intermediate of the acetal hydrolysis. This cation can be obtained in stable form as its fluoroborate salt by the alkylation of coumarin with triethyloxonium fluoroborate. The salt is relatively stable in 60% H_2SO_4 (half-life ca. 4 h). The uv spectrum in this acid is given in Fig. 2 and obviously bears a close resemblance to the spectrum of the transient species.

First-order rate constants for the formation of the pyrilium ion from coumarin diethyl acetal and its subsequent decomposition were measured, and are given in Table 1. The ion forms in a reaction which is first order in hydronium ion. The value of the second-order rate constant ($k_{H^+} = k_{obsd}/[H^+]$) is the same, within experimental error, as the rate constant $k_{H^+}{}^1$ obtained in the conversion of coumarin diethyl acetal to coumarin at high pH. The implication of this observation is that in the latter reaction the rate-limiting step in the overall conversion to coumarin is the formation of the pyrilium ion, all subsequent reaction steps being rapid. The pyrilium ion decays in a reaction which is independent of acidity. In simple terms, the pH-independent rate constant represents the hydration of the oxocarbonium ion, forming the hemiacetal.[2]

Perhaps the most significant aspect of our observation of the pyrilium ion intermediate is the very fact that it is observed. The life-times in general of the oxocarbonium ion intermediates of acetal and ortho ester hydrolysis have now been established to be short (16, 17) with the ion having a sufficient life-time to be seen only in cases where there is present some other structural feature which imparts unusual stability to the cation (18). There is such a stabilizing feature here, inasmuch as the present oxocarbonium ion is in fact an aromatic pyrilium ion. Herschfield and Schmir (3) have also suggested that cations of this type are unusually stable. The above authors propose that the extra stability provides the driving force for the cationic tetrahedral intermediate to break down to coumarin (protonated coumarin) rather than ring open.

Coumarinic Acid Ethyl Ester Intermediate

There is also observed a second longer-lived intermediate, whose structure we propose to be the ester **4**. This intermediate is most clearly observed, for reasons which will become apparent later, in dilute acids (pH 3–5). In Fig. 2 we display a uv spectrum obtained 20 s after dissolving coumarin diethyl acetal in 0.0005 *M* HCl. In this acid, the acetal has a half-life of about 3 s (based on $k_{H^+}{}^1$) and the pyrilium ion is also rapidly hydrated. The spectrum recorded, however, is not that of coumarin, although there is a slow spectral change (half-life 720 s in 0.0005 *M* HCl) resulting eventually in a spectrum identical to that of coumarin. Candidates for this second intermediate are the hemiacetal **5** and the ester **4**. The uv spectrum of the hemiacetal should be fairly similar to that of coumarin diethyl acetal, since the only structural difference involves the replacement of an ethoxy group by a hydroxy group. The spectrum observed, however, shows none of the characteristics of the acetal spectrum, and in fact bears a much closer resemblance to the spectrum of coumarin itself. The

[2]Neither of the observed products of this reaction are the hemiacetal itself. This means that the reaction being observed represents (at least) two stages, hydration to form hemiacetal, followed by the decomposition of this species. The interpretation that the rate of decay of pyrilium ion is equal to the hydration rate is valid only if the hydration stage is rate-limiting, that is, if the hemiacetal goes on to products rather than returns to ion.

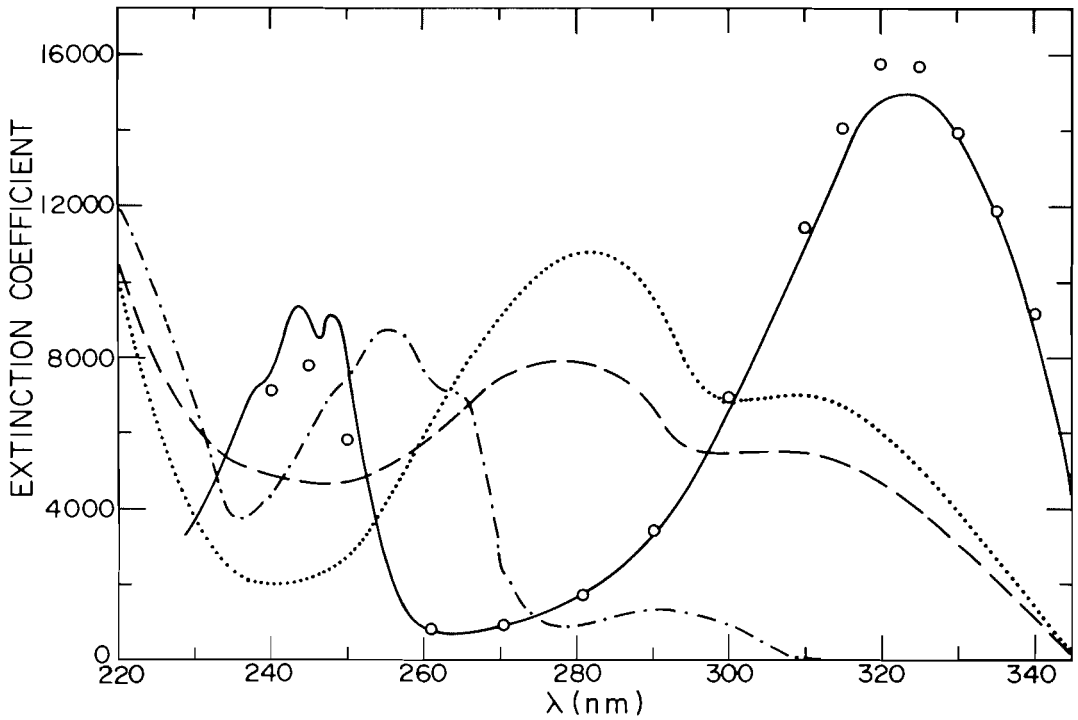

FIG. 2. Ultraviolet spectra. (---) Coumarin diethyl acetal, 0.001 *M* NaOH. (—) 6-Ethoxy-2,3-benzopyrilium borofluorate, 60% H_2SO_4. (○) Short-lived transient, based on absorbance readings obtained on the stopped-flow apparatus 5 ms after mixing coumarin diethyl acetal in 0.001 *M* NaOH with 1 *M* HCl. (- - -) Long-lived transient, spectrum obtained in 0.0005 *M* HCl. (····) Coumarin.

TABLE 1. First-order rate constants (25°C, ionic strength = 1.0 *M*) for the formation and decay of the 2-ethoxy-5,6-benzopyrilium ion

[HCl] (*M*)	k_{form} (s^{-1})	$k_{form}/[H^+]^a$ ($M^{-1}\ s^{-1}$)	$k_{decay}{}^b$ (s^{-1})
0.5	—	—	14.3
0.1	—	—	13.9
0.05	3.1×10^2	6.2×10^3	15.1
0.04	2.4×10^2	6.0×10^3	14.4
0.03	1.8×10^2	6.0×10^3	13.9
0.02	1.3×10^2	6.5×10^3	13.4

[a]Average, $6.2 \times 10^3\ M^{-1}\ s^{-1}$.
[b]Average 14.2 s^{-1}.

coumarinic acid ester, on the other hand, has the same basic chromophoric system as coumarin, and its uv spectrum should be similar.

As will become apparent, the intermediate spectrum discussed above represents a mixture (of the ester and coumarin), and thus our spectral argument for the identity of the intermediate might be open to question. A second, and perhaps more convincing, argument is based on a consideration of the kinetics of the conversion of the second intermediate to coumarin, a process which according to our proposal represents the lactonization of coumarinic acid ethyl ester. Our kinetic approach was to dissolve coumarin diethyl acetal in 0.0005 *M* HCl in order to generate the second intermediate. After waiting 20–30 s this solution was mixed with various acids or buffers, and rate constants obtained for the conversion to coumarin. The rate–pH profile is depicted in Fig. 3, where it also compared with the profile obtained by Herschfield and Schmir (3) for the lactonization of coumarinic acid. Although the actual numbers themselves are different, there is obviously a close similarity in these two profiles. In particular both include a break at pH 2–3 where a change in rate-determining step occurs (3). It is doubtful that hemiacetal decomposition would follow such a rate–pH profile (13–15), and obviously far more consistent if what we are following is the lactonization reaction.

We feel that in the previous study involving 3-phenylcoumarin diethyl acetal (5), the intermediate that was observed was also the coumarinic acid ester, and not the hemiacetal. Unfortunately the presence, and identity, of the intermediate in that study was based only on the fact that the hydrolysis of the acetal to 3-phenylcoumarin does not exhibit clean isobestic points. No detailed uv spectral analysis was presented. Rate constants, however, were reported for

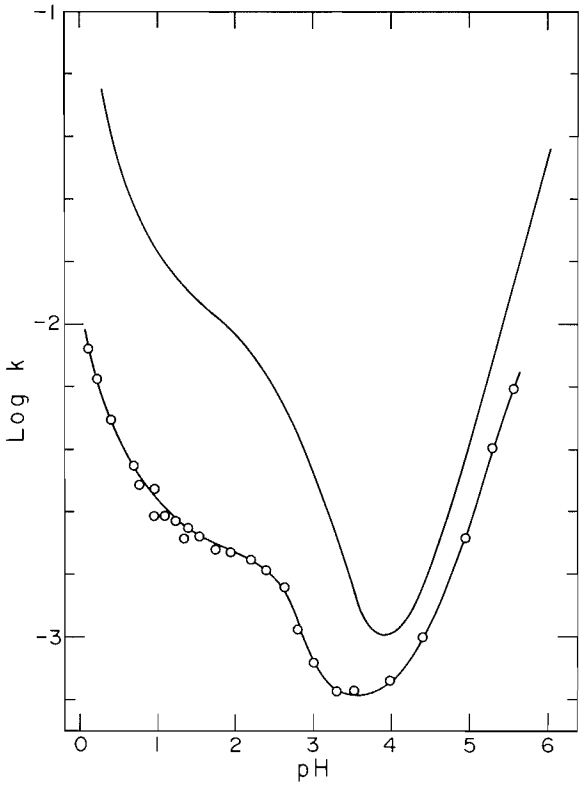

FIG. 3. First-order rate constants for the conversion of coumarinic acid ethyl ester to coumarin (25°C, μ = 1.0). The points are experimental, while the curve is based on the equation presented in the text (3). The upper curve represents first-order rate constants for the conversion of coumarinic acid to coumarin (3), in terms of the neutral substrate.

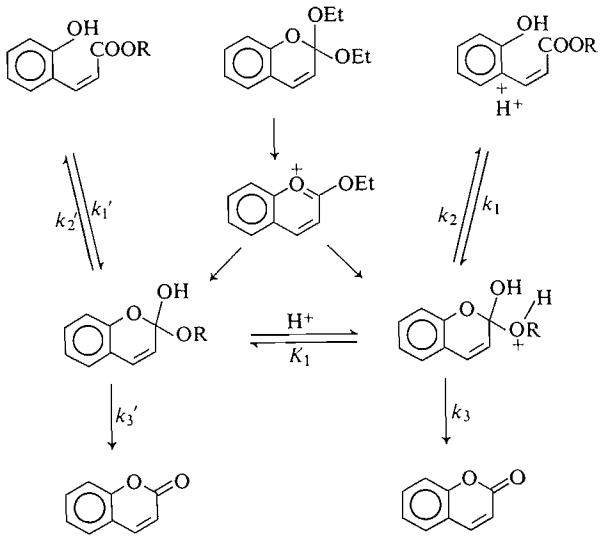

SCHEME 1

TABLE 2. Rate and equilibrium constants for the lactonization of coumarinic acid ethyl ester and coumarinic acid (μ = 1.0)

Constant	Coumarinic acid ethyl ester (25°C)	Coumarinic acid (30°C)[a]
pK'	2.79	2.63
P^+	0.993	0.983
P^0	0.045	0.042
k_1, s^{-1}	0.0079	0.078
k_{OH^-}, $M^{-1}\ s^{-1}$	1.1×10^6	1.8×10^6

[a]All data from ref. 3.

the conversion of the intermediate to 3-phenylcoumarin (5), and these are of the same order of magnitude as the rate constants that we obtain for the conversion of our second intermediate to coumarin.

Hemiacetal Partitioning – Lactonization

Herschfield and Schmir (3) propose that the break in the rate–pH profile for the lactonization of a coumarinic acid is caused by a change in rate-determing step. Scheme 1 shows the mechanism suggested by these workers, with the addition of a further route to the tetrahedral intermediate from the acetal. This scheme does not account for the base-catalyzed lactonization observed above pH 4. This mechanism for lactonization produces the steady-state rate equation

$$k_{obsd} = \frac{k_1([H^+]P^+ + K'P^0)([H^+] + K'(1 - P^0)/(1 + P^+))}{[H^+] + K'}$$

where $P^+(= k_3/(k_2 + k_3))$ and $P^0(= k_3'/k_2' + k_3'))$ are the partitioning ratios for the cationic and neutral tetrahedral intermediate respectively, and $K' = K_1(k_2' + k_3')/(k_2 + k_3)$. This equation contains four unknown constants. Values of these constants which best fit our experimental data are given in Table 2 along with the values for the lactonization of coumarinic acid (3). There is a close similarity in the two sets of data, consistent with our suggestion that the two processes are very similar. The one constant which differs significantly is k_1, which is 10 times smaller for the ester than for the acid. This refers to the acid-catalyzed nucleophilic addition of the phenol hydroxyl to the carbonyl. The difference in rate constant is probably just a reflection of the different susceptibilities of the acid and ester to nucleophilic attack. As another example, acid-catalyzed oxygen exchange of acetic acid (20) proceeds about an order of magnitude more rapidly than the acid-catalyzed hydrolysis of ethyl acetate (21).

The change in rate-determining step is most clearly seen in considering the partitioning ratios. In strongly acidic solution the cationic tetrahedral intermediate is the species which undergoes decomposition, and this breaks down preferentially to coumarin ($P^+ \approx 1$). The formation of the tetrahedral intermediate is therefore rate-determining in the lactonization. At higher pH, the neutral tetrahedral intermediate is involved, and this breaks down preferentially to coumarinic acid or its ester ($P^0 \approx 0$). The rate-determining step in the lactonization is therefore the breakdown of the tetrahedral intermediate to coumarin.

Hemiacetal Partitioning – Acetal Hydrolysis

This behaviour has important consequences when the initially formed products in the hydrolysis of the acetal are considered. There is little doubt that this hydrolysis proceeds with initial loss of one of the ethoxy groups, generating the intermediate pyrilium ion. This must then be followed by hydration of the ion to produce a hemiacetal, a species which is in fact the tetrahedral intermediate of the lactonization. With a change in rate-determining step in the lactonization, there should be a corresponding change in products in the acetal hydrolysis. This is indeed the case. In less acidic solutions, such as 0.0005 *M* HCl, the uv spectrum at the intermediate stage is significantly different from that of coumarin. This can be attributed to a significant amount of the ester intermediate being formed. In 0.1–1.0 *M* HCl, a spectrum very close to that of coumarin appears immediately. Since the ester is not converted to coumarin during the time required to record this spectrum, we can only conclude that there is little ester being formed in acid, that is, the hemiacetal breaks down preferentially to coumarin. (We verify here incidentally another suggestion of Herschfield and Schmir (3). The symmetry properties of the rate equation for the lactonization are such that it is not possible to assign the nature of the rate-limiting step at high pH and low pH on the basis of the kinetics alone; a second mathematical solution exists which equally satisfies the kinetic data, but which predicts the opposite modes of partitioning. The above authors assigned the nature of the rate-determining steps on the basis of analogy. Our results offer concrete proof that the assignment is correct.)

The partitioning of the intermediate of the acetal hydrolysis can be put on a more quantitative basis. To do this we have added acetal to a series of solutions of differing pH, and measured at 240 nm the apparent extinction coefficient (absorbance/concentration) after a time corresponding to six half-lives of the first reaction stage (based on $k_{H^+}[H^+]$). In solutions with pH < 4 this means that the measurement is being taken before a significant amount of ester can lactonize to coumarin, so that we are observing the actual partitioning of the intermediate. As is seen in Fig. 4 the experimental data trace out a sigmoidal titration curve; the curve drawn in the figure is based on the standard equation for such a curve, and represents the best fit of this equation to our data. This curve has limiting values of ε_{app} of 2020 and 5360 in acid and base respectively, with an inflection point at pH = 2.75.

In terms of Scheme 1, the following equation is produced:

$$\varepsilon_{app} = \frac{((1 - P^+)\varepsilon_E + P^+\varepsilon_C)[H^+] + ((1 - P^0)\varepsilon_E + P^0\varepsilon_C)K'}{[H^+] + K'}$$

where P^+, P^0, and K' are the same as defined previously, and ε_E and ε_C are the extinction coefficients at 240 nm of ester and coumarin respectively. This equation does take the form of a sigmoidal titration curve, with an inflection point at pH = pK'. It can immediately be noted that there is excellent agreement of the value of pK' obtained from the titration curve (2.75) and the pK' obtained in the kinetic analysis of the lactonization (2.79). The equation also predicts a limiting ε_{app} in acid of $(1 - P^+)\varepsilon_E + P^+\varepsilon_C$. The observed value is in fact very close to the extinction coefficient of coumarin itself, a value which can be accurately obtained using the same solutions used to determine ε_{app}, simply by allowing these solutions to stand until any ester is converted to coumarin (see the points △ in Fig. 4). The titration curve therefore predicts $P^+ \approx 1$, in agreement again with the more precisely determined kinetic value of $P^+ = 0.994$. The limiting value of ε_{app} at high pH is given by $(1 - P^0)\varepsilon_E + P^0\varepsilon_C$. Unfortunately we were unable to obtain a value of ε_E, since all attempts to prepare pure samples of this ester failed. This means that a value of P^0 cannot be calculated from the titration curve. The kinetic value is 0.045, so that the limiting ε_{app} in base must be close to ε_E.

Partitioning of Tetrahedral Intermediates Generated from Different Sources

However, simply on the basis of the agreement in the independently obtained pK' values we can con-

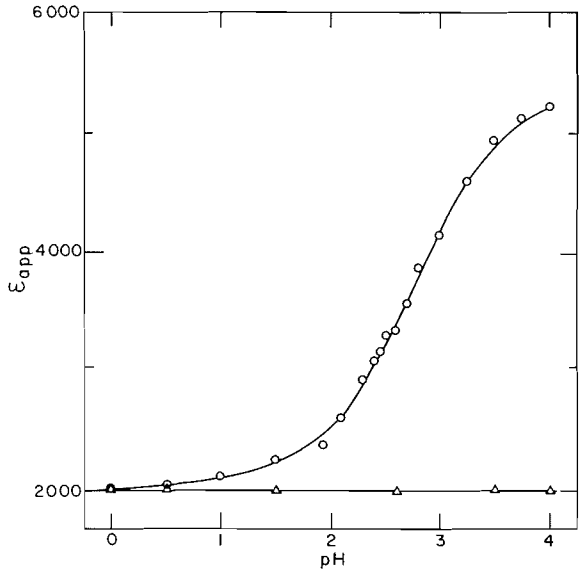

FIG. 4. Apparent extinction coefficient (240 nm) based on intermediate absorbance on dissolving coumarin diethyl acetal in aqueous solution (25°C, μ = 1.0). The points (○) are experimental; the curve is calculated (see text). The points (△) were obtained after a time corresponding to the complete conversion of any coumarinic acid ethyl ester to coumarin.

clude that the mode of partitioning of the tetrahedral intermediate is the same, regardless of whether the intermediate is generated in the lactonization of coumarinic acid ethyl ester or in the hydrolysis of coumarin diethyl acetal. Although this may seem a trivial point, there are cases where independently generated tetrahedral intermediates have been suggested to have different modes of breakdown. In a system closely related to that of this study, Deslongchamps *et al.* (22) have suggested that there may be a difference in the lone-pair orientation in tetrahedral intermediates generated in the hydrolysis of ortho esters (such as **6**) and in the lactonization of related hydroxy esters (such as **8**).

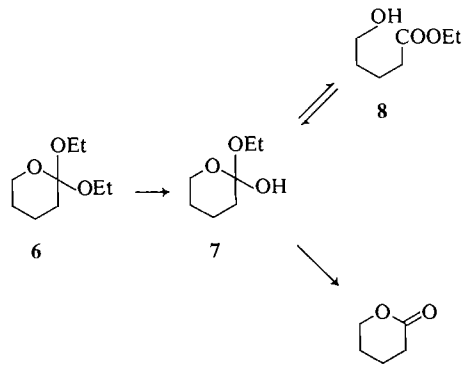

The intermediate in question (**7**) is very similar to that involved in our study. Our results suggest that its partitioning should be independent of its origin. Deslongchamps *et al.* based their conclusions principally on the basis of their observations that ortho esters such as **6** produce hydroxy esters as the initial products and not lactones.[3] Although this result is consistent with lone-pair orientation, an alternate explanation is simply that the tetrahedral intermediates **7** have a preference for ring opening. This latter suggestion leads to the prediction that the rate-determining step in the lactonization of the hydroxy ester is the breakdown of the tetrahedral intermediate to lactone. To our knowledge this has not been established for these simple lactonizations.

A case where more substantial evidence exists for a difference in modes of partitioning involves tetrahedral intermediates generated in imidate hydrolysis reactions and related ester ammonolysis reactions (23). These intermediates, although identical as to structure, are generated in different protonic forms, and it is proposed that they break down before protonic equilibrium is achieved. This is entirely reasonable since the life-times of these intermediates are exceedingly short (23). The tetrahedral intermediates of our study are probably also generated initially with the proton on different oxygens; our results suggest that they must have a sufficient life-time to equilibrate before breakdown. This is also entirely reasonable. We have established in several cases now (11–15) that hydrogen ortho ester life-times are relatively long, certainly long enough for acid–base equilibria to be established.

Acknowledgement

Financial support of the Natural Sciences and Engineering Research Council of Canada is gratefully acknowledged.

1. S. MILSTEIN and L. A. COHEN. J. Am. Chem. Soc. **92**, 4377 (1970); Proc. Natl. Acad. Sci. U.S.A. **67**, 1143 (1970); J. Am. Chem. Soc. **94**, 9158 (1972).
2. E. R. GARRETT, B. C. LIPPOLD, and J. C. MIELCK. J. Pharm. Sci. **60**, 396 (1971); B. C. LIPPOLD and E. R. GARRETT. J. Pharm. Sci. **60**, 1019 (1971).
3. R. HERSHFIELD and G. L. SCHMIR. J. Am. Chem. Soc. **95**, 7360 (1973).
4. R. HERSHFIELD and G. L. SCHMIR. J. Am. Chem. Soc. **95**, 8032 (1973).
5. R. KUHN and D. WEISER. Angew. Chem. **11**, 371 (1957).
6. M. L. BENDER. J. Am. Chem. Soc. **75**, 5986 (1953).
7. R. B. WOODWARD. Pure Appl. Chem. **9**, 49 (1964).
8. P. BLADON and G. C. FORREST. Chem. Commun. 481 (1966).
9. J. HINE, D. RICARD, and R. PERZ. J. Org. Chem. **38**, 110 (1973).
10. B. CAPON, J. H. HALL, and D. M. A. GRIEVE. J. Chem. Soc. Chem. Commun. 1034 (1974).

[3]Recent studies by Capon have found that this may not be entirely true. Substantial amounts of lactone are apparently also produced as the initial product (B. Capon, private communication).

11. M. AHMAD, R. G. BERGSTROM, M. J. CASHEN, A. J. KRESGE, R. A. McCLELLAND, and M. F. POWELL. J. Am. Chem. Soc. **99**, 4827 (1977).
12. R. A. McCLELLAND and M. AHMAD. J. Org. Chem. **44**, 1855 (1979).
13. M. AHMAD, R. G. BERGSTROM, M. J. CASHEN, Y. CHIANG, A. J. KRESGE, R. A. McCLELLAND, and M. F. POWELL. J. Am. Chem. Soc. **101**, 2669 (1979).
14. R. A. McCLELLAND, M. AHMAD, J. BOHONEK, and S. GEDGE. Can. J. Chem. **57**, 1531 (1979).
15. R. A. McCLELLAND and R. SOMANI. J. Chem. Soc. Chem. Commun. 407 (1979).
16. P. R. YOUNG and W. P. JENCKS. J. Am. Chem. Soc. **99**, 8238 (1977).
17. R. A. McCLELLAND and M. AHMAD. J. Am. Chem. Soc. **100**, 7031 (1978).
18. R. A. McCLELLAND and M. AHMAD. J. Am. Chem. Soc. **100**, 7027 (1978).
19. H. PERST. Oxonium ions in organic chemistry. Academic Press, New York, NY. 1971.
20. C. O'CONNOR and T. A. TURNEY. J. Chem. Soc. B, 1211 (1966).
21. C. A. LANE, M. F. CHEUNG, and G. F. DORSEY. J. Am. Chem. Soc. **90**, 6492 (1968).
22. P. DESLONGCHAMPS, R. CHENEVERT, R. J. TAILLEFER, C. MOREAU, and J. K. SAUNDERS. Can. J. Chem. **53**, 1601 (1975).
23. A. C. SATTERTHWAIT and W. P. JENCKS. J. Am. Chem. Soc. **96**, 7031 (1974).

Double layer structure at the mercury/dimethylformamide interface

W. RONALD FAWCETT, BRIAN M. IKEDA, AND JAMES B. SELLAN

Guelph–Waterloo Centre for Graduate Work in Chemistry, Guelph Campus, Department of Chemistry, University of Guelph, Guelph, Ont., Canada N1G 2W1

Received November 24, 1978

W. RONALD FAWCETT, BRIAN M. IKEDA, and JAMES B. SELLAN. Can. J. Chem. 57, 2268 (1979).

The differential capacity of the mercury/solution interface has been measured for various tetraalkylammonium and alkali metal perchlorates in dimethylformamide (DMF) at 25°C, and for tetraethylammonium perchlorate (TEAP) in DMF at −15°C, 0°C, and 40°C. On the basis of established analyses, it is shown that ionic specific adsorption at mercury from TEAP solutions in DMF is negligible. The properties of the inner layer are analyzed in detail on the basis of a statistical mechanical model in which the solvent molecules represented as hard polarizable spheres can occupy three orientations: with their dipole vectors towards the surface, away from the surface, and parallel to the surface. It is shown that this model provides a reasonable description of the electrostatic properties of the inner layer at the Hg/DMF interface.

W. RONALD FAWCETT, BRIAN M. IKEDA et JAMES B. SELLAN. Can. J. Chem. 57, 2268 (1979).

On a mesuré la capacité de l'interface mercure/solution des divers perchlorates de tétraalkylammonium et de métaux alcalins dans le diméthylformamide (DMF) à 25°C et de perchlorate de tétraéthylammonium (PTEA) dans le DMF à −15, 0 et 40°C. En se basant sur des analyses établies, on montre que l'adsorption spécifique ionique au niveau du mercure à partir de solutions de PTEA dans le DMF est négligeable. On a analysé en détail les propriétés de la couche intérieure en se basant sur un modèle mécanique statistique dans lequel les molécules de solvant représentées comme des sphères polarisables dures, peuvent occuper trois orientations; leurs vecteurs dipolaires peuvent être orientés vers la surface, à l'opposé de la surface et parallèle à la surface. On montre que ce modèle fournit une description des propriétés électrostatiques de la couche intérieure à l'interface Hg/DMF.

[Traduit par le journal]

Introduction

The thermodynamic properties of the mercury/dimethylformamide (DMF) interface were first examined by Minc *et al.* (1) who showed that the differential capacity – potential curves were rather featureless in comparison with those observed for many other solvents (2). In particular, the capacity hump which occurs at negative potentials for the protic amide solvents, and which is often attributed to solvent reorientation (3), is not found with DMF. Bezugly and Korshikov (4) studied the dependence of interfacial tension – potential curves on the nature of the ions in common 1–1 electrolytes; in the case of $LiClO_4$ solutions in DMF, the interfacial tension at the potential of zero charge (pzc) increased with increase in salt concentration, indicating that the relative ionic surface excesses decrease in the same direction. This behaviour is opposite to that observed for most salts at the mercury/solution interface. Damaskin and co-workers studied the adsorption of various inorganic ions (5, 6) and organic molecules (7, 8) from DMF solutions and compared the results with those obtained for water and other solvents. In addition, the adsorption of DMF at Hg from aqueous electrolyte solutions has been investigated by Bezugly and Korshikov (4) and by Payne (9). In the latter study, it was concluded that the DMF molecule is predominantly adsorbed at the pzc on Hg with its dipole vector parallel to the metal/solution interface. Under these circumstances, a capacity curve without a hump is expected in the pure solvent when ionic adsorption is absent (10).

Except for the electrocapillary curve for 0.1 *M* tetraethylammonium (TEA^+) iodide reported by Bezugly and Korshikov (4), the properties of the double layer for solutions of tetraalkylammonium salts (TAA^+) in DMF have not been investigated. These systems are of special interest in the area of organic electrochemistry since the Hg electrode may be polarized to very negative potentials, thereby permitting a study of the reduction of organic molecules to stable anion radicals and dianions (11). The purpose of the present study was to obtain double layer data for these electrolytes and to determine the extent of ionic adsorption especially at negative potentials. Inner layer capacity – potential curves obtained in the absence of specific adsorption in the temperature range −15 to 40°C are analyzed on the basis of a three state model for aprotic solvent structure at charged interfaces (10).

0008-4042/79/172268-10$01.00/0

Experimental

Differential capacity against potential data were obtained with an ac bridge operating at 1000 Hz as described previously (12). The cell, which was surrounded by a jacket through which a constant temperature fluid was circulated, consisted of two compartments, a working compartment and a reference electrode compartment, connected by fritted glass. The dropping mercury electrode was constructed from a fine capillary drawn from Pyrex tubing. The end of the capillary was bent through 180° so that the mercury emerged in an upwards vertical direction (Fig. 1) with a flow rate of ~ 0.1 mg s^{-1}. This unconventional design was chosen to avoid problems due to solution creep which are more troublesome in non-aqueous media. The electrode was stable over a long period of time and permitted data to be obtained with the reproducibility achieved with a normal dropping mercury electrode in aqueous systems. The area of the glass over which the emerging drop was formed was $\sim 2 \times 10^{-5}$ cm^2; this area was subtracted from the total area of the drop at balance (~ 0.01 cm^2) to obtain the area in contact with the solution. The bridge was normally balanced at 5 s after the beginning of drop growth except at far negative potentials where shorter periods were used because of the reduced natural life time of the drop. The counter electrode was a cylinder of Pt (~ 3 cm^2 area) which surrounded the dropping mercury electrode. The reference electrode (Ag/0.05 *M* $AgNO_3$, 0.1 *M* TEAP in DMF//) was placed in the reference electrode compartment which contained the same solution as the working compartment; the liquid–liquid junction was established in a fritted glass disc. The silver nitrate solution in this electrode was replaced daily because of the instability of Ag^+ in DMF to photoreduction. TAA^+ perchlorates (TEAP, tetrapropylammium perchlorate (TPAP) and tetra-*n*-butylammonium perchlorate (TBAP) were recrystallized several times from triply distilled water and dried *in vacuo* over P_2O_5 at 50°C. The alkali metal perchlorates were purified by the same procedure, the drying operation being carried out at 140°C. Spectroquality DMF (Matheson, Coleman and Bell) was dried with calcium hydride and stored over 4A molecular sieves. It was distilled at reduced pressure (1–2 mm Hg) under a nitrogen atmosphere before use. The experiments were carried out in a controlled atmosphere chamber (Vacuum Atmospheres) containing a nitrogen atmosphere which was continuously purged of oxygen and water. The temperature of the cell was maintained at temperatures in the range -15 to 40°C to ± 0.1°C by passing constant temperature methanol through the jacket surrounding the working and reference electrode compartments; the ambient temperature of the chamber was maintained close to that of the cell. The working solutions were degassed with purified nitrogen saturated with DMF prior to the experiment. Other details of the experiment are described elsewhere (12).

Results

Differential capacity – potential data were obtained for TEAP solutions in DMF in the concentration range 0.01 to 0.2 *M*. These data were numerically integrated as described previously to obtain values of electrode charge density σ for integral increments in σ. Typical capacity data plotted against σ are shown in Fig. 2. A diffuse layer minimum is apparent at the pzc indicating that specific adsorption is not important in this potential region. A shallow capacity

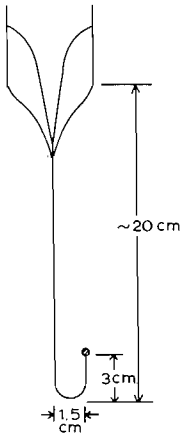

FIG. 1. Sketch of the rate determining portion of the thin walled capillary designed to prevent solution creep at the mercury/glass/solution interface. The shaded sphere at the end of the capillary represents an emerging Hg drop.

minimum is observed for large negative charge densities (-0.17 C m^{-2}) and a steep maximum at large positive charge densities (0.19 C m^{-2}). The capacity curves are similar to those observed for the Hg/acetonitrile (AN) interface (13) with the exception that data are reported at more positive charge densities in DMF. The absence of ionic specific adsorption in the vicinity of the pzc may be demonstrated on the basis of plots of the reciprocal of the experimental capacity $1/C$ against the reciprocal of the diffuse layer capacity $1/C_d$ as estimated by the Gouy–Chapman model for constant σ and varying electrolyte concentration (14). The fact that the slope of these plots is unity in the range $-0.04 \leq \sigma \leq +0.04$ C m^{-2} (Fig. 3) indicates that the inner layer capacity C_i is independent of electrolyte concentration for constant σ, and, therefore, that ionic specific adsorption is negligible. Since experimental activity coefficient data are not available for TEAP in DMF, the presence of specific adsorption at higher charge densities could not be tested by the method of Esin and Markov plots. However, under these conditions where $C_d \gg C_i$, the experimental capacity curves are almost independent of electrolyte concentration (Fig. 2), indicating that specific adsorption is not important. Thus, it is concluded that specific adsorption at the Hg/DMF interface may be neglected over the experimentally accessible potential range when the electrolyte is TEAP. The differential and integral capacities of the inner layer for this system are tabulated in Table 1.

It is interesting to examine the applicability of the Gouy–Chapman–Stern model to this system at the pzc on the basis of the test described earlier (15).

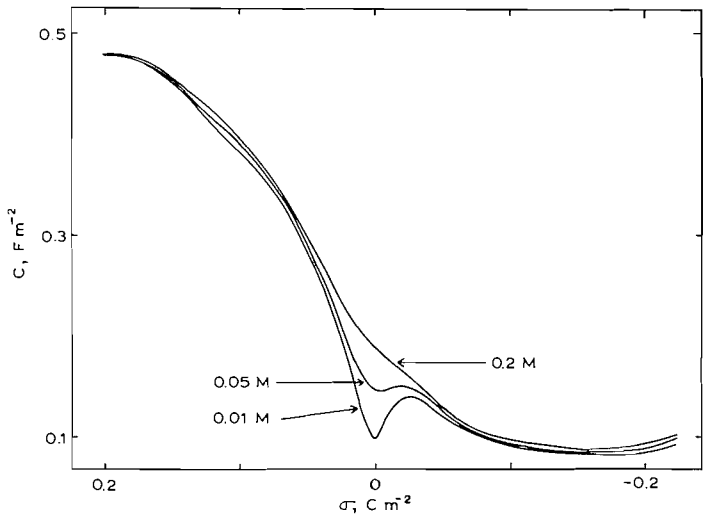

FIG. 2. Plots of differential capacity against electrode charge density for the mercury/dimethylformamide solution interface with various concentrations of tetraethylammonium perchlorate (TEAP) at 25°C. The concentration of TEAP is indicated for each curve.

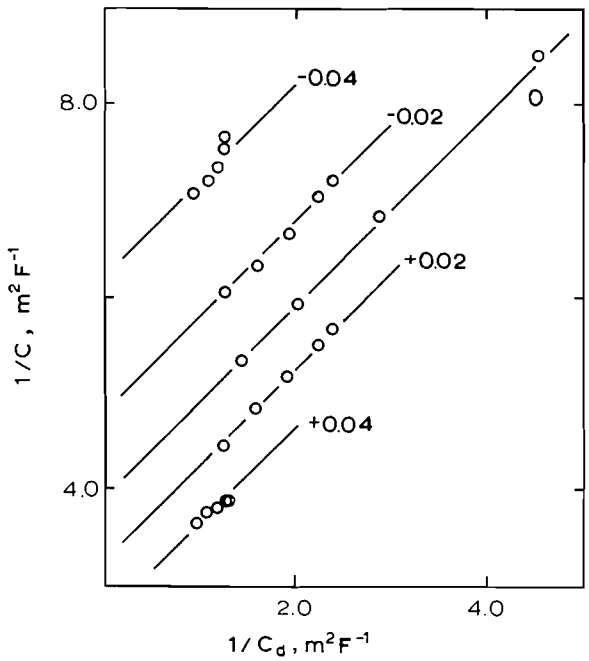

FIG. 3. Reciprocal of the differential capacity at constant electrode charge density plotted against the reciprocal of the diffuse layer capacity estimated by Gouy–Chapman theory for various concentrations of TEAP in DMF at 25°C. The integers adjacent to each curve indicate the value of the electrode charge density in C m^{-2}.

Accordingly,

$$[1] \quad 1/C_0 = 1/C_{i0} + 1/(f\theta\sqrt{c})$$

where C_0 is the capacity at pzc; C_{i0}, the corresponding inner layer capacity; c, the electrolyte concentration; $\theta^2 = 2RT\varepsilon\varepsilon_0$; and $f = F/RT$, ε being the dielectric constant of the solvent and ε_0 the permittivity of free space. A plot of $1/C$ against $1/\sqrt{c}$ for the TEAP data gave an excellent straight line (r = 0.999) with slope equal to 20.15 $m^{1/2}$ F^{-1} mol^{-1}. The corresponding value of the dielectric constant (37.0) agrees very well with published values for DMF (16). This result suggests that the Gouy–Chapman–Stern model provides a very good description of the Hg/DMF interface when TEAP is the electrolyte. Although one expects some lowering of the dielectric constant of the solvent especially in concentrated solutions (17), this effect is apparently not significant for TEAP in the concentration range considered. It should also be noted that the above analysis can be used to detect incomplete electrolyte

TABLE 1. Differential capacity C_i and integral capacity K_i of the inner layer as a function of electrode charge density σ for tetraethylammonium perchlorate solutions in dimethylformamide at mercury at 25°C

σ (C m^{-2})	C_i (F m^{-2})	K_i* (F m^{-2})	σ (C m^{-2})	C_i (F m^{-2})	K_i* (F m^{-2})
0.20	0.558	0.439	−0.02	0.211	0.234
0.18	0.557	0.428	−0.04	0.162	0.206
0.16	0.544	0.416	−0.06	0.127	0.179
0.14	0.530	0.402	−0.08	0.1065	0.157
0.12	0.509	0.388	−0.10	0.0972	0.142
0.10	0.491	0.371	−0.12	0.0927	0.131
0.08	0.463	0.351	−0.14	0.0899	0.123
0.06	0.427	0.328	−0.16	0.0884	0.118
0.04	0.372	0.301	−0.18	0.0882	0.113
0.02	0.304	0.271	−0.20	0.0901	0.110
0	0.254	0.254			

*K_i is defined by the equation $1/K_i = (\phi^m - \phi_0{}^m - \phi^d)/\sigma$ where ϕ^m is the electrode potential measured with respect to a given reference electrode, $\phi_0{}^m$, the corresponding value at the pzc, and ϕ^d, the potential drop across the diffuse layer estimated by the Gouy–Chapman equation.

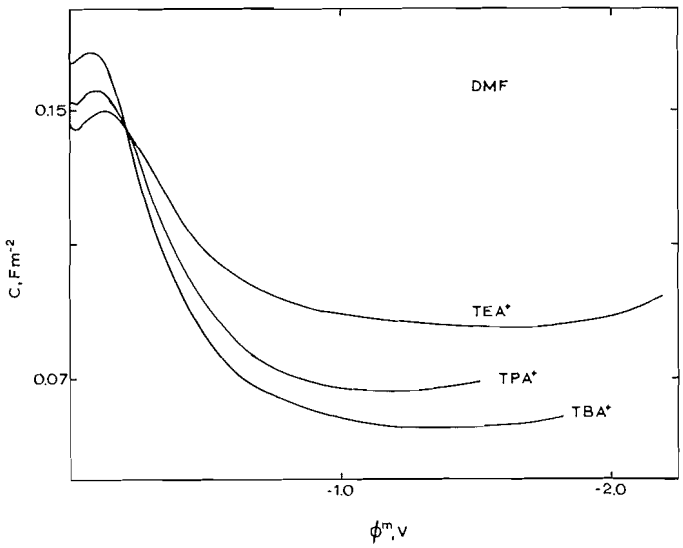

FIG. 4. Differential capacity of the Hg/solution interface plotted against electrode potential measured with respect to the potential of zero charge for various 0.05 *M* tetraalkylammonium perchlorate solutions in DMF. The cations involved are tetraethylammonium (TEA^+), tetrapropylammonium (TPA^+), and tetrabutylammonium (TBA^+) as indicated.

dissociation in non-aqueous solutions. Thus, Dzhaparidze and co-workers (18, 19) observed that the slopes of plots of $1/C$ against $1/\sqrt{c}$ were considerably higher than predicted by eq. [1] for $LiClO_4$ and KF solutions in ethylene glycol. In the present case, the above result indicates that TEAP is completely dissociated in DMF.

The effect of the size of the TAA^+ cation on the experimental differential capacity at negative potentials is illustrated in Fig. 4. As the size of the cation increases in the series $TEA^+ < TPA^+ < TBA^+$, the capacity decreases. This can be chiefly attributed to a corresponding increase in the thickness of the inner layer. However, as was observed earlier for the corresponding systems in AN (13), the ordering of capacities in the vicinity of the pzc is reversed. This suggests that the cation has an influence on the dielectric properties of the inner layer when the charge density on the electrode is low. One obvious way in which cation size effects dielectric properties is by changing the average number of solvent molecules per unit area in the inner layer, and, thus, the mean dielectric constant. As the field of the electrode increases, its influence on solvent dipole orientation predominates and the dielectric properties of the first solvent monolayer become the most important factor determining inner layer capacity.

The influence of alkali metal cations on capacity – potential curves in DMF is illustrated in Fig. 5. At sufficiently negative potentials, the capacity rises sharply in a potential region which becomes more negative as solvation of the cation increases, that is, in the order $Cs^+ < K^+ < Na^+ < Li^+$. This observation can be attributed to cation specific adsorption which is most pronounced in the case of Cs^+ (5). It is interesting to note that at less negative potentials where cation adsorption is not significant, the ordering of capacities is reversed, that is, $C(Li^+) > C(Na^+) > C(K^+)$. Although this effect is small, it is similar to the cation effects observed for formamide (20), *N*-methylformamide (15), *N*-methylacetamide (21), and dimethylsulphoxide (22). This ordering can be attributed to a dependence of both the dielectric properties and the thickness of the inner layer on the nature of the cation at the outer Helmholtz plane (oHp) (15).

The dependence of the interfacial capacity for the Hg/0.05 *M* TEAP system on temperature is illustrated in Fig. 6. It is interesting that the capacity is almost independent of temperature at far negative potentials. At far positive potentials, the capacity decreases with increase in temperature in the vicinity of the maximum. The present results may be compared with those obtained earlier for the Hg/H_2O (23, 24) and Hg/methanol interfaces (2). In the case of the aqueous system, the interfacial capacity varies markedly with temperature for positive charge densities on Hg and very little at negative charge densities. For the methanol interface where the capacity curve contains one minimum with no other extrema, very little variation in capacity with temperature is observed. On the basis of recent models (10, 25), the shape of capacity curves for non-aqueous systems in the absence of specific adsorption can be attributed to variation in dielectric properties of a solvent monolayer adjacent to the electrode with

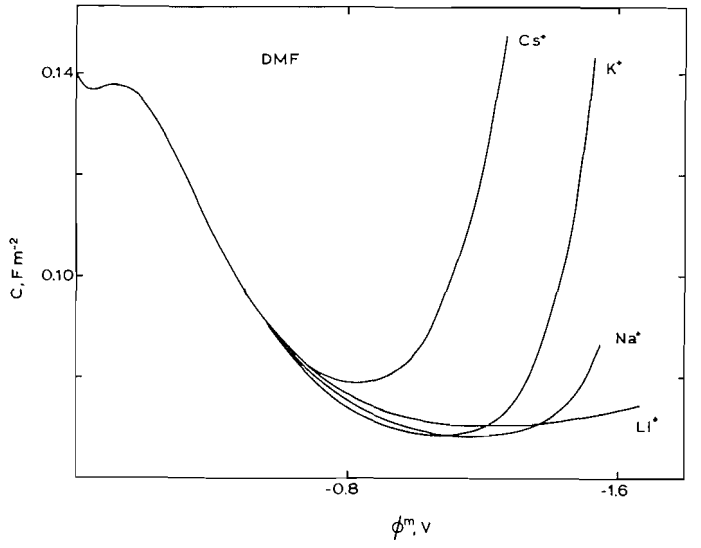

FIG. 5. Differential capacity of the Hg/solution interface plotted against electrode potential measured with respect to the potential of zero charge for various 0.05 *M* alkali metal perchlorate solutions in DMF. The nature of the cation is indicated adjacent to each curve.

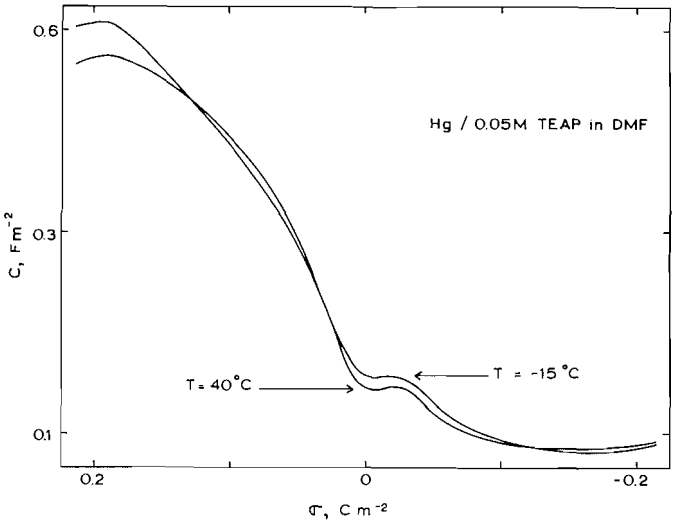

FIG. 6. Differential capacity of the Hg/0.05 *M* TEAP solution in DMF plotted against electrode charge density at −15°C and 40°C as indicated.

electrode charge density. The small variation in capacity with temperature is examined on the basis of these models below.

Discussion

Since the inner layer capacity curve for the Hg/DMF interface possesses two extrema, it does not fit clearly into the three categories discussed by Parsons (25). In previous investigations of this system (1, 3, 5), the maximum observed here at far positive potentials was not reported. Accordingly, DMF was classified together with solvents such as AN and acetone as a solvent with a featureless capacity curve characterized by a broad minimum. However, Borkowska (26) recently reported that a capacity maximum is also observed for the Hg/acetone interface when the electrolyte is chosen so that the electrode can be polarized to sufficiently positive potentials. According to the three state model proposed recently (10), the dielectric properties of these solvents at a polarizable interface can be accounted for if it is assumed that the solvent is predominantly adsorbed on the electrode with its dipole vector parallel to the surface. The other two states considered in the model

are solvent molecules adsorbed with the positive end of the dipole towards the metal ('up' orientation) and with the negative end towards the metal ('down' orientation) (10). If the electrode can be polarized over a sufficiently wide potential range, one would predict according to the three state model an inner layer capacity curve with three extrema, a central minimum and two maxima at far positive and negative potentials. The central minimum corresponds to the electrostatic condition at which the surface concentration of 'up' dipoles is equal to that of 'down' dipoles. As the electrode charge density is made more positive, the concentrations of 'parallel' and 'up' dipoles decrease and that of 'down' dipoles increases. The positive maximum then corresponds to the electrostatic condition at which the surface concentration of 'down' dipoles equals that of 'parallel' dipoles. The opposite situation holds at the negative maximum with the surface concentrations of 'up' and 'parallel' dipoles equal. On the basis of this model, the negative maximum is not observed at the Hg/DMF interface because reduction of the cation from the electrolyte limits the polarizable range of the electrode in the negative direction. An alternative explanation of the capacity curve might involve attributing the maximum observed at positive potentials to reorientation of 'up' dipoles which are strongly adsorbed at the pzc; the small increase in capacity at negative potentials could then be associated with electrostriction of solvent dipoles in the large negative electrode field (27). However, under these circumstances one would expect a large positive surface potential due to oriented dipoles at the pzc. In fact, the experimental evidence from studies of the adsorption of DMF at Hg from DMF–water solutions is that the solvent dipoles are predominantly adsorbed with their dipole vectors parallel to the surface (9). Thus, the first interpretation of the capacity offered above on the basis of the three state model is consistent with all experimental evidence obtained to date.

The equations defining the surface concentrations of 'up', 'down', and 'parallel' dipoles in a monolayer at the electrode/solution interface are (10)

$$[2] \quad N^{\uparrow} + N^{\downarrow} + N^{0} = N_{T}$$

$$[3] \quad kT \ln (N^{\uparrow}/N^{\downarrow}) = U_{r}^{\downarrow} - U_{r}^{\uparrow} - 2p(E + X)$$

and

$$[4] \quad kT \ln (N^{\downarrow}/N^{0}) = U_{r}^{0} - U_{r}^{\downarrow} + p(E + X)$$

$N^{\uparrow}$, $N^{\downarrow}$, and N^{0} are the number densities of solvent dipoles in the 'up', 'down', and 'parallel' orientations, respectively; $U_{r}^{\uparrow}$, $U_{r}^{\downarrow}$, and U_{r}^{0} are the corresponding residual energies which account for non-electrostatic contributions to interactions between the metal and solvent dipoles in each of the three states; E is the field due to the charge on the electrode, X, the mean field in the same direction at an average dipole site due to surrounding dipoles, p, the permanent dipole moment of the solvent molecule, and N_{T}, the total number of solvent molecules per unit area on the basis of hexagonal close packing of solvent molecules represented as hard spheres. On the basis of methods worked out by Levine *et al.* (28), it was shown that the dipole reaction field X is given by

$$[5] \quad X = c_{e}(pr - \alpha E)/Ad^{3}$$

where $r = (N^{\uparrow} - N^{\downarrow})/N_{T}$ and $A = 1 + c_{e}\alpha/d^{3}$; c_{e} is an effective coordination number for a dipole in the hexagonal array between the conducting electrode and the diffuse layer, α, the average molecular polarizability and d, the molecular diameter. Equations [2]–[4] form a set of non-linear equations in $N^{\uparrow}$, $N^{\downarrow}$, and N^{0} which may be solved iteratively. The total potential drop across the monolayer is

$$[6] \quad \Delta\phi = 4\pi\sigma d + (4\pi N_{T} d^{3} X/c_{e})$$

where σ is the charge density on the electrode. The differential capacity of the monolayer is then given by

$$[7] \quad \frac{1}{C_{i}} = \left(\frac{\partial \Delta\phi}{\partial \sigma}\right) = 4\pi d + \frac{4\pi N_{T} d^{3}}{c_{e}} \left(\frac{\partial X}{\partial \sigma}\right)$$

In order to determine $(\partial X/\partial\sigma)$, one must calculate the derivatives $(\partial N^{\uparrow}/\partial\sigma)$, $(\partial N^{\downarrow}/\partial\sigma)$, and $(\partial N^{0}/\partial\sigma)$; these are estimated on the basis of three equations derived from eqs. [2]–[4] by differentiation with respect to σ (10).

In order to determine whether eqs. [6] and [7] describe the electrostatic properties of the inner layer at the Hg/DMF interface one must determine values for the residual energies. As shown previously (10), these parameters may be estimated from the electrostatic properties of the interface at the extrema. In the present case, at the capacity minimum, $N^{\uparrow} = N^{\downarrow}$, and therefore from eqs. [3] and [5]

$$[8] \quad U_{r}^{\downarrow} - U_{r}^{\uparrow} = 2pE_{m}/A$$

where $E_{m} = 4\pi\sigma_{m}$, E_{m} and σ_{m} being the electrode field and charge density, respectively, at the minimum. At the maximum $N^{\downarrow} = N^{0}$ and assuming that $N^{\uparrow}$ is negligible, $N^{\downarrow}/N_{T} = N^{0}/N_{T} = 0.5$. From eqs. [4] and [5],

$$[9] \quad U_{r}^{\downarrow} - U_{r}^{0} = pE_{r}/A - 0.5c_{e}p^{2}/Ad^{3}$$

where E_{r} is the electrode field at the maximum. The values of the dipole moment and polarizability reported for DMF in the literature are 3.86 D (29) and

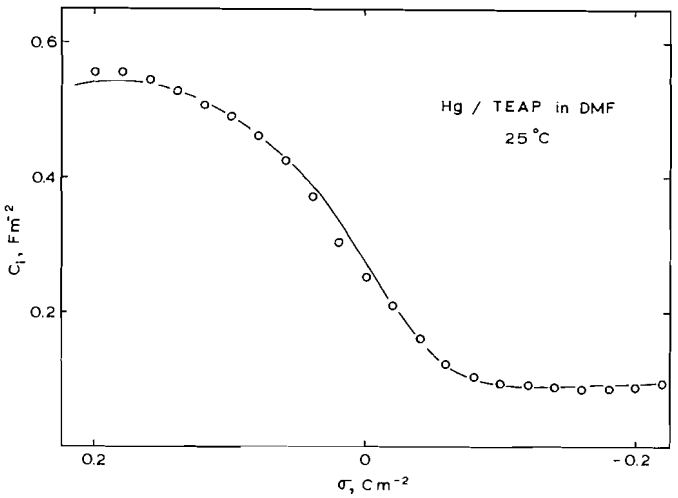

FIG. 7. Plot of the inner layer differential capacity C_i for the Hg/DMF interface with TEAP as electrolyte against electrode charge density at 25°C. The solid curve was calculated from the three state model as described in the text with $d = 0.340$ nm, $p = 3.86$ D, $\alpha = 7.81 \times 10^{-3}$ nm^3, $c_e = 14.84$, $U_r^{\downarrow} - U_r^{\uparrow} = -75.41$ kJ mol^{-1}, and $U_r^0 - U_r^{\downarrow} = 0.77$ kJ mol^{-1}.

7.81×10^{-24} cm^3 (30, 31), respectively. Thus, having chosen the parameters d and c_e, one can estimate the residual energy differences defined in eqs. [8] and [9].

Given the molecular parameters for the solvent (d, p, and α), effective coordination number c_e, and the residual energy differences $U_r^{\downarrow} - U_r^{\uparrow}$ and $U_r^{\downarrow} - U_r^0$, the dependence of $\Delta\phi$ and C_i on σ was determined as outlined previously (10). The calculated values of $\Delta\phi - \Delta\phi_0$, where $\Delta\phi_0$ is the potential drop across the dipole layer at the pzc, were compared with the rational potential drop across the inner layer ϕ^{md} (Table 1) determined experimentally; at the same time, the experimental and calculated values of C_i were compared. The criterion for the best values of the adjusted parameters d and c_e was a minimum in the standard deviations between experimental and calculated values of both C_i and $\Delta\phi - \Delta\phi_0$. The results of applying the three state model for the inner layer differential capacity data are shown in Fig. 7. From the values of the electrode charge density at the minimum (-0.17 C m^{-2}) and maximum (0.19 C m^{-2}), and using the best values of d (0.340 nm) and c_e (14.84), $U_r^{\downarrow} - U_r^{\uparrow} = -75.4$ kJ mol^{-1} and $U_r^{\downarrow} - U_r^0 = -0.77$ kJ mol^{-1}. It is apparent that an excellent fit to the experimental data can be made on the basis of the above model. It should be emphasized that only two parameters, namely d and c_e, were adjusted to achieve this fit. It was noted that very small variations in the effective coordination number c_e had a very large effect on the quality of the fit. Levine *et al.* (28) have shown the c_e should equal 15.2 for a monolayer of hexagonally close-packed spherical dipoles with all dipole vectors normal to the surface, and situated between a conducting electrode and electrolyte solution. The present result that the best fit was obtained with a lower value of c_e may be a reflection of the conclusion that a large fraction of the surface is covered by solvent dipoles in a 'parallel' orientation.

Calculated and experimental values of the integral capacity of the inner layer K_i which is defined by the equation

$$[10] \quad 1/K_i = (\Delta\phi - \Delta\phi_0)/\sigma$$

are shown in Fig. 8. Although the fit is quite good at negative charge densities, the calculated capacity is higher than the experimental values at positive charge densities. In comparing Figs. 7 and 8, it should be kept in mind that small discrepancies between calculated and experimental values of C_i are added in the integration process involved in calculating $\Delta\phi$ and thus K_i from C_i. Thus, the small differences between the experimental and calculated curves in Fig. 7 are much more apparent in Fig. 8.

On the basis of the above parameters one may estimate the fraction of the surface covered by each of the three species. Over most of the polarizable range, the majority of the Hg surface is covered by DMF molecules in a 'parallel' orientation, the concentration of 'up' dipoles being negligible (Fig. 9). As the electrode charge density becomes more positive, the fraction of solvent dipoles in the 'down' orientation, that is, with the oxygen atom towards the surface, increases at the expense of the 'parallel' orientation. On the basis of the Courtauld model and assuming that the dipole vector is approximately parallel to a

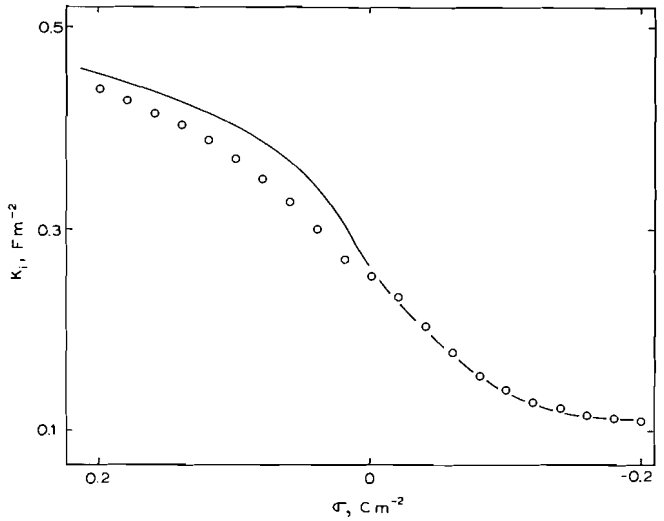

FIG. 8. Plot of the inner layer integral capacity K_i for the Hg/DMF interface with TEAP as electrolyte against electrode charge density at 25°C. The solid curve was calculated from the three state model as described in the text using the parameters given in the caption to Fig. 7.

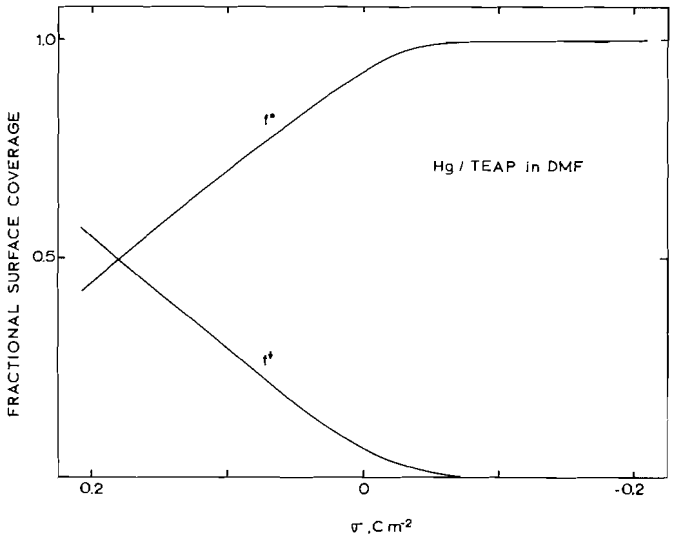

FIG. 9. Plot of the fractions of molecules in the down ($f^\downarrow$) and parallel (f^o) orientations against electrode charge density for a DMF monolayer at Hg. The parameters assumed in estimating these fractions are given in the caption to Fig. 7.

line drawn through the oxygen and nitrogen atoms in the DMF molecule (Fig. 10), the 'parallel' orientation corresponds to a solvent molecule positioned with its methyl groups on the surface. A similar conclusion was reached by Payne on the basis of a comparison of the potential shift of the pzc of aqueous solutions of DMF, *N*-methylformamide, and formamide with change in amide concentration (9). The value of the surface potential (−0.293 V) reflects the small net concentration of negatively oriented dipoles at the pzc. The distortional contribution to the effective inner layer dielectric constant ε_∞ estimated on the basis of the equation (10)

$$[11] \quad 1/\varepsilon_\infty = 1 - 4\pi\alpha N_T/Ad$$

is 3.71. In assessing these results one should keep in mind the fact that the isotropic polarizability has been used in the above calculations. Since the polarizability depends to some extent on molecular orientation (31) and electrode field (32), the effective polarizability is expected to vary somewhat with electrode charge density.

It is interesting to examine the predictions of the three state model regarding the temperature depen-

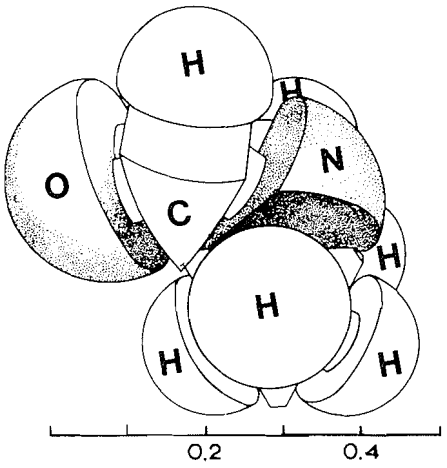

FIG. 10. Sketch of a dimethylformamide molecule on the basis of its Courtauld model. The scale defines the position of the surface in a 'parallel' orientation corresponding to the dipole vector parallel to the surface.

dence of $\Delta\phi$ and C_i. On the basis of eqs. [5] and [6],

$$[12]\quad \left(\frac{\partial\Delta\phi}{\partial\beta}\right)_\sigma = \frac{4\pi N_T d^3}{c_c}\left(\frac{\partial X}{\partial\beta}\right)_\sigma = \frac{4\pi N_T p}{A}\left(\frac{\partial r}{\partial\beta}\right)_\sigma$$

where $\beta = 1/kT$, and

$$[13]\quad \frac{\partial(1/C_i)}{\partial\beta} = \frac{4\pi N_T p}{A}\left(\frac{\partial^2 r}{\partial\beta\partial\sigma}\right)$$

From eqs. [2]–[4], it may be shown (10) that

$$[14]\quad r = (1 - a_1 e^{2y})/R$$

where $R = 1 + a_1 e^{2y} + a_2 e^{y}$, $a_1 = \exp[\beta(U_r^{\uparrow} - U_r^{\downarrow})]$, $a_2 = \exp[\beta(U_r^{\uparrow} - U_r^{0})]$, and $y = p\beta(E + X)$. Differentiating eq. [14] with respect to β at constant σ, one obtains

$$[15]\quad \left(\frac{\partial r}{\partial\beta}\right)_\sigma = \frac{-a_1 e^{2y}\Delta U_1}{R} - \frac{2a_1 e^{2y}}{R} \times \left[p(E + X) + \frac{c_c p^2\beta}{Ad^3}\left(\frac{\partial r}{\partial\beta}\right)_\sigma\right] - \frac{(1 - a_1 e^{2y})}{R^2}\left\{a_1 e^{2y}\Delta U_1 + a_2 e^{y}\Delta U_2 + (2a_1 e^{2y} + a_2 e^{y}) \times \left[p(E + X) + \frac{c_c p^2\beta}{Ad^3}\left(\frac{\partial r}{\partial\beta}\right)_\sigma\right]\right\}$$

where $\Delta U_1 = U_r^{\uparrow} - U_r^{\downarrow}$ and $\Delta U_2 = U_r^{\uparrow} - U_r^{0}$. Rearranging and setting $f^{\uparrow} = N^{\uparrow}/N_T = 1/R$, $f^{\downarrow} = N^{\downarrow}/N_T = a_1 e^{2y}/R$ and $f^{0} = N^{0}/N_T = a_2 e^{y}/R$, it is easily shown that

$$[16]\quad \left[\frac{1 + 2c_c p^2\beta f^{\downarrow}}{Ad^3} + r(2f^{\downarrow} + f^{0})\frac{c_c p^2}{Ad^3}\right]\left(\frac{\partial r}{\partial\beta}\right)_\sigma = -f^{\downarrow}\Delta U_1 - 2f^{\downarrow}p(E + X) - r[f^{\downarrow}\Delta U_1 + f^{0}\Delta U_2 + (2f^{\downarrow} + f^{0})p(E + X)]$$

At the minimum, $f^{\uparrow} = f^{\downarrow}$, $r = 0$, and therefore, on the basis of eq. [3], $\Delta U_1 = -2p(E + X)$. From eq. [16], it is apparent that $\partial r/\partial\beta = 0$ and thus $\partial(\Delta\phi)/\partial\beta = 0$ at the minimum. Similarly, for the present system, $f^{\downarrow} = f^{0} = 0.5$ at the maximum, and from eq. [4], $U_r^{0} - U_r^{\downarrow} = \Delta U_1 - \Delta U_2 = -p(E + X)$; on substituting these values into eq. [16], it is found that $\partial r/\partial\beta$ and $\partial(\Delta\phi)/\partial\beta$ are zero at the maximum. Thus, according to the three state model, the potential difference $(\Delta\phi)_m - (\Delta\phi)_r = (\phi^{md})_m - (\phi^{md})_r$ is independent of temperature where $(\Delta\phi)_m$ and $(\phi^{md})_m$ are the potential drops across the dipole layer according to the model, and as estimated from experiment on the basis of the rational potential, respectively, at the minimum, and $(\Delta\phi)_r$ and $(\phi^{md})_r$, the corresponding values at the maximum. From the experiments, $(\phi^{md})_m - (\phi^{md})_r = -1.923 \pm 0.006$ V, in the temperature range -15 to 40°C, that is, it is independent of temperature within experimental error. The above results suggest an effective way of defining an absolute potential scale for unassociated solvents at a polarizable electrode. If the principle extremum on the capacity curve observed with an electrolyte whose ions are not adsorbed occurs at the same charge density independent of temperature, one may assume that the absolute potential drop across the inner layer is also temperature independent and on this basis defines an absolute potential scale according to which the variation in surface potential with temperature is automatically accounted for.

On differentiating eq. [16] with respect to σ, one may derive an expression for the temperature dependence of the inner layer capacity C_i (eq. [13]). It can then be shown that the inner layer capacity does depend on temperature at the two extrema, although the temperature coefficient at the minimum is negligible in the present case. Comparison of calculated and experimental values of dC_i/dT (Fig. 11) reveals that the model gives the correct sign of the temperature dependence of the capacity at the maximum, but the coefficient calculated on the basis of the parameters given above is approximately twice that observed experimentally. In addition, the positive values of dC_i/dT observed for values of σ in the range $0.02 < \sigma < 0.14$ C m^{-2} are not predicted by the model. However, considering the fact that the variation in C_i with temperature is not large with

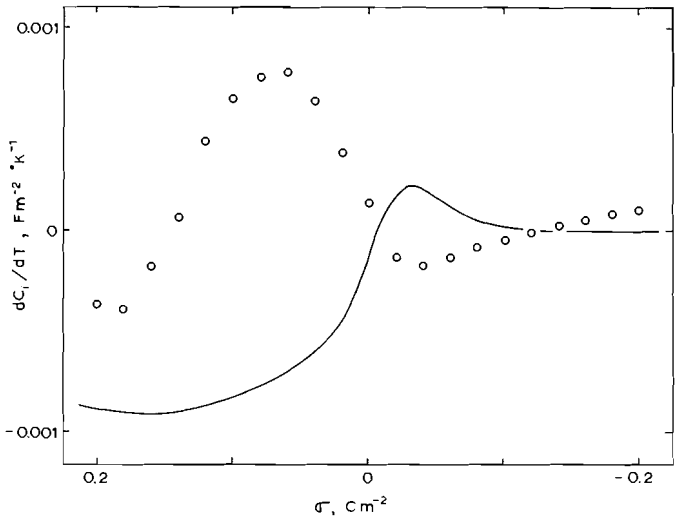

FIG. 11. The temperature derivative of the inner layer differential capacity dC_i/dT plotted against electrode charge density for data obtained at the Hg/DMF interface with TEAP as electrolyte in the temperature range −15 to 40°C. The solid curve was calculated from the three state model on the basis of the parameters given in the caption to Fig. 7.

respect to experimental error, one should not place great emphasis on the quantitative aspects of the above comparison. The present results may be compared with those obtained for the Hg/methanol interface where a small temperature coefficient was also observed (2).

Acknowledgements

The financial support of the National Research Council of Canada is gratefully acknowledged. B.M.I. acknowledges the receipt of an Ontario Graduate Scholarship.

1. S. MINC, J. JASTRZEBSKA, and M. BRZOSTOWSKA. J. Electrochem. Soc. **108**, 1160 (1961).
2. R. PAYNE. Adv. Electrochem. Electrochem. Eng. **7**, 1 (1970).
3. R. PAYNE. J. Phys. Chem. **73**, 3598 (1963).
4. V. D. BEZUGLY and L. A. KORSHIKOV. Elektrokhimiya, **1**, 1422 (1965); **3**, 390 (1967).
5. YA. DOYLIDO, R. V. IVANOVA, and B. B. DAMASKIN. Elektrokhimiya, **6**, 3 (1970).
6. I. M. GANZHINA, B. B. DAMASKIN, and R. V. IVANOVA. Elektrokhimiya, **6**, 709 (1970); **6**, 1540 (1970).
7. I. M. GANZHINA and B. B. DAMASKIN. Elektrokhimiya, **6**, 1715 (1970).
8. R. I. KAGANOVICH, B. B. DAMASKIN, and K. K. KAISHEVA. Elektrokhimiya, **6**, 1359 (1970); **8**, 1642 (1972); **9**, 94 (1973).
9. R. PAYNE. J. Electroanal. Chem. **47**, 265 (1973).
10. W. R. FAWCETT. J. Phys. Chem. **82**, 1385 (1978).
11. C. K. MANN and K. K. BARNES. Electrochemical reactions in nonaqueous systems. Marcel Dekker, New York. 1970.
12. W. R. FAWCETT and M. D. MACKEY. J. Chem. Soc. Faraday Trans. I, **69**, 634 (1973).
13. W. R. FAWCETT and R. O. LOUTFY. Can. J. Chem. **51**, 230 (1973).
14. R. PARSONS and F. G. R. ZOBEL. J. Electroanal. Chem. **9**, 333 (1965).
15. W. R. FAWCETT and R. O. LOUTFY. J. Electroanal. Chem. **39**, 185 (1972).
16. D. S. REID and C. A. VINCENT. J. Electroanal. Chem. **18**, 427 (1968).
17. H. BEHRET, F. SCHMITHALS, and J. BARTHEL. Z. Phys. Chem. N.F. **96**, 73 (1975).
18. DZH. I. DZHAPARIDZE and V. A. CHAGELISHVILI. The double layer and adsorption at solid electrodes, Proc. of the IVth Symposium, Tartu. 1975. p. 89.
19. V. A. CHAGELISHVILI, DZH. I. DZHAPARIDZE, and B. B. DAMASKIN. Elektrokhimiya, **13**, 1300 (1977).
20. B. B. DAMASKIN, R. V. IVANOVA, and A. A. SURVILA. Elektrokhimiya, **1**, 767 (1965).
21. R. PAYNE. J. Phys. Chem. **73**, 3598 (1969).
22. R. PAYNE. J. Am. Chem. Soc. **89**, 48 (1967).
23. D. C. GRAHAME. J. Am. Chem. Soc. **79**, 2093 (1957).
24. G. J. HILLS and R. PAYNE. Trans. Faraday Soc. **61**, 316 (1965).
25. R. PARSONS. Electrochim. Acta, **21**, 681 (1976).
26. Z. BORKOWSKA. J. Electroanal. Chem. **79**, 206 (1977).
27. J. R. MACDONALD. J. Chem. Phys. **22**, 1857 (1954).
28. S. LEVINE, G. M. BELL, and A. L. SMITH. J. Phys. Chem. **73**, 3534 (1969).
29. I. P. GOLDSHTEIN, YU. M. KESSLER, YU. M. POVAROV, and A. I. GORBANEV. Zh. Strukt. Khim. **4**, 445 (1963).
30. M. J. ARONEY, R. J. W. LEFÈVRE, and A. N. SINGH. J. Chem. Soc. 3179 (1965).
31. J. APPLEQUIST, J. R. CARL, and K. K. FUNG. J. Am. Chem. Soc. **94**, 2952 (1972).
32. A. D. BUCKINGHAM and B. J. ORR. Q. Rev. Chem. Soc. **21**, 195 (1967).

The photoelectron spectra of dimethylgermane, difluoro- and dichlorodimethyl germane

JOHN E. DRAKE, BORIS M. GLAVINĆEVSKI, AND KRYSTYNA GORZELSKA

Department of Chemistry, University of Windsor, Windsor, Ont., Canada N9B 3P4

Received March 15, 1979

JOHN E. DRAKE, BORIS M. GLAVINĆEVSKI, and KRYSTYNA GORZELSKA. Can. J. Chem. **57**, 2278 (1979).

He(I) and He(II) pe spectra of the series Me_2GeX_2 (X = H, F, Cl) are reported. Assignments are based on comparisons with the spectra of related Me_3GeX and $MeGeX_3$ series as well as semi-empirical CNDO/2 calculations.

JOHN E. DRAKE, BORIS M. GLAVINĆEVSKI et KRYSTYNA GORZELSKA. Can. J. Chem. **57**, 2278 (1979).

On rapporte les spectres pe de He(I) et He(II) dans une série de Me_2GeX_2 (X = H, F, Cl). On base les attributions sur des comparaisons avec des spectres de séries apparentées Me_3GeX et $MeGeX_3$ ainsi que sur des calculs semi-empiriques CNDO/2.

[Traduit par le journal]

Introduction

We recently reported (1, 2) the uv photoelectron spectra of the series of compounds Me_3GeX and $MeGeX_3$, where X = H, F, and Cl. This supplemented several earlier reports of the spectra of the germanium halides, germane, methylgermane, tetramethylgermane (3–9), and most recently, chlorotrimethylgermane (10). We complete the series by reporting the He(I) and He(II) spectra of the dimethylgermane derivatives, Me_2GeH_2, Me_2GeF_2, and Me_2GeCl_2. The spectra are relatively complicated because in C_{2v} local symmetry there are no degenerate orbitals. Thus, in addition to CNDO/2 calculations as an aid to assignment, particular use is made of correlation diagrams with the assignments for the $MeGeX_3$ and Me_3GeX series (1, 2).

Experimental

The spectra were recorded on a McPherson ESCA-36 photoelectron spectrometer, using both He(II) and He(I) excitation. The peaks were calibrated against the argon lines at 15.76 and 15.94 eV.

The CNDO/2 calculations utilized the program GEOM-FORTRAN IV (i.e. GEOMO, QCPE 290 (written in Fortran)) developed by Rinaldi (11). A non-standard basis, not including *d*-orbitals, was used for germanium and chlorine. The parameters that differ from those provided in the manual are the core integrals Cl(*s*)(19.235), Cl(*p*)(9.38) and Ge(*s*)(12.715), Ge(*p*)(6.845) (12) and the Slater exponents Cl(*s*)(2.3561) and Cl(*p*)(2.0387) (13). The coordinates of the atoms were calculated using bond lengths previously reported in the literature (14–17). All tetrahedral angles were assumed.

As in our earlier studies (1, 2), trial runs which included exact angles gave only small changes to eigenvalues and eigenvectors. This was also true of runs that utilized the optimisation routine so that this was also not used, resulting in considerable savings in computer time.

Materials

Dimethylgermane and difluorodimethylgermane were prepared by well-established methods (18, 19). Dichlorodimethylgermane was supplied by Laramie Chem. Co., WY. The samples were purified by vacuum fractionation and their purity was confirmed by ^1H nmr and vibrational spectroscopy (19–21).

Results and Discussion

The experimental vertical ionisation energies and the values of the orbitals calculated by the CNDO/2 method are recorded in Table 1, along with the designated symmetry and principal contributions to the molecular orbitals.

A comparison of the spectrum of Me_2GeH_2 (Fig. 1) with those of Me_3GeH (1) and $MeGeH_3$ (2) indicates similar features which, along with the CNDO/2 calculations, allows for a reasonable assignment. The calculations place the $3b_2$, $3b_1$, and $4a_1$ orbitals close together and three peaks can be clearly seen in the feature centred at 11.09 eV. In $MeGeH_3$, the $3a_1$ orbital (mainly Ge(*p*)—C(*p*)) was assigned to the lower energy peak because it was clearly sharper and less intense than the 2*e* (mainly Ge(*p*)—H(*s*)). Similarly, in Me_3GeH the broader, more intense band was assigned to 4*e* (now mainly Ge—C) which was the less stable orbital. Thus, in contrast to the CNDO predictions, the orbitals mainly involving Ge—H bonding are slightly more stable than those involving Ge—C bonding. The order of the orbitals in Me_2GeH_2 is assigned on the same basis in terms of the AO participation and the correlation diagram (Fig. 2) as $3b_1 < 4a_1 < 3b_2$. This order is identical to that proposed for Me_2SiH_2 (22). The transformation of the 2*e* orbital is from one that has predominantly H—Ge but some Ge—C character in $MeGeH_3$, to one of predominantly Ge—C character in Me_3GeH via the $3b_2$ and $3b_1$ orbitals. The former can be described as a Ge—H

0008-4042/79/172278-07$01.00/0

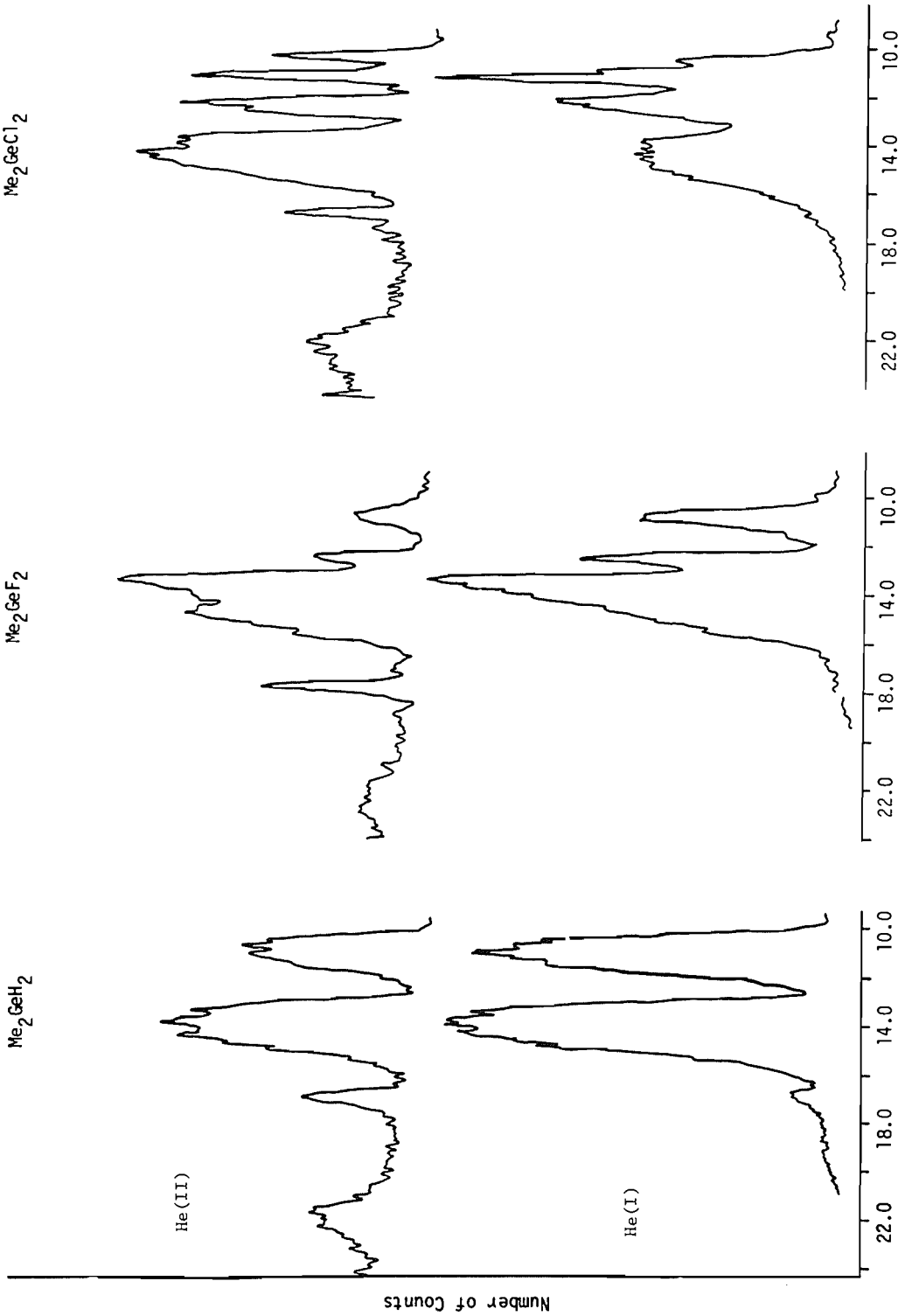

FIG. 1. Helium(I) and helium(II) photoelectron spectra of Me_2GeH_2, Me_2GeF_2, and Me_2GeCl_2.

TABLE 1. CNDO/2 calculated eigenvalues (eV), orbital symmetries, experimental ionization energies (eV), and parentage for Me_2GeF_2, Me_2GeCl_2, and Me_2GeH_2 (I)

H				F				Cl			
Orbital	CNDO/2	Exp.	Parentage	Orbital	CNDO/2	Exp.	Parentage	Orbital	CNDO/2	Exp.	Parentage
$3b_1$	15.46	10.74	Ge(p) 0.32 C(p) 0.52 H(s) 0.15	$4b_1$	15.17	10.45	Ge(p) 0.22 F(p) 0.19 C(p) 0.47 H(s) 0.10	$4b_1$	13.87	10.65	Ge(p) 0.12 Cl(p) 0.52 C(p) 0.29 H(s) 0.04
$4a_1$	15.51	11.04	Ge(p) 0.32 H(^1s) 0.24 C(p) 0.30 H(s) 0.15	$6a_1$	16.33	12.24	Ge(p) 0.15 F(p) 0.50 C(p) 0.26 H(s) 0.09	$6a_1$	14.53	11.20	Ge(p) 0.08 Cl(p) 0.75 C(p) 0.13 H(s) 0.04
$3b_2$	15.29	11.50	Ge(p) 0.27 H(^1s) 0.45 C(p) 0.11 H(s) 0.17	$4b_2$	17.00	13.16	Ge(p) 0.10 F(p) 0.75 C(p) 0.06 H(s) 0.08	$4b_2$	14.84	11.47	Ge(p) 0.05 Cl(p) 0.92
				$2a_2$	19.56	13.76	F(p) 0.92 C(p) 0.04	$2a_2$	15.65	12.40	Cl(p) 0.99 Cl(s) 0.03
				$3b_2$	19.59	13.88	F(p) 0.80 C(p) 0.10 H(s) 0.10	$3b_2$	16.70	12.75	Ge(p) 0.11 Cl(p) 0.63 C(p) 0.09 H(s) 0.12
				$5a_1$	20.18	14.30	Ge(p) 0.03 F(p) 0.75 C(p) 0.10 H(s) 0.09	$5a_1$	17.62	13.50	Ge(p) 0.14 Cl(s) 0.03 Cl(p) 0.58 C(p) 0.14 H(s) 0.10
				$3b_1$	19.77	14.56	F(p) 0.35 C(p) 0.33 H(s) 0.32	$3b_1$	17.80	13.90	Ge(p) 0.14 Cl(p) 0.37 C(p) 0.28 H(s) 0.20
$1a_2$	19.98	13.60	C(p) 0.50 H(s) 0.50	$1a_2$	20.66	14.80	F(p) 0.08 C(p) 0.47 H(s) 0.45	$1a_2$	20.36	14.78	C(p) 0.51 H(s) 0.43
$2b_1$	20.14	13.80	Ge(p) 0.06 C(p) 0.50 H(s) 0.44	$2b_1$	21.95	15.38	Ge(p) 0.12 F(p) 0.43 C(p) 0.25 H(s) 0.19	$2b_1$	20.92	15.20	Ge(p) 0.11 Cl(p) 0.08 C(p) 0.44 H(s) 0.34
$3a_1$	21.66	14.30	Ge(s) 0.09 Ge(p) 0.05 C(p) 0.48 H(s) 0.36	$4a_1$	22.64	15.80	Ge(p) 0.09 F(p) 0.12 C(p) 0.41 H(s) 0.34	$4a_1$	21.63	15.47	Ge(s) 0.16 Cl(s) 0.26 Cl(p) 0.20 C(p) 0.22 H(s) 0.15

TABLE 1 (*Concluded*)

H				F			Cl			
Orbital	CNDO/2	Exp.	Parentage	Orbital	CNDO/2	Exp.	Parentage	Orbital	CNDO/2	Exp.	Parentage
$2b_2$	22.62	14.90	Ge(p)0.20 H(^1s)0.10 C(p)0.39 H(s)0.32	$2b_2$	22.73	16.80	Ge(p)0.11 F(s)0.03 F(p)0.22 C(p)0.35 H(s)0.28	$2b_2$	21.80	16.35	Ge(p)0.05 Cl(s)0.20 Cl(p)0.09 C(p)0.35 H(s)0.30
$2a_1$	23.08	16.90	Ge(s)0.37 Ge(p)0.07 H(^1s)0.23 C(p)0.20 H(s)0.12	$3a_1$	22.84	17.52	Ge(s)0.36 F(s)0.04 F(p)0.29 C(p)0.22 H(s)0.08	$3a_1$	22.33	17.00	Ge(s)0.132 Ge(p)0.06 Cl(p)0.03 C(p)0.45 H(s)0.31

bonding orbital while the latter is best described as a Ge—C bonding orbital. In general, the energy of the Ge(p)—C bonding orbitals remains essentially constant in all three molecules which is consistent with the very similar Ge—C bond lengths that have been reported (14, 15). Also, there is an indication that the Ge—H bonding is not changing significantly along the series trihydride to monohydride which correlates with reported bond lengths of Ge—H in $MeGeH_3$ (1.529 Å) (15) and Me_3GeH (1.532 Å) (14). The predominantly CH_3-group bonding orbitals around 14 eV are relatively broad features in Me_2GeH_2 as was also observed for $MeGeH_3$ and Me_3GeH. There are, however, four fairly sharp peaks within the envelope which are assigned to the $1a_2$, $2b_1$, $3a_1$ and $2b_2$ orbitals in accord with the CNDO/2 predictions. The correlation diagram (Fig. 2) illustrates the similar energies in all three hydrides of these orbitals involving the methyl groups. Finally, the $2a_1$ orbital has the characteristic feature noted for the presence of the s-orbital of germanium (1, 2, 23), namely, the marked increase in its peak height in the He(II) spectrum relative to a virtually insignificant peak in the He(I) spectrum. Thus, its assignment at 17.0 eV is confirmed.

The He(I) and He(II) spectra of Me_2GeF_2 (Fig. 1) are assigned as shown in Table 1. The number of orbitals in Me_2GeF_2 increases as compared with Me_2GeH_2 because of the presence of the p orbitals of fluorine that are available for bonding. The $4b_1$ and $4b_2$ orbitals of Me_2GeF_2 are the central orbitals in the transition of the $5e$ orbital in $MeGeF_3$, which mainly involves fluorine and germanium orbitals, into the $5e$ orbital of Me_3GeF, where it essentially involves Ge—C bonding (Fig. 3). The $4b_1$ can be described as a Ge—C orbital and the $4b_2$ as a lone-pair orbital. This could account for the considerable splitting in their energies in contrast with the hydrides. The three remaining fluorine "lone-pair orbitals", the "methyl bonding orbitals", and the "Ge(p)—F(p) bonding orbitals", all fall relatively close together to form a large envelope, and the orbitals, with the exception of $2a_2$, have considerably mixed character. The lone-pair orbitals, $3b_2$ and $5a_1$, which include contributions from CH_3 bonding orbitals, are around the 14 eV region (Table 1). In the trifluoride, the corresponding orbitals are distinctly more stabilized while in the monofluoride, those that transform mainly as the lone-pairs are slightly destabilized. The $1a_2$ orbital in Me_2GeF_2, as well as the orbitals with which it is correlated in the series $MeGeF_3$, Me_2GeF_2, and Me_3GeF, are all found in the range of 15.5–14.2 eV. The gradual destabilization across the series correlated well with

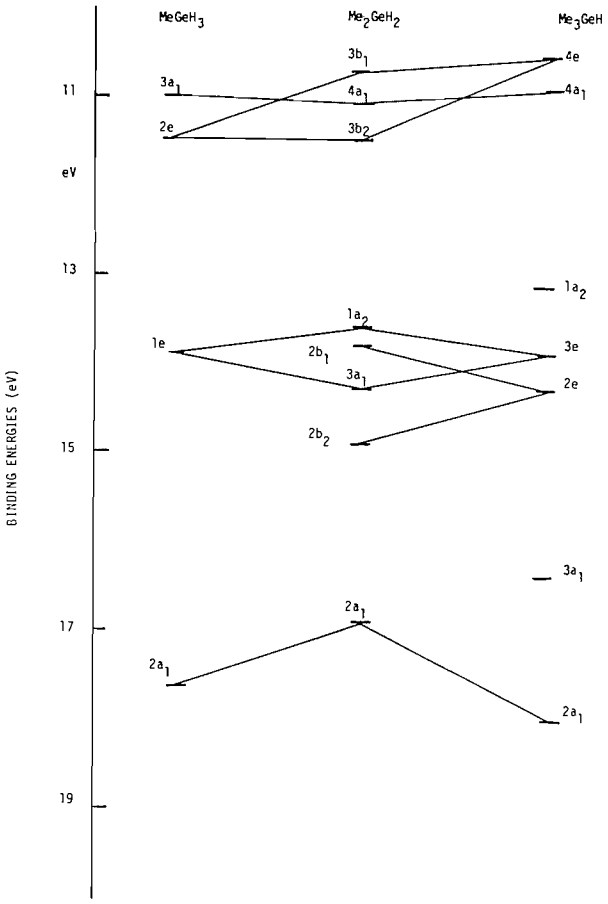

FIG. 2. Correlation of the binding energies across the series $MeGeH_3$, Me_2GeH_2, and Me_3GeH.

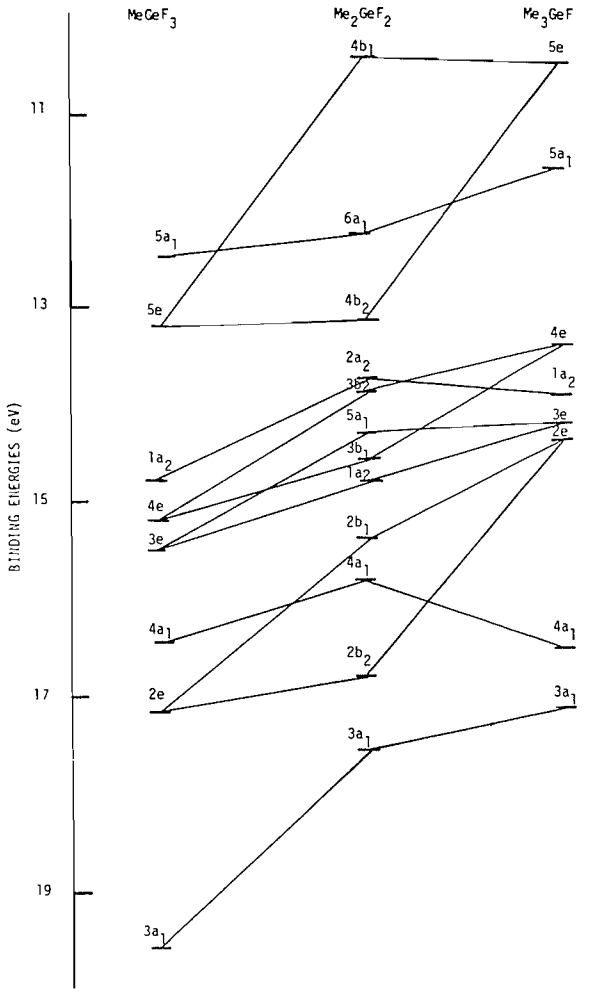

FIG. 3. Correlation of the binding energies across the series $MeGeF_3$, Me_2GeF_2, and Me_3GeF.

the successive substitution of methyl groups for fluorine. Thus, the predominantly fluorine lone-pair $3e$ orbital in $MeGeF_3$ at 15.5 eV, splits into the $5a_1$ (14.56 eV) and $1a_2$ (14.80) eV orbitals in Me_2GeF_2, both of which have increased CH_3 character. Further destabilization occurs when the $1a_2$ and $5a_1$ orbitals are correlated to the predominantly $CH_3(3e)$ orbital in Me_3GeF (14.2 eV). As in the case of the $4b_1$ and $4b_2$ orbitals, there is considerable splitting in energy between the $2b_1$ and $2b_2$ orbitals. The $4a_1$ orbital which according to the CNDO/2 calculations is the most stable of those involving mainly methyl groups, is assigned to the 13–15 eV region. The correlation diagram (Fig. 3) suggests that the assignment of the $4a_1$ orbital, which caused us some difficulties in Me_3GeF, should be in the region of 14.9–16.5 eV, rather than at 17.5, as we tentatively suggested in our earlier paper (1). The $3a_1$ orbital is assigned on the basis of the marked increase in its relative intensity in the He(II) spectrum which is expected from the CNDO/2 predictions of considerable contributions from the *s*-orbital of germanium. It is less stable than the most stable orbital assigned in $MeGeF_3$, but slightly stabilized relative to the corresponding orbital in Me_3GeF. There is a correlation between destabilization and increase in Ge—F bond length across the series ($MeGeF_3$, 1.714 Å; Me_2GeF_2, 1.739 Å; and Me_3GeF, 1.742 Å) (16).

The He(I) and He(II) spectra of Me_2GeCl_2 (Fig. 1) are assigned as indicated in Table 1. As in the fluorides there is a steady destabilization in the highest a_1 orbital along the $MeGeCl_3$, Me_2GeCl_2, and Me_3GeCl series (Fig. 4). The CNDO/2 calculations predict that there should be less energy difference between the $4b_1$ and $4b_2$ orbitals in Me_2GeCl_2 compared with Me_2GeF_2 and this is indeed the case. As with the fluoride, the b_2 orbital is closer in energy to the $5e$ orbital in $MeGeCl_3$ and the b_1 orbital is closer in energy to the $3e$ orbital in Me_3GeCl. There

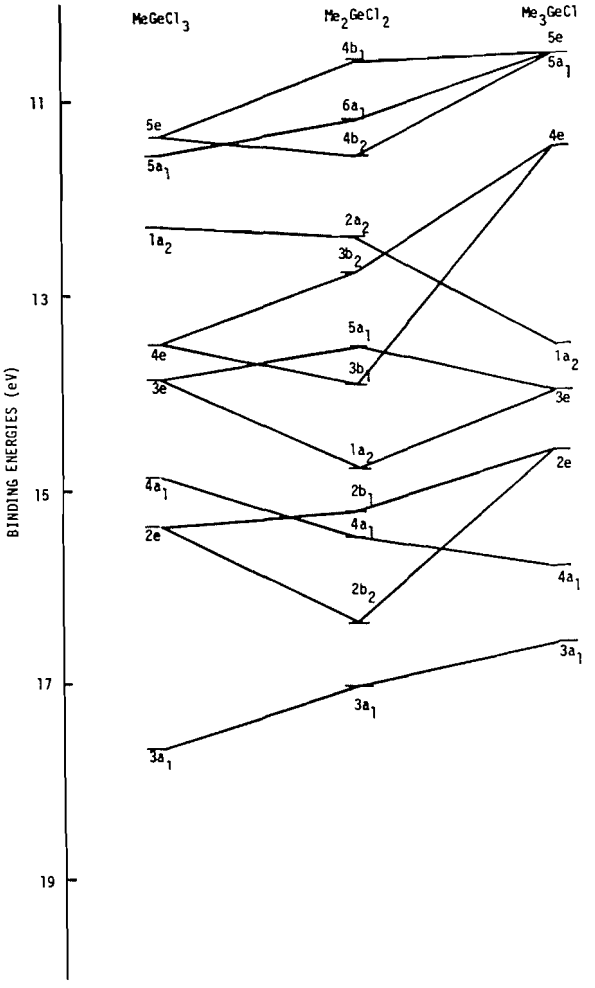

FIG. 4. Correlation of the binding energies across the series $MeGeCl_3$, Me_2GeCl_2, and Me_3GeCl.

is little change in the energy of the a_2 orbitals between $MeGeCl_3$ and Me_2GeCl_2 as both represent a lone-pair of chlorine (12.30 eV and 12.40 eV respectively). However, in Me_3GeCl the orbital is more stabilized as it now consists mainly of methyl group bonding (13.90 eV). The principal lone-pair chlorine orbitals, $2a_2$, $3b_2$, and $5a_1$ in Me_2GeCl_2 are clearly less energetically stable than those in the fluorides. The $2b_1$ and $2b_2$ orbitals show a noticeable degree of splitting. The latter orbital is apparently considerably stabilized because of contributions from the *s*-orbital of chlorine. This increasing participation of the *s*-orbitals also accounts for the fact that across the chloride series for the $4a_1$–$4a_1$–$4a_1$ sequence there is stabilization. The trend in the most stable valence orbitals involving the *s*-orbitals of germanium reverts to the sequence which shows increasing destabilization as chlorine is substituted by methyl groups. This essentially linear decrease in the energy of related orbitals was also noted for the series $MeSiCl_3$–Me_2SiCl_2–Me_3SiCl and also interpreted as indicating that the inductive effects of the Me and Cl groups predominate and that *d*-orbital participation need not be invoked (24). The lack of important involvement by *d*-orbitals was also indicated in work on silicon hydride derivatives (22, 25).

The first IP remains remarkably constant for all three molecules, Me_2GeX_2, X = H, F, Cl, suggesting that the Ge—C bonding characteristic predominates in all three cases despite the contributions from the F and Cl *p*-orbitals. The overlap integral matrices suggest that these *p*-orbitals of F and Cl are slightly anti-bonding and this factor apparently just overrides the general inductive stabilizing effect that might have been expected along the series Me_2Ge–(H_2)–(Cl_2)–(F_2). It is also interesting to note that the first IP in Me_2SiH_2 (11.2 eV) (22) is close to that in Me_2SiCl_2 (10.99 eV) (24) and both values are only slightly greater than those in the germanium analogues. Thus a change in the central atom from germanium to silicon causes only slight changes in the general features of the photoelectron spectra.

The plot of $-$CNDO/2 vs. experimental ionisation energies gives a slope of -1.40 and an intercept of 0.31 which compare very favourably with values reported for similar series (26) and for those we previously reported for Me_3GeX (1) and $MeGeX_3$ (2). In none of the calculations did we consider *d*-orbital participation by germanium. As with our earlier studies, we noted ill-defined features in the region above 20 eV which could correspond to the 2*s*-orbitals of carbon. In the spectra of Me_2GeCl_2 there were further peaks that probably indicate the 3*s*-orbitals of chlorine.

Acknowledgements

We thank the Natural Sciences and Engineering Research Council of Canada for financial support. One of us (J.E.D.) thanks Professor N. B. Jonathan and Dr. J. M. Dyke for providing space at the University of Southampton and for helpful discussions during a sabbatical leave.

1. J. E. DRAKE, B. M. GLAVINČEVSKI, and K. GORZELSKA. J. Electron Spectrosc. **16**, 331 (1979).
2. J. E. DRAKE, B. M. GLAVINČEVSKI, and K. GORZELSKA. J. Electron Spectrosc. To be published.
3. A. E. JONAS, G. K. SCHWEITZER, F. A. GRIMM, and T. A. CARLSON. J. Electron Spectrosc. **1**, 29 (1972/73).
4. J. C. GREEN, M. L. H. GREEN, P. J. JOACHIM, A. F. ORCHARD, and D. W. TURNER. Philos. Trans. R. Soc. London A, **269**, 111 (1970).
5. P. J. BASSETT and D. R. LLOYD. Chem. Phys. Lett. **3**, 22 (1969).

6. P. J. BASSETT and D. R. LLOYD. J. Chem. Soc. A, 641 (1971).
7. B. P. PULLEN, T. A. CARLSON, W. E. MODDEMAN, G. K. SCHWEITZER, W. E. BULL, and F. A. GRIMM. J. Chem. Phys. **53**, 768 (1970).
8. S. EVANS, J. C. GREEN, P. J. JOACHIM, A. F. ORCHARD, D. W. TURNER, and J. P. MAIER. Trans. Faraday Soc. II, **6**, 905 (1972).
9. R. BOSCHI, M. F. LAPPERT, J. B. PEDLEY, W. SCHMIDT, and B. T. WILKINS. J. Organomet. Chem. **50**, 69 (1973).
10. A. FLAMINI, E. SEMPRINI, F. STEFANI, S. SORRISO, and G. CARDACI. J. Chem. Soc. A, 731 (1976).
11. D. RINALDI. Université de Nancy. GEOMO, QCPE 290 available through Quantum Chemistry Program Exchange, University of Indiana.
12. J. HINZE and H. H. JAFFE. J. Am. Chem. Soc. **84**, 540 (1962); J. Phys. Chem. **67**, 1501 (1963).
13. E. CLEMENTI and D. L. RAIMONDI. J. Chem. Phys. **38**, 2686 (1963).
14. J. R. DURIG, M. M. CHEN, Y. S. LI, and J. B. TURNER. J. Phys. Chem. **77**, 227 (1973).
15. V. W. LAURIE. J. Chem. Phys. **30**, 1210 (1959).
16. J. E. DRAKE, R. T. HEMMINGS, J. L. HENCHER, F. M. MUSTOE, and Q. SHEN. J. Chem. Soc. Dalton, 394 (1976).
17. J. E. DRAKE, J. L. HENCHER, and Q. SHEN. Can. J. Chem. **55**, 1104 (1977).
18. J. E. DRAKE, B. M. GLAVINĆEVSKI, R. T. HEMMINGS, and H. E. HENDERSON. Inorg. Synth. **18**, 154 (1978).
19. J. W. ANDERSON, G. K. BARKER, A. J. F. CLARK, J. E. DRAKE, and R. T. HEMMINGS. Spectrochim. Acta, **30**A, 1081 (1974).
20. H. SCHMIDBAUR. Chem. Ber. **97**, 1639 (1964); J. E. GRIFFITHS. J. Chem. Phys. **38**, 2879 (1963); D. F. VAN DE VONDEL and G. P. VAN DER KELEN. Bull. Soc. Chim. Belg. **74**, 467 (1965).
21. G. K. BARKER, J. E. DRAKE, and R. T. HEMMINGS. Can. J. Chem. **53**, 2622 (1974); J. E. GRIFFITHS. Spectrochim. Acta, **20**A, 1335 (1964).
22. L. SZEPES, G. NARAY-SZABO, F. P. COLONNA, and G. DISTEFANO. J. Organomet. Chem. **117**, 141 (1976).
23. S. CRADOCK. Chem. Phys. Lett. **10**, 291 (1971).
24. M. C. GREEN, M. F. LAPPERT, J. B. PEDLEY, W. SCHMIDT, and B. T. WILKINS. J. Organomet. Chem. **31**, C55 (1971).
25. W. B. PERRY and W. L. JOLLY. J. Electron Spectrosc. **4**, 219 (1974).
26. H. BOCK. Angew. Chem. Int. Ed. **16**, 613 (1977).

The crystal and molecular structures of bromotricarbonyl(phenylbis(3,5-dimethylpyrazolyl)phosphine)rhenium(I) and tricarbonyl(phenylbis(3,5-dimethylpyrazolyl)phosphine)tungsten(0)

R. E. COBBLEDICK, L. R. J. DOWDELL, F. W. B. EINSTEIN,[1] J. K. HOYANO, AND L. K. PETERSON

Department of Chemistry, Simon Fraser University, Burnaby, B.C., Canada V5A 1S6

Received November 9, 1978

R. E. COBBLEDICK, L. R. J. DOWDELL, F. W. B. EINSTEIN, J. K. HOYANO, and L. K. PETERSON. Can. J. Chem. **57**, 2285 (1979).

Crystals of $[Re(CO)_3(P(Me_2pz)_2C_6H_5)Br]$ (where Me_2pz is 3,5-dimethylpyrazolyl) are monoclinic, space group $P2_1/c$, with $a = 8.964(4)$, $b = 14.441(10)$, $c = 18.156(8)$ Å, $\beta = 111.32(4)°$, and $Z = 4$. Crystals of $W(CO)_3(P(Me_2pz)_2(C_6H_5))$ are monoclinic, space group $P2_1/c$, with $a = 12.479(7)$, $b = 10.207(4)$, $c = 16.118(7)$ Å, $\beta = 98.77(2)°$, and $Z = 4$. In both structures there is irregular octahedral geometry about the metal atom with the carbonyl groups in a *fac* arrangement. The phenylbis(3,5-dimethylpyrazolyl)phosphine ligand, $[P(Me_2pz)_2(C_6H_5)]$, is coordinated to the tungsten atom through the two 2N nitrogen atoms of the pyrazolyl rings and to two carbon atoms of the phenyl ring so that the ligand is essentially tridentate. In the rhenium complex this ligand is bidentate with coordination via the 2N nitrogen atoms with a bromine atom occupying the sixth site.

R. E. COBBLEDICK, L. R. J. DOWDELL, F. W. B. EINSTEIN, J. K. HOYANO et L. K. PETERSON. Can. J. Chem. **57**, 2285 (1979).

Les cristaux de $[Re(CO)_3(P(Me_2pz)_2C_6H_5)Br]$ (où Me_2pz = diméthyl-3,5 pyrazolyle) sont monocliniques, groupe d'espace $P2_1/c$ avec $a = 8.964(4)$, $b = 14.441(10)$, $c = 18.156(8)$ Å, $\beta = 111.32(4)°$ et $Z = 4$. Les cristaux de $W(CO)_3(P(Me_2pz)_2(C_6H_5))$ sont monocliniques, groupe d'espace $P2_1/c$ avec $a = 12.479(7)$, $b = 10.207(4)$, $c = 16.118(7)$ Å, $\beta = 98.77(2)°$ et $Z = 4$. Dans les deux structures, la géométrie autour de l'atome de métal est octaédrique régulière et les groupes carbonyles sont dans un arrangement *fac*. Le ligand phénylbis(diméthyl-3,5 pyrazolyl)phosphine, $[P(Me_2pz)_2C_6H_5]$ est coordonné à l'atome de tungstène par les deux atomes d'azotes 2N des noyaux pyrazolyles et à deux atomes de carbone des noyaux phényles d'une façon telle que le ligand est essentiellement tridentate. Dans le complexe de rhénium, ce ligand est bidentate avec une coordination par l'intermédiaire des atomes d'azotes 2N avec un atome de brome occupant le sixième site.

[Traduit par le journal]

Introduction

The syntheses of a number of complexes of the set of ligands $\phi_x(R_2pz)_{3-x}$ ($x = 0$–2; R_2pz = pyrazolyl or 3,5-dimethylpyrazolyl, ϕ = phenyl) have been reported, together with structural assignments based on mass, infrared, ^1H, and ^{31}P nmr spectroscopic data (1). The modes of coordination of the pyrazolylphosphines are illustrated in structures **1**–**12**. The four-membered PNNM metallocycle in **1** was confirmed by an X-ray diffraction study (2). The PNNM metallocycles in the Mo(0) and W(0) derivatives (**3** and **4**) are more susceptible to ring opening reactions than in the Mn(I) and Re(I) analogues (**1** and **2**). Thus, the phosphorus bonded derivatives $[(\phi_2P(R_2pz))_2M(CO)_4]$ (M = Mo, W) are readily obtained, contrasting with the failure to obtain corresponding bis-phosphine analogues of Mn(I) and Re(I). In the remaining complexes **5**–**7**, the phosphorus atom does not appear to coordinate to the

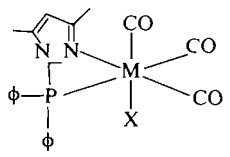

1, M = Mn, X = Cl
2, M = Re, X = Br
3, M = Mo, X = CO
4, M = W, X = CO

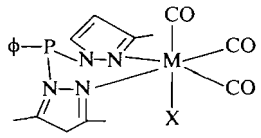

5, M = Mn, X = Cl
6, M = Re, X = Br
7, M = Mo, X = CO
8, M = W, X = CO

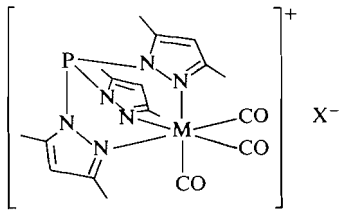

9, M = Mn, X = Cl
10, M = Re, X = Br
11, M = Mo, X not present
12, M = W, X not present

[1]To whom all correspondence should be addressed.

0008-4042/79/172285-07$01.00/0

TABLE 1. Data collection information

	Re cpd	W cpd
Radiation	Nb-filtered Mo Kα	Graphite monochromated Mo Kα
Scan	θ–2θ	θ–2θ
Scan rate	2° min^{-1} in 2θ	2° min^{-1} in 2θ
Base width	1.5° (increased for dispersion)	1.3° for 0° < 2θ ≤ 30° and 1.0° for 30° < 2θ ≤ 40° (both increased for dispersion)
Background count time	20 s at each side of scan	4 s for 0° < 2θ ≤ 30° and 10 s for 30° < 2θ ≤ 40° at each side of scan.
Maximum 2θ	40°	40°
Unique reflections recorded	2057	1901
Observed reflections	1362 with $I > 3\sigma(I)$	1467 with $I > 2.3\sigma(I)$
Number of parameters varied	132	138

metal centre; reduced basicity of the phosphorus atom has been attributed to the electron-withdrawing effects of the attached pyrazolyl rings. The *facial* structures **5** and **6** seem to be preferred over *meridial* structures containing *trans* CO groups. Compounds **7** and **8** give rise to tricarbonyl species $[\phi P(R_2pz)_2M(CO)_3]$, obtainable in two isomeric forms (red and yellow). These isomers give identical mass spectra, but show distinct infrared, ^1H, and ^{31}P nmr spectra. This work describes the structure determination of the red form of $[\phi P(Me_2pz)_2W(CO)_3]$ and of compound **6**. The X-ray diffraction study of $[\phi P(Me_2pz)_2W(CO)_3]$ (red) shows that a portion of the phenyl ring occupies one of the coordination sites of the six coordinate tungsten centre in a rather unusual fashion.

Tris-chelate structures analogous to **9–12** have been postulated for various pyrazolylborate complexes, including $[RB(R_2pz)_3Mn(CO)_3]$, $[B(R_2pz)_4Mn(CO)_3]$, and $[HB(Me_2pz)_3M(CO)_3]^-$ (M = Mo, W) (3). Based on ir data (ν_{CO} region), the ligands $P(Me_2pz)_3$ and $HB(Me_2pz)_3$ coordinate in essentially the same way to Mo(0) and W(0) in comparable tricarbonyl complexes. While the given tris-chelate structures for **9** and **10** are consistent with nmr and ir data, an alternative bis-chelate structure, containing covalently bound halogen and rapidly exchanging pyrazolyl groups, cannot as yet be ruled out.

The structural studies reported here were undertaken in order to corroborate proposed structures, and to help clarify the uncertainties described above.

Experimental

Structure Determination of $[Re(CO)_3(P(Me_2pz)_2C_6H_5)Br]$

A colourless crystal in the form of a rectangular prism of approximate dimensions 0.09 × 0.25 × 0.33 mm was used in the X-ray analysis. The space group was determined from the absent reflections on photographs taken with Cu Kα radiation. Unit cell parameters were obtained by least-squares refinement from the setting angles of 12 reflections centred on a Picker FACS-I automatic diffractometer using Mo Kα radiation.

Crystal data are shown below:

$C_{19}H_{19}N_4O_3PBrRe$ fw = 648.50
Monoclinic, $a = 8.964(4)$, $b = 14.441(10)$, $c = 18.156(8)$ Å, $\beta = 111.32(4)°$, $V = 2189.4$ Å^3, $Z = 4$, $\rho_c = 1.967$, $\rho_m = 1.94$ g cm^{-3} (by flotation), μ(Mo Kα) = 79.1 cm^{-1}, $T = 22°C$. Absent reflections: $h0l$, $l = 2n + 1$ and $0k0$, $k = 2n + 1$ uniquely define the space group $P2_1/c$.

Details concerning the collection of intensity data are shown in Table 1. Lorentz and polarization corrections were applied to the intensities but no absorption correction was made. The extreme error in F resulting from this is estimated to be ±18%.

The rhenium atom position was determined from a Patterson map and the remaining non-hydrogen atom positions were obtained from subsequent Fourier and electron density difference maps. Full-matrix least-squares refinement using anisotropic thermal parameters for the rhenium, bromine, and phosphorus atoms and isotropic ones for the remaining atoms gave a factor $R = 0.085$ (where $R = \sum ||F_o| - |F_c|| / \sum |F_o|$). An electron density difference map indicated regions of excess (1.4–2.2 e Å^{-3}) and deficient electron density ($\simeq -3.3$ e Å^{-3}) in the neighbourhood of the rhenium atom compared with $\simeq 6$ e Å^{-3} for a typical carbon atom. The map did not reveal the positions of the hydrogen atoms and these were omitted from the structure. There was no evidence of anisotropic motion of the lighter atoms and consequently the refinement was terminated at this stage. Unit weights were used through-

TABLE 2. Final fractional atomic coordinates

(*a*) Re complex ($\times 10^3$, except Re, Br, and P $\times 10^4$)

Atom	*x*	*y*	*z*
Re	−3(3)	2069(2)	817(1)
Br	−1766(9)	3334(5)	−145(4)
P	535(20)	2960(12)	2843(8)
N11	127(5)	323(3)	150(2)
N12	149(5)	347(3)	227(2)
C11	237(7)	419(4)	254(3)
C12	301(8)	452(5)	195(4)
C13	230(7)	390(4)	134(3)
C14	280(8)	464(5)	335(4)
C15	241(7)	394(4)	50(4)
N21	−169(4)	221(3)	145(2)
N22	−125(6)	271(4)	216(3)
C21	−270(7)	287(5)	229(3)
C22	−399(7)	245(5)	169(4)
C23	−320(8)	210(5)	128(4)
C24	−280(9)	331(5)	307(4)
C25	−422(7)	179(4)	34(4)
C31	145(6)	184(4)	309(3)
C32	314(7)	177(5)	339(4)
C33	392(7)	99(4)	370(3)
C34	303(7)	25(4)	379(3)
C35	141(7)	25(4)	352(3)
C36	61(7)	109(4)	317(3)
C1	−98(8)	109(5)	28(4)
O1	−175(6)	44(4)	−16(3)
C2	110(6)	199(4)	12(3)
O2	195(5)	186(3)	−24(2)
C3	124(6)	118(4)	147(3)
O3	225(6)	63(3)	179(3)

TABLE 2 (*Concluded*)

(*b*) W complex ($\times 10^4$, except W $\times 10^5$)

Atom	*x*	*y*	*z*
W	23839(9)	21814(9)	11095(6)
P	2998(6)	5166(6)	385(4)
N11	1411(13)	3335(16)	60(10)
N12	1845(14)	4555(18)	−154(11)
C11	1134(19)	5018(23)	−834(14)
C12	323(18)	4204(24)	−1028(14)
C13	488(17)	3151(22)	−449(13)
C14	1396(22)	6278(29)	−1244(17)
C15	−170(19)	1960(25)	−414(15)
N21	2348(13)	4147(17)	1769(10)
N22	2730(14)	5221(18)	1374(10)
C21	2669(17)	6280(23)	1925(14)
C22	2321(17)	5887(22)	2580(14)
C23	2107(16)	4491(21)	2486(13)
C24	3075(20)	7594(25)	1664(16)
C25	1672(19)	3627(25)	3078(15)
C31	3754(18)	3580(23)	443(14)
C32	3818(21)	2965(28)	−302(16)
C33	4624(26)	2078(33)	−325(20)
C34	5334(27)	1783(33)	361(23)
C35	5232(27)	2276(36)	1111(21)
C36	4470(25)	3252(31)	1140(19)
C1	3275(23)	1306(30)	2040(18)
O1	3758(21)	701(19)	2580(14)
C2	2479(19)	615(27)	412(15)
O2	2459(15)	−307(14)	17(10)
C3	1327(23)	1542(31)	1489(17)
O3	528(18)	912(17)	1752(11)
H121	−30	433	−148
H141	206	644	−142
H142	135	701	−87
H143	90	643	−175
H151	−82	208	−8
H152	27	121	−13
H153	−51	164	−99
H221	222	645	308
H241	383	772	191
H242	262	830	194
H243	290	769	100
H251	168	276	281
H252	90	395	304
H253	193	346	375
H321	322	313	−80
H331	467	169	−92
H341	592	114	28
H351	570	200	164
H361	437	360	171

out. Anomalous dispersion corrections were applied to the rhenium, bromine, and phosphorus atoms. Atomic scattering factors for rhenium were taken from ref. 4 and those of ref. 5 were used for the rest of the atoms. Crystallographic computer programs used in the analysis have been cited elsewhere (6).

Final positional parameters for both compounds are listed in Table 2 and the thermal parameters in Table 3. A listing of calculated structure factors and observed structure amplitudes has been deposited in the Depository of Unpublished Data.[2]

Structure Determination of $[W(CO)_3(P(Me_2pz)_2C_6H_5)]$

Unless otherwise stated in the text or Table 1 the experimental details are the same as for the rhenium compound. Crystals of the complex were obtained as red platelets elongated along the *b* axis. A plate-shaped crystal of dimensions 0.20 × 0.45 × 0.15 mm was used for the data collection. The crystal was mounted with the *b* axis offset from the ϕ axis of the diffractometer. No correction for absorption was applied to the data and, in extreme cases, the error in *F* could be ±7%.

Crystal data are shown below:

$C_{19}H_{19}N_4O_3PW$ fw = 566.23

Monoclinic, $a = 12.479(7)$, $b = 10.207(4)$, $c = 16.118(7)$ Å, $\beta = 98.77(2)°$, $V = 2029.0$ Å^3, $Z = 4$, $\rho_c = 1.853$, $\rho_m = 1.83$ g cm^{-3} (by flotation), Mo Kα radiation ($\lambda = 0.70926$ Å), μ(Mo Kα) = 61.2 cm^{-1}, $T = 23°$C. Absent reflections: $h0l$, $l = 2n + 1$ and $0k0$, $k = 2n + 1$ uniquely define the space group $P2_1/c$.

The coordinates of the tungsten atom were determined from the Patterson map and those of the remaining non-hydrogen atoms were determined from subsequent Fourier and difference maps. Anisotropic thermal parameters were introduced for those atoms indicating anisotropy on the difference maps. The coordinates of the 19 hydrogen atoms eventually were revealed by a difference map. These hydrogen atoms were included in the structure factor calculations but not allowed

[2]The listing is available, at a nominal charge, from the Depository of Unpublished Data, CISTI, National Research Council of Canada, Ottawa, Ont., Canada K1A 0S2.

TABLE 3. Final thermal motion parameters

(*a*) Anisotropic thermal parameters ($U_{ij} \times 10^3$ Å^2) except for ($U_{ij} \times 10^4$ Å) for W atom of the form exp $[-2\pi^2(h^2a^{*2}U_{11} + \cdots + 2hka^*b^*U_{12} + \cdots)]$

Atom	U_{11}	U_{22}	U_{33}	U_{12}	U_{13}	U_{23}
			Re complex			
Re	63(2)	38(1)	18(1)	10(2)	21(2)	−1(1)
Br	93(6)	62(5)	34(4)	25(4)	10(4)	9(3)
P	91(12)	42(10)	22(7)	5(10)	23(8)	2(8)
			W complex			
W	712(10)	155(9)	506(10)	18(6)	−81(5)	24(6)
P	81(5)	25(4)	52(4)	−11(4)	−1(4)	1(3)
O1	249(28)	45(13)	122(18)	30(16)	−106(19)	11(13)
O2	127(16)	11(9)	76(12)	9(10)	20(11)	−20(9)
O3	164(20)	42(11)	69(12)	2(13)	−8(13)	−24(10)

(*b*) Isotropic thermal parameters

Atom	$U \times 10^3$ Å^2	Atom	$U \times 10^3$ Å^2
	Re complex		
N11	36(12)	C25	67(19)
N12	40(12)	C31	39(14)
C11	54(16)	C32	60(19)
C12	71(20)	C33	56(17)
C13	53(16)	C34	58(17)
C14	73(21)	C35	57(17)
C15	67(18)	C36	55(17)
N21	28(10)	C1	70(20)
N22	66(15)	O1	90(15)
C21	68(18)	C2	45(15)
C22	67(18)	O2	60(12)
C23	67(18)	C3	38(14)
C24	88(23)	O3	81(14)
	W complex		
N11	39(5)	C23	41(6)
N12	51(5)	C24	70(8)
C11	56(7)	C25	64(7)
C12	57(7)	C31	52(6)
C13	50(7)	C32	77(8)
C14	86(9)	C33	106(11)
C15	65(7)	C34	111(11)
N21	40(5)	C35	113(11)
N22	48(5)	C36	98(10)
C21	49(6)	C1	83(9)
C22	48(6)	C2	56(7)
		C3	79(9)

to refine. The final R was 0.067 for the observed reflections. At this stage the only significant peaks (2.2–3.3 e Å^{-3}) were close to the tungsten atom. The maximum parameter shift was 0.15σ. Initially unit weights were used but in the later stages of refinement a weighting scheme was used with weights, $w = 1/\sigma^2(F)$. Anomalous dispersion factors were used for the tungsten atom and these and the atomic scattering factors were taken from ref. 7, except for the hydrogen atoms which were taken from ref. 8.

Results and Discussion

Perspective views of the rhenium and tungsten complex molecules are shown respectively in Figs. 1 and 2. Bond lengths and angles (excepting those involving hydrogen atoms) are listed in Tables 4 and 5. In both structures there is an irregular octahedral configuration around the central metal atom and in each case the three carbonyl groups have a *fac* arrangement. The phenylbis(3,5-dimethylpyrazolyl)-phosphine ligands coordinate via the two 2N nitrogen atoms of the pyrazolyl rings in both structures and the nitrogen atoms are *trans* to carbonyl groups. In the rhenium complex the sixth site is occupied by a bromine atom while in the tungsten complex the site is occupied by two carbon atoms of the phenyl group of the $P(Me_2pz)_2(C_6H_5)$ ligand. Both mole-

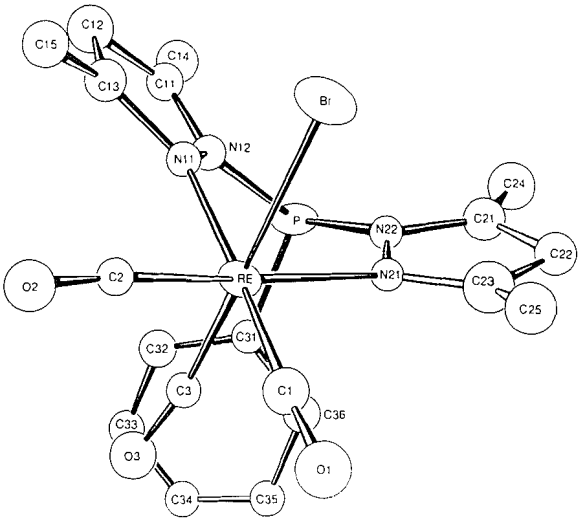

FIG. 1. Perspective view of $[Re(CO)_3(P(Me_2pz)_2C_6H_5)Br]$.

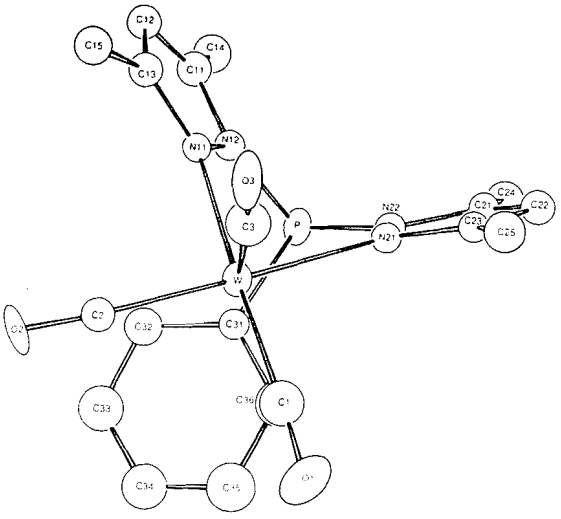

FIG. 2. Perspective view of $[W(CO)_3(P(Me_2pz)_2C_6H_5)]$.

cules have approximate non-crystallographic mirror symmetry about a plane containing atoms P, C3, O3 and the metal. The Re—Br distance is 2.623(7) Å and correction for the bromine riding motion on the metal atom gives 2.639 Å. The distance is intermediate in the range 2.469–2.769 Å reported for Re—Br distances (15). In both compounds there is little deviation from linearity of the carbonyl groups. As a result of the large errors, comparison of bond lengths and angles is of limited value. The carbon atom C3 in the tungsten complex behaved poorly in the least-squares refinement and the W—C3 bond length of 1.67(3) Å appears to be unreasonable. We attribute this to poor positioning of C3 (the C3—O3 distance is consequently long at 1.31(3) Å), despite various attempts to correct this

TABLE 4. Bond lengths (Å). Estimated standard deviations are given in parentheses

Bond	Length	
	Re complex	W complex
M—C1	1.76(7)	1.94(3)
M—C2	1.87(6)	1.97(3)
M—C3	1.83(6)	1.67(3)
M—N11	2.15(4)	2.26(2)
M—N21	2.21(4)	2.27(2)
M—Br	2.623(7)	—
M—C31	—	2.58(2)
M—C36	—	2.82(3)
P—N12	1.73(4)	1.68(2)
N11—N12	1.38(5)	1.42(2)
N12—C11	1.30(6)	1.38(3)
C11—C12	1.47(8)	1.31(3)
C12—C13	1.40(8)	1.42(3)
C13—N11	1.44(7)	1.32(2)
C11—C14	1.52(8)	1.50(3)
C13—C15	1.55(8)	1.47(3)
P—N22	1.67(5)	1.68(2)
N21—N22	1.41(6)	1.39(2)
N22—C21	1.42(7)	1.41(3)
C21—C22	1.41(8)	1.27(3)
C22—C23	1.32(8)	1.45(3)
C23—N21	1.28(7)	1.29(2)
C21—C24	1.59(9)	1.52(3)
C23—C25	1.67(9)	1.46(3)
C1—O1	1.27(7)	1.16(3)
C2—O2	1.19(6)	1.13(3)
C3—O3	1.18(6)	1.31(3)
P—C31	1.79(6)	1.87(2)
C31—C32	1.42(8)	1.37(3)
C32—C33	1.34(8)	1.36(4)
C33—C34	1.38(8)	1.34(4)
C34—C35	1.35(7)	1.33(4)
C35—C36	1.43(8)	1.38(4)
C36—C31	1.37(7)	1.37(3)

by placing it at a reasonable calculated starting position. Taking the W---O distances (2.97–3.10(5) Å) all three CO groups appear to be identical. The Re—N distances are 2.15(4), 2.21(4) Å while the W—N distances are 2.26(2) and 2.27(2) Å. In both structures the metal atom, the four nitrogen atoms, and the phosphorus atom form a six-membered ring with a boat configuration. In the rhenium compound the boat arrangement places the phenyl ring close to the carbonyl group *trans* to the bromine (C3---C31 = 3.04(7) Å). This interaction between the phenyl ring and the carbonyl group appears to displace the boat ring towards the bromine atom; the two N—Re—Br angles are 85(1)° and the two N—Re—C3 angles are 96(2)°. In the tungsten compound the boat ring is displaced in the opposite direction in such a way that C31 and C36 of the phenyl ring occupy the site occupied by the carbonyl group in the rhenium complex. The two N—W—C3 angles of 97(1) and 96(1)° indicate the displacement (cf. the comparable

N—Re—Br angles of 85(1)°). Another way of comparing the tilt of the boat ring is by examining the displacement of the ring atoms from the plane defined by the metal and the two carbonyl groups C2—O2 and C1—O1. Calculations for these and other relevant planes are shown in Table 6.

The W—C31 distance of 2.58(2) Å and the W—C36 distance of 2.82(2) Å, although longer than usual W—C contacts (e.g. 2.246 Å in bis-(η-cyclopentadienyl)bis-(3,5-dimethylbenzyl)tungsten (9)), are sufficiently short to suggest a weak interaction. In this way the tungsten atom could achieve an 18-electron configuration but, since the distances are long, the possibility of a 16-electron system certainly cannot be ruled out. All other W---C contacts with the phenyl ring are greater than 3.20 Å. The shorter contact involves the P-bonded carbon and the weaker interaction occurs with an *ortho* carbon. The assumed hydrogen atom on the *ortho* carbon atom does not point at the tungsten atom so the interaction is not similar to that observed in (diethyldi-1-pyrazolylborato)(trihapto-2-phenylallyl)-(dicarbonyl)molybdenum where the α carbon atom of an ethyl group is directed toward the molybdenum atom (10), giving it an effective 18-electron

TABLE 5. Bond angles (deg). Estimated standard deviations are given in parentheses

Bond	Angle Re complex	Angle W complex
Br—M—N11	85(1)	—
Br—M—N21	85(1)	—
Br—M—C1	98(2)	—
Br—M—C2	86(2)	—
Br—M—C3	178(2)	—
C31—M—N11	—	73.4(6)
C36—M—N11	—	101.6(8)
C31—M—N21	—	76.7(7)
C36—M—N21	—	74.6(8)
C31—M—C1	—	104(1)
C36—M—C1	—	75(1)
C31—M—C2	—	96.3(9)
C36—M—C2	—	100.9(9)
C31—M—C3	—	168(1)
C36—M—C3	—	157(1)
N11—M—N21	87(1)	81.0(6)
N11—M—C1	177(2)	176(1)
N11—M—C2	98(2)	93.9(8)
N11—M—C3	96(2)	97(1)
N21—M—C1	94(2)	95(1)
N21—M—C2	170(2)	172.2(8)
N21—M—C3	96(2)	96(1)
C1—M—C2	82(3)	89(1)
C1—M—C3	81(3)	86(1)
C2—M—C3	93(2)	91(1)
M—N11—N12	129(3)	117(1)
M—N11—C13	130(3)	135(1)
P—N12—N11	126(3)	122(1)
P—N12—C11	118(4)	133(2)
N11—N12—C11	116(4)	106(2)
N12—C11—C12	109(5)	111(2)
C11—C12—C13	101(5)	107(2)
C12—C13—N11	114(5)	109(2)
C13—N11—N12	100(4)	108(2)
N12—C11—C14	128(5)	119(2)
C12—C11—C14	123(5)	130(2)
N11—C13—C15	120(5)	122(2)
C12—C13—C15	126(6)	129(2)
M—N21—N22	121(3)	117(1)
M—N21—C23	136(4)	133(2)
P—N22—N21	131(4)	123(1)
P—N22—C21	122(4)	131(2)
N21—N22—C21	106(4)	105(2)
N22—C21—C22	111(5)	110(2)
C21—C22—C23	98(6)	108(2)
C22—C23—N21	124(6)	107(2)
C23—N21—N22	102(5)	110(2)
N22—C21—C24	124(5)	117(2)
C22—C21—C24	124(6)	133(2)
N21—C23—C25	115(5)	126(2)
C22—C23—C25	118(6)	127(2)
P—C31—C32	119(4)	117(2)
P—C31—C36	122(4)	121(2)
C31—C32—C33	123(6)	118(3)
C32—C33—C34	118(6)	122(3)
C33—C34—C35	123(6)	121(3)
C34—C35—C36	118(6)	118(3)
C35—C36—C31	121(5)	121(3)
C36—C31—C32	117(5)	119(2)
N12—P—N22	101(2)	103(1)
N12—P—C31	104(2)	95(1)
N22—P—C31	103(3)	99(1)
M—C1—O1	174(6)	175(3)
M—C2—O2	171(5)	175(2)
M—C3—O3	165(5)	173(3)

TABLE 6. Deviations of atoms (Å) from least-squares planes. The equations of the planes are referred to orthogonal axes with x along the a axis, y along the b axis, and z along the c^* axis

(*a*) Plane through C31, C32, C33, C34, C35, and C36[a]

	W complex	Re complex
C31	0.01(2)	0.01(5)
C32	−0.02(3)	−0.02(7)
C33	0.01(3)	0.02(5)
C34	0.04(3)	−0.02(5)
C35	−0.05(4)	0.01(5)
C36	0.02(3)	0.00(5)
P	0.577(7)	−0.346(14)
M	−2.479(1)	3.403(2)
	$\chi^2 = 4.70$	$\chi^2 = 0.49$

[a]W complex: $0.6634x + 0.7192y - 0.2067z - 5.5077 = 0$; Re complex: $0.2987x - 0.3273y - 0.8965z + 5.7812 = 0$.

TABLE 6 (*Concluded*)

(*b*) Plane through N11, N12, C11, C12, and C13[b]

	W complex	Re complex
N11	0.01(2)	0.02(4)
N12	−0.01(2)	−0.02(4)
C11	0.00(2)	0.03(6)
C12	0.01(2)	0.00(7)
C13	−0.02(2)	−0.02(6)
P	−0.050(7)	0.05(2)
C14	0.06(3)	0.04(7)
C15	0.02(2)	0.07(6)
	$\chi^2 = 1.51$	$\chi^2 = 0.58$

[b]W complex: $0.6115x - 0.4798y - 0.6292z + 0.6360 = 0$; Re complex: $-0.7039x + 0.6133y - 0.3583z - 1.8312 = 0$.

(*c*) Plane through N21, N22, C21, C22, and C23[c]

	W complex	Re complex
N21	0.01(2)	0.01(4)
N22	−0.01(2)	−0.01(6)
C21	0.01(2)	0.01(7)
C22	0.00(2)	0.00(7)
C23	0.00(2)	−0.02(7)
P	0.162(7)	−0.27(2)
C24	−0.05(3)	−0.17(7)
C25	0.01(2)	0.42(6)
	$\chi^2 = 0.55$	$\chi^2 = 0.25$

[c]W complex: $-0.8779x + 0.1974y - 0.4362z + 2.5901 = 0$; Re complex: $0.0385x + 0.8488y - 0.5274z - 1.3120 = 0$.

(*d*) Plane through M, O1, and O2[d]

	W complex	Re complex
P	2.208(7)	−1.12(2)
N11	0.04(2)	0.00(4)
N12	1.09(2)	−0.52(4)
N21	0.17(2)	0.20(4)
N22	1.24(2)	−0.11(5)
C31	2.47(2)	−2.68(5)

[d]W complex: $0.8934x + 0.3336y - 0.3010z - 2.6250 = 0$; Re complex: $-0.4079x + 0.6263y - 0.6643z - 1.1745 = 0$.

configuration. In the analogous (diphenyldipyrazolylborato)(2-methylallyl) (dicarbonyl)molybdenum where it might have been expected that the 18-electron configuration would be achieved by interaction with an *ortho* C—H bond of a phenyl group (11) no such interaction occurs and the metal atom remains with a 16-electron configuration. Cotton proposes that the apparent reason for this is that the attainment of a satisfactory conformation of the four rings about the boron atom (the two pyrazole rings are fixed in coordination to the molybdenum) is inconsistent with the orientation of one of the phenyl groups to give such an interaction.

Two platinum structures in which two adjacent carbon atoms of a substituted benzene ring are bonded to a metal are known (12, 13). The Pt—C distances lie in the range 2.05(2)–2.15(2) Å. In both these structures the C—C bond distances are alternately short and long (i.e. double and single bonds) with the exception of the double bond coordinated to the metal atom which has been appreciably lengthened. In the present structure, the estimated standard deviations are too large to establish the significance of differences in bonds of this type but the distances appear typical. The interaction does not appear to be of this type and is more similar to that occurring in the structure of tris(triphenylphosphine)rhodium(I) perchlorate (14) in which the Rh atom is 2.48(2) Å from the P-bonded carbon atom, 2.62(2) Å from the *ortho* carbon atom, and 2.56 Å from the assumed *ortho* hydrogen atom and in the structure of bis(2-methyl-2-phenylpropyl)-manganese(II) (16) where the Mn—C distances are ca. 2.7 Å with the *ortho* hydrogen atom close to the manganese atom.

Acknowledgement

The National Research Council of Canada is thanked for financial support.

1. J. K. HOYANO and L. K. PETERSON. Can. J. Chem. **54**, 2697 (1976); Can. J. Chem. In press.
2. R. E. COBBLEDICK and F. W. B. EINSTEIN. Acta Crystallogr. B**33**, 2020 (1977).
3. S. TROFIMENKO. J. Am. Chem. Soc. **91**, 588 (1969); F. A. COTTON and C. S. KRAIHANZEL. Inorg. Chem. **2**, 533 (1963); J. Am. Chem. Soc. **84**, 4432 (1962); F. A. COTTON. Inorg. Chem. **3**, 702 (1964).
4. International Tables for X-ray Crystallography. Vol. III. Kynoch Press, Birmingham. 1962.
5. D. T. CROMER and J. T. WABER. Acta Crystallogr. **18**, 104 (1965).
6. F. W. B. EINSTEIN and R. D. G. JONES. Inorg. Chem. **11**, 395 (1972).
7. International Tables for X-ray Crystallography. Vol. IV. Kynoch Press, Birmingham. 1974.
8. R. F. STEWART, E. F. DAVIDSON, and W. T. SIMPSON. J. Chem. Phys. **42**, 3175 (1965).
9. R. A. FORDER, I. W. JEFFERSON, and K. POUT. Acta Crystallogr. B**31**, 618 (1975).
10. F. A. COTTON, T. LA COUR, and G. STANISLOWSKI. J. Am. Chem. Soc. **96**, 754 (1974).
11. F. A. COTTON, B. A. FRENZ, and C. A. MURILLO. J. Am. Chem. Soc. **97**, 2118 (1975).
12. J. BROWNING and B. R. PENFOLD. J. Cryst. Mol. Struct. **4**, 335 (1974).
13. R. E. COBBLEDICK and F. W. B. EINSTEIN. Acta Crystallogr. B**34**, 1849 (1978).
14. Y. W. YARED, S. L. MILES, R. BAU, and C. A. REED. J. Am. Chem. Soc. **99**, 7076 (1977).
15. I. D. BROWN. Bond index to the determinations of inorganic crystal structures. Institute for Materials Research, McMaster University, Hamilton, Ontario. 1969–1977.
16. R. A. ANDERSEN, E. CARMONA-GUZMAN, J. F. GIBSON, and G. WILKINSON. J. Chem. Soc. Dalton, 2204 (1976).

A spectrophotometric study of the complex formation between cobalt(III) and *trans*-1,2-cyclohexanedinitrilotetraacetic acid (CyDTA)[1]

RITA K. HESSLEY

Department of Chemistry, The University of Texas at Arlington, Arlington, TX 76019, U.S.A.

AND

SHOBA WAYKOLE AND ROBERT L. SUBLETT

Department of Chemistry, Tennessee Technological University, Cookeville, TN 38501, U.S.A.

Received October 13, 1978

RITA K. HESSLEY, SHOBA WAYKOLE, and ROBERT L. SUBLETT. Can. J. Chem. 57, 2292 (1979).

An intriguing and unique system has been observed during the otherwise routine study of the cobalt(III) complex of *trans*-1,2-cyclohexanedinitrilotetraacetic acid (CyDTA). Using classical spectrophotometric methods to determine the stoichiometry and the stability of a complex, significant deviations from the predicted 1:1 complex were observed in a system buffered at pH = 4.6. It is postulated that in addition to the usual 1:1 complex, the propensity of the reactants to form complexes and the strong oxidizing conditions used in this investigation result in the formation of a second, higher order complex between Co(III) and CyDTA. When the concentration of CyDTA exceeds that of Co(III), the metal:ligand ratio for this complex is 1:2. A structure is proposed, and approximate stability constants of both complexes are discussed.

RITA K. HESSLEY, SHOBA WAYKOLE et ROBERT L. SUBLETT. Can. J. Chem. 57, 2292 (1979).

On a observé un système unique et curieux au cours d'une étude par ailleurs routinière des complexes du cobalt(III) avec l'acide cyclohexanedinitrilo-1,2 tétraacétique (CyDTA). Faisant appel à des méthodes spectrophotométriques pour déterminer la stoechiométrie et la stabilité du complexe et opérant dans un système tamponné à pH 4.6, on a observé des déviations importantes par rapport au complexe 1:1 prédit. On fait l'hypothèse qu'en plus du complexe 1:1 habituel, la propension des réactifs à former des complexes et les conditions très oxydantes utilisées au cours de cette étude conduisent à la formation d'un second complexe d'un ordre plus élevé entre le Co(III) et le CyDTA. Lorsque la concentration du CyDTA est supérieure à celle du Co(III), le rapport métal/ligand pour ce complexe est de 1:2. On propose une structure et on discute des constantes de stabilité approximative des deux complexes.

[Traduit par le journal]

Introduction

We had prepared a crystalline form of a Co(III)–CyDTA complex, and it was of interest to investigate the nature and the stability of the complex in solution. Previous work by Jacobsen and Selmer-Olsen showed that a 1:1 complex formed between these reactants, but that in the presence of excess cobalt(II) ion some of the ligand was oxidized (1). We had not observed an oxidation reaction, and a further study of the system was undertaken. It is known that Co(III) is a highly reactive species, but is stabilized by complex formation. Both Jacobsen and Selmer-Olsen (1), and Martinez and Mendoza (2), have used CyDTA to determine micro quantities of cobalt(III) ion in solution. Jacobsen and Selmer-Olsen carried out their investigation in solutions buffered at pH 4.6. Except when excess cobalt ion resulted in the partial oxidation of CyDTA, as noted above, an otherwise stable 1:1 complex was observed, regardless of the oxidant (1). Martinez and Mendoza determined that a 1:1 complex was formed in basic media using H_2O_2 as the oxidizing agent (2). They did not report an oxidation process such as Jacobsen observed. Working with ligands similar to CyDTA, Arribas and co-workers (3) have reported that two cobalt(III) complexes can form in solution. The aquated species, $Co(H_2O)Y^-$, is relatively unstable and loses a molecule of water to form the 'normal', CoY^-, complex. Flaschka and Ganchoff reported that these two complex species are characterized by absorbance maxima at two different wavelengths (4). Schwarzenbach showed that with cobalt(III) and a polydentate ligand such as EDTA, one co-ordination site can be freed from the primary ligand, and that substitution by a different ligand, such as a halogen or an hydroxyl ion, can occur (5). In the light of these studies, we wish to report a significant additional characteristic of the reaction between cobalt(III) and the polydentate ligand CyDTA.

[1]Presented at the 29th SERACS meeting, Tampa, FL, November 9–11, 1977.

0008-4042/79/172292-05$01.00/0

Experimental

Reagents

All reagents were of analytical reagent quality: $Co(NO_3)_2 \cdot 6H_2O$, Fisher Scientific; $KC_2H_3O_2$, Baker Chemical Co.; H_2O_2, 30%, Baker Chemical Co.; murexide indicator, Fisher Scientific; disodiumethylenedinitrilotetraacetic acid (Na_2EDTA), 99+%, Fisher Scientific; *trans*-1,2-cyclohexanedinitrilotetraacetic acid (CyDTA), 98%, Pflatz & Bauer (dec. > 210°C, homogeneous on tlc, nmr comparable to Aldrich spectrum No. 16A).

Apparatus

All spectrophotometric measurements were made with a Pye Unicam uv–visible spectrophotometer, model 2000, equipped with a thermostated cell and linear recorder. Perkin-Elmer 1.0 cm silica cells were used. A Corning pH meter, model 10, was used to determine the pH of all the reaction solutions.

Procedure

An aqueous stock solution of 0.025 *M* cobalt(II) nitrate hexahydrate was prepared by the direct weighing of the salt. The solution was standardized with 0.5 *M* EDTA using murexide indicator. An aqueous stock solution, 0.025 *M* in CyDTA and 0.1 *M* in potassium acetate, was prepared by the direct weighing of the salts. For all of the reaction solutions, the desired volume of each stock solution was measured accurately into 50 mL volumetric flasks. The ionic strength was held constant with potassium acetate, and the pH was adjusted to 4.6 with acetic acid, if necessary. Hydrogen peroxide (5 mL) was added to each solution and to a reference blank. The solutions were heated in a boiling water bath for at least 30 min. After cooling to room temperature, each solution was diluted to volume. The absorbance was recorded at 25°C, using the prepared blank as the reference. The slope-ratio method (*6a*), the mole ratio method (*6b*), and Job's method (*6c*) were carried out to investigate the molar composition and the stability of the cobalt(III)–CyDTA complex.

In each case, two series of solutions were prepared so that both the metal and the ligand concentration could be held constant with respect to the other. For the slope-ratio determination, millilitre increments of one reactant were added to reaction flasks containing 25 mL of the fixed component. For the mole ratio determination the concentration of one component was varied (1–12 mL; $2.50 \times 10^{-5} - 3.00 \times 10^{-4}$ mol). For Job's method, the volume of each component was varied in millilitre increments to maintain a concentration of 5.00×10^{-4} mol (20 mL).

Results and Discussion

Oxidized solutions of Co(II)–CyDTA have two absorbance maxima; the lower absorptivity is observed at 380 nm, the higher at 540 nm. The absorbance of aqueous solutions of CyDTA is negligible at these wavelengths. Solutions of Co(II) exhibit a very low absorbance at 540 nm. The absorbance of all the oxidized solutions was stable up to 8 days. No variation in the wavelength of maximum absorbance was observed when Co(II) or an unoxidized mixture of reactants was used as the reference.

The data in Fig. 1 constitute a slope-ratio determination (*6a*). Beer's law is obeyed at both wavelengths. In theory, the ratio of the slope of a pair of

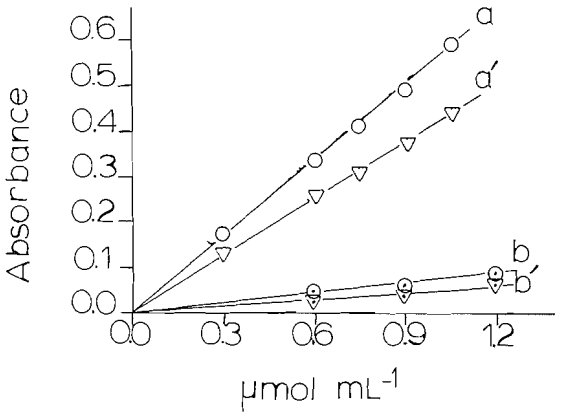

FIG. 1. The slope-ratio analysis of Co(III) with CyDTA at 540 nm (*a* and *b*), and at 380 nm (*a'* and *b'*). (*a*, *a*) per 7.5 mol mL^{-1} Co(II); (*b*, *b'*) per 7.5 mol mL^{-1} CyDTA; total volume, 50 mL; $\mu = 4.6$; 25°C; $\mu = 0.1$.

lines at a particular wavelength corresponds to the ratio of the components in a complex. Lines *a* and *a'* show the absorbance as a function of the CyDTA concentration. At 540 nm the molar absorptivity is 554 M^{-1} cm^{-1}, and at 380 nm the value is 404 M^{-1} cm^{-1} (lines *a* and *a'*, respectively). Jacobsen and Selmer-Olsen reported the molar absorptivity at 545 nm of only 305 M^{-1} cm^{-1}, but attributed low absorbance to the oxidation of ligand by excess Co(II) (1). We did not observe any oxidation of CyDTA. Lines *b* and *b'* show the change in the absorbance as a function of Co(II) ion concentration. The absorbance values for this series of solutions were expected to be identical to the first series (lines *a* and *a'*; assuming a 1:1 complex), because the limiting concentration was the same. The value calculated at 540 nm for line *b* is 73 M^{-1} cm^{-1}, and 47 M^{-1} cm^{-1} at 380 nm, a considerable difference from the complimentary series. There was no evidence that a more strongly absorbing species was formed initially, then decomposed. The ratio of the slope at each wavelength indicates a 1:8 Co(III):CyDTA complex. However, it is important to note that this method is valid only when one complex is formed.

Figures 2 and 3 show the absorbance values for the mole ratio determination (*6b*). When the concentration of CyDTA was fixed, the initial absorbance values were low, in accord with line *b* in Fig. 1. At the Co(II):CyDTA ratio 0.8, the absorbance of the solutions rose sharply, then became constant at a 1:1 mole ratio (Fig. 2). When the concentration of the Co(II) ion was fixed, the absorbance increased much more steeply, corresponding to line *a* in Fig. 1. The absorbance dropped suddenly, however, with the first increment of a molar excess of CyDTA. A second

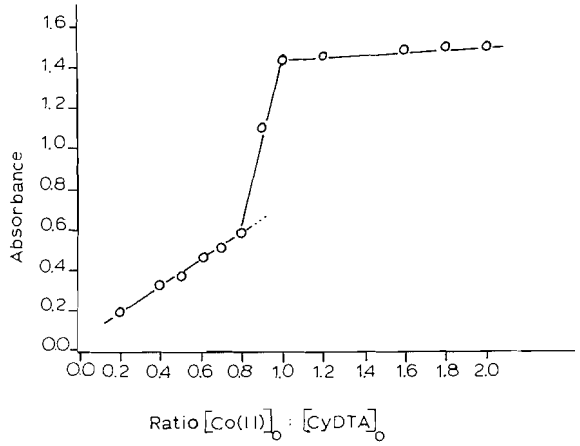

FIG. 2. The mole-ratio analysis of Co(III) with CyDTA at 540 nm. $[CyDTA]_0$ = 5 mL 0.025 *M* stock; total volume, 50 mL; pH = 4.6; 25°C, μ = 0.1.

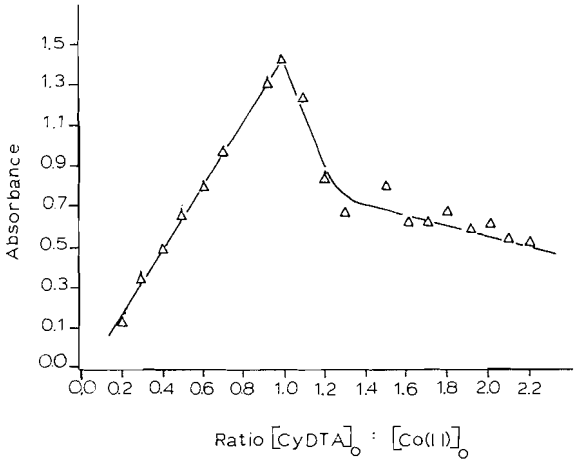

FIG. 3. The mole-ratio analysis of Co(III) with CyDTA at 540 nm. $[Co(II)]_0$ = 5 mL 0.025 *M* stock; total volume, 50 mL; pH = 4.6; 25°C, μ = 0.1.

inflection in the absorbance values was observed at the ratio 1.25 (Fig. 3). Repetition of these measurements at three wavelengths (380, 540, and 600 nm) and with different concentrations of reactants (using 4 mL and 6 mL of the fixed component in separate trials) gave the same results. There is some scatter in the data near the second inflection point in Fig. 3. This was also observed in the other trials. It is believed to be related to the instability of a second complex species.

When the mole fraction of CyDTA was increased according to Job's method (6*c*), the regularly increasing absorbance values dropped abruptly at a mole fraction 0.5, then decreased gradually. These data are shown in Fig. 4. When the mole fraction of Co(II) was increased, the trend in the absorbance rose sharply at mole fraction 0.5, then decreased steadily with excess Co(II).

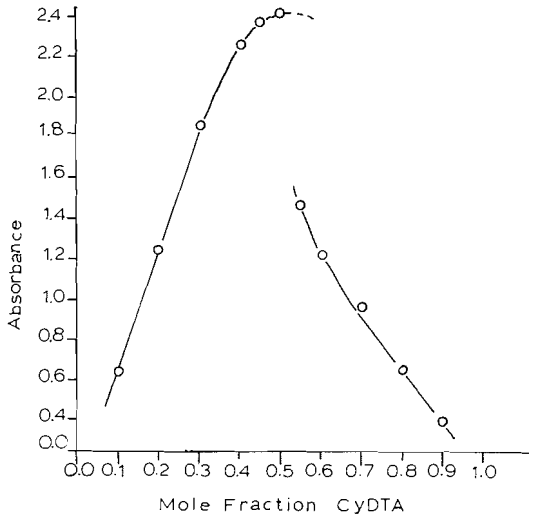

FIG. 4. The analysis of Co(III) with CyDTA by Job's method at 540 nm. Total volume, 50 mL; total concentration = 0.500 mmol (20 mL, 0.025 *M*); pH = 4.6; 25°C, μ = 0.1.

Several experimental variations were made to detect an artificial cause for these deviations from the expected behavior. In the light of Jacobsen and Selmer-Olsen's observations (1), separate solutions of Co(II) and CyDTA were allowed to react with hydrogen peroxide. When they were then mixed together and allowed to react, no loss of reactivity was detected. Complex formation between Co(II) and the acetate buffer ions was also investigated. When Co(II) was allowed to react with acetate ions under the same reaction conditions, no spectral evidence for a cobalt–acetate complex was observed. Because the analogous reaction between Co(II) and EDTA has been studied (7), that reaction was carried out under identical conditions of concentration and pH. The spectral data showed only that the known 1:1 complex was formed.[2]

These sets of data indicate, then, that more than one stable complex is being formed between Co(III) and CyDTA. Jakubiec and Boltz (8) observed similar data in a mole ratio determination of molybdate complexes with germanium, and Cheng and Goydish (9) reported absorbance minima in a Job's plot for palladium and mercury complexes with thio-Micheler's reagent. We believe that this is the first report of a higher order complex of a metal ion with a polyaminopolycarboxylic acid.

The work of Asmus and co-workers (10) which has been applied and extended by Langmyhr and co-workers (11) and others (12) treats data like those displayed in Fig. 4. Langmyhr and Stumpe (11*a*) found that when Job's curve exhibits an absorbance maxima at mole ratio 0.5, but shows inflection points

[2]Data were submitted to the referees.

in the absorbance curve near both limits, the molar co-efficients are equal but greater than one. In our case, such a parabolic inflection is observed only when the mole ratio favors the ligand, CyDTA. We believe that the Job's plot in Fig. 4 is reflecting the formation of two different complexes which form as the molar ratio of the reactants changes.

The method of Asmus and co-workers (10*a*) was used to resolve the stoichiometry and the equilibrium constant for the complex that forms between Co(III) and CyDTA when the ligand is in excess. The results are shown in Fig. 5. The data show clearly that 2 mol of CyDTA react with Co(II). From the intercept of the straight line, the value of the conditional formation constant was found to be $1.96 \times 10^5\ M^{-2}$ for the reaction in [2] below:

[1] $\text{Co(II)} + \text{CyDTA} \overset{K_1}{\rightleftharpoons} \text{Co(III)CyDTA}$

$\varepsilon = 554$ (540 nm)

[2] $\text{Co(II)} + 2\text{CyDTA} \overset{K_2}{\rightleftharpoons} \text{Co(III)(CyDTA)}_2$

$\varepsilon = 73$ (540 nm)

The spectral evidence for the 1:1 complex is clear from Figs. 2 and 3. This complex has a high molar absorptivity, and it is expected to have a large overall formation constant, characteristic of most CyDTA complexes (13). Jacobsen and Selmer-Olsen (1) calculated $\log K_f = 21.9$ for the 1:1 complex. Because of the abrupt inflection points which we recorded, the apparent formation constant cannot be determined accurately from these spectral data.

The description of this system is complicated by the effects which the absorbance and the formation constant of the higher order complex have on the 1:1 complex. Because the measured absorbance is an additive combination of both absorbing species, the calculated molar absorptivity values are undoubtedly high (1, 14). Secondly, the spectra indicate that excess

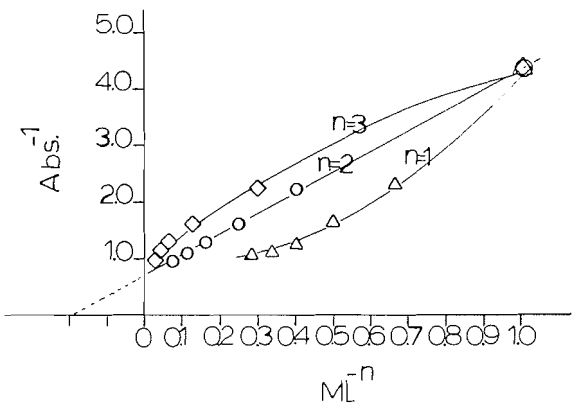

FIG. 5. The plot of absorbance^{-1} with mL^{-n} for 0.025 *M* CyDTA with 5.0 mL 0.025 *M* Co(II). Total volume, 50 mL; pH = 4.6; 25°C, $\mu = 0.1$.

ligand binds with a strongly absorbing species and diminishes its absorbance (presumably by forming a less strongly absorbing complex).

With reference to eqs. [1] and [2] above, in Fig. 1, lines *a* and *a'* show that when the concentration of Co(II) is sufficiently high, the formation of ML by eq. [1] is favored. Equilibrium [2] is suppressed by the concentration of Co(II) and K_1 expected $> K_2$.

Lines *b* and *b'* show that the high concentration of CyDTA enhances the effect of [2] to form the low absorbing ML_2 species at the expense of the 1:1 complex. Excess ligand, coupled with a relatively high stability constant, K_2, diminishes the concentration (absorbance) of the 1:1 complex (Fig. 2).

In Fig. 3, the strongly absorbing 1:1 species predominates initially. The presence of excess ligand shifts the equilibrium according to eq. [2] and decreases the concentration of the 1:1 complex.

From these data, and for a polydentate chelating agent, it is now only possible to speculate on a structure for a higher order complex. Yalman (15) has made an extensive study of Co(III) complexes with EDTA. He reported that both a monomeric Co(III) complex and a peroxodicobalt[(III), (III)] species can form during the oxidation with H_2O_2. Although the dimer exhibits a low molar absorptivity, these two complexes are characterized by different absorbance maxima. Also, the dimeric species forms in the presence of excess Co(II) ions, rather than with an excess of ligand as we have observed. Similarly, El-Awady and Hugus (16) reported that Co(III) can form a doubly bridged (through —OH) species with ethylenediamine, $Co(en)_4(OH)_2^{4+}$, in basic media.

We propose that the 1:2 Co(III):CyDTA complex can be formed in a chain structure. Using molecular models, it can be shown that one iminodiacetate 'arm' of the *trans*-CyDTA molecule can be directed away from the other sufficiently to be able to enter into complex formation with two different Co(III) ions (e.g. axial–axial C—N bonds in the 'boat' conformation). Two simplified arrangements of metal and ligand that could form in this manner are shown in **I** and **II** below.

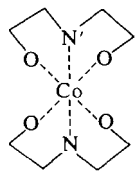

I

In **I** the four oxygen atoms occupy the equatorial positions, and are from two different CyDTA molecules (N and N'). The other iminodiacetate group of each molecule is directed toward other Co^{3+} ions. In the second arrangement, **II**, a nitrogen atom from

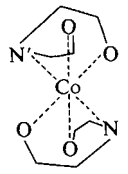

II

different CyDTA molecules occupies an equatorial position; oxygen atoms occupy the axial positions.

The paired inflection points at the M:L ratio 0.8 (Fig. 2) and L:M 1.25 (Fig. 3) suggest that the chain structure is composed of 4 metal atoms and 5 CyDTA molecules. The general M:L ratio, then, is M_nL_{n+1}.

Since both the 1:1 and the 1:2 complexes have absorbance maxima at the same wavelength, it might be that the structure shown in **II** is most like that of the 1:1 complex in which two equatorial positions are occupied by nitrogen atoms. Either structure is admittedly awkward. However, both of the reactants have a very strong propensity to enter into complex formation, and it is only when there is an excess of ligand and an extensive degree of protonation that the higher order complex is observed.

Our continuing study of this system will include an attempt to isolate both of the complexes in crystalline form. Molecular weight determination, X-ray analyses, and perhaps nmr studies will be very informative.

Acknowledgements

Acknowledgement is given to T. A. Furtsch and K. L. Brown for helpful discussions. S.W. thanks Tennessee Technological University for financial support.

1. E. Jacobsen and A. R. Selmer-Olsen. Anal. Chim. Acta, **25**, 476 (1961).
2. F. B. Martinez and R. R. Mendoza. Inf. Quim. Anal. Madrid, **12**, 160 (1958).
3. S. Arribas, R. Moro, M. L. Alverez, and C. Bahillo. Inf. Quim. Anal. **22**, 221 (1969).
4. H.A. Flaschka and J. Ganchoff. Talanta, **8**, 887 (1961).
5. G. Schwarzenbach. Helv. Chim. Acta, **32**, 839 (1949).
6. (*a*) A. S. Meyer and G. H. Ayres. J. Am. Chem. Soc. **79**, 49 (1957); (*b*) A. E. Harvey, Jr. and D. L. Manning. J. Am. Chem. Soc. **72**, 4488 (1950); (*c*) P. Job. Ann. Chim. **9**, 113 (1928).
7. C. N. Reilly, V. G. Scribner, and C. Temple. Anal. Chem. **28**, 450 (1965); N. Tanaka and H. Ogino. Bull. Chem. Soc. Jpn. **38**, 1054 (1965); J. Bond and D. B. Hobson. J. Chem. Soc. A, 2155 (1969).
8. R. Jakubiec and D. F. Boltz. Anal. Chem. **41**, 78 (1969).
9. K. L. Cheng and B. L. Goydish. Microchem. J. **10**, 158 (1966).
10. (*a*) E. Asmus, U. Hinz, K. Ohls, and W. Richly. Z. Anal. Chem. **178**, 104 (1960); E. Asmus. Z. Anal. Chem. (*b*) **183**, 321 (1961); (*c*) **183**, 401 (1961); (*d*) E. Asmus and P. Meyer. Z. Anal. Chem. **190**, 390 (1962); (*e*) E. Asmus and K. Ohls. Z. Anorg. Allg. Chem. **341**, 225 (1965).
11. (*a*) F. J. Langmyhr and T. Stumpe. Anal. Chim. Acta, **32**, 535 (1965); K. S. Klausen and F. J. Langmyhr. (*b*) Anal. Chim. Acta, **28**, 335 (1963); (*c*) **28**, 501 (1963).
12. L. Sommer and M. Hnilickova. (*a*) Anal. Chim. Acta, **27**, 241 (1962); (*b*) Coll. Czech. Chem. Commun. **27**, 439 (1962); (*c*) Talanta, **9**, 439 (1962); (*d*) G. F. Atkinson. Anal. Chem. **44**, 1098 (1972).
13. Stability constants. The Chemical Society of London, Burlington House, Special Publication No. 17, 698 (1964); Special Publication No. 25. 724 (1971).
14. H. A. Flaschka and A. J. Barnard, Jr. (*Editors*). Chelates in analytical chemistry. Marcel Dekker, New York, NY. 1976.
15. R. G. Yalman. J. Phys. Chem. **65**, 556 (1961).
16. A. A. El-Awady and Z. Z. Hugus. Inorg. Chem. **10**, 1415 (1971).

Specific binding of phenylalanine and tryptophan to β-nicotinamide adenine dinucleotide[1]

KLAUS J. NEUROHR AND HENRY H. MANTSCH

Division of Chemistry, National Research Council of Canada, Ottawa, Ont., Canada, K1A 0R6

Received March 7, 1979

KLAUS J. NEUROHR and HENRY H. MANTSCH. Can. J. Chem. 57, 2297 (1979).

This ^{1}H nmr study provides the first experimental evidence for specific complex formation between the coenzyme nicotinamide adenine dinucleotide (β-NAD^+) and the two aromatic amino acids phenylalanine and tryptophan. It is shown that the interaction is of the stacking type and occurs between the aromatic side chains of these amino acids and the adenine moiety of NAD^+. Binding parameters were obtained from dilution studies, taking into account the self-association of NAD^+. The apparent microscopic association constants for complex formation of phenylalanine and tryptophan with excess NAD^+ in aqueous solutions are 1.35 M^{-1} and 11.35 M^{-1}, respectively, indicating that the adenine moiety of NAD^+ can discriminate between phenylalanine and tryptophan by a stronger binding to the latter. The results are discussed with regard to the interaction of NAD^+ with dehydrogenases.

KLAUS J. NEUROHR et HENRY H. MANTSCH. Can. J. Chem. 57, 2297 (1979).

Dans ce travail, on rapporte les premières preuves expérimentales, basées sur une étude rmn ^{1}H, pour la formation de complexes spécifiques entre le dinucléotide de la nicotinamide et de l'adénine (β-DNA^+) et les deux acides aminés aromatiques phénylalanine et tryptophane. On montre que l'interaction en est une d'empilement et qu'elle se produit entre les chaînes latérales aromatiques de ces acides aminés et la portion adénine du DNA^+. On a obtenu les paramètres de liaison à partir d'études de dilution en tenant compte de l'auto-association du DNA^+. Les constantes d'association microscopiques apparentes pour la formation de complexes entre la phénylalanine et le tryptophane et un excès de DNA^+ en solutions aqueuses sont respectivement 1.35 M^{-1} et 11.35 M^{-1} ce qui indique que la portion DNA^+ peut distinguer la phénylalanine du tryptophane grâce au site de liaison plus fort avec ce dernier. On discute des résultats en rapport avec l'interaction de la DNA^+ avec les déshydrogénases.

[Traduit par le journal]

Introduction

Numerous nmr studies have been undertaken to investigate the dynamic conformation of β-nicotinamide adenine dinucleotide (NAD^+) in aqueous solution (1–19). A detailed discussion of the existing nmr literature on this subject was made recently by Ellis and co-workers (20). However, the results are often conflicting, the most argued question being the location of the two heterocyclic base moieties relative to each other and to the corresponding ribose moieties. While the nicotinamide moiety is known to be essential for the catalytic activity of all NAD^+-dependent dehydrogenases (21), the role of the somewhat remote adenine moiety is thought to be that of anchoring the NAD^+ molecule onto the corresponding enzyme (22, 23). This would require its recognition and (or) binding to a specific amino acid grouping on the enzyme.

In the present investigation we provide the first experimental evidence for specific complex formation between two aromatic amino acids, phenylalanine and tryptophan, and the adenine moiety of NAD^+.

Experimental Section

Materials and Sample Preparation

All chemicals were products of the highest available purity. Phenylalanine, tryptophan, and β-NAD^+ were from Sigma Chem. Co. The nmr samples were prepared in 99.8% D_2O containing 10 mM phosphate buffer, 1 mM NaCl, 1 mM *tert*-butanol, and 100 μM EDTA. The pH of the solutions was adjusted with NaOD or DCl to a "pH" (meter reading) of 7.3. The phenylalanine and tryptophan concentration was kept constant at 25 mM, while that of NAD^+ varied from 17 mM to 266 mM for complex formation and from 4 mM to 532 mM for the study of NAD^+ self-association. Individual NAD^+ concentrations were determined from the ultraviolet A_{260}, using ε_{max} = 17 900.

Nuclear Magnetic Resonance Measurements

All ^{1}H nmr spectra were taken with a Varian XL-100/12 spectrometer operating at 100 MHz under a 16 K Varian 620/L data system. The digital resolution was 0.25 Hz (0.0025 ppm); the 90° pulse-time was 20 μs. Between 20 and 12 000 transients were accumulated, depending on the dilution of the samples. Typically three, but at least two, independent measurements were made for each sample. The probe temperature was 32 ± 0.5°C. Chemical shifts were measured with respect to *tert*-butanol as internal reference.

Results and Discussion

The Self-association of NAD^+

In order to quantitate the interaction of phenylalanine and tryptophan with excess NAD^+, it is necessary to correct for the degree and influence of self-association of the latter under identical conditions. Therefore we have accurately measured the concentration dependence of the ^{1}H nmr chemi-

[1]NRCC No. 17491.

0008-4042/79/172297-05$01.00/0

TABLE 1. Concentration dependence of 100 MHz ^{1}H nmr chemical shifts σ (in ppm downfield from external TMS)[a] and chemical shift differences δσ (in Hz)[b] for all aromatic and the two 1′ ribose NAD^+ protons

NAD^+ (m*M*)[c]	σA8 δσA8	σA2 δσA2	σA1′ δσA′	σN2 δσN2	σN6 δσN6	σN4 δσN4	σN5 δσN5	σN1′ δσN1′
532	8.345	7.972	6.003	9.377	9.228	8.876	8.267	6.176
	7.4	21.2	3.4	−5.8	−7.7	−4.3	−7.6	−9.6
399	8.348	7.982	5.999	9.357	9.208	8.860	8.245	6.149
	7.1	20.1	3.8	−3.8	−5.6	−2.7	−5.4	−6.9
266	8.352	7.999	5.995	9.338	9.183	8.844	8.221	6.119
	6.7	18.5	4.2	−1.9	−3.2	−1.1	−3.0	−3.9
200	8.357	8.011	5.994	9.331	9.174	8.836	8.209	6.109
	6.2	17.3	4.3	−1.2	−2.2	−0.3	−1.8	−2.9
133	8.369	8.047	6.004	9.327	9.166	8.836	8.202	6.101
	5.0	13.7	3.3	−0.8	−1.4	−0.3	−1.1	−2.1
100	8.379	8.065	6.011	9.326	9.162	8.835	8.199	6.096
	4.0	11.9	2.6	−0.7	−1.1	−0.2	−0.8	−1.6
67	8.387	8.089	6.017	9.323	9.155	8.835	8.194	6.092
	3.2	9.5	2.0	−0.4	−0.4	−0.2	−0.3	−1.2
33	8.399	8.131	6.027	9.321	9.153	8.835	8.192	6.082
	2.0	5.3	1.0	−0.2	−0.1	−0.2	−0.2	−0.1
17	8.409	8.153	6.033	9.319	9.152	8.833	[e]	6.081
	1.0	3.1	0.4	0	0	0		0
8	8.414	8.172	[e]	9.319	9.152	8.833	[e]	[e]
	0.5	1.2		0	0	0		
4	8.416	8.178	[e]	9.319	9.152	8.833	[e]	[e]
	0.3	0.6		0	0	0		
0[d]	8.419	8.184	6.037	9.319	9.152	8.833	8.190	6.081
	0	0	0	0	0	0	0	0

[a]Chemical shifts were measured relative to internal *tert*-butanol and converted to the TMS scale by adding 1.24 ppm.
[b]Negative values indicate shifts to lower and positive values shifts to higher field compared to infinite dilution.
[c]Ultraviolet spectroscopically determined concentrations using $\varepsilon_{260}^{mM} = 17.9$.
[d]Zero concentration chemical shifts were obtained through extrapolation of experimental shifts.
[e]Due to overlap with other signals no accurate values could be given.

cal shifts for all aromatic protons of NAD^+. These are displayed in Table 1. Chemical shift assignments are based on those originally reported by Jardetzky and Wade-Jardetzky (2) and confirmed later unequivocally (13). The letters A and N are used to distinguish between protons located in the adenine (A) and the nicotinamide (N) moiety using the standard numbering scheme for the two bases. Over the concentration range investigated, from 4 m*M* to 532 m*M*, the adenine protons A2 and A8 undergo considerable upfield shifts with increasing concentration, while at the same time the nicotinamide protons N2, N4, N5, and N6 all undergo downfield shifts. It is interesting to note that the chemical shifts of the A1′ and N1′ protons of the contiguous bases also change in opposite directions, reflecting different shielding environments for the two bases.

While it is possible to rationalize the upfield shifts of the adenine protons with increasing concentration only in a unique situation in which two aromatic rings come close to each other, the corresponding downfield shifts of the nicotinamide protons could be associated with other intermolecular interactions such as hydrogen bonding or electrostatic (dipolar) interactions. The concentration profiles reported here for the A2 and A8 protons in NAD^+ are typical for intermolecular base-stacking interactions and resemble those observed with the A2 and A8 protons in adenine nucleotides (24). The existence of such intermolecular base-stacking interactions with adenine nucleotides in aqueous solutions has been demonstrated not only by nmr, but also by vapor pressure osmometry, microcalorimetry, sedimentation equilibrium, and ultraviolet hypochromism (25). It is generally agreed that this association proceeds beyond the dimer stage.

Earlier studies (4, 8, 13) had pointed out that the ^{1}H nmr chemical shifts of NAD^+ can vary with concentration; however, so far no attempts have been made to obtain equilibrium constants from the data. We have analyzed the concentration-dependent chemical shifts of the adenine NAD^+ protons by the isodesmic model of Dimicoli and Hélène (26). This takes into account both dimer and *n*-mer formation and is illustrated in Fig. 1 for the A2 and A8 protons of NAD^+. A plot according to this model of $(\delta\sigma/c_0)^{1/2}$ versus δσ (δσ being the difference between the individual chemical shifts at concentration c_0 and the corresponding chemical shift at infinite dilution) gave straight lines for both protons. From the slope of each of these, a micro-

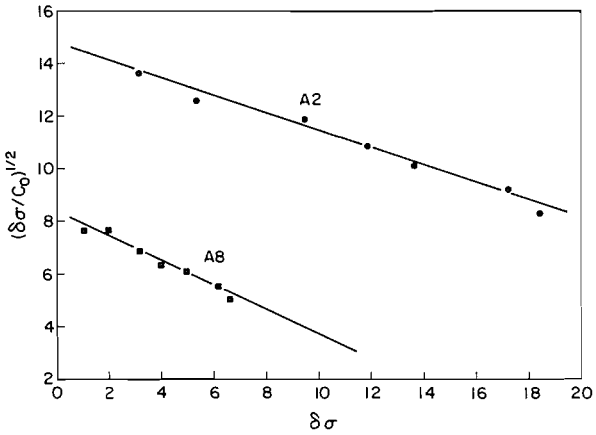

FIG. 1. Self-association of NAD^+ at 32°C and pH 7.3 as a plot of $(\delta\sigma/c_0)^{1/2}$ versus $\delta\sigma$ for the A2 and A8 protons of its adenine moiety.

scopic equilibrium constant (K_c) and the corresponding Gibbs energy change (ΔG^0) were obtained, while the x-axis intercept yielded the corresponding dimer shifts ($\delta\sigma_{A_2}$). The results shown in Table 2 also include the corresponding constants for the 5′-AMP self-association (28), evaluated on the basis of the same isodesmic model.

It is very interesting that the A2 and A8 proton-averaged apparent equilibrium constant for the self-association of NAD^+ ($\overline{K}_c = 4.62\ M^{-1}$) and the derived standard Gibbs energy change ($\overline{\Delta G}^0 = -3.85\ \text{kJ mol}^{-1}$) are more than twice those found for the self-association of 5′-AMP ($\overline{K}_c = 1.93\ M^{-1}$ and $\overline{\Delta G}^0 = -1.65\ \text{kJ mol}^{-1}$), which itself was thought to be strongly self-associated in concentrated aqueous solutions. Accordingly the tendency for self-association of NAD^+ is about 2.4 times greater than that of 5′-AMP.

While it is difficult to derive an accurate stacking geometry for the NAD^+ aggregates in aqueous solutions from only these data, it is possible to draw the following conclusions. (*i*) The adenine moiety of NAD^+ is involved in a base-stacking pattern. (*ii*) The nicotinamide moiety of NAD^+ does not participate in the stacking, but could be involved in the association through hydrogen bonding or dipole–dipole interactions. (*iii*) The association is intermolecular.

These conclusions are in very good agreement with the first X-ray study of NAD^+ recently reported by Saenger *et al.* (29) in which the authors showed that in the lithium complex, the crystal conformation of NAD^+ is "extended" due to an intermolecular base stacking, and not "folded" which would be the consequence of an intramolecular base stacking between the adenine and nicotinamide moieties.

TABLE 2. Microscopic equilibrium constants (K_c)[a], standard Gibbs energy changes (ΔG^0), and ^1H nmr dimer shifts[b] ($\delta\sigma_{A_2}$) for the self-association of NAD^+ and 5′-AMP at 32°C and pH 7.3

	K_c (M^{-1})	ΔG^0 (kJ mol^{-1})	$\delta\sigma_{A_2}$ (Hz)
NAD^+ (A2)	4.72	−3.9	22.7
NAD^+ (A8)	4.52	−3.8	8.2
5′-AMP (A2)	1.96	−1.67	44.6
5′-AMP (A8)	1.91	−1.63	18.0

[a]Both the equilibrium constants and the standard Gibbs energy changes reported here are based on concentrations as recommended by the ICSU Commission on Biothermodynamics (27).

[b]Dimer shifts were calculated according to the isodesmic model of Dimicoli and Hélène (26), which takes into account n-mer formation. This model considers the magnetic anisotropy of nearest neighbours only and assumes that the effects are additive. The change in chemical shift of a molecule located inside an n-mer, relative to the free molecule, is therefore twice that observed in the dimer.

Formation of Base-stacking Complexes between Phenylalanine or Tryptophan and NAD^+

We have monitored the ^1H nmr chemical shifts of individual protons located in the aromatic side groups of phenylalanine and tryptophan in the presence of varying amounts of NAD^+. Illustrated in Fig. 2 is the dependence on NAD^+ concentration of the H_c chemical shift of 25 mM tryptophan. The H_c singlet which is representative for the aromatic side group is easily distinguishable from the other aromatic protons of tryptophan and NAD^+. The resulting plot shows a steep decrease of the H_c chemical shift of tryptophan at low NAD^+ con-

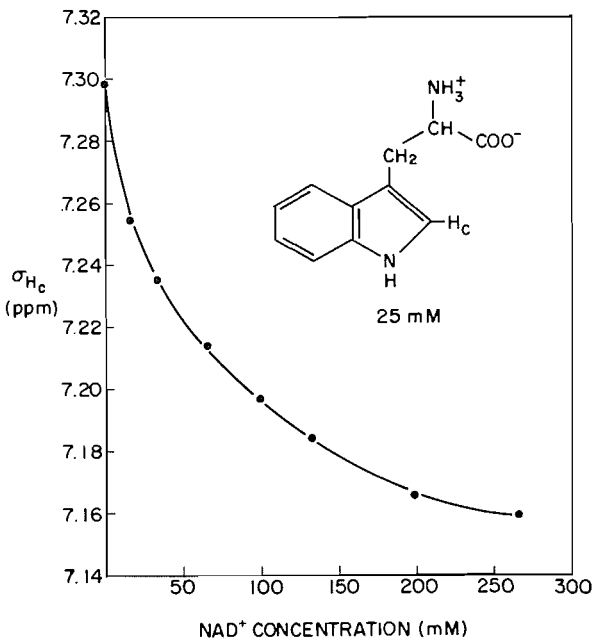

FIG. 2. Variation of the H_c chemical shift of 25 mM tryptophan as induced by complex formation with NAD^+ at 32°C and pH 7.3.

centrations, leveling off above 250 mM NAD^+. The H_c proton resonance of 25 mM tryptophan, in the absence of NAD^+, is at 7.30 ppm and the total chemical shift difference between "free" and "NAD^+-complexed" tryptophan is 14 Hz (0.14 ppm).

The five aromatic protons of phenylalanine are not resolved in the 100 MHz spectrum and appear as a singlet at 7.37 ppm in 25 mM phenylalanine. In the presence of an increasing NAD^+ concentration, this singlet undergoes an upfield shift similar to that displayed in Fig. 2 for the H_c resonance of tryptophan. For the NAD^+ concentration range investigated, the total chemical shift difference between "free" and "NAD^+-complexed" phenylalanine is also 14 Hz. However, the concentration profile of phenylalanine differs from that of tryptophan, which, as shown later, leads to different binding parameters. The similarity between the behavior of the two aromatic amino acids suggests that the observed upfield shifts of the aromatic protons are due to the same phenomenon, a base-stacking interaction with the NAD^+ molecule. Since the rate of exchange between the free and NAD^+-complexed amino acids is rapid on the ^1H nmr time-scale, only one resonance is observed for each proton monitored. Therefore, the measured chemical shifts in Fig. 2 represent the weighted average of chemical shifts for the free and NAD^+-complexed tryptophan molecules.

In order to extract the corresponding binding parameters, we have analysed these ^1H nmr chemical shift data by a modified Scatchard plot (28), using the mathematical model derived by Deranleau (30) and extended by Dimicoli and Hélène (26) to the case where the component in excess self-associates strongly.

$$[1]\quad \frac{\Delta\sigma}{\delta\sigma} = \left(\frac{K_c - k}{2K_c}\right)\frac{\Delta\sigma}{\delta\sigma_{A_2}} + \left(\frac{k}{2K_c}\right)\frac{\Delta\sigma_{BAB}}{\delta\sigma_{A_2}}$$

The variables in this equation have the following meaning. The parameters $\delta\sigma$, $\delta\sigma_{A_2}$, and K_c account for the self-association of NAD^+ and represent respectively the difference between the NAD^+ proton chemical shift at a given concentration and that at infinite dilution, the NAD^+ complex shift, and the microscopic association constant for NAD^+ self-association. $\Delta\sigma$ is the difference between the proton chemical shifts of the amino acids in the presence and absence of NAD^+. This is illustrated in Fig. 3 for the interaction of the two NAD^+ protons A2 and A8 with the H_c tryptophan proton. According to [1] a plot of $\Delta\sigma/\delta\sigma$ versus $\delta\sigma/\delta\sigma_{A_2}$ yielded straight lines, from the slope of which the microscopic association constant for complex formation, k, is calculated, while the complex shift $\Delta\sigma_{BAB}$ can be derived from the x-axis intercept. The k values obtained from the A2 and A8 NAD^+ protons are in good agreement (Table 3). A similar treatment of the experimental data obtained with 25 mM phenylalanine and excess NAD^+ yielded the corresponding constants given in Table 3.

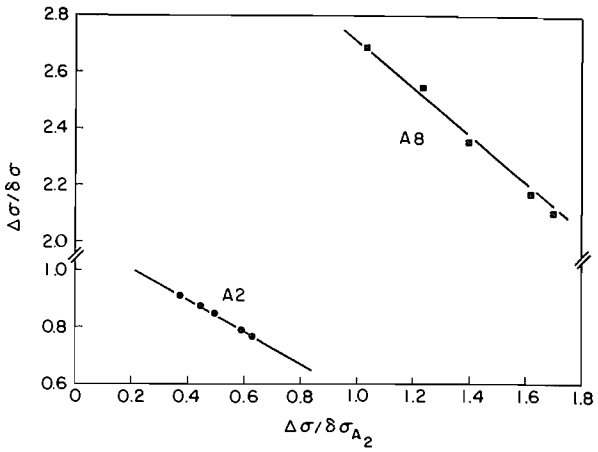

FIG. 3. Graphical evaluation of the constants for complex formation between 25 mM tryptophan and excess NAD^+, according to the formalism of Dimicoli and Hélène (26).

TABLE 3. Microscopic association constants (k) and standard Gibbs energy changes ($\overline{\Delta G}^0$) for the complex formation of phenylalanine and tryptophan with NAD^+ at 32°C and pH 7.3

	k		$\bar{k}$	$\overline{\Delta G}^0$
	A2	A8	(M^{-1})	(kJ mol^{-1})
Phenylalanine	1.4	1.3	1.35	−0.76
Tryptophan	10.1	12.6	11.35	−6.2

It is interesting that the proton-averaged association constant ($\bar{k}$) for complex formation of tryptophan with NAD^+ is an order of magnitude larger than that for the phenylalanine:NAD^+ complex. This is also revealed by the corresponding difference in binding strength as shown by the standard Gibbs energy changes in Table 3. These experimental data show that the adenine moiety of NAD^+ not only can recognize aromatic amino acids by a through-space base-stacking interaction, but can also discriminate between phenylalanine and tryptophan residues by a stronger binding to the latter.

Concluding Remarks

The largest group of biological redox reactions is catalysed by enzymes requiring NAD^+ as cofactor; so far over 150 different NAD^+-dependent dehydrogenases have been described (21–23). However, the forces involved in the recognition and binding

of NAD^+ to these dehydrogenases are far from understood. Recently Zens *et al.* (17) showed that the effective correlation time for the N4-NAD^+ proton was substantially shorter than that for the A8-NAD^+ proton when bound to chicken breast lactate dehydrogenase. Therefore they concluded that the adenine portion of NAD^+ is immobilized to a greater extent by the enzyme than the nicotinamide moiety, and that the latter does not interact with the enzyme to the extent as the adenine moiety in the absence of the substrate. These conclusions are strongly supported by the data from our present investigation which indicate that only the adenine moiety of NAD^+ is involved in the specific recognition through base-stacking interaction with individual aromatic amino acids.

In aqueous solutions NAD^+ is unlikely to possess a unique conformation such as the well-defined solid state stacking pattern in the Li–NAD^+ complex (29). Instead, due to an increased conformational flexibility about the pyrophosphate and (or) the glycosidic linkage, the adenine moiety of NAD^+ may be able to assume a geometry which optimizes both in-plane hydrogen bonding and out-of-plane base-stacking interactions with a given receptor macromolecule. The hydrophobic base-stacking interaction with suitable aromatic amino acyl groupings lining the NAD^+ binding site could be a major factor in fitting the adenine moiety into the hydrophobic pocket of NAD^+-dependent dehydrogenases.

Acknowledgments

The authors are grateful to Dr. Ian C. P. Smith for stimulating discussions and to the Deutsche Akademische Austausch-Dienst for a fellowship to K.J.N.

1. M. P. Schweizer, S. I. Chan, and P. O. P. Ts'o. J. Am. Chem. Soc. **87**, 5241 (1965).
2. O. Jardetzky and N. G. Wade-Jardetzky. J. Biol. Chem. **241**, 85 (1966).
3. R. H. Sarma, V. Ross, and N. O. Kaplan. Biochemistry, **7**, 3052 (1968).
4. W. A. Catterall, D. P. Hollis, and C. F. Walter. Biochemistry, **8**, 4032 (1969).
5. R. H. Sarma, M. Moore, and N. O. Kaplan. Biochemistry, **9**, 549 (1970).
6. R. H. Sarma and N. O. Kaplan. Biochemistry, **9**, 557 (1970).
7. J. Jacobus. Biochemistry, **10**, 161 (1971).
8. G. McDonald, B. Brown, D. P. Hollis, and C. F. Walter. Biochemistry, **11**, 1920 (1972).
9. B. Birdsall, N. J. M. Birdsall, and J. Feeney. J. Chem. Soc. D, 316 (1972).
10. B. Birdsall and J. Feeney. J. Chem. Soc. Perkin Trans. II, 1643 (1972).
11. P. D. Ellis, R. R. Fisher, R. B. Dunlap, A. P. Zens, T. A. Bryson, and T. J. Williams. J. Biol. Chem. **22**, 7677 (1973).
12. M. Blumenstein and M. A. Raftery. Biochemistry, **12**, 3585 (1973).
13. R. H. Sarma and R. J. Mynott. J. Am. Chem. Soc. **95**, 1641 (1973).
14. R. H. Sarma, R. J. Mynott, F. E. Hruska, and D. J. Wood. Can. J. Chem. **51**, 1843 (1973).
15. W. D. Hamill, R. J. Pugmire, and D. M. Grant. J. Am. Chem. Soc. **96**, 2885 (1974).
16. A. P. Zens, T. J. Williams, J. C. Wisowaty, R. R. Fisher, R. B. Dunlap, T. A. Bryson, and P. D. Ellis. J. Am. Chem. Soc. **97**, 2850 (1975).
17. A. P. Zens, P. T. Fogle, T. A. Bryson, R. B. Dunlap, R. R. Fisher, and P. D. Ellis. J. Am. Chem. Soc. **98**, 3760 (1976).
18. T. J. Williams, A. P. Zens, J. C. Wisowaty, R. R. Fisher, R. B. Dunlap, T. A. Bryson, and P. D. Ellis. Arch. Biochem. Biophys. **172**, 490 (1976).
19. R. M. Riddle, T. J. Williams, T. A. Bryson, R. B. Dunlap, R. R. Fisher, and P. D. Ellis. J. Am. Chem. Soc. **98**, 4286 (1976).
20. A. P. Zens, T. A. Bryson, R. B. Dunlap, R. R. Fisher, and P. D. Ellis. J. Am. Chem. Soc. **98**, 7559 (1976).
21. H. Sund. *In* Biological oxidations. *Edited by* T. P. Singer. Interscience, New York. 1968.
22. P. D. Boyer (*Editor*). The enzymes. Vol. 11. Academic Press, New York. 1975.
23. H. Sund (*Editor*). Pyridine nucleotide-dependent dehydrogenases. Springer, Berlin. 1970.
24. P. O. P. Ts'o. *In* Fine structure of proteins and nucleic acids. *Edited by* G. D. Fasman and S. N. Timasheff. Marcel Dekker, New York. 1970.
25. P. O. P. Ts'o. Basic principles in nucleic acid chemistry. Vols. 1–2. Academic Press, New York. 1974.
26. J. L. Dimicoli and C. Hélène. J. Am. Chem. Soc. **95**, 1036 (1973).
27. B. Dreyfus (*Editor*). Recommendations for measurement and presentation of biochemical equilibrium data. CODATA Bulletin, Vol. 20, Paris. 1976.
28. K. J. Neurohr and H. H. Mantsch. Can. J. Chem. **57**, 1986 (1979).
29. W. Saenger, B. S. Reddy, K. Mühlegger, and G. Weimann. Nature (London), **267**, 225 (1977).
30. D. A. Deranleau. J. Am. Chem. Soc. **91**, 4044 (1969).

Heats of vaporization and gaseous heats of formation of some five- and six-membered ring alkenes

RICHARD FUCHS AND L. ALAN PEACOCK

Department of Chemistry, University of Houston, Houston, TX 77004, U.S.A.

Received January 16, 1979

RICHARD FUCHS and L. ALAN PEACOCK. Can. J. Chem. 57, 2302 (1979).

The heats of vaporization of 1-methylcyclopentene, 3-methylcyclopentene, ethylidenecyclopentane, 1-ethylcyclopentene, methylenecyclohexane, allylcyclopentane, vinylcyclohexane, ethylidenecyclohexane, allylcyclohexane, 3,3-diethylpentane, 2,2,4,4-tetramethylpentane, and *trans*-2,2,5,5-tetramethyl-3-hexene have been measured by the gas chromatography – calorimetry method. These values have been combined with previously reported liquid heats of formation to give gaseous values of ΔH_f. The results indicate that the internal double bond is favored by about 0.5 kcal over the *exo* in both 5- and 6-membered rings, but the *endo–exo* differences are much smaller than previously believed. Several of the liquid heat capacities that were measured were not well predicted by group additivity schemes.

RICHARD FUCHS et L. ALAN PEACOCK. Can. J. Chem. 57, 2302 (1979).

Utilisant une méthode combinant la chromatographie en phase gazeuse et la calorimétrie, on a mesuré les chaleurs de vaporisation des hydrocarbures suivants: méthyl-1 cyclopentène, méthyl-3 cyclopentène, éthylidènecyclopentane, éthyl-1 cyclopentène, méthylènecyclohexane, allylcyclopentane, vinylcyclohexane, éthylidènecyclohexane, allylcyclohexane, diéthyl-3,3 pentane, tétraméthyl-2,2,4,4 pentane et tétraméthyl-2,2,5,5 hexène-3 *trans*. On a combiné ces valeurs avec les chaleurs de formation de ces liquides qui avaient été rapportées antérieurement afin d'en tirer les valeurs de ΔH_f en phase gazeuse. Les résultats indiquent que les doubles liaisons internes sont favorisées par environ 0.5 kcal/mol par rapport aux doubles liaisons *exo* dans les cycles à 5 et à 6 chaînons; toutefois la différence entre *endo* et *exo* est beaucoup plus faible que ce qu'on croyait antérieurement. En se basant sur les schémas d'additivité des groupes, il aurait été impossible de prédire adéquatement plusieurs des capacités calorifiques mesurées.

[Traduit par le journal]

A much discussed concept more than two decades ago was the idea that the internal (endocyclic) double bond is thermodynamically favored over the exocyclic double bond in six-membered ring systems, whereas the reverse was believed to be true in five-membered rings (1). However, Turner and Garner (2) measured the heat of hydrogenation (acetic acid solution, 25°C) of 1-methylcyclohexene, methylenecyclohexane, 1-methylcyclopentene, and methylenecyclopentane, and found that hydrogenation of the *exo* double bond is more exothermic in both the five-membered ring (by 3.7 kcal/mol) and six-membered ring (2.1 kcal/mol). Furthermore, treatment of methylenecyclopentane with acid converts it largely to 1-methylcyclopentene. It was concluded that 1-methylcyclopentene is the more stable of the two isomers, and this implies that the *endo* double bond is more stable than the *exo* in other cyclopentane derivatives as well.

This implication is open to possible criticism. First, methylenecyclohexane and methylenecyclopentane are dialkylethylenes, whereas 1-methylcyclohexene and 1-methylcyclopentene are trisubstituted. Open chain trialkylethylenes are known to be less exothermically hydrogenated than dialkyl isomers (3, 4), and this may be the source of the observed differences in the cyclic isomers. In a later paper (2), a comparison was also made of the heats of hydrogenation of ethylidenecyclopentane and 1-ethylcyclopentene, and of ethylidenecyclohexane and 1-ethylcyclohexene. The difference for each ring system was only 1.2–1.3 kcal/mol, but still suggested greater stability of the *endo* double bond. However, a second reservation arises from measurement of heats of hydrogenation in acetic acid solution, rather than in the gas phase.

The relationship between the gaseous and solution heats of hydrogenation as measured by Turner and Garner (2) is

$$\Delta H_{H_2}(g) = \Delta H_{H_2}(soln) + \Delta H_v(alkane) - \Delta H_v(alkene) + \Delta H_s(alkene) - \Delta H_s(alkane)$$

Without experimental measurement of the appropriate heats of solution in acetic acid and heats of vaporization and correction of the data to the gaseous state there is no assurance that valid conclusions will be drawn. It is usually assumed that the

0008-4042/79/172302-03$01.00/0

ΔH_v and ΔH_s effects are small, but in unpublished studies we have observed solution values in the range of 0.4 kcal/mol more exothermic to 2.5 kcal/mol less exothermic than gaseous values.

For this reason, the relative stabilities of *endo* and *exo* double bonds are still somewhat in doubt, particularly of the cyclopentane derivatives. It has occurred to us that comparisons of the gaseous heats of formation (ΔH_f(g)) of 1-ethylcyclohexene vs. ethylidenecyclohexane, and 1-ethylcyclopentene vs. ethylidenecyclopentane, all of which are trisubstituted ethylenes, might be a reasonable basis for comparison. Unfortunately, although heats of combustion and liquid heats of formation have been reported for these compounds (5), a value of ΔH_f(g) has been reported only for 1-ethylcyclohexene. Measurement of the values of ΔH_v required to convert ΔH_f(l) to ΔH_f(g) has therefore been undertaken by the gas chromatography – calorimetry technique (6–8) for ethylidenecyclohexane, 1-ethylcyclopentene, and ethylidenecyclopentane.

Values of ΔH_v have also been measured, and ΔH_f(g) calculated for the related alkene derivatives of cyclopentane and cyclohexane, 3-methylcyclopentene, methylenecyclohexane, allylcyclopentane, and vinylcyclohexane, and for the highly branched open chain hydrocarbons, *trans*-2,2,5,5-tetramethyl-3-hexene, 2,2,4,4-tetramethylpentane, and 3,3-diethylpentane. ΔH_v of allylcyclohexane has also been measured.

Experimental

Hydrocarbon samples were obtained from Chemical Samples Company, and were stated to be of 99% or greater purity. This purity was confirmed by gas chromatography. Heats of vaporization were measured using the technique, apparatus, and gc capillary column (II) previously described (7). The gc values of ΔH (v → DC-200) were corrected to 25°C using additivity rules to estimate liquid (9) and gaseous (10) heat capacities. Several liquid heat capacities were measured for compounds for which the calculated values of Shaw (9) and of Luria and Benson (11) show a large disparity. C_p(l) was measured in a 10 mL vacuum jacketed calorimeter, magnetically stirred, and immersed in a water bath at 25.00°C, regulated to ±0.002°C. C_p(l) values were calculated relative to water (17.98 cal/mol K) and *n*-heptane (53.77 cal/mol K). Each value (Table 1) was calculated from the mean of 4–10 heating curves which showed a standard deviation of 0.3% or less.

Results and Discussion

The experimental heats of vaporization of the 12 hydrocarbons, the measured liquid heat capacities, and the calculated liquid and gaseous heat capacities (9, 10) are listed in Table 1. The values of ΔH_v and previous values of ΔH_f(l) have been used (Table 2) to calculate ΔH_f(g).

TABLE 1. Heats of vaporization, heat capacities, and enthalpy data in DC-200 for unsaturated cyclic hydrocarbons

Compound	ΔH_s[a] (kcal mol^{-1})	C_p(l)[b] (cal mol^{-1} K^{-1})	C_p(g)[c] (cal mol^{-1} K^{-1})	ΔT (K)[d]	Slope[e]	$-\Delta H$(v → S)[f] (kcal mol^{-1})	ΔH_v[g] (kcal mol^{-1})
1-Methylcyclopentene	0.09	36.6	24.2	34.4	3.28819	6.96	7.80 ± 0.06
3-Methylcyclopentene	0.08	36.4	23.3	34.4	3.08585	6.58	7.42 ± 0.06
Ethylidenecyclopentane	0.15	43.3	29.2	34.8	3.95562	8.35	9.23 ± 0.06
1-Ethylcyclopentene	0.31	45.0	29.3	34.4	3.84130	8.17	9.21 ± 0.07
Methylenecyclohexane	0.16	42.4	30.1	34.4	3.67838	7.73	8.63 ± 0.07
Allylcyclopentane	0.19	48.5	34.4	34.8	4.15102	8.74	9.65 ± 0.06
Vinylcyclohexane	0.19	49.5[h]	35.1	35.6	4.05942	8.58	9.50 ± 0.06
Ethylidenecyclohexane	0.24	48.7	35.4	35.6	4.33042	9.08	10.04 ± 0.06
Allylcyclohexane	0.26	55.8	40.6	35.6	4.53367	9.55	10.51 ± 0.06
3,3-Diethylpentane	0.23	66.5	51.1	35.6	4.36827	9.23	10.17 ± 0.08
2,2,4,4-Tetramethylpentane	0.29	63.6[h]	51.4	33.9	3.91667	8.19	9.21 ± 0.07
trans-2,2,5,5-Tetramethyl-3-hexene	0.15	74.2[h]	54.2	34.5	4.27248	9.18	10.04 ± 0.06

[a]In DC-200 silicone fluid (100 cS) at 25°C. Estimated uncertainty ±0.02 kcal mol^{-1}.
[b]Experimental values (±0.5 cal mol^{-1} K^{-1}) unless otherwise indicated.
[c]Calculated from group values (10), estimated ±1.0 cal mol^{-1} K^{-1}.
[d]Mean temperature of gc retention time measurements 298.15 K.
[e]Of plot of ln gc corrected retention times vs. 1/*T*.
[f]Enthalpy of transfer from vapor to DC-200, corrected to 298.15 K.
[g]Corrected experimental heat of vaporization values at 298.15 K.
[h]Calculated from group values (9), estimated ±2.0 cal mol^{-1} K^{-1}.

TABLE 2. Gaseous heats of formation of unsaturated cyclic hydrocarbons

Compound	$\Delta H_f(l)^a$ (kcal mol^{-1})	ΔH_v^b (kcal mol^{-1})	$\Delta H_f(g)^c$ (kcal mol^{-1})
1-Methylcyclopentene	-8.66 ± 0.17	7.80 ± 0.06^d	-0.86 ± 0.18
3-Methylcyclopentene	-5.66 ± 0.16	7.42 ± 0.06^e	1.76 ± 0.17
Ethylidenecyclopentane	-13.56 ± 0.22	9.23 ± 0.06	-4.33 ± 0.23
1-Ethylcyclopentene	-13.93 ± 0.22	9.21 ± 0.07	-4.72 ± 0.23
Methylenecyclohexane	-14.7 ± 0.9	8.63 ± 0.07	-6.07 ± 0.90
Allylcyclopentane	-15.74 ± 0.25	9.65 ± 0.07	-6.09 ± 0.26
Vinylcyclohexane	-21.19 ± 0.21	9.50 ± 0.07	-11.69 ± 0.22
Ethylidenecyclohexane	-24.73 ± 0.18	10.04 ± 0.07	-14.69 ± 0.19
3,3-Diethylpentane	-65.82 ± 0.41	10.17 ± 0.08^f	-55.65 ± 0.42
2,2,4,4-Tetramethylpentane	-66.92 ± 0.34	9.21 ± 0.07^g	-57.71 ± 0.35
trans-2,2,5,5-Tetramethyl-3-hexene	-49.60 ± 0.64	10.04 ± 0.06	-39.56 ± 0.64

[a]Liquid heats of formation (5).
[b]Experimental values from Table 1.
[c]Gaseous heats of formation.
[d]Estimated (5) 8.1 ± 0.4 kcal mol^{-1}.
[e]Estimated (5) 7.7 ± 0.4.
[f]Estimated (5) 10.41 ± 0.10.
[g]Estimated (5) 9.12 ± 0.10.

From the data of Table 2 it may be seen that $\Delta H_f(g)$ for 1-ethylcyclopentene is 0.39 ± 0.33 kcal/mol more exothermic than $\Delta H_f(g)$ of ethylidenecyclopentane. Similarly, the value for 1-ethylcyclohexene (-15.16 ± 0.26 (5)) is 0.47 ± 0.32 kcal/mol more exothermic than that of ethylidenecyclohexane. Comparison of these two pairs of trialkylethylenes indicates that with comparably substituted double bonds the five- and six-membered ring systems show a similar preference for the *endo* double bond. This is a considerably smaller $\Delta H_f(g)$ difference than exists between 1-methylcyclohexene ($\Delta H_f(g) = -10.34 \pm 0.20$ kcal/mol (5)) and methylenecyclohexane (-6.07 ± 0.90 kcal/mol).

$\Delta H_f(g)$ for 1-methylcyclopentene is 2.62 ± 0.25 kcal/mol more exothermic than that of 3-methylcyclopentene. This is quite comparable to the 2.79 ± 0.22 kcal/mol difference in $\Delta H_f(g)$ (5), and the 2.7 kcal/mol difference in gaseous heats of hydrogenation (4), between 1-butene and *trans*-2-butene. This seems to be a matter of alkyl substitution differences rather than conformational stability differences.

Vinylcyclohexane is 3.47 ± 0.34 kcal/mol less exothermic in $\Delta H_f(g)$ than 1-ethylcyclohexene. This is very similar to the 3.51 ± 0.25 kcal/mol difference in $\Delta H_f(g)$, and 3.4 kcal/mol difference in $\Delta H_{H_2}(g)$ between 2-methyl-2-butene and 3-methyl-1-butene, again suggesting that the cyclic compounds differ in double bond substitution rather than conformational stability. The 5.60 ± 0.34 kcal/mol more exothermic $\Delta H_f(g)$ of vinylcyclohexane relative to allylcyclopentane is essentially identical to the ethylcyclohexane–propylcyclopentane difference (5), and is mainly a reflection of the 6.1 kcal/mol greater strain in the cyclopentane ring (12).

The observation that $\Delta H_f(g)$ for 3,3-diethylpentane is 0.99 ± 0.49 kcal/mol more exothermic than that of *n*-nonane is concordant with the observation that 3-ethylpentane and 3-ethylhexane have $\Delta H_f(g)$ values 0.4–0.5 kcal/mol more exothermic than the isomeric *n*-alkanes.

It is noteworthy that neither the Shaw (9) nor the Luria and Benson (11) liquid heat capacity group parameters very accurately predict values for the cyclic unsaturated compounds, and the calculated vs. experimental differences are as large as 4 cal/mol K.

Acknowledgments

This research was supported by the Robert A. Welch Foundation, Grant E-136. We wish to thank Professor N. L. Allinger for helpful discussion, and for furnishing a sample of 3-methylcyclopentene.

1. H. C. BROWN, J. H. BREWSTER, and H. SHECHTER. J. Am. Chem. Soc. **76**, 467 (1954).
2. R. B. TURNER and R. H. GARNER. J. Am. Chem. Soc. **79**, 253 (1957); **80**, 1424 (1958).
3. J. B. CONANT and G. B. KISTIAKOWSKY. Chem. Rev. **20**, 181 (1937).
4. J. L. JENSEN. Prog. Phys. Org. Chem. **12**, 189 (1976).
5. J. D. COX and G. PILCHER. Thermochemistry of organic and organometallic compounds. Academic Press, New York, NY. 1970.
6. L. A. PEACOCK and R. FUCHS. J. Am. Chem. Soc. **99**, 5524 (1977).
7. R. FUCHS and L. A. PEACOCK. Can. J. Chem. **56**, 2493 (1978).
8. P. P. S. SALUJA, L. A. PEACOCK, and R. FUCHS. J. Am. Chem. Soc. **101**, 1958 (1979).
9. R. SHAW. J. Chem. Eng. Data, **14**, 461 (1969).
10. S. W. BENSON. Thermochemical kinetics. 2nd ed. Wiley, New York, NY. 1976.
11. M. LURIA and S. W. BENSON. J. Chem. Eng. Data, **22**, 90 (1977).
12. E. M. ENGLER, J. D. ANDOSE, and P. v.R. SCHLEYER. J. Am. Chem. Soc. **95**, 8005 (1973).

Synthesis of potential DNA bisintercalative agents of the phenanthridinium class

J. WILLIAM LOWN, BRIAN C. GUNN,[1] KRISHNA C. MAJUMDAR,[1] AND E. MCGORAN[1]

Department of Chemistry, University of Alberta, Edmonton, Alta., Canada T6G 2G2

Received January 17, 1979

J. WILLIAM LOWN, BRIAN C. GUNN, KRISHNA C. MAJUMDAR, and E. MCGORAN. Can. J. Chem. 57, 2305 (1979).

The syntheses are described of certain bis(5-alkyl-3,8-diamino-6-phenylphenanthridinium)dichlorides linked through the 8-amino group with diamide bridges, as well as bis(5-alkyl-3,8-diamino-6-alkylphenanthridinium)dichlorides linked through the 6-position by methylene bridges, as potential double intercalators into duplex nucleic acids. The work explores the syntheses of bisethidium compounds via permissible points of attachment of the chromophore consistent with optimal fluorescence enhancement upon intercalation.

J. WILLIAM LOWN, BRIAN C. GUNN, KRISHNA C. MAJUMDAR et E. MCGORAN. Can. J. Chem. 57, 2305 (1979).

On décrit la synthèse de certains dichlorures de bis(alkyl-5 diamino-3,8 phényl-6 phénanthridinium) liés par le groupe amino en 8 à des ponts diamides ainsi que des dichlorures de bis(alkyl-5 diamino-3,8 alkyl-6 phénanthridinium) dont les positions 6 sont reliées par des ponts méthylènes; il s'agit de substances qui pourraient être doublement intercalées dans les acides nucléiques doubles. Le travail explore la synthèse des composés biséthidium par l'intermédiaire de points d'attaches permis pour un chromophore en accord avec une augmentation optimale de la fluorescence lorsque les produits sont intercalés.

[Traduit par le journal]

Introduction

There is accumulating evidence that many planar aromatic molecules including antibiotics, antimalarials, carcinogens, and mutagens intercalate, i.e., insert between the base pairs of double helical DNA (1–4). Among the most useful, in an analytical sense, has been the trypanocidal phenanthridinium derivative ethidium bromide **E** (3, 5). When the latter intercalates into duplex DNA its intrinsic fluorescence exhibits a quantum yield increase of about 25-fold (6). For this reason ethidium bromide has been widely used in spectrofluorimetric studies of nucleic acids (6–13). For example, ethidium bromide

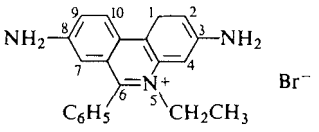

E

has been used to probe circular DNA structure (14), tRNA (9, 15), 5S RNA (16, 17), chromatin (18), and ribosomal RNA (19) as well as tRNA–protein interactions (20). Recently the fluorescence characteristics of ethidium have provided the basis of a number of useful and sensitive assays for the determination of the different types of chemical interaction of antitumor agents with nucleic acid cell targets (21–32).

The recognition of the concept of bisintercalation in the case of the quinoxaline antibiotic echinomycin (34) and in the synthetic bisintercalators of the bisacridine (35–42), bisacridinium (43), bisphenanthridinium (44–48), bisellipticine (49), and bisanthracycline (50) classes has led to increased binding upon interaction with DNA. The efficiency of DNA binding of such drugs is sensitively dependent on the nature of the linker, its length, and on its points of attachment to the two chromophores (43–46). In this paper we examine the synthesis of bisphenanthridinium compounds at different permissible points of attachment consistent with the requirements for good fluorescence enhancement upon DNA binding.

Experimental

Melting points were determined on a Fisher–Johns apparatus and are uncorrected. Infrared spectra were recorded on a Perkin-Elmer grating infrared spectrophotometer model 421 and generally only the principal peaks are reported. Absorption spectra were measured in either distilled water or 'spectro-grade' solvents and were run on either a Beckman DB spectrophotometer, a Gilford 250 spectrophotometer, or a Unicam SP1700 UV spectrophotometer. Proton magnetic resonance spectra were recorded on Varian A-60 and HA-100 analytical instruments and were generally measured on 10–15% (w/v) solutions of the compound in the appropriate deuterated solvent. The reference compound was tetramethylsilane (TMS). Line positions are reported in ppm from the reference. Mass spectra were determined with Associated Electrical Industries MS2, MS9, MS12, or MS50 (DS50) mass spectrometers. In general the ionization energy was 70 eV. Peak measurements were made by comparison with perfluo-

[1]University of Alberta Postdoctoral Fellows.

0008-4042/79/172305-09$01.00/0

rotributylamine at a resolving power of 1500. Kieselgel DF-5 (Camag, Switzerland) and Eastman Kodak precoated sheets were used for thin layer chromatography. Microanalyses were carried out by Mrs. D. Mahlow of this department.

Materials

The following α,ω-diacid chlorides required for this study were either available commercially or were synthesized from the appropriate dicarboxylic acids by established procedures. Each were purified by distillation under reduced pressure immediately before use: hexandioic, bp 116–118°C/12 Torr; heptandioic, bp 137°C/15 Torr; octandioic, bp 147–148°C/12 Torr; nonandioic, bp 158–159°C/12 Torr; decandioic, bp 192–193°C/11 Torr; undecandioic bp 198–199°C/11 Torr; dodecandioic acid chloride, bp 184–185°/10 Torr.

2-Acetamidobiphenyl

This acyl derivative was prepared in 97% yield by the method of Morgan and Walls (51).

4′-Nitro-2-acetamidobiphenyl ***1***

The foregoing acetamido derivative was nitrated with fuming nitric acid at 0°C to give the 4′-nitro-2-acetamidobiphenyl **1** in 55% yield by the procedure of Scarborough and Waters (52).

4′-Amino-2-acetamidobiphenyl

This amine, described by Finzi and Mangini (53), was prepared by treating 16.0 g (62 mmol) of the 4′-nitro-2-acetamidobiphenyl with 16.0 g (0.285 g-at.) of reduced iron powder in aqueous ethanol solution containing a trace of concentrated hydrochloric acid. After the work-up 10.5 g (75% yield) of the desired amine was obtained.

2,4′-Diaminobiphenyl ***2***

Hydrolysis of the above acetamido derivative by refluxing in ethanol containing 10% concentrated hydrochloric acid for 3 h yielded quantitatively the desired diaminobiphenyl **2**, mp 56°C (aqueous ethanol) (lit. (53) mp 56°C).

2,4-Diamino-4-nitrobiphenyl ***3***

A modification of the method of Finzi and Mangini (53) was used. A solution of 15 g (80 mmol) of 2,4-diaminobiphenyl in concentrated sulfuric acid (mixed at 0°C) was stirred in an ice–ethanol bath to a temperature of −2°C. Then 8.5 g (9 mL, 80 mmol) of *n*-propyl nitrate in 10 mL of glacial acetic acid was added dropwise such that the temperature did not rise above −2°C. Stirring was continued for 1 h and the mixture was poured into 250 g of ice and neutralized with saturated aqueous sodium carbonate solution. The resulting brown solid was collected and taken up in the minimum of concentrated hydrochloric acid and reprecipitated with concentrated ammonium hydroxide as a red solid. After collection and thorough washing with water the product **3** was recrystallized from aqueous ethanol as bright red rosettes, 10 g (55% yield), mp 177°C (aq. EtOH) (lit. (53) mp 177–178°C).

4′-Acetamido-2-benzamido-4-nitrobiphenyl ***4***

Benzoyl chloride (1.04 g, 7.4 mmol) was added dropwise with stirring to a solution of 2.0 g (7.4 mmol) of 4′-acetamido-2-amino-4-nitrobiphenyl in 25 mL of dry nitrobenzene. The mixture was heated at 140°C for 45 min and on cooling deposited crystals of the benzamido compound which were collected and washed with cold ether. The product was purified by recrystallization from aqueous pyridine as off-white needles, 2.3 g (83% yield), mp 185–187°C (lit. (54) mp 187°C).

8-Acetamido-3-nitro-6-phenylphenanthridine ***5***

4′-Acetamido-2-benzamido-4-nitrobiphenyl (1 g, 2.7 mmol) was cyclized to the corresponding phenanthridine by refluxing in 5 mL of phosphoryl chloride for 2 h. Upon cooling the mixture was cautiously poured onto ice and neutralized with ammonium hydroxide. The resulting yellow phenanthridine was collected, washed thoroughly with water, dried, and recrystallized from aqueous pyridine as yellow plates, 0.7 g (73% yield), mp 295–297°C (lit. (54) mp 297°C).

2-Amino-4′-carboethoxyamino-4-nitrobiphenyl 7

This urethane derivative was obtained in 76% yield together with a minor amount of the isomer **6** from the foregoing diaminonitrobiphenyl and ethyl chloroformate by a procedure similar to that described by Walls (55).

2-Benzamido-4′-carboethoxyamino-4-nitrobiphenyl

The foregoing amine was treated with benzoyl chloride in nitrobenzene to furnish the benzamide in 80% yield as described by Walls (55).

8-Carboethoxyamino-3-nitro-6-phenylphenanthridine ***8***

This phenanthridine was obtained in 42% yield by the treatment of the benzamido derivative with phosphoryl chloride at 120°C for 1 h (55).

8-Amino-3-nitro-6-phenylphenanthridine

Hydrolysis of the foregoing phenanthridine derivative with concentrated sulfuric acid at 140°C for 0.5 h afforded the free aminophenanthridine in almost quantitative yield, mp 228°C (EtOH) (lit. (55) mp 227–227.5°C).

N,N′-*[8,8′-Bis(3-nitro-6-phenyl)phenanthridinyl]sebacamide* ***9***

A dry benzene solution (10 mL) of 0.13 g (0.43 mmol) of 8-amino-3-nitro-6-phenylphenanthridine was treated with 52 mg (0.215 mmol) of decandioic acid chloride. An immediate precipitate formed and the mixture was heated under reflux for 2 h by which time evolution of hydrogen chloride ceased. The mixture was next treated with concentrated ammonium hydroxide until slightly basic and then concentrated *in vacuo*. The yellow gum which remained was triturated with 50% aqueous ethanol. Refluxing the solution for 15 min, cooling, and filtering afforded the amide **9** ($n = 8$). Recrystallization from aqueous pyridine gave pure **9** as orange-yellow crystals, mp 164–166°C, resolidifying at 170°C and remaining unmelted at 300°C. Infrared ($CHCl_3$) ν_{max}: 3320 (NH), 2840, 2920, 2980 (CH_2), 1660 (amide C=O), 1520, 1340 (NO_2), 1610 (aryl ring) cm^{-1}. *Anal.* calcd. for $C_{48}H_{20}N_6O_6$: N 9.48; found: N 9.63.

Similarly prepared by the above procedure was the corresponding dodecandiamide ($n = 10$) derivative **9** ($n = 10$) in 66% yield, mp 176°C, resolidifying at 180°C and unmelted at 300°C. Infrared ($CHCl_3$) ν_{max}: 3340 (NH), 2835, 2920, 2975 (CH_2), 1665 (amide CO), 1530, 1350 (NO_2), 1605 (aryl ring) cm^{-1}. *Anal.* calcd. for $C_{52}H_{48}N_6O_6$: N 9.85; found: N 9.75.

N,N′-*[8,8′-Bis(3-amino-6-phenyl)phenanthridinyl]sebacamide* ***10*** *(n = 8)*

This bisamine was prepared by treating the foregoing compound **9** ($n = 8$) with reduced iron powder in aqueous ethanol solution containing a trace of concentrated hydrochloric acid. After work-up as described in previous examples 80% yield of the bisamino compound **10** ($n = 8$) was obtained, mp 169°C. *Anal.* calcd. for $C_{48}H_{24}N_6O_2$: N 11.72; found: N 11.96.

8-Carboethoxyamino-5-methyl-3-nitro-6-phenylphenanthridinium Methyl Sulfate ***11***

8-Carboethoxyamino-3-nitro-6-phenylphenanthridine **8** was converted to the quaternary salt in 80% yield by the method of Walls, utilizing freshly distilled dimethyl sulfate in dry nitrobenzene at 180°C for 30 min. The crude salt was washed with ether to remove excess solvent and recrystallized from water as yellow plates (55).

8-Amino-5-methyl-3-nitro-6-phenylphenanthridinium Chloride

Removal of the carboethoxy group was accomplished as previously described by treating 0.6 g (1.16 mmol) of the above salt **11** with 2 mL of 70% sulfuric acid for 30 min at 135°C. After work-up the aminophenanthridinium salt was obtained in quantitative yield (0.5 g). Metathesis with saturated aqueous sodium chloride gave the corresponding chloride salt as brown-red plates (55).

N,N′-[*8,8′-Bis(5-methyl-3-nitro-6-phenyl-phenanthridinium)*]-*sebacamide Dichloride* ***12*** *(*n = *8)*

To a solution of 0.3 g (0.82 mmol) of 8-amino-5-methyl-3-nitro-6-phenylphenanthridinium chloride in 5 mL of dry nitrobenzene was added 0.098 g (0.41 mmol) of sebacyl chloride. When addition was completed the mixture was refluxed for 2 h until no more hydrogen chloride was evolved and then cooled to room temperature. Addition of ether precipitated the desired product as an orange-brown solid. Recrystallization from aqueous methanol afforded an orange amorphous solid, 0.21 g (48% yield), mp 110°C (resolidifies and remelts at 210°C). *Anal.* calcd. for $C_{50}H_{46}Cl_2N_6O_6$: C 66.88, H 5.12, Cl 7.91, N 9.36; found: C 66.53, H 5.18, Cl 8.02, N 9.57.

Similarly prepared by the above procedure was the corresponding dodecandiamide (*n* = 10) derivative **12** (*n* = 10) in 44% yield, mp 110°C (resolidifies and remelts at 215°C). *Anal.* calcd. for $C_{52}H_{50}Cl_2N_6O_6$: Cl 7.66, N 9.08; found: Cl 7.87, N 9.15.

N,N′-[*8,8′-Bis(3-amino-5-methyl-6-phenylphenanthridinium)*]-*sebacamide Dichloride* ***13***

A solution of 0.2 g (0.22 mmol) of *N,N′*-[8,8′-bis(5-methyl-3-nitro-6-phenylphenanthridinium)]sebacamide dichloride in 25 mL of 1:1 aqueous ethanol was mixed with 61.6 mg (1.1 mg-at.) of reduced iron powder and 1 drop of concentrated hydrochloric acid. The mixture was refluxed for 1.5 h, cooled, and filtered through Celite to give a purple filtrate. Concentration *in vacuo* and addition of sodium chloride resulted in precipitation of a red solid which was collected and recrystallized from aqueous ethanol as fine, deep-red crystals, 0.17 g (92% yield), mp > 300°C. Nmr (CD_3OD) δ: 1.24–1.8 (br, m, 12H, 6 CH_2), 2.18–2.4 (m, 4H, $2CH_2$), 4.45 (brs, 6H, $2CH_3$), 5.9 (brs, 4H, $2NH_2$), 7.25–8.73 (m, 22H, Ar), 9.45 (s, 2H, exch. NH). Infrared ($CHCl_3$) ν_{max}: 3450, 3420, 2930, 2865, 1670, 1450, 1245, 850 cm^{-1}. *Anal.* calcd. for $C_{50}H_{50}Cl_2N_6O_2$: C 71.68, H 5.97, Cl 8.48, N 10.03; found: C 71.24, H 6.02, Cl 8.57, N 10.25.

4,4′-Diamino-2-nitrobiphenyl ***15***

This nitrobenzidine was obtained in 84% yield by nitration of benzidine **14** with potassium nitrate in concentrated sulfuric acid according to the procedure of Leslie and Turner (55).

4,4′-Dicarboethoxyamino-2-nitrobiphenyl ***16***

The foregoing nitro compound was treated with ethyl chloroformate to furnish the diurethane in 87.5% yield as described by Leslie and Turner (56).

2-Amino-4,4′-dicarboethoxyaminobiphenyl ***17***

This compound was prepared from the corresponding nitro derivative in 75% yield by reduction by reduced iron metal in aqueous ethanol containing a trace of concentrated hydrochloric acid (56).

N,N′-*Di*[*2-(4,4′-dicarboethoxyamino)biphenyl*]*sebacamide* ***18*** *(*n = *8)*

To a solution of 1.7 g (5 mmol) of 2-amino-4,4′-dicarboethoxyaminobiphenyl in 20 mL of dry benzene was added dropwise with stirring 0.58 g (2.5 mmol) of decandioic acid chloride (sebacyl chloride). The resulting mixture was refluxed gently until the evolution of hydrogen chloride ceased, approx. 1 h. Then it was treated with ammonium hydroxide solution until just basic and heated under reflux again for a short period. The benzene was removed *in vacuo* to afford **18** (*n* = 8) as a cream colored solid which was purified by recrystallization from ethanol, 2.0 g (95% yield), mp 223°C. Mass spectrum *m/e* (% relative abundance): 369 (40.6) $\frac{1}{2}(P - C_8H_{18})$; 323 (64.6) $\frac{1}{2}(P - C_8H_{18}—C_2H_5OH)$; 277 (100) $\frac{1}{2}(P - C_8H_{18}—2C_2H_5OH)$. The ir spectrum ($CHCl_3$) ν_{max}: 3240–2410 (NH), 1695 (CO, carbamate), 1650 (CO, amide) cm^{-1}. The ^{1}Hmr spectrum ($(CD_3)_2SO$) δ: 9.6 (d, 4H, carbamate NH), 9.05 (s, 2H, amide NH), 7.14–7.65 (m, 14H, aryl protons), 4.16 (q, 8H, carbamate CH_2), 2.15 (br t, 4H, —amide CH_2), 1.26 (t, 12H, —carbamate CH_3), 1.05–1.68 (m, 12H, aliphatic $6CH_2$). *Anal.* calcd. for $C_{46}H_{56}N_6O_{10}$: C 64.79, H 6.59, N 9.85; found: C 64.62, H 6.9, N 10.27.

The additional bisamides in Tables 1 and 2 were prepared by the same general procedure.

1,4-Bis(3,8-dicarboethoxyaminophenanthridin-6-yl)butane ***19*** *(*n = *4)*

A solution of 2.0 g (2.5 mmol) of *N,N′*-bis(4,4′-dicarboethoxyamino-2-diphenylyl)adipamide in 7.0 mL of freshly redistilled phosphorus oxychloride was heated under reflux for 2.5 h. When cooled, the excess phosphorus oxychloride was removed under reduced pressure and the residue was poured into ice-water. Neutralization with concentrated ammonium hydroxide solution, followed by filtration and washing with water, gave the bisphenanthridine as an olive-green solid. Decolorization with charcoal and recrystallization from aqueous pyridine afforded the purified phenanthridine as a buff colored amorphous solid dec. > 300°C. The spectral and analytical data on this and related compounds are given in Tables 3 and 4.

1,4-Bis(3,8-diaminophenanthridin-5-yl)butane ***20*** *(*n = *4)*

This aminophenanthridine was prepared by treating 0.2 g (0.26 mmol) of 1,4-bis(3,8-dicarboethoxyaminophenanthridin-6-yl)butane with 2 mL of 70% sulfuric acid. After heating at 135°C for 1 h the mixture was diluted with water and neutralized with concentrated ammonium hydroxide solution. The resulting colloidal red precipitate was collected and dried. Recrystallization from aqueous dimethylformamide gave the product as fine red-brown needles, 0.1 g (85% yield), mp > 300°C with slow decomposition from 250°C. Nmr spectrum ($(CD_3)_2SO$) δ: 1.2–2.05 (br m, 4H, $2CH_2$), 3.1 (br m, 4H, $2CH_2$), 5–5.9 (br s, 8H, $4NH_2$), 6.87–8.35 (m, 2H, Ar). Infrared ($CHCl_3$) ν_{max}: 3455, 2924, 2860, 1480, 1245 cm^{-1}.

1,4-Bis(3,8-diamino-5-ethyl-6-phenanthridinium)butane dibromide ***21*** *(*n = *4)*

A solution of 0.28 g (0.36 mmol) of the 1,4-bis(3,8-dicarboethoxyaminophenanthridin-6-yl)butane in 8 mL of dry nitrobenzene was converted to the corresponding salt by treatment with 0.12 g (0.72 mmol) of diethyl sulfate at 180°C for 30 min. After cooling, the mixture was triturated with ice-cold ether. Continued washing with ether gave a dark-brown solid which was extracted with boiling water to remove it from a tarry material. The orange solution thus obtained was concentrated to 3 mL *in vacuo* and treated with 7 mL of concentrated sulfuric acid and the mixture heated at 110°C for 1 h. Upon cooling, the mixture was poured into water, and neutralized with concentrated ammonium hydroxide solution. Addition of potassium bromide precipitated a red-purple solid. Crystallization from water gave the phenanthridinium salt as small red-purple crystals, 45 mg (18% yield), mp > 300°C (slow decomposition from 230°C). Nmr spectrum ($(CD_3)_2SO$) δ: 1.3–1.9 (t, overlapping m, 10H, $2CH_3$, $2CH_2$), 2.4 (br m, 4H,

TABLE 1. *N,N'*-Di[2-(4,4'-dicarboethoxyamino)biphenylyl]alkylamides

No.	*n*	Crystallization solvent	Melting point (°C)	Yield (%)	Molecular formula	Calculated (%) C	H	N	Found (%) C	H	N
18*a*	4	$(CH_3)_2SO$, H_2O	238	92	$C_{42}H_{48}N_6O_{10}$	63.31	6.03	10.55	63.51	5.8	10.43
18*b*	5	Pyridine, EtOH	179–180	83	$C_{43}H_{50}N_6O_{10}$	63.70	6.17	10.37	64.21	5.69	10.59
18*c*	7	Pyridine, EtOH	174–177	95	$C_{45}H_{54}N_6O_{10}$	64.43	6.44	10.02	64.82	6.23	9.83
18*d*	10	Pyridine, EtOH	133–135	89	$C_{48}H_{60}N_6O_{10}$	65.45	6.81	9.54	65.73	6.34	9.46
18*e*	11	Pyridine, EtOH	155	87	$C_{49}H_{62}N_6O_{10}$	65.77	6.93	9.39	65.96	6.25	8.82
18*f*	12	Pyridine, EtOH	210–212	89	$C_{50}H_{64}N_6O_{10}$	66.07	7.04	9.25	65.83	6.71	9.62

TABLE 2. Spectral properties of *N,N'*-di-[2-(4,4'-dicarboethoxyamino)biphenyl]alkylamides

No.	Fourier transform infrared ($CHCl_3$) (cm^{-1})	Nuclear magnetic resonance (TMS–$(CD_3)_2SO$) δ CH_3	—(CH_2)—	—CH_2—C(=O)—	NH(amide)	NH(carbamate)	Aryl
18*a*	3280, 2975, 2920, 1699, 1655, 1597, 1500, 1240, 1070, 820, 770, 607	1.22 (t, 12H)	1.07–1.57 (m, 4H, CH_2) 2.1 (t, 4H, CH_2)	4.11 (q, 8H)	8.98 (s, 2H)	9.52 (d, 4H)	7.05–7.63 (m, 14H)
18*b*	3280, 2920, 2860, 1698, 1655, 1597, 1520, 1220, 1064, 810, 765	0.99–1.43 (m, 18H, CH_3, CH_2)		4.11 (q, 8H)	9.05 (s, 2H)	9.5 (s, 4H)	6.95–7.68 (m, 14H)
18*c*	3320, 2990, 2920, 2850, 1710, 1665, 1599, 1530, 1230, 1068, 760	1.02–1.41 (m, 22H, CH_3, CH_2)		4.1 (q, 8H)	9.0 (s, 2H)	9.4 (s, 4H)	6.8 –7.75 (m, 14H)
18*d*	3280, 2920, 2855, 1699, 1655, 1598 1520, 1220, 1070, 810, 770	0.98–1.35 (t, m, 28H, CH_3, CH_2)		4.1 (q, 8H)	9.0 (s, 2H)	9.55 (d, 4H)	7.05–7.61 (m, 14H)
18*e*	3280, 2920, 2850, 1700, 1655, 1599, 1510, 1220, 1065, 810, 770	1–1.50 (m, 30H, CH_3, CH_2)		4.13 (q, 8H)	9.07 (s, 2H)	9.62 (s, 4H)	7.08–7.68 (m, 14H)
18*f*	3280, 2920, 2860, 1720, 1650, 1600, 1520, 1220, 1060, 810, 765	0.95–1.63 (t, m, 32H, CH_3, CH_2)		4.12 (q, 8H)	8.55 (s, 2H)	9.63 (s, 4H)	6.89–7.8 (m, 14H)

$2CH_2$), 4.15 (q, 4H, NCH_2), 5.95, 6.3 (2s, br, exch. 8H, $4NH_2$), 7.2–8.7 (m, 12H, Ar). Infrared ($CHCl_3$) ν_{max}: 2945, 2895, 1480, 1245 cm^{-1}. *Anal.* calcd. for $C_{34}H_{38}Cl_2N_6$: C 67.87, H 6.37, Cl 11.79, N 13.97; found: C 67.95, H 6.24, Cl 11.93, N, 14.01.

Results

Our initial synthetic efforts towards potential bisintercalative phenanthridinium compounds were directed towards linkage through position 8 of the ethidium chromophore **E**. To permit discrimination between the 3 and 8 amino substituents the transformations in Scheme 1 were carried out. Selective acetylation occurs in the aniline ring of **3** since the nitro substituted ring is deactivated. The ring closure of **4** to **5** proceeds in only low yield but when ethyl chloroformate was employed for NH_2 protection, as in **6**, much improved yields resulted although the acylation was not completely selective (Scheme 2, **3** to **6** and **7**). Benzoylation followed by treatment of the acyl derivative with phosphorus oxychloride afforded the cyclization product **8**. Coupling of the free 8-NH_2 group of the product of acid hydrolysis of **8** with two diacyl chlorides proceeded smoothly to produce the 3-nitro bisphenanthridine compounds **9** in which the nitro groups could be reduced to the corresponding 3-aminoanalogues **10**.

The pair of compounds **9** resisted all attempts at quaternization of the phenanthridine nitrogen-5. In view of this the phenanthridine moiety was quatern-

TABLE 3. α,ω-Di(3,8-dicarboethoxyaminophenanthridin-6-yl)alkanes[a]

No.	*n*	Crystallization solvent	Melting point (°C)	Yield (%)	Molecular formula	Calculated (%) C	H	N	Found (%) C	H	N
19*a*	4	$C_6H_5NO_2$	>300	77	$C_{42}H_{44}N_6O_8$	66.31	5.78	11.05	66.25	5.41	10.71
19*b*	7	C_5H_5N, C_2H_5OH	>300	59	$C_{45}H_{50}N_6O_8$	67.33	6.23	10.47	66.86	6.04	10.8
19*c*	8	C_5H_5N, H_2O	>300	65	$C_{46}H_{52}N_6O_8$	—	—	10.29	—	—	10.5
19*d*	10	C_5H_5N, H_2O	222–225	67	$C_{48}H_{56}N_6O_8$	68.24	6.63	9.95	68.17	6.43	9.87
19*e*	11	C_5H_5N, H_2O	180–185	48	$C_{49}H_{58}N_6O_8$	68.53	6.75	9.79	68.23	6.64	9.6
19*f*	12	C_5H_5N, C_2H_5OH	194–197	60	$C_{50}H_{60}N_6O_8$	—	—	9.63	—	—	9.51

[a]All compounds showed a characteristic blue fluorescence when dissolved in concentrated H_2SO_4 and all were homogeneous by tlc (silica gel; 70% CH_3OH; 30% C_2H_5OH).

TABLE 4. Spectral properties of α,ω-di(3,8-dicarboethoxyaminophenanthridin-6-yl)alkanes

No.	Fourier transform infrared, cm^{-1}	Nuclear magnetic resonance (TMS–$(CD_3)_2SO$) δ CH_3 CH_2	Ar—CH_2	NH(carbamate)	Aryl
19*a*	3310, 2975, 2920,[a] 2845, 1693, 1613, 1205, 1055, 800, 759	1.1–1.9 (t, m, 16H, $4CH_3 + 2CH_2$)	3.2 (br, t, 4H, CH_2)	9.8 (d, 4H, NH)	6.95–8.68 (m, 12H, Ar)
19*b*	3320, 2920, 2860, 1708, 1598, 1524, 1220, 1068, 818	1.1–2.0 (t, m, 22H, $4CH_3 + 5CH_2$)	3.2 (br, t, 4H, CH_2)	9.9 (d, 4H, NH)	7.4–8.7 (m, 12H, Ar)
19*c*	3320, 2980, 2920,[b] 2850, 1700, 1620, 1210, 1060, 805, 760	1.1–2.08 (m, 24H, $4CH_3 + 6CH_2$)	3.2 (br, t, 4H, CH_2)	9.95 (d, 4H, NH)	7.1–8.72 (m, 12H, Ar)
19*d*	3320, 2970, 2928,[b] 2850, 1702, 1599, 1524, 1220, 1070, 818	1.12–2.1 (t, m, 28H, $4CH_3 + 8CH_2$)	3.21 (br, t, 4H, CH_2)	10 (d, 4H, NH)	7.64–8.8 (m, 12H, Ar)
19*e*	3340, 2920, 2845,[b] 1700, 1620, 1240, 810, 750	1.1–2.05 (t, m, 30H, $4CH_3 + 9CH_2$)	3.2 (br, t, 4H, CH_2)	9.95 (d, 4H, NH)	8.9 (m, 12H, Ar)
19*f*	3320, 2920, 2845,[b] 1700, 1615, 1220, 1070, 806, 760	1.1–2.0 (t, m, 32H, $4CH_3 + 10CH_2$)	3.2 (br, t, 4H, CH_2)	9.9 (d, 4H, NH)	7.42–8.86 (m, 12H, Ar)

[a]KBr disc.
[b]$CHCl_3$ film.

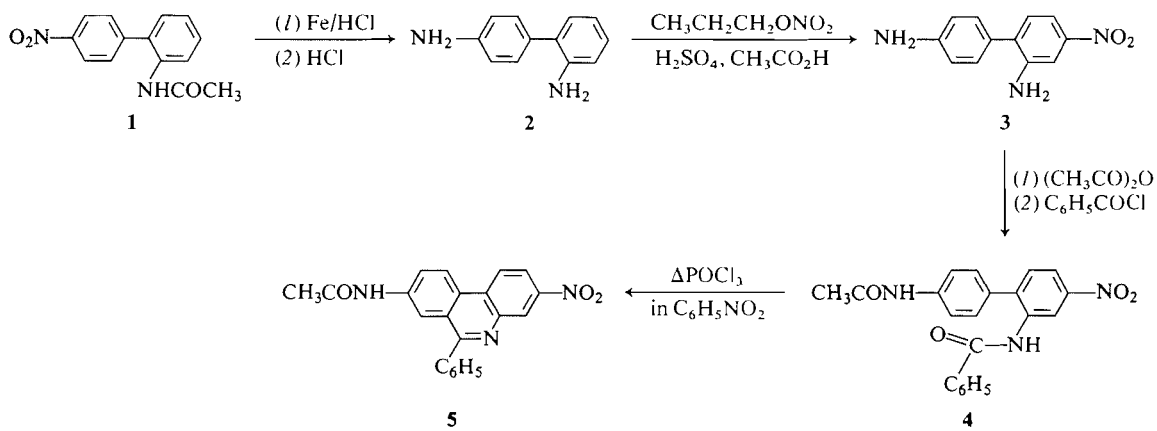

SCHEME I

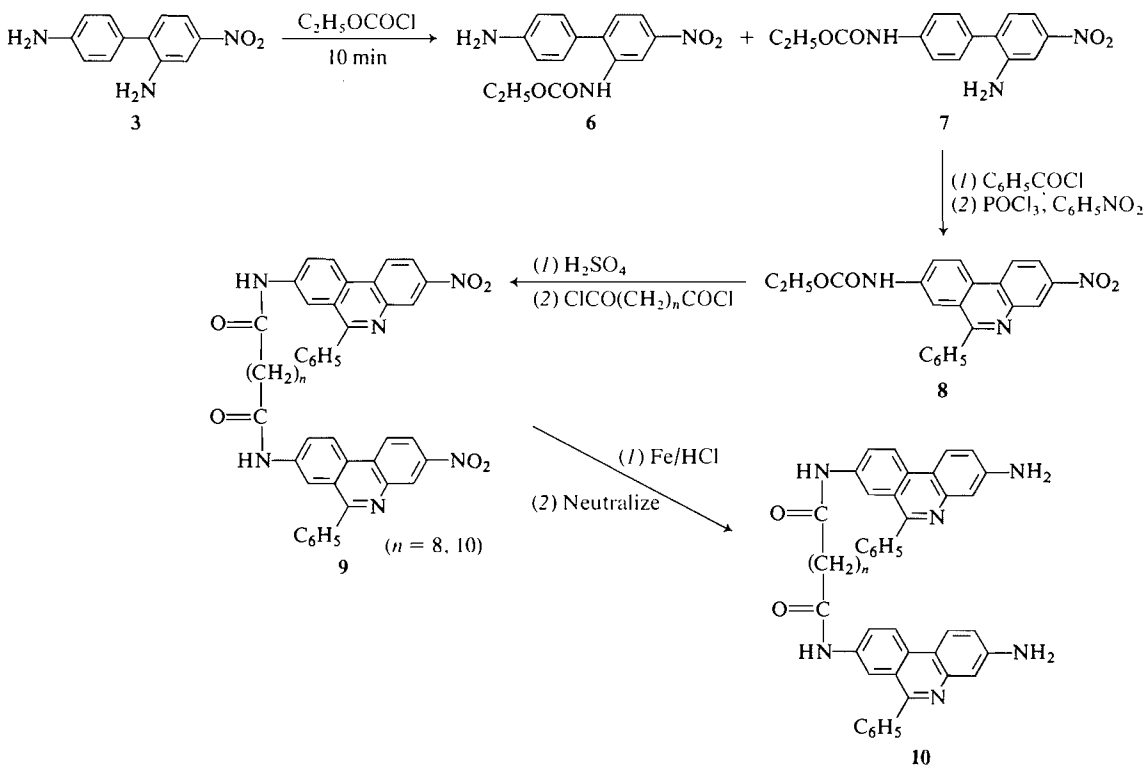

SCHEME 2

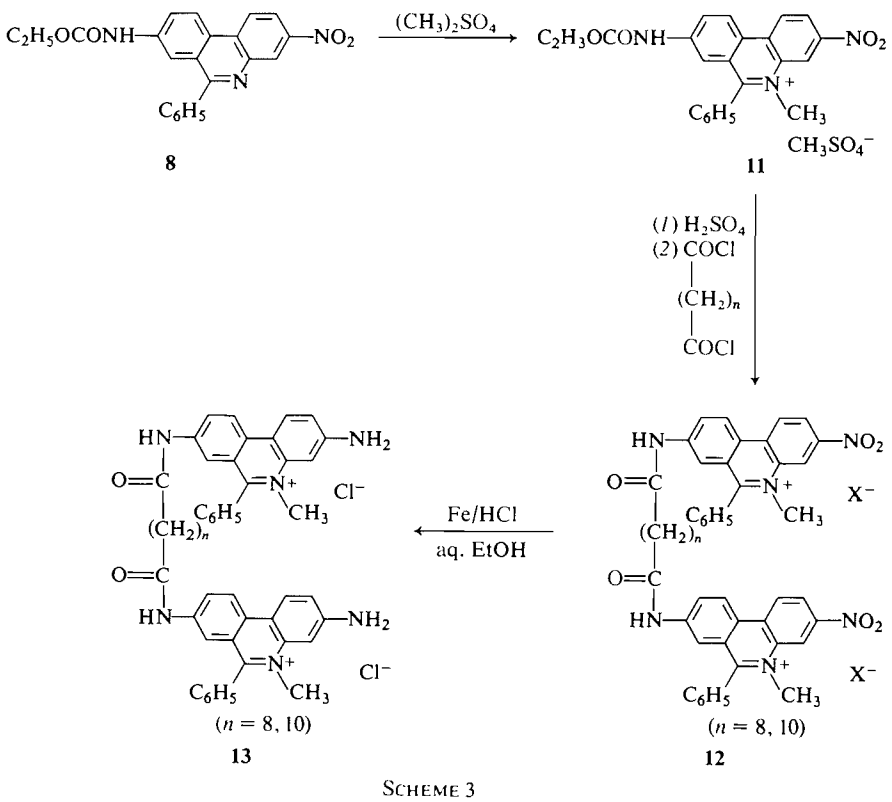

SCHEME 3

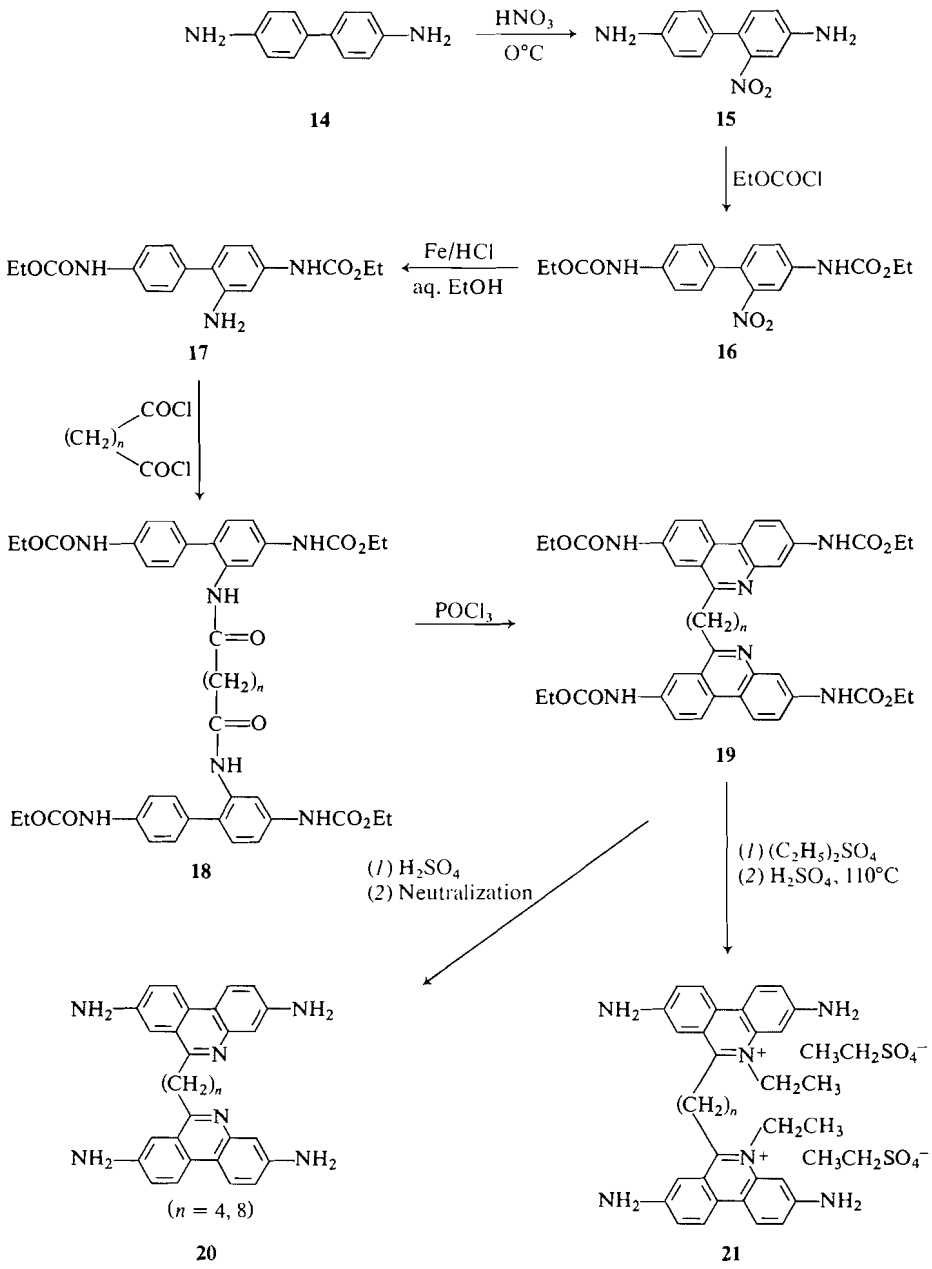

SCHEME 4

ized prior to coupling by alkylation of the relatively unhindered **8** with dimethyl sulfate to give **11** followed by acid generation of the free 8-amino group from **11** and condensation with two diacyl chlorides to give the compounds **12**. Reduction of the nitro group in **12** with iron and hydrochloric acid afforded the 8-linked bisphenanthridinium compounds **13** as outlined in Scheme 3.

Since our previous examination of the substituent requirements in the ethidium moiety for intercalation and fluorescence enhancement had also shown that the 6-aryl substituent may be replaced by an alkyl group without materially affecting the intercalative binding to DNA, a series of bisphenanthridinium compounds was prepared in which the chromophores were linked through the 6-position. Low temperature nitration of 4,4′-diaminobiphenyl **14** afforded compound **15** in 84% yield. Ethyl chloroformate gave the amino group product **16** in 87.5% yield. The nitro group in **16** was reduced in 75% yield by reduced iron metal in aqueous ethanol containing a trace of concentrated hydrochloric acid.

The selectively protected triamine **17** was condensed with diacyl chlorides to give the six 6-linked bisbiphenyl derivatives **18** where $n = 4, 5, 7, 10–12$, all in excellent yields. Ring closure was effected by heating each of the **18** compounds with phosphorus oxychloride to give the bisphenanthridines **19**. The best yields were obtained where $n = 4$, 8, and 10. In contrast to the previous example of **9**, quaternization of **19** with dimethyl sulfate proceeded normally. Deblocking of the 3 and 8 aminoacyl groups was effected smoothly with sulfuric acid at 110°C and afforded a new 6-linked bisphenanthridinium compound **21**. The synthetic plan is given in Scheme 4.

Discussion

The results of our previous studies indicated that among the permissible points of attachment of a linker in the projected synthesis of potential fluorescent bisintercalators on the ethidium chromophore **E** were the 8- and 6-positions (33). These allowed positions together with the requirement of N-5 alkylation are consistent with optimal fluorescence enhancement. The syntheses described here show it is feasible to prepare such bisphenanthridinium compounds linked through the 8- and 6-positions. One factor which influences the synthetic strategy is the resistance to N-5 quarternization noted in compounds **9**. It is possible that this is the result of steric hindrance as a result of stacking of the chromophores in solution for which there is spectroscopic evidence (46, 47). Consequently in the 8-position linked series it is recommended to quarternize the chromophore prior to condensation. By contrast, in the C-6 linked series it is evident that the topology of, for example **19**, is such that stacking of the phenanthridine moieties does not occur and consequently alkylation at N-5 can proceed normally. Le Pecq and co-workers have synthesized a bisphenanthridinium compound in which an alkylamino chain connects the ring nitrogen, and have concluded that it does not double-intercalate in DNA because of steric factors (45). By contrast, in the case of bisphenanthridinium compounds linked through either the *meta* (44) or *para* (48) positions of a 6-aryl substituent there is some evidence for double intercalation in DNA. It is evident then that steric constraints for effective double intercalation into DNA impose further restrictions on the chemical type, sites of attachment, and length of linkers in addition to those required for optimal fluorescence. These factors together with DNA binding characteristics of new bisphenanthridinium salts will be discussed in a subsequent paper.

Acknowledgements

This research was supported by grants to J.W.L. from the National Cancer Institute of Canada, the Natural Sciences and Engineering Research Council of Canada, and by the Department of Chemistry, University of Alberta.

1. L. S. Lerman. J. Mol. Biol. **3**, 18 (1961).
2. E. F. Gale, E. Cundliffe, P. E. Reynolds, M. H. Richmond, and M. J. Waring. *In* The molecular basis of antibiotic action. J. Wiley and Sons, Inc., New York. 1972. pp. 173–277.
3. M. J. Waring. *In* Mechanism of action of antimicrobial and antitumor agents. *Edited by* J. W. Corcoran and F. E. Hahn. Springer-Verlag, Heidelberg. 1975. pp. 151–165.
4. H. Kersten and W. Kersten. *In* Inhibitors of nucleic acid synthesis. Springer-Verlag, Heidelberg. 1974. pp. 74–81.
5. W. Fuller and M. J. Waring. Ber. Bunsenges. Physik. Chem. **68**, 805 (1964).
6. J. B. Le Pecq and C. Paoletti. J. Mol. Biol. **27**, 87 (1967).
7. R. L. P. Adams, R. H. Burton, A. M. Campbell, and R. M. S. Smellie. *In* The biochemistry of the nucleic acids. 8th ed. Academic Press, New York. 1976. p. 60.
8. M. J. Waring. J. Mol. Biol. **13**, 269 (1965).
9. R. Bittman. J. Mol. Biol. **46**, 251 (1969).
10. V. W. F. Burns. Arch. Biochem. Biophys. **133**, 420 (1969).
11. T. Tao, J. H. Nelson, and C. R. Cantor. Biochemistry, **9**, 3514 (1970).
12. J. B. Le Pecq. Methods Biochem. Anal. **20**, 41 (1971).
13. L. M. Angerer, S. Georghiou, and E. N. Moudrianakis. Biochemistry, **13**, 1075 (1974).
14. B. Hudson, W. B. Upholt, J. Devinny, and J. Vinograd. Proc. Natl. Acad. Sci. U.S.A. **62**, 813 (1969).
15. C. Urbanke, R. Romer, and G. Maass. Eur. J. Biochem. **33**, 511 (1973).
16. P. D. Gray and G. F. Saunders. Biochim. Biophys. Acta, **254**, 60 (1971).
17. J. Feunteun, R. Monier, R. Garrett, M. Le Bret, and J. B. Le Pecq. J. Mol. Biol. **93**, 535 (1975).
18. T. Ide and R. Baserga. Biochemistry, **15**, 600 (1976).
19. J. J. Lawrence and M. Daune. Biochemistry, **15**, 3301 (1976).
20. R. Rigler, E. Cronvall, M. Ehrenberg, U. Pachmann, R. Hirsch, and H. G. Zachau. F.E.B.S. Lett. **18**, 193 (1971).
21. R. Cone, S. K. Hasan, J. W. Lown, and A. R. Morgan. Can. J. Biochem. **54**, 219 (1976).
22. J. W. Lown, S. K. Sim, K. C. Majumdar, and R. Y. Chang. Biochem. Biophys. Res. Commun. **76**, 705 (1977).
23. J. W. Lown, K. C. Majumdar, A. I. Meyers, and A. Hecht. Bioorg. Chem. **6**, 453 (1977).
24. J. W. Lown, A. Begleiter, D. Johnson, and A. R. Morgan. Can. J. Biochem. **54**, 110 (1976).
25. J. W. Lown and C. K. Majumdar. Can. J. Biochem. **55**, 630 (1977).
26. J. W. Lown and G. L. Weir. Can. J. Biochem. **56**, 296 (1978).
27. M. H. Akhtar, A. Begleiter, D. Johnson, J. W. Lown, L. W. McLaughlin, and S. K. Sim. Can. J. Chem. **53**, 2891 (1975).
28. J. W. Lown and S. K. Sim. Can. J. Biochem. **54**, 446 (1976).
29. J. W. Lown and S. K. Sim. Can. J. Chem. **54**, 2563 (1976).
30. J. W. Lown and S. K. Sim. Biochem. Biophys. Res. Commun. **77**, 1150 (1977).
31. S. K. Sim and J. W. Lown. Biochem. Biophys. Res. Commun. **81**, 99 (1978).
32. J. E. Strong and S. T. Crooke. Cancer Res. **38**, 3322 (1978).

33. D. C. WARD, E. REICH, and I. H. GOLDBERG. Science, **149**, 1259 (1965).
34. H. T. CHEUNG, J. FEENEY, G. C. K. ROBERTS, D. H. WILLIAMS, G. UGHETTO, and M. H. WARING. J. Am. Chem. Soc. **100**, 46 (1978).
35. J. B. LE PECQ, M. LE BRET, J. BARBET, and B. P. ROQUES. Proc. Natl. Acad. Sci. U.S.A. **72**, 2915 (1975).
36. J. BARBET, B. P. ROQUES, S. COMBRISSON, and J. B. LE PECQ. Biochemistry, **15**, 2642 (1976).
37. E. S. CANELLAKIS, Y. H. SHAW, W. E. HANNERS, and R. A. SCHWARTZ. Biochim. Biophys. Acta, **418**, 277 (1976).
38. E. S. CANELLAKIS and R. A. BELLANTONE. Biochim. Biophys. Acta, **418**, 290 (1976).
39. E. S. CANELLAKIS, V. BONO, R. A. BELLATONE, J. S. KRAKOW, R. M. FICO, and R. A. SCHULZ. Biochim. Biophys. Acta, **418**, 300 (1976).
40. E. S. CANELLAKIS, R. M. FICO, A. H. SARRIS, and Y. H. SHAW. Biochem. Pharmacol. **25**, 231 (1976).
41. R. M. FICO and E. S. CANELLAKIS. Biochem. Pharmacol. **26**, 269, (1977); **26**, 275 (1977).
42. L. P. G. WAKELIN, M. ROMANOS, E. S. CANELLAKIS, and M. J. WARING. Stud. Biophys. **60**, 111 (1976).
43. J. W. LOWN, B. C. GUNN, R. Y. CHANG, K. C. MAJUMDAR, and J. S. LEE. Can. J. Biochem. **56**, 1006 (1978).
44. K. F. KUHLMANN, N. J. CHARBENEAU, and C. W. MOSHER. Nucleic Acids Res. **5**, 2629 (1978).
45. B. P. ROQUES, J. BARBET, R. OBERLIN, and J. B. LE PECQ. C. R. Acad. Sci. Ser. D, **283**, 1365 (1976).
46. B. P. ROQUES, J. BARBET, and J. B. LE PECQ. C.R. Acad. Sci. Ser. D, **283**, 1453 (1976).
47. K. ZACHARIASSE and W. KUHNLE. Z. Phys. Chem. N.F. **101**, 267 (1976).
48. P. B. DERVAN and M. M. BECKER. J. Am. Chem. Soc. **100**, 1968 (1978).
49. A. DELBARRE, B. P. ROQUES, and J. B. LE PECQ. C.R. Acad. Sci. Ser. D, **284**, 81 (1977).
50. G. TONG, D. G. KLEID, and D. W. HENRY. Presented at the 2nd Joint Conference, Chemical Institute of Canada and American Chemical Society, Montreal, June 2, 1977.
51. G. T. MORGAN and L. P. WALLS. J. Chem. Soc. 2447 (1931).
52. H. A. SCARBOROUGH and W. A. WATERS. J. Chem. Soc. 89 (1927).
53. C. FINZI and A. MANGINI. Gazzetta, **62**, 664 (1932).
54. A. G. CALDWELL and L. P. WALLS. J. Chem. Soc. 188 (1948).
55. L. P. WALLS. J. Chem. Soc. 3511 (1950); 67 (1947).
56. M. S. LESLIE and E. E. TURNER. J. Chem. Soc. 1588 (1933).

Identification des configurations relatives d'alcools secondaires α-cyclopropylidéniques et α-vinylcyclopropaniques. Attribution de structure aux éthyl-6 diméthyl-2,4 oxa-3 bicyclo [3.1.0^{1,5}]hexanes

MAURICE VINCENS, CLAUDE DUMONT ET MICHEL VIDAL

Laboratoire de Chimie Organique, Université Scientifique et Médicale de GRENOBLE – B.P. 53 Centre de Tri – 38041, France

Reçu le 3 janvier 1979

MAURICE VINCENS, CLAUDE DUMONT et MICHEL VIDAL. Can. J. Chem. **57**, 2314 (1979).

Dans le cadre d'une étude stéréochimique des alcools secondaires α-cycliques nous avons déterminé les configurations relatives des [éthyl-2 éthylidène-3 cyclopropyl(1*R**,2*R**)]-1 éthanol *E*, *R** et *S**. Le traitement en milieu basique de ces alcools secondaires diastéréoisomères conduit aux [éthyl-2 vinyl-3 cyclopropyl(1*R**,2*S**,3*S**)]-1 éthanol *R** et *S**; l'oxymercuration cyclisante de ces dérivés cyclopropaniques fournit les éthyl-6 diméthyl-2,4 oxa-3 bicyclo[3.1.0^{1,5}]hexanes *diendo*, *diexo*, et *exo–endo*. Les attributions de structure à ces éthers bicycliques, fondées sur des études en ir et rmn du ^{1}H et du ^{13}C, permettent d'attribuer les configurations relatives des alcools vinylcyclopropaniques et cyclopropylidéniques.

MAURICE VINCENS, CLAUDE DUMONT, and MICHEL VIDAL. Can. J. Chem. **57**, 2314 (1979).

During a stereochemical study of α-cyclic secondary alcohols, the relative configurations of the *E*, *R**, and *S** isomers of 1-(2-ethyl-3-ethylidene(1*R**,2*R**)cyclopropyl)ethanol was determined. Treatment in a basic medium of these secondary diastereomeric alcohols leads to the *R** and *S** isomers of 1-(2-ethyl-3-vinyl(1*R**,2*S**,3*S**)cyclopropyl)ethanol. Cyclic oxymercuration of these cyclopropanoic derivatives yields the di-*endo*, di-*exo*, and *exo–endo* derivatives of 6-ethyl-2,4-dimethyl-3-oxabicyclo[3.1.0.^{1,5}]hexane. The determination of the structure as bicyclic ethers, based on ir and ^{1}H and ^{13}C nmr studies, permits the assignment of the relative configurations of the vinylcyclopropanoic and cyclopropylidene alcohols.

[Journal translation]

Introduction

L'étude de l'induction asymétrique, au cours de la réduction des cétones α-cyclopropylidéniques et des transpositions en milieu acide des alcools secondaires qui résultent de cette réduction, nous a conduits à envisager l'identification par voie chimique des configurations relatives des [alkyl-2 éthylidène-3 cyclopropyl(1*R**,2*R**)]-1 éthanol *E*, *R** et *S**. Ce travail s'intègre, par ailleurs, dans l'élaboration d'une méthode générale d'identification chimique des configurations relatives d'alcools secondaires diastéréoisomères dans les séries vinylcyclopropanique, cyclopropanique et cyclopropénique. Ces attributions restent actuellement très délicates; la littérature ne mentionne, en effet, que quelques tentatives fondées généralement sur des données spectrophotométriques (1–3).

La méthode que nous avons utilisée comporte deux phases:

Une filiation chimique est établie entre les [éthyl-2 éthylidène-3 cyclopropyl(1*R**,2*R**)]-1 éthanol *E*, *S** et *R** (**1** et **2**) et les [éthyl-2 vinyl-3 cyclopropyl(1*R**, 2*S**,3*S**)]-1 éthanol *S** et *R** (**3** et **4**) ou les [éthyl-2 vinyl-3 cyclopropyl(1*R**,2*S**,3*R**)]-1 éthanol *S** et *R** (**5** et **6**). Cette filiation peut être facilement réalisée en provoquant la migration de la double liaison cyclopropylidénique de **1** et **2** en milieu basique (4)

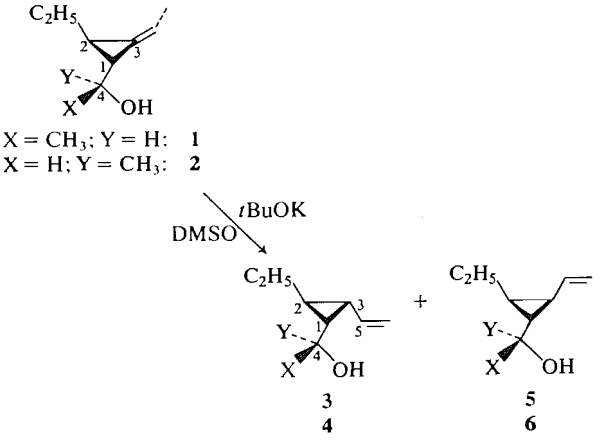

SCHÉMA 1

car, dans ces conditions expérimentales, les configurations relatives des carbones 1, 2 et 4 ne sont pas modifiées.

Les configurations relatives des alcools vinylcyclopropaniques **3** et **4** sont identifiées. La détermination des configurations relatives des carbones cyclopropaniques 1, 2 et 3 est fondée sur l'étude en résonance magnétique nucléaire du proton des glissements chimiques induits par un chélate des terres rares: Eu(dpm)$_3$ d'une part et les valeurs des constantes de couplage des protons cyclopropaniques d'autre part.

0008-4042/79/172314-07$01.00/0

Les configurations relatives des carbones 1 et 4 ont pu être établies en déterminant celles de ces deux centres de chiralité dans les éthyl-6 diméthyl-2,4 oxa-3 bicyclo[3.1.0^{1,5}]hexanes obtenus par oxymercuration cyclisante de ces alcools γ,δ-éthyléniques **3** et **4**.

L'oxymercuration des alcools γ,δ-éthyléniques, suivie d'une réduction par le borohydrure de sodium, fournit des oxolannes substitués (5–7). Cette cyclisation dépend du degré de substitution de l'atome de carbone terminal de la chaîne insaturée: une double substitution conduit à des hétérocycles à six chaînons, une monosubstitution à des hétérocycles à cinq et à six chaînons. Lorsque le carbone terminal n'est pas substitué et que l'on utilise l'acétate mercurique comme agent cyclisant, l'hétérocyclisation est spécifique; seule la structure tétrahydrofurannique est isolée (5). L'emploi de ce sel mercurique permet, en effet, d'éviter le réarrangement du cycle au cours de la réduction de l'organomercurique.

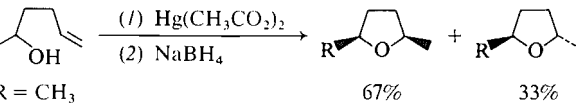

R = CH_3	67%	33%
R = *t*Bu	22%	78%

SCHÉMA 2

La proportion d'isomères *cis* et *trans* obtenus est très sensible à la taille des substituants portés par le carbone fonctionnel. Sans préjuger du mécanisme réactionnel, qui n'est pas totalement élucidé, tout se passe comme si une importante contrainte stérique était défavorable à la formation du dérivé *cis*. Il faut cependant noter que lorsque cette contrainte n'est pas trop importante (cas ou R = CH_3) le dérivé *cis* se forme majoritairement. Signalons enfin que la démercuration de l'organomercurique, réalisée en milieu basique par le borohydrure, conduit à des proportions de dérivés *cis* et *trans* souvent différentes de celles observées pour les organomercuriques (6). Compte tenu de l'ensemble de ces observations, l'oxymercuration des alcools vinylcyclopropaniques **3** et **4** suivie d'une réduction par $NaBH_4$ en milieu basique doit conduire respectivement aux éthers bicycliques **8**, **9** et **7**, **8**; la détermination des configurations relatives de **7** et **9** doit permettre de remonter à celles de **3** et **4** et par conséquent à celle des alcools secondaires cyclopropylidéniques **1** et **2**.

Partie expérimentale

Synthèse des (éthylidène-3 cyclopropyl) méthyl cétone E *et* Z *(**13** et **14**)*

Le diéthyl-2,3 cyclopropènecarboxylate d'éthyle **10** (0.5 mol) est traité par 1.8 mol de potasse dans le *n*-butanol (solution–suspension 6 *M*) pendant 20 h à 125°C. Après évaporation de l'alcool, le mélange réactionnel est amené à pH 2 par addition d'acide chlorhydrique 4 *N*. Après extraction à l'éther la distillation fournit le mélange des acides cyclopropylidéniques (**11** + **12**) avec un rendement de 80%.

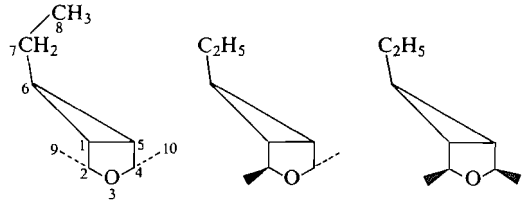

7 **8** **9**

SCHÉMA 3. Ethyl-6 diméthyl-2,4 oxa-3 bicyclo[3.1.0.^{1,5}]hexanes **7**, **8** et **9**.

A 0.2 mol de ce mélange d'acides, en solution dans 200 mL d'éther anhydre, on ajoute 0.4 mol de méthyllithium (0.8 *M* dans l'éther) en 30 min. Le mélange réactionnel est porté au reflux pendant 2 h après la fin de l'addition. Après hydrolyse à 0°C, en milieu acide (pH > 3) et extraction à l'éther, le mélange des cétones **13** et **14** est isolé par distillation (rdt = 75%). Ces composés sont séparés par cpv sur colonne Carbowax (20%) de 6 m (Chromosorb WAW 60/80, gaz vecteur: H_2, θ = 140°C).

*Cétone **13***: n_D^{20} 1.4620; ir (film): ν(C=O) = 1695, ν(C=C) = 1740 cm^{-1}; rmn (C_6D_6/TMS): δH_1 = 2.01 (1H, m), δH_2 = 1.90 (1H, m), δ(=—H) = 5.61 (1H, m), δ(CH_3—=) = 1.65 (3H, m), δ(CH_3—CH_2) = 0.82 (3H, t), δ(CH_3—CH_2) = 1.22 (2H, 5 raies), δ(CH_3—CO) = 2.05 ppm (3H, s). Les valeurs des constantes de couplage sont déterminées à partir d'une solution de **13** dans CCl_4 à laquelle on ajoute des quantités variables de Eu(dpm)$_3$ selon le couplage étudié: ^3J(=—H, =—CH_3) = 6.4 Hz, ^5J(=—CH_3, H_1) = ^5J(=—CH_3, H_2) = 1.9 Hz, ^4J(=—H, H_1) = ^4J(=—H, H_2) = 2.0 Hz, ^3J(CH_2, H_2) = 5.6 Hz, ^3J(CH_2, CH_3) = 6.5 Hz, ^3J(H_1, H_2) = 4.9 Hz.

*Cétone **14***: n_D^{20} 1.4630; ir (film): ν(C=O) = 1702, ν(C=C) = 1735 cm^{-1}; rmn (C_6D_6/TMS): δH_1 = 1.98 (1H, m), δH_2 = 1.90 (1H, m), δ(H—=) = 5.83 (1H, m), δ(CH_3—=) 1.55 (1H, m), δ(CH_3—CH_2) = 0.79 (3H, t), δ(CH_3—CH_2) = 1.17 (2H, 5 raies), δ(CH_3—CO) = 2.02 ppm (3H, s). Couplages (CCl_4, Eu(dpm)$_3$): ^3J(=—H, =—CH_3) = 6.3 Hz, ^5J(=—CH_3, H_1) = ^5J(=—CH_3, —H_2) = 1.7 Hz, ^4J(=—H, H_1) = ^4J(=—H, H_2) = 2.1 Hz, ^3J(CH_2, H_2) = 5.3 Hz, ^3J(CH_3, CH_2) = 6.6 Hz, ^3J(H_1, H_2) = 5.2 Hz.

[*Ethyl-2 éthylidène-3 cyclopropyl(1*R*,2R*)*]-1 éthanol* E, S* *(**1**) et* R* *(**2**)*

A une solution de 4 × 10^{-3} mol de cétone **13** dans 5 mL d'éther anhydre, on ajoute 10^{-2} mol de $AlLiH_4$ en solution–suspension dans l'éther. Le reflux est maintenu pendant 1 h après la fin de l'addition. Après hydrolyse, la phase organique est extraite à l'éther et le mélange d'alcools est récupéré par une distillation rapide. Les alcools cyclopropylidéniques **1** et **2** sont séparés par cpv sur colonne Carbowax (10%) de 4 m (Chromosorb P NAW 60/80, gaz vecteur: H_2, θ = 130°C).

*Alcool **1***: ir (film): ν(O—H) = 3360 ν(C=C) = 1640 cm^{-1}; rmn (CCl_4/TMS): δ(CH_3—CH_2) entre 1 et 1.4 ppm (3H), δ(=—H) = 5.78 (1H, m), δ(=—CH_3) = 1.79 (3H, 6 raies), δ(CH_3—CHOH—) = 1.16 (3H, d), δH_4 = 3.30 ppm (1H, m); ^3J(=—H, =—CH_3) = 6.4 Hz, ^3J(H_1, H_4) = 6.2 Hz.

*Alcool **2***: ir (film): ν(O—H) = 3360 ν(C=C) = 1640 cm^{-1}; rmn (CCl_4/TMS): δ(CH_3—CH_2) entre 1 et 1.4 ppm, δ(=—H) = 5.70 (1H, m), δ(=—CH_3) = 1.76 (3H, 6 raies), δ(CH_3—CHOH) = 1.17 (3H, d), δH_4 = 3.25 ppm (1H, m); ^3J(=—H, =—CH_3) = 6.1 Hz, ^3J(H_1, H_4) = 6 Hz.

Acides [éthyl-2 vinyl-3 cyclopropyl(1R,2S*)] carboxyliques 3R* (15) et 3S* (16)*

L'ester cyclopropénique **10** (22 mmol) est traité par 16 mmol de potasse en solution–suspension dans le *n*-butanol (12 *M*). Le mélange réactionnel est maintenu à 170°C pendant 10 h. Après évaporation de l'alcool et hydrolyse, les acides organiques sont précipités par addition d'une solution chlorhydrique 4 *N* (pH 2–3). Après extraction, la distillation fournit le mélange d'acides pé 65–70°C/0.2 Torr) qui sera utilisé brut pour l'étape suivante. Ces acides ont cependant été caractérisés sous forme d'esters obtenus en traitant une partie du mélange précédent par le diazométhane en solution éthérée. Ces esters sont alors séparés sur colonne Ucon Oil (20%) de 3.3 m (Chromosorb WAW 60/80, gaz vecteur: H_2, θ = 140°C).

Ester 1R, 2R*, 2S*, 3R**: ir (film): ν(=C—H) = 3080, ν(C=O) = 1723, ν(C=C) = 1634, ν(=C—H) = 905 cm^{-1}; rmn (CCl_4/TMS): δ(CO_2Me) = 3.65 (3H, s), δ(CH_3—CH_2) = 1.00 (3H, t), δ(CH_3—CH_2) = 1.45 (2H, m), δ(CH=CH_2) = 5.1–5.6 (3H, non analysable), $\delta H_{1,2}$ = 1.30–1.70 (2H, non analysable), δH_3 = 2.05 ppm (1H, m). Couplages (CCl_4, Eu(dpm)$_3$): $^3J(H_1, H_2)$ = 5.5 Hz, $^3J(H_1, H_3)$ = 5.5 Hz, $J(H_2, H_3)$ = 9.2 Hz.

Ester 1R, 2S*, 3S**: ir (film): ν(=C—H) = 3075, ν(C=O) = 1721, ν(C=C) = 1629, ν(=C—H) = 901 cm^{-1}; rmn (CCl_4/TMS): δ(CO_2Me) = 3.65 (3H, s), δ(CH_3—CH_2) = *1.02* (3H, t) et *1.40* (2H, m), δ(CH=CH_2) = 5.75 (1H, m), 5.17 (1H, m), 4.98 (1H, m), $\delta H_{1,2,3}$ = entre 1.3 et 1.9 ppm (3H, m). Couplages (CCl_4, Eu(dpm)$_3$): $^3J(H_1, H_2) \simeq {}^3J(H_2, H_3) \simeq 5$ Hz, $^3J(H_1, H_3)$ = 9.0 Hz.

[Ethyl-2 vinyl-3 cyclopropyl]-1 éthanol 3 à 6

Le mélange des acides (**15**, **16**) est réduit en cétones vinylcyclopropaniques par le méthyllithium dans l'éther anhydre selon le mode opératoire décrit pour la préparation des cétones **13** et **14**. Le mélange de cétones (**17**, **18**) ainsi obtenu est traité par $AlLiH_4$ (mode opératoire identique à celui décrit précédemment pour la préparation des alcools cyclopropylidéniques **1** et **2**); après hydrolyse et extraction à l'éther de la phase organique, le mélange d'alcools est distillé rapidement et utilisé brut pour le traitement par l'acétate mercurique. Ces alcools on été, par ailleurs, isolés par cpv sur colonne Carbowax (20%) de 4 m (Chromosorb P NAW 60/80, gaz vecteur: H_2, θ = 150°C).

Alcool 1R, 2S*, 3S*, S* (3)*: t_R (cpv) = 15 min; ir: ν(=CH_2) = 3078, ν(=C—H) = 2995, ν(C=C) = 1638, ν(=C—H) = 900 et 812 cm^{-1}; rmn (CCl_4/TMS): δ(CH=CH_2) = 5.54 (1H, m), 5.15 (1H, m), 4.95 (1H, m), δ(CH_3—CH_2, $H_{1,2,3}$) 0.90 à 1.30 (8H, m), δ(CHOH) = 3.34 (1H, 8 raies), δ(COH—CH_3) = 1.23 ppm (3H, d); couplages (CCl_4, Eu(dpm)$_3$): $^3J(CHOHCH_3)$ = 6.3 Hz, $^3J(CH$—$CHOH)$ = 8.7 Hz, $^3J(H_1, H_2)$ = 4.7 Hz.

Alcool 1R, 2S*, 3S*, R* (4)*: t_R(cpv) = 18 min; ir: ν(=CH_2) = 3078, ν(=CH) ≃ 3000, ν(C=C) = 1635, ν(=C—H) = 900 et 815 cm^{-1}; rmn (CCl_4/TMS): δ(CH=CH_2) = 4.80 à 5.40 (3H, m), δ(CH_3—CH_2, $H_{1,2,3}$) = 0.90 à 1.30 (8H, m), δ(CHOH) = 3.38 (1H, 8 raies), δ(COH—CH_3) = 1.17 ppm (3H, d); couplages: $^3J(CHOH$—$CH_3)$ = 6.1 Hz, $^3J(CH$—$CHOH)$ = 8.5 Hz, $^3J(H_1, H_2)$ = 5.2 Hz.

Alcool 1R, 2S*, 3R*, S* (5)*: t_R(cpv) = 24 min; ir: ν(=CH_2) = 3068, ν(=CH) = 2995, ν(C=C) = 1638, ν(=CH_2) = 900 à 920 cm^{-1}; rmn (CCl_4/TMS): δ(CH=CH_2) = 5.45 (1H, m), 5.08 (1H, m), 4.88 (1H, m), δ(CH_3—CH_2, $H_{1,2,3}$) = 0.95 à 1.40 (8H, m), δ(CHOH) = 3.20 (1H, 8 raies), δ(COH—CH_3) = 1.18 ppm (3H, d); couplages: $^3J(CHOH$—$CH_3)$ = 6.1 Hz, $^3J(CH$—$CHOH)$ = 8.5 Hz.

Alcool 1R, 2S*, 3R*, R* (6)*: t_R(cpv) = 25.5 min; ir: ν(=CH_2) = 3065, ν(=CH) = 2995, ν(C=C) = 1637, ν(=CH_2) = 900 à 920 cm^{-1}; rmn (CCl_4/TMS): δ(CH=CH_2) = 5.44 (1H, m), 5.17 (1H, m), 4.86 (1H, m) δ(CH_3—CH_2, $H_{1,2,3}$) = 0.90 à 1.40 (8H, m), δ(CHOH) = 3.24 (1H, 8 raies), δ(COH—CH_3) = 1.18 ppm (3H, d); couplages: $^3J(CHOH$—$CH_3)$ = 6.1 Hz, $^3J(CH$—$CHOH)$ = 6.6 Hz.

Hétérocyclisation des alcools secondaires vinylcyclopropaniques 3 et 4 par l'acétate mercurique

Préparation de l'organomercurique

A une solution de 2 mmol d'acétate mercurique dans 3 mL de THF sont ajoutés lentement 2 mmol d'alcool **3** (ou **4**). L'agitation est maintenue pendant 20 min (test à la soude négatif: absence d'ions Hg^{2+}).

Réduction de l'organomercurique in situ *par le borohydrure de sodium*

Après avoir refroidi le mélange réactionnel précédent dans un bain eau–glace, on ajoute lentement en agitant une solution de soude (10%) jusqu'à un pH neutre ou légèrement basique. La réduction s'effectue ensuite en ajoutant lentement 1.5 mmol de borohydrure de sodium en solution dans le minimum de soude à 10%. L'agitation est poursuivie pendant 3–4 h (jusqu'à obtention de mercure métallique). La phase organique est extraite à l'éther, lavée à l'eau et le THF est distillé lentement sous vide.

Le mélange de dérivés bicycliques **8** et **9** (ou 7 et **8**) est analysé par cpv analytique sur colonne Carbowax de 6.6 m, $\theta_{injecteur}$ 160°C, $\theta_{colonne}$ 80°C.

En fait la synthèse des composés **7**, **8** et **9** a été réalisée à partir du mélange d'alcools vinylcyclopropaniques **3** à **6** selon le même mode opératoire. La séparation de **7**, **8** et **9** se fait par cpv sur colonne Ucon Oil de 3.3 m, $\theta_{colonne}$ 70°C. Les alcools **5** et **6** sont récupérés inchangés en cpv. Leur présence rend difficile l'évaluation du rendement en composés bicycliques (≃80%).

Migration de la double liaison cyclopropylidénique des alcools 1 et 2

A 80°C, sous atmosphère anhydre, on ajoute à 0.03 mol de tertiobutylate de potassium dans 10 mL de DMSO anhydre 0.006 mol d'alcool **1** ou **2**. Après 5 h de réaction à 80°C, on hydrolyse à froid avec 80 mL d'eau, extrait à l'éther et sèche sur sulfate de sodium. On obtient le mélange d'alcools (**3** + **5**) ou (**4** + **6**), avec un rendement de 60% environ que l'on isole par cpv sur colonne Ucon Oil (20%) de 3.3 m (Chromosorb WAW 60/80, gaz vecteur: H_2, θ = 140°C).

Résultats et discussion

Identification par voie chimique des éthyl-2 éthylidène-3 cyclopropyl(1R,2R*)-1 éthanol E, S* (1) et R* (2)*

Alcools éthylidènecyplopropaniques 1 et 2

Le traitement en milieu basique du diéthyl-2,3 cyclopropènecarboxylate d'éthyle **10** conduit à un mélange des acides éthyl-2 éthylidène-3 cyclopropanecarboxyliques *Z* et *E* (**11** et **12**). La réduction de ce mélange d'acides en solution dans l'éther par le méthyllithium fournit les composés carbonylés **13** et **14**.

Ces composés **13** et **14** présentent en infrarouge les bandes d'absorption normalement attendues ν(=O)

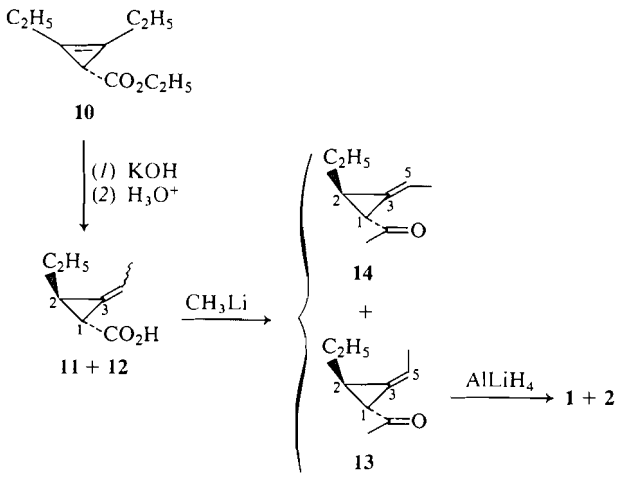

SCHÉMA 4

$\simeq$ 1700 cm^{-1} et $\nu(C{=}C) \simeq 1740\ cm^{-1}$. Dans ces dérivés la relation *trans* des protons cyclopropaniques **1** et **2** est démontrée sans ambiguité par la valeur de la constante de couplage $J_{H_1-H_2} \simeq 5$ Hz. Une relation *cis* se traduirait, en effet, par une valeur de cette constante de l'ordre de 8 Hz (9). Par ailleurs, les positions relatives du méthyle vinylique et du groupement fonctionnel qui différencient **13** et **14** sont déterminées par l'étude, en résonance magnétique nucléaire du proton, des glissements induits par un chélate de terre rare ($Eu(dpm)_3$). Compte tenu des positions relatives de ces deux groupes le glissement induit, observé pour le groupe méthyle dans **14**, doit être très nettement supérieur à celui observé dans le cas de **13**. Les valeurs expérimentales mesurées sont suffisamment différenciées pour permettre d'attribuer la configuration *E* à **13** et *Z* à **14**. En effet, les pentes (Δ) des courbes $\delta i = f(C\ Eu/(Co\ S)$, pour les méthyles et les hydrogènes vinyliques sont:

	13	**14**
$\Delta(=\!-Me)$	142	235
$\Delta(=\!-H)$	285	240

(δi est évalué en Hz, C Eu et Co S représentent respectivement la concentration en chélate et en dérivé carbonylé).

La réduction par l'aluminohydrure de lithium de la cétone cyclopropylidénique *E* (**13**) dans l'éther au reflux conduit au mélange des alcools stéréoisomères **1** et **2** (dans les proportions 43/57) qui sont isolés par cpv. Les carbones 1, 2, 3, 5 qui ne participent pas à la réaction de réduction présentent des configurations identiques à celle de **13**. Cette rétention de configuration est confirmée par la valeur des constantes de couplage $^3J_{H_1-H_2}$ voisine de 5 Hz dans les deux alcools d'une part et par l'étude des glissements induits par $Eu(dpm)_3$ qui, comme précédemment dans le cas de **13**, démontre que les dérivés **1** et **2** présentent bien une configuration *E*.

Alcools vinylcyclopropaniques 3 à 6

Les traitements de **1** et de **2** par le tertiobutylate de potassium dans le DMSO à 80°C conduisent respectivement aux mélanges d'isomères vinylcyclopropaniques **3** + **5** et **4** + **6**. Les dérivés **3** à **6** sont isolés par cpv. La migration de la double liaison cyclopropylidénique, le long de la chaîne éthylidénique, ne modifie pas les positions relatives des substituants portés par le cycle propanique. La relation *trans* des groupes éthyle et hydroxyméthyle est, en effet, facilement contrôlée par le valeur de la constante de couplage $^3J_{H_1-H_2}$ qui reste de l'ordre de 5 Hz. Cette méthode si elle permet d'assurer la filiation entre les alcools cyclopropylidéniques d'une part et les alcools vinylcyclopropaniques **3** ou **4** d'autre part est cependant difficile à mettre en oeuvre dans un but préparatif car elle nécessite la purification préalable en cpv de **1** et **2**. Pour cette raison, l'identification de **3** et **4**, fondée sur l'oxymercuration de ces alcools, a été réalisée à partir du mélange d'alcools **3** à **6** obtenu par la série de réactions suivantes.

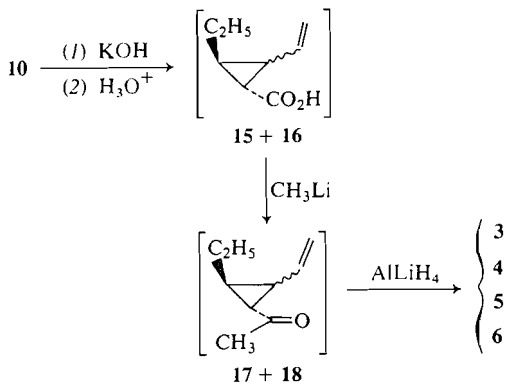

SCHÉMA 5

Traité par une solution suspension de potasse dans le *n*-butanol à 170°C, l'ester cyclopropénique **10** conduit au mélange d'acides vinylcyclopropaniques **15** + **16**; la réduction de ce mélange d'acides par le méthyllithium fournit les cétones **17** + **18** qui traitées par $AlLiH_4$ permettent d'accéder facilement aux mélanges d'alcools vinylcyclopropaniques **3** + **4** + **5** + **6**.

Identification des [*éthyl-2 vinyl-3 cyclopropyl(1*R*, *2*S*,*3*S*)]-*1 éthanol* S* *(3) et* R* *(4) et des* [*éthyl-2 éthylidène-3 cyclopropyl(1*R*,*2*R*)]-*1 éthanol* E,S* *(1) et* R* *(2)*

Le mélange des quatre diastéréoisomères **3** à **6**, sou-

TABLEAU 1. Déplacements chimiques dans $CDCl_3$/TMS en ppm

	H_2	H_1–H_5	H_4	H_6	$(CH_3)_2$	$(CH_3)_4$	CH_3—CH_2	CH_3—CH_2
7[a]	—	—	—	—	1.12	1.12	—	—
8[b]	4.05	Vers 1.25[c]	4.18	0.70	1.12	1.18	0.94	Vers 1.25[c]
9[c]	4.20	Entre 1.20[c] et 1.30	4.20	0.60	1.24	1.24	0.94	Entre 1.20 et 1.30

[a]Enregistré à 60 MHz.
[b]Enregistré à 250 MHz.
[c]Superposés, non analysables.

mis à l'oxymercuration cyclisante, fournit les trois éthers bicycliques **7**, **8** et **9**. Dans les conditions expérimentales que nous avons utilisées ($Hg(AcO)_2$/THF à 20°C), les alcools **5** et **6** restent inchangés et sont récupérés à la fin de la réaction. L'examen des modèles de Dreiding démontre que dans ces dérivés la distance OH-double liaison est supérieure à 3 Å; valeur trop élevée pour permettre l'oxymercuration cyclisante.

Par ailleurs, l'hétérocyclisation de chaque alcool diastéréoisomère **3** et **4**, isolé en cpv et traité séparément, conduit respectivement aux couples **8** + **9** et **7** + **8**

$$\mathbf{4} \rightarrow \mathbf{7}\ (15\%) + \mathbf{8}\ (85\%)$$

$$\mathbf{3} \rightarrow \mathbf{8}\ (25\%) + \mathbf{9}\ (75\%)$$

L'absence de composé **7** dans l'un des mélanges réactionnels et de composé **9** dans l'autre, démontre clairement que la réaction ne provoque pas d'épimérisation du carbone fonctionnel. Le substituant porté par le carbone du cycle tétrahydrofurannique situé en α de l'oxygène et provenant du groupe vinyle devant, selon la littérature (6), présenter la configuration *exo* et *endo*.

La connaissance de la configuration *diendo* ou *diexo* des composés **7** et **9** permet d'attribuer sans ambiguité aux diastéréoisomères **3** et **4** les configurations relatives qui suivent:

alcool vinylcyclopropanique **3**: 1*R**,2*S**,3*S**,4*S**

alcool vinylcyclopropanique **4**: 1*R**,2*S**,3*S**,4*R**

Comme nous l'avons vu, la migration de la double liaison en milieu basique dans les alcools cyclopropylidéniques **1** et **2** ne modifie pas les configurations des centres chiraux C_1 et C_2 ni évidemment celle de C_4. Il est donc possible d'affecter les configurations:

alcool cyclopropylidénique **1**: 1*R**,2*R**,4*S**

alcool cyclopropylidénique **2**: 1*R**,2*R**,4*R**

Identification des éthyl-6 diméthyl-2,4 oxa-3 bicyclo [3.1.0^{1,5}]hexanes diendo *7*, exo–endo *8*, diexo *9*

L'identification de ces dérivés est fondée sur leur étude en infrarouge et en résonance magnétique nucléaire du ^1H et du ^{13}C. Cependant l'hétérocycle **7**, instable à température élevée, n'a pû être isolé qu'en très faible quantité en cpv. Pour cette raison l'étude de ce dérivé en rmn du ^{13}C n'a pas été abordée; par ailleurs le spectre de rmn de ^1H réalisé sur une solution très diluée n'est que partiellement analysable.

Identification des composés 7 à 9 par résonance magnétique nucléaire de ^1H (Tableaux 1 et 2)

L'ensemble des données rmn est en accord avec les structures proposées: **8** et **9**. Notons, en particulier, que les spectres de ces composés révèlent la présence d'un cycle propanique (δH_6 = 0.60 et 0.70 ppm) et du groupe éthyle; la valeur des constantes de couplage $^3J_{H_1-H_6} \simeq {}^3J_{H_5-H_6} \simeq 3.4$ Hz établit la relation *trans* de H_6 d'une part et de H_1 et H_5 d'autre part.

La non équivalence des groupes méthyles doublets (δ = 1.12 et 1.18 ppm) et des hydrogènes (δ = 4.05 et 4.18 ppm), situés en position 2 et 4, permet d'affirmer que l'oxa-3 bicyclo[3.1.0^{1,5}]hexane **8** présente deux méthyles, l'un *endo*, l'autre *exo*. L'examen des modèles de Dreiding démontre que le cycle tétrahydrofurannique très contraint est plan; la rigidité de l'ensemble bicyclique due à la jonction cyclopropanique *cis* (en C_1 et C_2) ne permet pas d'envisager de déformations. D'après les modèles, les angles dièdres α = (H_2, C_2—C_1, H_1) et β = (H_5, C_5—C_4, H_4) du composé **8** valent 95° et 25° environ. Les valeurs trouvées pour les constantes de couplage $^3J \simeq 0$ et $^3J \simeq 3.8$ Hz ne peuvent être affectées, selon les courbes de Karplus, qu'aux angles dièdres α et β respectivement.

L'équivalence des groupes $(CH_3)_{2\text{ et }4}$ dans les composés **7** et **9** et de H_2 et H_4 (δ = 4.20 ppm) dans **9** caractérise l'existence d'un plan de symétrie. Ces deux hétérocycles ne peuvent donc présenter que des configurations *diexo* ou *diendo*. Dans le cas du composé **9** les constantes $^3J_{H_1-H_2}$ et $^3J_{H_4-H_5}$ sont nulles (raies fines). Les interactions stériques entre $(CH_3)_2$ et $(CH_3)_4$ restant très faibles dans les structures *diendo* et *diexo*, on peut affirmer que les angles dièdres α et β sont voisins de 95° et que le composé **9** présente une configuration *diexo*.

TABLEAU 2. Valeurs des constantes de couplage en Hz

	$J_{H_2-H_1}$	$J_{H_5-H_4}$	$J_{H_6-H_7}$	$J_{H_7-H_8}$	$J_{H_1-H_6}$ ou $J_{H_5-H_6}$	$J_{H_2-(CH_3)_2}$	$J_{H_4-(CH_3)_4}$
7	—	—	—	—	—	6.30	
8	0	3.8	6.8	7	3.4 en moyenne	6.10	5.90
9	0	0	6.8	7	3.4	6.30	

TABLEAU 3. Déplacement chimique et multiplicité des différents carbones en rmn du ^{13}C des composés **8** et **9** δ en ppm

C_1	C_2	C_4	C_5	C_6	C_7	C_8	C_9	C_{10}
				Composé **8**				
28.81 ou 30.05	76.58	72.41	28.81 ou 30.05	20.14	24.39	13.66	20.66	17.80
				Composé **9**				
31.32	77.58	77.58	31.32	25.90	24.70	13.45	24.47	24.47

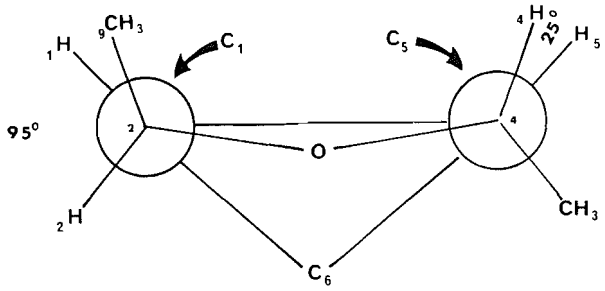

SCHÉMA 6. Angles dièdres du composé **8**. α = (H_2, C_2—C_1, H_1) et β = (H_5, C_5—C_4, H_4).

En conséquence la configuration de **7** qui possède un plan de symétrie est *diendo*.

Confirmation des attributions de structure à 8 et 9 par résonance magnétique nucléaire du ^{13}C (Tableau 3)

Lorsque l'on passe de la structure **9** à **8** puis à **7**, on remplace successivement les relations *trans* entre $(CH_3)_{2\text{ ou }4}$ et C_6 par des arrangements *cis* (gauches). On peut donc prévoir que l'on observera, chaque fois, un blindage de C_6 et du carbone de l'un des méthyles quelque soit, d'ailleurs, l'origine de cet effet γ-gauche (8). Il est alors particulièrement important d'attribuer avec certitude les sites de C_6 et des carbones des groupes $(CH_3)_{2\text{ et }4}$ C_9 et C_{10}.

L'examen des données expérimentales résumées dans le Tableau 3 implique les conclusions suivantes.

Composé 9: les multiplicités des pics dans le spectre hors-résonance, les intensités des signaux et l'effet α de l'oxygène permettent de réaliser une attribution très sûre pour tous les carbones. La présence de trois groupes de deux carbones équivalents (δ (ppm) = 24.47, 31.32 et 77.58) confirme l'existence d'un plan de symétrie.

Composé 8: les neuf atomes de carbones sont non équivalents; ce dérivé ne possède pas de plan de symétrie. Les pics de C_7, C_2 et C_4 sont identifiés respectivement à partir de la multiplicité des signaux et des glissements chimiques. Le carbone C_8, étant très éloigné du carbone qui subit une inversion de configuration (C_4), son signal peut être facilement identifié par comparaison des glissements chimiques des carbones de **8** et de **9**. Cet ensemble de données permet d'attribuer les pics de résonance des carbones C_9 et C_{10}.

La comparaison des glissements chimiques de C_9 et C_{10} démontre que l'un des signaux est, dans l'isomère asymétrique, considérablement blindé par rapport à sa position dans l'isomère symétrique; ce dernier doit donc présenter une configuration *diexo* (**9**). On doit alors observer, pour l'isomère asymétrique, un blindage important de l'un des carbones tertiaires cyclopropaniques par rapport aux valeurs déterminées pour l'isomère symétrique. C'est effectivement ce que l'on observe; ce résultat confirme l'attribution de la configuration *diexo* au composé **9**.

Conclusion

Les attributions de configuration aux éthyl-6 diméthyl-2,4 oxa-3 bicyclo[3.1.0^{1,5}] *exo–endo* et *diexo* réalisées en rmn ^1H sont confirmées par l'étude de ces dérivés en rmn ^{13}C.

Ces attributions sont en accord avec les prévisions que l'on pouvait formuler sur la stéréosélectivité de la réaction de cyclisation par oxymercuration. En effet, la contrainte stérique existant entre un méthyle *endo* et le carbone C_6 du cycle propanique défavorise le dérivé *exo–endo* par rapport au dérivé *diexo*; de

même, le dérivé *diendo* est fortement défavorisé devant l'isomère *exo–endo*.

Cette méthode permet de distinguer les [alkyl-2 vinyl-3 cyclopropyl(1*R**,2*S**,3*S**)]-1 éthanol *R** et *S** ou les[alkyl-2 éthylidène-3 cyclopropyl(1*R**,2*R**)]-1 ethanol *R** et *S**. Elle doit également permettre d'atteindre les configurations relatives des alcools secondaires α-cyclopropaniques (saturés), α-cyclopropéniques et α-spiropentaniques. Le travail en cours dans notre laboratoire permettra vraisemblablement d'établir une filiation chimique entre les alcools α-cycliques et les alcools cyclopropylidéniques de configuration connue à l'aide de réactions qui ne modifient pas les centres de chiralité (réduction par $AlLiH_4$, migration de la double liaison en milieu basique, pontages carbéniques).

1. F. ROCQUET, A. SEVIN et W. CHODKIEWICZ. C.R. Acad. Sci. **270C**, 848 (1970).
2. G. DESCOTES, A. MENET et F. COLLONGES. Tetrahedron, **29**, 2931 (1973).
3. R. MAURIN et M. BERTRAND. Bull. Soc. Chim. Fr. **6**, 2261 (1970).
4. M. VINCENS, C. DUMONT et M. VIDAL. C.R. Acad. Sci. **286C**, 717 (1978).
5. V. SPEZIALE, M. AMAT et A. LATTES. J. Heterocycl. Chem. 349 (1976).
6. V. SPEZIALE, J. ROUSSEL et A. LATTES. J. Heterocycl. Chem. 771 (1974).
7. T. HOSOKAWA, M. HIRATA, S. I. MURAHASHI et A. SONODA. Tetrahedron Lett. **21**, 1821 (1976).
8. H. BEIERBECK et J. K. SAUNDERS. Can. J. Chem. **54**, 2985 (1976).
9. J. L. PIERRE, M. VIDAL et P. ARNAUD. Bull. Soc. Chim. Fr. **4**, 1544 (1970).

Vibrational theory of polyatomic molecules: energy levels of CH_4/CD_4 and CH_3Cl/CD_3Cl

JAN BRON

Petrolite Corporation of Canada Ltd., Tretolite Division, 1145J-44th Ave, S.E., Calgary, Alta., Canada T2G 4X4

AND

R. WALLACE

Chemistry Department, University of Manitoba, Winnipeg, Man., Canada R3T 2N2

Received February 12, 1979

JAN BRON and R. WALLACE. Can. J. Chem. **57**, 2321 (1979).

A relatively simple model, previously used to describe polyatomic vibrations of nonlinear triatomic molecules, has been employed to evaluate the fundamentals, first overtones and combination bands of CX_4 and CX_3Cl (X = H, D). Relatively good agreement is obtained between calculated and observed frequencies. Interesting splittings of certain overtone and combination bands result from these calculations.

JAN BRON et R. WALLACE. Can. J. Chem. **57**, 2321 (1979).

On a utilisé un modèle relativement simple, employé antérieurement pour décrire les vibrations polyatomiques de molécules triatomiques qui ne sont pas linéaires, pour évaluer les bandes fondamentales, premières harmoniques et combinées du CX_4 et du CX_3Cl (X = H, D). On a obtenu un assez bon accord entre les fréquences calculées et observées. Des dédoublements intéressants de certaines bandes harmoniques et combinées découlent de ces calculs.

[Traduit par le journal]

Introduction

Efforts have recently been made by various researchers (1–7) to develop a model capable of describing large amplitude vibrations in molecules. The traditional normal mode theory (8) has proved rather cumbersome in this respect whereas an alternate starting point, involving internal coordinates and a "Morse" approximation of the molecular potential has proved to be quite successful, especially in accounting for the higher overtones of X—H bonds. Currently, attempts are being made to extend the domain of applicability of this approach by application to larger molecules containing bonds other than X—H, and by inclusion of the bending modes.

The present work is in many ways a complementary development to some studies (4) recently completed for the molecules CH_2X_2 (X = F, Cl, Br, I). In that study, only C—H and C—X stretching motions were included, but a large basis set (210 members) made possible the prediction of C—H stretches up to the sixth overtone. While agreement with observed transition energies was in general good, the principal shortcoming of the study appeared to be the omission of the bending modes. The present study also concerns molecules containing five atoms, includes the bending modes in a restricted fashion, and, because of the increase in the basis set this generates, limits itself to lower overtones, combination bands, and the effect of isotopic substitution, which is easily included.

The results to be presented have been derived using the model proposed by Wallace (7), and developed by Bron and Wallace in a series of papers (1). The only modification of that model is the explicit introduction of symmetry coordinates. This is required because the coordinate redundancy problem is more easily dealt with in symmetry coordinates. In addition, the Hamiltonian matrix attains a simpler form.

The importance of a method to determine the energies of excited states should not be overlooked. There is currently substantial practical interest in isotope effects (9) and the possibility of laser isotope separation (10).

Calculations

The equations presented in our recent paper (1*c*) can also be used for symmetry coordinates (i.e. linear combinations of internal coordinates) if the symbol R_i is replaced by S_i, where S_i represents symmetry coordinate *i*. Computational details follow.

From the molecular geometry and the atomic masses the **G** matrix with respect to internal coordinates is calculated by means of the defining matrix equations (11, 12)

$$[1] \quad \mathbf{G} = \mathbf{B}\mathbf{M}^{-1}\mathbf{B}^t; \quad \mathbf{R} = \mathbf{B}\mathbf{X}$$

In [1], **B** defines the transformation from Cartesian

0008-4042/79/172321-04$01.00/0

TABLE 1. Definitions and values of various parameters used in the calculations [a]

(*a*) CX_4 (X = H, D)

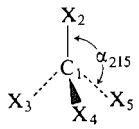

r(C—X) = 1.0936 Å
α(X—C—X) = 109.471222°

$R_1 = \Delta r_{12}$; $R_2 = \Delta r_{13}$; $R_3 = \Delta r_{14}$; $R_4 = \Delta r_{15}$;
$R_5 = \Delta\alpha_{314}$; $R_6 = \Delta\alpha_{415}$; $R_7 = \Delta\alpha_{315}$; $R_8 = \Delta\alpha_{213}$;
$R_9 = \Delta\alpha_{214}$; $R_{10} = \Delta\alpha_{215}$

$S_1^{(A)} = (R_1 + R_2 + R_3 + R_4)/2$; $S_2^{(F)} = (R_1 + R_4 - R_2 - R_3)/2$;
$S_3^{(F)} = (R_1 + R_2 - R_3 - R_4)/2$; $S_4^{(F)} = (R_1 + R_3 - R_2 - R_4)/2$;
$S_5^{(E)} = (2R_8 + 2R_6 - R_9 - R_7 - R_5 - R_{10})/\sqrt{12}$;
$S_6^{(E)} = (R_9 + R_7 - R_5 - R_{10})/2$; $S_7^{(F)} = (R_5 - R_{10})/\sqrt{2}$;
$S_8^{(F)} = (R_6 - R_8)/\sqrt{2}$; $S_9^{(F)} = (R_7 - R_9)/\sqrt{2}$
$F_{rr} = 5.234$ mdyn/Å; $F_{\alpha\alpha} = 0.62496$ mdyn Å
$F_{rr'} = 0.058$ mdyn/Å; $F_{\alpha\alpha'} = 0.1$ mdyn Å; $F_{\alpha\alpha}' = 0.127$ mdyn Å
$D_r = 8.09322 \times 10^{-12}$ erg; $D_\alpha = 48.7512 \times 10^{-12}$ erg

(*b*) CX_3Cl (X = H, D)

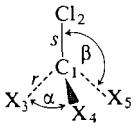

r(C—X) = 1.085 Å; r(C—Cl) = 1.780 Å
α(X—C—X) = 110.83°
β(X—C—Cl) = 108.07°

R_i's are defined the same as for CX_4

$S_1^{(A)} = (R_2 + R_3 + R_4)/\sqrt{3}$; $S_2^{(E)} = (2R_2 - R_3 - R_4)/\sqrt{6}$;
$S_3^{(E)} = (R_3 - R_4)/\sqrt{2}$; $S_4^{(A)} = R_1$;
$S_5^{(E)} = (2R_6 - R_7 - R_5)/\sqrt{6}$; $S_6^{(E)} = (R_7 - R_5)/\sqrt{2}$;
$S_7^{(E)} = (2R_8 - R_9 - R_{10})/\sqrt{6}$; $S_8^{(E)} = (R_9 - R_{10})/\sqrt{2}$;
$S_9^{(A)} = PS_{2a} - QS_{2b}$; $P = (1 + K)/(2 + 2K^2)^{1/2}$;
$Q = (1 - K)/(2 + 2K^2)^{1/2}$; $K = -3 \sin\beta \cos\beta/\sin\alpha$;
$S_{2a} = (A - B)/\sqrt{6}$; $S_{2b} = (A + B)/\sqrt{6}$;
$A = R_5 + R_6 + R_7$; $B = R_8 + R_9 + R_{10}$

$F_{ss} = 3.20$ mdyn/Å; $F_{rr} = 5.22$ mdyn/Å; $F_{rs} = 0.0$ mdyn/Å
$F_{rr'} = 0.061$ mdyn/Å; $F_{\alpha\alpha} = 0.533$ mdyn Å; $F_{\beta\beta} = 0.74$ mdyn Å
$F_{a\beta} = 0.1$ mdyn Å; $F_{\alpha\alpha'} = 0.047$ mdyn Å; $F_{\beta\beta'} = 0.1$ mdyn Å
$F_{a\beta}' = 0.1$ mdyn Å

$D_r = 8.09322 \times 10^{-12}$ erg; $D_s = 2.8953 \times 10^{-12}$ erg;
$D_\alpha = D_\beta = 48.7512 \times 10^{-12}$ erg

[a]See text for comments.

coordinates (**X**) to internal coordinates (**R**). The diagonal matrix, **M**, lists the masses of the atoms in the molecule; each atomic mass is repeated three times along the diagonal. From force constants in internal coordinates, which are defined by

$$[2] \quad 2V = \mathbf{R}^t\mathbf{F}\mathbf{R}$$

the force constants in symmetry coordinates can be calculated. The $\mathscr{G}$ and $\mathscr{F}$ matrices in symmetry coordinates can be obtained from the transformations

$$[3] \quad \mathscr{G} = \mathbf{U}\mathbf{G}\mathbf{U}^t; \quad \mathscr{F} = \mathbf{U}\mathbf{F}\mathbf{U}^t; \quad \mathbf{S} = \mathbf{U}\mathbf{R}$$

The **U** matrix defines the orthonormal transformation of internal coordinates to symmetry coordinates. It should be noted that, if in the equations presented previously, R_i is changed to S_i, the quantities F_{ij} and G_{ij} should be changed to $\mathscr{F}_{ij}$ and $\mathscr{G}_{ij}$.

It has been argued that the transformation of the "internal coordinate" model to a "symmetry coordinate" model is difficult to justify on the grounds that there is little reason to assume separability of the molecular potential in symmetry coordinates. Such arguments are countered by the following observations. (*1*) While the "internal coordinate" model has reflected the separability of the potential in internal

coordinates, its success does not depend upon that separability. It is assumed that the internal coordinate potential is approximately separable, but it must be remembered that the oscillators are coupled via kinetic energy terms in the Hamiltonian. Separability of the potential does not imply separability of the oscillators. (*2*) As its starting point, the normal coordinate model assumes separable harmonic oscillators in symmetry coordinates (i.e. both kinetic and potential energy terms are assumed separable). The "internal coordinate" model assumes symmetrized, coupled Morse oscillators in internal coordinates. The present model assumes coupled Morse oscillators in symmetry coordinates. The degree to which this assumption is useful is best judged a posteriori, by the results obtained.

In the present study only the first overtone and combination bands will be considered for the molecules CX_4 and CX_3Cl. The corresponding basis functions expressed in terms of symmetry coordinates can then be defined as

	Excitations	States	Permutations
	0	$\|000\ 000\ 000\rangle$	1
[4]	1	$\|100\ 000\ 000\rangle$	9
	2	$\|110\ 000\ 000\rangle$	36
	2	$\|200\ 000\ 000\rangle$	9

A total of 55 basis functions will therefore be included. Table 1 lists all the parameters that have been used to obtain the results to be presented. The quantities in Table 1 require further explanation. The geometries of methane (13) and methyl chloride (14) can be found in the literature. Definitions of symmetry coordinates have also been described (15, 16). For convenience, the parameters D_i have been given the same values in both internal and symmetry coordinates. This is not a good approximation, but does not seriously affect the lower states. From a "first estimate" of F_{ij}, the listed values for the force constants have been obtained by iterative fitting to the observed fundamentals of CH_4 and CH_3Cl. As before (2), the geometries, force constants, and D_i's have been taken equal for molecules differing only in isotopic substitution.

Results and Discussion

A comparison of the calculated and observed values for the fundamentals, overtone and combination levels for CH_4 and CD_4, as listed in Table 2, shows that agreement is generally good. In order to keep the number of parameters to a minimum, no interactions, via the potential energy, between the stretching and bending modes have been allowed. In other words, all force constants, F_{ij}, corresponding to stretch–bend interactions have been taken as zero. Bond stretch–bend interactions occur in the kinetic energy term of the Hamiltonian and, therefore, stretch–bend interactions have been included in a restricted sense. It is also notable that approximations such as setting the tetrahedral angle equal to 109.5°, rather than 109.47122°, lead to fictitious removal of degeneracies due to distortion of molecular symmetry.

TABLE 2. Comparison of observed and calculated energy levels of CH_4 and CD_4

	Energy level			
	CH_4		CD_4	
Assignment	Calcd	Obsd[a]	Calcd	Obsd[a]
ν_1	2919(1)[b]	2917	2109(1)	2108
ν_2	1535(2)	1534	1108(2)	1092
ν_3	3019(3)	3019	2301(3)	2259
ν_4	1309(3)	1306	1010(3)	996
$2\nu_1$	5714(1)	—	4132(1)	—
$2\nu_2$	3053(2)	—	2184(2)	—
	3058(1)	—	2186(1)	—
$2\nu_3$	5907(2)	6005	4510(2)	4496
	5907(1)	—	4511(1)	—
	6024(3)	—	4572(3)	—
$2\nu_4$	2601(2)	2600	1988(2)	1987
	2601(1)	—	1990(1)	—
	2604(3)	—	1990(3)	—
$\nu_1 + \nu_2$	4312(2)	—	3187(2)	—
$\nu_1 + \nu_3$	5925(3)	5861	4380(3)	4331
$\nu_1 + \nu_4$	4215(3)	4222	3089(3)	3105
$\nu_2 + \nu_3$	4541(6)	4546	3379(6)	3338
$\nu_2 + \nu_4$	2831(6)	2826	2088(6)	2084
$\nu_3 + \nu_4$	4314(6)	4313	3281(6)	3255
	4325(1)	—	3306(1)	—
	4441(2)	—	3278(2)	—

[a]Observed values are from ref. 15; unit of energy is cm^{-1}.
[b]The integer in brackets denotes the degeneracy of the energy level or sublevel.

The interesting splittings of overtone and combination bands, which are in accordance with the tables given by Herzberg (13), should be noted. These splittings have been obtained by numerical analysis and, therefore, without the explicit use of group theory. As the magnitudes of the splittings have not been reported in the literature, the accuracy of the calculated values cannot be assessed.

Table 3 lists the energy levels for CH_3Cl and CD_3Cl. Again, fair agreement between observed and calculated values is obtained. Not all of the bonds in these molecules are of the same type, there being three C—H(D) bonds and one C—Cl bond. In Table 1 it may be seen how complicated the definition of the symmetry coordinates is. As expected, splittings of certain overtone and combination bands result, but, once again, experimental data regarding these splittings are lacking.

As pointed out above, the force constants F_{ij} have been obtained from an iterative fitting. Better agree-

TABLE 3. Comparison of the calculated energy levels of CH_3Cl and CD_3Cl with observed values[a]

	Energy level			
	CH_3Cl		CD_3Cl	
Assignment	Calcd	Obsd	Calcd	Obsd
ν_1	2969(1)	2968	2189(1)	2160
ν_2	1347(1)	1355	1132(1)	1029
ν_3	734(1)	733	681(1)	701
ν_4	3040(2)	3039	2321(2)	2283
ν_5	1452(2)	1452	1073(2)	1060
ν_6	1017(2)	1017	792(2)	768
$2\nu_1$	5788(1)	—	4269(1)	—
$2\nu_2$	2655(1)	—	2189(1)	—
$2\nu_3$	1416(1)	—	1308(1)	—
$2\nu_4$	5970(2)	6014	4525(2)	—
	6041(1)	—	4589(1)	—
$2\nu_5$	2862(2)	2879	2090(2)	—
	2865(1)	—	2092(1)	—
$2\nu_6$	1994(1)	—	1528(1)	—
	1995(2)	—	1529(2)	—
$\nu_1 + \nu_2$	4280(1)	4229	3272(1)	—
$\nu_1 + \nu_3$	3666(1)	—	2816(1)	—
$\nu_1 + \nu_4$	5924(2)	5900	4456(2)	—
$\nu_1 + \nu_5$	4349(2)	—	3208(2)	—
$\nu_1 + \nu_6$	3948(2)	3979	2927(2)	—
$\nu_2 + \nu_3$	2049(1)	—	1754(1)	—
$\nu_2 + \nu_4$	4382(2)	4383	3399(2)	—
$\nu_2 + \nu_5$	2761(2)	—	2151(2)	—
$\nu_2 + \nu_6$	2326(2)	—	1869(2)	—
$\nu_3 + \nu_4$	3735(2)	—	2948(2)	—
$\nu_3 + \nu_5$	2147(2)	—	1699(2)	—
$\nu_3 + \nu_6$	1712(2)	—	1418(2)	—
$\nu_4 + \nu_5$	4453(1)	—	3339(1)	—
	4453(2)	—	3340(2)	—
	4455(1)	—	3346(1)	—
$\nu_4 + \nu_6$	4018(1)	4046	3058(1)	—
	4018(2)	—	3059(2)	—
	4023(1)	—	3068(1)	—
$\nu_5 + \nu_6$	2429(1)	2461	1810(1)	—
	2430(2)	—	1810(1)	—
	2438(1)	—	1814(1)	—

[a]Observed values are from refs. 13, 14; units of energy is cm^{-1}.

ment between calculated and observed values may be obtained by involving the force constants corresponding to bend–stretch interactions in the fitting process. Also, additional anharmonic higher order interaction terms in the potential energy expression may lead to improvement in agreement between observed and calculated frequencies. The main purpose of this paper is, in fact, to show that there is an alternative to the complex perturbation method traditionally used in this type of computation. Alternatives to the Morse potential will be the subject of future discussion. The calculations were not complicated by "resonances" as we used the variation method instead of second order perturbation theory. Nielsen points out (8) that resonances are artifacts of (second order) perturbation theory.

1. J. BRON and R. WALLACE. Can. J. Chem. (*a*) **55**, 2292 (1977); (*b*) **56**, 379 (1978); (*c*) **56**, 2167 (1978); (*d*) J. Chem. Soc. Faraday Trans. II, **74**, 611 (1978).
2. R. WALLACE and C. V. RAO. Z. Naturforsch. **32a**, 1450 (1977).
3. R. WALLACE. Chem. Phys. In press.
4. R. WALLACE and A. A. WU. Chem. Phys. In press.
5. M. L. ELERT, P. R. STANNARD, and W. M. GELBART. J. Chem. Phys. **67**, 5395 (1977).
6. R. L. SWOFFORD, M. E. LONG, and A. C. ALBRECHT. J. Chem. Phys. **65**, 179 (1976).
7. R. WALLACE. Chem. Phys. **11**, 189 (1975).
8. H. H. NIELSEN. Rev. Mod. Phys. **23**, 90 (1951).
9. J. BRON and M. WOLFSBERG. J. Chem. Phys. **57**, 2862 (1972).
10. R. N. ZARE. Sci. Am. **236**, 86 (1977).
11. E. B. WILSON, J. C. DECIUS and P. C. CROSS. Molecular vibrations. McGraw-Hill. 1955.
12. M. A. PARISEAU, I. SUZUKI, and J. OVEREND. J. Chem. Phys. **42**, 2335 (1965).
13. G. HERZBERG. Molecular spectra and molecular structure. Vol. II. Van Nostrand. 1955.
14. J. L. DUNCAN, A. ALLAN, and D. C. MCKEAN. Mol. Phys. **18**, 289 (1970).
15. I. M. MILLS. Spectrochim. Acta, **16**, 35 (1960).
16. J. BRON. Can. J. Chem. **52**, 3078 (1974).

Clionamide, a major metabolite of the sponge *Cliona celata* Grant

RAYMOND J. ANDERSEN AND RICHARD J. STONARD

Departments of Oceanography and Chemistry, University of British Columbia, Vancouver, B.C., Canada V6T 1W5

Received April 3, 1979

RAYMOND J. ANDERSEN and RICHARD J. STONARD. Can. J. Chem. 57, 2325 (1979).

Clionamide, the major metabolite of the burrowing sponge *Cliona celata*, has been isolated. The structure of clionamide (**1**) was shown to be (2*S*)-*N*-((1*E*)-5,6,7-trihydroxystyr-1-yl)-2-amino-3-(6-bromoindol-3-yl)propionamide by spectral analysis and by interconversion to its tetracetyl derivative **2**. The structure of **2** was determined from spectral data and extensive chemical degradation and was confirmed by the synthesis of its ultimate hydrogenation product, *N*-(5,6,7-triacetoxypheneth-1-yl)-2-acetamido-3-(indol-3-yl)propionamide (**11**).

RAYMOND J. ANDERSEN et RICHARD J. STONARD. Can. J. Chem. 57, 2325 (1979).

On a isolé le clionamide, le métabolite principal de l'éponge *Cliona celata*. Faisant appel à une analyse spectrale et au fait qu'il peut être transformé en son dérivé tétraacétylé **2**, on a démontré que la structure du clionamide (**1**) correspond au (2*S*)-*N*-(1*E*)-trihydroxy-5,6,7 styryl-1) amino-2 (bromo-6 indolyl-3)-3 propionamide. On a déterminé la structure de **2** à partir de données spectrales et d'une dégradation chimique élaborée et on l'a confirmée grâce à la synthèse de son produit ultime d'hydrogénation, le *N*-(triacétoxy-5,6,7 phénéthyl-1) acétamido-2 (indolyl-3)-3 propionamide. (**11**).

[Traduit par le journal]

Cliona celata, a cosmopolitan member of the Clionidae family of burrowing sponges, is found in British Columbia marine waters either free living or embedded in the calcium carbonate shells of the giant barnacle *Balanus nubilus* and the rock scallop *Hinnites multirugosus*. There has been considerable interest in the ability of the Clionidae to burrow into biogenic calcium carbonate (1). Frequently this burrowing is cited as a major source of coral reef erosion. Our interest in the antibiotic activity displayed by crude methanol extracts of *C. celata* (2) has prompted us to investigate the secondary metabolites associated with this sponge. We now wish to report the structure of clionamide (**1**), the major metabolite.

Initial attempts to purify crude *Cliona* metabolites involved silica gel, LH20, and reversed phase high pressure liquid chromatography. All such efforts failed due to the high polarity and instability of the compounds. Acetylation of the crude extracts facilitated the chromatographic purification of the derivatives on silica gel. The structure of the major acetylated metabolite, tetracetyl clionamide (**2**), has been described in a preliminary communication (3). A small-scale isolation using acetic anhydride-d_6 for derivatization produced tetracetyl clionamide-d_{12} (**3**), revealing that the phenol acetates and the acetamide were not natural features of clionamide. We have now been able to isolate pure clionamide (**1**) as a rather unstable yellow powder by a rapid acid extraction procedure followed by silica gel preparative thin layer chromatography (ptlc) (see

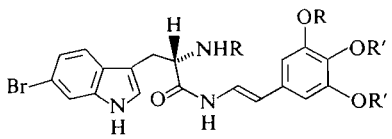

1 R = R′ = H
2 R = R′ = $COCH_3$
3 R = R′ = $COCD_3$
4 R = H; R′ = $>C(CD_3)_2$
5 R = H; R′ = $>C(CH_3)_2$

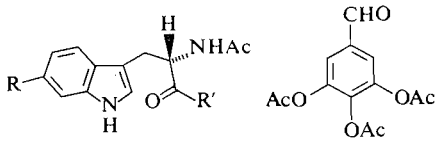

6 R = Br; R′ = NH_2
7 R = H; R′ = NH_2
8 R = Br; R′ = OCH_3

9

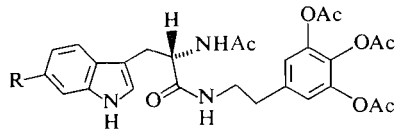

10 R = Br
11 R = H

Experimental). Dim lighting and an inert nitrogen atmosphere were absolutely essential to obtaining good yields of **1**.

Clionamide (**1**) gives positive ninhydrin and ferric chloride tests. It fails to show a parent ion in the electron impact mass spectrum and its infrared spectrum displays little of diagnostic value beyond a

0008-4042/79/172325-04$01.00/0

large OH/NH absorption at $\approx 3300\ cm^{-1}$ and a broad amide carbonyl absorption at $1635\ cm^{-1}$. Attempts to obtain a ^1H nmr spectrum of clionamide in acetone-d_6 resulted in the rapid and quantitative formation of the deuterated acetonide **4**. The acetonide methyl resonances appear at δ 1.42 and 1.47 in the nondeuterated acetonide **5**. A ^1H nmr spectrum of clionamide obtained in methanol-d_4 shows none of the exchangeable protons. The non-exchangeable protons are trivially assigned by analogy with the assigned signals for tetracetyl clionamide (**2**) (3). Clionamide (**1**) can be quantitatively tetracetylated to give **2**.

Tetracetyl clionamide (**2**), obtained as colourless needles, mp 209–211°C, has the molecular formula $C_{27}H_{26}Br\ N_3O_8$. The presence of a bromo indole residue was indicated by a strong fragment ion at *m/e* 208/210 (1:1) in the mass spectrum. The infrared spectrum (1760, 1627 cm^{-1}) and the ^{13}C nmr spectrum (δ 168.6 (1C), 169.3 (2C), 170.7 (1C), 171.2 (1C)) showed that **2** contained five carbonyls, two of them equivalent. The ^1H nmr spectrum indicated that one of the carbonyls belonged to an acetamide functionality (δ 1.84 (3H)) and that three others were associated with phenol acetates (δ 2.23 (9H)). The ^1H nmr spectrum also contained resonances at δ 6.09 (d, 1H, J = 15 Hz), 7.32 (q, 1H, J = 10, 15 Hz), and 8.64 (d, 1H, J = 10 Hz, D_2O exchange) appropriate for a *trans*-disubstituted olefin which has a heteroatom containing one exchangeable proton attached to one of the olefinic carbons.

Chemical degradation revealed the nature of the olefinic substituents. Ozonolysis of **2** followed by reductive work-up gave 3,4,5-triacetoxybenzaldehyde (**9**) which was identical to an authentic sample. Hydrolysis of **2** with hydrochloric acid in acetonitrile gave in low yield the bromo amide **6**. Hydrogenolysis of **6** converted it cleanly into the debromo amide **7**. Comparison of the debromo amide **7** to an authentic sample of 2-acetamido-3-(indol-3-yl)propionamide showed them to be identical. The absolute stereochemistry of **7** was determined to be *S* by comparison of its optical rotation with the literature value (4). Hence, the *trans*-disubstituted olefin must bear 3,4,5-triacetoxyphenyl and (2*S*)-2-acetamido-3-(bromoindol-3-yl)propionamidyl substituents.

The aromatic region in the ^1H nmr of the bromo methyl ester **8** (δ 7.16 (q, 1H, J = 8, 1.5 Hz), 7.50 (d, 1H, J = 8 Hz), and 7.58 (d, 1H, J = 1.5 Hz)), obtained by hydrolysis of **2** with concentrated sulfuric acid in methanol, indicated that the bromine atom must be attached to either carbon-5 or -6 of the indole ring. Comparison of the ^1H nmr of **8** to that of authentic *N*-acetyl-5-bromotryptophan methyl ester proved them different. Thus the bromine resides on carbon-6 and tetracetyl clionamide (**2**) must be (2*S*)-*N*-((1E)-5,6,7-triacetoxystyr-1-yl)-2-acetamido-3-(6-bromoindol-3-yl)propionamide.

Confirmation of the suggested structure for **2** was obtained by stepwise hydrogenation to give the diamides **10** and **11**. A synthetic sample of *N*-(5,6,7-triacetoxypheneth-1-yl)-2-acetamido-3-(indol-3-yl)-propionamide was shown to be identical to the diamide **11**.

Clionamide exhibits only very mild antibiotic activity which cannot account for the potency of the crude *Cliona* extracts. Structural studies on the more active *Cliona* metabolites are under way. The triphenolic portion of clionamide should possess good calcium chelating properties and we are currently investigating the possibility that it may play a role in the burrowing activities of the sponge.

Experimental

Melting points were determined on a Fisher-Johns apparatus and are uncorrected. ^1H nmr spectra were recorded on Varian XL-100, HA-100, and Nicolet-270 spectrometers. ^{13}C nmr spectra were recorded on a Varian CFT-20 spectrometer. TMS was used as an internal standard in all ^1H and ^{13}C nmr spectra. Low resolution mass spectra were obtained on an A.E.I. MS-902 spectrometer and high resolution mass spectra were recorded on an A.E.I. MS-50 spectrometer. Ultraviolet spectra were recorded on a Cary-14 spectrophotometer, ir spectra were recorded on a Perkin-Elmer Model 700B spectrophotometer, and optical rotations were measured on a Perkin-Elmer Model-141 polarimeter using a 1 cm cell unless otherwise indicated.

High pressure liquid chromatography (hplc) was performed on a Perkin-Elmer Series 2 instrument equipped with a Perkin-Elmer LC55 UV detector system. Merck silica gel 60 PF-254 was used for ptlc. The hplc solvents used were Fisher hplc grade, water was glass distilled; all other reagents and solvents were reagent grade.

Isolation of Clionamide (1)

Cliona celata was collected at 20 metres' depth in Barkley Sound and Howe Sound, British Columbia. The fresh sponge (~1 kg) was homogenized with methanol in a Waring Blendor and the solids were removed by filtration. The methanol extract was concentrated, partitioned between ethyl acetate and water, and the organic layer rapidly extracted with 1 *M* H_2SO_4. The acid layer was covered with fresh ethyl acetate; the two phases were mixed and deoxygenated by a rapid flow of nitrogen, and sodium bicarbonate was added until carbon dioxide evolution ceased. After drying over Na_2SO_4 and concentration, the ethyl acetate extract was purified by ptlc ($CHCl_3$–CH_3OH, 5:2) to give **1** (250 mg) as an unstable yellow powder; R_f (silica, $CHCl_3$–CH_3OH, 3:1) 0.24 ($FeCl_3$ and ninhydrin positive); $[\alpha]_D$ +32.1° (*c* 2.12, CH_3OH); uv(CH_3OH) λ_{max} (nm): 227 (ε 3.1 × 10^4), 291 (ε 1.1 × 10^4), 296 (ε 1.2 × 10^4), 311 (sh) (ε ≈ 9.4 × 10^3); ir (KBr), ν_{max}: 3350–3200 (b), 1635, 1605, 1500 cm^{-1}; ^{13}C nmr (CD_3OD): 30.4 (1C), 56.2 (1C), 106.1 (2C), 115.3 (1C), 116.1 (1C), 116.5 (1C), 116.7 (1C), 120.9 (2C), 123.2 (1C), 126.1 (1C), 127.6 (1C), 128.9 (1C), 129.2 (1C), 139.0 (1C), 147.2 (2C), 172.2 ppm (1C); ^1H nmr (100 MHz, $CD_3C{\equiv}N$–CD_3OD, 10:1) δ: 3.00 (dd, 1H, J = 7, 14 Hz, —CH_2CH<), 3.23 (dd, 1H, J = 5.5, 14 Hz, —CH_2CH<), 3.85 (t, 1H, J = 7 Hz, —CH_2CH<), 6.03 (d,

1H, J = 14.5 Hz, —*CH*=CHNH—), 6.39 (s, 2H, ϕ-*H*), 7.15 (s, 1H, indole, H-2), 7.17 (dd, 1H, J = 1.6, 7.5 Hz, indole, H-5), 7.20 (d, 1H, J = 14.5 Hz, —CH=*CH*NH—), 7.53 (d, 1H, J = 7.5 Hz, indole H-4), 7.57 (d, 1H, J = 1.6 Hz, indole H-7); spin decoupling (100 MHz, $CD_3C{\equiv}N$–CD_3OD, 10:1), $^1H_{obs}$ − {$^1H_{irr}$}, δ: 6.03(bs, 1H) − {7.20}, 7.17(s, 1H) − {7.53}, 7.53(s, 1H) − {7.17}, 7.57(s, 1H) − {7.17}. A 5 mg sample of **1** applied to a 0.65 cm disc of Schleicher and Schuell adsorbent paper gave a 1 mm zone of inhibition of the growth of *Staphylococcus aureus*.

Acetylation of Clionamide (1). A. With Acetic Anhydride

Excess acetic anhydride (10 mL) was added to a solution of **1** (100 mg) in pyridine (2 mL) and the reaction mixture was stirred overnight, at room temperature, under an atmosphere of nitrogen. Evaporation *in vacuo* and purification by ptlc ($CHCl_3$–CH_3OH, 10:1) gave tetracetyl clionamide (**2**, 82 mg), mp 209–211°C (THF – isopropyl ether); $[\alpha]_D$ +45° (*c* 0.7, acetone, 10 cm microcell); uv (CH_3OH) λ_{max} (nm): 227 (ε 5.9 × 10^4), 290 (ε 3.7 × 10^4); ir (KBr) ν_{max}: 3418, 3280, 1760, 1627 cm^{-1}; ^{13}C nmr ($CD_3C{\equiv}N$): 20.4 (1C), 20.9 (2C), 23.1 (1C), 28.3 (1C), 55.2 (1C), 111.3 (1C), 112.1 (1C), 115.1 (1C), 115.5 (1C), 118.3 (2C), 121.0 (1C), 122.7 (2C), 125.5 (2C), 127.7 (1C), 136.3 (1C), 138.4 (1C), 145.0 (2C), 168.1 (1C), 168.9 (2C), 171.0 (1C), 171.9 ppm (1C); ^1H nmr (100 MHz, $CD_3C{\equiv}N$) δ: 1.85 (s, 3H, —NH*Ac*), 2.23 (s, 9H, —O*Ac*), 3.06 (dd, 1H, J = 8, 14 Hz, —*CH*$_2$CH<), 3.24 (dd, 1H, J = 6, 14 Hz, —*CH*$_2$CH<), 4.59 (q, 1H, J = 7 Hz, D_2O − t, J = 7 Hz, —CH$_2$*CH*<), 6.09 (d, 1H, J = 15 Hz, —*CH*=CH—NH—), 6.70 (d, 1H, J = 7.5 Hz, D_2O exchange, —*NH*Ac), 7.06 (s, 2H, ϕ-*H*), 7.10 (s, 1H, indole, H-2), 7.15 (q, 1H, J = 2, 9 Hz, indole H-5), 7.32 (q, 1H, J = 10, 15 Hz, D_2O − d, J = 15 Hz, —CH=*CH*—NH—), 7.51 (d, 1H, J = 9 Hz, indole H-4), 7.67 (d, 1H, J = 2 Hz, indole H-8), 8.65 (d, 1H, J = 9 Hz, D_2O exchange, —CH=CH—*NH*—), 9.23 (b, 1H, D_2O exchange, indole H-1); spin decoupling (100 MHz, $CD_3C{\equiv}N$), $^1H_{obs}$ − {$^1H_{irr}$}, δ: 3.06 (d, 1H, J = 14 Hz) − {4.59}, 3.24 (d, 1H, J = 14 Hz) − {4.59}, 4.59 (d, 1H, J = 7.5 Hz) − {3.15}, 4.59 (t, 1H, J = 7 Hz) − {6.70}, 6.70 (bs, 1H) − {4.59}, 7.32 (d, 1H, J = 9 Hz) − {6.09}, 7.32 (d, 1H, J = 15 Hz) − {8.65}, 8.65 (bs, 1H) − {7.32}; ms *m/e*: 601/599 (9.3, M^+, 1:1), 542/540 (15.5, $M^+ - C_2H_5NO$, 1:1), 500/498 (9.5, $M^+ - C_2H_5NO - C_2H_2O$, 1:1), 210/208 (100, 1:1). *Exact Mass* calcd. for $C_{27}H_{26}{}^{81}Br\ N_3O_8$: 601.0874; found: 601.0889. *Anal.* calcd. for $C_{27}H_{26}BrN_3O_8$: C 54.01, H 4.36, N 7.00; found: C 53.89, H 4.40, N 7.09.

Higher yields of **2** could be obtained by acetylation of the initial crude ethyl acetate extract and purification by column chromatography (silica (Merck), CH_2Cl_2–EtOAc gradient).

Acetylation of Clionamide (1). B. With Acetic Anhydride-d_6

A small sample of the crude ethyl acetate extract (250 mg) was acetylated with acetic anhydride-d_6. Work-up as described for acetylation of clionamide (**1**) with acetic anhydride gave tetracetyl clionamide-d_{12} (**3**, 20 mg) which had a ^1H nmr spectrum identical to that of tetracetyl clionamide (**2**) except for the absence of signals at δ 1.85 (s, 3H) for acetamide and δ 2.23 (s, 9H) for three phenol acetates.

Clionamide Acetonide (5) and Clionamide Acetonide-d_6 *(4)*

Clionamide (**1**, 30 mg) was dissolved in acetone or acetone-d_6 for 1 h at room temperature. Concentration and purification by ptlc ($CHCl_3$–MeOH, 5:2) gave the acetonide **5** (19 mg) or the deuteroacetonide **4** respectively as stable oils; **5**: R_f ($CHCl_3$–CH_3OH, 3:1) 0.54 ($FeCl_3$ and ninhydrin positive); uv (CH_3OH) λ_{max} (nm): 229 (ε 2.5 × 10^4), 297 (ε 1.7 × 10^4), 315 (sh) (ε ≃ 1.4 × 10^4); ir (KBr) ν_{max}: 3300 (b), 2950, 1635 (b), 1605, 1508 cm^{-1}; ^1H nmr[1] (270 MHz, $(CD_3)_2CO$) δ: 1.42 (3H, s, acetonide-*CH*$_3$), 1.47 (s, 3H, acetonide-*CH*$_3$), 3.11 (dd, 1H, J = 7.5, 14.5 Hz), 3.31 (dd, 1H, J = 5, 14.5 Hz), 3.86 (dd, 1H, J = 5, 7.5 Hz), 6.50 (2H, s), 6.75 (d, 1H, J = 14.2 Hz), 6.83 (d, 1H, J = 14.2 Hz), 7.14 (dd, 1H, J = 2, 8.5 Hz), 7.28 (s, 1H), 7.57 (d, 1H, J = 2 Hz), 7.58 (d, 1H, J = 8.5 Hz), 10.09 (bs, 1H, D_2O exchange); ^{13}C nmr ($(CD_3)_2CO$): 27.6 (1C), 28.3 (1C), 30.3 (1C), 59.1 (1C), 105.7 (2C), 106.0 (1C), 110.1 (1C), 111.9 (1C), 114.9 (1C), 115.3 (1C), 116.6 (1C), 120.7 (1C), 121.3 (2C), 122.6 (2C), 125.6 (1C), 125.7 (1C), 129.5 (1C), 146.8 (1C), 174.2 ppm (1C); ms *m/e*: 475/473 (0.02, M^+, 1:1), 210/208 (100, 1:1). High resolution mass measurement was performed on the diacyl derivative of **5**; *Exact Mass* calcd. for $C_{26}H_{26}{}^{81}BrN_2O_6$: 557.0965; found: 557.0990.

The deuteroacetonide **4** was identical (tlc, uv, ^1H nmr, ms) to **5** with the exception of the absence of ^1H nmr signals at δ 1.42 (s, 3H) and δ 1.47 (s, 3H) for two acetonide methyl groups and the complex nature of the signals in the mass spectrum.

Ozonolysis of Tetracetyl Clionamide (2)

Ozone was passed through a solution of **2** (150 mg) in methanol (40 mL), at −78°C, for 5 min. The solution was flushed with oxygen, excess dimethyl sulfide was added, and the mixture allowed to warm to room temperature. Evaporation of the reaction mixture followed by purification by ptlc (EtOAc) gave the aldehyde **9** (60 mg) as a colourless oil.

The aldehyde **9** was identical in all respects (tlc, ir, ^1H nmr, ms) with 3,4,5-triacetoxybenzaldehyde prepared from gallic acid by acetylation, reaction with thionyl chloride, and Rosenmund reduction (6).

Hydrolysis of Tetracetyl Clionamide (2). A. With Hydrochloric Acid (7)

Tetracetyl clionamide (**2**, 145 mg) was dissolved in acetonitrile (15 mL, 0.1% H_2O) and concentrated HCl (0.25 mL in 2 mL $CH_3C{\equiv}N$) was added. After 48 h at room temperature the solvent was evaporated and the residue purified by ptlc ($CHCl_3$–CH_3OH, 5:1) to give the bromo amide **6** (21 mg); $[\alpha]_D$ +4.6° (*c* 3.2, CH_3OH); ^1H nmr (100 MHz, $(CD_3)_2CO$) δ: 1.87 (s, 3H), 3.13 (dd, 1H, J = 8.2, 14.2 Hz), 3.29 (dd, 1H, J = 6, 14.2 Hz), 4.71 (dd, 1H, J = 8.2, 6 Hz), 6.40 (b, 1H, D_2O exchange, —CON*H*$_2$), 6.93 (b, 1H, D_2O exchange, —CON*H*$_2$), 7.17 (dd, 1H, J = 8.8, 1.7, indole H-5), 7.20 (b, 1H, D_2O exchange, —*NH*Ac), 7.30 (s, 1H, indole H-2), 7.61 (d, 1H, J = 1.7 Hz, indole H-7), 7.64 (d, 1H, J = 8.8 Hz, indole H-4), 10.21 (b, 1H, D_2O exchange, indole H-1); ms *m/e*: 325/323 (2.9, M^+, 1:1), 266/264 (43.3, $M^+ - C_2H_5NO$, 1:1), 210/208 (100, $M^+ - C_4H_7N_2O_2$, 1:1), 129 (35.4), 128 (12.2). *Exact Mass* calcd. for $C_{13}H_{14}{}^{79}BrN_3O_2$: 323.0269; found: 323.0251.

Hydrogenolysis of the Bromo Amide 6

The procedure outlined for the hydrogenolysis of the bromo indole **10** was followed (5% Pd/C, 6 mg). Purification was performed by hplc (silica A, hexane – isopropyl alcohol gradient) to give the debromo amide **7** (8.4 mg from 31.3 mg of **6**); $[\alpha]_D$ +11° (*c* 1.0, CH_3OH) (lit. $[\alpha]_D{}^{23}$ +20 ± 1° (*c* 2%, CH_3OH) (4)). The debromo amide **7** was identical, except for optical rotation, with authentic 2-acetamido-3-(indol-3-yl)-propionamide prepared by ammonolysis of racemic *N*-acetyl tryptophan in the presence of DCC.

Hydrolysis of Tetracetyl Clionamide (2). B. With Sulphuric Acid – Methanol

Tetracetyl clionamide (**2**, 150 mg) was dissolved in CH_3OH –

[1]Amide N—H signals were not observed in acetone solution (see ref. 5).

H_2SO_4 (3:1) (10 mL) and stirred at room temperature until tlc indicated that **2** had been consumed. The reaction mixture was neutralized ($NaHCO_3$), concentrated, and the aqueous solution extracted with ethyl acetate. Concentration of the ethyl acetate layer followed by purification by ptlc (EtOAc) gave the bromo methyl ester **8** (25 mg); ^1H nmr (270 MHz, $(CD_3)_2CO$) δ: 1.88 (s, 3H), 3.14 (dd, 1H, J = 7, 15 Hz), 3.25 (dd, 1H, J = 6, 15 Hz), 3.63 (s, 3H), 4.80 (m, 1H), 7.16 (dd, 1H, J = 1.5, 8 Hz, indole H-5), 7.21 (s, 1H, indole H-2), 7.35 (b, 1H, D_2O exchange), 7.50 (d, 1H, J = 8 Hz, indole H-4), 7.58 (d, 1H, J = 1.5 Hz, indole H-7), 10.32 (b, 1H, D_2O exchange); ms *m/e*: 340/338 (16.6, M^+, 1:1), 281/279 (46.7, 1:1), 210/208 (100, 1:1).

The bromo methyl ester **8** differed (^1H nmr) from authentic 2-acetamido-3-(5-bromoindol-3-yl)propionic acid methyl ester prepared from racemic 5-bromo tryptophan; ^1H nmr (270 MHz, $(CD_3)_2CO$) δ: 1.89 (s, 3H), 3.14 (dd, 1H, J = 7, 15 Hz), 3.24 (dd, 1H, J = 6, 15 Hz), 3.63 (s, 3H), 4.76 (q, 1H, J = 7 Hz), 7.19 (dd, 1H, J = 1.5, 9 Hz, indole H-6), 7.24 (s, 1H, indole H-2), 7.34 (d, 1H, J = 9 Hz, indole H-7), 7.36 (b, 1H, D_2O exchange), 7.70 (d, 1H, J = 1.5 Hz, indole H-4), 10.33 (b, 1H, D_2O exchange).

Catalytic Hydrogenation of Tetracetyl Clionamide (**2**)

Palladium on charcoal catalyst (5%, 15 mg) was added to a solution of **2** (60 mg) in methanol (20 mL). The solution was stirred under an atmosphere of hydrogen overnight, filtered through Celite, concentrated, and purified by ptlc (EtOAc) to give **10** (26 mg) as a colourless oil; $[\alpha]_D$ +6.2° (*c* 4.37, acetone); uv (CH_3OH) λ_{max} (nm): 224 (ε 3.38 × 10^4), 283 (ε 6.02 × 10^3); ^1H nmr (100 MHz, $(CD_3)_2CO$) δ: 1.88 (s, 3H), 2.24 (s, 9H), 2.67 (t, 2H, J = 7 Hz, —CH_2CH_2NH—), 3.12 (m, 2H), 3.38 (m, 2H, D_2O − t, J = 7 Hz, —CH_2CH_2NH—), 4.63 (m, 1H), 6.94 (s, 2H), 7.11 (m, 1H), 7.24 (s, 1H), 7.60 (d, 1H, J = 2 Hz), 7.62 (d, 1H, J = 9 Hz), 10.40 (b, 1H, D_2O exchange); ms *m/e*: 603/601 (0.3, M^+, 1:1), 544/542 (2.7, M^+ − C_2H_5NO, 1:1), 210/208 (100, 1:1). *Exact Mass* calcd. for $C_{27}H_{28}{}^{81}BrN_3O_8$: 603.1040; found: 603.1020.

Hydrogenolysis of the Bromo Indole ***10***

Palladium on charcoal catalyst (5%, 10 mg) was added to a solution of **6** (26 mg) in CH_3OH (15 mL) containing 0.2% CH_3CO_2H. The reaction mixture was stirred at room temperature, under an atmosphere of hydrogen, for 72 h, filtered through Celite, concentrated, and purified by ptlc (EtOAc) to give **11** (8 mg) as a colourless oil; ir (KBr) ν_{max}: 3400, 1760, 1635 cm^{-1}; ^1H nmr (270 MHz, $(CD_3)_2CO$) δ: 1.81 (s, 3H), 2.25 (s, 9H), 2.64 (t, 2H, J = 7 Hz), 3.10 (m, 2H), 3.32 (m, 2H, D_2O − t, J = 7 Hz), 4.48 (m, 1H), 6.85 (s, 2H), 7.00 (t, 1H, J = 9 Hz, indole H-5), ~7.0 (1H, D_2O exchange), 7.06 (t, 1H, J = 9 Hz, indole H-6), 7.10 (s, 1H, indole H-2), 7.25 (d, 1H, J = 8 Hz, D_2O exchange), 7.35 (d, 1H, J = 8 Hz, indole H-7), 7.64 (d, 1H, J = 9 Hz, indole H-4), 10.14 (b, 1H, D_2O exchange, indole H-1); spin decoupling (100 MHz, $(CD_3)_2CO$–D_2O), $^1H_{obs}$ − {$^1H_{irr}$}, δ: 2.65 (s, 2H) − {3.36}, 3.12 (b, 2H) − {4.52}, 3.36 (s, 2H) − {2.65}, 4.52 (s, 1H) − {3.12}; ms *m/e*: 523 (0.3, M^+), 481 (0.5, M^+ − C_2H_2O), 464 (14.6, M^+ − C_2H_5NO), 422 (14.7), 380 (14.3), 130 (100). *Exact Mass* calcd. for $C_{27}H_{29}N_3O_8$: 523.1954; found: 523.1970.

Synthesis of the Secondary Amide ***11***

5-Hydroxydopamine hydrochloride (86.0 mg) was added, as a solid, to a solution of DCC (90.7 mg), (*S*)-*N*-acetyltryptophan (105.3 mg), and triethylamine (0.25 mL) in THF–$CH_3C{\equiv}N$ (10:1) (50 mL). The reaction mixture was stirred at room temperature overnight, filtered through Celite, and evaporated. The crude residue was acetylated ($(CH_3CO)_2O$–pyridine, 20:1), evaporated *in vacuo*, and purified twice by ptlc ($CHCl_3$–CH_3OH, 20:1) to give a colourless oil (66.5 mg) identical (tlc, uv, ^1H nmr, ir, ms) to the ultimate hydrogenation product **11** of tetracetyl clionamide (**2**).

Acknowledgments

The financial assistance of the National Science and Engineering Research Council of Canada is gratefully acknowledged. One of us (RJS) thanks the National Science and Engineering Research Council of Canada for a post-graduate scholarship. The authors would like to thank Sheila McDonald, Steve DeMora, and Mike LeBlanc for assistance in collecting the sponge.

1. (*a*) K. RUTZLER. Oecologia, **19**, 203 (1975); (*b*) T. F. GOREAU and W. D. HARTMAN. *In* Mechanisms of hard tissue destruction. Vol. 75. *Edited by* R. F. Sognnaes. American Association for the Advancement of Science. 1963. pp. 25–54; (*c*) D. F. FÜTTERER. J. Sediment. Petrol. **44**, 79 (1974); (*d*) P. WARD and M. J. RISK. J. Paleontol. **51**, 520 (1977).
2. S. JAKOWSKA and R. F. NIGRELLI. Ann. N.Y. Acad. Sci. **90**, 913 (1960).
3. R. J. ANDERSEN. Tetrahedron Lett. 2541 (1978).
4. H. T. HUANG and C. NIEMANN. J. Am. Chem. Soc. **73**, 1541 (1951).
5. G. T. CARTER, K. L. RINEHART, JR., L. H. LI, S. L. KUENTZEL, and J. L. CONNOR. Tetrahedron Lett. 4479 (1978).
6. R. P. BARNES. Org. Synth. Coll. Vol. III, 551 (1955).
7. A. KUTNER. J. Org. Chem. **26**, 3495 (1961).

Nuclear magnetic resonance reorientational correlation functions: the odd-valued spectral components

CATHERINE ELISABETH MARIE FOUQUES
Université de Provence, Chimie Organique, 13397 Marseille, Cedex 4, France
AND
LAWRENCE G. WERBELOW
Montana State University, Department of Chemistry, Bozeman, MT 59717, U.S.A.

Received February 26, 1979

CATHERINE ELISABETH MARIE FOUQUES and LAWRENCE G. WERBELOW. Can. J. Chem. **57**, 2329 (1979).

Practical consequences attributable to nonvanishing imaginary spectral components of the second rank spherical harmonic angular correlation function are described in detail. This analysis presumes the absence of macroscopic spatial anisotropies. Modulation frequency, anisotropy, and cross correlation of interaction between a nuclear spin and the extranuclear environment are considered. These findings permit a critical assessment of the second-order ultrafine dynamic frequency shift in the nuclear magnetic resonance experiment.

CATHERINE ELISABETH MARIE FOUQUES et LAWRENCE G. WERBELOW. Can. J. Chem. **57**, 2329 (1979).

Les conséquences pratiques attribuables à la valeur non-nulle des composantes spectrales imaginaires de la fonction de corrélation angulaire harmonique tensorielle de rang deux sont décrites en détails. Cette analyse suppose l'absence d'anisotropies spatiales macroscopiques. La fréquence de modulation, l'anisotropie et la corrélation croisée de l'interaction entre un spin nucléaire et l'environnement extranucléaire sont considérés. Ces résultats permettent un accès critique du déplacement de fréquence dynamique du deuxieme ordre dans l'expérience de résonance magnétique nucléaire.

Introduction

The interaction between a nuclear spin and the extranuclear environment (heat bath or lattice) can be written in the concise form

$$[1]\quad \mathscr{H}(t) = \mathscr{H}_0 + \sum_{\eta} \xi_{\eta} \sum_{k} (-1)^k T_{\eta}^{\,k} V_{\eta}^{\,-k}(t)$$

The indicated summation extends over all interactions (η) and projections of interaction (k). Equation [1] presumes that all nonspin degrees of freedom can be treated classically without loss of generality. The eigenstructure of $\mathscr{H}_0$ is manifest in chemical shift and multiplet structure parameters.

In marked contrast, the time dependent interactions are defined such that these perturbative terms vanish when ensemble averaged and hence do not contribute in first order to the spectral features of the nuclear magnetic resonance experiment. However, an iterative expansion of the Liouville equation retaining terms to second order in this perturbation demonstrates that whenever motional narrowing obtains, the perturbation-response characteristics of nuclear paramagnetism can be quantitatively described by rate constants of the functional form (1)

$$[2]\quad \text{Rate} \sim 2 \sum_{\eta} \sum_{\eta'} \underbrace{\xi_{\eta}\xi_{\eta'}} \sum_{k} \langle |T_{\eta}^{\,k}| \rangle \langle |T_{\eta'}^{\,-k}| \rangle \int_0^{\infty} \underbrace{\langle V_{\eta'}^{\,k}(t) V_{\eta}^{\,-k}(0) \rangle} (\cos \omega_k t - i \sin \omega_k t)\, dt$$

interaction strengths

lattice correlation of fluctuation

spin matrix elements "selection rules"

spectral density of fluctuation

For certain coherence rates, a summation over eigenbasis is also implied.

This illustrative expansion indicates that these rates are parameterized by an interaction strength, ξ, and a weighted sum of terms related to the fluctuation of interaction. Evaluation of the weighting

0008-4042/79/172329-04$01.00/0

factors, $\langle|T_\eta^k|\rangle$, is a straightforward exercise in the application of the quantum theory of angular momenta. Evaluation of the lattice correlation is much more difficult and is highly model dependent (2). As a prelude to ensuing discussion, it is sufficient to state that the lattice functions, V^k, for the chemical shift anisotropy, intramolecular dipole–dipole and quadrupolar interactions are the kth projections of the second rank spherical harmonic which define the relative orientation of the principal axis of interaction in the laboratory frame of reference. Hence, these interactions provide information on molecular reorientation and angular correlation. The random field, spin rotation, and scalar coupling mechanisms are sensitive to other lattice correlations which will not be discussed further in this work.

Inspection of [2] clearly reveals that the spectral representation of this lattice correlation function is complex valued. This of course does not necessarily imply that the correlation function itself is complex valued (3). Although various time inversion and time reversal arguments suggest that the correlation function is an even function of time, this function is introduced into magnetic relaxation theory in a causal manner and hence the odd (purely imaginary) component survives the one-sided Fourier transformation. Whereas the real component of this spectral representation is responsible for the randomization of phase coherence and the establishment of Boltzmann distributions, the imaginary component must be identified with an ultrafine second-order shift in the various single and multiple quantum coherences.

If extreme narrowing arguments obtain, it can be rationalized that this ultrafine shift is negligible. Likewise, if nonextreme narrowing arguments obtain, the adiabatic contribution to the linewidth renders the ultrafine shift negligible in a relative sense. However, for certain spin systems characterized by coincident Lorentzians, it is conceivable that because of cancellatory effects, the width of at least one spectral composite will be insensitive to the adiabatic term. The necessity to consider ultrafine dynamic frequency shifts has recently been illustrated for multiply degenerate spin one-half systems relaxed by dipolar interactions (4) and for multipolar spin systems relaxed by quadrupolar interactions (5).

It is the purpose of this work to expose the functional form of the dynamic frequency shift and subsequently discuss more fully the possible significance of this term in context of the nuclear magnetic resonance experiment.

Theory

The influence of dipolar, quadrupolar, shift anisotropy, and mutually interfering interactions can be described in terms of two complementary spectral density functions

$$[3]\quad \begin{Bmatrix} J_{\eta\eta'}(\omega) \\ Q_{\eta\eta'}(\omega) \end{Bmatrix} = \xi_\eta\xi_{\eta'} \begin{Bmatrix} \mathrm{Re} \\ \mathrm{Im} \end{Bmatrix} \int_0^\infty \langle Y_2^0(\Omega_\eta(t)) \times Y_2^0(\Omega_{\eta'}(0))\rangle \exp(-i\omega t)\,dt$$

It is assumed that the perturbation limit obtains necessitating consideration of only second-order terms. Absence of applied time dependent rf fields and macroscopic orienting potentials is implicit.

Although numerous dynamical models exist which enable microscopic parameterizations of the spherical harmonic correlation function (2), the present discussion assumes that molecular reorientation is described adequately by a diffusional-type process. Utilizing standard methods, it has been shown that the real component of the one-sided Fourier transform of the spherical harmonic correlation function introduced in [3] can be cast into the general form (6)

$$[4]\quad J_{\eta\eta'}(\omega)/\xi_\eta\xi_{\eta'} = \mathrm{Re}\int_0^\infty \langle Y_2^0(\Omega(t))\,Y_2^0(\Omega'(0))\rangle \times \exp(-i\omega t)\,dt = \left(\frac{1}{16\pi}\right)\sum_{k=-2}^{2} a_k b_k/(b_k^2+\omega^2)$$

where

$$a_0 = 3\sin^2\theta\sin^2\theta'\sin 2\phi\sin 2\phi'$$

$$a_{\pm1} = 12\cos\theta\cos\theta'\sin\theta\sin\theta' \begin{Bmatrix} \sin\phi\sin\phi' \\ \cos\phi\cos\phi' \end{Bmatrix}$$

$$a_{\pm2} = 3\sin^2\theta\sin^2\theta'\cos 2\phi\cos 2\phi' \begin{Bmatrix} \cos^2(\beta/2) \\ \sin^2(\beta/2) \end{Bmatrix} + (3\cos^2\theta - 1)(3\cos^2\theta' - 1) \begin{Bmatrix} \sin^2(\beta/2) \\ \cos^2(\beta/2) \end{Bmatrix} \pm \sqrt{3}\cos(\beta/2)\sin(\beta/2)[(3\cos^2\theta - 1) \times \sin^2\theta'\cos 2\phi' + (3\cos^2\theta' - 1) \times \sin^2\theta\cos 2\phi]$$

$$b_0 = 4D_1 + D_2 + D_3$$

$$b_{\pm1} = D_1 + \begin{Bmatrix} 4D_2 + D_3 \\ D_2 + 4D_3 \end{Bmatrix}$$

$$b_{\pm2} = 2(D_1 + D_2 + D_3) \pm 2(D_1^2 + D_2^2 + D_3^2 - D_1D_2 - D_1D_3 - D_2D_3)^{1/2}$$

$$\beta = \tan^{-1}\left(\frac{\sqrt{3}(D_2 - D_3)}{D_1 - D_2 - D_3}\right)$$

The ith component of the diagonalized diffusion tensor is denoted by D_i. The polar angles, $(\theta,\phi) \equiv \Omega$, position the vector interaction in this same frame.

Simplification of [4] results whenever symmetric top or spherical top approximations obtain.

The imaginary component of the one-sided Fourier transform of the spherical harmonic correlation function can be deduced from the absorption–dispersion relations, the Kramers–Kronig relations or, equivalently, from the realization that the Fourier transform of a causal function yields real and imaginary components related by a Hilbert transform (7),

$$[5]\quad Q_{\eta\eta'}(\omega) = (-\xi_\eta\xi_{\eta'}/\pi\omega) \star \mathrm{Re}\int_0^\infty \langle Y_2^{\,0}(\Omega(t)) \times Y_2^{\,0}(\Omega'(0))\rangle \exp(-i\omega t)\,dt = \left(\frac{-1}{\pi\omega}\right) \star J_{\eta\eta'}(\omega)$$

where $\star$ is the convolution operation.

Since convolution is a linear operation,

$$[6]\quad Q_{\eta\eta'}(\omega)/\xi_\eta\xi_{\eta'} = (16\pi)^{-1} \sum_{k=-2}^{2} a_k\omega b_k^{\,2}/(b_k^{\,2} + \omega^2)$$

The coefficients, a_k and b_k, are defined in [4]. This expression is valid for the general asymmetric top rotator in the absence of orienting potentials.

Discussion

The existing nmr literature provides very little discussion of the second-order dynamic frequency shift term. Explicit considerations of this term exist in a few scattered studies for some simple dipolar relaxed spin systems (8–10). In each of these instances, it was rationalized that the ultrafine corrections were insignificant and hence did not justify closer scrutiny. For example, the single quantum coherence rate for two identical spin one-half nuclei relaxed by dipolar interactions is given by the expression (10)

$$[7]\quad \langle I_+(t)\rangle/\langle I_+(0)\rangle = \mathrm{Re}\,[\exp(-t/T_2 + i\omega_0\tau_2 t/2T_1)]$$

Isotropic modulation of interaction (correlation time: τ_2) was assumed.

These studies in conjunction with other similar comments (11) have promulgated minimal interest in the second-order shift term. However, as noted in the introductory comments, certain instances have recently been exposed where these terms are indeed significant. Hence, a closer inspection of [6] is justifiable.

Well known features are readily apparent from expression [6]. Since $Q(\omega) = -Q(-\omega)$, whereas $J(\omega) = J(-\omega)$, all diagonal Redfield terms (spin–lattice relaxation),

$$[8]\quad R_{\alpha\alpha\beta\beta} \equiv \langle\alpha|T_\eta^{\,k}|\beta\rangle\langle\beta|T_{\eta'}^{\,-k}|\alpha\rangle\{J_{\eta\eta'}(\omega_{\alpha\beta}) + J_{\eta\eta'}(-\omega_{\alpha\beta}) + Q_{\eta\eta'}(\omega_{\alpha\beta}) + Q_{\eta\eta'}(-\omega_{\alpha\beta})\}$$

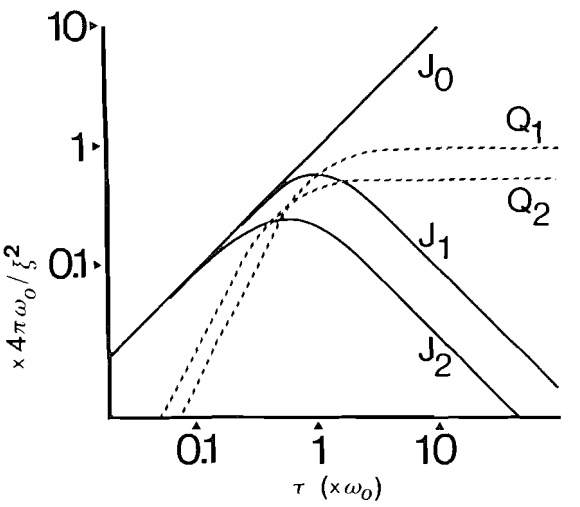

FIG. 1. Plot of $J_0(0)$, $J_1(\omega_0)$, $J_2(2\omega_0)$, $Q_1(\omega_0)$, and $Q_2(2\omega_0)$, measured in units of $\xi_\eta^{\,2}/4\pi\omega_0$ versus the reorientational correlation time τ, measured in units of $1/\omega_0$. It is assumed that the spherical harmonic angular correlation function is of the form

$$\langle Y_2^{\,k}(\Omega(t))\,Y_2^{\,-k}(\Omega(0))\rangle = (-1)^k\left(\frac{1}{4\pi}\right)\exp(-t/\tau).$$

This figure may also be utilized to deduce more general diffusional correlations where

$$\langle Y_2^{\,k}(\Omega(t))\,Y_2^{\,-k}(\Omega(0))\rangle = (-1)^k\left(\frac{1}{4\pi}\right) \times \sum_{i=1}^{5} \alpha_i\exp(-t/\tau_i);\quad \sum_i \alpha_i = 1.$$

For the cross correlation terms,

$$\sum_i \alpha_i = P_2(\cos(\Omega - \Omega')).$$

are unaffected by odd spectral components (12). Since Q is odd and continuous, the zero frequency shift, $Q(0)$, vanishes.

All other relevant features of the dynamic shift term can be easily deduced with the graphical aid of Fig. 1. This figure plots $J_k(k\omega_0)$ and $Q_k(k\omega_0)$, measured in the natural units of interaction, $\xi^2/4\pi$ inversely weighted by the Larmor frequency, $\omega_0 = \gamma B_0$, versus the reorientational correlation time, τ, measured in units of $1/\omega_0$. Assumed isotropic reorientation for this rudimentary plot is reflected by the occurrence of a single point of inflection in the J_1 and J_2 curves. For cross-correlation functions, the ordinate must be further scaled by the factor, $P_2(\hat{\eta}\cdot\hat{\eta}')$.

The left-hand portion of this figure corresponds to the extreme narrowing regime, $J_0 \simeq J_1 \simeq J_2$. In this same limit, it is important to note that the analogous ratio, Q_1/Q_2 does not equal unity. This feature suggests that conventional formulations of the extreme narrowing approximation when considering second-order shifts must be strengthened (4). In the viscous liquid regime of nmr (right-hand

portion of this figure), $Q_k = J_0 J_k$ ($\xi^2/4\pi\omega_0 \equiv 1$). Since Q_k is larger than J_k by the same factor by which it is smaller than J_0, evolution expressions for any quantum coherence which is independent of the adiabatic contribution will be dominated by the dynamic frequency shift term.

Since it is well known that anisotropic and internal motions radically influence the effectiveness of both T_1 and T_2 relaxation processes (for example, ref. 13), perhaps the singly most important question to be resolved is the importance of such motions on the dynamic shift term. In doing so, it must be remarked that [6] is equally valid for single internal rotations if this motion is coincident with any of the principal diffusion axes. Equations [4] and [6] are also amenable to other general interpretations with suitable identifications and assumptions (for example, see comments on papers in ref. 14).

Since T_2 is on the order of J_0 ($= \sum_k (1/b_k)$), whereas $\int_0^\infty J(\omega)\, d\omega$ is constant valued ($\xi^2/8$), the presence of high frequency reorientational anisotropies contribute very little to the density at zero frequency resulting in narrowed single quantum coherences. Likewise, for heteronuclear spin systems, it is well known that the longitudinal magnetization damping constants are on the order of J_1. Hence, in striking contrast, motional anisotropies may increase or decrease the effectiveness of the longitudinal damping rates depending on relative ratios of the various b_k's and ω_0; i.e., depending on whether the motions add to or subtract from the density at ω_0.

In previous studies (4, 5, 8–10), it has been demonstrated that the second-order shift behaves much like the imaginary counterpart of a heteronuclear T_1: there is no adiabatic contribution. However, it also behaves like a T_2 which is insensitive to modulation frequencies less than some critical frequency. For the dynamic shift, this critical frequency is the Larmor frequency. Thus, in nonextreme narrowing, internal motions and other high frequency anisotropies result in unaltered or diminished shifts. Enhancement is never realized.

These expressions may also prove helpful for the analysis of esr spectra where effects attributable to dynamic frequency shifts are well known.

Conclusions

Ramifications of a general expression for the second-order dynamic frequency shift are discussed in detail. It is clearly illustrated that the absence of the adiabatic linewidth contribution is the central criterion necessitating considerations of these shifts. It is noted that the dynamic shift demonstrates both conventional "T_1-stereotyped" and "T_2-stereotyped" reorientational response behavior. It is argued that the influence of motional anisotropies only diminishes the relative importance of the dynamic shift term. Within the framework provided by Fig. 1 and [6], the interested reader can assess the importance of the dynamic shift term for more specialized purposes.

1. A. G. REDFIELD. Adv. Magn. Reson. **1**, 1 (1965); P. S. HUBBARD. Rev. Mod. Phys. **33**, 249 (1961).
2. W. A. STEELE. Adv. Chem. Phys. **34**, 1 (1976), and references cited therein; K. A. VALIEV and E. N. IVANOV. Sov. Phys. Usp. **16**, 1 (1973), and references cited therein.
3. L. G. WERBELOW, D. M. GRANT, E. P. BLACK, and J. M. COURTIEU. J. Chem. Phys. **69**, 2407 (1978).
4. L. G. WERBELOW. J. Magn. Reson. **34**, 439 (1979); L. G. WERBELOW, A. THEVAND, and G. POUZARD. J. Chem. Soc. Faraday Trans. II. In press.
5. L. G. WERBELOW. J. Chem. Phys. In press.
6. L. G. WERBELOW and D. M. GRANT. J. Magn. Reson. **21**, 369 (1976); L. G. WERBELOW and D. M. GRANT. Adv. Magn. Reson. **9**, 189 (1977).
7. R. BRACEWELL. The Fourier transform and its applications. McGraw-Hill, New York, NY. 1968. Chapt. 12.
8. P. S. HUBBARD. Phys. Rev. **128**, 650 (1962).
9. D. GESCHKE. Z. Phys. **212**, 169 (1968).
10. L. G. WERBELOW. Ph.D. Thesis, University of British Columbia, Vancouver, B.C. 1974.
11. A. ABRAGAM. The principles of nuclear magnetism. Oxford Press, Clarendon, Engl. 1961. p. 279.
12. S. EMID. Physica (Utrecht), **70**, 616 (1973); **81B**, 137 (1976).
13. D. DODDRELL, V. GLUSHKO, and A. ALLERHAND. J. Chem. Phys. **56**, 3683 (1972); A. G. MARSHALL, P. G. SCHMIDT, and B. D. SYKES. Biochemistry, **11**, 3875 (1972); L. G. WERBELOW and A. G. MARSHALL. J. Am. Chem. Soc. **95**, 5132 (1973).
14. L. G. WERBELOW. J. Am. Chem. Soc. **96**, 4747 (1974); L. G. WERBELOW and D. M. GRANT. Can. J. Chem. **55**, 1558 (1977); L. G. WERBELOW and A. G. MARSHALL. J. Magn. Reson. **11**, 299 (1973).

Canadian Journal of Chemistry
Published by
THE NATIONAL RESEARCH COUNCIL OF CANADA

Journal canadien de chimie
Publié par
LE CONSEIL NATIONAL DE RECHERCHES DU CANADA

Volume 57 Number 18 September 15, 1979

Volume 57 numéro 18 15 septembre 1979

Comment: Ultrasonic velocities for deuterium oxide – water mixtures at 298.15 K

STEFAN ERNST AND JACEK GLINSKI
Institute of Chemistry, Wrocław University, ul. F. Joliot-Curie 14, 50-383 Wrocław, Poland

Received February 23, 1979

STEFAN ERNST and JACEK GLINSKI. Can. J. Chem. 57, 2333 (1979).

The results of highly precise measurements of ultrasonic velocity in mixtures of deuterium oxide with water by Kiyohara *et al.* were used to calculate and discuss the excess velocity of sound in this system.

STEFAN ERNST et JACEK GLINSKI. Can. J. Chem. 57, 2333 (1979).

Les résultats de mesures de haute precision de la vitesse ultrasonique en mélange d'oxide de deuterium et d'eau par Kiyohara *et al.* ont été utilisé pour calculer et discuter la vitesse excessible du son dans ce système.

Mixtures of H_2O with deuterium oxide are very interesting from the point of view of physicochemistry of solutions. Both the components (H_2O and D_2O) are very similar in almost all their physical properties. Their molecular radii and masses are close in value and the molecules have a similar symmetry and distribution of charges. Therefore, all the deviations of those mixtures from ideality are small and difficult to measure. Thus the results of sound velocity measurements in water–D_2O mixtures published recently (1) seem to be of particular interest. The high precision of those measurements makes it possible to calculate reliable values of two parameters characterizing deviations of the system from ideality: the 'excess' compressibility and 'excess' velocity of sound. The former was calculated by the authors on the basis of a thermodynamically justified and exact expression for the adiabatic compressibility of an ideal mixture (2). Moreover, deviations of the sound velocity from additivity were calculated:

$$[1] \quad \Delta u = u - \sum_i x_i u_i^0$$

where x_i is the mole fraction of the ith component; u_i^0, velocity of sound in the pure ith component; u, sound velocity in the mixture. In our opinion those deviations do not properly characterize the deviations of the acoustic properties of the mixture from ideality since according to the thermodynamic criterion of ideality of a mixture:

$$[2] \quad \bar{G} = \sum_i x_i \mu_i + RT \sum_i x_i \ln x_i$$

(where $\bar{G}$ is the mean molar free enthalpy and μ_i^0 is the chemical potential of the ith component) the sound velocity in an ideal mixture should differ from the molar fraction average of the velocities in the pure components. Since neither energy nor volume effects accompany the mixing of the components of an ideal mixture the time of propagation of a plane acoustic wave through an ideal mixture layer of thickness l should equal the sum of times the wave needs to pass through the separate layers of the pure components of thickness $lx_{v,i}$ (where $x_{v,i}$ is the volume fraction of the component i):

$$[3] \quad \frac{l}{u_{id}} = \sum_i \frac{lx_{v,i}}{u_i}$$

Thus

$$[4] \quad u_{id} = \left(\sum_i \frac{x_{v,i}}{u_i} \right)^{-1}$$

where u_{id} is the velocity of sound in the ideal mixture.

For a binary mixture eq. [4] can be written as

$$[5] \quad u_{id} = \frac{u_1 u_2}{x_{v,1} u_2 + x_{v,2} u_1}$$

Using the above relation, Natta and Baccaredda (3) interpolated sound velocity values for real mixtures which obviously cannot lead to exact results because of the nonideal behaviour of those mixtures.

0008-4042/79/182333-02$01.00/0

The 'ideal' sound velocity can also be calculated on the basis of the Laplace equation:

$$[6] \quad u_{id} = (1/\rho_{id}\beta_{id})^{1/2}$$

where ρ_{id} is the density and β_{id} the compressibility coefficient of the ideal mixture. The u_{id} values calculated from eq. [6] should be equal to those obtained by eq. [4].

The u_{id} values were calculated according to eqs. [4] and [6] using the data of Kiyohara, Halpin, and Benson (1) (the β_{id} values were calculated from β and β^E). The corresponding excess velocities $u^E = u - u_{id}$ are illustrated in Figs. 1 and 2, where the solid curves were calculated from

$$[7] \quad u^E = x(1-x)[A + B(2x-1) + C(2x-1)^2 + D(2x-1)^3]$$

with A, B, C, and D coefficients found numerically using the least-squares approximation: $A = -1.1126$, $B = -0.04925$, $C = 0.1932$, $D = -0.1378$ for u_{id} calculated from eq. [4] and $A = 0.1120$, $B = -0.2283$, $C = 0.2144$, $D = 0.01032$ for u_{id} calculated from eq. [6].

In spite of our expectations, the excess velocities calculated from eq. [4] in the whole concentration range differ from those calculated from eq. [6]. We suppose these differences result from errors in the parameter values used for calculating β_{id}. Even if the errors are small, they can seriously affect the excess velocity calculated from the relation:

$$[8] \quad u^E = u - u_{id} = \left(\frac{1}{\rho_{exp}\beta_{exp}}\right)^{1/2} - \left(\frac{1}{\rho_{id}\beta_{id}}\right)^{1/2}$$

because of the slight deviations of the H_2O–D_2O system from ideality. Therefore, the excess velocities calculated from

$$[9] \quad u^E = u - u_{id} = \frac{x_{v,1}u(u_2 - u_1) + u_1(u - u_2)}{x_{v,1}(u_2 - u_1) + u_1}$$

seem to be more reliable because their accuracy is affected only by the errors in the sound velocity measurements, which are extremely small in ref. 1 (standard deviation of 0.014 m s^{-1}).

The excess velocities calculated from the latter relation are negative in the whole concentration range and about ten times smaller than deviations from additivity on a mole fraction basis calculated by Kiyohara, Halpin, and Benson. Thus, like the adiabatic compressibilities, the velocities show only small negative deviations from the ideal values and a slight asymmetric variation with the mole fraction. This is probably due to the similarities of the structures and intermolecular interactions of both the components.

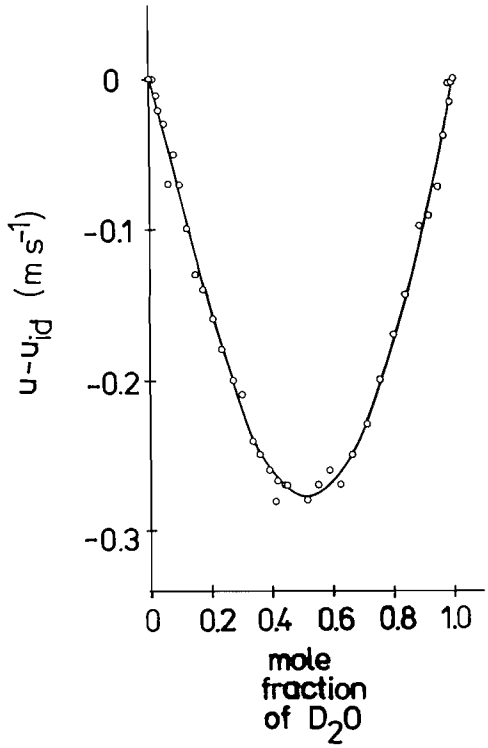

FIG. 1. The excess velocities of sound in mixtures of D_2O in H_2O. The ideal velocities calculated from eq. [4].

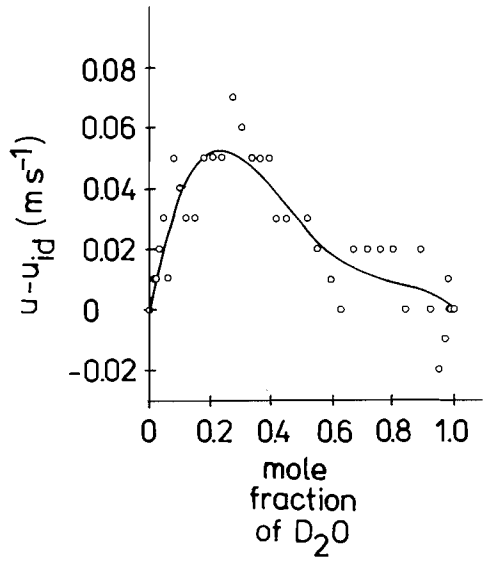

FIG. 2. The excess velocities of sound in mixtures of D_2O in H_2O. The ideal velocities calculated from eq. [6].

1. O. KIYOHARA, C. J. HALPIN, and G. C. BENSON. Can. J. Chem. **55**, 3544 (1977).
2. W. VAN DAEL. *In* Experimental thermodynamics. Vol. 2. *Edited by* B. LeNeindra and B. Vodar. Butterworths, London. 1974. Chapt. 11.
3. G. NATTA and M. BACCAREDDA. Atti Accad. Naz. Lincei, **4**, 360 (1948).

Reply to comment: Ultrasonic velocities for deuterium oxide – water mixtures at 298.15 K[1]

OSAMU KIYOHARA,[2] CARL J. HALPIN, AND GEORGE C. BENSON
Division of Chemistry, National Research Council of Canada, Ottawa, Ont., Canada K1A 0R6

Received March 19, 1979

OSAMU KIYOHARA, CARL J. HALPIN, and GEORGE C. BENSON. Can. J. Chem. 57, 2335 (1979).

The calculations of excess sound velocities in D_2O–H_2O mixtures by Ernst and Glinski are discussed and new results are presented.

OSAMU KIYOHARA, CARL J. HALPIN et GEORGE C. BENSON. Can. J. Chem. 57, 2335 (1979).

Les calculs de la vitesse excessive du son dans les mélanges D_2O–H_2O par Ernst et Glinski sont discuté et on présente quelques résultats récents.

[Traduit par le journal]

In their paper, Ernst and Glinski (1) have used results from an ultrasonic study in our laboratory (2) to calculate the excess velocities of sound in D_2O–H_2O mixtures. The twofold purpose of the present paper is to comment on the definition of excess sound velocity and to draw attention to a recent note (3) in which the derivation of excess isentropic compressibilities from our earlier results (2) is corrected.

The excess velocity u^E is the difference between the observed velocity u and the value u^{id} in the corresponding ideal mixture.

$$[1] \quad u^E = u - u^{id}$$

As pointed out by Ernst and Glinski, the concept of an ideal reference system is clearly defined for thermodynamic properties by

$$[2] \quad \mu_i^{id}(T,p,x_i) = \mu_i^0(T,p) + RT \ln x_i$$

where $\mu_i^{id}(T,p,x_i)$ is the chemical potential of component i in the mixture at temperature T, pressure p, and mole fraction x_i, and $\mu_i^0(T,p)$ is the chemical potential of the pure component at the same temperature and pressure. Unfortunately the velocity of sound in a mixture is not in general one of its thermodynamic properties.

Ernst and Glinski suggest two formulae for u^{id}. The first of these is

$$[3] \quad u^{id} = \left[\sum_i (\phi_i^0/u_i^0)\right]^{-1}$$

where u_i^0 is the velocity in pure component i, and

$$[4] \quad \phi_i^0 = x_i V_i^0/V^{id}$$

is the volume fraction of i in the mixture stated in terms of the unmixed components. In eq. [4], V_i^0 is the molar volume of pure component i and

$$[5] \quad V^{id} = \sum_i x_i V_i^0$$

is the molar volume of the ideal mixture. The second formula is

$$[6] \quad u^{id} = \left(V^{id}/\kappa_s^{id} \sum_i x_i M_i\right)^{1/2}$$

where κ_s^{id} is the isentropic compressibility of the ideal mixture, and M_i is the molar mass of component i. The authors express surprise that values of u^E calculated from eq. [3] and eq. [6] differ, and suggest that eq. [3] provides a better basis for the evaluation of u^{id}.

It appears to us that eq. [3], which depends on an intuitive model for the passage of a wave through layers of the unmixed components, is unsuitable for defining an ideal thermodynamic value of u. Equation [6], which follows from the Laplace equation under conditions where dispersion is negligible (waves of low frequency and small amplitude), is the correct way of relating u to thermodynamic properties and ideal thermodynamic behavior. In our paper on D_2O–H_2O (2), we fitted the deviation of u from linearity on a mole fraction basis, i.e.

$$[7] \quad \Delta u = u - x_1 u_1^0 - x_2 u_2^0$$

with a polynomial form to provide an algebraic representation of our results. We agree with Ernst and Glinski that Δu "does not properly characterize the deviations of the acoustic properties of the mixture from ideality", and we carefully avoided using the term excess velocity in discussing Δu. We believe that Δu provides a simple empirical way for summarizing the acoustic behavior of a mixture.

In applying eq. [6] to D_2O–H_2O mixtures, Ernst and Glinski used values of κ_s^{id} derived from data in

[1]NRCC No. 17512.
[2]National Research Council of Canada Research Associate.

0008-4042/79/182335-02$01.00/0

our paper (2). A recent note (3), which was not available to Ernst and Glinski, discusses the formulae which have been used in our laboratory to evaluate κ_s^{id}. In some of our earlier work we used the approximation

$$[8] \quad \kappa_s^{id} = \sum_i \phi_i^0 \kappa^0_{s,i}$$

where $\kappa^0_{s,i}$ is the isentropic compressibility of pure component i. In more recent work, including our paper on D_2O–H_2O (2), we used the expression

$$[9] \quad \kappa_s^{id} = \kappa_T^{id} C_v^{id}/C_p^{id}$$

with κ_T^{id}, the isothermal compressibility of the ideal mixture, equal to the volume fraction average of the values for the pure components

$$[10] \quad \kappa_T^{id} = \sum_i \phi_i^0 \kappa_{T,i}^0$$

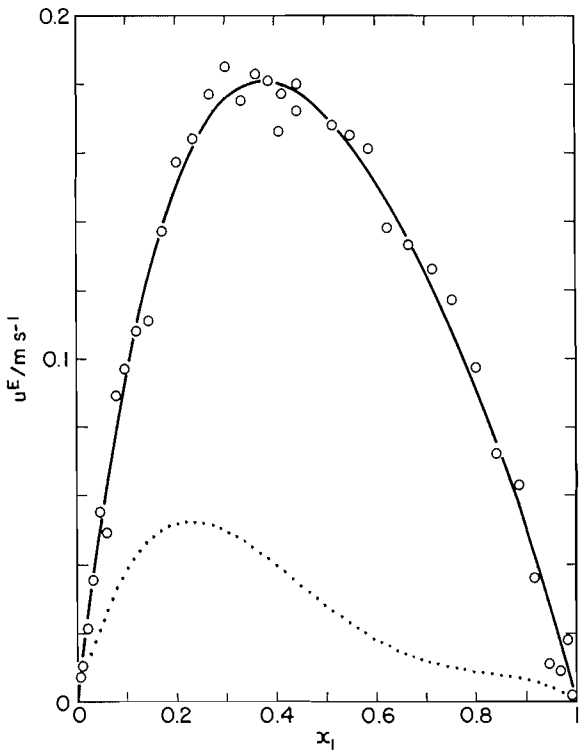

FIG. 1. Excess velocities of sound in $D_2O(1)$–$H_2O(2)$ mixtures at 298.15 K. Points, ○, derived from experimental results (2) using eq. [13] for κ_s^{id}. Curves: — least-squares representation by eq. [15]; ··· calculated by Ernst and Glinski (1) from our original κ_s^E values based on the approximation of C_v^{id} by eq. [12].

and C_p^{id}, the molar heat capacity of the ideal mixture at constant pressure, equal to the mole fraction average

$$[11] \quad C_p^{id} = \sum_i x_i C_{p,i}^0$$

Following Van Dael (4) we also adopted a mole fraction average for C_v^{id}, the molar heat capacity of the ideal mixture at constant volume,

$$[12] \quad C_v^{id} = \sum_i x_i C^0_{v,i}$$

and erroneously stated that this procedure was exact. We have since realized that eq. [12] is only approximate and that in some cases its use can alter the values of κ_s^{id} considerably. As indicated in our paper, the expression for κ_s^{id} which follows from eq. [2] is

$$[13] \quad \kappa_s^{id} = \kappa_T^{id} - TV^{id}(\alpha^{id})^2/C_p^{id}$$

where α^{id}, the coefficient of thermal expansion of the ideal mixture, is the volume fraction average of the values for the pure components

$$[14] \quad \alpha^{id} = \sum_i \phi_i^0 \alpha_i^0$$

and κ_T^{id}, V^{id}, and C_p^{id} are as given above.

Excess velocities of sound in D_2O–H_2O mixtures at 298.15 K, calculated from our experimental results (2) using eq. [13] to evaluate κ_s^{id}, are plotted against x_1, the mole fraction of D_2O, in Fig. 1. Also shown is their representation by the equation

$$[15] \quad u^E/\text{m s}^{-1} = x_1(1 - x_1)[0.684 + 0.300 \times (1 - 2x_1) + 0.196(1 - 2x_1)^2]$$

which has a standard deviation of 0.007 m s^{-1}. For comparison, the dotted curve in the same figure is that derived from our original κ_s^E values by Ernst and Glinski. The recalculated values of u^E are larger than those which depend on the approximate expression for C_v^{id} (eq. [12]), and the variation of u^E with mole fraction is less skewed.

1. S. ERNST and J. GLINSKI. Can. J. Chem. This issue.
2. O. KIYOHARA, C. J. HALPIN, and G. C. BENSON. Can. J. Chem. 55, 3544 (1977).
3. G. C. BENSON and O. KIYOHARA. J. Chem. Thermodyn. To be published.
4. W. VAN DAEL. *In* Experimental thermodynamics. Vol. 2. *Edited by* B. LeNeindre and B. Vodar. Butterworths, London. 1974. Chapt. 11.

The electron-donating properties of some phenylfurans. Charge transfer studies

RAFIE ABU-EITTAH AND MAHER M. HAMED

Department of Chemistry, Faculty of Science, University of Cairo, Giza, Egypt

Received November 20, 1978

RAFIE ABU-EITTAH and MAHER M. HAMED. Can. J. Chem. 57, 2337 (1979).

The formation of the molecular complexes of some phenylfurans with TCNE has been investigated by spectroscopic methods. The formation constants were determined by graphical and iterative procedures and some thermodynamic parameters were calculated. The formed molecular complexes were π ones. Diphenylfuran proved to be a much stronger electron donor than phenylfuran and the latter stronger than furan. Results at hand suggest that the donors investigated assume an all-planar conformation.

RAFIR ABU-EITTAH et MAHER M. HAMED. Can. J. Chem. 57, 2337 (1979).

Faisant appel à des méthodes spectroscopiques, on a étudié la formation de complexes moléculaires de quelques phénylfurannes avec le TCNE. On a déterminé les constantes de formation par des méthodes graphiques et itératives et on a calculé quelques paramètres thermodynamiques. Les complexes moléculaires qui se forment sont du type π. Le diphénylfuranne est un donneur d'électron beaucoup plus fort que le phénylfuranne et ce dernier est plus fort que le furanne. Les résultats obtenus suggèrent que les donneurs étudiés adoptent une conformation complètement plane.

[Traduit par le journal]

Introduction

The charge transfer interaction of some five-membered heterocycles with TCNE has been investigated and it has been found that these heterocycles act as π-electron donors (1–3). Ginns and Strong (4) studied the furan–iodine charge transfer complex in the gas phase. The band maximum of the charge transfer complex (~284 nm) was independent of furan pressure or temperature and was blue shifted (31 nm) from its position in the liquid phase complex. The 1:1 complex was exclusively formed.

The charge transfer interaction of furan, thiophene, and pyrrole with maleic anhydride was investigated (5). Sometimes two charge transfer transitions, from the highest MO's of the donors to the lowest vacant MO of the acceptors, were observed.

Dobrescu-Ciureanu and Sahini (6) applied a perturbation treatment to describe the electronic structure of molecular complexes formed by iodine with several five-membered heterocycles (including furan). Lang (7) has studied the iodine complexes of a number of heterocyclic donors.

The study of molecular complexes in which furan acts as an electron donor is rarely found in the literature. In this work the charge transfer complexes of some phenylfurans with TCNE were investigated. Measurements at different temperatures lead to the computation of some thermodynamic parameters of the molecular complex. The ionization potentials of the donors were calculated from the energies of the charge transfer bands.

Experimental

Materials

Tetracyanoethylene (TCNE, Fluka AG purum grade) was purified by crystallization from chlorobenzene. Chloroform (B.D.H. Analytical reagent) was used without further purification (scanning the spectra of a purified version of chloroform in which the stabilizer was removed gave the same values of band maxima and band intensity as those obtained when A.R. grade solvent was used without purification). Phenylfurans were prepared by the methods reported in literature (8–10).

Measurements

The absorption spectra were measured with a Beckman DK-1 spectrophotometer using 1.0 cm^3 fused silica cells.

Results and Discussion

(I) Equilibrium Studies

(i) 2-Phenylfuran + TCNE System

On mixing a solution of 2-phenylfuran (D) with that of TCNE (B), the following equilibrium is established for the 1:1 complex

$$D + B \rightleftharpoons D{\cdot}B$$

$$[1] \quad K = [DB]/[D][B] = [C]/([D]_0 - [C])([B]_0 - [C])$$

where [DB] = [C] = concentration of charge transfer complex, $[D]_0$ and $[B]_0$ = initial concentrations of the donor and acceptor respectively. If A is the absorbance of the mixture, if Beer's law is obeyed, and if a 1.0 cm optical path is used, eq. [1] can be transformed (11) to eq. [2]:

$$[2] \quad \frac{[D]_0[B]_0}{\Delta A} = \frac{1}{K\Delta\varepsilon} + \frac{[D]_0 + [B]_0}{\Delta\varepsilon} - \frac{[C]}{\Delta\varepsilon}$$

0008-4042/79/182337-05$01.00/0

where, ΔA = absorbance due to charge transfer complex only and $\Delta\varepsilon = \varepsilon_C - \varepsilon_D - \varepsilon_B$. Equation [2] is the Scott's (12) form of the Benesi–Hildebrand (13) relation. If one chooses a wavelength where absorbance is due only to the charge transfer complex then ΔA is replaced by A and $\Delta\varepsilon$ is replaced by ε_C in the above equation. Equation [2] is used to determine K and ε_C graphically (the relation between $[D]_0[B]_0/A$ is plotted against $[D]_0 + [B]_0$, from the slope and intercept one calculates ε_C, K). The results thus obtained are approximate (the last term of eq. [2] is neglected) and show some discrepancies. Iterative procedures eliminate the approximations. The Rosenbrock (14) optimization method is used to get accurate values of K and ε_C. This method depends on minimizing the sum of the squares of the differences between observed and calculated absorbances as outlined. Equation [2] is rearranged to

$$[3]\quad \frac{A}{\varepsilon_C} - \left([D]_0 + [B]_0 + \frac{1}{K}\right) + \frac{\varepsilon_C[D]_0[B]_0}{A} = 0$$

Equation [3] is a second order one and can be solved if K and ε_C are known. One defines the function $Y(K,\varepsilon_C)$ as

$$[4]\quad Y(K, \varepsilon_C) = \sum_{i=1}^{n} [A_{obs} - A_{calcd}]^2$$

where n is the number of experimental data.

The values of K and ε_C which give the minimum value of the function Y are the nearest to the correct values. Equation [3] is solved iteratively to get values of K and ε_C which minimize the value of the Y function. The entry values of K and ε_C are the ones obtained from the graphical method.

Figure 1 shows the absorption spectra (500–700 nm) of mixtures of 2-phenylfuran and TCNE at 18°C when chloroform was used as a solvent and a blank. A broad band with a maximum around 610 nm is observed and represents the maximum of a charge transfer transition since neither the donor nor the acceptor absorb light in that region. The formation of the molecular complex 2-phenylfuran–TCNE has been investigated at different temperatures. The observed increase of absorbance on cooling indicates the exothermic nature of the process of complex formation. The relation between $[D]_0[B]_0/A$ versus $[D]_0 + [B]_0$ is given in Fig. 2, the straight line relationship is apparent and approximate values of K and ε_C are calculated from the slope and intercept. The iteratively computed formation constants are given in Table 1, the decrease of the product $K\varepsilon_C$ with the increase of temperature is a further evidence that the process of complex formation is an exothermic one.

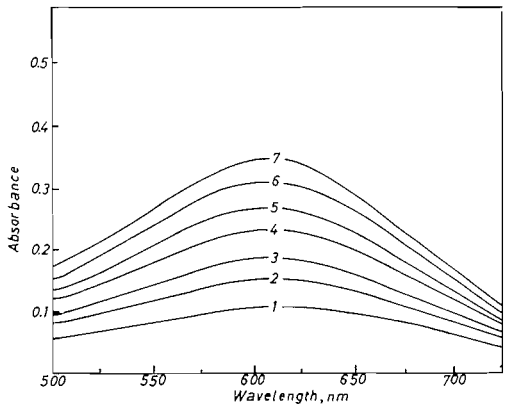

FIG. 1. Absorption spectra of pure TCNE(B) = 0.0027 M, 2-phenylfuran(D) = 0.0856 M, and their mixed solutions at 18.0°C. The concentrations of 2-phenylfuran are: (*1*) 0.0214 M, (*2*) 0.0321 M, (*3*) 0.0428 M, (*4*) 0.0535 M, (*5*) 0.0642 M, (*6*) 0.0749 M, (*7*) 0.0856 M; pure B and D show no absorbance. [TCNE] = 0.0027 M in all solutions.

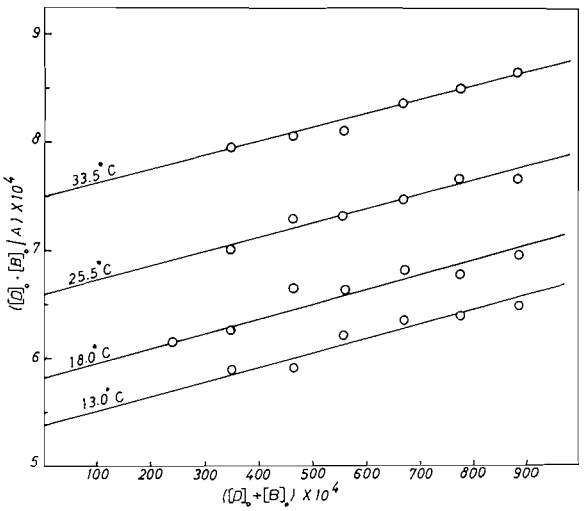

FIG. 2. Relation between $[D]_0[B]_0/A$ and $[D]_0 + [B]_0$ for 2-phenylfuran–TCNE system.

It may be interesting to compare the properties of the two molecular complexes: Furan–TCNE and 2-phenylfuran–TCNE. Yoshida and Kobayashi (5) have indicated that the molecular complex Furan–TCNE possesses two charge transfer transitions at 445 and 295 nm respectively. The determined value (graphically) of K was 0.35 ± 0.01. The broad band characteristic of the 2-phenylfuran + TCNE system makes it difficult to characterize two charge transfer bands analogous to those found when furan is the donor. In the latter case the two charge transfer transitions were assigned to transitions from the two highest occupied MO's of the donor to the lowest vacant MO of the acceptor.

TABLE 1. Values of the formation constants and molar extinction coefficients of the studied phenylfurans + TCNE complexes

Donor	Method*	$K_4\varepsilon_{ct}$	K_{ct} (M^{-1})	ε_{ct} (M^{-1} cm^{-1})	$\sum(D_{obsd} - D_{calcd})^2 \times 10^4$	T (°C)
2-Phenylfuran	Gr	1862	2.54	733		
	I	1844	2.32	795	0.15	13.0
	Gr	1708	2.34	730		
	I	1695	2.09	811	0.38	18.0
	Gr	1450	1.89	767		
	I	1496	1.76	850	0.17	25.5
	Gr	1331	1.70	783		
	I	1328	1.64	810	0.08	33.5
2-*p*-Tolylfuran	Gr	3570	3.57	1000		
	I	3497	3.02	1158	1.42	13.5
	Gr	3129	2.98	1050		
	I	3056	2.53	1208	1.70	19.0
	Gr	2701	2.42	1112		
	I	2682	2.10	1277	2.31	25.0
	Gr	2271	1.92	1183		
	I	2257	1.71	1320	0.30	34.5
2,5-Diphenylfuran	Gr	10650	21.30	500		
	I	10611	21.48	494	0.58	10.0
	Gr	7280	18.20	400		
	I	7278	17.58	414	0.57	13.0
	Gr	6240	16.00	390		
	I	6216	15.31	406	0.24	21.0
	Gr	7800	11.80	661		
	I	7760	11.60	669	0.63	25.0

*Gr = graphical, I = iterative.

The numerical value of K for the system 2-phenylfuran + TCNE is about five to six times larger than that for the system furan + TCNE. Therefore, the electron donating properties of 2-phenylfuran is much stronger than that of furan alone. Two important conclusions could be drawn from this result. First, the charge transfer complex in both systems is a π complex. If the n contribution has a significant role the basic (electron donor) properties of 2-phenylfuran should not differ from that of furan. Second, the π conjugation in 2-phenylfuran is pronounced (the molecule assumes an all-planar configuration). If the coplanarity of 2-phenylfuran is significantly distorted the charge transfer complex with TCNE should be of similar properties as that of furan + TCNE or benzene + TCNE; this similarity was not found in this work.

*(ii) 2-*p*-Tolylfuran + TCNE System*

To confirm the above results, complex formation between 2-*p*-tolylfuran, as a donor, and TCNE as an acceptor has been investigated by means of spectroscopic methods. The same procedures followed in studying 2-phenylfuran + TCNE were adopted. Results are given in Table 1.

(iii) 2,5-Diphenylfuran + TCNE System

Following the same procedures as above, the complex formation between 2,5-diphenylfuran and TCNE was studied. The charge transfer complex possesses a broad band with a maximum around 720 nm. The values of K and ε_C were calculated as before and results are given in Table 1. It can be seen that the electron donating property of the diphenyl isomer is very pronounced compared with that of the phenylfuran or the tolylfuran. Such a result gives evidence that the donors investigated in this work act as pure π donors and that their planarity is not apparently distorted. The large increase in the value of K for the complex 2,5-diphenylfuran–TCNE compared to those of both phenylfuran or tolylfuran with TCNE is evidence for the quazi rigid conformation of the donor. It also indicates that the size of the donor and acceptor plays a role in strengthening the overlap of the constituents of the molecular complex which in turn increases the stability of the complex.

The correlation between the planarity of the donor and the stability of the charge transfer complex is urged in the following way. Experimentally it is found that the charge transfer complex of either phenylfuran or tolylfuran is more pronounced than that of either furan or benzene with the same acceptor. Consequently, one concludes that phenylfuran and tolylfuran are stronger electron donors

than either furan or benzene. Since in all cases the molecular complex is a π one, then phenylfuran or tolylfuran would be stronger π donors (than benzene or furan) only if the conjugation on the molecule is not disturbed, that is, if the molecule is in an all-planar configuration. In these cases the donors (phenyl or tolylfurans) are described as being quazi rigid conformers and not free rotators. Molecular orbital calculations (15) on 2-phenylfuran supported such a conclusion and have shown that the height of the rotation barrier is of the order of 0.3 eV and that the all-planar conformer of 2-phenylfuran is the most stable one. Using the same way of reasoning one predicts the coplanarity of 2,5-diphenylfuran from the characteristics of its charge transfer complex with TCNE as compared to those of phenylfuran or tolylfuran with the same donor.

(II) Thermodynamic Properties of the Studied Complexes

The iteratively computed values of K at different temperatures were used to calculate ΔG^0 for the complex formation. The relation between $R \ln K$ and $1/T$ was plotted, the computed values of ΔH^0 and ΔS^0 are given in Table 2.

The interaction between the electron donor (D) and the electron acceptor (A) to form the molecular complex (D·A) has been described by Mulliken (16). The ground and excited states of the complex can be described by the wave functions.

$$\Psi_N = \lambda\psi_0(D, A) + \nu\psi_1 (D^+—A^-)$$

$$\Psi_E = \lambda^*\psi_1(D^+—A^-) - \nu^*\psi_0(D, A)$$

where ψ_0 refers to the nonbond wave function and ψ_1 corresponds to the dative-bond wave function. The ratio between the coefficient of the dative bond to the nonbond wave functions is given by (17–19)

$$\nu^2/\lambda^2 = -\Delta H^0/E_{ct}$$

This ratio varied between 0.07–0.19 (Table 2) for the aryl substituted furan + TCNE systems. The value of this ratio is high compared to that of many strong molecular complexes.

(III) Ionization Potentials of the Donors

A general expression deduced by Matsen (20) that relates the energy of the charge transfer transition for the complexes formed by a series of donors with the same acceptor to the donors ionization potential is

$$E_{ct} = mI_D + n$$

where m and n are constants. A number of equations of this form have been suggested to calculate the ionization potential of the donors (20–24). Aloisi *et al.* (25) determined the parameters m and n for a number of acceptors and substituted benzene and polynuclear hydrocarbons as donors. When TCNE is the acceptor, the relation is

$$I_D \text{ (eV)} = 5.21 + 1.65 \times 10^{-4}\nu \text{ (cm}^{-1}\text{)}$$

Ionization potentials calculated from this equation are given in Table 3, values calculated or measured by other methods are not available. However, the values obtained in this work (from charge transfer studies) seem to be reasonable (values do not differ significantly from theoretically calculated ones and the trend of the variation of the determined ionization potentials is in the right direction). A theoretical value for the lowest ionization potential of 2-phenylfuran was calculated from

$$[5] \quad I_D = \sum_{\mu,\nu} C_\mu F_{\mu\nu} C_\nu$$

where the C's are the SCF coefficients of the atomic orbitals and $F_{\mu\nu}$ are the off-diagonal elements of the F matrix (15). The off-diagonal elements, $F_{\mu\nu}$, were calculated using the relation

$$F_{\mu\nu} = \langle X_\mu|f|X_\nu\rangle - \tfrac{1}{2}P_{\mu\nu}\left\langle X_\mu X_\nu \left| \frac{1}{r_{12}} \right| X_\mu X_\nu \right\rangle$$

the symbols have their conventional meanings.

$$\beta_{\mu\nu}^{\text{core}} = \langle X_\mu|f|X_\nu\rangle$$

The resonance integral, $\beta_{\mu\nu}$, is calculated using the formula (26)

$$\beta_{\mu\nu} = [S_{\mu\nu}/(1 + S_{\mu\nu})]\,[(I_\mu + I_\nu)/2]$$

where I's are the appropriate ionization potentials for the atomic orbitals μ and ν. The zero differential overlap approximation was adopted and the electron-repulsion integrals were calculated using the Nishimoto–Mataga relation (27). The following

TABLE 2. Thermodynamic parameters calculated for the studied molecular complexes

Donor	$-\Delta H^0$	$-\Delta S^0$	ν^2/λ^2
2-Phenylfuran	3.13±0.14	9.30±0.49	0.07
3-*p*-Tolylfuran	4.56±0.16	13.72±0.79	0.10
2,5-Diphenylfuran	7.50±1.2	20.45±0.38	0.19

TABLE 3. Ionization potential of the studied phenylfuran calculated from ct results

Donor	$(\lambda_{max})_{ct}$ (nm)	E_{ct}	$h\nu$*	I_D (eV)
2-Phenylfuran	610	2.03	4.48	7.9
2-*p*-Tolylfuran	640	1.94	4.40	7.8
2,5-Diphenylfuran	720	1.72	3.83	7.5

*Energy of the lowest electronic transition of the donor.

parameters were used (28) (eV)

$$\alpha_C = -11.16, \alpha_O = -31.42$$

$$\gamma_{CC} = 11.13, \gamma_{OO} = -16.12$$

A value of 8.6 eV was obtained for the ionization potential of 2-phenylfuran which is slightly higher, but of the same order of magnitude, than the experimental one. The calculations, by means of eq. [5], were done on the basis that the highest occupied MO of 2-phenylfuran is a π one. The correspondance between the two values suggests that the charge transfer complex is a pure π charge transfer complex, that is the highest occupied MO of donors is a π molecular orbital.

A satisfactory empirical relationship exists between the free energy of formation of the complexes, ΔG^0, and the ionization potential of the donor, I_D. For the studied arylfurans + TCNE systems, the relation between ΔG^0 and I_D can be expressed by

$$[6] \qquad \Delta G^0 = 0.013 I_D - 3879 \text{ cal}$$

A linear relationship also exists between the energy of the charge transfer complex (E_{ct}) and ionization potential of the donor for the studied complexes, that may be expressed by the relationship

$$E_{ct} = 0.80 I_D - 4.3 \text{ eV}$$

which can be rearranged to read

$$I_D = 5.4 + 1.55 \times 10^{-4} \nu_{ct} (\text{cm}^{-1})$$

This equation does not differ significantly from that given by Aloisi *et al.* (25) for the molecular complexes of substituted benzene polynuclear hydrocarbons and TCNE.

1. A. R. Cooper, C. W. P. Crowne, and P. G. Farrell. Trans. Faraday Soc. **62**, 13 (1966).
2. R. Foster and P. Hanson. Tetrahedron, **21**, 255 (1965).
3. R. Foster and P. Hanson. Trans. Faraday Soc. **60**, 2189 (1964).
4. E. I. Ginns and R. L. Strong. J. Phys. Chem. **71**, 3059 (1967).
5. Z. Yoshida and T. Kobayashi. Tetrahedron, **26**, 267 (1970).
6. M. Dobrescu-Ciureanu and V. E. Sahini. Rev. Roum. Chim. **18**, 921 (1973).
7. R. P. Lang. J. Am. Chem. Soc. **84**, 4438 (1962).
8. D. C. Ayres and J. R. Smith. J. Chem. Soc. 2737 (1968).
9. W. J. Hale and L. Thorp. J. Am. Chem. Soc. **35**, 71 (1913).
10. S. Kapf and C. Paal. Ber. **21**, 3057 (1888).
11. R. Abu-Eittah and F. Al Sugeir. Can. J. Chem. **54**, 3705 (1976).
12. R. L. Scott. Recl. Trav. Chim. **75**, 787 (1956).
13. H. A. Benesi and J. H. Hildebrand. J. Am. Chem. Soc. **71**, 2703 (1949).
14. H. H. Rosenbrock. Compt. J. **3**, 175 (1960); H. H. Rosenbrock and C. Storey. Computational techniques for chemical engineers. Pergamon Press, London. 1966.
15. M. M. Hamed. Ph.D. Thesis. University of Cairo, Giza, Egypt. 1978.
16. R. S. Mulliken. J. Am. Chem. Soc. **72**, 600 (1950); **74**, 811 (1952); J. Phys. Chem. **56**, 801 (1952).
17. M. Tamres and M. Brandon. J. Am. Chem. Soc. **82**, 2134 (1960).
18. J. A. A. Ketelaar. J. Phys. Radium, **15**, 197 (1954).
19. G. Briegleb. Elektronen–Donator–Acceptor Komplexe. Springer Verlag, Berlin. 1961.
20. F. A. Matsen. J. Chem. Phys. **24**, 602 (1956).
21. R. Foster. Organic charge transfer complexes. Academic Press, London. 1969.
22. R. S. Mulliken and W. B. Person. Molecular complexes. A lecture and reprint volume. Wiley, New York. 1969.
23. (*a*) E. M. Voigt and C. Reid. J. Am. Chem. Soc. **86**, 3930 (1964); (*b*) G. Briegleb. Angew. Chem. Int. Ed. **3**, 617 (1964).
24. P. G. Farrell and J. Newton. J. Phys. Chem. **69**, 3506 (1965).
25. G. G. Aloisi, S. Santini, and S. Sorriso. J. Chem. Soc. Faraday, **70**, 1908 (1974).
26. G. Rasch. Z. Chem. **2**, 347 (1962).
27. I. Fischer-Hjalmars. *In* Molecular orbitals in chemistry, physics and biology. *Edited by* P. O. Lowdin. Academic Press, New York. 1964. p. 361.
28. R. L. Flurry, Jr. Molecular orbital theories of bonding in organic molecules. Marcel Dekker, Inc., New York. 1968.

Some reactions of 1,2-dihydropyridines with organic azides. Synthesis of diazabicylo-[4.1.0]hept-4-enes, 1,2,5,6-tetrahydropyridylidene-2-cyan (sulfon, carbon) amides, and piperidylidene-2-cyan (sulfon, carbon) amides

T. A. ONDRUS AND E. E. KNAUS[1]

Faculty of Pharmacy and Pharmaceutical Sciences, University of Alberta, Edmonton, Alta., Canada T6G 2N8

AND

C. S. GIAM

Department of Chemistry, Texas A & M University, College Station, TX 77843, U.S.A.

Received March 19, 1979

T. A. ONDRUS, E. E. KNAUS, and C. S. GIAM. Can. J. Chem. **57**, 2342 (1979).

The regiospecific 1,3-dipolarcycloaddition reaction of 1,2-dihydropyridines **1** with organic azides **2** afford 2,7-diazabicyclo[4.1.0]hept-4-enes **4**, whereas solutions of **1** also containing lithium hydroxide give predominately **4** along with the diazo product **6**. In contrast, the dimeric product **7** was obtained from the reaction of **1***a* with hydrazoic acid. Catalytic hydrogenation of **4** gives rise to a tautomeric mixture of **9** and **10**; when R^2 is methanesulfonyl or *p*-aminobenzenesulfonyl only **9** was obtained. Treatment of **4** with neutral alumina gives rise to the 1,2,5,6-tetrahydropyridylidenes **8** which are likewise reduced to a mixture of **9** and **10** or **9**.

T. A. ONDRUS, E. E. KNAUS et C. S. GIAM. Can. J. Chem. **57**, 2342 (1979).

La réaction de cycloaddition dipolaire-1,3 régiospécifique des dihydro-1,2 pyridines (**1**) avec les azotures organiques (**2**) conduit aux diaza-2,7 bicyclo[4.1.0]heptènes-4 (**4**) alors que des solutions de **1** contenant de l'hydroxyde de lithium conduisent à la formation prédominante de **4** aux côtés du diazo **6**. Par opposition, on obtient le produit dimère **7** lors de la réaction de **1***a* avec l'acide hydrazoïque. L'hydrogénation catalytique de **4** donne lieu à la formation du mélange tautomère de **9** et **10**; si R^2 est le méthanesulfonyle ou le *p*-aminobenzènesulfonyle, on n'obtient que le composé **9**. Si l'on traite **4** avec de l'alumine neutre, on obtient les tétrahydro-1,2,5,6 pyridylidènes (**8**) qui sont aussi réduits en un mélange de **9** et **10** ou **9**.

The 1,3-dipolarcycloaddition reaction of dienamines with organic azides is an attractive method for the synthesis of pharmacologically interesting bicyclic compounds. Mitomycin C is one of the few examples where a fused aziridine ring is an active alkylating agent. Most aziridinyl quinones active as antitumor agents possess multiple aziridinyl groups (1) and are known to cross-link DNA (2). It was therefore of interest to prepare bicyclic ring structures in which 1,2,3-triazoline or aziridine is fused to a tetrahydropyridine ring.

In earlier studies we showed that reaction of *N*-methoxycarbonyl (methanesulfonyl, acetyl)-1,2-dihydropyridines with cyanogen azide gave a 1:1 mixture of stereoisomers *E*- and *Z*-1,2,3,4-tetrahydropyridylidene-4-cyanamides (3). The regiospecific 1,3-dipolarcycloaddition reaction of dienamines **1** with organic azides **2** now provides a quantitative route to 2,7-diazabicyclo[4.1.0]hept-4-enes **4**. A preliminary account of this work has been published (4).

Reaction of 2-butyl-1,2-dihydropyridine **1***a* (lithium hydroxide free) with cyanogen azide **2***a* at 0°C under an atmosphere of nitrogen proceeds rapidly with evolution of nitrogen to yield 3-*n*-butyl-7-cyano-2,7-diazabicyclo[4.1.0]hept-4-ene **4***a* in quantitative yield (see Scheme 1).[2] Under similar conditions **1***b* gave **4***b* (100%). Although the cycloaddition reaction may occur at either the C3—C4 and (or) C5—C6 olefinic bonds no addition product other than **4** was detected (4). If the triazoline intermediate **3** is the product of electronic control the nitrogen atom bearing the R^2-substituent should be directed to the carbon of the enamine double bond bearing the enamine ring nitrogen (5). The reacting species in all of these reactions is the molecular organic azide since loss of nitrogen to give nitrenes occurs above 40°C (6). Similar reactions of 2-butyl-1,2-

[1]To whom inquiries should be addressed.

[2]The preparation of 1,2-dihydropyridines **1** by hydrolysis of the corresponding *N*-lithio-1,2-dihydropyridine with 1 equiv. of water produces 1 equiv. of lithium hydroxide. Although most of the lithium hydroxide rapidly precipitates out of anhydrous ether or tetrahydrofuran, about 5% remains suspended in the solvent. The suspended lithium hydroxide is completely removed if an excess of water is added followed by drying with anhydrous sodium sulfate.

0008-4042/79/182342-08$01.00/0

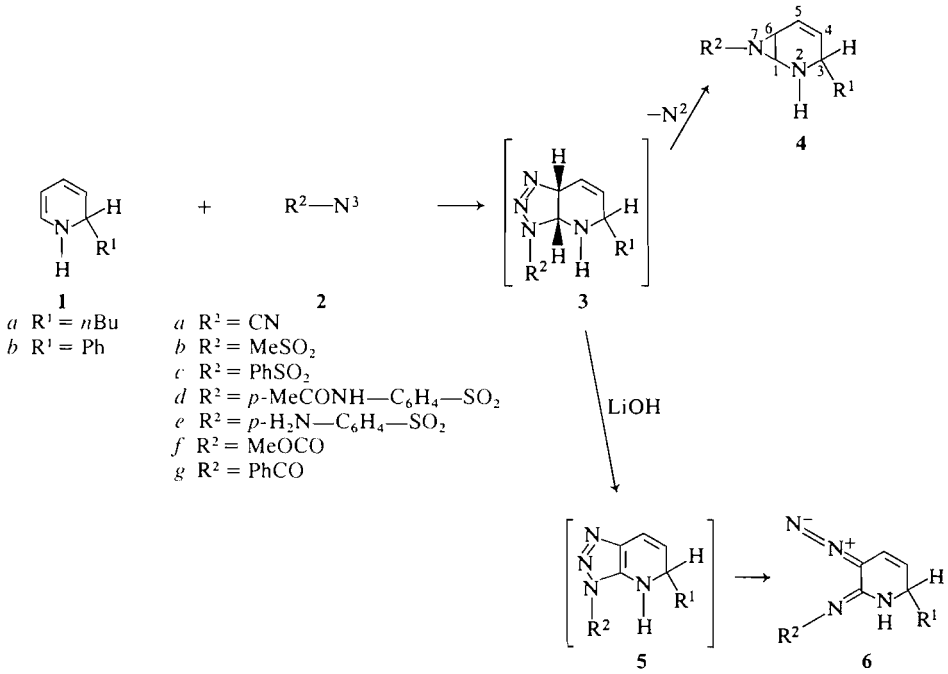

SCHEME 1. Substituents R^1 and R^2 for **4** and **6** are as illustrated in Table 1.

dihydropyridine **1***a* (lithium hydroxide free) with methanesulfonyl **2***b*, benzenesulfonyl **2***c*, *p*-acetamidobenzenesulfonyl **2***d*, *p*-aminobenzenesulfonyl **2***e*, and methoxycarbonyl **2***f* azides also afforded **4** in quantitative yields (see Table 1). On the other hand, reaction of **1***a* containing 0.05 equiv. lithium hydroxide[2] with sulfonyl azides **2***b–e* gave **4** as well as the unexpected 3-diazo-1,2,3,6-tetrahydropyridylidene-2-sulfonamides **6**. The most plausible mechanism for the formation of **6** involves base catalyzed proton abstraction of one of the bridgehead protons of the triazoline adduct **3**. Elimination of hydride would then afford the more aromatic 1,2-dihydropyridine triazole intermediate **5** which could ring open to give **6**. A similar mechanism has been proposed for opening of the adducts obtained from reactions of organic azides and ethoxyacetylene (7, 8).

The reaction of **1***a* with benzoyl azide **2***g* (5 equiv.) was also investigated. Although the ^1H nmr spectrum of the unpurified reaction product exhibited signals expected for 3-*n*-butyl-7-benzoyl-2,7-diazabi-

TABLE 1. Reaction of 1,2-dihydropyridines with organic azides

Compound	1,2-Dihydropyridine (R^1)	Organic azide (R^2)	Yield (%) 4	Yield (%) 6
a	*n*Bu	CN	100	
	*n*Bu[a]	CN	79	
b	Ph	CN	100	
c	*n*Bu	$MeSO_2$	100	
	*n*Bu[a]	$MeSO_2$	42.9	17.5
d	*n*Bu	$PhSO_2$	100	
	*n*Bu[a]	$PhSO_2$	40.7	34.1
e	*n*Bu	*p*-MeCONH—C_6H_4—SO_2	100	
	*n*Bu[a]	*p*-MeCONH—C_6H_4—SO_2	79	12.5
f	*n*Bu	*p*-H_2N—C_6H_4—SO_2	100	
	*n*Bu[a]	*p*-H_2N—C_6H_4—SO_2	78.5	1.3
g	*n*Bu	MeOCO	100	

[a]Solution of **1***a* contains 5% of the lithium hydroxide formed upon treatment of *N*-lithio-2-butyl-1,2-dihydropyridine with 1 equiv. water.

cyclo[4.1.0]hept-4-ene **4**, the only product recovered after preparative silica gel G tlc was the ring opened product **8** (R^1 = *n*Bu, R^2 = PhCO) (39.7%).

Treatment of **1***a* with hydrazoic acid yielded the unexpected 6,6′-di-*n*-butyl-1,2,3,6-tetrahydro-2,3′-dipyridyl **7** (64.7%) and 2-*n*-butylpyridine (12.2%). The most likely mechanism for the formation of **7** involves protonation of **1***a* at the C5 position by hydrazoic acid to give a 2,5-dihydropyridyl imminium species which could undergo nucleophilic attack at its highly electrophilic C6 position by **1***a*. Subsequent aromatization of the 2,5-dihydropyridine dimeric intermediate would afford **7**.

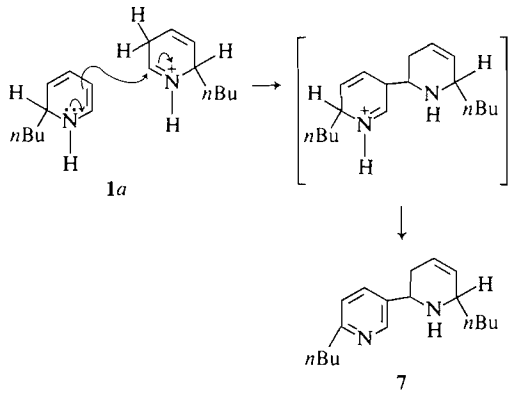

1*a* **7**

Neutral aluminum oxide chromatography (Brockman Activity 1) of the 2,7-diazabicyclo[4.1.0]hept-4-enes **4** gives rise to 1,2,5,6-tetrahydropyridylidene-2-cyan (sulfon) amides **8** in good yield (see Table 2). One possible mechanism for the formation of the alkylidene-2-cyan (sulfon) amides **8** may involve initial abstraction of the active C(1)H of **4** followed by opening of the aziridine ring and migration of the olefinic bond. Triethylamine also catalyzes the conversion of **4** to **8**. On the other hand, chromatography of **4***a* (R^1 = *n*Bu, R^2 = CN) on an acidic alumina (Brockman Activity 1) column gave **8***a* (7.7%) and unchanged **4***a* (92.3%). In contrast silica gel G tlc of **4***g* (R^1 = *n*Bu, R^2 = MeOCO) gives a quantitative yield of **8***e*.

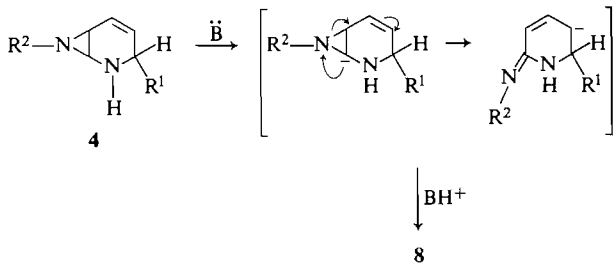

4 **8**

Hydrogenation of 7-cyano (methoxycarbonyl)-2,7-diazabicyclo[4.1.0]hept-4-enes **4** with 10% palladium on charcoal and hydrogen gas at 35 psi gives a tautomeric mixture of piperidylidene-2-cyan (methoxycarbonyl) amide **9** and 3,4,5,6-tetrahydropyridyl-2-cyan (methoxycarbonyl) amide **10** (see Scheme 2 and Table 2). The ultraviolet spectrum of the tautomeric mixture **9***f* ⇌ **10***f* (R^1 = *n*Bu, R^2 = CN) exhibited one band at 244 nm attributed to the Ṅ—C=N group. The infrared spectrum shows the presence of two NH bands. The piperidine NH of **9***f* exhibits an absorption at 3240 cm^{-1} while the cyanamide **10***f* displays a NH absorption at 3120 cm^{-1}. The spectrum also displays a cyano band at 2180 cm^{-1} and imine bands at 1605 cm^{-1} due to **9***f* and at 1645 cm^{-1} due to **10***f*. The existence of a similar tautomeric equilibrium between piperidylidene-2-ethoxycarbonylamide and 3,4,5,6-tetrahydropyridyl-2-ethoxycarbonylamide has been reported (9). On the other hand, catalytic hydrogenation of **4***c* (R^1 = *n*Bu, R^2 = $MeSO_2$) afforded 6-*n*-butylpiperidylidene-2-methanesulfonamide **9***h* (91.8%) and 6-*n*-butylpyridyl-2-methanesulfonamide **11** (7.5%). The infrared spectrum of **9***h* lacked those absorptions expected for tautomer **10***h*. 6-*n*-Butylpyridyl-2-methanesulfonamide **11** likely arises as a result of dehydrogenation of an intermediate **8***c* (9). In a similar reaction, hydrogenation of **4***f*, possessing an R^2 *p*-aminobenzenesulfonyl group, afforded **9***i* in quantitative yield.

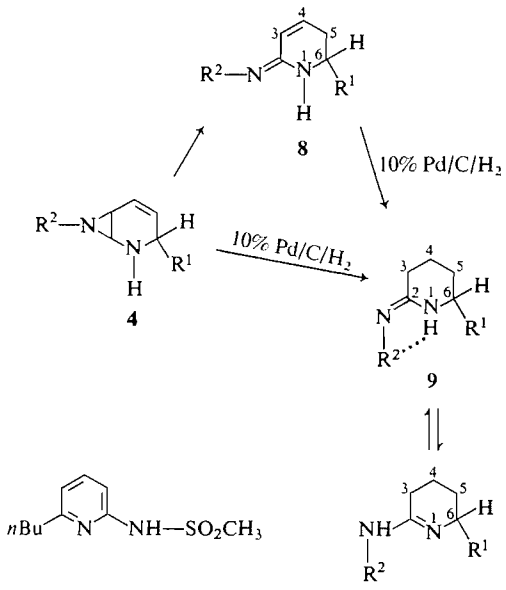

SCHEME 2. Substituents R^1 and R^2 for **8**, **9**, and **10** are as illustrated in Table 2.

Hydrogenation of 6-*n*-butyl-1,2,5,6-tetrahydropyridylidene-2-cyan (methanesulfon) amides **8** gave products identical to those obtained from reduction of **4**. For example, hydrogenation of **8***a* (R^1 = *n*Bu, R^2 = CN) gave a tautomeric mixture of **9***f* and **10***f*

TABLE 2. Chemical transformation of 3-substituted-2,7-diazabicyclo[4.1.0]hept-4-enes **4**

Compound	Procedure	R^1	R^2	Yield (%) 8	9 ⇋ 10	11
a	Neutral Al_2O_3 chrom. of **4**	*n*Bu	CN	79		
b	Al_2O_3 catalyzed opening of **4**	Ph	CN	100		
c	Neutral Al_2O_3 chrom. of **4**	*n*Bu	$MeSO_2$	100		
d	Neutral Al_2O_3 chrom. of **4**	*n*Bu	*p*-H_2N—C_6H_4—SO_2	92		
e	Silica gel G tlc of **4**	*n*Bu	MeOCO	100		
f	Pd/C/H_2 reduction of **4**	*n*Bu	CN		100	
g	Pd/C/H_2 reduction of **4**	Ph	CN		100	
h	Pd/C/H_2 reduction of **4**	*n*Bu	$MeSO_2$		91.8[a]	7.5
i	Pd/C/H_2 reduction of **4**	*n*Bu	*p*-H_2N—C_6H_4—SO_2		100[a]	
j	Pd/C/H_2 reduction of **4**	*n*Bu	MeOCO		63.4	
f	Pd/C/H_2 reduction of **8**	*n*Bu	CN		100	
h	Pd/C/H_2 reduction of **8**	*n*Bu	$MeSO_2$		91.5[a]	7.8

[a]The ir and ^{1}H nmr spectra exhibited absorptions only for tautomer **9**.

while hydrogenation of **8***c* (R^1 = *n*Bu, R^2 = $MeSO_2$) afforded **9***h* (91.5%) and the aromatic sulfonamide **11** (7.8%) (see Table 2).

Acid hydrolysis of a tautomeric mixture of **9***g* and **10***g* (R^1 = Ph, R^2 = CN) using a 10% H_2SO_4/MeOH solution (1:10 v/v) gave 6-phenyl-2-piperidone **12** (39%), thereby providing further evidence in support of structures **9** and **10**. The appearance

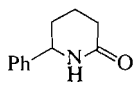

12

of the carbonyl band of **12** at 1640 cm^{-1} is in good agreement with that of 2-piperidone which appears at 1653 cm^{-1}. The carbonyl group of *N*-ethyl-3-piperidone hydrochloride appears at 1724 cm^{-1} (Aldrich Library of IR spectra).

The reactions of organic azides with 1,4-dihydropyridines are now in progress to broaden the scope of this reaction.

Experimental

Melting points were determined with a Büchi capillary apparatus and are uncorrected. Ultraviolet spectra were recorded on a Unicam SP 1800 spectrometer using absolute ethanol as solvent. Infrared spectra (potassium bromide unless otherwise noted) were taken on a Perkin-Elmer 267 or Unicam SP 1000 spectrometer. Nuclear magnetic resonance spectra were determined for solutions in deuterochloroform with TMS as internal standard with a Varian EM-360 spectrometer. Mass spectra were measured with an AEI-MS-50 mass spectrometer and these exact mass measurements are used in lieu of elemental analysis. All of the products described gave rise to a single spot on tlc using a solvent system less polar and more polar than the spectific solvent system described for purification of the reaction mixture. No residue remained after combustion of the products purified by the chromatographic procedures used. *Warning*: Cyanogen azide is a hazardous material. It should be handled only in solution. Concentration to pure material will result in violent detonation by heat or shock (10).

*2-*n*-Butyl-1,2-dihydropyridine (**1**a)*

To a solution of *n*-butyllithium (1.28 g, 20 mmol) in 50 mL anhydrous ether, under a nitrogen atmosphere at 0°C, pyridine (1.58 g, 20 mmol) was added dropwise with stirring. The resulting dark brown solution was stirred at 0°C for 35 min to afford *N*-lithio-2-*n*-butyl-1,2-dihydropyridine (20 mmol).

The dropwise addition of water (0.36 g, 20 mmol) with stirring at 0°C to the above solution afforded 2-*n*-butyl-1,2-dihydropyridine **1***a*. Removal of the supernatant via a syringe provided a solution of **1***a* containing about 0.05 equiv. suspended lithium hydroxide.

*2-*n*-Butyl-1,2-dihydropyridine (**1**a, Lithium Hydroxide Free)*

To a solution of *N*-lithio-2-*n*-butyl-1,2-dihydropyridine (4.29 g, 30 mmol), prepared from *n*-butyllithium (30 mmol) and pyridine (30 mmol) as described above, in 100 mL anhydrous ether under a nitrogen atmosphere, water (2.0 g, 110 mmol) was added dropwise with stirring at 0°C. The resulting pale yellow solution of **1***a* was stirred for 10 min, anhydrous sodium sulfate (25 g) was added, and the mixture was stirred for an additional 15 min at 0°C. The solution was allowed to stand without agitation for 5 min after which an aliquot of the supernatant containing the required amount of **1***a* was removed using a syringe under a nitrogen atmosphere.

*3-*n*-Butyl-7-cyano-2,7-diazabicyclo[4.1.0]hept-4-ene (**4**a)*

A solution of lithium hydroxide free **1***a* (2.74 g, 20 mmol) in 67 mL dry ether was added slowly with stirring to a solution of cyanogen azide (25 mmol), prepared from cyanogen bromide (2.65 g, 25 mmol) and sodium azide (8.125 g, 125 mmol) as reported previously (3), in 100 mL acetonitrile under a nitrogen atmosphere at 0°C. The reaction was allowed to proceed at 0°C for 1 h prior to warming to 25°C. Removal of the solvent *in vacuo* gave a light orange solid which on recrystallization from 100 mL ether–hexane (1:4 v/v) afforded **4***a* (3.54 g, 100%); mp 75°C; ir: 3225 (m, NH), 2180 (s, C≡N), and 1605 (s, C=C) cm^{-1}; ^{1}H nmr δ: 0.9 (t, J = 7 Hz, 3H, $CH_2CH_2CH_2CH_3$), 1.1–1.9 (m, 6H, $CH_2CH_2CH_2CH_3$), 3.21 (m, 1H, H-6), 3.3 (m, 1H, H-1), 4.17 (m, 1H, H-3), 5.8 (m, 2H, H-4, H-5), 8.63 (b s, 1, NH, exchanges with deuterium oxide). *Exact Mass* calcd. for $C_{10}H_{15}N_3$: 177.1266; found (high resolution ms): 177.1265. Reaction of **1***a* (20 mmol), containing lithium hydroxide (1 mmol), with cyanogen azide (40 mmol) as described above afforded **4***a* (79%).

*3-Phenyl-7-cyano-2,7-diazabicyclo[4.1.0]hept-4-ene (**4**b)*

A solution of lithium hydroxide free **1***b* (3.1 g, 20 mmol) in

100 mL dry tetrahydrofuran[3] was added slowly with stirring to a solution of cyanogen azide (20 mmol) in 100 mL acetonitrile under a nitrogen atmosphere at 0°C. The reaction was maintained at 0°C for 1 h and after warming to 25°C removal of the solvent *in vacuo* gave an orange solid. Recrystallization from 100 mL ether–hexane (1:4 v/v) yielded **4***b* (3.94 g, 100%); mp 147°C; ir: 3235 (m, NH), 2180 (s, C≡N), and 1610 (s, C=C) cm^{-1}; ^1H nmr δ: 3.2 (m, 1H, H-6), 3.3 (m, 1H, H-1), 5.08 (m, 1H, H-3), 5.77 (m, 2H, H-4, H-5), 7.26 (m, 5H, C_6H_5), 7.82 (b s, 1, NH, exchanges with deuterium oxide). *Exact Mass* calcd. for $C_{12}H_{11}N_3$: 197.0953; found (high resolution ms): 197.0954.

*3-*n*-Butyl-7-methanesulfonyl-2,7-diazabicyclo[4.1.0]hept-4-ene (**4**c) and 6-*n*-Butyl-3 diazo-1,2,3,6-tetrahydropyridylidene-2-methanesulfonamide (**6**c)*

A solution of **1***a* (2.74 g, 20 mmol) containing lithium hydroxide (0.024 g, 1 mmol) in 50 mL dry ether was added slowly with stirring to a solution of methanesulfonyl azide (2.42 g, 20 mmol) in 50 mL dry ether under a nitrogen atmosphere at 0°C. The reaction was allowed to proceed 1 h at 0°C before warming to 25°C. Addition of water (50 mL), extraction with chloroform (2 × 50 mL), drying (sodium sulfate), and removal of the solvent *in vacuo* afforded a reddish black semi-solid which was subjected to preparative tlc on six 8 in × 8 in. silica gel G plates, 0.75 mm in thickness, using benzene – ethyl acetate (2:1 v/v) as development solvent. Extraction with warm methanol (50 mL) of the band having R_f 0.59 gave **6***c* (0.894 g, 17.5%); ir: 3290 (m, NH), 2090 (s, N_2), and 1580 (s, C=N) cm^{-1}; ^1H nmr δ: 0.96 (t, J = 7 Hz, 3H, $CH_2CH_2CH_2CH_3$), 1.15–1.85 (m, 6H, $CH_2CH_2CH_2CH_3$), 3.02 (s, 3H, SO_2CH_3), 4.33 (m, 1H, H-6), 5.3 (d, $J_{4,5}$ = 10 Hz of d, $J_{5,6}$ = 4 Hz of d, $J_{1,5}$ = 1.5 Hz, 1H, H-5), 6.11 (d, $J_{4,5}$ = 10 Hz of d, $J_{4,6}$ = 1.5 Hz, 1H, H-4), 8.1 (b s, 1H, NH, exchanges with deuterium oxide). *Exact Mass* calcd. for $C_{10}H_{16}N_4O^{32}S$: 256.0994; found (high resolution ms): 256.0984. Extraction of the band with R_f 0.51 afforded 2-*n*-butyl pyridine (0.21 g, 7.7%). Extraction of the band with R_f 0.36 yielded **4***c* (1.974 g, 42.9%); ir: 3280 (m, NH) and 1600 (s, C=C) cm^{-1}; ^1H nmr δ: 0.9 (t, J = 7 Hz, 3H, $CH_2CH_2CH_2CH_3$), 1.1–1.8 (m, 6H, $CH_2CH_2CH_2CH_3$), 2.93 (s, 3H, SO_2CH_3), 3.06 (m, 2H, H-1, H-6), 4.05 (m, 1H, H-3), 5.76 (m, 2H, H-4, H-5), 8.40 (b s, 1, NH, exchanges with deuterium oxide). *Exact Mass* Calcd. for $C_{10}H_{18}N_2O_2{}^{32}S$: 230.1089; found (high resolution ms): 230.1085.

Reaction of lithium hydroxide free **1***a* (2.7 g, 20 mmol) in 67 mL dry ether with methanesulfonyl azide (2.42 g, 20 mmol) in 50 mL dry ether under a nitrogen atmosphere at 0°C was allowed to proceed for 1 h prior to warming to 25°C. Removal of the solvent *in vacuo* gave **4***c* (4.6 g, 100%); identical (ir, ^1H nmr) with the same product described above.

*3-*n*-Butyl-7-benzenesulfonyl-2,7-diazabicyclo[4.1.0]hept-4-ene (**4**d) and 6-*n*-Butyl-3-diazo-1,2,3,6-tetrahydropyridylidene-2-benzenesulfonamide (**6**d)*

A solution of **1***a* (2.74 g, 20 mmol) containing lithium hydroxide (0.024 g, 1 mmol) in 50 mL of dry ether was added slowly with stirring to a solution of benzenesulfonyl azide (3.67 g, 20 mmol) in 50 mL dry ether under a nitrogen atmosphere at 0°C. The reaction was allowed to proceed 1 h at 0°C before warming to 25°C. Addition of water (50 mL), extraction with chloroform (2 × 50 mL), drying (Na_2SO_4), and removal of the solvent *in vacuo* afforded a reddish black semi-solid which was subjected to preparative tlc using six 8 in. × 8 in. silica gel G plates, 0.75 mm in thickness, with benzene – ethyl acetate (4:1 v/v) as development solvent. Extraction of the band having R_f 0.68 using warm methanol (50 mL) gave **6***d* (2.17 g, 34.1%); mp: 103–104°C (dec. with evolution of gas); ir: 3280 (m, NH), 2090 (s, N_2), and 1570 (s, C=N) cm^{-1}; ^1H nmr δ: 0.85 (t, J = 7 Hz, 3H, $CH_2CH_2CH_2CH_3$), 1.05–1.8 (m, 6H, $CH_2CH_2CH_2CH_3$), 4.3 (m, 1H, H-6), 5.2 (d, $J_{4,5}$ = 10.5 Hz of d, $J_{5,6}$ = 4 Hz of d, $J_{1,5}$ = 1.5 Hz, 1H, H-5), 6.04 (d, $J_{4,5}$ = 10.5 Hz of d, $J_{4,6}$ = 1.25 Hz, 1H, H-4), 7.5 (m, 3, *meta* and *para* phenyl hydrogens), 7.98 (m, 2, *ortho* phenyl hydrogens), 8.26 (b s, 1, NH, exchanges with deuterium oxide). *Exact Mass* calcd. for $C_{15}H_{18}N_4O_2{}^{32}S$: 318.1150; found (high resolution ms): 318.1137. *Anal.* calcd. for $C_{15}H_{18}N_4O_2{}^{32}S$: C 56.58, H 5.70, N 17.6, O 10.05, S 10.07; found: C 56.48, H 5.72, N 17.6, O 9.87, S 10.04. Extraction of the band with R_f 0.53 afforded **4***d* (2.38 g, 40.7%); mp: 106°C; ir: 3205 (m, NH) and 1600 (s, C=C) cm^{-1}; ^1H nmr δ: 0.88 (t, J = 7 Hz, 3H, $CH_2CH_2CH_2CH_3$), 1.1–1.8 (m, 6H, $CH_2CH_2CH_2CH_3$), 3.06 (m, 2H, H-1, H-6), 4.07 (m, 1H, H-3), 5.72 (m, 2H, H-4, H-5), 7.5 (m, 3, *meta* and *para* phenyl hydrogens), 7.98 (m, 2, *ortho* phenyl hydrogens), 8.78 (b s, 1, NH, exchanges with deuterium oxide). *Exact Mass* calcd. for $C_{15}H_{20}N_2O_2{}^{32}S$: 292.1245; found (high resolution ms): 292.1232.

Reaction of lithium hydroxide free **1***a* (2.7 g, 20 mmol) in 67 mL dry ether with benzenesulfonyl azide (3.67 g, 20 mmol) in 50 mL dry ether under a nitrogen atmosphere at 0°C was allowed to proceed for 1 h prior to warming to 25°C. Removal of the solvent *in vacuo* gave **4***d* (5.84 g, 100%) identical (ir, ^1H nmr) with the same compound described above.

*3-*n*-Butyl-7-(N-acetyl)sulfanilyl-2,7-diazabicyclo[4.1.0]hept-4-ene (**4**e) and 6-*n*-Butyl-3-diazo-1,2,3,6-tetrahydropyridylidene-2-(N-acetyl)sulfanilamide (**6**e)*

A solution of **1***a* (1.37 g, 10 mmol) containing lithium hydroxide (0.012 g, 0.5 mmol) in 50 mL dry ether was added slowly with stirring to a solution of *N*-acetylsulfanilyl azide (2.42 g, 10 mmol) in 75 mL ether–acetonitrile (2:1 v/v) under a nitrogen atmosphere at 0°C. The reaction was allowed to proceed 1 h at 0°C before warming to 25°C. Addition of water (50 mL), extraction with chloroform (2 × 50 mL), drying (Na_2SO_4), and removal of the solvent *in vacuo* afforded a red semi-solid which was subjected to preparative tlc on six 8 in. × 8 in. silica gel G plates, 0.75 mm in thickness, using benzene – ethyl acetate (1:2 v/v) as development solvent. Extraction of the band having R_f 0.45 with warm methanol (50 mL) gave **6***e* (0.471 g, 12.5%); mp: 77°C (dec. with evolution of a gas); ir: 3300 (m, NH), 3180 (m, NH), 2090 (s, =N_2), and 1585 (s, C=N) cm^{-1}; ^1H nmr δ: 0.8 (m, 3H, $CH_2CH_2CH_2CH_3$), 1.05–1.8 (m, 6H, $CH_2CH_2CH_2CH_3$), 2.17 (s, 3H, $COCH_3$), 4.26 (m, 1H, H-6), 5.2 (d, $J_{4,5}$ = 10 Hz of d, $J_{5,6}$ = 4 Hz of d, $J_{1,5}$ = 1.25 Hz, 1H, H-5), 5.98 (d, $J_{4,5}$ = 10 Hz of d, $J_{4,6}$ = 1.25 Hz, 1H, H-4), 7.73 (m, 4H, C_6H_4), 8.1 (b s, 1, NH, exchanges with deuterium oxide), 8.68 (b s, 1, CONH, exchanges with deuterium oxide). *Exact Mass* calcd. for $C_{17}H_{21}N_3O_3{}^{32}S$: 347.1304 ($M^+$ − 28 due to loss of N_2); found (high resolution ms): 347.1304. Extraction of the band at R_f 0.26 yielded **4***e* (2.76 g, 79%), mp 126°C; ir: 3300 (m, NH), 3180 (m, NH), 1675 (s, C=O), and 1590 (s, C=C) cm^{-1}; ^1H nmr δ: 0.9 (t, J = 7 Hz), 3H, $CH_2CH_2CH_2CH_3$), 1.05–1.8 (m, 6H, $CH_2CH_2CH_2CH_3$), 2.18 (s, 3H, $COCH_3$), 3.06 (m, 2H, H-1, H-6), 4.1 (m, 1H, H-3), 5.75 (m, 2H, H-4, H-5), 7.8 (m, 4H, C_6H_4), 8.7 (b s, 1, NH, exchanges with deuterium oxide), 9.0 (s, 1H, CONH, exchanges with deuterium oxide). *Exact Mass* calcd. for $C_{17}H_{23}N_3O_3{}^{32}S$: 349.1460; found (high resolution ms): 349.1463.

Reaction of lithium hydroxide free **1***a* (0.685 g, 5 mmol) in 17 mL dry ether with *N*-acetylsulfanilyl azide **2***d* (1.2 g, 5 mmol) in 50 mL ether–acetonitrile (2:1 v/v) under a nitrogen

[3]Lithium hydroxide free 2-phenyl-1,2-dihydropyridine **1***b* is prepared by the same procedure as **1***a* except phenyllithium is used in place of *n*-butyllithium.

atmosphere at 0°C was allowed to proceed for 1 h prior to warming to 25°C. Removal of the solvent *in vacuo* gave **4***e* (1.75 g, 100%), identical (ir, ^{1}H nmr) with the same compound described above.

*3-*n*-Butyl-7-sulfanilyl-2,7-diazabicyclo[4.1.0]hept-4-ene (**4**f) and 6-*n*-Butyl-3-diazo-1,2,3,6-tetrahydropyridylidene-2-sulfanilamide (**6**f)*

A solution of **1***a* (1.37 g, 10 mmol) containing lithium hydroxide (0.012 g, 0.5 mmol) in 50 mL dry ether was added slowly with stirring to a solution of sulfanilyl azide **2***e* (1.98 g, 10 mmol) in 50 mL ether under a nitrogen atmosphere at 0°C. The reaction was allowed to proceed for 1 h at 0°C before warming to 25°C. Addition of water (50 mL), extraction with chloroform (2 × 50 mL), drying (Na_2SO_4), and removal of the solvent *in vacuo* afforded an orange solid which was subjected to preparative tlc on six 8 in. × 8 in. silica gel G plates, 0.75 mm in thickness, using benzene – ethyl acetate (1:2 v/v) as development solvent. Extraction of the fraction having R_f 0.88 using 50 mL warm methanol gave **6***f* (0.042 g, 1.3%), mp 134°C (dec. with evolution of a gas); ir: 3460 (m, NH_2), 3360 (m, NH_2), 3310 (m, NH), 2090 (s, N_2), and 1590 (s, C=N) cm^{-1}; ^{1}H nmr δ: 0.88 (t, J = 7 Hz, 3H, $CH_2CH_2CH_2CH_3$), 1.05–1.8 (m, 6H, $CH_2CH_2CH_2CH_3$), 4.27 (m, 3H, H-6, NH_2, exchanges with deuterium oxide), 5.2 (d, $J_{4,5}$ = 10 Hz of d, $J_{5,6}$ = 4 Hz of d, $J_{1,5}$ = 1.5 Hz, 1H, H-5), 6.0 (d, $J_{4,5}$ = 10 Hz of d, $J_{4,6}$ = 1.25 Hz, 1H, H-4), 6.68 (m, 2H, *ortho* amino phenyl hydrogens), 7.72 (m, 2H, *ortho* sulfonyl phenyl hydrogens), 8.16 (b s, 1, NH, exchanges with deuterium oxide). *Exact Mass* calcd. for $C_{15}H_{19}N_3O_2{}^{32}S$: 305.1194 ($M^+$ − 28 due to loss of N_2); found (high resolution ms): 305.1195. Extraction of the band having R_f 0.54 afforded **4***f* (2.41 g, 78.5%), mp 132°C; ir: 3460 (m, NH_2), 3360 (m, NH_2), 3290 (m, NH), and 1590 (s, C=C) cm^{-1}; ^{1}H nmr (DMSO-d_6) δ: 0.87 (t, J = 7 Hz, 3H, $CH_2CH_2CH_2CH_3$), 1.1–1.8 (m, 6H, $CH_2CH_2CH_2CH_3$), 3.0 (m, 2H, H-1, H-6), 4.1 (m, 1H, H-3), 4.8 (b s, 2H, NH_2, exchanges with deuterium oxide), 5.71 (m, 2H, H-4, H-5), 6.7 (m, 2H, *ortho* amino-phenyl hydrogens), 7.65 (m, 2H, *ortho* sulfonyl phenyl hydrogens), 8.6 (b s, 1H, NH, exchanges with deuterium oxide). *Exact Mass* calcd. for $C_{15}H_{21}N_3O_2{}^{32}S$: 307.1355; found (high resolution ms): 307.1353.

Reaction of lithium hydroxide free **1***a* (0.274 g, 2 mmol) in 7 mL dry ether with sulfanilyl azide **3***e* (0.396 g, 2 mmol) in 50 mL dry ether under a nitrogen atmosphere at 0°C was allowed to proceed for 1 h prior to warming to 25°C. Removal of the solvent *in vacuo* gave **4***f* (0.614 g, 100%), identical (ir, ^{1}H nmr) with the same compound described above.

*3-*n*-Butyl-7-methoxycarbonyl-2,7-diazabicyclo[4.1.0]hept-4-ene (**4**g)*

A solution of lithium hydroxide free **1***a* (1.37 g, 10 mmol) in 33 mL dry ether was added slowly with stirring to a solution of methoxycarbonyl azide **2***f* (1.01 g, 10 mmol) in 50 mL dry ether under a nitrogen atmosphere at 25°C. The reaction was allowed to proceed for 1 h and then completed as described previously to afford **4***g* (2.1 g, 100%); ir (neat): 3210 (m, NH), 1730 (s, C=O), and 1590 (s, C=C) cm^{-1}; ^{1}H nmr δ: 0.9 (t, J = 7 Hz, 3H, $CH_2CH_2CH_2CH_3$), 1.1–1.9 (m, 6H, $CH_2CH_2CH_2CH_3$), 3.1 (m, 2H, H-1, H-6), 3.75 (s, 3H, OCH_3), 4.1 (m, 1H, H-3), 5.82 (m, 2H, H-4, H-5), 9.8 (b s, 1, NH, exchanges with deuterium oxide). *Exact Mass* calcd. for $C_{11}H_{18}N_2O_2$: 210.1368; found (high resolution ms): 210.1365.

*6-*n*-Butyl-1,2,5,6-tetrahydropyridylidene-2-phenylcarbonyl-amide (**8**, R^1 = n*Bu*, R^2 = *PhCO*)*

A solution of lithium hydroxide free **1***a* (1.37 g, 10 mmol) in 67 mL dry ether was added slowly with stirring to a solution of benzoyl azide (7.35 g, 50 mmol) in 50 mL dry ether under a nitrogen atmosphere at 25°C. The reaction was allowed to proceed for 24 h before warming to 25°C. Addition of water (50 mL), extraction with chloroform (2 × 50 mL), drying (Na_2SO_4), and removal of the solvent *in vacuo* afforded a red oil which was subjected to preparative tlc on six 8 in. × 8 in. silica gel G plates, 0.75 mm in thickness, using benzene–ether (3:1 v/v) as development solvent. Extraction of the band having R_f 0.93 with 50 mL methanol afforded unreacted benzoyl azide (3.5 g, 47.7%). Extraction of the fraction having R_f 0.61 gave rise to **8** (1.02 g, 39.7%); ir: 3180 (m, NH), 1640 (s, C=O), 1595 (s, C=C), and 1560 (s, C=N) cm^{-1}; ^{1}H nmr δ: 0.9 (t, J = 7 Hz, 3H, $CH_2CH_2CH_2CH_3$), 1.1–1.9 (m, 6H, $CH_2CH_2CH_2CH_3$), 2.38 (m, 2H, H-5), 3.6 (m, 1H, H-6), 6.14 (d, $J_{3,4}$ = 10 Hz of d, $J_{3,5}$ = 2.0 Hz of d, $J_{3,5'}$ = 1.5 Hz, 1H, H-3), 6.6 (d, $J_{3,4}$ = 10 Hz of d, $J_{4,5}$ = 5.0 Hz of d, $J_{4,5'}$ = 3.5 Hz, 1H, H-4), 7.4 (m, 3H, *meta* and *para* phenyl hydrogens), 8.3 (m, 2H, *ortho* phenyl hydrogens), 10.6 (b s, 1H, NH, exchanges with deuterium oxide). *Exact Mass* calcd. for $C_{16}H_{20}N_2O$: 256.1576; found (high resolution ms): 256.1573. Extraction of the band having R_f 0.36 afforded 2-*n*-butylpyridine (0.208 g, 39.7%).

*6,6′-Di-*n*-butyl-1,2,3,6-tetrahydro-2,3′-dipyridyl (**7**)*

A solution of lithium hydroxide free **1***a* (2.74 g, 20 mmol) in 67 mL dry ether was added slowly with stirring to a solution of hydrazoic acid (34.4 mL of 5.8 *M*, 20 mmol) in 50 mL dry benzene under a nitrogen atmosphere at 25°C. The reaction was allowed to proceed for 24 h before warming to 25°C. Addition of water (50 mL), drying (Na_2SO_4), and removal of the solvent *in vacuo* gave a reddish brown oil. Preparative tlc was effected on six 8 in. × 8 in. silica gel G plates, 0.75 mm in thickness, using benzene–methanol (7:1 v/v) as development solvent. Extraction of the band having R_f 0.75 with 50 mL warm methanol afforded 2-*n*-butylpyridine (0.329 g, 12.2%). Extraction of the band having R_f 0.62 yielded **7** (0.873 g, 64.7%) which showed ir and ^{1}H nmr spectra identical to those of an authentic sample of **7** previously reported (11).

*6-*n*-Butyl-1,2,5,6-tetrahydropyridylidene-2-cyanamide (**8**a)*

Elution of **4***a* (0.406 g, 2.3 mmol) from a 2.5 cm × 33 cm neutral alumina column (Brockman Activity 1) using ethyl acetate (300 mL) gave a white solid which was subjected to preparative tlc on six 8 in. × 8 in. silica gel G plates, 0.75 mm in thickness, using ether – ethyl acetate (9:1 v/v) as development solvent. Extraction of the fraction having R_f 0.8 with 50 mL warm methanol gave 6-*n*-butyl-1,2,5,6-tetrahydropyridylidene-2-cyanamide **8***a* (0.321 g, 79%), mp 61°C; ir: 3240 (m, NH), 2180 (s, C≡N), 1645 (s, C=C), and 1575 (s, C=N) cm^{-1}; ^{1}H nmr δ: 0.9 (t, J = 7 Hz, 3H, $CH_2CH_2CH_2CH_3$), 1.1–2.0 (m, 6H, $CH_2CH_2CH_2CH_3$), 2.4 (m, 2H, H-5), 3.6 (m, 1H, H-6), 6.3 (m, 1H, H-3), 6.65 (m, 1H, H-4), 7.45 (m, 1H, NH, exchanges with D_2O). *Exact Mass* calcd. for $C_{10}H_{15}N_3$: 177.1266; found (high resolution ms): 177.1265.

*6-Phenyl-1,2,5,6-tetrahydropyridylidene-2-cyanamide (**8**b)*

A suspension of 5 g neutral alumina (Brockman Activity 1) in 25 mL chloroform containing **4***b* (0.216 g, 1.1 mmol) was stirred at 25°C for 72 h. Extraction with ethyl acetate (100 mL) and removal of the solvent *in vacuo* afforded **8***b* (0.218 g, 100%), mp 129°C; ir: 3190 (m, NH), 2180 (s, C≡N), 1650 (s, C=C), and 1580 (s, C=N) cm^{-1}; ^{1}H nmr δ: 2.6 (m, 2H, H-5), 4.65 (m, 1H, H-6), 6.35 (m, 1H, H-3), 6.56 (m, 1H, H-4), 7.25 (m, 5H, C_6H_5), 8.52 (b s, 1, NH, exchanges with D_2O). *Exact Mass* calcd. for $C_{12}H_{11}N_3$: 197.0953; found (high resolution ms): 197.0943.

*6-*n*-Butyl-1,2,5,6-tetrahydropyridylidene-2-methanesulfonamide (**8**c)*

Elution of **4***c* (0.364 g, 1.6 mmol) from a neutral alumina column (Brockman Activity 1) 2.5 cm × 20 cm using benzene –

ethyl acetate (4:1 v/v) (400 ml) gave **8***c* in quantitative yield; ir (neat): 3310 (m, NH), 1640 (s, C=C), and 1580 (s, C=N) cm^{-1}; ^1H nmr δ: 0.91 (t, J = 7 Hz, 3H, $CH_2CH_2CH_2CH_3$), 1.1–1.8 (m, 6H, $CH_2CH_2CH_2CH_3$), 2.42 (m, 2H, H-5), 2.97 (s, 3H, SO_2CH_3), 3.6 (m, 1H, H-6), 5.92 (m, 1H, H-3), 6.7 (d, $J_{3,4}$ = 10 Hz of d, $J_{4,5}$ = 5 Hz of d, $J_{4,5'}$ = 3.5 Hz, 1H, H-4). *Exact Mass* calcd. for $C_{10}H_{18}N_2O_2{}^{32}S$: 230.1089; found (high resolution ms): 230.1085.

6-n-*Butyl-1,2,5,6-tetrahydropyridylidene-2-sulfanilamide (***8***d)*

Elution of **4***f* (1.73 g, 5.6 mmol) from a neutral alumina column (Brockman Activity 1) 2.5 cm × 20 cm after standing for 1 week using chloroform – ethyl acetate (19:1 v/v) gave **8***d* (1.6 g, 92%), mp 162°C; ir: 3450 (m, NH_2), 3350 (m, NH_2), 3320 (m, NH), 1630 (s, C=C), and 1580 (s, C=N) cm^{-1}; ^1H nmr δ: 0.95 (t, J = 7 Hz, 3H, $CH_2CH_2CH_2CH_3$), 1.1–1.8 (m, 6H, $CH_2CH_2CH_2CH_3$), 2.34 (m, 2H, H-5), 3.55 (m, 1H, H-6), 4.2 (m, 2H, NH_2, exchanges with deuterium oxide), 5.95 (d, $J_{3,4}$ = 10 Hz of d, $J_{3,5}$ = 2 Hz, 1H, H-3), 6.6 (m, 1H, H-4), 6.65 (m, 2H, *ortho* amino phenyl hydrogens), 7.75 (m, 2H, *ortho* sulfonyl phenyl hydrogens), 8.1 (b s, 1H, NH, exchanges with deuterium oxide). *Exact Mass* calcd. for $C_{15}H_{21}N_3O_2{}^{32}S$: 307.1354; found (high resolution ms): 307.1364.

6-n-*Butyl-1,2,5,6-tetrahydropyridylidene-2-methoxycarbonylamide (***8***e)*

Preparative tlc of **4***g* (0.432 g, 2.06 mmol) was effected on six 8 in. × 8 in. silica gel G plates, 0.75 mm in thickness, using benzene – ethyl acetate (1:9 v/v) as development solvent. Extraction of the fraction having R_f 0.28 using methanol (50 mL) afforded **8***e* (0.432 g, 100%); ir (neat): 3260 (m, NH), 1650 (s, C=O), 1630 (s, C=C), and 1570 (s, C=N) cm^{-1}; ^1H nmr δ: 0.9 (t, J = 7 Hz, 3H, $CH_2CH_2CH_2CH_3$), 1.1–1.8 (m, 6H, $CH_2CH_2CH_2CH_3$), 2.4 (m, 2H, H-5), 3.6 (m, 1H, H-6), 3.73 (s, 3H, OCH_3), 6.0 (d, $J_{3,4}$ = 10 Hz of d, $J_{3,5}$ = 2.0 Hz of d, $J_{3,5'}$ = 1.5 Hz, 1H, H-3), 6.6 (d, $J_{3,4}$ = 10 Hz of d, $J_{4,5}$ = 5.0 Hz of d, $J_{4,5'}$ = 3.5 Hz, 1H, H-4), 9.6 (b s, 1H, NH, exchanges with deuterium oxide). *Exact Mass* calcd. for $C_{11}H_{18}N_2O_2$: 210.1368; found (high resolution ms): 210.1365.

6-n-*Butylpiperidylidene-2-cyanamide (***9***f) and 6*-n-*Butyl-3,4,5,6-tetrahydropyridyl-2-cyanamide (***10***f)*

Hydrogenation of **4***a* (0.12 g, 0.68 mmol) or **8***a* (0.123 g, 0.695 mmol) in 75 mL methanol using 45 mg 10% palladium on charcoal and hydrogen gas at 35 psi for 4 h at 25°C followed by filtration and removal of the solvent *in vacuo* afforded the tautomeric mixture 6-*n*-butylpiperidylidene-2-cyanamide (**9***f*) and 6-*n*-butyl-3,4,5,6-tetrahydropyridylidene-2-cyanamide (**10***f*) in quantitative yield (0.121 g and 0.124 g respectively); ir: 3240 (**9***f*) (m, NH), 3120 (**10***f*) (m, NH), 2180 (s, C≡N), 1645 (**10***f*) (s, C=N), and 1605 (**9***f*) (s, C=N) cm^{-1}; ^1H nmr δ: 0.9 (t, J = 7 Hz, 3H, $CH_2CH_2CH_2CH_3$), 1.1–2.3 (m, 10H, $CH_2CH_2CH_2CH_3$, H-4, H-5), 2.7 (m, 2H, H-3), 3.4 (m, 1H, H-6), 8.0 (b s, 1H, NH, exchanges with D_2O). *Exact Mass* calcd. for $C_{10}H_{17}N_3$: 179.1422; found (high resolution ms): 179.1418.

*6-Phenylpiperidylidene-2-cyanamide (***9***g) and 6-Phenyl-3,4,5,6-tetrahydropyridyl-2-cyanamide (***10***g)*

Hydrogenation of **4***b* (0.132 g, 0.67 mmol) or **8***b* (0.137 g, 0.695 mmol) in 75 mL methanol using 45 mg 10% palladium on charcoal and hydrogen gas at 35 psi for 4 h at 25°C followed by filtration and removal of the solvent *in vacuo* afforded the tautomeric mixture of **9***g* and **10***g* in quantitative yield; ir: 3230 (m, NH) (**9***g*), 3140 (m, NH) (**10***g*), 2170 (s, C≡N), 1600 (s, C=N) (**10***g*), and 1575 (s, C=N) (**9***g*) cm^{-1}; ^1H nmr δ: 1.5–2.3 (m, 4H, H-4, H-5), 2.7 (m, 2H, H-3), 4.6 (m, 1H, H-6), 7.3 (m, 5H, C_6H_5), 7.45 (b s, 1H, NH, exchanges with D_2O). *Exact Mass* calcd. for $C_{12}H_{13}N_3$: 199.1110; found (high resolution ms): 199.1100.

6-n-*Butylpiperidylidene-2-methanesulfonamide (***9***h) and 6*-n-*Butylpyridyl-2-methanesulfonamide (***11***)*

Hydrogenation of **4***c* (0.121 g, 0.526 mmol) or **8***c* (0.181 g, 0.787 mmol) in 75 mL methanol using 75 mg 10% palladium on charcoal and hydrogen gas at 35 psi for 4 h at 25°C, followed by filtration and removal of the solvent *in vacuo*, gave a colorless oil. Preparative tlc was effected on two 8 in. × 8 in. silica gel G plates, 0.75 mm in thickness, using benzene – ethyl acetate (1:2 v/v) as the development solvent. Extraction of the band having R_f 0.91 with 50 mL methanol afforded **11** (0.009 g, 7.5% and 0.014 g, 7.8% respectively); ir: 3240 (m, NH) cm^{-1}; ^1H nmr δ: 0.93 (t, J = 7 Hz, 3H, $CH_2CH_2CH_2CH_3$), 1.1–1.9 (m, 4H, $CH_2CH_2CH_2CH_3$), 2.7 (t, J = 7 Hz, 2H, $CH_2CH_2CH_2CH_3$), 3.17 (s, 3H, SO_2CH_3), 6.67 (d, $J_{3,4}$ = 7.5 Hz of d, $J_{3,5}$ = 1.0 Hz, 1H, H-3), 6.98 (d, $J_{4,5}$ = 9.0 Hz of d, $J_{3,5}$ = 1.0 Hz, 1H, H-5), 7.6 (d, $J_{4,5}$ = 9.0 Hz of d, $J_{3,4}$ = 7.5 Hz, 1H, H-4), 8.4 (b s, 1H, NH, exchanges with deuterium oxide). *Exact Mass* calcd. for $C_{10}H_{16}N_2O_2{}^{32}S$: 228.0932; found (high resolution ms): 228.0930. Extraction of the band having R_f 0.46 afforded **9***h* (0.112 g, 91.8% and 0.167 g, 91.5% respectively); ir: 3280 (m, NH), 1600 (s, C=N) cm^{-1}; ^1H nmr δ: 0.9 (t, J = 7 Hz, 3H, $CH_2CH_2CH_2CH_3$), 1.1–2.15 (m, 10H, $CH_2CH_2CH_2CH_3$, H-4, H-5), 2.46 (m, 2H, H-3), 2.95 (s, 3H, SO_2CH_3), 3.37 (m, 1H, H-6), 8.3 (b s, 1H, NH, exchanges with deuterium oxide). *Exact Mass* calcd. for $C_{10}H_{20}N_2O_2{}^{32}S$: 232.1245; found (high resolution ms): 232.1244.

6-n-*Butylpiperidylidene-2-sulfanilamide (***9***i)*

Hydrogenation of **4***f* (1.74 g, 5.6 mmol) or **8***d* (0.116 g, 0.38 mmol) in 100 mL methanol using 0.93 g 10% palladium on charcoal and hydrogen gas at 35 psi for 4 h at 25°C followed by filtration and removal of the solvent *in vacuo* gave **9***i* in quantitative yield, mp 136°C; ir: 3455 (m, NH_2), 3355 (m, NH_2), 3300 (m, NH), and 1590 (s, C=N) cm^{-1}; ^1H nmr δ: 0.86 (t, J = 7 Hz, 3H, $CH_2CH_2CH_2CH_3$), 1.1–2.1 (m, 10H, $CH_2CH_2CH_2CH_3$, H-4, H-5), 2.4 (m, 2H, H-3), 3.3 (m, 1H, H-6), 4.5 (b s, 2H, NH_2, exchanges with deuterium oxide), 6.6 (m, 2H, *ortho* amino phenyl hydrogens), 7.65 (m, 2H, *ortho* sulfonyl phenyl hydrogens), 8.37 (b s, 1H, NH, exchanges with deuterium oxide). *Exact Mass* calcd. for $C_{15}H_{23}N_3O_2{}^{32}S$: 309.1511; found (high resolution ms): 309.1516.

6-n-*Butylpiperidylidene-2-methoxycarbonylamide (***9***j) and 6*-n-*Butyl-3,4,5,6-tetrahydropyridyl-2-methoxycarbonylamide (***10***j)*

Hydrogenation of **4***g* (0.434 g, 2.07 mmol) in 75 mL methanol using 300 mg 10% palladium on charcoal and hydrogen gas at 35 psi for 4 h at 25°C followed by filtration and removal of the solvent *in vacuo* afforded a light brown oil. Preparative tlc was effected on six 8 in. × 8 in. silica gel G plates, 0.75 mm in thickness, using ethyl acetate – isopropanol (9:1 v/v) as development solvent. Extraction of the fraction having R_f 0.51 with 50 mL methanol afforded the tautomeric mixture of **9***j* and **10***j* (0.278 g, 63.4%); ir: (neat): 3210 (m, NH) (**9***j*) and 3150 (m, NH) (**10***j*), 1635 (s, C=O), and 1590 (s, C=N) cm^{-1}; ^1H nmr δ: 0.9 (t, J = 7 Hz, 3H, $CH_2CH_2CH_2CH_3$), 1.1–2.2 (m, 10H, $CH_2CH_2CH_2CH_3$, H-4, H-5), 2.48 (m, 2H, H-3), 3.45 (m, 1H, H-6), 3.71 (s, 3H, OCH_3), 10.2 (b s, 1H, NH, exchanges with deuterium oxide). *Exact Mass* calcd. for $C_{11}H_{20}N_2O_2$: 212.1525; found (high resolution ms): 212.1522.

*6-Phenyl-2-piperidone (***12***)*

A solution of the tautomeric mixture of **9***g* and **10***g* (0.2 g,

1.0 mmol) and 10 mL 10% sulfuric acid in 100 mL methanol was heated under reflux at 64°C for 20 h. The solution was neutralized to pH 7 using 10% aqueous sodium hydroxide, filtered, and the solution was heated *in vacuo* to remove the methanol. Extraction of the remaining aqueous mother liquor with chloroform (3 × 50 mL), drying (sodium sulfate), and removal of the solvent *in vacuo* afforded a tan colored solid. Recrystallization from petroleum ether (bp 30–60°C) gave 6-phenyl-2-piperidone (**12**) (0.068 g, 38.7%), mp 137°C; ir: 3180 (m, NH) and 1640 (s, C=O) cm^{-1}; ^1H nmr δ: 1.5–2.1 (m, 4H, H-4, H-5), 2.27 (m, 2H, H-3), 4.4 (m, 1H, H-6), 6.8 (m, 1H, NH, exchanges with D_2O), 7.21 (m, 5H, C_6H_5). *Exact Mass* calcd. for $C_{11}H_{13}NO$: 175.0997; found (high resolution ms): 175.1001.

Acknowledgement

We are grateful to the Medical Research Council of Canada (Grant No. MA-4888) for financial support of this work.

1. F. Chou, A. Hameed Khan, and J. S. Driscoll. J. Med. Chem. **19**, 1302 (1976).
2. M. H. Akhtar, A. Begleiter, D. Johnson, J. W. Lown, L. McLaughlin, and S. K. Kim. Can. J. Chem. **53**, 2891 (1975).
3. T. A. Ondrus, E. E. Knaus, and C. S. Giam. Can. J. Chem. **56**, 1026 (1978).
4. T. A. Ondrus, E. E. Knaus, and C. S. Giam. J. Heterocycl. Chem. **16**, 409 (1979).
5. J. F. Stephen and E. Marcus. J. Heterocycl. Chem. **6**, 969 (1969).
6. A. G. Anastassiou and H. E. Simmons. J. Am. Chem. Soc. **89**, 3177 (1967).
7. M. E. Hermes and F. D. Marsh. J. Am. Chem. Soc. **89**, 4760 (1967).
8. P. Grunanger and P. V. Finzi. Tetrahedron Lett. **26**, 1839 (1963).
9. E. Moriconi and R. Miser. J. Org. Chem. **34**, 3672 (1969).
10. M. E. Hermes and F. D. Marsh. J. Org. Chem. **37**, 2969 (1972).
11. E. E. Knaus, T. A. Ondrus, and C. S. Giam. J. Heterocycl. Chem. **13**, 789 (1976).

A room-temperature study of the kinetics of protonation of formaldehyde

SCOTT D. TANNER, GERVASE I. MACKAY, AND DIETHARD K. BOHME

Department of Chemistry and Centre for Research in Experimental Space Science, York University, Downsview, Ont., Canada M3J 1P3

Received April 4, 1979

SCOTT D. TANNER, GERVASE I. MACKAY, and DIETHARD K. BOHME. Can. J. Chem. **57**, 2350 (1979).

Rate constants measured with the flowing afterglow technique at 297 ± 2 K are reported for the protonation of CH_2O by H_3^+, N_2H^+, CH_5^+, HCO^+, $C_2H_5^+$, H_3O^+, H_3S^+, and $HCNH^+$ and for the subsequent deprotonation by NH_3. The rate constants are compared with predictions of various theories for ion–molecule collisions. The protonation was observed to proceed in the absence of competing channels and further decomposition and is discussed in terms of the energetics of the two sites of protonation and the energetics and mechanism of H_2 elimination. The rate measurements provide evidence for the room-temperature conversion of the adduct $C_2H_3^+ \cdot H_2$ to the more stable isomer derived from the direct protonation of C_2H_4.

SCOTT D. TANNER, GERVASE I. MACKAY et DIETHARD K. BOHME. Can. J. Chem. **57**, 2350 (1979).

Opérant à 297 ± 2 K et faisant appel à la technique de lueur d'écoulement résiduelle, on a mesuré les constantes de vitesse pour la protonation de CH_2O par H_3^+, N_2H^+, CH_5^+, HCO^+, $C_2H_5^+$, H_3O^+, H_3S^+ et $HCNH^+$ et la déprotonation subséquente par NH_3. On compare les constantes de vitesse avec celles que l'on peut prédire à l'aide de diverses théories relatives aux collisions ion–molécule. On a observé que la protonation se produit même s'il n'existe pas d'autres chemins en compétition et d'autres décompositions et on en discute en termes des énergies des deux sites de protonation et de l'énergie et du mécanisme d'élimination de H_2. Les mesures de vitesse fournissent des preuves à l'effet de la transformation, à température ambiante, de l'adduit $C_2H_3^+$ en son isomère plus stable dérivé de la protonation directe de C_2H_4.

[Traduit par le journal]

Introduction

Ion-molecule reactions of gaseous formaldehyde have been receiving an increasing amount of attention in the past few years. This is especially evident from the recent incorporation of formaldehyde into models of the ion chemistry proceeding in such diverse chemical environments as dense interstellar clouds (1), hydrocarbon flames (2), and planetary atmospheres, particularly the earth's stratosphere (3, 4). However, quantitative information on the rates of such reactions is still rather sparse. Here we present the results of a flowing afterglow study of the room-temperature kinetics of ion–molecule reactions which lead to the protonation of formaldehyde. Such reactions play an integral part in these chemical models. Their study also provides further fundamental insight into the kinetics of proton-transfer reactions in general.

Experimental

The measurements were carried out in a conventional flowing plasma mass-spectrometer (flowing afterglow) system in a manner which has been described previously (5).

Monomeric formaldehyde was prepared from paraformaldehyde (Fisher Scientific, Purified Grade) by an adaption of the method developed by Spence and Wild (6). Paraformaldehyde was distilled at low pressures at ~370 K. The formaldehyde was then dried by passing it through a cold trap at 195 K and frozen out at liquid nitrogen temperatures. A gaseous mixture of ~5% formaldehyde was used in these studies and the partial pressure of formaldehyde was maintained below 7 Torr to avoid polymerization. The monomer could be stored at these partial pressures for several days with negligible polymerization. It was introduced into the flowing afterglow sufficiently downstream of the ion production region to ensure that the reactant ions were thermalized by collisions with H_2 carrier gas molecules to the ambient temperature of 297 ± 2 K prior to reaction. The total pressure in the reaction region ranged from 0.29 to 0.68 Torr and the effective reaction length had values of 59 and 85 cm.

The gases used were hydrogen (Linde, Very Dry Grade, 99.95% H_2), methane (Matheson, Ultra High Purity, 99.97% CH_4), ethylene (Matheson, C.P. Grade, 99.5% C_2H_4), acetylene (Matheson, Purified Grade, 99.6% C_2H_2), carbon monoxide (Matheson, Coleman Grade, 99.99% CO), and nitrogen (Matheson, Prepurified Grade, 99.998% N_2).

Results and Discussion

The measurements were performed in H_2 carrier gas in which a variety of protonating agents with proton affinities intermediate between H_2 and CH_2O could be conveniently prepared upstream of the reaction region. This was accomplished for X = N_2, CO, CH_4, C_2H_4, H_2O, H_2S, and HCN through rapid proton transfer reactions of the type

0008-4042/79/182350-05$01.00/0

[1] $H_3^+ + X \rightarrow XH^+ + H_2$

the H_3^+ itself resulting from the reaction

[2] $H_2^+ + H_2 \rightarrow H_3^+ + H$

After their formation, the H_3^+ and XH^+ ions were allowed to undergo many thousands of collisions in the H_2 buffer gas upstream of the reaction region in order to establish Maxwell–Boltzmann energy distributions prior to reaction. Some ambiguity exists about the structure of the protonated heteroatomic species CO and HCN for which there are two possible sites of protonation. *Ab initio* molecular orbital calculations reported to date indicate that the proton affinity of the carbon site in the CO molecule is only ca. 18 kcal mol^{-1} higher than that of the oxygen site and that both the HCO^+ and COH^+ systems prefer a linear arrangement of nuclei in their ground states at equilibrium (7, 8). In the case of protonated HCN, calculations predict that the linear acetylene-like isomer, H—C≡N^+—H, lies ca. 70 kcal mol^{-1} lower in energy than the formaldehyde-like isomer, $\begin{matrix} H \\ \diagdown \\ C{=}N^+ \\ \diagup \\ H \end{matrix}$ (9). Consequently, it appears that two isomers are energetically accessible in the protonation of CO and HCN by H_3^+ according to reactions [3] and [4], where the exothermicity is given in kcal mol^{-1}. The experiments

[3] $H_3^+ + CO \rightarrow HCO^+ + H_2 + 42$
$\rightarrow COH^+ + H_2 + 28$

[4] $H_3^+ + HCN \rightarrow HCNH^+ + H_2 + 70$
$\rightarrow H_2CN^+ + H_2 + 0$

reported here do not provide any information about the extent of initial formation of the high energy isomer in either case. However, should such formation be occurring to any significant extent, we can expect isomerization to proceed to the low energy form, if not unimolecularly or by collision with H_2 carrier molecules, then by the proton transfer reactions

[5] $COH^+ + CO \rightarrow HCO^+ + CO + 18$

[6] $H_2CN^+ + HCN \rightarrow HCNH^+ + HCN + 70$

which would be encouraged to proceed by the presence of CO and HCN, respectively, upstream of the reaction region. Evidence for the ultimate preferential formation of the HCO^+ isomer under our experimental operating condition is given elsewhere (10). The $C_2H_5^+$ ions were prepared in two ways, either directly by proton transfer to C_2H_4 or indirectly through H_2 association

[7] $C_2H_3^+ + H_2 + M \rightarrow C_2H_5^+ + M$

preceded by proton transfer from H_3^+ to C_2H_2 (11).

Rate constants were measured in separate experiments in each of which the desired protonating agent was established as the major positive ion present in the flowing plasma. Figure 1 shows the decays of H_3^+, HCO^+, and H_3O^+ observed upon the addition of CH_2O into the reaction region under conditions of only partial conversion of H_3^+ to HCO^+ (relatively small additions of CO upstream). H_3O^+ results from proton transfer to H_2O impurity. The concomitant rise in the $m/e = 31$ signal is a manifestation of the production of protonated formaldehyde to which we have assigned the structure CH_2OH^+ (*vide infra*). The initial signal at $m/e = 31$ is accounted for by the ^{18}O isotope of HCO^+. No other primary product ions were observed. CH_2OH^+ appears to react further with CH_2O to form the cluster ion $CH_2OH^+ \cdot CH_2O$ presumably by three-body association. There was no evidence for the association of

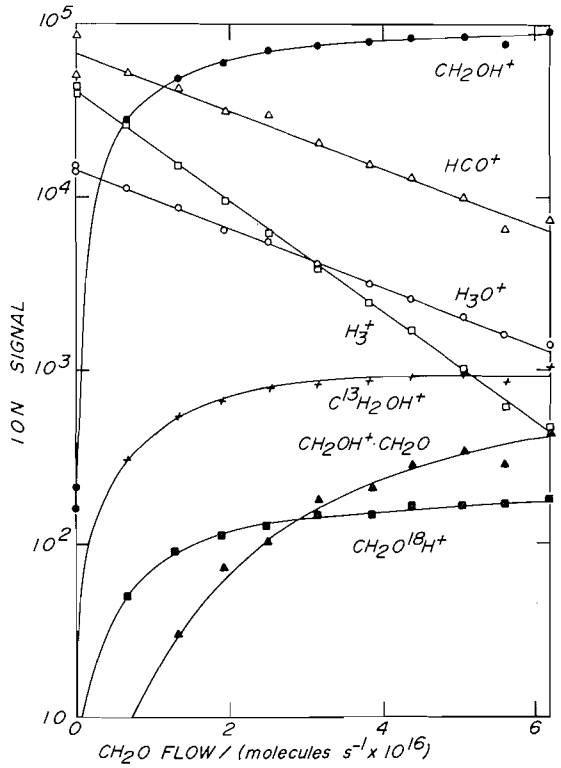

FIG. 1. The variation in the dominant ion signals recorded upon the addition of formaldehyde into a H_2–CO plasma in which HCO^+, H_3^+, and H_3O^+ are initial major ions: $T = 297$ K, $P = 0.421$ Torr, $v = 7.8 \times 10^3$ cm s^{-1}, $L = 60$ cm, and the flow of CO = 3.12×10^{16} molecules s^{-1}.

TABLE 1. Rate constants at 297 ± 2 K (in units of 10^{-9} cm^3 molecule^{-1} s^{-1}) for reactions of the type $XH^+ + CH_2O \rightarrow CH_2OH^+ + X$

XH^+	k_{expt}[a]	k_{AADO}[b]	k_{expt}/k_{AADO}	$-\Delta H_{298}$[c]
H_3^+	6.3±1.6(4)	6.68	0.94	70 ±2
N_2H^+	3.3±0.8(3)	2.87	1.1	54 ±2
CH_5^+	4.5±1.1(3)	3.35	1.3	40 ±3
HCO^+	3.3±0.8(4)	2.87	1.1	28 ±2
$C_2H_5^+$[d]	3.1±0.8(4)	2.87	1.1	12 ±4
H_3O^+	3.4±0.9(14)	3.23	1.1	5.1±0.8[e]
H_3S^+	2.2±0.6(3)	2.74	0.80	1.4±0.5[e]
$HCNH^+$	≥1.6	2.90	≥0.6	−0.1±0.4[e]

[a]The mean value together with the estimated accuracy of the measurements. The number of measurements is given in parentheses.
[b]The collision rate constant calculated using the angular momentum conserved-average dipole orientation theory with $C = 0.257$ (16), $\alpha = 2.81$ Å^3 (17), $\mu_D = 2.33$ D (18), and $I = 2.16 \times 10^{-39}$ g cm^2 (19).
[c]Standard enthalpy change based on PA(CH_2O) = 170.9 ± 1.2 kcal mol^{-1} (15, 20) and PA(H_2, N_2, CH_4, CO, C_2H_4) = 101 ± 1 (21), 117 ± 1 (unpublished results from this laboratory), 131 ± 2 (unpublished results from this laboratory), 143 ± 1 (23), and 159 ± 3 (24) kcal mol^{-1}, respectively.
[d]Derived from $H_3^+ + C_2H_4$ or $C_2H_3^+ + H_2 + M$.
[e]Standard enthalpy change based on equilibrium constant measurements performed in this laboratory (15).

CH_2OH^+ with the H_2 carrier gas molecules to form either the adduct $H_2COH^+ \cdot H_2$ or protonated methanol, $CH_3OH_2^+$. The observed rise in the $m/e = 33$ signal is completely accounted for by the ^{18}O isotope of CH_2OH^+. Our failure to observe $CH_2OH^+ \cdot H_2$ is consistent with the equilibrium constant measurements reported by Hiraoka and Kebarle (12) which suggest that this ion is stable only at low temperatures. Also, according to a recent study of the metastable decomposition of $CH_3OH_2^+$ (13), the formation of $CH_3OH_2^+$ from $CH_2OH^+ + H_2$ has an activation energy of 31 kcal mol^{-1}. The ^{18}O isotope also rules out significant formation (<0.2%) of $CH_3OH_2^+$ by the two-body reaction [8]

[8] $$CH_2OH^+ + CH_2O \rightarrow CH_3OH_2^+ + CO$$

which is 33 ± 4 kcal mol^{-1} exothermic and which appears to have been observed previously in the ion-cyclotron double resonance (ICR) experiments of Karpas and Klein (14). The CH_3O^+ in the ICR experiments was generated at relatively low pressures in CH_2O from CH_2O^+ and CHO^+ and was observed to produce not only CH_5O^+ but also a variety of $C_2H_xO_y^+$ ions. In fact, a number of these channels are endothermic so that it is necessary to surmise, as Karpas and Klein have done, that excited CH_3O^+ ions were present under their experimental conditions.

Table 1 summarizes the rate constants determined in this laboratory for the reactions of seven XH^+ ions with CH_2O. Measurements associated with the reactions of H_3S^+ and $HCNH^+$ with CH_2O have been reported previously in the context of a determination of their equilibrium constants (15). Very few other measurements appear to be available for comparison. Fehsenfeld and co-workers (4) have recently reported a flowing afterglow value of (2.2 ± 0.9) × 10^{-9} cm^3 molecule^{-1} s^{-1} for the reaction of H_3O^+ with CH_2O at room temperature which is somewhat lower than the value determined here, but there is agreement within the overall uncertainties of the two sets of measurements. Recent SIFT measurements in which HCO^+ was produced from CH_2O at low pressures indicated a rate constant of (3.2 ± 1.0) × 10^{-9} cm^3 molecule^{-1} s^{-1} which is in good agreement with the present result (25). Karpas and Klein (14) have reported a value of 6.1 × 10^{-10} cm^3 molecule^{-1} s^{-1} for the same reaction proceeding under the less well defined conditions of their ICR cell.

Figure 2 compares the measured rate constants with capture rate constants predicted by various ion–molecule collision theories: the Langevin theory which ignores the influence of the permanent dipole moment of CH_2O (26), the angular momentum-conserved average dipole orientation (AADO) theory (16), and the locked-dipole limit (27, 28). It is encouraging that the AADO theory predicts rate constants for the reactions studied here which are essentially within the uncertainty of the experimental measurements.

All of the reactions in Table 1 appeared to proceed predominantly by proton transfer unaccompanied by other competing channels and further decomposition of the protonated product. The isotopic labelling studies of Karpas and Klein (14) have shown that proton transfer and not H_2 transfer is responsible for the conversion of HCO^+ to CH_2OH^+. Some ambiguity exists regarding the actual site of protonation. Molecular orbital calculations have predicted an energy difference of at least 40 kcal mol^{-1} between the two tautomers corresponding to C and O protonation, viz. CH_3O^+ and CH_2OH^+ (9). Consequently it appears that two isomers may be energetically accessible in the protonation of CH_2O by H_3^+, N_2H^+, and possibly CH_5^+. For each of these ions the proton transfer reaction exothermicity

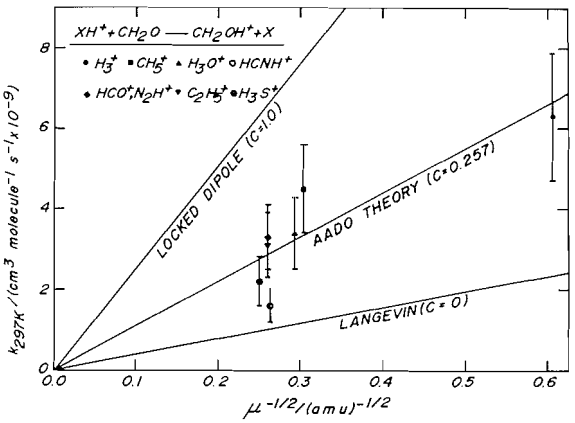

FIG. 2. A comparison of the measured rate constants with capture rate constants predicted by classical theories of collision for proton-transfer reactions with formaldehyde at 297 ± 2 K. The solid bars represent the estimated accuracy of the measurements.

>40 kcal mol^{-1} (see Table 1). The least endothermic route of decomposition of the CH_2OH^+ isomer corresponds to a symmetry-forbidden vicinal H_2 elimination which is ca. 28 kcal mol^{-1} endothermic and requires an excess energy of at least ca. 61 kcal mol^{-1} according to measurements of the kinetic energy release in the metastable decomposition of CH_2OH^+ (29). Such an excess energy is not available from any of the XH^+ ions used in this study except perhaps H_3^+:

[9a] $H_3^+ + CH_2O \rightarrow CH_2OH^+ + H_2 + 70$

[9b] $\hookrightarrow HCO^+ + H_2 - 28$

Also, Bowen and Williams have reported measurements which appear to indicate that the high energy CH_3O^+ tautomer loses H_2 in an exothermic symmetry-allowed reaction with a small activation energy (30). A second route of dissociative proton transfer can therefore be envisaged for the stronger acids H_3^+, N_2H^+, CH_5^+, e.g.,

[10a] $H_3^+ + CH_2O \rightarrow CH_3O^+ + H_2 + 30$

[10b] $\hookrightarrow HCO^+ + H_2 + 12$

Careful measurements of the $m/e = 29$ signal in the H_3^+ experiments, although complicated by the presence of N_2 and (or) CO impurities, provided an upper limit of ca. 1% to the occurrence of dissociation either via reaction [9b] or reaction [10b] under our experimental operating conditions.

The rate constant determined for the reaction of $C_2H_5^+$ with CH_2O was observed to be independent of the chemical history of this ion and there was no evidence for the formation of either CH_5O^+ or $C_3H_5O^+$ which may be conceived to proceed via "solvated" proton transfer according to

[11] $C_2H_3^+ \cdot H_2 + CH_2O \rightarrow CH_2OH^+ \cdot H_2 + C_2H_2$

or a switching reaction of the type

[12] $C_2H_3^+ \cdot H_2 + CH_2O \rightarrow C_2H_3^+ \cdot CH_2O + H_2$

Apparently the hydrogen adduct, $C_2H_3^+ \cdot H_2$, formed by the association of $C_2H_3^+$ with H_2 rearranges its structure at room temperature into that corresponding to the more stabler isomer derived from the direct protonation of C_2H_4 with H_3^+. This is in complete analogy with the behaviour proposed by Hiraoka and Kebarle for the corresponding isomers of $C_2H_7^+$ (31). These authors were able to characterise a loose hydrogen adduct, $C_2H_5^+ \cdot H_2$, approximately 8 kcal mol^{-1} less stable than the protonated ethane structure, $C_2H_7^+$. It was observed only at temperatures sufficiently low (−130 to −160°C) to prevent the interconversion which has a small activation energy. The facile formation at room temperature of the ethyl ion from $C_2H_3^+ + H_2$ is also in accord with observations of a small or negligible release of kinetic energy in what is conceived to be a concerted 1,1-elimination of H_2 from the ethyl cation to the vinylium ion (32). Theoretical treatments of the structures and relative energies of the ethyl and vinylium ions and possible transition states associated with their interconversion have recently been discussed and summarized by Dewar and Rzepa (33).

The reactions of protonated formaldehyde itself were not investigated in great detail. The recent SIFT measurements of Adams *et al.* (25) have shown that this ion is unreactive towards H_2, O_2, CO_2, COS, and CH_4 and reacts by proton transfer with NH_3 and CH_3OH which have proton affinities greater than that of CH_2O. We have studied the proton transfer reaction with NH_3 in these investigations and have determined a rate constant of $(1.7 \pm 0.4) \times 10^{-9}$ cm^3 molecule^{-1} s^{-1} which compares favorably with the SIFT value (2.0 ± 0.4), a previous flowing afterglow value (≃2), and an ICR value $(2.3 \pm 0.1) \times 10^{-9}$ cm^3 molecule^{-1} s^{-1} (22, 34).

Acknowledgement

We thank the Natural Sciences and Engineering Research Council of Canada for financial support.

1. W. D. WATSON. Rev. Mod. Phys. **48**, 513 (1976).
2. D. K. BOHME. *In* Kinetics of ion–molecule reactions. *Edited by* P. Ausloos. Plenum Press, New York, NY. 1979. p. 323.
3. F. ARNOLD, D. KRANKOWSKY, and K. M. MARIEN. Nature, **267**, 30 (1977).
4. F. C. FEHSENFELD, I. DOTAN, D. L. ALBRITTON, C. J. HOWARD, and E. E. FERGUSON. J. Geophys. Res. **83**, 1333 (1978).

5. D. K. BOHME, R. S. HEMSWORTH, H. W. RUNDLE, and H. I. SCHIFF. J. Chem. Phys. **58**, 3504 (1973).
6. R. SPENCE and W. WILD. J. Chem. Soc. 338 (1935).
7. P. J. BRUNS. Astrophys. Lett. **16**, 107 (1975).
8. P. J. BRUNS, S. D. PEYERIMHOFF, and R. J. BUENKER. Chem. Phys. **10**, 323 (1975).
9. W. A. LATHAN, L. A. CURTISS, W. J. HEHRE, J. B. LISTE, and J. A. POPLE. Prog. Phys. Org. Chem. **11**, 175 (1974).
10. S. D. TANNER, G. I. MACKAY, A. C. HOPKINSON, and D. K. BOHME. Int. J. Mass Spectrom. Ion Phys. **29**, 153 (1979).
11. G. I. MACKAY, K. TANAKA, and D. K. BOHME. Int. J. Mass Spectrom. Ion Phys. **24**, 125 (1977).
12. K. HIRAOKA and P. KEBARLE. J. Chem. Phys. **63**, 1688 (1975).
13. W. T. HUNTRESS, D. K. SEN SHARMA, K. R. JENNINGS, and M. T. BOWERS. Int. J. Mass Spectrum. Ion Phys. **24**, 25 (1977).
14. Z. KARPAS and F. S. KLEIN. Int. J. Mass Spectrom. Ion Phys. **16**, 289 (1975).
15. K. TANAKA, G. I. MACKAY, and D. K. BOHME. Can. J. Chem. **56**, 193 (1978).
16. T. SU, E. C. F. SU, and M. T. BOWERS. J. Chem. Phys. **69**, 2243 (1978).
17. E. W. ROTHE and R. B. BERNSTEIN. J. Chem. Phys. **31**, 169 (1959).
18. R. D. NILSON, D. R. LIDE, and A. A. MARJOTT. Natl. Stand. Ref. Data Ser. Natl. Bur. Stand. **10** (1966).
19. G. HERZBERG. Molecular spectra and molecular structure. Vol. 3. Van Nostrand Reinhold, Toronto. 1966.
20. K. M. A. REFAEY and W. A. CHUPKA. J. Chem. Phys. **48**, 5205 (1968).
21. A. J. DUBEN and J. P. LOWE. J. Chem. Phys. **55**, 4270 (1971).
22. W. T. HUNTRESS. Astrophys. J. Suppl. Ser. **33**, 495 (1977).
23. P. M. GUYON, W. A. CHUPKA, and J. BERKOWITZ. J. Chem. Phys. **64**, 1419 (1976).
24. H. M. ROSENSTOCK, K. DRAXL, B. W. STEINER, and J. T. HERRON. J. Phys. Chem. Ref. Data, **6** (1977).
25. N. G. ADAMS, D. SMITH, and D. GRIEF. Int. J. Mass Spectrom. Ion Phys. **26**, 405 (1978).
26. G. GIOUMOUSIS and D. P. STEVENSON. J. Chem. Phys. **29**, 294 (1958).
27. T. F. MORAN and W. H. HAMILL. J. Chem. Phys. **39**, 1413 (1963).
28. S. K. GUPTA, E. G. JONES, A. G. HARRISON, and J. T. MYHER. Can. J. Chem. **45**, 3107 (1967).
29. J. H. BEYNON, A. E. FONTAINE, and G. R. LESTER. Int. J. Mass Spectrom. Ion Phys. **1**, 1 (1968).
30. R. D. BOWEN and D. H. WILLIAMS. J. Chem. Soc. Chem. Commun. 378 (1977).
31. K. HIRAOKA and P. KEBARLE. J. Am. Chem. Soc. **98**, 6119 (1976).
32. D. H. WILLIAMS and G. HVISTENDAHL. J. Am. Chem. Soc. **96**, 6755 (1974).
33. M. J. S. DEWAR and H. S. RZEPA. J. Am. Chem. Soc. **99**, 7432 (1977).
34. F. C. FEHSENFELD, D. B. DUNKIN, and E. E. FERGUSON. Astrophys. J. **188**, 43 (1974).

The dual role of the coinitiator in the cationic polymerization of isobutene

KENNETH E. RUSSELL AND LINDA G. M. C. VAIL
Department of Chemistry, Queen's University, Kingston, Ont., Canada K7L 3N6

Received March 16, 1979

KENNETH E. RUSSELL and LINDA G. M. C. VAIL. Can. J. Chem. 57, 2355 (1979).

The influence of 2,4- and 2,6-dimethylphenol, 2,3,6- and 2,4,6-trimethylphenol, 2,3,4,6- and 2,3,5,6-tetramethylphenol, 2,6-diisopropylphenol, 2-*tert*-butyl-4-methylphenol and 2,4-di-*tert*-butylphenol on the stannic chloride initiated polymerization of isobutene has been investigated. At −78.5°C and with 0.185 *M* stannic chloride, these phenols act as coinitiators. Rates of polymerizaiton reach maximum values at phenol concentrations which depend greatly on the number and positions of alkyl substituents; molecular weights decrease continuously with phenol concentration. Phenols without 4-substituents are incorporated in polyisobutenes as end groups and those with 4-substituents give rise largely to olefinic end groups. Termination of polymerization occurs mainly by attack at a free 4-position or at the OH group. The initial *tert*-butyl carbenium ion is more readily terminated by 2,6-di-*tert*-butylphenol than the polymer carbenium ion.

The rate and molecular weight results are interpreted in terms of a simplified reaction scheme in which termination occurs spontaneously or by reaction with uncomplexed phenol. Rate constants for termination by methyl-substituted phenols are of the order of one tenth of the propagation rate constant while those for 2-*tert*-butyl-4-alkylphenols are about one hundredth of the propagation rate constant.

KENNETH E. RUSSELL et LINDA G. M. C. VAIL. Can. J. Chem. 57, 2355 (1979).

On a étudié l'influence des diméthyl-2,4 (et -2,6), des triméthyl-2,3,6 (et -2,4,6), des tétraméthyl-2,3,4,6 (et -2,3,5,6), du diisopropyl-2,6, du *tert*-butyl-2 méthyl-4 et du di-*tert*-butyl-2,4 phénols sur la polymérisation de l'isobutène catalysée par le chlorure stannique. A −78.05°C et avec 0.18 *M* de chlorure stannique, ces phénols agissent comme coinitiateurs. Les taux de polymérisation atteignent des valeurs maximales à des concentrations de phénols qui dépendent grandement du nombre et de la position des substituants alkyles; les poids moléculaires diminuent progressivement avec la concentration de phénol. Les phénols qui ne portent pas de substituants en position 4 sont incorporés dans les polyisobutylènes sous forme de groupes terminaux; ceux qui portent un substituant en position 4 donnent principalement lieu à des groupes terminaux portant des liaisons doubles. La terminaison de la polymérisation se produit principalement par une attaque au niveau de la position 4 vacante ou du groupe OH. Le carbocation *tert*-butyle initial est plus facilement piégé par le di-*tert*-butyl-2,6 phénol que le carbocation du polymère.

On interprète la cinétique et les poids moléculaires en termes d'un schéma réactionnel simplifié dans lequel la terminaison se produit spontanément ou par réaction avec un phénol qui n'est pas complexé. Les constantes de vitesse pour la terminaison par des phénols porteurs de groupes méthyles sont environ un dixième de la constante de vitesse de propagation alors que celles des *tert*-butyl-2 alkyl-4 phénols sont égales à un centième de la constante de vitesse de propagation.

[Traduit par le journal]

Introduction

Isobutene undergoes cationic polymerization in the presence of Lewis acids such as aluminum chloride (1), titanium tetrachloride (2), and stannic chloride (3). With most metal halides, a coinitiator such as water (3) or trichloracetic acid (2) is also required. Polymerizations proceed at measurable rates at −78.5°C with stannic chloride as the Lewis acid and alkylphenols as coinitiators (4); the polymerization mixtures are homogeneous over a wide range of reactant concentrations. Phenolic coinitiators have the advantage that the number, type, and position of alkyl substituents can be varied, and the influence of particular variables on the rate and degree of polymerization readily studied.

In earlier work it was shown that certain unhindered phenols increase the rate of polymerization of isobutene in ethyl chloride when stannic chloride is used as initiator (4). Over the concentration ranges studied, the rate continuously increased with phenol concentration for the coinitiators 2,6-dimethylphenol and 2,3,4,6-tetramethylphenol. On the other hand, 2-*sec*-butylphenol and 2,6-diisopropylphenol gave lower rates of polymerization as their concentrations were raised. Phenol itself caused a sharp rise in rate of polymerization at concentrations

0008-4042/79/182355-09$01.00/0

up to 0.02 *M* but addition of larger amounts caused the rate to go through a maximum and to decrease in the concentration range 0.025–0.07 *M*. It was predicted that the coinitiators 2,6-dimethylphenol and 2,3,4,6-tetramethylphenol would follow the same general behavior as phenol provided that the polymerization was studied over a sufficiently wide range of coinitiator concentrations. One objective of the present study was to determine whether this prediction was correct.

The proposed mechanism (4) includes a termination step in which the growing polymer carbenium ion reacts with free uncomplexed phenol, the phenol thereby becoming incorporated as a polymer end group. It was found that 2-*sec*-butylphenol and 2,6-diisopropylphenol were incorporated in the polyisobutene (5) but the fraction of polymer molecules with end groups derived from phenol was thought to be predominant. The position of attack of the polymer carbenium ion on the phenol was not firmly established. Recently it has been found that the polyisobutene chain is attached at the 4-position of 2,6-di-*tert*-butylphenol (6), a substance which acts as a strong retarder for the polymerization. Unhindered phenols which lack a substituent at the 4-position should also be susceptible to attack by polyisobutene carbenium ions. If the 4-position is blocked by a methyl or *tert*-butyl group, attack might occur at a 2- or 6-position, if free, or at the oxygen of the OH. The relative importance of these various termination steps can be investigated by means of rate and molecular weight studies and by end group analysis. The major objective of this work was then to obtain a more detailed understanding of the ways in which phenols act as terminating agents.

Experimental

Materials

Isobutene, ethyl chloride, and stannic chloride were purified by distillation on the vacuum line as described earlier (4). The solid phenols were recrystallized from methanol–water or ethanol–water mixtures and then sublimed at low pressure. The low melting solid, 2,6-di-*tert*-butylphenol, was purified by chromatography on a neutral alumina column with petroleum ether and benzene as eluents, followed by sublimation. The liquid phenols, 2,4-dimethylphenol and 2,6-diisopropylphenol were also subjected to chromatography.

2,4,6-Trimethylphenol-*d* and 2,3,5,6-tetramethylphenol-*d* were prepared by exchange with D_2O. A few drops of D_2O were added to a weighed amount of the phenol in the reaction tube which was then immersed in liquid nitrogen and evacuated. Ethyl chloride (0.3 mL) was condensed in the tube, the mixture was allowed to reach equilibrium, and the solvent and D_2O then removed by allowing them to vaporize repeatedly into a 100 mL volume and the vapor then pumped off. This treatment leads to effectively complete removal of water and no loss of phenol, the rate and degree of polymerization being unaffected when H_2O was used instead of D_2O.

Procedure

Polymerization mixtures for kinetic studies were prepared as described in an earlier study (4). The initial monomer concentration was 3.2 *M*, and the total stannic chloride concentration 0.185 *M*; the temperature was normally −78.5°C but some measurements were made at −63°C. Initial rates of polymerization obtained from dilatometric measurements were in good agreement with those determined by polymer precipitation. When required, the whole course of the polymerization could be followed by dilatometry. For molecular weight studies the polymer was precipitated after 10–20% reaction by addition of ethanol at −78.5°C, washing with cold ethanol, and drying in a vacuum oven at 40°C. High molecular weight samples for membrane osmometry were not reprecipitated but in polymerizations where the phenol concentration was high it was necessary to remove traces of free phenol by reprecipitation as its presence affected both molecular weight analysis by vapor pressure osmometry and spectroscopic analysis of phenol end groups.

Number average molecular weights, $\overline{M}_n$, of polyisobutenes of molecular weight greater than 8000 were determined by means of a Hewlett Packard HP-501 membrane osmometer with Sartorius SM 11536 or SM 11539 membranes; the latter allowed determination of $\overline{M}_n$ in the 8000 to 15 000 range with only a small correction because of polymer diffusion through the membrane. The solvent for these studies was toluene. Molecular weights less than 8000 were determined either by means of a Hewlett Packard 302B vapor pressure osmometer with carbon tetrachloride as solvent or by gel permeation chromatography. The gel chromatograph was a Water Associates GPC 200 instrument with toluene as eluent and the operating temperature was 60°C. Some recent studies were made by means of a Waters Associates ALC/GPC 244 chromatograph with refractive index and uv absorbance detection. The instruments were calibrated using standard polystyrene samples and molecular weights were calculated by the hydrodynamic volume method (7). The advantage of gel permeation chromatography is that it gives satisfactory estimates of molecular weight for samples containing small amounts of residual phenol; reprecipitation removes a little of the very low molecular weight polyisobutene in addition to free phenol.

Nuclear magnetic resonance spectra were obtained by means of a Bruker HFX-60 spectrometer. For studies of complexing between the phenols and stannic chloride the solvent was ethyl chloride or deuterated chloroform; with ethyl chloride, spectra were determined at temperatures down to 180 K and occasionally 143 K. The solutions containing the alkyl phenol (0.02–0.27 *M*) and stannic chloride (0.06–0.27 *M*) were made up on the vacuum line and stored at low temperatures.

End group analyses were made using three techniques. ^1H nmr spectra were obtained of polyisobutenes in deuterated chloroform or carbon tetrachloride solution. The presence of phenol end groups and the position of attack of the polymer carbenium ion on the phenol were investigated by means of absorptions in the δ = 6.4–7.2 ppm region. The presence of terminal olefinic groups was investigated using absorptions in the δ = 4.6–4.9 ppm region. The esr spectra of benzene solutions of polymers whose phenolic end groups had been oxidized by lead dioxide were determined by means of a Varian V4502 spectrometer. For concentration studies of radicals of long life, low microwave power was used and the standard was a solution of 2,2-diphenyl-1-picrylhydrazyl. Concentrations of phenolic end groups were normally estimated from uv spectra. Absorbances were measured at the higher wavelength maximum of the polymer substituted

phenol ($\lambda_{max} \sim 284$ nm) and the extinction coefficient was assumed to be that of the phenol under study with an alkyl substituent in the 4-position.

Results

Complex Formation between Alkylphenols and Stannic Chloride

Addition of stannic chloride to an ethyl chloride solution of a phenol causes the OH proton resonance to move to a lower field. The magnitude of the change increases with stannic chloride concentration and with decrease in temperature. After due allowance for phenol dimerization, the results are interpreted (4) in terms of complex formation between stannic chloride and the phenol.

[1] $SnCl_4 + ArOH \rightleftharpoons SnCl_4 \cdot ArOH$

The 1:1 complexes are favored at low concentrations of weak donors but if the phenol concentration is high and the temperature low, some 1:2 complex formation may also occur. The nmr data yield the following estimates of the equilibrium constant, K_X, for reaction [1] at -78.5°C: 2,6-dimethylphenol, 2.5 M^{-1}; 2,6-diisopropylphenol, 2 M^{-1}; 2,6-di-*tert*-butylphenol, 0.0 M^{-1}; 2,4-dimethylphenol, 15 M^{-1}; 2-*tert*-butyl-4-methylphenol, 2M^{-1}; 2,4-di-*tert*-butylphenol, 2 M^{-1}; 2,3,6-trimethylphenol, 3 M^{-1}; 2,4,6-trimethylphenol, 15 M^{-1}; 2,3,5,6-tetramethylphenol, 3 M^{-1}; 2,3,4,6-tetramethylphenol, 15 M^{-1}. It was not possible to observe directly, even at 143 K, the value of the chemical shift, δ, for the OH proton in the 1:1 complex, and the assumption was made that $\delta = 10.0$ ppm for all complexes (4). The uncertainty in the concentration of complex may be as high as 20% and the corresponding uncertainty in K_X approximately 40%. ΔH values for reaction [1] range from -1.3 kcal mol^{-1} for complex formation between stannic chloride and 2,6-diisopropylphenol to -3.2 kcal mol^{-1} for complex formation with 2,4,6-trimethylphenol. These values of K_X and ΔH are preferred to those determined earlier (4) because they apply to the same solvent as that used in kinetic experiments and to the same temperature range.

Rates of Polymerization

A typical plot of extent of reaction vs. time for a reaction mixture containing 3.2 *M* isobutene, 0.185 *M* stannic chloride in ethyl chloride, and 0.008 *M* 2,3,4,6-tetramethylphenol is shown in Fig. 1*a*. There is no observable induction period, the rate decreases continuously with time, and the apparent internal order with respect to monomer is close to one. This type of reaction curve was observed at all concentrations of 2,4,6-trimethylphenol and 2,3,4,6-tetramethylphenol and at all but the lowest concentrations of 2,4- and 2,6-dimethylphenol, 2,3,6-trimethylphenol, and 2,3,5,6-tetramethylphenol. At concentrations of these latter phenols less than 0.005 *M* there is some sigmoid character in the conversion–time curves. With 2-*tert*-butyl-4-methylphenol and 2,6-diisopropylphenol, deviations from first order behavior are apparent at all concentrations up to 0.2 *M* (Fig. 1*b*). The rates recorded are those observed for the initial stages of the polymerization and the detailed behavior at high conversion was not investigated.

The broad effect of phenol concentration on initial rate of polymerization is shown in Table 1. These alkylphenols increase the rate of polymerization of isobutene in the presence of stannic chloride at -78.5°C and are therefore all regarded as active coinitiators. 2,6-Diisopropyl phenol gives lower rates than those observed in an earlier study (4) but the recorded rates are believed to be due to the phenol and not to some very active remaining impurity. With the di-, tri-, and tetramethylphenols there is a common pattern of behavior. The initial rate of polymerization rises sharply at low phenol concentrations and then reaches a maximum value; at high phenol concentrations, the rate decreases as more phenol is added. The results for 2,3,5,6-tetramethylphenol are shown in Fig. 2*a*. At concentrations less than 0.005 *M*, this is a very active coinitiator whether judged on the basis of concentration of total phenol in the system or of 1:1 complex with stannic chloride. The rate reaches a maximum, however, at 0.007 *M* 2,3,5,6-tetramethlyphenol and drops to low values at concentrations in the 0.02–

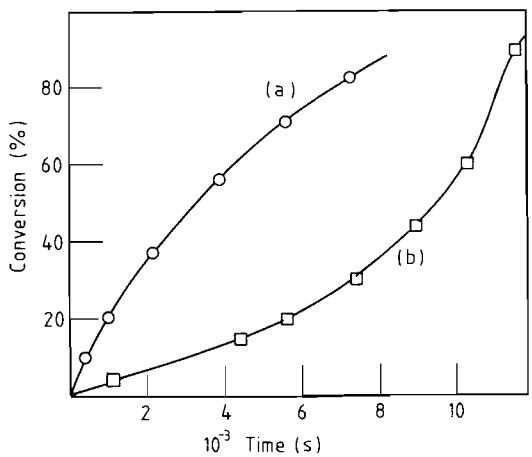

FIG. 1. Plots of conversion vs. time for (*a*) 0.008 *M* 2,3,4,6-tetramethylphenol; (*b*) 0.05 *M* 2-*tert*-butyl-4-methylphenol. Isobutene concentration 3.2 *M*; stannic chloride concentration 0.185 *M*; temperature -78.5°C.

TABLE 1. Effect of coinitiator on rate of polymerization and molecular weight

Phenol	Phenol concentration (M)	Polymerization rate $\times 10^4$ ($M\,s^{-1}$)	Molecular weight
2,4,6-Trimethyl-	0.006	6.6	210 000
	0.020	16.4	145 000
	0.063	78.0	93 000
	0.122	17.0	60 000
2,3,4,6-Tetramethyl-	0.006	7.6	200 000
	0.015	15.1	127 000
	0.023	12.6	110 000
	0.045	26.6	53 000
	0.061	14.9	47 000
2,3,6-Trimethyl-	0.004	3.5	185 000
	0.012	6.1	140 000
	0.030	2.2	62 000
	0.080	1.9	36 000
2,3,5,6-Tetramethyl-	0.002	2.3	230 000
	0.005	12.1	205 000
	0.020	3.0	94 000
	0.058	2.4	38 000
2,6-Dimethyl-	0.007	3.9	135 000
	0.011	6.4	124 000
	0.028	4.6	51 000
	0.050	3.0	39 000
	0.146	2.6	16 000
2,4-Dimethyl-	0.007	2.5	86 000
	0.017	4.2	94 000
	0.030	9.3	26 000
	0.073	4.5	14 000
	0.158	2.2	5 000
2,6-Diisopropyl-	0.012	0.5	43 000
	0.042	0.16	21 000
	0.12	0.04	6 400
2-*tert*-Butyl-4-methyl-	0.013	0.55	350 000
	0.028	0.9	280 000
	0.087	2.8	100 000
	0.157	4.9	64 000
	0.286	6.6	62 000
2,4-Di-*tert*-butyl-	0.006	1.8	275 000
	0.033	2.5	250 000
	0.120	11.2	150 000
	0.173	14.4	93 000
	0.245	12.5	84 000

0.06 M range. 2,4,6-Trimethylphenol shows a similar behavior (Fig. 2*b*), but the highest rates of polymerization are observed at a phenol concentration of 0.063 M. The optimum coinitiator concentrations are $<0.012\,M$ for 2,6-diisopropylphenol, 2,6-dimethylphenol, 2,3,6-trimethylphenol, and 2,3,5,6-tetramethylphenol, in the range 0.018–0.063 M for phenol (4), 2,4-dimethylphenol, 2,4,6-trimethylphenol, and 2,3,4,6-tetramethylphenol, and $>0.1\,M$ for 2,4-di-*tert*-butylphenol and 2-*tert*-butyl-4-methylphenol.

The hindered phenols, 2,6-di-*tert*-butyl-4-methylphenol and 2,4,6-tri-*tert*-butylphenol, do not increase the rate of polymerizaion of isobutene in the presence of stannic chloride. If they are added to polymerization mixtures containing coinitiators such as 2,6-dimethylphenol (0.009 M) or 2,4-di-*tert*-butylphenol (0.033 M), they have little or no effect on the rate of polymerization at concentrations of 2,6-di-*tert*-butyl-4-alkylphenol up to 0.06 M. The small decreases in rate observed at higher concentrations can probably be ascribed to these phenols acting as inert diluents.

At low concentrations, 2,4,6-trimethylphenol-*d* and 2,3,5,6-tetramethylphenol-*d* give rise to rates of polymerization which are close to 50% of the rates

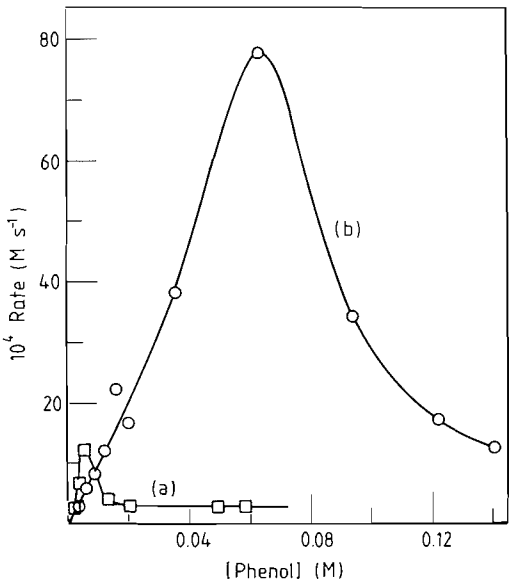

FIG. 2. The effect of total phenol concentration on the rate of polymerization: (*a*) 2,3,5,6-tetramethylphenol, (*b*) 2,4,6-trimethylphenol.

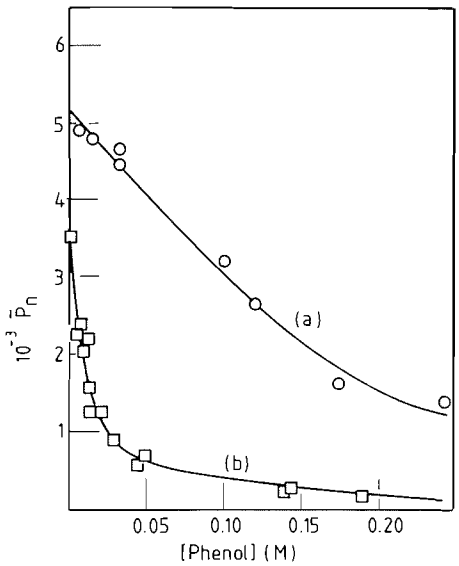

FIG. 3. The effect of phenol concentration on the degree of polymerization: (*a*) 2,4-di-*tert*-butylphenol, (*b*) 2,6-dimethylphenol.

observed with the normal phenols under similar conditions. At higher concentrations of 2,3,5,6-tetramethylphenol-*d* (0.01–0.1 *M*) the isotope effect on rate decreases, but with 2,4,6-trimethylphenol-*d* it is maintained at concentrations up to 0.1 *M*.

A brief study was made of the influence of temperature on the rate of polymerization with 2,4,6-trimethylphenol as coinitiator. At −63°C and at concentrations of added phenol in the range 0.09–0.3 *M*, the rates of polymerization were half the values observed at −78.5°C. Part of this decrease can be ascribed to the lower concentration of initiating complex at the higher temperature, but the overall reaction does appear to have a small negative activation energy.

Molecular Weight Studies

Addition of almost any phenol to a reaction mixture causes a decrease in the degree of polymerization, the magnitude of the effect increasing with concentration of added phenol. Two extreme types of behavior are exemplified by the coinitiators 2,4-di-*tert*-butylphenol and 2,6-dimethylphenol (Fig. 3). With 2,4-di-*tert*-butylphenol there is a slow but steady decrease in molecular weight as its concentration is increased from 0.006–0.25 *M*. In order to reduce the molecular weight to half its value at very low phenol concentration, it is necessary to add 2,4-di-*tert*-butylphenol at a concentration greater than 0.1 *M*. With 2,6-dimethylphenol on the other hand there is a much sharper drop in molecular weight as phenol is added. A reduction to one half the molecular weight is effected by addition of only 0.01 *M* 2,6-dimethylphenol and at 0.1 *M* the molecular weight is about one tenth of that at very low phenol concentration. Some typical values of the polymer molecular weights are given in Table 1. 2,6-Diisopropylphenol and 2,4-dimethylphenol are most active in reducing the molecular weight, followed closely by 2,6-dimethylphenol, 2,3,6-trimethylphenol, and 2,3,5,6-tetramethylphenol. 2,4,6-Trimethylphenol and 2,3,4,6-tetramethylphenol are slightly less active than the corresponding phenols which lack a 4-methyl substituent, and the least active phenols in the table are 2-*tert*-butyl-4-methylphenol and 2,4-di-*tert*-butylphenol.

2,6-Di-*tert*-butylphenol reduces the molecular weight of polyisobutene produced in the presence of an active coinitiator such as 2,6-dimethylphenol; for example, addition of 0.024 *M* 2,6-di-*tert*-butylphenol to a reaction mixture already containing 0.019 *M* 2,6-dimethylphenol reduces the molecular weight from 70 000 to 13 000. If however, the 2,6-di-*tert*-butylphenol possesses a methyl or a *tert*-butyl group at the 4-position, the molecular weight remains essentially unaffected at concentrations of hindered phenol up to 0.06 *M*. Deuteration of an active phenol does not significantly affect the extent to which it reduces the molecular weight of the polymer; 0.14 *M* 2,4,6-trimethylphenol-*d* gives a molecular weight of 150 000 and 0.058 *M* 2,3,5,6-tetramethylphenol-*d* a molecular weight of 40 000, values which are comparable to those obtained with the undeuterated phenols under similar conditions.

End Groups

Polyisobutenes obtained in the presence of 0.05 *M* 2,6-di-*tert*-butylphenol, 2,6-diisopropylphenol, 2,6-dimethylphenol, 2,3,6-trimethylphenol, and 2,3,5,6-tetramethylphenol possess a high proportion of phenolic end groups. Spectroscopic data provide strong evidence that the polyisobutene chain is attached at the 4-positions of these phenols. ^{1}H nmr spectra of polyisobutenes produced in the presence of 2,6-di-*tert*-butylphenol and 2,6-dimethylphenol show single resonances in the aromatic region, as would be anticipated if the end groups contained equivalent *meta* protons. Oxidation of the polymers produced in the presence of 2,6-di-*tert*-butyl-, 2,6-diisopropyl-, and 2,6-dimethylphenol by means of lead dioxide yields radicals whose stabilities and esr spectra are similar to those of the corresponding phenoxy radicals with a *tert*-butyl group in the 4-position. With 2,6-diisopropylphenol for example, a persistent radical is obtained whose hyperfine splittings can be assigned to the α-protons of the isopropyl groups (3.2 G) and the *meta*-protons of the ring (1.7 G); the relatively large splitting due to the *para*-proton in 2,6-diisopropylphenoxyl is absent from the spectrum of the oxidized polymer. The uv spectra of the polymers show maxima at 284 nm, consistent with alkyl substitution at the 4-position. The absorbance at 284 nm for the polymer produced in the presence of 0.012 *M* 2,6-diisopropylphenol indicates the presence of 30% phenolic end groups and for 0.05 *M* phenol in the reaction mixture this rises to 85%. For 0.05 *M* 2,6-dimethylphenol, the percentage of phenolic end groups is estimated to be 70% and for 0.05 *M* 2,3,5,6-tetramethylphenol only 42%, but in all cases the percentage increases with the concentration of phenol in the reaction mixture.

The 2,4-dialkylphenols give largely olefinic end groups even at a phenol concentration of 0.1 *M*. The presence of olefinic groups is indicated by resonances close to $\delta = 4.6$ and 4.8 ppm in the ^{1}H nmr spectrum (5); at the same time the resonances in the aromatic regions are weakened. The uv and nmr studies show that polyisobutene prepared in the presence of 0.15 *M* 2,4-dimethylphenol contains about 40% phenolic and 60% olefinic end groups. The phenolic groups arise mainly from attack of the polymer carbenium ion at the 6-position but some ether formation via simultaneous attack at the OH is not excluded. With the *ortho-tert*-butyl phenols studied, the end groups appear to be almost entirely olefinic even at high phenol concentration; the molecular weights of the isolated polymers are, however, relatively high and the error limits correspondingly large. The uv and nmr data for polymers produced in the presence of 2,4,6-trimethylphenol and 2,3,4,6-tetramethylphenol indicate that the end groups are olefinic. There is no significant absorbance at 284 nm but a weak absorbance in the 265–275 nm region suggests the presence of some phenol ether in the polymer.

Polyisobutenes with phenol end groups may have such end groups concentrated in a particular fraction or distributed evenly over the whole molecular weight range of the polymer. Gel permeation chromatography, with simultaneous uv and refractive index detection, of polyisobutenes with various phenolic contents shows that the percentage of phenolic end groups does not vary significantly with molecular weight. Gel permeation chromatography was also used to investigate the presence of very low molecular weight alkyl phenols in the products. In the standard technique for isolation and purification of the polymer such alkylphenols are removed along with the excess coinitiator. If, however, the reaction is stopped by the addition of a small amount of alcohol and the solvent and monomer removed, a product is obtained which contains the excess phenol and any other low molecular weight materials. In larger scale experiments with 0.2 *M* 2,6-di-*tert*-butylphenol in the reaction mixture, the number of moles of 2,4,6-tri-*tert*-butylphenol was over 5 times the number of moles of phenol-terminated polymer. The 2,4,6-tri-*tert*-butylphenol was initially identified by gel permeation chromatography, the μ-styragel columns resolving the 2,4,6-tri-*tert*-butylphenol from the reactant, 2,6-di-*tert*-butylphenol. In experiments where the 2,6-di-*tert*-butylphenol had almost completely reacted, low molecular weight phenol was sublimed from the product mixture and was shown by mp and mixture mp to be almost pure 2,4,6-tri-*tert*-butylphenol.

Discussion

The rate of polymerization of isobutene (3.2 *M*) in ethyl chloride initiated by stannic chloride (0.185 *M*) at −78.5°C is increased by the addition of any of the phenols studied except the 2,6-di-*tert*-butylphenols. The various 2,6-dimethylphenols increase the rate from less than $5 \times 10^{-6}\ M\ s^{-1}$ in the absence of phenol to $4\text{–}12 \times 10^{-4}\ M\ s^{-1}$ in the presence of 0.005 *M* phenol. Under these conditions the polymer molecular weights remained above 100 000 so that these alkyl phenols can be used at low concentrations to obtain greatly increased rates of polymerization without seriously reducing molecular weights. For reasons given earlier (4), the initiation reaction with phenol as coinitiator is con-

sidered to be reaction [2]:[1]

[2] $SnCl_4 \cdot ArOH \cdot CH_2{=}C(CH_3)_2 \rightarrow (CH_3)_3C^+ \cdot OAr^- \cdot SnCl_4$

The deuterium isotope effect on rate of polymerization indicates that the initiation step, involving proton transfer from phenol to monomer, is slow. At higher concentrations the rates for the various methyl-substituted phenols all reach maximum values, and further addition of these coinitiators causes a decrease in rate of polymerization. In the concentration range studied (0.012–0.12 *M*), increase of 2,6-diisopropylphenol concentration always decreases the rate of polymerization but since the rates are greater than that observed in the absence of added phenol, it is likely that 2,6-diisopropylphenol behaves like the methyl-substituted phenols with an optimum concentration less than 0.012 *M*.

The molecular weight of the polyisobutene is lowered by the addition of a phenol, the reduction becoming larger as the phenol concentration is raised. Phenols thus act as terminating or transfer agents in the polymerization of isobutene. 2,6-Di-*tert*-butylphenol reduces the rate and molecular weight to about the same extent and is therefore a terminating agent. With the other phenols the situation is more complicated because they act as coinitiators, but the simultaneous decrease in rate and molecular weight at higher concentrations of most phenols suggests that termination is again the more important chain breaking reaction.

Two types of end group are formed. Phenols with a vacant 4-position are incorporated in the polymer, the extent increasing with the concentration of added phenol; the preferred position of attack is the vacant 4-position. The 2,4,6-trimethylphenols give olefinic end groups and although some *O*-alkylation may occur, their main function is to increase the rate of proton transfer from the carbenium ion to the negative ion. The two termination steps are shown in [3] and [4].

[3] 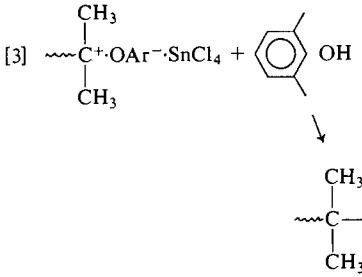

[4] 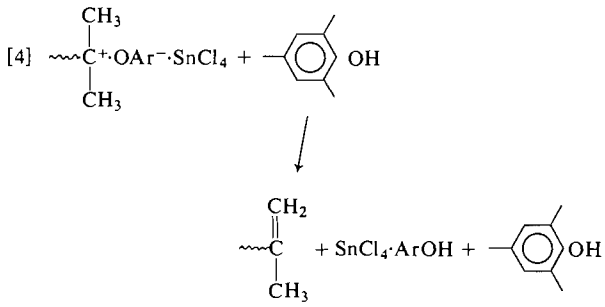

The extent to which phenols terminate by one or both of these mechanisms should be influenced by the basicities of the various sites and by steric factors. Information on the basicities comes from studies of the protonation of methyl-substituted phenols in FSO_3H (8, 9). When the *para*-position of the phenol is unsubstituted, as in 2,6-dimethyl-, 2,3,6-trimethyl-, and 2,3,5,6-tetramethylphenol, protonation occurs almost exclusively at this site. Relative to other centers on the phenol, the 4-position is thus strongly basic, and the polymer carbenium ion attacks at this position, provided that there are no major steric effects. Proton loss occurs from C-4 to give a polyisobutene chain terminated by phenol. Substitution of a methyl group on C-4 reduces the basicity of this carbon and protonation on C-2, C-6, or oxygen can now compete with *para*-protonation. 2,4,6-Trimethylphenol is protonated at oxygen and C-4, but the end groups in the polymerization are almost entirely olefinic and there is no evidence for displacement of the 4-methyl by the polyisobutene carbenium ion. 2,4-Dimethylphenol is largely protonated at oxygen and C-6; the polymerization product possesses both olefinic end groups and some resulting from attack of the carbenium ion at C-6. Reaction [4] appears to proceed most readily with a phenol which possesses a relatively basic oxygen atom.

Further information on the termination reactions is provided by the molecular weight studies. Addition of 2,6-di-*tert*-butyl-4-methylphenol does not affect the polymer molecular weight, thus providing confirmatory evidence that a methyl group at the 4-position prevents attack of the growing carbenium ion on this center in the phenol. It also shows that neither the oxygen in a highly hindered phenol nor a basic carbon (C-4) to which a methyl group is attached readily facilitates the termination reaction [4]. 2,4-Dimethylphenol at a total concentration of 0.1 *M* reduces the polymer molecular weight to below 10 000, while 2-*tert*-butyl-4-methyl- and 2,4-di-*tert*-butylphenol reduce it to about 100 000 at the same total concentration. This result strongly sug-

[1]A referee points out that analytical evidence for the initiating complex is desirable, since monomer complexing is unlikely to proceed to completion.

gests that it is the phenolic oxygen in 2,4-dimethylphenol which is largely responsible for the proton transfer reaction [4] because it is the main basic center to which access is restricted in the 2-*tert*-butylphenols.

The simple mechanism proposed in an earlier paper (4) includes initiation by reaction [2] with rate constant k_i, and termination by reaction [3] with rate constant k_{t2}. Spontaneous termination [5]

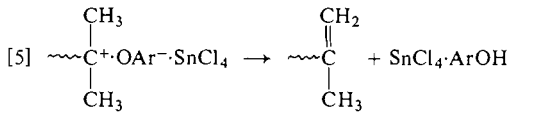

[5]

is also considered with rate constant k_{t1}. Chain propagation is assumed to have a rate constant, k_p, which does not vary with the substituents in the phenol. If these are the only important steps in the polymerization, the overall rate, R_p, is given by [6]

$$[6] \quad R_p = \frac{k_p k_i [X][M]}{k_{t1} + k_{t2}[ArOH]_f}$$

where X is the initiating complex and $[ArOH]_f$ is the concentration of free phenol in the polymerization mixture. The number average degree of polymerization, $\bar{P}_n$, is given by [7].

$$[7] \quad \bar{P}_n = \frac{k_p[M]}{k_{t1} + k_{t2}[ArOH]_f}$$

For 2,6-dimethyl-, 2,3,6-trimethyl-, 2,3,5,6-tetramethyl-, and 2,6-diisopropylphenol, plots of $[X]/R_p$ vs. $[ArOH]_f$ and of $1/\bar{P}_n$ vs. $[ArOH]_f$ are linear. The values of k_{t2}/k_p so obtained are respectively 0.13, 0.08, 0.09, and 0.28 at the reaction temperature of $-78.5°C$. In all cases k_{t1}/k_p was found to be close to 6×10^{-4} *M*. The rate constants for the initiation reaction, k_i, were estimated to be 3.2×10^{-5}, 1.7×10^{-5}, 1.9×10^{-5}, and 1.1×10^{-5} s^{-1} for 2,6-dimethyl-, 2,3,6-trimethyl-, 2,3,5,6-tetramethyl-, and 2,6-diisopropylphenol. The simple reaction scheme thus provides a satisfactory interpretation of the rate and molecular weight data and this is supported by the end group results. Termination by reaction [4] may also occur but because of the relatively high basicity of C-4, it is much less important than termination by reaction [3].

The maximum rates of polymerization for 0.063 *M* 2,4,6-trimethylphenol and 0.030 *M* 2,3,4,6-tetramethylphenol are higher than the maximum rates observed with the other phenols. These 2,4,6-trimethylphenols complex more strongly with stannic chloride and the higher rates can be partly ascribed to higher concentrations of initiating complex and lower concentrations of free phenol. Termination involving attack of the polyisobutene carbenium ion at C-4 does not occur to a significant extent. A major mode of termination has been removed and this too can contribute to relatively high rates of polymerization and polymer molecular weights. It is found, however, that the rates and molecular weights are significantly reduced at higher concentrations of these two phenols. The 4-methyl group increases the basicity of the oxygen which can then participate more readily in proton transfer from the carbenium ion and increase the rate of termination by reaction [4]. Quantitative analysis of the molecular weight results, assuming that reaction [4], rate constant k_{t3}, and reaction [5] are only important termination reactions, provides estimates of k_{t3}/k_p. The values for 2,4,6-trimethyl- and 2,3,4,6-tetramethylphenol are 0.04 and 0.10 respectively; k_{t1}/k_p is again close to 6×10^{-4} *M*. Plots of $[X]/R_p$ vs. $[ArOH]_f$ are not linear, however, and this casts doubt on the method of analysis. Similar difficulties are met with when 2,4-dialkylphenols are used as coinitiators. The molecular weight results lead to k_{t3}/k_p values of 0.25, 0.016, and 0.008 for 2,4-dimethyl-, 2-*tert*-butyl-4-methyl-, and 2,4-di-*tert*-butylphenol; the estimated error is $\pm 30\%$ and no allowance has been made for the simultaneous attack on C-6. The rate plots deviate from linearity and it is clear that 4-alkylphenols affect the reaction rate in more ways than are described in the simple reaction scheme. One factor which has been neglected is the possible formation of 1:2 stannic chloride – phenol complexes at higher concentrations of the more strongly basic phenols. A second is possible increased solvation of the growing carbenium ion by free phenol with a consequent change in its reactivity in propagation and termination reactions. Bywater and Worsfold (10), working with the boron trifluoride – water – diphenylethylene system, have shown that the concentration of carbenium ions passes through a maximum at room temperature when $[BF_3] = 2[H_2O]$, and drops fairly rapidly at higher concentrations of added water. If the stannic chloride – phenol – isobutene system were to behave in comparable fashion, the higher phenol concentrations would lead to a reduction in carbenium ion concentration rather than in its reactivity.

Polymerizations performed in the presence of high concentrations of 2,6-di-*tert*-butylphenol indicate that the initial carbenium ion may have an unusually high reactivity towards bases. With 0.2 *M* 2,6-di-*tert*-butylphenol, a high yield of 2,4,6-tri-*tert*-butylphenol is formed in addition to polymer with di-*tert*-butylphenol end groups. The *tert*-butyl carbenium ion appears to be more reactive towards 2,6-di-*tert*-butylphenol than monomer, whereas the reverse is true for the growing polymer carbenium ion. The coinitiators used in this study are somewhat

less basic than 2,6-di-*tert*-butylphenol but it is possible that they also reduce the concentration of carbenium ions by deactivating the initiating center before it adds a second monomer unit. In these circumstances the free phenol reduces the overall rate of polymerization by removing both the initial active centers and the growing carbenium ions and this may in part explain the surprisingly sharp drop in rate observed with some phenols as their concentrations are increased beyond the optimum values.

The dual role of the coinitiator has been recognized for some time. Water acts as a coinitiator in the polymerization of isobutene and its consumption during the reaction was thought to be, or to be associated with, a kinetic termination (11). Anisole cannot, like phenol, initiate polymerization but it has been shown to be a chain-breaking agent in the cationic polymerization of isobutene (12) and styrene (13). A significant conclusion from the present study is that the coinitiator terminates polymerization by aiding proton transfer from the polymer carbenium ion to the negative ion, in addition to becoming incorporated in the polymer. Knowledge of the concentrations of initiator–coinitiator complex and of free coinitiator leads to a rationalization of the observed rate, molecular weight, and end group data, but a fuller understanding must await better knowledge of the various species present and of the subtle effects exerted by the bases in solution.

Acknowledgements

The authors are grateful to the National Research Council of Canada for an operating grant and for the award of a scholarship. We thank Dr. C. C. Hsu for use of the GPC-200 chromatograph.

1. J. P. KENNEDY and R. M. THOMAS. J. Polym. Sci. **46**, 233 (1960).
2. P. H. PLESCH. J. Chem. Soc. 543 (1950).
3. R. G. W. NORRISH and K. E. RUSSELL. Trans. Faraday Soc. **48**, 91 (1952).
4. R. F. BAUER and K. E. RUSSELL. Can. J. Chem. **48**, 1251 (1970).
5. R. F. BAUER and K. E. RUSSELL. J. Polym. Sci. Part A, **9**, 1451 (1971).
6. K. E. RUSSELL and L. G. M. C. VAIL. J. Polym. Sci. Polym. Symp. **56**, 183 (1976).
7. Z. GRUBISIC, P. REMPP, and H. BENOIT. Polym. Lett. **5**, 753 (1967).
8. R. F. CHILDS and B. D. PARRINGTON. Can. J. Chem. **52**, 3303 (1974).
9. S. M. BLACKSTOCK, K. E. RICHARDS, and G. J. WRIGHT. Can. J. Chem. **52**, 3313 (1974).
10. S. BYWATER and D. J. WORSFOLD. Can. J. Chem. **55**, 85 (1977).
11. P. H. PLESCH. The chemistry of cationic polymerization. The MacMillan Company. New York. 1963. p. 193.
12. J. PENFOLD and P. H. PLESCH. Proc. Chem. Soc. 311 (1961).
13. G. F. ENDRES and C. G. OVERBERGER. J. Am. Chem. Soc. **77**, 2201 (1955).

Carbon-13 nuclear magnetic resonance studies of the cholesteryl ester – phosphatidylcholine system

ROBERT J. CUSHLEY AND BRUCE J. FORREST

Department of Chemistry, Simon Fraser University, Burnaby, B.C., Canada V5A 1S6

Received March 26, 1979

ROBERT J. CUSHLEY and BRUCE J. FORREST. Can. J. Chem. **57**, 2364 (1979).

Using difference spectroscopy, ^{13}C spin–lattice relaxation measurements on 40% egg phosphatidylcholine multilamellar liposomes (containing 25 mol% cholesteryl palmitate) – 60% D_2O indicate the ester contributes negligibly to the microviscosity of the acyl chains in the bilayers.

At 37°C, spin–spin and spin–lattice relaxation measurements have been obtained for 25 mol% cholesteryl linoleate in both egg phosphatidylcholine and dipalmitoyl phosphatidylcholine multilayers and indicate: (*a*) T_1 values of the linoleate ester chain are 0.5 times those of the lecithin chain carbons, and (*b*) $T_2^* = 16 \pm 6$ ms for *all* discernable linoleate carbons. At 52°C, cholesteryl ring carbons C5 and C6 yield T_2^* values of 23 and 20 ms, respectively. These studies suggest the esters reside in an environment whose "fluidity" approaches that found in very low density lipoprotein (VLDL).

ROBERT J. CUSHLEY et BRUCE J. FORREST. Can. J. Chem. **57**, 2364 (1979).

En se basant sur de la spectroscopie de différence, des mesures de relaxation spin–réseau ^{13}C sur des solutions à 40% de liposomes multicouches de phosphatidylcholine d'oeuf (contenant 25 mol% de palmitate de cholestéryle) dans 60% de D_2O indiquent que la contribution de l'ester à la microviscosité des chaînes acyles des doubles couches est négligeable.

A 37°C, on a obtenu des mesures de relaxation spin–spin et spin–réseau pour des solutions à 25% de linoléate de cholestéryle dans des multicouches de phosphatidylcholine d'oeuf ainsi que dephosphatidylcholine de dipalmitoyle et ces résultats indiquent: (*a*) que les valeurs T_1 de l'ester linoléate correspondent à 0.5 fois celles des carbones de la chaîne de lécithine et (*b*) que $T_2^* = 16 \pm 6$ ms pour *tous* les carbones de linoléate discernables. A 52°C, les valeurs T_2^* des carbones 5 et 6 du cholestérol sont respectivement 23 et 20 ms. Ces études suggèrent que l'ester se trouve dans un environnement dont "la fluidité" est semblable à celle que l'on trouve dans des lipoprotéines de très basse densité (LTBD).

[Traduit par le journal]

Introduction

Plasma lipoproteins provide the vehicle for the transport, and hence metabolism, of cholesterol and its fatty acid esters. Because of the key role played by lipoproteins, much effort has gone into determining composition, structure, and interactions of the various components. In particular, recent ^{13}C nmr studies on human high density lipoprotein (HDL), low density lipoprotein (LDL), and very low density lipoprotein (VLDL) (1–4) have established that high resolution spectra are obtained for the lipid components of lipoproteins. Use of model systems, including cholesteryl oleate (CO) and cholesteryl linoleate (CLa), neat and in $CHCl_3$ solution (1, 3), in mixture with the triglyceride triolein (4, 5), and in a lamellar liquid crystalline mixture with egg phosphatidylcholine (egg PC) (3), have established that the acyl chains of the lipid experience a microviscosity lower than found for phosphatidylcholine at the same temperature. That is, the lipid chains in lipoprotein could be said to be more "fluid" than the lipid chains in lecithin. The cholesterol, on the other hand, experienced a much higher microviscosity and, based on comparison of spin–spin and spin–lattice relaxation rates for cholesterol carbons, the cholesteryl moiety appears most likely to be undergoing rapid, anisotropic motions. However, the cholesteryl ring was said to demonstrate "a liquid rather than a liquid-crystalline mobility" in cholesteryl esters (1, 4). Unfortunately, because ^{13}C resonance signals of the acyl chains of cholesteryl esters, triglycerides, and phospholipids overlap, unique parameters attributed only to esters are difficult to attain.

A further significant feature of cholesteryl esters is their connection to the initiation process of atherosclerosis. The most significant changes in lipid content in aortic tissue is the increment in cholesteryl ester concentration (6). That cholesteryl ester accumulates more rapidly than free cholesterol has been shown by St. Clair *et al.* (7) to occur in pigeon aorta after 14 days of feeding cholesterol and in only 3 days in rabbit aorta (8). It has been reported that permeability to lactate, iodide, and

0008-4042/79/182364-07$01.00/0

glucose is much higher in sclerotic human aorta than in normal tissue (9, 10). The suggestion has been made that, even before morphological changes appear, certain areas of the artery are predisposed to lesions and these areas show increased cholesteryl ester content (11).

In this report, we present data on the interactions between cholesteryl esters and phospholipids. We have measured ^{13}C relaxation times for systems containing (*1*) the saturated ester cholesteryl palmitate (CP) in egg PC multibilayers, and (*2*) the unsaturated ester cholesteryl linoleate (CLa) in mixtures of either egg PC or dipalmitoyl phosphatidylcholine (DPPC) multibilayers. These studies were performed at temperatures of 37 and 52°C. The ratio of cholesteryl ester to phosphatidylcholine was set at 1:3 which is consistent with that found in aortic intima of young humans (12). This ratio is somewhat higher in HDL (1:1) and LDL (2:1); however, the general results apply equally to the lipoprotein case.

Data are obtained only for ester resonances by using difference spectra and mixtures of cholesteryl esters and phospholipids in combinations such that the gel → liquid crystalline phase transition temperature for phospholipids or the liquid crystalline → isotropic phase transition temperature for the ester are separated by the temperature of the nmr run.

Experimental

Egg yolk phosphatidylcholine (egg PC) was extracted from fresh egg yolks by the method of Singleton *et al.* (13). Thin layer chromatographic analysis ($CHCl_3$:MeOH:H_2O = 65:25:4) showed a single spot when sprayed with 50% H_2SO_4 and heated, or when exposed to I_2 vapour. The fatty acid composition was determined by glpc analysis of the corresponding methyl esters using the methylating agent, Methelute (methanolic trimethylanilinium hydroxide) 0.2 *M* (Aldrich). Peaks were identified by comparison with known standards. D,L-Dipalmitoylphosphatidylcholine (DPPC), 99%, cholesteryl palmitate (CP), 99%, and cholesteryl linoleate (CLa), 99%, were obtained from Sigma Chemical Co., and used without further purification.

Lecithin multilamellar liposomes, 40% w/v in either D_2O or 0.3 *M* sucrose in D_2O, were prepared by mechanical shaking of the dry lipid with a suitable volume of the aqueous phase. These dispersions were stabilized by approximately 6 heat–freeze–thaw cycles. Homogeneous, mixed dispersions of phosphatidylcholine:cholesteryl ester = 3:1 mole ratio were prepared in a similar manner by first co-dissolving both components in chloroform, solvent evaporation, and exhaustive pumping to obtain the dry lipid mixture.

Carbon-13 nmr spectra were determined at either 37 or 52°C at 25.2 MHz on a temperature controlled Varian XL-100-15 nmr spectrometer operating in the pulse Fourier transform mode using an internal ^2H field-frequency lock and an 8K dataset. T_1 relaxation times were measured using a $(\pi/2|_{0^\circ} - \tau - \pi/2|_{0^\circ} - AT)_n$ scheme. The data acquisition, AT, occurs at the conclusion of every two pulse sequence separated by a delay time, τ. A field spoiling pulse, duration = 50 μs, is applied during the delay time (14). The error in the T_1 and T_2^* relaxation times is ±10%. Chemical shifts (δ) are ppm downfield from external tetramethylsilane (TMS).

Results and Discussion

We have found that 25 mol% cholesteryl palmitate or linoleate could be suspended in 40% w/v egg PC or DPPC multilamellar liposomes prepared in D_2O (this is a 53 mol% solution of egg PC) for up to 12 h and in 0.3 *M* sucrose for several days. These samples appeared macroscopically homogeneous; however, in light of previous work (15–17), it is probable that ester in excess of approximately 5 mol% is present as a *separate phase*, either trapped between the "onion skin" layers of the egg PC liposomes, or as patches within the hydrophobic region of the bilayers.

The ^{13}C nmr spectrum of 40% w/v egg PC multilamellar liposomes in D_2O at 37°C is shown in Fig. 1*A*. Well resolved signals for carbonyl (δ 173–174), unsaturated carbons (δ 128–129), choline (δ 60–72), and acyl chain (δ 23–32) are found while the choline $N^+(CH_3)_3$ and fatty acid CH_3 groups are extremely sharp lines at δ 54.3 and δ 14.4, respectively. The spectrum is determined some 40°C above the gel to liquid crystalline phase transition for egg PC, and the resonances, although broad, are still resolved. This is so since the carbons undergo a rapid, coupled reorientation along the molecular long axis and thus reflect only the orientational order of the carbon nucleus in the bilayer and not the long correlation time for liposome rotation, ~0.1 s (18–21). Such an explanation is necessary and sufficient to explain the gradient in T_1 (see Table 1) along the acyl chain.

The intensities of the resonance signals in Fig. 1*A* are consistent with a 60:40 ratio of saturated to unsaturated fatty acids in egg PC. The glpc analysis gave 42.7% palmitic acid, 16.9% stearic acid, 27.7% oleic acid, 11% linoleic acid, and 1.6% palmitoleic acid.

The effect of adding 25 mol% CP to egg PC multilamellar liposomes (40% w/v in D_2O at 37°C) is shown in Fig. 1*B*. The spectra in Figs. 1*A* and 1*B* are very similar. The spin lattice relaxation times for the resonance signals in Fig. 1*A* (column 2) and for the signals in Fig. 1*B* (column 3) appear in Table 1. Within experimental error, the relaxation behaviour of the system is identical, whether the 25 mol% of cholesteryl palmitate is present or absent. The difference spectrum (Fig. 1*C*) yields a "baseline" indicating that the cholesteryl palmitate contributes negligibly to the observed intensity; i.e., the spectrum

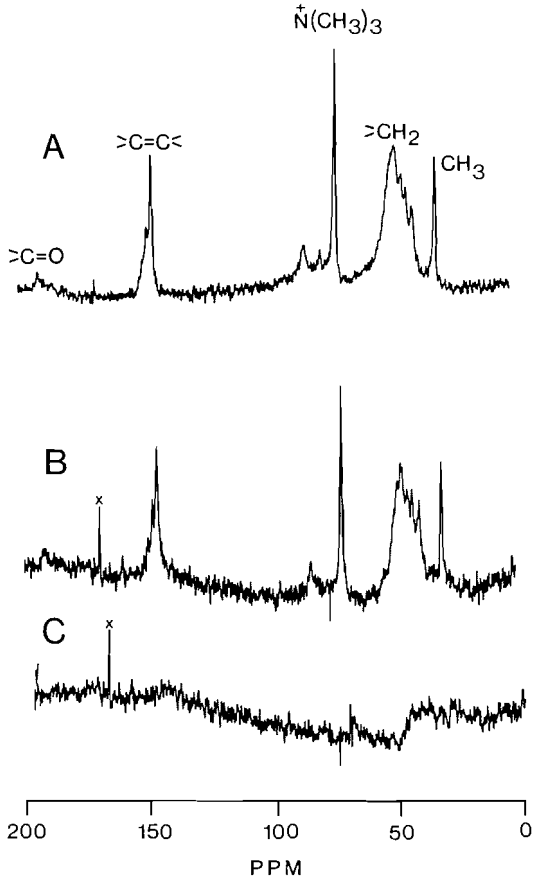

FIG. 1. (*A*) Proton noise decoupled ^{13}C nmr spectrum of a 40% w/v egg phosphatidylcholine multilamellar dispersion in D_2O at 37°C. Sweep width = 5000 Hz; rf pulse = 15 μs (60° flip angle); dataset = 8192; line broadening = 2 Hz. Field increases to the right. (*B*) Proton noise decoupled ^{13}C nmr spectrum of a 40% w/v egg phosphatidylcholine dispersion in D_2O containing 25 mol% cholesteryl palmitate at 37°C. Spectral parameters identical to (*A*). X is a spectrometer artifact. (*C*) Difference spectrum, (*B*) − (*A*).

is wholly due to the egg PC resonances. This is expected since, at 37°C, CP exists as a solid within the liposomes and the slow overall rotation of liposomes does not average out the ^{13}C–^{1}H dipolar interaction, hence, the ^{13}C resonance signals are significantly broadened and lost in the baseline noise. We conclude that there is no effect upon the microviscosity of the PC acyl chain by incorporation of large amounts of cholesteryl ester.

The ^{13}C nmr spectrum of a 40% w/v solution of egg PC liposomes containing 25 mol% cholesteryl linoleate in a 0.3 *M* sucrose solution in D_2O, and at 37°C, is featured in Fig. 2. The resonances of fatty acids esterified to cholesterol, and those esterified to lecithin overlap. Hence, the only peak which may be assigned to lecithin alone is that of $-N^+(CH_3)_3$ (δ 54.3).

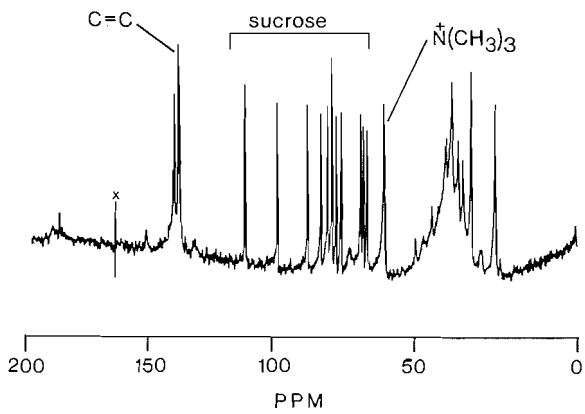

FIG. 2. Proton noise decoupled ^{13}C nmr spectrum of a 40% w/v dispersion of egg phosphatidylcholine plus 0.3 *M* sucrose in D_2O containing 25 mol% cholesteryl linoleate at 37°C. Spectral parameters as in Fig. 1.

In order to elucidate the origin of the sharp components of the spectrum of the egg PC-cholesteryl linoleate mixed liposomes, further experiments were undertaken using the fully saturated phospholipid, dipalmitoyl phosphatidylcholine (DPPC). The spectrum of a DPPC multilamellar dispersion in 0.3 *M* sucrose at 37°C is shown in Fig. 3*A*. Note that the only resonance resolved due to DPPC is that of the $N^+(CH_3)_3$ carbons. Even this resonance is severely broadened (width at half-height = 70 Hz) since the phospholipid is below the gel → liquid crystalline phase transition temperature (T_m = 41°C). (All of the sharp resonances downfield from the trimethylammonium resonance are due to sucrose.)

The spectrum in Fig. 3*A* may be compared with that obtained for DPPC multilamellar liposomes containing 25 mol% cholesteryl linoleate under identical conditions (Fig. 3*B*). At 37°C, the cholesteryl linoleate is in the isotropic liquid state (T_m = 35.5°C) while DPPC is in the gel state. While the lecithin trimethylammonium resonance is still extremely broad, the intensity and sharpness of the resonances in the olefinic region are clear. The δ 129.0 and δ 130.7 olefinic resonances may be unequivocally assigned to the 10,12 and 9,13 carbons, respectively, of the linoleate moiety of the cholesteryl ester since DPPC possesses two fully saturated fatty acid chains. In addition, a family of sharp lines is present upfield in the region of the alkyl carbons and must also be due to the cholesteryl ester. Figure 4*A* shows the ^{13}C nmr spectrum of pure DPPC multilamellar liposomes in 0.3 *M* sucrose at 52°C, 11 deg. above the gel → liquid crystalline transition temperature. In addition to the trimethylammonium resonance, three other very broad resonances are resolved. They are, moving to higher field, carbons 4–13 of the palmitate chains, the penultimate carbons

TABLE 1. Carbon-13 spin–lattice relaxation times (s) of 40% w/v egg phosphatidylcholine multilamellar dispersions in 0.3 *M* sucrose/D_2O (37°C)

Carbon	Egg PC	Egg PC + 25 mol% cholesteryl palmitate (CP)	Egg PC + 25 mol% cholesteryl linoleate (CLa)
$N^+(Me)_3$	0.52	0.44	0.50
$(CH_2)_n$	0.48	0.46	0.24
$C^*H_2CH_2CH_3$	[a]	[a]	0.51
$C^*H_2CH_3$	1.06	1.10	0.61
CH_3	2.83	2.43	1.98
C=C—C*—C=	0.55	0.62	0.28
C*—C=C	0.47	0.53	0.26
C*=C—C—C=C*	0.66	0.58	0.32
C=C*—C—C*=C	0.75	0.69	0.38

[a]Peaks not resolved.

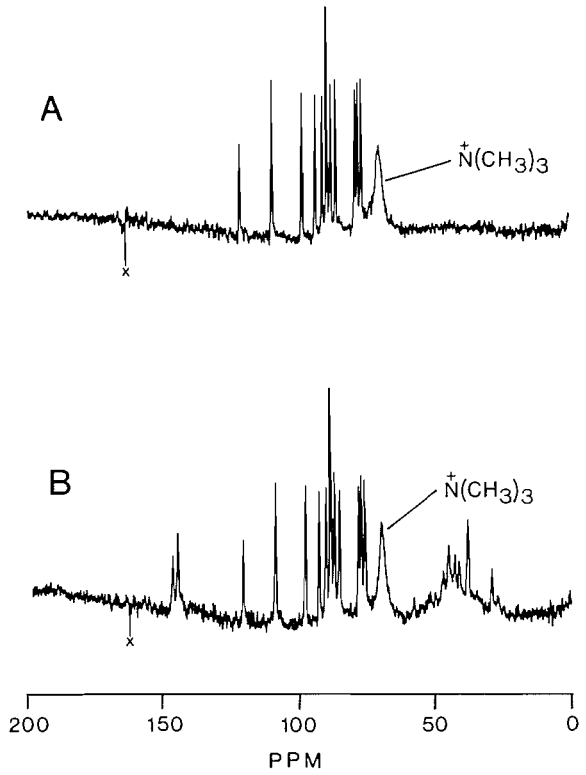

FIG. 3. (*A*) Proton noise decoupled ^{13}C nmr spectrum of a 40% w/v dipalmitoyl phosphatidylcholine dispersion plus 0.3 *M* sucrose in D_2O at 37°C. (*B*) Proton noise decoupled ^{13}C nmr spectrum of a 40% w/v dispersion of dipalmitoyl phosphatidylcholine plus 0.3 *M* sucrose in D_2O containing 25 mol% cholesteryl linoleate at 37°C. Spectral parameters as in Fig. 1.

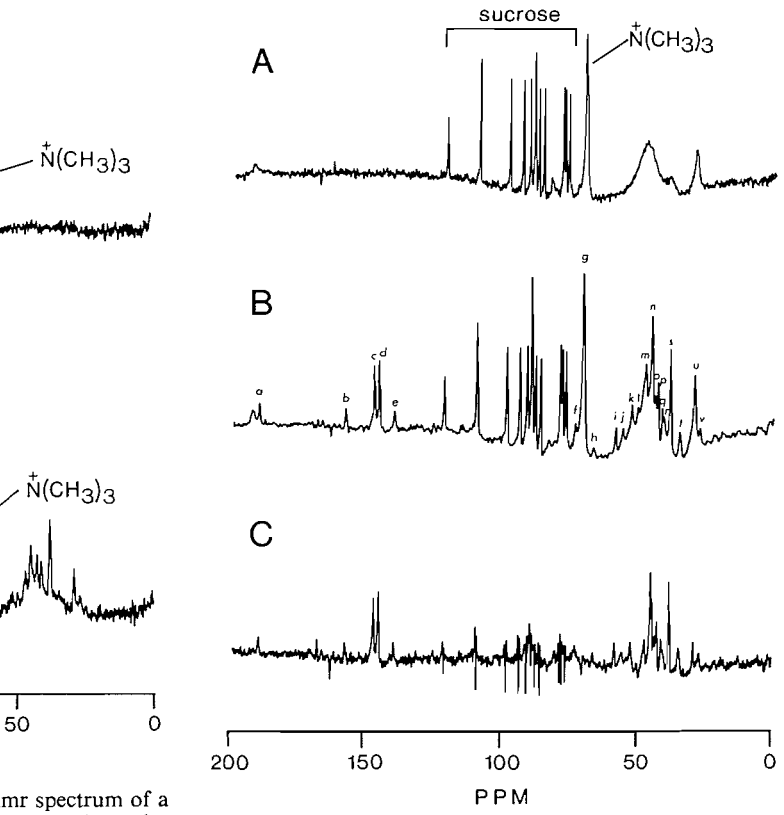

FIG. 4. (*A*) Proton noise decoupled ^{13}C nmr spectrum of a 40% w/v dispersion of dipalmitoyl phosphatidylcholine plus 0.3 *M* sucrose in D_2O at 52°C. (*B*) Proton noise decoupled ^{13}C nmr spectrum of a 40% w/v dipalmitoyl phosphatidylcholine dispersion plus 0.3 *M* sucrose in D_2O containing 25 mol% cholesteryl linoleate at 52°C. Spectral parameters as in Fig. 1. Peak assignments given in Table 2. (*C*) Difference spectrum, (*B*) − (*A*).

($\omega - 1$) of the palmitate chains which appear as a high field shoulder, and the terminal methyls (ω) – the resonance at highest field. The spectrum of a 3:1 mixture of DPPC – cholesteryl linoleate liposomes at 52°C is shown in Fig. 4*B*. In addition to sharp resonances due to the linoleate moiety, resonances are also resolved for carbons of the steroid nucleus, notably those of the unsaturated carbons C5 and C6 which flank the linoleate olefinic carbons. Assignments are given in Table 2. The difference spectrum, DPPC with cholesteryl linoleate minus DPPC, is shown in Fig. 4*C*. Even above the T_m of DPPC, therefore, the intensity of the sharp spectral lines is due only to the ester, although certain of

TABLE 2. Carbon-13 assignments of cholesteryl linoleate carbons in 40% w/v dispersions of dipalmitoyl phosphatidylcholine in 0.3 *M* sucrose/D_2O at 50°C (Fig. 4*B*). Primed numbers refer to carbons of the linoleate chain. Italicized numbers refer to carbons of the cholesteryl moiety

Peak	Assignment	Chemical shift (ppm)
a	C1′	171.1
b	*C5*	140.1
c	C13′, C9′	130.1
d	C10′, C12′	128.4
e	*C6*	122.5
f	*C14, C17*	57.3
g	$N^+(Me)_3$ of DPPC	54.7
h	*C9*	50.3
i	*C13*	42.6
j	*C12, C24*	39.9
k	*C1, C10, C20, C22*	36.8
l	C2′	34.4
m	C16′	31.9
n	C4′, C5′, C7′, C15′	29.8
o	*C16, C25*	28.3
p	C8′, C14′	27.6
q	C11′	26.0
r	*C15, C23*	25.2
s	C17′, *C26, C27*	23.0
t	*C19, C21*	19.1
u	C18′	14.3
v	*C18*	12.0

these peaks are superimposed on very broad phospholipid resonances.

The spin–lattice relaxation times for 40% w/v egg PC + 25 mol% cholesteryl linoleate were measured and appear in Table 1 (column 4). The relaxation times are much shorter than those obtained for the lecithin carbons alone or in the presence of 25 mol% cholesteryl palmitate with the exception of the lone resonance assigned to the phospholipid $N^+(CH_3)_3$ which yields a relatively unchanged relaxation time (0.52 vs. 0.50 s). The ^{13}C T_1 relaxation times for lecithin dispersions with incorporated cholesteryl linoleate reflect the motional freedom of the ester since it is only the ester carbons which contribute to the spectral intensity. The constancy of the spin–lattice relaxation time of the $N^+(CH_3)_3$ peak in free egg PC or egg PC with either cholesteryl palmitate or cholesteryl linoleate added indicates the ester is apparently not associated with the headgroup region.

It is interesting that the linoleate moiety of the cholesterol ester exhibits such low spin–lattice relaxation times. The T_1's are approximately half those observed for phospholipid fatty acid chains, although these values do increase as the chain terminus is approached. Relaxation times of 0.24, 0.51, 0.61, and 1.98 s were determined for the $(CH_2)_n$, $\omega - 2$, $\omega - 1$, and ω carbons, respectively. Thus, a fluidity gradient exists along the cholesteryl ester chain. However, the lower values indicate more limited mobility than experienced by phospholipid fatty acid chains at the same temperature. This phenomenon has been previously noted for a single linoleate carbon, C14, of enriched cholesteryl linoleate present in a turbid dispersion of lecithin, sphingomyelin, cholesterol, and cholesterol linoleate (22, 23). The value of 0.25 s determined for the relaxation time of C14 in the previous investigations is in excellent agreement with the value of 0.26 s determined for the lecithin – cholesteryl linoleate dispersion in this work. A comparison between the T_1's for CLa in egg PC multibilayers at 37°C and the "ester" T_1's for LDL and HDL at 36°C (1) indicates the relaxation times of CLa in egg PC are approximately 40% longer whereas they are only ~6% longer than the T_1's measured for VLDL (1). Comparison of spin–lattice relaxation of CLa in egg PC vs. relaxation of the related ester, cholesteryl oleate (CO), 0.56 *M* in $CHCl_3$ at 48°C (1), indicates that the CO spin–lattice relaxation times are >300% longer than those of CLa. A neat solution of CO, at 48°C, has T_1 = 240 ms for the unsaturated chain carbons C9 and C10 (5) which is from 25–37% shorter than the CLa unsaturated carbons (Table 1). In sum, the microviscosity of the acyl chain of CLa in model membranes composed of CLa:egg PC is essentially the same as the microviscosity one calculates for VLDL and lower than the microviscosity calculated for LDL and HDL. On the other hand, it is several times higher than the calculated microviscosity for CO in chloroform solution.

From the work of Janiak *et al.* (15) it may be reasonably assumed that less than 5% of the CLa is present in a homogeneous phospholipid–ester lamellar phase; i.e., where the ester molecules would be intercalated between PC molecules. The excess ester would be present as a separate phase.

At 37°C, this separate phase of CLa may be either present as small isotropic lipid droplets captured in the aqueous phase between the lamellae of the liposomes, or as patches of ester in the hydrocarbon interior of the bilayers. It has been reported (24) that extremely small quantities (0.1–0.5%) of cholesteryl esters may be suspended in aqueous solution above the melting point of the ester. Considering the large amounts of ester used in the present study, it is highly unlikely that the excess ester is suspended as droplets in the aqueous phase. Rather, it is more probable that small ester droplets are associated with the hydrophobic region of the phospholipid bilayer.

At 37°C, CLa is just above the cholesteric → isotropic phase transition (34–35°C). The average spin–spin relaxation time, T_2*, where $T_2^* = \pi\Delta\nu_{1/2}$ and $\Delta\nu_{1/2}$ is the linewidth at half-height, for *all* acyl chain carbons of CLa in DPPC multilayers at 37°C is 16 ms ± 6 ms (Table 3). The T_2* of phospholipid —$N(CH_3)_3$ = 5 ms, and of the high field sucrose resonance = 25 ms, in the same system. When the temperature is raised to 52°C, the acyl chain carbon T_2*'s increase only marginally to an average value of 18.5 ms, and this is seen to be due essentially to the olefinic carbons C9 to C13 (Table 3). At 52°C, T_2* for choline $\overset{*}{N}(CH_3)_3$ is increased to essentially equal that of the ester (14 ms). The linewidths of carbons of the rigid cholesteryl moiety of the ester are so large, e.g., for C5 and C6, that they are not observed at 37°C. Upon increasing the temperature to 52°C, however, C5 and C6 are visible with T_2* values of 23 and 20 ms, respectively. A comparison with the cholesteryl ester C5 and C6 positions in lipoproteins indicates that the microviscosity of the rigid steroid nucleus of CLa in egg DPPC at 37°C is approximately equal to that experienced in VLDL, while at 52°C the spectrum resembles that found for LDL and HDL. The lipoprotein spectra were determined at 40°C (2). For the only T_2* value reported for a cholesteryl ring carbon, T_2* of C6 was found to be ~30 ms and ~20 ms in LDL and HDL, respectively, at 36°C (1). The greater linewidths of the cholesteryl ring carbons at 37°C in the present study, i.e., broadened to the point of disappearance, are consistent with the fact that line narrowing anisotropic motion of the type encountered by the acyl chain carbons is not possible in the rigid steroid moiety (18–21).

TABLE 3. Carbon-13 spin–spin relaxation times (T_2*) of 25 mol% cholesteryl linoleate in 40% w/v DPPC dispersions at two temperatures

	T_2* (ms)	
Carbon	37°C	52°C
$N^+(Me)_3$	5	14
$(CH_2)_n$	13	11
$C^*H_2CH_2CH_3$[a]	14	16
$C^*H_2CH_3$[a]	14	15
CH_3	18	19
C=C—C*—C=	14	15
C*—C=C	16	13
C=C—C—C=C	16	27
C=C*—C—C*=C	22	32
C5[b]	—	23
C6	—	20
Sucrose	25	—

[a]Superimposed on *C26* and *C27*.
[b]Italicized numbers refer to carbons in the cholesteryl moiety.

Conclusion

Saturated and unsaturated cholesteryl esters form stable multilamellar systems with phosphatidylcholines up to ratios of PC:CE = 3:1. Even at the highest ester concentration, 25 mol%, there is no discernible effect of the ester on the PC acyl chain or head group motions as reflected by ^{13}C T_1 measurements. The microviscosity of the ester chain carbons, as estimated from the spin–lattice relaxation rates, indicates a medium just like that of VLDL.

The form of the ^{13}C spectrum for cholesteryl esters in PC bilayers depends critically on the cholesteric → isotropic phase transition temperature, T_m. The fact that the first visible signs of atherosclerotic lesions, the so-called stage I type (25), are fatty streaks and lipid crystals, suggests that there is an inhomogeneous distribution of esters in the lesions. The fatty streaks would be rich in unsaturated esters like cholesteryl linoleate, $T_m < 37°C$, while lipid crystals would be rich in saturated esters like cholesteryl palmitate, $T_m > 37°C$. That is, the abundance of various esters in the aorta may be less important than their distribution. The properties of the two forms, as shown by ^{13}C nmr, are quite different. Indeed, thermotropic birefringence studies have indicated significant heterogeneity between clusters of ester droplets in human aorta (26).

1. J. A. HAMILTON, C. TALKOWSKI, R. F. CHILDERS, E. WILLIAMS, A. ALLERHAND, and E. H. CORDES. J. Biol. Chem. **249**, 4872 (1974).
2. J. A. HAMILTON, C. TALKOWSKI, E. WILLIAMS, E. M. AVILA, A. ALLERHAND, E. H. CORDES, and G. CAMEJO. Science, **180**, 193 (1973).
3. B. SEARS, R. J. DECKELBAUM, M. J. JANIAK, G. G. SHIPLEY, and D. M. SMALL. Biochemistry, **15**, 4151 (1976).
4. J. A. HAMILTON, M. J. OPPENHEIMER, R. ADDLEMAN, A. O. CLOUSE, E. H. CORDES, P. M. STEINER, and C. J. GLUECK. Science, **194**, 1424 (1976).
5. J. A. HAMILTON, N. OPPENHEIMER, and E. H. CORDES. J. Biol. Chem. **252**, 8071 (1977).
6. D. G. CORNWELL, J. C. GEER, and R. V. PANAGANAMALA. *In* International encyclopedia of pharmacology and therapeutics. *Edited by* E. J. Masoro. Pergamon Press, Oxford. 1975. p. 449.
7. R. W. ST. CLAIR, H. B. LOFLAND, and T. B. CLARKSON. Circ. Res. **27**, 213 (1970).
8. A. J. DAY and J. W. PROUDLOCK. Atherosclerosis, **19**, 253 (1974).
9. J. E. KIRK and T. J. S. LAURSEN. J. Gerontol. **10**, 288 (1955).
10. J. E. KIRK. *In* Blood vessels and lymphatics. *Edited by* D. I. Abramson. Academic Press, New York. 1962. p. 587.
11. C. PRIES and F. B. KLYNSTRA. Lancet, **1**, 750 (1971).
12. E. B. SMITH, P. H. EVANS, and M. D. DOWNHAM. J. Atheroscler. Res. **7**, 171 (1967).
13. W. S. SINGLETON, M. S. GRAY, M. L. BROWN, and J. L. WHITE. J. Am. Oil Chem. Soc. **42**, 53 (1965).
14. G. G. MCDONALD and J. S. LEIGH, JR. J. Magn. Reson. **9**, 358 (1973).

15. M. J. JANIAK, C. R. LOOMIS, G. G. SHIPLEY, and D. M. SMALL. J. Mol. Biol. **86**, 325 (1974).
16. B. J. FORREST and R. J. CUSHLEY. Atherosclerosis, **28**, 309 (1977).
17. A. K. GROVER and R. J. CUSHLEY. Atherosclerosis, **32**, 87 (1979).
18. M. P. N. GENT and J. H. PRESTEGARD. Biochem. Biophys. Res. Commun. **58**, 549 (1974).
19. G. W. STOCKTON, C. F. POLNASZEK, A. P. TULLOCH, F. HASAN, and I. C. P. SMITH. Biochemistry, **15**, 954 (1976).
20. R. E. LONDON and J. AVITABLE. J. Am. Chem. Soc. **99**, 7765 (1977).
21. M. P. N. GENT and J. H. PRESTEGARD. J. Magn. Reson. **25**, 243 (1977).
22. W. STOFFEL, O. ZIERENBERG, B. D. TUNGGAL, and E. SCHREIBER. Hoppe-Seyler's Z. Physiol. Chem. **355**, 1381 (1974).
23. W. STOFFEL, O. ZIERENBERG, B. D. TUNGGAL, and E. SCHREIBER. Hoppe-Seyler's Z. Physiol. Chem. **355**, 1367 (1974).
24. B. LANDBERG. Chem. Phys. Lipids, **14**, 309 (1975).
25. P. D. LANG and W. INSULL. J. Clin. Invest. **49**, 1479 (1970).
26. G. H. HILLMAN and D. M. ENGELMAN. J. Clin. Invest. **58**, 1008 (1976).

Some reactions of 10-substituted-10*H*-pyrido[3,2-*b*][1,4]benzothiazine-*n*-butyllithium adducts with acyl and sulfonyl chlorides

FRANK M. PASUTTO AND EDWARD E. KNAUS[1]

Faculty of Pharmacy and Pharmaceutical Sciences, University of Alberta, Edmonton, Alta., Canada T6G 2N8

Received March 12, 1979

FRANK M. PASUTTO and EDWARD E. KNAUS. Can. J. Chem. **57**, 2371 (1979).

Reaction of 10*H*-pyrido[3,2-*b*][1,4]benzothiazines **1** possessing a 10-methyl **1***f*, 10-(3-dimethylaminopropyl) **1***b*, or 10-(2-dimethylaminopropyl) **1***c* substituent, with *n*-butyllithium and methyl chloroformate or diethyl chlorophosphate affords predominantly 1,2-dihydropyridines **11** and the 4-substituted derivatives **12**. The 1,7-disubstituted product **15***b* was obtained from reaction of the 10-methyl compound **1***f* with *p*-fluorobenzoyl chloride. On the other hand, treatment of the 10-methyl analog **1***f* with trifluoromethanesulfonyl chloride gave the unexpected 4-chloro derivative **12***c* and **13***c* which probably arises from the 1-trifluoromethanesulfonyl-1,2-dihydropyridine **11***c* via elimination of trifluoromethanesulfonic (sulfinic) acid. The N-10 dealkylated product **1***a* was obtained from reaction of the 10-(1-methyl-2-dimethylaminoethyl) analog **1***g* with *n*-butyllithium and methyl chloroformate, whereas a similar reaction employing the 10-(2-dimethylaminoethyl) derivative **1***h* gave rise to the *N*-methoxycarbonyl derivative **18**. On the other hand, reaction of **1***h* with *n*-butyllithium alone gave the N-10 *n*-hexyl product **19**. Mechanisms for the formation of **1***a*, **11**, **12**, **13**, **15**, **16**, and **19** are described.

FRANK M. PASUTTO et EDWARD E. KNAUS. Can. J. Chem. **57**, 2371 (1979).

La réaction des 10*H*-pyrido[3,2-*b*][1,4]benzothiazines **1** portant, en position 10, des groupes méthyle (**1***f*), diméthylamino-3 propyle (**1***b*), ou diméthylamino-2 propyle (**1***c*), avec du *n*-butyllithium et du chloroformate de méthyle ou du chlorophosphate de diéthyle conduit principalement aux dihydro-1,2 pyridines **11** et aux dérivés **12** substitués en position 4. On a obtenu le produit **15***b* disubstitué en 1,7 par réaction du composé **1***f* avec le chlorure de *p*-fluorobenzoyle. Par ailleurs, la réaction de **1***f* avec le chlorure di trifluorométhanesulfonyle conduit au dérivé chloro-4 inattendu (**12***c*) et à **13***c* qui provient probablement de la trifluorométhanesulfonyl-1 dihydro-1,2 pyridine **11***c* par élimination d'acide trifluorométhanesulfonique (sulfinique). On obtient le produit **1***a* qui ne porte pas de groupe alkyle sur l'azote N-10 par réaction de l'analogue (méthyl-1 diméthyl-amino-2 éthyl)-10 (**1***g*) avec le butyllithium et le chloroformate de méthyle alors qu'une réaction semblable avec le dérivé (diméthylamino-2 éthyl)-10 (**1***h*) conduit au dérivé **18** portant un *N*-méthoxycarbonyle. Par ailleurs, la réaction de **1***h* avec le *n*-butyllithium seul fournit le produit **19** portant un groupe *n*-hexyle sur l'azote en 10. On décrit des mécanismes pour la formation de **1***a*, **11**, **12**, **13**, **15**, **16** et **19**.

[Traduit par le journal]

10*H*-Pyrido[3,2-*b*][1,4]benzothiazine (**1***a*) is an analog of phenothiazine in which an annular nitrogen atom is incorporated into the ring system. Several N-10 derivatives of **1***a* in clinical use are more potent than their phenothiazine analogs. Prothipendyl (**1***b*) is a more useful antihistaminic agent than Promethazine while Isothipendyl (**1***c*), Pipazethate (**1***d*), and Pervetral (**1***e*) are employed as antihistaminic, antitussive, and antiemetic agents respectively (1).

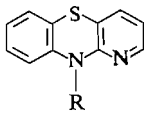

1

a R = H
b R = —$(CH_2)_3$—N—Me_2
c R = —CH_2—$CH(CH_3)$—N—Me_2
d R = —CO_2—$(CH_2)_2$—O—$(CH_2)_2$—N⟨ ⟩
e R = —$(CH_2)_3$—N⟨ ⟩N—$(CH_2)_2$—OH

In an earlier study we showed that reaction of 10-methyl-10*H*-pyrido[3,2-*b*][1,4]benzothiazine **1***f* with *n*-butyllithium affords a mixture of the C-4 proton abstraction product **12** (R = Me, R^1 = Li) and 2-*n*-butyl-4a-lithio-10-methyl-2,4a-dihydropyridyl[3,2-*b*]-[1,4]benzothiazine (**14**, R = Me, R^1 = Li) which results from nucleophilic addition at the C-2 position. Treatment of **12** and **14** with deuterium oxide gave the deuterated products **12** and **14** (R = Me, R^1 = D) in a ratio of 1:4.4 (2). We now describe the preparation of other N-10 substituted-10*H*-pyrido[3,2-*b*]-[1,4]benzothiazine-*n*-butyllithium adducts and their

[1]To whom inquiries should be addressed.

0008-4042/79/182371-08$01.00/0

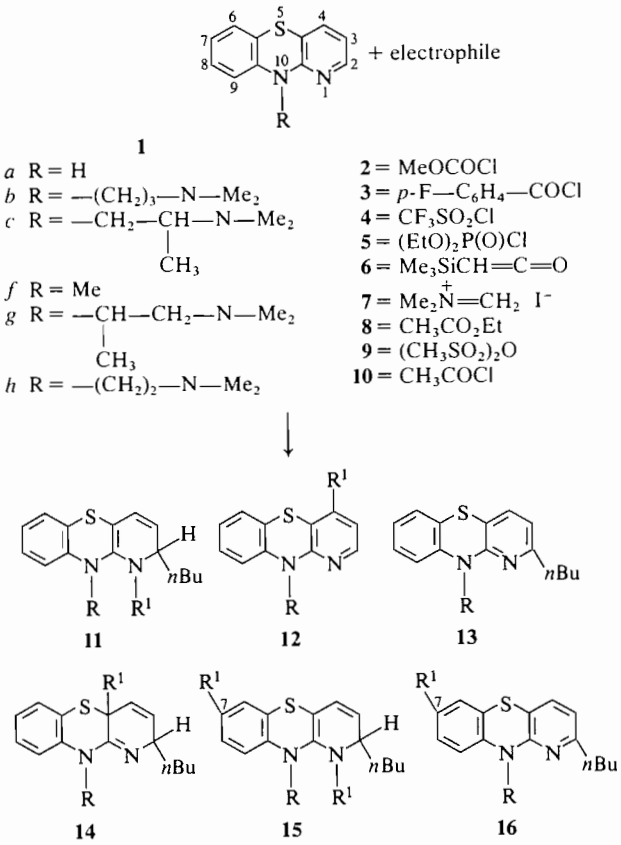

SCHEME 1. The R and R^1 substituents for products **11**–**16** are as illustrated in Table 1.

reactions with acyl and sulfonyl chlorides (see Scheme 1).

Reaction of **12** and **14** (R = Me, R^1 = Li), obtained from treatment of **1***f* with *n*-butyllithium (2), with methyl chloroformate (**2**) afforded the 1,2-dihydropyridyl derivative **11***a* (79.7%) and the 4-methoxycarbonyl product **12***a* (19.8%). Metalation at the C-4 position of **1***f* appears to be regiospecific since proton abstraction at C-6 was not observed (2). Abstraction of the C-4 rather than the C-2 proton of **1***f* is attributed to the known *ortho*-directing influence of the sulfur atom (3, 4).

Treatment of the 10-methyl derivative **1***f* with *n*-butyllithium and then *p*-fluorobenzoyl chloride (**3**) gave the 1,7-di-*p*-fluorobenzoyl-1,2-dihydropyridyl product **15***b* (35%) and the 2-*n*-butyl-7-*p*-fluorobenzoyl derivative **16***b* (2.5%) (see Table 1). The ^{1}H nmr spectrum (δ) of **15***b* exhibited a 12H multiplet at 6.64–7.82 attributed to the phenyl hydrogens and the C-4H. The C-2H and C-3H appeared as a 2H multiplet from 5.6–6.11 while the *N*-methyl signal was present as a 3H singlet at 3.08. The *n*-butyl absorption appeared as a 9H multiplet at 0.77–2.08. These assignments are consistent with the structure 1,7-di-*p*-fluorobenzoyl-2-*n*-butyl-10-methyl-1,2-dihydropyridyl[3,2-*b*][1,4]benzothiazine. The most plausible mechanism for the formation of **15***b* would involve initial formation of **11***b* which could undergo electrophilic substitution at C-7 to give 1,7-di-*p*-fluorobenzoyl-2-*n*-butyl-10-methyl-1,2-dihydropyridyl[3,2-*b*][1,4]benzothiazine **15***b*. The ^{1}H nmr spectrum (δ) of **16***b* exhibited a 2H doublet ($J_{2',3'}$ = 10) of doublets ($J_{2',F}$ = 6) at 7.8 due to the $C_{2'}$-H (*ortho*-benzoyl hydrogens), a 7H multiplet at 6.73–7.39 attributed to the remaining phenyl and pyridyl hydrogens, a 3H singlet at 3.5 due to the *N*-methyl group, a 2H triplet (J = 7) at 2.72 assigned to the α-methylene of the *n*-butyl group, and a 7H multiplet at 0.72–2.01 due to the remaining *n*-butyl hydrogens. These assignments are consistent with 2-*n*-butyl-7-*p*-fluoro-benzoyl-10-methyl-10*H*-pyrido[3,2-*b*][1,4]benzothiazine (**16***b*). Compound **16***b* could arise via the loss of the 1-*p*-fluorobenzoyl substituent from **15***b* as *p*-fluorobenzaldehyde.

Reaction of the 10-methyl analog **1***f* with *n*-butyllithium and trifluoromethanesulfonyl chloride (**4**) afforded the 4-chloro derivative **12***c* (14.5%) and **13***c* (44.4%). The high yield of **13***c* was unexpected since the reaction of 1-azaphenothiazines **1***b*, **1***c*, and **1***f* with other electrophiles as diethyl chlorophosphate, methyl chloroformate, and *p*-fluorobenzoyl chloride gave very low yields of **13**. In some reactions **13** was not detected (see Table 1). On the other hand, reactions of 1-azaphenothiazines **1***b* and **1***f* with trifluoromethanesulfonyl chloride gave **13***c* and **13***f* in 44.4% and 27.7% yield respectively. These high yields suggest that **13***c* arises from the 1,2-dihydropyridyl product **11***c* via fission of the N^1—S bond with loss of trifluoromethanesulfonic(sulfinic) acid, since this bond is expected to be quite labile due to the strong negative inductive effect of the trifluoromethyl group. Elimination of trifluoromethanesulfinic acid could occur spontaneously or trifluoromethanesulfonic acid as a result of reaction with water which is added in the workup procedure.

The ^{1}H nmr spectrum of **12***c* appeared initially to be consistent with the structure 4-trifluoromethanesulfonyl-10-methyl-10*H*-pyrido[3,2-*b*][1,4]benzothiazine (**12**, R^1 = SO_2CF_3). However, the mass spectral data did not agree. Elemental analysis subsequently indicated that the R^1-substituent was a chloro rather than a trifluoromethanesulfonyl substituent, which was also consistent with the mass spectral data. The most likely mechanism for the formation of **12***c* involves nucleophilic attack by **12** (R = Me, R^1 = Li) at chlorine, the driving force being elimination of sulfur dioxide and a trifluoromethyl carbanion which is stabilized by the strong negative inductive

TABLE 1. Reactions of 10-substituted-10*H*-pyrido[3,2-*b*][1,4]benzothiazine-*n*-butyllithium adducts with electrophiles

Electrophile	R	R^1	Yield (%) 11	12	13	14	15	16	Recovered 1
(*a*) MeOCOCl	Me	$-CO_2Me$	79.7	19.8	—	—	—	—	—
(*b*) *p*-F—C_6H_4—COCl	Me	*p*-F—C_6H_4—CO	—	—	—	—	35	2.5	10.2
(*c*) CF_3SO_2Cl	Me	—Cl	—	14.5	44.4	—	—	—	5.2
(*d*) MeOCOCl	$-(CH_2)_3N(Me)_2$	$-CO_2Me$	31.4[a]	7.5	—	—	—	—	12.3
(*e*) $(EtO)_2P(O)Cl$	$-(CH_2)_3N(Me)_2$	$(EtO)_2P(O)-$	16.7	9.3	—	2.5[b]	—	—	12.9
(*f*) CF_3SO_2Cl	$-(CH_2)_3N(Me)_2$	—Cl	—	8.3	27.7	—	—		3.1
(*g*) $(EtO)_2P(O)Cl$	$-CH_2-CHN(Me)_2$ | Me	$(EtO)_2P(O)-$	14.1	7.9	2.4	—[c]	—	—	—
(*h*) MeOCOCl	$-CH_2-CH(N(Me)_2)-$ | Me	$-CO_2Me$	38.5	8.5	—	—	—	—	12

[a]Purification by column chromatography on silica gel gave a 54.5% yield of 11*d*.
[b]The R^1-substituent of 14*e* is Et.
[c]Product 14*g* was also detected in the ^1H nmr spectrum of the thin-layer fraction (R_f 0.69) but it could not be isolated in sufficient amount to allow unequivocal characterization.

effect of the fluorine atoms. Alternatively **12***c* could arise via the *N*-methanesulfonylpyridinium chloride **17**.

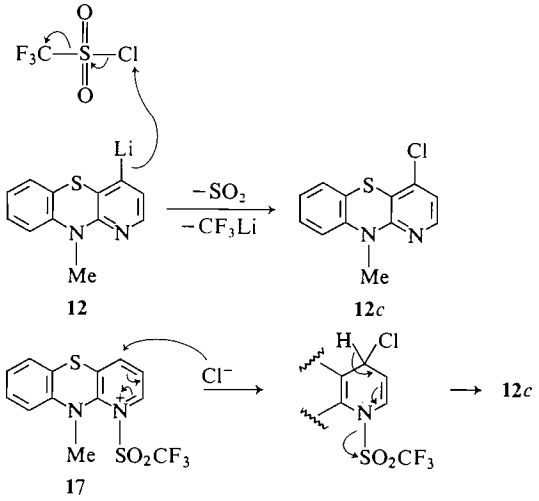

The ^1H nmr spectrum of the reaction mixture, obtained from treatment of the 10-(3-dimethylaminopropyl) analog **1***b* with *n*-butyllithium and then deuterium oxide was virtually identical in the 3.5–7 δ region to that reported for the 10-methyl derivative **1***f* (2). Reaction of **1***b* with *n*-butyllithium therefore gives rise to a mixture of **12** and **14** (R = $-(CH_2)_3-NMe_2$, R^1 = Li) which on treatment with methyl chloroformate afforded the 1,2-dihydropyridyl product **11***d* (31.4%) and 4-substituted product **12***d* (7.5%). A similar reaction employing diethyl chlorophosphate (**5**) yielded the 1,2-dihydropyridyl derivative **11***e* (16.7%), the 4-diethylphosphoryl derivative **12***e* (9.3%), and 2-*n*-butyl-4a-ethyl-10-(3-dimethylaminopropyl)-2,4a-dihydropyridyl[3,2-*b*][1,4]-benzothiazine (**14***e*, 2.5%). The most plausible mechanism for the formation of **14***e* involves nucleophilic attack by the C-4a carbanion of **14** (R = $-(CH_2)_3-NMe_2$, R^1 = Li) at the ethyl group of diethyl chlorophosphate as reported previously for **14** (R = Me, R^1 = Li) (2).

The reaction of the 10-(3-dimethylaminopropyl) analog **1***b* with trifluoromethanesulfonyl chloride gave rise to the 4-chloro product **12***f* (8.3%) and the 2-butyl derivative **13***f* (27.7%). It is expected that **12***f* and **13***f* arise via the same mechanisms proposed for the formation of **12***c* and **13***c*.

The reaction of the 10-(2-dimethylaminopropyl) analog **1***c* with *n*-butyllithium and diethyl chlorophosphate proceeded as expected to give low yields of **11***g* (14.1%), **12***g* (7.9%), and **13***g* (2.4%). Similarly, treatment with methyl chloroformate afforded **11***h* (38.5%) and **12***h* (8.5%). On the other hand, reaction of the isomeric 1-methyl-2-dimethylaminoethyl derivative **1***g* with *n*-butyllithium and methyl chloroformate afforded 10*H*-pyrido[3,2-*b*][1,4]benzothiazine (1*a*) (15.2%) as the only isolable product. Product 1*a* could arise following abstraction of the β-hydrogen and elimination as illustrated below or as a result of attack by *n*-butyllithium at the α-carbon of 1*g*.

The ^1H nmr spectrum of the reaction mixture, obtained from treatment of 10-(2-dimethylamino-

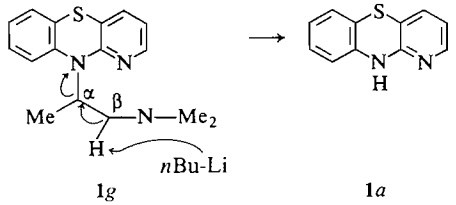

ethyl)-10*H*-pyrido[3,2-*b*][1,4]benzothiazine (**1***h*) with *n*-butyllithium and then deuterium oxide, was void of absorptions in the 3.5–7 δ region which would suggest that **14** (R = —$(CH_2)_2$—NMe_2, R^1 = Li) was not generated. Repetition of this reaction employing methyl chloroformate in place of deuterium oxide afforded the unexpected **18** (24.4%) and **1***h* (32.1%). Replacement of an *N*-methyl group by an alkoxycarbonyl group has been reported. Thus treatment of codeine (5), tropines (6, 7), and erythromycin (8) with ethyl chloroformate gave the corresponding *N*-ethoxycarbonyl products resulting from loss of the *N*-methyl substituent.

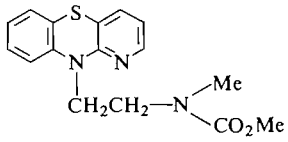

18

When the 10-(2-dimethylaminoethyl) derivative **1***h* was allowed to react with *n*-butyllithium, followed by quenching with water, the unexpected **19** (25.9%) was obtained probably as a result of nucleophilic attack by *n*-butyllithium at the β-carbon of **1***h* resulting in elimination of dimethylamine. The structure of **19** was confirmed by an unambiguous synthesis from reaction of **1***a* with sodium hydride and *n*-hexyl chloride.

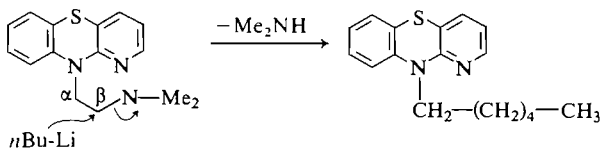

1*h* **19**

It is well documented that a Lewis base such as *N*,*N*,*N*^{1},*N*^{1}-tetramethylethylenediamine converts *n*-butyllithium into a coordinated monomeric reagent **20** (9). The 10-(2-dimethylaminoethyl)azaphenothiazine **1***h* has three nitrogens available for complexation with *n*-butyllithium, viz. N-1, N-10, and the side chain dimethylamino nitrogen. One could speculate that coordination of *n*-butyllithium could occur with the N-1 and side chain nitrogen as illustrated by structure **21**, the N-1 and N-10 nitrogens, or the N-10 and side chain nitrogen. The existence of a complex such as **21** may help to explain why the reaction of **1***h* with *n*-butyllithium gave rise to product **19**. The side chain nitrogen of **21** would attain some positive character thereby facilitating attack at the β-carbon and elimination of dimethylamine.

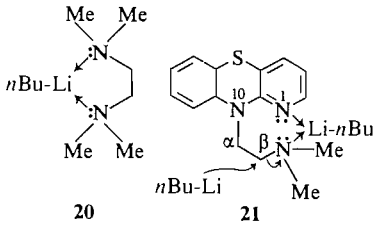

20 **21**

The observation that reaction of the 10-(2-dimethylaminopropyl) analog **1***c* with *n*-butyllithium and methyl chloroformate gave **11***g*, **12***g*, and **13***g*, while a similar 10-(1-methyl-2-dimethylaminoethyl) derivative **1***g* afforded only **1***a*, warrants comment. One would expect that steric repulsion between the α-methyl in **1***g* and the *peri* C-9H and the N-1 free electron pair would be greater than that of the β-methyl in **1***c*. If this is so, coordination of *n*-butyllithium with the N-1 and N-10 nitrogens of **1***g* as illustrated by **22** may be more favourable than coordination between N-1 and the side chain nitrogen. The coordination complex **22** would confer slight

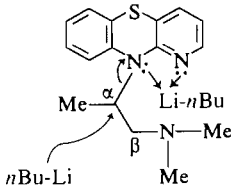

22

positive character to the N-10 nitrogen, facilitating attack at the α-position by *n*-butyllithium and elimination of 10*H*-pyrido[3,2-*b*][1,4]benzothiazine (**1***a*) as observed, thereby relieving steric repulsion between the α-methyl substituent and the *peri*-positions. Alternatively **1***a* could also arise as a result of nucleophilic attack at the β-hydrogen as described previously. These postulates are at best tenuous and are presented solely to rationalize the dependence of the reaction products obtained on the R-substituent of **1**. The possibility of intermolecular complexation also exists. No allowance has been made for the effect of conformational differences of **1** on chemical reactivity.

The reaction of adducts **14** (R = Me, —$(CH_2)_3$—N—Me_2, R^1 = Li) with methyl chloroformate and diethyl chlorophosphate affords 1,2-dihydropyridyl **11** and 4-substituted pyridyl derivatives **12** in good yield (See Table 1). On the other hand, treatment of a mixture of **12** and **14** (R = Me, R^1 = Li) with trimethylsilyketene **6** (10), dimethyl(methylene)ammonium iodide **7** (11), ethyl acetate **8**, methanesulfonic anhydride **9**, or acetyl chloride **10**, followed by quenching with deuterium oxide, gave a reaction product which exhibited a ^{1}H nmr spectrum identical to that of **12** and **14** (R = Me, R^1 = D). This indicated that the electrophilic reagents **6–10** were not

involved in the reaction. It could be proposed that any electrophile which is not able to form an iminium intermediate **23** would not react further to form a 1,2-dihydropyridyl derivative **11**. Although the intermediate **23** provides a plausible pathway to **11**, certain observations suggest that other, as yet unexplained, factors are also involved. Reaction of **14**

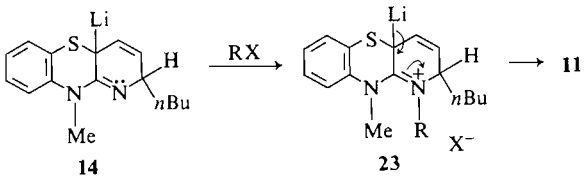

(R = Me, R^1 = Li) with acetyl chloride and methanesulfonyl chloride did not afford any isolable product other than the starting material **1***f*. Both reagents should be capable of forming intermediates **23**. It is also surprising that the 4-substituted product **12** expected from acylation of **12** (R = Me, R^1 = Li) was not produced. The absence of 1,2-dihydropyridines **11** in reactions employing electrophiles as dimethyl(methylene)ammonium iodide **7** and trimethylsilylketene **6** was previously rationalized in terms of their inability to form the iminium species **23**. However, there is no apparent explanation why the 4-substituted compounds **12** are not obtained with these electrophilic reagents.

Reactions of 2-, 3-, and 4-azaphenothiazines having varied functionality at the N-10 position with other organolithium reagents and electrophiles are now in progress to determine the generality and mechanisms of these reactions.

Experimental

Melting points were determined with a Büchi capillary apparatus and are uncorrected. Nuclear magnetic resonance spectra were determined for solutions in deuterochloroform with TMS as internal standard with a Varian EM-360A spectrometer. Infrared spectra (potassium bromide unless otherwise noted) were taken on a Unicam SP-1000 or Perkin Elmer 267 spectrometer. Mass spectra were measured with an AEI-MS-50 mass spectrometer and these exact mass measurements are used in lieu of elemental analyses. All of the products described gave rise to a single spot on tlc using a solvent system less polar and more polar than the specific solvent system described for purification of the reaction mixture. No residue remained after combustion of the products purified by tlc. Kieselgel silica gel DF-5 (Camag) was used for preparative thin-layer chromatography using 20 cm × 20 cm plates of 0.75 mm thickness.

*4-Lithio-10-substituted-10*H*-pyrido*[3,2-b][*1,4*]*benzothiazine* (***12***) *and 2-*n*-Butyl-4a-lithio-10-substituted-2,4a-dihydropyridyl*[3,2-b][*1,4*]*benzothiazine* (***14***) (*R^1 = Me, $-(CH_2)_3-N-Me_2$, $-CH_2-CH(CH_3)-N-Me_2$; R^1 = Li*)*

General Procedure

To a solution of ***1*** (5 mmol) in 125 mL anhydrous tetrahydrofuran, under a nitrogen atmosphere at 0°C, *n*-butyllithium (0.32 g, 5 mmol) was added dropwise with stirring. The reaction was stirred at 0°C for 1 h to afford a golden brown solution of ***12*** and ***14*** which was then cooled to −77°C and the appropriate electrophile (5–6 mmol) in 2 mL anhydrous tetrahydrofuran was added dropwise. The resulting solution was stirred at −77°C for 45–90 min before warming to room temperature over a 1–3 h period. The reaction products were isolated as described in individual cases.

*1-Methoxycarbonyl-2-*n*-butyl-10-methyl-1,2-dihydropyridyl-*[3,2-b][*1,4*]*benzothiazine* (***11***a) *and 4-Methoxycarbonyl-10-methyl-10*H*-pyrido*[3,2-b][*1,4*] *benzothiazine* (***12***a)

n-Butyllithium (0.32 g, 5 mmol), 10-methyl-10*H*-pyrido-[3,2-*b*][1,4]benzothiazine (**1***f*) (1.07 g, 5 mmol), and methyl chloroformate (0.567 g, 6 mmol) were stirred at −77°C for 1 h and allowed to warm to room temperature over a 3 h period as described in the general procedure. The resulting reddish-orange solution was treated with water (100 mL), extracted with dichloromethane (100 mL), and dried (Na_2SO_4). Evaporation of the solvent *in vacuo* gave a dark red oil (1.75 g) of which 1.1 g was subjected to preparative thin-layer chromatography on 12 silica gel plates using benzene – ethyl acetate (20:1 v/v) as the development solvent. Extraction of the silica gel fraction R_f 0.85 gave **11***a* as a dark yellow oil (0.827 g, 79.7%); ir(film): 1725 (s, C=O), 1632, and 1568 (s, C=C) cm^{-1}; ^{1}H nmr δ: 6.66–7.26 (m, 4H, Ph), 5.48–5.92 (m, 2H, H-3, H-4), 4.8 (m, 1H, H-2), 3.7 (s, 3H, OMe), 3.18 (s, 3H, NMe), 0.68–1.98 (m, 9H, *n*Bu). *Exact Mass* calcd. for $C_{18}H_{22}N_2O_2{}^{32}S$: 330.1397; found (high resolution ms): 330.1400. Extraction of the silica gel fraction R_f 0.53 gave a red solid (0.169 g, 19.8%). Recrystallization from hexanes (bp 68.4–68.9°C) gave **12***a* as a red solid; mp 118–120°C (dec.); ir: 1711 (s, C=O) cm^{-1}; ^{1}H nmr δ: 8.03 (d, $J_{2,3}$ = 5 Hz, 1H, H-2), 7.19 (d, $J_{2,3}$ = 5 Hz, 1H, H-3), 6.6–7.36 (m, 4H, Ph), 3.94 (s, 3H, OMe), 3.39 (s, 3H, NMe). *Exact Mass* calcd. for $C_{14}H_{12}N_2O_2{}^{32}S$: 272.0617; found (high resolution ms): 272.0615.

*1,7-Di-*p*-fluorobenzoyl-2-*n*-butyl-10-methyl-1,2-dihydropyridyl-*[3,2-b][*1,4*]*benzothiazine* (***15***b) *and 2-*n*-Butyl-7-*p*-fluorobenzoyl-10-methyl-10*H*-pyrido*[3,2-b][*1,4*]*benzothiazine* (***16***b)

n-Butyllithium (0.32 g, 5 mmol), 10-methyl-10*H*-pyrido-[3,2-*b*][1,4]-benzothiazine (**1***f*) (1.07 g, 5 mmol), and *p*-fluorobenzoyl chloride (0.875 g, 5.5 mmol) were stirred at −77°C for 1 h and allowed to warm to room temperature over a 2.5 h period as described in the general procedure. The resulting dark red solution was treated with water (60 mL), extracted with dichloromethane (3 × 50 mL), and dried (Na_2SO_4). Evaporation of the solvent *in vacuo* gave a dark red oil (2.037 g) of which 0.85 g was subjected to preparative thin-layer chromatography on 10 silica gel plates using benzene – ethyl acetate (25:1 v/v) as the development solvent. Extraction of the silica gel fraction R_f 0.94 gave **16***b* as a yellow waxy solid (0.02 g, 2.5%), mp 93–96°C; ir: 1660 (s, C=O) cm^{-1}; ^{1}H nmr δ: 7.8 (d, $J_{2',3'}$ = 10 Hz of d, $J_{2',F}$ = 6 Hz, 2H, H-2'), 6.73–7.39 (m, 7H, Ph, pyridyl hydrogens), 3.5 (s, 3H, NMe), 2.72 (t, $J_{CH_2CH_2}$ = 7 Hz, 2H, $-CH_2-C_3H_7$), 0.72–2.01 (m, 7H, $CH_2-C_3H_7$). *Exact Mass* calcd. for $C_{23}H_{21}N_2O^{32}SF$: 392.1354; found (high resolution ms): 392.1359. Extraction of the silica gel fraction R_f 0.58 gave a red oil (0.302 g) of which 0.2 g was rechromatographed on four silica gel plates using benzene as development solvent. This gave two fractions R_f 0.43 and R_f 0.31. Extraction of the silica gel fraction R_f 0.43 gave **1***f* as a yellow solid (0.03 g, 10.2%) identical (^{1}H nmr) with an authentic sample. Extrac-

tion of the silica gel fraction R_f 0.31 gave a red solid which was dissolved in chloroform and precipitated from solution by the addition of methanol. This gave **15***b* as a red solid (0.137 g, 35%); mp 84–86°C (dec.); ir: 1681 (s, C=O) and 1635 (s, C=C) cm^{-1}; ^1H nmr δ: 6.64–7.82 (m, 12H, Ph, H-4), 5.6–6.11 (m, 2H, H-2, H-3), 3.08 (s, 3H, NMe), 0.77–2.08 (m, 9H, *n*Bu). *Exact Mass* calcd. for $C_{30}H_{26}N_2O_2{}^{32}SF_2$: 516.1677; found (high resolution ms): 516.1680.

*4-Chloro-10-methyl-10*H*-pyrido[3,2-*b*][1,4]benzothiazine (**12**c) and 2-*n*-Butyl-10-methyl-10*H*-pyrido[3,2-*b*][1,4]benzothiazine (**13**c)*

n-Butyllithium (0.16 g, 2.5 mmol), 10-methyl-10*H*-pyrido-[3,2-*b*][1,4]benzothiazine (**1***f*) (0.535 g, 2.5 mmol), and trifluoromethanesulfonyl chloride (0.463 g, 2.75 mmol) were stirred at −77°C for 1 h and allowed to warm to room temperature over a 1.5 h period as described in the general procedure. The resulting dark yellow solution was treated with water (50 mL), extracted with dichloromethane (3 × 50 mL), and dried (Na_2SO_4). Evaporation of the solvent *in vacuo* gave a brownish red oil (0.819 g) of which 0.8 g was subjected to preparative thin-layer chromatography on 12 silica gel plates using benzene – ethyl acetate (10:1 v/v) as the development solvent. Extraction of the silica gel fraction R_f 0.97 gave **13***c* as a yellow oil (0.293 g, 44.4%) identical (^1H nmr) with an authentic sample (2). Extraction of the silica gel fraction R_f 0.64 gave a yellow semi-solid (0.143 g) which was rechromatographed on two silica gel plates using benzene as the development solvent. This gave two fractions R_f 0.41 and R_f 0.28. Extraction of the silica gel fraction R_f 0.28 gave **1***f* as a light yellow solid (0.027 g, 5.2%) identical (^1H nmr) with an authentic sample. Extraction of the silica gel fraction R_f 0.41 gave **12***c* as a light yellow solid (0.09 g, 14.5%), mp 74–75°C; ^1H nmr δ: 7.89 (d, $J_{2,3}$ = 5.5 Hz, 1H, H-2), 6.8–7.33 (m, 4H, Ph), 6.76 (d, $J_{2,3}$ = 5.5 Hz, 1H, H-3), 3.39 (s, 3H, NMe). *Exact Mass* calcd. for $C_{12}H_9N_2{}^{32}S^{37}Cl$: 250.0144; found (high resolution ms): 250.0141. *Exact Mass* calcd. for $C_{12}H_9N_2{}^{32}S^{35}Cl$: 248.0174; found (high resolution ms): 248.0168. *Anal.* calcd. for $C_{12}H_9N_2SCl$: C 57.95, H 3.65, N 11.26, S 12.88; found: C 57.95, H 3.73, N 11.24, S 12.83.

*1-Methoxycarbonyl-2-*n*-butyl-10-(3-dimethylaminopropyl)-1,2-dihydropyridyl[3,2-*b*][1,4]benzothiazine (**11**d) and 4-Methoxycarbonyl-10-(3-dimethylaminopropyl)-10*H*-pyrido[3,2-*b*][1,4]benzothiazine (**12**d)*

In a dry nitrogen atmosphere *n*-butyllithium (0.18 g. 2.81 mmol) was added dropwise with stirring to a solution of **1***b* (0.8 g, 2.81 mmol) in anhydrous tetrahydrofuran (125 mL) at 0°C. The resulting greenish brown solution was stirred at 0°C for 1 h, cooled to −77°C, and methyl chloroformate (0.318 g, 3.37 mmol) in anhydrous tetrahydrofuran (2 mL) was added dropwise. The reaction was stirred at −77°C for 1 h and allowed to warm to room temperature over a 2 h period. The resulting light brown solution was treated with water (75 mL), extracted with dichloromethane (4 × 50 mL), and dried (Na_2SO_4). Evaporation of the solvent *in vacuo* gave a brown oil (1.067 g) of which 0.65 g was subjected to preparative thin-layer chromatography on 12 silica gel plates using benzene – ethyl acetate (2:1 v/v) as the development solvent. Extraction of the silica gel fraction R_f 0.15 gave a yellow oil which was rechromatographed on four silica gel plates using ether–methanol (3:1 v/v) as the development solvent. This gave a single fraction R_f 0.87 which was extracted to give **11***d* as a yellow oil (0.215 g, 31.4%). Alternatively, chromatography of the reaction product on a 2.5 cm × 28 cm silica gel column and elution with ether (800 mL) gave **11***d* as a yellow oil (54.5%); ir (film): 1724 (s, C=O), 1635 (s, C=C) cm^{-1}; ^1H nmr δ: 6.7–7.34 (m, 4H, Ph), 5.42–5.93 (m, 2H, H-3, H-4), 4.79 (m, 1H, H-2), 3.52–3.88 (m, 2H, $CH_2CH_2CH_2NMe_2$), 3.69 (s, 3H, OMe), 2.14–2.45 (m, 2H, $CH_2CH_2CH_2NMe_2$), 2.14 (s, 6H, NMe_2), 0.69–2 (m, 11H, *n*Bu, $CH_2CH_2CH_2NMe_2$). *Exact Mass* calcd. for $C_{22}H_{31}N_3O_2{}^{32}S$: 401.2130; found (high resolution ms): 401.2135. Extraction of the silica gel fraction R_f 0.07 gave a yellowish brown oil (0.293 g) which was rechromatographed on four silica gel plates using chloroform–methanol (5:1 v/v) as the development solvent. This gave two fractions R_f 0.53 and R_f 0.45. Extraction of the silica gel fraction R_f 0.53 gave **12***d* as a bright yellow oil (0.044 g, 7.5%); ir (film): 1731 (s, C=O) cm^{-1}; ^1H nmr δ: 7.98 (d, $J_{2,3}$ = 5 Hz, 1H, H-2), 6.64–7.32 (m, 5H, Ph, H-3), 4.01 (m, 2H, $CH_2CH_2CH_2NMe_2$), 3.9 (s, 3H, OMe), 1.7–2.6 (m, 4H, $CH_2CH_2CH_2NMe_2$), 2.2 (s, 6H, NMe_2). *Exact Mass* calcd. for $C_{18}H_{21}N_3O_2{}^{32}S$: 343.1350; found (high resolution ms): 343.1348. Extraction of the silica gel fraction R_f 0.45 gave 10-(3-dimethylaminopropyl)-10*H*-pyrido[3,2-*b*][1,4]benzothiazine (**1***b*) as a light yellow oil (0.06 g, 12.3%) identical (^1H nmr) with an authentic sample.

*1-Diethylphosphoryl-2-*n*-butyl-10-(3-dimethylaminopropyl)-1,2-dihydropyridyl[3,2-*b*][1,4]benzothiazine (**11**e), 4-Diethylphosphoryl-10-(3-dimethylaminopropyl)-10*H*-pyrido[3,2-*b*][1,4]benzothiazine (**12**e), and 2-*n*-Butyl-4a-ethyl-10-(3-dimethylaminopropyl)-2,4a-dihydropyridyl-[3,2-*b*][1,4]benzothiazine (**14**e)*

In a dry nitrogen atmosphere *n*-butyllithium (0.213 g, 3.33 mmol) was added dropwise with stirring to a solution of **1***b* (0.79 g, 2.77 mmol) in anhydrous tetrahydrofuran (125 mL) at 0°C. The resulting greenish brown solution was stirred at 0°C for 45 min, allowed to warm to room temperature over a 0.5 h period, cooled to −77°C, and diethyl chlorophosphate (0.575 g, 3.33 mmol) in anhydrous tetrahydrofuran (2 mL) was added dropwise. The reaction was stirred at −77°C for 1.5 h and allowed to warm to room temperature over a 2 h period. The resulting dark yellow solution was treated with water (100 mL), extracted with chloroform (7 × 50 mL), and dried (Na_2SO_4). Evaporation of the solvent *in vacuo* gave a light brown oil (1.309 g) of which 0.72 g was subjected to preparative thin-layer chromatography on 10 silica gel plates using chloroform–methanol (5:1 v/v) as the development solvent. Extraction of the silica gel fraction R_f 0.87 gave **11***e* as a dark yellow oil (0.122 g, 16.7%); ir (film): 1271 (s, P=O), 1629, and 1568 (s, C=C) cm^{-1}; ^1H nmr δ: 6.67–7.38 (m, 4H, Ph), 5.4–5.95 (m, 2H, H-3, H-4), 4.43 (m, 1H, H-2), 3.53–4.32 (m, 6H, $(OCH_2CH_3)_2$, $—CH_2(CH_2)_2NMe_2$), 2.12–2.55 (m, 2H, $CH_2CH_2CH_2NMe_2$), 2.12 (s, 6H, NMe_2), 0.78–2.03 (m, 17H, *n*Bu, $CH_2CH_2CH_2NMe_2$), $(OCH_2CH_3)_2$). *Exact Mass* calcd. for $C_{24}H_{38}N_3O_3P^{32}S$: 479.2363; found (high resolution ms): 479.2354. Extraction of the silica gel fraction R_f 0.55 gave **14***e* as a yellow oil (0.014 g, 2.5%); ir (film): 1629 (s, C=N, C=C) cm^{-1}; ^1H nmr δ: 6.9–7.35 (m, 4H, Ph), 6.1 (d, $J_{3,4}$ = 10 Hz of d, $J_{2,3(4)}$ = 1.75 Hz, 1H, H-3 or H-4), 5.55 (d, $J_{3,4}$ = 10 Hz of d, $J_{2,3(4)}$ = 2 Hz, 1H, H-3 or H-4), 3.6–4.5 (m, 3H, H-2, $CH_2CH_2CH_2NMe_2$), 2.2 (s, 6H, NMe_2), 0.72–2.6 (m, 18H, *n*Bu, Et, $CH_2CH_2CH_2NMe_2$). *Exact Mass* calcd. for $C_{22}H_{33}N_3{}^{32}S$: 371.2388; found (high resolution ms): 371.2389. Extraction of the silica gel fraction R_f 0.05 gave **12***e* as a yellow oil (0.06 g, 9.3%); ir (film): 1266 (s, P=O) cm^{-1}; ^1H nmr δ: 8.09 (t, $J_{2,3}$ = $J_{2,31P}$ = 5 Hz, 1H, H-2), 6.72–7.3 (m, 5H, H-3, Ph), 3.74–4.5 (m, 6H, OCH_2CH_3, $CH_2CH_2CH_2NMe_2$), 1.62–2.65 (m, 4H, $CH_2CH_2CH_2NMe_2$), 2.22 (s, 6H, NMe_2), 1.32 (t, $J_{CH_2CH_3}$ = 7 Hz, 6H, OCH_2CH_3). *Exact Mass* calcd. for $C_{20}H_{28}N_3O_3P^{32}S$: 421.1582; found (high resolution ms): 421.1595. Extraction of silica gel fraction R_f 0.41 gave a brown oil (0.11 g) which was rechromatographed on two silica gel

plates using chloroform–methanol (2:1) as the development solvent. This gave a single fraction R_f 0.64 which was extracted to give **1***b* as a yellow oil (0.056 g, 12.9%) identical (^{1}H nmr) with an authentic sample.

*4-Chloro-10-(3-dimethylaminopropyl)-10*H*-pyrido[3,2-*b*][1,4]-benzothiazine (**12**f) and 2-*n*-Butyl-10-(3-dimethylaminopropyl)-10*H*-pyrido[3,2-*b*][1,4]benzothiazine (**13**f)*

In a dry nitrogen atmosphere *n*-butyllithium (0.122 g, 1.91 mmol) was added dropwise with stirring to a solution of **1***b* (0.534 g, 1.91 mmol) in anhydrous tetrahydrofuran (125 mL) at 0°C. The resulting greenish brown solution was stirred at 0°C for 1 h, cooled to −77°C, and trifluoromethanesulfonyl chloride (0.385 g, 2.29 mmol) in anhydrous tetrahydrofuran (2 mL) was added dropwise. The reaction was stirred at −77°C for 0.5 h and allowed to warm to room temperature over a 2 h period. The resulting lime green solution was treated with water (75 mL), extracted with dichloromethane (6 × 50 mL), and dried (Na_2SO_4). Evaporation of the solvent *in vacuo* gave a brown oil (0.683 g) of which 0.6 g was subjected to preparative thin-layer chromatography on nine silica gel plates using chloroform–methanol (5:1 v/v) as the development solvent. Extraction of the silica gel fraction R_f 0.79 gave **13***f* as a yellow oil (0.158 g, 27.7%); ^{1}H nmr δ: 6.74–7.4 (m, 4H, Ph), 7.1 (d, $J_{3,4}$ = 8 Hz, 1H, H-4), 6.57 (d, $J_{3,4}$ = 8 Hz, 1H, H-3), 4.1 (t, $J_{CH_2CH_3}$ = 7 Hz, 2H, CH_2CH_2-CH_2NMe_2), 0.69–2.81 (m, 13H, $CH_2CH_2CH_2NMe_2$, *n*Bu), 2.35 (s, 6H, NMe_2). *Exact Mass* calcd. for $C_{20}H_{27}N_3{}^{32}S$: 341.1920; found (high resolution ms): 341.1924. Extraction of the silica gel fraction R_f 0.46 gave a yellow oil (0.087 g) which was rechromatographed on two silica gel plates using chloroform–methanol (5:1 v/v) as the development solvent. This gave two fractions R_f 0.58 and R_f 0.5. Extraction of the silica gel fraction R_f 0.5 gave **1***b* as a yellow oil (0.015 g, 3.1%) identical (^{1}H nmr) with an authentic sample. Extraction of the silica gel fraction R_f 0.58 gave **12***f* as a yellow oil (0.051 g, 8.3%); ^{1}H nmr δ: 7.82 (d, $J_{2,3}$ = 5.5 Hz, 1H, H-2), 6.8–7.29 (m, 4H, Ph), 6.74 (d, $J_{2,3}$ = 5.5 Hz, 1H, H-3), 4.02 (t, $J_{CH_2CH_3}$ = 7 Hz, 2H, $CH_2CH_2CH_2NMe_2$) 1.76–2.57 (m, 4H, $CH_2CH_2CH_2NMe_2$), 2.2 (s, 6H, NMe_2). *Exact Mass* calcd. for $C_{16}H_{18}N_3{}^{32}S^{37}Cl$: 321.0877; found (high resolution ms): 321.0867. *Exact Mass* calcd. for $C_{16}H_{18}N_3{}^{32}S^{35}Cl$: 319.0907; found (high resolution ms): 319.0898.

*1-Diethylphosphoryl-2-*n*-butyl-10-(2-dimethylaminopropyl)-1,2-dihydropyridyl[3,2-*b*][1,4]benzothiazine (**11**g), 4-Diethylphosphoryl-10-(2-dimethylaminopropyl)-10*H*-pyrido[3,2-*b*][1,4]benzothiazine (**12**g), and 2-*n*-Butyl-10-(2-dimethylaminopropyl)-10*H*-pyrido[3,2-*b*][1,4]benzothiazine (**13**g)*

In a dry nitrogen atmosphere *n*-butyllithium (0.162 g, 2.53 mmol) was added dropwise with stirring to a solution of **1***c* (0.72 g, 2.53 mmol) in anhydrous tetrahydrofuran (125 mL) at 0°C. The resulting dark brown solution was stirred at 0°C for 1 h, cooled to −77°C, and diethyl chlorophosphate (0.524 g, 3.03 mmol) in anhydrous tetrahydrofuran (2 mL) was added dropwise. The reaction was stirred at −77°C for 1 h and allowed to warm to room temperature over a 2 h period. The resulting light orange solution was treated with water (100 mL), extracted with chloroform (6 × 50 mL), and dried (Na_2SO_4). Evaporation of the solvent *in vacuo* gave a dark reddish brown oil (0.984 g) of which 0.9 g was subjected to preparative thin-layer chromatography on 10 silica gel plates using chloroform–methanol (5:1 v/v) as the development solvent. Extraction of the silica gel fraction R_f 0.93 gave a yellow oil (0.256 g) which was rechromatographed on four silica gel plates using chloroform–methanol (5:1 v/v) as the development solvent. This gave two fractions R_f 0.88 and R_f 0.72. Extraction of the silica gel fraction R_f 0.88 gave **11***g* as a yellow oil (0.156 g, 14.1%); ir (film): 1270 (s, P=O), 1630, and 1565 (s, C=C) cm^{-1}; ^{1}H nmr δ: 6.8–7.23 (m, 4H, Ph), 5.4–5.92 (m, 2H, H-3, H-4), 3.3–4.67 (m, 7H, $(OCH_2CH_3)_2$, H-2, CH_2), 2.7 (m, 1H, CH), 2.23 (s, 6H, NMe_2), 0.71–1.86 (m, 15H, *n*Bu, $(OCH_2CH_3)_2$), 0.98 (d, J_{CH_3CH} = 6.5 Hz, 3H, Me). *Exact Mass* calcd. for $C_{24}H_{38}N_3O_3P^{32}S$: 479.2363; found (high resolution ms): 479.2369. Extraction of the silica gel fraction R_f 0.72 gave **13***g* as a yellow oil (0.019 g, 2.4%); ^{1}H nmr δ: 6.5–7.38 (m, 6H, Ph, H-2, H-3), 4.28 (d, J_{CH_2CH} = 6.5 Hz, 2H, CH_2), 3.1 (m, 1H, CH), 2.64 (d, $J_{CH_2CH_2C_2H_5}$ = 7 Hz, 2H, $CH_2C_3H_7$), 2.38 (s, 6H, NMe_2), 0.7–1.86 (m, 7H, $CH_2C_3H_7$), 1.06 (d, J_{CH_3CH} = 6.5 Hz, 3H, Me). *Exact Mass* calcd. for $C_{20}H_{27}N_3{}^{32}S$: 341.1920; found (high resolution ms): 341.1917. Extraction of the silica gel fraction R_f 0.61 gave a yellow oil (0.094 g) which was rechromatographed on one silica gel plate using chloroform–methanol (5:1 v/v) as the development solvent. This gave a single fraction R_f 0.67 which gave **12***g* as a yellow oil (0.077 g, 7.9%); ir (film): 1268 (s, P=O) cm^{-1}; ^{1}H nmr δ: 8.16 (t, $J_{2,3} = J_{2,31P}$ = 5 Hz, 1H, H-2). 6.89–7.5 (m, 5H, H-3, Ph), 3.96–4.51 (m, 6H, CH_2, $(OCH_2CH_3)_2$), 3.11 (m, 1H, CH), 2.33 (s, 6H, NMe_2), 1.36 (t, $J_{CH_2CH_3}$ = 7 Hz, 6H, $(OCH_2CH_3)_2$), 1.07 (d, J_{CH_3CH} = 6.5 Hz, 3H, CH_3). *Exact Mass* calcd. for $C_{20}H_{28}N_3O_3P^{32}S$: 421.1583; found (high resolution ms): 421.1580.

*1-Methoxycarbonyl-2-*n*-butyl-10-(2-dimethylaminopropyl)-1,2-dihydropyridyl[3,2-*b*][1,4]benzothiazine (**11**h) and 4-Methoxycarbonyl-10-(2-dimethylaminopropyl)-10*H*-pyrido[3,2-*b*][1,4]benzothiazine (**12**h)*

In a dry nitrogen atmosphere *n*-butyllithium (0.162 g, 2.53 mmol) was added dropwise with stirring to a solution of **1***c* (0.072 g, 2.53 mmol) in anhydrous tetrahydrofuran (125 mL) at 0°C. The resulting dark brown solution was stirred at 0°C for 1 h, cooled to −77°C, and methyl chloroformate (0.286 g, 3.03 mmol) in anhydrous tetrahydrofuran (2 mL) was added dropwise. The reaction was stirred at −77°C for 1 h and allowed to warm to room temperature over a 2 h period. The resulting light brown solution was treated with water (100 mL), extracted with chloroform (5 × 50 mL), and dried (Na_2SO_4). Evaporation of the solvent *in vacuo* gave a dark reddish brown oil (1.038 g) of which 0.9 g was subjected to preparative thin-layer chromatography on 12 silica gel plates using ethyl acetate – ether (5:1 v/v) as the development solvent. Extraction of the silica gel fraction R_f 0.34 gave **11***h* as a yellow oil (0.338 g, 38.5%); ir (film): 1726 (s, C=O), 1630 (s, C=C) cm^{-1}; ^{1}H nmr δ: 6.74–7.32 (m, 4H, Ph), 5.49–5.96 (m, 2H, H-3, H-4), 4.9 (m, 1H, H-2), 3.4–3.8 (m, 2H, CH_2), 3.72 (s, 3H, OMe), 3.0 (m, 1H, CH), 2.3 (s, 6H, NMe_2), 0.69–1.88 (m, 9H, *n*Bu), 1.07 (d, J_{CH_3CH} = 6.5 Hz, 3H, Me). *Exact Mass* calcd. for $C_{22}H_{31}N_3O_2{}^{32}S$: 401.2130; found (high resolution ms): 401.2146. Extraction of the silica gel fraction R_f 0.14 gave a dark yellow oil (0.25 g) which was rechromatographed on six silica plates using chloroform–methanol (5:1 v/v) as the development solvent. This gave two fractions R_f 0.8 and R_f 0.73. Extraction of the fraction R_f 0.8 gave **12***h* as a yellow oil (0.064 g, 8.5%); ir (film): 1729 (s, C=O) cm^{-1}; ^{1}H nmr δ: 8.0 (d, $J_{2,3}$ = 5 Hz, 1H, H-2), 6.7–7.32 (m, 4H, Ph), 7.16 (d, $J_{2,3}$ = 5 Hz, 1H, H-3), 4.08–4.3 (m, 2H, CH_2), 3.9 (s, 3H, OMe), 3.08 (m, 1H, CH), 2.29 (s, 6H, NMe_2), 1.0 (d, J_{CH_3CH} = 6.5 Hz, 3H, CH_3). *Exact Mass* calcd. for $C_{18}H_{21}N_3O_2{}^{32}S$: 343.1350; found (high resolution ms): 343.1347. Extraction of the silica gel fraction R_f 0.73 gave **1***c* as a yellow oil (0.075 g, 12%) identical (^{1}H nmr) with an authentic sample.

10H-Pyrido[3,2-b][1,4]benzothiazine (1a)

In a dry nitrogen atmosphere *n*-butyllithium (0.202 g, 3.16 mmol) was added dropwise with stirring to a solution of **1***g* (0.9 g, 3.16 mmol) in anhydrous tetrahydrofuran (125 mL) at 0°C. The resulting dark brown solution was stirred at 0°C for 1.5 h, cooled to −77°C, and methyl chloroformate (0.358 g, 3.79 mmol) in anhydrous tetrahydrofuran (2 mL) was added dropwise. The reaction was stirred at −77°C for 1 h and allowed to warm to room temperature over a 2 h period. The resulting orange-red suspension was treated with water (100 mL), extracted with chloroform (8 × 50 mL), and dried (Na_2SO_4). Evaporation of the solvent *in vacuo* gave a brown oil (0.856 g) of which 0.8 g was subjected to preparative thin-layer chromatography on 12 silica gel plates using benzene–ether (1:1 v/v) as the development solvent. Extraction of the silica gel fraction R_f 0.54 gave 10*H*-pyrido[3,2-*b*]-[1,4]benzothiazine (**1***a*) as a yellow solid (0.09 g. 15.2%) identical (^{1}H nmr, mp) with an authentic sample.

*10-(2-*N*-Methoxycarbonyl-2-*N*-methylaminoethyl)-10H-pyrido[3,2-b][1,4]benzothiazine (18)*

In a dry nitrogen atmosphere *n*-butyllithium (0.165 g, 2.58 mmol) was added dropwise with stirring to a solution of **1***h* (0.7 g, 2.58 mmol) in anhydrous tetrahydrofuran (30 mL) at 0°C. The resulting dark brown solution was stirred at 0°C for 40 min, cooled to −77°C, and methyl chloroformate (0.488 g, 5.17 mmol) in tetrahydrofuran (2 mL) was added dropwise. The resulting solution was stirred at −77°C for 0.5 h and allowed to warm to room temperature over a 3.5 h period. The resulting dark brown solution was treated with water (50 mL), extracted with ether (3 × 100 mL), and dried (Na_2SO_4). Evaporation of the solvent *in vacuo* gave a dark brown oil (0.711 g) of which 0.6 g was subjected to preparative thin-layer chromatography on seven silica gel plates using benzene–ether (5:1 v/v) as the development solvent. Extraction of the silica gel fraction R_f 0.40 gave **18** as a dark yellow oil (0.167 g, 24.4%); ir (film): 1710 (s, C=O) cm^{-1}; ^{1}H nmr δ: 8.0 (d, $J_{2,3}$ = 5 Hz of d, $J_{2,4}$ = 1.75 Hz, 1H, H-2), 6.59–7.34 (m, 6H, Ph, H-3, H-4), 4.29 (m, 2H, $CH_2CH_2NCH_3(CO_2Me)$, 3.51–3.95 (m, 2H, $CH_2CH_2NCH_3(CO_2Me)$, 3.74 (s, 3H, OMe), 3.04 (s. 3H, NMe). *Exact Mass* calcd. for $C_{16}H_{17}N_3O_2{}^{32}S$: 315.1038; found (high resolution ms): 315.1042. Extraction of the silica gel fraction R_f 0.15 gave **1***h* as a light brown oil (0.19 g, 32.1%) identical (^{1}H nmr) with an authentic sample.

*10-*n*-Hexyl-10H-pyrido[3,2-b][1,4]benzothiazine (19)*

In a dry nitrogen atmosphere **1***h* (0.8 g, 2.95 mmol) in anhydrous tetrahydrofuran (5 mL) was added dropwise with stirring to a solution of *n*-butyllithium (0.567 g, 8.86 mmol) in anhydrous tetrahydrofuran (50 mL) at 0°C. This solution was stirred at 0°C for 1 h and allowed to warm to room temperature over a 1 h period. The resulting dark brown solution was treated with water (50 mL), extracted with ether (2 × 100 mL), and dried (Na_2SO_4). Evaporation of the solvent *in vacuo* gave a reddish brown oil (1.084 g) of which 0.33 g was subjected to preparative thin-layer chromatography on seven silica gel plates using benzene–ether (5:1 v/v) as the development solvent. Extraction of the silica gel fraction R_f 1 gave a dark yellow oil which was rechromatographed on one silica gel plate using petroleum ether (bp 35–60°C) as the development solvent. This gave a single fraction R_f 0.05 which was extracted to give **19** as a yellow oil (0.066 g, 25.9%); ^{1}H nmr δ: 8.01 (d, $J_{2,3}$ = 5 Hz of d, $J_{2,4}$ = 1.75 Hz, 1H, H-2), 6.59–7.38 (m, 6H, Ph, H-3, H-4), 4.1 (t, $J_{NCH_2CH_2C_4H_9}$ = 7 Hz, 2H, $NCH_2C_5H_{11}$), 0.65–2.11 (m, 11H, $NCH_2C_5H_{11}$). *Exact Mass* calcd. for $C_{17}H_{20}N_2{}^{32}S$: 284.1343; found (high resolution ms): 284.1347. This material was identical (ir, ^{1}H nmr) with an authentic sample of **19** prepared from the reaction of **1***a* with sodium hydride and *n*-hexyl chloride described below.

10*H*-Pyrido[3,2-*b*][1,4]benzothiazine **1***a* (0.5 g, 2.5 mmol) was added to a suspension of sodium hydride (0.120 g, 5 mmol) in toluene (40 mL) and the mixture was heated under reflux for 1 h. A solution of *n*-hexylchloride (0.333 g, 2.75 mmol) in toluene (3 mL) was added dropwise and the mixture was allowed to reflux for a further 66 h. After cooling to 25°C, 15 mL methanol and then 50 mL water was added slowly. Extraction with methylene chloride (4 × 50 mL) and evaporation of the solvent gave a brown oil which was purified on a 2.5 cm × 23 cm silica gel column. Elution with petroleum ether (bp 37–57°C) (200 mL) gave a hydrocarbon oil which was discarded. Elution with petroleum ether – ether (1:1 v/v) (300 mL) gave **19** (0.278 g, 39.2%) identical (^{1}H nmr, ir) with the same product described previously. Further elution with the same eluant (300 mL) gave **1***a* (0.21 g, 42% recovery).

Acknowledgment

We are grateful to the Medical Research Council of Canada (Grant MA-4888) for financial support of this work.

1. C. O. Okafor. Int. J. Sulfur Chem. B, **6**, 237 (1971).
2. F. M. Pasutto and E. E. Knaus. Can. J. Chem. **56**, 2365 (1978).
3. H. Gilman and D. L. Esmay. J. Am. Chem. Soc. **75**, 233 (1953).
4. H. Gilman and S. Gray. J. Org. Chem. **23**, 1476 (1958).
5. M. M. Abdel-Monem and P. S. Portoghese. J. Med. Chem. **15**, 208 (1972).
6. G. Kraiss and K. Nador. Tetrahedron Lett. 57 (1971).
7. R. L. Clarke and M. L. Heckeler. J. Org. Chem. **43**, 4586 (1978).
8. E. H. Flynn, H. W. Murphy, and R. E. McMahon. J. Am. Chem. Soc. **77**, 3104 (1955).
9. J. M. Brown. Chem. Ind. (London), 454 (1972).
10. R. A. Ruden. J. Org. Chem. **39**, 3607 (1974).
11. J. Schreiber, H. Maag, N. Hashimoto, and A. Eschenmoser. Angew. Chem. Int. Ed. Engl. **10**, 330 (1971).

X-ray crystallographic study of Ni(II) bis(morpholine-*N*-carbodithioate) and epr studies of Cu(II) bis(morpholine-*N*-carbodithioate) and Cu(II) bis(pyrrolidine-*N*-carbodithioate)

F. G. HERRING, J. M. PARK, S. J. RETTIG, AND J. TROTTER

Department of Chemistry, The University of British Columbia, 2075 Wesbrook Mall, Vancouver, B.C., Canada V6T 1W5

Received November 30, 1978

F. G. HERRING, J. M. PARK, S. J. RETTIG, and J. TROTTER. Can. J. Chem. **57**, 2379 (1979).

Crystals of Ni(II) bis(morpholine-*N*-carbodithioate) are monoclinic, $a = 4.291(1)$, $b = 20.584(2)$, $c = 8.365(1)$ Å, $\beta = 97.39(2)°$, $Z = 2$, space group $P2_1/n$. The structure was solved by Patterson and Fourier syntheses and was refined by full-matrix least-squares procedures to $R = 0.036$ and $R_w = 0.044$ for 1800 reflections with $I \geq 3\sigma(I)$. The crystal structure consists of discrete molecules having approximate C_{2h} and exact (crystallographic) C_i symmetry. The nickel atom is coordinated to four sulphur atoms in a planar arrangement with Ni—S = 2.2122(7) and 2.2134(6) Å and S—Ni—S = 79.16(2) and 100.84(2)°.

The electron paramagnetic resonance spectra of ^{63}Cu(II) bis(morpholine-*N*-carbodithioate) and ^{63}Cu(II) bis(pyrrolidine-*N*-carbodithioate) doped in the respective Ni(II) analogues have been recorded at room temperature. The spin Hamiltonian parameters obtained from an analysis of the spectra of the polycrystalline samples have been used to investigate the bonding in these complexes. The results are compared to previous studies in carbodithioates.

F. G. HERRING, J. M. PARK, S. J. RETTIG et J. TROTTER. Can. J. Chem. **57**, 2379 (1979).

Les cristaux du bis(morpholine *N*-carbodithioate) Ni(II) sont monocliniques, $a = 4.291(1)$, $b = 20.584(2)$, $c = 8.365(1)$ Å, $\beta = 97.39(2)°$, $Z = 2$, groupe d'espace $P2_1/n$. On a résolu la structure par des synthèses de Patterson et de Fourier et on l'a affinée par la méthode des moindres carrés (matrice complète) jusqu'à une valeur de $R = 0.036$ et de $R_w = 0.044$ pour 1800 réflexions avec $I \geq 3\sigma(I)$. La structure cristalline comprend des molécules individuelles de symétrie approximative C_{2h} et de symétrie exacte (cristallographique) C_i. L'atome de nickel est coordonné à quatre atomes de soufre avec un arrangement planaire où Ni—S = 2.2122(7) et 2.2134(6) Å et S—Ni—S = 79.16(2) et 100.84(2)°.

Opérant à la température ambiante, on a enregistré le spectre de résonance paramagnétique électronique du ^{63}Cu bis(morpholine *N*-carbodithioate) et ^{63}Cu bis(pyrrolidine-*N*-carbodithioate) dopé avec son analogue au Ni(II). On a utilisé les paramètres Hamiltonien des spins provenant d'une analyse des spectres d'échantillons polycristallins pour étudier les liaisons dans ces complexes. On compare les résultats avec ceux obtenus dans des études antérieures de carbodithioates.

[Traduit par le journal]

The complexes formed by dithiocarbamates with transition metal ions have been the subject of many studies (1–4). These complexes have intriguing spectroscopic and structural properties arising from contributions of resonance structures which lead to an effective dianion electronic structure (1). The overall bonding to the transition metal is therefore very covalent leading to, for example, epr hyperfine parameters which are quite different from those in complexes where the donor atom is a harder base.

The binary complexes of dialkyldithiocarbamates with Cu(II) are very stable and their epr spectra have been widely investigated both in the solid state and frozen solution (5–8). Copper(II) bisdiethyldithiocarbamate has also been used to study fast Lewis acid–base reactions (9) as a probe of molecular motion in liquids (10). In order that a complex of Cu(II) can be used as a probe of molecular motion in liquids it is necessary that the anisotropies of the epr spin Hamiltonian be accurately determined. The g-tensor and hyperfine tensor can be obtained with sufficient accuracy from polycrystalline samples of the Cu(II) complex in the Ni(II) analogue; however, in doing so it is necessary to be sure that the environment in the host lattice does not include any dimeric interactions nor non-square planar coordination as, for example, in the case of the diethyldithiocarbamates of Zn(III) and Cu(II). In addition 'to accurately determine hyperfine parameters' it is desirable that the shape of the spin probe be as well defined as possible. To this end a dithiocarbamate ligand with the N-atom in a ring structure is suitable, and consequently we have investigated the utility of pyrrolidine-*N*-carbodithioate and morpholinecarbodithioate as ligands.

The present paper describes the epr of ^{63}Cu(II)-bis(pyrrolidine-*N*-carbodithioate) and ^{63}Cu(II) bis-(morpholine-*N*-carbodithioate) doped in their Ni(II) analogues together with the X-ray crystal structure analysis of the Ni(II) bis(morpholine-*N*-carbodi-

0008-4042/79/182379-07$01.00/0

thioate), that of the pyrrolidine-*N*-carbodithioate already having been determined (12). The results are used to compare the bonding in these compounds with that of the pyrrole analogue (13).

Experimental

Preparation of Compounds

Potassium morpholinecarbodithioate was prepared by mixing stoichiometric quantities of morpholine, carbon disulphide, and potassium hydroxide in water. The resultant salt was used to prepare the Ni(II) and ^{63}Cu(II) complexes by mixing the respective chloride and salt in water. The resultant precipitate was repeatedly washed and then recrystallized from chloroform. Crystals of Ni(II) bis(morpholinecarbodithioate) for the X-ray diffraction studies were obtained by slow evaporation at ambient temperature of a saturated chloroform solution.

The ^{63}Cu(II) bis(pyrrolidinecarbodithioate) was prepared as above using the ammonium salt which was obtained from Aldrich Chemicals. The $^{63}CuCl_2$ was prepared as described previously (10). All compounds studied in this work gave the correct microanalytical results for C, H, and N.

Electron Paramagnetic Resonance

Electron paramagnetic resonance (epr) spectra of polycrystalline samples of the ^{63}Cu(II) complex doped (1 : 1000) in the Ni(II) analogues were recorded at room temperature (22°C) in an X-band (9.05 GHz) spectrometer. The $NiCl_2$ used to prepare the Ni analogue of the carbodithioate under consideration often contained a high level of Cu(II) (mixed isotopes) which obscured the epr spectrum of the ^{63}Cu(II) carbodithioate doped in the Ni carbodithioate. This situation was remedied by coprecipitating the Cu(II) impurity with the Ni carbodithioate by pretreating a $NiCl_2$ solution with half an equivalent of the potassium carbodithioate. The resulting solution was filtered and the supernatant liquid, containing purified $NiCl_2$, used to prepare the Ni(II)bis(carbodithioate). The Ni complex prepared in this way proved to be free of Cu(II) at the operating levels of the epr spectrometer, and was subsequently used as a host for the Cu(II) complex.

The magnetic field of the epr spectrum was calibrated using a proton magnetometer and the microwave frequency was accurately measured using an HP 5425L counter equipped with an X-band plug-in.

The epr spectrum of ^{63}Cu(II) bis(morpholinecarbodithioate) is shown in Fig. 1. The g-tensor and hyperfine tensor were obtained by simulating the observed spectrum using a computer program described previously (14). The results of the simulations for the morpholine complex are shown in Fig. 2 and the spin Hamiltonian parameters used are presented in Table 1. The results for the pyrrolidine-*N*-carbodithioate are also included in Table 1.

X-ray Crystallographic Analysis of Ni(II) Bis(morpholine-N-carbodithioate)

The crystal chosen for study, grown by slow evaporation of a chloroform solution, was mounted with $(\bar{1}\bar{1}0)$ normal to the goniostat axis and had dimensions of ca. 0.6 × 0.2 × 0.35 mm. Unit-cell and space group data were obtained from film and diffractometer measurements. The unit-cell parameters were refined by least squares on 2 sin θ/λ values for 16 reflections measured on a diffractometer with MoK_α radiation (λ = 0.71073 Å). Crystal data (at 22°C) are:

$C_{10}H_{16}N_2NiO_2S_4$ fw = 383.22

Monoclinic, $a = 4.291(1)$, $b = 20.584(2)$, $c = 8.365(1)$ Å, $\beta = 97.39(2)°$, $V = 732.6(2)$ Å^3, $Z = 2$, $\rho_c = 1.737$ g cm^{-3}, $F(000) = 396$, $\mu(MoK_\alpha) = 18.6$ cm^{-1}. Absent reflections: $0k0$, $k = 2n$, $h0l$, $h + l \neq 2n$ define uniquely the space group $P2_1/n$ (alternate setting of $P2_1/c$, C_{2h}^5, No. 14).

Intensities were measured with zirconium-filtered MoK_α radiation on a Datex-automated General Electric XRD-6 diffractometer. A θ–2θ scan at 4° min^{-1} over a range of (1.80 + 0.86 tan θ)° in 2θ was employed. Background counts of 10 s were measured at each end of the scan. Data were measured to 2θ = 65°. The intensities of the check reflections, measured every 50 reflections throughout the data collection,

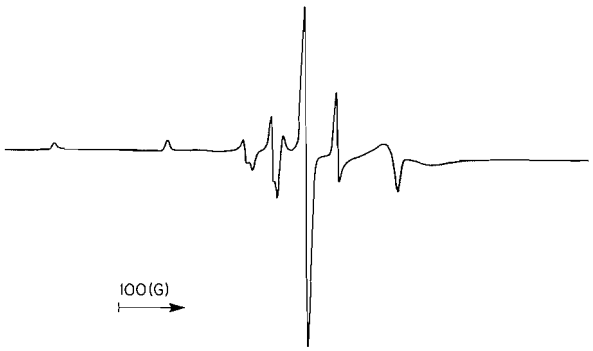

FIG. 1. The epr spectrum of copper(II)-63 bis(morpholine-*N*-carbodithioate) doped in the Ni(II) analogue.

FIG. 2. Simulated spectrum of copper(II)-63 bis(morpholine-*N*-carbodithioate).

TABLE 1. Spin Hamiltonian parameters determined from polycrystalline samples

Parameter	^{63}Cu(II) bis(morpholine-carbodithioate)	^{63}Cu(II) bis(pyrrolidine-carbodithioate)
A_{zz}†	−156.8 ±0.1	−158.0
A_{xx}	−35.8 ±0.2	−39.8
A_{yy}	−31.5 ±0.2	−35.3
g_{zz}	2.094±0.001	2.088
g_{xx}	2.025±0.001	2.022
g_{yy}	2.020±0.001	2.018

†cm^{-1} × 10^4.

decreased uniformly to final values which were 0.93 times the initial values and appropriate corrections were made. After data reduction, an absorption correction was applied using the Gaussian integration method (15, 16). Transmission factors ranged from 0.582 to 0.728. Of the 2656 independent reflections measured, 1800 (68%) had intensities greater than $3\sigma(I)$ above background where $\sigma^2(I) = S + B + (0.025S)^2$ with S = scan count and B = time-averaged background count.

The positions of the sulphur atoms were determined from the Patterson function assuming the nickel atom to be situated at the origin, and those of the O, N, and C atoms from a subsequent difference map. After full-matrix least-squares refinement of the non-hydrogen atoms with anisotropic thermal parameters to $R = 0.100$, a difference map gave the coordinates of all 8 independent hydrogen atoms, which were included in all subsequent cycles of refinement with isotropic thermal parameters. The scattering factors of ref. 17 were used for the non-hydrogen atoms and those of ref. 18 for hydrogen atoms. Anomalous scattering factors from ref. 19 were used for the Ni and S atoms. The weighing scheme, $w = (|F_o|/5.5)^2$ if $|F_o| < 5.5$, $w = 1$ if $5.5 \leq |F_o| \leq 25.0$, $w = (25.0/|F_o|)^2$ if $|F_o| > 25.0$, and $w = 0.144$ for the unobserved reflections, gave uniform average values of $w(|F_o| - |F_c|)^2$ over ranges of $|F_o|$ and was employed in the final stages of refinement. A type I anisotropic extinction correction (Thornley–Nelmes definition of mosaic anisotropy with a Lorentzian distribution) was applied (20–22). Extinction parameters are given in Table 2. Convergence was reached at $R = 0.036$ and $R_w = 0.044$ for 1800 reflections with $I \geq 3\sigma(I)$. For all 2656 planes $R = 0.061$ and $R_w = 0.051$.

On the final cycle of refinement the mean and maximum parameter shifts corresponded to 0.15 and 0.68σ respectively. The mean error in an observation of unit weight was 0.4784. The final positional and thermal parameters appear in Tables 3 and 4 respectively.[1] Measured and calculated structure factors have been placed in the Depository of Unpublished Data.[1]

The ellipsoids of thermal motion for the non-hydrogen atoms are shown in Fig. 3. Rigid-body thermal motion analysis (23) has been carried out using the computer program MGTLS. The rms standard error in the temperature factors σU_{ij} (derived from the least-squares analysis) is 0.0010 Å^2. Analysis of the 7-atom group consisting of C(1) plus the six morpholine ring atoms gave physically reasonable results (rms $\Delta U_{ij} = 0.0008$ Å^2). The appropriate bond lengths have been corrected for libration (24), using shape parameters q^2 of 0.08 for all atoms involved. Corrections to bonds involving atoms not included in the rigid-body were estimated using independent motion corrections based on the ΔU_{ij}. Corrected and uncorrected bond lengths are given in Table 5 and corrected bond angles in Table 6. Intra-annular torsion angles for the chelate and morpholine rings are given in Table 7.

Individual molecules of $Ni(S_2CNC_4H_8O)_2$ have exact (crystallographic) C_i symmetry with the nickel atoms located at the inversion centres (0,0,0) and $(\frac{1}{2},\frac{1}{2},\frac{1}{2})$. The molecule (Fig. 3) effectively has C_{2h} symmetry, the mirror plane being normal to the NiS_4 plane and containing Ni, C(1), N, and O. Bond lengths and angles are consistent with C_{2h} symmetry within experimental error but the C_{2h} symmetry is broken by a small twist of the morpholine ring with respect to the $C(1)S_2$ plane (the angle between normals to the C(1) and N coordination groups being 3.2°). This is assumed to be a result of packing forces.

The NiS_4 group is exactly planar as a result of the molecular inversion centre. Important mean[2] structural parameters are in excellent agreement with those found for related molecules (see Table 8). The relatively long mean Ni—S distance of 2.2128(6) Å is as expected for a dithiocarbamate ligand which generates a weak crystal field (32). Although the $Ni(S_2CNC_2)_2$ group is planar to within ±0.116 Å, deviations of this magnitude represent highly significant deviations from planarity. The four-membered chelate ring, NiS_2C, is slightly but significantly ($x^2 = 29.0$) non-planar as are the coordination groups of C(1) and N (displaced −0.011(2) and 0.073(2) Å respectively from the planes defined by their substituents). The morpholine ring adopts a nearly regular chair conformation, slightly distorted by the nearly planar coordination at nitrogen. Bond lengths

TABLE 2. Anisotropic extinction parameters, Lorentzian type I

Y	Thornley–Nelmes ($\times 10^{-8}$)
11	0.0045(5)
22	0.032(4)
33	0.41(5)
12	0.008(2)
13	0.04(1)
23	0.02(1)

Principal axes of mosaic spread (seconds of arc) and directions in orthogonal Å space referred to a, b, c^*

η_1	0.05	0.98	−0.18	0.05
η_2	0.58	0.19	0.98	−0.05
η_3	2.1	−0.04	0.06	0.99

TABLE 3. Final positional parameters (fractional $\times 10^5$, H $\times 10^3$) with estimated standard deviations in parentheses. Equivalent positions: $(x, y, z; 1/2 - x, 1/2 + y, 1/2 - z)$

Atom	x	y	z
Ni	50000	50000	50000
S(1)	67105(19)	50183(3)	26178(8)
S(2)	60886(20)	39638(3)	46864(8)
O	93529(54)	29171(10)	−6309(25)
N	82975(51)	37981(10)	18355(23)
C(1)	72301(58)	41989(11)	28842(27)
C(2)	93663(73)	40318(14)	3350(31)
C(3)	83374(80)	35637(15)	−10267(31)
C(4)	79695(89)	26976(15)	7450(38)
C(5)	90070(79)	31154(13)	22086(32)
H(2a)*	1175(8)	407(2)	55(4)
H(2e)	855(8)	443(2)	9(4)
H(3a)	593(8)	357(2)	−130(4)
H(3e)	920(8)	368(2)	−203(4)
H(4a)	556(9)	272(2)	44(4)
H(4e)	861(8)	227(2)	92(4)
H(5a)	1130(9)	307(2)	255(4)
H(5e)	793(8)	300(2)	304(4)

*a and e refer to axial and equatorial respectively.

[1]Structure factors and thermal parameters (Table 4) are available, at a nominal charge, from the Depository of Unpublished Data, CISTI, National Research Council of Canada, Ottawa, Ont., Canada K1A 0S2.

[2]Here and elsewhere in this report mean values refer to weighted means with rms deviations from the mean in parentheses.

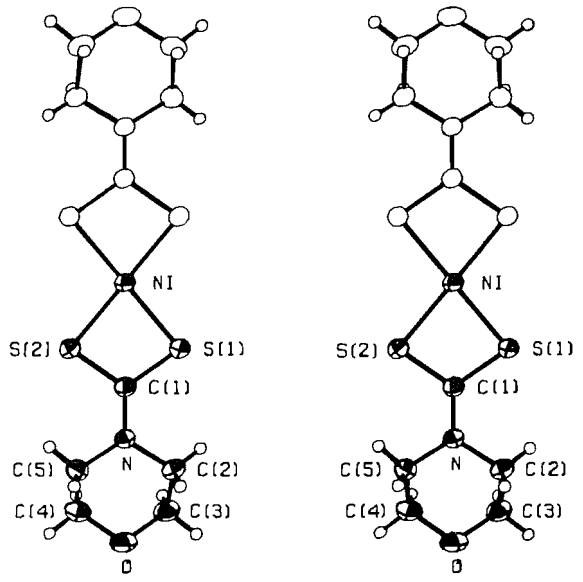

FIG. 3. Stereoview of the $Ni(S_2CNC_4H_8O)_2$ molecule. 50% thermal ellipsoids are shown for the non-hydrogen atoms; hydrogen atoms have been given artificially small temperature factors for the sake of clarity.

and angles in the morpholine ring are as expected. A possibly significant difference between the mean axial and equatorial C—H bond distance (1.02(2) vs. 0.93(4) Å) has been noted.

The crystal structure viewed along a^* is shown in Fig. 4. It has been noted that packing in compounds of this type is generally dominated by S···H and/or M···H contacts (11, 12, 29, 30, 32–34). The present structure is no exception, being made up of discrete molecules of $Ni(S_2CNC_4H_8O)_2$ linked by weak C—H···S interactions (S(2)···H(3e)(x, y, $1 + z$) = 2.95(3) and (S2)···H(4e)($x - \frac{1}{2}$, $\frac{1}{2} - y$, $\frac{1}{2} + z$) = 2.98(4) Å). All other intermolecular distances are greater than the sum of van der Waals radii. The shortest Ni···S contact is 3.847(1) Å (Ni···S(1) ($x - 1$, y, z and $2 - x$, $1 - y$, $1 - z$)), and does not represent any significant interaction.

Analysis of the epr Data for the Cu(II) Morpholine and Pyrrolidine N-carbodithioates

The spin Hamiltonian parameters obtained for the copper(II) complexes of the morpholinecarbodithioate and pyrrolidine-*N*-carbodithioate liquids are given in Table 1. The hyperfine and g-tensor show an orthorhombic character which can be attributed to a S(1)—Cu—S(2) angle of less than 90° and variations in Cu—S(1) and Cu—S(2) bond lengths; both of these distortions lead to symmetries less than D_{4h} and cause a splitting of the d_{xz} and d_{yz} orbitals producing the observed non-axial character. The magnitudes of the spin Hamiltonian parameters are typical for most dithiocarbamates with the possible exception of the pyrrolle-*N*-carbodithioate; this can be seen from Table 9 where the results for other complexes are collected. The parameters in Table 9 are all for the copper-63 complex doped in the nickel analogue with the exception of the pyrrole derivative (13). The crystal structures of the diethyl, morpholine, and pyrrolidine carbodithioates of Ni(II) are known (11, 12) and a summary of pertinent results is shown in Table 8. A consideration of the data in this table shows that only very weak axial interactions at the nickel atom occur in these lattices so that the spin Hamiltonian parameters obtained reflect a square planar environment free of additional interactions. This is not the case in Zn diethyldithiocarbamate, for example, where the environment is close to square pyramidal (11). The parameters for the Cu(II)-bis(pyrrole-carbodithioate) were obtained in the Cd(II) analogue and by use of mixed Cu isotopes; the latter fact leads to relatively inaccurate spin Hamiltonian parameters due to overlap of the ^{63}Cu and ^{65}Cu lines in the perpendicular region of the spectrum. The results for dimethyldithiocarbamate were obtained using Cu(II)-63 in the Ni(II) complex (25). Unfortunately the crystal structure for Ni(II) bis(dimethyldithiocarbamate) has not been determined so that the exact environment around the Ni(II) is not known and consequently absolutely reliable comparisons cannot be made, but the results are included for completeness.

The ligand environment around the Cu or Ni in dithiocarbamates corresponds to D_{2h} symmetry. A crystal field calculation by Choi *et al.* (26) for D_{2h} symmetry and four sulphur ligands shows as expected a $^2B_{1g}$ ground state. The application of group theory shows that the antibonding molecular orbitals are (27):

$$\psi_{B_{1g}} = \alpha d_{xy} - \tfrac{1}{2}\alpha'[-\sigma_{xy}^{(1)} + \sigma_{xy}^{(2)} + \sigma_{xy}^{(3)} - \sigma_{xy}^{(4)}]$$

$$\psi_{A_g} = \beta d_{x^2-y^2} - \tfrac{1}{2}\beta'[-p_{xy}^{(1)} - p_{xy}^{(2)} + p_{xy}^{(3)} + p_{xy}^{(4)}]$$

$$\psi_{A_g} = \gamma d_{z^2} - \tfrac{1}{2}\gamma'[\sigma_{xy}^{(1)} + \sigma_{xy}^{(2)} - \sigma_{xy}^{(3)} - \sigma_{xy}^{(4)}]$$

$$\psi_{B_{3g}} = \delta d_{yz} - \tfrac{1}{2}\delta'[p_z^{(1)} + p_z^{(2)} - p_z^{(3)} - p_z^{(4)}]$$

$$\psi_{B_{2g}} = \varepsilon d_{xz} - \tfrac{1}{2}\varepsilon'[p_z^{(1)} - p_z^{(2)} + p_z^{(4)} - p_z^{(3)}]$$

using the notation of Gersmann and Swalen (27). The magnetic parameters are:

[1] $g_{zz} = g_e - (\delta\lambda/\Delta E_{x^2-y^2})(\alpha^2\beta^2)$

[2] $g_{xx} = g_e - (2\lambda/\Delta E_{xz})(\alpha^2\varepsilon^2)$

TABLE 5. Bond lengths (Å) with estimated standard deviations in parentheses

(*a*) Non-hydrogen atoms

Bond	Uncorr.	Corr.	Bond	Uncorr.	Corr.
Ni—S(1)	2.2107(6)	2.2134	N—C(1)	1.328(3)	1.330
Ni—S(2)	2.2063(7)	2.2122	N—C(2)	1.471(3)	1.475
S(1)—C(1)	1.712(2)	1.717	N—C(5)	1.463(3)	1.469
S(2)—C(1)	1.714(2)	1.718	C(2)—C(3)	1.514(4)	1.517
O—C(3)	1.426(4)	1.432	C(4)—C(5)	1.515(4)	1.519
O—C(4)	1.434(4)	1.438			

(*b*) Bonds involving hydrogen atoms

C—H(axial), 0.99–1.03(3–4), mean 1.02(2)
C—H(equatorial), 0.90–0.99(3–4), mean 0.93(4) Å

TABLE 6. Bond angles (deg) with estimated standard deviations in parentheses

(*a*) Non-hydrogen atoms*

Bonds	Angle (deg)	Bonds	Angle (deg)
S(1)—Ni—S(2)	79.16(2)	S(1)—C(1)—S(2)	110.4(1)
S(1)—Ni—S(2)′	100.84(2)	S(1)—C(1)—N	125.2(2)
Ni—S(1)—C(1)	85.23(8)	S(2)—C(1)—N	124.5(2)
Ni—S(2)—C(1)	85.24(8)	N—C(2)—C(3)	109.9(2)
C(3)—O—C(4)	109.6(2)	O—C(3)—C(2)	111.6(2)
C(1)—N—C(2)	122.1(2)	O—C(4)—C(5)	111.1(3)
C(1)—N—C(5)	122.5(2)	N—C(5)—C(4)	109.9(2)
C(2)—N—C(5)	114.8(2)		

*Primed atom at $1-x, 1-y, 1-z$.

(*b*) Angles involving hydrogen atoms

R—C—H, 106–113(2–3), mean 109(2)°

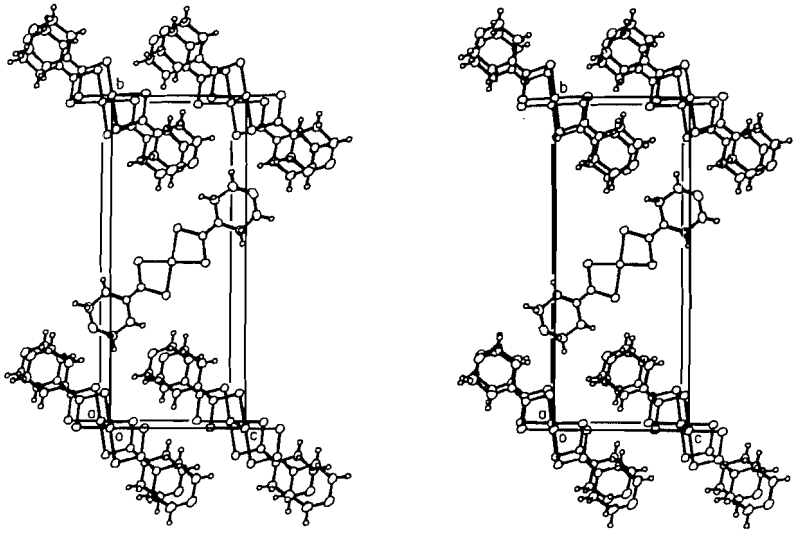

FIG. 4. The structure of $Ni(S_2CNC_4H_8O)_2$ viewed along a^*.

TABLE 7. Intra-annular torsion angles (deg)

Bond	Obs.	Bond	Obs.
N—C(2)	49.0(2)	Ni—S(1)	−0.40(8)
C(2)—C(3)	−54.3(2)	S(1)—C(1)	0.54(8)
C(3)—O	61.6(3)	C(1)—S(2)	−0.54(8)
O—C(4)	−61.9(3)	S(2)—Ni	0.40(8)
C(4)—C(5)	55.2(3)		
C(5)—N	−49.5(3)		

[3] $g_{yy} = g_e - (2\lambda/\Delta E_{yz})(\alpha^2\delta^2)$

[4] $A_{zz} = -K - \frac{4}{7}\alpha^2 P - 2\lambda\alpha^2 P\left(\frac{4\beta^2}{\Delta E_{x^2-y^2}} + \frac{3}{14}\frac{\delta^2}{\Delta E_{yz}} + \frac{3}{14}\frac{\varepsilon^2}{\Delta E_{xz}}\right)$

[5] $A_{xx} = -K + \frac{2}{7}\alpha^2 P - \frac{22}{14}\frac{\lambda\alpha^2\varepsilon^2}{\Delta E_{xz}}$

[6] $A_{yy} = -K + \frac{2}{7}\alpha^2 P - \frac{22}{14}\frac{\lambda\alpha^2\delta^2}{\Delta E_{yz}}$

These equations have been modified so that the Fermi contact term is represented by $-K$ and not $-\alpha^2 k$. The latter form is based upon the misconception that the Fermi contact term for d^9 systems is proportional to the square of the M.O. coefficient of the *d*-orbital in the single electron M.O.; this has been shown to be incorrect by McGarvey (28). The other symbols have their usual meaning and we adopt the values $\lambda = -828\ cm^{-1}$ and $P = 360 \times 10^{-4}\ cm^{-1}$.

The evaluation of the bonding parameters, α, β, δ, ε, and K requires a knowledge of the electronic spectrum of the dithiocarbamates of Cu(II). Recently Choi *et al.* (26) have performed an analysis of the electronic spectra of these complexes and the results can be summarized as the $d_{xy} \rightarrow d_{xz}$ and $d_{xy} \rightarrow d_{yz}$ occurring at ca. 2.30 μm^{-1}, $d_{xy} \rightarrow d_{x^2-y^2}$ at ca. 1.90 μm^{-1} and $d_{xy} \rightarrow d_{z^2}$ at ca. 1.60 μm^{-1}. The only disconcerting aspect of this interpretation is the very large extinction coefficient (or molar absorbtivity) of the band at 2.30 μm^{-1} which is unexpected for a *d–d* band. Choi *et al.* (26) provide a reasonable explanation of this large extinction coefficient and the orbital order is supported by crystal field calculations.

It is easy to show that the Fermi contact term can be obtained from:

$$-K = [(A_{xx} + A_{yy} + A_{zz}) - P(\Delta g_{xx} + \Delta g_{yy} + \Delta g_{xx})]/3$$

and α^2 from:

$$\alpha^2 = 7[-A_{zz} - K + P(\Delta g_{zz} + (3/14)\Delta g_{xx} + (3/14)\Delta g_{yy})]/(4P)$$

TABLE 8. Mean structural parameters for compounds of the type $(RR'NCS_2)_2M$, M = Ni(II) or Cu(II)

M	R	R′	Molecular symmetry	Bond lengths (Å)				Angles (deg)		Short non-bonded distances			Reference
				M—S	C—S	C(1)—N	N—C	S—Ni—S	Ni—S—C	M··S	M··H	S··H	
Ni	H	H	1	2.211(5)	1.69(1)	1.38(1)	—	78.5(1)	84.8(1)	3.599(8)	2.86	2.42	29
Ni	CH_3	H	$\bar{1}$	2.200(4)	1.71(1)	1.30(2)	1.47(2)	79.2(1)	85.5(2)	3.62(1)	—	2.66	30
Ni	i-C_3H_7	H	2	2.212(10)	1.69(3)	1.38(2)	1.46(2)	78.9(1)	84.5(11)	—	—	2.81	31
Ni	i-C_3H_7	i-C_3H_7	1	2.181(5)	1.70(1)	1.33(1)	1.50(2)	79.2(5)	85.7(4)	—	2.89	2.77	32
Ni	n-C_3H_7	n-C_3H_7	$\bar{1}$	2.203(6)	1.71(1)	1.33(1)	1.47(1)	79.3(1)	85.0(6)	—	3.24	2.88	33
Ni	C_2H_5	C_2H_5	$\bar{1}$	2.201(6)	1.707(7)	1.33(1)	1.49(1)	79.2(2)	85.1(3)	—	~2.8	~2.9	11
Ni	CH_3	C_6H_5	$\bar{1}$	2.203(5)	1.72(2)	1.30(1)	1.51(2)	79.3(1)	85.6(6)	—	3.06	2.85	34
Ni	$\frac{1}{2}(CH_2)_4$	$\frac{1}{2}(CH_2)_4$	$\bar{1}$	2.209(8)	1.710(3)	1.33(1)	1.50(1)	79.5(1)	84.6(2)	—	2.79	2.83	12
Ni	i-C_4H_9	i-C_4H_9	1	2.201(6)	1.719(2)	1.32(1)	1.50(1)	79.4(1)	85.4(3)	—	2.68	—	35
Ni	$\frac{1}{2}C_4H_8O$	$\frac{1}{2}C_4H_8O$	1	2.2128(6)	1.718(1)	1.330(3)	1.472(3)	79.16(2)	85.24(1)	3.847(1)	—	2.95	This work
Ni	$\frac{1}{2}(CH_2)_6$	$\frac{1}{2}(CH_2)_6$	$\bar{1}$	2.202(6)	1.72(1)	1.35(1)	1.48(1)	80.5(5)	84.0(5)	—	2.79	2.78	36
Cu	CH_3	CH_3	$\bar{1}$	2.311(9)	1.721(5)	1.31(1)	1.45(1)	77.0(1)	84.6(4)	3.159(3)	—	2.80	37
Cu	C_2H_5	C_2H_5	1	2.313(19)	1.717(13)	1.34(1)	1.47(1)	76.9(4)	84.6(10)	2.851(2)	2.86	—	11
Cu	n-C_3H_7	n-C_3H_7	1	2.325(4)	1.721(11)	1.32(1)	1.47(3)	76.5(2)	84.7(4)	2.741(3)	2.93	—	38
Cu	CH_3	C_6H_5	$\bar{1}$	2.302(27)	1.73(1)	1.31(2)	1.47(2)	77.7(1)	84.2(10)	—	3.08	2.94	34
Cu	$\frac{1}{2}(CH_2)_4$	$\frac{1}{2}(CH_2)_4$	$\bar{1}$	2.344(2)	1.728(8)	1.39(1)	1.51(1)	74.9(1)	86.9(1)	—	2.84	2.80	12
Cu	$\frac{1}{2}(CH_2)_6$	$\frac{1}{2}(CH_2)_6$	$\bar{1}$	2.297(1)	1.72	1.33	1.48	77.8	—	—	—	—	39

where $\Delta g_{xx} = g_{xx} - 2.0023$, etc., and the signs of A_{xx}, A_{yy}, and A_{zz} are taken to be negative. Once α^2 has been obtained β^2 can be obtained from eq. [1] with a knowledge of $\Delta E(xy \rightarrow x^2 - y^2)$ together with Δg_{xx} and Δg_{yy}. Finally we determined an average value of δ^2 by neglecting the slight orthorhombic character (i.e. setting $\delta^2 = \varepsilon^2$ and $\Delta E_{xz} \approx \Delta E_{yz}$) and using $g = \frac{1}{2}(g_{xx} + g_{yy})$ with the appropriate average of eq. [2] and eq. [3]. This was done since the electronic spectra do not permit a resolution of the $\Delta E(xy \rightarrow yz)$ transitions and this procedure is in accord with previous work where only $g_\perp$ is measured. We note that the above method of calculation of bonding parameters makes no assumptions as to the dependence of the Fermi contact term on α^2, nor does it assume that the Fermi contact term is a constant for all dithiocarbamates as is done in the method adopted by Bereman and Nalewajek (13). The results of the calculations are given in Table 9.

Discussion

It is appropriate to discuss our epr results in relation to previous studies. The most extensive epr studies have been carried out on $Cu(DEDTC)_2$ (5–8) and there is some variation in the spin Hamiltonian parameters. The variations in spin Hamiltonian parameters are well understood in terms of axial interactions or lowering of symmetry which cause $g_\parallel$ to increase and $A_\parallel$ to decrease (40). Thus if a study of the spectrum of $Cu(DEDTC)_2$ is made in even a mildly coordinating solvent quite large increases in $g_\parallel$ and decreases in $A_\parallel$ can be observed (40). This presumably accounts for the difference in hyperfine parameters observed for $Cu(DEDTC)_2$ in chloroform: toluene glass (10, 40), and $Cu(DEDTC)_2$ in the Ni analogue where axial interactions are minimal. We therefore feel that the hyperfine parameters obtained in the Ni(II) analogue reflect more closely those that would be obtained for the Cu(II) complex free of any non-specific interactions.

Weeks and Fackler (5) determined the spin Hamiltonian parameters of $Cu(DEDTC)_2$ in the Ni analogue and deduced from them the bonding parameters using various degrees of approximation. The results obtained by them using $\Delta E(xy \rightarrow x^2 - y^2) = 1.60\ \mu m^{-1}$ and $\Delta E(xy \rightarrow xz) = 2.0\ \mu m^{-1}$ are $\alpha = 0.74$, $\beta = 0.72$, and $\delta = 0.82$ which are in fair agreement with our results which were obtained using the electronic excitation energies of Choi *et al.* (14). Gersmann and Swalen (27) also determined the bonding parameters in $Cu(DEDTC)_2$ using the spin Hamiltonian parameters deduced from spectra recorded from samples in a frozen chloroform–toluene mixture. As mentioned above the g- and A-values obtained from this glass are subject to error and consequently they obtained bonding parameters that are substantially different in the π-bonding (δ) coefficient; they calculated $\alpha = 0.77$, $\beta = 0.74$, and $\delta = 0.94$. In like manner Bereman and Nalewajek (13) also computed erroneously high values of δ for $Cu(DEDTC)_2$, using the Gersmann and Swalen spin Hamiltonian parameters and the incorrect assump-

TABLE 9. Bonding parameters deduced from spin Hamiltonian and spectral parameters for some dithiocarbamates

Ligand amine	$g_{\parallel}$	$g_{\perp}$	$\lvert A_{\parallel}\rvert^a$	$\lvert A_{\perp}\rvert^a$	α	β	δ	K^a
Dimethylamine[b]	2.079	2.016	153.5	35.1	0.683	0.701	0.657	87.2
Diethylamine[c]	2.084	2.023	159.0	39.0	0.690	0.715	0.762	93.6
Pyrrolidine	2.0885	2.020	158.0	37.6	0.694	0.723	0.717	92.2
Morpholine	2.0936	2.023	156.8	33.7	0.705	0.741	0.750	90.5
Pyrrole[d]	2.11	2.02	144.8	30.5	0.699	0.792	0.775	85.7

[a]$cm^{-1} \times 10^4$ for ^{63}Cu.
[b]F. G. Herring and J. M. Park, unpublished results.
[c]Reference 5.
[d]Reference 3. The assignment of the electronic spectrum by Bereman and co-workers was used. $\Delta E(x^2 - y^2) = 1.89\ \mu m^{-1}$ and $\Delta E(xz) = 2.75\ \mu m^{-1}$.

tion that the Fermi contact term, K, is given by $(3/7)\alpha^2$ (28). In summary the results on $Cu(DEDTC)_2$ show that $\alpha = 0.69$ to 0.74, $\beta = 0.70$ to 0.74, and $\delta = 0.76$ to 0.82, i.e. a value of $\delta = 0.9$ is too high.

The spin Hamiltonian parameters for Cu bis-(pyrrole-*N*-carbodithioate) determined both in chloroform–toluene glass and the Cd analogue are somewhat different from the other compounds. This could reflect either that the environment of the complex contained axial interactions or that the π-bonding in this complex is truly different from the other dithiocarbamates as suggested by Bereman and Nalewajek. If we discard the former caution then the results of the calculations indicate that the bonding in these compounds is modified in both the σ-framework as exemplified by the variation in β- and the π-framework as exemplified by δ. However, in order to fully substantiate the claim of Bereman and Nalewajek (13) another investigation of the Cu bis(pyrrole-*N*-carbodithioate) should be carried out using a single isotope and a proven interaction free matrix.

Acknowledgements

We thank P. S. Phillips and the University of British Columbia Computer Centre for assistance. This work was supported by grants from the National Research Council of Canada.

1. D. CONCOUVANIS. Prog. Inorg. Chem. **11**, 294 (1970).
2. J. MCCLEVERTY. Prog. Inorg. Chem. **10**, 49 (1968).
3. R. EISENBERG. Prog. Inorg. Chem. **12**, 295 (1970).
4. G. THAN and R. LUDWIG. Dithiocarbamates and related compounds. Elsevier, New York, NY. 1962.
5. M. J. WEEKS and J. P. FACKLER. Inorg. Chem. **7**, 2548 (1968).
6. R. PETTERSSON and T. VÄNNGARD. Ark. Kemi, **17**, 249 (1951).
7. T. R. REDDY and R. SRINIVASAN. J. Chem. Phys. **43**, 1404 (1965).
8. A. K. GREGSON and S. MITRA. J. Chem. Phys. **49**, 3696 (1968).
9. F. G. HERRING and R. L. TAPPING. J. Phys. Chem. **78**, 316 (1974).
10. F. G. HERRING and R. L. TAPPING. Can. J. Chem. **52**, 4016 (1974).
11. M. BONAMICO, G. DESSY, A. VACIAGO, and L. ZAMBONELLI. Acta Crystallogr. **19**, 619 (1965); **19**, 898 (1965).
12. P. W. G. NEWMAN, C. L. RASTON, and A. H. WHITE. J. Chem. Soc. Dalton Trans. 1332 (1973).
13. R. D. BEREMAN and D. NALEWAJEK. Inorg. Chem. **16**, 2687 (1977).
14. F. G. HERRING, J. C. TAIT, and C. A. MCDOWELL. J. Chem. Phys. **57**, 4564 (1972).
15. P. COPPENS, L. LEISEROWITZ, and D. RABINOVICH. Acta Crystallogr. **18**, 1035 (1965).
16. W. R. BUSING and H. A. LEVY. Acta Crystallogr. **22**, 457 (1967).
17. D. T. CROMER and J. B. MANN. Acta Crystallogr. Sect. A, **24**, 321 (1968).
18. R. F. STEWART, E. R. DAVIDSON, and W. T. SIMPSON. J. Chem. Phys. **42**, 3175 (1965).
19. D. T. CROMER and D. LIBERMAN. J. Chem. Phys. **53**, 1891 (1970).
20. P. J. BECKER and P. COPPENS. Acta Crystallogr. Sect. A, **30**, 129 (1974); **30**, 148 (1974); **31**, 417 (1975).
21. P. COPPENS and W. C. HAMILTON. Acta Crystallogr. Sect. A, **26**, 71 (1970).
22. F. R. THORNLEY and R. J. NELMES. Acta Crystallogr. Sect. A, **30**, 748 (1974).
23. V. SCHOMAKER and K. N. TRUEBLOOD. Acta Crystallogr. Sect. B, **24**, 63 (1969).
24. D. W. J. CRUICKSHANK. Acta Crystallogr. **9**, 747 (1956); **9**, 754 (1956); **14**, 896 (1961).
25. F. G. HERRING and J. M. PARK. To be published.
26. S.-N. CHOI, E. R. MENZEL, and J. R. WASSON. J. Inorg. Nucl. Chem. **39**, 417 (1977).
27. H. R. GERSMANN and J. D. SWALEN. J. Chem. Phys. **36**, 3221 (1962).
28. B. R. MCGARVEY. J. Phys. Chem. **71**, 51 (1967).
29. G. F. GASPARRI, M. NARDELLI, and A. C. VILLA. Acta Crystallogr. **23**, 384 (1967).
30. P. W. G. NEWMAN and A. H. WHITE. J. Chem. Soc. Dalton Trans. 1460 (1972).
31. C. L. RASTON and A. H. WHITE. J. Chem. Soc. Dalton Trans. 1790 (1974).
32. P. W. G. NEWMAN and A. H. WHITE. J. Chem. Soc. Dalton Trans. 2239 (1972).
33. G. PEYRONEL and A. PIGNEDOLI. Acta Crystallogr. **23**, 398 (1967).
34. J. M. MARTIN, P. W. G. NEWMAN, B. W. ROBINSON, and A. H. WHITE. J. Chem. Soc. Dalton Trans. 2233 (1972).
35. C. L. RASTON and A. H. WHITE. Aust. J. Chem. **29**, 523 (1976).
36. Z. A. STARIKOVA, E. A. SUGAM, V. M. AGRE, and JU. V. OBOZENKO. Kristallografija, SSSR, **17**, 111 (1972).
37. F. W. B. EINSTEIN and J. S. FIELD. Acta Crystallogr. Sect. B, **30**, 2928 (1974).
38. G. PEYRONEL, A. PIGNEDOLI, and L. ANTOLINI. Acta Crystallogr. Sect. B, **28**, 3596 (1972).
39. Z. V. ZVONKOVA and V. I. JAKOVENKO. Kristallografija, SSSR, **13**, 169 (1968).
40. S. ANTOSIK, N. M. D. BROWN, A. A. MCCONNELL, and A. L. PANTE. J. Chem. Soc. A, 545 (1969).

Excess volumes of β-picoline and γ-picoline mixtures with some *n*-alcohols at 308.15 K

PREM P. SINGH
Department of Chemistry, Maharshi Dayanand University, Rohtak, India
AND
BUTA R. SHARMA[1] AND PARKASH C. CHOPRA
Department of Chemistry, D.A.V. College, Jullundur, India

Received January 11, 1979

PREM P. SINGH, BUTA R. SHARMA, and PARKASH C. CHOPRA. Can. J. Chem. 57, 2386 (1979).

Excess volumes, V^E, of binary mixtures of β-picoline and γ-picoline with ethanol, *n*-propanol, and *n*-butanol have been measured as a function of composition at 308.15 K by a dilatometric method. The V^E data are negative for all the mixtures studied here and suggest that the strong N---H—O interactions outweigh those due to the breaking of the O—H---O bonds.

PREM P. SINGH, BUTA R. SHARMA, and PARKASH C. CHOPRA. Can. J. Chem. 57, 2386 (1979).

Faisant appel à une méthode dilatométrique et opérant à 308.15 K, on a mesuré les volumes en excès, V^E, de mélanges binaires de β-picoline et de γ-picoline avec l'éthanol, le *n*-propanol et le *n*-butanol. Les données de V^E sont négatives pour tous les mélanges étudiés ici et suggèrent que les interactions N---H—O sont plus fortes que celles dues au bris des liaisons O—H---O.
[Traduit par le journal]

Introduction

Alcohols are strongly self-associated (1) but there is considerable disagreement as to the identification of the predominant associated species (2–5). Furthermore, for binary solution rich in alcohol, a three dimensional network of hydrogen-bonded alcohol molecules is believed to be present (6, 7). The purpose of the present investigation is to study the effect of β-picoline or γ-picoline on the excess volumes of their mixtures with some normal alcohols.

Experimental

Materials

Analytical grade β-picoline, γ-picoline, ethanol, *n*-propanol, and *n*-butanol were purified by standard procedures (8). Purities of the final samples were checked by measuring their densities at 298.15 ± 0.01 K, the results (except for *n*-butanol) agreed to within 0.00005 g cm^{-3} (0.00012 g cm^{-3} in the case of *n*-butanol) with those in the literature (9–12). Excess volumes as a function of composition[2] were determined dilatometrically (13) in a water bath controlled to ±0.01 K. The uncertainties in the V^E values is about 0.3%.

Results

The results at 308.15 ± 0.01 K are given in Table 1 and were fitted to the expression:

$$[1]\quad V^E/x_1x_2\ \text{cm}^3\ \text{mol}^{-1} = A + B(x_1 - x_2) + C(x_1 - x_2)^2$$

where A, B, and C are adjustable parameters and x_1 and x_2 are the mole fractions of components 1 and 2 in the mixture. These parameters were evaluated by fitting experimental values of V^E/x_1x_2 to eq. [1] by the method of least squares and are recorded together with the standard deviation, $\sigma(V^E)$, in Table 1.

Discussion

We are unaware of any data at 308.15 K with which to compare our results for these mixtures. Kowalski *et al.* (9) have determined the molar excess volumes of α-, β-, and γ-picolines (1) with some aliphatic alcohols (2) at 298.15 and 313.15 K. Assuming that V^E varies linearly in the temperature range 298.15–313.15 K for all the mixtures studied by these workers (9), we evaluated V^E values at 308.15 K for the mixtures studied in the present investigation. Our V^E values for β-picoline (1) + *n*-propanol (2) at 308.15 K are in excellent agreement (0.004 cm^3 mol^{-1}) with their V^E values for $x_{\beta\text{-picoline}} \geq 0.7$. In the rest of the β-picoline concentration range their values are consistently more negative than ours; the maximum difference being 0.02 cm^3 mol^{-1} at $x_{\beta\text{-picoline}} = 0.3$. For β-picoline (1) + *n*-butanol (2) our V^E values at 308.15 K are in excellent agreement with their V^E values (9) for $x_{\beta\text{-picoline}} \leq 0.15$ and $x_{\beta\text{-picoline}} \geq 0.6$. In the intermediate β-picoline concentration range their V^E values (9) are more negative than ours and differ by as much as 0.01 cm^3 mol^{-1} at $x_{\beta\text{-picoline}} = 0.3$. Furthermore our V^E data at 308.15 K for γ-picoline (1) + *n*-propanol (2) are in excellent agreement

[1]To whom all correspondence should be addressed.

[2]Complete set of the V^E data is available, at a nominal charge, from the Depository of unpublished Data, CISTI, National Research Council of Canada, Ottawa, Ont., Canada K1A 0S2.

0008-4042/79/182386-02$01.00/0

TABLE 1. Values of the parameters of eq. [1] for the various mixtures at 308.15 K; also given is the standard deviation $\sigma(V^E)$

Mixture	A	B	C	$\sigma(V^E)$ $cm^3\ mol^{-1}$
β-Picoline (1) + ethanol (2)	−1.5920	0.4089	0.0166	0.0007
β-Picoline (1) + *n*-propanol (2)	−1.3200	0.3452	−0.0496	0.0006
β-Picoline (1) + *n*-butanol (2)	−1.0720	0.2263	0.1175	0.0006
γ-Picoline (1) + ethanol (2)	−1.6400	0.6178	−0.0427	0.0006
γ-Picoline (1) + *n*-propanol (2)	−1.3320	0.4364	0.0782	0.0004
γ-Picoline (1) + *n*-butanol (2)	−1.0200	0.2367	0.2482	0.0006

($< 0.002\ cm^3\ mol^{-1}$) with their V^E values for $x_{\gamma\text{-picoline}} \leq 0.5$. However, for $x_{\gamma\text{-picoline}} \geq 0.5$, their V^E values are consistently more negative than ours; the maximum difference being $0.015\ cm^3\ mol^{-1}$ at $x_{\gamma\text{-picoline}} = 0.6$. For γ-picoline (1) + *n*-butanol (2) mixture, our V^E values at 308.15 K agree within $0.002\ cm^3\ mol^{-1}$ with the V^E values derived from the reported V^E data for this mixture at 298.15 and 313.15 K for $x_{\gamma\text{-picoline}} \geq 0.6$. In the rest of the γ-picoline concentration range, their V^E values are more negative than ours and differ by as much as 0.03 at $x = 0.2$. Again the excess volumes, V^E, for all the mixtures studied here are negative and the curves of V^E against x_1 are not symmetrical about $x_1 = 0.5$; they are slightly skewed towards the alkanol-rich end of the mole fraction scale. Furthermore V^E for an equimolar mixture increases in the order *n*-butanol > *n*-propanol > ethanol when the other component is β-picoline or γ-picoline at 308.15 K.

Various studies (14–16) indicate that alcohols are self-associated. The addition of the picoline would then cause rupture of some of the hydrogen bonds (since the picoline would try to adjust itself in the three dimensional hydrogen-bonded network and as such gives rise to increased steric repulsion between the alkyl chain of the alcohol and the picoline ring) so that the resulting alcohol chain fragments then interact with picolines. Since the observed V^E would be the cumulative sum of the contributions due to these factors, the observed V^E data for all these mixtures suggest that the contribution to V^E due to the O—H---N interactions always outweigh those due to the breaking of the O—H---O bonds. Furthermore, since self-association in alcohol varies in the order ethanol > *n*-propanol > *n*-butanol, the addition of a picoline would cause appreciable O—H---O bond rupture in *n*-propanol and *n*-butanol as compared to that in ethanol so that V^E for β- or γ-picoline (1) + *n*-butanol (2) would be more positive than that of β- or γ-picoline (1) + *n*-propanol (2). This has, in fact, been observed. Such a scheme of molecular interactions is also consistent with similar interpretation on the excess thermodynamic function data (17–20) on alcohol + amine mixtures.

Acknowledgments

B. R. Sharma thanks the University Grants Commission, New Delhi, for financial assistance and authorities of the D. A. V. College, Jullundur for laboratory facilities. Thanks are also due to two referees for their valuable suggestions.

1. F. FRANKS and D. J. G. IVES. Q. Rev. **20**, 1 (1966).
2. G. C. PIMENTEL and A. L. MCCLELLAN. The hydrogen bond. W. H. Freeman, San Francisco, CA. 1960.
3. K. B. WHETSEL and J. H. LADY. Spectrometry of fuels. Plenum Press, New York, NY. 1970. pp. 259–279.
4. E. M. WOOLLEY, J. G. TRAVERS, B. P. ERNO, and L. G. HEPLER. J. Phys. Chem. **75**, 3591 (1971).
5. J. R. JOHNSON, S. D. CHRISTIAN, and H. E. AFFSPRUNG. J. Chem. Soc. A, 764 (1967).
6. J. S. ROWLINSON. Liquid and liquid mixtures. 2nd ed. Butterworths, London. 1969. p. 159.
7. I. PRIGOGINE and R. DEFAY. Chemical thermodynamics. *Translated by* D. H. Everett. Longman Green & Co., London. 1953.
8. A. VOGEL. Practical organic chemistry. 3rd ed. Longmans, Green and Co. Ltd., London. 1968.
9. B. KOWALSKI, A. ORSZAGH, and S. CZERNIK. J. Chem. Thermodyn. **8**, 425 (1976).
10. J. P. E. GROLIER and A. VIALLARD. J. Chim. Phys. **68**, 1442 (1971).
11. G. C. BENSON and H. D. PFLUG. J. Chem. Eng. Data **15**, 382 (1970).
12. A. E. POPE, H. D. PFLUG, B. DACRE, and G. C. BENSON. Can. J. Chem. **45**, 2665 (1967).
13. R. K. NIGAM and P. P. SINGH. Trans. Faraday Soc. **65**, 950 (1969).
14. W. H. ZACHARIASEN, J. Chem. Phys. **3**, 158 (1935).
15. R. MECKE. Discuss. Faraday Soc. **9**, 161 (1950).
16. R. MECKE, A. REUTER, and R. SCHUPP. Z. Naturforsch. **4A**, 182 (1949).
17. K. NAKANISHI and H. SHIRAI. Bull. Chem. Soc. Jpn. **43**, 1634 (1970).
18. K. NAKANISHI, R. TOBA, and H. SHIRAI. J. Chem. Eng. Jpn. **2**, 4 (1969).
19. K. NAKANISHI, H. TOUHARA, and N. WATANABE. Bull. Chem. Soc. Jpn. **43**, 2671 (1970).
20. A. ORSZAGH and B. KOWALSKI. Roczniki Chem. **49**, 653 (1975).

Stereochemical aspects of the Pummerer reaction. Regioselectivity as a criterion for the differentiation of ylide and E2 pathways in the product-determining step of the reactions of benzyl methyl halo- and oxysulfonium cations

SAUL WOLFE AND PETER MICHAEL KAZMAIER

Department of Chemistry, Queen's University, Kingston, Ont., Canada K7L 3N6

Received December 11, 1978

SAUL WOLFE and PETER MICHAEL KAZMAIER. Can. J. Chem. 57, 2388 (1979).

The conversion of *p*-Y-$C_6H_4CH_2\overset{+}{S}(X)CH_3$ (X = Cl, OCH_3, $OCOCH_3$, $OCOCHCl_2$, $OCOCF_3$) to a regioisomeric mixture of *p*-Y-$C_6H_4CHXSCH_3$ and *p*-Y-$C_6H_4CH_2SCH_2X$ has been studied as a function of X, Y, and deuteration in the benzyl and methyl positions. The conclusion is reached that, when X is acyloxy, the transformation of the sulfonium cation to an α-thiocarbonium ion and thence to the products proceeds via an E2 pathway. Trifluoroacetic anhydride is a much more reactive reagent than acetic anhydride for Pummerer reactions of benzyl methyl sulfoxides. However, with other sulfoxides, this reagent is not as effective as acetic anhydride. Acetyl trifluoroacetate is not effective as a Pummerer reagent.

SAUL WOLFE et PETER MICHAEL KAZMAIER. Can. J. Chem. 57, 2388 (1979).

On a étudié l'influence de X et Y ainsi que de la deutération des positions benzyle et méthyle sur la conversion de *p*-Y-$C_6H_4CH_2\overset{+}{S}(X)CH_3$ (X = Cl, OCH_3, $OCOCH_3$, $OCOCHCl_2$, $OCOCF_3$) des mélanges régio-isomères de *p*-Y-$C_6H_4CHXSCH_3$ et *p*-Y-$C_6H_4CH_2SCH_2X$. On arrive à la conclusion que si X est un acyloxy, la transformation du cation sulfonium en un ion α-thiocarbonium, et donc en produit, s'effectue par une réaction E2. L'anhydride trifluoroacétique est beaucoup plus réactif que l'anhydride acétique pour les réactions de Pummerer des sulfoxydes de méthyle benzyle. Toutefois avec d'autres sulfoxydes ce réactif n'est pas aussi efficace que l'anhydride acétique. Le trifluoroacétate d'acétyle n'est pas efficace comme réactif de Pummerer.

[Traduit par le journal]

The Pummerer reaction, e.g., **1** → **2** (1), is an internal redox process, in which tetravalent sulfur (**1**, X = halogen, alkoxy, acyloxy) is reduced, and the adjacent carbon atom is oxidized. A vinylogous Pummerer reaction is also known (2). The sulfonium cation substrates **1** are prepared by halogenation of sulfides, or by alkylation or acylation of sulfoxides. In the Pummerer reactions of alkoxysulfonium salts (3), alkylation and redox can be performed in separate steps; however, when X is halogen (4) or acyloxy (5), the intermediate sulfonium cation is not isolable, and its intervention has to be inferred by indirect means.

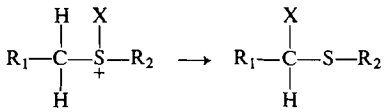

1 **2**

There is extensive evidence (1) that the conversion of **1** to **2** proceeds via the α-thiocarbonium ion **3**, and that intermolecular capture of this carbonium ion by X^- occurs, except in a few special cases (6, 7). One of these (6) is the transformation of benzyl-2-carboxyphenyl sulfoxide (**4**) to 2-benzyl-1,3-benzoxathian-6-one (**5**), which occurs (6*a*) with partial asymmetric induction in the formation of the C—O bond of the product. This interesting result has a number of practical and mechanistic implications, which have prompted the investigations reported in this and the following three papers.

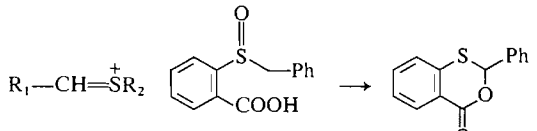

3 **4** **5**

Ab initio SCF-MO calculations (8) suggest that there is significant π-overlap between carbon and sulfur in an α-thiocarbonium ion, leading to a rather high barrier to rotation about the C—S bond. Therefore, if it is assumed that the α-thiocarbonium ion **6** is an intermediate in the conversion of **4** to **5**, the observed transfer of chirality from sulfur to carbon can be understood in terms of a preferential removal of one of the diastereotopic methylene protons of **4** (or a sulfonium cation derived from **4**), followed by C—O bond formation prior to rotation about the C—S bond of **6**. However, the direction and magnitude of such selectivity will depend upon the manner in which the elements of HX are eliminated

0008-4042/79/182388-09$01.00/0

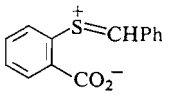

6

from the sulfonium cation to form the α-thiocarbonium ion.

If C—H bond-breaking precedes S—X bond-breaking, the reaction will proceed via a sulfonium ylide (1). On the other hand, when S—X bond-breaking precedes C—H bond-breaking, the reaction will proceed via a dication (9). Between these two extremes, an E2 process is operative. Each of these pathways has different stereochemical consequences.

In the case of a sulfonium cation such as **7**, the Pummerer reaction can lead to two regioisomers, viz., **8** and **9**, the regiochemistry being determined during the conversion of **7** to the mixture of α-thiocarbonium ions **10** and **11**. Interconversion of **10** and **11** prior to capture by X^- seems unlikely, since rearrangement of the α-thiocarbonium ion has not been observed even in the case of the substrate **12**, which affords **13** as the sole Pummerer product (10).

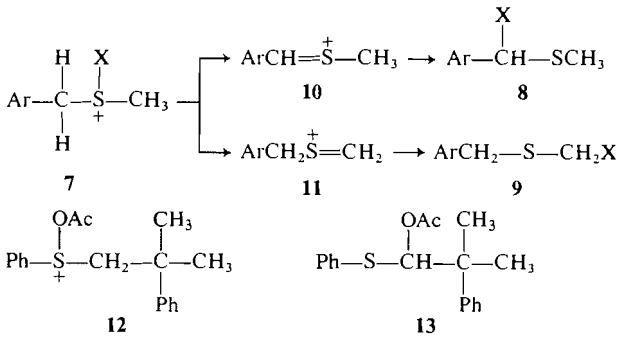

7 10 8 11 9

12 13

The proportions of **10** and **11** and, therefore, of **8** and **9**, that will be formed from an *ylide* precursor will depend upon the acidities of the benzyl and methyl protons. On the basis of the work of Johnson (3) and Wilson (4) and their collaborators, the relevant acidity here is the kinetic acidity. For example, no significant deuterium incorporation is observed when an alkoxysulfonium cation is rearranged to an α-alkoxysulfide in deuteriomethanol. In addition, conversion of the methoxyvinylsulfonium cation **14** to the sulfide **15** proceeds with only 8.3% incorporation of deuterium. Since it is well established (11) that the kinetic acidities of benzyl protons adjacent to sulfur are much higher than those of methyl protons adjacent to sulfur, it can be expected that, when the Pummerer reaction of **7** proceeds via an ylide intermediate, the benzyl-substituted regioisomer **8** will predominate.

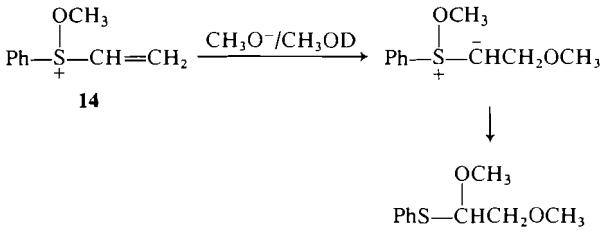

14 15

The same result is anticipated in the case of a dication mechanism. In this case, the regiochemistry of the deprotonation step is governed by the relative stabilities of α-thiobenzyl and α-thiomethyl *carbonium* ions.

The specific objectives of the present paper are to examine the regiochemistry of Pummerer reactions of **7** as a function of the electrophile X, the presence of deuterium in the methyl and benzyl positions, and the presence of *para*-substituents in the benzene ring. As one result of this work, the relationship between the ratio **8**/**9** and the mechanism of HX loss from **7** would appear to have the form shown in Fig. 1. It has also become clear that acyloxysulfonium cations having the general structure **7** undergo the Pummerer reaction via an E2 pathway.

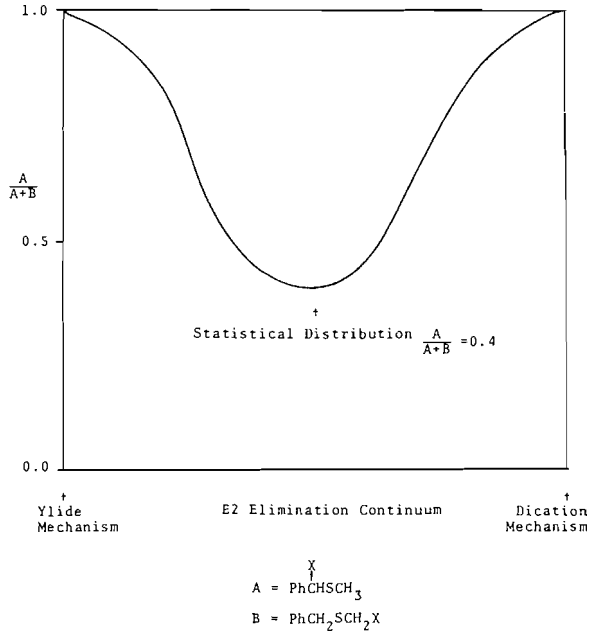

FIG. 1. Schematic representation of the ratio of regioisomers produced in the reaction **7** → **8** + **9**, as a function of C—H and S—X bond-breaking in the product-determining transition state. The 'statistical distribution' of 0.4 is the ratio of the number of benzylic hydrogens to the total number of hydrogens adjacent to sulfur.

TABLE 1. Reactions of benzyl methyl sulfide, benzyl methyl sulfoxide, and benzyl methyl methoxysulfonium fluoroborate with various electrophiles

Entry	Substrate	Pummerer reagent	Yield (%)	Temp. (°C)	Solvent	Product ratio		Ref.
1	$PhCH_2\overset{+}{S}(OCH_3)CH_3\ BF_4^-$	$CH_3ONa^{a,b}$	67[c]	25	MeOH	$PhCH(OCH_3)SCH_3$ (100)	$PhCH_2SCH_2OCH_3$	3
2	$PhCH_2S(=O)CH_3$	$CH_3C(=O)OC(=O)CH_3$[a]	—	80	C_6H_6	—	—	
3	$PhCH_2S(=O)CH_3$	$CH_3C(=O)OC(=O)CH_3$[a,b]	39[c]	130	Ac_2O	$PhCH(OAc)SCH_3$ (45)	$PhCH_2SCH_2OAc$ (55)	
4	$PhCH_2S(=O)CH_3$	$Cl_2CHC(=O)OC(=O)CH_2Cl$[a,b]	100	25	$CHCl_3$	$PhCH(OC(=O)OCHCl_2)SCH_3$ (53)	$PhCH_2SCH_2OC(=O)CHCl_2$ (47)	
5	$PhCH_2S(=O)CH_3$	$CF_3C(=O)OC(=O)CF_3$[a,b]	100	0	$CHCl_3$	$PhCH(OTFA)SCH_3$ (53)	$PhCH_2SCH_2OTFA$ (47)	
6	$PhCH_2S(=O)CH_3$	Br_2	73[c]	−20	C_5H_5N/ CH_3CN	$PhCH(Br)S(=O)CH_3$ (40)	$PhCH_2S(=O)CH_2Br$ (60)	12
7	$PhCH_2S(=O)CH_3$	$PhICl_2$	62[c]	−40	C_5H_5N	$PhCH(Cl)S(=O)CH_3$ (48)	$PhCH_2S(=O)CH_2Cl$ (52)	12
8	$PhCH_2SCH_3$	SO_2Cl_2[a,b]	86[c]	40	CH_2Cl_2	$PhCH(Cl)SCH_3$ (100)	$PhCH_2SCH_2Cl$ (0)	13

[a]Present work.
[b]Product ratio was determined by ^{1}Hmr.
[c]Isolated yields.

Results and Discussion

Table 1 summarizes the regioselectivity observed in the reactions of benzyl methyl sulfide, benzyl methyl sulfoxide, and benzyl methyl methoxysulfonium fluoroborate under various Pummerer conditions. With the exception of entries 1 and 8, no regioselectivity is evident in these reactions. We believe that the benzyl regioselectivity observed in entry 1 constitutes evidence for an ylide pathway, especially in view of the alkaline reaction conditions employed in this case. However, in the case of the benzyl regioselectivity observed in entry 8, either an ylide or a dication pathway is possible. For example, Tuleen and Stephens (14) have found that the chlorination of unsymmetrical sulfides with sulfuryl chloride or *N*-chlorosuccinimide (NCS) leads to substitution at the *more substituted* carbon atom (cf. eq. [1]). This result is incompatible with an ylide pathway, in which the relative proportions of the regioisomers are controlled by the relative acidities of methyl and isopropyl hydrogens (15).

[1] $CH_3-S-CH(CH_3)_2 \xrightarrow{NCS} ClCH_2S-CH(CH_3)_2 + CH_3S-C(Cl)(CH_3)_2$

~1 ~10

On the other hand, Kruse *et al.* (16) have reported that an ylide, assigned structure **16**, can be characterized spectroscopically as an intermediate in the chlorination of 1,3-dithiane with sulfuryl chloride in chloroform solvent, and that this ylide rearranges to 2-chloro-1,3-dithiane (**17**) at room temperature.

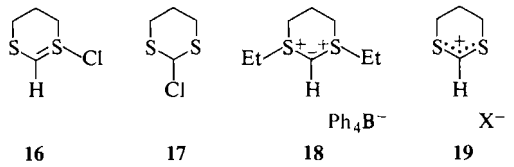

16 **17** **18** **19**

The assignment of structure **16** to this intermediate was based upon the appearance of a sharp singlet at δ 6.90 in the ^{1}Hmr spectrum, assigned to the C2 proton. However, if this assignment is correct, then the C2 proton of **16** is *almost 5 ppm further downfield* than the C2 proton of the 1,3-bissulfonium ylide **18**, which appears at 2.02 ppm (17). Chemical shifts near 2 ppm have also been observed for the C2 protons of a number of acyclic 1,3-bissulfonium fluoroborates (18) and tetraphenylborates (19).

The dithienium cation **19** (X = BF_4^-) has been described by Corey and Walinsky (20). Its ^{1}Hmr spectrum (in CD_3NO_2) shows the C2 proton at 11.10 ppm. This chemical shift is close to that (10.65) of the C2 proton of **17** in sulfur dioxide solvent at −50°C (21). According to Arai and Oki (21, 22), the nmr spectra of **17** and other α-chlorosulfides are very dependent upon the temperature and the solvent, because of the occurrence of the ionization process **17** ⇄ **19** (X = Cl^-). Since the C2 proton of **17** is found at 6.2 and 6.21 ppm in deuteriochloroform and carbon disulfide, respectively, a permissive reinterpretation of the observations of Kruse *et al.* is that the chlorosulfonium cation **20** is converted, by loss of HCl, to **19** (X = Cl^-), and that the 6.90 chemical shift of the C2 proton reflects the position of the **17** ⇄ **19** equilibrium in the presence of the small amounts of sulfur dioxide produced from the sulfuryl chloride reagent. A dication pathway would not be ruled out by this interpretation. Likewise, a dication pathway is not ruled out by the observation (4) that the product isotope effects (k_H/k_D) for the chlorination and bromination of 2,2-d_2-thiophane (**21**) are 5.1 and 3.6, respectively. Indeed, although their discussion differs somewhat from that given here, Wilson and Albert (4) consider that their bromination results are consistent with 'the El extreme transition state.'

Regardless of the precise interpretation to be given to the benzyl regioselectivity observed in entry 8 of Table 1, the lack of regioselectivity seen in entries

20 **21**

2–7 must be interpreted in terms of a mechanism in which neither an ylide nor a dication is an intermediate. It seems reasonable to suppose that an E2 process is operative in these cases, especially since the stereochemical course of the alpha-halogenation of sulfoxides has already been found to be best interpreted in terms of E2 elimination of HX from a haloxosulfonium cation (23) (eq. [2]).

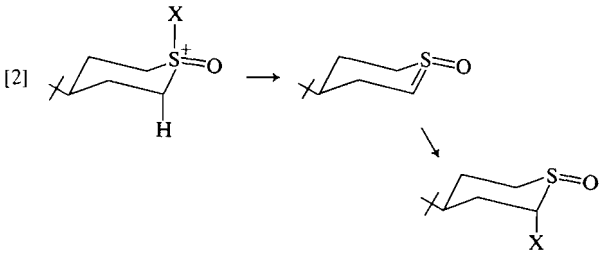

[2]

Table 2 shows the regioselectivities obtained in the Pummerer reactions of a series of deuterated benzyl methyl sulfoxides with trifluoroacetic anhydride (TFAA) in chloroform at 25°C. These results demonstrate that there is a significant hydrogen isotope effect in the product-determining step of the reaction. The magnitude of this effect (k_H/k_D) is calculated to be 4.0; this value is obtained by division of the **8**/**9** ratio of entry 5 by the **8**/**9** ratio of entry 1.

This result is consistent with the suggestion that the mechanistic change signalled by the lack of regioselectivity in the Pummerer reactions of the acyloxysulfonium and chloro- and bromosulfoxonium cations is a change to an E2 pathway. Such a conclusion is also supported by the observation that carbon–hydrogen bond-breaking occurs in the product-determining step of the reaction, and by the results of an examination of the effects of *para*-substituents upon the regioselectivity of the reaction. These results are presented in Table 3, and were obtained under the same conditions as those of Table 2. The Hammett σ–ρ plot for the effects of the *para*-substituents upon the regioselectivity of the reaction is shown in Fig. 2. This gives a ρ-value of 1.0.

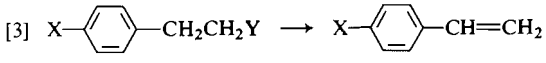

[3]

For E2 reactions of the type shown in eq. [3], ρ values range from +2.07 to +3.77 as the leaving group Y is varied from iodide to trimethylammonium (25). The increase in ρ for the poorer leaving group

TABLE 2. Effect of deuterium substitution upon the products of the reaction of trifluoroacetic anhydride with benzyl methyl sulfoxide[a,b]

Entry	Substrate[c]	% trifluoroacetoxybenzyl regioisomer[d] **8**	% trifluoroacetoxymethyl regioisomer[e] **9**
1	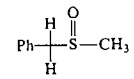	53	47
2	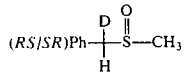	40	60
3	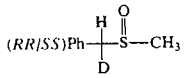	40	60
4	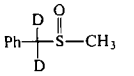	18	82
5	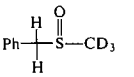	82	18
6	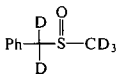	~50[f]	~50[f]

[a]All experiments were performed in $CDCl_3$ at 25°C with 1 equiv. of trifluoroacetic anhydride and a sulfoxide concentration of 0.32 *M*.
[b]The product deuterium isotope effect was estimated by dividing the **8**/**9** ratio of entry 5 by the **8**/**9** ratio of entry 1 to obtain a value of 4.0.
[c]See the Experimental for the syntheses of these compounds.
[d]Determined by integration of the proton nmr spectrum; ^{1}Hmr ($CDCl_3$) δ: 7.03 (1H, s, PhC*H*S), 2.13 (3H, s, SCH_3).
[e]Determined by integration of the proton nmr spectrum; ^{1}Hmr ($CDCl_3$) δ: 5.23 (2H, s, S—CH_2—O), 3.87 (2H, s, PhCH_2S).
[f]Estimated from the relative integrals of the phenyl peaks of the two regioisomers; ^{1}Hmr ($CDCl_3$) δ: 7.40 (5H, s, *Ph*CHS), 7.30 (5H, s, $PhCH_2S$).

TABLE 3. Substituent effects upon the regioselectivity of the Pummerer reaction of aryl methyl sulfoxides with trifluoroacetic anhydride[a]

Substituent	σ value[b]	Relative % of **8**[c]	Relative % of **9**[c]	Log (**8**/**9**)
p-NO_2	0.778	87	13	0.82
p-NO_2	0.778	88	12	0.87
p-Cl	0.227	61	39	0.19
p-Cl	0.227	63	37	0.23
p-H	0.00	53	47	0.052
p-H	0.00	57	43	0.049
p-CH_3	−0.170	34	66	−0.29

[a]Reactions were performed at 25°C in deuteriochloroform with 1 equiv. of trifluoroacetic anhydride, and a concentration of 0.32 *M*.
[b]The σ values were obtained from ref. 24.
[c]Determined by integration of the ^{1}Hmr spectra.

can be interpreted in terms of increased carbanionic character in the transition state. The application of these and other analogies to the elimination of trifluoroacetic acid from **7** (X = OTFA) leads to the expectation of a large positive ρ for an ylide mechanism, a small positive or negative ρ for an E2 mechanism (depending upon the degree of C—H and S—X bond-breaking in the transition state), a zero ρ for a cyclic *cis*-elimination mechanism (26), and a large negative ρ for a dication mechanism (27). The value 1.0 obtained in the present work appears to be consistent only with an E2 mechanism, with some carbanionic character in the transition state, and a very good leaving group.

Thus the interpretation of the results of Table 1 in terms of Fig. 1, the isotope effect studies of Table 2, and the *para*-substituent studies of Table 3, lead in each case to the conclusion that the Pummerer reactions of acyloxysulfonium cations proceed via an E2 pathway. The assumption that this E2 elimination process takes an *anti* stereochemical course has interesting consequences, as will be seen in the following two papers.

The use of trifluoroacetic anhydride (TFAA) as a reagent for Pummerer reactions is a relatively recent development (28). As seen in Table 1, this permits the reaction to be performed at much lower temperatures than is the case with acetic anhydride and, in the case of benzyl methyl sulfoxide as the substrate, the product is obtained in significantly higher yield. In a comparative study based upon the dis-

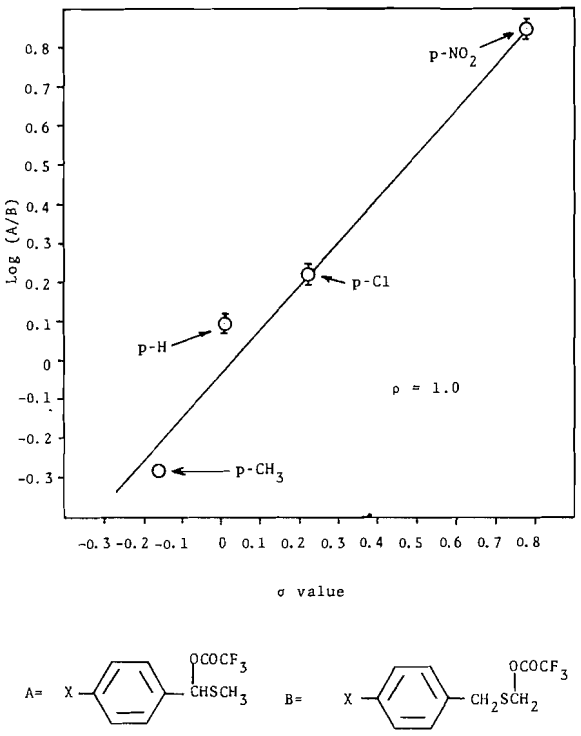

FIG. 2. Hammett plot showing the substituent effect upon the regioselectivity of the reaction of benzyl methyl sulfoxide with trifluoroacetic anhydride in chloroform at 25°C.

appearance of the sulfoxide, the reaction in acetic anhydride *solvent* was complete in 2 h at 130°C, while the reactions with dichloroacetic anhydride (1.4 equiv.) and TFAA (1.0 equiv.) were complete in 70 min and 5 min at 25°C, respectively. It was, therefore, of interest to examine the reactions of TFAA with other sulfoxides. These results and others taken from the literature are collected in Table 4.

Although the data are not extensive, the failures in the cases of thiophane sulfoxide and the phthalimidopenicillin sulfoxide are noteworthy. Since it is known that thiophane sulfoxides do react successfully with acetic anhydride (30), we suggest that TFAA may succeed as a Pummerer reagent when relatively acidic α-hydrogens are present, and when the α-thiocarbonium ion is sufficiently reactive for capture by the poorly nucleophilic trifluoroacetate anion. The rearrangement of the thiazolidine sulfoxide is reminiscent of the Morin rearrangement (31) of a penicillin sulfoxide to a Δ^3-cephem; however, the Morin rearrangement itself fails when TFAA is substituted for acetic anhydride because of rapid cleavage of the β-lactam by the trifluoroacetic acid product.

The mixed anhydride acetyl trifluoroacetate (ATFA) was also examined as a reagent for the

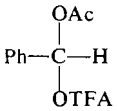

22

Pummerer reaction. However, the reaction of this compound with benzyl methyl sulfoxide led only to the mixed acylal **22**, identified by comparison with an authentic specimen prepared by the reaction of ATFA with benzaldehyde (32).

Experimental

General

Melting points were determined on Kofler hot-stage or Meltemp equipment, and are uncorrected. Refractive indices were measured on a Bausch and Lomb refractometer. The ^{1}Hmr spectra were obtained on Varian T60, Varian EM360, Varian HA100, or Bruker HX16 spectrometers; 10% solutions were employed. The ^{13}Cmr spectra were obtained on a Bruker HX16 spectrometer, equipped with a BSV 3PM pulse unit and a BNC-12 computer. Tetramethylsilane (TMS) or sodium 2,2-dimethyl-2-silapentane-5-sulfonate (DSS) were employed as internal standards, as required. Mass spectra were obtained on JEOL JMS-01SC, Hitachi Perkin Elmer RMU-6E or Dupont 21-491B mass spectrometers under electron impact conditions at 70 eV. Infrared spectra were recorded on either Perkin Elmer 180 or Acculab 6 instruments. Ultraviolet spectra were obtained on a Unicam SP800 spectrometer. Analyses are by Galbraith Laboratories, Knoxville, TN.

The ^{13}Cmr spectra were assigned by correlations within series of compounds. In some instances, ^{1}H–^{13}C coupling was used to confirm these assignments. Column chromatography was performed with 60 mesh silica gel (Merck). Thin layer chromatography was performed on silica gel plates containing a fluorescent indicator. Spots were observed under ultraviolet light, or were visualized with ninhydrin, 10% phosphomolybdic acid in ethanol, ceric sulfate in ethanol, or iodine vapour. Solvents were routinely distilled before use and dried as required by standard procedures. Materials were of reagent grade purity obtained from commercial sources.

The substrates benzyl methyl sulfoxide, *RS*/*SR*-benzyl-α-*d* methyl sulfoxide, *RR*/*SS*-benzyl-α-*d* methyl sulfoxide, benzyl-α,α-d_2 methyl sulfoxide, *p*-nitrobenzyl methyl sulfoxide, *p*-methoxybenzyl methyl sulfoxide, *p*-methylbenzyl methyl sulfoxide benzyl phenyl sulfoxide, and thiophane-*S*-oxide were synthesized by standard procedures (33–36). Only the synthesis of *p*-methylbenzyl methyl sulfoxide, a new compound, is reported here. The penicillin sulfoxide was obtained from Mr. R. J. Bowers, whom we thank.

p-*Methylbenzyl Methyl Sulfoxide*

Sodium *meta*-periodate (6.52 g, 33.7 mmol) was suspended in water/methanol (40 mL/10 mL). The solution was cooled to 0°C in a salt–ice bath and *p*-methylbenzyl methyl sulfide (5.12 g, 33.7 mmol) was added in one portion. After stirring at 0°C overnight, the reaction mixture was extracted with chloroform (5 × 20 mL) and the organic phase was dried (magnesium sulfate). After removal of the solvent, the syrupy product was chromatographed on silica gel (ether/methylene chloride, then methanol) to yield a crystalline product (5.21 g, 92%), mp 66°C; ^{1}Hmr ($CDCl_3$) δ: 7.13 (4H, s), 4.10, 3.87 (2H, AB, 12), 2.40 (3H, s), 2.33 (3H, s); ^{13}Cmr ($CDCl_3$) δ: 138.0, 136.7, 129.9, 129.6 (phenyl), 59.9 (PhCH_2SO), 37.2 ($SOCH_3$), 21.1 (CH_3); ir (KBr): 1025 (s, sulfoxide) cm^{-1}; uv (water, 25°C) λ_{max} (log ε): 231 (3.49).

TABLE 4. The reaction of trifluoroacetic anhydride with various sulfoxides

Sulfoxide	Solvent	Temp. (°C)	Yield (%)	Product(s)	Ref.
$PhCH_2S(O)CH_3$	$CDCl_3$	0	100[a]	$PhCH(OTFA)SCH_3$[b] + $PhCH_2SCH_2OTFA$	c
$PhCH_2S(O)Ph$	$CDCl_3$	0	100[a]	$PhCH(OTFA)SPh$[b]	c
$CH_3S(O)CH_3$	$CDCl_3$	−30	[d]	CH_3SCH_2OTFA	28
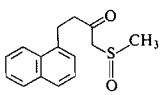	CH_3CN	80	58[e]	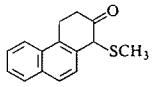	29
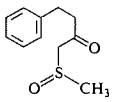	CH_3CN	80	42[e]	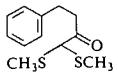	29
	CCl_4	0	—	[f]	c
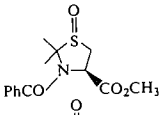	$CDCl_3$	25	100	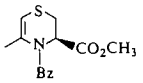	c
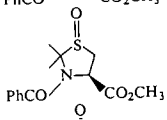	$CDCl_3$	−30	100	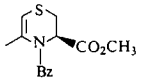	c
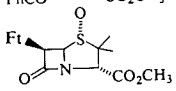	$CDCl_3$	0	—	[g]	c

[a]Yields were determined by ^{1}Hmr integration of crude reaction mixtures because the products were moisture-sensitive.
[b]These compounds were characterized on the basis of their spectral characteristics and by hydrolysis to benzaldehyde.
[c]Present work.
[d]Isolated as a by-product in an aminosulfurane synthesis.
[e]Isolated yields.
[f]A complex mixture of products resulted in this case.
[g]The reaction led to loss of the β-lactam ring.

Anal. calcd. for $C_9H_{12}OS$: C 64.24, H 7.19; found: C 64.69, H 7.51.

Reaction of Benzyl Methyl Methoxysulfonium Fluoroborate with Sodium Methoxide

In a dry box, carefully dried benzyl methyl sulfoxide (1.76 g, 11.4 mmol) in methylene chloride (5 mL) was added over a 5 min period to trimethyloxonium fluoroborate (2.35 g, 11.4 mmol). The reaction mixture was stirred for 1 h. Addition of ether afforded an oil, which crystallized upon standing in the refrigerator. After trituration of the crystals with ether, sodium methoxide in methanol (15.0 mL of 0.834 *N*) was added over a period of 5 min at 25°C. The reaction mixture was immediately evaporated to dryness, giving a milky oil. This was poured into brine (pH 7), to which a small portion of sodium carbonate had been added to raise the pH to 8.0. The mixture was extracted with ether (4 × 10 mL) and the combined extracts were dried over anhydrous sodium sulfate containing a small amount of sodium carbonate. Evaporation yielded a syrup (557 mg, 31%) consisting of a 2:1 mixture of α-methoxybenzyl methyl sulfide and benzyl methyl sulfide. Attempts to separate the two components by chromatography on Florisil were abandoned after some isomerization to α,α-dimethyl thiotoluene and α,α-dimethoxytoluene was detected.

Reaction of Benzyl Methyl Sulfoxide with Acetic Anhydride

Benzyl methyl sulfoxide (0.0969 g, 0.629 mmol) was dissolved in acetic anhydride (10 mL) and the solution was heated to 130°C for 2 h. After cooling, the reaction mixture was poured into saturated potassium bicarbonate. The aqueous solution was extracted with chloroform (4 × 20 mL). After drying (magnesium sulfate), and evaporation of the solvent, the product was isolated as a colourless syrup (48 mg, 39%). ^{1}Hmr indicated formation of the two isomers (α-acetoxybenzyl methyl sulfide/α-acetoxymethyl benzyl sulfide) in the ratio 45/55. α-Acetoxybenzyl methyl sulfide: ^{1}Hmr ($CDCl_3$) δ: 7.35 (5H, s), 6.95 (1H, s), 2.10 (3H, s), 2.15 (3H, s). α-Acetoxymethyl benzyl sulfide: ^{1}Hmr ($CDCl_3$) δ: 7.30 (5H, s), 5.05 (2H, s), 3.85 (2H, s), 2.03 (3H, s).

Reaction of Benzyl Methyl Sulfide with Sulfuryl Chloride

Sulfuryl chloride (8.1 mL, 13.5 g, 0.1 mol) was added drop-

wise (36 min) to a solution of benzyl methyl sulfide in methylene chloride (20 mL). After the addition was complete, the solution was refluxed (1 h). Evaporation of the solvent and distillation (bp 102–106°C/12 Torr (lit. (13) bp 118–121°C/14 Torr) yielded a colourless oil which rapidly turned orange (12.8 g, 86%); ^{1}Hmr ($CDCl_3$) δ: 7.40 (5H, m), 6.07 (1H, s), 2.32 (3H, s).

Reaction of Benzyl Methyl Sulfoxide with Dichloroacetic Anhydride

To benzyl methyl sulfoxide (90 mg, 0.6 mmol) in chloroform (0.5 mL) was added dichloroacetic anhydride (278 mg, 0.86 mmol). The reaction was followed by ^{1}Hmr at room temperature, and was complete in 70 min. There were two products, viz., α-dichloroacetoxybenzyl methyl sulfide and benzyl α-dichloroacetoxymethyl sulfide in the ratio 53/47. α-Dichloroacetoxybenzyl methyl sulfide: ^{1}Hmr ($CDCl_3$) δ: 7.45 (5H, s), 7.05 (1H, s), 6.05 (1H, s), 2.18 (3H,s). Benzyl α-dichloroacetoxymethyl sulfide: ^{1}Hmr ($CDCl_3$) δ: 7.38 (5H, s), 5.95 (1H, s), 5.23 (2H, s), 3.92 (2H, s).

Reaction of Benzyl Methyl Sulfoxide with Trifluoroacetic Anhydride

Benzyl methyl sulfoxide (25 mg, 0.16 mmol) was dissolved in carbon tetrachloride (0.5 mL) containing trifluoroacetic anhydride (0.16 mmol). After 5 min, a ^{1}Hmr spectrum of the reaction mixture indicated that the starting material had disappeared and that a mixture of the two regioisomeric trifluoroacetoxybenzyl methyl sulfides had been produced. The ratio of the two regioisomers (methyl α-trifluoroacetoxybenzyl sulfide/benzyl α-trifluoroacetoxymethyl sulfide) was 53/47. Methyl α-trifluoroacetoxybenzyl sulfide: ^{1}Hmr ($CDCl_3$) δ: 7.40 (5H, s), 7.03 (1H, s), 2.13 (3H, s). Benzyl α-trifluoroacetoxymethyl sulfide: ^{1}Hmr ($CDCl_3$) δ: 7.30 (5H, s), 5.23 (2H, s), 3.87 (2H, s).

General Procedure for the Reaction of Deuterated Benzyl Methyl Sulfoxides with Trifluoroacetic Anhydride

Trifluoroacetic anhydride (0.16 mmol) was added to benzyl methyl sulfoxide (0.16 mmol) in deuteriochloroform (0.5 mL) at ambient temperature. The ^{1}Hmr spectrum was run immediately and the proportions of the regioisomers were estimated from the peak integrals of undeuterated portions of the substrate. For benzyl methyl sulfoxide-d_5, the relative proportions of the two regioisomers were estimated from the integrals of the two phenyl peaks.

General Procedure for the Reaction of p-*Substituted Benzyl Methyl Sulfoxides with Trifluoroacetic Andydride*

Trifluoroacetic anhydride (0.16 mmol) was added to a solution of the sulfoxide (0.16 mmol) in deuteriochloroform (0.5 mL) and the ^{1}Hmr spectrum was run. The proportions of the two regioisomers were estimated from the integrals of the methine proton (δ ca. 7.0) of the benzyl substituted regioisomer and the SCH_2O methylene hydrogens (δ ca. 5.0) of the methyl substituted regioisomer.

Reaction of Benzyl Phenyl Sulfoxide with Trifluoroacetic Anhydride

Trifluoroacetic anhydride (0.3 mL, 2 mmol) was added to benzyl phenyl sulfoxide (40 mg, 0.19 mmol) in deuteriochloroform (0.5 mL) and the ^{1}Hmr spectrum was recorded immediately. This indicated a quantitative yield of α-trifluoroacetoxybenzyl phenyl sulfide; ^{1}Hmr ($CDCl_3$) δ: 7.0–7.5 (11H, m). This product proved very hygroscopic and, on exposure to moist air, the odour of benzaldehyde was apparent. Addition of 2,4-dinitrophenylhydrazine produced benzaldehyde-2,4-dinitrophenylhydrazone. Recrystallization from ethyl acetate yielded red crystals (202 mg, 31%), mp 234–239°C (lit. (37) mp 237°C).

*Reaction of Thiolane-*S*-Oxide with Trifluoroacetic Anhydride*

Thiolane-*S*-oxide (1.0 g, 9.6 mmol) was dissolved in carbon tetrachloride (9.6 mL). The mixture was cooled to 4°C and trifluoroacetic anhydride (1.4 mL, 9.6 mmol) was added in one portion. Within seconds, the reaction mixture had separated into two layers, the upper layer consisting of a deep red oil. The product was not investigated further.

Reaction of N-*Benzoyl-2,2-dimethyl-4*R-*methoxycarbonyl-1,3-thiazolidine-*S*-oxide with Trifluoroacetic Anhydride at 25°C and −30°C*

Trifluoroacetic anhydride (0.3 mL, 2 mmol) was added to *N*-benzoyl-2,2-dimethyl-4*R*-methoxycarbonyl-1,3-thiazolidine-*S*-oxide (38) (24 mg, 0.081 mmol) in deuteriochloroform (0.5 mL). There was an immediate change in the ^{1}Hmr spectrum and the sole product detectable by nmr was identified as *N*-benzoyl-2,3-dehydro-5-methoxycarbonyl-3-methyl-1,3-thiazine by comparison with an authentic sample (39); ^{1}Hmr ($CDCl_3$) δ: 7.52–7.57 (5H, s), 5.97 (1H, t, 3), 5.62 (1H, s), 3.82 (3H, s), 3.50 (2H, d, 3), 1.67 (3H, s). Repetition of the reaction at −30°C gave identical results.

Reaction of Methyl N-*Phthalimidopenicillinate-*R*-oxide with Trifluoroacetic Anhydride*

Trifluoroacetic anhydride (0.10 mL, 0.71 mmol) was added in one portion to a solution of methyl *N*-phthalimidopenicillinate-*R*-oxide (15.1 mg, 0.04 mmol) in deuteriochloroform (0.5 mL). After 1 min, the ^{1}Hmr spectrum showed the absence of the β-lactam protons (δ 4.0–6.0) and the reaction was not investigated further.

Acetyl Trifluoroacetate (40, 41)

Acetic anhydride (3.35 mL, 0.0355 mol) and trifluoroacetic anhydride (5.00 mL, 0.0355 mol) were dissolved in carbon tetrachloride (10 mL). The reaction was stirred at ambient temperature for 48 h, and the infrared spectrum was monitored periodically. During this period, the 1760 cm^{-1}/1820 cm^{-1} peaks of acetic anhydride and the 1800 cm^{-1}/1860 cm^{-1} peaks of trifluoroacetic anhydride were replaced by the 1780 cm^{-1}/1850 cm^{-1} peaks of acetyl trifluoroacetate. The yield was quantitative.

Reaction of Benzyl Methyl Sulfoxide with Acetyl Trifluoroacetate

Benzyl methyl sulfoxide (300 mg, 1.95 mmol) was dissolved in deuteriochloroform (2 mL). To this was added, dropwise, acetyl trifluoroacetate (0.25 mL, 2 mmol), and the progress of the reaction was monitored by ^{1}Hmr. The product of the reaction was α-acetoxy-α-trifluoroacetoxytoluene; ^{1}Hmr ($CDCl_3$) δ: 7.73 (1H, s), 7.42 (5H, s), 2.15 (3H, s); ir: 1785 cm^{-1}. Evaporation of the solvent below 20°C yielded a syrup (280 mg). 2,4-Dinitrophenylhydrazine (Brady's reagent) gave a positive aldehyde and ketone test, and the addition of semicarbazide hydrochloride and methanol (1 mL) followed by 10 drops of pyridine yielded the semicarbazone of benzaldehyde (45 mg, 15%), mp 211–213°C (lit. (37) mp 217°C).

α,α-Diacetoxytoluene

Benzaldehyde (14.3 g, 0.135 mol) and acetic anhydride (28.6 g. 0.277 mol) were mixed under nitrogen and cooled in an ice bath. Concentrated sulfuric acid (0.2 mL) was then added dropwise. A deep purple colour developed after the addition of the first drop. After 25 min, ^{1}Hmr indicated that all of the benzaldehyde had been consumed. The reaction mixture was poured into ice-cold saturated sodium bicarbonate solution, and stirred until gas evolution ceased (15 min). Extraction with methylene chloride (3 × 70 mL), drying over anhydrous sodium sulfate, and evaporation yielded a syrup, which crystallized upon cooling at −10°C (28.0 g, 99%). Recrystallization from ethanol yielded white needles (23.7 g,

84%); mp 39–44°C (lit. (32) mp 44–45°C); ir (Nujol): 1750 (s, acetate) cm^{-1}; ^{1}Hmr ($CDCl_3$) δ: 7.67 (1H, s), 7.43 (5H, s), 2.13 (6H, s); ^{13}Cmr ($CDCl_3$) δ: 168.6 (carbonyl), 135.6, 129.7, 128.6, 126.6 (phenyl), 89.7 (CH), 20.7 (CH_3).

α-Acetoxy-α-trifluoroacetoxytoluene

Benzaldehyde (14.3 g, 0.135 mol) and acetyl trifluoroacetate (32 mL, 0.280 mol) were mixed at 4°C, and concentrated sulfuric acid (0.2 mL) was added. The solution turned purple immediately. ^{1}Hmr showed that the reaction was complete within 5 min. The product was flash distilled to yield a colourless, water-white liquid (14.1 g, 40%), n_D^{24} 1.4376; ^{1}Hmr ($CDCl_3$) δ: 7.77 (1H, s), 7.48 (5H, s), 2.17 (3H, s); ir (film): 1785 (s, carbonyl) cm^{-1}.

α,α-Trifluoroacetoxytoluene

Benzaldehyde (14.3 g, 0.135 mol) and trifluoroacetic anhydride (40 mL, 0.280 mol) were mixed at 4° C. Concentrated sulfuric acid (ca 0.2 mL) was added and the solution turned dark purple. The progress of the reaction was followed by ^{1}Hmr. The reaction was complete after ca. 8 h. The product was flash distilled to yield a water-white liquid (33.7 g, 79%), n_D^{24} 1.3988; ^{1}Hmr ($CDCl_3$) δ: 7.82 (1H, s), 7.55 (5H, s); ^{13}Cmr ($CDCl_3$) δ: 156 (q, 44, carbonyl), 132.2, 129.8, 127.6 (phenyl), 115.1 (q, 285, CF_3), 94.6 (CH); ir (film): 1795 (s, $OCOCF_3$) cm^{-1}.

Acknowledgements

We thank the National Research Council of Canada for financial support of this work, and for the Award of a 1967 Science Scholarship.

1. R. Pummerer. Ber. **43**, 1401 (1910); L. Horner and P. Kaiser. Justus Liebigs Ann. Chem. **631**, 198 (1960); G. A. Russell and G. J. Mikol. *In* Mechanisms of molecular migrations. Vol. 1. *Edited by* B. S. Thyagarajan. Interscience, London. 1968. p. 157; T. Durst. Adv. Org. Chem. **6**, 285 (1969); S. Oae and T. Numata. *In* Isotopes in organic chemistry. Vol. 5. *Edited by* E. Buncel and C. C. Lee. Elsevier, Amsterdam. 1979. In press.
2. H. Kosugi, H. Uda, and S. Yamagiwa. J. Chem. Soc. Chem. Commun. 192 (1975); H. Kosugi, H. Uda, and S. Yamagiwa. J. Chem. Soc. Chem. Commun. 71 (1976); G. A. Koppel and L. J. McShane. J. Am. Chem. Soc. **100**, 288 (1978).
3. C. R. Johnson and W. G. Phillips. J. Org. Chem. **32**, 1926 (1967); C. R. Johnson and W. G. Phillips. J. Am. Chem. Soc. **91**, 682 (1969).
4. G. E. Wilson, Jr. and M. G. Huang. J. Org. Chem. **35**, 3002 (1970); G. E. Wilson, Jr. and R. Albert. J. Org. Chem. **38**, 2160 (1973).
5. S. Iwanami, S. Arita, and K. Takahashi. Yuki Gosei Kagaku Kyokai Shi. **26**, 375 (1968).
6. (*a*) B. Stridsberg and S. Allenmark. Acta Chem. Scand. Ser. B, **28**, 591 (1974); (*b*) B. Stridsberg and S. Allenmark. Acta Chem. Scand. Ser. B, **30**, 219 (1976); (*c*) S. Oae and T. Numata. Tetrahedron, **30**, 2641 (1974).
7. T. Numata and S. Oae. Tetrahedron Lett. 1337 (1977); T. Numata, O. Itoh, and S. Oae. Chem. Lett. 909 (1977).
8. F. Bernardi, I. G. Csizmadia, H. B. Schlegel, and S. Wolfe. Can. J. Chem. **53**, 1144 (1975).
9. S. Oae. Q. Rept. Sulfur Chem. **5**, 53 (1970).
10. W. E. Parham and L.D. Edwards. J. Org. Chem. **33**, 4150 (1968); see also T. P. Ahern, D. G. Kay, and R. F. Langler. Can J. Chem. **56**, 2422 (1978).
11. A. Rauk, E. Buncel, R. Y. Moir, and S. Wolfe. J. Am. Chem. Soc. **87**, 5498 (1965).
12. M. Cinquini and S. Colonna. J. Chem. Soc. Perkin Trans. I, 1883 (1972).
13. F. G. Bordwell and B. M. Pitt. J. Am. Chem. Soc. 77, 572 (1955).
14. D. L. Tuleen and T. B. Stephens. J. Org. Chem. **34**, 31 (1969).
15. S. Bory, R. Lett, B. Moreau, and A. Marquet. Tetrahedron Lett. 4921 (1972).
16. C. G. Kruse, N. L. J. M. Broekhof, A. Wijsman, and A. van der Gen. Tetrahedron Lett. 885 (1977).
17. I. Stahl and J. Gosselck. Tetrahedron, **29**, 2323 (1973); I. Stahl. Personal communication.
18. S. Wolfe, P. Chamberlain, and T. F. Garrard. Can. J. Chem. **54**, 2847 (1976).
19. C. P. Lillya and P. Miller. J. Am. Chem. Soc. **88**, 1560 (1966).
20. E. J. Corey and S. W. Walinsky. J. Am. Chem. Soc. **94**, 8932 (1972).
21. K. Arai and M. Oki. Bull. Chem. Soc. Jpn. **49**, 553 (1976).
22. M. Oki and K. Arai. Abstract W7. International Symposium on Stereochemistry. Kingston, Ont., Canada. 1976.
23. S. Bory, R. Lett, B. Moreau, and A. Marquet. C. R. Acad. Sci. Ser. C, **276**, 1323 (1973); S. Iriuchijima and G. Tsuchihashi. Bull. Chem. Soc. Jpn. **46**, 921 (1973); **46**, 929 (1973); T. Durst, K.-C. Tin, and M. J. V. March. Can. J. Chem. **51**, 1704 (1973); P. Calzavara, M. Cinquini, S. Colonna, R, Fornasier, and F. Montanari. J. Am. Chem. Soc. **95**, 7431 (1973); J. Klein. Chem. Lett. 359 (1979).
24. J. Hine. Physical organic chemistry. 2nd ed. McGraw-Hill, Toronto. 1962. p. 87.
25. W. H. Saunders. Jr. *In* The chemistry of alkenes. *Edited by* S. Patai. Interscience, London. 1964. p. 155.
26. G. G. Smith, F. D. Bagley, and R. Taylor. J. Am. Chem. Soc. **83**, 3647 (1961).
27. P. R. Wells. Linear free energy relationships. Academic Press, London. 1968.
28. A. K. Sharma and D. Swern. Tetrahedron Lett. 1503 (1974); A. K. Sharma, T. Ku, A. D. Dawson, and D. Swern. J. Org. Chem. **40**, 2758 (1975).
29. Y. Oikawa and O. Yonemitsu. Tetrahedron, **30**, 2653 (1974).
30. S. Glue, I. T. Kay, and M. R. Kipps. J. Chem. Soc. Chem. Commun. 1158 (1970); J. E. McCormick and R. S. McElhinney. J. Chem. Soc. Perkin Trans. I, 2533 (1976).
31. R. B. Morin, B. G. Jackson, R. A. Mueller, E, R. Lavagnino, W. B. Scanlon, and S. L. Andrews. J. Am. Chem. Soc. **91**, 1401 (1969); R. B. Morin, D. O. Spry, and R. A. Mueller. Tetrahedron Lett. 848 (1969).
32. M. J. Gregory. J. Chem. Soc. B, 1201 (1970).
33. A. Rauk. Ph.D. Thesis, Queen's University, Kingston, Ont., 1968.
34. P. M. Kazmaier. Ph.D. Thesis, Queen's University, Kingston, Ont., 1978.
35. I. D. Entwhistle, R. A. W. Johnstone, and B. J. Millard. J. Chem, Soc. C, 302 (1967).
36. Beilstein. Handbuch der Organischen Chemie. Erstes Ergänzungswerk. Vol. 6. Springer Verlag. 1931. p. 225.
37. H. T. Openshaw. A laboratory manual of qualitative organic analysis. 3rd ed. Cambridge University Press, Cambridge, England. 1955. p. 49.
38. A. W. A. Jeffrey. MSc Thesis, Queen's University, Kingston, Ont., 1975; S. Wolfe and A. W. A. Jeffrey. Unpublished results.
39. M. Iwakawa, B. M. Pinto, and W. A. Szarek. Can. J. Chem. **56**, 326 (1978).
40. T. G. Bonner and E. G. Gabb. J. Am. Chem. Soc. **85**, 3291 (1963).
41. E. J. Bourne, M. Stacey, J. C. Tatlow, and R. Worrall. J. Chem. Soc. 2006 (1954).

Stereochemical aspects of the Pummerer reaction. Diastereotopic selectivity in the deprotonation of oxysulfonium cations

SAUL WOLFE AND PETER MICHAEL KAZMAIER

Department of Chemistry, Queen's University, Kingston, Ont., Canada K7L 3N6

Received December 11, 1978

SAUL WOLFE and PETER MICHAEL KAZMAIER. Can. J. Chem. 57, 2397 (1979).

The diastereomeric *RS*/*SR*- and *RR*/*SS*-benzyl-α-*d* methyl sulfoxides have been subjected to the Pummerer reaction with acetic anhydride and with trifluoroacetic anhydride. The ethoxysulfonium fluoroborate derivatives of these sulfoxides have been subjected to the Pfitzner–Moffatt reaction with sodium hydride in tetrahydrofuran. The deuterium contents of the starting materials and of the Pfitzner–Moffatt product have been determined by mass spectrometry. The deuterium contents of the α-acyloxybenzyl methyl sulfoxides formed in the Pummerer reaction have been determined by ^{1}Hmr spectroscopy. The resulting data permit the calculation of the diastereotopic selectivities and isotope effects associated with the deprotonation of oxysulfonium cations. The selectivities are found to be lower by a factor of about 10 than those observed in the formation of the benzyl-α-*d* methyl sulfoxides by hydrogen–deuterium exchange of benzyl methyl sulfoxide. Nevertheless, the existence of selectivity in the Pummerer reactions rules out a sulfurane and a dication as sole product-determining intermediates. The factors contributing to this low selectivity are discussed.

SAUL WOLFE et PETER MICHAEL KAZMAIER. Can. J. Chem. 57, 2397 (1979).

On a soumis les benzyl α-*d*-méthylsulfoxydes diastéréomères *RS*/*SR* et *RR*/*SS* à la réaction de Pummerer sous l'influence des anhydrides acétique et trifluoroacétique. On a soumis les fluoroborates d'éthoxysulfonium dérivés de ces sulfoxydes à la réaction de Pfitzner–Moffatt avec l'hydrure de sodium dans le tétrahydrofuranne. Utilisant la spectroscopie de masse, on a déterminé les quantités de deuterium présentes dans les composés initiaux et dans les produits Pfitzner–Moffatt. Utilisant la spectroscopie rmn ^{1}H, on a déterminé les quantités de deutérium présentes dans les α-acyloxybenzyl méthylsulfoxydes qui se forment au cours de la réaction de Pummerer. Les données qui en découlent permettent de calculer les sélectivités diastéréotopes et les effets isotopiques associés à la déprotonation des cations oxysulfonium. On a trouvé que les sélectivités sont d'environ 10 fois plus faibles que celles observées lors de la formation de benzyl α-*d*-méthylsulfoxydes par échange hydrogène–deutérium du benzyl méthylsulfoxyde. Toutefois l'existence d'une sélectivité dans les réactions de Pummerer élimine la possibilité de l'existence d'un sulfuranne ainsi que d'un dication comme seuls intermédiaires conduisant à des produits. On discute des facteurs contribuant à cette faible sélectivité.

[Traduit par le journal]

When the alkoxysulfonium cation **1** is treated with base it is converted to a mixture of the benzyl sulfide **2**, by a Pfitzner–Moffatt reaction (1), and the benzaldehyde thioacetal **3**, by a Pummerer reaction (2). The proportions of the Pfitzner–Moffatt and Pummerer products depend upon the specific experimental conditions (3), but the alkoxysulfonium ylide **4** is an intermediate in both cases. Since sulfonium cations have a pyramidal configuration at sulfur (4), the methylene protons of **1** are diastereotopic, and some selectivity should, therefore, be expected in the deprotonation which forms the ylide (5), regardless of the subsequent chemical and (or) stereochemical fate of this species.

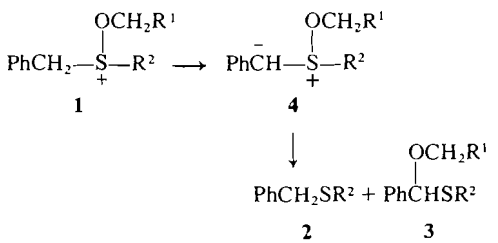

As discussed in the preceding paper (6), proton loss from the *acyloxysulfonium* cation **5** proceeds via an E2 process, which leads to a mixture of the α-thiocarbonium ions **6** and **7** and, thence, to the mixture of Pummerer products **8** and **9**. If it is assumed that the E2 elimination of acetic acid from **5** occurs with *anti*-periplanar stereochemistry, the Pummerer reaction of conformation **5***a* will involve loss of the pro-*S* hydrogen, and the reaction of conformation **5***b* will involve the loss of the pro-*R* hydrogen from the benzylic position.

If the transition states associated with the elimination of acetic acid from **5***a* and **5***b* differ in energy, then, according to the Curtin–Hammett principle (7), diastereotopic selectivity should again be ob-

0008-4042/79/182397-07$01.00/0

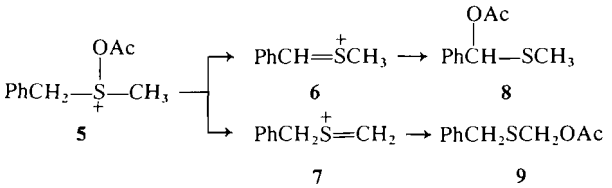

5

6 8

7 9

5a 5b

served in the removal of the methylene protons. Consequently, selectivity is expected, regardless of whether the deprotonation of an oxysulfonium cation follows an ylide or an E2 pathway. However, it is difficult to demonstrate this point experimentally in the Pfitzner–Moffatt and Pummerer reactions,[1] for a number of experimental and theoretical reasons.

For example, if selectivity exists in the deprotonation of an oxysulfonium cation, a transfer of chirality from sulfur to carbon in the Pummerer reaction is, in principle, possible. But, if a 'free' carbonium ion is formed subsequently, any stereochemical information gained in the deprotonation step would appear to be lost in the planar carbonium ion intermediate.

A transfer of chirality from sulfur to carbon might be demonstrable if selective deprotonation to form an ylide were followed by an intramolecular transfer of the oxy substituent. However, the barrier to rotation about the C—S bond of an acyclic sulfonium ylide is calculated (9) to be less than 10 kcal/mol, and pyramidal inversion at sulfur is much more rapid in a sulfonium ylide (10) than in a sulfonium cation. Thus it seems unlikely that the required intramolecular transfer from sulfur to carbon could compete successfully with stereomutation of the oxysulfonium ylide. In addition, when the sulfur substituent is alkoxy, the intramolecular transfer corresponds to a [1,2] sigmatropic rearrangement, and is predicted (11) to occur thermally in a concerted manner only with inversion of configuration at carbon. Such antarafacial processes have not been observed (12).

On the other hand, a suprafacial [2,3] sigmatropic rearrangement (11) is well established in the literature (13), and such a reaction is possible in the case of an acyloxysulfonium ylide (14). However, as already noted (6), acyloxysulfonium ylides do not appear to be intermediates in the Pummerer reactions of acyloxysulfonium cations such as **5**. Moreover, the conditions normally employed to generate an acyloxysulfonium cation from a sulfoxide also promote rapid epimerization at sulfur (15), which masks any potential asymmetric induction. For example, optically active benzyl methyl sulfoxide is racemized by 1 equiv. of trifluoroacetic anhydride at −65°C, but the Pummerer reaction with the same reagent is not observed below −30°C (16).

Despite these various problems, asymmetric induction in the Pummerer reaction has been achieved in a few systems. In the conversion of **10** to **11** (X = OBz) (14), only the epimer shown is produced. However, since **11** (X = OMs) is converted to **11** (X = Cl) with *retention* of configuration, it is apparent that asymmetric induction at C5 of the thiazolidine ring of this compound is controlled by the asymmetry at C4, and is not inherent in the Pummerer reaction itself.

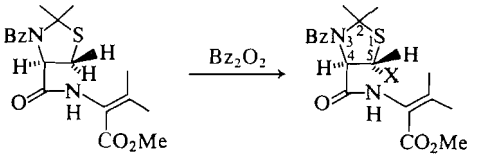

10 11

The conversion of (+)-**12** to (+)-**13** with dicyclohexylcarbodiimide (17) and to (−)-**13** with acetic anhydride (17, 18) and the conversion of optically active **14** to optically active **15** (19) with acetic anhydride are true examples of asymmetric induction in the Pummerer reaction. According to Stridsberg and Allenmark (17) the asymmetric induction observed in the formation of **13** is caused by the stereoselective removal of one of the methylene protons of **12**. However, Oae has argued (2*c*, 19) that the formation of optically active **15***a* cannot be explained in this manner if an ylide intervenes.

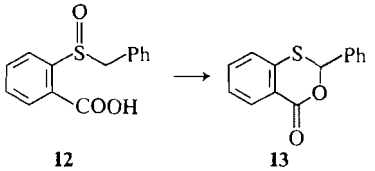

12 13

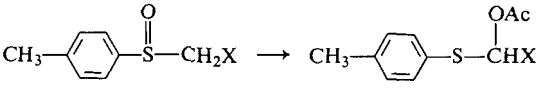

14 15

a X = CN
b X = C≡CH

The purpose of the present paper is to report that diastereotopic selectivity can be observed in the Pfitzner–Moffatt and Pummerer reactions of benzyl methyl ethoxy-, acetoxy-, and trifluoroacetoxysulfonium salts, by the use of the diastereomeric benzyl-α-*d* compounds (5*a*) as substrates. In the following paper, a similar procedure is employed to demon-

[1]Diastereotopic selectivity in the conversion of sulfoxides to α-halosulfoxides is well established (8).

strate that diastereotopic selectivity also exists in the conversion of **12** to **13**, and is responsible for the asymmetric induction.

For the present experiments, benzyl methyl sulfoxide, benzyl-α-d_2 methyl sulfoxide, and the *RS*/*SR*- and *RR*/*SS*-benzyl-α-*d* methyl sulfoxides were prepared by the procedures described previously (*5a*, *b*). Conversion to the acetoxy- and trifluoroacetoxysulfonium salts **16** and **17** was achieved *in situ* by reaction with acetic anhydride and trifluoroacetic anhydride, respectively. Conversion to the ethoxysulfonium salt **18** was accomplished with triethyloxonium fluoroborate (20).

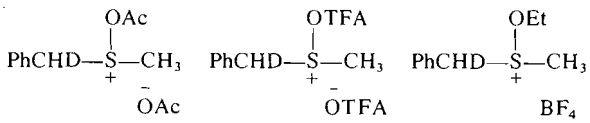

16 **17** **18**

Method

We employ the descriptors *A* and *B* to refer, respectively, to the more rapid and less rapid methylene sites of hydrogen–deuterium exchange of benzyl methyl sulfoxide in NaOD–D_2O (*5a*). Therefore, D_AH_B is the *RS*/*SR*-benzyl-α-*d* diastereomer (21), H_AD_B is the *RR*/*SS*-benzyl-α-*d* diastereomer, H_AH_B is the parent compound, and D_AD_B is the benzyl-α-d_2 compound. If k_A and k_B are the appropriate rate constants for the removal of H_A and H_B from H_AH_B, then the selectivity *S* is defined by $S = k_A/k_B$. To obtain this quantity for a Pfitzner–Moffatt or Pummerer reaction, it is necessary to work with the deuterated compounds D_AH_B and H_AD_B. This introduces a primary isotope effect, *I*, which must be taken into account. The assumption that the isotope effects at the two sites are equal (22) permits the calculation of *S* and *I* from eqs. [1] and [2] (23), where k_1/k_2 refers to the ratio k_A/k_B for D_AH_B, and k_1'/k_2' refers to the ratio k_A/k_B for H_AD_B.

$$[1] \quad S = (k_1/k_2)^{1/2}(k_1'/k_2')^{1/2}$$

$$[2] \quad I = (k_1'/k_2')^{1/2}(k_2/k_1)^{1/2}$$

For reactions of the type $PhCH_2\overset{+}{S}XCH_3 \rightarrow PhCHXSCH_3 + PhCH_2SCH_2X$, in which two regioisomers are formed, the ratios k_1/k_2 and k_1'/k_2' were determined by ^{1}Hmr. Within the accuracy of this method (10%), the substrate consisted entirely of either D_AH_B or H_AD_B. In such cases, the quantities k_1/k_2 and k_1'/k_2' could be calculated using eqs. [3] and [4],

$$[3] \quad k_1/k_2 = (d_1^{DAHB} - d_1^{S})/(d_1^{DAHB} - d_0^{S})$$

$$[4] \quad k_1'/k_2' = (d_1'^{HADB} - d_0'^{S})/d_1'^{HADB} - d_1'^{S})$$

where d_1^{DAHB} is the mole fraction of D_AH_B present in the starting sulfoxide sample (i.e., 1.0 in experiments analysed by ^{1}Hmr), d_1^{S} is the mole fraction of monodeuterated benzyl-substituted sulfide formed in the Pummerer reaction of D_AH_B, d_0^{S} is the mole fraction of undeuterated benzyl-substituted sulfide formed by the Pummerer reaction of D_AH_B, $d_1'^{HADB}$ is the mole fraction of H_AD_B present in the starting sulfoxide sample (i.e., 1.0 in experiments analysed by ^{1}Hmr), $d_1'^{S}$ is the mole fraction of monodeuterated benzyl-substituted sulfide formed in the Pummerer reaction of H_AD_B, and $d_0'^{S}$ is the mole fraction of undeuterated benzyl-substituted sulfide formed by the Pummerer reaction of H_AD_B.

The quantities d_1^{S}, d_0^{S}, $d_1'^{S}$, and $d_0'^{S}$ were determined by integration of the methine signal of the product (ca. δ 6.8) relative to an internal reference peak, usually the S-methyl peak at ca. δ 2.13.

For reactions of the type $PhCH_2\overset{+}{S}XCH_3 \rightarrow PhCHXSCH_3$, leading to a single regioisomer, analysis of the data was performed by mass spectrometry. If Z_m, Z_{m+1}, and Z_{m+2} are the heights of the *M*, *M* + 1, and *M* + 2 peaks of H_AH_B (normalized so that $Z_m + Z_{m+1} + Z_{m+2} = 1.00$), and Q_m, Q_{m+1}, and Q_{m+2} are the peak heights of a deuterated substrate, i.e., D_AH_B or H_AD_B, then

$$[5] \quad Q_m = Z_mD_0'$$

$$[6] \quad Q_{m+1} = Z_mD_1' + Z_{m+1}D_0'$$

$$[7] \quad Q_{m+2} = Z_mD_2' + Z_{m+1}D_1' + Z_{m+2}D_0'$$

where D_0', D_1', and D_2' are the mole fractions of the undeuterated, monodeuterated, and dideuterated species in the deuterated substrate. Equations [5]–[7] can be rearranged to give

$$[8] \quad D_0' = Q_m/Z_m$$

$$[9] \quad D_1' = (Q_{m+1} - Z_{m+1}D_0)/Z_m$$

$$[10] \quad D_2' = (Q_{m+2} - Z_{m+1}D_1 - Z_{m+2}D_0)/Z_m$$

The quantities Q_m, Q_{m+1}, and Q_{m+2} were obtained by measurement of the peak heights of the molecular ion cluster of the deuterated sample, and were normalized so that $Q_m + Q_{m+1} + Q_{m+2} = 1.0$. The quantities Z_m, Z_{m+1}, and Z_{m+2} could be determined by measurement of the peak heights of the molecular ion cluster of H_AH_B, but more accurate values were available by calculation using Beynon's equations (24). Table 1 lists the values of Z_m, Z_{m+1}, and Z_{m+2} calculated for benzyl methyl sulfoxide and benzyl methyl sulfide. The experimentally determined Z_m, Z_{m+1}, and Z_{m+2} values of benzyl methyl sulfoxide are included for comparison.

Equations [11] and [12] allow k_1/k_2 and k_1'/k_2' to be calculated,

$$[11]\quad k_1/k_2 = [d_1^{DAHB} - (d_1^{S} - d_2^{DADB})]/[d_1^{DAHB} - (d_0^{S} - d_0^{HAHB})]$$

$$[12]\quad k_1'/k_2' = [d_1'^{HADB} - (d_0'^{S} - d_0'^{HAHB})]/[d_1'^{HADB} - (d_1'^{S} - d_2'^{DADB})]$$

where d_2^{DADB}, d_1^{DAHB}, and d_0^{HAHB} are the relative amounts of dideuterated, monodeuterated, and undeuterated species in D_AH_B; $d_2'^{DADB}$, $d_1'^{HADB}$, and $d_0'^{HAHB}$ are the relative amounts of dideuterated, monodeuterated, and undeuterated species in H_AD_B, and d_0^{S}, d_1^{S}, and $d_0'^{S}$ and $d_1'^{S}$ are the corresponding quantities for the sulfide products from D_AH_B and H_AD_B.

Results and Discussion

Table 2 shows the results obtained in the Pummerer reactions of the benzyl-α-*d* methyl sulfoxides with acetic anhydride and with trifluoroacetic anhydride. Table 3 contains the deuterium analyses of the D_AH_B and H_AD_B benzyl methyl sulfoxides, and of the benzyl methyl sulfides formed from their derived ethoxysulfonium fluoroborates by reaction with sodium hydride in tetrahydrofuran. The selectivities and deuterium isotope effects calculated from these data are collected in Table 4.

TABLE 1. Relative abundances of Z_m, Z_{m+1}, and Z_{m+2} calculated from Beynon's equations

Compound	Molecular formula	Z_m	Z_{m+1}	Z_{m+2}
$PhCH_2\overset{O}{\overset{\|}{S}}CH_3$	$C_8H_{10}OS$	0.8695	0.08376	0.04674
$PhCH_2\overset{O}{\overset{\|}{S}}CH_3$[a]	$C_8H_{10}OS$	0.8680	0.0838	0.0440
$PhCH_2SCH_3$	$C_8H_{10}S$	0.8714	0.0836	0.04505

[a]Experimental results.

TABLE 2. Deuterium content of the α-acyloxybenzyl methyl sulfoxides formed in the Pummerer reactions of the D_AH_B and H_AD_B benzyl methyl sulfoxides[a]

Sulfoxide	Reagent	Temp. (°C)	d_0[b,c]	d_1[b,c]
D_AH_B	Ac_2O[d]	130	0.13	0.87
H_AD_B	Ac_2O[d]	130	0.19	0.81
D_AH_B	TFAA[e]	25	0.17	0.83
H_AD_B	TFAA[e]	25	0.14	0.86

[a]See text for the definitions of these isomers.
[b]Determined by ^{1}Hmr in CCl_4.
[c]The error in these measurements is 10% of the reported value.
[d]The solvent used was acetic anhydride with a sulfoxide concentration of 0.06 *M*.
[e]The solvent was CCl_4 with a sulfoxide concentration of 0.5 *M* and a TFAA concentration of 0.4 *M*.

In each case, the selectivity observed in the deprotonation of the oxysulfonium cation is opposite to that seen in the hydrogen–deuterium exchange which forms D_AH_B and H_AD_B, and is smaller by a factor of at least 10. However, the selectivities observed in the present work should be regarded as lower limits, for several reasons associated with the experimental conditions that were needed to obtain the results.

For example, as already mentioned (15), it is well established that the Pummerer reactions of acyloxysulfonium salts are complicated by a competing epimerization at sulfur. The relative rates of the two processes have been studied in several systems. Aryl benzyl sulfoxides are racemized in acetic anhydride at 100°C, a temperature at which the Pummerer reaction is not observed. For aryl methyl sulfoxides, the Pummerer reaction is faster than epimerization by a factor of 4.3 at 110°C. If epimerization is faster than the Pummerer reaction in the present work, D_AH_B (or H_AD_B) will be transformed to a 1:1 mixture of D_AH_B + H_AD_B, and all stereochemical information will be lost. Treatment of benzyl methyl sulfoxide with 1 equiv. of trifluoroacetic anhydride in methylene chloride at −65°C (25) followed, after 5 min, by addition of aqueous tetrahydrofuran, led to quantitative recovery of the compound. Repetition of this experiment with D_AH_B led to the recovery of a 1:1 mixture of the two diastereomers. Thus it is not surprising that little selectivity is evident in the Pummerer reaction when trifluoroacetic anhydride is employed as the reagent.

It is known (3) that the Pfitzner–Moffatt mode of decomposition of the oxysulfonium ylide derived from **18** is favoured in non-polar solvents. Therefore, this ylide was generated in tetrahydrofuran using sodium hydride as a non-nucleophilic base; these conditions avoid epimerization at sulfur and lead exclusively to the Pfitzner–Moffatt product. The high reactivity of sodium hydride, as can be seen from the negligible isotope effect which is observed in this case, would be expected to lead to reduced selectivity (26). In fact, the Pfitzner–Moffatt reaction exhibits the highest selectivity of the reactions studied in the present work.

In an attempt to find conditions that would lead to an increase in the selectivity of the Pfitzner–Moffatt reaction, the salt **19** was reacted with 2,6-lutidine in acetone, a solvent and base combination that is known (3) to minimize epimerization at sulfur. However, this reaction led, unexpectedly, to a 1:1 mixture of the acetal **20** and the dithioacetal **21**. It is suggested that this reaction proceeds via the sulfonium cation **22**, which is formed by the addition of the α-thiocarbonium ion **6** (an intermediate in the Pummerer reaction) to the thioacetal **23**. The mech-

TABLE 3. Deuterium analyses[a] of the D_AH_B and H_AD_B benzyl methyl sulfoxides[b], and of the benzyl methyl sulfides formed from their derived ethoxyfluoroborates[c] in the Pfitzner–Moffatt reaction

Starting material	Deuterium content of the starting material			Deuterium content of the Pfitzner–Moffatt product		
	d_0	d_1	d_2	d_0	d_1	d_2
D_AH_B	0.1094±0.0074	0.8090±0.0179	0.0861±0.0124[d]	0.3562±0.0326	0.5930±0.0322	0.0509±0.0044[e]
H_AD_B	0.5265±0.0228	0.4594±0.0079	0.0141±0.0035[f]	0.8029±0.0301	0.1908±0.0285	0.0063±0.0079[g]

[a]Analyses performed by mass spectrometry on Hitachi Perkin Elmer RMU-6E and Dupont 21-491B mass spectrometers under electron impact conditions at 70 eV.
[b]See text for the definitions of these isomers.
[c]Prepared from D_AH_B and H_AD_B by reaction with triethyloxonium fluoroborate.
[d]Average ± standard deviation of six determinations.
[e]Average ± standard deviation of three determinations.
[f]Average ± standard deviation of five determinations.
[g]Average ± standard deviation of four determinations.

TABLE 4. Stereoselectivity and deuterium isotope effects in the Pummerer and Pfitzner–Moffatt reactions of $PhCHSXCH_3^+$ salts

Substrate	Reagent	Temp. (°C)	S	I
$PhCH_2\overset{\overset{O}{\|}}{S}CH_3$	TFAA	25	0.89±0.14[a]	5.5 ±0.70[a]
$PhCH_2\overset{\overset{O}{\|}}{S}CH_3$	Ac_2O	130	0.80±0.12[a]	5.4 ±0.43[a]
$PhCH_2\overset{\overset{OEt}{\|}}{S}CH_3\ BF_4^-$	NaH	25	0.59±0.08[b]	1.09±0.21[b]

[a]Standard deviation based on three determinations.
[b]Standard deviation based on four determinations.

anism is written in this manner to account for the formation of a *mixture* of acetal and thioacetal (cf. ref. 27), and for the finding that **23** is stable to the action of 2,6-lutidine in acetone.

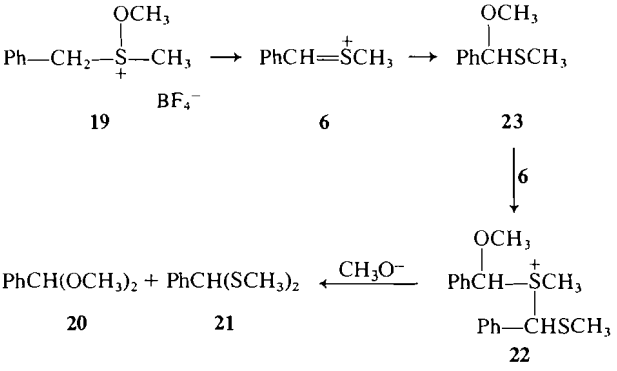

In the preceding paper (6), it was argued that a dication mechanism could not be ruled out for the reaction shown in eq. [13], which leads to the α-chlorobenzyl regioisomer exclusively. On the other hand, the Pummerer reactions of benzyl methyl acyloxysulfonium cations were considered to proceed via an E2 pathway. The observation of diastereotopic selectivity in the present work, while not proving the E2 pathway, is sufficient to rule out a dication mechanism for the acyloxysulfonium cations. The methylene protons of a dication are enantiotopic (28).

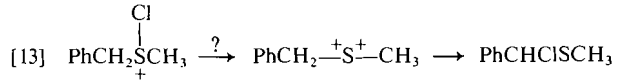

The same argument applies to the sulfurane **24**, which could be considered as an intermediate in the Pummerer reactions of the present work. The intervention of such species in Pummerer reactions has often been considered (2), but no definite evidence on this point has appeared. The sulfurane **24** is expected to exist in the trigonal bipyramidal geometry shown (29); the methylene protons of this molecule are *enantiotopic*. No selectivity between these protons could exist if the Pummerer reaction proceeds solely via **24**.

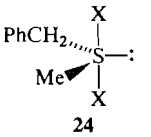

24

X = OAc, OTFA

Finally, it should be recognized that the selectivities reported here refer to acyclic molecules. Much higher selectivities are expected for cyclic, conformationally constrained systems (30). Extensions of the present work to appropriate molecules of this type are under active investigation.

Experimental

General experimental methods and syntheses of the *RS*/*SR*- and *RR*/*SS*-benzyl-α-*d* methyl sulfoxides have been described previously (5*a*, *b*, 6).

*Reaction of Benzyl-α-*d *Methyl Sulfoxide with Acetic Anhydride*

Benzyl-α-*d* methyl sulfoxide (D_AH_B or H_AD_B) (96 mg, 0.62 mmol) was dissolved in acetic anhydride (10 mL) and heated at 130°C for 2 h. The reaction mixture was poured into ice-cold saturated potassium bicarbonate. Extraction with chloroform (4 × 75 mL) and evaporation of the solvent after drying (magnesium sulfate) yielded a mixture of acetoxysulfides. The amount of hydrogen/deuterium on the methine carbon of α-acetoxybenzyl methyl sulfoxide was determined by integration using the acetoxy and SCH_3 protons as an internal reference.

*Reaction of Benzyl-α-*d *Methyl Sulfoxide with Trifluoroacetic Anhydride*

Benzyl-α-*d* methyl sulfoxide (D_AH_B or H_AD_B) (42 mg, 0.27 mmol) was suspended in carbon tetrachloride (0.5 mL), and trifluoroacetic anhydride (0.3 mL, 2 mmol) was added at 25°C. A ^{1}Hmr spectrum of the product was taken immediately, and the proton/deuterium content of the methine hydrogen of the α-trifluoroacetoxybenzyl methyl sulfide was measured by integration using the integral of the SCH_3 group as an internal reference.

*Reaction of Benzyl-α-*d *Methyl Ethoxysulfonium Fluoroborate with Sodium Hydride*

Benzyl-α-*d* methyl sulfoxide (0.500 g, 3.25 mmol) was weighed into a dry flask, and triethyloxonium fluoroborate (1.9 mL of 2.4 *M*, 4.56 mmol) in methylene chloride was added dropwise. After the solution was homogeneous, the sulfonium salt was precipitated with ether, and triturated further with ether. The ether was removed and dry tetrahydrofuran (10 mL) was added. To this was added sodium hydride (0.155 g, 50% dispersion, 3.23 mmol) in one portion, and the mixture was stirred at room temperature overnight. Then methanol (ca. 20 mL) was added, and the precipitated sodium fluoroborate was removed by filtration. The benzyl methyl sulfide was isolated by chromatography (silica gel, methylene chloride/petroleum ether (50–100) 5:1) and analysed by mass spectrometry.

*Epimerization of Benzyl-α-*d *Methyl Sulfoxide with Trifluoroacetic Anhydride at −65°C*

Benzyl-α-*d* methyl sulfoxide (D_AH_B) (100 mg, 0.65 mmol) was dissolved in methylene chloride (10 mL), and the solution was cooled to −65°C. Trifluoroacetic anhydride (0.4 mL of 1.63 *M*, 0.65 mmol) was added dropwise (2 min). The mixture became cloudy for a moment and then became clear. After 5 min, water (10 mL) and tetrahydrofuran (1 mL) were added and the mixture was allowed to warm to room temperature. Evaporation of the solvent led to a quantitative recovery of the sulfoxide. The ^{1}Hmr spectrum of this material showed two singlets (δ 4.20 and δ 3.88) in the benzyl region in the ratio 1:1, corresponding to a 1:1 mixture of D_AH_B and H_AD_B.

Acknowledgements

We thank the National Research Council of Canada for financial support of this work and for the Award of a 1967 Science Scholarship, and Mr. Peter Gordon and Dr. Peter Sipos, of the Dupont Research Centre, for assistance with the mass spectral analyses.

1. K. E. Pfitzner and J. G. Moffatt. J. Am. Chem. Soc. **85**, 3027 (1963); A. H. Fenselau and J. G. Moffatt. J. Am. Chem. Soc. **88**, 1762 (1966).
2. (*a*) G. A. Russell and G. J. Mikol. *In* Mechanisms of molecular migrations. Vol. 1. *Edited by* B. S. Thyagarajan. Interscience, London. 1968. p. 157; (*b*) T. Durst. Adv. Org. Chem. **6**, 285 (1969); (*c*) S. Oae and T. Numata. *In* Isotopes in organic chemistry. Vol. 5. *Edited by* E. Buncel and C. C. Lee. Elsevier, Amsterdam. 1979. In press.
3. C. R. Johnson and W. G. Phillips. J. Am. Chem. Soc. **91**, 682 (1969).
4. D. Darwish, S. H. Hui, and R. Tomilson. J. Am. Chem. Soc. **90**, 5631 (1968); K. Mislow. Rec. Chem. Progr. **28**, 217 (1967).
5. (*a*) A. Rauk, E. Buncel, R. Y. Moir, and S. Wolfe. J. Am. Chem. Soc. **87**, 5498 (1965); (*b*) T. F. Garrard. M.Sc. Thesis, Queen's University, Kingston, Ont. 1974; (*c*) G. Barbarella, A. Garbesi, A. Boicelli, and A. Fava. J. Am. Chem. Soc. **95**, 8051 (1973); (*d*) O. Hofer and E. L. Eliel. J. Am. Chem. Soc. **95**, 8045 (1973).
6. S. Wolfe and P. M. Kazmaier. Can. J. Chem. This issue.
7. J. I. Seeman and W. A. Farone. J. Org. Chem. **43**, 1854 (1978).
8. P. Calzavara, M. Cinquini, S. Colonna, R. Fornasier, and F. Montanari. J. Am. Chem. Soc. **95**, 7431 (1973); S. Bory, R. Lett. B. Moreau, and A. Marquet. C.R. Acad. Sci. Ser. C, **276**, 1323 (1973).
9. F. Bernardi, H. B. Schlegel, M.-H. Whangbo, and S. Wolfe. J. Am. Chem. Soc. **99**, 5633 (1977).
10. D. Darwish and R. L. Tomilson. J. Am. Chem. Soc. **90**, 5938 (1968); S. Wolfe, P. Chamberlain, and T. F. Garrard. Can. J. Chem. **54**, 2847 (1976).
11. R. B. Woodward and R. Hoffmann. The conservation of orbital symmetry. Verlag Chemie. Weinheim/Bergstrasse. 1970. p. 114.
12. J. E. Baldwin, W. F. Erickson, R. E. Hackler, and R. M. Scott. Chem. Commun. 576 (1970).
13. J. E. Baldwin, R. E. Hackler, and D. P. Kelly. Chem. Commun. 538 (1968).
14. J. E. Baldwin, A. Au, M. Christie, S. B. Haber, and D. Hesson. J. Am. Chem. Soc. **97**, 5957 (1975); G. A. Koppel, L. McShane, F. José, and R. D. G. Cooper. J. Am. Chem. Soc. **100**, 3933 (1978).
15. S. Oae, T. Kitao, S. Kawamura, and Y. Kitaoka. Tetrahedron, **19**, 817 (1963); S. Oae. Q. Rep. Sulfur Chem. **5**, 53 (1970); S. Oae and M. Kise. Tetrahedron Lett. 2261 (1968).
16. P. M. Kazmaier. Ph.D. Thesis, Queen's University, Kingston, Ont., 1978.
17. B. Stridsberg and S. Allenmark. Acta Chem. Scand. Ser. B, **28**, 591 (1974); **30**, 219 (1976).
18. S. Oae and T. Numata. Tetrahedron, **30**, 2641 (1974).
19. T. Numata and S. Oae. Tetrahedron Lett. 1337 (1977); T. Numata, O. Itoh, and S. Oae. Chem. Lett. 909 (1977); S. Glue, I. T. Kay, and M. R. Kipps. Chem. Commun. 1158 (1970).
20. C. R. Johnson and D. McCants, Jr. J. Am. Chem. Soc. **87**, 5404 (1965).

21. J. E. BALDWIN, R. E. HACKLER, and R. M. SCOTT. Chem. Commun. 1415 (1969).
22. R. R. FRASER and L. K. NG. J. Am. Chem. Soc. **98**, 4334 (1976).
23. D. Y. CURTIN and D. B. KELLOM. J. Am. Chem. Soc. **75**, 6011 (1953); E. L. ELIEL, A. ABATJOGLOU, and A. A. HARTMANN. J. Am. Chem. Soc. **94**, 4786 (1972).
24. J. H. BEYNON and A. E. WILLIAMS. Mass and abundance tables for use in mass spectroscopy. Elsevier, New York. 1963.
25. A. K. SHARMA and D. SWERN. Tetrahedron Lett. 1503 (1974); A. K. SHARMA, T. KU, A. D. DAWSON, and D. SWERN. J. Org. Chem. **40**, 2758 (1975).
26. B. GIESE. Angew. Chem. **89**, 162 (1977); A. PROSS. Adv. Phys. Org. Chem. **14**, 69 (1977).
27. H. J. BÖHME and H. J. GRAN. Justus Liebigs Ann. Chem. **577**, 68 (1952); R. F. LANGLER, W. S. MANTLE, and M. J. NEWMAN. Org. Mass Spectrom. **10**, 1135 (1975).
28. S. WOLFE. Acc. Chem. Res. **5**, 102 (1972).
29. J. C. MARTIN and T. M. BALTHAZER. J. Am. Chem. Soc. **99**, 152 (1977).
30. R. R. FRASER, F. J. SCHUBER, and Y. Y. WIGFIELD. J. Am. Chem. Soc. **94**, 8795 (1972); R. R. FRASER and P. J. CHAMPAGNE. J. Am. Chem. Soc. **100**, 657 (1978).

On the relationships between ^{18}O-transfer, diastereotopic selectivity, and asymmetric induction in an intramolecular Pummerer reaction

SAUL WOLFE, PETER MICHAEL KAZMAIER, AND HILLAR AUKSI
Department of Chemistry, Queen's University, Kingston, Ont., Canada K7L 3N6

Received December 19, 1978

SAUL WOLFE, PETER MICHAEL KAZMAIER, and HILLAR AUKSI. Can. J. Chem. 57, 2404 (1979).

The cyclization of benzyl 2-carboxyphenyl sulfoxide (**1**) to 2-benzylbenzoxathiane-6-one (**2**) has been examined by a combination of ^{18}O-labelling of the sulfoxide oxygen, stereoselective deuterium labelling in the benzylic position, and the use of optically active compounds. With dicyclohexylcarbodiimide (DCC) as the cyclizing agent, the reaction proceeds with 55.8% retention of the sulfoxide oxygen, 57.8% preference for abstraction of one of the diastereotopic methylene protons, and it produces a 61.4/38.6 mixture of enantiomers. It is proposed that all three experimental observables are controlled by the competition between initial attack of the DCC upon the sulfoxide oxygen and upon the carboxyl group, and a mechanism is proposed for the reaction which clarifies the relationship between these observables. In agreement with earlier work by Stridsberg and Allenmark, DCC affords **2** having the opposite sign of rotation from **1**, and acetic anhydride affords **2** having the same sign of rotation as **1**. Asymmetric induction in the latter reaction is significantly less than with DCC because of competing epimerization at sulfur, but the origin of the differences in the sign of rotation of **2** under the different conditions has been clarified by the finding that there is less than 40% retention of the sulfoxide oxygen with acetic anhydride as the reagent.

SAUL WOLFE, PETER MICHAEL KAZMAIER et HILLAR AUKSI. Can. J. Chem. 57, 2404 (1979).

On a étudié la cyclisation du benzyl carboxy-2 phényl sulfoxyde (**1**) en benzyl-2 benzoxathianone-6 (**2**) en combinant des méthodes de marquage de l'oxygène du sulfoxyde avec du ^{18}O et de marquage stéréosélectif au deutérium de la position benzylique ainsi que par l'utilisation de composés optiquement actifs. Lorsqu'on utilise la dicyclohexylcarbodiimide (DCC) comme agent de cyclisation, la réaction se produit avec 55.8% de retention de l'oxygène du sulfoxyde, avec une préférence de 57.8% pour l'enlèvement de l'un des protons diastéréomères du méthylène et il se forme un mélange 61.4/38.6 d'énantiomères. On suggère que les trois résultats expérimentaux observés sont contrôlés par une compétition entre une attaque initiale du DCC sur l'oxygène du sulfoxyde et sur le groupement carboxyle et on propose un mécanisme pour la réaction qui clarifie la relation entre ces observations. En accord avec les travaux antérieurs de Stridsberg et de Allenmark, le DCC fournit un composé **2** dont le signe de la rotation est inverse de celui de **1** alors que l'anhydride acétique conduit à un produit **2** dont la rotation est la même que celle de **1**. L'induction asymétrique dans cette dernière réaction est beaucoup moins importante qu'avec le DCC à cause de l'épimérisation au niveau du soufre qui est en compétition; toutefois on a pu clarifier l'origine des différences dans le signe de la rotation des produits **2** obtenus selon diverses conditions en trouvant que le taux de retention de l'oxygène du sulfoxyde est moins de 40% lorsque le réactif est l'anhydride acétique.
[Traduit par le journal]

The reaction of benzyl 2-carboxyphenyl sulfoxide (**1**) with acetic anhydride (1) or with dicyclohexylcarbodiimide (DCC) (2) leads to 2-benzyl-1,3-benzoxathian-6-one (**2**), via an intramolecular Pummerer reaction (3). On the basis of the mechanistic studies of Oae and Numata (1), the rate-determining step in this reaction is the formation of the cyclic acyloxysulfonium cation **3**. Stridsberg and Allenmark (2, 4) also consider **3** to be an intermediate in the reaction and, in their investigations of the stereochemical course of the reaction, these workers have demonstrated that the conversion of **3** to **2** proceeds with asymmetric induction. For example, the reaction of optically pure (+)−**1** with DCC in ethylene chloride solvent at 25°C gave (−)−**2** having 29.9% optical purity; in acetic anhydride solvent at 100°C, (+)−**1** afforded (+)−**2** having 11.2% optical purity. Both groups of workers propose that the product-determining step in the overall reaction is the deprotonation of **3** to the cyclic acyloxysulfonium ylide **4**. To account for the asymmetric induction, Stridsberg and Allenmark have suggested (4) that diastereotopic selectivity exists in this deprotonation step, and that the diastereomeric ylides thus formed are converted to different enantiomers of the product.

The two groups of workers propose different mechanisms for the formation of **3** from **1**. According to Oae and Numata, the reaction is initiated by activation of the carboxyl group (**1** → **5**), followed

0008-4042/79/182404-08$01.00/0

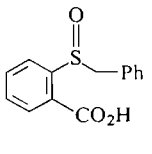

1

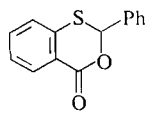

2

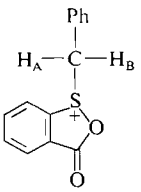

3

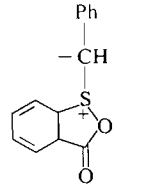

4

by rate-determining ring closure by the sulfoxide oxygen (**5** → **3**). On the other hand, Stridsberg and Allenmark, by analogy with the mechanism of the Pfitzner–Moffatt reaction (5), prefer an initial activation of the sulfoxide oxygen (**1** → **6**), followed by ring closure by the carboxyl group. These two pathways can be distinguished by ^{18}O-labelling experiments, since the sequence **1** → **5** → **3** predicts retention of the sulfoxide oxygen, and the sequence **1** → **6** → **3** predicts loss of the sulfoxide oxygen. One of the objectives of the present work is to provide the results of such experiments and to relate these results to the *direction* of the asymmetric induction observed under the different reaction conditions.

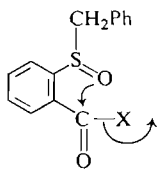

5

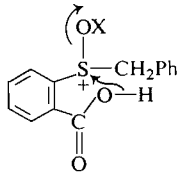

6

A second objective of the present work is to determine whether diastereotopic selectivity does exist in the deprotonation step of the reaction, and whether such selectivity can be related to the *magnitude* of the observed asymmetric induction. A third objective is to propose a new mechanism for the transformation of the cation **3** to the product **2**. This mechanism is consistent with experimental observations on the Pummerer reactions of acyloxysulfonium cations (6, 7), and it takes into account some theoretical calculations on the stereochemical properties of sulfonium ylides (8), which suggest that stereomutation of **4** would be sufficiently rapid to result in loss of the stereochemical integrity of diastereomers.

In the present mechanism, the deprotonation step is considered to proceed via an E2 pathway (6), with an *anti*-periplanar relationship between the C—H and S—O bonds. Thus conformation **3***a*[1] will lead to the α-thiocarbonium ion **7***a*, with loss of the pro-*S* benzylic proton, and conformation **3***b*[1] will lead to the α-thiocarbonium ion **7***b*, with loss of the pro-*R* benzylic proton. Because rotation about the C—S bond of an α-thiocarbonium ion is slow (9), in contrast to rotation about the C—S bond of a sulfonium ylide (8), collapse of the ion pair **7***a* is expected to lead to *S*-**2**, and collapse of the ion pair **7***b* is expected to lead to *R*-**2**, with net inversion of configuration at carbon. Since reactions **3***a* → **7***a* and **3***b* → **7***b* proceed via diastereomeric transition states, *S*-**2** and *R*-**2** will be produced in different amounts (10). Inspection of **7***a* and **7***b* suggests that the transition state leading to the latter α-thiocarbonium ion should be favoured significantly.

Consequently, *R*-**2** is expected to be the predominant enantiomer produced from the *R*-enantiomer of **3**, and it will be formed with loss of the pro-*R* benzylic proton. However, whether *R*-**3** or *S*-**3** is the intermediate in a reaction initiated from the *R*-enantiomer of **1** will depend upon which of the sequences **1** → **5** → **3** and **1** → **6** → **3** is operative under the specific reaction conditions. The above analysis will apply to a reaction initiated with *R*-**1** in which **3** is formed by the sequence **1** → **5** → **3**, with retention of configuration at sulfur (and retention of the sulfoxide oxygen). The analysis will also apply to a reaction initiated with *S*-**1**, in which **3** is formed by the sequence **1** → **6** → **3**, with *inversion* of configuration at sulfur (and *loss* of the sulfoxide oxygen).

Several aspects of this mechanistic proposal are, in principle, susceptible to experimental test. The first is the prediction that C—O bond formation occurs with net inversion of configuration at the benzylic carbon. To establish this point would require knowledge of the absolute configurations of **2**, **3**, and prochirally labelled **3**. None of this information is, as yet, available. A second is the prediction that the proportions of *R*-**2** and *S*-**2** are related to the relative rates of abstraction of the pro-*R* and pro-*S* methylene protons, respectively, and that these, in turn, are related to the fate of the sulfoxide oxygen of **1**.

Method

The procedure for the determination of diastereotopic selectivity in the deprotonation step was the same as that described in the preceding paper (7), using mass spectrometry, and was predicated upon

[1]The argument is presented for the *R*-enantiomer of **3**.

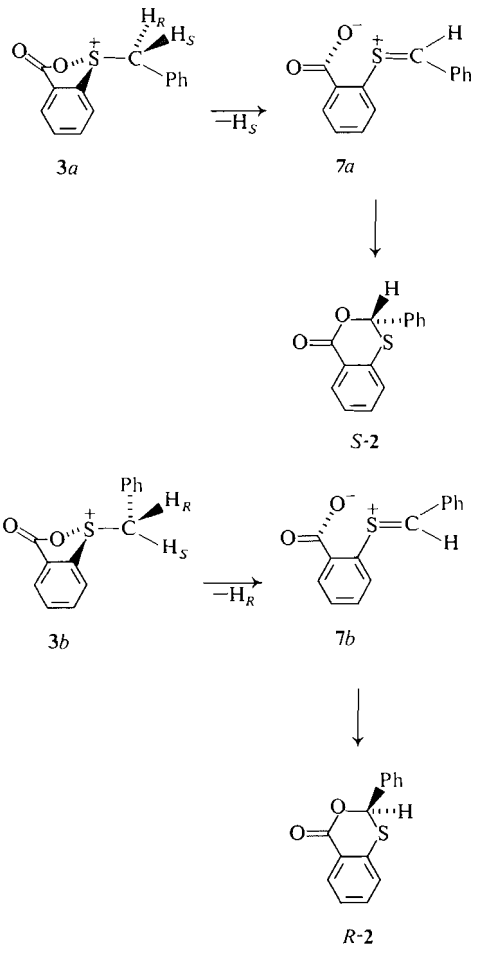

the assumption that the diastereomeric benzyl-α-*d* derivatives of **1** would be accessible by hydrogen–deuterium exchange. This assumption proved to be correct. In D_2O solvent at 30°C, the diastereotopic methylene protons of a 0.4 *M* solution of **1** were observed to be anisochronous (δ_A 4.32; δ_B 3.88). In *N* NaOD–D_2O, the downfield proton of the AB quartet (H_A) exchanged more rapidly than H_B, corresponding to the sequence of events $H_AH_B \rightarrow D_AH_B \rightarrow D_AD_B$. Such observations are now well established in the literature (11).

Figure 1 shows the results obtained in a typical experiment, in which the relative amounts of H_AH_B and D_AH_B were determined by integration of ^{1}Hmr spectra of the reaction mixture as a function of time. Scheme 1 is a simplified description of the processes which occur in this system. The rate of disappearance of H_AH_B provides $k_A + k_B$, where k_A and k_B are pseudo-first-order rate constants for the exchange of H_A and H_B, respectively. The rate of disappearance of D_AH_B provides k_B/J, where J is the secondary deuterium isotope effect. For $J = 1.34$,

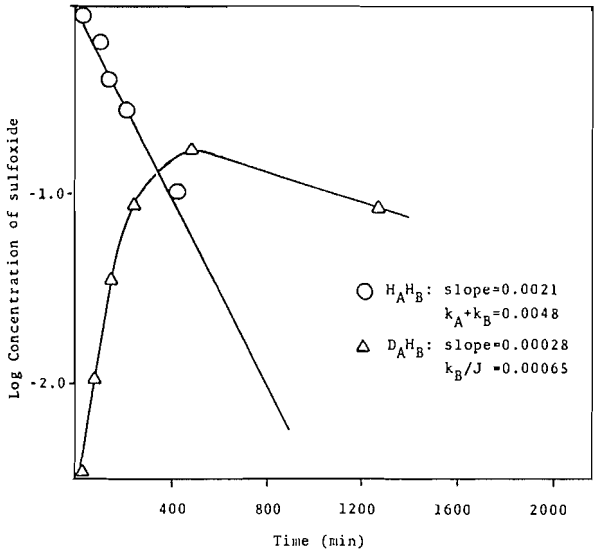

FIG. 1. Hydrogen–deuterium exchange of benzyl 2-carboxyphenyl sulfoxide (0.4 *M*) at 30°C in 1.0 *N* NaOD–D_2O.

the value observed in the hydrogen exchange of benzyl methyl sulfoxide (12), k_A and k_B were calculated to be 0.0040 min^{-1} and 0.00087 min^{-1}, respectively, leading to a ratio $k_A/k_B = 4.6$ at 30°C.

Although this result means that the D_AH_B diastereomer of **1** will be contaminated by H_AD_B, the proportions of the two are known, because the rate constants are known, and this permits appropriate corrections to be made to the selectivity results, as described below.

The H_AD_B diastereomer of **1** was synthesized by permitting the exchange of **1** to proceed to D_AD_B, and then carrying out a back exchange in NaOH–H_2O.

For the synthesis of ^{18}O-labelled **1**, benzyl 2-carboxyphenyl sulfide was oxidized with pyridinium perbromide in pyridine containing 12.678 at.% ^{18}O-enriched H_2O. Mass spectral analysis of the resulting sulfoxide indicated 13.08% ^{18}O-enrichment of the sulfoxide oxygen, based on analysis of M^+, and 12.56% enrichment, based on analysis of the *M*-91 peak. The average of these two values, 12.82 ± 0.55%, was used in the computation of the results.

Optically active **1** was prepared via the brucine salt, as described by Stridsberg and Allenmark (4).

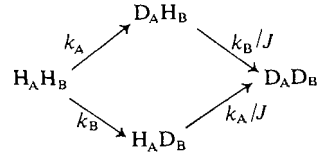

SCHEME 1

TABLE 1. Deuterium analyses[a] of the D_AH_B and H_AD_B diastereomers of **1** and of the cyclized product **2** obtained from these diastereomers under various conditions

Diastereomer[b,c]	Compound analyzed	Mode of formation	Deuterium content d_0	d_1	d_2
D_AH_B	**1**[d]		0.1794±0.0157	0.6378±0.0324	0.1829±0.0078
H_AD_B	**1**[e]		0.0994±0.0152	0.4405±0.0164	0.4601±0.0196
D_AH_B	**2**[f]	DCC[g]	0.3427±0.0190	0.6468±0.0272	0.0105±0.0102
H_AD_B	**2**[h]	DCC[g]	0.2563±0.0042	0.7307±0.0089	0.0130±0.0037
D_AH_B	**2**[i]	Ac_2O[j]	0.3446±0.0142	0.6387±0.0202	0.0167±0.0116
H_AD_B	**2**[k]	Ac_2O[j]	0.1919±0.0047	0.7486±0.0158	0.0595±0.0113
D_AH_B	**2**[l]	ATFA[m]	0.4286±0.0215	0.5691±0.0257	0.0023±0.0076
H_AD_B	**2**[n]	ATFA[m]	0.2587±0.0125	0.7199±0.0150	0.0214±0.0071

[a]Analyses performed by mass spectrometry on Hitachi-Perkin-Elmer RMU-6E and Dupont 21-491 B mass spectrometers under electron impact conditions at 70 eV.
[b]See text for definitions of these isomers.
[c]For reactions leading to **2**, this column refers to the nature of the starting sulfoxide.
[d]Average ± standard deviation of 11 determinations.
[e]Average ± standard deviation of 8 determinations.
[f]Average ± standard deviation of 9 determinations.
[g]Experiment performed in anhydrous 1,2-dichloroethane.
[h]Average ± standard deviation of 10 determinations.
[i]Average ± standard deviation of 15 determinations.
[j]Experiment performed in purified Ac_2O at 114°C.
[k]Average ± standard deviation of 11 determinations.
[l]Average ± standard deviation of 7 determinations.
[m]Experiment performed in CH_2Cl_2 solvent.
[n]Average ± standard deviation of 9 determinations.

However, in our hands, this led more readily to the *levo*-enantiomer.

The optically active sulfoxide and each of the isotopically labelled sulfoxides were converted to **2** in parallel experiments conducted using the same reagents and solvents.

Results and Discussion

Table 1 shows the deuterium analyses of the D_AH_B and H_AD_B diastereomers of **1** and of the cyclized product **2** obtained from these diastereomers under three sets of experimental conditions: (*i*) DCC in 1,2-dichloroethane, initially at 0°C for 1 h, and then at room temperature; (*ii*) acetyl trifluoroacetate (ATFA) in methylene chloride at 0°C for 1.5 h; (*iii*) acetic anhydride solvent at 114°C for 2 h. The selectivities and deuterium isotope effects calculated (7) from these data are collected in Table 2.

In the work of Oae and Numata (1), a kinetic isotope effect (k_H/k_D) of 1.07 was observed in the cyclization of **8**, a result consistent with the formulation **8** → **9** as the *rate*-determining step of the reaction. The isotope effects listed in Table 2 refer to the *product*-determining step, and are compatible with an E2 process.

Conversion of the selectivities shown in the second column of Table 2 to the true selectivities shown in the third column was achieved in the following manner. Solution of the differential equations for the exchange sequence $H_AH_B \rightarrow (D_AH_B + H_AD_B) \rightarrow D_AD_B$, and substitution of the

TABLE 2. Diastereotopic selectivities and deuterium isotope effects in the conversion of **1** to **2**

Reagent	Apparent selectivity[a]	True selectivity[b]	Isotope effect
DCC	0.782±0.028[c]	0.729±0.028[d]	2.13±0.29[c]
ATFA	1.00 ±0.078[c]	1.00 ±0.078	1.55±0.087[c]
Ac_2O	0.939±0.098[c]	0.923±0.098	2.44±0.17[c]

[a]Refers to k_A/k_B; see text for definitions of the A and B sites.
[b]Calculated by interpolation in Table 3.
[c]Standard deviation based on 4 determinations.
[d]Corresponds to a 57.2% preference for the abstraction of H_B.

values of k_A, k_B, and J provided an estimate of the ratio $[D_AH_B]/[H_AD_B]$ as a function of time. Evaluation of this expression for t = 402 min, the time at which D_AH_B was isolated, gave $[D_AH_B]/$

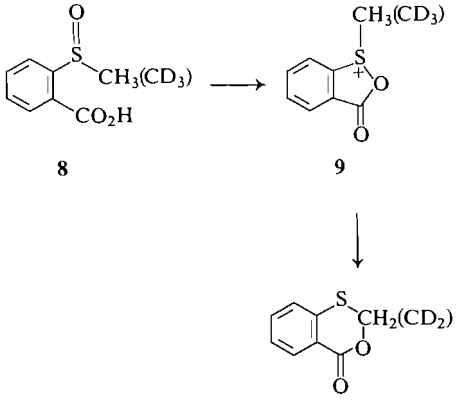

TABLE 3. Calculation of apparent selectivity as a function of true selectivity for a monodeuterated sample mixture containing 89% D_AH_B and 11% H_AD_B[a,b]

True selectivity (S')	Loss of deuterium[c]	Loss of hydrogen[c]	Apparent selectivity[d]
1.0	0.5000	0.5000	1.0000
0.9	0.4795	0.5205	0.9212
0.8	0.4567	0.5433	0.8405
0.7	0.4312	0.5688	0.7580
0.6	0.4025	0.5975	0.6736
0.5	0.3700	0.6300	0.5873
$10^{-\infty}$	0.1100	0.8900	0.1236

[a]Deuterium in this calculation is only a convenient label and the isotope effect is therefore taken to be 1.0.
[b]The relative proportions 0.89 and 0.11 were estimated from the solution of the differential equations (see text).
[c]The loss of deuterium and hydrogen were calculated by loss of deuterium $= S'/(1 + S')(0.89) + 1/(1 + S')(0.11)$ and loss of hydrogen $= 1/(1 + S')(0.89) + S'/(1 + S')(0.11)$.
[d]The apparent selectivity is the ratio of (loss of deuterium)/(loss o hydrogen).

$[H_AD_B] = 8.1$. Table 3 shows the apparent selectivity as a function of the true selectivity for a mixture of diastereomers having this composition. Interpolation in this table was used to obtain the true selectivities of Table 2.

The absence of selectivity in the case of ATFA as the Pummerer reagent is not surprising, since this reagent promotes rapid epimerization of sulfoxides (7). The same factor is responsible for the low selectivity observed with acetic anhydride (4, 7). For example, Stridsberg and Allenmark observed 31% racemization of optically active **1** after 3 min in acetic anhydride solvent at 100°C. In contrast, with DCC, we observed no racemization of optically active **1** after 1 h under the cyclization conditions.

The enantiomeric excesses predicted for **2** on the basis of the selectivity data of Table 2 are 15.7 ± 2% with DCC as the reagent and 4.0 ± 5% with Ac_2O as the reagent. When the standard deviation is taken into account, it can be seen that the direction of the lower selectivity observed under the latter conditions (and, therefore, whether the optically active **2** obtained from optically active **1** will have the same sign of rotation under the two sets of reaction conditions) cannot be determined by the present procedure.

The results of a number of experiments starting with the optically active sulfoxide are summarized in Table 4. In agreement with Stridsberg and Allenmark (4), DCC affords **2** having the opposite sign of rotation and Ac_2O affords **2** having the same sign of rotation as the sulfoxide; in addition, the selectivity is higher with DCC than with Ac_2O, in agreement with the earlier work and with the diastereotopic selectivity data. In the present work, the observed enantiomeric excesses are 23% with DCC and 5.7% with Ac_2O, under the conditions of the selectivity experiments. These various observations seem to be consistent with the view that the optical purity of the cyclized product is related to the diastereotopic selectivity exhibited in the deprotonation step.

The experiments with ^{18}O-labelled sulfoxide provide information concerning the question of whether the diastereotopic selectivity is itself determined by the mode of formation of **3**. The results of these experiments are summarized in Table 5. It is clear that both of the previously suggested sequences **1** → **5** → **3** and **1** → **6** → **3** are operative under both sets of reaction conditions. With Ac_2O as the reagent, the cyclized product retains less than 50% of the label and, with DCC as the reagent, more than 50% of the label. This indicates that the pathway via **5** is slightly preferred when the DCC conditions are employed, and the pathway via **6** is slightly preferred when the Ac_2O conditions are employed; **6** is also the intermediate in the competing racemization of **1** under the latter conditions (13). It is noteworthy that, with DCC, the preference for H_B (57.2%) and the retention of the sulfoxide oxygen (55.8%) are the same, within experimental error. Table 6 shows these data together with the optical activity data, expressed in the same manner.

In terms of the mechanistic proposals presented in the Introduction, the results of the ^2H, ^{18}O, and optical activity experiments permit the stereo-

TABLE 4. Asymmetric induction in the cyclization of optically active **1**

Reagent	Solvent	T (°C)	Reaction time (h)	$[\alpha]_D^{20}$ of product[a]	% optical purity[b]
Ac_2O	Ac_2O	130	1.0	−5.0[c]	3.4
Ac_2O	Ac_2O[d]	130	1.0	−2.0[c]	1.4
Ac_2O	Ac_2O	100	2.0	−3.0[e]	2.0
Ac_2O	Ac_2O	114	1.0	−8.8[e]	5.8
DCC	$ClCH_2CH_2Cl$[f]	25	38	+34.7[e]	22.9

[a]Determined at c 1.0 in ethanol
[b]Based on the literature determination of $[\alpha]_D^{25}$ ± 154.4 for optically pure **2** (4).
[c]The rotation of the starting sulfoxide was $[\alpha]_D^{20}$ −424 (c 0.5, EtOH) (94% optically pure (4)).
[d]The acetic anhydride was carefully purified to remove traces of acetic acid.
[e]The rotation of the starting sulfoxide was $[\alpha]_D^{20}$ −444 (c 0.5, EtOH) (98% optically pure).

TABLE 5. ^{18}O-retention in **2** prepared from **1** containing 12.82 ± 0.55% enrichment of the sulfoxide oxygen

Reagent	T (°C)	Reaction time (h)	^{18}O-content of **2**[a]	% retention of ^{18}O
Ac_2O	130	1.0	5.00±0.43	39.0±3.1
Ac_2O	130	0.5	3.97±0.42	31.3±3.5
Ac_2O	130	0.25	4.67±0.67	36.4±5.5
DCC	25	18.0	7.15±0.49[b]	55.8±4.5

[a]By mass spectral analysis of M^+.
[b]The dichloroethane solvent was carefully dried prior to reaction.

chemical course of the cyclization of **1** to **2** to be summarized as shown in Scheme 2. For a reaction initiated with *R*-**1**, the DCC conditions are predicted to lead to a preference for *R*-**2**, and the Ac_2O conditions are predicted to lead to a preference for *S*-**2**. We hope to report later concerning the absolute configurations of **1** and **2**.

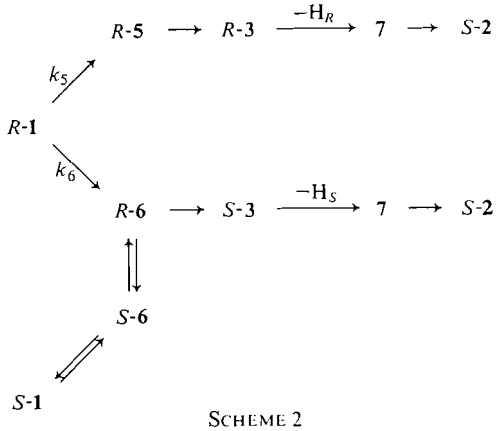

SCHEME 2

Experimental

General experimental methods and procedures have been described previously (6, 7). Optical rotations were measured on a Perkin Elmer 141 polarimeter. 1,2-Dichloroethane was dried by stirring over calcium hydride for 48 h at room temperature, followed by distillation under dry nitrogen; it was stored, under dry nitrogen, in a flask equipped with a serum cap.

Benzyl 2-Carboxyphenyl Sulfide

Thiosalicylic acid (10 g, 0.065 mol) was dissolved in 50% aqueous ethanol (40 mL) in a three-necked flask equipped with a mechanical stirrer, and sodium hydroxide pellets (5.2 g, 0.136 mol) were added. Benzyl chloride (8.2 mL, 0.071 mol) was then added dropwise to the light yellow solution over a period of 15 min. After one half of the benzyl chloride had been added, a white solid began to precipitate out of solution. This redissolved upon the addition of 50% ethanol (120 mL). The progress of the reaction was monitored by treating aliquots with potassium triiodide solution until the persistence of the purple colour indicated that all of the mercaptide had been consumed (3.5 h). After acidification with 3 *N* hydrochloric acid, extraction with methylene chloride and drying (sodium sulfate) yielded, after evaporation, a crystalline product. Recrystallization from hot ethanol afforded white needles (13.9 g, 88%), mp 187–188°C (lit. (1) mp 186–187°C); ^{1}Hmr ($CDCl_3$/DMSO-d_6 1:1) δ: 8.0–7.0 (9H, m), 4.13 (2H, s); ^{13}Cmr ($CDCl_3$/DMSO-d_6 1:1) δ: 167.6 (C=O), 141.7, 136.4, 132.1, 129.1, 128.4, 127.8, 127.1, 125.4, 123.7 (phenyls), 36.4 (PhCH_2); ir (KBr): 1660 (carboxyl) cm^{-1}.

Benzyl 2-Carboxyphenyl Sulfoxide

Benzyl 2-carboxyphenyl sulfide (10 g, 0.041 mol) was suspended in 50% aqueous pyridine (50 mL). Pyridinium perbromide (9.8 g, 0.041 mol) was added in one portion. The sulfide dissolved rapidly and the orange colour faded to a pale yellow (5 min). After cooling of the reaction mixture in ice, concentrated hydrochloric acid was added to bring the pH to 1. The pasty solution was extracted with methylene chloride (4 × 50 mL), and each organic extract was washed with copper(II) sulfate solution and with brine. To liberate the sulfoxide from the green copper complex, the combined methylene chloride extracts were treated with hydrogen sulfide and the black precipitate was removed by filtration through Celite. After evaporation of the solvent, the crude product was recrystallized from ethyl acetate to yield cubic crystals (4.12 g, 39%), mp 160–173°C (dec.) (lit. (1) mp 170°C (dec.)); ^{1}Hmr ($CDCl_3$/DMSO-d_6 1:1) δ: 7.4–8.5 (4H, m), 7.23 (5H, s), 4.38 (1H, d, 12), 3.75 (1H, d, 12); ^{13}Cmr ($CDCl_3$/DMSO-d_6 1:1) δ: 167.0 (C=O), 147.7, 132.9, 131.8, 130.9, 130.3, 128.0, 127.8, 124.6 (phenyls), 62.5 (PhCH_2); ir (KBr): 1680 (carboxyl), 1000 (sulfoxide) cm^{-1}.

Kinetics of Hydrogen–Deuterium Exchange in Benzyl 2-Carboxyphenyl Sulfoxide

Benzyl 2-carboxyphenyl sulfoxide (520 mg, 2 mmol) was dissolved in 1 *N* NaOD (5.0 mL). Sodium 2,2-dimethyl-2-silapentanesulfonate (50 mg) was added as an internal standard and the reaction mixture was kept at 30 ± 5°C. An aliquot was transferred to an nmr tube and kept at the same temperature. Periodically, the ^{1}Hmr sample was scanned. The results were evaluated by cutting and weighing.

Preparation of D_AH_B by Hydrogen–Deuterium Exchange of Benzyl 2-Carboxyphenyl Sulfoxide

Benzyl 2-carboxyphenyl sulfoxide (520 mg, 2 mmol) was dissolved in 1 *N* NaOD (5.0 mL) and DSS (50 mg) was added as an internal standard. The reaction mixture was warmed in a water bath at 31°C and an aliquot was examined by ^{1}Hmr. After 402 min, the product was isolated by addition of cold 2.5 *N* hydrochloric acid (5.0 mL) and immediate collection of the white crystalline product. This sample was recrystallized

TABLE 6. Diastereotopic selectivity, asymmetric induction, and ^{18}O-transfer in the conversion of **1** to **2**

Reagent	% optical purity	Diastereotopic selectivity	% ^{18}O-retention
DCC	22.9 (61.4±0.4)[a]	0.73±0.03 (57.8±1.0)	55.8±4.5
Ac_2O	5.7 (52.8±0.4)[b]	0.92±0.10 (52.0±3.0)	36.4±5.5

[a]Numbers in parentheses refer to the percent of the major enantiomer of 2 which corresponds to these data.
[b]The major enantiomers under the Ac_2O and DCC conditions have opposite absolute configurations.

from hot ethyl acetate (30 mL) to yield 453 mg (87%) of the D_AH_B diastereomer.

Preparation of D_AD_B by Hydrogen–Deuterium Exchange of Benzyl 2-Carboxyphenyl Sulfoxide

Benzyl 2-carboxyphenyl sulfoxide (520 mg, 2 mmol) was dissolved in 1 *N* sodium deuteroxide (5.0 mL) and DSS (50 mg) was added as an internal standard. The reaction mixture was warmed in a water bath at 30°C, and an aliquot was observed by ^{1}Hmr. After 4 days, the peaks corresponding to the benzyl AB quartet had completely disappeared. Addition of 2 *N* sulfuric acid (20 mL) allowed the isolation of a quantitative yield of D_AD_B.

Preparation of H_AD_B by Hydrogen–Deuterium Exchange of Benzyl 2-Carboxyphenyl Sulfoxide

Benzyl 2-carboxyphenyl sulfoxide (D_AD_B) (520 mg, 2 mmol) was dissolved in 1 *N* sodium hydroxide (5.0 mL). After warming to 30°C for 12 h, the sulfoxide was recovered by the addition of 2 *N* sulfuric acid (ca. 20 mL) and analyzed by ^{1}Hmr. The sample was subjected to another 4 h of exchange and then isolated in the same way. Recrystallization from ethyl acetate yielded 290 mg of H_AD_B (56%).

General Procedure for the Reaction of α-Deuteriobenzyl 2-Carboxyphenyl Sulfoxide (D_AH_B or H_AD_B) with Dicyclohexylcarbodiimide

Dicyclohexylcarbodiimide (103 mg, 0.5 mmol) was dissolved in 1,2-dichloroethane, and α-deuteriobenzyl 2-carboxyphenyl sulfoxide was added in one portion to the ice-cold solution. After stirring for 1 h, the crystalline sulfoxide had dissolved and amorphous dicyclohexyl urea had precipitated. After a further 17 h of stirring, 2 drops of acetic acid were added and the urea was collected (98.5 mg). The 2-phenyl-1,3-benzoxathian-6-one was purified by chromatography on silica gel ($CHCl_3$/pyridine 100:1). The deuterium content of the 2-phenyl-1,3-benzoxathian-6-one was analyzed by mass spectrometry.

General Procedure for the Reaction of α-Deuteriobenzyl 2-Carboxyphenyl Sulfoxide (D_AH_B or H_AD_B) with Acetyl Trifluoroacetate

α-Deuteriobenzyl 2-carboxyphenyl sulfoxide (110 mg, 0.42 mmol) was dissolved in dry methylene chloride, and acetyl trifluoroacetate (0.3 mL (1.5 *M*), 0.45 mmol) was added in one portion to the ice-cold methylene chloride solution. The sulfoxide dissolved in ca. 50 min. After 90 min, tlc ($CHCl_3$/pyridine 100:1) showed only 1 spot (R_f 0.50) corresponding to 2-phenyl-benzoxathian-6-one. The volatile components were evaporated and the resulting syrup was chromatographed on silica gel ($CHCl_3$/pyridine 100:1). The deuterium content of the product was analyzed by mass spectrometry.

General Procedure for the Reaction of α-Deuteriobenzyl 2-Carboxyphenyl Sulfoxide with Acetic Anhydride at 114°C

α-Deuteriobenzyl 2-carboxyphenyl sulfoxide (38 mg, 0.15 mmol) was suspended in acetic anhydride (0.5 mL) and heated to 114°C for 2 h. The acetic anhydride was removed in a desiccator over potassium hydroxide (50 Torr), and the product was purified by chromatography on silica gel ($CHCl_3$). The deuterium content of the 2-phenyl-1,3-benzoxathian-6-one was determined by mass spectrometry.

Synthesis of ^{18}O-labelled Benzyl 2-Carboxyphenyl Sulfoxide

Pyridinium perbromide (0.6362 g, 2.66 mmol) was added in one portion to a stirred suspension of benzyl 2-carboxyphenyl sulfide (0.6511 g, 2.66 mmol) in a mixture of $H_2{}^{18}O$ (0.5 mL, 12.678 at.% enriched) and pyridine (4.5 mL). The reaction mixture rapidly became homogeneous (2 min), and stirring was continued for an additional 6 min. Methylene chloride (15 mL) was then added and the resulting mixture was acidified to pH 1 with dilute hydrochloric acid. A reddish oil separated initially and redissolved with continued stirring. The organic layer was separated, washed with water (6 × 10 mL), and filtered to obtain a fine white precipitate. This was air dried and then dissolved in hot ethyl acetate (30 mL). The ethyl acetate solution was dried over anhydrous magnesium sulfate and then reduced in volume to 5 mL. Cooling to −15°C gave 272 mg of the sulfoxide as a white crystalline solid. Recrystallization from ethyl acetate at −15°C gave 204 mg of material; ir (KBr): 1000 (^{16}O-sulfoxide), 997, 963 cm^{-1}.

Reaction of ^{18}O-labelled Sulfoxide with Dicyclohexylcarbodiimide

The sulfoxide (0.0534 g, 0.205 mmol) was added in one portion to an ice-cold solution of DCC (0.0423 g, 0.205 mmol) in 1,2-dichloroethane (7 mL). The resulting heterogeneous solution was stirred at 0°C (ice-bath) for 1 h and then at room temperature for 53 h. The reaction was quenched with acetic acid (3 drops). Filtration, followed by removal of the solvent gave 0.0878 g of a white solid. This was dissolved in chloroform and purified by plc, using a 2 mm silica gel plate and three elutions with chloroform. The product was extracted from the plate with methylene chloride to give 39.7 mg (80%) of **2** as a white crystalline solid.

Reaction of ^{18}O-labelled Sulfoxide with Acetic Anhydride

A 0.1441 *M* solution of the sulfoxide (37.5 mg, 0.1441 mmol) in acetic anhydride (1.0 mL) was heated, under nitrogen, at 130°C for 15 min. The solvent was then removed in a desiccator under high vacuum to give a pale yellow solid. The residue was dissolved in ethyl acetate, and purified by plc on a 2 mm silica gel plate which was eluted with benzene. The product was extracted from the plate with ethyl acetate to give 31.0 mg (89%) of **2** as a white crystalline solid.

Resolution of Benzyl 2-Carboxyphenyl Sulfoxide

Racemic sulfoxide (2.86 g, 0.011 mol) and brucine (dihydrate; 4.74 g, 0.011 mol) were dissolved together in boiling ethyl acetate – acetone (6:1) (118 mL). The solution was left at room temperature for 24 h and the crystalline salt (3.75 g) was isolated. The salt was treated with 100 mL of boiling ethyl acetate and, after cooling to room temperature, was filtered and dried (2.87 g). A small quantity of this salt was converted to the acid, which showed $[\alpha]_D^{26}$ −414.1 (*c* 0.5, EtOH). This ethyl acetate extraction was repeated, using 33 mL of boiling ethyl acetate, to yield 2.70 g of salt. The brucine salt was dissolved in methylene chloride (200 mL), and water (100 mL) and dilute hydrochloric acid were added to give the aqueous layer a pH of 2. The organic layer was separated, extracted with water (2 × 100 mL), filtered, and evaporated to give 1.37 g of sulfoxide. Recrystallization from boiling ethyl acetate gave 1.31 g of sulfoxide, $[\alpha]_D^{25}$ −358 (EtOH), which contained a trace of brucine (^{1}Hmr). The sulfoxide was, therefore, redissolved in methylene chloride (250 mL) and extracted with 1 *N* HCl (2 × 100 mL) and water (2 × 100 mL). The organic layer was separated, filtered and evaporated to give 0.79 g of material. Recrystallization from hot ethanol gave 0.60 g of sulfoxide having $[\alpha]_D^{25}$ −421.7 (EtOH), which still contained some brucine (^{1}Hmr). The material was suspended in water (50 mL), and sufficient sodium bicarbonate was added to bring the sulfoxide into solution. The solution was extracted with ether (2 × 50 mL) and acidified to pH 1 with 3 *N* HCl. The white precipitate was collected and extracted with methylene chloride (300 mL). This extract was dried over anhydrous magnesium sulfate and evaporated to give 0.58 g of sulfoxide. Recrystallization from hot ethanol

gave 0.45 g of material, mp 159.0–160.0°C; $[\alpha]_D^{21}$ −444 (EtOH).

Acknowledgements

We thank the National Research Council of Canada for financial support of this research, for the award of a 1967 Science Scholarship, and for the award of a Postdoctoral Fellowship. All mass spectral determinations were performed at the Dupont Research Centre, Kingston; we are most grateful to Dr. Peter Sipos and Mr. Peter Gordon for their cooperation.

1. S. OAE and T. NUMATA. Tetrahedron, **30**, 2641 (1974).
2. B. STRIDSBERG and S. ALLENMARK. Acta Chem. Scand. Ser. B, **28**, 591 (1974).
3. S. OAE and T. NUMATA. *In* Isotopes in organic chemistry. Vol. 5. *Edited by* E. Buncel and C. C. Lee. Elsevier, Amsterdam. 1979. In press.
4. B. STRIDSBERG and S. ALLENMARK. Acta Chem. Scand. Ser. B, **30**, 219 (1976).
5. K. E. PFITZNER and J. G. MOFFATT. J. Am. Chem. Soc. **85**, 3027 (1963); A. H. FENSELAU and J. G. MOFFATT. J. Am. Chem. Soc. **88**, 1762 (1966).
6. S. WOLFE and P. M. KAZMAIER. Can. J. Chem. This issue.
7. S. WOLFE and P. M. KAZMAIER. Can. J. Chem. This issue.
8. F. BERNARDI, H. B. SCHLEGEL, M.-H. WHANGBO, and S. WOLFE. J. Am. Chem. Soc. **99**, 5633 (1977).
9. F. BERNARDI, I. G. CSIZMADIA, H. B. SCHLEGEL, and S. WOLFE. Can. J. Chem. **53**, 1144 (1975).
10. J. I. SEEMAN and W. A. FARONE. J. Org. Chem. **43**, 1854 (1978).
11. A. RAUK, E. BUNCEL, R. Y. MOIR, and S. WOLFE. J. Am. Chem. Soc. **87**, 5498 (1965).
12. T. F. GARRARD. MSc. Thesis, Queen's University, Kingston, Ont. 1974.
13. S. OAE. Q. Rep. Sulfur Chem. **5**, 53 (1970).

Cyclization of cysteinylglycine sulfoxides under Pummerer reaction conditions

SAUL WOLFE, PETER MICHAEL KAZMAIER, AND HILLAR AUKSI
Department of Chemistry, Queen's University, Kingston, Ont., Canada K7L 3N6

Received December 28, 1978

SAUL WOLFE, PETER MICHAEL KAZMAIER, and HILLAR AUKSI. Can. J. Chem. **57**, 2412 (1979).

A number of sulfoxides derived from 3-benzylthiopropionic acid, *S*-benzylcysteine, and *S*-phenylcystelne have been synthesized and exposed to typical Pummerer reaction conditions. Cyclization of the *S*-benzyl sulfoxides to six-membered or seven-membered heterocyclic rings (1,3-thiazin-4-ones and 1,3,6-oxathiazepines) is observed only in acetic anhydride solvent and only after conversion of the carboxyl group to an amide or peptide. Cyclization of *S*-phenylcysteinyl amides to β-lactams could not be achieved. The thiazolidine isomers of the six- and seven-membered rIngs have been synthesized and found not to be intermediates in the acetic anhydride reactions. The thiazolidines do rearrange to the six- and (or) seven-membered rings in anhydrous trifluoroacetic acid solvent. *S*-Benzylphthalimidocysteinylglycine sulfoxide, a 3:2 mixture of epimers at sulfur, affords a 3:2 mixture of isomeric thiazinones. A mechanism for these cyclizations is proposed, and it is suggested that the configuration at sulfur controls the configuration at the new asymmetric centre in the product.

SAUL WOLFE, PETER MICHAEL KAZMAIER et HILLAR AUKSI. Can. J. Chem. **57**, 2412 (1979).

On a synthétisé un certain nombre de sulfoxydes provenant de l'acide benzylthio-3 propionique, de la *S*-benzylcystéine et de la *S*-phénylcystéine et on les a soumis à des conditions typiques de la réaction de Pummerer. On a observé la cyclisation des *S*-benzylsulfoxydes en hétérocycles à six- ou sept-chaînons (thiazine-1,3 ones-4 et oxathiazépines-1,3,6) que lorsque l'on utilise l'anhydride acétique comme solvant et seulement après avoir transformé le groupe carboxyle en amide ou en peptide. On n'a pas pu effectuer la cyclisation des *S*-phénylcystéinylamides en β-lactames. On a synthétisé les isomères thiazolidines des hétérocycles à six et sept chaînons et on a trouvé qu'ils n'étaient pas des intermédiaires lors des réactions dans l'anhydride acétique. Les thiazolidines se transposent en hétérocycles à six et sept chaînons par traitement dans de l'acide trifluoroacétique anhydre comme solvant. Le sulfoxyde de la *S*-benzylphtalimidocystéinylglycine sous forme d'un mélange 3:2 d'épimères au niveau du soufre fournit un mélange 3:2 de thiazinones isomères. On propose un mécanisme pour ces cyclisations et on suggère que la configuration au niveau du soufre contrôle la configuration du nouveau centre asymétrique dans le produit.

[Traduit par le journal]

There are a number of reports in the literature concerning the synthesis of heterocyclic compounds by intramolecular capture of the α-thiocarbonium ion intermediate of the Pummerer reaction (eq. [1])

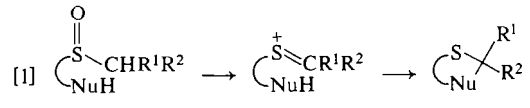

[1]

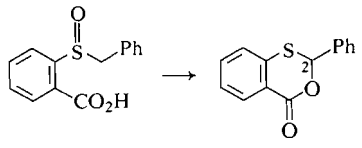

1 2

(1). A particularly interesting example is the conversion of benzyl 2-carboxyphenyl sulfoxide (**1**) to 2-phenyl-1,3-benzoxathian-6-one (**2**) (2, 3), which proceeds (2) with asymmetric induction. In connection with some other investigations in progress in this laboratory (4), we wished to know whether the latter reaction could be extended to more complex sulfoxides carrying a neighbouring carboxyl or carboxyl-derived functional group. This paper describes some preliminary results of a detailed investigation of the effects of structure and reaction conditions upon the dehydrative cyclization of a number of sulfoxides derived from cysteine and 3-mercaptopropionic acid.

The series of 19 sulfides **3***a*–**3***s* listed in Table 1 was synthesized via the appropriate Schemes 1–3, and 15 of these sulfides were converted to the sulfoxides **4***a*–**4***o*, shown in Table 2. The conversion **3** → **4** was achieved using one of the following procedures, as appropriate: (*A*) hydrogen peroxide in methanol; (*B*) hydrogen peroxide in acetone; (*C*) sodium *meta*-periodate; (*D*) *m*-chloroperbenzoic acid in chloroform or methylene chloride; (*E*) hydrogen peroxide in acetic acid.

The initial experiments were performed using *S*-benzyl-L-cysteine sulfoxide (**4***h*) as the substrate, and were uniformly unsuccessful. As can be seen from

0008-4042/79/182412-14$01.00/0

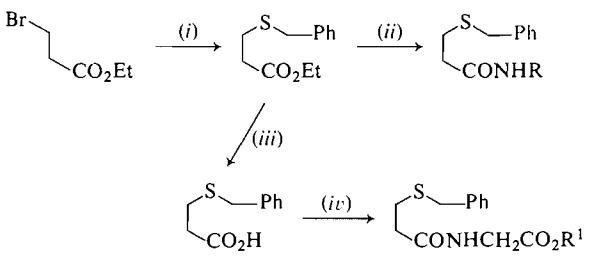

SCHEME 1
Reagents: (*i*) $PhCH_2SNa$, EtOH; (*ii*) RNH_2; (*iii*) KOH, EtOH; (*iv*) $H_2NCH_2CO_2R^1$, DCC.

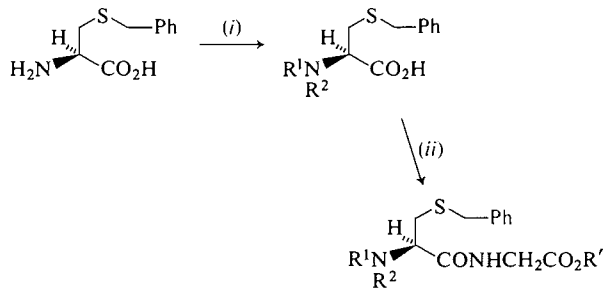

SCHEME 2
Reagents: (*i*) Ac_2O or PhCOCl or *o*-$C_6H_4(CO)_2NCO_2Et$; (*ii*) $H_2NCH_2CO_2Et$, EEDQ.

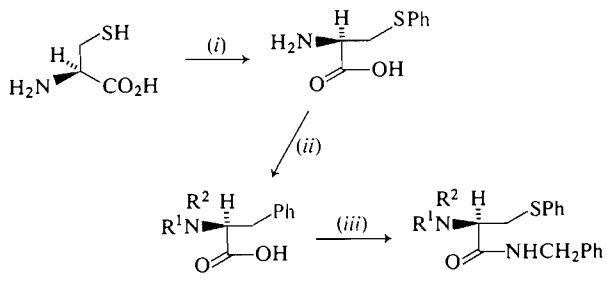

SCHEME 3
Reagents: (*i*) PhN_2^+, CuCl, (*ii*) Ac_2O or PhCOCl or *o*-$C_6H_4(CO)_2NCO_2Et$; (*iii*) $PhCH_2NH_2$, EEDQ.

the observations collected in Table 3, none of the reaction conditions and reagents known to be effective for inter- and intramolecular Pummerer reactions (2–4) leads to the cyclic compound **6**.

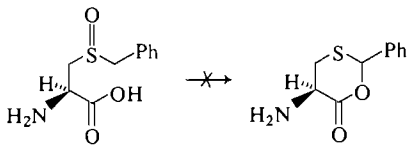

4*h* **6**

However, **4***h* differs from **1** as the substrate for an intramolecular Pummerer reaction in three important respects: (*i*) the presence of an amino group; (*ii*) the presence of a C—H bond beta to the sulfoxide; (*iii*) the absence of the conformational constraint imposed by the benzene ring. Clearly, the role of these structural variables required detailed examination under standard reaction conditions.

For the determination of the most appropriate reaction conditions, the cyclization **1** → **2** was re-examined, using acetic anhydride (Ac_2O), trifluoroacetic anhydride (TFAA), and acetyl trifluoroacetate (ATFA) as the dehydrating agents. The results of these experiments are shown in Table 4. The reactivities of the three anhydrides in the Pummerer reaction are TFAA > ATFA > Ac_2O (4*a*), but only in the latter case does the formation of **2** proceed cleanly. Therefore, acetic anhydride was selected as the reagent for all subsequent work.

The sulfoxide **4***a*, like **4***h*, afforded no cyclic product. Attention was next focused upon the effect of derivatization of the carboxyl group, and it was

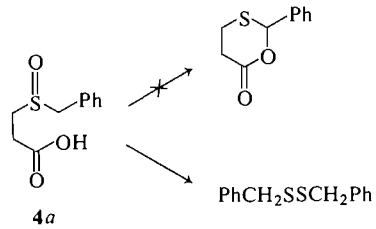

4*a*

found (cf. ref. 8) that cyclization to a perhydro-2-phenyl-1,3-*thiazin*-4-one (**8**) occurs when the carboxyl group of **4***a* is converted to a carboxamido derivative and the product (**4***c*, **4***d*, **4***e*, **4***f*) exposed to acetic anhydride. The results obtained in the cyclizations of **4***c*–**4***f* to **8** (R = H, CH_3, *n*-C_4H_9, CH_2CO_2Et) are collected in Table 5.

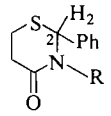

8

Following these observations, the reactions of cysteine derivatives with acetic anhydride were re-examined, this time after conversion to the glycyl peptides **4***k*–**4***m*. As can be seen in Table 6, the establishment of experimental conditions for the dehydrative cyclization of **4***k* required considerable effort. The product of this reaction, assigned the oxathiazepine structure **9***a*, was formed only in acetic anhydride solvent, and only in the temperature range 75–80°C. The same conditions were then used to prepare the benzamido analog **9***b* from **4***l*. However, the phthalimido compound **4***m* afforded a different skeleton, which is assigned the *thiazinone*

TABLE 1. Experimental data for substituted 3-mercaptopropionic acids

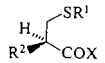

3

Compound	R^1	R^{2a}	X	Melting point (°C) Found	Melting point (°C) Reported	Ref.
a	$PhCH_2$	H	OEt	[b]	[b]	5
b	$PhCH_2$	H	OH	80–81	80–82	6
c	$PhCH_2$	H	NH_2	114–115	110–111	7
d	$PhCH_2$	H	$NHCH_3$	[c]	[c]	8
e	$PhCH_2$	H	$NH(CH_2)_3CH_3$	41–56	—	[d]
f	$PhCH_2$	H	$NHCH_2CO_2Et$	[c]	—	[d]
g	$PhCH_2$	H	$NHCH_2CO_2CHPh_2$	[c]	—	[d]
h	$PhCH_2$	AcNH	OH	143.5–147	[e]	9–11
i	$PhCH_2$	AcNH	$NHCH_2CO_2Et$	108–109	116.5–117.5	11
j	$PhCH_2$	PhCONH	OH	100–106	118–119	12
k	$PhCH_2$	PhCONH	$NHCH_2CO_2Et$	112–113	—	[d]
l	$PhCH_2$	Ft[f]	OH	[c]	—	[g]
m	$PhCH_2$	Ft[f]	$NHCH_2CO_2Et$	109–112	—	[h]
n	$PhCH_2$	$PhCH_2OCONH$	OH	92–93	93–94	13
o	Ph	NH_2	OH	162–165 (dec.)	170–172 (dec.)	14
p	Ph	AcNH	OH	127–129	142–143	14
q	Ph	AcNH	$NHCH_2Ph$	170–172	—	[i]
r	Ph	Ft[f]	OH	[c]	—	[d]
s	Ph	Ft[f]	$NHCH_2Ph$	131	—	[d]

[a]The configurations of all amino acids are L.
[b]Boiling point 134–136°C/0.23 Torr (reported 101–103°C/0.22 Torr).
[c]This compound was isolated as a syrup.
[d]This compound was characterized on the basis of spectroscopic evidence and by conversion to the sulfoxide.
[e]For this compound $[\alpha]_D^{26}$ −41.5 (*c* 1.0, 95% EtOH) (9).
[f]Ft represents phthalimido.
[g]This compound was characterized on the basis of the spectroscopic evidence and conversion to 3*m*.
[h]*Anal.* calcd. for $C_{22}H_{22}N_2O_5S$: C 61.95, H 5.20; found: C 62.00, H 5.16.
[i]*Anal.* calcd. for $C_{18}H_{20}N_2O_2S$: C 65.82, H 6.14; found: C 65.87, H 6.37.

structure **10***a*. This product was formed as a 3:2 mixture of stereoisomers. Close examination of the reaction conditions for the cyclizations of **4***l* and **4***m* revealed that, in the conversion **4***l* → **9***b*, the sulfoxide is consumed after 3 h *at 78–79°C*, but the conversion of **4***m* to **10***a* required more than 6 h at this temperature; longer reaction times could not be investigated because of decomposition of **10***a*.

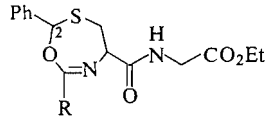

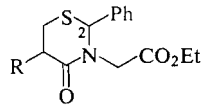

9*a* R = CH_3 (59% yield) **10***a* R = phthalimido (31% yield)
9*b* R = C_6H_5 (42% yield) **10***b* R = PhCONH

These observations are consistent with the general mechanism presented in Scheme 4, adapted from that proposed for the cyclization of **1** to **2** (2–4), in which the initial intermediate is the acetoxysulfonium cation **11**. With acetamido or benzamido substituents, this intermediate can be converted either to the six-membered cyclic oxysulfonium cation **12** or the five-membered cyclic oxysulfonium cation **13**. Only **13** is possible in the case of the phthalimido compound. Proton loss from **12** leads to the zwitterion **14**, which can cyclize by C—O bond formation to form an oxathiazepine (**9**), or by C—N bond formation to form a thiazolidine (**15**). Proton loss from **13** leads to the zwitterion **16**, which can cyclize to a thiazinone (**10**) or an imidate (**17**). The nature of the products and also the reaction times indicate that the six-membered ring **12** is formed more readily than the five-membered ring **13**.

The assignment of structure **10***a* to the dehydration product of **4***m* is based upon two features of its ^{1}Hmr spectrum and on detailed analysis of its high resolution mass spectrum. The ^{1}Hmr spectrum showed the H2 protons of the two stereoisomers at δ 6.03 and 5.63 ppm. These values can be compared to the H2 chemical shifts of the series of compounds **8**, which fall in the range 5.43–5.68δ. In compound **2**, which has a C—O bond, H2 appears at 6.53δ, and in compound **18** (4*a*), the tertiary proton appears at 6.95δ. The ^{1}Hmr spectrum of **10***a* also showed a large chemical shift difference between the diastereotopic methylene protons of the glycyl moiety (Δν = 1.94 and 0.94 ppm for the two isomers; J = 17 Hz in both cases). A similar non-equivalence was ob-

TABLE 2. Experimental data for substituted 3-mercaptopropionic acid sulfoxides

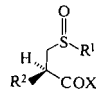

4

Compound	R^1	R^{2a}	X	Method of synthesis[b]	Yield (%)	Infrared (S=O) (cm^{-1})	Melting point (°C) Found	Reported	Ref.
a	$PhCH_2$	H	OH	*E*	27	982	147	—	[c]
b	$PhCH_2$	H	OEt	*E*	86	1018	62–63	—	[d]
c	$PhCH_2$	H	NH_2	*A*	52	1025	127–131	—	[e]
d	$PhCH_2$	H	$NHCH_3$	*B*	43	1015	134–135	138–140	8
e	$PhCH_2$	H	$NH(CH_2)_3CH_3$	*A*	63	1025	130 (dec.)	—	[f]
f	$PhCH_2$	H	$NHCH_2CO_2Et$	*A*	60	1020	91–97	—	[e]
g	$PhCH_2$	H	$NHCH_2CO_2CHPh_2$	*A*	84	1020	152–153 (dec.)	—	[g]
h	$PhCH_2$	NH_2	OH	*E*	81	1010	171–174 (dec.)	163–165	15
i	$PhCH_2$	AcNH	OH	*C*	85	1025	169–170 (dec.)	—	[f]
j	$PhCH_2$	Ft[h]	OH	*C*	95	—	88–96 (dec.)	—	[f]
k	$PhCH_2$	AcNH	$NHCH_2CO_2Et$	*A*	77	1025	148 (dec.)	—	[e]
l	$PhCH_2$	PhCONH	$NHCH_2CO_2Et$	*A*	82	1030	156–157 (dec.)	—	[e]
m	$PhCH_2$	Ft[h]	$NHCH_2CO_2Et$	*A*	76	1020	[i]	—	[e]
n	Ph	AcNH	$NHCH_2Ph$	*D*	100	1032	130–134 (dec.)	—	[e]
o	Ph	Ft[h]	$NHCH_2Ph$	*D*	100	1030	[i]	—	[e]

[a]The configurations of all amino acid derivatives are L.
[b]See text.
[c]*Anal.* calcd. for $C_{10}H_{12}O_3S$: C 56.59, H 5.70; found: C 55.79, H 6.23.
[d]*Anal.* calcd. for $C_{12}H_{16}O_3S$: C 60.00, H 6.71; found: C 60.37, H 7.03.
[e]Structural assignment is based on spectroscopic evidence.
[f]Satisfactory elemental analyses could not be obtained for these compounds.
[g]*Anal.* calcd. for $C_{25}H_{25}NO_4S$: C 68.94, H 5.79; found: C 68.78, H 5.97.
[h]Ft represents phthalimido.
[i]This compound was isolated as a syrup.

TABLE 3. Behaviour of *S*-benzyl-L-cysteine sulfoxide under Pummerer reaction conditions

Reagent	Solvent[a,b]	*T* (°C)	Product(s) (% yield)
Pyrolysis	None	180	$PhCH_2SSCH_2Ph$ (44)
TFAA[c]	CH_2Cl_2	3	$PhCH_2SSCH_2Ph$ (9)[d]
ATFA[e]	ATFA	28	[f]
DCC	CH_2Cl_2	28	[g] (100)
DCC–pyridine–TFA	CH_2Cl_2	28	[g] (93) + **5**[j] (30)
DCC–TFA	CH_2Cl_2	28	[g] (90) + **5**[j] (14)
DCC–TFA[h]	CH_2Cl_2	28	[g] (90) + **5**[j] (14)
TsOH	Benzene	80	[g] (100)
$SOCl_2$	CH_2Cl_2	28	[i]

[a]A concentration of 1.32 *M* was used, unless stated otherwise.
[b]One equivalent of reagent was added, unless stated otherwise.
[c]Five equivalents of trifluoroacetic anhydride were used.
[d]Benzaldehyde was also produced, but was not isolated.
[e]Acetyl trifluoroacetate was used in excess.
[f]No 2,4-dinitrophenylhydrazine-active products were present.
[g]Recovered starting material.
[h]Inverse addition, i.e., DCC added to sulfoxide and TFA.
[i]Benzaldehyde was isolated as its 2,4-dinitrophenylhydrazone.
[j]

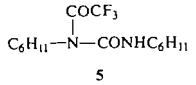

5

TABLE 4. Cyclization of benzyl 2-carboxyphenyl sulfoxide with various anhydrides

Anhydride	*T* (°C)	Solvent	Product(s) (% yield*)
Ac_2O	130	Ac_2O	**2** (92)
ATFA	4	CH_2Cl_2	**2** (73)+**1** (25)
TFAA	4	CH_2Cl_2	**2** (41)+7† (58)

*Isolated yield.
†

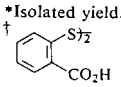

7

served in the ^{1}Hmr spectrum of **8** (R = CH_2CO_2Et) ($\Delta\nu$ = 1.37 ppm; J = 18 Hz).

The mass spectrum of **10***a* (see **19**) showed, in addition to M^+ (9.17%) (calcd. for $C_{22}H_{20}N_2O_5S$: 424.1093; found: 424.1097), peaks corresponding to fragmentation A (100%) (calcd. for $M - CH_2CO_2Et$: 337.0647; found: 337.0655), fragmentation B (26.87%) (calcd. for $C_6H_4(CO)_2NCH{=}CH_2$: 173.0477; found: 173.0482), and fragmentation C (20.73%) (calcd. for $C_6H_5C{=}S$: 121.0112; found: 121.0109).

That the cyclizations of **4***k* and **4***l* had proceeded in a different manner was immediately evident from the ^{1}Hmr spectra of **9***a* and **9***b*, and was confirmed by the high resolution mass spectra. In these compounds, H2 appeared at 6.10 and 6.18δ, but the glycyl methylene protons were found to be isochronous, and coupled to an adjacent NH proton. The mass spectrum of **9***a* (see **20**) showed, in addition to the molecular ion (2.90%) (calcd. for $C_{16}H_{20}N_2O_4S$: 336.1144; found: 336.1144), peaks corresponding to

TABLE 5. Cyclization of 3-benzylsulfinylpropionamides to perhydro-2-phenyl-1,3-thiazin-4-ones in acetic anhydride

Sulfoxide	T (°C)	Isolated yield (%)	^{1}Hmr[a]	^{13}Cmr[b]	Melting point (°C) Found	Reported	Ref.
4*c*	110	24[c]	6.88	57.2	[d]	—	[e]
4*d*	120	62	5.43	64.1	96	95–97	8
4*e*	114	28	5.52	61.9	[d]	—	[e]
4*f*	110	53	5.68	63.7	[d]	—	[e]

[a]Refers to H2.
[b]Refers to C2.
[c]The nitrogen atom was acetylated under the reaction conditions.
[d]Isolated as a syrup.
[e]Structure was assigned on the basis of the spectroscopic data.

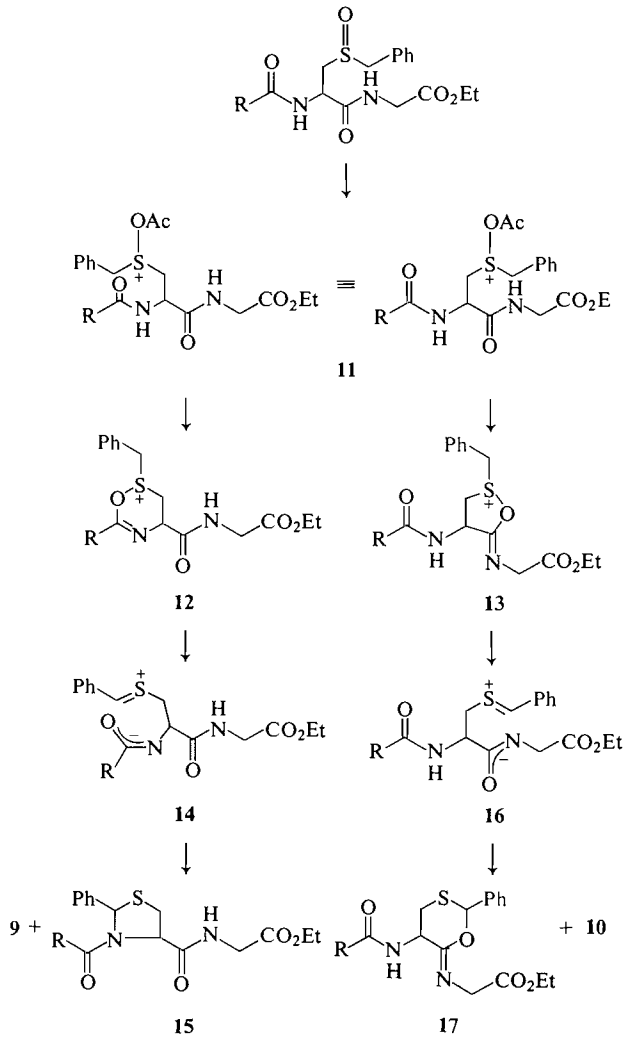

SCHEME 4
Mechanism proposed for the cyclizations of **4***k*–**4***m*.

fragmentation A (65.89%) (calcd. for C_9H_9NOS: 179.0405; found: 179.0405) and fragmentation B (17.59%) (calcd. for C_7H_5S: 121.0106; found: 121.0109). The mass spectrum of **9***b* (see **21**) also showed the molecular ion (0.80%) (calcd. for C_{21}-

TABLE 6. Attempted cyclization of 1 *M* solutions of *N*-acetyl-*S*-benzyl-L-cysteinylglycine-*S*-oxide (ethyl ester) under a variety of Pummerer conditions

Reagent	Solvent	T (°C)	Time[a]	Cyclization
ATFA	Ac_2O	25	8 min	–
Ac_2O[b]	Benzene	80	24 h	–
Ac_2O[b]	EtOAc	80	24 h	–
Ac_2O[b]	CH_3CN	80	24 h	–
Ac_2O[b]	EtOAc	Variable[c]	96 h	–
Ac_2O	Ac_2O	120	10 min	–
Ac_2O	Ac_2O	90	15 min	–
Ac_2O	Ac_2O	80	1 h	+
Ac_2O	Ac_2O	75	1 h	+
Ac_2O	Ac_2O	25	96 h	–

[a]The reaction was followed by tlc until the starting material had disappeared.
[b]Six equivalents of acetic anhydride were added.
[c]The temperature was increased gradually from 25–80°C.

$H_{22}N_2O_4S$: 398.1293; found: 398.1297) and the same two fragmentations as **9***a* (fragmentation A (100%): calcd. for $C_{14}H_{11}NOS$: 241.0567; found: 241.0564; fragmentation B (40.19%): found: 121.0122). Additional peaks identified in the mass

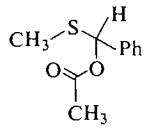

18

spectrum of **9***b* correspond to fragmentation C (18.90%) (calcd. for $C_{16}H_{14}NOS$: 268.0776; found: 268.0786) and fragmentation B + C (40.19%) (calcd. for C_9H_8NO: 146.0620; found: 146.0613).

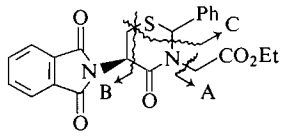

19

The ^{1}Hmr and mass spectral data just presented do not distinguish unequivocally between the thiazolidine structures **15** and the oxathiazepine structures **9**, and it was necessary, therefore, to

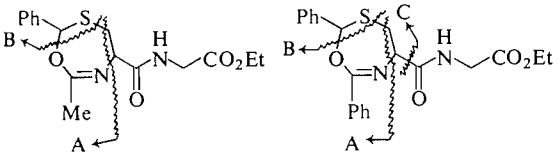

20 21

synthesize **15** (R = Me, Ph) by an alternative route for comparison with the products of the Pummerer reactions. The required thiazolidines were obtained by *N*-acylation of 2-phenylthiazolidine-4*R*-carboxylic acid (**22**) (16), followed by coupling with the ethyl ester of glycine. The non-identity of **9***a* and **15** (R = Me), and of **9***b* and **15** (R = Ph), was clearly evident from the different nmr, ir, and mass spectra, the different tlc behaviour, and from melting point and mixture melting point determinations of the pairs of isomers.

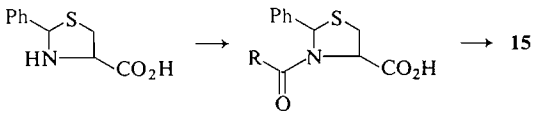

22 23

The thiazolidines **15** were stable to the Pummerer reaction conditions (Ac_2O, 79–80°C, 3 h). Consequently, these compounds cannot be intermediates in the Pummerer reactions. However, in anhydrous trifluoroacetic acid, the thiazolidines underwent rapid isomerization. The acetyl compound (**15**; R = Me) rearranged to **9***a*, identical in all respects to the material already described. The benzoyl compound (**15**; R = Ph) was converted to the *thiazinone* **10***b*. The ^{1}Hmr spectrum of **10***b* showed the characteristic large non-equivalence of the glycyl methylene protons ($\Delta\nu$ = 1.08 ppm; J = 17 Hz), and the mass spectrum (see **24**) showed the fragmentations indicated in A, B, and C.

Each of the five-membered, six-membered, and seven-membered heterocyclic rings of the present work has two asymmetric centres, so that two stereoisomers can exist in each case (cf. refs. 17, 18). A consideration of the configurations of **9**, **10**, and **15** is reserved for a subsequent publication (19). However, some comment concerning the formation of **10***a* as a 3:2 mixture of isomers seems pertinent at this point, since **4***m*, the sulfoxide precursor of **10***a*, was also found to have been formed as a 3:2 mixture of epimers at sulfur (based on integration of the phenyl region of the ^{1}Hmr spectrum). In terms of the mechanism presented in Scheme 4 and the stereochemical investigations of ref. 4, it is presently considered that **13** is formed from **11** with inversion of configuration at sulfur, that the transformation of **13** to **16** is an E2 elimination, which proceeds with stereospecific removal of one of the diastereotopic benzylic protons, and that the cyclization of **16** to **10***a* then leads to a single C2 epimer. It is noteworthy that only one epimer of **4***k* and **4***l* was apparently produced in the oxidations of each of the sulfides **3***i* and **3***k*, respectively, and only one epimer of **9***a* and **9***b* was detected in the Pummerer reactions of these sulfoxides. Attempts to secure a single epimer of **4***m* have not yet succeeded.

Finally, with the successful establishment of conditions for the cyclization of cysteinylglycine peptides to six- and seven-membered rings, a number of attempts were made to extend the reaction to the synthesis of β-lactams. For this purpose, the *S*-phenylcysteinylglycine sulfoxides **4***n* and **4***o* were prepared and subjected to the various reaction conditions summarized in Table 7. No evidence was obtained for the formation of **25** under these conditions. It seems probable, in any event, that the conditions required to form a β-lactam from **4***n* and **4***o* would also lead to rapid destruction of the product (20). To check this point, the methyl ester of phenylpenicillin was heated in acetic anhydride at

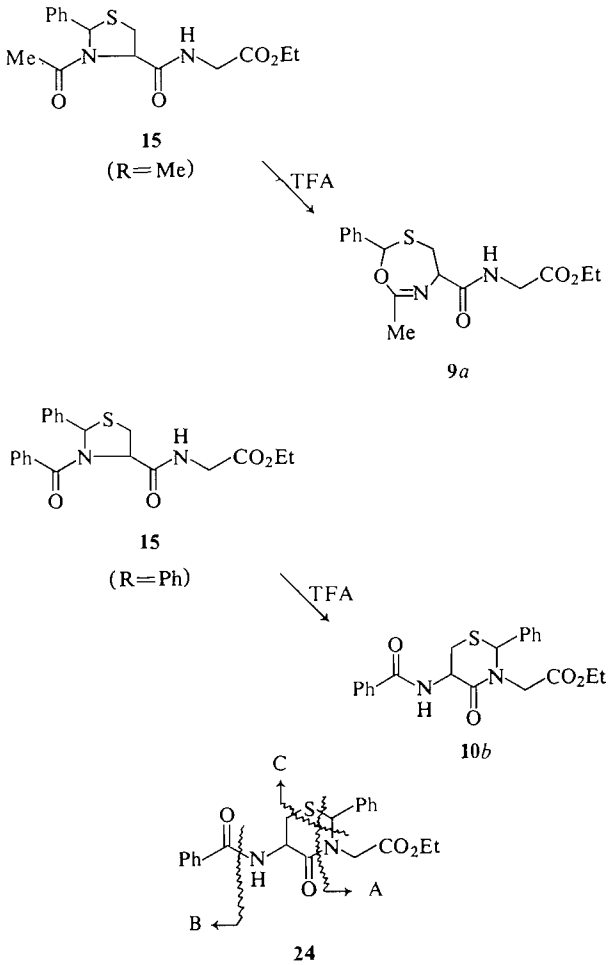

15 (R=Me) TFA 9*a*

15 (R=Ph) TFA 10*b*

24

TABLE 7. Attempted cyclization of **4***n* and **4***o* to β-lactams

Compound	Electrophile[a]	Solvent	*T* (°C)	Time[b]	Cyclization[c]
4*n*	Ac_2O	$CDCl_3$	100	3 h	No
4*n*	Ac_2O	$CDCl_3$	Variable[d]	30 h	No
4*n*	$Ac_2O/ClCH_2COOH$	$CDCl_3$	63	6 h	No
4*n*	TFAA	CH_2Cl_2	2	7 min	No
4*o*	Ac_2O	Ac_2O	75	20 min	No

[a]Acetic anhydride was used as cosolvent.
[b]Time for complete disappearance of the starting material.
[c]As judged by the absence of peaks in the 4.0–6.5δ region and C=O stretch at ca. 1780–1800 cm^{-1}.
[d]Temperature was varied from 25–65°C.

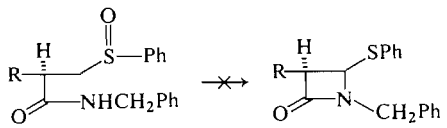

4*n* R = AcNH
4*o* R = phthalimido

25

80°C for 1.5 h. The β-lactam ring did not survive these conditions.

Experimental

General methods employed in this work have been described in refs. 4*a–c*. High resolution mass spectra were obtained on an AEI-MS 3074/DS 50 instrument.

Ethyl 3-Benzylthiopropionate (3a)

A solution of sodium metal (3.92 g, 0.170 g-atom) in absolute ethanol (50 mL) was treated dropwise at room temperature with benzyl mercaptan (20.0 mL, 0.170 mol) and then with ethyl 3-bromopropionate (21.2 mL, 0.170 mol). When thin-layer chromatography indicated that the reaction was complete (2 h), water (50 mL) was added and the product extracted with methylene chloride (4 × 50 mL). After flash evaporation, the product was distilled under high vacuum (bp 134–136°C/0.23 Torr, lit. (5) bp 101–103°C/0.22 Torr) to yield ethyl 3-benzylthiopropionate (32.5 g, 87%); ^{1}Hmr ($CDCl_3$)δ: 7.28 (5H, s), 4.12 (2H, q, 7), 3.72 (2H, s), 2.62 (4H, m), 1.25 (3H, t, 7); ir(NaCl film): 1730 (ester) cm^{-1}.

3-Benzylthiopropionic Acid (3b)

Ethyl 3-benzylthiopropionate (2.37 g, 10.5 mmol) was cooled to 4°C and potassium hydroxide in 95% ethanol (22 mL of 0.494 *M*, 10.8 mmol) was added. The reaction mixture was stirred at 4°C (4 h) and then at 25°C (12 h). The reaction mixture was acidified to pH 1.5 with 2.5 *N* hydrochloric acid and extracted with methylene chloride (5 × 20 mL). After drying over sodium sulfate, evaporation of the methylene chloride extract yielded a crystalline solid which, on recrystallization from ethyl acetate – petroleum ether, produced colourless needles (1.44 g, 70%), mp 80–81°C (lit. (6) mp 80–82°C); ^{1}Hmr ($CDCl_3$)δ: 7.30 (5H, s), 3.73 (2H, s), 2.63 (4H, s); ir(KBr): 1695 (s, carboxylic acid) cm^{-1}.

3-Benzylthiopropionamide (3c)

Ethyl 3-benzylthiopropionate (5.00 g, 22.2 mmol) and concentrated ammonium hydroxide (25 mL) were shaken together in a sealed flask (24 h). The milky white solution was extracted with methylene chloride (5 × 20 mL) and this extract was dried over sodium sulfate. Evaporation yielded a partially crystalline residue (4.94 g). Trituration to remove unreacted ester yielded a white crystalline product (882 mg, 21%), mp 114–115°C (lit. (7) mp 110–111°C); ^{1}Hmr ($CDCl_3$)δ: 7.33 (5H, s), 5.5 (2H, s), 3.73 (2H, s), 2.60 (4H, m); ir(KBr): 3320, 3180 (s, NH), 1648 (s, amide I), 1622 (amide II) cm^{-1}.

*3-Benzylthio-*N*-methylpropionamide (3d)*

Ethyl 3-benzylthiopropionate (5.00 g, 22.2 mmol) and methylamine (25 mL of 40% aqueous solution) were shaken together for 17 h. The milky emulsion was extracted with methylene chloride (4 × 20 mL) and the combined organic fractions dried over sodium sulfate. Evaporation yielded a light yellow syrup (3.79 g, 82%), ^{1}Hmr ($CDCl_3$)δ: 7.30 (5H, s), 6.13 (1H, s), 3.73 (2H, s), 2.75 (3H, d, 4), 2.5 (4H, m); ir(NaCl film): 3280 (NH), 1640 (amide I), 1550 (amide II) cm^{-1}.

n-*Butyl 3-Benzylthiopropionamide (3e)*

Neat ethyl 3-benzylthiopropionate (5.00 g, 0.0222 mol) and *n*-butylamine (11.1 mL, 0.111 mol) were mixed at 25°C. The progress of the reaction was monitored by infrared spectroscopy during a period of 7 days. Then excess *n*-butylamine was evaporated and the product was purified by trituration with petroleum ether to yield white crystals (4.71 g, 84%), mp 41–56°C; ^{1}Hmr ($CDCl_3$)δ: 7.32 (5H, s), 6.6 (1H, s), 3.73 (2H, s), 3.20 (2H, q, 6), 2.9–2.2 (4H, m), 2.7–0.9 (7H, m); ir(KBr): 3380 (s, NH), 1630 (s, amide I), 1345 (s, amide II) cm^{-1}.

Ethyl 3-Benzylthiopropionylglycinate (3f)

3-Benzylthiopropionic acid (1.57 g, 8 mmol) and glycine ethyl ester hydrochloride (1.12 g, 8 mmol) were suspended in ethyl acetate (10 mL). The mixture was cooled to −5°C in a brine ice bath, and triethylamine (1.12 mL, 8 mmol) was added. After 5 min of stirring at −5°C, dicyclohexylcarbodiimide (1.65 g, 8 mmol) in ethyl acetate (10 mL) was added in one portion. During the addition, the temperature rose to −3°C. After 1 h the ice bath was removed. When thin-layer chromatography indicated that the reaction was complete (1 h at room temperature), the precipitate was collected and washed thoroughly with ethyl acetate. The ethyl acetate solution was washed with 5% citric acid solution (1 × 20 mL), saturated potassium bicarbonate (1 × 20 mL), and water (1 × 20 mL). After drying (sodium sulfate), the ethyl acetate was removed by flash evaporation to yield a syrup (2.23 g, 90%). The ^{1}Hmr analysis revealed that the product contained ca. 10% of dicyclohexylurea. This product was used in the next step without further purification; ^{1}Hmr ($CDCl_3$)δ: 7.27 (5H, s), 6.7 (1H, t, 4), 4.17 (2H, q, 6), 3.95 (2H, d, 4), 2.4–2.8 (4H, m), 1.93 (3H, t, 6).

Diphenylmethyl Glycinate p-*Toluenesulfonic Acid Salt*

The *p*-toluenesulfonic acid salt of glycine (4.94 g, 20 mmol) was dissolved in dimethylformamide (5 mL). Diphenyldiazomethane in dimethylformamide was added dropwise (15 min) until the red colour of the diphenyldiazomethane persisted

(7.5 mL of 2.8 *M*, 21 mmol). After the addition of anhydrous ether (100 mL), a yellow syrup separated. On cooling to −20°C for 3 days, the syrup crystallized (5.94 g). Recrystallization from acetone – diethyl ether yielded a white crystalline product (2.71 g, 33%), mp 138°C (lit. (21) mp 140–142°C); ^{1}Hmr ($CDCl_3$)δ: 7.68, 7.12 (4H, AA′BB′, 8), 7.35 (10H, s), 6.88 (1H, s), 3.90 (2H, s), 2.33 (3H, s); ir(KBr): 1737 (s, ester) cm^{-1}.

Diphenylmethyl 3-Benzylthiopropionylglycinate (3g)

Diphenylmethyl 3-benzylthiopropionylglycinate was synthesized by the procedure used for ethyl 3-benzylthiopropionate. The compound was isolated as a syrup (100%); ^{1}Hmr ($CDCl_3$)δ: 7.30 (10H, s), 7.25 (5H, s), 6.92 (1H, s), 4.12 (2H, d, 6), 3.70 (2H, s), 2.55 (4H, m); ir(film): 3330 (s, NH), 1735 (s, ester), 1670 (s, amide I), 1530 (s, amide II) cm^{-1}.

N-*Acetyl*-S-*benzyl*-L-*cysteine (3h)*

S-Benzyl-L-cysteine (2.1 g, 9.9 mmol), water (12 mL), and sodium hydroxide (2.06 mL of 6.79 *N*, 14 mmol) were cooled to 7°C. The pH was monitored with a pH meter. Acetic anhydride (4 mL, 42.1 mmol) was added in eight portions and sodium hydroxide (6.79 *N*) was added dropwise so as to keep the pH in the range 8–10. After the addition was complete (20 min), the ice bath was removed and the solution was stirred at 25°C for 40 min. The pH was then lowered to 1.0 by the addition of sulfuric acid (6.04 *N*), and the mixture was cooled to 7°C. The precipitated crystals were collected by filtration and recrystallized from isopropanol/hexane (1:1) to yield colourless needles (1.94 g, 77%), mp 143.5–147°C; $[\alpha]_D^{24}$ −41.3 (*c* 1.0, 95% EtOH) (lit. (9) $[\alpha]_D^{26}$ −41.5 (*c* 1.0, 95% EtOH); ^{1}Hmr (DMSO-d_6)δ: 8.23 (1H, d, 8), 7.30 (5H, s), 4.42 (1H, m), 3.77 (2H, s), 3.6–3.8 (2H, m), 1.90 (3H, s); ^{13}Cmr (DMSO-d_6)δ: 172.1, 169.4 (carbonyl), 138.1, 128.8, 128.3, 126.8 (phenyl), 51.8 (CH), 35.5 (SCH_2Ph), 32.5 (SCH_2-CH), 22.3 (CH_3).

N-*Acetyl*-S-*benzyl*-L-*cysteinylglycine (Ethyl Ester) (3i)*

N-Acetyl-*S*-benzyl-L-cysteine (5.147 g, 0.0203 mol), EEDQ (5.18 g, 0.0203 mol), and glycine ethyl ester hydrochloride (2.83 g, 0.0203 mol) were suspended in methylene chloride (100 mL). Triethylamine (3.11 mL, 0.0406 mol) was added in one portion and the mixture was stirred overnight at room temperature. The solution was then washed successively with 1 *N* hydrochloric acid (3 × 20 mL), saturated sodium bicarbonate (2 × 20 mL), and water (2 × 20 mL). Drying over sodium sulfate and evaporation afforded a yellow syrup which crystallized from ethyl acetate/petroleum ether, with scratching, to yield a white crystalline product (5.72 g, 83%), mp 108–109°C, (lit. (11) mp 116.5–117.5°C); $[\alpha]_D^{18.2}$ −8.6 (*c* 1.0, ethyl acetate); ^{1}Hmr ($CDCl_3$)δ: 7.30 (6H, m), 6.83 (1H, d, 7), 4.67 (1H, q, 7), 4.17 (2H, q, 7), 3.98 (2H, d, 6), 3.75 (2H, s), 2.80 (2H, d, 7), 1.98 (3H, s), 1.27 (3H, t, 7); ^{13}Cmr ($CDCl_3$)δ: 171.0, 170.5, 169.4 (carbonyl), 138.1, 129.0, 128.6, 127.2 (phenyl), 61.4 (OCH_2), 52.3 (CH), 41.5 (N—CH_2-CO), 23.0 (acetyl), 14.1 (CH_3CH_2); ir(film): 3260 (NH), 1742 (ester), 1640 (amide I), 1550 (amide II) cm^{-1}.

N-*Benzoyl*-S-*benzyl*-L-*cysteine (3j)*

Sodium carbonate (5.16 g, 60 mmol) and *S*-benzyl-L-cysteine (4.22 g, 20 mmol) were suspended in water (60 mL). The mixture was cooled to −4°C and benzoyl chloride (2.32 mL, 20 mmol) was added dropwise. After the addition was complete (10 min), the ice bath was removed and the reaction mixture was stirred at 25°C for 40 min. It was then extracted with ether (2 × 20 mL). Dropwise addition of concentrated hydrochloric acid (7 mL) precipitated a white solid, which was removed by filtration. Recrystallization from ethyl acetate afforded 4.78 g (76%), mp 100–106°C (lit. (12) mp 118–119°C); $[\alpha]_D^{24.5}$ −35.4 (*c* 1.0, absolute EtOH); ^{1}Hmr ($CDCl_3$/DMSO-d_6 1:1)δ: 8.13 (1H, d, 8), 7.3–8.0 (5H, m), 7.25 (5H, s), 4.8 (1H, m), 3.75 (2H, s), 3.8–4.2 (2H, m); ^{13}Cmr ($CDCl_3$/DMSO-d_6 1:1)δ: 173.3, 166.4 (carbonyl), 138.4, 134.5, 131.0, 128.8, 128.1, 127.4, 126.6 (phenyl), 53.2 (CH), 35.9 ($PhCH_2$), 33.4 ($CHCH_2S$); ir(KBr): 3500 (m, COOH), 3320 (s, NH), 1720 (s, COOH), 1620 (s, amide I), 1520 (s, amide II) cm^{-1}.

N-*Benzoyl*-S-*benzyl*-L-*cysteinylglycine (Ethyl Ester) (3k)*

N-Benzoyl-*S*-benzyl-L-cysteine (3.813 g, 0.0121 mol) and glycine ethyl ester hydrochloride (1.70 g, 0.0121 mol) were suspended in methylene chloride (50 mL). Triethylamine (1.85 mL, 0.0242 mol) and EEDQ (2.99 g, 0.0121 mol) were added and the reaction mixture was stirred overnight. The organic layer was washed successively with 1 *N* hydrochloric acid (2 × 20 mL), saturated sodium bicarbonate (1 × 20 mL), and water (2 × 20 mL), dried over sodium sulfate and evaporated under reduced pressure. Recrystallization of the product from ethyl acetate/petroleum ether afforded a white crystalline solid (2.359 g, 51%), mp 112–113°C; $[\alpha]_D^{27.2}$ −52.6 (*c* 1.0, ethyl acetate); ^{1}Hmr ($CDCl_3$)δ: 7–8 (12H, m), 4.83 (1H, q, 6), 4.18 (2H, q, 7), 4.02 (2H, d, 5), 3.83 (2H, s), 3.1–2.8 (2H, m), 1.27 (3H, t, 7); ^{13}Cmr ($CDCl_3$)δ: 171.0, 169.4, 167.5 (carbonyl), 138.0, 133.6, 131.8, 129.0, 128.5, 127.3, 127.1 (phenyls), 61.4 (OCH_2), 52.7 (N—*CH*—C), 41.5 (N—CH_2CO), 36.5 ($PhCH_2$), 33.5 ($CHCH_2S$), 14.0 (CH_3); ir(KBr): 3280 (NH), 1732 (ester), 1650 (amide I), 1620 (amide I), 1515 (amide II) cm^{-1}.

S-*Phenyl*-L-*cysteine (3o)*

L-Cysteine hydrochloride (2.25 g, 15.7 mmol) was stirred under nitrogen with 1.5 *N* sulfuric acid (50 mL) and cuprous chloride (2.55 g, 25.4 mmol). As the cuprous chloride dissolved, the solution turned black and then green. A second portion of L-cysteine hydrochloride (2.25 g, 15.7 mmol) was added and the solution was cooled to 0°C. The diazonium salt prepared from aniline (5.0 mL, 28 mmol) was added rapidly enough to keep the reaction temperature at 3°C and nitrogen evolution at a moderate rate. After the addition was complete (1 h), the reaction mixture was allowed to warm to room temperature and stirring was continued overnight.

The following day, the reaction mixture was heated to 90°C, and hydrogen sulfide was introduced until a filtered aliquot no longer yielded a precipitate with hydrogen sulfide. The mixture was filtered through Celite and the filtrate was extracted with ether (2 × 20 mL) to remove phenol. The pH was then adjusted to 6 with ammonium hydroxide, whereupon yellow crystals precipitated from the solution. These were purified by recrystallization from water to yield pale yellow crystals (1.478 g, 27%), mp 162–165°C, (lit.(14) mp 170–172°C (dec.)); $[\alpha]_D^{24.2}$ 57.5 (*c* 1.0, 1 *N* HCl); ^{1}Hmr (CF_3COOD)δ: 7.47 (5H, m), 4.57 (1H, t, 6), 3.72 (2H, d, 6); ^{13}Cmr (CF_3COOD)δ: 173.6 (carbonyl), 134.0, 131.9, 131.4, 130.9 (phenyl), 54.8 (CH), 36.1 (SCH_2); ir(KBr): 3420 (NH_3^+), 1610 (amino acid I), 1575 (carboxylate), 1505 (amino acid II) cm^{-1}.

Ethyl-S-*benzyl*-N-*phthaloyl*-L-*cysteinylglycinate (3m)*

S-Benzyl-L-cysteine (4.22 g, 20 mmol) was suspended in 30 mL of aqueous 0.66 *M* sodium carbonate. To this suspension was added *N*-carboethoxyphthalimide (Nefkens' reagent) (4.5 g, 20.5 mmol) in one portion, and the mixture was stirred and monitored for the disappearance of the reagent. After 1.5 h at 25°C, the product was isolated by extraction with methylene chloride (6 × 20 mL), followed by drying (sodium sulfate) and evaporation of the solvent. Attempts to crystallize

the product failed and it was, therefore, carried on to the next step, as follows. The acid was dissolved in methylene chloride (100 mL), and glycine ethyl ester hydrochloride (2.70 g, 20 mmol), EEDQ (5.15 g, 20.2 mmol of 97%), and triethylamine (2.3 mL, 20 mmol) were added. The reaction mixture was stirred overnight at 25°C and then washed successively with 2.5 *N* hydrochloric acid (1 × 30 mL), water (1 × 30 mL), 10% sodium bicarbonate (1 × 30 mL), water (1 × 30 mL), and brine (1 × 30 mL). It was then dried (sodium sulfate) and evaporated to yield a white crystalline solid (7.56 g). This was recrystallized from ethyl acetate/hexane to yield 6.604 g (77%), mp 109–112°C; ^{1}Hmr ($CDCl_3$)δ: 7.82 (4H, m), 7.32 (5H, s), 6.9 (1H, b), 4.98 (1H, t, 7), 4.23 (2H, q, 7), 4.00 (2H, d, 6), 3.75 (2H, s), 3.26 (2H, d, 6), 1.25 (3H, t, 7); ^{13}Cmr ($CDCl_3$)δ: 169.4 (amide), 167.9 (imide carbonyls), 137.1, 134.4, 131.7, 129.0, 128.7, 127.3, 123.7 (phenyls), 61.5 (OCH_2), 52.7 (CH), 41.6 ($N—CH_2CO_2$), 38.7 (SCH_2Ph), 30.4 (SCH_2CH), 14.0 (CH_3); ir(KBr): 3360 (s, NH), 1768 (m, phthaloyl), 1737 (s, ester), 1695 (s, phthaloyl), 1680 (s, amide I), 1525 (s, amide II) cm^{-1}.

S-*Benzyl*-N-*carbobenzoxycysteine* (*3*n)

Sodium bicarbonate (4.20 g, 50 mmol) and *S*-benzyl-L-cysteine (4.22 g, 20 mmol) were suspended in water (40 mL) and stirred vigorously. Benzyl chloroformate (3.62 mL (95%), 24 mmol) was added in seven portions. After the addition was complete (30 min) the reaction mixture was stirred overnight. After filtration of the aqueous solution and extraction of the filtrate with ether (3 × 20 mL), the aqueous layer was acidified to pH 1.0 with concentrated hydrochloric acid and extracted with ethyl acetate (5 × 20 mL). Drying (sodium sulfate) and evaporation of the ethyl acetate extract gave a white solid. Recrystallization from ethyl acetate yielded 1.17 g (17%), mp 92–93°C (lit. (13) mp 93–94°C); ^{1}Hmr ($CDCl_3$)δ: 7.33 (5H, s), 7.27 (5H, s), 5.6 (1H, d, 8), 5.10 (2H, s), 4.6 (1H, m), 3.77 (2H, s), 2.93 (2H, d, 4); ^{13}Cmr ($CDCl_3$)δ: 175.3 (carbonyl), 156.1 (urethane), 137.5, 128.5, 128.3, 128.1, 127.2 (phenyls), 67.4 ($PhCH_2O$), 53.4 (CH), 36.7 ($PhCH_2S$), 33.3 (SCH_2CH); ir(KBr); 3250 (m, NH), 1710 (s, COOH), 1650 (s, urethane), 1535 (amide II) cm^{-1}.

N-*Acetyl*-S-*phenyl*-L-*cysteine* (*3*p)

S-Phenyl-L-cysteine (3.650 g, 18.5 mmol) was cooled in an ice bath, and sodium hydroxide (6.79 *N*) was added in small portions to dissolve the substrate and provide a pH of 10–11. After dissolution was complete, acetic anhydride (7.0 mL, 74 mmol) was added in eight portions (one portion every 4 min). The solution was agitated thoroughly and during this addition sodium hydroxide (6.79 *N*) was added to maintain the pH at 10–11. After the addition was complete, the reaction mixture was stirred at ambient temperature for 3.5 h and then cooled to 3°C, and sulfuric acid (6.04 *N*) added until the pH was 1.5. The oil was extracted with methylene chloride (6 × 30 mL) and this extract was dried (sodium sulfate) and evaporated. The resulting light yellow oil crystallized upon addition of ethyl acetate/hexane (1:1) and reevaporation. The crude yield was 2.471 g. The product was recrystallized by dissolving it in warm isopropanol (15 mL), followed by addition of hexane at room temperature (2.43 g, 51%), mp 127–129°C (lit. (14) mp 142–143°C);[1] $[\alpha]_D^{29.0}$ −3 (*c* 1, ethanol); ^{1}Hmr ($CDCl_3$)δ: 7.2–7.5 (5H, m), 6.3 (1H, bs), 3.93 (2H, s), 3.5 (2H, s), 1.95 (3H, s); ^{13}Cmr ($CDCl_3$/DMSO-d_6)δ: 171.8, 169.4 (carbonyl), 135.5, 129.0, 126.0 (phenyl), 51.8 (methine), 34.9 (CH_2S), 22.4 (acetyl); ir(KBr): 3330 (s, NH), 1728 (s, COOH), 1628 (s, amide I), 1568 (s, amide II) cm^{-1}.

[1]The reported values refer to the anhydrous compound.

S-*Phenyl*-N-*phthaloyl*-L-*cysteine* (*3*r)

Anhydrous sodium carbonate (473 mg, 5.5 mmol) and *S*-phenyl-L-cysteine (986 mg, 5 mmol) were suspended in water (20 mL) and Nefkens' reagent (1.424 g, 6.5 mmol) was added in one portion. After stirring of this mixture for 2 h at ambient temperature, some greyish brown solid remained in the flask. The mixture was filtered, the filtrate extracted with methylene chloride (3 × 20 mL) and this extract was discarded. The aqueous phase was acidified with 3 *N* hydrochloric acid to pH 1.0 and again extracted with methylene chloride (5 × 20 mL). Drying (sodium sulfate) and evaporation of this extract gave a yellow syrup (1.209 g) which was purified by column chromatography (silica gel, ethyl acetate) to yield *S*-phenyl-*N*-phthaloyl-L-cysteine as a syrup (633 mg, 39%); ^{1}Hmr ($CDCl_3$)δ: 10.48 (1H, s), 7.75 (4H, s), 7.2 (5H, m), 5.0 (1H, m), 3.4–3.9 (2H, m); ir ($CHCl_3$, 5%): 1775, 1720 (s, Ft) cm^{-1}.

N-*Acetyl*-N′-*benzyl*-S-*phenyl*-L-*cysteinamide* (*3*q)

N-Acetyl-*S*-phenyl-L-cysteine (1.14 g, 5.76 mmol) and EEDQ (1.47 g (97%), 5.76 mmol) were suspended in methylene chloride (25 mL). Benzylamine (0.63 mL, 5.76 mmol) was added in one portion followed by triethylamine (0.08 mL, 5.76 mmol). After stirring for 12 h, the reaction mixture was washed successively with 2.5 *N* hydrochloric acid (2 × 20 mL), water (20 mL), saturated sodium carbonate (20 mL), and water (2 × 30 mL), and the organic phase was dried over anhydrous sodium sulfate and evaporated. The residual solid (1.25 g) was recrystallized from ethyl acetate (711 mg, 71%), mp 170–172°C; $[\alpha]_D^{24.8}$ +2.4 (*c* 0.5, $CHCl_3$); ^{1}Hmr ($CDCl_3$/DMSO-d_6 1:1)δ: 8.3–8.6 (2H, m), 7.23 (10H, m), 4.87 (1H, q, 7), 4.28 (2H, d, 6), 3.0–3.4 (2H, m), 1.88 (3H, s); ^{13}Cmr ($CDCl_3$/DMSO-d_6)δ: 170.0, 169.7 (carbonyl), 138.9, 136.0, 128.8, 128.7, 128.2, 127.2, 126.8, 126.5 (phenyl), 52.6 (CH), 42.6 (NCH_2Ph), 22.7 (CH_3); ir (KBr): 3280 (s, NH), 1625 (s, amide I), 1530 (s, amide II) cm^{-1}. *Anal.* calcd. for $C_{18}H_{20}N_2O_2S$: C 65.82, H 6.14; found: C 65.87, H 6.37.

N′-*Benzyl*-S-*phenyl*-N-*phthaloyl*-L-*cysteinamide* (*3*s)

S-Phenyl-*N*-phthaloyl-L-cysteine (628 mg, 1.92 mmol) was dissolved in methylene chloride (100 mL). Then EEDQ (495 mg, 2.0 mmol) was added in one portion, followed by benzylamine (0.209 mL, 1.92 mmol). The solution was stirred overnight. The next day, the light yellow solution was washed successively with 2.5 *N* hydrochloric acid (1 × 20 mL), water (1 × 20 mL), saturated sodium bicarbonate (1 × 20 mL), water (1 × 20 mL), and brine (1 × 20 mL), and it was then dried (sodium sulfate) and evaporated. The residue was dried under high vacuum to yield an off-white semicrystalline solid (622 mg, 78%). The product was recrystallized from ethyl acetate/hexane at room temperature to yield a white crystalline solid (317 mg, 40%), mp 131°C; ^{1}Hmr ($CDCl_3$)δ: 7.73 (4H, s), 7.27 (10H, m), 6.6 (1H, s), 4.93 (1H, t, 7), 4.40 (2H, d, 6), 3.83 (2H, d, 7). Exchange with D_2O confirmed the NH assignment (δ 6.6); ^{13}Cmr ($CDCl_3$)δ: 167.7, 167.5 (carbonyls), 137.7, 134.2, 131.6, 131.1, 129.0, 128.7, 127.6, 127.1, 123.5 (phenyls), 54.0 (CH), 43.7 (NCH_2Ph), 33.7 (SCH_2CH); ir(KBr): 3380 (m, NH), 1772 (m, *antisym* phthalimido), 1710 (s, *sym* phthalimido), 1640 (s, amide I), 1530 (m, amide II) cm^{-1} $[\alpha]_D^{25.0}$ −70.0 (*c* 1.0, $CHCl_3$).

Ethyl Benzylsulfinylpropionate (*4*b) (*Method* E)

Ethyl 3-benzylthiopropionate (30.00 g, 0.134 mol) was dissolved in glacial acetic acid (50 mL). Hydrogen peroxide (11.5 mL of 30%, 0.134 mol) was added dropwise to the reaction mixture at 10°C. After the addition was complete (10 min), the reaction mixture was stirred at 25°C for 1 h. The solvent was evaporated and the viscous residue was poured into saturated sodium bicarbonate (50 mL) and extracted with methylene chloride (4 × 50 mL). The organic

phase was washed with brine, dried (sodium sulfate), and concentrated to a viscous syrup. The compound was crystallized by solution in ether, cooling to 4°C, and addition of hexane with vigorous stirring (27.72 g, 86%), mp 62–63°C; ^{1}Hmr ($CDCl_3$)δ: 7.23 (5H, s), 4.12 (2H, q, 7), 3.98 (2H, s), 2.82 (4H, s), 1.25 (3H, t, 7); ^{13}Cmr ($CDCl_3$)δ: 171.1 (carbonyl), 130.1, 128.8, 128.2 (phenyl), 60.8 (OCH_2), 58.2 (CH_2Ph), 45.4 ($SOCH_2CH_2$), 26.29 (CH_2CO), 14.1 (CH_3); ir(KBr): 1718 (s, ester), 1018 (s, sulfoxide) cm^{-1}. *Anal.* calcd. for $C_{12}H_{16}O_3S$: C 60.00, H 6.71; found: C 60.37, H 7.03.

*Benzylsulfinylpropionic Acid (**4**a)*

Ethyl 3-benzylsulfinylpropionate (4.00 g, 16.7 mmol) was dissolved in absolute ethanol, and the solution was cooled to 4°C. Then potassium hydroxide (1.50 g, 27 mmol) was added in three portions. The reaction was complete within 10 min (tlc, $CHCl_3$/MeOH 5:1). After a further 15 min, the pH was lowered to 1.0 by the addition of 3 *N* hydrochloric acid, and the solid product was collected by filtration (1.81 g). Recrystallization from ethanol produced white needles (961 mg, 27%), mp 147°C; ^{1}Hmr ($CDCl_3$/DMSO-d_6 1:1)δ: 7.02 (5H, s), 3.68 (2H, s), 3.0–2.4 (4H, m); ir(KBr): 1710 (s, COOH), 982 (s, sulfoxide) cm^{-1}. *Anal.* calcd. for $C_{10}H_{12}O_3S$: C 56.59, H 5.70; found: C 55.79, H 6.23.

*3-Benzylsulfinylpropionamide (**4**c) (Method* A*)*

3-Benzylthiopropionamide (855 mg, 4.38 mmol) was dissolved in methanol/water (2.5 mL/2.5 mL) and the solution was stirred at 4°C. Then hydrogen peroxide (0.25 mL of 50%, 4.4 mmol) was added in one portion. The reaction was monitored by tlc (ethyl acetate) and was complete after 3 days. Solid sodium bisulfite was added at this time until a negative starch–iodide test was obtained. Evaporation of the solvent and recrystallization of the residue from ethyl acetate yielded colourless needles (408 mg, 52%), mp 127–131°C; ^{1}Hmr ($CDCl_3$)δ: 7.33 (5H, s), 4.00 (2H, ABq), 6.7 (2H, s), 2.4–3.3 (4H, m); ir(KBr): 3378, 3178, (s, NH), 1645 (s, amide I), 1620 (s, amide II), 1025 (s, sulfoxide) cm^{-1}.

*3-Benzylsulfinyl-*N*-methylpropionamide (**4**d) (Method* B*)*

3-Benzylthio-*N*-methylpropionamide (3.79 g, 18.1 mmol) was dissolved in acetone (25 mL), hydrogen peroxide (2.0 mL of 30%, 22 mmol) was added in one portion, and the mixture was shaken until it became homogeneous. After 5 days, thin-layer chromatography indicated that the reaction was not yet complete. Acetic acid (1.0 mL) was added and, in about 10 min, a white precipitate appeared. Solid sodium bicarbonate (ca. 500 mg) was added, and the product was recovered by evaporation of the solvent. Proton magnetic resonance indicated that the reaction was still incomplete. The product was purified by column chromatography (chloroform/methanol 6:1). Crystallization from ethyl acetate afforded a white crystalline solid (2.00 g, 43%), mp 134–135°C, (lit. (8) mp 138–140°C); ^{1}Hmr ($CDCl_3$)δ: 7.37 (6H, s), 4.00 (2H, s), 2.2–3.2 (7H, m); ^{13}Cmr ($CDCl_3$)δ: 170.7, (carbonyl), 130.0, 129.6, 129.0, 128.4 (phenyl), 58.4 (PhCH_2SO), 46.3 (CH_2-CH_2SO), 28.7 (CH_2CON), 26.2 (NCH_3); ir(KBr): 3295 (NH), 1630 (amide I), 1540 (amide II), 1020–1010 (sulfoxide) cm^{-1}.

*3-Benzylsulfinyl-*N*-butylpropionamide (**4**e)*

3-Benzylthio-*N*-butylpropionamide (4.34 g, 17.3 mmol) was oxidized by method *A* to give, after recrystallization from ethyl acetate, white flakes (2.74 g, 63%), mp 130°C; ^{1}Hmr ($CDCl_3$)δ: 7.33 (5H, s), 4.00 (2H, s), 2.5–3.4 (6H, m), 1.7–0.9 (7H, m); ^{13}Cmr ($CDCl_3$)δ: 170.0 (carbonyl), 130.1, 129.8, 128.8, 128.4 (phenyl), 58.2 (PhCH_2), 46.5 (CH_2CH_2SO), 39.3 (NCH_2), 31.4 (NCH_2CH_2), 28.7 (CH_2CO), 20.1 (CH_2CH_3), 13.7 (CH_3); ir(KBr): 3275 (s, NH), 1638 (s, amide I), 1550 (m, amide II), 1025 (s, sulfoxide) cm^{-1}.

*3-Benzylthiopropionylglycine-*S*-oxide (Ethyl Ester) (**4**f)*

3-Benzylthiopropionylglycine (2.23 g, 90% pure, 7.2 mmol) was oxidized by method *A* to give, after recrystallization from ethyl acetate, a white crystalline solid (1.287 g, 60%), mp 91–97°C; ^{1}Hmr ($CDCl_3$)δ: 7.35 (5H, s), 7.2 (1H, s), 4.17 (2H, q, 7), 4.03 (2H, s), 3.95 (2H, d, 5), 2.6–3.1 (4H, m), 1.27 (3H, t, 7); ^{13}Cmr ($CDCl_3$)δ: 170.8, 169.7 (carbonyl), 130.1, 129.8, 128.8, 128.3 (phenyl), 61.2 (OCH_2), 57.9 (PhCH_2), 45.8 (CH_2SO), 41.3 (NCH_2CO), 28.2 (CH_2CO), 14.1 (CH_3); ir(KBr): 3300 (NH), 1730 (ester), 1635 (amide I), 1545 (amide II), 1020 (sulfoxide) cm^{-1}.

*Diphenylmethyl 3-Benzylsulfinylpropionylglycinate (**4**g)*

Diphenylmethyl 3-benzylthiopropionylglycinate (1.20 g, 2.86 mmol) was oxidized by method *A* to give 1.05 g (84%), mp 152–153°C (dec.). *Anal.* calcd. for $C_{25}H_{25}NO_4S$: C 68.94, H 5.79; found: C 68.78, H 5.97.

S-*Benzyl-*L*-cysteine-*S*-oxide (**4**h)*

S-Benzyl-L-cysteine (5.00 g, 23.7 mmol) was oxidized by method *E* to give, after recrystallization from 30% ethanol, 4.36 g (81%) of product, mp 171–174°C (lit. (15) mp 163–165°C); $[\alpha]_D^{24}$ +5.8 (*c* 1.0, 0.1 *N* NaOH); ^{1}Hmr (D_2O)δ: 7.4 (5H, m), 4.50 (2H, m), 3.43 (2H, m); ir(Nujol): 1010 (s, sulfoxide) cm^{-1}.

Ethyl N*-Acetyl-*S*-benzyl-*L*-cysteinylglycinate-*S*-oxide (**4**k)*

Ethyl *N*-acetyl-*S*-benzyl-L-cysteinylglycinate (5.72 g, 0.017 mol) was oxidized by method *A* to give, after recrystallization from ethyl acetate, 4.438 g (77%), mp 148°C (dec.); ^{1}Hmr ($CDCl_3$/DMSO-d_6 1:1)δ: 8.34 (1H, m), 7.30 (5H, s), 5.2 (1H, s), 4.70 (1H, m), 4.23 (2H, q, 7), 4.12 (2H, s), 4.02 (2H, d, 6), 3.00 (2H, d, 7), 1.89 (3H, s), 1.22 (3H, t, 7); ir(KBr): 3275 (NH), 1725 (ester), 1640 (amide I), 1540 (amide II), 1025 (sulfoxide) cm^{-1}; ^{13}Cmr ($CDCl_3$/DMSO-d_6 1:1)δ: 170.5, 170.1, 169.8, (C=O), 131.0, 130.9, 130.3, 128.5, 127.8 (Ph), 60.6 (OCH_2), 57.9, (PhCH_2SO), 53.7 (CH), 47.8 (CH_2SO), 41.1 (NCH_2CO), 22.7 (CH_3CO), 14.0 (CH_3CH_2).

N-*Benzoyl-*S*-benzyl-*L*-cysteinylglycine-*S*-oxide (Ethyl Ester) (**4**l)*

N-Benzoyl-*S*-benzyl-L-cysteinylglycine (ethyl ester) (1.736 g, 4.49 mmol) was oxidized by method *A* to give, after recrystallization from ethyl acetate 1.533 g (82%), mp 156–157°C (dec.); ^{1}Hmr ($CDCl_3$/DMSO-d_6 1:1)δ: 7.2–8.1 (7H, m), 7.33 (5H, s), 5.1 (1H, m), 4.17 (2H, q, 7), 4.02 (2H, s), 3.90 (2H, d, 5), 3.3 (1H, m), 1.23 (3H, t, 7); ^{13}Cmr ($CDCl_3$/DMSO-d_6 1:1)δ: 170.1, 169.3, 166.7 (carbonyl), 133.8, 130.9, 131.4, 130.3, 128.5, 128.1, 127.6 (phenyl), 60.6 (OCH_2), 53.1 ($NCHCO$), 41.2 (NCH_2CO), 14.0 (CH_3); ir(KBr): 3270 (NH), 1735 (ester), 1655 (amide I), 1625 (amide I), 1520 (amide II), 1030 (sulfoxide) cm^{-1}.

S-*Benzyl-*N*-phthaloyl-*L*-cysteinylglycine-*S*-oxide (**4**m)*

Ethyl-*S*-benzyl-*N*-phthaloyl-L-cysteinylglycinate (4.26 g, 10 mmol) was oxidized by method *A* to give a colourless foam (3.362 g, 76%); ^{1}Hmr ($CDCl_3$)δ: 7.80 (4H, m), 7.35 (3H, s), 7.32 (2H, s), 5.43 (1H, t, 6), 4.08 (2H, q, 7), 4.08 (2H, s), 3.93 (2H, d, 6), 3.0–3.8 (2H, m), 1.23 (3H, t, 7); ir($CHCl_3$, 5%): 3380 (b, NH), 1780 (m, *antisym* phthalimido), 1730 (s, ester), 1700 (s, *sym* phthalimido), 1020 (m, sulfoxide) cm^{-1}.

N-*Acetyl-*N′*-benzyl-*S*-phenyl-*L*-cysteinamide-*S*-oxide (**4**n) (Method* D*)*

N-Acetyl-*N*′-benzyl-*S*-phenyl-L-cysteinamide (152 mg, 0.5 mmol) was dissolved in methylene chloride (25 mL) and *m*-chloroperbenzoic acid (101 mg of 85%, 0.5 mmol) was added. The reaction mixture was shaken until the peracid dissolved. After 22 h at 25°C the solution was washed with saturated sodium bicarbonate (4 × 7 mL) and brine (1 × 7 mL). It was

then dried (sodium sulfate) and evaporated to yield the sulfoxide (176 mg, 100%), mp 130–134°C; ^{1}Hmr ($CDCl_3$)δ: 7.58 (5H, s), 7.30 (5H, s), 7.9–7.3 (2H, m), 5.0 (1H, m), 4.45, 4.42 (2H, d + d), 3.2 (2H, s), 2.07, 1.93 (3H, s); ir(KBr): 3280 (s, NH), 1635 (s, amide I), 1530 (s, amide II), 1032 (s, sulfoxide) cm^{-1}.

N-*Phthaloyl*-N′-*benzyl*-S-*phenyl*-L-*cysteinamide*-S-*oxide* (**4o**)

N-Phthaloyl-*N*′-benzyl-*S*-phenyl-L-cysteinamide (165 mg, 0.399 mmol) was oxidized by method *D* to yield a syrup (175 mg, 100%); ^{1}Hmr ($CDCl_3$)δ: 7.73 (4H, s), 7.60 (1H, b), 7.46 (5H, s), 7.20 (5H, s), 5.2 (1H, m), 4.30 (2H, d, 6), 3.7 (2H, m); ^{13}Cmr ($CDCl_3$)δ: 167.9, 167.3, 166.6 (carbonyls), 137.4, 134.5, 134.2, 131.8, 131.4, 129.6, 129.4, 128.7, 128.1, 127.6, 127.4, 124.2, 123.8, 123.5 (aromatic), 55.8, 52.7 (CH), 49.2, 46.3 (SCH_2); ir($CHCl_3$, 5%): 3280 (m, NH), 1770, 1715 (s, Ft), 1680 (s, amide I), 1510 (s, amide II), 1030 (m, sulfoxide) cm^{-1}.

Cyclization of Benzyl 2-Carboxyphenyl Sulfoxide with Acetic Anhydride

Benzyl 2-carboxyphenyl sulfoxide (500 mg, 2.05 mmol) was suspended in acetic anhydride (5 mL) under nitrogen and heated to 125–150°C in an oil bath. When thin-layer chromatography indicated that the reaction was complete (75 min), the volatile components were removed under high vacuum. Column chromatography on silica gel (petroleum ether/ethyl acetate 5:1) yielded a pale yellow crystalline product (427 mg, 92%), mp 89.5–90°C (lit. (2, 3) mp 90–91°C); ^{1}Hmr ($CDCl_3$)δ: 8.3–6.5 (9H, m), 6.53 (1H, s); ^{13}Cmr ($CDCl_3$)δ: 163.7 (C=O), 138.7, 134.8, 133.7, 132.7, 129.8, 128.7, 127.4, 126.7, 124.3 (phenyl), 83.5 (CH); ir(KBr): 1720 (ester) cm^{-1}.

Cyclization of Benzyl 2-Carboxyphenyl Sulfoxide with Acetyl Trifluoroacetate

Benzyl 2-carboxyphenyl sulfoxide (500 mg, 2.05 mmol) was suspended in dry methylene chloride (1.46 mL) and cooled to 4°C under dry nitrogen. Acetyl trifluoroacetate (0.22 mL, 1.9 mmol) was added in one portion. The reaction mixture was stirred at 4°C for 30 min. After evaporation of the solvent, the pale yellow residue was chromatographed on silica gel (chloroform → chloroform/methanol 9:1). The first component eluted from the column corresponded to 2-phenyl-1,3-benzoxathian-6-one (314 mg, 73%) while the second component was identified as benzyl 2-carboxyphenyl sulfoxide (123 mg, 25%). Both compounds were identified by comparison with authentic samples.

Cyclization of Benzyl 2-Carboxyphenyl Sulfoxide with Trifluoroacetic Anhydride

Benzyl 2-carboxyphenyl sulfoxide (500 mg, 1.92 mmol) was suspended in dry methylene chloride (1.46 mL) under dry nitrogen. Trifluoroacetic anhydride (0.27 mL, 1.9 mmol) was added dropwise to this ice-cold solution over a period of 1 min. The ice bath was then removed and the first thin-layer chromatogram indicated that all of the starting sulfoxide had reacted (3–4 min). After evaporation of the solvent, the white crystalline residue was purified by column chromatography (silica gel). The first component (chloroform) was identified as 2-phenyl-1,3-benzoxathian-6-one (191 mg, 41%) by comparison with an authentic sample. The second component (chloroform/methanol 9:1) was identified as 2,2′-dithiosalicylic acid (170 mg, 58%) by comparison of its ir spectrum with that of an authentic sample; mp >260°C (lit. (22) mp 287–290°C); ^{1}Hmr ($CDCl_3$)δ: 7.1–8.2 (8H, m); ir(Nujol): 1670 (carboxyl) cm^{-1}.

Cyclization of 3-Benzylsulfinylpropionamide (**8**; *R* = *Ac*)

3-Benzylsulfinylpropionamide (3.7 mg, 1.5 mmol), and acetic anhydride (1.14 mL) were heated at 110°C for 30 min. The reaction mixture was then placed in a desiccator over potassium hydroxide under high vacuum to remove the solvent. The product was isolated by column chromatography on silica gel (benzene/ethyl acetate 3:1) followed subsequently by preparative thick-layer chromatography (chloroform) to yield a syrup (86 mg, 24%); ^{1}Hmr ($CDCl_3$)δ: 7.33 (5H, s), 6.88 (1H, s), 2.80 (4H, m), 2.60 (3H, s); ^{13}Cmr ($CDCl_3$)δ: 128.7, 127.7, 126.1 (phenyl), 57.2 (methine), 36.1 (SCH_2), 27.3 (CH_2CO), 21.9 (acetyl); ir(5% CCl_4 solution): 1695 cm^{-1}.

Cyclization of 3-Benzylsulfinyl-N-*methyl propionamide* (**8**; *R* = CH_3)

3-Benzylsulfinyl-*N*-methylpropionamide (500 mg, 2.36 mmol) was suspended in acetic anhydride (1.8 mL) and heated under nitrogen to 114–120°C. When thin-layer chromatography indicated that the reaction was complete (30 min), the reaction mixture was transferred to a vacuum desiccator and the solvent was removed over potassium hydroxide pellets. Purification by column chromatography on silica gel (benzene/ethyl acetate 3:1 to ethyl acetate by gradient elution) yielded a crystalline product (302 mg, 62%), mp 96°C (lit. (8) mp 95–97°C) after recrystallization from ether/hexane; ^{1}Hmr ($CDCl_3$)δ: 7.33 (5H, m), 5.43 (1H, s), 2.97 (3H, s), 2.80 (4H, m); ^{13}Cmr ($CDCl_3$)δ: 169.4 (C=O), 139.0, 128.7, 128.2, 126.4 (Ph), 64.1 (Ph*CH*), 35.5 (CH_2CH_2CO and NCH_3), 34.6, 22.2; ir(KBr): 1620 (amide I) cm^{-1}.

Cyclization of S-*Benzylsulfinyl*-N-*butylpropionamide* (**8**; *R* = n-C_4H_9)

S-Benzylsulfinyl-*N*-butylpropionamide (500 mg, 2 mmol) was suspended in acetic anhydride (1.5 mL) and heated at 114°C for 30 min. The acetic anhydride was then removed in a vacuum desiccator over potassium hydroxide pellets. The product was purified by column chromatography on silica gel (benzene to benzene/ethyl acetate 3:1 by gradient elution) to yield a syrup (139 mg, 28%); ^{1}Hmr ($CDCl_3$)δ: 7.33 (5H, s), 5.52 (1H, s), 3.0–0.8 (13H, m); ^{13}Cmr ($CDCl_3$)δ: 169.2 (carbonyl), 139.7, 128.6, 128.1, 126.6 (phenyl), 61.9 (methine), 47.8 (NCH_2), 34.4 (SCH_2), 29.6 (NCH_2CH_2), 21.9, 20.3 (CH_2CO + CH_2CH_3), 13.8 (CH_3); ir(KBr): 1630 (amide I) cm^{-1}.

Cyclization of Ethyl 3-Benzylsulfinylpropionylglycinate (**8**; *R* = CH_2CO_2Et)

Ethyl 3-benzylsulfinylpropionylglycinate (595 mg, 2 mmol) was suspended in acetic anhydride (2.6 mL) and the suspension was heated to 110°C. When tlc (ethyl acetate) indicated that the reaction was complete (30 min), the excess acetic anhydride was removed in a vacuum desiccator over potassium hydroxide pellets. Chromatography on silica gel (benzene → ethyl acetate) afforded *N*-(ethoxycarbonylmethyl)-perhydro-*S*-phenyl-1,3-thiazin-6-one as a syrup (295 mg, 53%); ^{1}Hmr ($CDCl_3$)δ: 7.33 (5H, s), 5.68 (1H, s), 4.70, 3.33 (2H, AB, 18), 4.25 (2H, q, 6), 2.87, (4H, s), 1.23 (3H, t, 6); ^{13}Cmr ($CDCl_3$)δ: 170.3, 168.8 (carbonyl), 138.9, 128.9, 127.1 (phenyl), 63.7, 61.2 (CH and OCH_2), 47.8 (NCH_2CO), 35.0 (SCH_2), 23.2 (CH_2-CO), 14.1 (CH_3); ir(KBr): 1735 (ester), 1640 (s, amide I) cm^{-1}.

Cyclization of **4**k *to* **9**a

A 0.323 *M* suspension of **4***k* (0.80 g, 2.26 mmol) in acetic anhydride (7.0 mL) was heated under nitrogen at 75–80°C for 3.75 h. The acetic anhydride was removed in a vacuum desiccator over potassium hydroxide pellets to give a yellow solid. Purification by column chromatography on silica gel using gradient elution (benzene → benzene/methanol 5:1) afforded two major fractions. The slower moving band (0.37 g) was unreacted sulfoxide. The faster moving band (0.43 g) was mainly **9***a* (^{1}Hmr), although it was a yellow oil.

The oil was dissolved in benzene (4 mL), and white crystals of **9***a* formed when the solution was allowed to stand at room temperature. The crystals (83 mg) were collected by suction filtration. Recrystallization from acetone (2.5 mL) at −11°C gave 25 mg of **9***a* as a white crystalline solid, mp 184.0–184.2°C. In a second experiment, 416 mg (59%) of **9***a* were obtained from 708 mg of **4***k*; ^{1}Hmr ($CDCl_3$)δ: 8.0–7.6 (1H, bs, N*H*), 7.53–6.87 (5H, m, Ph), 6.10 (1H, s, PhC*H*), 5.35–5.10 (1H, m, =N—C*H*), 4.22 (2H, q, J = 7 Hz, CH_2-CH_3), 4.06 (2H, d, J = 5.5 Hz, N—CH_2—CO; D_2O, 2H, s), 3.60–3.20 (2H, m, CH_2S), 1.97 (3H, s, CH_3), 1.30 (3H, t, J = 7 Hz, CH_2CH_3); ^{13}Cmr ($CDCl_3$)δ: 170.6, 169.8 (carbonyl), 134.5, 129.2, 128.3, 124.6 (phenyl), 66.4, 65.0, 61.6, 41.5 (NCH_2CO), 30.9 (SCH_2), 23.9 (CH_3) 14.2 (CH_3); ir (KBr): 3328, 1735, 1655, 1635, 1530 cm^{-1}; ms (50°C, 70 eV) *m/e* (relative intensity): 336.1144 (3), 179.0405 (66), 165.0326 (10.7), 164.0230 (100), 158.0318 (11.8), 137.0306 (13.7), 121.0109 (17.6), 118.0608 (13.6), 106.0116 (16.5), 104.0080 (15.5). *Anal.* calcd. for $C_{16}H_{20}N_2O_4S$: C 57.13, H 5.99, N 8.32, S 9.53; found: C 57.05, H 6.11, N 8.08, S 8.75.

Cyclization of **4***l* *to* **9**b

A suspension of **4***l* (200 mg, 0.5 mmol) in acetic anhydride (1.2 mL) was heated under nitrogen for 3 h at 78–79°C. The excess acetic anhydride was removed in a vacuum desiccator over potassium hydroxide pellets and the resulting syrup was chromatographed on silica gel (benzene → benzene/methanol 5:1) to yield 138 mg of a light yellow syrup which, on standing, solidified to an amorphous solid. Recrystallization from acetone at −78°C for 3 h and overnight at −15°C gave a pale yellow crystalline solid (61.7 mg). Recrystallization from acetone afforded 50.4 mg of **9***b* as a white solid, mp 118–121°C; ^{1}Hmr ($CDCl_3$)δ: 8.07–7.67 (1H, bs), 7.7–6.8 (5H, m), 7.26 (5H, s), 6.18 (1H, s), 5.38 (1H, t, J = 4.5 Hz), 4.22 (2H, q, J = 7 Hz), 4.07 (2H, d, J = 5.5 Hz; D_2O, 2H, s), 3.43 (2H, d, J = 4.5 Hz), 1.29 (3H, t, J = 7 Hz); ^{13}Cmr ($CDCl_3$)δ: 129.8, 129.1, 128.7, 127.4 (phenyl), 61.5, 59.2, 53.9 (*C*HCO), 41.8 (NCH_2CO), 31.8 (SCH_2), 14.2 (CH_3); ir($CHCl_3$, 5%): 1735 1670, 1650, 1500 cm^{-1}; ms (50°C, 70 eV) *m/e* (relative intensity): 398.1297 (0.8), 294.0009 (10), 268.0786 (18.9), 242.0596 (17.2), 241.0564 (100), 158.0300 (12.1), 146.0613 (40.2), 121.0122 (8.9).

Cyclization of **4**m *to* ***10***a

A suspension of **4***m* (0.735 g, 1.73 mmol) in acetic anhydride (5.2 mL) was heated under nitrogen at 75–80°C for 6 h, by which time tlc analysis indicated that, although **4***m* had not been consumed, some decomposition of the product was occurring. Evaporation of the solvent followed by drying under high vacuum gave 0.68 g of a deep yellow oil. This was chromatographed on silica gel using benzene/methanol to give 0.58 g of a pale yellow semi-solid which was rechromatographed on silica gel (benzene → 5% methanol/benzene) to give 0.42 g of a bright yellow oil. This was chromatographed again on silica gel and eluted with 1% methanol/benzene to give 0.13 g of a pale yellow oil. Preparative layer chromatography (benzene/ethyl acetate 5:1, four elutions) afforded 9.9 mg of material with mp 179.5–185°C. In a second experiment, 852 mg (2 mmol) of **4***m* was heated under nitrogen in acetic anhydride (6.06 mL) at 73–75°C for 20 min. Removal of the solvent in the usual manner yielded a syrup which was chromatographed on silica gel (benzene → benzene/methanol 5:1) to yield two components. The slower component proved to be unreacted sulfoxide (493 mg, 56%). The faster component was recrystallized from acetone to give 120 mg (31%) of **10***a*; ^{1}Hmr ($CDCl_3$)δ: 7.78 (4H, d), 7.42 (5H, s), 6.03 (0.6 H, s), 5.63 (0.4H, s), 5.43 (0.4H, t, J = 6 Hz), 5.22 (1H, t, J = 6 Hz), 4.83 (d, J = 17 Hz), 4.38 (d, J = 17 Hz), 4.18 (q, J = 7 Hz), 4.12 (q, J = 7 Hz), 3.58 (1H, q, J = 13, 12 Hz), 3.44 (d, J = 17 Hz), 3.29 (d, J = 17 Hz), 2.88 (1H, q, J = 13, 5Hz), 1.24 (t, J = 7 Hz), 1.22 (t, J = 7 Hz); ^{13}Cmr ($CDCl_3$)δ: 168.2, 167.5, 155.0 (carbonyl), 134.2, 132.1, 129.8, 129.2, 129.0, 127.6, 123.7 (aromatic), 65.4 (S*C*H(H)Ph), 62.5, 61.4 (OCH_2), 51.6, 51.1 (Ft*CH*), 49.2, 47.4 (NCH_2CO), 28.9 (SCH_2), 14.1 (CH_3); ir(KBr): 1770 (Ft), 1730 (ester), 1715 (Ft), 1667 (amide I) cm^{-1}; ms (50°C, 70 eV) *m/e* (relative intensity): 424.1097 (9), 338.0694 (20.7), 337.0655 (100), 200.0099 (41.7), 173.0482 (26.9), 172.0401 (24.5), 121.0109 (20.7), 118.0658 (78), 104.0293 (28.8).

Synthesis of ***15*** *(R = CH_3)*

L-Cysteine hydrochloride monohydrate (10.0 g, 57.1 mmol) was dissolved in 50% ethanol (175 mL) under nitrogen, benzaldehyde (7.0 mL, 63 mmol) was added in one portion, and the flask was sealed under nitrogen. The thiazolidine **22** began to crystallize out after 3.5 h and the flask was then stored for 16 h at −10°C. The product was collected by filtration (8.32 g, 70%), mp 163–164.5°C (lit. (16) mp 159–160°C). In a second preparation, L-cysteine hydrochloride (10.0 g) and potassium acetate (6.0 g, 61.5 mmol) were added to 50% aqueous ethanol (175 mL). Benzaldehyde (7.0 mL, 7.29 g, 68.7 mmol) was added to the suspension, and the resulting mixture was stirred for 5 min at room temperature to give a clear, homogeneous solution. Stirring was continued at room temperature for an additional 25 min during which time a white crystalline material began to precipitate. The reaction mixture was transferred to an ice-water bath and allowed to stand at 0°C for 24 h. The compound was then collected by filtration and air dried. The crystals were dissolved in hot ethanol (800 mL), the solution was filtered, and the filtrate allowed to cool to room temperature and then overnight in an ice-water bath. Filtration afforded 8.93 g (75%), mp 163–165°C (dec). The material was identical in all respects with that prepared above.

The thiazolidine **22** (2.68 g, 12.87 mmol) was added to water (20 mL), and the suspension was cooled to 0°C. Aqueous sodium hydroxide (10.9 *N*) was added dropwise until the mixture became homogeneous and the pH reached 8.0–9.0. Acetic anhydride (5.26 g, 51.48 mmol) was then added to the solution over a 20 min period, in five portions. During the addition the pH was maintained in the range 8–10 by addition of sodium hydroxide. After the addition of acetic anhydride was complete, the reaction mixture was removed from the ice-water bath and stirred at room temperature for 40 min, the pH being maintained at 8–10 by addition of sodium hydroxide. Acidification to pH 2 with dilute hydrochloric acid precipitated a white solid, which was collected and air dried. The material was dissolved in 20 mL of hot ethanol, filtered to remove some insoluble material and evaporated. The residue was dissolved in 70 mL of water/ethanol (10:1), hot water (55 mL) was added, and the solution was allowed to cool to room temperature. Further cooling in an ice-water bath precipitated 1.26 g (39%) of **23** (R = CH_3) as a white crystalline solid, mp 151–152°C; ^{1}Hmr ($CDCl_3$/DMSO-d_6)δ: 7.8–7.2 (5H, m), 6.20 (1H, s), 4.8 (1H, m), 3.3 (2H, m), 1.87 (3H, s); ^{13}Cmr (0.1 *N* NaOD)δ: 176.3, 175.5, 173.0 (carbonyl), 67.8, 67.1 (methines), 34.3, 32.3 (SCH_2), 22.6, 22.2 (acetyl); ir(KBr): 1715 (carboxyl), 1610 (amide) cm^{-1}.

The thiazolidine **23** (R = CH_3) (1.08 g, 4.30 mmol) was dissolved in methylene chloride (50 mL). *N*-Ethoxycarbonyl-2-ethoxy-1,2-dihydroquinoline (EEDQ) (1.06 g, 4.30 mmol) and then glycine ethyl ester hydrochloride (0.60 g, 4.30 mmol) were added to the methylene chloride solution (this particular order of mixing appears to be essential). Triethylamine (0.44 g, 4.30 mmol) was then added and the suspension was

stirred at room temperature for 16 h. The methylene chloride solution was extracted with aqueous 5% sodium bicarbonate (2 × 30 mL) and aqueous 5% hydrochloric acid (2 × 30 mL). The organic layer was dried over anhydrous magnesium sulfate, filtered, evaporated, and dried under high vacuum to give 1.40 g of crude **15** (R = CH_3) as a yellow-white foam. Crystallization from hot ethyl acetate (10 mL) followed by recrystallization from hot ethyl acetate gave 0.98 g (68%) of **15** (R = CH_3) as a white crystalline solid, mp 147.5–148.5°C; ^{1}Hmr ($CDCl_3$, 340 K)δ: 7.7–7.1 (6H, m), 6.12 (1H, bs), 5.10 (1H, dd, J = 6, 5 Hz), 4.24 (2H, q, J = 7 Hz), 4.07 (2H, d, J = 5 Hz), 3.65 (q, J = 5, 12 Hz), 3.18 (q, J = 6, 12 Hz), 2.00 (3H, s), 1.28 (3H, t, J = 7 Hz); ^{1}Hmr ($CDCl_3$, 300 K)δ: 7.8–7.2 (6H, m), 6.05 (1H, bs), 5.14 (1H, dd, J = 5, 6 Hz), 4.24 (2H, q, J = 2, 7 Hz), 4.12 (2H, d, J = 6 Hz), 3.66 (1H, q, J = 5, 12 Hz), 3.18 (1H, q, J = 6, 12 Hz), 2.00 (3H, s), 1.28 (3H, t, J = 7 Hz); ^{13}Cmr ($CDCl_3$)δ: 171.5, 169.9, 169.5 (carbonyl), 139.9, 128.9, 128.4, 126.7 (phenyl), 67.2, 65.0 (methine carbons), 61.4 (OCH_2), 31.3 (SCH_2), 23.0 (acetyl), 14.2 (CH_2CH_3); ir(KBr): 3395 (NH), 1738 (ester) cm^{-1}; ms (50°C, 70 eV) *m/e* (relative intensity >20%): 336 (M^+, 6), 293 ($M - CH_2CO$, 10), 206 ($C_{10}H_{10}N_2OS^+$, 3), 179 (30), 164 (44), 43 (100). *Anal.* calcd. for $C_{16}H_{20}N_2O_4S$: C 57.12, H 5.99; found: C 56.87, H 6.05.

*Synthesis of **15** (R = Ph)*

The thiazolidine **22** (5.77 g, 25.57 mmol) was added to water (30 mL), and the resulting suspension was cooled to 0°C and aqueous sodium hydroxide (13.4 *N*) was added until the mixture became homogeneous and the solution had a pH of 8.0–9.0. Benzoyl chloride (15.58 g, 110.8 mmol) was then added with stirring at a rate of 0.25 mL/min. During this addition the pH of the mixture was maintained in the range 8–10 by addition of sodium hydroxide solution. After the addition was complete, the reaction mixture was removed from the ice-water bath and stirred at room temperature for 40 min, the pH being maintained at 8–10. Filtration, followed by acidification to pH 2 with dilute hydrochloric acid, precipitated a light yellow product which was collected and air dried. The crude product was dissolved in hot ethanol (150 mL), the solution was filtered, and the filtrate reduced in volume to 50 mL. Cooling to 0°C gave 5.31 g of **23** (R = Ph) as a white crystalline solid. Recrystallization from hot ethanol (45 mL) gave 4.62 g (53%) as a white crystalline solid, mp 156.5–158°C; ^{1}Hmr ($CDCl_3$)δ: 11.13 (1H, s), 7.28 (10H, b), 6.13 (1H, bs), 5.13 (1H, t, J = 7 Hz), 3.34 (2H, d, J = 7 Hz); ir (KBr): 3300–2100, 1710, 1590, 1602 cm^{-1}.

The thiazolidine **23** (R = Ph) (2.24 g, 7.15 mmol) was dissolved in methylene chloride (100 mL). EEDQ (1.77 g, 7.15 mmol) and then glycine ethyl ester hydrochloride (1.00 g, 7.15 mmol) were added to the methylene chloride solution. The thiazolidine and EEDQ dissolved instantly, but the glycine ethyl ester hydrochloride remained in suspension. Triethylamine (0.73 g, 7.15 mmol) was added to the suspension, and the reaction mixture was stirred at room temperature for 17.5 h. The methylene chloride solution was extracted with aqueous 5% sodium bicarbonate (2 × 50 mL) and aqueous 5% hydrochloric acid (2 × 50 mL). The organic layer was dried over anhydrous magnesium sulfate, filtered, evaporated, and the residue dried under high vacuum to give 2.26 g of material as a white foam. Crystallization from ethyl acetate/petroleum ether at −15°C gave 1.09 g (38%) of **15** (R = Ph) as a white crystalline solid, mp 156.5–157.5°C; ^{1}Hmr ($CDCl_3$)δ: 7.70 (1H, bs), 7.30 (10H, s), 6.16 (1H, bs), 5.17 (1H, t, J = 7.5 Hz), 4.19 (2H, q, J = 7 Hz), 4.06 (2H, d, J = 7.5 Hz), 3.67 (1H, q, J = 8, 12 Hz), 3.20 (q, J = 7, 12 Hz), 1.27 (3H, t, J = 7 Hz); ir (KBr): 3270(s), 3066(m), 2967(w), 2917(w), 1751 and 1747(s), 1724(s), 1687(s), 1614(s), 1568(s) cm^{-1}.

*Stability of **15** (R = CH_3) in Acetic Anhydride*

The thiazolidine (0.1081 g) was dissolved in 1.0 mL of Ac_2O and the solution was heated for 3 h at 79–80°C. The solvent was then removed under high vacuum. The ^{1}Hmr spectrum of the residue was identical to that of **15** (R = CH_3).

*Rearrangement of **15** (R = CH_3) to **9**a in TFA*

The thiazolidine (0.0668 g) was dissolved in anhydrous trifluoroacetic acid (1 mL), and the solution was allowed to stand at room temperature for 1 h. The solvent was then removed and the residue dried under high vacuum and purified by plc (silica gel, four developments with benzene/methanol 5:1) to give three bands. The leading band (7.5 mg), R_f 0.54–0.62, was **15** (R = CH_3). The middle band (32.6 mg), R_f 0.33–0.50, was ***9a***. The trailing band, R_f 0.23–0.30, contained insufficient material for characterization.

*Rearrangement of **15** (R = Ph) to **10**b in TFA*

The thiazolidine (0.2002 g) was dissolved in anhydrous trifluoroacetic acid (2.0 mL), and the solution was allowed to stand at room temperature for 1 h. The solvent was then removed and the residue dried under high vacuum and subjected to plc (silica gel, three developments with benzene/methanol 5:1) to give three bands. The trailing band, R_f 0.59–0.66, was unreacted thiazolidine. The leading band (55.9 mg), R_f 0.79–0.88, was identified as ***10b***; ^{1}Hmr ($CDCl_3$)δ: 7.93–6.60 (6H, m, 1H exchanges with D_2O), 7.36 (5H, s), 5.78 (1H, s), 4.97 (1H, sextet, J = 5, 6, 13 Hz), 4.47 (1H, d, J = 17 Hz), 4.15 (2H, q, J = 7 Hz), 3.39 (1H, d, J = 17 Hz), 3.33 (2H, *AB*X, J = 13, 13, 6 Hz), 1.23 (3H, t, J = 7 Hz); ir (KBr): 3340 (m), 1737 (s), 1663 (s), 1627 (s) cm^{-1}; ms *m/e* (relative intensity >10%): 398 (M^+, 4.5), 277 (12), 192 (48), 190 (50), 118 (25), 105 (100), 91 (41), 77 (43), 51 (10).

Acknowledgements

We thank the National Research Council of Canada for financial support of this research, for the award of a 1967 Science Scholarship, and for the award of a Postdoctoral Fellowship. We also thank Mr. J. D. Kronis for assistance with the high resolution mass spectra.

1. (*a*) Y. Oikawa and O. Yonemitsu. J. Chem. Soc. Perkin Trans. I, 1479 (1976), and references cited therein; (*b*) H. L. Yale. J. Heterocycl. Chem. **15**, 331 (1978).
2. B. Stridsberg and S. Allenmark. Acta Chem. Scand. B, **28**, 591 (1974); **30**, 219 (1976).
3. S. Oae and T. Numata. Tetrahedron, **30**, 2641 (1974).
4. (*a*) S. Wolfe and P. M. Kazmaier. Can. J. Chem. **57**, 2388 (1979); (*b*) **57**, 2397 (1979); (*c*) S. Wolfe, P. M. Kazmaier, and H. Auksi. Can. J. Chem. **57**, 2404 (1979).
5. E. A. Steck. J. Am. Chem. Soc. **74**, 5547 (1952).
6. C. Berse and G. Dupuis. Can. J. Chem. **43**, 2174 (1965).
7. R. Ponci, A. Baruffini, and F. Gialdi. Farmaco Ed. Sci. **18**, 305 (1963); Chem. Abstr. **59**, 7370d (1963).
8. I. Nagakura, H. Oka, and Y. Nitta. Heterocycles, **3**, 453 (1975).
9. B. V. De Pamphilis, B. A. Averill, T. Herskovitz, L. Que, Jr., and R. H. Holm. J. Am. Chem. Soc. **96**, 4159 (1974).
10. V. du Vigneaud, J. L. Wood, and O. J. Irish. J. Biol. Chem. **129**, 171 (1939).
11. W. D. Cash. J. Org. Chem. **27**, 3329 (1962).

12. C. M. STEVENS, C. A. JOHNSON, and R. WATANABE. J. Biol. Chem. **212**, 49 (1955).
13. D. B. HOPE, V. V. S. MURTI, and V. DU VIGNEAUD. J. Am. Chem. Soc. **85**, 3686 (1963).
14. L. GOODMAN, L. O. ROSS, and B. R. BAKER. J. Org. Chem. **23**, 1251 (1958).
15. A. STOLL and E. SEEBECK. Helv. Chim. Acta, **32**, 866 (1949).
16. M. SCHUBERT. J. Biol. Chem. **114**, 347 (1936).
17. R. PARTHASARATHY, B. PAUL, and W. KORYTNYK. J. Am. Chem. Soc. **98**, 6634 (1976).
18. L. SZILÁGYI and Z. GYÖRGYDEÁK. J. Am. Chem. Soc. **101**, 427 (1979).
19. H. AUKSI and S. WOLFE. To be published.
20. S. KUKOLJA, R. D. G. COOPER, and R. B. MORIN. Tetrahedron Lett. 3381 (1969); S. WOLFE, C. FERRARI, and W. S. LEE. Tetrahedron Lett. 3385 (1969).
21. A. A. ABODERIN, G. R. DELPIERRE, and J. S. FRUTON. J. Am. Chem. Soc. **87**, 5469 (1965).
22. Aldrich catalog handbook of organic and biochemicals. The Aldrich Chemical Company, Ltd., Milwaukee, WI. 1974. p. 334.

Conformational analysis of acyclic compounds with oxygen–sulphur interactions. Part VI.[1] Some 1-thioderivatives of 2-propanol and its acetates

FELIPE ALCUDIA, JOSÉ L. GARCÍA RUANO, AND JESÚS RODRÍGUEZ

Departamento de Química Orgánica, Facultad de Ciencias, Universidad Autónoma de Madrid, Spain

AND

FÉLIX SÁNCHEZ

Instituto de Química Orgánica, (C.S.I.C.), Madrid-6, Spain

Received January 12, 1979

FELIPE ALCUDIA, JOSÉ L. GARCÍA RUANO, JESÚS RODRÍGUEZ, and FÉLIX SÁNCHEZ. Can. J. Chem. **57**, 2426 (1979).

A conformational study of 1-X-2-propanol (X = SH, SMe, SOMe, SO_2Me, $^+SMe_2$) and their *O*-acetyl derivatives (X = SMe, SOMe, SO_2Me, and $^+SMe_2$) is reported. From the relative values of the vicinal coupling constants in ^1H nmr spectra it has been possible to establish the conformational preference. When a density of opposite charge is supported by heteratoms, polar factors determined a great predominance of that conformation in which the sulphur function has an *anti*-relationship with respect to the methyl group. In thiol and thioethers the conformational preference is not so marked.

FELIPE ALCUDIA, JOSÉ L. GARCÍA RUANO, JESÚS RODRÍGUEZ et FÉLIX SÁNCHEZ. Can. J. Chem. **57**, 2426 (1979).

On rapporte une étude conformationnelle des X-1 propanols-2 (X = SH, SMe, SOMe, SO_2Me, $^+SMe_2$) et de leurs dérivés *O*-acétylés. A partir des valeurs relatives de leurs constantes de couplage vicinal dans les spectres rmn ^1H, on a pu établir la préférence conformationnelle. Lorsque les hétéroatomes supportent des densités opposées de charges, des facteurs polaires favorisent une grande prédominance de la conformation dans laquelle la fonction sulfurée se trouve dans une relation *anti* par rapport au groupe méthyle. Dans le cas du thiol et du thioéther, la préférence conformationnelle n'est pas aussi marquée.

[Traduit par le journal]

Introduction

The conformational analysis of some 2-thioderivatives of 1-phenylethanol and 1,2-diphenylethanol has been previously reported by us (1–4). Conformational preferences could be explained by taking into account polar and steric factors. However, we have made a theoretical study by CNDO/2 of 2-methylsulphonyl-1-phenylethanol (5) in which the results obtained suggest that stabilizing interactions between the phenyl group and the sulphur atom must also be considered. On the other hand, contrary to the experimental evidence, the intramolecular hydrogen bonding makes an important contribution to the conformational stability of rotamers around the C-S bond.

In the present paper, the conformational analysis of compounds **1–9** are reported in order to clarify these points.

The solubility of these compounds is greater than that in previous series and, as well, the phenyl group has been substituted by a methyl one. This suggests that their conformational study would throw some light on the above questions.

[1]For Parts I–V, see refs. 1–5.

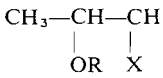

1 R = H, X = SH
2 R = H, X = SCH_3
3 R = H, X = $SOCH_3$
4 R = H, X = SO_2CH_3
5 R = H, X = $^+S(CH_3)_2$
6 R = Ac, X = SCH_3
7 R = Ac, X = $SOCH_3$
8 R = Ac, X = SO_2CH_3
9 R = Ac, X = $^+S(CH_3)_2$

Results and Discussion

The synthesis of compounds **1–9** was carried out as indicated in Scheme 1 by means of procedures described in the Experimental.

The reaction of compound **2** with metaperiodate yields a mixture of two diastereomers. In this paper only one of them has been isolated and studied, but its configuration has not yet been determined. Compound **7** has been obtained from this isomer.

The method used for evaluating the conformational populations was the study of coupling constants[2] of the protons on C-1 and C-2. The possible

[2]The δ values are of little use in this analysis due to the difficulty in predicting substituent effects and the lack of comparable model systems.

0008-4042/79/182426-08$01.00/0

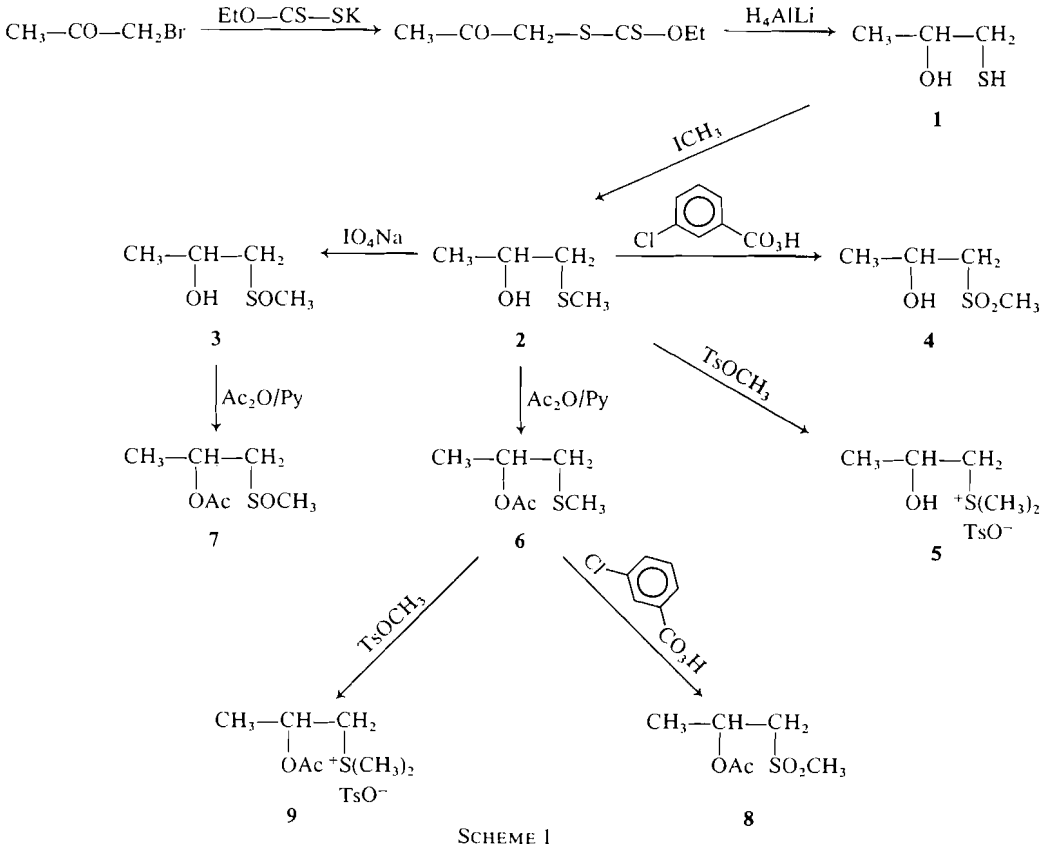

SCHEME 1

conformations of compounds **1–9** are given in Fig. 1. From the equilibrium shown in this figure and taking into account that $J_{trans} \gg J_{gauche}$, it may be deduced that very different values of the vicinal coupling constants are only compatible with a marked preference for conformations *A* or *B*.

The observed spectral parameters suggest a different conformational behaviour of compounds **1**, **2**, and **6** with respect to the others and so an independent study of both types of compounds was undertaken.

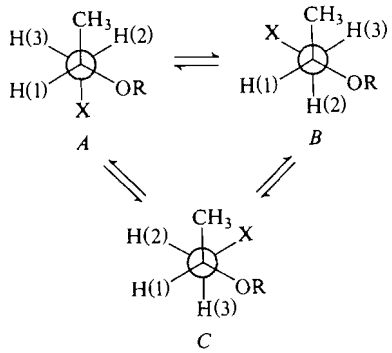

FIG. 1. Conformational equilibria of compounds **1–9** around the C(1)—C(2) bond.

The δ and *J* values obtained from computer analysis of the ^{1}H nmr spectra for compounds **3–5**, recorded in $CDCl_3$ and DMSO-d_6 at several concentrations, are given in Table 1.

The $J_{1,2}$ value is larger than $J_{1,3}$ in all cases, which is compatible with a marked predominance of either *A* or *B* conformations. In all other cases similar values for the two vicinal coupling constants were observed.

The spectra for sulphone **4** in DMSO-d_6 have shown that the proton on C-2, which appears at lower field (considered to be *gauche* with respect to H-1 from the J_{vic} values), is further coupled to the hydroxy proton ($^4J_{H-C-C-O-H} \simeq 0.5$ Hz). This atom sequence is typical in carbohydrate compounds in which the long range coupling constants are only observed when a *W* planar arrangement between involved protons becomes possible (6, 7). In compound **4**, this arrangement is only possible in the *A* conformer (Fig. 2). In addition, only one of the two methylene protons appears split as a consequence of this coupling and so we can exclude the possibility

TABLE 1. Chemical shifts and coupling constants of compounds **3–5**

Compound	Solvent	Concentrations (% w/v)	Chemical shifts (δ)				Coupling constants (J/Hz)						
			H-1	H-2	H-3	H-4	$J_{1,2}$	$J_{1,3}$	$J_{2,3}$	$J_{1,4}$	$J_{3,4}$	$J_{Me,*2}$	$J_{Me,*3}$
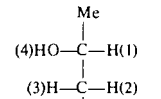 **3**	$CDCl_3$	10	4.366	2.829	2.783	4.673	10.8	1.7	−13.1	—	—	—	—
		5	4.406	2.842	2.774	4.491	10.5	1.9	−13.1	—	—	—	—
		1	4.511	2.879	2.719	3.333	9.7	2.3	−13.2	—	—	—	—
	$^2H_6DMSO$	10	4.037	2.734	2.697	4.984	10.5	2.1	−12.9	5.1	—	—	—
		5	4.037	2.730	2.695	4.981	10.5	2.2	−13.0	5.7	—	—	—
		1	4.034	2.726	2.693	4.976	10.9	1.8	−12.9	5.3	—	—	—
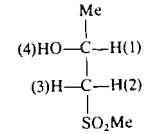 **4**	$CDCl_3$	15	4.370	3.202	3.070	3.470	9.5	2.4	−14.5	—	—	0.4	0.9
		10	4.429	3.205	3.064	3.191	9.6	2.3	−14.5	—	—	0.5	0.8
		5	4.450	3.188	3.065	2.949	9.6	2.2	−14.5	—	—	0.6	0.8
		1	4.474	3.163	3.070	1.971	10.3	1.7	−14.4	—	—	0.5	0.7
		0.1	4.485	3.165	3.075	1.820	9.8	1.8	−14.5	—	—	0.7	0.6
	$^2H_6DMSO$	10	4.116	3.277	3.114	5.066	8.6	3.5	−14.7	5.2	0.4	0.6	0.4
		5	4.113	3.222	3.038	5.087	8.5	3.4	−14.7	5.2	0.4	0.7	0.5
		1	4.106	3.226	3.047	5.124	8.6	3.4	−14.3	5.7	0.5	0.6	0.5
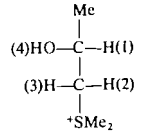 **5**	$^2H_6DMSO$	10	4.089	3.329	3.345	5.586	9.3	3.2	−12.8	5.0	—	—	—
		5	4.097	3.324	3.432	5.596	9.3	3.3	−12.9	5.0	—	—	—
		1	4.090	3.319	3.416	5.570	9.3	3.3	−12.8	5.0	—	—	—

*Methyl of the methylsulphonyl group.

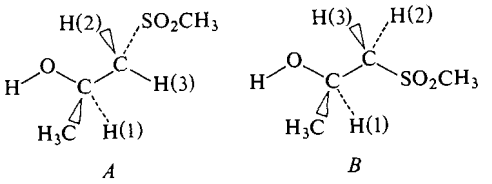

FIG. 2. Spatial arrangement of the H(3) and hydroxylic protons in conformations *A* and *B*.

of *B* being the preferred rotamer. On the other hand, this long range coupling permits us to carry out the unequivocal assignment of H-2 and H-3.

In previous studies (1–4), sulphoxides, sulphones, and the sulphonium salts showed a similar conformational preference. Therefore, it seems reasonable to assume that in sulphoxide **3** and in sulphonium salt **5**, the *A* conformation should be the most stable, as was observed in sulphone **4**.

The predominance of the *A* conformation can be explained assuming a strong electrostatic attraction between the heteroatoms, since the sulphur atom supports some positive charge. The intramolecular hydrogen bonding contribution is not negligible, at least in sulphone **4**, where conformational preference, deduced from the relative values of coupling constants, increases with dilution and decreases when the spectra were recorded in DMSO-d_6, as can be expected. On the other hand, the influence of the polarity change can be explained by taking into account the different association of solvents with conformers *A* and *B*. Nevertheless, the preference shown by salt **5** suggests that the relative contribution of the intramolecular hydrogen bonds, with respect to the electrostatic interaction, may be unimportant.

Another interesting feature is based on the long range coupling constants $^4J_{H-C-S-CH_2}$, observed in sulphone **4**. The staggered conformations around the C—S bond are indicated in Fig. 3. The $^4J_{Me,H(2)}$ and $^4J_{Me,H(3)}$ values are indicative of conformational populations of A_2 and A_1 respectively, as the most favourable spatial arrangement (*W*) between involved protons is present in these conformations. These values indicate that there is a preference for conformation A_1 in concentrated solutions of $CDCl_3$. This situation has been previously reported (1, 8) and has been attributed to an Me–OH attraction as a result of the delocalization of positive charge from the sulphur on the methyl group. The decrease in preference for A_1 with dilution, however, suggests that the shift of conformational equilibrium is the result of an inter/intramolecular interaction balance since rotamer A_1 presents the most favourable arrangement for an Me–OH attraction and intermolecular association by hydrogen bonds, whereas in A_2 and A_3 intramolecular hydrogen bonding is possible. This could explain the disagreement between the theoretical calculations (5) and the experimental finding (1) on 2-methylsulphonyl-1-phenylethanol. The theoretical study showed that rotamers A_2 and A_3 in the vapour state were more stable than A_1, due to the possibility of forming intramolecular hydrogen bonds.

The ^{1}H nmr parameters of compounds **7**–**9** are given in Table 2. From the relative values of vicinal coupling constants it can be deduced that the preference for conformation *A* in the *O*-acetyl derivatives **7** and **8** is less marked than in **3** and **4**. This can be explained by differences in steric and hydrogen bond effects between both types of compounds. However, the small influence of hydrogen bonds (deduced from the results obtained in sulphone **4** in DMSO-d_6) and the steric effect (as indicated by the results in salt **9** with respect to salt **5**), suggest additional factors, such as the electrostatic interactions between oxygen of the acetyl group and the heteroatoms in the sulphur function. These interactions ought to be stabilizing in salt **9** and more destabilizing in sulphone **8** than in sulphoxide **7**. Clearly, the relative contribution of the electrostatic interactions will be less in DMSO-d_6 as solvent. Taking into account the three mentioned effects the results obtained can be satisfactorily explained.

From the $^4J_{Me,H(2)}$ and $^4J_{Me,H(3)}$ values, the major contribution of the A_1 rotamer in the equilibrium $A_1 \rightleftharpoons A_2 \rightleftharpoons A_3$ can be deduced. Accordingly, the dilution effect is very small, since the intermolecular associations are less important in the acetoxy sulphone **8**, whereas the intramolecular ones will destabilize conformations A_2 and A_3 by electrostatic repulsion.

The ^{1}H nmr parameters of compounds **1**, **2**, and **6** are given in Table 3. The results can be rationalized according to the following points.

(*i*) There are no important differences in the $J_{1,2}$ and $J_{1,3}$ values in compounds **1** and **2**, and so only a slight preference for *A* or *B* conformations can be established.

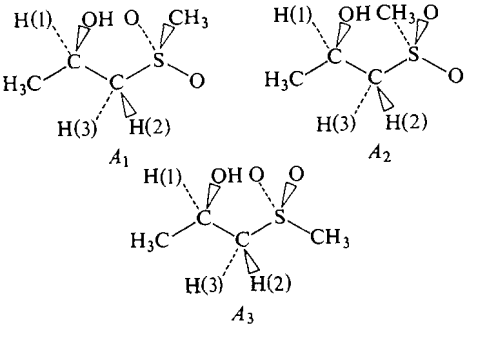

FIG. 3. Rotamers of compounds **6** around the C—S bond.

TABLE 2. Chemical shifts and coupling constants of compounds **7–9**

Compound	Solvent	Concentrations (% w/v)	Chemical shifts (δ)			Coupling constants (*J*/Hz)				
			H-1	H-2	H-3	$J_{1,2}$	$J_{1,3}$	$J_{2,3}$	$J_{Me,*3}$	$J_{Me,*2}$
7	$CDCl_3$	10	5.313	2.956	2.886	8.8	3.9	−13.3	—	—
		5	5.313	2.943	2.882	9.0	4.1	−13.3	—	—
		1	5.309	2.931	2.881	8.9	3.7	−13.2	—	—
	$^2H_6DMSO$	10	5.145	3.054	2.909	9.4	3.5	−13.5	—	—
		5	5.141	3.052	2.907	9.4	3.5	−13.4	—	—
		1	5.140	3.050	2.905	9.4	3.5	−13.4	—	—
8	$CDCl_3$	10	5.369	3.389	3.152	7.6	4.5	−14.8	0.8	0.5
		5	5.367	3.374	3.127	7.4	4.6	−14.9	0.9	0.5
		1	5.365	3.366	3.115	7.3	4.7	−14.8	0.9	0.5
	$^2H_6DMSO$	10	5.238	3.539	3.391	8.1	4.0	−14.8	0.7	0.5
		1	5.233	3.540	3.394	8.3	4.0	−14.8	0.8	0.5
9	$CDCl_3$	10	5.135	3.595	3.857	8.9	2.9	−13.6	—	—
		5	5.151	3.611	3.916	9.2	2.7	−13.6	—	—
		1	5.174	3.616	3.992	9.1	2.5	−13.7	—	—
	$^2H_6DMSO$	5†	5.174	3.620	3.620	12.0‡		—	—	—

*Methyl of the methylsulphonyl group.
†Deceptively simple spectra were obtained in all concentrations.
‡$J_{1,2} + J_{1,3}$ value.

TABLE 3. Chemical shifts and coupling constants of compounds **1**, **2**, and **6**

Compound	Solvent	Concentrations (% w/v)	Chemical shifts (δ) H-1	H-2	H-3	H-4	H-5	Coupling constants (J/Hz) $J_{1,2}$	$J_{1,3}$	$J_{2,3}$	$J_{1,4}$	$J_{2,5}$	$J_{3,5}$
Me (4)HO—C—H(1) (3)H—C—H(2) SH(5) **1**	$CDCl_3$	30	3.659	2.374	2.464	3.409	1.370	6.7	4.6	−13.5	—	8.5	8.5
		10	3.804	2.498	2.672	2.658	1.400	7.3	4.1	−13.5	—	8.9	8.4
		5	3.774	2.489	2.690	2.435	1.376	7.4	4.0	−13.5	—	8.9	8.4
		1	3.806	2.488	2.714	2.160	1.371	7.5	4.0	−13.6	—	9.2	8.3
		0.25	3.805	2.488	2.714	1.915	1.359	7.5	3.9	−13.7		9.2	8.2
	$^2H_6DMSO$	5*	3.645	2.454	2.454	4.697	—	12.0†		—	4.9	—	—
Me (4)HO—C—H(1) (3)H—C—H(2) SMe **2**	$CDCl_3$	40	3.549	2.321	2.378	—	—	7.1	5.4	−13.5	—	—	—
		10	3.857	2.479	2.640	—	—	8.4	4.0	−13.6	—	—	—
		5	3.850	2.462	2.652	—	—	8.7	3.8	−13.6	—	—	—
		1	3.854	2.463	2.663	—	—	8.7	3.7	−13.7	—	—	—
	$^2H_6DMSO$	10	3.734	2.406	2.502	4.601	—	6.4	6.0	−13.2	4.8	—	—
		5	3.746	2.401	2.497	4.634	—	6.4	5.9	−13.1	4.8	—	—
		1	3.746	2.403	2.499	4.610	—	6.4	6.0	−13.2	4.8	—	—
Me AcO—C—H(1) (3)H—C—H(2) SMe **6**	$CDCl_3$	10	5.045	2.580	2.676	—	—	6.2	6.3	−13.8	—	—	—
		5	5.050	2.583	2.678	—	—	6.2	6.3	−13.8	—	—	—
		1	5.052	2.582	2.678	—	—	6.2	6.3	−13.8	—	—	—
	$^2H_6DMSO$	5*	4.915	2.620	2.620	—	—	12.1†		—	—	—	—

*Deceptively simple spectra were obtained in all concentrations.
†$J_{1,2} + J_{1,3}$ value.

TABLE 4. O—H stretching frequency of compounds **1** and **2** ($c < 10^{-2}$ *M*) in CCl_4

Compound	Free O—H (cm^{-1})	Intramolecular bonded O—H (cm^{-1})	$\Delta\nu$ (cm^{-1})
1	3616	3550	66
2	3614	3522	92

Infrared spectra recorded in CCl_4 at low concentration ($<10^{-2}$ *M*) have shown the presence of intramolecular hydrogen bonds in these compounds. The relative intensity of the associated OH band is larger than the free OH one (see Table 4) in both compounds and gives rise to the idea that the *A* rotamer is the most populated (9), as the intramolecular associations are not possible in *B*.

The variation of the J_{vic} values with changes in concentration and in solvent polarity supports the above assumption. Thus, the conformational preference increased with dilution (greater differences between vicinal coupling constants are observed) due to the predominance of intra- over intermolecular interactions. On the other hand, this preference disappears in compounds **2**[3] when DMSO-d_6 is used as a solvent.

(*ii*) In thioether **6** values of the vicinal coupling constants are in agreement with the impossibility of forming intramolecular hydrogen bonds and the small influence of dilution suggests that steric interactions may now be responsible for the conformational equilibrium shift. On the other hand, the values $J_{1,2} + J_{1,3}$ in compounds **1**, **2**, and **6** remain constant with dilution in all studied solvents. This is only possible if the contribution of the conformation *C* to the equilibrium is small or zero, due probably to steric effects.

(*iii*) Comparison of the $J_{1,2}$ and $J_{1,3}$ values for compound **6** with those for 2-thiomethyl-1-phenylethanol **10**, previously studied (2), is of great interest. In the latter compound the preference for conformation *B* could be proved although the population of *A* was also important ($J_{1,3} = 7.9$ and $J_{1,2} = 5.5$), whereas in compound **6** there is no preference ($J_{1,2}$ and $J_{1,3} = 6.2$–6.3). From the analysis of the interactions in compounds **6** and **10** it can be deduced that conformation *A* is equally stabilized in both compounds, but the rotamer *B* has an Me–SMe interaction in **6** and a Ph–SMe one in **10**; this latter interaction must be more stabilizing than Me–SMe. Taking into account that the steric hindrance of the phenyl group is larger than that of methyl (10), other factors have to be invoked to explain stability differences which must also be independent of solvent polarity.

The theoretical calculations by CNDO/2 of the different conformations of 2-methylsulphonyl-1-phenylethanol (5) showed a stabilizing interaction Ph–SO_2Me (ca. 4 kcal) due to d-π overlap of the sulphur atom with the phenyl group. Similar interactions may be responsible for the lower destabilization of the *gauche* Ph–SMe interaction with respect to the Me–SMe one.

[3]Compound **1** shows a deceptively simple spectrum in DMSO-d_6 at any concentration and so it is only possible to know the $J_{1,2} + J_{1,3}$ value.

Experimental

^{1}H nmr spectra were recorded on a Varian XL-100-15 spectrometer operating at 100 MHz by Fourier transform technique, using 16K of core in a Nicolet 1180 stored programme computer. The signal of the deuterated solvent was employed for deuterium field-frequency lock and TMS as an internal reference. The analyses of the spectra were carried out using a LAOCOON III programme (11, 12) on a Nicolet 1180 computer. We estimate the reliability of all values as 0.1 Hz, and the root mean square deviations for the calculated and the experimental lines were usually better than 0.05 Hz. Infrared spectra were recorded on a Pye-Unicam SP-1100 spectrometer. The studies on the intramolecular hydrogen bondings were carried out on a Beckman IR-4240 spectrophotometer. Mass spectra were obtained using a Hitachi Perkin Elmer RMU-6M spectrometer at 70 eV. Melting points were determined on a Kofler hot-stage and are, like the boiling points, uncorrected.

1-Mercapto-2-propanol ***1***

This compound was prepared by reaction of potassium ethylxanthate with bromoacetone following the procedure reported by Djerassi (13) for similar compounds; bp 50–52°C/10 Torr (lit. (14) bp 51°C/8 Torr).

1-Methylthio-2-propanol ***2***

A solution of **1** (7.99 g, 0.087 mol) in absolute ethanol (90 mL) was slowly added to a solution of sodium (2 g) in anhydrous ethanol (200 mL) and cooled at 0°C. It was then treated with a solution of methyl iodide (12 g, 0.087 mol) in ethanol and the reaction mixture was allowed to stand overnight at room temperature with constant stirring. Water (160 mL) was added and it was extracted with chloroform (3 × 75 mL). The chloroform extracts were dried ($MgSO_4$) and concentrated (rotary evaporator) to yield 7.1 g (77%) of **2**; bp 60–62°C/15 Torr (lit. (15) bp 55–58°C/10 Torr).

The Acetyl Derivative ***6***

This compound was prepared with acetic anhydride and pyridine, distilled at 68–70°C/15 Torr (lit. (16) 64–65°C/10 Torr).

1-Methylsulphonyl-2-propanol ***3***

To an ice-cooled solution of 3.2 g (0.015 mol) of sodium metaperiodate in 20 mL of water was added 1.62 g (0.015 mol) of **2**. The reaction mixture was stirred at 0°C for 4 h and was then allowed to stand overnight at room temperature. Ethanol (30 mL) was added and the sodium iodate formed was filtered. The solution was evaporated and treated with 50 mL of chloroform. The chloroform extracts were dried (Na_2SO_4) and concentrated to afford 1.8 g (97%) of **3** as a mixture of two diastereomers (two signals of similar intensity for the methyl group bonded to the sulphur atom in the ^{1}H nmr spectrum). The isolation of one of the diastereomers was carried out by repeated recrystallization from benzene, mp 89–91°C (lit. (17)

mp 89–90°C); ν_{max} (Nujol): 3277 and 1010 cm^{-1}; δ($CDCl_3$, 10%): 1.31 (3H, d, J = 6.2 Hz, CH_3—C), 2.63 (3H, s, CH_3—S), 2.83 (2H, m, —CH_2—), 4.35 (1H, m, —CH—), and 4.67 (1H, s, broad, OH). *Anal.* calcd. for $C_4H_{10}O_2S$: C 39.33, H 8.25, S 26.20; found: C 39.49, H 8.41, S 26.43.

The Acetyl Derivative **7**

This compound was prepared by reaction of isolated diastereomer **3** with acetic anhydride and pyridine; ν_{max} (Nujol): 1745, 1250, and 1010 cm^{-1}; δ($CDCl_3$, 10%): 1.39 (3H, d, J = 6.2 Hz, CH_3—CH), 2.03 (3H, s, CH_3—CO), 2.60 (3H, s, CH_3—S), 2.85 (2H, m, —CH_2—), 5.31 (1H, m, —CH—); significant peaks in ms *m/e*: 164 (M^+), 149, 121, 101 (base peak), 63, and 61.

1-Methylsulphonyl-2-propanol **4**

A solution of *m*-chloroperoxibenzoic acid (2.24 g, 0.013 mol) and 1-methylthio-2-propanol, **2** (0.53 g, 0.005 mol), in chloroform (50 mL) was stirred at room temperature for ca. 10 h. The solution was then washed with saturated aqueous sodium bicarbonate (200 mL), dried ($MgSO_4$), and concentrated to give 0.54 g (79%) of **4**. The solid was recrystallized from benzene, mp 67–69°C (lit. (18) mp 47–51°C); ν_{max} (Nujol): 3330, 1290, and 1125 cm^{-1}; δ($CDCl_3$, 10%): 1.32 (3H, d, J = 6.2 Hz, CH_3—C), 3.02 (3H, s, CH_3—S), 3.14 (2H, m, —CH_2—), 3.19 (1H, s, OH), and 4.41 (1H, m, —CH—). *Anal.* calcd. for $C_4H_{10}O_3S$: C 34.78, H 7.29, S 23.19; found: C 34.01, H 7.49, S 23.09.

The Acetyl Derivative **8**

This derivative was similarly obtained by reaction of **6** with *m*-chloroperoxibenzoic acid and recrystallized from CCl_4, mp 54–55°C; ν_{max} (Nujol): 1745, 1130, and 1050 cm^{-1}; δ($CDCl_3$, 10%): 1.41 (3H, d, J = 6.0 Hz, CH_3—CH), 2.06 (3H, s, CH_3—CO), 2.96 (3H, s, CH_3—S), 3.27 (2H, m, —CH_2—), and 5.37 (1H, m, —CH—).

Dimethyl(2-hydroxypropyl)sulphonium p-*Toluenesulphonate* **5**

A mixture of **2** (0.56 g, 0.0047 mol) and methyl *p*-toluenesulphonate (2 mL) was stirred at 30°C for 18 h. The reaction mixture was washed with ether (5 × 20 mL) and filtered to give 1.31 g (85%) of **5**. It was recrystallized from methanol, mp 120–122°C; ν_{max} (Nujol): 3330 cm^{-1}; δ(DMSO-d_6, 10%): 1.19 (3H, d, J = 6.0 Hz, CH_3—C), 2.27 (3H, s, CH_3—Ar), 2.87 (3H, s, CH_3—S), 2.89 (3H, s, CH_3—S), 3.35 (2H, m, CH_2), 4.09 (1H, m, OH), 5.57 (1H, d, CH), 7.07, and 7.45 (4H, AB system, J_{AB} = 8 Hz, aromatic H's). *Anal.* calcd. for $C_{12}H_{20}O_4S_2$: C 49.31, H 6.89, S 21.91; found: C 49.40, H 7.04, S 22.06.

The Acetyl Derivative **9**

This compound was similarly prepared from compound **6** by reaction with methyl *p*-toluenesulphonate. The purification of this compound by crystallization has not been possible due to its hydroscopic character. However, the spectroscopic data and the synthesis process are in accordance with its structure; ν_{max} (Nujol): 1750 cm^{-1}; δ($CDCl_3$, 10%): 1.27 (3H, d, J = 6.0 Hz, CH_3—CH), 1.99 (3H, s, CH_3—Ar), 3.07 (6H, s, $(CH_3)_2$—S), 3.75 (2H, m, CH_2), 5.13 (1H, m, CH), and 7.10–7.65 (4H, m, aromatic H's).

1. F. Alcudia, F. Farina, J. L. Garcia Ruano, and F. Sanchez. J. Chem. Soc. Perkin Trans. 2, 412 (1978).
2. F. Alcudia, F. Farina, J. L. Garcia Ruano, J. Rodriguez, and F. Sanchez. An. Quim. **74**, 481 (1978).
3. F. Alcudia, J. L. Garcia Ruano, J. Rodriguez, F. Farina, and F. Sanchez. J. Chem. Soc. Perkin Trans. 2, 564 (1979).
4. F. Alcudia, J. L. Garcia Ruano, J. Rodriguez, and F. Sanchez. An. Quim. **75**, 375 (1979).
5. F. Alcudia, J. L. Garcia Ruano, and C. Sieiro. J. Mol. Struct. **52**, 135 (1979).
6. J. C. Jochims, A. Seeliger, P. Lutz, and H. E. Driesen. Tetrahedron Lett. 4363 (1967).
7. J. C. Jochims and G. Taigel. Tetrahedron Lett. 5483 (1968).
8. M. K. Kaloustian, N. Dennis, S. Mager, S. A. Evans, F. Alcudia, and E. L. Eliel. J. Am. Chem. Soc. **98**, 956 (1976).
9. A. R. H. Cole and P. R. Jefferies. J. Chem. Soc. 4391 (1956).
10. E. L. Eliel, N. L. Allinger, S. J. Angyal, and G.A. Morrison. Conformational analysis. Interscience-Wiley, New York. 1965. pp. 44–45; M. Hanack. Conformational theory. Academic Press, New York. 1965. pp. 103–104.
11. A. A. Bothner-By and S. M. Castellano. J. Chem. Phys. **41**, 3863 (1964).
12. S. M. Castellano. $LAOCN_3$ in computer programs for chemistry. Vol. 1. *Edited by* D. F. Detar. Benjamin, New York. 1968. p. 10.
13. C. Djerassi, M. Gorman, F. X. Markley, and E. B. Oldenburg. J. Am. Chem. Soc. **77**, 568 (1955).
14. A. D. B. Sloan. J. Chem. Soc. C, 1252 (1969).
15. J. K. Kim, M. C. Findlay, C. Meredith, W. G. Henderson, and M. C. Caserio. J. Am. Chem. Soc. **95**, 2184 (1973).
16. K. S. Boustany and A. Jacot-Gillarmod. Chimia. **23**, 31 (1969).
17. M. Axelrod, P. Bichart, J. Jacobus, M. M. Green, and K. Mislow. J. Am. Chem. Soc. **90**, 4835 (1968).
18. M. Numata, M. Yamaoka, and K. Masuda. Chem. Pharm. Bull. **18**, 221 (1970).

The nature of the NADP complex with manganese(II) ions as studied by proton and phosphorus magnetic resonance[1]

M. KIRK GREEN AND GEORGE KOTOWYCZ

Department of Chemistry, University of Alberta, Edmonton, Alta., Canada T6G 2G2

Received February 1, 1979

M. KIRK GREEN and GEORGE KOTOWYCZ. Can. J. Chem. **57**, 2434 (1979).

Proton and phosphorus magnetic resonance techniques have been applied to study the conformation of the complex formed between Mn(II) ions and nicotinamide adenine dinucleotide phosphate (NADP) in aqueous solutions at a pH of 7.5 and 20°C. The dipolar correlation time (τ_c) for the Mn(II)–NADP complex at 20°C was calculated to be 1.7×10^{-10} s, based on the measurement of proton longitudinal relaxation time ratios and a literature value of τ_c for nicotinamide adenine dinucleotide (NAD). The τ_c, as well as the ^1H and ^{31}P relaxation data together with the measured stability constant for this complex, were used to calculate the distances from the ^1H and ^{31}P nuclei to the Mn(II) ion. These distances are 3.8 Å to A8, 5.0 Å to A2, 4.5 Å to A1′, 5.3 Å to N2, 5.4 Å to N6, 5.5 Å to N5, 5.8 Å to N1′, and 6.3 Å to N4. The distances to the linkage ^{31}P nuclei are 3.7 Å, and 3.3 Å to the adenosine ribose 2′-phosphate. Based on these distances, a model is proposed for the Mn(II)–NADP complex. In this complex, the Mn(II) ion is bonded to the oxygens of all three phosphates, and the adenine and nicotinamide bases are 7–8 Å apart and parallel. Hence the Mn(II) ion is located between and to one side of the two bases but is distinctly closer to the adenine base. The adenine base is in the *anti* conformation, whereas the nicotinamide moiety can be either *syn* or *anti*. Hence there is little or no close stacking of the two bases in the complex. The addition of Mg(II) ions to a solution of free NADP caused no observable shift of the aromatic proton peaks, indicating no differences in shielding effects. Hence the rings are probably similarly oriented in both free NADP and the metal–NADP complex. Effects on the transverse relaxation rates due to the paramagnetic metal ion (T_{2p}^{-1}) were also measured from the ^{31}P linewidths as a function of temperature. The lifetime of the metal ion in the complex is $4.0 \pm 0.5 \times 10^{-6}$ s and $\Delta H^{\neq}$ for the exchange process is 13.7 ± 0.5 kcal/mol.

M. KIRK GREEN et GEORGE KOTOWYCZ. Can. J. Chem. **57**, 2434 (1979).

On a appliqué les techniques de la résonance magnétique du proton et du phosphore pour étudier la conformation de complexes formés entre des ions Mn(II) et le phosphate de dinucléotide de la nicotinamide et de l'adénine (PDNA) en solutions aqueuses, à un pH de 7.5 et à 20°C. On a calculé que le temps de corrélation dipolaire (τ_c) du complexe Mn(II)–PDNA est de 1.7×10^{-10} s en se basant sur la mesure de rapports de temps de relaxation longitudinale protonique et sur une valeur de τ_c pour le dinucléotide de nicotinamide et d'adénine (DNA) trouvée dans la littérature. On a utilisé cette valeur de τ_c de même que des données de relaxation ^1H et ^{31}P ainsi que la constante de stabilité mesurée pour ce complexe pour calculer les distances entre les noyaux ^1H et ^{31}P de l'ion Mn(II). Ces distances sont 3.8 Å de A8, 5.0 Å de A2, 4.5 Å de A1′, 5.3 Å de N2, 5.4 Å de N6, 5.5 Å de N5, 5.8 Å de N1′ et 6.3 Å de N4. Les distances du noyau ^{31}P de liaison sont de 3.7 Å et 3.3 Å du phosphate-2′ de l'adénosine de ribose. En se basant sur ces distances, on propose un modèle pour le complexe Mn(II)–PDNA. Dans ce complexe, l'ion Mn(II) est lié aux oxygènes des trois phosphates et les bases adénine et nicotinamide sont parallèles et à 7–8 Å de distance. Donc le Mn(II) est situé entre les deux bases et beaucoup plus près de l'adénine. L'adénine est dans une conformation *anti* alors que la nicotinamide peut être soit *syn* ou *anti*. Donc il n'y a que peu ou pas de superposition entre ces deux bases dans le complexe. L'addition d'ions Mg(II) à une solution de PDNA ne provoque pas de déplacements appréciables des raies des protons aromatiques ce qui indique qu'il n'y a pas de différences dans les effets de blindage. Donc les cycles sont probablement orientés d'une façon similaire tant dans le PDNA que dans le complexe métal–PDNA. On a aussi mesuré les effets, sur les taux de relaxation transversale, des ions métalliques paramagnétiques (T_{2p}^{-1}) en se basant sur les largeurs de raies ^{31}P en fonction de la température. Le temps de vie de l'ion métallique dans le complexe est de $4.0 \pm 0.5 \times 10^{-6}$ s et le $\Delta H^{\neq}$ du processus d'échange est de 13.7 ± 0.5 kcal/mol.

[Traduit par le journal]

[1]This is paper No. XIII in a series of studies of metal ion interactions with nucleotides and coenzymes. Paper No. XII is ref. 13. This study was presented at the Annual Conference and Exhibition of the Chemical Institute of Canada, Vancouver, B.C., June 3–6, 1979.

0008-4042/79/182434-10$01.00/0

Introduction

Several nuclear magnetic resonance (nmr) studies of the solution conformation of nicotinamide adenine dinucleotide (NAD) and nicotinamide adenine dinucleotide phosphate (NADP)[2] (Fig. 1) have been performed (refs. 1–6 and references therein). Chemical shift measurements suggest that these coenzymes exist in an equilibrium involving folded and extended forms at room temperature and neutral pH (1, 3). Bose and Sarma (5) have evaluated the solution conformations of free NAD and NADP. It has been established that molecular association occurs between the nicotinamide and the adenine rings of NAD in a folded conformation in aqueous solution (7); however, Zens *et al.* (6) conclude from proton longitudinal relaxation time measurements that, for a time comparable to the reorientation correlation time for NAD, the aromatic rings do not get closer than 4.5 Å. X-ray studies of the lithium–NAD complex (8) indicate that this complex exists as a "dimer" of two NAD molecules arranged head-to-tail. Li^+ is coordinated tetrahedrally to adenine N7 and to three of the four pyrophosphate oxygens. The adenine is stacked intermolecularly on nicotinamide, and the conformation of NAD is "extended" as found in holoenzyme complexes. The planes of the adenine and nicotinamide rings are almost perpendicular to each other and separated by about 11.5 Å. Saenger and co-workers (9) have compared, in a very elegant manner, the conformation of NAD in solution, in the Li^+ complex, and in holoenzymes.

Enzymes involved in oxidative decarboxylations require Mg(II) or Mn(II) ion. Maloney and Dennis (10) have shown, for example, that the reverse reaction of the NADP-specific isocitrate dehydrogenase from pea stems is activated by Mn(II) ions and not Mg(II) ions. Westheimer (11) describes experiments involving mechanisms of enzymic decarboxylations, and finds that enzymic decarboxylations follow two mechanisms: (*a*) the compound is converted to a Schiff base salt; (*b*) a metal ion is bonded to a carbonyl oxygen atom in order to activate it.

The stability constant K_s for the Mn(II)–NADP complex has been determined previously (10, 12, 13). The stability constant is strongly pH dependent in the pH region of 6.1 where the 2′-phosphate ionizes. A value of K_s equal to $370 \pm 50\ M^{-1}$ that was previously obtained (13) is used to interpret the present results, since it was measured under the same experimental conditions that are used in the present study. Previous nmr studies of Co(II) binding to NAD and NADP (14, 15) indicate direct binding of the Co(II) ion to the pyrophosphate oxygens.

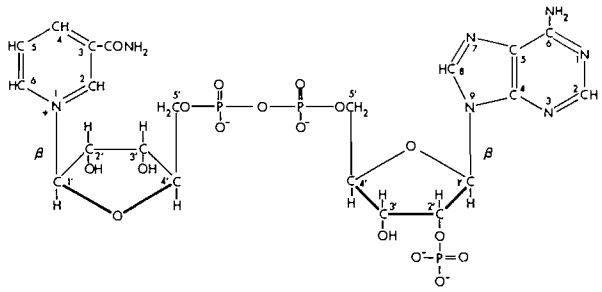

FIG. 1. Structure of NADP at a pH of 7.5. The related coenzyme NAD has a hydrogen instead of the PO_3^{2-} group at the adenine ribose 2′-position.

We have studied the solution conformation of NADP using the paramagnetic Mn(II) ion probe and ^1H and ^{31}P magnetic resonance relaxation techniques. These data for the Mn(II)–NADP complex are used to calculate the distances from the bound Mn(II) ion to eight protons and to three phosphorus nuclei of NADP in the complex. The value of the correlation time measured for NAD by Ellis and co-workers (6) was used for the calculation of τ_c for the complex. These distances give a picture of the conformation of the Mn(II)–NADP complex in solution. In addition, the temperature dependence of the ^{31}P transverse relaxation rates due to the paramagnetic metal ion (T_{2p}^{-1}) gives a value for the lifetime of the Mn(II) ion in the complex (τ_M) as well as the enthalpy of activation ($\Delta H^{\ddagger}$) for this process.

Experimental

Materials

The coenzymes NADP (monosodium salt) and NAD (free acid) were purchased from Sigma Chemical Co. They were purified to eliminate trace metal contaminants by passing a solution through a column of Chelex 100 (from Bio-Rad Laboratories) of mesh 100 to 200 and then lyophilizing the effluent solution. The purified coenzymes were then dissolved in 99.7% D_2O and lyophilized two to three times from D_2O. The resin was treated following standard procedures as recommended by the manufacturer. It was rinsed with 1 *N* HCl, methanol, and then 1 *N* NaOH, followed by equilibration with $NaKHPO_4$ buffer at a pH of 7 and extensive rinsing with doubly distilled deionized water until the effluent was of pH > 9. The D_2O that was used was vacuum distilled to eliminate paramagnetic impurities.

N-ethyl morpholine from Eastman Organic Chemicals was vacuum distilled for the nmr experiments. $MnCl_2 \cdot 4H_2O$ from Fisher Scientific Co. Ltd. and KCl from J. T. Baker Chemical Co. were used without further purification. For all experiments, 40 m*M* *N*-ethyl morpholine was used as the buffer.

[2]NAD, nicotinamide adenine dinucleotide; NADP, nicotinamide adenine dinucleotide phosphate; NMN, nicotinamide mononucleotide; T_{1p}^{-1}, effect on the longitudinal relaxation rate due to the paramagnetic metal ion; T_{2p}^{-1}, effect on the transverse relaxation rate due to the paramagnetic metal ion.

Methods

The NAD and NADP concentrations were measured by monitoring the solution absorbance at 260 nm using a Unicam SP2600 spectrophotometer. The samples for the proton and phosphorus magnetic resonance experiments were prepared in D_2O at a pH of 7.9 (uncorrected for D_2O solvents) to ensure that all of the phosphate moieties of NADP are deprotonated (net charge on the NADP anion is -3 (Fig. 1)). The measurements were carried out at 293 K. The KCl concentration was 0.153 *M* and the NADP concentration was 4.5–4.6 $\times$ 10^{-3} *M*, whereas the Mn(II) ion concentration ranged from 0–6 $\times$ 10^{-6} *M*. The Mn(II) stock solutions for both the nmr and the epr experiments used in the previous study (13) were prepared by weighing out the Mn(II) salt, and the solutions for the nmr experiments were prepared using H. E. Pedersen micropipets for maximum accuracy. The effects on the longitudinal relaxation rates of the observed nuclei due to the paramagnetic metal ions T_{1p}^{-1} were calculated according to [1]

$$[1] \quad 1/T_{1p} = (1/T_{1,Mn}) - (1/T_{1,0})$$

where $1/T_{1,Mn}$ denotes the relaxation rate of the NADP nuclei in solution in the presence of the paramagnetic species and $1/T_{1,0}$ denotes the relaxation rate of the same nuclei but in the absence of the Mn(II) ions. All proton magnetic resonance longitudinal relaxation times (T_1) were measured using the Varian HA-100-15 nmr spectrometer (100.0 MHz) interfaced with the Digilab FTS/NMR-3 Fourier transform system including the pulse unit (FTS/NMR 400-2) and the Nova 1200 computer. The temperature was maintained at 293 K using the Bruker B-ST 100/700 temperature controller. The T_1 measurements were carried out using the (180° $-$ τ $-$ 90°) two-pulse sequence and 50–200 pulse sequences were collected. The deuterium signal from D_2O was used for the lock signal. All T_1 calculations are based on measurements of peak heights. However, for the nicotinamide protons N4 and N6, average peak heights of the multiplets were used, whereas for the nicotinamide N5 proton and the adenine and nicotinamide A1′ and and N1′ protons, the peak height of one peak of each multiplet could only be measured.

The nuclear Overhauser effect experiments were run under conditions that were identical to the other nmr samples except that the NADP concentration was 0.05 *M* and the temperature was 304 K. The measurements were also carried out on the Digilab system at 100 MHz.

The ^{31}P nmr T_1 experiments were carried out at 110 MHz and 146 MHz using the Bruker 270 and 360 MHz nmr spectrometers. These measurements were carried out by Dr. B. D. Sykes and Dr. W. E. Hull, respectively. The measurements of the T_1 values at 110 MHz were carried out using the two-pulse sequence at 28°, whereas the T_1 experiments at 146 MHz were carried out using saturation recovery techniques at 25°. The effects on the transverse relaxation rates due to the paramagnetic metal ion T_{2p}^{-1} were measured from the linewidths at half height of the ^{31}P nmr spectra obtained at 36.43 MHz using the Bruker HFX-90 nmr spectrometer. $1/T_{2p}$ was calculated from the data using the relationship

$$[2] \quad 1/T_{2p} = \pi(\Delta\nu_{Mn} - \Delta\nu_0)$$

where $\Delta\nu_{Mn}$ is the linewidth at half-height of the given resonance in the presence of the Mn(II) ions and $\Delta\nu_0$ is the linewidth at half-height of the same resonance in the absence of the metal ion. The samples were prepared in the same way as for the ^1H nmr measurements.

Distance Calculations from the ^1H Nuclear Magnetic Resonance Data

Swift and Connick (16) obtained the relationship between the observed transverse relaxation time due to the paramagnetic ion T_{2p} and the inner sphere relaxation rate $1/T_{2M}$. This relationship is given by [3],

$$[3] \quad 1/T_{2p} = f_M/(T_{2M} + \tau_M)$$

Similarly, Luz and Meiboom (17) obtained the relationship between the observed longitudinal relaxation time due to the paramagnetic ion T_{1p} and the inner sphere relaxation rate $1/T_{1M}$. This is given by

$$[4] \quad 1/T_{1p} = f_M/(T_{1M} + \tau_M)$$

where f_M = [bound metal ion]/[observed ligand] and τ_M is the exchange lifetime. The theoretical expressions for T_{1M} and T_{2M} are given by Solomon and Bloembergen (18–20). For high magnetic field strengths, the contact term in the Solomon–Bloembergen equation for T_{1M} is negligible. In the fast exchange region ($\tau_M \ll T_{1M}$), a general equation for the calculation of r (distance between the paramagnetic centre and the proton under study) can be obtained from the dipolar term in T_{1M}. This equation may be written as (21)

$$[5] \quad r(\text{in Å}) = C[T_{1M}F(\tau_c)]^{1/6} = C\left[T_{1M}\left(\frac{3\tau_c}{1 + \omega_I^2\tau_c^2} + \frac{7\tau_c}{1 + \omega_s^2\tau_c^2}\right)\right]^{1/6}$$

where C is a physical constant equal to 812 for protons and 601 for phosphorus, ω_I is the nuclear magnetic resonance frequency (rad/s), and ω_s is the electron magnetic resonance frequency at the same field strength. The dipolar correlation time, τ_c, is given by $1/\tau_c = (1/\tau_r) + (1/\tau_s) + (1/\tau_M)$ where τ_r is the rotational correlation time and τ_s is the electron relaxation time.

Both [3] and [4] have an additional term arising from outer sphere relaxation. A contribution from this term, $1/T_{1,os}$, to T_{1p}^{-1} must be known before distances can be calculated using [5]. Comparison of the T_1 values for the *N*-ethyl morpholine proton resonances in a pure NADP solution with those measured for *N*-ethyl morpholine in a solution containing 1.0 μM Mn(II) ions gave a value of $1/T_{1p}$ for these resonances of about 0.05 s^{-1}. As *N*-ethyl morpholine complexes very weakly with Mn(II) ions (22), this value may be regarded as an upper limit on $1/T_{1,os}$ for the NADP protons. A comparison of this number with $1/T_{1p}$ for the NADP protons under the same conditions shows that outer sphere relaxation will not significantly affect any of the distances calculated from $1/T_{1p}$.

In a recent article, Koenig (23) has presented a novel derivation of the Solomon–Bloembergen equations and points out the difficulties involved in deriving reliable values for the number of water molecules bound to the Mn(II) ion in Mn(II)–protein complexes. However, in the present study, we are not concerned with the number of water molecules in the Mn(II)–NADP complex, as we have an independent method for obtaining a value of τ_c.

Results

A typical proton magnetic resonance spectrum for the aromatic and anomeric protons of NADP is shown in the top half of Fig. 2. The proton assignments are based on the work of Jardetzky and Wade-Jardetzky (1). However, there are different assignments, depending on the experimental conditions, in the literature concerning the adenine A1′ and the nicotinamide N1′ anomeric protons (1, 5, 24). We

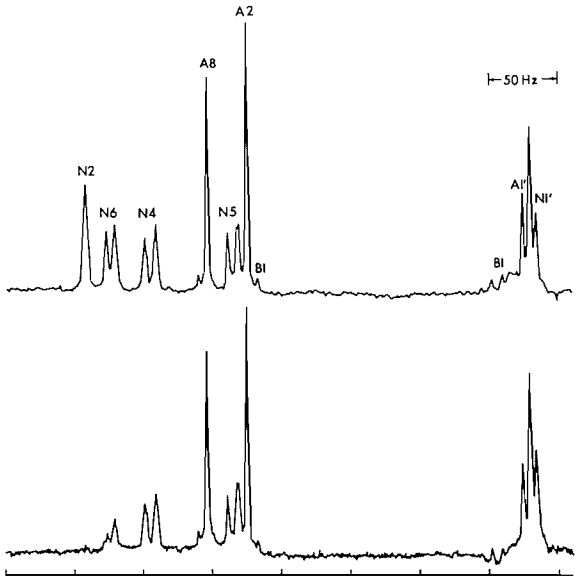

FIG. 2. The results of the nuclear Overhauser effect experiments on NADP. The aromatic nicotinamide (labelled N) and adenosine (labelled A) proton resonances as well as the anomeric proton resonances are shown. The top spectrum was obtained before irradiation, while for the bottom spectrum the irradiation frequency is centred on the N2 resonance. Peaks labelled B1 are images of the buffer peaks occurring at 1.1 and 2.4 ppm to low field of TMS. The temperature was 304 K.

have assigned these two anomeric protons on the basis of nuclear Overhauser effect (nOe) experiments (Fig. 2, bottom spectrum).

Egan *et al.* (25) observed an nOe of 0.14 for proton N1′ when proton N2 was irradiated, and 0.17 when proton N6 was irradiated in nicotinamide mononucleotide (NMN) at neutral pH and at 35°C. In the present experiments, the saturating irradiation frequency was centred on the N2 proton resonance, but also partially saturated the N6 proton. As was observed for NMN, an increase in intensity of about 30% was observed for the high field singlet of the triplet corresponding to the anomeric protons (an nOe due to both protons N2 and N6). This confirms that the N1′ proton resonance is to high field of the A1′ proton resonance. This assignment has been found to be valid over a very large concentration range of NADP (24). For NAD, the anomeric proton assignments are reversed (1, 5, 24). This suggests that the addition of the 2′-phosphate group, in comparing NAD to NADP, has a deshielding effect on the A1′ proton.

A typical set of proton T_1 inversion recovery spectra are shown in Fig. 3. The results of the T_1 measurements for the metal-free solutions, for NADP solutions containing Mn(II) ions, and for the calculated T_{1M} values obtained using [4], are given in Table 1.

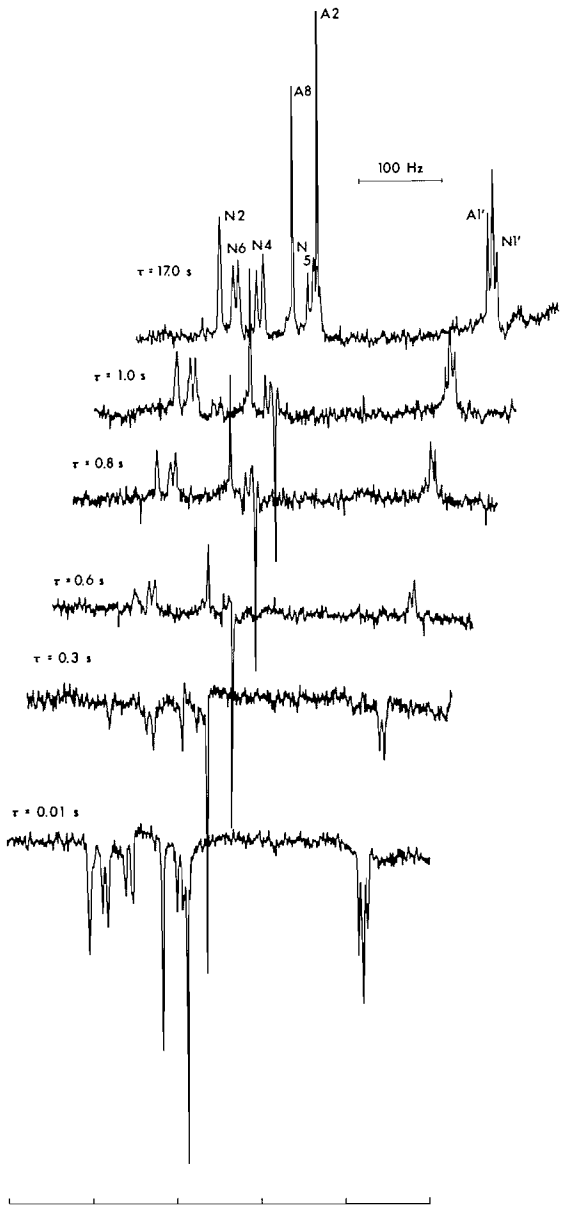

FIG. 3. Proton longitudinal relaxation time inversion recovery spectra for pure NADP (aromatic and anomeric proton region) at 20°C. Each spectrum consists of 50 pulse sequences.

The experimental ^{31}P, $T_{1,Mn}$ and $T_{1,0}$ data, together with the calculated T_{1M} values, are listed in Table 2. A plot of ln $1/fT_{2p}$ vs. $1/T$, based on ^{31}P linewidth measurements, is shown in Fig. 4. The fT_{2p} results for the ^{31}P nuclei are in the slow exchange limit ($\tau_M > T_{1M}$) and the lifetime τ_M for the metal ion in the complex is equal to $4.0 \pm 0.5 \times 10^{-6}$ s for all three phosphate groups. In addition, the enthalpy of activation $\Delta H^{\ddagger} = 13.7$ kcal/mol.

In order to use [5] to calculate the distances between the Mn(II) ion and the individual proton and

TABLE 1. Experimental $T_{1,0}$ and $T_{1,Mn}$ data for Mn(II)–NADP solutions together with calculated T_{1M} values (s)[a]

Sample No.	[Mn(II)] (μM)	Variable	N2	N6	N4	A8	N5	A2	A1′	N1′
1	0	$T_{1,0}$	0.72	0.63	1.18	0.65	0.79	4.22	0.98	0.53
2	0	$T_{1,0}$	0.70	0.43	1.09	0.66	0.53	3.16	1.02	0.65
2	0	$T_{1,0}$	0.66	0.50	1.13	0.57	0.71	3.16	0.82	0.47
Average		$T_{1,0}$	0.69	0.52	1.13	0.63	0.68	3.51	0.94	0.55
3	0.5	$T_{1,Mn}$	0.55	0.42	1.02	0.212	0.48	1.12	0.41	0.48
		T_{1M}	1.87	1.51	7.24	0.221	1.13	1.13	0.50	2.61
3	0.5	$T_{1,Mn}$	0.49	0.40	0.76	0.176	0.54	0.96	0.41	0.46
		T_{1M}	1.17	1.19	1.60	0.169	1.31	0.91	0.50	1.94
4	1.0	$T_{1,Mn}$	0.46	0.38	0.82	0.125	0.52	0.69	0.28	—
		T_{1M}	1.93	1.97	4.18	0.218	3.09	1.20	0.56	—
4	1.0	$T_{1,Mn}$	0.40	0.37	0.70	0.134	0.43	0.50	0.27	0.39
		T_{1M}	1.33	1.79	2.58	0.238	1.63	0.82	0.53	1.88
5	1.0	$T_{1,Mn}$	0.37	0.29	0.85	0.113	0.45	0.67	0.26	0.30
		T_{1M}	1.10	0.92	4.73	0.190	1.83	1.14	0.49	1.14
6	1.5	$T_{1,Mn}$	0.36	0.30	0.67	0.092	0.51	0.47	0.25	0.39
		T_{1M}	1.56	1.56	3.41	0.223	4.23	1.13	0.71	2.78
6	1.5	$T_{1,Mn}$	0.38	0.35	—	0.099	0.38	0.51	0.23	0.34
		T_{1M}	1.86	2.42	—	0.243	1.79	1.24	0.63	1.84
7	1.5	$T_{1,Mn}$	0.32	0.32	0.73	0.094	0.42	0.56	0.25	0.41
		T_{1M}	1.24	1.73	4.28	0.230	2.23	1.38	0.71	3.34
8	6.0	$T_{1,Mn}$	0.185	0.192	3.99	0.034	—	0.137	0.089	0.215
		T_{1M}	2.09	2.51	5.10	0.297	—	1.18	0.82	2.92
8	6.0	$T_{1,Mn}$	0.173	0.163	—	—	0.105	0.149	0.077	0.275
		T_{1M}	1.90	1.96	—	—	1.02	1.29	0.69	5.48
Average			1.61	1.75	4.14	0.225	2.03	1.14	0.61	2.66
$T_{1M}(\sigma)$[b]			(0.37)	(0.50)	(1.70)	(0.036)	(1.04)	(0.17)	(0.11)	(1.25)
%σ			23	29	41	16	51	15	19	47

[a]The T_{1M} values are multiplied by 10^4. The temperature is 20°C. A total of eight separate samples were prepared and many of them were run twice.
[b]The standard deviation in T_{1M} is designated by σ.

^{31}P nuclei for which the relaxation times due to the paramagnetic metal ion were measured (Tables 1 and 2), the fast exchange limit for fT_{1p} must be applicable, i.e., $T_{1M} > \tau_M$, at 20°C. For the ^1H data, this was shown to be valid from a study of the temperature dependence of proton fT_{1p} values (26). In fact, at 20°C the adenine A8 proton has the greatest contribution from τ_M to T_{1M}. A comparison of the magnitudes of fT_{1p} ($=T_{1M} + \tau_M$) for this proton at 20°C ($T_{1M} = 2.25 \times 10^{-5}$ s) (Table 1) with the value for τ_M of 4×10^{-6} s obtained from the ^{31}P data, shows that τ_M is less than 20% of the value of fT_{1p} at 20°C.

TABLE 2. Experimental ^{31}P $T_{1,0}$ and $T_{1,Mn}$ data for Mn(II)–NADP solutions together with the calculated T_{1M} values (s)[a]

Sample No.	[Mn(II)] (μM)	Variable	Ribose ^{31}P	Low field linkage ^{31}P	High field linkage ^{31}P
1[b]	0	$T_{1,0}$	2.57	1.53	1.39
2	0	$T_{1,0}$	3.16	1.86	1.74
3	0.2	$T_{1,Mn}$	1.37	1.14	1.20
		T_{1M}[c]	8.3	12.2	25.6
4	0.33	$T_{1,Mn}$	0.82	0.88	0.86
		T_{1M}[c]	5.2	7.8	7.9
5	0.5	$T_{1,Mn}$	0.75	0.90	0.94
		T_{1M}[c]	7.4	15.2	20.8

[a]T_{1M} values are multiplied by 10^5.
[b]Samples 1, 3, and 5 were measured at 146 MHz at 25°C; samples 2 and 4 were obtained at 110 MHz at 28°C.
[c]T_{1M} values are calculated using the blank value of $T_{1,0}$ obtained at the same frequency as $T_{1,Mn}$.

For the ^{31}P fT_{1p} data, a comparison of the results in Table 2 with the $1/fT_{2p}$ data in Fig. 4 indicates that, for all three ^{31}P nuclei, the ratio of $1/fT_{2p}$ to $1/fT_{1p}$ is greater than 13, i.e., $(T_{1M} + \tau_M)/\tau_M > 13$ and therefore τ_M is less than 10% of $1/fT_{1p}$. Although the ^{31}P fT_{2p} values are in the slow exchange region, the fT_{1p} values are in the fast exchange region. Hence [5] can readily be applied to the ^1H and ^{31}P fT_{1p} data to calculate r.

In using [5], a value for the dipolar correlation time τ_c must be known. Assuming that $\tau_c = \tau_r$, this was accomplished by comparing our T_1 data for NADP under the present experimental conditions (0.005 M NADP, pD 7.9, 20°C) with the T_1 data obtained by Zens *et al.* (6, 27) (Table 3) for NAD (0.005 M NAD in phosphate buffer, pD 7.0, 5°C). Zens *et al.* (6) measured the τ_c equal to 2.8×10^{-10} s for NAD. Assuming that the predominant intramolecular relaxation mechanism is dipolar, then $T_1 \propto 1/\tau_c$, and the ratio of the T_1 data allows us to calculate a value for τ_c for NADP since the structures

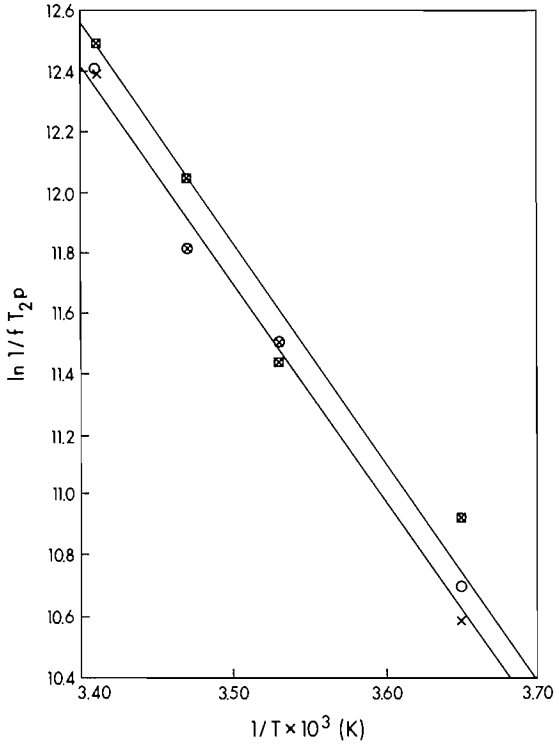

FIG. 4. A plot of the transverse relaxation rate ln $1/fT_{2p}$ vs. $1/T$ for the ^{31}P nuclei of NADP in the Mn(II)–NADP complex. The linewidth measurements were carried out on samples 2 and 4 (Table 4). The symbols represent the ^{31}P nuclei as follows: (⊠) ribose 2′-phosphorus; (○) low field diphosphate ^{31}P; (×) high field diphosphate ^{31}P.

of NADP and NAD are very similar. The results of these calculations are given in Table 3. For six of the eight protons which may be compared, $T_{1,NADP}/T_{1,NAD} \simeq 1.7$; hence $\tau_{c,NADP}/\tau_{c,NAD} = 0.60$ and τ_c for 0.005 M NADP at 20°C is then $0.60 \times 2.8 \times 10^{-10}$ s $= 1.7 \times 10^{-10}$ s. The ratio of 1.7 arises mainly from the fact that the experiments were carried out at two temperatures. Since τ_M is 4×10^{-6} s and τ_s is about 10^{-9} s (21), the short value of τ_c is dominated by τ_r as the other two correlation times are much longer, i.e., $\tau_c = \tau_r$.

The smaller $T_{1,NADP}/T_{1,NAD}$ ratios for the A8 and A1′ protons are likely due to the fact that NADP contains the PO_3^{2-} group at the adenosine ribose 2′-position, whereas in NAD this group is not present. The ^{31}P nucleus is expected to decrease the relaxation times of these two protons.

The temperature dependence of the dipolar correlation time τ_c is given by

$$[6] \quad \tau_c = \tau_0 \exp(-E_a/RT)$$

where E_a is the activation energy corresponding to the rotational correlation time (τ_r). For $T_1 \propto 1/\tau_c$, the above equation can be rearranged into the form

$$T_{1,a} = T_{1,b} \exp(E_a/R[1/T_b - 1/T_a])$$

where $T_{1,a}$ is the longitudinal relaxation time at temperature T_a, and $T_{1,b}$ is the relaxation time at temperature T_b. T_1 data for NADP were obtained at 20 and 30°C (Table 3) and these have been used to estimate a value for E_a equal to 4.9 ± 0.4 kcal/mol. This is in very good agreement with the value of 4.6 ± 0.3 kcal/mol obtained by Zens *et al.* (27) for NAD, and lends further support to our approach for calculating the correlation time. The value for τ_r is not expected to vary significantly between free NADP and the metal complex.

Alternative methods of calculating the correlation time for the complex such as using the T_{1M}/T_{2M} ratio or the frequency dependence of the ^{31}P T_{1M} data proved unsatisfactory. The former method proved unreliable for protons because accurate measurements of the proton linewidths could not be obtained due to signal overlap and a poor signal to noise ratio, especially in the presence of Mn(II) ions. T_{1M}/T_{2M} ratios for the ^{31}P data were not used because fT_{2p} values are in the slow exchange limit. The latter method proved unsatisfactory because of the inconsistency of the calculated τ_c values since the experiments were performed in two different laboratories. The calculated r values are not as sensitive to the variation of the T_{1M} data since they depend on the sixth root of T_{1M} and τ_c.

Using a value of 1.7×10^{-10} s for the correlation time and $F(\tau_c)$ at 100 MHz of 5.0×10^{-10} s^{-1} (20°C), the Mn(II) ion distances to the adenosine (A) and the nicotinamide (N) protons were calculated using [5] and are given in Table 4. From the table it is seen that all the distances to the adenosine moiety are shorter than those to the nicotinamide moiety. The error limits in the distance based on the standard deviation in T_{1M} are smaller than the 10% error limits that are quoted. The 10% error limits in r are based on a theoretical and experimental error analysis carried out by Mildvan (28). If τ_M contributes to fT_{1p}, then r (calculated) is greater than r (actual) by 0.1 Å. This is much smaller than the quoted error limits. The fact that the values of T_{1M} vary between each experiment for a given proton is due to the fact that the experiments were carried out on 0.005 M NADP solutions, and it was not always easy, working at such low concentrations, to obtain the optimum signal to noise ratio. In addition, when Mn(II) ions are added and the lines broaden, the overlap of resonances is more serious. This is the main reason for the range of T_{1M} values in Table 1. However, many experiments with a wide range of metal ion concentrations were carried out to reduce our standard deviation for T_{1M} for each proton.

The distance calculations based on the ^{31}P data

TABLE 3. Comparison of T_1 data for NAD and NADP

Proton	Values of Zens *et al.* (1975, 1976) for 0.005 *M* NAD at 5°C	Values obtained in present study for 0.005 *M* NADP at 20°C	$\frac{T_{1,NADP}\ (20°C)}{T_{1,NAD}\ (5°C)}$	Values obtained in present study for 0.005 *M* NADP at 30°C	E_a for τ_c (kcal/mol)
N2	0.41	0.70	1.70	0.98	6.0
N6	0.28	0.52	1.86	0.67	4.5
N4	0.66	1.13	1.71	1.46	4.5
A8	0.45	0.63	1.40	0.87	5.7
N5	0.40	0.68	1.70	0.88	4.6
A2	2.13	3.51	1.65	4.57	4.7
N1′	0.32	0.55	1.72	0.74	5.3
A1′	0.87	0.94	1.08	1.18	4.0
				Mean E_a 4.9±0.4 kcal/mol[a]	

[a]The error limits represent one standard deviation.

in Table 2 are given in Table 5. For the data at 110 MHz, τ_c equals 1.4×10^{-10} s at 28°C and $F(\tau_c) = 4.0 \times 10^{-10}\ s^{-1}$. For the 146 MHz data, obtained at 25°C, $\tau_c = 1.5 \times 10^{-10}$ s and $F(\tau_c) = 4.4 \times 10^{-10}\ s^{-1}$. These correlation times were obtained at the two temperatures using [6] and are slightly shorter due to the higher temperatures used for these experiments. The binding constant as a function of temperature was determined in our previous study (13) for the Mn(II)–NADP complex, so that the ratio f_M was determined also at both temperatures for use in [4]. The Mn(II) ion to ^{31}P distances were then calculated using [5].

In order to assess the effect of metal ion binding on the NADP conformation, and to compare this conformation with that of free NADP, proton chemical shifts of 0.003 *M* NADP in the absence and presence of Mg(II) ions at a concentration of 0.006 *M* were obtained. Maloney and Dennis (10) observed that the ratio of stability constants for the Mg(II)–NADP complex to that for the Mn(II)–NADP complex is $430\ M^{-1}/760\ M^{-1} = 0.56$. By applying this ratio of stability constants to our experimental conditions, about 1/2 of the NADP should be complexed in the presence of Mg(II). However, shifts greater than 0.5 Hz were not observed.

TABLE 4. T_{1M} values and calculated Mn(II)—proton distances for Mn(II)–NADP

Proton	$T_{1M} \times 10^4$ (σ)[a] (s)	r (Å) (σ)[b]
N2	1.61(0.37)	5.3(0.5)
N6	1.75(0.50)	5.4(0.5)
N4	4.14(1.7)	6.2(0.6)
A8	0.225(0.039)	3.8(0.4)
N5	2.03(1.04)	5.4(0.5)
A2	1.14(0.17)	5.0(0.5)
A1′	0.61(0.11)	4.5(0.5)
N1′	2.66(1.25)	5.7(0.6)

[a]σ is one standard deviation.
[b]Distances are calculated using $\tau_c = 1.7 \times 10^{-10}$ s.

TABLE 5. T_{1M} values and calculated Mn(II)—^{31}P nuclei distances for the Mn(II)–NADP complex

Variable	Ribose ^{31}P	Low field linkage ^{31}P	High field linkage ^{31}P
$T_{1M} \times 10^5$ (110 MHz) (1)[a]	5.2	7.8	7.9
$T_{1M} \times 10^5$ (146 MHz) (2)	7.85	13.8	23.2
r (Å) (110 MHz)[b]	3.2	3.4	3.4
r (Å) (146 MHz)[c]	3.4	3.8	4.1
r (Å) (average)	3.3±0.3	3.6±0.4	3.8±0.4

[a]The values in parentheses refer to the number of measurements.
[b]The correlation time τ_c equals 1.4×10^{-10} s at 28°C.
[c]The correlation time τ_c equals 1.5×10^{-10} s at 25°C.

Discussion

The previously measured value of $K_s = 370 \pm 50\ M^{-1}$ (13) for the first stability constant is used for the interpretation of the nmr relaxation time data since the nmr samples were prepared with essentially the same Cl^- ion concentration as was used in the previous epr study.

From the structure of NADP, the two *primary* metal ion binding sites per NADP can readily be located. These are the oxygen atoms of the diphosphate linkage and the oxygen atoms of the 2′-phosphate group. Distinct primary binding sites at either the nicotinamide C=O oxygen or with the adenine N7 nitrogen are unlikely, as these would normally act as secondary binding sites compared with the phosphate oxygens. Under the experimental conditions required for the nmr relaxation time measurements, [Mn(II)] ≪ [NADP], we postulate that for these low Mn(II) ion concentrations, one Mn(II) ion binds simultaneously to the oxygens of both the 2′-phosphate group and the diphosphate linkage. From an examination of molecular models, this is possible if the adenine ribose is in the 2′-*endo* conformation in the complex. This conclusion is also further supported by the ^{31}P nmr relaxation time data. The measurements carried out at 110 and

146 MHz indicate that the Mn(II) ion is between 3.3 and 3.8 Å from all three phosphorus nuclei, and is slightly closer to the ribose phosphorus than to the linkage phosphates. Finally, the data in Fig. 4 show equal exchange lifetimes, τ_M, for the three phosphorus nuclei. These results all indicate the presence of one metal ion in the Mn(II)–NADP complex which binds with the oxygens of the three phosphate groups.

In view of these results, the ^1H distances in Table 4 together with the Mn(II) to ^{31}P distances in Table 5 may now be analyzed. The Mn(II) to the N4 (6.2 Å) and to the N1′ (5.7 Å) distances are independent of the *syn–anti* ratio of the nicotinamide ring and these two distances can be used to place the Mn(II) ion about 4.5 Å from the ring centre. The Mn(II)—N2 and the Mn(II)—N(6) distances are equal (5.3–5.4 Å) and, together with the distance to N5, place the vector from the centre of the ring to the Mn(II) ion within $\pm 30°$ of the normal to the ring plane; i.e., the Mn(II) ion is located more or less directly above the plane of the ring. According to these data, the *syn* or *anti* conformation for the nicotinamide ring is possible.

All of the adenosine protons are closer to the Mn(II) ion (Mn(II)—A8 = 3.8 Å, Mn(II)—A2 = 5.0 Å, and Mn(II)—A1′ = 4.5 Å) than are the nicotinamide mononucleotide protons. This result is not surprising, considering the presence of the positive charge on the nicotinamide ring and the presence of the 2′-phosphate on the adenine ribose to which the Mn(II) ion also binds.

The adenine A8 and A1′ proton distances can be used to locate the metal ion. However, the distance of 5.0 Å to A2 is too short. This can be explained in terms of the 90% *anti*,10% *syn* ratio for NADP as has been observed for NAD in considering the adenine-ribose glycosidic linkage (6, 27). The distance that is measured is an average value $\langle 1/r^6 \rangle$. Hence, if for the *syn* conformation the A2 proton is 3.5–4 Å away from the metal, and in the *anti* conformation it is greater than 5 Å away, a value of 5 Å will still be observed, since the average value will be heavily weighted by the shorter distance. A similar calculation for A8 will change the distance by less than 0.1 Å.

The calculated Mn(II) to ^{31}P distances (Table 5) are 3.3 ± 0.3 Å to the 2′-ribose ^{31}P nucleus and 3.6 to 3.8 ± 0.4 Å to the linkage ^{31}P nuclei. As X-ray and other data indicate that these distances should be near 3.0 Å for inner sphere complexes (29, 30), the present Mn(II) to ^{31}P distances are interpreted in terms of a distorted inner sphere complex (29). This could arise from the simultaneous coordination of the Mn(II) ion by the diphosphate as well as by the ribose phosphate oxygens. Secondly, as discussed by Sloan *et al.* (31), if a rapid equilibrium between inner sphere and second sphere complexes were present, a time-averaged distance would be observed. At present, these two possibilities cannot be distinguished, but the distorted inner sphere complex is favored.

Blumenstein and Raftery (32) tentatively assigned the high field of the AB quartet to the linkage phosphorus resonance corresponding to the ^{31}P nucleus nearest the adenine base. These ^{31}P to Mn(II) ion distances, together with the Mn(II)–proton distances, allow us to consider the conformation of the Mn(II)–NADP complex. First of all, the Mn(II) ion sits in a pocket between the three phosphate groups and is bound to one oxygen from each of the linkage phosphates and to one, or two, of the ribose phosphate oxygens. The adenine ring is above the plane formed by the three phosphorus atoms and is tilted over this plane. The centre of the nicotinamide ring is about 4.5 Å from the Mn(II) ion. Since the nicotinamide ring can move in an arc with respect to the phosphate-bound Mn(II) ion, a family of conformations where both rings are parallel to each other and about 7–8 Å apart, to a conformation where the nicotinamide ring is roughly perpendicular to the adenine ring, and close to it, is possible. The former conformation is shown in Fig. 5. Hence, for the Mn(II)–NADP complex, we conclude that there is essentially no close stacking of the two rings in NADP. This is in agreement with the conclusions of Zens *et al.* (6) who concluded, based on the effects of deuteration on the proton T_1 values, that the two rings in free NAD are at least 4.5 Å apart. Even though distances are being measured for a molecule which is thought to exist in an equilibrium of folded and extended forms (1, 3), our results are not consistent with the presence of an equilibrium involving a folded form with closely stacked rings unless the folded form exists for only a short fraction of the time. Consequently, there appears to be no significant stacking of the two rings in the complex.

Finally, a comparison is drawn between the NADP conformation in the complex with that of free NADP in solution. In uncomplexed NADP, both aromatic rings may be in either the *syn* or *anti* conformation with respect to their contiguous ribose groups. Zens *et al.* (6) summarize the results of the experiments carried out on NAD (at 5°C) and find that the components within NAD behave in a manner analogous to 5′-AMP and NMN. Both the nicotinamide and adenine rings have a significant amount of flexibility about the glycosidic bond. Their results indicate that the adenine ring is about 92% in the *anti* conformation in the two-state microdynamic model. With regard to the pyridyl-ribose glycosidic linkage, nearly equal populations have been measured by Zens *et al.*

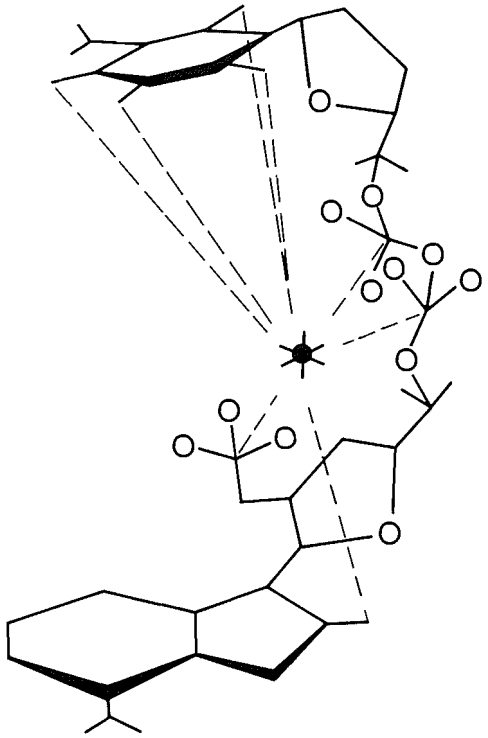

FIG. 5. The solution conformation of the Mn(II)–NADP complex. The nicotinamide ring may move in an arc perpendicular to the plane of the paper.

(27), whereas Sarma and Mynott (24) estimate that the nicotinamide ring is predominantly *syn* in NAD. In NMN, Egan *et al.* (25) observed nearly equal populations of the *syn* and *anti* conformers with a slight preference for the *anti*. Finally, Thornton and Bayley (33) have carried out conformational energy calculations on NAD. Two of their main conclusions are as follows. (*a*) *In vacuo*, the most stable structures exhibit *either* stacking interactions between the two rings *or* electrostatic interactions between the positive charge on the nicotinamide and the negatively charged pyrophosphate backbone. This latter interaction has been observed previously (32). (*b*) A variety of different conformations are observed for the electrostatically stabilized structures which are relatively extended compared to the stacked states.

As mentioned in the Results, binding of Mg(II) ions to NADP did not change the proton chemical shifts by more than 0.5 Hz. However, proton chemical shifts for the adenine and nicotinamide protons of 0.1–0.3 ppm to high field relative to those observed for NMN, 5′-AMP, and adenosine diphosphoribose have been observed (1, 24) and indicate the presence of intramolecular ring current diamagnetic shielding in the coenzyme with respect to its constituents. The absence of a change in the chemical shifts of the protons in the present experiment for the Mg(II)–NADP complex indicates no differences in shielding effects. Hence the rings probably have the same time-averaged spatial relationship both in the metal ion complex and in free NADP in solution. As the complete ribose spectrum could not be examined at 100 MHz, conclusions cannot be drawn with respect to changes in the conformation of the remainder of the molecule on Mg(II) ion binding.

Acknowledgements

The authors acknowledge the assistance of Dr. B. D. Sykes, University of Alberta, and Dr. W. E. Hull of Bruker-Physik AG at Karlsruhe, Germany, for measuring the high-field ^{31}P nmr spectra, and Dr. R. E. D. McClung for his assistance with the computations. This research was supported by the Natural Sciences and Engineering Research Council of Canada and the University of Alberta, for which the authors express their appreciation.

1. O. JARDETZKY and N. G. WADE-JARDETZKY. J. Biol. Chem. **241**, 85 (1966).
2. J. JACOBUS. Biochemistry, **10**, 161 (1971).
3. G. MCDONALD, B. BROWN, D. P. HOLLIS, and C. WALTER. Biochemistry, **11**, 1920 (1972).
4. M. BLUMENSTEIN and M. A. RAFTERY. Biochemistry, **12**, 3585 (1973).
5. K. S. BOSE and R. H. SARMA. Biochem. Biophys. Res. Commun. **66**, 1173 (1975).
6. A. P. ZENS, T. A. BRYSON, R. B. DUNLAP, R. R. FISHER, and P. D. ELLIS. J. Am. Chem. Soc. **98**, 7559 (1976).
7. J. L. CZEISLER and D. P. HOLLIS. Biochemistry, **14**, 2781 (1975).
8. W. SAENGER, B. S. REDDY, K. MUHLEGGER, and G. WEIMANN. Nature, **267**, 225 (1977).
9. W. SAENGER, B. S. REDDY, K. MUHLEGGER, and G. WEIMANN. *In* Pyridine nucleotide-dependent dehydrogenases. 2nd FEBS International Symposium, University Konstanz, Konstanz, Germany. *Edited by* H. Sund. Walter de Gruyter, Berlin. 1977. pp. 222–236.
10. R. J. MALONEY and D. T. DENNIS. Can. J. Biochem. **55**, 928 (1977).
11. F. H. WESTHEIMER. Mechanism of enzymic decarboxylation. *In* Proceedings Robert A. Welch Foundation Conferences on Chemical Research. XV. Bio-organic Chemistry and Mechanisms, Houston, Texas, November 1–3, 1971. Vol. 15. 1972. p. 7.
12. R. F. COLMAN. Anal. Biochem. **46**, 358 (1972).
13. M. K. GREEN and G. KOTOWYCZ. Can. J. Biochem. **57**, 995 (1979).
14. J. TORREILLES and A. CRASTES DE PAULET. Biochimie, **55**, 1077 (1973).
15. J. TORREILLES, A. CRASTES DE PAULET, and N. PLATZER. Org. Magn. Reson. **9**, 584 (1977).
16. T. J. SWIFT and R. E. CONNICK. J. Chem. Phys. **37**, 307 (1962).
17. E. LUZ and S. MEIBOOM. J. Chem. Phys. **40**, 2686 (1964).
18. I. SOLOMON. Phys. Rev. **99**, 559 (1955).
19. N. BLOEMBERGEN. J. Chem. Phys. **27**, 572 (1957).
20. N. BLOEMBERGEN and L. O. MORGAN. J. Chem. Phys. **34**, 842 (1961).

21. A. S. MILDVAN and J. L. ENGLE. *In* Methods in enzymology. Vol. 26. *Edited by* C. H. W. Hirs and S. N. Timasheff. Academic Press, New York. 1972. pp. 654–682.
22. W. J. O'SULLIVAN and M. COHN. J. Biol. Chem. **241**, 3104 (1966).
23. S. H. KOENIG. J. Magn. Reson. **31**, 1 (1978).
24. R. H. SARMA and R. J. MYNOTT. *In* Conformation of biological molecules and polymers. The Jerusalem Symposia on Quantum Chemistry and Biochemistry. Vol. 5. 1973. pp. 591–626.
25. W. EGAN, S. FORSEN, and J. JACOBUS. Biochemistry, **14**, 735 (1975).
26. M. K. GREEN. M.Sc. thesis, University of Alberta, Edmonton, Alta. 1979.
27. A. P. ZENS, T. J. WILLIAMS, J. C. WISOWATY, R. R. FISHER, R. B. DUNLAP, T. A. BRYSON, and P. D. ELLIS. J. Am. Chem. Soc. **97**, 2850 (1975).
28. A. S. MILDVAN. Acc. Chem. Res. **10**, 246 (1977).
29. A. S. MILDVAN and C. M. GRISHAM. Struct. Bonding (Berlin), **20**, 1 (1974).
30. E. A. MERRITT, M. SUNDARALINGAM, R. D. CORNELIUS, and W. W. CLELAND. Biochemistry, **17**, 3274 (1978).
31. D. L. SLOAN, L. A. LOEB, A. S. MILDVAN, and R. J. FELDMANN. J. Biol. Chem. **250**, 8913 (1975).
32. M. BLUMENSTEIN and M. A. RAFTERY. Biochemistry, **11**, 1643 (1972).
33. J. M. THORNTON and P. M. BAYLEY. Biopolymers, **16**, 1971 (1977).

Transition state geometry in the scission and formation of cyclopentane and cyclohexane oxiranes. Use of the dilatometer in studying mixed reactions of different orders

JOHN W. BOVENKAMP,[1] EDWARD J. LANGSTAFF, AND ROBERT Y. MOIR
Department of Chemistry, Queen's University, Kingston, Ont., Canada K7L 3N6
AND
ROBERT A. B. BANNARD
Defence Research Establishment Ottawa, Ottawa, Ont., Canada K1A 0Z4
Received December 7, 1978

JOHN W. BOVENKAMP, EDWARD J. LANGSTAFF, ROBERT Y. MOIR, and ROBERT A. B. BANNARD. Can. J. Chem. **57**, 2444 (1979).

Two methods, one more accurate, the other more convenient, were developed by which the dilatometer could be used with concurrent reactions of the second and third order. The more accurate method, employing a dilatometer of high specific surface area and equipped with a stable and responsive thermometer, was used in studying as many as six simultaneous oxirane scissions in acid solution. Interlocking double comparisons were made between cyclohexane and cyclopentane ring systems, between systems possessing or lacking a methoxyl substituent and between others having the substituent in varying orientations, between charged and uncharged nucleophiles, and between transition states of different degrees of protonation. Searching experimental checks were therefore possible in four main areas: (*i*) a quantitative dissection of the inductive effect from steric and conformational effects, and from dipole–ion or dipole–dipole interactions with the nucleophile, (*ii*) a quantitative demonstration of three main differences between transition states based on 5- and 6-membered rings, (*iii*) a proof that *syn*-1,3-effects in the transition states are very charge dependent, being large and positive with unfavourably arranged dipoles, and small or perhaps negative with favourable arrangements, and (*iv*) a rejection of certain proposed ion-pair alternatives to the A2 mechanism.

JOHN W. BOVENKAMP, EDWARD J. LANGSTAFF, ROBERT Y. MOIR et ROBERT A. B. BANNARD. Can. J. Chem. **57**, 2444 (1979).

On a développé deux méthodes, l'une précise et l'autre plus commode, faisant appel à un dilatomètre pour étudier des réactions concurrentes du deuxième et du troisième ordre; la méthode la plus précise, qui fait appel à un dilatomètre à grande surface spécifique équipé d'un thermomètre stable et sensible a été utilisée pour étudier jusqu'à 6 réactions de scissions simultanées d'oxiranne en solution acide. On a fait des comparaisons de recouvrement double entre les systèmes cyclopentanique et cyclohexanique, entre des systèmes avec ou sans substituants méthoxyles, entre d'autres systèmes portant le substituant dans diverses orientations entre des nucléophiles chargés ou non et entre des états de transition à divers degrés de protonation. Il a été possible de faire des vérifications expérimentales dans quatre domaines principaux; (*i*) une dissection quantitative entre l'effet inductif et les effets stériques et conformationnels ou les interactions dipole–ion ou dipole–dipole avec le nucléophile, (*ii*) une démonstration quantitative de trois différences principales entre les états de transition portés par des cycles à 5 et à 6 chaînons, (*iii*) une preuve que les effets *syn*-1,3, dans les états de transition dépendent beaucoup sur la charge; les effets étant importants et positifs lorsque les dipoles sont dans un arrangement non favorable et petits ou peut être négatifs lorsque les arrangements sont favorables et (*iv*) un rejet de certaines paires d'ions proposées comme alternative au mécanisme A2.

[Traduit par le journal]

Introduction

Theories of oxirane scission (1, 2) attempt explanations in terms of polar, steric, and conformational effects. In the previous paper (3), a method was proposed which led to the recognition and measurement of certain polar effects in a particularly simple way. The simultaneous attack of two nucleophiles, under rigidly standardized conditions, was observed for each of the oxiranes **1** to **6**, and the relative yields of the products accurately measured. A simple double comparison technique (4) was then used to show that the rate of scission was very dependent both on the relative charge of nucleophile

[1]Present address: Defence Research Establishment Ottawa, Ottawa, Ont., Canada K1A 0Z4.

0008-4042/79/182444-14$01.00/0

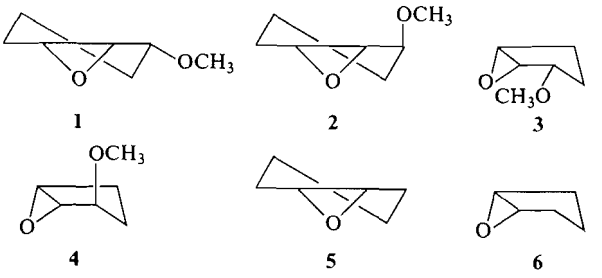

and substituent and on their orientation to each other in the transition state.[2] Surprisingly far reaching implications arose from these experiments. They suggested a dissection of the inductive effect and a method of attack upon the conformational parameters, both of which are continued in the present paper. Presumably they will bring about a reversal in current opinion as to the importance of charge effects in the formation of bridged intermediates during the reactions of olefins (6).

In our view, the concept of inductive effect should be separated from substituent–nucleophile interactions such as those discussed above. However, it has not been easy to separate polar effects from steric and conformational effects. Many years ago (7) it was suggested that **2** was preferentially attacked by nucleophiles at the position more remote from methoxyl because of the more unfavourable inductive effect at the nearer position. This view is now generally accepted (1, 2, 5, 8) but alternative explanations are still being offered (9). For example, it has been supposed that nucleophile, oxirane carbon, and leaving oxirane oxygen are nearly colinear in an oxirane-like transition state (see diagram below; contrary to the standard *trans*-diaxial picture), and that therefore steric interference occurs with the substituent in attack upon the nearer position of **2**, but not for that at the position more remote from methoxyl.[3] However, the idea fails completely to explain the similar results for the corresponding *cis*-oxirane **1**, as indeed had already been pointed out (7).

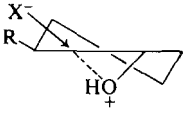

[2]The effect has been observed qualitatively, for a particular orientation of positive pyridinium and negative bromine, in a somewhat similar reaction (5).

[3]Three-dimensional models show that in **2**, anything resembling colinear attack at the oxirane position nearer the substituent is physically impossible. Colinear attack at the more remote position is not consistent with the very large charge effects observed (3). The transition states are in fact product-like rather than reactant-like (3, 10).

A similar lack of consistency applies to the suggestion (11) that the inhibition at the nearer position could be explained by conformational factors.[4] However, it was obviously imperative to provide a convincing and quantitative dissection of the inductive effect. In the present work, this was done in several ways, perhaps most directly in the comparison of pairs of compounds in which each member of a pair possessed exactly the same steric configuration, but a different positional structure, with respect to its partner. In the interval, Berti and his co-workers (9, 12) have described a most elegant solution to the problem. In the 3,4-epoxytetrahydropyrans, the ring oxygen has the same relation to the oxirane function as does the methoxyl oxygen in **1** to **4** but the steric effects are much smaller. Although the resulting dissection of the inductive effect differs from ours in important respects, there is no doubt that this is a most promising approach.[5]

In the previous work (3), an A2 mechanism was assumed for acid-catalyzed oxirane scission (13). In only a few instances (for example refs. 14 and 15 and the present work) has the third-order kinetics, required for the mechanism, been demonstrated. Indeed, the A1 mechanism has been frequently proposed in its place, and as frequently rejected (16). Recently (17), a more formidable challenge has appeared in the proposal of certain ion-pair mechanisms. Doubts have been expressed in regard to these (9, 18) and in the present work it is demonstrated that the A2 mechanism is still clearly preferable.

Second- and third-order differences form the basis of the present and the previous work (3). The importance of experimental accuracy cannot therefore be too strongly emphasized. In the gas–liquid chromatographic analysis, for example, "constant" errors due to nonlinearity in the detector and to baseline effects are much larger than the random errors which alone are reported in contemporary papers on mechanism. In our work (3), standard

[4]The suggestions arose from valid explanations offered for the 3-*tert*-butylcyclohexene oxides. However, substituent methoxyl lacks the size necessary either to impose the twist-boat conformation or to provide the steric blockage required in the explanations. Unpublished work (R. C. Cathcart and R. Y. Moir) shows how the chair and twist-boat conformations in the transition states may be distinguished.

[5]The value deduced for the inductive effect is less than half that calculated in the present work. In the tetrahydropyran work, effects caused by (*i*) the nucleophile-oxygen interactions and by (*ii*) the (field) effect due to the fact that the more remote oxirane position is much closer to the ring oxygen of the tetrahydropyrans than it is to the functionally similar methoxyl group in **1** to **4** are neglected. The relation of the nearer oxirane position to the electron withdrawing oxygen is the same in both series.

TABLE 1. Rate constants for the attack of charged and uncharged nucleophiles upon related oxiranes in acid solution[a,b]

Oxirane (and point of attack)[c]	Acid added	Initial molarity of acid	Apparent rate constant for attack at a single centre by: Chloride ($L^2 mol^{-2} min^{-1}$)	Methanol ($L mol^{-1} min^{-1}$)	Water ($L mol^{-1} min^{-1}$)
		Cyclohexane series			
trans-3-Methoxy **2**					
Position 1	$HClO_4$	0.15	—	0.0307	0.0330
	HCl	0.15	0.0570	0.0293	0.0300
Position 2[d]	$HClO_4$	0.15	—	0.00147	0.00177
	HCl	0.15	0.00467	0.00137	0.00175
cis-3-Methoxy **1**					
Position 1	$HClO_4$	0.015	—	0.112	0.147
	HCl	0.015	1.59	0.113	0.148
		0.015[e]	1.63	0.116	0.152
		0.15[f]	1.68	0.113	0.148
Unsubstituted **5**	$HClO_4$	0.015	—	1.20	1.42
(at a single centre)	HCl	0.015	11.0[g]	1.21	1.43
		0.015[e]	11.5[g]	1.23	1.46
		Cyclopentane series			
trans-3-Methoxy **4**	$HClO_4$	0.15	—	0.00195	0.00159
	HCl	0.15[h]	0.00453	0.00195	0.00159
cis-3-Methoxy **3**					
Position 1	$HClO_4$	0.15	—	0.00184	0.00184
	HCl	0.15[h,i]	0.0224	0.00184	0.00184
Position 2[d]	$HClO_4$	0.15	—	9.78×10^{-5}	6.78×10^{-5}
	HCl	0.15	0.00180	9.78×10^{-5}	6.78×10^{-5}
Unsubstituted **6**[j]	$HClO_4$	0.015	—	0.0583	0.0521
(at a single centre)[k]	HCl	0.015	0.405	0.0576	0.0515

[a]The initial concentration of oxirane was 0.06 *M* and the initial ionic strength was adjusted to 0.215 *M* with sodium perchlorate. All reactions were carried out at 2.43°C in 50 wt.% aqueous methanol.
[b]Corrected results from the multi-tube dilatometers gave the composite rate constants k_N (for attack by chloride) and k_s (for attack by methanol and water). The individual rate constants were then calculated from the analysis of the reaction mixtures (3).
[c]Position 1 is the oxirane carbon more remote from methoxyl.
[d]Observed simultaneously with the corresponding attack at position 1.
[e]These solutions were 0.035 *M* in added sodium chloride.
[f]The temperature–time graph had the same form as that of the next entry.
[g]The temperature–time graph was assumed to be the same as the average graph for the corresponding perchloric acid system.
[h]k_s was assumed to be equal to that for the corresponding perchloric acid systems. The mixture was kept at reaction temperature for 9 days.
[i]k_s was assumed to be equal to that for the corresponding perchloric acid systems. The mixture was kept at reaction temperature for 7 days.
[j]One of 14 rate experiments employing $HClO_4$ was rejected, the rest showing, in six groups, an average standard deviation of the mean of 0.72% in k_s. Two of 19 experiments in which HCl was used were rejected, the rest showing, in 7 groups, a corresponding error figure of 0.46% in k_N and of 0.76% in k_s. At least 56% of the reaction (as judged by the acidity) was used for the direct measurement of k_N, 70–80% being usual.
[k]Experimental rate constants for oxiranes 5 and 6 were twice those reported in the table.

samples were therefore adjusted to have as nearly as possible the *same* composition as each unknown, and the success of the corrections was demonstrated by two independent methods of analysis. Similarly, although in the present work, good reproducibility in rate measurements (Table 1) has been obtained, more attention has been paid to those errors which, constant for any one reaction, increase rapidly with the rate of reaction, and which are almost totally neglected in current work. Our purpose was to ensure and to demonstrate the reliability of the values of the second- and third-order differences derived from the rate constants (Tables 2 and 3). In so doing a method for employing the dilatometer in reactions of higher order has been developed that hopefully will be of general interest and utility.

Comparison of the rates of scission of an oxirane by different nucleophiles under exactly the same conditions was, in brief, our whole method. It was therefore necessary to solve the general kinetic problem of simultaneous reactions which separately were of the second and third order (3) (by numerical integrations). Experimentally it was necessary to demonstrate that the method of solution was unaffected by extraneous sources of curvature in the rate plot. For example, ionic strengths varied slightly

TABLE 2. Effects of neighbouring methoxyl upon the rates of scission and formation of cyclohexane oxiranes[a]

Example	Oxirane	Related chlorohydrin[b]	Related transition state[c]	$\Delta^2F_s^{\ddagger d}$ (for scission)	$\Delta_s^{3\ddagger}$	$\Delta^2F_f^{\ddagger d,e}$ (for formation)	$\Delta_f^{3\ddagger}$	$(\Delta^2F_s^{\ddagger} - \Delta^2F_f^{\ddagger})$
1	*Cis*[f]	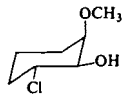	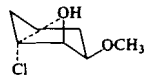	1.05	3.21	−0.76	2.68	1.81
	1	7						
2	*Trans*[g]	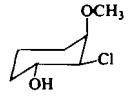	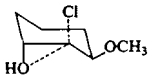	4.26	1.37	1.92		2.34
	2	8						
3	*Trans*[f]	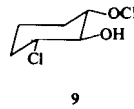	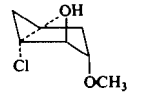	2.89		1.32	2.64	1.57
	2	9						
4	*Cis*[g]	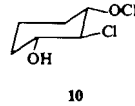	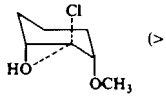	(>4)[h]		3.96		
	1	10						

[a]All numerical values are given in kcal/mol.
[b]The chlorohydrin was either formed from the epoxide in "acid-catalyzed" scission by chloride ion, or was converted to the same oxirane by base. For clarity in exposition different enantiomers of the oxiranes have been used in illustrating different reactions.
[c]Shown for the "acid-catalyzed" scissions, symbols for electric charge being omitted. For the corresponding formation reactions, —OH in these transition states is replaced by $—O^-$.
[d]$\Delta F^{\ddagger}$ for the reaction related to the indicated oxirane *minus* $\Delta F^{\ddagger}$ for that related to cyclohexene oxide. See [1] and [2].
[e]Values given were obtained by extrapolation of the experimental values from 20–2.43°C by the Arrhenius equation, and from 44–50 wt.% methanol by assuming that all free energies of activation suffered the same net change. By experiment, $\Delta F_f^{\ddagger}$ for compound 7 decreased by 7.5% when the solvent was changed from 87–44 wt.% methanol, whereas $\Delta F_f^{\ddagger}$ for cyclohexene chlorohydrin decreased by 7.6% on the same change of solvent.
[f]This example corresponds to attack at position 1 of the oxirane (that more remote from methoxyl), as in Table 1.
[g]Attack at position 2 of the oxirane.
[h]Reaction too slow to be observed.

during each reaction, and the constraints of the problem (3) did not allow us to swamp out the resulting effects completely. A large amount of experimental work was required to measure the effects of this variation upon the rate constants, and was justified less by its estimate of this very small quantity[6] than by the demonstration that the rate constants could be extracted without difficulty in the presence of this extraneous source of curvature. The same work was used in the comparison of two methods for compensation of temperature errors.

Oxirane scissions are exothermic, and the resulting rise in temperature may produce three main errors. With care, the first error, the direct effect upon the rate constant itself, is negligible (19). The second, larger error, here called the Tong–Olson effect (20), is discussed below. The third error applies especially to the dilatometry of concurrent reactions of different order. For these reactions (unlike first-order reactions) one must know the chemical sensitivity for each of the reaction orders involved and, in our method, one of these sensitivities must be obtained from a related first-order reaction. In such reactions, even when the Tong–Olson effect upon the rate constant is only 2–3%, the sensitivity, uncorrected for temperature rise, is commonly in error by more than 100%. Even though the resulting error in the rate constants is less by an order of magnitude, it is clear that corrections must be applied and verified. The agreement of two different methods of temperature compensation, one based on direct measurement and the other on the form of the observed capillary height – time curve, therefore completed our demonstration of the utility of the dilatometer in reactions of higher order.

Our work also applies to the use of the dilatometer in first-order reactions. Most workers appear to believe that the temperature effect is transient, its

[6]Fixed errors due to the neglect of activity coefficients in Table 1 cancelled essentially exactly for solvent, catalyst, and nucleophile, and perhaps largely for substrate, in the comparisons of Tables 2 and 3.

TABLE 3. Effect of neighbouring methoxyl on the rates of scission and formation of cyclopentane oxiranes[a]

Example	Oxirane	Related chlorohydrin[b]	Related transition state[c]	$\Delta^2F_s^{\ddagger d}$ $\Delta_s^{3\ddagger}$ (for scission)	$\Delta^2F_f^{\ddagger d,e}$ $\Delta_f^{3\ddagger}$ (for formation)	$(\Delta^2F_s^{\ddagger} - \Delta^2F_f^{\ddagger})$
1	*Cis*[f]	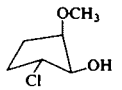	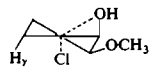	1.59	−0.08	1.67
	3	**11**			3.13	
2	*Trans*[g]	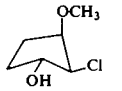	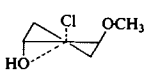	(>5.5)[h]	3.05	—
	4	**12**				
3	*Trans*[f]	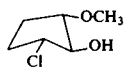	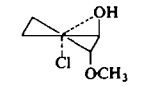	2.47	0.95	1.52
	4	**13**		0.50	0.85	
4	*Cis*[g,h]	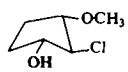	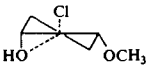	2.97	1.80	1.17
	3	**14**				

[a,b,c]As in Table 2.

[d]$\Delta F^{\ddagger}$ for the reaction related to the indicated oxirane *minus* $\Delta F^{\ddagger}$ for that related to cyclopentene oxide.

[e]Values given were obtained by extrapolation of the experimental values from 14.91–2.43°C, assuming the same change in $\Delta F^{\ddagger}$ as the average change in the cyclohexane series over the same range (acceptable because of the small variation in $\Delta S_f^{\ddagger}$ in the latter) and from 87–50 wt.% methanol by assuming a 5% reduction in $\Delta F_f^{\ddagger}$ for all examples. By experiment, $\Delta F_f^{\ddagger}$ declined by 6.035% for compound **12** and by 6.04% for compound **14**, when the solvent was changed from 87–44 wt.% methanol.

[f,g]As in Table 2.

[h]Interpretation of the drawings of the transition states may be aided by noting: (*i*) A 1,3-*syn*-diaxial-like relation does not exist between methoxyl and hydroxyl in example 4, though one does exist between methoxyl and chlorine in 3. (*ii*) Chlorine is nearly eclipsed by the pseudo-axial methoxyl in example 2. In all other examples, the corresponding relationship of chlorine is with H_y, and since this relation also exists in the reference reaction related to cyclopentene oxide, its primary effects cancel. See text. (*iii*) The degree of eclipsing between hydroxyl and methoxyl in example 1 is less severe than the effect between chlorine and methoxyl in example 2. (*iv*) Although drawn in the twist conformations the transition states are actually distorted to allow a surprisingly great degree of staggering of vicinal groups throughout the structures.

end signified by the onset of a pure first-order law of capillary rise (or fall). Tong and Olson (20) showed instead that temperature and reaction decay together (the source of the third error above), and moreover that the later part of the curve may very closely obey the first-order law and still yield a grossly erroneous rate constant. Simulated rate curves confirm the deceptive nature of this effect. The error is highly reproducible, not appearing in the experimental statistics. Moreover, its onset is sudden.[7,8] All these factors have led to a neglect of the Tong–Olson effect. Indeed, one may say that the resulting large and widespread errors have had a damaging effect on mechanism studies. The necessary temperature corrections may be made either by direct measurement or by Tong–Olson theory. In the latter method, a correction must be applied to their work (see Experimental).

[7]The first-order, corrected Tong–Olson theory agreed well with the observed overall temperature–time curves, though it missed details. Simulations were based on the corrected theory, random numbers being used to imitate the dispersion of the capillary readings. One simulation agreed well with a particular experiment performed in the cylindrical dilatometer (see Experimental); the simulated rate constant obtained from a straight part of the first-order rate plot was in error (with respect to the theoretical input) by only 0.49%, the correlation coefficient being −0.9999. A fourfold increase in the rate constant changed these values to 10.1% and −0.9990 respectively. Such a change could easily have been exceeded, for example, in an attempt to enforce first-order kinetics with excess hydrochloric acid. In a simulation of the faster of these reactions in the multi-tube dilatometer, the error was only 0.14% (in place of 10.1%), and the correlation coefficient −0.9999, showing the immense advantage of a mere doubling of the cooling constant (see Experimental).

[8]The cylindrical dilatometer had a cooling constant about four times better than that thought to be typical of traditional designs (20) which are not reviewed here. Furthermore our reactions were not especially fast. Nevertheless, the maximum temperature rise in the slower of the simulated reactions above was 0.24°C. Clearly, temperature rises of over 1 deg have often occurred in literature studies of the entropies of reaction. The largest maximum temperature rise observed in the multi-tube dilatometer was 0.110°C.

Discussion

Very great simplifications are made possible by the familiar method of double comparison. For the oxirane scission reaction [A],

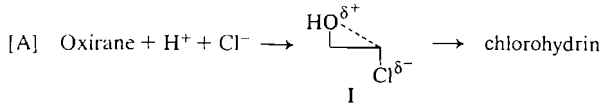

I

$$\Delta F_s^{\ddagger} = F_s^{\ddagger} - F_{ox}{}^0 - F_{H^+}{}^0 - F_{Cl^-}{}^0$$

(with $F_s^{\ddagger}$ as the standard free energy[9] of **I**), several ground state terms survive in the experimental quantity $\Delta F_s^{\ddagger}$. Some of these are removed by comparing the expression with that for a standard oxirane, so that, from the difference of the two values of $\Delta F_s^{\ddagger}$,

$$[1] \quad \Delta^2 F_s^{\ddagger} = \Delta F_s^{\ddagger} - \Delta F_{s^0}{}^{\ddagger} = (F_s^{\ddagger} - F_{s^0}{}^{\ddagger}) - (F_{ox}{}^0 - F_{ox^0}{}^0)$$

(s^0 and ox^0 refer to *the standard oxirane*). More important is the fact that the oxirane under investigation (e.g., example 1, Table 3, epoxide **3**) shares many characteristics in common with the corresponding standard (**6**). The influence of these characteristics cancels in $\Delta^2 F_s^{\ddagger}$ (see footnote *h* to Table 3).

The usefulness of the quantities $\Delta^2 F_s^{\ddagger}$ is much increased by comparing them with similar quantities derived from the related oxirane formation reactions [B], whose rates we have also measured,

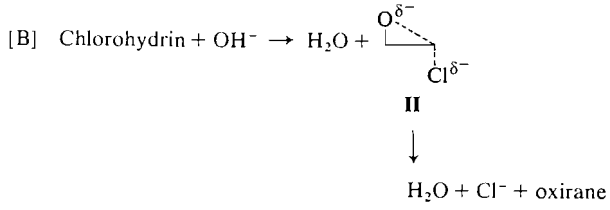

$$[2] \quad \Delta^2 F_f^{\ddagger} = (F_f^{\ddagger} - F_{f^0}{}^{\ddagger}) - (F_{Ch}{}^0 - F_{Ch^0}{}^0)$$

where $F_f^{\ddagger}$ is the standard free energy of the transition state **II** belonging to the particular reaction under investigation, and $F_{Ch^0}{}^0$ is the standard free energy of the reference chlorohydrin (cyclohexene chlorohydrin for the examples in Table 2). The quantity $\Delta^2 F_f^{\ddagger}$ is the direct physical measure of the effect upon the rate of oxirane formation brought about by placing a substituent at a given position and orientation in the parent chlorohydrin. The analogous measure of the effect of a substituent on the rate of "acid-catalyzed" oxirane scission by a given nucleophile is given by $\Delta^2 F_s^{\ddagger}$. Values are listed in Tables 2 and 3.

The cancellation of effects possible in the use of these quantities is often startling. For reaction [B] of example 1 (Table 2), the chlorohydrin **7**, in moving to its transition state, has to be converted from one chair form to another, a process aided by the methoxyl group's change from the axial to the equatorial position. Since the *A* value for methoxyl is known to be 0.77 kcal/mol (21), it is evident from the experimental value for $\Delta^2 F_f^{\ddagger}$ that this conformational effect is the *only* surviving effect of methoxyl in the particular configuration of **7**. Obviously, the increased ease of deprotonation of the hydroxyl group caused by the methoxyl group must have been offset by the decreased nucleophilicity of the oxyanion in **II** due to the same cause. In contrast, both corresponding polar effects would be expected to work together to decrease the rate of the corresponding reaction [A] by which **7** is formed. In agreement with the postulated importance of these factors, it can be seen from $\Delta^2 F_s^{\ddagger}$ (1.05 kcal/mol) (example 1, Table 2) that methoxyl strongly decreases the rate of scission, whereas (from $\Delta^2 F_f^{\ddagger} = -0.76$ kcal/mol) it notably increases the rate of the corresponding formation of oxirane.

An interesting dissection for isolation of the inductive effect is possible. In the comparison of values of $\Delta^2 F^{\ddagger}$ for examples 1 and 2, or for examples 3 and 4 (Table 2), compounds similar in geometry both in the ground state and in the transition state are paired together, so that steric and conformational effects might be expected to cancel. The differences in $\Delta^2 F_f^{\ddagger}$ values might therefore be regarded as a measure of the polar effects of methoxyl upon the developing positive charge at the carbon being attacked by the oxyanion.[10] Confirmation of this analysis is seen in the fact that the two values of $\Delta_f{}^{3\ddagger}$ (2.60 and 2.68 kcal/mol) for the two very different transition state geometries, are in close agreement. Indeed, one may go further. In the previous paper (3), the geometrical orientation of the ring carbon – methoxyl dipole with respect to the C ··· Cl partial bond was shown to have a profound

[9]The Gibbs free energy is represented by *F* in these papers, to avoid confusion with the symbol *G* used for the *gauche* effect.

[10]Both this definition and the method of dissection of the inductive effect exclude a number of dipole–dipole interactions, included later in the conformational parameters. Close examination supports the simplicity of the dissection. For example, ground state hydrogen bonding terms (22) in hydroxylic solvents are thought to be small (3). Similarly, the inductive effect quoted is actually the difference between the effect in a 1,2-chloromethoxy compound and that in a 1,3-compound, but it has been argued (1) that the latter effect is nearly zero.

effect upon the rates of scission. Consideration of this fact together with the transition state geometries of Table 2 shows that the similar values quoted for $\Delta_f^{3\ddagger}$ in the two comparisons cannot be understood unless *the oxyanion and the leaving chloride bear almost equal charges in the transition states leading to the formation of the oxiranes* (reaction [B]). An important point in the analysis is that this is emphatically *not* the case in the corresponding transition states for reactions [A].[11,12]

The existence of a large inductive effect deduced from the base-catalyzed reactions [B] is confirmed in two independent ways. The true reverse reactions of [A] are the solvolysis of the chlorohydrins. In a previous paper (18), a study of the solvolysis of analogues of **8** and **9**, in which chlorine had been replaced by the tosyloxy group, was carried out. In spite of its large conformational advantage, the tosylate corresponding to **8** solvolyzed about 10 times slower than did the isomer corresponding to **9**, evidence for a very large inductive effect involving transition states exactly analogous to **I**. Reactions [A] allowed a more quantitative comparison. Comparison of $\Delta^2F_s^{\ddagger}$ values for examples 1 and 2 (Table 2) gave a value for the inductive effect of 3.21 plus "other effects" (e.g., different starting epoxides). A long and difficult analysis suggested that the sum of the "other effects" was small. This was confirmed by the more accurate comparison of $\Delta^2F_s^{\ddagger}$ values for examples 2 and 3 (Table 2), for which experimental errors are at a minimum[12] and ground state contributions vanish exactly. In this way, the inductive effect was found to be 1.37 plus an amount due to a large conformational effect in the transition state. In this case, the conformational effect could be estimated accurately by a method to be explained in a later paper,[13] giving a value for the inductive effect in the "acid-catalyzed" scissions [A] of 3.0 to 3.2 kcal/mol.

Intuitively one would expect (12) that the inductive effect would be larger in reactions [A] than in [B] because of the greater positive charge expected on oxirane carbon in the transition state of the former. However, the difference cannot be large, on account of the similarity of the ratios of yields of normal and abnormal products in acid- and base-catalyzed scissions in the present system (ref. 24 and this paper). Thus the quantitative separation of the inductive effect from steric and conformational effects is supported both by theory and by experiments made with different ground states and under very different conditions of scission, formation, and solvolysis.

One may use the well defined cyclohexane conformations as references to which the less regular cyclopentanes may be compared. Inspection of Table 1 shows that scission of the cyclohexane oxiranes is usually much faster than that of the corresponding cyclopentane derivatives. This fact has been noticed before (23, 25), and ascribed to the relatively greater increase in eclipsing interactions in going from oxirane to transition state in the cyclopentanes. By referring each oxide to its unsubstituted parent, most of these effects are removed, allowing those that remain to become clearly evident. When this is done, the reasons for the present confusion in the literature on cyclopentane conformations become immediately apparent. At times, the behaviour of the two ring systems can be similar indeed. As shown in the previous paper (3), the response of each ring system to dipole orientations is nearly the same. In the rate experiments, the closest similarity lies in examples 3 (Tables 2 and 3); for these both $\Delta^2F_s^{\ddagger}$ and $\Delta^2F_f^{\ddagger}$ are only slightly lower in value for the cyclopentanes than for the cyclohexanes. In particular, both ring systems show large 1,3-*syn*-like interactions in the transition states for either scission or formation of the oxiranes.

In contrast, there is a large difference in examples 4 of the two series. The quantity $\Delta_f^{3\ddagger}$ for examples 3 and 4 (i.e., from comparing $\Delta^2F_f^{\ddagger}$ for examples 4 and 3) is 2.60 kcal/mol for the cyclohexanes, but only 0.85 kcal/mol for the cyclopentanes. This difference amounts to a numerical verification of the previous conclusion (10) that cyclopentanes of the configuration shown in example 4 (Table 3) are able to avoid *syn*-1,3-like interactions in the transition states, whereas cyclohexane transition states of the same configuration (example 4, Table 2) are not able to avoid them. The reasons for the different behaviour in examples 3 and 4 have been given (10). Still another important source of confusion as to

[11]The dissection does not ignore the difference in ground state free energies between examples 1 and 2 due to the different chemical neighbour of methoxyl in each. Every ground state is compared with the transition state of the same positional structure. In view of footnote 10, the differences which survive the comparison essentially constitute the inductive effect.

[12]The extended comparisons are often aided by a cancellation of experimental errors. Each value quoted for $\Delta_f^{3\ddagger}$ and $\Delta_s^{3\ddagger}$ in the tables involves no more error contributions than those of a single $\Delta^2F_f^{\ddagger}$ or $\Delta^2F_s^{\ddagger}$ value, respectively. In two comparisons of $\Delta^2F_s^{\ddagger}$, namely of examples 2 and 3 in Table 2, and of 1 and 4 of Table 3, the cancellation is more extensive, each comparison involving an error equivalent to that of a single chemical analysis alone. In the least favourable comparison of the paper, the standard deviation is considerably less than that in tables of conformational parameters (23).

[13]Unpublished work with E. J. Langstaff.

the ability of the cyclopentane system to support *syn*-1,3-interactions is described below.

The second major difference between the cyclopentanes and cyclohexanes is illustrated by comparing examples 2 (Tables 2 and 3). Here $\Delta^2F_f^{\ddagger}$ is greater for the cyclopentane compound by 1.13 kcal/mol, and $\Delta^2F_s^{\ddagger}$ by at least 1.2 kcal/mol[14] than for the corresponding quantities in the cyclohexanes. Clearly these effects belong to the transition states, and a source is readily found in the near-eclipsing of chlorine and pseudo-axial methoxyl forced by the geometry of the cyclopentane transition state (10) but not by that of the cyclohexane series. In all the other examples, the corresponding effect is the interaction between chloride and pseudo-axial H_y (cf. example 1, Table 3), and the primary effect of this interaction cancels because of the method of comparison (see footnote *h*, Table 3) in examples 1, 3, and 4 (Table 3). A relatively large secondary effect appears in one of these. For example 1, oxirane formation is less favoured in the cyclopentanes than in the cyclohexanes (Table 2) by 0.68 kcal/mol, as measured by $\Delta^2F_f^{\ddagger}$. Model studies show that attempts to relieve the Cl/H_y interactions in the transition states result in a series of adjustments leading to the appearance of a smaller than normal dihedral angle between the ring carbon – methoxyl bond and the adjacent carbon–oxygen bond. This *extended gauche effect*, the third of the major differences brought to light in the present studies, serves further to emphasize that the relative behaviour of the two ring systems is strongly dependent upon the arrangement of the substituents.

The importance of polar effects in altering the main conformational parameters is made clearest by an approach which also underlines the fact that the dissections of the paper are based upon large and significant differences. Attack of chloride ion upon the *cis*-oxide **1** is (from Table 1) 29.5 times faster than the corresponding attack upon the *trans*-oxide **2**. With methanol as the nucleophile, reaction of the *cis*-oxide is only 3.9 times as fast as that of the *trans*. In other words, chloride ion is 7.6 times more selective than methanol, though it is much the more nucleophilic reagent. Polar effects have clearly upset the literal applicability of Hammond's hypothesis (26), and the influence of unfavourably oriented dipoles (3) is further shown by the fact that in the cyclopentane series, the reaction with methanol is actually slower with the *cis*-oxide **3** than it is with **4**.

[14]Tables 2 and 3 each contain one $\Delta^2F_s^{\ddagger}$ value given as a lower limit, estimated from the sensitivity of the glc method of analysis (3).

In the dissection already made, it has been repeatedly seen that transition state effects evident in reactions [A] appear also in those for reactions [B], experimental support for the intuitive idea that these states (**I** and **II**) differ mainly in the presence of an acidic proton in the former. This idea is easily made quantitative, and leads to a useful dissection of the polar effects (27).

If $\Delta F_p^{\ddagger}$ is the standard free energy for the (composite) reaction transferring a proton from solvent to transition state **II** (yielding **I**), and if $\Delta^2F_p^{\ddagger} = \Delta F_p^{\ddagger} - \Delta F_{p^0}^{\ddagger}$ is the corresponding comparison made with the transition states from the unsubstituted compounds, then

$$[3] \quad (\Delta^2F_s^{\ddagger} - \Delta^2F_f^{\ddagger}) = \Delta^2F_p^{\ddagger} + (F_{Ch}^{0} - F_{Ch^0}^{0}) - (F_{ox}^{0} - F_{ox^0}^{0})$$

where the other symbols are as in [1] and [2]. The values given in the final columns of Tables 2 and 3 do not correlate with any transition state effects, and it is now shown that they do correlate very well with certain ground state terms expected in [3]. Ignoring other effects, one would expect on conformational principles that chlorohydrins possessing a predominantly axial methoxyl in the ground state (such as **7** and **8**) would show higher values of F_{Ch}^{0} than, e.g., **9** and **10**. Similarly, one would expect the *trans*-oxides **2** and **4** to possess lower F_{ox}^{0} values than the corresponding *cis*-oxides **1** and **3**. All six tabulated values of $(\Delta^2F_s^{\ddagger} - \Delta^2F_p^{\ddagger})$ agree qualitatively with the hypothesis that these are the dominant surviving effects. This number of agreements is too large to be due to chance, and moreover the separate numerical values are all reasonable. The most convincing comparison is that of examples 2 and 3, Table 2, for which the experimental errors are at a minimum,[12] and for which the ground state contributions of the oxiranes to [3] vanish exactly. If the whole of the difference $(\Delta_p^{3\ddagger})$ between the two values of $(\Delta^2F_s^{\ddagger} - \Delta^2F_f^{\ddagger})$ is then attributed to ground state effects in the chlorohydrins **8** and **9**, and if every difference between **8** and **9** is ignored except the work required to convert methoxyl from the axial to the equatorial position, then $\Delta_p^{3\ddagger}$ would be calculated to have the *A* value for methoxyl, viz. −0.77 kcal/mol. This is exactly the experimental difference between the two values of $(\Delta^2F_s^{\ddagger} - \Delta^2F_f^{\ddagger})$ given in Table 2 for the comparison of 2 and 3.

The assumption that this wholesale cancellation of effects also applies to the comparisons of examples 1 and 2 (Table 2) and of 1 and 3 (Table 3) leads to a self-consistent quantitative conformational analysis

of the entire set of reactions given in Table 1.[15] Within the set, the analysis retains its quantitative value even if the assumption is in error, but for comparisons outside the system, errors in the assumption do affect the results. A careful inspection of the observed cancellations of the previous paragraph with respect to those assumed in this shows that ground state errors are small, but that a significant error[16] due to dipole orientations in the transition states is present. Although the error could be estimated, it seems better to say that with favourable orientations of the dipoles (as in the acid-catalyzed methanolysis of the *trans*-oxide **2**) the value of the conventional Z effect in the transition state is at most a small positive number, and may well be negative.

Among the rather far-reaching implications of this generalization may be mentioned an explanation for the observations of Berti and co-workers (28) on the preferential formation of certain "*cis*-onium" ions in, for example, addition reactions of 3-methoxycyclohexene. It also serves to remove a reservation previously expressed (2) regarding our conclusion that large positive values are possible for *syn*-1,3-like interactions in transition states of the cyclopentane series. Examination of the experimental basis for the objection (29) shows that it involves reactions of cyclopentane compounds having favourably arranged dipoles, i.e., a situation in which the corresponding cyclohexane compounds would also have failed to show a large positive Z effect.[17]

Lamaty and co-workers (17) felt they had obtained evidence supporting an ion-pair mechanism for oxirane scission, in place of the familiar A2 (1, 13, 31). Reactions with hydrogen chloride which showed the expected third-order kinetics in ionizing solvents were second order in less polar solvents. They proposed a kinetic scheme in which the rate-determining steps involved the formation of different ion-pairs in the two cases. Many other interpretations are possible including several which support the A2 mechanism.[18] In addition, double comparison allows us to remove from consideration one interesting class of ion-pair reactions. No one doubts that drawings like those of this paper represent very well the product determining states, whatever the mechanism. But the postulation of additional transition states and intermediates is possible, and as Wylde and co-workers have pointed out (17), one type would serve to separate the rate- and product-determining steps, thus making easier the union of theory and experiment, while at the same time remaining "invisible" kinetically and (from Curtin–Hammett theory) having no direct effect upon product distribution. Such intermediates may be thought of as doubly bridged, with both the oxirane oxygen and the incoming nucleophile bonded approximately symmetrically to the two oxirane carbons (in order to avoid immediate product determination at a rate-determining step). Species like these arise naturally from the ion-pair theory, and are prominent in several currently accepted mechanisms (18).

If the incoming nucleophile is water, and if proton transfers with the solvent remain rapid with respect to reactions of the intermediates, then it is easily seen (in contrast to the transition states shown in Fig. 1) that the incoming oxygen and the oxirane oxygen will be very similarly situated in such an intermediate. It is possible (and in our view likely) that in such an intermediate the distinction between the two oxygens would be lost. Dramatic support for the existence of these intermediates would therefore arise if two different oxiranes could be shown to proceed to the same product through a common intermediate.

Experiment shows that this is emphatically not the case. Each of the two diols (**15** and **16**) was formed in two different ways. Ground state effects cannot be important contributors to the $\Delta^2F^{\ddagger}$ values of Fig. 1 since in one case the *cis*-oxide leads to a very positive value and in the other to a

[15]For example, the experimentally accurate comparison of examples 1 and 4, Table 3, then leads to the estimate of 0.50 kcal/mol for the ground state A value of methoxyl in the cyclopentanes. From the rates of oxirane scission by methanol given in Table 1, one can estimate a value for the *syn*-1,3-interaction (Z effect) of substituent methoxyl and incoming methanol in the transition state of -0.57 kcal/mol. This value forms an interesting contrast with the uniformly high positive values of Z in the few examples known (23) for the ground state.

[16]The errors are such as to cause the quoted value for $Z(CH_3OH/OCH_3)$ to be too negative, and the quoted A value for methoxyl in the cyclopentanes to be too small, the error being much smaller in the second of these values.

[17]Surviving criticisms of our work point to the anomalies experienced when the methoxyl group is replaced by alkyl radicals (ref. 30, but see ref. 12). Unpublished work with R. C. Cathcart suggests that these are to be explained on the basis of polarization of the alkyl group by the incoming nucleophile.

[18]The difficulty is to avoid postulating a switch to acid-catalyzed A1 in the *less* polar solvents, the obvious way to do this being the suggestion of initial attack on the oxirane by un-ionized HCl, or the equivalent. Several versions of the A2 mechanism then show second-order kinetics and insensitivity to added chloride in the less polar solvents. J. Wylde, in a private communication, strongly doubts this explanation for the less polar solvents, but expresses complete agreement that A2 is the mechanism in aqueous methanol.

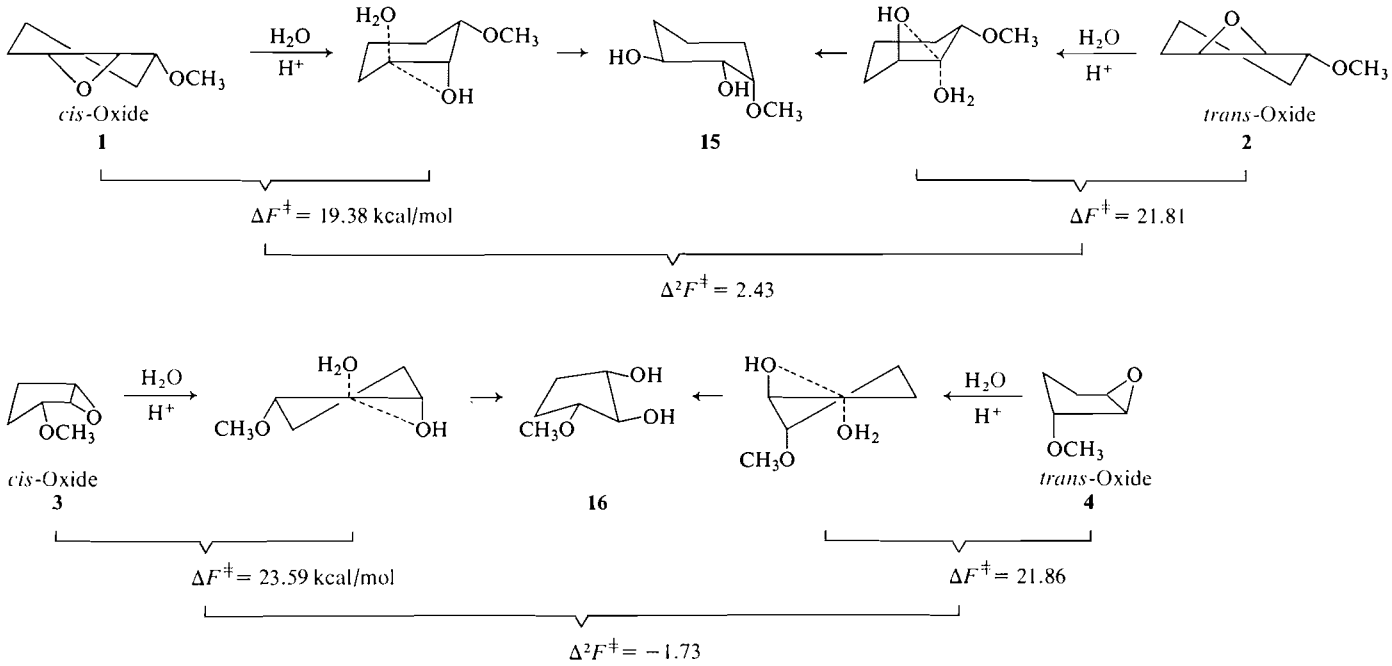

FIG. 1. Formation of the same product by two different routes.

very negative value of $\Delta^2F^{\ddagger}$, and in view of the dissections made above. Obviously the transition states must all be very unsymmetrical, maintaining throughout the reactions a strong distinction between the incoming hydroxyl group and the oxirane oxygen. Of course, the ion-pair theory could be adjusted to fit this evidence, but the fact remains that the A2 fits the evidence automatically, as it has all the other tests of these papers.

Experimental

Preparation and purification of the compounds mentioned in this paper, and the identification of reaction products in the scission and formation of the oxiranes, have been described previously (3, 7, 10, 24, 32). The methods of analysis of the reaction products in scission are described in the previous paper (3). Rates of oxirane formation were observed by a method resembling that of McCabe and Warner (33). Reactions of scission and of formation were conducted in an insulated Sargent bath equipped with a proportional heating control; temperatures varied less than 0.006 deg throughout the bath. The working differential thermometer was referred to a standard thermocouple calibrated with freezing mercury and with decomposing sodium sulfate decahydrate. It was checked at the freezing point of benzene, yielding 5.486°C during the "formation" work, and 5.481°C, during the "scission" work; the literature value (34) is 5.483°C. The initial operations of preparing and mixing the reaction sample and of filling the dilatometer have been described (3).

Dilatometry

The Multi-tube Dilatometers (See Fig. 2)

Good heat transfer, active convection, mechanical strength, and ease of filling were all obtained by forming the reservoir from six connecting tubes, five outlining the surface of a spheroid, the sixth being axial. The reaction dilatometer had a volume of 81.7 mL and, when filled with 50 wt.% aqueous methanol at 2.43°C, a thermal sensitivity of 6.63 cm deg^{-1} and a passive cooling constant of about 1.01 min^{-1}. These characteristics very closely matched those of the reference dilatometer. A thermistor (Yellowstone Instruments precision, 10 kΩ at 25°C) was placed, together with a little silicone oil, in a thermometer well present in each dilatometer, the thermistors being connected by shielded cable to opposite arms of a Wheatstone bridge. In view of the difficulties previously reported in the use of high impedance thermistors (19), care was taken to avoid ground loops and common ground pathways, and to isolate the bridge from the recorder (Varian model A-25) with an operational amplifier. Circuit analysis showed, however, that the principal difficulty lay in differential heating effects in the bridge resistors, temperature measurements stable to 0.001°C requiring the resistors to be matched in temperature within a few thousandths of a degree. Ordinary control circuits being ineffective, temperature oscillations in the bridge were prevented by (*i*) cementing the elements to a heat sink of high thermal capacity, (*ii*) using as heating elements of very low thermal capacity the actual resistors and transistors of the heating circuit, (*iii*) careful placement of the heating and sensing elements, and (*iv*) providing a dual "fast" and "slow" proportional control for the heater. No oscillations (to a sensitivity of 0.2% in voltage) could be detected in the heater drive, and no short or long term variations in the recorder output, due to the bridge, could be detected up to several hours at a sensitivity of 0.001°C. Calibration of the system agreed well with the theoretical analysis in showing a sensitivity at the recorder input of 0.40 V deg^{-1} and in verifying the expected very satisfactory linearity up to a temperature difference of at least 0.24°C. Roux and Viallard (35) have reported an interesting variation for a different purpose.

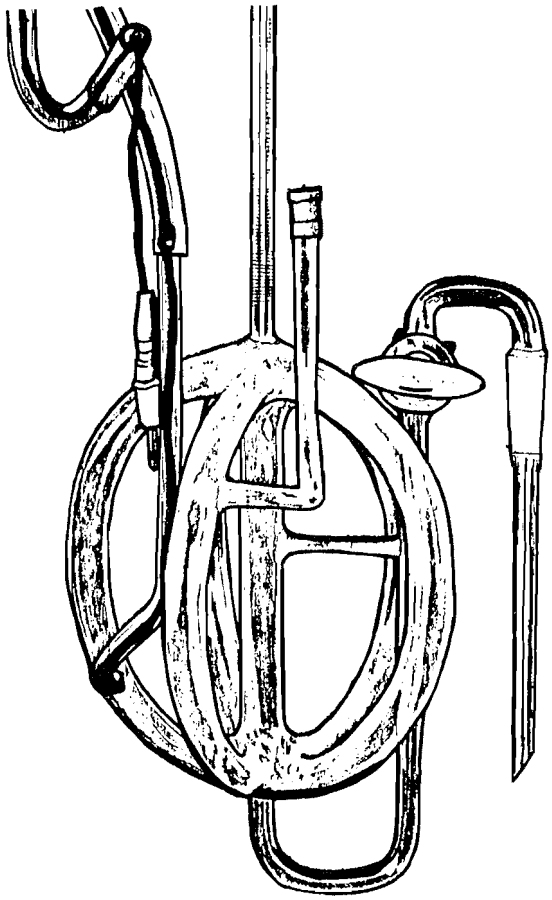

FIG. 2. The multi-tube dilatometer.

During a reaction, 95–197 points were observed beginning at 3.0 min after the mixing of the reactants for those observed at 0.5 and 1.0 min intervals and at 5 min for those observed at 5 min intervals. The kinetic bath was protected against air currents and strong light. Readings from the reaction dilatometer were corrected (*i*) by comparison with those of the reference dilatometer, (*ii*) for emergent stem temperature effects, if necessary, and (*iii*) for differential temperature effects detected by the thermistor, if the maximum temperature rise within the run was greater than 0.003°C. None of the experiments with cyclopentane derivatives but nearly all of those with cyclohexane compounds required the last correction (Table 1).

Cylindrical Dilatometers

The *cylindrical dilatometers* were of Eastham's pattern (36), modified to allow transfer from the mixing vessel to occur under the surface of the bath liquid. The reaction dilatometer, closely matched by its reference dilatometer, had a volume of

35.5 mL, a thermal sensitivity of 6.76 cm deg^{-1}, and an active cooling constant of about 0.64 min^{-1}. Temperature corrections were made by a modified Tong–Olson theory (see below) (20).

Determination of Pseudo-first-order Constants for Solvolysis. Perchloric Acid

The results in Table 1 were obtained by applying Guggenheim's method (37) to the corrected observations from the multi-tube dilatometers. From 31–97 pairs of points were used. With the faster reactions, all of the readings were taken in 1 day and there was at most one point between the two intervals. With the slower reactions, the readings of the first interval were taken one day while those of the second interval were taken on the next. In general, points prior to 5 min (or to 6.5 min in faster reactions) were not used in the fittings. Another method, reported below, was employed for the cylindrical dilatometers.

Determination of the Chemical Sensitivities of the Dilatometer for Use in Reactions of Mixed Order. Modification of the Tong–Olson Theory

For a reaction *at constant temperature* of an oxirane with aqueous methanolic hydrochloric acid, the capillary readings y_i at times t_i obey

$$[4] \quad y_i = y_0 + u_N[\mathrm{Ch}] + u_s D$$

where y_0 is the hypothetical reading at zero time, [Ch] the amount of oxirane (in mol L^{-1}) which has been converted to chlorohydrin at time t_i, and D the corresponding conversion by solvolysis. The final capillary reading (obtained as in the Guggenheim method) is y_f. For mixed reactions not of the same order, one must know the chemical sensitivities, u_N and u_s, in order to determine the rate constants k_N and k_s of the corresponding reactions. One of these sensitivities (u_s) was obtained by applying [4] to the solvolysis in perchloric acid, where [Ch] = 0. The procedure was straightforward for very slow reactions, or for reactions in which temperature corrections could be determined from thermistor readings. Values of u_s for the multi-tube dilatometer were found to be in the cyclohexane series, for solvolysis of the *trans-*, *cis-*, and unsubstituted oxiranes of Table 1, −151.8, −134.9, −138.5, and in the cyclopentane series, −130.7, −129.6, and −119.8 cm mol^{-1} L respectively.[19]

Temperature corrections for the cylindrical dilatometers were made by a curve fitting technique. For two sets of solvolyses of cyclohexene oxide at different acidities, differential least-squares curve fitting to the first-order Tong–Olson (20) eq. [5] in the four variables C_a, C_b, k, and g, gave

$$[5] \quad y_i - y_f = C_a e^{-kt} + C_b e^{-gt}$$

rapid convergences, stable to large perturbations in the initial estimates, and reproducible from run to run. As a by-product, the fittings gave values for the active cooling constant g, and for the first-order rate constant k, corrected for the Tong–Olson effect. In the neglect of thermal effects, the desired chemical sensitivity (u_s) can be obtained from $u_s = -C_a/[\mathrm{Ox}]_0$, where $[\mathrm{Ox}]_0$ is the initial concentration of oxirane. Tong and Olson suggested $u_s = -(C_a + C_b)/[\mathrm{Ox}]_0$, but this value is also grossly in error, since [5] neglects the initial events of mixing and transfer. A step-function calculation gave the remarkable result that in [6] the value of u_s is independent

$$[6] \quad -u_s[\mathrm{Ox}]_0 = C_a + \frac{(C_a' - C_a)(g - k')}{g(1 - k'/k)}$$

(under suitable circumstances) of these early events. From values of C_a and k obtained by fitting [5] to results from a solvolysis in 0.03 M aqueous methanolic perchloric acid, and values of C_a' and k' obtained from a similar solvolysis in 0.015 M acid, u_s for cyclohexene oxide was found to be −135.8 cm mol^{-1} L. Since a value of −136.0 was found from a very slow run in 0.0015 M acid, the method was confirmed.

Determination of the Rate Constants for Oxirane Scissions in Aqueous Methanolic Hydrochloric Acid

Curve fittings were performed with iterative differential least-squares routines (38), the required numerical integrations being carried out with a simple predictor-corrector (39). No more than three adjustable parameters were used, in order to avoid parameter sliding (40). The input data included the capillary readings, the chemical sensitivity (u_s), the initial oxirane concentration ($[\mathrm{Ox}]_0$), the initial acidity (A_0) and the final acidity (A_f), determined experimentally by titrations in triplicate of the spent reaction mixture at a definite temperature (usually 27.0°C) and corrected to obtain A_f at 2.43°C (the temperature at which all of the kinetic runs were carried out). Points prior to 5 min (6.5 min in the fastest reactions) were ignored in the curve fittings. The rate constants of Table 1 were obtained by application of the "main program" (see below) to corrected results from the multi-tube dilatometers. In this program, mechanism A2 was assumed, and the effect of changes in ionic strength during a reaction was ignored. Later, subsidiary programs were applied to reject A1 and similar mechanisms, and to show that the effect of changes in the ionic strength were negligible. Finally, it was shown that the experimentally more convenient method, in which temperature effects are not measured, may be used even for mixed nonlinear reactions, with varying ionic strength, and with temperature effects which cannot be neglected.

(a) The "Main Program"[20,21]: A2 Mechanism, Neglecting the Variations in Ionic Strength within Each Run

The equations of the mechanism are $\mathrm{d}D/\mathrm{d}t = -k_s[\mathrm{Ox}]A$ and $d[\mathrm{Ch}]/\mathrm{d}t = -k_N[\mathrm{Ox}]A(A + S)$, where [Ox] is the concentration of oxirane, A the titrable acidity, and S the concentration of added sodium chloride. Both rate constants are composite. In solving the system, it was not assumed that k_s had the same value as in perchloric acid. Instead, the parameter was eliminated by the use of [7] (3), which also served (together with elementary stoichiometry) to give [Ox], [Ch], and D (eq. [4]) and consequently the capillary readings y_i, as functions of the single chemical variable A. In this way [8]

[19]Rate constants obtained from the dilatometer are of very little value unless accompanied by values of the chemical sensitivity, thermal sensitivity, and cooling constant (see Introduction).

[20]Details are available from the authors.

[21]Extensive sets of further numerical integrations served to verify the adequacy of the mathematical procedure, and provided estimates for the closeness of fitting and of the errors in k_s and k_N caused by experimental errors in the fixed input parameters u_s, A_0, A_f, and $[\mathrm{Ox}]_0$; these errors turned out to be adequately represented by the external standard deviations (Table 1). A striking feature of the integration (illustrated later) was the absorption of errors into the dummy parameters u_N. A useful test was the fact that the value of k_N obtained from the end reaction independently of the main program, and of u_s and u_N, always agreed approximately with the final value of the program.

was obtained as an expression for the A2 mechanism. This differs from that derived for the A1 mechanism (eq. [9]):

$$[7] \quad k_N/k_s = \ln[(A_0 + S)/(A_f + S)]/[[Ox]_0 + A_f - A_0]$$

$$[8] \quad dA/dt = -f(A)$$

$$[9] \quad dA/dt = -kf(A)/[k_s + k_N(A + S_O)]$$

In [8] and [9],[22] $f(A)$ was a particular function of the time-variable acidity A, the adjustable constant k_N, and experimental constants. The corresponding equation for the capillary readings involved only k_N, u_N, and y_f as adjustable parameters. Convergence was consequently rapid. Initial estimates of the parameters (except y_f) were made by the program itself under the assumption, subsequently refined, that the end-reaction was pseudo first order.

(b) Rejection of the A1 Mechanism for the Attack of Chloride upon Oxirane

Although several other possibilities were considered, space can be given only to the limiting mechanism (13, 17). Its equation for the product ratios had exactly the same form as that of [7] applying to the A2 mechanism. Transformation of the rate equations led to [9] and since the denominator did not vary much within a single run, [9] was also almost indistinguishable from [8] for a single reaction. Indeed when [9] was applied to the same three sets of reactions (seven experiments in all) for *cis*-3-methoxycyclohexene oxide (**1**) which had given the results for the A2 mechanism reported in Table 1, the curve fittings gave average standard deviations per point in the capillary readings of only 0.011, 0.010, and 0.015 cm, close to the values for the A2 fitting of 0.010, 0.010, and 0.014 cm respectively. Careful inspection showed that there was little to choose between the two excellent fittings. Further, the average standard deviation of the mean value of the first-order rate constant k for the A1 fitting was only 0.44% within each set. The unsuitability of the A1 mechanism was shown by the change in rate constants between sets. The variation in k between the sets was 70%, increasing roughly with initial concentration of chloride ion. The same data gave for the A2 fittings a variation in k_N of only 5.2% and in k_s of only 2.7% with the same variation in the initial conditions (Table 1). Similar results were obtained with cyclohexene oxide.

(c) Inclusion of the Variation in Ionic Strength during a Reaction within the Rate Laws for A2

The approximations of [10] could easily be incorporated into the existing programs without an increase in the number of adjustable parameters. Because of the small variations within any one reaction, they were also sufficiently accurate,

$$[10] \quad \begin{aligned} k_s &= k_1 + k_2(A + S + W)^{1/2} \\ k_N &= k_s[k_3 + k_4(A + S + W)^{1/2}] \end{aligned}$$

where W is the concentration of added sodium perchlorate. Rate constants determined for solvolysis of cyclohexene oxide in aqueous methanolic perchloric acid, using both the cylindrical and the multi-tube dilatometers, gave a good fit to the experimental values of k_s for $k_1 = 3.359$ and $k_2 = 4.04$. For reactions in aqueous methanolic hydrochloric acid, the latter value was held fixed, but the value for k_1 was used only as an initial estimate. Variations in the product ratio with ionic strength, reported in the previous paper (3) for cyclohexene oxide, were fitted by a network procedure[20] to find values of k_3 and k_4. Suitable values of k_4 ranged from -15.0 at low ionic strength to -10.0 at the higher. The appropriate value (-11.0 for cyclohexene oxide under the conditions of Table 1) was supplied to the program as a fixed constant. The corresponding value of k_3 had to be calculated for each separate reaction with hydrochloric acid in an initial iterative routine, since [7] did not apply. The suitably altered "main program" then performed iterations with y_f, u_N, and k_1 as adjustable parameters. For the two sets of data for cyclohexene oxide used in Table 1, the new values for k_N and k_s at "half-reaction" (as judged by the acidity) differed from those reported in Table 1 by less than 0.6%. The difference in ionic strength to which each constant of Table 1 applies is therefore significant only for the *cis*-oxide **1**, and for it, the difference is negligible in the comparisons of Tables 2 and 3, as shown by similar curve fittings.

(d) Ionic Strength Effects in Parallel Reactions of Different Order. Comparison of Two Different Methods of Temperature Compensation

Conditions were purposely chosen so that temperature effects on the rate constant would be small, the more severe comparisons in u_N being used. Solvent, temperature, and initial oxirane concentration were as in Table 1, the added acid being hydrochloric. The reactions were conducted in the "cylindrical" dilatometers. Temperature corrections were made by a linearized Tong–Olson approximation. Points prior to 7 min were ignored in fitting the results to the "variable ionic strength" program described above, with $k_4 = -15.0$. Set 1 (4 trials, 0.03 M HCl, no added salts) gave $k_N = 31.0$ L^2 mol^{-2} min^{-1}, $k_s = 3.97$ L mol^{-1} min^{-1}, and $u_N = -55.4$ cm mol^{-1} L. Set 2 (3 trials, 0.015 M HCl, no added salts) gave values of 33.5, 3.85, and -68.0, respectively, and set 3 (4 trials, 0.015 M HCl, 0.03 M $NaClO_4$) gave 27.7, 4.11, and -55.2, respectively. The average external standard deviations of the mean for k_N and k_s were 0.69% and 0.68%. For comparison, temperature corrected results from the "multi-tube" dilatometer, obtained as in the previous section, were (*i*) (0.015 M HCl, 0.2 M $NaClO_4$), $k_N = 22.0$, $k_s = 5.31$, and $u_N = -57.5$ and (*ii*) (0.015 M HCl, 0.035 M NaCl, 0.165 M $NaClO_4$), 23.4, 5.48, and -54.9, respectively. These results lead one to expect a value of u_N for the *cylindrical* dilatometer of -55.0, close to that reported just above.

Fitted *without* temperature correction, the same three sets of data for the cylindrical dilatometer gave standard deviations in y_i very slightly higher than before. Values for k_N were 2–3% higher, and for k_s, lower by the same percentage, with respect to the corrected results. However, values for u_N (-447, -357, and -424) were about eight times the corrected values, illustrating the efficiency of this parameter in absorbing temperature errors.

Formation of Minor Isomers in Acid- and Base-catalyzed Scissions

Analysis of scission products formed from the *trans*-oxide **2** and the *cis*-oxide **3**, under the conditions of Table 1, have been reported (3). With hot aqueous perchloric acid, **2** gave 6.6% of minor isomer (by calibrated gas–liquid chromatography) in a heterogeneous reaction and **3** gave 6.7%. No minor isomer could be detected for the *cis*-oxide **1** under acid catalysis at 2.43°C, but hot aqueous base gave about 0.3% of minor isomer, easily detected by glc, in a heterogeneous

[22]Equation [9] is written to emphasize the resemblance in form to [8]. The symbols k_N and k_s do not have the same physical meaning in eqs. [8] and [9] since two different mechanisms are involved.

reaction. ("Minor isomer" corresponds to attack at position 2. See Table 2.)

Blank Experiments

No temperature rise occurred when cyclohexene oxide and solvent were mixed in the mixing vessel of the dilatometer. The capillary level did not fall over several hours (i.e., many half-lives for the acid-catalyzed reaction) after the mixture was forced into the dilatometer. Thus both the heat of mixing and the uncatalyzed solvolysis were negligible. A comparison run using sodium hydroxide as the catalyst was too slow for accurate measurement, but the slight capillary fall observed in 5 days corresponded to a rate constant no greater than 0.00012 L mol^{-1} min^{-1}. Reactions with methoxide in boiling methanol are also extremely slow (*7a*). By analogy, therefore, the uncatalyzed reaction with chloride ion was also negligible even in the least favourable of our examples. Solutions of aqueous methanol and hydrochloric (or perchloric) acid maintained titration values unchanged at least for several days, as did spent reaction mixtures; analytical (glc) values of the latter were also stable with time. Reactions concurrent with, or subsequent to, the acid-catalyzed scissions were therefore also negligibly slow.

Acknowledgements

The aid of the National Research Council of Canada, in financial support of this work and in the grant of studentships to J.W.B. and E.J.L., is gratefully acknowledged. We wish to thank Mr. C. Levay for his excellent glassblowing work on the dilatometers.

1. R. E. Parker and N. S. Isaacs. Chem. Rev. **59**, 737 (1959).
2. H. Z. Sable and J. G. Buchanan. *In* Selective organic transformations. Vol. 2. *Edited by* B. S. Thyagarajan. Wiley-Interscience, New York, NY. 1972.
3. J. W. Bovenkamp, R. Y. Moir, and R. A. B. Bannard. Can. J. Chem. **55**, 4144 (1977).
4. R. W. Taft. *In* Steric effects in organic chemistry. *Edited by* M. S. Newman. John Wiley and Sons, New York, NY. 1956. Chapt. 13, p. 556.
5. (*a*) P. L. Barili, G. Bellucci, F. Marioni, and V. Scartoni. J. Org. Chem. **40**, 3331 (1975); (*b*) J. W. Lown and A. V. Joshua. J. Chem. Soc. Perkin Trans. I, 2680 (1973).
6. C. Anselmi, G. Berti, G. Catelani, L. Lecce, and L. Monti. Tetrahedron, **33**, 2271 (1977).
7. (*a*) J. A. McRae, R. Y. Moir, J. W. Haynes, and L. G. Ripley. J. Org. Chem. **17**, 1621 (1952); (*b*) R. U. Lemieux, R. K. Kullnig, and R. Y. Moir. J. Am. Chem. Soc. **80**, 2237 (1958).
8. P. L. Barili, G. Bellucci, G. Berti, M. Golfarini, F. Marioni, and V. Scartoni. Gazz. Chim. Ital. **104**, 107 (1974).
9. G. Bellucci, G. Berti, G. Ingrosso, A. Vatteroni, G. Conti, and R. Ambrosetti. J. Chem. Soc. Perkin Trans. II, 627 (1978).
10. E. J. Langstaff, R. Y. Moir, R. A. B. Bannard, and A. A. Casselman. Can. J. Chem. **46**, 3649 (1968).
11. J.-C. Richer and C. Freppel. Tetrahedron Lett. 4411 (1969).
12. G. Berti, G. Catelani, M. Ferretti, and L. Monti. Tetrahedron, **30**, 4013 (1974).
13. J. F. Pritchard and F. A. Long. J. Am. Chem. Soc. **78**, 2667 (1956).
14. J. K. Addy and R. E. Parker. J. Chem. Soc. (*a*) 915 (1963); (*b*) 644 (1965).
15. J. N. Brönsted, M. Kilpatrick, and M. Kilpatrick. J. Am. Chem. Soc. **51**, 428 (1929).
16. Y. Pocker and B. P. Ronald. J. Am. Chem. Soc. **100**, 3122 (1978).
17. G. Lamaty, R. Maleq, C. Selve, A. Sivade, and J. Wylde. J. Chem. Soc. Perkin Trans. II, 1119 (1975).
18. R. C. Cathcart, J. W. Bovenkamp, R. Y. Moir, R. A. B. Bannard, and A. A. Casselman. Can. J. Chem. **55**, 3774 (1977).
19. R. P. Bell and J. C. Clunie. Proc. R. Soc. London, Ser. A, **212**, 16 (1952).
20. L. K. J. Tong and A. R. Olson. J. Am. Chem. Soc. **65**, 1704 (1943).
21. D. S. Noyce and L. J. Dolby. J. Org. Chem. **26**, 3619 (1961).
22. J. W. Bovenkamp, R. Y. Moir, A. A. Casselman, and R. A. B. Bannard. J. Chromatogr. **118**, 345 (1976).
23. E. L. Eliel, N. L. Allinger, S. J. Angyal, and G. A. Morrison. Conformational analysis. Interscience Publishers, Inc., New York, NY. 1965.
24. R. A. B. Bannard, A. A. Casselman, E. J. Langstaff, and R. Y. Moir. Can. J. Chem. **46**, 35 (1968).
25. (*a*) F. V. Brutcher and T. Roberts. Abstracts, 127th meeting of the American Chemical Society, Cincinnati, Ohio, 1955. p. 39-N; (*b*) Abstracts, 126th meeting of the American Chemical Society, New York, NY. 1954. p. 64-O.
26. J. A. Hirsch. Concepts in theoretical organic chemistry. Allyn and Bacon, Boston, MA. 1974.
27. J. L. Kurz. Acc. Chem. Res. **5**, 1 (1972).
28. G. Bellucci, G. Berti, R. Bianchini, G. Ingrosso, and E. Mastrorilli. Gazz. Chim. Ital. **106**, 955 (1976).
29. (*a*) J. A. Franks, B. Tolbert, R. Steyn, and H. Z. Sable. J. Org. Chem. **30**, 1440 (1965); (*b*) A. Hasegawa and H. Z. Sable. J. Org. Chem. **31**, 4161 (1966); (*c*) R. Steyn and H. Z. Sable. Tetrahedron, **25**, 3579 (1969).
30. B. C. Hartma and B. Rickborn. J. Org. Chem. **37**, 4246 (1972).
31. J. Biggs, N. B. Chapman, and V. Wray. J. Chem. Soc. B, 71 (1971).
32. E. J. Langstaff, E. Hamanaka, G. A. Neville, and R. Y. Moir. Can. J. Chem. **45**, 1907 (1967).
33. (*a*) J. E. Stevens, C. Lae, C. L. McCabe, and J. C. Warner. J. Am. Chem. Soc. **70**, 2449 (1948); (*b*) C. L. McCabe and J. C. Warner. J. Am. Chem. Soc. **70**, 4031 (1948).
34. T. W. Richards and J. W. Shipley. J. Am. Chem. Soc. **36**, 1825 (1914).
35. A. H. Roux and A. Viallard. Bull. Soc. Chim. 189 (1977).
36. R. K. Brown and A. M. Eastham. Can. J. Chem. **38**, 2039 (1960).
37. E. A. Guggenheim. Philos. Mag. **2**, 538 (1926).
38. W. E. Wentworth. J. Chem. Educ. **42**, 97 (1965).
39. L. Fox and D. F. Mayers. Computing methods for scientists. Clarendon Press, Oxford. 1968.
40. D. Edelson. J. Chem. Educ. **52**, 642 (1975).

On the reliability of the inversion of the Arrhenius rate law

ANDREW W. YAU[1] AND HUW O. PRITCHARD

Centre for Research in Experimental Space Science, York University, Downsview, Ont., Canada M3J 1P3

Received December 14, 1978

ANDREW W. YAU and HUW O. PRITCHARD. Can. J. Chem. 57, 2458 (1979).

A numerical test of the reliability of the Slater–Forst procedure for the inversion of the Arrhenius rate law is presented using the theoretical data for the reactions $N_2O \rightarrow N_2 + O$ and $CO_2 \rightarrow CO + O$ reported previously: the test results are positive. The sensitivity of the procedure to variations in the Arrhenius parameters is also examined.

ANDREW W. YAU et HUW O. PRITCHARD. Can. J. Chem. 57, 2458 (1979).

Faisant appel à des données théoriques relatives aux réactions $N_2O \rightarrow N_2 + O$ et $CO_2 \rightarrow CO + O$ rapportées antérieurement, on présente une méthode numérique permettant de mettre à l'épreuve l'exactitude de la méthode de Slater–Forst pour l'inversion de la loi de vitesse d'Arrhénius: les résultats de nos essais sont positifs. On examine aussi la sensibilité de la méthode aux variations des paramètres d'Arrhénius.

[Traduit par le journal]

I. Introduction

In an earlier publication (1), the microscopic reaction probability functions $k(E)$ for the spin-forbidden reactions

[1] $N_2O(\tilde{X}^1\Sigma^+) \rightarrow N_2(X^1\Sigma_g^+) + O(^3P)$

and

[2] $CO_2(\tilde{X}^1\Sigma_g^+) \rightarrow CO(X^1\Sigma^+) + O(^3P)$

were calculated in the framework of the theory of radiationless transitions. The calculation was two-dimensional, incorporating the two stretching degrees of freedom in a modified form of Rosen's relative co-ordinate system (2); also, all of the microscopic parameters required for the calculation were derived from spectroscopic data, and there were no adjustable parameters in the formulation. The computed $k(E)$ functions were of "kinetic accuracy": for both reactions, the high-pressure reaction rates calculated from the $k(E)$ functions were in reasonable agreement with experiment (3–5). The pre-exponential factor and activation energy were also computed: they vary only moderately with temperature, except at very low temperature for N_2O. Indeed, over a long range of temperature, the reaction rates may be very well approximated by a strict Arrhenius expression, viz.

[3] $k_\infty(T) \doteq A_\infty \exp(-E_\infty/RT)$

with $A_\infty = 1.41 \times 10^{12}\ s^{-1}$ and $E_\infty = 65.10$ kcal mol^{-1} for reaction [1] and $A_\infty = 1.80 \times 10^{12}\ s^{-1}$ and $E_\infty = 127.3$ kcal mol^{-1} for reaction [2] (1).

The inversion procedure of (experimental) high-pressure rate laws such as eq. [3] to obtain the microscopic reaction probability function $k(E)$ was first discussed by Slater (6) and was later re-derived and developed for unimolecular fall-off calculations by Forst (7). Despite the success to date (8) of the Slater–Forst procedure in unimolecular rate calculations, concerns have been voiced in the past regarding its validity: (*i*) that the experimental rate law is necessarily approximate; (*ii*) that the inversion procedure may be very sensitive to the fine structure of $k_\infty(T)$, and the loss of the latter through experimental scatter precludes obtaining even the overall shape of the $k(E)$ function; (*iii*) that (in the case of the strict Arrhenius rate law, eq. [3]), E_∞ is *not* equal to E_0, the critical energy of reaction; and that (*iv*) the $k(E)$ function is expected to be very sensitive to the assumed Arrhenius parameters, particularly near the threshold. Regarding (*i*), the $k(E)$ function obtained by the inversion of an approximate rate law is necessarily approximate; the question is how approximate is the function? As to (*ii*), we have argued previously (8) using the linearity property of Laplace Transform, that the loss of the fine-structure in $k_\infty(T)$ would mean a corresponding loss in the fine-structure, but not the overall shape, of $k(E)$ in the inversion procedure. Case (*iii*) actually arises out of an over-interpretation of eq. [3]: insofar as the inversion procedure is concerned, both A_∞ and E_∞ are *empirical* quantities and no assumption is made that E_∞ is equal to E_0. At this juncture, we note that

[1]Present address: Herzberg Institute of Astrophysics, National Research Council of Canada, Ottawa, Ont., Canada K1A 0R6.

0008-4042/79/182458-06$01.00/0

no *realistic* kinetic data (either theoretical or experimental) of $k(E)$ and $k_\infty(T)$ yet exist which may be used to examine (*iv*) in particular and to investigate the validity of the Slater–Forst procedure in general: hence, the present work using the $k(E)$ and $k_\infty(T)$ data in ref. 1.

II. Theory

We begin with an outline of the relevant theoretical results.

We define, for a discrete reactive state i, g_i as its degeneracy, ε_i as its energy, and k_i as its microscopic decay rate constant to product. The infinite-pressure rate constant $k_\infty(\beta)$ at inverse temperature β $(= 1/kT)$ is then (8)

$$[4] \qquad k_\infty(\beta) = \sum_j F(E_j) \exp(-\beta E_j)/Q(\beta)$$

where $Q(\beta)$ is the molecular partition function, the j-summation is over all energy levels, and

$$[5] \qquad F(E_j) = \sum_i k_i g_i$$

the i-summation being over states at energy E_j. $F(E_j)$ may thus be obtained as the inverse Laplace Transform of $k_\infty(\beta)Q(\beta)$, whence

$$[6] \qquad F(E_j) = \mathscr{L}^{-1}\{k_\infty(\beta)Q(\beta)\}$$

and, if the rate law is strict Arrhenius in form, i.e., eq. [3],

$$[7] \qquad F(E_j) = A_\infty P(E_j - E_\infty)$$

where $P(E_j)$ is the state-degeneracy at energy E_j.

Equations [4] and [7] may be compared with their corresponding solutions for a continuous system, where

$$[8] \qquad k_\infty(\beta) = \int_0^\infty f(E) \exp(-\beta E)\, dE/Q(\beta)$$

$$[9] \qquad f(E) = \rho(E)k(E)$$

and, in the case of the strict Arrhenius rate law,

$$[10] \qquad f(E) = A_\infty \rho(E - E_\infty)$$

$\rho(E)$ being the state-density at energy E and $k(E)$ the reaction probability function.

From a computational standpoint, eqs. [4]–[7] and eqs. [8]–[10] are equivalent.[2] This is because in unimolecular rate calculations, the reactant level spectrum is grouped into energy grids and the relevant integrations are carried out by stepwise summations over the energy grids. Thus, the quantity of computational interest is

$$[11a] \qquad \phi_k = \int_{E_k}^{E_{k+1}} f(E)dE/\Delta E$$

where ΔE is the grid size and E_k is the energy of the kth grid. Equivalently,

$$[11b] \qquad \phi_k = \sum F(E_j)/\Delta E$$

where the summation is over energy levels between E_k and E_{k+1}. It is obvious that at high energy $(E_k \gg E_\infty)$, eqs. [11*a*] and [11*b*] are very similar and ϕ_k varies only slightly with the assumed grid size ΔE. At low energy $(E_k \gtrsim E_\infty)$ on the other hand, the behaviour of ϕ_k may be expected to depend more strongly on ΔE. In particular, when ΔE becomes comparable with (or smaller than) the mean energy spacing near the zero point energy, the non-uniform distribution of energy levels there would imply, according to [7], a highly oscillatory distribution of ϕ_k which varies drastically with ΔE. However, this constitutes no serious problem in practical applications, cf. Section IV.

III. Reaction Probability Function ϕ_k

In the theoretical calculation (1) of the microscopic reaction probability, the reactant state is characterised, in the notation of ref. 1, by (v_{b1}, v_{b2}, v_{bend}, J, M_J) where v_{b1} and v_{b2} refer to the two stretching co-ordinates; v_{bend} denotes the doubly-degenerate bending quantum number, and J and M_J the rotational quantum numbers. The reaction probability $k_{v_{b1}\, v_{b2}\, v_{bend}\, J\, M_J}$ from the reactant state is assumed to be independent of v_{bend}, J, and M_J, whence

$$[12] \qquad k_{v_{b1}\, v_{b2}\, v_{bend}\, J\, M_J} = k_{v_{b1}\, v_{b2}\, 0\, 0\, 0}$$

with

$$[13] \qquad k_{v_{b1}\, v_{b2}\, 0\, 0\, 0} \equiv k_{v_{b1}\, v_{b2}} = \sum k^{u,\varepsilon_{u1},v_{u2}}_{b,v_{b1},v_{b2}}$$

where $k^{u,\varepsilon_{u1},v_{u2}}_{b,v_{b1},v_{b2}}$ is the microscopic reaction probability from the bound (b) reactant state (v_{b1}, v_{b2}) to the unbound (u) product state (ε_{u1}, v_{u2}) and the summation is over all accessible product states (ε_{u1}, v_{u2}). As discussed in ref. 1, the reaction probability $k_{v_{b1}\, v_{b2}}$ is a randomly fluctuating function of the reactant state energy. Nevertheless, the convolution of the bending and rotational motions has the effect of smoothing out these apparent fluctuations: of course, the reaction probability $k_{v_{b1}\, v_{b2}\, v_{bend}\, J\, M_J}$ still varies erratically as a function of the reactant state

[2]We have discussed previously (8) the conceptual difficulty associated with the state-density near the zero point energy in eq. [10], which does not arise in eq. [7].

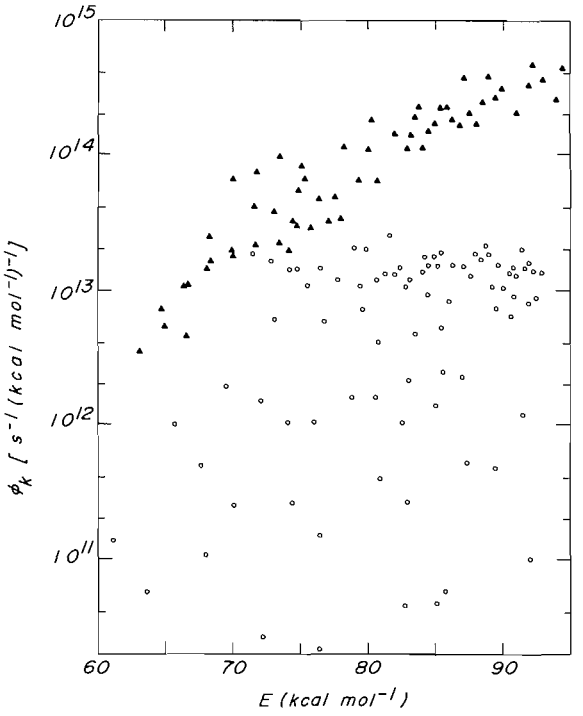

FIG. 1. Grained reaction probability function ϕ_k for the dissociation of N_2O calculated using eq. [11*b*] with $\Delta E = 0.05$ kcal mol^{-1}. E is the energy of the reactant state relative to the zero point energy. Open circles: bending and rotational motions excluded, eq. [14*a*]; solid triangles: bending motion included, eq. [14*b*].

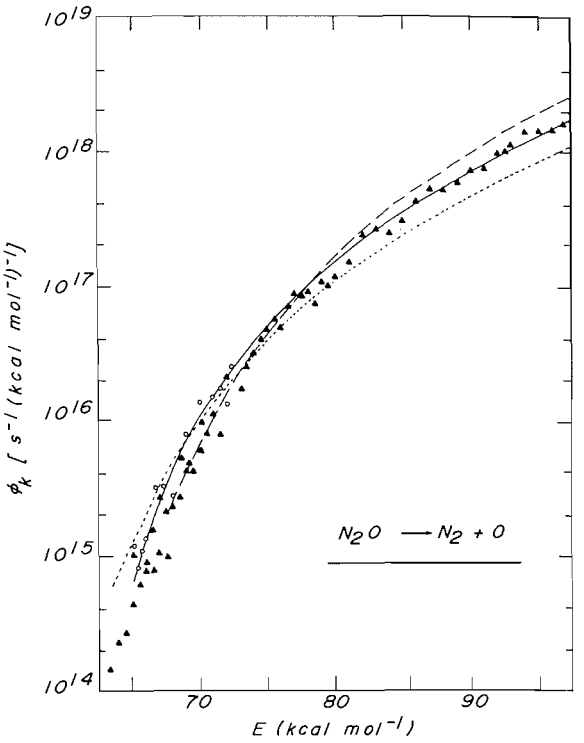

FIG. 2. Grained reaction probability function ϕ_k for the dissociation of N_2O, with $\Delta E = 0.05$ kcal mol^{-1}. E is the energy of the reactant state relative to the zero point energy. Solid triangles: exact probabilities from eq. [14*c*]; solid curve: approximation from inversion of Arrhenius rate law with $A_\infty = 1.41 \times 10^{12}$ s^{-1} and $E_\infty = 65.10$ kcal mol^{-1}, eq. [15]; dotted curve: eq. [15*a*] with $A_\infty' = 7.05 \times 10^{11}$ s^{-1} and $E_\infty' = 63.25$ kcal mol^{-1}; dashed curve: eq. [15*b*] with $A_\infty'' = 2.82 \times 10^{12}$ s^{-1} and $E_\infty'' = 67.87$ kcal mol^{-1}. The open circles indicate fluctuations of $\phi_{k,app}$ near the threshold.

energy, but now the enormous increase in the reactant state density means that over a typical energy range of ΔE ($\sim$0.1 kcal mol^{-1}), the *apparent* reaction probability distribution is smoothed out considerably. This is illustrated in Fig. 1 for the N_2O reaction, where we sum up the reaction probabilities from states in energy grids of 0.05 kcal mol^{-1}. When neither the bending nor the rotational motions are included, i.e.

$$[14a] \quad \phi_k = \{\sum g_{v_{b1}\, v_{b2}\, 0\, 0\, 0} k_{v_{b1}\, v_{b2}\, 0\, 0\, 0}\}/\Delta E$$

where the summation is over the (v_{b1}, v_{b2}, 0, 0, 0) states within E_k and E_{k+1}, the grained reaction function ϕ_k exhibits random fluctuations (open circles). On the other hand, as soon as the bending motions are included, i.e.

$$[14b] \quad \phi_k = \{\sum g_{v_{b1}\, v_{b2}\, v_{bend}\, 0\, 0} k_{v_{b1}\, v_{b2}\, v_{bend}\, 0\, 0}\}/\Delta E$$

the summation being over the (v_{b1}, v_{b2}, v_{bend}, 0, 0) states within E_k and E_{k+1}, the smoothing of ϕ_k immediately becomes apparent (filled triangles: note that in this case, only a representative fraction of data points is shown in the figure for the sake of clarity). The further smoothing of ϕ_k with the convolution of the rotational states, i.e.

$$[14c] \quad \phi_k = \{\sum g_{v_{b1}\, v_{b2}\, v_{bend}\, J\, M_J} k_{v_{b1}\, v_{b2}\, v_{bend}\, J\, M_J}\}/\Delta E$$

the summation being over the (v_{b1}, v_{b2}, v_{bend}, J, M_J) states within E_k and E_{k+1}, is shown by the quasi-smooth array of solid triangles in Fig. 2. Similar results are obtained for the CO_2 reaction; they will not be presented here.

IV. The "Arrhenius" Reaction Probability Function

Given the relevant spectroscopic parameters (Table 1 of ref. 1), it is a simple matter to calculate the reactant state-sum $G(E)$ and, combining eqs. [7] and [11*b*], the grained reaction probability function $\phi_{k,app}$,

$$[15] \quad \phi_{k,app} = A_\infty[G(E_{k+1} - E_\infty) - G(E_k - E_\infty)]/\Delta E$$

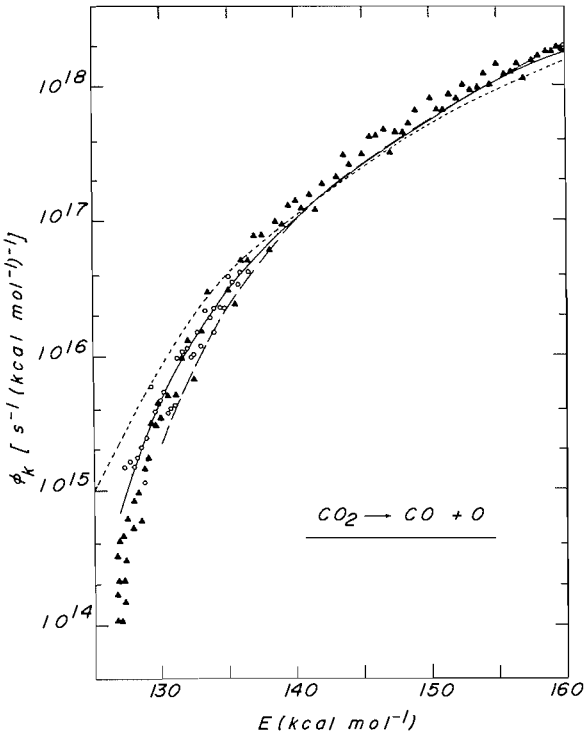

FIG. 3. Grained reaction probability function ϕ_k for the dissociation of CO_2 with $\Delta E = 0.05$ kcal mol^{-1}. See captions in Fig. 2: $A_\infty = 1.80 \times 10^{12}$ s^{-1}, $E_\infty = 127.3$ kcal mol^{-1}; $A_\infty' = 1.20 \times 10^{12}$ s^{-1}, $E_\infty' = 124.8$ kcal mol^{-1}; $A_\infty'' = 2.70 \times 10^{12}$ s^{-1} and $E_\infty'' = 129.8$ kcal mol^{-1}.

Equation [15] has been calculated using the Arrhenius parameters obtained in ref. 1 and compared with ϕ_k in Fig. 2 for N_2O and in Fig. 3 for CO_2. In both figures, the values of ϕ_k are represented by solid triangles, while $\phi_{k,app}$ is shown as a smooth curve: near the threshold, the $\phi_{k,app}$ values actually exhibit some fluctuations, as indicated by the open circles. The remarkable agreement between the solid curve and the triangles in the intermediate energy range (between 10 and 30 kcal mol^{-1} above the Arrhenius activation energy) should not be surprising: the strict Arrhenius law approximates the exact rates best at the medium temperatures (1000–3000 K in N_2O and 2000–5000 K in CO_2) where the reactive state population distribution (i.e., $F(E_j)$ exp $(-\beta E_j)$ in eq. [4]) peaks within this energy range. It is interesting to note that the high energy region of ϕ_k is important only at very high temperature, where the concept of an infinite pressure rate constant (in the Tolman sense (9)) becomes less well-defined (8). Conversely, the low energy region (near the threshold) of ϕ_k is important only at very low temperature (for recombination studies); hence we may expect the largest departure between ϕ_k and $\phi_{k,app}$ in this energy region. A flow chart illustrating the principal computational steps in this comparison is given in Fig. 4.

Figures 2 and 3 show that, at least for the two reaction systems studied here, the inversion of the strict Arrhenius rate law (eqs. [3] and [7]) does lead to a reasonable approximation to the exact reaction

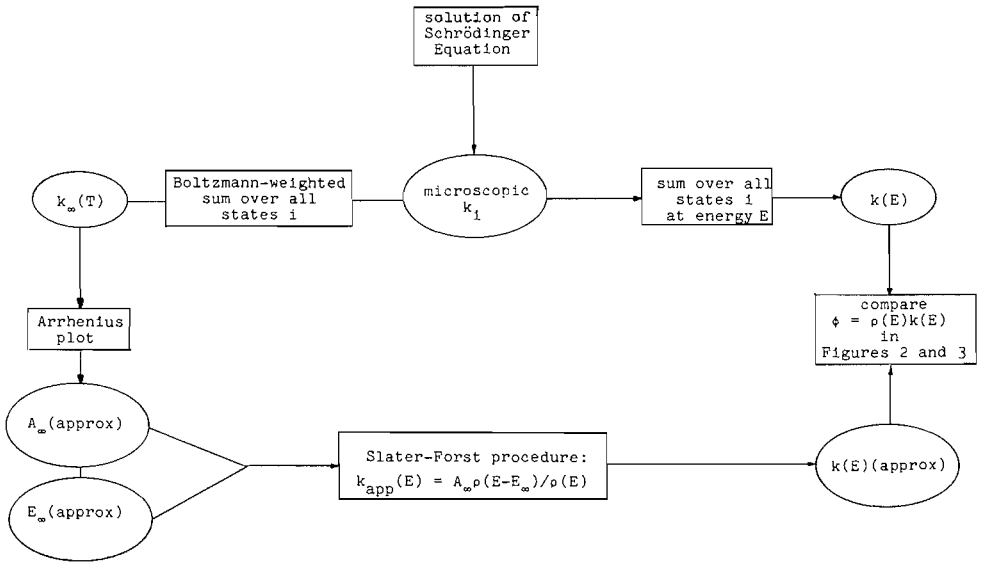

FIG. 4. Schematic flow chart of the test procedure.

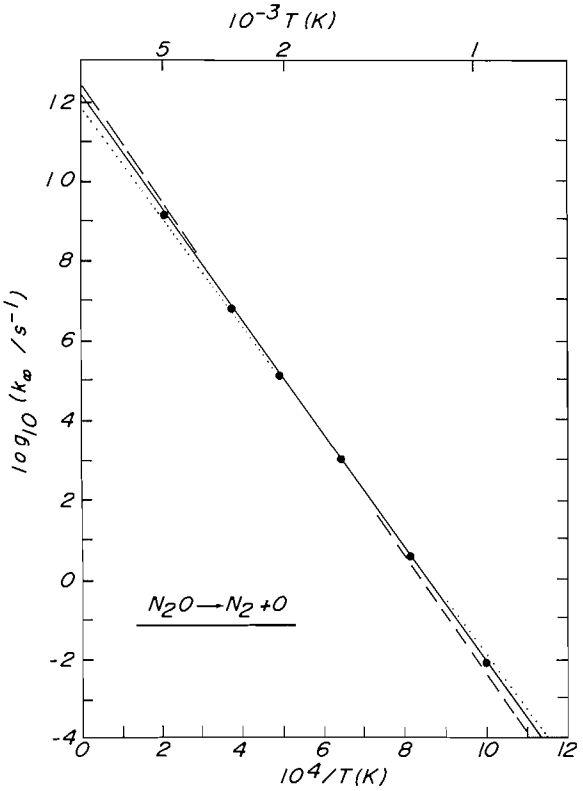

FIG. 5. Arrhenius plot of the infinite pressure rate constant for the dissociation of N_2O. Solid circles: computed (exact) rates from ref. 1; solid line: Arrhenius rate law with A_∞ = 1.41 × 10^{12} s^{-1} and E_∞ = 65.10 kcal mol^{-1}; dotted line: Arrhenius rate law with A_∞' = 7.05 × 10^{11} s^{-1} and E_∞' = 63.25 kcal mol^{-1}; dashed line: Arrhenius rate law with A_∞'' = 2.82 × 10^{12} s^{-1} and E_∞'' = 67.87 kcal mol^{-1}.

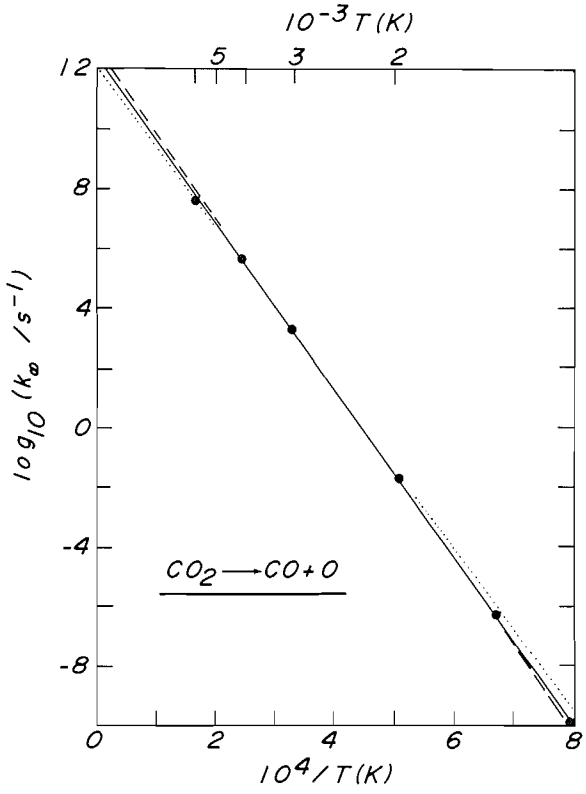

FIG. 6. Arrhenius plot of the infinite pressure rate constant for the dissociation of CO_2. Solid circles: computed (exact) rates from ref. 1; solid line: Arrhenius rate law with A_∞ = 1.80 × 10^{12} s^{-1} and E_∞ = 127.3 kcal mol^{-1}; dotted line: Arrhenius rate law with A_∞' = 1.20 × 10^{12} s^{-1} and E_∞' = 124.8 kcal mol^{-1}; dashed line: Arrhenius rate law with A_∞'' = 2.70 × 10^{12} s^{-1} and E_∞'' = 129.8 kcal mol^{-1}.

probability function. It is important to assess the sensitivity of the inversion procedure to variations of the Arrhenius parameters. For each reaction, two additional pairs of parameters have been chosen to test this sensitivity. For N_2O, A_∞' = 7.05 × 10^{11} s^{-1}, E_∞' = 63.25 kcal mol^{-1} and A_∞'' = 2.82 × 10^{12} s^{-1}, E_∞'' = 67.87 kcal mol^{-1}; for CO_2, A_∞' = 1.20 × 10^{12} s^{-1}, E_∞' = 124.8 kcal mol^{-1} and A_∞'' = 2.70 × 10^{12} s^{-1}, E_∞'' = 129.8 kcal mol^{-1}. They are compared with the "best" parameters (A_∞ = 1.41 × 10^{12} s^{-1} and E_∞ = 65.1 kcal mol^{-1} for N_2O and A_∞ = 1.80 × 10^{12} s^{-1} and E_∞ = 127.3 kcal mol^{-1} for CO_2) and the exact reaction rates in Figs. 5 (for N_2O) and 6 (for CO_2).

Going back to Figs. 2 and 3, the dotted curves denote the grained reaction probability functions $\phi_{k,app}'$ obtained using A_∞' and E_∞':

$$[15a] \quad \phi_{k,app}' = A_\infty'[G(E_{k+1} - E_\infty') - G(E_k - E_\infty')]/\Delta E$$

the dashed curves denote $\phi_{k,app}''$ obtained from A_∞'' and E_∞'':

$$[15b] \quad \phi_{k,app}'' = A_\infty''[G(E_{k+1} - E_\infty'') - G(E_k - E_\infty'')]/\Delta E$$

In both figures, these two curves intersect with the solid curve ($\phi_{k,app}$, eq. [15]) and with each other in the intermediate energy region. In other words, both $\phi_{k,app}'$ and $\phi_{k,app}''$ approximate the exact function best in this energy region. This is to be expected since both sets of Arrhenius parameters approximate the exact rates k_∞ best in the medium temperature range. As we have discussed previously (8), this is simply a consequence of the linearity property of the Laplace Transform.

Likewise, the divergent departure between $\phi_{k,app}'$ and $\phi_{k,app}''$ at very high energy is related to the corresponding departure between the respective Arrhenius expressions at very high temperature.

Here, it is pleasing to note that in the case of N_2O (Fig. 2), a factor of 4 variation in the pre-exponential factor results in only a factor of 2 variation of $\phi_{k,app}$ at 30 kcal mol^{-1} above E_∞. In experiments where a factor of 2 uncertainty in the A-factor is not atypical, the variation of $\phi_{k,app}$ in the corresponding energy region may be expected to be even smaller, as is illustrated in the case of CO_2 (Fig. 3).

Discrepancies between the respective $\phi_{k,app}$'s are most drastic near E_∞, but even here, the difference in absolute magnitude between $\phi_{k,app}'$ and $\phi_{k,app}''$ at and above E_∞'' is not phenomenal (a factor of 2 at E_∞'' for a variation of 4.6 kcal mol^{-1} in the Arrhenius activation energy in N_2O; a factor of 3 at E_∞'' for a variation of 5 kcal mol^{-1} in the Arrhenius activation energy in CO_2). Notice that even in this energy region, $\phi_{k,app}$ gives the best approximation to ϕ_k. The most serious difficulty is that $\phi_{k,app}$ is zero between the critical energy of reaction E_0 and the activation energy E_∞ ($E_\infty > E_0$) whereas ϕ_k is not. Note, however, that $\phi_{k,app}$ is *not* zero at E_∞; also, ϕ_k is small between E_0 and E_∞. Hence, the discrepancy between ϕ_k and $\phi_{k,app}$ in this region is unlikely to magnify in rate calculations of typical physical systems (unless the latter sample predominantly this energy region). From a computational standpoint, we may catagorise reaction systems into two classes: those in which ($E_\infty - E_0$) is large (such as N_2O), where ϕ_k is extremely small between E_∞ and E_0 (see ref. 1) and may therefore be well approximated by zero, and those in which E_0 and E_∞ are close to one another (such as CO_2), where simple procedures may be employed to interpolate between the zero value of $\phi_{k,app}$ at E_0 and the non-zero values of $\phi_{k,app}$ at and above E_∞. Alternatively, the overall fit to ϕ_k may be improved by a linear combination of more than one Arrhenius expression as suggested previously (8).

Conclusions

The present work represents a first attempt to test the sensitivity and reliability of the Slater–Forst procedure for inverting the strict Arrhenius rate law using purely theoretical (and realistic) rate data (1); at a later date, similar tests should be made for some adiabatic reactions, but we see no reason to expect that the results will be any less encouraging since the non-adiabatic reactions can be expected, in general, to be more non-Arrhenius. For the two reactions studied, the test results are indeed positive in the sense that (*i*) given the "best" Arrhenius parameters, the inversion procedure yields faithfully a very good approximation to the exact probability function. It is important to recognise the nature of the test we are making: if we simply take the exact computed $k_\infty(T)$ function and perform an inverse Laplace Transform, then we should (barring rounding errors) recover the original $k(E)$; however, the function upon which we apply the inverse Laplace Transform is not $k_\infty(T)$, but an approximate parametrisation of it, viz. $k_\infty(T) = A_\infty \exp(-E_\infty/RT)$. Moreover, by assuming that E_∞ can only be determined to within ± 2 or 3 kcal mol^{-1}, we have shown that (*ii*) reasonably approximate (experimental) rate laws would lead to reasonable approximations to the exact reaction probability function $k(E)$. It should also be noted that we are guaranteed approximate coincidence between the original theoretical and the doubly transformed values of $k(E)$ around the mean reaction energy, but what is remarkable about Figs. 2 and 3 is the fact that (*iii*) for these two reactions the inverse Laplace Transform approximation is uniformly satisfactory at all energies above the activation energy E_∞, including the very high energies which make little contribution to the reaction rate in the temperature ranges considered (1). Finally, it would appear that if it proves necessary (*iv*) simple interpolation procedures should prove adequate for synthesising approximate values of $k(E)$ between E_∞ and E_0 (the critical energy of the reaction), both when E_∞ and E_0 are far apart (e.g. N_2O) and when they are close to one another (e.g. CO_2).

Acknowledgements

This work has been supported by the National Research Council of Canada. We would also like to thank Galina Diker for computational assistance.

1. A. W. YAU and H. O. PRITCHARD. Can. J. Chem. **57**, 1731 (1979).
2. N. ROSEN. J. Chem. Phys. **1**, 319 (1933).
3. H. A. OLSCHEWSKI, J. TROE, and H. GG. WAGNER. Ber. Bunsenges. Phys. Chem. **70**, 450 (1966).
4. H. A. OLSCHEWSKI, J. TROE, and H. GG. WAGNER. Ber. Bunsenges. Phys. Chem. **70**, 1060 (1966).
5. H. GG. WAGNER and F. ZABEL. Ber. Bunsenges. Phys. Chem. **78**, 705 (1974).
6. N. B. SLATER. Proc. Leeds Philos. Lit. Soc. Sci. Sect. **6**, 259 (1955).
7. W. FORST. J. Phys. Chem. **76**, 342 (1972).
8. A. W. YAU and H. O. PRITCHARD. Can. J. Chem. **56**, 1389 (1978).
9. R. C. TOLMAN. Statistical mechanics with applications to physics and chemistry. Chemical Catalog Co., New York. 1927.

Active surface centres in vanadium pentoxide/alkali metal sulphate heterogeneous catalysts for 2-propanol decomposition

DAVID VICTOR FIKIS, WILLIAM JOHN MURPHY,[1] AND ROBERT ANDERSON ROSS[2]

Department of Chemistry, Lakehead University, Thunder Bay, Ont., Canada P7B 5E1

Received December 11, 1978

DAVID VICTOR FIKIS, WILLIAM JOHN MURPHY, and ROBERT ANDERSON ROSS. Can. J. Chem. 57, 2464 (1979).

Infrared spectra of the surfaces of vanadium pentoxide and vanadium pentoxide containing 9.09 mol% caesium and potassium, as sulphates, have been determined after exposure to 2-propanol for various times. Interpretation of the spectra leads to the proposal that the principal source of catalyst activity may be associated with surface hydrogen and hydroxyl groups on V^{5+} and V^{4+} sites. The "stability" of the catalysts towards reduction by the alcohol was consistent with the activity series derived from kinetic measurements: V_2O_5 (pure) < V_2O_5 (Cs) < V_2O_5 (K). The degree of sample reduction has also been assessed qualitatively by measurements of the ratio of surface area before to that after reaction and the same catalyst sequence was established. The trend in surface area ratios was similar to that shown by the surface "Tammann" temperatures of vanadium pentoxide and alkali metal sulphates which has been taken to imply that the ease and (or) extent with which the sulphates enter into inter-solid reactions with the oxide in the preparation stage may exert influence on the subsequent reducibility of the individual members of the catalyst series.

DAVID VICTOR FIKIS, WILLIAM JOHN MURPHY et ROBERT ANDERSON ROSS. Can. J. Chem. 57, 2464 (1979).

On a déterminé les spectres infrarouges de surfaces de pentoxyde de vanadium et de pentoxyde de vanadium contenant 9.09 mol% de césium et de potassium, sous formes de sulfates, après les avoir exposées à du propanol-2 pour des temps variés. L'interprétation des spectres permet de suggérer que la source principale de l'activité catalytique est associée avec les hydrogènes et les groupes hydroxyles à la surface des sites V^{5+} et V^{4+}. La stabilité des catalyseurs vis-à-vis la réduction par l'alcool est en accord avec la suite d'activité dérivée de mesures cinétiques: V_2O_5 (pur) < V_2O_5 (Cs) < V_2O_5 (K). On a aussi déterminé qualitativement le degré de réduction d'échantillon à l'aide de mesures de rapports de surface avant et après la réaction et on a déterminé que l'ordre des catalyseurs est le même. La tendance dans les rapports des surfaces est semblable à celle obtenue grâce aux températures de surface "Tammann" du pentoxyde de vanadium et des sulfates de métaux alcalins; on en déduit que la facilité ou le degré de réactions inter-solides entre les sulfates et l'oxyde lors de la préparation peut influencer la facilité subséquente de la réduction de membres individuels de la série des catalyseurs.

[Traduit par le journal]

Introduction

We have recently reported the results of a kinetic study of 2-propanol decomposition on vanadium pentoxide and alkali metal promoted vanadium pentoxide catalysts (1). Mechanisms based on elimination-type reactions were proposed and some evidence of a relationship between catalyst activities and the presence of "acidic" species on the solid surface was presented. Similar preparations have been examined in a number of surface reactions including oxidation and oxygen-exchange systems (2–5) where catalyst activity trends can be explained in terms of variations in the surface mobility of the catalyst oxygen with the additive activity series: V_2O_5 (none) < Li_2SO_4 < Na_2SO_4 < K_2SO_4 < Rb_2SO_4 < Cs_2SO_4 (2–6).

Variations of the additive positions in this series were observed in studies of oxygen exchange from $O_2/C^{18}O_2$ systems (7) and, in particular, the sequence was not obtained for the heterogeneous decomposition of 2-propanol (1). The latter investigation has now been extended to include an infrared spectroscopic study of the catalyst surfaces in an attempt to identify active sites and to monitor the catalyst reduction process.

Experimental

Samples of vanadium pentoxide (>99.9% pure; Ventron, MA) and catalysts containing 9.09 mol% alkali metal sulphate (>99.9% pure; Ventron, MA) were prepared as previously described (1).

[1]Now at: Research Department, Imperial Oil Ltd., Sarnia, Ontario.

[2]To whom all correspondence should be addressed.

0008-4042/79/182464-06$01.00/0

Certified grade helium (> 99.9% pure; Canadian Liquid Air, Toronto) was passed through a series of saturators containing 2-propanol (Fisher "Spectranalyzed" grade) to obtain the required partial pressure of reactant and then directed through a Pyrex-lined tube furnace where samples were contained in Pyrex boats. Temperature was maintained at 300 ± 0.5°C by means of a "Thermo Electric 400" indicating controller. Samples were removed by quenching to room temperature after various exposure times prior to measurement of infrared spectra. Experiments in which hydrogen (> 99.9% pure; Canadian Liquid Air, Toronto) was substituted for 2-propanol were carried out in a similar manner.

Transmission infrared spectra of both used and fresh samples were determined using the KBr disc method. Specimens were prepared by grinding a mixture of the appropriate solid with KBr in an agate mortar and then pelletizing in the usual manner. The time during which water adsorption from the atmosphere could have occurred was kept to a minimum and the absence of water confirmed by scanning at ~3400 cm^{-1}. Pellets containing caesium and potassium sulphates had 0.95 mg of catalyst/200 mg KBr while pure V_2O_5 pellets contained 0.60 mg V_2O_5/200 mg KBr. Infrared spectra were measured using a Beckman IR-12 spectrometer. This method gave better defined spectra than those obtained with infrared ATR spectroscopy in parallel experiments.

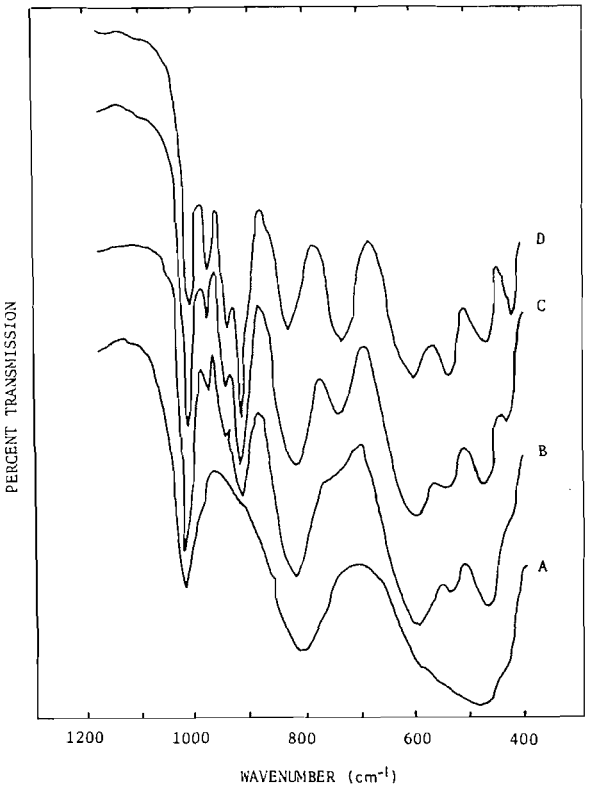

FIG. 1. Infrared spectra of vanadium pentoxide samples before and after exposure to 2 Torr (0.267 kPa) of 2-propanol at 300°C: (A) unexposed; (B) exposed for 7.5 min; (C) exposed for 15 min; and (D) exposed for 60 min.

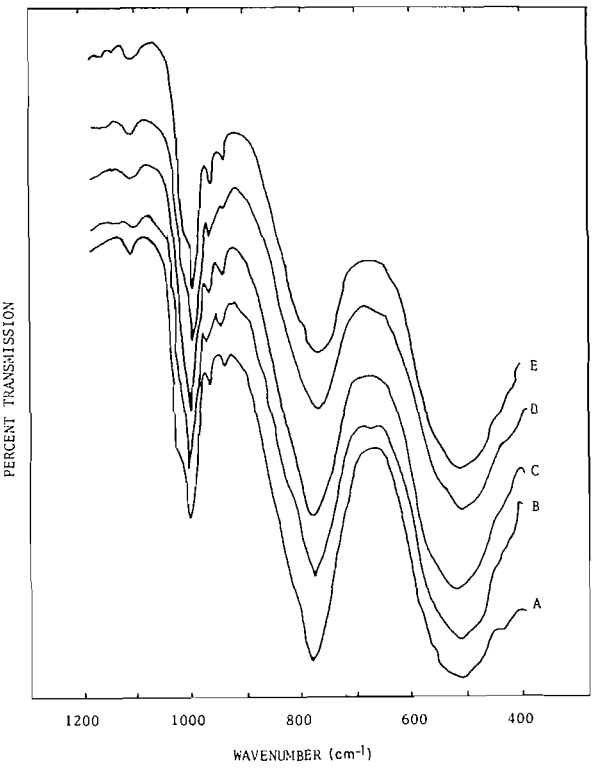

FIG. 2. Infrared spectra of potassium-promoted vanadium pentoxide samples before and after exposure to 2 Torr (0.267 kPa) of 2-propanol at 300°C: (A) unexposed; (B) exposed for 7.5 min; (C) exposed for 15 min; (D) exposed for 45 min; and (E) exposed for 90 min.

Results

Figures 1–3 show infrared spectra of V_2O_5 and V_2O_5 promoted with 9.09 mol% K_2SO_4 and Cs_2SO_4 before and after exposure to 2-propanol at 300°C. Figure 4 shows the infrared spectra of V_2O_5 after exposure to hydrogen at 300°C.

V_2O_5 exhibits a very characteristic spectrum before reaction (Fig. 1A), with three major peaks at 1020, 825, and 450–600 cm^{-1}, identified, respectively, as a V=O stretching vibration, a V—O—V stretching vibration, and possibly a V—O—V rocking vibration (7–10). After exposure to 2-propanol all three bands split into multiplets, Fig. 1B–D.

Prior to the action of 2-propanol, the potassium and caesium catalysts show splitting of the characteristic vanadium–oxygen peaks (Figs. 2A and 3A). The splitting is more clearly defined for the caesium sample and, unlike the potassium-promoted catalyst, includes the V—O—V bands.

The caesium sample shows an increase in splitting in step with increased exposure to 2-propanol (Fig. 2)

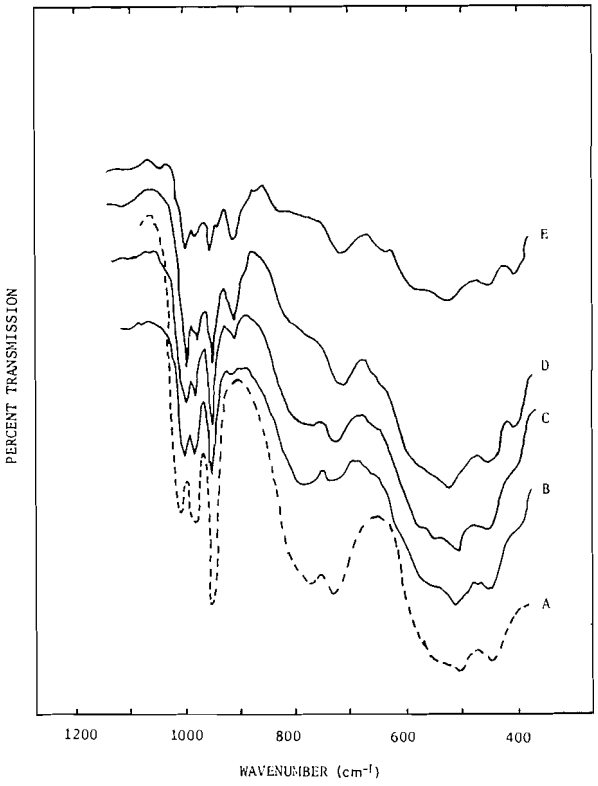

FIG. 3. Infrared spectra of caesium-promoted vanadium pentoxide samples before and after exposure to 2 Torr (0.267 kPa) of 2-propanol at 300°C: (A) unexposed; (B) exposed for 7.5 min; (C) exposed for 15 min; (D) exposed for 45 min; and (E) exposed for 90 min.

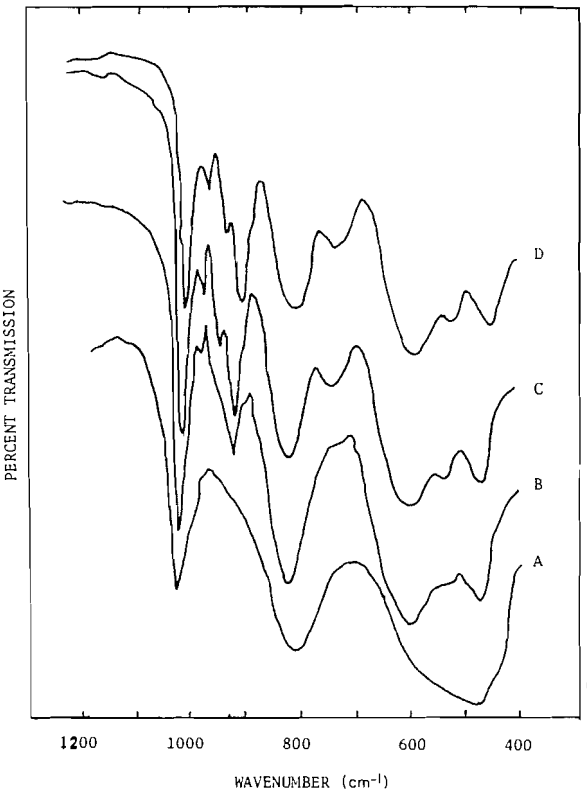

FIG. 4. Infrared spectra of vanadium pentoxide samples before and after exposure to hydrogen at 300°C: (A) unexposed; (B) exposed for 15 min; (C) exposed for 30 min; and (D) exposed for 45 min.

similar to V_2O_5 (Fig. 1), while the catalyst containing potassium appears unaffected (Fig. 3).

V_2O_5 exposed to hydrogen at 300°C (Fig. 4) does not show the rapid, extensive splitting characteristic of V_2O_5 exposed to 2-propanol under similar conditions (Fig. 1). Although both hydrogen and 2-propanol produce new bands at 925 and 750 cm^{-1}, the latter exhibits a longer induction period with hydrogen treatment.

Surface areas of the catalysts obtained during kinetic studies under similar conditions (1) are compared in Fig. 5 as a ratio of the values obtained before and after reaction. The figure includes data on the surface "Tammann" temperature, $0.3T_m$ (11) of V_2O_5 and all of the alkali metal sulphate additives studied here and previously (1).

Discussion

Characterisation of the Vanadium/Oxygen Species

The infrared spectra of freshly prepared samples of V_2O_5 and V_2O_5 containing alkali metal promoters have been reported (7) and the major bands, i.e., 1020, 825, and 600 cm^{-1}, correlated with the stretching frequencies of the V=O and V—O—V groups and with the frequency of the V—O—V group in a rocking vibration, in agreement with the literature (8, 12). In the present studies, the appearance of bands ranging from 1000–920 cm^{-1} on reaction of promoted and pure vanadium pentoxide samples with both hydrogen and 2-propanol may indicate that entities with structural similarities to V=O and V—O—V network species in V_2O_5 have been created. However, the V=O and V—O—V bonding states in V_2O_5 are not readily trackable (7) since the observed frequencies are influenced significantly by the lattice environments of the species.

The stretching frequency of "monomeric" V=O has been reported (13) at 987 cm^{-1} in pure $VOSO_4$, whereas that for $VOCl_3$ was 1035 cm^{-1} (9, 10). Recently, the V=O stretching frequencies for a series

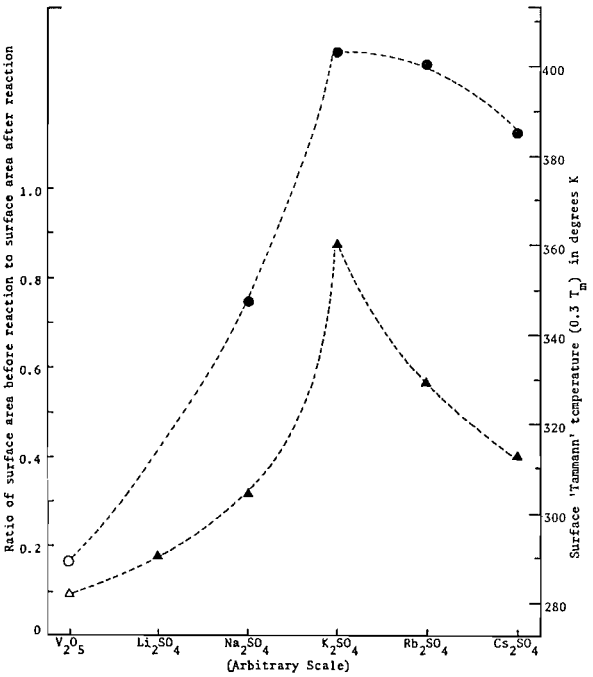

FIG. 5. Correlation diagram showing the ratio of surface area before and after reaction ((△) V_2O_5; (▲) melts containing 9.09 mol% alkali metal sulphate) and the surface "Tammann" temperature ($0.3T_m$) for V_2O_5 (○) and the added alkali metal sulphates (●).

of vanadyl complexes have been observed in which the ν(V—O) varied from 979 to 955 cm^{-1} (14) while the infrared frequencies of VO^{2+} in alkali halides have been shown to vary from 765 to 825 cm^{-1} (15). The displacement in V=O frequency may be a consequence of d_π–p_π metal–oxygen interactions which act to produce a stronger bond and hence a higher ν(V—O) (14, 15). Thus any lattice modification which enhances the d_π–p_π interactions would be expected to increase bond strength with the corollary that a diminution in d_π–p_π interactions would result in a weaker bond and lower ν(V—O).

Comparison of spectra A in Figs. 1–3 and, in particular, the stretching frequencies of the "V=O species" in these solids (Table 1) suggests that inclusion of an alkali metal in the pentoxide lattice affects the electron delocalisation of the surface. This phenomenon has been shown to have a marked effect on the catalytic activity (7) associated with V=O, probably through enhancement of d_π–p_π metal–oxygen interactions. However, such inclusions modify the crystal structure to an extent dependent, *inter alia*, on the size of the included atom and

TABLE 1. Stretching frequencies of the "V=O species"

Sample	ν(V—O) (cm^{-1})
V_2O_5	1020
V_2O_5 (K promoted)	1020, 1015, 1005
V_2O_5 (Cs promoted)	1020, 995, 965

results in the "V=O species" ν(V—O) being split into a triplet, the splitting increasing with the size of the added metal atom (Table 1). This effect is parallelled by a corresponding splitting in the V—O—V stretching and rocking vibration frequencies as might be expected (Fig. 3A).

An examination of the structure of V_2O_5 indicates that V=O and V—OH are surface groups not found in the bulk material. On the other hand, the V—O—V species is present both on the surface and in the bulk. Comparison of transmission and reflectance (ATR) infrared spectra showed a minimal difference in the relative intensities associated with the V=O and V=OH entities thus confirming the allocation of the present data to surface species. (The ATR results were not so intense overall owing to light loss in the attachment.)

Decomposition of 2-Propanol

Figure 1 shows that with increase in exposure time of 2-propanol on V_2O_5 from 0 to 15 min, an increase in the intensity of the V=O band is observed, accompanied by a slight increase in the band frequency from 1020 to 1025 cm^{-1}. An increase of band intensity would suggest that the population of the species has increased which would generally have been expected to occur along with a decrease in the band width, as was observed initially (Fig. 1A, B). The frequency increase may be indicative of a decrease in the extent of delocalisation due to adsorption of 2-propanol on V^{4+} and V^{5+} sites as recently proposed (1, 12). Adsorption on the V^{4+}

[1]

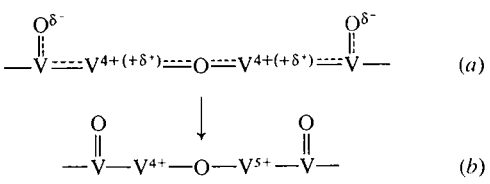

SCHEME I

and V^{5+} sites would tend to reduce the extent of delocalisation and promote d_π–p_π metal–oxygen overlap through increased donation of electrons into *d* orbitals of vanadium.

We have proposed previously (1) that 2-propanol initially decomposes on vanadium pentoxide by a

dehydration mechanism which may proceed from the intermediate

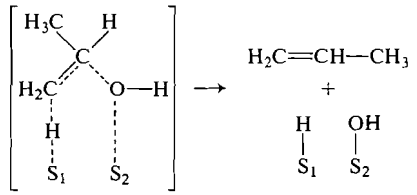

where S_1 and S_1 are V^{4+} and V^{5+}, respectively, thus yielding

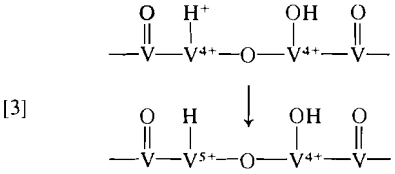

surface arrangements (2). The formation of

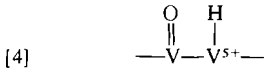

would be expected to decrease d_π–p_π metal–oxygen overlap in the V=O system due to the electron-accepting propensity of the vacant d orbital in V^{5+} which is adjacent to the V=O species. Such a mechanism could lead to a decrease in the metal–oxygen bond strength and a corresponding decrease in the ν(V—O). The appearance of the new band at 925 cm^{-1} may then be explained by the formation of a destabilised V=O species. The appearance of this band is also observed on reduction of V_2O_5 with H_2 (Fig. 4), indicating that it is unlikely to be ascribed to the presence of chemisorbed organic entities on the catalyst surface.

The appearance of the bands at 750 cm^{-1} may be related to the formation of surface hydroxide (16),

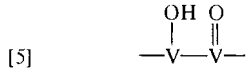

which would increase in degree of surface coverage with the progress of the reaction.

It was observed earlier that propane and acetone became significant decomposition products as the exposure time of V_2O_5 to the alcohol was increased and mechanisms of the type shown in [6] were proposed (1) to account for the formation of both products:

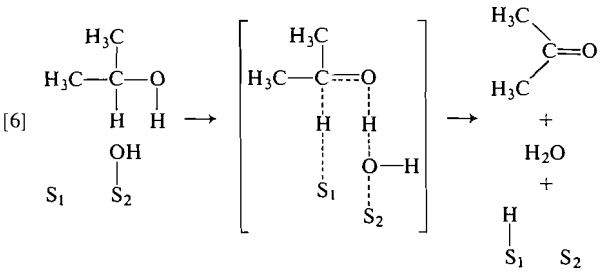

Now, if S_1 is V=O and S_2 is V^{4+} then this scheme could account for the gradual decrease in intensity of the 1020 cm^{-1} band and hence the number of V=O groups in the catalyst. Similarly, the active sites for propane formation may contribute to catalysis, thus

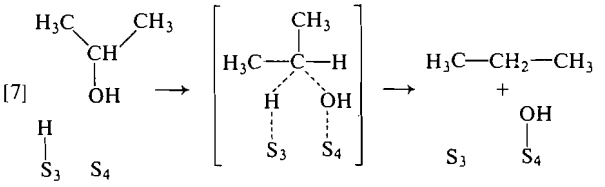

and if S_3 is V^{5+} adjacent to a V=O and S_4 is V^{5+} then the end result would be an increase in the surface population of V^{4+}—OH as indicated by the growth of the 750 cm^{-1} band with time (Figs. 1, 3).

Although the direct reaction of hydrogen on V_2O_5 produces both the 925 and 750 cm^{-1} band (Fig. 4), the former continues to grow with increase in exposure time, whereas the 750 cm^{-1} band appears to reach a steady level. The V—OH species, which gives rise to the 750 cm^{-1} band, can only be produced by hydrogen reaction with V=O and not, as in the case of the band at 925 cm^{-1}, by straight adsorption on V^{4+} sites.

Trends in the extent of reduction by hydrogen of a similar series of catalysts have been related to changes in the mobility of catalyst oxygen (6). Reduction of the present catalysts by exposure to 2-propanol did not exhibit such a relationship.

The infrared spectra of the promoted catalysts, before reaction, show splitting of the V=O and V—O—V bands which have been attributed to bond destabilization (7). The degree of bond destabilization and hence catalyst reduction, on exposure to 2-propanol, should be reflected by the extent of splitting in the infrared bands. Figures 1–3 show that the caesium- and potassium-promoted catalysts are less susceptible to reduction than pure vanadium pentoxide. Thus, the "stability" of the catalysts with respect to reduction by 2-propanol appears to be

[8] V_2O_5 (no additive) < V_2O_5 (Cs) < V_2O_5 (K)

The above trend parallels the catalyst activity series previously reported for 2-propanol decomposition (1). Minor variations in the levels of activity shown by other members of the series of alkali metal promoted catalysts may be related to the presence of different phases in the solid solutions and (or) changes in the extent of delocalization and destabilization of surface V=O and V—O—V bonds (7).

Recently, "atomic" hydrogen has been shown to be a more effective reducing agent for vanadium pentoxide than "molecular" hydrogen (17) which suggests that differences in reported reduction patterns for similar catalyst series based on V_2O_5 (1, 6) may be related to variations in the bonding level of adsorbed hydrogen, itself influenced by the redox potential of surface sites and by the form of dissociation on adsorption from the gaseous reactant.

The degree of catalyst reduction as related to solid sintering has also been demonstrated by measurements of surface area changes. If the ratio of surface area before reaction to that after reaction is taken as a broad qualitative measure of catalyst "stability", then the same series as that given by the infrared spectra is apparent (Fig. 5).

The similar trends shown by the surface "Tammann" temperatures (11) and the surface area ratios (Fig. 5) are taken simply to indicate the relative ease or extent with which the alkali metal sulphates and vanadium pentoxide enter into inter-solid reactions in the preparative melts which may later influence the reducibility and perhaps activity of the catalyst in a given reaction.

Figure 3 shows that similar general trends to those shown by V_2O_5 are observed with the reaction of 2-propanol on caesium-promoted samples. Initially, the population of the stronger V=O band, 1020 cm^{-1}, increases while that at 995 cm^{-1} decreases. No frequency shift was observed in the position of the V=O bands on reaction with 2-propanol probably through the modification of electronic features related to the incorporation of caesium in the pentoxide lattice. This feature would also explain the observation that the intensity of the 925 cm^{-1} band is not as large as that in pure V_2O_5 nor does it increase much with exposure time. Ultimately, however, the 750 cm^{-1} band intensity does increase significantly until it becomes the predominant V—O stretching band through the continual buildup of V—OH.

Figure 2 shows that the reaction of 2-propanol on potassium-promoted samples does not create new bands to any significant extent and so no new surface species of any permanency can be anticipated. The 1020 cm^{-1} band and the lower frequency bands all decrease in intensity at the same rates.

We conclude that the decomposition of 2-propanol on V_2O_5 and caesium-promoted V_2O_5 produces V—H and V—OH species in close proximity on the surface and that these remain there in a chemisorbed state after reaction. It has been proposed (12) elsewhere, however, that such species may react to give water,

$$[9]\quad \begin{matrix} H^+ & & OH \\ | & & | \\ V^{4+}—O—V^{4+}—O \end{matrix} \longrightarrow V^{5+}—O—V^{4+} + H_2O$$

which would mean that (*a*) the V=O species would not be destabilised since there would be a continual removal of adjacent V^{4+} and (*b*) the 750 cm^{-1} band would not be observed since the concentration of V—OH on the surface at any given time would be very small. Thus, it may be that variations observed in the surface structures of vanadium pentoxide and promoted catalysts with time of exposure to 2-propanol are related to kinetic differences in surface mechanisms such as the rate at which the latter reaction takes place with respect to the other steps involved in the overall decomposition.

1. D. V. Fikis, W. J. Murphy, and R. A. Ross. Can. J. Chem. **56**, 2530 (1978).
2. V. N. Bibin and L. A. Kasatkina. Kinet. Catal. **5**, 653 (1964).
3. A. P. Dzisyak, G. K. Boreskov, L. A. Kasatkina, and V. E. Kochurikhin. Kinet. Catal. **2**, 727 (1961).
4. P. Jiru, D. Tomkova, V. Jara, and J. Wankova. Z. Anorg. Allg. Chem. **121**, 303 (1960).
5. B. W. Krupay and R. A. Ross. J. Catal. **50**, 220 (1977).
6. D. G. Klissurski and N. T. Abadzhieva. Khim. Ind. (Sofia), **46**, 250 (1974).
7. D. V. Fikis, K. W. Heckley, W. J. Murphy, and R. A. Ross. Can. J. Chem. **56**, 3078 (1978).
8. Y. Kera and K. Hirota. J. Phys. Chem. **73**, 3973 (1969).
9. H. I. Eichhoff and F. Weigel. Z. Anorg. Allg. Chem. **275**, 268 (1954).
10. R. A. Millar and L. R. Cousins. J. Chem. Phys. **26**, 329 (1957).
11. S. J. Gregg. The surface chemistry of solids. Chapman and Hall Ltd., London. 1965. p. 158.
12. D. K. Chakrabarty, D. Guha, and A. B. Biswas. J. Solid State Chem. **22**, 263 (1977).
13. C. G. Barnaclough, J. Lewis, and R. S. Nyholm. J. Chem. Soc. 3552 (1959).
14. M. Y. Al-Janabi and N. J. Ali. Z. Naturforsch. **31a**, 1696 (1976).
15. S. Radhakrishna, B. V. R. Chowdari, and A. Kasiviswanath. Chem. Phys. Lett. **44**, 121 (1976).
16. W. P. Griffith and T. D. Wickins. J. Chem. Soc. A, 1087 (1966).
17. N. I. Il'chencko, V. A. Lavrenka, G. I. Golodets, V. L. Tikush, V. S. Zenkov, and V. M. Vereshchak. Teor. Eksp. Khim. **14**, 36 (1978).

Ionization of ethylene glycol in isodielectric acetonitrile + ethylene glycol mixtures at 25°C

KUMARDEV BOSE AND KIRON K. KUNDU[1]

Physical Chemistry Laboratories, Jadavpur University, Calcutta-700032, India

Received August 15, 1978[2]

KUMARDEV BOSE and KIRON K. KUNDU. Can. J. Chem. 57, 2470 (1979).

The autoprotolysis constants (K_s^m) of ethylene glycol in isodielectric acetonitrile + ethylene glycol mixtures have been determined at 25°C from emf measurements on the cell

Pt, H_2(g, 1 atm)|Na–glycoxide(m_1), NaCl(m_2), solvent|AgCl–Ag.

From these values, those of $\delta\Delta G^0$, the free energy of ionization of ethylene glycol in these mixed solvents relative to that in pure glycol, have been computed. The nature of variation of $\delta\Delta G^0$ with solvent composition has been compared with that in two other mixed systems: water + ethylene glycol and methanol + 1,2-propanediol and the intrinsic differences between the solvation characteristics of the various solvents have been pointed out. The standard free energies of transfer of the glycoxide ion, $\Delta G_t^0(OEg^-)$, from pure glycol to acetonitrile + glycol mixtures have also been estimated using $\Delta G_t^0(H^+)$ values obtained earlier. The glycoxide ion is increasingly desolvated as the acetonitrile content of the solvent increases, as indicated by increasingly positive values of $\Delta G_t^0(OEg^-)$. This behaviour has been compared with those of $\Delta G_t^0(H^+)$ and $\Delta G_t^0(Cl^-)$ determined previously.

KUMARDEV BOSE et KIRON K. KUNDU. Can. J. Chem. 57, 2470 (1979).

Opérant à 25°C, on a déterminé les constantes d'autoprotolyse (K_s^m) de l'éthylèneglycol dans des mélanges isodiélectriques acétonitrile–éthylèneglycol en se basant sur des mesures de fem de la cellule

Pt, H_2(g, 1 atm)/glycolate de Na(m_1), NaCl(m_2), solvant/AgCl–Ag

A partir de ces valeurs, on a calculé l'énergie libre d'ionisation, $\delta\Delta G^0$, de l'éthylèneglycol dans ces solvants mixtes par rapport au glycol pur. On a comparé la nature de la variation du $\delta\Delta G^0$ en fonction de la composition du solvant avec celle observée dans deux autres systèmes mixtes; eau–éthylèneglycol et méthanol–propanediol-1,2 et on identifie les différences intrinsèques entre les caractéristiques de solvatation de divers solvants. On a aussi évalué les énergies libres standard de transfert de l'ion glycolate, $\Delta G_t^0(EgO^-)$, du glycol pur à des mélanges acétonitrile–glycol en se basant sur les valeurs de $\Delta G_t^0(H^+)$ obtenues antérieurement. Quand la proportion d'acétonitrile dans le solvant mixte augmente, l'ion glycolate se désolvate progressivement et cet effet se reflète par des valeurs de $\Delta G_t^0(EgO^-)$ qui sont de plus en plus positives. On compare ce comportement avec ceux de $\Delta G_t^0(H^+)$ et $\Delta G_t^0(Cl^-)$ déterminés antérieurement.

[Traduit par le journal]

Introduction

The free energy of transfer, ΔG_t^0, of a solute from a standard state (usually the infinitely dilute solution) in a reference solvent to a standard state (also one of infinite dilution) in a second solvent is recognized as one of the most important quantities reflecting the intensity of solute–solvent interactions taking place in the chemical milleau under consideration. However, when a charged species, like an ion, is transferred from solvent A to solvent B, a sizeable contribution to the observed ΔG_t^0 arises from the difference in the dielectric constants of A and B. This so-called Born contribution (1) to ΔG_t^0 is due to the long-range coulombic interaction between the ion and the solvent regarded as a continuum. Solution chemists are much more interested in the remaining "non-Born" part of ΔG_t^0, often called the "chemical" part, which measures the specific and short-range interactions between the ion and its neighbouring solvent molecules.

To estimate and allow for the Born part and hence to determine the chemical part is a task involving too many unknowns and uncertainties, as has been pointed out (1, 2), and it would be unwise to interpret results obtained so tentatively. One, although admittedly not a general, way of solving this problem is to choose the solvents A and B in such a manner that their dielectric constants are more or less equal. The transfer of an ion between such isodielectric solvents entails no significant changes in the long-range ion–solvent interactions and the

[1]To whom all correspondence should be addressed.

[2]Revision received May 18, 1979.

0008-4042/79/182470-06$01.00/0

magnitude of the Born contribution is therefore negligibly small. Thus, ΔG_t^0 of an ion in an isodielectric solvent system is all 'chemical'' and so faithfully reflects the short-range and specific interactions which are of paramount interest in solution chemistry.

Lately, our attention has been focussed on several such isodielectric solvent systems, one being the acetonitrile (ACN) + ethylene glycol (EgOH) system. In previous papers (3) we have determined the ΔG_t^0's of various electrolytes and estimated those of some individual ions in these mixed solvents, the reference solvent being EgOH. It has been pointed out that in this isodielectric system consisting of a protic (EG) and a dipolar aprotic (ACN) solvent, the nature of short-range ion–solvent interactions as well as the essential difference between the solvation characteristics of the two solvent types should be clearly revealed.

Extensive studies (4–11*a*) of proton transfer equilibria and reaction kinetics have shown that the basicity in a protic solvent is greatly enhanced by the addition of a dipolar aprotic solvent. In the ACN + EgOH system, specifically, Kundu and Aiyar (8) have demonstrated that the H_- function increases as the ACN content of the solvent mixture increases. The most important reason for this type of behaviour is that dipolar aprotic solvents are extremely poor solvators of anions (2, 12, 13), especially those anions which can interact with solvents only through hydrogen bonding (besides coulombic forces). Such an anion is the glycoxide ion (OEg^-), and the present paper aims to present thermodynamic evidence for its varying solvation behaviour with regard to EgOH, a protic solvent, and ACN, a dipolar aprotic one, from the determination of autoprotolysis constants in ACN + EgOH mixtures.

Since both the acidic and the basic character of ACN are very weak (2, 6, 13), we are concerned with the single equilibrium

[A] $EgOH(s) \rightleftharpoons H^+(s) + OEg^-(s)$

i.e. the ionization of EgOH. Here s indicates that the reacting species are in the standard state in the given solvent (14) and $H^+(s)$ counts all H^+(solvated) that are seen by the electrode. Cell [B],

[B] Pt, H_2(g, 1 atm)|Na–glycoxide(m_1), NaCl(m_2), solvent|AgCl–Ag

was used for emf measurements at 25°C and the solvent contained 0, 20, 40, or 60 wt.% ACN; m_1, m_2 represent molalities.

Experimental

Purification of the solvents has been described earlier (3*a*). G. R. Merck grade sodium chloride was used after drying at 300°C. Clean bits of sodium metal were dissolved in pure EgOH and the solvent composition was adjusted to requirement by adding ACN (stock 1). Direct addition of sodium to a mixed solvent was avoided as this caused a vigorous reaction leading to undesirable products. Stock 1 was mixed with a NaCl solution in the solvent (stock 2) in such suitable proportion as to keep the ratio $m_{OG^-}:m_{Cl^-} \approx 1$ in the resulting mixture (stock 3). The OEg^- ion concentration in stock 3 was determined by titration with a standard HCl solution. Solutions for emf measurement were prepared by dilution (by weight) of stock 3 with the solvent. Two sets of solution were prepared for each solvent, each set having a different value of the $m_1:m_2$ ratio. Assuming that the salts are completely dissociated in the dilute solutions the ionic strength $\mu \approx (m_1 + m_2)d_s$, where d_s is the solvent density, was generally maintained between 0.01 and 0.05. Adequate care was taken to avoid absorption of moisture and CO_2 during preparation and handling of the solutions, using a dry-box whenever possible.

Cell design, electrode preparation, experimental procedure etc. have been described earlier (3*a*, 15). No poisoning of the platinum electrodes was observed. Equilibrium was reached in 5 h in pure EgOH and in 8–10 h in the mixed solvents. The equilibrium emf was only slightly affected by the hydrogen bubbling rate and could be reproduced to within ±0.5 mV by introducing a freshly platinized electrode.

Results and Discussion

The emf values were corrected to a hydrogen pressure of 1 atm as earlier (3*a*). The corrected emf values (E) recorded in Table 1 are accurate to within ±0.5 mV. The extrapolation function pK_s' given by [1] was then constructed;

$$[1] \quad pK_s' = \frac{F(E - E^0)}{(\ln 10)RT} - \log\frac{m_1}{m_2}$$

$$= pK_s^m - \log\frac{\gamma_{Cl^-} \cdot a_{EgOH}}{\gamma_{OEg^-}} = pK_s^m + f(\mu)$$

where the symbols carry their usual meaning (11*a*). The standard state is so chosen that at infinite dilution in a given solvent, $\gamma_{Cl^-} = \gamma_{OEg^-} = a_{EgOH} = 1$. The linear plots of pK_s' vs. μ (Fig. 1) were extrapolated to $\mu = 0$ to obtain values of pK_s^m (molal scale). Values of E^0 and d_s were taken from a previous paper (3*a*). The uncertainties in the pK_s^m values (Table 2) are ±0.01 for pure EgOH and ±0.02 for the mixed solvents. The values of pK_s' in each of the solvents when fitted to linear form by the method of least squares, furnish identical values of pK_s as well as their standard deviations as noted above.

In a mixed solvent system having at least one protic component ROH it is possible to define the ionization constant of ROH, i.e. the equilibrium constant for the general reaction [A], in a variety of ways depending on the standard state of ROH chosen. Hepler and co-workers (17) have derived

TABLE 1. Electromotive force data for cell [B] in ACN + EgOH mixtures at 25°C

μ	m_{OEg^-}	m_{Cl^-}	E/V	μ	m_{EOg^-}	m_{Cl^-}	E/V
	Pure EgOH				20% ACN		
0.0105	0.00487	0.00457	0.9589	0.00524	0.00255	0.00254	0.9641
0.0200	0.0110	0.00701	0.9702	0.00772	0.00376	0.00374	0.9648
0.0302	0.0140	0.0132	0.9613	0.0102	0.00495	0.00493	0.9660
0.0398	0.0219	0.0140	0.9708	0.0200	0.00974	0.00971	0.9683
0.0502	0.0233	0.0219	0.9620	0.0249	0.0103	0.0139	0.9569
0.0600	0.0330	0.0211	0.9711	0.0400	0.0165	0.0223	0.9620
0.0697	0.0324	0.0304	0.9619				
	40% ACN				60% ACN		
0.00528	0.00241	0.00311	0.9780	0.00518	0.00298	0.00284	0.9991
0.0103	0.00475	0.00598	0.9793	0.0101	0.00580	0.00554	1.0012
0.0199	0.00925	0.0116	0.9798	0.0161	0.00865	0.00943	0.9978
0.0248	0.0113	0.0146	0.9821	0.0220	0.0132	0.0115	1.0029
0.0397	0.0184	0.0231	0.9807	0.0327	0.0197	0.0171	1.0047
0.0596	0.0276	0.0347	0.9852	0.0439	0.0264	0.0229	1.0062

useful conclusions regarding the ionization of water in a number of mixed aqueous solvents by considering the quantity

$$[2] \quad K_{a/c} = C_H C_{OR} (y_\pm)^2 / C_{ROH}$$

where C_H, C_{OR}, and C_{ROH} represent the molar concentrations of H^+, OR^-, and ROH in the mixed solvent and $y_\pm$ is the mean molar activity coefficient. (For mixed aqueous solvents, ROH = H_2O.)

$K_{a/c}$ is related to our operational constant K_s^m by (14)

$$[3] \quad K_{a/c} = K_s^m d_s^2 / C_{ROH}$$

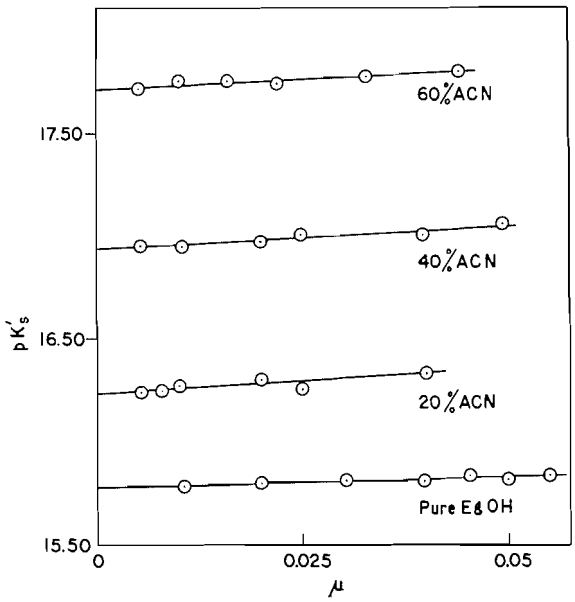

FIG. 1. Variation of pK_s' with μ in ACN + EgOH mixtures at 25°C.

where d_s is the density of the solvent. In terms of free energies, the ionization process may then be described by the quantity (14, 17)

$$[4] \quad \delta\Delta G^0 = {}_s\Delta G_{a/c} - {}_r\Delta G_{a/c}$$
$$= (\ln 10)RT\,[p({}_sK_{a/c}) - p({}_rK_{a/c})]$$

where $\Delta G_{a/c}$ is the free energy of ionization of ROH, and the subscripts s and r refer to quantities relating to the process occurring in a mixed solvent (s) and a "reference" solvent (r). It is usual to choose the pure solvent ROH as the reference solvent.

For the ACN + EgOH system (where ROH = EgOH), we have calculated the values of $\delta\Delta G^0$ using eqs. [3] and [4]; Fig. 2 shows the variation of $\delta\Delta G^0$ with mol% ACN. Moreover, as it was felt that a comparison of the behaviour of this system with that of others is likely to prove interesting, $\delta\Delta G^0$ values were also calculated for the H_2O + EgOH (ROH = EgOH) and the MeOH (methanol) + PgOH (1,2-propanediol) (ROH = PgOH) system, for which K_s^m data are available (15*a*, 16, 18). In Fig. 2, $\delta\Delta G^0$ is shown plotted against mol% H_2O and MeOH for the H_2O + EgOH and MeOH + PgOH systems respectively.

$\delta\Delta G^0$ plots for H_2O + EgOH and ACN + EgOH systems relate to the variation of the extent of ionization of EgOH in the presence of two different types of co-solvent. The decrease in $\delta\Delta G^0$ values for the former system may in part be accounted for by the increase in dielectric constant with increasing water content and the consequently greater ease of ionization; the remaining contribution is likely to arise from the greater net stability attained by the H^+ and OEg^- ions through increased solvation by water molecules. On the other hand, in the isodi-

TABLE 2. Values of autoprotolysis constants and the related free energies of transfer in ACN + EgOH mixtures at 25°C

Wt.% ACN	pK_s^m	$p({}_sK_{a/c})$	$\delta\Delta G^0$ (kJ mol^{-1})	ΔG_t^0(EgOH–EgOH)$_{sys}$ (kJ mol^{-1})	$\Delta G_t^0(H^+)^b$ (kJ mol^{-1})	$\Delta G_{t,app}^0(OEg^-)$ (kJ mol^{-1})	$-RT \ln x_{EgOH}$ (kJ mol^{-1})	$\Delta G_t^0(OEg^-)$ (kJ mol^{-1})
0	15.77 (15.84)[a]	16.93	0	0	0	0	0	0
20	16.23	17.33	2.26	3.10	0.3	2.8	0.8	3.6
40	16.93	17.93	5.72	7.54	0.7	6.8	1.7	8.5
60	17.71	18.57	9.35	12.41	1.7	10.7	2.9	13.6

[a]Value from ref. 16.
[b]Values from ref. 3*d*.

electric ACN + EgOH system, the dielectric constant effect on $\delta\Delta G^0$ is negligibly small, but ACN being a dipolar aprotic solvent has little tendency to solvate either ion and ionization becomes more difficult with the progressive addition of ACN to EgOH, as shown by the rapidly increasing values of $\delta\Delta G^0$. The MeOH + PgOH system besides being isodielectric is also a protic–protic combination and as such there is little change in $\delta\Delta G^0$; whereas by comparison, the large change in dielectric constant accounts for a large part of the rapidly changing $\delta\Delta G^0$ in the H_2O + EgOH system, as indicated above. Again, ACN + EgOH and MeOH + PgOH are each an isodielectric system, and their average dielectric constants differ by only about 10 units; moreover EgOH and PgOH are much alike in chemical nature. Yet one observes a totally different nature of $\delta\Delta G^0$ plots for the two systems. This is because of the strongly contrasting solvation characteristics of MeOH and ACN: the protic MeOH is a good solvator for the hydrogen bonding ions while the dipolar aprotic ACN is not.

Informative as the above discussion might be,

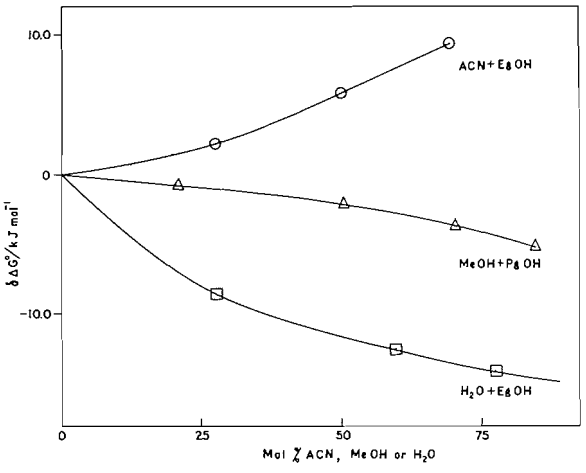

FIG. 2. Variation of $\delta\Delta G^0$ with mol% cosolvent at 25°C.

$\delta\Delta G^0$ plots can reflect no more than the overall solvation of the H^+ and OR^- ions. As shown earlier (14, 18), a knowledge of the ionic components of free energies should provide a clearer picture of specific ion–solvent interactions involved in the process. The evaluation and interpretation of the free energies of transfer of the OEg^- ion, $\Delta G_t^0(OEg^-)$, in ACN + EgOH mixtures are therefore in order.

The standard free energy on the mole fraction scale, corresponding to the process [A] in a mixed solvent ($_s\Delta G^0$) relative to that in pure EgOH ($_g\Delta G^0$) was computed by [5].

$$[5]\quad {}_s\Delta G^0 - {}_g\Delta G^0 = (\ln 10)RT[p({}_sK_s^m) - p({}_gK_s^m)] - 2RT \ln M_s/M_g$$

In this isodielectric system, the quantity ($_s\Delta G^0 - {}_g\Delta G^0$) is expected to reflect only the effects of the acidity and the basicity of the solvent (11*a*). This quantity is identical with ΔG_t^0(EgOH–EgOH)$_{sys}$, the free energy of transfer of EgOH molecules acting as an acid–base system from pure EgOH to a mixed solvent, i.e. the free energy change accompanying the process [C] (11*a*),

$$[C]\quad EgOH(S) + H^+(G) + OEg^-(G) \rightarrow EgOH(G) + H^+(S) + OEg^-(S)$$

which may be written as the sum of the processes [D] and [E],

$$[D]\quad H^+(G) \rightarrow H^+(S)$$

$$[E]\quad OEg^-(G) + EgOH(S) \rightarrow OEg^-(S) + EgOH(G)$$

In [C], [D], and [E], (G) and (S) denote that the species concerned are in the standard state in pure EgOH and the mixed solvent respectively. $\Delta G_t^0(H^+)$ and $\Delta G_{t,app}^0(OEg^-)$ are defined as the free energy changes for the processes [D] and [E] respectively, so that

$$[6]\quad {}_s\Delta G^0 - {}_g\Delta G^0 = \Delta G_t^0(EgOH-EgOH)_{sys} = \Delta G_t^0(H^+) + \Delta G_{t,app}^0(OEg^-)$$

When the standard state of EgOH molecules is referred to the particular solvent concerned, $\Delta G_{t,app}^{0}$-(OEg^-) is identical to $\Delta G_t^0(OEg^-)$, the standard free energy of transfer of the OEg^- ion from EgOH to that solvent, i.e. the free energy change for the process [F].

[F] $OEg^-(G) \rightarrow OEg^-(S)$

However, with pure EgOH as the standard state, these two quantities are related by [7] (11*a*),

[7] $\Delta G_t^0(OEg^-) = \Delta G_{t,app}^0(OEg^-) - RT\ln(a_{EgOH})_g^s$

where $(a_{EgOH})_g^s$ is the activity of EgOH in the mixed solvent referred to pure EgOH as the standard state. Assuming as earlier (3*a*) that Raoult's law is obeyed by this solvent system, we have $a_{EgOH} \approx x_{EgOH}$, the mole fraction of EgOH in the solvent, and combining [6] and [7], we get

[8] $\Delta G_t^0(OEg^-) = \Delta G_t^0(EgOH-EgOH)_{sys} - \Delta G_t^0(H^+) - RT\ln x_{EgOH}$

Substituting the value of $\Delta G_t^0(H^+)$ for each solvent mixture from an earlier paper (3*d*) and knowing the values of the other two terms on the right side of [8], those of $\Delta G_t^0(OEg^-)$ on the mole fraction scale were calculated; $\Delta G_t^0(EgOH\text{–}EgOH)_{sys}$ and $\Delta G_t^0(OEg^-)$ values are reported in Table 2.

$\Delta G_t^0(OEg^-)$ is shown plotted against mol% ACN in Fig. 3. Plots of $\Delta G_t^0(Cl^-)$ and $\Delta G_t^0(H^+)$, taken from a previous paper (3*d*), are also shown in Fig. 3, and are seen to be qualitatively similar to the $\Delta G_t^0(OEg^-)$ plot. The fact that all three increase with increasing proportions of ACN indicates a progressive desolvation of these ions as the solvent becomes richer in ACN. It is to be noted further that the relative desolvation of the anions OEg^- and Cl^- is greater than that of the H^+ ion. Such behaviour arises from a very typical characteristic of dipolar aprotics like ACN, namely, the marked inability to solvate small anions which interact wholly through hydrogen bonds and ion–dipole forces (2, 12, 13). In the case of ACN, in spite of the considerable polarization of the C≡N bond (19), the positive end of the dipole is located at an unfavourable position for interaction with anions (19, 20) and the hydrogen-bond donating capacity of the molecule is only very feeble (2, 13, 20). The relative desolvation of the OEg^- ion is the most marked, probably because in pure EgOH it undergoes the strongest stabilization through hydrogen-bonding and fits most easily into the solvent structure.

Similar, incidentally, is the case of the dimethylsulphoxide (DMSO) + water system (11) — another protic–dipolar aprotic combination, where solvation effects are more important than dielectric constant effects at least up to 60 wt.% DMSO. Thus, as the positive charge centre of DMSO molecule is surrounded by bulky groups and therefore not easily approachable, increasing addition of DMSO to water causes increasing desolvation of anions (11, 21). Again, the greater propensity of the protophilic OH^- (compared to Cl^-, say) to take part in the solvent structure through hydrogen-bonding stabilizes OH^- more than the Cl^- ion in water, and consequently $\Delta G_t^0(OH^-)$ is observed to be more positive than $\Delta G_t^0(Cl^-)$ for a given solvent mixture.

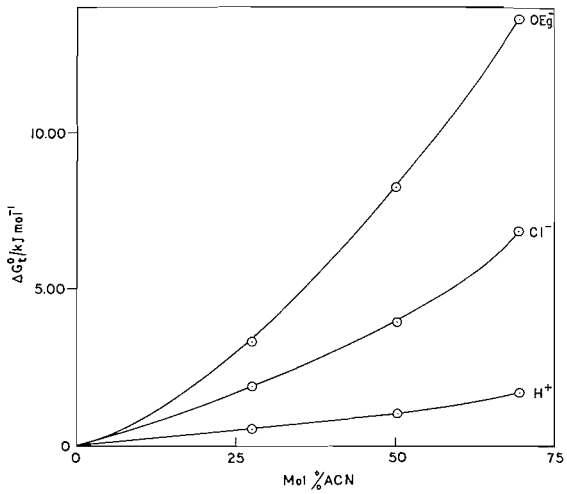

FIG. 3. Variation of ΔG_t^0 of various ions in ACN + EgOH mixtures at 25°C.

Acknowledgement

The authors wish to thank the National Council of Educational Research and Training for granting an N.S.T.S. Scholarship to one of them (K.B.).

1. R. G. BATES. *In* Hydrogen-bonded solvent systems. *Edited by* A. K. Covington and P. Jones. Taylor and Francis, London. 1968. p. 49.
2. R. G. BATES. *In* Solute–solvent interactions. *Edited by* J. F. Coetzee and C. D. Ritchie. Marcel Dekker, New York. 1969. p. 45.
3. K. BOSE and K. K. KUNDU. (*a*) J. Chem. Soc. Faraday Trans. 1, 284 (1977); (*b*) J. Solution Chem. 8, 175 (1979); (*c*) Indian J. Chem. In press; (*d*) Can. J. Chem. This issue.
4. K. BOWDEN. Chem. Soc. Rev. **66**, 119 (1966).
5. C. H. ROCHESTER. Q. Rev. Chem. Soc. **20**, 511 (1966).
6. C. D. RITCHIE. *In* Solute–solvent interactions. *Edited by* J. F. Coetzee and C. D. Ritchie. Marcel Dekker, New York, 1969. p. 219.
7. J. R. JONES. Chem. Br. **7**, 336 (1971).
8. K. K. KUNDU and L. AIYAR. J. Chem. Soc. Perkin Trans. **2**, 715 (1972).

9. R. STEWART, J. P. O'DONNELL, D. J. CRAM, and B. RICKBORN. Tetrahedron, **18**, 917 (1962).
10. D. DOLMAN and R. STEWART. Can. J. Chem. **45**, 911 (1967).
11. A. K. DAS and K. K. KUNDU. (*a*) J. Chem. Soc. Faraday Trans. 1, **69**, 730 (1973); (*b*) **70**, 1452 (1974).
12. A. J. PARKER. Q. Rev. Chem. Soc. **16**, 163 (1962); Chem. Soc. Rev. **69**, 1 (1969).
13. E. PRICE. *In* The chemistry of nonaqueous solvents. Vol. 1. *Edited by* J. J. Lagowski. Academic Press, New York. 1966. p. 67.
14. A. K. DAS and K. K. KUNDU. J. Phys. Chem. **79**, 2604 (1975).
15. (*a*) S. K. BANERJEE, K. K. KUNDU, and M. N. DAS. J. Chem. Soc. A, 166 (1967); K. K. KUNDU and M. N. DAS. J. Chem. Eng. Data, (*b*) **9**, 82 (1964); (*c*) **9**, 87 (1964).
16. K. K. KUNDU, P. K. CHATTOPADHYAY, D. JANA, and M. N. DAS. J. Phys. Chem. **74**, 2633 (1970).
17. E. M. WOOLLEY, D. G. HURKOT, and L. G. HEPLER. J. Phys. Chem. **74**, 3908 (1970).
18. K. K. KUNDU, A. L. DE, and M. N. DAS. J. Chem. Soc. Dalton Trans. 378 (1972).
19. M. SALOMON. Can. J. Chem. **54**, 1487 (1976).
20. R. YAMDAGNI and P. KEBARLE. J. Am. Chem. Soc. **94**, 2940 (1972).
21. K. H. KHOO. J. Chem. Soc. A, 2932 (1971).

Free energies of transfer of some single ions from ethylene glycol to its isodielectric mixtures with acetonitrile at 25°C

KUMARDEV BOSE AND KIRON K. KUNDU[1]

Physical Chemistry Laboratories, Jadavpur University, Calcutta 700032, India

Received August 15, 1978[2]

KUMARDEV BOSE and KIRON K. KUNDU. Can. J. Chem. 57, 2476 (1979).

Free energies of transfer (ΔG_t^0) of the reference electrolyte Ph_4AsBPh_4 (Ph = phenyl) from ethylene glycol to its approximately isodielectric mixtures with acetonitrile have been determined at 25°C from the measurement of the solubilities of KPi, Ph_4AsPi, and KBPh (Pi = picrate) in these solvents. Using the assumption $\Delta G_t^0(Ph_4As^+) = \Delta G_t^0(Ph_4B^-) = \frac{1}{2}\Delta G_t^0(Ph_4AsBPh_4)$, ΔG_t^0 values for the individual ions K^+, Pi^-, Ph_4As^+, and Ph_4B^- have been estimated. These, in conjunction with previously determined values of ΔG_t^0 for MCl (M = Li, Na, K, Rb, Cs, and H), KBr and KI have provided ΔG_t^0 values for Cl^-, Br^-, I^-, and M^+ ions. Ionic ΔG_t^0's have been interpreted in terms of specific ion–solvent interactions. The contrasting behaviour of ethylene glycol and acetonitrile in ion-solvation is shown to be characteristic of the protic and dipolar aprotic solvent types respectively.

KUMARDEV BOSE et KIRON K. KUNDU. Can. J. Chem. 57, 2476 (1979).

Opérant à 25°C et faisant appel à des mesures de solubilité de KPi, Ph_4AsPi et $KBPh_4$ (Pi = picrate) dans ces solvants, on a déterminé les énergies libres de transfert (ΔG_t^0) de l'électrolyte de référence, Ph_4AsBPh_4 (Ph = phényle), de l'éthylèneglycol à ses mélanges qui sont approximativement isodiélectriques avec de l'acétonitrile. Faisant l'hypothèse que $\Delta G_t^0(Ph_4As^+) = \Delta G_t^0(Ph_4B^-) = \frac{1}{2}\Delta G_t^0(Ph_4AsBPh_4)$, on a évalué les valeurs de ΔG_t^0 des ions individuels K^+, Pi^-, Ph_4As^+ et PhB^-. Ces valeurs, utilisées de concert avec les valeurs de ΔG_t^0 déterminées antérieurement pour MCl (M = Li, Na, K, Rb, Cs et H), KBr et KI permettent de déterminer les valeurs ΔG_t^0 des ions Cl^-, Br^-, I^- et M^+. On a interprété les valeurs de ΔG_t^0 ioniques en termes d'interactions spécifiques ion–solvant. On démontre que les contrastes entre les comportements de l'éthylèneglycol et l'acétonitrile vis-à-vis la solvatation ionique sont respectivement caractéristiques de types de solvants protiques et aprotiques dipolaires.

[Traduit par le journal]

Introduction

The importance of isodielectric solvent systems is being increasingly recognized in thermodynamic studies of ion–solvent interactions. This is because while "Born-type" electrostatic contributions (1) to thermodynamic transfer parameters, e.g. the free energy of transfer (ΔG_t^0), of ions and electrolytes in non-isodielectric systems, being difficult to estimate and to correct for, mask the effect of "true" or short-range ion–solvent interactions, the ΔG_t^0 in isodielectric systems wholly reflects the extent of ion-stabilization through such short-range interactions since "Born-type" contributions are non-existent or negligibly small in the latter systems.

In addition, great interest lies in the study of binary solvent mixtures containing a protic and a dipolar aprotic component. Thus, with the progressive increase in the proportion of the dipolar aprotic solvent (DAS) in the mixture, the solvent character undergoes gradual but material change, with hydrogen-bond donating properties of the protic solvent (PS) weakening and giving way to radically different forces like soft–soft (2), dispersion (1) and π-overlap (3) interactions. In such a mixed solvent system, therefore, the modes of specificity in the solvation behaviour of the two components are expected to show up in sharp contrast.

In previous papers (4) we have indicated that the solvent system acetonitrile (ACN) + ethylene glycol (EG) constitutes a PS–DAS combination which is also approximately isodielectric and have determined the ΔG_t^0's of various electrolytes from EG to ACN + EG mixtures. These values, however, reflect the solvent effect on the sum of the interactions undergone by the ions with the solvent without revealing the nature of solvation of the individual ions. For a better understanding of the solvation of single ions, we now proceed to split the composite ΔG_t^0's into individual ionic contributions, using the most popular extrathermodynamic assumption (5–7):

$$[1] \quad \Delta G_t^0(Ph_4As^+) - \Delta G_t^0(Ph_4B^-) = \tfrac{1}{2}\Delta G_t^0(Ph_4AsBPh_4)$$

where Ph = phenyl.

[1]To whom all correspondence should be addressed.

[2]Revision received May 18, 1979.

0008-4042/79/182476-06$01.00/0

Recently, Treiner (8) has calculated the ΔG_t^0 values for the Ph_4As^+ ion between water and several pure non-aqueous solvents using the scaled-particle theory (SPT) (9) according to which contribution to ΔG_t^0 comes from two parts — one due to solute–solvent interactions, ΔG_t^0(int), and the other due to cavity formation in the solvent, ΔG_t^0(cav). Thus,

$$[2] \quad \Delta G_t^0 = \Delta G_t^0(\text{int}) + \Delta G_t^0(\text{cav})$$

In calculating ΔG_t^0, a necessary approximation is to equate the relatively unknown ΔG_t^0(int) to zero. When theoretical and experimental (5*c*) values are compared, this approximation is shown to be generally invalid for DAS, the reason being correctly attributed to strongly increased ion–solvent interactions in passing from water to DAS and a corresponding large negative value for ΔG_t^0(int). However, it does not necessarily follow, as Treiner assumes (8), that with increasing strength of interaction with the solvent, the difference in solvation of the Ph_4As^+ ion and the Ph_4B^- ion becomes appreciable and hence that [1] becomes invalid. All that the SPT calculations reveal is the rather expected result that ΔG_t^0(int) values for these two large ions are highly negative. They cannot be used to make predictions about the equality or inequality of these values. Therefore, it seems unjustified to recommend, as Treiner does, against the use of [1]. Amidst the controversy raging over the "best" extrathermodynamic assumption (7*b*), [1] still remains one of the few most reliable assumptions for the determination of single ion ΔG_t^0 values. A recent paper by Kim (10) also strongly supports this contention.

ΔG_t^0 values at 25°C for the "reference electrolyte" Ph_4AsBPh_4 have been determined from [3]:

$$[3] \quad \Delta G_t^0(Ph_4AsBPh_4) = \Delta G_t^0(Ph_4AsPi) + \Delta G_t^0(KBPh_4) - \Delta G_t^0(KPi)$$

(where Pi = picrate) using the corresponding values for Ph_4AsPi, $KBPh_4$, and KPi obtained from solubility measurements.

Experimental

The purification of the solvents EG and ACN (4*a*) as well as the preparation of the salts KPi (11), Ph_4AsPi (12*a*), and $KBPh_4$ (12*b*) have been described. The concentration of water in the solvents determined by Karl Fischer titrations was found, as before (4*a*), to lie between 0.01 and 0.015 mol dm^{-3}. It was shown in an earlier paper (4*a*) that in presence of such small concentrations of water, even protons, which have normally a strong tendency to be hydrated, are preferentially solvated by EG. The possibility of selective solvation by water of the much larger and less hydrophilic ions presently under study was therefore considered to be remote.

For solubility measurements, small quantities of the salt was added with shaking to 25 mL of the solvent taken in a Jena bottle until no further visible dissolution occurred. Since prolonged contact with oxygen also affects its stability (12*b*), the dissolution of $KBPh_4$ as well as each subsequent withdrawal of its solution for analysis were performed under a flush of dry nitrogen. The solutions were thermostatted at 25 ± 0.05°C and allowed to equilibriate. At two-day intervals aliquots of each solution were withdrawn, appropriately diluted, and analyzed using a Beckmann DU-2400 model spectrophotometer. The solvents used for dilution and the pertinent λ_{max} and ε_{max} values are indicated below.

	Diluting solvent	Dilution	λ_{max} (nm)	ε_{max}
KPi (12*b*) and Ph_4AsPi (1*b*2)	Water	200–5000	355	1.44×10^4
$KBPh_4$ (7*a*)	ACN	100	266	3.2×10^3
			274	2.1×10^3

It may be noted that ε_{max} values of the samples when checked in the respective diluting solvents were found to lie within 1% of the literature values cited above. So was the solubility of $KBPh_4$ in pure ACN, which was found to be 0.0528 ± 0.0006 *M* compared to 0.0533 *M* reported by Popovych (7*a*). Saturation was reached 8–10 days after which the measured concentrations of the solutions showed no further change beyond the experimental error of about 1%. The reported concentrations (Table 1) are the mean of two sets of measurements agreed to within 1%.

Results

The thermodynamic solubility products of each of the salts on the molar scale were calculated by [4]:

$$[4] \quad pK_{sp}^c = -\log \{C(1-\alpha)y_\pm\}^2$$

where C is the observed concentration in mol dm^{-3}, α is the degree of association of the salt into ion-pairs, and $y_\pm$ is the mean molar activity coefficient of the salt. Values of α were calculated by [5]:

$$[5] \quad \alpha = \frac{(2CK_Ay_\pm^2 + 1) - (4CK_Ay_\pm^2 + 1)^{1/2}}{2CK_Ay_\pm^2}$$

using previously reported values (4*c*) of K_A, the association constant. $y_\pm$ values were obtained from [6] by interactive calculations with the help of B-6700 computer using FORTRAN programmes

$$[6] \quad -\log y_\pm = \frac{1}{2}\frac{A_0B_0d_s^{-1/2}C_1^{1/2}}{\ln 10} \times [(1 + a_0^+B_0d_s^{-1/2}C_1^{1/2})^{-1} + (1 + a_0^-B_0d_s^{-1/2}C_1^{1/2})^{-1}] + \log\left(1 + 0.002\frac{C_1M_s}{d_s}\right)$$

where $C_1 = C(1-\alpha)$ and the other parameters

TABLE 1. Parameters of [4] and free energies of transfer in ACN + EG mixtures at 25°C

Wt.% ACN	C (mol dm^{-3})	K_A (dm^3 mol^{-1})[b]	α	$y_\pm$	pK_{sp}^c	ΔG_t^0 (kJ mol^{-1})
			KPi			
0	0.0722	4.5±0.1	0.082±0.002	0.546	2.88	—
20	0.1383	5.5±0.2	0.143±0.004	0.505	2.44	−2.40
40	0.1607	9.2±0.5	0.221±0.008	0.496	2.41	−2.50
60	0.1318	10.1±0.7	0.207±0.010	0.498	2.60	−1.37
100[a]	—	—	—	—	5.28	13.41
			Ph_4AsPi			
0	0.0037	20.3±0	0.048±0.0	0.845	5.07	—
20	0.0318	11.5±0.2	0.132±0.002	0.692	3.44	−9.19
40	0.0843	9.3±0.3	0.184±0.005	0.593	2.78	−12.89
60	0.1298	4.3±0.5	0.117±0.010	0.517	2.45	−14.72
100[a]	—	—	—	—	3.83	−6.80
			Ph_4BK			
0	0.0077	18.2±0.1	0.075±0.001	0.794	4.50	—
20	0.0596	9.5±0.2	0.159±0.002	0.630	2.99	−8.50
40	0.1321	4.7±0.3	0.134±0.004	0.537	2.42	−11.69
60	0.1518	0.0	0.0	0.490	2.26	−12.35
100[a]	—	—	—	—	4.10	−2.00

[a]Calculated from ref. 7*a*.
[b]Reference 4*c*.

TABLE 2. Single ion free energies of transfer from EG to ACN + EG mixtures at 25°C

	ΔG_t^0 (kJ mol^{-1})										
Wt.% ACN	H^+	Li^+	Na^+ t	K^+	Rb^+	Cs^+	Cl^-	Br^-	I^-	Pi^-	Ph_4As^+/Ph_4B^-
20	0.3	0.0	−0.4	−0.9	−1.1	−1.1	2.1	1.5	1.1	−0.5	−7.6
40	0.7	1.0	0.3	−0.6	−0.8	−0.9	4.3	3.7	2.5	−1.1	−11.0
60	1.7	2.8	1.3	0.4	0.0	−0.2	0.8	6.3	4.3	−1.3	−12.9
100	—	—	—	8.9	—	—	—	—	—	5.1	−10.9

carry their usual meaning (4*a*). The ion-size parameters, a_0^+ and a_0^-, for the cation and the anion respectively, were assumed to have the following values (7*a*):

$$a_0^{K^+} = a_0^{Pi^-} = 0.3 \text{ nm}$$

$$a_0^{Ph_4As^+} = a_0^{Ph_4B^-} = 0.5 \text{ nm}$$

Values of C, $y_\pm$, and pK_{sp}^c are listed in Table 1. Uncertainties in α values were obtained by using two sets of pK_A values as limited by their respective standard deviations, in the interactive calculations of α and $y_\pm$ values. Since the errors in the measured solubilities and those in the effective ionic concentrations $C_i = C(1 - \alpha)$ arising from the uncertainties in α values as well, lie within 2%, pK_{sp}^c values could be taken to be correct to within ±0.02 unit. pK_{sp}^c values for pure ACN computed from a previous work (7*a*) are also given. Free energies of transfer of each salt on the mole fraction scale (ΔG_t^0) were calculated using [7]

$$[7] \quad \Delta G_t^0 = (\ln 10)\, RT\, [(pK_{sp})_s^c - (pK_{sp})_g^c] + 2\,(\ln 10)\, RT \log M_g d_s / M_s d_g$$

where $T = 298.15$ K, and the subscripts g and s refer to EG and the mixed solvent respectively. ΔG_t^0 values reported in Table 1 are accurate to within ±0.1 kJ mol^{-1}.

Single ion free energies of transfer ΔG_t^0(i), estimated by means of the basic assumption [1] using [3], [8]–[11], are given in Table 2.

$$[8] \quad \Delta G_t^0(Pi^-) = \Delta G_t^0(Ph_4AsPi) - \Delta G_t^0(Ph_4As^+)$$

$$[9] \quad \Delta G_t^0(K^+) = \Delta G_t^0(KBPh_4) - \Delta G_t^0(Ph_4B^-)$$

$$[10] \quad \Delta G_t^0(X^-) = \Delta G_t^0(KX) - \Delta G_t^0(K^+)$$

$$[11] \quad \Delta G_t^0(M^+) = \Delta G_t^0(MCl) - \Delta G_t^0(Cl^-)$$

Values of ΔG_t^0(KX) (X = Br or I) and ΔG_t^0(MCl) (M = Li, Na, Rb, Cs, or H) were obtained from previous papers (4*a*, *b*).

Discussion

Plots of ΔG_t^0(i) against mol% of ACN are shown in Fig. 1. Certain distinct trends, each characterizing a group of ions, are observed and may be considered to reflect features peculiar to a protic + dipolar aprotic solvent system.

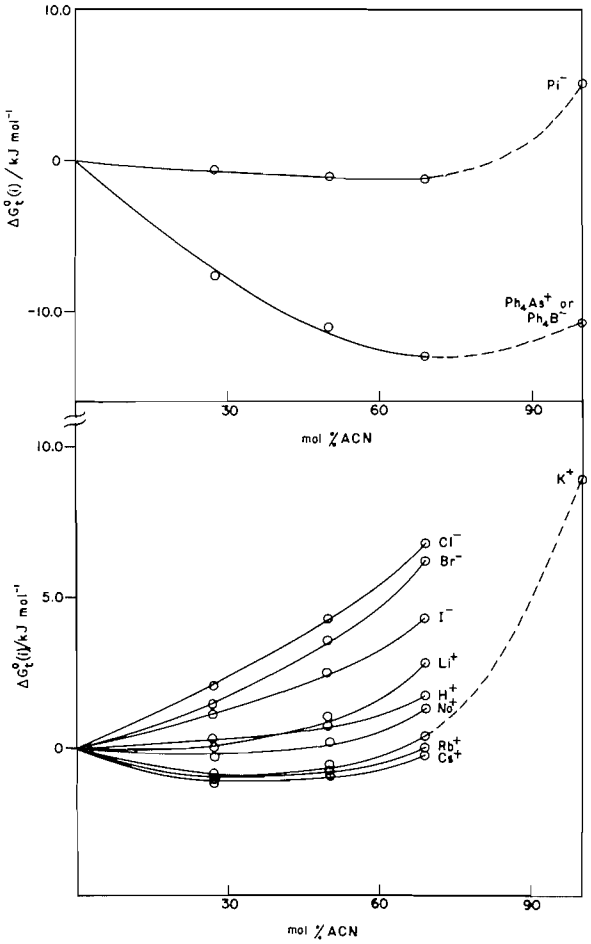

FIG. 1. Variation of ΔG_t^0(i) with solvent composition in ACN + EG mixtures at 25°C.

The simple anions, viz. the halide ions, are relatively strongly solvated by EG through hydrogen-bonding whereas their interaction with the very weakly acidic hydrogen atoms of ACN, although possible (13), is very weak. Increasing loss of hydrogen-bonded stability is seen reflected in the monotonic rise of $\Delta G_t^0(X^-)$ with increasing ACN content of the solvent. The observed order $\Delta G_t^0(Cl^-) > \Delta G_t^0(Br^-) > \Delta G_t^0(I^-)$ for any given solvent is the combined result of decreasing strength of H-bonded interaction (with EG) and increasing strength of "soft–soft" (2, 14) and dispersion interactions (5*c*, 15) (with ACN) with increasing anion size. A recent study (13*a*) indicates that steric requirements of H-bonding between X^- and ACN may also be partly responsible for this order: it has been suggested (13*a*) that the X^- ion approaches the ACN molecule along the C_3 axis of the latter and bonding occurs symmetrically through all three hydrogen atoms; and that therefore the overall strength of such H-bonds increases as the ion becomes larger and more accommodative.

The alkali metal cations have highly positive ΔG_t^0's between pure EG and pure ACN as typified by the behaviour of the K^+ ion. Apparently, in spite of its high dipole moment (16) and a considerable localization of negative charge density on its nitrogen atom (17), ACN is a poorer cation solvator compared to EG. This suggests an explanation in terms of ion–solvent interactions of a specific type, as outlined below.

The geometry of the EG molecule is such as to favour its functioning as a bidentate ligand towards alkali metal ions (M^+). Infrared studies (18) indicate that the predominant configuration of the EG molecule in the liquid state at room temperature is the *gauche* form with intramolecular H-bonding (**A**).

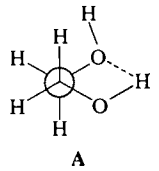

A

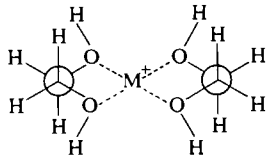

B

It may be assumed that the loss of stability accompanying the rupture of the H-bond during M^+ ion solvation is compensated by the possible formation of four essentially electrostatic bonds in solvates of the type $M(EG)_2^+$ (**B**). It should be apparent from a molecular model that when the four M—EG bonds in solvate (**B**) are coplanar, the eight-atom ring C—O—O—C—O—O—C surrounding the M atom is less puckered and hence more stable than when the M—EG bonds are not coplanar. The use of the Neumann projection (19) shows clearly that besides possessing reflection symmetry at the plane N, this solvate must also be centrosymmetric about M^+. Incidentally, for 1,2-dimethoxyethane, where the hydroxyl H atoms of EG have been substituted by CH_3 groups thereby making the O atoms more basic, alkali metal ions have been shown to be strongly solvated (20) and for cyclic ethers stable M^+ solvates have been isolated (21). The powerful solvation of M^+ by 1,2-dimethoxyethane has been believed to arise from its behaviour as a bidentate ligand (20*c*) through the electrostatic interaction of

the basic O atoms with the M^+ ion. In this light, to assume the existence of $M(EG)_2^+$ solvates, if only in solution, does not seem unreasonable. Such an assumption can moreover offer a plausible explanation for the interesting parts of the $\Delta G_t^0(M^+)$ curves: the noticeable minima for K^+, Rb^+, and Cs^+; $\Delta G_t^0(Li^+)$ has no minimum at all, and $\Delta G_t^0(Na^+)$ is a typical borderline case.

As indicated above, from symmetry and bond-strain considerations, the four M—EG bonds in the $M(EG)_2^+$ solvates may be expected to be more or less coplanar, so that in mixed solvents of low ACN content, ACN molecules approach the central ion from above and below the plane of the solvate and undergo ion–dipole and/or soft–soft interactions with the ion; an octahedral solvate (**C**) is thus

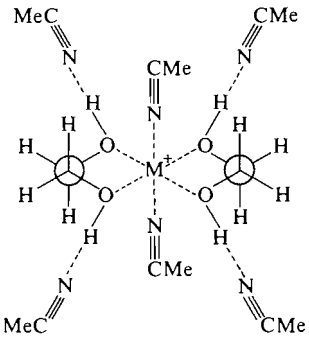

C

formed. Moreover, the well-known tendency of ACN to form hydrogen bonds with protic solvents (22–26) should lead to the stabilization of (**C**) through interaction of its "acidic" hydroxyl H atoms (1) with ACN molecules. An earlier study (27) involving the shift in ir stretching vibration frequencies has in fact indicated the formation of similar $M^+\cdots ODH\cdots N{\equiv}$ CMe associates in aqueous ACN solutions.

Note, however, that hexa-coordination of the M^+ ion in the above manner can be achieved only when its size is large enough, for example, in the case of K^+, Rb^+, and Cs^+. For Na^+, hexa-coordination would be possible but unfavourable; for Li^+ tetra-coordination is only just feasible while hexa-coordination is impossible from steric considerations. Apart from this, the increasing stability of **C** with increasing ionic size also stems from the fact that ACN, being a soft base (17), interacts more and more strongly with M^+ as its radius and hence its polarizability ("softness") increases. The two factors together explain the negative absolute magnitudes which increase in the order $K^+ < Rb^+ < Cs^+$. With increasing proportions of ACN, however, structure **C** should no longer be so stable. It is possible that EG, which, like water, has two donor centres for H-bonding (viz. its two hydroxyl hydrogen atoms) forms with ACN a H-bonded complex of the type EG·2ACN analogous to $H_2O{\cdot}2ACN$ which has been shown to exist in aqueous ACN solutions (23). The formation of such complexes probably forces structure **C** to fall apart "from both sides" with a resultant destabilization of the M^+ ion and an increase in $\Delta G_t^0(M^+)$ values. Above 70 mol% ACN, $\Delta G_t^0(M^+)$ rises sharply up to pure ACN where any tendency to establish ion–dipole interactions between M^+ and ACN is probably opposed by the formation of dimers of the type

$$H_3C{-}C{\equiv}N \quad (+\ -)$$
$$N{\equiv}C{-}CH_3 \quad (-\ +)$$

which ir studies in pure ACN have shown to exist (28, 29).

The Li^+ ion and the H^+ ion (and to a lesser degree, the Na^+ ion) behave similarly on transfer from EG to the mixed solvents. The uniform increases in ΔG_t^0 is indicative of a rather stable state of solvation in pure EG which is progressively broken up upon addition of ACN. As mentioned above, steric reasons oppose the entry of ACN molecules in the primary solvation zone of Li^+ and Na^+ ions, although H-bonding of the solvate **B** by ACN is still possible. This H-bonded stabilization of **B**, slowing down the initial rate of increase of $\Delta G_t^0(Li^+)$ and $\Delta G_t^0(Na^+)$ is rapidly overcome as further amounts of added ACN break up structure **B** in the manner described above and a rapid increase in ΔG_t^0 is observed. The relatively slower increase of $\Delta G_t^0(H^+)$ suggests that as in other amphiprotic solvents, the proton is "chemically" solvated by EG, and that this "glycolated" proton has a structure strong enough to retain its existence even in solvents rich in ACN.

The case of the Pi^- ion is in some ways similar to that of the larger M^+ ions. In pure EG, the Pi^- ion is stabilized by H-bonded solvation through all or some of its seven oxygen atoms, each of which has its share of the negative charge delocalized over the aromatic nucleus. The flat shape of the ion, however, allows the π-electron cloud of the nucleus to undergo dispersion interactions with an ACN molecule approaching in a perpendicular direction. Such interactions continue to stabilize the Pi^- ion till about 70 mol% ACN after which desolvation, caused by the rapid breakdown of the Pi^-—EG H-bonds, is probably more important than solvation through Pi^-—ACN dispersion interactions which are likely to reach saturation instead of increasing further in

strength. In pure ACN itself, the characteristic anion-desolvating property of ACN (1, 3, 15, 30) outweighs the effect of dispersion interactions and there occurs an overall destabilization of the Pi^- ion relative to pure EG or ACN + EG mixtures.

It is interesting to note, however, that the relative destabilization of the Pi^- ion in ACN-rich solvents is much less compared to that of the K^+ ion, although in general dipolar aprotic solvents are poorer solvators of anions than cations. This is certainly because the dispersion interactions of Pi^- with ACN are stronger than the "soft–soft" interactions of K^+ with ACN, a contention which is in agreement with the observation that $\Delta G_t^0(Pi^-)$ exhibits a more pronounced minimum than $\Delta G_t^0(K^+)$ at intermediate solvent compositions (1, 3).

Finally, the behaviour of $\Delta G_t^0(Ph_4As^+)$ or $\Delta G_t^0(Ph_4B^-)$ offers what looks like a straight case of solvation through dispersion interactions. With their four phenyl groups, such interactions with ACN must be very strong, whereas in pure EG these same groups effectively prevent any "classical" interactions with the ionic charge buried deep inside. This causes the very sharp and very large decrease of ΔG_t^0 upto 80% ACN after which saturation is probably reached and the inherent ion-desolvating tendency of ACN causes ΔG_t^0 to increase slightly from 80–100% ACN.

Acknowledgements

The authors wish to thank the National Council of Educational Research and Training for granting a N.S.T.S. scholarship to one of them (K.B.) and Mr. Indra N. Basu Mullick for carrying out the necessary computer analysis of the data.

1. R. G. Bates. *In* Solute–solvent interactions. *Edited by* J. F. Coetzee and C. D. Ritchie. Marcel Dekker, New York. 1969. p. 45.
2. R. G. Pearson. J. Am. Chem. Soc. **85**, 3533 (1963).
3. A. J. Parker. (*a*) Q. Rev. Chem. Soc. **16**, 163 (1962); (*b*) Chem. Rev. **69**, 1 (1969).
4. K. Bose and K. K. Kundu. (*a*) J. Chem. Soc. Faraday Trans. 1, **73**, 284 (1977); (*b*) J. Solution Chem. **8**, 175 (1979); (*c*) Indian J. Chem. In press.
5. (*a*) R. Alexander and A. J. Parker. J. Am. Chem. Soc. **89**, 5549 (1967); (*b*) R. Alexander, A. J. Parker, J. H. Sharp, and W. E. Waghorne. J. Am. Chem. Soc. **94**, 1148 (1972); (*c*) B. G. Cox, G. R. Hedwig, A. J. Parker, and D. W. Watts. Aust. J. Chem. **27**, 477 (1974); (*d*) A. J. Parker and R. Alexander. J. Am. Chem. Soc. **90**, 3313 (1968).
6. I. M. Kolthoff and M. K. Chantooni, Jr. (*a*) J. Phys. Chem. **76**, 2024 (1972); (*b*) Anal. Chem. **44**, 194 (1972); (*c*) J. Am. Chem. Soc. **93**, 7104 (1971).
7. (*a*) O. Popovych, A. Gibofsky, and D. H. Berne. Anal. Chem. **44**, 811 (1972); (*b*) O. Popovych. Crit. Rev. Anal. Chem. **1**, 73 (1970).
8. C. Treiner. Can. J. Chem. **55**, 682 (1977).
9. R. A. Pierotti. J. Phys. Chem. **67**, 1840 (1963); **69**, 281 (1965).
10. J. I. Kim. J. Phys. Chem. **82**, 191 (1978).
11. P. Salomaa and M. Mattsen. Acta Chem. Scand. **25**, 361 (1971).
12. (*a*) D. H. Berne and O. Popovych. J. Chem. Eng. Data, **17**, 178 (1972); (*b*) O. Popovych and R. M. Friedman. J. Phys. Chem. **70**, 1671 (1966).
13. (*a*) R. Yamdagni and P. Kebarle. J. Am. Chem. Soc. **94**, 2940 (1972); (*b*) J. P. Roche and P. Van Huong. J. Chem. Phys. Physicochem. Biol. **67**, 211 (1970); (*c*) I. Gerzberg, V. I. Derevskaya, D. G. Traber, and I. Yu. Tseretli. Zh. Fiz. Khim. **44**, 227 (1970).
14. D. Feakins and P. J. Voice. J. Chem. Soc. Faraday Trans. I, **68**, 1390 (1972).
15. J. F. Coetzee and W. R. Sharpe. J. Soln. Chem. **1**, 77 (1972).
16. A. K. Covington and T. Dickinson (*Editors*). Physical chemistry of organic solvent systems. Plenum Press, London. 1973.
17. M. Salomon. Can. J. Chem. **54**, 1487 (1976).
18. P. J. Kruenger and H. D. Mettee. J. Mol. Spectrosc. **18**, 131 (1965); P. Buckley and P. A. Giguere. Can. J. Chem. **45**, 397 (1967).
19. E. L. Eliel. Stereochemistry of carbon compounds. McGraw-Hill, New York. 1962.
20. (*a*) J. Ugelstad and O. A. Rokstad. Acta Chem. Scand. **18**, 474 (1964); (*b*) L. L. Chan and J. Smid. J. Am. Chem. Soc. **89**, 4547 (1967); (*c*) T. E. Hogen-Esch and J. Smid. J. Am. Chem. Soc. **92**, 1955 (1970).
21. C. Pederson. J. Am. Chem. Soc. **89**, 2495 (1967).
22. O. D. Bonner and Y. S. Choi. J. Phys. Chem. **78**, 1727 (1974).
23. A. Le Narvor, E. Gentric, and P. Saumagne. Can. J. Chem. **49**, 1933 (1971).
24. V. N. Narziev and A. I. Sidorova. Vestn. Leningrad Univ. Fiz. Khim. 64 (1969); Strukt. Rol Vody Zhivom Organizme, 15 (1968).
25. L. Singurel. An Stiint Univ. 'Al I. Cuza' Iasi, Sect. Ib, **15**, 41 (1969).
26. P. A. Clarke and N. F. Hepfinger. J. Org. Chem. **35**, 3249 (1970).
27. I. S. Perelygin and N. R. Sifiullina. Tepl. Dvizhnie Mol. Mezmol Vsimodeistvie Zhidk. Rastvorakh 180 (1969).
28. E. L. Zukova. Opt. Spectrosk. **4**, 750 (1958).
29. A. M. Saum. J. Polym. Sci. **42**, 57 (1960).
30. E. Price. *In* The chemistry of nonaqueous solvents. Vol. I. *Edited by* J. J. Lagowski. Academic Press, New York. 1966. p. 67.

The thermal isomerisation of allyl isocyanide

MARSHA T. J. GLIONNA AND HUW O. PRITCHARD
Chemistry Department, York University, Downsview, Ont., Canada M3J 1P3

Received March 23, 1979

MARSHA T. J. GLIONNA and HUW O. PRITCHARD. Can. J. Chem. 57, 2482 (1979).

The thermal isomerisation of allyl isocyanide to allyl cyanide has been studied in the gas phase over the temperature range 130–200°C. The reaction is homogeneous and first order, and at high pressure (20 Torr) has an activation energy of 40.8 ± 0.6 (2sdm) kcal mol^{-1}; the corresponding range of frequency factor is $10^{14.77\pm0.30}$ s^{-1}.

MARSHA T. J. GLIONNA et HUW O. PRITCHARD. Can. J. Chem. 57, 2482 (1979).

Opérant en phase gazeuse, à des températures allant de 130 à 200°C, on a étudié l'isomérisation thermique de l'isocyanure d'allyle en cyanure d'allyle. La réaction est homogène et du premier ordre; à pression élevée (20 Torr), l'énergie d'activation est 40.8 ± 0.6 (2sdm) kcal mol^{-1} et le facteur de fréquence correspondant est $10^{14.77\pm0.30}$ s^{-1}.

[Traduit par le journal]

Introduction

In our recent exploratory study of the reactions of methylene radicals with isocyanides (1), we noticed that allyl isocyanide appeared to be somewhat less readily isomerised than were methyl or ethyl isocyanides: since this isomerisation appears to take place through the insertion of the methylene radical into the R—NC bond, followed by its elimination, this might suggest that the R—NC bond in allyl isocyanide is slightly stronger than a normal aliphatic R—NC bond. The origin of such a strengthening could be rationalised in terms of some residual conjugation between the π-electrons in the C=C and N=C bonds and if this were the case, the activation energy for isomerisation to cyanide would be expected to be larger than normal: the activation energies for isomerisation at infinite pressure for methyl and ethyl isocyanides are both 38.4 kcal mol^{-1} (2, 3) whereas for vinyl isocyanide where there is full conjugation between the two π-electron systems, the activation energy for isomerisation is estimated to be about 70 or 80 kcal mol^{-1} (4).

On the other hand, allyl isocyanide could conceivably isomerise by a head-to-tail intramolecular mechanism, which would almost certainly have a lower activation energy than normal. Consequently, it is of some interest to determine the activation energy for the thermal isomerisation of allyl isocyanide to allyl cyanide.

Experimental

Allyl isocyanide was prepared from allylamine by standard methods (1) and was purified by preparative-scale gas chromatography. Allyl cyanide, required for calibration purposes, was prepared by carrying the thermal decomposition of a sample of our allyl isocyanide to completion: a commercial sample (Aldrich) appeared to be a mixture of two isomeric substances which we were unable to resolve sufficiently well to provide an analytical standard.

Reaction was carried out in a 100 mL spherical Pyrex bulb immersed in an oil bath; reaction was initiated by admitting a (nominal) pressure of 20 Torr of allyl isocyanide vapour into the bulb, already immersed in the bath, and was terminated by removing the bulb from the bath and quenching it. Auxiliary tests using fine thermocouples inside the reaction vessel showed that the maximum uncertainty in the measured reaction time was ±3 s; this is negligible, since the reaction times ranged from 3–4 days near 130°C to 15 min near 200°C.

Reaction temperature was measured by chromel–alumel thermocouple with a Digitemp digital display: the instrument was calibrated at 0, 100, and 327°C, and its linearity in the experimental interval was checked by comparison against a mercury in glass thermometer; the precision of the temperature control during any experiment was ±0.1°C, with an absolute accuracy of ±1°C.

Analysis of the reaction products was carried out by gas chromatography using a Pennwalt 223 column at 70°C and thermal conductivity detectors: due to the tailing of the isocyanide peak, the precision of these analyses was about ±5%, and this represents the major source of uncertainty in these experiments.

Results

The cleanliness of the reaction was demonstrated by the experiment, noted above, to prepare allyl cyanide from allyl isocyanide: apart from a trace of HCN, which is typical in these isomerisations (5, 6), there was about 1% of an unidentified product of retention time intermediate between that of the isocyanide and the cyanide; we cannot tell whether this was present in the original isocyanide, or whether it was a byproduct. Also, a separate series of experiments was undertaken at 175°C to show that the calculated rate constant, which we have assumed to be first order and at its high-pressure limit, was independent of the initial pressure, the

0008-4042/79/182482-02$01.00/0

TABLE 1. The thermal isomerisation of allyl isocyanide at 18 Torr in the temperature range 128.7–201.8°C

T (K)	Time (s)	% reaction	k_∞ (s^{-1})
401.9	2.55×10^{5}	0.96	3.8×10^{-8}
404.2	3.55×10^{5}	1.76	5.0×10^{-8}
415.3	7.75×10^{4}	1.51	2.0×10^{-7}
419.4	1.53×10^{5}	5.06	3.4×10^{-7}
422.5	6.36×10^{4}	2.85	4.6×10^{-7}
431.1	2.88×10^{4}	3.11	1.1×10^{-6}
440.3	1.35×10^{4}	3.87	2.9×10^{-6}
449.9	3.74×10^{3}	3.07	8.3×10^{-6}
458.2	3.73×10^{3}	7.63	2.1×10^{-5}
467.5	1.73×10^{3}	8.60	5.2×10^{-5}
475.0	9.43×10^{2}	8.69	9.6×10^{-5}

reaction time and the surface-to-volume ratio: all the rate constants fell within a range of $\pm6\%$, with no apparent trends, as would be expected for a well behaved reaction with the analytical precision attainable.

The results of a series of experiments to determine the activation energy, all made at the same pressure (18 Torr), are shown in Table 1; assigning equal weight to each determination, the least-squares treatment yields an activation energy of 40.81 kcal mol^{-1} with a standard deviation (7) of ±0.29 kcal mol^{-1}; the corresponding range in the frequency factor is $10^{14.77\pm0.15}$ s^{-1}.

The activation energy for the isomerisation of allyl isocyanide appears to be about 2.4 ± 1 kcal mol^{-1} greater than that for the analogous isomerisation of methyl isocyanide (2, 8) or than that for ethyl isocyanide (3). This supports the supposition that there may be a small enhancement of the strength of the R—NC bond in the allyl compound, and that the alternative head-to-tail intramolecular mechanism is not important: the latter conclusion is also supported by the relatively high value we find for the frequency factor, since the head-to-tail mechanism would require a cyclic transition state, and would probably have a rather lower frequency factor on this account. A definitive determination of the mechanism of this reaction could be made by using isotopically labelled allyl isocyanide; unfortunately, suitably deuteriated allyl compounds are not readily available.

Acknowledgement

This research is supported by the National Research Council of Canada.

1. M. T. J. GLIONNA and H. O. PRITCHARD. Can. J. Chem. **57**, 1229 (1979).
2. F. W. SCHNEIDER and B. S. RABINOVITCH. J. Am. Chem. Soc. **84**, 4215 (1962).
3. K. M. MALONEY and B. S. RABINOVITCH. J. Phys. Chem. **73**, 1652 (1969).
4. J. B. MOFFAT. J. Phys. Chem. **81**, 82 (1977).
5. C. K. YIP and H. O. PRITCHARD. Can. J. Chem. **48**, 2942 (1970).
6. T. FUJIMOTO, F. M. WANG, and B. S. RABINOVITCH. Can. J. Chem. **50**, 3251 (1972).
7. N. C. BARFORD. Experimental measurements: precision, error and truth. Addison-Wesley, London. 1967. p. 62.
8. J. L. COLLISTER and H. O. PRITCHARD. Can. J. Chem. **54**, 2380 (1976).

Absolute rate constants for hydrocarbon autoxidation. 26. Rate constants for reaction of the *tert*-butylperoxy radical with 1-bromo-2-methylbutane and 1-bromo-3-methylbutane and some related substituted butanes[1]

J. A. HOWARD AND J. H. B. CHENIER

Division of Chemistry, National Research Council of Canada, Ottawa, Ont., Canada K1A 0R9

Received January 29, 1979

J. A. HOWARD and J. H. B. CHENIER. Can. J. Chem. 57, 2484 (1979).

Rate constants and Arrhenius parameters for reaction of the *tert*-butylperoxy radical with 1-bromo-2-methylbutane and 1-bromo-3-methylbutane in solution from 30–80°C have been estimated. The magnitude of these kinetic parameters are consistent with activation of the tertiary hydrogen vicinal to the bromine substituent and the involvement of a "bridged" transition state in the hydrogen atom transfer reaction.

Chloro, trimethylsilyl, and trimethylstannyl substituents also activate a vicinal tertiary hydrogen and activation increases in the order trimethylsilyl ~ trimethylstannyl < chloro < bromo.

J. A. HOWARD et J. H. B. CHENIER. Can. J. Chem. 57, 2484 (1979).

On a évalué les constantes de vitesse et les paramètres d'Arrhénius de la réaction du radical *tert*-butylpéroxy avec les bromo-1 méthyl-2 et bromo-1 méthyl-3 butanes en solution à des températures allant de 30 à 80°C. L'ordre de grandeur de ces paramètres cinétiques est en accord avec une activation de l'hydrogène tertiaire vicinal par rapport au brome et une implication d'un état de transition "ponté" dans la réaction de transfert de l'atome d'hydrogène.

Des substituants chloro, triméthylsilyle et triméthylstannyle activent aussi un hydrogène tertiaire vicinal et l'activation augmente dans l'ordre triméthylsilyle ~ triméthylstannyle < chloro < bromo.

[Traduit par le journal]

Introduction

Several papers have appeared recently in support of the concept that rates of hydrogen atom abstraction by free-radicals ($Y^{\cdot}$) are enhanced by certain substituents (X) attached to the β-carbon of the substrate (reaction [1]) (for reviews dealing with anchimeric assistance, see ref. 1).

$$[1]\quad -\overset{|}{C}H—CH_2X + Y^{\cdot} \rightarrow -\overset{|}{\underset{\cdot}{C}}—CH_2X + YH$$

where Y is, for example, Br$^{\cdot}$ and t-$BuO_2^{\cdot}$ and X is Cl, Br, and I.

Thus Wagner and Sedon (2) have shown that δ-bromo and -iodo groups enhance the rate of triplet state γ-hydrogen abstraction during photolysis of δ-halovalerophenones while Everly, Schweinsberg, and Traynham (3) have concluded that a β-chloro substituent assists removal of a tertiary hydrogen by the bromine atom. Furthermore we have reported (4) that the tertiary hydrogen in 1-bromo-2-methylbutane is 2.6 times more reactive to the *tert*-butylperoxy radical at 30°C than the tertiary hydrogen in 3-methylpentane.

These enhanced rates have generally been rationalized in terms of an interaction between the neighbouring substituent and the reactive centre in the form of a bridged transition state.

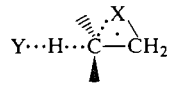

I

The involvement of a bridged species such as **I** should be reflected in a decrease in both the enthalpy and entropy of activation for reaction because the bridged radical will have more resonance stabilization energy than the unbridged radical while the probability of forming **I** must be less than the probability of forming a transition state without bridging (5, 6). Unfortunately most of the work on anchimeric assistance by β-substituents has been performed at one temperature and the relation between rate enhancement and the activation parameters has not been generally established. Skell and co-workers (5, 6) have, however, reported that the enthalpy and entropy of activation for removal of a secondary hydrogen β to the bromo substituent in 1-bromobutane are ~3 kcal mol^{-1} and ~6 cal deg^{-1} mol^{-1} smaller than the corresponding parameters for removal of a secondary hydrogen from propane.

[1]NRCC No. 17535.

0008-4042/79/182484-07$01.00/0

Moreover, Cain and Solly (7) found that the activation energy for thermal ring opening of 1-bromomethyl-4-chlorobicyclo[2.2.0]hexane is 2.9 kcal mol^{-1} smaller than it is for 1-ethyl-4-chlorobicyclo [2.2.0]hexane although in this case the pre-exponential factors were identical within experimental error.

In the present paper we report a full kinetic and product study of the autoxidation of 1-bromo-2-methylbutane and its co-oxidation with 3-methylpentane, both reactions being performed in the presence of *tert*-butyl hydroperoxide. This work enables us to report kinetic parameters for abstraction of the tertiary hydrogen atom from 1-bromo-2-methylbutane by the *tert*-butylperoxy radical. These parameters will of course be influenced by deactivation by inductive electron withdrawal by the bromo substituent as well as activation by anchimeric assistance. Separation of these two effects has been achieved by comparing kinetic parameters for reaction of 1-bromo-2-methylbutane and 1-bromo-3-methylbutane with $t\text{-}BuO_2^{\bullet}$.

In addition we have investigated the effect of vicinal chloro, trimethylsilyl, and trimethylstannyl substituents on the rate of H-atom transfer to the *tert*-butylperoxy radical because β-chloro, β-trialkylsilyl, and β-trialkylstannyl-alkyl radicals are known to have a preferred conformation in which the heteroatom is eclipsed by the *p* orbital of the radical centre (8).

Experimental

Materials

1-Bromo-2-methylbutane (Chemical Procurement Labs. Inc.), *1-bromo-4-methylpentane* (Chemical Samples Co.), and *1-bromo-3-methylbutane* (Eastman) were purified by preparative gas chromatography to >99.9% *1-Chloro-2-methylbutane* and *1-chloro-3-methylbutane* (Chemical Samples Co.) were purified by distillation and were passed down a column of basic alumina before use.

2-Methyl-1-trimethylsilylbutane. 1-Bromo-2-methylbutane (61.1 g, 0.4 mol) in dry tetrahydrofuran (125 mL) was added dropwise with stirring to magnesium turnings (9.83 g) in dry THF (50 mL). After addition of the alkyl bromide the mixture was stirred and refluxed under argon for 1 h. Chlorotrimethylsilane (12.5 g, 0.4 mol) in dry THF (100 mL) was added dropwise and the reaction mixture was stirred for a further 16 h. Excess Grignard reagent was destroyed by the addition of water and dilute HCl was added until two layers were formed. The THF layer was washed three times with equal volumes of water and dried over anhydrous sodium sulphate. Distillation gave 15 g of 2-methyl-1-trimethylsilylbutane, bp 131–133°C.

2-Methyl-1-trimethylstannylbutane was prepared from 1-bromo-2-methylbutane and chlorotrimethylstannane by the method used for 2-methyl-1-trimethylsilylbutane.

1-Bromo-2-methylbutan-2-ol, *1-bromo-3-methylbutan-2-ol*, *1-chloro-2-methylbutan-2-ol*, and *1-chloro-3-methylbutan-2-ol* were prepared from 2-methylbut-1-ene and 3-methylbut-1-ene by the method of Suter and Zook (9).

Addition of the hypohalous acid to 2-methylbut-1-ene gave the expected 1-halo-2-methylbutan-2-ol whereas addition of hypobromous acid to 3-methylbut-1-ene gave 1-bromo-3-methylbutan-2-ol, 2-bromo-3-methylbutan-1-ol, and 1,2-dibromo-3-methylbutane and addition of hypochlorous acid to 3-methylbut-1-ene gave 1-chloro-3-methylbutan-2-ol and 2-chloro-3-methylbutan-1-ol. These products were separated by preparative gas chromatography and identified by mass spectrometry.

1,2-Dibromo-2-methylbutane and *1,2-dibromo-3-methylbutane* were prepared by reaction of molecular bromine with 2-methylbut-1-ene and 3-methylbut-1-ene.

Kinetic Procedure

Rate constants for reaction of the substituted butanes with the *tert*-butylperoxy radical were obtained either by the *direct* method which involved measuring substrate oxidizability in the presence of *tert*-butyl hydroperoxide (0.5–2 *M*) and 2,6-di-*tert*-butyl-4-methylphenol ($\sim 2 \times 10^{-4}$ *M*) or by the *indirect* method whereby relative reactivities were determined from competitive autoxidations in the presence of *tert*-butyl hydroperoxide using 3-methylpentane as the reference compound. More detailed experimental details for these two methods are given in previous publications in this series (10, 11).

Product Analysis

Oxidized samples were quantitatively reduced with a slight excess of triphenylphosphine and the products were analysed after distillation by gas chromatography employing a Varian 2800 chromatograph equipped with 12 ft × 1/8 in. OV-101 and FFAP on chromosorb W (60–80 mesh) columns and thermal conductivity and flame ionization detectors.

Alcohols were identified and their absolute and relative yields determined by comparing gas chromatographic retention times and integrated areas with those of authentic standard samples. When samples of the alcohols were not commercially available or readily synthesized they were separated from the reaction mixture by gas chromatography and identified by mass spectrometry. For example, the mass spectrum of 1-bromo-3-methylbutan-3-ol contained the following fragments with *m/e* values in order of decreasing intensity 59 ($m - CH_2CH_2Br$), 151 ($m - CH_3$), 153 ($m - CH_3$), 107 ($m - (CH_3)_2COH$), 109 ($m - (CH_3)_2COH$).

Results

1-Bromo-2-methylbutane (1)

1-Bromo-2-methylbutane (8.08 *M*) containing α,α′-azo-bisisobutyronitrile (0.18 *M*) absorbed oxygen slowly at 30°C and 720 Torr of oxygen and the kinetic chain length was ~3. The overall rate of autoxidation was 1.2 times faster at 100 Torr of oxygen suggesting the involvement of bromine atoms, produced by β-scission of 1-bromo-2-methylbutyl radicals (reaction [2]), in rate controlling propagation reactions (reaction [3]).

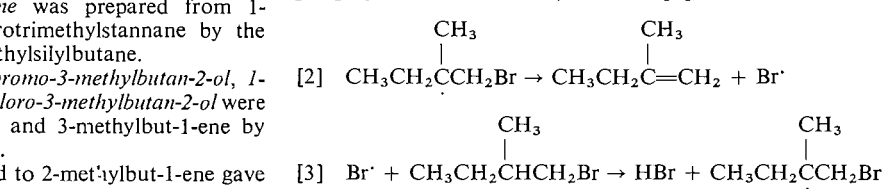

TABLE 1. Kinetic data for autoxidation of 1-bromo-2-methylbutane (**1**) in the presence of *tert*-butyl hydroperoxide at 30°C[a]

[**1**] (M)	[*t*-BuOOH][b] (M)	$10^7 R_i$[c] ($M\,s^{-1}$)	$10^7(-d[O_2]/dt)_{obs}$ ($M\,s^{-1}$)	$10^7(-d[O_2]/dt)_{corr}$ ($M\,s^{-1}$)	$10^4(k_p^1/(2k_t)^{1/2})$[d] ($M^{-1/2}\,s^{-1/2}$)
8.08	—	0.19	0.6	0.6	0.54
7.3	1.0	1.13	12.6	15.5	6.3
6.46	2.0	1.33	8.7	12.2	5.2
6.7	2.0	16	11.0	52.6	6.2
7.3	1.0	0.17	4.9	5.3	5.6
3.24[e]	1.0	0.155	1.95	2.36	5.8

[a]All runs were performed in the presence of α,α′-azobisisobutyronitrile (0.18 M) and 2,6-di-*tert*-butyl-4-methoxyphenol (1×10^{-4} to 1×10^{-3} M).
[b]Total hydroperoxide concentration.
[c]Rate of free-radical chain initiation.
[d]Calculated from the rate expression $(-d[O_2]/dt)_{corr} = k_p^1[1]R_i^{1/2}/(2k_t)^{1/2}$.
[e]Solvent: *tert*-butylbenzene.

The kinetic chain length was about 10 times longer in the presence of *tert*-butyl hydroperoxide (0.5–2 M) and $-d[O_2]/dt$ was independent of the oxygen pressure. This means that although β-scission still occurred the accelerating effect bromine atoms had on the rate of propagation was eliminated by chain transfer with the hydroperoxide (12).

[4] $Br^{\cdot} + (CH_3)_3COOH \rightarrow HBr + (CH_3)_3COO^{\cdot}$

Kinetic data for autoxidation of 1-bromo-2-methylbutane are presented in Table 1 and the average oxidizability in the presence of *tert*-butyl hydroperoxide, $k_p^1/(2k_t)^{1/2}$, is $5.8 \pm 0.4 \times 10^{-4}$ $M^{-1/2}\,s^{-1/2}$ where k_p^1 is the *overall* rate constant for reaction of *t*-$BuO_2^{\cdot}$ with **1** and $2k_t$ is the termination rate constant for *t*-$BuO_2^{\cdot}$. The experimental value of $2k_t$ in this system was 1.4×10^3 $M^{-1}\,s^{-1}$ which is equal, within experimental error, to our best value of 1.2×10^3 $M^{-1}\,s^{-1}$ (13) indicating that *t*-$BuO_2^{\cdot}$ were the only radicals involved in rate controlling propagation and termination reactions. From the rate constant ratio $k_p^1/(2k_t)^{1/2}$, k_p^1 can be calculated to be $5.8 \times 10^{-4} \times (1.2 \times 10^3)^{1/2} = 0.02 \pm 0.002$ $M^{-1}\,s^{-1}$.

Product analyses established that >90% of the oxygen absorbed by 1-bromo-2-methylbutane gave 1-bromo-2-hydroperoxy-2-methylbutane. Interestingly 1,2-dibromo-2-methylbutane was formed in low yield and it probably arose by bromination of 2-methylbut-1-ene, formed in [2], with molecular bromine produced by reduction of the bromine atom formed in [2] to HBr followed by oxidation with excess *t*-BuOOH.

The high yield of products derived from abstraction of the tertiary hydrogen implies that the overall propagation rate constant should be equivalent to the rate constant for abstraction of the tertiary hydrogen

$$[5]\quad (CH_3)_3COO^{\cdot} + CH_3CH_2\overset{CH_3}{\overset{|}{C}}HCH_2Br \xrightarrow{k_p^1} (CH_3)_3COOH + CH_3CH_2\overset{CH_3}{\overset{|}{C}}CH_2Br$$

There was no evidence for the formation of secondary alcohols from **1** almost certainly because of deactivation of the secondary C—H bonds on C-1 and C-3 by the bromine substituent.

Co-oxidation of **1** (3.23 M) and 3-methylpentane (3.85 M) gave $k_p/(2k_t)^{1/2} = 2.9 \times 10^{-4}$ $M^{-1/2}\,s^{-1/2}$ where $k_p = ak_p^1 + bk_p^{ref}$(overall) and a and b are the mole fractions of **1** and 3-methylpentane and k_p^{ref}(overall) is the overall reactivity of 3-methylpentane to the *tert*-butylperoxy radical. Since k_p^{ref}(overall) = 0.008 $M^{-1}\,s^{-1}$ (11) $k_p^1 = 0.012$ $M^{-1}\,s^{-1}$. Oxygen (0.073 M) was absorbed to give 1-bromo-2-methylbutan-2-ol (0.041 M) and 3-methylpentan-3-ol (0.036 M) as the major reaction products indicating that k_p^1 (per *t*-C—H) = $1.35 \times 0.007 = 0.0094$ $M^{-1}\,s^{-1}$. Repetitive experiments at 30°C suggested that the tertiary hydrogen in **1** is 1.32 ± 0.16 times more reactive than the tertiary hydrogen in 3-methylpentane and k_p^1 (per *t*-C—H) = 0.009 ± 0.001 $M^{-1}\,s^{-1}$.

The value of k_p^1 obtained from these co-oxidation experiments is a factor of 2 smaller than the directly determined value from the autoxidation of **1** which is well outside our usual experimental error. At the present time we are inclined to favour the lower value because the errors involved in measuring $k_p/(2k_t)^{1/2}$ are greater than those involved in measuring ratios of alcohols.[2]

[2]We have previously reported a rate constant for reaction of *t*-$BuO_2^{\cdot}$ with 1-bromo-2-methylpropane at 30°C of 0.017_5 $M^{-1}\,s^{-1}$ determined by the direct method (12). Application of the co-oxidation method to this substrate gave the somewhat lower value of 0.013 $M^{-1}\,s^{-1}$. Interestingly the *t*-C—H

TABLE 2. Relative yields of 1-bromo-2-methylbutan-2-ol and 3-methylpentan-3-ol produced by co-oxidation of 1-bromo-2-methylbutane (**1**) and 3-methylpentane in the presence of *tert*-butyl hydroperoxide

Temperature (°C)	$[C_6H_{14}]_0$ (*M*)	$[\mathbf{1}]_0$ (*M*)	p_{O_2} (atm)	$[(CH_3)_3COOH]$ (*M*)	$[C_5H_{11}BrO]^a$ (*M*)	$[C_6H_{14}O]^b$ (*M*)	k_p^1/k_p^{ref}
30	4.4	2.65	13	1	0.022	0.0235	1.55
30	3.08	3.24	1	2	0.11	0.1	1.1
30	3.09	3.24	1	2	0.16	0.12	1.3
30	3.85	3.23	1	1	0.041	0.036	1.35
30	3.85	3.23	100	1	0.032	0.029	1.3
50	2.31	4.86	5	1	0.069	0.03	1.1
50	4.63	2.42	5	1	0.03	0.053	1.1
80	3.41	3.6	100	1	0.11	0.094	1.12
80	4.63	2.42	5	1	0.022	0.046	0.92
80	2.31	4.86	5	1	0.050	0.022	1.08
80	4.63	2.42	5	1	0.13	0.2	1.24
80	4.63	2.42	5	1	0.15	0.31	0.92

[a] 1-Bromo-2-methylbutan-2-ol.
[b] 3-Methylpentan-3-ol.

Co-oxidations of **1** and 3-methylpentane in the presence of *t*-BuOOH were performed from 30 to 80°C and the results are presented in Table 2. A least-squares treatment of the relative reactivities of these two substrates over this temperature range yielded the Arrhenius equation

$$\log (k_p^1/k_p^{ref}) = (-0.56 \pm 0.21) + (0.93 \pm 0.3)/\theta$$

where $\theta = 2.303RT$ kcal mol^{-1} and $k_p^{ref} = k_p$ (per *t*-C—H) for 3-methylpentane. This implies $\Delta S^{\ddagger}(ref) - \Delta S^{1\ddagger} \sim 2$ cal deg^{-1} mol^{-1} and $E_p^{ref} - E_p^1 \sim 900$ cal mol^{-1}, i.e., both the entropy and energy of activation are negative relative to the values for 3-methylpentane.

Incidentally the relative reactivity of 1-bromo-2-methylbutane and 3-methylpentane did not change when the oxygen pressure was increased from 1 to 100 atm. Relative reactivities of these substrates are, therefore, not influenced by reversal of the rate controlling propagation reaction (14).

1-Bromo-3-methylbutane, **2**, absorbed oxygen about 4 times slower than 1-bromo-2-methylbutane in the presence of *t*-BuOOH at 30°C. The oxidizability of **2**, $k_p^2/(2k_t)^{1/2}$, was 1.4×10^{-4} $M^{-1/2}$ s$^{-1/2}$ suggesting that k_p^2(overall) = 0.0048 M^{-1} s^{-1}. The principal reaction products, after reduction, were 1-bromo-3-methylbutan-3-ol and 1,2-dibromo-3-methylbutane, which were identified by their mass spectra. The relative concentration of these two products, [1-bromo-3-methylbutan-3-ol]/[1,2-dibromo-3-methylbutane] was ~15. There was also a low yield of 1-bromo-3-methylbutan-2-ol and at least 5 other products in very low yields with gas chromatographic retention times close to those for the major reaction products.

Production of 1,2-dibromo-3-methylbutane indicates abstraction of a secondary hydrogen from C-2 by the *tert*-butylperoxy radical followed by β-scission of the 1-bromo-3-methyl-2-butyl radical (reactions [6] and [7]).

[6] $t\text{-BuO}_2\cdot + (CH_3)_2CHCH_2CH_2Br \rightarrow t\text{-BuO}_2H + (CH_3)_2C\dot{C}HCH_2Br$

[7] $(CH_3)_2C\dot{C}HCH_2Br \rightarrow (CH_3)_2CHCH{=}CH_2 + Br\cdot$

Molecular bromine is evidently formed by autoxidation of **2** because reaction mixtures were usually yellowish-brown and became colorless immediately upon addition of $(C_6H_5)_3P$.

The rate of autoxidation of a mixture of **2** (4.95 *M*) and 3-methylpentane (2.15 *M*) in the presence of *t*-BuOOH (1 *M*) and the free radical initiator 2,2,3,3-tetraphenylbutane (0.0046 *M*) at 30°C gave $k_p/(2k_t)^{1/2} = 1.7 \times 10^{-4}$ $M^{-1/2}$ s$^{-1/2}$, a value consistent with the individual oxidizability of the substrates and their mole fraction. Oxygen (0.11 *M*) was absorbed in 10 days and the major reaction products were 3-methylpentan-3-ol (0.024 *M*), 3-methylpentan-2-ol (0.003 *M*), 1-bromo-3-methylbutan-3-ol (0.0085 *M*), and 1,2-dibromo-3-methylbutane (0.00064 *M*) to give a product yield of only 32% based on the oxygen absorbed. This extremely low yield of oxidation products is somewhat disturbing since we usually obtain yields in excess of 90% from most oxidations. There were, however, no major reaction products to account for this discrepancy.

bond in 1-bromo-2-methylpropane is ca. 1.4 times more reactive than the *t*-C—H bond in 1-bromo-2-methylbutane, perhaps because of a higher percentage of the rotomer with the substituent eclipsing the developing unoccupied orbital, i.e., the least favoured conformation.

TABLE 3. Product and kinetic data for co-oxidation of 1-bromo-3-methylbutane **2** and 3-methylpentane in the presence of *tert*-butyl hydroperoxide (1 *M*)

Temperature (°C)	$[C_6H_{14}]_0$ (*M*)	[**2**] (*M*)	p_{O_2} (atm)	$\frac{[C_5H_{11}BrO]^a}{[C_6H_{14}O]}$	$10^3k_p^2$(*t*-C—H) $(M^{-1}\ s^{-1})^b$
30	2.3	4.79	1	0.25	0.90
30	3.47	3.6	1	0.11	
30	2.15	4.95	1	0.35	
50	2.3	4.79	5	0.32	4.9
50	3.47	3.6	5	0.19	
80	2.3	4.79	5	0.35	56
80	3.47	3.6	5	0.25	
80	1.54	5.6	100	0.89	

[a][1-Bromo-3-methylbutan-3-ol]/[3-methylpentan-3-ol].
[b]Relative to $k_p^{ref} = 0.007\ M^{-1}\ s^{-1}$ at 30°C, 0.03 $M^{-1}\ s^{-1}$ at 50°C, and 0.26 $M^{-1}\ s^{-1}$ at 80°C (11).

TABLE 4. Rate constants for reaction of some substituted methylbutanes with the *tert*-butylperoxy radical at 30°C

Substrate	$10^4k_p/(2k_t)^{1/2}$ [a] $(M^{-1/2}\ s^{-1/2})$	10^3k_p[b] $(M^{-1}\ s^{-1})$	10^3k_p(*t*-C—H)[c] $(M^{-1}\ s^{-1})$
$CH_3CH_2CH(CH_3)CH_2Cl$	1.5	5.4	3.5
$(CH_3)_2CHCH_2CH_2Cl$	—	—	3.0
$CH_3CH_2CH(CH_3)CH_2Si(CH_3)_3$	6.75	23	22
$CH_3CH_2CH(CH_3)CH_2Sn(CH_3)_3$	6.1	22	—

[a]Oxidizability in the presence of *tert*-butyl hydroperoxide.
[b]Overall reactivity to *t*-BuO_2.
[c]Reactivity of the tertiary hydrogen relative to the tertiary hydrogen in 3-methylpentane.

If the concentrations of 1-bromo-3-methylbutan-3-ol, 1,2-dibromo-3-methylbutane, and 1-bromo-3-methylbutane-2-ol are used to calculate rate constants for **2**, we find that k_p^2(per *t*-C—H) = 0.001 $M^{-1}\ s^{-1}$ and k_p^2(per *s*-C—H on C-2) $\simeq 4 \times 10^{-5}$ $M^{-1}\ s^{-1}$ and k_p(overall) determined directly is 3 times larger than k_p^2 per (*t*-C—H) + $2k_p^2$(per *s*-C—H on C-2).

The results of co-oxidations of **2** and 3-methylpentane at various temperatures are gathered in Table 3 and yielded the following Arrhenius equation for the relative reactivities of the tertiary hydrogens of these substrates.

$$\log k_p^2(\text{per } t\text{-C—H})/k_p^{ref} = (0.75 \pm 0.4) - (2.3 \pm 0.6)/\theta$$

This equation implies that $\Delta S(\text{ref})^{\ddagger} - \Delta S_4^{\ddagger} \sim -3.5$ cal deg^{-1} mol^{-1} and $E_p^{ref} - E_p^2 \sim -2.3$ kcal mol^{-1}.

1-Chloro-2-methylbutane **3** and *1-chloro-3-methylbutane* **4** undergo autoxidation to give, after reduction, mainly 1-chloro-2-methylbutan-2-ol and 1-chloro-3-methylbutan-3-ol, respectively. Kinetic data obtained by the direct and indirect methods for **3** and **4** are summarized in Table 4.

2-Methyl-1-trimethylsilylbutane (5) and 2-Methyl-1-trimethylstannylbutane (6). Both these compounds in the presence of *t*-BuOOH absorb oxygen about 3 times faster than 3-methylpentane and $k_p^5/(2k_t)^{1/2} = 6.75 \times 10^{-4}\ M^{-1/2}\ s^{-1/2}$ and $k_p^6/(2k_t)^{1/2} = 6.1 \times 10^{-4}\ M^{-1/2}\ s^{-1/2}$ giving $k_p^5 = 0.023\ M^{-1}\ s^{-1}$ and $k_p^6 = 0.021\ M^{-1}\ s^{-1}$. 2-Methyl-1-trimethylsilylbutane is oxidized almost exclusively to 2-methyl-1-trimethylsilylbutan-2-ol and the indirect method gave $k_p^5 = 0.022\ M^{-1}\ s^{-1}$. We were unable to show that 2-methyl-1-trimethylstannylbutan-2-ol was the principal reaction product formed by oxidation of **6** and we could not confirm the value of k_p^6 by the indirect method. There is a slow reaction between **6** and *t*-BuOOH which probably accounts for the difficulties that we experienced in analyzing for the oxidation products of this compound.

Discussion

It is a little disturbing that the rate constants for reaction of *t*-$BuO_2^{\bullet}$ with 1-bromo-2-methylbutane and 1-bromo-3-methylbutane obtained directly and indirectly differ by as much as a factor of 3 whereas these two methods gave identical results for 3-methylpentane (11) and a variety of aralkanes (14). Since part of the aim of this work was to investigate the influence of a β-bromo substituent on absolute

reactivity towards t-$BuO_2^{\cdot}$ we have concluded that the *lower* rate constants obtained by the indirect method are more accurate than the directly determined values. There is some justification for this conclusion in that the errors involved in estimating relative rate constants by the direct method are greater than those involved in the indirect method.

With this limitation in mind, a tertiary hydrogen β to a bromine substituent is ~10 times more reactive than a tertiary hydrogen γ to this substituent ($k_p^1/k_p^2 = 0.009/0.0009$) whereas it would be less reactive if the substituent performs only in a deactivating capacity. The reactivity of a β position in the absence of anchimeric assistance relative to the tertiary position in 3-methylpentane can be estimated to be 0.03–0.07 from the rate constant for abstraction of the tertiary hydrogen from 1-bromo-4-methylpentane by t-$BuO_2^{\cdot}$ at 30°C (0.0017 M^{-1} s^{-1}) using the arguments of Shea, Lewis, and Skell (6). The magnitude of the anchimeric effect is, therefore, at least 30 if we consider that bridging can only occur for the radical derived from the thermodynamically least favoured rotomer.

A comparison of the activation parameters for 1-bromo-2-methylbutane and 1-bromo-3-methylbutane relative to those for 3-methylpentane reveals that the activation energy for 1-bromo-2-methylbutane is ~3 kcal mol^{-1} lower than activation energy for 1-bromo-3-methylbutane and $\Delta S^{2\ddagger} - \Delta S^{1\ddagger} =$ 4–5 cal deg^{-1} mol^{-1}. These parameters are quite consistent with the intermediacy of a "bridged" 1-bromo-2-methyl-2-butyl radical and a normal 1-bromo-3-methyl-3-butyl radical in the H-atom transfer reaction to a peroxy radical.

Deactivation by a β-chloro substituent overshadows activation by anchimeric assistance because the t-C—H in 1-chloro-2-methylbutane is ~0.5 times as reactive as the t-C—H in 3-methylpentane. There must, however, be activation by anchimeric assistance because the t-C—H in 1-chloro-2-methylbutane is slightly more reactive than the t-C—H in 1-chloro-3-methylbutane.

The secondary hydrogens on C-2 of 1-bromo-3-methylbutane are of course β to the bromo substituent and they will be deactivated by inductive electron withdrawal and may be activated by anchimeric assistance. We have previously estimated a rate constant for reaction of the secondary hydrogen on C-3 of 2-methylpentane = 1×10^{-4} M^{-1} s^{-1} (11) which, when compared with a value of 4×10^{-5} M^{-1} s^{-1} for **2** indicates that activation of a secondary hydrogen by a β-bromo substituent is overshadowed by deactivation.

The kinetic data reported in this paper suggest that the peroxy radical shows much less preference than the bromine atom for a tertiary position vicinal to bromo and chloro substituents. Thus a β-bromo substituent enhances the rate of abstraction of a tertiary hydrogen by the bromine atom by a factor of 8–27 at 30°C (6) whereas the rate enhancement for a peroxy radical is only 1.35 at this temperature. In addition a s-C—H bond β to a bromo substituent and a t-C—H bond β to a chloro substituent exhibit enhanced reactivity to Br· whereas these bonds are less reactive than the corresponding bonds in an alkane to $RO_2^{\cdot}$.

We have previously concluded that Br· and $RO_2^{\cdot}$ have approximately the same selectivity to aliphatic s-C—H and t-C—H bonds whereas rates of abstraction of benzylic hydrogens by Br· are more sensitive to meta and para electron donating and withdrawing substituents than the rates of reaction of the *tert*-butylperoxy radical with ring substituted toluenes (15). This latter difference has been attributed to the greater electron affinity of Br·. Similar polar effects can perhaps be invoked to explain the selectivity difference between $RO_2^{\cdot}$ and Br· towards C—H bonds vicinal to bromo and chloro substituents in alkanes.

In conclusion, trimethylsilyl and less unambiguously trimethylstannyl substituents activate vicinal tertiary hydrogens and these groups in an *overall* sense are more effective than bromine. Trimethylsilyl does not deactivate a vicinal hydrogen by inductive electron withdrawal and it can tentatively be concluded that bromine and almost certainly chlorine are better bridging groups than trimethylsilyl and trimethylstannyl.

1. (*a*) P. S. Skell. Chem. Soc. Spec. Publ. No. 19, 131 (1964); (*b*) P. S. Skell and K. J. Shea. Israel J. Chem. **10**, 493 (1972); (*c*) P. S. Skell and K. J. Shea. *In* Free radicals. Vol. 2. *Edited by* J. K. Kochi. Wiley, New York, NY. 1973. Chapt. 26; (*d*) W. A. Thaler. Methods Free-Radical Chem. **2**, 166 (1966); (*e*) L. Kaplan. Bridged free radicals. Dekker, New York, NY. 1972. Chapt. 6.
2. P. J. Wagner and J. H. Sedon. Tetrahedron Lett. 1927 (1978).
3. C. R. Everly, F. Schweinsberg, and J. G. Traynham. J. Am. Chem. Soc. **100**, 1200 (1978).
4. J. A. Howard. Proc. 278th Colloqu. International (C.N.R.S.) 467 (1978).
5. P. S. Skell and K. J. Shea. J. Am. Chem. Soc. **94**, 6550 (1972).
6. K. J. Shea, D. C. Lewis, and P. S. Skell. J. Am. Chem. Soc. **95**, 7768 (1973).
7. E. N. Cain and R. K. Solly. J. Chem. Soc. Chem. Commun. 148 (1974).
8. J. K. Kochi. Adv. Free Radical Chem. **5**, 189 (1975).
9. C. M. Suter and H. D. Zook. J. Am. Chem. Soc. **66**, 738 (1944).

10. J. H. B. CHENIER, S. B. TONG, and J. A. HOWARD. Can. J. Chem. **56**, 3047 (1978).
11. J. A. HOWARD, J. H. B. CHENIER, and D. A. HOLDEN. Can. J. Chem. **56**, 170 (1978) and previous papers in this series.
12. J. H. B. CHENIER, J. P.-A. TREMBLAY, and J. A. HOWARD. J. Am. Chem. Soc. **97**, 1618 (1975).
13. S. KORCEK, J. H. B. CHENIER, J. A. HOWARD, and K. U. INGOLD. Can. J. Chem. **50**, 2285 (1972).
14. J. A. HOWARD and S. B. TONG. Unpublished results.
15. J. A. HOWARD and J. H. B. CHENIER. J. Am. Chem. Soc. **95**, 3054 (1973).

Ab initio configuration interaction study of the $A^2A_1-{}^2B_1$ transition of PH_2 and PD_2

MILJENKO PERIC

Institut za Fizicku Hemiju, Prirodno-Matematickog Fakulteta, 11000 Beograd, Yugoslavia

ROBERT J. BUENKER

Lehrstuhl für Theoretische Chemie, Gesamthochschule Wuppertal, Gaußstraße 20, D-5600 Wuppertal 1, Germany

AND

SIGRID D. PEYERIMHOFF

Lehrstuhl für Theoretische Chemie, Universität Bonn, Wegelerstraße 12, D-5300 Bonn 1, Germany

Received February 5, 1979

MILJENKO PERIC, ROBERT J. BUENKER, and SIGRID D. PEYERIMHOFF. Can. J. Chem. **57**, 2491 (1979).

The potential surfaces for the X^2B_1 and A^2A_1 states of PH_2 are calculated by means of an *ab initio* CI method. These results are then used to obtain vibrational levels and wavefunctions for each electronic state in both PH_2 and PD_2, whereby a two-dimensional treatment of the associated bending modes is carried out; the resulting vibrational frequencies are found to agree with the corresponding experimental findings (where available) to within 25 cm^{-1} in each case. The discrepancy in the calculated 0–0 transition energy is 0.06 eV and the variation in $\Delta G_{v_2'+1/2}$ values parallels quite closely that obtained experimentally. Finally the electronic transition moment is calculated as a function of the internuclear angle and this information is combined with the above vibrational wavefunctions to describe the intensity distribution in this electronic system; a maximum intensity is obtained for $v_2' = 4$ in the bending mode for PH_2, in agreement with the observed findings, and is predicted to occur for $v_2' = 6$ in PD_2.

MILJENKO PERIC, ROBERT J. BUENKER et SIGRID D. PEYERMIHOFF. Can. J. Chem. **57**, 2491 (1979).

Faisant appel à une méthode CI *ab initio*, on a calculé les surfaces de potentiel des états X^2B_1 et A^2A_1 de PH_2. On a alors utilisé ces résultats dans le but obtenir les niveaux vibrationnels et les fonctions d'onde de chaque état électronique de PH_2 et PD_2 alors que l'on a effectué un traitement bi-dimentionnel des modes de vibrations associés; on note que les fréquences de vibration qui en résultent sont en bon accord avec les valeurs expérimentales correspondantes (lorsqu'elles sont disponibles) à 25 cm^{-1} dans chaque cas. La différence avec l'énergie de transition 0–0 calculée est de 0.06 eV et la variation dans les valeurs de $\Delta G_{v_2'+1/2}$ sont parallèlles à celles obtenues expérimentalement. Enfin on a calculé le moment de la transition électronique en fonction de l'angle internucléaire et on combine cette information avec les fonctions d'onde décrites plus haut afin de décrire la distribution d'intensité de ce systeme électronique; on obtient un maximum d'intensité pour $v_2' = 4$ dans le mode de déformation de PH_2 ce qui est en accord avec les valeurs observées; on prédit que ce maximum sera associé au $v_2' = 6$ dans le cas de PD_2.

[Traduit par le journal]

Introduction

The absorption spectrum of the free radical PH_2 was first observed by Ramsay (1) during flash photolysis of phosphine. It consists of a long progression of bands with complicated fine structure (eleven peaks have been found for PH_2 in the 3600–5500 Å region and 13 have been seen in the same energy range for PD_2) and the main features are attributed to excitation of successive quanta of the bending vibration v_2' of the upper state. Further studies (2) found that the solid state spectrum taken at 4.2 K corresponds closely to the spectrum in the gas phase and that the emission spectrum obtained from electrical discharges in PH_3 and PD_3 (3, 4) also shows the same pattern, whereby several progressions $(0v_2'0)$–$(0v_2''0)$ with $v_2' = 0$–5 and $v_2'' = 0$–9 could be identified.

In analogy to the situation in NH_2 (5, 6) the ground state electronic configuration of PH_2 is assigned as $^2B_1$, while the first excited state is taken to be of $^2A_1$ symmetry. Nevertheless, there is a major difference between the two radicals NH_2 and PH_2 since investigations (5, 7) of NH_2 clearly indicate a quasi-linear excited state conformation for NH_2, while the early experimental results (8, 9) for PH_2 already spoke in favor of a decidedly bent upper species.

A number of rotational analyses for the $(0v_2'0$–

0008-4042/79/182491-07$01.00/0

000) bands with v_2' running from 1 to 8 in the absorption spectrum (10, 11) and for the (000–020) and (000–030) bands of PH_2 in emission (12) have led to accurate predictions of various molecular constants; an internuclear angle of 91°40′ has been deduced in this manner for the $^2B_1$ electronic ground state and an opening of the internuclear angle upon excitation to 123° 4′ has also been extracted therefrom. Similar to the situation in NH_2 (7) numerous rotational perturbations are found in the excited state levels and it has been concluded (11) that these perturbations are caused by high vibrational levels of the ground state, since no other electronically excited PH_2 states are found below the A^2A_1 species.

Various new and refined experimental techniques (13–15) have been employed recently for the further study of the PH_2 free radical, whereby the greater emphasis was placed on its electronic ground state. Zittel and Lineberger (15) have observed a small peak in the photoelectron spectrum of PH_2^- at approximately 2270 ± 80 cm^{-1} relative to the (000) level of the ground state and have assigned this feature to the (100–000) transition, although they point out that this energy is similar to twice the PH_2 bending frequency ($\bar{\nu}_2' = 1102$ cm^{-1}). To our knowledge there are no experimental results available which allow a determination of the other vibrational frequencies $\bar{\nu}_3$ in PH_2 or $\bar{\nu}_1$ and $\bar{\nu}_3$ in PD_2.

In contrast to the numerous experimental investigations very few theoretical studies are available for this system; the most recent thereof is an *ab initio* SCF calculation (16) for the ground state of PH_2, but no *ab initio* treatment of the excited PH_2 states has appeared to our knowledge thus far. Hence it is the goal of the present paper to treat the PH_2 molecule in its X^2B_1 and $^2A_1$ excited states in a similar manner as has been undertaken recently for the related NH_2 molecule (17), whereby particular emphasis will be placed on the calculation of the vibrational features of the A^2A_1–X^2B_1 transition.

Technical Details of the Treatment

The AO basis set employed in the present calculations is similar to that used in a previous treatment of the PH_5 molecule (18): six *s* and four *p* groups in the contraction (6,2,1,1,1,1|4,2,1,2) given by Veillard (19) are employed to represent the P atom, in addition to two sets of cartesian *d* functions ($\alpha_1 = 0.85$, $\alpha_2 = 0.30$); the hydrogen atoms are described in the same manner as in NH_2 (17), i.e. by two *s* groups (20) with four and one components each (with a scaling factor of $\eta^2 = 2$) augmented by a single *p* function ($\alpha = 0.735$). Furthermore one *s* and one *p* function ($\alpha(s) = 0.14$ and $\alpha(p) = 0.18$) located in each of the PH bonds are added so that the entire AO basis consists of 48 contracted cartesian gaussian functions.

The configuration interaction treatment is of the standard MRD-CI type with configuration selection and energy extrapolation as described elsewhere (21, 22). A core of five MO's corresponding to the 1*s*, 2*s*, and 2*p* shells of phosphorous is kept doubly occupied in all configurations, the corresponding five complementary MO's with the highest orbital energies are entirely excluded from consideration; all other MO's are in principle allowed variable occupation. For both states, X^2B_1 and A^2A_1 only one reference species has been employed in order to generate the double-excitation configuration space since all other species appear with small coefficients (less than 0.3%) in the final CI expansion. This procedure led to configuration spaces of roughly 6000 symmetry-adapted functions (in C_{2v} symmetry), while the sizes of the secular equations actually diagonalized were in the order of 2000. It should be pointed out, however, that the respective SCF orbitals are always taken as the MO basis. The energy contribution of higher than double-excitation configurations is also estimated according to the formula (23), $\Delta E_{Quad} = (1 - C_0^2)(E_{SCF} - E_{CI})$, which upon addition to the corresponding CI result is referred to as the full-CI limit in the ensuing discussion.

The basic vibrational treatment has been discussed in detail recently (method 1 of ref. 24) for the examples HCN and O_2. A functional basis of Hermite polynomials is employed in order to form a matrix representation of the Schrödinger equation for the symmetric and antisymmetric stretching modes (generally 15 such basis functions), while harmonic oscillator functions of the form

$$[1a] \quad \psi(r, \phi) = e^{iK\phi}R(r)$$

whereby

$$[1b] \quad R_{v,K}(\rho) = N_{v,K}\, e^{-\beta\rho/2}(\beta\rho)^{K/2}L^K_{(v+K)/2}(\beta\rho)$$

are chosen for the corresponding description of the two-dimensional bending mode.[1] Since a large number of bending vibrational levels are of interest in the present study, a basis of 50 $R_{v,K}(\rho)$ functions is supplied for the treatment of this mode. In all

[1]In this notation *r* is directly proportional to the bending angle α and $\rho = r^2$ ($0 \le \rho \le \infty$), whereby $L^K_{(v+K)/2}$ are the associated Laguerre polynomials and the quantity β is used as a variational parameter. The bending Hamiltonian used explicitly in this case is of the form

$$\left\{-\frac{1}{2\mu}\left[\frac{\partial^2}{\partial r^2} + \frac{1}{r}\frac{\partial}{\partial r} + \frac{1}{r^2}\frac{\partial^2}{\partial\phi^2}\right] + V(r)\right\}\psi(r, \phi) = E\psi(r, \phi)$$

whereby a different potential energy function is used for each of the two electronic states.

cases cubic-spline fitting techniques are used to represent the *ab initio* potential energy data, as described in detail in ref. 24.

In essence the present treatment thus employs a matrix representation of the global Hamiltonian in terms of a basis set of conventional vibronic product functions. The calculations are carried out entirely within the Born–Oppenheimer framework, i.e. cross terms involving derivatives of electronic wavefunctions with respect to nuclear variables are neglected, so that the Renner effect is not considered in this work. It should be pointed out, however, that the vibrational functions of eq. [1*a*] already contain the factor $e^{iK\phi}$, where K is the total vibronic angular momentum quantum number. This procedure should be distinguished from that used in previous treatments of the bending vibration in triatomic molecules in which vibrational functions containing the factor $e^{il\phi}$ (l being a pure vibrational quantum number) are first obtained as eigenfunctions of a zeroth-order Schrödinger equation (one which uses the same potential energy function for both electronic states) for the bending mode, which are then multiplied with $e^{\pm i\Lambda\phi}$ (Λ being the pure electronic angular momentum quantum number) in order to give the final eigenfunctions of the form $e^{iK\phi}$.

Results and Discussion

Potential Energy Curves

The potential energy curves for HPH bending are obtained for angles of 180, 160, 140, 120, 100, 91.7, 80, 60, and 40 deg at the SCF and the CI (except at 40°) level and are presented in Fig. 1 together with the results corresponding to the full-CI limit in the given AO basis. The PH bond length is thereby held fixed at 2.67967 au, i.e. the experimental equilibrium value (11) for the PH_2 ground state. The total SCF energy for the ground state minimum is -341.85943 hartree compared to the best previous value in the literature (16) of -341.85720 hartree with a comparable AO basis set. The CI energy is -342.0016 hartree, while the contribution of higher excitation species is estimated to amount to roughly 0.01 hartree. From the overall appearance of the curves in Fig. 1 it is seen that the SCF treatment already gives a good approximation to the true potential curves, although a closer analysis shows that CI is more effective for the linear arrangement of nuclei (Δ(SCF,CI) is 0.1518 au at 180°, for example, and only 0.1407 au at 100° for the X^2B_1 state, while the corresponding differences are 0.1520 au and 0.1448 au for the $^2A_1$ excited species), thereby reducing the ground state barrier by about 2400 cm^{-1}. The curve for the estimated full-CI energy runs to a large extent parallel to the ground and excited state double-

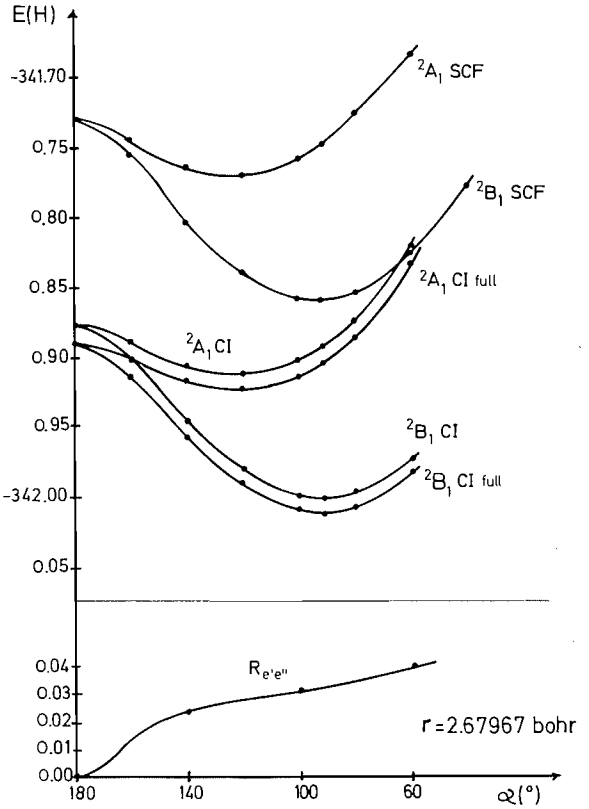

FIG. 1. Angular potential curves for the X^2B_1 and A^2A_1 electronic states of PH_2 obtained at various levels of treatment (see text for details); energy values are given in units of hartree (27.21 eV). The variation of the electronic transition moment (atomic units) between these two states is also given at the bottom of the figure.

excitation CI counterpart, although a small change in the same direction as the correction from SCF to CI can be noted (i.e. the difference between double-excitation CI and the full-CI estimate is 0.0136 au at 180° and only 0.0094 au at 100° for $^2B_1$, with the equivalent values of 0.0137 au and 0.0114 au for the $^2A_1$ species).

The calculated curves for the symmetric and asymmetric stretching mode of the PH_2 molecule are plotted in Figs. 2 and 3 respectively. In this case the $^2A_1$ upper state is treated at three different internuclear angles (91.7, 123, and 180 deg) in order to determine the coupling between the symmetric stretching and bending motion in this state, but the roughly parallel appearance of the curves indicates a relatively weak interdependence of the ν_1 and ν_2 modes in this instance. The calculations are again carried out at all three levels of treatment, but only the values corresponding to the full-CI estimate are given explicitly.

Finally, the various characteristic data for the $^2B_1$

TABLE 1. Calculated equilibrium data for PH_2 and PD_2 in their ground and first electronically excited states and comparison with experiment

	Value			
	X^2B_1		A^2A_1	
Parameter	This work	Expt.	This work	Expt.
P—H (Å)	1.420	1.428 (25) 1.418 (11)	1.399	1.403 (25) 1.389 (11)
∠HPH (degree)	91.1	91.5 (25) 91.7 (11)	122.1	123.1 (25) 123.2 (11)
PH_2[a] $\bar{\nu}_1(cm^{-1})$	2330	2270 ± 80 (15)	2430	—
$\bar{\nu}_2(cm^{-1})$	1110	1102 (25) 1103 (4)[b]	973	951.3 (25) 949.12 (11)[c]
$\bar{\nu}_3(cm^{-1})$	2495	—	2660	—
PD_2[a] $\bar{\nu}_1(cm^{-1})$	1675	—	1756	—
$\bar{\nu}_2(cm^{-1})$	800	803.5 (4)	710	689.5 (4)
$\bar{\nu}_3(cm^{-1})$	1785	—	1927	—

[a]The calculated values are always obtained as the difference between $\varepsilon(v = 1)$ and $\varepsilon(v = 0)$.
[b]An alternative value of 1107.26 cm^{-1} (12) is also given for $\bar{\nu}_2$ from an extrapolation procedure.
[c]Alternative values given by other authors are 951 cm^{-1} (4) and 956 cm^{-1} (12).

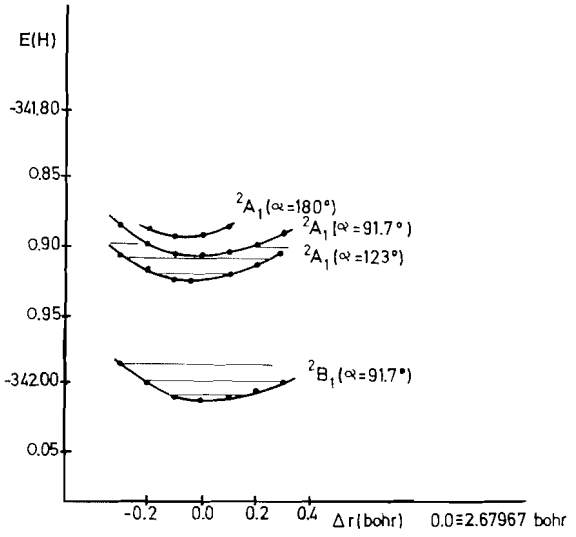

FIG. 2. Symmetric stretch potential curves and calculated vibrational levels for the X^2B_1 and A^2A_1 states of PH_2; in the upper state potential curves are shown for a series of three fixed internuclear angles (energy given in units of hartree).

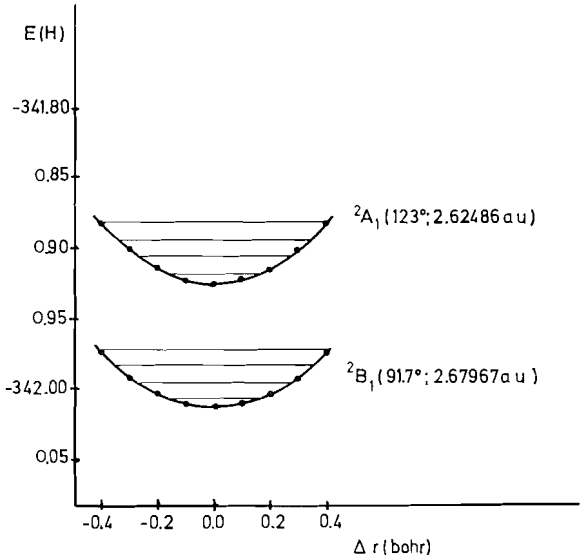

FIG. 3. Antisymmetric stretch potential curves and calculated vibrational levels for the X^2B_1 and A^2A_1 states of PH_2; results are obtained for fixed internuclear angle and average PH bond length, as given in parentheses (energy in hartree units).

and $^2A_1$ potential surfaces obtained by polynomial fits to the data points of Figs. 1–3 are collected in Table 1 and are compared with corresponding experimental data whenever available. It is seen that extremely good agreement between the structural data and the vibrational frequencies obtained from the *ab initio* potential energy surfaces and the corresponding quantities derived from experiments is achieved; discrepancies in the bond-angle determination are only 1.0 deg (or less), deviations in bond lengths are at most 0.01 Å, while experimental and theoretical vibrational frequencies agree to within 25 cm^{-1}.

The A^2A_1–X^2B_1 *Transition and Its Vibrational Structure*

The calculated energy difference between the two minima of the X^2B_1 and $^2A_1$ potential energy curves is $\Delta E_e = 18\,760\ cm^{-1}$. This value taken together

TABLE 2. Calculated Franck–Condon factors for the symmetric (ν_1) and asymmetric (ν_3) stretching modes in the A^2A_1–X^2B_1 electronic transition of PH_2 and PD_2

(*a*) PH_2

	$\nu_1' = 0$	$\nu_1' = 1$	$\nu_1' = 2$
$\nu_1'' = 0$	0.980	1.96×10^{-2}	4.1×10^{-5}
$\nu_1'' = 1$	1.93×10^{-2}	0.946	0.033
$\nu_1'' = 2$	3.7×10^{-4}	0.032	0.939
	$\nu_3' = 0$	$\nu_3' = 1$	$\nu_3' = 2$
$\nu_3'' = 0$	0.999	0.0	5.5×10^{-4}
$\nu_3'' = 1$	0.0	0.998	0.0
$\nu_3'' = 2$	5.5×10^{-4}	0.0	0.997

(*b*) PD_2

	$\nu_1' = 0$	$\nu_1' = 1$	$\nu_1' = 2$
$\nu_1'' = 0$	0.996	3.6×10^{-3}	1.3×10^{-4}
$\nu_1'' = 1$	3.7×10^{-3}	0.987	9.0×10^{-3}
$\nu_1'' = 2$	3.7×10^{-5}	9.2×10^{-3}	0.982
	$\nu_3' = 0$	$\nu_3' = 1$	$\nu_3' = 2$
$\nu_3'' = 0$	0.999	0.0	7.1×10^{-4}
$\nu_3'' = 1$	0.0	0.998	0.0
$\nu_3'' = 2$	7.1×10^{-4}	0.0	0.996

with the calculated frequencies for the zeroeth level of each vibrational mode yields an estimate for $\Delta E_{000,000}$ of 18 820 cm^{-1} (or 2.33 eV), which must be compared with the T_0 value of 18 276.6 cm^{-1} (25) or 18 272.6 cm^{-1} (26) (2.27 eV) deduced from experiment. Thus there remains a discrepancy of 0.06 eV.

The various calculated vibrational energy levels for the symmetric and asymmetric stretching modes[2] of PH_2 are also indicated for ground and excited states in Figs. 2 and 3. The calculated Franck–Condon factors (Table 2) support the qualitative conclusion which can be drawn from Figs. 2 and 3, namely that the 0–0 transition is by far the strongest in each of the two modes, so that one strong peak rather than a long progression in one of the stretching coordinates should be observed in the spectrum.

The calculated vibrational energy levels for the bending mode of PH_2 and PD_2 are contained in Figs. 4 and 5 respectively; the values for $K = 0$ (symmetric) and $K = 1$ (antisymmetric) are explicitly shown therein. It is seen that the K-type splitting is very small for the low-lying levels inside the potential well which exhibit the characteristic rotational structure; this splitting becomes a distinctive factor in the neighborhood of the potential maximum, however, and above this barrier the vibrational term pattern which is typical for a linear molecule becomes dominant. Levels corresponding to higher K values

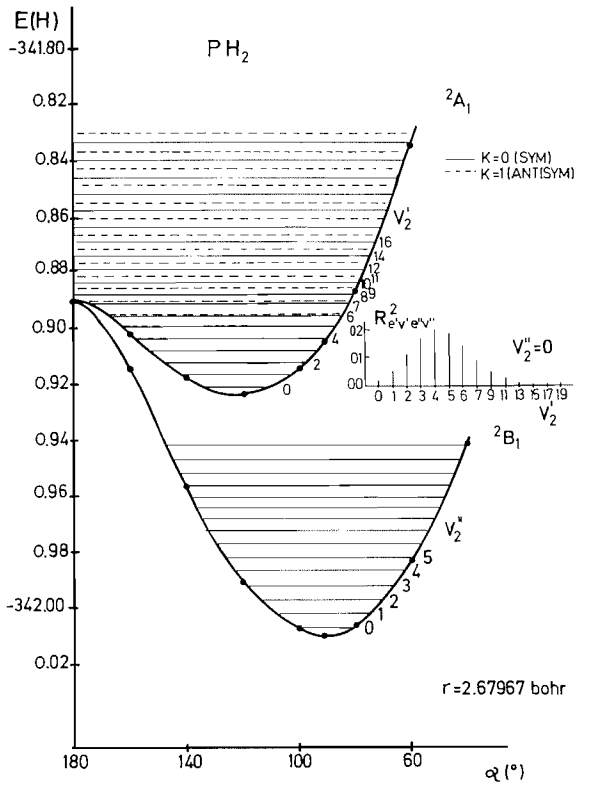

FIG. 4. Calculated CI angular potential curves and corresponding vibrational levels for the two lowest electronic states of PH_2; results are given for two different values of the rotational quantum number K in the upper state. The values of the square of the electronic moment connecting the various levels of the upper state with the $v_2'' = 0$ species of X^2B_1 are also given.

have also been calculated but are not plotted since they behave in the expected way (24).[3]

It is also interesting that the calculated differences ΔG between consecutive levels (of the same K quantum number) in the upper state decrease from (0–1) to (6–7) in PH_2 (and until (8–9) in PD_2), just as has been found in the observed ($K' = 1$) spectrum (see Fig. 6) (1), whereas the vibrational intervals increase thereafter with further increase in v_2'. Dixon (8) has interpreted this behavior as being caused by the barrier in the $^2A_1$ state potential function for the higher vibrations, and indeed Figs. 4 and 5 support this deduction quantitatively.

The intensity distribution for transitions between various vibrational levels of the $^2B_1$ and $^2A_1$ state has also been calculated and the resulting data,

[2]The potential energy curve for symmetric stretch is thereby represented via a fit with terms up to $(R - R_0)^5$, while the asymmetric curve is approximated by a polynomial of 4th order; 15 vibrational basis functions are chosen in each case.

[3]The calculated CI points have been supplemented by the spline technique so that the potential is represented by a polynomial of order 30; technical details are contained in ref. 24.

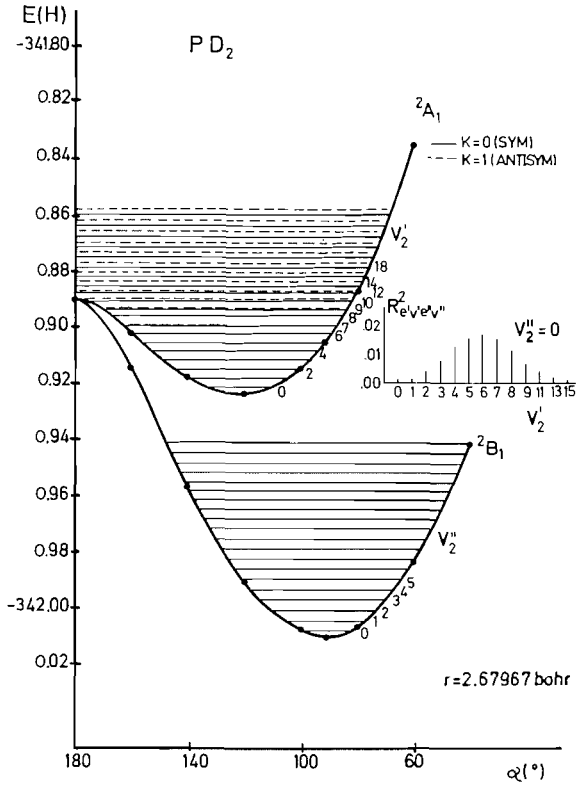

FIG. 5. Calculated CI angular potential curves and corresponding vibrational levels for the two lowest electronic states of PD_2; results are given for two different values of the rotational quantum number K in the upper state. The values of the square of the electronic transition moment connecting the various levels of the upper state with the $v_2'' = 0$ species of X^2B_1 are also given.

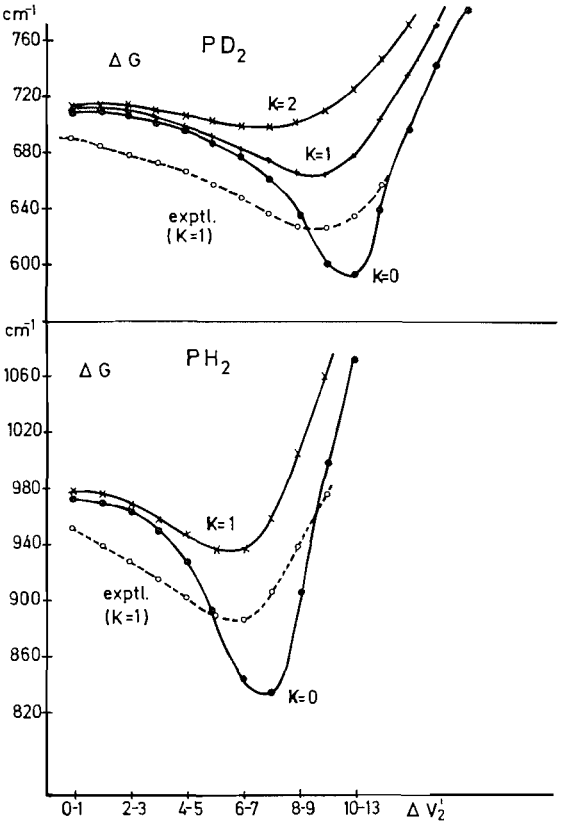

FIG. 6. Comparison of calculated and experimental ΔG values in cm^{-1} for the v_2' bending mode of the $^2A_1$ state of PH_2 (bottom) and PD_2 (top); theoretical results for several series with the same rotational quantum number K are given, while the experimental curve corresponds to $K = 1$ (for the vibrational numbering see Figs. 4, 5).

which correspond to the absorption spectrum of PH_2 and PD_2, are also plotted in Figs. 4 and 5. In this case simple Franck–Condon factors have not been evaluated but rather the actual expression

$$R^2_{e'v'e''v''} = [\int R_{v_2',K'}(\rho)\{\int \Psi_{e',\mu}\Psi_{e''}\,d\tau_e\}R_{v_2'',K''}(\rho)\,d\tau_v]^2$$

since the electronic transition moment $R_{e'e''}$ is found to depend strongly on the internuclear angle (Fig. 1). The intensity maximum for absorption is calculated to occur for $v_2' = 4$ in PH_2 in complete accord with known experiments (9); it is predicted to occur for $v_2' = 6$ in the PD_2 radical. In comparison to NH_2 the maximum occurs at much smaller quantum numbers (in NH_2 at $v_2' = 9$) because of the fact that the equilibrium internuclear angle is decidedly smaller (more bent) for the PH_2 $^2A_1$ state than for the (quasi-linear) NH_2 $^2A_1$ radical. Thus altogether it is seen that the calculations describe the long progression in the bending mode in an almost quantitative manner.

Summary and Conclusion

The present *ab initio* CI calculations have dealt with the calculation of the vibrational structure of the A^2A_1–X^2B_1 electronic transition of the PH_2 (and PD_2) radical. They predict the nuclear geometry of this system to within errors of 1.0 deg and 0.01 Å respectively in both electronic states, and also obtain the bending frequencies for both states and both isomers with deviations of less than 25 cm^{-1} from the corresponding experimental data. Furthermore they predict the frequencies for symmetric and asymmetric stretching vibrations of both ground and excited states, which have not yet been determined from experiments. Calculation of the vibrational intensity distribution shows that the 0–0 transitions in both symmetric and asymmetric stretch are highly favored over excitations to levels with higher quantum numbers. On the other hand, the long progression in the bending mode deduced from the observed

spectra is reproduced very satisfactorily by the calculations, both with respect to vibrational spacing and intensity distribution. Hence it is demonstrated that the fairly detailed structure of the PH_2 (or PD_2) electronic spectrum between 3600 and 5500 Å can be reproduced almost quantitatively by means of present-day *ab initio* CI calculations. The investigation of small perturbations of vibrational levels in the upper state, which are also observed in the measured spectrum and are thought to be caused by the presence of vibrational levels of the ground electronic state, i.e. effects of the Renner–Teller splitting or further terms not present in the Born–Oppenheimer approximation, would thus seem to be the next realistic step in upgrading the theoretical treatment of the molecular spectra of such systems.

Acknowledgements

We wish to thank the Deutsche Forschungsgemeinschaft for financial support given to part of this work. The services and computer time made available by the RHRZ at the University of Bonn are also gratefully acknowledged.

1. D. A. RAMSAY. Nature, London, **178**, 374 (1956).
2. G. W. ROBINSON and M. MCCARTY. J. Chem. Phys. **30**, 999 (1959).
3. H. GUENEBAUT and B. PASCAT. J. Chim. Phys. **61**, 592 (1964).
4. H. GUENEBAUT, B. PASCAT, and J. M. BERTHOU. J. Chim. Phys. **62**, 867 (1965).
5. G. W. ROBINSON and M. MCCARTY. J. Chim. Phys. **56**, 723 (1959).
6. D. A. RAMSAY. J. Chem. Phys. **25**, 188 (1956).
7. J. W. C. JOHNS, D. A. RAMSAY, and S. C. ROSS. Can. J. Phys. **54**, 1804 (1976).
8. R. N. DIXON. Trans. Faraday Soc. **60**, 1363 (1964).
9. R. N. DIXON, G. DUXBURY, and D. A. RAMSAY. Proc. R. Soc. A, **296**, 137 (1967).
10. B. PASCAT, J. M. BERTHOU, H. GUENEBAUT, and D. A. RAMSAY. C. R. Paris, **B263**, 1397 (1966).
11. J. M. BERTHOU, B. PASCAT, H. GUENEBAUT, and D. A. RAMSAY. Can. J. Phys. **50**, 2265 (1972).
12. B. PASCAT, J. M. BERTHOU, J. C. PRUDHOMME, H. GUENEBAUT, and D. A. RAMSAY. J. Chim. Phys. **65**, 2022 (1968).
13. K. C. SMYTH and J. I. BRAUMAN. J. Chem. Phys. **56**, 1132 (1972).
14. P. B. DAVIES, D. K. RUSSEL, and B. A. THRUSH. Chem. Phys. Lett. **37**, 1 (1976).
15. P. F. ZITTEL and W. C. LINEBERGER. J. Chem. Phys. **65**, 1236 (1976).
16. J. R. BALL and C. THOMSON. Int. J. Quantum Chem. **14**, 39 (1978).
17. M. PERIC, R. J. BUENKER, and S. D. PEYERIMHOFF. To be published.
18. S.-K. SHIH, S. D. PEYERIMHOFF, and R. J. BUENKER. J. Chem. Soc. Faraday II, **75**, 379 (1979).
19. A. VEILLARD. Theor. Chim. Acta. **12**, 405 (1968).
20. S. D. PEYERIMHOFF, R. J. BUENKER, and L. C. ALLEN. J. Chem. Phys. **45**, 734 (1966).
21. R. J. BUENKER and S. D. PEYERIMHOFF. Theor. Chim. Acta, **39**, 217 (1975); **35**, 33 (1974).
22. R. J. BUENKER, S. D. PEYERIMHOFF, and W. BUTSCHER. Mol. Phys. **35**, 771 (1978).
23. S. T. ELBERT and E. R. DAVIDSON. Int. J. Quantum Chem. **8**, 857 (1974).
24. M. PERIC, R. RUNAU, J. RÖMELT, S. D. PEYERIMHOFF, and R. J. BUENKER. J. Mol. Spectrosc. In press.
25. G. HERZBERG. Molecular spectra and molecular structure. Vol. III. D. van Nostrand Co. 1966.
26. R. N. DIXON and G. DUXBURY. Chem. Phys. Lett. **1**, 330 (1967).

Pentagonal pyramidal lead coordination in the crystal structure of dimeric diaquopyridine-2,6-dicarboxylatolead(II) pyridine-2,6-dicarboxylic acid monohydrate

K. A. BEVERIDGE AND G. W. BUSHNELL

Chemistry Department, University of Victoria, Victoria, B.C., Canada V8W 2Y2

Received December 22, 1978

K. A. BEVERIDGE and G. W. BUSHNELL. Can. J. Chem. 57, 2498 (1979).

The crystal structure of dimeric diaquopyridine-2,6-dicarboxylatolead(II) pyridine-2,6-dicarboxylic acid monohydrate, empirical formula and asymmetric unit $C_{14}H_{14}N_2O_{11}Pb$, has been solved and refined to $R = 0.081$, $R_w = 0.100$. The space group was $P\bar{1}$ with $a = 1073.8(3)$, $b = 1123.2(5)$, $c = 705.0(3)$ pm, $\alpha = 101.28(8)°$, $\beta = 95.42(6)°$, $\gamma = 92.80(7)°$, $\rho = 2.37$ g cm^{-3} (meas.). Measurements were done on an automatic 4-circle diffractometer ($MoK_{\bar{a}}$ radiation, $\lambda = 71.069$ pm), and corrected for absorption. The lead complex is dinuclear with an inversion point at the centre of the double bridging. Each lead atom has distorted pentagonal pyramidal coordination with a water molecule at the apex. The basal ligands are water and terdentate pyridine-2,6-dicarboxylate. The double bridging is by one of the coordinated carboxylic oxygen atoms and its inverse. The electron pair geometry is assumed to be pentagonal bipyramidal with a stereochemically active lone pair occupying considerable solid angle in an axial position. Bond lengths (±2 pm) are: Pb—OH_2 (apex), 259; Pb—OH_2 (basal), 273; Pb—O, 251, 258, 273; Pb—N, 259. The mean of the bond angles at Pb involving the apical oxygen is 77°. The unit cell contains two water and two dicarboxylic acid molecules of crystallisation which are involved in an H-bonding network with one bond for each hydrogen attached to oxygen in the structure.

K. A. BEVERIDGE et G. W. BUSHNELL. Can. J. Chem. 57, 2498 (1979).

On a résolu la structure cristalline du monohydrate dimère du diaquopyridinecarboxylato-2,6 plomb(II) acide pyridinedicarboxylique de formule empirique et unité asymétrique $C_{14}H_{14}N_2O_{11}Pb$ et on l'a affinée jusqu'à des valeurs de $R = 0.081$ et $R_w = 0.100$. Le groupe d'espace est $P\bar{1}$ avec $a = 1073.8(3)$, $b = 1123.2(5)$, $c = 705.0(3)$ pm, $\alpha = 101.28(8)°$, $\beta = 95.42(6)°$, $\gamma = 92.80(7)°$, $\rho = 2.37$ g cm^{-3} (mes). On a effectué les mesures sur un diffractomètre automatique à 4 cercles (radiation $MoK_{\bar{a}}$, $\lambda = 71.069$ pm) et elles sont corrigées pour l'absorption. Le complexe de plomb est dinucléaire avec un point d'inversion au centre du double pont. La coordination de chaque atome de plomb est assimilée à une pyramide pentagonale déformée portant une molécule d'eau à son sommet. Les ligands à la base de la pyramide sont l'eau et le pyridinedicarboxylate-2,6 tridentate. Le double pont est assuré par un des atomes d'oxygène du carboxylate coordonné et de son inverse. On fait l'hypothèse que la géométrie de la paire d'électrons est bipyramidale pentagonale et qu'elle porte une paire libre d'électrons active du point de vue stéréochimique qui occupe un angle solide important dans la position axiale. Les longueurs des liaisons (±2 pm) sont: Pb—OH_2 (sommet), 259; Pb—OH_2 (base), 273; Pb—O, 251, 258, 273; Pb—N, 259. L'angle de valence moyen autour du Pb impliquant l'oxygène au sommet est 77°. La maille unitaire contient deux molécules d'eau et deux molécules d'acide dicarboxylique de cristallisation qui sont impliquées dans un réseau de liaison H dans lequel il y a une liaison pour chaque hydrogène qui est attachée à un atome d'oxygène de la structure.

[Traduit par le journal]

Introduction

Lead and its compounds are toxic and give rise to many serious industrial hazards. The smelting of lead produces metal fumes and flue dusts. In manufacturing processes nearly one million American workers are exposed to lead in various chemical forms. Some uses of lead compounds ensure that the element is widely distributed near to man, for example the inclusion of tetraethyllead in motor fuel formulations and the use of hydroxycarbonate as a white paint pigment. The toxicology of lead has been intensively studied (1). However, the structural chemistry of plumbous compounds which might be relevant to situations in living systems is relatively undeveloped. Existing X-ray crystallographic results indicate the variability of both the coordination number of the plumbous ion and its stereochemistry. The inert pair of electrons usually influences the stereochemistry, often by occupying one side of the lead atom opposite to the ligands.

The anion of pyridine-2,6-dicarboxylic acid (dipicolinate) is a ligand of some biochemical interest. It is produced by all bacterial spores and some fungi. The heat resistance and metabolic dormancy of the

0008-4042/79/182498-06$01.00/0

spores are thought to depend on the calcium salt of this acid. The crystal structures of calcium pyridine-2,6-dicarboxylate trihydrate (2) and strontium pyridine-2,6-dicarboxylate tetrahydrate (3) have been determined.

A recent series of papers on metal purpurate complexes (4) contains a summary of crystallographic studies on pyridine-2,6-dicarboxylates, and two eight coordinate Pb(II) purpurate complexes. The crystal structure of pyridine-2,6-dicarboxylic acid monohydrate has been published (5).

Experimental

A mixture of crystals was obtained by diffusion of aqueous solutions of lead nitrate into pyridine-2,6-dicarboxylic acid. The densities were found to be 3.16 g cm^{-3} for the flat lathes and 2.37 g cm^{-3} for the rods thus prepared. The mixture was separated by flotation in a carbon tetrachloride/1,1,2,2-tetrabromoethane solution. Analysis of the lathes gave: C 22.55, H 0.80, N 3.75%. Calculated for Pb dipic: C 22.58, H 0.81, N 3.76%. Analysis of the rods gave: C 26.8, H 2.19, N 4.68%. Calculated for Pb dipic·H_2 dipic·$3H_2O$: C 28.3, H 2.38, N 4.72. The structure of the rod shaped crystals is reported in this paper.

The crystal system is triclinic, space group $P\bar{1}$. The Delaunay reduced cell has parameters $a = 1073.8(3)$, $b = 1123.2(5)$, $c = 705.0(3)$ pm, $\alpha = 101.28(8)°$, $\beta = 95.42(6)°$, $\gamma = 92.80(7)°$, $V_{cell} = 0.8281(5)$ nm^3. The cell was refined by the method of least squares with Picker diffractometer centering measurements at $\pm 2\theta$ in pairs using $MoK_{\bar{\alpha}}$ radiation ($\lambda = 71.069$ pm). Formula $C_{14}H_{14}N_2O_{11}Pb$, $M = 593.47$, $n = 2$, ρ(calc) = 2.38 g cm^{-3}. Crystal dimensions 0.037, 0.041, 0.478 mm along x, y, z respectively; mounting direction, z. The absorption coefficient for $MoK_{\bar{\alpha}}$ was 96.9 cm^{-1}. Reflections were scanned in 50 steps of 0.04° in 2θ counting for 2 s at each step. Background counts were for 50 s at each extremity. Three standards were measured before each batch of 50 reflections. A total of 4156 measurements were made up to $2\theta = 50°$, ($h \geq 0$), and of these 2355 reflections (and 192 standards) had $I > 3\sigma(I)$. The crystal changed from colourless to pale smoky yellow in the X-radiation, and the intensities of the standards dropped approximately 12% during data collection. Lorentz, polarisation, and crystal decomposition/instrument variation factors were applied, and absorption corrections were done using a program derived from that of Coppens, Lieserowitz, and Rabinovich (6), and tested by the procedure of Cahen and Ibers (7). Transmission factors were in the range 0.65–0.72. After sorting the reflections and merging any duplicate or equivalent measurements 2206 intensities remained.

Structure Determination

The structure was solved by the Patterson function and heavy atom methods. The atomic scattering factors and the anomalous dispersion correction for Pb were taken from the International Tables (8). The light atoms were located by means of difference maps. The structure was refined uneventfully by minimising $\sum w(|F_o| - |F_c|)^2$ using full matrix least-squares. A weighting scheme devised to eliminate systematic variations of $w\Delta^2$ took the form $w = (A + Bx + Cx^2 + Dx^3)^{-1}$ where $x = |F_o|$, $A = 2.3208$, $B = -1.950 \times 10^{-2}$, $C = -6.4 \times 10^{-5}$, $D = 2 \times 10^{-6}$. The final agreement factors were $R = 0.081$, $R_w = 0.100$ where $R_w = (\sum w\Delta^2 / \sum w|F_o|^2)^{1/2}$. The final difference map had peaks and troughs

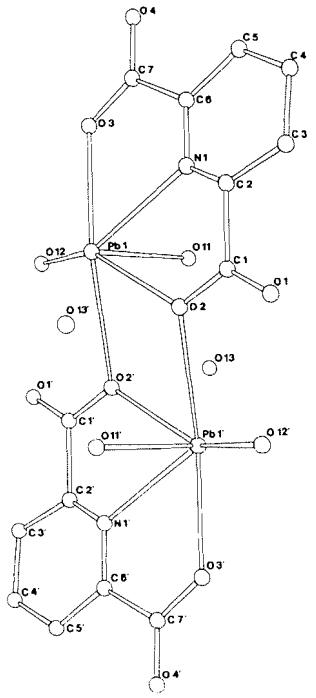

FIG. 1. The dimeric lead complex.

less than 2×10^{-6} e pm^{-3} except in the vicinity of Pb, where max = $+4.3 \times 10^{-6}$ e pm^{-3} and min = -3.2×10^{-6} e pm^{-3} both 105 pm from the metal atom.

The hydrogen atom peaks were poorly defined. Calculations were done using a set of programs supplied by Dr. B. R. Penfold of the University of Canterbury, Christchurch, New Zealand. The structure factor and other tables are in the Depository for Unpublished Data.[1]

Results and Discussion

The fractional atomic coordinates are given in Table 1. The asymmetric unit consists of half of the dimeric lead(II) complex shown in Fig. 1, a molecule of pyridine-2,6-dicarboxylic acid of crystallisation, and a water molecule containing O(13). The crystal packing is shown in Fig. 2. The numbering scheme of the free acid molecule can be derived by adding 7, 1, and 4 to the numbers of the corresponding C, N, and O atoms in Fig. 1. The only differences between the ligand and non-ligand molecules which are possibly significant are between the C—O bond lengths. In the ligand C(1)—O(2) = 128(3), C(1)—O(1) = 120(3), C(7)—O(3) = 128(3), C(7)—O(4) = 125(3) pm. The oxygen bound to Pb has the longer C—O length. The non-ligand has C(8)—O(6) = 119(3), C(8)—O(5) = 132(3), C(14)—O(7) = 128(3),

[1]Copies may be obtained, at a nominal charge, from the Depository of Unpublished Data, CISTI, National Research Council of Canada, Ottawa, Ont., Canada K1A 0S2.

TABLE 1. Atomic parameters*

Atom	x	y	z	U_{iso}
Pb	−21.8(1)	850.3(1)	150.6(2)	—
O(11)	−11(2)	741 (2)	−207 (3)	37(4)
O(12)	−246(2)	721 (2)	17 (3)	47(5)
O(13)	−166(2)	796 (2)	−525 (3)	48(5)
O(1)	330(2)	1062 (2)	58 (3)	42(5)
O(2)	133(2)	1003 (2)	73 (3)	47(5)
O(3)	19(2)	634 (2)	204 (3)	37(4)
O(4)	150(2)	484 (2)	222 (3)	37(4)
O(5)	700(2)	−28 (2)	443 (3)	38(4)
O(6)	878(2)	72 (2)	412 (3)	51(5)
O(7)	872(2)	470 (2)	278 (3)	47(5)
O(8)	709(2)	577 (2)	353 (3)	48(5)
N(1)	205(2)	784 (2)	134 (3)	29(5)
N(2)	755(2)	270 (2)	361 (3)	30(5)
C(1)	251(2)	987 (2)	79 (3)	19(5)
C(2)	290(2)	859 (2)	129 (3)	9(4)
C(3)	414(2)	839 (2)	110 (4)	26(5)
C(4)	448(3)	720 (2)	135 (4)	37(6)
C(5)	354(2)	640 (2)	158 (4)	28(5)
C(6)	231(2)	676 (2)	164 (4)	28(5)
C(7)	126(2)	589 (2)	197 (4)	26(5)
C(8)	767(3)	66 (2)	413 (4)	37(6)
C(9)	689(2)	170 (2)	381 (4)	28(5)
C(10)	559(2)	160 (2)	388 (4)	37(6)
C(11)	490(3)	265 (2)	373 (4)	37(6)
C(12)	559(3)	368 (2)	353 (4)	36(6)
C(13)	688(2)	366 (2)	342 (4)	34(6)
C(14)	761(3)	482 (2)	328 (4)	36(6)

*Fractional atomic coordinates $\times 10^{-3}$ are given. U_{iso} values to be multiplied by 10 to give mean square amplitudes in pm². For Pb in pm²: $U_{11} = 278(5)$, $U_{22} = 191(5)$, $U_{33} = 544(7)$, $U_{12} = 64(4)$, $U_{23} = 117(4)$, $U_{31} = 120(4)$. Estimated standard deviations, given in parentheses, in units of the least significant digit.

C(14)—O(8) = 122(3) pm, showing asymmetry in the C(8) carboxyl group reversed with respect to that of the ligand. Hydrogen atoms on O(5) and O(7) are consistent with the hydrogen bonding scheme to be proposed. The mean C—C single bond length is 154 pm, and the mean O—C—O angle = 125°. Other bond lengths and angles of the pyridine groups are of little interest and have been deposited with the structure factor tables.

The lead atom is six coordinate with approximately pentagonal pyramidal geometry. The water molecule containing O(11) is at the apex of the pyramid. Interatomic distances are given in Table 2(*a*). The last three entries are distances from lead to its next nearest neighbours, and the bonding if present would be weak. We presume that the lone pair of electrons on the plumbous ion occupies the position below the pyramid base, opposite O(11). The electron pair geometry is thus pentagonal bipyramidal. As expected from valence shell electron pair repulsion theory, the lone pair occupies a greater solid angle than a bonding pair and the angles in Table 3(*a*) involving O(11) are all less than 85° (mean 77.0°). The bridging to an inverted pyramid is through O(2) and O(2′), an arrangement similar to that in calcium pyridine-2,6-dicarboxylate trihydrate (2). The centre of the bridge is a crystallographic inversion centre.

The hydrogen bonding scheme is illustrated in Fig. 3. Eight hydrogen bonds were found, one for each hydrogen attached to oxygen in the structure. The lengths of the hydrogen bonds are given in Table 2(*b*). The water molecule containing O(13) bridges the non-coordinated acid molecules in the y direction using hydrogen bonds to O(5) and O(8) which are at the extremities of these molecules. O(13) is also hydrogen bonded to O(11) at the apex of the pentagonal pyramid and lies beneath a neighbouring pyramid (not shown in Fig. 1) only 302(2) pm from its lead atom. O(4) at the end of the dimeric complex is hydrogen bonded to O(11) and O(12) of the next molecule in the y direction. The hydrogen bond to O(7) links the uncoordinated dicarboxylic acid and the dimeric unit. The distance O(11)—O(7) = 285(3) pm, but O(7) was rejected as an H atom receptor in favour of N(2), since angle O(4′)—O(11)—O(7) = 65°. The O(12)—O(1) hydrogen bond is intramolecular to the lead complex. O(6) is not involved in hydrogen bonding. The hydrogen atom attachments

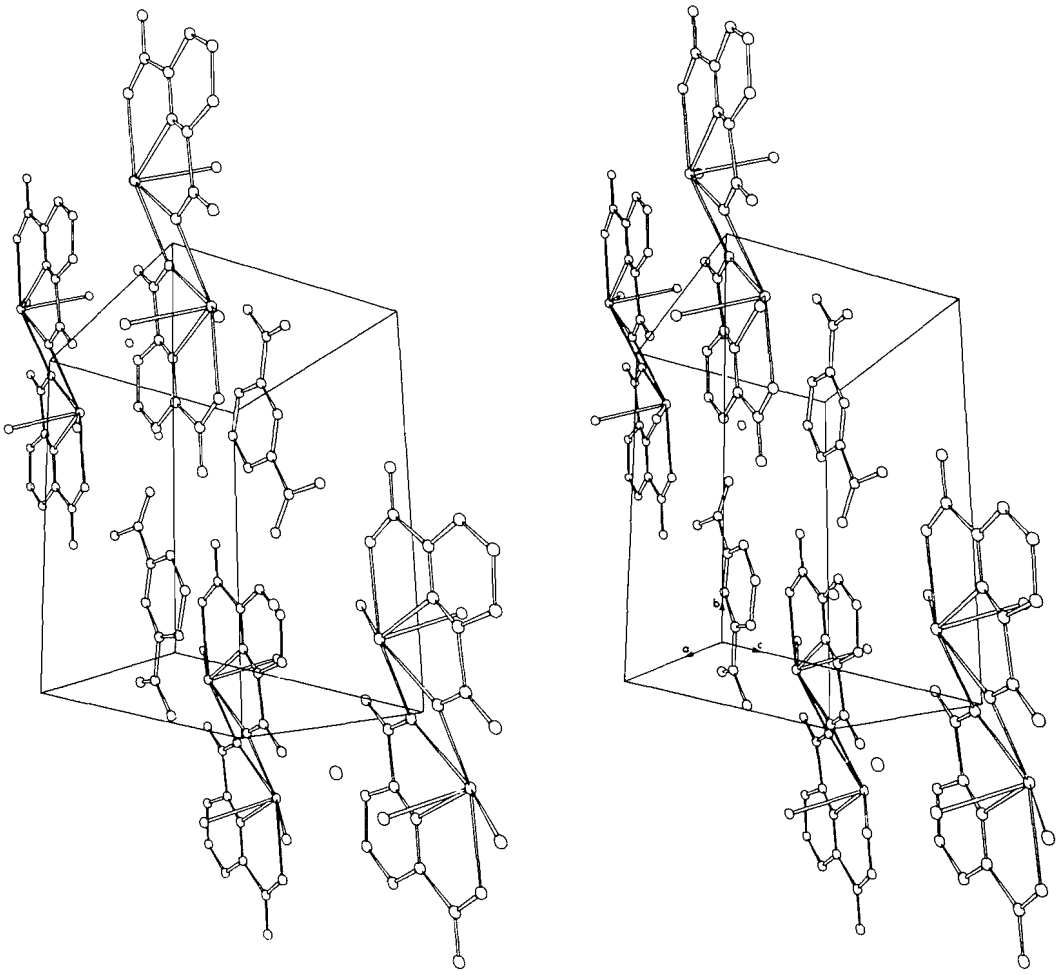

FIG. 2. The crystal packing diagram as a stereoscopic pair.

suggested in Table 2(*b*) were derived from the carboxyl C—O bond lengths, and are consistent with three water molecules and an undissociated dicarboxylic acid molecule in the asymmetric unit. Angles relevant to the hydrogen bonding scheme are given in Table 3(*b*).

The results of the mean plane calculations are given in Table 4. Both pyridine rings are planar. The carboxylate groups, particularly O(7) and O(8), are slightly out of the pyridine ring planes, which are mutually parallel. The coordination geometry of the lead atom is only approximately a pentagonal pyramid. The basal pentagon has significant deviations from planarity. The lead atom is at a perpendicular distance of 60.0 pm from the least-squares plane.

The pentagonal bipyramidal electron pair geometry has been found for two lead(II) complexes having sulfur atoms coordinated. In the crystal structure of tetraethylammonium tris(ethylxanthato)lead(II), $Et_4N^+[Pb(EtOCS_2)_3]^-$, the lead atom has an axial lone pair (9). Each ligand has one short (284–295 pm) and one long (312–313 pm) Pb–S bond. A next nearest neighbour lies at 368 pm from Pb. In the crystal structure of polymeric lead(II) *O,O'*-diisopropylphosphonodithionate, $\{Pb[(Pr^iO)_2PS_2]_2\}_\infty$, the lone pair position is equatorial (10). The axial lengths are 298.5 and 302.7 pm and the equatorial lengths are 276.1, 277.2, 317.5, and 323.2 pm, with the greater lengths adjacent to the lone pair. These two compounds establish the Pb—S lengths to be expected.

D-Penicillamine has been used in chelation therapy for lead poisoning. In the crystal structure of D-Penicillaminatolead(II) (11), the amino acid is a terdentate chelating ligand to one lead atom: Pb—O, 244 pm; Pb—N, 244 pm; Pb—S, 272 pm. Weaker interactions to two other lead atoms have lengths:

TABLE 2. Interatomic distances (pm)

(*a*) Lead coordination

Atoms	Distance (pm)	Coordinates of 2nd atom*
Pb—O(11)	259(2)	
Pb—O(12)	273(2)	
Pb—O(2′)	273(2)	$-x, 2-y, -z$
Pb—O(2)	251(2)	
Pb—N(1)	259(2)	
Pb—O(3)	258(2)	
Pb—O(13)	302(2)	$x, y, 1+z$
Pb—O(6)	310(2)	$x-1, y+1, z$
Pb—O(6)	325(2)	$1-x, 1-y, 1-z$

(*b*) Hydrogen bonds

Atoms	Distance (pm)	Coordinates of 2nd atom*
O(13) ... H—O(5)	254(3)	$x-1, y+1, z-1$
O(13)—H ... O(8)	269(3)	$x-1, y, z-1$
O(13)—H ... O(11)	284(3)	
O(4) ... H—O(11)	286(2)	$-x, 1-y, -z$
N(2) ... H—O(11)	305(3)	$1-x, 1-y, -z$
O(7)—H ... O(3)	253(3)	$x+1, y, z$
O(12)—H ... O(1)	276(3)	$-x, 2-y, -z$
O(12)—H ... O(4)	288(3)	$-x, 1-y, -z$

*Given with respect to x, y, z values of Table 1.

Pb—S, 316 and 348 pm; Pb—O, 277 pm. If the very long Pb—S bond is accepted, the electron pair geometry is distorted pentagonal bipyramidal with the lone pair equatorial, and adjacent to the long Pb—S bonds.

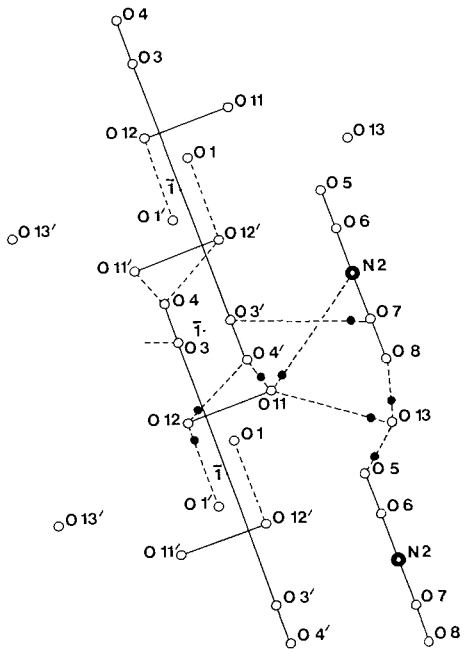

FIG. 3. The hydrogen bonding scheme.

The range of bond lengths in the literature for Pb(II) to N and O is wide with lengths from about 240 to 300 pm being common. The variability of the Pb(II) stereochemistry and the use of macrocyclic ligands are probable causes for this. Our bond lengths are near the middle of the range.

The stereochemical activity of the lone pair of

TABLE 3. Bond angles

(*a*) Lead coordination

Atoms	Angle (deg)	Atoms	Angle (deg)
O(11)—Pb—O(2)	84.1(6)	O(2) —Pb —N(1)	64.5(6)
O(11)—Pb—N(1)	74.2(6)	N(1) —Pb —O(3)	62.7(6)
O(11)—Pb—O(3)	80.5(6)	O(3) —Pb —O(12)	76.6(6)
O(11)—Pb—O(12)	71.7(6)	O(12)—Pb —O(2′)	78.5(6)
O(11)—Pb—O(2′)	74.3(6)	O(2′) —Pb —O(2)	68.1(7)
		Pb —O(2)—Pb′	111.9(7)

(*b*) Hydrogen bonding

Atoms	Angle (deg)	Atoms	Angle (deg)
Pb —O(11)—O(4)	101.7(7)	Pb —O(12)—O(1)	85.9(7)
Pb —O(11)—N(2)	118.1(7)	Pb —O(12)—O(4)	97.8(7)
Pb —O(11)—O(13)	122.8(8)	O(1) —O(12)—O(4)	132.9(9)
O(4) —O(11)—N(2)	117.2(8)	O(8) —O(13)—O(5)	113.1(9)
N(2) —O(11)—O(13)	102.2(8)	O(5) —O(13)—O(11)	132.5(9)
O(13)—O(11)—O(4)	93.0(8)	O(11)—O(13)—O(8)	98.4(8)
C(7) —O(4) —O(11)	137(2)	C(13)—N(2) —O(11)	118(2)
C(7) —O(4) —O(12)	133(2)	C(9) —N(2) —O(11)	122(2)
C(7) —O(3) —O(7)	106(2)	C(1) —O(1) —O(12)	117(2)
C(14)—O(7) —O(3)	127(2)	C(14)—O(8) —O(13)	123(2)
C(8) —O(5) —O(13)	112(2)		

TABLE 4. Results of mean plane calculations

(*a*) Definition of sets of atoms

Plane	Atoms	Description
1	N(1), C(2)–C(6)	The coordinated pyridine ring
2	N(2), C(9)–C(13)	The uncoordinated pyridine ring
3	O(2′), O(2), N(1), O(3), O(12)	The basal pentagon

(*b*) Equations of least-squares planes through selected sets of atoms: $Ax + By + Cz = D$ (pm)*

Plane	*A*	*B*	*C*	*D*	χ^2†
1	−0.0468	−0.1107	−0.9928	−199.79	17.2
2	−0.0287	−0.1105	−0.9935	−295.72	1.2
3	0.2345	−0.2641	−0.9356	−302.04	379.5

*The axis system used has x along the a-axis, y in the (a, b) plane, and z along the c^* axis.
†$\chi^2 = \Sigma_i (P_i^2/\sigma^2(P_i))$ where P_i is the perpendicular distance of atom i from the plane.

(*c*) Perpendicular distances in pm of atoms from the planes

Plane	Atoms and distances
1	Pb, −2.5(1); C(1), 15(2); O(1), 16(2); O(2), 22(2); C(7), −9(2); O(3), −14(2); 0(4), −14(2)
2	C(8), −11(3); O(5), −17(2); O(6), −15(2); C(14), −5(3); O(7), 26(2); O(8), −32(2)
3	Pb, −60.0(1); O(2′), 6(2); O(2), −20(2); N(1), 28(2); O(3), −16(2); O(12), 7(2)
Angles between normals to the planes: 1,2 = 1.04°; 2,3 = 17.85°; 1,3 = 18.73°	

electrons on a Pb(II) ion cannot be taken for granted. In $(\pi\text{-}C_6H_6)Pb(AlCl_4)_2 \cdot C_6H_6$ the coordination geometry is pentagonal bipyramidal, with benzene occupying one site, and the lone pair position is not evident (12). In $[Pb(SCN)_2C_{12}H_{26}N_2O_4]$, containing the 1,7,10,16-tetraoxa-4,13-diazacyclooctadecane ligand, the Pb(II) ion is eight coordinate and the lone pair has only a minor stereochemical effect (13).

The crystal structure reported here establishes pentagonal pyramidal lead(II) with oxygen and nitrogen donors, in an interesting doubly bridged dimeric structure, the lone pair on each lead atom being stereochemically active.

Acknowledgements

We wish to acknowledge operating grants from the National Science and Engineering Research Council of Canada and the University of Victoria Faculty Research Committee. The illustrative photography was done by Mr. Blaine Hawkins.

1. H. B. ELKINS. The chemistry of industrial toxicology. 2nd ed. John Wiley, New York. 1959.
2. G. STRAHS and R. E. DICKERSON. Acta Crystallogr. B**24**, 571 (1968).
3. K. J. PALMER, R. Y. WONG, and J. C. LEWIS. Acta Crystallogr. B**28**, 223 (1972).
4. A. H. WHITE and A. C. WILLIS. J. Chem. Soc. Dalton, **14**, 1362 (1977).
5. F. TAKUSAGAWA, K. HIROTSU, and A. SHIMADA. Bull. Chem. Soc. Jpn. **46**, 2020 (1973).
6. P. COPPENS, L. LIESEROWITZ, and D. RABINOVICH. Routines for the CDC 1604, Rehovoth, Israel.
7. D. CAHEN and J. A. IBERS. J. Appl. Crystallogr. **5**, 298 (1972).
8. J. A. IBERS and W. C. HAMILTON (*Editors*). International tables for X-ray crystallography. Vol. IV. Kynoch Press, Birmingham. 1974. Tables 2.2A and 2.3.1.
9. W. G. MUMME and G. WINTER. Inorg. Nucl. Chem. Lett. **7**, 505 (1971).
10. S. L. LAWTON and G. T. KOKOTAILO. Inorg. Chem. **11**, 363 (1972).
11. H. C. FREEMAN, G. N. STEPHENS, and I. F. TAYLOR. J. Chem. Soc. Chem. Commun. 366 (1974).
12. A. G. GASH, P. F. RODESILER, and E. L. AMMA. Inorg. Chem. **13**, 2429 (1974).
13. B. METZ and R. WEISS. Acta Crystallogr. B**29**, 1088 (1973).

The conformations of furanosides. A ^{13}C nuclear magnetic resonance study

NATSUKO CYR[1] AND ARTHUR S. PERLIN

Department of Chemistry, McGill University, Montreal, P.Q., Canada H3A 2A7

Received March 19, 1979

NATSUKO CYR and ARTHUR S. PERLIN. Can. J. Chem. 57, 2504 (1979).

A study of the conformations of 15 methyl aldohexo- and pentofuranosides in aqueous solution has been carried out, based primarily on measurements of coupling by ^{13}C-1 and ^{13}C-2 with protons of the five-membered ring. From these stereochemically-dependent data, and their correspondence with vicinal ^1H–^1H couplings, the conformation favored by each glycoside has been deduced. Although, in general, the coupling patterns exhibited by homologous pairs of hexoses and pentoses are closely similar, the α-*gluco* and α-*xylo* pair provide an exception: their data indicate that the latter favors the ^2E conformation, whereas the glucoside is characterized by interconverting E_4 and ^3E conformers. It appears that a *quasi*-equatorial exocyclic side chain and a *quasi*-axial C-1,O-1 bond (anomeric effect) are equally important stabilizing factors in furanosides. In a number of instances, the current findings differ from those obtained in earlier studies for configurationally-related furanose derivatives in organic media.

NATSUKO CYR et ARTHUR S. PERLIN. Can. J. Chem. 57, 2504 (1979).

On a effectué une étude des conformations de 15 aldohéxo- et pentofurannosides de méthyle en solutions aqueuses; cette étude est basée principalement sur des mesures de couplage entre les ^{13}C-1 et ^{13}C-2 avec les protons du cycle à cinq chaînons. A partir de ces données qui dépendent de la stéréochimie et de leur similitude avec les couplages vicinaux ^1H–^1H, on en déduit la configuration favorisée par chaque glycoside. Quoique, d'une façon générale, les couplages des paires homologues d'hexoses et de pentoses se ressemblent, la paire α-*gluco* et α-*xylo* correspond à une exception: leurs données indiquent que le dernier favorise une conformation ^2E alors que le glucoside est caractérisé par des conformères E_4 et ^3E en interconversion. Il semble qu'une chaîne latérale exocyclique *quasi*-équatoriale et une liaison C-1,O-1 *quasi*-axiale (effet anomère) soient aussi des facteurs stabilisants importants dans les furannosides. Dans un certain nombre de cas, nos résultats diffèrent de ceux obtenus au cours d'études antérieures effectuées sur les dérivés furannosides configurationnellement apparentés mais en solution dans des solvants organiques.

[Traduit par le journal]

Introduction

It has been known for many years that furanose sugars adopt conformations in which the five-membered ring is puckered. In 1947, an X-ray study by Beevers and Cochran (1) demonstrated that the D-fructofuranose residue in sucrose sodium bromide dihydrate has an envelope conformation in which C-4′ is displaced above the plane of the other four ring atoms. With developments in nucleic acid chemistry, extensive studies have been carried out on the solid state conformations of the ribo- and deoxyribofuranose moieties in these polymers and related nucleotides and nucleosides. Generally, either C-2′ or C-3′ of these compounds is displaced out of the plane of the furanose ring by 0.5–0.6Å, and a puckering angle in the vicinity of 35° is commonly observed (2, 3).

The conformations of diastereomeric furanoses and derivatives in solution are expected (4–8) to differ from each other in ways that reflect minimal non-bonded interactions between the ring substituents. However, for a given diastereomer (8, 9) there may be several pseudorotating envelope and twist conformations (10). Much of the evidence dealing with conformational isomerism in solution comes from the measurement of ^1H–^1H coupling constants (9, 11–17). For example, a small coupling constant (0–1 Hz) for vicinal *trans* protons is taken to indicate that the corresponding torsional angle is close to 90°, rather than 120°, whereas a large value of ^3J (~5 Hz) implies that the angle is closer to 180° than to 120°. However, less information is available as to the sense in which direction the ring is puckered from coupling data for vicinal *cis* protons, and the contributions to ^3J of factors other than torsional angle are difficult to assess. Hence many of the results available are tentative in nature.

In this study, we introduce an alternate criterion of furanose conformation, namely the stereochemical dependence of two-bond and three-bond ^{13}C–^1H coupling constants. Another aspect of the study con-

[1]Present address: Alberta Research Council, Edmonton, Alta.

0008-4042/79/182504-08$01.00/0

cerns the specific question of conformational isomerism in aqueous solution. That is, various methyl aldohexofuranosides and pentofuranosides in D_2O solution are dealt with here, whereas most of the earlier literature describes the characteristics of ester derivatives in organic solvents. We have also measured $^3J_{H,H}$ values for many of the glycosides which, in general, are shown to reinforce the conclusions based on the ^{13}C–^1H coupling data obtained.

Results and Discussion

^{13}C–^1H Coupling Constants, and the Conformational Analysis of Furanosides

From the data available on saturated systems, the ^1H-coupled ^{13}C spectrum of an aldofuranoside is expected to exhibit spin–spin splitting due to coupling across one, two, or three bonds (^1J, ^2J, ^3J) but not four or more bonds. All of these couplings are stereochemically dependent (20, 21). Hence, in order to study the ring conformation, carbons-1 and -2 are of primary interest because the multiplicities of their signals are affected only by protons of the ring, whereas carbons-3 and -4 can couple with exocyclic protons (e.g., H-5) and thereby introduce the additional problem of side-chain conformations. Generally, therefore, only the C-1 and C-2 portions of ^{13}C spectra are described here. Since C-1 resonates far downfield of the other carbons (18, 19), its signal always can be examined readily, although the C-2 signal of most of the compounds examined (19) also proved to be adequately well separated from the others. It is noteworthy, as will be seen below, that many of the C-1 and C-2 signals have the appearance of simple multiplets. Aside from this indication that the contributing couplings involved are often of the same magnitude, another simplifying factor is likely to be the low limit of resolution obtainable over the many hours of accumulation time required.

Three-bond Coupling, ^3J

The relationship between $^3J_{CH}$ and torsional (dihedral) angle is expressed by a Karplus type curve (18, 20–23). However, only vicinal coupling >2–2.5 Hz is directly observable in ^1H-coupled ^{13}C spectra of carbohydrate derivatives (20, 24, 25), although it may be detected as line broadening. According to the data for $^3J_{CCCH}$ or $^3J_{COCH}$ available from studies on carbohydrates (20–22, 26–28), this means that the signal multiplicities due to ^3J reported here must arise from torsional angle relationships >120° associated with puckering of the furanose ring.

Considering envelope forms (for simplicity, a twist form may be regarded as a combination of two envelope forms) several different dihedral angles may be envisaged between ^{13}C—C (or ^{13}C—O) and

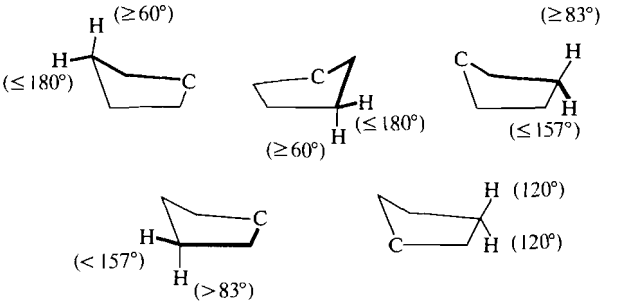

SCHEME 1. Dihedral angles between ^{13}C—C and C—^1H bonds in envelope conformations of furanosides. Heavy lines denote pathways expected to give rise to clearly observable values (~4–5 Hz) of $^3J_{CH}$.

C—^1H bonds under varying circumstances, as shown in Scheme 1. The maxima and minima listed are for extreme puckering of the ring (29), so that if the puckering is less pronounced the real angle would be be between 120° and the value given. Hence, only coupling pathways having the geometries represented by the heavy lines (Scheme 1) should be associated with an observable splitting (~4–5 Hz) of the C-1 or C-2 signal, due to interaction with H-3 and (or) H-4.

Two-bond Coupling, ^2J

Coupling between ^{13}C and ^1H nuclei separated by two bonds also is stereochemically dependent (20, 21, 25, 30, 31). Three categories of ^2J involving C-1 and C-2 nuclei have been recognized (21, 30, 31), according to the number and disposition of proximal oxygen atoms.

(*a*) *C-1,H-2*—Coupling between C-1 and H-2 is observed (~4–5 Hz) when the torsional angle between the two anomeric C—O bonds and the C-2—H-2 bond are similar (as in **1** and **2**) but not, as in **3**, when the angles are very different. According to molecular models, the arrangement of nuclei in **1** can be attained only in a 1,2-*trans* anomer, through extreme puckering; for the arrangement in **2**, eclipsing in a 1,2-*cis* anomer is required.

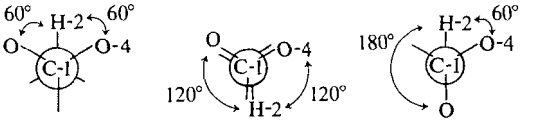

1 **2** **3**

(*b*) *C-2,H-1*—Coupling between C-2 and H-1 may be as large as 8 Hz when the dihedral angle between the C-2—O-2 and C-1—H-1 bonds is close to 180°C, and decreases with decreasing angle size to a value of ~0 Hz at 60°. On this basis, there should be observable coupling for arrangements of nuclei illustrated in Scheme 2, which are confined to 1,2-*cis* isomers.

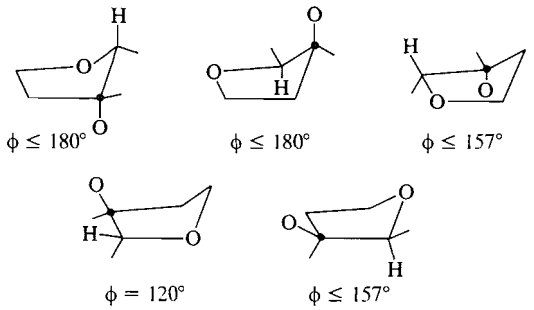

SCHEME 2. Orientations of C-1,^{1}H-1 and ^{13}C-2,O-2 bonds expected to give rise to clearly observable values (4–5 Hz) of $^2J_{CH}$ between ^{13}C-2 and ^{1}H-1 in furanosides.

(*c*) *C-2,H-3*—A coupling of ~5 Hz between C-2 and H-3 has been demonstrated when the angle between the ^{13}C-2—O-2 and C-3—^{1}H-3 bond is 60°, whereas ^2J is ~0 Hz when the angle is ≥ 120°. Therefore, if coupling between C-2 and H-3 is observed in a furanoside, O-2 and O-3 of that isomer must be close to *trans,gauche*.

Analyses of the ^{1}H-coupled Spectra of ^{13}C-1 and ^{13}C-2

Because $^1J_{CH}$ is large, each signal consists of two roughly equivalent segments separated by 150–175 Hz (24, 25). In a number of instances, only one of these segments could be examined because the second was obscured by overlap with other signals. Estimates of ^3J and ^2J were made from the spacings observed. Although some of these values could differ appreciably from the true J values, owing to second order effects (32), the discrepancies are assumed to be sufficiently small (32) so as not to invalidate the general conclusions reached. Furthermore, many of the spectra have been simplified, and the source of coupling confirmed, by the use of regioselectively deuterated glycosides.

Signal analyses for four methyl aldohexofuranosides are described below, as representative examples. The pentosides gave C-1 and C-2 signals closely resembling those of their six-carbon homologs, with one exception: the C-1 signal of methyl α-D-xylofuranoside was distinctly different from that of methyl α-D-glucofuranoside, and hence it is dealt with separately as a fifth example.

Methyl α-D-*Glucofuranoside (**4**)*

C-1 signal: (*a*) quintet, indicating coupling with one proton in addition to the three methyl protons; (*b*) a closely similar quintet was produced by the 4-deutero analog of **4**; (*c*) the 3-deutero analog of **4** produced a quartet. Therefore, C-1 couples with H-3; observed spacing, 4.5 Hz.

C-2 signal: (*a*) a triplet; (*b*) a closely similar triplet was produced by the 4-deutero analog of **4**; (*c*) the 3-deutero analog of **4** produced a doublet. Therefore, C-2 couples with H-2 and H-3; observed spacings, 4.0 Hz each.

Methyl α-D-*Mannofuranoside (**8**)*

C-1 signal: (*a*) broad septet, indicating coupling with two protons in addition to the methyl protons; confirmed by selective decoupling of latter protons, whereupon the signal became a triplet (centre peak broader than outside peaks); (*b*) quintet observed on selective decoupling of H-3; (*c*) quintet observed on selective decoupling of H-2 *plus* H-4 (overlapping signals); (*d*) selective decoupling, using the 3,5,6,6′-tetradeutero analog of **8** (33) showed that H-1 is coupled to C-4; in such circumstances, according to molecular models, there should not simultaneously be an observable coupling between C-1 and H-4.

Therefore, C-1 couples with H-2 and H-3; observed spacings, ~3 Hz and ~5 Hz, respectively.

C-2 signal: sharp singlet.

Therefore, C-2 does not couple with H-1, -3, or -4.

Methyl β-D-*Galactofuranoside (**11**)*

C-1 signal: quartet.

Therefore, C-1 does not couple with H-2, -3, or -4.

C-2 signal: doublet; according to Scheme 2, since O-2 and O-3 are *trans*, H-3 is suitably positioned for coupling (i.e., analogous to the *gluco* isomers).

Therefore, C-2 couples with H-3; observed spacing, 4.0 Hz.

Methyl α-D-*Allofuranoside (**6**)*

C-1 signal: (*a*) quintet, indicating coupling with one proton in addition to the methyl protons; (*b*) a closely similar quintet was produced by the 4-deutero analog; (*c*) the 3-deutero analog of **6** produced a quartet. Therefore, C-1 couples with H-3; observed spacing, 4.5 Hz.

C-2 signal: overlap with C-5 signal; appears to be sharp singlet.

Therefore, C-2 (probably) does not couple with H-1, -3, or -4.

Methyl α-D-*Xylofuranoside (**12**)*

C-1 signal: (*a*) quartet, attributable to coupling with methyl protons; (*b*) singlet produced by methyl-d_3 glycoside.

Therefore C-1 does not couple with H-2, -3, or -4.

Data obtained for 15 methyl furanosides, including values of $^1J_{CH}$, are presented in Tables 1 and 2.

Conformational Analysis of Furanosides

In selecting conformational possibilities consistent with the ^{13}C–^{1}H couplings observed and the various coupling pathways outlined in Schemes 1 and 2, the following procedure was adopted. For each of the ^3J

TABLE 1. ^{13}C-^{1}H coupling constants (Hz)[a] of methyl aldohexofuranosides

	α-*Gluco* (4)	β-*Gluco* (5)	α-*Allo* (6)	β-*Allo* (7)	α-*Manno* (8)	β-*Manno* (9)	α-*Galacto* (10)	β-*Galacto* (11)
$^{1}J_{C-1,H-1}$	174.0	172.5	174.5	174.0	172.4	175.0	174.0	172.0
$^{2}J_{C-1,H-2}$	0	0	0	0	~3	0	3.0[b]	0
$^{3}J_{C-1,H-3}$	4.0	4.5	4.5	0	~5	4	0[b]	0
$^{3}J_{C-1,H-4}$	0	0	0	~4	0	0	0	0
$^{2}J_{C-2,H-1}$	4.0	0	[c]	0	0	0	0	0
$^{2}J_{C-2,H-3}$	4.0	3.0	[c]	0	0	0	4.5	4.0
$^{3}J_{C-2,H-4}$	0	0	[c]	0	0	0	0	0

[a]Spacings measured directly from the ^{1}H-coupled ^{13}C spectra; a value of 0 Hz is reported when splitting was not observable.
[b]Coupling assignments may be reversed.
[c]C-2 signal obscured by overlap.

TABLE 2. ^{13}C-^{1}H coupling constants (Hz)[a] of methyl aldopentofuranosides

	α-*Xylo* (12)	β-*Xylo* (13)	α-*Ribo* (14)	β-*Ribo* (15)	α-*Lyxo* (16)	β-*Arabino* (17)	α-*Arabino* (18)
$^{1}J_{C-1,H-1}$	173.0	174.0	173.0	174.0	171.0	174.0	173.0
$^{2}J_{C-1,H-2}$	0	0	0	0	0	3.0[b]	0
$^{3}J_{C-1,H-3}$	0	4.0	4.0	0	4.0	0[b]	0
$^{3}J_{C-1,H-4}$	0	0	0	4.0	0	3.0	0
$^{2}J_{C-2,H-1}$	>3	0	[c]	0	0	0	0
$^{2}J_{C-2,H-3}$	>3	3.5	[c]	0	0	>4	3.5
$^{3}J_{C-2,H-4}$	0	0	[c]	0	0	0	0

[a]Spacings measured directly from the ^{1}H-coupled ^{13}C spectra; a value of 0 Hz is reported when splitting was not observable.
[b]Coupling assignments may be reversed.
[c]C-2 signal obscured by overlap.

TABLE 3. Conformations of methyl β-allofuranoside (7) compatible with observed values of ^{13}C–^{1}H coupling

	^{3}J (Hz)	Possible conformations
C-1,H-3	0	$^{1}\underline{E}$, E_2, ^{3}E, E_4, ^{0}E, E_0
C-1,H-4	4.5	$^{1}\underline{E}$, E_3, ^{4}E, E_0
C-2,H-4	0	$^{1}\underline{E}$, E_2, ^{3}E, E_4, ^{0}E, E_1

values involving C-1 and C-2 (i.e., due to coupling of C-1 with H-3 and (or) H-4, and coupling of C-2 with H-4) all possible conformations were examined, and those consistent with all of the ^{3}J values were judged to be feasible conformations. Two-bond coupling of C-1 with H-2 and C-2 with H-1 was then evaluated, in a number of instances, as a cross check.[2] An example of the procedure is given for methyl β-D-allofuranoside **7** in Table 3, which shows that only the ^{1}E conformer (C-1 is displaced upwards from the plane) is consistent with all of the observations. This conclusion also is compatible with the fact that neither C-1 nor C-2 of **7** exhibited two-bond coupling.

[2]Applied to methyl β-D-mannofuranoside, this form of analysis also served to identify H-3 as a source of coupling with H-1; details are presented as an addendum to the Experimental section.

Conformational possibilities deduced in this way for each of the furanosides are listed in the second column of Table 4. More than one choice is given for most compounds, although it is noteworthy that each grouping contains only immediate E neighbors in the pseudorotational itinerary defined for furanose rings (8, 9). Hence energy barriers within each chosen group should be sufficiently small to allow for ready conformational interconversions.

To narrow the choice of possibilities further, corresponding vicinal ^{1}H–^{1}H coupling constants have been evaluated. The latter values, obtained from 220 MHz ^{1}H spectra (with the aid of computer simulation), are collected in Table 4 together with the pertinent vicinal ^{1}H–^{1}H projected angles (29). When the observed values of $^{3}J_{HH}$ are inconsistent with a conformation listed, the latter is regarded as less of a possibility. For example, an E_2 or ^{3}E conformation for methyl α-D-mannofuranoside (**8**) is not in accord with the intermediate value of 3.0 Hz found for $J_{1,2}$ (Table 4), because these conformations are characterized by relatively large H-1, H-2 torsional angles corresponding (34) to ^{3}J values of >5 Hz. By contrast, an E_4 conformer would be more consistent with all of the data for **9**. A similar process of selection leads to the conclusion that an E_4 conformation is not an important contributor to the pseudorota-

TABLE 4. Conformational possibilities for methyl furanosides, corresponding dihedral angles ($\phi°$), and related $^3J_{H,H}$ values (Hz) obtained experimentally

Isomer	Conformations	$\phi_{1,2}$	$^3J_{1,2}$	$\phi_{2,3}$	$^3J_{2,3}$	$\phi_{3,4}$	$^3J_{3,4}$
α-*Gluco*	E_2	≤60		≥60		0	
	^3E	≤37	4.5	≥60	3.3	≤60	4.7
	E_4[a]	0		≥83		≤60	
β-*Gluco*	E_2[a]	≥60		≥60		0	
	^3E[a]	≥83	1.1	≥60	1.0	≤60	4.6
	E_4	120		≥83		≤60	
α-*Allo*	E_1	≤60	4.5	≤37	5.5	120	3.0
β-*Allo*	^1E	≥60	1.3	≤37	4.7	120	4.6
α-*Manno*	E_2	≤180		≤60		≤37	
	^3E	≤157	3.0(3.0)[b]	≤60	5.0(5.0)[b]	≤60	3.5(4.2)[b]
	E_4[a]	120		≤37		≤60	
β-*Manno*	E_2	≤60		≤60		≤37	
	^3E	≤37	4.9	≤60	5.0	≤60	3.8
	E_4[a]	0		≤37		≤60	
α-*Galacto*	^1E	≤60		≥83		120	
	E_3[a]	≤37	4.0	≤180	~5	≤180	—
	^4E[a]	0		≤157		≤180	
β-*Galacto*	E_0	≤180		120		120	
	E_3[a]	≤157	~2.0	≤180	—	≤180	—
	^4E[a]	120		≤180		≤180	
α-*Xylo*	^2E	≤60	4.5(4.4)	≤180	5.0(6.4)	<37	7.0(6.8)
β-*Xylo*	E_2[a]	≥60		≥60		<37	
	^3E[a]	≥83	0.7(<0.5)	≥60	1.6(1.8)	<60	4.4(5.3)
	E_4	120		≥83		<60	
α-*Ribo*	E_1	≤60	−(4.3)	≤37	−(6.5)	120	−(2.3)
β-*Ribo*	^1E	≥60	−(<0.5)	≤37	−(4.6)	120	−(7.0)
α-*Lyxo*	E_2	≤180		≤60		≤37	
	^3E	≤157	−(1.5)	≤60	−(5.2)	≤60	−(5.4)
	E_4[a]	120		≤37		≤60	
β-*Arabino*	^1E	≤60		≤83		120	
	E_3[a]	≤37	4.3(4.5)	≤180	7.5(7.2)	≤180	7.5(5.1)
	^4E[a]	0		≤157		≤180	
α-*Arabino*	E_0[a]	≤180		120		120	
	E_3	≤157	2.0(<0.5)	≤180	4.0(1.6)	≤180	6.5(4.9)
	^4E[a]	120		≤180		≤180	

[a]Conformational possibility more compatible with ^1H–^1H coupling data.
[b]These and other bracketed values are for peracetates.

tional itinerary of methyl β-D-glucofuranoside (**5**), and that this isomer is represented by interconverting E_2 and ^3E conformations.

An overall evaluation of our findings is presented in Scheme 3 in terms of the orientation of ring substituents in each of the furanosides. Two features are particularly prominent, i.e., very frequently the C-1—O-1 bond favours a *quasi* axial orientation, and the exocyclic C-4—C-5 bond a *quasi* equatorial orientation. Both of these features are consistent with well known stabilizing influences. The latter corresponds to the *quasi* equatorial preference of the methyl group of methylcyclopentane (4), and the former to operation of the anomeric effect (6–8, 35) which, in pyranoses, accounts for the stability of axial C-1—OR bonds. Noteworthy with respect to this general preference for a *quasi* axial orientation of the methoxyl function of the furanosides, is the fact (Table 1) that there is little variation in the magnitude of coupling between C-1 and H-1: all of the values are between 172 and 175 Hz. This is in contrast to the difference of ~10 Hz in $^1J_{C\text{-}1-H\text{-}1}$ that characterizes an axial, equatorial anomeric pair of pyranoses (20, 21, 36), and hence supports the conclusion above that the C-1 substituents of furanosides *tend* to be oriented in the same (axial) manner.

The process of ruling out certain conformational possibilities on the basis of the ^1H–^1H coupling data

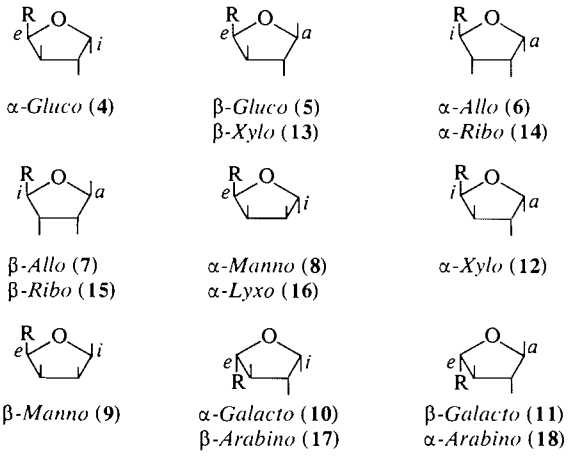

SCHEME 3. Orientations favored by ring substituents in methyl D-aldohexo- and pentofuranosides; **17** and **18** are L-enantiomers. For hexosides **4–11**, R = $CHOHCH_2OH$; for pentosides **12–18**, R = CH_2OH. Axial (*a*), equatorial (*e*), isoclinal (*i*).

helped materially in arriving at an overall consistency. For example, an α-*gluco* E_4 conformation appears preferable to an E_2 because it would incorporate an equatorial C-5, whereas O-1 would be equatorial in the E_2 conformation. However, an E_2 conformation is a more attractive possibility for the β-glucoside because this would be more compatible with the anomeric effect.

Hexofuranoside vs. Pentofuranoside

In almost all instances, the coupling patterns exhibited by C-1 and C-2 of the 6- and 5-carbon homologs are closely similar. This is true also of their vicinal ^1H–^1H coupling characteristics. Therefore, it is valid to assume that the ring conformation of a pentoside is essentially the same as that of the configurationally-related hexoside. The α-*gluco* (**4**) and α-*xylo* (**12**) pair provide an exception to this consistent picture; whereas C-1 of the former shows coupling with H-3 the analogous interaction is not observed for the xyloside, and the ^1H spectra of the two differ strikingly also in the magnitude of $^3J_{2,3}$ and $^3J_{3,4}$. Consequently, these compounds have been depicted (Table 4 and Scheme 3) by geometries that are remote from each other in the conformational itinerary of the furanoside ring (8, 9), i.e., $E_4 \rightleftarrows {}^3E$ for **4** and ^2E for **12**. The latter is characterized by an axial O-1 substituent, and the former by an equatorial side chain.

By considering all 15 compounds, it is seen (Scheme 3) that 10 favor a conformation in which the exocyclic side chain is equatorial, and 9 compounds favour a conformation in which O-1 is axial, whereas the β-*galacto*,α-*arabino* and β-*gluco*,β-*xylo* pairs incorporate both features. Hence, neither of these stabilizing orientations is predominant in determining the conformations of furanosides. A related consideration is the fact that when C-5 and O-3 are *cis*, puckering of the ring so as to orient C-5 equatorially eliminates eclipsing at the 3,4-position; similarly, *cis*-1,2 substituents are staggered (*quasi a,e*) when O-1 is axial. The α-*gluco* and α-*xylo* pair is distinguished from the other pairs of hexo- and pentofuranosides in having *cis* arrangements of substituents at both the 1,2- and 4,5-positions. Either of the associated eclipsing arrangements may be alleviated by suitable puckering of the ring, but not both simultaneously. There is evidence (19) that the —$CHOHCH_2OH$ moiety of **4** introduces substantially greater steric crowding than does the —CH_2OH of **12**. That is, aldohexofuranosides in which C-5 and O-3 are *cis* exhibit notable C-5 and C-4 upfield shifts as compared with their pentose homologs. Conceivably, then, this difference is sufficient to favor an equatorial orientation and staggered 4,5-substituents in the α-glucoside whereas, on balance, the anomeric effect and concomitant staggering of the 1,2-substituents may be the overriding factor for the α-xyloside.

TABLE 5. A comparison of conformational choices proposed for aldopentofuranose derivatives in different studies

	Present study	Bishop and Cooper (5)	Stevens and Fletcher (15)	Hall and co-workers (9)
α-*Xylo*	^2E	$^2T_3$	$^2T_3$	
β-*Xylo*	E_2, ^3E	$^2T_3$	$^3T_2$	E_2, ^3E
α-*Ribo*	E_1	^2E	^2E, $^2T_1$	^3E, E_3
β-*Ribo*	^1E	^3E	$^3T_2$	E_2, ^3E
α-*Arabino*	E_0, ^4E	$^2T_3$, $^3T_2$	$^0T_1$	E_3
β-*Arabino*	E_3, ^4E	E_2	$^1T_2$, E_2	
α-*Lyxo*	E_4	E_3	E_3	

The present findings may be compared with the results of ^1H nmr studies cited above. This is of interest particularly because the latter studies, in contrast to the current ones, have employed ester derivatives in organic media. The various data are compiled in Table 5; they deal only with aldopentofuranoses because hexose derivatives were not included in the earlier investigations. Also given in Table 5 are Bishop and Cooper's results of conformational analysis of methyl pentosides, based on thermodynamic data (5). All of the envelope (E) and twist (T) conformations represented in the Table appear within the following segment of the furanoid pseudorotational itinerary (8, 9); for simplicity, each T form is listed on the lower line between the two most closely related E forms:

$$\begin{array}{ccccccccccccccccccc} {}^4E & \rightleftarrows & E_0 & \rightleftarrows & {}^1E & \rightleftarrows & E_2 & \rightleftarrows & {}^3E & \rightleftarrows & E_4 & \rightleftarrows & {}^0E & \rightleftarrows & E_1 & \rightleftarrows & {}^2E & \rightleftarrows & E_3 \\ & & {}^4T_0 & & {}^1T_0 & & {}^1T_2 & & {}^3T_2 & & {}^3T_4 & & {}^0T_4 & & {}^0T_1 & & {}^2T_1 & & {}^2T_3 \end{array}$$

TABLE 6. Conformations of methyl β-mannofuranoside (**9**) compatible with observed values of ^{13}C–^1H coupling

		J (Hz)	Possible conformations
Case 1	C-1,H-3	4.5	^1E, $\underline{E}_2$, $^3\underline{E}$, $\underline{E}_4$
	C-1,H-4	0	E_1,[a] $\underline{E}_2$, ^2E,[b] $^3\underline{E}$, $\underline{E}_4$, ^0E
	C-1,H-2	0	Ring puckered at C-1,C-2
Case 2	C-1,H-3	0	E_1, ^2E, E_3, ^4E, ^0E, E_0
	C-1,H-4	0	E_1, ^2E, E_2, ^3E, E_4, ^0E
	C-1,H-2	4.5	Ring not puckered at C-1,C-2
Case 3	C-1,H-3	0	E_1, ^2E, E_3, ^4E, ^0E, E_0
	C-1,H-4	4.5	^1E, E_3, ^4E, E_0
	C-1,H-2	0	Ring puckered at C-1,C-2
Case 4	C-2,H-1	0	Not ^2E,[b] not E_1[a]
	C-2,H-1	0	^1E, E_1,[a] $\underline{E}_2$, $^3\underline{E}$, $\underline{E}_4$, ^0E

[a] E_1 eliminated by case 4.
[b] ^2E eliminated by case 4.

Since the various sets of data in Table 5 have all been obtained with different derivatives and (or) under different conditions, there is no reason a priori to expect general agreement as to the favored conformation associated with a given diastereomer. Nevertheless, a substantial number of consistencies are found. In four out of seven instances, the pentosides in water appear to adopt essentially the same conformations as do the corresponding ester derivatives examined by Stevens and Fletcher. Closely similar conclusions have been reached also for three out of the four diastereomers examined, as esterified glycosyl halides, by Hall and co-workers, and for four out of the seven evaluated by Bishop and Cooper. However, the degree of conformational variability for a given diastereomeric furanose is apparent from the fact that only the α-*ribo* species exhibits a consistent geometric preference throughout.

Experimental

Nuclear Magnetic Resonance Spectra

Proton-coupled ^{13}C spectra were recorded at 22.63 MHz with a Bruker WH-90 Ft spectrometer, using gated ^1H irradiation. The repetition time was ~2.5 s, the decouple time ~0.6 s, and the pulse width ~16 μs (~90°). Spectral widths of 1800–2400 Hz were used, giving a digital resolution of 0.5–0.6 Hz after Fourier transformation (4K real data points).

Proton nmr spectra were recorded at 220 MHz, by Dr. A. A. Grey of the Canadian 220 MHz NMR Centre.

Deuterium oxide was the solvent for unsubstituted compounds and $CDCl_3$ for their acetate derivatives, generally at concentrations of 0.2–0.4 g/mL.

Methyl Glycofuranosides

The preparation of these glycosides and monodeuterated analogs has been described earlier (19). Methyl-d_3 α-D-xylofuranoside was kindly furnished by Dr. J. E. Shin.

Assignment of ^{13}C–^1H Coupling in Methyl β-D-Mannofuranoside, and Conformational Analysis

The C-1 signal (downfield-half observed) was a quintet showing that, in addition to coupling with the methyl protons, C-1 couples (J = 4.5 Hz) with H-2, -3, or -4. These three possibilities (cases 1, 2, and 3) are associated in Table 6 with various envelope conformations of the glycoside. The additional fact that the C-2 signal (downfield-half observed) was a singlet, introduces two additional conditions to be satisfied. Complete correspondence is found only between the conformations in this latter group and those of case 1. Therefore, H-3 gives rise to the 4.5 Hz coupling with C-1 and, accordingly, the glycoside is expected to favor conformations E_2, ^3E, and (or) E_4, which are common to both sets.

Acknowledgments

Generous support by the Faculty of Graduate Studies and Research, McGill University, and by the National Research Council of Canada is gratefully acknowledged. The authors also express their thanks to Drs. R. G. S. Ritchie and J. E. Shin for valuable assistance, and to Dr. A. A. Grey for recording the 220 MHz ^1H spectra.

1. C. A. BEEVERS and W. COCHRAN. Proc. R. Soc. London, Ser. A, **190**, 257 (1947).
2. C. ALTONA and M. SUNDARALINGAM. J. Am. Chem. Soc. **94**, 8205 (1972).
3. G. A. JEFFREY and M. SUNDARALINGAM. Adv. Carbohydr. Chem. Biochem. **34**, 345 (1977), and references cited therein.
4. K. S. PITZER and W. E. DONATH. J. Am. Chem. Soc. **81**, 3213 (1959).
5. C. T. BISHOP and F. P. COOPER. Can. J. Chem. **41**, 2743 (1963).
6. R. U. LEMIEUX. *In* Molecular rearrangements. *Edited by* P. de Mayo. Wiley-Interscience, New York. 1963. p. 713.
7. (*a*) S. J. Angyal. Angew. Chem. Int. Ed. Engl. **8**, 157 (1969); (*b*) E. L. Eliel, N. L. Allinger, S. J. Angyal, and G. A. Morrison. Conformational analysis. Interscience, New York. 1965. p. 378.
8. J. F. STODDART. Stereochemistry of carbohydrates. Wiley-Interscience, New York. 1971. p. 97.
9. L. D. HALL, P. R. STEINER, and C. PEDERSEN. Can. J. Chem. **48**, 115 (1970).
10. J. E. KILPATRICK, K. S. PITZER, and R. SPITZER. J. Am. Chem. Soc. **75**, 5634 (1953).
11. C. D. JARDETSKY. J. Am. Chem. Soc. **82**, 229 (1960); **83**, 2919 (1961); **84**, 62 (1962).
12. R. U. LEMIEUX. Can. J. Chem. **39**, 116 (1961).
13. R. J. ABRAHAM, L. D. HALL, L. HOUGH, and K. A. MCLAUCHLAN. J. Chem. Soc. 3699 (1962).
14. A. S. PERLIN. Can. J. Chem. **42**, 1365 (1964).
15. J. D. STEVENS and H. G. FLETCHER, JR. J. Org. Chem. **33**, 1799 (1968).
16. J. ALFÖLDI, C. PECIAR, R. PALOVCIK, and P. KOVAC. Carbohydr. Res. **25**, 249 (1972).
17. C. ALTONA and M. SUNDARALINGAM. J. Am. Chem. Soc. **95**, 2333 (1973).

18. A. S. PERLIN, N. CYR, H. J. KOCH, and B. KORSCH. Ann. N.Y. Acad. Sci. **222**, 935 (1973).
19. R. G. S. RITCHIE, N. CYR, B. KORSCH, H. J. KOCH, and A. S. PERLIN. Can. J. Chem. **53**, 1424 (1975).
20. A. S. PERLIN and B. CASU. Tetrahedron Lett. 293 (1969).
21. J. A. SCHWARCZ and A. S. PERLIN. Can. J. Chem. **50**, 3667 (1972).
22. R. U. LEMIEUX, T. L. NAGABHUSHAN, and B. PAUL. Can. J. Chem. **50**, 773 (1972).
23. R. WASYLISHEN and T. SCHAEFER. Can. J. Chem. **50**, 2710 (1972).
24. A. S. PERLIN, N. CYR, R. G. S. RITCHIE, and A. PARFONDRY. Carbohydr. Res. **37**, C1 (1974).
25. A. S. PERLIN. *In* International review of science. Org. Chem. Ser. 2, Vol. 7. *Edited by* G. O. Aspinall. 1976. p. 21.
26. K. BOCK and C. PEDERSEN. Acta Chem. Scand. Ser. B, **31**, 354 (1977).
27. T. E. WALKER, R. E. LONDON, T. W. WHALEY, R. BARKER, and N. A. MATWIYOFF. J. Am. Chem. Soc. **98**, 5807 (1976).
28. G. K. HAMER, F. BALZA, N. CYR, and A. S. PERLIN. Can. J. Chem. **56**, 3109 (1978).
29. B. COXON. Methods Carbohydr. Chem. **6**, 527 (1972).
30. J. A. SCHWARCZ, N. CYR, and A. S. PERLIN. Can. J. Chem. **53**, 1872 (1975).
31. N. CYR, G. K. HAMER, and A. S. PERLIN. Can. J. Chem. **56**, 297 (1978).
32. N. CYR, R. G. S. RITCHIE, T. M. SPOTSWOOD, and A. S. PERLIN. Can. J. Spectrosc. **19**, 190 (1974).
33. F. BALZA, N. CYR, G. K. HAMER, A. S. PERLIN, H. J. KOCH, and R. S. STUART. Carbohydr. Res. **59**, C7 (1977).
34. M. KARPLUS. J. Chem. Phys. **33**, 316 (1960).
35. J. T. EDWARD. Chem. Ind. (London), 1102 (1955).
36. K. BOCK and C. PEDERSEN. J. Chem. Soc. Perkin Trans. II, 293 (1974).

The normal and the retro-Boulton–Katritzky rearrangement of hydroxy- and nitro-substituted benzofuroxans

ERWIN BUNCEL, NOEMI CHUAQUI-OFFERMANNS, AND ALBERT R. NORRIS

Department of Chemistry, Queen's University, Kingston, Ont., Canada K7L 3N6

Received April 16, 1979

ERWIN BUNCEL, NOEMI CHUAQUI-OFFERMANNS, and ALBERT R. NORRIS. Can. J. Chem. **57**, 2512 (1979).

The demethylation of 7-methoxy-4-nitrobenzofuroxan by aqueous KOH gives rise to 7-hydroxy-4-nitrobenzofuroxan as well as 5-hydroxy-4-nitrobenzofuroxan, the latter being formed via a retro-Boulton–Katritzky rearrangement. The retro rearrangement also occurs on heating the potassium salt of 7-hydroxy-4-nitrobenzofuroxan in the solid state. In basic aqueous solution 5-hydroxy-4-nitrobenzofuroxan undergoes the normal Boulton–Katritzky rearrangement to yield 7-hydroxy-4-nitrobenzofuroxan. These processes are rationalized on the basis of a balance between electrostatic and steric interactions in the reactants and the products of rearrangement.

ERWIN BUNCEL, NOEMI CHUAQUI-OFFERMANNS et ALBERT R. NORRIS. Can. J. Chem. **57**, 2512 (1979).

La déméthylation du méthoxy-7 nitro-4 benzofuroxanne par le KOH aqueux conduit à l'hydroxy-7 nitro-4 benzofuroxanne aux côtés de l'hydroxy-5 nitro-4 benzofuroxanne; ce dernier composé se forme par une transposition retro-Boulton–Katritzky. La transposition rétro se produit aussi par chauffage du sel de potassium de l'hydroxy-7 nitro-4 benzofuroxanne à l'état solide. En solutions aqueuses basiques, l'hydroxy-5 nitro-4 benzofuroxanne subit la transposition normale de Boulton–Katritzky et conduit à l'hydroxy-7 nitro-4 benzofuroxanne. On rationalise ces processus en se basant sur un équilibre entre les interactions stériques et électrostatiques dans les réactifs et les produits de la transposition.

[Traduit par le journal]

During our study (1–3) of σ-complex formation and reactivity in the nitrobenzofuroxan series (see also refs. 4–7), we observed that the compound **1** reacts with methoxide ion in methanol solution by competitive attack at the aryl carbon to give the σ-complex **2**, and at the aliphatic carbon to give the displacement product **3**, Scheme 1 (1). In order to ascertain whether demethylation could also be effected in a less activated system, we have extended the study to the mononitro analog **4**. We have in fact identified conditions under which demethylation does occur readily with this compound. However, unexpectedly, we found that the demethylated product **7** undergoes a retro-Boulton–Katritzky rearrangement to yield **5**, while under other conditions **5** undergoes a normal Boulton–Katritzky rearrangement (8–14) to give **7**. The observations are unlike previous reports of the simultaneous occurrence of the normal and retro-Boulton–Katritzky rearrangement processes.

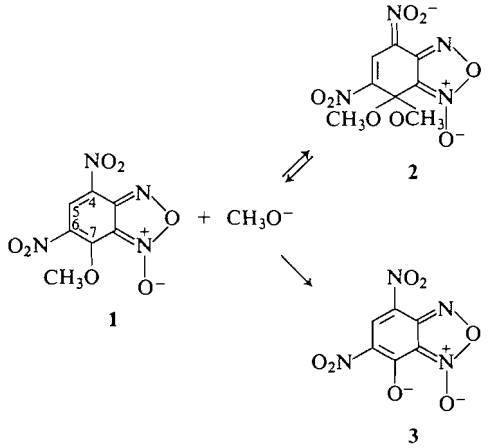

SCHEME 1

Results and Discussion

7-Methoxy-4-nitrobenzofuroxan (**4**) on heating at 55°C with aqueous KOH for 45 min, followed by acidification to pH 1, yielded a suspension consisting of a red solid and an orange colored solution. The separated red solid, after treatment with chloroform to remove traces of orange material, was recrystallized from water to yield a red crystalline material which was shown to be the potassium salt of 7-hydroxy-4-nitrobenzofuroxan (**7**). The orange filtrate was further acidified, extracted with chloroform, and worked up to yield a yellow solid shown to be 5-hydroxy-4-nitrobenzofuroxan (**5**). The following evidence was obtained as structure proof for the reaction scheme given in

0008-4042/79/182512-04$01.00/0

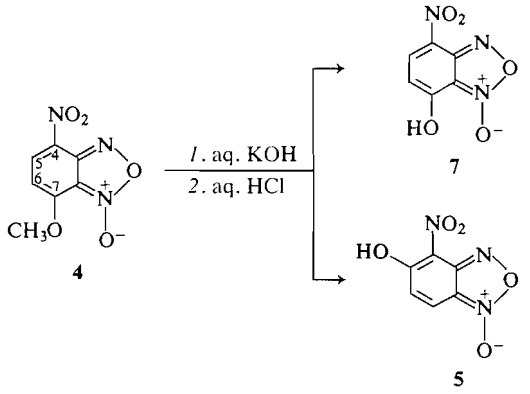

SCHEME 2

Scheme 2 (details of analytical data, etc. are given in the Experimental).

7-Hydroxy-4-nitrobenzofuroxan (7) and its Potassium Salt (7-K)

The red solid obtained as above exhibited in the nmr spectrum (Table 1) in DMSO-d_6 resonances (δ ppm), H_A 8.10 (d), H_B 5.60 (d), J_{AB} 10 Hz, assignable respectively to the protons adjacent to the NO_2 and O^- functions of **7**-K. For a series of 7-substituted 4-nitrobenzofuroxans the differences in the chemical shifts between the A and B protons, Δ_{AB}, has been found to range between 1.5 and 2.0 ppm (10). In the present system, the larger difference of 2.5 ppm is attributed to the greater shielding effect of the O^- function compared to the uncharged substituents examined in previous work (10). Acidification of the solution of the potassium salt in DMSO-d_6 with CF_3CO_2D led to a shift in the resonances, that is H_A 8.47 (d), H_B 6.52 (d), J_{AB} 9 Hz. The Δ_{AB} value of 1.95 ppm is now quite comparable to that (1.77 ppm) observed in **4** and related compounds and is in accord with the acid conversion of **7**-K to **7**. On treatment of the solution of the potassium salt in DMSO-d_6 with methyl iodide and monitoring by nmr, the characteristic spectrum of 7-methoxy-4-nitrobenzofuroxan (**4**) gradually evolved, that is H_A 8.61 (d), H_B 6.84 (d), J_{AB} 9 Hz, CH_3O 4.13 (s), thus providing definitive proof of structure.

5-Hydroxy-4-nitrobenzofuroxan (5)

The nmr spectral characteristics of the yellow solid in DMSO-d_6/CF_3COOD are given in Table 1. The assignment of the 7.88 resonance to H-7 and of the 7.24 resonance to H-6 of **5** is in accord with results in the literature for a number of 5-substituted 4-nitrobenzofuroxans (10). The difference in chemical shifts for the A and B protons, Δ_{AB} 0.64 ppm, compares with corresponding literature values of 0.3–0.8 ppm (10) reported for similar compounds. The reduced Δ_{AB} value in **5** compared with **7** can be accounted for by the weaker deshielding effect of the N(O) function relative to NO_2. The ir spectrum of **5** (KBr) presents the characteristic stretching absorption for intramolecular hydrogen-bonded hydroxyl at 3400–3600 cm^{-1}.

The Rearrangement Processes

The most plausible and consistent explanation of our experimental findings is that demethylation of **4** occurs by direct nucleophilic displacement to yield **7**, which then undergoes a retro-Boulton–Katritzky rearrangement to yield **5**. The possibility that a prior rearrangement of **4** had occurred to yield 5-methoxy-4-nitrobenzofuroxan can be discounted by the work of Ghosh (10), who showed that this compound readily undergoes the normal Katritzky–Boulton rearrangement at ambient temperature.

Interestingly, Ghosh observed (10) that 7-anilino-4-nitrobenzofuroxan (**6**) on heating above 150°C in the dry state changed, without melting, into the isomeric 5-anilino-4-nitrobenzofuroxan (**8**) (eq. [1]).

[1] 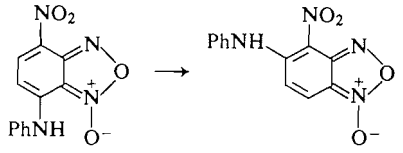

The compound **6** provided the only case of the retro-Boulton–Katritzky rearrangement in the course of examination of about a dozen 7-substituted 4-nitrobenzofuroxan derivatives. Ghosh suggested that the likelihood of a stronger NH···O_2N hydrogen bond in **8** compared with **6** (NH···ON distance 1.9 Å in **8** versus 2.3 Å in **6**) would compensate for the increased steric interactions in **8** compared with **6**. In accord with this explanation, the normal Boulton–Katritzky rearrangement (**8** → **6**) was found to occur in DMSO, which can act as a hydrogen bond acceptor (15, 16), but not in protic solvents (10).

In view of these proposals and the dearth of information concerning the factors which promote the retro-Boulton–Katritzky rearrangement (10), as well as current interest in the limits of the normal Boulton–Katritzky rearrangement (14), we decided to investigate further the interconversion of **5** and **7**.

When the solid potassium salt **7**-K was heated at 50°C under *vacuo* for 24 h, a color change from red to deep orange was observed. The uv–visible absorption spectrum of the resulting material was identical to that of the oxyanion of **5** (i.e., **5**-K), indicating the occurrence of the retro-Boulton–Katritzky rearrange-

TABLE 1. Nuclear magnetic resonance spectral characteristics of the hydroxy- and nitro-substituted benzofuroxans and their anions

Compound	H_A δ (ppm)	H_B δ (ppm)	Δ_{AB} δ (ppm)	J_{AB} (Hz)	Solvent
7-K 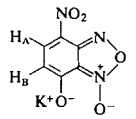	8.10	5.60	2.50	10.0	DMSO-d_6
7[a] 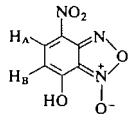	8.47	6.52	1.95	9.0	DMSO-d_6/CF_3CO_2D (80/20 v/v)
5-K[b] 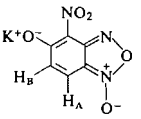	7.25	6.46	0.79	9.6	DMSO-d_6
5 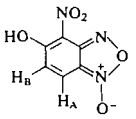	7.88	7.24	0.64	9.7	DMSO-d_6/CF_3COOD (80/20 v/v)

[a]Spectrum recorded following acidification of solution of 7-K in DMSO-d_6.
[b]Spectrum of material obtained from retro-Boulton–Katritzky rearrangement of 7-K (see text). A pure sample of 5-K, dissolved in DMSO-d_6 at room temperature, rapidly yields an equilibrium mixture of 5-K and 7-K in which 7-K is present in approximately 10-fold excess over 5-K.

[2] 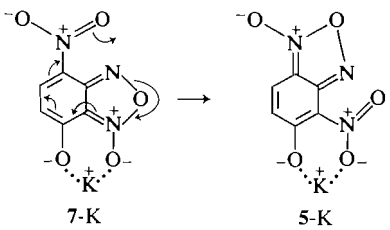
7-K 5-K

ment (eq. [2]). The nmr data for **5**-K are included in Table 1 and are in accord with the structural formulation of the rearranged material. It is noteworthy that this rearrangement could be brought about ~100° below the temperature required in the case of the transformation **6** → **8** (10).

As a contrasting experiment, it was of interest to examine the behaviour of the rearrangement product in aqueous solution. Thus a solution of **5** in a buffer of pH 10.3 was found to undergo the spectral changes which are illustrated in Fig. 1. These changes are characteristic of the conversion **5** → **7** (i.e., **5**-K → **7**-K, at pH 10.3) and indicate that a normal Boulton–Katritzky rearrangement is occurring. It is recalled that the anilino compound **8** showed no spectral changes in solutions of protic solvents (10).

The experiments described above show that we are dealing here with a reversible system, **7**-K ⇄ **5**-K, representing a retro- and a normal Boulton–

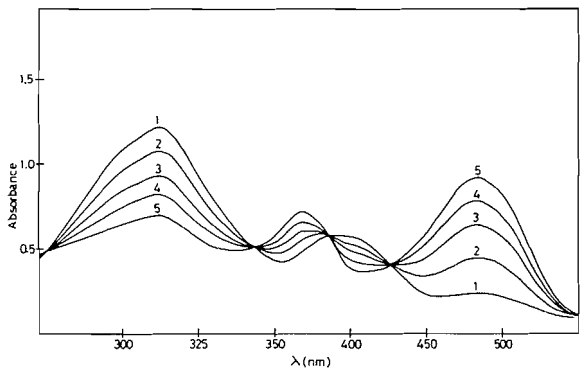

FIG. 1. Spectral scans of a solution of 5-hydroxy-4-nitrobenzofuroxan (7.14×10^{-5} *M*) at pH 10.3, 25°C, showing the transformation to 7-hydroxy-4-nitrobenzofuroxan. Scan times: (*1*) 1 min; (*2*) 30 min; (*3*) 75 min; (*4*) 135 min; (*5*) 16 h.

Katritzky rearrangement in the forward and reverse directions, respectively. Our present results can be explained by invoking electrostatic interactions as having a major influence on the type of process which occurs. In the solid state, the increased electrostatic attraction between K^+ and the two oxygen atoms in **5**-K, compared with the situation in **7**-K, will tend to overcome the unfavorable steric interactions in the former, so that the retro-Boulton–Katritzky rearrangement, **7**-K → **5**-K, is favored. In aqueous solution the free oxy anion will no longer be

TABLE 2. Ultraviolet–visible absorption spectral characteristics of hydroxy-nitrosubstituted benzofuroxans and their anions

Species	Medium	λ_{max} (ε), nm (L mol^{-1} cm^{-1})		
7	8*M* HCl	435 (7 370)	320 (5 630)	300 sh (5 600)
7-K	pH 10.3	484 (11 700)	371 (8 300)	312 (8 100)
5	7*M* HCl	402 (7 300)	320 (7 200)	277 (5 950)
5-K	pH 10.3	394 (6 720)	—	312 (15 500)

subject to influence from the potassium counterion, thus allowing the normal Boulton–Katritzky rearrangement, **5**-K → **7**-K, to occur. This explanation of the importance of electrostatic interactions is similar in principle to that invoked by Ghosh (10), even though in that system the normal Boulton–Katritzky rearrangement was not observed in aqueous solution, unlike the present case. We intend to study the kinetics of the rearrangement processes in these systems in order to shed more light on the normal as well as the retro-Boulton–Katritzky rearrangement.

Experimental

7-Methoxy-4-nitrobenzofuroxan (0.5 g, 2.4 mmol), prepared as described previously (3), was heated with 31 mL of 0.1 *N* KOH (3.2 mmol) at 55°C for 45 min. Cooling to 0°C, acidification with 1 *N* HCl to pH 1, and filtration yielded a red precipitate and an orange colored filtrate. The filtrate was further acidified with concentrated HCl, extracted with chloroform, the solvent evaporated, and the solid recrystallized from chloroform to yield **5** as yellow crystals, mp 170–172°C (dec.), *m/e* 197. *Anal.* calcd. for $C_6H_3N_3O_5$: C 36.57, H 1.53, N 21.32; found: C 36.56, H 1.51, N 21.17. The nmr data (Bruker 60 MHz HFX-60, with tetramethylsilane as internal standard) are given in Table 1.

The red solid obtained above was agitated with chloroform, to remove residual **5** as well as any unreacted **4**, and recrystallized from water to yield the potassium salt of **7**, i.e., **7**-K, as red crystals of the monohydrate, mp 275–277°C (dec.). *Anal.* calcd. for $C_6H_2N_3O_5K \cdot H_2O$: C 28.46, H 1.59, N 16.60, K 15.44; found: C 28.96, H 1.74, N 16.32, K 13.17.

For the methylation of **7**-K the red solid (0.066 mmol) was placed in an nmr tube, dissolved in 0.4 mL DMSO-d_6, treated with methyl iodide (0.12 mmol), and the nmr spectrum monitored with time. After 6 days at room temperature the characteristic resonances of **4** appeared (3) and a precipitate of potassium iodide was formed.

The uv–visible absorption spectra of **5** and **7** were obtained for the neutral and anionic forms. The spectral characteristics are given in Table 2. The *n*-butylamine/HCl buffer solution used in the experiment shown in Fig. 1 was prepared according to procedures outlined in ref. 17.

Acknowledgements

We gratefully acknowledge financial support of this research by the National Science and Engineering Research Council and the McLean Foundation (A.R.N.).

1. E. BUNCEL, N. CHUAQUI-OFFERMANNS, R. Y. MOIR, and A. R. NORRIS. Can. J. Chem. **57**, 494 (1979).
2. E. BUNCEL, N. CHUAQUI-OFFERMANNS, B. K. HUNTER, and A. R. NORRIS. Can. J. Chem. **55**, 2852 (1977).
3. E. BUNCEL, N. CHUAQUI-OFFERMANNS, and A. R. NORRIS. J. Chem. Soc. Perkin Trans. I, 415 (1977).
4. P. B. GHOSH, B. TERNAI, and M. W. WHITEHOUSE. J. Med. Chem. **15**, 255 (1972).
5. L. DINUNNO, S. FLORIO, and P. E. TODESCO. J. Chem. Soc. Perkin Trans. II, 1469 (1975).
6. F. TERRIER, F. MILLOT, A. P. CHATROUSSE, M. J. POUET, and M. P. SIMONNIN. Org. Magn. Reson. **8**, 56 (1976).
7. F. TERRIER, F. MILLOT, and W. P. NORRIS. J. Am. Chem. Soc. **98**, 5883 (1976).
8. A. J. BOULTON, P. B. GHOSH, and A. R. KATRITZKY. Angew. Chem. Int. Ed. Engl. **3**, 693 (1964); J. Chem. Soc. B, 1004 (1966).
9. F. B. MALLORY, S. L. MANATT, and C. S. WOOD. J. Am. Chem. Soc. **87**, 5433 (1965).
10. P. B. GHOSH. J. Chem. Soc. B, 334 (1968).
11. R. SOSA and L. PAOLONI. Tetrahedron, **25**, 4197 (1969).
12. A. J. BOULTON, I. J. FLETCHER, and A. R. KATRITZKY. J. Chem. Soc. C, 1193 (1971).
13. A. GASCO and A. J. BOULTON. J. Chem. Soc. Perkin Trans. II, 1613 (1973).
14. H. BALLI and S. GUNZENHAUSER. Helv. Chim. Acta, **61**, 2628 (1978).
15. A. J. PARKER. Q. Rev. Chem. Soc. **16**, 163 (1962).
16. E. BUNCEL and H. WILSON. Adv. Phys. Org. Chem. **14**, 133 (1977).
17. D. D. PERRIN and B. DEMPSEY. Buffers for pH and metal ion control. Chapman and Hall, London. 1974.

COMMUNICATIONS

Subtilisin Carlsberg, a chiral catalyst: an organic co-solvent

JOHN F. BECK AND JOHN F. MCMULLAN

Department of Chemistry, St. Francis Xavier University, Antigonish, N.S., Canada B2G 1C0

Received May 22, 1979

JOHN F. BECK and JOHN F. MCMULLAN. Can. J. Chem. 57, 2516 (1979).

The kinetics of subtilisin Carlsberg catalyzed hydrolyses of typical substrates in the presence of isopropanol indicate that this secondary alcohol could serve as a suitable organic co-solvent in synthetic applications of this enzyme.

JOHN F. BECK et JOHN F. MCMULLAN. Can. J. Chem. 57, 2516 (1979).

La cinétique d'hydrolyse de substances typiques catalysées par la subtilisine Carlsberg en présence d'alcool isopropylique indique que cet alcool secondaire peut servir de co-solvant organique idéal lorsque cet enzyme est utilisé en synthèse.

[Traduit par le journal]

The use of an enzyme as an asymmetric catalyst in an organic reaction sequence is contingent on the predictability of that enzyme acting on a foreign substrate, under conditions required to solubilize the substrate in the aqueous medium of the enzyme. Data providing this predictability are currently available for only a few enzymes, notably some mammalian hydrolases and various alcohol dehydrogenases (1, 2). The bacterial serine hydrolases, the subtilisins, possess a constitutional specificity which is potentially broader than all of the mammalian serine hydrolases (1), and have displayed a greater organic solvent stability while retaining a high degree of stereospecificity (3, 4). Because its reaction rates are higher than the other subtilisins (4, 5) we chose to investigate subtilisin Carlsberg as a potential organic reagent. We found that although data have begun to accumulate as to its action on foreign substrates (4–9), the organic co-solvents employed in these studies were either DMSO, dioxane, or primary alcohols. These are effective inhibitors of the enzyme (6, 10) and in the case of the alcohols, transesterification has also been shown to occur (4). Isopropanol being a secondary alcohol does not lead to transesterification due to steric factors and has, in fact, been reported to enhance the activity of the enzyme (4). Moreover, it has good solubilizing characteristics and can be easily purified and easily separated from the reaction products (compare DMSO).

The reaction kinetics of the subtilisin Carlsberg mediated hydrolyses of *N*-acetyl-L-tyrosine ethyl ester (NATEE) and of α-*N*-benzoyl-L-arginine ethyl ester (BAEE) were determined employing pH-stat methods (6) at pH 8 and 25°C. All reaction solutions were 0.1 *M* with respect to KCl and 0.02 *M* or 0.04 *M* NaOH solutions were used as titrants. Enzyme concentrations of about 1.8×10^{-8} *M* and 3.6×10^{-8} *M* were used for NATEE and BAEE respectively, while the substrate concentrations varied from 5.0×10^{-4} *M* to 9×10^{-3} *M*. Four isopropanol concentrations (1%–20% v/v) were compared to the essentially alcohol free conditions. The Michaelis–Menten constants were obtained using Lineweaver–Burke and least-squares regression analyses. All experiments were duplicated.

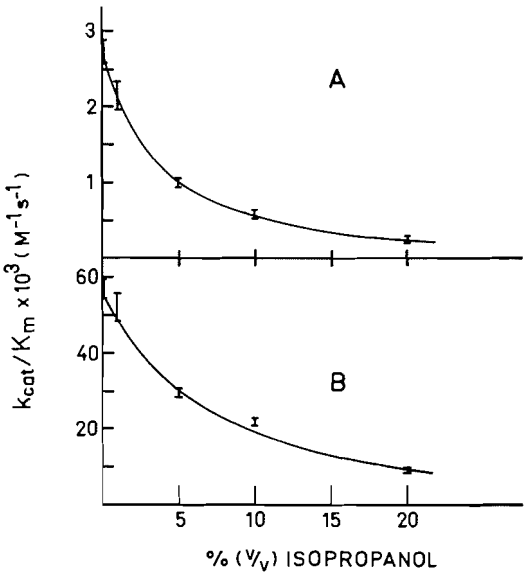

FIG. 1. k_{cat}/K_M (m^{-1} s^{-1}) versus isopropanol concentration (% v/v), pH 8, 25°C, 0.1 *M* KCl; (*A*) BAEE, (*B*) NATEE.

The results, presented in Fig. 1, indicate that the susceptibility (1) of both the NATEE and the BAEE

0008-4042/79/182516-02$01.00/0

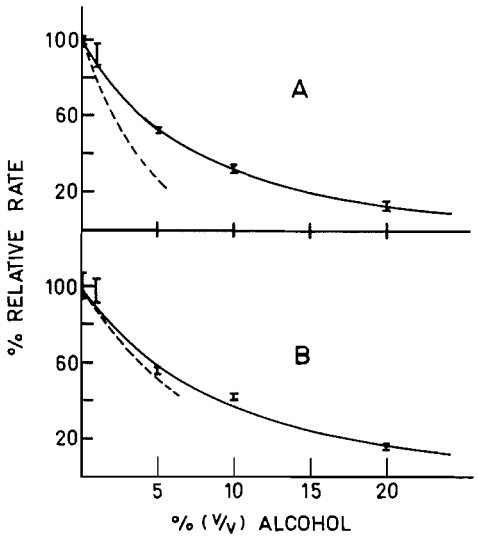

FIG. 2. % Relative rate versus alcohol concentration (% v/v) at a substrate concentration of 2.5×10^{-3} *M*, pH 8, 25°C, 0.1 *M* KCl. (*A*) BAEE with isopropanol (—); *p*-tosyl-argine methyl ester with methanol or ethanol (---) (10), (*B*) NATEE with isopropanol (—), with methanol or ethanol (---) (10).

to enzyme catalysis decreases as the isopropanol concentration increases. The effect over the range studied is greater for the more polar BAEE (ca. 11-fold decrease) compared to the less polar NATEE (ca. 6.4-fold decrease). This is due largely to a greater increase in K_M for BAEE (2.7-fold) than for NATEE (1.2-fold) and compares favourably with previous reports (10, 11) which conclude that the substrate binding forces in subtilisin Carlsberg are primarily hydrophobic in nature. As the alcohol concentration rises the solvation of these hydrophobic substrate binding sites (12) by the isopropanol stabilizes the enzyme, hindering substrate interactions (13). The NATEE competes more effectively with the isopropanol than does the BAEE, hence the above results.

The only published compilation (10) of solvent effects on subtilisin Carlsberg activity employing conditions similar to those used here is limited to reporting the relative rates versus solvent concentration. The primary alcohols are the least inhibitory solvents (10) and in order to compare the effects of isopropanol the reaction rates at a substrate concentration of 2.5×10^{-3} *M*, taken as a percent of the aqueous medium rates, were plotted versus alcohol concentration (Fig. 2). As is evident for NATEE, the isopropanol effects the catalysis somewhat less than the methanol or ethanol, which are the least inhibitory of the primary alcohols (10). In the case of the arginine derivatives the effects are more dramatic but it must be borne in mind that the interaction of the *p*-tosyl-arginine methyl ester will differ from that of the BAEE at the amide binding region (14) of the enzyme. This binding dissimilarity will account (1) for some of the observed difference in the rate profiles. Nevertheless, the more polar substrate displays a relative rate profile very similar to that of the less polar one, which is not the case for subtilisin Carlsberg inhibited by primary alcohols (10).

It would thus appear that the use of isopropanol with subtilisin Carlsberg offers the advantages of an organic co-solvent which is less inhibitory than the primary alcohols, but will not lead to transesterification (4) and is somewhat of a better solvent than ethanol or methanol.[1]

Acknowledgements

This research was supported by the National Research Council of Canada and by St. Francis Xavier University.

1. J. B. JONES and J. F. BECK. *In* Applications of biochemical systems in organic chemistry. Vol. X. *Edited by* J. B. Jones, D. Perlman, and C. J. Sih. J. Wiley and Sons, New York. 1976. p. 107.
2. C. J. SIH, E. ABUSHANAB, and J. B. JONES. Annu. Rep. Med. Chem. **12**, 298 (1977).
3. T. N. PATTABIRAMAN and W. B. LAWSON. Biochem. J. **126**, 645 (1972); **126**, 659 (1972).
4. A. N. GLAZER. J. Biol. Chem. **241**, 635 (1966).
5. A. N. GLAZER. J. Biol. Chem. **242**, 433 (1967).
6. M. OTTESEN and I. SVENDSEN. Methods Enzymol. **XIX**, 199 (1970).
7. F. S. MARKLAND, JR. and E. L. SMITH. The enzymes. Vol. III. *Edited by* P. D. Boyer. Academic Press, New York. 1971. p. 562.
8. M. S. MATTA and D. D. STALEY. J. Biol. Chem. **249**, 732 (1974).
9. Y. KARASAKI and M. OHNO. J. Biochem. Tokyo, **84**, 531 (1978).
10. I. SVENDSEN. C. R. Trav. Lab. Carlsberg, **38**, 385 (1971).
11. M. OTTESEN and I. SVENDSEN. C. R. Trav. Lab. Carlsberg, **38**, 369 (1971).
12. G. B. RALSTON. C. R. Trav. Lab. Carlsberg, **39**, 25 (1972).
13. R. P. BELL, J. C. CRITCHLOW, and M. I. PAGE. J. Chem. Soc. Perkin Trans. II, 66 (1974).
14. S. G. COHEN. Trans. N.Y. Acad. Sci. **31**, 705 (1969).

[1]In the present study NATEE was found to dissolve easily in a 1% (v/v) isopropanol–water solution but only with difficulty in 2% methanol or ethanol solutions.

Variable-temperature Raman spectroscopy as a probe of the supermolecular structure of ionomers

A. NEPPEL, I. S. BUTLER, AND A. EISENBERG
Department of Chemistry, McGill University, Montreal, P.Q., Canada H3A 2K6

Received May 24, 1979

A. NEPPEL, I. S. BUTLER, and A. EISENBERG. Can. J. Chem. 57, 2518 (1979).

Raman spectroscopy has been used for the first time to show the presence of multiplets and clusters of ion pairs in ethyl acrylate – sodium acrylate and styrene – sodium methacrylate ionomers and to determine the relative concentrations of ion pairs in these two different kinds of sites.

A. NEPPEL, I. S. BUTLER et A. EISENBERG. Can. J. Chem. 57, 2518 (1979).

La spectroscopie Raman a été utilisée pour la première fois dans le but de montrer d'une part, la présence de multiplets et des groupes de paires d'ions dans les ionomères suivants; acrylate d'éthyle – acrylate de sodium, et styrène – méthacrylate de sodium, et pour déterminer d'autre part la concentration relative des paires d'ions dans ces deux différentes sortes de sites.
[Traduit par le journal]

The state of aggregation of the ions in ion-containing polymers such as the copolymers of acrylic and methacrylic acid salts with ethylene, butadiene, and styrene is known to have a strong influence of the mechanical and rheological properties of the polymers (1, 2). Ion pairs are thought to be formed between the ionic sites on the polymer chains and the metal ions, and these ion pairs are further believed to conglomerate into groups of a few ion pairs called *multiplets* and into somewhat larger entities called *clusters* (3). Evidence for multiplet and cluster formation in styrene-based ionomers has come from such measurements as small angle X-ray scattering (4), water saturation experiments (5), dynamic mechanical (4) and dielectric loss studies (6), and far-infrared spectroscopy (7). We report here the first use of Raman spectroscopy to show the presence of multiplets and clusters in ionomers and, more importantly, how Raman intensity data can be used to determine the relative concentrations of ion pairs in the two different kinds of sites. This latter information is of importance in the designed synthesis of ionomers with specific properties and is not readily available by any other method.

The Raman spectra of powdered samples of ethyl acrylate – sodium acrylate and styrene – sodium methacrylate ionomers containing various mol% of ionic component have been investigated in the 22–250°C temperature range. Both series of ionomers exhibit characteristic weak Raman bands at ~ 250 and $\sim 170\ cm^{-1}$ which are not present in the spectra of the homopolymers and which, on the basis of previous far-infrared work on the styrene samples (7), can be assigned to multiplets and clusters of ion pairs, respectively. Unlike the infrared bands where it was impossible to measure their intensities because of strong overlapping with bands due to the polymer backbones, the intensities of the Raman bands could be readily determined. These intensities were obtained by measuring the areas of the two peaks and then correcting these areas for instrument response by comparison to suitable reference peaks of the host polymer. The Raman measurements were made on a Jarrell-Ash 25-300 spectrometer using 488.0 nm Ar^+ laser excitation (~ 85 mW at the samples) and the intensities of the bands at ~ 250 and $\sim 170\ cm^{-1}$ were determined for all the samples at 22, 150, 200, and 250°C.

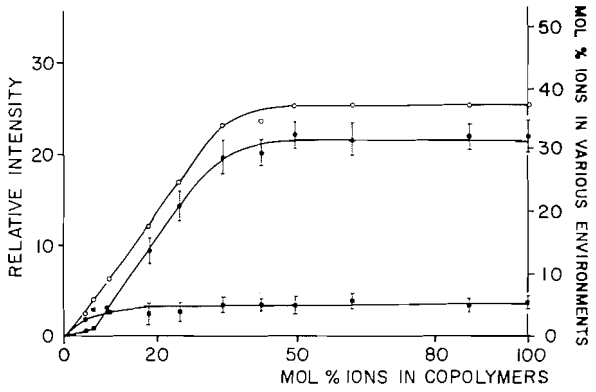

FIG. 1. Plots of the relative Raman intensities of the multiplet (■) and cluster (●) bands, and their sum (○), in the series of ethyl acrylate – sodium acrylate copolymers investigated at 22°C vs. mol% sodium acrylate.

In the case of the ethyl acrylate – sodium acrylate copolymers, at all four temperatures, the intensities of the multiplet and cluster Raman bands increase steadily with increasing sodium acrylate content up

0008-4042/79/182518-02$01.00/0

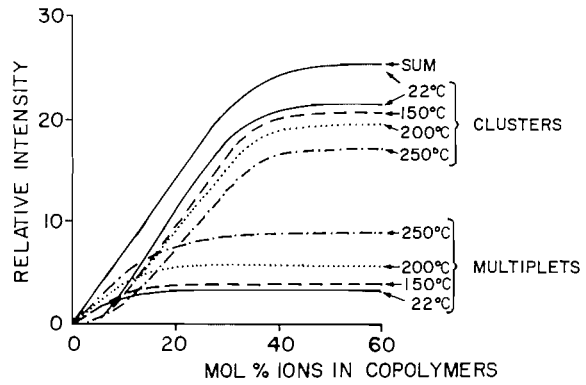

FIG. 2. Plots of the relative Raman intensities of the multiplet and cluster bands in the ethyl acrylate – sodium acrylate copolymers at four different temperatures vs. mol% sodium acrylate. Since their sum is essentially the same at all four temperatures, only that at 22°C is shown. The graphs follow the same monotonous trends from 60 to 100 mol% ions in the copolymers.

to about 10 and 35 mol%, respectively (Fig. 1). With increasing temperature, the multiplet band intensity increases while the cluster band intensity decreases for the complete composition range investigated (Fig. 2). This behaviour is in qualitative accord with earlier theoretical predictions (3) but has not been verified experimentally before the present study. The quantitative relations between the peak areas and the ion contents assumed in the above analysis can be deduced from the following considerations. As is seen in Fig. 1, the sum of the relative intensities of the multiplet and cluster bands between 0 and ~30 mol% gives an excellent linear correlation ($\bar{r}$ = 0.992) with the total ion content. This suggests that all the ions are accounted for by this technique. Furthermore, since in Raman spectroscopy the band intensities are directly proportional to the ion contents, and since the sums correlate so well with the total ion content, the individual band intensities are expected to show the same relation.

Throughout the temperature range investigated, the intensities of the multiplet and cluster Raman bands in the styrene – sodium methacrylate ionomers are essentially invariant to changes in temperature. Moreover, the intensity data reveal that at comparable total ion contents at room temperature the total number of ion pairs in multiplets is greater in the ethyl acrylate ionomers than in the styrene ones. For the ethyl acrylate ionomers, the multiplet saturation limit is reached at ~5 mol% of ionic groups, while for the styrene ionomers this limit is reached at ~2 mol%. Clearly, the multiplet solubility limit is a function of the host polymer and is most probably a direct consequence of the dielectric constant of the polymer backbone (poly(ethyl acrylate): ε = ~4.0; polystyrene: ε = ~2.5 (8)).

The sum of the relative intensities of the multiplet and cluster bands in the ethyl acrylate – sodium acrylate ionomers remains essentially constant above about 35–40 mol% of ionic groups. This suggests that at this approximate total ion content the matrix becomes saturated with clusters, just as it became saturated with multiplets at ~10 mol% of ionic groups. It appears, therefore, that above ~10 mol% ionic concentration, any additional ion pairs go into clusters, and that above the cluster solubility limit (~40 mol%), all further ionic groups go into a hitherto unsuspected third type of structure which has not as yet been detected by Raman spectroscopy.

In conclusion, Raman spectroscopy is an extremely useful technique for studying the supermolecular structure of ionomers and we are currently investigating the spectra of several other types of these industrially important copolymers.

Acknowledgements

One of us (A.N.) thanks the Social Sciences and Humanities Research Council of Canada for the award of a graduate scholarship. We acknowledge the research support of the Natural Sciences and Engineering Research Council of Canada, the Government of Quebec, and the U.S. Army Research Office.

1. L. HOLLIDAY. Ionic polymers. Halsted Press, Division of Wiley and Sons, New York. 1975. Chapt. 1.
2. A. EISENBERG and M. KING. Ion-containing polymers. Academic Press, New York. 1977.
3. A. EISENBERG. Macromolecules, 3, 147 (1970).
4. A. EISENBERG and M. NAVRATIL. Macromolecules, 7, 90 (1974).
5. A. EISENBERG and M. NAVRATIL. Macromolecules, 6, 604 (1973).
6. I. M. HODGE and A. EISENBERG. Macromolecules, 11, 283 (1978).
7. G. B. ROUSE, W. M. RISEN, JR., A. T. TSATSAS, and A. EISENBERG. J. Polym. Sci., Polym. Phys. Ed. 17, 81 (1979).
8. J. BRANDRUP and E. H. IMMERGUT (*Editors*). Polymer handbook. Interscience Publishers, New York. 1966.

Solution structures of dimeric methylpyrazolyl and indazolyl dimethyl-derivatives of boron, gallium, and indium from ^{1}H nuclear magnetic resonance data

LOUIS K. PETERSON[1]

Department of Chemistry, Simon Fraser University, Burnaby, B.C., Canada V5A 1S6

AND

KWAT I. THÉ

Departmento de Quimica, Universidade Federal da Paraiba, Joao Pessoa, Paraiba, Brazil

Received April 3, 1979

LOUIS K. PETERSON and KWAT I. THÉ. Can. J. Chem. **57**, 2520 (1979).

Trimethylboron and trimethylgallium react with 3-methylpyrazole to yield isomer pairs of dimeric products $[Me_2E(Mepz)]_2$ (E = B, Ga; Mepz = 3-methylpyrazolyl), in the approximate ratios 4:3 (E = B) and 9:1 (E = Ga), while trimethylindium gives a single species. Reactions of indazole with trimethylgallium and trimethylindium also yield a single structural isomer of the dimer $[Me_2Eind]_2$ (E = Ga, In; ind = indazolyl). Solution structures were interpreted on the basis of ^{1}H nmr data.

LOUIS K. PETERSON et KWAT I. THÉ. Can. J. Chem. **57**, 2520 (1979).

Le triméthylbore et le triméthylgallium réagissent avec la méthyl-3-pyrazole pour donner des paires d'isomères de produits dimères $[Me_2E(Mepz)]_2$ (E = B, Ga; Mepz = méthyl-3 pyrazolyle) dans les rapports approximatifs de 4:3 (E = B) et 9:1 (E = Ga), alors que le triméthylindium donne des espèces monomères. Les réactions de l'indazole avec le triméthylgallium et le triméthylindium donnent également un seul isomère structural du dimère $[Me_2Eind]_2$ (E = Ga, In; ind = indazolyle). L'attribution des structures a été faite sur la base des données de la rmn du proton.

[Traduit par le journal]

There is considerable interest in the coordination properties of the pyrazolyl derivatives of the Group III elements (1–7). The neutral, coordinatively saturated dimeric species $[R^1{}_2E(R_2pz)]_2$ (E = B, Al, Ga; R^1 = hydrogen, alkyl, aryl, or halogen; R = H, in pyrazolyl, or R = CH_3, in 3,5-dimethylpyrazolyl) are readily converted to monoanions $R^1{}_2E(R_2pz)_2^-$ which function as chelating ligands in a wide variety of metal complex systems (1–11). Structurally, the species $[R^1{}_2E(R_2pz)]_2$ and $[R^1{}_2E(R_2pz)_2M]$ (M = metal atom or ion plus associated ligands) contain a central, six-membered $[E(N—N)_2E]$ or $[E(N—N)_2M]$ metallocycle with representative structures ranging from relatively flexible boat configurations to planar or even shallow chair conformations (4, 12) for the six atoms.

We report here the preparation of $[Me_2E(Mepz)]_2$ (E = B, Ga, and In; Mepz = 3-methylpyrazolyl) and $(Me_2Eind)_2$ (E = Ga, In; ind = indazolyl) by the reaction of 3-methylpyrazole or indazole with the appropriate trimethyl–Group III derivative (see Experimental section).

The boron and gallium derivatives $[Me_2E(Mepz)]_2$ were obtained as isomeric pairs of products, in the approximate ratios 4:3 (E = B) and 9:1 (E = Ga), as determined from ^{1}H nmr spectra. Only one isomer of $[Me_2In(Mepz)]_2$ was observed.

The largest mass spectral fragment observed for all three $[Me_2E(Mepz)]_2$ compounds was M − 15, corresponding to the loss of one methyl group from the parent ion. A similar loss of a single alkyl group from the parent ion of $(Me_2Gapz)_2$ and $(Et_2Gapz)_2$ (6) and $(Me_2Inpz)_2$ has been observed,[2] and details of the fragmentation of 1-pyrazolylboranes (pyrazaboles) have been published (13).

From ^{1}H nmr evidence (see Table 1) the pseudoaxial and pseudoequatorial methyl—E groups of the more abundant isomer **1** of $[Me_2E(Mepz)]_2$ (E = B, Ga) are magnetically equivalent. In addition, the pairs of groups 3-Me/3′-Me, 4-H/4′-H, and 5-H/5′-H are equivalent. Consequently, the rapidly inverting structure A is assigned to isomer **1**. An alternative inverting chair structure would also satisfy the nmr evidence, but seems less likely on account of an independent X-ray crystal structure analysis which indicates a boat form for isomer **1** of $[Me_2Ga(Mepz)]_2$ (5). The boat inversion process in $(Me_2Gapz)_2$ has been shown to be rapid on the nmr time scale, even at −100°C (6).

Structure B is assigned to the less abundant isomer

[1]To whom all correspondence should be addressed.

[2]K. I. Thé. Unpublished results.

0008-4042/79/182520-03$01.00/0

TABLE 1. ^{1}H nmr data for isomers **1** and **2** of $[Me_2E(Mepz)]_2$[a,b]

(*a*) Isomer **1**

	τ			
E	Me_2E	3-Me 3′-Me	4-H 4′-H	5-H 5′-H
B	9.83s	7.62s	3.83d[c]	2.41d[c]
Ga	10.13s	7.63s	3.83d[d]	2.45d[d]
In	10.10s	7.63s	3.83d[e]	2.45d[e]

(*b*) Isomer **2**[f]

Me_2B[g]		3-Me 5′-Me	4-H 4′-H	3′-H 5-H
9.95s	9.72s	7.58s	3.83d[h]	2.50d[h]

[a]Spectra were run in $CDCl_3$, and data quoted are τ values relative to internal TMS, τ = 10.0.
[b]Mepz = 3-methylpyrazolyl.
[c]$J_{4,5}$ = 2.2 Hz.
[d]$J_{4,5}$ = 2.1 Hz.
[e]J = 2.0 Hz.
[f]The Me_2Ga resonances occurred at τ 10.03 and 10.18. Other ^{1}H resonances were not resolved from those of isomer **1** for $[Me_2Ga(Mepz)]_2$.
[g]τ 9.95 is assigned to the Me_2B protons proximal to the 3-Me and 5′-Me groups; τ 9.72 is assigned to Me_2B proximal to 3′-H and 5-H.
[h]$J_{4,5} = J_{3,4}$ = 2.2 Hz.

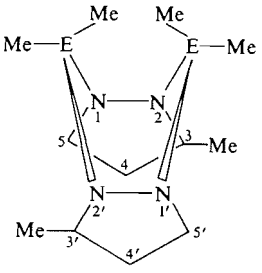

Structure A

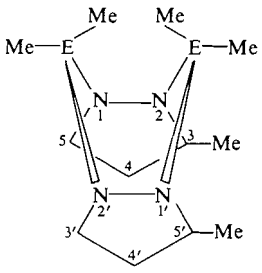

Structure B

2 of $[Me_2E(Mepz)]_2$ (E = B, Ga), on the basis of the observed magnetic distinction between the two sets of Me_2E groups. The six protons of the pairs of methyl groups are equivalent, however, by virtue of rapid inversion of boat forms, as are the pairs of groups 3-Me/5′-Me, 4-H/4′-H, and 5-H/3′-H. For isomer **2** of $[Me_2B(Mepz)]_2$, the more upfield resonance (at τ 9.95) is assigned to the Me_2B group proximal to the electron-releasing 3-Me and 5′-Me groups, while the second resonance (at τ 9.72) is due to Me_2B proximal to 5-H and 3′-H. The Me_2Ga groups of isomer **2** of $[Me_2Ga(Mepz)]_2$ are distinguished in a similar fashion. The chemical shift for the twelve equivalent Me_2E protons of structure A is the mean of the two distinct shifts for the protons of the two different Me_2E groups of structure B.

While structure A satisfies the ^{1}H nmr data obtained for the unique form of $[Me_2In(Mepz)]_2$, a

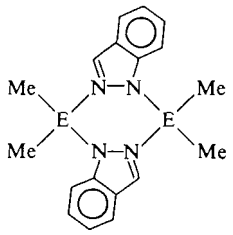

Structure C

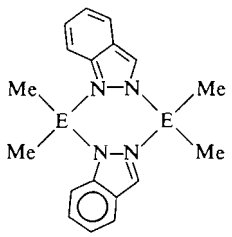

Structure D

completely planar $[In(N—N)_2In]$ bimetallocycle cannot be ruled out. Planar or near planar metallocycles have been found or proposed for $[Et_2B(4\text{-}Brpz)]_2$ (1), $[Me_2Ga(Me_2pz)]_2$ (4), $[Me_2Ga(Me_2pz)_2\text{-}Cu]$ (9), $[(pz)HBpz]_2$ (12), and $[(\phi_2PCH_2CH_2P\phi_2)\text{-}Pt(pz)_2\ Ni]^{2+}$ (14). It appears that boat configurations are generally preferred because of favourable bond angles about the Group III atom, and maximized delocalization of the π-electrons of the planar pyrazolyl rings in these structures (4). The flattening of the boat configuration is a function of the nature of the metal atoms within the metallocycle, and the need to minimize intramolecular steric repulsions (1, 4, 5, 12).

In principle, six structures are possible for the indazolyl derivatives $(Me_2Eind)_2$ (E = Ga, In), viz., boat, chair, and planar metallocycle configurations based upon structures C and D. In fact, the ^{1}H nmr solution spectra of the gallium and indium derivatives $(Me_2Eind)_2$ showed that the twelve Me—E protons were equivalent, thus eliminating structures based on D, and indicating a rapidly inverting boat or chair configuration C, or planar C. Of these possibilities, the chair conformation is least preferred, since the pyrazolyl rings would lose planarity to some extent, with a consequent loss of π-electron delocalization energy (4). In the solid phase, an independent X-ray diffraction study has shown that $(Me_2Gaind)_2$ adopts a boat configuration, based on structure C (5).

Experimental

All materials were handled using a high vacuum system or a nitrogen-filled drybox. 3-Methylpyrazole and indazole (K & K) were dried and sublimed before use. Me_3B (15) was made from BCl_3 (K & K), and Me_3In (16) from $InCl_3$ (K & K), according to published methods. Solvents were dried and distilled under nitrogen before use (17).

Analyses for C, H, and N were performed by the Departmental analyst, Simon Fraser University. Melting points were measured on samples in sealed capillaries, using a Gallenkamp instrument, and are uncorrected. In several cases, samples softened several degrees before melting, in a manner already described in the literature (18, 19). Mass spectra were determined with a double focusing RMU-6E Hitachi Perkin-Elmer instrument, and nmr spectra with the Varian XL100 spectrophotometer.

Preparation of $[Me_2E(Mepz)]_2$ *(E = B, Ga, In)*[3]

Reactions between 3-methylpyrazole (~1.5 mmol) and Me_3E (E = B, Ga, In; ~3 mmol) were carried out in sealed tubes, using ether as solvent in all cases except Me_3B. Reaction temperatures (and times) were: Me_3B, 100°C (~24 h); Me_3Ga, 80°C (3 days); Me_3In, 40°C (~24 h). Products were separated on a vacuum line. The derivatives $[Me_2E(Mepz)]_2$ were purified by sublimation under high vacuum, and were identified by elemental analysis, mass spectra, ^1H nmr (see Table 1), and ir spectroscopy.

$[Me_2B(Mepz)]_2$, yield, 90%. *Anal.* calcd. for $C_{12}H_{22}B_2N_4$: C 59.1, H 9.08, N 23.0; found: C 59.3, H 9.30, N 23.2.

$[Me_2Ga(Mepz)]_2$, yield, 80%, mp (isomer **1**) 47–48°C. *Anal.* calcd. for $C_{12}H_{22}B_2N_4$: C 39.8, H 6.09, N 15.5; found: C 40.1, H 6.20, N 15.2. Isomer **1** was obtained pure by repeated crystallization (from hexane) and repeated sublimation.

$[Me_2In(Mepz)]_2$, yield, 90%, mp 58–61°C. *Anal.* calcd. for $C_{12}H_{22}In_2N_4$: C 31.9, H 4.87, N 12.4; found: C 32.2, H 4.90, N 12.3.

Preparation of $[Me_2Eind]_2$ *(E = Ga, In)*

The procedure was similar to that described above, except that indazole was used in place of 3-methylpyrazole, and reaction temperatures were: Me_3Ga, 110°C; Me_3In, 80°C. Products were purified by sublimation under vacuum.

$[Me_2Gaind]_2$, yield, 90–100%, mp 125–128°C. *Anal.* calcd. for $C_{18}H_{22}Ga_2N_4$: C 49.8, H 5.08, N 12.9; found: C 49.9, H 5.03, N 13.0. ^1H nmr spectrum (in $CDCl_3$), τ 10.90 (s, 12H, Me—Ga), and a multiplet of ring protons (10H), centred at τ 3.17.

$[Me_2Inind]_2$, yield, 90–100%, mp 108–110°C. *Anal.* calcd. for $C_{18}H_{22}In_2N_4$: C 41.2, H 4.20, N 10.7; found: C 41.1, H 4.10, N 10.7. ^1H nmr spectrum (in $CDCl_3$), τ 10.77 (s, 12H, Me—In), and a multiplet (10H), centred at τ 3.17, for the ring protons.

[3]Reaction between 3-methylpyrazole and Me_3Al gave $[Me_2Al(Mepz)]_2$, sublimable when freshly prepared but rapidly becoming non-volatile. The product did not melt sharply, and analyses for C, H, and N were poor.

Acknowledgment

We thank the National Research Council of Canada for financial support of this research.

1. S. TROFIMENKO. Adv. Chem. Ser. **150**, 289 (1976).
2. S. TROFIMENKO. Chem. Rev. **72**, 497 (1972).
3. S. TROFIMENKO. Acc. Chem. Res. **4**, 17 (1971).
4. D. F. RENDLE, A. STORR, and J. TROTTER. Can. J. Chem. **53**, 2944 (1975).
5. D. F. RENDLE, A. STORR, and J. TROTTER. Can. J. Chem. **53**, 2930 (1975).
6. A. ARDUINI and A. STORR. J. Chem. Soc. Dalton, 503 (1974).
7. D. F. RENDLE, A. STORR, and J. TROTTER. Chem. Commun. 189 (1973).
8. K. R. BREAKELL, D. J. PATMORE, and A. STORR. J. Chem. Soc. Dalton, 749 (1975).
9. D. J. PATMORE, D. F. RENDLE, A. STORR, and J. TROTTER. J. Chem. Soc. Dalton, 718 (1975).
10. F. G. HERRING, D. J. PATMORE, and A. STORR. J. Chem. Soc. Dalton, 711 (1975).
11. D. F. RENDLE, A. STORR, and J. TROTTER. J. Chem. Soc. Dalton, 176 (1975).
12. N. W. ALCOCK and J. F. SAWYER. Acta Crystallogr. B**30**, 2899 (1974).
13. C. E. MAY, K. NIEDENZU, and S. TROFIMENKO. Z. Naturforsch. Anorg. Chem. Org. Chem. **31B**, 1662 (1976).
14. G. MINGHETTI, G. BANDITELLI, and A. F. BONATI. Chem. Ind. 123 (1977).
15. H. C. BROWN. J. Am. Chem. Soc. **67**, 374 (1945).
16. H. C. CLARK and A. L. PICKARD. J. Organomet. Chem. **8**, 427 (1967).
17. A. WEISSBERGER. Technique of organic chemistry. Vol. VIII. Organic solvents. Interscience Publishers, Inc., New York. 1955.
18. O. T. BEACHLEY, G. E. COATES, and G. KOHNSTAM. J. Chem. Soc. 3248 (1965).
19. H. C. CLARK and A. L. PICKARD. J. Organomet. Chem. **13**, 61 (1967).

A facile procedure for the introduction of a hydroxyethyl group. *S,S'*-Diethyl dithiomalonate as masked ethanol carbanion

HSING-JANG LIU AND HOI KIONG LAI

Department of Chemistry, University of Alberta, Edmonton, Alta., Canada T6G 2G2

Received June 22, 1979

HSING-JANG LIU and HOI KIONG LAI. Can. J. Chem. **57**, 2522 (1979).

A general procedure for the introduction of a hydroxyethyl group has been developed. *S,S'*-Diethyl dithiomalonate (**1**) readily undergoes substitution with a variety of electrophiles to give dithiomalonates $RR'C(COSEt)_2$ which on treatment with W-2 Ra-Ni afford ethanol derivatives $RR'CHCH_2OH$.

HSING-JANG LIU et HOI KIONG LAI. Can. J. Chem. **57**, 2522 (1979).

On a mis au point une méthode générale d'introduction du groupe hydroxyéthyle. Divers agents électrophiles provoquent des réactions de substitution sur le *S,S'*-dithiomalonate d'éthyle (**1**) et conduisent aux dithiomalonates $RR'C(COSEt)_2$. Ces derniers, traités par du Ni de Raney W-2 se transforment en dérivés de l'éthanol $RR'CHCH_2OH$.

[Traduit par le journal]

0008-4042/79/182522-04$01.00/0

Preparation of $[Me_2E(Mepz)]_2$ *(E = B, Ga, In)*[3]

Reactions between 3-methylpyrazole (~1.5 mmol) and Me_3E (E = B, Ga, In; ~3 mmol) were carried out in sealed tubes, using ether as solvent in all cases except Me_3B. Reaction temperatures (and times) were: Me_3B, 100°C (~24 h); Me_3Ga, 80°C (3 days); Me_3In, 40°C (~24 h). Products were separated on a vacuum line. The derivatives $[Me_2E(Mepz)]_2$ were purified by sublimation under high vacuum, and were identified by elemental analysis, mass spectra, ^1H nmr (see Table 1), and ir spectroscopy.

$[Me_2B(Mepz)]_2$, yield, 90%. *Anal.* calcd. for $C_{12}H_{22}B_2N_4$: C 59.1, H 9.08, N 23.0; found: C 59.3, H 9.30, N 23.2.

$[Me_2Ga(Mepz)]_2$, yield, 80%, mp (isomer **1**) 47–48°C. *Anal.* calcd. for $C_{12}H_{22}B_2N_4$: C 39.8, H 6.09, N 15.5; found: C 40.1, H 6.20, N 15.2. Isomer **1** was obtained pure by repeated crystallization (from hexane) and repeated sublimation.

$[Me_2In(Mepz)]_2$, yield, 90%, mp 58–61°C. *Anal.* calcd. for $C_{12}H_{22}In_2N_4$: C 31.9, H 4.87, N 12.4; found: C 32.2, H 4.90, N 12.3.

Preparation of $[Me_2Eind]_2$ *(E = Ga, In)*

The procedure was similar to that described above, except that indazole was used in place of 3-methylpyrazole, and reaction temperatures were: Me_3Ga, 110°C; Me_3In, 80°C. Products were purified by sublimation under vacuum.

$[Me_2Gaind]_2$, yield, 90–100%, mp 125–128°C. *Anal.* calcd. for $C_{18}H_{22}Ga_2N_4$: C 49.8, H 5.08, N 12.9; found: C 49.9, H 5.03, N 13.0. ^1H nmr spectrum (in $CDCl_3$), τ 10.90 (s, 12H, Me—Ga), and a multiplet of ring protons (10H), centred at τ 3.17.

$[Me_2Inind]_2$, yield, 90–100%, mp 108–110°C. *Anal.* calcd. for $C_{18}H_{22}In_2N_4$: C 41.2, H 4.20, N 10.7; found: C 41.1, H 4.10, N 10.7. ^1H nmr spectrum (in $CDCl_3$), τ 10.77 (s, 12H, Me—In), and a multiplet (10H), centred at τ 3.17, for the ring protons.

[3]Reaction between 3-methylpyrazole and Me_3Al gave $[Me_2Al(Mepz)]_2$, sublimable when freshly prepared but rapidly becoming non-volatile. The product did not melt sharply, and analyses for C, H, and N were poor.

Acknowledgment

We thank the National Research Council of Canada for financial support of this research.

1. S. TROFIMENKO. Adv. Chem. Ser. **150**, 289 (1976).
2. S. TROFIMENKO. Chem. Rev. **72**, 497 (1972).
3. S. TROFIMENKO. Acc. Chem. Res. **4**, 17 (1971).
4. D. F. RENDLE, A. STORR, and J. TROTTER. Can. J. Chem. **53**, 2944 (1975).
5. D. F. RENDLE, A. STORR, and J. TROTTER. Can. J. Chem. **53**, 2930 (1975).
6. A. ARDUINI and A. STORR. J. Chem. Soc. Dalton, 503 (1974).
7. D. F. RENDLE, A. STORR, and J. TROTTER. Chem. Commun. 189 (1973).
8. K. R. BREAKELL, D. J. PATMORE, and A. STORR. J. Chem. Soc. Dalton, 749 (1975).
9. D. J. PATMORE, D. F. RENDLE, A. STORR, and J. TROTTER. J. Chem. Soc. Dalton, 718 (1975).
10. F. G. HERRING, D. J. PATMORE, and A. STORR. J. Chem. Soc. Dalton, 711 (1975).
11. D. F. RENDLE, A. STORR, and J. TROTTER. J. Chem. Soc. Dalton, 176 (1975).
12. N. W. ALCOCK and J. F. SAWYER. Acta Crystallogr. B**30**, 2899 (1974).
13. C. E. MAY, K. NIEDENZU, and S. TROFIMENKO. Z. Naturforsch. Anorg. Chem. Org. Chem. **31B**, 1662 (1976).
14. G. MINGHETTI, G. BANDITELLI, and A. F. BONATI. Chem. Ind. 123 (1977).
15. H. C. BROWN. J. Am. Chem. Soc. **67**, 374 (1945).
16. H. C. CLARK and A. L. PICKARD. J. Organomet. Chem. **8**, 427 (1967).
17. A. WEISSBERGER. Technique of organic chemistry. Vol. VIII. Organic solvents. Interscience Publishers, Inc., New York. 1955.
18. O. T. BEACHLEY, G. E. COATES, and G. KOHNSTAM. J. Chem. Soc. 3248 (1965).
19. H. C. CLARK and A. L. PICKARD. J. Organomet. Chem. **13**, 61 (1967).

A facile procedure for the introduction of a hydroxyethyl group. *S,S'*-Diethyl dithiomalonate as masked ethanol carbanion

HSING-JANG LIU AND HOI KIONG LAI

Department of Chemistry, University of Alberta, Edmonton, Alta., Canada T6G 2G2

Received June 22, 1979

HSING-JANG LIU and HOI KIONG LAI. Can. J. Chem. **57**, 2522 (1979).

A general procedure for the introduction of a hydroxyethyl group has been developed. *S,S'*-Diethyl dithiomalonate (**1**) readily undergoes substitution with a variety of electrophiles to give dithiomalonates $RR'C(COSEt)_2$ which on treatment with W-2 Ra-Ni afford ethanol derivatives $RR'CHCH_2OH$.

HSING-JANG LIU et HOI KIONG LAI. Can. J. Chem. **57**, 2522 (1979).

On a mis au point une méthode générale d'introduction du groupe hydroxyéthyle. Divers agents électrophiles provoquent des réactions de substitution sur le *S,S'*-dithiomalonate d'éthyle (**1**) et conduisent aux dithiomalonates $RR'C(COSEt)_2$. Ces derniers, traités par du Ni de Raney W-2 se transforment en dérivés de l'éthanol $RR'CHCH_2OH$.

[Traduit par le journal]

0008-4042/79/182522-04$01.00/0

We recently observed that β-keto thiolesters undergo facile dealkylthiocarbonylation reaction when treated with Raney nickel under virtually neutral conditions (1).[1] An extrapolation of these results suggested that treatment of a 1,3-dithiol ester with Ra-Ni could induce the removal of one thiolester group with concomitant reduction of the other to the aldehyde or the alcohol level (2). On this basis, a general procedure has been developed for the introduction of a hydroxyethyl function, a process which is of considerable importance in organic synthesis. The overall transformation can be considered as the replacement of one or two β-protons of ethyl alcohol by electrophile(s) involving no more than three operationally simple steps using *S,S'*-diethyl dithiomalonate (**1**) as a latent ethanol carbanion according to the following general scheme.

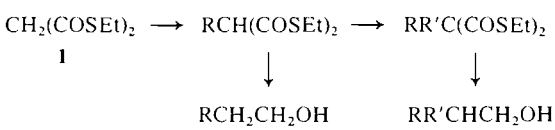

S,S'-Diethyl dithiomalonate (**1**), bp 105–106°C/3 Torr (lit. (3) bp 135°C/10 Torr), was readily prepared in 95% yield by the reaction of malonyl dichloride and ethanethiol (1.5 equiv.) in ether at room temperature for 16 h.[2] Dithiomalonate **1** was shown to react cleanly with a variety of alkyl halides[3] in the presence of sodium hydride in 1,2-dimethoxyethane (Table 1). Monoalkylation (Entries 1–4) could be achieved using one equivalent of base. When dialkylation with two identical substituents (Entry 5) or ring formation (Entry 6) are desired, substitution could be accomplished in one operation by using two equivalents of base. The incorporation of two different substituents (Entries 7–9) was best done via isolation and purification of the intermediate monosubstituted material followed by the second alkylation step. Electrophiles other than electrophilic carbon can also be used.[4] For example, treatment of the carbanion derived from dithiomalonate **2** with benzoyl peroxide in benzene produced the benzoyloxy derivative **4** in 97% yield (Entry 9).

Table 1 also summarizes the results of the reactions of the dithiomalonates with W-2 Ra-Ni[5] (9), all of which were carried out in benzene solution at room temperature under an atmosphere of nitrogen. In all cases, the dithiomalonate function was effectively reduced to a hydroxyethyl group and ethanol derivatives were obtained in good yields. Two especially noteworthy examples are the reductions of the dithiomalonates **3** and **4**. In each case, the reduction occurred smoothly with the *O*-ester group intact.

The preparation of 3-phenyl-1-propanol shown below illustrates the general procedure used.

To a suspension of sodium hydride (50% oil dispersion; 48 mg, 1 mmol) in 1,2-dimethoxyethane (5 mL) was added a solution of *S,S'*-diethyl dithiomalonate (192 mg, 1 mmol) in 1,2-dimethoxyethane (3 mL). The reaction mixture was stirred at room temperature under a nitrogen atmosphere for 10 min and a solution of benzyl chloride (163 mg, 1.3 mmol) in 1,2-dimethoxyethane (3 mL) was introduced. The resulting mixture was refluxed for 6 h. After cooling to room temperature, it was poured into ice-cold 1 *N* aqueous hydrochloric acid and extracted with ether. Column chromatography of the crude product obtained after the usual work-up of the extracts on silica gel with *n*-hexane elution resulted in the removal of the mineral oil from sodium hydride. Further elution with benzene–*n*-hexane (1:1) gave dithiomalonate **2** (244 mg, 87% yield): ir (neat) 1697, 1668 (thiolester), 1602, and 1585 (phenyl) cm^{-1}; nmr (CCl_4) δ: 7.13 (t, 5H, C_6H_5), 3.91 (t, 1H, CH), 3.15 (d, 2H, benzylic CH_2), 2.82 (q, 4H, $J = 8$ Hz, $COSCH_2$), and 1.23 (t, 6H, $J = 8$ Hz, CH_3); ms M^+: 282.0749 (calcd. for $C_{14}H_{18}O_2S_2$: 282.0749). To a solution of dithiomalonate **2** (95 mg, 0.34 mmol) in benzene (5 mL) was added 1 mL (settled volume) of W-2 Raney nickel suspended in benzene (5 mL). After stirring at room temperature under a nitrogen atmosphere for 1 h, the mixture was filtered and the residue washed thoroughly with benzene. Concentration of the filtrate gave an oil which was purified by column chromatography on silica gel. Elution with a solution of 30% ether in benzene afforded 35 mg (76% yield) of 3-phenyl-1-propanol.

In an attempt to extend the method to the direct synthesis of aldehydes, we examined the reaction of dithiomalonate **2** with Ra-Ni which had been

[1] We have since found that β-keto thiolesters readily undergo *C*-alkylation, and the dealkylthiocarbonylation of fully substituted β-keto thiolesters is equally effective. Results will be published elsewhere.

[2] For other methods, see refs. 3–5.

[3] Alkylation of dithiomalonate **1** has been previously studied using sodium in pyridine (6). Dithiomalonate **1** is also known to undergo Michael additions with ethyl acrylate and acrylonitrile (5) as well as reactions with diazomethane (5), aldehydes (7), and acid chlorides (8).

[4] See ref. 5 for bromination of dithiomalonate **1**.

[5] The rate of reduction was found to be sensitive to the quality of the Raney nickel. Slight variation of the procedure for preparation of the catalyst or storage of the catalyst for a period of time gave decreased reaction rates, however the reaction yields were unchanged.

TABLE 1. Substitution and reduction of dithiomalonates

		Substitution[a]				Reduction[b]		
Entry	Malonate	Reagent	Time (h)	Product[c]	(% yield)	Time (h)	Product[c]	(% yield)
1	**1**	$C_6H_5CH_2Cl$	6[d]	$C_6H_5CH_2CH(COSEt)_2$ **2**	(87)	1	$C_6H_5(CH_2)_3OH$	(76)
2	**1**	$C_6H_5CH_2Br$	20	**2**	(76)	—	—	—
3	**1**	$CH_3(CH_2)_4CH_2I$	48	$CH_3(CH_2)_5CH(COSEt)_2$	(78)	1	$CH_3(CH_2)_7OH$	(84)
4	**1**	$BrCH_2COOEt$	4	$EtOOCCH_2CH(COSEt)_2$ **3**	(90)	12	$EtOOC(CH_2)_3OH$	(77)
5	**1**	$C_6H_5CH_2Br$[e]	16	$(C_6H_5CH_2)_2C(COSEt)_2$	(100)	1.5	$(C_6H_5CH_2)_2CHCH_2OH$	(79)
6	**1**	$Br(CH_2)_5Br$[f]	48[d]	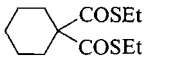	(91)	16	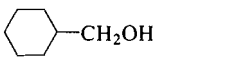	(84)
7	**2**	CH_3I	6	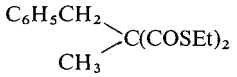	(100)	1	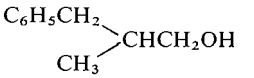	(66)
8	**2**	$(CH_3)_2CHI$	48[d]	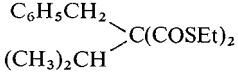	(61)	1	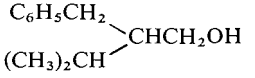	(81)
9	**2**	$(C_6H_5COO)_2$[g]	24	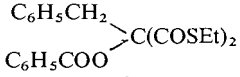 **4**	(97)	3	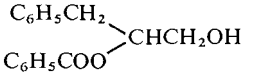	(72)

[a]Unless otherwise specified, substitution reactions were carried out at room temperature in 1,2-dimethoxyethane using 1 equiv. of NaH and 1.3 equiv. of the reagents listed.
[b]Without exception, reductions were performed in benzene at ambient temperature using ca. 10 mL (settled volume) of Ra-Ni (W-2)/g of substrate.
[c]All new compounds were adequately characterized by spectroscopic methods and by exact mass measurement and (or) elemental analysis.
[d]The reaction was carried out in refluxing 1,2-dimethoxyethane.
[e]2.2 equiv. of NaH and 2.4 equiv. of the reagent were used.
[f]2 equiv. of NaH was used.
[g]Benzene was used as a solvent.

deactivated with acetone (2) to various degrees (room temperature reflux for 0.5–3 h). However the results were unpromising; the best obtained was a 2:3 mixture of 3-phenylpropanal and the corresponding alcohol.

Acknowledgments

We are grateful to the Natural Science and Engineering Research Council of Canada and the University of Alberta for financial support.

1. H. J. Liu and H. K. Lai. Tetrahedron Lett. 1193 (1979).
2. E. Mosettig. Org. React. **8**, 229 (1954).
3. J. E. Purvis, H. O. Jones, and H. S. Tasker. J. Chem. Soc. **97**, 2289 (1910).
4. L. B. Dashkevich and V. A. Pechenyuk. Zh. Org. Khim. **3**, 636 (1967).
5. S. Scheithauer and R. Mayer. Chem. Ber. **100**, 1413 (1967).
6. V. A. Pechenyuk and L. B. Dashkevich. Izobret., Prom. Obraztsy, Tavarnye Znaki. **45**, 23 (1968); Chem. Abstr. **69**, 35465g (1968).
7. V. A. Pechenyuk and L. B. Dashkevich. Otkytiya, Izobret., Prom. Obraztsy, Tavarnye Znaki. **47**, 30 (1970); Chem. Abstr. **74**, 41933C (1971).
8. L. B. Dashkevich and L. V. Kouovalova. Zh. Org. Khim. **8**, 2269 (1972).
9. R. Mozingo. Org. Synth. Coll. Vol. **3**, 181 (1955).

Canadian Journal of Chemistry
Published by
THE NATIONAL RESEARCH COUNCIL OF CANADA

Journal canadien de chimie
Publié par
LE CONSEIL NATIONAL DE RECHERCHES DU CANADA

Volume 57 Number 19 October 1, 1979 Volume 57 numéro 19 1 octobre 1979

Ipso nitration XXI.[1] Nitration of *p*-tolylalkanoic acids and derivatives: spiro adducts

ALFRED FISCHER, DAVID R. A. LEONARD, and ROLF RÖDERER
Department of Chemistry, University of Victoria, Victoria, B.C., Canada V8W 2Y2

Received March 2, 1979

ALFRED FISCHER, DAVID R. A. LEONARD, and ROLF RÖDERER. Can. J. Chem. **57**, 2527 (1979).

Nitration of 4-(*p*-tolyl)butyric acid and of 3-(*p*-tolyl)propionic acid in acetic anhydride gives good yields of the diasteriomeric spiro lactone adducts **1** and **12**, respectively. Nitration of methyl 4-(*p*-tolyl)butyrate, 4-(*p*-tolyl)butanol, and 4-(*p*-tolyl)butyl acetate gives nitronium acetate adducts but does not give spiro adducts.

ALFRED FISCHER, DAVID R. A. LEONARD et ROLF RÖDERER. Can. J. Chem. **57**, 2527 (1979).

La nitration de l'acide (*p*-tolyl)-4 butyrique et de l'acide (*p*-tolyl)-3 proprionique dans l'anhydride acétique conduit avec de bons rendements aux spiro lactones diastéréoisomères **1** et **12**. La nitration du (*p*-tolyl)-4 butyrate de méthyle, du (*p*-tolyl)-4 butanol et de l'acétate de (*p*-tolyl)-4 butyle conduit aux adduits acétates de nitromium mais non pas aux adduits spiro.
[Traduit par le journal]

Nitration, in acetic anhydride, of aromatic compounds containing an activated *ipso* position, leads to the formation of nitronium acetate adducts (1–5). Such adducts are formed in particularly high yield from *p*-xylene and other *p*-dialkylbenzenes (6–11). The compounds studied in the present work: 4-(*p*-tolyl)butyric acid, methyl 4-(*p*-tolyl)butyrate, 4-(*p*-tolyl)butan-1-ol, 4-(*p*-tolyl)butyl acetate, 3-(*p*-tolyl)-propionic acid, and *p*-tolylacetic acid may be regarded as side-chain derivatives of dialkylbenzenes. Formation of significant amounts of adducts is therefore to be expected from these substrates.

Results and Discussion

Nitration of 4-(*p*-tolyl)butyric acid in acetic anhydride gave a crude product which contained 65% of dienes. Recrystallization gave one diastereoisomer of the lactone of 4-(1′-hydroxy-4′-methyl-4′-nitrocyclohexa-2,5-dienyl)butyric acid (**1***a*) and the other diastereoisomer **1***b* was obtained on chromatography. Formation of the adduct 4-(4′-acetoxy-4′-methyl-1′-nitrocyclohexa-2,5-dienyl)butyric acid (**2**) also apparently occurred since a diene with a methyl peak at δ 1.45 ppm was evident in a late (polar) column fraction. The higher field methyl group is typical of a methyl *ipso* to acetate (10). In **1***a* and **1***b* the methyl groups (*ipso* to nitro) are at lower field, δ 1.78 and 1.72 ppm. The methyl peak at 1.45 ppm was also evident in the spectrum of the crude reaction product, as was another smaller peak at 1.32 ppm (possibly from a diastereoisomer). The 1.45 ppm peak was ca. one third of the height of the peaks at 1.72 and 1.78 ppm and thus nitration *ipso* to the methyl group is favoured over nitration *ipso* to the butyric acid side-chain. Nitration *ipso* to the methyl was found to be preferred to nitration *ipso* to other alkyl groups (8–10), a result attributed to the increase of steric hindrance with size of the alkyl group. A similar explanation is applicable in the present case. Formation of the lactone **1** in preference to nitronium acetate adduct **4** shows that in the intermediate cyclohexadienyl cation **6** the carboxylic acid group competes effectively with the external nucleophile (acetic acid or acetic anhydride) in adding to the tertiary carbonium ion centre. Other reaction products include the expected 4-(4′-methyl-2′-nitrophenyl)-butyric acid and its 3′-nitro isomer and the lactone of 4-hydroxy-4-(*p*-tolyl)butyric acid

[1]For Part XX, see ref. 5.

0008-4042/79/192527-06$01.00/0

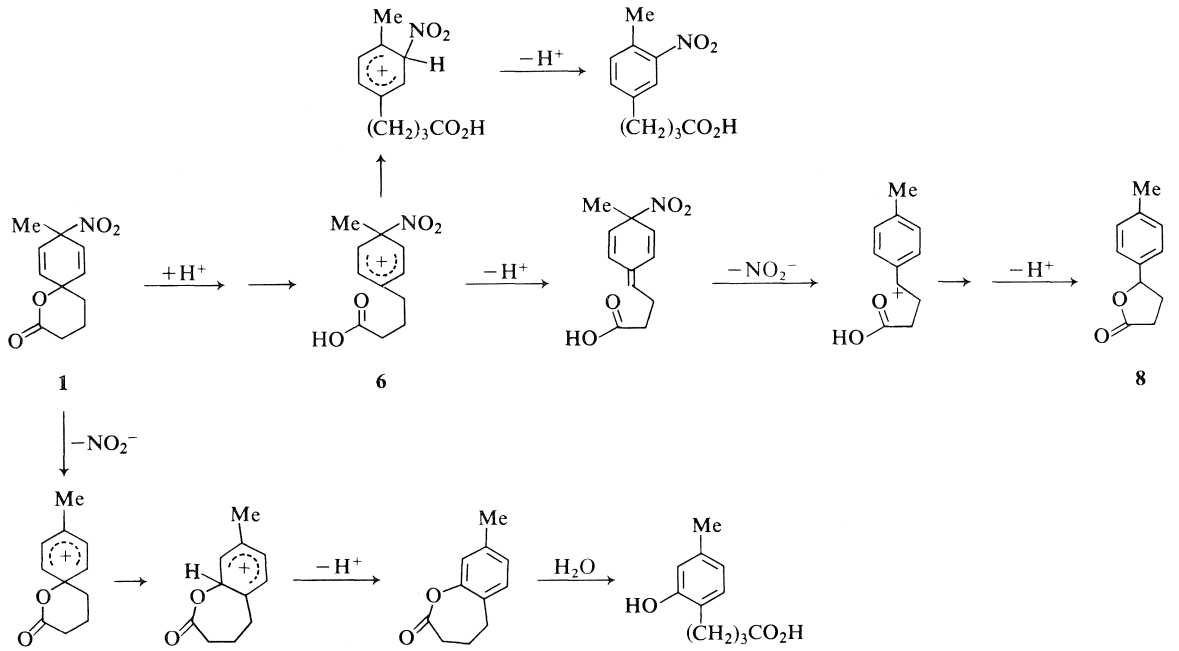

SCHEME 1. Reactions of lactone **1**.

(**8**). Formation of lactone **8** is a parallel to the reactions leading to side-chain derivatives commonly observed accompanying the nitration of polymethylbenzenes containing *para* alkyl groups (12). The probable mechanism is shown in Scheme 1, **6** → **8**.

Nitration of methyl 4-(*p*-tolyl)butyrate gave 40% of diene adducts. Four isomers appeared to be present in the crude reaction product, two with lower field methyl groups (δ 1.77 and 1.70 ppm) which are assigned as the diastereoisomers of **5** with nitro *ipso* to methyl, and two with higher field methyl groups (δ 1.46 and 1.48 ppm), presumably the diastereoisomers of **3**. Dienes **5** were present in greater amount. The dienes were partially separated by chromatography but only one of them, one diastereoisomer of **5**, was able to be crystallized and thus obtained pure. In this case the nitronium acetate adduct is formed in preference to the lactone **1** and it appears that the methoxy carbonyl function is not able to compete effectively with the solvent nucleophile in adding to the tertiary cation centre of **7**. However, it is also possible that ring closure by the ester function of **7** is fast but that demethylation of the resulting cation **9** is slow relative to its reversion to **7** and eventual reaction of the latter with solvent.

Nitration of 4-(*p*-tolyl)butanol followed a similar pattern to that of the butyrate ester in that adducts were obtained with nitro *ipso* to methyl in the predominant pair of diastereoisomers and with nitro *ipso* to the tetramethylene side-chain in the minor

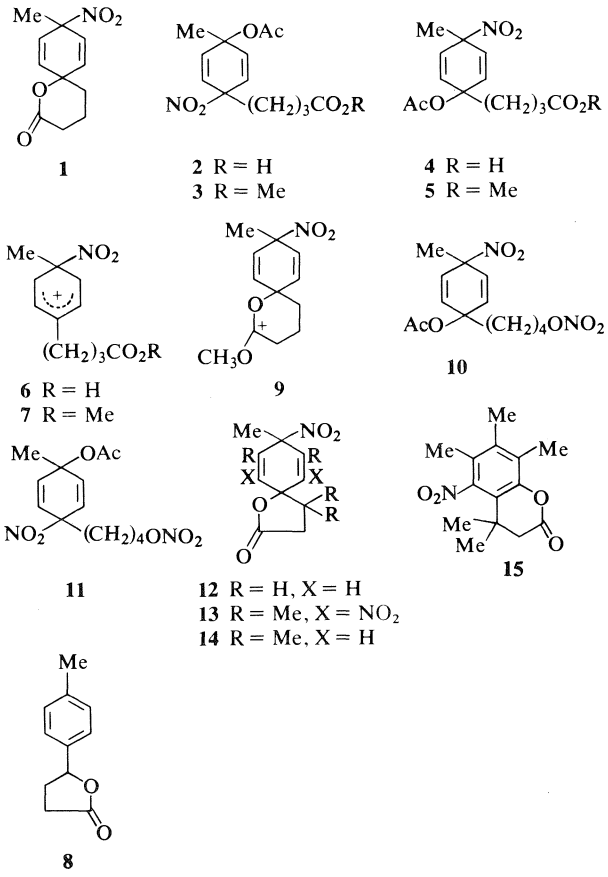

pair of diastereomers (Table 1). No spiro ether product resulting from ring closure in the nitrocyclohexadienyl cation was observed. This observation does not necessarily mean that the intramolecular addition of hydroxyl to the cationic centre is not competitive with the attack by the solvent nucleophile, since the alcohol function was converted into the nitrate ester in the course of the reaction and this may have preceded the addition of nitronium ion to the aromatic ring.

Nitration of 4-(*p*-tolyl)butyl acetate gave ~60% of diene adducts. Only partial separation of the diene adducts was achieved on chromatography. However, it was possible to recognise at least three different dienes in the various fractions. Two of the dienes had nitro *ipso* to methyl since the methyl peak in each was at lower field, δ 1.77 and 1.71 ppm, respectively. The third, with a methyl peak at δ 1.48 ppm, evidently had nitro *ipso* to the butyl acetate side-chain and acetate *ipso* to methyl. All of the fractions exhibited two peaks in the acetate region (δ 1.96 and 2.02 ppm) and there was no evidence for the formation of spiro product.

Nitration of 3-(*p*-tolyl)propionic acid gave ~70% of diene adducts. The diastereoisomeric diene lactones **12***a* and **12***b* were isolated from the reaction mixture. The mother liquid remaining after isolation of the dienes was heated with acetic acid to decompose any residual dienes. From this the normal nitration products, 3-(4′-methyl-2′-nitrophenyl)propionic acid and 3-(4′-methyl-3′-nitrophenyl)propionic acid were isolated and, in addition, a compound tentatively assigned as 7-methyldihydrocoumarin. The last is the product that would be expected to be obtained on solvolysis of diene **12**, by analogy with the solvolytic conversion of the adduct of *p*-xylene to 2,5-dimethylphenyl acetate. Shinoda and Suzuki (13) obtained lactone **13** on nitration of methyl 3-methyl-3-(3′,4′,5′-trimethylphenyl)butyrate and proposed lactone **14** as an intermediate in the formation of the dihydrocoumarin **15** which is also obtained in the nitration (14).

TABLE 1. Dienes from nitration of 4-(*p*-tolyl)butanol

Diene[a]	Yield[b] (%)	^{1}H nmr (CCl_4) δ/ppm[c]
11*a*	12	1.43, 1.91, 4.37, 6.01, 6.06
10*a*	50	1.75, 1.92, 4.35, 5.95, 6.00
11*b*	8	1.48, 1.93, 4.36, 6.11, 6.12
10*b*	30	1.68, 1.93, 4.36, 6.16, 6.17

[a]Dienes listed in order of elution.
[b]Percentage of total diene product formed.
[c]Peaks from left to right are assigned as (1′ or 4′)-CH_3(s), $OCOCH_3$(s), CH_2ONO_2(s), 2′-*H*, 3′-*H*, 5′-*H*, and 6′-*H* (q, J = 10 Hz). The peaks of 2-CH_2, 3-CH_2, and 4-CH_2 were not clearly resolved.

Nitration of *p*-tolylacetic acid gave a low yield (~20%) of diene products which were not further investigated.

Shift reagent studies using tris(1,1,1,2,2,3,3-heptafluoro-7,7-[$^2H_6$]dimethyl-4,6-[$^2H_3$]octanedionato)europium(III)(Eu([$^2H_9$]fod)$_3$) with the diene lactones **1***a*, **1***b*, **12***a*, and **12***b* gave the results shown in Table 2. Studies with secondary acetate adducts have been useful in assigning the stereochemistry of adducts (15). However, in the case of tertiary acetate adducts (from 1-methyl-4-alkylbenzenes), the shifts of the 4-methyl protons in the diastereoisomers are closely similar and it has not been possible to assign the stereochemistry (7, 8). The shifts of the 4′-methyl protons in the lactones **1***a* and **1***b*, and also in the lactones **12***a* and **12***b*, are similar and the differences between them are not larger than those between other pairs of corresponding protons. Nevertheless, a tentative stereochemical assignment can be proposed. The *a* isomers in each case exhibit a smaller relative gradient for the 4′-methyl protons than the *b* isomers. The *a* isomers were eluted first in chromatography and the *a* isomers have higher melting points than the *b* isomers. In the nmr spectra the 3-(or 4-)methylene and the 4′-methyl protons are lower field in the *a* isomers than in the *b* isomers. The chemical shift difference between the 2′- and 3′-protons is smaller in the *a* isomers than in the *b* isomers. These parallels strongly suggest that the *a* isomers have the same stereochemistry and, correspondingly, the two *b* isomers have the same stereochemistry opposite to that of the *a* isomers. The consistent smaller shift gradient of the 4′-methyl protons in the *a* isomers indicates that these have the europium *trans* to methyl, i.e., *cis* nitro and lactone groups, and thus the *b* isomers have *trans* nitro and lactone functions.

Rearomatization of lactone **1** was studied under both acidic and solvolytic (aqueous acetic acid) conditions. Lactone **8** was formed under both acidic and solvolytic conditions. It was the only product in acetic acid containing acetic anhydride and sulfuric acid and the major product in deuteriochloroform containing borontrifluoride etherate. It was a minor

TABLE 2. Relative gradients (gradient 2-CH_2 = 1.00) of proton chemical shifts for diene lactones from the addition of Eu([$^2H_9$]fod)$_3$

Lactone	3-H[a]	2′-H	3′-H	4′-CH_3
1*a*	0.33	0.35	0.15	0.103
1*b*	0.32	0.37	0.18	0.121
12*a*	0.41	0.37	0.20	0.117
12*b*	0.40	0.42	0.18	0.130

[a]The 3-CH_2 and 4-CH_2 groups in **1***a* and **1***b* were not resolved from each other.

product in aqueous acetic acid. The major products were a mixture of acids which were not further identified but which appeared (nmr spectrum) to include nuclear nitro-substituted 4-*p*-tolylbutyric acid(s) and phenolic acid(s). Nuclear magnetic resonance absorptions in the δ 6.5–7.0 ppm region suggested the presence of the phenol derivatives. The mechanism proposed for formation of lactone **8** is depicted in Scheme 1 (centre). A 1,2 migration of the nitro group in the *ipso* cation **6** would, after deprotonation, give 4-(4′-methyl-3′-nitrophenyl)butyric acid (Scheme 1, upper). Expulsion of the nitro group as nitrite anion followed by migration of the carboxylate group, deprotonation, and hydrolysis of the resulting lactone would give 4-(2′-hydroxy-4′-methylphenyl)butyric acid (Scheme 1, lower). Parallels for these reactions exist in the reactions of adducts obtained from alkylbenzenes (4, 7, 16, 17).

Electrophilic addition at an *ipso* position coupled with internal nucleophilic participation was first noted by Corey *et al.* They obtained the bromolactone **16** on bromination of the salt of α-*p*-tolyloxyisobutyric acid (18). If the carbonyl group is accepted as a two-membered ring then there are many other (and earlier) examples of electrophilic addition coupled with internal nucleophilic participation provided by the nitration and halogenation of *p*-cresol and its derivatives to form *ipso*-nitro- and halocyclohexadienones (19–22). The spirolactone **17** is ob-

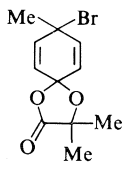

16

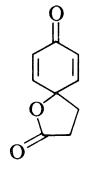

17

tained on both chemical oxidation (23) and electrooxidation (24) of 3-(*p*-hydroxyphenyl)propionic acid. On treatment with acid, **17** gives a mixture of 6- and 7-hydroxydihydrocoumarins in which either isomer can be made to predominate depending upon the conditions. Migration of the carboxylate function to give the 7-hydroxydihydrocoumarin is not intramolecular but apparently involves an initial Michael-like addition of a solvent nucleophile to the dienone system (23). It is possible that solvolysis of **12** could also involve a competition between the migration of the methylene group (to form 6-methyldihydrocoumarin) and the formal migration of the carboxylate group (to form 7-methyldihydrocoumarin), i.e., the compound tentatively identified above as 7-methyldihydrocoumarin could be the 6-isomer or a mixture of the two. In this connection it should be noted that the facile migration of an acetate group in the solvolysis of nitrocyclohexadienyl acetates is not necessarily a good analogy for the migration of the carboxylate group in either **12** or **1** (Scheme 1). In the case of the dienyl acetates the carbonyl oxygen can bond to the neighbouring carbon atom allowing the acetate to migrate via a cyclic transition state. An analogous transition state is impossible for the diene lactones.

Experimental

General experimental methods have been described previously (7).

*Nitration of 4-(*p*-Tolyl)butyric Acid*

A solution of nitric acid (15.7 g, 0.25 mol) in acetic anhydride (100 cm^3) at −78°C was added to a stirred mixture of 4-(*p*-tolyl)butyric acid (17.8 g, 0.1 mol) in acetic anhydride (200 cm^3) at −50°C. The temperature was maintained between −45 and −50°C for 1.5 h, the mixture becoming homogenous after 20 min. The solution was then added to ether (1.5 dm^3) at −78°C and quenched with ammonia, keeping the temperature below −60°C. Excess ammonia was aspirated and the ethereal solution washed with water, dried, and the ether evaporated to yield the crude product (12.1 g) containing 65% of dienes by nmr. Recrystallization from acetone–ether yielded one diastereomer of the lactone of 4-(1′-hydroxy-4′-methyl-4′-nitrocyclohexa-2′,5′-dienyl)butyric acid (**1***a*, 2.2 g) as colourless needles, mp 138.0–138.5°C; ir (Nujol): 1730, 1240 (δ-lactone), 1555 (NO_2) cm^{-1}; nmr ($CDCl_3$) δ: 1.78 (s, 3, C*H*$_3$), 1.95 (m, 4, 3-C*H*$_2$, 4-C*H*$_2$), 2.60 (m, 2, 2-C*H*$_2$), 6.17 (s, 4, 2′-*H*, 3′-*H*, 5′-*H*, 6′-*H*) ppm, on addition of Eu([$^2H_9$]fod)$_3$ the 6.17 ppm singlet split into a quartet, J = 10 Hz. *Anal.* calcd. for $C_{11}H_{13}NO_4$: C 59.18, H 5.87, N 6.28; found: C 59.26, H 6.21, N 6.14.

Chromatography of the mother liquor residues from the recrystallizations on neutral alumina (400 g deactivated with 10% (w/w) water), at −45°C and elution with ether–pentane and then ether gave the *lactone* of *4-hydroxy-4-(*p*-tolyl)butyric acid* (**8**, 0.38 g), mp 71–72.5°C (lit. (25) mp 72–73°C); ir (Nujol): 1765 (γ-lactone) cm^{-1}; nmr ($CDCl_3$) δ: 2.34 (s, 3, C*H*$_3$), 2.6 (m, 4, C*H*$_2$C*H*$_2$), 5.42 (t, 1, J = 7 Hz, C*H*CH$_2$), 7.18 (s, 4, Ar*H*) ppm; ms (70 eV) *m/e* (relative intensity): 176 (33, M), 161 (23, M − CH_3), 121(52), 119(43), 117(43), 115(20), 91(68), 28(100).

Further elution with ether afforded diene **1***a*, and then mixtures of the diastereomers **1***a* and **1***b* in approximately equal proportions. Elution with dichloromethane gave a further amount of the mixture of diastereomers. The mixtures were combined (2.1 g) and recrystallized from chloroform–pentane to give colourless prisms of the second diastereomer of the *lactone* of *4-(1′*-hydroxy-4′-methyl-4′-nitrocyclohexa-2′,5′-dienyl)butyric acid (**1***b*), mp 113.5–114.0°C (dec.); ir (Nujol): 1730 (δ-lactone), 1545 (NO_2) cm^{-1}; nmr ($CDCl_3$) δ: 1.72 (s, 3, C*H*$_3$), 1.87 (m, 4, 3-C*H*$_2$ and 4-C*H*$_2$), 2.60 (m, 2, 2-C*H*$_2$), 6.20 (nq, 2, J = 10 Hz, 2′-*H* and 6′-*H*), 6.27 ppm (nq, 2, J = 10 Hz, 3′-*H* and 5′-*H*). *Anal.* calcd. for $C_{11}H_{13}NO_4$: C 59.18, H 5.87, N 6.28; found: C 58.76, H 6.18, N 6.07.

Elution with methanol gave a mixture of 4-(nitro-*p*-tolyl)butyric acids and dienes (4.0 g). This appeared to contain a third diene, presumably 4-(4′-acetoxy-4′-methyl-1′-nitrocyclohexa-2,5-dienyl)butyric acid, but the mixture was not further resolved.

The aqueous washings were acidified with hydrochloric acid and extracted with methylene chloride to yield a mixture (4.2 g) containing 4-(nitro-*p*-tolyl)butyric acids; ir: 1705 (CO), 1525 (NO_2) cm^{-1}; nmr δ: 7.25, 7.75 ppm. Another component

present was probably 4-(hydroxy-*p*-tolyl)butyric acid; nmr δ: 6.85, 7.0, 7.05 ppm. Chromatography on silica did not resolve the mixture and it did not crystallize.

*Nitration of Methyl 4-(*p*-Tolyl)butyrate*

A solution of nitric acid (15.8 g, 0.25 mol) in acetic anhydride (100 cm^3) at −78°C was added to a slurry of methyl 4-(*p*-tolyl)butyrate (19.2 g, 0.1 mol) in acetic anhydride (100 cm^3) also at −78°C. The mixture was warmed to −50°C and stirred for 2 h. After quenching with ammonia and work-up the product contained 40% of dienes, by nmr. On chromatography at least four different dienes could be recognized in various fractions but only that obtained in largest amount could be crystallized and obtained pure. Methyl 4-(1′-acetoxy-4′-methyl-4′-nitrocyclohexa-2′,5′-dienyl)butyrate (**5**) was recrystallized from ether–pentane, m.p. 62–63°C; ir (Nujol): 1740, 1240 ($OCOCH_3$), 1735, 1180 ($COOCH_3$) 1540 (NO_2) cm^{-1}; nmr ($CDCl_3$) δ: 1.74 (m, 4, 3-CH_2 and 4-CH_2), 1.77 (s, 3, CH_3), 1.97 (s, 3, $OCOCH_3$), 2.29 (t, 2, J = 6 Hz, 2-CH_2), 3.62 (s, 3, OCH_3), 6.04, and 6.07 ppm (q, 4, J = 10 Hz). *Anal.* calcd. for $C_{14}H_{19}NO_6$: C 56.56, H 6.44, N 4.71; found: C 56.35, H 6.41, N 4.51.

*Nitration of 4-(*p*-Tolyl)butanol*

Nitric acid (6.3 g, 0.1 mol) in acetic anhydride (50 cm^3) was added to a stirred solution of the alcohol (8.2 g, 0.05 mol) in acetic anhydride (50 cm^3) at −40°C. After 2.5 h the solution was quenched and worked up yielding an oil (13.7 g) which contained 20% of starting material and 55% of dienes, by nmr. Repeated chromatography at low temperature on 5 and 3% aqueous deactivated neutral alumina afforded fractions containing four isomers of 4-(1′ or 4′)-acetoxy-4′-methyl(4′ or 1′)-nitrocyclohexa-2′,5′-dienyl)butyl nitrate (**11** and **10**, Table 1). Only the major isomer, 4-(1′-acetoxy-4′-methyl-4′-nitrocyclohexa-2′,5′-dienyl)butyl nitrate (**10***a*) was clearly separated from the others, as an oil; ir (film): 1740, 1240 ($OCOCH_3$), 1630, 1280 (ONO_2), 1545 (NO_2) cm^{-1}; nmr (CCl_4) δ: 1.70 (m, 6, 2-CH_2, 3-CH_2, 4-CH_2), 1.75 (s, 3, 4′-CH_3), 1.92 (s, 3, $OCOCH_3$), 4.35 (t, 2, J = 6 Hz, CH_2ONO_2), 5.95, 6.00 (q, 4, J = 10.4 Hz, 2′-*H*, 3′-*H*, 5′-*H*, 6′-*H*) ppm.

*Nitration of 3-(*p*-Tolyl)propionic Acid*

A solution of nitric acid (1.98 cm^3, 47 mmol) in acetic anhydride (9 cm^3) was added to a solution of 3-(*p*-tolyl)propionic acid (5 g, 30 mmol) in acetic anhydride (9 cm^3) at −78°C and the mixture warmed to 0°C. Evaporation of the solvent under reduced pressure gave a residue containing 70% of (two) dienes and 30% of aromatic compounds, by nmr. Crystallization from acetone–pentane gave one diastereomer of the lactone of 4-(1′-hydroxy-4′-methyl-4′-nitrocyclohexa-2′,5′-dienyl)propionic acid (**12***a*) which, after recrystallization from chloroform, had mp 138–139°C (dec.); ir (Nujol): 1790, 1180 (γ-lactone), 1530 (NO_2) cm^{-1}; nmr ($CDCl_3$) δ: 1.78 (s, 3, 4′-CH_3), 2.24 (t, 2, J = 7 Hz, 3-CH_2), 2.68 (t, 2, J = 7 Hz, 2-CH_2), 6.14 (nq, 2, J = 10.7 Hz, 2′-*H* and 6′-*H*), 6.20 (nq, 2, J = 10 Hz, 3′-*H* and 5′-*H*) ppm; ms (chemical ionization, methane) *m/e* (relative intensity): 192 (15, M − OH), 165 (15), 164 (100), 163 (80). Recrystallization of the residue from acetone–ether gave the second diastereomer of the dienyl lactone **12***b* which had mp 82–84°C (dec.); ir (Nujol): 1775, 1190 (γ-lactone), 1540 (NO_2) cm^{-1}; nmr ($CDCl_3$) δ: 1.71 (s, 3, 4′-CH_3), 2.15 (t, 2, 3-CH_2), 2.66 (t, 2, 2-CH_2), 6.08 (nq, 2, J = 10 Hz, 2′-*H* and 6′-H), 6.30 (nq, 2, J = 10 Hz, 3′-*H* and 5′-*H*) ppm; ms (chemical ionization, methane) *m/e* (relative intensity): 192 (15, M − OH), 165 (15), 164 (100), 163 (100).

The mother liquor from which the dienyl lactones had been crystallized was heated with acetic acid on the steam bath and, after work-up, chromatographed on silica gel using ether–pentane (20:80) for elution. The early fractions contained a component tentatively assigned the structure of 7-methyldihydrocoumarin; ms *m/e*: 162 (95, M) 134 (90, M − CO), 119 (65), 91 (100, $C_7H_7^+$), 77 (35), 39 (56). Later fractions contained mixtures of 3-(4′-methyl-3′-nitrophenyl)propionic acid and its 2′-nitro isomer with the former being present in greater amount in the final fractions. Recrystallization of the fractions and hand sorting of the crystals obtained gave 3-(4′-methyl-2′-nitrophenyl)propionic acid, nmr ($CDCl_3$) δ: 2.39 (s, CH_3), 2.74 (t, J = 7 Hz, 2-CH_2), 3.17 (t, J = 7 Hz, 3-CH_2), 7.28 (nq, J = 8 Hz, 6′-*H*), 7.34 (nq, J = 8 Hz, 5′-*H*), 7.76 (b s, 3′-*H*) ppm; and 3-(4′-methyl-3′-nitrophenyl)propionic acid, nmr ($CDCl_3$) δ: 2.54 (s, CH_3), 2.69 (t, J = 7 Hz, 2-CH_2), 2.99 (t, J = 7 Hz, 3-CH_2), 7.28 (nq, J = 8 Hz, 5′-*H*), 7.35 (nq, J = 8 Hz), 7.83 (b s, 2′-*H*) ppm.

The dienyl lactones were also isolated by neutralization of the nitration mixture with ammonia at low temperatures followed by extraction with ether and low temperature chromatography of the extract.

Nitration of p*-Tolylacetic Acid*

A solution of nitric acid (1.26 g, 20 mmol) in acetic anhydride (5 cm^3) was added to *p*-tolylacetic acid (1.5 g 10 mmol) in acetic anhydride (5 cm^3) at 0°C and the mixture stirred for 2 h. The nmr of the reaction mixture indicated that most of the *p*-tolylacetic acid had reacted and ca. 20% of diene products had been formed. A reaction carried out in which methylene chloride (10 cm^3) was added to increase the solubility of the *p*-tolylacetic acid gave a similar yield of dienes.

Rearomatization of Lactone **1***a*

A solution of lactone **1***a* (90 mg) in $CDCl_3$ (0.2 cm^3) at −78°C was treated with boron trifluoride etherate (0.4 cm^3) and warmed to ambient temperature. After work-up, ir and nmr showed that the product was mainly the lactone of 4-hydroxy-4-(*p*-tolyl)butyric acid (**8**). The minor product appeared to be 4-(4′-methyl-3′-nitrophenyl)butyric acid (δ 7.75 ppm).

Reaction, at 0°C, of lactone **1***a* with a solution of acetic anhydride in acetic acid (1:9 v/v) containing 0.05% sulfuric acid gave only lactone **8**.

Reaction, at 100°C of lactone **1***a* with aqueous acetic acid (1:9 v/v) gave a mixture of lactone **8** and carboxylic acids. The reaction was repeated on a 1 mmol scale. The carboxylic acids (~0.7 mmol) were extracted with aqueous bicarbonate and appeared to consist of a mixture of 4-(4′-methyl-3′-nitrophenyl)butyric acid (δ 7.25, 7.75 ppm) and 4(4′-methyl-2′-hydroxyphenyl)butyric acid (δ 6.85, 7.0, 7.05 ppm). The neutral fraction was lactone **8** (0.3 mmol).

Lactone **1***a* was recovered unchanged on refluxing for 1 h in benzene and also in methanol.

1. D. J. Blackstock, A. Fischer, K. E. Richards, J. Vaughan, and G. J. Wright. Chem. Commun. 641 (1970).
2. R. C. Hahn and M. B. Groen. J. Am. Chem. Soc. **95**, 6128 (1973).
3. R. B. Moodie and K. Schofield. Acc. Chem. Res. **9**, 287 (1976).
4. T. Banwell, C. S. Morse, P. C. Myhre, and A. Vollmar. J. Am. Chem. Soc. **99**, 3042 (1977).
5. A. Fischer and K. C. Teo. Can. J. Chem. **56**, 1758 (1978).
6. D. J. Blackstock, J. Cretney, A. Fischer, M. P. Hartshorn, K. E. Richards, J. Vaughan, and G. J. Wright. Tetrahedron Lett. 2793 (1970).
7. A. Fischer and J. N. Ramsay. Can. J. Chem. **52**, 3960 (1974).
8. A. Fischer and R. Röderer. Can. J. Chem. **54**, 423 (1976).
9. A. Fischer and R. Röderer. Can. J. Chem. **54**, 3978 (1976).

10. A. FISCHER, G. N. HENDERSON, and R. J. THOMPSON. Aust. J. Chem. **31**, 1241 (1978).
11. A. H. CLEMENS, M. P. HARTSHORN, K. E. RICHARDS, and G. J. WRIGHT. Aust. J. Chem. **30**, 103 (1977).
12. D. J. BLACKSTOCK, A. FISCHER, K. E. RICHARDS, and G. J. WRIGHT. Aust. J. Chem. **26**, 775 (1973).
13. M. SHINODA and H. SUZUKI. J. Chem. Soc. Chem. Commun. 479 (1977).
14. L. I. SMITH and W. W. PRICHARD. J. Am. Chem. Soc. **62**, 780 (1940).
15. A. FISCHER and J. N. RAMSAY. J. Chem. Soc. Perkin Trans. II, 237 (1973).
16. P. C. MYHRE. J. Am. Chem. Soc. **94**, 7921 (1972).
17. H. W. GIBBS, R. B. MOODIE, and K. SCHOFIELD. J. Chem. Soc. Perkin Trans. II, 1145 (1978).
18. E. J. COREY, S. BARCZA, and G. KLOTMANN. J. Am. Chem. Soc. **91**, 4782 (1969).
19. V. V. ERSHOV, A. A. VOLOD'KIN, and G. N. BOGDANOV. Russ. Chem. Rev. **32**, 75 (1963).
20. A. J. WARING. Adv. Alicyc. Chem. **1**, 172 (1966).
21. D. J. BLACKSTOCK, M. P. HARTSHORN, A. J. LEWIS, K. E. RICHARDS, J. VAUGHAN, and G. J. WRIGHT. J. Chem. Soc. B, 1212 (1971).
22. A. FISCHER and G. N. HENDERSON. Can. J. Chem. **57**, 552 (1979).
23. J. S. DAVIES, C. H. HASSALL, and J. A. SCHOFIELD. Chem. Ind. (London), 740 (1963).
24. A. I. SCOTT, P. A. DODSON, F. MCCAPRA, and M. B. MEYERS. J. Am. Chem. Soc. **85**, 3703 (1963).
25. S. MITSUI, Y. ISHIKAWA, and Y. TAKEUCHI. Nippon Kaguku Zasshi, **81**, 286 (1960); Chem. Abstr. **56**, 437c (1962).

Enzymes in organic synthesis 17.[1] Oxidoreductions of alcohols, aldehydes, and ketones using chemically modified horse liver alcohol dehydrogenase

J. BRYAN JONES AND DAVID R. DODDS

Department of Chemistry, University of Toronto, Toronto, Ont., Canada M5S 1A1

Received April 12, 1979

J. BRYAN JONES and DAVID R. DODDS. Can. J. Chem. **57**, 2533 (1979).

The substrate specificity of acetimidylated (A-HLADH) and hydroxybutyrimidylated horse liver alcohol dehydrogenase (HB-HLADH) has been evaluated for the ethanol–acetaldehyde, *trans*-2-hexenol – *trans*-2-hexenal, furfural – furfuryl alcohol, benzaldehyde – benzyl alcohol, cyclobutanol–cyclobutanone, cyclopentanol–cyclopentanone, cyclohexanol–cyclohexanone, and cycloheptanol–cycloheptanone substrate couples. The pH-optima of A- and HB-HLADH are similar to that of native enzyme (~pH 7) for the reduction mode, but are displaced from the broad ~8–10.5 range for the native enzyme to ~11.8 for the modified enzymes in the oxidative mode. However, because of coenzyme instability, the practical pH optimum for oxidations remains 9 for both native and modified HLADH's. The modified enzymes provide limited synthetic advantages for the substrates evaluated.

J. BRYAN JONES et DAVID R. DODDS. Can. J. Chem. **57**, 2533 (1979).

On a évalué la spécificité de la déshydrogénase d'alcool extraite du foie de cheval à laquelle on a fixé des groupes acétymidyle (A-HLADH) et hydroxybutyrimidyle (HB-HLADH) vis-à-vis les systèmes de substrat éthanol/acétaldéhyde, hexène-2 ol-*trans*/hexène-2 al-*trans*, alcool furfurylique/furfural, alcool benzylique/benzaldéhyde, cyclobutanol/cyclobutanone, cyclopentanol/cyclopentanone, cyclohexanol/cyclohexanone et cycloheptanol/cycloheptanone. Les pH optima des A- et HB-HLADH sont semblables à celui (~pH = 7) de l'enzyme naturel pour le mode de réduction mais ils sont déplacés, dans le mode oxydant, de la large région ~8–10.5 applicable à l'enzyme naturel vers ~11.8 pour les enzymes modifiés. Toutefois due à l'instabilité du coenzyme, le pH optimum pratique pour les oxydations demeure 9 tant pour l'enzyme naturel que pour ses modifications. Les enzymes modifiés fournissent des avantages synthétiques limités pour les substrats évalués.

[Traduit par le journal]

The practicality of exploiting the chiral catalytic properties of enzymes for effecting asymmetric syntheses of broad organic chemical interest is well recognised (1, 2). Alcohol dehydrogenases are among the synthetically most useful enzymes, with the best documented of this group being the enzyme from horse liver, HLADH.[2] HLADH is a commercially available NAD^+/H-dependent alcohol dehydrogenase which catalyzes $CH(OH) \rightleftharpoons C{=}O$ oxidoreductions for a broad spectrum of substrates (1, 2). The oxidoreductions generally proceed via the ordered Theorell–Chance pathway, as represented in eq. [1] (3*a*). For many good substrates, E.NAD/H

$$[1]\quad E + NAD^+ \rightleftharpoons E.NAD^+ + S_{OH} \rightleftharpoons E.NAD^+.S_{OH} \rightleftharpoons E.NADH.S_{CO} \rightleftharpoons S_{CO} + E.NADH \rightleftharpoons E + NADH$$

dissociation is the rate-determining step (1*b*, 3*a*).

Although HLADH is one of the most versatile enzymes of proven practical value, experimental problems are encountered during preparative-scale oxidoreductions of slowly transformed substrates. Such reactions can take many days to go to completion, during which time extensive degeneration of the enzyme, the nicotinamide coenzymes, and the coenzyme recycling systems (1*b*) may occur. This can add considerably to the amounts of the biological materials which must be used in order to achieve complete conversion of a poor substrate to the desired product.

Some of the substrates of most organic chemical interest fall into the poor substrate category. In fact, many are oxidoreduced so slowly that preparative-scale reactions are currently impractical. Clearly the value of HLADH as an asymmetric synthetic catalyst would be greatly enhanced if the catalytic activity of the enzyme towards slow substrates could be increased. The enhanced catalytic activities observed by Plapp and co-workers (4) for chemically modified HLADH presented an attractive possibility in this regard. Accordingly, we have carried out a comparative study of A-HLADH[2]- and HB-HLADH[2]-catalyzed oxidoreductions of a selected structural

[1]For Part 16, see ref. 1*a*.

[2]Abbreviations used: HLADH, horse liver alcohol dehydrogenase; NAD^+ and NADH, oxidized and reduced forms respectively of nicotinamide adenine dinucleotide; S_{OH}, alcohol substrate; S_{CO} carbonyl substrate; A-HLADH, acetimidylated HLADH; HB-HLADH, hydroxybutyrimidylated HLADH.

0008-4042/79/192533-06$01.00/0

range of acyclic and cyclic alcohols, aldehydes, and ketones.

Results

A-HLADH and HB-HLADH were prepared by modification of native HLADH with ethyl acetimidate and 4-bromobutyramide respectively (4*b*, *d*, *f*). The modified enzymes were found to possess 7-fold (A-HLADH) and 19-fold (HB-HLADH) the activity of native HLADH with respect to catalysis of ethanol oxidation.[3] The modified enzymes were somewhat less stable than native HLADH when stored at 4°C in 0.05 *M* Tris/HCl buffer pH 7.4. Both A- and HB-HLADH lost up to 35% of their activity during 1 week under these conditions, as determined by acetaldehyde reduction and ethanol oxidation assays at pH 7 and 9 respectively. The stabilities of the modified enzymes were not improved by the addition of up to 0.5 m*M* EDTA. The loss of activity was slightly greater when phosphate buffer was used. However, when A-HLADH stored as described above at pH 7.4 for 3 weeks was assayed in its oxidation mode at pH 11, >90% of activity was retained.

The pH-profiles were determined for both modified enzymes using acetaldehyde and ethanol as substrates. The results are summarized in Fig. 1.

The kinetics of oxidoreduction of the alcohol, aldehyde, and ketone substrates selected for study were determined at pH 7 for reduction and pH 9 for oxidation. The results obtained with each enzyme are summarized in Tables 1 and 2.

Discussion

A wide selection of reagents has been used to modify HLADH (4, 5–11). In contrast, the range of substrates used to evaluate the oxidoreduction properties of the modified enzymes has been restricted to those of the ethanol ⇌ acetaldehyde, benzyl alcohol ⇌ benzaldehyde, and cyclohexanol ⇌ cyclohexanone reactions. A more extended structural specificity data base was clearly needed in order to evaluate the organic synthetic advantages of the modified enzymes. With this aim in mind, structurally more diverse substrates encompassing a representative range of acyclic and cyclic aliphatic and aromatic structures (Tables 1 and 2) were selected for examination. Achiral compounds only were considered at this stage, leaving the important question of the effect of the enzyme modifications on stereospecificity to be examined subsequently with appropriate chiral substrates.

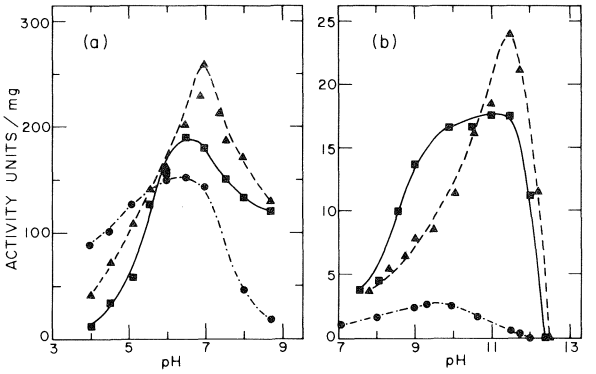

FIG. 1. pH Profiles for HLADH (●), A-HLADH (▲), and HB-HLADH (■)-catalyzed (*a*) reduction of acetaldehyde and (*b*) oxidation of ethanol. Close to optimum substrate concentrations[3] were used for each profile.

Various degrees of activation, or inactivation, can be induced by different chemical modifications of HLADH (4, 5–11). The highest activation levels are achieved by imidylation of the ε-amino group of Lys-228 (4*c*). Acetimidylation and hydroxybutyrimidylation were selected as two simply effected activations permitting comparisons of the consequences of introducing both a small (A) group and a larger, conformationally flexible, one (HB). Such modifications effect activation of HLADH by increasing the velocity of the, for many substrates, rate-limiting dissociation of coenzyme from the E.NAD/H binary complex (4).

The activations were performed in triethanolamine–HCl buffer pH 8 (4*b*, *d*).[4] The 7- and 19-fold[3] levels of activation achieved for A-HLADH and HB-HLADH respectively were in accord with the literature values (4*f*). Modifications performed at pH 10 (12) in phosphate buffer were less satisfactory, giving ≤3-fold activations only. In our hands, the modified enzymes were less stable than previously reported (4*d*). In contrast to native enzyme, which is unaffected by ≥2 weeks storage at pH 7.4 at 4°C, both A- and HB-HLADH lost up to 5% of their activity every 24 h under the same storage conditions. Accordingly, all kinetic data for the modified enzymes were obtained with freshly prepared, <1 day old, A- and HB-HLADH.

[3]The assays were performed as recommended (4*a*) under conditions favourable to the modified enzymes, i.e., with [EtOH] at 550 m*M*. Native HLADH is subject to substrate inhibition at this EtOH level, and retains only 40% of its activity in the standard assay, in which [EtOH] is 9 m*M* (3*b*). The activation levels of the modified enzymes relative to native HLADH would therefore be ~3-fold (A-HLADH) and ~7.5-fold (HB-HLADH) if the activity of each under its individual optimum assay conditions were used as the basis of comparison.

[4]HLADH modifications performed in phosphate buffer of the same pH in the absence of triethanolamine gave a 60%-*deactivated* enzyme preparation. B.V. Plapp (personal communication) has also found phosphate alone to be a poor buffer.

TABLE 1. Kinetic data for HLADH-, A-HLADH-, and HB-HLADH-catalyzed reductions[a]

Substrate	K_m (mM)			k_{cat} (s^{-1})		
	HLADH[b]	A-HLADH[c]	HB-HLADH[c]	HLADH[b]	A-HLADH[c]	HB-HLADH[c]
CH_3CHO	0.33	1.18	2.24	132.3	136.7	175.9
$CH_3(CH_2)CH{=}CHCHO$	0.16	0.61	1.24	20.0	35.8	44.3
Furfuraldehyde	0.20	13.8	2.25	110.8	209.5	37.6
Benzaldehyde	0.03	0.29	0.69	53.1	35.7	46.2
Cyclobutanone	9.06	42.2	12.1	5.88	10.0	4.4
Cyclopentanone	2.77	>1.5M	47.0	0.32	13.3	0.72
Cyclohexanone	3.71	9.05	4.54	35.2	24.6	11.2
4-Methylcyclohexanone	3.66	9.32	8.07	7.58	4.63	3.8
Cycloheptanone	2.53	28.8	4.9	0.68	0.67	0.27

[a]Determined at 25°C in 0.1 M phosphate buffer pH 7.0, [NADH] 0.2 mM.
[b][S] 0.01–10 mM.
[c][S] 0.01–100 mM.

TABLE 2. Kinetic data for HLADH-, A-HLADH-, and HB-HLADH-catalyzed oxidations[a]

Substrate	K_m (mM)			k_{cat} (s^{-1})		
	HLADH[b]	A-HLADH[c]	HB-HLADH[c]	HLADH[b]	A-HLADH[c]	HB-HLADH[c]
CH_3CH_2OH	0.28	1.92	19.14	2.08	11.7	35.8
$CH_3(CH_2)_2CH{=}CHCH_2OH$	0.04	0.06	0.33	4.45	13.9	68.9
Furfuryl alcohol	0.07	0.10	0.19	1.38	1.68	2.14
Benzyl alcohol	0.04	0.36	0.39	1.86	5.32	5.85
Cyclobutanol	0.02	0.03	0.09	1.47	0.85	0.71
Cyclopentanol	0.07	0.27	0.14	0.54	0.55	0.38
Cyclohexanol	0.69	1.86	10.0	3.15	12.2	21.5
cis-4-Methylcyclohexanol	0.15	0.81	1.42	1.87	4.02	3.47
trans-4-Methylcyclohexanol	0.15	1.21	1.41	0.99	3.17	2.02
Cycloheptanol	0.28	1.26	2.03	4.73	12.3	16.7

[a]Determined at 25°C in 0.1 M glycine–NaOH buffer pH 9.0.
[b][NAD^+] 0.5 mM, [S] 0.01–10.0 mM.
[c][NAD^+] 2.0 mM, [S] 0.01–10.0 mM.

The rate of loss of activity on storage was found to be sensitive to the pH at which the assays were performed. For example, A-HLADH kept at pH 7.4 at 4°C for three weeks lost only 10% of its activity with respect to ethanol oxidation at pH 11. This observation, and the fact that HB-HLADH showed a monotonic increase in activity up to pH 9.9 with benzyl alcohol as substrate (4*h*), prompted the pH-activity profile study summarized in Fig. 1 for the acetaldehyde $\rightleftharpoons$ ethanol substrate couple. The results for both oxidation and reduction are remarkable in that the modified enzymes show much higher activities at elevated pH's than does the native enzyme. The oxidation mode is the more noteworthy, with the pH-optima for A- and HB-HLADH occurring at ~11.8. The data at pH > 10 required increasingly large corrections for the pseudo-base reaction of NAD^+ (13).[5] At pH > 12, the rate of this reaction became the limiting factor, and the apparent loss of activity at pH ≥ 12.5 is due to the effectively instantaneous conversion of NAD^+ to its pseudo-base under these conditions. As a result, the practical pH-maximum for routine assays or preparative-scale reactions remains 9 for both native and modified HLADH.

For the reductive mode (Fig. 1*a*), the inflection points of each curve occur at about the same pH's, viz. ~6.4 and ~7.8 (14). This implies that the ionizing groups responsible for the characteristic pK_a's of HLADH-catalyzed reduction of acetaldehyde (4*g–i*, 10*a*, 14–17) are not affected by Lys-228 imidylation, and that the modified Lys-228 does not exert any electronic effects during reduction. This is in accord with the conclusion that the imidylated HLADH's continue to follow the mechanistic pathway outlined in eq. [1] (4*a*,*f*). On the other hand, the pH profile of ethanol oxidation (Fig. 1*b*) shows a large shift to higher pK_a for the modified enzymes, from ~6.3 for the native enzyme (14) to ~9 for HB-HLADH and ~10 for A-HLADH. The current data are insufficient to enable the reasons for these shifts to be identified. Electronic effects due to the conversion of the lysine residues of the native enzyme

[5]At pH 10.5, the half-life of NAD^+ under our assay conditions was ≤4 h.

($pK_a \sim 10.5$) to guanidine-like groups ($pK_a \sim 12$ (18)) on imidylation, together with accompanying conformational, isomerization, and steric changes (4*e–h*, 8, 11, 18–21) may all contribute. In addition, these factors may also account collectively for the need to increase [NAD^+] in oxidations involving modified HLADH's (Table 2). For reductions, all the pH-profiles have the same form and no corresponding [NADH] increase is required when assaying the modified enzymes (Table 1).

The kinetic constants of Tables 1 and 2 do not follow a simple pattern. Under reductive mode conditions (Table 1) only two of the substrates, acetaldehyde and furfuraldehyde, have k_{cat} values consistent with NAD^+ dissociation from the E.NAD^+ complex (eq. [1]) being rate-determining in native enzyme-catalyzed reductions (3*a*). HLADH-mediated reductions of the other substrates are significantly (up to 400-fold) slower, presumably reflecting the fact that the hydride transfer step, or product–alcohol dissociation (22), have become at least partly rate-limiting.

With the exception of the 41-fold increased k_{cat} of A-HLADH-catalyzed reduction of cyclopentanone, fairly modest rate increases only are observed for modified enzyme-mediated reductions of the Table 1 substrates. In fact, for several substrates the k_{cat} values are more or less the same for all three enzymes and, in one or two cases, for example HB-HLADH-catalyzed reductions of cyclohexanone and benzaldehyde, the modified enzymes are slightly less effective than HLADH itself.

The situation with respect to oxidation is quite different. In contrast to their Table 1 carbonyl counterparts, the alcohol substrates of Table 2 are generally significantly more efficiently oxidized in the presence of the imidylated HLADH preparations than with the native enzyme. The only exceptions are cyclobutanol and cyclopentanol, both of which are poor substrates of unmodified HLADH also. The increases in oxidative mode k_{cat} values with modified HLADH's are greatest for alcohols such as ethanol, *trans*-2-hexenol, cyclohexanol, and cycloheptanol, which are also good substrates for native HLADH. This is as expected since E.NADH dissociation is rate-limiting for good substrates of this kind, and the imidylation of the Lys-228 residue in the A- or HB-modifications of HLADH has been shown to increase the rate of this limiting dissociation step (4). For the remaining Table 2 alcohols, all of which are somewhat poorer substrates than the four mentioned above, the normal k_{cat} values are augmented to a smaller degree by A- or HB-modification of HLADH. This is again as expected since the rates of hydride-transfer or substrate-diffusion steps become dominant for poorer substrates (3*a*, 4*f*, 11*c*, 16*b*, 19, 20), thus reducing, or even eliminating, the impact of Lys-228 modifications, which have their greatest impact on the E.NADH dissociation step.

For all the carbonyl and alcohol substrates examined, the K_m values are higher, often considerably so, for the modified enzyme oxidoreductions than for the corresponding native enzyme-catalyzed reactions. While the K_m values recorded in the Tables are not Michaelis constants as usually defined (23), they are considered to reflect relative binding affinities of the substrates under the saturating coenzyme concentration conditions employed in the assays. Each substrate is clearly less well bound by A- and HB-HLADH than by the native enzyme (4*e*, *f*, *h*).

While many of the kinetic questions arising from the current study remain to be answered, the results obtained do provide a clear perspective with regard to our main objective of assessing the preparative potentials of the modified enzymes.

In both reduction and oxidation modes, the modified HLADH's can be expected to show significant rate enhancements for good substrates where E.NAD/H dissociation (eq. [1]) remains rate determining. Primary alcohols and aldehydes, and many cyclic six- and seven-membered ring alcohols, will be in this category. For poorer substrates, into which group most alcohols and ketones of organic chemical interest will fall, modest rate enhancements may be anticipated in the oxidation mode. At present, A- or HB-HLADH do not appear to offer any significant advantages over the native enzyme for effecting reductions of slower substrates of this kind.

Experimental

HLADH (EC 1.1.1.1) is commercially available from Worthington or Boehringer. NAD^+ (>99% purity) and NADH (>98% purity) were purchased from Sigma. All substrates were obtained from Aldrich or Fisher and were purified prior to use.

Preparation of A-HLADH and HB-HLADH

A-HLADH

The general procedure of Plapp and co-workers (4*b*, *d*) was used. Ethyl acetimidate (1 g (24)) in water (2 mL) was brought to pH 8.0 with concentrated aqueous sodium hydroxide to a final volume of 4 mL of a 2.1 *M* solution. An aliquot (100 μL) of this solution was added every 15 min to HLADH (5 mg) dissolved in triethanolamine–HCl buffer (2 mL, 0.5 *M*, pH 8.0) at 25°C. (It is recommended that the ethyl acetimidate solution be freshly made up prior to each addition.) After four additions (1 h), the mixture was passed through a Sephadex G-50 (1.5 cm × 30 cm) column and eluted with 0.05 *M* Tris-HCl buffer, pH 7.4. The protein-containing fractions were monitored at 280 nm, with an OD of 0.455 taken as 1 mg/mL. The A-HLADH obtained consistently assayed (4*a*) for 6.5–7.0 μ/mg. This corresponds to ~7-fold activation

with respect to native enzyme, which showed 0.92 μ/mg activity under these modified enzyme assay conditions. The modified enzyme was stored as its pH 7.4 solution at 4°C.

HB-HLADH

The procedure described above was used, with 4-bromobutyramide (45 mg (4*d*)) added all at once and using a reaction period of 2 h. The HB-HLADH obtained consistently showed activity of 17.5–18.0 μ/mg, corresponding to ~19-fold activation. It was stored as for A-HLADH at 4°C.

Kinetic Studies

Reductions

Kinetic runs were carried out at 25°C in 0.1 *M* phosphate buffer pH 7.0 with [NADH] 0.2 m*M*. The reactions were initiated by the addition of 10–40 μL of enzyme solution having an OD of 0.400 at 280 nm to make a final volume of 3.0 mL in a 1 cm-pathlength quartz cuvette. This was up-ended briefly to ensure mixing and the absorbance change at 340 nm measured using a Unicam SP 1800 spectrophotometer. The initial rates at each substrate concentration were analyzed in a Lineweaver–Burk manner by the least squares method. Correlation coefficients were ≥0.995 in each case. The k_{cat} values were obtained taking the molecular weight of HLADH as 80 000 and the extinction coefficient of NADH as 6 220. The substrate concentration ranges used, for HLADH, A-HLADH, and HB-HLADH, respectively, were (in m*M*): acetaldehyde (0.04–0.3; 0.6–1.5; 0.3–2.7), *trans*-2-hexenal (0.03–0.4; 0.06–1.5; 0.3–2.0), furfuraldehyde (0.012–0.036; 0.006–0.33; 0.03–0.33), benzaldehyde (0.013–0.13; 0.006–0.14; 2.0–20.0), cyclobutanone (1.5–11.0; 4.0–40.0; 4.0–40.0), cyclopentanone (1.3–9.0; 10.0–100.0; 10.0–180.0), cyclohexanone (1.3–7.5; 0.6–5.5; 0.6–6.0), 4-methylcyclohexanone (0.3–5.0; 1.5–10.5; 0.6–11.0), and cycloheptanone (0.3–3.3; 4.0–30.0; 1.3–9.3). The results obtained are recorded in Table 1.

Oxidations

The procedures described above were applied using 0.1 *M* glycine–NaOH buffer pH 9.0. [NAD^+] was 0.5 m*M* for HLADH and 2.0 m*M* for A- and HB-HLADH. The substrate concentration ranges used, in m*M*, for HLADH, A-HLADH, and HB-HLADH, respectively, were: ethanol (0.03–0.6; 0.3–6.0; 0.1–2.0), *trans*-2-hexenol (0.01–0.08; 0.02–1.2; 0.02–1.2), furfuryl alcohol (0.01–0.25; 0.01–0.15; 0.016–0.5), benzyl alcohol (0.007–0.07; 0.016–0.4; 0.03–0.33), cyclobutanol (0.007–0.1; 0.01–0.06; 0.016–0.1), cyclopentanol (0.01–0.13; 0.13–2.3; 0.03–0.3), cyclohexanol (0.06–1.0; 0.09–11.0; 0.3–4.0), *cis*-4-methylcyclohexanol (0.06–1.0; 0.1–0.7; 0.1–1.5), *trans*-4-methylcyclohexanol (0.01–0.16; 0.1–1.0; 0.1–2.5), and cycloheptanol (0.06–0.6; 0.16–2.0; 0.06–0.17). The results obtained are recorded in Table 2.

pH-Profiles

The pH-profiles were determined using the standard assay procedure (3*a*) with 0.1 *M* phosphate buffer for the pH range 4.0–8.7 and 0.1 *M* glycine–NaOH for pH >7.5. Acetaldehyde and ethanol were used as substrates for the reductive and oxidative modes respectively. The substrate concentrations were 9 m*M* for HLADH and 550 m*M* for the modified enzymes. The corresponding coenzyme concentrations employed were: reductions, [NADH] 0.2 m*M*; oxidations, [NAD^+] 0.5 m*M* with HLADH, 2.0 m*M* with A- and HB-HLADH.

Acknowledgements

Support of this work by NSERC is gratefully acknowledged. We also express our gratitude to Hoffmann-La Roche for additional financial aid and for a generous gift of enzyme, and to Ogilvie Flour Mills Ltd. for the award of a Kenneth Armstrong Memorial Fellowship (to D.R.D.).

1. (*a*) J. DAVIES and J. B. JONES. J. Am. Chem. Soc. In press; (*b*) J. B. JONES and J. R. BECK. Tech. Chem. (N.Y.), **10**, 107 (1976); (*c*) J. B. JONES. *In* Enzymic and nonenzymic catalysis. *Edited by* P. Dunnill. Ellis Horwood Press, Chichester. U.K. 1979. In press; (*d*) J. B. JONES and K. P. LOK. Can. J. Chem. **57**, 1025 (1979), and references cited therein.
2. B. J. ABBOTT. Adv. Appl. Microbiol. **20**, 203 (1976); Ann. Repts. Ferment. Proc. **1**, 205 (1977); **2**, 91 (1978).
3. (*a*) K. DALZIEL. *In* The enzymes. Vol. 11. 3rd ed. *Edited by* P. D. Boyer. Academic Press, New York. 1975. p. 1; (*b*) K. DALZIEL. Acta Chem. Scand. **11**, 397 (1957).
4. (*a*) B. V. PLAPP. J. Biol. Chem. **245**, 1727 (1970); (*b*) R. L. BROOKS, J. D. SHORE, and B. V. PLAPP. J. Biol. Chem. **248**, 3470 (1973); (*c*) R. T. DWORSCHACK, G. TARR, and B. V. PLAPP. Biochemistry, **14**, 200 (1975); (*d*) R. W. FRIES, D. P. BOHLKEN, R. T. BLAKLEY, and B. V. PLAPP. Biochemistry, **14**, 5233 (1975); (*e*) M. ZOLTBROCKI, J. C. KIM, and B. V. PLAPP. Biochemistry, **13**, 899 (1974); (*f*) R. T. DWORSCHACK and B. V. PLAPP. Biochemistry, **16**, 111 (1977); **16**, 2716 (1977); (*g*) D. M. PARKER, M. J. HARDMAN, B. V. PLAPP, J. J. HOLBROOK, and J. D. SHORE. Biochem. J. 173 (1978); 269 (1978); (*h*) R. T. DWORSCHACK and B. V. PLAPP. *In* Alcohol and aldehyde metabolizing systems. Vol. 2. *Edited by* R. G. Thurman. Academic Press, New York. 1977. p. 43; (*i*) B. V. PLAPP, H. EKLUND, and C.-I. BRANDEN. J. Mol. Biol. **122**, 23 (1978).
5. R. H. BAUER. Biochemistry, **1**, 41 (1961).
6. (*a*) C. H. REYNOLDS and J. S. MCKINLEY-MCKEE. Acta Chem. Scand. **15**, 1811 (1961); (*b*) Arch. Biochem. Biophys. **168**, 145 (1975); (*c*) K. H. DAHL and J. S. MCKINLEY-MCKEE. Eur. J. Biochem. **81**, 223 (1977).
7. P. WOOLLEY. Nature, **258**, 677 (1975).
8. E. ZEPPEZAUER, H. JORNVALL, and I. OHLSSON. Eur. J. Biochem. **58**, 95 (1975).
9. M. J. HARDMAN. Eur. J. Biochem. **66**, 401 (1976).
10. (*a*) J. T. MCFARLAND, J. CHEN, M. WNUK, M. C. DETRAGLIA, T. Y. LI, R. PETERSEN, J. W. JACOBS, J. SCHMIDT, B. FEINBERG, and K. L. WATER. J. Mol. Biol. **115**, 355 (1977); (*b*) J. T. MCFARLAND and Y.-H. CHU. Biochemistry, **14**, 1140 (1975); (*c*) M. C. DETRAGLIA, J. SCHMIDT, M. F. DUNN, and J. T. MCFARLAND. J. Biol. Chem. **252**, 433 (1977).
11. (*a*) C. S. TSAI. Bioorg. Chem. **6**, 117 (1977); (*b*) C. S. TSAI, Y.-H. TSAI, G. LAUZON, and S. T. CHENG. Biochemistry, **13**, 440 (1974); (*c*) C. S. TSAI. Can. J. Biochem. **46**, 381 (1968).
12. D. T. BROWNE and S. B. H. KENT. Biochem. Biophys. Res. Commun. **67**, 133 (1975).
13. S. L. JOHNSON and C. C. GUILBERT. Biochemistry, **16**, 335 (1977).
14. H. THEORELL, A. P. NYGAARD, and R. BONNICHSEN. Acta Chem. Scand. **9**, 1148 (1955).
15. (*a*) C.-I. BRANDEN, H. JORNVALL, H. EKLUND, and B. FURUGREN. *In* The enzymes. Vol. 11. 3rd ed. *Edited by* P. D. Boyer. Academic Press, New York. 1975. p. 104; (*b*) C.-I. BRANDEN. *In* Alcohol and aldehyde metabolizing systems. Vol. 2. *Edited by* R. G. Thurman. Academic Press, New York. 1977. p. 17.
16. (*a*) J. D. SHORE, H. GUTFREUND, R. L. BROOKS, D. SANTIAGO, and P. SANTIAGO. Biochemistry, **13**, 4185 (1974); (*b*) R. L. BROOKS and J. D. SHORE. Biochemistry, **10**, 3855

(1971); R. L. BROOKS, J. D. SHORE, and H. GUTFREUND. J. Biol. Chem. **247**, 2382 (1972); (*c*) J. D. SHORE, H. HALVORSON, and K. LUCAST. *In* Pyridine nucleotide dependent dehydrogenases. *Edited by* H. Sund. Springer-Verlag, Berlin. 1970.
17. S. TANIGUCHI, H. THEORELL, and A. AKESON. Acta Chem. Scand. **21**, 1903 (1967).
18. P. TEUNGLER. Biochem. Biophys. Acta, **484**, 1 (1977).
19. P. A. GURR, P. M. BRONSKILL, C. S. HANES, and J. F.-T. WONG. Can. J. Biochem. **50**, 1376 (1972); C. S. HANES, P. M. BRONSKILL, P. A. GURR, and J. T.-F. WONG. Can. J. Biochem. **50**, 1385 (1972).
20. (*a*) G. R. AINSLIE and W. W. CLELAND. J. Biol. Chem. **247**, 946 (1972); (*b*) C. C. WRATTEN and W. W. CLELAND. Biochemistry, **11**, 1486 (1972).
21. S. SUBRAMANIAN and P. D. ROSS. Biochem. Biophys. Res. Commun. **78**, 461 (1977); Biochemistry, **17**, 2193 (1973).
22. S. A. BERNHARD, M. F. DUNN, P. L. LUISI, and P. SCHACK. Biochemistry, **9**, 185 (1970); J. T. MCFARLAND and S. BERNHARD. Biochemistry, **11**, 1486 (1972).
23. M. DIXON and E. C. WEBB. Enzymes. 2nd ed. Longmans, London. 1964. p. 65.
24. M. J. HUNTER and M. L. LUDWIG. Methods Enzymol. **25**, 585 (1972).

Erratum: Cobalt(II), nickel(II), and copper(II) complexes of di- and tetrapeptides containing tyrosine and glycine residues

MOHAMED S. EL-EZABY, JASSIM M. AL-HASSAN, NAMEK F. EWEISS, AND FARIDA AL-MASSAAD
Department of Chemistry, Faculty of Science, University of Kuwait, Kuwait

Received May 31, 1979
(Ref.: Can. J. Chem. **57**, 104 (1979))

The name of the first author should read Mohamed S. El-Ezaby.
Equation [2] should read

$$[2] \qquad pK_W = \frac{E_A - E_B}{K_2} + \log \frac{C_4}{C_3 C_1^2} = -\log C_H C_{OH}$$

Reference 21 should read L. G. VAN UITERT and C. G. HAAS. J. Am. Chem. Soc. **75**, 451 (1953).

Electronic spectroscopy of aromatic Schiff's bases. III. Luminescence in some *p*-substituted benzylideneaniline molecules

MICHEL BELLETÊTE AND GILLES DUROCHER

Département de Chimie, Université de Montréal, C.P. 6210, Station A, Montréal (Qué.), Canada H3C 3V1

Received April 6, 1979

MICHEL BELLETÊTE and GILLES DUROCHER. Can. J. Chem. **57**, 2539 (1979).

Fluorescence and phosphorescence spectra of a few *p*-substituted benzylideneaniline (BA) molecules have been obtained in the EPA solvent. Results show that the ϕ_p/ϕ_f ratio increases regularly with an increase in the static dipole moment of the molecules except for the most polar molecule where the fluorescence is much more intense.

Moreover, it has been shown that the interaction of the BA molecules with aprotic polar solvents is solvatochromic in origin, meaning that no specific solute–solvent interactions had been detected. It has been shown that the BA molecules behave like the D—Ar—A molecular type as far as the photophysical aspect is concerned.

MICHEL BELLETÊTE et GILLES DUROCHER. Can. J. Chem. **57**, 2539 (1979).

Les spectres de fluorescence et de phosphorescence de quelques molécules de benzylideneaniline (BA) *para*-substituées ont été obtenus dans l'EPA utilisé comme solvant. Les résultats démontrent que le rapport ϕ_p/ϕ_f augmente régulièrement en fonction du moment dipolaire de l'état fondamental des molécules de BA étudiées à l'exception de la molécule de BA la plus polaire où la fluorescence est plus intense.

Il est de plus démontré qu'un effet solvatochrome normal explique l'interaction entre les BA et un solvant polaire aprotique. Aucune interaction spécifique soluté–solvant n'a pu être mise en évidence dans ces solvants. Il est démontré que le comportement photophysique des BA est semblable à celui des molécules plus connues du type D—Ar—A.

Introduction

The absorption spectroscopy of the para-substituted benzylideneaniline (BA) molecules has been studied in recent years and for a review of the literature we refer the reader to parts I and II of this series of papers (1, 2). Very few papers exist on the emission spectroscopy of these molecules (3–6). In order to carry on our work on the intramolecular charge transfer states in these kind of molecules, we had to investigate their emission properties. The purpose of this paper is two-fold; first of all, we would like to establish the conditions where molecular emissions can be detected and secondly, we would like to propose a mechanism by which the highly polar excited states in those molecules interact with polar solvents. The molecules studied here are the following using the same notation as described in an earlier paper (2):

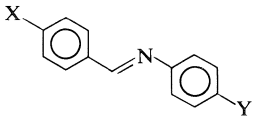

6: X = $N(CH_3)_2$, Y = NO_2
5: X = OCH_3, Y = NO_2
3: X = H, Y = NO_2
2: X = OCH_3, Y = H
4: X = OCH_3, Y = OCH_3

Experimental

The BA molecules have been synthesized and purified as described previously (1, 2). The EPA solvent (5:5:2 mixture of diethyl ether, isopentane, and ethanol) was prepared in the laboratory. Diethyl ether and ethanol were purified as described previously (2). Isopentane (pure grade from Phillips Petroleum Co.) was distilled over concentrated sulfuric acid, washed with triply distilled water, and distilled again over sodium. Methylcyclohexane (pure grade from Phillips Petroleum Co.) was distilled over concentrated sulfuric acid, washed with distilled water, distilled again over sodium, then chromatographed on a 5 ft silica gel column and stored in the dark. Acetonitrile and dimethylformamide (DMF) (reagent grade, Anachemia Chemicals Ltd.) were purified as described previously (2).

The emission spectra (fluorescence and phosphorescence) were measured with a Fluorispec Baird Atomic Model SF-1 spectrofluorometer modified to accommodate a 1000 W Xenon arc lamp at the entrance of the excitation monochromator (7). The fluorescence spectra have been recorded with all samples at room temperature and at 77 K and the phosphorescence spectra have been recorded with all samples at liquid nitrogen temperature. The EPA solvent was used for the latter and the sample concentrations were of the order of 5×10^{-5} *M*.

Results and Discussion

Among the *p*-substituted BA molecules studied earlier (2), only those molecules with substituents favoring an electron migration from X to Y, that is to say stabilizing the intramolecular charge transfer state, have been shown to give any measurable emission: fluorescence or phosphorescence.

0008-4042/79/192539-03$01.00/0

TABLE 1. Fluorescence and phosphorescence peak maxima and the ϕ_p/ϕ_F ratios in some *p*-substituted BA molecules in EPA solvent at 77 K

Molecules	X	Y	$\bar{\nu}_F$ (cm^{-1})	$\bar{\nu}_p$ (cm^{-1})	ϕ_p/ϕ_F	μ_g* (D)
6	$N(CH_3)_2$	NO_2	19 700	—	$<2\times10^{-5}$†	8.6
5	OCH_3	NO_2	22 500	19 000	3100	7.7
3	H	NO_2	—	19 400	≥3000†	5.5
2	OCH_3	H	29 900	22 500	25	2.6
4	OCH_3	OCH_3	26 900	22 200	2.3	1.6

*Following ref. 2.
†Only indicative of the limiting value.

Results are given in Table 1 in which the phosphorescence to fluorescence quantum yield ratios (ϕ_p/ϕ_f) have been obtained through excitation in the first absorption peak maximum of each solute molecule and by further correction for the sensitivity of the emission monochromator–PM system versus the emission wavelength. Results show clearly that the ϕ_p/ϕ_f ratio increased regularly with an increase in the static dipole moment of the molecules except for molecule **6** where the fluorescence is much more intense than for other molecules and the phosphorescence has hardly been observed. McGlynn *et al.* obtained the same kind of behavior in their study of the luminescence of polar molecules of the type D—Ar—A (8). The dipole moment of the ground states of these molecules varies as *p-* > *m-* > *o-*. The low energy highly polar excited states of these molecules are referred to as "charge transfer" states and the phosphorescence intensity as well as the S_1–T_1 intersystem crossing efficiency vary in the order *p-* > *m-* > *o-*. In less polar aniline derivatives, the intersystem crossing is apparently not quite as efficient and weak fluorescence can be observed. Moreover, *N*-methylation of *p*-nitroaniline by lowering the effective ionization potential of the amino group (makes it a better electron donor and increases the dipole moment of the molecule) has a pronounced effect on the luminescence behavior of *p*-nitroaniline. The efficiency of intersystem crossing seems to decrease to a point where fluorescence again is observable.

The intramolecular charge transfer states in the benzylideaniline molecules seems to have the same photophysical behavior as the smaller aniline derivatives. Substitution effect greatly alters the energies and the polarities of the various electronic excited states which in turn are responsible for the various non-radiative probabilities between the excited states and the ground state.

Are there any specific interactions between the excited BA molecules and polar solvents? In view of the fact that the excited dipole moments of the BA molecules are quite large (2), exciplex formation with highly polar solvents may be possible at room temperature (9). Molecule **6** which possesses the highest static dipole moment in the ground state was dissolved in methylcyclohexane (MCH) and their absorption and fluorescence peak maxima were studied with various amounts of ethanol, acetonitrile, and DMF added to the MCH solution.

The fluorescence peak maxima of molecule **6** dissolved in a non-polar solvent like MCH is at 21 300 cm^{-1} compared to 19 200 cm^{-1} when it is dissolved in EPA which is a 5:5:2: mixture of ether, isopentane, and ethanol. Since no fluorescence could have been detected when molecule **6** is dissolved in ether alone, we can say that ethanol is the solvent responsible in EPA for the fluorescence observed. When ethanol is added to a MCH solution of molecule **6**, a red shift in the fluorescence peak maximum is observed but no new fluorescence emission which might be assigned to an exciplex (9) could be detected. Moreover, the fluorescence intensity does not change much with the addition of ethanol. On the other hand the relation of Lippert–Mataga on the solvatochromic shift does not hold (10–12).

Since the polarizability function $F(D,n)$ in the Lippert–Mataga equation (10–12) is about the same for ethanol, acetonitrile, and DMF, it would be interesting to compare the effect of adding the last two solvents to a MCH solution of molecule **6**.

Results for DMF are reported in Table 2. The absorption peak maximum of molecule **6** is not much influenced by these small amounts of DMF added to the MCH solution.

Table 2 shows that the fluorescence intensity at the peak maximum markedly increases with the amount of DMF added. This behavior is contrary to that observed when exciplex formation is present in that there is normally a quenching of the fluorescence and appearance of a new emission band at lower energies (9). McGlynn *et al.* (8) also observed an increase in the fluorescence intensity of the D—Ar—A type of molecules they have studied. Table 2 also shows that the fluorescence is red-shifted for the relatively small amounts of DMF added.

In order to verify whether this shift is solvato-

TABLE 2. Effect of small amounts of DMF added to the MCH solution of 4-dimethylaminobenzylidene-4′-nitroaniline (**6**) on the first electronic absorption and fluorescence peak maxima

%DMF (V/V)	$\bar{\nu}_A$ (cm^{-1})	$\bar{\nu}_F$ (cm^{-1})	I_F (r. unit)	$\bar{\nu}_A - \bar{\nu}_F$ (cm^{-1})	$F(D,n)$
0	26 500	21 300	18	5 200	0.003
0.66	26 500	21 100	30	5 400	0.046
0.99	26 500	20 800	32	5 700	0.068
1.31	26 300	20 600	36	5 700	0.088
1.64	26 300	20 500	39	5 800	0.107
2.28	26 200	19 900	51	6 300	0.139
2.91	26 100	19 500	67	6 600	0.167
3.54	26 000	19 200	85	6 800	0.192
4.15	26 000	19 000	92	7 000	0.213

chromic in nature, we have calculated the excited state dipole moment of molecule **6** using the method proposed by Lippert (10) and Mataga *et al.* (11, 12). The slope of the graph, $\bar{\nu}_A - \bar{\nu}_F$ vs. $F(D,n)$ $[\equiv (D-1)/(2D+1) - (n^2-1)/(2n^2+1)]$, where D and n are respectively the dielectric constants and the refraction index of the medium, gives access to the excited state dipole moment when the ground state dipole moment along with the cavity radius of the solute molecule are known (2, 10–12). From the results contained in Table 2, an excited state dipole moment of 39 D has been calculated. This value is in very good agreement with that of 38 D already published by Lippert *et al.* (10). So, the red-shifted fluorescence observed when molecule **6** is dissolved in DMF is only due to a normal solvatochromic effect (10–12). Exactly the same behavior has been observed with acetonitrile. We take this as another proof, apart from the fluorescence intensity behavior, to conclude that no specific interaction exists between the highly polar benzylideneaniline molecules and the aprotic polar solvents. Ethanol does not behave like aprotic solvents and work is still in progress in order to be sure that some specific interactions do exist with the BA molecules.

Conclusions

The emission spectroscopy of the *p*-substituted BA molecules with substituents favoring an electron migration from X to Y seems to be similar in many respects to the spectroscopy of polar molecules of the type D—Ar—A in that the photophysical behavior seems to be the same and, moreover, the interaction of the BA molecules with aprotic polar solvents seems to be solvatochromic in origin.

Acknowledgements

This work was supported by the National Research Council of Canada and also by the "Ministère de l'Education du Québec, FCAC". One of us (M.B.) acknowledges the National Research Council of Canada and the "Ministère de l'Education du Québec" for research scholarships.

1. B. SCHEUER-LAMALLE and G. DUROCHER, Can. J. Spectrosc. **21**, 165 (1976).
2. M. BELLETÊTE, B. SCHEUER-LAMALLE, L. BARIL, and G. DUROCHER. Can. J. Spectrosc. **22**, 31 (1977).
3. E. LIPPERT. Z. Elektrochem. **61**, 962 (1957).
4. O. A. OSIPOV, YU. A. ZHDANOV, M. I. KNYAZHANSKII, V. I. MINKIN, A. GAVNOVSKII, and I. D. SADEKOV. Russ. J. Phys. Chem. **41**, 322 (1967).
5. E. B. AGRACHEVA and V. F. GACHKOVSKII. Zh. Obshch. Khim. **40**, 191 (1970).
6. N. A. VASILENKO, R. N. NURMUKHAMETOV, and A. N. PRAVEDNIKOV. Dokl. Phys. Chem. **223**, 1098 (1975).
7. M. BELLETÊTE. Master thesis. Université de Montréal, Montréal, Qué. 1977.
8. C. J. SELISKAR, O. S. KHALIL, and S. P. MCGLYNN. Excited states. Vol. 1. *Edited by* E. C. Lim. Academic Press. 1970. p. 237.
9. E. A. CHANDROSS. The exciplex. *Edited by* M. Gordon and W. R. Ware. Academic Press. 1975. p. 187.
10. E. LIPPERT. Z. Naturforsch. **10**a, 541 (1955); Z. Elektrochem. **61**, 962 (1957).
11. N. MATAGA, Y. KAIFU, and M. KOIZUMI. Bull. Chem. Soc. Jpn. **28**, 690 (1955); **29**, 465 (1956).
12. N. MATAGA and T. KUBOTA. Molecular interactions and electronic spectra. Marcel Dekker, Inc., New York. 1970. p. 371.

Osmotic and activity coefficients of lithium chloride in water from 50 to 150°C

ALAN N. CAMPBELL AND OM N. BHATNAGAR

Department of Chemistry, University of Manitoba, Winnipeg, Man., Canada R3T 2N2

Received April 18, 1979

ALAN N. CAMPBELL and OM N. BHATNAGAR. Can. J. Chem. **57**, 2542 (1979).

The activity coefficients of lithium chloride in aqueous solution at temperatures of 50, 75, 100, 125, and 150°C and concentrations varying from 0.5 to 3 *m* have been determined. The method used was the application of the Gibbs–Duhem theorem, i.e., the activity of the solvent water was the quantity actually determined. The experimental determination was that of the vapour pressure of the solution using a differential manometer. At all temperatures the activity coefficient passes through a minimum and then increases progressively.

ALAN N. CAMPBELL et OM N. BHATNAGAR. Can. J. Chem. **57**, 2542 (1979).

On a déterminé les coefficients d'activité de solutions aqueuses de chlorure de lithium à 50, 75, 100, 125 et 150°C et à des concentrations allant de 0.5 à 3.0 *m*. On a fait appel à une méthode basée sur le théorème de Gibbs–Duhem c'est à dire que l'on a déterminé de fait l'activité de l'eau agissant comme solvant. On a déterminé expérimentalement la tension de vapeur de la solution en utilisant un manomètre différentiel. A toutes les températures, le coefficient d'activité passe par un minimum avant de croître d'une façon progressive.

[Traduit par le journal]

Introduction

It is not necessary to stress the importance of osmotic and activity coefficients in the study of solutions of electrolytes. Because of this importance a wealth of data has accumulated since the concept of activity was first introduced some seventy years ago. Most of these data, however, were obtained at room temperature (say 25°C). Knowledge of activity at elevated temperatures is perhaps even more important than at room temperature but the amount of such data is small. The reason obviously lies in the experimental difficulty of the work at temperatures above 100°C.

Some thermodynamic work has been done at higher temperatures (1, 2) but in many instances the data lack precision. Osmotic coefficients for NaCl solutions have been reported up to 270°C by Gardner and co-workers (3, 4). In their admirable work, Liu and Lindsay (5, 6) carried out a detailed and systematic study of osmotic and activity coefficients of aqueous sodium chloride solutions up to 300°C and from a concentration of 0.1 *m* to saturation. These workers also investigated to a limited extent salts such as LiCl, CsCl, $MgCl_2$, $MgSO_4$, etc. Their technique was essentially that of the present study, viz. determination of the vapour pressure of the solvent or, more correctly, the difference between the vapour pressure of solvent in solution and in the pure state. Application of the Gibbs–Duhem theorem then yields the activity of the electrolyte.

Soldano and co-workers (7–10) have reported the osmotic coefficients of a number of electrolytes at temperatures up to 165°C in the concentration range 0.5 up to 8 *m* using the isopiestic method.

The whole study of the thermodynamic properties of electrolytic solutions above 100°C is in a fragmentary state, and it seemed to us that systematic work should be done on these properties as functions of temperature and concentration. We have chosen to study the osmotic and activity coefficients of 1:1, 1:2, and 2:2 electrolytes. Our first report deals with lithium chloride at temperatures from 50 to 150°C and over a concentration range from 0.5 to 3.0 *m*.

Experimental

Analytical grade lithium chloride was used without further purification. The concentrations of the solution were determined by gravimetric analysis as silver chloride. The solvent was triply distilled conductance water. To avoid contact with air, the solutions were prepared by the method of Lindsay and Liu (11). The vapour pressures of the solutions were measured by means of a differential manometer (Fig. 1), one limb of which contained the solution and the other pure water or, in the case of concentrated solutions, a solution of lithium chloride or sodium chloride, whose vapour pressure had previously been determined. The latter procedure was inevitable because, with concentrated solutions, the difference in vapour pressure from that of pure water was so great that it exceeded the pressure range of the manometer. The liquids in the manometer were degassed by freezing in liquid nitrogen, pumping down, melting, refreezing, and so on.

The differential manometer was enclosed in a stainless steel pressure bomb, with windows of pressure resistant glass. The glass used for these windows was obtained from Corning Glass Works, Corning, NY. Effectually to remove the manometer itself from high pressure, pure water was always placed at the bottom of the bomb. Thus, the only high pressure developed was that on the interior of the bomb.

0008-4042/79/192542-04$01.00/0

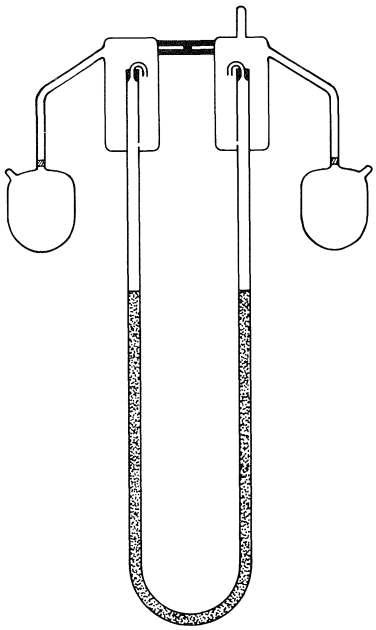

FIG. 1. Differential manometer.

The bomb, which was very heavy, was raised by means of a crane and lowered into a large oil bath, also furnished with glass windows, and containing about 25 gallons of oil.[1] The bath was stirred by two stirrers. Temperature control was obtained by means of a Sargent Thermonitor, model ST, temperature control unit. The temperature of the oil bath was constantly monitored using multijunction thermocouples. An exploration with a thermocouple at different points in the bath showed that the temperatures at different points did not differ by more than ± 0.05°C. The temperature was constant to ± 0.05 up to 100°C, and to ± 0.1°C between 100 and 150°C. In order to check the reproducibility of our equipment and technique, we measured the vapour pressure of 1 *m* NaCl at 75 to 150°C. Our values of osmotic coefficients were within 1% of those reported by Liu and Lindsay (5) for 1 *m* NaCl solutions.

Results

At each temperature several readings of vapour pressure were taken, over a time period of a few hours, after equilibrium had been reached. For each temperature, the readings were taken twice, once after the temperature had been raised and once after cooling from a higher temperature. If the two readings did not agree within 1%, the results were rejected. Otherwise, the two readings were averaged to give the pressure difference (ΔP). The manometric liquid was mercury throughout and the ΔP values were corrected to the density of mercury at 0°C. The solutions were analyzed after each experiment, and it was these concentrations which were used in the calculations. These concentrations were then corrected to the appropriate temperature, as suggested by Lindsay and Liu (11).

The osmotic coefficients were calculated from the following:

$$[1]\quad \phi = \frac{1000}{\nu m M_1 RT}\left[RT \ln \frac{P^0}{P} - \int_P^{P^0} \xi \mathrm{d}p - V_1{}^0(\mathrm{l})\Delta P\right]$$

where ϕ is the osmotic coefficient, T is the absolute temperature, R the gas constant, M_1 the molecular weight of the solvent water, m the molality, ν the number of ions resulting from the complete ionisation of one molecule, P^0 the vapour pressure of pure water, and P the vapour pressure of the solution (solute assumed non-volatile).

The first term in the brackets gives the osmotic coefficient at low vapour pressures, the second term gives the corrections for the deviations of the vapour from the perfect gas law, and the third term is an adequate approximation for the isothermal compression of the solution from its own vapour pressure to that of pure water. The integrand, ξ, was calculated using the equation given by Smith, Keyes, and Gerry (12). $V^0(\mathrm{l})$, the molar volume of pure water and P^0 were calculated from the equations given in ref. 12. As usual, $V^0(\mathrm{l})$ is used instead of $\bar{V}_1(\mathrm{l})$, the partial molar volume of water, because under these conditions the difference is negligibly small. The osmotic coefficients obtained from eq. [1] are listed in Table 1.

The mean ionic activity coefficients, $\gamma\pm$, were calculated using the osmotic coefficients of Table 1 from eq. [2].

$$[2]\quad \ln \gamma\pm = -2\int_0^{m^{1/2}} \frac{1-\phi}{m^{1/2}} \mathrm{d}m^{1/2} - (1-\phi)$$

The Debye–Hückel limiting values were used to evaluate the above integral in the dilute region; the integration was done graphically. The results for mean ionic activity coefficients are also given in Table 1.

In Fig. 2, we have plotted our results for osmotic coefficients vs. the square root of concentration. Our values from 1 *m* lithium chloride at 125 and 150°C are in good agreement with those of Lindsay and Liu (11). The results of Soldano *et al.* refer to temperatures of 99.6 and 151.4°C (7, 10). Our values for 100 and 150°C are in reasonable agreement at lower concentrations, but, at higher concentrations the agreement with Soldano is poor.

In all cases, the osmotic coefficients increase with

[1]We are indebted to Atomic Energy of Canada, Pinawa, for this oil.

TABLE 1. Osmotic and activity coefficients of LiCl in water from 50 to 150°C

t (°C)	Molality	$\Delta P = P^\circ - P$ (mm Hg)	Osmotic coefficient (ϕ) at $P = P^\circ$	Activity coefficient ($\gamma\pm$)
50.0	0.4479	1.44	0.9735	0.7634
	1.0039	3.37	1.0220	0.7984
	1.4000	4.84	1.0624	0.8435
	1.8961	6.88	1.1109	0.9094
	2.9354	11.04	1.1967	1.0598
	3.2014	13.04	1.2236	1.1130
75.0	0.4479	4.50	0.9640	0.7726
	1.0039	10.31	0.9955	0.7831
	1.4000	14.67	1.0237	0.8086
	1.8961	20.38	1.0615	0.8505
	2.9354	33.13	1.1415	0.9626
	3.2014	36.51	1.1610	0.9951
100.0	0.4479	14.23	0.9503	0.7104
	1.0040	27.11	0.9881	0.7188
	1.4003	39.23	1.0239	0.7473
	1.8969	53.71	1.0591	0.7845
	2.9359	88.88	1.1580	0.9082
	3.2020	99.73	1.1854	0.9504
125.0	0.4491	27.24	0.9470	0.6863
	1.0049	61.59	0.9670	0.6770
	1.4010	87.07	0.9889	0.6897
	1.8980	122.54	1.0385	0.7269
	2.9365	188.59	1.0959	0.7835
	3.2030	230.61	1.1145	0.8018
150.0	0.4500	55.29	0.9186	0.6353
	1.0064	123.11	0.9235	0.5997
	1.4052	173.52	0.9399	0.5979
	1.9018	242.93	0.9827	0.6170
	2.9416	385.47	1.0312	0.6469
	3.2075	452.51	1.0429	0.6733

concentration and with temperature up to about 100°C, after which temperature they decrease. Similar behaviour is observed with sodium chloride (5) although here the temperature of the maximum is about 65°C.

We are unable to understand Soldano's curves in the lower part of his Fig. 1 (10) for 151.4°C since it is necessary for all such curves to have their origin at $\phi = 1.0000$, at $m = 0$.

Discussion

In Fig. 3 (a comparison of the osmotic coefficients of lithium chloride and of sodium chloride at 75 and at 150°C) it appears that the difference in the osmotic coefficients of the two salts becomes small at 150°C. When ϕ is plotted against $m^{1/2}$, the results of Soldano show the curves for LiCl at 151.40 intersecting but our results show no intersection up to 3.2 m at 150°C.

Lindenbaum *et al.* (13) reported the osmotic coefficients of a number of ternary alkyl ammonium salts. They found the order of magnitude to be $(C_4H_9)_4NCl > (C_3H_7)_4NCl > (CH_3)_4NCl$ at 25°C,

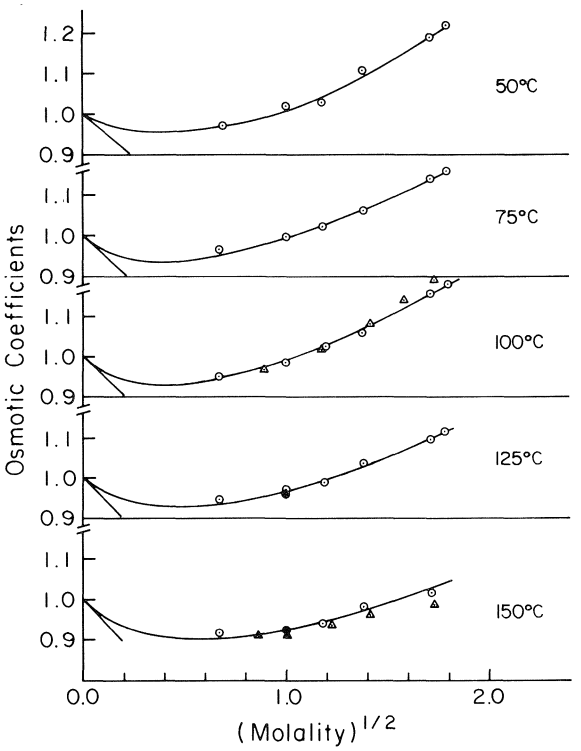

FIG. 2. Osmotic coefficient (ϕ) vs. (molality)$^{1/2}$: ○, present work; ●, data from ref. 11; △, data from refs. 7, 10 at 99.6 and 151.4°C.

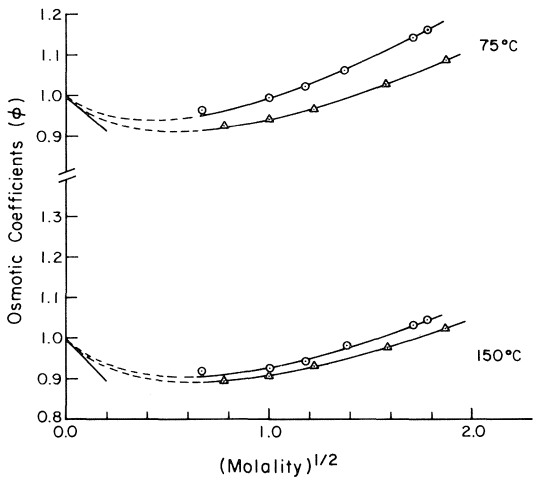

FIG. 3. Osmotic coefficients of NaCl (△) ref. 11, LiCl (○) in water.

i.e., the osmotic coefficient increased with increasing molecular weight, while the order was reversed at 65°C. On the other hand, they found that the osmotic coefficient of $(CH_3)_4NI$ is greater than that of $(C_3H_7)_4NI$ both at 25 and 65°C. It is perhaps unreasonable to draw conclusions from the tetraalkyl ammonium salts since the ion-solvent interaction

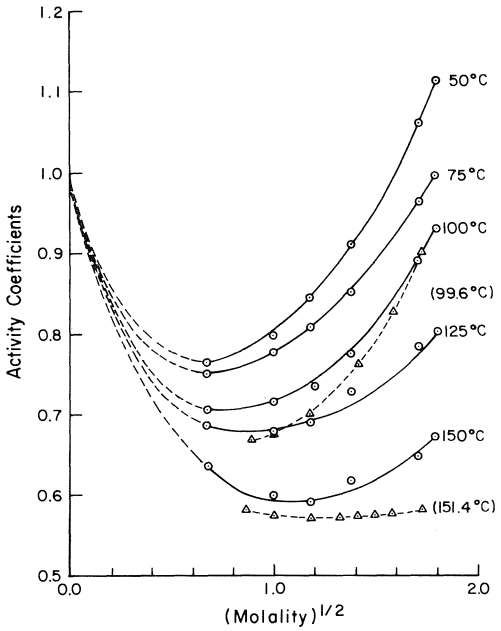

FIG. 4. Activity coefficients of LiCl in water; ○, present work; △, calculated from the osmotic coefficient data from refs. 7 and 10.

must be very different from that of the alkali halides, but it is significant that the osmotic coefficient of lithium chloride is always greater than that of sodium chloride at 25 to 150°C.

The activity coefficients of lithium chloride are in general much lower than those of sodium chloride at corresponding temperatures and concentrations. Figure 4 reproduces the activity coefficients calculated as above. By way of comparison, we have calculated the activity coefficients from the results of Soldano for osmotic coefficients at 99.6 and 151.4°C. At 100°C, our results are generally larger than those of Soldano, while the agreement at 150°C is very poor, even allowing for the slight difference in temperature. Our results show a considerable concentration dependence, similar to the behaviour of sodium chloride, as reported by Lindsay and Liu (6). No such concentration dependence is exhibited by Soldano's results, at 151.4°C.

Åkerlöf (13) has reported the activity coefficients of lithium chloride in water–methanol mixtures at 25°C. Addition of methanol to water lowers the dielectric constant progressively. Similarly, raising the temperature of water lowers its dielectric constant in much the same way. A 50% mixture of water–methanol has almost the same dielectric constant (55.9) as water at 100°C (56). The plot of activity coefficient vs. the square root of molality in water–methanol mixtures is quite similar to that reported by us for water at 100°C although the $\gamma\pm$ values for LiCl are much lower than in water having the same dielectric constant (at 100°C). This seems to show that, in addition to ion association and solvation processes, the activity coefficient is also dependent on some other factor or factors.

Acknowledgments

We are indebted to the National Research Council of Canada for a grant to one of us (A.N.C.) from which the expense of this research has been paid and to Mr. M. Tomlinson, Director, Chemical and Materials Science Division, Atomic Energy of Canada Ltd., Pinawa, Man. for suggesting to us the problem and for the loan of some equipment.

1. W. L. GARDNER, R. E. MITCHELL, and J. W. COBBLE. J. Phys. Chem. **73**, 2025 (1969).
2. C. M. CRISS and J. W. COBBLE. J. Am. Chem. Soc. **86**, 5385 (1964).
3. E. R. GARDNER, P. J. JONES, and H. J. DE NORDWALL. Trans. Faraday Soc. **59**, 1994 (1963).
4. E. R. GARDNER. Trans. Faraday Soc. **65**, 91 (1969).
5. C. LIU and W. T. LINDSAY, JR. J. Phys. Chem. **74**, 341 (1970).
6. C. LIU and W. T. LINDSAY, JR. J. Solution Chem. **1**, 45 (1972).
7. C. S. PATTERSON, L. O. GILPATRIC, and B. A. SOLDANO. J. Chem. Soc. 2730 (1960).
8. B. A. SOLDANO and C. S. PATTERSON. J. Chem. Soc. 937 (1962).
9. B. A. SOLDANO and M. MEEK. J. Chem. Soc. 4424 (1963).
10. B. A. SOLDANO and P. B. BIEN. J. Chem. Soc. A, 1825 (1966).
11. W. T. LINDSAY and C. LIU. Vapour pressure lowering of aqueous solutions at elevated temperatures. OSW Research and Development Progress Report No. 347.
12. L. B. SMITH, F. G. KEYES, and H. T. GERRY. Proc. Am. Acad. Arts Sci. **69**, 137 (1934).
13. G. ÅKERLÖF. J. Am. Chem. Soc. **52**, 2353 (1930).
14. S. LINDENBAUM, L. LEIFER, G. E. BOYD, and J. W. CHASE. J. Phys. Chem. **74**, 761 (1970).

Analysis of trace metal impurities in phthalocyanine pigments

RAFIK O. LOUTFY AND CHENG-KUO HSIAO

Xerox Research Centre of Canada, 2480 Dunwin Drive, Mississauga, Ont., Canada L5L 1J9

Received April 24, 1979

RAFIK O. LOUTFY and CHENG-KUO HSIAO. Can. J. Chem. **57**, 2546 (1979).

An analytical procedure was developed to determine the content of metallic impurities in metal-free phthalocyanine (H_2Pc) pigments. The technique involves dissolving the pigment in concentrated sulfuric acid, followed by oxidative degradation using hydrogen peroxide. Phthalimide was the only organic oxidation product. The remaining trace metals in the solution were determined using plasma atomic emission. The trace metals content in a commercial α polymorph of phthalocyanine pigment (ICI-Monolite Fast Blue GS) was monitored as a function of purification processes. Experiment showed that Monolite Fast Blue contains 2500 ppm Na; 350 ppm Ca, and 370 ppm Fe. Purification of this material by extraction with hot dimethylformamide gave β-H_2Pc, which contained 300 ppm Na, 110 ppm Ca, and 310 ppm Fe. Sulfuric acid purification (acid pasting) reduced the content of non-transition elements, but inincreased the content of transition metals.

These results were compared to the trace metal content in H_2Pc pigment which were synthesized.

RAFIK O. LOUTFY et CHENG-KUO HSIAO. Can. J. Chem. **57**, 2546 (1979).

On a développé une méthode analytique permettant de déterminer les quantités d'impuretés métalliques contenues dans des pigments de phtalocyanine (H_2Pc) sans métaux. La technique implique la dissolution du pigment dans de l'acide sulfurique concentré suivie d'une dégradation oxydante faisant appel au peroxyde. La phtalimide est le seul composé organique résiduel. On détermine les traces métalliques résiduelles à l'aide d'émission atomique des plasmas. On a déterminé les quantités de métaux à l'état de trace de la forme polymorphe α d'un pigment phtalocyanine commercial (ICI-Monolite Fast Blue GS) en fonction des méthodes de purification. L'expérience montre que le Monolite Fast Blue contient 2500 ppm de Na, 350 ppm de Ca et 370 ppm de Fe. La purification de ce produit par extraction avec de la diméthylformamide à l'ébullition conduit à la β-H_2Pc qui contient 300 ppm de Na, 110 ppm de Ca et 310 ppm de Fe. Une purification par de l'acide sulfurique (formation de pate acide) augmente le contenu en éléments de transition mais diminue les quantités des autres éléments.

On compare ces résultats à ceux obtenus relativement aux quantités de métaux à l'état de trace contenus dans des pigments H_2Pc obtenus par synthèse.

[Traduit par le journal]

Introduction

Phthalocyanine and its metal complexes possess unique semiconducting (1), photoconducting (2), and dielectric properties (3) and have found many practical applications in electrophotographic imaging systems (4). These materials have the potential to replace inorganic semiconductors and photoconductors in many applications. Metal-free phthalocyanine (H_2Pc) is now known to exist in three distinct polymorphic forms. The face centred monoclinic β-H_2Pc, the tetragonal α-H_2Pc, and the hexagonal *x*-H_2Pc have substantially differing dielectric conductivity and photoactivities (3). These phthalocyanines are normally prepared by methods involving reductive condensation of phthalonitrile. Seldom has a commercial phthalocyanine been found to be electrically useful. Extensive purification was always required to produce materials which possess these semiconducting and photoconducting properties. Workers (1, 2) often assume that extensive solvent extraction, acid pasting, or sublimation procedures will yield high purity materials and thus neglect to measure the nature, concentration, and distribution of any remaining impurity. Therefore, the differences and irreproducible electrical results reported in the literature are not surprising.

Often, insufficient attention is paid to the chemical purity of organic semiconductors. Many investigators (1–3) have used phthalocyanine, purified in different ways, without an exact determination of the amount and nature of the impurities present, even though impurities are known to greatly influence the measured electrophysical properties.

The aim of this work is to describe a method which was developed for the analysis of trace metal impurities in phthalocyanines. We have chosen for this investigation all the three polymorphs of metal-free phthalocyanines (α, β, and *x*-H_2Pc), the commercial

0008-4042/79/192546-03$01.00/0

TABLE 1. Results[a] of plasma atomic emission analysis of trace metal impurities (μg/g) in phthalocyanines

	Concentration								
	Group I	Group II		Group III	Transition metals				
	Na	Mg	Ca	Al	Fe	Cu	Zn	Mn	Co
1. ICI-α-H_2Pc Monolite Fast Blue	2500	46	350	—	380	7	—	—	—
2. β-H_2Pc	300	48	110	27	310	19	19	4.5	1.4
3. α-H_2Pc-1	151	49	940	50	1550	190	30	15.0	1.2
4. *x*-H_2Pc	60	12	114	24	620	35	30	5.4	—
5. Synthesized *x*-H_2Pc	12	—	7	6	47	3.5	8	—	—

[a]Standard deviation is better than 3%.

precursor material (ICI Monolite Fast Blue GS) and a synthesized *x*-H_2Pc. Full details of the method and the results are described below.

Methodology

Phthalocyanine pigments, in particular the metal-free compounds, are highly intractable materials insoluble in most common solvents. This renders analytical examination for trace impurities difficult. Metal-free phthalocyanines are soluble in concentrated H_2SO_4 although the resulting solutions are quite viscous. Because of the high viscosity it is difficult to analyze for trace metals by plasma emission spectroscopy where nebulization of the solution is required. On dilution with water, the phthalocyanine and its metal complexes precipitate. In order to resolve this dilemma, we decided to oxidize the phthalocyanine with peroxides before dilution. In this way, all the trace metals will remain in the solution, but the macrocyclic tetrazoporphin ring system will suffer oxidative degradation. The following general procedure was used.

(a) Sample Test Solution

Metal-free phthalocyanine (5 g) was dissolved in 16.7 mL concentrated sulfuric acid (36 *N*, BDH Aristar 98%). This was followed by drop-wise addition of hydrogen peroxide (30 Volume, Baker) to the cooled solution until the colour of the solution changed from dark green to pale yellow (~10 mL H_2O_2). The volume of the solution was then brought up to 50 mL using dionized water. N.B.: all the glassware was washed with (1:1) dilute nitric acid, deionized water, and dried. The product of the oxidation, phthalimide (3.45 g, 60%), identified using infrared spectroscopy and mixed melting point, precipitated on cooling.

The solution was filtered before plasma emission analysis.

(b) Blank Solution

A blank solution was prepared, which contained the same volume of sulfuric acid, hydrogen peroxide, and deionized water as the test solution. This solution was used to determine and cancel the background atomic emission level.

(c) Standard Solution

The standard solutions were prepared using the same amount of sulfuric acid (16.7 mL), hydrogen peroxide (10 mL), and a known volume of BDH standard metal ion solution: 5 mL of 1000 ppm iron, 0.5 mL of 1000 ppm each of calcium, sodium, magnesium, aluminum, copper, zinc, manganese, cobalt, and barium, The total volume was brought up to 50 mL using deionized water to give a standard solution of 100 ppm Fe, 10 ppm of Ca, Na, Al, Mg, Cu, Zn, Mn, Co, and Ba.

Plasma Emission Analysis

The trace metal analysis was carried out using a Spectrametrics Incorporated (Boston), model Spectrospan III, DC Argon plasma atomic emission instrument. The standard solution was nebulized into the argon ion plasma and the strongest atomic emission line of the particular element under investigation was selected using the instrument echelle grating. The slit position and width, photomultiplier sensitivity and wavelength were optimized to give the best signal/noise ratio. Then the microprocessor was activated to optimize the signal output and to accept it as the high standard 100 ppm for iron and 10 ppm for other metals. This was followed by nebulizing the blank solution at exactly the same rate and instrument setting, thus allowing the microprocessor to accept the emission signal output as background which is used for normalization. The test solution was then nebulized and the atomic emission signal (accumulation time 10 s, average of two runs) was processed by the microprocessor in reference to the high standard and blank samples to directly give the metallic content of the sample in ppm. For each element an average of three to four runs were performed. A linear curve resulted using the method of standard additions.

Results and Discussion

In the present work trace metal impurities in a number of metal-free phthalocyanines were determined using the procedure described above. Results are given in Table 1. The relative precision of the determination is 2–3%, which is much better than that reported by Kiryukhin and co-workers (6).

Table 1 shows that the unpurified commercial material, α-H_2Pc Monolite Fast Blue GS, contains large amounts of sodium (2500 ppm) and lesser amounts of the commonly used metals (Fe, Ca, Mg). This material was probably synthesized using the ICI-patented phthalonitrile – sodium amylate – amyl-alcohol method (7).

Monolite Fast Blue GS was purified by extraction with hot dimethylformamide solvent. Three extractions were required to remove all soluble organic

contaminants. During this treatment the material was converted to the β polymorph. The product was washed twice with isopropanol, dried, then preground to submicron size. This purification procedure reduced the sodium and calcium content significantly to 300 ppm and 110 ppm, respectively, as indicated by the trace metal analysis.

The α-H_2Pc polymorph was prepared by dissolving β-H_2Pc in cold, concentrated sulfuric acid and slowly reprecipitating the phthalocyanine by adding the solution to a large volume of ice water. The resulting α-H_2Pc, after filtering, was washed successively with ammonia and methanol, and then dried at 70°C. Several batches of α-H_2Pc were prepared from β-H_2Pc using the acid pasting process. A dramatic difference in the content of metallic impurities between these batches was noted. The greatest differences are in the content of the transition metals such as iron and the alkaline earths such as calcium. These differences were attributed to the purity and quantity of the sulfuric acid used in the acid pasting process.

The attempts to purify phthalocyanine by reprecipitation from concentrated sulfuric acid reduce only the labile metals such as sodium. However, the content of the heavy metals, Fe, Cu, Zn, and Mn, and organic impurities (decomposition products), are usually increased. The difficulty of eliminating many metals is associated with the fact that phthalocyanine complexes are formed in the synthesis together with the main product. Furthermore, these complexes possess very similar physiochemical properties. The most important effect of the acid pasting process is the morphological change in the pigment structure and in the particle size.

x-H_2Pc polymorph was prepared by dry milling α-H_2Pc-11 with flint stones for a week, followed by a methanol wash to remove organic impurities which are either formed by or released during grinding. The final product is microcrystalline material, submicron in size (1000 Å particles). The metallic content in *x*-H_2Pc is shown in Table 1. The most abundant metal is iron (600 ppm) followed by calcium (110 ppm) and lesser amounts of a variety of other metals.

Synthesized *x*-H_2Pc was prepared using Brach's methods (8) which involves heating phthalonitrile in 2-dimethylaminoethanol (DMAE) at 140°C for 1 h. When the temperature of the reaction mixture reached 130°C, 3% by weight of *x*-H_2Pc was added as seed, then the temperature was raised to 140°C and maintained for 1 h. The dark blue solution was filtered while hot, and the product was washed repeatedly with hot DMF, then with isopropanol, then dried, to yield 44% of crystalline material. The crystal structure was determined to be *x*-H_2Pc using visible and ir spectroscopy and from X-ray powder diffraction methods (5). The mean particle size was 36 μm.

Trace metal analysis of synthesized *x*-H_2Pc indicated that this material is very pure. This *x*-H_2Pc contained 50 ppm iron, originating from DMAE (contains 50 ppm Fe) and ~10 ppm Al, originating from the phthalonitrile, and very little of other metals.

In conclusion, tests showed that the content of metallic impurities in phthalocyanine pigments is highly dependent on the synthetic route and the purification procedures. High purity metal-free phthalocyanine can be obtained by reductive condensation of purified phthalonitrile in dimethylaminoethanol.

The presence of metallic impurities — most likely as metal phthalocyanines — could greatly influence the electrical properties of phthalocyanines. Impurities may act as exciton or carrier traps. The influence of these impurities would be observed in charge-carrier generation, carrier mobility, electron spin resonance signals and perhaps in other spectroscopic measurements, such as fluorescence emission and singlet exciton lifetime. We are at present studying the effect of these impurities on the electrical and photoelectrical properties of metal-free phthalocyanines.

Acknowledgements

The authors are indebted to Dr. T. Martin for the use of the plasma atomic emission instrument and to Dr. J. H. Sharp for his support and interest in the work.

1. (*a*) K. Wihksne and A. E. Newkirk. J. Chem. Phys. **34**, 2184 (1961); (*b*) S. E. Harrison and K. H. Ludewig. J. Chem. Phys. **45**, 343 (1966); (*c*) S. E. Harrison and J. M. Assour. J. Chem. Phys. **40**, 365 (1963).
2. (*a*) C. F. Hackett, J. Chem. Phys. **55**, 3178 (1971); (*b*) D. Day and R. J. P. Williams. J. Chem. Phys. **42**, 4049 (1965); (*c*) Z. Popovic and J. H. Sharp. J. Chem. Phys. **66**, 5076 (1977).
3. M. A. Abkowitz and A. I. Lakatos. J. Chem. Phys. **57**, 5033 (1972).
4. R. Luebbe, M. Maltz, G. Reinis, and W. G. Van Vorn. Photogr. Sci. Eng., Second International Conference on Electrophotography, 1974. p. 43.
5. J. H. Sharp and M. Lardon. J. Phys. Chem. **72**, 3230 (1968).
6. I. A. Kiryukhin, K. N. Lobanova, Yu. A. Popov, Y. Kh. Shaulov, and V. A. Benderskii. Russ. J. Phys. Chem. **50**, 380 (1976).
7. I. M. Heilbron, F. Irving, and R. P. Linstead. U.S. patent 2, 116, 602 (1938).
8. P. Brach and H. Six. German Patent Geroffen 1942701 (1970).

Insertion of an acetylene into the platinum–iodide bond

N. CHAUDHURY AND R. J. PUDDEPHATT[1]

Donnan Laboratories, The University of Liverpool, P.O. Box 147, Liverpool L69 3BX, U.K.

N. CHAUDHURY and R. J. PUDDEPHATT. Can. J. Chem. **57**, 2549 (1979).

Reaction of [PtIMe(2,2′-bipyridine)], **I**, with $MeO_2CC{\equiv}CCO_2Me$ gives first a 5 co-ordinate π-complex [PtIMe($MeO_2CC{\equiv}CCO_2Me$)(bipy)], **II**, and then the product of insertion into the PtI bond [PtMe{$C(CO_2Me){=}C(CO_2Me)I$}(bipy)], **III**. A study of the kinetics of dissociation of **II** to **I** and free alkyne shows that reaction occurs largely by dissociation of iodide followed by loss of alkyne from the resulting cationic alkyne complex. Formation of **III** may involve nucleophilic attack by I^- on the co-ordinated alkyne of this cationic intermediate.

N. CHAUDHURY et R. J. PUDDEPHATT. Can. J. Chem. **57**, 2549 (1979).

La réaction du [PtIMe(bipyridine-2,2′)], **I**, avec le $MeO_2CC{\equiv}CCO_2Me$ conduit en premier lieu à un complexe π penta coordonné [PtIMe($MeO_2CC{\equiv}CCO_2Me$)(bipy)], **II**, puis au produit d'insertion dans la liaison PtI [PtMe{$C(CO_2Me){=}C(CO_2Me)I$}bipy], **III**. Une étude de la cinétique de la dissociation de **II** en **I** et en alcyne libre montre que la réaction se produit en grande partie par une dissociation de l'iodure suivie par une perte de l'alcyne par le complexe alcyne cationique qui en résulte. La formation de **III** peut impliquer une attaque nucléophile par le I^- sur l'alcyne coordonné de cet intermédiaire cationique.

[Traduit par le journal]

Introduction

There has been considerable interest in insertion reactions of alkenes and akynes into the Pt—X bond where X = H, CH_3, or Cl (1–7). Generally such reactions involve intermediates in which the alkene or alkyne and the group X are in mutually *cis* co-ordination sites in a square planar molecule, for then migration of X to the co-ordinated alkene or alkyne is particularly favorable (1) Such reactions give *cis* addition to alkynes. However, attack by external nucleophiles on co-ordinated alkenes or alkynes is also possible and *trans* addition then occurs (8–10). During investigations of alkyl(2,2′-bipyridine)platinum(II) complexes with alkenes and alkynes (4, 5, 11), a reaction was discovered in which an alkyne underwent insertion into a Pt—I bond of [PtIMe(bipy)], bipy = 2,2′-bipyridine, rather than into the PtMe bond as was expected. This paper describes an investigation into the mechanism of this reaction.

Results

Characteristics of Products

Yellow solutions of [PtIMe(bipy)], **I**, in acetone, benzene, or methanol were rapidly decolorised by addition of $MeO_2CC{\equiv}CCO_2Me$, and the almost colorless adduct [PtIMe($MeO_2CC{\equiv}CCO_2Me$)(bipy)], **II**, could be isolated after short reaction times. However, in acetone or benzene the solutions became yellow in color after a few minutes at room temperature and from such solutions the yellow product [PtMe{$C(CO_2Me){=}C(CO_2Me)I$}(bipy)], **III**, could be isolated.[2]

Many 5 co-ordinate platinum–alkyne complexes analogous to **II** are now known and characterisation was straight-forward (11–17). The infrared spectrum contained a strong band at 1818 cm^{-1} due to ν(C≡C) of the co-ordinate alkyne as well as ν(CO) stretching vibrations at 1700 cm^{-1}. The uv–visible spectrum of a freshly-prepared solution contained no MLCT band in the region 400–500 nm, and this is typical of 5 co-ordinate alkene or alkyne complexes or of (2,2′-bipyridine)platinum(IV) complexes; 2,2′-bipyridine complexes of platinum(II) with square planar stereochemistry have a prominent band in this region due to excitation of an electron from a filled 5*d*-orbital of platinum to a π*-orbital of 2,2′-bipyridine (18). However, dissociation of the alkyne occurred readily and the characteristic MLCT band of **I** was observed after a short time. Attempts to record the ^1H nmr spectrum of **II** in $CDCl_3$ were unsuccessful due to dissociation to **I** (δ(MePt) 1.22 ppm, ^2J(PtH) 78 Hz) and free alkyne (δ(MeO) 3.81 ppm). However, a spectrum was obtained by adding excess alkyne to a solution of **I** in $CDCl_3$, when a methylplatinum resonance appeared (δ(MePt) 0.58 ppm, ^2J(PtH) 68 Hz) due to **II**. The decrease in the coupling constant $^2J(PtCH_3)$ is typical of such com-

[1]To whom all correspondence should be addressed. Present address: Department of Chemistry, The University of Western Ontario, London, Ont., Canada N6A 5B7.

[2]In methanol this product was not formed and the observed product was an oil which could not be purified. Nuclear magnetic resonance studies suggested that a methoxy group from the solvent was incorporated.

0008-4042/79/192549-06$01.00/0

pounds (19, 20). The resonances due to the equilibrium mixture of **I** and **II** then slowly decayed as further reaction to give **III** occurred.

The ^{1}H nmr spectrum of **III** contained a methylplatinum resonance (δ(MePt) 0.84 ppm, ^2J(PtH) 82 Hz) characteristic of square planar methyl(2,2′-bipyridine)platinum(II) complexes (18, 21), and two equal intensity methoxy resonances (δ 3.80 ppm, J(PtH) 3 Hz; δ 3.65 ppm). The low-field methoxy resonance with distinct coupling to ^{195}Pt is assigned to the CO_2Me group α to a platinum (6, 7, 20). The uv–visible spectrum contained an MLCT band with typical dependence of energy on solvent polarity (390 mn in CH_3CN, 402 and 414 nm in acetone, 422 and 436 nm in benzene). The presence of this MLCT band indicates that the product is a square planar platinum(II) complex. The infrared spectrum gave strong peaks due to ν(CO) at 1700 cm^{-1}, but no peaks due to a co-ordinated alkyne. A band at 568 cm^{-1} was assigned to ν(PtMe) but the expected weak band at around 1550 cm^{-1} due to ν(C≡C) was not observed and was presumably obscured by a strong band due to the ligand 2,2′-bipyridine in this region. Unfortunately, the spectroscopic data cannot distinguish between the *cis* and *trans* orientations of the CO_2Me groups about the C≡C bond of **III**, and attempts to grow single crystals suitable for X-ray structural determination have been unsuccessful due to crystal twinning. Overall the reaction of **I** with $MeO_2CC{\equiv}CCO_2Me$ can be represented by reaction [1] where N⌒N = bipy, R = CO_2Me.

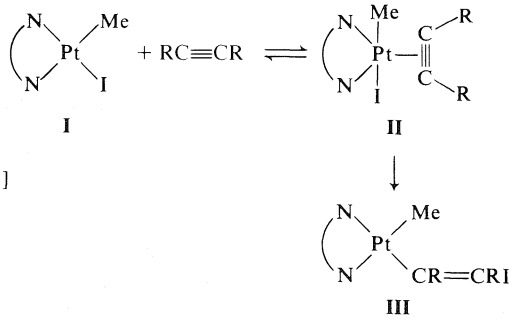

[1]

Kinetic Studies

Complex **II** decomposed quantitatively to **I** and free alkyne when dissolved in organic solvents, and we have studied the kinetics of this process using uv–visible spectrophotometry. Thus the growth of the MLCT band due to **I** can be used to monitor the reaction rate. A typical uv–visible spectrum is shown in Fig. 1. The reactions followed first-order kinetics in benzene, tetrahydrofuran, and acetone solvents. The rates were higher in the more polar solvents as measured by Reichardt's E_T parameter of solvent polarity (Table 1), suggesting a polar reaction intermediate (22). In acetone solution the reaction was retarded by addition of free iodide (Table 1). Concentrations of I^- were calculated from the concentrations of Bu_4NI added after allowing for ion-pairing using the equilibrium constant given by Winstein and co-workers (23). A graph of k_{obs} vs. $1/[I^-]$ gave an intercept at $1/[I^-] = 0$ of approximately 1.7×10^{-3} s^{-1}, indicating that there was a component of the reaction rate which was independent of the concentration of iodide. Good agreement was obtained using the expression for k_{obs}:

$$k_{obs} = k_1 + 1/(a[I^-] + b)$$

or

$$1/(k_{obs} - k_1) = a[I^-] + b$$

The constants $k_1 = 1.53 \times 10^{-3}$ s^{-1}, $a = 3.85 \times 10^5$ L mol^{-1} s, and $b = 21$ s were then determined (24).

The above results strongly support the mechanism of Scheme 1 (11).

If the stationary state approximation is made for

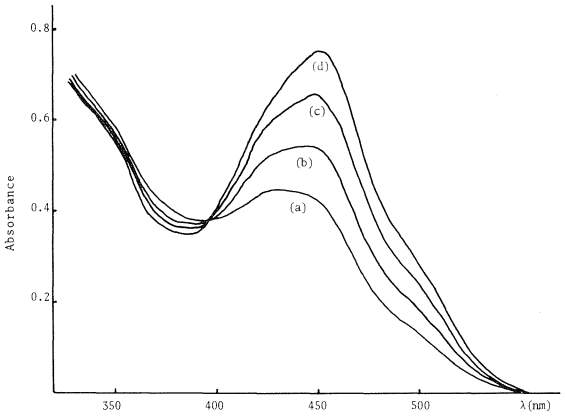

FIG. 1. Ultraviolet–visible spectra recorded during the decomposition of **II** → **I** in tetrahydrofuran at 40°C. Spectra recorded after: (*a*), 3 min; (*b*), 8 min; (*c*), 17 min; (*d*), 40 min.

TABLE 1. First order rate constants for the thermal decomposition of **II** at 40°C

Solvent	E_T	10^3 [$Bu_4N^+I^-$] (M)	$10^3 k_{obs}$ (s^{-1})
Benzene	34.1	0	2.0
Tetrahydrofuran	37.4	0	2.3
Acetone	42.4	0	6.3
		1.25	3.3
		2.50	2.8
		5.00	2.2
		10.0	2.0
		20.0	1.8

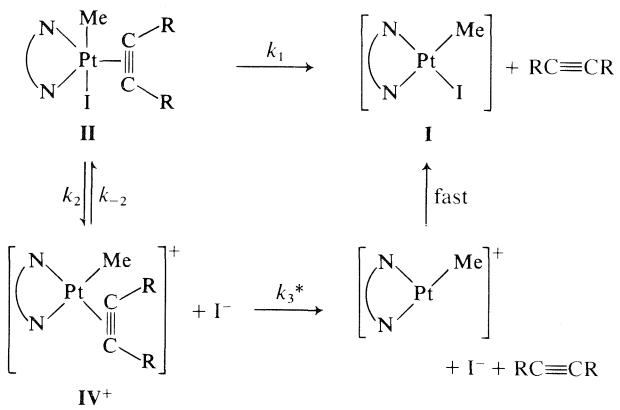

SCHEME 1. N⌒N = bipy, R = CO_2Me. The k_3 step is written as a dissociative step (for which precedents are known (25)) but could well involve displacement of alkyne by solvent. The reverse reaction **I** → **II** is negligible under the experimental conditions, and hence the reaction proceeds essentially to completion as shown

the ionic intermediate **IV** then the expected rate expression is:

$$-d[\mathbf{II}]/dt = [\mathbf{II}][k_1 + k_2k_3/(k_{-2}[I^-] + k_3)]$$

This is consistent with all the experimental data and the values $k_1 = 1.53 \times 10^{-3}$ s^{-1}, $k_2 = 4.77 \times 10^{-3}$ s^{-1}, and $k_{-2}/k_3 = 1.8 \times 10^3$ L mol^{-1} can be calculated for the reaction in acetone solution at 40°C. We were unable to obtain reliable kinetic data for the reverse reaction leading to formation of **II** from **I**, but this must involve the same intermediates.

Examination of typical uv–visible spectra obtained after addition of $MeO_2CC{\equiv}CCO_2Me$ to a solution of **I** again leads to the conclusion that reaction proceeds in two separate steps (Figs. 2 and 3). The first rapid step leads to decay of the MLCT band of **I** as the rapid equilibrium with **II** is achieved (graphs (*a*)–(*c*) in Figs. 2 and 3). It was not possible to obtain reliable kinetic data for this step since it was too rapid, but approximate values of the equilibrium constants for π-complex formation were obtained; the mean values were 4.1 ± 0.5 L mol^{-1} in acetone and 5.4 ± 0.6 L mol^{-1} in benzene. The second stage of reaction leads to growth of a new MLCT band due to **II** and clear isosbestic points are observed during this reaction. The formation of **III** from the quilibrium mixture of **I** and **II** followed good first order kinetics in solvents benzene, acetone, and methylcyanide and rate constants in these solvents with a fixed concentration of alkyne are given in Table 2. There is a significant increase in rate with solvent polarity suggesting a polar intermediate or transition state. The rate of reaction in benzene or acetone solution increased with concentration of alkyne, reaching

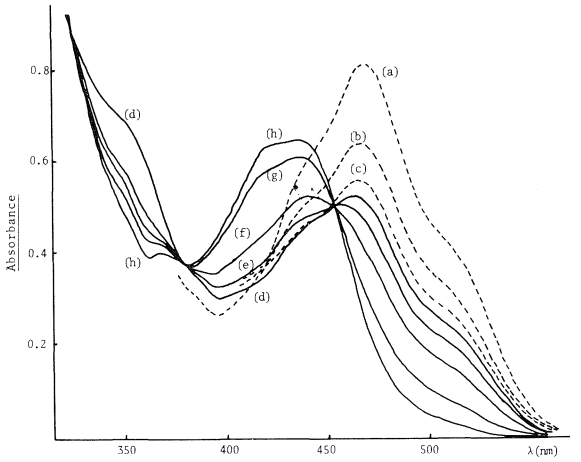

FIG. 2. Ultraviolet–visible spectra recorded during the reaction of **I** with $MeO_2CC{\equiv}CCO_2Me$ (0.076 *M*) in benzene at 40°C. Spectra recorded after: (*a*), time zero; (*b*), 3 min; (*c*), 10 min; (*d*), 30 min; (*e*), 75 min; (*f*), 154 min; (*g*), 318 min; (*h*), 375 min.

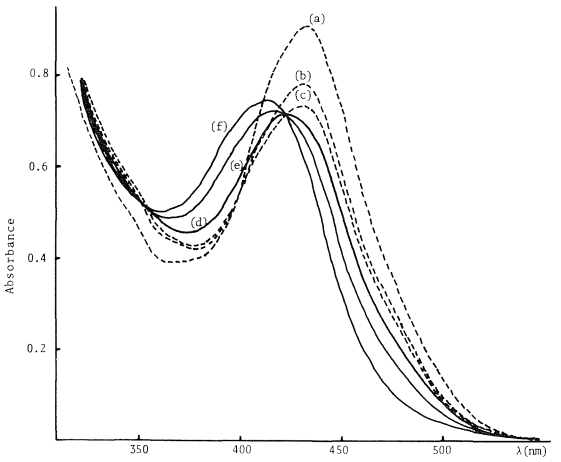

FIG. 3. Ultraviolet–visible spectra recorded during the reaction of **I** with $MeO_2CC{\equiv}CCO_2Me$ (0.074 *M*) in acetone solution at 40°C. Spectra recorded after: (*a*), 1 min; (*b*), 2 min; (*c*), 3 min; (*d*), 9 min; (*e*), 18 min; (*f*), 74 min.

a limiting value at high alkyne concentration. The data gave good agreement with the expression

$$k_{obs} = [RCCR]/(a + b[RCCR])$$

or

$$1/k_{obs} = a/[RCCR] + b$$

Thus graphs of $1/k_{obs}$ vs. 1/[RCCR] gave good linear plots (Fig. 4) and the parameters resulting are given in Table 3.

Attempts to study the kinetics of formation of **III** in the presence of free I^- were unsuccessful since different, unidentified products were formed under these conditions. The rate was not affected by the

TABLE 2. Observed first order rate constants for formation of **III** at 40°C

Solvent	E_T	$[MeO_2CC{\equiv}CCO_2Me]$ (M)	$10^4\ k_{obs}$ (s^{-1})
C_6H_6	34.1	0.144	1.47
Me_2CO	43.2	0.144	18.5
MeCN	46.0	0.144	51.2
C_6H_6	34.1	0.058	0.80
C_6H_6		0.076	0.90
C_6H_6		0.104	1.12
C_6H_6		0.226	2.0
C_6H_6		0.500	2.67
Me_2CO	43.2	0.0337	5.5
Me_2CO		0.0750	10.3
Me_2CO		0.100	12.8
Me_2CO		0.1440	18.5
Me_2CO		0.3240	21.5

TABLE 3. Kinetic parameters for formation of **III** at 40°C

Solvent	a (L^{-1} mol s)[a]	b (s)[a]	b/a (L mol^{-1})	K (L mol^{-1})[b]
Benzene	588	2700	4.6±0.4	5.4±0.6
Acetone	54	240	4.4±0.2	4.1±0.5

[a]For definition see the text.
[b]Equilibrium constants for formation of **II** from **I** and alkyne measured directly.

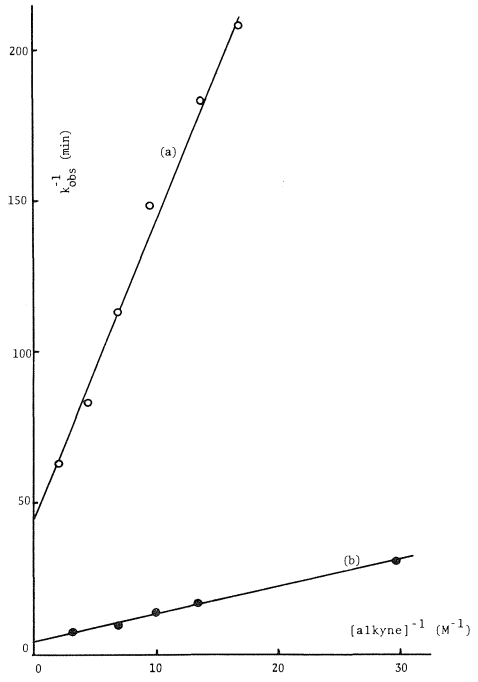

FIG. 4. Graph of the reciprocal of the observed rate constant for formation of **III** at 40°C vs. reciprocal of the concentration of alkyne: (*a*), in benzene solution; (*b*), in acetone solution.

presence of free 2,2′-bipyridine, indicating that dissociation of 2,2′-bipyridine at an intermediate stage does not occur. This type of ligand dissociation was observed in the reaction of diethyl(2,2′-bipyridine)-platinum(II) with methyl acrylate (5).

Discussion

The kinetic data for dissociation of alkyne from **II** shows clearly that the dominant pathway involves preliminary reversible dissociation of I^- to give a cationic intermediate **IV**, which then releases the alkyne as shown in Scheme 1. The mechanism is strongly supported by the retardation of the reaction by free iodide and is also supported by the increased rate in more polar solvents. There is also a component of the reaction for which the rate is independent of the concentration of free iodide. This could involve simple dissociation of the alkyne from **II**, or could involve the intermediacy of a tight ion pair $\mathbf{IV}^+I^-$, or could involve the direct displacement of alkyne from $\mathbf{IV}^+$ by I^-.

The mechanism by which the product of insertion of the alkyne into the Pt—I bond, **III**, is formed is more difficult to elucidate, particularly because other reactions occurred in the presence of free I^- and hence the dependence of the reaction rate on $[I^-]$ could not be determined. The observed rate dependence on the concentration of alkyne is consistent with any one of the routes *A*, *B*, or *C* shown in Scheme 2. Route *A* involves direct insertion of the alkyne into the Pt—I bond of **I**, route *B* involves nucleophilic attack by I^- on the co-ordinated alkyne of $\mathbf{IV}^+$ while route *C* involves intramolecular migration of co-ordinated iodide to the co-ordinated alkyne of **II**. If the equilibrium between **I** and **II** is established rapidly compared with the rate of formation of **III** and, in the case of route *B*, if the stationary state approximation is made for $\mathbf{IV}^+$, then each route will give an expression for k_{obs} of the general form observed experimentally, and in each case the ratio of parameters b/a should give an independent measure of the equilibrium constant, K, for formation of **II** from **I** and RCCR. The relevant data are given in Table 3 and satisfactory agreement is found between the values of the equilibrium constants measured directly and those deduced from the kinetic data.

The considerable increase in rate of formation of **III** in more polar solvents strongly suggests a polar intermediate or transition state and this can be taken as evidence in favor of route *B* above. This would be expected to give a product with *trans* stereochemistry about the C=C bond. We were unable to determine this stereochemistry, but insertion of $MeO_2CC{\equiv}CCO_2Me$ into a PtCl bond of

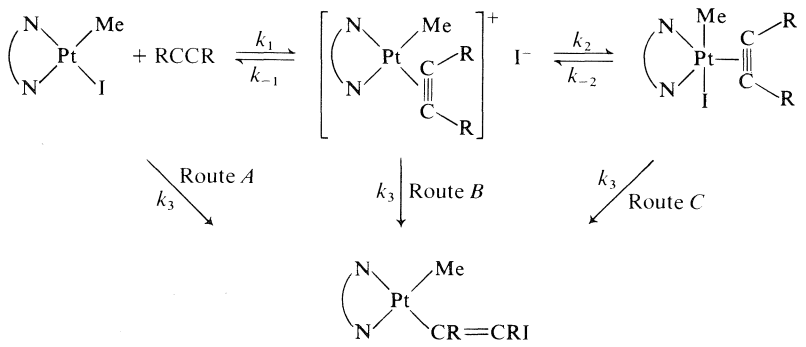

SCHEME 2. This scheme shows the possible mechanisms of the formation of **III**. The mechanism of interconversion of **I** ⇌ **II** has been simplified for clarity (see Scheme 1 for details)

$[Pt(CO)_2Cl_2]$ is known to give this *trans* stereochemistry although it was suggested that the *cis* isomer might be formed first followed by rapid isomerisation (6). Curiously, the reaction of [PtClMe(bipy)] with $MeO_2CC{\equiv}CCO_2Me$ gives the adduct $[PtClMe(MeO_2CC{\equiv}CCO_2Me)(bipy)]$ but this does not readily rearrange to give the product of insertion into either the PtMe or PtCl bond. Slow reaction does occur, but there is always an induction period in solvents acetone, CH_2Cl_2, or tetrahydrofuran and a free-radical process, perhaps like that discovered by Clark and co-workers (20), appears to operate. This reaction gave a mixture of products which were difficult to identify, and the kinetics were not reproducible. It was therefore not studied further. The difference in reactivity could be due to the greater nucleophilicity of iodide than of chloride.[3]

Experimental Section

[PtIMe(COD)], COD = 1,5-cyclo-octadiene, was prepared by the literature method (21). ^1H nmr spectra were recorded at 60 MHz using a Perkin-Elmer R12B instrument. Ultraviolet–visible spectra were recorded using a Unicam SP8000 spectrophotometer, with an electrically heated thermostatted (to ±0.2°C) cell compartment.

Iodo(methyl)(2,2′-bipyridine)platinum(II) [PtIMe(COD)] (0.316 g) and 2,2′-bipyridine (0.196 g) were each dissolved in benzene (5 cm^3). The solutions were mixed and heated under reflux for 2 h, then cooled to 0°C for several hours. The orange crystals of the product were filtered off, washed with ether, and dried under vacuum. Yield 0.314 g; mp 255–264°C (dec.). *Anal.* calcd. for $C_{11}H_{11}IN_2Pt$: C 26.80, H 2.33; found: C 26.85, H 2.39. Nmr ($CDCl_3$) δ(CH_3Pt) 1.22 ppm, ^2J(PtH) 78 Hz.

[PtIMe(MeO₂CC≡CCO₂Me)(2,2′-bipyridine)]

[PtIMe(2,2′-bipyridine)] (0.205 g) was dissolved in the minimum volume of warm acetone (~50 cm^3). This solution was then cooled in ice and $MeO_2CC{\equiv}CCO_2Me$ (0.2 cm^3) was added. The mixture was allowed to react at 0°C for 15 min and the solvent was then evaporated under high vacuum. The product was washed with ether and dried *in vacuo*. Yield 0.2374 g, mp 160°C (dec.). *Anal.* calcd. for $C_{17}H_{17}IN_2O_4Pt$: C 32.20, H 2.68, Pt 30.70; found: C 32.06, H 2.97, Pt 31.30. The pure product is almost colourless, and can also be prepared conveniently in methanol solution.

[PtMe{C(CO₂Me)=C(CO₂Me)I}(2,2′-bipyridine)]

[PtIMe(2,2′-bipyridine)] (0.110 g) was dissolved in warm acetone (25 cm^3) and $MeO_2CC{\equiv}CCO_2Me$ (0.115 g) was then added. The solution was stirred for 3 h at room temperature. The yellow crystals which formed were filtered off, washed with ether, and dried under vacuum. Yield 0.054 g; mp 173–183°C (dec.). *Anal.* calcd. for $C_{17}H_{17}IN_2O_4Pt$: C 32.20, H 2.68, I 20.00, Pt 30.70; found: C 32.13, H 2.74, I 20.12, Pt 30.77.

Kinetic Studies

(a) Decomposition of Complexes II

The complex **II** (0.002–0.003 g) was dissolved in the required solvent and the volume was made up to 25 cm^3 in a volumetric flask. The solution was rapidly transferred to the 1 cm quartz uv cell held in the thermostatted cell compartment of the spectrophotometer. Spectra were recorded at intervals as the reaction proceeded. Naturally some decomposition occurred before the first spectrum could be recorded but this does not affect the form of the kinetics. Absorbance changes were taken at 465 nm in benzene, 450 nm in tetrahydrofuran, and 432 nm in acetone solution, these values being close to the maximum absorbance due to the MLCT band of [PtIMe(bipy)] in these solvents.

(b) Kinetics of Formation of III

$MeO_2CC{\equiv}CCO_2Me$ (0.04–0.5 g) was weighed accurately into a 5 cm^3 volumetric flask. [PtIMe(bipy)] (0.0015 g) was weighed out separately, dissolved in the required solvent, and the volume made up to 25 cm^3. This solution was added to the volumetric flask containing the alkyne and the volume was made up to 5 cm^3. The solution was mixed and transferred rapidly to the 1 cm quartz uv cell held in the thermostatted cell compartment of the spectrophotometer. Spectra were then recorded at intervals as the reaction proceeded.

[3]We thank a referee for this suggestion.

1. D. L. THORN and R. HOFFMANN. J. Am. Chem. Soc. **100**, 2079 (1978).
2. H. C. CLARK and C. S. WONG. J. Am. Chem. Soc. **96**, 7213 (1974); H. C. CLARK and C. A. JABLONSKI. Inorg. Chem. **13**, 2213 (1974).
3. H. C. CLARK and K. VON WERNER. J. Organomet. Chem. **101**, 347 (1975).

4. N. CHAUDHURY, M. G. KEKRE, and R. J. PUDDEPHATT. J. Organomet. Chem. **73**, C17 (1974).
5. N. CHAUDHURY and R. J. PUDDEPHATT. J. Chem. Soc. Dalton, 915 (1976).
6. F. CANZIANI, L. GARLASCHELLI, and M. C. MALATESTA. J. Organomet. Chem. **146**, 179 (1978).
7. F. CANZIANI, A. ALBINATI, L. GARLASCHELLI, and M. C. MALATESTA. J. Organomet. Chem. **146**, 197 (1978).
8. T. G. APPLETON, H. C. CLARK, and R. J. PUDDEPHATT. Inorg. Chem. **11**, 2074 (1972).
9. M. H. CHISHOLM and H. C. CLARK. Acc. Chem. Res. **6**, 202 (1973).
10. J. K. STILLE and D. E. JAMES. J. Organomet. Chem. **108**, 401 (1976).
11. N. CHAUDHURY and R. J. PUDDEPHATT. J. Organomet. Chem. **87**, C45 (1975).
12. T. THEOPHANIDES and P. C. KONG. Can. J. Chem. **48**, 1084 (1970).
13. B. W. DAVIES, R. J. PUDDEPHATT, and N. C. PAYNE. Can. J. Chem. **50**, 2276 (1972).
14. B. W. DAVIES and N. C. PAYNE. Inorg. Chem. **13**, 1843 (1974).
15. L. MARESCA, G. NATILE, M. CALLIGARIS, P. DELISE, and L. RANDACCIO. J. Chem. Soc. Dalton, 2386 (1976).
16. G. NATILE, L. MARESCA, L. CATTALINI, U. BELLUCO, P. UGUAGLIATI, and U. CROATTO. Inorg. Chim. Acta, **20**, 49 (1976).
17. I. AL-NAJJAR and M. GREEN. J. Chem. Soc. Chem. Commun. 212 (1977).
18. N. CHAUDHURY and R. J. PUDDEPHATT. J. Organomet. Chem. **84**, 105 (1975).
19. H. C. CLARK and R. J. PUDDEPHATT. Inorg. Chem. **10**, 18 (1971).
20. T. G. APPLETON, M. H. CHISHOLM, H. C. CLARK, and K. YASUFUKU. J. Am. Chem. Soc. **96**, 6600 (1974).
21. H. C. CLARK and L. E. MANZER. J. Organomet. Chem. **57**, 411 (1973).
22. K. DIMROTH, C. REICHARDT, T. SIEPMANN, and F. BOHLMANN. Ann. Chem. **661**, 1 (1963); C. REICHARDT. Angew. Chem. Int. Ed. Engl. **4**, 29 (1965).
23. S. WINSTEIN, L. G. SAVEDOFF, S. SMITH, I. D. R. STEVENS, and J. S. GALL. Tetrahedron Lett. **9**, 24 (1960).
24. A. R. STEIN. J. Chem. Educ. **52**, 303 (1975).
25. R. ROMEO, D. MINNITI, and M. TROZZI. Inorg. Chem. **15**, 1134 (1976).

Structure of a new crystalline modification of dithiocyanato(triphenylphosphine)-mercury(II)

RAMESH C. MAKHIJA, ROLAND RIVEST, AND ANDRÉ L. BEAUCHAMP[1]

Département de Chimie, Université de Montréal, C.P. 6210, Succ. A, Montréal (Qué.), Canada H3C 3V1

Received April 4, 1979

RAMESH C. MAKHIJA, ROLAND RIVEST, and ANDRÉ L. BEAUCHAMP. Can. J. Chem. **57**, 2555 (1979).

Crystals of the β-form of the title compound are monoclinic, space group $P2_1/c$, a = 21.071(5), b = 17.716(5), c = 11.285(3) Å, β = 101.66(5)°, and Z = 8. The structure was refined on 2741 independent observed reflections to an R factor of 0.042.

The crystals consist of two types of infinite chains with backbones of thiocyanate-bridged mercury atoms. In chain 1, mercury shows the same (3 + 2) coordination as observed in the α-form. It is bound to P of triphenylphosphine (Hg—P = 2.429(4) Å) and two S-bonded thiocyanate ligands (Hg—S = 2.491(5), 2.519(5) Å) in the equatorial plane of a distorted trigonal bipyramid. The axial positions are occupied by weakly-bonded N atoms from adjacent units (Hg—N = 2.74(1), 2.89(1) Å). Chain 2 contains four-coordinated mercury with an approximate tetrahedral geometry. A bridging SCN group links successive Hg atoms in the chain by moderately strong Hg—S (2.648(5) Å) and Hg—N (2.40(1) Å) bonds. The coordination sphere also includes phosphorus (Hg—P = 2.432(4) Å) and a unidentate S-bonded thiocyanate group (Hg—S = 2.454(5) Å). The chains are held together by normal van der Waals contacts.

RAMESH C. MAKHIJA, ROLAND RIVEST et ANDRÉ L. BEAUCHAMP. Can. J. Chem. **57**, 2555 (1979).

Les cristaux de la forme β du composé étudié appartiennent au système monoclinique, groupe d'espace $P2_1/c$, a = 21.071(5), b = 17.716(5), c = 11.285(3) Å, β = 101.66(5)° et Z = 8. La structure a été affinée au moyen de 2741 réflexions observées indépendantes jusqu'à un facteur R de 0.042.

Les cristaux sont constitués de deux sortes de chaînes infinies dans lesquelles les atomes de mercure sont reliés par des ponts thiocyanates. Dans la première sorte de chaîne, le mercure possède la même coordination (3 + 2) que dans la forme α. Il s'y trouve entouré du phosphore de la triphénylphosphine (Hg—P = 2.429(4) Å) et de deux groupes SCN liés par le soufre (Hg—S = 2.491(5), 2.519(5) Å) dans le plan équatorial d'une bipyramide triangulaire déformée. Les sites axiaux sont occupés par des atomes d'azote faiblement liés appartenant à des motifs voisins (Hg—N = 2.74(1), 2.89(1) Å). L'autre sorte de chaîne renferme du mercure tétracoordiné selon une géométrie à peu près tétraédrique. Un groupe SCN relie deux atomes de mercure successifs par des liaisons Hg—S (2.648(5) Å) et Hg—N (2.40(1) Å) moyennement fortes. La sphère de coordination comprend aussi un atome de phosphore (Hg—P = 2.432(4) Å) et un groupe SCN monodentate lié par le soufre (Hg—S = 2.454(5) Å). Les chaînes sont retenues normalement par des forces de van der Waals.

Introduction

In a previous paper, we have shown that mercury has a (3 + 2) trigonal bipyramid coordination in the 1:1 adduct of $Hg(SCN)_2$ with triphenylarsine (1). The three strongly-bonding equatorial positions are occupied by the soft donors (2 S and 1 As), whereas the apical sites are filled with two weakly-bonded N atoms from SCN groups acting as bridging ligands. Recently, the crystals obtained from a 1:1 mixture of $Hg(SCN)_2$ and triphenylphosphine (Ph_3P) in *ethanol* (referred to hereafter as the α-form) were shown to be isomorphous with the As analog (2). These results seemed to disagree with those of Plane and coworkers (3), who interpreted the ir spectrum of $Hg(SCN)_2 \cdot Ph_3P$ in terms of both bridging and nonbridging SCN groups. However, when the compound was prepared from *acetone* as originally described by Plane *et al.* (3), its composition remained unchanged but it was crystallographically different. The crystal structure of this new modification (the β-form) is described in the present paper.

Experimental Section

Preparation

$Hg(SCN)_2$ and triphenylphosphine (1:1 ratio) were mixed in acetone. Crystals suitable for X-ray work were obtained by slow evaporation at room temperature.

Crystal Data

$C_{20}H_{15}HgN_2PS_2$ fw = 579.05

Monoclinic, $P2_1/c$, a = 21.071(5), b = 17.716(5), c = 11.285(3) Å, β = 101.66(5)°, V = 4125.7 Å^3, Z = 8, D_c =

[1]To whom all correspondence should be addressed.

0008-4042/79/192555-05$01.00/0

1.864 g cm^{-3}, μ(MoKα) = 77.3 cm^{-1}, λ(MoKα̃) = 0.71069 Å (graphite monochromator), t = 23°C.

Crystallographic Measurements

The crystal selected for X-ray work was an elongated plate with the following distances between pairs of opposite faces: 0.10 mm (100 and $\bar{1}00$), 0.17 mm ($1\bar{1}0$ and $\bar{1}10$), and 0.47 mm (011 and $0\bar{1}\bar{1}$). Space group $P2_1/c$ was unambiguously determined from a set of precession photographs. The crystal was mounted on an Enraf-Nonius CAD4 diffractometer and the cell parameters were obtained from least-squares fit of the setting angles for 25 reflections centered in the counter aperture. Intensity data were collected using the ω/2θ scan technique. A fixed slit of 4 × 4 mm^2 was used and the scan range (ω) was (1.0 + 0.347 tan θ)° extended 25% on either side for backgrounds. Scan speed between 16.7 and 1.0 deg min^{-1} was automatically selected to make $I/\sigma(I)$ = 100, but maximum scan time was limited to 120 s. Prescans at 10° min^{-1} were made and all reflections having $I/\sigma(I) < 1$ were labeled "weak" and not remeasured. Three standard reflections used as a check on instrument and crystal stability showed only random fluctuations. Crystal orientation was checked every 100 reflections by recentering three axial reflections. If a difference > 0.2° was found between any scattering vector and the corresponding direction deduced from the orientation matrix, a new matrix was defined.

A total of 5401 independent hkl and $\bar{h}kl$ reflections (2θ ≤ 45°) were measured using Enraf–Nonius option FLAT, a procedure to measure intensity at the ψ position where absorption is minimum. Net intensity I was calculated from $I = (P - 2B)S$ where P is the peak count, B is the total background counted during one half of scanning time, and S is the scan rate. The standard deviation was obtained from $\sigma^2(I) = (P + 4B)S^2 + (0.04I)^2$. A set of 2741 reflections with $I > 2.5\sigma(I)$ was retained for structure determination. An absorption correction was applied (Gaussian integration, grid 10 × 10 × 10, Program NRC-3, Ahmed and Singh). For 95% of the data, the transmission factor was in the range 0.25–0.50, but factors as low as 0.12 were found in the remaining 5% of the data for which diffractometer geometry did not permit measurement at the most favorable ψ angle. The data were finally corrected for Lp.

TABLE 1. Refined fractional coordinates (× 10^3, Hg × 10^5, P, S × 10^4) of Hg(SCN)$_2$(triphenylphosphine), β-form

Atom	x	y	z
Hg(1)	43141(3)	19036(4)	5979(6)
Hg(2)	7590(4)	69506(4)	3516(6)
S(1)	5376(2)	2067(3)	−21(4)
S(2)	3946(3)	3205(3)	1051(4)
S(3)	1229(3)	8278(2)	−125(4)
S(4)	−387(3)	7067(3)	472(5)
P(1)	3650(2)	801(2)	749(4)
P(2)	1321(2)	5969(2)	−536(4)
N(1)	506(1)	309(1)	−196(1)
N(2)	362(1)	288(1)	330(1)
N(3)	127(1)	804(1)	−254(1)
N(4)	−36(1)	742(1)	287(2)
C(1)	518(1)	268(1)	−118(1)
C(2)	373(1)	301(1)	234(2)
C(3)	125(1)	812(1)	−154(1)
C(4)	−37(1)	727(1)	192(2)
C(11)	284(1)	108(1)	81(1)
C(12)	246(1)	67(1)	144(2)
C(13)	184(1)	89(1)	149(2)
C(14)	159(1)	152(1)	92(2)
C(15)	196(1)	193(1)	29(2)
C(16)	256(1)	170(1)	21(2)
C(21)	393(1)	23(1)	206(1)
C(22)	392(1)	52(1)	322(2)
C(23)	411(1)	9(1)	425(2)
C(24)	435(1)	−63(1)	413(2)
C(25)	438(1)	−91(1)	300(2)
C(26)	417(1)	−49(1)	201(1)
C(31)	360(1)	19(1)	−56(1)
C(32)	413(1)	15(1)	−111(1)
C(33)	413(1)	−34(1)	−209(2)
C(34)	359(1)	−79(1)	−247(2)
C(35)	309(1)	−77(1)	−189(2)
C(36)	308(1)	−27(1)	−95(2)
C(41)	200(1)	634(1)	−105(1)
C(42)	212(1)	623(1)	−221(1)
C(43)	268(1)	656(1)	−254(2)
C(44)	306(1)	703(1)	−173(2)
C(45)	295(1)	716(1)	−63(2)
C(46)	243(1)	681(1)	−27(2)
C(51)	160(1)	519(1)	45(1)
C(52)	128(1)	495(1)	132(2)
C(53)	149(1)	433(1)	199(2)
C(54)	198(1)	391(1)	180(2)
C(55)	231(1)	413(1)	93(2)
C(56)	213(1)	478(1)	26(2)
C(61)	76(1)	560(1)	−183(1)
C(62)	48(1)	607(1)	−273(1)
C(63)	−2(1)	584(1)	−365(1)
C(64)	−20(1)	510(1)	−367(1)
C(65)	9(1)	462(1)	−283(2)
C(66)	57(1)	485(1)	−190(1)

Structure Determination

The structure was solved by the heavy-atom method and refined by full-matrix least-squares in the early stages. Both independent Hg atoms were positioned from a Patterson synthesis and the remaining nonhydrogen atoms were located from a subsequent Fourier synthesis. Isotropic refinement using unit weights led to $R = \sum ||F_o| - |F_c||/\sum |F_o| = 0.076$. Refinement was continued using block-diagonal least-squares. Anisotropic temperature factors were refined for all nonhydrogen atoms. Hydrogens were held fixed at the calculated positions (assuming sp^2 hybridization and a C—H distance of 0.95 Å) with isotropic temperature factors U of 0.076 Å^2 (B = 6.0 Å^2), and their coordinates were recalculated after each cycle. Individual weights based on counting statistics $w = 1/\sigma^2(F)$ were applied in the last least-squares cycles. Anisotropic refinement of all nonhydrogen atoms, together with scale factor and isotropic extinction coefficient (g = −5.4(4) × 10^3) converged to R = 0.042 and $R_w = [\sum w(|F_o| - |F_c|)^2/\sum w|F_o|^2]^{1/2}$ = 0.046. The goodness-of-fit ratio was 1.55. The general background in the final ΔF map was 0.5 e Å^{-3}, except around mercury, where a few peaks of 0.7–1.2 e Å^{-3} were left.

The form factors used were those of Cromer and Waber (4), except for hydrogen (5). Anomalous dispersion terms f' and f'' were used for Hg, S, and P (6).

The refined coordinates are listed in Table 1. Anisotropic temperature factors and hydrogen coordinates are part of the unpublished material.[2]

[2]The supplementary material includes lists of temperature factors, structure factors, interatomic distances and bond angles in the triphenylphosphine ligands and hydrogen coordinates. Complete set of data is available, at a nominal charge, from the Depositiory of Unpublished Data, CISTI, National Research Council of Canada, Ottawa, Ont., Canada K1A 0S2.

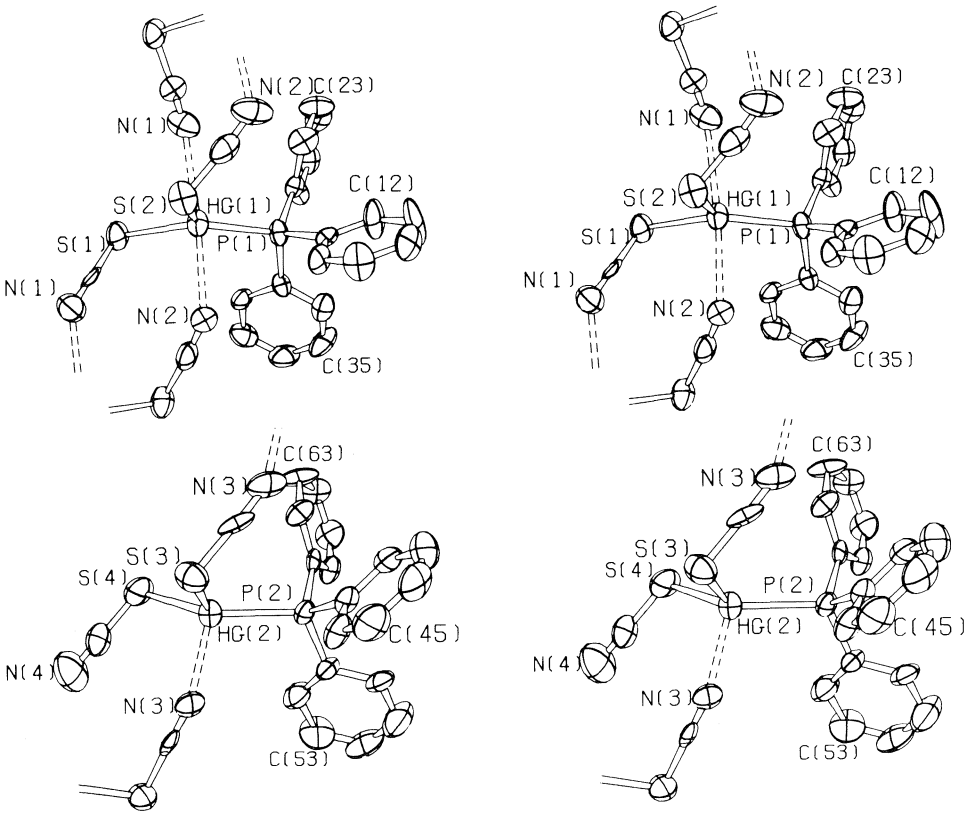

FIG. 1. Stereoscopic view of the two non-equivalent $Hg(SCN)_2$(triphenylphosphine) units and their surroundings. Dashed sticks represent chain-propagating Hg—N bonds. The ellipsoids correspond to 50% probability.

Description of the Structure and Discussion

Figure 1 shows both non-equivalent $Hg(SCN)_2 \cdot Ph_3P$ units. Selected interatomic distances and bond angles are listed in Table 2.

Mercury Coordination

The environment of Hg(1) is essentially the same as in the α-form of $Hg(SCN)_2 \cdot Ph_3P$ (2): a (3 + 2) trigonal bipyramid in which the equatorial positions are filled with three strongly-bonded soft donors. Hg(1) is only 0.02 Å above the PSS plane and the Hg—S (2.491(5), 2.519(5) Å) distances are normal. The Hg—P distance (2.429(4) Å) is slightly smaller than in the α-form (2.461 Å), but both of these bonds are longer than those of $(Hg(NO_3)_2 \cdot Ph_3P)_n$ (7) and $(Hg(NO_3)_2(\text{tricyclohexylphosphine}))_2$ (2.359 Å) (8), where hard nitrate groups act as anions. The S(1)—Hg(1)—S(2) angle (106.4(2)°) is much smaller than the S—Hg—P angles (132.5(2), 121.1(1)°) as a consequence of steric hindrance from phenyl groups. Two weak axial Hg—N bonds (2.74(1), 2.89(1) Å) are approximately perpendicular to the HgS_2P plane (Table 2).

In contrast with the above unit, where both SCN groups are bridging, there is only one bridging SCN group attached to Hg(2) which is four-coordinated with a distorted tetrahedral geometry. The Hg(2)—P(2) distance (2.432(4) Å) is the same as above, but the Hg(2)—S(4) bond length with the unidentate SCN group is shorter (2.454(5) Å). The nitrogen end of the bridging group is much more strongly bonded to mercury (2.40(1) Å) at the expense of the Hg(2)—S(3) bond which is considerably lengthened (2.648(5) Å). A similar type of coordination has been observed in the $[Ph_4P]^+$ salt of $[Hg(SCN)_3]^-$, with the difference that Ph_3P is replaced by another unidentate S-bonded SCN group (9). As in the present case, a bridging SCN group forms a moderately strong Hg—N bond and weakened Hg—S bond. The shortest intermolecular Hg(2)...N(4) contact with the other SCN group is >3.4 Å.

The Ligands

The S—C (ave. 1.65(2) Å) and C—N (ave. 1.14(2) Å) distances are normal and the angles at sulfur are around 100° as usual (Table 2). The angles at nitrogen are 132(1)° and 138(1)° for weak bridging. It is noteworthy that the most strongly bonded nitrogen is the one with the C—N—Hg angle (152(1)°) closest to 180°. The P—C bond lengths (ave.

TABLE 2. Selected interatomic distances and bond angles

Bond	Length (Å)	Bonds	Angle (deg)
Hg(1)—S(1)	2.491(5)	S(1)—Hg(1)—S(2)	106.4(2)
Hg(1)—S(2)	2.519(5)	S(1)—Hg(1)—P(1)	132.5(2)
Hg(2)—S(3)	2.648(5)	S(2)—Hg(1)—P(1)	121.1(2)
Hg(2)—S(4)	2.454(5)	N(1)[a]—Hg(1)—S(1)	85.5(3)
Hg(1)—P(1)	2.429(4)	N(1)[a]—Hg(1)—S(2)	86.1(3)
Hg(2)—P(2)	2.432(4)	N(1)[a]—Hg(1)—P(1)	98.5(3)
Hg(1)—N(1)[a]	2.89(1)	N(2)[b]—Hg(1)—S(1)	93.4(4)
Hg(1)—N(2)[b]	2.74(1)	N(2)[b]—Hg(1)—S(2)	86.5(4)
Hg(2)—N(3)[c]	2.40(1)	N(2)[b]—Hg(1)—P(1)	88.3(4)
P(1)—C(11)	1.80(2)	N(2)[b]—Hg(1)—N(1)[a]	177.8(5)
P(1)—C(21)	1.78(2)	S(3)—Hg(2)—S(4)	110.5(2)
P(1)—C(31)	1.82(2)	S(3)—Hg(2)—P(2)	108.5(2)
P(2)—C(41)	1.78(2)	S(3)—Hg(2)—N(3)[c]	94.7(4)
P(2)—C(51)	1.80(2)	S(4)—Hg(2)—P(2)	130.5(2)
P(2)—C(61)	1.80(2)	S(4)—Hg(2)—N(3)[c]	101.0(4)
S(1)—C(1)	1.68(1)	P(2)—Hg(2)—N(3)[c]	105.0(4)
S(2)—C(2)	1.64(2)	Hg(1)—S(1)—C(1)	101.9(6)
S(3)—C(3)	1.64(1)	Hg(1)—S(2)—C(2)	98.1(7)
S(4)—C(4)	1.67(2)	Hg(2)—S(3)—C(3)	97.7(6)
C(1)—N(1)	1.13(2)	Hg(2)—S(4)—C(4)	104.1(7)
C(2)—N(2)	1.18(2)	S(1)—C(1)—N(1)	178(2)
C(3)—N(3)	1.15(2)	S(2)—C(2)—N(2)	176(2)
C(4)—N(4)	1.11(2)	S(3)—C(3)—N(3)	178(1)
		S(4)—C(4)—N(4)	178(2)
		C(1)[a]—N(1)[a]—Hg(1)	138(1)
		C(2)[b]—N(2)[b]—Hg(1)	132(1)
		C(3)[c]—N(3)[c]—Hg(2)	152(1)

[a] x, $1/2 - y$, $1/2 + z$.
[b] x, $1/2 - y$, $-1/2 + z$.
[c] x, $3/2 - y$, $1/2 + z$.

1.80(2) Å) are the same as in Ph_3P itself (10). The Hg—P—Ring angles average 111.5(5)° and the Ring—P—Ring angle (ave. 107.4(7)°) are larger than in Ph_3P (103.0°), where the lone pair is free. Phenyl rings have normal geometry within experimental errors.[2]

Packing

Figure 2 shows the two varieties of chains running along the *c* direction. All mercury atoms in a given chain are of the same type and chain propagation is consequently achieved by the same bridging pattern. Interchain interactions are restricted to van der Waals contacts, none of which are unusually short.

Discussion

Chain propagation by single bridging involves strong bonding from both donor atoms of the SCN group. In the doubly-bridged chain, mercury interacts with one extra donor, but the N ends of both ligands are only weakly bonded. These bridging patterns presumably do not greatly differ in energy, because they result from only slight changes in preparative conditions and they coexist within the same crystal.

A few years ago, Plane and co-workers (3) reported for $Hg(SCN)_2 \cdot Ph_3P$ infrared results that could not be satisfactorily interpreted with our crystallographic results on the α-form. The β-form, which is most likely the one used by these authors, is more consistent with their results. Two bands were observed in the C—S stretching region: one at 680 cm^{-1} is typical of unidentate S-bonded ligands and another at 760 cm^{-1} can be assigned to bridging groups (11). The C—N stretching region was not so clear, but the presence of a many-component band pointed to more than one type of SCN groups. Crystals of the β-form contain one unambiguously recognizable bridging group (# 3) and one unidentate S-bonded group (# 4). Because the N end of the two remaining ligands (# 1 and # 2) interact only weakly with mercury, we expect them not to differ greatly from unidentate ligands in the ir spectrum. Indeed, similarly weak intermolecular Hg—N contacts (2.80 Å) exist in $Hg(SCN)_2$ itself (12), and there is no evidence of bridging in its ir spectrum (13).

The simple dimeric structure proposed by Plane and co-workers (3) incorporated all structural features deduced from ir spectra. However, the present work shows more complicated patterns which have also been found in other compounds

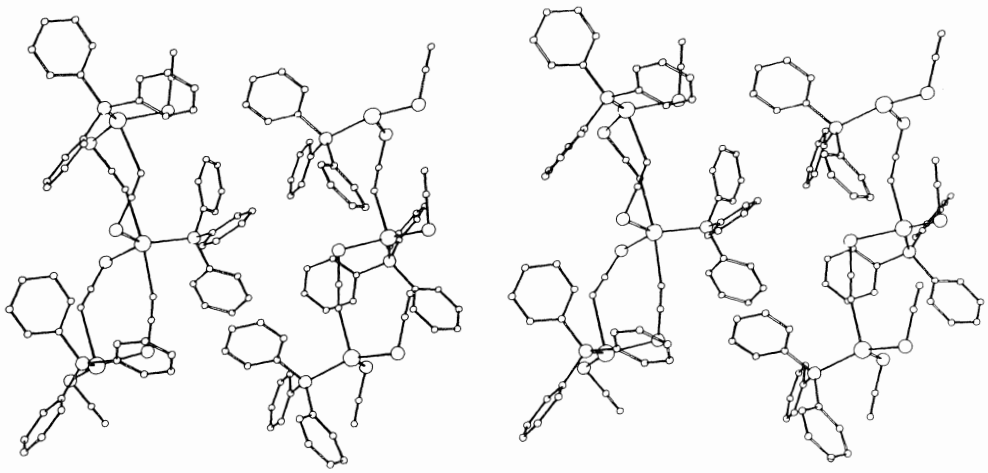

FIG. 2. Stereoscopic view of the two types of infinite chains in crystals of $Hg(SCN)_2$(triphenylphosphine), β-form. The chains are oriented along the *c* axis. The plane represented here goes through the origin and bisects the γ angle.

(1, 2, 9). Therefore, it is quite possible that other 1:1 adducts of $Hg(SCN)_2$ believed to be dimeric, also form in the solid state infinite chains similar with those observed in the present compound.

Acknowledgment

We wish to thank the National Research Council of Canada for financial support.

1. J. HUBERT, A. L. BEAUCHAMP, and R. RIVEST. Can. J. Chem. **53**, 3383 (1975).
2. C. GAGNON and A. L. BEAUCHAMP. Acta Crystallogr. B**34**, 166 (1979).
3. A. R. DAVIS, C. J. MURPHY, and R. A. PLANE. Inorg. Chem. **9**, 423 (1970).
4. D. T. CROMER and J. T. WABER. Acta Crystallogr. **18**, 104 (1965).
5. J. STEWART, R. DAVIDSON, and A. SIMPSON. J. Chem. Phys. **42**, 3175 (1965).
6. D. T. CROMER. Acta Crystallogr. **18**, 17 (1965).
7. S. H. WHITLOW. Can. J. Chem. **52**, 198 (1974).
8. E. C. ALYEA, S. A. DIAS, G. FERGUSON, and R. J. RESTIVO. Inorg. Chem. **16**, 2329 (1977).
9. A. SAKHRI and A. L. BEAUCHAMP. Inorg. Chem. **14**, 740 (1975).
10. J. J. DALY. J. Chem. Soc. 3799 (1964).
11. R. A. BAILEY, S. L. KOZAK, T. W. MICHELSEN, and W. N. MILLS. Coord. Chem. Rev. **6**, 407 (1971).
12. A. L. BEAUCHAMP and D. GOUTIER. Can. J. Chem. **50**, 977 (1972).
13. R. P. J. COONEY and J. R. HALL. Aust. J. Chem. **22**, 2117 (1969).

Isopotential points in the electrosorption of selenite, selenate, selenide, and tellurite at the platinum rotating disc electrode

HÉLIO C. CHAGAS

Instituto de Quimica, Universidade de S. Paulo, S. Paulo, C.P. 20780, Brasil

Received March 14, 1979

HÉLIO C. CHAGAS. Can. J. Chem. **57**, 2560 (1979).

Electrosorption at the platinum rotating disc electrode in sulfuric acid solutions of selenite, selenate, selenide, and tellurite gives rise to isopotential points in the potential range where oxidation of platinum occurs. The data are analyzed with the framework of the model put forward by Untereker and Bruckenstein. Since similar behavior is observed for the selenite, selenate, and selenide systems, it is tentatively inferred that a common electrosorbed species, possibly selenium itself, may be involved in these systems.

HÉLIO C. CHAGAS. Can. J. Chem. **57**, 2560 (1979).

L'électrosorption sur une électrode de platine à disque tournant dans des solutions sulfuriques de sélénite, de sélénate, de sélénure et de tellurite donne lieu à des points isopotentiels dans l'écart de potentiel où l'oxydation du platine se produit. On analyse les données dans le cadre du modèle proposé par Untereker et Bruckenstein. Puisque l'on observe des comportements semblables avec les systèmes sélénite, sélénate et sélénure, on en déduit provisoirement qu'il existe peut être une espèce électrosorbée commune, possiblement du sélénium lui-même, dans tous ces systèmes.

[Traduit par le journal]

Introduction

The occurrence of isopotential points in a family of current–potential curves facilitates detection and analysis of surface processes at solid electrodes. Such isopotential points (IP) are the electrochemical counterparts of isobestic points in absorption spectrophotometry. The relevant parameters are: the current (or charge) passed at the electrode, the potential, and a factor related to the nature of the temporal dependence of the potential variation (e.g., the sweep rate in linear voltammetry).

The model developed by Untereker and Bruckenstein (1) to rationalize the occurrence of IP is applicable when the following experimental conditions hold: (*a*) all the current–potential curves of a given family correspond to the same electrode potential – time program; (*b*) the electrode surface, at the onset of potential–time program is covered with at least one electrosorbed or electrodeposited species in quantities which differ for each curve of the family; (*c*) the electrode surface behaves as if it were composed of at least two electrochemically independent regions of areas A_1 and A_2 whose sum remains constant throughout the entire period during which the potential sweep is applied.

The existence of IP was verified in studies of the electrodeposition of metals at platinum (1, 2) and gold (3) rotating disc electrodes and of electrosorption of species such as sulfite on the platinum rotating disc electrode (RDE) (1).

In the present work, we report an investigation of the electrosorption of selenite, selenate, selenide, and tellurite at the platinum RDE in sulfuric acid medium, taking advantage of information derived from the occurrence of IP in the systems.

This electrosorption process is of special interest in view of the technological importance of these substances as additives for improving the current yield in electrodeposition of manganese (4–6). Moreover, the electrosorption of selenium has been employed to increase the activity of platinum electrodes in studies of oxidation processes of organic compounds (7).

Experimental

Apparatus

The potentiostat used to control the electrode potential, the potential programmer, and the electromechanical system which controls the electrode rotation rate have been previously described (8, 9). A Pyrex cell with volume of ca. 200 mL was employed throughout. Electrical contact between the SCE reference electrode and the electrolytic solution was achieved by means of a Luggin capillary situated near the working electrode. All potentials were referenced against the saturated calomel electrode (SCE).

Materials

Electrolytic solutions were prepared with triple-distilled water. The supporting electrolyte was 0.2 *M* H_2SO_4 (Baker Reagent grade) in all experiments. Sodium selenite was prepared by careful neutralization of a water solution of SeO_2 (BDH A.R. grade) with reagent grade sodium hydroxide; sodium selenate was prepared in a similar fashion using an aqueous selenic acid solution (10). Sodium selenide (K & K

0008-4042/79/192560-04$01.00/0

Lab., Inc.) was used as received. Sodium tellurite was prepared by the method of Brauer (11). The final concentration of all stock solutions was $5 \times 10^{-4} M$.

All solutions were deaerated by purging with purified nitrogen and all electrochemical measurements performed under a nitrogen atmosphere.

Methods

Prior to all experiments the platinum RDE was polished by hand with 0.05 μm alumina powder and subjected to an electrochemical pretreatment in the supporting electrolyte solution. This pretreatment consisted of repeated cycling of the potential of the working electrode between +1.40 and −0.25 V and maintaining the electrode rotation frequency (36 Hz) and the potential sweep rate (200 mV/s), until reproducible current–potential curves were obtained (10–20 cycles). Following this treatment, appropriate aliquots of the stock solution of the electroactive species of interest were added to the supporting electrolyte solution already in the electrolytic cell.

Families of current–potential curves were obtained utilizing a potential program of the type $E(t) = E_i + vt$, where E_i represents the initial potential and $v = dE/dt$ the (constant) sweep rate. The sign of v was reversed at the extremes of the potential sweep, i.e., at +1.40 and −0.25 V. The quantity of the chemical species under investigation electrosorbed at the electrode surface was varied by maintaining the electrode at a potential $E_i = 0$ V and a rotation frequency of 9 Hz for different periods of time. At the end of this electrosorption period, the electrode was swept from $E_i = 0$ V to a more cathodic potential up to a potential of −0.25 V, at which point the sweep was reversed to the anodic direction. Between each successive curve, the electrode was oxidized for 60 s at a potential of +1.30 V. At the end of this oxidation, the electrode potential was jumped to $E_i = 0$ V for a new electrosorption. The initial fractional coverage θ_R of the electrode surface by the electrosorbed species was calculated from the relative decrease in the area of the hydrogen desorption peaks in the presence and absence of the electrosorbed species according to the general procedure of Untereker and Bruckenstein (1).

Results and Discussion

Figure 1 exhibits a family of current–potential curves for a 3.3×10^{-6} M solution of sodium selenite in 0.2 M H_2SO_4. Each curve corresponds to the oxidation of a different quantity of the electrosorbed species at the electrode surface. Of particular importance is the presence of an isopotential point IP-I at $E_{IP\text{-}I} = 0.75$ V, i.e., in the potential range where oxidation of platinum occurs. Indeed, the electrode surface may be considered to consist of two independent electrochemical regions; one of area A_1 corresponding to the platinum itself and a second of area A_2 corresponding to a submonolayer of the electrosorbed species. Thus, the relevant Faradaic processes occurring in the potential range around IP-I are: (*a*) the oxidation of platinum in area A_1

[1] $Pt \rightarrow PtO_x + n_1e$

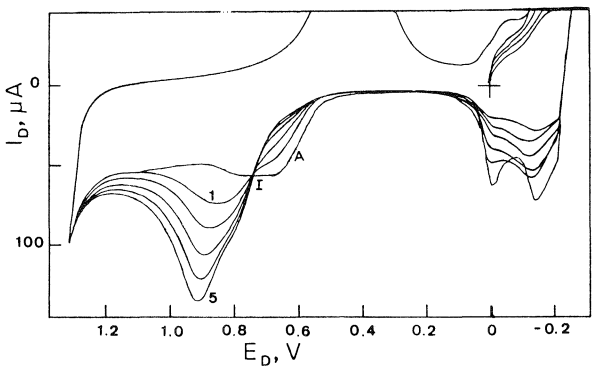

FIG. 1. *I–E* curves for oxidation of various quantities of the electrosorbed species at the platinum rotating disc electrode in the selenite system: $[SeO_3^{2-}] = 3.3 \times 10^{-6}$ M, $[H_2SO_4] = 0.2$ M, $f = 9$ Hz, $v = 200$ mV/s, $E_{IP\text{-}I} = 0.75$ V/SCE, electrode area = 0.162 cm². Fractional monolayer coverages of electrosorbed species at the electrode surface for *I–E* curves are: (*1*) 0.14, (*2*) 0.22, (*3*) 0.37, (*4*) 0.49, (*5*) 0.61; *A* = absence of SeO_3^{2-}.

and (*b*) oxidation of the electrosorbed species, represented as $R(H_2SeO_3)$, in area A_2.

[2] $R(SeO_3^{2-}) \rightarrow Ox_2 + n_2e$

That the species $R(SeO_3^{2-})$ is electrosorbed at both the weakly and strongly bound hydrogen atom electrosorption sites is indicated by the corresponding decrease of both current peaks characteristic of hydrogen desorption with increasing fraction of coverage θ_R.

Families of current–potential curves for 3.3×10^{-6} M sodium selenate and 3.75×10^{-6} M sodium selenide in 0.2 M H_2SO_4 are presented in Figs. 2 and 3, respectively. As in the case of selenite, isopotential points (IP-II at $E_{IP\text{-}II} = 0.75$ V in Fig. 2 and IP-III at $E_{IP\text{-}III} = 0.75$ V in Fig. 3) are observed in the potential range where oxidation of platinum occurs. Thus the faradaic processes associated with these IP may be represented by equations entirely analogous to [1] and [2]. In the hydrogen desorption potential range, the electrosorbed species $R(Se^{2-})$ of Fig. 3 exhibits roughly equal preference for the hydrogen binding sites; on the other hand, the electrosorbed species $R(SeO_4^{2-})$ of Fig. 2 exhibits a slight preference for the sites corresponding to strong binding of hydrogen. Curve *A* of Fig. 2, obtained for the supporting electrolyte in the absence of the electroactive species, fails to pass through the point IP-II observed in the presence of the electroactive species. This departure from the expected behavior is most readily interpretable in terms of a small constant amount of "irreversible" electrosorption of a nonoxidable species at the electrode surface resulting in

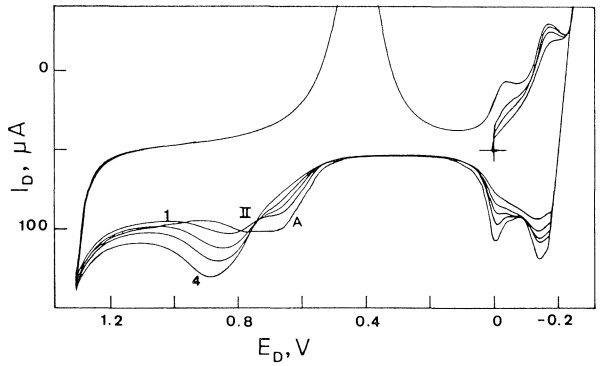

FIG. 2. *I–E* curves for oxidation of various quantities of the electrosorbed species at the platinum rotating disc electrode in the selenate system: $[SeO_4^{2-}] = 3.3 \times 10^{-6}$ *M*, $[H_2SO_4]$ = 0.2 *M*, *f* = 9 Hz, *v* = 200 mV/s, $E_{IP\text{-}II}$ = 0.75 V/SCE, electrode area = 0.162 cm². Fractional monolayer coverages of electrosorbed species at the electrode surface for *I–E* curves are: (*1*) 0.15, (*2*) 0.18, (*3*) 0.24, (*4*) 0.35; *A* = absence of SeO_4^{2-}.

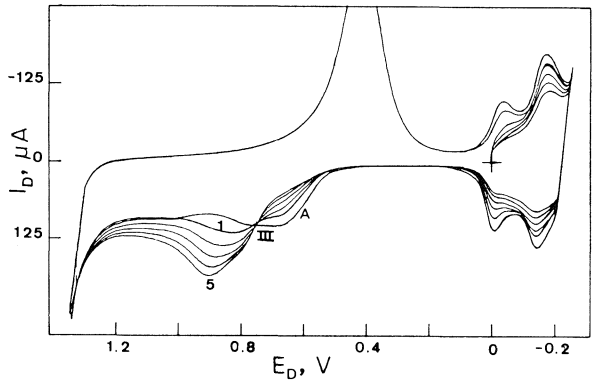

FIG. 3. *I–E* curves for oxidation of various quantities of the electrosorbed species at the platinum rotating disc electrode in the selenide system: $[Se^{2-}] = 3.75 \times 10^{-6}$ *M*, $[H_2SO_4]$ = 0.2 *M*, *f* = 9 Hz, *v* = 200 mV/s, $E_{IP\text{-}III}$ = 0.75 V/SCE, electrode area = 0.280 cm². Fractional monolayer coverages of the electrosorbed species at the electrode surface for *I–E* curves are: (*1*) 0.09, (*2*) 0.19, (*3*) 0.27, (*4*) 0.33, (*5*) 0.42; *A* = absence of Se^{2-}.

a net reduction of the available electrode surface in the presence of selenate. This phenomenon is much less pronounced for the selenite and selenide systems (Figs. 1 and 3 respectively).

Families of current–potential curves similar to those of Figs. 1–3 were obtained in experiments carried out under the same conditions but with different potential sweep rates. The dependence of the current density at the potential points (IP-I, IP-II, and IP-III) on the potential sweep rate (*v*) for each of these three systems is shown in Fig. 4. Linear dependences are observed with slopes of 1.74, 1.62, and 1.77 μA s/(cm² mV) for selenite, selenate, and selenide systems, respectively. The potential (E_{IP}) at

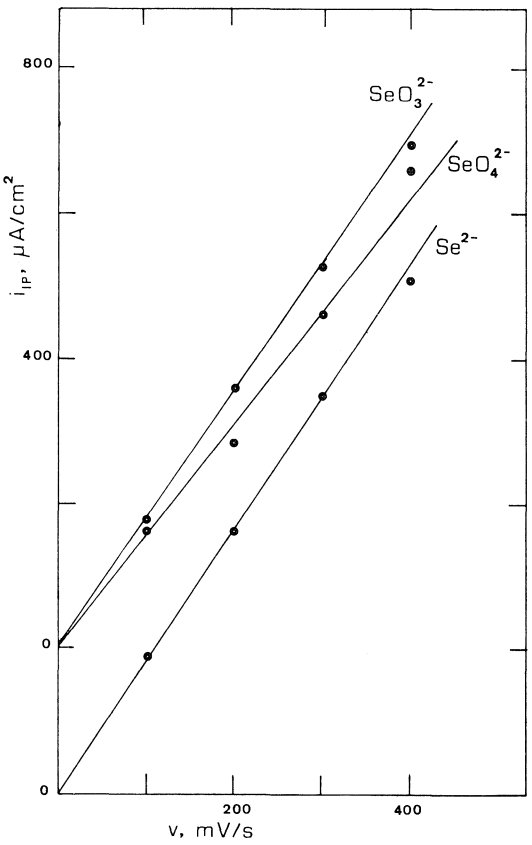

FIG. 4. Plot of the current density at the isopotential points versus potential sweep rate for selenite, selenate, and selenide systems.

which the points IP-I to IP-III occur varies very little (<2%) over the range of potential sweep rates (*v*) employed.

Figure 5 exhibits a family of current–potential curves for 3.3×10^{-6} *M* sodium tellurite in 0.2 *M* H_2SO_4. In this case, the current peaks corresponding to oxidation of electrosorbed species occur at a less anodic potential and are much sharper than those observed for selenium systems.

For the tellurite we don't observe isopotential points. In the potential range for hydrogen desorption this system exhibits the same behavior as the selenite and selenide systems.

Conclusions

The currents are sufficiently high at the experimental isopotential points for the selenite, selenate, and selenide systems ($I_{IP\text{-}I}$ to $I_{IP\text{-}III}$) that we may conclude that these points result from equal current densities for oxidation of platinum (i_{Pt}^0) in area A_1 and oxidation of a submonolayer of electrosorbed species (i_k^0) in area A_2.

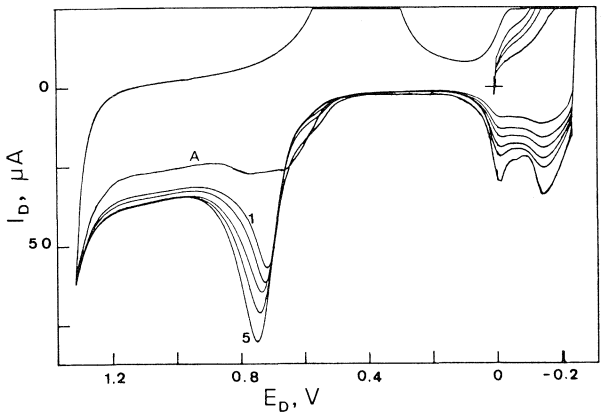

FIG. 5. *I–E* curves for oxidation of various quantities of the electrosorbed species at the platinum rotating disc electrode in the tellurite system: $[TeO_3^{2-}] = 3.3 \times 10^{-6}$ *M*, $[H_2SO_4] = 0.2$ *M*, $f = 9$ Hz, $v = 100$ mV/s, electrode area = 0.162 cm². Fractional monolayer coverages of the electrosorbed species at the electrode surface for *I–E* curves are: (*1*) 0.16, (*2*) 0.24, (*3*) 0.36, (*4*) 0.48, (*5*) 0.63; *A* = absence of TeO_3^{2-}.

According to the theory of Untereker and Bruckenstein (1), this current I_{IP} may be expressed as

$$[3] \quad I_{IP} = A|(\partial Q_k/\partial E)_t v + (\partial Q_k/\partial t)_E|$$

where A is the total area of the electrode and

$$Q_k = \int_0^\tau i_k^0 \, dt$$

represents the charge density necessary for oxidation of platinum or of the electrosorbed submonolayer during the time interval 0–τ (or, for a linear potential sweep, between two potentials). The observation of a linear relationship between $i_{IP} = I_{IP}/A$ and v for the three selenium systems (Fig. 4) permits us to conclude from [3] that

$$(\partial Q_k/\partial E)_t v \gg (\partial Q_k/\partial t)_E$$

The corresponding slopes thus furnish values of $(\partial Q_k/\partial E)_t$ for the two Faradaic processes responsible for the existence of the isopotential points. These slopes are comparable for the selenite and selenide systems. In addition, the potentials E_{IP} for these two systems, as well for selenate system, are quite similar. In this regard, the overall similarity of the families of current–potential curves for the three systems (Figs. 1–3) is noteworthy. These considerations lead us to infer that the species R electrosorbed at the electrode surface may well be the same, and possibly selenium itself, in all three cases, particularly in the selenite and selenide systems. This inference, though still tentative in the absence of additional corroborating evidence, is supported by the standard potentials (12) for the reactions

$H_2SeO_3 + 4H^+ + 4e = Se(0) + 3H_2O$	$E^0 = 0.74$ V
$H_2SeO_3 = H^+ + HSeO_3^-$	$k = 2.7 \times 10^{-3}$
$HSeO_3^- = H^+ + SeO_3^{2-}$	$k = 2.5 \times 10^{-7}$
$SeO_4^{2-} + 4H^+ + 2e = H_2SeO_3 + H_2O$	$E^0 = 1.15$ V
$HSeO_4^- = H^+ + SeO_4^{2-}$	$k = 8.9 \times 10^{-3}$
$Se(0) + 2H^+ + 2e = H_2Se$	$E^0 = -0.40$ V

which suggest that, in acid medium, the reductions Se(IV) → Se(0) and Se(VI) → Se(IV) → Se(0) and the oxidation Se^{2-} → Se(0) should be possible.

Acknowledgments

Dr. Ivo Giolito is gratefully acknowledged for supplying some of the reagents employed in this work. The author also wishes to acknowledge Dr. Frank H. Quina for assistance in the preparation of the manuscript.

1. D. F. UNTEREKER and S. BRUCKENSTEIN. Anal. Chem. **44**, 1009 (1972).
2. S. H. CADLE and S. BRUCKENSTEIN. Anal. Chem. **44**, 1993 (1972).
3. S. H. CADLE. Anal. Chem. **46**, 587 (1974).
4. J. E. LEWIS, P. H. SCAIFE, and D. A. SWINKELS. J. Appl. Electrochem. **6**, 453 (1976).
5. N. P. SHUL'GINA and M. N. POLUKAROV. Uch. Zap. Permsk. Gos. Univ. **141**, 86 (1966); Chem. Abstr. **68**, 8364q (1968); **68**, 8364r (1968); **68**, 8364s (1968).
6. P. RADHAKRISHNAMURTHY and A. K. N. REDDY. J. Appl. Electrochem. **7**, 113 (1977).
7. H. BINDER, A. KÖLING, and G. SANDSTEDE. Nature, **214** 268 (1968).
8. H. C. CHAGAS. Cienc. Cult. (Sao Paulo), **29**, 601 (1976).
9. H. C. CHAGAS. An. Acad. Bras Cienc. **49**, 567 (1977).
10. L. I. GILBERTSON and G. B. KNIG. Inorganic syntheses. McGraw Hill, New York. 1950.
11. G. BRAUER (*Editor*). Handbook of preparative inorganic chemistry. Vol. I. Academic Press, New York. 1963.
12. W. M. LATIMER. *In* The oxidation states of the elements and their potential in aqueous solutions. 2nd ed. Prentice-Hall, New York. 1952.

Stereoselectivity in Diels–Alder reactions

MASATOSHI KAKUSHIMA

Department of Chemistry, University of New Brunswick, Fredericton, N.B., Canada E3B 5A3

Received March 30, 1979

MASATOSHI KAKUSHIMA. Can. J. Chem. **57**, 2564 (1979).

Two competing effects, secondary attractive interactions and closed-shell repulsions, provide the main control of *endo–exo* stereoselectivity of Diels–Alder cycloadditions.

MASATOSHI KAKUSHIMA. Can. J. Chem. **57**, 2564 (1979).

Deux effets compétitifs, les interactions attractives secondaires et les répulsions des couches complètes d'électrons, procurent le contrôle principal de la stéréosélectivité *endo–exo* des cycloadditions de Diels–Alder.

[Traduit par le journal]

In the course of our endeavors in the total synthesis of natural products, some results from our concurrent studies on the Diels–Alder reaction (1, 2, 3) have enabled us to systematize several factors which we believe may contribute to a better understanding of the regio- and stereoselectivity of this reaction (4, 5).

In the schematic Diels–Alder reaction shown in Scheme 1, four isomeric adducts are possible. Examples of the reaction between some 1-substituted dienes and acrylates are presented in Table 1. The *ortho* isomers **5** and **6** are predominant or exclusive in all cases (6). Frontier molecular orbital (FMO) theory using terminal (7, 8) and secondary (9) attractive interactions has been applied to rationalize these phenomena. For example, an electron-donating substituent at C-1 of the diene increases the difference in the magnitudes of the terminal HOMO coefficients (C-1 and C-4) of the diene (Table 2), resulting in a high regioselectivity in the reaction (Table 1).

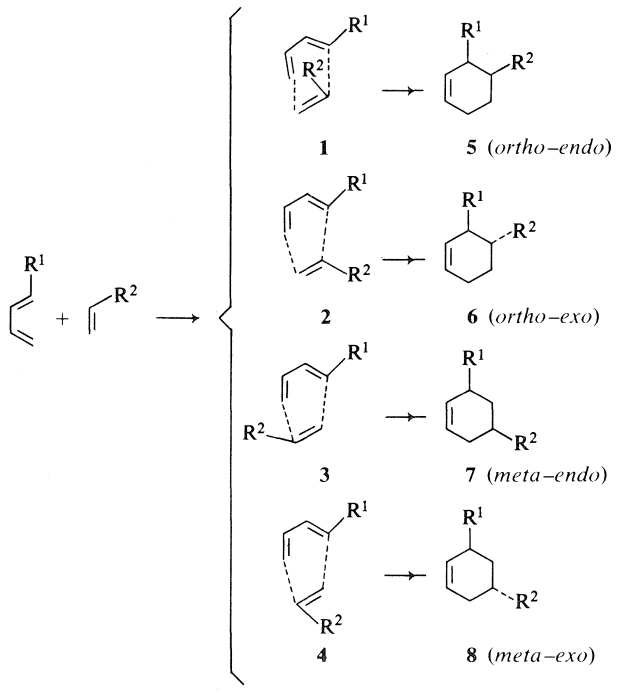

SCHEME 1

However, controversy has arisen on the subject of the importance of secondary overlap on the stereochemical outcome of the reaction (8, 9, 10). Experimental results show that an alkoxycarbonyl group on the dienophile fails to control *endo* stereoselectivity in reactions with highly electron-rich 1-substituted dienes (Table 1). As shown in Table 2, an electron-donating substituent at C-1 of the diene not only increases the difference in the magnitudes of the secondary HOMO coefficients (C-2 and C-3), but also increases the exclusion shell[1] (the gross orbital charge of $2P_z^2$) at C-2. The *ortho–endo* isomer **5** must be favored through increased secondary attractive interactions (9), while at the same time the same isomer **5** must be disfavored through increased closed-shell repulsions (3). Clearly, both for preparative and for theoretical reasons, it is important to assess the relative magnitudes of these two opposing interactions.

In order to examine the balance between secondary attractive interactions and closed-shell repulsions more closely, we have focused on the reaction between some 1-substituted dienes and dimethyl fumarate (**9**) (Scheme 2), because in this case ter-

[1]The larger the π charge density on an atom, the larger the size of the "exclusion shell" into which other electrons are forbidden to penetrate (11).

[2]Since the coefficients of $2P_z$ orbitals are discussed for attractive interactions by FMO theory (7, 8, 9), the gross orbital charges of $2P_z$ orbitals should be considered for repulsive interactions.

0008-4042/79/192564-05$01.00/0

TABLE 1. The addition of *E*-1-substituted-1,3-butadienes to acrylates

Diene R^1	Dienophile R^2	Regioselectivity % *ortho* (5 + 6)	Stereoselectivity[a] % *endo* 5	% *exo* 6
CO_2H	CO_2H	81	72	28[b]
CO_2H	CO_2CH_3	83	74	26[b]
CH_3	CO_2H	>98	70	30[c]
$NHCOCCl_3$	CO_2CH_3	>98	77	23[b]
$NHCO_2C_6H_5$	CO_2CH_3	>98	81	19[b]
C_6H_4—*p*-NO_2	CO_2CH_3	>98	72	28[d]
C_6H_5	CO_2CH_3	>98	62	38[d]
C_6H_4—*p*-OCH_3	CO_2CH_3	>98	57	43[d]
SC_6H_5	CO_2CH_3	>98	50	50[e]

[a]For the formation of *ortho* adducts.
[b]Reference 12.
[c]Reference 13.
[d]Reference 14.
[e]Reference 15.

TABLE 2. Computed data[a] for dienes

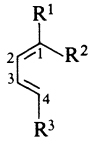

Diene R^1	Diene R^2	Diene R^3	HOMO Eigenvalues (au)[b]	HOMO Eigenvectors ($2P_z$) C-1	C-2	C-3	C-4
CO_2CH_3	H	H	−0.249	0.525	0.384	−0.366	−0.498
CH_3	H	H	−0.232	0.528	0.428	−0.373	−0.533
OCH_3	H	H	−0.206	0.441	0.496	−0.297	−0.503
OCH_3	CH_3	CH_3	−0.193	0.453	0.463	−0.332	−0.496
CO_2CH_3	CH_3	CH_3	−0.232	0.519	0.392	−0.372	−0.488

Diene R^1	Diene R^2	Diene R^3	LUMO Eigenvalues (au)[b]	LUMO Eigenvectors ($2P_z$) C-1	C-2	C-3	C-4
CO_2CH_3	H	H	0.182	0.505	−0.523	−0.311	0.542
CH_3	H	H	0.232	0.629	−0.436	−0.451	0.617
OCH_3	H	H	0.241	0.644	−0.396	−0.468	0.609
OCH_3	CH_3	CH_3	0.260	0.652	−0.413	−0.410	0.618
CO_2CH_3	CH_3	CH_3	0.190	0.494	−0.512	−0.292	0.536

Diene R^1	Diene R^2	Diene R^3	Exclusion shells Gross orbital charges ($2P_z$)[c] C-1	C-2	C-3	C-4
CO_2CH_3	H	H	1.046	0.929	1.005	0.977
CH_3	H	H	0.973	1.027	0.987	1.022
OCH_3	H	H	0.992	1.101	0.975	1.055
OCH_3	CH_3	CH_3	1.003	1.100	1.032	0.985
CO_2CH_3	CH_3	CH_3	1.025	0.957	1.034	0.958

[a]MO method: *ab initio* STO-3G (16, 17); standardized geometrical parameters were used (18).
[b]1 au = 620 kcal.
[c]In units of electrons.

TABLE 3. Computed data[a] for dienophiles

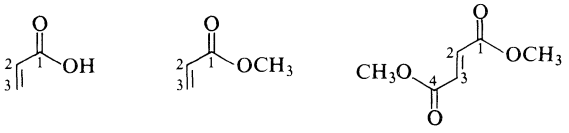

Dienophile	HOMO Eigenvalues (au)[b]	HOMO Eigenvectors ($2P_z$) C-1	C-2	C-3	C-4
Acrylic acid[c]	−0.314	0.240	−0.456	−0.495	
Methyl acrylate	−0.313	0.225	−0.435	−0.471	
Dimethyl fumarate	−0.306	0.175	−0.430	−0.430	0.175

Dienophile	LUMO Eigenvalues (au)[b]	LUMO Eigenvectors ($2P_z$) C-1	C-2	C-3	C-4
Acrylic acid[c]	0.231	0.471	0.482	−0.678	
Methyl acrylate	0.234	0.475	0.489	−0.674	
Dimethyl fumarate	0.179	0.321	0.532	−0.532	−0.321

Dienophile	Exclusion shells: Gross orbital charges ($2P_z$)[d] C-1	C-2	C-3	C-4
Acrylic acid[c]	0.918	1.029	0.940	
Methyl acrylate	0.911	1.025	0.946	
Dimethyl fumarate	0.924	0.974	0.974	0.924

[a]MO method: *ab initio* STO-3G (16, 17); standardized geometrical parameters were used (18).
[b]1 au = 620 kcal.
[c]Monomer; the data for hydrogen-bridged acrylic acid (dimer) are different.
[d]In units of electrons.

minal interactions can be ignored due to the symmetric nature of this dienophile (Table 3). The difference in the magnitudes of the secondary HOMO coefficients (C-2 and C-3) of *E*-1-methoxybutadiene

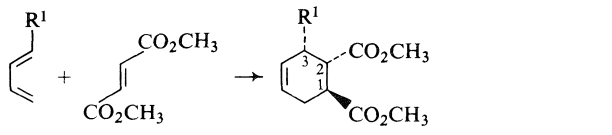

9 **10***a*: $R^1 = CH_3$; **10***b*: $R^1 = OCOCH_3$; **10***c*: $R^1 = OCH_3$

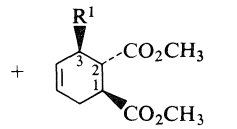

11*a*: $R^1 = CH_3$; **11***b*: $R^1 = OCOCH_3$; **11***c*: $R^1 = OCH_3$

SCHEME 2

is much larger than that in the magnitudes of the secondary HOMO coefficients (C-2 and C-3) of *E*-piperylene (*E*-penta-1,3-diene) (Table 2); as a result, the selectivity (**10**:**11**) in the addition of *E*-1-methoxybutadiene to **9** should be greater than that in the addition of *E*-piperylene to **9**. However, a very small difference in the selectivity of these reactions is observed (Table 4), which suggests that the increase in secondary attractive interactions must be counteracted by a nearly equal increase in closed-shell repulsions. Interestingly, Fleming *et al.* (10) have reported that the addition of 1-methoxycyclohexa-1,3-diene (**12**) to **9** or **13** produces the isomer of type **10** as the minor adduct (Scheme 3), which indicates that in these cases the secondary attractive interactions fail to overcome the closed-shell repulsions due to the large exclusion shell at C-2 of **12**. The exclusion shell at C-2 of **12** is similar to that at C-2 of *E*-1-methoxybutadiene, while the difference in the magnitudes of the secondary HOMO coefficients (C-2 and C-3) of **12** is smaller than the difference in

TABLE 4. The addition of *E*-1-substituted-1,3-butadienes to **9**

Diene R^1	Molar ratio Diene:**9**	Conditions	Total yield (%)	Product ratio (%)
CH_3	5:1	$C_6H_5CH_3$, 90°C, 17 h	96	**10***a* (53) **11***a* (47)
$OCOCH_3$	Excess diene	$(CH_3CO)_2O$, C_6H_6, 130°C, 4 h	73	**10***b* (62.5) **11***b* (37.5)[a]
OCH_3	4:1	$C_6H_5CH_3$, 90°C, 19 h	96	**10***c* (67) **11***c* (33)

[a]Reference 19.

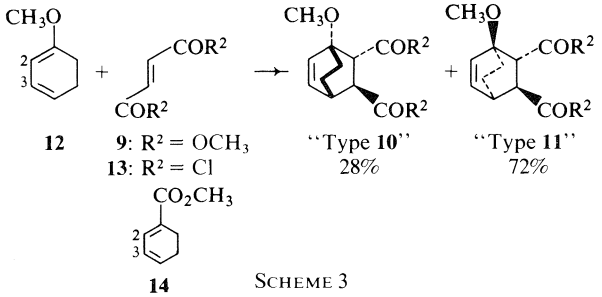

SCHEME 3

the magnitudes of the secondary HOMO coefficients (C-2 and C-3) of *E*-1-methoxybutadiene.[3]

A simple prediction can be made to test this explanation: the addition of a diene such as **14** to **9** should produce the isomer of type **10** as the major adduct. The methoxycarbonyl group of **14** should significantly decrease the exclusion shell at C-2 of **14**, while retaining a larger secondary HOMO coefficient at this carbon.[4]

A quantitative assessment of the two opposing effects considered above is clearly difficult. It is hoped, however, that experimental results and MO calculations of the type reported here together with further predictions and their testing will make it possible to achieve better stereo-control of Diels–Alder cycloadditions in the future.

Experimental

The ir spectra were recorded in CCl_4 solution on a Perkin-Elmer 457 ir spectrophotometer. The nmr spectra were recorded in $CDCl_3$ solution using TMS as an internal standard on a Varian T-60 spectrometer. The 220 MHz nmr spectra were obtained from the Canadian 220 MHz NMR Centre, University of Toronto. Proton chemical shifts (ppm) are expressed relative to TMS. The high resolution mass spectra were obtained from the Department of Chemistry, University of Alberta.

Chromatographic columns were packed with Merck silica gel H (type 60) under a positive nitrogen pressure, and Merck precoated silica gel 60 F-254 plates (0.25 mm) were used. *E*-Piperylene (99%) and *E*-1-methoxybutadiene (practical grade) were purchased from the Aldrich Chemical Co. and were used without purification. Dimethyl fumarate (Eastman Kodak Co.) was washed with an aqueous $NaHCO_3$ solution, extracted with benzene, dried over anhydrous K_2CO_3, concentrated, and recrystallized. Ethyl acetate and hexanes were distilled. Toluene was distilled from $LiAlH_4$. $Eu(fod)_3$ was purchased from the Aldrich Chemical Co. Diels–Alder reactions were performed under a nitrogen atmosphere in the presence of hydroquinone (catalytic amount) in a 200 mL pressure bottle. The adducts were concentrated *in vacuo* and passed through a chromatographic column using the solvent system of ethyl acetate–hexanes (1:9). Conditions and product ratios (**10**:**11**) are summarized in Table 4. The product ratios were found to be constant at temperatures from 40 to 140°C. Prolonged heating of the isomers (**10***c* and **11***c*) at 140°C for 90 h did not affect the ratio.

Analysis of Diels–Alder Adducts

Compounds **10***a* and **11***a* ($R^1 = CH_3$) gave values for ir: 1735, 1195, 1175, and 1162 cm^{-1}; *m/e* (% int.): 181.0859(31) ($M^+ - CH_3O$, $C_{10}H_{13}O_3$ requires 181.0865); 180.0787(39) ($M^+ - CH_3OH$, $C_{10}H_{12}O_3$ requires 180.0786); 152.0836(49) ($M^+ - CO_2CH_3-H$, $C_9H_{12}O_2$ requires 152.0837). The product ratio (**10***a* and **11***a*) was determined by comparison of the 220 MHz nmr spectrum of the adducts with that of the authentic sample (**10***a*:**11***a* = 11:5), which was prepared from the adducts of *E*-piperylene with methyl *E*-4-oxobutenoate (2, 3). Nuclear magnetic resonance for **10***a* δ: 2.87 (J = 12, 11.5, 5 Hz, C1—H), 3.03 (J = 12, 6 Hz, C2—H), 2.70 (multiplet, C3—H), 0.88 (J = 7 Hz, C3—CH_3); for **11***a* δ: 1.05 (J = 7 Hz, C3—CH_3).

For compounds **10***c* and **11***c* ($R^1 = OCH_3$), ir: 1735, 1195, 1175, and 1160 cm^{-1}; *m/e* (% int.): 196.0735(100) ($M^+ - CH_3OH$, $C_{10}H_{12}O_4$ requires 196.0736); 168.0788(70) ($M^+ - CO_2CH_3-H$, $C_9H_{12}O_3$ requires 168.0787). The nmr spectrum of the product (adducts **10***c* and **11***c*; 54 mg) with $Eu(fod)_3$ (67 mg) shows two sets of three methyl singlets, the integration of which indicates that the product ratio is approximately 2:1. The integration of the product (54 mg) when combined with an authentic sample (**10***c*:**11***c* = 5:1; 52 mg) indicates that the major isomer in the product is **10***c*. The authentic sample was prepared from the adducts of *E*-1-methoxybutadiene with methyl *E*-4-oxobutenoate (3).

Acknowledgements

The author would like to express his sincere appreciation to Professor Z. Valenta for his encouragement, helpful suggestions, and ample financial support. He also thanks Professor F. Grein, University of New Brunswick, for helping him with the computations, and Dr. I. Fleming, Cambridge University, and Mr. D. J. Burnell of this Department, for several enlightening discussions concerning FMO theory. Miss J. P. Smolinski, a senior student in this Department, has helped with computations.

[3]The computed data for the diene ($R^1 = OCH_3$; R^2, $R^3 = CH_3$) are used for the description of **12** (Table 2).

[4]The computed data for the diene ($R^1 = CO_2CH_3$; R^2, $R^3 = CH_3$) are used for the description of **14** (Table 2). The LUMO (diene)/HOMO (dienophile) secondary attractive interactions also predict the formation of the isomer of type **10** as the major adduct.

1. R. A. DICKINSON, R. KUBELA, G. A. MACALPINE, Ž. STOJANAC, and Z. VALENTA. Can. J. Chem. **50**, 2377 (1972); Ž. STOJANAC, R. A. DICKINSON, N. STOJANAC, R. J. WOZNOW, and Z. VALENTA. Can. J. Chem. **53**, 616 (1975); N. STOJANAC, A. SOOD, Ž. STOJANAC, and Z. VALENTA. Can. J. Chem. **53**, 619 (1975).
2. M. KAKUSHIMA, J. ESPINOSA, and Z. VALENTA. Can. J. Chem. **54**, 3304 (1976).
3. M. KAKUSHIMA and D. G. SCOTT. Can. J. Chem. **57**, 1399 (1979).
4. J. SAUER. Angew. Chem. Int. Ed. Engl. **6**, 16 (1967).
5. H. WOLLWEBER. Diels–Alder Reaktion. Georg Thieme Verlag, Stuttgart, Germany. 1972.
6. K. ALDER and G. STEIN. Angew. Chem. **50**, 510 (1937).
7. K. N. HOUK. J. Am. Chem. Soc. **95**, 4092 (1973); Acc. Chem. Res. **8**, 361 (1975).
8. O. EISENSTEIN, J. M. LEFOUR, N. T. ANH, and R. F. HUDSON. Tetrahedron, **33**, 523 (1977).
9. P. V. ALSTON, R. M. OTTENBRITE, and D. D. SHILLADY. J. Org. Chem. **38**, 4075 (1973); P. V. ALSTON and R. M. OTTENBRITE. J. Org. Chem. **40**, 1111 (1975); P. V. ALSTON, R. M. OTTENBRITE, and T. COHEN. J. Org. Chem. **43**, 1864 (1978).
10. I. FLEMING, J. P. MICHAEL, L. E. OVERMAN, and G. F. TAYLOR. Tetrahedron Lett. 1313 (1978).
11. L. SALEM. J. Am. Chem. Soc. **90**, 543 (1968); **90**, 553 (1968); R. E. TOWNSHEND, G. RAMUNNI, G. SEGAL, W. J. HEHRE, and L. SALEM. J. Am. Chem. Soc. **98**, 2190 (1976).
12. L. E. OVERMAN, G. F. TAYLOR, K. N. HOUK, and L. N. DOMELSMITH. J. Am. Chem. Soc. **100**, 3182 (1978).
13. V. K. ALDER and W. VOGT. Justus Liebigs Ann. Chem. **564**, 120 (1949).
14. M. F. ANSELL and A. H. CLEMENTS. J. Chem. Soc. C, 275 (1971).
15. T. COHEN, A. J. MURA, JR., D. W. SHULL, E. R. FOGEL, R. J. RUFFNER, and J. R. FALCK. J. Org. Chem. **41**, 3218 (1976).
16. W. J. HEHRE, W. A. LATHAN, R. DITCHFIELD, M. D. NEWTON, and J. A. POPLE. Program No. 236, Quantum Chemistry Program Exchange **10**, 236 (1973).
17. W. J. HEHRE, R. F. STEWART, and J. A. POPLE. J. Chem. Phys. **51**, 2657 (1969); W. J. HEHRE. Acc. Chem. Res. **9**, 399 (1976).
18. J. A. POPLE and M. GORDON. J. Am. Chem. Soc. **89**, 4253 (1967).
19. V. F. KUCHEROV, N. YA. GRIGOR'EVA, and I. N. NAZAROV. Izv. Akad. Nauk S.S.S.R., Otd. Khim. Nauk, 849 (1959).

The occurrence of ergosterol and (22*E*,24*R*)-24-ethylcholesta-5,7,22-trien-3β-ol in the unicellular chlorophyte *Dunaliella tertiolecta*[1]

JEFFREY L. C. WRIGHT

Atlantic Regional Laboratory, National Research Council of Canada, 1411 Oxford St., Halifax, N.S., Canada B3H 3Z1

Received May 7, 1979

JEFFREY L. C. WRIGHT. Can. J. Chem. **57**, 2569 (1979).

Using ^{13}C nuclear magnetic resonance spectroscopy the major sterols of the unicellular chlorophyte *Dunaliella tertiolecta* were found to be ergosterol and a closely related C_{29} trienol. Apparently the absence of a cell wall in *D. tertiolecta* does not significantly affect the type of sterol produced since other unicellular chlorophytes which possess a cell wall produce similar sterols containing an unsaturated side chain and a 24[*R*]-alkyl substituent.

JEFFREY L. C. WRIGHT. Can. J. Chem. **57**, 2569 (1979).

Faisant appel à la rmn ^{13}C, on a trouvé que les principaux stérols du chlorophyte monocellulaire, *Dunaliella tertiolecta*, sont l'ergostérol et un triénol en C_{29} qui lui est intimement apparenté. Il semble que l'absence de paroi cellulaire dans le *D. tertiolecta* n'affecte pas beaucoup le type stérol produit puisque d'autres chlorophytes monocellulaires possédant une paroi cellulaire fournissent des stérols semblables portant une chaîne latérale qui n'est pas saturée et un substituant alkylé [*R*] en 24.

[Traduit par le journal]

Introduction

The distribution of sterols in marine algae is of phylogenetic interest to phycologists (1–4). Although patterns have emerged for major sterols within certain phyla (e.g., cholesterol in Rhodophyceae; fucosterol in Phaeophyceae) there is much variety among the Chlorophyceae. It arises through biogenetic alkylation at C-24 and modification of the tetracyclic ring system. Thus a range of Δ^5, Δ^7, and $\Delta^{5,7}$ compounds with methyl or ethyl substituents at C-24 have been reported as major sterols in Chlorophyceae (1, 4). Recently we used ^{13}C nmr spectroscopy to determine the structure and C-24 configuration of several alkyl sterols (5). This technique has now been applied in a study of the sterols of *Dunaliella tertiolecta* Butcher, a unicellular chlorophyte which is unusual in lacking a cell wall.

Results and Discussion

Sterols were separated from the non-saponifiable fraction of *D. tertiolecta* by silica gel chromatography. Gas–liquid chromatographic analysis (1.5% OV-17) of the combined sterol fractions showed two major components (Peaks B and E) and five minor ones. (Peaks A, C, D, F, and G). When the sterol mixture was acetylated the minor sterols were eluted together, before the two major sterols, from a silver nitrate – silica gel column. The major sterols, although freed from the minor components, could not be separated from each other by repeated argentation chromatography either as the parent compounds or as their acetates. The uv absorption of the mixture indicated that at least one contained an ergosterol-type nucleus. The smaller component (Peak B) had the same gas–liquid chromatography (glc) retention time as ergosterol (**1**) or its C-24 epimer. Gas chromatography – mass spectral (gc–ms) analysis of the acetate gave a mass spectrum identical (6) with that of ergosterol acetate (**2**) and high resolution mass spectral data of the free sterol established the molecular formula as $C_{28}H_{44}O$.

The glc retention time of the more abundant component (Peak E) corresponded with that for a C_{29} sterol (7), and the high resolution mass spectrum indicated a molecular formula of $C_{29}H_{46}O$. The gc–ms analysis of the acetate gave a mass spectral fragmentation pattern like that of ergosterol acetate but with the most abundant ions above *m/e* 355 at 14 mass units higher. Ions at *m/e* 392 and 377 correspond to loss of acetic acid and additional loss of methyl, but further cleavage yielded fragments at *m/e* 355, 341, 281, and 253, as found in ergosterol acetate. The striking similarity in mass spectral fragmentation patterns of the two sterol acetates including the common ion at *m/e* 253 which arises through loss of the complete side chain (6) indicates that the compounds differ only by an extra carbon in the side chain.

The ^{13}C nmr spectrum of the free sterol mixture contained 39 signals of varying intensity (Table 1). The sixteen most intense signals could be assigned to C-1 through C-19 of an ergosterol nucleus (8), though the signals for C-15, C-16, and C-17 appeared

[1]NRCC No. 17601.

0008-4042/79/192569-03$01.00/0

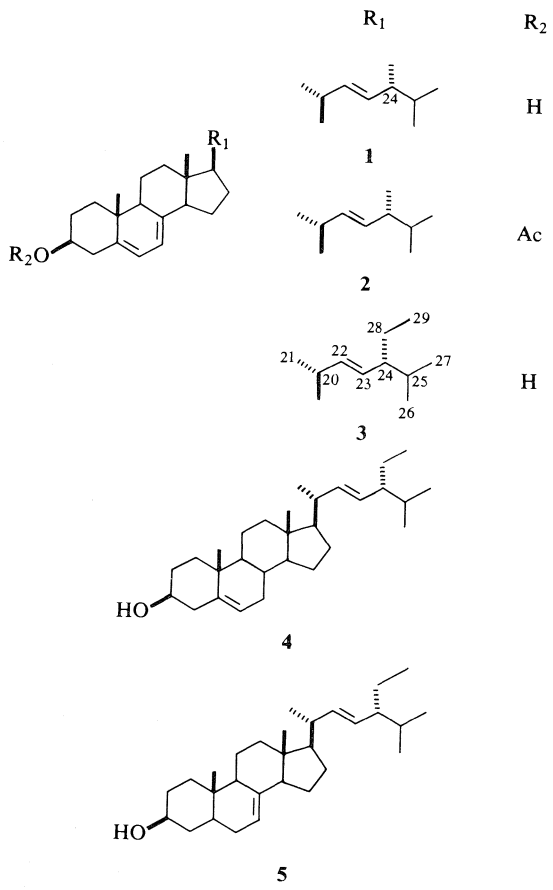

as pairs with components in the approximate ratio 1:2. Thus, both sterols share a common ergosterol-type nucleus but differences in the side-chain cause a perturbation of some resonances in ring D.

The seven least intense signals in the spectrum (δ_c 135.62, 132.05, 40.44, 33.13, 19.97, 19.67, and 17.64) can be assigned to an ergosterol side chain (Table 1). Resonances for C-21, (δ_c 21.16) and C-24 (δ_c 42.88) overlap with those for C-11 and C-13. The characteristic shift at δ_c 17.64,[2] assigned to C-28, establishes the configuration at C-24 as *R* (5) and hence ergosterol (**1**) as a major sterol of *D. tertiolecta*. The ten remaining resonances (δ_c 138.05, 129.66, 51.27, 40.73, 31.86, 25.41, 21.35, 20.94, 18.98, and 12.44) are accommodated by a Δ^{22} unsaturated side-chain containing an ethyl substituent at C-24 (Table 1). In this case the chemical shifts of C-28 (δ_c 25.41) and C-29 (δ_c 12.44)[3] indicate that the configuration at C-24 is also *R* (5), and thus identify (22*E*,24*R*)-24-ethylcholesta-5,7,22-trien-3β-ol (**3**) as the second major sterol. A similar trienol has been reported as a minor constituent in the prokaryotic blue-green alga *Phormidium luridum* (9), the unicellular chlorophyte *Chlamydomonas reinhardi* (10), and the unicellular chrysophyte *Ochromonas danica* (11), though in all cases the configuration at C-24 was not established.

The occurrence of ergosterol in *D. tertiolecta* and other Chlorophyceae (1) is interesting, since it is more generally recognised as a major sterol of fungi and yeast (12). However, the latter organisms biosynthesize it via a 24-methylene derivative (12) (Scheme 1, *a*) whereas the Chlorophyceae use an alternative route (e.g., Scheme 1, *b*) which may not include an unsaturated intermediate (2, 13, 14). The occurrence of (**1**) and (**3**) as major sterols in *D. tertiolecta* corresponds to the distribution in other unicellular chlorophytes (1, 4) of (**1**), poriferasterol (**4**), and chondrillasterol (**5**) which all possess a Δ^{22} side-chain and a 24[*R*]-alkyl substituent. Clearly the absence of a cell wall in *D. tertiolecta* does not drastically affect the

TABLE 1. ^{13}C nuclear magnetic resonance chemical shift data (δ_c TMS) for *D. tertiolecta* sterols, ergosterol (**1**), ergosterol acetate (**2**), and poriferasterol (**4**) in C^2HCl_3

	D. tertiolecta sterols					
	(**1**)	(**2**)*	Peak B		Peak E	(**4**)†
C-1	38.45	37.88		38.43		
C-2	32.07	28.10		32.06		
C-3	70.51	72.66		70.50		
C-4	40.88	36.62		40.86		
C-5	139.81	138.25		139.83		
C-6	119.65	120.04		119.65		
C-7	116.35	116.16		116.36		
C-8	141.32	141.16		141.37		
C-9	46.32	46.02		46.32		
C-10	37.09	37.06		37.08		
C-11	21.14	21.07		21.16		
C-12	39.18	39.00		39.16		
C-13	42.89	42.78		42.88		
C-14	54.62	54.45		54.62		
C-15	23.04	23.01	23.04		23.10	
C-16	28.29	28.10	28.31		28.61	
C-17	55.85	55.66	55.81		55.73	
C-18	12.08	12.06		12.06		
C-19	16.32	16.13		16.32		
C-20	40.42	40.40	40.44		40.73	40.45
C-21	21.17	21.07	21.16		20.94	20.95
C-22	135.60	135.25	135.62		138.05	138.28
C-23	132.06	131.76	132.05		129.66	129.37
C-24	42.89	42.78	42.88		51.27	51.25
C-25	33.14	33.04	33.13		31.86	31.87
C-26	19.97	19.96	19.97		18.98	18.97
C-27	19.67	19.67	19.67		21.35	21.20
C-28	17.63	17.63	17.64		25.41	25.42
C-29					12.44	12.43

*Reported in ref. 8.
†Reported in ref. 5.

[2]The resonance for C-28 of the 24*S*-isomer appears at δ_c 18.08 (5).

[3]The resonances for C-28 and C-29 of the 24*S*-isomer appear at δ_c 25.44 and δ_c 12.27 respectively (5).

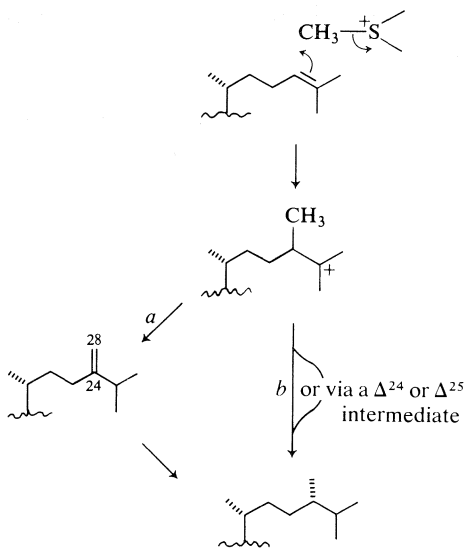

SCHEME 1

type of sterol produced. Phylogenetically it is interesting that ergosterol and related $\Delta^{5,7}$ sterols have not been reported in multicellular species of green algae which, in fact, usually produce isofucosterol (1, 4).

Experimental

Gas–liquid chromatographic analysis was carried out with a Hewlett-Packard model 5750 chromatograph equipped with a flame-ionization detector and a packed column (3 m × 0.4 mm id) containing 1.5% OV-17 on Gas Chrom Q. The injector port was at 260°C, the detector at 260°C, the oven at 240°C; helium carrier gas was at 22 psi, flow 15 mL/min. The gc-ms analysis was performed with a Finnigan Model 4000; glc conditions: glass column (2 m × 0.4 mm id) containing 3% OV-1 on Gas Chrom Q, injector port 180°C, oven 250°C, He carrier gas, flow 30 mL/min. Mass spectral conditions: glass jet separator, probe at 250°C, 70 eV; ionising energy, scan limits 60 to 500 amu. Mass spectra were obtained with a DuPont model 21-110B double-focusing spectrometer used in the electrical detection mode; 8 kV accelerating voltage, 70 eV ionising energy. Accurate mass measurements were made by peak matching against a perfluorokerosene reference. ^{13}C nuclear magnetic resonance spectra were recorded with a Varian XL 100/15 Fourier transform spectrometer under the conditions already described (5). Sample concentration was 5–15 mg/mL in C^2HCl_3. Ultraviolet and infrared absorption spectra were recorded with GCA McPherson Series 700 and Perkin-Elmer model 237 spectrophotometers respectively.

Dunaliella tertiolecta Butcher (15) was maintained in an enriched seawater medium containing (per L) $NaNO_3$ 850 mg, NaH_2PO_4 7.66 mg, P–I metals (16) 10 mL, EDTA (Na Salt) 541 mg, ferric citrate 28.6 mg, $MgSO_4 \cdot 7H_2O$ 116 mg, at 25°C with constant illumination. Cultures were transferred every two weeks. For production one to two week old cultures (100 mL) were added to the above medium (30 L) in a sterilised glass culture tank designed and constructed in this laboratory.[4] The culture was grown aseptically at 25°C for five days with constant illumination (16 fluorescent tubes, 100 W) and pH was maintained at 7.6 by buffering with CO_2. The cells were harvested by centrifugation, freeze dried (14 g), saponified under reflux in methanol:water (3:7) containing 10% KOH for 2 h and the lipid fraction extracted with ether to yield a yellowish oil (286 mg.) Chromatography on a silica gel column (1.2 cm × 25 cm) using hexane and hexane–ether mixtures yielded a sterol fraction (35 mg) which by glc analysis showed peaks A, B, C, D, E, F, and G in the proportion 1, 27, 4, 15, 37, 5, and 11. Chromatography of the sterol acetates (pyridine and acetic anhydride, 16 h) on a 25% silver nitrate – silica gel column eluted with hexane–benzene mixtures yielded a fraction which glc analysis showed to contain five components corresponding to peaks A, C, D, F, and G of the original mixture and another fraction with two components corresponding to peaks B and E of the original mixture. The gc–ms analysis gave the following data: *m/e* (relative intensity) for peak B: 378 (13), [*M* − 60], 363 (6.6) [*M* − (60 + 15)], 355 (5) [*M* − 83], 341 (5) [*M* − 97], 281 (30) [*M* − (97 + 60)], 253 (23) [*M* − (125 + 60)]; peak E: 392 (15) [*M* − 60], 377 (10) [*M* − (60 + 15)], 355 (5) [*M* − 97], 341 (6.6) [*M* − 111], 281 (31.6) [*M* − (111 + 60)], 253 (30) [*M* − (139 + 60)]. Accurate mass measurement of the free sterol mixture: peak B, 396.3379 (M^+, calculated for $C_{28}H_{44}O$, 396.3392); peak E, 410.3545 (M^+, calculated for $C_{29}H_{46}O$, 410.3548); 392.3436 (*M* − H_2O, calculated for $C_{29}H_{44}$, 392.3443); λ_{max} (EtOH) 215.6, 271.6, 282.2, 293.8 nm; ν_{max} (KBr disc) 3600–3100, 1450, 1370, 1050, 1033, 965, and 830 cm^{-1}.

[4]M. V. Laycock and J. L. C. Wright, unpublished results.

Acknowledgements

I thank Mrs. Cheryl Craft for technical assistance and Mr. Don Smith and Dr. John Walter for recording the nmr spectra.

1. G. W. PATTERSON. Lipids, **6**, 120 (1971).
2. L. J. GOAD, J. R. LENTON, F. F. KNAPP, and T. W. GOODWIN. Lipids, **9**, 582 (1974).
3. L. J. GOAD and T. W. GOODWIN. Prog. Phytochem. **3**, 113 (1972).
4. T. W. GOODWIN. *In* Algal physiology and biochemistry. *Edited by* W. D. P. Stewart. University of California Press, Los Angeles. 1974. p. 266.
5. J. L. C. WRIGHT, A. G. MCINNES, S. SHIMIZU, D. G. SMITH, J. A. WALTER, D. IDLER, and W. KHALIL. Can. J. Chem. **56**, 1898 (1978).
6. B. A. KNIGHTS. J. Gas Chromatogr. **5**, 273 (1967).
7. G. W. PATTERSON. Anal. Chem. **43**, 1165 (1971).
8. R. J. CUSHLEY and J. D. FILIPENKO. Org. Magn. Reson. **8**, 308 (1976).
9. N. J. DE SOUZA and W. R. NES. Science, **162**, 363 (1968).
10. M. BARD, K. J. WILSON, and R. M. THOMPSON. Lipids, **13**, 533 (1978).
11. M. C. GERSHENGORN, A. R. H. SMITH, G. GOULSTON, L. J. GOAD, T. W. GOODWIN, and T. H. HAINES. Biochemistry, **7**, 1698 (1968).
12. N. J. MCCORKINDALE. *In* The fungi. Vol. 2. *Edited by* J. E. Smith and D. R. Berry. Edward Arnold Publishers, London. 1976. p. 369.
13. Y. TOMITA, A. VOMORI, and E. SAKURAI. Phytochemistry, **10**, 573 (1971).
14. L. J. GOAD, F. F. KNAPP, J. R. LENTON, and T. W. GOODWIN. Biochem. J. **129**, 219 (1972).
15. J. MCLACHLAN. Can. J. Microbiol. **6**, 367 (1960).
16. J. MCLACHLAN. *In* Handbook of phycological methods: culture methods and growth measurements. *Edited by* J. R. Stein. Cambridge University Press, London. 1973. p. 25.

Réarrangement du squelette de la catharanthine. IV.[1] Nor-5 catharanthine et couplage avec la vindoline.[2]

RATREMANIAINA ZO ANDRIAMIALISOA, NICOLE LANGLOIS, YVES LANGLOIS, PIERRE POTIER
Institut de Chimie des Substances Naturelles, C.N.R.S., 91190, Gif-sur-Yvette, France
ET
PETER BLADON
University of Strathclyde, Glasgow, Ecosse

Reçu le 21 mars 1979

RATREMANIAINA ZO ANDRIAMIALISOA, NICOLE LANGLOIS, YVES LANGLOIS, PIERRE POTIER et PETER BLADON. Can. J. Chem. **57**, 2572 (1979).

La nor-5 catharanthine **3** est préparée à partir de la catharanthine **5**. Le couplage du N_b-oxyde correspondant **10** avec la vindoline **4**, dans les conditions de la réaction de Polonovski modifiée, conduit à deux dimères sans fragmentation du squelette.

L'obtention de nor-5 desméthoxycarbonyl-16 catharanthine **20** par clivage d'un des produits de couplage (**18**) de la vindoline **4** et du N_b-oxyde de desméthoxycarbonyl-16 catharanthine **17** corrobore la structure **18** qui avait été assignée à ce dimère dans notre laboratoire.

RATREMANIAINA ZO ANDRIAMIALISOA, NICOLE LANGLOIS, YVES LANGLOIS, PIERRE POTIER, and PETER BLADON. Can. J. Chem. **57**, 2572 (1979).

5-Norcatharanthine **3** was prepared from catharanthine **5**. The coupling of the corresponding N_b-oxide **10** with vindoline **4**, under modified Polonovski reaction conditions, led to two dimers without breaking the structural framework.

The isolation of 5-nor-16-demethoxycarbonylcatharanthine **20** by cleavage of one of the coupling products (**18**) of vindoline **4** and the N_b-oxide of 16-demethoxycarbonylcatharanthine **17** corroborates the structure **18** which was assigned to this dimer by our laboratory.

[Journal translation]

L'application de la réaction de Polonovski modifiée (2) au N_b-oxyde d'anhydrovinblastine **1**[3] se traduit par une compétition entre l'élimination d'un proton en C21′ et une fragmentation de la liaison C5′—C6′ (3). Cette dernière s'effectue avec participation de l'atome d'azote indolique ($N_{a'}$) et conduit, après hydrolyse des intermédiaires, perte de formol et cyclisation (Schéma 1) à la nor-5′ anhydrovinblastine **2** (3). L'accès, par cette méthode, à de nouveaux composés bis-indoliques du type norvinblastine nous a incités à étendre aussi ces résultats à la préparation des dérivés nor d'alcaloïdes monoindoliques. En particulier, il nous a semblé intéressant d'obtenir la nor-5 catharanthine **3** et d'étudier le couplage de ce nouveau composé avec la vindoline **4**.

Nous avons déjà montré (4) que la chaîne tryptaminique du N_b-oxyde **6** de la catharanthine **5** et d'autres composés du même type se fragmente dans les conditions de la réaction de Polonovski proprement dite (5) pour conduire, après addition d'un nucléophile en C6 tel qu'un ion acétate et cyclisation, à des composés tels que **8**, comportant l'enchaînement N_a—CH_2—N_b (Schéma 2).

Les essais d'hydrolyse du bis-immonium **7** impliqué dans cette réaction n'ont pas permis d'obtenir directement la nor-5 catharanthine **3**. En effet, la cyclisation $N_a \rightarrow C5$ s'effectue plus facilement que l'addition d'un hydroxyle sur le carbone 5 suivie de perte de formol et seul le composé **9** est obtenu.

Toutefois, des conditions acides plus énergiques (HCl 10%, 110°C) provoquent rapidement la réouverture de ce cycle et la nor-5 catharanthine **3** s'obtient alors avec 66% de rendement. Il est possible que le bis-immonium **7** soit régénéré au cours de cette réaction avec participation de l'azote N_b selon le Schéma 2, mais on ne peut pas exclure l'éventualité d'une protonation de l'azote N_b suivie de la participation de l'azote indolique qui conduirait au même résultat.

L'analyse spectrale de **3** prouve la structure indiquée. En particulier, l'analyse en haute résolution de l'ion moléculaire $M^{+\cdot}$ à *m/e* 322.1634 en spectrométrie de masse ($C_{20}H_{22}N_2O_2$), l'identification de tous les signaux en rmn du ^1H à haut champ (6) et en rmn du ^{13}C où le déplacement chimique du C6 se situe à 50.0 ppm (appariccine δ C6 = 54.3 ppm (7))

[1]Pour partie III voir réf. 1.

[2]Ce travail est dédié à la mémoire du Professeur R. H. F. Manske.

[3]P. Mangeney. A paraître.

0008-4042/79/192572-06$01.00/0

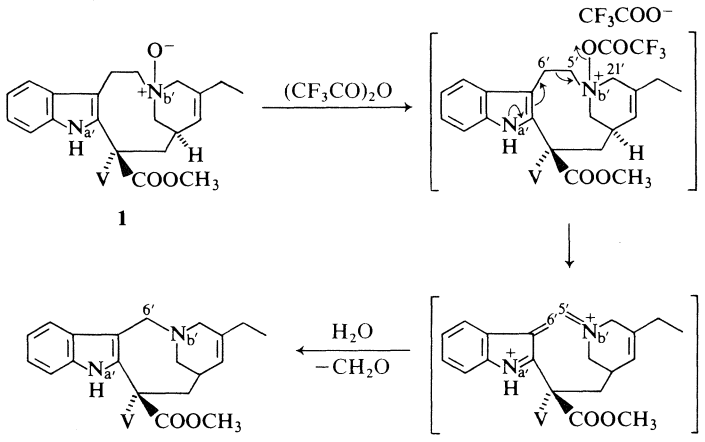

1 **2** V = vindolinyl-10

SCHÉMA 1

et celui du C16 à 45.1 ppm (catharanthine δ C16 ~ 55.5 ppm (8, 9)).

Le N_b-oxyde de nor-5 catharanthine **10** en présence d'anhydride trifluoroacétique et de vindoline **4** (10) n'évolue que très lentement à basse température (−70°C). Si la même réaction est effectuée à 0°C, la

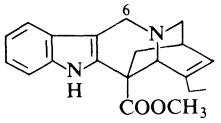

3

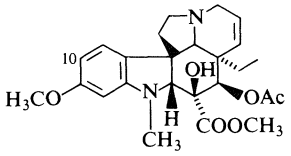

4 vindoline

formation de deux composés est détectée en ccm avant l'addition de borohydrure de sodium, ce qui indique l'absence d'immonium en fin de réaction. L'analyse des deux dimères obtenus permet de leur attribuer respectivement les structures **12** et **14**, ce qui corrobore le fait précédent. Le dimère **12** résulte de l'addition de la vindoline **4** sur l'immonium **11** formé par élimination inhabituelle d'un des protons en C3 (Schéma 3, I) comme en témoignent, en particulier, la composition de l'ion *a* (35%) à *m/e* 562.2890 en spectrométrie de masse, et la présence d'un système AB attribuable à un méthylène de type gramine dans le spectre de rmn du ^1H. L'élimination d'un des protons en C6, en α de l'indole, conduit à l'immonium **13**, précurseur du dimère **14** (Schéma 3, II). Pour ce composé également, le spectre de masse (composition de l'ion *b* (100%) à *m/e* 668.2958) et le spectre de rmn du ^1H (absence de système AB vers

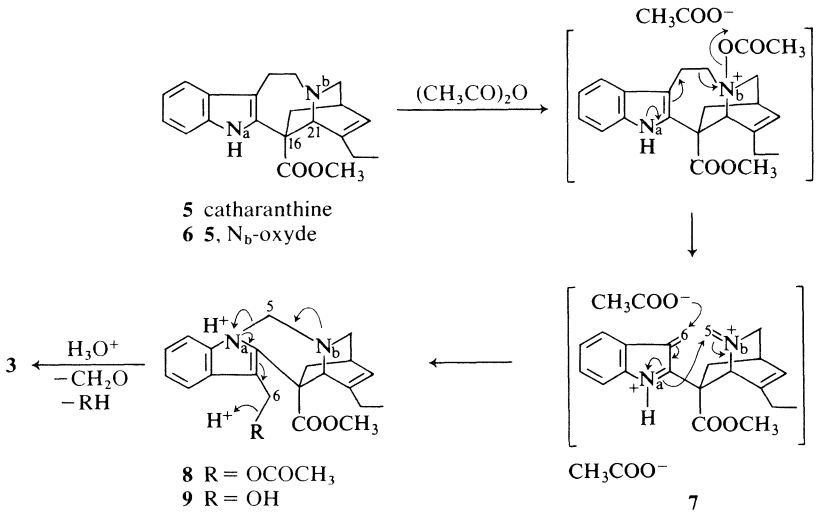

5 catharanthine
6 **5**, N_b-oxyde

8 R = $OCOCH_3$
9 R = OH
15 R = vindolinyl-10

7

SCHÉMA 2

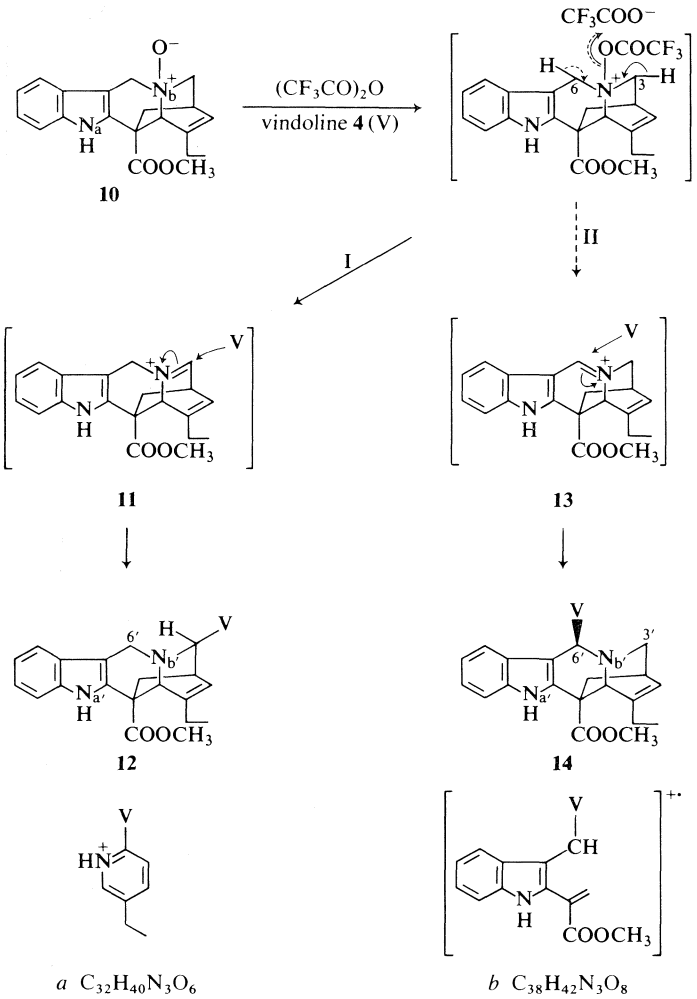

SCHÉMA 3

4 ppm et présence d'un singulet d'un proton à 5.58 ppm attribué à C6′—H) sont les plus caractéristiques. L'examen des modèles moléculaires est en faveur des configurations respectives en 3′ et 6′ indiquées sur les formules.

Aucun dimère résultant de la fragmentation C16—C21, majoritaire dans le cas du N_b-oxyde de catharanthine **6** (10, 11), n'a été observé. Dans le composé **10**, la rupture de cette liaison qui fait partie d'un cycle à 6 atomes est donc très défavorisée.

Lors du couplage de la vindoline **4** et du N_b-oxyde de catharanthine **6** dans les conditions de la réaction de Polonovski modifiée, la fragmentation décrite dans le Schéma 2 constitue une réaction secondaire (4%) conduisant au "dimère" **15** (10*b*). Avec certains dérivés de **6** comme le N_b-oxyde **17** de la desméthoxycarbonyl-16 catharanthine **16** (12), cette réaction est plus importante et le dimère **18** est obtenu avec un rendement d'environ 16% (13). Nous avons établi sa structure par analyse spectrale (13, 14). Cette structure **18** est très différente de celle (**19**) assignée par Kutney et collaborateurs, qui ont préparé un dimère présentant les mêmes caractéristiques en appliquant notre méthode de couplage (11). Leur argument principal reposait notamment sur l'identification du produit obtenu par coupure en milieu acide à la desméthoxycarbonyl-16 catharanthine **16**.

La possibilité de fragmenter en milieu acide les composés à enchaînement $—N_a—CH_2—N_b—$ tels que **8** et **9** (Schéma 2) nous a conduits à reproduire l'expérience de clivage du dimère **18** dans les conditions décrites par ces auteurs (11). Le seul composé indolique isolé de cette réaction s'est révélé différent de **16** en ccm et ses données spectrales sont en accord avec la structure nor-5 desméthoxycarbonylcatharanthine **20**. On observe en particulier dans le spectre de rmn du ^1H enregistré à 400 MHz[4] le système AB engendré par le méthylène de type gramine (C6—H_2)

[4]S. K. Kan *et al.* A paraître.

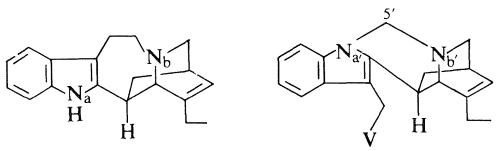

16
17 **16**,N_b-oxyde

18 V = vindolinyl-10

$-CH_2O$ | H_3O^+
$-$**4**

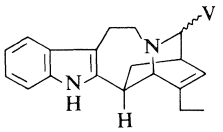

19 V = vindolinyl-10

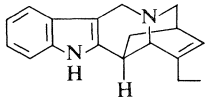

20

à 4.44 et 4.11 ppm. Ceci corrobore la structure **18** que nous avions attribuée au dimère précurseur.

Contrairement au N_b-oxyde de catharanthine **6**, le N_b-oxyde de nor-5 catharanthine **10** ne subit pas de fragmentation C16—C21 dans les conditions de la réaction de Polonovski modifiée en présence de vindoline **4** mais on observe une compétition entre l'élimination d'un proton en C3 et C6. Les deux dimères obtenus seront soumis aux tests systématiques pour évaluer leur rôle éventuel d'inhibiteur de polymérisation de la tubuline (15).

Partie expérimentale

Les points de fusion ont été pris sur bloc Kofler et sont corrigés. Les pouvoirs rotatoires ont été mesurés au moyen du polarimètre électronique Perkin-Elmer 141 MC. Les spectres ir (ν cm^{-1}, $CHCl_3$, sauf indication contraire) ont été enregistrés sur spectromètre Perkin-Elmer 257, les spectres uv (EtOH, λ_{max} nm (ε)) sur appareil Bausch et Lomb Spectronic 505 et les courbes de dc [EtOH, λ_{max} nm (Δε)] sur dichrographe Roussel-Jouan. Les spectres de rmn (sauf mention contraire dans $CDCl_3$, avec le TMS comme indicateur interne δ = 0 ppm) ont été effectués, pour le ^1H sur appareils IEF 240 MHz (6) ou 400 MHz[4] (les constantes de couplage sont exprimées en Hz, les lettres s, d, t, dd et m désignent respectivement les singulets, doublets, triplets, doublets de doublets et multiplets), et, pour le ^{13}C sur appareil Brüker HX 90 E ou Caméca 250 MHz. Les spectres de masse ont été enregistrés sur spectrographe AEI type MS 9, MS 50 ou MS 902. Les chromatographies sur couches épaisses (cce) ont été effectuées avec le Kieselgel HF 254 + 366 Merck.

Préparation de la nor-5 catharanthine **3**

A une solution de N_b-oxyde de catharanthine (200 mg, 0.57 mmol) préparé comme décrit (10*b*), dans 25 mL de chlorure de méthylène sec, maintenue à 0°C sous atmosphère inerte, on ajoute 2.5 mL d'anhydride acétique. Le mélange est agité à température ambiante pendant 1.5 h. Le solvant et l'excès de réactif sont évaporés sous vide. Une solution du résidu dans 40 mL d'acide chlorhydrique aqueux à 10% est ensuite chauffée sous argon à 110°C pendant 10 min. Le milieu réactionnel refroidi à 0°C est alcalinisé par NH_4OH concentrée et extrait par du chloroforme. Après séchage (Na_2SO_4) et évaporation du solvant sous pression réduite (traitements habituels), on obtient la nor-5 catharanthine **3** (180 mg) qui est purifiée par cce de silice (éluant: acétate d'éthyle, cuve saturée de NH_3), 120 mg (66%); $[\alpha]_D$ 0° (*c* 0.69, $CHCl_3$); chlorhydrate $[\alpha]_D$ −17° (*c* 0.63, CH_3OH); ir: 3400, 2950, 1730 cm^{-1}; uv (CH_3OH): 228(34 000), 276(ep 10 800), 284(11 000), 291(9700); uv (CH_3OH–HCl): 224-(31 800), 260(12 100), 272(ep 11 600), 288(9500); dc (CH_3OH): 230 (+1.5), 275 (+1.1); sm pics à *m/e* (%): 322.1634 (33), $C_{20}H_{22}N_2O_2$ calc.: 322.1629; 214(100); 154.0659 (42), $C_{11}H_8N$ calc.: 154.0659; 131.0740 (13), C_9H_9N calc.: 131.0741; 121.0911 (3), $C_8H_{11}N$ calc.: 121.0913; 109.0891 (57), $C_7H_{11}N$ calc.: 109.0891; 108.0819 (51), $C_7H_{10}N$ calc.: 108.0820. Les données rmn du ^1H (attributions après expériences de double irradiation) δ: 8.16 (s, 1H, N_a—H), 7.32–6.90 (m, 4H, aromatiques), 5.93 (m, 1H, C15—H), 4.21 (d, 1H, $J_{6a,6b}$ = 15, C6—H_a), 3.89 (d, 1H, $J_{6a,6b}$ = 15, C6—H_b), 3.70 (s, 1H, C21—H), 3.69 (s, 3H, CO_2CH_3), 3.00 (dd élargi par couplage en W, 1H, $J_{3a,3b}$ = 8 et $J_{3a,14}$ = 3, C3—H_a), 2.53 (m, 1H, C14—H), 2.40 (d, 1H, $J_{3a,3b}$ = 8, C3—H_b), 2.31 (m, 2H, C19—H), 2.06 (dd élargi par couplage en W, $J_{17a,17b}$ = 12.5, C17—H_a), 1.82 (dd, $J_{17a,17b}$ = 12.5 et $J_{14,17b}$ = 2.5, C17—H_b), 1.09 (t, 3H, $J_{18,19}$ = 7.5, C18—H); rmn du ^{13}C δ: 175.0 (C=0), 148.2 (C20), 136.7 et 136.2 (C2 et C13), 126.6 (C8), 124.6 (C15), 122.2, 119.8 et 118.5 (C10, C11 et C9), 111.2 (C12), 105.2 (C7), 58.8 (C21), 52.4 (OCH_3), 50.0 et 48.8 (C6 et C3), 45.2 (C16), 39.2 (C17), 30.1 (C14), 26.7 (C19), 11.0 (C18).

N_b-oxyde de nor-5 catharanthine ***10***

A une solution de nor-5 catharanthine **3** (48 mg, 0.15 mmol) dans du chlorure de méthylène anhydre (2 mL) maintenue sous argon, on ajoute à 0°C et sous agitation 30 mg (0.17 mmol) d'acide *m*-chloroperbenzoïque. Après 5 min d'agitation à 0°C, le milieu réactionnel est alcalinisé par une solution aqueuse de Na_2CO_3 à 10%, puis extrait par du chloroforme. Après traitements habituels, le N-oxyde de nor-5 catharanthine **10** est purifié par cce de silice (éluant: chloroforme–méthanol 94:6, sat. NH_3), on isole 31 mg (rdt 62%) de N_b-oxyde **10**.

Infrarouge: 3400, 2950, 1740 cm^{-1}; uv: 225, 276, 286, 292; inchangé en milieu acide; sm *m/e*: 338 ($M^{+\cdot}$), 322, 294, 234, 214 (100%), 158, 154, 130, 109, 108; rmn du ^1H (Varian 60 MHz) δ: 9.10 (s, 1H, N_a—H), 7.53–7.0 (m, 4H aromatiques), 6.33 (m, 1H, C15—H), 4.83 (m, 2H, C6—H), 4.50 (s élargi, 1H, C21—H), 3.80 (s, 3H, CO_2CH_3), 1.13 (t, 3H, *J* = 7.0, C18—H).

Couplage du N_b-oxyde de nor-5 catharanthine ***10*** *avec la vindoline* ***4***

A une solution de N_b-oxyde **10** (310 mg, 0.92 mmol) et de vindoline **4** (450 mg, 0.98 mmol) dans du CH_2Cl_2 anhydre (2.5 mL) maintenue sous argon à 0°C, on ajoute, sous agitation, l'anhydride trifluoroacétique (0.345 mL, 2.4 mmol). Le mélange est agité à 0°C pendant 45 min, puis le solvant et l'excès d'anhydride sont évaporés sous vide. Le résidu en solution dans du méthanol (20 mL) est réduit par un excès de $NaBH_4$. Après 10 min, le milieu réactionnel est dilué par de l'eau distillée et extrait par du chloroforme. Après traitements habituels, on obtient 700 mg de résidu qui est chromatographié sur cce de silice (éluant: acétate d'éthyle – méthanol 99.25:0.75, 2 migrations de 20 cm). On isole le dimère **12** (200 mg, 0.26 mmol, rdt 28%), la vindoline **4** (200 mg, 44%), la nor-5 catharanthine **3** (40 mg, 13%) et le dimère **14** (160 mg, rdt 23%).

Dimère ***12*** *(vindolinyl-3′ nor-5 catharanthine)*

Ce dimère présente les caractéristiques suivantes: $[\alpha]_D$ +80° (*c* 0.62, $CHCl_3$); ir: 3450, 2950, 1750 cm^{-1}; uv: 225 (53 400), 258 (17 200), 286 (10 700), 293 (10 800) et 307 (inflexion); milieu acide: 262 (20 800), 281 (10 800), 288 (10 800) et 308 (6500); dc: 205 (−4.5), 225 (+3.8), 255 (+3.8)

et 305 (+1.2); sm *m/e* (%): 776.3756 (100), $C_{45}H_{52}N_4O_8$ calc.: 776.3785; 616.3381 (5), $C_{39}H_{44}N_4O_3$ calc.: 616.3413; 563.2941 (23), $C_{32}H_{41}N_3O_6$ calc.: 563.2995; 562.2890 (35), $C_{32}H_{40}N_3O_6$ calc.: 562.2917; 282.1352 (5), $C_{14}H_{20}NO_5$ calc.: 282.1341; 214.0858 (7), $C_{13}H_{12}NO_2$ calc.: 214.0868; 135.1074 (6), $C_9H_{13}N$ calc.: 135.1048; 122.1015 (3), $C_8H_{12}N$ calc.: 122.0970. Les données rmn du ^1H δ: 9.74 (s large, 1H, C16—OH), 8.35 (s, 1H, $N_{a'}$—H), 7.35 (2H aromatiques), 7.24 (s, 1H, C9—H), 7.2–7.0 (2H aromatiques), 5.97 (s, 1H, C12—H), 5.85 (dd, 1H, $J_{14,15}$ = 10 et $J_{3,14}$ = 3, C14—H), 5.66 (d, 1H, $J_{14',15'}$ = 7.5, C15′—H), 5.45 (s, 1H, C17—H), 5.25 (d, 1H, $J_{14,15}$ = 10, C15—H), 4.07 (d, 1H, $J_{6'a,6'b}$ = 15, C6′—H_a), 3.87 (s, 1H, C21′—H), 3.79 et 3.75 (2s, 6H, OCH_3), 3.72 (s, 1H, C2—H), 3.68 (s, 3H, OCH_3 + d, 1H, $J_{6'a,6'b}$ = 15, C6′—H_b), 2.75 (s, 1H, C21—H), 2.68 (s, 3H, N_a—CH_3), (2.10 (s, 3H, $OCOCH_3$), 1.80 (q, 2H, $J_{18',19'}$ = 7.5, C19′—H), 1.16 (t, 3H, $J_{18',19'}$ = 7.5, C18′—H), 0.60 (t, 3H, $J_{18,19}$ = 7, C18—H); rmn du ^{13}C δ: 174.9 (C16′—*C*OOCH$_3$), 172.9 et 170.7 (*O*COCH$_3$ et C16—CO_2CH_3), 158.0 (C11), 152.4 (C13), 147.8 (C20′), 136.7 et 135.1 (C2′ et C13′, 131.0 (C15), 127.0 (C8′), 124.5, 123.2 et 123.1 (C15′, C9, C10, C8 et C14), 121.9 (C10′), 119.6 et 118.5 (C11′ et C9′), 111.0 (C12′), 105.9 (C7′), 92.7 (C12), 83.9 (C2), 79.0 (C16), 77.0 (C17), 67.2 (C21), 59.7 (C21′), 56.9 (C3′), 55.3 (C11—*O*CH$_3$), 53.2–51.1 (C7, C3, C5 et 2CO_2*C*H$_3$), 47.3 (C6′), 44.4 (C16′), 44.2 (C6), 43.2 (C20), 40.0 (C17′), 38.9 (N_a—CH_3), 36.1 (C14′), 31.0 et 27.3 (C19 et C19′), 21.0 (CO*C*H$_3$), 12.7 (C18′), 7.5 (C18).

*Dimère **14** (vindolinyl-6′ nor-5′ catharanthine)*

Ce dimère présente les caractéristiques suivantes: $[\alpha_D]$ −21° (*c* 0.56, $CHCl_3$); ir: 3400, 2950, 1740 cm^{-1}; uv: 223(70 000), 263(26 600), 275(18 400), 283(17 000), 298(7700); milieu acide: 221(77 600), 272(32 000), 281(20 000), 299(11 600); dc: 205(−60.1), 220(+60.0), 260(+18.7), 295(−7.5) et 300(+1.9); sm *m/e* (%): 776.3770(7), $C_{45}H_{52}N_4O_8$ calc.: 776.3785; 668.2958(100), $C_{38}H_{42}N_3O_8$ calc.: 668.2972; 617.3473(4), $C_{39}H_{45}N_4O_3$ calc.: 617.3491; 616.3377(3), $C_{39}H_{44}N_4O_3$ calc.: 616.3413; 282.1344(23), $C_{14}H_{20}NO_5$ calc.: 282.1341; 135.1047-(23), $C_9H_{13}N$ calc.: 135.1048; 122.0970(8), $C_8H_{12}N$ calc.: 122.0970; 121.0901(7), $C_8H_{11}N$ calc.: 121.0891; 107.0740(18), C_7H_9N calc.: 107.0735. Les données rmn du ^1H: 9.62 (s large, 1H,C16—OH), 8.31 (s, 1H, $N_{a'}$—H), 7.29 (d, 1H, *J* = 7.5 aromatique), 7.05 (2H aromatiques), 6.89 (dd, 1H, *J* = 7.5 aromatique), 6.52 (s, 1H, C9–H), 6.15 (s, 1H, C12—H), 6.00 (d, 1H, $J_{14',15'}$ = 7.5, C15′—H), 5.70 (dd, 1H, $J_{14,15}$ = 10 et $J_{3,14}$ = 3, C14—H), 5.58 (s, 1H, C6′—H), 5.35 (s, 1H, C17—H), 5.17 (d, 1H, $J_{14,15}$ = 10, C15—H), 3.95 (s, 3H, OCH_3), 3.82 (s, 1H, C21′—H), 3.75 (s, 6H, OCH_3), 3.69 (s, 1H, C2—H), 2.71 (s, 3H, N_a—CH_3), 2.05 (s, 3H, $OCOCH_3$), 0.88 (t, 3H, *J* = 7.5, C18′—H) et −0.35 (t, 3H, *J* = 7.5, C18—H); rmn du ^{13}C δ: 174.9 (C16′—*C*O_2CH_3), 172.9 (*O*COCH$_3$), 170.6 (C16—*C*O_2CH_3), 158.1 et 151.9 (C11 et C13), 146.1 (C20′), 136.2 (C2′ ou C13′), 130.9 (C15), 126.1 (C8′), 125.7, 123.8, 123.2 et 122.2 (C15′, C14, C9 et C10), 122.7 (C8), 120.0, 119.5 (C10′, C11′ et C9′), 111.1 et 110.6 (C7′ et C12′), 94.7 (C12), 83.6 (C2), 80.0 (C16), 77.7 (C17), 66.0 (C21), 56.7 (C11—*O*CH$_3$), 55.3 (attribué à C21′), 54–50 (C6′, C7, 2 CO_2*C*H$_3$, C3, C5 et C3′), 45.4 (C16′), 44.6 (C6), 43.0 (C20), 38.8 (C17′ et N_a—CH_3), 30.8 (C14′), 30.6 et 26.9 (C19 et C19′), 21.1 (COCH$_3$), 10.9 (C18′) et 6.8 (C18).

*Desméthoxycarbonyl-16 catharanthine **16***

Une solution d'acide catharanthinique (350 mg, 1.09 mmol préparé quantitativement à partir de **5** (3, 13)) dans de l'acide trifluoroacétique (30 mL) est agitée sous argon à température ordinaire pendant 30 min. Après évaporation sous pression réduite à la même température et alcalinisation par une solution aqueuse de Na_2CO_3, la desméthoxycarbonyl-16 catharanthine **16** est extraite par du chloroforme et purifiée par cce de silice (éluant éther–cyclohexane–méthanol 70:20:10). On obtient 273 mg de desméthoxycarbonyl-16 catharanthine **16** (rdt 90%) déjà connue (12).

Infrarouge: absence de carbonyle; uv: 228(16 500), 284(7500), 292(5700); dc(CH_3OH): 230 (+1.4), 240(−3.1), 305 (−0.2); sm *m/e*: 278, 170, 156, 143, 135(100%), 122, 121, 107; rmn du ^1H δ: 7.80 (s, 1H, N_a—H), 7.4–7.0 (aromatiques), 5.80 (d large, 1H, $J_{14,15}$ = 8, C15—H), 3.17 (m, 1H, C21—H), 2.14 (m, 2H, C19—H), 1.87 (m, 1H, C16—H), 0.90 (t, 3H, $J_{18,19}$ = 7, C18—H); rmn du ^{13}C (13).

*Dimère **18***

Le dimère **18**, préparé comme décrit (11, 13, 14) présente les caractéristiques suivantes: $[\alpha]_D$ −26° (*c* 0.33); ir: 1745, 1620 cm^{-1}; uv: 214 (45 200), 222 (épaulement 36 700), 254 (13 000), 286 (9000), 295 (8500), 304 (épaulement 7000); dc: 250 (+16.9), 295 (+0.2), 305 (+0.4); sm pics à *m/e*: 732 ($M^{+\cdot}$), 673, 672, 624, 573, 571, 465, 464, 357, 343, 324, 282, 178, 135 (pic de base), 122, 121; rmn du ^1H (240 MHz) δ: 7.43–7.03 (m, 4H aromatiques), 6.53 (s, 1H, C9—H), 6.12 (s + m, 2H, C12—H et C15′—H), 5.82 (dd, 1H, $J_{14,15}$ = 10 et $J_{3,14}$ = 3.5, C14—H), 5.40 (s, 1H, C17—H), 5.20 (d, 1H, $J_{14,15}$ = 10, C15—H), 5.18 (d, 1H, J_{AB} = 12.8, C5′—H_a), 4.94 (d, 1H, J_{AB} = 12.8, C5′—H_b), 3.90 et 3.80 (2s, 6H, C11—OCH_3) et C16—CO_2CH_3), 2.71 (s, 3H, N_a—CH_3), 2.11 (s, 3H, $OCOCH_3$), 1.13 (t, 3H, $J_{18',19'}$ = 7, C18′—H), 0.27 (t, 3H, $J_{18,19}$ = 7, C18—H).

*Clivage du dimère **18***

Le dimère **18** (60 mg, 0.08 mmol) est traité par de l'acide chlorhydrique à 10% en présence d'étain et de chlorure d'étain comme décrit (11).

La séparation des produits obtenus par cce de silice (acétate d'éthyle – méthanol 96:4, cuve saturée de NH_3) permet d'isoler, à côté de vindoline **4**, de son dérivé désacétylé, de dimère **18** qui n'a pas réagi et de produits polaires, la nor-5 desméthoxycarbonyl-16 catharanthine **20** (10 mg, 46%).

Infrarouge: 3400, 2950; uv (CH_3OH): 228, 276, 282, 290; sm *m/e*: 264, 182, 156 (100), 154, 149, 139, 110, 108; rmn du ^1H (400 MHz) δ: 8.15 (m, 1H, N_a—H), 7.4–7.0 (m, 4H aromatiques), 6.15 (d élargi, 1H, $J_{14,15}$ ~ 5, C15—H), 4.44 (d, 1H, $J_{6a,6b}$ = 15, C6—H_a), 4.11 (d, 1H, $J_{6a,6b}$ = 15, C6—H_b), 1.10 (t, 3H, $J_{18,19}$ = 7, C18—H).

Remerciements

Nous remercions la Ligue Nationale Française contre le Cancer pour l'attribution d'une bourse (R. Z. Andriamialisoa), le Dr. J. Y. Lallemand (École Normale Supérieure, Paris) pour l'enregistrement de spectres de RMN sur Caméca (250 MHz), C. Marazano pour des discussions concernant les spectres de masse et les Laboratoires Eli Lilly pour la fourniture de catharanthine.

1. P. Mangeney et Y. Langlois. Tetrahedron Lett. 3015 (1978).
2. A. Cavé, C. Kan-Fan, P. Potier et J. Le Men. Tetrahedron, **23**, 4681 (1967).
3. P. Mangeney. Thèse de Doctorat ès Sciences. Orsay. 1979.
4. N. Langlois, F. Guéritte, Y. Langlois et P. Potier. Tetrahedron Lett. 1487 (1976).
5. M. Polonovski et M. Polonovski. Bull. Soc. Chim. Fr. 1190 (1927).

6. S. KAN, P. GONORD, C. DURET, J. SALSET et C. VIBET. Rev. Sci. Instrum. **44**, 1725 (1973).
7. M. DAMAK. Thèse de Doctorat ès Sciences. Orsay. 1977.
8. M. DAMAK, C. POUPAT et A. AHOND. Tetrahedron Lett. 3531 (1976).
9. E. WENKERT, D. W. COCHRAN, H. E. GOTTLIEB, R. B. FILHO, F. J. DE ABREU MATOS et M. I. L. MACHADO MADRUGA. Helv. Chim. Acta, **59**, 2437 (1976).
10. (*a*) P. POTIER, N. LANGLOIS, Y. LANGLOIS et F. GUÉRITTE. J. Chem. Soc. Chem. Commun. 670 (1975); (*b*) N. LANGLOIS, F. GUÉRITTE, Y. LANGLOIS et P. POTIER. J. Am. Chem. Soc. **98**, 7017 (1976).
11. J. P. KUTNEY, T. IBINO, E. JAHNGEN, T. OKUTANI, A. H. RATCLIFFE, A. M. TREASURYWALA et S. WUNDERLY. Helv. Chim. Acta, **59**, 2858 (1976).
12. (*a*) M. GORMAN et N. NEUSS. Ann. Chim. (Rome), **53**, 43 (1963); (*b*) M. GORMAN, N. NEUSS et N. J. CONE. J. Am. Chem. Soc. **87**, 93 (1965).
13. R. Z. ANDRIAMIALISOA, Y. LANGLOIS, N. LANGLOIS et P. POTIER. C. R. Acad. Sci. Ser. C, **284**, 751 (1977).
14. R. Z. ANDRIAMIALISOA. Thèse de Doctorat ès Sciences. Orsay. 1978.
15. F. ZAVALA, D. GUÉNARD et P. POTIER. Experientia, **34**(11), 1497 (1978).

Polar radicals XIII.[1] A reinvestigation of the polar effects reported for the hydrogen transfer reactions of the 1-ethylpentyl radical

DENNIS D. TANNER, ROBERTO HENRIQUEZ,[2] AND DARWIN W. REED

Department of Chemistry, University of Alberta, Edmonton, Alta., Canada T6G 2G2

Received March 23, 1979

DENNIS D. TANNER, ROBERTO HENRIQUEZ, and DARWIN W. REED. Can. J. Chem. **57**, 2578 (1979).

The relative kinetics obtained from the decomposition products of *tert*-butyl-2-ethylperhexanoate, BEPH, (0.1 *M*) in mixtures of toluene and carbon tetrachloride were reinvestigated. Relative reactivities calculated from the ratios of heptane to 3-chloroheptane formed from BEPH decompositions in a variety of substituted toluenes, with added carbon tetrachloride, gave a similar Hammett correlation to that previously reported, but with a rather poor correlation coefficient ($r = 0.88$, $\rho = 0.68$).

From a material balance of the products formed it was determined that very few if any of the 1-ethylpentyl radicals formed ultimately abstract a benzylic hydrogen from toluene or a substituted toluene. The small amounts of heptane found (<0.7%) at any of the kinetically meaningful ratios of substrates, $ArCH_3/CCl_4$ 2.1 to 16.3, could have potentially arisen from radical disproportionation. No appreciable amount of aromatic substitution product could be detected under these conditions.

Decompositions of BEPH carried out in neat toluene only yielded small amounts (~0.4%) of addition product; however, the absolute amounts of heptane produced in reactions run in *p*-cyanotoluene were less than those formed in reactions carried out in toluene. These observations do not argue strongly for the authenticity of a relatively large positive ρ value (previously reported, +0.7) arising either from benzylic abstraction, or from addition to the aromatic ring.

DENNIS D. TANNER, ROBERTO HENRIQUEZ et DARWIN W. REED. Can. J. Chem. **57**, 2578 (1979).

On a étudié les cinétiques relatives à partir des produits de décomposition de l'éthyl-2 perhexanoate de *tert*-butyle, EPHB (0.1 *M*), dans des mélanges de toluène et de tétrachlorure de carbone. Les réactivités relatives calculées à partir des rapports d'heptane: chloro-3 heptane formés par décomposition de EPHB dans des toluènes substitués auxquels on a ajouté du tétrachlorure de carbone conduisent à des corrélations de Hammett semblables à celles rapportées antérieurement; le coefficient de corrélation est toutefois médiocre ($r = 0.88$, $\rho = 0.68$).

En se basant sur un bilan pondéral des produits formés, on peut déterminer que les radicaux éthyl-1 pentyles formés n'enlèvent que peu d'hydrogènes benzyliques du toluène ou des toluènes substitués. Les faibles quantités de pentane trouvées (<0.7%) à tous les rapports de substrat présentant une signification cinétique $ArCH_3/CCl_4$: 2.1 à 16.3, pourraient provenir d'une dismutation du radical. Dans ces conditions on n'a pas pu détecter des quantités appréciables de produits de substitution aromatique.

Les décompositions du EPHB effectuées dans le toluène pur ne conduisent qu'à de faibles quantités, ~0.4%, de produit d'addition; toutefois les quantités absolues d'heptane produites lors de réactions effectuées dans le *p*-cyanotoluène sont plus faibles que celles obtenues lorsque les réactions sont effectuées dans le toluène. Ces observations ne correspondent pas beaucoup à une valeur de ρ relativement très positive (rapportée antérieurement à +0.7) provenant soit de l'enlèvement benzylique ou d'une addition au noyau aromatique.

[Traduit par le journal]

Introduction

Substituent effects observed in the hydrogen transfer reactions of substituted toluenes have generally been explained as arising from the contribution of dipolar structures to the stabilities of the transition states for these reactions, i.e., polar effects (1).

Several years ago an interesting alternative proposal for these substituent effects was proposed by Zavitsas and Pinto (2). These authors suggested that polar effects were unnecessary considerations in rationalizing the relative rates of these reactions, but that the effects observed could be explained solely on the basis of the effect of the substituent on the bond dissociation energy of the benzylic carbon–hydrogen bond. Since a large number of radical abstraction reactions from substituted toluenes had been shown to have negative Hammett ρ values, it followed from their proposal that only negative ρ values could be obtained from these abstraction

[1]For Part XII, see ref. 11.

[2]Postdoctoral Fellow, University of Alberta, 1977–1978.

0008-4042/79/192578-07$01.00/0

reactions since the nature of the abstracting species could not affect the ordering of the bond dissociation energies.

Evidence against the Zavitsas proposal was subsequently reported (3, 4), but the most convincing arguments against these ideas were the publication of the positive ρ values obtained from the kinetic studies of a number of alkyl radicals, undecyl (5, 6) (ρ, +0.5), isopropyl (7) (ρ, +0.8), 1-ethylpentyl (8) (ρ, +0.7), and *tert*-butyl (7, 9) (ρ, +1.0), generated in the presence of a series of substituted toluenes. The validity of the reported ρ value for the primary undecyl radical has been seriously questioned by Zavitsas (10). In a reinvestigation of the ρ value obtained for the *tert*-butyl radical, the ρ value previously reported was shown to be an artifact of a competing reaction, cage disproportionation, since the production of the isobutane formed from the radicals was governed by the viscosity of the toluene (solvent) in which the radical source, 2,2′-azoisobutane, was decomposed (11).

In order to substantiate whether any authentic positive ρ values have been determined for alkyl radicals it has become necessary to reinvestigate the reaction previously reported for the two still unchallenged, secondary radicals. The study of the isopropyl radical (7) was carried out in a manner similar to that for *tert*-butyl, and its reactions are presently being reinvestigated. The results of the reinvestigation of the 1-ethylpentyl radical is the subject of this report.

The method used by the previous author was to generate the 1-ethylpentyl radical (R·) by the thermolysis, at 80°C, of *tert*-butyl-2-ethylperhexanoate (BEPH) in a mixture of a toluene (QH) and carbon tetrachloride (8).

$$\text{Perester} \rightarrow \text{R}\cdot \text{ and other products}$$

$$\text{R}\cdot + \text{QH} \xrightarrow{k_H} \text{RH} + \text{Q}\cdot$$

$$\text{R}\cdot + \text{CCl}_4 \xrightarrow{k_{Cl}} \text{RCl} + \text{CCl}_3\cdot$$

The values for k_H/k_{Cl} were obtained from plots of [RH]/[RCl] vs. [QH]/[CCl_4] and from these values, assuming that k_{Cl} is constant with different QH toluenes, the relative values of k_H/k_H^0 could be determined. The method assumes that the only source of RH is from abstraction by the 1-ethylpentyl radical (R·) from a substrate toluene.

Results and Discussion

Although Henderson did not report the [QH]/[CCl_4] ratios used in his kinetic studies (8) it became immediately apparent, upon the repetition of the reported reactions, that the range that could conceivably have been used must have been quite limited. When the BEPH decompositions were carried out in substrate mixtures having ratios of [QH]/[CCl_4] of 2.13 (QH, toluene) very little heptane, <0.5%, could be detected ([RH]/[RCl], 8.3×10^{-3}), while at a larger [QH]/[CCl_4] ratio, 16.3, the value of [RH]/[RCl] that was determined, 11.0×10^{-3}, did not appear to change appreciably from those obtained at the lower ratio. Even at the larger ratio only 0.75% of heptane (RH) was formed during a typical decomposition carried out in toluene and carbon tetrachloride (0.5 *M*), see Table 1.

At the larger [QH]/[CCl_4] ratio, 16.3, a material balance was obtained (QH, toluene) which accounted for 98% of the products resulting from the BEPH decomposition, see Table 1.

The small values of [RH]/[RCl] found in the perester decompositions were expected and are predictable, since the competitive abstraction reactions of 1-hexyl radicals from substrate mixtures of toluene and carbon tetrachloride had previously been reported by DeTar and Wells (12). These authors carried out the decomposition reactions of *n*-heptanoyl peroxide in mixtures of toluene and carbon tetrachloride, [QH]/[CCl_4], ranging from 4.17–0.265 and found, for the less selective primary 1-hexyl radical, values of [RH]/[RCl] of from 59×10^{-3} to 25×10^{-3}. From these values the relative rates of transfer between toluene and carbon tetrachloride, k_H/k_{Cl}, could be approximated, after an estimated correction for cage disproportionation had been applied, to be $6 \times 10^{-2} \pm 10^{1}$. The smaller values obtained for the more selective 1-ethylpentyl radical, 6.6×10^{-4}, are not unreasonable in light of the small value previously reported for the 1-hexyl radical.

Reactions carried out at the higher [QH]/[CCl_4] ratio, 16.3, with a variety of QH solvents gave simi-

TABLE 1. Products from the thermolysis of BEPH (0.1 *M*) in toluene and 0.52 *M* carbon tetrachloride, 80°C (starting material BEPH (186 mmol × 10^3, 9.30×10^{-2} *M*))

Products	Yield (mmol × 10^3) (%)
Carbon dioxide	184 (98.8)
Heptane	1.4 (0.75)
2-Heptene	6.0 (3.2)
3-Heptene	6.7 (3.6)
3-Chloroheptane	129.0 (69.4)
3-*tert*-Butoxyheptane	38.8 (20.9)
tert-Butyl alcohol	144.0 (77.4)
Bibenzyl	84.0
Chloroform	136.0
Benzyl chloride	14.5
trans-Stilbene	2.3
1,1,1-Trichloro-2-phenylethane	32.8

TABLE 2. Product yields from the thermolysis of BEPH in mixtures of QH and carbon tetrachloride

X—$C_6H_4CH_3$	Starting materials (mol/L × 10^2) (mmol)			Products (mmol)					Material balance (%)
	BEPH	CCl_4	$ArCH_3$						
H	9.30 (0.186)	52.3	855	0.0014	0.0060	0.0067	0.129	0.0388	97.5
p-CH_3	9.30 (0.186)	54.4	738	0.0025	0.0093	0.0115	0.140	0.0119	94.2
m-CH_3	9.90 (0.198)	60.7	735	0.0017	0.0136	0.0165	0.0165	0.0065	102.7
p-Cl	9.30 (0.186)	54.7	769	0.0015	0.0076	0.0092	0.124	0.040	97.7
m-Cl	9.40 (0.188)	57.6	773	0.0013	0.0067	0.0082	0.157	0.0156	100.4
p-CN	9.70 (0.188)	61.0	759	0.0020	0.0082	0.0088	0.0861	—	

larly small ratios of [RH]/[RCl], 11×10^{-5} to 23×10^{-3}, over the entire range of substrates previously used by Henderson (substituted toluenes with σ values of -0.17 to 0.63) (8) (see Table 2). The yield of heptane in these reactions ranged from 0.75–1.4%. The relative rates calculated from the [RH]/[RCl] ratios obtained from these reactions, although very reproducible, gave a poor fit to the Hammett equation, $\rho = 0.56$, $r = 0.88$ (see Table 3).

The Hammett parameters, however, are quite similar to those reported by Henderson (8), $\rho = 0.70 \pm 0.09$ ($r = 0.94$). The supposition that the heptane was produced solely by radical abstraction from toluene must be questioned since accompanying the heptane were three products arising from hydrogen transfer reactions, 2-heptene, 3-heptene, and a substituted stilbene. The ratio of olefinic products to heptane in the reaction run in toluene was 10.7 (see Table 1). Similar values, >7.2–12.8, were obtained for the reactions run in the other substrates; amounts of substituted stilbenes were not included in these calculations, as only stilbene itself was determined quantitatively (see Table 2).

An average material balance of 99 ± 2% was obtained for the radicals produced from the decomposition of the BEPH in all solvents.

From an analysis of the products formed from the decomposition of BEPH in the toluene–carbon tetrachloride mixture a reasonable picture can be formulated for the decomposition of the perester and for the subsequent reactions of its radical products.

A plethora of reactions must be considered due to the complexity of the reaction mixture (see Fig. 1). The formation of heptane by disproportionation as well as abstraction, need be considered (see reactions [12]–[14]); however, heptane's disproportionation partner, heptene (reaction [14]), cannot only be formed external to the solvent cage (reactions [14] and [15]) but within the solvent cage (reaction [2]). In order to establish the potentiality of disproportionation (reaction [14]) as a source of the small

TABLE 3. Relative rates of reaction for BEPH decompositions in various substituted toluenes, ·QH

QH	k_H/k_{Cl}[a]	k_H/k_H^0
Toluene	$3.66 \times 10^{-4} \pm 0.06$	1
p-Methyltoluene	$5.18 \times 10^{-4} \pm 0.32$	1.42
m-Methyltoluene	$4.05 \times 10^{-4} \pm 0.09$	1.11
p-Chlorotoluene	$7.79 \times 10^{-4} \pm 0.09$	2.13
m-Chlorotoluene	$6.98 \times 10^{-4} \pm 0.19$	1.91
p-Cyanotoluene	$11.9 \times 10^{-4} \pm 0.1$	3.25
$\rho = 0.66$; $r = 0.88$; $S_{y \cdot x} = 0.102$		

[a]Average values from duplicate experiments. The errors listed are average deviations from the mean value.

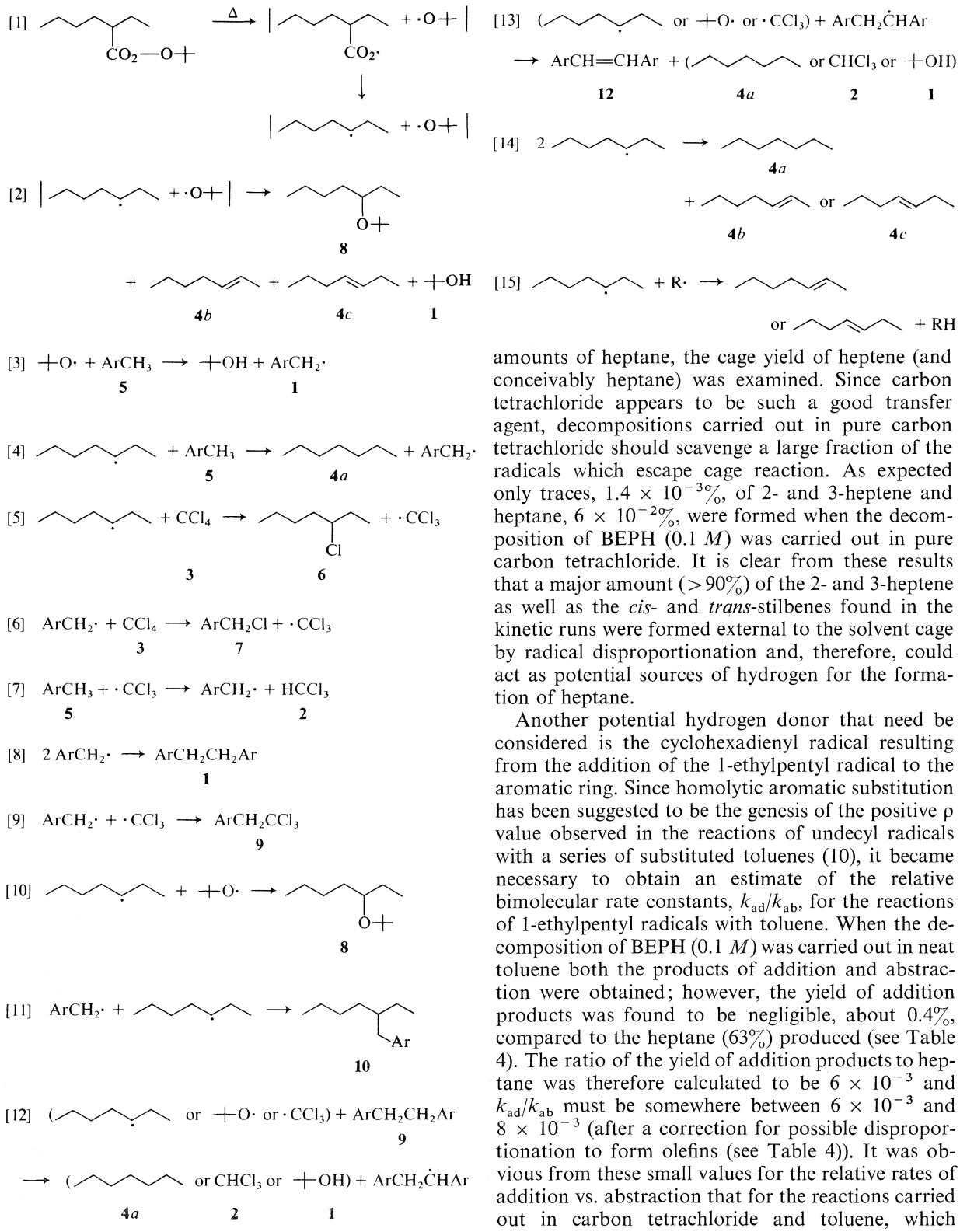

amounts of heptane, the cage yield of heptene (and conceivably heptane) was examined. Since carbon tetrachloride appears to be such a good transfer agent, decompositions carried out in pure carbon tetrachloride should scavenge a large fraction of the radicals which escape cage reaction. As expected only traces, $1.4 \times 10^{-3}\%$, of 2- and 3-heptene and heptane, $6 \times 10^{-2}\%$, were formed when the decomposition of BEPH (0.1 *M*) was carried out in pure carbon tetrachloride. It is clear from these results that a major amount (>90%) of the 2- and 3-heptene as well as the *cis*- and *trans*-stilbenes found in the kinetic runs were formed external to the solvent cage by radical disproportionation and, therefore, could act as potential sources of hydrogen for the formation of heptane.

Another potential hydrogen donor that need be considered is the cyclohexadienyl radical resulting from the addition of the 1-ethylpentyl radical to the aromatic ring. Since homolytic aromatic substitution has been suggested to be the genesis of the positive ρ value observed in the reactions of undecyl radicals with a series of substituted toluenes (10), it became necessary to obtain an estimate of the relative bimolecular rate constants, k_{ad}/k_{ab}, for the reactions of 1-ethylpentyl radicals with toluene. When the decomposition of BEPH (0.1 *M*) was carried out in neat toluene both the products of addition and abstraction were obtained; however, the yield of addition products was found to be negligible, about 0.4%, compared to the heptane (63%) produced (see Table 4). The ratio of the yield of addition products to heptane was therefore calculated to be 6×10^{-3} and k_{ad}/k_{ab} must be somewhere between 6×10^{-3} and 8×10^{-3} (after a correction for possible disproportionation to form olefins (see Table 4)). It was obvious from these small values for the relative rates of addition vs. abstraction that for the reactions carried out in carbon tetrachloride and toluene, which

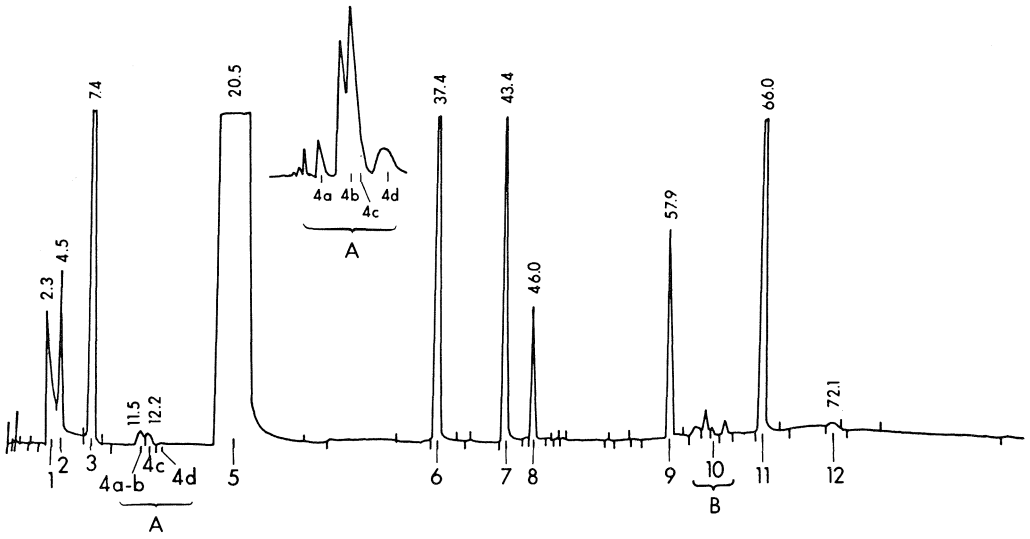

FIG. 1. Glc chromatogram and peak assignments for the reaction mixture from the thermolysis (80°C) of BEPH (0.1 *M*) in a mixture of toluene and carbon tetrachloride (0.5 *M*). The chromatogram was obtained using the SE-30 column, while the insert portion (A) was obtained using the Carbowax 400 column. **1**, *tert*-Butanol; **2**, chloroform; **3**, carbon tetrachloride; **4***a*, heptane; **4***b*, 2-heptene; **4***c*, 3-heptene; **4***d*, —; **5**, toluene; **6**, 3-chloroheptane; **7**, benzyl chloride; **8**, *tert*-butyl-3-heptyl ether; **9**, 1,1,1-trichloro-2-phenylethane; **10**, 3-benzylheptane; **11**, bibenzyl; **12**, *t*-stilbene.

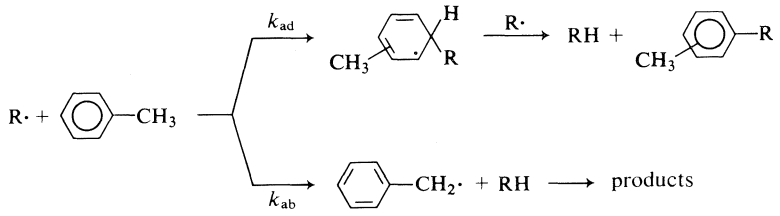

showed so little abstraction, no detectable amount of addition would be found.

When BEPH (0.1 *M*) was thermolyzed (80°C) in neat *p*-cyanotoluene the absolute amount of heptane (40.8%) formed in the BEPH decompositions carried out in the supposedly more hydrogen donating solvent, *p*-cyanotoluene, was less than 2/3 that formed when the decomposition was carried out in toluene.

TABLE 4. Products from the thermolysis (80°C) of BEPH (0.1 *M*) in toluene

Products	Yield (mol/mol BEPH)[a]	%
Heptane	0.632±0.035	63.2
2- and 3-Heptene	0.112±0.004	11.2
1-(3-Heptyl)-3- and -4-methylbenzene	0.004±0.001	0.4
3-*tert*-Butoxyheptane	0.056±0.011	5.6
Bibenzyl	0.528±0.022	
tert-Butyl alcohol	0.791±0.009	79.1
3-Benzylheptane	0.124±0.001	12.4

[a]Errors are average deviations from the mean values for duplicate experiments.

Conclusion

Toluene (or a substituted toluene) as a donor of benzylic hydrogen appears to compete quite poorly with carbon tetrachloride, as a transfer reagent, at all practical concentrations, for reaction with secondary alkyl radicals. Kinetic methods based on these competitive rates have very little possibility of being definitive since other sources of hydrogen, kinetically more favorable, are available to the alkyl radicals. In kinetic runs the formation of disproportionation products, olefins, far outweighs the heptane produced. The olefinic products produced in the reaction were shown to be formed, primarily, external to the solvent cage, and thus their precursor radicals are established as a potential source of hydrogen for the formation of heptane.

Decompositions of BEPH carried out in pure toluene demonstrated that addition to the aromatic ring is negligibly competitive with benzylic abstraction. Addition products only accounted for the reaction of ca. 0.4% of the 1-ethylpentyl radicals that were produced, while the absolute amount of heptane

produced in the reaction was less for the reactions run in *p*-cyanotoluene than the reactions carried out in toluene. These observations do not argue strongly for a relatively large, $\rho = +0.7$, positive ρ value caused either from benzylic abstraction (8), or from addition to the aromatic ring (10).

A calculation of the relative rates of reaction of the substituted toluenes obtained using the competitive method of Henderson (8) gave relative rate constants which showed a poor correlation with their Hammett substitution constants ($r = 0.88$, $\rho = +0.66$). Since under the most favorable conditions the yield of heptane amounts to only from <0.5–0.75% of the 3-ethylpentyl radicals produced, and since under these reaction conditions it was not experimentally possible to determine the genesis of this small amount of heptane, the nucleophilicity (8) or electrophilicity (10) of a secondary alkyl radical has not as yet been experimentally demonstrated.

Experimental

Materials

Toluene and *p*-xylene (Phillips 66, research grade, >99.9%) were used without further purification. *m*-Xylene and *m*-chlorotoluene (Eastman Chemical Co.) were fractionally distilled (24 in. teflon spinning band column) before use. *p*-Cyanotoluene and *p*-chlorotoluene (Aldrich Chemical Co.) were purified by repeated low temperature fractional recrystallization followed by fractional distillation, using a 24 in. teflon spinning band column. Carbon tetrachloride (Baker Chemical Co., spectral grade), was fractionally distilled before use. All these materials were shown by glpc (10 ft × 1/4 in. 10% QF-1 on 60/80 Chromosorb P AW DMCS, glass column) to be >99.9% pure.

tert-Butyl-2-ethylperhexanoate (BEPH) was prepared according to an adaptation of the method reported in the literature for *tert*-butyl perpivalate (13). The perester was purified by column chromatography on activated alumina at 0°C, using dry ether as eluent. *Anal.* calcd. for $C_{12}H_{24}O_3$: C 66.63, H 11.18; found: C 66.83, H 11.02.

3-Chloroheptane (**6**) was prepared using the general method for preparation of secondary halides with thionyl chloride and 3-heptanol in pyridine as solvent (14). The chloride was fractionally distilled through a 24 in. teflon spinning band column and shown to be one compound by glpc (7.5% SE-30 Chromosorb PAW 60/80 10 ft × 1/4 in. column and on the QF-1 column); bp 144°C/751 Torr. *Anal.* calcd. for $C_7H_{15}Cl$: C 62.42, H 11.22; found: C 62.53, H 11.37.

tert-Butyl-3-heptyl ether (**8**) was prepared according to the method of Henry (15); bp 164–166°/740 Torr. Its glpc (SE-30, column) retention time and mass spectral cracking pattern (*m/e* 143 M^+, base peak 57, $C_4H_9^+$) and ir spectra were identical to those obtained from the product (assigned this structure) which was formed in the perester decomposition reaction.

1-(3-Heptyl)-4-methylbenzene, 1-(3-heptyl)-3-methylbenzene, and 3-benzylheptane (**10**) were synthesized by the hydrogenation of the olefins obtained from the dehydration of the alcohols which were obtained from the reaction of 3-heptanone with the appropriate Grignard reagent (16).

Thermolysis of tert*-Butyl-2-ethylperhexanoate (BEPH)*

Aliquot solutions of BHP (0.1 *M*), the appropriate toluene (7–8 *M*), and carbon tetrachloride (0.5–0.6 *M*) were placed in Pyrex ampoules, degassed by the freeze–thaw method, and sealed. The sealed ampoules were thermostated at 80 ± 0.1°C for 76 h.

One of the reactions was carried out in an ampoule fitted with a break seal. After the reaction the ampoule was opened to a vacuum line and the CO_2 produced in reaction was fractionated, measured, and identified by its glpc retention time and mass spectrum, all in the manner previously described (13). The decomposition was found to have proceeded essentially to completion since 98.8% of the theoretical carbon dioxide was isolated.

After thermolysis the ampoules were opened and a weighed amount of internal standard (*p*-nitrotoluene) was added and the mixture was then subjected to glpc analysis using the SE-30 column. A typical chromatogram (toluene as substrate) is given in Fig. 1. The glpc chromatogram indicated the presence of a large number of products. The identity of the products (compounds **1**–**4***b*, **5**–**8**, and **10**–**12**) was established by a comparison of their glpc retention times, mass spectral cracking patterns, and ir spectra with those of authentic samples. The structure of the compound corresponding to **4***c* (see Fig. 1), 3-heptene, was tentatively assigned on the basis of the following observations. In the course of the synthesis of 3-chloroheptane several olefinic products are formed. One of these corresponded (identical glpc retention time and mass spectral cracking pattern) to 2-heptene, while the other olefin corresponded to the compound assigned the structure 3-heptene. The products with lower retention times, heptane, 2-heptene, and 3-heptene, were analysed by glpc using a second column (10% Carbowax 400 Diotoport WAW 60-80 mesh 20 ft × 1/8 in. ss column) (see insert A in Fig. 1).

An aliquot of the reaction mixture (with toluene as substrate) was treated with a small amount of bromine in the absence of light for about 5 min; glpc analysis using both the SE-30 and Carbowax 400 columns showed the disappearance of the peaks corresponding to 2-heptene, 3-heptene, and *trans*-stilbene.

The identity of the chromatographic peak corresponding to 3-heptene was assigned on the basis of the reaction of the compound with molecular bromine and because of the similarity of its mass spectral cracking pattern with that of its isomer 2-heptene. Analysis by glpc–ms showed ions at *m/e* 98 (M^+, 20.4%) and 55 ($M^+ - C_3H_7$, 100%), while 2-heptene gave *m/e* 98 (M^+, 22.9%) and 41 ($M^+ - C_4H_9$, 100%).

The structure of 1,1,1-trichloro-2-phenylethane (**9**) was assigned according to its mass spectral cracking pattern, which showed weak intensity parent ions, *m/e* 212, 210, 208 (M^+) whose relative intensities were consistent with the ratios produced for three chlorine atoms (calcd. 0.01, 0.13, 0.42, 0.43; found: 0.0, 0.12, 0.42, 0.45), base peak *m/e* 91 corresponding to $C_7H_7^+$, and its ir spectra which showed aromatic absorption at 3080, 3040, 705, and 768 cm^{-1}, and CH_2 absorption at 2940 and 1460 cm^{-1}.

The chromatographic peaks on either side of **10** (see section B, Fig. 1) did not compare (ir, mass spectral cracking pattern, or glpc retention times) with either of the two substitution products, 1-(3-heptyl)-4-methylbenzene or 1-(3-heptyl)-3-methylbenzene. The first peak (section B, Fig. 1) had the same retention time as the two substitution products, but ir and mass spectra were different than those of the authentic materials.

The thermolyses of BEPH in neat solvents, carbon tetrachloride, toluene, and *p*-cyanotoluene were carried out in the same manner as the reactions that were run in the mixed substrates. The products identified (see Table 4) were assigned the structures listed on the basis of a comparison of their glpc retention times, SE-30 and Carbowax 400 columns, and their mass spectra with those of authentic samples.

Gas–Liquid Partition Chromatographic Analyses

The quantitative glpc analyses were carried out using both the SE-30 and Carbowax 400 columns (see Fig. 1). The area ratios of the product and an added standard were obtained using a HP-3380A integrator. The mole ratios of products were determined using standard calibration curves obtained using known mixtures of the authentic materials. For the compounds listed below, the authentic materials were not available and the calibration factors obtained from model compounds were used: 3-heptene (model compound 2-heptene); 1,1,1-trichloro-2-phenylethane (calibration factor 1).

Gas–Liquid Partition Chromatographic – Infrared Analyses

The glpc–ir analyses were carried out on kinetic reaction mixtures from the reaction of 0.1 *M* BEPH and 0.5 *M* carbon tetrachloride in toluene. The spectrum for each compound was obtained using a Nicolet 7199 FT-IR interfaced to a Nicolet series 7000 gas chromatograph fitted with a 6 ft × 1/8 in. OV-1, 3%, ss column. The spectrum of each component was compared with that of the authentic material.

Acknowledgements

The authors wish to thank the National Research Council of Canada and the University of Alberta for their generous support of this work. We would further like to express our appreciation to Dr. R. L. Julian of the Nicolet Instrument Corporation for carrying out the gc–ir analyses in their laboratory.

1. (*a*) C. WALLING. Free radicals in solution. Wiley, New York, NY. 1957. Chapt. 8; (*b*) G. A. RUSSELL. *In* Free radicals. Vol. 1. *Edited by* J. Kochi. Wiley, New York, NY. 1973. pp. 293–298; (*c*) C. WALLING and B. MILLER. J. Am. Chem. Soc. **79**, 4181 (1957); (*d*) G. A. RUSSELL. J. Org. Chem. **23**, 1407 (1958).
2. A. A. ZAVITSAS and J. A. PINTO. J. Am. Chem. Soc. **94**, 7390 (1972).
3. D. D. TANNER, R. J. ARHART, E. V. BLACKBURN, N. C. DAS, and N. WADA. J. Am. Chem. Soc. **96**, 829 (1974).
4. J. A. HOWARD and H. H. B. CHENIER. J. Am. Chem. Soc. **95**, 3055 (1973).
5. W. A. PRYOR and W. H. DAVIS, JR. J. Am. Chem. Soc. **96**, 7557 (1974).
6. R. W. HENDERSON and R. D. WARD, JR. J. Am. Chem. Soc. **96**, 7556 (1974).
7. W. H. DAVIS, JR. and W. A. PRYOR. J. Am. Chem. Soc. **99**, 6365 (1977).
8. R. W. HENDERSON. J. Am. Chem. Soc. **97**, 213 (1975).
9. W. A. PRYOR, W. H. DAVIS, JR., and J. P. STANLEY. J. Am. Chem. Soc. **95**, 4754 (1973).
10. A. A. ZAVITSAS and G. M. HANNA. J. Org. Chem. **40**, 3782 (1975).
11. D. D. TANNER, P. W. SAMAL, T.C-S. RUO, and R. HENRIQUEZ. J. Am. Chem. Soc. **101**, 1168 (1979).
12. D. F. DETAR and D. V. WELLS. J. Am. Chem. Soc. **82**, 5839 (1960).
13. D. D. TANNER, H. YABUUCHI, and H. LUTZER. Can. J. Chem. **55**, 612 (1977).
14. A. I. VOGEL. Practical organic chemistry. 3rd ed. Longman. 1956. pp. 270–274.
15. L. HENRY. Recl. Trav. Chim. Pays-Bas Belg. **23**, 329 (1904).
16. A. I. VOGEL. Practical organic chemistry. 3rd ed. Longman. 1956. pp. 474, 517.

Partial molal volumes of organic compounds in carbon tetrachloride. IV. Ketones, alcohols, and ethers

JOHN T. EDWARD, PATRICK G. FARRELL, AND FEREIDOON SHAHIDI[1]

Department of Chemistry, McGill University, 801 Sherbrooke St. W., Montreal, P.Q., Canada H3A 2K6

Received January 11, 1979

JOHN T. EDWARD, PATRICK G. FARRELL, and FEREIDOON SHAHIDI. Can. J. Chem. **57**, 2585 (1979).

The partial molal volumes $\bar{V}^0$ in carbon tetrachloride at 25°C of 13 ketones, 18 alcohols, and 17 mono- or poly-functional ethers, all acyclic, have been determined. Results are in reasonable agreement with $\bar{V}^0$ calculated from an equation developed previously, using previous parameters plus the following: increments (in mL mol^{-1}) of 8.72 for carbonyl, 6.1 for hydroxyl, 4.4 for oxygen in a monofunctional ether, and 5.8 for oxygen in a polyfunctional ether; decrements δ (in mL mol^{-1}) of -1.68 for $g_{C-C}^{CO/C}$, -2.22 for $g_{C-C}^{O/C}$, -0.90 for $g_{C-C}^{O/O}$, -3.27 for $g_{O-C}^{C/C}$, and -1.93 for $g_{O-C}^{C/O}$. The increments for carbonyl and hydroxyl are smaller than the van der Waals volumes of these groups, and indicate some degree of complexation to carbon tetrachloride. Only a roughly linear relation is found between $\bar{V}^0$ of alcohols in water and $\bar{V}^0$ in carbon tetrachloride, possibly because of the intrusion of additional effects such as structure-promotion in water.

JOHN T. EDWARD, PATRICK G. FARRELL et FEREIDOON SHAHIDI. Can. J. Chem. **57**, 2585 (1979).

On a déterminé le volume molaire partiel, $\bar{V}^0$, dans le tétrachlorure de carbone à 25°C, de 13 cétones, 18 alcools, et de 17 éthers mono ou polyfonctionnels, tous acycliques. Les résultats sont raisonnablement en accord avec $\bar{V}^0$ calculé à partir des équations développées antérieurement en utilisant les paramètres déjà mentionnés, ainsi que les suivants: des incréments (en mL mol^{-1}) de: 8.72 pour le carbonyle, 6.1 pour l'hydroxyle, 4.4 pour l'oxygène des éthers monofonctionnels, et 5.8 pour l'oxygène des éthers polyfonctionnels; des décréments δ (en mL mol^{-1}) de: -1.68 pour $g_{C-C}^{CO/C}$, -2.22 pour $g_{C-C}^{O/C}$, -0.90 pour $g_{C-C}^{O/O}$, -3.27 pour $g_{O-C}^{C/C}$ et -1.93 pour $g_{O-C}^{C/O}$. Les incréments pour le carbonyle et l'hydroxyle sont plus petits que les volumes de van der Waals de ces groupes et indiquent quelque degré de complexation au carbone du tétrachlorure. On a seulement trouvé une grossière relation linaire entre $\bar{V}^0$ des alcools dans l'eau et $\bar{V}^0$ dans le tétrachlorure de carbone, probablement à cause de l'intrusion d'effets additionnels, telle l'accroissement de structure dans l'eau.

[Traduit par le journal]

Introduction

The partial molal volumes $\bar{V}^0$ of straight- and branched-chain alkanes (1) and alkyl halides (2) in carbon tetrachloride at 25°C may be calculated with reasonable accuracy using the equation

$$[1] \quad \bar{V}^0 = V_c + \sum_1^m n^k I^k + \sum_1^n Z_g{}^l \delta^l$$

where V_c is a covolume of 11.61 mL mol^{-1}, n^k is the number of atoms or groups of type k and I^k is the volume increment associated with this type, Z_g^l is the mol fraction of *gauche* interactions of type l found in the solute molecules (3) and δ^l is the decrement associated with this interaction. In the present paper we test the validity of [1] for 13 aliphatic ketones, 18 alcohols, and 17 ethers, whose $\bar{V}^0$ values we have determined and listed in Tables 1, 4, and 5.

To calculate $\bar{V}^0$, we must first calculate Z_g^l, following the procedure described by Mann (3) for straight- and branched-chain alkanes. For the compounds discussed in this paper, particularly ethers, the calculations become complex, and so are described in some detail.

Calculation of Z_g

Following Flory (4), we adopt the extended, all *anti* (*a*) conformation[2] as the reference state of A—B—C—D. Rotation about the B—C bond can convert this conformation into either of two chiral *gauche* conformations, g^- and g^+:

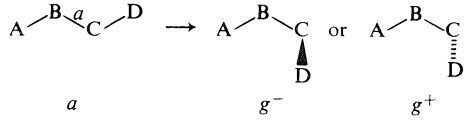

Accompanying the change $a \rightarrow g$ is an enthalpy change $\Delta H_{g(B-C)}^{A/D}$ and a change in partial molal

[1]Present address: Lash Miller Chemical Laboratory, University of Toronto, 80 St. George Street, Toronto, Ont., Canada M5S 1A1.

[2]Flory uses the term *trans* instead of *anti*; our usage is that preferred by most stereochemists (5*a*).

0008-4042/79/192585-08$01.00/0

TABLE 1. Calculated and experimental partial molal volumes $\bar{V}^0$ (in mL mol^{-1}) of ketones in carbon tetrachloride at 25°C

Ketones	$Z_g^{CO/C}$	$Z_g^{C/C}$	$\bar{V}^0_{calcd}$*	$\bar{V}^0_{exptl}$
1 Acetone	0	0	73.6	74.7±0.7
2 2-Butanone	0	0.38	90.0	90.0±0.2
3 2-Pentanone	0.41	0.32	106.8	107.7±0.2
4 3-Pentanone	0	0.66	106.7	106.2±0.2
5 3-Methyl-2-butanone	0	1.13	108.0	108.2±0.6
6 2-Hexanone	0.36	0.65	123.5	122.3±0.8
7 4-Methyl-2-pentanone	1.14	0.20	125.8	125.6±0.6
8 2-Heptanone	0.97	0.82	139.4	140.8±0.6
9 2-Methyl-3-hexanone	0.44	1.28	141.6	140.4±0.3
10 5-Methyl-3-hexanone	1.15	0.52	142.3	141.7±0.2
11 2,2-Dimethyl-3-pentanone	0	2.00	143.1	142.6±0.4
12 2,4-Dimethyl-3-pentanone	0	2.00	143.0	142.9±0.1
13 4,4-Dimethyl-2-pentanone	2.00	0	144.7	144.5±0.5

*Calculated from [1] using parameters of Tables 2 and 6.

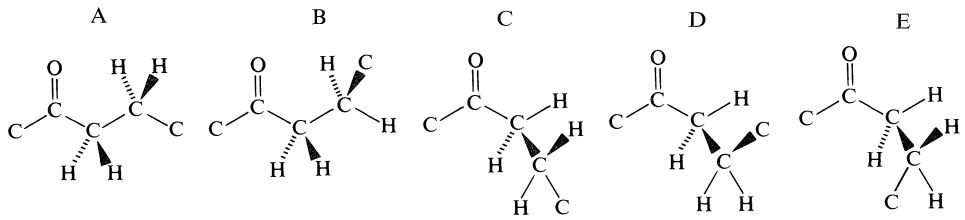

	a a	*a g*$^+$	*g*$^-$*a*	*g*$^-$*g*$^-$	*g*$^-$*g*$^+$
$z_g^{CO/C}_{(C-C)}$	0	1	0	1	1
$z_g^{C/C}_{(C-C)}$	0	0	1	1	1
γ	0.365	0.317	0.221	0.096	~0
$\gamma z_g^{CO/C}_{(C-C)}$	0	0.317	0	0.096	~0
$\gamma z_g^{C/C}_{(C-C)}$	0	0	0.221	0.096	~0

SCHEME 1

volume $\delta^{A/D}_{(B-C)}$: the superscripts and subscripts define completely the nature of the *gauche* arrangement.

As an illustration of the calculation of Z_g^l of a ketone, let us consider 2-pentanone (**3** in Table 1). The stable conformations of ketones are those in which the carbonyl double bond is eclipsed by a neighbouring C—H or C—C bond (5*b*, 6, 7), so that we can write down the five staggered conformations A—E of Scheme 1. Various lines of evidence (6) indicate the *anti–anti* (*aa*) conformation A to be the most stable. The *anti–gauche* (*ag*$^+$) arrangement B should be less stable because of *gauche* interaction between the C(2) (carbonyl) and the C(5) (methyl) carbons, denoted $g^{CO/C}_{C-C}$. The enthalpy difference $\Delta H^{CO/C}_{g(C-C)}$ between *a* and $g^{CO/C}_{C-C}$ is discussed below. (The enantiomeric *ag*$^-$ conformation will have the same enthalpy as *ag*$^+$.) The *g*$^-$*a* conformation C will be less stable than A because of a *gauche* interaction $g^{C/C}_{C-C}$ between the C(1) methyl and the C(4) methylene carbons. The enthalpy difference between C and A will approximate $\Delta H^{C/C}_{g(C-C)}$ between *gauche* and *anti* alkanes (700 cal mol^{-1} (1, 3)). (It may be slightly smaller because of the different geometry of methylene (sp^3) and carbonyl (sp^2) carbons.) Accompanying C is an enantiomeric *g*$^+$*a* conformation. Next, enantiomeric *g*$^-$*g*$^-$ (D) and *g*$^+$*g*$^+$ conformations are possible. As before (1–3) we assume that ΔH of D is given by the sum of $\Delta H^{C/C}_{g(C-C)}$ for each individual *gauche* interaction. This assumption however fails for *g*$^-$*g*$^+$ (E) and *g*$^+$*g*$^-$ arrangements, which are of excessively high enthalpy (1–3) because of the close approach of the terminal methyl groups. Conformations containing such arrangements form a very small proportion of the molecular population and may be ignored.

We estimate the $\Delta H^{CO/C}_{g(C-C)}$ recorded in Table 2 from ΔH (1360 cal mol^{-1}) for the *cis* to *trans* epimerization of 3,5-dimethylcyclohexanone (5*c*, 8), which results in two additional *gauche* interactions (one $g^{C/C}_{C-C}$, one $g^{CO/C}_{C-C}$). This compares with 1700

TABLE 2. Enthalpy (ΔH_g) and volume (δ) effects associated with first-order interactions in acyclic ethers and alcohols

Interaction	ΔH_g (cal mol^{-1})	δ (mL mol^{-1})
$g^{C/C}_{C-C}$	700*	−2.50
$g^{CO/C}_{C-C}$	500	−1.68
$g^{O/C}_{C-C}$	−200†	−2.22
$g^{O/O}_{C-C}$	−430†	−0.90
$g^{C/C}_{O-C}$	900†	−3.27
$g^{C/O}_{O-C}$	~−1500†	−1.93

*From ref. 1.
†From ref. 4.

cal mol^{-1} for the change from equatorial to axial methyl in cyclohexane (5*d*), due to two additional $g^{C/C}_{C-C}$ interactions. Assuming additivity of conformational effects, this indicates ΔH = 850 cal mol^{-1} for $g^{C/C}_{C-C}$ and 500 cal mol^{-1} for $g^{CO/C}_{C-C}$.[3]

Using these ΔH values, the mol fraction γ of the conformations *aa*, ag^+, g^+a, and g^+g^+ may be calculated in the usual way (1–3) (taking account of the different multiplicities of A, B, C, and D). Values of γ are shown in Scheme 1, along with the numbers of *gauche* interactions z^l_g of type *l* in each conformation. The mole fractions of *gauche* conformation of each type are then given by $Z^l_g = \Sigma\gamma\, z^l_g$, and are recorded in Table 1. Also recorded are Z^l_g values for the other twelve ketones, which were calculated in a similar way.

Rotation about the C—O bond of alcohols encounters a three-fold barrier (10, 11), so that in alcohols three kinds of *gauche* arrangements are possible, illustrated in the conformations G, H, and I of 1-butanol:

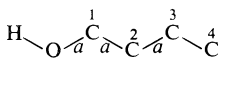

F

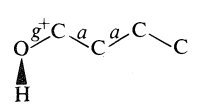

G

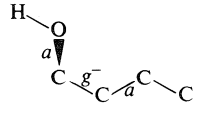

H

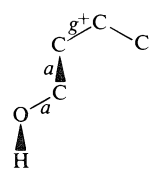

I

For reasons discussed below, we ignore *gauche* arrangements of the type found in G, and consider only those found in H and I. We assume that in alcohols, as in ethers (4), the enthalpy of the $g^{O/C}_{C-C}$ arrangement in H is 200 cal mol^{-1} lower than that of the *anti* arrangement in F (see Table 2). (Probably for similar reasons, the *gauche* form of *n*-propyl fluoride is more stable than the *anti* (5*e*); oxygen and fluorine have similar van der Waals radii (12).)

The superior stability of the *gauche* form in H is possible because attractive and repulsive forces between O---C_3 can be brought into balance by a small increase above 60° in the O—C1/C2—C3 dihedral angle, with only a small increase in torsional strain. This is not possible in isobutyl alcohol in the conformation J; the rotation about C1—C2 to relieve the O---C_3 repulsion would only increase the O---C_4 repulsion (cf. ref. 5*f*), and this conformation with two *gauche* arrangements (O/C3, O/C4) should be less stable than the alternative conformations with only one *gauche* (O/C3 or O/C4) arrangement.[4] The published data for isobutyl chloride (5*f*) show that this "isobutyl effect" results in an increase

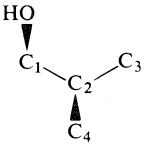

J

of 540 cal mol^{-1} over that calculated from the simple addition of ΔH_g values as prescribed by Mann (3). We have adopted the same value for the isobutyl effect in alcohols, although because of the different dimensions of oxygen and chlorine (5*g*) it is likely to be too high.

Gauche interactions are an example of first-order interactions, the interacting groups A/D being separated by three bonds. Second-order interactions can occur between groups separated by four bonds (4). In alkane sequences g^+g^+ or g^-g^-, second-order interactions are negligible (1, 3), and ΔH for such sequences is approximately $2\Delta H_g$. However, sequences g^+g^- or g^-g^+ (I in Table 3) bring the methyl or methylene carbons intolerably close together (~2.54 Å), so that ΔH for such sequences is very much higher than $2\Delta H_g$; the additional enthalpy ΔH_ω due to the second-order interaction is about 2200 cal mol^{-1} (4). However, the smaller size of oxygen as compared with methyl or methylene causes the second-order interaction II of Table 3 to

[3]The $g^{C/C}_{C-C}$ interactions for axial methyl in cyclohexane are evidently of higher energy than $g^{C/C}_{C-C}$ interactions in flexible chain alkanes, probably because in the latter, but not the former, minor torsional adjustments are possible to reduce torsional strain (9). It is accordingly possible that $\Delta H_g{}^{CO/C}_{(C-C)}$ of 500 cals mol^{-1} is slightly too high for flexible chain molecules. However, this will be compensated to some extent by having $\delta^{CO/C}_{C-C}$ (see below) also slightly too high.

[4]A similar argument applies to cyclohexanol, which is more stable in the equatorial than in the axial conformation (5*d*), in spite of the fact that the latter has two *gauche* O/C arrangements.

TABLE 3. Enthalpy (ΔH_ω) associated with second-order interactions

Interaction	Structure	ΔH_ω (cal mol^{-1})
I $g^{+C/C}_{C-C}\ g^{-C/C}_{C-C}$	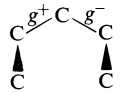	~2200
II $g^{+O/C}_{C-C}\ g^{-C/C}_{C-C}$	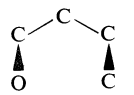	340
III $g^{+C/C}_{O-C}\ g^{-O/C}_{C-C}$	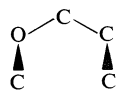	>2200
IV $g^{+C/C}_{C-O}\ g^{-C/C}_{O-C}$	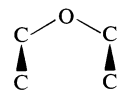	>2200
V $g^{+O/C}_{C-O}\ g^{-C/C}_{O-C}$	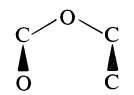	350
VI $g^{+O/O}_{C-C}\ g^{-C/C}_{C-O}$	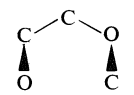	350
VII $g^{+O/C}_{C-C}\ g^{-C/O}_{C-C}$	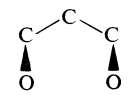	250
VIII $g^{+C/O}_{O-C}\ g^{-O/C}_{C-O}$	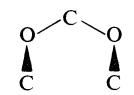	>2200

be no longer prohibitively crowded, so that ΔH_ω is modest. Consequently, such arrangements must be taken into account in calculations of Z_g. The value of ΔH_ω for II shown in Table 3 is taken from Flory (4) (who was considering the conformations of ethers).

The mol fractions $Z^{O/C}_{g(C-C)}$ and $Z^{C/C}_{g(C-C)}$ of the simpler *n*-alkanols were calculated from these ΔH_g and ΔH_ω values by usual methods and are listed in Table 4. Calculations of $Z^{C/C}_{g(C-C)}$ of the *n*-alkanols **3**, **5**, **8**, and **15** showed that it varied with the number n of carbon atoms according to the equation (cf. ref. 1):

$$Z^{C/C}_{g(C-C)} = 0.5 + 0.29(n - 3)$$

and hence this equation was used to obtain $Z^{C/C}_{g(C-C)}$ for **16**, **17**, and **18**, for which computations otherwise would be tedious. For 1-butanol and higher alcohols $Z^{O/C}_{g(C-C)}$ remained constant at 0.72.

Ethers have been shown by extensive investigations (summarized by Flory (4)) also to have a threefold rotational barrier about the C—O bond, and so they also exist in various staggered conformations. Examination of these conformations reveals many more types of *gauche* arrangements ($g^{O/O}_{C-C}$, $g^{C/C}_{O-C}$, $g^{C/O}_{O-C}$) when we consider the various mono- and polyfunctional ethers of Table 5. The mol fractions Z_g of these various types have been calculated using ΔH_g values in Table 2 and ΔH_ω values in Table 3. Four of the ΔH_g values and seven of the ΔH_ω values are from Flory (4); ΔH_ω for the second-order interaction V of Table 3 represents our guess. This is likely to be not grossly in error, because ΔH_ω values have about the expected magnitude when account is taken of (*a*) the van der Waals radius of oxygen, which is smaller than that of methyl or methylene (12), and which accounts in part for the much smaller ΔH_ω of II as compared with I; (*b*) the length of the C—O bond (smaller than C—C) and the size of the C—O—C bond angle (smaller than C—C—C), which accounts for the more severe methyl/methylene interactions in III, IV, and VIII as compared with I; and (*c*) the electrostatic repulsion between oxygen atoms, which causes ΔH_ω of VII to be only slightly smaller than ΔH_ω of II, in spite of much smaller van der Waals repulsions. (Explanation of the first-order effects of Table 2 is less straightforward. The low ΔH_g of $g^{O/O}_{C-C}$ is a manifestation of the "*gauche* effect" (15), and of $g^{C/O}_{O-C}$ of the anomeric effect (16).)

Results and Discussion

Using the values of Z_g listed in Table 1, and increments (Table 6) and decrement $\delta^{C/C}_{C-C}$ (Table 2) already reported (1), the increment I of the carbonyl group (Table 6) and the decrement $\delta^{CO/C}_{C-C}$ (Table 2) were obtained by a least-squares fitting of the experimental data of Table 1 to [1]. It was then possible to calculate $\bar{V}^0$ of the ketones of Table 1 by this equation. Agreement between calculated and experimental values is good considering the various approximations necessary. Thus $\bar{V}^0$ values calculated for the isomeric ketones $C_7H_{14}O$ (**8**–**13** of Table 1) reproduce at least qualitatively the trends in $\bar{V}^0$ found by experiment. Any of the other purely additive schemes in vogue at present ignore conformational as well as more subtle effects (e.g., variation in the volume of primary, secondary, and tertiary hydrogen (1)), and would yield identical values of $\bar{V}^0$ for all six ketones **8**–**13**.

A similar procedure yielded the increments for hydroxyl and ether oxygen (Table 6) and the decrements for the various *gauche* arrangements found in alcohols and ethers (Table 2). An increment of 5.57 mL mol^{-1} for ether oxygen was established by a least-squares fitting of all of the experimental data of Table 5 to [1]. However, the values of $\bar{V}^0$ calculated using this value of I tended to be systematically high for monoethers (compounds **1**–**8** of

TABLE 4. Calculated and experimental partial molal volumes ($\bar{V}^0$, in mL mol^{-1}) of alcohols in carbon tetrachloride at 25°C

Alcohol	$Z_{g(C-C)}^{O/C}$	$Z_{g(C-C)}^{C/C}$	$\bar{V}^0_{calcd}$	$\bar{V}^0_{exptl}$
1 Methanol	—	—	44.6	41.4±0.5[a,b]
2 Ethanol	—	—	61.9	60.2±0.2[c,d]
3 1-Propanol	0.74	—	77.6	77.7±0.1[e]
4 2-Propanol	—	—	81.9	80.1±0.3[f]
5 1-Butanol	0.72	0.34	94.2	94.3±0.3[g]
6 2-Methyl-1-propanol	1.2	—	96.5	96.4±0.1
7 2-Methyl-2-propanol	—	—	101.7	100.1±0.3
8 1-Pentanol	0.72	0.64	110.9	110.9±0.3[h]
9 2-Pentanol	0.86	0.58	113.1	113.1±0.3
10 3-Pentanol	1.30	0.61	112.1	111.9±0.4[i]
11 2-Methyl-1-butanol	1.24	1.11	111.0	111.5±0.3[j]
12 3-Methyl-1-butanol	0.68	1.11	112.2	112.1±0.5[k]
13 3-Methyl-2-butanol	1.30	1.16	113.2	113.2±0.3
14 2,2-Dimethyl-1-propanol	2.0	—	114.6	114.9±0.3
15 1-Hexanol	0.72	0.92	127.5	128.6±0.4
16 1-Heptanol	0.72	1.21	144.1	144.3±0.2[l]
17 1-Octanol	0.72	1.50	160.7	161.9±0.2[m]
18 1-Hexadecanol	0.72	3.82	293.8	292.6[n]

Literature values: [a]45.2 (ref. 13); [b]41.3 (ref. 14); [c]59.9 (ref. 13); [d]59.8 (ref. 14); [e]76.6 (ref. 13); [f]79.1 (ref. 13); [g]95.1 (ref. 13); [h]111.9 (ref. 13); [i]111.5 (ref. 13); [j]109.6 (ref. 13); [k]110.5 (ref. 13); [l]145.1 (ref. 13); [m]163.0 (ref. 13); [n]from ref. 14.

TABLE 5. Partial molal volumes ($\bar{V}^0$, in mL mol^{-1}) of ethers in carbon tetrachloride at 25°C

Ether	$Z_{g(C-C)}^{C/C}$	$Z_{g(C-C)}^{O/C}$	$Z_{g(C-C)}^{O/O}$	$Z_{g(O-C)}^{C/C}$	$Z_{g(O-C)}^{C/O}$	$\bar{V}^0_{calcd}$	$\bar{V}^0_{exptl}$
1 Diethyl ether	—	—	—	0.54	—	102.6*	103.4±0.4
2 Ethyl *n*-propyl ether	—	0.71	—	0.47	—	118.3*	117.9±0.5
3 Methyl *n*-butyl ether	0.34	0.69	—	0.22	—	118.6*	117.0±0.2
4 Methyl *tert*-butyl ether	—	—	—	2.00	—	120.1*	118.4±0.4
5 Ethyl *n*-butyl ether	0.34	0.69	—	0.45	—	135.3*	136.2±0.7
6 Di-*n*-propyl ether	—	0.41	—	0.40	—	136.9*	136.0±0.3
7 Di-isopropyl ether	—	—	—	2.00	—	137.6*	141.5±0.5
8 Di-*n*-butyl ether	0.71	1.34	—	0.42	—	170.4*	169.6±0.9
9 Dimethoxymethane	—	—	—	—	1.86	90.7†	92.4±0.9
10 1,1-Dimethoxyethane	—	—	—	1.02	1.97	107.4†	107.0±0.2
11 1,2-Dimethoxyethane	—	—	0.78	0.55	—	109.4†	110.3±0.9
12 2,2-Dimethoxypropane	—	—	—	2.02	1.98	123.8†	121.5±0.1
13 Diethoxymethane	—	—	—	0.51	1.86	124.0†	125.0±0.2
14 2,2-Diethoxypropane	—	—	—	2.20	2.00	157.9†	159.0±0.2
15 Trimethoxymethane	—	—	—	—	4.00	110.9†	112.0±0.1
16 1,1,2-Trimethoxyethane	—	—	2.00	1.11	2.00	126.7†	126.2±0.2
17 Tetramethoxymethane	—	—	—	—	8.00	128.3†	135.4±0.2

*Using I = 4.40 mL mol^{-1} for ether O.
†Using I = 5.80 mL mol^{-1} for ether O.

Table 5) and systematically low for polyethers (compounds **9**–**17** of Table 5). Consequently we have adopted I = 4.40 mL mol^{-1} for monoethers and I = 5.80 mL mol^{-1} for polyethers (see Table 6).

Results for eighteen alcohols are given in Table 4. $\bar{V}^0$ values for twelve have been reported in the literature,[5] and we have checked eleven of them, with generally fair agreement; $\bar{V}^0$ values for six alcohols are (to our knowledge) reported for the first time. If we ignore the small molecules **1**, **2**, **4**, and **7**, agreement between calculated and experimental $\bar{V}^0$ is astonishingly good, and often within experimental error. Particularly impressive is the agreement for the seven isomeric alcohols $C_5H_{11}OH$ (**8**–**14**).

The agreement between calculated and experimental $\bar{V}^0$ for ethers is considerably poorer. If we scrutinize the series of isomeric ethers $C_5H_{12}O$ (**2**, **3**, and **4** in Table 5), we see that [1] gives values of $\bar{V}^0$ following only roughly the experimental values. The

[5]The values reported by Longsworth (14) are in fact for apparent molal volumes ϕ of the alcohols in very dilute (0.1–0.5 *m*) solution. At this dilution the difference between ϕ and $\bar{V}^0$ is small, as shown by comparison with values in Table 1.

TABLE 6. Van der Waals volumes V_w and increments I (both in mL mol^{-1}) of atoms or groups

Atom or group	V_w*	I_{calcd}†	I	Atom or group	V_w*	I_{calcd}†	I
$-CH_3$	13.67	26.2	26.85‡	—Br	14.4	26.6	19.53§
$>CH_2$	12.23	18.2	17.36‡	>O	3.7	7.2	4.4, 5.8
>CH	6.78	10.1	10.35‡	>C=O	11.70	21.1	8.32
—C—	3.4	3.4	3.4‡	—OH	8.04	16.6	6.1

*From ref. 12.
†From [2].
‡From ref. 1.
§From ref. 2.

same is true for the isomers $C_6H_{14}O$ (**5**, **6**, **7**), $C_4H_{10}O_2$ (**10**, **11**), and $C_5H_{12}O_2$ (**12**, **13**).

Several possible reasons for the less regular behaviour of ethers present themselves. Second-order interactions are of negligible importance for alkyl but not for ether chains. Hence ethers can suffer more extensive folding, which may affect $\bar{V}^0$. The dipole moments of the ether groups may tend to cancel out in some polyethers, so that the interaction with the induced dipole of the solvent may be less for polyethers than monoethers. (This would account fot different I values.) Finally, because there are many different types of *gauche* conformations, the δ values of Table 2 are based on a small number of experimental values for each different type, and become more liable to experimental error.

It accordingly seems possible that [1] may not apply too well to certain classes of polyfunctional compounds. This has already been found true for 1,2-, but not 1,3-dibromoalkanes (2). However, the same defects will be found *a fortiori* in other additive schemes for calculating molecular volumes.

Relation of Increments to van der Waals Volumes

We now consider the relation of the increments I listed in Table 6 for carbonyl, hydroxyl, and ether oxygen to their van der Waals volumes. The loose packing of the roughly spherical molecules of carbon tetrachloride results in a molar volume of the liquid 84% greater than the van der Waals volume V_w at 25°C. This additional volume has been termed *empty volume* (V_e) by Bondi (17). The introduction of one mol of solute into a very large volume of carbon tetrachloride increases the volume by $\bar{V}^0$, part made up by the van der Waals volume V_w of N (Avogadro number) solute molecules, part by an increase in $V_e \equiv Nv_e$ which depends on how closely the solvent molecules pack about N solute molecules; v_e would be expected to be proportional to the area A (12) of the solute molecule, and hence to A of the groups making it up (18). This expectation is fulfilled for methyl, methylene, and methine groups, for which an approximate value of I may be calculated by

$$[2] \quad I_{calc} = V_w + 5.9 \times 10^{-9} A$$

as shown in Table 6.[6] However, the experimental increment I for bromine and ether oxygen (Table 6) is less than I_{calc}, although still greater than V_w. Attractive forces due to dipole-induced dipole effects evidently lead to closer packing of carbon tetrachloride molecules about bromine and oxygen than about alkyl groups, so that V_e and thence I are diminished.

For carbonyl and hydroxyl groups I actually becomes smaller than V_w. Such a decrease is greater than can be accounted for by dipole-induced dipole effects, and points to some degree of complexation of these groups with carbon tetrachloride (19). Such complexation has already been indicated for dinonyl ketone by thermodynamic studies (20), and for a large number of alcohols by a variety of techniques (21–27).

Complexation of the hydroxyl group with the bulky carbon tetrachloride molecule would tend to bias conformations about the O—C bond towards *anti* (e.g., F) and away from *gauche* (e.g., G) arrangements, which was our reason for ignoring possible effects of $g_{O-C}^{H/C}$ (e.g., G) conformations. The smaller values of $\bar{V}^0$ found for the smaller alcohols **1**, **3**, **4**, and **7** of Table 4, in which the proportion of OH to inert hydrocarbon is higher, and which would consequently be more effective in hydrogen-bonding, can be explained by either (*a*) stronger hydrogen-bonding to carbon tetrachloride, or (*b*) stronger self-association by hydrogen-bonding, so that even in the most dilute solutions studied some methanol (**1**), etc., is in the form of dimers. It is noteworthy that

[6]Close agreement between I and I_{calc} cannot be expected, because we have ignored small differences in attractive forces between solvent and CH_3, CH_2, and CH (1). These should affect v_e and hence I.

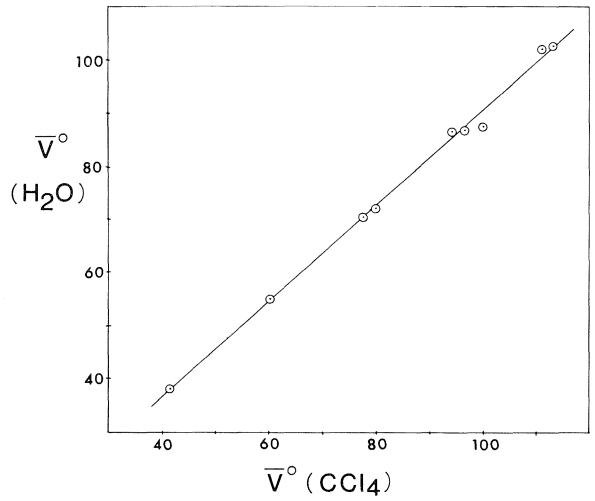

FIG. 1. Relation between the partial molal volumes $\overline{V}^0$ (in mL mol^{-1}) of alcohols **1–9** of Table 4 in carbon tetrachloride and in water. Straight line given by [3].

Duboc's $\overline{V}^0$ for methanol (13), found by fitting excess volumes to a polynomial function of concentration, is close to our calculated value.

Partial Molal Volumes of Alcohols in Water

While our preliminary studies show that [1] is successful with other organic solvents, it seems likely that it will be less successful with water as solvent. This is shown by our studies of $\overline{V}^0$ of alcohols **1–14**[7] in water at 25°C. These $\overline{V}^0$ values prove to be roughly linearly related to $\overline{V}^0$ in carbon tetrachloride, as shown for alcohols **1–9** by the straight line of Fig. 1, which is defined by

[3] $\overline{V}^0(H_2O) = 0.90\ \overline{V}^0(CCl_4)$

The smaller volumes in water may be explained by the greater internal pressure (29) or cohesive energy density (30, 31) of this solvent. However, while [3] serves as a rough guide to correlate $\overline{V}^0$ (H_2O) and $\overline{V}^0$ (CCl_4), its limitations are shown in Fig. 2, in which the data for the seven isomeric alcohols $C_5H_{11}OH$ (**8–14** of Table 4) are plotted on a larger scale. It would seem that factors other than those accommodated in [1] (perhaps solvent structure-making or structure-breaking[8]) obtrude in water.

[7]Values of $\overline{V}^0$ (in mL mol^{-1}) of alcohols **1–14** in water at 25°C were obtained from ref. 28, except for the following, which were determined for this work: **8**, 102.1; **9**, 102.5; **11**, 101.3; **12**, 101.7; **13**, 100.5.

[8]These factors have occasionally been invoked (cf. ref. 32) to explain different $\overline{V}^0$ values of isomeric alcohols in water. It is apparent from the results in this paper that at least a part, probably the major part, of such differences arises from structural (I) and constitutional (Z_g) factors, and that only when these have been accounted for should the residual effects be explained in terms of solvent perturbation.

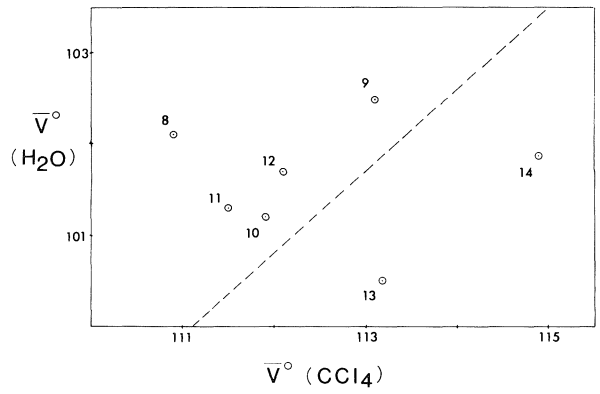

FIG. 2. Relation between partial molal volumes $\overline{V}^0$ (in mL mol^{-1}) of alcohols **8–14** of Table 4 in carbon tetrachloride and in water. Straight line given by [3].

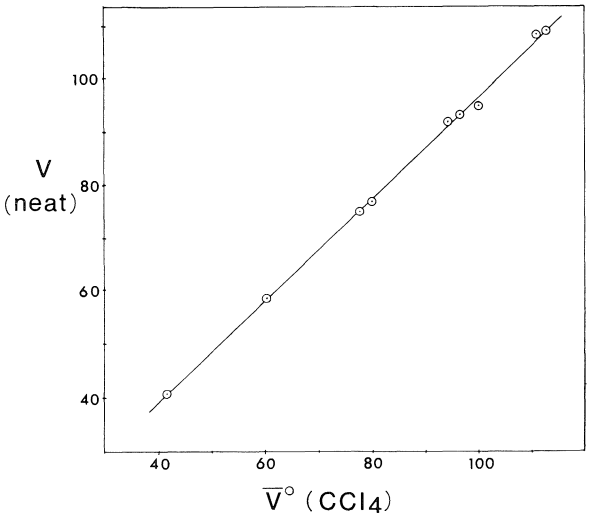

FIG. 3. Relation between molar volumes V of neat alcohols **1–9** (Table 2) and their partial molal volumes $\overline{V}^0$ in carbon tetrachloride, both in mL mol^{-1}. Straight line given by [4].

The same is likely to be true for molar volumes V of the neat alcohols (calculated from data in ref. 33), as shown by deviations from linearity in the plot in Fig. 3. The straight line is defined by

[4] $V = 0.968\ \overline{V}^0(CCl_4)$

the slope being closer to unity because the internal pressures (30–32) of the various alcohols are not so far removed from that of carbon tetrachloride as is the internal pressure of water.[9]

Experimental

Materials

The ketones, alcohols, and ethers were all commercial

[9]The success of Mann's treatment (3) for the neat hydrocarbons probably arises from the fact that all of them have low and comparable internal pressures.

products, for the most part from Aldrich Co. They were distilled before use, and the middle fraction retained for experimental work. Purification of carbon tetrachloride and the procedure for density measurements using a Paar digital precision density meter have been described previously (1). Densities were determined at 8–21 different concentrations, ranging usually from about 0.03 to 0.20 *M*. Plots of the apparent molal volume ϕ_v against concentration were linear, and $\overline{V}^0$ was obtained by extrapolation to zero concentration.[10]

Acknowledgments

We are grateful to the Natural Sciences and Engineering Research Council of Canada for financial support, and the Faculty of Graduate Studies and Research of McGill University for assistance towards the purchase of a precision density meter.

1. J. T. EDWARD, P. G. FARRELL, and F. SHAHIDI. J. Phys. Chem. **82**, 2310 (1978).
2. F. SHAHIDI, P. G. FARRELL, and J. T. EDWARD. J. Phys. Chem. **83**, 419 (1979).
3. G. MANN. Tetrahedron, **23**, 3375 (1967).
4. P. J. FLORY. Statistical mechanics of chain molecules. Interscience, New York. 1964.
5. E. L. ELIEL, N. L. ALLINGER, S. J. ANGYAL, and G. A. MORRISON. Conformational analysis. Interscience, New York. 1965. (*a*) p. 10; (*b*) p. 19; (*c*) p. 114; (*d*) p. 44; (*e*) p. 15; (*f*) p. 17; (*g*) p. 452.
6. G. J. KARABATSOS and D. J. FENOGLIO. Topics in stereochemistry. Vol. 5. *Edited by* E. L. Eliel and N. L. Allinger. Wiley-Interscience, New York, NY. 1970. pp. 167–203.
7. R. J. ABRAHAM and E. BRETSCHNEIDER. Internal rotation in molecules. *Edited by* W. J. Orville-Jones. John Wiley, London. 1974. p. 537.
8. N. L. ALLINGER and L. A. FREIBURG. J. Am. Chem. Soc. **84**, 2201 (1962).
9. N. L. ALLINGER, J. A. HIRSCH, M. A. MILLER, I. J. TYMINSKI, and F. A. VANCATLEDGE. J. Am. Chem. Soc. **90**, 1199 (1968); R. H. BOYD. J. Am. Chem. Soc. **97**, 5353 (1975).
10. M. S. GORDON. J. Am. Chem. Soc. **91**, 3122 (1969).
11. N. L. ALLINGER and D. Y. CHUNG. J. Am. Chem. Soc. **98**, 6798 (1976).
12. A. BONDI. J. Phys. Chem. **68**, 441 (1964).
13. G. DUBOC. Bull. Soc. Chim. Fr. 2260 (1969).
14. L. G. LONGSWORTH. J. Colloid Interface Sci. **22**, 3 (1966).
15. S. WOLFE. Acc. Chem. Res. **5**, 102 (1972).
16. F. A. L. ANET and I. YAVARI. J. Am. Chem. Soc. **99**, 6752 (1977).
17. A. BONDI. J. Phys. Chem. **58**, 929 (1954).
18. J. T. EDWARD and P. G. FARRELL. Can. J. Chem. **53**, 2965 (1975).
19. W. J. JEPSON and J. S. ROWLINSON. J. Chem. Soc. 1278 (1956).
20. E. F. MEYER and F. A. BAIOCCHI. J. Am. Chem. Soc. **99**, 6206 (1977).
21. A. N. FLETCHER. J. Phys. Chem. **73**, 2217 (1969).
22. J. H. SPENCER, J. R. SWEIGART, M. E. BROWN, R. L. BENSING, T. L. HASSINGER, W. KELLY, D. L. HOUSEL, and G. W. REISINGER. J. Phys. Chem. **80**, 811 (1976).
23. T. GRAMSTAD. Acta Chem. Scand. **15**, 1337 (1961).
24. T. GRAMSTAD and W. J. FUGELVIK. Acta Chem. Scand. **16**, 6 (1962).
25. T. GRAMSTAD and O. MUNDHEIM. Spectrochim. Acta, Part A, **28**, 1405 (1972).
26. W. C. DUER and G. L. BERTRAND. J. Am. Chem. Soc. **92**, 2587 (1970).
27. A. N. FLETCHER and C. A. HELLER. J. Phys. Chem. **71**, 3742 (1967).
28. J. T. EDWARD, P. G. FARRELL, and F. SHAHIDI. J. Chem. Soc. Faraday Trans. I, **73**, 705 (1977).
29. A. F. M. BARTON. J. Chem. Educ. **48**, 156 (1971).
30. J. H. HILDEBRAND and R. L. SCOTT. Regular solutions. Prentice-Hall, Inc., Englewood Cliffs, NJ. 1962.
31. M. R. J. DACK. J. Chem. Educ. **51**, 231 (1974).
32. F. FRANKS and H. T. SMITH. Trans. Faraday Soc. **63**, 2586 (1967); **64**, 2962 (1968).
33. J. A. RIDDICK and W. B. BUNGER. Techniques of chemistry. Vol. II. Organic solvents. Wiley-Interscience, NY. 1970. pp. 520–528.

[10]A tabulation of the experimental data (number of determinations, concentration range, slope of plot) is available at nominal charge from the Depository of Unpublished Data, CISTI, National Research Council, Ottawa, Ont., Canada K1A 0R6.

Cyanoethylation of the salts of cyanoguanidine in aprotic solvents

PIOTR ALEKSANDROWICZ, MARIA BUKOWSKA, MIECZYSŁAW MACIEJEWSKI, AND JAN PREJZNER[1]

Institute of Organic Chemistry and Technology, Warsaw Technical University, 75 Koszykowa St., 00-662 Warsaw, Poland

Received March 13, 1979

PIOTR ALEKSANDROWICZ, MARIA BUKOWSKA, MIECZYSŁAW MACIEJEWSKI, and JAN PREJZNER. Can. J. Chem. **57**, 2593 (1979).

The reactions of lithium or sodium salts of cyanoguanidine (**1**) with acrylonitrile in aprotic solvents result in the rapid formation of *N,N*-bis(2-cyanoethyl)-*N'*-cyanoguanidine (**3**) followed by a slower intramolecular cyclization of **3** leading to 4-amino-1-(2-cyanoethyl)-5,6-dihydro-2-pyrimidinylidenecyanamide (**4**). A tentative assignment of the tautomeric forms to the cyclic derivatives of (β-cyanoethyl) cyanoguanidines and the products of their hydrolysis is described.

PIOTR ALEKSANDROWICZ, MARIA BUKOWSKA, MIECZYSŁAW MACIEJEWSKI et JAN PREJZNER. Can. J. Chem. **57**, 2593 (1979).

L'addition de sels de lithium et de sodium de la cyanoguanidine (**1**) sur l'acrylonitrile en milieu non protique conduit à la formation rapide de la *N,N*-bis(cyano-2 ethyl)cyanoguanidine (**3**) qui subit une cyclisation intramoléculaire plus lente pour donner l'amino-4 cyanimino-2-(cyano-2 ethyl)-1 dihydro-5,6 pyrimidine (**4**). Les formes tautomères de dérivés cycliques de (cyano-2 ethyl)cyanoguanidines et de produits de leur hydrolyse sont discutées.

The present investigations have been made in consideration of cyanoguanidine derivatives as monomers to make them available for polyguanamine synthesis (1).

The reaction of cyanoguanidine with acrylonitrile in the presence of strong alkaline bases such as sodium hydroxide was employed to prepare syrups suitable for the impregnation of textiles (2). All our attempts to isolate or identify distinct products of this reaction were unsuccessful; complex reaction mixtures resulted apparently from several competitive and consecutive reactions such as conjugate additions, inter- and intramolecular cyclizations, etc. On the basis of preliminary experiments it appeared to us that the cyanoethylation process should be favored with respect to others by a high concentration of cyanoguanidine anion providing the reaction time was sufficiently short. To confirm this prediction we have carried out the cyanoethylation of lithium and sodium salts of **1** in dipolar aprotic solvents. Cyanoguanidine, a weak acid of $pK_a^{25} = 12$ (3), was converted into its lithium or sodium salt by reaction with lithium or sodium hydride, respectively, in dimethylformamide or dimethyl sulfoxide. Upon rapid addition of an equimolar amount of acrylonitrile an exothermic reaction occurred which subsided after 1–2 min; stirring was continued for another 8–13 min, followed by quenching the reaction with an equimolar amount of an acid. A crude product was proved to consist only, apart from starting material, of the 1:2 adduct **4** of cyanoguanidine (**1**) and acrylonitrile. The same reaction brought about under milder conditions resulted in a main product **3** of the same molecular weight but for which both the melting point and spectra were quite different from those for **4**. On the basis of spectra and chemical behaviour **3** was identified as *N,N*-bis(2-cyanoethyl)-*N'*-cyanoguanidine. The ir spectrum of **3** shows four intense bands in the N—H stretching vibration region. The strong sharp band at 3438 cm^{-1} is likely related to the NH_2 group. If this is so, the strong band at 1660 cm^{-1} which disappears on deuteration will be the NH_2 scissoring band. Two weak absorptions at 2258 and 2249 are due to the C≡N stretching vibration in the cyanoethyl group, although the nature of this splitting is not clear. The strong band at 2174 with a shoulder at 2185 cm^{-1} is undoubtedly due to the stretching vibration of the =N''—CN grouping and may be compared to the similar bands in **1**; similarly, the NCN' and NCN'' asymmetric vibrations may be tentatively assigned to a broad strong band with maxima at 1554 and 1523 cm^{-1} (4). A proper choice of structure **3** among three possible bis(2-cyanoethyl)-cyanoguanidines was confirmed by treatment of **3** with barium hydroxide. The resulting monobarium salt of iminodipropionic acid was converted into monoammonium salt which was identical with the product of the independent synthesis (5).

Before discussing the nmr spectrum of **3**, which is not contradictory with the proposed structure, it seems that the nmr spectra of cyanoguanidine and 5,6-dihydropyrimidine derivatives described in this paper merit some general comment. Unlike the nmr spectra of some 5,6-dihydropyrimidine derivatives (6), so far as we know, those of cyanoguanidines have

[1]To whom all correspondence should be addressed.

0008-4042/79/192593-06$01.00/0

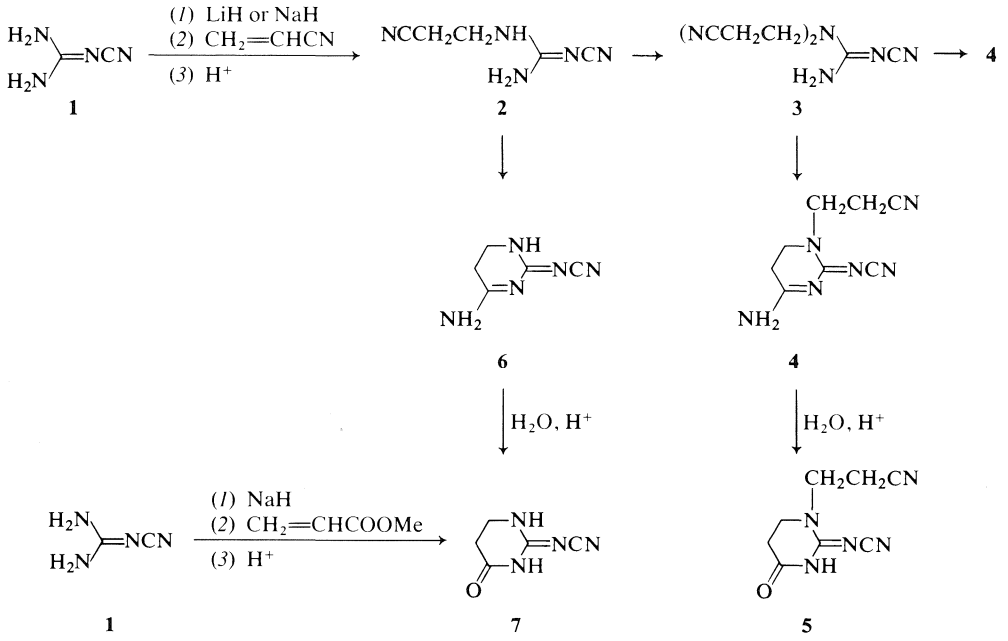

SCHEME 1

not been studied yet. It seems, generally, that for both cyanoguanidines and dihydropyrimidines a N—H proton exchange in aprotic solvents is slow on the nmr time scale, and this is probably due to both low acidity and basicity of these compounds. On the other hand, quadrupolar relaxation appears to be rather efficient, leading to relatively narrow signals of the N—H resonances in these types of compound unless the NH group is adjacent to a carbonyl function, and therefore, in some cases to a splitting of these resonances resulting from coupling to α-carbon protons (7). In the course of another investigation it was found, e.g., that the N—H protons in *N*-(methyloxymethyl)-*N'*-cyanoguanidine in $(CD_3)_2SO$ show a triplet at 7.64 ppm and a singlet at 6.98 ppm which correspond to the —NH— and $—NH_2$ groups, respectively. The N—methylene resonance appears as a doublet resulting from coupling to the NH proton which itself, therefore, constitutes a triplet.[2]

The nmr spectrum of **3** in $(CD_3)_2SO$ reveals a single peak at 7.36 ppm due to two protons of the NH_2 group and pair of triplets at 3.63 and 2.74 ppm due to the CH_2N and CH_2CN groups, respectively, coupled to each other (J = 6.9 Hz).

A close relationship between **3** and **4** was established by the observation that **3** was easily converted to **4** on being heated above its melting point. In the infrared spectrum of **4**, in addition to strong bands at 3403 and 1665 cm^{-1} due to the NH_2 group, the high intensity doublet at 2172 and 2189 cm^{-1} related to the N''—CN grouping, and the medium-weak intensity band at 2255 cm^{-1} due to the aliphatic nitrile, there are several additional strong bands in the region 1300–1600 cm^{-1}. Some of these bands may be assigned to a dihydropyrimidine ring although this assignment must still be regarded as tentative. The above data suggest that **4** is the product of intramolecular cyclization in which the amino and cyano groups are involved. The cyclic product **4** could, in principle, exist in three tautomeric forms, **4***a*–**4***c*, but it appears that its infrared spectrum rules out, at least in the solid state, **4***b* and **4***c* (Scheme 2).

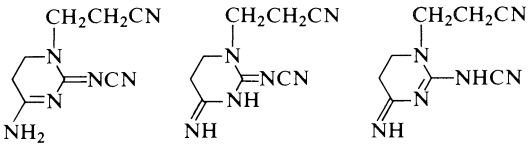

SCHEME 2

In the nmr spectrum of **4** there are two pairs of triplets in the methylene region. Assuming that the cyclization does not affect essentially the chemical shifts of methylenes in the cyanoethyl group in **4** with respect to those in **3** we have assigned the triplets at 3.62 and 2.76 ppm to the CH_2N and CH_2CN groups, respectively, in the cyanoethyl group. Some support for this assignment has been obtained from the observation that the addition of a drop of trifluoroacetic acid does not affect these

[2]M. Bukowska and M. Maciejewski. Unpublished results.

resonances. The other two triplets at 3.42 and ca. 2.5 ppm we have assigned to the CH_2N and $CH_2C{=}$ groups of the 5,6-dihydropyrimidine ring. The fact that these resonances appear as triplets instead of as more complex multiplets due, e.g., to an AA′BB′ system might be perhaps explained on a stereochemical basis as has been done for dihydrouracil (6). In the NH region there are two singlets at 8.05 and 8.34 ppm ($w_{1/2}$ ca. 6 Hz) each integrating for one proton. If **4** had structure **4***b* or **4***c* it would be difficult to explain this relatively high deshielding of an imine proton, for it is known that in somewhat similar structures the imine proton resonances occur at ca. 6 ppm (8, 9). On the other hand, structure **4***a* can be assigned from its nmr spectrum, assuming that the nonequivalence of the two amino protons results from hindered rotation about the C—NH_2 bond owing to its partial double bond character. Both the restricted rotation and the relatively high deshielding of the amino protons can be attributed to a marked contribution of structure **4***a*′ to a resonance hybrid. Nuclear magnetic resonance temperature variation experiments and uv spectra support also the structure of 4-amino-1-(2-cyanoethyl)-2(1*H*)-pyrimidinylidenecyanamide (**4***a*) (*vide infra*).

Several runs performed with variation of molar ratio of reactants, time, and temperature led us to the supposition that (cyanoethyl)cyanoguanidine anion resulting from addition of the guanidine anion to acrylonitrile undergoes addition to another molecule of acrylonitrile, with the formation of the asymmetric derivative **3**, at a rate much higher than that of the first step. The subsequent intramolecular cyclization reaction evidently occurs more slowly than the cyanoethylation reaction under these conditions. Analysis by nmr spectroscopy of samples withdrawn at various reaction times offered some support for this assumption. The nmr spectrum of a sample taken after 3 min (starting with the addition of acrylonitrile at room temperature, molar ratio 1:1) revealed in the NH region, apart from the cyanoguanidine peak, three signals at 6.9, 7.0, and 7.4 ppm which might be attributed to the NH resonances of bis(2-cyanoethyl)- and probably (2-cyanoethyl)cyanoguanidine (**2**) (Scheme 1). The lack of cyclic products in this earlier stage of the reaction was also shown in the methylene region where there were only two multiplets centered at 3.67 and 2.79

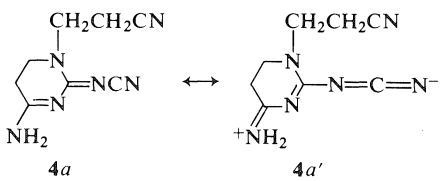

4*a* **4***a*′

SCHEME 3

ppm. On continuing the reaction (7–17 min) the above mentioned NH resonances disappeared and the new ones appeared in the 8 ppm region; also in the methylene region there appeared two pairs of triplets as those in **4**. Longer reaction times (45 min and more) led to substantial changes in both the NH and methylene regions of the nmr spectrum, and gave unidentifiable syrups.

Isolation of cyanoethylation products was generally difficult due to their low solubility in common solvents and to the unstable nature of the cyclic products to hydrolysis (*vide infra*). All our attempts to isolate *N*-(2-cyanoethyl)-*N*′-cyanoguanidine (**2**) failed. In the course of the laborious and tedious process of multiple crystallizations the NH signals of the supposed monocyanoethyl derivative **2** disappeared and new signals in the 8 ppm region appeared. In fact, we have only been able to obtain a very small amount of crystalline product, presumably a side effect of the isolation procedure, assigning to it structure **6**. Microanalysis and mass spectrometric measurement show a molecular composition for **6** consistent with that of a 1:1 adduct of **1** and acrylonitrile. The ir spectrum of **6** displays no band in the aliphatic nitrile region and, therefore, indicates clearly the absence of the cyanoethyl group in the molecule. The strong bands at 3435 and 1666 cm^{-1}, disappearing on deuteration, indicate the presence of the amino group and this suggests that **6**, at least in the solid state, is similar to **4** and exists in the tautomeric form with the amino group at C-4. This excludes from further considerations two of four possible tautomeric forms, and the choice between the other two, the cyanoimino **6***a* and the cyanoamino form **6***b* may also be made tentatively by

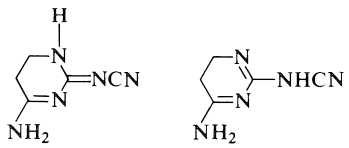

6*a* **6***b*

SCHEME 4

means of its ir spectrum. The former appears to be the more likely, based on the observed low frequency of a high intensity band at 2165 cm^{-1} due to the —NC≡N grouping as compared with an expected higher frequency of the —NHC≡N group, reinforced by a cross-conjugation in **6***b* (10, 11). The uv spectra of **4** and **6** are consistent with structures **4***a* and **6***a* in that a strong absorption at ca. 250 nm may provide evidence for the presence of a conjugated cyanoguanidine chromophore in their molecules. Indicative of a more conjugated system in **4** than in its open-chain precursor **3** is a bathochromic shift

of the wavelength maximum, $\Delta\lambda = 32$ nm, in the ultraviolet spectrum after cyclization.

The nmr spectrum of **6** reveals a pair of triplets at 2.44 and 3.22 ppm which we have assigned to the $CH_2C{=}$ and CH_2N groupings, respectively. The NH protons give rise to three peaks at 8.32 ($w_{1/2}$ ca. 14 Hz), 8.07 ($w_{1/2}$ ca. 14 Hz), and 7.84 ($w_{1/2}$ ca. 7 Hz), each with an area due to one proton. The two lower field peaks are attributable, by analogy to **4**, to two protons of the amino group with hindered rotation due to partial double bond character in structure **6***a*. The different nature of these protons with respect to that at 7.84 ppm can be shown by temperature variation experiment. The two lower field resonances coalesce in $(CD_3)_2SO$ at around 80°C, while the higher field peak may be distinctly seen even at 110°C. Similarly, the NH proton resonances in **4** coalesce at about 80°C. Some ambiguity remains in assignment of the higher field NH peak and, therefore, in the choice between structures **6***a* and **6***b* for this compound in a DMSO solution. First of all, tautomeric structure **6***a* might be expected to reveal coupling between H-1 and H-6, and the lack of splitting of the CH_2N resonance due to this coupling, if not fortuitous, might show evidence for **6***b*. On the other hand, the NHCN proton resonance in **6***b* might be expected to occur at lower field than that experimentally determined. Since, intuitively, chemical resonance in **6***b* does not seem to be sufficiently significant to hinder a rotation of the amino group, we have tentatively assigned structure **6***a* to this compound in the DMSO solution too.

A striking difference between the cyanoethyl derivative of cyanoguanidine **3** and the cyclic products of cyanoethylation, **4** and **6**, can be seen in their hydrolytic behaviour. Compounds **4** and **6** are rapidly converted into the 4-pyrimidinone derivatives, **5** and **7**, respectively, under the influence of dilute mineral acid. In contrast, **3** is quite stable under these conditions. The labile nature of **4** and **6** is likely attributable to a facile protonation of N-3 resulting in some increase of positive charge at C-4. This, consequently, would facilitate the attack of a water molecule at C-4. This suggestion may be somewhat substantiated by the nmr spectrum of **4** in which, upon the addition of a drop of trifluoroacetic acid to its $(CD_3)_2SO$ solution, the NH_2 doublet collapses into a broad singlet and the $CH_2C{=}$ resonance is shifted a little downfield. Both **5** and **7** show a strong carbonyl band at ca. 1730 cm^{-1} which is only slightly shifted towards the lower frequency on deuteration. The relatively high values of the C=O and N—C≡N stretching frequencies in **5** and **7** could be likely attributed to a cross-conjugation between the carbonyl and cyanoguanidine moieties in these compounds. Their uv spectra are consistent with that conclusion. In contrast to **4** and **6** which exhibit only one band at λ_{max} ca. 250 nm due to a conjugation of cyanoguanidine chromophore, **5** and **7** display two bands at λ_{max} ca. 215 and 240 nm.

The cyclic structure of **5** and **7** was also confirmed chemically by the reaction of the sodium salt of **1** with methyl acrylate (12) resulting in a product which was identical with that obtained by acid hydrolysis of **6** (Scheme 1).

The nmr spectrum of **5** exhibits in the methylene region two pairs of triplets integrating for eight protons; these centered at 3.74 ($J = 7.0$ Hz) and 2.67 ppm we have assigned to NCH_2 and CH_2CO of the 5,6-dihydro-4-pyrimidinone ring, respectively, and the other two centered at 3.64 and 2.82 ppm ($J = 6.7$ Hz) to NCH_2 and CH_2CN, respectively, of the cyanoethyl group. A broad band at 10.9 ppm integrating for one proton can be attributed to the N-3 proton adjacent to the C=O and C=NCN groups. This accounts for a marked deshielding of this proton. The nmr spectrum of **7** shows a pair of triplets at 3.42 (3H, $J = 7$ Hz) and ca. 2.5 ppm partly obscured by residual DMSO due to the CH_2N and CH_2CN groups respectively. In the NH region there is a broad featureless resonance at 10.65 and the other at 8.72 ($w_{1/2} = 20$ Hz), each integrating for one proton, assigned to the N-3 and N-1 protons, respectively. Although a tentative choice between the cyanoimimo- and cyanoamino tautomer in favour of the former was based on the ir and uv spectra, some ambiguity persists in that the N-1 proton is more strongly deshielded than might be expected as compared with similar structures, and in the lack of splitting of the NCH_2 resonances due to coupling to this proton.

Experimental

All melting points are uncorrected. Dimethylformamide and dimethyl sulfoxide were dried by refluxing over calcium hydride and distilled *in vacuo* in an argon atmosphere. Acrylonitrile was distilled just before use. Reagent grade cyanoguanidine was used without further purification.

Ultraviolet spectra were measured in water with a Cary Model 118 C spectrophotometer. Infrared spectra were recorded on a Perkin-Elmer Model 577 spectrometer. Proton magnetic resonance spectra were recorded with a JEOL JMN-MH 100 spectrometer in δ values with $(CD_3)_2SO$ as solvent and tetramethylsilane as an internal reference standard. Mass spectra were determined with a LKB-9000 instrument (70 eV, direct inlet system). The elemental analyses were made on an Elemental Analyser Perkin-Elmer CHNO 240.

Preparation of the Lithium Salt of Cyanoguanidine

A solution of 0.1–0.2 mol of **1** in 50 cm^3 of DMSO or DMF was added to a suspension of an equimolar amount of lithium hydride in 50 cm^3 of the same solvent. The mixture was stirred and heated at 50–60°C under argon until no further evolution of hydrogen was observed.

Preparation of the Sodium Salt of Cyanoguanidine

A solution of 0.1–0.2 mol of **1** was added with stirring and cooling to a solution of an equimolar amount of the sodium salt of dimethyl sulfoxide prepared from DMSO and sodium hydride by heating at 70°C in an argon atmosphere. The sodium salt of **1** was prepared prior to use.

4-Amino-1-(2-cyanoethyl)-5,6-dihydro-2(1H)-pyrimidinylidene-cyanamide (4)

A. Acrylonitrile (5.3 g, 0.1 mol) was added rapidly to 50 cm^3 of a DMSO solution of 0.1 mol of the lithium salt of **1** with stirring and water cooling under an argon atmosphere. The temperature rose immediately to 67°C and began rapidly to fall. After 10–15 min the reaction mixture was poured into 150 cm^3 of ice-chilled tetrahydrofuran. The resulting slurry mixture was centrifuged to remove an amorphous precipitate. Tetrahydrofuran and most of the dimethyl sulfoxide were distilled off *in vacuo*. A semisolid residue was triturated with ethanol yielding 6.5 g of crystalline product **4**, mp 226–229°C (yield 68%).

B. Acrylonitrile (10.6 g, 0.2 mol) was added rapidly to 50 cm^3 of a DMSO solution containing 0.1 mol of the sodium salt of **1**. The temperature rose to 86°C. After 10 min the reaction mixture was subject to the same work-up as described in *A*, yielding **4** in 86% yield. Crystallization from water gave an analytical sample of mp 233–234°C; ir (KBr) ν_{max}: 3403 (NH_2), 3340, 3165 (NH), 2255 (C≡N), 2172 and 2189 (N—C≡N), 1665 (NH_2) cm^{-1}; uv λ_{max} (log ε): 255 (4.42); ms *m/e*: 190 (M^+); nmr δ: ca. 2.5 (CH_2C=), 3.42 (t, 2H, J = 7 Hz, ring CH_2N), 2.76 (t, 2H, J = 6.6 Hz, CH_2CN), 3.62 (t, 2H, J = 6.6 Hz, CH_2N), 8.05 (s, $w_{1/2}$ = 6.6 Hz, 1H, NH), 8.34 (s, $w_{1/2}$ = 6.6 Hz, 1H, NH). *Anal.* calcd. for $C_8H_{10}N_6$: C 50.52, H 5.30, N 44.18; found: C 50.85, H 5.45, N 43.59.

N,N-*Bis(2-cyanoethyl)*-N′-*cyanoguanidine (3)*

To a stirred solution of 0.118 mol of the lithium salt of **1** in 100 cm^3 of dimethylformamide at 3°C under argon was added dropwise 12.5 g (0.236 mol) of acrylonitrile in 30 cm^3 of DMF. The reaction mixture was stirred for 1 h at around 3°C, and then poured into 200 cm^3 of chilled tetrahydrofuran with 0.06 mol of sulfuric acid. After centrifuging an amorphous solid and evaporating the solvents *in vacuo*, a semisolid residue was triturated with 100 cm^3 of acetone yielding 18.6 g of **3** (yield 82%). Crystallization from water gave an analytical sample of mp 166–167°C; ir (KBr) ν_{max}: 3438, 3320 (NH_2), 3192, 3164 (NH), 2258, 2249 (C≡N), 2174, 2185 (sh N—C≡N), 1660 (NH_2), 1554, 1523 cm^{-1}; uv λ_{max} (log ε): 223 (4.29) nm; nmr δ: 2.74 (t, 2H, J = 6.9 Hz, CH_2CN), 3.63 (t, 2H, J = 6.9 Hz, CH_2N), 7.36 (s, 2H, NH_2); ms *m/e*: 190 (M^+). *Anal.* calcd. for $C_8H_{10}N_6$: C 50.52, H 5.30, N 44.18; found: C 50.49, H 5.26, N 44.30.

4-Amino-5,6-dihydro-2(1H)-pyrimidinylidenecyanamide (6)

To a stirred solution of 0.08 mol of the salt of **1** in 35 cm^3 of dimethyl sulfoxide was added dropwise 4.27 g (0.08 mol) of acrylonitrile. Throughout the addition the mixture was cooled in a water bath and the temperature did not rise above 30°C. When the exothermic reaction subsided the mixture was removed from the water bath, stirred for 30 min at room temperature, and then poured into a chilled solution of 0.08 mol of sulfuric acid in 80 cm^3 of acetone. A crystalline material was recrystallized from water yielding 3.4 g of **4**. The filtrate was concentrated *in vacuo* yielding a material which was found to be a mixture of **1**, **3**, **4**, and an alleged monocyanoethyl derivative **2** (see the text). The multiple crystallizations from acetone gave, apart from **3** and **4**, a small amount (60 mg) of **6**, mp 250–252°C; ir (KBr) ν_{max}: 3455 (NH_2), 3235, 3145 (NH), 2165, 2170 (sh, N—C≡N), 1666 (NH_2) cm^{-1}; uv λ_{max} (log ε): 253 (4.31) nm; nmr δ: ca. 2.44 (CH_2C=), 3.22 (t, 2H, J = 7 Hz, CH_2N), 7.84 (s, $w_{1/2}$ = 9 Hz, 1H, NH), 8 07 (s, $w_{1/2}$ = 14 Hz, 1H, NH), 8.32 (s, $w_{1/2}$ = 14 Hz, 1H, NH); ms *m/e*: 137 (M^+). *Anal.* calcd. for $C_5H_7N_5$: C 43.79, H 5.14, N 51.07; found: C 43.56, H 5.17, N 50.77.

Conversion of 3 into 4

One hundred milligrams of **3** was heated above its melting point. After several seconds the liquid substance began to resolidify yielding 100 mg of a crystalline product which was proved to be identical with **4**.

Hydrolysis of 3 with Barium Hydroxide

A mixture of 0.58 g (0.003 mol) of **3** and 3 g of barium hydroxide octahydrate in 20 cm^3 of water was heated under reflux until the evolution of ammonia ceased. The mixture was saturated with carbon dioxide and the precipitate was filtered off. The filtrate was evaporated *in vacuo* to dryness. The resulting monobarium salt was dissolved in a small amount of water and treated with an equivalent amount of ammonium sulfate. After filtering off barium sulfate the filtrate was concentrated and diluted with methanol. The precipitate was recrystallized twice from aqueous methanol yielding a crystalline product, mp 178–179°C, which was proved to be identical with the ammonium salt of β,β′-iminobispropionic acid obtained by alkaline hydrolysis of β,β′-iminobispropanenitrile.

Hydrolysis of 6

An equivalent amount of hydrochloric acid was added dropwise, as it was consumed, to a stirred suspension of 0.027 g (2×10^{-4} mol) of **6** in 3 cm^3 of water at 40°C. The addition was continued until a slight excess of hydrochloric acid was present. The colorless crystals were filtered off and washed with water yielding 0.024 g of tetrahydro-4-oxo-2(1*H*)-pyrimidinylidenecyanamide (**7**), mp 273–274°C; ir (KBr) ν_{max}: 3200, 3095, 3060 (NH), 2200, 2185 (sh, N—C≡N), 1725 (C=O) cm^{-1}; uv λ_{max} (log ε): 216 (4.22), 239 (4.17) nm; nmr δ: ca. 2.5 (CH_2CO), 3.42 (t, 2H, J = 7 Hz, CH_2N), 8.72 (s, $w_{1/2}$ ca. 20 Hz, 1H, NH), 10.65 (br s, 1H, NHCO); ms *m/e*: 138 (M^+). *Anal.* calcd. for $C_5H_6N_4O$: C 43.48, H 4.38, N 40.56; found: C 43.28, H 4.65, N 40.46.

Hydrolysis of 4

Compound **4** (0.19 g) was hydrolysed in a similar way to that described above for **6** yielding 0.17 g of 1-(2-cyanoethyl)-tetrahydro-4-oxo-2(1*H*)-pyrimidinylidenecyanamide (**5**), mp 148–149°C; ir (KBr) ν_{max}: 3175 (NH), 2256 (C≡N), 2196 (N—C≡N), 1731 (C=O) cm^{-1}; uv λ_{max} (log ε): 218 (4.16), 244(4.17) nm; nmr δ: 2.67 (t, 2H, J = 6.6 Hz, CH_2CO), 3.74 (t, 2H, J = 6.6 Hz, CH_2N ring), 2.82 (t, 2H, J = 6.7 Hz, CH_2CN), 3.64 (t, 2H, J = 6.7 Hz, CH_2N), 10.92 (br s, 1H, NH); ms *m/e* 191 (M^+). *Anal.* calcd. for $C_8H_9N_5O$: C 50.26, H 4.75, N 36.63; found: C 50.31, H 4.71, N 36.44.

1. T. SEO, T. KAKURAI, and T. NOGUCHI. Kobunshi Ronbunshu, Engl. Ed. **31**, 401 (1974).

2. J. HECHENBLEIKNER. U.S. Patent No. 2,489,181 (1949); Chem. Abstr. **44**, 1750a (1950).
3. N. KAMEYAMA. Kogyo Kagaku Zasshi (J. Chem. Soc. Jpn., Ind. Chem. Sect.), **24**, 1263 (1921).
4. W. J. JONES and W. J. ORVILLE-THOMAS. Trans. Faraday Soc. **55**, 193 (1959).
5. J. H. FORD. J. Am. Chem. Soc. **67**, 876 (1945).
6. H. CHABRE, D. GAGNAIRE, and C. NOFRE. Bull. Soc. Chim. Fr. 108 (1966).
7. F. A. BOVEY. NMR spectroscopy. Academic Press, New York. 1969. p. 237.
8. W. WIERENGA and J. A. WOLTERSOM. J. Org. Chem. **43**, 529 (1978).
9. H. MAEHR, J. SMALLHEER, and V. TOOME. J. Heterocycl. Chem. **14**, 687 (1977).
10. N. B. COLTHUP, L. H. DALY, and S. E. WIBERLEY. Introduction to infrared and Raman spectroscopy. Intern. ed. Academic Press, New York and London. 1964. p. 204.
11. G. R. REVANKAR, R. K. ROBINS, and R. L. TOLMAN. J. Org. Chem. **39**, 1256 (1974).
12. K. SUGINO, R. KITAWAKI, and M. AKITANI. Jpn. Patent No. 7,033,897 (1970); Chem. Abstr. **74**, 88031x (1971).

Characterization of autohydrolysis aspen (*P. tremuloides*) lignins. Part 2. Alkaline nitrobenzene oxidation studies of extracted autohydrolysis lignin

MORRIS WAYMAN AND MIRANDA G. S. CHUA

Department of Chemical Engineering and Applied Chemistry, University of Toronto, Toronto, Ont., Canada M5S 1A4

Received February 19, 1979

MORRIS WAYMAN and MIRANDA G. S. CHUA. Can. J. Chem. **57**, 2599 (1979).

Alkaline nitrobenzene oxidation of the lignins extracted from extractive-free aspen wood meal after autohydrolysis at 195°C for periods varying from 5 min to 2 h indicated that these lignins were structurally more condensed in terms of an increase in new carbon–carbon bonds than aspen milled wood lignin. The degree of condensation generally increased with longer autohydrolysis times. It is postulated that condensation involved materials from both the carbohydrate and lignin components of the wood which were generated during the autohydrolysis. The molar ratio of syringaldehyde to vanillin of extracted lignin on oxidation was observed to decrease with increasing autohydrolysis time. It is suggested that syringyl units are preferentially extracted as low molecular weight material.

MORRIS WAYMAN et MIRANDA G. S. CHUA. Can. J. Chem. **57**, 2599 (1979).

L'oxydation par le nitrobenzène alcalin de lignines extraites de sciures de bois de tremble sans principes extractifs et soumises à une autohydrolyse à 195°C pour des périodes allant de 5 min à 2 h indiquent que ces lignines sont, du point de vue structural, plus condensées en termes d'une augmentation de nouvelles liaisons carbone–carbone que la lignine de bois de tremble broyé. Le degré de condensation augmente généralement en fonction des temps d'autohydrolyse. On suppose que la condensation implique des substances provenant autant de la portion carbohydrate que de la lignine qui est générée au cours de l'autohydrolyse. On a observé que les rapports molaires de syringaldéhyde à vanilline obtenus par oxydation des lignines extraites diminuent lorsque le temps d'autohydrolyse augmente. On suggère que les unités syringyles sont extraites d'une façon préférentielle sous forme de substances de bas poids moléculaires.

[Traduit par le journal]

Introduction

Alkaline nitrobenzene oxidation of wood and of extracted lignin has been widely used for characterizing protolignin, as well as for studying the effects of isolation procedures on the structure of lignin (1–3). The composition and quantity of the aromatic aldehydes obtained reflect the structural features of the side chain and the extent of carbon–carbon linkages present in the lignin (4). Studies of model compounds (5–7) have indicated that lignin structures which are condensed gave lower aromatic aldehyde yields. In this alkaline nitrobenzene oxidation study of the lignins extracted from aspen wood meal after autohydrolysis at 195°C for periods varying from 5 min to 2 h, a decrease in aromatic aldehyde yield is attributed mainly to condensation reactions and only to a minor extent to modification of the side chain of the lignin. Condensation also adequately explains the changes in the chemical composition and molecular weight distribution of the extracted lignins (8). Kratzl and co-workers (9–11) showed that even after only a short pretreatment with water at elevated temperature and pressure, the total aldehyde yield from wood on alkaline nitrobenzene oxidation was considerably decreased, which has been attributed to condensation.

Results

Alkaline nitrobenzene oxidation of aspen milled wood lignin (MWL) and extracted lignin (XL) was modified in the determination of vanillin and syringaldehyde according to the procedure of Stone and Blundell (12) i.e., by simultaneous spectrophotometric analysis (13). The reproducibility of the yields of vanillin and syringaldehyde by the modified procedure is shown in Table 1. The autohydrolysis XL have lower yields of vanillin and syringaldehyde than MWL, the reference protolignin, except for XL-5 which has a slightly higher syringaldehyde yield. This apparent increase in syringaldehyde for XL-5 can probably be attributed to a lower value of uncondensed syringyl units determined for MWL than originally present in wood. After 40 min of autohydrolysis, the vanillin yield remained constant but the syringaldehyde yield fluctuated $\pm 12\%$ of that of XL-40.

As shown in Table 2, at longer autohydrolysis times, the decrease in aromatic aldehyde yield was small,

0008-4042/79/192599-04$01.00/0

TABLE 1. Reproducibility of the modified method for alkaline nitrobenzene oxidation

Sample	% Vanillin (V)* (1)	(2)	(3)	Average	% Variation
MWL	6.210	6.162	6.084	6.152	+0.9 to −1.1
XL-5	4.056	4.069	4.282	4.136	+3.5 to −2.1
XL-10	4.016	3.972	3.898	3.962	+1.4 to −1.6
XL-20	3.129	3.092	3.015	3.079	+1.6 to −2.1
XL-30	2.730	2.671	2.615	2.672	+2.1 to −2.1
XL-40	1.553	1.547	1.533	1.544	+0.6 to −0.7
XL-60	1.461	1.515	1.601	1.526	+4.9 to −4.2
XL-90	1.553	1.574	1.580	1.569	+0.7 to −1.0
XL-120	1.586	1.501	1.640	1.576	+4.1 to −4.8
Sample	% Syringaldehyde (S)* (1)	(2)	(3)	Average	% Variation
MWL	9.602	9.844	9.783	9.743	+1.0 to −1.4
XL-5	10.259	10.276	10.113	10.216	+0.5 to −1.0
XL-10	7.841	7.604	8.036	7.827	+2.6 to −2.9
XL-20	5.280	5.010	5.093	5.128	+3.0 to −2.3
XL-30	4.396	4.318	4.153	4.289	+2.5 to −3.2
XL-40	2.025	2.126	2.225	2.125	+4.7 to −4.7
XL-60	1.954	1.968	2.045	1.989	+2.8 to −1.8
XL-90	2.570	2.356	2.438	2.455	+4.7 to −4.0
XL-120	2.341	2.311	2.334	2.329	+0.5 to −0.8

*% yield by weight, based on lignin on a carbohydrate-free basis.

TABLE 2. Total yield and molar ratio of vanillin and syringaldehyde

Sample	Total (V + S)*	Molar ratio S/V
MWL	15.89	1.32
XL-5	14.36	2.07
XL-10	11.79	1.65
XL-20	8.21	1.39
XL-30	6.96	1.34
XL-40	3.67	1.16
XL-60	3.52	1.08
XL-90	4.02	1.31
XL-120	3.91	1.23

*% yield by weight, based on lignin on a carbohydrate-free basis.

and after going through a minimum at about 60 min, the S/V ratio increased to that of MWL.

Discussion

The observed marked decreasing yield of aromatic aldehyde from the XL with increasing autohydrolysis time is attributed mainly to condensation reactions involving the formation of new carbon–carbon bonds, resulting in a lignin structure which is much less amenable to oxidation to phenolic aldehydes. Chang and Allen (4) have suggested that the yields and nature of the oxidation products may be determined by the structural features of the aliphatic side chains. This possibility may contribute to the observed decreased yields of aromatic aldehydes, but it is difficult to relate it to the syringyaldehyde to vanillin molar ratio trends and molecular weight distribution patterns (8).

A lower yield of aromatic aldehyde can also be partly attributed to physical or chemical incorporation of non-lignin materials such as carbohydrate degradation products. It is highly probable that these reaction intermediates, namely furfural and its precursors, participate in the lignin condensation reactions (14), resulting in the formation of new carbon–carbon bonds, thereby contributing to the condensed nature of XL.

The methoxyl content of MWL was 21.54%, 1.47 MeO/C_9 unit, which represents a syringyl-to-guaiacyl ratio, taking into account both condensed and uncondensed units, of 1:1. The S/V ratio found after oxidation, 1.32:1, indicates more uncondensed syringyl than guaiacyl, and conversely preferential condensation of guaiacyl units in the protolignin.

Our explanation for the variation in S/V ratio for XL is depicted in Scheme 1. The observed high S/V ratio after 5 min of autohydrolysis is due to preferential condensation of guaiacyl units and preferential extraction of syringyl units during autohydrolysis. From studies of the reactivity of the aromatic sites in lignin (15–17), it has been established that acid-catalyzed condensation reactions proceed most rapid-

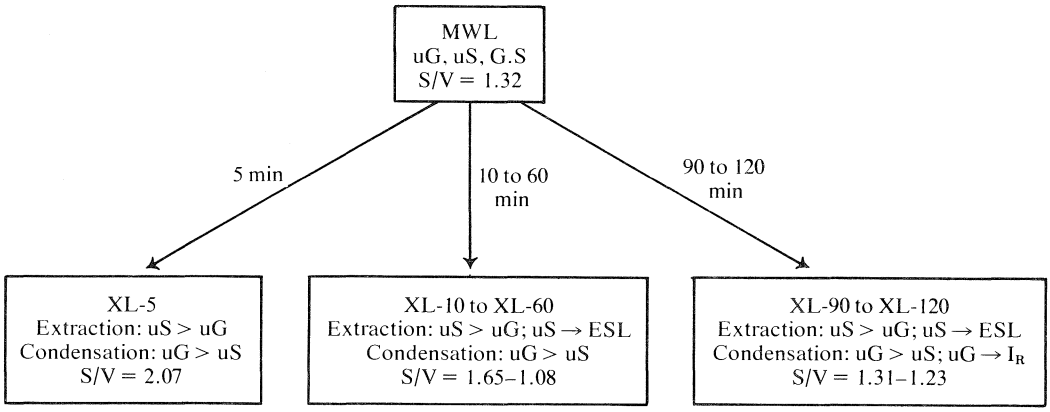

SCHEME 1. Explanation of variation of S/V ratio with autohydrolysis time; uG = uncondensed guaiacyl; uS = uncondensed syringyl; G.S = condensed guaiacyl/syringyl; S/V = molar ratio of syringaldehyde-to-vanillin; ESL = ether-soluble extracted lignin; I_R = reactive intermediate.

ly at the C-6 position (structures **1**, **2**, and **3**). The syringyl unit because of the additional methoxyl group at the C-5 position would represent a configuration sterically hindered to condensation at C-6. This would also account for the preferential extraction of syringyl units during lignin fragmentation. Stone (18) and Marth (19) in their alkaline nitrobenzene oxidation studies of the spent sulphite pulping liquors and pulps of aspens found that the ratio of syringaldehyde-to-vanillin in the liquor continually increased during the heating, whereas the syringaldehyde-to-vanillin ratio of the pulp decreased. These results support the suggestion that syringyl-containing units of lignin are more easily extracted. The observed decrease in syringyl units for XL-10 to XL-60 may be attributed to the removal of syringyl units into the ether-soluble fraction during purification of the lignin, which is supported by the high methoxyl content of 23.1% found for this fraction.

After 60 min of autohydrolysis the S/V ratio increased. At this stage of autohydrolysis, lignin and non-lignin degradation products, termed reactive intermediates, are becoming prominent. These reactive intermediates are postulated to be Hibbert ketones (20), *p*-hydroxybenzoic acids (21, 22), syringic acid (23), vanillic acid (23), and furfural, hydroxymethyl furfural, and their precursors (14). From molecular weight distribution studies (8), XL-90 and XL-120 are essentially low molecular weight materials but are highly condensed in the sense of having high proportions of carbon–carbon bonds, as indicated by the very low aromatic aldehyde yield on alkaline nitrobenzene oxidation. An explanation for the increase in S/V ratio is that remaining uncondensed guaiacyl can react with the reactive intermediates resulting in new carbon–carbon bonds and consequently contributing to the increase in S/V ratio.

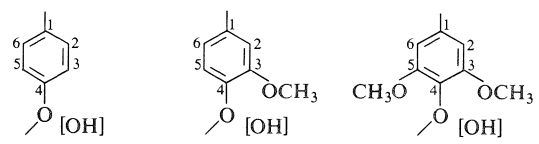

p-Hydroxybenzyl unit **1** Guaiacyl unit **2** Syringyl unit **3**

Experimental

Preparation of Autohydrolysis Extracted Lignin (XL)

For details refer to ref. 8. Extractive-free aspen wood meal was autohydrolysed at 195°C for periods varying from 5 min to 2 h. The lignocellulosic residue was then extracted with 90% dioxane at 70°C and the extracted lignin purified and recovered by precipitation into ether, followed by subsequent washings with benzene and petroleum ether.

Alkaline Nitrobenzene Oxidation of Autohydrolysis Extracted Lignin

The modified procedure is described in detail in ref. 13. It consisted essentially of subjecting the extracted lignin to alkaline nitrobenzene oxidation at 180°C for 2 h, recovering the oxidation products by paper chromatography, and determining the vanillin and syringaldehyde contents by simultaneous spectrophotometric analysis.

Acknowledgements

The authors wish to thank the National Research Council of Canada for both the award of an NRCC postgraduate scholarship to one of them (M.G.S.C.) and for a research grant which supported this investigation. The authors also wish to thank Mr. J. H. Lora for the sample of milled wood lignin used in this work, and for helpful discussion of the results.

1. A. KLEMOLA and G. A. NYMAN. Suom. Kemistil. B, **38**, 92 (1965).
2. J. M. PEPPER and M. SIDDIQUELLAH. Can. J. Chem. **39**, 1454 (1961).

3. I. A. PEARL. For. Prod. J. **14**, 435 (1964).
4. H. M. CHANG and G. G. ALLAN. *In* Lignins. *Edited by* K. V. Sarkanen and C. H. Ludwig. Wiley Interscience, NY. 1971. pp. 433–444.
5. B. LEOPOLD. Acta Chem. Scand. **4**, 1523 (1950).
6. B. LEOPOLD. Sven. Kem. Tidskr. **64**, 18 (1952).
7. B. LEOPOLD and I. L. MALMSTROM. Acta Chem. Scand. **5**, 936 (1951).
8. M. G. S. CHUA and M. WAYMAN. Can. J. Chem. **57**, 1141 (1979).
9. K. KRATZL. Pap. Puu, **43**, 643 (1961).
10. K. KRATZL, K. BUCHTELA, J. GRATZL, J. ZAUNER, and O. ETTINGSHAUSEN. Tappi, **45**, 113 (1962).
11. K. KRATZL and H. SILBERNAGEL. Monatsh. Chem. **83**, 1022 (1952).
12. J. E. STONE and M. J. BLUNDELL. Anal. Chem. **23**, 771 (1951).
13. M. G. S. CHUA and M. WAYMAN. Tappi, **62** (3), 103 (1979).
14. A. KLEMOLA and G. A. NYMAN. Pap. Puu, **48**, 595 (1966).
15. K. V. SARKANEN, B. ERICSSON, and J. SUZUKI. Tappi, **50**, 572 (1967).
16. K. V. SARKANEN and C. W. DENCE. J. Org. Chem. **25**, T15 (1960).
17. B. ERICSSON; B. NIST, and K. V. SARKANEN. Chim. Biochim. Lignine, Cellulose, Hemicelluloses. Actes Symp. Intern., Grenoble, France. 1964. p. 59.
18. J. E. STONE. Tappi, **38**, 610 (1955).
19. D. E. MARTH. Tappi, **42**, 301 (1959).
20. A. KLEMOLA. Suom. Kemistil. B, **41**, 83 (1968).
21. I. PEARL and D. BEYER. Tappi, **40**, 45 (1957).
22. D. C. C. SMITH. J. Chem. Soc. 2347 (1955).
23. D. A. STANEK. Tappi, **41**, 601 (1958).

Characterization of autohydrolysis aspen (*P. tremuloides*) lignins. Part 3. Infrared and ultraviolet studies of extracted autohydrolysis lignin

MIRANDA G. S. CHUA AND MORRIS WAYMAN

Department of Chemical Engineering and Applied Chemistry, University of Toronto, Toronto, Ont., Canada M5S 1A4

Received February 19, 1979

MIRANDA G. S. CHUA and MORRIS WAYMAN. Can. J. Chem. **57**, 2603 (1979).

Infrared and ultraviolet studies of the lignins extracted from extractive-free aspen wood meal after autohydrolysis at 195°C for periods varying from 5 min to 2 h indicated that these lignins were functionally modified and different from aspen milled wood lignin. The extracted lignins changed from a guaiacyl–syringyl type lignin to a syringyl-deficient type lignin with increasing autohydrolysis time. Extracted lignins were also observed to contain unconjugated β-ketone groups and conjugated carboxylic acid groups. It is proposed that the unconjugated β-ketone groups resulted from the depolymerization reactions of the lignin macromolecule under acidic conditions which formed monomeric, dimeric, and oligomeric/polymeric lignin fragments with Hibbert's ketone side chains. The conjugated carboxylic acid group observed to be present was attributed to *p*-hydroxybenzoic acid. *p*-Hydroxybenzoic acid has been postulated as contributing to the extractability of aspen lignin by acting as a blocking agent in the repolymerization of lignin fragments to form insoluble lignin.

MIRANDA G. S. CHUA et MORRIS WAYMAN. Can. J. Chem. **57**, 2603 (1979).

Des études infrarouge et ultraviolette de lignines extraites de sciures de bois de tremble sans principes extractifs et soumises à une autohydrolyse à 195°C pour des périodes allant de 5 min à 2 h indiquent que ces lignines sont modifiées du point de vue fonctionnel et sont différentes de la lignine de bois de tremble broyé. Si l'autohydrolyse se prolonge, les lignines extraites changent d'un type guaiacyl–syringyle à un type déficient en syringyle. On a aussi observé que les lignines extraites contiennent des groupes β-cétoniques qui ne sont pas conjugués et des groupes carboxyliques conjugués. On suggère que les groupes β-cétoniques qui ne sont pas conjugués proviennent de réactions de dépolymérisation de la macromolécule de lignines sous l'influence des conditions acides qui forment des fragments de lignines monomères, dimères et oligomère/polymère avec des chaînes latérales cétoniques de Hibbert. On attribue le groupe acide carboxylique conjugué observé à la présence d'acide *p*-hydroxybenzoique. On suppose que l'acide *p*-hydroxybenzoique contribue à la facilité d'extraction de la lignine de tremble en agissant comme agent qui bloque la repolymérisation des fragments de lignine conduisant à de la lignine sous forme insoluble.

[Traduit par le journal]

Introduction

During autohydrolysis (steaming) of wood, the reactions that occur in the lignin fraction, as well as in the hemicellulose and cellulose components of wood, are a result of the prevailing acidic condition and the high temperature. In many respects, the effects of autohydrolysis on the lignin fraction are similar to those obtained on acidolysis (1–3) and ethanolysis (4–8). As reported in an earlier paper (9), the changes in elemental composition and decrease in methoxyl content of the lignin extracted from extractive-free aspen wood meal autohydrolysed at 195°C for periods varying from 5 min to 2 h were similar to those observed for aspen lignin on acidolysis. Alkaline nitrobenzene oxidation studies suggested that the extracted autohydrolysis lignins were condensed in structure which was in accordance with the molecular weight changes observed for extracted lignin (9). Acidolysis lignin has also been found to have undergone condensation (10, 11). Lundquist in a comprehensive study of acidolysis (12–18) using spruce and birch Bjorkman milled wood lignins and model compounds has, by identifying the reaction products of the acid-catalyzed degradation, proposed cleavage mechanisms which have proved useful in the elucidation of the structure of lignin. Autohydrolysis at elevated temperatures, although lower in acidity (pH of liquor approximately 3.0), is more drastic in terms of cleavage of lignin–lignin and lignin–carbohydrate bonds than mild acidolysis due to the higher temperatures involved. In addition, in autohydrolysis, the depolymerized lignin fragments remain in the proximity of condensation sites in the wood matrix, and are more liable to recondense than in acidolysis, where degradation products go into solution. Klemola (19) obtained only the more stable Hibbert ketones in the degradation products on steam hydrolysis of birch at 185°C for 2 h. Nimz (20, 21) on mild hydrolysis of finely powdered wood with percolating water at 100°C succeeded in

0008-4042/79/192603-09$01.00/0

TABLE 1. Assignment of infrared absorption bands in the region 800 cm^{-1} to 2000 cm^{-1} for aspen milled wood lignin (MWL) and for extracted autohydrolysis lignins (XL)

MWL (cm^{-1})	XL (cm^{-1})	Overall trend in XL	Comment
845	845	Decreases	Aromatic C—H out-of-plane deformation, attributed to the presence of 1,2,3,5-tetrasubstituted aromatic rings, i.e., uncondensed syringyl units
920	915	Increases	Aromatic C—H out-of-plane deformation of syringyl units
1035	1035	Decreases	Aromatic C—H in-plane deformation, assigned as characteristic of uncondensed guaiacyl units
1128	1125–1115	Decreases	Aromatic C—H in-plane deformation, attributed to contribution from both guaiacyl and syringyl units
1225	1215	Constant (Variation ±10%)	Ring breathing with C—O stretching in syringyl and guaiacyl units
1270	1270	Decreases	Ring breathing with C—O stretching in uncondensed guaiacyl units
1325	1325	Decreases	Ring breathing with C—O stretching in syringyl unit
1420	1425	Decreases	Aromatic skeletal vibrations. Strongly coupled by C—H in-plane deformation and sensitive to the nature of ring substituents
1460	1460	Decreases	Asymmetric C—H deformation in methyl and methylene groups, apparently considerably affected by methoxyl groups
1505	1510	Constant	Aromatic skeletal vibrations. Found to have minimal intensity variation with structure, therefore used as internal standard
1590	1595–1605	Decreases	Aromatic skeletal vibrations. Affected by aromatic C—O stretching mode and by conjugation with α-carbonyl groups
1670	—	—	Stretching of conjugated aryl carbonyl, i.e., aryl—C(=O^{α})—C—, aryl—C=C—C(=O)—
1720	1710–1705	Increases	Carbonyl stretching of unconjugated β-ketone, i.e., aryl—C—C(=O^{β})—C— and conjugated acids/esters, i.e., aryl—C(=O^{α})—O— in the lignin unit
1735	—	—	Attributed to unconjugated acids/esters, i.e., aryl—C—C(=O^{β})—O—

hydrolysing specifically the more labile benzyl ether linkages, and reduced recondensation reactions and rearrangements in the aliphatic side chain.

The purpose of these infrared and ultraviolet studies of the extracted autohydrolysis lignin was to follow the changes in functional groups taking place during the acid-catalyzed degradation of lignin. Thus, together with the results obtained from the earlier studies and also supplemented by the findings of the above-mentioned researchers, insight can be gained into the mechanisms involved in lignin reactions during autohydrolysis.

Results

Infrared Spectra of Aspen Milled Wood Lignin (MWL) and Extracted Lignin (XL)

The positions and assignments for the infrared absorption bands for aspen MWL and XL are tabulated in Table 1. The assignments in Table 1 follow essentially those summarized by Hergert (22, 23) supplemented by the work of Sarkanen and Chang (24–26).

Comparing the spectra of XL with MWL as shown in Fig. 1, significant differences are observed. The spectra of MWL indicated absorption at 1720 cm^{-1} with a shoulder at 1735 cm^{-1} attributed to unconjugated acids/esters and a band at 1670 cm^{-1} due to α-carbonyl groups.

In XL, a sharp increase in the 1705–1710 cm^{-1} band with increasing autohydrolysis time is observed, which because of its broadness (1650–1720 cm^{-1}) may indicate some absorption at 1670 cm^{-1}. The 1705–1720 cm^{-1} band may be attributed to unconjugated ketone carbonyl groups and conjugated acids/esters (23, 27–31). To evaluate the nature of the absorption in this region, the lignins were reduced with sodium borohydride under mildly alkaline conditions and the percentage decrease in the 1705–1720 cm^{-1} tabulated in Table 2. The results show that MWL contains unconjugated acids/esters (elimination of 1735 cm^{-1} band) and conjugated acids/esters (1720 cm^{-1} remaining after reduction), but no unconjugated ketones. The 1670 cm^{-1} band in MWL attributed to conjugated

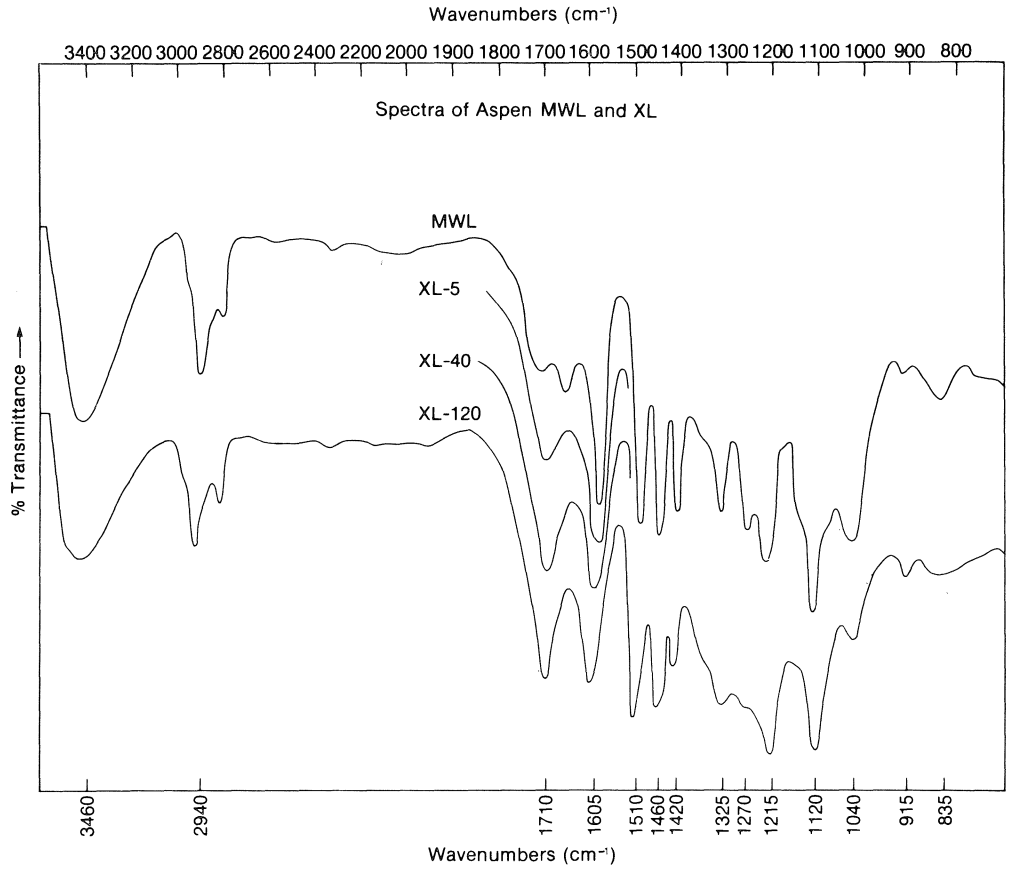

FIG. 1. Spectra of aspen MWL and XL.

TABLE 2. Analyses of infrared spectra of sodium borohydride reduced aspen MWL and XL

Sample	%Change after $NaBH_4$ reduction		
	1590–1610 cm^{-1}	1705–1720 cm^{-1}	1670 cm^{-1}
Reduced MWL	Small	Significant change in 1735 cm^{-1} region Insignificant change in 1720 cm^{-1} region	−12.2
Reduced XL-5	+11.9	−27.0	Absent
Reduced XL-40	+16.1	−47.6	Absent
Reduced XL-120	+23.8	−60.0	Absent

carbonyl groups was decreased by only 12% on reduction. The XL is seen to contain both unconjugated carbonyl structures (reduced portion) as well as conjugated acids/esters (unreduced portion). The band remaining after reduction is more likely to be due to carboxylic acid groups than esters, since the labile ester bonds would have been cleaved by the prevailing hydrolytic conditions. On saponification, the XL could only be precipitated at pH 4 or below and the infrared spectra of the saponified XL showed a decrease in the 1705–1720 cm^{-1} band. This is indicative of carboxylic acid groups.

There is also observed a shift from a lower to a higher frequency of absorption from MWL to XL in the aromatic skeletal vibrations, from 1420–1425 cm^{-1}, 1505–1710 cm^{-1}, and 1590–1605 cm^{-1}, corresponding to a change from a guaiacyl–syringyl type lignin (MWL) to a syringyl-deficient type lignin (XL) (ref. 22, p. 272). This transition is also substantiated by the ratio of absorptivities of the 1600–

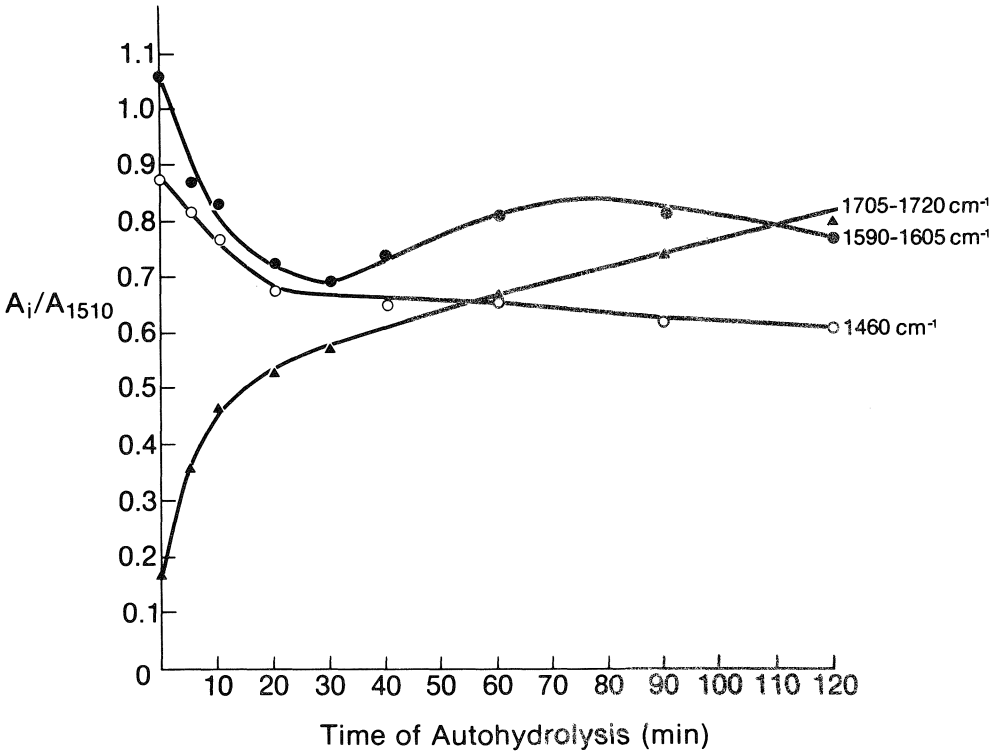

FIG. 2. Trends for absorption bands at 1705–1720 cm^{-1}, 1590–1605 cm^{-1}, and 1460 cm^{-1} for MWL and XL.

1500 cm^{-1} band, which decreases from 1.05 for MWL to approximately 0.8 for XL. The former value is characteristic of hardwood (guaiacyl–syringyl) lignin and the latter softwood (guaiacyl) unit. Furthermore, the band at 1460 cm^{-1} affected by absorption of methoxyl groups (25, 32, 33) is observed to decrease with increasing autohydrolysis time, supporting the observation that XL is tending towards a softwood lignin structure. Figure 2 shows in greater detail the increase in the 1705–1720 cm^{-1} band and the decrease in the 1600 and 1460 cm^{-1} bands.

Ultraviolet Spectra of Aspen Milled Wood Lignin (MWL) and Extracted Lignin (XL)

Aspen lignin has been found by many researchers (26, 34, 35) to give abnormally high ionization difference absorption ($\Delta\varepsilon_i$) due to the presence of *p*-hydroxybenzoate groups. For this reason, the $\Delta\varepsilon_i$ (ionization difference) and $\Delta\varepsilon_r$ (borohydride reduction difference) curves obtained for MWL and XL will be qualitatively interpreted only.

The presence of a maximum at 360 nm for MWL and 366 nm for XL shown in Fig. 3 indicates that both contain phenolic hydroxyls conjugated to α-carbonyl groups, carbon–carbon double bonds, or biphenyl groups. The shift in frequency indicates that the type and proportion of these conjugated structures differ for MWL and XL. From Fig. 4, the phenolic hydroxyl content increases with increasing autohydrolysis time as indicated by the increase in $\Delta\varepsilon_i$ at 255 nm and 296 nm. However, the absorption at these wavelengths is affected by conjugation. Sodium borohydride reduced samples, $\Delta\varepsilon_r$, were run but the trends obtained were difficult to explain, although still indicative of higher phenolic hydroxyl content. It can also be concluded from the 366 nm absorption that increasing amounts of conjugated phenolic structures are being formed on autohydrolysis. From the reduction difference spectra, $\Delta\varepsilon_r$, it appears that only a portion of the conjugated structures can be reduced by sodium borohydride, and this implies the presence of both conjugated carbonyl groups (reduced portion) and conjugated ethylenic group and conjugated acid/esters (unreduced portion).

Discussion

In order to explain the results of the infrared and ultraviolet studies and to relate these to the earlier work on molecular weight distribution (9) and degree of condensation of XL,[1] the possible mechanisms of lignin depolymerization and repolymerization proposed are outlined in Scheme 1.

Scheme 1 shows all possible cleavages of ether

[1]Part 2 in this series of papers.

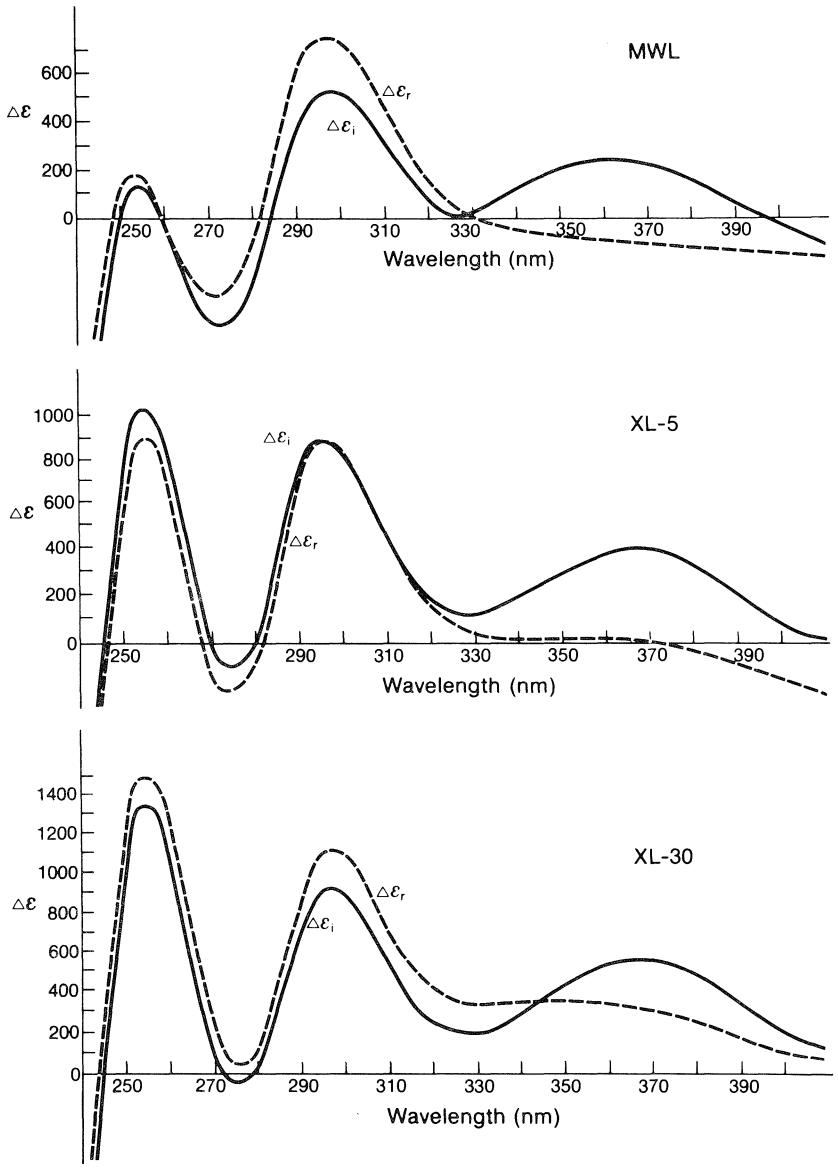

FIG. 3. Ultraviolet ionization ($\Delta\varepsilon_i$) and reduction ($\Delta\varepsilon_r$) curves for MWL and XL.

linkages under acidic conditions of a representative portion of beech hardwood lignin structure as proposed by Nimz (36), with generation of monomeric aromatic (**I***a* and **I***b*) and monomeric aliphatic (**I***c*), dimeric (**II***a* and **II***b*) and oligomeric/polymeric (**III***a* and **III***b*) lignin degradation products. Legend 1 explains the groupings and the subsequent products obtained under the prevailing acidic conditions after the initial hydrolysis.

The depolymerization scheme in Scheme 1 shows that on acidic hydrolysis the monomeric, dimeric, and also oligomeric/polymeric products formed contain aliphatic side chains similar to Hibbert's ketones, namely, with carbonyl and hydroxyl groups. The presence of these compounds is supported by the infrared studies which showed increasing formation of unconjugated β-ketones in the XL, from the 1705–1720 cm^{-1} band with increasing autohydrolysis time. Also the ultraviolet studies have indicated the presence of α,β-diketone, and conjugated ethylenic groups, which may be indicative of phenylcoumarone and stilbene structures. Klemola (19) has also found the more stable Hibbert's ketones and guaiacyl and syringyl derivatives with 3 or less carbon side chain compounds such as acetoguaiacone, acetosyringone, guaiacol, and syringol, in the low molecular weight

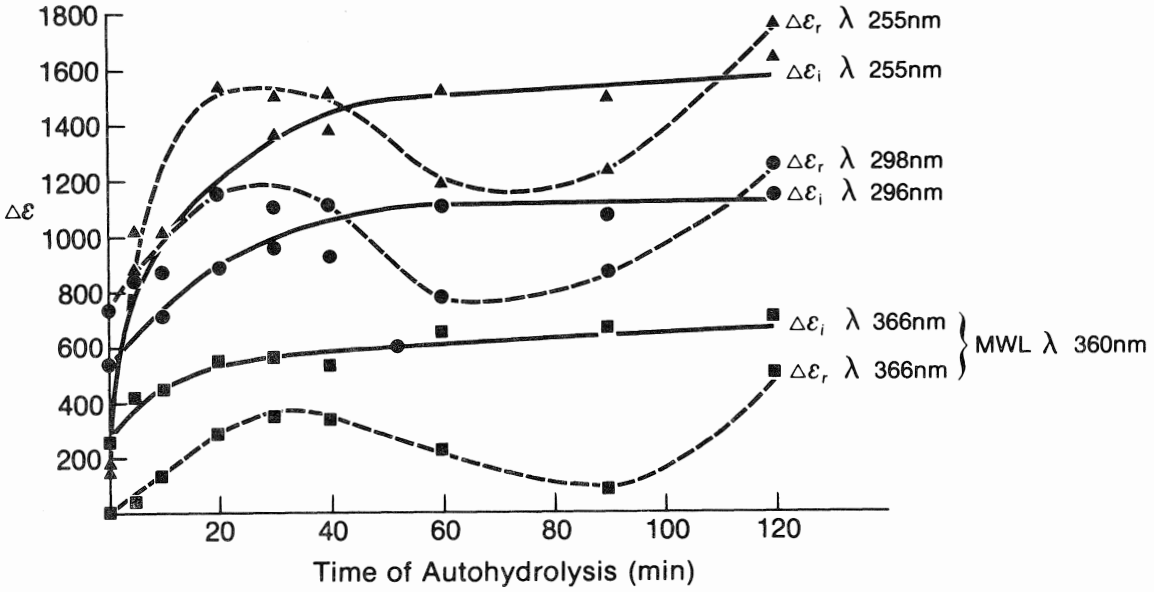

FIG. 4. Trends in ionization ($\Delta\varepsilon_i$) and reduction ($\Delta\varepsilon_r$) curves for MWL and XL.

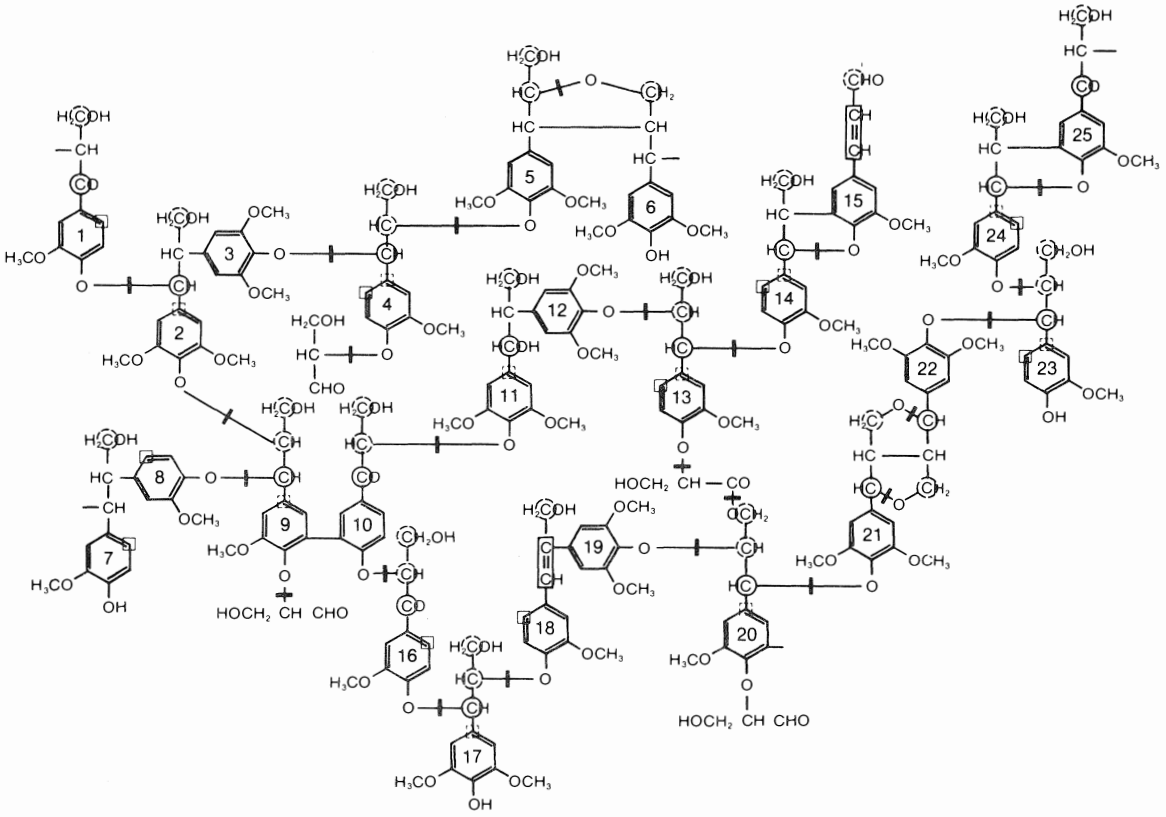

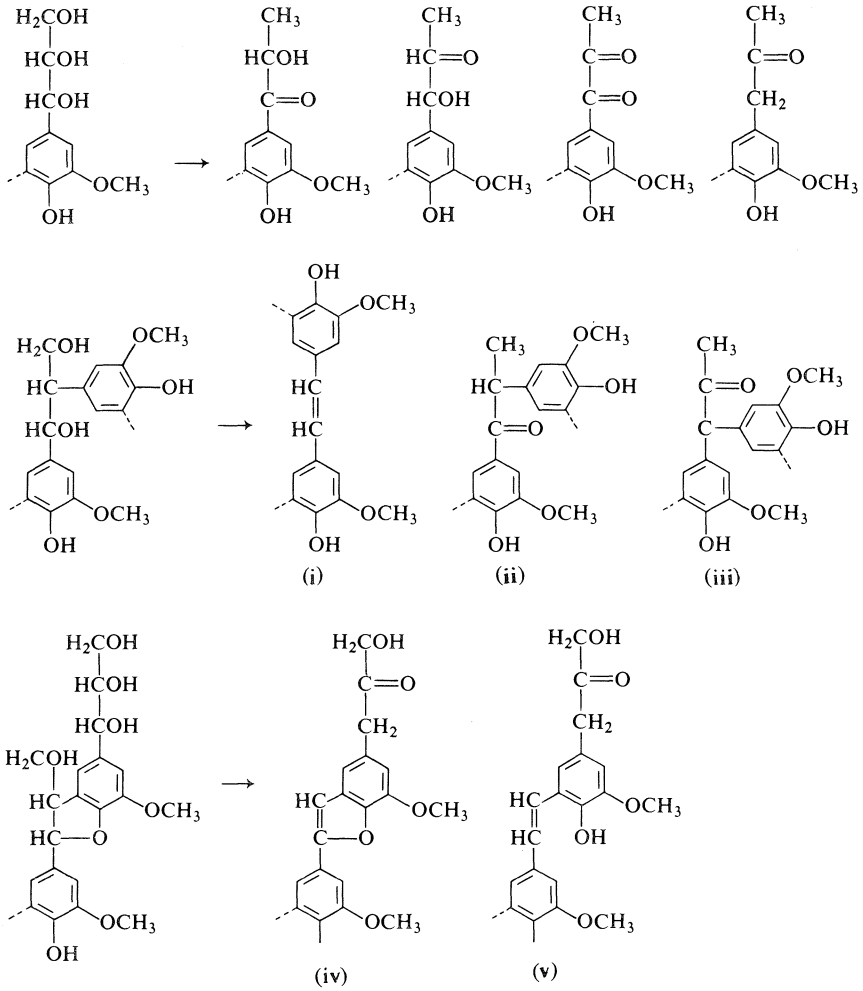

SCHEME 1. Schematic representation of (*a*) depolymerization and (*b*) repolymerization of a representative portion of hardwood lignin under acidic conditions.

(*a*) Depolymerization (indicated by bond cleavage (/)): aromatic ring number → lignin degradation products are 1 → I*a* or III; 2/3 → III*a*; 4 → I*b*, I*c*; 5/6 → II*b* or III; 7/8 → II*b* or III; 9/10 → I*c*, II*b*; 11/12 → II*a*; 13 → I*b*, I*c*; 14/15 → II*b*; 16 → I*a*; 17 → I*b*; 18/19 → II*b*; 20 → I*c*, III*a*; 21/22 → II*b*; 23 → I*b*; 24/25 → II*b* or III.

I*a* = Monomeric guaiacyl and syringyl derivatives with 3 or less carbon atom aliphatic side chains, carrying C=C double bond, carbonyl or hydroxyl groups.

I*b* = Guaiacylglycerol and syringylglycerol structures, which from acidolysis studies are known to form Hibbert's ketones under acidic conditions.

I*c* = Monomeric aliphatic compounds. Lundquist (13) has found pyruvaldehyde, formaldehyde, and methanol in acidolysis liquor.

II*a* = 1,2-Bisguaiacyl-1,3-propandiol and 1,2-bissyringyl-1,3-propandiol structures, which from acidolysis studies have been found to form the following compounds: 4,4′-dihydroxy-3,3′-dimethoxy stilbene (**i**), 1,2-bisguaiacyl-1-propanone (**ii**), and 1,1-bisguaiacyl-2-propanone (**iii**) (or their syringyl analogues).

II*b* = Dimeric guaiacyl or syringyl structures originating from dimers present in the lignin, for example, phenylcoumaran and pinoresinol type of structures (or their syringyl analogues). From acidolysis studies it has also been shown that phenylcoumaran structures which on hydrolysis have a glyceryl side chain form dimeric products with Hibbert's ketone side chains: phenylcoumarone ketone (**iv**) and *o,p*′-dihydroxystilbene (**v**).

III = These represent oligomeric/polymeric products which are not degraded to monomers or dimers because of carbon–carbon linkages.

III*a* = Oligomeric/polymeric products with Hibbert's ketone side chains which on hydrolysis contain glyceryl side chains.

III*b* = Repolymerization (indicated by reactive centres): electrophilic sites ◯, strong; ◌, weak; nucleophilic sites □, strong; ⬚, weak.

fraction on steam hydrolysis of birch. Kratzl *et al.* (37), Sears *et al.* (38), and Goldschmid (39) in their prehydrolysis studies have found besides the Hibbert's ketones, aldehydes such as vanillin *p*-coumaraldehyde and coniferylaldehyde. Stanek (40) in his hydrolysis studies of aspen has found vanillic, syringic, and *p*-hydroxybenzoic acids, the latter in larger amounts than the former two. Smith (27) has found that *p*-hydroxybenzoate groups are present in aspen, up to 10% by weight, which on hydrolysis of the ester linkages form *p*-hydroxybenzoic acid. Furthermore, Nakano and co-workers (41) have shown that at least a part of the *p*-hydroxybenzoate groups are located at the α-position of the lignin side chain. It is also worth stressing that during autohydrolysis the hemicellulose fraction is also being hydrolysed, followed by subsequent dehydration of the sugars to generate reactive furfural, hydroxymethylfurfural, and their precursors. Sugars, furfural, and 5-hydroxymethylfurfural, evidently derived from the carbohydrate constituents of the wood, have been found together with the monomeric lignin degradation products in the hydrolysis liquor of hemlock at 175°C by Goldschmid (39).

The cleavage of lignin linkages under the acidic conditions of autohydrolysis is viewed as only one of two types of opposing reactions occurring simultaneously. Hydrolytic degradation results in depolymerization of lignin, which accounts for its subsequent extractability by various solvents, and condensation reactions result in repolymerization of the lignin fragments and insolubility.

Condensation reactions in lignin under acidic conditions involve an electrophile reacting with a nucleophile to form carbon–carbon bonds. In Scheme 1, part *b*, strong and weak electrophilic and nucleophilic sites have been marked and these represent positions of condensation in the lignin macromolecule. Lignin electrophiles are essentially carbonium ions generated as a result of the cleavage of ether bonds or aliphatic side chain carbon with hydroxyl or carbonyl groups capable of forming carbonium ions. Lignin nucleophiles are the unsaturated aromatic rings with a high electron density at C-6 and C-1 and the unsaturated aliphatic side chains. It is further suggested that some of the lignin degradation products **I**, **II**, and **III**, are also reactive electrophiles and nucleophiles and recondense with the reactive centres in the lignin macromolecule. In addition, furfural, hydroxymethylfurfural, and their precursors, because of the aldehyde group and C=C double bonds in the furan ring, are electrophilic and can also participate extensively in lignin condensation reactions. All these condensations result in the formation of higher molecular weight lignin, leading eventually to the formation of insoluble residual lignin. In aspen lignin, it is proposed that the formation of insoluble residual lignin has to a large extent been prevented, as is seen by the ease of extractability of aspen lignin compared with other hardwoods, by the action of *p*-hydroxybenzoic acid acting as a blocking agent. *p*-Hydroxybenzoic acid acting as a nucleophile reacts at the position *ortho* to the phenolic hydroxyl with electrophilic lignin carbonium ions, thus preventing further condensation towards the formation of insoluble lignin. This is substantiated by these infrared studies, which have indicated the presence of conjugated carboxylic acid in the XL.

Experimental

Preparation of Autohydrolysis Extracted Lignin (XL)

For details refer to ref. 9. Extractive-free aspen wood meal was autohydrolysed at 195°C for periods varying from 5 min to 2 h. The lignocellulosic residue was then extracted with 90% dioxane at 70°C and the extracted lignin purified and recovered by precipitation into ether, followed by subsequent washings with benzene and petroleum ether.

Infrared Spectra

Infrared spectra of milled wood lignin (MWL) and extracted autohydrolysis lignin (XL) were determined in potassium bromide pellets on the Beckman IR-9. Lignin samples and spectrophotometric-grade potassium bromide were dried before use to ensure moisture-free pellets. Lignin (1 mg) was mixed and thoroughly ground with 300 mg of potassium bromide to reduce particle size and to obtain uniform dispersion of the sample in the pellet. The lignin sample was then determined against a pure potassium bromide pellet on the IR-9 operated on a double-beam mode.

Borohydride-reduced MWL and XL were prepared (26) by dissolving 60 mg of lignin in a mixture of 2.0 mL of ethanol and 1.0 mL of 0.1 *N* sodium hydroxide in a nitrogen atmosphere. To the mixture 20 mg of sodium borohydroxide was added, followed by 2.0 mL of water. After 7 days, the solution was acidified to pH 4 with dilute hydrochloric acid, and the precipitated lignin collected by centrifugation. The reduced lignin samples were washed twice with water, dried in a vacuum desiccator, and the infrared spectra determined as in the previous procedure.

XL's were saponified (26) by dissolving 200 mg of lignin in 5% NaOH in a nitrogen atmosphere at room temperature. After 24 h, the solution was acidified to pH 4 with dilute hydrochloric acid. The precipitated lignin was recovered by centrifugation, washed twice with water, dried in a vacuum desiccator, and the infrared spectra determined.

Ultraviolet Spectra

For the determination of ultraviolet spectra (26) of MWL and XL, 5 mg of lignin was dissolved in 7.5 mL of methylcellosolve and diluted with 95% ethanol to 25 mL. The neutral solution was prepared by diluting 10 mL of this solution to 50 mL with 95% ethanol. The alkaline solution was prepared by adding 5 mL of 1 *N* NaOH to 10 mL of the initial solution and diluting to 50 mL with distilled water. The alkaline-neutral difference spectra, $\Delta\varepsilon_i$, were determined by running the alkali solution against the neutral solution. Similarly the reduction difference spectra, $\Delta\varepsilon_r$, were determined as in the above procedure using sodium borohydride reduced MWL and XL.

Acknowledgements

The authors wish to thank the National Research Council of Canada for both the award of an NRCC postgraduate scholarship to one of them (M.G.S.C.) and for a research grant which supported this investigation. The authors also wish to thank Mr. J. H. Lora for the sample of milled wood lignin used in this work, and for helpful discussion of the results.

1. E. ADLER, K. LUNDQUIST, and G. E. MIKSCHE. Adv. Chem. Ser. **59**, 22 (1966).
2. E. ADLER, J. M. PEPPER, and E. ERIKSON. Ind. Eng. Chem. **49**, 1391 (1957).
3. K. LUNDQUIST. Acta Chem. Scand. **18**, 1316 (1964).
4. K. SARKANEN and C. SCHUERCH. J. Am. Chem. Soc. **79**, 4203 (1957).
5. E. WEST, A. S. MACINNES, and H. HIBBERT. J. Am. Chem. Soc. **65**, 1187 (1943).
6. W. S. MACGREGOR, T. H. EVANS, and H. HIBBERT. J. Am. Chem. Soc. **66**, 41 (1944).
7. E. ADLER and B. D. LINDGREN. Sven. Papperstidn. **55**, 563 (1952).
8. E. ADLER and S. YLLNER. Sven. Papperstidn. **55**, 238 (1952).
9. M. G. S. CHUA and M. WAYMAN. Can. J. Chem. **57**, 1141 (1979).
10. J. M. PEPPER and M. SIDDIQUELLAH. Can. J. Chem. **39**, 1454 (1961).
11. K. R. KAVANAGH and J. M. PEPPER. Can. J. Chem. **33**, 24 (1955).
12. K. LUNDQUIST and K. HEDLUNG. Acta Chem. Scand. **21**, 1750 (1967).
13. K. LUNDQUIST. Acta Chem. Scand. **24**, 889 (1970).
14. K. LUNDQUIST and L. ERICSSON. Acta Chem. Scand. **24**, 3681 (1970).
15. K. LUNDQUIST and T. K. KIRK. Acta Chem. Scand. **25**, 889 (1971).
16. K. LUNDQUIST and K. HEDLUNG. Acta Chem. Scand. **25**, 2199 (1971).
17. K. LUNDQUIST and R. LUNDGREN. Acta Chem. Scand. **26**, 2005 (1972).
18. K. LUNDQUIST. Acta Chem. Scand. **27**, 2597 (1973).
19. A. KLEMOLA. Suom. Kemistil. B, **41**, 83 (1968).
20. H. H. NIMZ. Chem. Ber. **98**, 533 (1965).
21. H. H. NIMZ. Holzforschung, **20**, 105 (1966).
22. K. V. SARKANEN and C. H. LUDWIG. Lignins. Wiley Interscience, NY. 1971.
23. H. J. HERGERT. J. Org. Chem. **25**, 405 (1960).
24. H. M. CHANG and K. V. SARKANEN. Tappi, **56**, 133 (1973).
25. K. V. SARKANEN, H. M. CHANG, and B. ERICSSON. Tappi, **50**, 572 (1967).
26. K. V. SARKANEN, H. M. CHANG, and G. G. ALLEN. Tappi, **50**, 583 (1967).
27. D. C. C. SMITH. J. Chem. Soc. 2347 (1955).
28. D. C. C. SMITH. Nature, **176**, 927 (1955).
29. A. J. MICHELL. Aust. J. Chem. **19**, 2285 (1966).
30. K. H. EKMAN and J. J. LINDBERG. Papper och Trä, **1**, 21 (1960).
31. S. KOLHOE and O. ELLEFSEN. Tappi, **45**, 163 (1962).
32. C. Y. LIANG, K. H. BASSET, E. A. MCGINNES, and R. H. MARCHESSAULT. Tappi, **43**, 1017 (1960).
33. D. E. BLAND and A. F. LOGAN. Biochem. J. **95**, 515 (1965).
34. G. AULIN-ERDTMAN and H. SANDEN. Paper and Timber, Helsinki, **43**, 671 (1961).
35. M. A. BUCHANAN, F. E. BRAUNS, and R. L. LEAF. J. Am. Chem. Soc. **71**, 1297 (1949).
36. H. H. NIMZ. Angew. Chem. **13**, 31 (1974).
37. K. KRATZL, W. KISSER, J. GRATZL, and H. SILBERNAGEL. Monatsh. Chem. **90**(6), 771 (1959).
38. K. D. SEARS, A. BEELIK, R. L. CASEBIER, R. J. ENGEN, J. K. HAMILTON, and H. L. HERGERT. J. Polym. Sci. **36**, 425 (1971).
39. O. GOLDSCHMID. Tappi, **38**, 728 (1955).
40. D. A. STANEK. Tappi, **41**, 601 (1958).
41. J. NAKANO, A. ISHIZU, and N. MIGITA. Tappi, **44**, 30 (1961).

Characterization of autohydrolysis aspen (*P. tremuloides*) lignins. Part 4. Residual autohydrolysis lignin

MORRIS WAYMAN AND MIRANDA G. S. CHUA

Department of Chemical Engineering and Applied Chemistry, University of Toronto, Toronto, Ont., Canada M5S 1A4

Received March 21, 1979

MORRIS WAYMAN and MIRANDA G. S. CHUA. Can. J. Chem. **57**, 2612 (1979).

Lignocellulosic residue remaining after autohydrolysis of extractive-free aspen wood meal at 195°C for periods of time varying from 5 to 120 min followed by extraction with 90% dioxane was subjected to enzymatic hydrolysis to obtain residual lignin. Infrared studies indicated that in the early stages of autohydrolysis residual lignin resembles protolignin, but as autohydrolysis proceeds it changes to resemble more and more the extracted lignin. Residual lignin was found to be higher in carbon but lower in hydrogen and oxygen than aspen milled wood lignin. The methoxyl content was also lower than the reference lignin. From alkaline nitrobenzene oxidation, residual lignin is seen to become more condensed with increasing autohydrolysis time. The insolubility of residual lignin is attributed to the existence of strong bonds between this lignin and carbohydrate.

MORRIS WAYMAN et MIRANDA G. S. CHUA. Can. J. Chem. **57**, 2612 (1979).

On a soumis le résidu lignocellulosique provenant d'une autohydrolyse de sciures de bois de tremble sans principes extratifs à 195°C pour des périodes allant de 5 à 120 min et suivie d'une extraction par du dioxanne à 90%, à une hydrolyse enzymatique dans le but d'en retirer la lignine résiduelle. Des études infrarouges indiquent qu'au début de l'autohydrolyse la lignine résiduelle ressemble à la protolignine, mais au fur et à mesure que l'autohydrolyse progresse la lignine se transforme pour resembler de plus en plus à la lignine extraite. On a trouvé que la lignine résiduelle contient plus de carbone et moins d'hydrogène et d'oxygène que la lignine de bois de tremble broyé. La quantité de méthoxyle est aussi plus faible que la lignine de référence. En se basant sur l'oxydation alcaline par le nitrobenzène, on observe que la lignine résiduelle devient plus condensée lorsque le temps d'autohydrolyse augmente. On attribue l'insolubilité de la lignine résiduelle à l'existence de la présence de liaisons fortes entre cette lignine et les hydrates de carbone.

[Traduit par le journal]

Introduction

Studies of the protolignin in wood and the reactions of lignin during various pulping processes have centred mainly on the lignin which is extractable. Characterization of these isolated lignins, for example, milled wood lignin, kraft lignin, and lignosulphonate, have enabled lignin researchers to achieve some understanding of lignin structure and to postulate the mechanisms involved in lignin reactions. Recently however, interest is being focussed on the non-extractable lignin fraction, the residual lignin, as indicated by investigations (1, 2) into the characterization of the residual lignin in kraft and NSSC pulps.

The problems associated with the study of residual lignin are two-fold. First, residual lignin is generally insoluble in most solvents, or if it dissolves under more drastic conditions there is inadvertent modification of the lignin structure. This has limited the characterization of residual lignin to methods which utilise the lignin in the solid form. The second factor contributing to the difficulties involved in analysing residual lignin is the strong association of lignin with carbohydrate in wood (3–11) and wood-pulp (12–17), making it impossible to obtain residual lignin free of carbohydrate or conversely a carbohydrate fraction free of lignin. This has led to the prevailing concept of the existence of lignin–carbohydrate bonds and the presence of lignin–carbohydrate complexes in wood.

In our study of the effects of autohydrolysis on the lignin in wood to elucidate the mechanism whereby lignin becomes solvent-soluble during autohydrolysis, there is the need to account for the inextractability of the residual lignin.

Extractive-free aspen wood meal was autohydrolyzed at 195°C for periods of time varying from 5 to 120 min, and the soluble lignin extracted with 90% dioxane at 70°C.[1] The extracted lignocellulosic residue (ER) was then treated with cellulase enzyme to recover the residual lignin (RL), which was analysed for elemental composition and methoxyl content, for infrared absorption, and subjected to alkaline nitrobenzene oxidation.

[1]Refer to Parts 1, 2, and 3 of this series. Part 1 is ref. 18.

0008-4042/79/192612-05$01.00/0

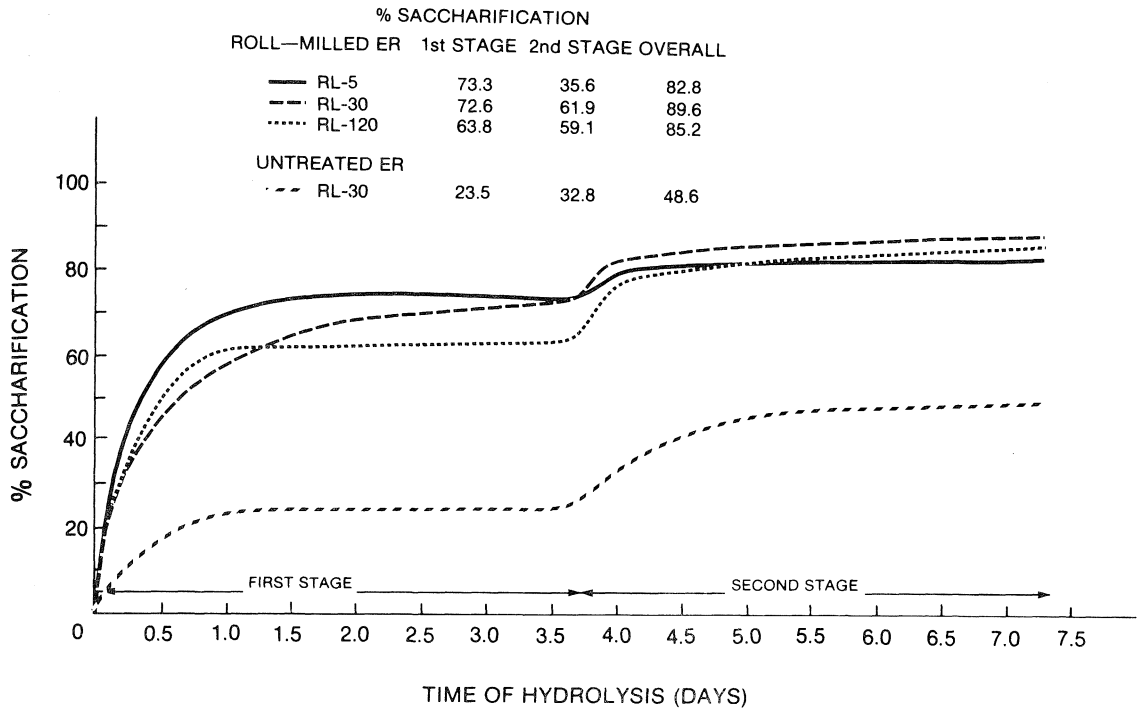

FIG. 1. Enzymatic hydrolysis of extracted lignocellulosic residue (ER) to obtain residual lignin (RL) (based on sugars in liquor after post-hydrolysis).

Results

Saccharification of Extracted Lignocellulosic Residue (ER)

The two-stage saccharification of the extracted lignocellulosic residue (ER) by cellulase enzyme, as shown in Fig. 1, resulted in saccharification yields of 83–90% based on the sugar in the liquor after post-hydrolysis. A mechanical pretreatment of the ER before hydrolysis affected greatly the percentage saccharification, as seen from the untreated ER and roll-milled samples. The effectiveness of mechanical pretreatment in enhancing reactivity of cellulosic materials is due to the alteration of the cellulose crystalline structure thereby increasing accessibility of the cellulose to enzyme or chemicals (19). By comparison, the saccharification yields calculated from Klason lignin determinations of ER and RL were between 92–97%. The higher saccharification yields were attributed to the solubilization under the concentrated acid conditions of Klason analysis of the carbohydrate portion which is not hydrolyzable by cellulase enzyme. The RL contained between 12–34% carbohydrate.

Elemental Analyses of Residual Lignin (RL)

The elemental composition of residual lignin (RL), shown in Table 1, indicated that RL has higher carbon content and lower hydrogen and oxygen contents than aspen milled wood lignin (MWL). Similar changes in C, H, and O were observed for the extracted lignin (XL) (18). These changes suggest that condensation reactions with formation of carbon–carbon bonds and elimination of water have taken place in the lignin in wood during autohydrolysis. The low oxygen content of RL-5 is attributed to the hydrolysis of *p*-hydroxybenzoate groups in MWL with subsequent removal of *p*-hydroxybenzoic acid ($C_7H_6O_3$) with its high oxygen content.

The observed decrease in OCH_3/C_9 unit for RL with increasing autohydrolysis time was quantitatively very similar to that for XL (18). It can be attributed to demethoxylation, inclusion of non-lignin components such as carbohydrate degradation products, and to variation of the proportion of syringyl to guaiacyl units.

Alkaline Nitrobenzene Oxidation of Residual Lignin (RL)

As shown in Table 2, the total aromatic aldehyde yield on alkaline nitrobenzene oxidation of RL decreased with increasing autohydrolysis time

TABLE 1. Elemental analyses of residual lignin (RL) (carbohydrate-free-basis)*

Sample	Carbohydrate in RL (%)	Analysis (%) C	H	O	OCH_3	C_9 formula	Molecular weight C_9 unit
MWL	2.5	59.50	6.25	34.25	21.54	$C_9H_{8.70}O_{3.05}(OCH_3)_{1.47}$	211.2
RL-5	18.2	62.29	6.09	31.62	21.49	$C_9H_{7.93}O_{2.57}(OCH_3)_{1.39}$	200.2
RL-20	25.4	60.54	6.19	33.27	18.51	$C_9H_{8.81}O_{3.00}(OCH_3)_{1.21}$	202.5
RL-30	34.5	61.07	6.09	32.84	18.24	$C_9H_{8.56}O_{2.93}(OCH_3)_{1.18}$	200.1
RL-40	16.5	62.07	6.02	31.91	18.32	$C_9H_{8.25}O_{2.76}(OCH_3)_{1.16}$	196.5
RL-90	14.3	62.08	5.75	32.17	15.54	$C_9H_{8.10}O_{2.91}(OCH_3)_{0.97}$	192.7
RL-120	12.8	62.55	5.64	31.81	15.77	$C_9H_{7.79}O_{2.83}(OCH_3)_{0.97}$	191.5

*Elemental composition for extracted lignin (XL) at corresponding autohydrolysis time is found in ref. 18.

TABLE 2. Alkaline nitrobenzene oxidation of residual lignin (RL)*

Sample	Vanillin (V)† (%)	Syringaldehyde (S)† (%)	Total (V+S) (%)	Molar ratio S/V
MWL	6.15	9.74	15.89	1.32
RL-5	6.74	10.22	16.96	1.27
RL-40	2.07	2.67	4.74	1.08
RL-120	1.42	1.39	2.81	0.80

*Alkaline nitrobenzene oxidation yields for extracted lignin (XL) at corresponding autohydrolysis time is found in Part 2 of this series.
†% yield by weight, based on lignin on a carbohydrate-free basis.

suggesting that RL became increasingly more condensed in structure as autohydrolysis proceeded. Very similar results were obtained for the XL of the same autohydrolysis periods. The slightly higher aromatic aldehyde yield of RL-5 than for MWL is attributed to modification during MWL preparation. The total aromatic aldehyde yield on alkaline nitrobenzene oxidation of aspen wood meal has been found to be much higher than our value of 15.9% for MWL (20).

The decreasing molar ratio of syringaldehyde to vanillin (S/V) for RL with increasing autohydrolysis time is attributed to the preferential removal of syringyl units as low molecular weight compounds into the ether-soluble fraction during purification. The ether-soluble fraction has a high methoxyl content of 23.1%. This trend of decreasing S/V ratio with increasing autohydrolysis time was also observed for the extracted lignin.[2]

Infrared Spectra of Residual Lignin (RL)

The infrared spectra of RL shown in Fig. 2 will be only qualitatively treated because of the presence of carbohydrate in RL. This is indicated in the spectra of RL-30, which had the highest carbohydrate content, by the two peaks at 1060 cm^{-1} and 1165 cm^{-1} attributed to C—O and C—O—C stretching vibrations respectively, in cellulose and hemicellulose (11, 15, 21–23).

In the region 1600–1800 cm^{-1}, the 1670 cm^{-1} band attributed to α-conjugated carbonyl group is present for RL-5 to RL-40, whereas the 1705–1715 cm^{-1} band attributed to β-unconjugated ketone group is present in RL-90 and RL-120. The 1670 cm^{-1} band is present in MWL spectra whilst the 1705–1715 cm^{-1} band is observed to increase prominently with increasing autohydrolysis time for extracted lignin (XL).[3]

A prominent band at 810 cm^{-1} is observed to be present in the spectrum of RL-120 only but absent from the other RL and XL spectra. The presence of furans or furan-related compounds cannot explain the observed 810 cm^{-1} band, because although 2-methylfurfural and furfuryl alcohol show strong absorption around 810 cm^{-1}, the 730 cm^{-1} band associated with the ring deformation of the furan nucleus is absent (24, 25). It was also noted that the 675 cm^{-1} band is present in the spectra of all XL and RL-5 to RL-40, but absent from RL-90 and RL-120.

Discussion

In the early stages of autohydrolysis RL resembles MWL (or protolignin) but as autohydrolysis proceeds it is seen to resemble more and more extracted lignin. This is clearly suggested from the infrared studies by the presence of the 1670 cm^{-1} band (present in MWL[3]) and the absence of the 1705–1715 cm^{-1} band (present in XL) in the spectra of RL-5 to RL-40, whereas for the samples at longer autohydrolysis times, RL-90 and RL-120, the reverse is true. The elemental analyses also show this tran-

[2]Part 2 of this series.

[3]Part 3 of this series.

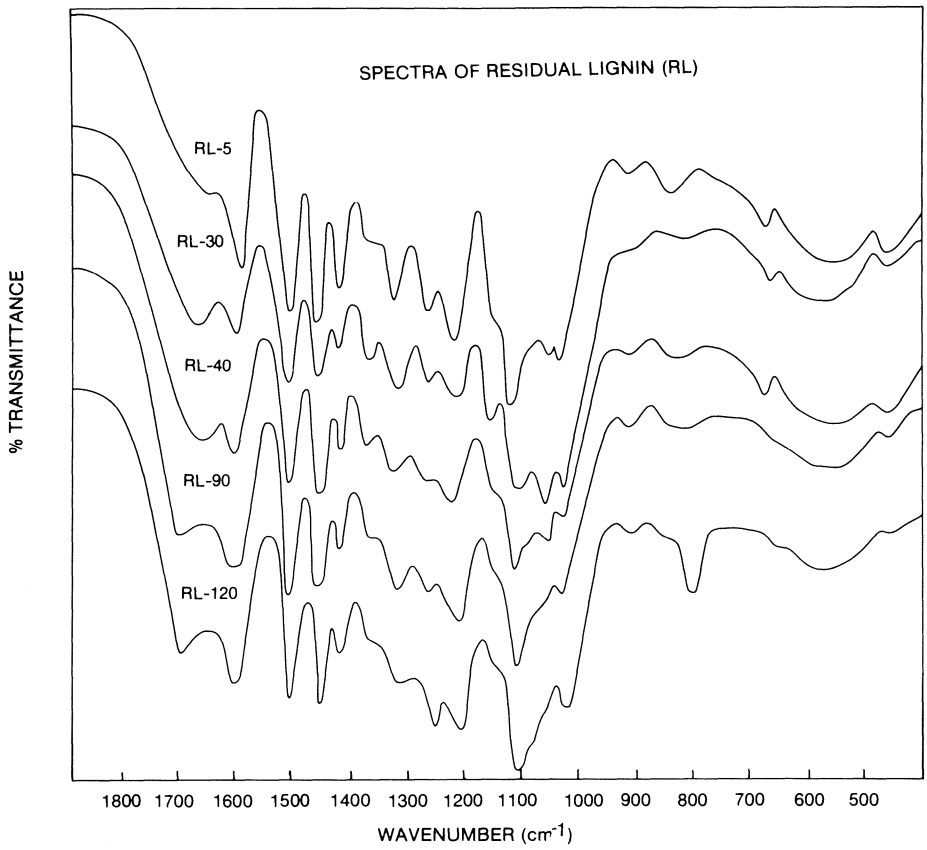

FIG. 2. Spectra of residual lignin (RL).

sition from a protolignin-type residual lignin to an extracted lignin-type residual lignin, as is indicated by the composition of RL-120 being more similar to XL-120 (18) than to MWL.

Alkaline nitrobenzene oxidation has proved to be most illuminating with regard to the concept of simultaneous depolymerization and repolymerization. It has shown that during autohydrolysis besides depolymerization, resulting in extractable lignin, condensation has also taken place even as early as during the first 5 min of autohydrolysis. In addition, condensation is observed to be taking place to almost the same extent in the RL and in the XL of the same autohydrolysis time, as indicated by their similar total aromatic yield.

The mechanism of the reactions of lignin in wood during autohydrolysis may be viewed as in Scheme 1. It shows that on autohydrolysis the original insoluble protolignin (PL) in wood was depolymerized resulting in formation of extracted lignin (XL) and leaving a protolignin-type residual lignin (PRL) presumably firmly bound to the carbohydrate. The XL was shown from molecular weight distribution studies (18) to consist of low and high molecular weight lignins (LMXL and HMXL). The soluble LMXL repolymerizes to form soluble HMXL. For the first 40 min of autohydrolysis, the yield of PRL decreased resulting in formation of more extracted lignin (XL). As a result of condensation and also of reaction with carbohydrates and their degradation products as autohydrolysis proceeded, most of the lignin became insoluble as observed by the increase in yield of extracted lignin-type residual lignin (XRL). This increase in XRL is seen to correspond to a decrease in soluble HMXL, which is postulated to be the intermediate in a succession of condensa-

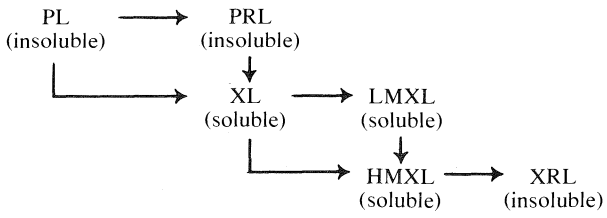

SCHEME 1. Formation of residual lignin and extracted lignin: PL = insoluble protolignin, PRL = protolignin-type residual lignin, LMXL = low molecular weight extracted lignin from XL, HMXL = high molecular weight extracted lignin from XL, XRL = extracted lignin-type residual lignin.

tion reactions of lignin fragments leading eventually to the formation of insoluble lignin (18).

From the saccharification studies, the presence of a portion of carbohydrate which is not saccharified by cellulase enzyme suggests the existence of strong lignin–carbohydrate linkages. The insolubility of residual lignin during autohydrolysis is attributed to these strong bonds between this lignin and carbohydrate.

Experimental

Residual Lignin (RL) from Extracted Lignocellulosic Residue (ER)

The extracted lignocellulosic residue (ER) which remained after extraction of autohydrolysed extractive-free aspen wood meal at 195°C for periods varying from 5 min to 2 h with 90% dioxane (18), was subjected to cellulase hydrolysis to recover the residual lignin (RL). For most experiments, ER was mechanically pretreated before enzymatic hydrolysis, by passing through a two roll mill 3 times for 1-min cycles (processed by the U.S. Army Natick Development Laboratory, Natick, MA) as this was found to enhance cellulose saccharification. Cellulase enzyme (*Trichoderma reesei*) supplied by courtesy of Dr. C. Massey of Natick Laboratory with an activity of 0.125 IU/mg was used for the hydrolysis.

Following the Natick procedure, 5 g of substrate (ER) in 95 mL of citrate buffer pH 4.8 was hydrolysed using 0.7 g of cellulase (enzyme activity in solution was 1 IU per mL) in 250 mL shake flasks at 50°C. Samples of the solution (5 mL) were withdrawn at various time intervals and analysed for sugar content after post-hydrolysis by the dinitrosalicylic acid method of Miller (26) as modified by Natick Laboratory (27). Post-hydrolysis consisted of subjecting the hydrolysis solution to 4% H_2SO_4 in an autoclave at 16 psig for 1 h to ensure that oligomers or dimers are completely hydrolysed to glucose. The difference between the glucose content determined before and after posthydrolysis was less than 6%. The hydrolysis was stopped after 3.5 days, the remaining substrate centrifuged, washed thoroughly with distilled water, and subjected to a second hydrolysis. After another 3.5 days, the solid remaining from the 2-stage hydrolysis, termed residual lignin (RL) was recovered by centrifugation, washed thoroughly with distilled water, and freeze-dried.

Elemental Analyses, Methoxyl Determination of Residual Lignin and % Carbohydrate in the Residual Lignin

Lignin samples were analysed for C, H, and methoxyl content by Schwarzkopf Microanalytical Laboratory, Inc., New York.

The % carbohydrate in the residual lignin was determined by measuring the amount of sugar present in the final hydrolysis liquor after Klason analysis by the dinitrosalicylic acid method.

Alkaline Nitrobenzene Oxidation

The modified procedure for alkaline nitrobenzene oxidation is described in detail in ref. 28.

Infrared Spectra

Infrared spectra of residual lignin were determined in potassium bromide pellets on the Beckman IR-9. Lignin (1 mg) was mixed and thoroughly ground with 300 mg of potassium bromide to reduce particle size and to obtain uniform dispersion of the sample in the pellet. The lignin sample was then determined against pure potassium bromide on the Beckman IR-9.

Acknowledgments

The authors wish to thank the National Research Council of Canada for both the award of an NRCC postgraduate scholarship to one of them (M.G.S.C.) and for a research grant which supported this investigation. The authors also wish to thank Mr. J. H. Lora for the sample of milled wood lignin used in this work, and for helpful discussion of the results.

1. J. H. Lin, C. L. Chen, H-m. Chang, and J. S. Gratzl. Abstracts, Cellulose, Paper and Textile Division, American Chemical Society, Spring Meeting, Appleton. 1978.
2. W. G. Glasser, H. R. Glasser, C. A. Barnett, and N. Morohoshi. Abstracts, Cellulose, Paper and Textile Division, American Chemical Society, Spring Meeting, Appleton, 1978.
3. J. C. Pew. Tappi, **40** (7), 553 (1957).
4. J. C. Pew and P. Weyna. Tappi, **45** (3), 247 (1962).
5. K. P. Kringstad and C. W. Cheng. Tappi, **52** (12), 2382 (1969).
6. J. W. T. Merewether. Holzforschung, **8**, 116 (1954).
7. A. Bjorkman. Sven. Papperstidn. **59**, 447 (1956).
8. A. Bjorkman. Sven. Papperstidn. **60**, 243 (1957).
9. H. H. Brownell. Tappi, **48** (9), 513 (1965).
10. F. Yaku, Y. Yamada, and T. Koshijima. Holzforschung, **30** (5), 148 (1976).
11. H-m. Chang, E. B. Cowling, and W. Brown. Holzforschung, **29** (5), 153 (1975).
12. J. Polcin and B. Bezuch. Wood Sci. Technol. **12**, 149 (1978).
13. A. J. Michell, A. J. Watson, and H. G. Higgins. Tappi, **48** (9), 520 (1965).
14. H. I. Bolker. Nature, **197**, 489 (1963).
15. H. I. Bolker and N. G. Somerville. Pulp Pap. Mag. Can. **64**, T187 (1963).
16. K. J. Harrington, H. G. Higgins, and A. J. Michell. Holzforschung, **18**, 108 (1964).
17. C. Y. Liang, K. H. Bissett, E. A. McGinnes, and R. H. Marchessault. Tappi, **43**, 1017 (1960).
18. M. G. S. Chua and M. Wayman. Can. J. Chem. **57**, 1141 (1979).
19. M. A. Millett, A. J. Baker, and L. D. Satter. *In* Enzymatic Conversions of Cellulosic Materials: Technology and Applications. Biotechnology and Bioengineering Symposium No. 6. Interscience Publishers, New York. 1976. p. 125.
20. J. M. Pepper, M. Manolopoulo, and R. Buton. Can. J. Chem. **40**, 1976 (1962).
21. M. Wayman, M. R. Azhar, and Z. Koran. Wood Fiber, **3** (3), 53 (1971).
22. H. G. Higgins, C. M. Stewart, and K. J. Harrington. J. Polym. Sci. **51**, 59 (1961).
23. C. Y. Liang and R. H. Marchessault. J. Polym. Sci. **39**, 269 (1959).
24. C. J. Pouchert. The Aldrich Library of IR spectra. 2nd ed. Aldrich Chemical Co., Milwaukee. 1975.
25. H. A. Szymanski. Interpreted infrared spectra. Vol. 3. Plenum Publishing Corp., New York. 1967.
26. G. L. Miller. Anal. Chem. **31**, 426 (1959).
27. M. H. Mandels and D. Sternberg. Recent Advances in Cellulase Technology. Cellulose Technology, **54** (4), 267 (1967).
28. M. G. S. Chua and M. Wayman. Tappi, **62** (3), 103 (1979).

Electrochemical oxidation of trifluoroacetic acid anion. IV. Synthesis and stereochemistry of products of trifluoromethyl radical addition to some mono- and disubstituted olefins[1]

ROGER N. RENAUD, PHILIPPE J. CHAMPAGNE,[2] AND MARC SAVARD[3]

Division of Chemistry, National Research Council of Canada, Ottawa, Ont., Canada K1A 0R6

Received September 18, 1978[4]

ROGER N. RENAUD, PHILIPPE J. CHAMPAGNE, and MARC SAVARD. Can. J. Chem. **57**, 2617 (1979).

The trifluoromethylation of mono- and disubstituted ethylene molecules was performed in good yields via the electrochemical oxidation of sodium trifluoroacetate. The relative quantities of monomeric and dimeric products are a function of the concentration of the substrate.

The stereoisomers of the products were separated and identified and, when possible, their stereochemistry was determined by Hnmr and Fnmr spectroscopies.

ROGER N. RENAUD, PHILIPPE J. CHAMPAGNE et MARC SAVARD. Can. J. Chem. **57**, 2617 (1979).

La trifluorométhylation par voie électrochimique de molécules d'éthylène mono et disubstituées fut étudiée. A partir de radicaux trifluorométhyles formés par oxydation anodique d'acétate de sodium, il est démontré qu'il est possible de trifluorométhyle la double liaison en bons rendements. La quantité relative des produits monomériques et dimériques formés est en fonction de la concentration du substrat dans le milieu réactionnel.

Les stéréoisomères des produits formés furent séparés et identifiés, et, dans quelques cas, la stéréochimie fut établie par spectroscopie de rmn du proton et du fluor.

Trifluoromethylation of olefinic compounds via the photolysis of trifluoroiodomethane (1) or hexafluoroazomethane (2) has been the subject of very extensive studies. The results showed that only monotrifluoromethylated products were obtained. More recently, trifluoromethylation of olefins by electrochemical oxidation of trifluoroacetic acid anion gave bis-trifluoromethylated monomeric and dimeric products (3–5) according to Scheme 1.

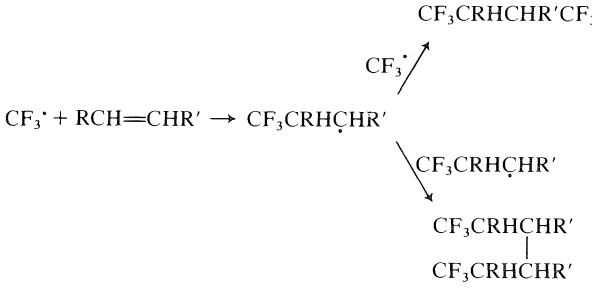

SCHEME 1

The present paper concerns the electrochemical trifluoromethylation of a few monosubstituted, disubstituted, and heterocyclic olefinic compounds (**1–5**) in order to study the generality of the reaction.

The stereoisomers of the products were separated and their physical properties were determined. In some cases the stereochemistry of the isomers was also determined. These results were compared with those obtained for the equivalent methylation reactions (6).

1 CH_2=$CHCOCH_3$

2 CH_3CO_2CH=CH_2

3 EtO_2CCH=$CHCO_2Et$ (*trans* and *cis*)

4

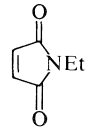

5

Experimental

All starting compounds were commercially available and were further purified by fractional distillation or sublimation. The Pr-optishift-II nmr reagent was obtained from Willow Brook Labs Inc. All melting points are uncorrected. The electrolytic cell has been shown before (6). Gas–liquid chromatographic analyses were done on a Fisher/Victoreen apparatus Series 4400 and preparative glc was carried out using an Aerograph Autoprep model A-700 with a 20 ft × 3/8 in. column, 30% SE30 on 45/60 chromosorb P. A LKB 7000 Ultrorac Fraction collector was utilized for the silica gel chromatographic column separation. Proton magnetic resonance spectra were taken in deuteriochloroform on a Varian Associates spectrometer model EM 360 and are reported in the δ scale. Fnmr spectra were obtained in $CHCl_3$, unless otherwise noted, on a Varian Associates XL 100A spectrometer equipped with a Nicolet Instrument TT 100A FT accessory. The spectra are reported in ppm using $CFCl_3$ as reference. The mass spectra were obtained either from a Finnigan 4000 GC-MS or a Hitachi Perkin-Elmer RMU-6D mass spectrometer.

[1]NRCC No. 17666.

[2]Present address: Department of Energy, Mines and Resources, Canmet, Energy Research Laboratories, Coal Liquefaction Section.

[3]Summer student 1976 and 1977.

[4]Revision received July 11, 1979.

0008-4042/79/192617-04$01.00/0

Electrolysis of Sodium Trifluoroacetate in the Presence of the Olefinic Substrate (General Procedure)

A solution of NaOH (6 g) in TFA (45 mL) was added to the anodic compartment containing a mixture of acetonitrile (180 mL) and water (75 mL). The cathodic compartment was charged with a 1.0 *M* solution of NaOH in water. A current of 1.8 A was passed through the solution for a period of 15 min. The temperature of the reaction mixture was maintained at 22°C using a cold ethanol bath. Then the substrate (0.01 to 0.1 mol) was added and the electrolysis was continued for 7 h at a current of 1.8 A, which is equivalent to a current density of 0.15 A/cm^2.

Purification and Physical Properties of the Products

*(A) From Methyl Vinyl Ketone (**1**)*

The solution after electrolysis of 0.1 mol of freshly distilled methyl vinyl ketone was poured into water (600 mL), a heavy brown oil separating from the aqueous phase. The mixture was extracted with three 75 mL portions of methylene chloride. After the evaporation of the solvent on a rotary evaporator, a brown oil (6.3 g) was obtained. This crude oil was distilled under reduced pressure (10^{-2} Torr) at 50°C into a liquid N_2 trap. The analytical vpc of the distillate showed a mixture of at least six minor peaks and one major one. This mixture was fractionally distilled first under reduced pressure (10^{-2} Torr) at room temperature and the colorless high vapor pressure distillate, collected in a liquid N_2 trap, corresponded to impure 1,2-bis(trifluoromethyl)ethyl methyl ketone. Fnmr: 94.60 (d), 96.55 (t). The ketone could not be obtained pure as it turned dark brown on standing for a few hours at 5°C.

The low vapor pressure fraction, which distilled at 50°C, was collected in an ice trap. The semi-solid distillate proved to be a 1:1 stereoisomeric mixture of *meso*- and *dl*-3,4-bis(βββ-trifluoroethyl)hexane-2,5-dione (3.3 g; 24%). A final purification of the mixture was done on the preparative glc. Fnmr: −68.26 (t), −68.10 (t). *Anal.* calcd. for $C_{10}H_{12}F_6O_2$: C 43.19, H 4.32; found: C 42.57, H 4.36. The solid phase was separated from the above mixture either by centrifuge in a Craig tube or by a simple washing with ether. The oil could not be obtained absolutely free from the solid isomer. The Fnmr showed the presence of about 5% of the solid isomer. The melting point of the white solid isomer was 86–87°C. Fnmr −68.00 (t). *Anal.* found for $C_{10}H_{12}F_6O_2$: C 43.29, H 4.28.

*(B) From Vinyl Acetate (**2**)*

Freshly distilled vinyl acetate (0.1 mol) was trifluoromethylated as described above. The anodic solution was concentrated on a rotary evaporator and the remaining 75 mL was poured into water (600 mL). The resulting aqueous solution was extracted 4 times with 75 mL of methylene chloride. The residue after the evaporation of the solvent was distilled under a pressure of 10^{-2} Torr into a liquid N_2 trap. A yellowish oil (2.8 g) was obtained and shown by analytical vpc to be a mixture of at least three minor and three major compounds. The oil was fractionally distilled at 50°C in a Späth bulb under a pressure of 10^{-2} Torr. The colorless high vapor pressure distillate collected in a liquid N_2 trap was so unstable that it turned dark blue as it warmed up to room temperature. The colorless oil collected in the bulb at room temperature corresponded to a nearly pure 1:1 stereoisomeric mixture of *meso*- and *dl*-3,4-diacetyl-1,1,1,6,6,6-hexafluorohexane (1.6 g; 13.5%). The large difference in retention times of the isomers on the preparative glc allowed them to be separated in pure form. The compound corresponding to the first peak was an oil at room temperature. Fnmr −67.23 (t). *Anal.* calcd. for $C_{10}H_{12}F_6O_4$: C 38.71, H 3.87; found: C 38.62, H 3.96. The second fraction was a solid melting at 61–62°C. Fnmr −67.43 (t). *Anal.* found for $C_{10}H_{12}F_6O_4$: C 38.74, H 4.04.

*(C) From Diethyl Fumarate (**3**)*

The solution after electrolysis of 0.1 mol of substrate was poured into water (600 mL) and the heavy oil that separated was collected (22.5 g). This oil was washed once with water (200 mL) and fractionally distilled at 10^{-2} Torr in a vacuum manifold. Two main fractions were collected as follows:

High Vapor Pressure Fraction

This fraction which was distilled at room temperature and was collected in a liquid N_2 trap consisted of almost pure *meso*- and *dl*-diethyl-2,3-bis(trifluoromethyl)succinate (14.5 g; 47%); Hnmr 1.32 (6H, 2t, methyls), 3.86 (2H, m, methines), 4.27 (4H, q, methylenes); Fnmr −68.10 (d), −68.79 (d); ms *m/e* 310 $(M)^+$, 283 $(M - C_2H_3)^+$ (7), 265 $(M - OC_2H_5)^+$, 237 $(M - CO_2C_2H_5)^+$. *Anal.* calcd. for $C_{10}H_{12}F_6O_4$: C 38.71, H 3.87; found: C 39.32, H 4.12.[5]

The two stereoisomers, obtained in a ratio of 2:1, were separated and identified by the following procedure. The mixture was placed in a Craig tube and cooled to 0°C for 12 h. Under these conditions one of the isomers crystallized out. The cold mixture was then centrifuged in order to separate the two phases. The solid phase (4.7 g) melted at 56–58°C and was nearly pure *meso* isomer according to vpc analysis and nmr spectroscopy: Hnmr 1.34 (6H, t, methyls),[6] 3.80 (2H, m, methines), 4.26 (4H, q, methylenes);[6] Fnmr −68.80 (d).[7] *Anal.* found for $C_{10}H_{12}F_6O_4$ (after recrystallization and sublimation): C 38.40, H 3.83. The liquid phase obtained from the separation of the solid phase by centrifuge still contained about 6% of the *meso* isomer. A purity of over 98% was attained after a second treatment in the Craig tube. The yield of this isomer (shown below to be the *dl* isomer)[8] was 9.3 g; Hnmr 1.32 (6H, t, methyls), 3.78 (2H, m, methines), 4.23 (4H, q, methylenes);[9] Fnmr −68.10 (d).[10] *Anal.* found for $C_{10}H_{12}F_6O_4$: C 38.68, H 3.89.

Low Vapor Pressure Fraction

This fraction was distilled at 100°C (10^{-2} Torr) and was determined by vpc analysis and nmr spectroscopy to be nearly pure 1,4-bis(trifluoromethyl)-1,2,3,4-tetracarboethoxybutane (6.4 g; 26.6%):[11] Fnmr (series of doublets of unequal intensities indicating a mixture of isomers). *Anal.* calcd. for $C_{18}H_{24}F_6O_8$: C 44.81, H 4.98; found: C 44.89, H 5.07. When the isomeric mixture was cooled in a Craig tube for 24 h some crystals were formed. These were separated from the liquid phase by centrifuge and were shown by Fnmr spectroscopy to contain only one of the stereoisomers (mp 68–69°C): Fnmr −69.10 (d). *Anal.* found for $C_{18}H_{24}F_6O_8$: C 44.88, H 4.98.

---

[5]The elemental analysis is a little over the acceptable limit. However, it is introduced in order to indicate that even after a simple distillation the compound is nearly pure.

[6]The triplet and the quartet shifted upfield in the presence of Pr-optishift-II nmr reagent but remained as a triplet and a quartet indicating the presence of the *meso* isomer.

[7]The doublet remained a doublet in the presence of optishift reagent, which also indicates the presence of the *meso* isomer.

[8]A sample of the *dl* isomer in the presence of a trace of triethylamine epimerized into a 1:1 *meso*:*dl* isomeric mixture after 1 min.

[9]The quartet split into two quartets in the presence of optishift reagent indicating the presence of the *dl* isomer.

[10]Some splitting of this doublet could be seen due to long range coupling. The doublet split into two doublets in the presence of the optishift reagent. This result also indicates the presence of the *dl* isomer.

[11]The dimeric product was nearly eliminated by reducing the initial concentration of diethyl fumarate to 0.01 mol.

(D) From Diethyl Maleate (3)

Essentially the same result as with diethyl fumarate was obtained using diethyl maleate as the trifluoromethyl radical acceptor.

(E) From N-*Ethylmaleimide (4)*

The solution obtained from the electrolysis of 0.02 mol of substrate was concentrated on a rotary evaporator and the residue was poured into water (600 mL). The aqueous solution was extracted three times with 75 mL of methylene chloride. The organic solution on concentration gave a colorless oil which was fractionally distilled at 10^{-2} Torr. The fraction which distilled slowly at room temperature (2.5 g) was collected in a liquid N_2 trap and determined by vpc analysis and nmr spectroscopy to be a mixture of 85% of *trans*-2,3-bis(trifluoromethyl)-*N*-ethylsuccinimide[12] and 3% of a peak which was attributed to the *cis* isomer[13] and 12% of starting material. Pure 2,3-bis(trifluoromethyl)-*N*-ethylsuccinimide (mp 29–30°C) was obtained from preparative glc separation. Hnmr 1.20 (3H, t methyl), 3.62 (4H, 2 unresolved q, methylene and methines). Fnmr −71.32 (d, J = 7.36 Hz);[14] ms *m/e* 263 $(M)^+$, 248 $(M - CH_3)^+$, 236 $(M - C_2H_3)^+$ (7), 220 $(M - NCH_2CH_3)^+$. *Anal.* calcd. for $C_8H_7F_6NO_2$: C 36.50, H 2.66, N 5.32; found: C 36.62, H 2.87, N 5.73.

(F) From 2,5-Dihydrothiophene-1,1-dioxide (5)

Freshly sublimed 2,5-dihydrothiophene-1,1-dioxide (0.02 mol) was trifluoromethylated as described above. After concentration of the anodic solution on a rotary evaporator, the residue (≈ 75 mL) was poured into water (600 mL) and the solution was extracted with four 75 mL portions of methylene chloride. A viscous oil was obtained on evaporation of the solvent. The crude material (3.0 g) was distilled at 65°C under a pressure of 10^{-2} Torr into a liquid N_2 trap leaving an unidentified sticky oil in the distilling flask (0.4 g). The analytical vpc of the distillate showed three peaks, one of which corresponded to the starting compound. The Fnmr spectrum of this distillate in acetone showed the presence of four fluorinated compounds whose absorptions were centered at −72.09, −70.76, −68.59, and −67.50 in a ratio of 0.5:1:0.2:0.9 respectively. On heating an aliquot of the mixture at 160°C for 2 min, the peak corresponding to the starting compound on the vpc and the broad singlet at −68.59 in the Fnmr spectrum disappeared. This singlet corresponds most likely to 3-trifluoromethyl-2,5-dihydrothiophene-1,1-dioxide.

The distillate obtained above was dissolved in boiling ether and allowed to cool to 0°C in a Craig tube. The white solid that precipitated was separated by centrifuge. This product, melting at 135–136°C, corresponded to one of the two stereoisomers of 3,4-bis(trifluoromethyl)tetrahydrothiophene-1,1-dioxide. Fnmr −67.50 (2d, J = 4.13 and 4.45 Hz); ms *m/e* 256 $(M)^+$, 207 $(M - HSO)^+$, 192 $(M - SO_2)^+$. *Anal.* calcd. for $C_6H_6F_6O_2S$: C 28.13, H 2.34, S 12.50; found: C 28.34, H 2.45, S 12.34.

The residual oil from above was subjected to column chromatography on silica gel. Elution of the column with a 4:1 hexane – ethyl acetate mixture afforded three main fractions. The first fraction was a solid (0.82 g; 16%) subliming on melting at 104–108°C. It corresponded to the other stereoisomer of 2,3-bis(trifluoromethyl)tetrahydrothiophene-1,1-dioxide. Fnmr −70.72 (broad s); ms *m/e* 256 $(M)^+$. *Anal.* found for $C_6H_6F_6O_2S$: C 28.37, H 2.47, S 12.39. The second fraction corresponded to the same compound obtained from the crude mixture in ether (total yield 0.79 g; 15.4%). The third fraction was an oil (0.49 g; 13%) corresponding to 3-trifluoromethyl-4,5-dihydrothiophene-1,1-dioxide. Hnmr 3.35 (m, 2H, methylene), 3.91 (m, 1H, methine), 6.63 and 6.90 (2H, m, CH=CH). Fnmr −72.10 (d, J = 8.91 Hz); ms *m/e* 186 $(M)^+$. *Anal.* calcd. for $C_5H_5F_3O_2S$: C 32.26, H 2.67, S 17.20; found: C 32.38, H 2.78, S 17.03.

[12]The *trans* isomer was detected by Hnmr analysis. In the presence of optishift reagent, the quartet for the methylene protons split into two quartets as expected for the *trans* isomer.

[13]The compound corresponding to the minor peak was not isolated but showed a doublet in Fnmr at −71.93 ppm. It disappeared after 15 min at room temperature in the presence of trimethylamine presumably by epimerization to the more stable *trans* isomer.

[14]The doublet split into two doublets in the presence of optishift reagent, indicating the presence of the *trans* isomer.

Results and Discussion

The trifluoromethylation of activated ethylene molecules by the electrochemical technique was found to give, in most cases, good yields of 1,2-bis(trifluoromethyl) derivatives and, under certain experimental conditions such as high concentration of the substrate, to give acceptable yields of dimeric products.

The behaviour of the two monosubstituted substrates was similar to that observed previously for ethyl acrylate (4) but in both cases the monomeric products were too unstable to allow them to be isolated in pure form. The dimers, however, are stable. The yields of 3,4-bis(βββ-trifluoroethyl)hexane-2,5-dione and 3,4-diacetyl-1,1,1,6,6,6-hexafluorohexane are acceptable for a one step reaction. The stereoisomers were separated but their configurations were not determined.

Both diethyl fumarate and diethyl maleate give rise to a mixture of *meso* and *dl* isomers in a ratio of 1:2 respectively. Efforts to change this ratio either by varying the current densities or by varying the concentration of the substrate even by a factor of ten were unsuccessful. In order to determine whether epimerization of the products was occurring under the conditions of electrolysis, a run was carried out in which diethyl fumarate was replaced by pure *dl*-diethyl-2,3-bis(trifluoromethyl)succinate. The *dl*-succinate compound was quantitatively recovered unchanged. Therefore, it can be concluded that no epimerization occurred after the product formation. Furthermore, the thermodynamic ratio was found to be 1:1 (*meso*:*dl*) in the presence of triethylamine.

The trifluoromethylation of *N*-ethylmaleimide gives practically only *trans*-*N*-ethyl 2,3-bis(trifluoromethyl)succinimide. The small amount of product which was attributed to the *cis* isomer epimerized readily in the presence of triethylamine to the thermodynamically more stable of the two possible isomers. A slow acid-catalyzed epimerization might also be occurring during the electrolysis, but this fact can only be clarified with the availability of the *cis* isomer.

The trifluoromethylation of 2,5-dihydrothiophene-

1,1-dioxide is an example of a radical addition to an unactivated double bond. The *cis* and *trans* stereoisomers of the 3,4-bis(trifluoromethyl)tetrahydrothiophene-1,1-dioxide, obtained in a ratio of 1:1, were separated and identified but their stereochemistry was not determined. This work is in progress. Important quantities of Δ^2 and Δ^3 unsaturated monotrifluoromethylated products were also obtained. The Δ^2 compound behaves in a similar fashion to the starting compound in that it decomposes on heating to 160°C, presumably to SO_2 and 2-trifluoromethylbutadiene, whereas the Δ^3 isomer is stable at this temperature.

The yields from methylation of olefins activated by electron withdrawing groups (6) are consistently higher than the yields from trifluoromethylation, while the methyl radical did not react at all with the unactivated double bond in 2,5-dihydrothiophene-1,1-dioxide under the present conditions. This can be explained in terms of the much stronger electrophilicity of the trifluoromethyl radical over the slightly nucleophilic methyl radical (8). The CF_3 radical, therefore, reacts more slowly with electron poor olefins and more quickly with electron rich olefins than does the methyl radical.

Acknowledgements

The authors wish to thank Mr. H. Séguin for the elemental analysis, Mr. M. E. Bednas for the mass spectral determinations, Dr. S. Brownstein and Mr. J. Bornais for the Fnmr spectra, and Dr. R. R. Fraser and Mr. R. Capoor for the Hnmr spectra.

1. R. N. HASZELDINE, D. W. KEEN, and A. E. TIPPING. J. Chem. Soc. C, 414 (1970).
2. A. P. STEFANI, L. HERK, and M. SZWARC. J. Am. Chem. Soc. **83**, 4732 (1961).
3. C. J. BROOKES, P. L. COE, D. M. OWEN, A. E. PEDLER, and J. C. TATLOW. J. Chem. Soc. Chem. Commun. 323 (1974).
4. R. N. RENAUD and P. J. CHAMPAGNE. Can. J. Chem. **53**, 529 (1975).
5. V. A. GRINBERG, V. R. POLISHCHUK, E. I. MYSOV, L. S. GERMAN, L. S. KANEVSKII, V. V. TSODIKOV, and Y. B. VASILEV. Bull. Acad. Sci. USSR, Div. Chem. Sci. **26**, 2615 (1978).
6. R. N. RENAUD and P. J. CHAMPAGNE. Can. J. Chem. **57**, 990 (1979).
7. J. H. BEYNOV, R. A. SAUNDERS, and A. E. WILLIAMS. The mass spectra of organic molecules. Elsevier. 1968. p. 250.
8. (*a*) I. M. WHITTEMORE, A. P. STEFANI, and M. SZWARC. J. Am. Chem. Soc. **84**, 3799 (1962); (*b*) S. W. CHARLES, J. T. PEARSON, and E. WHITTLE. Trans. Faraday Soc. **59**, 1156 (1963).

The kinetics and mechanisms of the gas phase pyrolyses of *exo*-2-norbornyl chloride and cyclopentyl chloride

J. L. HOLMES, D. L. MCGILLIVRAY,[1] AND D. YUAN

Chemistry Department, University of Ottawa, Ottawa, Ont., Canada K1N 9B4

Received April 12, 1979

J. L. HOLMES, D. L. MCGILLIVRAY, and D. YUAN. Can. J. Chem. 57, 2621 (1979).

The gas phase pyrolyses of *exo*-2-norbornyl chloride and cyclopentyl chloride were studied in the temperature range 570–670 K. The results obtained show that these compounds behave as typical secondary halides insofar as the kinetics of their hydrogen chloride elimination reactions are concerned. Labelling experiments showed that in the formation of *both* norbornene and cyclopentene, a *cis*-1,2 elimination with a deuterium isotope effect of ~3 was involved. Nortricyclene also was produced from *exo*-2-norbornyl chloride, via a *trans* 1,3 elimination; this process is analogous to a fragmentation of the ionized molecule. No gas phase Wagner–Meerwein rearrangement was involved in the formation of either norbornene or nortricyclene.

J. L. HOLMES, D. L. MCGILLIVRAY et D. YUAN. Can. J. Chem. 57, 2621 (1979).

On a étudié dans l'intervalle de température 570–670 K la pyrolyse en phase gazeuse des chlorures de *exo*-norbornyl-2 et de cyclopentyle. Les résultats obtenus montrent que ces composés se comportent comme des halogénures secondaires typiques dans la mesure ou les cinétiques de leur réactions d'élimination de chlorure d'hydrogène sont impliqués. Les expériences de marquage isotopique montrent que dans la formation des *deux* produits: norbornène et cyclopentène, une élimination *cis* 1,2 est impliquée avec un effet isotopique du deutérium d'environ 3. Par une élimination *trans* 1,3, on aboutit au nortricyclène à partir du chlorure de *exo*-norbornyl-2; ce procédé est analogue à une fragmentation de la molécule ionisée. Aucun réarrangement de Wagner–Meerwein en phase gazeuse n'est impliqué lors de la formation du norbornène ou du nortricyclère.

[Traduit par le journal]

Introduction

The nature of the transition state in the unimolecular gas phase elimination of hydrogen halide from halogen substituted hydrocarbons has been investigated for many years. No direct experimental test has been made as to whether the process occurs as a *cis* or *trans* 1,2 elimination. Maccoll's (1) ion pair theory would allow both a *cis* and a *trans* process, while Benson's semi-ion pair theory (2) would not permit the latter.

We have investigated this mechanistic problem by studying the gas phase pyrolyses of *exo*-2- norbornyl chloride and cyclopentyl chloride using compounds specifically labelled with deuterium.

exo-2-Norbornyl chloride was chosen for this investigation because of its rigid structure and in the belief that the only hydrocarbon product was norbornene.

The gas phase pyrolysis of *exo*-2-norbornyl chloride has been mentioned by Herndon *et al.* (3, 4). They also reported (5) that norbornene rapidly underwent a retro-Diels–Alder reaction yielding ethylene and cyclopentadiene; they measured the kinetics of this reaction in the temperature range 573 K to 673 K.

The gas phase pyrolyses of specifically deuterium labelled cyclopentyl chlorides were also studied in the present work for comparison with the more complex pyrolysis of *exo*-2-norbornyl chloride. The gas phase pyrolysis of the former has been described by Swinbourne (6) who presented the rate expression for the elimination of hydrogen chloride in the temperature range 582 K to 649 K. Herndon *et al.* (3, 4) showed that the rates of elimination of hydrogen chloride from the cyclopentyl compound were similar to those for cyclohexyl chloride.

Experimental

Materials

Hydrogen chloride, deuterium chloride, and deuterium oxide, norbornene, norcamphor, 5-norbornene-2-ol, cyclopentanol, cyclopentanone, and cyclopentyl chloride were obtained commercially.

We have previously reported (7) the preparation of *exo*-2-norbonyl chloride, a mixture of 56% *exo*-3-d_1 and 44% *syn*-7-d_1 *exo*-2-norbornyl chloride and *exo*-2-norbornyl chloride-3,3-d_2. *exo*-2-Norbornyl chloride-*exo*-5-*exo*-6-d_2 was obtained by treating the corresponding alcohol (8) with triphenyl-phosphine as described by Downie and Lee (9). The extent and location of the deuterium was determined by mass spectrometry (7, 10) and nmr analysis (11). Nortricyclene was

[1]Present address: Chemistry Department, University of Victoria, Victoria, B.C., Canada V8W 2Y2.

0008-4042/79/192621-05$01.00/0

prepared by a Bamford-Stevens reaction on the tosyl-hydrazone of norcamphor (12).

Cyclopentyl chloride-*cis*-2-d_1 was prepared by chlorination of the brosylate of cyclopentyl alcohol-*trans*-2-d_1 with tetramethylammonium chloride in dimethyl sulphoxide. Cyclopentyl alcohol-*trans*-2-d_1 was obtained by $LiAlD_4$ reduction of cyclopentene oxide, prepared from cyclopentene and *meta*-chloroperoxybenzoic acid in ether. Using the same method of chlorination, cyclopentyl alcohol-*cis*-2-d_1, prepared from cyclopentene and hexa-deuterodiborane plus hydrogen peroxide in alkaline solution, was converted to cyclopentyl chloride-*trans*-2-d_1. The mono-labelled compounds (95% d_1) were purified by gas chromatography. Repeated deuteration of cyclopentanone with anhydrous sodium acetate in deuterium oxide, followed by $LiAlH_4$ reduction and chlorination by triphenylphosphine dichloride in dimethylformamide gave cyclopentyl chloride-2,2,5,5-d_4 (94%), purified by trap-to-trap distillation. The deuterium content of the labelled compounds was determined from mass spectra obtained at low ionising electron energies.

Apparatus and Procedures

The decompositions were studied in a static Pyrex glass vacuum system of conventional design. The gas chromatographic apparatus consisted of a Gowmac thermal conducitivity detector and a 1 m column containing 10% by weight of di-isodecylphthalate on chromosorb P; helium was used as carrier gas.

A typical pyrolysis was carried out by expanding a vaporised sample into the reaction vessel and measuring the initial pressure using a null glass-diaphragm gauge. The reaction was studied by continually monitoring the pressure of the reaction mixture. In the case of *exo*-2-norbonyl chloride the extent of reaction was also followed by titration of the hydrogen chloride produced and by gas chromatography of the reaction products.

The pyrolysis products of the labelled norbornyl chlorides were trapped as they left the glc column. The olefins produced from the mono-labelled cyclopentyl chlorides were removed from undecomposed starting material by means of two cold traps. The deuterium content of the products was determined by mass spectrometry.

Results and Discussion

Kinetics

(a) exo-*2-Norbornyl Chloride*

The production of hydrogen chloride and cyclopentadiene (and ethylene) in the pyrolysis of *exo*-2-norbornyl chloride were found to follow first order kinetics. If any free radical reactions were present they would be inhibited by the cyclopentadiene produced (13). The first order rate coefficients were independent of pressure (range 10–80 Torr) and the homogeneity of the reaction was established by comparing the rate of formation of HCl in unpacked (s/v 1:1 cm^{-1}) and packed (s/v 5:1 cm^{-1}) reaction vessels (see Table 1). The rate of formation of cyclopentadiene, which is equal to the rate of formation of norbornene (because the rate of the retro-Diels–Alder reaction (5) is very much faster than the rate of formation of norbornene) is shown in Table 1 for the temperature range 573 K to 643 K. The results yield the Arrhenius equation $k_{HCl} = 13.79 \pm 0.70 \exp(-208 \pm 8)/RT\ s^{-1}$, for $C_5H_6(C_7H_{10})$ $\log A = 12.97 \pm 0.70$ and E_a was the same as for the HCl production.

The discrepancy between the rates of formation of the two products is due to the presence of another primary elimination product, nortricyclene. Its presence was confirmed by comparing the gc retention time and mass spectrum of a synthetic sample with that of the pyrolysis product. That the two C_7H_{10} isomers, nortricyclene and norbornene, do not intercovert under pyrolysis conditions was shown as follows. A sample of norbornene placed in the reaction vessel was observed to produce a very rapid pressure increase due to the fast retro-Diels–Alder reaction (5); the reaction products contained *only* ethylene and cyclopentadiene. A sample of nortricyclene similarly treated produced *no* pressure change with or without HCl, and the recovered material contained *only* nortricyclene.

Thus, the gas phase pyrolysis of *exo*-2-norbornyl chloride can be represented as shown below

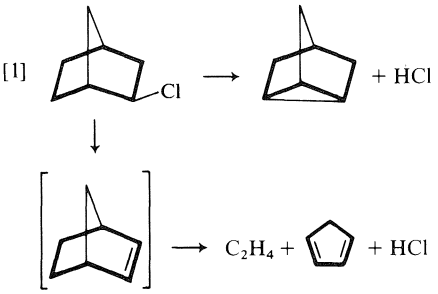

At each temperature it was observed that the rate of formation of cyclopentadiene was a constant fraction of the rate of formation of hydrogen chloride (see Table 1). Owing to the solubility of nortricyclene in *exo*-2-norbornyl chloride and the difficulty of completely sweeping excess chloride into the gas chromatograph, it was not possible to measure accurately the absolute rate of formation of nortricyclene. This was therefore determined indirectly, from the difference in the rates of formation of hydrogen chloride and cyclopentadiene at each temperature. The Arrhenius parameters for nortricyclene generation are $k = 13.29 \pm 0.70 \exp(-207 \pm 8)/RT\ s^{-1}$.

For a similar system, *endo*-2-bornyl chloride, the results have been interpreted as involving appreciable surface induced reactions (14). However, surface catalyzed eliminations of hydrogen halide have much lower activation energies (ca. 85 kJ mol^{-1}) (15) than that observed here for the nortricyclene production. We therefore propose that this reaction is indeed homogeneous.

It is not possible to determine the rates of the

TABLE 1. Rate constants[a] for the formation of hydrogen chloride, cyclopentadiene, and nortricyclene[b] at various temperatures in the range 569 K to 643 K

T (K)	First order rate constant (s^{-1}) for the formation of		
	Hydrogen chloride	Cyclopentadiene	Nortricyclene
569	6.3×10^{-6}	—	—
583	1.5×10^{-5}	1.0×10^{-5}	0.5×10^{-5}
595	3.3×10^{-5}	—	—
603	7.1×10^{-5}	4.7×10^{-5}	2.4×10^{-5}
608	1.2×10^{-4}	—	—
611	1.1×10^{-4}	—	—
612[c]	1.3×10^{-4}	—	—
612.5[c]	1.4×10^{-4}	—	—
614[c]	1.9×10^{-4}	—	—
614.5	1.8×10^{-4}	—	—
619	1.6×10^{-4}	—	—
619.5	2.1×10^{-4}	—	—
623	2.3×10^{-4}	1.4×10^{-4}	0.9×10^{-4}
625	2.9×10^{-4}	—	—
633	5.2×10^{-4}	—	—
639[c]	10×10^{-4}	—	—
643	7.0×10^{-4}	4.5×10^{-4}	2.5×10^{-4}

[a]Rate constants are the average of five or more runs.
[b]Determined from the difference between the rate of formation of hydrogen chloride and cyclopentadiene (see text).
[c]Packed reaction vessel (s/v ratio 5:1).

TABLE 2. Rate coefficients and Arrhenius parameters for the gas phase pyrolysis of cyclopentyl chloride

Cyclopentyl chloride	10^5k (s^{-1})[b]			E (kJ mol^{-1})	A (s^{-1})
	613 K	643 K	663 K		
Unlabelled[a]	12.2 (3.00)	82.4 (2.67)	278 (2.65)	217.0	14.17
trans-2-d_1	12.1 (2.97)	81.5 (2.64)	264 (2.51)	216.7	14.27
cis-2-d_1	8.26 (2.03)	59.1 (1.91)	215 (2.05)	213.7	13.96
2,2,5,5-d_4	4.07 (1)	30.9 (1)	105 (1)	218.5	14.96

[a]Rate constants at 613, 643, and 663 K from Swinbourne (6) were 15.5, 100, and 309 $\times$ 10^{-5} s^{-1}, respectively.
[b]The values in parentheses are the variation of rate ratios with temperature. The rate for the 2,2,5,5-d_4 compound has been taken as unity at each temperature.

individual reactions from the pressure data alone. However, using the rates of formation of hydrogen chloride, cyclopentadiene, and nortricyclene from Table 1 and assuming the norbornene concentration to be negligible, pressure changes were calculated using the equation appropriate for two first order concurrent reactions. Calculated and observed pressure changes agreed to within 10% over conversion ranges from ~10 to 40%.

(b) Cyclopentyl Chloride

The variation of the rate coefficients with temperature and the Arrhenius parameters are shown in Table 2 together with the ratios of the pyrolysis rate coefficients for unlabelled and labelled cyclopentyl chlorides. The results can be explained by invoking an isotope effect of 3 for the elimination of HCl at 613 K; the magnitude of the isotope effect decreases slightly with increasing temperature. This isotope effect is similar to that reported by Blades *et al.* (16, 17) who found an isotope effect of 2.20 for the elimination of HCl from ethyl chloride compared with that of DCl loss from deuterium labelled ethyl chloride at 773 K, and a value of 2.17 for the corresponding process in ethyl bromide. The results show that deuterium in the *trans* position is not involved in the elimination, that in the *cis* position being specifically lost. Thus the pyrolysis of cyclopentyl chloride proceeds by a *cis*-1,2 unimolecular elimination of hydrogen chloride via a four-centered transition state.

Analyses for the deuterium content of the olefin produced from several pyrolyses at low conversions of *trans* and *cis*-2-d_1-cyclopentyl chlorides at temperatures of 613 K and 663 K are shown in Table 3. The isotope content of the olefin produced in the pyrolysis of the *cis* isomer agreed with that calculated assuming an exclusively *cis* elimination. These

TABLE 3. Ratios of labelled and unlabelled cyclopentenes produced from the pyrolysis of *trans* and *cis*-2-d_1-cyclopentyl chloride

(*a*) Found

Cyclopentyl chloride	2% Pyrolysis		10% Pyrolysis	
	C_5H_7D	C_5H_8	C_5H_7D	C_5H_8
	At 613 K			
trans-2-d_1	94.6	5.4	94.7	5.3
cis-2-d_1	69.1	30.9	69.7	30.3
	At 663 K			
trans-2-d_1	94.6	5.4	93.1	6.9
cis-2-d_1	66.5	33.5	65.7	34.4

(*b*) Calculated[a]

Cyclopentyl chloride	613 K		663 K	
	C_5H_7D	C_5H_8	C_5H_7D	C_5H_8
trans-2-d_1	95.0	5.0	95.0	5.0
cis-2-d_1	69.5	30.5	67.4	32.6

[a]The compounds were 95%-d_1, 3.0 was taken as the isotope effect at 613 K and 2.65 at 663 K. Calculation based on the assumption that the pyrolysis proceeded solely via a *cis*-elimination.

results confirm retention of label in the *trans* isomer, proving that *trans* elimination does not occur to greater than 5%.

Labelling Experiments with exo-*2-Norbornyl Chloride*

The extent of *cis* or *trans* elimination in the formation of norbornene can directly be determined by placing a deuterium atom in the *exo* or *endo*-3 position of the halide and measuring the deuterium content of the cyclopentadiene. Similarly, by pyrolysing appropriately labelled compounds and then measuring the deuterium content of the nortricyclene, it should be possible to determine which hydrogen atom(s) is involved in its formation. However, first it was necessary to show whether a Wagner–Meerwein rearrangement took place under pyrolysis conditions. *exo*-2-Norbornyl chloride-3,3-d_2 was prepared and analyzed both for deuterium content and the positional integrity of the label atoms by a specific mass spectrometric method previously reported by ourselves (7, 8). It was found that 11.5% Wagner–Meerwein reaction had occurred during the preparation of the compound and that the deuterium content of the halide was 92% d_2, 8% d_1. This compound was then pyrolyzed and the deuterium content of the products determined mass spectrometrically; the results are shown in Table 4. The deuterium content of the cyclopentadiene was then calculated (assuming a *cis* elimination) using the deuterium content and the Wagner–Meerwein analysis of the starting material. An isotope effect of 3 was assumed for the relative elimination rates of HCl and DCl. For the 3,3-d_2 compound the calculated deuterium contents of the cyclopentadiene products were d_2 = 24%; d_1 = 73%; d_0 = 3% in very good agreement with the experimental results 24%, 71%, and 5% respectively (see Table 4). Thus, only the hydrogen atoms on C-3 are involved in the elimination of hydrogen chloride which yields norbornene. This therefore rules out the involvement of any Wagner–Meerwein rearrangement in the pyrolysis system. The nortricyclene formed in the above pyrolyses was found to have the same deuterium content as the parent chloride indicating that the hydrogen atoms on C-3 were *not* involved in its formation viz.:

[2] 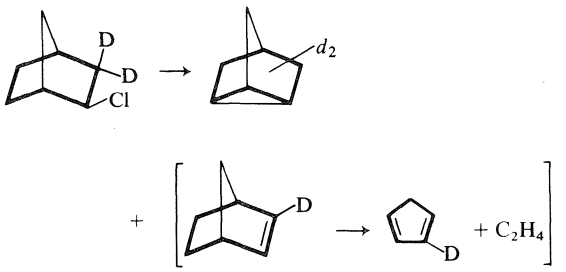

exo-2-Norbornyl chloride, prepared by the addition of deuterium chloride to norbornene (shown by metastable peak analysis (7, 10) to contain 56% *exo*-2-norbornyl chloride-*exo*-3-d_1 and 44% *exo*-2-norbornyl chloride-*syn*-7-d_1), was pyrolyzed and the deuterium content of the products is also shown in Table 4. The deuterium content of the cyclopentadienes, calculated in the same manner as above, were d_1 = 65% and d_0 = 35%. This agrees well with the experimental results (see Table 4) and again is compatible with a *cis* elimination of HCl in the formation of norbornene. Furthermore, the deuterium content of the nortricyclene was again the same as that of the parent compound showing that hydrogen atoms in the *exo*-3 and *syn*-7 positions were not involved in the formation of nortricyclene.

In order to determine whether the *exo* and *endo*-6 hydrogen atoms are involved in nortricyclene formation, the pyrolysis of *exo*-2-norbornyl chlorine-*exo*-5-*exo*-6-d_2 was similarly studied. These results are

[3] 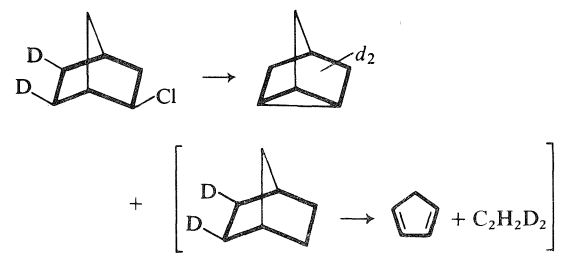

TABLE 4. Deuterium content of the pyrolysis products of various labelled *exo*-2-norbornyl chlorides

Compound	Label %	Wagner–Meerwein in syntheses %	Pyrolysis products	Label %
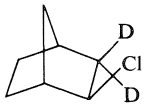	92 d_2 8 d_1	11.5	Cyclopentadiene Ethylene Nortricyclene	24 d_2, 71 d_1, 5 d_0 0 d_2, 2.5 d_1, 97.5 d_0 92 d_2, 5 d_1, 3 d_0
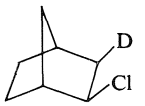	94 d_1 6 d_0	44	Cyclopentadiene Ethylene Nortricyclene	62 d_1 38 d_0 0 d_1, 100 d_0 94 d, 6 d_0
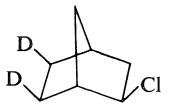	30 d_2 40 d_1 30 d_0	0	Cyclopentadiene Ethylene Nortricyclene	0 d_2, 0 d_1, 100 d_0 31 d_2, 40 d_1, 29 d_0 28 d_2, 41 d_1, 31 d_0
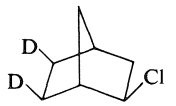	72 d_2 22 d_1 6 d_0	15[a]	Cyclopentadiene Ethylene Nortricyclene	4 d_2, 7 d_1, 89 d_0 63 d_2, 24 d_1, 13 d_0 57 d_2, 34 d_1, 10 d_0

[a]From metastable peak analysis of the chloride it is clear that some 5% of the label is in the 2 and 3 positions. A Wagner–Meerwein rearranged reactant would contain a further 5% deuterium in the 1 and 7 positions. These factors contribute to the discrepancy in the results.

also given in Table 4. The ethylene produced had the same deuterium content as the parent chloride showing that the hydrogen atoms on the *exo*-5 and *exo*-6 positions were *not* involved in the formation of norbornene. The deuterium content of the nortricyclene was the *same* as that of the chloride. We therefore propose that *only* the *endo*-6 hydrogen atom is involved in the formation of nortricyclene; i.e. that a *trans* elimination takes place in this reaction. This pyrolysis was repeated using a sample of *exo*-2-norbornyl chloride – *exo*-5-*exo*-6-d_2 which was richer in deuterium and these results are given in Table 4. They agree with the previous results.

Additional support for the above proposal comes from our study of the elimination of a chloroethyl radical from the molecular ion of *exo*-2-norbornyl chloride (10), where it was shown that the reaction specifically involved the *endo*-6 H atom.

[4] 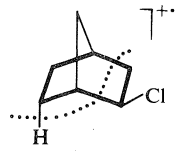 $\longrightarrow C_5H_7^+ + C_2H_4Cl^{\cdot}$

1. A. MACCOLL. *In* Theoretical organic chemistry. Butterworth and Co. Ltd., London. 1958.
2. S. W. BENSON and A. N. BOSE. J. Chem. Phys. **39**, 3463 (1963).
3. W. C. HERNDEN, J. M. SULLIVAN, and M. B. HENLEY. J. Phys. Chem. **67**, 2842 (1963).
4. W. C. HERNDEN, J. M. SULLIVAN, M. B. HENLEY, and J. M. MARION. J. Am. Chem. Soc. **86**, 5691 (1964).
5. W. C. HERNDEN, W. C. COOPER, and M. J. CHAMBERS. J. Phys. Chem. **68**, 2016 (1963).
6. E. S. SWINBOURNE. J. Chem. Soc. 2371 (1960).
7. J. L. HOLMES, D. MCGILLIVRAY, and N. S. ISAACS. Can. J. Chem. **48**, 2791 (1970).
8. J. L. HOLMES and D. MCGILLIVRAY. Org. Mass Spectrom. **7**, 559 (1973).
9. I. M. DOWNIE and J. B. LEE. Tetrahedron, **23**, 359 (1967).
10. J. L. HOLMES and D. MCGILLIVRAY. Org. Mass Spectrom. **5**, 1339 (1971).
11. J. M. BROWN and M. C. MCIVOR. Chem. Commun. 239 (1969).
12. A. NICKON and N. H. WERSTIUK. J. Am. Soc. **88**, 4543 (1966).
13. A. MACCOLL. Chem. Rev. **69**, 53 (1969).
14. S. W. BENSON and H. E. O'NEAL. Kinetic data on gas phase unimolecular reactions. National Bureau of Standards, Washington. 1970.
15. S. S. SHAPIRO, E. S. SWINBOURNE, and B. C. YOUNG. Aust. J. Chem. **17**, 217 (1964).
16. A. T. BLADES, P. W. GILDERSON, and M. G. H. WALLBRIDGE. Can. J. Chem. **40**, 1526 (1962).
17. A. T. BLADES, P. W. GILDERSON, and M. G. H. WALLBRIDGE. Can. J. Chem. **40**, 1533 (1962).

Electron scattering cross sections of gaseous pentanes and hexanes[1]

GORDON R. FREEMAN, ISTVÁN GYÖRGY, AND SAM S.-S. HUANG
Chemistry Department, University of Alberta, Edmonton, Alta., Canada T6G 2G2

Received May 15, 1979

GORDON R. FREEMAN, ISTVÁN GYÖRGY, and SAM S.-S. HUANG. Can. J. Chem. **57**, 2626 (1979).

Electron scattering cross sections σ_v have been estimated as functions of electron velocity v for six gaseous pentanes and hexanes. The scattering cross section of each compound has a minimum in the vicinity of $v = (2\text{–}3)\ 10^7$ cm/s, corresponding to an electron energy of 0.1–0.2 eV. For the pentanes, the scattering cross sections on the low energy side of the minimum increase with increasing sphericity of the molecules, while the minimum tends to shift to higher energies. The same is true of the hexanes.

GORDON R. FREEMAN, ISTVÁN GYÖRGY et SAM S.-S. HUANG. Can. J. Chem. **57**, 2626 (1979).

Les sections transversales σ_v de diffusion électronique sont évaluées comme étant des fonctions de la vitesse v de l'électron pour six pentanes et hexanes à l'état gazeux. Pour chaque composé la section transversale de diffusion a un minimum, au voisinage de $v = (2\text{–}3)\ 10^7$ cm/s, correspondant à une énergie électronique de 0.1–0.2 eV. Pour les pentanes, du côté de basse énergie du minimum, les sections transversales de diffusion augmentent avec le sphéricité des molécules, pendant que le minimum tend à glisser vers de plus grandes énergies. On observe la même tendance pour les hexanes.

[Traduit par le journal]

The effects of density and temperature on thermal electron transport in gaseous and liquid hexanes (1) and pentanes (1, 2) have recently been reported. The treatment of electron scattering by molecules in the low density limit involved the assumption that the scattering cross section σ_v for electrons of velocity v could be approximated by eq. [1] over the limited range of velocities used.

$$[1] \quad \sigma_v = A_\alpha v^{-\alpha}$$

where A_α is a constant whose value depends on α. It has been found that for some of the butenes eq. [1] is inadequate to describe the behavior over the temperature range 300–500 K (3). The pentane and hexane results have therefore been subjected to a more detailed numerical analysis, using trial and error to extract σ_v as a function of v from plots of mobility against temperature. The cross section of each compound has a minimum in the vicinity of $v = (2\text{–}3)\ 10^7$ cm/s, corresponding to an electron energy of 0.1–0.2 eV. The same result had been found earlier for simpler alkanes (4).

When the velocity distribution is Maxwellian and scattering is mainly elastic,[2] the low density limit of the mobility μ_{1d} (cm^2/V s) may be represented (3, 5) by eq. [2].

$$[2] \quad \mu_{1d} = (5.23 \times 10^{-14}/nT^{2.5}) \times \int_0^\infty (v^3/\sigma_v) \exp(-3.30 \times 10^{-12} v^2/T)\, dv$$

where n (molecule/cm^3) is the gas density and T (K) is the temperature.

A first approximation to σ_v as a function of v was obtained using eq. [1] in the manner described previously (1, 2). A plot of σ_v against v thus obtained was then adjusted to improve the agreement of values of μ_{1d} calculated numerically from eq. [2] with those observed over a range of temperatures.

The mobilities normalized for gas density, $n\mu_{1d}$, are shown as functions of temperature in Fig. 1. The experimental data for each compound display curvature towards the T axis, with the exception of those for n-pentane and neopentane. We believe that curvature in the n-pentane results is obscured by the experimental scatter.

Cross sections derived from the mobilities are

[1]Assisted financially by the National Science and Engineering Research Council and the International Atomic Energy Agency.

[2]At the low energies involved in the present work, the magnitude of the elastic scattering cross section is much greater than that of the inelastic scattering cross section (see, for example, ref. 4). The mobility is restricted by collisions that change the direction of flight of the electrons. The flight direction is changed by both elastic and inelastic collisions, but under the present conditions the former dominate. The amount of energy exchanged during the elastic collisions is small, however, and the relatively infrequent inelastic collisions govern the electron energies in the present systems (2). This explains the conclusion that "... the electrons are cooled predominantly by inelastic collisions with the hydrocarbons, in contrast to the behavior with the monatomic molecules of xenon" (1), that had been derived from consideration of the ratio v_d(threshold)/c_0.

0008-4042/79/192626-03$01.00/0

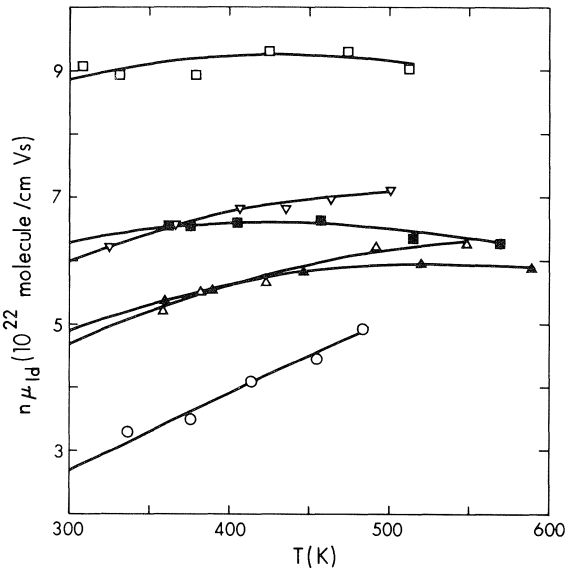

FIG. 1. Temperature dependence of density normalized mobilities $n\mu_{1d}$ of thermal electrons in low density pentane and hexane gases. □, *n*-pentane; ▽, isopentane; ○, neopentane; △, cyclopentane; ■, *n*-hexane; ▲, cyclohexane. Mobilities from ref. 2 were decreased by a factor of 1.21 and those from ref. 1 were increased by a factor of 1.08 (hexanes) or 1.03 (cyclopentane) to correct for errors in measurement of the gap between the electrodes. The lines represent the mobilities calculated from the cross sections displayed in Fig. 2.

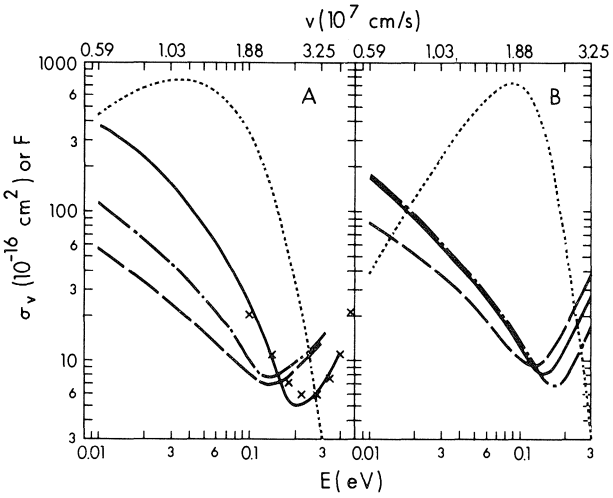

FIG. 2. Electron scattering cross sections σ_v of pentane and hexane molecules, as functions of electron velocity v or energy E. *A*: ---, *n*-pentane; ·····, isopentane; —, neopentane; ×, neopentane cross sections from ref. 7; ··· Maxwellian E and v distribution at 400 K, $F = (1.36 \times 10^{-7} v^2/T^{1.5}) \exp(-3.3 \times 10^{-12} v^2/T)$. *B*: ---, *n*-hexane; ·····, cyclopentane; —, cyclohexane; ···, scattering probability distribution for *n*-hexane at 400 K, $F = 2 \times 10^{-33}(v^3/\sigma_v) \exp(-3.3 \times 10^{-12} v^2/T)$. The factors F are the true values multiplied by 10^{10} in *A* and 2×10^{-33} in *B* to fit the displayed scale.

given in Fig. 2. Mobilities calculated from these cross sections are represented by the lines in Fig. 1.

To designate the energy region of main interest, the Maxwellian distribution of electron velocities and energies at 400 K is shown in Fig. 2*A*, and the scattering probability distribution for *n*-hexane at 400 K is given in Fig. 2*B*. The energy region of greatest sensitivity in the curve fitting procedure is in the vicinity of the maximum in the scattering probability curve (Fig. 2*B*). Under the present conditions the region ranges from about 0.04–0.14 eV for *n*-hexane and *n*-pentane to about 0.05–0.22 eV for neopentane. The cross section curves become progressively more uncertain with increasing distance from this region.

The most accurate portion of each σ_v curve in Fig. 2 lies on the low energy side of the minimum. The scattering cross sections of the pentanes in this region increase with increasing sphericity of the molecules, while the minimum tends to shift to higher energies. The same is true of the hexanes. The reason for the correlation between the scattering properties and molecular sphericity is not known. The correlation for the low density gases is different from that for the normal liquids of the same compounds (2, 6).

The cross sections for neopentane are in satisfactory agreement with those reported recently by McCorkle *et al.* (7), in the region of overlap.

When scattering cross sections derived from mobilities are averaged for comparison of one molecule with another, the appropriate weight is placed on the most sensitive region of velocities by using eq. [3].

[3] $$\sigma_{ave} = \langle v \rangle / \langle v/\sigma_v \rangle = 4.59 \times 10^{22} T^2 \Big/ \int_0^\infty (v^3/\sigma_v) \exp(-3.30 \times 10^{-12} v^2/T)\, dv$$

The simple average $\langle \sigma_v \rangle$ is commonly used, but it tends to emphasize the larger values of σ_v, where the curve fitting is least accurate.

[4] $$\langle \sigma_v \rangle = 4\pi (m/2\pi kT)^{3/2} \int_0^\infty \sigma_v v^2 \exp(-mv^2/2kT)\, dv$$

$$= 1.35 \times 10^{-17} T^{-1.5} \int_0^\infty \sigma_v v^2 \exp(-3.30 \times 10^{-12} v^2/T)\, dv$$

TABLE 1. Average scattering cross sections at 300 K[a]

Molecule	σ_{ave}[b]	$\langle\sigma_v\rangle$[c]
n-C_5H_{12}	15.7	31.8
	(15.1[d])	(23.2[d])
i-C_5H_{12}	23.2	60.5
neo-C_5H_{12}	52.0	200.0
c-C_5H_{10}	29.6	91.0
n-C_6H_{14}	22.1	48.6
	(21.2[d])	(31.0[d])
c-C_6H_{12}	28.4	86.0

[a]From Fig. 2 unless otherwise noted. In units of 10^{-16} cm^2.
[b]Equation [3]. Recommended.
[c]Equation [4]. This type of average is not recommended when σ_v has been estimated from mobility data.
[d]Using eq. [1] with $\alpha = 1.0$, inserted in eq. [2].

The difference between σ_{ave} and $\langle\sigma_v\rangle$ is illustrated in Table 1. The mobilities in *n*-pentane and *n*-hexane over the present range of temperatures can be reproduced moderately well by using eq. 1 for σ_v with $\alpha = 1.0$. The values of σ_{ave} so obtained are nearly the same as those obtained from Fig. 2 (see Table 1). However, the values of $\langle\sigma_v\rangle$ are greatly different for the two forms of σ_v (Table 1). The average scattering powers of molecules should be compared through σ_{ave}, not through $\langle\sigma_v\rangle$, when σ_v has been estimated from mobility data.

Acknowledgement

We thank Norman Gee for writing the computer programs used in this work.

1. S. S.-S. HUANG and G. R. FREEMAN. Can. J. Chem. **56**, 2388 (1978).
2. I. GYÖRGY and G. R. FREEMAN. J. Chem. Phys. **70**, 4769 (1979).
3. T. WADA and G. R. FREEMAN. To be published.
4. C. W. DUNCAN and I. C. WALKER. J. Chem. Soc. Faraday II, **70**, 577 (1974).
5. L. H. G. HUXLEY and R. W. CROMPTON. The diffusion and drift of electrons in gases. Wiley, New York. 1974. p. 69.
6. J.-P. DODELET and G. R. FREEMAN. Can. J. Chem. **50**, 2667 (1972).
7. D. L. MCCORKLE, L. G. CHRISTOPHOROU, D. V. MAXEY, and J. G. CARTER. J. Phys. B**11**, 3067 (1978).

Hydrogen bond assisted reactions: *C*- and *O*-alkylations, sulphenylations, and Michael additions aided by polymer immobilized fluoride ion

JACK M. MILLER,[1] STEPHEN R. CATER,[2] AND KWOK-HUNG SO[3]
Chemistry Department, Brock University, St. Catharines, Ont., Canada L2S 3A1
AND
JAMES H. CLARK
Department of Chemistry, University of York, Heslington, York, England Y01 5DD

Received April 23, 1979

JACK M. MILLER, STEPHEN R. CATER, KWOK-HUNG SO, and JAMES H. CLARK. Can. J. Chem. 57, 2629 (1979).

Hydrogen bond assisted *C*- and *O*-alkylations, sulphenylations, and Michael additions have been carried out with the aid of fluoride ion immobilized on strongly basic anion exchange resins.

JACK M. MILLER, STEPHEN R. CATER, KWOK-HUNG SO et JAMES H. CLARK. Can. J. Chem. 57, 2629 (1979).

On a effectué des réactions de *C*- et *O*-alkylations, de sulphénylations et d'additions de Michael facilitées par des liaisons hydrogènes en faisant appel à l'ion fluorure immobilisé sur des résines échangeuses anioniques fortement basiques.

[Traduit par le journal]

Introduction

We have previously shown that the fluoride ion is capable of behaving as an electron source in hydrogen bonds formed with a wide variety of protic organic compounds (1). From a chemical reactivity point of view, the nucleophilicity of the electron acceptors in these H-bonds is enhanced. This prompted us to investigate a number of alkali metal fluoride and tetraalkylammonium fluoride assisted organic reactions carried out under heterogeneous and homogeneous conditions including *C*-alkylations (2, 3), *O*-alkylations (1, 4–6), *N*-alkylations (1), sulphenylations (7), and Michael additions (3, 8). The results of these investigations clearly demonstrated the fluoride ion method to be a viable alternative to more conventional base-assisted processes.

In the last few years, functionalized insoluble polymers have been developed for a variety of sequential and one-step organic syntheses (9–11). These include a number of reactions using polymer supported phase transfer catalysts often prepared from Merrifield type DVB crosslinked chloromethylated polystyrene resin (12–18). One recent article on this subject described the fluoride ion assisted preparation of Merrifield resin ester (19). The realization that strongly basic ion exchange resins are simply insoluble quaternary ammonium salts led us to investigate the possibility of carrying out typically fluoride-ion mediated reactions in the presence of commercial strongly basic anion exchange resins converted to their fluoride form (20*a*). Another communication published during the writing of this paper describes the synthesis of phthalimidomethyl esters of *N*-protected amino acids using the strongly basic anion exchange resin, Amberlyst A-26, containing fluoride ions (20*b*).

Other reported examples of the synthetic use of anion exchange resins include the synthesis of nitrites (21), the *C*-alkylation of malonic esters and related compounds (22), fluorinations (23, 24), alkylations (25, 26), and reductions (27). Our preliminary work (20*a*) showed that while the fluoride forms of commercial analytical type resins such as Amberlite[4] IRA-400 and Dowex[5] 1-X8 and lower crosslinked resins such as Dowex 1-X2 were not particularly effective, the fluoride forms of Dowex MSA-1 macroporous resin and Amberlyst A-26 and A-27 macroreticular resins, which are designed for use in non-aqueous solvents, gave satisfactory results. We now report our detailed results for H-bond assisted reactions using the fluoride forms of these resins. The results have been optimized in terms of the resin, solvent, temperature, and regenerative capability of the resin.

[1]To whom all correspondence should be addressed.
[2]Undergraduate Summer Assistant.
[3]Abstracted in part from the M.Sc. thesis of K. H. So, Brock University, 1978.

[4]Amberlyte and Amberlyst are ion exchange resin tradenames used by Rohm and Hass Co.
[5]Dowex is an ion exchange resin tradename used by Dow Chemical Co.

0008-4042/79/192629-04$01.00/0

TABLE 1

(*a*) Summary of reactions

Reactants	Product	Time (h)	*T* (°C)	Solvent	Resin[b]	Yield[a] (%)
		C-Alkylations				
$[MeC(O)]_2CH_2$ + MeI	$[MeC(O)]_2CHMe$	24	20	THF	A-26	60
		24	20	THF	A-26	52
		24	20	DMF	A-26	32
		24	65	THF	A-26	57
		24	60	DMF	A-26	35
		24	20	THF	A-26[c]	53
		24	20	THF	A-26[e]	35
		24	20	THF	A-27	70
		24	20	THF	A-27	65
		12	20	THF	A-27	60
		24	60	THF	A-27	65
		24	20	DMF	A-27[d]	35
		24	20	THF	A-27	50
		24	20	THF	MSA-1	0
		48	60	DMF	MSA-1	70
		24	20	THF	IRA-900	42
		O-Alkylation				
PhOH + MeI	PhOMe	24	60	DMF	A-26	65
		24	60	DMF	MSA-1	50
		24	65	THF	A-26	40
p-$NO_2C_6H_4OH$ + MeI	p-$NO_2C_6H_4OMe$	24	60	DMF	A-26	65
		24	60	DMF	MSA-1	50
		24	65	THF	A-26	40
		Sulphenylation				
$[MeC(O)]_2CH_2$ + PhSH + air	$[MeC(O)]_2CH(SPh)$	24	60	DMF	MSA-1	75
		24	60	DMF	A-26	20
		24	60	DMF	IRA-900	20
		24	65	THF	A-26	15
		24	65	THF	A-27	15
		24	80	Benzene	A-27	15
		24	20	DMF	A-27	15
		24	20	THF	A-26	15
		24	60	DMF	A-27	11
		24	100	DMF	A-26	7
$[MeC(O)]_2CH_2$ + Ph_2S_2		24	60	DMF	MSA-1	75
		Michael addition				
$MeC(O)CH{=}CH_2$ + PhSH	$MeC(O)CH_2CH_2SPh$	24	20	THF	MSA-1	80
		24	20	THF	A-26	75
		24	65	THF	A-26	70
		24	20	THF	A-26	63[c]
		24	20	DMF	A-27	58
		24	20	DMF	A-26	53
		24	20	DMF	None	40

[a]Yields were determined by ^1H nmr peak intensities for products and starting material and by gc peak areas. Known compounds were identified by ^1H nmr and gc/ms.
[b]Characteristics of the commercial strongly basic anion exchange resins in their chloride forms taken from manufacturer's literature (see Table 1(*b*)).
[c]Resin was regenerated from used resin.
[d]Only 15 mL resin used.
[e]Resin was previously used in a Michael addition reaction.

Experimental

^1H nmr spectra were recorded in $CDCl_3$ on a Varian A60 (60 MHz) spectrometer ($SiMe_4$ internal standard). Mass spectra were obtained on a AEI MS-30 double beam double focussing mass spectrometer interfaced to a Pye 104 G.C. via a Biemann separator. Samples were introduced either via a solids probe or via the gas chromatograph (6 ft × 1/4 in. column, 3% SE30 on Chromosorb W).

The resins were converted to their fluoride forms by the following general procedure. The resins were obtained in their chloride forms and were first treated with an excess of 10% sodium bicarbonate followed by at least five bed volumes of 10% NaOH solution over a period of 1.25 h to convert the resins to their hydroxide forms. The resins were washed with water until neutral and in order to determine the capacity of the resin, a sample was washed with acetone and ether, dried, and weighed. The sample was then reacted with excess 1.000 *M*

TABLE 1 (*Concluded*)

(*b*) Characteristics of commercial anion exchange resins from manufacturer's literature

Resin	Designation	Moisture capacity (%)	Ion exchange capacity[c]		Effective size (mm)	Av. pore diameter[d] (Å)	Surface area (m^2/g)	Max *T* (°C)	
			Dry resin (meq/g)	Wet resin (meq/mL)				Cl^-	OH^-
Amberlyst[a] A-26	Macroreticular	61–65	4.1–4.4	0.95–1.1	0.45–0.55	400–700	25–30	90	60
Amberlyst[a] A-27	Macroreticular	56–62	2.6 min	0.7 min	0.4–0.5	400–800	60–70	N.A.	N.A.
Amberlite[a] IRA-900	Macroreticular	60–64	4.2 min	1.0 min	0.43–0.52	N.A.	N.A.	77	60
Dowex[b] MSA-1	Macroporous	57–63	3.8–4.2	1.2	20–50 mesh	N.A.	N.A.	150	50

[a]Rohm & Haas; active group quaternary ammonium; cross linkage (% DVB) not defined.
[b]Dow; active group trimethylbenzylammonium; cross linkage (% DVB) not defined.
[c]Min. = minimum exchange capacity.
[d]N.A. = not available.

HCl, filtered off, and washed. The resulting solution was back-titrated with 1.000 *M* NaOH to a bromothymol blue end point. The calculated capacities of the Amberlyst resins were between 0.83 and 0.97 meq/cm^3 of moist resin. The hydroxide resins were converted to their fluoride forms with 1 *M* HF solution, a slight excess of acid being used. It was also possible to convert the chloride form of the resin to the fluoride form by direct exchange with a KF solution although we preferred the more quantitative neutralization procedure. Once in the fluoride form, the resin was washed with water until neutral, followed by several bed volumes of methanol, then washed with the solvent that was to be used in the proceeding reaction. Regeneration of used resins followed a similar procedure. The A-26 resin appeared to be particularly easy to regenerate whereas the A-27 resin appeared to break down, at least physically, after some of the reactions.

In an attempt to determine the extent of resin fluorination after a typical conversion, samples of dried resin were reacted with α-bromoacetophenone, α-fluoroacetophenone being the expected product. Some chloroacetophenone was also produced, suggesting that some unconverted chloride resin was also present. Typical F/Cl ratios were 9:1.

In a typical reaction, 2,4-pentanedione (0.01 mol) was added to 40 cm^3 of A-27 F^- resin (ca. 0.035 mol F^-) in 50 cm^3 THF. After stirring for several minutes, iodomethane (0.01 mol) was added and reaction was allowed to proceed with stirring, at room temperature for 24 h. At the end of this time, the resin was filtered off and washed with several portions of diethyl ether. The combined filtrates were evaporated yielding 0.95 g of material which was shown by nmr and gc/ms to be the starting diketone (20–25 mol%) and the 3-methyl derivative (75–80 mol%). This corresponds to a yield of 65% based on diketone used. Somewhat better yields could be obtained by using a 10% excess of iodomethane.

Results and Discussion

The results of our detailed investigations into the efficiency of fluoride resins in some typically base-assisted organic reactions are summarized in Table 1. There are essentially three important aspects of these results to be considered: the relative efficiencies of the resins used, the loss in efficiency on using a regenerated resin, and the choice of solvent.

Overall, there does not seem to be one particular resin which consistently gives the best yields although some definite trends are apparent. In particular, MSA-1 F^- resin seems to be a particularly effective catalytic resin in that it is clearly the best choice for both Michael additions and sulphenylations. The latter reactions are especially sensitive to the choice of resin in that only the MSA-1 F^- resin gives a satisfactory yield. In an attempt to isolate the cause of this apparent anomaly, we attempted to convert the thiolalone to the disulphide in the presence of the A-26 F^- resin and found that 100% reaction occurred within 24 h at room temperature. This leads us to believe that the efficiency of the A-26 and A-27 F^- resins may be impaired by the presence of water (produced in the thiol oxidation step) and we are presently investigating the possibility as part of a general project into the effect of water on fluoride ion mediated reactions.

While the MSA-1 F^- resin is superior for catalytic reactions, alkylations (where the resin undergoes chemical reaction), and in particular *C*-alkylation, are best carried out using A-26 and A-27 F^- resins. IRA-900 F^- resin gave moderate yields of product in *C*-alkylation experiments. We found that IRA 938 resin and Whatman DE32 ion exchange cellulose were only converted to their F^- forms with considerable difficulty and we did not attempt any reactions with them.

In most reactions, a 2- to 4-fold excess of resin was used. Doubling the quantity of resin did not significantly affect the yields for *C*- and *O*-alkylations. In the absence of resin or in the presence of resin in its Cl^- form, no *C*- or *O*-alkylation was observed although some reaction did occur in the Michael additions.

We have found that with regard to the reusability and efficiency of regeneration of the F^- resins, the A-26 is superior and we report *C*-alkylation yields

using regenerated resin and resin that was previously used in a (catalytic) Michael addition (Table 1). While the regenerated resin is of comparable efficiency to the fresh sample, the previously used resin gives noticeably lower product yields which implies significant loss in activity but not appreciable physical degeneration on reaction.

With regard to the choice of solvent, it would seem that those reactions which proceed smoothly at or near room temperature are best carried out in THF whereas the higher boiling DMF is preferred for those reactions requiring higher temperatures. Reaction times were usually kept at 24 h although where reaction monitoring was attempted, optimum yields seemed to occur at 12 h or less.

Analysis of the product mixtures did reveal the presence of some side-products, in particular the disulphide (strictly an intermediate) in the sulphenylations and Michael additions and also the olefin dimer for the latter reactions.

In general, the yields reported here are comparable or slightly poorer than those obtained using soluble tetraalkylammonium fluoride (2, 3, 6–8), silica supported tetraalkylammonium fluoride (28), or KF supported on Celite (29). One possible explanation for some of the low yields obtained in reactions with the F^- resins is that it is often difficult to ensure complete extraction of products from the resin. Despite such shortcomings, the overall success of the method, demonstrated here and by independent research (20*b*), suggests that fluoride resins are useful and inexpensive aids to the synthetic chemist.

Acknowledgements

The authors wish to thank the Natural Sciences and Engineering Research Council of Canada and Imperial Oil Limited for financial support (J.M.M.), N.A.T.O. for a collaborative research travel grant (J.H.C. and J.M.M.), and Mr. T. R. B. Jones for running the mass spectra.

1. J. H. CLARK and J. M. MILLER. J. Am. Chem. Soc. **99**, 498 (1977).
2. J. H. CLARK and J. M. MILLER. J. Chem. Soc. Perkin Trans. I, 1743 (1977).
3. J. H. CLARK, J. M. MILLER, and K. H. SO. J. Chem. Soc. Perkin Trans. I, 941 (1978).
4. J. H. CLARK, H. L. HOLLAND, and J. M. MILLER. Tetrahedron Lett. 3361 (1976).
5. J. H. CLARK and J. M. MILLER. Tetrahedron Lett. 599 (1977).
6. J. M. MILLER, K. H. SO, and J. H. CLARK. Can. J. Chem. **57**, 1887 (1979).
7. J. H. CLARK and J. M. MILLER. Can. J. Chem. **56**, 141 (1978).
8. J. H. CLARK and J. M. MILLER. J. Chem. Soc. Perkin Trans. I, 2063 (1977).
9. C. C. LEZNOFF. Chem. Soc. Rev. **3**, 65 (1974).
10. C. G. OVERBERGER and K. N. SANNES. Angew. Chem. Int. Ed. Engl. **13**, 99 (1974).
11. C. C. LEZNOFF. Acc. Chem. Res. **11**, 327 (1978).
12. S. L. REGEN. J. Am. Chem. Soc. **97**, 5956 (1975).
13. J. M. BROWN and J. A. JENKINS. J. Chem. Soc. Chem. Commun. 458 (1976).
14. H. MOLINARI, F. MONTANARI, and P. TUNDO. J. Chem. Soc. 639 (1977).
15. W. M. MCKENZIE and D. C. SHERRINGTON. J. Chem. Soc. Chem. Commun. 541 (1978).
16. M. TUMOI, M. IKEDA, and H. KAKIUCHI. Tetrahedron Lett. 3757 (1978).
17. P. TUNDO. Synthesis, 315 (1978).
18. S. COLONNA, R. FORNASIER, and U. PFEIFFER. J. Chem. Soc. Perkin Trans. I, 8 (1978).
19. K. HORIKI, K. IGANO, and K. INOUYE. Chem. Lett. 165 (1978).
20. (*a*) J. M. MILLER, K. H. SO, and J. H. CLARK. J. Chem. Soc. Chem. Commun. 466 (1978); (*b*) K. HORIKI. Synth. Commun. **8**, 515 (1978).
21. M. GORDON, D. L. PAMPHILIS, and C. E. GRIFFIN. J. Org. Chem. **28**, 698 (1963).
22. K. SHIMO and S. WAKAMATSU. J. Org. Chem. **28**, 504 (1963).
23. C. L. BORDERS, JR., D. L. MACDONELL, and J. L. CHAMBERS, JR. J. Org. Chem. **37**, 3544 (1972).
24. G. CAINELLI and F. MANESCALCHI. Synthesis, 472 (1976).
25. G. CAINELLI and F. MANESCALCHI. Synthesis, 723 (1975).
26. G. GELBARD and S. COLONNA. Synthesis, 113 (1975).
27. H. W. GIBSON and F. COURTNEY BAILEY. J. Chem. Soc. Chem. Commun. 815 (1977).
28. J. H. CLARK. J. Chem. Soc. Chem. Commun. 789 (1978).
29. T. ANDO and J. YAMAWAKI. Chem. Lett. 45 (1979).

Rare-gas sensitized radiolysis of gaseous isobutene: ionic processes

JAN A. HERMAN

Département de chimie et Centre de Recherches sur les Atomes et les Molécules, Université Laval, Québec (Qué.), Canada G1K 7P4

Received May 3, 1979

JAN A. HERMAN. Can. J. Chem. **57**, 2633 (1979).

Irradiation of isobutene at low pressure in the presence of suitable scavengers or mixed with the rare gases Ar, Kr, and Xe shows that 2-methyl-but-2-ene is partially formed in ionic processes. These processes involve polymeric ions of isobutene formed in "head-to-head" reactive encounters with neutral isobutene. The resulting ionic species, which have internal structural tension, can isomerize with a subsequent elimination of ethylene, or decompose to give 2-methyl-but-2-ene. The rare-gas sensitized radiolysis confirms the already established reaction channels for formation of the main products.

JAN A. HERMAN. Can. J. Chem. **57**, 2633 (1979).

L'irradiation de l'isobutylène à basse pression et présence d'intercepteurs adéquats, de même que la radiolyse sensibilisée aux gaz nobles Ar, Kr et Xe, de ce même composé, indique que le 2-méthyl-butène-2 est formé en partie par voie ionique. Ce processus est la conséquence de réaction "tête-à-tête" entre les ions polymériques et l'isobutylène neutre. L'intermédiaire ainsi formé peut, soit isomériser avec élimination de l'éthylène, soit se décomposer en donnant du 2-méthyl-butène-2. La radiolyse sensibilisée aux gaz nobles confirme les voies réactionnelles déjà établies de formation des produits principaux.

Introduction

In a recent mass-spectrometric investigation of ion/molecule reactions in gaseous isobutene it was assumed that the condensed ionic species formed during the polymerization processes may decompose to give neutral ethylene and branched pentenes, as depicted in Scheme 1 (1). Such decomposition processes result from "head-to-head" bonding between the condensed ion and the tertiary carbon of the neutral isobutene, giving rise to the formation of a species with internal structural strain,

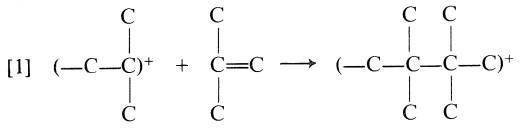

This ion decomposes on reactive encounter,

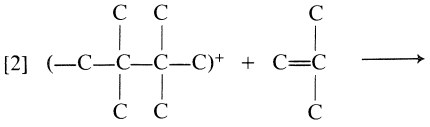

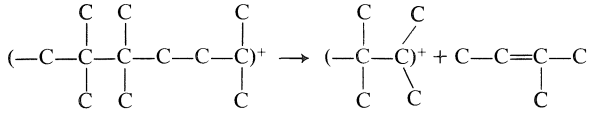

or isomerizes with the subsequent elimination of an ethylene molecule,

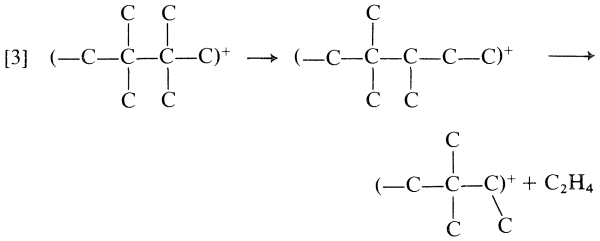

On the other hand, radiolysis experiments on gaseous isobutene with added nitric oxide as radical scavenger suggested that all condensed C_5 products were formed by radical processes (2). However, the choice of NO as a radical scavenger is not unambiguous, because of the possibility of charge transfer between ionized isobutene (ionization potential, IP = 9.23 eV) and/or its fragmentary ions and the NO molecule (IP = 9.26 eV) (3), even if this process is known to be a slow one (4). Therefore, it seems useful to investigate again the possibility of the formation of ethylene and pentenes in ionic processes, using this time a radical scavenger for which the charge transfer process from iso-$C_4H_8^+$ is not allowed.

The mass-spectrometric investigations of ion/molecule reactions were conducted in systems at low pressure (< 3 Torr) and normally the γ-ray radiolysis should also be carried out at these pressures in order to avoid doubtful extrapolation of results from high to low densities of gas. However, the γ-ray doses needed for accumulation of reasonable amounts of products in low pressure isobutene samples were

0008-4042/79/192633-07$01.00/0

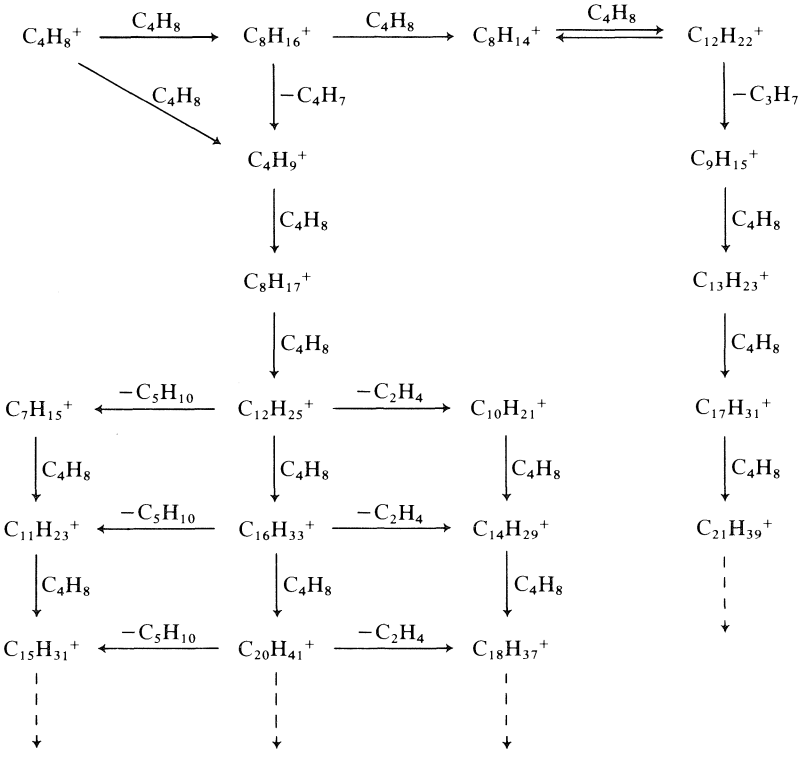

SCHEME 1

unduly long for the available ^{60}Co γ-ray irradiator. Therefore, only a few radiolyses of pure isobutene at 10 Torr or less were performed, most of the irradiations being done on high-pressure samples of rare gases containing small amounts of iso-C_4H_8 ($\simeq 1\%$); under these conditions the irradiation time was shortened to only several hours. Besides this practical aspect of the rare-gas sensitized radiolysis, there is another feature of this kind of experiment that is useful to the comprehension of the observed behaviour of the irradiated system. In the rare-gas sensitized radiolysis the spread of the energy transferred from the excited or ionized noble gas atom to the molecule of interest is much narrower, limited usually to the energy of the metastable states and the fundamental ionic state of the rare gas atom or molecular ion (ref. 5, part 4, p. 211). Under these conditions one can expect that the extent of fragmentation of parent ions is limited to only a few fragment ions as compared to the direct radiolysis, and that the identification of reaction paths for products originating in ionic processes might be less ambiguous (6).

Experimental

Matheson Co. C.P. Grade isobutene (minimum purity 99.0%) was gas-chromatographically purified and the remaining impurities consisted of isobutane (<0.01%) and butene-1 (0.31%). Oxygen (99.995%) from Union Carbide and ammonia (99.99%) from the Matheson Co. were used without further purification. Matheson rare gases, Ar, Kr, and Xe (minimum purity 99.995%), were dried and deoxygenated on pulverised metallic sodium for at least 24 h prior to mixing with isobutene in the reaction cell.

Pyrex irradiation cells were spherical with a volume of 270 ± 10 mL. Break seals allowed the gases to be recovered after irradiation.

The products of radiolyses were analyzed by gas-chromatography equipped with a flame ionization detector. The products were separated on a 9 m squalane or on a 6 m Ucon column.

The samples were irradiated at room temperature (~25°C) in a Gammacell 220 irradiator (Atomic Energy of Canada Ltd) at a dose-rate of approximately 2.21×10^5 rad/h. The total doses absorbed ranged between 2.8×10^{17} eV ($\sim 10^{21}$ eV mol^{-1}) for low-pressure pure isobutene samples and 1.3×10^{19} eV ($\sim 10^{22}$ eV mol^{-1} of rare gas) in rare-gas sensitized radiolysis experiments. The dosimetry was carried out by measuring the acetylene formed in irradiated ethylene at 600 Torr, whose radiolytical yield is 3.6 (7).

Results

Partial results for direct radiolysis and rare-gas sensitized irradiations are presented in Table 1. The radiolytic yields are expressed in $G(X)$ values, which represent the number of molecules X formed per 100 eV of energy absorbed by the system. The only correction made for energy absorbed directly by iso-C_4H_8 in the rare-gas sensitized radiolysis consists of subtracting the yields of products formed in pure

TABLE 1. Radiochemical yields of products formed in isobutene (with and without scavengers) and in isobutene + rare-gas mixtures

Component	Composition (Torr)						
iso-C_4H_8	10.0	10.0	10.0	1.0	1.0	1.0	1.0
Rare gas	—	—	—	Xe:100	Kr:100	Ar:100	Ar:200
Oxygen	—	0.62	0.61	—	—	—	—
Ammonia	—	—	1.0	—	—	—	—
Product	**Yield**						
CH_4	1.41[a]	0.59	0.56	0.82[b]	1.7±0.4	2.35	1.18
C_2H_2	0.73	0.71	0.73	0.19	0.14	0.91	0.38
C_2H_4	1.02	1.00	0.91	0.60	0.93	1.32	0.90
C_2H_6	0.38	0.04	0.02	0.57	1.16	1.80	0.60
C_3H_6	1.56	1.43	1.29	0.63	0.94	1.06	0.68
Propyne	0.90	0.90	0.93	0.59	0.75	0.81	0.60
Allene	1.31	1.30	1.30	0.85	1.01	0.90	0.85
iso-C_4H_{10}	3.25	1.74	0.86	2.26	1.92	2.42	1.77
$(CH_3)_4C$	0.22	—[f]	—	0.48	0.72	n.m.	0.73
$(CH_3)_2CHCH_2CH_3$	0.53	—	—	0.10	0.10	0.10	0.08
3MB1[c]	0.10	—	—	0.02	0.03	0.02	0.03
2MB1[d]	0.88	—	—	0.32	0.30	0.30	0.23
2MB2[e]	0.49	0.29	—	0.32	0.23	0.22	0.17
$\sum G$	12.5			7.75	9.54±0.4	12.2	

[a] G-values calculated relative to the energy absorbed by isobutene.
[b] G-values calculated relative to the energy absorbed by the rare gas.
[c] 3-Methyl-but-1-ene.
[d] 2-Methyl-but-1-ene.
[e] 2-Methyl-but-2-ene.
[f] — indicates undetected.

iso-C_4H_8 at 1 Torr irradiated for the same length of time. This correction is actually very small, being less than 1%. The results in Table 1, with the exception of Xe-sensitized irradiations, are mean values of several experiments. They are reproducible within 12% for the main compounds.

In Table 1 are shown yields for these products which are relevant for the discussion. The following products are not indicated: propane (whose yield is around 0.1), *cis*- and *trans*-butene-2, butene-1, 1,2-butadiene ($G \simeq 0.04$), and some minor unsaturated C_6, whose $G < 0.01$. All these compounds, with the exception of the butenes, are scavenged completely by oxygen. The yields of methane in krypton-sensitized irradiations were less reproducible than in other experiments, as indicated by the range of variation of the G-value. Special care was undertaken in the analyses by gc of the C_5 condensation products. The reported yields for these compounds in the presence of oxygen and ammonia, although very low, correspond to measurable amounts and are meaningful (Tables 1 and 2). In the radiolysis of isobutene at low pressure (without or with oxygen) the radiochemical yields of 2-methyl-but-2-ene (2MB2) are not very reproducible, the likely reason being that neither isobutene nor oxygen was thoroughly dried and traces of water vapor introduced into the system appear to affect the polymerization yield (8).

In rare-gas sensitized irradiations the presence of additives, oxygen and/or ammonia, diminishes the G-values of products formed from isobutene because of the partitioning of transferred energy from the rare gas, among the components of the mixture. This effect is shown by the G-values of allene in Table 2 (11th row). On the other hand, it is well established that allene and propyne are formed with yields which are independent of radical scavenger concentrations (8–10). Therefore, at constant pressure the yield of allene, as well as that of propyne, can be used as an internal reference for calculation of the amount of energy transferred from the rare-gas atom to isobutene. This property is used to estimate the relative yields of products formed in the presence of ammonia and oxygen in the rare-gas sensitized radiolysis as a function of G(allene); the results are presented in Table 2.

Inspection of Table 2 shows that the presence of oxygen has a strong effect on the yields of methane, ethane, isobutane, 2,2-dimethylpropane, and the methyl-butenes. The simultaneous presence of oxygen and ammonia almost completely suppresses the formation of isobutane and 2MB2, and influences strongly the yields of ethylene and propene in the case of the Ar-sensitized radiolysis.

Discussion

The radiochemical yields for irradiations of pure iso-C_4H_8 or iso-C_4H_8 + O_2 mixtures at 10 Torr or

TABLE 2. Relative yields of products formed in isobutene + rare-gas mixtures[a]

Component	Composition (Torr)										
iso-C_4H_8	1.0	1.0	1.0	1.0	1.0	1.0	1.0	1.0	1.0	1.0	1.0
Rare gas	Xe:100	Xe:100	Xe:100	Kr:100	Kr:100	Kr:100	Ar:100	Ar:200	Ar:200	Ar:200	Ar:200
Oxygen	—	0.5	0.5	—	0.5	0.5	—	0.5	—	0.5	0.5
Ammonia	—	—	0.2	—	—	0.3	—	—	—	—	0.25
Product	**Yield**										
CH_4	96	45	47	170±40	130±20	100±20	261	126	139	93	68
C_2H_2	22	30	34	14	18	16	101	93	45	48	43
C_2H_4	71	100	102	92	100	94	147	147	106	119	43
C_2H_6	67	—	—	115	—	—	200	5	70	5	3
C_3H_6	74	81	70	93	90	83	118	140	80	100	55
Propyne	75	66	78	81	71	74	98	100	69	71	80
Allene $G(C_3H_4)$	(0.85)	(0.63)	(0.47)	(1.01)	(0.91)	(0.69)	(0.90)	(0.58)	(0.85)	(0.75)	(0.60)
Allene Relative	100	100	100	100	100	100	100	100	100	100	100
iso-C_4H_{10}	266	87	17	190	56	4	269	86	208	64	3
$(CH_3)_4C$	56	—[b]	—	71	—	—	n.m.	—	86	—	—
$(CH_3)_2CHCH_2CH_3$	12	—	—	10	—	—	11	—	9	—	—
3MB1	2	—	—	3	—	—	—	—	4	—	—
2MB1	38	—	—	30	—	—	33	—	27	—	—
2MB2	38	11	—	23	6	—	24	10±4	20	5	2

[a]The yields were calculated relative to the energy absorbed by the rare gas.
[b]— indicates undetected.

lower pressure are those expected from extrapolation of G-values already published (2, 9, 10). They are strongly pressure dependent, decreasing with increasing density of the gas.

Ionic Processes

As established by Sieck and Ausloos (12), the formation of isobutane in an ionic process (accounting for approximately 50% of all iso-C_4H_{10} formed in irradiation of pure isobutene) consists of a H_2 transfer from the $(C_8H_{16})^+$ ion to neutral isobutene,

[4] $C_8H_{16}^+ + \text{iso-}C_4H_8 \rightarrow C_8H_{14}^+ + \text{iso-}C_4H_{10}$

Our results are consistent with this mechanism, as shown by the action of oxygen and ammonia (Tables 1 and 2). Here ammonia acts as a proton or charge acceptor from the ionic species formed in the iso-C_4H_8 system, in competition with ion/molecule reaction of hydrocarbon ions leading to ionic isobutane (13). However, one can see that the addition of NH_3 in an amount corresponding to 10% of that of iso-C_4H_8 at 10 Torr is not sufficient to inhibit completely the formation of the $(C_8H_{16})^+$ species, which react very efficiently with neutral iso-C_4H_8 (reaction [4]). In the rare-gas sensitized radiolysis, where the relative concentrations of isobutene and ammonia are similar, one can see that isobutane is almost completely scavenged when O_2 and NH_3 are both present in the system (Table 2).

The new result of this study, as compared to ref. 2, is the proof that 2MB2 is partially formed in ionic processes. This observation is particularly evident from the data obtained by irradiation of isobutene at low pressure in the presence of oxygen (acting as a radical scavenger) and ammonia (acting as a proton acceptor). Assuming that $G_{ion}(2MB2) = 0.29$ represents the yield of 2-methyl-but-2-ene formed at 10 Torr in the detachment process form successive condensation ion products,

[5] $[C_4H_9(C_4H_8)_n]^+ \rightarrow [C_7H_{15}(C_4H_8)_{n-2}]^+ + C_5H_{10}$

one can compare this yield with the extrapolated yield of $[C_7H_{15}(C_4H_8)_p]^+$ ($p = 0, 1, 2, \ldots$) at 10 Torr from mass-spectrometric measurements (1). Taking $W = 23.8$ eV (14) as the energy required for the formation of one pair of ions in gaseous isobutene, the total radiochemical yield for ion species should be G_{total} (ion) = 4.2. The yield G_{ion} (2MB2) = 0.29 constitutes 7% of the G_{total} (ion), which is in very good agreement with the extrapolated percentage of $[C_7H_{15}(C_4H_8)_p]^+$ ions observed by mass-spectrometry (1).

The formation of only 2MB2 in the ionic process [5], with the exclusion of the two other methylbutenes (2MB1 and 3MB1) indicates that the reactive site is on the methylene position of the neutral isobutene, which is in accordance with a polymerization mechanism.

Following the reaction Scheme 1, some of the ethylene should be formed by the reactions

[6] $[C_4H_9(C_4H_8)_n]^+ \rightarrow [C_{10}H_{21}(C_4H_8)_{n-2}]^+ + C_2H_4$

The mass-spectrometric investigation shows that the

corresponding ion species $[C_{10}H_{21}(C_4H_8)_q]^+$ ($q = 0$, 1, 2, ...) account for $\sim 2\%$ at 3 Torr of the total ion concentration, which corresponds to a $G_{ion}(C_2H_4) \simeq 0.08$ (1). This yield seems to be pressure independent (or very nearly) and its value is probably unchanged at 10 Torr. There is actually a small decrease in $G(C_2H_4)$ in irradiated isobutene at 10 Torr in the presence of O_2 and NH_3 (Table 1). However, this decrease is within the limits of the experimental errors, and, on the basis of the present data, reaction [6] cannot be confirmed.

The rare-gas sensitized irradiations confirm the occurrence of ionic reactions leading to the 2MB2 formation. However, the dilution of the reacting hydrocarbon makes this reaction path less effective; only around 25% of the 2MB2 is formed in reaction [5], compared to $\sim 60\%$ in the case of pure isobutene. If this lower effectiveness to ionic polymerization of isobutene in rare gases is real, then the formation of C_2H_4 in reaction [6] should be even more difficult to establish, as suggested by inspection of Table 2.

Rare-gas Sensitized Radiolysis

A general view of how the energy of excited or ionized isobutene is disposed after the energy transfer processes from the rare gas metastable and ionic species can be inferred from the sum of the radiochemical yields, $\sum G$, for unscavenged radiolysis experiments (Table 1). Even if the quoted $\sum G$ values do not include yields of isomerization and polymerization processes, the general trend is maintained, and, as expected, $\sum G$ increases with increasing IP and/or metastable-state energy of the noble gas atoms.

In rare-gas sensitized radiolysis experiments the occurrence of less exothermic charge-transfer reactions from dimer rare-gas ions must be taken into account, when added compound is present at low concentration. To what extent dimerization of rare-gas ion, X^+, via

[7] $X^+ + 2X \rightarrow X_2^+ + X$

occurs at pressures of 100 Torr and higher in the presence of added compound whose concentrations are around 1%, can be estimated from the rate coefficients of reaction [7] for Ar, Kr, and Xe (15–17). With a typical value of $k = 10^{-31}$ cm^6 s^{-1} at a pressure of 100 Torr, a positive atomic ion is converted to a molecular ion with a frequency of approximately 10^6 s^{-1}. On the other hand, the frequency of collision of an atomic ion, X^+, with iso-C_4H_8 at 1 Torr is roughly 10^7 s^{-1}. Therefore, it can be assumed that the contribution of molecular rare-gas ions, X_2^+, in charge transfer reaction on isobutene,

[8] $X_2^+ + \text{iso-}C_4H_8 \rightarrow \text{iso-}C_4H_8^+ + 2X$

is not very important in the present experiments.

The Hornbeck–Molnar process

[9] $X^{**} + X \rightarrow X_2^+ + e$

is another possibility of formation of molecular rare-gas ions. (The appearance potentials of X_2^+ (X = Ar, Kr, Xe) species in HM process (ref. 5, p. 196) or the ionization potentials of X_2 van der Waals molecules (19) are the same within 0.1 eV. Their values are within ± 0.1 eV: $AP(Ar_2^+) = 14.6$ eV, $AP(Kr_2^+) = 12.9$ eV, and $AP(Xe_2^+) = 11.2$ eV.) It is difficult to assess the importance of HM processes in the present experiments. A kinetic study of associative excitation in argon indicates that the limiting quantum yields for reaction [9] are rather less than unity, because evidence was found for a competitive quenching (20)

[10] $X^{**} + X \rightarrow X^+ + X$

However, reaction [10] can occur with states X** that lie very close (~ 0.1 eV) to the ionization continuum, but the HM region extends to 1 eV or more from the continuum. On the other hand, theoretical calculations of the contribution of HM processes to the W-value of pure Ar, Kr, and Xe indicate that they account for less than 10%, as estimated on the basis of the optical approximation (21). Based on this information we shall neglect the formation of X_2^+ species in the HM process under the present experimental conditions, and we shall assume that their contribution to reaction [8] seems not to be important in the radiolysis.

Therefore, we assume that the charge transfer only from atomic rare-gas ions

[11] $X^+ + \text{iso-}C_4H_8 \rightarrow \text{iso-}C_4H_8^+ + X$

contributes to the formation of the isobutene ions. The iso-$C_4H_8^+$ ions can also be formed in Penning reactions involving the metastable states of the rare-gas atoms,

[12] $X^* + \text{iso-}C_4H_8 \rightarrow \text{iso-}C_4H_8^+ + e + X$

Assuming that the lowest metastable states of rare-gas atoms are participating in the energy exchange reaction [12], only the $^3P_2(Ar) = 11.5$ eV and the $^3P_2(Kr) = 9.9$ eV states contribute to the parent ion formation.

The iso-$C_4H_8^+$ ions formed either in reaction [11] or [12] carry away an excess energy which is approximately equal to the differences $[IP(X^+) - IP(\text{iso-}C_4H_8^+)]$ or $[^3P_2(X) - IP(\text{iso-}C_4H_8^+)]$. (The exoergicity of reactions [11] and [12] is carried away solely by the iso-$C_4H_8^+$ ions, if the electrons formed have zero energy. However, Penning electron

spectroscopy shows that the electrons can carry away some of the exoergicity.)

The excited parent ion can be collisionally deactivated or, if it contains enough energy to overcome the internal-potential barriers, it can isomerize or decompose. The fragment ions formed in the monomolecular decomposition of iso-$C_4H_8^+$ species having the lowest AP are $C_4H_7^+$ (AP = 11.41 eV), $C_3H_5^+$(AP = 11.45 eV) (22), and $C_2H_4^+$(AP = 12.0 ± 0.25 eV) (23). As already established, the allyl ion, $C_3H_5^+$, leads to propene formation by an H^- transfer reaction (10),

[13] $C_3H_5^+ + \text{iso-}C_4H_8 \rightarrow C_3H_6 + C_4H_7^+$

In photolysis experiments at 8.4 eV (where photoionization does not occur) and at 11.6–11.8 eV (where the photoionization quantum yield = 0.31) the ratios of yields $r_1 = \phi(C_2H_4)/\phi(\text{allene}) = 0.10 \pm 0.03$ and $r_2 = \phi(C_3H_6)/\phi(\text{allene}) = 0.16 \pm 0.03$ seem to be independent of the photon energy (11). This suggests a non-ionic origin of ethylene and propene formation. In the rare-gas radiolyses the similar ratios are higher and they increase with the IP of the rare gases: $r_1^{Xe,Kr,Ar} = 1.0, 1.0, 1.47$ and $r_2^{Xe,Kr,Ar} = 0.8, 0.9$, and 1.47, respectively. These differences in behaviour in photolysis and rare-gas irradiations suggest strongly that an important fraction of both propene and ethylene originates in ionic reactions, such as [13] and [14]

[14] $C_4H_7^+ + \text{iso-}C_4H_8 \rightarrow C_5H_9^+ + C_3H_6$

in the case of C_3H_6 (24). Ethylene is formed probably in charge-exchange reaction of the $C_2H_4^+$ fragmentary ion with neutral isobutene

[15] $C_2H_4^+ + \text{iso-}C_4H_8 \rightarrow C_2H_4 + \text{iso-}C_4H_8^+$

a very efficient reaction, as measured by Abramson and Futrell (24). For each rare gas used the transferred energy in process [11] is sufficient to decompose the isobutene parent ion into fragmentary ions, $C_4H_7^+$, $C_3H_5^+$, and $C_2H_4^+$, which can undergo ion/molecule reactions (13–15).

The decrease of $G^{Ar}(C_2H_4)$ in the presence of oxygen and ammonia in Ar-sensitized irradiations suggests an additional ionic reaction channel of formation of this molecule, involving a fragmentary ion, which is not formed in Xe- and Kr-sensitized radiolyses.

The formation of allene and propyne proceeds from excited neutral isobutene through splitting of the β(C—H) bond or the α(C—C) bond, respectively,

[16] $\text{iso-}C_4H_8^{**} \rightarrow H + CH_2{-}C(CH_3){=}CH_2^*$

[16a] $\downarrow \quad CH_2{=}C{=}CH_2 + CH_3$

[17] $\text{iso-}C_4H_8^{**} \rightarrow CH_3 + CH_3{-}C{=}CH_2^*$

[17a] $\downarrow \quad CH_3{-}C{\equiv}CH + H$

The ratio β(C—H)/α(C—C) is equal to 1.3 ± 0.1, as found by Collin (24) in the photolysis of the butene isomers at 8.4 eV (xenon resonance line) and this value is in agreement with the experimental ratio of photochemical yields: φ(allene)/φ(propyne) = 1.53 (11) at this wavelength. The ratio of radiochemical yields G(allene)/G(propyne) is 1.5 for Xe-sensitized irradiations, indicating that the same mechanisms of formation of allene and propyne are involved in both cases, the required energy of excitation coming from 8.4 eV photons or through $^3P_2$(Xe) metastable state atoms. When transferred energy originates from higher metastable states of Kr and Ar, the ratio G(allene)/G(propyne) decreases to 1.4 and 1.0, respectively. This result suggests that other excited states of neutral isobutene may be involved in α(C—C) splitting with increasing excitation energy. The decrease of the $G(CH_4)$ value in Kr- and Ar-sensitized radiolysis in the presence of both O_2 and NH_3 is probably due to the competition of NH_2· radicals with oxygen for methyl radicals.

Acknowledgements

The author is indebted to Dr. Z. Łuczynski and Dr. G. Collin for valuable discussion and to Mrs. Hélène Gagnon-Deslaurier for gas-chromatographic analyses. This work was made possible through the financial assistance of the National Research Council of Canada.

1. Z. Łuczynski and J. A. Herman. Int. J. Mass Spectrom. Ion Phys. In press.
2. J. A. Herman. Can. J. Chem. **48**, 3446 (1970).
3. H. M. Rosenstock, K. Draxl, B. W. Steiner, and J. T. Herron. J. Phys. Chem. Ref. Data, **6**, Suppl. 1 (1977).
4. L. W. Sieck and J. H. Futrell. J. Chem. Phys. **48**, 1409 (1968).
5. D. H. Stedman and D. W. Setser. Prog. React. Kinet. **6**, 211 (1971).
6. E. Lindholm. *In* Ion–molecule reactions. Vol. 2. Plenum Press, New York. 1972. p. 457.
7. G. G. Meisels and T. J. Sworski. J. Phys. Chem. **69**, 815 (1965).
8. K. O. Okamoto, K. Fueki, and Z. Kuri. J. Phys. Chem. **71**, 3222 (1967).
9. G. Collin and J. A. Herman. Can. J. Chem. **45**, 3097 (1967).
10. G. Collin and J. A. Herman. Can. J. Chem. **47**, 3837 (1969).
11. J. A. Herman, K. Herman, and P. Ausloos. J. Chem. Phys. **52**, 28 (1970).
12. L. W. Sieck and P. Ausloos. J. Chem. Phys. **56**, 1010 (1972).
13. Z. Łuczynski and J. A. Herman. Unpublished results.

14. R. LEBLANC and J. A. HERMAN. J. Chim. Phys. **63**, 1055 (1966).
15. D. SMITH and P. R. CROMEY. J. Phys. B, Proc. Phys. Soc. **1**, 638 (1968).
16. C. L. CHEN. Phys. Rev. **131**, 2550 (1963).
17. P. KEBARLE, R. M. HAYNES, and S. K. SEARLES. J. Chem. Phys. **47**, 1684 (1967).
18. G. COLLIN. Rev. Chem. Intermediates. In press.
19. C. Y. NG, D. J. TREVOR, P. H. MAHAN, and Y. T. LEE. J. Chem. Phys. **66**, 446 (1977).
20. R. E. HUFFMAN and D. H. KATAYAMA. J. Chem. Phys. **45**, 138 (1966).
21. G. S. HURST and C. E. KLOTS. *In* Advances in radiation chemistry. Vol. 5. *Edited by* J. Wiley and Sons, New York. 1976. p. 17.
22. F. P. LOSSING. Can. J. Chem. **50**, 3973 (1972).
23. G. G. MEISELS, J. Y. PARK, and B. G. GIESSNER. J. Am. Chem. Soc. **92**, 254 (1970).
24. F. P. ABRAMSON and J. H. FUTRELL. J. Phys. Chem. **72**, 1994 (1968).

The correlation between O—H stretching frequencies and hydrogen bond distances in a crystalline sugar monohydrate[1]

J. UMEMURA, G. I. BIRNBAUM, D. R. BUNDLE, W. F. MURPHY, H. J. BERNSTEIN, AND H. H. MANTSCH
Division of Chemistry and Division of Biological Sciences, National Research Council of Canada, Ottawa, Ont., Canada K1A 0R6

Received May 14, 1979

J. UMEMURA, G. I. BIRNBAUM, D. R. BUNDLE, W. F. MURPHY, H. J. BERNSTEIN, and H. H. MANTSCH. Can. J. Chem. **57**, 2640 (1979).

The Raman and infrared spectra of crystalline methyl 3,6-dideoxy-β-D-*ribo*-hexopyranoside monohydrate in the O—H stretching region have been studied at room temperature and lower temperatures. Four bands have been identified and correlated with the corresponding O...O distances of the four distinct hydrogen bonds obtained from X-ray data. The assignments were substantiated by a deuterium isotopic dilution study.

J. UMEMURA, G. I. BIRNBAUM, D. R. BUNDLE, W. F. MURPHY, H. J. BERNSTEIN et H. H. MANTSCH. Can. J. Chem. **57**, 2640 (1979).

On a étudié, à la température ambiante et à de plus basses températures, les spectres Raman et infra rouge du méthyle 3,6-didésoxy-β-D-*ribo*-hexopyranoside monohydrate cristalline dans la région d'élongation du O—H. On a identifié 4 bandes et on les a relié aux distances O...O correspondantes de 4 liaisons hydrogènes distinctes obtenues à partir des données des rayons X. On a corroboré ces assignations par l'étude de dilution isotopique du deutérium.
[Traduit par le journal]

Introduction

The 3,6-dideoxyhexoses are characteristic cell wall components of Gram-negative bacteria (1, 2), and immunodominant sugars of O-antigens.

The crystal structure of such a 3,6-dideoxyhexose, methyl 3,6-dideoxy-β-D-*ribo*-hexopyranoside (methyl paratoside) monohydrate has been recently published by two of the present authors (3). The crystals are monoclinic, belonging to the space group $P2_1$; the unit cell contains two molecules of sugar and two water molecules. There are four distinct intermolecular hydrogen bonds whose O...O distances range from 2.652 to 2.960 Å. The relation between hydrogen bonded O...O distances and the corresponding O—H stretching frequencies has been investigated by several authors (4–9). Since this crystalline sugar monohydrate has four distinct O...O distances, its OH vibrational spectra should be particularly amenable to analysis using such a relationship.

In this study we measured the Raman and infrared spectra; the results obtained at room temperature and at lower temperatures are discussed in relation to the individual hydrogen bond distances.

Experimental

Materials

Methyl 3,6-dideoxy-β-D-*ribo*-hexopyranoside was synthesized and crystallized as described elsewhere (3, 10). For the isotopic dilution experiment, 500 mg of methyl paratoside were dissolved in 5 mL of water containing 10% v/v of deuterium oxide. The solution was evaporated to dryness at 40°C under reduced pressure and then treated once more with the 10% deuterium oxide solution. The crystalline mass was then dissolved in 5 mL of ethyl acetate and seeded (3) with a single crystal of methyl paratoside. After 2 h at room temperature the resulting colourless crystals were filtered, washed with ethyl acetate, and dried under a stream of dry nitrogen.

Spectra

For Raman measurements, a single crystal with dimensions of 5 × 3 × 1 mm was attached to the end of a glass rod with epoxy cement. It was mounted in a variable temperature cell (11) such that the *b* (5 mm) axis was parallel to the direction of the incident beam. Raman scattering was obtained using 400 mW of 488.0 nm radiation from a Spectra Physics model 166-03 argon ion laser. Polarized spectra were recorded at a spectral resolution of about 4 cm^{-1} using a Jarrell-Ash 25-102 double monochromator, a cooled RCA C31034 photomultiplier, and a photon counting system.

For infrared measurements, a flurolube mull was prepared between NaCl plates using a stream of dry nitrogen to prevent further hydration. It was mounted in a liquid nitrogen cooled low temperature cell. The partially deuterated sample was investigated as a KBr pellet. Spectra were recorded using a Perkin–Elmer 180 spectrophotometer, with resolution better than 2.8 cm^{-1}.

Results and Discussion

O—H Stretching Bands

Figure 1 shows Raman spectra in the O—H stretching region of the single crystal of methyl paratoside. In the spectrum taken at room temperature there are two bands clearly evident at 3442 and 3216 cm^{-1} and a weaker feature at 3530 cm^{-1}. In Table 1, the correlation diagram for the methyl paratoside crystal is given. Each of the four distinct OH stretching vibrations (two of free methyl paratoside and two of free water) split into a pair of

[1]NRCC No. 17633.

0008-4042/79/192640-06$01.00/0

TABLE 1. Correlation diagram for methyl 3,6-dideoxy-β-D-*ribo*-hexopyranoside monohydrate[a]

Free sugar C_1	Site C_1	Unit cell C_2^2	Site C_1	Free H_2O C_{2v}
$2A$	$2A$	$2A(2)\ T_b;\ \alpha_{aa}, \alpha_{bb}, \alpha_{cc}, \alpha_{ac}$	$A(2)$	$A_1(1)$
				$A_2(0)$
		$2B(2)\ T_a, T_c;\ \alpha_{ab}, \alpha_{bc}$		$B_1(1)$
				$B_2(0)$

[a]Numbers preceding the species notations refer to the number of the O—H stretching modes in methyl paratoside; those in parentheses refer to that of the water molecule.

components having A and B symmetry under the factor group C_2^2. All of these are active in both the Raman and infrared spectra. For the Raman spectra shown in Fig. 1, the electric vectors of both the incident and scattered light were parallel to the γ axis, which lies in the *ac* plane. Therefore, the scattering geometry can be identified as $b(\gamma\gamma)\perp\gamma$. Since the *b*-axis is perpendicular to the γ axis, the *ab* or *bc* components will not be observed; and the spectra will consist of bands belonging only to the A species of the factor group C_2^2.

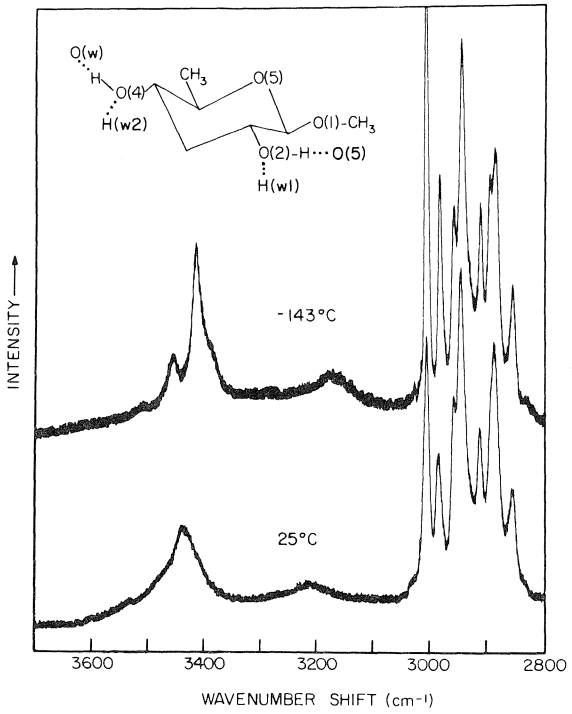

FIG. 1. Polarized Raman spectra of a single crystal of methyl paratoside at two different temperatures: polarization $b(\gamma\gamma)\perp\gamma$. The γ-axis is in the *ac*-plane and the spectrum thus consists of the (*aa*), (*cc*), and (*ac*) components.

Since all four OH vibrations have components of A symmetry, each of them should be observable under our experimental conditions. However, differences in the inherent scattering activity for the four bands will make some easier to observe than others. Also, since the properties of each type of OH bond are actually the average of those of a distribution of bonds, the vibrational band due to a given OH species will be broadened to an extent dependent on the range of the distribution associated with that bond.

These distributions are expected to sharpen at reduced temperatures, so, in order to try to observe spectral features associated with each type of OH bond, the Raman spectrum was recorded at a reduced temperature. The resulting spectrum is also shown in Fig. 1. The strongest feature in the OH region of the low temperature spectrum is a narrow band at 3413 cm^{-1}. However, because this band is so sharp, we prefer to identify it with a combination band which becomes more evident at reduced temperatures due to a decrease in bandwidth. Similar enhancement of combination bands at reduced temperature has been observed previously (12, 13). In addition to the 3413 cm^{-1} band, the low temperature OH stretching region consists of (*i*) a weak band at 3508 cm^{-1} (corresponding to the feature at 3530 cm^{-1} in the room temperature spectrum), (*ii*) a band at 3454 cm^{-1} which may be identified with the high frequency shoulder (at about 3470 cm^{-1}) of the 3442 cm^{-1} band in the room temperature spectrum of Fig. 1, (*iii*) a 3405 cm^{-1} shoulder on the strong 3413 cm^{-1} peak associated with the room temperature feature at 3442 cm^{-1}, and (*iv*) the broad feature centered at 3170 cm^{-1}. The observed OH stretching frequencies are collected in Table 2.

Other polarized components of the Raman spectrum were also measured; however, the band intensities were weaker and the spectra thus noisier. Bands of B symmetry were observed at 3437, 3198,

TABLE 2. O—H (O—D) stretching vibrational frequencies (cm^{-1}) in crystalline methyl paratoside monohydrate

Band No.	Raman[a], single crystal		Infrared[c], polycrystalline					
	25°C	−143°C	23°C	ν_{OH}/ν_{OD}	−193°C	ν_{OH}/ν_{OD}	Assignment[d]	$R_{O...O}$ (Å)[e]
I	3530 vw[b]	3508 vw	3527 sh (~2592, sh)	1.361	3503 sh (2575, sh)	1.360	$\nu_{O(4)-H}$	2.960
II	~3470 sh	3454 w	3467 sh (2553, vs)	1.358	3439 vs (2531, vs)	1.359	$\nu_{O(w)-H(w1)}$	2.827
III	3442 m	~3405 sh	3439 vs (2502, m)	1.375	~3395 sh (2479, s)	1.370	$\nu_{O(w)-H(w2)}$	2.797
IV	3216 w	3170 w	3196 s (2399, vs)	1.332	3130 s (2364, vs)	1.324	$\nu_{O(2)-H}$	2.652

[a]*A* species ($\gamma\gamma$), where the γ-axis is in the *ac*-plane; for *B* species see text.
[b]The symbols vw, w, m, s, vs, and sh stand for very weak, weak, medium, strong, very strong, and shoulder, respectively.
[c]Values in parentheses refer to the corresponding O—D stretching frequencies obtained from the deuterium isotopic dilution experiment.
[d]Notation is that used in ref. 3; see also inset in Fig. 1.
[e]Distances from X-ray data, ref. 3.

and 3160 cm^{-1} corresponding to *A* symmetry components at 3442, 3216, and 3170 cm^{-1}, respectively.

In order to confirm the Raman results, infrared spectra were run at room temperature and at a reduced temperature. In the room temperature spectrum in Fig. 2, there are two broad features centered at 3439 and 3196 cm^{-1}. In the low temperature infrared spectrum, we observe bands at 3503(I), 3439(II), 3404, ~3395(III), and 3130(IV) cm^{-1}, corresponding to the Raman bands at 3508(I), 3454(II), 3414, 3405(III), and 3170(IV) cm^{-1}. A careful re-examination of the room temperature infrared spectrum reveals shoulders at 3527 and ~3467 cm^{-1}, corresponding to the 3503(I) and 3439(II) cm^{-1} features in the low temperature infrared spectrum. These frequencies are all included in Table 2. The discrepancies between the frequencies observed in the Raman and infrared spectra are likely due to the fact that modes transforming to both the *A* and *B* symmetry species are observed in the infrared spectra of the polycrystalline sample. Since the *A* and *B* species bands for the individual transitions are broad, they are not resolved in the observed spectra, but act only to shift the peak frequencies. In addition, for the low temperature spectra, these frequency discrepancies are also associated with the difference in the sample temperature. The OH stretching frequencies were observed to decrease with decreasing temperature, e.g. as has been reported for *l*-ascorbic acid (14).

In spectra taken at intermediate temperatures, the 3404 cm^{-1} band sharpens with decreasing temperature and remains almost unchanged in frequency, in contrast to the shifts of the bands I–IV. This feature is thus assigned to a combination band, the ir counterpart of the 3413 cm^{-1} Raman feature. The very weak band at 3285 cm^{-1} in the low temperature infrared spectrum is presumably another combination band corresponding to a feature at 3270 cm^{-1} in the low temperature Raman spectrum. The shoulder band at about 3180 cm^{-1} in the low temperature infrared spectrum is probably also a combination band. The assignment of this feature as an *A* species band corresponding to the *B* species band at 3130 cm^{-1} is unlikely in view of the observed frequency separation of 10 cm^{-1} for those bands in the polarized Raman spectra of the single crystal.

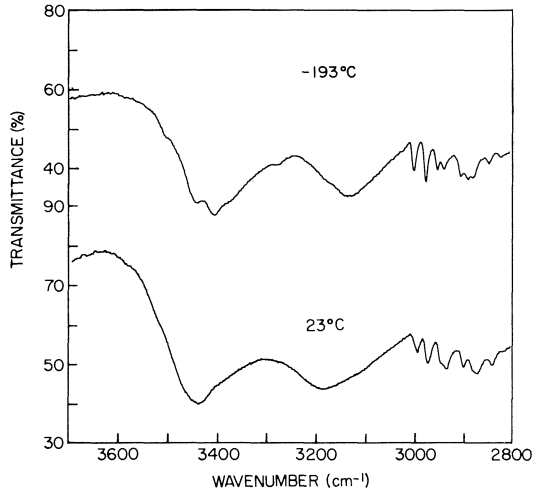

FIG. 2. Infrared spectra of polycrystalline methyl paratoside monohydrate (fluorolube mull) at two temperatures.

O—D Stretching Bands

Since there was some uncertainty in the identification of the OH stretching bands, infrared spectra of the OD stretching region of a 10% v/v deuterated sample were recorded at room temperature and at a reduced temperature (Fig. 3). The three strong bands at 2553, 2502, and 2399 cm^{-1} in the room temperature spectrum shift to 2531, 2479, and 2364 cm^{-1}, respectively, at low temperature. These frequency shifts are characteristic of OH stretching bands as previously stated. Thus, these bands are easily identified with bands II, III, and IV, respectively, in the undeuterated compound (see Table 2). As shown in Table 2, the ratios of the OH/OD frequencies for this assignment agree fairly well for the two temperatures. They also agree quite well with the average

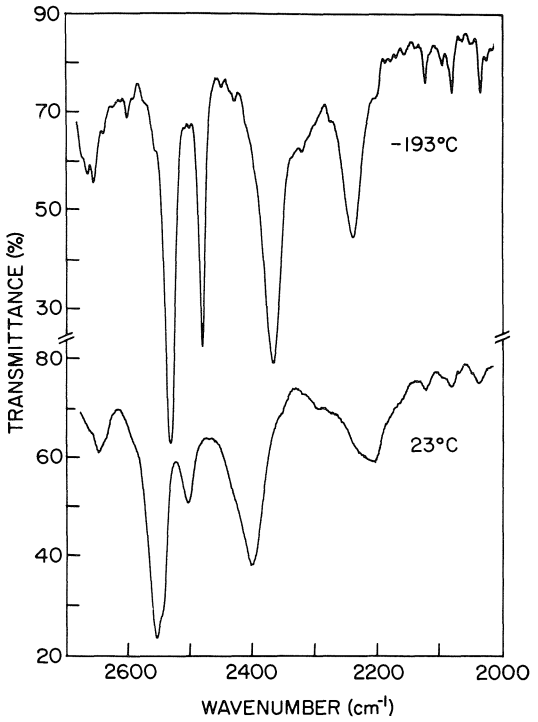

FIG. 3. Infrared spectra of partially deuterated (10% v/v deuterium) polycrystalline methyl paratoside monohydrate (KBr pellet) at two temperatures.

value of 1.355 obtained from a large collection of data, mainly ices and hydrates.[2]

The broad band at 2210 cm^{-1} cannot be assigned to an OD stretching mode since it shifts to 2236 cm^{-1} at low temperature, contrary to the expected behaviour. Furthermore, this band appears in the undeuterated methyl paratoside spectrum, and consequently may be assigned as a combination band whose intensity compares to that of the OD stretching bands because of the dilute deuterium concentration.

It is important to note that there is no feature in the OD stretching region corresponding to the strong band in the OH spectrum identified as a combination band. That assignment thus appears to be justified.

It remains to identify a feature in the OD spectrum corresponding to band I. For shoulders at 2592 cm^{-1} at room temperature and 2575 cm^{-1} at low temperature, an agreement is found for the OH/OD frequency ratios at two temperatures, similar to the behaviour of these ratios for the bands II, III, and IV. Other weak features in the room temperature spectrum shift to higher frequencies, if they shift at all, and are due to combination bands; in particular, the shoulder at 2544 cm^{-1} in the room temperature spectrum shifts to 2556 cm^{-1} at low temperature. We are thus led to the above tentative assignment of band I in the isotopically diluted sample. However, this weak band is clearly identified in the Raman and ir spectra of the undeuterated methyl paratoside.

[2]M. Falk. Private communication.

Correlation of OH/OD Stretching Frequencies with O...O Distances

For an identification of the individual stretching frequencies with specific OH bonds in the crystal, we have considered the available correlations between hydrogen bonded O...O distances and OH frequency shifts (5–7). It has been found that in all cases the OH frequency shifts monotonically to lower frequencies as the O...O distance is decreased, i.e., as the hydrogen bond strength increases. In our case, the frequencies of the two types of isolated OH bonds (alcoholic and aqueous) are close enough that we may initially consider the four bonds on the same basis. The frequency of the free aqueous OH bond is taken to be that of HOD vapour, 3707 cm^{-1} (15), and that of the free alcoholic bond as that of methanol vapour, 3682 cm^{-1} (16). In this case, the observed frequencies may be related to individual OH bonds on the basis of their associated $R_{O...O}$ distances. This has been done in Table 2, where the notation is that of ref. 3, and the atoms involved are identified in the insert to Fig. 1.

From the O...O distance correlation, it is obvious that the alcoholic OH modes should have frequencies at the extremes of the allowed range. This suggests that the $\nu_{O(4)—H}$ frequency should be the highest one observed (band I). For an $R_{O...O}$ distance of 2.652 Å, however, previously proposed relations predict that $\nu_{O(2)—H}$ should be observed at 3075 cm^{-1} (7) or even at 2830 cm^{-1} (5). This would then suggest that $\nu_{O(2)—H}$ is overlapped with CH stretching modes and that band IV may not be ascribed to that OH vibration. However, this possibility is readily eliminated by the isotopic dilution results, since the ν_{OH}/ν_{OD} value for the above assignment is clearly consistent with the corresponding ratios for the other bands. Furthermore, we can find no strong band ascribable to the OD stretching modes in the region below 2399 cm^{-1}. The assignment of bands I and IV, which differ so much in intensity, to the two alcoholic modes is reasonable in light of previous findings that intensities of the OH stretching bands increase significantly with increasing hydrogen bond length (14).

This assignment of the alcoholic OH(OD) stretching modes leads us to the conclusion that bands II and III are due to aqueous OH(OD) stretching modes. In the general case of a hydrated crystal (17–20) water is treated as a vibrationally distorted molecule. For a water molecule which occupies an asymmetric site,

the concept of symmetric and antisymmetric stretching modes breaks down and the two OH stretching modes become partially decoupled. Then the maximum separation between the two modes would be appreciably less than in the fully coupled case. There, e.g., in water vapour, the frequency separation is $\nu_3 - \nu_1 = 3756 - 3654 = 102\ cm^{-1}$ (21, 22). Thus we expect the frequencies of the aqueous OH stretching modes in methyl paratoside to differ by significantly less than this amount. In fact, the frequency separation between bands II and III ranges from 28 to 49 cm^{-1} (about 50 cm^{-1} for the isotopically diluted sample). This confirms the identification of bands II and III with the aqueous OH stretching modes, with band II being associated with the OH bond having the large O...O distance. The alternate assignment of band I to one of these modes is less reasonable because of the difference in intensities between that band and band II or III.

As stated above, there have been several studies of the relationship between the hydrogen bonded O...O distance and OH stretching frequencies obtained from vibrational spectra (4–9). The best correlation was found for isotopically dilute samples, where coupling between adjacent OH bonds is eliminated (8). As deduced from theoretical arguments (5), it is preferable to correlate the O...O distance with the shift in OH stretching frequency from that for the corresponding free OH bond.

We have made such a correlation for the present case. From the free aqueous and alcoholic frequencies given above and our observed Raman data (room temperature and using the average frequencies for *A* and *B* symmetry species, when available), we have calculated $\Delta\nu_{OH} = (\nu_{OH,free} - \nu_{OH,bonded})$. These are plotted against the O...O distance in Fig. 4. Also included in Fig. 4 are $\Delta\nu_{OH}$ frequencies calculated from the room temperature ν_{OD} data, using the relation $\Delta\nu_{OH} = 1.355\Delta\nu_{OD}$.[2] For comparison, we have also included three of the correlations previously presented in the literature. One of these (9) was given in terms of $\Delta\nu_{OD}$, and we converted it to $\Delta\nu_{OH}$ using the relation given above.

The present data points fall close to the previously derived relation; it must be pointed out that the latter curves are the average of data which were scattered due to the diversity of the systems studied. Further, the frequencies for methyl paratoside are likely to be affected by interactions within the crystal including coupling between adjacent OH bonds.

It is clearly more appropriate to correlate the O—H stretching frequencies directly with O—H bond lengths rather than with O...O distances in an O—H...O hydrogen bond. However, hydrogen positions obtained from X-ray analyses are poorly

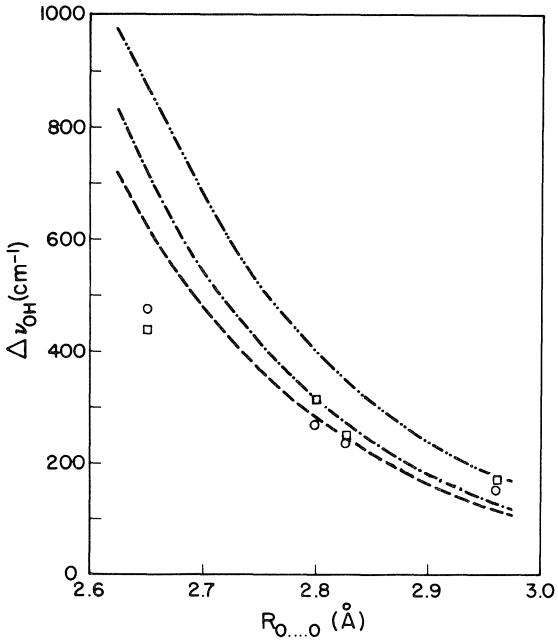

FIG. 4. Correlation between the O...O distance and $\Delta\nu_{OH}$ ($\nu_{OH,free} - \nu_{OH,bonded}$) in crystalline methyl paratoside monohydrate (○, from observed OH spectra; □, converted from observed OD spectra), in comparison with similar correlations proposed by Lippincott and Schroeder (-··) ref. 5, Bellamy and Owen (---) ref. 7, and Falk (-·) ref. 9.

defined; O—H distances so derived are an order of magnitude less precise than corresponding O...O distances. Furthermore, the O—H...O angle may deviate appreciably from linearity. In the case of the four hydrogen bonds of methyl paratoside monohydrate (3), these deviations range from 2 to 16°, but they can be as large as 40° (23). Accurate O—H distances are obtainable from neutron diffraction, but the number of such studies is as yet relatively small. A comparison between neutron diffraction and corresponding X-ray data has been reviewed recently for a number of carbohydrate crystals (24). Unfortunately, neutron diffraction studies have not been made for many compounds which have been well characterized spectroscopically, and vice versa. As more such data become available, the direct correlation of O—H stretching frequencies with O—H distances will have to be reinvestigated.

Acknowledgements

We are grateful to Dr. M. Falk for his useful suggestions and discussion of this work. Thanks are also due to Dr. D. G. Cameron for making the low-temperature infrared cell available to us, and to Dr. L. V. Haley for help in setting up the low-temperature Raman cell.

1. O. WESTPHAL and O. LÜDERITZ. Angew. Chem. **72**, 881 (1960).
2. O. LÜDERITZ, A. M. STAUB, and O. WESTPHAL. Bacteriol. Rev. **30**, 192 (1966).
3. G. I. BIRNBAUM and D. R. BUNDLE. Biochim. Biophys. Acta, **582**, 515 (1979).
4. K. NAKAMOTO, M. MARGOSHES, and R. E. RUNDLE. J. Am. Chem. Soc. **77**, 6480 (1955).
5. E. R. LIPPINCOTT and R. SCHROEDER. J. Chem. Phys. **23**, 1099 (1955).
6. H. RATAJCZAK and W. J. ORVILLE-THOMAS. J. Mol. Struct. **1**, 449 (1967–68).
7. L. J. BELLAMY and A. J. OWEN. Spectrochim. Acta, **25A**, 329 (1969).
8. A. NOVAK. Struct. Bond. **18**, 177 (1974).
9. M. FALK. *In* Chemistry and physics of aqueous gas solutions. The Electrochemical Society, New York. 1975. p. 19.
10. D. R. BUNDLE. J. Chem. Soc. Perkin I, in press.
11. S. SUNDER and R. E. D. MCCLUNG. Chem. Phys. **2**, 467 (1973).
12. S. HAYASHI and J. UMEMURA. J. Chem. Phys. **63**, 1732 (1975).
13. J. UMEMURA. J. Chem. Phys. **68**, 42 (1978).
14. M. FALK and M. J. WOJCIK. Spectrochim. Acta, in press.
15. W. S. BENEDICT, N. GAILAR, and E. K. PLYLER. J. Chem. Phys. **24**, 1139 (1956).
16. D. G. BURKHARD and D. M. DENNISON. J. Mol. Spectrosc. **3**, 299 (1959).
17. J. SCHIFFER and D. F. HORNIG. J. Chem. Phys. **49**, 4150 (1968).
18. V. SEIDL, O. KNOP, and M. FALK. Can. J. Chem. **47**, 1361 (1969).
19. R. KLING and J. SCHIFFER. J. Chem. Phys. **54**, 5331 (1971).
20. B. BERGLUND, J. LINDGREN, and J. TEGENFELDT. J. Mol. Struct. **21**, 135 (1974).
21. J. M. FLAUD and C. CAMY-PEYRET. J. Mol. Spectrosc. **55**, 278 (1974).
22. W. A. P. LUCK. *In* The hydrogen bond. Vol. 2. *Edited by* P. Schuster, G. Zundel, and C. Sandorfy. North-Holland Publishing, New York. 1976. p. 526.
23. G. I. BIRNBAUM and S. R. HALL. J. Am. Chem. Soc. **98**, 1926 (1976).
24. G. A. JEFFREY and S. TAKAGI. Acc. Chem. Res. **11**, 264 (1978).

The mechanism of the solvolysis of *p*-methoxybenzyl chloride in aqueous acetone containing pyridine or thiourea. Evidence for concurrent substitution by unimolecular and bimolecular processes

ALAN QUEEN

Parker Chemical Laboratory, University of Manitoba, Winnipeg, Man., Canada R3T 2N2

Received December 20, 1978

ALAN QUEEN. Can. J. Chem. **57**, 2646 (1979).

The overall rate of reaction of *p*-methoxybenzyl chloride with 70% aqueous acetone is increased by the addition of pyridine but the rate of hydrolysis is decreased. Comparison of these data with those for benzhydryl chloride under the same conditions shows that the rate of hydrolysis of *p*-methoxybenzyl chloride is less than the rate of ionisation. These results are discussed in terms of concurrent operation of the S_N1 mechanism and a bimolecular process. Similar results are obtained when thiourea is used instead of pyridine.

ALAN QUEEN. Can. J. Chem. **57**, 2646 (1979).

La vitesse globale de la réaction du chlorure de *p*-méthoxybenzyle avec l'aceétone aqueux à 70% est augmentée par l'addition de pyridine, mais la vitesse d'hydrolyse est diminuée. La comparaison de ces résultats avec ceux du chlorure de benzhydryle dans les mêmes conditions montre que la vitesse d'hydrolyse du chlorure de *p*-méthoxybenzyle est plus faible que celle d'ionisation. On discute de ces résultats en termes de l'opération concurrente d'un mécanisme S_N1 et d'un processus bimoléculaire. On a obtenu des résultats semblables quand on utilise la thiourée au lieu de la pyridine.

[Traduit par le journal]

Introduction

During the last few years considerable attention has been given to the mechanisms of nucleophilic displacement reactions of substituted benzyl compounds (1–3). Kohnstam has presented evidence that benzyl chloride hydrolyses in aqueous solvents by the S_N2 mechanism (4) that *p*-methoxybenzyl chloride solvolyses by the S_N1 route and that a progressive change from the bimolecular mechanism to the unimolecular pathway is observed as the para-substituent is changed in the order NO_2, Cl, H, CH_3, CH_3O (1, 5). The intermediate situation for *p*-methylbenzyl chloride is sometimes referred to as "borderline" solvolysis and several possibilities have been proposed. Kohnstam (1) has argued that S_N1 and S_N2 processes occur side by side. Although it is difficult to demonstrate this for purely solvolytic reactions, evidence has been presented that azide attack on *p*-methoxybenzyl chloride involves concurrent operation of the two mechanisms (6). Other workers have preferred some sort of intermediate mechanism involving either a "loose" S_N2 type of transition state (7) or ion-pairs (8, 9). The extreme view of the situation has been that of Sneen (10, 11) who has proposed that all nucleophilic substitutions proceed through a single ion-pair intermediate. Although this view has been accepted by some workers (12–14), it has been criticized by others (15–17). Reviews of the S_N1–S_N2 borderline region have been published (18–20).

Graczyk and Taylor (21) have measured the effect of azide ions on the chlorine isotope effect for the reaction of *p*-methoxybenzyl chloride in aqueous acetone. They concluded that their results support Sneen's mechanism. Although this interpretation has not been specifically discarded, it seems to have been modified in a recent paper (22) to admit concurrent substitution through a free carbocation.

The present trend in dealing with solvolytic reactions is to discuss them in terms of the mechanism (scheme [I]) originally proposed by Winstein *et al.* (23) for solvolytic reactions in acetic acid.

[I] $RX \rightleftharpoons |R^+ \ X^-| \rightleftharpoons R^+ // X^- \rightleftharpoons R^+ + X^-$

intimate ion-pair; external ion-pair; free carbocation

Products

Aronovitch and Pross (24) have applied the concept of reactivity–selectivity relationships (25, 26) to the solvolyses of benzyl compounds in aqueous ethanol and have concluded that a truncated form of the Winstein scheme, which excludes the kinetic involvement of the free carbocation, can account for the behaviour of all these systems.

0008-4042/79/192646-06$01.00/0

TABLE 1. The effects of electrolytes on the rates of solvolysis of *p*-methoxybenzyl chloride in aqueous ethanol

T (°C)	Solvent	Salt	[Salt] (M)	$10^4 k$ (s^{-1})	$k/k^{0\,b}$
19.44	80% ethanol	None		7.125 ± 0.031^a	
		NaCl	0.5470	7.133 ± 0.024	1.001
		$NaClO_4$	0.04971	8.610 ± 0.034	1.210
10.03	70% ethanol	None		6.734 ± 0.024	
		NaCl	0.05580	6.711 ± 0.024	0.997
		$NaClO_4$	0.05767	8.043 ± 0.029	1.169

[a] $k = k^0$.
[b] Calculated for 0.05 M salt.

It is our view that the conclusions of these two sets of workers are not correct for the case of *p*-methoxybenzyl chloride. Both ignore the well documented retardation of the rate of solvolysis of this compound by chloride ions in aqueous acetone (1, 6). This effect strongly supports the participation of the free carbocation in the solvolytic reaction (18, 27). It seems unlikely that solvent would be able to react with any form of ion-pair and yet be unreactive towards the free carbonium ion. The magnitude of the common ion rate depression is the same as that for the corresponding reaction of benzhydryl chloride, a classical S_N1 case (28, 29). Support for the view that the rate decrease in the presence of chloride ion is a mass-law effect is provided by the observation that similar retardations are observed for the solvolyses of substituted benzhydryl chlorides and that the effect increases as the electron releasing capacity of the substituent increases (30). While it is true that common-ion retardation of solvolysis has not been previously reported for the reaction of benzyl compounds in aqueous ethanol, the data in Table 1 show similar features to those reported for aqueous acetone. The very large differences in the effects of sodium chloride and sodium perchlorate indicate, in the absence of contrary evidence, that carbonium ions are formed in the solvolysis of *p*-methoxybenzyl chloride in aqueous ethanol.

If free carbocations are present in the reaction mixtures, any discussions of mechanism which ignore them would seem to be incomplete. Further information about nucleophilic substitutions in aqueous organic media can often be obtained by adding competitive nucleophiles to the reaction mixtures and measuring the rates of formation of the various products. A number of such studies have been carried out using ionic reagents but little data is available for nonionic nucleophiles. A notable exception has been the use of thiourea as a competitive nucleophile to study the supposedly borderline reactions of 2-octyl mesylate. The results are entirely consistent with reaction by the S_N2 mechanism (31).

This paper presents data for the reaction of *p*-methoxybenzyl chloride with 70% aqueous acetone containing either pyridine or thiourea.

Results and Discussion

The ion-pair scheme [II] was proposed by Sneen and Larsen (10) as a unifying mechanism for all nucleophilic substitution reactions.

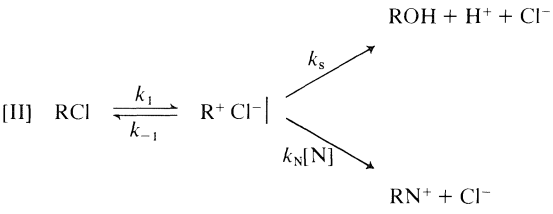

The overall rate of reaction is defined by eq. [III] and the rate of hydrolysis by eq. [IV]

$$[III] \quad d[Cl^-]/dt = k_{Cl}[RCl]$$

$$[IV] \quad d[H^+]/dt = k_H[RCl]$$

The experimental instantaneous rate constants are:

$$[V] \quad k_{Cl} = \frac{k_1(1 + m[N])}{1 + x + m[N]}$$

$$[VI] \quad k_H = \frac{k_1}{1 + x + m[N]}$$

where $x = k_{-1}/k_s$; $m = k_N/k_s$. In the absence of added nucleophile, but in the presence of an appropriate amount of non-nucleophilic salt or non-electrolyte, depending on the nature of the nucleophile used, a rate constant k_{NA} can be defined by eq. [VII]:

$$[VII] \quad k_{NA} = k_1/(1 + s)$$

TABLE 2. The effect of non-electrolytes on the rate of reaction of benzhydryl chloride in 70% aqueous acetone at 20°C

T (°C)	Adduct	Concentration (M)	$10^4\,k$ (s^{-1})	k/k^0	[RN]/[ROH]
20.02	None		2.724±0.021[a]		
	Acetone	1.0884	2.080±0.022	0.7637	
	Benzene	0.5606	1.732±0.016	0.6360	
	Ethanol	0.8707	2.561±0.020	0.9402	
	2,6-Lutidine	0.5142	2.109±0.007	0.7743	
	Pyridine	0.2502	2.605±0.026	0.9563	
		0.4932	2.472±0.020	0.9075	0.08
		0.7487	2.374±0.020	0.8715	
19.44	None		2.441±0.018[a]		
	Urea	0.1040	2.692±0.020	1.103	
	Thiourea	0.0720	2.984±0.027	1.222	0.24
		0.1035	3.198±0.024	1.310	0.34
		0.1435	3.559±0.035	1.458	0.51
		0.2061	4.062±0.037	1.664	0.74

[a] $k = k^0$.

TABLE 3. The effects of non-electrolytes on the rate of reaction of *p*-methoxybenzyl chloride in 70% aqueous acetone at 20°C

T (°C)	Adduct	Concentration (M)	$10^4\,k$ (s^{-1})	k/k^0	[RN]/[ROH]
20.02	None		2.507±0.018[a]		
	Acetone	1.0884	1.906±0.018	0.7602	
	Benzene	0.5606	1.945±0.020	0.7759	
	Ethanol	0.8707	2.255±0.016	0.8995	
	2,6-Lutidine	0.5143	1.954±0.008	0.7794	
	Pyridine	0.2472	2.573±0.020	1.0263	0.18
		0.4942	2.606±0.019	1.0395	0.40
		0.7420	2.660±0.020	1.0610	0.65
19.44	None		2.249±0.020[a]		
	Urea	0.1040	2.514±0.024	1.118	
	Thiourea	0.0704	3.617±0.015	1.608	0.78
		0.1008	4.173±0.036	1.855	1.14
		0.1394	5.037±0.036	2.240	1.74
		0.2024	6.243±0.051	2.776	2.63

[a] $k = k^0$.

It can be seen that eqs. [V] and [VI] lead to eq. [VIII]:

$$[\text{VIII}] \quad k_{Cl}/k_H = 1 + m[N]$$

Table 4 gives values of m calculated from the data for the reaction of *p*-methoxybenzyl chloride with pyridine (Table 3). The values of m increase markedly with the concentration of pyridine. Since comparatively large amounts of this reagent were used, the water content of the solvent was also considerably decreased and the changes in m are in the expected direction.

Equations [V] and [VII] can be combined to give eq. [IX]:

$$[\text{IX}] \quad \frac{k_{Cl}}{k_{NA}} = \frac{(1 + x)(1 + m[N])}{1 + x + m[N]}$$

Unfortunately, values of k_{NA} cannot be obtained directly. Sneen, for his work with ionic nucleophiles, carried out model experiments with non-nucleophilic salts and assumed that the salts had non-specific effects. This is not justified (32, 33). The results shown in Tables 2 and 3 show that different inert solvents and non-ionic reagents also have specific effects on the rates of hydrolysis of both *p*-methoxybenzyl chloride and benzhydryl chloride. On the other hand, these non-nucleophilic adducts have very similar effects on the rates of hydrolysis of the

TABLE 4. The effect of pyridine on the rate of reaction of *p*-methoxybenzyl chloride in 70% aqueous acetone at 20.02°C

[Pyridine] (M)	$10^4 k_{Cl}$ (s^{-1})	$10^4 k_H$ (s^{-1})	m	$10^4 k_i$ (s^{-1})	$10^4 k_{2N}$ ($M^{-1} s^{-1}$)
0	2.507±0.018	2.507±0.018		2.507±0.018	
0.2472	2.573±0.020	2.172±0.021	0.747±0.022	2.399±0.035	0.704±0.040
0.4942	2.606±0.019	1.865±0.020	0.804±0.023	2.275±0.030	0.670±0.036
0.7420	2.660±0.020	1.611±0.017	0.878±0.024	2.187±0.030	0.637±0.036

two chlorides. Kohnstam and co-workers (6) have used the salt effects of nucleophiles on the rate of solvolysis of benzhydryl chloride to estimate the corresponding effects for the reactions with *p*-methoxybenzyl chloride. There is considerable justification for this approach from the observation that both reactions are equally affected by non-nucleophilic acids and salts, by changes in water content of the solvent and by the addition of chloride ions (1, 6). On the other hand, the application of this method to [II] requires either that m is the same for both reactions or that $m = 0$ for benzhydryl chloride. The data in Tables 2 and 3 show that neither condition is satisfied. In fact, it is not possible to adequately test eq. [IX] with any data available at the present time. The same problems apply to the studies carried out using thiourea as the nucleophile. McLennan (31) used the inert substance urea to obtain the medium effects for his reactions. Since these effects were very small for his reactions, this method was probably justified. The data in Table 2 show that this is not the case in the present studies.

Since the ion-pair mechanism cannot be adequately tested, a different approach has been used. This attempts to see if the results are consistent with the operation of two independent mechanisms. It is justified by the fact that common-ion rate depression of the rate of solvolysis indicates the presence of reactive free carbocations in the reaction mixture. Moreover, there is at least one case (34) where the strongly nucleophilic azide ions react bimolecularly with an organic chloride in 70% aqueous acetone even though the hydrolysis follows the S_N1 route.

The solvolytic reactions of benzhydryl chloride and *p*-methoxybenzyl chloride show a number of similarities. Mass law and salt effects have already been mentioned. The ratio $\Delta C_p^{\neq}/\Delta S^{\neq}$ for both reactions are the same and the values are much larger than those for bimolecular solvolyses (1). Many studies have shown that benzhydryl chloride is sterically hindered to bimolecular attack, even by powerful reagents such as azide ions (35). On the other hand, although the solvolytic reactions of *p*-methoxybenzyl chloride follow an S_N1 route, more powerful reagents may be able to react by a bimolecular process. The simplest reaction scheme, which uses only the S_N1 and S_N2 pathways, is shown in [X].

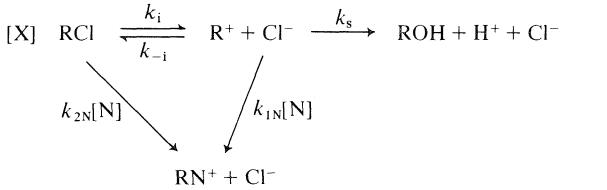

As before, overall substitution can be measured by the rate constant, k_{Cl}, and hydrolysis, by k_H. A complete treatment of mechanism [X] leads to eq. [XI], where $\alpha = k_{-i}/k_s$ and $\beta = k_{1N}/k_s$.

$$[XI] \quad k_{Cl} = \frac{k_i(1 + \beta[N])}{1 + \alpha[Cl^-] + \beta[N]} + k_{2N}[N]$$

When the concentration of the substrate is low, $\alpha[Cl^-] \ll (1 + \beta[N])$, so that eq. [XI] reduces to eq. [XII]:

$$[XII] \quad k_{Cl} = k_i + k_{2N}[N]$$

The rate constant for hydrolysis is given by eq. [XIII]

$$[XIII] \quad k_H = \frac{k_i}{1 + \alpha[Cl^-] + \beta[N]} \approx \frac{k_i}{1 + \beta[N]}$$

In the absence of strong nucleophiles, $k_{Cl}^0 = k_H^0 = k_i^0$. Equations [XII] and [XIII] may be combined to give eq. [XIV].

$$[XIV] \quad k_{Cl}/k_i = 1 + k_{2N}[N]/k_i$$

The ratio k_{Cl}/k_i is the analogue of the term k_{Cl}/k_{NA} used by Sneen, but in this case it is possible to correct k_i^0 for medium effects in order to obtain k_i. The evidence for this will be discussed for the reactions in the presence of pyridine.

Pyridine has a low polarity and dielectric constant compared to water. Thus, its addition to aqueous acetone would be expected to decrease the ionising power of the solvent and the rates of S_N1 reactions should be less than those in the pure solvent. This expectation is confirmed for the reaction of benzhydryl chloride in 70% aqueous acetone (Table 2). This compound is known to react less rapidly as the water content of aqueous organic solvents is

TABLE 5. The effect of thiourea on the rate of reaction of *p*-methoxybenzyl chloride in 70% aqueous acetone at 19.44°C

[Thiourea] (M)	$10^4 k_{Cl}$ (s^{-1})	$10^4 k_H$ (s^{-1})	m	$10^4 k_i$ (s^{-1})	$10^4 k_{2N}$ ($M^{-1} s^{-1}$)
0	2.249±0.020	2.249±0.020		2.249±0.020	
0.0704	3.617±0.015	2.030±0.029	10.7±0.2	2.738±0.040	12.5±0.6
0.1008	4.173±0.036	1.946±0.026	10.9±0.2	2.928±0.040	12.4±0.5
0.1394	5.037±0.036	1.839±0.018	11.9±0.2	3.250±0.049	12.8±0.4
0.2024	6.243±0.051	1.722±0.024	12.5±0.2	3.716±0.055	12.4±0.4

decreased (1, 28). The effects of benzene, ethanol, and 2,6-lutidine on the rate of reaction of benzhydryl chloride are also shown in Table 2.

Table 3 lists results obtained for the corresponding reactions of *p*-methoxybenzyl chloride under the same conditions. For every case except those involving pyridine, the rate of reaction is decreased by the addition of a non-ionic material to the solvent. The reactions with 2,6-lutidine are particularly interesting because this compound, apart from the large amount of steric hindrance around the nucleophilic nitrogen atom, is structurally similar to pyridine. Thus, although it would be a poor nucleophile compared to water or pyridine, its medium effects should be similar in type to those of pyridine. It can be seen that 2,6-lutidine decreases the rates of solvolysis of benzhydryl chloride and *p*-methoxybenzyl chloride to the same extent. These results indicate that experiments with benzhydryl chloride and pyridine provide a very close measure of the rate of ionisation of *p*-methoxybenzyl chloride under the same conditions.

In contrast to the results obtained with 2,6-lutidine, the overall rate of reaction of *p*-methoxybenzyl chloride is increased by the addition of pyridine to the reaction mixture, despite the decrease in ionising power and water content. Consequently, pyridine must be able to react by a pathway that does not involve the free carbocation. If S_N1 substitution by pyridine also occurs, the rate of hydrolysis, $k_H[RCl]$, will be less than the rate of ionisation, $k_i[RCl]$. The value of k_i can be obtained from model experiments with benzhydryl chloride in the presence of pyridine, as described in the last paragraph. Table 4 shows that the rate of hydrolysis is indeed less than that of ionisation.

A plot of k_{Cl}/k_i against pyridine concentration is linear, as required by eq. [XIV]. The values of k_{2N} are given in Table 4. They show an apparent drift of about 20%, but this is within the combined experimental errors. The results are, therefore, consistent with the concurrent operation of unimolecular and bimolecular mechanisms for the reaction of pyridine with *p*-methoxybenzyl chloride.

The data for reaction in the presence of thiourea also support the concurrent operation of two mechanisms. The data in Table 2 show that both urea and thiourea increase the rate of reaction of benzhydryl chloride, but to different extents. On the other hand, urea has very nearly the same effects on the rates of hydrolysis of benzhydryl and *p*-methoxybenzyl chlorides. This indicates that the reactions of benzhydryl chloride can be used to obtain the medium effects for the reactions *p*-methoxybenzyl chloride with thiourea. The results of these calculations are listed in Table 5. Thiourea is much more nucleophilic than pyridine and lower concentrations of this nucleophile could be used. The m values for the ion-pair scheme increase with thiourea concentration whereas k_{2N} values for scheme [X] are constant. In addition, the values of k_H are less than those of k_i, indicating that thiourea also reacts with the free carbocation.

It is concluded that at least two independent pathways of substitution are concurrently involved in the reaction of *p*-methoxybenzyl chloride with pyridine and thiourea. One of these routes involves a free carbocation and corresponds to the classical S_N1 mechanism. The other may involve one or more ion-pair intermediates and/or the undissociated substrate. The literature contains many conflicting views concerning the importance of ion-pairs and unionised substrates in bimolecular processes. The present results do not resolve the difficulties of the problem. At the present time it seems to be necessary to consider nucleophilic substitution reactions in terms of the full Winstein mechanism. The actual species involved in a particular reaction will depend on the solvent and the nucleophiles involved.

Experimental

Solvents

Aqueous acetone (70%) was made up using 30 volumes of water and 70 volumes of acetone, as previously described (36). Ethanol was Fisher Certified Reagent which was used without further purification. Benzene and petroleum ether (60–80°C) were washed several times with concentrated sulphuric acid and 5% sodium carbonate solution. They were dried over anhydrous magnesium sulphate and fractionally distilled from sodium. Pyridine, bp 115°C and 2,6-lutidine, bp 144–145°C were fractionally distilled from potassium hydroxide.

Weighed samples of the non-electrolytes were accurately made up to volume with 70% aqueous acetone.

Kinetics

Solvolytic rate constants were determined in two ways. The first method involved titration of acid with 0.01 *M* sodium hydroxide solution using lacmoid as indicator. An equivalent method involved titration of chloride ions using a glass electrode and a silver electrode attached to a sensitive pH meter. Samples were drawn from the reaction mixtures at intervals throughout at least three half-lives and the reaction quenched with an excess of dry, neutral acetone. The second method used a conductance technique (37). Reaction cells were calibrated individually by measuring the resistance of a large number of solutions of known composition and concentration of completely reacted benzhydryl chloride. Large scale graphs of resistance against concentration were drawn.

For reactions involving pyridine and 2,6-lutidine, the rates were also determined in two ways. Quenched samples of the reaction mixtures in dry acetone were potentiometrically titrated for acid and chloride ions using a glass electrode and silver electrode as described above. When only the total rate or reaction was required, the reactions were monitored by the conductance method.

In the reactions with thiourea, samples (10 mL) of the reaction mixture were quenched by adding them to ice-cold petroleum ether (50 mL) and water (5 mL). After thoroughly shaking, the aqueous layer was isolated. Separate samples (5 mL) were titrated with 0.01 *M* sodium hydroxide solution using a mixed methylene blue, methyl red indicator. One of the samples was titrated without further treatment while the other was first passed through a column of amberlite IR 120 resin to remove cations.

Thermostats were controlled at 20°C to within $\pm 0.01°$, as measured by a platinum resistance thermometer.

Rate Constants

Overall rate constants are defined by eq. [XV] and integrated values were obtained in the usual way from the integrated form of this equation. Hydrolysis rate constants were obtained from eq. [XVI] by numerical integration.

$$[XV] \quad d[Cl^-]/dt = k_{Cl}[RCl] = k_{Cl}([Cl^-]_\infty - [Cl^-]_t)$$

$$[XVI] \quad d[H^+]/dt = k_H[RCl] = k_H([Cl^-]_\infty - [Cl^-]_t)$$

1. G. KOHNSTAM. Adv. Phys. Org. Chem. **5**, 121 (1967).
2. J. W. HILL and A. FRY. J. Am. Chem. Soc. **84**, 2763 (1962).
3. V. J. SHINER, JR., M. W. RAPP, and H. R. PINNICK. J. Am. Chem. Soc. **92**, 232 (1970).
4. B. BENSLEY and G. KOHNSTAM. J. Chem. Soc. 4747 (1957).
5. G. R. COWIE, J. R. FOX, H. J. M. FITCHES, K. A. HOOTON, D. M. HUNT, G. KOHNSTAM, and B. SHILLAKER. Proc. Chem. Soc. 222 (1967).
6. G. KOHNSTAM, B. SHILLAKER, and A. QUEEN. Proc. Chem. Soc. 157 (1959).
7. M. P. FRIEDBERGER and E. R. THORNTON. J. Am. Chem. Soc. **98**, 2861 (1976).
8. H. A. GOERING and J. F. LEVY. J. Am. Chem. Soc. **86**, 120 (1964).
9. V. J. SHINER, JR., R. D. FISHER, and W. DOWD. J. Am. Chem. Soc. **91**, 7748 (1969).
10. R. A. SNEEN and A. W. LARSEN. J. Am. Chem. Soc. **91**, 6031 (1969).
11. R. A. SNEEN. Acc. Chem. Res. **6**, 46 (1973).
12. L. P. HAMMETT. Physical organic chemistry. McGraw-Hill, New York. 1970.
13. D. J. RABER, J. M. HARRIS, R. E. HALL, and P. v. R. SCHLEYER. J. Am. Chem. Soc. **93**, 4821 (1971).
14. A. R. STEIN. J. Org. Chem. **41**, 519 (1976).
15. B. J. GREGORY, G. KOHNSTAM, A. QUEEN, and D. J. REID. Chem. Commun. 797 (1971).
16. M. H. ABRAHAM. J. Chem. Soc. B, 299 (1971); Chem. Commun. 51 (1973).
17. P. J. DAIS and G. A. GREGORIOU. Tetrahedron Lett. 3827 (1974).
18. J. M. HARRIS. Prog. Phys. Org. Chem. **11**, 89 (1974).
19. D. J. MCLENNAN. Acc. Chem. Res. **9**, 281 (1976).
20. D. J. RABER, J. M. HARRIS, and P. v. R. SCHLEYER. Ions and ion-pairs in organic reactions. Vol. 2. *Edited by* M. Szwarc. Wiley, New York. 1974.
21. D. G. GRACZYK and J. W. TAYLOR. J. Am. Chem. Soc. **96**, 3255 (1974).
22. D. G. GRACZYK, J. W. TAYLOR, and C. R. TURNQUIST. J. Am. Chem. Soc. **100**, 7333 (1978).
23. S. WINSTEIN, E. CLIPPINGER, A. H. FAINBERG, and G. C. ROBINSON. J. Am. Chem. Soc. **76**, 2597 (1954).
24. H. ARONOVITCH and A. PROSS. J. Chem. Soc. Perkin II, 540 (1978).
25. A. PROSS. Adv. Phys. Org. Chem. **14**, 69 (1977).
26. B. GIESE. Angew. Chem. Int. Ed. **16**, 125 (1977).
27. A. STREITWIESER, JR. Solvolytic displacement reactions. McGraw-Hill, New York. 1962.
28. L. C. BATEMAN, M. G. CHURCH, E. D. HUGHES, C. K. INGOLD, and N. A. TAHER. J. Chem. Soc. 979 (1940).
29. G. KOHNSTAM. J. Chem. Soc. 2066 (1966).
30. T. H. BAILEY, J. R. FOX, E. JACKSON, G. KOHNSTAM, and A. QUEEN. Chem. Commun. 122 (1966).
31. D. J. MCLENNAN. Tetrahedron Lett. 4689 (1975).
32. E. F. DUYNSTEE, E. GRUNWALD, and M. L. KAPLAN. J. Am. Chem. Soc. **82**, 5654 (1960).
33. C. A. BURTON, T. W. DEL PESCO, A. M. DUNLOP, and Y-U. YANG. J. Org. Chem. **36**, 887 (1971).
34. A. QUEEN, D. M. MCKINNON, and A. W. BELL. Can. J. Chem. **54**, 1906 (1976).
35. C. K. INGOLD. Structure and mechanism in organic chemistry. 2nd ed. Cornell University Press. 1969. Chapt. 7.
36. D. M. MCKINNON and A. QUEEN. Can. J. Chem. **50**, 1401 (1972).
37. R. E. ROBERTSON. Prog. Phys. Org. Chem. **4**, 213 (1967).

Substituent effects on the zero-field splitting parameters of diarylmethylene. Evidence for merostabilization in appropriately substituted diphenylmethylenes[1]

ROBERT W. R. HUMPHREYS AND DONALD R. ARNOLD[2]

The Photochemistry Unit, Department of Chemistry, University of Western Ontario, London, Ont., Canada N6A 5B7

Received March 20, 1979

ROBERT W. R. HUMPHREYS and DONALD R. ARNOLD. Can. J. Chem. **57**, 2652 (1979).

An analysis of the temperature dependence (4–30 K) of the electron spin resonance (esr) spectra of substituted diphenylmethylenes (e.g. *para*-, *para'*-; methoxy, cyano, dimethylamino, and nitro) indicates all of these species have a triplet ground state. The variation in the zero-field splitting parameter D for this series of methylenes provides evidence that the average separation of the unpaired electrons is greatest for the unsymmetrically substituted derivatives, those having a strong *para*-electron-withdrawing substituent and a strong *para'*-electron-donating substituent. This result is explained in terms of a favourable contribution of charge-separated valence-bond structures, i.e., merostabilization.

ROBERT W. R. HUMPHREYS et DONALD R. ARNOLD. Can. J. Chem. **57**, 2652 (1979).

Une analyse de la relation entre la température (4–30 K) et les spectres de résonance paramagnétique électronique des diphénylméthylènes substitués (i.e. *para*-, *para'*-; méthoxy, cyano, diméthylamino et nitro) indique que toutes ces espèces ont un état fondamental triplet. Pour ces séries de méthylènes, la variation du paramètre D de dédoublement du champ zéro fournit la preuve que la séparation moyenne des électrons non appariés est plus grande pour les dérivés substitués d'une façon dissymétrique en particulier ceux ayant en *para* un substituant fortement électroattracteur et en *para'* un substituant fortement électrodonneur. On explique ces résultats en termes d'une contribution favorable de structure, de liaison de valence dont les charges sont séparées, i.e. mérostabilisation.

[Traduit par le journal]

Introduction

It has been recognized for some time that radicals which are appropriately substituted with strong resonance electron-withdrawing and -donating groups exhibit unusual spectral properties and stability when compared to the unsubstituted systems. The first explanation for these observations was provided by Walter (1), who classified radicals as "S" or "O" based on whether electron-withdrawing and donating substituents have the same or opposite effects on the spectral properties of the radical in question. Katritzky and co-workers (2) classified as "merostabilized" those radicals for which favourable, charge-separated resonance structures can be drawn by virtue of the appropriate substitution of the radical with a strong electron-withdrawing and a strong electron-donating group. The predictive value of the approach of Katritzky and co-workers was exemplified by the design and synthesis of new, stable radicals (2*b*).

Both of these classification systems are based on simple resonance theory and concepts of radical stabilization through three-electron bonding. Illustrative examples of merostabilized radicals are Kosower's radical, nitroxides, and diphenylpicrylhydrazyl. The importance of delocalization to the stability of these radicals becomes evident on examination of Kosower's radical and related systems. For instance, 4-carbomethoxy-1-methylpyridinyl (**1**) dimerizes very slowly in solution at room temperature, whereas 4-carbomethoxy-1,3,5-trimethylpyridinyl (**2**) dimerizes very rapidly under identical conditions (3). Delocalization involving charge-separated resonance structures is possible only in the former in which the carbonyl and pyridinyl π-systems can approach coplanarity (Fig. 1). These charge-separated canonical forms are important in the overall resonance description of merostabilized radicals.

Increased delocalization should result in a change in the spin density distribution in merostabilized radicals compared to similar systems lacking such stabilization. This effect has been observed in the electron spin resonance (esr) of *para*-substituted α-carbomethoxy-α-cyanobenzyl radicals (4).

While it is now generally accepted that resonance involving charge-separated structures and three-electron bonding can play an important part in both the spectral properties and stability of free radicals,

[1]Contribution No. 224 from the Photochemistry Unit, University of Western Ontario, London, Ont., Canada.

[2]To whom all correspondence should be addressed. Present address: Department of Chemistry, Dalhousie University, Halifax, N.S., Canada B3H 4J3.

0008-4042/79/192652-10$01.00/0

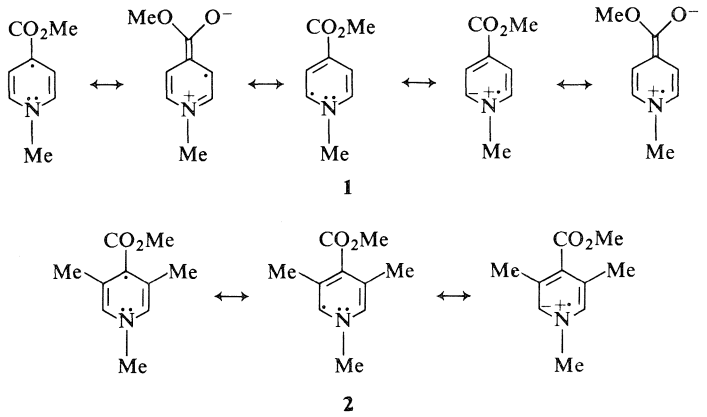

FIG. 1. Merostabilization and increased delocalization.

these concepts had not been applied to other electron deficient species containing unpaired electrons. It occurred to us that diphenylmethylene should be an appropriate system for the investigation of the effects of merostabilization in divalent carbon species. Electron spin resonance (5) and visible and fluorescence spectroscopic studies (6) have shown that the diphenylmethyl radical provides a reasonable model for the electronic structure of diphenylmethylene. Both molecules possess a 13-π-electron odd-alternant hydrocarbon system and exhibit absorption and emission spectra in accord with this structure. The other unpaired electron in diphenylmethylene occupies an orbital (the σ-orbital) situated in the plane of the molecule and the nodal plane of the π-system.

Examination of diphenylmethyl in light of the arguments of Walter and Katritzky leads to the prediction that substitution of this molecule with a strong *para*-electron-donating group and a strong *para'*-electron-withdrawing group should lead to a merostabilized system. Similar substitution in diphenylmethylene should result in a significant redistribution of the unpaired electron spin density of the π-system. This effect is shown in Fig. 2 for (*p*-dimethylaminophenyl) - (*p* - nitrophenyl)methylene (**3***l*). It can be seen that, by virtue of the favourable charge-separated resonance structures, the unpaired electron in the π-system can be delocalized into positions *ortho* to the substituents, that is, *meta* to the divalent carbon.

The experimental verification of this change in spin density distribution in appropriately substituted (merostabilized) diphenylmethylenes should be possible by examination of the magnitude of the zero-field splitting (ZFS) parameter *D* as a function of substitution. *D* can be calculated from the esr spectrum of the diphenylmethylene triplet and it can be shown that the magnitude of *D* is related to the inverse of the cube of the distance between the unpaired electrons in the triplet (7). Any effect which increases the average distance between the unpaired electrons in the triplet causes a corresponding decrease in *D*. The increased delocalization in appropriately substituted (merostabilized) diphenylmethylenes should lead to an increased separation between the unpaired electrons with a concomitant decrease in *D* (see Discussion for further details).

We have studied the esr spectra of an extensive series of *para*- and *para,para'*-substituted diphenylmethylenes and, in this paper, we report the first examples of significant and predictable substituent effects on the ZFS parameter *D* of diphenylmethylene. These effects can be explained in terms of the simple resonance theory discussed above. The diphenylmethylenes studied are listed in Table 1.

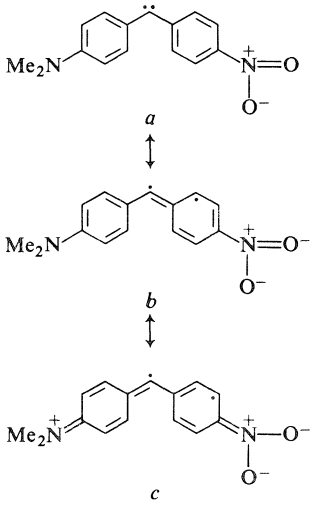

FIG. 2. Merostabilization in a diphenylmethylene (**3***l*).

TABLE 1. *para,para'*-Disubstituted diphenylmethylenes (**3**)

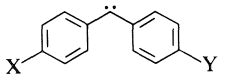

Compound label	X	Y
a	H	H
b	H	OMe
c	OMe	OMe
d	H	CN
e	CN	CN
f	CN	OMe
g	H	NMe_2
h	NMe_2	NMe_2
i	NMe_2	OMe
j	H	NO_2
k	NO_2	NO_2
l	NO_2	NMe_2
m	NO_2	Me
n	NO_2	MeO
o	CN	NMe_2

In addition, we have a continuing interest in the ground state multiplicity of diphenylmethylene as a function of substitution. It has been suggested recently that the separation between the ground state triplet and first excited singlet state of diphenylmethylene may be as small as 3 kcal mol^{-1} (8). We felt that an energy separation of this magnitude might be significantly affected by appropriate substituents, possibly to the extent that the singlet would become the ground state of the system. The rationale behind this hypothesis has been dealt with in detail in a previous publication (9*a*) in which it was shown that the ground state of the diphenylmethylenes **3***a–f* is the triplet. Although the effects of *p*-methoxy and *p*-cyano-substituents were not large enough to invert the order of states in diphenylmethylene, we were reluctant to abandon this objective. Therefore, we have determined the ground state multiplicity of diphenylmethylenes **3***g–o* substituted with the stronger resonance electron-withdrawing and -donating groups nitro and dimethylamino, respectively, by temperature dependent esr studies and application of the Curie law.

Results

Diphenylmethylenes **3***a–o* were generated by irradiation of the corresponding diazo compounds. The substituted diphenyldiazomethanes (**4**) (Table 2) were prepared by one of two general methods. The first method involved the oxidation of the corresponding benzophenone hydrazone with yellow mercuric oxide in the presence of base in a manner previously described (9, 10). This procedure was found to be quite satisfactory for diphenyldiazomethanes **4***a–i*.

Diphenyldiazomethanes **4***j–o* were prepared by the thermal decomposition of the potassium salt of the tosylhydrazone of the corresponding benzophenone. This was essentially a modification of the general procedure of Bamford and Stevens (11) and was adopted because of difficulties encountered in the preparation and/or oxidation of the hydrazone precursors to **4***j–o*. The tosylhydrazone salts could be prepared in large quantities and were stable when stored in a refrigerator. The diazo compounds were generally prepared by allowing the solid salt to stir in the dark at room temperature in *n*-pentane or diethyl ether. In most cases, the decomposition of the salt was a slow process and accumulation of significant amounts of the diazo compound required a considerable period of time (up to one week). The tosylhydrazone salts of *p*-dimethylamino-*p'*-nitrobenzophenone and *p*-cyano-*p'*-dimethylamino-benzophenone decomposed rapidly and reasonable amounts of the diazo compounds could be accumulated overnight.

The diphenyldiazomethanes **4***a–o* were characterized by ir, ^{1}Hmr, and visible spectroscopy. The long-wavelength visible absorption band was particularly useful for the proof of structure of these compounds. A good correlation was found between the position of the visible absorption maximum and the Hammett substituent parameter $\sum\sigma_p$. The visible absorption maxima along with $\sum\sigma_p$ values are listed in Table 2 and the Hammett plot is shown in Fig. 3. The λ_{max} values for the nitro compounds **4***j–n* are plotted in ranges of 10 nm. The long-wavelength absorption for these compounds occurs as a shoulder on a far more intense band and, thus, the exact position is difficult to estimate. The line drawn in Fig. 3 is the least-squares line obtained by using the midpoint of the 10 nm range for **4***j–n*, and the points for the other compounds. The utility of this relationship in identifying the diazo compounds, particularly the less stable ones, should be obvious. A similar correlation has been reported between the diazo stretching frequency in the infrared and Hammett σ_p^+ (12, 13).

The preparations of the diphenyldiazomethanes **4***a–f* have been described elsewhere (9*a*). The preparations of diphenyldiazomethanes **4***g–o* are described in the Experimental section. All of the tosylhydrazones and their salts are new compounds, as are the diphenyldiazomethanes **4***i*, *l*, *n*, and *o*. The preparation of bis(*p*-nitrophenyl)diazomethane has been reported previously (13), but the hydrazone of the corresponding benzophenone is required, for

TABLE 2. Long-wavelength λ_{max} for *para,para'*-disubstituted diphenyldiazomethanes (**4**) and Hammett $\sum\sigma_p$ values

Compound label	Substituent		$\sum\sigma_p$	λ_{max} (nm)	Solvent
	para	*para'*			
a	H	H	0	523	Methylcyclohexane
b	H	OMe	−0.27	529	Methylcyclohexane
c	OMe	OMe	−0.54	543	Methylcyclohexane
d	H	CN	+0.66	503	Methylcyclohexane
e	CN	CN	+1.22	488	Methylcyclohexane
f	CN	OMe	+0.39	511	Methylcyclohexane
g	H	NMe_2	−0.83	538	Methylcyclohexane
h	NMe_2	NMe_2	−1.66	566	Methylcyclohexane
i	NMe_2	OMe	−1.11	550	*n*-Pentane
j	H	NO_2	+0.78	495–505	Diethylether
k	NO_2	NO_2	+1.56	480–490	Diethylether
l	NO_2	NMe_2	−0.05	515–525	*n*-Pentane
m	NO_2	Me	+0.61	500–510	Methylcyclohexane
n	NO_2	OMe	+0.51	505–515	Diethylether
o	CN	NMe_2	−0.17	524	Diethylether

which a preparation was not described. The preparation of this hydrazone is apparently not straightforward (14).[3]

Generation of diphenylmethylenes **3***a–i* in the esr cavity at ca. 5 K was performed by irradiating the appropriate diazo precursor in a rigid glass with a high pressure mercury arc lamp (1 kW). Once generated, these diphenylmethylenes seemed to be stable to further irradiation. A variety of precursors was used to generate diphenylmethylenes **3***j–o*. In an initial experiment, it was found that the esr spectrum of diphenylmethylene could be generated by irradiating the solid potassium salt of benzophenone tosylhydrazone at 77 K. Based on this result, **3***j–o* were generated and characterized by irradiating the corresponding tosylhydrazone salt under similar conditions. This procedure was found to be unsuccessful for **3***k* and *l*. Prolonged irradiation of the salts of these tosylhydrazones produced no signals which could be assigned to **3***k* or *l* at either liquid nitrogen or liquid helium temperatures. Thus, attempts to generate **3***k* and *l* by this method were abandoned in favour of the diazo precursors.

Methylene triplet signals were assigned in terms of the Hamiltonian

$$[1] \quad \hat{H} = g\beta \boldsymbol{H} \cdot \hat{S} + D(\hat{S}_z^2 - \tfrac{1}{3}\hat{S}^2) + E(\hat{S}_x^2 - \hat{S}_y^2)$$

The ZFS parameters were obtained from the observed spectra by employing an iterative computer program and are summarized in Table 3. Accurate field positions for all diphenylmethylenes were obtained by employing the esr field standard $[Cr(NH_3)_5Cl]Cl_2$ diluted in $[Co(NH_3)_5Cl]Cl_2$ (15) (see Experimental for details).

The ZFS parameters for **3***a–f* were obtained by irradiating the diazo compound in a rigid glass (4:1 methylcyclohexane:isopentane). The ZFS parameters for **3***g–o* were obtained in a number of matrices and at varying temperatures. The field positions for **3***l* were obtained in a tetrahydrofuran (THF) matrix at liquid helium temperature. This low temperature was required because of the difficulty in generating even moderately strong signals for this species at liquid nitrogen temperature. It should be noted that although THF does not form a glass, spectra of diphenylmethylenes obtained in a matrix of this solvent did conform to those expected for randomly oriented triplets (i.e., rotating the sample caused no noticeable shift in field positions).

For diphenylmethylenes generated from the tosylhydrazone salt, a powdered salt was used in all cases and the spectra obtained again conform to those of randomly oriented triplets; the ZFS parameters for all diphenylmethylenes except **3***l* were obtained at 77 K.

For **3***a–g* and **3***k*, spectra were intense enough that four lines could be observed (H_{z_1}, H_{x_2}, H_{y_2}, H_{z_2}). For the other diphenylmethylenes, the H_{z_2} line was not observed or was so weak and broad that assignment of the field position was impossible.

Temperature dependence studies were carried out on diphenylmethylenes **3***g–o* using the H_{x_2} line in every case. The experiments were performed in the same glass or matrix used to obtain the ZFS parameters. Temperatures were varied over the range of 5–30 K. The temperature was monitored by using the

[3]Preparation of *p,p'*-dinitrobenzophenone hydrazone required prior preparation of the thioketone P_2S_5 (14).

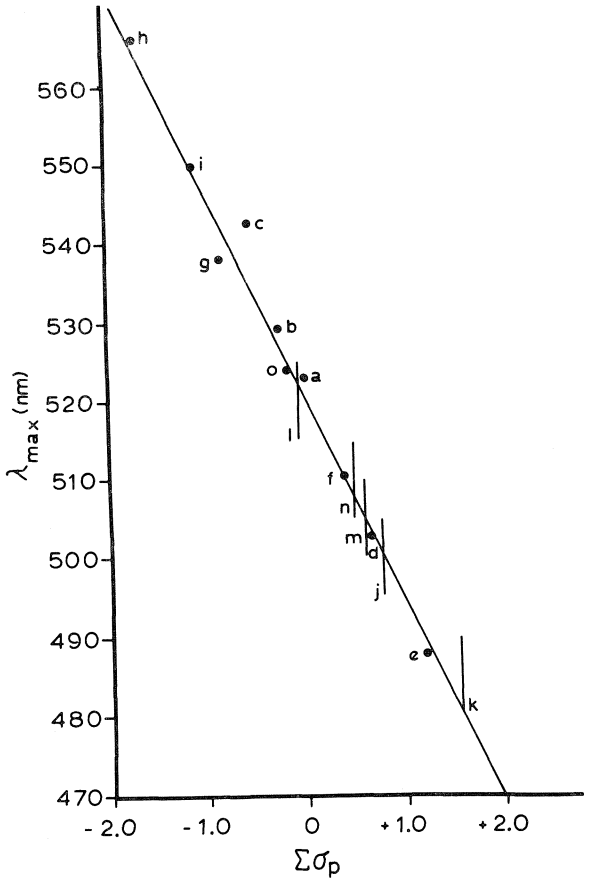

FIG. 3. Graph of λ_{max} (nm) vs. $\Sigma\sigma_p$ for diphenyldiazomethanes (4).

high field line of phenylnitrene as an internal standard in a manner described previously (16).

The observed signal intensity (peak-to-peak height of the H_{x_2} line) as a function of temperature for two of the diphenylmethylenes (**3***h*, *k*) is shown in Fig. 4. As can be seen, the plots are linear over the entire temperature range. These results were typical of those for all of the diphenylmethylenes listed in Table 1.

Discussion

In a simple model, the ZFS parameters D and E for a triplet depend on the distance between electrons with parallel spins as given by eq. [2]:

$$[2a] \quad D = \tfrac{3}{4}g^2\beta^2\left\langle\frac{r^2 - 3z^2}{r^5}\right\rangle$$

$$[2b] \quad E = \tfrac{3}{4}g^2\beta^2\left\langle\frac{y^2 - x^2}{r^5}\right\rangle$$

where the angular brackets imply an average value (7). These equations assume that any spin–orbit coupling contribution to D and E is small and thus, that D and E arise from a predominantly dipolar interaction between the two unpaired electrons. D is essentially a measure of the interaction between the two unpaired electrons along the z-magnetic axis of the molecule while E is a measure of the x,y-interaction. E is relatively small for the methylenes measured here and, although the approximation is crude, it facilitates the discussion somewhat if D is assumed to be related to $1/r^3$ (i.e., cylindrical symmetry is assumed and E is ignored).

Two trends become obvious when the D-values for **3***a–o* are compared (Table 3). First, substitution generally causes a decrease in D over that in the parent molecule **3***a*. Second, the decrease in D is largest when the diphenylmethylene is substituted with one *para*-electron-withdrawing group and one *para'*-electron-donating group. The decrease in D in these unsymmetrically disubstituted diphenylmethylenes is always larger than that predicted by taking the sum of the effects in the mono-substituted derivatives (e.g., compare **3***g*, **3***j*, and **3***l*).

The substituent effects on D are not large, but an explanation can be formulated for the observed trends. The ZFS parameters are directly related to the spin density distribution in the molecule. In the accepted model for diphenylmethylene, one unpaired electron is localized at the divalent carbon atom in the σ-orbital, which means that the spin density at the divalent carbon due to this unpaired electron is essentially one. Obviously, then, any change in D due to substitution must result from a change in the spin density distribution in the π-system containing the other unpaired electron.

The D values in Table 3 indicate that mono- and symmetrical disubstitution both cause a decrease in D and that the effect of disubstitution is greater than (but not double) that of monosubstitution by the same substituent in all cases. The small substituent effect on D was predictable based on the results obtained for the substituent effects on the esr hyperfine splittings of substituted benzyl radicals. For all substituents, the hyperfine splitting constant of the benzyl protons was found to be similar and, thus, substitution has little effect on the spin density at the benzyl carbon (17). A similar conclusion was reached from INDO calculations on the diphenylmethylene system (14). The calculations indicate that substituents had very little effect on the spin density at the divalent carbon and that any change in D was due to a spin density change in other regions of the molecule. Unfortunately, only mono- and symmetrically disubstituted systems were investigated, but the results agree with those in this study for similar systems.

The effect on D of disubstitution of diphenylmethylene with a strong electron-withdrawing group

TABLE 3. Zero-field splitting parameters for diphenylmethylenes (3)

Compound label	Substituent *para*	Substituent *para'*	D (cm^{-1})	E (cm^{-1})	Precursor	Glass or matrix[a]
a	H	H	0.4088	0.0170	Diazo compound	MCIP
			(0.4050)[b]	(0.0194)[b]	Diazo compound	—
b	H	OMe	0.4043	0.0191	Diazo compound	MCIP
			(0.3989)[b]	(0.0192)[b]	Diazo compound	MCIP
			(0.4042)[b]	(0.0194)[b]	Diazo compound	—
c	OMe	OMe	0.4022	0.0189	Diazo compound	MCIP
			(0.4065)[b]	(0.0193)[b]	Diazo compound	—
d	H	CN	0.3906	0.0193	Diazo compound	MCIP
			(0.3854)[b]	(0.0193)[b]	Diazo compound	MCIP
e	CN	CN	0.3879	0.0178	Diazo compound	MCIP
			(0.3818)[b]	(0.0179)[b]	Diazo compound	MCIP
f	CN	OMe	0.3774	0.0172	Diazo compound	MCIP
g	H	NMe_2	0.3876	0.0168	Diazo compound	THF
h	NMe_2	NMe_2	0.3748	0.0180	Diazo compound	4:1 MC:THF
i	OMe	NMe_2	0.3994	0.0178	Diazo compound	THF
j	H	NO_2	0.3778	0.0173	Tosylhydrazone salt	Solid salt
			(0.3765)[b]	(0.0175)[b]	Diazo compound	—
k	NO_2	NO_2	0.3773	0.0177	Diazo compound	Slurry, THF
l	NO_2	NMe_2	0.3351	0.0164	Diazo compound	THF
m	NO_2	Me	0.3711	0.0176	Tosylhydrazone salt	Solid salt, MC slurry
			0.3696	0.0171	Diazo compound	THF
n	NO_2	OMe	0.3599	0.0159	Tosylhydrazone salt	Solid salt, MC slurry
			0.3611	0.0172	Diazo compound	THF
o	CN	NMe_2	0.3518	0.0163	Tosylhydrazone salt	Solid salt

[a]MCIP = 4:1 methylcyclohexane:isopentane; MC = methylcyclohexane; THF = spectral grade tetrahydrofuran.
[b]Previously reported values, ref. 5*a*.

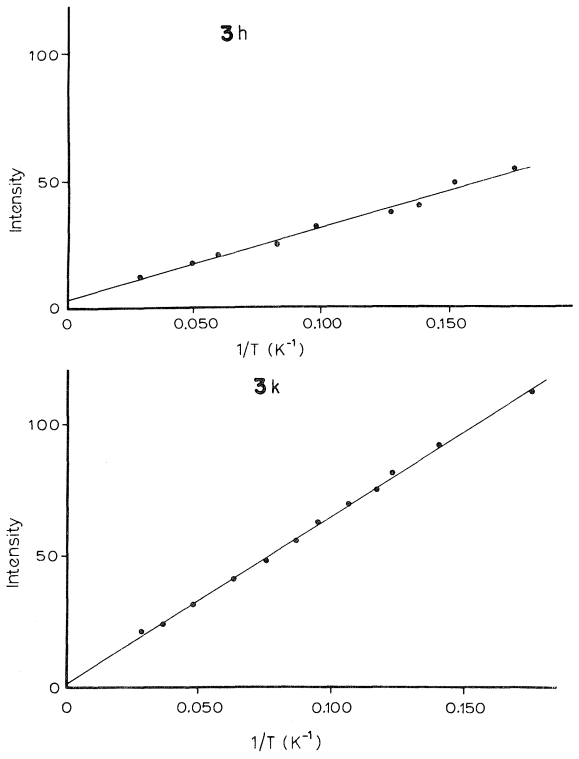

FIG. 4. Curie law plots for the diphenylmethylenes 3*h* and 3*k*.

and a strong electron-donating group can be explained in a different way. For all of the diphenylmethylenes which fall into this class (3*f*, *l*, *m*, *n*, *o*), the D value is smaller than that predicted by taking the sum of the effects in the mono-substituted systems. A simple explanation involving resonance theory allows these results to be explained and is illustrated in Fig. 2 for 3*l*. The appropriate substitution leads to systems which, by Katritzky's definition, can be classified as merostabilized. It should be obvious from Fig. 2 that this type of resonance interaction in symmetrically disubstituted or monosubstituted diphenylmethylenes leads to canonical forms of type "*c*" which would be of relatively high energy. Such canonical forms contribute very little to the overall resonance description of these symmetrically substituted systems. However, for diphenylmethylenes disubstituted with a strong *para*-electron-withdrawing and a strong *para'*-electron-donating group, canonical forms of type "*c*" should contribute significantly to the overall resonance description of these systems. The result is increased delocalization of the unpaired electron occupying the π-system of these diphenylmethylenes. The experimental result is a significant decrease in D compared to systems lacking merostabilization.

The increased delocalization of the *p*-electron in these diphenylmethylenes will result in a spin density

redistribution throughout the π-system. From Fig. 2, it can be seen that merostabilization of diphenylmethylene should result in a significant decrease in the negative spin density at positions *ortho* to the substituents compared to the parent molecule. Unfortunately, the large linewidths (ca. 80 G) of the esr spectra of these randomly oriented triplets preclude the resolution of the appropriate proton hyperfine coupling constants. Nevertheless, the concept of merostabilization is completely consistent with the observed trends in D as a function of substitution.

Although the ZFS parameters for a number of *para*-substituted diphenylmethylenes have been reported (*5a*), the substituents were chosen in a random fashion and no consistent trend in D as a function of substitution was apparent. In addition to providing a clear picture of the effects of substitution on D, this work indicates the importance of resonance and merostabilization in the interaction between the unpaired electrons of a triplet species such as diphenylmethylene.

The temperature dependence studies indicate that the intensity of the esr signals for the diphenylmethylenes **3***g–o* follow the Curie law over the entire temperature range studied. Therefore, **3***g–o* have triplet ground states and the singlet state is not populated to any significant extent at the maximum temperature of the experiment for any of the systems studied. An alternative possibility is that the singlet is the ground state of these species and it is separated by such a small energy from the upper triplet (< 5 cal mol^{-1}) as to be in thermal equilibrium with this upper state even at the lowest temperature studied. The latter explanation seems highly unlikely for **3***g–o*.

Temperature dependence studies have been carried out on the parent molecule (*8a*) and there is no doubt that this molecule has a triplet ground state. Although the chemistry of diphenylmethylene at room temperature seems to involve both the singlet and the triplet states (19), no spectroscopic observation of the singlet state has been reported. From the studies described in this paper, it is not possible to place a lower limit on the triplet–singlet energy separation for any of the diphenylmethylenes **3***g–o* because of the experimental difficulty in detecting deviations from Curie law behaviour due to population of an upper singlet state (16). It is possible that the triplet–singlet separation was lowered significantly in some of the derivatives and that this effect was not detected. It can, however, be concluded that the effects of *p*-methoxy, *p*-cyano, *p*-nitro, and *p*-dimethylamino substituents are not large enough to invert the order of states in diphenylmethylene.

Experimental

General

[1]Hmr spectra were obtained on a Varian T-60 spectrometer, usually in deuterochloroform, and are reported in units of δ ppm relative to tetramethylsilane as an internal standard. Infrared spectra were obtained on a Beckman IR-5A, Beckman "Acculab 4", or Perkin-Elmer 621 Grating Infrared Spectrometer and were calibrated with a polystyrene film. Infrared spectra were obtained in chloroform or carbon tetrachloride in potassium bromide solution cells and are quoted in μm. Visible and ultraviolet spectra were obtained on a Cary 118 spectrometer using quartz cuvettes. Melting points were obtained on a Sybron Corporation Thermolyne melting point apparatus and are corrected.

Electron spin resonance spectra were obtained from a Varian E-12 esr spectrometer. Temperature dependence studies were performed with an Air Products Model LTD-3-110 "Heli-tran" liquid helium Dewar and transfer system. Samples were placed in Suprasil esr tubes and were irradiated with a Hanovia 1 kW high-pressure mercury arc lamp.

Sample preparation varied and depended on the precursor used to generate the methylene. When the diazo compound was used as the precursor, 10–20 mg was dissolved in 1 mL of the appropriate solvent. If the diazo compound was stable, degassing was carried out by the freeze–pump–thaw method. If the diazo compound was unstable, no attempt was made to degas the sample.

In some cases, the potassium salt of the tosylhydrazone of the corresponding benzophenone was used as a convenient precursor for the generation of the methylene. Usually, the solid salt was packed in an esr tube to the appropriate height. In some cases, it was found that only the outer surface of the salt was irradiated under these conditions, and thus the salt was added to an esr tube as a slurry in dry THF and was quickly placed in the esr cavity and frozen before settling could occur. This procedure allowed more complete irradiation to occur and, thus, produced larger signals.

Phenylazide was added to samples used in temperature dependence studies. When the diazo compound was used as the methylene precursor, about 6–8 mg phenylazide was added to the esr sample. When the tosylhydrazone salt was used, a solution of about 40 mg phenylazide in 1 mL methylcyclohexane was added to the salt in the esr tube and was allowed to mix with the salt.

Irradiations in the esr cavity were generally carried out through a Corning O-53 (≥ 280 nm) or O-54 (≥ 300 nm) filter. Under these conditions, large methylene (and nitrene) signals could be produced quickly from either precursor.

Temperature dependence studies on all diarylmethylenes were carried out using a procedure identical to that described previously (9, 16, 20). Temperature measurement at liquid helium temperatures was carried out by including phenylazide in the sample and monitoring the nitrene signal intensity as a function of temperature.

Zero-field Splitting Parameters

Accurate field positions for the diphenylmethylenes **3***a–o* were determined by employing the inorganic field standard $[Cr(NH_3)_5Cl]Cl_2$ as a 2% mixture in $[Co(NH_3)_5Cl]Cl_2$ (15). Accurate field positions for this standard have been provided, along with the appropriate microwave frequency corrections.

Calculations of the zero-field splitting parameters from the esr field positions were performed by employing an iterative computer program described previously (16). The line position was taken as the maximum, minimum, or midpoint, depending on the line shape (21).

Preparation of the Diphenyldiazomethanes

The preparation of **4***a–f* has been described in full (9). The general procedure for **4***g–i* involved the preparation of the corresponding benzophenone hydrazone (10) from the ketone, and subsequent oxidation with yellow mercuric oxide in the presence of base. **4***j–o* were prepared by decomposition of the tosylhydrazone salt.

The visible absorption maxima for the diazo compounds are listed in Table 2.

Preparation of the Hydrazones

A 100 mL round-bottom flask equipped with a magnetic stirring bar, reflux condenser, nitrogen inlet tube, and bubbler was purged with nitrogen. The ketone (ca. 2.0 g) and hydrazine hydrate (50 mL) were added and the contents were heated to reflux using an oil bath. Vigorous stirring was employed. After heating at reflux overnight, the reaction mixture was cooled. An oil settled to the bottom of the flask and solidified and crystals formed in the hydrazine hydrate. The solid was collected by vacuum filtration. The hydrazine hydrate was extracted with chloroform (100 mL) and the chloroform was removed on a rotary evaporator to give an oil. This oil was combined with the solid and solidified on standing.

p-*Dimethylaminobenzophenone Hydrazone*

The ^{1}Hmr spectrum showed that both *E* and *Z* isomers were present (yield = 2.0 g, 99%). ^{1}Hmr ($CDCl_3$): δ 2.80, 2.86 (s, 6H total); δ 5.10, 5.27 (2 br. s, 2H total); δ 6.60 (m, AA′BB′, 4H); δ 7.18 (m, 5H).

*Bis-(*p*-dimethylamino)benzophenone Hydrazone*

The product was recrystallized from absolute alcohol to give yellow needles, mp 150–152°C. ^{1}Hmr ($CDCl_3$): δ 2.84 (s, 3H); δ 2.92 (s, 3H); δ 5.07 (s, br., 2H); δ 6.86 (m, 8H); ir ($CHCl_3$): 2.90, 3.31, 6.20, 6.60, 6.75, 6.91, 7.37, 8.39, 8.47, 9.40, 10.57, 12.17.

p-*Dimethylamino*-p′-*methoxybenzophenone Hydrazone*

The product was recrystallized from absolute alcohol to give light yellow needles, mp 166–170°C. ^{1}Hmr ($CDCl_3$): δ 2.86, 2.92 (2s, 6H); δ 3.72, 3.80 (2s, 3H); δ 5.20, 5.32 (2s br., 2H); δ 6.92 (m, 8H); ir ($CHCl_3$): 2.92, 3.31, 3.56, 6.19, 6.60, 7.33, 7.43, 7.97, 8.49, 9.62, 11.90, 12.12.

Anal. calcd. for $C_{16}H_{19}N_3O$: C 71.34, H 7.11; found: C 71.12, H 7.06.

Oxidation of the Hydrazone

The hydrazone (ca. 1.0 g), anhydrous ether (60 mL), anhydrous sodium sulfate (3.0 g), yellow mercuric oxide (3.3 g, 15 mmol) and saturated ethanolic potassium hydroxide (3 mL) were placed in a 150 mL round-bottom flask equipped with a magnetic stirring bar and drying tube. The mixture was allowed to stir in the dark at room temperature for 11 h. After filtering by gravity into a round-bottom flask covered with aluminum foil, the solvent was removed on a rotary evaporator with the water bath at room temperature.

*(*p*-Dimethylaminophenyl)phenyldiazomethane (***4***g)*

A purple solid was obtained, the ^{1}Hmr, ir, and visible spectra of which were consistent with **4***g*. ^{1}Hmr (CCl_4): δ 2.92 (s, 6H); δ 6.83 (m, AA′BB′, 4H); δ 7.10 (m, 5H); ir ($CHCl_3$): 3.38, 4.93, 6.23, 6.61, 6.71, 6.93, 7.73, 9.58.

*Bis-(*p*-dimethylaminophenyl)diazomethane (***4***h)*

As above, with the exception that dry tetrahydrofuran was substituted for anhydrous ether; **4***h* was obtained as a grey-blue solid. ^{1}Hmr (CH_2Cl_2): δ 2.90 (s, 12H); δ 6.78 (m, AA′BB′, 8H); ir ($CHCl_3$): 3.31, 4.91, 6.20, 6.60, 6.92, 7.35, 12.24.

*(*p*-Dimethylaminophenyl)(*p*-methoxyphenyl)diazomethane (***4***i)*

As above, with the exception that *n*-pentane was substituted for anhydrous tetrahydrofuran. A deep blue solid was obtained. ^{1}Hmr (CD_2Cl_2): δ 2.96 (s, 6H); δ 3.83 (s, 3H); δ 6.96 (m, 8H); ir ($CHCl_3$): 3.31, 3.50, 4.93, 6.19, 6.61, 8.00, 8.26, 9.62.

p-*Cyano*-p′-*dimethylaminobenzophenone*

This compound was prepared by a modification of the procedure of Shah, Deshpande, and Chaubal (22). Phosphorus oxychloride (11.8 mL, 0.13 mol), *N*,*N*-dimethylaniline (36 mL, 0.28 mol) and *p*-cyanobenzanilide (21 g, 0.095 mol) were placed in a 1 L round-bottom flask equipped with a reflux condenser and thermometer with the bulb extending below the surface of the reaction mixture. The flask was placed in an oil bath and the bath was heated slowly. At about 120°C, an exothermic reaction began and the flask was cooled in ice-water as soon as the temperature reached 180°C. A thick brown syrup was obtained. After adding 10% HCl (700 mL), the mixture was heated on a steam bath and the brown product was hydrolyzed. The resulting yellow solid was collected by vacuum filtration and recrystallized several times from absolute alcohol. Yellow plates (3.0 g, 20%) of *p*-cyano-*p*′-dimethylaminobenzophenone were obtained, mp 178–179°C. ^{1}Hmr ($CDCl_3$): δ 3.07 (s, 6H); δ 7.07 (m, 4H); δ 7.63 (m, 4H); ir ($CHCl_3$): 3.32, 4.37, 6.00, 6.20, 6.40, 7.20, 7.48, 7.65, 8.65, 10.69, 11.66, 12.03.

Anal. calcd. for $C_{16}H_{14}N_2O$: C 76.78, H 5.64; found: C 76.68, H 5.48.

p-*Nitrobenzophenone Tosylhydrazone*

A mixture of *p*-nitrobenzophenone (23) (5.0 g, 0.022 mol), *p*-toluenesulfonhydrazide (8.2 g, 0.044 mol), and benzene (200 mL), in a 500 mL round-bottom flask equipped with a reflux condenser, was heated at reflux for 3 days. The solution was cooled and the benzene was removed on a rotary evaporator to give a yellow oil containing some solid. Methanol (50 mL) was added and the mixture was warmed to dissolve the oil and then cooled in ice. Crystals were collected in a sintered glass funnel and recrystallized by dissolving in benzene, adding ethanol, and boiling off most of the solvent. A total of 4.0 g (46%) *p*-nitrobenzophenone tosylhydrazone was obtained, mp 130–138°C. ^{1}Hmr ($CDCl_3$): δ 2.45 (s, 3H); δ 7.75 (m, 14H); ir ($CHCl_3$): 3.03, 3.23, 6.24, 6.58, 6.91, 7.20, 7.73, 7.60, 8.58, 9.38, 10.19, 11.42, 11.72, 11.80.

Anal. calcd. for $C_{20}H_{17}N_3O_4S$: C 60.75, H 4.33; found: C 60.92, H 4.44.

p-*Methyl*-p′-*nitrobenzophenone Tosylhydrazone*

Light yellow needles (1.18 g from 1 g of the ketone (24), 70%) mp 130–200°C (dec.) were obtained after recrystallization from benzene–alcohol. ^{1}Hmr ($CDCl_3$): δ 2.30, 2.40 (2s, 6H); δ 7.47 (m, 13H); ir ($CHCl_3$): 3.04, 3.28, 3.41, 6.26, 6.61, 7.24, 7.45, 7.62, 8.61, 9.38, 10.21, 11.41, 11.63, 12.16.

Anal. calcd. for $C_{21}H_{19}N_3O_4S$: C 61.61, H 4.68; found: C 61.42, H 4.62.

p-*Methoxy*-p′-*nitrobenzophenone Tosylhydrazone*

Yellow crystals (3.0 g from 4.0 g of the ketone (18), 45%), mp 191–192°C were obtained after recrystallization from chloroform–methanol. ^{1}Hmr ($CDCl_3$): δ 2.40 (s, 3H); δ 3.72, 3.83 (2s, 3H total); δ 7.50 (m, 13H); ir ($CHCl_3$): 3.03, 3.27, 3.39, 3.52, 6.22, 6.60, 7.39, 7.62, 7.96, 8.60, 10.19, 11.63.

Anal. calcd. for $C_{21}H_{19}N_3O_5S$: C 59.29, H 4.50; found: C 59.51, H 4.82.

p,p′-*Dinitrobenzophenone Tosylhydrazone*

Yellow needles (1.17 g from 1.0 g of the ketone, 84%), mp 198–201°C (dec.) were obtained after recrystallization from benzene–ethanol. ^{1}Hmr (acetone-d_6): δ 2.39 (s, 3H); δ 7.74 (m, 13H); ir ($CHCl_3$): 3.03, 3.30, 6.25, 6.58, 7.44, 7.63, 8.60, 9.35, 10.21, 11.41, 11.64, 11.88.

Anal. calcd. for $C_{20}H_{16}O_6N_4S$: C 54.55, H 3.66; found: C 54.30, H 3.72.

p-*Dimethylamino*-p′-*nitrobenzophenone Tosylhydrazone*

Benzene (250 mL), *p*′-dimethylamino-*p*′-nitrobenzophenone (24) (20 g, 0.074 mol), and *p*-toluenesulfonylhydrazide (16.6 g, 0.089 mol, 20% excess) were placed in a 500 mL round-bottom flask equipped with a reflux condenser, Dean–Stark trap, and drying tube. The reaction mixture was heated at reflux for 3 days, during which time approximately 1 mL water accumulated in the D–S trap. The reaction mixture was allowed to cool and the benzene was removed on a rotary evaporator to give a thick, dark orange oil. Absolute alcohol (100 mL) was added and the mixture was warmed on a steambath until the oil had dissolved. A light orange solid precipitated. After cooling in ice, the orange solid was collected by vacuum filtration. After recrystallization from tetrahydrofuran – absolute alcohol, orange crystals (17.2 g, 53%) of *p*-dimethylamino-*p*′-nitrobenzophenone tosylhydrazone were obtained.

Recrystallization from benzene – petroleum ether (30–60) resulted in two crystal forms; one, dark red cubes, and the other, an orange powder. The ^{1}Hmr spectra indicated that the two crystalline forms were composed of different ratios of *E* and *Z* isomers of the tosylhydrazone. ^{1}Hmr ($CDCl_3$): δ 2.40 (s, 3H); δ 3.00 (s, 6H); δ 7.24 (m, 13H); ir ($CHCl_3$): 3.05, 3.41, 6.23, 6.60, 7.45, 7.63, 8.61, 9.40, 10.24, 11.41, 11.64, 11.77, 12.22.

Anal. calcd. for $C_{22}H_{22}N_4O_4S$: C 60.27, H 5.06; found: C 60.15, H 5.21.

p-*Cyano*-p′-*dimethylaminobenzophenone Tosylhydrazone*

Yellow crystals (435 mg from 500 mg of the ketone, 52%), mp 178–179°C, were obtained from benzene–alcohol. ^{1}Hmr ($CDCl_3$): δ 2.42 (s, 3H); δ 3.03 (s, 6H); δ 7.30 (m, 13H); ir ($CHCl_3$): 3.04, 3.51, 4.48, 6.21, 6.93, 7.33, 7.61, 8.57, 9.35, 10.21, 11.41, 11.83, 12.21.

Anal. calcd. for $C_{23}H_{22}N_4O_4S$: C 66.01, H 5.30; found: C 65.84, H 5.43.

(p-*Dimethylaminophenyl*)-(p-*nitrophenyl*)*diazomethane* (**4**l)

In a 250 mL Erlenmeyer flask equipped with a magnetic stirring bar, *p*-dimethylamino-*p*′-nitrobenzophenone tosylhydrazone (760 mg, 1.74 mmol) and anhydrous diethyl ether (100 mL) were placed and the mixture was stirred for several minutes to allow as much as possible of the tosylhydrazone to dissolve. Potassium *tert*-butoxide (215 mg, 1.91 mmol, 10% excess) was added and the colour of the ether changed slowly from light orange to a deep red-orange. The flask was loosely corked and the reaction mixture was allowed to stir for 1 h in the dark. The red potassium salt of the tosylhydrazone was separated from the ether by gravity filtration, giving an orange ether solution and a deep red solid in the filter paper. The red salt was washed back into the Erlenmeyer flask with *n*-pentane and a total of 200 mL *n*-pentane was added. The flask was corked lightly and allowed to stir at room temperature in the dark. After 5 h, the mixture was filtered by gravity into a round-bottom flask covered with aluminum foil, giving an orange pentane solution and leaving the red salt behind in the filter paper. The pentane was removed on a rotary evaporator using a cold water bath. A red orange solid was obtained, the ir and visible absorption spectra of which indicated the presence of the desired (*p*-dimethylaminophenyl)-(*p*-nitrophenyl)diazomethane. The diazo compound was stored in a freezer at ca. −20°C. The potassium salt was washed back into the Erlenmeyer flask and more *n*-pentane (200 mL) was added. This process could be repeated until all of the salt had decomposed. However, since only small amounts of the diazo compound were required for the esr experiments and since **4***l* was found to be unstable, the salt decomposition was never carried to completion.

The purity of the (*p*-dimethylaminophenyl)-(*p*-nitrophenyl)-diazomethane was checked by both ^{1}Hmr and thin layer chromatography (tlc). The ^{1}Hmr spectrum showed one large singlet for the methyls of the dimethylamino group of the diazo compound and two much smaller singlets at approximately the same chemical shift, assigned to impurities. The purity was checked by tlc using alumina plates and benzene elution. The diazo compound in *n*-pentane, before solvent removal, showed one dark orange spot which moved rapidly and faded to pale yellow when exposed to room light. A faint spot with a much smaller R_f was also observed. The dark orange spot was assigned to the diazo compound. The red-orange solid obtained after removal of the pentane was also tested by tlc under identical conditions. Again, a dark orange spot with large R_f was observed. Two lighter spots of lower R_f, one visible only under uv light, were also observed. However, the diazo compound was the major spot. Based on ^{1}Hmr and tlc results, the diazo compound was estimated to be ca. 80% pure. ^{1}Hmr (CH_2Cl_2): δ 2.83 (s, 6H); δ 7.30 (m, 8H); ir ($CHCl_3$): 3.28, 3.40, 4.90, 6.22, 6.30, 7.43, 7.51, 8.35, 8.89.

Bis-(p-*nitrophenyl*)*diazomethane* (**4**k)

In a 25 mL round-bottom flask equipped with a magnetic stirring bar and drying tube, *p*,*p*′-dinitrobenzophenone tosylhydrazone (1.00 g, 2.27 mmol) and dry tetrahydrofuran (7 mL) were placed and the tosylhydrazone was allowed to dissolve. The solution was stirred slowly and potassium *tert*-butoxide (0.28 g, 2.5 mmol) was added. The solution turned deep orange immediately and an orange precipitate formed. After approximately 5 min, the orange potassium salt of the tosylhydrazone was collected in a Buchner funnel and washed with anhydrous ether. The salt was transferred to a 250 mL Erlenmeyer flask covered with aluminum foil and equipped with a magnetic stirring bar, anhydrous ether (200 mL) was added and the flask was loosely corked and allowed to stir at room temperature. After stirring overnight, the reaction mixture was filtered by gravity into a round-bottom flask covered with aluminum foil, giving a light yellow ether solution and leaving the orange salt in the filter paper. The ether was removed on a rotary evaporator to give a small amount of an orange solid, the ir of which showed a strong diazo stretching band at ca. 4.9 μm (2040 cm^{-1}). The salt was rinsed back into the Erlenmeyer flask, more ether was added, and the process was repeated. This procedure was continued until enough bis-(*p*-nitrophenyl)-diazomethane was accumulated for the experiments of interest to be performed. ^{1}Hmr (CH_2Cl_2): δ 7.83 (m, AA′BB′); ir ($CHCl_3$): 3.31, 4.85, 6.28, 6.58, 7.41, 7.50, 8.95, 11.75.

(p-*Nitrophenyl*)*phenyldiazomethane* (**4**j)

In a 100 mL round-bottom flask equipped with a magnetic stirring bar and drying tube, *p*-nitrobenzophenone tosylhydrazone (1.00 g, 2.52 mmol) and dry tetrahydrofuran (10 mL) were added and the tosylhydrazone was allowed to dissolve. The solution was stirred slowly and potassium *tert*-butoxide (0.31 g, 2.9 mmol) was added. The reaction mixture immediately turned deep red and, after a few minutes, the potassium salt of the tosylhydrazone began to precipitate. After about 10 min, anhydrous ether (60 mL) was added. The salt precipitated completely and was collected in a Buchner funnel and washed several times with anhydrous ether. The orange salt was transferred to a 250 mL Erlenmeyer flask equipped with a magnetic stirring bar and covered with aluminum foil. Anhydrous ether (150 mL) was added, the flask was loosely corked, and the mixture was allowed to stir at room temperature. After stirring overnight, the reaction was filtered by gravity to yield a light yellow ether layer. The ether solution was placed in a round-bottom flask covered with aluminum foil and the solvent was removed on a rotary evaporator with the water bath at room temperature. A small amount of orange solid was obtained, the ir spectrum of which showed a diazo stretching band at 4.88 μm as the strongest band in the spectrum.

The salt was rinsed from the filter paper back into the Erlenmeyer flask. More ether was added and the entire process was repeated until enough diazo compound was accumulated to perform the desired experiments. ^{1}Hmr (CD_2Cl_2): δ 7.14 (m, 5H); δ 7.62 (m, AA′BB′, 4H); ir ($CHCl_3$): 3.28, 4.88, 6.29, 6.62, 7.49, 8.31, 9.00.

*(*p*-Methylphenyl)-(*p*-nitrophenyl)diazomethane (4*m*)*

This compound was prepared by a method similar to that used to prepare **4***i*. ^{1}Hmr (CD_2Cl_2): δ 2.30 (s, 3H); δ 7.19 (s, 5H); δ 7.56 (m, AA′BB′, 4H); ir ($CHCl_3$): 3.33, 3.46, 4.87, 6.27, 6.61, 7.50, 8.32, 8.98.

*(*p*-Methoxyphenyl)-(*p*-nitrophenyl)diazomethane (4*h*)*

The same procedure was used as for **4***i*. ir ($CHCl_3$): 3.30, 3.50, 4.89, 6.29, 6.63, 7.50, 8.01, 9.00, 9.67.

*(*p*-Cyanophenyl)-(*p*-dimethylaminophenyl)diazomethane (4*o*)*

In a 125 mL Erlenmeyer flask equipped with a magnetic stirring bar, 400 mg (0.96 mmol) *p*-cyano-*p*′-dimethylaminobenzophenone tosylhydrazone and 15 mL dry tetrahydrofuran were added and the tosylhydrazone was allowed to dissolve. The solution was stirred slowly and 118 mg (1.05 mmol, 10% excess) potassium *tert*-butoxide was added. The solution slowly changed from light yellow to a deep yellow. After 15 min stirring, 50 mL *n*-pentane was added. The potassium salt of the tosylhydrazone precipitated and the yellow solid was allowed to settle. The solvent was decanted and the salt was washed once with 50 mL anhydrous ether. The Erlenmeyer flask was covered with aluminum foil and 100 mL anhydrous ether was added. The flask was loosely corked and the reaction mixture was allowed to stir at room temperature for 3 h. The reaction mixture was filtered by gravity into a round-bottom flask covered with aluminum foil, giving a light pink ether solution. The ether was removed on a rotary evaporator, using a cold water bath. A purple solid was obtained by the above procedure. The ir and uv spectra confirmed the formation of **4***o*. This compound was found to be comparatively unstable and was kept in a freezer until needed (ca. −20°C). ir ($CHCl_3$): 3.34, 3.49, 4.49, 4.90, 6.24, 6.60, 8.25.

1. R. I. Walter. J. Am. Chem. Soc. **88**, 1923 (1966).
2. (*a*) R. W. Baldock, P. Hudson, and A. R. Katritzky. J. Chem. Soc. Perkin I, 1422 (1974); (*b*) A. R. Katritzky and F. Soti. J. Chem. Soc. Perkin I, 1427 (1974).
3. M. Itoh and S. Nagakura. Bull. Chem. Soc. Jpn. **39**, 369 (1966).
4. (*a*) H. A. P. de Jonge, C. R. H. I. de Jonge, and W. J. Mijs. J. Org. Chem. **36**, 3160 (1971); (*b*) H. A. P. de Jonge, C. R. H. I. de Jonge, H. J. M. Sinnige, W. J. de Klein, W. G. B. Huysmans, W. J. Mijs, W. J. van den Hoek, and J. Smidt. J. Org. Chem. **37**, 1960 (1972); (*c*) W. J. van den Hoek, B. A. C. Rousseeuw, J. Smidt, W. G. B. Huysmans, and W. J. Mijs. Chem. Phys. Lett. **13**, 429 (1972).
5. (*a*) A. M. Trozzolo and E. Wasserman. *In* Carbenes. Vol. 2. *Edited by* R. A. Moss and M. Jones, Jr. John Wiley and Sons, New York. 1975, and references cited therein; (*b*) R. W. Brandon, G. L. Closs, C. E. Davoust, C. A. Hutchison, Jr., B. E. Kohler, and R. Silbey. J. Chem. Phys. **43**, 2006 (1965); (*c*) E. Wasserman, A. M. Trozzolo, W. A. Yager, and R. W. Murray. J. Chem. Phys. **40**, 2408 (1964); (*d*) C. A. Hutchison, Jr. and B. E. Kohler. J. Chem. Phys. **51**, 3327 (1969).
6. A. M. Trozzolo. Acc. Chem. Res. **1**, 329 (1968).
7. J. E. Wertz and J. R. Bolton. Electron spin resonance. McGraw-Hill, New York. 1972. Chapt. 10.
8. (*a*) G. L. Closs. *In* Carbenes. Vol. 2. *Edited by* M. Jones, Jr. and R. A. Moss. John Wiley and Sons, Inc., New York. 1975; (*b*) G. L. Closs and B. E. Rabinow. J. Am. Chem. Soc. **98**, 8190 (1976).
9. (*a*) R. W. R. Humphreys and D. R. Arnold. Can. J. Chem. **55**, 2286 (1977); (*b*) D. R. Arnold and R. W. R. Humphreys. J. Chem. Soc. Chem. Commun. 181 (1978).
10. L. I. Smith and K. L. Howard. Org. Syn. Coll. Vol. 3. J. Wiley and Sons, Inc., New York. 1955. p. 351.
11. W. R. Bamford and T. S. Stevens. J. Chem. Soc. 4735 (1952).
12. S. Stankovsky and S. Kovac. Chem. Zvesti. **28**, 238 (1974).
13. P. Yates, B. L. Shapiro, N. Yoda, and J. Fugger. J. Am. Chem. Soc. **79**, 5756 (1957).
14. J. H. Hall. Private communication.
15. W. T. M. Andriessen. J. Magn. Reson. **23**, 339 (1976).
16. D. R. Arnold, R. W. Humphreys, W. J. Leigh, and G. E. Palmer. J. Am. Chem. Soc. **98**, 6225 (1976).
17. P. Neta and R. H. Schuler. J. Phys. Chem. **77**, 1368 (1973).
18. B. Jones. J. Chem. Soc. 1854 (1936).
19. G. L. Closs. Top. Stereochem. **3**, 193 (1968).
20. R. W. R. Humphreys. Ph.D. Thesis, University of Western Ontario, London, Ont. 1978.
21. E. Wasserman, L. C. Snyder, and W. A. Yager. J. Chem. Phys. **41**, 1763 (1964).
22. R. C. Shah, R. K. Deshpande, and J. S. Chaubal. J. Chem. Soc. 642 (1932).
23. G. Schroeter. Chem. Ber. **42**, 3356 (1909).
24. H. Limpricht and E. Samietz. Ann. **286**, 321 (1895).

Some thermodynamic aspects of dissolution of solid solutions of hydroxylapatites of phosphorus and arsenic

T. S. B. NARASARAJU[1] AND U. S. RAI

Department of Chemistry, Banaras Hindu University, Varanasi-221005, India

Received March 20, 1979

T. S. B. NARASARAJU and U. S. RAI. Can. J. Chem. 57, 2662 (1979).

The solubility equilibria of synthetic samples of hydroxylapatite, its arsenic isomorph, and a series of their solid solutions, spread over the entire compositional range, were investigated at 37°C in the pH range 5.0 to 7.6 in buffered systems through microanalytical determinations of calcium, phosphorus, and arsenic in their saturated solutions. From the ionic products of the samples so determined their stoichiometric dissolution was established and their free energies of solution evaluated.

T. S. B. NARASARAJU et U. S. RAI. Can. J. Chem. 57, 2662 (1979).

Opérant à 37°C, à des pH allant de 5.0 à 7.6 dans des systèmes tamponnées et faisant appel à des déterminations microanalytiques du calcium, du phosphore et de l'arsenic dans leurs solutions saturées, on a étudié les équilibres de solubilité d'échantillons de synthèse de l'hydroxylapatite, de son isomorphe contenant de l'arsenic et d'une série de leurs solutions solides variant sur toute l'échelle de composition. Sur la base des produits ioniques déterminés pour ces échantillons, on a établi leur dissolution stoechiométrique et on a évalué leurs énergies libres de solution.

[Traduit par le journal]

Introduction

Phosphorus hydroxylapatite (PHA), $Ca_{10}(PO_4)_6(OH)_2$, the principal inorganic constituent of human bones and teeth (1), undergoes several anionic and cationic substitutions, significant among which from the point of view of arsenic poisoning (2, 3) being the replacement of PO_4^{3-} by AsO_4^{3-} resulting in the formation of its isomorph, arsenic hydroxylapatite (AsHA). It is evident that incomplete progress of such a substitution leads to the formation of a series of solid solutions of these isomorphs as shown by Montel and co-workers (4). Since bone processes, calcification and resorption, the deposition and dissolution respectively of PHA at the bone/body-fluid interface are controlled by its solubility, it was considered desirable to investigate the pH-dependence of solubilities of PHA, AsHA, and a series of their solid solutions over the entire compositional range under simulated biological conditions to throw light on the mechanism of arsenic incorporation and its likely reversal. The present paper which deals with such a series of investigations in the pH range 5.0 to 7.6 adopts a new approach towards the evaluation of their solubility products from which their free energies of solution have been calculated.

Experimental

The experimental details of preparation, characterization, and determination of solubilities of PHA, AsHA, and a series of their solid solutions were reported elsewhere (5–10), particular attention being paid to provide evidence for the homogeneity of the solid solutions based on the validity of Vegard's law. The solubility of each one of the samples was determined by analyses of its saturated solution at a few chosen pH values in the range 5.0 to 7.6, using suitable buffer combinations (10), the final pH of each system being measured using a pH meter (PHM 29, Radiometer, Copenhagen). To overcome the complications involved in the microdetermination of the products of dissolution of the samples of apatites, three different analytical procedures were adopted for the analyses of the saturated solutions of (*i*) PHA, (*ii*) AsHA, and (*iii*) solid solutions of (*i*) and (*ii*). While the method adopted for (*i*) is the same as that reported earlier (11, 12), solutions of (*ii*) could be analysed by an extension of method (*i*) to a combination of calcium and arsenic instead of calcium and phosphorus, the only difference being that the reduction of the corresponding heteropoly acid to molybdenum blue was by heating the solution for about 15 min over a water bath since the process is considerably slower for arsenic than for phosphorus at ordinary temperatures.

While saturated solutions of PHA and AsHA could be analysed for calcium and phosphorus or arsenic as described above, complications arose in the case of systems involving the solid solutions. Consequent upon the similarity in the behaviour of phosphorus and arsenic towards their spectrophotometric determination based on the formation of molybdenum blue, a combined determination of the two elements in the saturated solution of the systems involving the solid solutions of PHA and AsHA was attempted. Concentration of arsenic was then obtained by subtracting the phosphorus content determined by masking (13) of arsenic as mentioned above from the combined value. Such an indirect procedure had to be adopted for the analysis of the systems of the solid solutions since alternative techniques were not available for the purpose.

Results and Discussion

The weight percent errors in the quantitative

[1]Present address: Chemistry Department, North-Eastern Hill University, Shillong, India.

0008-4042/79/192662-03$01.00/0

determinations of calcium, phosphorus, and arsenic when present together were found to be ± 0.6, ± 1.7, and ± 2.5 respectively. The details of the analytical data of Ca^{2+}, PO_4^{3-}, and AsO_4^{3-}, the associated calculations (6) as well as the pH range used, leading to the evaluation of the ionic product, K_{ip} (represented as pK_{ip}, equal to $-\log K_{ip}$) and the free energy of solution, ΔG_{soln}, of each sample have been included in the Depository of Unpublished Data.[2] From the average pK_{ip} values of the samples obtained from the analysis of their saturated solution, values of ΔG_{soln} were calculated; a consolidated account of these two sets of values is given in columns 3 and 4 respectively of Table 1. The details of the theoretical implications involved in considering the ionic products of these solutes to be synonymous with their corresponding solubility products have been mentioned earlier (14, 15).

The present investigations could establish that the solubilities of PHA, AsHA, and their solid solutions increased with increasing hydrogen ion concentration of the medium of dissolution.[2] This could be justified on the basis of the establishment of a series of simultaneous equilibria in the saturated solutions of these samples and their dependence (15) on the H_3O^+ ion activity of the medium. It may be mentioned that the set of equilibria operative in the case of AsHA is analogous to that of PHA while both sets are established in the case of their solid solutions.

It can be concluded from the pK_{ip} values given in column 3 of Table 1 that the solubilities of the samples increased with an increase in the proportion of AsHA. This could be explained on the basis of the higher dissociation constants (6, 10) of H_3AsO_4 ($K_1 = 4.0 \times 10^{-3}$, $K_2 = 1.0 \times 10^{-7}$, and $K_3 = 3.2 \times 10^{-12}$) over the corresponding values of H_3PO_4 ($K_1 = 7.51 \times 10^{-3}$, $K_2 = 6.33 \times 10^{-8}$, and $K_3 = 4.73 \times 10^{-13}$). An additional theoretical substantiation of this experimental finding can be made on the basis of alterations in lattice and solvation energies of ionic crystals brought about by anionic replacement, the rest of the ions being left undisturbed. The tetrahedral covalent radius (16) of AsO_4^{3-} (1.18 Å) being higher than that of PO_4^{3-} (1.10 Å) the lattice of AsHA can be supposed to be less firmly bound than that of PHA. Solvation energies of the constituent ions of the two lattices being nearly the same, loose packing associated with the lattice of AsHA can account for its higher solubility. That AsHA is relatively less stable than PHA is evident from the experimental ΔG_{soln} values given in column 4 of Table 1. The reported (17) increase in the solubilities of sodium halides in the order NaF, NaCl, NaBr, and NaI may be suggested to justify this observation. However, solubilities of RbF and RbI do not follow this sequence. It is evident that ΔG_{soln} depends exclusively on the balance of entropy and enthalpy terms and hence the above argument does not merit a generalization.

In accordance with the earlier observations (15, 18–21) the analytical data of the saturated solutions of the samples could establish stoichiometric dissolution on the basis of the proximity of the Ca/(P or As or both) values to the theoretical value of 1.67 (as indicated by materials in the Depository of Unpublished Data). In addition, as is to be expected from the variation in lattice energies of the samples with a replacement of PO_4^{3-} by AsO_4^{3-}, a fairly systematic gradation of ΔG_{soln} values with increase in the proportion of PHA could be observed, absence of regularity in this gradation being attributed to the fluctuations in the determination of pK_{ip} values which amount to about $\pm$ 1.5. Since the difference in the ΔG_{soln} values of the end members (PHA and AsHA) is about 20, which is much above the limits of fluctuation, the above conclusion can be justified.

TABLE 1. Ionic products and free energies of solution of hydroxylapatites of phosphorus and arsenic and their solid solutions*

Sample Number	Molecular formula of the sample	Average pK_{ip}	ΔG_{soln} (kcal/mol)
1	$Ca_{10}(PO_4)_6(OH)_2$	107.8	153.9
2	$Ca_{10}(PO_4)_{5.4}(AsO_4)_{0.6}(OH)_2$	107.9	154.1
3	$Ca_{10}(PO_4)_{4.8}(AsO_4)_{1.2}(OH)_2$	108.1	154.3
4	$Ca_{10}(PO_4)_{4.2}(AsO_4)_{1.8}(OH)_2$	107.9	154.1
5	$Ca_{10}(PO_4)_{3.6}(AsO_4)_{2.4}(OH)_2$	105.6	150.8
6	$Ca_{10}(PO_4)_{3.0}(AsO_4)_{3.0}(OH)_2$	105.1	150.1
7	$Ca_{10}(PO_4)_{2.4}(AsO_4)_{3.6}(OH)_2$	102.0	145.6
8	$Ca_{10}(PO_4)_{1.8}(AsO_4)_{4.2}(OH)_2$	99.9	142.6
9	$Ca_{10}(PO_4)_{1.2}(AsO_4)_{4.8}(OH)_2$	98.9	141.2
10	$Ca_{10}(PO_4)_{0.6}(AsO_4)_{5.4}(OH)_2$	96.6	137.9
11	$Ca_{10}(AsO_4)_6(OH)_2$	94.5	134.9

*Details of analytical data of Ca^{2+}, PO_4^{3-}, and AsO_4^{3-}, the associated calculations as well as the pH ranges used have been included in the Depository of Unpublished Data.

Acknowledgements

Thanks are due to Professor O. P. Malhotra, former Head, Chemistry Department, Banaras Hindu University, for providing necessary facilities. Financial assistance given to one of us (U.S.R.) by UGC (India) is also gratefully acknowledged.

[2]A complete set of data is available, at a nominal charge, from the Depository of Unpublished Data, CISTI, National Research Council of Canada, Ottawa, Ont., Canada K1A OS2.

1. A. S. POSNER. *In* Phosphorus and its compounds. Vol. II. *Edited by* J. R. Van Wazer. Interscience Publisher Inc., NY. 1961. pp. 1429–1459.

2. C. P. STEWART and A. STOLMAN. Toxicology. Mechanism and analytical methods. Academic Press, NY. 1960. p. 202.
3. W. B. DEICHMANN and H. W. GERARDE. Toxicology of drugs and chemicals. Academic Press, NY. 1969. p. 113.
4. M. MASSUYAS, J. C. TROMBE, G. BONEL, and G. MONTEL. Bull. Chem. **7**, 2308 (1969).
5. T. S. B. NARASARAJU, N. S. CHICKERUR, and R. P. SINGH. J. Inorg. Nucl. Chem. **33**, 3194 (1971).
6. T. S. B. NARASARAJU and V. L. N. RAO. Z. Phys. Chem. Leipzig, **255**, 655 (1974).
7. T. S. B. NARASARAJU, V. L. N. RAO, M. LAL, and U. S. RAI. Indian J. Chem. **13**, 369 (1975).
8. N. S. CHICKERUR, R. P. SINGH, and T. S. B. NARASARAJU. Naturwissenschaften, **56**, 282 (1969).
9. T. S. B. NARASARAJU, K. K. RAO, and U. S. RAI. Indian J. Chem. In press.
10. T. S. B. NARASARAJU, K. K. RAO, U. S. RAI, and B. K. KAPOOR. Indian J. Chem. **14**A, 1014 (1977).
11. R. P. SINGH, N. S. CHICKERUR, and T. S. B. NARASARAJU. Z. Anal. Chem. **237**, 117 (1968).
12. T. S. B. NARASARAJU, R. P. SINGH, and V. L. N. RAO. Z. Anal. Chem. **251**, 300 (1970).
13. P. D. GOULDEN and P. B. BANK. Limnol. Oceanogr. **19**(4), 705 (1974).
14. V. K. LA MER. J. Phys. Chem. **66**, 973 (1962).
15. T. S. B. NARASARAJU, K. K. RAO, and U. S. RAI. Can. J. Chem. In press.
16. L. V. AZAROFF. Introduction to solids. TMH Ed., Tata McGraw-Hill Publishing Company Ltd., India. 1960. p. 440.
17. D. L. LEUSSING. *In* Treatise on analytical chemistry. Part I. Vol. I. *Edited by* I. M. Kolthoff, P. J. Elving, and E. B. Sandell. The Interscience Encyclopaedia, Inc., NY. 1959. p. 675.
18. J. S. CLARK. Can. J. Chem. **33**, 1696 (1955).
19. E. C. MORENO, T. M. GREGORY, and W. E. BROWN. J. Res. Natl. Bur. Stand. Sect. A, **72(6)**, 773 (1968).
20. D. R. WIER, S. H. CHIEN, and C. A. BLACK. Soil Sci. **111(2)**, 107 (1971).
21. A. N. SMITH, A. M. POSNER, and J. P. QUIRK. J. Colloid. Interface Sci. **48(3)**, 442 (1974).

Thermochemistry of tantalum(V) bromide

ALAN D. WESTLAND

Department of Chemistry, University of Ottawa, Ottawa, Ont., Canada K1N 9B4

Received May 8, 1979

ALAN D. WESTLAND. Can. J. Chem. 57, 2665 (1979).

The enthalpy of formation of crystalline $TaBr_5$ is found by solution calorimetry to be -142.9 ± 0.4 kcal mol^{-1}. Estimates of entropies and heat capacities lead to thermochemical quantities for the liquid and gaseous compound as well.

ALAN D. WESTLAND. Can. J. Chem. 57, 2665 (1979).

On a trouvé, par calorimétrie en solution, que l'enthalpie de formation du composé cristallin $TaBr_5$ est de -142.9 ± 0.4 kcal mol^{-1}. Des évaluations des entropies et des capacités calorifiques permettent de déduire les quantités thermochimiques des composés à l'état liquide et à l'état gazeux.

[Traduit par le journal]

In the course of measuring the bromide ion affinity of gaseous $TaBr_4$ it was necessary to obtain the standard enthalpy of formation of the compound and this in turn required a knowledge of the enthalpy of formation of the pentabromide. The literature contains two values which are not in good agreement. The present work was undertaken in order to resolve the question.

Shchukarev *et al.* reported a value of -145.6 ± 1.0 kcal mol^{-1} for the enthalpy of formation of $TaBr_5$ which was based upon measurement of the enthalpy of hydrolysis of the compound (1). When their value is revised by making use of the most recent auxiliary data (2) a value of -147.0 kcal mol^{-1} is obtained. Gross *et al.* subsequently determined the enthalpy of formation by direct combustion and obtained the value -142.96 kcal mol^{-1} (3). The combustion measurements carried out on other systems by the latter workers have been of generally high quality. However, in favour of the Russian work is the accuracy of their value of ΔH_f^0 for $TaCl_5$ which they reported in the same publication (1) and which was based in part on some of the same data which led to the pentabromide value. Moreover, we have found that if the combustion of tantalum is momentarily inefficient, a refractory tribromide is formed which does not subsequently brominate easily to $TaBr_5$. McCarley and Boatman reported a similar finding (4). Gross *et al.* indeed found the reaction with bromine to be so sluggish that it was necessary to operate the calorimeter at 110°C and correct the value so obtained to 298 K with the aid of estimated heat capacities.

It was decided to employ an independent method based on the dissolving of $TaBr_5$ and tantalum metal in aqueous hydrofluoric acid. The procedure devised by Schäfer and Kahlenberg and used by them to examine the pentachloride (5) was followed exactly. In following Schäfer and Kahlenberg it was possible to verify some of their data for partial processes common to the chloride and bromide thermal cycles and this served to minimize some of the uncertainty associated with solution calorimetry where many terms may have to be added in the cycle.

Experimental

Calorimeter

The calorimeter consisted of a Dewar vessel and attachments which was immersed in a water thermostat maintained at 25.00 ± 0.05°C. The Dewar volume was 600 cm^3. The top of the calorimeter had five inlets which contained respectively a spiral stirrer, a thermistor, a calibration heater, a sample container, and a cooling well. All glass surfaces were coated with a wax composed of 90% paraffin and 10% butyl rubber sealant (Lepage's Ltd).

The thermistor (Sargent-Welch Model S81750-12) was immersed in oil in a thin-walled well. The thermistor resistance was measured by means of a Sargent-Welch Model 81601 thermometric bridge connected to a Wheelco 1 mV recorder. The sensitivity was ±0.001°C. Non-linearity of the thermistor was compensated for by calibrating after each run over the same temperature interval as in the dissolution process. This was achieved by evaporating small quantities of liquid nitrogen in the cooling well by which means the calorimeter could be brought back to its original temperature before the electrical heating was begun.

The heater was a spiral of No. 30 constantan wire which was immersed in oil. Its resistance was 4.160 ± 0.003 ohms. The leads were No. 22 gauge copper wire. Current for the heater was drawn from a large 2 V accumulator. The current was measured by means of a potentiometer (Derritron Electronics Model No. E4224) connected across a 0.2 ohm standard resistance.

Solid samples were contained in thin-walled quartz bulbs which were crushed on a silver spike mounted in a plastic housing. The exterior surface of the bulbs was coated with wax. A blank experiment showed that the operation of crushing the bulb generated negligible heat (≤ 0.2 cal).

In order to measure the enthalpy of dilution of concentrated hydrofluoric acid solutions, the bulb-breaking device was re-

0008-4042/79/192665-04$01.00/0

placed by a cylindrical silver vessel (2.5 × 11 cm) mounted on a Teflon sleeve. The bottom of this cup was affixed with wax and could be knocked out in order to allow the contained liquid to mix with the outer liquid. When the concentrated acid contained platinum, the silver cup was also coated with wax.

Reaction periods lasted no longer than 2 min. Errors in the corrections for heat loss or gain during the reaction period were estimated to be no greater than 0.1%. The operation of the calorimeter was checked by measuring the heat of neutralization of tris(hydroxymethyl)aminomethane (THAM) (6). This indicated that the electrical circuitry and timer were correctly calibrated to ±0.2%.

Materials

Tantalum Pentabromide

Tantalum foil (99.95%) was supplied by Fansteel Metals, Inc. The bromide was prepared by heating the metal in purified bromine vapour in a previously evacuated, sealed system. The product was handled in a dry nitrogen atmosphere and stored in sealed ampoules. Bromine in the samples was determined by totally hydrolyzing the compound in a closed container with aqueous hydroxide and completing the determination by the Volhard method. *Anal.* calcd. for $TaBr_5$: Br 68.83; found: Br 68.73.

Hydrofluoric Acid

Two solutions were prepared from the concentrated acid (Analar). The concentrations were established by alkalimetric titration of weighed portions. A standardized burette was employed. (*a*) Hydrofluoric acid containing 26.97 ± 0.04% w/w HF. The 40.00 g portions of this acid used later contained 0.5391 mol HF and 1.621 mol H_2O. (*b*) Hydrofluoric acid containing 3.47 ± 0.01% w/w HF. A 349.7 g portion of this was used as a solvent for $TaBr_5$. This portion contained 0.6064 mol HF and 18.74 mol H_2O.

Hydrobromic Acid

A dilute solution which contained 0.7285 ± 0.0003% w/w HBr was used as a calorimeter liquid in the study of partial process [II] (*vide infra*). A 306.9 g portion contained 0.02763 mol HBr and 16.91 mol H_2O.

H_2PtCl_6-solution

A platinum catalyst solution identical to that used by Schäfer and Kahlenberg was prepared (5).

The Partial Processes

A thermal cycle analogous to that described by Schäfer and Kahlenberg was employed (5). The first step of this cycle involves the dissolving of tantalum metal in aqueous HF. This was done by Schäfer and Kahlenberg who employed 1.0 g of 6 μm thick foil. In order that the previous authors' value for the heat of solution of tantalum could be used in the present work, acids of the same concentration were used throughout.[1] The following list of partial processes therefore corresponds to that of the German workers.

Reactions [II] to [IV] were examined experimentally in this laboratory. The enthalpy of reaction [I] was taken from ref. 5. The enthalpies of reactions [V] to [VIII] were obtained from standard literature sources (2, 7).

The quantities shown in the following reactions refer to 1 mol of tantalum. The quantities contained in braces denote solution compositions in terms of moles of the solutes and the solvent water. The quantities used in the actual calorimeter runs are given in the details which follow these equations.

[I] $Ta(c) + \{109.7; 0.00165H_2PtCl_6; 331.7H_2O\} \xrightarrow{\Delta H_1} \{TaF_5; 104.7HF; 0.0369HCl; 331.7H_2O\} + 0.00615Pt + (2.5\text{–}0.0123)H_2(g)$

[II] $\{TaF_5; 104.7HF; 0.0369HCl; 331.7H_2O\} + \{5.00HBr; 3060H_2O\} \xrightarrow{\Delta H_2} \{TaF_5; 104.7HF; 5HBr; 0.0369HCl; 3391.7H_2O\}$

[III] $\{TaF_5; 104.7HF; 5.00HBr; 0.0369HCl; 3391.7H_2O\} \xrightarrow{\Delta H_3} TaBr_5(c) + \{109.7HF; 0.0369HCl; 3391.7H_2O\}$

[IV] $\{109.7HF + 3390.06H_2O\} \xrightarrow{\Delta H_4} \{109.7HF; 330.06H_2O\} + 3060H_2O\,(l)$

[V] $2.5H_2(g) + 2.5Br_2(l) + 3060H_2O(l) \xrightarrow{\Delta H_5} \{5.00HBr; 3060H_2O\}$

[VI] $\{0.0369HCl; 1.64H_2O\} + 0.00615Pt \xrightarrow{\Delta H_6} \{0.00615H_2PtCl_6; 1.64H_2O\} + 0.0123H_2(g)$

[VII] $\{109.7HF; 330.06H_2O\} + \{0.00615H_2PtCl_6; 1.64H_2O\} \xrightarrow{\Delta H_7} \{109.7HF; 0.00615H_2PtCl_6; 331.7H_2O\}$

[VIII] $\{109.7HF; 0.0369HCl; 3391.7H_2O\} \xrightarrow{\Delta H_8} \{0.0369HCl; 1.64H_2O\} + \{109.7HF; 3390.06H_2O\}$

The sum of these partial processes yields

$$Ta(c) + 2.5\,Br_2(l) = TaBr_5(c)$$

for which

$$\Delta H_f^0(TaBr_5(c)) = \sum_1^8 \Delta H_i$$

Process [I]: Dissolving of Tantalum in Hydrofluoric Acid

Schäfer and Kahlenberg (5) dissolved 1.000 g tantalum foil in a mixture of 45.00 g hydrofluoric acid (0.6065 mol HF +

[1]This was done for economy. A quotation of $200 per g for 10 μm foil led us to abandon our intention to repeat the measurements for the first process.

1.824 mol H_2O) with 0.170 cm^3 of H_2PtCl_6 solution (34×10^{-6} mol H_2PtCl_6 + 9.05×10^{-3} mol H_2O). Their mean value was $\Delta H_1 = -99.66 \pm 0.1$ kcal/mol. This value includes a correction for the heat of evaporation of the hydrofluoric acid caused by the evolution of hydrogen. The platinum catalyzes the reaction.

Process [II]: Dilution of the Tantalum Solution from Process [I]

In the present work, tantalum solutions {TaF_5; 104.7HF; 0.0369HCl; 331.7H_2O} were prepared from 0.1 mm thick tantalum foil. The dissolving process was too slow with foil of this thickness for a calorimetric study. The metal (0.889 g) was dissolved in 40.00 g of 26.97% HF to which was added 0.15 g of the H_2PtCl_6-solution. After the solution had been allowed to stand for 2 days[2] it was thoroughly mixed and a 41.04 g portion diluted in the calorimeter with 272.8 g of 0.7285% hydrobromic acid. The mean of three values of the enthalpy of dilution gave $\Delta H_2 = -22.7 \pm 0.2$ kcal based on 1.0 mol of tantalum.

Process [III]: Dissolving of Tantalum(V) Bromide

Owing to the extreme moisture sensitivity of $TaBr_5$, the product was inevitably hydrolyzed to a slight extent. The enthalpies of solution were corrected by dividing by the purity where purity = observed % Br/calculated % Br. This assumes that a given quantity of moisture totally hydrolyzes an equivalent amount of the halide:

$$n\mathrm{TaBr_5} + 5\mathrm{H_2O} \rightarrow \mathrm{Ta_2O_5} + (n-2)\mathrm{TaBr_5} + 10\mathrm{HBr}$$

This is perhaps an oversimplification.

It was not convenient to work with exactly 3.208 g portions of $TaBr_5$ as indicated by the ideal partial reaction [III]. Instead, various quantities were dissolved in 3.47% hydrofluoric acid and the mean value chosen. The data shown in Table 1 indicate that enthalpies of solution are independent, within experimental error, of the quantity of $TaBr_5$ taken; thus, the compound behaves in solution as if it were infinitely dilute. The results give $\Delta H_3 = +96.04 \pm 0.12$ kcal mol^{-1}.

The solution so obtained, when referred to 1 mol of tantalum, must still be mixed with the solution {0.0369HCl; 0.7H_2O} in order for the above reaction to correspond to partial process [III]. This would entail a negligible heat of mixing (< 0.1 kcal).

Process [IV]: Dilution of Hydrofluoric Acid

Portions (40.00 g) of 26.97% hydrofluoric acid were diluted with 270.8 g portions of water. The mean of four determinations gave $+27.9 \pm 0.2$ kcal. This is 0.1 kcal less than the value reported by Schäfer and Kahlenberg. A possible reason for this difference may be the presence of silica in the acid used in the former work. It was common for acid to contain silica. The acid used in the present study was reported by the manufacturer to contain 0.1% SiF_4. In any case, the error would appear also in ΔH_2 with a reversed sign. Thus $\Delta H_2 + \Delta H_4 = 5.2$ kcal in both the present and the former work of Schäfer and Kahlenberg.

Process [V]: Enthalpy of Formation of Hydrobromic Acid

Interpolation of the literature data (2) gives $\Delta H_5 = -144.68$ kcal. The preamble to ref. 2 suggests that the uncertainty in this figure is no greater than ± 0.10 kcal.

[2]Although Schäfer and Kahlenberg report that foil of 6 μm thickness dissolved rapidly to form Ta(V), we found that the thicker metal led to the formation of brown–yellow solutions which became colourless only after several hours. Schäfer and Kahlenberg observed such an effect with niobium (8). The coloured species was believed to be metal in the 3+ oxidation state.

TABLE 1. Enthalpy of solution of $TaBr_5$

Sample weight (g)	$-\Delta H$ (kcal mol^{-1})
0.6480	96.22
1.0244	96.06
1.2059	96.03
1.3128	95.88
2.5335	96.01
	Mean 96.04 ± 0.12

TABLE 2. Enthalpies of partial processes

Enthalpy	Value
ΔH_1	-99.66 ± 0.15
ΔH_2	-22.7 ± 0.2
ΔH_3	$+96.04 \pm 0.12$
ΔH_4	$+27.9 \pm 0.2$
ΔH_5	-144.68 ± 0.15
ΔH_6	$+0.43 \pm 0.02$
ΔH_7	-0.23
ΔH_8	~ 0

Process [VI]: Reduction of the H_2PtCl_6-solution

The literature data yield the value $\Delta H_6 = -0.43 \pm 0.02$ kcal (2).

Process [VII]: Enthalpy of Dilution

We neglect the small H_2PtCl_6 content. The enthalpy of dilution of the hydrofluoric acid is then $\Delta H_7 = -0.23$ kcal (2).

Process [VIII]: Enthalpy of Mixing

The literature does not contain data for the mixing of hydrochloric and hydrofluoric acids. However, Schäfer and Kahlenberg (5) have bracketed the value and find $\Delta H_8 < 0.1$ kcal.

The partial process enthalpies are summarized in Table 2. The sum of the partial enthalpies gives:

$$\Delta H_f^0(\mathrm{TaBr_5(c)}\ 298\ \mathrm{K}) = -142.9 \pm 0.4\ \mathrm{kcal\ mol^{-1}}$$

It is possible to estimate the quantities shown in Table 3.

Estimates of entropies and heat capacities were based on data for similar reference compounds which are available in standard compilations (2, 6). The heat capacities were derived from $ZrBr_4$(c) and $TiBr_4$(g) by an application of Kopp's Law. The halogen contribution was obtained by subtracting the heat capacities of the metals at 298 K. The heat capacity of tantalum metal was then added to the halogen contribution extrapolated to five atoms of bromine.

The entropies of crystalline compounds likewise obey an additivity law which is a corollary of Kopp's Law. The related compounds $TaCl_5$, UCl_4, UCl_5, UBr_4, and $ThBr_4$ permit us to infer the standard entropies of $TaBr_5$ by making use of the following approximate principles: (*i*) The contribution of the halogen in a pentahalide is taken to be 5/4 that for a tetrahalide. (*ii*) Given the value of S_{298}^0 for a chloride, the increment in entropy which would result by replacing Cl by Br is the same in all analogous compounds, e.g. in UCl_4 and UBr_4.

The heat of fusion, 10.9 kcal mol^{-1} (9, 10), affords the value of ΔH_f^0 for the liquid. Two sets of workers have measured the sublimation pressures of $TaBr_5$(c) over a range of temperature extending from 453 to 540 K (10, 11). These data lead to enthalpies of sublimation of 25.4 and 25.8 kcal mol^{-1} respectively. We estimate from the heat capacities given in Table 3 a correction of +1.3 kcal mol^{-1} in converting from 498 K to

TABLE 3. Thermochemical data for $TaBr_5$ at 298 K

State	ΔH_f^0 (kcal mol^{-1})	S^0 (eu)	ΔG_f^0 (kcal mol^{-1})	C_p
Crystalline	-142.9 ± 0.4	67 ± 2	-133	$29+19\times10^{-3}T$
Liquid	-132.0 ± 0.4			
Gaseous	-116.0 ± 0.6	115 ± 3	-120	$31-2\times10^{5}T^{-2}$

298 K. We thus propose ΔH(subl. 298 K) = 26.9 kcal mol^{-1}. From the same vapour pressure data we obtain ΔS(subl. 498 K) = 44.0 cal deg^{-1} mol^{-1}. The heat capacity correction (+3.5 cal deg^{-1} mol^{-1}) therefore gives ΔS(subl. 298 K) = 47.5 cal deg^{-1} mol^{-1}.

The empirical formula of Geiseler (12) gives the value $S^0(TaBr_5(g)$ 298 K) = 116.9 cal deg^{-1} mol^{-1} which agrees well with the estimate recorded in Table 3.

Hill, Worsley, and Hepler have provided estimates of entropies which are very close to ours (13).

Acknowledgements

The author wishes to thank Fansteel Metals Inc. for a gift of tantalum metal.

1. S. A. SHCHUKAREV, E. K. SMIRNOVA, I. V. VASIL'KOVA, and L. L. LAPPO. Vestn. Leningrad Univ. Ser. Fiz. Khim. **15**, 113 (1960).
2. D. D. WAGMAN, W. H. EVANS, V. B. PARKER, I. HALOW, S. M. BAILEY, and R. H. SCHUMM. Selected values of chemical thermodynamic properties. Technical note 270-3. National Bureau of Standards, Washington, DC. 1968.
3. P. GROSS, C. HAYMAN, D. L. LEVI, and G. L. WILSON. Trans. Faraday Soc. **58**, 890 (1962).
4. R. E. MCCARLEY and J. C. BOATMAN. Inorg. Chem. **4**, 1486 (1965).
5. H. SCHÄFER and F. KAHLENBERG. Z. Anorg. Allg. Chem. **294**, 242 (1958).
6. R. J. IRVING and I. WADSÖ. Acta Chem. Scand. **18**, 195 (1964).
7. F. D. ROSSINI. Selected values of chemical thermodynamic properties. Circular 500. National Bureau of Standards, Washington, DC. 1952.
8. H. SCHÄFER and F. KAHLENBERG. Z. Anorg. Allg. Chem. **305**, 291 (1960).
9. K. M. ALEXANDER and F. FAIRBROTHER. J. Chem. Soc. S223 (1949).
10. E. L. WISEMAN and N. W. GREGORY. J. Am. Chem. Soc. **71**, 2344 (1949).
11. S. S. BERDONOSOV, A. V. LAPITSKII, and E. K. BAKOV. Russ. J. Inorg. Chem. **10**, 173 (1965).
12. G. GEISELER. Z. Phys. Chem. **202**, 424 (1954).
13. J. O. HILL, I. G. WORSLEY, and L. G. HEPLER. Chem. Rev. **71**, 127 (1971).

Photochemical ring expansion of a bridged cyclobutanone. Crystal and molecular structure of the photoproduct acetal

TREVOR J. GREENHOUGH, JOHN R. SCHEFFER, JAMES TROTTER, AND LEUEEN WALSH

Department of Chemistry, University of British Columbia, Vancouver, B.C., Canada V6T 1W5

Received December 8, 1978

TREVOR J. GREENHOUGH, JOHN R. SCHEFFER, JAMES TROTTER, and LEUEEN WALSH. Can. J. Chem. **57**, 2669 (1979).

The photochemistry of the bridged cyclobutanone system 1,3,4,6,8,9-hexamethyltricyclo-[4.4.0.0^{3,10}]decane-2,5-dione has been studied. Irradiation in methanol leads to a single ring-expanded cyclic acetal whose structure was determined by X-ray crystallography. The reaction represents the first example of oxacarbene formation in a bridged cyclobutanone. Rationalization of the observed regioselectivity on the basis of alkyl substitution effects on radical stability following α-cleavage is inappropriate since the starting cyclobutanone bears equal α and α′ substitution. An alternative explanation involving alkyl radical angle strain and hyperconjugation effects is advanced.

TREVOR J. GREENHOUGH, JOHN R. SCHEFFER, JAMES TROTTER et LEUEEN WALSH. Can. J. Chem. **57**, 2669 (1979).

On a étudié la photochimie du système cyclobutanone ponté hexaméthyl-1,3,4,6,8,9 tricyclo[4.4.0.0^{3,10}] décanedione-2,5. L'irradiation dans le méthanol conduit à la formation d'un seul acétal cyclique, résultant d'une extention de cycle dont la structure a été déterminée par diffraction des rayons-X. Cette réaction correspond au premier exemple de formation du oxacarbène dans une cyclobutanone pontée. Il ne serait pas approprié de rationaliser la régiosélectivité observée en utilisant les effets de substitution alkyle sur la stabilité des radicaux provenant d'un clivage α puisque les substituants en α et en α′ de la cyclobutanone de départ sont semblables. On propose une autre explication impliquant la tension angulaire alkyl-radical et des effets d'hyperconjugaison.

[Traduit par le journal]

Introduction

The photochemistry of cyclobutanones is a subject of continuing interest and investigation (1–3). For monocyclic or fused bicyclic cyclobutanones, three major photochemical pathways have been identified, (*a*) reverse 2 + 2 fragmentation (cycloelimination) to yield ketenes and olefins, (*b*) decarbonylation, and (*c*) ring expansion via oxacarbenes to afford (in alcoholic solvents) cyclic acetals.

This latter process is favored by increasing alkyl substitution at the α-carbon atoms of the four membered ring as well as by substituents (e.g., β-cyclopropyl) which increase the cyclobutanone internal angle strain. Also effective in directing reaction toward this pathway are cyclobutanone substituents which electronically stabilize the product oxacarbene, for example α-ethylenic and α-cyclopropyl moieties.

Both biradical (initial alkyl–acyl cleavage) and concerted mechanisms have been considered in oxacarbene formation owing to the fact that the reaction exhibits features characteristic of each. For example, oxacarbene formation is regiospecific, the major product generally (but not always (4)) being explicable in terms of formation of the more stable of the two possible biradical intermediates. On the other hand (and consistent with a concerted process), oxacarbene formation is generally found to be stereospecific (1–3), the reaction proceeding with retention of configuration at the cyclobutanone α-carbon atom. To accommodate these and other experimental observations, Morton and Turro (1) have suggested a "biradical-like" transition state (and not a freely rotating acyl–alkyl biradical) as the direct precursor of the oxacarbene species.

Perusal of the literature reveals that oxacarbene formation has never been observed for cyclobutanone systems which are *bridged* across positions 2 and 4. Of the few substrates of this type which have been irradiated, one undergoes decarbonylation (ref. 5, as quoted in ref. 1, footnote 89), one takes part in unsaturated aldehyde formation (6), and the others (which are bridged β,γ-unsaturated cyclobutanones) either rearrange via 1,3-acyl shifts (7), decarbonylate (7*a*), or undergo cyclo-elimination (8). The source of this avoidance of oxacarbene formation is not apparent, and in order to clarify the situation, we have undertaken a study of the photochemistry of the bridged cyclobutanone 1,3,4,6,8,9-hexamethyltricyclo[4.4.0.0^{3,10}]decane-2,5-dione (**1**, Scheme 1). The present paper describes the high yield formation of an oxacarbene-derived product from irradiation of **1**

0008-4042/79/192669-08$01.00/0

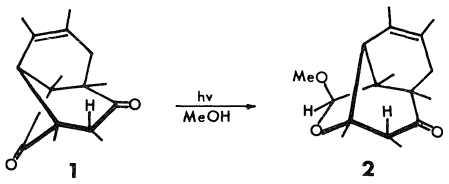

SCHEME 1

in methanol and summarizes the elucidation of the photoproduct structure via X-ray crystallography.

Results

Cyclobutanones having the basic tricyclo-[4.4.0.0^{3,10}]decane-2,5-dione structure of **1** are readily available through irradiation ($\lambda > 340$ nm) of Diels–Alder adducts between duroquinone and acyclic 1,3-dienes (9); the substrate **1** is derived from the 2,3-dimethylbutadiene–duroquinone adduct (9*a*). Photolysis of cyclobutanone **1** (uv n $\rightarrow \pi^*\lambda_{max}^{MeOH}$ 300 nm, ε 66) in methanol solvent through Pyrex rapidly and cleanly afforded a single major photoproduct in 70–80% yield. More than a dozen minor photoproducts could be detected by flame ionization glc but were present in amounts too small to permit isolation.

The photoproduct is isolated as a colorless solid, mp 49.5–51.5°C, ir, (KBr) 5.89 (C=O) μ; nmr (270 MHz, $CDCl_3$) δ 1.03 (d, 3H, J = 7 Hz), 1.05 (s, 3H), 1.36 (s, 3H), 0.92 (s, 3H), 1.64 (broad s, 3H), 1.79 (broad s, 3H), 2.12 and 1.69 (calculated) (AB q, J = 18.5 Hz), 2.41 (q, 1H, J = 7 Hz), 2.44 (s, 1H), 3.32 (s, 3H), and 4.40 (s, 1H); mass spectrum parent (70 eV) *m/e* 278.

These data clearly indicate that the photoproduct has an oxacarbene-derived cyclic acetal structure. They do not, however, allow one to distinguish between the structure **2** and its "opposite" in which the cyclic ether oxygen atom and the methoxyl bearing carbon atom are interchanged. In addition the data do not permit a definitive assignment of the stereochemistry at the methoxyl bearing carbon. For these reasons a direct method X-ray crystal structure investigation was undertaken. The results of this study, the details of which are given below, unequivocally identify **2** as the structure of the major photoproduct.

X-ray Crystal Structure Determination

Crystallization of the photoproduct **2** from hexane afforded well-formed colorless plates suitable for X-ray examination. Initial unit cell parameters and the space group were established from a series of precession photographs. A crystal of dimensions ca. 0.18 × 0.18 × 0.09 mm was mounted with the normal to (10$\bar{1}$) approximately parallel to the φ axis of the goniometer. Accurate unit-cell dimensions were obtained by a least-squares analysis of the setting angles of 25 reflections ($60 < 2\theta < 80°$) automatically located and centered in the counter of an Enraf Nonius CAD-4F diffractometer using Ni filtered CuK_α radiation.

Crystal data for 1α,4,5α,7α,9,10-hexamethyl-2β-methoxy-3-oxatricyclo[5.4.0.0^{4,11}]undec-9-ene-6-one (**2**):

$C_{17}H_{26}O_3$ fw = 278.4
Monoclinic, a = 13.9190(8), b = 8.5880(12), c = 13.6506(7) Å, β = 105.02(1)°, V = 1576.0(1) Å^3, Z = 4, ρ_c = 1.173 g cm^{-3}, $F(000)$ = 608 (22°C, CuK_α, λ = 1.5418 Å, μ = 5.9 cm^{-1}). Absent reflections: 0k0, $k \neq 2n$, and h0l, $l \neq 2n$, space group $P2_1/c$ (C_{2h}^5, No. 14).

Diffractometer data provided a total of 3252 independent reflections out to $2\theta_{max}$ = 150° using an ω–2θ scan with variable scan width and scan speed. The ω scan angle was set to (1.10 + 0.5 tan θ)°, the midpoint being calculated using the average wavelength $(\lambda\alpha_1 + \lambda\alpha_2)/2$, with a 25% extension each side for background determination. The scan speed for each reflection was determined by a prescan using a speed of 20.0116/NPIPRE deg/min with NPIPRE set to 2. This prescan gives I_{net} = INT − 2(BGL + BGR) and $\sigma(I_{net})$ = (INT + 4(BGL + BGR))$^{1/2}$ where INT is the scan total and BGL and BGR are the left and right background count totals. For reflections giving more than 30 000 counts/s the reflected beam was attenuated (factor 26.92) and the scan repeated at the same speed; for all other reflections the final scan speed was determined by SIGPRE, SIGMA, and ITMAX. SIGPRE, the prescan acceptance parameter, was set to 0.5 so that reflections giving $\sigma(I_{net})/I_{net} > 0.5$ were considered unobserved; SIGMA was set to 0.05 leading to acceptance of the prescan data when $\sigma(I_{net})/I_{net} \leq 0.05$. All other reflections were rescanned at speeds determined by these parameters and ITMAX, the maximum scan time which was set to 120 s. The final scan speed of 20.0116/NPI was determined from NPI = NPIPRE((σ(I_{net})/I_{net})/SIGMA)^2 with NPI_{max} calculated from NPI_{max} = ITMAX/3(SCAN ANGLE). Thus, using the prescan information, reflections more than 20σ above background were collected at 2°/min, very strong intensities being attenuated, those less than 2σ above background were considered unobserved, and those in between were collected at speeds inversely proportional to the relative σ(I)/I down to a minimum of NPI = 23 or 0.91°/min. The intensities of three check reflections remained constant to within ±3% throughout the data collection, and reorientation, set to take place

when a deviation of 0.05° or more from the calculated position of the scattering vectors of any of three orientation control reflections occurred, was not required.

Lorentz and polarization corrections were applied in the usual manner along with check reflection scaling, and the derived structure amplitudes were corrected for absorption by the Gaussian integration method using the program BICABS, which gave maximum and minimum transmission factors for the correction of F^2 of 0.9088 (15,2,4) and 0.8048 ($0,\bar{2},\bar{16}$). Of the 3252 reflections measured, 1305 had $I < 3\sigma(I)$ where $\sigma^2(I) = S + B + (0.07S)^2$ with S = scan count and B the time averaged background count.

Structure Analysis

The structure was solved by direct methods. A total of 449 $|E|$-values greater than 1.5 was used to determine eight sets of signs by Sayre relationships in an iterative procedure (10). One set of signs was outstanding with a consistency index of 0.77, and an E map computed from the 216 positive and 233 negative values of E in this set contained twenty large peaks which accounted for the non-hydrogen atoms. Three cycles of isotropic followed by three cycles of anisotropic full-matrix least-squares refinement of the C and O atoms gave $R = 0.10$ using unit weights, and a subsequent difference-Fourier synthesis allowed 19 of the 26 hydrogen atoms to be located. After further refinement including the hydrogen positional parameters, R was 0.067 and the outstanding hydrogen atoms were located from a difference-Fourier synthesis. The final cycles of least-squares refinement included the isotropic thermal parameters of the hydrogen atoms and an isotropic extinction parameter g (11) and gave the final R-index of 0.043 for 1943 observed reflections. The function minimized was $\sum w(|F_o| - |F_c|)^2$ where F_c is extinction corrected. The chosen weights were $1/\sigma^2(F)$ and weighting analyses confirmed their suitability, the final value of $R_w = [\sum w(|F_o| - |F_c|)^2/\sum w|F_o|^2]^{1/2}$ being 0.058 and the standard deviation of an observation of unit weight (σ_1) 1.04. A difference-Fourier synthesis calculated after the final cycle of refinement showed maximum fluctuations of ± 0.25 e/Å^3, the greatest parameter shift being 0.176σ and the average 0.008σ on the final cycle. Atomic scattering factors for C and O were taken from ref. 12 and those for H from ref. 13. The final positional and thermal parameters are given in Tables 1 and 2[1] respectively. Measured and calculated structure factors have been placed in the Depository of Unpublished Data.[1]

TABLE 1. Final positional parameters (fractional × 10^4, H × 10^3) with estimated standard deviations in parentheses

Atom	x	y	z
C(1)	2117(1)	3683(2)	520(1)
C(2)	2987(2)	4662(3)	366(1)
O(3)	3852(1)	3758(2)	733(1)
C(4)	3592(2)	2187(2)	979(1)
C(5)	3689(2)	2174(3)	2132(1)
C(6)	3083(2)	3527(3)	2360(1)
C(7)	2053(1)	3825(2)	1641(1)
C(8)	1353(2)	2542(3)	1853(2)
C(9)	1374(2)	985(3)	1358(2)
C(10)	1903(2)	744(3)	687(2)
C(11)	2492(1)	2049(2)	384(1)
C(21)	3565(3)	6007(4)	−879(2)
O(21)	2837(1)	4971(2)	−679(1)
C(41)	4279(2)	1061(3)	657(2)
C(51)	4758(2)	2215(4)	2787(2)
O(61)	3398(1)	4373(2)	3084(1)
C(71)	1670(2)	5408(3)	1886(2)
C(91)	767(3)	−247(5)	1705(3)
C(101)	1950(3)	−805(4)	178(3)
C(110)	1129(2)	4063(3)	−239(2)
H(2)	308(1)	569(2)	71(1)
H(5)	338(2)	130(3)	229(2)
H(81)	64(2)	296(3)	167(2)
H(82)	150(2)	234(3)	257(2)
H(11)	251(2)	190(3)	−31(2)
H(211)	327(3)	630(4)	−161(3)
H(212)	370(3)	697(5)	−46(3)
H(213)	579(3)	454(4)	74(3)
H(411)	495(2)	127(3)	94(2)
H(412)	412(2)	105(3)	−10(2)
H(413)	414(2)	−1(4)	84(2)
H(511)	514(2)	123(4)	273(2)
H(512)	476(2)	233(3)	351(3)
H(513)	510(3)	307(4)	261(3)
H(711)	97(2)	564(4)	149(2)
H(712)	163(2)	544(3)	261(2)
H(713)	215(2)	624(3)	186(2)
H(911)	55(3)	−105(5)	125(3)
H(912)	20(3)	15(5)	174(3)
H(913)	118(4)	−76(6)	224(4)
H(101)	142(3)	−157(5)	13(3)
H(102)	255(4)	−152(6)	58(4)
H(103)	216(3)	−72(5)	−37(3)
H(111)	95(2)	523(3)	−28(2)
H(112)	56(2)	348(4)	−10(2)
H(113)	114(2)	375(4)	−95(2)

Thermal Motion Analysis and Molecular Geometry Correction

The thermal motion of the molecule was analyzed in terms of rigid-body translation (**T**), libration (**L**), and screw motion (**S**) (14) using the computer program RIGIDB. Different sets of atoms contributing to the assumed rigid body were inspected, omitting hydrogen atoms. Approximating the whole molecule to a rigid-body gave rms $\Delta U_{ij} = 0.0040$ Å^2 com-

[1]The structure factor table and Tables 2 and 3 (thermal parameters) are available, at a nominal charge, from the Depository of Unpublished Data, CISTI, National Research Council of Canada, Ottawa, Ont., Canada K1A 0S2.

TABLE 4. Bond lengths (Å) with estimated standard deviations in parentheses

(*a*) Nonhydrogen atoms

Bond	Length		Bond	Length	
	Uncorrected	Corrected		Uncorrected	Corrected
C(1)—C(2)	1.533(3)	1.538	C(8)—C(7)	1.547(3)	1.551
C(2)—O(3)	1.411(2)	1.414	C(4)—C(11)	1.540(3)	1.545
O(3)—C(4)	1.458(3)	1.462	C(2)—O(21)	1.412(2)	1.414
C(4)—C(5)	1.545(3)	1.549	O(21)—C(21)	1.427(3)	1.429
C(5)—C(6)	1.515(3)	1.519	C(6)—O(61)	1.213(3)	—
C(6)—C(7)	1.535(3)	1.540	C(4)—C(41)	1.503(3)	1.505
C(7)—C(1)	1.560(3)	1.565	C(5)—C(51)	1.525(3)	1.526
C(1)—C(11)	1.525(3)	1.529	C(7)—C(71)	1.529(3)	1.531
C(11)—C(10)	1.508(3)	1.512	C(1)—C(110)	1.527(3)	1.530
C(10)—C(9)	1.332(3)	1.334	C(10)—C(101)	1.510(4)	—
C(9)—C(8)	1.502(3)	1.506	C(9)—C(91)	1.504(4)	1.505

(*b*) Bonds involving hydrogen atoms

Bond	Length	Bond	Length
C(2)—H(2)	1.00(2)	C(51)—H(513)	0.95(4)
C(5)—H(5)	0.92(2)	C(71)—H(711)	1.00(3)
C(8)—H(81)	1.02(3)	C(71)—H(712)	1.00(3)
C(8)—H(82)	0.96(3)	C(71)—H(713)	0.99(3)
C(11)—H(11)	0.96(2)	C(91)—H(911)	0.92(4)
C(21)—H(211)	1.01(4)	C(91)—H(912)	0.87(4)
C(21)—H(212)	1.00(4)	C(91)—H(913)	0.92(5)
C(21)—H(213)	0.99(4)	C(101)—H(101)	0.98(4)
C(41)—H(411)	0.94(3)	C(101)—H(102)	1.06(5)
C(41)—H(412)	1.00(3)	C(101)—H(103)	0.87(4)
C(41)—H(413)	0.99(3)	C(110)—H(111)	1.03(3)
C(51)—H(511)	1.01(3)	C(110)—H(112)	1.00(3)
C(51)—H(512)	0.99(3)	C(110)—H(113)	1.01(3)

pared to the rms deviation in U_{ij} of 0.0012 Å^2. The agreement between observed and calculated U_{ij} for this model was particularly poor for C(101) and O(61), and omitting these atoms from the model gave rms ΔU_{ij} = 0.0026 Å^2, indicating a reasonable rigid body approximation. The analysis results are given in Table 3.[1] **T** is roughly isotropic and the principal axes of **L** are oriented 4° from the C(5)—C(2) vector (L_1), 14° from O(3)—O(61) (L_2) and 16° from O(3)—C(1) (L_3).

Bond distances corrected for libration (15) using shape parameters q^2 of 0.08 for all atoms are included in Table 4 along with the uncorrected distances. The libration corrections are all less than twice the esd of the uncorrected bond length and bond distances referred to in the discussion are the uncorrected values.

Discussion of the X-ray Crystal Structure

Figure 1 shows a stereoscopic view of the molecule and the atomic numbering scheme. Bond lengths and angles are given in Tables 4 and 5. Selected dihedral angles are given in Table 6. The structure analysis shows that the major photoproduct has the tricyclic acetal structure **2** (Scheme 1).

The six-membered ring containing the carbonyl group is in the chair conformation with C(1), C(4), C(5), and C(7) in plane and C(6) and C(11) displaced above and below the plane by 0.51 and 0.89 Å, respectively. The carbonyl group is slightly nonplanar, with O(61) displaced by 0.012 Å (6σ) from the C(5) to C(7) plane. The methyl group C(51) is in the equatorial configuration with respect to this ring, consistent with maximizing intramolecular contact distances in this molecular conformation.

The other six-membered ring, C(1) and C(7) to C(11), is in a half-chair conformation with C(8) to C(11) in plane and C(1) and C(7) on opposite sides of the plane displaced by 0.59 and 0.17 Å, respectively. The torsion about the C(9)=C(10) double bond is 1.1(2)°. The five-membered ring is in a slightly twisted envelope conformation (see Table 6) with C(11) displaced by 0.65 Å from the mean plane of C(1), C(2), O(3), C(4).

The bond lengths generally agree well with expected values, with mean C(sp^3)—C(sp^3) 1.533 and

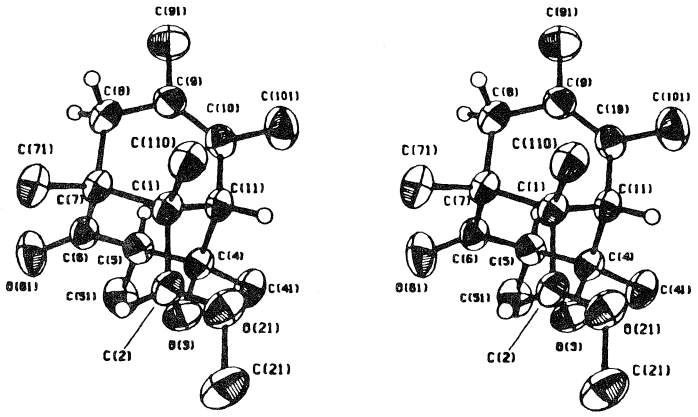

FIG. 1. Stereoscopic view of photoproduct **2**. The methyl hydrogen atoms have been omitted for clarity.

TABLE 5. Bond angles (deg) with estimated standard deviations in parentheses (nonhydrogen atoms)

Bonds	Angle
C(2)—C(1) —C(7)	109.9(2)
C(2)—C(1) —C(11)	100.4(1)
C(2)—C(1) —C(110)	113.2(2)
C(7)—C(1) —C(11)	107.4(2)
C(7)—C(1) —C(110)	112.2(2)
C(11)—C(1) —C(110)	113.0(2)
C(1)—C(2) —O(3)	106.3(2)
C(1)—C(2) —O(21)	109.1(2)
O(3)—C(2) —O(21)	110.7(2)
C(2)—O(3) —C(4)	110.6(1)
O(3)—C(4) —C(5)	106.2(2)
O(3)—C(4) —C(11)	102.8(2)
O(3)—C(4) —C(41)	108.3(2)
C(5)—C(4) —C(11)	110.4(2)
C(5)—C(4) —C(41)	113.5(2)
C(11)—C(4) —C(41)	114.7(2)
C(4)—C(5) —C(6)	107.3(2)
C(4)—C(5) —C(51)	114.3(2)
C(6)—C(5) —C(51)	111.8(2)
C(5)—C(6) —C(7)	118.3(2)
C(5)—C(6) —O(61)	121.7(2)
C(7)—C(6) —O(61)	120.1(2)
C(1)—C(7) —C(6)	109.4(2)
C(1)—C(7) —C(8)	109.0(2)
C(1)—C(7) —C(71)	113.3(2)
C(6)—C(7) —C(8)	106.9(2)
C(6)—C(7) —C(71)	109.3(2)
C(8)—C(7) —C(71)	108.7(2)
C(7)—C(8) —C(9)	117.6(2)
C(8)—C(9) —C(10)	121.7(2)
C(8)—C(9) —C(91)	114.0(2)
C(10)—C(9) —C(91)	124.3(3)
C(9)—C(10)—C(11)	120.6(2)
C(9)—C(10)—C(101)	123.4(2)
C(11)—C(10)—C(101)	115.9(2)
C(1)—C(11)—C(4)	101.0(2)
C(1)—C(11)—C(10)	115.0(2)
C(4)—C(11)—C(10)	116.7(2)
C(2)—O(21)—C(21)	112.5(2)

TABLE 6. Intraannular dihedral angles (deg)

Ring	Angle	Ring	Angle
C(1)—C(7)	−58.0(2)	C(1)—C(11)	−72.8(2)
C(7)—C(8)	36.3(2)	C(11)—C(4)	74.8(2)
C(8)—C(9)	−6.1(2)	C(4)—C(5)	−58.6(2)
C(9)—C(10)	−1.1(2)	C(5)—C(6)	43.1(2)
C(10)—C(11)	−24.4(2)	C(6)—C(7)	−44.2(2)
C(11)—C(1)	53.8(2)	C(7)—C(1)	58.7(2)
C(1)—C(2)	−32.0(2)	C(1)—C(2)	81.0(2)
C(2)—O(3)	8.2(2)	C(2)—O(3)	8.2(2)
O(3)—C(4)	19.0(2)	O(3)—C(4)	−97.0(2)
C(4)—C(11)	−38.2(2)	C(4)—C(5)	52.2(2)
C(11)—C(1)	42.1(2)	C(5)—C(6)	43.1(2)
		C(6)—C(7)	−44.2(2)
		C(7)—C(1)	−49.7(2)

mean C(sp^2)—C(sp^3) 1.509 Å compared to normal values of 1.534 (16) and 1.510 Å (17), respectively; C=C is 1.332(3), C=O 1.213(3), and mean C—H 0.98 Å. The lengthening of the C(1)—C(7) distance, 1.560(3) Å, is possibly due to the intramolecular crowding (see Table 7); the bond lengths and angles in general do not indicate a large amount of strain in the molecule. The C(sp^3)—O bond distances average 1.427 Å with C(21)—O(21) as expected at 1.427(3) Å (17) and C(4)—O(3), O(3)—C(2), and C(2)—O(21) at 1.458(3), 1.411(2), and 1.412(2) Å, differing by +0.031, −0.016, and −0.015 Å from the mean value. It is interesting that the variations in the C—O bond distances are similar to those observed in the methyl acetal groups of methyl α-pyranoses such as methyl α-D-galactopyranoside monohydrate and methyl α-D-altopyranoside (18), where the bond distances comparable to C(4)—O(3), O(3)—C(2), and C(2)—O(21) are 1.439, 1.418, 1.405 and 1.440, 1.416, 1.405 Å respectively. A shortening of −0.016 Å for the two C—O bonds associated with the anomeric carbon in methyl α-pyranoses has

TABLE 7. Selected intra- and intermolecular* contacts

Intramolecular		Intermolecular	
Atoms	Distance (Å)	Atoms	Distance (Å)
C(1)···C(4)	2.365(3)	C(41)—O(61)[1]	3.427(3)
C(1)···O(3)	2.357(2)	O(61)—H(411)[2]	2.85(3)
C(1)···O(21)	2.400(2)	C(110)—H(711)[3]	2.99(3)
O(3)···C(11)	2.344(3)	H(113)—H(82)[4]	2.39(5)
O(3)···O(21)	2.321(2)	H(102)—H(2)[5]	2.50(5)
C(2)···C(11)	2.349(3)		
C(6)···C(8)	2.477(3)		
C(7)···C(11)	2.487(3)		
C(7)···C(2)	2.533(3)		
O(3)···H(2)	1.97(2)		
C(6)···H(5)	1.97(2)		
O(21)···H(2)	1.94(2)		

*X—X < 3.5 Å, X—H < 3.0 Å, H—H < 2.5 Å (X = C, O). Superscripts refer to atoms at positions [1] $-x, -y, -z-1$; [2] $1-x, 1/2+y, 1/2-z$; [3] $-x, 1-y, -z$; [4] $x, 1/2-y, z-1/2$; [5] $x, y-1, z$.

been predicted (19). In the β-pyranoses the predicted shortening is −0.009 (in ring) and −0.041 Å (equatorial anomeric C—O), in general agreement with observed values such as those in methyl β-cellobioside-methanol (20). In the oxolane ring, described as intermediate between envelope and twist, of the tricyclic photoproduct $C_{15}H_{24}O_3$ (21) the torsion angles and C—O bond distances are similar to those found here, with the equivalents of C(4)—O(3), O(3)—C(2), C(2)—O(21), and O(21)—C(21) at 1.435(4), 1.417(5), 1.403(6), and 1.430(5) Å. The fact that C(4)—O(3) here (1.458(3) Å) is significantly longer than those compared above may be due to the same intramolecular steric effects which give the C(1)—C(7) distance of 1.560(3) Å (see Table 7).

The C(1)—C(2)—O(21)—C(21) torsion angle is 174.1° with C(21) *trans* to C(1) corresponding to the preferred orientation in methyl glycosides (18) and to that predicted for this group in the 2-alkoxyhydropyrans (22). The bond angles at C(1), C(11), and C(4) within the five-membered ring are all well below tetrahedral values at 100.4(1), 101.0(2), and 102.8(2)°, respectively. Selected intermolecular contact distances, which correspond to van der Waals interactions, and intramolecular non-bonded distances are given in Table 7.

Discussion of the Photochemical Results

The present photochemical results indicate that there is no inherent difference in photochemical reactivity between bridged cyclobutanones and their fused or monocyclic counterparts and that all can take part in oxacarbene formation. The observation of a *single* ring-expanded cyclic acetal in the case of cyclobutanone **1** is, however, intriguing and worthy of further comment.

There are at least three possible explanations for the preference for formation of cyclic acetal **2** rather than its regioisomer **7** (Scheme 2). In order to discuss these possibilities we adopt Morton and Turro's (1) notion of an acyl–alkyl biradical-like transition state (**3** and **5**) as leading to the two possible intermediate oxacarbenes **4** and **6** respectively. (*A*) We first consider the possibility that the relative amounts of **2** and **7** could be governed by the rates of reaction of methanol with oxacarbene intermediates **4** and **6** respectively. This explanation appears unlikely, however, in view of the close structural similarities between these latter two species. (*B*) Secondly, the possibility exists that oxacarbene intermediate **6** could be reverting to **1** faster than the analogous return of oxacarbene **4** to **1**. While we cannot at present rigorously rule this possibility out, we deem it unlikely since there is good reason to believe (*vide infra*) that the forward process **1** → **3** → **4** is associated with a lower activation energy than the **1** → **5** → **6** sequence. Microscopic reversibility plus the realization that **4** and **6** should have very nearly equal energies thus renders explanation (*B*) improbable. (*C*) It thus appears most likely that the relative amounts of final products **2** and **7** are controlled by the relative rates of rearrangement of photoexcited **1** to oxacarbenes **4** and **6**, i.e., by the relative energetics of biradicaloid transition states **3** and **5** respectively.

It should be noted at the outset that the standard explanation of preferential α-cleavage of the more highly substituted acyl–alkyl carbon–carbon bond does not suffice in the case of cyclobutanone **1**; both carbon atoms α to the four-membered ring carbonyl group of **1** are equally substituted with two ring residues and one methyl group. However, one obvious difference between biradicaloids **3** and **5** involves the location of the alkyl radical portion in

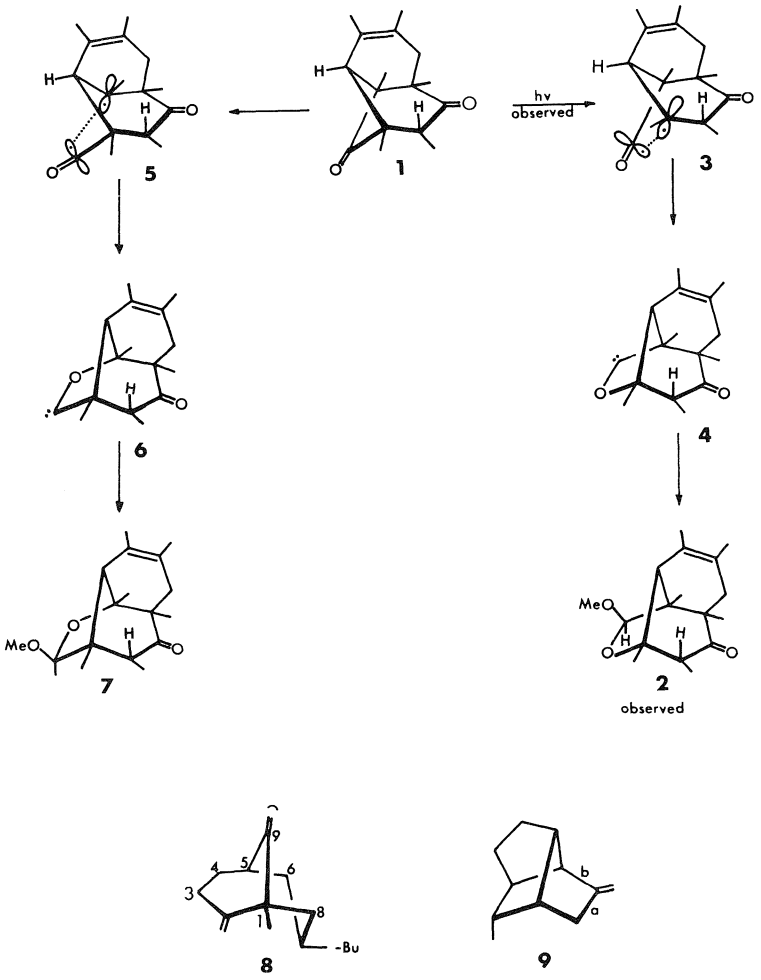

SCHEME 2

each. In **5** it is situated on the one-carbon bridge of a bicyclo[3.3.1]nonyl system whereas in species **3** the developing *p*-orbital is located on one of the three-carbon bridges. We suggest that one significant factor involved in favoring transition state **3** over transition state **5** concerns the angle strain experienced by the incipient alkyl radical centers in each. While the requirement for trigonal, planar geometry is less stringent for free radicals as compared to carbocations, it does seem reasonable to suggest that **3** will be able to approach this favorable arrangement more easily than **5**. This idea is borne out by X-ray crystal structure data on bicyclo[3.3.1]nonyl systems. A good example is provided by diketone **8** (23) (Scheme 2) in which the C(1)—C(9)—C(5) angle (112.5°, model for transition state **5**) is considerably distorted from the ideal of 120° relative to the C(1)—C(2)—C(3) angle (116.7°, model for transition state **3**). Analogous effects are presumably involved in the preference for oxacarbene formation via cleavage of bond (*a*) rather than bond (*b*) in the photolysis of ketone **9** (24) (Scheme 2).

A second important factor which favors transition state **3** over transition state **5** involves the extra stabilization afforded **3** by hyperconjugation of the alkyl radical center with its adjacent non-methyl β-hydrogen atom. Such delocalization is of course not possible in biradicaloid **5** due to the bridgehead nature of the relevant β-hydrogen atom involved. The existence of radical hyperconjugation is clearly indicated by esr measurements on alkyl radicals bearing β-hydrogen atoms which show large β-hyperfine coupling constants (25).

One final point concerns the stereoselectivity of the reaction of methanol with the intermediate oxacarbene **4**. It could be argued that such stereoselectivity indicates approach of methanol from the *exo* face with concerted insertion of the carbene into the oxygen–hydrogen bond. Such an interpretation, while speculative, is in accord with (*a*) the preferred

direction of approach of most reagents to the bicyclo[2.2.1] system (incorporated in the oxacarbene portion of **4**) and (*b*) the singlet nature of the photochemical oxacarbene-forming reactions of cyclobutanones (1, 3).

Experimental

Photolysis of Cyclobutanone 1

Cyclobutanone **1** was prepared as described in ref. 9*a*, uv $n \rightarrow \pi^* \lambda_{max}^{MeOH}$ 300 nm, ε 66. A solution of 101 mg of **1** in 170 mL of methanol containing 1.4 g of sodium carbonate (to avoid acid-catalyzed reactions) was irradiated through Pyrex using a 450 W medium pressure mercury lamp and immersion well apparatus. The reaction was monitored by glc (5 ft × 1/8 in. stainless steel column packed with 5% OV-17 on 80/100 Chromosorb W, column temperature 175°C) which showed the buildup of one major photoproduct and at least a dozen minor products. After 10.7 h of photolysis the mixture consisted of 53% of photoproduct **2** and 25% of starting material **1**; none of the other photoproducts was present in amounts greater than 7% (product percentages are estimated without use of internal standards and are approximate only). Cyclic acetal **2** was isolated by preparative glc (5 ft × 1/4 in. stainless steel column packed with 5% OV-17 on 80/100 Varaport 30 operating at 160°C) and exhibited the physical and spectroscopic data outlined in the text. Large clear single crystals were grown from concentrated hexane solutions. *Anal.* calcd. for $C_{17}H_{26}O_3$: C 73.35, H 9.41; found: C 73.29, H 9.56.

Acknowledgments

Acknowledgment is made to the donors of the Petroleum Research Fund, administered by the American Chemical Society, for partial support of this research. We thank the National Research Council of Canada for financial support, and the University of British Columbia Computing Center for assistance.

1. D. R. Morton and N. J. Turro. Adv. Photochem. **9**, 197 (1974).
2. W.-D. Stohrer, P. Jacobs, K. H. Kaiser, G. Wiech, and G. Quinkert. Fortschr. Chem. Forsch. **46**, 181 (1974).
3. P. Yates and R. O. Loutfy. Acc. Chem. Res. **8**, 209 (1975).
4. R. D. Miller and V. Y. Abraitys. J. Am. Chem. Soc. **94**, 663 (1972).
5. H. Hart. Unpublished results.
6. J. Doyle. Ph.D. Thesis. Oxford University. 1970. ref. 125.
7. (*a*) W. F. Erman. J. Am. Chem. Soc. **89**, 3828 (1967); (*b*) W. F. Erman and H. C. Kretschmar. J. Am. Chem. Soc. **89**, 3842 (1967).
8. J. J. Hurst and G. H. Whitman. J. Chem. Soc. 2864 (1964).
9. (*a*) J. R. Scheffer, K. S. Bhandari, R. E. Gayler, and R. A. Wostradowski. J. Am. Chem. Soc. **97**, 2178 (1975); (*b*) J. R. Scheffer, B. M. Jennings, and J. P. Louwerens. J. Am. Chem. Soc. **98**, 7040 (1976).
10. R. E. Long. Ph.D. Thesis. University of California at Los Angeles, Los Angeles, CA. 1965.
11. P. J. Becker and P. Coppens. Acta Crystallogr. (*a*) A**30**, 129 (1974); (*b*) A**31**, 417 (1975); (*c*) P. Coppens and W. C. Hamilton. Acta Crystallogr. A**26**, 74 (1970).
12. D. T. Cromer and J. B. Mann. Acta Crystallogr. A**24**, 321 (1968).
13. R. F. Stewart, E. R. Davidson, and W. T. Simpson. J. Chem. Phys. **42**, 3175 (1965).
14. V. Schomaker and K. N. Trueblood. Acta Crystallogr. B**24**, 63 (1968).
15. D. W. J. Cruikshank. Acta Crystallogr. **9**, 747 (1956); **9**, 754 (1956); **14**, 896 (1961).
16. O. Bastiansen and M. Traetteberg. Tetrahedron, **17**, 147 (1962).
17. L. E. Sutton. Chemical Society Special Publication No. 18, London: The Chemical Society.
18. B. M. Gatehouse and B. J. Poppleton. Acta Crystallogr. B**27**, 654 (1971); B**27**, 871 (1971).
19. G. A. Jeffrey, J. A. Pople, and L. Radom. Carbohydrate Res. **25**, 117 (1972).
20. J. T. Ham and D. G. Williams. Acta Crystallogr. B**26**, 1373 (1970).
21. G. Bernardinelli and R. Gerdil. Helv. Chim. Acta, **57**, 1846 (1974).
22. A. J. deHoog, H. R. Boys, C. Altona, and E. Havinga. Tetrahedron, **25**, 3365 (1969).
23. P. W. Hickmott, P. J. Cox, and G. A. Sim. J. Chem. Soc., Perkin I, 2544 (1974).
24. J. C. Tam. Ph.D. Thesis, University of Toronto, Toronto, Ont. 1974.
25. T. H. Lowry and K. S. Richardson. Mechanism and theory in organic chemistry. Harper and Row, New York, NY. 1976. p. 466.

COMMUNICATION

Thermal explosions of methyl isocyanide: a re-examination of the data

HUW O. PRITCHARD

Chemistry Department, York University, Downsview, Ont., Canada M3J 1P3

Received June 4, 1979

HUW O. PRITCHARD. Can. J. Chem. 57, 2677 (1979).

By the use of an improved interpolation method for the rate constants for the thermal isomerisation of methyl isocyanide, it is found that a pattern emerges in the previously unexplained scaling behaviour of the critical explosion parameter (δ_c). At low Rayleigh number (where δ_c should be constant) the ratio $(\delta/Ra)_c$ for a fixed temperature is approximately constant for seven spherical vessels of volumes 0.3 to 5 L. Also, in the limit of very large vessels, or very high temperatures, it appears that the Arrhenius temperature coefficient of $(\delta/Ra)_c$ tends to the activation energy of the reaction.

HUW O. PRITCHARD. Can. J. Chem. 57, 2677 (1979).

L'emploi d'une méthode améliorée d'interpolation des constantes de vitesse dans l'isomérisation thermique de l'isocyanure de méthyle a permis de faire la lumière sur la tendance à l'augmentation, non expliquée précédemment, du paramètre d'explosion critique (δ_c). Pour des valeurs faibles des nombres de Rayleigh (où δ_c doit être constant) le rapport $(\delta/Ra)_c$ à température donnée est approximativement constant pour sept récipients sphériques dont le volume varie de 0.3 à 5 L. Dans le cas limite de très grand récipients ou de très hautes températures, il apparait également que la valeur du coefficient de température d'Arrhénius $(\delta/Ra)_c$ tend vers l'énergie d'activation de la réaction.

[Traduit par le journal]

In the two existing studies of the thermal explosions of methyl isocyanide vapour (1, 2) the rate constants for the isomerisation reaction in the explosion temperature range were estimated by extrapolation procedures: in the former study, the rough-and-ready assumption was made that the shape of the unimolecular fall-off curve for 230°C could be taken as constant and used to estimate the rate constants in the range 280–350°C; in the latter study, empirical extrapolation formulae were generated (3) from conventional static and flow experiments at lower temperature. Tyler (4) has shown that near 280°C, such extrapolated values are in error by some 25%, and we have found that the formulae of ref. 3 do not give monotonically varying rate constants above 300°C. However, it is known (3, 5) that at infinite pressure and in the absence of self-heating, the rate constant for the isomerisation of methyl isocyanide is strict-Arrhenius in form. Moreover, we are now able to calculate unimolecular fall-off from these infinite-pressure rates with considerable confidence (5); hence all the required rate constants have been recalculated in this way, and the results are shown in Table 1. Also shown in this table are the recalculated values of the critical explosion parameter δ_c and the Rayleigh number Ra: the thermal conductivity data used in these calculations are our own (2), the viscosity data are those of Vines and Bennett (6) for methyl cyanide extrapolated linearly into the interesting temperature range; the heat capacity, likewise, is that of methyl cyanide.

Apart from some alterations to the actual numbers,[1] the pattern of the δ_c values differs little from

[1]The data from ref. 1 are not included in Table 1 since, in general, they do not fall at the tabulated temperature values. The revised rate constants and values of δ_c and Ra, recalculated from newer enthalpy and thermal conductivity data (2), and values of $(\delta/Ra)_c$, are as follows

T (°C)	10^2k (s^{-1})	δ_c	Ra	$(\delta/Ra)_c$
285	1.18	13.9	(2540)	(6)
292	1.56	11.6	(1087)	(11)
300	2.08	11.1	(612)	(18)
312	3.39	11.1	240	46
323	5.04	11.1	119	93
335	7.47	10.8	55	195
344	9.60	10.1	32	319
351	12.0	10.2	22	468

At an earlier stage (2), we suspected that there could be a temperature discrepancy between the works of refs. 1 and 2: for example, an error in the temperature of 2°C would change δ_c by about 10%, and these values of δ_c seem to be 10–20% below those for the 1.0 L vessel in Table 1. However, the values of $(\delta/Ra)_c$ of 93 and 319 at $T = 323$ and 344°C respectively are not out of line with the values in Table 1 of about 80 and about 260 at 320 and 340°C respectively, so that, despite appearances, both sets of data could be quite consistent.

0008-4042/79/192677-03$01.00/0

TABLE 1. Summary of interpolated rate constants (k in s^{-1}), values of δ_c, Ra, and $(\delta/Ra)_c$ recalculated for the thermal explosion data of Collister and Pritchard, Table 1 of ref. 2: see top left-hand panel for method of data presentation*

Nominal volume (L)	Temperature of explosion											
	260°C		280°C		300°C		320°C		340°C		360°C	
0.3	$10^3 \times k$	δ_c					64.8	*13.5*	123	*11.2*	260	*15.4*
	Ra	$10^3 \times (\delta/Ra)_c$					157	**86**	35	**320**	17	**930**
0.5							58.7	*13.5*	116	*12.6*	217	*13.0*
							163	**83**	43	**290**	15	**880**
1.0							48.9	*13.1*	94.2	*12.1*	180	*13.5*
							172	**76**	47	**260**	18	**750**
1.5					(24.3	*22.1*)	48.3	*17.2*	91.9	*15.4*	167	*15.4*
					(1504	**15**)	261	**66**	68	**230**	23	**670**
2.0					16.0	*6.63*	33.5	*6.88*	64.0	*6.82*	117	*7.21*
					297	**22**	83	**83**	26	**260**	10	**720**
3.0					14.9	*7.69*	30.9	*7.99*	53.9	*6.45*	102	*7.77*
					386	**20**	110	**73**	28	**230**	12	**620**
5.0	(2.01	*4.31*)	4.07	*2.56*	9.17	*2.89*	17.8	*2.83*	27.3	*1.89*	58.4	*3.03*
	(4210	**1**)	416	**6**	123	**23**	36	**80**	8	**240**	5	**610**

*The rate constants are calculated from the infinite-pressure data of Collister and Pritchard (3) viz. $A_\infty = 10^{13.35}$ s^{-1}, $E_\infty = 38.2$ kcal/mol, together with the procedures of Yau and Pritchard (5); the entries in parentheses have Ra significantly greater than 400, see final paragraph of Discussion section.

that already published in Table 1 of ref. 2, and the conclusions remain the same, i.e., (*i*) for a given vessel, and provided that Ra is below 400–500, δ_c is independent of temperature, but there is some considerable scatter, well outside the limits of the precision of the experiments. (*ii*) with the exception of the 5 L vessel, for which δ_c appears to be a little lower than the theoretical value for a sphere (7) of about 3.75, all the values of δ_c are very much higher than expected.

The fourth number for each tabular entry in Table 1 is the ratio $(\delta/Ra)_c$ and it can be seen that, for a fixed temperature, this ratio is remarkably constant, if one excludes points with $Ra \gg 400$; the data for $T = 320$°C are particularly impressive.

It appears that there are two regimes in these thermal explosions. The first is a high-pressure regime for which $Ra > 400$: below this Rayleigh number, the critical temperature rise ΔT_c is correctly predicted by standard theory, but above this value, the temperature profiles cease to be uniform (8) and the observed values of ΔT_c fall considerably below the theoretical values (1, 8). However, in the low-pressure regime, the critical explosion conditions are defined, not by δ_c = constant for all r and T, but by $(\delta/Ra)_c$ = constant for all r (r being the radius of the vessel).

In normal circumstances, it is conventional to plot $R \ln p_c/T^3$ vs. T^{-1} whence[2] the slope is the activation energy E of the reaction (9): for the data described here (cf. Table 1 of ref. 2) the slopes lie in the range 20–23 kcal/mol, fortuitously (?) close to the value of Q, the exothermicity of the reaction. On the other hand, plots of $R \ln (\delta/Ra)_c$ vs. T^{-1} are reasonable straight lines, with slopes in the range 36–39 kcal/mol. The reason for this is fairly clear at high temperature or for large volumes: in this temperature range $Ra \sim$ constant $\times r^3 p_c^2/\lambda T^4$ (the extra power of T arises because the viscosity $\sim cT$) and $\delta_c \sim$ constant $\times r^2 p_c k/\lambda T^3$ (where k is the rate constant and λ is the thermal conductivity); thus $(\delta/Ra)_c \sim$ constant $\times k r^{-1} p_c^{-1} T^{-1}$. Now, for very large vessels or for very high temperatures, the explosion pressure changes very little with temperature, so that for fixed r, the temperature coefficient of $(\delta/Ra)_c$ is dominated (especially since p_c and T vary in opposite senses) by that of the rate constant k itself, i.e., E, the activation energy, which is about 36 kcal/mol at these low pressures (5).

It is not clear at the present time why it should be that standard explosion theory can predict the correct temperature rise in these systems, provided Ra is low, but that it cannot predict the critical explosion pressure. If the present correlation of δ_c with Ra is significant, then clearly we have to consider other as yet unsuspected energy transport mechanisms which alone, or severally, cause an inhibition of the explosion in small vessels, but perhaps also make the explosion somewhat easier in very large vessels. It does not seem likely that the fault lies in the neglect of convection, as might be signalled by the correlation of δ_c with Ra: the onset of convective effects, which destroy the ideal temperature profiles above $Ra = 400$, are clearly seen both in this system (1) and in others (8). It seems more likely that the

[2]This relationship assumes that the thermal conductivity is independent of temperature: since λ is roughly proportional to T, this will introduce a small difference of the order of RT.

present correlation of δ_c with Ra is accidental in the sense that the hitherto unsuspected mechanism is not convection, but some other transport process which when taken together with the thermal conductivity gives a net transport rate which appears to scale roughly with the Rayleigh number.

I have chosen, for the time being, to exclude from consideration those results for which Ra $\gg$ 400 for two reasons: one, that the principal problem at the moment is to understand the explosion behaviour in the range Ra $<$ 400 where δ_c should be constant; two, that in the convective explosions when Ra $\gg$ 400, the calculation of Ra itself (using for example, as in ref. 1, a constant value of ΔT_c) is a considerable oversimplification. However, when one considers that the values of Ra in parentheses in Table 1 and in footnote 1 are somewhat too large, it is not entirely impossible that all the values of $(\delta/\mathrm{Ra})_c$ conform to a single pattern — compare the value for 285°C (in footnote 1) with that for 280°C (in Table 1), or the five values for $T = 300$°C.

Acknowledgements

This work was supported by the Natural Sciences and Engineering Research Council of Canada, and owes much to a series of discussions with B. J. Tyler.

1. H. O. Pritchard and B. J. Tyler. Can. J. Chem. **51**, 4001 (1973).
2. J. L. Collister and H. O. Pritchard. Can. J. Chem. **55**, 3815 (1977).
3. J. L. Collister and H. O. Pritchard. Can. J. Chem. **54**, 2380 (1976).
4. B. J. Tyler. Private communication.
5. A. W. Yau and H. O. Pritchard. Can. J. Chem. **56**, 1389 (1978).
6. R. G. Vines and L. A. Bennett. J. Chem. Phys. **22**, 360 (1954).
7. B. J. Tyler and T. A. B. Wesley. Eleventh Symposium (International) on Combustion, The Combustion Institute, Pittsburgh, PA. 1967. p. 1115.
8. P. G. Ashmore, B. J. Tyler, and T. A. B. Wesley. Eleventh Symposium (International) on Combustion, The Combustion Institute, Pittsburgh, PA. 1967. p. 1133.
9. D. H. Fine, P. Gray, and R. Mackinven. Twelfth Symposium (International) on Combustion, The Combustion Institute, Pittsburgh, PA. 1969. p. 545.

Canadian Journal of Chemistry
Published by
THE NATIONAL RESEARCH COUNCIL OF CANADA

Journal canadien de chimie
Publié par
LE CONSEIL NATIONAL DE RECHERCHES DU CANADA

Volume 57 Number 20 October 15, 1979 Volume 57 numéro 20 15 octobre 1979

Ketone or diazoalkane formation from Δ^3-1,3,4-oxadiazolin-2-ones. Details of two competing thermolysis mechanisms[1]

ANTHONY JAMES PAINE[2] AND JOHN WARKENTIN[2]
Department of Chemistry, McMaster University, Hamilton, Ont., Canada L8S 4M1

Received April 5, 1979

ANTHONY JAMES PAINE and JOHN WARKENTIN. Can. J. Chem. **57**, 2681 (1979).

The title compounds thermolyse at 50–100°C in a variety of solvents via two (and only two) competing unimolecular pathways, one producing a diazoalkane and carbon dioxide, the other a ketone, carbon monoxide, and dinitrogen. Diazoalkane formation is favoured by polar solvents and electron-donating substituents, with a Hammett ρ of −1.93 for seven *p*-substituted 5-methyl-5-phenyloxadiazolinones. Moderate solvent polarity effects, secondary kinetic isotope effects (2.1 ± 0.3% per D for **2***b*-d_6), the Hammett ρ, and Frontier Molecular Orbital Theory, all support concerted diazoalkane formation through a transition state with non-synchronous bond rupture.

Neither decomposition mode shows any correlation with Taft steric parameters, E_s, and ketone formation does not correlate with inductive parameters. The enthalpy change during the exothermic three piece fragmentation was calculated to be only -30 ± 2 kcal mol^{-1}, precluding chemiluminescence. A vigorous search for intermediates by esr, ms, CIDNP, trapping, and racemization experiments leads to the conclusion that ketone formation must also be concerted.

A new oxidation procedure using lead tetraacetate in the presence of five equivalents of trifluoroacetic acid was useful in the synthesis of oxadiazolinones from ketone semicarbazones which would not cyclize under normal LTA oxidation conditions.

ANTHONY JAMES PAINE et JOHN WARKENTIN. Can. J. Chem. **57**, 2681 (1979).

Les composés mentionnés subissent la thermolyse à 50–100°C dans différents solvants par l'intermédiaire de deux (et seulement deux) processus unimoléculaires compétitifs. L'un de ces processus fournit un diazoalcane et du dioxyde de carbone, l'autre produit une cétone, du dioxyde de carbone et de l'azote. La formation du diazoalcane est favorisée par les solvants polaires et les substituants électrodonneurs, avec un paramètre de Hammett ρ = −1.93 pour sept méthyl-5 phényl-5 oxadiazolinones substituées en position *para*. Tous les facteurs suivants: l'effet des solvants modérément polaires, l'effet cinétique isotopique (2.1 ± 0.3% par D pour **2***b*-d_6), le paramètre ρ de Hammett et la théorie des orbitales moléculaires frontières militent en faveur de la formation concertée du diazoalcane par l'intermédiaire d'un état de transition impliquant une rupture asynchrone de la liaison.

Aucune méthode de décomposition ne correspond aux paramètres stériques de Taft, E_s, et la formation de la cétone ne correspond pas aux paramètres d'induction. La réaction de fragmentation en trois parties est exothermique et la faible valeur de $\Delta H = -30 \pm 2$ kcal mol^{-1} obtenue par les calculs exclut la possibilité d'une réaction chimiluminescente. Une recherche approfondie des intermédiaires au moyen de diverses techniques d'analyse, telles la rpe, la spectrométrie de masse, la CIDNP, l'isolation des produits et la racémisation, a permis de conclure que la formation de la cétone est également concertée.

Un nouveau processus d'oxidation qui utilise du tétraacétate de plomb en présence de cinq equivalents d'acide trifluoroacétique a aidé à la synthèse d'oxydiazolinones à partir de semicarbazones de cétone qui ne se cyclisent pas sous des conditions normales d'oxidation par tétraacetate de plomb (TAP).

[Traduit par le journal]

[1]This work was presented, in part, at the Chemical Institute of Canada Conference in Montreal, Canada (June, 1977).
[2]Address correspondence to either author.

0008-4042/79/202681-15$01.00/0

Introduction

Δ^3-1,3,4-Oxadiazolin-2-ones (**2**, Scheme 1) are the most reactive of a series of heterocyclic compounds of general structure **3** under study in this laboratory. The ring system **3** is characterized by two possible thermolysis modes, one generating $R_1R_2C{=}Y$, together with N_2 and $:C{=}X$, and another producing a diazoalkane ($R_1R_2C{=}\overset{+}{N}{=}\overset{-}{N}$) concomitant with $X{=}C{=}Y$. The former reaction has been shown to produce carbon monosulfide from 5,5-dimethyl-1-phenyl-Δ^3-1,3,4-triazolin-2-thione (**3**; X = S, Y = NPh) (1). Generation of diazoalkanes bestows synthetic utility upon the two piece fragmentation, and thermolyses of oxadiazolinones (**2**) as well as phenyliminooxadiazolines (**3**; X = NPh, Y = O) have recently been exploited, the first as a good alternative method for the conversion of α,β-epoxyketones to acetylenic carbonyl compounds (2) and the second as an alternative route to oxindoles, hydantoins, and related heterocycles (3).

The title oxadiazolinones are easily prepared from ketone semicarbazones by oxidative cyclization with lead tetraacetate (LTA), followed by acid hydrolysis (Scheme 1) (4). When both R groups are alkyl, isolated yields of oxadiazolinones are near 80%, based on semicarbazone, but if aldehyde semicarbazones are used, tautomerization of the intermediate iminooxadiazoline (**1**) prevents the desired reaction (5).

The oxadiazolinone ring system undergoes competing unimolecular fragmentations at modest temperatures (less than 100°C). One of these produces diazoalkane by carbon dioxide loss, the other ketone

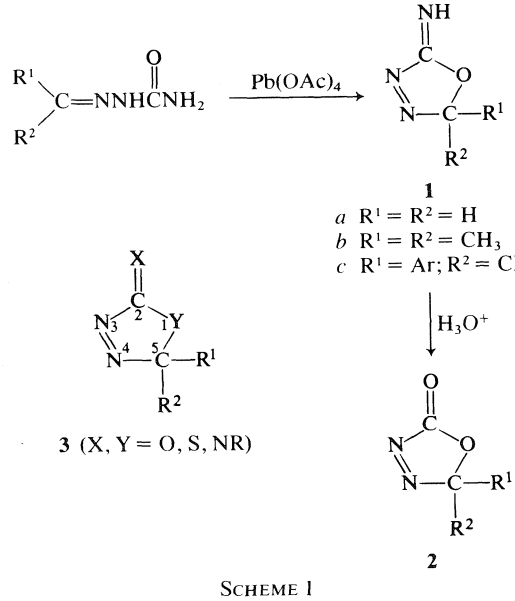

SCHEME 1

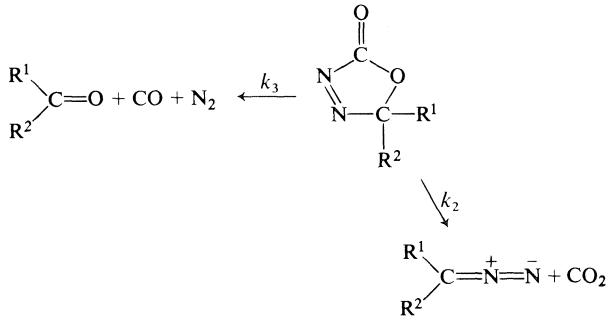

Some possible intermediates—

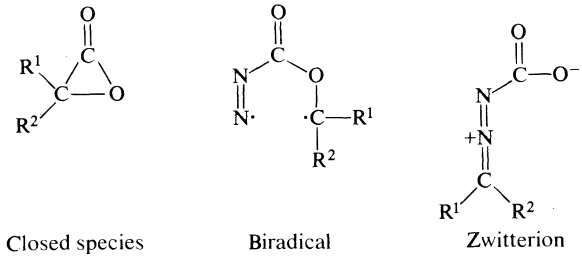

Closed species Biradical Zwitterion

SCHEME 2

by carbon monoxide and nitrogen extrusion (Scheme 2) (6).

A preliminary kinetic study (6) suggested that the balance between the two decomposition modes is dependent on solvent polarity, for the yield of diazoalkane increased on changing solvent from carbon tetrachloride to methanol. Solvent effects on the individual rate constants were qualitatively assessed in terms of a nonpolar ketone-forming transition state and a polar diazoalkane-forming transition state. We now wish to report the results of more detailed mechanistic studies which provide considerable insight on the transition state structures for these reactions. By exposing the underlying factors controlling the balance between the rates of these competing reactions, comprehensive mechanistic information permits partial control of the diazoalkane-forming reaction for synthetic purposes. In addition, it illuminates one example of a relatively rare chemical phenomenon — a three piece fragmentation to stable molecules.

Methods, Results, and Discussion

There are several, a priori, mechanistic alternatives for these thermolyses. Either one or both reactions could be completely concerted, for both thermal reactions are symmetry allowed. Diazoalkane and carbon dioxide are produced by what is formally a 1,3-dipolar cycloreversion, while ketone, carbon monoxide, and nitrogen arise from a $\sigma 2s + \sigma 2s + \sigma 2s$ cycloreversion (7). Among stepwise alternatives, there exists a plethora of possibilities because either

of the two bonds broken during diazoalkane formation could be broken in the rate determining step, while any one or two of three bonds broken in the ketone formation might be broken in the slow step. The possible alternatives may be grouped according to the type of intermediate involved. As Scheme 2 exemplifies, these might include zwitterions (such as that from O1—C5 bond heterolysis) or biradicals (for example, from homolysis of the N4—C5 bond) or even closed-shell molecules. It is important to remember that these two competing decomposition modes each have several possible intermediates of each of the three types in Scheme 2 from which a choice must be made; those structures in the Scheme are only a few reasonable examples.

The kinetic analysis of this reacting system is straightforward. From the disappearance of the starting oxadiazolinone, as monitored by its uv absorption at 360 nm (azo n $\rightarrow \pi^*$) or its ir carbonyl stretch at 1835 cm^{-1}, excellent concentration-independent, first order plots for the total rate constant, $k_T = k_2 + k_3$, are obtained. To dissect this further into the two individual rate constants, the product distribution is required. Since the diazoalkane formed on thermolysis is usually subject to several different fates (none of which ultimately produce ketone), only the time infinity ketone yield was quantitatively analysed by calibrated gas chromatography or infrared spectroscopy. From the fraction of ketone formed, k_3 is easily calculated, and hence k_2 by difference.

That only two primary processes occur can be verified by trapping the diazoalkane with a few percent trifluoroacetic acid (TFA). In these experiments, monitored by nmr, only ketone and trifluoroacetic acid ester are observed, indicating that the other, often unidentified, products formed in the absence of TFA, arose from subsequent reactions of diazoalkane, usually with itself or with solvent. Furthermore, even though only ketone was quantitatively assayed, better linear-free energy relationship correlations (*vide infra*) were always obtained for diazoalkane formation. Had an unknown third process been operative, large systematic errors would have surfaced in the diazoalkane correlations.

Product Distributions

Relevant to the synthetic potential of oxadiazolinones as diazoalkane precursors are the data pictorialized in Fig. 1. The two lines show how the delicate balance between the two competing decomposition routes is affected by solvent polarity. To facilitate comparison to current literature on cycloaddition and cycloreversion reactions, the polarity parameter used here is Dimroth's E_T value

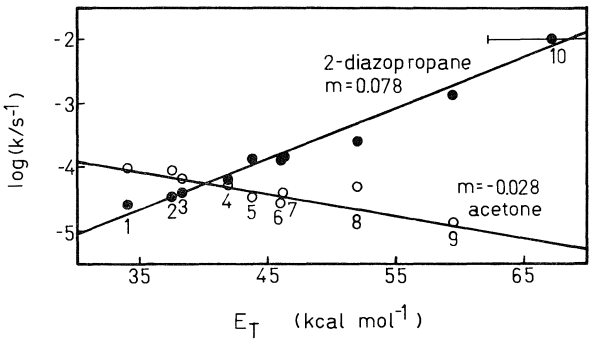

FIG. 1. Effect of solvent polarity on rates of 2-diazopropane (k_2) and of acetone (k_3) formation from **2***b* at 85.0°C. The solvents are: 1 (toluene), 2 (chlorobenzene), 3 (DME), 4 (DCE), 5 (DMF), 6 (acetonitrile), 7 (nitromethane), 8 (acetic acid), 9 (TFE), and 10 (TFA). The E_T value for TFA is estimated in Appendix I. Product composition as a function of E_T can be estimated for untried solvents from this plot. For example, it is 50:50 at the E_T value where the regression lines intersect, and 91:9, or 9:91 at the E_T values for which the ordinates of the two lines differ by one log unit. The slopes of the lines are given by *m*.

(see ref. 8 for an excellent review of solvent polarity parameters). An E_T value for TFA was estimated from correlations with other polarity parameters (see Appendix I). For the 5,5-dimethyl compound, the diazoalkane yield increases from about 20% in toluene, up through chlorobenzene, 1,2-dimethoxyethane (DME), 1,2-dichloroethane (DCE), nitrobenzene, dimethylformamide (DMF), nitromethane, acetonitrile, acetic acid, and 1,1,1-trifluoroethanol (TFE) to TFA where one obtains diazoalkane exclusively.

The effect of substituent polarity, as measured by the Hammett σ parameter, on the product distribution from *para*-substituted 5-phenyl-5-methyloxadiazolinones, can be determined from Fig. 2. Even weak electron donors such as methyl and phenyl strongly favour the diazoalkane route, although a relatively polar solvent, acetonitrile, was used to obtain these data. Note also that these compounds were thermolysed at 50°C compared to 85°C for the 5,5-dialkyl oxadiazolinones. These are unstable compounds indeed, and many could only be purified by column chromatography at Dry Ice temperatures.

Substituted acetophenone semicarbazones, in which the *para*-substituent is strongly electron withdrawing (NO_2, CN, or CF_3) would not cyclize under normal oxidation conditions (LTA in methylene chloride at room temperature, 2 h). For these compounds and for other semicarbazones especially insoluble in methylene chloride (e.g., *p*-C_6H_5), addition of five equivalents of trifluoroacetic acid boosted the oxidative capability and a rapid reaction

occurred at lower temperatures. This mixed oxidizing system gave unique results not observed with lead tetratrifluoroacetate itself. For details see the Experimental section.

Kinetic Investigations

Solvent Effects (Table 5)

The degree of charge separation at the transition state, as reflected in solvent effects on the reaction rate, is a particularly useful mechanistic probe. In Fig. 1, the log of an individual rate constant for diazopropane or acetone formation, from 5,5-dimethyloxadiazolinone, is plotted against the E_T parameter: toluene is on the low E_T end and TFE and TFA are on the high E_T end. It is noteworthy that a similar plot of log k_T (the total rate constant) is not at all linear, but shows an overall U-shape. That the dissection of k_T into two competing processes gives linear correlations supports the contention that these are independent primary processes and that both products do not originate from a common intermediate, produced in the rate determining step, whose subsequent product determining steps are solvent sensitive.

The slopes of the solvent correlation lines are small. The sign of the slope means that the transition state for diazopropane formation is more polar than the starting material, while that for ketone is less polar. The actual respective values of 0.08 and -0.03 mol kcal^{-1} may be compared to the very much larger value of $+0.29$ observed by Huisgen for a known stepwise 2 + 2 cycloaddition; that of tetracyanoethylene to butyl vinyl ether which proceeds via a zwitterionic intermediate (ref. 9, eq. [1]):

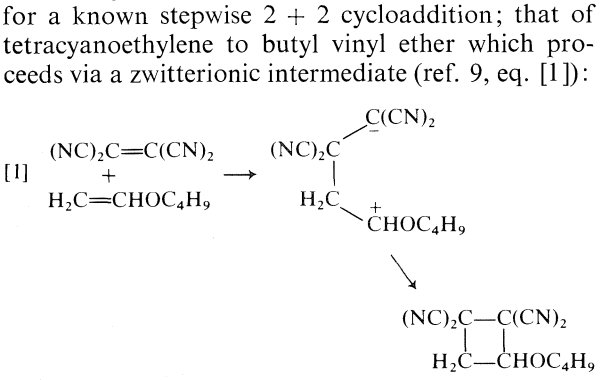

From the data in Fig. 1, oxadiazolinone decomposition in either mode via zwitterionic intermediates is ruled out.

Thermochemistry and Activation Parameters (Tables 1 and 2)

A brief look at the thermochemistry of these two processes is in order inasmuch as it relates to the position of the transition state on the reaction coordinate and is germane to discussion of the activation parameters. The heat of combustion of 5,5-dimethyloxadiazolinone was measured and used to calculate its heat of formation in the gas phase at room temperature (see Experimental). With a crude estimate for the entropy, data from standard tables, and the additivity principles of Benson (10), changes in the thermodynamic variables were calculated for each process. These are summarized in Table 1. From the lower part of the table, it is plain that the thermodynamic entropy changes, ΔS^0, are quite large; about $+26$ and $+58$ entropy units for the two and three piece fragmentations, respectively. The calculated free energy changes of -7 and -48 kcal mol^{-1} differ by 41 kcal. This may be contrasted with the difference in the free energies of activation, a difference of about 1 kcal mol^{-1} in the nonpolar solvent, toluene.

A further consequence of the thermodynamic estimates from Table 1 is that, exothermic as it is, fragmentation to the three very stable products — acetone, carbon monoxide, and nitrogen — is not sufficiently exothermic to populate excited states of any products. The lowest available electronically excited state would be the acetone $n\pi^*$, with respective singlet and triplet energies of 85 and 78 kcal mol^{-1} above the ground state (11). Dioxetane thermolysis produces triplet acetone (with a few percent singlet) whose phosphorescence (and minor fluorescence) can be observed in degassed samples (11). Using a single photon counting apparatus, we observed no chemiluminescence in the thermolysis of **2***b*. Based on that experiment, an upper limit to the yield of excited state acetone was set at 10^{-7} to 10^{-8}% (see Experimental section for details).

Historically, activation parameters have often been employed as a guide to the mechanism of similar unimolecular fragmentations (7, 12). It is not uncommon for concerted cycloreversions (for example, the retro-Diels–Alder reaction) to show small or even negative entropies of activation as bonds are only partially broken at the transition state. For ketone formation, very little of the large positive thermodynamic entropy change of $+58$ entropy units is realized at the transition state: $\Delta S^{\ddagger}$ varies from $+2$ to $+10$ eu (Table 2). Although the entropy of activation is expected to be positive if the reaction proceeds through a floppy biradical intermediate, it should not be as large as the ΔS^0 for the whole fragmentation process. It is impossible to say, a priori, where, in the range $0 < \Delta S^{\ddagger} < +58$ eu, the borderline between a concerted mechanism and a stepwise alternative, via a biradical intermediate, would lie. For this reason, we sought other types of evidence.

For diazoalkane formation, the activation entropies (-5 to -10 eu) have neither the sign nor the

TABLE 1. Gas phase thermochemistry of 5,5-dimethyl-Δ^3-1,3,4-oxadiazolin-2-one[a]

	Me_2CNN +	CO_2	← **2***b* →	N_2 +	CO +	Me_2CO
ΔH_f^0 (gas)	47 ± 5[b]	−94.1	-48 ± 2	0	−26.4	−51.7
S_{298}^0	75[c]	51.1	ca. 100 ± 10[d]	45.8	42.2	70.5
ΔH^0			1 ± 7 -30 ± 2			
ΔS^0			26 ± 10 58 ± 10			
ΔG_{298}^0			-7 ± 10 -48 ± 5			
ΔG_{358}^0			-9 ± 11 -51 ± 6			
ΔH_{max}[e]			-26 ± 7 -60 ± 2			
ΔG_{max}[e]			-38 ± 12 -79 ± 7			

[a]Data for acetone, CO, N_2, and CO_2 from ref. 36. Units are kcal mol^{-1} (ΔH, ΔG) or cal mol^{-1} K^{-1} (ΔS, S) throughout.
[b]$\Delta H_f^0(Me_2CNN) = \Delta H_f^0(H_2CNN) + \Delta H_f^0(Me_2CO) - \Delta H_f^0(H_2CO) = 71 \pm 5 - 51.7 + 27.7 = 47.0 \pm 5$ kcal mol^{-1} (10).
[c]Analogous to footnote [b], for $S_{298}^0 = 58.1 + 70.5 - 53.7 = 74.9$ cal mol^{-1} K^{-1} (10).
[d]Compare to S_{298}^0(cyclopentane) = 70.0, (1,1-dimethylcyclopentane) = 85.4, and (cyclopentene) = 69.2 cal mol^{-1} K^{-1} (10).
[e]Energy difference between transition state and products at 85°C, assuming $\Delta H^{\ddagger}$ and $\Delta G^{\ddagger}$ for toluene (Table 2) apply to the gas phase.

TABLE 2. Activation parameters for thermolysis of 5,5-dimethyloxadiazolinone over the temperature range 50–95°C[a]

	Diazopropane formation		Acetone formation	
Solvent	$\Delta H^{\ddagger}$	$\Delta S^{\ddagger}$	$\Delta H^{\ddagger}$	$\Delta S^{\ddagger}$
Toluene	27.1 ± 0.4	-4.7 ± 1.0	30.3 ± 0.3	7.4 ± 0.9
Acetonitrile	25.1 ± 1.0	-6.3 ± 2.7	29.3 ± 1.7	1.8 ± 4.7
Trifluoroethanol	23.4 ± 0.15	-6.6 ± 0.4	32.3 ± 1.5	8.5 ± 4.3
Trifluoroacetic acid	20.8 ± 0.5	-9.9 ± 1.4	—	—

[a]Crude data found in Table 6. All errors are those returned by linear least-squares analysis. Units are kcal mol^{-1} and cal mol^{-1} K^{-1} for ΔH and ΔS, respectively.

magnitude of the thermodynamic value of +28 eu. Here, the increasingly negative values of $\Delta S^{\ddagger}$, as solvent polarity increases, could be interpreted as arising from increased ordering of the solvent shell around the moderately polar transition state for this process. In this case, biradicals could not account for the trend.

Secondary Deuterium Kinetic Isotope Effects (Table 7)

The β-deuterium kinetic isotope effects measured for **2***b*-d_6 were 2.1 ± 0.3 and 1.3 ± 0.4% per deuterium for diazopropane-d_6 and acetone-d_6 formation, respectively. Although small, these values are significant (13) and imply that a bond involving C5 is broken in the rate-determining step of each process. These would be the O1—C5 and N4—C5 bonds, respectively. There are no reasonable transition states which do not involve rupture of a bond to C5 but which could account for this isotope effect. Steric or ponderal effects of isotopic substitution are ruled out by the absence of an alkyl steric effect on either process (*vide infra*).

Alkyl Substituent Effects (Table 8)

There is no correlation of rate constants for nine 5,5-dialkyl substituted oxadiazolinones with Taft steric parameters, E_s (14), for either ketone formation or diazoalkane formation. The reason for the scatter plots obtained is that some of the data are much better fitted by inductive parameters, σ^*, for the alkyl substituents. For diazoalkane formation, $\rho^* = -1.27 \pm 0.06$ ($r = 0.993$), but there is no significant correlation of the rate of ketone formation with σ^* — much like the Hammett plot for that reaction.

Aryl Substituent Effects (Table 3)

For the seven *para* substituted 5-aryl-5-methyloxadiazolinones studied, both electron withdrawing and electron donating substituents mildly accelerate ketone formation. The range of rate is only a factor of two, and the rho value is not significantly different from zero: -0.13 ± 0.12 ($r = -0.402$). This erratic behaviour is not unlike that observed from bis-(phenylmethyl)diazene fragmentation to benzyl radicals (15) and could be interpreted as suggesting that ketone formation involves rate determining creation of a radical centre at C5. On the other hand, scatter plots are to be expected from any mechanism if the isokinetic temperature lies in the range studied (50–85°C).

In complete contrast, diazoalkane formation gives an excellent fit to inductive parameters. A rho value of −1.93 is obtained with log k plotted against a

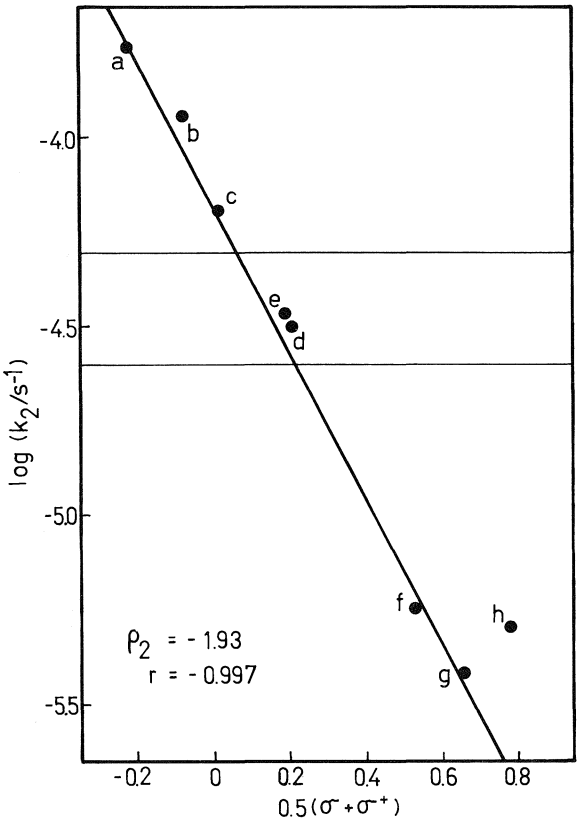

FIG. 2. Hammett plot for diazoalkane formation from *p*-substituted 5-methyl-5-phenyloxadiazolinones (**2***c*) thermolysed at 50.0°C in acetonitrile. Substituents are X = CH_3 (a), C_6H_5 (b), H (c), Br (d), Cl (e), CF_3 (f), CN (g), NO_2 (h). The horizontal band corresponds to the range of rate constants for ketone formation (which do not correlate with σ, σ^+, or the "improved" $\sigma^\cdot$ (40)). From this band, and the regression line, product compositions may be estimated for untried substituents, by a procedure analogous to that of Fig. 1.

50/50 mixture of sigma and sigma plus (Fig. 2). The utility of blending the sigma parameters in cases where a full positive charge is not achieved in the products has been discussed elsewhere (16).

Mechanism of Diazoalkane Formation

At first sight, a build-up of positive charge at C5 of the transition state is quite difficult to rationalize as CNDO calculations (see Experimental) confirm that the corresponding carbon of the diazoalkane is most definitely negative in net charge density relative to C5 of the oxadiazolinone. For the hypothetical **2***a* in Scheme 1, the calculations give a net charge density of +0.17 at C5 (17) while in diazomethane, the same carbon is −0.26 in net charge. Notwithstanding the fact that the calculations only refer to gas phase molecules, a rho value of −1.93 measured in acetonitrile must surely mean that the net charge on C5 increases and passes through a value greater than +0.17 at the transition state. This is only consistent with some degree of O1—C5 bond heterolysis at the transition state. Both the solvent effects and the intermediate size of this Hammett rho rule out a zwitterionic intermediate sporting a full positive charge at C5. The reaction must therefore be concerted with more O1—C5 than C2—N3 cleavage at the transition state (Fig. 3).

Consideration of the reverse of fragmentation, cycloaddition, tends to confirm this deduction. Fragmentation to give carbon dioxide and diazoalkane is formally a retro-1,3-dipolar cycloaddition. Thanks to the work of Fukui (18), Houk (19), and Huisgen (20), the stereoselectivity of the cycloaddition reaction is understandable in terms of Frontier Molecular Orbital (FMO) theory and a concerted mechanism.

Examination of the frontier orbitals of CO_2 and diazomethane shown in Fig. 3 predicts that their major cyclization product (path *a*) would be the wrong regioisomer (**4**), resulting from the largest orbital extension between the two biggest lobes, on the carbon atoms. However, by the Principle of Microscopic Reversibility, the fragmentation in question must share the same transition state as the cyclization to give that regioisomer (path *b*). Now the greatest frontier density is found between the CO_2 carbon and the terminal nitrogen, predicting a transition state with more C2—N3 than O1—C5 bond formation, in precise agreement with the experimental deduction of transition state structure. We conclude, therefore, that diazoalkane formation occurs via a non-synchronous but concerted mechanism.

Mechanism of Ketone Formation

A large number of possible mechanisms are still consistent with the information presented so far. A few reasonable alternatives to a fully concerted mechanism are: prior loss of one of the three stable fragments to give either a biradical or a closed shell species which rapidly decays to products; or a pre-equilibrium one bond scission to give a biradical.

Even at ambient temperature (ca. 50°C) and low ionizing voltages (ca. 10 eV), the mass spectrum of **2***b* shows no evidence for fragment ions at P − 28 (loss of N_2 or CO), nor any metastables for P → P − 28. A parent ion is also not observed. Like the parent ion, if such intermediates occur, their lifetimes must be of the order of a microsecond (21). If they do not occur for ionized oxadiazolinone at 10^{-5} Torr in the gas phase, it seems unlikely they could be significant in the solution thermolysis of oxadiazolinones.

Both a stepwise process via reasonable biradicals like **5** or **6** or a concerted mechanism would be con-

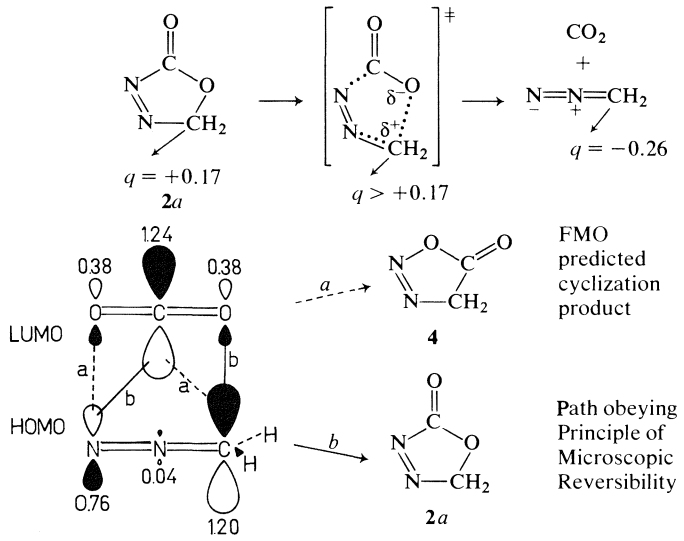

FIG. 3. Charge densities (q) and Frontier MO's for cycloaddition. Frontier densities are given by $2\sum C_{\mu i}^2$.

sistent with the observed solvent effects and β-deuterium kinetic isotope effect. The Hammett plot misbehaviour slightly favours a biradical, while the low activation entropies tend to favour a concerted mechanism. No esr signals attributable to intermediate radicals or biradicals were observed when **2***b* was thermolysed in the presence or absence of nitrosobenzene. Furthermore, chemically induced dynamic nuclear polarization (CIDNP) effects (22) were not observed in decompositions performed in either chlorobenzene or methylene iodide solvent (heavy atoms expected to enhance singlet–triplet mixing (25)), even in ^{13}C spectra obtained during decomposition of 90% C5 labelled substrate.

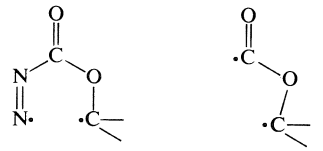

5 **6**

Most reasonably, any diradical formed in thermolysis would be born singlet, and would, therefore, have to intersystem cross and then fragment to triplet products for CIDNP to be observed. In the fifteen year history of the phenomenon, CIDNP from 1,5-biradicals has only been reported for biradicals born as triplets (23–25). However, the singlet 1,5-biradical **5** has unusual potential to display CIDNP effects by intersystem crossing and fragmentation, because one of the products (ketone) has a low-lying triplet state. When both C5 substituents are methyl, the thermochemistry suggests that there is actually insufficient energy for formation of triplet ketone. Nevertheless, other heterocyclic ring systems which do show chemiluminescence might be a source for this, as yet unrecognized, type of CIDNP from thermally generated biradicals. Photo-CIDNP may be more likely if 1,5-biradicals are intermediates in the photodecomposition of oxadiazolinones.

If the biradical **5** were reversibly formed, racemization might occur during decomposition of starting material optically active at C5. To this end, the two oxadiazolinones, **7** (Scheme 3), were prepared from the semicarbazone of *d*-camphor. Their stereochemistry was assigned on the basis of a large downfield shift of the signal corresponding to the *syn* methyl group at C7 of the *exo*-azo isomer, **7***a*. Models show that these protons spend time in the deshielding region of the azo pi bond and so absorb at an extra 0.5 ppm downfield from the analogous protons in the *endo*-azo isomer, **7***b* (see Appendix

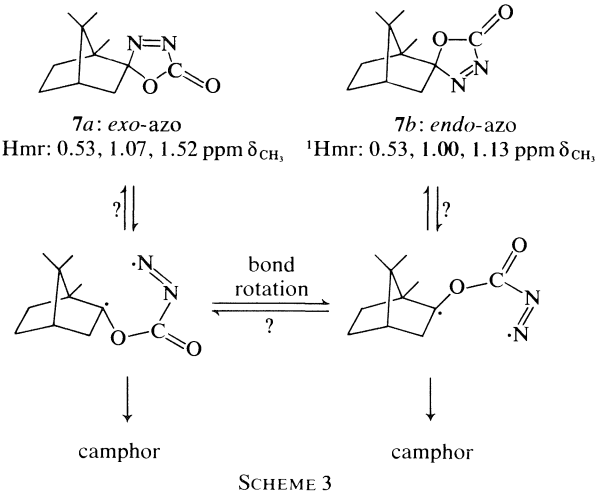

SCHEME 3

II). If biradicals were formed reversibly and if bond rotation (and inversion, for a non-planar radical centre) competed with decomposition, interconversion of *exo*-azo and *endo*-azo isomers could occur during decomposition (Scheme 3). Such interconversion was not observed by ^{1}Hmr during thermolysis of the pure *exo*-azo isomer, suggesting that rotation/inversion *with* return does not occur, although either rotation/inversion *or* return might occur.[3]

Finally, it is instructive to consider the effect of phenyl substitution on k_3. From the activation parameter data reported in Table 2, k_3 for **2***b* in acetonitrile at 50°C is computed to be 2.54×10^{-7} s^{-1}. Thus, $k_3(\mathbf{2}c)/k_3(\mathbf{2}b) = 170$, corresponding to $\Delta\Delta G^{\ddagger} = -3.3$ kcal mol^{-1}. For comparison, values of $\Delta\Delta G^{\ddagger}$ of -5.8, -6.3, and -5.8 kcal mol^{-1} per phenyl group replacing a methyl group may be calculated for two sets of symmetrical *trans*-diazenes and one set of *trans*-3,5-disubstituted pyrazolines.[4] If thermolyses of these three model diazene sets are assumed to involve concerted nitrogen loss to form two radical centres, then the $\Delta\Delta G^{\ddagger}$ per phenyl group for the models is twice as large as for oxadiazolinone. If the model extrusions were stepwise (one CN bond ruptured at the transition state), then the oxadiazolinone effect would be even more discrepant!

Clearly, ketone formation does not behave like these classical radical forming reactions and, after eliminating all other mechanistic alternatives and failing to detect (or even infer the existence of) possible intermediates in numerous experiments, a concerted mechanism is compellingly implicated.

Experimental

General

Melting points were determined on a Thomas Hoover capillary melting point apparatus and are uncorrected. Infrared (ir) spectra (CCl_4 solutions unless otherwise noted) were obtained on a Perkin-Elmer model 283 spectrophotometer. ^{1}Hmr and Cmr spectra were taken on Varian EM-390 and Brüker WH-90 instruments, respectively, all with TMS internal reference unless otherwise indicated. Mass spectra (ms) were recorded on either a CEC-21-110B spectrometer at 70 eV or an Hitachi Perkin-Elmer RMU-6A instrument at lower ionizing voltages. Ultraviolet–visible (uv–vis) measurements were obtained from a Cary 14 instrument. Gas chromatographic (glc) analyses were performed on a column (10 ft × 1/4 in.) packed with 20% Carbowax 20M on 60–80 mesh Chromosorb P, using a Varian Aerograph model 920 gas chromatograph equipped with thermal conductivity detection and model 485 digital integration. Chlorocarbon extracts were dried over anhydrous sodium sulfate and diethyl ether or light petroleum extracts over anhydrous magnesium sulfate. Light petroleum refers to the fraction boiling between 30–45°C; pentane to "Fisher Certified, IR Spectranalysed" *n*-pentane; hexane to "Baker Analysed" reagent, bp 68.5–69.3°C.

Materials

Because of an aqueous decomposition mechanism,[5] good first order kinetics could not be obtained using wet solvents. 1,2-Dimethoxyethane (DME) and toluene were each fractionated at high reflux ratio (ca. 5:1) from calcium hydride and a two-thirds centre cut stored over fresh 4 Å molecular sieves. The following solvents were fractionated from Drierite ($CaSO_4$, Hammond Co.) and the centre cut stored over molecular sieves: chlorobenzene, 1,2-dichloroethane (DCE), and trifluoroethanol (TFE); acetonitrile and nitromethane were each pretreated by passage through a column of neutral alumina (30 g L^{-1}); nitrobenzene and dimethylformamide (DMF) were fractionated at reduced pressure (10–20 Torr). Trifluoroacetic acid (TFA) and acetic acid (HOAc) were each fractionated prior to use and ca. 1% of the respective anhydride added to keep them dry. In all cases, glc analysis showed water to be less than 0.05%.

Lead tetraacetate (LTA) refers to the material stabilized with 10% acetic acid, as sold by Ventron Corp.

Synthesis

General Procedure for LTA Oxidation of Dialkyl Ketone Semicarbazones (Method A)

LTA (10.0 g, 0.021 mol) was added in one portion to a stirred suspension of the semicarbazone (0.020 mol) in dry CH_2Cl_2 (150 mL) at 0°C. There was an immediate development of a yellow colour. The ice bath was then removed for a period of 0.5–2 h during which time the solution gradually became colourless and a white precipitate formed. The ice bath was returned and a mixture of 2.4 *N* HCl (50 mL) and ice (150 g) was added. After 15 min the reaction mixture was filtered through Celite (Johns-Manville Ltd.), the organic phase was separated, and the aqueous phase extracted with ice cold CH_2Cl_2 (3 × 50 mL). The organic extracts were com-

[3]A referee has pointed out that the isomerization of **7***a* to **7***b* is inherently unlikely because bicycloheptyl radicals are known to react preferentially from the *exo* side (see, for example, ref. 37). There are three reasons why we expect that preference to be unimportant in the present case. First, the reclosure to either **7***a* or **7***b* is a radical coupling reaction rather than a chain transfer step. *Exo* preference has been established for chain transfer steps, which must have a higher activation energy, and presumably greater *exo*/*endo* selectivity, than coupling reactions. Second, reclosures to either **7***a* or **7***b* are intramolecular steps with a restricted approach angle for attack at C2 of the bicycloheptyl skeleton, because the new ring formed is 5-membered. Intramolecularity should reduce the normal *exo* preference because the more severely hindered approach avenues from the *endo* side (which cut down bimolecular *endo* rate constants) are irrelevant to intramolecular closure. Third, the presence of the C7 methyl group should mitigate potential *exo* preference. The alternative test, isomerization from **7***b*, could not be performed because pure **7***b* was unavailable. Also, it is noteworthy that no Δ^1-pyrazoline has ever demonstrated internal return with isomerization (38, 39).

[4]$\Delta G^{\ddagger}$ values, in kcal mol^{-1}, computed at 50°C from ln (k/T) vs. T^{-1} plots of the original kinetic data are: di-*t*-butyldiazene (37.0); dicumyldiazene (25.4); diisopropyldiazene (42.3); bis(α-phenylethyl)diazene (29.6); *trans*-3,5-dimethyl-Δ^1-pyrazoline (37.5); and *trans*-3,5-diphenyl-Δ^1-pyrazoline (25.9) (refs. 41–46, respectively).

[5]Manuscript in preparation.

TABLE 3. ^{1}Hmr data for dialkyl substituted oxadiazolinones

R^1	R^2	Melting point (°C)	^{1}Hmr (δ)[a]
CH_3	CH_3	39.5–40.0	1.67 (s, $2CH_3$)
CH_3	CH_2CH_3	Oil	0.83 (t, J = 7.5 Hz, 3H, CH_3) 1.66 (s, 3H, CH_3) 2.11 (q, J = 7.5 Hz, 2H, CH_2)
CH_3	$CH_2CH_2CH_3$	Oil	1.60 (s, 3H, CH_3) 1.8–2.2 (m, 3H, CH_3) 2.2–2.4 (m, 2H, CH_2) 3.4–3.7 (m, 2H, CH_2)
CH_3	$CH(CH_3)_2$	Oil	0.94 and 1.09 (both d, J = 6.9 Hz, 6H, diastereotopic CH_3) 1.62 (s, 3H, CH_3) 2.25 (septet, J = 6.9 Hz, 1H, CH)
CH_3	$CH_2CH(CH_3)_2$	Oil	0.92 and 0.98 (both d, J = 6.4 Hz, 6H, diastereotopic CH_3) 1.4–2.2 (m, 3H, CH_2CH) 1.63 (s, 3H, CH_3)
CH_3	$C(CH_3)_3$	36–36.5	1.05 (s, 9H, t-Bu) 1.56 (s, 3H, CH_3)
CH_3	CH_2OCH_3	Oil	1.65 (s, 3H, CH_3) 3.31 (s, 3H, OCH_3) 3.71 and 3.93 (2d, J = 11.3 Hz, 2H, diastereotopic AB set in ratio 2:1, CH_2)
CH_3	$CH_2C_6H_5$	108 (dec)	1.63 (s, 3H, CH_3) 3.28 (s, 2H, CH_2) 6.95–7.4 (m, 5H, aromatic H)[b]
$CH_2C_6H_5$	$CH_2C_6H_5$	105 (dec)	3.38 and 3.53 (both d, J = 15 Hz, 4H, diastereotopic AB set in ratio 4:1, $2CH_2$) 6.95–7.4 (m, 10H, aromatic H)[b]
$CH(CH_3)_2$	$CH(CH_3)_2$	Oil	0.91 and 1.06 (both d, J = 6.9 Hz, 12H, diastereotopic CH_3) 2.72 (septet, J = 6.9 Hz, 2H, 2CH)

[a] CCl_4 solution, except where noted.
[b] $CDCl_3$ solvent.

bined and washed with a cold, saturated solution of sodium bicarbonate (50 mL), and with water (3 × 50 mL). Drying and removal of the solvent under reduced pressure gave crude oxadiazolinone in about 80–90% yield.

The crude material was purified by one or more of the following three methods. Dimethyl- and methyl-*t*-butyl-oxadiazolinones were twice sublimed at 0.01 Torr from 0°C to a Dry Ice/acetone cold finger. The methylbenzyl and dibenzyl compounds were recrystallized from light petroleum. All other alkyl-substituted substrates were distilled at 0.01 to 0.001 Torr at room temperature (higher temperatures lead to decomposition), then repeatedly recrystallized from pentane at low temperature (ca. −20 to −80°C) until magnified ir spectra of the carbonyl region showed less than 0.5% of ketone impurity. Overall yields at the end of the first purification step were 70 to 80%, in most cases. Table 3 lists the melting points and ^{1}Hmr data obtained for this series.

Isotopically labelled dimethyloxadiazolinones (5-^{13}C and perdeutero-) were synthesized from the semicarbazones of acetone-2-^{13}C (90% enriched, Merck, Sharpe and Dohme Ltd.) and acetone-d_6 (99+% D, Aldrich Co.). The deuterium content of the latter oxadiazolinone was taken to be identical to that measured for the semicarbazone (98.4 ± 0.2% D by ms comparison to unlabelled material).

LTA Oxidation of Semicarbazones of p-*Substituted Acetophenones (Method B)*

As Table 4 summarizes, Method A was successfully used to synthesize the *p*-H, Br, Cl, and CH_3 substituted 5-methyl-5-phenyloxadiazolinones. Although a change of oxidation solvent (to light petroleum) permitted ir observation of the oxadiazolinone from *p*-methoxyacetophenone, evaporation of the solvent was followed by rapid decomposition to the corresponding diazoalkane and subsequent products. Method B was used in cases where Method A was not successful because the semicarbazones would not cyclize at low temperature and the oxidation products were unstable if oxidation was attempted at higher temperatures.

An oxidizing mixture of 0.21 *M* Pb(IV) containing approximately 1:1 acetate and trifluoroacetate was prepared by dissolving lead tetraacetate (90%, 102.5 g) and TFA (76 mL) in dry CH_2Cl_2 (1 L). Qualitatively, this solution gave the best results: more TFA led to more decomposition, less meant incomplete cyclization. No effort was made to determine if

TABLE 4. Synthesis and decomposition of *p*-substituted acetophenone oxadiazolinones (**2***c*)

p-Substituent (σ, σ^+,[a] synthetic method,[b] crude yield,[c] ν_{CO}[d])	Melting point (°C)	f_{oxa}[e]	$10^5\ k_T$[f,g]	% Ketone[g,h]	$10^5\ k_3/s^{-1}$	$10^5\ k_2/s^{-1}$
CH_3(−0.17, −0.13, A, 60, 1834)	Oil	0.866	57.01±0.17	15.5±0.6	8.84±0.34	48.17±0.37
C_6H_5(−0.01, −0.17, B, 55, 1832)	68–70	0.926	39.98±0.48	21.0±1.6	8.40±0.65	31.58±0.74
H(0.00, 0.00, A, 70, 1835)	Oil	0.858	21.96±0.15	19.7±0.8	4.33±0.18	17.63±0.21
Cl(0.23, 0.11, A, 60, 1837)	Oil	0.754	14.91±0.10	36.9±1.5	5.49±0.23	9.42±0.23
Br(0.23, 0.15, A, 60, 1837)	Oil	0.878	13.64±0.15	35.6±1.7	4.86±0.24	8.78±0.25
CF_3(0.54, 0.52, B, 75, 1837)	Oil	0.799	6.34±0.05	75.9±3.0	4.81±0.19	1.53±0.19
CN(0.66, 0.66, B, 55, 1837)	109–10 (dec)	0.844	7.16±0.02	85.1±3.4	6.10±0.24	1.06±0.24
NO_2(0.78, 0.79, B, 60, 1840)	103–4 (dec)	0.793	7.00±0.05	79.9±3.2	5.59±0.23	1.41±0.21
$CONH_2$[i](—, —, B, 50, 1836)	110–11 (dec)					

[a]Reference 32.
[b]See text for details of methods A and B.
[c]^{1}Hmr integration prior to purification (%).
[d]Infrared in CH_3CN (cm^{-1}).
[e]^{1}Hmr assay for oxadiazolinone purity (see text). Standard deviations are 2–3%.
[f]Total first-order rate constant, k_T, at 50.0°C in CH_3CN (s^{-1}).
[g]Errors are standard deviations of the mean, usually from triplicates.
[h]Calibrated ir spectroscopy, slow scan.
[i]Not used in kinetics.

the enhanced oxidation rate was due to increased semicarbazone solubility or to formation of a mixed acetate/trifluoroacetate Pb(IV) species of higher oxidizing power. Lead tetratrifluoroacetate (LTTFA) (26) in either CH_2Cl_2 or TFA/TFAA did not result in oxidative cyclization, even though the latter solution was completely homogeneous.

In a typical experiment, three separate solutions were cooled to −15°C for 0.5 h in an ice/salt or ice/alcohol bath: a stirred slurry of semicarbazone (0.010 mol) in dry CH_2Cl_2 (50 mL) in a stoppered flask (250 mL); oxidizing solution (50 mL, 0.0105 mol) in a stoppered flask; and 2.4 *N* HCl (50 mL). The oxidant was rapidly added to the semicarbazone slurry and the now-homogeneous reaction mixture stirred 3–5 min before the aqueous acid was added. Hydrolysis times of about 1 min were adequate and filtration through Celite followed by ice-cold workup was identical to that in Method A above. ^{1}Hmr spectra of the crude reaction product indicated that oxadiazolinone accounted for more than 50% of this material (yields of crude products, Table 4).

Purification of the crude material was done as follows. For the *p*-NO_2, $CONH_2$, and CN compounds, the crude solid was extracted from a residue of unreacted semicarbazone with a minimum of CH_2Cl_2, then recrystallized from $CHCl_3$. The separation of the oxadiazolinones bearing *p*-CH_3, C_6H_5, H, Cl, Br, and CF_3 substituents from their decomposition products formed in synthesis, mostly ketone and trifluoroacetic acid ester, could only be achieved without further decomposition by low temperature column chromatography. In an evacuated, Dry Ice/acetone filled, jacketting Dewar, a column of 2.5 cm × 30 cm was packed with silica gel (Baker, 60–300 mesh, ca. 90 g for one gram of crude material). Generally, 15–20% diethyl ether in light petroleum was used as the eluant. In spite of problems inherent in this technique — trying to keep things dry, low solubility (gumming of the sample at the top of the column), and rapid elution — magnified ir spectra of the carbonyl region for each fraction allowed selection of a small cut of reasonably clean material. In all cases but the *p*-C_6H_5, an oil was obtained which could not be further purified. 5-Methyl-5-*p*-biphenylyloxadiazolinone was recrystallized from diethyl ether/hexane.

Because none of the acetophenone oxadiazolinones was very pure, each was assayed by low temperature (−30°C) ^{1}Hmr in CCl_4 or acetone-d_6 by careful integration of the methyl group against anisole as internal standard. This information is also contained in Table 4. The assay was applied as a correction factor, f_{oxa}, when determining starting oxadiazolinone concentrations for product analysis. Fortunately, the reaction rates were independent of any impurities remaining in these samples after the above purification step. All samples (neat or CH_3CN solution) were stored in the freezer (−25°C) prior to use, and none was kept for more than 10 days after preparation.

LTA Oxidation of d-*Camphor Semicarbazone*

The crude reaction product obtained using Method A contained about 60% ketone and 40% oxadiazolinones (ir). This material was chromatographed at −20°C on silica gel (Baker, 60–300 mesh, 50 g per gram), from which it was eluted with 1% diethyl ether in light petroleum. Although the two isomeric oxadiazolinones (**7***a* and **7***b*) were completely separated from the ketone, they were not well separated from each other. Fractions containing more than 75% *exo*-azo isomer (**7***a*; by ^{1}Hmr, see Appendix II) were combined and the white solid fractionally crystallized five times from pentane to give **7***a* (ca. 0.1 g, mp 83–84°C) in 1.5% overall yield. The *endo*-azo isomer (**7***b*) remained an oil and further attempts to isolate it from its contaminant (30% of **7***a*) were unsuccessful.

Kinetics

General

Rate constants k_3 and k_2, respectively, for ketone and diazoalkane formation, were determined by applying the product assay for fraction of ketone formed (see below) to the total rate constant for disappearance of starting material, $k_T = k_2 + k_3$. Each value of k_T was measured in triplicate and the results averaged. The bath temperature was maintained to ±0.10°C or better and the average k_T had a typical standard deviation of the mean of less than 1%.

Ultraviolet Method

A kinetic method employing uv analysis of removed aliquots was utilized for the solvent effects (Table 5), activation parameters (Tables 2 and 6), β-deuterium kinetic isotope effect (Table 7), and alkyl substituent effect studies (Table 8) in all but TFE and TFA. After a warming period of 20 min, aliquots of 6 mL (3–5 m*M* in oxadiazolinone) were withdrawn by syringe from capped 100 mL volumetric reaction flasks and quenched in liquid N_2. Two time infinity (10 half-lives) samples were taken for each run and then all 12–14 samples were allowed to warm to room temperature for uv–vis analysis of absorption at λ_{max} of the azo $n \rightarrow \pi^*$ transition (ca. 360–380 nm, slightly solvent variable, $\varepsilon_{max} \sim 200$–$400\ M^{-1}\ cm^{-1}$).

TABLE 5. Solvent effects on thermolysis of **2***b* at 85.0 ± 0.1°C

Solvent	E_T[a]	$10^5\ k_T$[b,c]	Kinetic method[c,d]	% Ketone[c]	Analytical method[e]	$10^5\ k_3/s^{-1}$	$10^5\ k_2/s^{-1}$
Toluene	33.9	12.23±0.11	A	79.1±1.2	GC	10.03±0.11	2.20±0.09
Chlorobenzene	37.5	11.90±0.12	A	71.3±0.8	GC	8.48±0.13	3.42±0.10
1,2-Dimethoxyethane	38.2	10.60±0.11	A	60.8±1.7	GC	6.44±0.19	4.16±0.19
1,2-Dichloroethane	41.9	11.75±0.08	S	44.3±0.65	IR	5.21±0.08	6.54±0.08
Dimethylformamide	43.8	16.60±0.20	A	19.9±0.7	GC	3.30±0.05	13.30±0.16
Acetonitrile	46.0	17.40±0.17	A	16.5±0.2	GC	2.82±0.06	14.58±0.15
Nitromethane	46.3	18.3 ±0.8	A	21.9±0.6	GC	4.01±0.13	14.3 ±0.3
Acetic acid	51.9	28.62±0.19	A	13.3±0.15	GC	3.81±0.05	24.81±0.46
1,1,1-Trifluoroethanol	59.5	139.4 ±0.6	S	0.9±0.15	GC	0.35±0.14	139.1 ±0.6
Trifluoroacetic acid	66±7[f]	1045 ±20	S	0.4±0.25	NMR	—	1041 ±20
Nitrobenzene[g]	42.0	17.7 ±0.5	NMR	38 ±2	NMR	—	—

[a]Reference 8.
[b]Total first-order rate constant, k_T (s^{-1}).
[c]Errors are estimated standard deviations of the mean, usually of triplicates.
[d]A = 100 mL volumetric flask in bath; 6 mL aliquots withdrawn and quenched in liq. N_2; analysed in 1 cm uv cells near 360–380 nm. S = individual sealed tubes suspended in bath; removed and quenched; analysed in 0.1 cm uv cells near 360 nm. NMR = Varian EM-390 spectrometer operated at 85 ± 2°C.
[e]GC = calibrated gas chromatography with internal standard. IR = calibrated ir spectroscopy, slow scan speed.
[f]Calculated from correlations among E_T and other solvent polarity parameters. See Appendix I.
[g]A ^{1}Hmr experiment, meaningful only for product distribution.

TABLE 6. Kinetic data for the activation parameters in thermolysis of **2***b*

Solvent	Temperature[a]	$10^5\ k_T$[b,c]	% Ketone[c,d]	$10^5\ k_3/s^{-1}$	$10^5\ k_2/s^{-1}$
Toluene	94.0	35.26±0.38	84.0 ±0.8	29.62±0.43	5.64±0.29
	89.0	19.84±0.07	82.4 ±0.4	16.35±0.10	3.49±0.08
	85.0	12.23±0.1	82.0 ±0.5	10.03±0.11	2.20±0.09
	81.0	7.50±0.04	81.1 ±0.5	6.08±0.05	1.42±0.04
	77.0	4.69±0.015	80.8 ±0.5	3.79±0.03	0.90±0.02
Acetonitrile	89.0	24.3 ±0.8	16.5 ±0.3	4.01±0.15	20.3 ±0.7
	85.0	17.4 ±0.17	16.2 ±0.3	2.82±0.06	14.58±0.15
	81.0	11.01±0.08	15.2 ±0.1	1.67±0.02	9.34±0.07
	77.0	6.98±0.03	14.0 ±0.2	0.98±0.01	6.00±0.03
Trifluoroethanol	85.0	139.4 ±0.6	0.25±0.10	0.35±0.14	139.1 ±0.6
	70.6	34.21±0.14	0.30±0.10	0.10±0.03	34.11±0.14
	60.3	11.55±0.06	0.40±0.10	0.046±0.012	11.50±0.06
	51.6	4.24±0.04	0.90±0.15	0.038±0.006	4.20±0.04
Trifluoroacetic acid	85.0	1045 ±20	[e]		1041 ±20
	77.15	517 ±13	[e]		515 ±13
	70.6	320 ± 5	[e]		319 ±5
	60.3	116.5 ±1.0	[e]		116.0 ±1.0
	51.6	46.0 ±0.3	[e]		45.8 ±0.3

[a]Temperatures measured by National Research Council of Canada calibrated thermometer (°C, ±0.1°).
[b]Total first-order rate constant, k_T (s^{-1}).
[c]Errors are estimated standard deviations of the mean, usually from triplicates.
[d]Calibrated gas chromatography with internal standard.
[e]Not measurable; put at 0.4 ± 0.25.

The data were treated by a standard linear least-squares procedure and the calculated total first order rate constants (k_T) were obtained with typical correlation coefficients of 0.999 for up to 5 or more half-lives. Increasing the concentration by a factor of 20 or adding 1% aniline had no effect on the measured rate constants. TFE and TFA runs were done using 0.5 mL aliquots individually sealed in glass tubes and uv analysis was accomplished in cells of 0.1 cm path length.

The β-deuterium kinetic isotope effect, k_H/k_D, for each process was measured at 85.0°C in toluene and acetonitrile by the uv method. For labelled and unlabelled **2***b*, k_T was simultaneously determined, each in duplicate to eliminate possible errors arising from minor temperature variations. Duplicate k_T's for 3 half-lives agreed within their estimated standard deviations ($\lesssim 0.3\%$). Product analysis by calibrated glc employed acetone-d_6 in a fashion analogous to that described below. Although the total isotope effects, $k_T(H)/k_T(D)$ were nearly the same for both solvents (1.1 for all 6D), only k_H/k_D for ketone formation in toluene and for diazoalkane formation in acetonitrile are ultimately reported since the propagated error for the minor pathway in each case renders the value of k_H/k_D for that pathway unreliable (see Table 7).

Infrared Method

The uv method was unsuitable for the *para*-substituted 5-methyl-5-phenyloxadiazolinones because a pink to red colouration develops during decomposition, presumably from the diazoalkane. Oxadiazolinone (ca. 0.050 g) was carefully

TABLE 7. β-Deuterium secondary kinetic isotope effects in thermolysis of **2***b* at 85.0°C[a]

Solvent	Substrate	$10^5\ k_T$[b,c]	% Ketone[c,d]	$10^5\ k_3$	$10^5\ k_2$	$k_3(H)/k_3(D)$[e]	$k_2(H)/k_2(D)$[e]
Toluene	**2***b*	12.12±0.05	80.6±1.5	9.77±0.19	2.35±0.18	1.078±0.024	1.199±0.110
	2*b*-d_6	11.02±0.04	82.2±0.9	9.06±0.10	1.96±0.10	[1.013±0.004 per D]	[1.031±0.018 per D[f]]
Acetonitrile	**2***b*	17.4 ±0.2	16.5±0.3	2.82±0.06	14.58±0.18	1.041±0.041	1.131±0.020
	2*b*-d_6	15.6 ±0.2	17.4±0.5	2.71±0.09	12.89±0.17	[1.007+0.007 per D[f]]	[1.021±0.003 per D]

[a]For each solvent, each substrate was done in duplicate, all four runs simultaneously.
[b]Total first-order rate constant, k_T (s^{-1}).
[c]Errors are standard deviations of the mean of duplicates.
[d]Calibrated glc with internal standard.
[e]$k(H)/k(D)$ (per D) = $(k(H)/k(D)\ (obs.))^{1/6}$.
[f]For the minor pathway, the propagated error is large (see text). This value may, therefore, not be reliable.

TABLE 8. Alkyl substituent effects on thermolysis of oxadiazolinones in 1,2-dichloroethane at 85.0°C[a]

R^1	R^2	$\Sigma\sigma^{*b,c}$	ΣE_s^b	$10^5\ k_T$[d]	% Ketone	$10^5\ k_3/s^{-1}$	$10^5\ k_2/s^{-1}$
CH_3	CH_3	0.00	0.00	11.75±0.08	44.3±0.6	5.21±0.08	6.54±0.08
CH_3	$CH_3CH_2CH_2$	−0.115	−0.36	17.43±0.17	50.9±1.7	8.87±0.31	8.56±0.31
CH_3	$(CH_3)_2CH$	−0.19	−0.47	16.05±0.19	42.4±0.6	6.81±0.13	9.24±0.14
CH_3	$(CH_3)_3C$	−0.30	−1.54	21.02±0.12	28.4±0.5	5.97+0.11	15.05±0.14
CH_3	$(CH_3)_2CHCH_2$	−0.125	−0.93	36.6 ±1.7	43.0±1.5	15.7 ±0.9	20.9 ±1.1
CH_3	$C_6H_5CH_2$	+0.215	−0.38	8.39±0.09	66.8±1.0	5.60±0.10	2.79±0.09
CH_3	CH_3OCH_2	+0.52	−0.19	3.41±0.01	97 ±3	3.31±0.10	0.10±0.10
$(CH_3)_2CH$	$(CH_3)_2CH$	−0.38	−0.94	25.84±0.22	24.7±0.6	6.38±0.16	19.46±0.23
$C_6H_5CH_2$	$C_6H_5CH_2$	+0.43	−0.76	6.36±0.10	69.9±0.5	4.45±0.08	1.91±0.04

[a]Kinetics and product distributions by ir spectroscopy, errors are standard deviations for the mean of triplicates.
[b]Reference 14.
[c]Correlation of $\log(k_2/k_2(CH_3/CH_3)) = \sigma^*\rho^*$ has $\rho^* = -1.27 \pm 0.06$ ($r = -0.993$). $\log(k_3/k_3(CH_3/CH_3)) = \sigma^*\rho^*$ has $\rho^* = -0.28 \pm 0.11$ ($r = -0.686$).
[d]Total first-order rate constant, k_T (s^{-1}).

weighed and dissolved in dry CH_3CN (10.00 mL). Portions of about 0.2 mL were transferred by syringe to glass tubes (12 cm long by 2 mm id), filling about 45 of them to a depth of 5 cm. This amount of sample was exactly sufficient to fill a 0.5 mm CaF_2 ir solution cell. The tubes were quickly sealed and stored in the freezer at −25°C until used for either kinetics or product analysis.

In a typical kinetic run, 12 to 16 sample tubes were withdrawn from the bath at intervals calculated to give roughly equal concentration differences up to 3 to 5 half-lives. The reaction was quenched by cooling with liquid N_2. For the ir analysis, the spectrophotometer was operated in the absorbance mode on a very slow scan speed and a large wavelength expansion setting at 1835 cm^{-1}. Calibration plots using ketones showed that measured absorbances were a linear function of concentration, and first order fits of the disappearance of ν_{co} of oxadiazolinone gave correlation coefficients typically better than 0.9995 (see Table 4).

Product Analysis

Diazoalkanes generated in oxadiazolinone thermolyses often react in a variety of ways to give several products, some incorporating solvent (^{1}Hmr, glc). The addition of a few drops of TFA per mL of solvent effectively traps the diazoalkane as the trifluoroacetic acid ester, the only other product observed by ^{1}Hmr and glc being ketone. Under the reaction conditions employed in these thermolysis studies, neither diazopropane nor any of its subsequent reaction products (principally acetone azine) were hydrolysed or otherwise converted to the ketone. This means that accurate determination of the product distribution may be inferred from quantitative assay of ketone only.

For the solvent effects (Table 5), activation parameters (Table 6), and β-deuterium kinetic isotope effects (Table 7) (cases where very pure starting material was available), the time infinity acetone concentration was measured by integrated glc, calibrated against internal standard 2-butanone. Typically 8–15 injections of each of several calibrant solutions and reaction mixtures were used to obtain an average of the fraction of ketone formed in each case, f_{co}, and this result had an estimated standard deviation of the mean of about 1–2%.

Ketone measurements by ir carbonyl absorption for dialkyl and acetophenone oxadiazolinones were obtained under conditions of slow scan speed and large wavelength scale magnification. Seven to ten calibration solutions of twice recrystallized or redistilled ketone demonstrated excellent linearity between absorbance and concentration. By measuring the time infinity ketonic carbonyl absorption and correcting for any ketonic impurity at time zero, the concentration, and hence the fraction, f_{co}, of ketone formed was computed. From a knowledge of the nmr purity assay, f_{oxa} (see above), a correction to the starting concentration of acetophenone oxadiazolinone was made:

$$f_{co} = \frac{([\text{ketone}]_\infty - [\text{ketone}]_0) \times MW_{oxa} \times Vol}{\text{weight}_{oxa} \times f_{oxa}}$$

For alkyl substituted oxadiazolinones, f_{oxa} was taken to be unity though it may have been as low as 0.95 in rare cases.

The product distribution in nitrobenzene was obtained by ^{1}Hmr.

For the camphor oxadiazolinones, the product ratios (ir) were obtained as a function of the *exo*/*endo* ratio (^{1}Hmr) in seven mixtures. Least-squares analysis gave $f_{co}(exo) = 8.4 \pm 0.4\%$ and $f_{co}(endo) = 26.2 \pm 1.1\%$.

Thermochemistry: $\Delta H_f^0(oxa)_g$

At 25°C, the energy released by combustion of 1 g pellets of 5,5-dimethyloxadiazolinone was measured in a Parr Oxygen Bomb Calorimeter and found to be 526.0 ± 0.2 kcal mol^{-1}. An enthalpy of combustion was computed from the stoichiometry,

$$C_4H_6N_2O_{2(s)} + 4\tfrac{1}{2}O_{2(g)} \rightarrow 4CO_{2(g)} + N_{2(g)} + 3H_2O_{(L)}$$

then corrected for the ca. 2% nitrogen combustion (27). This gave $\Delta H_c^0 = -525.1 \pm 0.4$ and $\Delta H_f^0(oxa)_s = -56.05 \pm 0.4$ kcal mol^{-1}. Determination of the gaseous heat of formation necessitated approximating the heat of sublimation, ΔH_s^0, to a crude estimate for the heat of vaporization, ΔH_v^0, obtained from Benson's empirical formula (10):

$$\Delta H_v^0(298\ K) = 22(1.76 \times 10^{-3} \times T_b(°C) + 0.253)$$

Although the boiling point, T_b, of dimethyloxadiazolinone is unknown, it is a reasonably volatile solid of mp 39.5–40.0°C, so a bracketted guesstimate of $40 < T_b < 100$°C generated error limits in $\Delta H_v^0 = 8.3 \pm 1.2$ kcal mol^{-1}. With $\Delta H_s^0 \sim 8.3 \pm 2.0$, $\Delta H_f^0(oxa)_g = -47.7 \pm 2.0$ kcal mol^{-1}. Admittedly, several very crude assumptions are involved in the value chosen for ΔH_s^0, and hence $\Delta H_f^0(oxa)_g$, but very generous error limits appended to the final value do reflect the uncertainty.

Chemiluminescence

Attempts to observe chemiluminescence employed a single photon counting apparatus calibrated with luminol (28). Event signals from a 14 stage Amperex 56 DUVP/03 photomultiplier tube in a PRA-510 housing operated at −1990 V were run through an ORTEC 9301 fast preamp to an ORTEC 454 timing filter and out to a Hewlett-Packard 60 MHz frequency counter. The dark current was 13 Hz.

A solution of dimethyloxadiazolinone in hexane (0.3 *M*) was degassed in a cylindrical quartz tube by three freeze–pump–thaw cycles and heated to 100–110°C in an oil bath for three min prior to transferral to the sample chamber of the single photon counting apparatus. Counting was initiated immediately. In only a few minutes, the sample had cooled to ca. 50°C, but at no time was any chemiluminescence apparent. No signal above background dark current was observed. The experiment was repeated in the presence of anthracene with identical results. Another sample, 0.02 *M* in 5-methyl-5-(*p*-chlorophenyl)-Δ^3-1,3,4-oxadiazolinone, also gave no additional counts. A detection limit of a 20% increase over background counts would have meant the fraction of acetone excited states formed near 50°C had been $\sim 2 \times 10^{-10}$.

CNDO/2 Calculations

The computer program and method have been described previously (17). The following structural parameters were used: CO_2 (29), $r_{CO} = 1.162$ Å; diazomethane (30), $r_{CH} = 1.08$, $r_{CN_1} = 1.32$, $r_{N_1N_2} = 1.12$, all in Å, and $\angle HCH = 127°$. Eight of twelve CNDO/2 LCAO orbitals for carbon dioxide are occupied, giving rise to zero order net charge densities of +0.536 and −0.268 on the carbon and each oxygen, respectively. A pair of degenerate HOMO's with π symmetry at −15.70 eV have a node on carbon and coefficients of ±0.707 on the oxygens. The LUMO is also a degenerate pair of π-type orbitals, at 5.14 eV, each with coefficients: C(+0.795), O(−0.429). The Frontier orbital densities of Fig. 3 are calculated for atom A in orbital *i* as $2 \sum_{\mu}^{on\ A} C_{\mu i}^2$.

In the case of diazomethane, eight of fourteen LCAO orbitals are occupied, and net charge densities computed to be: H(+0.045), C(−0.261), N_1(+0.306), N_2(−0.136). At −11.05 eV, the HOMO has π symmetry, with orbital coefficients: C(−0.780), N_1(−0.125), N_2(+0.613). The LUMO, at 4.35 eV, is found to have σ symmetry, but the π-type NLUMO at 4.45 eV has orbital coefficients: C(+0.506), N_1(−0.704), N_2(+0.499). In cycloaddition reactions, the regiochemistry is very often controlled by the HOMO–LUMO interaction of smallest energy gap (18), which would be HOMO(CH_2N_2) − LUMO(CO_2), at 16.19 eV. The calculations predict the HOMO(CO_2) − NLUMO(CH_2N_2) gap to be 20.15 eV.

Electron Spin Resonance

Electron spin resonance signals were not observed during thermolysis of degassed chlorobenzene solutions 0.5 *M* in dimethyloxadiazolinone at a temperature of 100°C in the probe of a JEOL JES-3BS-X spectrometer. When the experiment was repeated in the presence of doubly sublimed nitrosobenzene, the esr spectrum of diphenyl nitroxide was obtained (a_N = 10.0 g; a_H = 0.9 g). The same spectrum was observed from nitrosobenzene in the absence of oxadiazolinone, and the splitting parameters agree with those in the literature (31).

Chemically Induced Dynamic Nuclear Polarization

In a biradical of structure **5**, formed from 5,5-dimethyloxadiazolinone, coupling of the methyl protons to the unpaired electron at C5 might produce enhanced absorption or emission in the ^{1}H nmr during decomposition, but such effects were not observed at ca. 100°C in chlorobenzene.

In some cases, ^{13}C nmr is more sensitive to CIDNP phenomena (e.g., ref. 24*b*), but with as much as 0.25 g of sample, the carbonyl carbons of oxadiazolinone and product acetone could not be detected above baseline noise because too few scans were accumulated during the key minutes of the reaction. To overcome this problem, 90% enriched 5,5-dimethyl-Δ^3-1,3,4-oxadiazolin-2-one-5-^{13}C was synthesized from acetone-2-^{13}C (Merck, Sharpe and Dohme of Canada Ltd.). Even though C5 and acetone carbonyl could be easily observed from 0.050 g of the labelled oxadiazolinone, the thermolysis at 100°C in either chlorobenzene or methylene iodide failed to generate emission or enhanced absorption in the Cmr spectrum. The CIDNP experiment was negative.

Proton Magnetic Resonance Test of Interconversion of **7**a *and* **7**b

The sample of pure **7***a* was assayed by 90 MHz ^{1}Hmr to contain ≤0.2% **7***b*. This detection limit was determined from scans of the 0.6 to 1.1 ppm region under conditions which did not saturate signals (low rf power and moderate scan speed). Excellent Gaussian lineshapes were always obtained. Cut-and-weight integration procedures established for assay of mixtures of **7***a* and **7***b* proved that a peak of 0.5% of the total intensity in this region was easily measured. Hence, a detection limit of about 40% of this level was inferred as reasonable.

Oxadiazolinone **7***a* (0.030 g) in dry CCl_4 (0.5 mL) was sealed into a tube and thermolysed at 85°C for 80 min (ca. 30% decomposition). The sample was cooled, transferred to an nmr tube, and the ^{1}Hmr obtained. To the high field side of the *anti*-C7 methyl protons of **7***a* (1.07 ppm), a complex series of absorptions obscured one possible C7 methyl of the *endo* isomer, **7***b* (1.00 ppm). However, the low field side of the **7***a* absorption was remarkably clear and revealed no observable change in baseline attributable to the 1.13 ppm methyl in **7***b*. On this evidence, interconversion of **7***a* and **7***b* was ruled out.

Acknowledgements

The National Research Council of Canada (now the National Science and Engineering Research Council) supported this work through an operating grant and through postgraduate scholarships to A.J.P.

1. D. C. FROST, N. P. C. WESTWOOD, N. H. WERSTIUK, L. CABELKOVA-TAGUCHI, and J. WARKENTIN. Can. J. Chem. **55**, 3677 (1977).
2. G. A. MACALPINE and J. WARKENTIN. Can. J. Chem. **56**, 308 (1978).
3. J. B. FULTON. Ph.D. Thesis. Department of Chemistry, McMaster University, Hamilton, Ont. 1979.
4. S. L. LEE, G. B. GUBELT, A. M. CAMERON, and J. WARKENTIN. Chem. Commun. 1074 (1970).
5. P. KNITTEL. Ph.D. Thesis. Department of Chemistry, McMaster University, Hamilton, Ont. 1976.
6. S. L. LEE, A. M. CAMERON, and J. WARKENTIN. Can. J. Chem. **50**, 2326 (1972).
7. T. L. GILCHRIST and R. C. STORR. Organic reactions and orbital symmetry. Cambridge University Press, London, Engl. 1972.
8. C. REICHARDT. Angew. Chem. Int. Ed. Engl. B4, 29 (1965); **18**, 98 (1979).
9. R. HUISGEN. Acc. Chem. Res. **10**, 117 (1977).
10. S. W. BENSON, F. R. CRUICKSHANK, D. M. GOLDEN, G. R. HAUGEN, H. E. O'NEIL, A. S. ROGERS, R. SHAW, and R. WALSH. Chem. Rev. **69**, 279 (1969).
11. N. J. TURRO, P. LECHTKEN, N. W. SCHORE, G. SCHUSTER, H.-C. STEINMETZER, and A. YEKTA. Acc. Chem. Res. **7**, 97 (1974).
12. H. KWART and K. KING. Chem. Rev. **68**, 415 (1968).
13. E. A. HALEVI. Prog. Phys. Org. Chem. **1**, 109 (1963).
14. T. H. LOWRY and K. S. RICHARDSON. Mechanism and theory in organic chemistry. Harper and Row, New York, NY. 1976. p. 67.
15. B. K. BANDLISH, A. W. GARNER, M. L. HODGES, and J. W. TIMBERLAKE. J. Am. Chem. Soc. **97**, 5856 (1975).
16. Y. YUKAWA and Y. TSUNO. Bull. Chem. Soc. Jpn. **32**, 971 (1959).
17. A. J. PAINE and N. H. WERSTIUK. Can. J. Chem. **56**, 1319 (1978).
18. (*a*) K. FUKUI. Top. Curr. Chem. **15**, 1 (1970); (*b*) K. FUKUI, T. YONEZAWA, and C. NAGATA. J. Chem. Phys. **27**, 1247 (1957); (*c*) Bull. Chem. Soc. Jpn. **27**, 423 (1954).
19. K. N. HOUK, Y.-M. CHANG, and P. S. ENGEL. J. Am. Chem. Soc. **97**, 1824 (1975).
20. R. HUISGEN. J. Org. Chem. **33**, 2291 (1968).
21. F. W. MCLAFFERTY. Interpretation of mass spectra. 2nd ed. W. A. Benjamin, Inc., Reading, MA. 1973. p. 189.
22. (*a*) R. KAPTEIN. Adv. Free-Radical Chem. **5**, 319 (1975); (*b*) G. L. CLOSS. Adv. Magn. Reson. **7**, 157 (1974); (*c*) A. R. LEPLEY and G. L. CLOSS. Chemically induced magnetic polarization. John Wiley and Sons, New York, NY. 1973; (*d*) J. H. FREED and J. B. PEDERSEN. Adv. Magn. Reson. **8**, 1 (1976).
23. G. L. CLOSS and C. E. DOUBLEDAY. J. Am. Chem. Soc. **95**, 2735 (1973).
24. (*a*) G. L. CLOSS. J. Am. Chem. Soc. **93**, 1546 (1971); (*b*) R. KAPTEIN, R. FREEMAN, and H. D. W. HILL. Chem. Phys. Lett. **26**, 104 (1974).
25. G. L. CLOSS and C. E. DOUBLEDAY. J. Am. Chem. Soc. **94**, 9248 (1972).
26. R. E. PARTCH. J. Am. Chem. Soc. **89**, 3662 (1967).
27. F. D. ROSSINI. Experimental methods in thermochemistry. Wiley Interscience, New York, NY. 1956.
28. J. LEE and H. H. SELIGER. Photochem. Photobiol. **4**, 1015 (1965).
29. I. L. KARLE and J. KARLE. J. Chem. Phys. **17**, 1052 (1949).
30. G. HERZBERG. Molecular spectra and molecular structure. D. Van Nostrand Co., New York, NY. 1966.
31. K. MUKAI, N. NISHIGUCHI, K. ISHIZU, Y. DEGUCHI, and H. TAKAKI. Bull. Chem. Soc. Jpn. **40**, 2731 (1967).
32. E. M. KOSOWER. An introduction to physical organic chemistry. Wiley and Sons Inc., New York, NY. 1968.
33. T. W. BENTLEY and P. v. R. SCHLEYER. J. Am. Chem. Soc. **98**, 7667 (1976).
34. Sadtler Standard NMR Spectra. Sadtler Research Labs., Philadelphia, PA. 1972. (*a*) No. 6023; (*b*) No. 425.
35. J. B. STOTHERS. Carbon-13 nmr spectroscopy. Academic Press, New York, NY. 1972.
36. M. K. KARAPET'YANTS and M. L. KARAPET'YANTS. Thermodynamic constants of inorganic and organic compounds. Ann Arbor-Humphrey Science Pub., Ann Arbor, Michigan. 1970.
37. P. I. ABEL. *In* Free radicals. Vol. 2. *Edited by* J. K. Kochi. Wiley Interscience, New York, NY. 1973. p. 73.
38. R. J. CRAWFORD, D. M. CAMERON, and H. TOKUNAGA. Can. J. Chem. **52**, 4025 (1974).
39. S. PATAI (*Editor*). The Chemistry of the hydrazo, azo, and azoxy groups. Wiley Interscience, New York, NY. 1975.
40. S. DINCTURK, R. A. JACKSON, and M. TOWNSON. J. Chem. Soc. Chem. Commun. 172 (1979).
41. J. C. MARTIN and J. W. TIMBERLAKE. J. Am. Chem. Soc. **92**, 978 (1970).
42. S. F. NELSON and P. D. BARTLETT. J. Am. Chem. Soc. **88**, 137 (1966).
43. M. J. PERONA, P. C. BEADLE, and D. M. GOLDEN. Int. J. Chem. Kinet. **5**, 495 (1973).
44. S. G. COHEN, S. J. GROSZOS, and D. B. SPARROW. J. Am. Chem. Soc. **72**, 3947 (1950).
45. R. J. CRAWFORD and A. MISHRA. J. Am. Chem. Soc. **88**, 3963 (1966).
46. J. W. TIMBERLAKE and B. K. BANDLISH. Tetrahedron Lett. 1393 (1973).

Appendix I. Estimation of an E_T Value for TFA

Protonating solvents remove the solvatochromic absorption band of the pyridinium *N*-phenolbetaine used to define the E_T scale. In order to include trifluoroacetic acid in the reported solvent polarity correlations, an E_T value was estimated from linear correlations with other solvent polarity parameters (8).

Solvolysis data on 2-adamantyl tosylate ($k_{2\text{-AdOTs}}$) in TFA, TFE, HCOOH, HOAc, EtOH, MeOH, and $(CF_3)_2CHOH$ (33) were correlated with the solvent polarity parameter called log k_{ion} (8) to estimate a value of log k_{ion}(TFA), and then that value was plugged into a correlation of log k_{ion} with E_T:

$$\log k_{2\text{-AdOTs}} = (2.193 \pm 0.096) \log k_{ion} - (2.269 \pm 0.154) \qquad r = 0.990$$

$$\log k_{ion} = (0.195 \pm 0.016)E_T - (13.17 \pm 0.75) \qquad r = 0.964$$

$$\log k_{2\text{-AdOTs}}(\text{TFA}) = -3.05$$

Therefore E_T(TFA) = 65.7 ± 6.6.

In spite of the necessary use of two correlations, instead of one (because log $k_{2\text{-AdOTs}}$ data are available only for very few solvents with measured E_T

TABLE 9. Nuclear magnetic resonance assignment of stereochemistry in camphor oxadiazolinones[a]

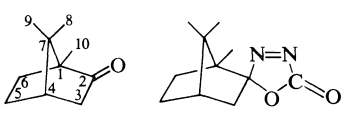

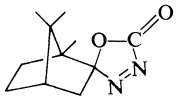
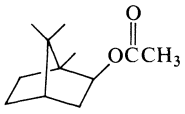
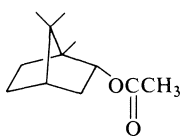

		d-Camphor	7*a*	7*b*	Borneol acetate	Isoborneol acetate
^{1}Hmr, methyls	C8	(0.85)	1.52	(1.00)	(0.83)	(0.82)
	C9	(0.92)	1.07	(1.13)	(0.90)	(0.82)
	C10	(0.97)	0.53	0.53	(0.95)	(0.96)
	Reference	This work	This work	This work	34*a*	34*b*
Cmr, methyls	C8	(19.3)	20.5	(19.4)		
	C9	(19.0)	20.5	(19.7)		
	C10	9.5	9.4	8.6		
	Reference	35	This work	This work		

[a]Bracketed values may not be correctly assigned. Chemical shifts are in ppm relative to internal standard TMS, in CCl_4 solvent.

values), the error propagation suggests quite reasonable confidence limits. The same procedure converts log $k_{2\text{-AdOTs}}$(TFE) = −5.821 (33) to an E_T(TFE) = 59.2 ± 6.2, only 0.3 units below the measured value (8*b*).

Appendix II. Nuclear Magnetic Resonance Assignment of Stereochemistry in the Diastereomers of *d*-Camphor Oxadiazolinones

Selective decoupling of the methyl protons at 0.53 ppm of either isomer of **7** caused collapse of the quartet at 8.6 or 9.4 ppm in the Cmr spectrum (see Table 9), indicating that the upfield protons were on C10. In both isomers, these protons spend time in the shielding region above the plane of the azo pi bond and appear about 0.5 ppm upfield of their usual position at ca. 1 ppm. The opposite downfield shift of the C8 methyl protons to 1.52 ppm in one isomer cannot be due to the oxygen lone pairs nor to the carbonyl group since such an effect is absent in borneol and isoborneol acetates (Table 9). Models show that free rotation of the C8 methyl group of 7*a* permits the protons to spend time in the deshielding region in the plane of the azo pi bond. In the *endo*-azo isomer, this effect is not possible and the C8 methyl hydrogens appear in their usual position, at about 1 ppm.

Synthesis of 1,3-dihydro-2*H*-benzo-1,4-diazepin-2-ones and 1,2-dihydropyrazin-2-ones via iminophosphoranes. Mass spectra of 1,5-disubstituted-1,2-dihydropyrazin-2-ones[1,2]

JACK ACKRELL,[3] EDVIGE GALEAZZI, AND JOSEPH M. MUCHOWSKI[3]

Research Laboratories, Syntex, S.A., Apartado Postal 10-820, Mexico 10, D.F.

AND

LASZLO TÖKÉS

Syntex Research, Institute of Organic Chemistry, 3401 Hillview Avenue, Palo Alto, CA 94304, U.S.A.

Received February 15, 1979

JACK ACKRELL, EDVIGE GALEAZZI, JOSEPH M. MUCHOWSKI, and LASZLO TÖKÉS. Can. J. Chem. **57**, 2696 (1979).

The azido ketones **4***c–e* and **10***a–d* reacted with triphenylphosphine under mild conditions to give the benzo-1,4-diazepin-2-ones **7***c–e* and the 1,2-dihydropyrazin-2-ones **12***a–d*, respectively.

The electron impact induced fragmentation of the 1,5-disubstituted-1,2-dihydropyrazin-2-ones was shown to occur by extensive skeletal rearrangement. The 1,5-diaryl derivatives **12***a–c* fragmented via 1,4-diarylimidazole species produced by the expulsion of CO from the molecular ion. In contrast, the 1-cyclohexyl-5-phenyl derivative **12***d* fragmented almost entirely via a 2-hydroxypyrazine intermediate derived from the molecular ion by McLafferty cleavage.

JACK ACKRELL, EDVIGE GALEAZZI, JOSEPH M. MUCHOWSKI et LASZLO TÖKÉS. Can. J. Chem. **57**, 2696 (1979).

Les azido cétones **4***c–e* et **10***a–d* réagissent, dans des conditions douces, avec la triphénylphosphine pour conduire respectivement aux benzodiazépine-1,4 ones-2 **7***c–e* et aux dihydro-1,2 pyrazinones-2 **12***a–d*.

On a montré que, pour les composés dihydro-1,2-pyrazinones-2 disubstitués en positions 1,5, la fragmentation induite par impact électronique se produit avec une transposition profonde du squelette. Les dérivés diary-1,5 **12***a–c* se fragmentent par l'*intermédiaire* d'une espèce diaryl-1,4 imidazole produite par l'élimination du CO de l'ion moléculaire. A l'opposé le dérivé cyclohexyl-1 phényl-5, **12***d* se fragmente presqu'entièrement via un intermédiaire pyrazinol-2 provenant de l'ion moléculaire selon un clivage de McLafferty.

[Traduit par le journal]

Iminophosphoranes, the isoelectronic analogues of phosphonium ylids, have been known (1) for sixty years, and the chemistry of this class of compounds has been investigated extensively. Whereas the intermolecular synthesis of imines from iminophosphoranes and aldehydes or ketones is well known (1–3), examples of the intramolecular version of this reaction are rare. The synthesis (4) in low yield (11%) of the alkaloid nigrifactine **2** from the azido ketone **1** and triphenylphosphine is one instance of a reaction which may proceed in the above manner. In contrast, Nomura *et al.* (5) have shown that *N*-(2-acylphenyl)iminophosphoranes did not cyclize to benzazetes. Recently (6), the synthesis of diazepam **7***a* and nitrazepam **7***b* from the azidoacetanalides **4***a* and **4***b* and triphenylphosphine or triethylphosphite (Scheme 1) was described in a patent. Our work, which had been carried out independently, confirms and extends the observations published in a recent patent (6).

The intramolecular reaction between an iminophosphorane and a carbonyl moiety was first applied to the synthesis of benzo-1,4-diazepines. Thus, the addition of a slight excess of triphenylphosphine to a toluene solution of 2-azidoacetamidobenzaldehyde **4***c* (see Table 1) caused the occurrence of an exothermic reaction and the rapid precipitation of 1,3-dihydro-2*H*-benzo-1,4-diazepin-2-one **7***c* in greater than 50% yield. The other benzo-1,4-diazepines **7***d*, *e* were prepared (see Table 2) in a similar way from the azides **4***d*, *e*, but in these cases the intermediate iminophosphoranes **5** could be detected as polar intermediates by thin layer chromatography (tlc). Indeed, in one instance (**5***e*), the iminophosphorane was stable at room temperature and could be isolated as the hydrochloride salt. The transformation of this substance into **7***e* could then be effected at a higher temperature after liberation from its salt with sodium hydride.

---

[1]Contribution No. 465 from the Syntex Institute of Organic Chemistry and contribution No. 1 from the Analytical Research Division.

[2]Presented in part at the 59th Canadian Chemical Conference of the Chemical Institute of Canada, London, Ont., June 7–9, 1976.

[3]Presently at Palo Alto, California, address.

0008-4042/79/202696-07$01.00/0

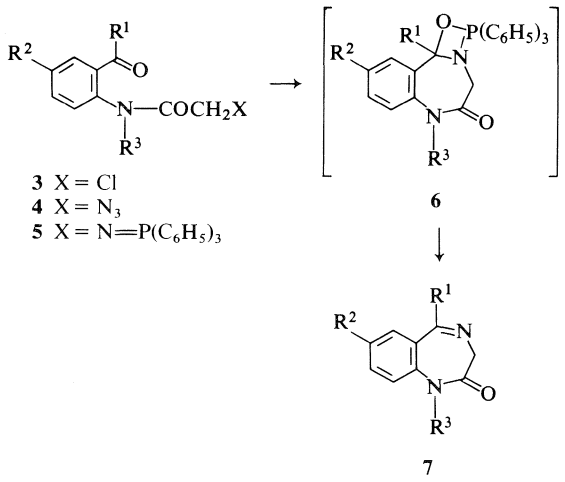

	R^1	R^2	R^3
a	C_6H_5	Cl	CH_3
b	C_6H_5	NO_2	H
c	H	H	H
d	C_6H_5	H	CH_3
e	C_6H_5	Cl	H

SCHEME 1

A process analogous to that described above when applied to the azidoketone **10***a* (Scheme 2 and Table 1), derived from the corresponding phenacyl amine **8***a*, gave 1,5-diphenyl-1,2-dihydropyrazin-2-one **12***a* (35% yield) and not the expected tetrahydropyrazin-2-one **11***a*. The oxidation which took place was not aerial in nature (7) because the dihydro compound **12***a* was also formed (40% yield) when the reaction was effected in a nitrogen atmosphere. Indeed, a careful examination of the course of the reaction by tlc revealed only the presence of the unstable, but isolable, intermediate iminophosphorane, the product **12***a*, and triphenylphosphine oxide. The other 1,5-disubstituted-1,2-dihydropyrazin-2-ones **12***b–d* (Table 2) were likewise formed in 34–54% yields from the azidoketones **10***b–d*.[4] Although unexceptional, these yields are not worse than those obtained when dihydropyridazin-2-ones are synthesized by the ammonolysis of the bromoacetamides of α-aminoketones (7).

The mildness and formal neutrality of the intramolecular Schiff base synthesis described herein make this a highly attractive process for the construction of nitrogen containing cyclic systems.

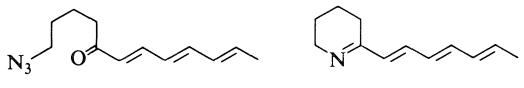

1 2

[4]These compounds were examined for general central nervous system depressant activity but did not possess significant activity in this regard.

Compounds **12***a–d* were characterized by their elemental analysis and spectral characteristics. The nmr spectra had the expected (8) low field absorption (δ 8.15 ± 0.05) for H-3 which was long range coupled ($J \approx 1.5$ Hz) to H-6. The mass spectra (see Table 3), in addition to the expected molecular ions, possessed several interesting and notable features which are discussed in detail below.

The electron impact induced behaviour of the 1,5-diaryl-1,2-dihydropyrazin-2-ones **12***a–c* is typified by the mass spectrum of the diphenyl derivative **12***a* (Fig. 1). These compounds exhibited extensive skeletal rearrangements during the course of fragmentation and the major cleavage patterns, the supporting metastable ion measurements, as well as some mechanistic considerations are summarized in Scheme 3.[5]

The primary fragmentation of **12***a–c* occurs by the expulsion of CO from the molecular ion (a process which has analogy in the mass spectra of pyridazones and phthalazones (12*a*)) to yield the 1,4-diarylimid-

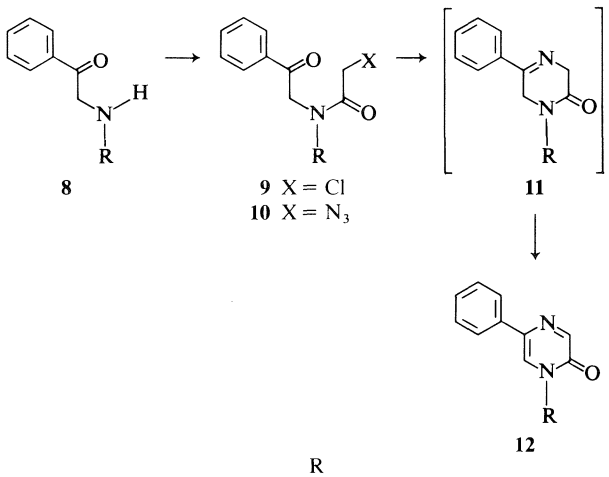

R
a C_6H_5
b 4-CH_3—C_6H_4
c 3-Cl—C_6H_4
d C_6H_{11}

SCHEME 2

[5]The empirical formulae of all the ions shown in Scheme 3 were established by high resolution analysis. The nature of the transitions marked with symbols (see below) was supported by one or more of the following metastable ion measurements; (*) metastable peaks, (†) scanning the accelerating voltage with a fixed electric sector voltage and a constant magnetic field, (‡) scanning the electric sector voltage with a fixed accelerating voltage and a constant magnetic field (using an instrument with reversed Nier–Johnson geometry).

TABLE 1. Yields and physical constants of the chloro and azido amides

Compound	Cryst. solvent	Yield (%)[a]	Melting point (°C)	Analysis % Calculated C	H	N	% Found C	H	N
3*c*	Dichloromethane–hexane	69–78.5	99–102.5	54.70	4.07	7.08	54.48	4.02	7.02
4*c*	Hexane	89	67.5–68.5	52.94	3.95	27.44	52.75	3.85	27.57
4*d*	Ether	78	106–108	65.29	4.79	19.03	65.41	4.85	18.96
4*e*	Hexane	72	76.5–77.5	57.24	3.52	17.80	57.05	3.55	17.78
9*a*	Ether–acetone	50	114–115	66.79	4.97	4.86	66.67	4.84	4.86
9*b*	Acetone–hexane	75	84–86	67.66	5.34	4.63	67.67	5.31	4.74
9*c*	Acetone–hexane	70	89–91	59.64	4.06	4.34	59.82	4.00	4.21
10*a*	Ether–acetone	83	75–77	65.29	4.79	19.03	65.36	4.68	18.92
10*b*	Ether–hexane	86	68–70	66.21	5.23	18.17	66.23	5.24	18.12
10*c*	Ether–hexane	71	56–59	58.45	3.98	17.04	58.45	4.01	16.93

[a]Yield of once crystallized products.

TABLE 2. Yields and physical constants of some 1,3-dihydro-2*H*-benzo-1,4-diazepin-2-ones **7** and 1,2-dihydropyrazin-2-ones **12**

Compound	Cryst. solvent	Yield (%)[a]	Melting point (°C)	Analysis % Calculated C	H	N	% Found C	H	N
7*c*	Methanol	52–54	223–225[b]						
7*d*	Dichloromethane–hexane	76	156.5–157.5[c]						
7*e*	Ether–hexane	80	214–216[d]						
12*a*	Acetone–methanol	35	133–134	77.39	4.87	11.28	77.16	4.88	11.17
12*b*	Acetone–hexane	34	127–128	77.83	5.36	10.68	77.87	5.32	10.67
12*c*	Acetone–hexane	36	130–131	67.96	3.92	9.91	67.68	4.02	10.02
12*d*	[e]	54	57–60	75.55	7.13	11.00	75.75	7.19	11.11

[a]Yield of once crystallized products.
[b]Lit. (9) mp 223–225°C.
[c]Lit. (10) mp 154–156°C.
[d]Lit. (11) mp 214–216°C.
[e]Difficult to recrystallize; purified by column chromatography on alumina.

TABLE 3. Mass spectra* of 1,5-disubstituted 1,2-dihydropyrazin-2-ones **12***a–d*

Mass spectra *m/e* (% relative intensity) ion type			
12*a*	**12***b*	**12***c*	**12***d*
248 (100) $M^{+\cdot}$	262 (100) $M^{+\cdot}$	282† (100) $M^{+\cdot}$	254 (34) $M^{+\cdot}$
220 (50) *b*	234 (62) *b*	254† (78) *b*	172 (100) *o*
193 (6) *e*	207 (7) *e*	227† (8) *e*	144 (41) *p*
192 (3) *f*	206 (11) *f*	226† (3) *f*	117 (8)
165 (12) *g*	179 (4) *g*	218 (3) *b* − HCl	116 (7)
117 (30) *c*	178 (5)	199† (3) *g*	105 (8)
116 (13) *h*	165 (10)	192 (13) *e* − Cl	103 (11)
110 (4) b^{++}	131 (57) *c*	191 (8) *e* − HCl	92 (13)
104 (3) *k*	130 (14) *c* − H	190 (7) *f* − HCl	91 (17)
90 (19) *d*	117 (11) b^{++}	165 (23)	77 (8)
89 (13) *i*	116 (24) *h*	151† (40) *c*	57 (9)
77 (17) *l*	104 (28) *d*	124† (8) *d*	55 (17)
63 (5) *j*	91 (30) *l*	116 (49) *c* − Cl	43 (25)
51 (14) *m*	90 (16)	111† (24) *l*	41 (23)
	89 (31) *i*	90 (24)	
	77 (8)	89 (52) *i*	
	65 (35) *m*	75 (35) *l* − HCl	
	63 (14) *j*	63 (23) *j*	
	51 (9)	51 (25)	

*Uncorrected for ^{13}C and (or) ^{37}Cl isotope contributions.
†These peaks are accompanied by the 25% ^{37}Cl isotope peaks.

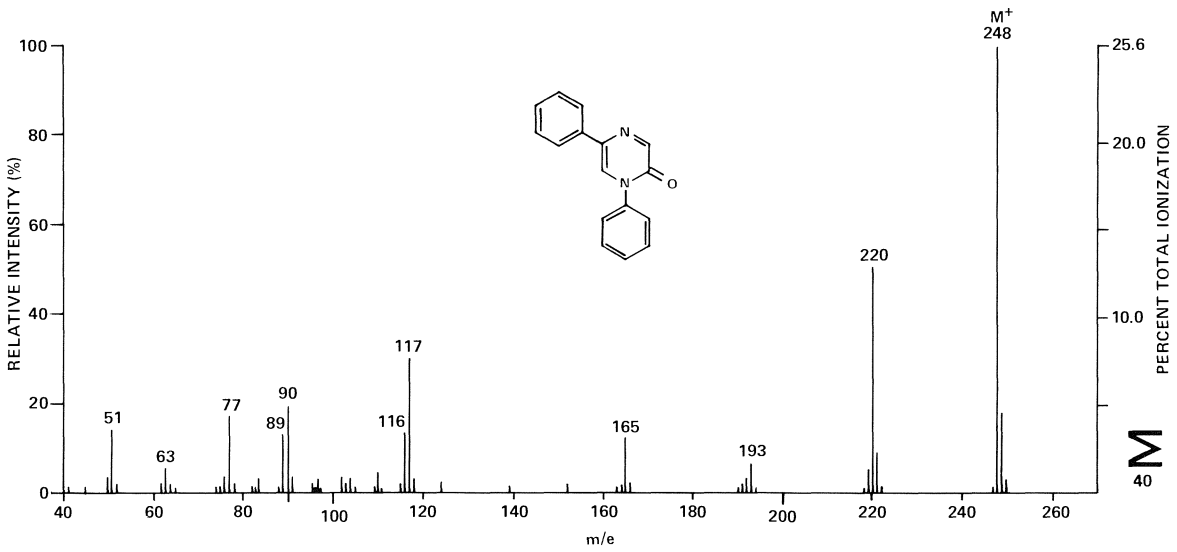

FIG. 1. Mass spectrum of 1,5-diphenyl-1,2-dihydropyrazin-2-one (**12***a*).

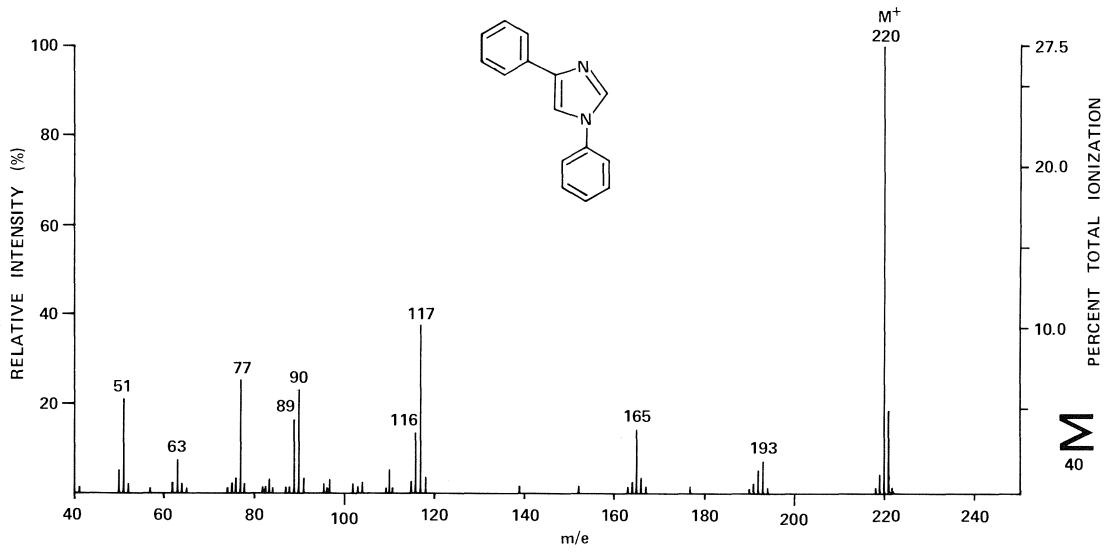

FIG. 2. Mass spectrum of 1,4-diphenylimidazole.

azole ion b_1. The structure assignment of this ion is based on the observation that the spectrum from this point (i.e., *m/e* 220) downward is identical to that of authentic (13) 1,4-diphenylimidazole (cf. Figs. 1 and 2). The predominant mode of fragmentation of b_1 is the loss of benzonitrile, presumably via a valence isomer such as b_2. The ion c_1, thus produced, retains the *N*-aryl substituent in **12***b* and **12***c* and the deuterium labels in 1,4-diphenylimidazole-2,5-d_2. Ion c_1 then undergoes a 1,2-shift of the phenyl group from nitrogen to carbon and loss of HCN (from c_2) to give the $C_7H_6^{+\cdot}$ species (*d*). This pathway is only partially responsible for the genesis of *d* because the spectra of **12***b* and **12***c* contain the $C_7H_6^{+\cdot}$ species as well as the expected substituted ions (i.e., *m/e* 104 and 124, respectively; see Table 3).

Another important fragmentation of the 1,4-diarylimidazole species b_1 takes place by the loss of HCN to give an ion the most probable structure of which is e_1. This type of cleavage is common to both unsubstituted (12*b*, 14) and substituted (15) imidazoles and the site specificity thereof is dependent on the substitution pattern of the imidazole moiety (12*b*). The fragmentation behaviour of the diphenylazirine radical ion e_1 is very complex. Thus, when derived from **12***a* or **12***b* a hydrogen radical is lost,

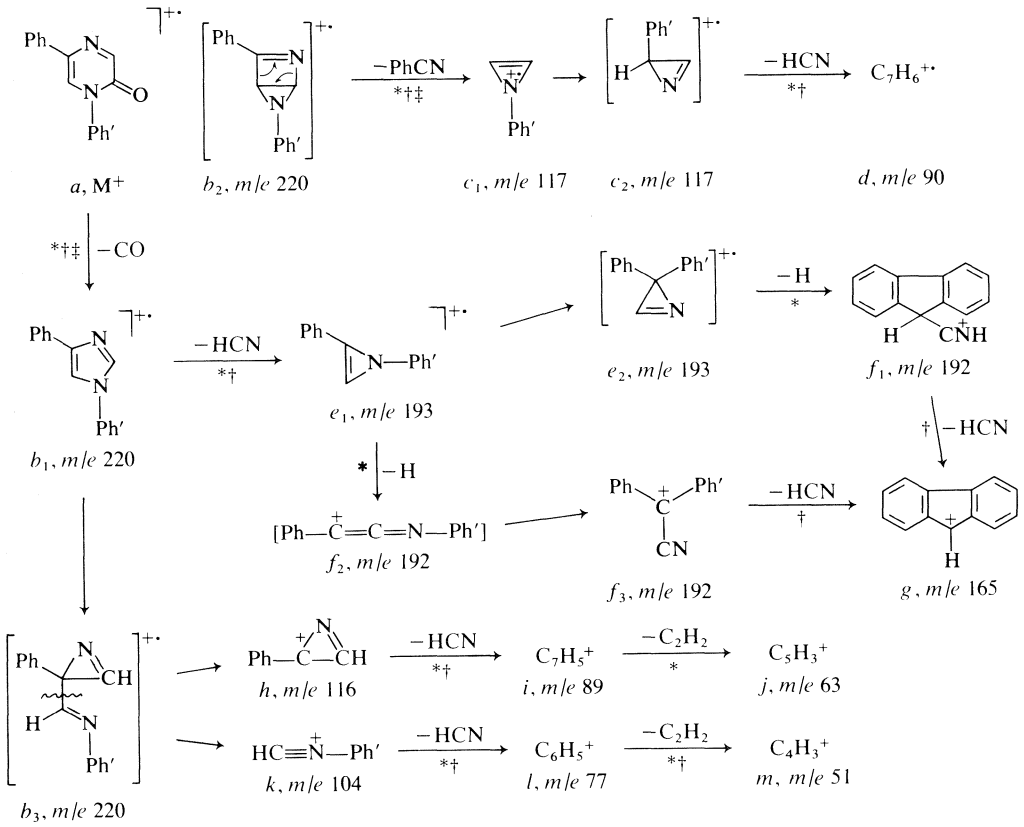

SCHEME 3

whereas either a hydrogen or the *meta* chloro group is liberated from the ion which stems from **12***c*. The species obtained via hydrogen elimination (i.e., f_1 or f_3) then lose HCN, which indicates that this fragmentation process involves a 1,2-migration of the nitrogen substituent to the carbon atom bearing the phenyl group. The $C_{13}H_9^+$ fragment (*m/e* 165) obtained in this way from **12***a*, and for which the fluorenyl cation structure has been suggested, has also been observed for several other diphenyl substituted heterocyclic systems containing two heteroatoms (16, 17). Other fragmentation pathways, in addition to the two shown, contribute to the formation of *g* from e_1. Thus, the *m/e* 165 species is also formed from **12***b* and **12***c*, and furthermore, metastable ion measurements indicate that it is, in part, formed directly from *e*. For **12***b* and **12***c*, this requires the loss of HCN and the substituent from the 1-aryl group instead of an *ortho* hydrogen involved in $e \rightarrow g$. In addition, about 50% of one of the deuterium atoms is retained in the *m/e* 165 ion derived from 1,4-diphenylimidazole-2,5-d_2, an observation which implicates exchange of the imidazole and phenyl hydrogens prior to fragmentation of the diheteroatomic system (17).

The formation of the other fragment ions in these systems do not require the invervention of skeletal rearrangements. The genesis thereof can be rationalized in terms of simple cleavages of valence isomer b_3 of the diarylimidazole. The fragmentation modes $h \rightarrow i$–j and $k \rightarrow l$–m (Scheme 3) are supported by the expected mass shifts in the spectrum of 1,4-diphenylimidazole-2,5-d_2 and by metastable ion measurements on **12***a*–*c*, although the parent ions of

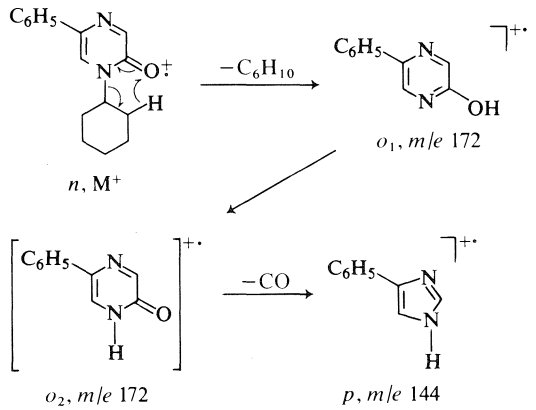

SCHEME 4

h and *k* could not be identified. It is noteworthy, however, that the aryl cation *l* is derived almost entirely from the *N*-aryl groups, an observation which may be of value for structure elucidation purposes.

The mass spectrum of the 1,5-disubstituted-1,2-dihydropyrazin-2-ones changes completely when the nitrogen substituent is a cyclohexyl group as in **12***d* (see Table 3). It is suggested that the fragmentation of this compound can be rationalized in terms of an initial McLafferty cleavage of the molecular ion as shown in Scheme 4. The expulsion of CO does take place to a significant extent, but only after the McLafferty cleavage has occurred (i.e., $n \rightarrow o_1 \rightarrow o_2$–$p$)

Experimental

The melting points were determined in a Mel-Temp apparatus and are corrected. The ir spectra were measured with a Perkin-Elmer model 237 grating infrared spectrophotometer. The nmr spectra were recorded with a Varian T-60 spectrometer. The low resolution mass spectra were measured on Varian-MAT CH-7 and AEI MS-9 mass spectrometers at 70 eV ionizing voltage. The high resolution analyses and metastable ion measurements were carried out on a Varian-MAT 311A mass spectrometer at 70 eV ionizing voltage, 10 000 resolution (10% valley), and ±2 ppm accuracy.

*Preparation of the Chloroacetamido Compounds **3** and **9***

These compounds were prepared by the method of Petersen and Lakowitz (18) except that dioxan was used as the solvent instead of chloroform. Compounds **3***d* (19) and **3***e* (10) have been described previously. The yields, melting points, etc. for the unknown chlorides are given in Table 1.

*Synthesis of the Azidoamides **4** and **10***

These compounds were synthesised from the chlorides and sodium azide by the method of Petersen and Lakowitz (18) except that dimethylsulfoxide was used as the solvent and the reaction was conducted at room temperature. The yields, melting points, etc. for these compounds are compiled in Table 1.

*Synthesis of the 1,3-Dihydro-2*H*-benzo-1,4-diazepin-2-ones **7***

To a stirred solution of the azide (1 equiv.) in anhydrous toluene (20–100 mL/g of the azide) was added triphenylphosphine (1.1 equiv.). Agitation was continued for the times and at the temperatures specified below. The progress of the cyclizations was followed by tlc.

Synthesis of 7c

The addition of triphenylphosphine to a toluene solution of the azide **4***c* caused an exothermic reaction to take place and a solid separated from solution. The mixture was kept at room temperature for 0.5 h (reaction apparently complete at this time) and at reflux temperature for 2.5 h.

Synthesis of 7d

The reaction was complete after 4 h at room temperature.

Synthesis of 7e *and Isolation of the Iminophosphorane* 5e

The solution was stirred at room temperature for 1 h and at reflux temperature for 18 h at the end of which time the iminophosphorane was no longer present.

To isolate the iminophosphorane hydrochloride, the solution obtained after 1 h at room temperature was evaporated to dryness *in vacuo*, and a 10% hydrochloric acid solution was added to the residue. The aqueous solution was decanted from the gummy residue, and the addition of ethyl acetate to this material caused crystallization to occur. The solid was collected by filtration, washed with water, and dried *in vacuo*. Crystallization of this substance from chloroform – ethyl acetate gave a white solid (83%) with mp 217–219°C dec. Recrystallization from ethyl acetate gave the analytical specimen, mp 222–224°C dec. *Anal.* calcd. for $C_{33}H_{26}ClN_2O_2P{\cdot}HCl$: C 67.69, H 4.65, N 4.79; found: C 67.85, H 4.51, N 4.76; ir ($CHCl_3$) ν_{max}: 3330, 2730, 2640, 2440, 1695, 1650 cm^{-1}; nmr ($CDCl_3$) δ: 3.73 (d, CH_2N, J_{PH} = 14.4 Hz), 7.15–8.05 (m, aromatic H's), 9.35 (s, HNP, W_H = 16 Hz, exchanged with D_2O), 10.93 (s, NHCO, W_H = 4 Hz, exchanged with D_2O).

To cyclize the iminophosphorane, an equimolar amount of the hydrochloride and sodium hydride was stirred at room temperature with anhydrous toluene (60 mL toluene/g of iminophosphorane hydrochloride) until hydrogen evolution had ceased. The mixture was stirred at reflux temperature for 4 h, during which period only a slight conversion to the cyclized material had occurred. At this time, 0.1 molar equivalents of triphenylphosphine (the catalytic effect of triphenylphosphine is not understood) was added, and stirring at reflux temperature was continued for 18 h. The reaction was worked up as described below to give a 96% yield of the crude (homogeneous by tlc) benzodiazepinone **7***e*. One crystallization of this material from ether–hexane gave the pure product mp 214–215°C (67%).

The isolation of the benzodiazepinones was carried out in the manner described below.

Compound **7***c* was very insoluble in toluene. When the reaction mixture had cooled to room temperature, this substance was collected by filtration and dried.

To isolate the other benzodiazepinones, the solvent was removed *in vacuo*, the residue was dissolved in ethyl acetate, and this solution was extracted with 10% hydrochloric acid. The acidic extract was cooled, made alkaline with 20% sodium hydroxide solution, and the product was extracted into ethyl acetate. The extract was washed with water, dried over sodium sulfate, and evaporated *in vacuo*. The residue was crystallized from an appropriate solvent.

The yields, melting points, etc., of the benzodiazepinones are compiled in Table 2. The identity of these compounds was ascertained from their characteristic nmr spectra (20) and from the good agreement of the observed melting points with those recorded in the literature. In addition, the ir spectrum of compound **7***c* was identical to that of an authentic specimen, and the mixture mp's of **7***d* and **7***e* with authentic samples were undepressed.

*Synthesis of the 1,2-Dihydropyrazin-2-ones **12***

*Synthesis of **12***a–c

A solution of the azide (1 equiv.) and triphenylphosphine (1.2 equiv.) in anhydrous toluene (10 mL/g of azide) was stirred at room temperature for 20 h. The solvent was removed *in vacuo* and the residue was then purified as described below.

Compound **12***a* was obtained pure by tlc of the mixture on silica gel using chloroform–acetone (95:5) as the developing solvent.

Compound **12***b* was separated from the reaction mixture by column chromatography on Florisil (100 g, for a 7.7 mmol scale reaction). The column was developed (100 mL fractions) with hexane (200 mL), hexane – ethyl acetate, 95:5 (400 mL), and hexane – ethyl acetate, 90:10 (600 mL). The product was contained in fractions 8–10.

Compound **12***c* was also purified by column chromatography on Florisil (50 g, for a 3.1 mmol scale reaction). The column was developed (100 mL fractions) in exactly the same

manner as described for **12***b*. The product was found in fractions 9–11.

Synthesis of **12**d

The synthesis of **12***d* was effected without purification of any of the intermediates.

Cyclohexylamine (5.8 mL, 50 mmol) was added, at −10°C, to a stirred solution of phenacyl bromide (5.0 g, 25 mmol) in anhydrous dichloromethane (100 mL) maintained in a nitrogen atmosphere. The reaction temperature was allowed to rise to 15°C and the mixture was stirred at this temperature for 1 h 40 min. The mixture was filtered, and chloroacetyl chloride (4.6 mL, 60 mmol) was added to the filtrate at room temperature. After a few minutes the solution was concentrated to a small volume *in vacuo*, water was added, and the mixture was extracted with ethyl acetate. The extract was washed with water, dried over sodium sulfate, and evaporated *in vacuo*. The residue was dissolved in benzene, the solution was washed with aqueous sodium carbonate solution, and then with water. The solution was dried, evaporated *in vacuo*, and the residue was chromatographed on alumina (250 g, Act. II, 200 mL fractions). The column was eluted with hexane (600 mL), hexane – ethyl acetate, 95:5 (1000 mL), hexane – ethyl acetate, 90:10 (100 mL), and hexane – ethyl acetate, 85:15 (2200 mL). The chloroamide **9***d* (2.25 g, 32% overall) was isolated as an oil from fractions 17–23. This substance had ν_{max} ($CHCl_3$): 1708, 1650 cm^{-1}, and was used directly in the next step.

The chloroamide was converted into the azido amide **10***d* in the manner described previously. The crude, oily azide (ν_{max} ($CHCl_3$): 2075, 1708, 1655 cm^{-1}) was obtained in 98% yield and was used immediately in the next step.

The azido compound was transformed into the corresponding pyrazin-2-one in the manner described above. The crude product was chromatographed on alumina (100 g for a 6.6 mmol reaction; Act II, 100 mL fractions). The column was eluted with hexane (300 mL) and hexane – ethyl acetate, 95:5 (1400 mL). The product was contained in fractions 8–12.

The 1,5-diaryl-1,2-dihydropyrazin-2-ones showed four intense ir ($CHCl_3$) bands at 1672 ± 2, 1616 ± 2, 1605 ± 3, and 1595 ± 5 cm^{-1}. Compound **12***d* had ν_{max} ($CHCl_3$): 1657, 1595 cm^{-1}. The yields, melting points, etc., for these compounds are compiled in Table 2.

2,5-Diphenylimidazole-2,5-d_2

A solution of 1,4-diphenylimidazole (10 mg) (13) in methanol-OD (5 mL, 99% d_1) containing sodium methoxide (prepared from sodium (50 mg)) was boiled under reflux for three days (nitrogen atmosphere) the progress of the exchange being followed by gc–ms analysis of periodically removed aliquots (0.1 mL). The solution was poured onto a mixture of ice and ether, the ether phase was washed with water, dried over sodium sulfate, and evaporated *in vacuo*. The crystalline residue exhibited 17% d_1 and 83% d_2.

When the exchange was carried out in MeOD–D_2O (9:1), in the presence of NaOD, the first deuterium was incorporated in ca. 20 h, presumably at position 2 (21). The exchange of the second hydrogen took place much more slowly.

Acknowledgements

We are grateful to Dr. H. Yamamoto, Sumitomo Chemical Co. Ltd., Osaka, Japan, for the ir and nmr spectra of **7***c*, and Dr. W. E. Scott, Hoffmann-La Roche Inc., Nutley, New Jersey, for a generous gift of compounds **7***d* and **7***e*. Also, we thank Dr. D. H. Smith, Stanford University, for recording the AEI MS-9 mass spectra. Finally, the skillful technical assistance of P. Demaree, H. Schären, and D. K. Cho of this Institute is gratefully acknowledged.

1. H. Staudinger and J. Meyer. Helv. Chim. Acta, **2**, 635 (1919).
2. A. W. Johnson. Ylid chemistry. Academic Press, New York. 1966. pp. 226–236.
3. S. Trippet. Organophosphorous chemistry. The Chemical Society, London. Vol. 1. 1970. pp. 209, 210; Vol. 2. 1971. pp. 187–189; Vol. 3. 1972. p. 185; Vol. 4. 1973. p. 203; Vol. 5. 1974. pp. 197, 198.
4. M. Pailer and E. Haslinger. Monatsh. Chem. **101**, 508 (1970).
5. Y. Nomura, Y. Kikuchi, and Y. Takeuchi. Chem. Lett. 575 (1974).
6. Ger. Patent No. 2,504,937 (1975); Chem. Abstr. **84**, 44186d (1976).
7. Y. A. Tota and R. C. Elderfield. J. Org. Chem. **7**, 313 (1942); R. A. Baxter, G. T. Newbold, and F. S. Spring. J. Chem. Soc. 370 (1947).
8. R. H. Cox and A. A. Bothner-By. J. Phys. Chem. **72**, 1646 (1968).
9. S. Inaba, T. Hirohashi, I. Maruyama, T. Izumi, and Y. Yamamoto. Jpn. Patent No. 7,141,315 (1971); Chem. Abstr. **76**, 46224y (1972).
10. L. H. Sternbach, R. I. Fryer, W. Metlesies, E. Reeder, G. Sach, G. Saucy, and A. Stempel. J. Org. Chem. **27**, 3788 (1962).
11. S. C. Bell, T. S. Sulkowski, G. Gochman, and S. C. Childress. J. Org. Chem. **27**, 562 (1962).
12. (*a*) J. H. Bowie, R. G. Cooks, P. F. Donaghue, J. A. Halleday, and H. J. Rodda. Aust. J. Chem. **20**, 2677 (1967); (*b*) J. H. Bowie, R. G. Cooks, S. O. Lawesson, and G. Schroll. Aust. J. Chem. **20**, 1613 (1967).
13. R. M. Dodson and F. Ross. J. Am. Chem. Soc. **72**, 1478 (1950).
14. R. Hodges and M. R. Grimmet. J. Am. Chem. Soc. **21**, 1085 (1968); K. J. Klebe, J. J. van Houte, and J. van Thuijl. Org. Mass Spectrom. **6**, 1363 (1972).
15. L. Birkofer, M. Franz, and G. Schmidtberg. Org. Mass Spectrom. **8**, 347 (1974); G. Cooper and W. J. Irwin. Org. Mass Spectrom. **10**, 885 (1975).
16. J. H. Bowie and T. K. Bradshaw. Aust. J. Chem. **23**, 1431 (1970); B. K. Simons, B. Nussey, and J. H. Bowie. Org. Mass Spectrom. **3**, 925 (1970); T. Blumenthal and J. H. Bowie. Org. Mass Spectrom. **6**, 1083 (1972); G. L. Aldous and J. H. Bowie. Org. Mass Spectrom. **10**, 64 (1975).
17. J. H. Bowie, P. F. Donaghue, H. J. Rodda, and B. K. Simons. Tetrahedron, **24**, 3965 (1968); B. K. Simons, R. K. M. R. Kallury, and J. H. Bowie. Org. Mass Spectrom. **2**, 739 (1969).
18. J. B. Petersen and K. H. Lakowitz. Acta Chem. Scand. **23**, 971 (1969).
19. N. C. Hindlay and T. M. McClymont. Ger. Patent No. 2,233,482 (1973); Chem. Abstr. **78**, 111385j (1973).
20. P. Nuhn and W. Bley. Pharmazie, **22**, 532 (1967); W. Bley, P. Nuhn, and G. Benndorf. Arch. Pharm. **301**, 444 (1968).
21. Y. Takeuchi, H. J. C. Yeh, K. L. Kirk, and L. A. Cohen. J. Org. Chem. **43**, 3565 (1978).

Phase transformation studies on $K_2Cr_2O_7$

MAHADEVA NATARAJAN AND ETALO A. SECCO[1]

Chemistry Department, St. Francis Xavier University, Antigonish, N.S., Canada B2G 1C0

Received June 6, 1979

MAHADEVA NATARAJAN and ETALO A. SECCO. Can. J. Chem. 57, 2703 (1979).

The phase transformations occurring in $K_2Cr_2O_7$ have been examined by differential thermal analysis (DTA), differential scanning calorimetry (DSC), specific heat measurements, electrical conductivity technique, and X-ray diffractometry. The results show that the polymorphic behavior of $K_2Cr_2O_7$ is very sensitive to the thermal and preparative history of the sample.

MAHADEVA NATARAJAN et ETALO A. SECCO. Can. J. Chem. 57, 2703 (1979).

A l'aide des méthodes suivantes: l'analyse thermique différentielle (DTA) la calorimétrie par balayage différentiel (DSC) les mesures de chaleur spécifique, la technique de conductivité électrique et la diffraction par rayons X, on a examiné les transformations de phase se produisant dans le $K_2Cr_2O_7$. Les résultats montrent que le comportement polymorphique du $K_2Cr_2O_7$ est très sensible au mode de préparation de l'échantillon et aux conditions thermiques utilisées.

[Traduit par le journal]

Introduction

Polymorphism in $K_2Cr_2O_7$ has been the subject of a number of studies (1–5). The room temperature (RT) stable structure of $K_2Cr_2O_7$ is triclinic (6) space group $P\bar{1}$ with cell constants $a = 13.376$ Å, $b = 7.376$ Å, $c = 7.445$ Å, $\alpha = 90.75°$, $\beta = 96.21°$, and $\gamma = 97.96°$.[2]

The triclinic form A transforms at ~270°C to a monoclinic form C, space group $P2_1/n$; the cell parameters reported (4) at 300°C are $a = 13.45$ Å, $b = 7.52$ Å, $c = 7.55$ Å, and $\beta = 91.68°$. Below 240°C monoclinic C transforms to a metastable monoclinic form B, probable space group $C2/c$, with lattice constants $a = 13.06$ Å, $b = 7.37$ Å, $c = 7.43$ Å, and $\beta = 91.85°$. The B → C transition was noted to occur at 255°C. However, the existence of a distinct monoclinic B phase in $K_2Cr_2O_7$ is questioned (5).

Our interest in phase transformation phenomena (7, 8) prompted us to investigate the polymorphic changes occurring in $K_2Cr_2O_7$. This paper presents the results of such an investigation using differential thermal analysis, differential scanning calorimetry, X-ray diffractometry, electrical conductivity, and infrared techniques.

Experimental

Certified ACS potassium dichromate (Fisher Scientific, ≥99.95% purity) was used in this work. The stock material was passed through a standard sieve (0.297 mm mesh) to obtain samples of uniform particle size for this study.

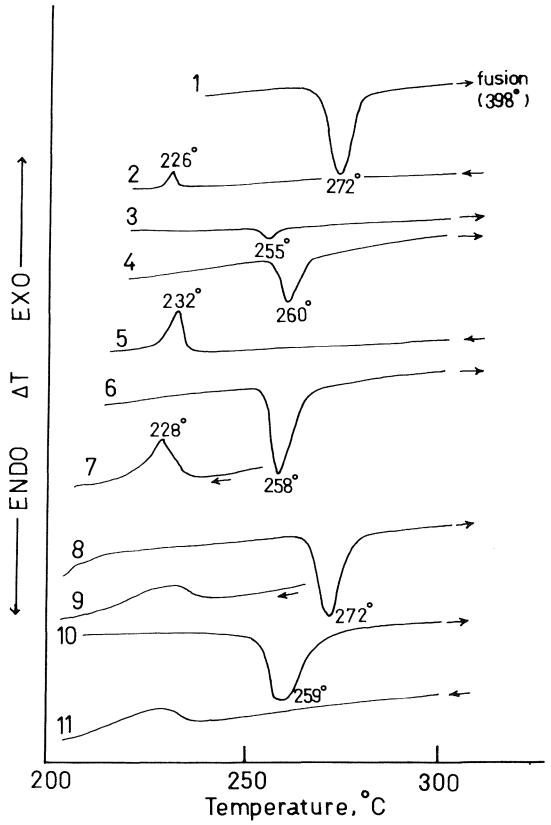

FIG. 1. DTA traces; *1*, stock triclinic $K_2Cr_2O_7$ in heat mode to fusion; *2*, fused product in cool mode; *3*, residue from *2* in heat mode; *4*, product from *3* after remaining at RT for 2 h in heat mode; *5*, product from *4* in cool mode; *6*, after remaining at RT for 48 h in heat mode; *7*, product from *6* in cool mode; *8*, stock triclinic $K_2Cr_2O_7$ in heat mode to 350°C below fusion; *9*, product in cool mode; *10*, residue from *9* in heat mode; *11*, product from *10* in cool mode.

[1]To whom all correspondence should be addressed.

[2]The cell constants quoted in the convention adopted in ref. 1 to facilitate comparisons.

0008-4042/79/202703-04$01.00/0

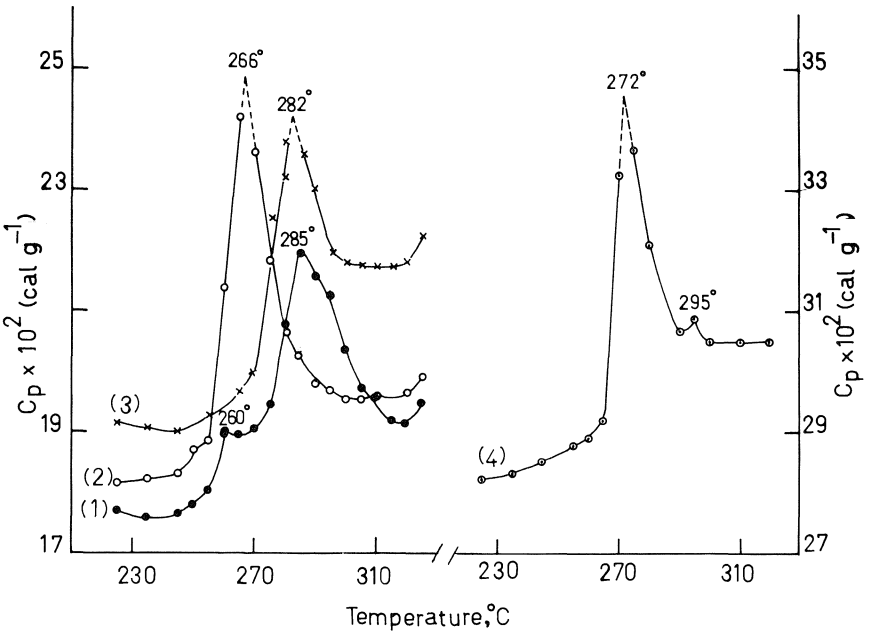

FIG. 2. Specific heat plots: *1*, stock triclinic $K_2Cr_2O_7$ fused and cooled to RT; *2*, reheat residue from *1*; *3*, $K_2Cr_2O_7$ precipitated slowly from aqueous solution; *4*, $K_2Cr_2O_7$ by heating aqueous solution to dryness.

Differential thermal analysis (DTA) and differential scanning calorimetric (DSC) traces were recorded on a duPont Model 990 Thermal Analyzer module with the appropriate attachments (9). Al_2O_3 was used as the reference material and the heating rate was 10° min^{-1}. The transition enthalpies were evaluated using the enthalpy of fusion for Sn as standard (ΔH_f = 14.14 mcal mg^{-1} at 231.9°C). Specific heat measurement traces with the DSC attachment used sapphire crystal as calibration standard.

X-ray diffraction patterns were recorded using a Norelco diffractometer, calibrated with Si standard, using CuK_α radiation (λ = 1.5418 Å) as previously described (10).

The procedure for the electrical conductivity measurements on compressed polycrystalline discs using General Radio impedance bridge GR-1608A has already been described (7, 11). Heating rate was 20° h^{-1}.

The infrared spectra of samples were recorded in the 4000–250 cm^{-1} region on Perkin-Elmer Model 180 spectrophotometer using the standard disc technique with KBr or KCl as matrix.

Results and Discussion

DTA traces are presented in Fig. 1. Curve *1* represents the heat mode for stock triclinic $K_2Cr_2O_7$ undergoing a sharp transition to stable monoclinic structure at 272°C; the enthalpy for this A → C transition was determined to be 385 ± 10 cal mol^{-1}. Curve *2* represents the cool mode of the fused product from curve *1*; the weak exotherm at 226°C assigned to the C → B transition corresponds to an enthalpy of 30 ± 5 cal mol^{-1}. Immediate reheating of this residue, curve *3*, yields a weak endotherm at 255°C with an enthalpy of 30 ± 5 cal mol^{-1}. After remaining at RT for 2 h, the sample gave curve *4* in the heat mode with the endotherm at 260°C and curve *5* in the cool mode with the exotherm at 232°C. Curves *6* and *7* represent heat and cool modes of the sample, respectively, after remaining at RT for 48 h — standing at RT sharpens the thermal effects and shifts the peak temperatures.

Curve *8* represents stock triclinic $K_2Cr_2O_7$ heated to 350°C, identical thermal effect as curve *1*. Curve *9* represents the cool mode of the product from curve *8* with an exotherm extending over the temperature range 202–238°C; the broad exotherm suggests a slow C → B transformation rate. Reheating the residue, curve *10*, produces the endotherm at 259°C and re-cooling the sample yields curve *11*; further heat–cool cycles do not alter significantly the DTA traces of this sample.

The transition enthalpy at 270°C for well-powdered (ground in mortar) stock triclinic $K_2Cr_2O_7$ was determined to be 180 ± 10 cal mol^{-1} in contrast to 385 cal mol^{-1} for "as bottled" sample; the enthalpy of this sample attains the value of 380 cal mol^{-1} after repeated heat–cool cycles. The lower enthalpy indicates that a partial conversion of form A to form C had occurred on grinding. Since the three forms of $K_2Cr_2O_7$ have been correlated (1) with different layer arrangements of the basic Cr_2O_7 unit it is most probable that the A → C transition, occurring via a displacive mechanism is effected by the grinding shear energy.

The specific heat curves *1–4*, Fig. 2, clearly show

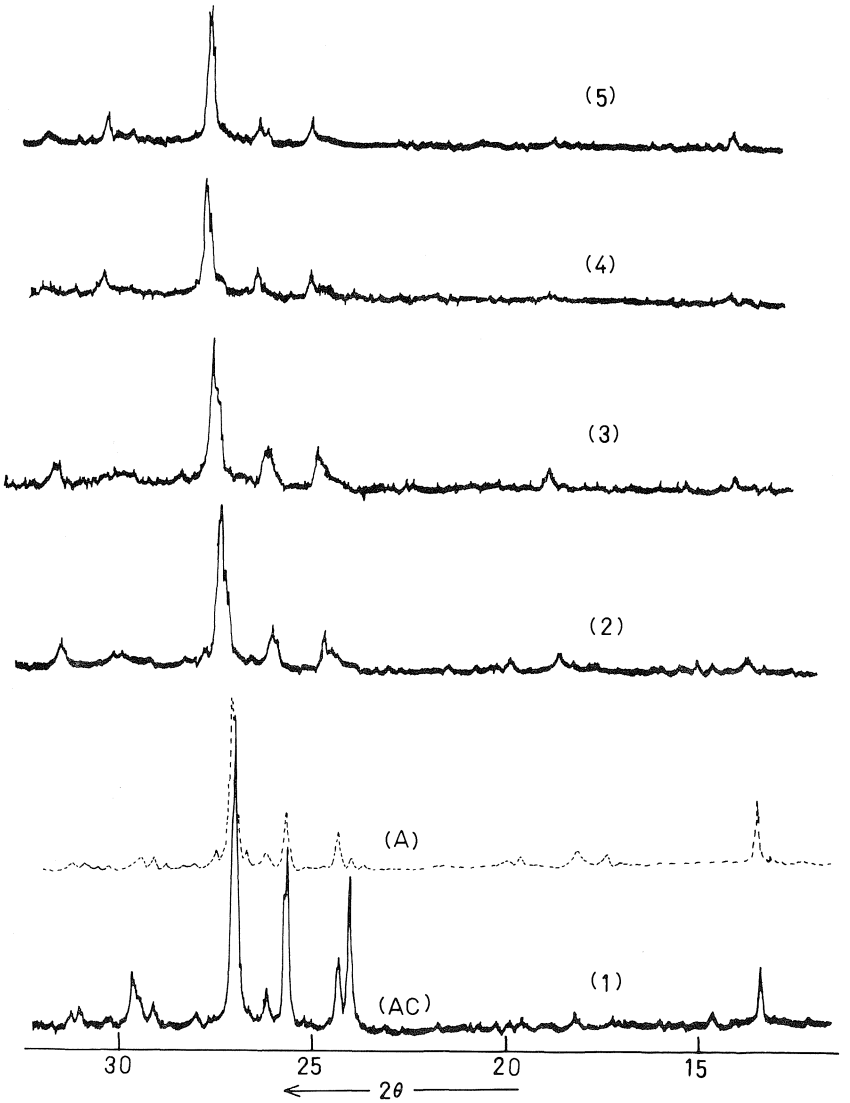

FIG. 3. X-ray diffractograms at RT: A, stock triclinic $K_2Cr_2O_7$; AC, well powdered stock $K_2Cr_2O_7$; *1*, identical to AC; *2*, after heating *1* to 300°C; *3*, after remaining 3 h at RT; *4*, after reheating *3* to 300°C; *5*, after remaining 17 h at RT.

distinct features of the different samples.[3] Curve *1*, stock sample fused and cooled to RT, exhibits a weak anomaly at 260 ± 2°C interpreted as a small fraction of B transforming to C with an intense anomaly at 285°C assigned to triclinic A conversion to monoclinic C. Reheating this cooled sample revealed a single sharp anomaly at 266 ± 2°C, curve *2*, interpreted as the pure A → C transition. The specific heat behavior of $K_2Cr_2O_7$ precipitated slowly from aqueous solution, curve *3*, produces a single sharp anomaly at 282°C. On the other hand, $K_2Cr_2O_7$ obtained by gently heating an aqueous solution to dryness, curve *4*, reveals an intense anomaly at 272 ± 2°C along with a very weak one at 295°C.

The X-ray diffractograms of $K_2Cr_2O_7$ exposed to specific anneal conditions are presented in Fig. 3. The stock sieved sample produces pattern A, with peaks characteristic of triclinic A, whereas the well-powdered stock sample gives pattern AC, with peaks characteristic of both triclinic A and monoclinic C forms. The sequence of X-ray diffractograms, curves *1–5*, shows the progress of the characteristic peaks as a function of anneal and storage variables.

[3]Comment added in proof: The additional contribution to the specific heat of sample 4, Fig. 2, relative to samples 1–3 could originate with an ionic complex, e.g. $(CrO_4 \cdot CrO_3)^{2-}$?

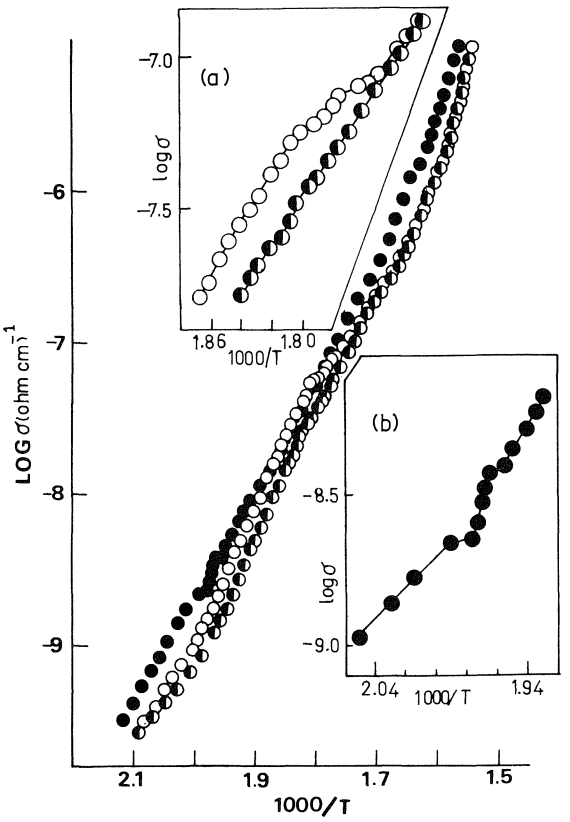

FIG. 4. Logarithm of conductivity, σ, versus $10^3/T$ K plots at reduced pressure, $\sim 10^{-2}$ Torr: ○, stock well-powdered $K_2Cr_2O_7$ in heat mode; ●, heated product in cool mode; ◐, quenched $K_2Cr_2O_7$ in heat mode.

Figure 4 presents the conductivity versus temperature plots for $K_2Cr_2O_7$. The conductivity for stock well-powdered $K_2Cr_2O_7$ (unfilled circles) in the heat mode shows a break from linearity in the temperature region 279–288°C, inset (*a*). The conductivity behavior in the cool mode (filled circles) shows a discontinuity over the temperature range 240–230°C, inset (*b*), with higher conductivity values. The conductivity data for a quenched sample in the heat mode (half-filled circles) are lower for lower temperature region but merge with the stock sample data at elevated temperatures — a barely discernible break occurs in the region 276–282°C, inset (*a*). All the conductivity data are reproducible well within the limits of the bridge sensitivity and therefore, the discontinuities are to be viewed with a high degree of confidence.

Since the infrared spectra of all samples were identical no additional structural correlation was evident.

DTA traces obtained on single crystals of $K_2Cr_2O_7$, grown by slow evaporation (10 days) of aqueous solutions, exhibited non-reproducible extraneous thermal effects in the heat mode, including an exotherm. The extraneous effects, most likely due to lattice strain energy, were absent after the single crystal had been powdered.

In summary, this study shows that the polymorphic behavior in $K_2Cr_2O_7$ is not straightforward and very sensitive to the thermal and preparative history of the sample as evident by the results from DTA, calorimetry, specific heat, electrical conductivity, and X-ray diffraction. The phase relationships with transition temperature ranges and transition ΔH values are presented below:

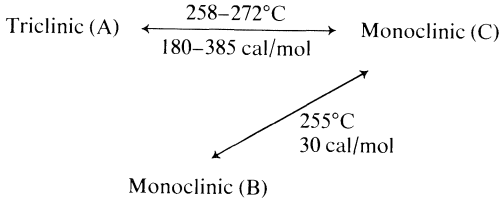

The coexistence of mixed A and C phases produces a range in transition temperatures and ΔH values. Although monoclinic B exists at RT it does not transform to RT stable triclinic directly but only via monoclinic C. The low transition ΔH values observed for $K_2Cr_2O_7$ relative to Na_2SO_4 (8) suggest that the $K_2Cr_2O_7$ phases are energetically quite similar.

Acknowledgments

Grateful acknowledgment is made to the Natural Sciences and Engineering Research Council of Canada for financial support of this research program.

1. I. D. BROWN and C. CALVO. J. Solid State Chem. **1**, 173 (1970).
2. YU. I. VESNIN and L. A. KHRIPIN. Russ. J. Inorg. Chem. **11**, 1188 (1966).
3. C. W. F. T. PISTORIUS. Z. Phys. Chem. **35**, 109 (1962).
4. J. JAFFRAY and A. LABARY. Compt. Rend. **242**, 1421 (1956).
5. U. KLEMENT and G. M. SCHWAB. Z. Kristallogr. **114**, 170 (1960).
6. J. K. BRANDON and I. D. BROWN. Can. J. Chem. **46**, 933 (1968).
7. M. NATARAJAN and E. A. SECCO. Can. J. Chem. **52**, 712 (1974).
8. R. MACL. MURRAY and E. A. SECCO. Can. J. Chem. **56**, 2616 (1978).
9. K. RAJESHWAR and E. A. SECCO. Can. J. Chem. **54**, 2509 (1976).
10. E. A. SECCO. Can. J. Chem. **42**, 2143 (1964).
11. M. NATARAJAN and E. A. SECCO. Can. J. Chem. **53**, 1542 (1975).

Factor analysis as a complement to band resolution techniques. VI. Complex formation between pentachlorophenol-OD and acetone

J. KORPPI-TOMMOLA AND H. F. SHURVELL

Department of Chemistry, Queen's University, Kingston, Ont., Canada K7L 3N6

Received May 4, 1979

J. KORPPI-TOMMOLA and H. F. SHURVELL. Can. J. Chem. 57, 2707 (1979).

Complex formation between pentachlorophenol-OD (PCP-OD) and acetone and acetone-d_6 in CCl_4 solution has been studied. Digitized infrared spectra in the O—D stretching region ν(OD) of PCP-OD and the C—O stretching region ν(CO) of acetone have been recorded from solutions of various concentrations. The present results are compared with previous work on complex formation between PCP and the same acceptor molecules.

In the ν(OD) region, factor analysis (principal component analysis) and a concentration study of the areas of the resolved band components suggest that two (1:1) complexes occur in solution. The equilibrium constant obtained for one of the complexes shows an isotope effect due to deuteration of the proton donor. In the ν(CO) region, only one band due to complexed species was resolved. Equilibrium constants calculated using the results from the ν(OD) and ν(CO) regions are in good agreement with each other.

J. KORPPI-TOMMOLA et H. F. SHURVELL. Can. J. Chem. 57, 2707 (1979).

On a étudié, en solution dans le CCl_4, la formation de complexe entre le pentachlorophénol-OD (PCP-OD) et l'acétone, et l'acétone-d_6. A partir de solutions à différentes concentrations, on a enregistré les spectres numériques ir dans la région d'élongation du O—D ν(OD) du PCP-OD et la région d'élongation du C—O ν(CO) de l'acétone. On a comparé ces résultats à ceux de travaux antérieurs sur la formation de complexes entre le PCP et les mêmes molécules "accepteurs".

Dans la région ν(OD), le facteur d'analyse (analyse du constituant principal) et l'étude de concentration des surfaces des bandes résolues des constituants suggérent que deux complexes (1:1) se forment en solution. La constante d'équilibre obtenue pour l'un de ces complexes montre un effet isotopique due à la deutération du donneur de proton. Dans la région ν(CO) seule une bande due à l'espèce complexe a été résolue. Les constantes d'équilibre calculées en utilisant les résultats obtenus à partir des régions de ν(OD) et ν(CO) sont en parfait accord avec l'une et l'autre.

[Traduit par le journal]

Introduction

Self-association of alcohols and phenols and complex formation with other proton acceptors in solution have been studied extensively by infrared spectroscopy. In earlier work (1, 2), equilibrium constants have been obtained from the concentration dependence of the monomer hydroxyl stretching band only, while the band due to association or complex formation was usually ignored. The application of factor analysis (principal component analysis) to digitized infrared spectra leads to the determination of the number of absorbing components in a complex band (3). Subsequent band resolution and the calculation of band areas and molar absorption coefficients allows various models of complex formation to be tested and equilibrium constants to be calculated (3, 4). Additional quantities such as wavenumber maxima and half-widths of bands assigned to complexed species can be obtained. These quantities, together with the equilibrium constants, provide a qualitative as well as quantitative picture of association or complex formation in solution and utilize fully the data recorded in a given spectral region.

Fundamental bands associated with the vibrations of the functional groups involved in hydrogen bonding are subject to both frequency and intensity changes in the vibrational spectrum. In some cases, direct study of the hydrogen-bond stretching modes is possible (5). Several matrix-isolation infrared self-association studies have shown that hydrogen bonding manifests itself in all three vibrational modes of the hydroxyl group in alcohols (6, 7). When complex formation occurs between alcohols or phenols and ketones, both the ν(OH) band and the ν(CO) band show concentration dependencies (4). In principle, any band in the vibrational spectrum, which undergoes changes due to hydrogen bonding can be used to calculate the equilibrium constants. One purpose of the present study was to compare the calculated parameters of the bands due to complexed species and the equilibrium constants obtained from studies of two separate regions of the infrared spectrum.

In our recent study of complex formation between PCP and acetone in CCl_4 solution (4), conflicting results were obtained from factor analysis and band

0008-4042/79/202707-07$01.00/0

resolution. In the ν(OH) region, factor analysis indicated three absorbing components, whereas the band resolution procedure gave a better fit when four components were used. It was therefore of interest to see if this conflict would also arise in the ν(OD) region of the spectra of PCP-OD/acetone mixtures.

We have recorded infrared spectra of pentachlorophenol-OD (PCP-OD) and acetone and PCP-OD and acetone-d_6 in CCl_4 solution in the O—D stretching region of PCP-OD and in the carbonyl stretching region of acetone. The spectra were digitized and factor analysis and band resolution were carried out. The molar absorption coefficients were calculated for each set of solutions and equilibrium constants were then calculated. The results are compared to those obtained earlier for normal PCP/acetone and acetone-d_6 complexes (4) and to those reported previously for phenol and phenol-OD/acetone complexes (8–10).

Experimental

Deuterated pentachlorophenol (PCP-OD) was synthesized by shaking a warm PCP/carbon tetrachloride solution with D_2O and re-crystallizing the deuterated phenol, which precipitates on cooling. The procedure was repeated several times until deuteration was better than 90%. Samples were contained in Beckman- R.I.I.C. variable pathlength cells and the spectra were recorded on a Perkin-Elmer 180 spectrometer. Pathlengths were determined using the fringe method from 0.05 to 0.2 mm and linearity of micrometer readings with pathlength was assumed over the range used in this work. When recording the spectra in the ν(OD) region the spectrometer was flushed with nitrogen gas to minimize absorption by carbon dioxide. The same solutions were used in both ν(OD) and ν(CO) regions, with the pathlengths adjusted accordingly. Concentrations were corrected for the thermal expansion of CCl_4 due to heating of the sample by the infrared beam of the spectrometer.

A spectrum of PCP-OD in CCl_4 solution was recorded and areas of the ν(OH) and ν(OD) bands were measured. These areas were used to estimate the isotopic concentration ratio k, given by:

$$[1] \qquad k = \frac{C_{OD}}{C_{OH} + C_{OD}} = \frac{A_{OD}}{A_{OD} + (\varepsilon_{OD}/\varepsilon_{OH})A_{OH}}$$

where C_{OD} and C_{OH} are the concentrations of PCP-OD and PCP and A_{OD} and A_{OH} are the areas of the ν(OD) and ν(OH) bands respectively. The observed spectra were digitized at 2.5 cm^{-1} intervals in the ν(OD) region giving 281 data points, while in the ν(CO) region the digitization inverval was 1.0 cm^{-1} giving 151 data points per spectrum. The digitizing procedure and the further computational processing of the data are reported in detail in ref. 4. The details of the solutions and the pathlengths are not given here, but these are available from the authors on request.

PCP is unusual in that it does not undergo self association in CCl_4 solution (11). Thus no complication of the spectra in the OD stretching region is expected from self association and any absorption in addition to the free ν(OD) band must be due to formation of complexes.

The possibility of interference from water in the phenol, or the solvents has been considered. Independent experiments indicate that small added amounts of moisture do not significantly perturb the OH stretching band. Nevertheless, as a precaution, all solvents were stored over molecular sieves and all manipulations, except weighing, were carried out in a dry box.

Chemical Equilibrium

Our previous results in the ν(OH) region of PCP (4) and the present results in the ν(OD) region of PCP-OD suggest that there are two 1:1 pentachlorophenol–acetone complexes in CCl_4 solution. In the PCP-OD case, the solutions always contain some of the non-deuterated phenol and its complexes. The calculation of the equilibrium constants accordingly becomes somewhat complicated. The total initial concentration of donor OH or OD groups (C_d^T) is distributed among six species at equilibrium as follows:

$$[2] \qquad C_d^T = C_d^{OH} + C_d^{OD} + \sum_{i=1}^{4} C_{11}{}^i$$

where C_d^{OH} and C_d^{OD} are the equilibrium concentrations of uncomplexed donor species PCP and PCP-OD and $C_{11}{}^i$ is the concentration of the ith 1:1 complex (either a PCP-OD or a PCP complex). Using the Beer–Lambert law:

$$[3] \qquad A = \varepsilon C l$$

where A = absorbance, ε = molar absorption coefficient, and l = pathlength. We can rewrite eq. [2] as:

$$[4] \qquad C_d^T = \frac{A_{OD}}{\varepsilon_{OD} l} + \frac{A_{OH}}{\varepsilon_{OH} l} + \sum_{i=1}^{4} \frac{A_i}{\varepsilon_i l}$$

where A_i and ε_i are the absorbance and molar absorption coefficients respectively of the ith 1:1 complex (either a PCP-OD or a PCP complex).

The concentration (C_a) of the uncomplexed acceptor species (acetone) at equilibrium is given by:

$$[5] \qquad C_a = C_a^T - \sum_{i=1}^{4} C_{11}{}^i$$

and from eq. [2] we obtain:

$$[6] \qquad C_a = C_a^T - C_d^T + C_d^{OH} + C_d^{OD}$$

Using the isotopic concentration ratio k from eq. [1] we can write:

$$[7] \qquad C_a = C_a^T - C_d^T + C_d^{OD}/k$$

Again using the Beer–Lambert law eq. [7] becomes:

$$[8] \qquad C_a = C_a^T - C_d^T + A_{OD}/\varepsilon_{OD} k l$$

For the equilibrium between PCP-OD and acetone we can write:

$$[9] \qquad K_{11}{}^i = C_{11}{}^i / C_d^{OD} C_a$$

where i = 1 or 2 for the first or second 1:1 complex respectively.

Finally, eq. [9] can be written as

$$[10] \qquad K_{11}{}^i = A_i \varepsilon_{OD} / A_{OD} \varepsilon_i C_a$$

In the ν(CO) region, the calculations were made in the same way, except that only one complex band was assumed to occur in solution and the monomeric donor concentration (C_d^{OD}) was considered as an unknown in eq. [6] instead of the monomeric acceptor concentration. For comparison, 1:1 equilibrium constants were also calculated using the areas of the monomer ν(OD) band.

Results and Discussion

Typical concentration behaviour of the ν(OD) band is seen in Fig. 1. For a fixed PCP-OD initial concentration the sharp monomer band at 2608 cm^{-1} decreases in intensity relative to the broad complex band on the lower frequency side as the acetone concentration is increased. For the PCP-OD/acetone complex band shown in Fig. 1 there are no interfering ν(CH) bands and the concentration dependence is similar to that of the PCP/acetone complex bands in ref. 4. On the other hand, it is seen in Fig. 2 that the concentration behaviour in the ν(CO) region is reversed. The monomer band at 1718 cm^{-1} increases in intensity relative to the complex band which appears as a shoulder on the lower frequency side as the acetone concentration is increased. This kind of behaviour is expected, since at fixed PCP-OD concentration a decreasing proportion of acetone molecules forms complexes as the acetone concentration is increased.

Factor Analysis

In the ν(OD) region, factor analysis (principal component analysis) indicates three absorbing components for both sets of solutions studied (i.e. for PCP-OD/acetone and PCP-OD/acetone-d_6 in CCl_4). Three absorbing components were also found previously for non-deuterated PCP/acetone solutions in the ν(OH) region. To illustrate the method, the results of the factor analysis are given here for the PCP-OD/acetone system. Similar results were obtained for the PCP-OD/acetone-d_6 system.

The number of absorbing components NC in a complex band is taken as the number of statistically non-zero eigenvalues of the matrix $\mathbf{Q} = \mathbf{A}^T\mathbf{A}$ (3), where $\mathbf{A}$ is the absorbance matrix for all solutions studied and $\mathbf{A}^T$ is its transpose. Details of four statistical tests to determine the number of non-zero eigenvalues of $\mathbf{Q}$ are given in ref. 3.

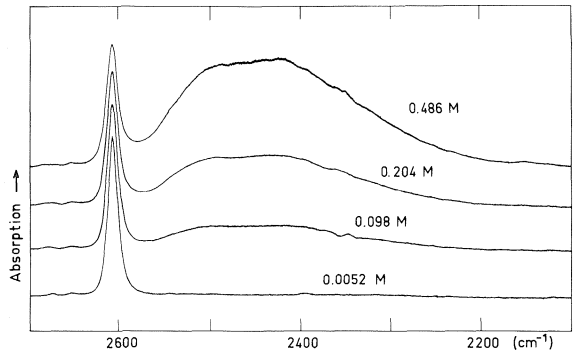

FIG. 1. Infrared spectra in the ν(OD) region of various solutions of PCP-OD/acetone in CCl_4. Acetone concentrations are shown on the figure. The PCP-OD concentration was 0.045 *M*.

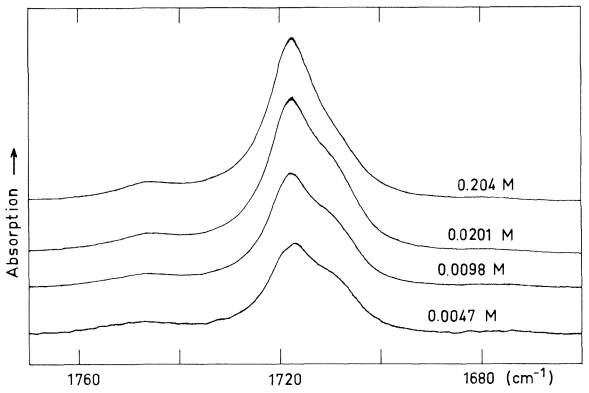

FIG. 2. Infrared spectra in the ν(CO) region of various solutions of PCP-OD/acetone in CCl_4. Acetone concentrations are shown on the figure. The PCP-OD concentration was 0.045 *M*.

The matrix $\mathbf{A}$ is an NW by NS matrix, where NW is the number of digitized points in the spectrum and NS is the number of solutions studied. The results of two statistical tests are given in Table 1. When the residual standard deviation (S_k) is calculated using two eigenvalues, then S_2 is greater than the experimental error in the absorbance measurements (DA). On the other hand, S_3 is less than DA. This indicates that NC = 3. There is also a leveling off of the eigenvalues below the third entry. The square root of the estimated variance criterion also indicates that NC is three, since the variance of the fourth eigenvalue is more than three times larger than the eigenvalue itself.

Table 2 summarizes the results of a regeneration of the absorbance matrix using m eigenvectors ($m = 1, 2, \ldots, NS$) for DA = 0.01. The smallest number of eigenvectors to give a satisfactory fit with the experimental A is equal to NC. When three eigenvectors are used to regenerate the absorbance matrix, only 72 points out of 2529 deviate by more

TABLE 1. Factor analysis of nine CCl_4 solutions of PCP-OD and acetone in the ν(OD) region using the residual standard deviation and square root of eigenvalue variance criteria (3)

No. of solutions	Eigenvalue	Residual standard deviation[a]	Square root of estimated variance[a]
1	232.9919	0.11463	0.13626
2	32.7410	0.01218	0.07634
3	0.3251	0.00436	0.13828
4	0.0218	0.00321	0.06484
5	0.0109	0.00243	0.07318
6	0.0053	0.00195	0.07142
7	0.0043	0.00144	0.05640
8	0.0032	0.00087	0.05607
9	0.0019	—	0.05800

[a]Experimental absorbance error DA = 0.01.

TABLE 2. Factor analysis of nine CCl_4 solutions of PCP-OD and acetone in the ν(OD) region. Comparison of the observed and regenerated absorbance matrix[a] and the χ^2 criterion (3)

No. of eigenvalues	Distribution of misfit (number of points) for number of standard deviations						χ_m^2	Expectation value of χ_m^2
	0–1	1–2	2–3	3–4	4–5	> 5		
1	487	435	366	229	163	849	331136	2240
2	1695	534	258	34	5	3	3726	1953
3	2444	72	9	3	1	0	475	1663
4	2489	29	7	4	0	0	256	1385
5	2506	19	4	0	0	0	147	1104
6	2512	15	2	0	0	0	94	825
7	2524	4	1	0	0	0	51	548
8	2529	0	0	0	0	0	19	273
9	2529	0	0	0	0	0	0	0

[a]Experimental absorbance error DA = 0.01.

than two standard deviations from the experimental values. Adding the fourth eigenvector does not markedly improve the fit. Thus, it is concluded that NC = 3. A final criterion is the calculation of χ_m^2 using from one to nine eigenvectors of **Q** and comparing these with the expectation values, given by $(NW - m)(NS - m)$. It is seen that χ_3^2 is smaller than the corresponding expectation value, while χ_2^2 is larger, which indicates that NC = 3.

In the ν(CO) region, factor analysis indicates again three absorbing components. However, the interpretation here is different. There are two monomer bands and only one complex band in the spectra, as indicated by the concentration study. It can be seen in Fig. 2 that there is a broad shoulder on the high frequency side of the main ν(CO) peak. The intensity of this shoulder increases with increasing acetone concentration. In acetone-d_6 a Fermi doublet (12, 13) is observed, while the complex band is found as an asymmetry on the lower frequency side. These features are illustrated in Fig. 3, where CALCOMP plots of the various resolved components are shown.

Band Contour Resolution

A band resolution programme (PC 116) originally written by Jones *et al.* (14) was modified to perform the calculations in absorbance units. Baseline subtraction and band area computation subroutines have been added to the program. Three Gauchy–Gauss product functions were used to reproduce the experimental spectrum in the ν(OD) region. Plots of typical resolved spectra are shown in Fig. 4.

When the number of components NC is not known, components are added sequentially to an initial trial fit, at the position of greatest difference between observed and calculated contours, until an acceptable fit is obtained. The criterion of an

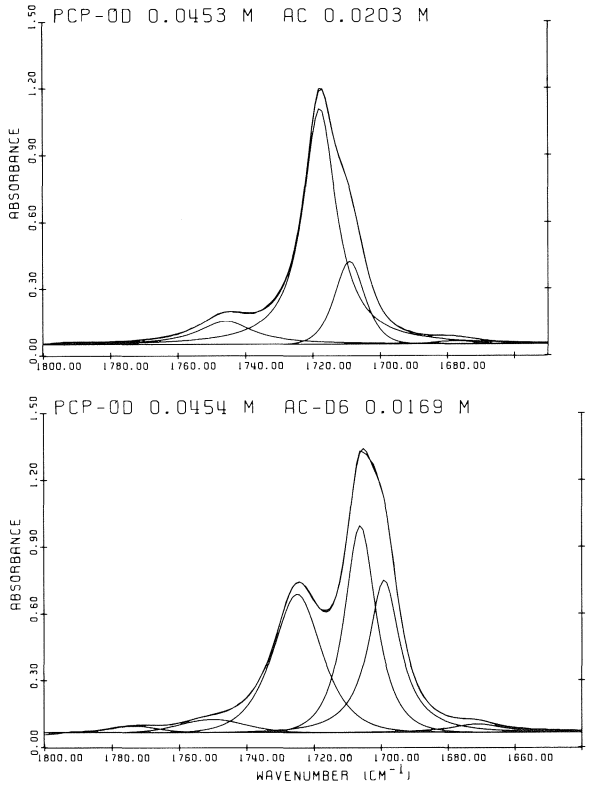

FIG. 3. Resolution of a typical ν(CO) band of PCP-OD/acetone (upper) and of PCP-OD/acetone-d_6 in CCl_4 (lower).

acceptable fit is found from the sum of the squares of the differences between experimental and computed absorbance values at each of the NW points in the digitized spectrum. When this sum is approximately equal to $S_A^2 \cdot NW$ (where S_A is the standard deviation in the absorbance measurements) then the fit is good. Addition of further components would improve the fit beyond experimental error. For the

band fitting program, it is assumed that all bands are symmetric and in the present case it is also assumed that only the OD stretching modes of the species present contribute to the overall contour. However, in the presence of extraneous absorption, due perhaps to weak overtone or combination bands, or an asymmetry in one or more of the component bands, which could arise from the presence of "hot" bands,[1] the criterion for a good fit may not be satisfied by only NC components. In such cases additional components will improve the fit but may not be reasonable from the point of view of the chemistry of the system under study. The OD stretching band of solutions of PCP-OD with acetone in CCl_4 provides an example of this problem. The three band fits shown in Fig. 4 give a sum of squares of errors greater than $S^2 \cdot NW$, whereas addition of a fourth component gives an excellent fit with the experimental spectrum, as may be seen in Fig. 5. For a four-band fit, the areas of the three resolved bands due to complexed species each show a linear relationship to the area of the monomer ν(OD) band. This result requires that three (1:1) complexes be present in solution. However, we reject this conclusion for several reasons. First, factor analysis clearly indicates that only three components contribute to the absorption in the ν(OD) region. Secondly, it was not possible to obtain a consistent set of molar absorption coefficients for the four-component model and finally, it is difficult to find chemically reasonable structures for three 1:1 complexes. We therefore believe that the three-component fit for the ν(OD) band is correct.

Average wavenumber maxima and half-widths of the resolved bands of the three-band fit are given in Table 3. The standard deviations indicate that the monomer ν(OD) bands have an excellent wavenumber position and half-width consistency.

Four- and six-component fits were carried out in the ν(CO) regions of acetone and acetone-d_6, respectively. These fits are illustrated in Fig. 3. However, only the three main components, as suggested by factor analysis, were used to calculate the equilibrium constants. In the ν(CO) region the wavenumber maxima and half-width consistency of the resolved band components are also excellent, as is seen in Table 3.

To illustrate the frequency changes typical of the modes involved in hydrogen bonding, we have tabulated Δν values in Table 4 ($\Delta\nu = \nu_0 - \nu_i$, where ν_0 and ν_i are the wavenumbers of bands due to the free and the *i*th complexed species, respectively).

[1] "Hot" bands arise from transitions for which the lower state is not the ground state.

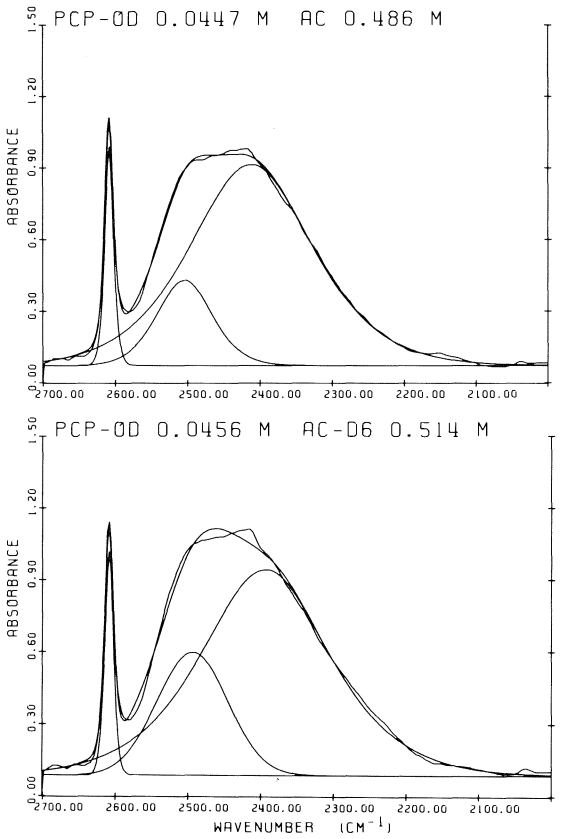

FIG. 4. Resolution using a three-component fit of a typical ν(OD) band of PCP-OD/acetone in CCl_4 (upper) and of PCP-OD/acetone-d_6 (lower).

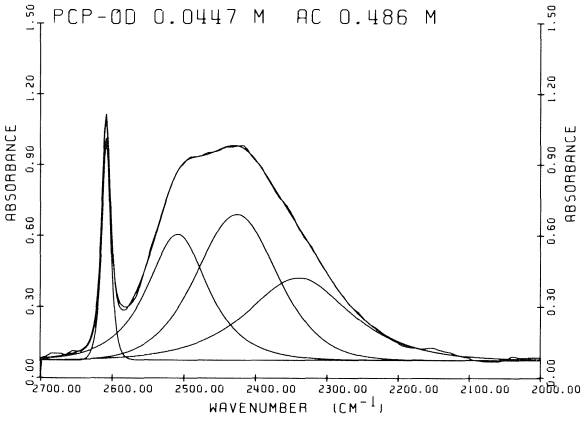

FIG. 5. Resolution using a four component fit of a typical ν(OD) band of PCP-OD/acetone in CCl_4.

Relative wavenumber perturbations $\Delta\nu/\nu_0$ and half-widths in each complex band studied are also included in Table 4. Our Δν values for the two (1:1) complexes in the PCP/acetone and PCP-OD/acetone systems in the hydroxyl stretching region are higher

TABLE 3. Computed average parameters for the ν(OD) and ν(CO) band components[a]

(*a*) PCP-OD . . . Ac (7 solutions)

	Component	ν (cm^{-1})	$\Delta\nu_{1/2}$ (cm^{-1})	ε (mol^{-1} m^2)
ν(OD)	Monomer	2607.8(0.1)	13.6(0.2)	376(20)
	(1:1)[1] complex	2508 (8)	96 (8)	1134(950)
	(1:1)[2] complex	2409 (12)	202 (17)	1860(280)
ν(CO)	Combination	1746 (1)	20.3(1.7)	656(600)
	Monomer	1717.5(0.4)	11.7(0.1)	744(180)
	(1:1) complex	1709.5(1.1)	11.2(1.1)	599(500)

(*b*) PCP-OD . . . Ac-d_6 (5 solutions)

	Component	ν (cm^{-1})	$\Delta\nu_{1/2}$ (cm^{-1})	ε (mol^{-1} m^2)
ν(OD)	Monomer	2607.8(0.2)	14.0(0.2)	349(21)
	(1:1)[1] complex	2504 (15)	109 (11)	1249(260)
	(1:1)[2] complex	2401 (18)	195 (35)	1861(110)
ν(CO)	Monomer, F.R. comp.	1724.6(0.1)	17.1(0.4)	1035(420)
	Monomer, F.R. comp.	1706.1(0.1)	10.9(0.3)	708(270)
	(1:1) complex	1699.2(0.4)	11.3(0.6)	574(130)

[a]The numbers given in parentheses are standard deviations. F.R. refers to Fermi resonance.

TABLE 4. Comparison of the Δν values (cm^{-1}) and the relative frequency perturbations $\Delta\nu/\nu_0$ (%) for PCP acetone complexes[a] in CCl_4 solution

	ν(OH) or ν(OD) region				ν(CO) region (1:1) complex	
	(1:1)[1] complex		(1:1)[2] complex			
Complex	Δν	$\Delta\nu/\nu_0$	Δν	$\Delta\nu/\nu_0$	Δν	$\Delta\nu/\nu_0$
PCP . . . Ac[b]	168	4.77	324	9.19	7.2	0.42
PCP . . . Ac-d_6[b]	172	4.88	326	9.25	6.4	0.38
PCP-OD . . . Ac	100	3.83	199	7.63	8.0	0.47
PCP-OD . . . Ac-d_6	104	3.99	207	7.94	6.9	0.40

[a]The notation (1:1)[1] and (1:1)[2] is that used in ref. 4 and refers to the two different (1:1) complexes.
[b]These results are from ref. 4. The frequency of the monomer band is ν_0.

than those reported for phenol/acetone (135 and 235 cm^{-1}) and phenol-OD/acetone (90 and 160 cm^{-1}) respectively (9). Larger Δν values in PCP complexes could be interpreted as an indication of stronger complexing of acetone with the chlorinated proton donor.

The isotopic frequency ratio ν_{OH}/ν_{OD} for the monomer band of PCP is 1.350, while for the bands due to complexes, ν_{OH}/ν_{OD} is ~1.335. Using eq. [3] from p. 20 of ref. 7, it appears that for PCP/acetone complexes, O—H···O bonding is slightly stronger than O—D···O bonding. This result is independent of the deuteration of acetone. In the ν(CO) region the Δν values are larger for acetone/PCP complexes than for acetone-d_6/PCP complexes, independent of PCP deuteration. The values of Δν are compared in Table 4.

The relative frequency perturbation ($\Delta\nu/\nu_0$) in the ν(OH) region seems to be higher than that in the ν(OD) region. A similar result has been reported previously for some phenol complexes (15). From Tables 3 and 4 it can be seen that for the bands in the ν(CO) region, changes in half-width on complex formation as well as $\Delta\nu/\nu_0$ are an order of magnitude less than corresponding quantities in the hydroxyl stretching regions. This observation indicates that hydrogen bonding results in a considerable perturbation of the hydroxyl stretching mode of the proton donor, while the influence on the ν(CO) mode of the proton acceptor is small, but not negligible.

It seems reasonable to conclude that the hydrogen-bond energy originates mainly from the functional group of the proton donor.

Equilibrium Constants

Before proceeding to calculate the molar absorption coefficients by a linear regression program, the band resolution was carried out for a second time. A chemical requirement, that each of the complexes should absorb at a particular wavenumber independent of its concentration in the solution, was introduced into the calculation by fixing the wave-

TABLE 5. Equilibrium constants (mol^{-1} m^3) at 30°C for the isotopically different PCP acetone complexes in CCl_4 solution[a]

Complex	ν(OH) or ν(OD) regions		ν(CO) region	$K_{11} \times 10^3$ calculated from "free" ν(OH) or ν(OD) bands
	$K_{11}^{(1)} \times 10^3$	$K_{11}^{(2)} \times 10^3$	$K_{11} \times 10^3$	
PCP . . . Ac[b]	3.2 (0.8)	5.4 (1.2)	11.0 (1.9)	8.8 (1.6)
PCP . . . Ac-d_6[b]	2.6 (1.5)	5.3 (0.4)	6.2 (1.1)	7.1 (1.0)
PCP-OD . . . Ac	4.0 (0.7)	5.5 (1.0)	8.9 (1.6)	8.9 (1.1)
PCP-OD . . . Ac-d_6	2.9 (0.7)	4.4 (1.3)	10.5 (0.2)	8.1 (1.0)

[a]The initial PCP concentration was about 0.05 *M* in all solutions studied. The numbers given in parentheses are standard deviations.
[b]These data are from ref. 4.

numbers of the monomer and the resolved complex bands to the average wavenumbers obtained previously for each set of solutions (Table 3). Only the peak height and band shape parameters were allowed to change in the second iteration process. The fixing of the wavenumbers resulted in slightly worse fits, but more consistent sets of band areas were obtained for each set of solutions, especially at low complex concentrations. The linear regression method, used to calculate the molar absorption coefficients, seemed to be very sensitive to the actual values of the band areas, as is indicated by fairly large standard deviations of the values of ε in Table 3. In each set of solutions the complex-band areas showed a linear relationship with the corresponding monomer-band areas, indicating that only (1:1) complexes occur in solution. According to our assignments, we have two (1:1) complexes in solution. Individual bands for each of these complexes have been obtained in the ν(OD) region, and from the areas of these bands, equilibrium constants $K_{11}^{(1)}$ and $K_{11}^{(2)}$ can be calculated for the formation of the two complexes labelled $(1:1)^1$ and $(1:1)^2$. The calculated values of $K_{11}^{(1)}$ and $K_{11}^{(2)}$ are given in Table 5.

Only one complex band can be resolved in the ν(CO) region and from the concentration dependence of the area of this band a combined equilibrium constant, K_{11}, can be calculated. This implies that there is no difference, from the point of view of the ν(CO) band of the acceptor molecule, between the two (1:1) complexes. A calculation of K_{11} can also be made using the concentration dependence of the free ν(OD) band. The results of these calculations are shown in the last two columns of Table 5.

From the algebraic expressions for $K_{11}^{(1)}$ and $K_{11}^{(2)}$, it follows that $K_{11} = K_{11}^{(1)} + K_{11}^{(2)}$. By adding the values of $K_{11}^{(1)}$ and $K_{11}^{(2)}$ from columns 2 and 3 of Table 5 and comparing these sums with the corresponding values of K_{11} in columns 4 and 5, it is seen that this simple relationship does appear to hold.

Conclusions

The calculated equilibrium constants $K_{11}^{(1)}$, $K_{11}^{(2)}$, and K_{11} show standard deviations of less than 20%, which gives a rough picture of the accuracy of the method used. The equilibrium constants in the hydroxyl stretching region show two isotopic effects. The value of $K_{11}^{(1)}$ increases slightly when PCP is deuterated for complex formation with either acetone or acetone-d_6. On the other hand, the value of $K_{11}^{(1)}$ is lowered when deuterated acetone replaces normal acetone as the acceptor. The value of $K_{11}^{(2)}$ is either almost unchanged or slightly lowered when PCP is deuterated. Examination of the ratio $K_{11}^{(2)}/K_{11}^{(1)}$ leads to the conclusion that the $(1:1)^2$ complex is favoured by deuteration of acetone, while the $(1:1)^1$ complex is favoured by deuteration of PCP.

Acknowledgements

This work was supported by grants from the National Research Council of Canada. One of the authors (J.K.-T.) acknowledges a Fellowship granted under the Cultural Exchange Programme between Canada and Finland.

1. U. LIDDEL and E. D. BECKER. Spectrochim. Acta, **16**, 70 (1957).
2. J. NEEL, P. PINEAU, and O. QUIVORON. J. Chim. Phys. **62**, 37 (1965).
3. J. T. BULMER and H. F. SHURVELL. J. Phys. Chem. **77**, 256 (1973); **77**, 2085 (1973).
4. J. KORPPI-TOMMOLA and H. F. SHURVELL. Can. J. Chem. **56**, 2959 (1978).
5. S. G. W. GINN and J. L. WOOD. Spectrochim. Acta, **23A**, 611 (1967).
6. A. J. BARNES and H. E. HALLAM. Trans. Faraday Soc. **66**, 1920 (1970); **66**, 1932 (1970).
7. J. KORPPI-TOMMOLA. J. Mol. Struct. **40**, 13 (1977).
8. S. SINGH and C. N. R. RAO. Can. J. Chem. **44**, 2611 (1966).
9. H. FRITZSCHE. Spectrochim. Acta, **21**, 799 (1964).
10. J. W. BOETTER and R. S. DRAGO. J. Chem. Phys. **78**, 429 (1974).
11. J. W. ROHLEDER and B. JAKUBOWSKI. Acta Phys. Pol. **31**, 1047 (1967).
12. M. T. FOREL and M. FOUASSIER. Spectrochim. Acta, **23A**, 1977 (1967).
13. M. MAILLOUX, J. WEINMAN, and S. WEINMAN. C.R. Acad. Sci. Paris, **276**, 379 (1973).
14. R. N. JONES *et al.* National Research Council of Canada, Computer Programmes for Infrared Spectroscopy. 1974.
15. PHAM VAN HUONG, M. COUZI, and J. LASCOMBE. C.R. Acad. Sci., Paris, **266B**, 172 (1968).

Preparation of copper(1) carbonyl hexafluoroarsenate, $CuCO^+AsF_6^-$, and copper(1) trifluorophosphine hexafluoroarsenate, $CuPF_3^+AsF_6^-$

C. David Desjardins, D. Brian Edwards, and Jack Passmore

Department of Chemistry, University of New Brunswick, P.O. Box 4400, Fredericton, N.B., Canada E3B 5A3

Received April 23, 1979

C. David Desjardins, D. Brian Edwards, and Jack Passmore. Can. J. Chem. **57**, 2714 (1979).

PF_3 and CO react with $CuAsF_6$ in SO_2 solution to form 1:1 addition compounds, the vibrational spectra of which are consistent with the formulations $[CuPF_3]^+[AsF_6]^-$ and $[CuCO]^+[AsF_6]^-$. The latter has a ν[CO] stretch at 2180 ± 5 cm^{-1}, the highest yet observed for a monocarbonyl.

C. David Desjardins, D. Brian Edwards et Jack Passmore. Can. J. Chem. **57**, 2714 (1979).

La trifluorophosphine et le monoxyde de carbone réagissent avec l'hexafluoroarsenate de cuivre dans une solution de bioxyde de soufre pour conduire aux composés d'addition 1:1. Les spectres de vibration de ces produits d'addition permettent de conclure à la formation de composés de type: $[CuPF_3]^+[AsF_6]^-$ et $[CuCO]^+[AsF_6]^-$. Ce dernier a une élongation ν[CO] à 2180 ± 5 cm^{-1} la plus grande valeur observée jusqu'à présent pour un composé monocarbonylé.
[Traduit par le journal]

We previously described the preparation of $CuAsF_6$ containing the Cu^+ ion in a very weakly basic environment (1). In such an environment Cu^+ and related transition metal ions are potentially powerful electron acceptors towards a variety of ligands (2, 3). In general, $[Cu^IL]^+$ complexes are unstable unless other ligands are present. For example, although complexes containing phosphorus ligands are well known (4–6), no simple $[CuPF_3]^+$ complexes have been reported. Also, the ready formation of $[Cu^I(am)_3CO]^+$ complexes (am_3 = ammine ligand(s) occupying 3 coordination sites (7)) is in contrast to the simple triatomic $[CuCO]^+$, known so far only in $[Cu^ICO]^+[CF_3CO_2]^-$ (8) in which there is likely to be strong cation–anion interaction. We report below the preparation of $[CuPF_3]^+[AsF_6]^-$ and $[CuCO]^+[AsF_6]^-$.

Experimental Section

Chemicals, experimental procedures, and the preparation of $CuAsF_6$ have been described (1). Phosphorous trifluoride (Pfaltz and Bauer) and carbon monoxide (Matheson, 99.5%) were used directly. Analytical results were obtained from Alfred Bernhardt Microanalytical Laboratories. A Raman spectrum of $CuAsF_6 \cdot PF_3$ was obtained by use of a Spex Industries 1400 spectrometer and a Spectra-Physics 140 Argon-ion laser at liquid nitrogen temperatures.

Preparation of $CuAsF_6 \cdot PF_3$

In a typical reaction $CuAsF_6$ (2.2 g, 8.7 mmol) was dissolved in sulphur dioxide (ca. 5 g) and then reacted with excess PF_3 (1.5 g, 17.0 mmol) in a glass vessel (ca. 80 mL) equipped with a medium glass fritted disc and a "Rotaflo" valve. On warming to room temperature from −196°C, the reddish brown $CuAsF_6$ solution immediately became colourless. After 1 h, all volatiles were removed under dynamic vacuum leaving a solid white product (2.79 g) which corresponds to formation of a 1:1 adduct. Analytical results obtained (*Anal.* calcd. for $CuAsF_6 \cdot PF_3$: F 50.22, Cu 18.67, As 22.01, P 9.10; found: F 50.43, Cu 18.51, As 21.70, P 9.24) support this formulation. The ir spectrum showed peaks, in addition to those of Nujol, at 960(sh), 919(s), 714(s, br), 587 (w), 519(s), 389(m, br) cm^{-1}. The Raman spectrum gave peaks at 940(m), 715(m), 680(s), 577(w), 373(w), 245(w), 145(m), 122(s), 104(s) cm^{-1}. An X-ray powder diffraction photograph of $CuAsF_6 \cdot PF_3$ indicated that neither unreacted $CuAsF_6$ nor elemental copper were present. Reaction times exceeding 1 h resulted in disproportionation (i.e. the solution changed to light brown with formation of a brown unidentified precipitate). This result may parallel that obtained by Dean and Ibbott (2) who observed disproportionation of Hg_2^{2+} in the presence of excess ligand (i.e. $PPh_3:Hg^{2+} > 1$). Reactions completed without solvent at low pressures of PF_3 (ca. 2–3 atm) gave varying product ratios due to incomplete reaction. Unreacted $CuAsF_6$ was observed in the X-ray powder diffraction photographs of these products. Adducts containing higher ratios of $PF_3:CuAsF_6$ (i.e. $2PF_3:CuAsF_6$) were obtained at low temperatures (i.e. −78°C) in SO_2 solution but these higher adducts slowly lost PF_3 on warming and were not further investigated. $CuPF_3^+AsF_6^-$ did not change on storage in a sealed vessel for several weeks at room temperature.

Preparation of $CuAsF_6 \cdot CO$

In a reaction similar to that described above, $CuAsF_6$ (1.33 g, 5.27 mmol) was dissolved in SO_2 (ca. 6 g) and an excess of CO was added. The reactants were warmed to room temperature. After a day, the volatiles were removed and the remaining solid was ground, and pumped to dryness yielding a yellow solid. Analytical results obtained (*Anal.* calcd. for $CuAsF_6 \cdot CO$: C 4.28, F 40.64, Cu 22.66, As 26.71; found: C 4.31, F 40.36, Cu 22.99, As 26.83) were consistent with formation of a 1:1 adduct. An ir spectrum of the adduct excluding peaks due to Nujol gave a CO stretch at 2180 ± 5 cm^{-1} and peaks attributable to AsF_6^- (700, 389 cm^{-1}). Solid $CuAsF_6 \cdot CO$ stored under anhydrous conditions changed colour slowly indicating either decomposition or disproportionation.

0008-4042/79/202714-02$01.00/0

Results and Discussion

PF_3 Adduct

PF_3 reacted with $CuAsF_6$ in SO_2 solution at room temperature to form a 1:1 adduct. The vibrational spectrum is consistent with the presence of AsF_6^- (ir 714, 389 cm^{-1}; Raman 715, 680, 577, 373 cm^{-1}), although the symmetry is less than octahedral (9), and coordinated (approximately C_{3v}) PF_3 (ir 919ν_{as}, 519δ_s; Raman 940ν_s). The increase in the P—F stretching frequency relative to PF_3 itself (892ν_s, 860ν_{as}) (10) is consistent with other related PF_3 adducts (i.e. $Hg_2PF_3^{2+}$ (2), $AgPF_3^+$ (2), and $M(PF_3)_x$ (M = Ni, Pd, Pt, etc. (6, 11))) but not as marked as that for $AsF_5 \cdot PF_3$ (12) (953ν_s, 1003, and 1027ν_{as}). Presumably arsenic pentafluoride is a better acceptor than the copper(+1) cation and back donation is absent in $F_3P \cdot AsF_5$. The vibrational spectra, reaction stoichiometry, and solubility of the product in SO_2 indicate the presence of a $[CuPF_3]^+$ ion (though this may be fluorine bridged to a neighbouring AsF_6^- (or to SO_2 in solution)). However, a formulation such as $(CuPF_3^+)_x(AsF_6^-)_x$ (or $(CuCO^+)_x(AsF_6^-)_x$) cannot be totally excluded.

CO Adduct

The reaction of $CuAsF_6$ with CO at room temperature results in the formation of a 1:1 adduct. The most noteworthy property of the $[CuCO]^+[AsF_6]^-$ complex is the extremely high ν(CO) stretch, 2180 $\pm$ 5 cm^{-1}, the highest yet observed for a monocarbonyl (free carbon monoxide has ν(CO) at 2143 cm^{-1} (13), $[CuCO][CF_3CO_2]$ at 2155 cm^{-1} (8), $CuCO^+$ at 2168 cm^{-1} in H_2SO_4–BF_3–H_2O solution (14), $Cu_4(F_3C_2O_2)_4 \cdot 4CO$ at 2120 cm^{-1} (15), $BH_3 \cdot CO$ at 2165 cm^{-1} (10), and normal $[Cu(am_3)(CO)]^+$ complexes have νCO at 2080 cm^{-1} (7)).

The increase in ν(CO) stretching frequency (relative to free CO) may be attributed to a kinematic effect, the donation of the slightly antibonding lone pair (16) towards the cuprous ion, and to an increase in positive charge on carbon which results in an increase in CO bond order. Presumably there is only weak back donation in $CuCO^+$.

Acknowledgements

We thank the National Research Council of Canada for financial assistance and Dr. Frank Bottomley for useful discussions.

1. C. D. Desjardins and J. Passmore. J. Fluorine Chem. **6**, 379 (1975).
2. P. A. W. Dean and D. G. Ibbott. Can. J. Chem. **54**, 177 (1976).
3. P. A. W. Dean, D. G. Ibbott, and J. B. Stothers. Can. J. Chem. **54**, 166 (1976).
4. M. B. Dines. Inorg. Chem. **11**, 2949 (1972).
5. O. Stelzer. Top. Phosphorus Chem. **9**, 1 (1977).
6. J. F. Nixon. Adv. Inorg. Chem. Radiochem. **13**, 363 (1970) and references therein.
7. M. Pasquali, F. Marchetti, and C. Floriani. Inorg. Chem. **17**, 1684 (1978) and references therein.
8. A. F. Scott, L. L. Wilkening, and B. Rubin. Inorg. Chem. **8**, 2533 (1969).
9. (*a*) F. O. Sladkey, P. A. Bulliner, and N. Bartlett. J. Chem. Soc. A, 2179 (1969); (*b*) K. O. Christe and W. Sawodny. Inorg. Chem. **6**, 313 (1967); (*c*) C. Lau and J. Passmore. J. Chem. Soc. Dalton Trans. 2528 (1973).
10. K. Nakamoto. Infrared spectra of inorganic and coordination compounds. 2nd ed. Wiley-Interscience, New York. 1970. pp. 93, 193 and references therein.
11. H. G. M. Edwards and L. A. Woodward. Spectrochim. Acta, **26**A, 897 (1970).
12. G. S. H. Chen and J. Passmore. J. Chem. Soc. Dalton. In press.
13. G. E. Ewing and G. C. Pimentel. J. Chem. Phys. **35**, 925 (1961).
14. Y. Matsushima, T. Koyano, T. Kitamura, and S. Wada. Chem. Lett. 433 (1973).
15. P. F. Rodesiler and E. L. Amma. J. Inorg. Nucl. Chem. **39**, 1229 (1977).
16. J. Chatt, D. P. Melville, and R. L. Richards. J. Chem. Soc. A, 2841 (1969) and references therein.

Density and temperature effects on electron mobilities in gaseous butene isomers[1]

TOSHINORI WADA AND GORDON R. FREEMAN

Chemistry Department, University of Alberta, Edmonton, Alta., Canada T6G 2G2

Received June 4, 1979

TOSHINORI WADA and GORDON R. FREEMAN. Can. J. Chem. **57**, 2716 (1979).

The density normalized mobilities μn at low electric field strengths in the low density gases fall in the order *trans*-2- > *cis*-2- > 1- > isobutene. The respective values in the saturated vapors at 297 ± 1 K were 10.7, 4.4, 3.8, and 1.84 (10^{22} molecules/cm V s). The scattering cross section σ_v has a Ramsauer–Townsend-like minimum at an electron energy of 0.085 eV in *trans*-2-butene, 0.13 eV in *cis*-2-butene, 0.12 eV in 1-butene, and 0.16 eV in isobutene. The mobilities in the last three isomers increase with increasing temperature (300–500 K) and field strength ($\gtrsim$ 1 Td). Temperature and field effects were smaller in *trans*-2-butene. The ratio of the field effect threshold drift velocity to the speed of sound in the low density gas is 14, 19, 20, and > 50 in iso-, 1-, *cis*-2-, and *trans*-2-butene, respectively, at 297 K. The electrons are de-energized mainly by inelastic collisions. Quasilocalization occurs to a similar extent in each of the isomers at densities $\gtrsim 1 \times 10^{21}$ molecules/cm^3 and temperatures near the coexistence curve. Quasi-localization is characterized by large, negative values of ΔH and ΔS, and a small value of ΔG over a small temperature range.

TOSHINORA WADA et GORDON R. FREEMAN. Can. J. Chem. **57**, 2716 (1979).

Les mobilités normalisées pour la densité μn à de faibles champs électroniques pour les gaz de faible densité, décroissent dans l'ordre 2-*trans* > 2-*cis* > 1- > isobutène. Les valeurs respectives pour les vapeurs saturées à 297 ± 1 K sont 10.7, 4.4, 3.8 et 1.84 (10^{22} molécules/cm V s). La section efficace σ_v de diffusion passe par un minimum de Ramsauer–Townsend à une énergie électronique de 0.085 eV pour le produit 2-*trans*, de 0.13 eV pour le 2-*cis*, de 0.12 eV pour le 1- et de 0.16 eV pour l'isobutène. Les mobilités des trois derniers isomères augmentent avec la température (300–500 K) et la force du champ ($\gtrsim$ 1 Td). Les effets de la température et du champs sont plus faibles pour le butène-2 *trans*. Les rapports entre la vitesse de dérivé du seuil d'effet de champ et la vitesse du son dans les gaz de faible densité, à 297 K sont respectivement 14, 19, 20 et > 50 pour les dérivés iso-, 1-, 2-*cis* et butène-2 *trans*. Les électrons subissent principalement une perte d'énergie à cause de collisions non élastiques. Une quasi-localisation se produit d'une manière similaire dans chacun des isomères à des densités $\gtrsim 1 \times 10^{21}$ molécules/cm^3 et à des températures voisines de la courbe de concomitance. La quasi-localisation est caractérisée par une grande valeur négative de ΔH et ΔS et une faible valeur de ΔG dans une zone de température assez limitée.

[Traduit par le journal]

Introduction

The mobilities of electrons in the liquid isomeric butenes are vastly different from each other at room temperature (1), but they are similar near the melting points and in the critical fluids (2). At temperatures near the critical temperature and pressures equal to the vapor pressure, the mobilities are more affected by the changing fluid density than by the changing temperature (2). It was therefore desirable to extend the study to the gas phase, with densities ranging from the critical to the dilute gas. The results are reported herein.

Experimental

Materials and Apparatus

The Phillips Research Grade butenes were further purified under vacuum as described earlier (2).

The conductance cell was of the heavy walled type which could contain a pressure of 60 bar (3). The gap between the parallel electrodes was $l = 0.32$ cm. The purified butene was distilled into the cell at 77 K and sealed under a vacuum of 10^{-4} Pa.

The sample was placed in a well grounded Faraday cage and irradiated by a 110 ns pulse of X rays, which delivered 7×10^9 eV/g to the gas. The pulse shape is shown in Fig. 1*a*. A dc voltage was applied to the high voltage electrode by a Fluke (up to 6 kV) or Spellman (up to 30 kV) power supply through low pass filters. The electron conductance transient (ECT, Fig. 1*b*) was measured using amplifier #8 (4) and a Tektronix 7623 oscilloscope; a 7A22 plug-in was used for decay times > 50 μs and a 7A13 for shorter times.

The temperature control system and other experimental procedures were the same as in refs. 2 and 3.

Physical Properties of the Fluids

The densities n (molecules/cm^3) of the saturated vapors were calculated from the law of rectilinear diameters (6) and the liquid densities (5, 6). The critical constants listed in refs. 5–7 were averaged (Table 1). Dipole moments were taken from ref. 8.

Determination of the Electron Mobility μ

The mobility was determined from the flight time of the

[1]Assisted financially by the National Research Council of Canada.

0008-4042/79/202716-11$01.00/0

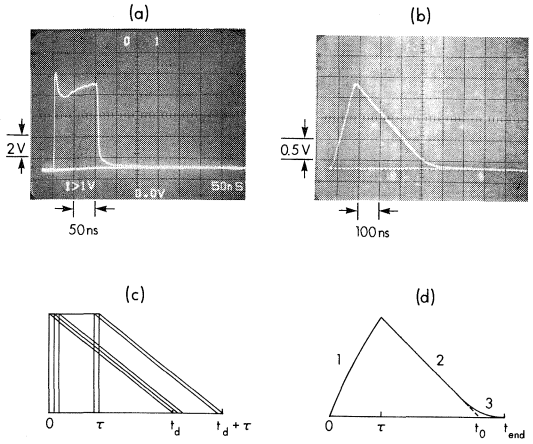

FIG. 1. (*a*) Pulse shape, measured using a 7A24 plug-in with 350 MHz bandwidth. (*b*) ECT signal in *cis*-2-butene, $E = 31$ kV/cm, $n = 2.06 \times 10^{21}$ molecules/cm^3. (*c*) Growth and decay of signal from small portions of a pulse. (*d*) Sum of the portions in part *c*.

electrons between parallel electrodes, using eq. [1].

$$[1] \qquad \mu = l^2/Vt_d$$

where l is the distance between the electrodes, V is the applied voltage, and t_d is the time required for the electrons to drift the distance l. An ECT obtained at a high field strength is shown in Fig. 1*b*. This ECT is composed of three parts; (*i*) the rising part during the radiation pulse, (*ii*) the linear decay part, and (*iii*) the tail for which it is not easy to determine the real end. The length of the tail is similar to the pulse width. To determine the drift time t_d, we divide the square radiation pulse width τ into many narrow parts. Each part produces a small individual ECT which decays linearly for the drift time t_d (Fig. 1*c*). The whole ECT obtained by summation of the small ECT's is shown in Fig. 1*d*, which is very similar to the experimental ECT in Fig. 1*b*. For $\tau < t_d$ the electron current during the three portions of the ECT is: (*i*) $ct(1 - [t/2t_d])$, $t \leq \tau$; (*ii*) $c\tau(t_d + [\tau/2] - t)/t_d$, $\tau \leq t \leq t_d$; (*iii*) $c(t_d + \tau - t)^2/2t_d$, $t_d < t < t_d + \tau$; c is a constant that depends on the energy absorption rate by the sample and the free ion yield. The drift time may be determined experimentally from eq. [2] or [2′].

$$[2] \qquad t_d = t_0 - (\tau/2)$$

$$[2'] \qquad t_d = t_{end} - \tau$$

where t_0 is the time when an extension of the linear decay crosses the base line, and t_{end} is the time when the ECT actually reaches zero. Equation [2] was used to obtain t_d because t_0 is more accurately determined than t_{end}.

At sufficiently low fields and large values of t_d, the decay of the ECT was no longer linear. Random diffusion of the electrons during the drift to the collecting electrode spreads the tail of the ECT. This effect is taken into consideration by replacing l in eq. [1] with $(l + \Delta x)$, where Δx is the mean distance of diffusion opposed to the field direction during the time t_d and is given by $(2Dt_d)^{1/2}$. It is assumed that the diffusion coefficient D of the electrons is represented by the Einstein relation $D = (kT/e)\mu$, and eq. [1] is used as a zero order approximation of the mobility. The corrected electron mobility is then:

$$[3] \qquad \mu = l^2[1 + (2kT/eV)^{1/2}]/Vt_d$$

where k is Boltzmann's constant, T is the absolute temperature, and e is the electron charge. For an ECT measured at $V = 10$ V and $T = 500$ K the correction for the diffusion is $(2kT/eV)^{1/2} = 0.09$.

Results

Electron mobilities were measured as functions of electric field strength, temperature, and vapor density. The range of the density-normalized electric field strength E/n was 0.03 – 4 Td (Td = 10^{-17} V cm^2/molecule). The saturated vapors were measured from room temperature to the critical temperature T_c, with densities from $0.025n_c$ to the critical n_c. The gases were further heated above the coexistence curves at several fixed densities.

Low Density

The density normalized mobilities μn at low fields fell in the order *trans*-2-butene > *cis*-2-butene > 1-butene > isobutene (Fig. 2). The respective values at 297 ± 1 K in the saturated vapors were 10.7, 4.4, 3.8, and 1.84 (10^{22} molecules/cm V s).

The mobilities in three of the saturated vapors increased with field strength at $E/n \gtrsim 1$ Td as shown in Fig. 2. The drift velocity at the threshold of the field dependent region was 3 km/s in isobutene, and 4 km/s in 1-butene and *cis*-2-butene. The experimental arrangement did not have sufficient time resolution to permit measurement of the threshold in *trans*-2-butene.

Increasing the temperature of isobutene vapor at constant density increased the electron mobility and the threshold of the field effect (Fig. 3). The same was true in *cis*-2-butene vapor (Fig. 4). Temperature and field effects were smaller in low density *trans*-2-butene and 1-butene (see below).

Effect of Density

Along the coexistence curve. The increasing density of the saturated vapor with increasing temperature resulted in a decrease of mobility (half filled points in Figs. 5–8). The density normalized mobility μn decreased gently with increasing density over most of the vapor range (Fig. 9). However, as the critical density was approached μn either increased (isobutene and *cis*-2-butene) or decreased more sharply (1-butene and *trans*-2-butene). The liquid phase results from ref. 2 are included in Fig. 9 for completeness. The curve for *trans*-2-butene plunges through the curves for the other compounds in the vicinity of the critical region.

Electron mobilities in the critical fluids were 17,

TABLE 1. Physical properties of butene isomers

Property	Value			
	trans-Butene	*cis*-Butene	1-Butene	Isobutene
T_c (K)[a]	428	433	419	418
n_c (10^{21} molecules/cm^3)[a]	2.56	2.57	2.50	2.51
P_c (MPa)[a]	4.1	4.2	4.0	4.0
Dipole moment (10^{-18} esu cm)[b]	0.0	0.3	0.34	0.50
Average polarizability (10^{-24} cm^3)[c]	7.88	7.88	7.83	7.88

[a]References 5–7.
[b]Reference 8.
[c]Landolt-Bornstein, Zahlenwerte and Funktionen, 6 Auflage, I Bd., 3 Teil, Springer-Verlag, Berlin. 1951. p. 515.

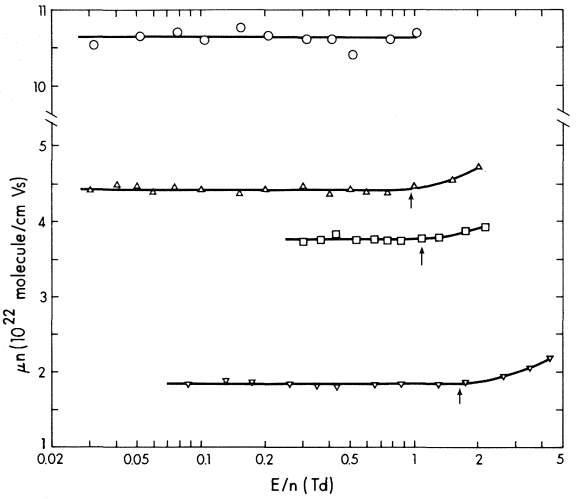

FIG. 2. Effect of E/n on μn in low density, saturated vapors. The temperatures and densities (K, 10^{19} molecule/cm^3) are: ○, *trans*-2-butene (298, 6.0); △, *cis*-2-butene (297, 6.2); □, 1-butene (298, 7.2); ▽, isobutene (296, 7.1).

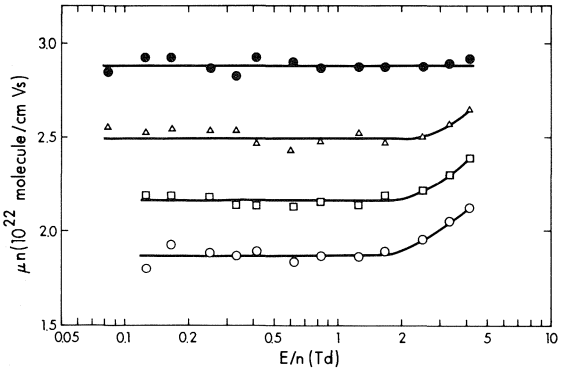

FIG. 3. Effect of E/n on μn in low density isobutene vapor at different temperatures $n = 7.5 \times 10^{19}$ molecule/cm^3. ○, 308 K; □, 360 K; △, 432 K; ●, 537 K.

14, 8.7, and 7.4 cm^2/V s for *cis*-2-, *trans*-2-, 1-, and isobutene, respectively.

On the temperature coefficient at constant density. In low density *trans*-2-butene vapor the Arrhenius temperature coefficient was nearly zero. The coefficient was slightly positive near the coexistence curve and

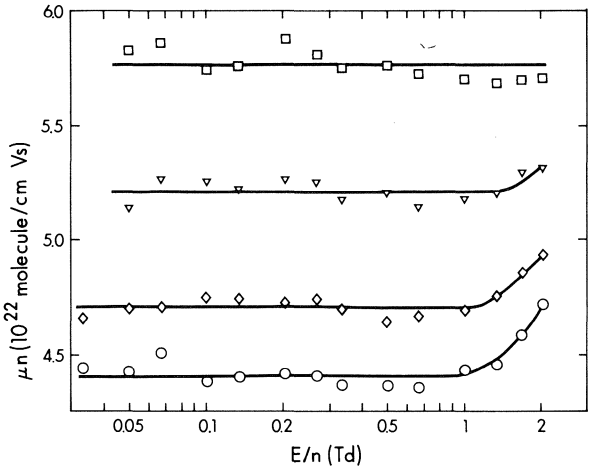

FIG. 4. Effect of E/n on μn in low density *cis*-2-butene vapor at different temperatures $n = 9.3 \times 10^{19}$ molecule/cm^3. ○, 317 K; ◇, 347 K; ▽, 417 K; □, 518 K.

slightly negative at high temperatures (Fig. 5). At high densities the coefficient was more positive.

In the other isomers the temperature coefficients were positive at all temperatures at low density, and increased with density (Figs. 6–8). At each density the coefficient tended to decrease with increasing temperature.

The temperature coefficients at a given n/n_c and T/T_c were in the order iso- $\gtrsim$ *cis*-2- > 1- > *trans*-2-butene. For example, at $n/n_c = 1.00$ and $T/T_c = 1.01$ the respective Arrhenius temperature coefficients are 0.69, 0.69, 0.56, and 0.48 eV. Although at very low densities the Arrhenius model is not appropriate, to indicate the magnitude of the change of temperature coefficient with density, at $n/n_c = 0.03$ and just above the coexistence temperature the respective coefficients are 0.024, 0.020, 0.011, and 0.008 eV.

On the field effect. In the saturated vapors of 1-, *cis*-2-, and *trans*-2-butene the field effect remained essentially the same from low densities up to the critical. The uncertainty in the threshold values of E/n was about 30%. In isobutene the threshold remained at ~1.5 Td up to $n/n_c = 0.2$, but decreased at higher densities and reached ~0.7 Td at $n/n_c = 1.0$.

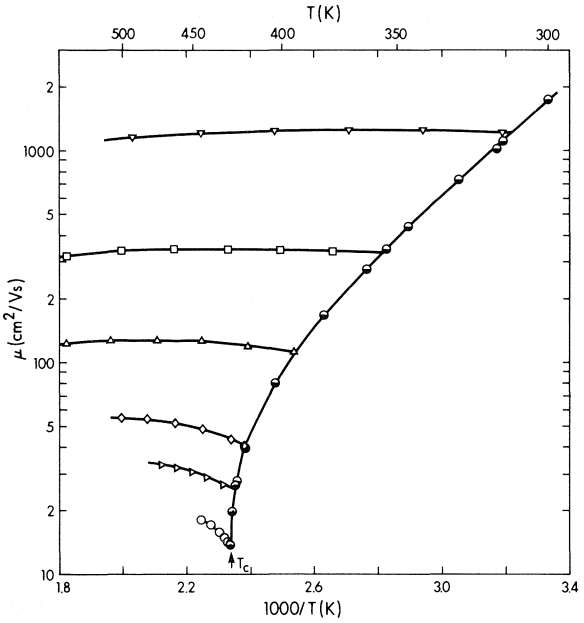

FIG. 5. Arrhenius plots of electron mobilities in *trans*-2-butene vapor at different densities n (10^{20} molecule/cm^3). ▽, 0.90, the curve was calculated by eq. [6] with cross sections from Fig. 11; □, 2.91; △, 6.98; ◇, 14.4; ▷, 20.2; ○, n_c = 25.6; ◒, coexistence vapor.

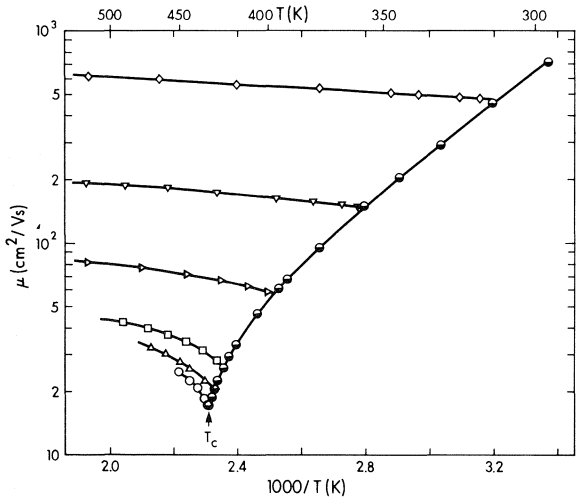

FIG. 6. Arrhenius plots of electron mobilities in *cis*-2-butene vapor at different densities n (10^{20} molecules/cm^3). ◇, 0.93, the curve was calculated by eq. [6] with cross sections from Fig. 11; ▽, 2.95; ▷, 7.32; □, 14.4; △, 18.8; ○, n_c = 25.7; ◒, coexistence vapor.

In the supercritical gases at $n/n_c = 1.00$ and $T/T_c = 1.04$ the magnitudes of the field effects at 1.0 Td in 1-, iso-, and *cis*-2-butene were somewhat smaller than those in the critical fluids. In the corresponding supercritical *trans*-2-butene the mobility decreased gently at $E/n > 0.07$ Td, so the field effect

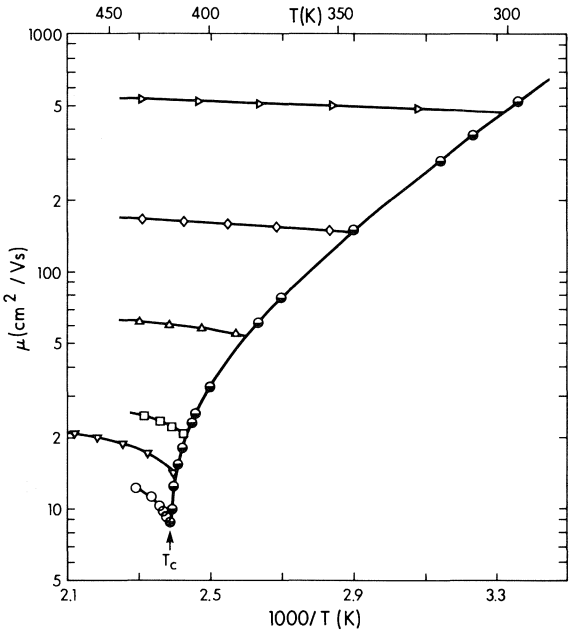

FIG. 7. Arrhenius plots of electron mobilities in 1-butene vapor at different densities n (10^{20} molecules/cm^3). ▷, 0.78, the curve was calculated by eq. [6] with cross sections from Fig. 11; ◇, 2.16; △, 5.42; □, 13.6; ▽, 18.9; ○, n_c = 25.0; ◒, coexistence vapor.

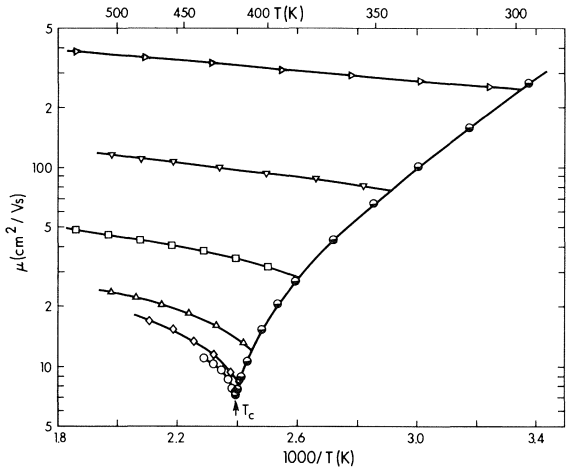

FIG. 8. Arrhenius plots of electron mobilities in isobutene vapor at different densities n (10^{20} molecules/cm^3). ▷, 0.75, the curve was calculated by eq. [6] with cross sections from Fig. 11; ▽, 2.26; □, 5.75; △, 12.2; ◇, 18.2; ○, n_c = 25.1; ◒, coexistence vapor.

has the opposite sign to those in the other butenes (Fig. 10).

Discussion

Low Density

Electrons gain energy by acceleration in the field and lose it by collisions with molecules. At low field strengths the average amount of energy gained be-

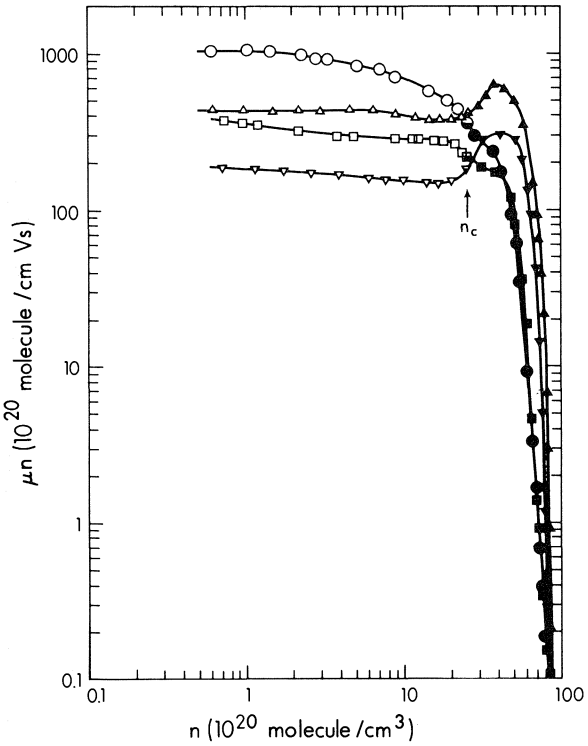

FIG. 9. Plots of μn against n in the coexistence fluids. ○, *trans*-2-butene; △, *cis*-2-butene; □, 1-butene; ▽, isobutene. Open symbols, vapors; filled symbols, liquids (ref. 2); half-filled symbols, critical fluids.

tween collisions is less than that normally exchanged during a collision, so the electrons remain in thermal equilibrium with the medium. At moderate field strengths the electrons gain more energy between collisions than they normally exchange, so they increase in velocity until a new steady state is reached. If the electron collision frequency changes as a result of the increased velocity, the mobility changes.

The velocity also increases with temperature, so the field effect at moderate field strengths is in the same direction as the temperature effect.

The mobility μ_{ld} at low densities can be expressed as (9–11):

$$[4] \quad \mu_{ld} = -\frac{4\pi}{3}\frac{e}{mn}\int_0^\infty \frac{v^2}{\sigma_v}\frac{df_0}{dv}\,dv$$

where e and m are the charge and mass of the electron, respectively, σ_v is the scattering cross section of the molecules for electrons of velocity v, and f_0 is the spherically symmetric term in the series expansion of the electron velocity distribution function. For a Maxwellian distribution one has

$$[5] \quad f_0 = (m/2\pi kT)^{3/2}\exp(-mv^2/2kT)$$

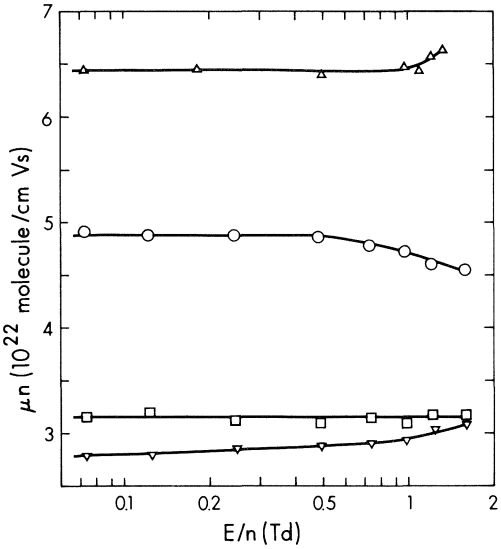

FIG. 10. Effect of E/n on μn in the supercritical gases at $n = n_c$ and $T/T_c = 1.04$. ○, *trans*-2-butene; △, *cis*-2-butene; □, 1-butene; ▽, isobutene.

and

$$[6] \quad \mu_{ld} = (5.23 \times 10^{-14}/nT^{2.5})\int_0^\infty (v^3/\sigma_v) \times \exp(-3.30 \times 10^{-12}v^2/T)\,dv$$

where k is Boltzmann's constant.

Scattering Cross Sections

The value of σ_v as a function of v was determined for each butene by fitting eq. [6] to the mobilities in the uppermost curve in each of Figs. 5–8. Equation [6] was integrated numerically, using 22 logarithmic steps between $v = 5.9 \times 10^6$ and 3.2×10^7 cm/s, which was the sensitive range (0.01–0.3 eV). An initial estimate of σ_v was made by assuming $\sigma_v \approx A_\alpha v^{-\alpha}$, which gives eq. [7].

$$[7] \quad \mu_{ld} \approx \left[1.32 \times 10^{15}\left(1 + \frac{\alpha}{2}\right)!/nA_\alpha\right] \times (3.03 \times 10^{11}T)^{(\alpha-1)/2}$$

The values of α and A_α were obtained from the slope and intercept of a plot of log μ_{ld} against log T. A plot of log σ_v against log v was then made and adjusted to give the best agreement with the array of experimental (μ_{ld}, T) values, through iterative calculations with eq. [6]. The cross sections so obtained are displayed in Fig. 11, plotted against energy in the traditional manner. Cross sections estimated earlier (12) for 1-butene are shown for comparison; mobilities had been measured at only two temperatures.

The Maxwellian distribution of E and v is indi-

cated in Fig. 11*a*. The energy range of greatest sensitivity in the curve fitting procedure is that near the maximum in the scattering probability curve, which ranges from about 0.04–0.20 eV in isobutene (Fig. 11*b*) to about 0.03–0.13 eV in *trans*-2-butene. The accuracy of the estimated cross section decreases with increasing distance from this central region.

The density normalized mobilities $n\mu_{ld}$ in the low density gases are plotted on an expanded scale in Fig. 12 to show the extent to which the values calculated from eq. [6] with the cross sections in Fig. 11 match those determined experimentally.

When cross sections σ_v that have been derived from mobilities are averaged to compare values for different molecules, the appropriate weight is placed on the most sensitive region of velocities by using eq. [8] (13, 14).

$$[8] \quad \sigma_{ave} = \langle v \rangle / \langle v/\sigma_v \rangle$$

For a Maxwellian distribution of velocities eq. [8] becomes

$$[9] \quad \sigma_{ave} = 4.59 \times 10^{22} T^2 \Big/ \int_0^\infty (v^3/\sigma_v) \times \exp(-3.30 \times 10^{-12} v^2/T)\, dv$$

It may be noted that multiplying eq. [6] by

$$1 = 4.59 \times 10^{22} T^2 \Big/ \sigma_{ave} \int_0^\infty (v^3/\sigma_v) \times \exp(-3.3 \times 10^{-12} v^2/T)\, dv$$

from eq. [9] gives [10].

$$[10] \quad \mu_{ld} = 2.40 \times 10^9 / nT^{1/2} \sigma_{ave}$$

This is equivalent to the expression derived by Lorentz using a cross section that was independent of v (15).

The values of σ_{ave} fall in the order *trans*- < *cis*- $\lesssim$ 1- < isobutene (Table 2). The molecular electric dipole moments lie in the same order (Table 1). One may therefore suggest that the scattering power of a butene molecule contains contributions from a stiff central core and the dipolar electric field.

The simple model of electron scattering by the induced dipole (16) is not adequate for the central core component, because the value of σ_{ave} predicted by the model for the nonpolar *trans*-2-butene is seventeen times larger than the observed value. The repulsive interaction between the projectile electron and the imperfectly polarizable molecular electrons cancels most of the attractive interaction between the charge and the induced dipole.

For scattering by a point-dipole potential $(-eD/r^2)$

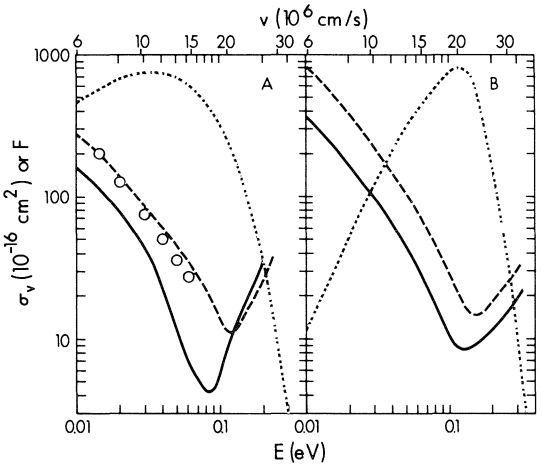

FIG. 11. Scattering cross sections σ_v of the low density vapors as functions of electron energy E or velocity v. *A*:—, *trans*-2-butene; ---, 1-butene; ○, 1-butene from ref. 12; ···, Maxwellian distribution of E and v at 400 K, $F = (1.36 \times 10^{-7}\ v^2/T^{1.5}) \exp(-3.30 \times 10^{-12}\ v^2/T)$; *B*: —, *cis*-2-butene; ---, isobutene; ···, scattering probability distribution for isobutene at 400 K, $F = 6 \times 10^{-33}\ (v^3/\sigma_v) \exp(-3.30 \times 10^{-12}\ v^2/T)$. The factors F are the true values multiplied by 10^{10} in *A* and 6×10^{-33} in *B* to fit the displayed scale.

$\times \cos\theta$, the Born approximation model of Altshuler (17) gives:

$$[11] \quad \sigma_v(\text{Alt}) = (8\pi/3)(eD/\hbar v)^2$$

where D is the dipole moment and $h = 2\pi\hbar$ is Planck's constant. The cross section averaged over a Maxwellian distribution in the manner of eq. [8] is:

$$[12] \quad \sigma_{\text{Alt},T} = 2.86 \times 10^{24} D^2/T$$

Values of $\sigma_{\text{Alt},300\text{ K}}$ are given in Table 2. They are roughly three-fold smaller than the observed cross sections for the polar butenes. Taking σ_{ave} of *trans*-2-butene to represent the contribution of the stiff core for each of the butenes, and making the crude assumption that contributions of two processes are approximately additive when one does not completely dominate the other, the net ratio $[(\sigma_{ave} - 12.5)/\sigma_{Alt}]_{300\text{ K}}$ is still greater than unity (Table 2). The dipole field makes a significant contribution to scattering by the polar butenes, but some other force is greater. The dipole field tends to dominate only for molecules with $D \gtrsim 1.0 \times 10^{-18}$ esu cm (18).

An additional factor in scattering by the butenes is the as yet unexplained effect of the degree of sphericity of the molecules. The scattering cross section for low energy electrons increases with increasing sphericity of isomeric hydrocarbons (19). The degrees of sphericity of the butenes are in the order *trans*- < 1- < *cis*- < isobutene, and the cross sections tend to

TABLE 2. Electron scattering parameters of the gaseous butenes

Parameter	Value			
	trans-Butene	*cis*-Butene	1-Butene	Isobutene
n (10^{19} molecules/cm^3)	9.0	9.3	7.8	7.5
$\sigma_{ave,300\ K}$ (10^{-16} cm^2)	12.5	33	38	75
$\sigma_{ave,500\ K}$ (10^{-16} cm^2)	10.3	19	24	39
$\sigma_{Alt,300\ K}$ (10^{-16} cm^2)	0	8.6	11.0	24
$[(\sigma_{ave} - 12.5)/\sigma_{Alt}]_{300\ K}$	—	2.3	2.3	2.6
$E_{\sigma min}$ (eV)	0.085	0.13	0.12	0.16

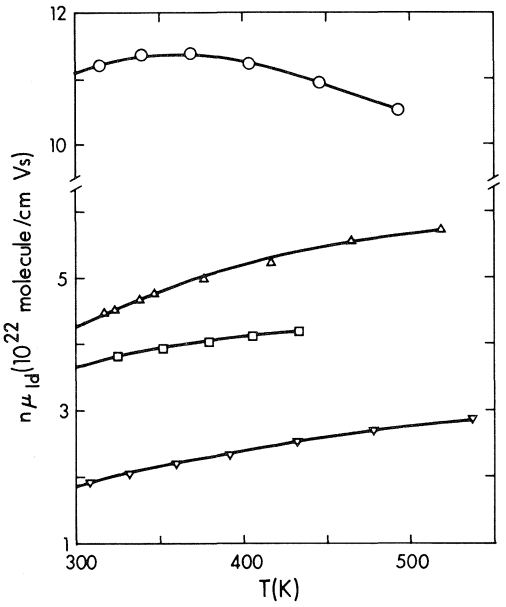

FIG. 12. Comparison of the calculated and experimental values of the density normalized mobilities $n\mu_{td}$ in the low density gases at different temperatures. ○, *trans*-; △, *cis*-; □, 1-; ▽, isobutene. The lines were calculated by eq. [6] with cross sections from Fig. 11.

increase in the same order (Table 2). This rationalizes the apparent anomaly that the butene with the largest dipole moment, isobutene, has a value of $[(\sigma_{ave} - 12.5)/\sigma_{Alt}]$ larger than those of the other polar butenes (Table 2). For a dipole field superimposed upon a stiff core, the ratio might have been expected to be closest to unity for the isomer with the largest dipole moment.

In terms of the less accurate but simpler eq. [7], the sphericity effect displays itself as a larger value of α for more spherelike molecules. The present results for the low density butene gases give $\alpha \approx 0.7$, 1.6, 2.0, and 2.5 for *trans*-, 1-, *cis*-, and isobutene, respectively, which is in the same order as the degree of sphericity estimated visually from space-filling molecular models. Similarly, for the isomeric pentanes the values of α were 1.1, 1.5, and 3.2 for *n*-, iso-, and neopentane, respectively (13).

The sphericity effect includes a tendency for the minimum in σ_v to lie at a higher energy for a more sphere-like isomer (Fig. 11 and Table 2). In the pentane isomers the value of $E_{\sigma min}$ was 0.13 eV for *n*- and isopentane and 0.21 eV for neopentane (19).

Simple models of electron scattering by induced or permanent dipoles (9, 16, 17) do not fit scattering by hydrocarbons. A better interpretation of the results might involve the Ramsauer–Townsend effect or transient negative ion states. However, it is not yet known how to interpret the sphericity effect in those terms.

Field Dependence Thresholds

Elastic scattering of electrons by individual molecules in the gas is kinetically equivalent to scattering by phonons (20, 21). The effective mass M^* of a phonon is given by:

$$[13] \quad M^* c_0^2 = kT$$

where c_0 is the velocity of low frequency sound. In the low density gas $c_0 = (\gamma kT/M)^{0.5}$, where γ is the heat capacity ratio and M is the molecular mass (22). One therefore obtains $M^* = M/\gamma \approx 0.9\,M$ in the low density butenes (5). When elastic scattering is the dominant process that moderates the electron energy, the electron drift velocity v_d should become nonlinear with field strength when $v_d \approx c_0$ (20). The velocity of sound is therefore a useful parameter in assessing electron scattering processes even in the single scatterer regime.

The value of c_0 in the low density butene vapors at 297 K is 221 m/s. The threshold drift velocities, v_d(threshold), for field dependent mobilities were 3.1, 4.2, 4.4, and >11 km/s in iso-, 1-, *cis*-2-, and *trans*-2-butene, respectively (Fig. 2). The respective values of the ratio v_d(threshold)/c_0 are 14, 19, 20, and >50 at 297 K. These large values imply that the electrons in the butenes are cooled predominantly by inelastic collisions. Values of the ratio in other gases are: xenon, 0.7 (4); methane, 1.0 (23); neopentane, 5 (13); cyclopentane, 11 (14); isopentane, 15 (13); *n*-pentane, >100 (13). The ratio increases with decreasing sphericity of the molecules. We conclude

that the sphericity contribution to electron scattering tends to be an elastic process.

The values of v_d(threshold) in iso- and *cis*-2-butene increase with increasing temperature (Figs. 3 and 4). So do the values of c_0 and v_d(threshold)/c_0. At 530 K the values in both gases are v_d(threshold) > 11 km/s, $c_0 = 290$ m/s and v_d(threshold)/$c_0 > 40$. The higher electron energies at the higher temperature enhance the contribution of inelastic collisions. The higher vibrational–rotational states of the molecules in the hotter gas might also be better energy sinks than the lower states for inelastic collisions with low energy electrons.

Effect of Density

The effects of density on μn in the coexistence vapor and liquid of 1-butene are similar to those in *trans*-2-butene; each curve contains a negatively sloped inflection near 3×10^{21} molecules/cm^3 (Fig. 9). The density effects in isobutene are similar to those in *cis*-2-butene; each curve contains a shallow minimum near 2×10^{21} molecules/cm^3 and a maximum near 4×10^{21} molecules/cm^3 (Fig. 9). The plots for *cis*- and *trans*-2-butene cross near the critical region, as do those for iso- and 1-butene. A detailed description of the behaviors in *cis*- and *trans*-2-butene will therefore apply qualitatively to those in iso- and 1-butene as well.

The temperature coefficient of the mobility in the high density gas varies with the density and the temperature. The coefficient is taken as $\theta_{n,T} = (\partial \log \mu/\partial \log T)_{n,T}$; values are plotted against n for two fixed temperatures, T_c and $1.05T_c$, in Fig. 13. The value of $\theta_{n,T}$ becomes independent of n and T at low n, where an electron interacts with only one molecule at a time. The low density limit of θ is related to the α in eq. [7] through the relation $\theta = (\alpha - 1)/2$. As the density is increased above about 7×10^{20} molecules/cm^3, θ_{n,T_c} increases rapidly, becoming roughly proportional to n^2. Heating the vapor to $1.05T_c$, an increase of only 21 K, greatly reduces the temperature coefficient at high densities (Fig. 13); the reduction is by a factor of 3.4 in *trans*-2-butene at n_c, while the mobility itself increases by only a factor of 1.3 (Fig. 5).

The great difference between the temperature dependence of the *mobility* and that of the *temperature coefficient of the mobility* indicates that the extent of localization is relatively small. The electrons are only shallowly trapped and the temperature coefficient is associated mostly with the concentration of trapping sites, that is, with the density fluctuations in the fluid. The process is termed quasilocalization (4, 13, 14, 24).

Values of μn at several values of constant T are plotted against n for *trans*- and *cis*-2-butene in Figs. 14 and 15, respectively. Moderate heating of the gas at constant density greatly decreases the degree of quasilocalization, and at $1.15T_c$ it is virtually destroyed in both gases. At this temperature μn increases with density at $n > 7 \times 10^{20}$ molecules/cm^3

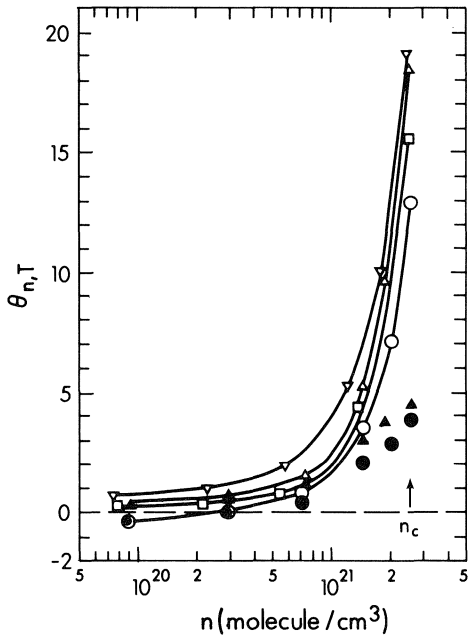

FIG. 13. Effect of density on the temperature coefficient of mobility at temperature T. $\theta_{n,T} \equiv (\partial \log \mu/\partial \log T)_{n,T}$. ▽, isobutene; △, ▲, *cis*-2-butene; □, 1-butene; ○, ●, *trans*-2-butene. Open symbols and solid lines represent $T = T_c$. Closed symbols represent $T = 1.05T_c$.

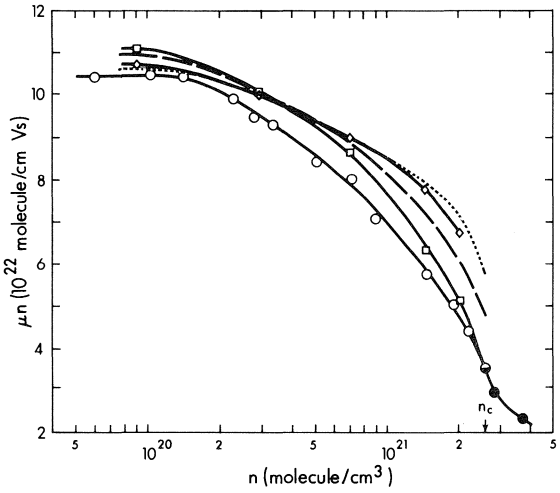

FIG. 14. Plots of μn against density in *trans*-2-butene at different temperatures. ○, coexistence vapor; ◒, critical fluid; ●, coexistence liquid; □, 428 K (T_c); ---, 450 K ($1.05T_c$); ◇, 471 K ($1.10T_c$); ···, 492 K ($1.15T_c$), with points at 10^{-20} n = 20.2 and 25.7 obtained by extrapolation of data in Fig. 5.

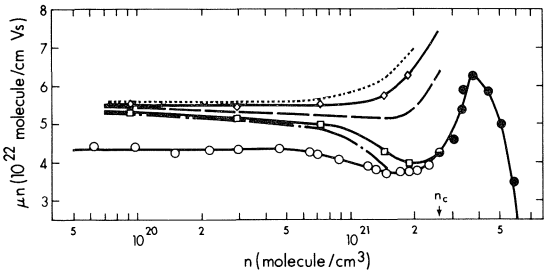

FIG. 15. Plots of μn against density in *cis*-2-butene at different temperatures. ○, coexistence vapor; ◒, critical fluid; ●, coexistence liquid; ·-·-·-·, 426 K ($0.98T_c$); □, 433 K (T_c); ---, 455 K ($1.05T_c$); ◇, 476 K ($1.10T_c$), with points at 10^{-21} $n = 1.88$ and 2.57 obtained by extrapolation of data in Fig. 6; ···, 498 K ($1.15T_c$), with a point at 1.88×10^{21} molecules/cm^3 obtained by extrapolation of data in Fig. 6.

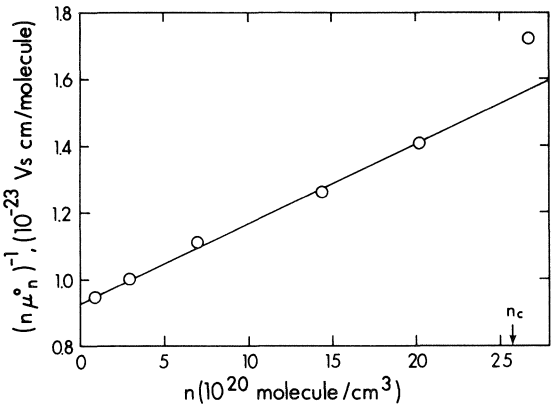

FIG. 16. Plot of $(n\mu_n^0)^{-1}$ against density in *trans*-2-butene vapor at $1.15T_c = 492$ K.

in *cis*-2-butene, while in the *trans* isomer it decreases at $n > 2 \times 10^{20}$ molecules/cm^3. The increase in *cis*-2-butene is due to the mutual partial cancellation of long range scattering interactions, such as charge–dipole and charge – induced dipole, by the several molecules that interact simultaneously with an electron. *trans*-2-Butene is nonpolar, but the mutual inference of the charge – induced dipole interactions would still tend to make μn increase at high densities. The observed decrease must have a different cause, probably transient anion formation (25, 26).

$$[14] \quad e_{qf}^- + M \underset{\tau^{-1}}{\overset{\nu_1}{\rightleftharpoons}} M^-$$

where e_{qf}^- represents a quasifree electron. The attachment rate is represented by $\nu = \nu_1 n$, and the anion ionization lifetime by τ. The forward and reverse reactions have orders that differ by one, which might be either 2 and 1 or 3 and 2, respectively.

The mobility μ_{qf} of a quasifree electron is much greater than that of an anion, so reaction [14] leads to eq. [15].

$$[15] \quad n\mu_n^0 = n\mu_{qf}/(1 + \nu_1\tau n)$$

where μ_n^0 refers to the mobility in the absence of quasilocalization (see later) in the fluid of density n. In Fig. 16 the reciprocal of $n\mu_n^0$ at $1.15T_c$ is plotted against n. The relation is linear for $n < 0.8n_c$, with $n\mu_{qf} = 1.08 \times 10^{23}$ molecules/cm V s and $\nu_1\tau = 2.6 \times 10^{-22}$ cm^3/molecule.

The forward and reverse rates of [14] depend on the energies of the species. The energy dependence of the attachment cross section is probably different from that of the total scattering cross section. However, taking the average attachment cross section as a fraction κ of the average scattering cross section σ_{ave} one obtains

$$[16] \quad \nu_1 \approx \kappa\sigma_{ave}\langle v\rangle$$

Thus, for *trans*-2-butene at $n < 0.8n_c$ and $T = 1.15T_c$, with $\langle v\rangle = 1.2 \times 10^7$ cm/s and $\sigma_{ave} = 1.04 \times 10^{-15}$ cm^2 one obtains

$$[17] \quad \tau \approx 2.1 \times 10^{-14}/\kappa$$

At $n > 0.8n_c$, the mobility decreases more rapidly than is suggested by [14] and [15]. Higher order processes contribute at high densities.

The present results support the suggestion that transient anions are the lower energy state in the two-state electron transport mechanism in liquid *trans*-2-butene (2).

Quasilocalization is a different process than the transient attachment represented by [14]. The former is much more sensitive to temperature and occurs over a narrower density range than the latter. At vapor densities and temperatures near the coexistence curve van der Waals clusters of molecules form, some of which can temporarily capture an electron. In general, the clusters may be considered as density fluctuations in the fluid. A fluctuation of appropriate depth and width is a possible localization site for an electron.

$$[18] \quad \text{Medium} \rightleftarrows \text{site}$$

$$[19] \quad e_{qf}^- + \text{site} \rightleftarrows e_{loc}^-$$

The density normalized mobility at any value of n and T is:

$$[20] \quad \mu n = n\mu_n^0 f$$

where

$$[21] \quad f = [e_{qf}^-]/([e_{qf}^-] + [e_{loc}^-]) = (1 + [\text{site}]K_{19})^{-1}$$

where [site] is the concentration of sites and K_{19} is the equilibrium constant of reaction [19]. One may write

$$[22] \quad [\text{Site}] = \exp(\Delta S_{18}^0/R)\exp(-\Delta H_{18}^0/RT)$$

[23] $K_{19} = \exp(\Delta S_{19}^0/R)\exp(-\Delta H_{19}^0/RT)$

and

[24] $(n\mu_n^0/\mu n) - 1 = \exp(\Delta S'/R)\exp(-\Delta H'/RT)$

where $\Delta S' = \Delta S_{18}^0 + \Delta S_{19}^0 \approx \Delta S_{18}^0$ and $\Delta H' = \Delta H_{18}^0 + \Delta H_{19}^0 \approx \Delta H_{18}^0$ (see below).

The density fluctuations, and hence the concentration of sites, are largest in the coexistence vapor. They diminish as the gas is heated at constant density.

It may be shown that the Arrhenius temperature coefficient of mobility, E_μ, is related to $\theta_{n,T}$ by[2]

[25] $E_\mu = kT\theta_{n,T}$

The Arrhenius temperature coefficient in *trans*-2-butene at n_c and just above T_c is 0.47 eV, or 46 kJ/mol. However, the value of μn in the critical fluid is 0.5 of $n_c\mu_{n_c}^0$ and is 0.3 of the low density limit $n_c\mu_{qf}$. The total amount of localization by both [14] and [19] is relatively small and the localization free energy is in each case a bit less than kT, ~3 kJ/mol. Thus ~6% of the temperature coefficient is due to [19] and ~94% is attributable to [18].

A plot of the log of the left side of eq. [24] against $1/T$ is given in Fig. 17 for *trans*-2-butene, using $n_c\mu_{n_c}^0 = 7 \times 10^{22}$ molecules/cm V s. The slope at $1.002T_c$ gives $\Delta H' = -85$ kJ/mol and the extrapolated intercept indicates $\Delta S' = -198$ J/mol K. Thus $\Delta G' \approx 0$ kJ/mol at 429 K, corresponding to the relatively small extent of quasilocalization.

The values of $\Delta H'$ and $\Delta S'$ decrease rapidly in magnitude with increasing temperature away from the coexistence curve. For $n = n_c$ and $T = 1.04T_c$, $\Delta H' = -47$ kJ/mol and $\Delta S' = -110$ J/mol K. These are only 55% of the values at $T = 1.002T_c$.

The quasilocalization behavior is similar in each of the isomers. For electron transport in the high density gas near the coexistence curve, the enthalpy and entropy changes associated with quasilocalization are large and negative and are due to step [18], while the energy and extent of [19] are small.

Returning now to the behavior of μn as a function of n in the coexistence vapor and liquid of *trans*-2-butene (Fig. 9), at $n > n_c$ there is an inflection in the curve. The inflection is attributed to a tendency of interactions of the several molecules interacting simultaneously with an electron to partially counteract each other at the distances in question. In the more globular hydrocarbons, such as *cis*-2- and isobutene, this tendency causes μn to increase (Fig. 9). Finally, at $n/n_c > 1.5$ in *trans*-2-butene μn plunges, due to the formation of increasingly stable localized states. The greater stability is caused by the existence of deeper traps in the denser fluid and by the concomitant lower temperature of the liquid with higher n.

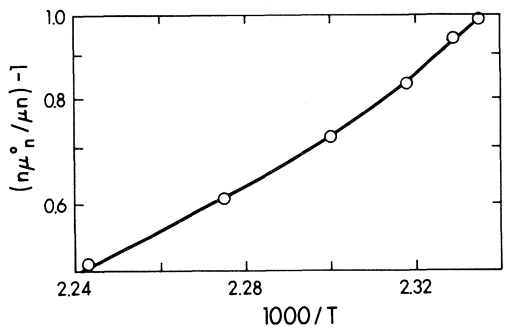

FIG. 17. Plot of eq. [24] for *trans*-2-butene at n_c, with $n\mu_n^0 = 7 \times 10^{22}$ molecules/cm V s.

The rapid plunge of μn occurs at $n/n_c > 1.5$ in *trans*-2-, 1.8 in 1-, and 2.0 in iso- and *cis*-2-butene (Fig. 9). This correlates with the degree of sphericity of the molecules and the associated difficulty of forming a stable localized state of the electron in the liquid.

Quasilocalization and Molecular Structure

The quasilocalization process does not reflect differences in molecular structure as much as do the processes in the dilute gases or normal liquids. For a series of substances ranging from xenon (4) and methane (23) to *n*-pentane (13) and 1-butene, quasilocalization occurs to a similar extent in the dense, coexistence vapors, independent of whether in the normal liquids of the same substances the electrons become quasifree or more deeply trapped.

Acknowledgement

We would like to thank the staff of the Radiation Research Center for help with the electronics.

1. J.-P. DODELET, K. SHINSAKA, and G. R. FREEMAN. J. Chem. Phys. **59**, 1293 (1973).
2. J.-P. DODELET and G. R. FREEMAN. Can. J. Chem. **55**, 2893 (1977).
3. J.-P. DODELET and G. R. FREEMAN. Can. J. Chem. **55**, 2264 (1977).
4. S. S.-S. HUANG and G. R. FREEMAN. J. Chem. Phys. **68**, 1355 (1978).
5. R. W. GALLANT. Physical properties of hydrocarbons. Vol. 1. Gulf Publishing Co., Houston, TX. 1968.
6. R. R. DREISBACH. Physical properties of chemical compounds. Adv. Chem. Ser. Vol. 22. 1959.
7. J. TIMMERMANS. Physico-chemical constants of pure organic compounds. Elsevier Publishing Co., Amsterdam. Vol. 1, 1950; Vol. 2, 1965.
8. R. D. NELSON, JR., D. R. LIDE, JR., and A. A. MARYOTT. Selected values of electric dipole moments for molecules in the gas phase. NSRDS-NBS 10, U.S. Gov't. Printing Office, Washington, DC. 1967.
9. H. S. W. MASSEY and C. B. O. MOHR. Proc. R. Soc. London, A**144**, 188 (1934).
10. L. S. FROST and A. V. PHELPS. Phys. Rev. **127**, 1621 (1962).
11. L. G. H. HUXLEY and R. W. CROMPTON. The diffusion and

[2] $\mu = A_\mu \exp(-E_\mu/kT) = A_\theta T^\theta$; $d(\ln\mu)/dT = E_\mu/kT^2 = \theta/T$.

drift of electrons in gases. Wiley, New York. 1974. Chapts. 3 and 13.
12. C. R. BOWMAN and D. E. GORDON. J. Chem. Phys. **46**, 1878 (1967).
13. I. GYÖRGY and G. R. FREEMAN. J. Chem. Phys. **70**, 4769 (1979).
14. S. S.-S. HUANG and G. R. FREEMAN. Can. J. Chem. **56**, 2388 (1978).
15. H. A. LORENTZ. The theory of electrons. Dover Publications, New York. 1952. pp. 267–274.
16. E. W. MCDANIEL. Collision phenomena in ionized gases. Wiley, New York. 1964. Chapt. 3.
17. S. ALTSHULER. Phys. Rev. **107**, 114 (1957).
18. L. G. CHRISTOPHOROU and A. A. CHRISTODOULIDES. J. Phys. B, **2**, 71 (1969).
19. G. R. FREEMAN, I. GYÖRGY, and S. S.-S. HUANG. Can. J. Chem. This issue.
20. W. SHOCKLEY. Bell System Tech. J. **30**, 990 (1951); **30**, 1018 (1951).
21. M. H. COHEN and J. LEKNER. Phys. Rev. **158**, 305 (1967), and references therein.
22. E. HAUSMANN and E. P. SLACK. Physics. Van Nostrand, New York. 1944. p. 412.
23. N. GEE and G. R. FREEMAN. Phys. Rev. A. In press.
24. N. GEE and G. R. FREEMAN. Chem. Phys. Lett. **60**, 439 (1979).
25. R. H. RITCHIE and J. E. TURNER. Z. Phys. **200**, 259 (1967).
26. L. FROMMHOLD. Phys. Rev. **172**, 118 (1968).

Reactions of 4-phenyl-3*H*-1,2,4-triazole-3,5 (4*H*)-dione with alcohols and amines

LÊ H. DAO[1] AND DONALD MACKAY

The Guelph–Waterloo Centre for Graduate Work in Chemistry, Waterloo Campus, Department of Chemistry, University of Waterloo, Waterloo, Ont, Canada N2L 3G1

Received April 20, 1979

LÊ H. DAO and DONALD MACKAY. Can. J. Chem. **57**, 2727 (1979).

Two equivalents of the title compound (**1**) react with one equivalent of primary alcohols to give good yields of nitrogen and 1-alkoxycarbonyl-2-*N*-phenylcarbamoyl-4-phenyl-1,2,4-triazolidine-3,5-diones (**3**). With secondary alcohols or benzyl alcohol the major products are the ketone or benzaldehyde, while **3** are minor products. The latter can, however, be made the major products if pyridine is used to catalyze the reaction. Compound **3***a* dissociates on heating or in pyridine solution into the 1-methoxycarbonyltriazolidinedione **4**.

If alcohols are absent **1** is converted by pyridine or other tertiary amines into nitrogen and the bicyclic compound **9**; if diethyl azodicarboxylate is present in the reaction compound **13** can be trapped.

Primary and secondary amines react very rapidly with **1** to give nitrogen and complex products. It is likely that these are 1,2-dicarbamoyl-4-phenyltriazolidine diones, analogous to **3**, and that they are very prone to dissociate in solution.

LÊ H. DAO et DONALD MACKAY. Can. J. Chem. **57**, 2727 (1979).

Deux équivalents du composé (**1**) réagissent avec un équivalent d'alcools primaires pour conduire, avec de bons rendements, à l'azote et à l'alkoxycarbonyl-1-*N*-phénylcarbamoyl-2-phényl-4-triazolidine-1,2,4,diones-3,5 (**3**). Avec les alcools secondaires ou l'alcool benzylique, les produits principaux sont la cétone ou la benzaldéhyde, tandis que **3** sont des produits secondaires. Cependant, ces derniers peuvent devenir des produits principaux si on utilise la pyridine comme catalyseur de la réaction. Par chauffage ou dans une solution de pyridine, le composé **3***a* se dissocie en méthoxycarbonyl-1-triazolidinedione **4**.

S'il n'y a pas d'alcools, **1** est transformé par la pyridine ou d'autres amines tertiaires en azote et en composé bicyclique **9**; si l'azodicarboxylate de diéthyle est présent dans la réaction, le composé **13** peut être isolé.

Les amines primaires et secondaires réagissent très rapidement avec **1** pour conduire à l'azote et à des produits complexes. Il est probable que ces produits soient des dicarbamoyl-1,2-phényl-4-triazolidine diones semblables à **3** et qu'ils aient une grande tendance à se dissocier en solution.

[Traduit par le journal]

As a class the 4-substituted 3*H*-1,2,4-triazole-3,5(4*H*)-diones[2] are probably the most powerful dienophiles known, but they show a wide range of other reactivity as well. A large variety has now been synthesized, though the 4-phenyl derivative **1** has been the most widely studied, references to it outnumbering those to all others combined.

As well as Diels–Alder additions many other reactions of compound **1** with unsaturated substrates have been investigated. Among these are "ene" reactions with alkenes (1), dienes (2), and primary enamines (3), insertion reactions in tropolone (4), cycloaddition to alkenes (5, 6), formation of reactive dipoles with vinyl ethers (7), vinyl azides (8), vinyl esters (6, 9, 10), and diazoacetic ester (11), addition to 1,3-dipoles (12), and insertion in N—H in pyridones (13). It has also been shown to oxidize alcohols to carbonyl compounds (14).

Despite its great reactivity to such a range of substrates, **1** is remarkably stable to strong acids, as its synthesis from the 4-phenylurazole **2** with N_2O_4 attests (15). It is unaffected by atmospheric exposure for long periods, and its solutions in chlorinated or saturated hydrocarbon solvents remain deeply colored and free of precipitate almost indefinitely. We noticed, however, that its solutions in methanol rapidly decolorized. In concentrated solution the reaction was exothermic with the formation of a precipitate. We expected this to be the urazole **2**, formed by oxidation of the alcohol. In fact it was a product $C_{17}H_{14}N_4O_5$ resulting from the reaction of one molecule of methanol and two molecules of **1** with loss of one molecule of nitrogen.

In view of the proven ability of **1** to oxidize secondary alcohols (14) we decided to examine its reaction with a range of representative alcohols: methanol, ethanol, 1-butanol, 2-propanol, cyclopentanol, and benzyl alcohol. Some of our results have been published in a preliminary form (16), and are now

[1]Present address: Department of Chemistry, York University, Downsview, Ont., Canada M3J 1P3.

[2]The nomenclature is that of Chemical Abstracts.

0008-4042/79/202727-07$01.00/0

presented in more detail along with other related reactions of **1**.

The identity of the product from methanol as **3***a* followed from its spectra, its reactions, and its rational synthesis. The ^{1}Hmr spectrum included a MeO singlet at 5.95τ and one exchangeable proton. The ir spectrum (Nujol) had an NH absorption at 3398 and an intense broad complex absorption in the CO region with maxima at 1828, 1760, and 1700 cm^{-1}. It had no well defined mp, decomposing between 180 and 187°C to a solid and a liquid. The solid was readily identified as **4** by comparison with an authentic sample made from **2** by treatment with sodium hydride or pyridine, followed by methyl chloroformate. If **2** was treated with one equivalent of sodium hydride, and then in turn with phenyl isocyanate and methyl chloroformate, **3***a* was produced in a good yield. The liquid was phenyl isocyanate identified as ethyl *N*-phenylcarbamate. The latter was also formed when **3***a* was refluxed in ethanol. The behaviour of **3***a* in solution was examined by ^{1}Hmr spectroscopy. In benzene-d_6 or chloroform-*d* there was no evidence of decomposition, but in pyridine-d_5 the equilibrium in eq. [1] was rapidly established. (K_{eq} = 0.75 for a 0.17 *M* solution of **3***a*.) Addition of chloroform-*d* reversed the reaction, which could be moved in either direction by varying the proportions of chloroform and pyridine. Examples of such urethane–isocyanate equilibria have been noted previously (17).

[1] **3***a* ⇌ **4***a* + PhNCO

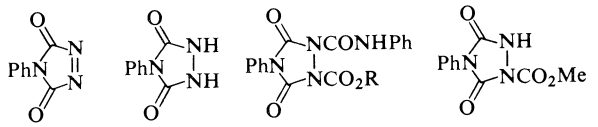

1 **2** **3** **4**

a R = Me
b R = Et
c R = *n*-Bu
d R = *i*-Pr
e R = *c*-C_5H_{10}
f R = $PhCH_2$

In general compounds **3***a–f* were prepared by stirring equimolar amounts of **1** and the alcohol (0.1 *M* each) in benzene at room temperature for 2 days. Alternatively a large excess of the alcohol was used in methylene chloride as solvent, in which case the reaction was much more rapid (~30 min). In either case the reaction mixture was evaporated and the residue treated with chloroform to remove traces of insoluble polymer or the urazole **2**. The chloroform-soluble material was worked up to give **3**, purified by conventional crystallization techniques.

The isolated yields were close to the actual in those cases where the latter were determined by gas–liquid chromatography (glc); glc was also used to analyze for benzaldehyde and cyclopentanone. The determination of other carbonyl compounds was made by ^{1}Hmr analysis.

The yields of products, and the melting points, spectroscopic properties, and elemental analyses are shown in Table 1. The yields of **3** are seen to be good to excellent for the oxidation of primary alcohols; aldehydes were not detected. From benzyl alcohol and both secondary aliphatic alcohols examined the yields of **3** were low, benzaldehyde or the ketone being the major product.

The mechanism for the oxidation reactions of **1** with alcohols is not certain, though initiation through α-hydrogen atom abstraction by the azo group seems likely. Other instances of oxidation of 2-propanol to acetone by carbonylazo compounds have been noted (18, 19). In the case of benzoylphenyldiimine (18) the intervention of radicals by homolysis of the intermediate phenyldiimine was clearly established.

For the formation of compounds **3** we propose (Scheme 1) an initial addition of alcohol at the carbonyl group, followed by deprotonation to the nucleophilic species **5** (or its *N*-acyl anion equivalent if loss of nitrogen precedes further reaction of **5**). Attack on a second molecule of **1** to give **6**, cyclization to **7**, and cleavage of the C to N—Ph bond completes the reaction. The sequence **6** to **7** to **3** in effect transposes the methoxycarbonyl group from one nitrogen to another. Migrations of this general type to a nucleophilic centre have been reviewed (20). The resonance stabilized amide anion is predictably a better leaving group from **7** than is alkoxide ion. We tried to synthesize compound **8**, the protonated form of **6** (R = Me) to test whether the 1,4-shift of methoxycarbonyl to give **3** occurred under the reaction conditions. *N*,*N*-Dimethoxycarbonylaniline was treated with the anion of the urazole **2**, but neither NaH nor KO*t*-Bu was able to effect the condensation to **8** in a variety of solvents. This failure is perhaps not surprising since it requires the displacement of methoxide by amide anion.

Pyridine had a strong catalytic effect on the reac-

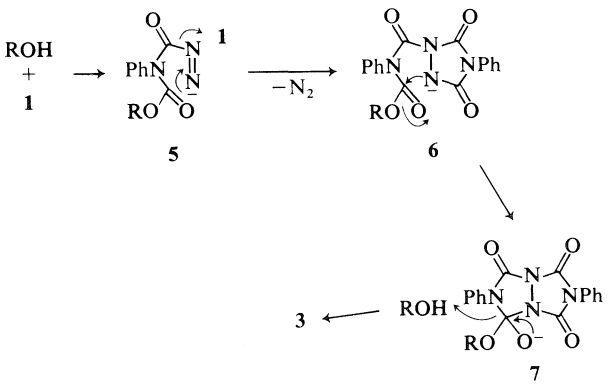

SCHEME 1

TABLE 1. Reaction of equimolar amounts of **1** and alcohol in benzene at 25°C with and without pyridine

ROH	Pyridine (equiv.)	Aldehyde or ketone[a] (%)	Compd 3	Yield[b] (%)	Mp[g] (°C)	ν(Nujol) NH, C=O (cm^{-1})	τ($CDCl_3$) (ppm)[l] R	Ph[m]	Analysis Compound	C	H	N
MeOH	—	0[c]	*3a*	95[e]	180–187[h]	3398, 1828, 1760, 1700	5.95(s, 3H, OMe)	2.3–2.8, 2.4	$C_{17}H_{14}N_4O_5$	Calcd.: 57.63	3.98	15.81
	1.0	0[c]	*3a*	96[e]						Found: 57.61	4.13	15.75
EtOH	—	0[c]	*3b*	95[e]	140–142[h]	3338, 1810, 1755, 1730	8.60(t, 3H, Me), 5.50(q, 2H, OCH_2)	2.2–2.8, 2.5	$C_{18}H_{16}N_4O_5$	Calcd.: 58.69	4.38	15.21
										Found: 58.75	4.31	15.07
n-BuOH	—	0[c]	*3c*	60[e]	134–135[i]	3358, 1805 1755, 1720	9.00(distorted t, 3H, Me), 8.1–8.7 (m, 4H, CH_2CH_2), 5.50(t, 2H, OCH_2)	2.3–2.7, 2.4	$C_{20}H_{20}N_4O_5$	Calcd.: 60.60	5.09	14.13
										Found: 60.64	5.21	14.17
i-PrOH	—	64,[c] 68[d]	*3d*	17,[e] 20[f]	129–130[j]	3333, 1797, 1772, 1752, 1738	8.80(d, 6H, Me), 4.87(s, 1H, OCH)	2.4–3.1, 2.6	$C_{19}H_{18}N_4O_5$	Calcd.: 59.68	4.74	14.65
										Found: 59.59	4.65	14.72
	0.5	8[c]	*3d*									
	1.0	5[c,d]	*3d*	90[c]								
	2.0, 10	3[c]	*3d*									
c-C_5H_9OH	—	60[d]	*3e*	28,[e] 30[f]	140–142	3357, 1804, 1771, 1740	7.8–8.6(b, 8H, $(CH_2)_4$,), 4.60(m, 1H, OCH)	2.3–2.8, 2.5	$C_{21}H_{20}N_4O_5$	Calcd.: 61.76	4.94	13.72
										Found: 61.59	4.85	14.02
	1.0	20[d]	*3e*	60[e]								
$PhCH_2OH$	—	80[d]	*3f*	18,[e] 20[f]	180–182[k]	3180, 1810 1770, 1710	4.52(s, 2H, OCH_2)	2.2–2.8 (15 H)	$C_{24}H_{18}N_4O_5$	Calcd.: 64.18	4.22	13.02
	1.0	30[d]	*3f*	60[f]						Found: 63.89	4.18	12.92

[a]Based on the reaction of 1 mol of **1** with 1 mol of alcohol.
[b]Based on the reaction of 1 mol of **1** with 0.5 mol of alcohol.
[c]Analysis by ^{1}Hmr (±4%).
[d]Analysis by glc (±2%).
[e]Isolated.
[f]The unreacted alcohol was measured by glc. The balance of the alcohol was assumed to be the yield of **3**.
[g]In all cases accompanied by decomposition. Compound **3***d* re-solidified above its mp; melting occurred again between 260–290°C.
[h]Recrystallization from $CHCl_3$.
[i]Recrystallization from C_6H_6.
[j]Recrystallization from C_6H_6–isooctane.
[k]Recrystallization from CCl_4.
[l]The NH absorption was variable, but in general occurred between 0.0 and 1.0 τ.
[m]The phenyl protons absorbed in general as a broad multiplet, dominated by a strong singlet, each containing 5H.

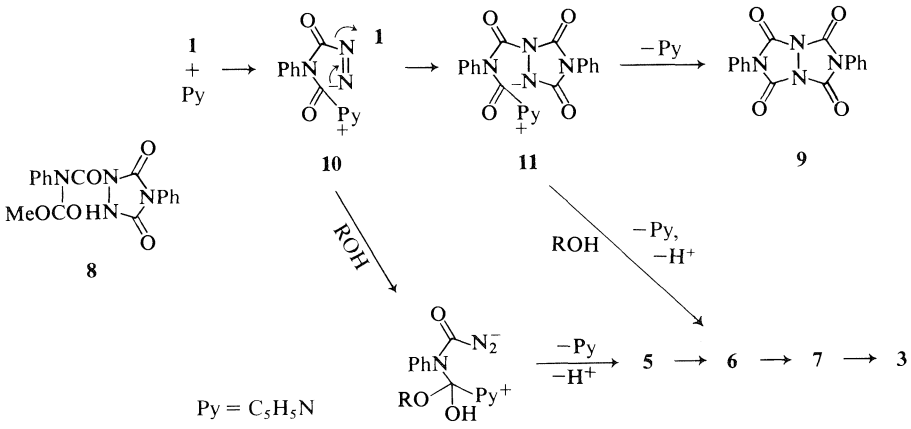

SCHEME 2

tion of **1** with alcohols. Thus when benzene solutions were made 1 *M* in pyridine, as well as in **1** and in methanol, decolorization was complete within minutes, **3***a* being again formed in an excellent yield. Likewise attack on benzyl alcohol and the secondary alcohols to give compounds **3** was accelerated, much more so than the oxidation reaction. The results are also shown in Table 1, from which it is clear that the conversion of alcohols in general into compounds **3** can be made the dominant reaction by inclusion of pyridine where necessary. A series of reactions in 2-propanol (Table 1) showed that the yields of **3***d* and acetone were almost independent of pyridine concentration over the range 0.5 to 10 *M*.

In the absence of alcohols, solutions of **1** containing pyridine, or alternatively triethylamine or 1,5-diazabicyclo[4.3.0]nonene-5, still reacted readily with evolution of nitrogen to give a sparingly soluble solid in good yield. This product, which was not observed in the alcohol reactions,[3] was shown to be the tetrazabicyclo[3.3.0]octane derivative **9**. It is the pyrolysis product of **1**, first obtained by Stollé (21). It has also been made by reaction of **2**, either with phenyl isocyanate (22) or with **1**, in what has been interpreted as a radical chain process (23).

The role of the pyridine was examined on a somewhat more quantitative basis by visible spectroscopy. A solution in methylene chloride 0.02 *M* in each of **1** and pyridine[4] had a half life (measured at the λ_{max} of **1** at 550 nm) of 40 min at 30°C. When a similar solution was also made 0.04 *M* in methanol the half life was reduced to 23 min. The uncatalyzed reaction of **1** (0.02 *M*) and methanol (0.04 *M*) is relatively very much slower with a half life of 1–1.5 days.

The formation of **3** or **9** in the presence of pyridine can be accounted for by a variation of the uncatalyzed reaction in which nucleophilic attack by pyridine leads to the ring-opened species **10** (Scheme 2), analogous to **5**. In the absence of alcohol the reaction proceeds through **10** to **11** to **9**. When alcohol is present it may attack **10** to give **5**, or **11** to give **6**, and thence compound **3** in either case, a reaction faster than the sequence leading to **9**. The latter is *not* an intermediate in the formation of **3**, control reactions showing that it is not opened by, for example, methanol alone or methanol and pyridine.

Bicyclic structures of type **9** are recognized thermal decomposition products of 5-membered cyclic azodicarbonyl compounds. They have been found with other triazolinediones (21, 24), while pyrazolinediones also give analogous products (25).

Formally **9** is the result of cycloaddition of **1** to 2-phenylaziridinedione or an open dipolar or diradical equivalent of it (**12***a*, *b*, *c*). We examined the possibility of other cycloadditions of **12**. Treatment of **1** with an excess of diethyl azodicarboxylate gave an isolated yield of 28% of **13**, whose identity was proven by its synthesis from the urazole **2** with 2 equiv. of sodium hydride and ethyl chloroformate. No reaction was detected with dimethyl maleate or stilbene, only compound **9** being produced; dimethyl acetylenedicarboxylate gave a methoxy-containing polymer, as well as **9**.

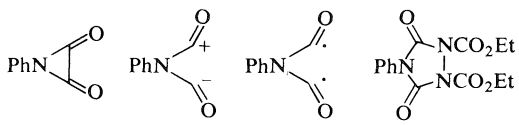

a *b* *c*

12 **13**

[3]It was a minor product in the pyridine-catalyzed reactions of the *sec* alcohols.

[4]The lower concentrations, one tenth that used in the preparative runs, were necessary for the spectrophotometric experiment. Methylene chloride, rather than benzene, was chosen as solvent since separation of solid products in the cell only occurred in the late stages of the reaction.

The greater reactivity towards the azo bond than towards -ene or -yne bonds may reside in the greater ability of nitrogen than carbon to stabilize negative charge in the product precursor, as in **11**. Azo adducts must also benefit from the stabilization inherent in the creation of two amide groups.

The reaction of **1** with primary and secondary amines was also examined to see if compounds **14** (R^1 = H or R^1 = R) might be formed, analogous to **3** from alcohols. With *tert*-butylamine, pyrrolidine, or dimethylamine, decomposition of **1** was fast and exothermic, but work-up led to intractable gums. Compound **9** was evidently not a product. The reaction of **1** with dimethylamine in C_6D_6 was followed by ^{1}Hmr spectroscopy, but the methyl signals were at all times broad and complex.

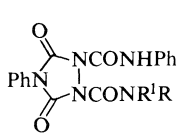

14

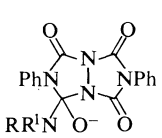

15

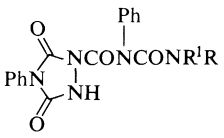

16

An intermediate like **15** does not have the special bias towards cleavage of the C to N—Ph bond found in **7**. Cleavage to **16** must also compete with that to **14**. Furthermore the amines presumably catalyze the dissociation of **14** (cf. pyridine and compound **3**) to PhNCO and, when R^1 = H, to RNCO. These, on recombination with the urazole ring system can lead to multiplication of products. Compound **16** may similarly dissociate when R^1 = H.

Experimental

The following spectrometers were used: for ir a Beckman IR 10, all values given being determined in Nujol mulls; for uv a Unicam SP 800 B; for ^{1}Hmr a Varian T-60. Melting points are uncorrected.

*1-Alkoxycarbonyl-2-*N*-phenylcarbamoyl-4-phenyl-1,2,4-triazolidine-3,5-diones (3)*

Uncatalyzed Reactions

(*a*) The deep red solution of the azo compound **1** (15) (1.75 g, 10 mmol) and the alcohol (10 mmol) in benzene (100 mL) was stirred for about 2 days at room temperature, by which time the color had faded to a pale yellow. The benzene was evaporated under reduced pressure and the pasty residue treated with chloroform (5 mL). A small amount of undissolved material (the urazole **2** or polymer) was filtered off. The solution was evaporated till crystallization occurred or otherwise to dryness. In the latter case the residue was crystallized from an appropriate solvent.

(*b*) To a solution of **1** (10 mmol) in methylene chloride (10 mL) was added a large excess of the alcohol (10 mL). The reaction was exothermic, vigorous evolution of nitrogen was observed, and after about 30 min the red had given place to a straw color. The solution was evaporated and the residue worked up as before.

To confirm the absence of aldehyde (methanol, ethanol, 1-butanol reactions) and to determine the yield of acetone in the 2-propanol reaction, the alcohol and **1** (0.1 mmol each) were dissolved in C_6D_6 (0.3 mL) in an nmr tube. When the reaction was complete toluene was added as an internal standard and the peaks for it and the carbonyl compound were integrated (±4%).

To estimate the amounts of benzaldehyde and cyclopentanone produced, and of benzyl alcohol and cyclopentanol unreacted, solutions of alcohol and **1** (1.0 mmol each) in benzene (3 mL) were allowed to react and then analyzed by glc (6 ft × 1/8 in., 10% SE 30, 90°C), using mesitylene as internal standard (±2%). From the amount of reacted alcohol the yields of **3***e* and *f* (and in one case **3***d*) were determined. The latter were only slightly higher than the isolated yields obtained in the work-up. Gas–liquid chromatography (70°C) was similarly used as an alternative for measuring the yields of acetone.

The melting points, solvents of crystallization, yields, and elementary analyses of **3**, as well as the yields of aldehyde or ketones, are listed in Table 1.

Pyridine-catalyzed Reactions

These experiments were in general done on a 1 mmol scale as described above for the glc analyses. One equivalent of pyridine (in the case of the 2-propanol reaction variable amounts, see Table 1), the alcohol, and **1** reacted rapidly in benzene, decolorization being complete within one hour.

The work-up and the determination of yields were carried out as described above. Compound **9** (see below) was a minor insoluble product in the reaction with 2-propanol or cyclopentanol.

The yields of **3** and of the corresponding carbonyl compounds are also given in the table.

Kinetics

The disappearance of the chromophore at 550 nm in 0.02 *M* solutions of **1** in methylene chloride (1 cm quartz cell, 30°C) was followed in each of the following experiments by repeated scanning of the visible region: (*i*) 0.04 *M* in methanol, $t_{1/2}$ = 1–1.5 days; (*ii*) 0.02 *M* in pyridine, $t_{1/2}$ = 40 min; (*iii*) 0.04 *M* in methanol, 0.02 *M* in pyridine, $t_{1/2}$ = 23 min.

1-Methoxycarbonyl-4-phenyl-1,2,4-triazolidine-3,5-dione (4)

(a) From **3**a

When **3***a* (100 mg) was heated just above its mp in a small test tube it decomposed to a solid and a liquid which condensed on the upper walls. Careful washing out of this liquid and treatment of it with ethanol gave ethyl *N*-phenylcarbamate, identified by comparison with an authentic sample. The solid was identified as **4** by crystallizing it from ethanol.

Alternatively, when **3***a* was refluxed in ethanol for 30 min and the solution concentrated and cooled, compound **4** separated out. Ethyl *N*-phenylcarbamate was identified in the mother liquor.

Equilibrium between **3**a *and* **4**

Solutions of **3***a* in chloroform-*d* showed no evidence of the presence of **4** when examined by ^{1}Hmr spectroscopy. Addition of pyridine-d_5 caused the appearance of compound **4**. In neat C_5D_5N the equilibrium constant for **3***a* ⇌ **4** was 0.75 (**3***a* and **4** having τ for OMe at 3.82 and 3.92 ppm respectively) but it could be reduced by the addition of $CDCl_3$.

(b) By Synthesis from **2**

To a suspension of 50% sodium hydride – mineral oil (0.50 g, 11 mmol) in dry tetrahydrofuran (40 mL) was added **2** (1.77 g, 10 mmol) followed by methyl chloroformate (0.91 g, 10 mmol). After one hour the mixture was evaporated and the residue washed free of oil with hexane. Decomposition with water gave **4** (1.98 g, 84%), purified by crystallization from ethanol, mp 229–230°C.

Pyridine could also be used in place of sodium hydride.

Compound **4** had ν: 3350 (NH), 1800, 1754 (C=O) cm^{-1}; τ(CD_3COCD_3): 2.45 (m, 5H phenyl), 6.05 (s, OMe) ppm.

Anal. calcd. for $C_{10}H_9N_3O_4$: C 51.07, H 3.86, N 17.87; found: C 51.03, H 3.99, N 17.61.

Synthesis of **3***a from* **2**

Addition of **2** (1.77 g, 10 mmol) to a suspension of 50% sodium hydride – mineral oil (0.50 g, 11 mmol) in dry tetrahydrofuran (40 mL) caused vigorous effervescence. Phenyl isocyanate (1.19 g, 10 mmol) and then methyl chloroformate (0.91 g, 10 mmol), each in tetrahydrofuran (5 mL), were added and the mixture kept for 1 h at room temperature. Addition of water (30 mL) gave a colorless solid which was washed with water and ether and then dried (80%). It was identified as **3***a* by comparison with the product from the reaction of **1** with methanol.

*3,7-Diphenyl-1,3,5,7-tetrazabicyclo[3.3.0]octan-2,4,6,8-tetraone (***9***)*

Pyridine (3 mL) was added to a solution of **1** (1.75 g, 10 mmol) in methylene chloride (10 mL). Decolorization was rapid, nitrogen was copiously evolved, and a solid separated. Filtration and washing with cold alcohol gave **9** (1.30 g, 80%) in high purity, mp 234–235°C. It could be recrystallized on a small scale from a large volume of ethanol. It was identical with material prepared by pyrolysis, as described by Stollé (21); ν (Nujol): 1790, 1757 (C=O) cm^{-1}.

Triethylamine or 1,5-diazabicyclo[4.3.0]nonene-5 in place of pyridine also led to **9** in high yields.

Stability of **9** *to Methanol and Pyridine*

A suspension of **9** (50 mg) in methanol (10 mL) was refluxed for 12 h and evaporated to dryness. The ir spectrum of the residue was identical with that of starting material.

Pyridine (2 mL) containing **9** (50 mg) was brought to its boiling point and methanol (2 mL) was added. The milky suspension was then kept at room temperature for 4 h and the solvents completely removed. The residue was pure **9**.

*1,2-Diethoxycarbonyl-4-phenyl-1,2,4-triazolidine-3,5-dione (***13***)*

(a) By Trapping with **1** *in the Presence of Pyridine*

To a suspension of **1** (1.75 g, 10 mmol) and diethyl azodicarboxylate (8.7 g, 50 mmol) in dry ether (30 mL) was added pyridine (10 mL). The mixture was stirred until the azo color had disappeared and evolution of nitrogen had stopped. The ethereal suspension was washed with water, hydrochloric acid (2 *N*), water again, and dried. Evaporation of the ether gave an oil which was chromatographed on silica gel with benzene as eluent, affording **13** as a colourless solid (0.9 g, 28%) identical with material synthesized in (*b*) below.

(b) Direct Synthesis

Compound **2** (1.77 g, 10 mmol) and a 50% sodium hydride – mineral oil suspension (0.92 g, 20 mmol) were stirred in dry dimethoxyethane (50 mL) for 4 h at room temperature. Ethyl chloroformate (2.16 g, 20 mmol) was added dropwise and the mixture was stirred for 12 h. Work-up as in (*a*) gave a residue which readily crystallized (2.0 g, 62%). It was recrystallized from benzene–iso-octane as needles, mp 120–120.5°C; ν (Nujol): 1767, 1734 (C=O) cm^{-1}; τ($CDCl_3$): 2.58 (5H phenyl, s), 5.58 ($2OCH_2$, q, J = 7.2 Hz), 8.65 ($2CH_3$, t) ppm. *Anal.* calcd. for $C_{14}H_{15}N_3O_6$: C 52.34, H 4.71, N 13.08; found: C 52.46, H 4.68, N 12.88.

Attempted Trapping Experiment with **1** *in the Presence of Pyridine*

Solutions of **1** (0.175 g, 1 mmol) in methylene chloride (5 mL) were treated with 1 mmol of either stilbene, dimethyl maleate, or dimethyl acetylenedicarboxylate, followed in each case by pyridine (1 mL). When nitrogen evolution had ceased the solvent was removed. The stilbene reaction produced only unreacted stilbene and compound **9**. The involatile residue from the dimethyl maleate reaction was devoid of methoxy-containing material (^{1}Hmr). In the acetylene ester reaction the residue contained material which gave a broad methoxy signal in the ^{1}Hmr spectrum, suggesting that polymeric material had been produced. Compound **9** was the major product.

Reaction with Amines

(a) tert-*Butylamine*

A solution of the amine (73 mg, 1 mmol) in methylene chloride (5 mL) was slowly added to a solution of **1** (175 mg, 1 mmol) in methylene chloride (5 mL). The reaction was highly exothermic and deep colors developed through light to deep purple and then to brown. Evaporation to a sticky residue and trituration with cold ether – methylene chloride gave a tan solid (200 mg) which was sparingly soluble in $CDCl_3$; τ: 2.3–2.9 (Ph), 4.4–5.1 (NH), and 8.7–9.0 (*tert* Bu) ppm, all very broad and in the approximate ratios of 5:2:9.

(b) Pyrrolidine

Solutions of pyrrolidine (51 mg, 1 mmol) and **1** (175 mg, 1 mmol), each in methylene chloride (5 mL), were mixed. There was immediate decolorization of the azo compound. The residue on evaporation was a gum soluble in $CDCl_3$; τ: 2.1–3.1 (5H phenyl), 6.0 (1H, broad), 6.5 (3H, slightly broadened q), 8.1 (3H, broad), 8.8 (2H, t) ppm. Attempted purification gave fractions of increased complexity in their ^{1}Hmr spectra.

(c) Dimethylamine

Equimolar solutions (0.3 mmol) of the amine and **1** were mixed as in (*b*) in a total of 5 mL of methylene chloride. The brown residue obtained on evaporation was mostly soluble in $CDCl_3$; τ: 2.3–3.0 (Ph), 6.37, 6.60, 6.83, 6.93, 7.04, 7.62 (Me and ? NH, 6 singlets of widely varying intensity, 1.2 times area of Ph peak) ppm.

The reaction was followed by ^{1}Hmr spectroscopy in C_6D_6 by gradually adding **1** to a solution of the amine. The Me region was complex before and after the stoichiometric point.

1. W. H. Pirkle and J. C. Stickler. J. Chem. Soc. Chem. Commun. 760 (1967).
2. J. Brynjolffsen, A. Emke, D. Hands, J. M. Midgley, and W. B. Whalley. J. Chem. Soc. Chem. Commun. 633 (1975); K. Hayakawa and H. Schmid. Helv. Chim. Acta, **60**, 1551 (1977).
3. H. Wamhoff and K. Wald. Ber. **110**, 1716 (1977).
4. T. Sasaki, K. Kanematsu, and K. Hayakawa. J. Chem. Soc. C, 2142 (1971).
5. E. K. von Gustorf, D. V. White, B. Kim, D. Hess, and J. Leitich. J. Org. Chem. **35**, 1155 (1970); D. J. Pasto, A. F.-T. Chen, and G. Binsch. J. Am. Chem. Soc. **95**, 1553 (1973); R. H. Rynbrandt. J. Hetero. Chem. **11**, 787 (1974).
6. K. B. Wagener, S. R. Turner, and G. B. Butler. J. Org. Chem. **37**, 1454 (1972).
7. S. R. Turner, L. J. Guilbault, and G. B. Butler. J. Org. Chem. **36**, 2838 (1971).
8. A. Hassner, D. Tang, and J. Keogh. J. Org. Chem. **41**, 2102 (1976).
9. K. B. Wagener and G. B. Butler. J. Org. Chem. **38**, 3070 (1973).
10. A. E. Baydar, G. V. Boyd, R. L. Monteil, P. F. Lindley, and M. M. Mahmoud. J. Chem. Soc. Chem. Commun. 650 (1976).
11. R. A. Izydore and S. McLean. J. Am. Chem. Soc. **97**, 5611 (1975).

12. E. CAWKILL, W. D. OLLIS, C. A. RAMSDEN, and G. P. ROWSON. J. Chem. Soc. Chem. Commun. 439 (1976).
13. N. P. SHUSHERINA and M. SAID. Dokl. Akad. Nauk SSSR, **233**, 606 (1977); Chem. Abstr. **87**, 39382x (1977).
14. R. C. COOKSON, I. D. R. STEVENS, and E. WATTS. J. Chem. Soc. Chem. Commun. 744 (1966).
15. J. C. STICKLER and W. H. PIRKLE. J. Org. Chem. **31**, 3444 (1966).
16. L. H. DAO and D. MACKAY. J. Chem. Soc. Chem. Commun. 326 (1976).
17. D. L. KLAYMAN, J. J. MAUL, and G. W. A. MILNE. J. Hetero. Chem. **5**, 517 (1968); S. J. LOVE and J. A. MOORE. J. Org. Chem. **33**, 2361 (1968).
18. S. J. COHEN and J. NICHOLSON. J. Org. Chem. **30**, 1162 (1965).
19. D. MACKAY, U. F. MARX, and W. A. WATERS. J. Chem. Soc. 4793 (1964).
20. R. M. ACHESON. Acc. Chem. Res. **4**, 177 (1971).
21. R. STOLLÉ. Ber. **45**, 273 (1912).
22. L. CAPUANO and K. MÜLLER. Ber. **110**, 1691 (1977).
23. H. WAMHOFF and K. WALD. Ber. **110**, 1699 (1977).
24. R. F. SMITH, S. B. KALDOR, E. D. LAGANIS, and R. F. OOT. J. Org. Chem. **40**, 1854 (1975).
25. B. T. GILLIS and R. A. IZYDORE. J. Org. Chem. **34**, 3181 (1969); A. B. ENVIN, A. Y. LAM, J. J. MAHER, and J. J. BLYSKAL. Tetrahedron Lett. 4497 (1969).

Synthesis and spectroscopic studies of the pyrimidine-2(1*H*)thione derivatives

FAROUK H. AL-HAJJAR,[1] YUSUF A. AL-FARKH, AND HAYAT S. HAMOUD

Petroleum and Petrochemicals Department, Kuwait Institute for Scientific Research, P.O. Box 24885, Safat, Kuwait

Received April 12, 1979

FAROUK H. AL-HAJJAR, YUSUF A. AL-FARKH, and HAYAT S. HAMOUD. Can. J. Chem. **57**, 2734 (1979).

1,3-Diaryl-2-propen-1-ones **1** reacted with thiourea in the presence of sodium ethoxide to give 4,6-diaryl-3,4-dihydropyrimidine-2(1*H*)thiones **5** which upon dehydrogenation with 3 mol of ethanolic sodium ethoxide yielded the corresponding 4,6-diarylpyrimidine-2(1*H*)thiones **9**. The *N*-acetyl derivatives of the former thiones were prepared. Infrared, nuclear magnetic resonance, and ultraviolet spectral data of the above compounds were tabulated and discussed.

FAROUK H. AL-HAJJAR, YUSUF A. AL-FARKH et HAYAT S. HAMOUD. Can. J. Chem. **57**, 2734 (1979).

La réaction des diaryl-1,3 propène-2 ones-1 avec la thiourée en présence d'éthylate de sodium fournit les diaryl-4,6 dihydro-3,4 1*H*-pyrimidinethiones-2 (**5**) qui par déshydrogénation par 3 mole d'éthylate de sodium en milieu éthanolique conduisent aux diaryl-4,6 1*H*-pyrimidine thiones-2 (**9**) correspondantes. On a aussi préparé les dérivés *N*-acétylés des thiones. On rapporte et discute les données spectrales ir, rmn et uv des composés préparés.

[Traduit par le journal]

Introduction

The reaction of acetylenic ketones with thiourea and its derivatives has been known to give 4,6-diarylpyrimidine-2(1*H*)thione derivatives (1, 2). The condensation of 1,3-diaryl-2-propen-1-ones with thiourea in the presence of sodium ethoxide under reflux for 10 h has been reported to give the corresponding 4,6-diaryl-5,6-dihydropyrimidine-2(1*H*)thiones (3).

The present work was intended to study the reaction of 1,3-diaryl-2-propen-1-ones **1** with thiourea and to account for the manipulated methods and reasoning in establishing the mechanism of the reaction as well as the structure of the products.

Experimental

Infrared (ir) spectra were measured on a Perkin Elmer 577 spectrophotometer (KBr). Nuclear magnetic resonance (nmr) spectra were measured on a JEOL-PMX 60 spectrometer using TMS as internal standard. Ultraviolet spectra (uv) were measured on a Beckman spectrophotometer ACTA MVI (ethanol). The purity of the analytical samples was checked by thin-layer chromatography (tlc) (silica gel). Melting points were taken in a BÜCHI 510 melting point in open capillary tubes and are uncorrected. Microanalyses for N, S, and Cl were determined by the Chemical Analytical Laboratory (KISR), however, C and H were determined by Alfred Bernhardt, West Germany. All evaporations were performed on evaporators *in vacuo*.

*Reaction of 1,3-Diaryl-2-propen-1-one **1** with Thiourea*

General Procedure

1,3-Diaryl-2-propen-1-one **1** (0.03 mol) and thiourea (0.03 mol) were added successively to a solution of sodium ethoxide (0.03 mol) in absolute ethanol (100 mL). The reaction mixture was heated under reflux for 1 h. The solvent was evaporated and the residue was dissolved in water (150 mL). The alkaline solution was acidified with acetic acid (10 mL) and the precipitated solid was separated by filtration. Crystallization of the crude products from suitable solvents gave the corresponding 4,6-diaryl-3,4-dihydropyrimidine-2-(1*H*)thione **5** as colorless crystals. The results are reported in Table 1. Heating of the thiones **5***a–f* with 3 mol of sodium ethoxide in absolute ethanol for 2 h afforded the corresponding 4,6-diarylpyrimidine-2(1*H*)thione **9***a–f* approximately in quantitative yield (mp, mixed mp, and ir spectra).

The thiones **5***a–c* are insoluble in both hot and cold NaOH solutions. All the attempts to prepare the *N*-methyl, *S*-methyl, or the disulfide derivatives from the corresponding thiones **5***a–l* were unsuccessful.

*1-Acetyl-4,6-diaryl-3,4-dihydropyrimidine-2(1*H*)thiones **8**a–l*

General Procedure

The thione **5** (2.0 gm) was heated with acetic anhydride (3 mL) on a boiling water-bath for 30 min. The product, which precipitated on addition of cyclohexane, was crystallized from a suitable solvent to give the corresponding 1-acetyl derivative which upon heating for 5 min with 3 mol of sodium ethoxide in ethanol gave the corresponding thione **5** (mp, mixed mp, and ir spectra). However, when the heating was continued for 2 h, it gave the corresponding 4,6-diarylpyrimidine-2(1*H*)thione **9**. The results are reported in Table 2.

Results and Discussion

When 1,3-diaryl-2-propen-1-ones **1***a–l* were refluxed with thiourea in the presence of sodium ethoxide in ethanol for one hour, they gave the corresponding 4,6-diaryl-3,4-dihydropyrimidine-2-(1*H*)thiones **5***a–l* and not 4,6-diaryl-5,6-dihydropyrimidine-2(1*H*)thione **4**, as described previously by Sammour *et al.* (3). The reaction proceeds either by (*i*) 1:2-addition or (*ii*) 1:4-addition of the anion (A) to the ketone, followed by cyclization of the intermediates **2** and **3** (Scheme 1). Route (*ii*) seems more

[1]To whom all correspondence should be addressed.

0008-4042/79/202734-09$01.00/0

TABLE 1. 4,6-Diaryl-3,4-dihydropyrimidine-2(1*H*)-thiones (**5***a–l*)

Compound	Empirical formula	Yield (%)	Melting point[a] (°C)	Elemental analysis					
				Calculated (%)			Found (%)		
				N	S	Cl	N	S	Cl
5*a*	$C_{16}H_{14}N_2S$	97	183–184[b]	10.52	12.04	—	10.31	12.11	—
5*b*	$C_{16}H_{13}ClN_2S$	95	162–163[c]	9.31	10.66	11.79	9.61	10.44	11.93
5*c*	$C_{17}H_{16}N_2S$	91	199–200[b]	9.99	11.42	—	9.90	11.61	—
5*d*	$C_{16}H_{13}ClN_2S$	93	193–194[c]	9.31	10.66	11.79	9.41	10.53	11.82
5*e*	$C_{16}H_{13}ClN_2S$	88	181–182[c]	9.31	10.66	11.79	9.71	10.73	11.63
5*f*	$C_{17}H_{16}N_2OS$	85	179–180[d]	9.45	10.82	—	9.33	10.91	—
5*g*	$C_{17}H_{14}N_2O_2S$	87	194–195[d]	9.03	10.33	—	8.96	10.41	—
5*h*	$C_{18}H_{18}N_2OS$	92	190–191[c]	9.02	10.33	—	8.85	10.51	—
5*i*	$C_{17}H_{15}ClN_2OS$	93	177–178[c]	8.47	9.69	10.72	8.71	9.37	10.62
5*j*	$C_{16}H_{12}Cl_2N_2S$	90	152–153[c]	8.36	9.56	21.15	8.26	9.62	21.30
5*k*	$C_{18}H_{18}N_2O_2S$	81	195–196[c]	8.58	9.80	—	8.26	9.77	—
5*l*	$C_{17}H_{13}ClN_2O_2S$	87	186–187[d]	8.12	9.28	10.28	7.95	9.37	10.13

[a]Reported melting points for the compounds **5***a*, **5***c*, and **5***h* are 177, 195, and 189°C, respectively (3).
[b]Crystallized from methanol.
[c]Crystallized from benzene.
[d]Crystallized from methanol–benzene.

likely by analogy to the reaction of α,β-unsaturated ketones with nitrogen compounds (1, 4) and an active methylene group (5, 6).

The structure of the above products was established spectroscopically and chemically. Thus, the ir spectra of these compounds (Table 3) were devoid of ν SH, which excluded structures **6** and **7**. The presence of a broad band in the region 3360–3140 cm^{-1} (ν NH) and a strong band in the region 1180–1155 cm^{-1} (ν C=S) (7) indicated that these compounds have structure **5**. The nmr spectra of these compounds reflect a strong evidence for the suggested structure (Table 3). They show a multiplet or two doublets in the region δ 5.22–5.07 correlated to the neighbouring methine and methylene protons. The spectra also show a broad signal attributed to two NH protons exchangeable with D_2O. This fact was established by running the nmr spectrum of **5***j* in $CDCl_3$, $CDCl_3$/DMSO-d_6 1:3, and DMSO-d_6, respectively (cf. Fig. 1), in which the broad signal was split into two broad ones, exchangeable with D_2O, and the distance between them depends on the ratio of the more polar solvent added. Natural abundance ^{13}C nmr spectra for the thiones (**5***a*, *f*) gave further support for the reported structure. They show signals attributable for CS, $\geqslant$CH, and =CH— (Table 4). Further evidence for the structure of these compounds was obtained from their uv spectra. They show absorption bands which can be attributed to π–π* transition of the styrene moiety (6). Also the uv spectra of these compounds in polar and non-polar solvents such as ethanol, chloroform, and carbon tetrachloride (cf. Table 5) show that the red shift in the position of the absorption bands varies inversely with the polarity of the solvent. This may be attributed to the stabilizing influence of the hydrogen bonding on the thione form **5**; however, in the non-polar solvents the other form (thiol form, **6** or **7**) is favoured, similar to the phenomenon observed in the case of pyrimidine-2(1*H*)thione (1) and β-diketones (8). The ms spectrum of **5***f* affords an additional support for the assigned structure, since it shows peaks at the following *m/e* (relative intensity): 296 (63.2)]M]$^+$, 219 (27.2) [M − C_6H_5]$^+$, 194 (17.2) [M − $C_6H_5C{\equiv}CH$]$^+$, and 77 (100) [C_6H_5]$^+$.

Chemical behaviour of these compounds gives further evidence for the assigned structure. Thus, compounds **5***a–g* gave, upon refluxing for 2 h with 3 mol of sodium ethoxide in methanol, the corresponding 4,6-diarylpyrimidine-2(1*H*)thiones **9** (Scheme 2) approximately in quantitative yield identical with the products separated from the reaction of acetylenic ketones with thiourea (2). Acetylation of the thiones **5***a–l* with acetic anhydride afforded the corresponding *N*-acetyl derivatives **8***a–l*. The structure of the latter compounds was established by their ir, nmr, uv, and ms spectra (Table 6). Thus, their ir spectra (KBr) show a strong band in the region 1660–1650 cm^{-1} (ν $NCOCH_3$) and two broad bands in the region 3370–3140 cm^{-1} (ν NH) (Table 6). When the ir spectrum of **8***a* was run in chloroform solution, a sharp band at 3410 cm^{-1} (free NH) was obtained. Their nmr spectra (Table 5), however, show two doublets in the regions δ 6.33–6.19 and δ 5.91–5.71 (J = 7 Hz) attributable to the neighbouring methine and olefinic protons. These assignments were con-

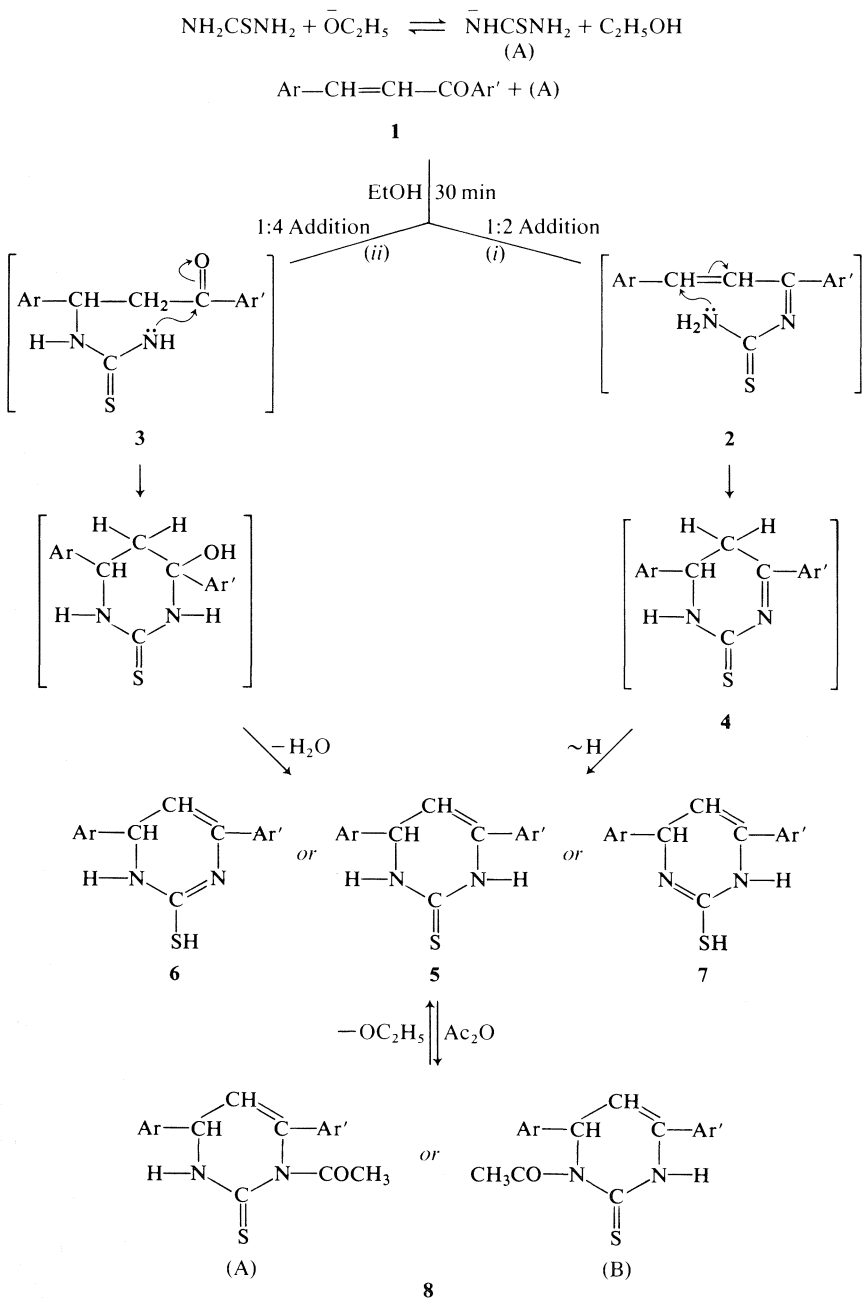

SCHEME 1

a: Ar = Ar′ = C_6H_5
b: Ar = C_6H_5, Ar = *p*-Cl·C_6H_4
c: Ar = *p*-$CH_3C_6H_4$, Ar′ = C_6H_5
d: Ar = *m*-Cl·C_6H_4, Ar′ = C_6H_5
e: Ar = *p*-Cl·C_6H_4, Ar′ = C_6H_5
f: Ar = *p*-$CH_3OC_6H_4$, Ar′ = C_6H_5
g: Ar = 3,4-$OCH_2OC_6H_3$, Ar′ = C_6H_5
h: Ar = *p*-$CH_3C_6H_4$, Ar′ = *p*-$CH_3OC_6H_4$
i: Ar = *p*-$CH_3OC_6H_4$, Ar′ = *p*-Cl·C_6H_4
j: Ar = Ar′ = *p*-Cl·C_6H_4
k: Ar = Ar′ = *p*-$CH_3OC_6H_4$
l: Ar = 3,4-$OCH_2OC_6H_3$, Ar′ = *p*-Cl·C_6H_4

firmed by double irradiation experiments, e.g., on irradiation at the frequency of the olefinic proton, the doublet of the methine proton collapsed to a singlet. The differences in the proton shifts for the methine and olefinic protons in the compounds **5***a–l* as compared with the acetylated products **8***a–l* are due to the fact that the NH group possesses more +R effect than the $-NCOCH_3$ group, accordingly it will increase the electron density on the olefinic CH more than the $NCOCH_3$ group, i.e., it will cause a decrease in the δ-value (upfield shift) (cf. Scheme 3). These structures show, in addition, a singlet signal in the region δ 2.83–2.75 (3,$COCH_3$) and a broad signal at δ 8.82–8.42 (1,NH) exchangeable with D_2O. The ^{13}C nmr spectra for **8***a*,*f* (Table 4) show signals attributable to CS and $COCH_3$ groups. The uv spectra of these compounds are identical, which reflects their structural analogy (Table 6). Further support for the assigned structure was gained from the ms spectrum **8***f* which shows peaks at the following *m*/*e* (relative intensity): 338 (13.15) $[M]^+$, 323 (3.28) $[M - CH_3]^+$, 295 (98) $[M - COCH_3]^+$, and 236 (100) $[M - C_6H_5C{\equiv}CH]^+$. The absence of the $[M - SCOCH_3]^+$ peak in the spectrum gave further evidence for the structure. All the spectral data of these compounds show that structure **8**(A) is more probable than the other one **8**(B) because the

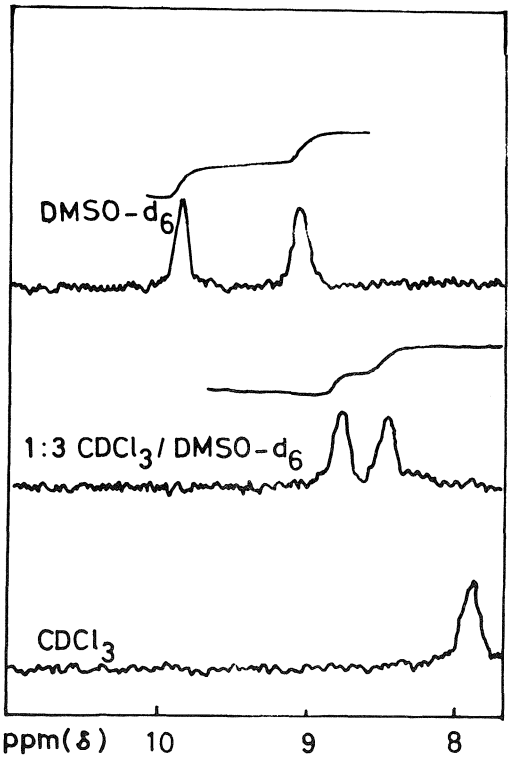

FIG. 1. Nuclear magnetic resonance spectrum for **5***j*.

TABLE 2. 1-Acetyl-4,6-diaryl-3,4-dihydropyrimidine-2(1*H*)thiones (**8***a–l*)

Compound	Empirical formula	Yield (%)	Melting point (°C)	Elemental analysis									
				Calculated (%)					Found (%)				
				C	H	N	S	Cl	C	H	N	S	Cl
8*a*	$C_{18}H_{16}N_2OS$	78	154–155[a]	—	—	9.08	10.40	—	—	—	9.11	10.33	—
8*b*	$C_{18}H_{15}ClN_2OS$	76	164–165[a]	63.06	4.41	8.17	9.35	10.34	63.04	4.22	8.31	9.52	10.61
8*c*	$C_{19}H_{18}N_2OS$	80	158–159[a]	70.78	5.63	8.69	9.94	—	71.00	5.73	8.71	9.73	—
8*d*	$C_{18}H_{15}ClN_2OS$	81	179–180[a]	63.06	4.41	8.17	9.35	10.34	62.86	4.23	8.01	9.15	10.67
8*e*	$C_{18}H_{15}ClN_2OS$	73	164–165[a]	63.06	4.41	8.17	9.35	10.34	63.44	4.17	8.22	9.25	10.41
8*f*	$C_{19}H_{18}N_2O_2S$	75	158–160[a]	67.43	5.36	8.28	9.47	—	67.28	5.26	8.11	9.63	—
8*g*	$C_{19}H_{16}N_2O_3S$	80	170–171[a]	64.76	4.58	7.95	9.10	—	64.57	4.43	8.17	9.21	—
8*h*	$C_{20}H_{20}N_2O_2S$	68	168–169[b]	68.16	5.72	7.95	9.10	—	68.01	5.69	7.88	9.33	—
8*i*	$C_{19}H_{17}ClN_2O_2S$	78	171–172[a]	—	—	7.51	8.60	9.51	—	—	7.41	8.73	9.69
8*j*	$C_{20}H_{20}Cl_2N_2OS$	75	180–181[a]	—	—	7.43	8.5	18.80	—	—	7.51	8.43	19.20
8*k*	$C_{20}H_{20}N_2O_3S$	79	155–156[a]	65.20	5.47	7.60	8.70	—	64.78	5.29	7.81	8.62	—
8*l*	$C_{19}H_{15}ClN_2O_3S$	88	173–174[c]	58.99	3.91	7.24	8.29	9.17	59.24	3.86	7.35	8.41	9.33

[a]Crystallized from methanol.
[b]Crystallized from methanol–benzene.
[c]Crystallized from benzene.

TABLE 3. Infrared and nuclear magnetic resonance spectral data of 4,6-diaryl-3,4-dihydropyrimidine-2(1*H*)-thiones (**5***a–l*)

Compound	Infrared bands (KBr)		Nuclear magnetic resonance values ($CDCl_3$)	
	ν (cm^{-1})	Assignments	δ	Assignments (No. of protons)
5*a*	3180 (br)	NH	7.82 (br)	(2) NH
	1640 (m)	C=C or C=N	7.60–6.93 (m)	(10) ArH + NH
	1590 (m), 1540 (s)	C=C	5.2 (m)	(2) —CH= + ≥CH
5*b*	3140 (br)	NH	7.92 (br)	(2) NH
	1640 (m)	C=C or C=N	7.68–7.18 (m)	(9) ArH
	1520 (s)	C=C	5.22 (m)	(2) —CH= + ≥CH
5*c*	3180 (br)	NH	7.70 (br)	(2) NH
	1650 (w)	C=C or C=N	7.58–6.85 (m)	(9) ArH
	1540 (s)	C=C	5.20 (m)	(2) —CH= + ≥CH
			2.35 (s)	(3) ArCH
5*d*	3140 (br)	NH	*8.23 (br)	(2) NH
	1645 (m)	C=C or C=N	7.65–7.15 (m)	(9) ArH
	1550 (s)	C=C	5.22	(2) —CH= + ≥CH
5*e*	3150 (br)	NH	7.83 (br)	(2) NH
	1645 (m)	C=C or C=N	7.63–6.63 (m)	(9) ArH
	1595 (m), 1535 (s)	C=C	5.18 (m)	(2) —CH= + ≥CH
5*f*	3180 (br)	NH	7.65 (br)	(2) NH
	1650 (m)	C=C or C=N	7.55–6.68 (m)	(9) ArH
	1590 (m), 1540 (s)	C=C	5.20 (m)	(2) —CH= + ≥CH
			3.78 (s)	(3) ArOCH
5*g*	3320 (br), 3150 (br)	NH	*8.50 (br)	(1) NH
			8.37 (br)	(1) NH
	1648 (m)	C=C or C=N	7.63–6.53 (m)	(8) ArH
	1520 (s)	C=C	5.93 (s)	(2) OCH_2O
			5.15 (m)	(2) ≥CH + —CH=
5*h*	3180 (br)	NH	7.62 (br)	(2) NH
	1648 (m)	C=C or C=N	7.52–6.63 (m)	(8) ArH
	1585 (s), 1545 (s)	C=C	5.17 (d)	(1) —CH=
			5.07 (d)	(1) ≥CH
			3.80 (s)	(3) $ArOCH_3$
			2.33 (s)	(3) $ArCH_3$
5*i*	3360 (br), 3160 (br)	NH	7.85 (br)	(2) NH
			7.55–6.75 (m)	(8) ArH
	1648 (m)	C=C or C=N	5.18 (m)	(2) —CH= + ≥CH
	1585 (m), 1540 (s)	C=C	3.80 (s)	(3) $ArOCH_3$
5*j*	3360 (br), 3180 (br)	NH	7.70 (br)	(2) NH
			7.57–7.0 (m)	(8) ArH
	1648 (m)	C=C or C=N	5.20	(2) —CH= + ≥CH
	1525 (s)	C=C		
5*k*	3180 (br)	NH	7.65 (br)	(1) NH
	1650 (m)	C=C or C=N	7.52–6.75 (m)	(9) ArH + NH
			5.18 (d)	(1) —CH=
	1585 (s), 1545 (s)	C=C	5.08	(1) ≥CH
			3.82 (s)	(6) $ArOCH_3$
5*l*	3320 (br), 3160 (br)	NH	*8.90 (br)	(1) NH
			8.40 (br)	(1) NH
	1648 (w)	C=C or C=N	7.70–6.63 (m)	(7) ArH
	1530 (s)	C=C	5.95 (s)	(2) OCH_2O
			5.13 (m)	(2) —CH= + ≥CH

*In $CDCl_3$ + D_6MSO.

TABLE 4. ^{13}C nuclear magnetic resonance chemical shifts of the thiones (**5***a*,*f*) and (**8***a*,*f*) in $CDCl_3$

Compound	Chemical shift[a] $\delta(C_2)$	$\delta(C_5)$	$\delta(C_6)$	δ Other carbon atoms
5*a*	174.985	100.626	57.112	142.238, 133.958, 133.225, 129.475, 129.085, 128.937, 128.500, 126.894, 125.237 (Ar)
5*f*	174.985	100.774	56.722	55.357 (OCH_3) and 159.781, 134.441, 133.763, 133.272, 129.475, 128.984, 128.204, 125.089, 114.419 (Ar)
8*a*	173.621	105.499	54.188	178.790 (CO), 27.727 (CH_3), and 139.073, 135.665, 132.055, 129.865, 129.085, 128.742, 128.063, 126.601, 125.382 (Ar)
8*f*	173.521	105.694	55.211	178.689 (CO), 53.700 and 27.727 (CH_3 groups), and 159.392, 135.517, 132.102, 130.988, 129.818, 129.132, 128.259, 125.334, 114.126 (Ar)

[a]In ppm downfield from TMS.

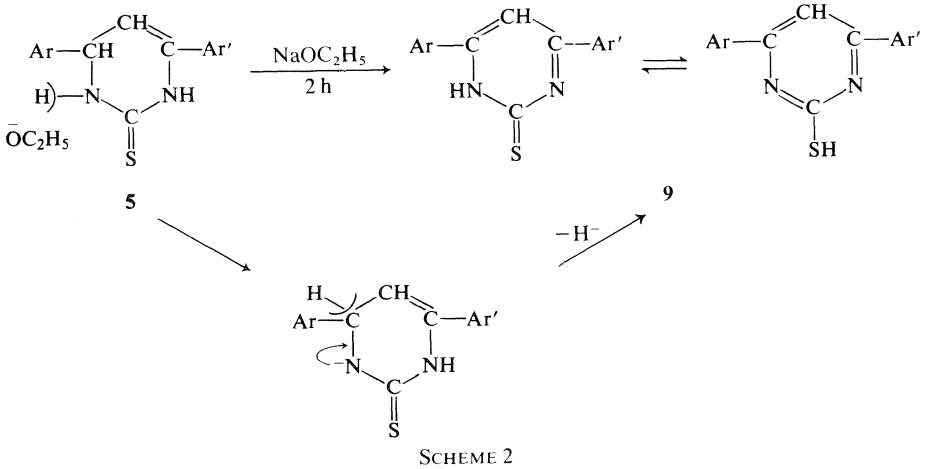

SCHEME 2

TABLE 5. Ultraviolet absorption bands of substituted pyrimidine-2(1*H*)thione (**5***a–l*)[a]

Compound	λ_{max} (nm) (log ε)		
	Ethanol	Chloroform	Carbon tetrachloride
5*a*	267 (4.18) 226 (4.36)	275 (4.16)	313–286 (sh) (4.14) 282 (4.15)
5*b*	253 (4.28) 232 (4.32)	272 (4.20)	279 (4.05)
5*c*	265 (4.18) 224 (4.36)	281–273 (sh) (4.16) 272 (4.16)	291 (4.14) 258 (4.13)
5*d*	267 (4.09)	274 (4.09)	300 (4.07)
5*e*	267 (4.12) 230 (4.36)	274 (4.08)	300 (4.05)
5*f*	272–258 (sh) (4.14) 247 (4.22) 225 (4.31)	272 (4.16)	307–287 (sh) (4.11) 278 (4.14)
5*g*	296–279 (sh) (4.09) 257 (4.16)	298–283 (sh) (4.19) 276 (4.20)	293 (4.20) 260 (4.17)
5*h*	270–257 (sh) (4.32) 250 (4.40)	273 (4.31) 251 (4.37)	285 (4.24)
5*i*	253 (4.31) 232 (4.35)	271 (4.22)	309–288 (sh) (4.12) 279 (4.20) 260 (4.24)
5*j*	275–255 (sh) (4.17) 238 (4.35)	274 (4.23)	309–291 (sh) (4.13) 285 (4.17) 282–274 (sh) (4.16)
5*k*	271–261 (sh) (4.31) 253 (4.40)	274 (4.25) 253 (4.3)	282 (4.21)
5*l*	260 (4.33) 234 (4.39)	292 (4.20) 282–272 (sh) (4.14)	297 (4.20) 261 (4.18)

[a]Abbreviation: sh = shoulder.

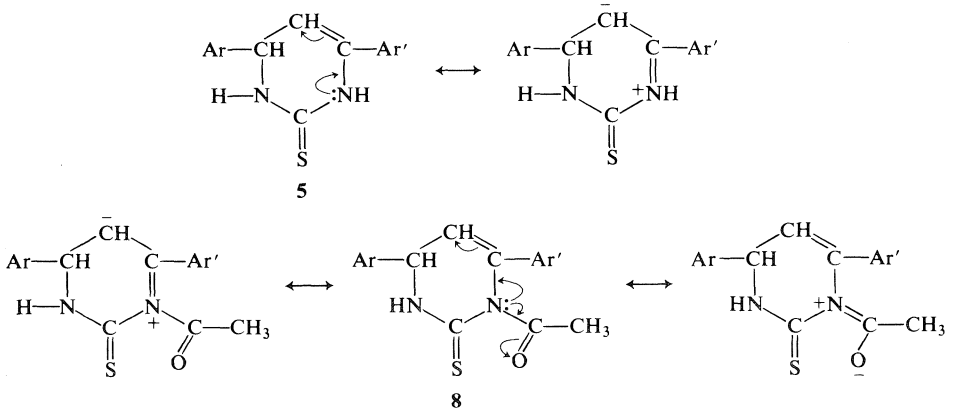

5

8

SCHEME 3

TABLE 6. Infrared, ultraviolet, and nuclear magnetic resonance spectral data of 1-acetyl-4,6-diaryl-3,4-dihydropyrimidine-2(1*H*)thiones (**8***a–l*)

	Infrared bands (Nujol)		Ultraviolet bands (EtOH)	Nuclear magnetic resonance values ($CDCl_3$)	
Compound	$\nu(cm^{-1})$	Assignments	λ_{max} (nm) (log ε)	δ	Assignments (No. of protons)
8*a*	3200 (br) 3140 (br)	NH	327 (4.00) 243 (4.35)	8.63 (br) 7.67–7.23 (m)	(1) NH (10) ArH
	1650 (s)	$COCH_3$		6.3 (d) 5.88 (d) 2.80 (s)	(1) —CH= (1) >CH (3) $COCH_3$
8*b*	3370 (br) 3210 (br)	NH	325 (4.11) 244 (4.41)	8.42 (br) 7.68–7.10 (m)	(1) NH (9) ArH
	1650 (s)	$COCH_3$		6.28 (d) 5.86 (d) 2.80 (s)	(1) —CH= (1) >CH (3) $COCH_3$
8*c*	3220 (br) 3150 (br)	NH	325 (3.9) 238 (4.32)	8.78 (br) 7.77–6.83 (m)	(1) NH (9) ArH
	1660 (s)	$COCH_3$		6.33 (d) 5.91 (d) 2.82 (s) 2.33 (s)	(1) —CH= (1) >CH (3) $COCH_3$ (3) $ArCH_3$
8*d*	3200 (br) 3140 (br)	NH	327 (4.01) 242 (4.37)	8.55 (br) 8.05–6.72 (m)	(1) NH (9) ArH
	1655 (s)	$COCH_3$		6.31 (d) 5.89 (d) 2.83 (s)	(1) —CH= (1) >CH (3) $COCH_3$
8*e*	3210 (br) 3150 (br)	NH	326 (4.08) 242 (4.44)	8.57 (br) 7.73–7.10 (m)	(1) NH (9) ArH
	1655 (s)	$COCH_3$		6.27 (d) 5.87 (d) 2.82 (s)	(1) —CH= (1) >CH (3) $COCH_3$
8*f*	3200 (br) 3140 (br)	NH	330 (4.06) 281–253 (sh) (4.15)	8.82 (br) 7.83–6.63 (m)	(1) NH (9) ArH
	1650 (s)	$COCH_3$	239 (4.39)	6.3 (d) 5.88 (d) 3.78 (s) 2.80 (s)	(1) —CH= (1) >CH (3) $ArOCH_3$ (3) $COCH_3$
8*g*	3310 (br) 1660 (br)	NH $COCH_3$	328 (3.99) 291–253 (sh) (4.17) 239 (4.42)	8.60 (br) 7.90–6.57 (m) 6.23 (d) 5.87 (d) 5.92 (s) 2.80 (s)	(1) NH (8) ArH (1) —CH= (1) >CH (2) OCH_2O (3) $COCH_3$
8*h*	3210 (br) 3130 (br)	NH	329 (3.92) 259 (4.42)	8.43 (br) 7.70–6.73 (m)	(1) NH (8) ArH
	1660 (s)	$COCH_3$		6.23 (d) 5.73 (d) 3.80 (s) 2.78 (s) 2.30 (s)	(1) —CH= (1) >CH (3) $ArOCH_3$ (3) $COCH_3$ (3) $ArCH_3$
8*i*	3180 (br) 3140 (br)	NH	328 (3.97) 281–255 (sh) (4.18)	8.58 (br) 7.68–6.62 (m)	(1) NH (8) ArH
	1640 (s)	$COCH_3$	245 (4.34)	6.23 (d) 5.83 (d) 3.75 (s) 2.77 (s)	(1) —CH= (1) >CH (3) $ArOCH_3$ (3) $COCH_3$

TABLE 6 (*Concluded*)

Compound	Infrared bands (Nujol) ν (cm^{-1})	Assignments	Ultraviolet bands (EtOH) λ_{max} (nm) (log ε)	Nuclear magnetic resonance values ($CDCl_3$) δ	Assignments (No. of protons)
8*j*	3200 (br)	NH	326 (4.06)	8.65 (br)	(1) NH
	1650 (s)	$COCH_3$	248 (4.47)	7.72–7.02 (m)	(8) ArH
				6.28 (d)	(1) $\geqslant$CH=
				5.86 (d)	(1) —CH
				2.78 (s)	(3) $COCH_3$
8*k*	3210 (br) }	NH	329 (3.95)	8.68 (br)	(1) NH
	3140 (br) }		259 (4.45)	7.75–6.58 (m)	(8) ArH
	1650 (s)	$COCH_3$		6.19 (d)	(1) —CH=
				5.71 (d)	(1) $\geqslant$CH
				3.80 (s)	(3) $ArOCH_3$
				3.73 (s)	(3) $ArOCH_3$
				2.75 (s)	(3) $COCH_3$
8*l*	3200 (br)	NH	326 (3.85)	8.82 (br)	(1) NH
	1660 (s)	$COCH_3$	294–255 (sh) (4.12)	7.80–6.60 (m)	(7) ArH
			244 (4.32)	6.21 (d)	(1) —CH=
				5.81 (d)	(1) $\geqslant$CH
				5.92 (s)	(2) OCH_2O
				2.78	(3) $COCH_3$

values of $COCH_3$ group generally are not changed by the substituent (Tables 4 and 6).

Heating of the *N*-acetyl derivatives **8***a–l* with 3 mol sodium ethoxide for 5 min afforded the corresponding thiones **5***a–l*. However, when the heating was continued for 2 h, they gave the corresponding 4,6-diarylpyrimidine-2(1*H*)thiones **9***a–l*.

1. F. G. BADDAR, F. H. AL-HAJJAR, and N. R. EL-RAYYES. J. Heterocycl. Chem. **13**, 257 (1976).
2. F. G. BADDAR, F. H. AL-HAJJAR, and N. R. EL-RAYYES. J. Heterocycl. Chem. **15**, 105 (1978).
3. A. SAMMOUR, M. I. B. SELIM, M. M. NOUR EL-DEEN, and M. ABD-EL-HALIM. U. A. R. J. Chem. **13**, 7 (1970).
4. Y. AL-FARKH, F. H. AL-HAJJAR, F. S. AL-SHAMALI, and H. S. HAMOUD. Chem. Pharm. Bull. (Tokyo), **27**, 264 (1979).
5. R. CONNOR and D. B. ANDREWS. J. Am. Chem. Soc. **56**, 2713 (1934).
6. Y. A. AL-FARKH, F. H. AL-HAJJAR, and H. S. HAMOUD. J. Heterocycl. Chem. **16**, 1 (1979).
7. L. J. BELLAMY. The infrared spectra of complex molecules. Methuen, London. 1966. p. 355.
8. NEIL S. ISAACS. Experiments in physical organic chemistry. The Macmillan Company, London. 1970. p. 133.

An unusual carbomethoxyl migration from nitrogen to carbon. Formation of a 2*H*-pyrrole from $AlCl_3$-promoted reaction of 1-carbomethoxy-2,5-dimethylpyrrole with dimethyl acetylenedicarboxylate[1,2]

R. A. F. MATHESON, A. W. MCCULLOCH, A. G. MCINNES, AND D. G. SMITH

Atlantic Regional Laboratory, National Research Council of Canada, Halifax, N.S., Canada B3H 3Z1

Received May 4, 1979

R. A. F. MATHESON, A. W. MCCULLOCH, A. G. MCINNES, and D. G. SMITH. Can. J. Chem. 57, 2743 (1979).

The $AlCl_3$-promoted reaction of methyl 2,5-dimethylpyrrole-1-carboxylate **1** with dimethyl acetylenedicarboxylate affords under certain conditions a low yield of 2,5-dimethyl-2-tricarbomethoxyvinyl-2*H*-pyrrole **3**. The structure of the latter was established on the basis of detailed ^1H and ^{13}C nmr studies, and confirmed by conversion to dimethyl 5-methyl-5-(3-oxobutyl)-3-pyrrolin-2-one-3,4-dicarboxylate **4**.

R. A. F. MATHESON, A. W. MCCULLOCH, A. G. MCINNES et D. G. SMITH. Can. J. Chem. 57, 2743 (1979).

La réaction du diméthyl-2,5-pyrrole carboxylate de méthyle-1 (**1**) avec l'acétylène dicarboxylate de méthyle catalysée par $AlCl_3$ conduit sous certaines conditions avec un faible rendement au diméthyl-2,5-tricarbométhoxyvinyl-2-2*H* pyrrole **3**. La structure de ce dernier est établie à partir d'études détaillées en rmn du proton et du ^{13}C, et confirmée par sa transformation en méthyl-5-(3-oxobutyl)-5-pyrrolin-3-one-2-dicarboxylate de méthyle-3,4 (**4**).

[Traduit par le journal]

Introduction

We have previously reported the $AlCl_3$-promoted Diels–Alder addition of 1-carbomethoxy-2,5-dimethylpyrrole **1** to dimethyl acetylenedicarboxylate (DMAD) to give trimethyl 1,4-dimethyl-7-azabicyclo-[2.2.1]2,5-heptadiene-2,3,7-tricarboxylate **2** (1). Further investigation of the reaction between **1** and DMAD (see Experimental) led to the isolation of an additional product (max. yield 15%). In this note we describe the structural elucidation of this new compound, which has been identified as 2,5-dimethyl-2-tricarbomethoxyvinyl-2*H*-pyrrole **3**.

Results and Discussion

Mass spectral analysis of **3** established the molecular formula $C_{14}H_{17}NO_6$, indicating a 1:1 product. The ^1H nmr spectrum (Table 1) showed that the seventeen hydrogens were accounted for by resonances for three chemically non-equivalent carbomethoxy methyl groups, two chemically non-equivalent methyl groups, both on quaternary carbons, and two olefinic hydrogens which were vicinally coupled to one another (J = 4.8 Hz). Irradiation of the low-field *C*-methyl (δ 2.14) caused a 14% nuclear Overhauser enhancement of the signal for the high-field olefinic hydrogen, whereas irradiation of the high-field methyl (δ 1.39) caused a 19% enhancement of the signal for the olefinic hydrogen at low field. These results established that each olefinic hydrogen was vicinal to a methyl group.

When 1-carbomethoxy-3,4-dideutero-2,5-dimethylpyrrole was substituted for **1** in the reaction with DMAD, the product obtained had ^1H nmr resonances for five methyl groups identical to those of **3**, but had no olefinic signals. Thus the olefinic hydrogens of **3** are derived directly from the comparable hydrogens (H-3 and H-4) of **1**. In other words, the intact carbon chain of the 2,4-hexadiene moiety of **1** is incorporated into **3**, as suggested by the nOe experiments.

Further evidence for structure **3** was derived from ^{13}C nmr measurements (Table 2).[3] On the basis of characteristic chemical shifts, multiplicities, and $^1J_{CH}$ values it was possible to unequivocally assign resonances due to the two methyl, six carbomethoxyl, and two olefinic methine carbons. The remaining four resonances were all for quaternary carbons. The chemical shift (δ 82.06) of one of these indicated a saturated carbon (C-2) deshielded by an attached nitrogen, while the low-field shift (δ 173.60) of a second was characteristic of an imino carbon (C-5) forming part of a cyclic structure (cf. ref. 2). Single frequency decoupling experiments (irradiation in

[1]Issued as NRCC No. 17637.

[2]Taken, in part, from the Ph.D. thesis of R.A.F.M. (supervisor, A.G.McI.), Dalhousie University, Halifax, N.S. 1973.

[3] ^{13}C nmr data for **1** and **2** are included for purposes of comparison.

0008-4042/79/202743-04$01.00/0

TABLE 1. ^{1}H nmr data (δ_H TMS)

Compound	Hydrogen				
	CH_3 (s, 3H)	OCH_3 (s, 3H)	H-1	H-3, H-4	H-6, H-7
3 $CDCl_3$	1.52 (at C-2) 2.23 (at C-5)	3.72 3.84 3.86	—	AXq, centered at 6.78, $\Delta\nu_{3,4}$ = 102.0 $J_{3,4}$ = 4.8 Hz; H-4 at higher field than H-3	—
3[a] DMSO-d_6	1.39 (at C-2) 2.14 (at C-5)	3.67 3.74 3.78	—	AXq, centered at 6.84, $\Delta\nu_{3,4}$ = 88.2, $J_{3,4}$ = 4.8 Hz; H-4 at higher field than H-3	—
4	1.56 (at C-5) 2.11 (C-9)	3.86 3.89	8.01 (bs, exch. with D_2O)	—	2.20–2.35 (4H)
5	1.44 (at C-2) 2.01 (at C-5)	3.75 3.82 3.85	—	2.00–2.70 (4H)	—

[a]Using a 5% solution of **3** in degassed DMSO-d_6, the following nuclear Overhauser enhancements were observed (irradiated hydrogens in parentheses): H-3 (CH_3 at C-2) 19%, H-4 (CH_3 at C-5) 14%, H-3 (CH_3 at C-5) 0%, H-4 (CH_3 at C-2) 0%.

turn of each olefinic hydrogen and of the hydrogens of each *C*-methyl group) established that each of C-2 and C-5 was directly bonded to a methyl group and *trans* ($^3J_{CH}$ = 11.5 Hz) to an olefinic hydrogen. The combined evidence, together with the high $^1J_{CH}$ values observed for C-3 and C-4 (3), is consistent with a 2-substituted 2,5-dimethyl-2*H*-pyrrole moiety.

The only possible arrangement of the three carbomethoxyl groups and two unassigned quaternary olefinic carbons is as a tricarbomethoxyvinyl group, which must therefore be the C-2 substituent. The carbon resonating at δ 147.02 was coupled ($^3J_{CH}$ = 4.1 Hz) only to the hydrogens of the methyl group at C-2 and can thus be readily assigned to C-6. As expected, C-7 (δ 124.98), which is bonded to and

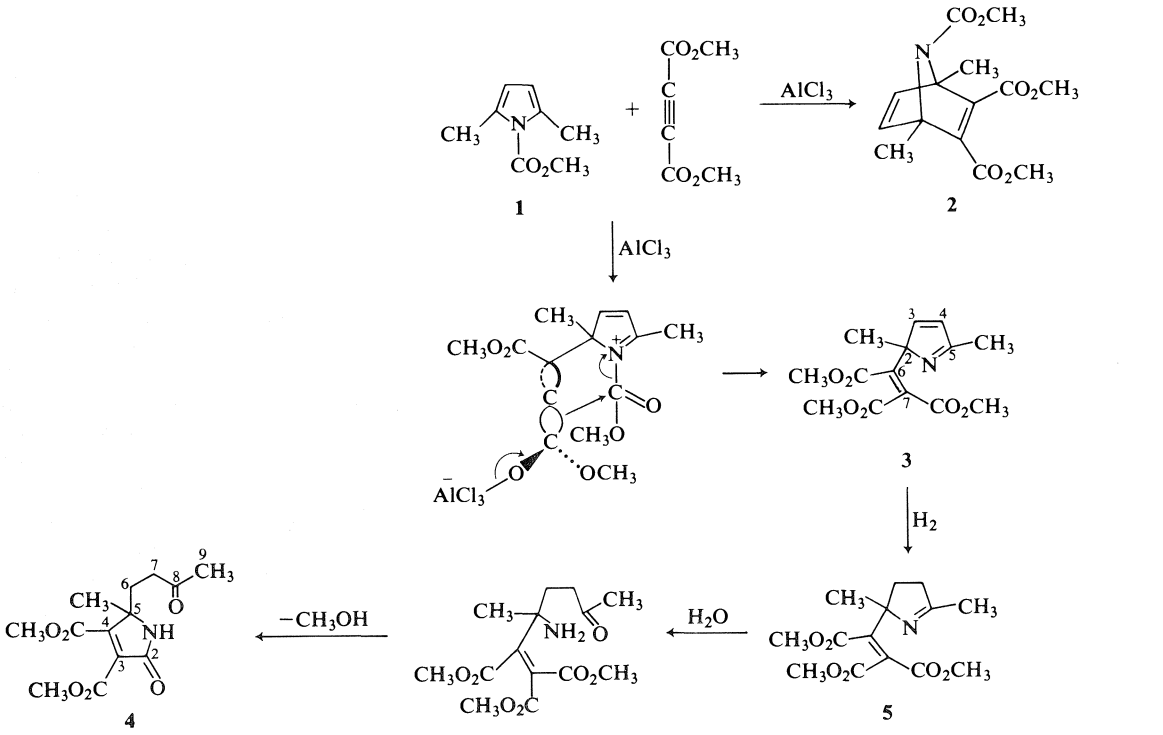

SCHEME 1

geminal to quaternary centers, showed no discernible coupling. For similar reasons no coupling other than that with the methoxyl hydrogens ($^3J_{CH} \sim 4$ Hz) would be expected or was observed in any of the three carbonyl carbon resonances.

Chemical confirmation of the structure of **3** was provided by its conversion to the pyrrolinone **4**. Catalytic reduction of **3** afforded the sensitive 3,4-dihydro derivative **5**, which was not fully characterized. During chromatography **5** underwent imine hydrolysis; spontaneous cyclization of the resulting aminoketone (not isolated) gave **4**.

The ^{1}H nmr spectrum of **5** (Table 1) showed signals for two chemically non-equivalent methyl groups attached to quaternary centers, four methylene hydrogens, and three chemically non-equivalent methoxyl groups, but none for olefinic hydrogens. The spectrum of **4** was similar except that there were signals for only two chemically non-equivalent methoxyl groups, and there was now an NH signal.

Mass measurement of **4** established the molecular formula $C_{13}H_{17}NO_6$ and also the facile cleavage of the 3-oxobutyl side-chain. The ^{13}C nmr spectrum of **4** (Table 2) contained signals for the carbons of two methyl, two methylene, and two carbomethoxyl groups, and for two quaternary olefinic carbons. The three remaining resonances could be readily assigned to a saturated carbon (C-5; δ 63.27) deshielded by nitrogen, and to amide (C-2; δ 166.60) and ketone (C-8; δ 207.43) carbonyls. The high-resolution ^{13}C data are compatible only with structure **4**. The lack of coupling in the two carbomethoxyl carbonyls once again indicated that both these carbons were bonded to and geminal to quaternary carbons. Couplings of the amide proton with the adjacent carbonyl ($^2J_{CH}$ 2.3 Hz) and with the ring carbon C-3 ($^3J_{CH}$ 7.2 Hz) were confirmed by running the spectrum after exchange of the NH with deuterium.

The formation of **3** involves a novel 1,3-migration of an intact carbomethoxyl group from nitrogen to carbon. Although migrations of ester groups to nucleophilic centers have been observed (4), this appears to be the first example of such a migration from nitrogen to carbon. A plausible intramolecular transfer pathway is shown (Scheme 1). An alternative mechanism would be an intermolecular process involving methyl chloroformate: we were, however, unable to detect the latter in the reaction mixture or products.

Experimental

The ^{1}H nmr spectra of **4** and **5** were recorded in $CDCl_3$ on a Varian A-60A spectrometer; spectra of **3** (in $CDCl_3$ and DMSO-d_6) were obtained using a Varian HA-100D spectrometer.

The ^{13}C spectra of **1**, **2**, and **4** were recorded in $CDCl_3$ on a Varian XL-100-15 spectrometer under the following condi-

TABLE 2. ^{13}C nmr (δ_C TMS, multiplicity[a], $^nJ_{CH}$ Hz)

Compound	Ester OCH_3 (q)	Ester C=O (q)	CH_3	C-1	C-2	C-3	C-4	C-5	C-6	C-7	C-8
					Carbon						
1	53.04	152.66	16.24	—	131.49	110.92	as	as	—	—	—
	^1J 147.8	b, ^3J 3.8	qt, ^1J 128.1		sext. ^2J_q	dqu, ^1J 169.4,	C-3	C-2			
			$^3J \approx {}^4J \approx 1.1$		$= {}^2J = {}^3J = 7.0$	$^2J = {}^3J = 4.2$					
2	52.41	164.73	16.24	77.83	155.44	as	as	148.23	as	—	—
	^1J 147.7	^3J 4.0	q, ^1J 129.4	tq, $^2J = {}^3J =$	q, ^3J 4.3	C-2	C-1	dqu, ^1J 181.9	C-5		
	52.41	155.44 155.93		8.2, $^2J = 5.3$	or			$^2J = {}^3J_q = 4.9$			
	^1J 147.0	or			155.93						
		^3J 4.3 ^3J 3.8			q, ^3J 3.8						
3	52.40	162.96	18.76 (at C-5)	—	82.06	156.33	128.50	173.60	147.02	124.98	—
	^1J 147.4	^3J 4.0	q, ^1J 127.5		ddq, ^3J 11.5	dqu, ^1J 176.1	ddq, ^1J 171.3	dqu, ^3J 11.5	bq, ^3J 4.1	s	
	52.60	165.03	22.79 (at C-2)		^2J 7.8,	$^2J = {}^3J = 3.5$	^2J 5.6, ^3J 2.8	$^2J = {}^2J_q = 7.0$			
	^1J 147.8	^3J 4.0	bq, ^1J 132.0		^2J_q 4.2						
	52.80	167.34									
	^1J 148.1	^3J 4.1									
4	52.79	161.89	24.50 (at C-5)	—	166.60	134.44	153.47	63.27	30.79	207.43	
	^1J 148.1	^3J 4.1	bq, ^1J 130.1		d, ^2J 2.3	d, ^3J 7.2	bm	bm	btm (^1J 130)	bm	
	52.87	162.38	30.05 (C-9)						37.53		
	^1J 148.4	^3J 4.4	q, ^1J 127.3						btm (^1J 127)		

[a]b = broad, s = singlet, d = doublet, t = triplet, q = quartet, qu = quintet.

tions: frequency 25.16 MHz; acquisition time 0.8 or 1.6 s (data accuracy ± 0.6 or ± 0.3 Hz); spectral width 5120 Hz (5400 Hz in case of **4**); flip angle 30°; internal ^{2}H lock to solvent; temperature about 30°C. ^{1}H irradiation at 100 MHz: (*a*) $\gamma H_2/2\pi$ ca. 3800 Hz, broadband irradiation by 0–180° phase modulation at 150 Hz; (*b*) as for *a*, but irradiation only applied for 1.6 s between data acquisition periods (high-resolution spectrum with retained nOe). ^{13}C spectra of **3** (100 mg/0.4 mL $CDCl_3$) were recorded on a Varian FT 80 spectrometer under the following conditions: frequency 20 MHz; acquisition time 0.99 or 1.98 s (data accuracy ± 0.5 or ± 0.25 Hz); spectral width 4132 Hz; flip angle 25° or 50°; internal ^{2}H lock to solvent; temperature about 35°C. ^{1}H irradiation at 80 MHz: (*a*) $\gamma H_2/2\pi$ ca. 4000 Hz, bandwidth 2000 Hz (broadband decoupling); (*b*) $\gamma H_2/2\pi$ ca. 2900 Hz, bandwidth 1000 Hz, field applied for 2 s between data acquisitions to retain nOe (high-resolution spectrum); (*c*) as for *b*, but with additional constant ^{1}H irradiation $\gamma H_2/2\pi$ 196 Hz at frequencies of individual ^{1}H resonances (single frequency decoupling with nOe retained at all resonances).

Infrared absorptions were measured on Perkin-Elmer 521 or 180 spectrometers. High-resolution mass spectral measurements were made with a Dupont-CEC 21-110B double-focussing mass spectrometer, using electrical detection for mass measurements.

2,5-Dimethyl-1,3,4-trideuteropyrrole

A solution of concentrated H_2SO_4 (400 mg) in D_2O (100 mL) was added directly to 2,5-dimethylpyrrole (20 g) and the mixture stirred for 30 min at room temperature. An excess of solid K_2CO_3 was then added and the mixture extracted with benzene. Evaporation of solvent from the dried (Na_2SO_4) extract afforded an oily residue which was distilled. The product (71%) was obtained as a colorless oil; ^{1}H nmr analysis indicated 93% of the title compound.

1-Carbomethoxy-2,5-dimethylpyrrole ***1***

This compound was prepared in the manner described by Gabel (5). Its 3,4-dideutero derivative was similarly prepared from 2,5-dimethyl-1,3,4-trideuteropyrrole.

*2,5-Dimethyl-2-tricarbomethoxyvinyl-2*H*-pyrrole* ***3***

A solution of **1** (1.53 g, 0.01 mol) in CH_2Cl_2 (50 mL) was added dropwise with stirring to a mixture of DMAD (2.90 g, 0.02 mol) and $AlCl_3$ (1.40 g, 0.01 mol) in CH_2Cl_2 (100 mL). The mixture was refluxed for 30 min. The dark red reaction mixture was then washed with ice water. The organic layer was dried and evaporated to give a dark red oily residue (4.26 g) which was chromatographed (200 g SiO_2; $CHCl_3$ as eluant). This gave (*a*) DMAD (1.93 g), (*b*) trimethyl 1,4-dimethyl-7-azabicyclo[2.2.1]2,5-heptadiene-2,3,7-tricarboxylate **2** (0.09 g) (1), and (*c*) slightly contaminated **3**. Fraction (*c*) was subjected to preparative tlc (2 mm SiO_2; 70% petroleum ether/ethyl acetate as eluant). This afforded **3** (0.45 g, 15%) as a cream-colored solid, mp 77–79°C. Repeated tlc raised the mp to 82–84°C. Molecular ion at *m/e* 295.1056 ($C_{14}H_{17}NO_6$ requires 295.1057). Infrared ν_{max} ($CHCl_3$): 1722, 1636, 1613 cm^{-1}.

A similar experiment was conducted using 1-carbomethoxy-3,4-dideutero-2,5-dimethylpyrrole in place of **1**. The same work-up procedure gave 3,4-dideutero-2,5-dimethyl-2-tricarbomethoxyvinyl-2*H*-pyrrole.

An estimated (from ^{1}H nmr) 10% yield of **3** was obtained by reacting **1**, DMAD, and $AlCl_3$ (molar ratio 1:1:5) in CH_2Cl_2 for 30 min at −10°C.

Care must be exercised during the work-up of **3**, particularly when high concentrations of $AlCl_3$ are used. The compound is sensitive to aqueous acid and the reaction mixture must therefore be quenched cautiously with ice. Compound **3**, in addition, deteriorates on standing, even under refrigeration.

Gas chromatography (Perkin-Elmer 910; OV-101; capillary column 25 m × 0.27 mm id; column temp. 40°C) did not show any methyl chloroformate in either the reaction or products.

*3,4-Dihydro-2,5-dimethyl-2-tricarbomethoxyvinyl-2*H*-pyrrole* ***5***

A sample (170 mg) of **3** in methanol (75 mL) was hydrogenated over 5% Pd/C (90 mg) for 5 min only. Filtration and evaporation gave **5** as a pale yellow oil (166 mg). It was important to restrict uptake of H_2 to only one mole.

Dimethyl 5-methyl-5(3-oxobutyl)-3-pyrrolin-2-one-3,4-dicarboxylate ***4***

The crude **5** (166 mg) obtained above was applied to two 20 cm × 20 cm × 2 mm prep. tlc plates, which were then eluted twice with 5% MeOH/$CHCl_3$. Extraction of the major band (R_f 3) afforded **4** as an almost colorless oil (102 mg, 62% overall from **3**), which crystallized on standing at 0°C. Recrystallization from ethyl acetate/petroleum ether gave colorless needles, mp 104.5–106°C. Molecular ion at *m/e* 283.1055 ($C_{13}H_{17}NO_6$ requires 283.10559); base peak at *m/e* 180.0293 ($C_8H_6NO_4$ requires 180.02968); strong ion at *m/e* 212.0565 ($C_9H_{10}NO_5$ requires 212.05590). Infrared ν_{max} (liq. film): 3270 (br), 1740 (sh), 1700 (br), 1645 (sh) cm^{-1}.

Acknowledgements

We wish to thank Mrs. M. G. Flack for her valuable technical assistance. We also thank D. J. Embree for the mass spectra and P. F. Seto for infrared measurements. The assistance of Dr. J. A. Walter with the single-frequency decoupling experiments is gratefully acknowledged.

1. R. C. Bansal, A. W. McCulloch, and A. G. McInnes. Can. J. Chem. **48**, 1472 (1970).
2. Sadtler Standard Carbon-13 NMR Spectra, No. 3167 Sadtler Research Laboratories, Philadelphia, PA 19104.
3. E. Breitmaier and W. Voelter. ^{13}C nmr spectroscopy. Verlag Chemie, Weinheim. 1974. p. 97.
4. R. M. Acheson. Acc. Chem. Res. **4**, 177 (1971).
5. N. W. Gabel. J. Org. Chem. **27**, 301 (1962).

A new method for the determination of the relative acidities of alcohols in alcoholic solutions. The nucleophilicities and competitive reactivities of alkoxides and phenoxides[1]

WILKINS REEVE, CHARLES M. ERIKSON, AND PATRICK F. ALUOTTO
Department of Chemistry, University of Maryland, College Park, MD 20742, U.S.A.

Received January 4, 1979

WILKINS REEVE, CHARLES M. ERIKSON, and PATRICK F. ALUOTTO. Can. J. Chem. **57**, 2747 (1979).

A new semiquantitative method has been developed for measuring the relative acidities of methanol, ethanol, isopropyl alcohol, and *tert*-butyl alcohol in mixed hydroxylic solvents. A solution of the alkoxides of two alcohols in an excess of the two alcohols is allowed to react with *n*-butyl bromide to form a mixture of two ethers. The composition of the ether mixture is a measure of the "competitive reactivity" of the two alkoxides. This can be measured directly, and in theory can be factored into two components: the relative nucleophilicity and the relative basicity of the two alkoxides. Relative nucleophilicities are determined by using solutions in which phenol is one component. Knowing the competitive reactivities and nucleophilicities, the relative acidities of methanol, ethanol, isopropyl alcohol, and *tert*-butyl alcohol in alcoholic media are shown to be 4.4, 1.0, 0.24, and 0.21, respectively. The relative nucleophilicities of hydroxide, methoxide, ethoxide, isopropoxide, *tert*-butoxide, phenoxide, and *m*-cresoxide are 0.08, 0.82, 1.0, 0.4, 0.04, 0.46, and 0.57 respectively.

WILKINS REEVE, CHARLES M. ERIKSON et PATRICK F. ALUOTTO. Can. J. Chem. **57**, 2747 (1979).

On a développé une nouvelle méthode semi-quantitative pour mesurer les acidités relatives du méthanol, de l'éthanol, des alcools isopropylique et tertiobutylique dans un mélange de solvants hydroxyliques. On a fait réagir une solution d'alkoxydes de deux alcools en présence d'un excès de ces alcools avec le bromure de *n*-butyle pour obtenir un mélange de deux éthers. La composition du mélange d'éther est une mesure de la "réactivité compétitive" des deux alkoxydes. Ceci peut être mesuré directement et en théorie peut être décomposer en deux composantes: la nucléophilie et la basicité relative des deux alkoxydes. Les nucléophilies relatives sont déterminées en utilisant des solutions où le phénol est un constituant. Connaissant les réactivités compétitives et les nucléophilies, les acidités relatives du méthanol, de l'éthanol et des alcools isopropylique et tertiobutylique sont établies respectivement à 4.4, 1.0, 0.24 et 0.21. Les nucléophilies relatives des méthoxyde, isopropoxyde, *tert*-butoxyde, phenoxyde et *m*-crésoxyde sont respectivement: 0.08, 0.82, 1.0, 0.4, 0.04, 0.46 et 0.57.

[Traduit par le journal]

There has been much interest recently in the relative acidities of alcohols in the gas phase (1), but little progress has been made in developing new methods for determining acidities of alcohols in protic solvents. We report here a new, semi-quantitative method for measuring the relative acidities of methanol, ethanol, isopropyl alcohol, and *tert*-butyl alcohol in mixtures of these alcohols. The presence of small amounts of water does not affect the results, but it does not follow that the acidity values reported here necessarily apply to dilute aqueous solutions where the three dimensional structure of pure water might have an effect.

During the past fifty years, many investigators have studied the acidities of methanol and ethanol and, to a lesser extent, some secondary and tertiary alcohols. The alcohols are weak acids and the methods used to measure their acidities often gave conflicting results (2). It is recognized that new independent approaches are needed to determine acidity values more accurately, and to provide independent evidence as to the correctness of the acidity values measured by the different methods (3).

We have now developed a new method for measuring the proton-transfer acidities of alcohols. It depends upon the determination of what we call the competitive reactivity (C.R.) of two alkoxides, and also the relative nucleophilicity (R.N.) of these two alkoxides. These properties are related by the simple equation:

$$[1] \quad C.R._{RO^-/R'O^-} = (R.N._{RO^-/R'O^-}) \times (\text{Relative acidities of ROH/R'OH})$$

where the competitive reactivity of two alkoxides, RO^- and $R'O^-$, is measured with respect to a certain substrate, and the relative nucleophilicity of the two alkoxides is also measured with respect to the same substrate. Knowing the C.R. and the R.N., the

[1]Taken in part from the doctoral theses of C.M.E. (1974) and P.F.A. (1967).

0008-4042/79/202747-08$01.00/0

relative acidities of the two alcohols can be calculated. We will now discuss our method for determining competitive reactivities and relative nucleophilicities in detail.

Competitive Reactivity

Consider an experiment in which an atom of sodium is dissolved in a mixture of 10 mol of methanol and 10 mol of ethanol to yield the two alkoxides, each in equilibrium with each other and with the two alcohols, which are present in large excess.

[2] $CH_3OH + C_2H_5O^- \rightleftarrows CH_3O^- + C_2H_5OH$

[3] $K = [CH_3O^-][C_2H_5OH]/[CH_3OH][C_2H_5O^-]$

We will show later that the equilibrium constant, K, has a value of 4.4, and we therefore say that methanol is 4.4 times as strong an acid as ethanol and the concentration of methoxide anion will be 4.4 times as great as the concentration of ethoxide anion in a solution prepared as described above. Our definition of acidity in this work is as above. If a mole of *n*-butyl bromide is now added to the solution, the two alkoxide anions will competitively react with it to form a mixture of methyl *n*-butyl ether and ethyl *n*-butyl ether. If the two alkoxide anions had identical nucleophilicities, the methyl and ethyl ethers would be formed in the same ratio as the concentrations of the two alkoxide anions. However, methoxide is only 0.82 times as nucleophilic as ethoxide (as we will show later) so the amount of methyl *n*-butyl ether formed is reduced by this amount. Accordingly, the competitive reactivities of methoxide versus ethoxide in the above experiment is 4.4 times 0.82 which equals 3.6. Experimentally, the ratio in which these ethers are formed can be determined by analyzing a sample of the reaction mixture by glc.

We see from the above discussion that competitive reactivity is a measure of how two nucleophiles, in the presence of their conjugate acids, compete with each other for a common substrate. Experimentally it can be measured directly, and in theory it can be factored into two components, relative nucleophilicity of the alkoxides and the relative acidity of the alcohols. For this approach to be theoretically sound, the reactions with the substrate must be irreversible so that kinetic control is in effect. It follows that the molar ratio of the final products is also the ratio of the reaction rates by which they are formed.

The experimental results in Table 1 were obtained using *n*-butyl bromide as substrate. In all cases the alcohols were present in seven-fold to thirty-fold excess over the corresponding alkoxide concentrations. The initial concentration of the *n*-butyl bromide was the same or a little less than that of the initial total alkoxide concentration. The reactions were carried out at 26°C, and 25 h were required for 50% of the *n*-butyl bromide to react. Less than 3% of the *n*-butyl bromide is converted to 1-butene, and this has no effect on the product ratios. In the absence of base, there was no measurable reaction.

All of the competitive reactivity values given in Table 1 are the averaged values of at least duplicate experiments, and are accurate to at least 10%. The internal consistency of the data is striking. Changing the ratios of the alcohols caused little change in the measured competitive reactivities if a concentration term was included so as to give the following equation which corrects for mass action.

[4] $C.R._{RO^-/R'O^-} = (\text{mole ratio ROBu/R'OBu}) \times (\text{mole ratio R'OH/ROH})$

The concentration term in eq. [4] is a valid correction as long as the alcohols are present in large excess relative to the base. On varying the ratios of allyl alcohol to methanol over a fifteen-fold range (#5, 6, 7 in Table 1), the measured competitive reactivities were constant within experimental error. Furthermore, the same value was obtained in a mixture containing three alcohols (#11), and the addition of 20% of water (#12) had no effect. This strongly indicates that the influence of ion-pairing, changes in the dielectric constant, and other solvent effects are small. In any case, the concentrations used are characteristic of practical synthetic work, so the results obtained do have practical significance.

Since competitive reactivities are ratios of rate constants, it is possible to multiply or divide one by another and obtain a new competitive reactivity. Thus, dividing the allyloxide/ethoxide competitive reactivity value by the allyloxide/methoxide value gives 4.4 as the value for the methoxide/ethoxide competitive reactivity, and this is in reasonable agreement with the more accurate value of 3.6 obtained by a direct comparison of methoxide and ethoxide anions. Multiplying the nominal competitive reactivity of *t*-BuO^-/*i*-PrO^- by that of *i*-PrO^-/EtO^- gives the nominal competitive reactivity of *t*-BuO^-/EtO^- equal to (0.11) (0.11) or 0.012.

The comparison of ethanol with isopropyl alcohol and of isopropyl alcohol with *tert*-butyl alcohol are special cases in that the 0.2 mol of minor alcohol in each mixture was in only two-fold excess of the metal (0.1 atom of metal was used in runs 3 and 4), whereas normally there was a five- to ten-fold excess of the minor alcohol. In the first case, after correcting for

TABLE 1. Competitive reactivities of various alkoxides reacting with *n*-butyl bromide at 26°C

Run	Comparison	Moles of alcohols	Composition of ether mixture (mol%)	Competitive reactivity	
1	MeO^-/EtO^-	1.0:1.0	79.5:20.5		3.9
2	MeO^-/EtO^-	0.5:1.4	54:46		3.3
11	MeO^-/EtO^-	See below			3.7
				Best value:	3.6
3[a]	$i\text{-}PrO^-/EtO^-$	2.0:0.2	52.4:47.6	(0.11)[b]	0.092[c]
4[a,d]	$t\text{-}BuO^-/i\text{-}PrO^-$	2.0:0.2	52.5:47.5	(0.11)[b]	0.097[c]
5	$C_3H_5O^-$[e]$/MeO^-$	0.5:0.5	47:53		0.90
6	$C_3H_5O^-$[e]$/MeO^-$	0.3:2.0	14:86		1.1
7	$C_3H_5O^-$[e]$/MeO^-$	1.18:0.5	71:29		1.0
11	$C_3H_5O^-$[e]$/MeO^-$	See below			1.0
				Best value:	0.95
8	$C_3H_5O^-$[e]$/EtO^-$	0.5:0.5	80:20		4.0
9	$C_3H_5O^-$[e]$/EtO^-$	0.3:1.4	48:52		4.4
11	$C_3H_5O^-$[e]$/EtO^-$	See below			3.8
				Best value:	4.2
10	OH^-/EtO^-	1.66:1.2	12:88		0.1
11	$C_3H_5O^-$[e]$:MeO^-:EtO^-$	1:1:1	45:44:11.7	Allyl[e]/EtO =	3.8
				MeO/EtO =	3.7
				Allyl[e]/MeO =	1.0
12	$C_3H_5O^-$[e]$:MeO^-:EtO^-:OH^-$	0.5:0.5:0.5:1.1	44:45:11:near zero	Allyl[e]/EtO =	4.0
				MeO/EtO =	4.1
				Allyl[e]/MeO =	1.0

[a]At 25°C.
[b]Nominal value from eq. [4].
[c]Recalculated value, see text.
[d]Potassium rather than sodium was the cation.
[e]Allyloxide anion.

the amount of alcohol converted to the alkoxide by using eq. [3] and acidity values calculated later, the ratio of the two neutral alcohols present at the beginning of the reaction was calculated to be 11.17 instead of the nominal 10.0. At the end of the reaction, the ratio was 12.78 because an appreciable fraction of the minor alcohol was consumed in product formation. Using an average value of 11.97 in eq. [4], the C.R. was recalculated to be 0.0917. A similar treatment of the isopropyl alcohol in *tert*-butyl alcohol data changes the nominal C.R. of 0.11 to 0.097. A more detailed explanation is in the Experimental section.

Benzyl bromide has also been studied as a substitute for the *n*-butyl bromide substrate (4), and the results are in Table 2. The time for 50% reaction with the benzyl bromide was approximately 15 min.

The agreement between the various competitive reactivity ratios using *n*-butyl bromide and benzyl bromide is outstanding. Benzyl bromide is known to be capable of reacting by either the S_N1 or S_N2 mechanism, but the experimental conditions employed here (good nucleophile in non-aqueous solvent) favors the S_N2 mechanism (5), and so both substrates are reacting by the S_N2 pathway.

Relative Nucleophilicity

Nucleophilicity relates to the kinetics of covalent bond formation. We have used only *n*-butyl bromide as a substrate, so relative nucleophilicity (R.N.) in our studies is the ratio of the rates with which two nucleophiles enter into an S_N2 displacement reaction with *n*-butyl bromide. Consider an experiment in which 0.1 mol *n*-butyl bromide is added to an ethanol solution containing 0.1 mol sodium ethoxide and 0.1 mol sodium phenoxide. Since phenol is a million times stronger as an acid than ethanol, all of the phenol in the reaction mixture will always be present as phenoxide and we therefore know the ratio of the concentrations of the two nucleophiles at the start of the reaction. As the reaction proceeds, *n*-butyl ethyl ether and *n*-butyl phenyl ether are competitively formed by S_N2 attack of ethoxide and phenoxide on the *n*-butyl bromide, and the ratio of the ethers formed, determined by glc analyses, is a measure of the R.N. of the two nucleophiles.

In the above experiment, the moles of the butyl ethyl ether and butyl phenyl ether present at the completion of the reaction was 0.063 and 0.037 respectively. Ethoxide is clearly the better nucleophile, but one must consider the relative amounts of

TABLE 2. Competitive reactivities of some alkoxides with benzyl bromide at 26°C

Run	Comparison	Moles of alcohols	Composition of ether mixture (mol%)	Competitive reactivity
1	MeO^-/EtO^-	0.5:0.5	76:24	3.2
2	MeO^-/EtO^-	0.5:1.4	58:42	3.8
9	MeO^-/EtO^-	See below		4.0
3	$C_3H_5O^-$[a]/MeO^-	0.5:0.5	47:53	0.89
4	$C_3H_5O^-$[a]/MeO^-	1.2:0.5	17:33	0.83
5	$C_3H_5O^-$[a]/MeO^-	0.3:2.0	12:88	0.93
8	$C_3H_5O^-$[a]/MeO^-	See below		0.84
6	$C_3H_5O^-$[a]/EtO^-	0.5:0.5	79:21	3.8
7	$C_3H_5O^-$[a]/EtO^-	0.3:1.4	49:51	4.5
9	$C_3H_5O^-$[a]/EtO^-	See below		3.3
8	OH^-/EtO^-	1.7:1.3	8:92	0.073
9	$C_3H_5O^-$[a]:MeO^-:EtO^-	0.5:0.5:0.5	40:48:12	Allyl[a]/EtO = 3.3 MeO/EtO = 4.0 Allyl[a]/MeO = 0.84
10	$C_3H_5O^-$[a]:MeO^-:EtO^-:OH^-	0.5:0.5:0.5:1.1	42:46:12:near zero	Allyl[a]/EtO = 3.4 MeO/EtO = 3.8 Allyl[a]/MeO = 0.91

[a]Allyloxide anion.

the two nucleophiles present during the course of the reaction before a R.N. is calculated. At the start of the reaction, the nucleophiles were present in equal amounts, but the amounts present at the end of the reaction were 0.037 mol for ethoxide and 0.063 mol for phenoxide due to the two ethers being formed in unequal amounts. An approximate R.N. can be calculated using average concentrations of the nucleophiles present during the course of the reaction to correct for the effects of mass action, but an exact solution follows.

$$[5] \quad EtO^- + BuBr \xrightarrow{k_1} EtOBr$$

$$[6] \quad PhO^- + BuBr \xrightarrow{k_2} PhOBu$$

let x = [EtOBu], and y = [PhOBu] at any time, t. The values for [EtO^-] and [PhO^-] at $t = 0$ will be A_0 and B_0.

$$[7] \quad dx/dt = k_1[EtO^-][BuBr]$$

$$[8] \quad dy/dt = k_2[PhO^-][BrBr]$$

Dividing, substituting, and rearranging terms gives

$$[9] \quad \frac{dx}{[A_0 - x]} = \left(\frac{k_1}{k_2}\right)\left(\frac{dy}{[B_0 - y]}\right)$$

Integrating between $x = 0$ and $x = x_{final}$ gives

$$[10] \quad \frac{k_1}{k_2} = \frac{\log \dfrac{[\text{initial } EtO^-]}{[\text{final } EtO^-]}}{\log \dfrac{[\text{initial } PhO^-]}{[\text{final } PhO^-]}}$$

For the experiment described, R.N. = k_1/k_2 = 2.14.

In the above manner, nucleophilicities of methoxide, ethoxide, isopropoxide, and *tert*-butoxide were determined relative to phenoxide. Methoxide and ethoxide were also measured against *m*-cresoxide, and phenoxide and *m*-cresoxide in ethanol were also compared directly. The results are in Table 3. As before, all runs were at least in duplicate and most were repeated several times. Standard deviations were calculated for all glc analyses and were usually under 2%. The error in the final calculated R.N. is believed not to exceed 5%. The time for 50% of the *n*-butyl bromide to react was approximately 20 h at

TABLE 3. Measured relative nucleophilicities of alkoxides versus phenoxide or *m*-cresoxide reacting with *n*-butyl bromide[a] at 25°C

Comparison	Composition of ether mixture (mol%)	Relative nucleophilicity
1. MeO^-/PhO^-	61:39	1.90
2. EtO^-/PhO^-	64:36	2.20
3. *i*-PrO^-/PhO^-	47.1:52.9	0.85
4.[b] *t*-BuO^-/PhO^-	16:84	0.095
5.[c] *m*-CrO^-/PhO^-	29:24	1.30
6. MeO^-/*m*-CrO^-	55.4:44.6	1.36
7. EtO^-/*m*-CrO^-	60:40	1.75
5.[c] PhO^-/*m*-CrO^-	24:29	0.77

[a]Reaction mixture consisted of 0.1 mol sodium phenoxide or *m*-cresoxide, 0.1 mol sodium alkoxide, and 0.1 mol *n*-butyl bromide in 1.8 to 2.7 mol of the alcohol corresponding to alkoxide.
[b]Potassium salts used.
[c]Three nucleophiles (0.1 mol *m*-cresoxide, 0.1 mol phenoxide, 0.1 mol ethoxide) competing for 0.1 mol *n*-butyl bromide in 2.65 mol of ethanol solvent.

25°C, and the reactions were allowed to run for about 2 weeks.

An experiment was devised to demonstrate that the composition of the ether mixture is dependent on the relative concentrations of the alkoxides present, that is, that the nucleophile which forms the new oxygen–carbon bond is the alkoxide ion itself rather than solvating neutral molecules clustered around the alkoxide ion. Two moles of ethanol were allowed to react with 0.1 atom of sodium; 0.11 mol of phenol was then added, and finally 0.10 mol of *n*-butyl bromide. This mixture should consist initially of essentially 100% phenoxide ion, solvated with ethanol, since phenol is 10^6 more acidic than alcohol. The ether mixture obtained was 98% *n*-butyl phenyl ether and 2% *n*-butyl ethyl ether. The small amount of the latter shows the neutral alcohol molecules interfere to only a minor extent; less than the 5% error observed in measuring the relative nucleophilicities. A similar experiment substituting methanol for ethanol gave 96% *n*-butyl phenyl ether and 4% *n*-butyl methyl ether. Again this error is within the experimental limits. If these side reactions are treated as competitive side reactions and the data recalculated, the relative nucleophilicities of MeO^-/PhO^- and EtO^-/PhO^- given in Table 3 are decreased from 1.90 to 1.70 and 2.20 to 2.10 respectively. These changes are within the experimental error and are too small to affect the subsequent calculations of acidity appreciably.

Since relative nucleophilicities are ratios of reaction rates, they can be combined by multiplication or division and new ratios obtained, some of which cannot be measured directly. In Table 4, the validity of this approach is demonstrated with the *m*-CrO^-/PhO^- ratio which is calculated from two different sets of data and compared with the value obtained by direct measurement.

Relative Acidity

Knowing the competitive reactivities and the relative nucleophilicities of the alkoxides, the relative acidities of the alcohols in mixed hydroxylic solvents can be calculated using eq. [1]. We believe these relative acidities are valid for the conditions under which they are measured, namely, in alcoholic media with the ionic strength in the range of 0.5 to 1.5. Table 5 gives the results and summarizes the C.R. and R.N. data from Tables 1, 3, and 4.

Comparisons with Prior Data

Alet and England (8) compared the rates of the S_N2 reaction of hydroxide, methoxide, and ethoxide with methyl iodide in various dioxane–alcohol mixtures, and extrapolated the results to pure dioxane to calculate relative nucleophilicities of 0.21, 0.64, and 1.0 respectively. They also summarized the earlier work of others on the MeO^- in MeOH vs. EtO^- in EtOH ratios of individual reaction rate constants against a variety of substrates; the ratios varied from 0.1 to 0.5. Murto (9) has made a thorough study of the rates of competitive displacement reactions of hydroxide, methoxide, and ethoxide with methyl iodide, as well as other substrates in solvents of varying composition, and has calculated the reaction rate constants for these reactions by a lengthy mathematical analysis of his data. The relative nucleophilicities with methyl iodide substrate were calculated to be 0.08:0.6:1.0 respectively. It is apparent both of these earlier studies are in agreement with our work (0.08:0.82:1.0) in that hydroxide was found to be a weak nucleophile relative to ethoxide and that methoxide was intermediate in nucleophilicity. We believe our results are more accurate, in part because ours is a more simple and direct approach. Data on many studies of the reactions of phenoxide and ethoxide with alkyl halides have been summarized by Streitwieser *et al.* (10). Again there is qualitative agreement with our work in that the ratio of the reaction rate constants in the literature indicate the PhO^-/EtO^- relative nucleo-

TABLE 4. Calculated relative nucleophilicities

Comparison	Calcd. from Table 3, runs #	Relative nucleophilicity
m-CrO^-/PhO^-	5	1.30
m-CrO^-/PhO^-	1/6	1.40
m-CrO^-/PhO^-	2/7	1.26
MeO^-/EtO^-	1/2	0.86
MeO^-/EtO^-	6/7	0.78
		Best value taken as 0.82
i-PrO^-/EtO^-	3/2	0.39
t-BuO^-/EtO^-	4/2	0.043

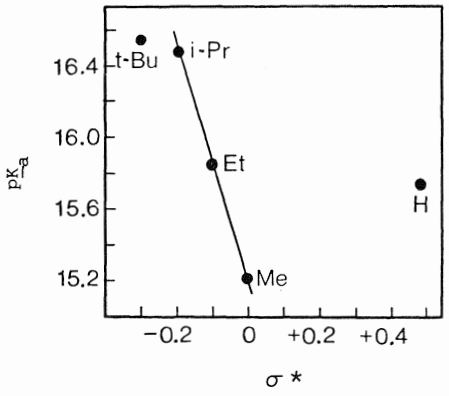

FIG. 1. Plot of pK_a values of alcohols versus Taft's σ* values.

TABLE 5. Competitive reactivities and relative nucleophilicities of alkoxides, and relative acidities of the alcohols in mixed hydroxylic solvents

Alkoxide	Competitive reactivity	Relative nucleophilicity	Relative acidity of alcohols
Hydroxide	0.1	(0.08)[a]	1.3[b]
Methoxide	3.6	0.82	4.4
Ethoxide	1.0	1.0	1.0
Isopropoxide	0.092	0.39	0.24
tert-Butoxide	0.0089	0.043	0.21
Phenoxide	—	0.46	(10^6)[c]
m-Cresoxide	—	0.57	(10^6)[c]

[a]Calculated value using literature acidity value of ref. 6.
[b]Reference 6.
[c]Reference 7.

philicity has an average value of 0.2 for methyl iodide substrate, 0.5 for ethyl iodide, and 0.6 for *n*-propyl iodide, all in ethanol solution. For *n*-butyl bromide, we found the relative nucleophilicity to be 0.46.

Although there is a voluminous literature on the acidity and basicity of organic compounds in general (3, 11), there are only eight quantitative studies on the acidity of methanol (6, 9, 12–15, 20, 21), ten on ethanol (6, 9, 14–21), four on isopropyl alcohol (6, 15, 20, 21), and three on *tert*-butyl alcohol (15, 20, 21). All investigators now agree that methanol is more acidic than water by a factor of two- (12) to seven- (13) fold. Unmack's 1928 work (12), based on conductivity, solubility, freezing points, and reaction rate data, suggested methanol was three to five times more acidic than water, but emf measurements suggested it was less than twice as acidic. The most accurate work appears to be that of Hine and Hine (6) who established their acidity scale in isopropyl alcohol by the indicator method using *p*-nitrodiphenylamine. The pioneering work with an indicator (etioporphyrin) was done by McEwen (15), and his work is still often cited in textbooks. He took methanol as his standard and assigned it a pK_a of 16 based on the work of Unmack (12). The conductivity method of Ballinger and Long (14) established the pK_a scale relative to water.

Ethanol has been studied thoroughly by emf (16), conductivity (14, 17), indicator (6, 15, 18), titration (19, 20), and reaction-kinetic methods (9). Caldin and Long's indicator procedure (18) gave ethanol as either 2 or 0.2 times as strong an acid as water depending on whether their data were extrapolated to pure ethanol or water, respectively. Their data as recalculated by Murto (ref. 9; p. 29) give ethanol 0.56 as acidic as water. Again, the most reliable work appears to be that of Hine and Hine (6) who studied water, methanol, ethanol, and other alcohols by their indicator method. The reaction-kinetic method used by Murto (9) represents a new approach. Methods based on emf measurements or titration data give erratic results. Ballinger and Long could not measure the acidity of ethanol directly by their conductivity method, and extrapolation of their data using a σ^* relationship was necessary (14).

Arnett and Small (21) have measured the heat of deprotonation of alcohols in dimethyl sulfoxide and calculated the following pK_a values: water, 27.5; methanol, 27.9; ethanol, 28.2; isopropyl alcohol, 29.3; and *tert*-butyl alcohol, 29.4. This corresponds to relative acidities of 2:1:0.08:0.063 for these alcohols in this aprotic solvent. Comparisons between our results in protic solvents and these results in an aprotic solvent must be made very cautiously, but it is noteworthy that methanol here also is more acidic than ethanol, and *tert*-butyl alcohol is only a little less acid than isopropyl alcohol.

There is remarkably good agreement between our work and that of Hine and Hine (6), Murto (9), and Long and Ballinger (14), with respect to the relative acidities of methanol and ethanol, especially in view of the four different experimental approaches. Our measured acidity of *tert*-butyl alcohol relative to ethyl or isopropyl alcohols is surprising, but the only values our data can be compared against are those of McEwen (15) and Arnett and Small (21). Perhaps the common belief that *tert*-butyl alcohol is much less acidic than isopropyl alcohol arises from the low nucleophilicity of the *tert*-butoxy anion (see Table 5).

Streitwieser *et al.* (22) have shown that a plot of Taft's σ^* values (23) against the pK_a values of a series of 9-alkylfluorenes yields a straight line for the methyl, ethyl, and isopropyl members of this series, but not for *tert*-butyl and hydrogen. A plot of our pK_a values (see Table 6) against the σ^* values gives a plot similar to that of Streitwieser *et al.*, and reinforces our belief in the validity of our data.

Experimental Section

The alcohols were pure as measured by glc. Reference samples of the ethers were prepared by standard procedures

TABLE 6. Comparison of relative acidities with literature values

Compound	This work: Relative value	This work: pK_a[a]	McEwen[b] pK_a	Hine and Hine[c] relative values	Long[d] pK_a	Murto[f] relative values
Water	—	15.74	—	1.27	15.74	1.27
Methanol	4.4	15.21	16	4.22	15.5	3.2
Ethanol	1.0	15.85	18	1.0	(15.9)[e]	1.0
Isopropyl alcohol	0.24	16.48	18	0.079		
tert-Butyl alcohol	0.21	16.54	19			

[a]Using water as the reference solvent, following ref. 14, and taking the H_2O:EtOH K_a ratio as 1.3.
[b]Initial indicator method using etioporphyrin (ref. 15).
[c]Indicator method using 4-nitrodiphenylamine (ref. 6).
[d]Conductivity method (ref. 14).
[e]Extrapolated value from a plot of acidities vs. σ^*.
[f]Reaction kinetic method with methyl iodide substrate (ref. 9, p. 62).

and used to determine the instrumental response factor for the mixtures analyzed. Gas–liquid chromatographic analyses were carried out on either a F and M model 300 with a thermistor detector (used for the competitive reactivity work) or a Hewlett-Packard 5750 instrument with flame ionization (used for runs 3 and 4 in Table 1 and for the relative nucleophilicity work), using 2 m columns packed with 10% isodecyl phthalate, 20% Lutensol (an oxyethylation product of nonylphenol manufactured by Supelco Inc., Supelco Park, Bellefonte, PA), or Apiezon-L (for the benzyl ethers). Programs and retention times are in the thesis of C.M.E. Erratic results were avoided by using a syringe which minimized blow-by (Glenco Micro Syringe, Glenco Scientific, Houston, Texas).

Typical Competitive Reactivity Determination

To a mixture of 40.4 mL (1 mol) of methanol and 58.2 mL (1 mol) of ethanol was added 1.4 g (0.06 g-atom) of freshly cut sodium. Following the dissolution of the sodium, 5.4 mL (0.05 mol) of *n*-butyl bromide was added, and the mixture was allowed to stand for a month in a stoppered flask at 26 ± 1°C. Samples of the reaction mixture were then directly and repeatedly analyzed by glc and the area ratios of the two ethers measured. Application of the response factor gave the ether compositions listed in Table 1, and the competitive reactivities were calculated by eq. [4]. With benzyl bromide, the reaction is complete in a few hours, but the mixtures were allowed to stand for 3 weeks.

The *i*-PrO^-/EtO^- C.R. ratio (run #3 in Table 1) differed from the others in that the two alcohols were employed in a nominal 10:1 ratio with the more acidic alcohol being the minor component, and with 0.1 atom of metal per 0.2 mol of minor alcohol. The data were treated initially in the usual way and the relative acidity of *i*-PrOH to EtOH was calculated to be 0.282 from the C.R. value of 0.11 divided by the R.N. value of 0.39 (Table 5). Equation [3] was then set up as follows:

$$\text{Acidity of } i\text{-PrOH/EtOH} = 0.282 = [PrO^-][EtOH]/[PrOH][EtO^-] = [PrO^-][0.2 - EtO^-]/[2 - PrO^-][EtO^-]$$

Knowing $[EtO^-] + [i\text{-}PrO^-] = 0.1$, the equation was solved to give $[i\text{-PrOH}] = 1.925$ and $[EtOH] = 0.1755$, or a ratio of these alcohols of 10.98 at the start of the reaction. No base is left at the completion of the reaction, and the ratio of the two alcohols can be calculated from the initial concentrations of 2.0 and 0.2 minus what was consumed by formation of the two ethers. These concentrations are calculated to be 1.948 and 0.1524 or a ratio of 12.78. Accordingly the average ratio of the two alcohols present during the course of the reaction is 11.9. If this value is used in eq. [4] the C.R. changes from its first calculated value of 0.11 to 0.0925, and the relative acidity changes from 0.282 to 0.237. Repeating the calculations again using the new relative acidity causes little change; a new C.R. value of 0.0917 is obtained, from which a new relative acidity of 0.236 is calculated.

The *t*-BuO^-/*i*-PrO^- data in Tables 1 and 5 were likewise treated twice in a reiterative manner and the nominal C.R. of *t*-BuO^-/*i*-PrO^- of 0.111 was recalculated successively as 0.0972 and 0.0969. The nominal relative acidity of *t*-BuOH/*i*-PrOH of 0.993 was recalculated successively as 0.872 and 0.869. Multiplying the relative acidity of *i*-PrOH/EtOH of 0.236 by the *t*-BuOH/*i*-PrOH relative acidity of 0.869 gives the corrected relative acidity of *t*-BuOH/EtOH of 0.205 as given in Table 5.

Typical Relative Nucleophilicity Determination

Freshly cut sodium (0.2 atom) was added to the alcohol (2 mol) in an oversized test tube (3.5 × 30 cm) and after dissolution was complete, the phenol (0.1 mol) (or *m*-cresol) was added and the solution thoroughly mixed. The *n*-butyl bromide (0.1 mol) was added from a burette, and the solution was again thoroughly mixed. The test tube was stoppered, sealed with "Parafilm", and placed in a bath thermostated at 25 ± 0.1°C. The reaction was considered to be complete when *n*-butyl bromide could no longer be detected by glc. Two aliquots were removed and each was analyzed by glc using multiple injections. For example, in the experiment using ethanol and phenol, the program (Lutensol column) involved holding the column at 30°C for 10 min, raising the temperature to 150°C at 30°C/min, and holding the column at this final temperature. The *n*-butyl ethyl ether and *n*-butyl phenyl ether retention times were 7 and 25 min, respectively. The area data from six injections (three from each aliquot) for the peaks representing BuOEt and BuOPh as read by the disc integrator follows: 2335/2204, 2362/2340, 2450/2430, 2492/2370, 2868/2815, and 2730/2784. These data give an average area ratio of 1.02 with a standard deviation of 0.01. Two other experiments carried out four months later gave average area ratios of 1.02 ± 0.01 and 0.992 ± 0.006. The instrument response factor was determined from known mixtures to be 1.67 and the mole ratio of the BuOEt and BuOPh ethers was therefore 1.70, or 63:37. (The 64:36 value given in Table 3 is an averaged value and includes data from runs in which a phenol – *m*-cresol mixture in ethanol solution reacted with *n*-butyl bromide.) The

initial concentrations of EtO^- and PhO^- were each 0.1 mol per volume of the reaction mixture, and the final concentrations were 0.037 and 0.063, respectively. Applying eq. [10] gives the relative nucleophilicity of EtO^-/PhO^- as 2.15 for this set of data.

1. E. M. ARNETT, L. E. SMALL, R. T. MCIVER, and J. S. MILLER. J. Am. Chem. Soc. **96**, 5638 (1974); J. I. BRAUMAN and L. K. BLAIR. J. Am. Chem. Soc. **93**, 4315 (1971) and ref. 2 therein.
2. E. M. ARNETT. *In* Progress in physical organic chemistry. *Edited by* S. G. Cohen *et al.* Interscience Publishers, New York, NY. 1963. p. 353.
3. R. F. COOKSON. Chem. Rev. **74**, 5 (1974).
4. W. REEVE and P. F. ALUOTTO. Tetrahedron Lett. 2557 (1968).
5. C. W. L. BEVAN, E. P. HUGHES, and C. K. INGOLD. Nature, **171**, 301 (1953).
6. J. HINE and M. HINE. J. Am. Chem. Soc. **74**, 5266 (1952).
7. A. I. BIGGS and R. A. ROBINSON. J. Chem. Soc. 388 (1961).
8. I. R. ALET and B. D. ENGLAND. J. Chem. Soc. 5259 (1961).
9. J. MURTO. Ann. Acad. Sci. Fenn. Ser. A, II, **117**, 57 (1962); **117**, 62 (1962); **117**, 64 (1962); **117**, 77 (1962); J. Murto. *In* The chemistry of the hydroxyl group. Part 2. *Edited by* S. Patai. Interscience Publishers, New York, NY. 1971. p. 1104.
10. A. STREITWIESER. Chem. Rev. **56**, 582 (1956).
11. K. BOWDEN. Chem Rev. **66**, 119 (1966).
12. A. UNMACK. Z. Phys. Chem. **129**, 349 (1927); **131**, 371 (1928); **133**, 45 (1928).
13. J. KOSKIKALLIO. Suom. Kemistil. **30**B, 111 (1957); Chem. Abstr. **51**, 17356 (1957).
14. F. A. LONG and P. BALLINGER. *In* Electrolytes. *Edited by* B. Pesce. Pergamon Press Ltd., Oxford. 1962. p. 152; P. BALLINGER and F. A. LONG. J. Am. Chem. Soc. **81**, 1050 (1959).
15. W. K. MCEWEN. J. Am. Chem. Soc. **58**, 1124 (1936).
16. P. S. DANNER. J. Am. Chem. Soc. **44**, 2832 (1922).
17. P. S. DANNER and J. H. HILDEBRAND. J. Am. Chem. Soc. **44**, 2824 (1922).
18. E. F. CALDIN and G. LONG. J. Chem. Soc. 3737 (1954).
19. C. W. ROBERTS, E. T. MCBEE, and C. E. HATHAWAY. J. Org. Chem. **21**, 1369 (1956).
20. A. P. KRESHKOV, L. N. BYKOVA, Z. G. BLAGODATSKAYA, and V. D. ARDASHNIKOVA. Zh. Anal. Khim. **23**, 271 (1968); Chem. Abstr. **69**, 2725*z* (1968); L. N. BYKOVA and S. I. PETROV. Zh. Anal. Khim. **25**, 5 (1970); Chem. Abstr. **72**, 104581*t* (1970).
21. E. M. ARNETT and L. E. SMALL. J. Am. Chem. Soc. **99**, 808 (1977).
22. A. STREITWIESER, C. J. CHANG, and D. M. E. REUBEN. J. Am. Chem. Soc. **94**, 5730 (1972).
23. R. W. TAFT, JR. *In* Steric effects in organic chemistry. *Edited by* M. S. Newman. Wiley, New York, NY. 1956. p. 619.

Absolute rate constants for hydrocarbon autoxidation. 27. On the question of a reversible rate controlling propagation reaction[1]

J. A. HOWARD AND SHIU BOR TONG[2]

Division of Chemistry, National Research Council of Canada, Ottawa, Ont., Canada K1A 0R9

Received January 29, 1979

J. A. HOWARD and SHIU BOR TONG. Can. J. Chem. **57**, 2755 (1979).

Autoxidations of cumene, 3-methylpentane, cyclopentane, and cyclohexane have been performed to high conversion in the presence of $(CH_3)_3COOD$ from 0.1 to 1 atm of oxygen and it has been found that very low yields of $C_6H_5C(CH_3)_2D$, $C_6H_{13}D$, *c*-C_5H_9D, and *c*-$C_6H_{11}D$ are produced. Furthermore, autoxidation of $C_6H_5C(CH_3)_2D$ in the presence of $(CH_3)_3COOH$ does not give detectable concentrations of $C_6H_5C(CH_3)_2H$ and relative reactivities of cumene and 3-methylpentane to the *tert*-butylperoxy radical in solution do not depend on the pressure of oxygen above the liquid from 1 to 100 atm. These results have been interpreted in term of a slow reaction of the alkyl radical with alkyl hydroperoxide outside the solvent cage in competition with a fast reaction of the alkyl radical with oxygen. A rate constant for the former reaction has been estimated from the relative yields of 5-hexene and methylcyclopentane produced by decomposition of 5-hexenylformyl peroxide in an inert solvent containing *tert*-butyl hydroperoxide.

The relative reactivity of the tertiary hydrogens in cumene and 3-methylpentane to the *tert*-butylperoxy radical in the gas phase is about 0.8 times the value in solution. This relative reactivity difference between the two phases is probably due to the involvement of *tert*-butoxy radicals in rate controlling propagation reactions in the gas phase rather than to significant reversal of the H-atom transfer reaction between the peroxy radical and the substrate inside the solvent cage.

J. A. HOWARD et SHIU BOR TONG. Can. J. Chem. **57**, 2755 (1979).

On a réalisé l'autoxydation du cumène, du méthyl-3 pentane du cyclopentane et du cyclohexane, avec de très bons rendements en présence du $(CH_3)_3COOD$ sous une pression d'oxygène allant de 0.1 à 1 atmosphère et on a trouvé qu'il se forme de très faibles quantités de $C_6H_5C(CH_3)_2D$, $C_6H_{13}D$, *c*-C_5H_9D et *c*-$C_6H_{11}D$. De plus l'autoxydation du $C_6H_5(CH_3)_2D$ en présence du $(CH_3)_3COOH$ ne produit pas des quantités décelables de $C_6H_5C(CH_3)_2H$ et les réactivités relatives du cumène et du méthyl-3 pentane par rapport au radical *tert*-butylperoxy en solution ne dépend pas de la pression de l'oxygène au-dessus du liquide entre 1 et 100 atmosphères. On a interprété ces résultats en fonction d'une réaction lente du radical alkyle avec l'hydroperoxyde d'alkyle à l'intérieur de la cage du solvant, en compétition avec une réaction rapide du radical alkyle avec l'oxygène. On a évalué la constante de vitesse de la première réaction à partir des rendements en hexène-5 et en méthylcyclopentane produits par la décomposition du peroxyde d'hexenyl-5 formyle dans un solvant inerte contenant de l'hydroperoxyde de *tert*-butyle.

La réactivité relative des hydrogènes tertiaires du cumène et du méthyl-3 pentane par rapport au radical *tert*-butylperoxy dans la phase gazeuse est environ 0.8 fois la valeur en solution. Cette différence de réactivité relative entre les deux phases est due probablement à l'entrée en jeu des radicaux *tert*-butylperoxy dans l'étape déterminante des réactions de propagation dans la phase gazeuse plutôt qu'à une inversion significative de la réaction de transfert d'un atome d'hydrogène entre le radical peroxy et le substrat à l'intérieur de la cage du solvant.

[Traduit par le journal]

Introduction

It has been reported that rates of free-radical bromination of alkanes and alkyl halides (RH) in solution are influenced by reaction of the chain carrying alkyl radical (R•) with hydrogen bromide both inside and outside the solvent cage, reactions [−1] and [2], and with HBr_3•, reaction [3] (1–4),

$$[1] \quad Br^{\bullet} + RH \underset{k_{-1}}{\overset{k_1}{\rightleftharpoons}} (BrH + R^{\bullet})_{cage}$$

$$[2] \quad R^{\bullet} + HBr \xrightarrow{k_2} RH + Br^{\bullet}$$

$$[3] \quad R^{\bullet} + HBr_3 \longrightarrow RH + Br_3^{\bullet}$$

Thus the relative reactivity of two substrates to the bromine atom obtained from the yields of alkyl bromides produced by competitive brominations will

[1]NRCC No. 17735.

[2]NRCC Research Associate 1977–1979.

0008-4042/79/202755-06$01.00/0

be in error if the rates of reactions [−1], [2], and [3] depend on the structure of R.

Now the heat of the reaction of an alkylperoxy radical with RH is very similar to ΔH for reaction [1] because the strength of the O—H bond in an alkyl hydroperoxide (5) is almost equal to D(H—Br) (6). Hydrocarbon autoxidations in the presence of large concentrations of *tert*-butyl hydroperoxide (*t*-BuOOH) may, therefore, be influenced by reversal of the rate controlling propagation reaction as shown in Scheme 1.

$$[4] \quad t\text{-BuO}_2^{\bullet} + \text{RH} \underset{k_{-4}}{\overset{k_p}{\rightleftharpoons}} (t\text{-BuOOH} + \text{R}^{\bullet})_{\text{cage}}$$

$$[5] \quad (t\text{-BuOOH} + \text{R}^{\bullet})_{\text{cage}} \xrightarrow{k_5} t\text{-BuOOH} + \text{R}^{\bullet}$$

$$[6] \quad \text{R}^{\bullet} + \text{O}_2 \xrightarrow{k_O} \text{RO}_2^{\bullet}$$

$$[7] \quad \text{RO}_2^{\bullet} + t\text{-BuOOH} \xrightarrow{k_7} \text{ROOH} + t\text{-BuO}_2^{\bullet}$$

$$[8] \quad \text{R}^{\bullet} + t\text{-BuOOH} \xrightarrow{k_r} \text{RH} + t\text{-BuO}_2^{\bullet}$$

SCHEME 1

where $RO_2^{\bullet}$ and ROOH are the peroxy radical and hydroperoxide derived from the hydrocarbon RH and t-$BuO_2^{\bullet}$ is the *tert*-butylperoxy radical.

Reactions [4] to [8] along with the usual chain initiation and termination reactions give the following expression for the rate of autoxidation,

$$[9] \quad \frac{-\text{d}[\text{O}_2]}{\text{d}t} = \frac{k_5 k_p [\text{RH}] R_i^{1/2} k_O [\text{O}_2]}{(k_{-4} + k_5)(2k_t)^{1/2}(k_O[\text{O}_2] + k_r[t\text{-BuOOH}])}$$

where k_p and $2k_t$ are the rate controlling propagation and termination rate constants and R_i is the rate of chain initiation.

Clearly absolute values of k_p calculated from the usual rate expression [10] (7)

$$[10] \quad \frac{-\text{d}[\text{O}_2]}{\text{d}t} = \frac{k_p[\text{RH}]R_i^{1/2}}{(2k_t)^{1/2}}$$

will be in error if reactions [−4] and [8] are important. It also follows that relative reactivities obtained from competitive autoxidations (7, 8) could be influenced by reversible rate controlling propagation reactions.

We have attempted to resolve this problem by employing the experimental techniques used by Tanner and co-workers (1–4) to demonstrate the importance of reversal in free-radical bromination. Thus we have studied the autoxidation of cumene, 3-methylpentane, cyclohexane, and cyclopentane in the presence of *t*-BuOOD to high conversion and analyzed the unreacted hydrocarbon for incorporation of deuterium. We have also investigated the autoxidation of cumene-α-d_1 in the presence of *t*-BuOOH and the co-oxidation of cumene and 3-methylpentane in solution at oxygen pressures from 1 to 100 atm and in the gas phase. The results of this study, which are reported here, indicate that reversible hydrogen atom transfer has no significant influence on kinetic data obtained from autoxidations in the presence of high concentrations of hydroperoxide.

In addition, we have estimated the rate constant for reaction of an alkyl radical with a hydroperoxide, k_r, by measuring the yields of 5-hexene and methylcyclopentane produced by decomposition of 5-hexenylformyl peroxide in the presence of *tert*-butyl hydroperoxide.

Experimental

Materials

Cumene (Anachemia) was washed with concentrated sulphuric acid, 10% aqueous sodium bicarbonate, and water; it was then dried over anhydrous magnesium sulphate and distilled. Analysis by gas chromatography showed it to be >99.8% and it did not contain any α-cumyl alcohol It was stored under argon at −20°C. Cumene-α-d_1 was obtained from Merck, Sharpe, and Dohme (Canada) Limited. 3-Methylpentane (Chemical Samples Co.), cyclohexane (Fischer Scientific Co.), and cyclopentane (Phillips Research Grade) were >99.9% pure and contained no alcoholic impurity. These substrates were used without further purification. *tert*-Butyl hydroperoxide (Aldrich) was fractionally distilled at reduced pressure. The fraction with bp 39–40°C at 20 Torr was collected and was 99.9% pure by gas chromatography. $(CH_3)_3COOD$ was prepared by shaking $(CH_3)_3COOH$ with an equal volume of 99% D_2O (9). The D_2O was then removed and the procedure repeated until the O—H band in the infrared spectrum (ν = 3530 cm^{-1}) was replaced by the O—D band (ν = 2610 cm^{-1}). A sample of $(CH_3)_3COOD$ (99% pure by nmr) was kindly provided by Professor D. D. Tanner (University of Alberta). 5-Hexenylformyl peroxide was prepared from 6-heptenoic acid (K and K) by Staab's carbonyldiimidazole route (10, 11). 2,2′-Azoisobutane was prepared from *tert*-butyl amine by the method of Stevens (12). *tert*-Butyl hyponitrite was prepared by the method of Kiefer and Traylor (13).

Procedure

Liquid-phase Autoxidations

Reactions at 1 atm of oxygen and below were performed in the automatic recording gas apparatus described previously (14). In a typical experiment cumene (6.45 *M*) containing α,α′-azo-bis-isobutyronitrile (0.05 *M*), $(CH_3)_3COOD$ (1.1 *M*) and D_2O (0.5 mL) was shaken with oxygen at 720 Torr and 30°C. Oxygen (0.69 *M*) was absorbed in 120 h and the hydroperoxides in the reaction mixture were reduced with triphenylphosphine. Volatile products were pumped into a trap maintained at the temperature of liquid nitrogen and the concentration of α-cumyl alcohol was determined by gas chromatography (Varian 2800 chromatograph equipped with a 12 ft 12% OV-101 on Chromosorb W column and flame ionization detector). High pressure experiments were conducted in a glass tube in a stainless steel bomb. Oxygen concentrations in the

various hydrocarbons were calculated using solubility data from the literature (15).

Gas-phase Autoxidations

Solutions of 3-methylpentane, cumene, initiator (2,2′-azoisobutane or di-*tert*-butyl hyponitrite), and *tert*-butyl hydroperoxide were injected through a serum cap into a 1-litre reaction vessel containing oxygen (400 Torr). The reaction vessel was immersed in an oil bath maintained at a constant temperature, and for azoisobutane initiated reactions the reaction mixture was irradiated with a Westinghouse 275W Sun-lamp for 160–260 h. The reaction mixture was then pumped into a trap maintained at the temperature of liquid nitrogen, and enough triphenylphosphine was added to reduce all the hydroperoxides present. The reduced sample was distilled into a cold trap and analyzed by gas chromatography.

Decomposition of 5-Hexenylformyl Peroxide

These reactions were performed at 50°C in degassed carbon tetrachloride or chlorobenzene containing *tert*-butyl hydroperoxide. The volatile products were distilled from the reaction mixture and analyzed by gas chromatography.

Mass Spectroscopic Analysis

Percentages of monodeuterated hydrocarbon in cumene, 3-methylpentane, cyclohexane, and cyclopentane and normal cumene in $C_6H_5C(CH_3)_2D$ after autoxidation were determined from a comparison of the mass spectrum of the starting material and the spectrum of the recovered unreacted hydrocarbon after at least 10% conversion. Mass spectra were obtained with a Finnigan 4000 automated gas chromatograph–mass spectrometer system.

Results and Discussion

Cumene

Oxygen at a pressure of 720 Torr was absorbed very rapidly by cumene (6.45 *M*) at 30°C containing AIBN (0.05 *M*), *t*-BuOOD (1 *M*), and D_2O (0.5 mL). In 93 h 0.69 *M* of oxygen had been absorbed and α-cumene hydroperoxide (0.69 *M*) was the major reaction product. The unoxidized cumene was found to contain ~1.5% cumene-α-d_1.

If this autoxidation is described by the reactions shown in Scheme 1 with R = $C_6H_5C(CH_3)_2$ the rate of formation of cumyl hydroperoxide is given by

$$\frac{d[C_6H_5C(CH_3)_2OOH]}{dt} = k_O[C_6H_5\dot{C}(CH_3)_2][O_2]$$

and the rate of formation of $C_6H_5C(CH_3)_2D$ by

$$\frac{d[C_6H_5C(CH_3)_2D]}{dt} = k_r[C_6H_5\dot{C}(CH_3)_2][(CH_3)_3COOD]$$

The concentration of monodeuterated cumene will, therefore, be governed by

$$[11]\quad \frac{k_r}{k_O} = \frac{[C_6H_5C(CH_3)_2D]_t[O_2]_0}{[C_6H_5C(CH_3)_2OOH]_t[(CH_3)_3COOD]_0}$$

where $[C_6H_5C(CH_3)_2D]_t$ and $[C_6H_5C(CH_3)_2OOH]_t$ are the concentrations after time *t* and the subscript 0 refers to initial concentrations.

In order to calculate the rate constant ratio k_r/k_O from [11] it is necessary to know $[(CH_3)_3COOD]_0$. Now it is not known whether cumyl radicals will react with the associated form of the hydroperoxide. We have, therefore, assumed for the purpose of this work that reaction only occurs with free hydroperoxide, the concentration of which has been calculated from the thermodynamic data provided by Walling and Heaton (9).

Substitution of the reactant concentrations and the yields of α-cumyl hydroperoxide and $C_6H_5C(CH_3)_2D$ reported above in eq. [11] gives $k_r/k_O \sim 2 \times 10^{-4}$.

The rate constant ratio k_r/k_O should be proportional to the first-power of the oxygen concentration and inversely proportional to the first-power of the hydroperoxide concentration. The latter concentration exponent could not be confirmed experimentally because below a hydroperoxide concentration of 1 *M* the percentage of deuterated cumene in unreacted cumene was too low to be measured accurately while above 1 *M* most of the hydroperoxide was associated by hydrogen bonding.

In an attempt to determine the oxygen concentration exponent reactions were performed at low oxygen pressures (95 Torr) and the percentage cumene-α-d_1 was found to be identical, within experimental error, to the percentage at 720 Torr. This unexpected result probably reflects the difficulty in accurately determining low percentages of deuterated cumene by mass spectrometry rather than a zero-order dependence on the oxygen concentration.

The results of several experiments conducted under different experimental conditions are listed in Table 1 and suggest that $k_r/k_O < 10^{-3}$ which means that if k_O is $10^{9.5}$ M^{-1} s^{-1} (16), $k_r < 10^{6.5}$ M^{-1} s^{-1}.

Cumene-α-d_1

This compound was oxidized at 30°C under 700 Torr of oxygen in the presence of *t*-BuOOH (2 *M*) to approximately 10% conversion. The mass spectrum of the unoxidized cumene was identical with that obtained from the starting material indicating negligible loss of deuterium by reaction of cumyl radicals with the hydroperoxide.

Alkanes

3-Methylpentane (6.94 *M*) containing AIBN (0.09 *M*), *t*-BuOOD (1.1 *M*), and D_2O (0.3 mL) was allowed to react with oxygen (5 atm) at 30°C for 29 days. After this length of time ~10% of the alkane had been oxidized. There was, however, no evidence for $CH_3CH_2C(CH_3)DCH_2CH_3$ in the unreacted alkane.

In an attempt to increase the percentage yield of monodeuterated alkane cyclopentane and cyclo-

TABLE 1. Reactant concentrations and product yields for the liquid-phase autoxidation of cumene in the presence of $(CH_3)_3COOD$ at 30°C

$[Cumene]_0$ (*M*)	$[(CH_3)_3COOD]_0$[a] (*M*)	$10^2[O_2]$ (*M*)	10^3[Cumene-α-d_1]$_f$ (*M*)	ΔO_2[b] (*M*)	$[Cumyl\ alcohol]_f$ (*M*)	$10^4\frac{k_r}{k_O}$[c]
6.45	0.57	0.83	8.4	0.69	—	2
5.74	0.64	0.83	21	0.46	0.3	9
5.2	0.76	0.83	16	0.44	0.57	3
5.74	0.64	0.13	10–21	—	0.6	0.25–0.5

[a]Monomer concentration.
[b]Total concentration of oxygen absorbed.
[c]Calculated on the assumption that cumyl radicals only react with monomeric $(CH_3)_3COOD$.
[d]Subscripts 0 and f refer to initial and final concentrations.

hexane were used instead of 3-methylpentane, the oxygen pressure was decreased to 1 atm and the temperature was increased to 50°C. Data obtained for these substrates are summarized in Table 2 and it can be seen from these data that the percentage yields of monodeuterated cyclane were so low that the reproducibility was extremely poor. In fact the only conclusion that can be drawn from these data is that k_r/k_O is somewhat less than 10^{-2}.

Co-oxidation of Cumene and 3-Methylpentane

The relative reactivity of cumene and 3-methylpentane to t-$BuO_2^{\bullet}$ obtained from co-oxidations in the presence of high concentrations of t-BuOOH would depend on the concentration of oxygen dissolved in the reaction mixture if the rate controlling propagation reactions are reversible and the rate of the reverse reaction depends on the nature of R. We have therefore determined the relative reactivity of these substrates at 1, 10, and 100 atm of oxygen at 30°C and find that k_p(cumene)/k_p^{ref} (where k_p^{ref} is the reactivity of the t-C—H bond in 3-methylpentane) = 21.8 at 1 atm, 22.6 at 10 atm, and 19.9 at 100 atm. Clearly this rate constant ratio is unchanged over a 100-fold variation in the oxygen concentration.

Gas-phase Autoxidation

Although the experiments described above indicate that reaction of an alkyl or substituted alkyl radical with alkyl hydroperoxide outside the solvent cage (reaction [7]) is not important enough to effect either rates of autoxidation or product ratios from co-oxidations, they give no indication of the importance of cage reversal (reaction [5]) on these rates and product ratios. Thus the efficiency with which an alkyl radical escapes the solvent cage will depend on the rate of its reaction with ROOH inside the cage. Now the strength of the t-C—H bond in 3-methylpentane is at least 10 kcal mol^{-1} stronger than the strength of the t-C—H bond in cumene (17) and the 3-methyl-3-pentyl radical could in theory react more rapidly than the cumyl radical with ROOH. Therefore, if cage reversal is important cumyl radicals will escape the solvent cage more efficiently than 3-methyl-3-pentyl radicals and k_p(cumene)/k_p^{ref} will be anomalously large in solution because a disproportionate amount of cumyl hydroperoxide will be formed.

We have attempted to assess the importance of cage reversal by investigating the co-oxidation of cumene and 3-methylpentane in the presence of t-BuOOH initiated by thermolysis of di-*tert*-butyl hyponitrite and by photolysis of 2,2′-azoisobutane in the gas phase and comparing the results with those obtained in solution.

The di-*tert*-butyl hyponitrite (0.009 *M*) initiated autoxidation of cumene (0.86 *M*) and 3-methylpentane (6.32 *M*) containing $(CH_3)_3COOH$ (0.6 *M*) at 45°C in the gas phase gave 3-methylpentan-3-ol (0.0043 *M*), α-cumyl alcohol (0.0094 *M*), and di-*tert*-butyl peroxide (0.264 *M*) as the major reaction products. The relative yield of these two alcohols gives k_p(cumene)/k_p^{ref} = 16. The kinetic chain length (ν), based on the total alcohol yield and the yield of di-*tert*-butyl peroxide was, however, only 0.02.

When this reaction was conducted in the liquid phase at 45°C the product yields were 3-methylpentan-3-ol (0.035 *M*), cumyl alcohol (0.076 *M*), and di-*tert*-butyl peroxide (0.004 *M*), giving k_p(cumene)/k_p^{ref} = 16, cf., k_p(cumene)/k_p^{ref} = 20 (7), and the kinetic chain length was 14.

TABLE 2. Reactant concentrations and product yields for the liquid-phase autoxidation of cyclopentane and cyclohexane in the presence of $(CH_3)_3COOD$ at 50°C and 1 atm of oxygen[a]

Substrate (*M*)	$[(CH_3)_3COOD]$[b] (*M*)	$[RD]_f$ (*M*)	$[ROH]_f$ (*M*)
Cyclopentane (8.47)	0.75	0.024	0.1
Cyclopentane (9.62)	0.45	0.17	0.11
Cyclopentane (9.62)	0.45	0	0.25
Cyclopentane (10.1)	0.29	0.09	0.19
Cyclohexane (8.34)	0.45	0.016	0.076
Cyclohexane (8.73)	0.29	0.029	0.093
Cyclohexane (8.95)	0.17	0.065	0.05

[a]$[O_2] = 1.3 \times 10^{-2}$ *M*.
[b]Monomer concentration.

These di-*tert*-butyl hyponitrite initiated co-oxidations were repeated several times and the average relative reactivities were $k_p(\text{cumene})/k_p^{ref} = 15 \pm 2$ in the gas phase ($\nu = 0.01$–0.6) and $k_p(\text{cumene})/k_p^{ref} = 19 \pm 3$ in the liquid phase ($\nu = 13$–35).

2,2′-Azoisobutane initiated gas phase autoxidations gave $k_p(\text{cumene})/k_p^{ref} = 15.5$ at 45°C ($\nu = 0.2$) and 10 at 55°C ($\nu = 4$).

It would, therefore, appear from these experiments that $k_p(\text{cumene})/k_p^{ref}$ in the gas phase is about 0.8 times the relative reactivity in solution, which could be interpreted as being indicative of cage reversal in solution. Kinetic chain lengths for the gas phase reactions were, however, very short and it is quite possible that the gas phase rate constant ratios are low because of H-atom abstraction by *tert*-butoxy radicals formed by nonterminating interactions of *tert*-butylperoxy radicals. These radicals are more reactive and less selective than *tert*-butylperoxy radicals and would be expected to lower the reactivity difference between cumene and 3-methylpentane.

Measurement of k_r

The kinetic data given in Table 2 suggest that the rate constant ratio k_r/k_O is $<10^{-2}$ for the cyclopentyl and cyclohexyl radicals, and since k_O is $\sim 10^{9.5}$ (16) k_r is $<10^{7.5}\ M^{-1}\ s^{-1}$. On the other hand yields of $C_6H_5C(CH_3)_2D$ obtained from autoxidation of cumene in the presence of $(CH_3)_3COOD$ suggest that k_r for cumyl radicals is $<10^{6.5}$.

It should be possible to estimate the value of k_r from the relative concentrations of 5-hexene and methylcyclopentane produced by decomposition of 5-hexenylformyl peroxide in the presence of *tert*-butyl hydroperoxide. This peroxide decomposes readily at 50°C to give the 5-hexenyl radical which either abstracts the hydroperoxidic hydrogen to give 5-hexene or isomerizes to the cyclopentylmethyl radical which picks up a hydrogen atom to give methylcyclopentane.

[12] 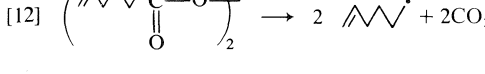

[13] 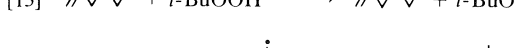

[14] 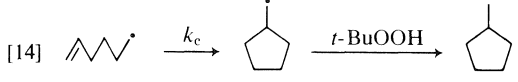

The rate constant ratio k_c/k_r is given by

[15] $$\frac{k_c}{k_r} = \frac{[\text{cyclopentyl}][t\text{-BuOOH}]}{[\text{5-hexenyl}]}$$

and since $k_c = 2.36 \times 10^5\ s^{-1}$ at 50°C (18) k_r can be calculated from the relative concentrations of the two hydrocarbons formed by reaction with the hydroperoxide and the concentration of *tert*-butyl hydroperoxide.

Methylcyclopentane and 5-hexene were formed in the ratio 1.72 ± 0.02 after decomposition of 5-hexenylformyl peroxide (0.05 *M*) in degassed chlorobenzene containing *t*-BuOOH (0.9 *M*). There is, however, no way of estimating from this experiment the amount of hydrocarbon formed via reactions [13] and [14] and the amount formed by other processes, such as radical–radical disproportionation reactions. In order to resolve this problem 5-hexenylformyl peroxide was decomposed in the presence of 2.0 *M* *t*-BuOOD (and a trace of D_2O) and the yields of monodeuterated methylcyclopentane and 5-hexene relative to C_6H_{12} were measured by mass spectrometry. This experiment gave 10.15 ± 0.4 for the total ratio of methylcyclopentane to 5-hexene and indicated that 92% of the methylcyclopentane was $C_6H_{11}D$ whereas only 35% of the 5-hexene was $C_6H_{11}D$. Clearly most of the methylcyclopentane was formed by abstraction of the hydroperoxidic deuterium while a significant fraction of 5-hexene was formed by another route. Calculation of k_r from the formula

$$\frac{k_c}{k_r} = \frac{[\text{D-cyclopentyl}]\,[t\text{-BuOOD}]_{monomer}}{[\text{5-hexenyl-D}]} = 27 \times 0.75$$

gave $k_r = 8.7 \times 10^3\ M^{-1}\ s^{-1}$ and a slightly larger value if the alkyl radicals react with deuterium bonded hydroperoxide.

Abstraction of a hydroperoxidic hydrogen by an alkyl radical probably has a primary deuterium isotope effect no greater than 2 and we can conclude that k_r for normal *tert*-butyl hydroperoxide is $\sim 2 \times 10^4\ M^{-1}\ s^{-1}$.

Conclusions

It is apparent from the results presented in this paper that reversal of the rate controlling propagation reaction for hydrocarbon autoxidation in the presence of large amounts of alkyl hydroperoxide is not important enough to influence the magnitude of cross-propagation rate constants determined by the hydroperoxide method (7, 8, 17).

The rate constant for reaction of an alkyl radical with *t*-BuOOH in solution is about five orders of magnitude smaller than the rate constant for reaction of the alkyl radical with oxygen and the former reaction is unimportant even at hydroperoxide to oxygen ratios of 100:1. Consequently it is not surprising that estimates of k_r/k_O made from the

yields of c-$C_6H_{11}D$ and c-C_5H_9D produced by autoxidation of c-C_6H_{12} and c-C_5H_{10} in the presence of *tert*-BuOOD (Table 2) were erratic. The maximum mole fraction of monodeuterated cyclane that could be expected if $k_r = 2 \times 10^4\ M^{-1}\ s^{-1}$ is 5×10^{-6} which is outside the limits of detection by mass spectrometry.[3]

In contrast, Tanner *et al.* (2) have found that the cyclohexyl radical is only about 0.3 times less reactive to HBr than it is to Br_2. This difference between autoxidation and bromination may be because a peroxy radical is less reactive to a hydroperoxide than a bromine atom is to HBr or because an alkyl radical is more reactive to oxygen than it is to bromine.

Acknowledgements

The authors were prompted to perform the experiments described in this paper by discussions with Professor D. D. Tanner. They also wish to thank Mr. M. Bednas for mass spectroscopic analyses and a referee for helpful suggestions.

[3]NOTE ADDED IN PROOF: Reanalysis of oxidized cyclopentane and cyclohexane in the presence of $(CH_3)_3COOD$ using a capillary column in the gas chromatograph gave even *lower* yields of monodeuterated cyclane than the values reported in Table 2.

1. D. D. TANNER, T. OCHIAI, and T. PACE. J. Am. Chem. Soc. **97**, 6162 (1975).
2. D. D. TANNER, T. PACE, and T. OCHIAI. J. Am. Chem. Soc. **97**, 4303 (1975).
3. D. D. TANNER, T. PACE, and T. OCHIAI. Can. J. Chem. **53**, 2202 (1975).
4. D. D. TANNER, Y. KOSUGI, R. ARHART, N. WADA, T. PACE, and T. RUO. J. Am. Chem. Soc. **98**, 6275 (1976).
5. L. R. MAHONEY and M. A. DAROOGE. J. Am. Chem. Soc. **92**, 4063 (1970).
6. J. A. KERR and A. F. TROTMAN-DICKENSON. Handbook of chemistry and physics. 58th ed. Chem. Rubber Publ. Co., Cleveland, OH. 1977–1978.
7. J. A. HOWARD, J. H. B. CHENIER, and D. A. HOLDEN. Can. J. Chem. **56**, 170 (1978) and previous papers in this series.
8. J. A. HOWARD and J. H. B. CHENIER. Can. J. Chem. **57**, 2484 (1979).
9. C. WALLING and L. HEATON. J. Am. Chem. Soc. **87**, 38 (1965).
10. H. A. STAAB. Angew. Chem. Int. Ed. Engl. **1**, 351 (1962).
11. P. SCHMID and K. U. INGOLD. J. Am. Chem. Soc. **100**, 2493 (1978).
12. T. E. STEVENS. J. Org. Chem. **26**, 2531 (1961).
13. H. KIEFER and T. G. TRAYLOR. Tetrahedron Lett. 6163 (1966).
14. J. A. HOWARD and K. U. INGOLD. Can. J. Chem. **47**, 3809 (1969).
15. E. WILHELM and R. BATTINO. Chem. Rev. **73**, 1 (1973).
16. J. A. HOWARD. Free radicals. Vol. II. *Edited by* J. K. Kochi. Wiley, New York, NY. 1973. Chapt. 12.
17. S. KORCEK, J. H. B. CHENIER, J. A. HOWARD, and K. U. INGOLD. Can. J. Chem. **50**, 2285 (1972).
18. P. SCHMID, D. GRILLER, and K. U. INGOLD. Int. J. Chem. Kinet. **11**, 333 (1979).

Organometallic peroxy radicals. Part 5. Trialkylsilylperoxy and trialkylstannylperoxy radicals[1]

JAMES ANTHONY HOWARD,[2] JOHN CHARLES TAIT,[3] AND SHIU BOR TONG[4]

Division of Chemistry, National Research Council of Canada, Ottawa, Ont., Canada K1A 0R9

Received March 6, 1979

JAMES ANTHONY HOWARD, JOHN CHARLES TAIT, and SHIU BOR TONG. Can. J. Chem. **57**, 2761 (1979).

A variety of organosilylperoxy and organostannylperoxy radicals, $R_3MO_2^{\bullet}$ (R = Me, Et, *n*-Bu, *t*-Bu, and Ph and M = Si and Sn) have been prepared and studied by electron spin resonance spectroscopy. Trialkylsilylperoxy radicals exist in equilibrium with a tetroxide at temperatures below 233 K with $\Delta H^0 = -11 \pm 2$ kcal mol^{-1} and $\Delta S^0 < -30$ cal deg^{-1} mol^{-1}. Above 233 K these radicals decay either with first-order, one half-order, or zero-order kinetics depending on the radical and its concentration. Trialkylstannylperoxy radicals do not exist in reversible equilibrium with a dimer below ambient temperature and they undergo self-reaction with second-order kinetics. Tri-*n*-butylstannylperoxy radicals react with 2,6-di-*tert*-butyl-4-methylphenol and cobalt(II) acetylacetonate and Arrhenius parameters for these two reactions are reported. The structure of $R_3SiO_2^{\bullet}$ resembles the structure of alkylperoxy radicals whereas the two oxygen nuclei of $R_3SnO_2^{\bullet}$ are magnetically equivalent and the peroxy group becomes a bidentate ligand. This structural difference has a significant effect on radical reactivity.

JAMES ANTHONY HOWARD, JOHN CHARLES TAIT et SHIU BOR TONG. Can. J. Chem. **57**, 2761 (1979).

On a préparé et étudié par résonance paramagnétique électronique une série de radicaux organosilylperoxy et organostannylperoxy $R_3MO_2^{\bullet}$ (R = Me, Et, *n*-Bu et M = Si et Sn). Les radicaux trialkylperoxy existent en équilibre avec le tétroxyde à des températures inférieures à 233 K avec un $\Delta H^0 = -11 \pm 2$ kcal mol^{-1} et un $\Delta S^0 < -30$ cal deg^{-1} mol^{-1}. Au dessus de 233 K, ces radicaux se désintègrent avec des cinétiques soit de premier ordre, d'ordre égal à une demi ou à zéro, dépendant du radical et de sa concentration. Les radicaux trialkylstannylperoxy n'existent pas en équilibre avec le dimère au dessous de la température ambiante et subissent une auto-réaction avec une cinétique de second ordre. On rapporte les paramètres d'Arrhénius pour les réactions des radicaux tri-*n*-butylstannylperoxy avec le di-*tert*-butyl-2,6 méthyl-4 phénol et l'acétylacétonate de cobalt(II). La structure de $R_3SiO_2^{\bullet}$ s'apparente à la structure des radicaux alkylperoxy où les deux noyaux d'oxygène du $R_3SnO_2^{\bullet}$ sont magnétiquement équivalents et où le groupe peroxy devient un ligand bidentate. Cette différence structurale a un effet significatif sur la réactivité du radical.

[Traduit par le journal]

Introduction

Recent reports from this laboratory have been concerned with kinetic and spectroscopic properties of the peroxy radicals resulting from addition of oxygen to group 4b organometallic radicals, $R_3M^{\bullet}$, where M is silicon, germanium, tin, and lead and R is methyl, *n*-butyl, and phenyl. Thus we have shown that spectroscopic *g*-factors can be used to identify these radicals (1), that trimethylgermylperoxy and triphenylgermylperoxy radicals at low temperatures exist in equilibrium with their tetroxides and decay irreversibly by a first-order process (2), and that the two oxygen atoms of the tri-*n*-butylstannylperoxy radical are magnetically equivalent rather than, as is usually found for peroxy radicals, nonequivalent (3).

In the first part of this series (1) we reported briefly on the spectroscopy of the trimethylsilylperoxy radical and the kinetics of the self-reaction of the trimethylstannylperoxy radical. Here we report a more thorough study of the free-radical chemistry of these and related radicals.

Experimental

Materials

Trimethylsilane (Chemical Procurement Labs Inc.), triethylsilane (Columbia Organic Chemicals Inc.), tri-*n*-butylsilane (K and K), triphenylsilane, tri-*n*-butyltin hydride, and hexa-*n*-butylditin (Ventron, Alfa Division) were purified by standard methods. Trimethyltin hydride was prepared from trimethyltin bromide and tri-*n*-butyltin hydride. Triphenyltin hydride was synthesized by reduction of tri-phenyltin bromide with $LiAlH_4$ (4). Tri-*tert*-butyl silane was a gift from Dr. K. U. Ingold.

[1]NRCC No. 17631.

[2]To whom all correspondence should be addressed.

[3]NRCC Research Associate 1975–1977. Present address: A.E.C.L., Pinawa, Manitoba.

[4]NRCC Research Associate.

0008-4042/79/202761-06$01.00/0

Procedure

The peroxy radicals were prepared directly in the cavity of a Varian E-4 EPR spectrometer by photolysis of the appropriate hydride in an oxygen saturated solvent (cyclopropane, CF_2Cl_2, toluene, CF_3Cl) containing di-*tert*-butyl peroxide.

$$[1]\quad t\text{-BuOOBu-}t \xrightarrow{h\nu} 2t\text{-BuO}^{\bullet}$$

$$[2]\quad t\text{-BuO}^{\bullet} + R_3MH \rightarrow t\text{-BuOH} + R_3M^{\bullet}$$

$$[3]\quad R_3M^{\bullet} + O_2 \rightarrow R_3MO_2^{\bullet}$$

where R = Me, Et, *n*-Bu, and Ph and M = Si and Sn or, in the case of the trialkylstannylperoxy radicals, by photolysis of hexaalkylditin in oxygen or air saturated toluene.

The kinetics of irreversible decay and the thermochemistry of reversible dimerization of $R_3MO_2^{\bullet}$ were investigated by following the influence of time and temperature on the radical concentration after the initiating light was masked (2). Absolute radical concentrations were measured relative to a standard solution of 2,2-diphenyl-1-picrylhydrazyl (DPPH).

Peroxy radicals tagged with ^{17}O were prepared from oxygen enriched to 60% in this isotope (Yeda Research and Development Company).

Results and Discussion

Trialkylsilylperoxy Radicals

The electron spin resonance parameters of the radicals which were formed when triethylsilane, tri-*n*-butylsilane, and tri-*t*-butylsilane were photolyzed in an oxygen saturated solvent containing di-*t*-butyl peroxide (DTBP) are summarized in Table 1. All three silanes gave two radicals, a trialkylsilylperoxy radical centred at $g = 2.027$ to 2.0294 and an alkylperoxy radical near $g = 2.015$. The esr spectrum of the alkylperoxy radical produced from Et_3SiH consisted of two lines separated by ~ 5 G indicating that the unpaired electron was interacting with one proton on the carbon adjacent to the peroxy group (5). An almost identical coupling constant was obtained for the alkylperoxy radical from *n*-Bu_3SiH. These radicals were almost certainly α-substituted secondary alkylperoxy radicals which were generated as shown in reaction [4]

$$[4]\quad t\text{-BuO}^{\bullet} + (RCH_2)_3SiH \rightarrow \begin{cases} (RCH_2)_2SiH\dot{C}HR \xrightarrow{O_2} (RCH_2)_2SiH\underset{\displaystyle R}{C}HO_2^{\bullet} \\ (RCH_2)_3Si^{\bullet} \xrightarrow{O_2} (RCH_2)_3SiO_2^{\bullet} \end{cases}$$

The spectrum of the alkylperoxy radical from *t*-Bu_3SiH had no hyperfine structure and the radical was extremely persistent at low temperatures (~ 173 K). These two observations suggest that this radical was *t*-$BuO_2^{\bullet}$.

The esr spectrum from tri-*tert*-butylsilylperoxy radical tagged with ^{17}O consisted of three superimposed spectra, a central line from *t*-$Bu_3SiO_2^{\bullet}$ and two sets of six lines from *t*-$Bu_3Si^{17}OO^{\bullet}$ and *t*-$Bu_3SiO^{17}O^{\bullet}$. The two oxygen coupling constants are 14.6 and 25.4 G indicating nonequivalent oxygen nuclei. The spectrum with the larger coupling constant can be assigned to *t*-$Bu_3SiO^{17}O^{\bullet}$ and this hyperfine interaction is ~ 1.2 G larger than a_0 for the terminal oxygen in *t*-$BuO_2^{\bullet}$ (6). The smaller oxygen coupling constant is from *t*-$Bu_3Si^{17}OO^{\bullet}$ and it is approximately 3 G smaller than a_0 for *t*-$Bu^{17}OO^{\bullet}$. These differences can be interpreted in terms of a trialkylsilylperoxy radical that has a larger π spin density on the terminal oxygen and a smaller π spin density on the inner oxygen than *t*-$BuO_2^{\bullet}$ (7).

Since the publication of our paper on organogermylperoxy radicals (2) we have measured ^{17}O hyperfine coupling constants for $Ph_3GeO^{17}O^{\bullet}$ ($a_0 = 24.9$ G, $A_{xx} = 91.8$ G) and $Ph_3Ge^{17}OO^{\bullet}$ ($a_0 = 15.4$ G and $A_{xx} = 64.5$ G). The isotropic parameters for this radical are closer to the values of a_0 for *t*-$Bu_3SiO_2^{\bullet}$ than they are to the values of a_0 for *t*-$BuO_2^{\bullet}$, implying that organogermyl- and organosilyl-peroxy radicals have about the same distribution of unpaired spin in the peroxy group and probably the same geometry.[5]

The secondary alkylperoxy radicals prepared from Et_3SiH and *n*-Bu_3SiH decayed more rapidly than $R_3SiO_2^{\bullet}$ and could be removed from the system by annealing at 193 K. $Et_3SiO_2^{\bullet}$ and *n*-$Bu_3SiO_2^{\bullet}$ were extremely persistent between 183 and 223 K and in this temperature range an increase in temperature gave an increase in the radical concentration while a decrease in temperature produced a decrease in the radical concentration with no apparent irreversible radical decay. Trialkylsilylperoxy radicals, therefore, behave like $RO_2^{\bullet}$ (8), $Me_3GeO_2^{\bullet}$, and $Ph_3GeO_2^{\bullet}$ (2) at low temperatures and must exist in equilibrium with bistrialkylsilyl tetroxide.

$$[5]\quad 2R_3SiO_2^{\bullet} \rightleftharpoons R_3SiO_4SiR_3$$

Plots of 2 log $[R_3SiO_2^{\bullet}]$ against the reciprocal of the absolute temperature gave $\Delta H^0 = -11 \pm 2$ kcal mol^{-1} for $Et_3SiO_2^{\bullet}$ and *n*-$Bu_3SiO_2^{\bullet}$. This value for the enthalpy change associated with [5] is very

[5]We were unable to obtain anisotropic parameters for ^{17}O labelled *t*-$Bu_3SiO_2^{\bullet}$ because of extremely low radical concentrations in the frozen solution. The ^{17}O anisotropic interactions associated with g_{yy} and g_{zz} for $Ph_3GeO_2^{\bullet}$ were too small to be resolved (3).

TABLE 1. Electron spin resonance parameters for the peroxy radicals from trialkylsilanes

Silane	Radicals
Et_3SiH	$Et_3SiO_2^{\bullet}$, $g = 2.028$; $Et_2SiCH(Me)O_2^{\bullet}$, $g = 2.0155$, $a_H(1) = 5$ G
n-Bu_3SiH	n-$Bu_3SiO_2^{\bullet}$, $g = 2.027$; n-$Bu_2SiHCH(n$-$Pr)O_2^{\bullet}$, $g = 2.015$, $a_H(1) = 5$ G
t-Bu_3SiH	t-$Bu_3SiO_2^{\bullet}$, $g = 2.0294$, $a_{^{17}O}(1) = 25.4$ G, $a_{^{17}O}(1) = 14.6$ G; t-$BuO_2^{\bullet}$, $g = 2.015$, $a_{^{17}O}(1) = 23.25$ G, $a_{^{17}O}(1) = 17.65$ G

similar to the value for $Me_3GeO_2^{\bullet}$ and $Ph_3GeO_2^{\bullet}$ (2) and it would appear that the central O—O bond strength in $R_3SiO_4SiR_3$ is of the order of 11 kcal mol^{-1} and is about 3 kcal mol^{-1} stronger than the central O—O bond strength in di-*tert*-alkyl tetroxides (8). As is the case with most peroxy radicals ΔS^0 for $R_3SiO_2^{\bullet}$ could only be estimated to be < -30 cal deg^{-1} mol^{-1} because irreversible radical decay commenced before complete dissociation of the dimer.

Triethylsilylperoxy decayed irreversibly at temperatures above 223 K with first-order kinetics and steady-state radical concentrations were linearly dependent on the light intensity. Values of the first-order rate constant $k_{epr}^{(1)}$ are given in Table 2. This radical has a half-life ($\tau_{1/2}$) = 27 s at 252 K and it is about 10 times more persistent than $Me_3GeO_2^{\bullet}$ at this temperature (2). Decays of n-$Bu_3SiO_2^{\bullet}$ exhibited even more unusual kinetics in that plots of the square root of the radical concentration against time in the temperature range 243–273 K were linear indicating an overall concentration exponent of 0.5.

We have previously concluded (2) that the unusual irreversible decay kinetics exhibited by $Me_3GeO_2^{\bullet}$ and $Ph_3GeO_2^{\bullet}$ are caused by the fact that these radicals are in equilibrium with substantial concentrations of dimer and decay irreversibly with true first-order kinetics.

[6] $R_3GeO_2^{\bullet} + R_3GeO_2^{\bullet} \rightleftharpoons R_3GeO_4GeR_3$

[7] $R_3GeO_2^{\bullet} \xrightarrow{k_7}$ non-radical products

$$[8] \quad \frac{-d[R_3GeO_2^{\bullet}]}{dt} = \frac{k_7[R_3GeO_2^{\bullet}]}{1 + 4K_6[R_3GeO_2^{\bullet}]}$$

TABLE 2. Rate constants, $k_{epr}^{(1)}$, for irreversible first-order decay of $Et_3SiO_2^{\bullet}$

Temperature (K)	$k_{epr}^{(1)}$ (s^{-1})
242	0.008
252	0.026
261	0.19
271	0.44

where K_6 is the equilibrium constant for [6] and k_7 is either a true or pseudo-first-order rate constant. The results presented above for $Et_3SiO_2^{\bullet}$ suggest that irreversible decay of this radical can be rationalized by an expression analogous to [8].

It should, however, be noted that a change from zero- to first-order kinetics cannot be invoked to explain the apparent half-order kinetics for the decay of n-$Bu_3SiO_2^{\bullet}$ because even if ΔS_5^0 is -25 cal deg^{-1} mol^{-1} and $\Delta H_5^0 = -11$ kcal mol^{-1} the concentrations of n-$Bu_3SiO_2^{\bullet}$ were too low for $K_5[n$-$Bu_3SiO_2^{\bullet}]$ to approach 1. It is possible that in this case radical decays after the light was switched off were influenced by a thermally unstable compound which accumulated during the light period (9).

We have had little success to date identifying the products from decay of $R_3SiO_2^{\bullet}$ and $R_3GeO_2^{\bullet}$. Ph_3GeOOH undergoes free-radical induced decomposition initiated by thermolysis of di-*tert*-butyl hyponitrite in PhCl at 50°C. The major organogermanium product appeared to be $(Ph_3Ge)_2O$ which offered no clues with regards to reaction mechanisms. Interestingly little or no oxygen was evolved by this reaction supporting a pseudo rather than true first-order radical decay. It should, however, be noted that kinetic electron spin resonance spectroscopy has indicated first-order decay for some tertiary alkylperoxy radicals (10, 11) which are generally believed to undergo bimolecular self-reactions with second-order kinetics (8). Anomalous decay kinetics of this nature have so far not been explained.

Somewhat surprisingly photolysis of oxygen saturated solutions of DTBP and Me_3SiH did not give an esr spectrum even though an intense spectrum is obtained from $Me_3Si^{\bullet}$ in the absence of oxygen (12–15). There was some evidence for a very broad singlet at $g = 2.024$ if the oxygen pressure was reduced below 100 Torr. The signal intensity was, however, much too low for kinetic studies to be performed on this radical. Intuitively it seems very odd that $Me_3SiO_2^{\bullet}$ is so extremely difficult to detect by the esr method while very intense spectra from t-$BuO_2^{\bullet}$ and $Me_3GeO_2^{\bullet}$ are readily obtained.

$Ph_3SiO_2^{\bullet}$ ($g = 2.0271$) was readily prepared from Ph_3SiH and decayed rapidly at temperatures in the range 233 to 183 K with second-order kinetics and $k_{epr}^{(2)} = 1 \times 10^7$ M^{-1} s^{-1} at 167 K and 4.3×10^7 M^{-1} s^{-1} at 218 K. Superficially this radical would appear to decay with kinetics that are different to those for $Ph_3GeO_2^{\bullet}$ and $R_3SiO_2^{\bullet}$. The values of $k_{epr}^{(2)}$ for $Ph_3SiO_2^{\bullet}$ are, however, almost certainly rate constants for reversible dimerization and not rate constants for irreversible decay. Although this radical disappeared rapidly when the light was masked, temperature jump experiments did indicate the presence of a radical–dimer equilibrium.

The aralkylsilylperoxy radical $MeSiPh_2O_2^{\bullet}$ (g = 2.026) was prepared from $MeSiHPh_2$ but photolysis of $PhSiMe_2H$ gave a singlet at g = 2.004. The intensity of this spectrum was, however, too weak to determine the number of oxygen nuclei, if any, associated with this radical by ^{17}O tagging experiments.

Trialkylstannylperoxy Radicals

The esr spectrum from $Me_3SnO_2^{\bullet}$ (g = 2.024), n-$Bu_3SnO_2^{\bullet}$ (g = 2.025), and $Ph_3SnO_2^{\bullet}$ (g = 2.020) consisted of a rather broad singlet with no evidence, even under optimum conditions of high intensity and narrow line width, for satellite lines from interaction of the unpaired electron with ^{119}Sn and ^{117}Sn nuclei. The narrowest line width that we obtained was 8 G and since A_0 is ~15 500 G for Sn (16) the 5s spin density on this nucleus is <0.05% which is at least one tenth the 2s spin density on the central carbon of the *tert*-butylperoxy radical (17).

The line width of n-$Bu_3SnO_2^{\bullet}$ increased from 8 G at 183 K to 15 G at 153 K whereas the line width of alkylperoxy radicals (18) and organogermylperoxy radicals decrease with decreasing temperature in this temperature range. In this respect n-$Bu_3SnO_2^{\bullet}$ behaves (at these temperatures) like most other radicals and line broadening from reduced averaging of anisotropic processes must overshadow line narrowing from spin–orbit relaxation mechanisms (18).

n-$Bu_3SnO_2^{\bullet}$ was extremely long-lived below 193 K and the radical concentration was independent of the temperature in the range 193 to 143 K (Table 3). Clearly this radical does not undergo reversible dimerization at low temperatures. Similar experiments demonstrated that $Me_3SnO_2^{\bullet}$ and $Ph_3SnO_2^{\bullet}$ do not exist in equilibrium with their tetroxides at low temperatures.

Above 183 K $Me_3SnO_2^{\bullet}$ decayed irreversibly with *second-order* kinetics and the second-order rate constant $k_{epr}^{(2)}$, given in Table 4, can be represented by the Arrhenius equation

$$\log (k_{epr}^{(2)}/M^{-1}\,s^{-1}) = (11.8 \pm 1.0) - (7.8 \pm 0.7)/\theta$$

where $\theta = 2.303RT$ kcal mol^{-1}, which is very close to our original preliminary equation (1).

n-$Bu_3SnO_2^{\bullet}$ is more persistent than $Me_3SnO_2^{\bullet}$ and did not begin to decay irreversibly until about 213 K. This radical decayed with second-order kinetics and $\log (k_{epr}^{(2)}/M^{-1}\,s^{-1}) = (12.0 \pm 1.0) - (13 \pm 1)/\theta$. It is, therefore, more persistent than $Me_3SnO_2^{\bullet}$ because of a larger activation energy for self-reaction.

$Ph_3SnO_2^{\bullet}$ also decayed irreversibly with second-order kinetics and $k_{epr}^{(2)} = 6.3 \times 10^4\ M^{-1}\ s^{-1}$ at 238 K, $2.6 \times 10^3\ M^{-1}\ s^{-1}$ at 223 K, and $7.3 \times 10^2\ M^{-1}\ s^{-1}$ at 213 K.

TABLE 3. The concentration of n-$Bu_3SnO_2^{\bullet}$ in the dark as a function of temperature[a]

Temperature (K)	$10^4[n\text{-}Bu_3SnO_2^{\bullet}]$ (M)
143	1.9
153	1.9
163	1.9
173	1.7
183	1.7
188	1.7
193	1.9

[a]In cyclopropane after the initiating light was switched off.

TABLE 4. Second-order rate constant for irreversible decay $Me_3SnO_2^{\bullet}$

Temperature (K)	$10^{-3}(k_{epr}^{(2)})/M^{-1}\,s^{-1}$
179	0.16
183	0.32
197	1.75
203	2.0
223	16
225	15

The low reactivity of n-$Bu_3SnO_2^{\bullet}$ towards self-reaction has enabled us to determine absolute reactivities of this radical to two typical alkylperoxy radical scavengers, 2,6-di-*tert*-butyl-4-methylphenol (BMP) and cobalt(II) acetylacetonate. In both cases radical decays were first-order in the presence of excess scavenger (A) and pseudo-first-order rate constants were linearly dependent on the concentration of the scavenger. The second-order rate constants for reaction of n-$Bu_3SnO_2^{\bullet}$ with BMP (k_{BMP}) and $Co(acac)_2$ ($k_{Co(acac)_2}$) were determined over a temperature range and

$$\log (k_{BMP}/M^{-1}\,s^{-1}) = (7.5 \pm 1) - (7 \pm 1)/\theta$$

and

$$\log (k_{Co(acac)_2}/M^{-1}\,s^{-1}) = (12 \pm 1) - (11.5 \pm 1)/\theta$$

The corresponding Arrhenius equations for reaction of t-$BuO_2^{\bullet}$ with BMP and $Co(acac)_2$ are

$$\log (k/M^{-1}\,s^{-1}) = (4.6 \pm 0.2) - (0.8 \pm 0.2)/\theta \quad \text{(ref. 16)}$$

and

$$\log (k/M^{-1}\,s^{-1}) = (8.9 \pm 1) - (4.7 \pm 0.5)/\theta$$

respectively (19, 20).

The reaction of n-$Bu_3SnO_2^{\bullet}$ with BMP must involve the rate determining transfer of the phenolic hydrogen to the peroxy radical because rate constants for 2,6-di-*tert*-butyl-4-methyl O—D were smaller than rate constants for normal BMP. This was

substantiated by the observation that 2,6-di-*tert*-butyl-4-methylphenoxy (g = 2.0046, $a_H^{CH_3}(4)$ = 11.23 G, $a_H(3) = a_H(5)$ = 1.64 G) was produced when n-$Bu_3SnO_2^{\bullet}$ ($\sim 10^{-4}$ M) was destroyed in the dark at 200 K by 2,6-di-*tert*-butyl-4-methylphenol (0.08 M). It is probable that a total of two n-$Bu_3SnO_2^{\bullet}$ were destroyed by each molecule of BMP. The overall reaction can probably be represented by

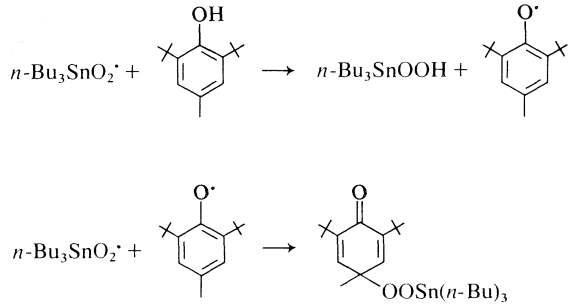

although we have no unambiguous experimental evidence for a stoichiometric factor of 2, or for the production of tri-*n*-butylstannyl hydroperoxide and 1-methyl-1-tri-*n*-butylstannylperoxy 3,5-di-*tert*-butylcyclohexadiene-2,5-dione.

It is apparent from this work that pre-exponential factors and activation energies for reaction of $R_3SnO_2^{\bullet}$ with itself and with a peroxy radical scavenger are significantly larger than the corresponding parameters for reactions of the *tert*-butylperoxy radical. We have previously concluded (3) from ^{17}O labelling experiments that n-$Bu_3SnO_2^{\bullet}$ has a pentacoordinate, trigonal bipyramidal structure in which the vacant Sn 5*d* orbitals are used to form a dative bond with the lone pair of electrons on the terminal oxygen of the peroxy function. Now it is possible that this structure (**I**) is in equilibrium with the more usual structure for a peroxy radical (**II**)

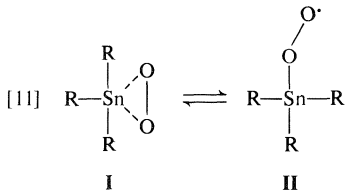

I **II**

and it is the acyclic form which undergoes self-reaction and reaction with BMP and $Co(acac)_2$.

If this is the case, the overall rate constant for self-reaction $k_{epr}^{(2)} = 2K_{11}k_t$ where K_{11} is the equilibrium constant for [11] and $2k_t$ is the termination rate constant for **II**. If we then assume that $2k_t$ has the normal pre-exponential factor of 10^9 M^{-1} s^{-1} and a low activation energy of 2 kcal mol^{-1} we can calculate values of $\Delta S_{11}^0 \sim 5.5$ cal deg^{-1} mol^{-1} and $\Delta H_{11}^0 = 6$ kcal mol^{-1}. Extending this argument to reaction of n-$Bu_3SnO_2^{\bullet}$ with BMP and $Co(acac)_2$ it is possible that the large activation parameters for these reactions result from the fact that k_{BMP} and $k_{Co(acac)_2}$ are made up of K_{11} and the rate constant for reaction of **II** with the scavenger.

Summary

Trialkylsilylperoxy radicals behave like alkylperoxy and organogermylperoxy radicals at low temperatures and exist in equilibrium with a tetroxide. The thermodynamic parameters for this reversible dimerization are closer to the values for organogermylperoxy radicals than alkylperoxy radicals. Irreversible radical decays follow first or lower order kinetics and in this respect they behave like organogermylperoxy radicals.

^{17}O hyperfine splitting constants indicate that the two oxygen nuclei in $R_3SiO_2^{\bullet}$ are magnetically nonequivalent and that these radicals have more π spin density on the terminal oxygen than alkylperoxy radicals.

Trialkylstannylperoxy radicals do not exist in equilibrium with bistrialkylstannyl tetroxide and decay irreversibly with clean second-order kinetics. These radicals react with typical alkylperoxy radical scavengers but they do so more slowly than alkylperoxy radicals. Arrhenius parameters and activation energies for self-reaction and destruction by a radical scavenger suggest that $R_3SnO_2^{\bullet}$ exist primarily in a form in which both oxygen atoms are bonded to the tin atom and that this peroxide structure is in equilibrium with the more usual acyclic peroxy structure.

On the basis of the magnetic resonance parameters for n-$Bu_3SnO_2^{\bullet}$ it is possible to conclude that the unpaired electron occupies a π orbital made up exclusively of $O(2p_z)$ atomic orbitals and that the two oxygen nuclei are equivalent. These radicals which can be considered to have a formal valency of $Sn^{IV}O_2^-$ are not analogous to cobalt, iron, or chromium dioxygen complexes which have a high spin density on nonequivalent oxygens (21, 22) or to manganese dioxygen complexes which have low spin density on equivalent oxygen nuclei (23). Trialkylstannylperoxy radicals can, therefore, be considered to be examples of a new class of dioxygen–metal complexes.[6]

1. J. E. Bennett and J. A. Howard. J. Am. Chem. Soc. **94**, 8244 (1972).
2. J. A. Howard and J. C. Tait. Can. J. Chem. **54**, 2669 (1976).
3. J. A. Howard and J. C. Tait. J. Am. Chem. Soc. **99**, 8349 (1977).
4. H. G. Kuivila and O. F. Beaumel, Jr. J. Am. Chem. Soc. **83**, 1246 (1961).

[6]We wish to thank a referee for bringing this point to our attention.

5. J. E. BENNETT and R. SUMMERS. J. Chem. Soc. Faraday 2, **69**, 1043 (1973).
6. J. A. HOWARD. Can. J. Chem. **50**, 1981 (1972).
7. E. MELADMUD and B. L. SILVER. J. Phys. Chem. **77**, 1896 (1973).
8. J. A. HOWARD. Am. Chem. Soc. Symp. Ser. **69**, 413 (1978).
9. J. E. BENNETT, J. A. EYRE, C. P. RIMMER, and R. SUMMERS. Chem. Phys. Lett. **26**, 69 (1974).
10. K. U. INGOLD and J. R. MORTON. J. Am. Chem. Soc. **86**, 3400 (1964).
11. S. FUKUZUMI and Y. ONO. J. Chem. Soc. Perkin Trans. 2, 622 (1977).
12. S. W. BENNETT, C. EABORN, A. HUDSON, H. A. HUSSAIN, and R. A. JACKSON. J. ORGANOMET. Chem. **16**, 36 (1969).
13. P. J. KRUSIC and J. K. KOCHI. J. Am. Chem. Soc. **91**, 3938 (1969).
14. P. T. FRANGOPOL and K. U. INGOLD, J. Organomet. Chem. **25**, C9 (1970).
15. G. B. WATTS and K. U. INGOLD. J. Am. Chem. Soc. **94**, 491 (1972).
16. J. R. MORTON and K. F. PRESTON. J. Magn. Res. **30**, 577 (1978).
17. J. A. HOWARD. Can. J. Chem. **57**, 253 (1979).
18. J. R. THOMAS. J. Am. Chem. Soc. **88**, 2064 (1966).
19. J. A. HOWARD and E. FURIMSKY. Can. J. Chem. **51**, 3738 (1973).
20. J. A. HOWARD and S. B. TONG. Unpublished results.
21. E. F. VANSANT and J. H. LUNSFORD. Adv. Chem. Ser. **121**, 441 (1973).
22. R. K. GUPTA, A. S. MILDVAN, T. YONETANI, and T. S. SRIVASTAVA. Biochem. Biophys. Res. Commun. **67**, 1005 (1975).
23. B. M. HOFFMAN, T. SZYMANSKI, T. G. BROWN, and F. BASOLO. J. Am. Chem. Soc. **100**, 7253 (1978).

Conformations of bridged diphenyls. XIV. Crystal structure of 2-(4′-carbomethoxy-2′aminophenoxy)-1,3,5-trimethylbenzene and endocylic angles in bridged diphenyls

RAMANATHAN GOPAL, W. DAVID CHANDLER, AND BEVERLY E. ROBERTSON[1]

Faculty of Science, University of Regina, Regina, Sask., Canada S4S 0A2

Received October 10, 1978[2]

RAMANATHAN GOPAL, W. DAVID CHANDLER, and BEVERLY E. ROBERTSON. Can. J. Chem. **57**, 2767 (1979).

The structure of 2-(4′-carbomethoxy-2′-aminophenoxy)-1,3,5-trimethylbenzene, $C_{17}H_{19}NO_3$, has been determined by X-ray diffraction. The crystals are monoclinic, $a = 23.895(9)$, $b = 7.821(4)$, $c = 16.641(8)$ Å, $\beta = 99.26(3)$, $C2/c$, $Z = 8$. The integrated intensities of 3540 independent reflections were measured on a four-circle diffractometer. A total of 2403 of these reflections was used in the refinement to give a final least-squares weighted residual of 0.069 and a conventional R factor of 0.096. The molecule adopts the skew-amino-*distal* conformation as does the analogous *ortho*-nitro-substituted compound. The lengths of the bonds from the amino substituted ring and the mesityl ring are 1.404(3) and 1.376(4) Å respectively and the torsional angles about those bonds are ± 5.8 and $\mp 79.5°$. The angle subtended at the bridging oxygen atom is 120.1°. Variations in the endocyclic angles subtended at substituted ring carbon atoms in this and other bridged diphenyls may be understood in terms of a combination of hybridization effects, and the spatial requirements of the bonds to substituents.

RAMANATHAN GOPAL, W. DAVID CHANDLER et BEVERLY E. ROBERTSON. Can. J. Chem. **57**, 2767 (1979).

Par diffraction de rayons-X, on a déterminé la structure du (carbométhoxy-4′-aminophénoxy-2′)-2 triméthyl-1,3,5 benzène, $C_{17}H_{19}NO_3$. Les cristaux sont monocliniques $a = 23.895(9)$, $b = 7.821(4)$, $c = 16.641(8)$ Å, $\beta = 99.26(3)$, $C2/c$, $Z = 8$. On a mesuré, avec un diffractomètre à quatre cycles, les intensités totales de 3540 réflexions indépendantes. On a utilisé avec soins 2403 de ces réflexions pour obtenir par la méthode des moindres carrés un résidu moyen final de 0.069 et un facteur conventionnel de 0.096. La molécule adopte la conformation amine-*gauche* la plus *éloignée* comme le font les composés ayant un substituant nitro en position *ortho*. Dans les cycles substitués par une amine et dans le cycle mésityle, les longueurs de liaisons sont respectivement 1.404(3) et 1.375(4) Å et les angles de torsion autour de ces liaisons sont de ± 5.8 et $\mp 79.5°$. L'angle sous-tendu à l'atome d'oxygène du pont est de 120.1°. Les variations des angles endocycliques sous-tendus aux atomes de carbone du cycle substitué dans ce composé et dans d'autres diphényles pontés peuvent être compris en fonction d'une combinaison d'effets d'hybridation et d'arrangements spatiaux des liaisons par rapport aux substituants.

[Traduit par le journal]

Introduction

In previous parts of this series we have considered the role of substituents and the bridging group in determining the conformation of bridged diphenyl compounds (1) and have established that in most cases proton chemical shifts may be used to infer the approximate conformation of bridged diphenyl compounds and to study their internal rotations (2). Most of the compounds studied to date have been tri-*ortho*-substituted with the single *ortho* substituent on one ring being a nitro group. In the compound whose structure is reported here the single substituent is an amino group. The electronic properties of the latter substituent are quite different from those of the nitro group and we therefore will expect a change in the ring distortions associated with these effects and in the interaction between the NH_2 group and the bridging group.

Paulus has recently determined the structures of 3-trifluoromethyl-1-(2′-carboxy-6′-methylanilino)-benzene (**I**) and 3-trifluoromethyl-1-(2′-carboxy-4′-methylanilino)benzene (**II**) (3). Both compounds show evidence of an intramolecular N—H---O hydrogen bond. The strength of the hydrogen bond is not the same in the two compounds, as manifested both by their biological activity and by differences in their observed conformations. The six-atom ring formed by the NH bridge, the carbonyl group, and the two ring carbon atoms, to which the NH and COOH groups are bonded, is planar in **II**. This causes one of the torsional angles (associated with

[1]To whom all correspondence should be addressed.

[2]Revision received July 10, 1979.

0008-4042/79/202767-08$01.00/0

the COOH substituted ring) to be 35.9° while the other ring is nearly coplanar with the bridging plane, with a torsional angle of 8.6°. Using our nomenclature the conformation is planar-carboxy-*distal*-trifluoromethyl-*proximal*, but borders on the twist conformation.

The formation of the hydrogen bond is therefore crucial in determining the conformation of the aforementioned molecule. In **I** the methyl group prevents the formation of a planar six-membered ring and weakens the hydrogen bond, thereby changing the biological activity of this compound from that of the former. The torsional angle associated with the COOH substituted ring becomes 60.1° and that associated with the other ring 14.1°. The conformation then is skew-trifluoromethyl-*distal*, but also borders on the twist conformation. Intramolecular hydrogen bonding involving the bridging group is therefore a factor that must be considered in determining the probable conformation of bridged diphenyl compounds. The bridged diphenyl whose structure is reported here offers the possibility for the formation of an intramolecular hydrogen bond with the bridging atom playing the role of the hydrogen bond acceptor.

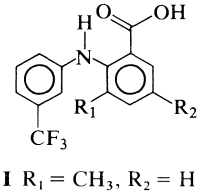

I $R_1 = CH_3$, $R_2 = H$
II $R_1 = H$, $R_2 = CH_3$

In previous reports of the structures of bridged diphenyls we have noted systematic deviations in the symmetry of the phenyl groups from the D_{6h} symmetry of unsubstituted benzene. We have argued that, in large part, these deviations are associated with the electronic properties of the substituents of the ring. A comprehensive treatment of the relation between electronic properties and ring distortion has appeared recently in a series of papers by Domenicano, Vaciago, Coulson and co-workers (4). They find that spatial effects, conjugation, and perturbations to the hydridization of ring carbon atoms associated with the properties of the substituent at that carbon atom may all affect the endocyclic angle. We will attempt to rationalize the systematic variations in the endocyclic angles of 2-(4′-carbomethoxy-2′-aminophenoxy)-1,3,5-trimethylbenzene and the other bridged diphenyl compounds whose structures have been reported in earlier papers of this series.

Experimental

2-(2′-Nitro-4′-carbomethoxyphenoxy)-1,3,5-trimethylbenzene was reduced to 2-(4′-carbomethoxy-2′-aminophenoxy)-1,3,5-trimethylbenzene using W2 Raney nickel and hydrogen in absolute ethanol according to the method used by Bergman and Chandler (5). The mp after four recrystallizations from absolute ethanol was 115–116°C. A colourless rectangular sample with approximate dimensions 0.4 × 0.4 × 0.7 mm was chosen for data collection on a Picker FACS I automated four-circle diffractometer equipped with a graphite monochromator. The cell constants were determined by a least-squares fit to the positions of 22 reflections between the 2θ settings of 37 and 43° where the MoKα_1 and MoKα_2 peaks were well resolved. The estimated standard deviations in the cell constants are taken directly from the least squares.

The crystal data are as follows:

$C_{17}H_{19}NO_3$ fw = 285.19
Monoclinic, $C2/c$, a = 23.895(9), b = 7.821(4), c = 16.641(8) Å, β = 99.26(3)°, ρ_o = 1.23(1) g cm^{-3} (flotation), ρ_c = 1.237 g cm^{-3}, Z = 8, $F(000)$ = 1216 e, μ(MoKα) = 0.875, λ(MoKα_1) = 0.70926 Å, T = 22 ± 2°C.

The integrated intensities of 3540 independent reflections with 2θ values between 2 and 55° were collected with MoKα radiation using the θ–2θ scan mode, a minimum base width of 3.0° in 2θ and 40 s background counts at each limit of the scan, and a scan rate of 2° min^{-1}. The data were reduced to structure factors using standard procedures. No corrections were made for extinction or absorption. The standard deviation in $|F_o|$, $\sigma(F_o)$, was calculated from $\sigma(F_o) = 1.0 + 0.01|F_o| + \sigma'(F_o)$ where $\sigma'(F_o)$ is based on counting statistics.

The scattering factors for carbon, oxygen, and nitrogen atoms were taken from those given by Cromer and Mann (6). The scattering factor for hydrogen was taken from Stewart, Davidson, and Simpson (7). The systematic extinctions ($h + k = 2n + 1$; $h0l$, $l = 2m + 1$) indicate the space groups $C2/c$ or Cc. The average values of $|E|$ and $|E^2 - 1|$ were 0.739 and 1.041 respectively, and therefore $C2/c$ was assumed to be the correct space group. The 446 reflections with $|E| > 1.48$ were used to solve the structure using the logical symbolic addition method.[3] The E-map calculated from the solution with the highest figures of merit yielded all the non-hydrogen positions. The structure was refined anisotropically by least-squares and the hydrogen atoms were then found from a difference Fourier map. The 2459 reflections for which $|F_o| > \sigma(F_o)$ were used in the final cycles of refinement with the least-squares weight, w, calculated as $w = \sigma(F_o)^{-2}$.

The final values of R_w and the conventional R factor were 0.069 and 0.096 respectively. The relatively large residuals reflect the low counting rates used during data collection and the inclusion of many weak reflections in the least squares. The observed and calculated structure factors have been placed in the Depository of Unpublished Data.[4] The final positional and thermal parameters are listed in Table 1, with standard deviations. The bond lengths, bond angles, and atomic numbering are given in Fig. 1.

Discussion of the Structure

The angles between the planes of 2-(4′-carbomethoxy-2′-aminophenoxy)-1,3,5-trimethylbenzene

[3]The direct methods program LSAM, written by Germain and Woolfson (8), was used for structure solution. The program FORDAP written by Zalkin (9) was used for all Fourier calculations. The program ORFLS, written by Busing *et al.* (10), was used for least-squares refinement. Stereograms were prepared with the aid of the program ORTEP, written by Johnson (11).

[4]Complete set of tabular data is available, at a nominal charge, from the Depository of Unpublished Data, CISTI, National Research Council of Canada, Ottawa, Ont., Canada K1A 0S2.

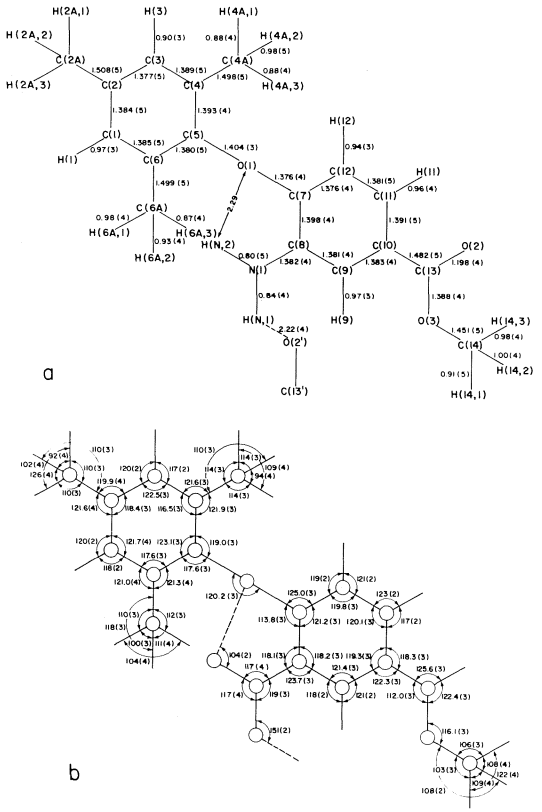

FIG. 1. (*a*) Bond lengths (Å) and atom labeling. (*b*) Bond angles (deg). The numbers in parentheses are estimated standard deviations.

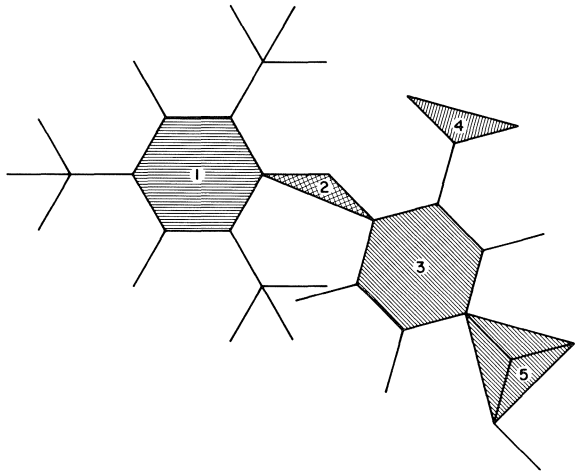

FIG. 2. Labeling of the least-squares planes.

as defined in Fig. 2 are given in Table 2. The molecule has the skew-amino-*distal* conformation. The packing of the molecules is shown in Fig. 3. The molecules pack in pairs with the amino-substituted rings of a pair coplanar and separated by 3.4 Å. The pairs are repeated by the centers of symmetry at $[\frac{1}{2}00]$ and $[\frac{1}{2}0\frac{1}{2}]$ to form a continuous stack in the *c* direction. The dihedral angles *1,2* and *2,3* which correspond to the torsional angles ϕ[C(7)—O(1)—C(5)—C(4)] and ψ[C(5)—O(1)—C(7)—C(12)] are $\pm 79.5°$ and $\mp 5.8°$ respectively. The two sets of signs refer to the two enantiomers which must be present in a centrosymmetric space group. In all of the structures which we have studied to date the angles occur in (+,+) and (−,−) pairs (1). In all conformations, the pairing of equivalent signs reduces the steric interaction between *ortho* hydrogen atoms or substituents and the π electrons and *ortho* hydrogen atoms or substituents of the other ring.

A feature of the structure which relates to the unusual pairing of the signs of the torsional angles is the nature of the distortions of the phenyl rings from idealized symmetry. The distance of the *proximal-ortho* hydrogen atom above the plane of the mesityl ring is 2.40 Å, which is similar to the value in other bridged diphenyls, even though the signs of the torsional angles in the other compounds are more favourably disposed to maintaining this distance at an adequate value. The distance would also be increased by (*i*) increasing the C(5)—O(1)—C(7) angle, and (*ii*) a bending of the amino-substituted ring at the bridgehead carbon [C(7)] away from the mesityl ring over the value that would occur in an undistorted molecule. The C(5)—O(1)—C(7) angle (120.1°) compares with an average of 119.0° for the eight other independent bridged diphenyl ether molecules whose structures have been determined as part of this series. The bending at the bridgehead carbon atom is 5.6° which compares with an average of 2.8° for the other eight ether molecules. Therefore both effects appear to be present.

The aforementioned large bending angle at the bridgehead carbon atom would appear to be facilitated by the presence of the amino group in the *distal-ortho* position. The amino group itself is bent 2.8(4)° towards the ether oxygen atom. {([N(1)—C(8)—C(9)] − [N(1)—C(8)—C(7)])/2 = 2.8°.} In other cases of small *ortho* substituents (Cl or CH_3) in bridged diphenyl ethers the equivalent angle differs insignificantly from zero. For nitro groups, carbomethoxy groups, or large aryl groups, the sense of the bending is away from the ether oxygen atom. The bending of the groups at both C(7) and C(8) therefore suggests a positive interaction between those groups; i.e. between the atom H(N2) and the lone pair on O(1). Other relevant parameters are: [H(N2)—O(1)] = 2.29(4) Å, [N(1)—O(1)] = 2.606(4) Å, [N(1)—H(N2)—O(1)] = 104(2)°.

We compare this geometry with a related one in 4-hydroxy-L-proline, the structure of which has been determined by neutron diffraction (12). The [H—O] distance and N—H---O angle are 2.082(3) Å and 113.2(2)° respectively, indicating the presence of an

TABLE 1. Structural parameters of 2-(4′-carbomethoxy-2′-aminophenoxy)-1,3,5-trimethylbenzene

(*a*) Fractional atomic coordinates (esd in parentheses) of non-hydrogen atoms ($\times 10^4$)

Atom	*x*	*y*	*z*
C(1)	2090(2)	4375(5)	585(2)
C(2)	2623(2)	4955(5)	927(2)
C(3)	2753(2)	5050(5)	1763(2)
C(4)	2368(1)	4614(4)	2272(2)
C(5)	1836(1)	4062(4)	1894(2)
C(6)	1689(1)	3914(4)	1060(2)
C(2A)	3057(2)	5471(8)	409(3)
C(4A)	2523(2)	4696(6)	3180(3)
C(6A)	1120(2)	3243(7)	681(3)
C(7)	1119(1)	4633(4)	2726(2)
C(8)	708(1)	3869(4)	3119(2)
C(9)	365(1)	4918(4)	3496(2)
C(10)	409(1)	6679(4)	3466(2)
C(11)	819(2)	7410(4)	3067(2)
C(12)	1174(2)	6383(4)	2699(2)
C(13)	19(2)	7829(5)	3818(2)
C(14)	−731(2)	7978(6)	4589(3)
N(1)	681(2)	2104(4)	3130(3)
O(1)	1444(1)	3482(3)	2378(2)
O(2)	−11(1)	9348(3)	3729(2)
O(3)	−314(1)	6970(3)	4252(2)

(*b*) Thermal parameters (U_{ij}) for non-hydrogen atoms ($\times 10^3$)

Atom	U_{11}	U_{22}	U_{33}	U_{12}	U_{13}	U_{23}
C(1)	51(2)	62(2)	48(2)	8(2)	9(2)	−6(2)
C(2)	47(2)	55(2)	51(2)	3(2)	18(2)	0(2)
C(3)	37(2)	49(2)	59(3)	−5(2)	7(2)	−2(2)
C(4)	47(2)	40(2)	44(2)	−2(2)	9(2)	−3(2)
C(5)	43(2)	35(2)	60(2)	5(2)	23(2)	1(2)
C(6)	39(2)	47(2)	61(3)	7(2)	8(2)	−4(2)
C(2A)	64(3)	115(4)	69(3)	−2(3)	35(3)	15(3)
C(4A)	74(3)	64(3)	54(3)	−17(3)	5(2)	0(2)
C(6A)	48(3)	79(3)	87(4)	−3(2)	0(3)	−20(3)
C(7)	38(2)	36(2)	52(2)	−2(2)	13(2)	2(2)
C(8)	35(2)	34(2)	54(2)	−2(2)	8(2)	6(2)
C(9)	36(2)	43(2)	51(2)	−3(2)	14(2)	8(2)
C(10)	39(2)	40(2)	51(2)	−5(2)	12(2)	−4(2)
C(11)	54(2)	33(2)	74(3)	−6(2)	28(2)	−1(2)
C(12)	54(2)	39(2)	74(3)	−6(2)	36(2)	6(2)
C(13)	50(2)	47(2)	56(2)	−8(2)	19(2)	−7(2)
C(14)	83(4)	66(3)	102(4)	2(3)	60(3)	−8(3)
N(1)	56(2)	38(2)	116(3)	−5(2)	43(2)	12(2)
O(1)	55(2)	37(1)	81(2)	0(1)	38(1)	3(1)
O(2)	93(2)	40(2)	127(3)	−5(2)	70(2)	−8(2)
O(3)	59(2)	50(2)	79(2)	−1(1)	40(2)	0(1)

intramolecular hydrogen bond. In 2-(4′-carbomethoxy-2′-aminophenoxy)-1,3,5-trimethylbenzene the amount by which the [H(N2)—O(1)] distances is less than the sum of Van der Waals radii of the two atoms involved (ca. 0.1 Å) is not sufficient to indicate the presence of a hydrogen bond, according to the usual conventions of nomenclature. Nevertheless, the interaction appears to be of sufficient strength to affect the conformation of the molecule and perhaps thereby its molecular packing.

The other amino hydrogen atom forms a hydrogen bond to the carbonyl oxygen atom, O(2), of an adjacent molecule removed by one *b* translation from the first. The [N(1)—O(2)] and [H(N1)—O(2)] distances are 2.984(4) and 2.22(4) Å respectively. The next shortest intermolecular distance involving at

TABLE 1 (*Concluded*)

(*c*) Fractional atomic coordinates of hydrogen atoms ($\times 10^3$)

Atom	*x*	*y*	*z*	*B* (Å²)
H(1)	200(1)	423(4)	0(2)	5(1)
H(3)	309(1)	545(4)	200(2)	3(1)
H(4A1)	243(2)	378(6)	343(3)	7(2)
H(4A2)	239(2)	577(7)	339(3)	10(2)
H(4A3)	289(2)	492(6)	335(2)	7(2)
H(6A1)	105(2)	213(6)	91(3)	8(2)
H(6A2)	107(2)	296(5)	13(2)	6(3)
H(6A3)	84(2)	388(6)	79(3)	7(2)
H(2A1)	305(2)	467(7)	−4(3)	11(2)
H(2A2)	293(2)	636(6)	6(3)	7(3)
H(2A3)	340(2)	534(6)	68(3)	8(2)
H(N1)	41(2)	164(5)	331(2)	5(1)
H(N2)	80(2)	162(6)	278(3)	8(3)
H(9)	10(1)	438(4)	380(2)	4(1)
H(11)	84(2)	863(5)	306(2)	6(1)
H(12)	144(1)	686(4)	240(2)	5(1)
H(14,1)	−90(2)	720(6)	488(3)	9(2)
H(14,2)	−52(2)	885(5)	497(2)	7(2)
H(14,3)	−95(2)	859(6)	413(3)	11(2)

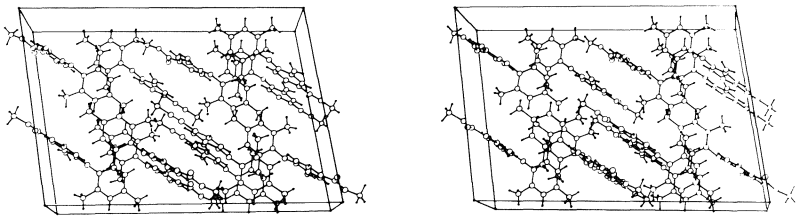

FIG. 3. Stereoscopic view of the molecular packing. The *a* axis points to the right, the *b* axis is into the page, and the *c* axis points up.

least one non-hydrogen atom is 2.71(4) Å. The [C(13)—O(2)] bond length is 1.198(4) Å which compares with 1.187(3) Å in the similar nitro-substituted compound (1) where there is no opportunity for hydrogen bonding.

Substituent Effects and Endocyclic Angles

The difference in the bond lengths from the bridgehead carbon atoms to the ether oxygen atom is 0.028 Å. This value [Δ(C—G)] is compared with others from related bridged biphenyls in Table 3 which also summarizes the endocyclic angles of several bridged diphenyl compounds. Compound **4** in Table 3 is that reported here. The details of the structure of compound **2** will be reported shortly (13). The structures of all the other compounds have been reported previously (1). The angles and substituent positions in Table 3 are defined in Fig. 4. Some values given in Table 3 are averages from two molecules in the asymmetric unit. The average standard deviation in a bond length is 0.003 Å. The average standard deviation in a bond angle is 0.3°.

Among the diphenyl ethers of Table 3 (compounds **1** through **5**), the C—O distances to the bridging oxygen atoms (and therefore the values of Δ(C—O)) appear to be related to the electron withdrawing or donating ability of substituents on the phenyl ring to which the C atom belongs.

The electron withdrawing or donating ability of a substituent may be inferred from the concept of charge dependent electronegativity as expounded by Huheey (14). The electronegativity is given by $\chi = a + b\delta$ where δ is the transferred partial charge, *a* is the inherent electronegativity, and *b* is the charge coefficient. The electron withdrawing or donating ability (i.e., the value of δ) is then determined by both the difference in inherent electronegativities and the charge coefficient of the substituent, with small values of the charge coefficient leading to large values of δ.

We observe that the compound whose structure is reported here (compound **4**) has weakly electron withdrawing substituents R_2 and R_3 and the largest C_7—O length among the ethers. Compound **1** has

TABLE 2. Least-squares planes

(*a*) Equations of planes $Ax + By + Bz = D$. Coordinates refer to the directions of the ***a***, ***b***, and ***c**** axes. The planes are defined in Fig. 2

Plane	*A*	*B*	*C*	*D*
1	−0.3361	0.9411	−0.0379	1.5598
2	−0.5836	−0.0497	−0.8105	−4.9434
3	−0.5278	0.0244	−0.8491	−4.7369
4	−0.5441	0.4917	−0.6799	−3.1151
5	−0.5597	−0.1181	−0.8202	−5.3155

(*b*) Dihedral angles

Planes	Angle (deg)
1,2	79.5
1,3	76.6
2,3	5.8
3,4	28.8
3,5	8.5

two strong electron withdrawing substituents and has the shortest C_7—O distance. The largest C_5—O distance occurs for compound **1** for which R_1 is the electron donor $(CH_3)_3C$, and which has a very low charge coefficient. The shortest C_5—O distance occurs with compound **3** for which R_1 is Cl which is weakly electron withdrawing. We attribute this variation in bond lengths to the bridging oxygen atom to variation in the conjugative effects between electrons on the oxygen atom and the π electrons of the ring. The unsubstituted ring (compound **2**) shows a C_5—O distance similar to that of the mesityl rings (compounds **4** and **5**).

In the case of the C=O and CH_2 bridging groups, the variations in the bond lengths to the bridging atom are small as expected. In the case of the SO and SO_2 bridges, the greater interaction is between the electron donating phenyl ring and the bridge. The shorter bond length is therefore between the mesityl ring and the bridging atom.

Several authors have recognized the effect of the electronegativity of the substituent on the hybridization of the substituted carbon atom and on its endocyclic angles, but the most complete discussion of this and related phenomena is probably that of Domenicano and co-workers (4). They identify (*i*) a spatial effect which reduces the endocyclic angle at substituents by 2.0 to 2.5°, (*ii*) a hybridization effect, previously described by Bent and by Walsh (15), that increases the endocyclic angle at electron withdrawing substituents and decreases it at electron donating substituents, and (*iii*) a conjugation effect which decreased the endocyclic angle at all substituents which conjugate with the π electrons in the ring. We would add a fourth (*iv*) effect which is based on the fact that in a planar six-membered ring, the angles must add up to 720°.

We now wish to determine if these four phenomena can be used to explain adequately the deviation of the endocyclic angles from 120° in the ten compounds listed in Table 3, and if so, their relative importance.

We note first the values of ϕ_2 and the average of the two similarly affected angles, ϕ_4 and ϕ_6, in compounds **4** to **10** inclusive. These angles may be influenced by the spatial effect, the hybridization effect, and for $(\phi_4 + \phi_6)/2$, the deviations of angle ϕ_5 from 120°. In compound **2** only the latter effect applies. It would appear that substitution by a methyl group or an increase in ϕ_5 from 120° cause similar and small decreases in the average of ϕ_4 and ϕ_6. The angle ϕ_2 is also decreased slightly by the substitution of methyl at C_2. The relative importance of the spatial effect and the hybridization effect for methyl substituents cannot be inferred from these observations. However, the greater deviations of the angles ϕ_2 and $(\phi_4 + \phi_6)/2$ in the case of compound **1** can be attributed to the greater electron donating ability of *tert*-butyl over that of the methyl substituents. In compound **1**, the Cl substituents are electron acceptors and lead to angles greater than 120°. The average of the two similar angles ϕ_1 and ϕ_3 adjusts to accommodate the changes at the substituted carbons (fourth effect).

Among the five diphenyl ethers, the angle ϕ_5 correlates closely with the length of the C_5—O bond. In compounds **1**, **2**, **4**, and **5** the angle is large and it would appear that the bridging oxygen atom, the other ring, and its electron withdrawing substituents are, from the point of view of C_5, a large electron withdrawing substituent with a low charge coefficient.

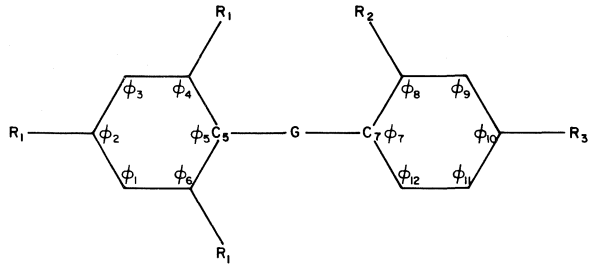

FIG. 4. Labeling of substituents and endocyclic angles.

In the Cl substituted ether (compound **3**), $(\phi_4 + \phi_6)/2$ is greater than 120°, thus forcing ϕ_5 to be smaller than 120°. In the other five bridged diphenyls the electron withdrawing effect at C_5 is smaller and the value of ϕ_5 appears to be more closely dependent on $(\phi_4 + \phi_6)/2$. The large value of ϕ_5 for the ethers reinforces the decrease of $(\phi_4 + \phi_6)/2$ below 120° with the result that $\phi_2 - (\phi_4 + \phi_6)/2$ averages to 1.6° and for the remaining bridged diphenyls it averages to 0.1°.

Carbomethoxy substituents tend to give endocyclic angles less than 120° even though carbomethoxy is a weakly electron withdrawing substituent. We therefore assume the presence of a combination of the spatial effect and the hybridization effect with the former being the larger. Other endocyclic angles at substituted ring carbon atoms are presumably influenced in a similar manner and the electron withdrawing or donating substituents should therefore be viewed as promoting deviations from a base endocyclic angle of approximately 118°, a value consistent with the observations of Domenicano and co-workers (4). Therefore the angles ϕ_8 and ϕ_{10} properly reflect the electronegativity of the substituents at their respective carbon atoms. Furthermore they do not seem to be affected in any systematic way by other substituents or the bridging group. An examination of those endocyclic angles which might be expected to be affected by conjugation (ϕ_2 and ϕ_5 for compounds **7** and **8**, ϕ_7 and ϕ_{10} for compounds **1** through **5**) yields no evidence of conjugation effects.

We conclude that the most important factors in determining distortions in endocyclic angles in these compounds is the hybridization effect of electron donating or withdrawing substituents. The spatial demands of the bonds from the substituent to the ring and the indirect effect of highly distorted endocyclic angles on neighboring endocyclic angles have secondary importance.

TABLE 3. Variations in the bridging bond lengths and endocyclic angles associated with substituent effects. The angles (deg) and atomic distances (Å) are labeled in Fig. 4

No.	**1**	**2**	**3**	**4**	**5**	**6**	**7**	**8**	**9**	**10**
G	O	O	O	O	O	S	SO	SO_2	CH_2	CO
R_1	$(CH_3)_3C$	H	Cl	CH_3	CH_3	CH_3	CH_3	CH_3	CH_3	CH_3
R_2	NO_2	NO_2	$COOCH_3$	NH_2	NO_2	NO_2	NO_2	NO_2	NO_2	NO_2
R_3	NO_2	$COOCH_3$	NO_2	$COOCH_3$	$COOCH_3$	$COOCH_3$	$COOCH_3$	$COOCH_3$	$COOCH_3$	$COOCH_3$
$[C_5—G]$	1.430	1.409	1.384	1.404	1.413	1.785	1.798	1.774	1.514	1.503
$[C_7—G]$	1.350	1.352	1.368	1.376	1.360	1.759	1.819	1.806	1.522	1.502
$\Delta[C—G]$	0.080	0.057	0.016	0.028	0.053	0.026	−0.021	−0.032	−0.008	0.001
ϕ_2	117.4	119.8	122.0	118.4	118.3	117.8	118.4	118.2	117.9	118.7
$(\phi_4 + \phi_6)/2$	115.3	118.2	120.8	117.0	116.5	117.8	117.6	117.4	119.2	118.4
$\phi_2 - (\phi_4 + \phi_6)/2$	2.1	1.6	1.2	1.4	1.8	0.0	0.8	0.8	−1.3	0.3
ϕ_5	124.4	122.4	119.2	123.1	123.8	121.5	121.6	121.5	119.5	120.6
$(\phi_1 + \phi_3)/2$	123.4	120.6	118.5	122.1	122.5	122.6	122.3	122.6	122.1	122.0
$\phi_5 - (\phi_1 + \phi_3)/2$	1.0	1.8	0.7	1.0	1.3	−1.1	−0.7	−1.1	−2.6	−1.4
ϕ_7	118.0	117.3	120.8	121.2	118.2	115.5	117.9	117.7	114.8	116.7
ϕ_8	120.8	121.1	118.0	118.2	121.3	122.7	122.6	122.1	123.1	123.1
ϕ_{10}	121.9	118.5	122.0	119.3	118.8	118.7	119.9	119.6	119.2	119.7

Acknowledgements

The authors thank the National Research Council of Canada for support in the form of Operating Grants, the University of Regina for the provision of computer time, and the Alexander von Humboldt

Foundation of West Germany for a fellowship to B.E.R.

1. E. A. H. GRIFFITH, W. D. CHANDLER, and B. E. ROBERTSON. Can. J. Chem. **50**, 2963 (1972); **50**, 2972 (1972); **50**, 2979 (1972); **52**, 182 (1974); S. P. N. VAN DER HEIJDEN, E. A. H. GRIFFITH, W. D. CHANDLER, and B. E. ROBERTSON. Can. J. Chem. **53**, 2084 (1975); K. GURTU, W. D. CHANDLER, and B. E. ROBERTSON. Can. J. Chem. **53**, 2093 (1975); S. P. N. VAN DER HEIJDEN, W. D. CHANDLER, and B. E. ROBERTSON. Can. J. Chem. **53**, 2102 (1975); **53**, 2108 (1975); **53**, 2115 (1975); **53**, 2127 (1975).
2. J. J. BERGMAN, E. A. H. GRIFFITH, B. E. ROBERTSON, and W. D. CHANDLER. Can. J. Chem. **51**, 162 (1973); H. BENJAMINS and W. D. CHANDLER. Can. J. Chem. **52**, 597 (1974); H. BENJAMINS, F. H. DAR, and W. D. CHANDLER. Can. J. Chem. **52**, 3297 (1974).
3. E. F. PAULUS. Private communication.
4. A. DOMENICANO, A. VACIAGO, and C. A. COULSON. Acta Crystallogr. B**31**, 221 (1975); B**31**, 1630 (1975); A. DOMENICANO, P. MAZZEO, and A. VACIAGO. Tetrahedron Lett. **13**, 1029 (1976).
5. J. J. BERGMAN and W. D. CHANDLER. Can. J. Chem. **50**, 353 (1972).
6. D. T. CROMER and J. B. MANN. Acta Crystallogr. A**24**, 321 (1968).
7. R. F. STEWART, E. R. DAVIDSON, and W. T. SIMPSON. J. Chem. Phys. **42**, 3175 (1965).
8. G. GERMAIN and M. M. WOOLFSON. Acta Crystallogr. B**24**, 91 (1968).
9. A. ZALKIN. FORDAP, A Fortran program for Fourier calculations. University of California, Berkeley, CA.
10. W. R. BUSING, K. O. MARTIN, and H. A. LEVY. ORFLS, Report ORNL-TM-305. Oak Ridge National Laboratory, Oak Ridge, TN. 1962.
11. C. K. JOHNSON. ORTEP, Report ORNL-3794. Oak Ridge National Laboratory, Oak Ridge, TN. 1965.
12. T. F. KOETZLE, M. S. LEHMAN, and W. C. HAMILTON. Acta Crystallogr. B**29**, 231 (1973).
13. R. GOPAL, W. D. CHANDLER, and B. E. ROBERTSON. To be published.
14. J. E. HUHEEY. J. Phys. Chem. **69**, 3284 (1965); **70**, 2086 (1966).
15. A. D. WALSH. Discuss. Faraday Soc. **2**, 18 (1947); H. A. BENT. Chem. Rev. **61**, 275 (1961); J. Inorg. Nucl. Chem. **19**, 43 (1961).

Further studies on the use of the thallium salt of *N*-hydroxysuccinimide for the preparation of succinimidyl esters[1]

ALENKA PAQUET

Food Research Institute, Canada Department of Agriculture, Ottawa, Ont., Canada K1A 0C6

Received April 6, 1979

ALENKA PAQUET. Can. J. Chem. **57**, 2775 (1979).

An efficient preparation of four alkyl (ethyl, *tert*-butyl, *p*-nitrobenzyl, trichloroethyl) succinimidyl carbonates from the thallium salt of *N*-hydroxysuccinimide and corresponding chloroformates is described. The general utility of trichloroethyl succinimidyl carbonate is demonstrated by its reaction with glycine to give trichloroethoxycarbonylglycine. The preparation of succinimidyl esters of numerous fatty acids using the thallium salt of *N*-hydroxysuccinimide and the corresponding acid chlorides is described. The advantage of this method over the *N*,*N*′-dicyclohexylcarbodiimide method for the preparation of these esters is demonstrated. Succinimidyl *p*-toluenesulfonate and chloroacetate were also prepared.

ALENKA PAQUET. Can. J. Chem. **57**, 2775 (1979).

On décrit une préparation efficace de quatre alkylcarbonates de *N*-hydroxysuccinimide (éthyle, *tert*-butyle, *p*-nitrobenzyle, trichloroéthyle) à partir des sels de thallium de la *N*-hydroxysuccinimide et des chloroformates correspondants. On utilise la préparation de la trichloroéthoxycarbonylglycine à partir de trichloroéthylcarbonate de *N*-hydroxysuccinimide pour faire ressortir l'utilité de ce dernier. On décrit également la préparation des esters de *N*-hydroxysuccinimide de plusieurs acides gras à partir du sel de thallium de la *N*-hydroxysuccinimide et des chlorures d'acide correspondants. On met en évidence l'avantage de cette méthode sur celle à la *N*,*N*′-dicyclohexylcarbodiimide. On a également préparé les *p*-toluènesulfonate et chloroacétate de *N*-hydroxysuccinimide.

[Traduit par le journal]

We have recently described a simple preparation of the thallium salt of *N*-hydroxysuccinimide (TlONSu) and its reaction with acid chlorides, which affords the corresponding succinimidyl (ONSu) esters in high yields (1). Within the extension of the research in this laboratory, we have explored the TlONSu for further preparation of various succinimidyl esters.

Alkyl succinimidyl carbonates (**1**) can be used for facile introduction of urethane type (ROCONH—) protecting groups in amino acid chemistry, essentially as described for acylation of amino acids by ONSu esters (2–4). The TlONSu provides a convenient starting material for the preparation of these compounds. We report here the preparation of two known compounds, ethyl succinimidyl carbonate, **1***a* (5), and *tert*-butyl succinimidyl carbonate, **1***b* (5, 6), and two new analogues, *p*-nitrobenzyl succinimidyl carbonate, **1***c*, and trichloroethyl succinimidyl carbonate, **1***d*. The succinimidyl carbonates (**1***a–d*) were prepared from corresponding chloroformates and TlONSu in an inert solvent as described previously for the preparation of benzyl succinimidyl carbonate (1). All chloroformates were commercially available except for *tert*-butyl chloroformate, which was prepared *in situ* from phosgene, *tert*-butanol, and pyridine at −30°C (7, 8). In addition, **1***b* was prepared by reaction of succinimidyl chloroformate with *tert*-butanol. The succinimidyl chloroformate was obtained in 90% yield from TlONSu and phosgene. This yield is superior to that reported for the preparation of this compound using KONSu and phosgene (5). The compounds **1** are described in Table 1.

The utility of **1***a* and **1***b* has been demonstrated previously (5, 6, 9). The compound **1***d* could be used instead of trichloroethyl chloroformate for the introduction of the trichloroethoxycarbonyl group (10, 11), namely for the selective protection of an amino group in the presence of a hydroxy group. A general example of the utility of **1***d* is described in this communication by its reaction with glycine in the presence of 1 equivalent of sodium bicarbonate giving an 85% yield of trichloroethoxycarbonylglycine.

The TlONSu was also found to be useful for the preparation of ONSu esters of fatty acids (**2**). Its reaction with corresponding acid chlorides does not give any side products and affords high yields. Thus, succinimidyl butyrate (**2***a*) and succinimidyl caproate (**2***b*) were prepared by refluxing equivalent amounts of TlONSu and butyryl and caproyl chlorides for 2–4 h giving yields of 88 and 90%, respectively. When working with long and medium chain fatty

[1]Contribution No. 388 from the Food Research Institute, Agriculture Canada, Ottawa, Ont., Canada.

0008-4042/79/202775-04$01.00/0

TABLE 1. Alkyl succinimidyl carbonates **1** (ROCONSu)[a]

	R	Melting point (°C) Found	Ref. 5	Yield (%)	Molecular formula	Analysis (%) C Calcd.	C Found	H Calcd.	H Found	N Calcd.	N Found
1*a*	Ethyl	50–51	50–52	90	—						
1*b*	*tert*-Butyl	98–101	98–100	75[b] 64[c]	—						
1*c*	*p*-Nitrobenzyl	130	—	90	$C_{12}H_{10}N_2O_7$	48.98	48.68	3.42	3.49	9.51	9.26
1*d*	Trichloroethyl	113[d]	—	90	$C_7H_6Cl_3NO_5$	28.94	28.91	2.08	2.11	4.81	4.69

[a]Infrared and nmr spectra of all compounds were in accord with their structures.
[b]From the reaction of *tert*-butyl chloroformate and TlONSu.
[c]From the reaction of succinimidyl chloroformate and *tert*-butanol.
[d]Softens at 108°C.

acids, milder reaction conditions (room temperature and shorter reaction time) can be used, giving the pure ONSu esters in 92–95% yields after recrystallization from ethanol.

We have found that the TlONSu method is superior to the *N*,*N*′-dicyclohexylcarbodiimide (DCC) method for the synthesis of these esters. The DCC method gives high yields of ONSu esters of acylamino acids (2, 3, 4), but it is less convenient for work with the less reactive fatty acids. When fatty acids were coupled with *N*-hydroxysuccinimide using DCC, several side products were formed in all cases. Moreover, complete removal of the *N*,*N*′-dicyclohexylurea (DCU) was not always possible. Purification of ONSu esters by repeated crystallization gave satisfactory results with medium and long chain fatty acids (starting with caprylic), but was not efficient when working with shorter fatty acids. For example, succinimidyl butyrate (**2***a*) was prepared from butyric acid and *N*-hydroxysuccinimide, using DCC in ethyl acetate, according to the usual procedure for the preparation of ONSu esters of acylamino acids (2, 3, 4). The DCU was separated by filtration and the material remaining in solution was isolated by fractional crystallization. The first compound which crystallized was identified as *N*-butyryl-*N*,*N*′-dicyclohexylurea on the basis of its melting point, infrared spectrum, and elemental analysis. The low melting **2***a* could not be completely freed from *N*-acylurea, despite the fact that only a small amount of it was formed during the reaction. Attempts to purify **2***a* by means of column chromatog-

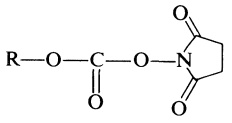

1

a R = C_2H_5
b R = $(CH_3)_3C$
c R = $(p\text{-}NO_2)C_6H_4CH_2$
d R = Cl_3CCH_2

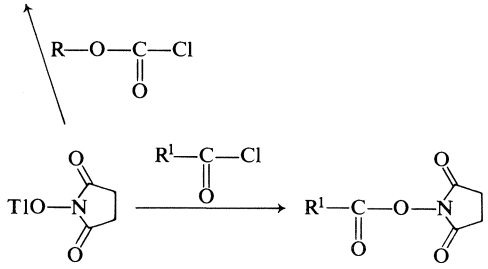

2

a $R^1 = C_3H_7$ *f* $R^1 = C_{13}H_{27}$
b $R^1 = C_5H_{11}$ *g* $R^1 = C_{15}H_{31}$
c $R^1 = C_7H_{15}$ *h* $R^1 = C_{17}H_{35}$
d $R^1 = C_9H_{19}$ *i* $R^1 = ClCH_2$
e $R^1 = C_{11}H_{23}$ *j* $R^1 = (p\text{-}CH_3)C_6H_4SO_2$

TABLE 2. Succinimidyl esters **2** (RCONSu)[a]

RCO—	Melting point (°C) Found	Ref. 19	Molecular Formula	Analysis (%)[b] C Calcd.	C Found	H Calcd.	H Found	N Calcd.	N Found
2*a* Butyrate	36–38	—	$C_8H_{11}NO_4$	51.89	51.73	5.98	6.11	7.56	7.70
2*b* Caproate	55–57	—	$C_{10}H_{15}NO_4$	56.32	56.19	7.09	7.03	6.57	6.43
2*c* Caprylate	63	63	—						
2*d* Caprate	69–70	—	$C_{14}H_{23}NO_4$	62.43	62.52	8.61	8.52	5.20	5.05
2*e* Laurate	76–77	75	—						
2*f* Myristate	85–86	—	$C_{18}H_{31}NO_4$	66.43	66.29	9.60	9.76	4.30	4.43
2*g* Palmitate	91	90	—						
2*h* Stearate	93–94	93	—						
2*i* Chloroacetate	120	—	$C_6H_6ClNO_4$	37.62	37.63	3.16	3.10	7.31	7.39
2*j p*-Toluensulfonate	138	—	$C_{11}H_{11}NO_5S$	49.06	48.93	4.11	3.88	5.19	4.92

[a]Infrared and nmr spectra of all compounds were in accord with their structures. Compounds 2*c*–2*h* prepared using DCC method were obtained in yields 85–88%. Compounds 2*a*–2*j* prepared using TlONSu method were obtained in yields 90–95%.
[b]The elemental analyses of ONSu esters were obtained by analyzing products from the TlONSu method. The esters obtained using DCC method were identified by comparing their R_f values on tlc, physicochemical constants, and infrared spectra with the products obtained using the TlONSu method.

raphy failed due to its partial decomposition. Thus, sufficient quantities of pure **2***a* for further work could not be obtained using the DCC method.

N-Acylurea formation has previously been observed during peptide synthesis (12, 13). It arises from the intermediate *O*-acylisourea by internal nucleophilic substitution (14). It is likely that the formation of fatty *N*-acylurea assumes the same pathway. The fatty acid chain must interfere with the reaction of the intermediate *O*-acylisourea with the *N*-hydroxysuccinimide, thus promoting intramolecular reaction to give the *N*-acylurea.

When **2***a* was prepared in dioxane, another side-product precipitated out together with the *N*-acylurea and was isolated by fractional crystallization from dioxane. On the basis of its melting point and elemental analysis, this compound is considered to be the succinimidyl ester of succinimidoxycarbonyl-β-alanine, a compound previously isolated by others during the preparation of ONSu esters of less reactive amino acids (15). The structure of this compound has been established by Gross and Bilk (16), who also showed that it is formed from *N*-hydroxysuccinimide, itself, in the presence of DCC, and that it can be expected to form during the conversion of slowly reacting acids into their ONSu esters using DCC.

Succinimidyl ester of succinimidoxycarbonyl-β-alanine was also detected by tlc during the preparation of **2***a* in ethyl acetate, but was not isolated.

The next even chain fatty acid derivative, succinimidyl caproate (**2***b*) behaved similarly to **2***a* during purification. Compound **2***b* was eventually obtained in a pure state, in 78% yield after three recrystallizations from ethanol. However, yields varied due to partial decomposition during repeated crystallization. The esters obtained by the two different methods are described in Table 2.

Two other esters, succinimidyl chloroacetate (**2***i*) and *p*-toluenesulfonate (**2***j*) were also obtained in high yields using TlONSu and chloroacetyl and *p*-toluenesulfonyl chloride respectively. Compound **2***i* may in some cases conveniently replace chloroacetyl chloride for the introduction of the chloroacetyl group in amino acid chemistry (17). Furthermore, there exist claims in the patent literature to the use of succinimidyl chloroacetate as a starting material for the preparation of succinimidyl esters of various acids (18). Thus, the simple preparation of **2***i* may bring some improvement in this field as well.

We have previously described the acylation of the side chain amino group of α-unprotected lysine using succinimidyl palmitate in the presence of triethylamine (1). Further studies have shown that for work with shorter fatty acids, sodium hydroxide should be used instead of triethylamine in some cases (results to be published). Reinvestigation of the previously reported reaction between lysine and benzyl succinimidyl carbonate in the presence of methanolic potassium hydroxide (1) leads us to the conclusion that the yield reported (85%) was higher than that which can actually be obtained. The product of the reaction was not, in fact, homogeneous.

Experimental

Melting points were determined on a Koffler Block and are uncorrected. Nuclear magnetic resonance spectra were recorded on a Varian T-60 spectrometer in deuteriochloroform. Infrared spectra were determined with a Beckman-IR-20 spectrometer in chloroform. Thin layer chromatography was carried out on precoated plates (Analtech, Inc., Newark, DE,

U.S.A.). Fatty acid chlorides were purchased from NU CHEK PREP, Inc., Elysian, MN, U.S.A.

Derivatives **2***b* and **2***c* were synthesized using the TlONSu method as indicated for **2***a*. The esters **2***d–h* were prepared using this method as described for the preparation of succinimidyl myristate **2***f*. The preparations of ONSu esters using DCC were carried out as described for the preparation of succinimidyl myristate **2***f*.

*Succinimidyl Butyrate (***2**a*)*

To a stirred solution of 2.13 g (20 mmol) of freshly distilled butyryl chloride in 25 mL of dry methylene chloride was added 6.36 g (20 mmol) of TlONSu in small portions. The mixture was refluxed and stirred under a stream of nitrogen for 3–4 h (until the tlc analysis did not show any chloride present). The thallium chloride was removed by filtration through a Celite pad, resuspended in methylene chloride, and filtered. The combined filtrate was washed with 10% aqueous sodium bicarbonate and water, dried over sodium sulfate, and the solvent was evaporated under reduced pressure. The oily residue upon addition of ether and chilling gave 32.5 g (88%) of **2***a*.

*Succinimidyl Myristate (***2**f*) using TlONSu*

A mixture of 2.46 g (10 mmol) of myristyl chloride and 3.18 g (10 mmol) of TlONSu in 20 mL of dry methylene chloride was stirred at room temperature for 1–2 h (until the tlc analysis did not show any chloride present). Workup as described for **2***a* followed by crystallization from ethanol gave **2***f* in 95% yield.

*Succinimidyl Myristate (***2**f*) using DCC*

To a stirred solution of 5.8 g (50 mmol) of *N*-hydroxysuccinimide and 11.42 g (50 mmol) of myristic acid in 75 mL of dioxane was added 10.3 g (50 mmol) of DCC in small portions. The mixture was kept overnight at 0°C and then DCU was filtered off. The solvent was removed under reduced pressure and the crude product was recrystallized twice from ethanol to give 13.8 g (85%) of **2***f*.

Isolation of N-*Butyryl*-N,N′-*dicyclohexylurea*

To a suspension of 26.4 g (0.23 mol) of *N*-hydroxysuccinimide in 980 mL of ethyl acetate, 20.2 g (0.23 mol) of freshly distilled butyric acid and 4.74 g (0.23 mol) of DCC were added. The mixture was stirred at room temperature for 1 h and kept at 5°C overnight. The DCU was removed by filtration, and two further crops were separated from the concentrated filtrate. Three crystallizations of the residue from ether gave 3.77 g of *N*-butyryl-*N*,*N*′-dicyclohexylurea. A sample, recrystallized from dioxane had mp 149°C. Infrared: 1510–1540, 1660, 1705 cm^{-1}. *Anal.* calcd. for $C_{17}H_{30}N_2O_2$: C 69.34, H 10.27, N 9.51; found: C 69.33, H 10.13, N 9.70.

*Isolation of Succinimidyl Ester of Succinimidoxycarbonyl-*β*-alanine*

This compound was isolated from the attempt to synthesize **2***a* in dioxane using 0.023 mol of each reagent essentially as described above for the synthesis of **2***f* using DCC. After the removal of DCU by filtration and concentration of the filtrate, 370 mg of a mixture of *N*-acylurea, DCU, and succinimidoxycarbonyl-β-alanine *N*-hydroxysuccinimide ester was obtained. Fractional crystallization from dioxane gave 250 mg of the pure β-alanine derivative, mp 163–165°C (lit. (16) mp 156–163°C, dioxane–ether or acetonitrile–ether). *Anal.* calcd. for $C_{12}H_{13}N_3O_8$: N 12.83; found: N 12.48.

*Succinimidyl Chloroacetate (***2**i*)*

A suspension of 112.9 mg (1 mmol) of chloroacetyl chloride and 318.4 mg (1 mmol) of TlONSu in 3 mL of dry chloroform was stirred at room temperature for 2–3 h. The thallium chloride was filtered off, resuspended in chloroform, and filtered. The combined filtrate was washed with 10% aqueous sodium bicarbonate and water, dried over sodium sulfate, and evaporated to dryness. The crude product was recrystallized from ether to give 176.3 mg (92%) of the product.

Succinimidyl p-*Toluensulfonate (***2**j*)*

A mixture of 190.6 mg (1 mmol) of *p*-toluenesulfonyl chloride and 318.4 mg (1 mmol) of TlONSu in 5 mL of dry chloroform was stirred at room temperature for 2–3 h. Work-up as described for **2***i*, followed by crystallization from chloroform–hexane gave 242.5 mg (90%) of **2***j*.

Trichloroethoxycarbonylglycine

To the stirred solution of 450 mg (6 mmol) of glycine and 540 mg (6 mmol) of sodium bicarbonate in a mixture of water (12 mL) and tetrahydrofuran (3 mL) was added 1.74 g (6 mmol) of **1***d*. After stirring overnight, the mixture was acidified, and then concentrated to a small volume *in vacuo*. Addition of a small amount of water and chilling afforded 1.26 g (84%) of crystalline trichloroethoxycarbonylglycine; mp 126–127°C. *Anal.* calcd. for $C_5H_6O_4Cl_3N$: C 23.97, H 2.41, N 5.59; found: C 24.00, H 2.48, N 5.58.

Acknowledgements

The author is grateful to Dr. L. Benoiton for discussing this work, to Mr. G. Morris (Analytical Services, C.B.R.I., Agriculture Canada) for elemental analyses, and to Mr. G. Khanzada for technical assistance.

1. A. Paquet. Can. J. Chem. **54**, 733 (1976).
2. G. W. Anderson, J. E. Zimmerman, and F. M. Callahan. J. Am. Chem. Soc. **85**, 3039 (1963).
3. G. W. Anderson, J. E. Zimmerman, and F. M. Callahan. J. Am. Chem. Soc. **86**, 1839 (1964).
4. G. W. Anderson. U.S. Patent 3,317,559. 1967.
5. H. Gross and L. Bilk. Ann. Chem. **725**, 212 (1969).
6. M. Frankel, D. Ladkany, C. Gilon, and Y. Wolman. Tetrahedron Lett. 4765 (1966).
7. R. B. Woodward, K. Heusler, J. Costeli, P. Naegeli, W. Oppolzer, R. Ramage, S. Ranganathan, and H. Vorbrüggen. J. Am. Chem. Soc. **88**, 852 (1966).
8. S. Sakakibara, I. Honda, and K. Takada. Bull. Chem. Soc. Jpn. **42**, 809 (1969).
9. M. Bodanszky, Y. S. Klausner, and M. A. Ondetti. *In* Peptide synthesis. 2nd ed. J. Wiley, New York. 1976. p. 32.
10. T. B. Windholz and D. B. R. Johnston. Tetrahedron Lett. 2555 (1967).
11. H. Yajima, H. Watanabe, and M. Okamoto. Chem. Pharm. Bull. **19**, 2185 (1971).
12. H. G. Khorana. Chem. Ind. 1087 (1955).
13. F. Weygand, D. Hoffmann, and E. Wünsch. Z. Naturforsch. **21**b, 426 (1966).
14. J. M. Jones. Chem. Ind. 723 (1974).
15. M. Löw and L. Kisfaludy. Acta Chim. Hung. **44**, 61 (1965).
16. H. Gross and L. Bilk. Tetrahedron, **24**, 6935 (1968).
17. J. P. Greenstein and M. Winitz. *In* Chemistry of amino acids. Vol. 2. Wiley, New York. 1951. p. 920.
18. A. Hagitani, T. Muramatsu, S. Sakakibara, J. Abe, and T. Watanabe. U.S. Patent 3,880,823. 1975.
19. Y. Lapidot, S. Rappoport, and Y. Wolman. J. Lipid Res. **8**, 142 (1967).

Electron spin resonance of Mn^{2+} impurity ions in MoO_3–pumice catalyst

K. C. KHULBE, R. S. MANN, AND N. TAN

Department of Chemical Engineering, University of Ottawa, Ottawa, Ont., Canada K1N 9B4

AND

A. MANOOGIAN

Department of Physics, University of Ottawa, Ottawa, Ont., Canada K1N 9B4

Received April 26, 1979

K. C. KHULBE, R. S. MANN, N. TAN, and A. MANOOGIAN. Can. J. Chem. **57**, 2779 (1979).

The electron spin resonance of Mn^{2+} impurities in the MoO_3–pumice system is studied along with the behavior of the system in the oxidation of methanol to formaldehyde. The intensity of the Mn^{2+} esr lines and the rate of catalytic conversion were both found to pass through a maximum at the same catalyst concentration. The results can be qualitatively explained in terms of the ion sites at the MoO_3–pumice surface.

K. C. KHULBE, R. S. MANN, N. TAN et A. MANOOGIAN. Can. J. Chem. **57**, 2779 (1979).

On a étudié le spectre de résonance paramagnétique électronique des ions Mn^{2+} contenus comme impureté dans le système de catalyseur MoO_3 déposé sur de la ponce ainsi que le comportement de ce dernier lors de l'oxydation du méthanol en formaldéhyde. On a trouvé que l'intensité des lignes spectrales des ions Mn^{2+} et la vitesse de conversion catalytique atteignent un maximum pour la même concentration de catalyseur. Ces résultats peuvent être expliqués qualitativement en fonction de la position des ions à la surface du système MoO_3–ponce.

[Traduit par le journal]

Catalysts based on molybdenum oxide are widely used in oxidation, hydrodesulfurization, and hydrocarbon reactions (1–7). A mixture of two or more metal oxides has been found to be very useful for obtaining high yields of formaldehyde from methanol oxidation. Molybdenum on several supports was studied by electron spin resonance (esr) and a number of correlations were obtained between catalytic activity and intensity of the molybdenum esr signal (1, 5, 7). No esr studies have been reported for MoO_3–pumice catalyst even though pumice is widely used as a support material. The purpose of the present work is to study the esr of Mn^{2+} impurities which exist in the MoO_3–pumice system, and to correlate the results with the behavior of the catalysts in the oxidation of methanol to formaldehyde, which is also studied.

Pumice is a hard glossy lava of volcanic origin, and is a complex silicate of sodium, potassium, magnesium, iron, and aluminum. It has a low surface area, is a porous material, and is a relatively inert support. Manganese is a natural impurity in pumice but it exists in a valence state which does not produce any esr lines. However, when MoO_3 is added to pumice the esr lines of Mn^{2+} are observed. Mn^{2+} ($S = 5/2$, $I = 5/2$) produces five fine structure esr lines, each of which is split into six hyperfine lines due to the interaction term $A\boldsymbol{I}\cdot\boldsymbol{S}$, where A is the hyperfine parameter. In powders only the central fine structure line ($M_s = 1/2 \rightarrow -1/2$) with its sextet of hyperfine lines is normally observed, since its position is nearly independent of the external magnetic field direction. The outer four fine structure lines are broadened due to their strong magnetic field dependence in crystalline electric fields with symmetry lower than cubic. The esr spectrum due to these lines is usually observed as only a broad hump superimposed on the resolved central line. The esr was done at X-band microwave frequency (~9.4 GHz) using a commercial spectrometer. Most of the measurements were performed at room temperature but some were done at liquid nitrogen temperature (−196°C) in order to check for extra lines which might appear more favorably at low temperature.

In the preparation of the catalyst, pumice (Fisher, size 8 mesh sieve) was ground and only 30–40 mesh size grains were used. The grains were washed with concentrated hydrochloric acid and then with distilled water until no precipitate was formed after applying a silver nitrate solution. They were then dried overnight in an oven at 110°C. The molybdenum doped pumice was prepared by impregnating the required amount of pumice with a calculated amount of ammonium molybdate solution in water. The mixture was then slowly dried over a hot water bath and then dried further for 3 h at 110°C. It was finally calcined from 200 to 650°C by raising the temperature continuously at the rate of 100°C/h and then heating continuously for 18 h at 650°C. The catalytic air oxidation of methanol was investigated

0008-4042/79/202779-04$01.00/0

in an isothermal fixed bed integral flow reactor, using an apparatus described previously (8).

Chemical analysis of pumice was carried out in order to determine the impurity concentration of manganese. In the analysis procedure 0.0789 g pumice was dissolved in a mixture of 2 mL perchloric acid plus 5 mL hydrochloric acid, and the solution was evaporated to dryness. The residue was dissolved in 5 mL of 6 *N* HCl and the volume was then increased to 30 mL by adding distilled water. The manganese concentration of the solution was measured quantitatively by atomic absorption spectroscopy and found to be 0.053 wt.% in the pumice. The ammonium molybdate was also analyzed for manganese content but no trace of the impurity was found.

The esr spectrum of pumice itself did not show the presence of any Mn^{2+} esr lines. Only two broad low intensity humps were observed, one at $g \simeq 4$ and the other at $g \simeq 2$, which are likely due to Fe^{3+} impurities. Figure 1*a* shows the esr spectrum obtained when 10 wt.% of MoO_3 was doped on pumice. The six line spectrum can be attributed to Mn^{2+} ions which are likely formed from non-paramagnetic manganese impurities originating in the pumice. The six lines have nearly equal spacings and intensities, and are due to the hyperfine splitting of the Mn^{2+} $M_s = 1/2 \rightarrow -1/2$ fine structure line. The hump on which the six lines are superimposed is due to the broadened $M_s = \pm 3/2 \rightarrow \pm 5/2$ fine structure lines. This result indicates that the crystalline electric field at the Mn^{2+} site contains a small non-cubic component. From the average magnetic field position of the hyperfine lines the Mn^{2+} *g*-value was calculated to be 2.000. The average separation of the hyperfine lines is 81 (10^{-4}) cm^{-1} and, to first order in perturbation theory, this spacing represents the magnitude of the hyperfine parameter *A*. The *A* value can be used to give information about the number and type of ligands surrounding the Mn^{2+} ion in the material. From a plot of the average value of the hyperfine parameter vs. the covalency parameter divided by the number of coordinated ligands (9) it is seen that the value of $A = 81$ (10^{-4}) cm^{-1} corresponds to an environment of six O^{2-} ions. When the esr spectrum was run at low temperature (−196°C) it was observed that sharp low intensity doublet lines exist between each pair of hyperfine lines. This is the pattern expected for Mn^{2+} first-forbidden hyperfine lines ($\Delta M_I = \pm 1$) for the $M_s = 1/2 \rightarrow -1/2$ transition.

Figure 2 shows the relative intensity of the Mn^{2+} allowed hyperfine lines for various concentrations of MoO_3 on pumice. It is observed that the intensity of the Mn^{2+} lines increases steadily up to 6.9 wt.% of MoO_3, after which it declines. It was also noted during the course of the experiment that the color of the 6.9 wt.% MoO_3 catalyst was creamish brown while the others were yellow grey to dark yellow grey, depending on the concentration of MoO_3. When the MoO_3–pumice catalyst was calcined further at 700°C the esr spectrum changed as shown in Fig. 1*b*. The Mn^{2+} lines become superimposed on a large broad line centered at $g = 1.965$. There is no effect on the Mn^{2+} line intensities due to the calcination. The broad line can be attributed to Mo^{5+} or Mo^{3+} ions, which are paramagnetic and have *g*-values known to be near the measured value of 1.965 (1, 7, 10).

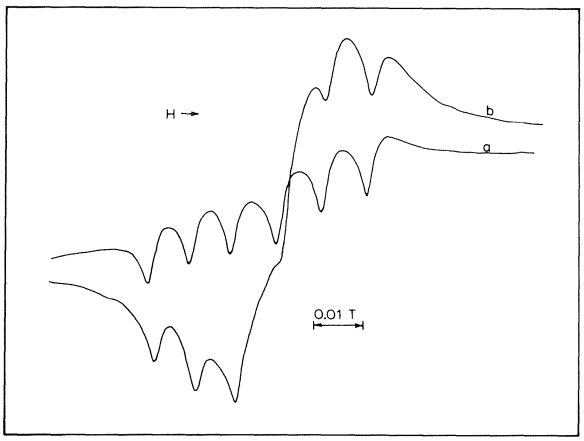

FIG. 1. (*a*) Electron spin resonance spectrum of Mn^{2+} impurities in 10 wt.% of MoO_3 doped on pumice, and (*b*) esr spectrum obtained when calcined further at 700°C.

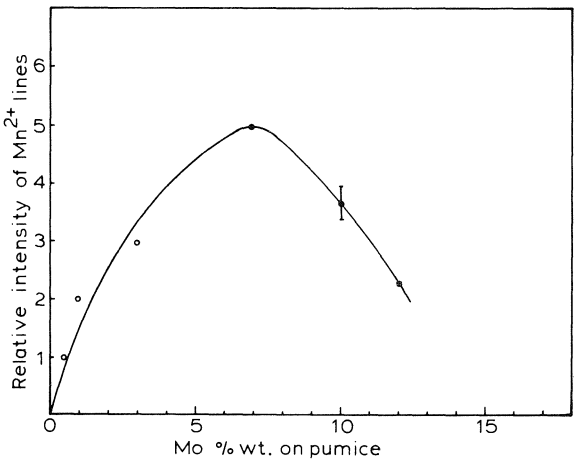

FIG. 2. Relative intensity of Mn^{2+} esr lines for various concentrations of MoO_3 on pumice.

In the conversion of methanol to formaldehyde it was observed that the relative conversion increased with increasing MoO_3 concentration on pumice up to a maximum of 6.9 wt.% MoO_3 and then decreased (Fig. 3). The selectivity of formaldehyde formation for the catalysts was always 100% since only formaldehyde could be detected after reaction. Figures 2 and 3 show that both the Mn^{2+} esr line intensities and the conversion rate maximize at the same catalyst concentration. It was observed in the used catalysts that the Mn^{2+} line intensities did not change after reaction.

In order to check if the existence of manganese ions in the Mn^{2+} state was dependent on the doping material, catalysts of 1 wt.% Mn, Cu, Ni, and Fe doped on pumice were prepared in a similar way as for the MoO_3–pumice catalyst. However, no esr signals due to Mn^{2+} ions were observed in any of these systems. This result suggests that the close relationship which was found to exist between the Mn^{2+} esr line intensities and the catalytic activity of the MoO_3–pumice system is dependent on the Mo ion or on the nature of the Mo ion sites.

We also studied the esr spectrum of 2 wt.% MoO_3 doped on kieselguhr. The catalyst was prepared in a similar way as that described for MoO_3–pumice. Kieselguhr is a naturally occurring low surface area material and is derived from marine life. It has a diatomic cellular structure and is composed entirely of semi-amorphous silica. The esr spectrum obtained (Fig. 4) is due to Mn^{2+} ions and is similar to that obtained in pumice except that the hyperfine lines are now broadened. The broadening may be due to a spread in A values for the Mn^{2+} ions, but the average A value is the same as that obtained in the MoO_3–pumice catalyst. No Mn^{2+} lines were observed in undoped kieselguhr.

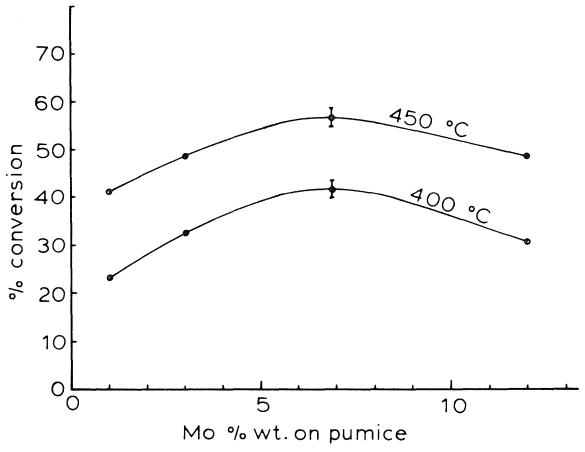

FIG. 3. Percent conversion of methanol to formaldehyde vs. the concentration of MoO_3 on pumice.

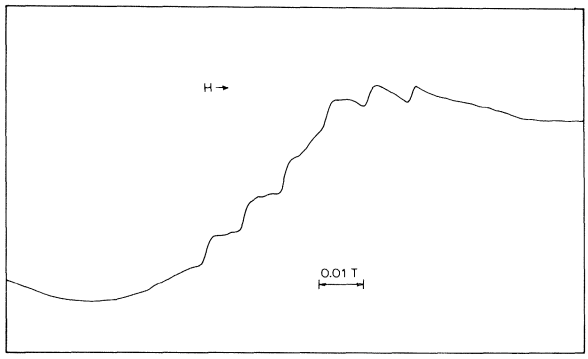

FIG. 4. Electron spin resonance spectrum of 2% MoO_3 on kieselguhr.

A qualitative explanation can be made regarding the behavior of the MoO_3–pumice catalyst. When molybdenum oxide is added to the support it forms a chemical bond with the surface atoms. For low dopant concentrations the molybdenum oxide likely forms a monolayer on the pumice surface, with Mo atoms in tetrahedral ($Mo{\cdot}4O^{2-}$) and octahedral ($Mo{\cdot}6O^{2-}$) sites, as is its usual habit (5). As the molybdenum oxide concentration is increased then normal MoO_3 is formed (5). This material possesses a rhombic lattice and consists of Mo^{6+} ions in strongly deformed octahedra of oxygens. A correlation between catalytic activity and Mn^{2+} esr line intensities can be made if the Mn^{2+} sites are located in the MoO_3–pumice interface structure. As the loading of MoO_3 increases, the exposed surface area of MoO_3 will increase up to the point where all the pumice surface is covered. The increasing MoO_3 surface area will account for the increased catalytic activity up to the point of maximum coverage. The area of the MoO_3–pumice interface also increases up to this point, hence accounting for the increased Mn^{2+} ion content. Beyond the point of maximum loading the state of the molybdenum oxide layer is likely affected by the thickness of the layer, causing both the catalytic activity and the Mn^{2+} presence to decrease.

Acknowledgments

The authors thank the National Research Council of Canada for financial assistance for the project A-1125. The authors would also like to thank Mrs. Diane Garrett, Department of Geology, University of Ottawa, Ottawa, for the quantitative analysis of pumice and ammonium molybdate.

1. M. NIWA, M. MIZUTANI, and Y. MURAKANI. Chem. Lett. Jpn. **8**, 1295 (1975).
2. B. I. PARSONS and M. TERNAN. Proc. 6th Int. Congr. Catal. Vol. 2. 1976. p. 965.
3. M. STEIJNS, P. KOOPMAN, B. NIENWENHUIJSE, and P. MARS. J. Catal. **42**, 96 (1976).
4. P. JIRU, B. WICHTERLOVA, and J. TICHY. Proc. 3rd Int. Congr. Catal. Vol. 1. 1964. p. 199.
5. G. K. BORESKOV, G. D. KOLOVERTNOV, L. M. KEFELI, L. M. PLYASOVA, L. G. KARAKCHIEV, V. N. MASTIKHIN, V. I. POPOV, V. A. DZIS'KO, and D. V. TARASOVA. Kinet. Katal. **7**, 144 (1966); Engl. Transl. p. 125.
6. M. DENTE, R. POPPI, and I. PASQUON. Chim. Ind. Milan, **46**, 1326 (1964).
7. K. S. SESHADRI and L. PETRAKIS. J. Phys. Chem. **74**, 4102 (1970).
8. R. S. MANN, S. K. JAIN, and M. K. DOSI. J. Appl. Chem. Biotechnol. **27**, 198 (1977).
9. B. KIGGINS and A. MANOOGIAN. Can. J. Phys. **49**, 3174 (1971).
10. R. I. MAKSIMOVSKAYA, V. F. ANUFRIENKO, and G. D. KOLOVERTNOV. Kinet. Katal. **9**, 1186 (1968); Engl. Transl. p. 984.

Rate–acidity profiles for exchange of the 4-methyl protons in amino, imino, and keto pyrimidines

ROSS STEWART, STEWART J. GUMBLEY, AND R. SRINIVASAN

Department of Chemistry, University of British Columbia, Vancouver, B.C., Canada V6T 1W5

Received April 24, 1979

ROSS STEWART, STEWART J. GUMBLEY, and R. SRINIVASAN. Can. J. Chem. **57**, 2783 (1979).

The rate of exchange of deuterium for protium in the 4-methyl groups of 2-imino-1,4-dimethyl-1,2-dihydropyrimidine (**1**), 1,4-dimethyl-2-pyrimidone (**2**), and 4-methyl-2-amino-pyrimidine (**3**) has been determined in aqueous solution over an acidity range of some 21 pH(H_0) units. The various exchange routes involve attack by base (water, hydroxide ion, buffer anion) on substrate (neutral, singly protonated, doubly protonated) and the identities of the principal components across the acidity spectrum have been established for all three compounds. The Brønsted slope, kinetic isotope effect, and activation parameters for **1** have also been determined. Protonating **1** activates it toward exchange by a factor of 10^3; addition of a second proton has a further effect of $> 10^5$. The activating effects of the imino group, the carbonyl group, and the protonated imino group in these compounds are in the ratio $10^{-1}:1:10^2$.

ROSS STEWART, STEWART J. GUMBLEY et R. SRINIVASAN. Can. J. Chem. **57**, 2783 (1979).

On a déterminé, en solution aqueuse sur une large échelle d'acidité de quelque 21 unités de pH(H_0), la vitesse d'échange des protons par des deutérium des groupes méthyl-4 de l'imino-2 diméthyl-1,4 dihydro-1,2 pyrimidine (**1**), de la diméthyl-1,4, pyrimidone-2 (**2**) et de la méthyl-4 amino-2 pyrimidine. Les différentes voies d'échange impliquent l'attaque du substrat (neutre, simplement ou doublement protoné) par une base (eau, ion hydroxyle, tampon anionique) et on a identifié les principaux composants à travers le spectre d'acidité des trois composés. On a également déterminé pour le composé **1** la courbe de Brønsted, l'effet isotopique cinétique et les paramètres d'activation. La protonation de **1** l'active vis-à-vis de l'échange par un facteur de 10^3, l'addition d'un second proton a un effet plus grand de l'ordre $> 10^5$. Dans ces composés, les effets d'activation des groupements imine, carbonyle et des groupements imines protonés sont dans un rapport $10^{-1}:1:10^2$.

[Traduit par le journal]

Introduction

Proton loss from an activated carbon–hydrogen bond is the critical step in enolization, and thus is the step that initiates a number of important reactions of organic chemistry and biochemistry. The usual activating unit in the enolization process is the carbonyl group, either free or protonated, and the activation that accompanies protonation of the carbonyl group has been the subject of a number of papers from this laboratory (1–6).

In 1964 Bender and Williams (7) pointed out that the equilibrium concentration of protonated ketone would be too low to provide effective activation at physiological pH and they considered the possibility that the protonated imino analog (protonated ketimine or Schiff's base) might fulfill this role. They estimated that a typical protonated ketimine is 10^3 times less reactive than the protonated ketone with respect to proton loss from the methyl group, but 10^8 times more reactive than the ketone itself. Hine (8), Spencer (9), and others have also been concerned with this alternative mode of activation and their results suggest that the latter factor is only of the order of 10^3 (8*b*, 9*b*).

The present work examines three derivatives of pyrimidine, the imino and keto compounds **1** and **2**, and the fully aromatic aminopyrimidine **3**. All have a methyl group at the 4-position that undergoes exchange in D_2O, brought about by attack of base on the neutral substrates or their conjugate acids. Comparing the rate of reaction of **2** with that of the conjugate acid of **1** will give the relative effectiveness of the carbonyl and protonated imino groups at activating the 4-methyl group with respect to proton loss. We have shown elsewhere (6) that the proton activating factor, **paf**, for **2** is 3×10^3, that is the 4-methyl group in the conjugate acid of **2** reacts 3×10^3 times faster with bases than does **2** itself. It should be noted that the conjugate acids of **1** and **2** have the quite different structures **1***a* and **2***a*, the former closely resembling **3***a*, one of the tautomeric

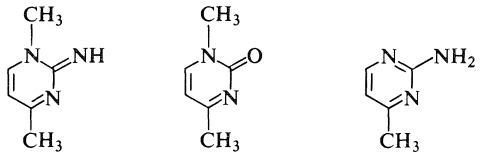

1 **2** **3**

0008-4042/79/202783-07$01.00/0

pair that are the conjugate acids of the true pyrimidine **3**.

Compounds **1** and **3** are of interest since they should behave quite differently in their neutral forms but almost identically in their cationic forms **1***a* and **3***a*.

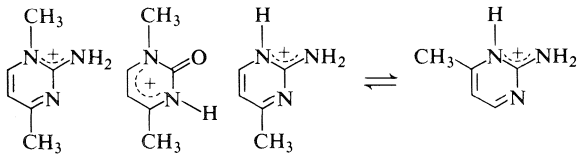

We herein report the rate–acidity profiles for exchange of the 4-methyl groups in **1**–**3** in D_2O over an acidity range that covers some 21 pH(H_0) units (10). It is not clear which acidity function is the most appropriate for the present systems and we have chosen to use D_0, the analog of H_0, throughout, partly because of its familiarity and partly because the principal alternative function H_A has not been determined for deuterated media.

Results and Discussion

The effect of acidity on the rate of exchange of the 4-methyl groups in **1**, **2**, and **3** is shown in Figs. 1 and 2. The measurements for the points in Fig. 1 were made in 0.2 *M* aqueous phosphate buffer over most of the acidity range; aqueous sulfuric acid was used in the strongly acidic (D_0) region, and aqueous sodium hydroxide for solutions more basic than pD 12.

Since the reactions are subject to general acid and general base catalysis the rate at any acidity will depend on the identity and concentration of the buffer acids present, and the curves in Fig. 1 can be considered as simple log (rate) vs. pD profiles in which the only acids and bases involved in the exchange would be D^+, DO^-, and D_2O, on which are superimposed contributions from the buffer components and from self-catalysis. The latter phenomenon, in which the neutral heterocycle acts as the base in removing the exchanging proton from the conjugate acid, can be important at acidities near the pK of the substrate.

Figure 2 refers to solutions in which no buffer was used. Control of acidity in these experiments depended to a large extent on the buffering ability of the substrates, which in turn varied considerably across the pD spectrum. By measuring pD before and after exchange with a glass electrode reasonably reliable values of the acidity could be obtained.

*1,4-Dimethyl-2-imino-1,2-dihydropyridine (**1**)*

Acid and base catalyzed exchange in D_2O of the

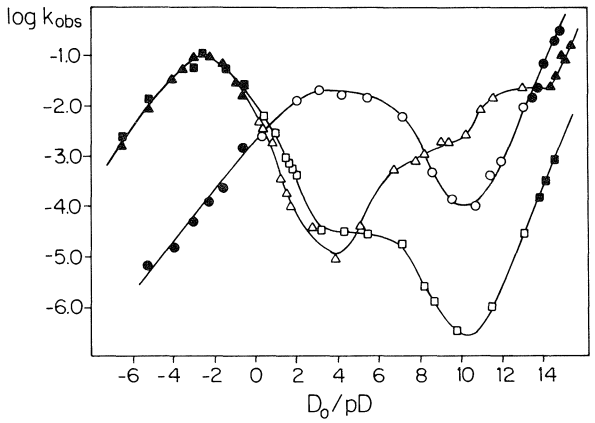

FIG. 1. Log rate–acidity profiles for **1** (triangles), **2** (circles), and **3** (squares) in D_2O containing 0.2 *M* phosphate buffer, except for points represented by closed symbols, which contain D_2SO_4 or NaOD instead of buffer; k_{obs} in units of min^{-1}; substrate concentrations 0.2 *M*.

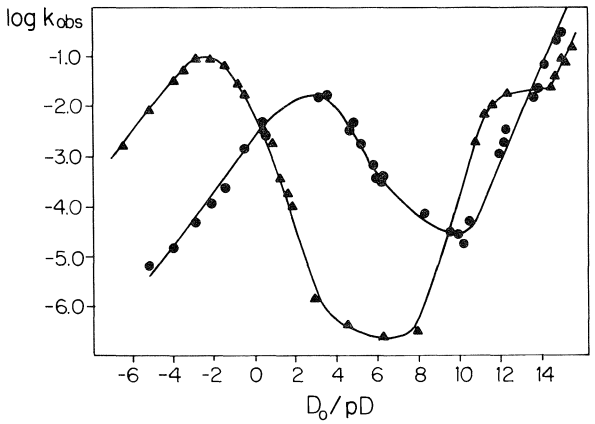

FIG. 2. Log rate–acidity profiles for **1** (triangles) and **2** (circles) in unbuffered D_2O using D_2SO_4, DCl, or NaOD to control the acidity; k_{obs} in units of min^{-1}; substrate concentrations 0.2 *M*.

4-methyl group in this compound has previously been observed by Batterham, Brown, and Paddon-Row, who produced a partial rate–acidity profile for the closely related 1,4,6-trimethyl compound (11). Their results for the latter compound are compatible with our more extensive study of **1**.

The curves in Fig. 1 (buffered) and Fig. 2 (unbuffered) represent essentially the three exchange mechanisms shown in eqs. [1]–[3]. Only the immediate exchanging intermediate formed in the rate-controlling step when base removes a proton from the 4-methyl group is shown in each case. For the sake of convenience the hydrogen atoms attached to oxygen and nitrogen atoms in the formulas are represented by the symbol H rather than D. The bases that contribute significantly to the three reac-

tions are identified in parentheses below the arrows, the various buffer anions being represented by the symbol A^-.

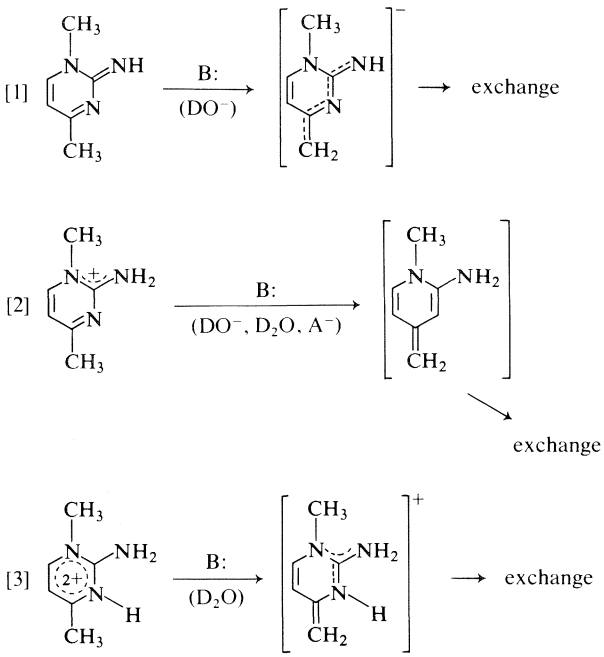

In the most basic systems studied the principal exchange reaction for **1**, $pK_{BD^+} = 11.4$, is given by [1]. The rate is roughly proportional to the deuteroxide ion concentration, as can be seen from the results of Fig. 2 where the straight line has been drawn with unit slope. The plateau near pD 12 presumably corresponds to the contribution from pathway [2] with the role of base being played by deuteroxide ion. This reaction will be pD-independent in solutions in which the concentration of the conjugate acid is small, i.e., when the pD is greater than about 12.

The **paf** (1) for **1**, that is the ratio of the rate constants for **1***a* and **1** reacting with the same base, is determined from the curve in Fig. 2, as follows. For hydroxylic catalysis, routes [1] and [2] make equal contributions to the rate of exchange when the overall rate is twice that at the plateau, that is at about pD 14.5. At this point eq. [4] is satisfied and, thus, **paf** is equal to $10^{-11.4}/10^{-14.5}$ or $10^{3.1}$. In other words, protonating **1** to give **1***a* activates the molecule towards prototropic exchange at the 4-methyl group by a factor of about one thousand.

$$[4] \quad \mathbf{paf} = K_{ZH^+}/[H^+]$$

This value is about one-third that previously observed (6) for the analogous keto compound **2**, a very modest difference in view of the dissimilar charge distributions in the two cations **1***a* and **2***a*.

As the basicity is reduced below the pK_{BD^+} (11.4) the rate drops in both the buffered and unbuffered systems as a result of the hydroxide ion concentration decreasing while the concentration of **1***a* remains the same. The slope of the log k vs. pD plot is linear in the pD region 7–11 in the unbuffered systems but a large contribution from buffer catalysis and possibly self-catalysis is apparent from the curve in Fig. 1. At pD 8 the uncatalyzed rate is less than 1% of the buffer catalyzed rate. The more thorough analysis of buffer catalysis and self-catalysis that was made for **2** is described in the next section.

The rate minimum for **1** occurs near pD 4 in phosphate buffer and near 6 in the unbuffered systems. As the acidity is increased the rate of exchange rises and the difference between the unbuffered and buffered system vanishes. We assign this exchange path to reaction of the dication with water, eq. [2]. The slope of the line between pD 0 and 2 is close to unity, as required for such a reaction path. We have measured the $pK_{BH_2^{2+}}$ for **1** by nmr and find the position of half-protonation to be at -2.61 on the H_0 scale. It is clear from Figs. 1 and 2 that this pK (which will not be drastically different in the deuterated system) is somewhere near the peak of the curve. The principal cause of the decrease in rate as the acidity is further increased is almost certainly the decrease in activity of the base, water, as the sulfuric acid concentration is raised. In going from 46.2% to 74.3% D_2SO_4 the observed rate of exchange decreases by a factor of 52 while the D_2O activity decreases by a factor of 30 (12). A plot of log k_{obs} (ordinate) against the logarithm of a_{D_2O} is linear with a slope of 1.35 (Fig. 3).

The second **paf**, that is the difference in the rate constants for reactions [2] and [3] with the same base, can be estimated from the curve in Fig. 2. The trough of the curve represents the maximum rate for reaction [3] with water acting as the base. This difference is at least a factor of 10^5 and may be considerably more, since the depth of the trough is not easily measured and since the water activity has already begun to drop at the rate maximum. It is thus clear that the second **paf** is larger than the first for **1**, that is, the second proton has a greater effect than the first in activating the 4-methyl group toward bases. This effect is presumably a result of the second unit of positive charge being located near the exchanging methyl group. (Compare the cations in [2] and [3].)

The reaction of **1** in aqueous buffers in the pH region 3.6–6.0 was examined using iodometry. This technique allows very low substrate concentrations to be used and hence avoids any interference by self-catalysis. In addition, isotope effects can be

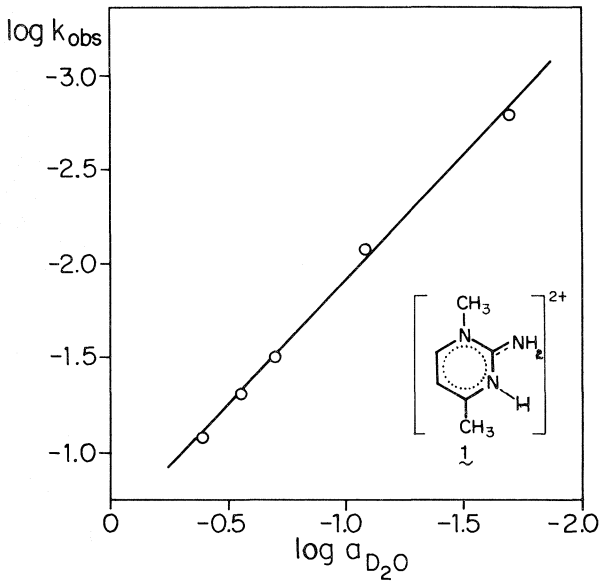

FIG. 3. Logarithm of rate of exchange of **1** in sulfuric acid as a function of the activity of D_2O; slope = 1.35; k_{obs} in units of min^{-1}; substrate concentration 0.2 *M*.

TABLE 1. Reaction of compound **1** with various bases in H_2O as determined by iodometry; T = 25°C, ionic strength = 0.7

Base	pK_{HA} (corr)[a]	k_2 (corr)[a] 10^5 L mol^{-1} min^{-1}
3,3-Dimethylglutarate (dianion)	6.04	80
Succinate (dianion)	5.18	36
Glutarate (dianion)	5.12	21
Propionate	4.88	22
Acetate	4.76	13
Phenylacetate	4.31	14
Benzoate	4.20	9.9
m-Fluorobenzoate	3.86	7.1
Nicotinamide	3.63	5.6
Methoxyacetate	3.57	3.5

[a]Statistical corrections made as heretofore (4).

determined since the solvent is H_2O rather than D_2O.

The data for the reaction of **1** with buffer acids HA are given in Table 1. Considering the pK_{BH^+} of **1** (11.1) (ref. 15) and the acidities used, the rate constants actually refer to the reaction of **1***a* with the buffer anions A^-. The Brønsted plot shown in Fig. 4 thus refers to the general base-catalyzed removal of a proton from the 4-methyl group of the conjugate acid of the substrate. The value of β is 0.50.

The isotope effect for the reaction of the conjugate acid of the 4-CD_3 analog of **1***a* with acetate ion is 7.4 at 25°C; $\Delta H^{\dagger}$ is 100.0 kJ mol^{-1} and $\Delta S^{\dagger}$ is -17.6 J $mol^{-1}K^{-1}$ for the reaction of **1***a* with the same base.

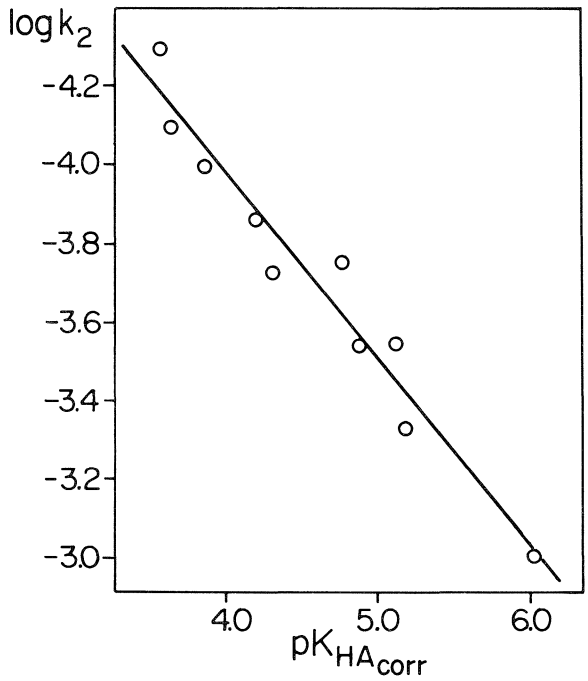

FIG. 4. Brønsted plot for the reaction of **1** with anionic bases in H_2O. From right to left the bases follow the order of descent in Table 1. Brønsted slope = 0.50; k_2 in units of M^{-1} min^{-1}.

The Brønsted slope, the isotope effect, and the activation parameters all appear to be unexceptionable.

1,4-Dimethyl-2-pyrimidone (2)

In D_2O this compound undergoes exchange of the hydrogens of the 4-methyl group by the following reaction paths.

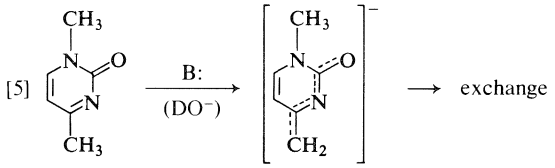

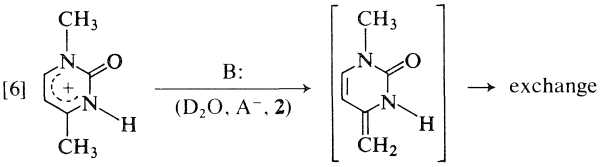

In solutions more basic than pD 11 the rate is first-order in hydroxide ion and there is virtually no buffer catalysis. (See Fig. 5 where the straight line in this region of the curve has been drawn with unit slope.)

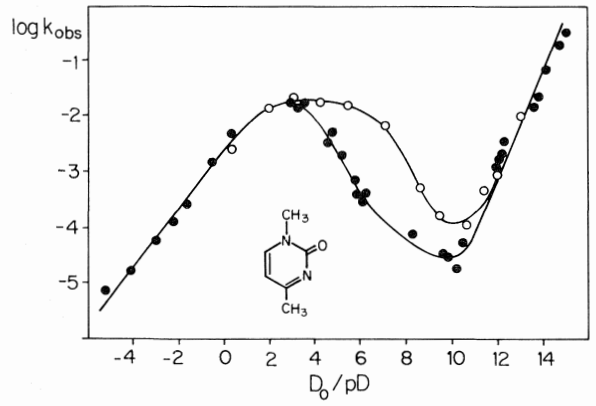

FIG. 5. Log rate–acidity profile for **2** in buffered (0.2 *M* phosphate, open circles) and unbuffered (D_2SO_4, NaOD, closed circles) solution; k_{obs} in units of min^{-1}; substrate concentration 0.2 *M*.

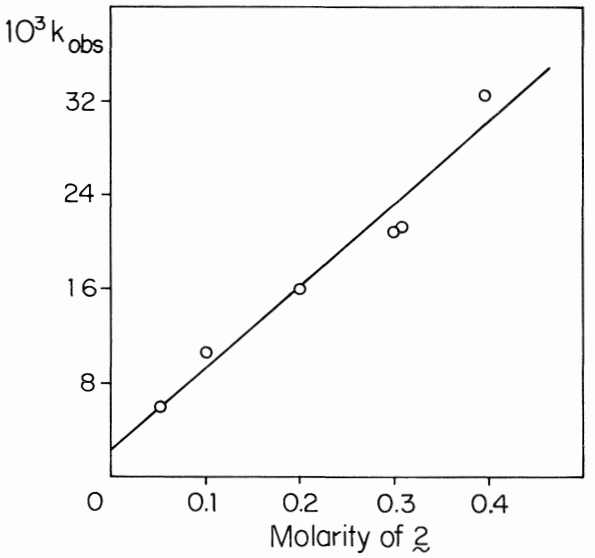

FIG. 6. Dependence on the rate of reaction of **2** on the compound's concentration; pD 3.4–3.5; k_0(intercept) = 2.1 × 10^{-3} min^{-1}.

A minimum occurs in both buffered and unbuffered systems near pH 10 and as the solution is made more acidic pathway [6] becomes dominant, with phosphate buffer catalysis being clearly evident in the pD region between 3 and 11. The pK_{BD^+} of **2** is 3.60 and if water and phosphate anions were the only bases involved in deprotonating cation **2***a* the rate should level off at a pD value about one unit below the p*K* and remain unchanged until the solution is made so acidic that the activity of water begins to drop. However, a decrease in the rate of exchange occurs long before the latter effect should be evident, as can be seen from the curves in Fig. 5. This effect has been traced to self-catalysis by the pyrimidine, which can itself act as the base in deprotonating its conjugate acid. This route will be most important at the p*K* of the substrate, 3.60. Decreasing the concentration of **2** markedly lowers the exchange rate in unbuffered solution in the pD region 3.4–3.5; even though acidity control was a problem at low substrate concentrations it was possible to show (Fig. 6) that the exchange rate is markedly dependent on solute concentration. Thus the drop in the curve in Fig. 5 as the acidity is increased is due to self-catalysis becoming less important as the pD moves away from the pK_{BD^+}, with the continuing decrease that occurs in the sulfuric acid region being due to the drop in water activity. The line in this region is roughly parallel to that observed with **1**, the imino analog.

4-Methyl-2-aminopyridine (3)

The first and second conjugate acids of this compound differ from those of **1** only in having a hydrogen atom instead of a methyl group on one of the ring nitrogen atoms. Experience tells us that such substitution should have only a minor effect on the reactivity of the 4-methyl group (2) and the close correspondence of the curves for **1** and **3** in the acid region is in agreement with this expectation (Fig. 1). The pK_{BD^+} of **3** is approximately 4.6 ($1.005\,pK_{BH^+}$ + 0.48) (13) and the two curves diverge sharply near this point. Whereas the cationic form of **1** predominates up to pD 11, **3** exists principally as the less reactive neutral molecule above pD 6 and the decrease in the rate of exchange of the 4-methyl group as the solution is made basic can be attributed to this factor. Buffer catalysis and self-catalysis probably contribute to the exchange in the region pD 3–5.

The increase in rate with increasing acidity beginning near pD 3 culminates in the curves for **1** and **3** merging. The diprotonated form of **3** is doubtless the reactive intermediate here (eq. [7]) since we have found the $pK_{BH_2^{2+}}$ value of **3** to be very close to the value of −2.61 that we obtain for **1**.

At the minimum in the curve, near pD 10, the reaction shown in eq. [8] gives way to that shown in eq. [9].

At the minimum of the curve, just above pD 10 the concentration of the cation **3***a* (or **3***a*′) has been reduced to 10^{-6} times that of the neutral compound **3** and the latter takes over as the principal exchanging intermediate. The increase in the rate as the solution is made more basic is directly proportional to the increase in hydroxide concentration (see Fig. 2 where the straight line in this region is drawn with unit slope). The reaction, therefore, is that shown in eq. [9].

It is clear that ionization of the amino group does not have a significant effect on the exchange of the

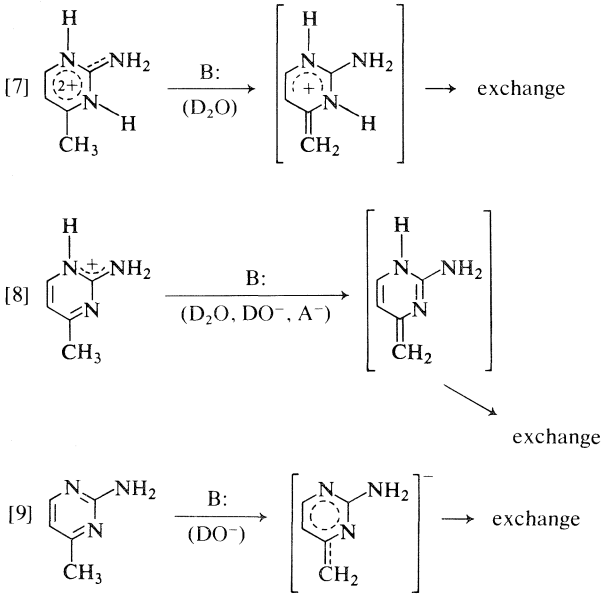

4-methyl protons even under the most basic conditions we have used, since the pK_{HA} of 2-aminopyrimidine is 20.5 (14) and the presence of the 4-methyl group will raise this value to about 20.9 (16).

The bottom of the trough in the rate vs. pD profile near pD 10 provides us with the maximum value possible for the rate of the reaction of cation **3***a* (and **3***a'*) with hydroxide ion, a pH-independent reaction. Now the principal exchange route of **1** at this acidity is also the reaction between hydroxide ion and a cation, **1***a*, which is, moreover, identical to **3***a* except for the replacement of methyl by hydrogen. The very large effective rate difference for these virtually identical reactions ($>10^5$) is due to **1** being largely protonated whereas **3** is protonated to only a minute degree at this acidity.

The minimum in the trough that occurs at pD 10 also gives us the maximum rate for the reaction of **3** with water. Were this the principal pH-independent route, rather than the kinetically equivalent counterpart discussed in the previous paragraph or the reaction with buffer anions, then at pD 10 the hydroxide- and water-catalyzed routes would be equally productive and hydroxide ion would be 10^6 times as effective as water at the same concentration. This quantity, called the deprotonating factor (1) **dpf**, is given for reactions of protium compounds by eq. [10] where $[H^+]^*$ is the hydrogen ion concentration where the two routes make equal contributions (1).

$$[10]\quad \mathbf{dpf} = [H^+]^*/1.8 \times 10^{-16}$$

Most **dpf** (HO^-/H_2O) values previously observed are 10^8 or greater and it is thus probable that the water-catalyzed route does not make a major contribution to the exchange even at the rate minimum at pD 10. An exact profile of the trough is not readily obtained since reaction half-life at the minimum is many years.

Activation by Carbonyl and Imino Groups

In strongly basic solution compounds **1** and **2** undergo exchange by identical mechanisms: hydroxide ion removes a proton from the 4-methyl group of the neutral substrates. The lines in Fig. 2 are parallel in this region with that for **2** being displaced above that for **1** by 1.0 logarithmic units. Thus the carbonyl group is more effective than the imino group in activating the 4-methyl group by a factor of about ten. This is a rather modest difference and it may be that the two ring nitrogen atoms provide such a large degree of activation that the effect of the other groups is damped.

The activating effect of the protonated imino group in these compounds is, of course, greater than that of imino but is also greater than that for the carbonyl group, in agreement with previous observations on aliphatic systems (7–9). The relative effects of carbonyl and protonated imino can be simply determined from the crossover point of the curves for **1** and **2** that occurs at pD 13.5. At this point **2** is completely in the neutral form, whereas **1** (pK_{BD^+} 11.4) is only about 1% protonated. Since the protonated form is responsible for essentially all of the exchange at this basicity, the protonated imino group is 100 times more reactive than the carbonyl group. This number is much closer to the values of Hine *et al.* (8*b*) and Spencer *et al.* (9*b*), $\sim 10^3$, than to that of Bender and Williams (7), 10^8. It should be noted, however, that all their values refer to aliphatic compounds, whereas ours refers to a heterocyclic system in which there is resonance stabilization of both the carbonyl and protonated imino groups.

Experimental

Materials

1,4-Dimethyl-1,2-dihydro-2-iminopyrimidine (**1**) was prepared as the hydrochloride salt essentially by the method of Brown and Paddon-Row (15). 2-Amino-4-methylpyrimidine was methylated with methyl iodide to give pale yellow needles mp 257°C (dec.) (lit (13) 253–254°C (dec.)), and the iodide exchanged for chloride using Dowex 1-X8 (Cl^-) resin, mp of chloride 257°C (dec.) (lit (15) 227°C (dec.)).

1,4-Dimethyl-2-pyrimidone (**2**) was prepared by methylating 2-hydroxy-4-methylpyrimidine, essentially by the method of Brown and Foster (16) except that the reaction was conducted at room temperature. Chromatographic purification (chloroform/alumina and methanol – carbon tetrachloride/silica gel) gave deep yellow crystals, mp 159.5–160.5°C (lit. (16) 156–157°C).

2-Amino-4-methylpyrimidine (**3**) was obtained commercially and sublimed twice before use, mp 161.5°C (lit. (17) 159–160°C).

Kinetics

The compounds were dissolved in solutions of the appropriate pD/D_0 to a concentration of 0.2 *M* and the rate of exchange measured by nmr or by iodometry at 36°C, essentially as previously described (3, 4, 6).

Ionization Constants

The pK_{BD^+} values of **1** and **2** were determined by spectrophotometry at 335 and 309 nm respectively in 0.05 *M* sodium phosphate in D_2O. They were found to be 11.4 and 3.66, respectively.

The second protonation constants, $pK_{BH_2^{2+}}$, for **1** and **3** were determined by the change in the nmr chemical shift of the 4-methyl peak in aqueous H_2SO_4 solution. They were found to be −2.61 and −2.65, respectively, using the H_0 acidity function.

Acknowledgement

The financial support of the National Research Council of Canada is gratefully acknowledged.

1. R. Stewart and R. Srinivasan. Acc. Chem. Res. **11**, 271 (1978).
2. R. Stewart and R. Srinivasan. Can. J. Chem. **53**, 224 (1975); **53**, 2906 (1975).
3. R. Srinivasan and R. Stewart. J. Am. Chem. Soc. **98**, 7648 (1976).
4. R. Srinivasan and R. Stewart. J. Chem. Soc. Perkin Trans. II, 674 (1976).
5. R. Stewart and J. M. McAndless. J. Chem. Soc. Perkin Trans. II, 376 (1972).
6. R. Stewart, S. J. Gumbley, and R. Srinivasan. Tetrahedron, **35**, 1257 (1979).
7. M. L. Bender and A. Williams. J. Am. Chem. Soc. **88**, 2502 (1966).
8. (*a*) J. Hine. Acc. Chem. Res. **11**, 1 (1978); (*b*) J. Hine, B. C. Menon, J. H. Jensen, and J. Mulders. J. Am. Chem. Soc. **88**, 3367 (1966).
9. T. A. Spencer. *In* Biorganic chemistry. Vol. 1. *Edited by* E. E. Van Tamelen. Academic Press, New York. 1977; (*b*) D. J. Hupe, M. C. R. Kendall, and T. A. Spencer. J. Am. Chem. Soc. **94**, 1254 (1972).
10. C. H. Rochester. Acidity functions. Academic Press, London. 1970.
11. T. J. Batterham, D. J. Brown, and M. N. Paddon-Row. J. Chem. Soc. B, 171 (1967).
12. J. Bus, H. Steinberg, and Th. J. De Boer. Recl. Trav. Chim. **87**, 609 (1968).
13. I. R. Bellobono and E. Diani. J. Chem. Soc. Perkin Trans. II, 1707 (1972).
14. M. G. Harris and R. Stewart. Can. J. Chem. **55**, 3800 (1977).
15. D. J. Brown and M. N. Paddon-Row. J. Chem. Soc. C, 1928 (1967).
16. D. J. Brown and R. V. Foster. Aust. J. Chem. **19**, 2321 (1966).
17. S. Gabriel and J. Colman. Chem. Ber. **32**, 2925 (1899).

Electrophilie du ligande η^3-allylique de complexes η^3-allyl-dicarbonyl-nitrosyl-fer

J. L. A. ROUSTAN ET F. HOULIHAN

Faculté des Sciences et de Génie, Département de Chimie, Université d'Ottawa, Ottawa, Ont., Canada K1N 9B4

Reçu le 22 mai 1979

J. L. A. ROUSTAN et F. HOULIHAN. Can. J. Chem. **57**, 2790 (1979).

Les complexes neutres η^3-allyl-dicarbonyl-nitrosyl-fer réagissent rapidement dans le THF à température ambiante avec des nucléophiles du type doublement activé tel l'anion malonate. Les composés organiques de monoallylation sont obtenus avec de bons rendements (80–95%). Avec des ligandes η^3-allyliques dissymmétriques le carbone le moins substitué est alkylé préférentiellement.

J. L. A. ROUSTAN and F. HOULIHAN. Can. J. Chem. **57**, 2790 (1979).

Neutral η^3-allyl-dicarbonyl-nitrosyl iron complexes react rapidly in THF at room temperature with nucleophiles of the doubly activated type such as malonate anion. Monoallylated organic products are obtained in good yields (80–95%). With unsymmetrical η^3-allyl ligands the less substituted carbon is alkylated preferentially.

Introduction

L'augmentation de l'électrophilie d'un ligande organique η^2-oléfinique ou η^3-allylique, par coordination sur un centre métallique approprié, est une propriété bien documentée (1, 2).

Le plus souvent la réaction s'effectue au niveau d'un complexe cationique (3–6) ou s'accompagne de l'expulsion d'un ligande négativement chargé (7); il en résulte un complexe η^1-alkyl ou η^2-oléfinique globalement électriquement neutre. Dans les cas beaucoup plus rares où la réaction s'effectue sur un complexe neutre (tel un complexe η^2-oléfinique (8)) un complexe anionique est formé.

Dans une telle réaction mettant en jeu un ligande η^3-allylique (schéma 1), la facilité d'approche du nucléophile ainsi que la stabilisation du complexe anionique intermédiaire doivent augmenter en même temps que la capacité des ligandes auxiliaires L_n à délocaliser la charge négative qui apparaît sur le métal.

Le ligande nitrosyle NO véritable "puit d'électrons" (9) apparaît parfaitement approprié à jouer ce rôle. Pour examiner la validité de cette hypothèse les complexes η^3-allyliques du dicarbonyl-nitrosyl-fer, aisement accessibles à partir d'halogénures (10) ou de diènes 1–3 (11) ont été sélectionnés et opposés à divers nucléophiles du type doublement activé.

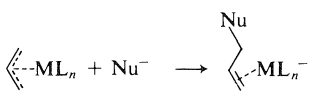

SCHÉMA 1

Partie expérimentale

Le THF est distillé sur $LiAlH_4$ avant usage. Les complexes η^3-allyliques sont préparés selon des modes opératoires déjà décrits (10).

Réactions d'alkylation

Les anions du type utilisé dans cette étude sont préparés dans le THF à température ambiante par la réaction de NaH avec le composé organique approprié en quantité stoechiométrique. A la solution contenant le nucléophile est ajoutée une quantité stoechiométrique de complexe η^3-allylique en solution dans le même solvant à température ambiante et sous CO. Après agitation durant 30 min, les composés organométalliques présents (seul $Fe(CO)_3NO^-$, Na^+ est détecté par ir) sont oxydés par barbotage d'air dans la solution durant 30 min. Le THF est évaporé, remplacé par l'éther diéthylique, puis le milieu est hydrolysé. Après séchage sur $MgSO_4$, le solvant est évaporé et l'huile obtenue est analysée par ^1H nmr, ^{13}C nmr et chromatographie en phase vapeur (colonne DEGS 10% sur Chromosorb W, $T = 130°C$, oxalate d'éthyle comme étalon interne).

Dans le cas de la réaction d'alkylation du complexe η^3-crotylique ***1b*** par le diéthyl malonate de sodium (un excès de 20% de diéthyl malonate est utilisé dans cette réaction) deux produits isomères de monoallylation sont formés. Ils sont séparés du diéthyl malonate en excès et d'une trace de produits de bis allylation par chromatographie sur colonne de silice (60–200 mesh) en éluant avec un mélange hexane – chlorure de méthylène (25–75).

Résultats

Les résultats sont présentés dans les tableaux 1 et 2. Dans tous les cas étudiés la réaction principale est la réaction de monoallylation du nucléophile qui s'effectue avec de bons rendements (schéma 2). La seule réaction secondaire qui a été mise en évidence est une bis allylation du nucléophile.

La réaction est effectuée à température ambiante,

0008-4042/79/202790-02$01.00/0

TABLEAU 1. Réaction de **1***a* avec divers nucléophiles Nu^-

Nu^- X	$^-CH(X)(X')$	Rendement % en produit de monoallylation 
—CO—CH_3	—COOEt	85
—COOEt	—COOEt	83; 80*
—$COOCH_3$	—SO_2—C_6H_5	95
—CN	—COOEt	77

*Rendement du produit de monoallylation si la réaction est effectuée sous argon.

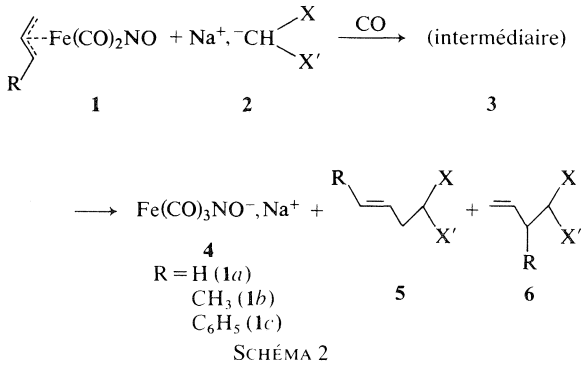

SCHÉMA 2

sous atmosphère de CO, dans le THF anhydre. Le complexe η^3-allylique solubilisé dans le THF est ajouté à la solution contenant le nucléophile. L'évolution du milieu réactionnel est suivie par un examen périodique de la solution par spectroscopie infrarouge.

La présence de substituants sur le ligande allylique n'a que peu d'influence sur la vitesse de disparition des complexes **1** qui est complète en moins de 10 min. De même que lors de la réduction électrochimique ou chimique du complexe **1***a* (R = H) dans l'acétonitrile (12), un intermédiaire réactionnel **3** est détecté (THF, $\nu(cm^{-1})$: CO = 1950, 1870, NO = 1630). Sa structure reste pour le moment spéculative. Il se décompose par la suite en anion **4**.

L'étude de la distribution des produits de monoallylation **5** et **6** issus de la réaction des complexes η^3-allyliques substitués **1***b* (R = CH_3) et **1***c* (R = C_6H_5) révèle une régiosélectivité marquée (tableau 2), le carbone le moins substitué du ligande allylique réagissant préférentiellement. Un effet analogue avait déjà été constaté dans les réactions de complexes η^3-allyliques cationiques du fer (4).

TABLEAU 2. Réaction de **1***b* (R = CH_3) et **1***c* (R = C_6H_5) avec l'anion diéthyl malonate Nu^- = $^-CH(COOEt)_2$

R	 (%)	 (%)
—CH_3	78	16
—C_6H_5	89	0

En conclusion, cette étude démontre la possibilité d'utiliser des fragments métalliques neutres pour réaliser l'activation de ligandes η^3-allyliques vis-à-vis de réactifs nucléophiles.

Le prolongement naturel de ce travail est l'incorporation dans un cycle catalytique de la séquence réactionnelle précédente établie à l'échelle stoechiométrique, afin de réaliser une alkylation catalytique de substrats allyliques peu réactifs tel que les acétates ou les formates.

Les résultats positifs obtenus dans ce contexte seront publiés ultérieurement.

Remerciements

Les auteurs remercient vivement le Conseil de Recherches en Sciences Naturelles et Génie du Canada ainsi que l'Université d'Ottawa pour l'aide financière apportée sous forme d'octrois.

1. S. G. DAVIES, M. L. H. GREEN et D. M. P. MINGOS. Tetrahedron, **34**, 3047 (1978).
2. B. M. TROST. Tetrahedron, **33**, 2515 (1977).
3. B. E. R. SCHILLING, R. HOFFMAN et J. W. FALLER. J. Am. Chem. Soc. **101**, 592 (1979).
4. T. H. WHITESIDES, R. W. HART et R. W. SLAVEN. J. Am. Chem. Soc. **95**, 5792 (1973).
5. P. L. LENNON, A. M. ROSAN et M. ROSENBLUM. J. Am. Chem. Soc. **99**, 8426 (1977).
6. B. M. TROST, L. WEBER, P. E. STREGE, T. J. FULLERTON et T. J. DIETSCHE. J. Am. Chem. Soc. **100**, 3416 (1978).
7. J. TSUJI. Acc. Chem. Res. **2**, 144 (1969).
8. B. W. ROBERTS et J. WONG. J. Chem. Soc. Chem. Commun. 20 (1977).
9. N. G. CONNELLY. Inorg. Chim. Acta Rev. 47 (1972).
10. G. CARDACI et A. FOFFANI. J. Chem. Soc. Dalton, 1809 (1974).
11. F. M. CHAUDHARI, G. R. KNOW et P. L. PAUSON. J. Chem. Soc. C, 2255 (1967).
12. G. PALIANI, S. M. MURGIA et G. CARDACI. J. Organomet. Chem. **30**, 221 (1971).

Canadian Journal of Chemistry
Published by
THE NATIONAL RESEARCH COUNCIL OF CANADA

Journal canadien de chimie
Publié par
LE CONSEIL NATIONAL DE RECHERCHES DU CANADA

Volume 57 Number 21 November 1, 1979 Volume 57 numéro 21 1 novembre 1979

The commutative property of strong-transition rate matrices

HUW O. PRITCHARD AND ARUNACHALAM LAKSHMI
Centre for Research in Experimental Space Science, York University, Downsview, Ont., Canada M3J 1P3

Received March 23, 1979

HUW O. PRITCHARD and ARUNACHALAM LAKSHMI. Can. J. Chem. **57**, 2793 (1979).

The $(n - 1)$-fold degenerate set of transition probabilities used in our recent reformulation of unimolecular reaction theory is operationally equivalent to the set of effective strong-transition probabilities introduced recently by Nordholm. We have found that the relaxation matrix corresponding to these transition probabilities commutes with *any* other relaxation matrix which will drive the same system to a Boltzmann distribution at infinite time. Some useful results stemming from this commutative property are presented; we expect that these results will help to clarify further the nature of the assumptions underlying strong- and effective strong-collision theories.

HUW O. PRITCHARD et ARUNACHALAM LAKSHMI. Can. J. Chem. **57**, 2793 (1979).

L'ensemble des probabilités de transition qui sont dégénérées $(n - 1)$ fois que nous avons utilisé dans notre récente reformulation de la théorie des réactions unimoléculaires est opérationnellement équivalent à l'ensemble des probabilités de fortes transitions efficaces introduit récemment par Nordholm. Nous avons trouvé que la matrice de relaxation correspondant à ces probabilités de transition s'échange avec toute autre matrice de relaxation qui conduira le même système à une distribution de Boltzmann à temps infini. Nous présentons quelques résultats pratiques issus de cette propriété commutative; nous espérons que ces résultats aideront à clarifier d'avantage la nature des hypothèses sous-jacentes aux théories des collisions fortes et des collisions fortes efficaces.

[Traduit par le journal]

Introduction

Nordholm, Freasier, and Jolly (1) have recently given a somewhat more precise definition of a strong collision as it appears in the description of unimolecular reactions. In quantum form, the transition probabilities corresponding to strong collisions may be written as

$$[1] \quad p_{j\to i} = \exp(-\beta E_i)/\sum \exp(-\beta E_i)$$

where E_i is the energy, $\beta = (kT)^{-1}$, and the summation is over all possible states. Transition rates given by [1] are about an order of magnitude larger than the accepted rates, and subsequently Nordholm (2) replaced the usual collision frequency by an effective collision frequency defined so as to allow the correct relaxation rate of the internal energy to be reproduced.

Meanwhile, as a result of examining information theoretic aspects of bulk relaxation, we (3) had constructed a set of transition rates for which the decay of both the total energy *and* all the populations is pure exponential; the elements of the relaxation matrix **A** are given by (4)

$$[2] \quad a_{ij} = \mu\{(1 - \delta_{ij})\tilde{n}_i - \delta_{ij}(1 - \tilde{n}_i)\}$$

where μ is a constant of proportionality, $\tilde{n}_i$ is the equilibrium population of state i, with $\sum \tilde{n}_i$ normalised to unity, and δ_{ij} is either zero or one. The meaning of eq. [2] is that for $i \neq j$

$$[3] \quad p_{j\to i} = \mu\tilde{n}_i/Z[\mathrm{M}]$$

and is clearly the same as eq. [1] apart from the proportionality factor $\mu/Z[\mathrm{M}]$; since μ is the time constant for relaxation, Z is the collision number, and [M] is the particle density, eq. [2] is equivalent to the "effective strong collision" modification of [1] introduced by Nordholm (2) as far as energy-transfer rates are concerned.

0008-4042/79/212793-05$01.00/0

The only point of difference between the two approaches is in the qualitative description of the fraction of events which leave the molecule unchanged, i.e. $p_{i\to i}$: according to eq. [1], it is always the same fraction of the collisions because the collision number is made proportional to the relaxation rate, whereas according to eq. [2], the fraction of collisions leaving the molecule of interest in an unchanged state increases as the relaxation rate constant μ decreases. However, at the simplest levels of theory, this distinction has no operational consequences, as can easily be seen algebraically by considering a chemical activation process.

We may represent the steady-state chemical activation experiment by the set of simultaneous equations

$$[4]\quad \frac{dn_i}{dt} = \sum_j a_{ij}n_j + d_i n_i + R_i \equiv [\mathbf{A} + \mathbf{D}]\mathbf{n} + \mathbf{R} = 0$$

where R_i is the rate of production of each state i by chemical activation, and d_i is (minus) the rate constant for the decay of state i to products, and the subscripts denote groups of levels or grains. This equation cannot be solved as it is unless one of two assumptions is made, either that **R** contains a sink term for the stabilised products, or the temperature is assumed to be so low that once products are stabilised, they can never again become interesting; the former approach is difficult to implement, and the latter is the one generally used. Treating the stabilised products as one grain and labelling it $i = 0$, we simply write all $p_{0\to i} = 0$ and discard the equation for dn_0/dt, giving

$$[5]\quad [\mathbf{A}' + \mathbf{D}']\mathbf{n}' + \mathbf{R}' = 0$$

where the prime indicates that the first row and the first column, representing transfers into and out of the stabilised state, are missing from all matrices. The submatrix **A**′ differs from a normal relaxation matrix for the subset of levels because it still contains in each diagonal element the term $-\mu\tilde{n}_0$, corresponding to the rate of transfer of molecules at that level out of the subsystem. Consequently, eq. [5] is equivalent to the standard strong-collision treatment of chemical activation processes (5, 6), except that ω, the collision rate, is replaced by $\mu\tilde{n}_0$; likewise, in the effective strong-collision case, ω would be replaced by $\lambda\omega$ (2).

Recognising this, it becomes clear that there is a very close connection between our reformulation of unimolecular reaction theory (4) and Nordholm's effective strong-collision modification of RRKM theory (2), and this renders it possible to place the former in its proper position in the hierarchy of unimolecular reaction theories. Standard RRKM theory uses an (independent channel) generalised Lindemann expression (eq. [27] of ref. 4), and is usually used in a scaled form which renders it an effective strong-collision theory (2). On the other hand, our reformulation (4) is an effective strong-collision theory in which proper allowance is made for the mutual perturbation of the competing reaction channels,[1] through a more complicated generalised Lindemann expression (eq. [46] of ref. 4). It would appear that if iterated to convergence, the first term in eq. [22] of ref. 2 would yield the same numerical results as this latter generalised Lindemann form: the second term in this equation allows for the possibility of differing collisional efficiencies for molecules of different internal energies, for which there is no counterpart in our formulation. Other intermediate levels of approximation are described in eqs. [16], [18], and [20] of ref. 2.

In the following sections, we first describe the commutative property of eq. [2] for non-reacting systems: then we show briefly how reacting systems, treated as a perturbation of [2], behave; finally, we try to predict some uses for, and to give a physical description of, this commutative property. We believe that this short exposition will not only complement the efforts of Nordholm, Freasier, and Jolly (1, 2) in trying to clarify the relationship between strong- and weak-collision theories, but that the algebraic properties we describe could be helpful in the construction of explicit formulae for strong-collision models of reaction rates.

Non-reacting Systems

Let **M** be the symmetrised form of **A**, viz.,

$$[6]\quad \mathbf{M} = \mathbf{E}^{-1/2}\mathbf{A}\mathbf{E}^{1/2}$$

where $e_{ij} = \tilde{n}_i\delta_{ij}$, and let **L** be the symmetrised form of *any* other relaxation matrix **B** for the same system of energy levels. **L** has a set of eigenvalues defined by

$$[7]\quad \mathbf{L} = \mathbf{S}\Lambda\mathbf{S}^{\mathrm{T}}$$

where[2]

$$[8]\quad 0 = \lambda_0 \gg \lambda_1 > \lambda_2 > \ldots > \lambda_{n-1}$$

and

$$[9]\quad S_{i,0} = \tilde{n}_i^{1/2}$$

M has the eigenvalues

$$[10]\quad 0 = m_0 \text{ and } m_1 = m_2 = \ldots = m_{n-1} = -\mu$$

[1]In the strong-collision regime, the neglect of the mutual perturbation between reactive channels has only a small effect, but it becomes progressively more serious as the collisions become weaker.

[2]Note the change of subscript ordering from all of our previous works.

The two matrices share one common eigenvector, $S_{i,0}$, given by eq. [9], but the other $(n-1)$ eigenvectors of **M** are undetermined.

While studying the relaxation behaviour of a model molecule diluted in a heat bath consisting of a mixture of two gases (7), the relaxation matrix $[(1-x)\mathbf{L} + x\mathbf{M}]$ (where x is the mole fraction) was examined and it was found that for all $x \neq 1$ and $i \neq 0$

$$[11] \quad [(1-x)\mathbf{L} + x\mathbf{M}]\boldsymbol{S}_i = [(1-x)\lambda_i - x\mu]\boldsymbol{S}_i$$

Thus, $[\mathbf{L} + \mathbf{M}]$ commutes with **L**, whence it follows that **M** commutes with **L**, and **A** with **B**. Following this discovery, it was demonstrated numerically that

$$[12] \quad \mathbf{M}\boldsymbol{S}_i = -\mu\boldsymbol{S}_i \qquad i \neq 0$$

to machine accuracy for several other relaxation matrices **L**, where the $\boldsymbol{S}_i$ were *any* of the vectors of the respective **L** matrices.

We have presented the commutative property of the relaxation matrix **A** (or its symmetrical form **M**) in this way, since this is the manner in which we discovered the property. Both referees have suggested that a formal proof should be given, and, in hindsight, such a proof is almost trivial. We may use the property (8) that *if* **A** *is a simple matrix with* s *distinct eigenvalues, every matrix which commutes with* **A** *has at least* s *independent right eigenvectors in common with* **A**. In our case, **A** has two distinct eigenvalues, 0 and $-\mu$, and we know that it shares one common eigenvector (cf. eqs. [8]–[10]) with **B** (when $\lambda_{\mathbf{B}} = 0$). Since the remaining eigenvectors of **A** corresponding to $\lambda_{\mathbf{A}} = m_i = -\mu$ are completely arbitrary except for the fact that they must be orthogonal to the known common eigenvector, we may choose any vector of **B** as the second vector of **A**; thus, the commutative property is established. Even more trivially, **A** and **B** share one common vector, and we may choose an acceptable second vector for **A** to be one of the remaining vectors of **B**; a third vector of **A** must be orthogonal to the first two, and so a third vector of **B** will be acceptable, and so on. Consequently, the vector set of **B** is an acceptable set for **A**. Likewise, vector sets of other matrices **C**, **D**, etc. are also acceptable sets of vectors for **A**: thus **A** will commute with **B**, **C**, **D**, etc. where **A**, **B**, **C**, **D**, etc. all refer to the relaxation of the same physical system at the same temperature (otherwise, they would not share a common eigenvector).

Reacting Systems

In our earlier paper (4), the rate constant for a unimolecular decomposition k_{uni} was taken as minus the eigenvalue of smallest numerical magnitude (i.e. $-\gamma_0$ in the present notation) of the perturbed relaxation matrix $[\mathbf{A} + \mathbf{D}]$ (unsymmetrised) or $[\mathbf{M} + \mathbf{D}]$ (symmetrised). If, for example, the system were grained so that all the bound states constitute one grain, **D**, the matrix of decay rate constants, would have the form diag$|0, -k_1, -k_2, \ldots, -k_{n-1}|$. Thus **D** would have one zero eigenvalue, but it does not commute with **A** or **M** since **D** will not drive the system to a Boltzmann distribution: the final distribution obtained by operating with **D** is that all reactive states are removed, but the bound-state population remains unchanged; in other words, the eigenvector corresponding to the zero eigenvalue is not [9], but is $\{1, 0, 0 \ldots\}$. Consequently, the eigenvalues of $[\mathbf{A} + \mathbf{D}]$ are not given exactly by the analogue of [11], viz.

$$[13] \quad \gamma_i = -(k_i + \mu),\ i \neq 0, \text{ or zero, } i = 0$$

However, under those conditions, i.e.

$$[14] \quad |\gamma_0| \ll k_i$$

when $\gamma_0 = -k_{\text{uni}}$ is adequately represented by eq. [46] of ref. 4, all the other γ_i fall in a sequence

$$[15] \quad \gamma_i = -(k_i + \mu - \delta_i) \qquad i \neq 0$$

with[3]

$$[16] \quad \delta_i > \delta_{i+1} \quad \text{and} \quad \sum_{i=1}^{n-1} \delta_i = k_{\text{uni}} = -\gamma_0$$

A further set of examples of the commutation of **M** with all other **L** (and the absence of extreme ill-conditioning in practical application) is provided by examination of the key equation (eq. [20*a*]) of ref. 4 for the eigenvectors ψ of the perturbed matrix $[\mathbf{M} + \mathbf{D}]$, i.e.

$$[17] \quad \psi_{ki} = \sum_l \sum_m \frac{S_{km} S_{lm}}{\gamma_i - \lambda_m} d_l \psi_{li}$$

where the γ_i are the true eigenvalues of $[\mathbf{M} + \mathbf{D}]$, the λ_m are those of **M** (i.e. 0 or $-\mu$) and **S** can now be the eigenvectors of any matrix **L** which commutes with **M**. We examined this relationship for three sets of surrogate vectors **S**, one for a full matrix **L** of arbitrary transition probabilities, one for a matrix **L** corresponding to the tridiagonal sum rule (3), and one for the continuant matrix [18] described below; in each case [17] held to machine accuracy.

Equation [17] is difficult to use, of course, if the γ_i are not known. However, $\gamma_0 = -k_{\text{uni}}$ is given explicitly by eq. [46] of ref. 4 and under all conditions where this is valid, the remaining γ_i, $i \neq 0$ may be very accurately approximated using [13] since by [14] and [16] *all* the δ_i are necessarily very small compared with the k_i.

[3]With the reactive region grained according to [18] and [19], it appears that $\delta_{i+1} \simeq c\delta_i$ with c typically about 0.5 or 0.6.

Possible Applications of Commuting Relaxation Matrices

Any computational advantage of using the commutative property will emerge only when one is interested in problems requiring a knowledge of the eigenvectors, e.g. the population distributions during a reaction, or the behaviour during the transient period, i.e. induction or incubation period. In isolated calculations, one would normally solve for the eigenvalues and eigenvectors of the relaxation matrix in the usual way, but when a series of very similar models is to be compared, eq. [17] (with [13] as an approximation for the γ_i, $i \neq 0$) would have real advantages.

In the strong- or effective strong-collision case, where we can have no significant information about the transients, we may be limited to comparing population distributions in the long-time regime: at infinite pressure, such information follows directly from eq. [22] of ref. 4, but in the fall-off region, all the eigenvectors would be required to evaluate the population evolution, using eq. [11] of ref. 4. According to [17], we need the eigenvalues and eigenvectors of *any* matrix **B** which commutes with **A**, and we are free to choose the most simple and convenient form of **B** (or **L**) if we wish to describe a coupled relaxation and reaction process governed by **A** (and **M**). One form which has interesting possibilities for unimolecular reaction theory is the continuant

$$[18] \quad \mathbf{L} = \begin{pmatrix} 1 & 1 & 1 & & 1 \\ d_0 & d_1 & d_2 & d_3 \ldots . & d_{n-1} \\ 1 & 1 & 1 & & 1 \end{pmatrix}$$

This implies that the elements of the unsymmetrised surrogate transition probability matrix are

$$[19] \quad p_{i\rightarrow j} = \tilde{n}_i{}^{-1/2}\tilde{n}_j{}^{1/2} \times \text{constant} \times (\delta_{i-1,j} + \delta_{i+1,j})$$

and the diagonal elements of **B** (or **L**) are then

$$[20] \quad d_j = -\tilde{n}_j{}^{-1/2}(\tilde{n}_{j-1}{}^{1/2} + \tilde{n}_{j+1}{}^{1/2}) \times \text{constant}$$

with $\tilde{n}_{-1}$ and $\tilde{n}_n$ taken to be zero. Suppose that we now grain the system in such a way that all $\tilde{n}_j/\tilde{n}_{j+1}$ $(0 \leq j < n-1)$ are constant, this causes all the d_j (except d_0 and $d_{n-1} = d_0{}^{-1}$) to be constant: we then subtract d_1 from all the diagonal elements in [18] to give

$$[21] \quad \mathbf{L}^* = \begin{pmatrix} 1 & 1 & 1 & & 1 \\ d_0{}^* & 0 & 0 & 0 \ldots . & d_{n-1}{}^* \\ 1 & 1 & 1 & & 1 \end{pmatrix}$$

If $d_0{}^*$ and $d_{n-1}{}^*$ were also zero, then the eigenvalues of $\mathbf{L}^*$ would be (9)

$$[22] \quad \lambda_j{}^0 = 2\cos[(j+1)\pi/(n+1)] \qquad j = 0, 1, 2, \ldots, n-1$$

$\mathbf{L}^*$, in fact, corresponds to a Hückel molecular orbital determinant for a polyene with two terminal hetero-atoms, one of higher and one of lower electronegativity, and the true eigenvalues λ_j' can be calculated by known methods (10); they will not be very different from the values given by [22], and the correspondence between the true eigenvalues λ_j' and the approximations $\lambda_j{}^0$ is shown in Fig. 1. The proper values λ_j of the eigenvalues of **L** are then found by adding d_1 to all the λ_j', and the un-normalised surrogate vectors are themselves simple continuants (11, 12), i.e.

$$[23] \quad S_{ij} = \begin{pmatrix} -1 & -1 & -1 & & -1 \\ a_i & -\lambda_j' & -\lambda_j' & -\lambda_j' \ldots . & a_0 \\ -1 & -1 & -1 & & -1 \end{pmatrix} S_{0j}$$

where $a_i = d_i{}^* - \lambda_j'$. A slightly simpler result, more appropriate for high temperatures, would be obtained by choosing the grain sizes so that all the $\tilde{n}_i$ were equal.

At the present time, unimolecular reaction theories are classified generally as strong-collision or weak-collision theories, and the intermediate ground between these two extremes is not well understood (1, 2). It has been suggested (13) that the transition from weak-collision to strong-collision behaviour could be explored using a reaction matrix

$$[24] \quad \mathbf{R} = \mathbf{E}^{-1/2}[x\mathbf{A} + (1-x)\mathbf{B} + \mathbf{D}]\mathbf{E}^{1/2} = [x\mathbf{M} + (1-x)\mathbf{L} + \mathbf{D}]$$

where x is now simply a weighting factor and **A** and **B** are respectively the strong- and weak-collision transition rate matrices. As a result of [11], only one set of eigenvalues and eigenvectors, those of **L** itself, are required for the implementation of [17] over the whole range of x, i.e., the transition from weak- to strong-collision behaviour.

The Physical Meaning of Commuting Relaxation Matrices

In quantum mechanics, the commutation of two operators gives rise to very specific conclusions about simultaneous observation, and is a very powerful conceptual tool. It does not appear that in chemical kinetics, commutation of operators (i.e. relaxation matrices) is of such far-reaching importance.

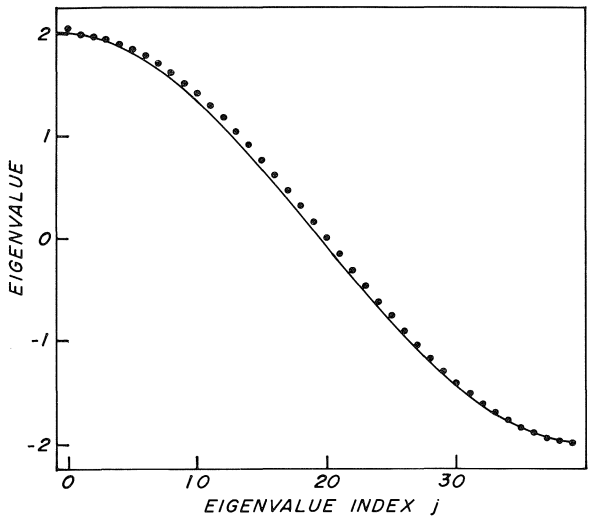

FIG. 1. Comparison of the eigenvalues of the shifted matrix **L*** of eq. [21] with the values given by the formula of Moffitt and Coulson, eq. [22].

In the absence of reaction, the relaxation of a system under the simultaneous influence of a transition matrix **B** and the $(n - 1)$-fold degenerate matrix **A** always has the form of the relaxation by **B** alone, in the sense that the eigenvectors of [**A** + **B**] are those of **B**, and these determine the form of the relaxation through the normal modes (14).

The important feature of the transition rates described by [2], as far as the commutation relationships are concerned, is that (3, 4)

$$[25] \quad n_i(t) = \tilde{n}_i + [n_i(0) - \tilde{n}_i]\, e^{-\mu t}$$

and, in fact, it is this property that renders the master-equation reformulation of unimolecular reactions (4) at all tractable. If we partition the nonstationary distribution at any time during a relaxation into a part which is Boltzmann for the temperature of the heat bath and a remainder, the operation of **A** on the remainder does not alter the ratios of population within the remainder, it simply shrinks all the unbalanced populations towards a Boltzmann distribution with the same time constant μ, according to eq. [25]. Thus, no matter what the form of **B**, **A** does not *interfere* with it, but simply changes the time constant according to eq. [11], and provides the only condition under which the linear mixture rule can be obeyed rigorously; similarly, the linear mixture rule for chemical reaction is only obeyed rigorously when the *reaction* matrices commute (15).

Notice also that eq. [25] provides one of the only two known idealised conditions under which a relaxation time can be defined uniquely (3, 4) whereas for all real molecular systems, the apparent relaxation time must depend somewhat upon the method of measurement (13, 14, 16).

In the reaction case, at least when k_{uni} is slow compared with the specific dissociation rate constants k_i, we would have, according to [15], a series of consecutive processes of time constant approximately $(k_i + \mu)$, and it is the smallness of the coupling terms δ_i (which together make up the rate constant [16]) which accounts for the fact that there is very little difference in numerical magnitude between the master-equation and RRKM generalised Lindemann forms (4); [15] and [16] may also be used to understand the convergence properties of eq. [22] of ref. 2.

Acknowledgements

This work was supported by the National Research Council of Canada; we would also like to thank A. W. Yau and S. Nordholm for help and criticisms.

1. S. NORDHOLM, B. C. FREASIER, and D. L. JOLLY. Chem. Phys. **25**, 433 (1977).
2. S. NORDHOLM. Chem. Phys. **29**, 55 (1978).
3. A. W. YAU and H. O. PRITCHARD. Can. J. Chem. **55**, 737 (1977).
4. A. W. YAU and H. O. PRITCHARD. Can. J. Chem. **56**, 1389 (1978).
5. M. HOARE. J. Chem. Phys. **38**, 1630 (1963).
6. P. J. ROBINSON and K. A. HOLBROOK. Unimolecular reactions. John Wiley, London. 1972.
7. H. O. PRITCHARD, N. I. LABIB, and A. LAKSHMI. Can. J. Chem. **57**, 1115 (1979).
8. P. LANCASTER. Theory of matrices. Academic Press. 1969. pp. 264–266.
9. W. E. MOFFITT and C. A. COULSON. Trans. Faraday Soc. **44**, 81 (1948).
10. R. DAUDEL, R. LEFEBVRE, and C. MOSER. Quantum chemistry. Academic Press, New York. 1959. pp. 539–546 and references therein.
11. T. MUIR. The theory of determinants in the historical order of development. Vol. 4. St. Martin's Press, London. 1923. p. 400.
12. T. MUIR and W. H. METZLER. A treatise on the theory of determinants. Dover Publications, New York. 1960. p. 528.
13. A. W. YAU. Ph.D. Thesis, York University, Downsview, Ont. 1978.
14. H. O. PRITCHARD and N. I. LABIB. Can. J. Chem. **54**, 329 (1976).
15. R. K. BOYD. Can. J. Chem. **55**, 802 (1977).
16. A. W. YAU and H. O. PRITCHARD. J. Phys. Chem. **83**, 134 (1979).

Apparent molar heat capacities and volumes of aqueous electrolytes at 25°C: $Cr(NO_3)_3$, $LaCl_3$, $K_3Fe(CN)_6$, and $K_4Fe(CN)_6$

JAN J. SPITZER, INGER V. OLOFSSON,[1] PREM PAUL SINGH,[2] AND LOREN G. HEPLER

Department of Chemistry, University of Lethbridge, Lethbridge, Alta., Canada T1K 3M4

Received March 19, 1979

JAN J. SPITZER, INGER V. OLOFSSON, PREM PAUL SINGH, and LOREN G. HEPLER. Can. J. Chem. **57**, 2798 (1979).

We have used a flow calorimeter and a flow densimeter for measurements at 25°C of heat capacities and densities of aqueous solutions of four electrolytes of high charge type: $LaCl_3$, $Cr(NO_3)_3$, $K_3Fe(CN)_6$, and $K_4Fe(CN)_6$. Results of these measurements have been used for calculating corresponding apparent molar heat capacities and apparent molar volumes, which have been extrapolated to infinite dilution to obtain the corresponding standard state apparent molar and partial molar properties. Uncertainties resulting from extrapolations of heat capacities are discussed. Results of our measurements are compared with those of earlier related investigations.

JAN J. SPITZER, INGER V. OLOFSSON, PREM PAUL SINGH et LOREN G. HEPLER. Can. J. Chem. **57**, 2798 (1979).

Nous avons utilisé un calorimètre et un densimètre à flux continu pour mesurer, à 25°C, les capacités calorifiques et les densités de solutions aqueuses de quatre électrolytes de type fortement chargés: $LaCl_3$, $Cr(NO_3)_3$, $K_3Fe(CN)_6$ et $K_4Fe(CN)_6$. Les résultats de ces mesures ont été utilisés pour calculer les capacités calorifiques molaires apparentes et les volumes molaires apparents correspondants. Par extrapolation à dilution infinie on obtient les propriétés molaires apparentes et molaires partielles apparentes de l'état fondamental correspondant. Nous discutons des incertitudes résultants des extrapolations des capacités calorifiques. Les résultats de nos mesures sont comparés à ceux obtenus au cours de recherches antérieures apparentées.

[Traduit par le journal]

Introduction

As part of our continuing program of measurements leading to thermal and volumetric properties of aqueous solutions, we have made calorimetric measurements leading to apparent molar heat capacities and density measurements leading to apparent molar volumes of four electrolytes of high charge type.

These heat capacities and volumes of solutes are useful for calculation of the temperature and pressure dependences of various thermodynamic properties; this usefulness has provided one reason for undertaking these measurements on electrolytes of high charge type, for which there are relatively few reliable volumes and even fewer heat capacities.

Experimental

Heat capacity measurements were made with a flow calorimeter of the Picker type that has been described previously (1). A small systematic error in some of the measurements has been identified and corrected as recently described (2, 3). Densities of solutions have been measured with a flow densimeter that has also been described (4). All results obtained with these instruments refer to 25.00 ± 0.01°C; temperatures were controlled to ±0.001°C during each measurement.

A few solutions of $K_3Fe(CN)_6$ and $K_4Fe(CN)_6$ were prepared by mass from distilled water and BDH Analar salts that had been dried to constant mass at 110°C. Most solutions of these electrolytes were prepared by mass from distilled water and BDH Analar salts that had been recrystallized from distilled water and then dried to constant mass at 105°C.

Fisher certified "$LaCl_3 \cdot 6H_2O$" samples were recrystallized from distilled water and then dissolved in distilled water to form two solutions that were close to 0.1 *M* lanthanum chloride with pH = 5.3. Small known amounts of hydrochloric acid were added to these solutions to lower the pH values to 4.9 and 4.3. These solutions were then analyzed gravimetrically for Cl^- by precipitation of AgCl; allowances were made for the very small amounts of added Cl^- in the calculations of concentrations of lanthanum in the solutions.

Fisher certified $Cr(NO_3)_3 \cdot 9H_2O$ was recrystallized from dilute nitric acid. Two different samples of the recrystallized material were dissolved in distilled water containing a little added nitric acid to form stock solutions. Aliquots of these stock solutions were analyzed for chromium as previously described (5). The two stock solutions were found to be 0.1159 *M* (pH = 2.2) and 0.3373 *M* (pH = 1.2). Further solutions for measurements of heat capacities and densities were prepared by dilution with distilled water; knowledge of densities permitted expression of final composition of solutions in terms of molalities of $Cr(NO_3)_3$(aq).

Results and Discussion

Apparent molar properties of solutions (ϕ_Y) are defined by

$$[1] \quad \phi_Y = [Y(\text{soln}) - n_1 Y_1^0]/n_2$$

in which the symbols have the following meanings:

[1]Visiting scientist from Chemical Center, University of Lund, Lund, Sweden.

[2]Visiting scientist from Department of Chemistry, Punjab Agricultural University, Ludhiana, India.

0008-4042/79/212798-06$01.00/0

TABLE 1. Apparent molar heat capacities and volumes

m / mol kg^{-1}	ϕ_C / J K^{-1} mol^{-1}	ϕ_V / cm^3 mol^{-1}	m / mol kg^{-1}	ϕ_C / J K^{-1} mol^{-1}	ϕ_V / cm^3 mol^{-1}
	$LaCl_3$			$Cr(NO_3)_3$*	
0.013967	−419.7	17.05	0.01738	−206.5	48.36
0.017906	−415.1	17.05	0.02316	−215.7	48.83
0.018609	−410.9	16.56	0.03477	−225.5	48.69
0.026898	−417.2	16.83	0.04638	−231.5	49.23
0.027946	−412.1	17.31	0.05807	−225.9	49.57
0.027949	−406.6	17.77	0.03370	−223.6	49.81
0.035838	−408.4	17.34	0.05057	−229.4	49.12
0.037227	−403.8	17.73	0.06740	−226.6	49.66
0.037231	−409.0	17.51	0.1012	−224.7	49.67
0.044908	−404.0	17.92	0.1350	−219.1	49.93
0.046625	−401.7	17.97	0.1690	−213.4	49.97
0.053826	−398.6	17.81			
0.071695	−393.5	18.32		$K_4Fe(CN)_6$	
0.089901	−386.8	18.65			
0.089901	−386.7	18.70	0.007526	−383.1	117.53
			0.013040	−362.8	119.10
	$K_3Fe(CN)_6$		0.022280	−337.8	120.76
			0.024516	−330.1	121.97
0.02003	−152.6	149.49	0.029576	−324.4	122.60
0.03105	−141.2	151.43	0.034545	−312.2	123.58
0.04863	−126.8	152.02	0.041080	−311.6	123.25
0.06025	−119.9	151.62	0.049830	−287.6	125.09
0.08212	−109.8	151.97	0.070083	−273.0	125.55
0.10299	−100.0	152.73	0.079670	−254.4	125.82
0.15588	−85.7	153.88	0.099630	−232.4	129.39
			0.13219	−218.8	128.07

*Stock solution for the first five measurements was 0.1159 M $Cr(NO_3)_3$ and had initial pH = 2.2; stock solution for the last six measurements was 0.3373 M $Cr(NO_3)_3$ and had initial pH = 1.2. In both cases, solutions used in the measurements were prepared by dilution with distilled water.

Y is the property (heat capacity or volume for our purposes) of a specified quantity of solution, n_1 is the number of moles of solvent in this specified quantity of solution, Y_1^0 is the property (heat capacity or volume) of 1 mol of pure solvent, and n_2 is the number of moles of specified solute in the specified quantity of solution.

Our experimental results (compositions of solutions, heat capacities, densities) have been used to obtain apparent molar heat capacities (ϕ_C) and apparent molar volumes (ϕ_V) that are listed in Table 1. In obtaining these tabulated quantities we have used $c_p^0 = 4.1793$ J K^{-1} g^{-1} and $d_1^0 = 0.997044$ g cm^{-3} for the heat capacity and density of pure water. Rather than tabulate our experimental heat capacities and densities of various solutions, we point out that these quantities can be recovered from the tabulated m, ϕ_C, and ϕ_V values by way of

$$[2] \quad c_p = (m\phi_C + c_p^0)/(1 + mM_2)$$

and

$$[3] \quad d = (1 + mM_2)d_1^0/(1 + md_1^0\phi_V)$$

Apparent molar properties of dilute aqueous solutions of strong electrolytes are accurately described by equations of the form

$$[4] \quad \phi_Y = \phi_Y^0 + A_Y(d_1^0 m)^{1/2} + B_Y m$$

in which ϕ_Y^0 is the limiting value of ϕ_Y at infinite dilution (identical to the corresponding partial molar property $\bar{Y}^0$), A_Y is the limiting slope derived from the Debye–Hückel theory, and B_Y is an adjustable parameter. We begin by applying [4] to our apparent molar volumes and then turn to similar application to our apparent molar heat capacities.

Millero (6) has thoroughly reviewed the applicability of the Debye–Hückel theory and eq. [4] to apparent molar volumes and also evaluated the limiting slopes. Following Millero (6) we use $A_V(d_1^0)^{1/2} = 27.413$ cm^3 mol$^{-3/2}$ kg$^{1/2}$ for electrolytes of 3:1 charge type and $A_V(d_1^0)^{1/2} = 58.984$ cm^3 mol$^{-3/2}$ kg$^{1/2}$ for electrolytes of 4:1 charge type. Least-squares analysis of our ϕ_V values in Table 1 in terms of eq. [4] leads to the ϕ_V^0 ($= \bar{V}^0$) and B_V values that are summarized in Table 2.

We do not know of any previous measurements on aqueous chromic nitrate leading to a ϕ_V^0 value to compare with our result in Table 2. We can, how-

TABLE 2. Volumetric parameters for eq. [4]

Solute	ϕ_V^0 / cm^3 mol^{-1}	B_V / cm^3 mol^{-2} kg
$Cr(NO_3)_3$	45.4	−41.1
$K_3Fe(CN)_6$	146.6	−24.6
$LaCl_3$ (all points)	13.8	−39.4
($m < 0.04$)	14.3	−54.9
$K_4Fe(CN)_6$	113.3	−43.4

ever, make indirect comparisons of our result with those of earlier workers by way of conventional ionic volumes based on $\phi_V^0(H^+) = 0$. Using $\phi_V^0(NO_3^-)$ from Millero (6) with our ϕ_V^0 from Table 2 leads us to our conventional $\phi_V^0(Cr^{3+}) = -41.6$ cm^3 mol^{-1}. Millero (6) has previously listed $\phi_V^0(Cr^{3+}) = -39.5$ cm^3 mol^{-1} based on earlier work. Lumme (7) has used densities of relatively concentrated (0.40 to 1.99 *M*) solutions of chromic perchlorate to calculate a ϕ_V^0 that we combine with $\phi_V^0(ClO_4^-)$ from Millero (6) to obtain a conventional $\phi_V^0(Cr^{3+}) = -47$ cm^3 mol^{-1}. We judge that our ϕ_V^0 for aqueous chromic nitrate and that our derived conventional $\phi_V^0(Cr^{3+})$ are the best ones available for this solute.

As shown in Table 2, we have analyzed our results for lanthanum chloride in two ways, obtaining ϕ_V^0 values that differ by 0.5 cm^3 mol^{-1}. We judge that the value based only on solutions with $m < 0.04$ mol kg^{-1} is better than the other value, which is based on these results *and* on those for more concentrated solutions. As can be seen from a graph of our ($\phi_V - 27.413m^{1/2}$) against m, there is a hint of a slight "break" or change in slope in the concentration range near 0.04 mol kg^{-1}. We therefore select $\phi_V = 14.3$ cm^3 mol^{-1} as the best value to be obtained from our measurements on aqueous lanthanum chloride and combine with the conventional $\phi_V^0(Cl^-)$ from Millero (6) to obtain a conventional $\phi_V^0(La^{3+}) = -39.2$ cm^3 mol^{-1}.

Dilatometric measurements by Dunn (8) have led him to $\phi_V^0 = 14.28$ cm^3 mol^{-1} for aqueous lanthanum chloride. Density measurements by two methods have led Spedding *et al.* (9, 10) to report $\phi_V^0 = 14.51$ and 14.688 cm^3 mol^{-1} for aqueous lanthanum chloride; we judge the first of these values to be better than the second because the first is based on densities for more dilute solutions than is the second.

We can also compare our conventional $\phi_V^0(La^{3+})$ from aqueous lanthanum chloride with similar conventional $\phi_V^0(La^{3+})$ values derived from ϕ_V^0 values for other salts of lanthanum. Results of this comparison, for which we have used $\phi_V^0(Cl^-$, ClO_4^-, and $NO_3^-)$ from Millero (6), are presented in Table 3. On the basis of our assessments of all of the investigations cited in Table 3, with particular

TABLE 3. Conventional $\phi_V^0(La^{3+})$ values

$\phi_V^0(La^{3+})$ / cm^3 mol^{-1}	Solute	Source
−39.7	$LaCl_3$	This work, all points
−39.2	$LaCl_3$	This work, $m < 0.04$
−39.2	$LaCl_3$	Reference 8
−39.0	$LaCl_3$	Reference 9
−38.8	$LaCl_3$	Reference 10
−39.0	$La(ClO_4)_3$	Reference 11
−38.8	$La(ClO_4)_3$	Reference 12
−37	$La(ClO_4)_3$	Reference 13
−37.6	$La(NO_3)_3$	Reference 9
−37.5	$La(NO_3)_3$	Reference 14
−39	$La(NO_3)_3$	Reference 15

bias in favor of ϕ_V^0 values derived from measurements on the most dilute solutions, we choose $\phi_V^0(La^{3+}) = -39.1$ cm^3 mol^{-1} as the best available conventional ionic volume for La^{3+}(aq) at 25°C.

For aqueous $K_3Fe(CN)_6$, a 3:1 electrolyte, we have $\phi_V^0 = 146.4$, 146.2, and 146.8 cm^3 mol^{-1} from previous investigations (16–18), all in excellent agreement with our present $\phi_V^0 = 146.6$ cm^3 mol^{-1}.

Previous investigations of aqueous $K_4Fe(CN)_6$, a 4:1 electrolyte, have led to the following. Hepler, Stokes, and Stokes (18) obtained $\phi_V^0 = 110$ cm^3 mol^{-1} by way of measurements with a dilatometer.[3] More recently, Billi *et al.* (16) have reported $\phi_V^0 = 108.5$ cm^3 mol^{-1}, based on similar measurements; it is desirable to recalculate their results by way of an equation like [4], but their results are not presented in a way that permits such recalculation. Still other dilatometric measurements by Curthoys and Matheson (17) have led them to report $\phi_V^0 = 112.3$ cm^3 mol^{-1}; our recalculation (omitting the ϕ_V for their most dilute solution, for reasons discussed by Curthoys and Matheson) leads us to $\phi_V^0 = 112.7$ cm^3 mol^{-1}. Our present $\phi_V^0 = 113.3$ cm^3 mol^{-1} is not in ideal agreement with any of the previous results, which are not in good agreement with one another. There is, at present, no way to make a rational selection of a best ϕ_V^0 for aqueous $K_4Fe(CN)_6$.

Previous experience here and elsewhere with flow densimeters of the type we have used has provided good evidence that total uncertainties in derived ϕ_V^0 values are usually less than ± 0.5 cm^3 mol^{-1}. The agreement of our present ϕ_V^0 values for aqueous $LaCl_3$ (see Table 3) and aqueous $K_3Fe(CN)_6$ (discussed in the text earlier) is consistent with a similar estimate of our present uncertainties in ϕ_V^0 values for these solutes.

Because previous results for salts of Cr^{3+}(aq) have

[3]In ref. 18 we reported $\phi_V^0 = 147.8$ cm^3 mol^{-1} for aqueous $K_3Fe(CN)_6$; R. A. Robinson has kindly pointed out errors in our calculations and has provided a corrected $\phi_V^0 = 146.8$ cm^3 mol^{-1}.

quite large uncertainties, we are unable to use comparisons as a guide in estimating the uncertainty in our ϕ_V^0 for aqueous $Cr(NO_3)_3$. Instead, we estimate that the uncertainties in our *density measurements* are about the same as for other solutions, and also recognize that there is an additional source of uncertainty in the derived ϕ_V and ϕ_V^0 values. Because of the tendency of Cr^{3+}(aq) to hydrolyze to such species as $CrOH^{2+}$(aq), it was necessary for us to work with solutions that contained some nitric acid as well as the chromic nitrate of interest to us. The resulting additional uncertainty associated with treatment of our experimental data leads us to estimate that the *total* uncertainty in our reported ϕ_V^0 for aqueous $Cr(NO_3)_3$ is about ± 1.2 cm^3 mol^{-1}.

Uncertainties in ϕ_V^0 values based on dilatometric measurements of the type used in the three earlier investigations (16–18) of aqueous $K_4Fe(CN)_6$ are typically less than ± 0.5 cm^3 mol^{-1}, as they are for the flow densimeter we have used. It is obvious from the range of reported values (108.5, 110, 112.3 or 112.7, and 113.3 cm^3 mol^{-1}) that true uncertainties for at least some of these results are larger than normally found in this kind of work. We have no reliable way of selecting the best value or of assessing individual uncertainties.

In connection with our previous investigations of heat capacities of aqueous electrolytes of charge types 1:1 and 2:1 we have used $A_C(d_1^0)^{1/2} = 28.95$ and 150.4 J K^{-1} mol$^{-3/2}$ kg$^{1/2}$. These values are based on the earlier analyses of Philip and Desnoyers (19) and Leduc, Fortier, and Desnoyers (20), and have been used in connection with many similar investigations at the Université de Sherbrooke and elsewhere. Calculations by Spitzer (22) and by Silvester and Pitzer (23) have led to values of $A_C(d_1^0)^{1/2}$ about 10% and about 25% larger, respectively, than the values quoted above. Nearly all of the differences between these limiting slopes can be attributed to differences in the second derivatives of the dielectric constant of water with respect to temperature that have been selected by the various investigators (19, 20, 22, 23). Desnoyers and co-workers (19–21) and Spitzer (22) have tried to obtain the best limiting slopes for 25°C and other "ordinary" temperatures, all at 1 atm, while Silvester and Pitzer (23) have tried (24) to obtain the best complete set of limiting slopes for a much wider range of temperatures and pressures. These different approaches have necessarily been substantially based on different sets of dielectric constants and have therefore led to different second derivatives, which accounts for part of the discrepancy in $A_C(d_1^0)^{1/2}$ values.

If it were possible to make heat capacity measurements of sufficient accuracy on *very* dilute solutions, it would then be possible to obtain accurate ϕ_C^0 values and also limiting slopes by simply plotting ϕ_C against $m^{1/2}$. Since this simple approach is made unsatisfactory by our inability to make sufficiently accurate heat capacity measurements on sufficiently dilute solutions, we are forced to make use of some approach based on an equation like [4]. Application of eq. [4] with *three adjustable* parameters (ϕ_C^0, A_C, and B_C) to presently available heat capacities is generally unsatisfactory because it is possible to fit the experimental results with a range of values of the three parameters that is unacceptably large. We note, however, that modest improvements in our ability to measure heat capacities of dilute solutions may suffice to make one of the approaches described in this paragraph useful in the future.

Our best presently available approach to analysis of heat capacities of dilute solutions is based on eq. [4] with limiting slope derived from the Debye–Hückel theory and the properties (density and dielectric constant) of water. In the following discussion of this approach, we will focus on the slopes from Desnoyers and co-workers (19, 20) and from Silvester and Pitzer (23) because Spitzer's limiting slope falls in between these other values.

Application (25) of eq. [4] to typical heat capacities of 1:1 electrolytes at 25°C is not critically dependent on whether we use Desnoyers' (19, 20) or Pitzer's (23) limiting slope because derived ϕ_C^0 values ordinarily differ by only about 1 J K^{-1} mol^{-1}, which is about one-third of the commonly estimated uncertainty associated with heat capacities obtained recently in both Sherbrooke and Lethbridge. Similar application (25) of eq. [4] to heat capacities of solutions of 2:1 electrolytes shows that ϕ_C^0 values derived on the basis of the two different limiting slopes under present consideration differ by about 6 J K^{-1} mol^{-1}, which is a little larger than previously estimated uncertainties in these values. Because of the way (19, 20, 22, 23) in which electrolyte charge enters A_C, we anticipate that the ϕ_C^0 values derived from applications of eq. [4] to our present heat capacities of solutions of electrolytes of 3:1 and 4:1 charge types will depend significantly on our choice of limiting slope.

Our calculations with eq. [4] for 3:1 electrolytes have been based on $A_C(d_1^0)^{1/2} = 425.5$ and 523 J K^{-1} mol$^{-3/2}$ kg$^{1/2}$ from Desnoyers and co-workers (19, 20) and from Silvester and Pitzer (23), respectively. Similar calculations for the 4:1 electrolyte $K_4Fe(CN)_6$ have been done with $A_C(d_1^0)^{1/2} = 915.5$ and 1126 J K^{-1} mol$^{-3/2}$ kg$^{1/2}$ from the same sources. Results of all of these calculations are summarized in Table 4.

We do not know of any heat capacities of solutions of $Cr(NO_3)_3$, $K_3Fe(CN)_6$, or $K_4Fe(CN)_6$ that can be compared with our results in Tables 1 and 4.

TABLE 4. Heat capacity parameters for eq. [4]

Solute		Desnoyers' limiting slope		Pitzer's limiting slope	
		ϕ_C^0 / J K^{-1} mol^{-1}	B_C / J K^{-1} mol^{-2} kg	ϕ_C^0 / J K^{-1} mol^{-1}	B_C / J K^{-1} mol^{-2} kg
$LaCl_3$	all points	−465	−580	−475	−805
	$m < 0.04$	−456	−898	−464	−1203
$Cr(NO_3)_3$	$m < 0.04$	−223	−2337	−231	−2644
	$m < 0.06$	−242	−1628	−251	−1887
	visual	−230		−240	
$K_3Fe(CN)_6$		$-206._5$	−300	$-218._7$	−478
$K_4Fe(CN)_6$		−460	−688	−481	−1141

Spedding and Jones (26) have measured heat capacities of aqueous solutions of lanthanum chloride, all having molalities greater than 0.1 mol kg^{-1}, and have treated their results with an equation of the form of

$$[5] \quad \phi_C = A + Bm^{1/2} + Cm + Dm^{3/2} + Em^2$$

in which A, B, C, D, and E are adjustable parameters. They report $A = -466$ J K^{-1} mol^{-1}. It is our opinion that the uncertainty in this value (mostly due to a lack of data below 0.1 m) is too large to justify its use in choosing between the various ϕ_C^0 values listed for aqueous $LaCl_3$ in Table 4.

We also note that heat capacities of solutions of $La(NO_3)_3$ and $La(ClO_4)_3$ have been measured (27, 28) at concentrations above 0.1 mol kg^{-1}. Extrapolations of the results to infinite dilution by way of equations like [5] have led (27, 28) to $\phi_C^0 = -286$ J K^{-1} mol^{-1} for aqueous $La(NO_3)_3$ and to $\phi_C^0 = -222$ J K^{-1} mol^{-1} for aqueous $La(ClO_4)_3$. Combinations of these values with conventional ϕ_C^0 values (29) for aqueous Cl^-, NO_3^-, and ClO_4^- leads to $\phi_C^0 = -448$ and -525 J K^{-1} mol^{-1} for aqueous $LaCl_3$. Again we are unable to use these results from other investigations to help us choose between the various ϕ_C^0 values listed in Table 4.

Heat capacities of solutions of a few other MCl_3 salts are worth mentioning. Measurements by Vasilev and co-workers (30, 31) have led to $\phi_C^0 = -418$ J K^{-1} mol^{-1} for aqueous YCl_3 and to $\phi_C^0 = -466$ J K^{-1} mol^{-1} for aqueous $CeCl_3$. Spedding, Walters, and Baker (32) have measured heat capacities of solutions of eight different rare earth chlorides and have reported corresponding ϕ_C^0 values ranging from -434 to -519 J K^{-1} mol^{-1}; we particularly note their $\phi_C^0 = -493$ J K^{-1} mol^{-1} for aqueous $GdCl_3$. Jekel, Criss, and Cobble (33) have used enthalpies of solution at several temperatures to derive $\phi_C^0 = -435$ J K^{-1} mol^{-1} for aqueous $GdCl_3$ at 25°C. Once again we are unable to use these results from other investigations to help us choose between the various ϕ_C^0 values listed in Table 4.

In spite of the uncertainties in our measurements and those from our calculations based on different limiting slopes in the heat capacity eq. [4], we believe that our ϕ_C^0 values in Table 4 are the best ones now available for aqueous electrolytes of 3:1 and 4:1 charge types.

NOTE ADDED IN PROOF: Bradley and Pitzer (33) have reported results of their new calculations of Debye–Hückel parameters. Because the "best" A_C now appears to be intermediate between values we have used, corresponding "best" ϕ_C^0 values are probably intermediate between values listed in Table 4.

Bottomley, Glossop, and Staunton (34) have reported a new and apparently reliable $\phi_V^0 = 111.7$ cm^3 mol^{-1} for aqueous $K_4Fe(CN)_6$.

Acknowledgements

We all thank the National Research Council of Canada for support of this research and I.V.O. also thanks the Canada Council for a scholarship.

1. P. PICKER, P.-A. LEDUC, P. R. PHILIP, and J. E. DESNOYERS. J. Chem. Thermodyn. **3**, 631 (1971).
2. G. PERRON, N. DESROSIERS, and J. E. DESNOYERS. Can. J. Chem. **54**, 2163 (1976).
3. J. E. DESNOYERS, C. DE VISSER, G. PERRON, and P. PICKER. J. Solution Chem. **5**, 605 (1976).
4. P. PICKER, E. TREMBLAY, and C. JOLICOEUR. J. Solution Chem. **3**, 377 (1974).
5. L. H. JOHNSON, L. G. HEPLER, C. E. BAMBERGER, and D. M. RICHARDSON. Can. J. Chem. **56**, 446 (1978).
6. F. J. MILLERO. *In* Water and aqueous solutions: structure, thermodynamics, and transport processes. *Edited by* R. A. Horne. Wiley-Interscience, New York, NY. 1972. Chapt. 13.
7. P. LUMME. Trans. Royal Inst. Tech. Stockholm, Pure and Appl. Chem. **34**, No. 293, 575 (1972).
8. L. A. DUNN. Trans. Faraday Soc. **62**, 2348 (1966).
9. F. H. SPEDDING, M. J. PIKAL, and B. O. AYERS. J. Phys. Chem. **70**, 2440 (1966).
10. F. H. SPEDDING, V. W. SAEGER, K. A. GRAY, P. K. BONEAU, M. A. BROWN, C. W. DEKOCK, J. L. BAKER, L. E. SHIERS, H. O. WEBER, and A. HABENSCHUSS. J. Chem. Eng. Data, **20**, 72 (1975).

11. F. H. SPEDDING, P. F. CULLEN, and A. HABENSCHUSS. J. Phys. Chem. **78**, 1106 (1974).
12. F. H. SPEDDING, L. E. SHIERS, M. A. BROWN, J. L. DERER, D. L. SWANSON, and A. HABENSCHUSS. J. Chem. Eng. Data, **20**, 81 (1975).
13. J. E. ROBERTS and N. W. SILCOX. J. Am. Chem. Soc. **79**, 1789 (1957).
14. F. H. SPEDDING, L. E. SHIERS, M. A. BROWN, J. L. BAKER, L. GUITIERREZ, L. S. MCDOWELL, and A. HABENSCHUSS. J. Phys. Chem. **79**, 1087 (1975).
15. F. D. LEIPZIGER and J. E. ROBERTS. J. Phys. Chem. **62**, 1014 (1958).
16. A. BILLI, F. MALATESTA, R. ZAMBONI, and A. INDELLI. J. Chem. Phys. **61**, 4787 (1974).
17. G. CURTHOYS and J. G. MATHESON. J. Chem. Eng. Data, **22**, 225 (1977).
18. L. G. HEPLER, J. M. STOKES, and R. H. STOKES. Trans. Faraday Soc. **61**, 20 (1965).
19. P. R. PHILIP and J. E. DESNOYERS. J. Solution Chem. **1**, 353 (1972).
20. P.-A. LEDUC, J.-L. FORTIER, and J. E. DESNOYERS. J. Phys. Chem. **78**, 1217 (1974).
21. P.-A. LEDUC and J. E. DESNOYERS. Private communication.
22. J. J. SPITZER. Unpublished calculations.
23. L. F. SILVESTER and K. S. PITZER. J. Phys. Chem. **81**, 1822 (1977).
24. K. S. PITZER. Private communication.
25. L. G. HEPLER. To be published.
26. F. H. SPEDDING and K. C. JONES. J. Phys. Chem. **70**, 2450 (1966).
27. F. H. SPEDDING, J. L. BAKER, and J. P. WALTERS. Private communication.
28. F. H. SPEDDING, J. L. BAKER, and J. P. WALTERS. J. Chem. Eng. Data, **20**, 189 (1975).
29. A. ROUX, G. M. MUSBALLY, G. PERRON, J. E. DESNOYERS, P. P. SINGH, E. M. WOOLLEY, and L. G. HEPLER. Can. J. Chem. **56**, 24 (1978).
30. M. KH. KARAPET'YANTS, V. A. VASILEV, and S. N. NOVIKOV. Russ. J. Phys. Chem. **50**, 622 (1976).
31. V. A. VASILEV, S. N. NOVIKOV, and M. KH. KARAPET'YANTS. Russ. J. Phys. Chem. **49**, 1137 (1975).
32. F. H. SPEDDING, J. P. WALTERS, and J. L. BAKER. J. Chem. Eng. Data, **20**, 438 (1975).
33. D. J. BRADLEY and K. S. PITZER. J. Phys. Chem. **83**, 1599 (1979).
34. G. A. BOTTOMLEY, L. G. GLOSSOP, and W. P. STAUNTON. Aust. J. Chem. **32**, 699 (1979).

Erratum: Phase-transfer catalyzed synthesis of activated cyclopropanes

JOHN M. MCINTOSH AND HAMDY KHALIL
Department of Chemistry, University of Windsor, Windsor, Ont., Canada N9B 3P4

(Ref.: Can. J. Chem. **56**, 2134 (1978))
Received August 20, 1979

The experimental directions regarding the amounts of reagents and solvent are in error. Thus the first three sentences of the experimental procedure should read:

To a mixture of 40 mL of methylene chloride and 4.1 mL of 9.5 *N* aqueous sodium hydroxide (0.04 mol) was added ca. 100 mg of benzyltriethylammonium chloride (TEBAC). The system was cooled to 0°C in an ice–salt bath. To this solution was added a mixture of 0.04 mol of each of the acceptor and donor molecules at 0°C with good stirring.

Mechanistic and theoretical studies of the photochemistry of 5,6-dihydro-2-cyanobenzobarrelene

CHRISTOPHER OWEN BENDER AND SEAMUS F. O'SHEA

Department of Chemistry, University of Lethbridge, Lethbridge, Alta., Canada T1K 3M4

Received May 1, 1979

CHRISTOPHER OWEN BENDER and SEAMUS F. O'SHEA. Can. J. Chem. **57**, 2804 (1979).

The direct ($\Phi_6 = 0.04$) or acetone sensitized ($\Phi_6 = 0.51$) photolysis of 2-cyano-1,4-dihydro-1,4-ethanonaphthalene (**5**) yields 1-cyanobenzotricyclo[3.3.0.0^{2,8}]octa-3-ene (**6**). Deuterium labelling studies suggest that **6** derives from a Zimmerman di-π-methane rearrangement and not from the McCullough 1-cyanocyclohexene rearrangement. The observed rearrangement and regioselectivity are in accord with predictions based upon CNDO-CI calculations of changes in atom–atom interaction energies on excitation to the S_1 and T_1 excited states of **5**.

CHRISTOPHER OWEN BENDER et SEAMUS F. O'SHEA. Can. J. Chem. **57**, 2804 (1979).

La photolyse directe ($\Phi_6 = 0.04$) ou sensibilisée par l'acétone ($\Phi_6 = 0.51$) du cyano-2 dihydro-1,4 éthano-1,4 naphtalène (**5**) conduit au cyano-1-benzotricyclo[3.3.0.0^{2,8}]octa-3-ène (**6**). Des études de marquages au deuterium suggèrent que **6** dérive d'un réarrangement di-π méthane de Zimmerman et non pas par un réarrangement cyano-1 cyclohexène de McCullough. Le réarrangement et la régiosélectivité observés sont en accord avec les prédictions qui proviennent de calculs des changements d'energies d'interactions atome–atome sur excitation à l'état singulet (S_1) et à l'état triplet (T_1) de **5**.

Introduction

The topic of photo-regioselectivity in triplet sensitized di-π-methane rearrangements of polar-substituted dihydrobenzobarrelene and related (e.g., benzonorbornadiene) derivatives is of current theoretical and experimental interest (1). Since cases where the polar substituent is on the alkene moiety have not been reported we undertook the study of the photochemistry of the cyanolated dihydrobenzobarrelene **5**. The choice of the cyano group as substituent was prompted by the recent discovery of McCullough and Manning that the 1-cyanocyclohexene derivatives **1***a*, *b* photorearrange to bicyclo[3.1.0]hexane-1-carbonitriles (**3***a*, *b*) according to the general mechanism proposed in Scheme 1 (2).[1] Thus

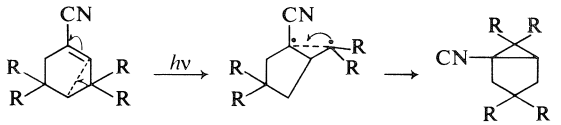

1*a* (R = H)
1*b* (R = CH_3)

2*a*,*b*

3*a*,*b*

SCHEME 1

in addition to providing regioselectivity information the investigation of **5** was conceived to examine the intramolecular competition between the 1-cyanocyclohexene and di-π-methane rearrangements.

Results

Compound **5** was isolated as a colourless solid from the diimide reduction of the less polar double bond of the known (3) 2-cyanobenzobarrelene (**4**) (see Scheme 2). The nmr data support the structure assigned to **5**: δ6.60–7.05 (m, 5H, H-3 and aromatics), δ3.76–4.03 (m, 2H, bridgeheads), and δ1.12–1.80 (m, 4H, methylenes). Particularly informative is the Eu(fod)$_3$ shifted spectrum, which, after the addition of 12 mol% of the LIS reagent, reveals one olefinic hydrogen, H-3, at δ7.70 (d, $J_{3,4} = 6.0$ Hz), coupled, as shown by double irradiation techniques, to H-4 at δ4.30 (broad d, $J = 6.0$ Hz); H-1 is a broad singlet at δ4.65 and the four methylene protons at C-5 and C-6 occur as a complex multiplet centred at δ1.83. In further accord with the structure, the deshielding effect of the cyano group on the adjacent coplanar vinyl proton, H-3, (δ6.90 in the absence of Eu(fod)$_3$; one limb of the doublet is hidden by the aromatic multiplet) relative to the corresponding proton in 2,3-dihydrobenzobarrelene (4) is 0.74 ppm which compares well with the reported chemical shift substituent constant of 0.8 for the *cis* proton of acrylonitrile (5).

On direct irradiation at 254 nm **5** gave the dihydrosemibullvalene derivative **6** as the major product isomeric with starting material; variable

[1]The experimental evidence does not exclude a concerted $2\sigma_a + 2\pi_a$ conversion of **1***a*, *b* to **3***a*, *b* (2).

0008-4042/79/212804-08$01.00/0

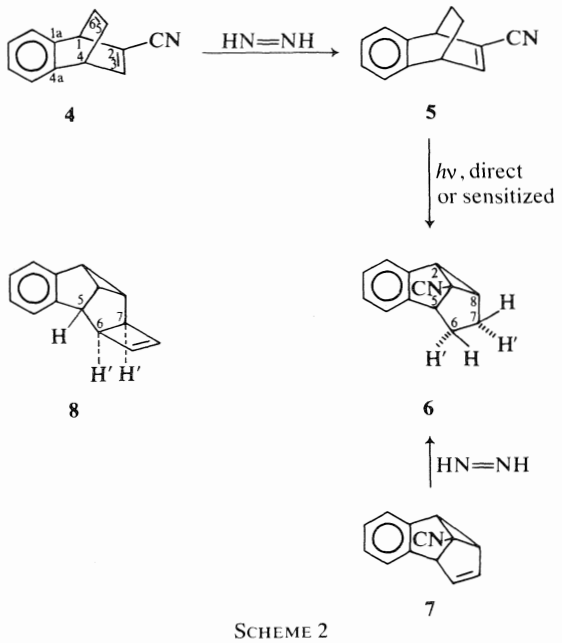

4 5 8 6 7

SCHEME 2

amounts of polymer were also formed together with minor amounts of other products which polymerized during work-up. By contrast, the acetone sensitized irradiation of **5** at 313 nm yielded only **6**. Photoproduct **6** is identical to the unique product isolated from the diimide reduction of the known (3) 1-cyanobenzosemibullvalene **7**.

The interpretation of the 400 MHz nmr spectrum of **6** is straightforward. In addition to the aromatic proton signals which occur as two sets of multiplets at δ7.20 (3H) and δ7.02 (1H) the spectrum contains seven distinctly separated nearly first order one-proton resonances for the seven non-aromatic protons (see Experimental).

The couplings between protons were confirmed by double irradiation techniques. The fact that H-5 occurs as a doublet, being coupled to H-6 (J = 5.0) but not to H-6′, is not unexpected since the dihedral angle between H-5 and H-6′ is 90° (Drieding Model). Furthermore, Paquette and co-workers have reported that H-5 and H-6′ are also not coupled in the semibullvalene derivative **8** (*6*).

Support for the proton assignments was provided by observing the effect of $Eu(fod)_3$ addition to the nmr solution of **6** (see Fig. 1). The hydrogens at C-2, C-5, and C-8 are closest and approximately equidistant from the cyano group, and consequently their signals are shifted the most and to approximately the same extent; the signals of the methylene hydrogens H-6 and H-7 *syn* to the cyano group are

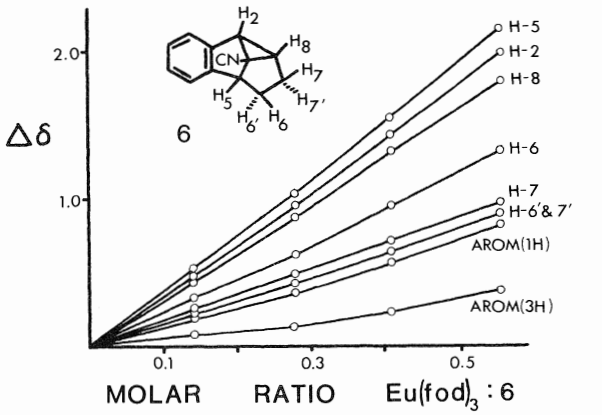

FIG. 1. Variation of chemical shift for the protons in **6** with increasing addition of the shift reagent $Eu(fod)_3$.

shifted more than those of the H-6′ and H-7′ *anti* methylene hydrogens.

Quantum Yields and S_1 *and* T_1 *Energies of* **5**

The quantum yields for the transformation of **5** to **6** were investigated to ascertain the relative efficiencies of the sensitized and unsensitized processes; in cyclohexane with 254 nm light the appearance Φ for **6** is 0.04 whereas in neat acetone with 313 nm light Φ is 0.51.

The singlet energy of **5** in cyclohexane solution at room temperature was determined to be 102 kcal mol^{-1} from intersection of the absorption and fluorescence spectra. The triplet energy of **5** could not be obtained spectrometrically since no phosphorescence in isopentane – methylcyclohexane glass at 77 K could be detected. However, an "effective" triplet energy at room temperature in cyclohexane solution of $74 \gtrsim E_T > 69$ kcal mol^{-1} is suggested by triplet sensitization experiments; the conversion of **5** to **6** can be sensitized efficiently by acetone (Φ = 0.51; E_{T_1} = 78 kcal mol^{-1}), less efficiently by acetophenone (Φ = 0.16; E_{T_1} = 74 kcal mol^{-1}) but apparently not by benzophenone (E_{T_1} = 69 kcal mol^{-1}) or by thioxanthone (E_{T_1} = 65 kcal mol^{-1}).

Mechanistic Considerations

The formation of **6** from **5** can be accounted for in terms of the McCullough 1-cyanocyclohexene rearrangement (Scheme 3, route *i*, stepwise; route *ii*, concerted, $2\sigma_a + 2\pi_a$), or the Zimmerman di-π-methane rearrangement (7) (Scheme 3, route *iv*, stepwise; route *iii*, concerted, $2\sigma_a + 2\pi_a$). A means of determining the route *i* (or *ii*) versus route *iv* (or *iii*) competition was provided by examining the photolyses of the mixture of deuterated dihydrobarrelenes **5***a*. Mixture **5***a* was prepared from the diimide

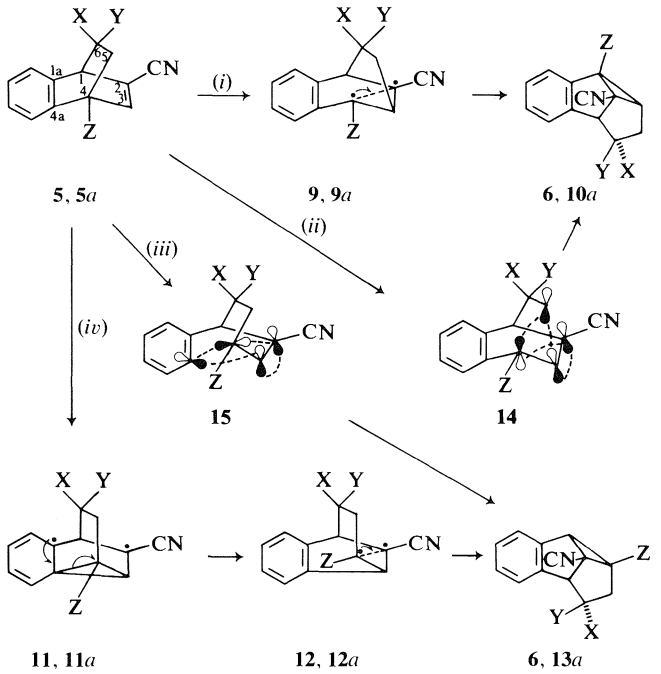

SCHEME 3. For **5**, **6**, **9**, **11**, and **12**, X = Y = Z = H. For series *a*, individual structures represent a 1:0.6:0.4 mixture of three component isotopes, **20**, **21**, and **22** respectively (see Scheme 4), each singly labelled with deuterium at the positions designated by Z, X, and Y.

reduction of the previously available (3) 50:50 mixture of deuterated barrelenes **18** and **19** (containing 94 ± 3% *d*, at C-4 and 92 ± 4% *d*, at C-6 respectively) obtained from the addition of benzyne to *meta* deuterobromobenzene followed by treatment with cuprous cyanide (see Scheme 4).

Nuclear magnetic resonance evidence indicates that this synthetic sequence leads to the formation of three isotopes **20**, **21**, and **22**. Comparison of the integrated areas of the bridgehead (H-1, H-4) and the methylene proton signals in the Eu(fod)$_3$ shifted spectrum reveals that the total deuterium content of mixture **5***a* is 94 ± 5% (assuming 0%-d_1 in the aromatics) and that the ratio of **20**:(**21** + **22**) is ca. 1.0:1.0. The relative amounts of **21** and **22** present in the mixture could not be ascertained directly from the nmr data of **5***a* because of overlap of the methylene proton signals. However, a ratio of 1.5 (**21**):1.0(**22**) is suggested from inspection of the nmr spectrum of the deuterated dihydrosemibullvalene photoproducts **13***a* (*vide infra*).

The hydrogen distributions of the dihydrosemibullvalene material isolated from the direct, acetone and acetophenone sensitized, irradiations of the deuterated mixture **5***a* are the same within experimental error (see Table 1); half of the deuterium is located at C-8 and the other half at C-6, i.e., consistent with **13***a*. Thus the McCullough 1-cyanocyclohexene rearrangement (routes *i* and *ii*, Scheme 3) does not participate in the formation of **6** during direct or sensitized irradiations of **5**.

Inspection of Table 1 also reveals that the H-6:H-6′ ratio accords with a distribution of 1.5:1.0 (*anti*:*syn*) for the deuterium on C-6, a result that suggests that the ratio of **21**:**22** is also 1.5:1.0 in the deuterated starting mixture **5***a* (assuming that no deuterium scrambling at C-6 occurs during the course of rearrangement to **13***a*), which in turn implies that the reduction of **4** is 60% stereoselective in favour of the vinyl–vinylcyano rather than benzo–vinyl approach of diimide.

Discussion

The excited state of **5** yielding **6** upon sensitized irradiations with acetone or acetophenone is assumed to be T_1. This assumption is based on the finding that when either sensitizer is used the deuterated dihydrobarrelene **5***a* gives dihydrosemibullvalene product containing the same label distributions, i.e., **13***a*. The observation that the quantum yield for the formation of **6** (Φ = 0.51) is much higher in the case of acetone (E_{T_1} = 78 kcal mol^{-1}) sensitization than

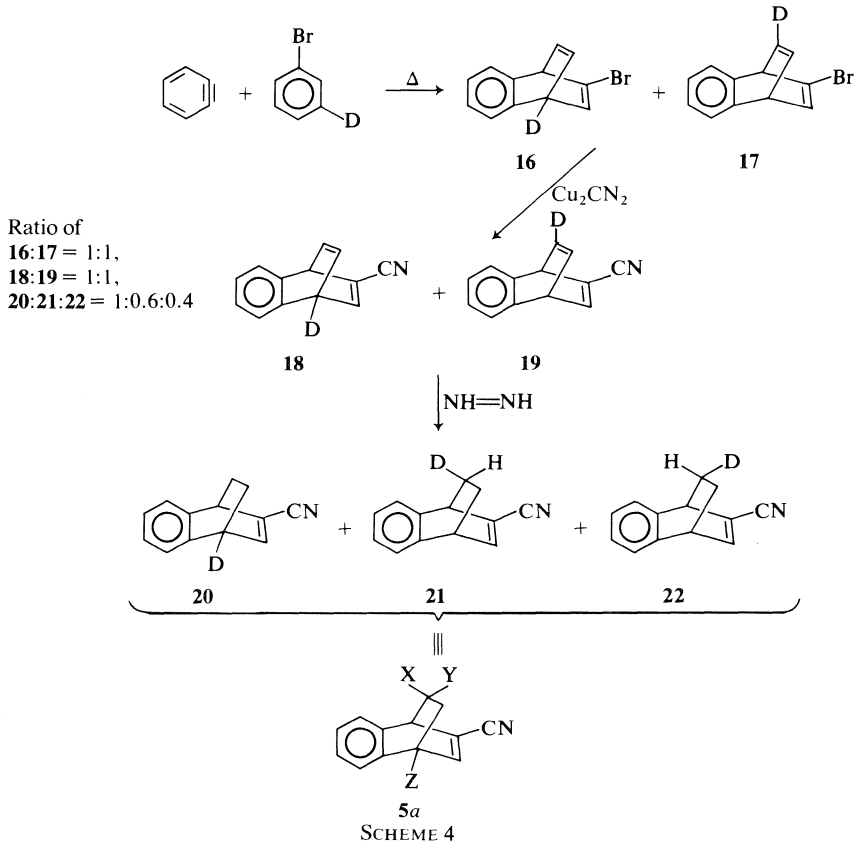

SCHEME 4

in acetophenone sensitization ($\Phi = 0.16$) is taken to mean that T_1 of **5** is close to T_1 of acetophenone, i.e., 74 kcal mol^{-1}.[2]

In the case of the direct irradiation of **5** the excited state leading to **6** is not clear. T_1 is a reasonable candidate on the grounds that (*a*) the formation of **6** from the direct irradiation of **5** ($\Phi = 0.04$) is much less efficient than in the case of acetone sensitized runs ($\Phi = 0.51$) as expected for a process involving intersystem crossing, and (*b*) the deuterium labelled mixture **5***a* leads to dihydrosemibullvalene material (i.e., **13***a*) containing the same label distributions from direct and sensitized irradiations. However, there is no evidence to rule out involvement of S_1. In fact our CNDO/2-CI calculations (*vide infra*) suggest that S_1 should follow the same overall mechanistic course as T_1.

With respect to the mechanistic considerations, the observed preference for route *iii* (or *iv*) over route *i* (or *ii*) (Scheme 3) is in excellent agreement with predictions derived from CNDO/2-CI calculations of changes of atom–atom interaction energies in the singlet (S_1) and triplet (T_1) excited states of **5** (see Table 2). In these calculations (3) (see Experimental) the electronic excitation energy for the lowest singlet and triplet states are rewritten as sums of changes in single-atom energies and atom-pair interaction energies. By interpreting these changes in interaction energies as forces which give rise to initial nuclear motion and by assuming that in rigid systems[3] these motions determine the ultimate products, we can make predictions about preferences between competing processes.

For the non-concerted transformations (Scheme 3, routes *i* and *iv*) of **5** to **6** the calculations suggest that for both the S_1 and T_1 excited states of **5** the largest attractive 1,3 non-bonded carbon–carbon interaction is that between C-3 and C-4a (case 1) while the greatest weakening in existing bonds occurs between C-2 and C-3 (case 13) and between C-1a and C-4a

[2]Interestingly, theoretical calculations (CNDO/2-CI, *vide infra*) for the lower excited states of **5** give relative theoretical energy ratios of $1.000(S_1):0.709(T_1):1.070(S_2):0.927(T_2)$. Since the singlet ($S_1$) energy of **5** was determined to be 102 kcal mol^{-1} (*vide supra*) the following scaled estimates for the energies of the other excited states can be obtained: $T_1 = 72$ kcal mol^{-1}, $S_2 = 109$ kcal mol^{-1}, and $T_2 = 95$ kcal mol^{-1}.

[3]Zimmerman and co-workers have recently reported similar calculations on excited states of some non-rigid systems (8).

TABLE 1. Observed[a] and theoretical hydrogen distributions for deuterated dihydrosemibullvalenes from photolyses of **5***a*

Case	Hydrogen distributions						
	H-2	H-5	H-6	H-6′	H-7	H-7′	H-8
1. Mechanism *i* or *ii*,[b] calcd.[c]	0.54±0.04	1.00	0.81±0.04	0.72±0.04	1.00	1.00	1.00
2. Mechanism *iii* or *iv*,[b] calcd.[c]	1.00	1.00	0.81±0.04	0.72±0.04	1.00	1.00	0.54±0.04
3. Direct, exptl.[d,e]	0.97±0.04	0.99±0.03	0.80±0.05	0.71±0.04	1.02±0.03	1.01±0.04	0.54±0.03
4. Acetone sensitized, exptl.[d,e]	0.98±0.02	0.98±0.02	0.81±0.04	0.71±0.04	1.04±0.03	1.02±0.03	0.52±0.04
5. Acetophenone sensitized, exptl.[d,e]	1.00±0.04	0.97±0.03	0.79±0.04	0.72±0.04	1.03±0.03	1.00±0.04	0.57±0.04

[a]$CDCl_3$ solvent.
[b]See Scheme 3 for mechanisms *i–iv*.
[c]Corrected for the presence of the three singly labelled isotopes **20** (50%), **21** (30%), and **22** (20%) in mixture **5***a*.
[d]Errors estimated from scatter of nmr signal integrations.
[e]Hydrogen distributions were normalized on the assumption that the aromatic multiplet at δ7.02 represents 1.00H.

TABLE 2. Changes[a,b] in atom–atom interaction energies (eV) resulting from electronic excitation to the lowest singlet (S_1) and triplet (T_1) states of reactant **5** in its equilibrium geometry[c,d]

Changes between 1,3-non-bonded atoms				Changes between bound atoms			
Case	Atom–atom	T_1	S_1	Case	Atom–atom	T_1	S_1
1	3–4a	−0.782	−2.303	13	2–3	10.681	5.127
2	1a–2	−0.689	−1.887	14	1a–4a	0.808	2.670
3	3–5	−0.339	0.324	15	4a–4	0.715	0.891
4	2–6	−0.334	0.243	16	1–1a	0.650	−0.060
5	1–3	−0.154	−0.092	17	5–6	0.598	0.254
6	2–4	−0.151	−0.109	18	4–5	0.490	−0.128
7	1a–6	−0.128	0.136	19	1–6	0.402	−0.060
8	5–4a	−0.124	0.149	20	1–2	−0.752	−0.142
9	1–4a	0.047	0.017	21	3–4	−0.852	−0.263
10	1–5	0.047	0.020				
11	1a–4	0.050	0.018				
12	4–6	0.051	0.025				

[a]Calculated by the CNDO/CI method using the theoretical parametization (11).
[b]Negative values are interpreted as "forces" tending to bring the atoms together, while positive values cause the atoms to move further apart.
[c]Calculations on the full molecule **5** were performed; only values for the dihydrobarrelene portion are given here.
[d]The numbering of the atoms is that given in Scheme 3.

(case 14). These predictions precisely coincide with the initial bonding reorganizations that would be engendered in the formation of the first diradical intermediate **11** in the di-π-methane mechanism (route *iv*). The formation of the initial diradical **9** in the 1-cyanocyclohexene mechanism (route *i*) is seen by inspection of Table 2 (cases 3, 13, and 18) to be less favourable.

Likewise, for the concerted alternatives for the transformations of **5** to **6** (Scheme 3, routes *ii* and *iii*) the di-π-methane rearrangement ($2\sigma_a + 2\pi_a$ version, route *iii*) is, according to the calculations, more favourable than the 1-cyanocyclohexene rearrangement ($2\sigma_a + 2\pi_a$ version, route *ii*) (cf. cases 1, 6, 13, and 15 with cases 3, 6, 13, and 18 respectively).

Turning now to the topic of di-π-methane regioselectivity, it should be noted that Paquette and coworkers have reported the striking control on the directionality of benzo–vinyl bonding exerted by the cyano group when substituted in the aromatic ring of the dihydrobenzobarrelene **23** (Scheme 5); in the case of the *meta* cyano derivative (**24***a*) the di-π-methane rearrangement proceeds with complete regiospecificity, to give **26***a* (1*a*) while for the *ortho* cyano derivative (**24***b*) it proceeds with high regioselectivity to produce 91% **28***b* and 9% **26***b* (1*b*). In the case of **5** where the cyano group is on the alkene moiety its effect is also profound; the triplet di-π-methane rearrangement is regiospecific, proceeding via C_3—C_{4a} bonding. Inspection of Table 2 (case 1) reveals that the CNDO/2-CI atom–atom approach predicts a preference for the observed initial C_3—C_{4a} bonding over the alternative di-π-methane initial C_{1a}—C_2 bonding option (case 2).

Experimental

The nmr spectra were recorded on Bruker 400 MHz or Varian (EM-360) 60 MHz instruments with TMS as internal standard. The ir spectra were recorded on a Perkin-Elmer 337 spectrometer, the uv spectra on a Cary 15 spectrophotometer, and the mass spectra on an MS 9 (A.E.I.). All melting points are uncorrected. Elemental analyses were performed by Galbraith Labs. Inc., Knoxville, TN. Cyclohexane solvent was

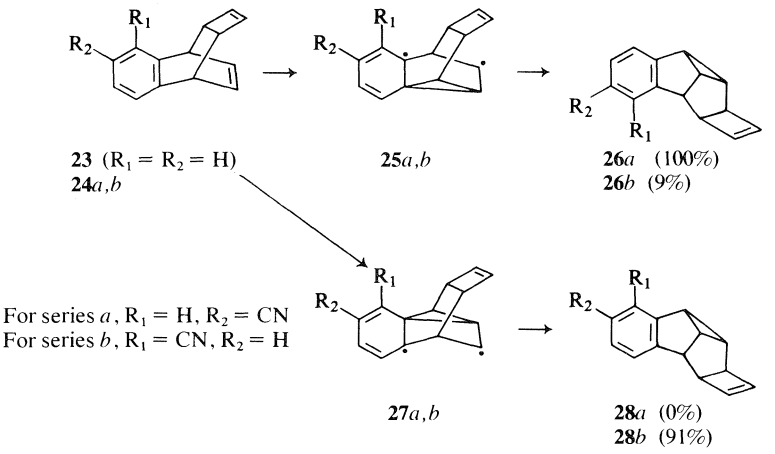

SCHEME 5

prepared for photolyses by scrubbing with 10% of its volume of 30% fuming sulfuric acid, followed by washing with 10% aqueous sodium hydroxide, drying ($MgSO_4$), and finally distilling from calcium hydride. Solid triplet sensitizers were sublimed and recrystallized prior to use, and acetophenone was distilled. Acetone sensitizer was obtained by refluxing spectroscopic grade acetone with neutral potassium permanganate, followed by distillation and then redistillation from anhydrous potassium carbonate. Nuclear magnetic resonance chemical shifts are given in δ units and J values in hertz; uv maxima are given in nanometers (ε); ir bands are given in reciprocal centimeters. Thin-layer chromatographic separations were carried out on Merck plates, 20 cm × 20 cm, 0.25 mm layer of Silica Gel 60 F-254.

2-Cyano-1,4-dihydro-1,4-ethanonaphthalene (5)

To a stirred mixture of 741.7 mg (4.2 mmol) of **4** (3) and 1.6858 g of potassium azodicarboxylate (8.7 mmol) in 30 mL of methanol at −30°C, 1.5 mL of acetic acid was added in one portion. The reaction mixture was allowed to warm to room temperature during 1.5 h after which time the solution was added to 300 mL of cyclohexane and was washed with 5% aqueous sodium hydroxide (200 mL) followed by water (2 × 200 mL). The cyclohexane solution was dried ($MgSO_4$), concentrated *in vacuo*, and the residue column chromatographed on silicic acid (100–200 mesh) with 1% ether–cyclohexane. Crystallization of the contents of the first band from hexane gave 175.2 mg (23%) of colourless **5**, mp 66–68°C; ir (KBr): 2200, C≡N; uv (cyclohexane): 222 sh (6200), 238 sh (1120), 253 sh (720), 260 (540), 267 (330), and 269 (280); nmr (60 MHz, CCl_4): 6.60–7.05 (m, 5H, H-3 and aromatics), 3.76–4.03 (m, 2H, bridgeheads), and 1.12–1.80 (m, 4H, methylenes); LIS nmr (60 MHz) with 11.1 mg of **5** and 8.3 mg of Eu(fod)$_3$ in 0.25 mL CCl_4: 7.70 (d, 1H, H-3, $J_{3,4}$ = 6.0), 7.24 (m, 4H, aromatics), 4.65 (br s, 1H, H-1), 4.30 (br d, 1H, H-4, $J_{3,4}$ = 6.0), and 1.83 (m, 4H, methylenes); spin-decoupling experiments on LIS spectrum: irradiation of H-3 collapsed H-4 to a broad singlet. Mass spectrum (70 eV, direct inlet) showed molecular ion at m/e 181.0892 (10%), $C_{13}H_{11}N$ requires 181.0891. *Anal.* calcd. for $C_{13}H_{11}N$: C 86.15, H 6.12, N 7.73; found: C 85.91, H 6.13, N 7.63.

Crystallization (hexane) of the contents of the second band from the column chromatography yielded 554.0 mg (75%) of recovered starting material (**4**).

1-Cyanobenzotricyclo[3.3.0.0^{2,8}]octa-3-ene (6)

To a stirred mixture of 113.1 mg (0.62 mmol) of **7** (3) and 650.2 mg of potassium azodicarboxylate (3.4 mmol) in 30 mL of methanol at −30°C, 1.5 mL of acetic acid was added in one portion. The reaction mixture was allowed to warm to room temperature during 1.5 h and was then worked up and chromatographed as described for the preparation of **5** (*vide supra*). Crystallization (hexane) of the contents of the first band off the column gave 42.6 mg (37%) of colourless **6**, mp 64–66°C; ir (KBr): 2230, C≡N; uv (cyclohexane): 220 sh (4070), 257 sh (260), 262 (440), 267 sh (600), 268 (680), and 276 (830); nmr (400 MHz, $CDCl_3$): 7.20 (m, 3H, aromatic), 7.02 (m, 1H, aromatic), 3.87 (d, 1H, H-5, $J_{5,6}$ = 5.0, $J_{5,6'}$ = 0.0), 3.15 (d, 1H, H-2, $J_{2,8}$ = 8.0), 2.60 (m, 1H, H-8, $J_{2,8}$ = 8.0, $J_{7,8}$ = 2.0, $J_{7',8}$ = 6.6), 2.45 (m, 1H, H-6, $J_{6,7}$ = 11.5, $J_{5,6}$ = 5.0, $J_{6,6'}$ = 10.8, $J_{6,7'}$ = 8.5), 2.01 (m, 1H, H-7′, $J_{7',8}$ = 6.6, $J_{6',7'}$ = 0.0, $J_{6,7'}$ = 8.5, $J_{7,7'}$ = 11.0), 1.76 (q, 1H, H-6′, $J_{6',7}$ = 6.0, $J_{6',7'}$ = $J_{5,6'}$ = 0, $J_{6,6'}$ = 10.8), and 1.20 (m, 1H, H-7, $J_{7,8}$ = 2.0, $J_{6',7}$ = 6.0, $J_{6,7}$ = 11.5, $J_{7,7'}$ = 11.0); spin-decoupling experiments: irradiation of H-7 collapsed H-6′ to a d ($J_{6,6'}$ = 10.8), collapsed H-8 to a q ($J_{2,8}$ = 8.0, $J_{7',8}$ = 6.6), and modified the H-7′ and H-6 multiplets; irradiation of H-6′ collapsed H-7 to a broad t ($J_{7,7'}$ = 11.0, $J_{6,7}$ = 11.5, $J_{7,8}$ = 2.0) and modified the H-6 m; irradiation of H-7′ collapsed H-8 to a broad doublet ($J_{2,8}$ = 8.0, $J_{7,8}$ = 2.0) and modified the H-6 and H-7 multiplets; irradiation of H-6 collapsed H-5 to an s, collapsed H-6′ to a d ($J_{6',7}$ = 6), and modified the H-7 and H-7′ multiplets; irradiation of H-8 collapsed H-2 to an s, collapsed H-7′ to a q ($J_{7,7'}$ = 11.0, $J_{6,7'}$ = 8.5), and modified the H-7 m; irradiation of H-2 collapsed H-8 to two doublets ($J_{7,8}$ = 2, $J_{7',8}$ = 6.6); irradiation of H-5 collapsed H-6 to six lines (1:1:2:2:1:1) ($J_{6,7}$ = 11.5, $J_{6,7'}$ = 8.5, $J_{6,6'}$ = 10.8). Mass spectrum (70 eV, direct inlet) showed molecular ion at m/e = 181.0886 (13%). *Anal.* found: C 86.16, H 6.22, N 7.58.

The second band off the column yielded 61.7 mg (55%) of starting material (**7**).

Effect of Lanthanide Shift Reagent on the Nuclear Magnetic Resonance Spectrum of 6

The nmr spectrum of **6** was recorded (60 MHz) in CCl_4 (0.40 mL containing 1% TMS) in the presence of increasing amounts of a solution of Eu(fod)$_3$ in CCl_4 (28.8 mg in 0.10 mL). The results are summarized in Fig. 1.

*Deuterio 2-Cyano-1,4-dihydro-1,4-ethanonaphthalene Mixture 5*a

The 50:50 mixture of deuterated barrelenes **18** and **19**, containing 94 ± 3% *d*, at C-4 and 92 ± 4% *d*, at C-6, respectively, was available from a previous study (3). To a stirred

solution of 355.9 mg (2.0 mmol) of the 50:50 mixture of **18** and **19** in 35 mL methanol at −30°C, 957.8 mg (4.9 mmol) of potassium azodicarboxylate was added followed by 2 mL of acetic acid. The reaction mixture was allowed to warm to room temperature during 2 h and was worked up as previously described for the preparation of **5**; 82.1 mg (23%) of colourless **5***a*, mp 66–68°C, was obtained along with 254.6 mg (72%) of recovered starting material. The LIS nmr spectrum (60 MHz) with 11.9 mg of **5***a* and 27.4 mg of $Eu(fod)_3$ in 0.25 mL CCl_4: 7.80–8.03 (m, 0.98 ± 0.04 H, H-3), 6.25–6.93 (m, 4.00 H, aromatics), 4.96 (broad s, 1.01 ± 0.03 H, H-1), 3.73–3.98 (m, 0.53 ± 0.03 H, H-4), and 1.00–1.93 (m, 3.54 ± 0.03 H, methylenes), i.e., this corresponds to a ratio of ca. 1.0:1.0 for **20**:(**21** + **22**), **20** containing 94 ± 6% *d*, at C-4 and **21** + **22** containing a total of 92 ± 6% *d*, at C-6.

Preparative and Quantum Yield Apparatus for Sensitized Irradiations

The apparatus consisted of a "merry-go-round" fitted with a 450W Hanovia medium pressure mercury arc which was surrounded by a water-cooled quartz immersion well. Light of wavelength 313 nm was isolated by a two compartment quartz cell fitting concentrically around the immersion well. The first compartment contained a 2.0 cm path length of a solution of 306 g of cobaltous sulfate heptahydrate and 552 g of nickel sulfate hexahydrate per litre of 5% aqueous H_2SO_4. The second compartment contained a 0.2 cm path length of a solution of 1 g of potassium chromate in 300 mL of 1% aqueous sodium carbonate. This combination showed transmittance between 302–323 nm with a maximum at 313 nm (20%).

Before irradiation, solutions (35 mL) of reactants contained in calibrated 20 mm × 150 mm quartz test-tube-like photolysis cells were deoxygenated by flushing with argon. The tubes were sealed under a positive pressure of argon which was maintained throughout the course of the irradiation.

Acetone Sensitized Photolysis of **5**

A solution of 29.0 mg (0.16 mmol) of **5** in 35 mL of acetone was photolysed with 313 nm light for 137 min. The photolysate was concentrated *in vacuo* and the residue was applied to a tlc plate; after two irrigations with 6% ether–cyclohexane, 13.0 mg (45%) of recovered starting material was obtained from the first band, and 11.7 mg (40%) of a colourless solid from the second band, which after crystallization from hexane gave 8.2 mg of material, mp 64–66°C, which was identical in all respects to **6**.

Sensitized Photolyses of Deuterated Dihydrobarrelene Mixture **5**a

(a) With Acetone

A solution of 30.4 mg (0.17 mmol) of mixture **5***a* in 35 mL of acetone was photolysed with 313 nm light for 183 min. The photolysate was worked up as in the undeuterated case to give 10.4 mg (34%) of starting material and 13.0 mg (43%) of deuterated dihydrosemibullvalene mixture **13***a*, mp 64–66°C; see Table 1 (case 4) for the nmr H distributions.

(b) With Acetophenone

A solution of 53.3 mg (0.29 mmol) of mixture **5***a* and 326.1 mg of acetophenone in 35 mL of cyclohexane was photolysed with 313 nm light for 453 min. The photolysate was concentrated *in vacuo* and the acetophenone sensitizer was removed by short-path distillation at 30°C/0.1 Torr. The residue was thereafter worked up as in the case of the acetone sensitized run, except that two tlc plates were employed, to give 32.7 mg (61%) of starting material and 4.2 mg (8%) of deuterated dihydrosemibullvalene mixture **13***a*, mp 64–66°C; see Table 1 (case 5) for the nmr H distributions.

Sensitized Quantum Yield Determinations

Sensitized quantum yields for the conversion of **5** to **6** with 313 nm light were determined on the "merry-go-round" apparatus. Sample solutions (35 mL) of ca. 0.3 mmol of **5** and ca. 6.0 mmol of the sensitizer (acetophenone, benzophenone, or thioxanthone; acetone sensitizer was used neat) were contained in separate, calibrated (for differences in light transmittance) test-tube-like cells and were irradiated in the same run. The lamp output was determined by potassium ferrioxalate actinometry (9). The photolysates were concentrated *in vacuo*, a known quantity of **4** was added as internal standard and the product compositions were determined by nmr analysis. In all cases nmr peak areas were calibrated against authentic mixtures of similar constitution. Conversions were kept below 18% and the quantum yields were determined from the average of two runs. The Φ for the appearance of **6** were: Φ(acetone) = 0.51 ± 0.05, Φ(acetophenone) = 0.16 ± 0.04, Φ(benzophenone) < 0.01, Φ(thioxanthone) < 0.01.

Direct Irradiation of **5**

A solution of 46.1 mg (0.25 mmol) of **5** in 250 mL of cyclohexane contained in a 250 mL water cooled photolysis well was stirred under an argon atmosphere and irradiated for 247 min with Vycor-filtered light provided by a 2 W U-shaped Hanovia cold cathode low pressure Mercury discharge lamp (>90% of emitted light is 254 nm). The photolysate was concentrated *in vacuo* and the residue was applied to two tlc plates; after two irrigations with 6% ether–cyclohexane 21.7 mg (47%) of recovered starting material was obtained from the first major band and 7.8 mg (17%) of **6**, mp 64–66°C, from the second. Variable amounts of polymer are formed during the reaction depending on the conversion; the direct irradiation of photoproduct **6** also gives rise to the efficient formation of polymer.

Direct Irradiation of Deuterated Dihydrobarrelene Mixture **5**a

A solution of 51.6 mg (0.29 mmol) of **5***a* in 250 mL of cyclohexane was photolysed for 250 min with 254 nm light (provided as described for the direct irradiation of **5**). The photolysate was worked up as in the undeuterated case to give 22.4 mg (43%) of recovered **5***a* and 6.7 mg (13%) of **13***a*, mp 64–66°C; see Table 1 (case 3) for the nmr H distributions.

Quantum Yield Apparatus and Measurement for Direct Irradiation of **5**

Quantum yields were performed on an optical bench. Light from a fan-cooled 450 W Hanovia medium pressure lamp was roughly focussed by 4 cm diameter quartz biconvex lens (focal length 5.0 cm) located at one end of a collimating tube of 10 cm length and 4 cm diameter. At the other end of the collimating tube a square (5 cm × 5 cm) Ealing-TFP Interference Filter (20% transmission at 254 nm, 20 nm band width at half-height) was located. The light was beamed onto a cell holder (15 cm from lamp) containing a calibrated 20 mm × 150 mm quartz test-tube-like photolysis cell. The light entered the cell via a narrow slotted window (3 cm × 1 cm, 1 cm deep). In a typical run, a solution of 0.15 mmol of **5** in 25 mL of cyclohexane was deoxygenated by flushing with argon and sealed under a slightly positive pressure. The magnetically stirred solution was irradiated for ca. 65 h. The lamp output was determined via potassium ferrioxalate actinometry (9) prior to, several times during, and after irradiation of the sample solution of **5**. The light fluctuations were found to be less than 20% during the course of irradiations. After irradiation, the photolysate was worked up and analyzed by nmr spectroscopy as described for the sensitized quantum yield determinations. The Φ for the appearance of **6**, determined from the average of three runs of less than 10% conversion, was 0.04 ± 0.02.

Fluorescence and Phosphorescence Studies of Dihydrobarrelene **5**

The fluorescence spectrum of **5** was measured in cyclohexane solution at room temperature on an Aminco-Bowman Spectrometer. Intersection of the fluorescence (λ_{max} = 360 nm) and absorption spectra of **5** occurred at 280 nm, suggesting a singlet energy of 102 kcal mol^{-1}.

The phosphorescence study was carried out on a modified Aminco-Bowman apparatus (10) in an isopentane–methylcyclohexane (1:4) glass at 77 K. No detectable phosphorescence peak could be observed.

Calculations

The calculations were performed on a DEC-20 system computer using a modified version of the CNDO/M-CI program (QCPE #315) of Jaffé and co-workers (11); the theoretical parametization was used. The lowest singlet and triplet excited states were calculated using a limited CI (60 determinants) in the virtual orbital approximation.

As a result of the CI each excited state is written as a mixture of configurations; each configuration is constructed by removing electrons from MO's occupied in the ground state and placing them in MO's which are vacant in the ground state. Using the CI mixing coefficients, and the coefficients of expansion of the molecular orbitals in terms of the atomic basis functions, the energies of both the ground and excited states can be written as a sum of energies of interaction between pairs of orbitals and shifts in single orbital energies. In the zero differential overlap approximation used in CNDO, INDO, etc., interactions involving three or more orbitals simultaneously are assumed to be zero. By summing the appropriate groups of orbital–orbital energies one can write the state energies in terms of atom–atom interactions energies and single atom energies, as is done for the ground state energy in ref. 12. By subtraction of ground and excited state energies, or directly resolving the excitation energy, one can calculate the changes in the atom–atom interactions resulting from excitation. These changes reflect the decreased (positive values) or increased (negative values) bonding between atoms. When the bonding is reduced the distance between the atoms is assumed to increase and vice versa. The pattern of changes in atom–atom energies can thus be interpreted as a pattern of initial molecular distortion. The atomic basis set used in these calculations is the unhybridized valence set normally employed in CNDO calculations. This atom–atom energy approach was developed because in non-planar molecules such as **5** σ–π separation is not strictly valid. Further details of the calculations are available from the authors.

Acknowledgements

The authors thank the Spectroscopic Services Laboratory of the University of Alberta for the 400 MHz nmr and mass spectra, Professor Bryan Henry of the University of Manitoba for phosphorescence studies, and the University of Lethbridge Computing Centre for use of the DEC-20 system computer. Financial support from the Natural Sciences and Engineering Research Council of Canada is gratefully acknowledged.

1. (*a*) L. A. PAQUETTE, D. M. COTTRELL, and R. A. SNOW. J. Am. Chem. Soc. **99**, 3723 (1977); (*b*) R. A. SNOW, D. M. COTTRELL, and L. A. PAQUETTE. J. Am. Chem. Soc. **99**, 3734 (1977); (*c*) C. SANTIAGO, E. J. MCALDUFF, K. N. HOUK, R. A. SNOW, and L. A. PAQUETTE. J. Am. Chem. Soc. **100**, 6149 (1978).
2. J. J. MCCULLOUGH and C. MANNING. J. Org. Chem. **43**, 2839 (1978).
3. C. O. BENDER, D. W. BROOKS, W. CHENG, D. DOLMAN, S. F. O'SHEA, and S. S. SHUGARMAN. Can. J. Chem. **56**, 3027 (1978).
4. K. TORI, Y. HATA, R. MUNEYUKI, Y. TAKANO, T. TSUJI, and H. TANIDA. Can. J. Chem. **42**, 926 (1964).
5. C. PASCUAL, J. MEIR, and W. SIMON. Helv. Chim. Acta, **49**, 164 (1966).
6. L. A. PAQUETTE, M. J. KUKLA, and J. C. STOWELL. J. Am. Chem. Soc. **94**, 4290 (1972).
7. S. S. HIXSON, P. S. MARIANO, and H. E. ZIMMERMAN. Chem. Rev. **73**, 531 (1973).
8. (*a*) H. E. ZIMMERMAN, W. T. GRUENBAUM, R. T. KLUN, M. G. STEINMETZ, and T. R. WELTER. J. Chem. Soc. Chem. Commun. 228 (1978); (*b*) H. E. ZIMMERMAN and M. G. STEINMETZ. J. Chem. Soc. Chem. Commun. 230 (1978); (*c*) H. E. ZIMMERMAN, M. G. STEINMETZ, and C. L. KREIL. J. Am. Chem. Soc. **100**, 4146 (1978); (*d*) H. E. ZIMMERMAN and T. P. CUTLER. J. Org. Chem. **43**, 3283 (1978).
9. C. G. HATCHARD and C. A. PARKER. Proc. R. Soc. London, Ser. A, **235**, 518 (1956).
10. B. HENRY and J. MORRISON. J. Mol. Spectrosc. **55**, 311 (1975).
11. J. DEL BENE and H. H. JAFFÉ. J. Chem. Phys. **48**, 1807 (1968); **48**, 4050 (1968); **49**, 1221 (1968); **50**, 1126 (1969).
12. J. A. POPLE and D. L. BEVERIDGE. Approximate molecular orbital theory. McGraw-Hill, New York, N.Y. 1971.

Photochemical α-cleavage and hydrogen abstraction in deoxybenzoin: a laser spectroscopy investigation

JEAN-PIERRE FOUASSIER AND ANDRÉ MERLIN

Laboratoire de Photochimie Générale, Equipe de recherche Associée au C.N.R.S. no 386, Ecole Nationale Supérieure de Chimie, 68093 Mulhouse Cedex, France

Received May 8, 1979

JEAN-PIERRE FOUASSIER and ANDRÉ MERLIN. Can. J. Chem. **57**, 2812 (1979).

Transient absorptions in the range 380–500 nm in deoxybenzoin are investigated for the first time by nanosecond laser spectroscopy. This study gives evidence for absorption by a triplet state, and by benzoyl and benzyl radicals. Photoreduction of the triplet state and generation of a ketyl radical are also obtained. This enables some peculiar results of the polymerization of vinyl monomers photoinduced by deoxybenzoin to be explained. Our results show that deoxybenzoin exhibits a peculiar behaviour since the two photoprocesses occur with the same efficiency. Hydrogen abstraction and α-cleavage rate constants, quenching rate constants of the species by oxygen, lifetimes of the transients, and absorption spectra are derived. The influence of the solvent is discussed as a function of the excited states involved. A complete diagram of the evolution of the energy levels is thus obtained.

JEAN-PIERRE FOUASSIER et ANDRÉ MERLIN. Can. J. Chem. **57**, 2812 (1979).

Les absorptions transitoires dans la désoxybenzoine sont étudiées pour la première fois dans la région de 380 à 500 nm, à l'aide de la spectroscopie laser au nanoseconde. Cette étude fournit la preuve que l'absorption se fait par un état triplet et par les radicaux benzoyle et benzyle. On a également obtenu la photoréduction de l'état triplet et la génération du radical cétyle. Ceci permet d'expliquer quelques résultats particuliers obtenus lors de la polymérisation photoinduite des monomères vinyliques par la désoxybenzoine. Nos résultats montrent que la désoxybenzoine fait preuve d'un comportement particulier puisque les deux processus photochimiques se produisent avec la même efficacité. On a déduit les constantes de vitesse de l'élimination de l'hydrogène et du clivage en α, les constantes de vitesse de l'inhibition des espèces par l'oxygène, les durées de vie des espèces transitoires et leurs spectres d'absorption. On a discuté de l'influence des solvants comme étant une fonction des états excités impliqués. On a ainsi obtenu un diagramme complet des nivaux d'énergie et de l'évolution des états excités.

[Traduit par le journal]

Introduction

For a long time, it has been known that ketones in solution can undergo photochemical α-cleavage (Norrish type I) or/and hydrogen abstraction yielding a ketyl radical. The latter process was extensively studied by laser spectroscopy and under steady state conditions. In contrast, most of the substantial work devoted recently to the photochemistry of aromatic acyloins has been carried out using continuous light illumination (1–2) and accurate information has been derived concerning the formation of the photoproducts.

These molecules represent an important group of initiators, and under uv light they produce radicals which initiate the polymerization of vinyl monomers (3). In the case of deoxybenzoin, which was studied by Lewis *et al.* (4), it was postulated that the origin of the photolysis products could be explained by the formation of a benzoyl–benzyl radical pair (reaction [1]).

However, a preliminary investigation of this molecule under laser excitation (5) and recent experiments

[1] 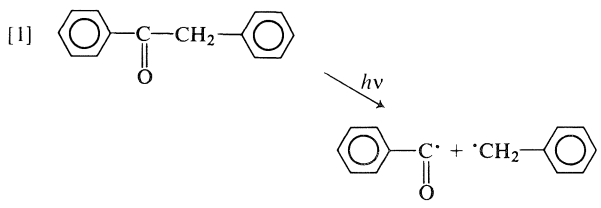

on the photoinduced polymerization of methylmethacrylate by deoxybenzoin (6) suggest also the formation of a ketyl radical (reaction [2]) which has never been mentioned to occur by laser spectroscopy of this molecule. However, the formation of pinacol under continuous uv light illumination suggests a ketyl radical as intermediate (7).

Since there are both practical and fundamental interest to this problem, the present investigation by laser spectroscopy is devoted to direct evidence for the Norrish type I photoscission and for the hydrogen abstraction reaction. It provides a better insight into the evolution of the excited states and permits subsequent discussion on the mechanism of the polymerization initiation.

0008-4042/79/212812-06$01.00/0

[2] 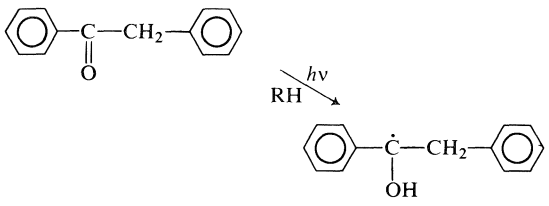

Experimental

Deoxybenzoin was purchased from Kodak Eastman Company. Benzene was a commercial product of the highest grade (99.9%). THF was purified before use. The nanosecond laser apparatus and the analyzing system were described previously (8). The excitation consisted of a train of 6 pulses (200 ps FWHM, 10 ns separated). The output energy density was about 50 mJ cm^{-2} at 347 nm.

Results and Discussion

Solvent Effect upon the Transients

Laser excitation of deoxybenzoin (DB) in benzene solution leads to transient absorptions in the near uv and visible wavelength range. A typical oscilloscope trace is shown in Fig. 1. According to previous experiments (5), the first part of the relaxation curve may be ascribed to the triplet state decay of DB. The second part of the curve appears to be the sum of two absorptions. On a longer time scale of evolution (> 10 μs), a residual absorption appears: it is due to a transient we call *LLR* (*L*ong *L*ived *R*adical). In the time range of some hundred nanoseconds, the absorption curve can be accounted for by the relaxation of a transient which decays according to a second order kinetics, the rate constant of which at 430 nm in nitrogen atmosphere is about $k/\varepsilon l = 38 \times 10^7$ s^{-1}. This transient will be called *SLR* (*S*hort *L*ived *R*adical). We note that the absorption seems also to follow a first order kinetics ($k = 1.4 \times 10^6$ s^{-1}): the precision of the kinetic treatment is not sufficient to decide between the two possibilities. It can be concluded that the relaxation of the transient obeys rather complex kinetics (see the explanation suggested below).

In aerated solutions, the time scale of evolution of the transient SLR is shortened. This demonstrates a quenching process by oxygen which becomes the major deactivation pathway of this species. If we assume that the bimolecular deactivation is negligible, a first order law will hold. Indeed first order kinetics is obtained and the lifetime of the radical is about 380 ns. Thus the quenching rate constant $k_q^{O_2}$ is 1.3×10^9 M^{-1} s^{-1} (a lower value of k_q is determined if a first order rate constant is assumed for the relaxation in nitrogen atmosphere: $k_q^{O_2} = 0.6 \times 10^9$ M^{-1} s^{-1}). First order plots are also obtained for the first part of the relaxation curves which lead to triplet state values of 240 ns in nitrogen atmosphere and 115 ns in aerated solution. The separation of the two contributions (triplet and SLR) is very difficult and the estimated error is large (~30%). Moreover, we believe that 240 ns is the lower limit of the triplet lifetime. The quenching rate constant of the triplet state $k_q^{O_2}$ is about 2×10^9 M^{-1} s^{-1} (Table 1). This value is close to the diffusion limit for benzene $k_q = 5 \times 10^9$ M^{-1} s^{-1} (9). Values with a similar order of magnitude have also been obtained in previous experiments upon carbonyl compounds (7). The triplet lifetime in degassed benzene solution appears to be lower than the value calculated from the Stern–Volmer plot reported by Lewis and Heine (4). In fact, irradiation of DB in presence of naphthalene gives Stern–Volmer plot for quenching of benzaldehyde formation. The slope is about 3100 ± 1500 M^{-1}. A direct measurement of the quenching rate constant (5) gives $k_q = (5 \pm 0.5) \times 10^9$ M^{-1} s^{-1} which is in agreement with the value commonly used. The deduced triplet lifetime is 600 ± 300 ns which is slightly higher than our value. A quenching by an hydrogen donating impurity seems to be ruled out since one should have $k_q[Q] \sim 1.6 \times 10^6$ s^{-1} and $[Q] \sim 1.2$ M if we use the bimolecular rate constant of the photoreduction of benzophenone by isopropanol ($k_r = 1.2 \times 10^6$ M^{-1} s^{-1}).

As the relative concentrations of the triplet and of SLR are a function of the oxygen concentration in the solution (Fig. 1), the following reaction scheme holds in benzene solution (reaction [3]).

[3] ^{3}DB triplet $\xrightarrow{k_\alpha}$ SLR

^{3}DB triplet $\xrightarrow{k_q[O_2]}$ O_{DB+O_2}

Thus the ratio between the concentrations of the radical SLR and of the triplet generated by the picosecond pulse number i can be expressed by:

$$[SLR]_i/[Triplet]_i = k_\alpha/(k_\alpha + k_q[O_2])$$

The total amount of SLR created by the whole train of picosecond pulses is

$$[SLR] = \frac{k_\alpha}{k_\alpha + k_q[O_2]} \sum_i [Triplet]_i$$

Thus

$$\left(\frac{[SLR]}{[Triplet]}\right)_{air} \Big/ \left(\frac{[SLR]}{[Triplet]}\right)_{N_2} = \frac{k_\alpha}{k_\alpha + k_q[O_2]_{air}}$$

where $[O_2]_{air}$ is the oxygen concentration in an aerated solvent solution. As the triplet and the radical relax during the running time of the pumping train

TABLE 1. Kinetic parameters of the triplet state and radical transient of deoxybenzoin as a function of the solvent

Solvent	Triplet state			SLR			LLR		
	τ_T^0 (ns)	τ_T (ns)	$k_q^{O_2}$ (M^{-1} s^{-1})	τ_T^0 (ns)	τ_T (ns)	$k_q^{O_2}$ (M^{-1} s^{-1})	τ_T^0 (ns)	τ_T (ns)	$k_q^{O_2}$ (M^{-1} s^{-1})
Benzene	240	115	2×10^9	710	380	0.6×10^9	—	—	—
THF	—	—	—	370	200	1.1×10^9	—	470	1×10^9
Isopropanol	90	60	2.5×10^9	460	—	—	—	—	—
Methanol	140	80	2.4×10^9	—	—	—	—	—	—

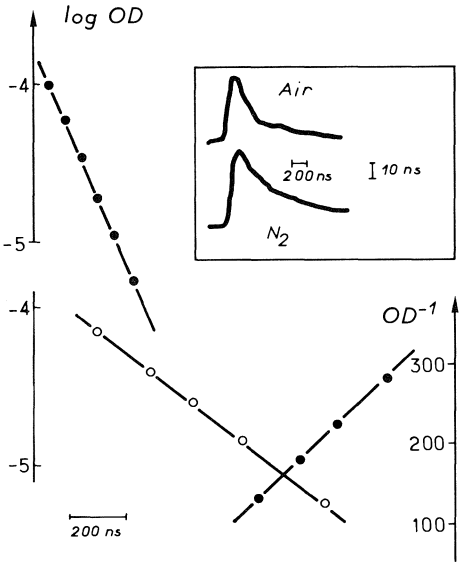

FIG. 1. Typical oscilloscope trace of the transient absorptions observed after laser excitation of deoxybenzoin in benzene under nitrogen atmosphere (λ = 430 nm). First order plot of the triplet relaxation (upper curve). First and second order plot of the fast decaying radical transient (lower curve).

of pulses, the concentrations are corrected to take into account the evolution of the populations between the moment where the *i*th pulse strikes the sample and a chosen value of time (at which the optical densities are measured, t = 100 ns), according to a formula developed elsewhere (10). A corrected value of 0.48 is calculated which is very close to the ratio calculated from the values of k_α, k_q, and $[O_2] = 2 \times 10^{-3}$ M (this value is 0.5). This value corroborates the proposed reaction scheme. Similar results are obtained for LLR. It may be concluded that both SLR and LLR are generated through the triplet state.

In a mixture of benzene and THF (9/1), DB exhibits three transients (Fig. 2). As in benzene, the first one corresponds to the triplet state but its lifetime is shortened, which means that a photoreduction with the solvent occurs as mentioned previously (5). The two other transients are ascribed to radicals. One of them seems to exhibit a very long decay time

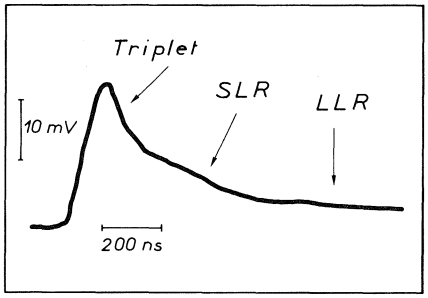

FIG. 2. Typical oscilloscope trace of the transient absorptions observed after laser excitation of deoxybenzoin in aerated solution of a mixture THF–benzene (λ = 430 nm): triplet state, benzoyl radical (SLR), benzyl and ketyl radicals (LLR).

and is still called LLR; its nature will be described later.

By increasing the concentration of THF in benzene, one observes that the relaxation times of both the triplet and the SLR decrease whereas the LLR seems unaffected. From the plot of Fig. 3, a value of the quenching rate constant of the triplet state by THF may be calculated; its value is 4×10^6 M^{-1} s^{-1}. For higher values of the THF concentration, no calculations are available since the triplet absorption at the end of the laser excitation decreases drastically due to the short lifetime of the transient.

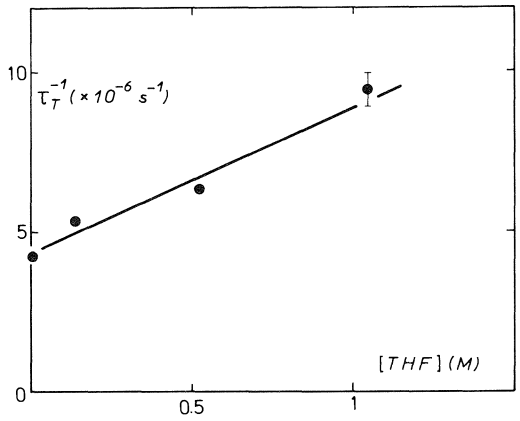

FIG. 3. Stern–Volmer plot of the triplet state lifetime of deoxybenzoin in deaerated benzene solutions as a function of the THF concentration (λ = 430 nm).

The quenching by both O_2 and an hydrogen donating solvent, the value of the lifetime of SLR, and the results of steady state experiments strongly suggest that the SLR radical is the benzoyl radical which is known to yield benzil and benzaldehyde (4) through the reactions

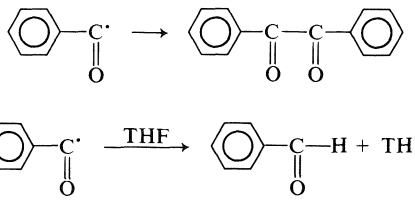

The LLR may be attributed to the benzyl radical. Thus in benzene, it is not surprising that the relaxation of the SLR radical obeys complex kinetics since it has been shown (4) that the quantum yields of benzaldehyde and benzil have the same order of magnitude: the relaxation follows a mixture of a first order law (quenching by benzene) and a second order law (bimolecular recombination). No Stern–Volmer plot can be drawn for the quenching of SLR by THF, in the range of the low THF concentrations, because of the superposition of at least three transients (triplet, benzoyl, benzyl).

In pure THF, we observed mainly the two radicals whose lifetimes are 200 ns for SLR and 470 ns for LLR in aerated solutions, and 370 ns for SLR and in the >10 μs range for LLR in degassed solutions. It is reasonable to assume that the value of 370 ns corresponds to the reciprocal value of the quenching rate constant of SLR by THF. A value of $k_q^{THF} = 2.1 \times 10^5\ M^{-1}\ s^{-1}$ can be derived (a lower value can also be calculated if we take into account the relaxation of the benzoyl radical: $k_q^{THF} = 1.1 \times 10^5\ M^{-1}\ s^{-1}$). The quenching rate constants by oxygen estimated for the two radicals are $1.1 \times 10^9\ M^{-1}\ s^{-1}$ and $1 \times 10^9\ M^{-1}\ s^{-1}$ for SLR and LLR, respectively.

Similar experiments were performed in isopropanol. We observed a triplet state (its lifetime is 90 ns and 60 ns in degassed and aerated solutions, respectively) and two radicals of the same type, a short-lived radical and a long-lived radical. Both of them are quenched by oxygen. The lifetime of SLR in degassed solution is 460 ns which leads to a quenching rate constant of the radical by isopropanol of $1.6 \times 10^5\ M^{-1}\ s^{-1}$, a value which is of the same order of magnitude as the rate constant of the quenching by THF.

The relative values of the α-cleavage and the hydrogen abstraction rate constants can be deduced from the above experiments. With $k_\alpha = 4.2 \times 10^6\ s^{-1}$, values of the rate constant k_r of the photoreduction are estimated to be $2.8 \times 10^6\ s^{-1}$, $6.8 \times 10^6\ s^{-1}$, and $50 \times 10^6\ s^{-1}$ in methanol, isopropanol, and THF respectively (a similar high rate constant in THF, compared with isopropanol, is observed during the photoreduction of benzophenone (9)).

The Ketyl Radical

If we consider the relative concentration of the two radicals originating from the triplet state after the laser excitation, it is found that their ratio is not constant, the concentration of LLR increasing with the hydrogen donating character of the solvent (Table 2). The same phenomenon is observed in the mixture of benzene–THF (Fig. 4). As mentioned above, in benzene solution, the long-lived radical LLR is the benzyl radical resulting from Norrish type I cleavage which appears concomitant to the benzoyl radical. However, the ratio of the concentration of the benzoyl and benzyl radicals must not depend upon the solvent. In agreement with the decrease of the lifetime of the triplet state in hydrogen donating solvents, it is deduced that a ketyl radical formation is observed in these solvents as in benzophenone systems. Thus, the long-lived radical should be the

TABLE 2. Ratio of the absorbances of the short- and the long-lived radicals as a function of the solvent

Solvent	Absorbance
Benzene	0.35
Benzene + THF (1:1)	3.4
THF	3.8
Isopropanol	3.7

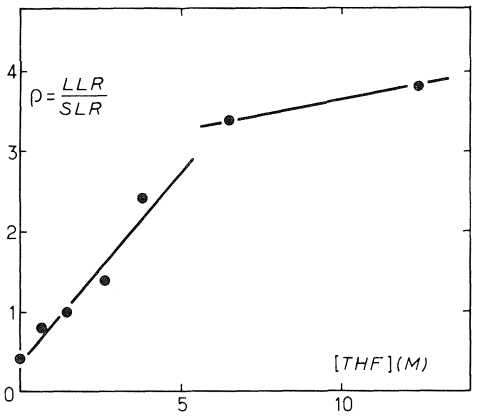

FIG. 4. Ratio of the absorbances of the short and long lived radicals (SLR and LLR) in benzene solutions, under nitrogen atmosphere, as a function of the THF concentrations (λ = 430 nm). The absorbances are taken at $t = 100$ ns and are corrected as in ref. 8. It is assumed that the extinction coefficients of the transients are not (or slightly) dependent upon the wavelength. This is reasonable by considering the shape of the transient absorption band (cf. Fig. 5*b*).

superposition of the two benzyl and ketyl radicals. The following reaction scheme may be written:

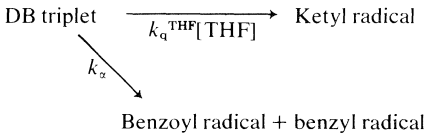

From experiments performed in benzene solution, we conclude that the ratio of the absorption of these two radicals (benzyl and benzoyl) is about 0.35 at 430 nm. Thus, the absorbances of the three transients may be expressed as follows:

$$\frac{\varepsilon_1[\text{benzyl}] + \varepsilon_2[\text{ketyl}]}{\varepsilon_3[\text{benzoyl}]} = \frac{\varepsilon_2 k_q^{THF}[THF] + 0.15\varepsilon_3 k_\alpha}{\varepsilon_3 k_\alpha} = \frac{LLR}{SLR}$$

where LLR and SLR are related to the absorbances of the radicals. With $k_\alpha = 4.2 \times 10^6\ s^{-1}$ (reciprocal value of the triplet lifetime in degassed benzene solution) and $k_q^{THF} = 4 \times 10^6\ M^{-1}\ s^{-1}$, the ratio LLR/SSR is at a first approximation a linear function of the THF concentration; the slope of the straight line is $0.95 \times \varepsilon_2\varepsilon_3^{-1}$. The experimental value is 0.45 (Fig. 4), which means that $2\varepsilon_2 = \varepsilon_3$ at 430 nm. At higher concentrations ($> 6\ M$), the ratio seems to reach a limiting value. This can be interpreted on the assumption that the benzoyl and the benzyl radicals can escape from the solvent cage more easily in THF than in benzene, which increases the benzoyl concentration at the same moment as the ketyl concentration increases. This assumption is in agreement with the conclusion of Lewis *et al.* (4) about the existence of an early transition state with a moderate degree of ionic character depicted as follows:

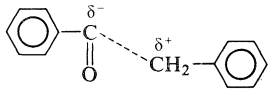

Absorption spectra of the triplet state in benzene and of the radicals in THF are reported in Fig. 5*a* and *b*. The main contribution to the absorption of LLR is due to the ketyl radical, the benzyl radical exhibiting a very low absorption in the visible wavelength range (as observed by recording the absorption spectrum in benzene) which is in agreement with the very weakly structured transition observed in the 4500 Å region (11) (the main absorptions are in the 3100 and 2600 Å regions). Moreover, the lifetime of LLR determined previously in THF can be attributed to the ketyl radical (a lifetime of the same order of magnitude was also measured for the ketyl radical of benzophenone (12)).

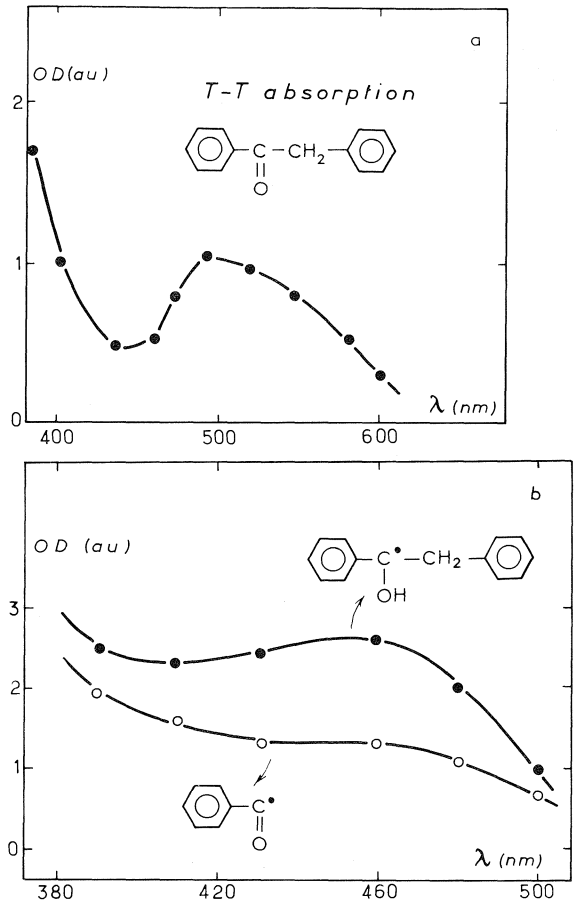

FIG. 5. (*a*) Transient absorption spectrum of deoxybenzoin: triplet state in benzene. (*b*) Transient absorption spectra of deoxybenzoin: benzoyl and ketyl radicals in THF.

DB is known to initiate the uv light induced polymerization of methylmethacrylate (MMA). By adding MMA to solutions of DB in benzene, one observes a substantial decrease of the triplet state lifetime (a quenching rate constant $k_q^{MMA} = 6 \times 10^8\ M^{-1}\ s^{-1}$ is calculated) whereas the relaxations of the radicals seem to be only slightly affected in the concentration range used (10^{-3}–$10^{-1}\ M$). Complete results about the initiation process of the polymerization of MMA will be published elsewhere.

The overall results are summarized in Fig. 6 which shows the evolution of the excited states of DB after uv light excitation. This allows us to explain the photochemistry of DB in benzene solution (4), the influence of the hydrogen donating system, the reactivity of DB in photocrosslinking reactions (13), and the ability of DB to initiate the polymerization of MMA under uv light excitation (6).

After this work had been submitted to publication

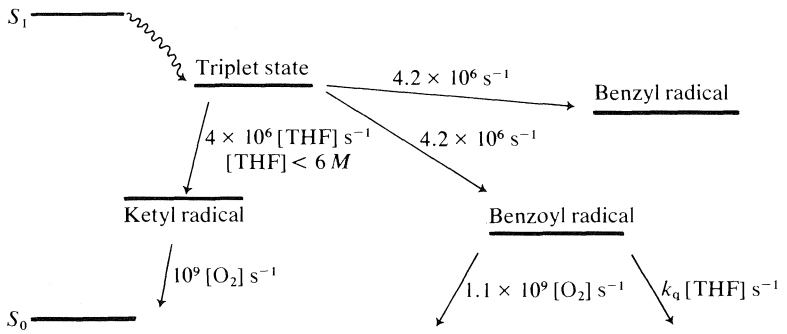

FIG. 6. Diagram showing the evolution of the excited states of deoxybenzoin.

we noted a paper (14) in which the reaction between deoxybenzoin compounds and thiol was investigated. Some measurements were also performed in benzene and in THF which give evidence for the ketyl radical as previously determined (5). However, the benzoyl radical is not observed whereas the absorption of the benzyl radical is reported. This is in contrast with our present work and with measurements on 2,2-dimethoxy-2-phenylacetophenone (15).

Acknowledgments

The authors wish to express their appreciation to Professor J. Faure for helpful comments. We greatly appreciated the help of F. Wieder in operating the ruby laser.

1. F. D. LEWIS, R. T. LAUTENBACH, H. G. HEINE, W. HARTLANN, and H. RUDOLPH. J. Am. Chem. Soc. **97**, 1510 (1975).
2. M. R. SANDNER and C. L. OSBORN. Tetrahedron Lett. **5**, 415 (1974).
3. M. R. SANDNER, C. L. OSBORN, and D. J. TRECKER. J. Polym. Sci. Polym. Chem. Ed. **10**, 3173 (1972); L. H. CARLBLOM and S. P. PAPPAS. J. Polym. Sci. Polym. Chem. Ed. **15**, 1381 (1977); A. LEDWITH. Pure Appl. Chem. **49**, 431 (1977); H. G. HEINE, H. RUDOLPH, and H. J. ROSENKRANZ. J. Polym. Sci. Appl. Polym. Symp. **26**, 157 (1975).
4. F. D. LEWIS, C. H. HOYLE, J. G. MAGYAR, H. G. HEINE, and W. HARTMANN. J. Org. Chem. **40**(4), 488 (1975).
5. J. P. FOUASSIER, D. J. LOUGNOT, and J. FAURE. C.R. Acad. Sci. Paris, **284**, 643 (1977).
6. A. MERLIN and J. P. FOUASSIER. J. Polym. Sci. Polym. Lett. Ed. In press.
7. J. H. STOCKER and D. H. KERN. J. Org. Chem. **33**, 1271 (1968).
8. J. FAURE, J. P. FOUASSIER, D. J. LOUGNOT, and R. SALVIN. Nouv. J. Chim. **1**, 15 (1977).
9. P. J. WAGNER and A. E. KEMPPAINEN. J. Am. Chem. Soc. **91**, 3085 (1969).
10. J. P. FOUASSIER, D. J. LOUGNOT, and J. FAURE. J. Photochem. **7**, 17 (1977).
11. P. M. JOHNSON and A. C. ALBRECHT. J. Chem. Phys. **48**, 851 (1967).
12. J. P. FOUASSIER and A. MERLIN. Unpublished data.
13. J. A. BOUSQUET, J. B. DONNET, J. FAURE, J. P. FOUASSIER, B. HAÏDAR, and A. VIDAL. J. Polym. Sci. Polym. Chem. Ed. **17**, 1685 (1979).
14. G. AMIRZADEH, R. KUHLMANN, and W. SCHNABEL. J. Photochem. **10**, 133 (1979).
15. J. P. FOUASSIER and A. MERLIN. J. Photochem. In press.

A synthetic route to 4-*C*-methyl-*xylo*-furanose

TIM FAT TAM AND BERT FRASER-REID

Guelph–Waterloo Centre for Graduate Work in Chemistry, University of Waterloo, Waterloo, Ont., Canada N2L 3G1

Received May 7, 1979

TIM FAT TAM and BERT FRASER-REID. Can. J. Chem. **57**, 2818 (1979).

3-*O*-benzyl-1,2-isopropylidene-α-D-*xylo*-pentodialdofuranose could not be α-methylated by direct or indirect methods. The aldol product from reaction of the dialdofuranose with formaldehyde could not be trapped, but underwent a Cannizzaro reaction to give the *C*-4-bis-hydroxymethyl product. The latter can be regioselectively sulfonated at the pro-(*S*) hydroxymethyl group. Reduction with lithium aluminum hydride then affords 3-*O*-benzyl-1,2-isopropylidene-4-*C*-methyl-α-D-*xylo*-furanose as the major isomer, the configuration of which is proved by transformation into an oxetane.

TIM FAT TAM et BERT FRASER-REID. Can. J. Chem. **57**, 2818 (1979).

L'utilisation des méthodes directe ou indirecte ne permet pas de méthyler en position α le *O*-benzyl-3 isopropylidène-1,2 α-D-*xylo*-pentodialdofurannose. La réaction du dialdofurannose avec le formaldéhyde conduit à un aldol qui n'a pu être isolé, mais qui, par une réaction de Cannizzaro, peut être transformé en un produit bis-hydroxyméthylé en position C-4. Ce composé peut être sulfoné d'une façon régiosélective au niveau du groupe hydroxyméthyl-pro (*S*). La réduction par l'hydrure double d'aluminium et de lithium conduit alors au composé *O*-benzyl-3 isopropylidène-1,2 *C*-4-méthyl α-D-*xylo*-furannose comme isomère principal. La transformation de cet isomère en oxétanne fournit la preuve de sa configuration.

[Traduit par le journal]

During the past few years there have been impressive developments in the syntheses of *C*-glycofuranosides (1), prompted undoubtedly by the fact that these substances provide easy access to *C*-nucleosides which are chemotherapeutic agents of considerable promise (2). In addition to this substantive goal, these *C*-glycofuranosides may also be viewed as chiral synthons of tetrahydrofuran compounds having functionalized alkyl substituents at positions 2 and 5 which occur in a variety of natural products. Examples of the latter are nonactic acid (3) and many polyether ionophores (4).

A structural feature which presents an added complication is the existence of a methyl group at position 2 (or 5) as shown in the part-structures **1**, **2**, and **3** (Scheme 1) which occur respectively in ipomeamarone and its congeners (5), liatrin (6), and a large number of elemanolides (7). The presence of methyl groups at both positions 2 and 5 (**4**) is found, for example, in citreaviridin (8), and the structural element of jatropone (9), **5**, which may be viewed as an elaborate congener of **3**, presents an even higher degree of complexity.

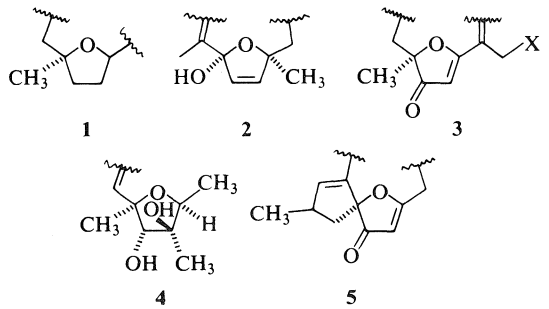

SCHEME 1

In view of the foregoing, we have been investigating synthetic routes to furanose derivatives bearing methyl and (or) functionalized methyl groups at C-4 which might provide access to structures such as those in Scheme 1. It would of course be imperative to know the orientation of the methyl group, and this paper reports some of our work related to this study.

The only example that we could find of a furanose derivative having different functionalized geminal substituents at C-4, was that obtained by Rosenthal and Ratcliffe from photoamidation of a 3-enofuranose (10). Unfortunately the conversions in this otherwise excellent procedure were low and so we decided to examine other substrates.

We turned our attention to the bis-hydroxymethyl derivatives such as **8***a* whose preparation from the readily available aldehyde **7***a* had been reported by Schaffer (11). This reaction indicated that it was possible for a suitable electrophile to capture the enolate derived from **7***a*. However all attempts to α-methylate **7***b* by direct (e.g., LDA/HMPA/MeI) or indirect (Stork enamine alkylation (12)) methods caused the substrate to decompose. Evidently alkylation of **7***b* requires an electrophile which is stronger than methyl iodide.

0008-4042/79/212818-05$01.00/0

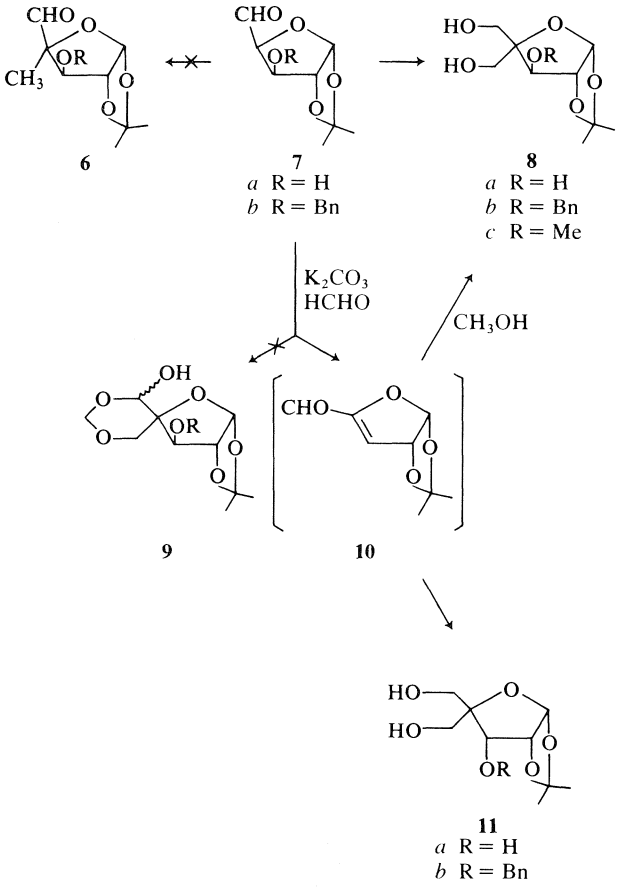

6 7 8
a R = H *a* R = H
b R = Bn *b* R = Bn
c R = Me

9 10

11
a R = H
b R = Bn

SCHEME 2

The work of Just and coworkers summarized in Scheme 3 had shown that by using *potassium carbonate* as base, the initial aldol product (**12**) could be captured as the acetal **13** and therefore prevented from undergoing the Cannizzaro reaction (13). In confirmation of this, Ho had subsequently found that 2,3-*O*-isopropylidene ribose upon treatment with formaldehyde and *potassium carbonate* gave the 2-hydroxymethyl adduct without any Cannizzaro

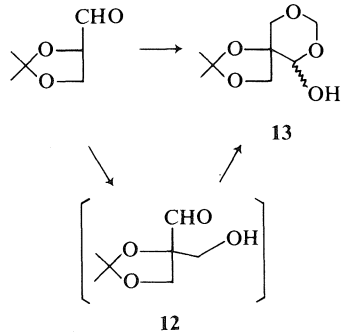

13

12

SCHEME 3

product (14). If **7***b* could be induced to undergo a similar reaction, the product would be **9** which, in view of the different oxidation levels of the two C-4 substituents, would be an attractive synthon for the structures in Scheme 1. However application of these conditions to **7***b* gave, instead of **9**, two products whose structures were shown to be **8***b* and **8***c*.

Identification of the *O*-benzyl derivative **8***b* is based upon an agreeable elemental analysis, and assignment of L-*threo* rather than D-*erythro* (i.e., **11***b*) configuration follows from the fact that the latter, which has recently been prepared by Moffatt and coworkers (15), melts at 101–102°C while our compound **8***b* melts at 73–74°C.

With regard to the *O*-methyl derivative **8***c*, elemental analysis was in agreement with the assigned structure, and from a comparison of the 220 MHz nmr parameters with those of **8***b* (Table 1), it was apparent that both compounds were configurationally related. The formation of **8***c* is most readily explained by invoking the intermediacy of **10**. In fact Leland and Kotick had reported that **7***a* upon treatment with base had given both **8***a* and **11***a*; compound **10** also accounts for their observed "epimerisation" (16). The fact that Just *et al.* (13) (Scheme 3) and Ho (14) observed no comparable unsaturated products is undoubtedly due to the circumstance that the anion in their cases is at position 4 of a dioxolane residue and therefore not well aligned for β-elimination.

In contrast to the foregoing, when sodium hydroxide was used as the base for the condensation on **7***b*, compound **8***b* was obtained in 61% yield without any evidence of products (**8***a* or **11***a*) arising from the elimination–addition sequence. Since the two hydroxyl groups of **8***b* are in very different steric environments it seemed that they might react regioselectively. Consequently the molecule was treated with one equivalent of *p*-toluenesulfonyl chloride.

The product (Scheme 4) consisted of unreacted **8***b*, the disulfonate **14***c* which was obtained in crystalline form, and a mixture of monosulfonates **14***a* and **14***b*. These proved to be unresolved in a variety of tlc systems but an analysis of the 220 MHz spectrum (Experimental) did indicate that an unequal mixture of both had been produced. Based on the integrated ratio of H-1 protons, the two isomers were present in the ratio of 2.2:1.

Some regioselectivity between the two hydroxymethyl groups of **8***b* was therefore possible, but at this stage we were unable to determine whether it was the pro-(*R*) or pro-(*S*) group that had been preferentially sulfonated. This question was answered in the following manner.

The mixture of monotosylates **14**(*a* + *b*) was

TABLE 1. 220 MHz proton magnetic resonance parameters. The carbon atoms are labelled as follows:

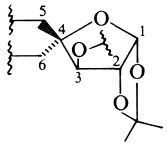

Compound	Chemical shifts (ppm)								Coupling constants (Hz)			
	H-1	H-2	H-3	H-5	H-6	pH CH_2	CH_3CCH_3	Others	$J_{1,2}$	$J_{2,3}$	$J_{5,5'}$	$J_{6,6'}$
8*b*	6.03	4.79	4.12	3.36 – 3.82		4.56–4.79	1.35, 1.55		4.2	2.0	n.d.	n.d.
8*c*	6.00	4.78	3.91	3.59 – 3.77			1.34, 1.55	OCH_3 3.47	5.0	2.0	n.d.	n.d.
14*c*	5.84	4.61	3.82	4.13		4.52, 4.68	1.27, 1.36	ArCH_3 2.45, 2.48	4.0	0	10	
16*b**	6.04	4.66	4.22	3.75	1.39	—	1.36, 1.59	—	4.0	0	12.0	—
16*c*	5.86	4.60	3.95	3.89, 4.11	1.39	—	1.30, 1.48	$ArCH_3$ 2.45	4.0	0	10.0	—
15	6.25	4.72	4.95	4.45, 4.56	1.59	—	1.39, 1.55	—	4.0	0	8.0	—
17*c*	5.86	4.56	4.20	1.33	3.9, 4.23	—	1.23, 1.33	ArCH_3 2.46	4.0	0	10.0	—

*Assignment is based on an 8:1 enriched mixture of **16***b*:**17***b*.

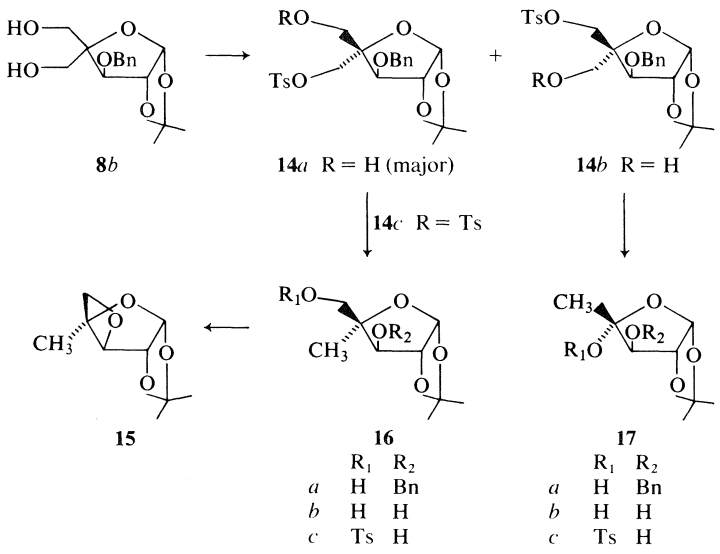

SCHEME 4

reduced with lithium aluminum hydride which afforded another mixture judged to be the *C*-methyl substances **16***a* and **17***a*. This mixture also proved to be non-crystalline and unresolvable on tlc, however debenzylation with sodium in liquid ammonia afforded the mixture of diols, **16***b* and **17***b* in the ratio 2.2:1, as a crystalline material. Fractional crystallization gave a batch of new crystals which was shown by gc analysis to be a 8:1 mixture of **16***b* and **17***b*; in the mother liquors the ratio of the isomers was 1:2, showing an enrichment in the minor product.

The major component of this recrystallized mixture was shown to be **16***b* by transformation into an oxetane by means of a procedure patterned after the work of Hough and Otter (17). Thus the (8:1) diol mixture, **16***b* and **17***b*, was selectively sulfonated at the primary positions, and the crystalline monotosylates obtained, **16***c* and **17***c*, were treated with sodium methoxide in methanol. Only the major component reacted and the newly formed substance was shown to be the oxetane **15**. The unreacted sulfonate **17***c* was recovered and crystallized.

The foregoing results would seem to indicate that in the processing of the mixture **14***a* + **14***b*, the former gave **16***a* while the latter gave **17***a*. However it is conceivable (Scheme 5) that upon treatment with lithium aluminum hydride, both **14***a* and **14***b* react to give the same oxetane **18** as an intermediate which is then cleaved to give the *C*-methyl substances **16***a* and **17***a*.[1] The sequence in Scheme 4 was supported by observing that the relative intensities for

[1]We are grateful to a referee for suggesting this alternative.

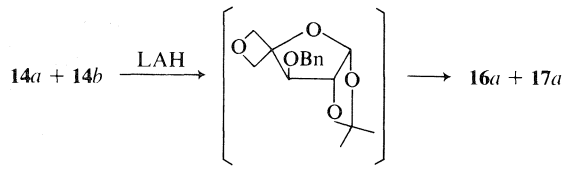

18

SCHEME 5

the anomeric protons (H-1) in the 220 MHz spectra were the same (2.2:1) in the crude mixture of **14**(*a* + *b*) as in the deoxygenated mixtures (**16***a* + **17***a*) and debenzylated mixtures (**16***b* + **17***b*). On the other hand the proposition in Scheme 5 is excluded by our observation that the mixture **14**(*a* + *b*) was recovered unchanged after treatment for five days with sodium methoxide, conditions which had been used for preparing compound **15**. The fact that the oxetane **18** was not formed under these favourable conditions makes it very unlikely that it would have been produced in the manner indicated in Scheme 5.

Other approaches to the preparation of *C*-alkyl furanoses related to the structures in Scheme 1 are being explored in our laboratory and will be reported in due course.

Experimental

General

Melting points were determined on a Fisher-Johns heating stage or a Mel-Temp apparatus, and are uncorrected. The nmr spectra were determined, unless otherwise stated, in deuteriochloroform containing 1% tetramethylsilane as internal standard with a Varian HR 220 or a Varian T-60 spectrometer. Coupling constants were obtained by measuring spacings of spectra judged to be first order.

Thin-layer chromatography (tlc) was performed on precoated 0.2 mm silica gel sheets (E. Merck, F-254) and developed with the solvent indicated. The chromatograms were first viewed under ultraviolet light, then sprayed with concentrated sulfuric acid and heated in an oven for complete visualization.

For column chromatography, E. Merck silica gel (0.05–0.20 mm, 70–325 mesh A.S.T.M.) was used.

Microanalyses were done by the Microanalyses Laboratory, Toronto.

*3-O-Benzyl-4-C-(hydroxymethyl)-1,2-O-isopropylidene-*β*-*L*-threo-pentofuranose* **8***b and its 3-O-Methyl Analogue* **8***c*

(*a*) To a solution of 3-*O*-benzyl-1,2-isopropylidene-α-D-*xylo*-pentodialdofuranose, **7***b* (18) (2.1 g, 7.55 mmol) in methanol (15 mL) was added potassium carbonate (3.6 g, 26 mmol) in water (8 mL) and 14 mL of 37% formaldehyde (172 mmol). The mixture was stirred at room temperature for 16 h at which time tlc in ether indicated that all of the starting material had disappeared. The methanol was removed by evaporation and the residue partitioned between water and methylene chloride. Standard processing afforded a syrup which was chromatographed over silica gel using ether as eluant. In addition to some benzyl alcohol, 0.5 g of **8***b* (24%) and 0.5 g of **8***c* (28%) were obtained, each of which was recrystallized from ether – petroleum ether (30–60°C) mixtures.

For **8***b* mp 73–74°C; $[\alpha]_D^{23}$ −347.7° (*c* 0.26, $CHCl_2$); R_f(ether): 0.55; (ether–benzene (1:1)): 0.16.^{13}Cmr data (TMS): 104.9 (C-1), 84.8 (C-2), 86 (C-3), 89.8 (C-4), 63.4, 63.6 (C-5/C-6), 72.7 (Ph—Ch_2), 26.8, 113.1, 27.4 (CH_3—C—CH_3), 127.6, 128, 128.5 (Ph). *Anal.* calcd. for $C_{16}H_{22}O_6$: C 61.93, H 7.10; found: C 61.87, H 7.24.

For **8***c* mp 86–87°C; $[\alpha]_D^{23}$ −341.5° (*c* 0.7, $CHCl_3$); R_f (ether): 0.30. ^{13}Cmr data (TMS): 104.9 (C-1), 87.1 (C-2), 85.5 (C-3), 89.9 (C-4), 63.4 (C-5/C-6), 26.3, 113.1, 27.3 (CH_3—C—CH_3), 58.3 (O—CH_3). *Anal.* calcd. for $C_{10}H_{18}O_6$: C 51.20, H 7.69; found: C 51.21, H 7.63.

220 MHz nmr data for **8***b* and **8***c* are shown in Table 1.

(*b*) The aldehyde **7***b* (5.0 g; 18 mmol) dissolved in dioxane (10 mL) was treated with formaldehyde (5 mL of 37%; 61.6 mmol) and sodium hydroxide (1.5 g; 37.5 mmol) in water (10 mL) was added, After 2 h at room temperature the solution was neutralized with acetic acid and extracted with methylene chloride. The latter phase was washed with water and sodium bicarbonate and dried (Na_2SO_4). Evaporation afforded a crystalline residue which was recrystallized from ether – petroleum ether (30–60°C) mixture and was found identical to **8***b* obtained in part (*a*). The yield was 3.42 g, 61%.

*3-O-Benzyl-4-C(hydroxymethyl)-1,2-O-isopropylidene 5-O-p-toluenesulfonyl-*α*,D-xylo-furanose* **14**b, *its* β-L-Arabino-*furanose Analogue* **14**a, *and 3-O-Benzyl-4-C-(p-toluenesulfonyloxymethyl)-1,2-O-isopropylidene-5-O-p-toluenesulfonyl-*β*-L-threo-pentofuranose* **14**c

The diol **8***b* (3.42 g, 11 mmol) was dissolved in a mixture of pyridine (5 mL) and dry methylene chloride (10 mL) and a solution of *p*-toluenesulfonyl chloride (2.5 g; 13.2 mmol) dissolved in a small amount of dry methylene chloride was added. The solution was allowed to stand in the freezing compartment of a refrigerator for 20 h and then poured into aqueous sodium bicarbonate. Extraction with methylene chloride and standard processing yielded a syrup which was freed from traces of pyridine by azeotroping with toluene. Column chromatography over silica gel using ether–toluene (1:1) as eluant gave the ditosylate **14***c* (0.7 g, 10.3%), a mixture of monotosylates **14**(*a* + *b*) (2.31 g; 46%), and 0.70 g of unreacted starting material.

The mixture of monotosylates **14**(*a* + *b*) ($M^+ - CH_3$ = 605) failed to crystallize, but the ditosylate **14***c* did, and was recrystallized from hexane.

For **14***c*: mp 81–82°C; $[\alpha]_D^{23}$ −284.8° (*c* 0.4, $CHCl_3$). *Anal.* calcd. for $C_{30}H_{34}O_{10}S_2$: C 58.25, H 5.5, S 10.42; found: C 58.10, H 5.44, S 10.31.

For **14**(*a* + *b*) spectral data, nmr 220 MHz, δ: 4.75 (m, H-2), 4.15 (m, H-3), 3.63 (t, —CH_AH_BOH), 3.84 (d, —CH_AH_BOH, J_{AB} = 15 Hz), 4.08–4.22 (m, —CH_2OTs), 4.56 (d, PhCH_AH_B, J_{AB} = 12 Hz), 4.82 (m, PhCH_AH_B), 1.32, 1.42 (2s, $(CH_3)_2$C).

Tentative assignments for **14***a*: 6.01 (d, H-1, J_{12} = 4.5 Hz); 2.45 (s, Ar—CH_3); for **14***b*: 5.95 (d, H-1, J_{12} = 4.5 Hz); 2.43 (s, Ar—CH_3). Based on the integrated intensities of H-1 protons, the two monotosylates were formed in about 2.2:1 ratio.

*1,2-O-Isopropylidene-4-C-methyl-*α*,D-xylo-furanose* **16**b *and 1,2-O-Isopropylidene-4-C-methyl-*β*,L-arabino-furanose* **17**b

The monotosylate mixture **14**(*a* + *b*) (9.57 g, 20.62 mmol) was dissolved in dry dimethoxyethane (0.30 mL) and lithium aluminum hydride (1.0 g; 26.3 mmol) was added slowly. After hydrogen evolution ceased, the mixture was refluxed for 2.5 h when tlc indicated that all the starting material had disappeared. The solution was diluted with ether and poured into 60 mL of ice cold 2% dilute hydrochloric acid. Ether extraction and evaporation gave a syrupy mixture of **16***a* and **17***a* (3.65 g, 60.5%) which was unresolved on tlc; R_f: 0.5 (15% ether in methylene chloride).

For **16***a* and **17***a* spectral data, nmr 220 MHz, δ: 4.73 (d, H-2), 3.93 (s, H-3), 3.45–3.75 (m, —CH_2OH), 4.56 (d, $PhCH_AH_B$, J_{AB} = 12 Hz), 4.68 (m, $PhCH_AH_B$), 1.55 (s, CH_3). Tentative assignments for **16***a*: 6.05 (d, H-1, J_{12} = 4.5 Hz); 1.38, 1.34 (2s, $(CH_3)_2C$). For **17***a*: 5.91 (s, H-1), 1.27, 1.32 (2s, $(CH_3)_2C$). Mass spectra *m/e*: 279 (M^+—CH_3), 263 (M^+—CH_2OH). Based on the integrated intensities of H-1 protons the two methyl isomers are in 2.2:1 ratio.

The mixture of benzyl ethers **16***a* and **17***a* (3.65 g; 12.5 mmol) was dissolved in dry dimethoxyethane (10 mL) and liquid ammonia (~30 mL) at −40°C. Small pieces of clean sodium were added slowly until a deep blue colour persisted. Solid ammonium chloride was then added until the blue colour disappeared. The solution was allowed to warm up slowly to room temperature and then diluted with ether (25 mL). The ethereal solution was washed twice with water (10 mL) and dried (Na_2SO_4). Evaporation afforded a crystalline residue. Based on the integrated intensities of the H-1 protons, the ratio of the two isomers remained 2.2 to 1.

The residue was recrystallized from ether – petroleum ether (30–60°C) (1.85 g, 73% from **16***a* and **17***a*). Gas–liquid chromatographic analysis of the recrystallized product indicated the presence of the two components **16***b* and **17***b* in the ratio of 8:1. Evaporation of the mother liquors afforded a pale yellow semi-solid syrup. Analysis (glc) of this residue showed the presence of the two isomers in the ratio of 1:2.

For **16***b* and **17***b* (8:1 mixture) mp 92–93°C. ^{13}Cmr data for major isomer (TMS): 105.4 (C-1), 88.6 (C-2), 81.8 (C-3), 87.2 (C-4), 67.2 (C-5), 22.7 (C-6), 26.3, 112.5, 26.8 (CH_3—C—CH_3). *Anal.* calcd. for $C_9H_{16}O_5$: C 52.94, H 7.8; found: C 53.06, H 7.78.

R_f(10% methanol CH_2Cl_2): 0.55 (major isomer); 0.30 (minor isomer).

*1,2-*O*-Isopropylidene-4-*C*-methyl-5-*O*-*p*-toluenesulfonyl-*α*,*D*-xylo-furanose* **16***c and 1,2-*O*-Isopropylidene-4-*C*-methyl-5-*O*-*p*-toluenesulfonyl-*β*-*L*-arabino-furanose* **17**c

A portion (0.646 g; 3.17 mmol) of the recrystallized mixture of the diols **16***b* and **17***b* (8:1 ratio) was dissolved in a mixture of dry pyridine (3 mL) and methylene chloride (5 mL), and *p*-toluenesulfonyl chloride (0.664 g; 3.39 mmol) in methylene chloride (5 mL) was added. The solution was stored in the freezing compartment of a refrigerator for 16 h and then worked up as described above for **14**(*a* + *b*). Column chromatography on silica using a 7:3 mixture of ethyl acetate and petroleum ether (30–60°C) afforded 0.751 g of the monotosylate mixture **16***c* and **17***c*, and 0.229 g of unreacted starting material. Although the 220 MHz nmr spectrum was consistent with the mixture as assigned, the material did crystallize from ether – petroleum ether (30–60°C) mixtures and was recrystallized from ether–hexane.

For **16***c* + **17***c* mp 99–102°C. *Anal.* calcd. for $C_{16}H_{22}O_7S$: C 53.63, H 6.14, S 8.94; found: C 53.35, H 6.23, S 8.54.

*3,5-Anhydro-1,2-*O*-isopropylidene-4-*C*-methyl-*α*,*D*-xylo-furanose* **15**

Clean sodium (0.360 g) was dissolved in dry methanol (25 mL) and the mixture of sulfonates (0.704 g; 1.97 mmol) was added. After standing at room temperature for 30 h, tlc (35% ethyl acetate in petroleum ether) indicated the formation of a major new substance. The reaction mixture was evaporated to dryness and the syrupy residue partitioned between water and ether. The ether extract was washed with water, dried (Na_2SO_4), and evaporated to yield a pale syrup which was chromatographed on a column of silica gel using 35% ethyl acetate in petroleum ether as eluant. The oxetane **15** (R_f (35% EtOAc in petroleum ether): 0.55) was isolated in 71% yield and 81 mg of the monotosylate **17***c* (R_f (35% EtOAc in petroleum ether): 0.32 (30–60°C)), was recovered unchanged.

Compound **17***c* was recrystallized from ether – petroleum ether (30–60°C), mp 134–135°C; $[\alpha]_D^{23}$ −186.2° (*c* 0.34, $CHCl_3$).

For **15** $[\alpha]_D^{23}$ −33.7° (*c* 1.34, $CHCl_3$); *m/e*: 186 (M^+), 171 ($M^+ - CH_3$), 156 ($M^+ - 2CH_3$), 128 ($M^+ - CH_3$-$COCH_3$).

Nuclear magnetic resonance data for **15** and **17***c* are shown in Table 1.

Acknowledgements

We are grateful to the Natural Sciences and Engineering Research Council of Canada, Merck, Sharp, and Dohme (Rahway), and Bristol Laboratories (Syracuse) for financial support. We are indebted to the Canadian 220 MHz NMR Centre for determining the spectra.

1. S. Hanessian and A. G. Pernet. Adv. Carbohydr. Chem. Biochem. **33**, 111 (1976); G. Just and A. Martel. Tetrahedron Lett. 1517 (1973); L. Kalvoda, J. Farkas, and F. Sorm. Tetrahedron Lett. 2297 (1970); J. G. Buchanan, A. D. Dunn, and A. R. Edgar. J. Chem. Soc. Perkin Trans. I, 68 (1976); H. Ohrui, G. H. Jones, J. G. Moffatt, M. L. Maddox, A. T. Christensen, and S. K. Byram. J. Am. Chem. Soc. **97**, 4602 (1975).
2. K. Gerzon, D. C. Delong, and J. C. Kline. Pure Appl. Chem. **28**, 489 (1971); R. J. Suhadolnik. Nucleoside antibiotics. Wiley-Interscience, New York. 1970; J. J. Fox, K. A. Watanabe, and A. Bloch. Prog. Nucl. Acad. Mol. Biol. **5**, 251 (1966).
3. W. Keller-Schierhein and H. Gerlach. Fortschr. Chem. Org. Naturst. **26**, 161 (1978).
4. N. D. Jones, M. O. Chaney, J. W. Chamberlin, R. L. Hamill, and S. Chen. J. Am. Chem. Soc. **95**, 3399 (1973); T. J. Petcher and H. P. Weber. Chem. Commun. 697 (1974); N. Otake, M. Koenunia, H. Kinashi, S. Sato, and Y. Saito. Chem. Commun. 92 (1975).
5. I. Vritani and T. Akazawa. Science, **121**, 216 (1955); T. Kametani, H. Nemoto, and K. Fukumoto. Heterocycles, 1365 (1977).
6. S. M. Kupchan, V. H. Daves, T. Fujita, M. R. Cox, R. J. Restivo, and R. F. Bryan. J. Org. Chem. **38**, 1853 (1973).
7. R. F. Raffanf, P. K. C. Huang, P. W. Le Quesne, S. B. Levery, and T. F. Brennan. J. Am. Chem. Soc. **97**, 6884 (1975); W. Vichnewski, S. J. Sarti, B. Gilbert, and W. Herz. Phytochemistry, **15**, 191 (1976); A. R. De Vivar. C. Guerrero, E. Diaz, E. A. Bratoeff, and L. Jimenez. Phytochemistry, **15**, 525 (1976).
8. N. Sakabe, T. Goto, and Y. Hirata. Tetrahedron Lett. 1825 (1964).
9. S. M. Kupchan, C. W. Sigel, M. J. Matz, C. J. Gilmore, and R. F. Bryan. J. Am. Chem. Soc. **98**, 2295 (1976).
10. A. Rosenthal and M. Ratcliff. Carbohydr. Res. **54**, 61 (1977).
11. R. Schaffer. J. Am. Chem. Soc. **81**, 5452 (1959).
12. G. Stork and S. R. Dowd. J. Am. Chem. Soc. **85**, 2178 (1963); J. M. Conia and P. Briet. Bull. Soc. Chim. Fr. 3881 (1966); 3888 (1966).
13. G. Just, B. T. Chung, G. Ruseberg, and M. Dupre. Can. J. Chem. **54**, 1260 (1976).
14. P. T. Ho. Tetrahedron Lett. 1623 (1978); Can. J. Chem. **57**, 381 (1979); **57**, 384 (1979).
15. R. Youssefyeh, D. Tegg, J. P. H. Verheyden, G. H. Jones, and J. G. Moffat. Tetrahedron Lett. 435 (1977).
16. D. L. Leland and M. P. Kotick. Carbohydr. Res. **28**, C9 (1974).
17. L. Hough and B. A. Otter. Carbohydr. Res. **4**, 126 (1967).
18. R. C. Anderson. Ph.D. Thesis, University of Waterloo, Waterloo, Ont. 1978.

Structure et réactivité. IV.[1] Diastéréosélectivité de la réduction de cétones par le borohydrure de sodium. De l'influence de l'effet de champs de substituants polaires éloignés

JEAN-PIERRE AYCARD ET RONALD LAFRANCE

Laboratoire de Chimie Organique Structurale, Université de Provence, 13397 Marseille Cedex 4, France

ET

BERNARD BOYER

Laboratoire de Chimie Organique Physique, Université des Sciences et Techniques du Langue doc 34060 Montpellier Cedex, France

Reçu le 17 avril 1979

JEAN-PIERRE AYCARD, RONALD LAFRANCE et BERNARD BOYER. Can. J. Chem. **57**, 2823 (1979).

L'influence d'un substituant cyano est étudiée à travers la réduction par $NaBH_4$ des *R*-3 cyano-4 cyclohexanones *cis* et *trans*, nulle pour R = H, la diastéréosélectivité est respectivement de 74 et 62% (R = CH_3), et de 74 et 50% (R = $(CH_3)_3C$), avec formation préférentielle de l'isomère thermodynamiquement le plus stable. Ces stéréosélectivités sont justifiées à partir des valeurs expérimentales des différences d'enthalpie libre entre conformères et des diastéréosélectivités observées pour les *t*-butyl-3 (et 4) cyclohexanones et les *cis* dimethyl-3,5 et trimethyl-3,3,5 cyclohexanones sans qu'il soit nécessaire de tenir compte d'une influence spécifique du groupement cyano. La diminution de la diastéréosélectivité pour R = $(CH_3)_3C$, isomère *trans*, est associée aux déformations issues des contraintes stériques entre les substituants.

JEAN-PIERRE AYCARD, RONALD LAFRANCE, and BERNARD BOYER. Can. J. Chem. **57**, 2823 (1979).

The cyano group effect on diastereoselectivity is studied through the reduction of *cis* and *trans* 3-*R* 4-cyano cyclohexanones with $NaBH_4$; the diastereoselectivity (zero for R = H) is 74 and 62% respectively (R = CH_3) and 74 and 50% (R = $(CH_3)_3C$), the more stable isomer being always the major one. These stereoselectivities are rationalized from the experimental values of free enthalpy between conformers and from the diastereoselectivities of the 3-*t*-butyl (and 4-*t*-butyl) cyclohexanones, *cis* 3,5-dimethyl and 3,3,5-trimethyl cyclohexanones, without taking account of a cyano group specific effect. The decrease in diastereoselectivity for R = $(CH_3)_3C$ (*trans* isomer) is associated with deformation induced by steric strain between the substituents.

Introduction

Depuis les travaux d'Akhrem et ses collaborateurs sur la réduction des *t*-butyl-3 méthoxy-4 cyclohexanones *cis* et *trans* (2), il est généralement admis que la position conformationnelle du substituant polaire en 4 influence sérieusement la diastéréosélectivité de la réduction des cyclohexanones qui évolue de 76 à 40% en passant de l'isomère *cis* à l'isomère *trans*. Ce point de vue a été renforcé par les travaux de Moreau (3) portant sur la réduction des *t*-butyl-2 X-4 cyclohexanones *cis* et *trans*.

Cependant, dans ces deux exemples, les auteurs considèrent uniquement une structure chaise classique des substrats. Or, il a été montré que pour les *t*-butyl-3 X-4 cyclohexanones *trans* (4, 5), qui présentent une forte interaction stérique entre les substituants, les conformères twist (6) sont appréciablement peuplés. De même, en relation avec le second exemple, nous devons rappeler que la *t*-butyl-2 cyclohexanone présente un équilibre conformationnel correspondant à une différence d'enthalpie libre de 1.6 kcal mol^{-1} (7).[2] De plus, dans ce type de structure, le groupement *t*-butyl vicinal du centre de réaction exerce très certainement dans les états de transition des contraintes stériques très importantes (8, 1).

Dans ces conditions, et au vu de plusieurs travaux récents faisant intervenir des chemins réactionnels issus de conformères de haute énergie (9, 10), l'influence de la position conformationnelle du substituant polaire sur la diastéréosélectivité reste un problème ouvert que nous pouvions aborder aisément compte tenu de nos études conformationnelles sur les *R*-3 cyano-4 cyclohexanones isomères (5).

Résultats et discussion

A partir des pourcentages des alcools mesurés par cppv (cf. partie expérimentale), nous précisons dans

[1]Pour partie III voir ref. 1.

[2]Il est possible d'envisager ici, l'existence d'un conformère de structure twist 1,4 avec un pseudo axe C_2 passant par les carbones C_1 et C_4.

0008-4042/79/212823-04$01.00/0

TABLEAU 1. Diastéréosélectivités expérimentales des réductions par $NaBH_4$; ( ) valeurs calculées

	R	X	%2	%5	%2–%3	%5–%6
a	H	CN	50		0	
b	CH_3	CN	87	81	74 (72)	62 (60)
c	$(CH_3)_3C$	CN	87	75	74 (76)	50
d(2)	$(CH_3)_3C$	OCH_3	88	70	76 (76)	40
e	$(CH_3)_3C$	H	85		70	
f(12)	H	$(CH_3)_3C$	83		66	

le tableau 1, les diastéréosélectivités de la réduction de nos composés (voir schéma 1), ainsi que celles obtenues lors de la réduction des *t*-butyl-3 méthoxy-4 cyclohexanones et des *t*-butyl-4 (11) et *t*-butyl-3 cyclohexanones (12).

Dans ce tableau, les valeurs indiquées entre parenthèses ont été calculées à partir de l'équation d'Eliel (13, 14), en considérant une structure chaise des différents conformères. Ces valeurs sont obtenues en utilisant les valeurs des équilibres conformationnels déterminés pour les différentes cétones (4, 5) et les diastéréosélectivités de cétones modèles (*t*-butyl-3 et *t*-butyl-4 cyclohexanones pour les cétones **1***c*, **1***d*, **4***c* et **4***d*; diméthyl-3,5 cyclohexanone *cis* (12) et triméthyl-3,3,5 cyclohexanone (12) pour les cétones méthylées **1***b* et **4***b*).

Dans ces conditions, la diastéréosélectivité nulle observée pour la réduction de la cyano-4 cyclohexanone **1***a* peut s'expliquer facilement en tenant compte de la valeur de la différence d'enthalpie libre conformationnelle de ce composé ($\Delta G^0 = 0$ kcal·mol^{-1}). Un calcul identique effectué à partir de la chloro-4 cyclohexanone qui présente 67% de forme axiale (15), conduit à une diastéréosélectivité de 28% (32% expérimentalement (16)).

La deuxième remarque que nous pouvons faire est le bon accord observé entre les valeurs calculées, sans tenir compte d'un effet spécifique du groupement CN, et les valeurs expérimentales issues de la réduction des cétones bloquées **1***c* et **1***d*, ou présentant un équilibre entre deux conformations chaises (**1***b* et **4***b*).

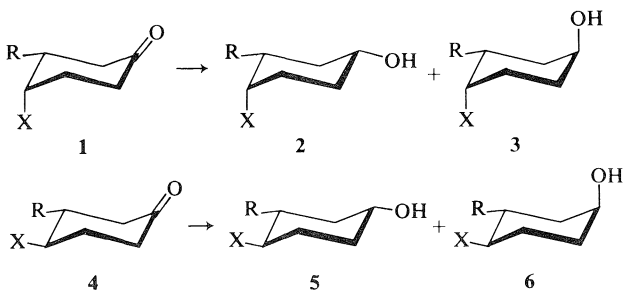

	a	*b*	*c*	*d*	*e*	*f*
R	H	CH_3	$(CH_3)_3C$	$(CH_3)_3C$	$(CH_3)_3C$	H
X	CN	CN	CN	OCH_3	H	$(CH_3)_3C$

SCHÉMA 1. Numérotation des composés.

Cette concordance des valeurs montre que contrairement au cas des cétones portant un substituant polaire en position 3, et en particulier un groupement cyano (17, 18), l'existence d'un tel substituant en position 4 ne modifie aucunement la diastéréosélectivité de la réduction du carbonyle par $NaBH_4$.

Dans ces conditions, la diminution observée pour les cétones **4***c* et **4***d* (cf. tableau 1) par rapport à **1***c* et **1***d* ne peut être imputée à un effet de champ du groupement polaire en position 4. Par contre, pour ces cétones, l'existence d'une importante interaction *gauche* entre les groupements *t*-butyle et X-4 conduit à la présence d'un équilibre conformationnel entre une forme chaise à substituants diéquatoriaux et une forme twist (6).

On peut donc considérer que pour ces composés la perte de diastéréosélectivité peut, soit être due à une intervention importante des conformères twist, soit à une diminution de l'entrée axiale dans le conformère chaise.

Afin de vérifier ces deux hypothèses, nous avons effectué une étude cinétique de la réduction des cétones **1***a*, **1***c* et **4***c* et comparé les valeurs obtenues (cf. tableau 2) aux résultats de Rickborn et Wuesthoff (19) et Boyer (20).

La première observation que nous pouvons faire au vu des résultats du tableau 2, est l'effet d'accélération du groupement cyano; cet effet est par ailleurs analogue à celui d'un groupement chlore placé dans une situation semblable (16).

De plus, nous devons noter que cet effet d'accélération est peu dépendant de la position conformationnelle du groupement CN puisque les rapports k(**1***c*)/k(**1***e*) et k(**1***a*)/k(cyclohexanone) sont voisins et égaux à 11.8 et 14.3 respectivement. En effet, alors que **1***c* possède un groupement CN axial, la préférence conformationnelle de ce groupement est nulle dans **1***a*. Donc, ici encore l'effet d'un substituant polaire en position 4 est très différent de celui observé lorsqu'il est en position 3, position pour laquelle Agami *et al.* (18) ont montré qu'il existait

TABLEAU 2. Constantes de vitesse expérimentales

Cétones	k (M^{-1} s^{-1})	k (relatif)
Cyclohexanone (16)	0.173	100
1*e*	0.105	61
1*a*	2.469	1427
Chloro-4 cyclohexanone (16)	2.34	1352
1*c*	1.242	7.8
4*c*	0.641	371
tert-Bu-3,5 cyclohexanone *cis* (20)	0.00139	0.80

une accélération de 100 environ pour l'attaque équatoriale d'un carbonyle substitué en β par un groupement cyano.

Si nous considérons maintenant la valeur de la constante de vitesse obtenue pour **4***c* ($k = 0.641\ M^{-1}\ s^{-1}$), nous voyons qu'elle est pratiquement de l'ordre de grandeur des constantes de vitesse obtenue pour la cyclohexanone et la *t*-butyl-3 cyclohexanone **1***e* ($k = 0.173$ et $0.105\ M^{-1}\ s^{-1}$ respectivement); mais cent fois plus grande que celle obtenue lors de la réduction d'une cétone de conformation twist, la *t*-butyl-3,5 cyclohexanone *cis* ($k = 0.139 \times 10^{-1}\ M^{-1}\ s^{-1}$) (20). Par contre, si nous considérons la cétone **4***c* comme un mélange équimolaire de forme chaise et de forme twist, nous obtenons une constante de vitesse

$$k = \frac{k\ \text{twist}}{2} + \frac{k\ \mathbf{1}c}{2} = 0.622\ M^{-1}\ s^{-1}$$

soit une valeur très proche de la valeur expérimentale.

Dans ces conditions et en accord avec les travaux de Geneste *et al.* (21), nous devons considérer que **4***c* a une réactivité trop grande par rapport à celle d'une forme croisée, et que seule doit intervenir dans la réaction de réduction la conformation chaise. Aussi devons nous attribuer la perte de diastéréosélectivité de **4***c* et vraisemblablement celle de **4***d* à une réactivité particulière du conformère chaise de ces dérivés, due aux contraintes stériques existant entre les substituants *trans* diéquatoriaux. En effet, il faut rappeler que ce type de dérivés cyclohexaniques présentant un groupement *t*-butyle *trans* d'un substituant X-vicinal est fortement déstabilisé par rapport à leur isomères *cis* (22).

Conclusion

Ce travail nous a permis de montrer que la perte de diastéréosélectivité observée lors de la réduction des *t*-Bu-3 X-4 cyclohexanones n'est pas due à un effet de champ spécifique du groupement polaire en position 4, mais très certainement à une modification de réactivité issue des contraintes stériques existant dans ce type de composés.

Partie expérimentale

Synthèse des composés

La réduction des cétones est effectuée dans un mélange eau/méthanol (50/50) à température ambiante.

Dans un ballon de 100 cc pourvu d'une agitation magnétique, et contenant 0.02 mol de $NaBH_4$ dans 10 cc du mélange eau/méthanol 50/50, on verse 10 cc d'une solution $2 \times 10^{-4}\ M$ de cétone. L'avancement de la réaction est suivi par cppv. Lorsque toute la cétone a réagi, le mélange est hydrolysé, puis extrait à l'éther. La phase organique est séchée sur $MgSO_4$ puis évaporée.

Les pourcentages d'alcool sont mesurés par cppv à l'aide d'un intégrateur LTT 4000, et corrigés de l'effet de réponse par l'utilisation de mélanges étalons. Dans tous les cas, nous avons vérifié que le pourcentage n'évoluait pas dans le mélange réactionnel. Les différents alcools sont séparés par cppv puis identifiés par rmn et ir.

Conditions d'analyses

Les analyses chromatographiques ont été effectuées sur un appareil GIRDEL 3000 à 160°C sur une colonne de longueur 3m, diamètre 3.5 mm, phase stationnaire Carbowax 4000 10% sur chromosorb W 60/80.

La séparation des composés est effectuée sur un appareil Aérograph 90 P.

Identification des composés

Pour les composés **2***a* et **5***a*, ainsi que pour les dérivés *t*-butylés **2***c* et **5***c* l'identification a été effectuée à partir des spectres rmn des alcools deutériés en position 2,2,6,6 (23).

L'infrarouge (ir)

2*a*: 3600, 3450, 2960, 2880, 2240 cm^{-1}; **5***a*: 3600, 3460, 2980, 2960, 2240 cm^{-1}; **2***c*: 3610, 3460, 2960, 2860, 2240 cm^{-1}; **5***c*: 3610, 3490, 2980, 2870, 2240 cm^{-1}; **6***c*: 3620, 3490, 2990, 2880, 2440 cm^{-1}.

La résonance magnétique nucleaire (rmn)

L'étude rmn des alcools **2***a*, **5***a*, **2***c* et **5***c* spécifiquement deutériées en positions 2,2,6,6 a été décrite par ailleurs (23). Tous les spectres ont été enregistrés à température ambiante sur un appareil EM 360 en solution dans $CDCl_3$. **2***b* CH_3 1.8, *H*—C—CN 2.45–2.7, CH_2 et *H*—C—R 1.1–2.1, *H*—COH 3.6; **3***b* CH_3 1.2; **5***b* CH_3 1.15, *H*—CN, CH_2 et *H*—C—R 1.1–2.4, *H*—C—OH 3.6; **6***b* CH_3 1.1, *H*—CN, CH_2 et *H*—CR 1.1–2.4, *H*—C—OH 4.0; **3***c* $C(CH_3)_3$ 4.0; **6***c* $C(CH_3)_3$ 1.0, *H*—C—CN 2.2, CH_2 et *H*—C—R 1.1–2, *H*—CO—H 4.0. Les produits **3***b* et **3***c* en trop petite quantité n'ont pas pu être isolés.

Conditions cinétiques

Les conditions de concentration et de solvant sont les mêmes que celles de Geneste et Lamaty (24): eau–dioxanne 50/50 en volume, 0.05 *N* en soude. La réaction est suivie à 25.0 ± 0.1°C par spectrophotométrie uv à une longueur d'onde ($\lambda = 285$ nm) pour laquelle seule la cétone de départ absorbe. Les constantes de vitesse d'addition de BH_4^- ont été mesurées selon un procédé décrit par ailleurs (25). Pour chaque produit nous avons effectué 6 mesures.

1. M. MONNIER et J. P. AYCARD. Can. J. Chem. **57**, 1257 (1979).
2. A. A. AKHREM, A. V. KAMERNITSKII et A. M. PROKHODA. Zh. Org. Khim. **3**, 46 (1967); **3**, 57 (1967).
3. G. MOREAU. Bull. Soc. Chim. 2814 (1972).
4. R. D. STOLOW, T. GROOM et D. I. LEWIS. Tetrahedron Lett. 913 (1969).
5. R. LAFRANCE, J. P. AYCARD, J. BERGER et H. BODOT. Org. Magn. Reson. **8**, 95 (1976).
6. R. VIANI, J. LAPASSET, J. P. AYCARD, R. LAFRANCE et H. BODOT. Acta Crystallogr. Sect. B, **34**, 1190 (1978).

7. N. L. ALLINGER et H. M. BLATTER. J. Am. Chem. Soc. **83**, 994 (1961).
8. J. C. RICHER et D. EUGENE. Can. J. Chem. **47**, 2387 (1969).
9. D. C. WIGFIELD, S. FEINER et D. J. PHELPS. J. Org. Chem. **40**, 2533 (1975).
10. D. C. WIGFIELD et D. J. PHELPS. J. Am. Chem. Soc. **96**, 543 (1974).
11. H. HANDEL et J. L. PIERRE. Tetrahedron Lett. 2029 (1976).
12. T. WIPKE et P. GUND. J. Am. Chem. Soc. **98**, 8107 (1976).
13. E. L. ELIEL. Stereochemistry of carbon compounds. McGraw Hill, New York. 1962. p. 238.
14. R. O. HUTCHINS. J. Org. Chem. **42**, 920 (1977).
15. R. D. STOLOW et T. W. GIANTS. Chem. Commun. 529 (1971).
16. H. KWART et T. TAKESHITA. J. Am. Chem. Soc. **84**, 2833 (1962).
17. W. NAGATA, T. WAKABAYASHI, N. NARISADA et Y. HAYASE. J. Chem. Soc. C, 2415 (1971).
18. (*a*) C. AGAMI, A. KAZAKOS et J. LEVISALLES. Tetrahedron Lett. 2035 (1975); (*b*) 4073 (1977).
19. B. RICKBORN et M. T. WUESTHOFF. J. Am. Chem. Soc. **92**, 6894 (1970).
20. B. BOYER. Thèse d'état. Université des Sciences et Techniques du Languedoc, Montpellier. 1978.
21. P. GENESTE, G. LAMATY et J. P. ROQUE. Tetrahedron Lett. 5007 (1970).
22. J. P. AYCARD et H. BODOT. Can. J. Chem. **51**, 741 (1973).
23. J. P. AYCARD et R. LAFRANCE. Soumis pour publication.
24. P. GENESTE et G. LAMATY. Bull. Soc. Chim. Fr. 669 (1968).
25. B. BOYER, G. LAMATY, J. P. ROQUE et P. GENESTE. Recl. Trav. Chim. Pays-Bas, **93**, 260 (1974).

The structure and fragmentation of protonated carboxylic acids in the gas phase

NORA E. MIDDLEMISS AND ALEX. G. HARRISON

Department of Chemistry, University of Toronto, Toronto, Ont., Canada M5S 1A1

Received May 28, 1979

NORA E. MIDDLEMISS and ALEX G. HARRISON. Can. J. Chem. **57**, 2827 (1979).

Gaseous protonated acids fragment in the first drift region of a double focussing mass spectrometer to yield the corresponding acylium ion and water. The metastable peaks for this fragmentation reaction have been recorded for the protonated acids from acetic to valeric and the kinetic energy release distributions evaluated from the metastable peak shapes. The protonated acids were produced by dissociative ionization of the ethyl, propyl, and butyl esters. The results provide evidence for two structures for gaseous protonated acids. Fragmentation of the hydroxyl protonated structure, a minor contributor to the metastable peak intensity, shows a low kinetic energy release (T(most probable) = 0.02 eV) as would be expected for a simple bond fission reaction. Fragmentation of the carbonyl protonated acid, which represents the major part of the metastable peak, is accompanied by a much larger kinetic energy release (T(most probable) = 0.30 to 0.43 eV). This result is interpreted in terms of an activation barrier for fragmentation of the carbonyl protonated acid which is considerably greater than the reaction endothermicity, with the excess energy being partitioned between internal energy and kinetic energy of the fragments. The results indicate that the addition of the acylium ion to water in the gas phase to produce the carbonyl protonated acid has an activation energy barrier.

NORA E. MIDDLEMISS et ALEX G. HARRISON. Can. J. Chem. **57**, 2827 (1979).

Les acides protonés à l'état gazeux se fragmentent dans la première région de dérive d'un spectromètre de masse à double champ en donnant les ions acylium correspondants et de l'eau. On a enregistré les pics métastables provenant de la fragmentation d'une série d'acides protonés allant de l'acide acétique à l'acide valérique et on a évalué, à partir de la forme de ces pics, les distributions de l'énergie cinétique libérée. Les acides protonés proviennent d'une dissociation ionique des esters éthylique, propylique et butyrique. Ces résultats prouvent que les acides protonés existent sous deux formes structurales. La fragmentation de la forme protonée au niveau du groupe hydroxyle, forme qui contribue faiblement à l'intensité du pic métastable, libère une faible énergie cinétique (T = 0.02 eV probablement) ce qui correspond à l'énergie libérée lors d'une simple rupture de liaison. La fragmentation de l'acide protoné au niveau du groupe carbonyle, forme qui contribue principalement à l'intensité du pic métastable, est accompagnée d'une plus grande libération d'énergie cinétique (T = 0.30 à 0.43 eV probablement). On interprète ces résultats en fonction d'une barrière d'énergie d'activation, de la réaction des acides protonés au niveau du carbonyle considérablement plus élevée que l'endothermicité de la réaction. L'excès d'énergie étant réparti entre l'énergie interne et l'énergie cinétique des fragments. Ces résultats révèlent que la formation de l'acide protoné au niveau du groupe carbonyle, par suite de l'addition de l'ion acylium à l'eau dans la phase gazeuse, a une barrière d'énergie d'activation.

[Traduit par le journal]

Introduction

A common fragmentation reaction in the electron impact mass spectra of carboxylic esters is the double hydrogen transfer reaction [1], leading to formation of the protonated acid ion $RCO_2H_2^+$.

[1] $RCO_2R' + e \rightarrow RCO_2H_2^+ + [R' - 2H] + 2e$

Although both the mechanisms[1] and the energetics (2–5) of the rearrangement process have been studied extensively, only recently has it been established (6) that the ion formed at the appearance potential threshold has the carbonyl protonated structure *a*,

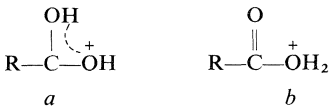

a

b

rather than the hydroxyl protonated structure *b*, although the results do not preclude the formation of *b* at higher electron energies. From proton affinity – O(1*s*) ionization energy correlations it has been established (7) that structure *a* is more stable than *b* by $\gtrsim$ 1 eV.

Protonated carboxylic acid ions also are observed (8–13) as major fragment ions in the chemical ionization mass spectra of ethyl and higher esters. Although the structure of these fragment ions is not known

[1]The earlier mechanistic studies are summarized in refs. 1*a* and *b*, more recent studies are reported in refs. 1*c* and *d*.

0008-4042/79/212827-07$01.00/0

arguments have been presented (12) which support the carbonyl protonated structure *a*.

As expected, protonated carboxylic acid ions are observed (14, 15) in the chemical ionization mass spectra of carboxylic acids, and from the effect of *ortho* substituents on the CI mass spectra of benzoic acid it has been suggested that H_2O elimination from the carbonyl protonated structure has a high activation barrier. Kebarle and co-workers (16) have observed protonated acetic acid in high-pressure studies of the equilibrium

[2] $CH_3—C{\equiv}O^+ + H_2O \leftrightharpoons CH_3CO_2H_2^+$

for which they obtained $\Delta H^0 = -25$ kcal mol^{-1}. This reaction exothermicity is compatible only with the carbonyl protonated structure *a* for the $CH_3CO_2H_2^+$ ion.

More recently Mackay *et al.* (17) have reported a study of dissociative proton transfer to formic acid and acetic acid in the gas phase. They observed significant fragmentation by reaction [3]

[3] $RCO_2H_2^+ \rightarrow R—C{\equiv}O^+ + H_2O$

and, by analogy with the unimolecular acyl oxygen, $A_{Ac}1$, mechanism commonly invoked for the cleavage of esters, amides, and carboxylic acids in acid solution (18), they proposed protonation at the hydroxylic hydrogen (structure *b*) for those ions undergoing fragmentation. As they pointed out the alternative of initial protonation at the carbonyl oxygen to give *a*, followed by [1,3]-hydrogen migration to form *b* also is possible, however, there is some evidence (19–21) that such hydrogen shifts have high activation barriers in excess of the reaction endothermicity.

In summary, although there is direct evidence for structure *a* for protonated carboxylic acids, the evidence for structure *b* is only indirect. We have observed that a major fragmentation route for protonated carboxylic acids generated by the dissociative ionization reaction [1] involves the loss of H_2O (reaction [3]) and that this fragmentation reaction is accompanied by a metastable peak. The utility of metastable ion studies, particularly those involving ion kinetic energy spectroscopy, in the elucidation of ion structures and fragmentation mechanisms is well established (22–24). Further, it has been amply demonstrated (21, 25, 26) that these fragmentation reactions which have an activation energy in excess of the reaction endothermicity (i.e., a reverse activation energy) usually show a large kinetic energy release in the ion decomposition reaction. It appeared that a detailed study of the kinetic energy release associated with the fragmentation reaction [3] occurring in the drift region of a double focussing mass spectrometer not only could provide evidence concerning the structure(s) of the fragmenting protonated carboxylic acid ions but also should provide direct information concerning the presence of an activation barrier for the interconversion of *a* and *b*.

Experimental

Fragmentation reactions occurring in the drift region between the ion source and the electric sector of an AEI MS-902 mass spectrometer were studied using the ion accelerating voltage scan technique (27) at constant electric sector voltage and constant magnetic field. Unless otherwise noted all experiments were done at 70 eV ionizing electron energy, a source temperature of 180°C, and a β (energy defining) slit width of 0.008 in.

For the metastable ion scans the electric sector voltage was supplied by a separate power supply (Northeast Scientific Model PQE-0503). The starting ion accelerating voltage was set by adjusting the reference input voltage to the high voltage supply of the MS-902. An adjustable linear ramp voltage from an external generator was applied to the reference input thus scanning the ion accelerating voltage. By adjustment of the constant input voltage and the ramp voltage amplitude any desired ion accelerating voltage range could be repetitively scanned. The ion signal output was accumulated in a 1024-channel signal averager (Varian Associates C-1024). The kinetic energy release distribution was obtained from the metastable ion peak shape, with correction for the main beam width, using the analytical method of Holmes and Osborne (28).

The acetate and propionate esters were commercially available. The remaining esters were prepared by reaction of the appropriate acid and alcohol with purification by fractional distillation. The ethyl-d_5 alcohol was obtained from Merck, Sharp and Dohme. Samples were admitted to the ion source using an all-glass heated inlet system at 150°C.

Results and Discussion

The fragmentation reactions investigated were

[4] $CH_3CO_2H_2^+ \rightarrow CH_3—C{\equiv}O^+ + H_2O$

[5] $C_2H_5CO_2H_2^+ \rightarrow C_2H_5—C{\equiv}O^+ + H_2O$

[6] $n\text{-}C_3H_7CO_2H_2^+ \rightarrow n\text{-}C_3H_7—C{\equiv}O^+ + H_2O$

[7] $n\text{-}C_4H_9CO_2H_2^+ \rightarrow n\text{-}C_4H_9—C{\equiv}O^+ + H_2O$

with the fragmenting ions in each case being prepared from several different precursor esters. A typical trace of the metastable ion signal as a function of ion accelerating voltage is shown in Fig. 1 for reaction [5] for ions produced by 70 eV electron impact on *n*-butyl propionate. The metastable peak clearly is composite with a major broad component and a minor narrow component. All metastable peaks observed exhibited this characteristic shape as is shown by the kinetic energy release distributions presented in Figs. 2 to 6. In each case the distribution is normalized to $n(T) = 1$ at the maximum and in several figures the vertical scale has been displaced for clarity.

The presence of two components is indicative of two structures for the fragmenting $RCO_2H_2^+$ ions. We assign the minor component with a small ki-

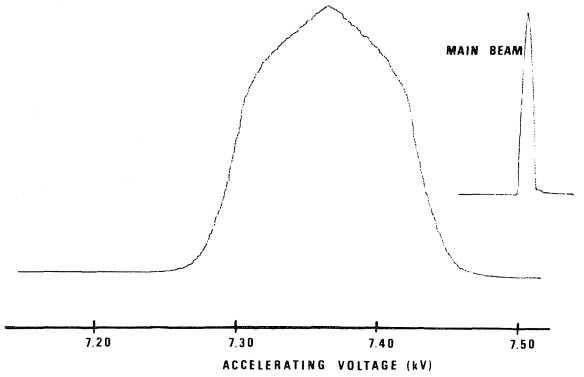

FIG. 1. Metastable peak for $C_2H_5CO_2H_2^+ \rightarrow C_2H_5CO^+ + H_2O$, *n*-butyl propionate. Summation of 50 scans. Main beam peak shown on same voltage scale.

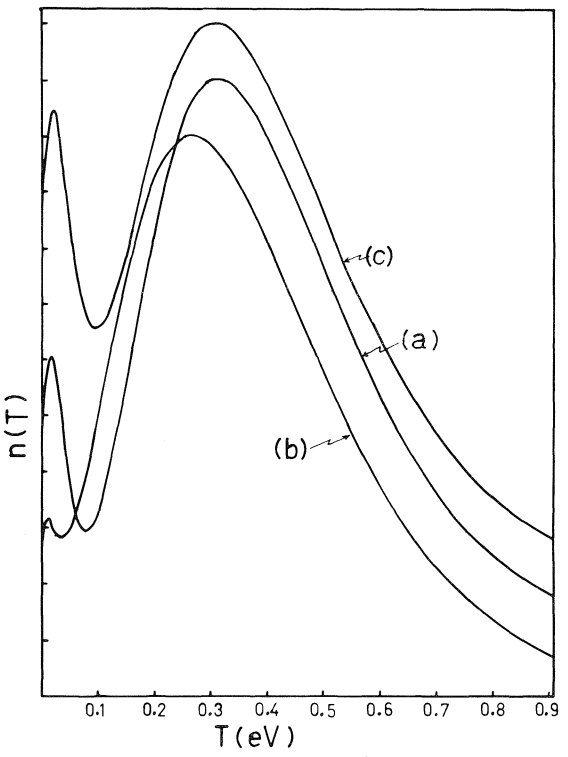

FIG. 2. Energy release distributions for $CH_3CO_2H_2^+ \rightarrow CH_3CO^+ + H_2O$. Precursors (*a*) $CH_3CO_2C_2H_5$, (*b*) $CH_3CO_2C_3H_7$, (*c*) $CH_3CO_2C_4H_9$.

netic energy release to the fragmentation reaction.

[8] $R—\overset{\overset{O}{\|}}{C}—\overset{+}{O}H_2 \rightarrow R—C\equiv O^+ + H_2O$

and the major component with the larger kinetic energy release to the fragmentation reaction.

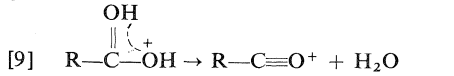

[9] $R—\overset{\overset{OH}{\|}}{C}—\overset{+}{O}H \rightarrow R—C\equiv O^+ + H_2O$

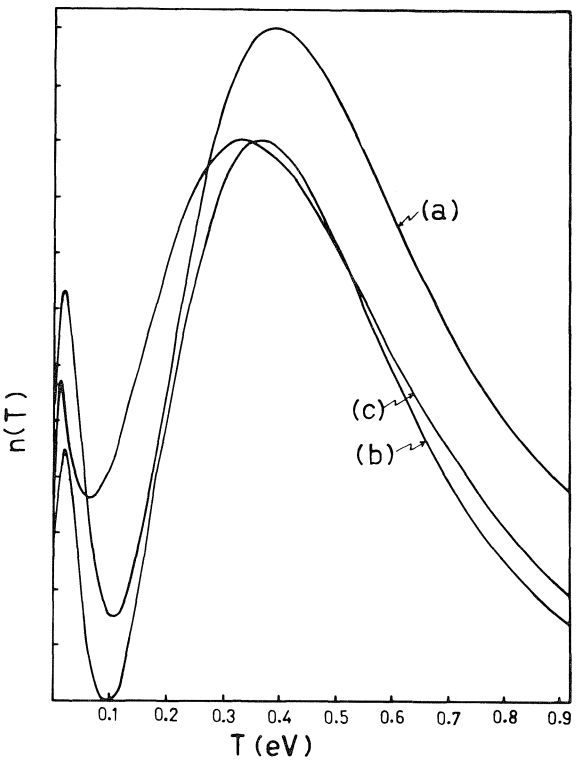

FIG. 3. Energy release distributions for $C_2H_5CO_2H_2^+ \rightarrow C_2H_5CO^+ + H_2O$. Precursors (*a*) $C_2H_5CO_2C_2H_5$, (*b*) $C_2H_5CO_2C_4H_9$, (*c*) $C_2H_5CO_2C_5H_{11}$.

The reasoning for these assignments is given below. The alternatives of two structures for the product ion, i.e., $R''CH_2—C\equiv O^+$ and $R''CH=C=OH^+$, is precluded by the observations that the $CD_3CO_2H_2^+$ ion produced from *n*-propyl acetate-d_3 showed a metastable peak for loss of H_2O only, while the $C_3H_7CO_2D_2^+$ ion produced from ethyl-d_5 butyrate showed a metastable peak for loss of D_2O only.

The individual fragmentation reactions are discussed in detail below in relation to their thermochemistry.

[4] $CH_3CO_2H_2^+ \rightarrow CH_3—C\equiv O^+ + H_2O$

From $\Delta H_f^0(CH_3CO_2H) = -103.3$ kcal mol^{-1} (29) and $PA(CH_3CO_2H) = 187$ kcal mol^{-1} (30), referring to protonation of the carbonyl oxygen (12, 31–33), we derive $\Delta H_f^0(CH_3C(OH)_2^+) = 76$ kcal mol^{-1}. From the PA–IE(O1*s*) correlation (12) we derive a proton affinity of 161 kcal mol^{-1} for the hydroxylic oxygen of CH_3CO_2H leading to ΔH_f^0-

$(CH_3—\overset{\overset{O}{\|}}{C}—\overset{+}{O}H_2) = 102$ kcal mol^{-1}. Although the standard compilation (34) lists a value $\Delta H_f^0(CH_3—C\equiv O^+) = 151$ kcal mol^{-1}, on the basis of an or-

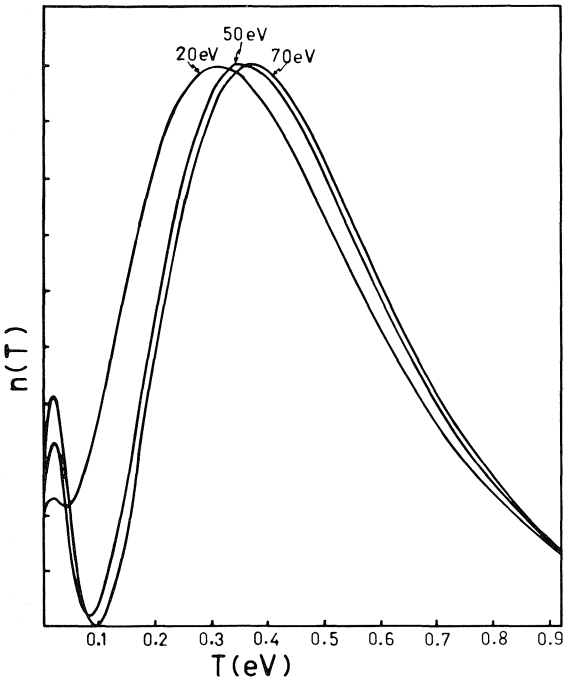

FIG. 4. Energy release distributions for $C_2H_5CO_2H_2^+ \rightarrow C_2H_5CO^+ + H_2O$ for ions produced from *n*-propyl propionate, effect of electron energy variation.

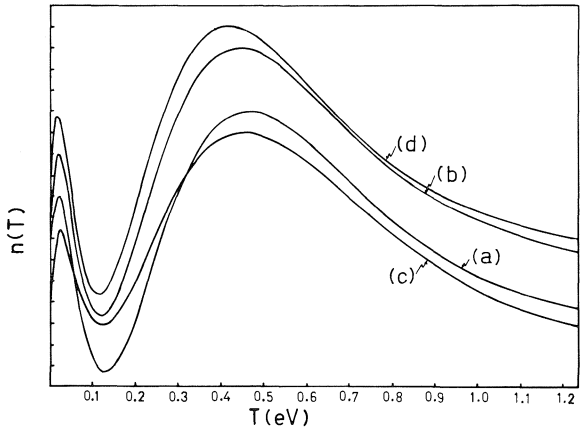

FIG. 5. Energy release distributions for $C_3H_7CO_2H_2^+ \rightarrow C_3H_7CO^+ + H_2O$. Precursors (*a*) $C_3H_7CO_2C_2D_5$, (*b*) $C_3H_7CO_2C_3H_7$, (*c*) $C_3H_7CO_2C_4H_9$, (*d*) $C_3H_7CO_2C_5H_{11}$.

dering of the stabilities of carbonium ions based on ion–molecule reaction studies Beauchamp and co-workers (35) derived $\Delta H_f^0(CH_3—C\equiv O^+) = 158$ kcal mol^{-1}. This higher value is supported by two recent measurements (16, 36) of the proton affinity of ketene which yield, as an average, $\Delta H_f^0(CH_3—C\equiv O^+) = 160$ kcal mol^{-1}. Using this value along with the data above and $\Delta H_f^0(H_2O) = -58$ kcal mol^{-1} (29) we derive the thermochemistry

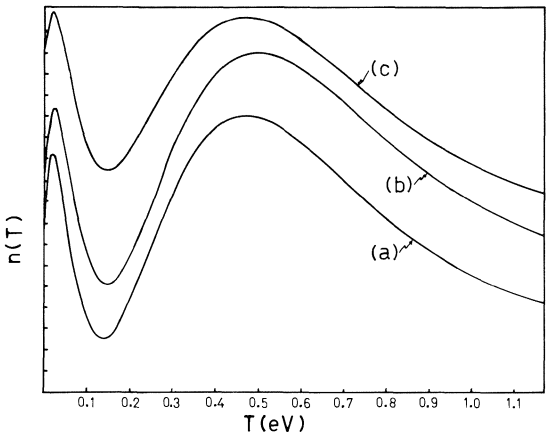

FIG. 6. Energy release distributions for $C_4H_9CO_2H_2^+ \rightarrow C_4H_9CO^+ + H_2O$. Precursor (*a*) $C_4H_9CO_2C_2H_5$, (*b*) $C_4H_9CO_2C_3H_7$, (*c*) $C_4H_9CO_2C_4H_9$.

[10] $CH_3—\overset{\overset{OH}{\|}}{C}—\overset{+}{O}H \rightarrow CH_3—C\equiv O^+ + H_2O$

$\Delta H^0 = +26$ kcal mol^{-1}

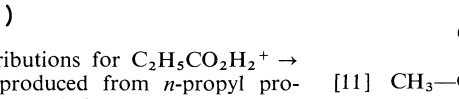

[11] $CH_3—\overset{\overset{O}{\|}}{C}—OH_2^+ \rightarrow CH_3—C\equiv O^+ + H_2O$

$\Delta H^0 = 0$ kcal mol^{-1}

The simple bond fission reaction [11], which is essentially thermoneutral, should show only a very small kinetic energy release and is identified with the low kinetic release component of Fig. 2 (T(most probable) = 0.02 eV). Indeed, it is rather surprising to observe a metastable for the thermoneutral reaction and the small number of *b* ions fragmenting in the drift region presumably reflect a slow formation of $R\overset{\overset{O}{\|}}{C}—OH_2^+$ by dissociation of the ester molecular ion. The variations in metastable ion abundance presumably reflect the variations in the fraction of ester ions which fragment by the energetically disfavoured route to give $CH_3—\overset{\overset{O}{\|}}{C}—OH_2^+$.

The broad metastable component (T(most probable) = 0.3 eV (6.9 kcal mol^{-1})) must be assigned to fragmentation reaction [10]. The large kinetic energy release is characteristic of a fragmentation reaction with a reverse activation energy (24–26) with partitioning of this excess energy between internal modes and translational modes of the product species. The results therefore provide direct evidence that the elimination of H_2O from protonated carboxylic acids of structure *a* has an activation energy in excess of the endothermicity of the reaction. This

activation barrier presumably refers to the symmetry-forbidden (1,3)-H migration converting structure *a* to structure *b* with fragmentation occurring from *b*.

[5] $C_2H_5CO_2H_2^+ \rightarrow C_2H_5C{\equiv}O^+ + H_2O$

From $\Delta H_f^0(C_2H_5CO_2H) = -108.4$ kcal mol^{-1} (29) and PA($C_2H_5CO_2H$) = 189 kcal mol^{-1} (30) we derive $\Delta H_f^0(C_2H_5{-}\overset{\overset{OH}{|}}{C}{-}\overset{+}{O}H) = 69$ kcal mol^{-1}, while from the PA–IE(O1*s*) correlation (12) we estimate the hydroxyl oxygen proton affinity of $C_2H_5CO_2H$ to be 161 kcal mol^{-1} leading to $\Delta H_f^0(C_2H_5{-}\overset{\overset{O}{\|}}{C}{-}OH_2^+) = 97$ kcal mol^{-1}. From photon impact studies $\Delta H_f^0(C_2H_5{-}C{\equiv}O^+) = 144$ kcal mol^{-1} has been derived (34), however, from ion–molecule reaction studies Beauchamp *et al.* (35) have derived $\Delta H_f^0(C_2H_5{-}C{\equiv}O^+) = 151$ kcal mol^{-1} (for a similar discrepancy see discussion of $CH_3{-}C{\equiv}O^+$ (above). Using the latter value we derive the thermochemistry

[12] $C_2H_5{-}\overset{\overset{OH}{|}}{C}{-}\overset{+}{O}H \rightarrow C_2H_5{-}C{\equiv}O^+ + H_2O$

$\Delta H^0 = +24$ kcal mol^{-1}

[13] $C_2H_5{-}\overset{\overset{O}{\|}}{C}{-}OH_2^+ \rightarrow C_2H_5{-}C{\equiv}O^+ + H_2O$

$\Delta H^0 = -4$ kcal mol^{-1}

The kinetic energy release distribution curves (Figs. 3 and 4) show a minor component with a most probable kinetic energy release of ~0.02 eV (0.5 kcal mol^{-1}) which we identify with the simple bond fission reaction [13]. Although this reaction is probably slightly exothermic it has been suggested (37) that for such reactions very little of the exothermicity will appear as kinetic energy of the fragments. The metastable peak shapes for reaction [5] for ions produced from *n*-propyl propionate were studied as a function of ionizing electron energy with the results shown in Fig. 4. With decreasing electron energy the contribution of the low kinetic energy release component decreases. This is consistent with its identification with reaction [13] since the onset potential for formation of $C_2H_5\overset{\overset{O}{\|}}{C}{-}OH_2^+$ is >1 eV higher than the onset potential for formation of $C_2H_5{-}C(OH)_2^+$, the fragmenting ion in reaction [12].

There is a small shift to lower values in the most probable kinetic energy release of the broad component as the contribution of the narrow component decreases (Fig. 4), although the shift is not much greater than the reproducibility of the measurements. It is not clear whether this is a real phenomenon or an artefact arising from the curve fitting routine. Trials with artifically constructed curves of similar shapes showed a similar behaviour suggesting that the shift is an artefact arising from the analytical procedure used to derive the $n(T)$ distribution. The dominant metastable peak component, identified with reaction [12], has a most probable kinetic energy release of ~0.35 eV (8.1 kcal mol^{-1}) somewhat larger than that associated with reaction [10]. The distribution curve also extends to slightly higher kinetic energy release values.

[6] n-$C_3H_7CO_2H_2^+ \rightarrow$ n-$C_3H_7{-}C{\equiv}O^+ + H_2O$

The kinetic energy release distribution curves for this fragmentation reaction are shown in Fig. 5. For the ethyl ester the fragmentation of $C_3H_7CO_2D_2^+$ (produced from ethyl-d_5 butyrate) was studied to avoid interference from the isotopic peak of the intense metastable for H_2O loss from $[M - C_2H_4]^+$ ($CH_2{=}C(OH)OC_2H_5^+$). Two components are clearly visible in the metastable peak. The minor component, with a most probable kinetic energy release of ~0.02 eV, is associated with fragmentation of structure *b* (reaction [14]) while the major component with T(most probable) = 0.45 eV (10 kcal mol^{-1}) is identified with fragmentation of structure *a* (reaction [15]).

[14] n-$C_3H_7{-}\overset{\overset{O}{\|}}{C}{-}OH_2^+ \rightarrow n$-$C_3H_7{-}C{\equiv}O^+ + H_2O$

[15] n-$C_3H_7{-}\overset{\overset{OH}{|}}{C}{-}\overset{+}{O}H \rightarrow n$-$C_3H_7{-}C{\equiv}O^+ + H_2O$

Neither the proton affinities of butyric acid nor $\Delta H_f^0(n$-$C_3H_7{-}C{\equiv}O^+)$ are reliably established, however, by analogy with the acetic and propionic acid systems, reaction [14] undoubtedly is thermoneutral or slightly exothermic while reaction [15] will be endothermic. It should be noted that T(most probable) for [15] is larger than for the similar fragmentations of protonated acetic and propionic acids and the kinetic energy distribution extends to higher values.

[7] n-$C_4H_9CO_2H_2 \rightarrow$ n-$C_4H_9{-}C{\equiv}O^+ + H_2O$

The kinetic energy release distribution curves for this fragmentation reaction are shown in Fig. 6. As for the lower analogues two components to the metastable peak are clearly seen. The low kinetic energy release component (T(most probable) = 0.025 eV) is identified with the structure *b* and the

major component with T(most probable) = 0.48 eV (11 kcal mol^{-1}) is identified with fragmentation of protonated butyric acid of structure *a*. Thermochemical data are almost completely absent for this system.

In summary, the metastable peak shapes and the kinetic energy release distributions calculated therefrom show clear evidence for two structures for protonated carboxylic acids fragmenting in the first drift region of the double focussing mass spectrometer. Fragmentation of the hydroxyl protonated structure *b* proceeds with little release of kinetic energy, consistent with a simple bond fission reaction of low or negligible activation energy. The relative importance of this fragmentation reaction increases as the size of the alkyl group in $RCO_2H_2^+$ increases. This probably is attributable to the increase in the degrees of freedom of the ion which will increase its mean lifetime with the result that a larger proportion will fragment in the drift region. Fragmentation of the carbonyl protonated structure *a* proceeds with a much greater kinetic energy release (T(most probable) = 0.3–0.48 eV). This kinetic energy release is too large to be associated with partitioning of the non-fixed energy of the fragmenting species between internal and translational modes and is consistent only with a reaction for which there is a reverse activation energy, with this energy in excess of the endothermicity being partitioned between internal and translational modes. In the absence of detailed knowledge of this partitioning the magnitude of the reverse activation energy cannot be estimated from the present data, however, the magnitude of the T(most probable) values would indicate that it must be at least 1 eV (23 kcal mol^{-1}).

Both the range of kinetic energy released and the most probable kinetic energy release increase through the series from protonated acetic acid to protonated butyric acid. The most likely rationale is that the activation energy for H_2O loss from *a* remains essentially constant through the series while the reaction endothermicity decreases, thus leading to an increase in the reverse activation energy. If the fraction of the reverse activation energy partitioned into kinetic energy remains constant the kinetic energy released will increase through the series.

Olah and White (38) have determined an enthalpy of activation of 16.3 kcal mol^{-1} for dissociation of protonated acetic acid into the acetyl ion and water in solution. As Kebarle and co-workers (16) have noted this is considerably smaller than the gas phase reaction endothermicity of 26 kcal mol^{-1}, indicative of strong solvent participation. The present results indicate that the activation energy for the gas phase reaction is considerably greater than the endothermicity. Kinetic studies of the addition of water to acyl ions in the gas phase (reaction [2]) in addition to equilibrium studies such as reported by Kebarle and co-workers (16) would be of interest in evaluating the magnitude of this activation energy.

Acknowledgements

The authors are indebted to the National Research Council of Canada for financial support and to Professor J. L. Holmes for making available a copy of the programme for obtaining kinetic energy release distributions. Dr. F. M. Benoit carried out the initial experiments using propyl acetate-d_3. The assistance of D. W. Priddle, W. Panning, P. P. Dymerski, and J. Hegedüs Vajda in developing and testing the repetitive accelerating voltage scan systems is gratefully acknowledged.

1. (*a*) H. Budzikiewicz, C. Djerassi, and D. H. Williams. Mass spectrometry of organic compounds. Holden-Day, San Francisco. 1967; (*b*) D. G. I. Kingston, J. T. Bursey, and M. M. Bursey. Chem. Rev. **74**, 215 (1974); (*c*) F. M. Benoit and A. G. Harrison. Org. Mass. Spectrom. **11**, 1056 (1976); (*d*) F. Borchers, K. Levsen, G. Eckhardt, and G. W. A. Milne. Adv. Mass Spectrom. **7**, 162 (1978).
2. D. Van Raalte and A. G. Harrison. Can. J. Chem. **41**, 2054 (1963).
3. M. S. B. Munson and J. L. Franklin. J. Phys. Chem. **65**, 3191 (1964).
4. A. G. Harrison and E. G. Jones. Can. J. Chem. **43**, 960 (1965).
5. A. G. Harrison, A. Ivko, and D. Van Raalte. Can. J. Chem. **44**, 1625 (1966).
6. F. M. Benoit, A. G. Harrison, and F. P. Lossing. Org. Mass Spectrom. **12**, 78 (1977).
7. F. M. Benoit and A. G. Harrison. J. Am. Chem. Soc. **99**, 3980 (1977).
8. M. S. B. Munson and F. H. Field. J. Am. Chem. Soc. **88**, 4337 (1966).
9. B. L. Jelus, J. Michnowicz, and B. Munson. J. Org. Chem. **39**, 2130 (1974).
10. C. V. Pescheck and S. E. Buttrill, Jr. J. Am. Chem. Soc. **96**, 6027 (1974).
11. A. G. Harrison and C. W. Tsang. Can. J. Chem. **54**, 2029 (1976).
12. F. M. Benoit and A. G. Harrison. Org. Mass Spectrom. **13**, 128 (1978).
13. H. E. Audier, A. Millet, C. Perret, J. C. Tabet, and P. Varenne. Nouveau J. Chim. **1**, 269 (1978).
14. R. J. Weinkam and J. Gal. Org. Mass Spectrom. **11**, 188 (1976).
15. H. Ichikawa and A. G. Harrison. Org. Mass Spectrom. **13**, 389 (1978).
16. W. R. Davidson, Y. K. Yau, and P. Kebarle. Can. J. Chem. **56**, 1016 (1977).
17. G. I. Mackay, A. C. Hopkinson, and D. K. Bohme. J. Am. Chem. Soc. **100**, 7640 (1978).
18. K. Yates. Acc. Chem. Res. **4**, 136 (1971).
19. M. A. Winnik. Org. Mass Spectrom. **9**, 220 (1974).
20. W. J. Bouma, D. Poppinger, and L. Radom. J. Am. Chem. Soc. **99**, 6443 (1977).
21. H. Schwarz, D. H. Williams, and C. Wesdemiotis. J. Am. Chem. Soc. **100**, 7052 (1978).
22. R. G. Cooks, J. H. Beynon, R. M. Caprioli, and G. R. Lester. Metastable ions. Elsevier, Amsterdam. 1973.

23. R. G. COOKS and J. H. BEYNON. *In* Mass spectrometry, MTP international review of science, physical chemistry, Series II, Vol. 5. *Edited by* A. MacColl. Butterworth's, London. 1975.
24. K. LEVSEN. Fundamental aspects of mass spectrometry. Verlag Chemie, New York. 1978.
25. D. H. WILLIAMS and G. HVISTENDAHL. J. Am. Chem. Soc. **96**, 6753 (1974).
26. D. H. WILLIAMS. Acc. Chem. Res. **10**, 280 (1977).
27. M. BARBER and R. M. ELLIOTT. Paper presented at 12th Annual Conference on Mass Spectrometry and Allied Topics, Montreal, Canada, 1964.
28. J. L. HOLMES and A. D. OSBORNE. Int. J. Mass Spectrom. Ion Phys. **23**, 189 (1977).
29. J. D. COX and R. PILCHER. Thermochemistry of organic and organometallic compounds. Academic Press, NY. 1970.
30. R. YAMDAGNI and P. KEBARLE. J. Am. Chem. Soc. **98**, 1320 (1976).
31. T. X. CARROLL, S. R. SMITH, and T. D. THOMAS. J. Am. Chem. Soc. **97**, 659 (1975).
32. B. E. MILLS, R. L. MARTIN, and D. A. SHIRLEY. J. Am. Chem. Soc. **98**, 2380 (1976).
33. S. R. SMITH and T. D. THOMAS. J. Am. Chem. Soc. **100**, 5459 (1978).
34. H. M. ROSENSTOCK, K. DRAXL, B. W. STEINER, and J. T. HERRON. J. Phys. Chem., Ref. Data, **6**, Suppl. 1 (1977).
35. R. H. STALEY, R. D. WIETING, and J. L. BEAUCHAMP. J. Am. Chem. Soc. **99**, 5964 (1977).
36. J. VOGT, A. D. WILLIAMSON, and J. L. BEAUCHAMP. J. Am. Chem. Soc. **100**, 3478 (1978).
37. J. R. CHRISTIE, P. J. DERRICK, and G. J. RICKARD. J. Chem. Soc. Faraday Trans. II, **74**, 304 (1978).
38. G. A. OLAH and A. M. WHITE. J. Am. Chem. Soc. **89**, 3591 (1967); **89**, 7072 (1967).

The thermal decomposition of 1-(2′-cyano-2′-propoxy)-4-oxo-2,2,6,6-tetramethylpiperidine[1]

D. W. GRATTAN,[2] D. J. CARLSSON, J. A. HOWARD, AND D. M. WILES
Division of Chemistry, National Research Council of Canada, Ottawa, Ont., Canada K1A 0R9

Received May 14, 1979

D. W. GRATTAN, D. J. CARLSSON, J. A. HOWARD, and D. M. WILES. Can. J. Chem. **57**, 2834 (1979).

The thermal decomposition of 1-(2-cyano-2′-propoxy)-4-oxo-2,2,6,6-tetramethylpiperidine in solution has been studied as a function of solvent, temperature, and the presence of radical scavengers. In the absence of a scavenger, decomposition produces a hydroxylamine and methacrylonitrile, whereas in the presence of a scavenger such as oxygen, a nitroxide and 2-cyano-2-propyl radicals result. Decomposition in the presence of a scavenger is ~50 times more rapid than decomposition in its absence. By using various free radical scavengers, scission of the NO—C bond is confirmed, that is the reverse of the normal nitroxide – alkyl radical reaction. Increasing solvent polarity causes a marked decrease in thermal stability, both in the presence or absence of radical traps. The importance of the thermal decomposition reactions in the interpretation of nitroxide scavenging of radicals is discussed.

D. W. GRATTAN, D. J. CARLSSON, J. A. HOWARD et D. M. WILES. Can. J. Chem. **57**, 2834 (1979).

La décomposition thermique du (cyano-2′-propoxy-2′)-1-oxo-4-tétraméthyl-2,2,6,6-pipéridine en solution est étudiée en fonction du solvant, de la température et de la présence de pièges à radicaux. En l'absence de piège, la décomposition produit une hydroxylamine et de la méthacrylonitrile, tandis qu'en présence d'un piège tel que l'oxygène, un nitroxyde et des radicaux cyano-2-propyl-2 sont produits. La décomposition en présence d'un piège est ~50 fois plus rapide que la décomposition sans piège. En utilisant différents pièges à radicaux libres, on a confirmé la scission de la liaison NO—C, ce qui est l'inverse d'une réaction normale de radical nitroxyde – alkyle. L'augmentation de la polarité du solvant provoque une diminution marquée dans la stabilité thermique et ce, en l'absence ou en présence de pièges à radicaux. On a discuté de l'importance des réactions de décomposition thermique dans l'interprétation de l'action des nitroxydes comme pièges à radicaux.

[Traduit par le journal]

Nitroxides derived from the hindered amine 2,2,6,6-tetramethylpiperidine have been widely used to scavenge alkyl or aralkyl free radicals, both in kinetic studies of free radical processes (1–4) and in the stabilization of hydrocarbons and polymers against oxidative degradation (5–9). Nitroxide scavenging produces an O-substituted hydroxylamine (reaction [1]) (5, 6). The use of the nitroxide in kinetic studies usually involves the implicit assumption that the >NOR species is stable. In addition

[1] $>NO\cdot + R\cdot \rightarrow >NOR$

this species may well play an important role in preventing further oxidative degradation of polymers (10, 11) and in the "catalytic inhibition" of the autoxidation of hydrocarbons (9). However, the O-substituted hydroxylamines have been reported to be thermally unstable (4, 9, 12) which is not entirely unexpected in view of the low values of the O—H bond strength in hydroxylamines (13). In an early study Kovtun *et al.* (4) used electron spin resonance (esr) spectroscopy to show that nitroxide can be reformed under certain conditions. More recently Bolsman *et al.* (9) have monitored the production of the unsubstituted hydroxylamine and olefin from the decomposition of *N,N,O*-tri-*tert*-butylhydroxylamine. In the most thorough analytical study of >NOR decomposition, Howard and Tait (12) showed that hydroxylamine and olefin resulted from the slow decomposition of O-aralkyl substituted hydroxylamine in the absence of O_2, whereas nitroxide was formed rapidly in the presence of O_2. Indirect evidence indicated the intermediacy of the aralkyl radical in the presence of O_2.

In this paper, the thermal decomposition reactions of an O-alkyl-substituted hydroxylamine (1-(2′-cyano-2′-propoxy)-4-oxo-2,2,6,6-tetramethylpiperidine, **1**) are examined in various solvents, both in the presence and absence of oxygen. This compound is quite similar to the species expected from the nitroxide scavenging of macro-radicals during polyolefin

[1]Issued as NRCC No. 17629.

[2]Present address: The Canadian Conservation Institute, Ottawa.

0008-4042/79/212834-09$01.00/0

oxidative degradation (6, 7), and it is important to understand the behaviour of >NOR species both in hydrocarbon and highly polar environments, simulating respectively the unoxidized and oxidized regions of the polymer.

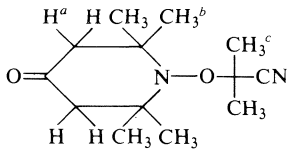

1

Experimental

Preparation of O-substituted Hydroxylamines

Heating a hexane solution of 4-oxo-2,2,6,6-tetramethylpiperidine-*N*-oxyl (**2**) with an excess of α,α′-azo-bis-*iso*-butyronitrile at 55°C gave 1-(2′-cyano-2′-propoxy)-4-oxo-2,2,6,6-tetramethylpiperidine **1**, as described previously (11, 14). 1-Cyclohexyloxy-4-oxo-2,2,6,6-tetramethylpiperidine (**3**) solutions were prepared by the photolysis of di-*tert*-butyl peroxide in a cyclohexane solution of **2** under nitrogen until colourless (11). Gas chromatography (gc) showed the steady loss of **2** and formation of **3**.

Other Materials

The unsubstituted hydroxylamine (1-hydroxyl-2,2,6,6-tetramethylpiperidine-4-one, **4**) was prepared for comparison with the products from **1**. Hydrogenation of **2** (0.09 g) in isooctane (17 mL) over 5% palladium on charcoal (0.2 g) with H_2 at 1 atmosphere for ~30 min gave a mixture of **4** (~70%), **2** (~10%), and 4-oxo-2,2,6,6-tetramethylpiperidine **5** (~20%). Prolonged hydrogenation gave a quantitative yield of **5**. The hydroxylamine oxidized steadily back to the nitroxide, so that the pure product was not isolated in quantity. However, gas chromatography – mass spectrometry (gc–ms) analysis during the hydrogenation gave firm evidence for the **2** → **4** → **5** conversion, and the characteristic mass spectrum of **4** was obtained.

The nitroxide **2** (Aldrich) was recrystallized from methanol. 4-Oxo-2,2,6,6-tetramethylpiperidine (**5**) was obtained from Eastman.

For the radical trapping experiments, 2-methyl-2-nitrosopropane (a gift from K. U. Ingold) was prepared by the method of Stowell (15) and benzenethiol was supplied by Fisher. For comparison with products from the nitroso compound, 2-methylpropyl-2,2′-cyano-2′-propyl nitroxide **6** was prepared from the decomposition of α,α′-azo-bis-*iso*-butyronitrile in the presence of the nitroso compound in degassed cyclohexane. This preparation also produced the 2-cyano-2-propyl adduct to **6** (*O*,*N*-di-(2-cyano-2-propyl)-*N*-2′-methyl-2′-propyl hydroxylamine, **7**).

Thermal Decompositions

Degassed or air saturated aliquots (0.5 mL) of **1** (1.35×10^{-2} *M*) were heated in sealed ampules at preselected temperatures. Decomposition under air employed a large air/liquid volume ratio so that an excess of oxygen was available. After each set decomposition period, tubes were quenched in liquid nitrogen and stored at −15°C. For analysis, the samples were warmed to room temperature, the ampules broken open and analysed within ~5 min.

Product Analysis

Products from the thermal decompositions of **1** were analysed by a combination of liquid chromatography (hplc), gc, gc – ms, and esr spectroscopy. The liquid chromatograph was a Waters ALC 201 fitted with both uv and refractive index detectors and an SiO_2 column (Waters 0.65 cm id × 27 cm, Micro-Porasil, 10 μm particles). Isochratic elutions were made with isopropanol (3 vol%) in *n*-hexane at 1.0 mL min^{-1}. For gc separations, a Hewlett-Packard 5730A (flame ionization detector) was fitted with a 10% UCW-982 coated, Chromosorb W column (20 in. × 1/8 in. od); gc-ms analysis used a similar column with a Finnigan 4000 automated gas chromatograph/EI-CI mass spectrometer system, operated in the electron impact mode.

Electron spin resonance spectra of the nitroxides were measured on a Varian E-4 spectrometer. For unsubstituted hydroxylamines, the highly sensitive triphenyltetrazolium chloride (TTZC) test of Snow (16) was used to quickly identify products and hplc fractions containing free hydroxylamines. When benzenethiol was used to trap radical products from the decomposition of **1**, perdeuterobenzene (Merck, Sharp, and Dohme) was used as solvent and the products analysed by gc, esr, or by nmr spectroscopy at 60 MHz using a Varian EM360 spectrometer. Chemical shifts of products and of **1** were compared with standards in the thiol–C_6D_6 mixture. Shift values are given in ppm relative to tetramethylsilane as internal standard.

Results

Thermal decomposition of **1** in various O_2-free solvents gave a >90% yield of the unsubstituted hydroxylamine **4** and ~80% yield of methacrylonitrile. The loss of **1** and accumulation of **4** at various temperatures in cyclohexane are shown in Fig. 1. Decomposition products were separated by gc and lc and confirmed by gc–ms. The effect of different solvents at constant temperature (82°C) is shown in Fig. 2. Blank experiments showed that methacrylonitrile was unchanged after 20 h at 82°C in the O_2-free solvents used; **4** is also quite stable, decomposing only slowly to **2** (Fig. 2). However, hydroxylamines are destroyed very rapidly in the presence of hydroperoxides (2). This was confirmed by addition of *tert*-butyl hydroperoxide to reaction products containing **4**. Gas chromatographic analysis showed the immediate (<10 s at 25°C) quantitative conversion of **4** to **2**. Hydroperoxide impurities in the solvents

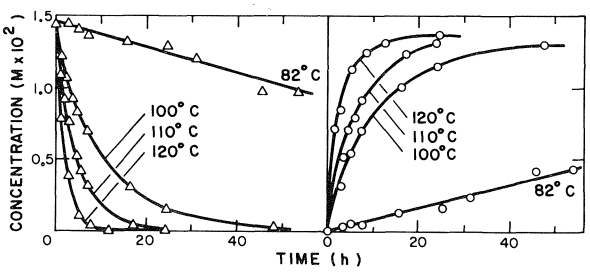

FIG. 1. Thermal decomposition of **1**, cyclohexane solution, O_2-free. Concentrations of **1** (△) and **4** (○) from lc and gc.

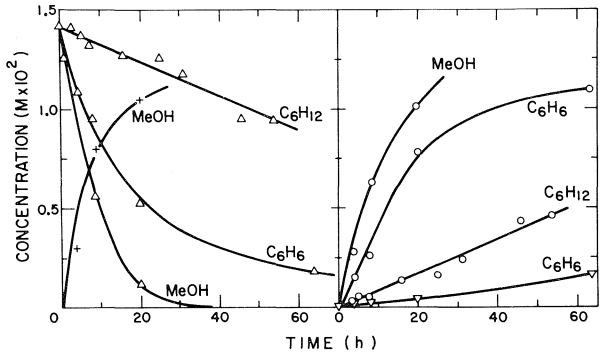

FIG. 2. Effects of solvents on the thermal decomposition of **1** in the O_2-free solvents shown at 82°C. Concentrations of **1** (△), **4** (○), methacrylonitrile (+), and **2** (▽) from gc and lc.

had the same effect. Deliberate addition of *tert*-butyl hydroperoxide to hydroxylamine-containing mixtures was used as a cross check on the assignment of the hydroxylamine gc peak initially identified by a comparison of the retention time with that of the hydroxylamine synthesized by hydrogeneration of the parent nitroxide.

In the air-saturated solutions, decomposition of **1** is much faster than in O_2-free solutions, and the products are distinctly different. Decomposition of **1** at two temperatures in cyclohexane is shown in Fig. 3, with O_2-free data included for comparison. The major product from **1** is now **2** (~80%); **4** is not detected (<2% yield) despite being fairly stable in blank experiments. For example, the half life for decomposition of **4** to **2** in air-saturated solvents at 82°C was ~4 h. Appreciable amounts of a second substituted hydroxylamine **3** accumulated in the presence of oxygen (Fig. 3). High yields of **2** were also observed in methanol and *tert*-butyl hydroperoxide (Fig. 4).

Only trace amounts of methacrylonitrile (~2%) were found after the complete decomposition of **1** in each air-saturated solvent despite the olefin being quite stable either in pure solvents at the temperatures studied, or in decomposing **1** solutions in the presence of oxygen. A new product from the butyronitrile moiety of **1** was 2-cyanopropan-2-ol, found in ~50% yield in the first few hours of **1** decomposition in air-saturated solutions but in much lower yields at higher conversions. Control experiments showed that 2-cyanopropan-2-ol is quite unstable in dilute solutions, decomposing to a quantitative yield of acetone (and presumably HCN), with a half life of ~6 h in methanol at 50°C. Increasing acetone concentrations were found during the decomposition of **1** in the presence of O_2. The combined accumulation of acetone and 2-cyanopropan-2-ol is shown in Fig. 4.

In air-saturated cyclohexane, methanol, or *tert*-butyl hydroperoxide, decomposition of **1** was sufficiently rapid that loss of **1** and formation of **2** could be measured at room temperature. (The half life of **1** at 23°C was ~9 days in the polar solvents.)

Saturation of solutions of **1** with oxygen gave the same products and rates as found with air-saturated solutions.

Decomposition of **1** in air-saturated benzene again produces **2**, but in only ~50% yield at 82°C (Fig. 4). Another major product (~30% of **1**) and a minor (~10% of **1**) product were found by gc. Their mass spectra were quite similar to those from **5** (the minor product) and **2** (the major product) although their gc retention times were much greater than both of these compounds. Electron spin resonance confirmed only the nitroxide level equivalent to the **2** yield observed by gc. Other possible products precluded by

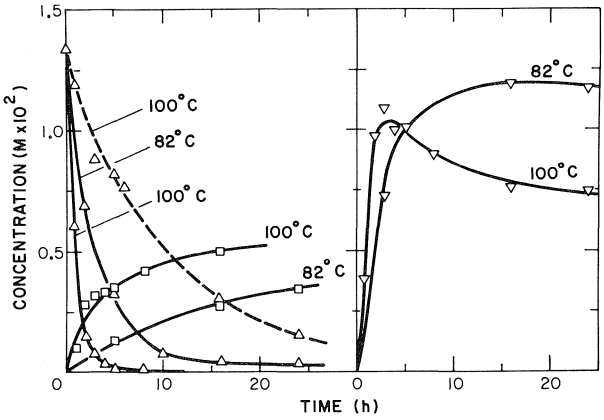

FIG. 3. Effects of temperature on the thermal decomposition of **1**, (—) in air-saturated cyclohexane; (---) in O_2-free cyclohexane for comparison. Concentrations of **1** (△), **2** (▽), and **3** (□) from gc and lc.

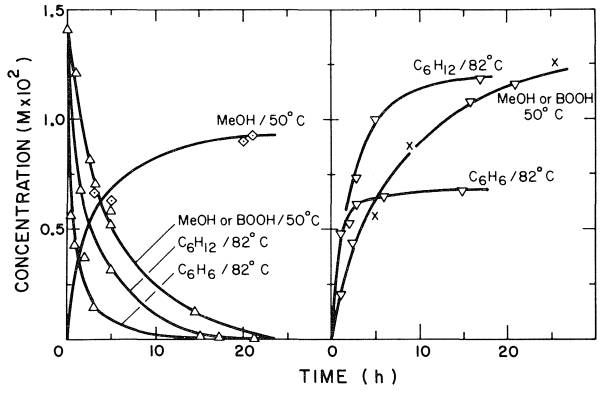

FIG. 4. Decomposition of **1** in various air-saturated solvents. Concentrations of **1** (△), **2** (▽), and acetone + 2-cyanopropane-2-ol (◇) determined by lc and gc. Concentrations of **2** (×) also determined by esr after reactions in methanol.

gc–ms included phorone and 1-methoxy-4-oxo-2,2,6,6-tetramethylpiperidine. The major unidentified product from the decomposition of **1** in benzene was also found in small amounts (~5%) after the decomposition of **1** in other solvents, and as an impurity in commercial **2**.

To investigate the possibility of O_2 acting as a trap for free radical decomposition products from **1**, the spin traps 2-methyl-2-nitrosopropane (16) or benzenethiol were added to O_2-free solutions of **1** at 55°C. The formation of **2** and 2-methyl-2-propyl-2′-cyano-2′-propyl nitroxide **6** in the presence of 2-methyl-2-nitrosopropane were indicated by gc and esr (a_N = 14.7 and 15.2 G respectively). In the presence of the nitroso spin trap, the O_2-free decomposition of **1** was found to proceed initially at a rate very close to the rate observed in air-saturated cyclohexane at the same temperature to give **2** together with a similar yield of **6**. This implies that the nitroso compound is not trapping radicals from a minor side reaction (17), but a product from the main decomposition mechanism of **1**. However, after virtually complete decomposition of **1**, only ~10% of the theoretical yield of **6** was observed, with a large yield of the adduct **7** (~60%, based on 2-cyano-2-propyl radicals from the decomposition of **1**).

In the presence of the nitroso compound, neither the parent piperidine **5**, nor the substituted hydroxylamine **3**, nor 2-methyl-2-propyl-2′-cyano-2′-propoxyl nitroxide (which should have been easily detectable by esr because a_N = 27.25 G, despite being somewhat unstable (18)) were detected after the decomposition of O_2-free solutions of **1**.

The decomposition of **1** at 55°C in O_2-free benzenethiol/perdeuterobenzene (1:2 by volume) produced a quantitative yield of **5** and 2-cyanopropane as shown by nmr and gc. The well characterized nmr spectrum of **1** ($4H^a$ multiplet at 2.14; $12H^b$ doublet at 1.05, 1.10; $6H^c$ singlet at 1.32 ppm) (14) was replaced by the combined spectrum of **5** ($4H^a$ singlet at 1.96; $12H^b$ singlet at 0.96) (19) and 2-cyanopropane ($6H^c$ doublet at 0.79, 0.68; 1H septet at 2.23, 2.12, 1.99, 1.88, 1.78, 1.68, 1.57 — but only 1.88, 1.78, 1.57 clear of other absorptions in the reaction mixture). Examination of the reaction mixture by nmr at high amplification showed the absence (<5% based on **1** decomposed) of methacrylonitrile and 2-cyanopropan-2-ol. Addition of **2** to degassed C_6H_5SH–C_6D_6 at 23°C also gave a quantitative yield of **5** within seconds of solution as shown by nmr, gc, and the loss of the esr nitroxide signal, together with a high yield of diphenyl disulfide.

Discussion

Rates of decomposition of **1** measured over a concentration range of $1 - 100 \times 10^{-4}$ *M* were found to follow first order kinetics (Fig. 5), with rate constants in a given solvent which were independent of the method of concentration determination (gc, lc, or esr). Some of the calculated rate constants are collected in Table 1.

Decomposition of **1** in O_2-free solvents can be rationalized in terms of a unimolecular homolysis (reaction [2]). The process is strongly solvent

[2] 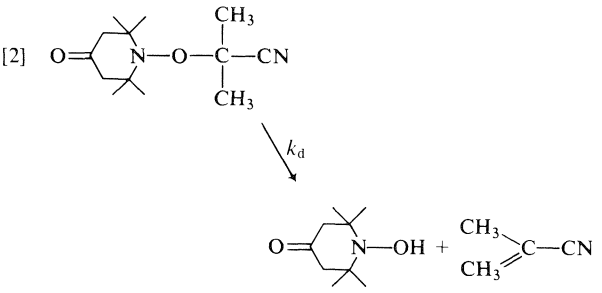

dependent (Fig. 2). Arrhenius plots for the data in cyclohexane and methanol are shown in Fig. 6. Activation energies and pre-exponential factors are collected in Table 2, together with other literature values. The slow generation of nitroxide from **4** in the absence of O_2 (Fig. 2) probably occurs by the process (2)

$$\text{>NOH} + \text{HON<} \rightarrow \text{>NO}\cdot + H_2O + \cdot\text{N<}$$

Keana *et al.* (20) have reported that the substituted hydroxylamine 1-benzyloxy-4-hydroxyl-2,2,6,6-tetramethylpiperidine is stable at 170°C. However this substituted hydroxylamine has no reactive β-hydrogens and so cannot undergo reaction [2].

Superficially, the thermal decomposition of **1** in the presence of O_2 appears to follow a different mechanism from reaction [2]. In the presence of O_2, the observed products (nitroxide and some 2-cyano-

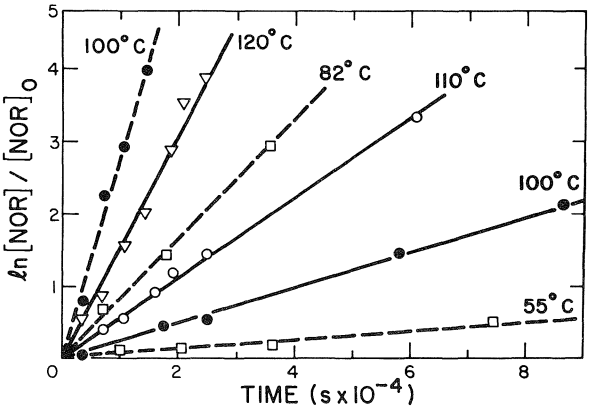

FIG. 5. First order kinetic dependence of the decomposition of **1** in cyclohexane, O_2-free (—) or air-saturated (---).

TABLE 1. Rate constants (k_d) for the thermal decomposition of **1**

Solvent	Temperature (°C)	Initial [**1**] M	$k_d^a \times 10^4$ (s^{-1})
	O_2-free solutions		
Cyclohexane	120	1.42×10^{-2}	1.50
Cyclohexane	100	1.42×10^{-2}	0.24
Cyclohexane	82	1.42×10^{-2}	0.021
Benzene	82	1.42×10^{-2}	0.13
Methanol	82	1.42×10^{-2}	0.34
	Air saturated solutions		
Cyclohexane	82	1.34×10^{-2}	0.84
Cyclohexane	82	1.11×10^{-2}	0.71[b]
Cyclohexane	61	1.30×10^{-3}	0.11[b]
			0.10[b,c]
Cyclohexane	55	5.54×10^{-4}	0.061[b]
Cyclohexane	55	1.34×10^{-3}	0.062[b,d]
Cyclohexane	23	5.13×10^{-4}	0.0015[b]
Benzene	82	1.42×10^{-2}	2.06
Methanol	63	1.42×10^{-2}	0.71
Methanol	63	1.09×10^{-4}	0.79[b]
Methanol	50	1.42×10^{-2}	0.39
Methanol	23	1.09×10^{-4}	0.0091[b]
tert-Butyl hydroperoxide	50	1.40×10^{-2}	0.40

[a]Data from gc and lc measurements unless otherwise specified.
[b]Data from esr measurements.
[c]O_2-free, but in the presence of I_2 (2.2×10^{-3} M or 4.4×10^{-2} M).
[d]O_2-free, but in the presence of 8.5×10^{-3} M 2-methyl-2-nitrosopropane.

propan-2-ol) are consistent with reaction [3] followed by [4*a*] where RH is the solvent.

The progressive production of **3** in cyclohexane (Fig. 3) probably results from the scavenging of an alkyl radical (from reactions [4*a* and *b*]) by the nitroxide (3, 10, 11, 17). In the absence of an effective scavenger such as O_2 to remove radicals produced in reaction [3], **2** will rapidly recombine with this radical with a rate constant k_{-d} of $\sim 4 \times 10^8$ M^{-1} s^{-1} to reform **1** (3, 10, 11, 17).

The products from the decomposition of **1** in the presence of 2-methyl-2-nitrosopropane (but in the absence of O_2) are also consistent with reaction **3**. This nitroso compound is known to trap alkyl (or alkoxy) radicals, with the formation of a new nitroxide (16) (**6** in reaction [5], $k_5 \sim 1 \times 10^7$ M^{-1} s^{-1} at 55°C (17)) together with **2** from reaction [3]. Further scavenging of the 2-cyano-2-propyl radicals by **6** gives the tri-alkyl substituted hydroxylamine **7**. The adduct **7** appeared to be quite stable at 55°C in comparison with **1**. The k_d value for reaction [3] in the presence of 2-methyl-2-nitrosopropane was very similar to that found in the presence of air, and is listed in Table 1. The quantitative production of

[3] 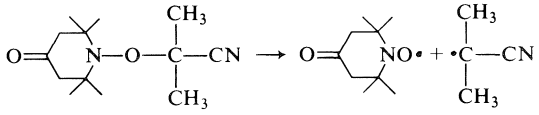

[4] 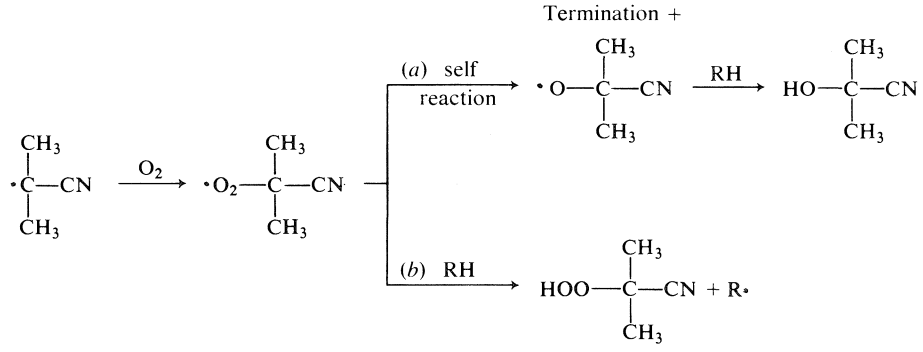

[5] 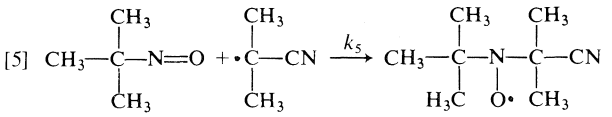

6

2-cyanopropane from the decomposition of **1** in O_2-free C_6H_5SH–C_6D_6 is again consistent with [3], followed by hydrogen abstraction from the thiol. In addition the production of **5** from this decomposition can be explained by the known reaction of nitroxide with a thiol (21).

Two other processes might lead to the products observed from the decomposition of **1** in the presence of O_2. These are scission at the N—O link (rather than the O—C link as in [3]) or the homolysis [2] followed by a rapid reaction of the hydroxylamine with hydroperoxides (from the thermal oxidation of the solvent) to give **2** (2). This latter route to nitroxide formation is, however, precluded by the absence of methacrylonitrile from the decomposition of **1** in C_6H_5SH and the immediate accumulation of **2** (Figs. 3 and 4) even in benzene (Fig. 4) which cannot peroxidize. However Toda *et al.* (22) have observed products from radical attack on nitroxides and shown that the 3-position is particularly vulnerable in **2**. Thus the two new products from the decomposition of **1** found in appreciable quantities only in C_6H_6 most likely result from some attack of 2-cyano-2-propyl or peroxy on the piperidine species, favoured by the resistance of the solvent itself to attack. The slow decomposition of **1** to give **4** must obviously still occur in the presence of O_2. However, $-d[\mathbf{1}]/dt$ is 20–30 times faster in the presence of O_2 (cf. Fig. 6). The detection of only traces of **4** must in part be due to the rapid reaction of **4** with peroxy radicals (2) and other oxidizing species. Scission at the N—O bond of **1** to give an amine radical and a 2-cyano-2-propoxy radical is not consistent with the products observed in the presence of either 2-methyl-2-nitrosopropane or benzenethiol.

The ability of nitroxide radicals to scavenge many alkyl radicals in oxidations has been suggested to result from the attack of peroxy radicals on the O-alkyl hydroxylamine (reaction [6]) (4, 9, 11). This

$$[6]\quad R'O_2\cdot + \mathbf{1} \xrightarrow{k_1} \mathbf{2} + [ROOR']$$

could contribute to the loss of **1** in the presence of O_2. However $-d[\mathbf{1}]/dt$ was unaffected by the presence of an efficient peroxy radical scavenger (2,6-di-*tert*-butyl-4-methylphenol at 4.5×10^{-4} *M*, $[\mathbf{1}]_0 = 5 \times 10^{-4}$ *M* at 75°C). Similarly the published rate constants for reactions [6] (11) and [4*a*] (23) imply that **6** can only account for the loss of **1** and

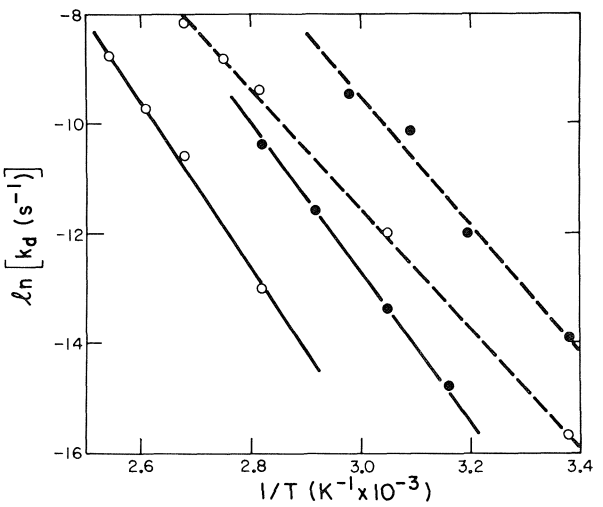

FIG. 6. Temperature dependence of the decomposition of **1** in cyclohexane (○) and methanol (●), O_2-free (—) or air-saturated (---).

reaction [3] appears to be the dominant decomposition route.

In any one O_2-free solvent, the rate of decomposition of **1** is very much slower than in air-saturated solutions (Fig. 3 and cf. Figs. 2 and 4). In air-saturated methanol and cyclohexane, the activation energies and pre-exponential factors shown in Table 2 were derived from the Arrhenius plots in Fig. 6. Both the activation energies and pre-exponential factors were appreciably lower than the air-free values for the respective solvents. This contrasts with the behaviour of the aralkyl substituted hydroxylamine shown in Table 2, where only the activation energy is influenced by solvent. The rates of decomposition of **1** via [2] or [3] increase with changing solvents in the sequence cyclohexane < benzene < methanol ≃ *tert*-butyl hydroperoxide. Both solvent viscosity decrease and polarity increase follow the order cyclohexane < benzene < methanol, and both effects could influence the reaction rates. The reaction rates in methanol (low viscosity) and *tert*-butyl hydroperoxide (high viscosity) are, however, very similar, implying that solvent polarity is the key factor. This was substantiated when the decomposition of **1** in cyclohexane and in Nujol was compared (air-saturated solutions at 55°C). From esr spectroscopy, k_d was only marginally slower (~10%) in Nujol despite the wide difference in viscosities (about 0.7–90 cp (24)). Kiefer and Traylor (24) have reported a four-fold decrease in the rate of photodissociation of di-*tert*-butyl peroxide on going from pentane to Nujol as solvent. However the rate constant for *tert*-butoxy radical self-combination may be close to diffusion controlled (23), about 10 times

TABLE 2. Collected Arrhenius parameters for thermal decomposition of O-substituted hydroxylamines

O-Substituted hydroxylamine $\rangle N—O—R$	Products	Solvent	E_d (kcal mol^{-1})	A, s^{-1} [log (A/s^{-1})]
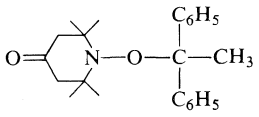	$\rangle NOH + \rangle C{=}C\langle$	$CDCl_3$	29.4 ± 0.8[a]	6.3×10^{14}[a] [14.8 ± 0.5]
	$\rangle NO\cdot + (\cdot O_2R)$	C_6H_5Cl/O_2	24.5 ± 0.8[a]	6.3×10^{14}[a] [14.8 ± 0.5]
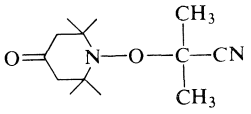	$\rangle NOH + \rangle C{=}C\langle$	C_6H_{12}	30 ± 2[b]	1.1×10^{13}[b] [13.0 ± 0.8]
		CH_3OH	27 ± 0.4[b]	2.1×10^{12}[b] [12.3 ± 0.5]
	$\rangle NO\cdot + \cdot O_2—R$	C_6H_{12}/O_2	22 ± 0.5[b]	1.3×10^{9}[b] [9.1 ± 0.5]
		CH_3OH/O_2	23 ± 3[b]	1.2×10^{11}[b] [11.1 ± 2]
$(t\text{Bu})_2NO(t\text{Bu})$	$\rangle NO\cdot + \rangle C{=}C\langle$	C_6D_5Br	23[c]	1.5×10^{9}[c] [9.2]
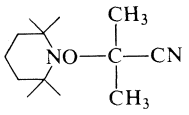	$\rangle NO\cdot + (I—R)$	C_6H_5Cl/I_2	25.0[d]	4.2×10^{12}[d] [12.62]

[a]From ref. 12.
[b]This work.
[c]From ref. 9.
[d]From ref. 4.

faster than the nitroxide – alkyl radical constant for reaction [1] (3, 10–12). The accelerating effect of increasing solvent polarity on decomposition reactions has been extensively reviewed by Martin (25). The similarity in solvent effects on the rates of product formation from O_2-free and O_2-containing solutions might result from a common precursor. This could be the NO—C cleavage (reaction [3]) followed by either recombination (dominant unless a scavenger is present) or disproportionation of the radicals from [3] to give hydroxylamine and olefin, i.e., equivalent to reaction [2].

The thermal stability of O-substituted hydroxylamines has been suggested to be markedly dependent on the nature of the substituent (4), and this is confirmed by the calculated data collected in Table 3. In particular the O-alkyl substituted compounds shown are at least 18 times more stable than the O-aralkyls in the presence of O_2. Such a large difference in thermal stability implies that the transition state for decomposition occurs early in the reaction coordinate and that the stability of O-alkylhydroxylamines is governed principally by strain in the ground state of the molecule (26). Our k_d in the absence of O_2 for **1** is within a factor of 2 of the value found by Bolsman *et al.* (9) for *N,N,O*-tri-(2-methyl-2-propyl)hydroxylamine decomposition (Table 3) with very similar Arrhenius parameters (Table 3). However these latter workers failed to appreciate the effects of O_2 and solvent on the decomposition process, and consequently were unable to explain the catalytic inhibition by nitroxide in terms of the (relatively) low k_d under O_2-free conditions. Kovtun *et al.* (4) observed only the scavenger I_2-assisted decomposition of **1** (reaction [3]), and ignored the formation of a hydroxylamine in the absence of a scavenger. Their reported k_d values in the presence of I_2 are all 16–20 times higher than our values found with O_2, I_2, or 2-methyl-2-nitrosopropane scavenging. This may result from complicating side reactions in the presence of I_2. For example, in contradiction to the data of Kovtun *et al.* (4), we found no effect of I_2 concentration (Table 1) on k_d, but found gross deviations from first order kinetics for the decomposition of **1** in the presence of I_2 at >10% conversion with only ~30% of the theoretical yield of **2** after ~4 half lives of **1** at 61°C.

The thermal instability of $\rangle NOR$ compounds has

TABLE 3. Comparison of k_d for various O-substituted hydroxylamines

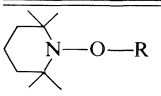	Solvent	k_d ($s^{-1} \times 10^4$)	Origin of data
	O_2-free at 100°C		
R = 	$CDCl_3$	37	Ref. 12
R = 	t-$C_4H_9C_6H_5$	0.53	Ref. 12
R = 	c-C_6H_{12}	0.29	This work
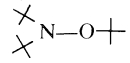	C_6D_5Br	0.58	Ref. 9
	Under O_2 at 60°C		
R = 	C_6H_5Cl	550	Ref. 12
R = 	C_6H_5Cl	0.9	Ref. 12
R = 	c-C_6H_{12}	0.10	This work
(R =  /I_2)	C_6H_5Cl	1.64	Ref. 4

some very important implications for the interpretation of published data on nitroxide or >NOR scavenging of radicals. In several instances, >NOH (10, 27) or >NO· (28–30) formation from >NOR decomposition must have played a part in the observed kinetics. For example, Sudnik *et al.* have reported rate constant values for reaction [6] (28) and the rate constant for nitroxide scavenging of alkyl radicals (29), both derived from experiments at temperatures where the substituted hydroxylamine can be expected to have a half life of below 1.0 h. Similarly, the reaction conditions used by Kovtun *et al.* (27) (amine or alcohol solvents at 75°C) in the nitroxide reaction with alkyl radicals would rapidly decompose any >NOR to give the observed hydroxylamine, rather than their suggestion of direct nitroxide attack on the amine or alcohol. It is also worth emphasizing that stabilization by nitroxides at low O_2 levels will give >NOR which would decompose to olefin and >NOH. The latter can then rapidly scavenge a peroxy radical (2) and regenerate >NO· so that many chains would be terminated by each nitroxide molecule (9). However, at high O_2 pressures, >NOR may function as an initiator, and the nitroxide would lose some of its overall scavenging efficiency.

Acknowledgements

The authors thank Mr. R. T. Pon for assistance with syntheses and analytical procedures and Mr. M. E. Bednas for performing the gc–ms work. We are indebted to Dr. K. U. Ingold for a gift of the 2-methyl-2-nitrosopropane. The authors are grateful to both referees for valuable comments.

1. E. G. ROZANTSEV. Free nitroxyl radicals. Plenum Press, New York. 1970.
2. I. T. BROWNLIE and K. U. INGOLD. Can. J. Chem. **45**, 2427 (1967).
3. S. NIGAM, K. D. ASMUS, and R. L. WILLSON. J. Chem. Soc. Faraday Trans. I, **72**, 2324 (1976).
4. G. A. KOVTUN, A. L. ALEKSANDROV, and V. A. GOLUBEV. Izv. Akad. Nauk SSSR, Ser. Khim. 2197 (1973).
5. J. J. USILTON and A. R. PATEL. Adv. Chem. Ser. **169**, 116 (1978).
6. V. Y. SHLYAPINTOKH, V. B. IVANOV, O. M. KHVOSTACH, A. B. SHAPIRO, and E. G. ROZANTSEV. Dokl. Akad. Nauk SSSR, **225**, 1132 (1975).
7. D. J. CARLSSON, D. W. GRATTAN, T. SUPRUNCHUK, and D. M. WILES. J. Appl. Polym. Sci. **22**, 2217 (1978).
8. M. S. KHLOPLYANKINA, A. L. BUCHACHENKO, M. B. NEIMAN, and A. G. VASILEVA. Kinet. Katal. **6**, 394 (1965).
9. T. A. B. M. BOLSMAN, A. P. BLOK, and J. H. G. FRIJNS. Recl. Trav. Chim. Pays-Bas, **97**, 313 (1978).
10. V. B. SHILOV and E. T. DENISOV. Vysokomol. Soedin. Ser. A, **16**, 2313 (1974).
11. D. W. GRATTAN, D. J. CARLSSON, and D. M. WILES. J. Polym. Deg. Stab. **1**, 69 (1979).
12. J. A. HOWARD and J. C. TAIT. J. Org. Chem. **43**, 4279 (1978).
13. L. R. MAHONEY, G. D. MENDENHALL, and K. U. INGOLD. J. Am. Chem. Soc. **95**, 8610 (1973).
14. K. MURAYAMA, S. MORIMURA, and T. YOSHIOKA. Bull. Chem. Soc. Jpn. **42**, 1640 (1969).
15. J. C. STOWELL. J. Org. Chem. **36**, 3055 (1971).
16. G. A. SNOW. J. Chem. Soc. 2588 (1954).
17. P. SCHMIDT and K. U. INGOLD. J. Am. Chem. Soc. **99**, 6434 (1977).
18. M. J. PERKINS and B. P. ROBERTS. J. Chem. Soc. Perkin Trans. II, 297 (1974).
19. M. J. ARONEY, C-Y. CHEN, R. J. W. LEFEVRE, and A. N. SINGH. J. Chem. Soc. B, 98 (1966).
20. J. F. W. KEANA, R. J. DINERSTEIN, and F. BAITIS. J. Org. Chem. **36**, 209 (1971).
21. K. MURAYAMA and T. YOSHIOKA. Bull. Chem. Soc. Jpn. **42**, 1942 (1969).
22. T. TODA, E. MARI, H. HORIUCHI, and K. MURAYAMA. Bull. Chem. Soc. Jpn. **45**, 1802 (1972).
23. J. A. HOWARD. Adv. Free-Radical Chem. **4**, 49 (1972).
24. H. KIEFER and T. G. TRAYLOR. J. Am. Chem. Soc. **89**, 6667 (1967).
25. J. C. MARTIN. *In* Free radicals. Vol. 2. *Edited by* J. C. Kochi. Wiley, New York. 1973. Chapt. 20.
26. C. RUCHARDT. Angew. Chem. Int. Ed. Engl. **9**, 830 (1970).
27. G. A. KOVTUN, V. A. GOLUBEV, and A. L. ALEKSANDROV. Izv. Akad. Nauk SSSR, Ser. Khim. 793 (1974).
28. M. V. SUDNIK, M. F. ROMANTSEV, A. B. SHAPIRO, and E. G. ROZANTSEV. Izv. Akad. Nauk SSSR, Ser. Khim. 2813 (1975).
29. M. V. SUDNIK, M. F. ROMANTSEV, A. B. SHAPIRO, and E. G. ROZANTSEV. Izv. Akad. Nauk SSSR, Ser. Khim. 45 (1977).
30. E. M. PLISS and A. L. ALEKSANDROV. Izv. Akad. Nauk SSSR, Ser. Khim. 753 (1977).

Molecular and group relaxation studies in parasubstituted benzenes in various media

J. CROSSLEY, J. P. SHUKLA, S. P. TAY, M. S. WALKER, AND S. WALKER
Department of Chemistry, Lakehead University, Thunder Bay, Ont., Canada P7B 5E1

Received February 16, 1979

J. CROSSLEY, J. P. SHUKLA, S. P. TAY, M. S. WALKER, and S. WALKER. Can. J. Chem. **57**, 2843 (1979).

Dielectric absorption studies have been made on molecules of the type X—aromatic—Y where X—Y is —OCH_3, —$COCH_3$, —CH_2Cl, and —CH_2CN. The molecules have been dissolved in (*a*) a polystyrene matrix and (*b*) in the viscous liquid *o*-terphenyl. For 1,4-dimethoxybenzene the group process dominates in both media, and estimates have been made of the activation enthalpy for group relaxation. For 1,4-dimethoxybenzene in benzene, decalin, Nujol, and *o*-terphenyl solutions, however, there appears to be a small contribution from the molecular process. No such contribution was detected in the matrix studies on this solute molecule. For 1,4-diacetylbenzene, 1,4-bis(chloromethyl)benzene, and 1,4-bis(cyanomethyl)benzene in *o*-terphenyl solution it again seems that the group and molecular processes overlap. However, in polystyrene the enthalpies of activation which emerge are characteristic of the group relaxation process as determined by the nmr approach. Altogether, the work illustrates that *o*-terphenyl may be a useful solvent in helping to decide whether a solute has contributions from an intramolecular motion.

J. CROSSLEY, J. P. SHUKLA, S. P. TAY, M. S. WALKER et S. WALKER. Can. J. Chem. **57**, 2843 (1979).

On a effectué des études d'absorbtion diélectrique sur des molécules du type X—aromatique—Y où X—Y représente —OCH_3, —$COCH_3$, —CH_2Cl et —CH_2CN. On a dissous les molécules dans (*a*) une matrice de polystyrène et (*b*) un liquide visqueux, le *o*-terphényle. Dans le cas du diméthoxy-1,4 benzène le mouvement des groupes domine dans les deux milieux et on a évalué l'enthalpie d'activation pour la relaxation du groupe. Dans le cas du diméthoxy-1,4 benzène en solution dans le benzène, la décaline, le Nujol ou le *o*-terphényle, il semble que le processus moléculaire fournit une petite contribution. On n'a pas détecté de telles contribution lors des études dans des matrices de cette molécule de soluté. Dans les cas des diacétyl-1,4, bis(chlorométhyl)-1,4 et bis(cyanométhyl)-1,4 benzènes en solution dans le *o*-terphényle, il semble de nouveau que les processus impliquant les groupes et la molécule se recouvrent. Toutefois dans le polystyrène les enthalpies d'activation qui se dégagent sont caractéristiques d'un processus de relaxation de groupe, tel que déterminé par une méthode rmn. Dans l'ensemble, le travail illustre que le *o*-terphényle peut être un solvant utile pour déterminer si un soluté a des contributions dues à un mouvement intramoléculaire.

[Traduit par le journal]

Introduction

Molecules which have a flexible group attached to an aromatic ring have been widely studied by dielectric techniques. Usually the molecules have been examined either as a pure liquid or as a solute in a dilute solution of a non-polar solvent, and the dielectric absorption has been observed in the microwave region. In all cases the absorption due to the molecular and group reorientations overlap, and the relaxation times for these processes must be deduced from a Budó analysis (1). Such analyses are often subject to appreciable errors which in turn lead to serious uncertainties in the enthalpies of activation obtained for the intramolecular processes.

It has been found possible in a number of cases studied by Davies *et al.* (2, 3) and Walker *et al.* (4–6) to separate completely the absorption due to the intramolecular and molecular processes for molecules by dispersing the solute in a polystyrene matrix. The enthalpies of activation for the intramolecular process have, on the whole, compared quite well with those from the other direct methods of nmr and ultrasonics (7).

A number of dielectric studies (8–10) has been made of acetyl group relaxation in aromatic compounds dissolved in non-polar solvents of low viscosity (~ 1 cP). Typically, the enthalpy of activation for group relaxation in such solvents is ~ 5 kJ mol^{-1}. However, for similar solutes dispersed in a polystyrene matrix (6) the corresponding values are ~ 30 kJ mol^{-1}, and these are of the same order as that estimated for acetophenone by Grindley, Katritzky, and Topsom (11, 12) who obtained a value of 26 kJ mol^{-1}.

0008-4042/79/212843-05$01.00/0

Studies of group relaxation in five aromatic methoxy compounds in a polystyrene matrix yielded ΔH_E values between 11 and 14 kJ mol^{-1} for methoxy group relaxation (13). However, dielectric studies on similar solutes in non-polar solvents (14, 15) gave values of ~6 kJ mol^{-1}. This significant difference in the enthalpies of activation for the acetyl and methoxy groups between these two different dielectric approaches merited further study. The molecules chosen for investigation were of the type X—aromatic—X (Y, Y) ; such molecules have a common feature in that the fixed component of the main dipole along the main principal axis is zero; thus, if molecular relaxation is to be detected, it has to result from a (temporary) stable isomer which has a dipole component perpendicular to this long axis (e.g. a *cis* or *gauche* form). More information on molecular relaxation contributions in X—aromatic—X (Y, Y) systems — or their absence — was also sought.

Experimental and Results

Studies in o-*Terphenyl Solvent*

All the solutes were purified before use. The *o*-terphenyl solvent (Polyscience Inc.) was used without further purification. The apparatus and procedure used in the *o*-terphenyl studies to determine the permittivity (ε') and the dielectric loss (ε'') at frequencies between 1 and 6 GHz have been described previously (16). The low frequency permittivity (ε_0) was measured at 2 MHz with a WTW Dipolmeter. The refractive index (n_D) was measured with an Abbé refractometer and the viscosities (η) determined by means of calibrated Ubbelohde type viscometers and density bottles.

The dielectric data for all the solutions were analyzed in terms of a Cole–Cole symmetrical distribution function for a mean relaxation time τ_0 and a distribution parameter α. The dielectric loss due to the solvent was comparable to the experimental error for these dielectric data. The very high frequency permittivity values, ε_∞, obtained from the Cole–Cole analyses, were similar to $n_D{}^2$.

Dipole moments μ were calculated by means of the equation:

$$\mu = 0.012812\left[\frac{3T(\varepsilon_0 - \varepsilon_\infty)M_2}{(\varepsilon_1 + 2)^2 w_2 d_1}\right]^{1/2}$$

where M_2 and w_2 are the molecular weight and weight fraction respectively of the solute and ε_1 and d_1 the permittivity and density of the solvent respectively at the absolute temperature T.

The mean relaxation times, τ_0, distribution parameters, α, viscosities and dipole moments are listed in Table 1.

Enthalpies of activation for dielectric relaxation (ΔH_E) and viscous flow ($\Delta H_\eta{}^*$) were obtained from the plots of $\log \tau T$ against T^{-1} and $\log \eta$ against T^{-1} respectively and are presented in Table 2.

Studies in Polystyrene Matrix

Dielectric measurements on solutes dispersed in a polystyrene matrix and the evaluation of the results have been described previously (4–7). The polystyrene matrix was prepared in the way described by Davies and Swain (2). We have also adopted their experimental and analytical procedures for obtaining relaxation times and distribution parameters by means of the Fuoss–Kirkwood equation and the enthalpy of activation from the Eyring equation. The polystyrene used here had a weight average molecular weight, $\bar{M}_w$, of 230 000. The relaxation data and the results of Eyring equation analyses of these data are given in Table 3.

Standard statistical techniques were employed to fit the function of temperature data to the Eyring equation. The 95% confidence intervals on ΔH_E were typically ±10% of the nominal values or ±3 kJ mol^{-1} whichever is the greater and in agreement with the work of Davies *et al.* (2, 3). For the ΔS_E term, these confidence intervals were of the order of ±50% of the nominal values in some cases, since this term is often a small part of the intercept, $\{\ln(h/k_B) - \Delta S_E/R\}$, of the $\ln(T\tau)$ versus $(1/T)$ plot.

TABLE 1. Relaxation times (τ_0), solution viscosities (η), distribution parameters (α), and dipole moments (μ) for some polar solutes in liquid *o*-terphenyl at four temperatures and weight fraction ($\bar{w}_2$)

T (K)	τ_0 (ps)	α	η (cP)	μ (D)
1,4-Dimethoxybenzene (w_2 = 0.1498)				
329	21.6	0.14	10.8	1.5
333	19.7	0.12	9.1	1.5
338	16.8	0.14	7.5	1.5
343	16.1	0.11	6.2	1.5
1,4-Diacetylbenzene (w_2 = 0.0713)				
328	178	0.24	25.7	2.71
333	154	0.22	19.4	2.78
338	121	0.19	14.7	2.80
343	108	0.17	11.3	2.83
1,4-Bis(cyanomethyl)benzene (w_2 = 0.0237)				
333	96.4	0.39	21.56	3.88
338	73.7	0.35	16.06	3.93
343	52.8	0.30	12.58	3.79
1,4-Bis(chloromethyl)benzene (w_2 = 0.0995)				
328.6	17.2	0.42	14.62	2.09
333	13.5	0.41	11.91	2.09
338	12.2	0.35	9.56	2.09
343	9.4	0.32	7.88	2.09

TABLE 2. Activation energy data* for solutes in *o*-terphenyl above its melting point

Solute	ΔH_η* (kJ mol^{-1})	ΔH_E (kJ mol^{-1})
1,4-Bis(cyanomethyl)benzene	51.3	57
1,4-Bis(chloromethyl)benzene	40.3	37
1,4-Diacetylbenzene	51.2	33
1,4-Dimethoxybenzene	36.5	20

*See text for discussion of these ΔH_E values since when overlap of the group and molecular processes occurs then the values are not meaningful in terms of a particular process.

Discussion

1,4-Dimethoxybenzene and 4,4'-Dimethoxybiphenyl

Both these solute molecules were examined in a polystyrene matrix, but only the 1,4-dimethoxybenzene proved soluble in *o*-terphenyl above its melting point and only one set of symmetrical absorption peaks were detected. However, the enthalpies of activation for both solutes resulting from this process are virtually identical (Table 3). The ΔH_E values shown are very similar to the 11 kJ mol^{-1} determined by Katritzky *et al.* (11, 12) for methoxy group rotation in anisole and to values obtained in previous studies on five aromatic methoxy compounds dispersed in a polystyrene matrix (13). It is to be noted that values of ΔH_E of about 13 to 14 kJ mol^{-1} are quite unacceptable for molecular relaxation in these compounds. Molecular relaxation enthalpies are quite sensitive to the length of the long axis of the molecule, e.g. ΔH_E values for 4-bromotoluene and 4-iodobiphenyl are 42 and 102 kJ mol^{-1} respectively. These rigid solute molecules are, in fact, fairly similar in size to 1,4-dimethoxybenzene and 4,4-dimethoxybiphenyl respectively. The fact that the two molecules of such a different size have enthalpies of activation, which are virtually identical, indicates that molecular relaxation makes a negligible contribution to their dielectric absorption.

The study of 1,4-dimethoxybenzene in *o*-terphenyl yielded an Eyring activation enthalpy of 20 $\pm$ 5 kJ mol^{-1} which is almost of the same order as the value obtained in polystyrene. Further, the free energies of activation estimated at 333 K for this solute in polystyrene and *o*-terphenyl, 12 and 14 kJ mol^{-1} respectively, are virtually identical.

Grubb and Smyth favoured a small contribution from the molecular process ($C_1 \sim 0.15$) for 1,4-dimethoxybenzene in Nujol and also in decalin solution (14). A comparison of the relaxation times at 333 K in benzene ($\eta \sim 0.5$ cP), $\tau_0 = 4.6$ ps with that in *o*-terphenyl solution ($\eta \sim 25$ cP), $\tau_0 = 19.7$ ps, strongly supports contributions from both group and molecular processes. The approximately four-fold increase in τ_0 cannot be accounted for by an intramolecular process, and the τ_0 values are too short to be attributed solely to molecular relaxation. In fact, the sequence of τ_0 values with increasing solvent viscosity is quite revealing (see Table 4).

It is evident from Table 4 that τ_0 lengthens quite appreciably with increasing viscosity. The most likely explanations are *either*: (*a*) the presence of a molecular process which is significantly dependent on the viscosity; *or* (*b*) the hindrance of group rotation with increasing viscosity so that the role of molecular relaxation becomes enhanced. Since the diameter of the sphere swept out by methoxy group rotation is not appreciably greater than the thickness of the benzene ring little perturbation of the surrounding solvent molecules would be expected. Hence explanation (*a*) is preferred.

Comparison of the τ_0 values in Nujol and *o*-terphenyl suggests that, despite the appreciably greater macroscopic viscosity in Nujol, it is *o*-terphenyl which has the larger microscopic viscosity. This could be accounted for by much closer packing of the solvent molecules in the *o*-terphenyl case.

1,4-Diacetylbenzene

This molecule had been examined previously in a polystyrene matrix (6) and as the pure solid (6). The enthalpies of activation for group relaxation were 27 and 29 kJ mol^{-1} respectively. The former value is similar to that for acetyl group relaxation in 4-acetylbiphenyl (6) where both group and molecular relaxations were separated and established. For 1,4-diacetylbenzene in the solid phase it seems likely that only group relaxation would occur. Certainly the ΔH_E value of 29 kJ mol^{-1} is a typical value for acetyl group relaxation as determined by the dielectric matrix approach and also from nmr data (6).

The study of 1,4-diacetylbenzene in liquid *o*-terphenyl has yielded a very similar enthalpy of activation (33 kJ mol^{-1}). However, 4-ethylbromobenzene, which is a fairly similar-sized rigid (effectively from the dielectric point of view) molecule, in *o*-terphenyl gives a similar enthalpy of activation of 32 kJ mol^{-1}. Thus, the ΔH_E value of 33 kJ mol^{-1} for 1,4-diacetylbenzene in *o*-terphenyl could be accounted for by either group or molecular relaxation or an overlap of the two processes. However, a comparison of the τ_0 values of 1,4-diacetylbenzene in benzene (16.2 ps) and *o*-terphenyl (154 ps) at 333 K reveals that there is an appreciable increment between the two solvents. Such lengthening of the observed relaxation time for an increase in macroscopic viscosity from $\sim$0.6 to $\sim$25 cP clearly indicates a substantial contribution from the molecular reorientation process. This is in agreement with the findings of Fong and Smyth (9) who attributed a weight factor of $\sim$0.9 to the molec-

TABLE 3. Relaxation data and Eyring activation parameters for some solutes dispersed in a polystyrene matrix

Solute	Temperature range (K)	Relaxation time (s) at 200 K	ΔG_E (kJ mol^{-1}) at 200 K	ΔH_E (kJ mol^{-1})	ΔS_E (J K^{-1} mol^{-1})
1,4-Bis(cyanomethyl)benzene	99–194	1.6×10^{-6}	26	3	−114
1,4-Bis(chloromethyl)benzene	158–196	9.6×10^{-6}	29	8.5	−103
1,4-Diacetylbenzene (6)	133–168	9.7×10^{-8}	22	29	36
4-Acetylbiphenyl (6)	146–177	2.4×10^{-7}	23	30	35
1,4-Dimethoxybenzene	85– 99	1×10^{-8}	13	13	2
4,4′-Dimethoxybiphenyl	85–102	1.7×10^{-8}	14	14	2

TABLE 4. Mean relaxation time values at 333 K of 1,4-dimethoxybenzene in various solvents of appreciably different viscosity

Solvent	η (cP)	τ_0 (ps)	Reference
Benzene	0.45	4.6	15
Decalin	2.61	9.8	14
Nujol	211	11.6	14
o-Terphenyl	~25	19.7	16

ular process. It would seem likely that for 1,4-diacetylbenzene in *o*-terphenyl the group and molecular processes overlap.

1,4-Bis(cyanomethyl)benzene

This solute, when examined in a polystyrene matrix, yielded only one set of absorption peaks and a very low enthalpy of activation (3 kJ mol^{-1}). If this value is compared with the enthalpy of activation of 38 kJ mol^{-1} for a fairly similar-sized rigid molecule, 4-bromoethylbenzene, it is apparent that the value for 1,4-bis(cyanomethyl)benzene is to be ascribed to —CH_2CN group relaxation. For this same solute in *o*-terphenyl ΔH_E is 57 kJ mol^{-1} (Table 2) whereas ΔH_E for 4-bromoethylbenzene in *o*-terphenyl (18) is 32 kJ mol^{-1}. This suggests, at the very least, an appreciable contribution from a molecular relaxation process in 1,4-bis(cyanomethyl)benzene. In addition, the difference between the τ_0 values at 333 K in *o*-terphenyl, 96 ps (Table 1), and in benzene, 4.6 ps, for this solute cannot be accounted for solely by an intramolecular process. Similarly, comparison of the τ_0 in *o*-terphenyl solution at 333 K (Table 1) with that for 4-bromoethylbenzene (203 ps) at the same temperature (18) reveals that the process is not solely molecular. Clearly in this case there is an overlap of the group and molecular processes for 1,4-bis(cyanomethyl)benzene in *o*-terphenyl.

Thus, in this instance, it is apparent for 1,4-bis(cyanomethyl)benzene in *o*-terphenyl solution that, although the dipole moment components along the long principal axis cancel, there must be some temporary restriction of the —CH_2CN groups in the potential energy troughs which leads to molecular dipole moment reorientation.

1,4-Bis(chloromethyl)benzene

Smyth *et al.* (19) examined this solute in benzene solution and obtained a very short relaxation time of 3.72 ps at 333 K. This indicated the predominance of a —CH_2Cl group relaxation process. However, the relaxation time observed for this solute in *o*-terphenyl is 13.5 ps at this temperature. Such a lengthening would suggest that the absorption is not entirely due to an intramolecular process. One possibility is that the proportion of polar isomers increased in *o*-terphenyl over benzene solution. The ΔH_E value of 37 kJ mol^{-1} in *o*-terphenyl is to be compared with the molecular relaxation value of 32 kJ mol^{-1} for the somewhat smaller molecule, 4-bromoethylbenzene, and contrasted with the value of 8.8 kJ mol^{-1} obtained by Schaeffer *et al.* (17) for group rotation in benzylchloride. Clearly, there is at least an appreciable contribution from a molecular process for 1,4-bis(chloromethyl)benzene in *o*-terphenyl.

The dielectric absorption of this solute in a polystyrene matrix gives one symmetrical absorption peak at each temperature in the low temperature region. The enthalpy of activation of 9 kJ mol^{-1} is in excellent agreement with the value obtained by Schaeffer *et al.* (20) and is to be ascribed to CH_2Cl group reorientation.

Conclusions

For 1,4-dimethoxybenzene, in a polystyrene matrix, non-polar low viscosity solvents and in the relatively high viscosity *o*-terphenyl a group reorientation process dominates the dielectric absorption. In polystyrene and *o*-terphenyl the enthalpies of activation for methoxy group relaxations are quite similar and are of the order of the literature values for a direct method. However, the enthalpy value in the non-polar low viscosity solvents is significantly lower.

For 1,4-diacetylbenzene, 1,4-bis(chloromethyl)benzene, and 1,4-bis(cyanomethyl)benzene in *o*-terphenyl it seems probable that the group and molecular pro-

cesses overlap. It is possible that the proportion of isomers differs in this solvent from that in the non-polar solvents such as benzene. Further, the enthalpies of activation which emerge from the slope of the $\ln \tau T$ versus $1/T$ plots are more characteristic of the molecular than of the group process.

For the 1,4-diacetylbenzene and 1,4-bis(chloromethyl)benzene dispersed in a polystyrene matrix the enthalpies of activation are consistent with the literature values for group rotation as determined from nmr data.

It is concluded that in favourable cases the dielectric approach employing the matrix technique yields accurate ΔH_E values for a group relaxation process.

It is to be noted that liquid *o*-terphenyl is a most useful solvent in dielectric work and sometimes may assist in deciding whether a solute has contributions from both intramolecular and molecular relaxation processes. It is apparent that the host medium, *o*-terphenyl, exerts a pronounced effect on the relaxation data. This is to be attributed to the macroscopic tending more to the microscopic (16) than is the case for solvents of relatively low viscosity such as benzene, *p*-xylene, and cyclohexane.

1. A. Budó. Phys. Z. **39**, 706 (1938).
2. M. Davies and E. Edwards. Trans. Faraday Soc. **63**, 2163 (1967).
3. M. Davies and J. Swain. Trans. Faraday Soc. **67**, 1637 (1971).
4. S. P. Tay and S. Walker. J. Chem. Phys. **63**, 1634 (1975).
5. S. P. Tay, J. Kraft, and S. Walker. J. Phys. Chem. **82**, 303 (1976).
6. C. K. McLellan and S. Walker. Can. J. Chem. **55**, 583 (1977).
7. S. P. Tay, S. Walker, and E. Wyn-Jones. Adv. Mol. Relaxation Interact. Processes, **13**, 47 (1978).
8. F. K. Fong and C. P. Smyth. J. Am. Chem. Soc. **85**, 548 (1963).
9. F. K. Fong and C. P. Smyth. J. Am. Chem. Soc. **85**, 1565 (1963).
10. D. B. Farmer, P. F. Mountain, and S. Walker. J. Phys. Chem. **77**, 714 (1973).
11. T. B. Grindley, A. R. Katritzky, and R. D. Topsom. Tetrahedron Lett. **26**, 2643 (1972).
12. A. R. Katritzky and R. D. Topsom. Chem. Rev. **77**, 639 (1977).
13. M. A. Mazid, J. P. Shukla, and S. Walker. Can. J. Chem. **56**, 1800 (1978).
14. E. L. Grubb and C. P. Smyth. J. Am. Chem. Soc. **83**, 4873 (1961).
15. E. Forest and C. P. Smyth. J. Am. Chem. Soc. **86**, 3474 (1964).
16. J. Crossley, S. P. Tay, M. S. Walker, and S. Walker. J. Chem. Phys. **69**, 1980 (1978).
17. T. Schaeffer, L. J. Kruczynski, and W. E. Parr. Can. J. Chem. **54**, 3210 (1976).
18. J. Crossley, D. Gourlay, M. Rujimethabhas, S. P. Tay, and S. Walker. In press.
19. W. P. Purcell, K. Fish, and C. P. Smyth. J. Am. Chem. Soc. **82**, 6299 (1960).

Erratum: Nuclear magnetic resonance studies of the solvation of phosphorus(V) selenides, 1,2-bis(diphenylphosphino)ethane, and tris(dimethylamino)phosphine telluride by sulfur dioxide

Philip A. W. Dean
Department of Chemistry, University of Western Ontario, London, Ont., Canada N6A 5B7

Received July 11, 1979
(Ref: Can. J. Chem. **57**, 754 (1979))

In Table 1 left column on p. 755 the next to the last and last entries should be $[Ph_2P(Se)(CH_2)_2]_2P(Se)Ph$ and $[Ph_2P(Se)(CH_2)_2]_2P(Se)Ph$ respectively. On p. 760, left column, the second formula on line 14 and the formula on line 18 should be $[SePPh_2(CH_2)_2]_2P(Se)Ph$.

Relation entre structure et réactivité dans les réactions d'addition nucléophile sur les dérivés carbonylés: influence des interactions diaxiales-1,3 sur la réactivité de cyclanones et cyclanols stériquement encombrés

BERNARD BOYER, GÉRARD LAMATY[1] ET CLAUDE MOREAU

Laboratoire de Chimie Organique Physique, Université des Sciences et Techniques du Languedoc, 34060 Montpellier Cedex, France

ET

PATRICK GENESTE

Laboratoire de Chimie Organique Physique Appliquée, Ecole Nationale Supérieure de Chimie de Montpellier, 34080 Montpellier Cedex, France

Reçu le 1 mai 1979

BERNARD BOYER, GÉRARD LAMATY, CLAUDE MOREAU et PATRICK GENESTE. Can. J. Chem. **57**, 2848 (1979).

Les constantes de vitesse d'addition du borohydrure de sodium sur les cyclanones stériquement encombrées, triméthyl-3,3,5 cyclohexanone (**2**), tétraméthyl-3,3,5,5 cyclohexanone (**3**), bicyclo[3,2,1]octanone-3 (**4**), tricyclo[5,2,1,$0^{3,8}$]décanone-3 (**5**), tricyclo[5,3,1,$0^{3,8}$]undécanone-5 (**6**) et bicyclo[3,3,1]nonanone-3 (**7**), ont été mesurées dans un mélange H_2O/dioxanne 50/50 en volumes, à 25.0°C. Elles mettent en évidence les énergies dues aux interactions diaxiales-1,3, interactions qui apparaissent lorsque l'on passe de l'état initial à l'état de transition. Les énergies d'activation mesurées, représentant presque la totalité de l'énergie conformationnelle correspondant à ces interactions, sont significatives d'un état de transition tardif.

La comparaison des constantes de vitesse de réduction de ces cétones, où le carbone siège de la réaction passe d'une hybridation sp^2 à une hybridation sp^3, avec les vitesses d'oxydation chromique des alcools correspondants, qui implique le changement d'hybridation opposé, montre que l'importance des interactions diaxiales-1,3 peut servir de critère pour déterminer la position de l'état de transition le long du chemin réactionnel.

Les différences de réactivité observées peuvent en outre contribuer à l'élucidation de problèmes conformationnels.

BERNARD BOYER, GÉRARD LAMATY, CLAUDE MOREAU, and PATRICK GENESTE. Can. J. Chem. **57**, 2848 (1979).

The rate constants for the addition of sodium borohydride to the sterically hindered cyclic ketones, 3,3,5-trimethylcyclohexanone (**2**), 3,3,5,5-tetramethylcyclohexanone (**3**), bicyclo[3,2,1]-3-octanone (**4**), tricyclo[5,2,1,$0^{3,8}$]-3-decanone (**5**), tricyclo[5,3,1,$0^{3,8}$]-5-undecanone (**6**) and bicyclo[3,3,1]-3-nonanone (**7**) have been determined at 25°C in a 50/50 by volume mixture of water and dioxane. The values demonstrate energies due to 1,3-diaxial interactions that arise on passing from the initial to the transition states. The measured energies of activation represent almost the total conformational energy corresponding to these interactions, suggesting a late transition state.

Comparison of the rates of reduction of these ketones where the carbon atom at the site of attack passes from sp^2 to sp^3 hybridisation, with the rates of chromic acid oxidation of the corresponding alcohols showing therefore the opposite change in hybridisation, indicates that the magnitude of the 1,3-diaxial interactions can serve to determine the position of the transition state along the reaction coordinate.

The observed differences in reactivity can also contribute to the elucidation of conformational problems.

[Journal translation]

Introduction

L'interprétation des résultats obtenus dans les réactions d'addition nucléophile sur les dérivés carbonylés est souvent rendue difficile à cause de la diversité et de la multiplicité des facteurs mis en jeu (1), à l'origine de la controverse concernant la position de l'état de transition dans la réduction des cétones par le borohydrure de sodium; à la suite des travaux effectués dans notre laboratoire, l'hypothèse d'un état de transition tardif a été émise pour cette réaction (2). Cette hypothèse, critiquée par certains auteurs (3), a reçu un accueil beaucoup plus favorable ces dernières années (4).

Le recours à des composés cycliques et polycycliques rigides permet d'utiliser plus rationnellement les données conformationnelles; il permet dans

[1]Auteur à qui toute correspondance doit être adressée.

0008-4042/79/212848-05$01.00/0

le travail que nous présentons ici de faire varier sélectivement un seul facteur de réactivité: les interactions diaxiales-1,3. Les modèles, dont le squelette est une cyclohexanone chaise, ont en effet été choisis de façon à maintenir constants les autres facteurs de réactivité tels que la tension angulaire, l'hyperconjugaison ou les barrières de torsion.

Notre étude a porté sur la réduction des cyclanones stériquement encombrées **1** à **7** et sur la comparaison avec l'oxydation chromique des cyclanols correspondants **8** à **13**, résultats obtenus dans notre laboratoire (5) ou cités par d'autres auteurs (6).

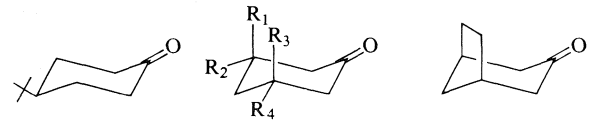

1 **2** $R_1 = R_2 = R_4 = CH_3$, $R_3 = H$ **4**

3 $R_1 = R_2 = R_3 = R_4 = CH_3$

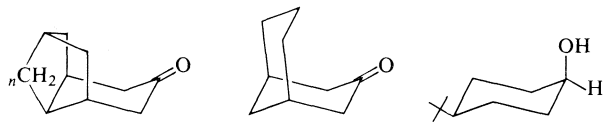

5 $n = 1$ **7** **8**

6 $n = 2$

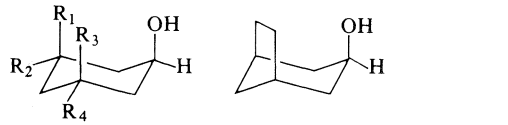

9 $R_1 = R_2 = R_4 = CH_3$, $R_3 = H$ **10**

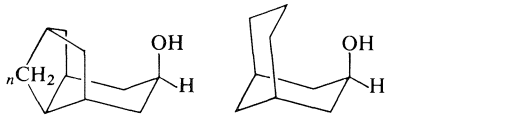

11 $n = 1$ **13**

12 $n = 2$

Résultats expérimentaux

Les constantes de vitesse d'addition du borohydrure de sodium ont été déterminées à 25.0°C, dans un mélange eau/dioxanne 50/50 en volumes, la phase aqueuse contenant 0.05 mol/L de soude; dans ces conditions les solutions de BH_4Na sont stables (2).

Les constantes de vitesse partielles correspondant à l'attaque équatoriale, k_e, ont été calculées à partir des constantes de vitesse totales k et des résultats stéréochimiques obtenus dans la réduction des cétones **1** à **7** ($k_e = k \times$ % alcool axial), malgré les réserves que ce genre de calculs a suscitées (7).

Nos résultats expérimentaux sont rassemblés dans le tableau 1.

Interprétation des résultats expérimentaux et discussion

Nous admettons en première approximation que les cycles portant la fonction cétone ont une conformation chaise. Les différentes méthodes physiques (rmn ^1H et ^{13}C, Rayons X sur les cétones ou les oximes) ont montré que ces cycles étaient des chaises peu déformées (11–14).

Bien que la conformation chaise de la tétraméthyl-3,3,5,5 cyclohexanone (**3**) ne fasse, à l'heure actuelle, aucun doute, il n'était cependant pas déraisonnable, étant donné la présence de deux méthyles axiaux, d'envisager dans l'attaque équatoriale de l'ion borohydrure, une conformation réagissante autre que chaise, en particulier une forme croisée qui permet de diminuer les interactions diaxiales-1,3 entre les deux groupes Me et le groupe OH qui se forme.

Pour différencier entre la conformation stable et la conformation réagissante, nous avons synthétisé les cétones tricycliques **5** et **6** qui sont des modèles rigides de **3** (15). Le fait que les vitesses de réduction de ces cétones soient du même ordre de grandeur que celle de **3** est une forte indication que ce dernier composé, chaise à l'état fondamental, reste chaise dans le complexe activé.

Par comparaison avec les pourcentages obtenus dans la réduction des cétones **5** et **6** ces deux modèles permettent d'estimer à environ 70% le pourcentage d'attaque équatoriale sur la tétraméthyl-3,3,5,5 cyclohexanone (**3**).

Une approche de l'évaluation du pourcentage d'attaque équatoriale a déjà été tentée par Wigfield *et al.* (16) mais elle a l'inconvénient d'introduire un dipôle en position 4 qui peut modifier *et* la vitesse *et* la stéréochimie de la réduction par BH_4Na.

TABLEAU 1. Constantes de vitesse de réduction des cétones **1** à **7** par BH_4Na dans le mélange H_2O/dioxanne 50/50 en volumes à 25.0°C

Cétones	$k \times 10^3$ (M^{-1} s^{-1})	% Attaque équatoriale	$k_e \times 10^3$ (M^{-1} s^{-1})	$\delta\Delta G_{red}^{\neq}$ [a] (kcal/mol)
1	188.5	20 (8)	37.7	0
2	3.35	55 (7)	1.84	1.8
3	0.213	$\simeq 70$[b]	0.149	3.3
4	0.245	40 (9)	0.098	3.5
5	0.240	67	0.161	3.3
6	0.116	72	0.084	3.6
7	0.00109	88 (10)	0.00096	6.2

[a] $\delta\Delta G_{red}^{\neq} = -RT \ln k_e(n)/\ln k_e(1)$; $n = 2, 3, 4, 5, 6, 7$.
[b] Estimation de l'attaque équatoriale (voir texte).

Si les cycles cétoniques ont une conformation chaise, l'influence sur la vitesse des hydrogènes axiaux en 2 et 6 sera pratiquement la même. Si l'état de transition est tardif et si nous considérons les vitesses d'addition équatoriale k_e (schéma 1) les différences d'énergies $\delta\Delta G_{red}^{\neq}$ doivent correspondre aux interactions diaxiales-1,3 qui se développent entre l'état initial et l'état de transition et ce quelle que soit la structure, linéaire ou cyclique, que l'on admette pour le complexe activé (17).

La présence d'un méthyle axial, cas de la triméthyl-3,3,5 cyclohexanone (**2**), nécessite une énergie supplémentaire de 1.8 kcal/mol par rapport à la *t*-butyl-4 cyclohexanone (**1**) pour passer de l'état initial à l'état de transition. Les valeurs de ΔG^0 données par la littérature pour les interactions diaxiales-1,3 Me ··· OH, et qui se manifestent en totalité dans l'état final, varient de 1.9 à 2.4 kcal/mol (18); la valeur $\delta\Delta G_{red}^{\neq} = 1.8$ kcal/mol constitue donc un nouvel argument en faveur d'un état de transition tétragonal dans l'addition nucléophile de BH_4^- sur les dérivés carbonylés (2). Les mêmes calculs faits à partir des données de Wigfield et Phelps (7), de Rickborn et Wuesthoff (19) et de Calvet et Levisalles (20) conduisent respectivement à 1.6, 1.7 et 1.6 kcal/mol pour l'interaction diaxiale-1,3 qui apparaît dans le complexe activé; les derniers auteurs concluent également à un état de transition tardif.

La présence d'un second méthyle axial, cas de la tétraméthyl-3,3,5,5 cyclohexanone (**3**), nécessite 1.5 kcal/mol de plus par rapport à la triméthyl-3,3,5 cyclohexanone (**2**), valeur plus faible puisque la répulsion entre les méthyles axiaux tend à diminuer les interactions diaxiales-1,3 Me ··· OH; l'étude radiocristallographique de l'oxime de la tétraméthyl-3,3,5,5 cyclohexanone montre que les méthyles axiaux sont distants de 3.24 Å alors qu'ils seraient à

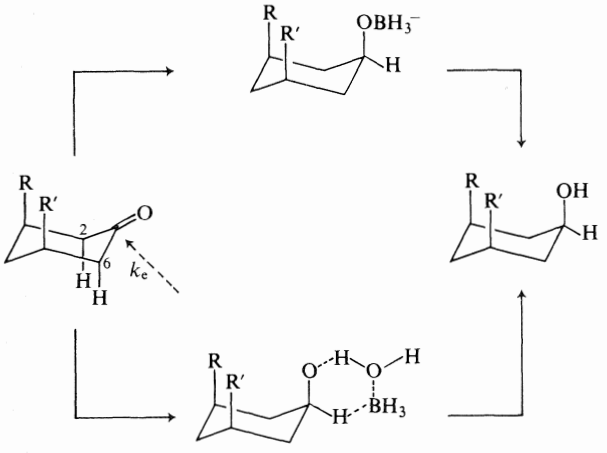

SCHÉMA 1

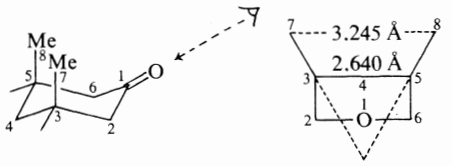

SCHÉMA 2

une distance de 2.64 Å si les deux liaisons C_3—Me et C_5—Me étaient parfaitement parallèles.[2]

La présence de deux méthyles axiaux nécessite donc une énergie d'activation supplémentaire de 3.3 kcal/mol pour la tétraméthyl-3,3,5,5 cyclohexanone (**3**) par rapport à la *tert*-butyl-4 cyclohexanone (**1**). Si l'on compare avec les systèmes rigides correspondants, bicyclo[3,2,1]octanone-3 (**4**), tricyclo[5,2,1,$0^{3,8}$]décanone-5 (**5**) et tricyclo[5,3,1,$0^{3,8}$]undécanone-5 (**6**), les différences d'énergies dues aux interactions diaxiales-1,3 sont respectivement égales à 3.5,3.6 et 3.3 kcal/mol. La réactivité de la tétraméthyl-3,3,5,5 cyclohexanone, comparable à celle d'autres cétones rigides, confirme donc la conformation chaise préférentielle de cette cétone même dans le complexe activé.

L'étude de la réactivité permet ainsi de résoudre des problèmes conformationnels puisqu'elle est directement liée à la conformation des molécules étudiées et que, dans le cas présent, un seul facteur influence de façon prépondérante la réactivité. La relation existant entre réactivité et conformation, démontrée dans le cas de la tétraméthyl-3,3,5,5 cyclohexanone, peut également s'appliquer au cas de la bicyclo[3,3,1]nonanone-3.

L'étude conformationnelle du bicyclo[3,3,1]nonane fait apparaître deux conformations: double-chaise (c.c.) et chaise-bateau (c.b.) (schéma 3, X = H_2) (21).

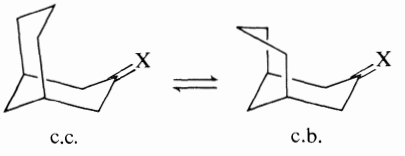

SCHÉMA 3

Des études rmn sur l'oxime de la bicyclo[3,3,1]nonanone-3 ont montré que le cycle portant la fonction cétone existait sous une conformation chaise (11); il n'existe donc que deux conformations possibles pour cette cétone (schéma 3, X = O): double-chaise et chaise-bateau.

Si la bicyclo[3,3,1]nonanone-3 existe sous la conformation chaise-bateau sa réactivité devrait alors être comparable à celle de la bicyclo[3,2,1]octanone-3

[2]J. Lapasset, S. Toure, B. Boyer et G. Lamaty. Acta Crystallogr. Sect. B. Envoyé pour publication.

TABLEAU 2. Constantes de vitesse relatives de réduction des cétones **1** à **7** et d'oxydation des alcools correspondants **8** à **13**

Cétones	k_e rel.	$\delta\Delta G_{red}^{\neq}$ (kcal/mol)	$\delta\Delta G_{ox}^{\neq}$ (kcal/mol)	k_{ox} rel.	Alcools
1	1	0	0	1 (5)	**8**
2	0.049	1.8	−1.5	14 (6)	**9**
3	0.0040	3.3	—	—	—
4	0.0026	3.5	−2.1	38 (6)	**10**
5	0.0043	3.3	−2.7	94	**11**
6	0.0022	3.6	−2.9	132	**12**
7	0.000025	6.2	−1.4	12 (6)	**13**

(**4**) ou des deux cétones tricycliques **5** et **6**: $\delta\Delta G_{red}^{\neq} \simeq$ 3.5 kcal/mol. Les résultats expérimentaux (6.2 kcal/mol) sont incompatibles avec une telle conformation chaise-bateau et sont en faveur de la conformation double-chaise (21).

Comparaison avec l'oxydation chromique des alcools

La comparaison de la réactivité des cyclanones vis-à-vis de BH_4^-, où le carbone siège de la réaction passe d'une hybridation sp^2 à une hybridation sp^3, avec la réaction inverse c'est-à-dire l'oxydation chromique des alcools secondaires correspondants (5) qui implique le changement d'hybridation opposé met en évidence un comportement symétrique (22). L'origine des différences de réactivité entre les substrats dans chaque cas provient principalement du changement dans la tension interne (I-strain) qui accompagne le changement d'hybridation en allant de l'état initial à l'état de transition.

Il était donc intéressant de comparer les réactivités dans le cas de nos composés et à côté de nos résultats obtenus dans la réduction des cétones nous avons fait figurer les résultats relatifs à l'oxydation chromique des alcools correspondants, résultats obtenus dans notre laboratoire (5) ou cités par d'autres auteurs (6) (Tableau 2).

Ce tableau montre qu'à une diminution de la vitesse de réduction correspond une augmentation de la vitesse d'oxydation. Si les interactions diaxiales-1,3 Me ··· OH sont responsables du ralentissement observé dans la réduction des cétones **2** à **7** elles doivent être également responsables de l'accélération de l'oxydation des alcools **9** à **13**; c'est ce que l'on constate en portant sur un diagramme $\delta\Delta G_{ox}^{\neq}$ en fonction de $\delta\Delta G_{red}^{\neq}$ (Fig. 1).

Une exception apparaît cependant avec le bicyclo-[3,3,1]nonanol-3 (**13**). L'oxydation chromique procède environ 500 fois moins vite que ce que l'on était en droit d'attendre si la conformation de cet alcool était double-chaise (○ voir Fig. 1) ce qui correspond à une perte d'énergie d'environ 3.5 kcal/mol. Or des études physiques ont montré

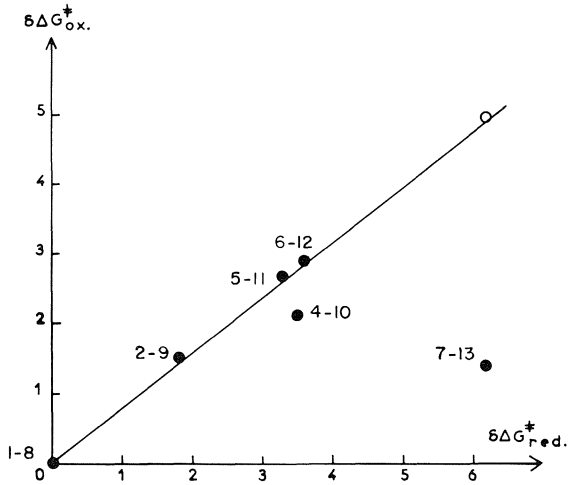

FIG. 1. Variation de $\delta\Delta G_{ox}^{\neq}$ en fonction de $\delta\Delta G_{red}^{\neq}$ (kcal/mol).

que l'alcool (**13**) existait préférentiellement sous une forma chaise-bateau plutôt que double-chaise (10), la différence de tension entre les deux formes étant justement de l'ordre de 4 kcal/mol (6, 23). Dans ces conditions le résultat expérimental (● voir Fig. 1) correspond bien à la conformation préférentielle chaise-bateau.

Conclusion

L'utilisation de systèmes rigides judicieusement choisis permet de limiter certains facteurs de réactivité pour n'en dégager qu'un seul. Dans le travail présenté nous avons mis en évidence par des méthodes cinétiques les interactions diaxiales-1,3 qui se développent ou disparaissent entre l'état initial et l'état de transition aussi bien dans l'addition de BH_4Na sur des cyclanones stériquement encombrées que dans l'oxydation des alcools correspondants. Les résultats expérimentaux confirment donc les hypothèses émises sur la position de l'état de transition dans la réduction des cétones par le borohydrure de sodium.

Partie expérimentale

Synthèse des produits

Les cétones **1**, **2** et **3** sont des produits commerciaux (Aldrich). La synthèse des autres cétones est décrite dans la littérature: **4** (24), **5** et **6** (15) et **7** (25).

La réduction de la cétone **5** par $AlLiH_4$ conduit à l'alcool **11** (OH axial, 67%) et à son isomère (OH équatorial, 33%); dans les mêmes conditions la réduction de la cétone **6** permet d'obtenir l'alcool **12** (OH axial, 72%) et de l'isomère (OH équatorial, 28%). Les isomères ont été séparés par chromatographie préparative sur plaques de silice. L'attribution de structure a été effectuée à partir des spectres rmn ^1H (Varian HA 100 MHz, $CDCl_3$) et ^{13}C (Bruker 20, 115 MHz, $CDCl_3$) (26). Alcool **11** (OH axial): H5, multiplet centré à 4.12 ppm; C5, 67.0 ppm. Isomère (OH équatorial): H5, multiplet centré à 3.88 ppm; C5, 63.6 ppm. Alcool **12** (OH axial): H5, multiplet centré à 4.13 ppm; C5, 67.3 ppm. Isomère (OH équatorial): H5, massif centré à 3.97 ppm; C5, 64.1 ppm.

Pour les alcools **8**, **9**, **10** et **13**, nous avons utilisé les données de la littérature (5, 6).

Méthodes cinétiques

Les études cinétiques de réduction et d'oxydation ont été effectuées par spectrophotométrie uv selon les méthodes déjà décrites dans la littérature (5, 27).

1. (*a*) D. C. WIGFIELD. Tetrahedron, **35**, 449 (1979); (*b*) H. C. BROWN et K. ICHIKAWA. Tetrahedron Lett. 221 (1957); (*c*) H. C. BROWN et J. MUZZIO. J. Am. Chem. Soc. **88**, 2811 (1966).
2. (*a*) P. GENESTE et G. LAMATY. Bull. Soc. Chim. Fr. 669 (1968); (*b*) P. GENESTE, G. LAMATY, C. MOREAU et J. P. ROQUE. Tetrahedron Lett. 5011 (1970).
3. (*a*) M. CHEREST et H. FELKIN. Tetrahedron Lett. 2205 (1968); (*b*) D. C. WIGFIELD et D. J. PHELPS. Can. J. Chem. **50**, 388 (1972).
4. (*a*) R. D. BURNETT et D. N. KIRK. J. Chem. Soc. Perkin Trans. II, 1523 (1976); (*b*) D. J. PASTO et B. LAPESKA. J. Am. Chem. Soc. **98**, 1091 (1976); (*c*) E. A. HILL et S. A. MILOSEVICH. Tetrahedron Lett. 3013 (1976); (*d*) D. C. WIGFIELD et F. W. GOWLAND. Can. J. Chem. **56**, 786 (1978); Communication IV° Conference U.I.C.P.A. de Chimie Organique Physique. York, Angleterre. 1978; (*e*) B. CARO, E. GENTRIC, D. GRANDJEAN et G. JAOUEN. Tetrahedron Lett. 3009 (1978).
5. (*a*) R. DURAND, P. GENESTE, G. LAMATY et J. P. ROQUE. Recl. Trav. Chim. Pays-Bas, **94**, 131 (1975); (*b*) R. DURAND, P. GENESTE, G. LAMATY, C. MOREAU, O. POMARES et J. P. ROQUE. Recl. Trav. Chim. Pays-Bas, **97**, 42 (1978).
6. P. MULLER et J. C. PERLBERGER. J. Am. Chem. Soc. **98**, 8407 (1976).
7. D. C. WIGFIELD et D. J. PHELPS. J. Org. Chem. **41**, 2396 (1976).
8. H. KWART et T. TAKESHITA. J. Am. Chem. Soc. **84**, 2833 (1962).
9. E. VOLPI, G. BIGGI et F. RIETRA. J. Chem. Soc. Perkin Trans. II, 571 (1973).
10. M. HARTMANN et U. GRAEFE. Z. Chem. **7**, 305 (1967).
11. R. DURAND, P. GENESTE, C. MOREAU et A. A. PAVIA. Org. Magn. Reson. **6**, 73 (1974).
12. J. B. STOTHERS et C. T. TAN. Can. J. Chem. **52**, 308 (1974).
13. S. TOURE et J. LAPASSET. Acta Crystallogr. Sect. B, **33**, 1998 (1977).
14. P. GENESTE, R. DURAND, J. M. KAMENKA, H. BEIERBECK, R. MARTINO et J. K. SAUNDERS. Can. J. Chem. **56**, 1940 (1978).
15. B. BOYER, P. DUBREUIL, G. LAMATY, J. P. ROQUE et P. GENESTE. Tetrahedron Lett. 2919 (1974).
16. D. C. WIGFIELD, G. W. BUCHANAN, C. A. ASHLEY et S. FEINER. Can. J. Chem. **54**, 3536 (1976).
17. D. C. WIGFIELD, S. FEINER et F. W. GOWLAND. Tetrahedron Lett. 3377 (1976).
18. E. L. ELIEL, N. L. ALLINGER, S. J. ANGYAL et G. A. MORRISON. Conformational analysis. J. Wiley and Sons, NY. 1965. p. 117.
19. B. RICKBORN et M. T. WUESTHOFF. J. Am. Chem. Soc. **92**, 6894 (1970).
20. A. CALVET et J. LEVISALLES. Tetrahedron Lett. 2157 (1972).
21. H. CALDARADU et M. MORARU. J. Am. Chem. Soc. **96**, 149 (1974).
22. P. GENESTE, M. BONNET et M. RODRIGUEZ. J. Catal. **57**, 147 (1979).
23. M. FISCH, S. SMALLCOMBE, J. C. GRAMAIN, M. A. MCKERVEY et J. E. ANDERSON. J. Org. Chem. **35**, 1886 (1970).
24. B. WAEGELL et C. W. JEFFORD. Bull. Soc. Chim. Fr. 844 (1964).
25. H. K. HALL, JR. J. Org. Chem. **28**, 3213 (1963).
26. J. B. STOTHERS et C. T. TAN. Can. J. Chem. **55**, 841 (1977).
27. B. BOYER, G. LAMATY, J. P. ROQUE et P. GENESTE. Recl. Trav. Chim. Pays-Bas, **93**, 260 (1974).

The synthesis of bicyclo[2.2.2]octenones via intramolecular Diels–Alder reactions of modified Wessely oxidation products[1]

PETER YATES AND HILLAR AUKSI

Lash Miller Chemical Laboratories, University of Toronto, Toronto, Ont., Canada M5S 1A1

Received May 4, 1979

PETER YATES and HILLAR AUKSI. Can. J. Chem. **57**, 2853 (1979).

"Modified" Wessely oxidation of 2,6-dimethylphenol with lead tetraacetate in the presence of acrylic acid, cinnamic acid, *cis*-β-bromoacrylic acid, *trans*-β-bromoacrylic acid, methyl hydrogen maleate, methyl hydrogen fumarate, and tiglic acid followed by intramolecular cycloaddition gives *exo*-6-hydroxy-4,6-dimethyl-5-oxobicyclo[2.2.2]oct-7-ene-*exo*-2-carboxylic acid lactones. Analogous products have been obtained from *o*-cresol. Structural assignments have been made on the basis of the ir, uv, and ^{1}H nmr spectra of the products; analysis of the last shows that the geometry of the bicyclo[2.2.2]octenone system is distorted by the presence of the lactone ring. Chemical transformations of two of the products from the "modified" Wessely oxidation – intramolecular cycloaddition sequence have demonstrated that this route may be used to prepare regioisomers or stereoisomers of products obtained by the conventional Wessely oxidation – intermolecular cycloaddition sequence.

PETER YATES et HILLAR AUKSI. Can. J. Chem. **57**, 2853 (1979).

En présence des acides suivants: acrylique, cinnamique, β-bromoacrylique *cis* et *trans*, l'hydrogénomaléate de méthyle, l'hydrogénofumarate de méthyle et l'acide tiglyque, l'oxygénation de Wessely "modifiée" du diméthyl-2,6-phénol par le tétraacétate de plomb, suivi d'une cycloaddition intramoléculaire conduit aux *exo*-hydroxy-6-diméthyl-4,6-oxobicyclo-[2,2,2]oct-5-ène-7-*exo*-carbolactones-2. Des produits semblables sont obtenus à partir du *o*-crésol. Les structures des produits ont été établies à partir des spectres ir, uv et rmn du proton; l'analyse des derniers spectres met en évidence une distorsion du système bicyclo[2 2,2] octénone en présence du cycle de la lactone. Les transformations chimiques de deux des produits obtenus par la séquence oxydation de Wessely "modifiée" – cycloaddition intramoléculaire ont démontré que cette méthode peut être utilisée pour préparer les régioisomères et les stéréoisomères des produits de la séquence normale oxydation de Wessely – cycloaddition intermoléculaire.

[Traduit par le journal]

The oxidation of *o*- or *p*-substituted phenols with lead tetraacetate in acetic acid to give 2,4-cyclohexadienones and 2,5-cyclohexadienones was first reported by Wessely and Sinwel in 1950 (2); thus mesitol (**1**) was observed to give the dienones **2** and **3**.

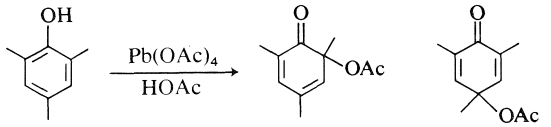

1 **2** **3**

In addition to products of these types quinones and bimolecular oxidation products may also be formed (2, 3). Because the Wessely oxidation provides a simple one-step route to 2,4-cyclohexadienones from *o*-substituted phenols, it is one of the best methods for the synthesis of such compounds, in spite of the fact that in some cases only modest yields are obtained because of the accompanying formation of the other types of products referred to above.

The 2,4-cyclohexadienones obtained in this way can serve as the diene component in Diels–Alder reactions, as demonstrated by Wessely and Budzikiewicz; thus 2-methyl-*o*-quinol acetate **4**, formed by oxidation of *o*-cresol with lead tetraacetate, gives with dimethyl acetylenedicarboxylate an adduct **5** (4). They can also serve as the dienophile component in Diels–Alder reactions and thus can undergo Diels–Alder dimerization (5). The formation of adducts of type **5** in two steps from phenols represents one of the simplest entries into the bicyclo[2.2.2]octenone series.

It was recently found (6) that reaction of **1** with lead tetraacetate in the presence of an excess of acrylic acid gave a mixture of **6** and **7**.[2] When the

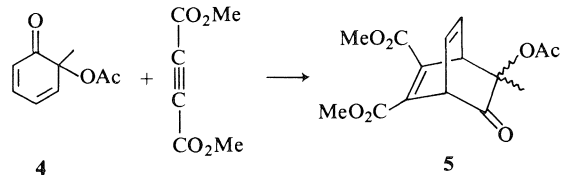

4 **5**

[1]For a preliminary account of part of this work, see ref. 1.

[2]Introduction of a *saturated* acyloxy group other than acetoxy had earlier been observed when **1** was treated with lead tetraacetate in propionic acid to give the propionyloxy analogue of **2** (3).

0008-4042/79/212853-11$01.00/0

mixture was heated in boiling benzene, **6** underwent an *intramolecular* Diels–Alder reaction to give **8**, which could readily be separated from the remaining, unchanged **7**. An analogous product was shown to be formed by similar treatment of 4-methyl-3-xanthenol. We now report on an investigation that has established the generality of this route for the synthesis of bicyclo[2.2.2]octenones, with particular reference to variation of the α,β-unsaturated acid used in the "modified" Wessely oxidation. We also describe some reactions of the products obtained.

2,6-Dimethylphenol (**9**) was chosen as the phenolic substrate for most of the modified Wessely oxidation

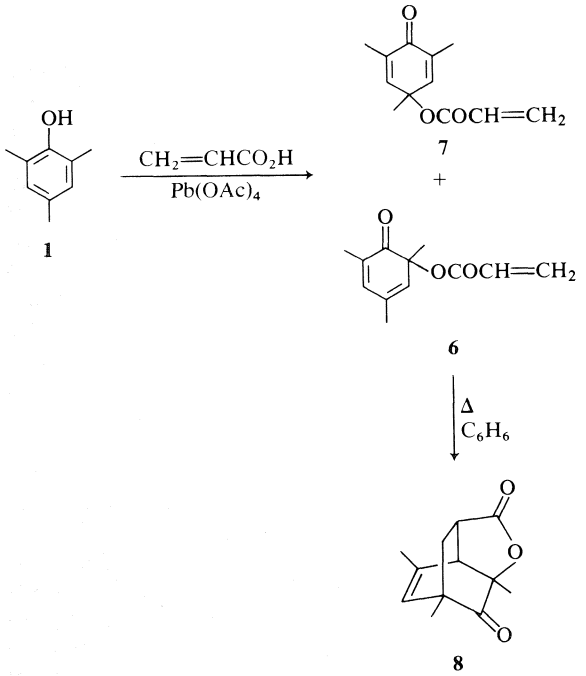

reactions because it is the most readily available *o,o'*-disubstituted phenol with identical substituents and is known to undergo the conventional Wessely oxidation in good yield (3). Its reaction with acrylic acid and lead tetraacetate was investigated first to establish that this is analogous to the reaction of **1**. Addition of **9** to a solution of lead tetraacetate and a large excess of acrylic acid in dichloromethane gave a mixture of **10** and **11**, identified by ir and ^{1}H nmr spectroscopy (an authentic sample of **11** was prepared by oxidation of **9** with lead tetraacetate in acetic acid (3)). The products were not separated, but when the mixture was heated in boiling benzene **10** was converted to the intramolecular Diels–Alder product **12**, which was isolated in 45% yield based on **9**. The structural assignment **12** is based on the product's spectra (*vide infra*) and their similarities to those of **8** (6). Hydrogenation of **12** over palladium/carbon proceeded rapidly and cleanly to give the

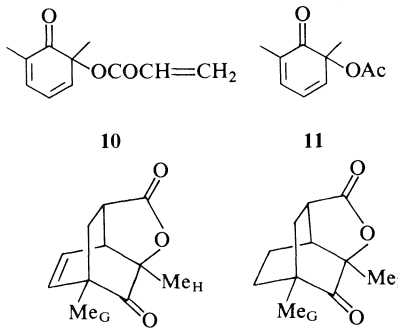

dihydro compound **13**, whose ^{1}H nmr spectrum shows methyl singlets at δ 1.05 and 1.50. These are assigned to Me_G and Me_H, respectively; the chemical shift of the latter is similar to that of Me_H in **12** (δ 1.45), while the signal of the former is at significantly higher field than that of Me_G in **12** (δ 1.32).

Similar modified Wessely oxidation followed by intramolecular cycloaddition of **9** in the presence of cinnamic acid (**14**), *cis*-β-bromoacrylic acid (**15**), *trans*-β-bromoacrylic acid (**16**), methyl hydrogen maleate (**17**), methyl hydrogen fumarate (**18**), and tiglic acid (**19**) gave the corresponding keto lactones **20**–**25**. In some cases the Wessely oxidation products underwent spontaneous cycloaddition and it was unnecessary to heat them in boiling benzene. The yields based on **9** were 30–62%, except in the case of **25**, derived from the trisubstituted ethylene **19**, where the yield was reduced to 14%. Similar reaction sequences with *o*-cresol and **16** and **17** gave **26** and **27**, respectively, monomethyl analogs of **22** and **23**, in low yield.

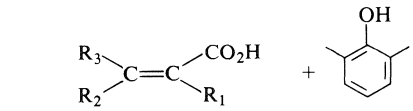

14 $R_1 = R_3 = H$, $R_2 = C_6H_5$
15 $R_1 = R_2 = H$, $R_3 = Br$
16 $R_1 = R_3 = H$, $R_2 = Br$
17 $R_1 = R_2 = H$, $R_3 = CO_2Me$
18 $R_1 = R_3 = H$, $R_2 = CO_2Me$
19 $R_1 = R_2 = Me$, $R_3 = H$

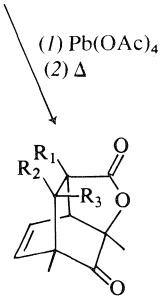

20 $R_1 = R_3 = H$, $R_2 = C_6H_5$
21 $R_1 = R_2 = H$, $R_3 = Br$
22 $R_1 = R_3 = H$, $R_2 = Br$
23 $R_1 = R_2 = H$, $R_3 = CO_2Me$
24 $R_1 = R_3 = H$, $R_2 = CO_2Me$
25 $R_1 = R_2 = Me$, $R_3 = H$

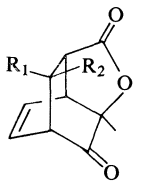

26 $R_1 = Br, R_2 = H$
27 $R_1 = H, R_2 = CO_2Me$

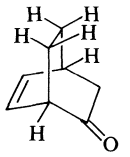

28

The structures of compounds **12** and **20–27** are assigned on the basis of their spectra (Tables 1–3). Their ir spectra show two carbonyl-stretching bands in the regions 5.56–5.63 and 5.70–5.76 μm. The former band is assigned to the lactonic and the latter to the ketonic carbonyl group (superimposed on the ester band in the cases of **23**, **24**, and **27**). They are at lower wavelength than normal for simple γ lactones and bicyclo[2.2.2]octenones (7), which is attributed to strain and dipolar effects. The uv spectra of **12** and **20–27** show maxima in the region 308–316 nm (ε 100–130) ascribed to the enhanced intensity $n \rightarrow \pi^*$ absorption characteristic of bicyclo[2.2.2]octenones (8). As expected the enhancement is greater in the case of **8**, which has a methyl substituent on the ethylenic double bond, and is much reduced or absent in the case of the dihydro compound **13** (λ_{max} 306 nm (ε 35)). The maxima of **12** and **20–27** occur at significantly longer wavelengths than those of simple bicyclo[2.2.2]octenones (9) and this can be attributed to the presence of the lactone ring which exerts a bathochromic effect similar to that of an axial α-acetoxy substituent in cyclohexanones (9); this effect is also evident in the case of **13**. An interesting aspect of the uv spectra is that compounds **21**, **23**, and **27**, which have a bromo or carbomethoxy substituent *syn* with respect to the ketone show two similar maxima in the 308–316 nm region whereas all of the other compounds, including the *anti* isomers of **21** and **23**, show a single maximum.

In most cases 220 MHz ^{1}H nmr spectra were used for analysis of the coupling patterns and assignment of the signals and coupling constants (Tables 2, 3). The vinyl protons of **12** and **20–25** give signals in the ranges δ 5.8–6.2 (H_A) and 6.3–6.6 (H_B). The signals of the H_A and H_B protons in the parent bicyclo[2.2.2]octenone (**28**) occur at δ 6.20 and 6.42, respectively, and the difference in their chemical shifts has been attributed to a homoconjugative effect (10). It is of interest that if it were not for shielding of H_A by the C—Me_G bond (11)[3] in **12**, **21**, and **23** the H_A signal would be very similar in position to the H_B signal (this conclusion is in accord with the relationship of the vinyl proton signals of **23** and **27**, although individual assignments could not be made in the latter case). This effect could arise, at least in part, from a diminution of homoconjugation resulting from the distortion in geometry in the bicyclo[2.2.2]-octenone system engendered by the lactone ring (*vide infra*). It may be noted that a related effect is observed in the ^{13}C nmr spectra of these compounds.[4] The H_C signals of **12** and **20–24** fall in the narrow range δ 3.5–3.7; the corresponding signals for **26** and **27** have similar chemical shifts although overlap with the H_G signals precludes exact assignments. These signals may be compared with the bridgehead proton signals of **28**, which give rise to overlapping multiplets at δ ~ 3.1. The downfield shift is presumably associated with the inductive and the geometrical effect of the lactone ring referred to above. The C—Me_H bond may also exert an effect in the opposite sense; the relationship of this bond to H_C is similar to that of the C—Me_D bond in **26**, where the H_C signal is shifted upfield to δ 3.02. The H_D signal of **12** appears at δ 2.83 and is shifted downfield to δ 3.1–3.25 by phenyl, bromine, or carbomethoxy substituents on the adjacent carbon in **20–24** and **26–27**. The H_E and H_F signals of **12** at δ 1.85 and 2.01, respectively, are also shifted downfield in **20–24** by these substituents, but with a much greater range of effects, as expected for substituents on the same carbon as the protons. It is noteworthy that although the absence of the Me_G group in **26** results in a downfield shift of the H_F signal relative to that in **22** (Δδ 0.32), the difference in the chemical shifts of the H_E signals of **23** and **27** (Δδ 0.03) is negligible. This may be accounted for in terms of the geometry of these lactones (*vide infra*) which results in different dihedral angles between the C—Me_G bond and the C—H_E and C—H_F bond and thus leads to greater anisotropic shielding by the C—Me_G bond in the latter case (11). The signal of the Me_G protons of **12** at δ 1.32 is shifted to δ 1.47–1.48 in the spectra of **21** and **22**, presumably largely as a result

TABLE 1. Infrared and ultraviolet spectra of *exo*-6-hydroxy-5-oxobicyclo[2.2.2]octene-*exo*-2-carboxylic acid lactones

Compound	$\nu_{max}^{CHCl_3}$, μm	λ_{max}^{EtOH}, nm (ε)
12	5.60, 5.76	309 (110)
20	5.59, 5.75	310 (100)[a]
21	5.56, 5.70	308 (104), 314 (103)
22	5.60, 5.74	315 (120)
23	5.61, 5.75	306 (115), 312 (115)
24	5.61, 5.76	310 (100)
25	5.62, 5.74	309 (100)
26	5.58, 5.74	316 (130)
27	5.63, 5.75	308 (114), 313 (109)

[a]Also has B bands at 252–270 nm (see Experimental).

[3]The shielding of H_A by the C—Me_G bond is estimated to be ~0.3 ppm (10).

[4]The ^{13}C nmr spectra of **12**, **13**, and **20–27**, which will be discussed elsewhere, are in full accord with the structural assignments.

TABLE 2. ^{1}H nmr chemical shifts of *exo*-6-Hydroxy-5-oxobicyclo[2.2.2]octene-*exo*-2-carboxylic acid lactones[a]

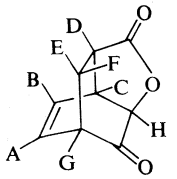

	$^H\delta^{CDCl_3}$								
	12	**20**	**21**	**22**	**23**	**24**	**25**[b]	**26**	**27**
H_A	6.17	5.83	6.16	5.97	6.11	5.97	5.90	6.3–6.6[c]	6.1–6.7[c]
H_B	6.27	6.56	6.39	6.45	6.30	6.32	6.28	6.3–6.6[c]	6.1–6.7[c]
H_C	3.52	3.66	3.63	3.59	3.56	3.55	3.02	3.5–4.0[d]	3.4–3.7[d]
H_D	2.83	3.18	3.20	3.25	3.14	3.24	—	3.14	3.13
H_E	1.85	—	4.11	—	2.82	—	—	—	2.85
H_F	2.01	3.25	—	4.27	—	2.95	2.13	4.59	—
H_G	—	—	—	—	—	—	—	3.5–4.0[d]	3.4–3.7[d]
Me_G	1.32	1.18	1.47	1.48[e]	1.33	1.46[e]	1.31	—	—
Me_H	1.45	1.51	1.49	1.48[e]	1.49	1.46[e]	1.40	1.47	1.47
OMe	—	—	—	—	3.69	3.69	—	—	3.71

[a]The signal intensities and multiplicities (cf. Table 3) are in accord with the assignments.
[b]Me_D and Me_E signals at δ 1.19 and 0.88, respectively.
[c]H_A and H_B signals overlap.
[d]H_C and H_G signals overlap.
[e]Me_G and Me_H signals superimposed.

TABLE 3. ^{1}H nmr coupling constants of *exo*-6-hydroxy-5-oxobicyclo[2.2.2]octene-*exo*-2-carboxylic acid lactones

Coupled protons[a]	*J*, Hz								
	12[b]	**20**	**21**	**22**	**23**	**24**	**25**	**26**[c]	**27**[c]
AB	8.5	8	8	8	8	8	8		
AC	2	2	2.5	2	2	2	2		
AF	[d]	2	—	1	—	[d]	1		
BC	6.5	6.5	6	6	6	7	7.5		
CD	5.5	5	5	5.5	5	5	—	5	4.5
DE	10.5	—	9	—	10	—	—	—	10
DF	1	2	—	0	—	1.5	—	0	—
FG, EG	—	—	—	—	—	—	—	4	1

[a]Proton designations are given in Table 2.
[b]J_{EF} = 13.5 Hz.
[c]Spectrum not fully analyzed.
[d]Signal broadening indicates unresolved coupling.

of an inductive effect of the bromine atom, which is independent of the stereochemistry. In the case of **23** and **24**, however, while the carbomethoxy substituent shifts the Me_G signal in the latter downfield to δ 1.46, it has little effect on that of the former (δ 1.33), a difference that must stem from a difference in the anisotropic effect of the carbomethoxy group in the two locations. The Me_H signals of **12** and **20–27** all fall in the narrow range δ 1.4–1.5, reflecting the isolation of this group from the sites at which the changes are rung.

Examination of molecular models indicates that the presence of the three sp^2 carbon atoms in bicyclo[2.2.2]octenone makes the molecule much more rigid than bicyclo[2.2.2]octane and as a result it has the eclipsed geometry shown in **28**. Introduction of the lactone ring in compounds **12** and **20–27** results in a significant distortion of the skeletal geometry, as represented in **29**, and allusion has already been made to some possible manifestations of this. The resulting changes in certain of the dihedral angles would be expected to evidence themselves also in abnormal H—H coupling constants, although electronegativity and strain effects are also expected to influence these. Indeed, such abnormalities have been observed in systems of type **30** (12). The coupling constants in the spectra of **12** and **20–25** are given in Table 3. The vicinal J_{AB} and J_{BC} and the allylic J_{AC} values, 8–8.5, 6–7.5, and 2–2.5 Hz, respectively, are similar to those observed for simple bicyclo[2.2.2]octenones (7, 10, 13). This is expected since the relevant dihedral angles, all ~0°, are very similar in both **28** and **29**. The J_{CD} values, 5–5.5 Hz, are larger than the expected value of ~3 Hz for **28** and are considered to reflect the decrease of the ~60° dihedral angle in **28** to ~45° in **29**. Similarly the J_{DF} values are reduced to

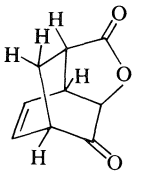

29

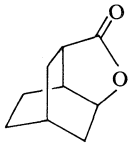

30

1–2 Hz in accord with the decrease of the ~120° dihedral angle in **28** to ~100° in **29**: exceptionally, no coupling is observed in the case of **22**, perhaps because of an electronegativity effect on the coupling constant. The J_{DE} values, 9–10.5 Hz, are also reduced from the value of ~12 Hz expected for **28** (12, 14), in accord with the increase in the dihedral angle from ~0° to ~20°. An unusual long range coupling is observed in the spectra of **20**, **22**, and **25** between the ethylenic H_A and the *anti* H_F protons, the values of J_{AF} falling in the range 1–2 Hz; an analogous, but unresolved, coupling occurs in the spectra of **12** and **24**, as vouchsafed by signal broadening. Again it may be suggested that this arises as a result of geometrical distortion, which leads to a closer approach of the two protons involved to the W pattern that favors long range coupling (15). The spectra of **26** and **27** are more complex than those of the compounds with the Me_G group and have not been analyzed fully; where coupling constants can be extracted they are similar to those found for **12** and **20–25**. It may be noted that **26**, like **22**, shows no coupling between H_D and H_F. Two additional coupling constants are observed in the spectra of **26** and **27**, J_{FG} = 4 Hz and J_{EG} = 1 Hz, and once again these reflect the distorted geometry of the ring system. As expected $J_{FG} < J_{CD}$ since the introduction of the lactone ring has a greater effect on the H_C–H_D dihedral angle than on the H_F–H_G dihedral angle. It may finally be pointed out that the sole geminal coupling constant, J_{EF} in **12**, has the normal value 13.5 Hz, suggesting that little of the strain in the system is felt at the carbon bearing these hydrogens (12).

Base-induced Reactions of 22 and 23

Treatment of **22** with 1,1-dimethylhydrazine in boiling methanol gave a product, $C_{12}H_{14}O_4$, that is assigned structure **31**. Its ir spectrum shows a hydroxyl-stretching band at 2.87 μm together with carbonyl-stretching bands at 5.80 and 5.84 μm, assigned to the ketonic and α,β-unsaturated ester carbonyl groups. Its ^{1}H nmr spectrum (Table 4) shows three three-proton singlets corresponding to the two C(sp^3)—Me groups and the CO_2Me group. The only other C(sp^3)—H signal occurs at δ 4.35 and is assigned to the bridgehead proton; it shows the expected vicinal coupling with a single vinyl proton and equivalent allylic coupling with two vinyl protons. The chemical shifts and multiplicities of the three vinyl protons are in accord with structure **31** when account is taken of accidentally equivalent coupling of H_B with H_A and H_C. The uv spectrum of **31** shows the large enhancement of the intensity of the ketonic $n \rightarrow \pi^*$ band, 312 nm (ε 360), expected for bicyclo[2.2.2]octadienones (16). Treatment of **22** with 1,1-dimethylhydrazine in boiling ethanol gave **32**, the ethyl ester corresponding to **31** (see Table 4).

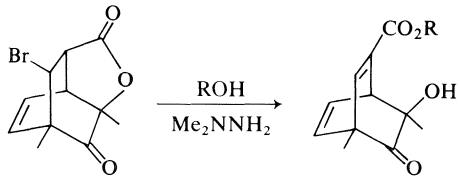

22

31 R = Me
32 R = Et

Reaction of **22** with slightly more than 2 equivalents of aqueous sodium hydroxide followed by acidification gave an acid, $C_{11}H_{12}O_4$, that was converted with ethereal diazomethane to the corresponding methyl ester, isomeric with **31**. These compounds are assigned structures **33** and **34**, respectively. The ir spectrum of the acid shows bands at 3–4, 5.66, and 5.88 μm characteristic of carboxylic acid and γ-lactone functions. Its ^{1}H nmr spectrum (CD_3OD) was not fully interpreted because of extensive long range coupling; however, the following features can be discerned. A three-proton singlet at δ 1.71 and a three-proton signal with fine splitting at δ 1.77 can be assigned to the C(sp^3)—CH_3 and C(sp^2)—CH_3 groups, respectively, the latter showing allylic and homoallylic coupling. The vinylic proton involved in the former coupling gives rise to a multiplet at δ 5.4, while the other vinylic protons give rise to a complex two-proton multiplet at δ 5.5–6.0. The two C(sp^3)—H methine proton signals each appear as doublets at δ 3.23 and 3.70 (J = 13

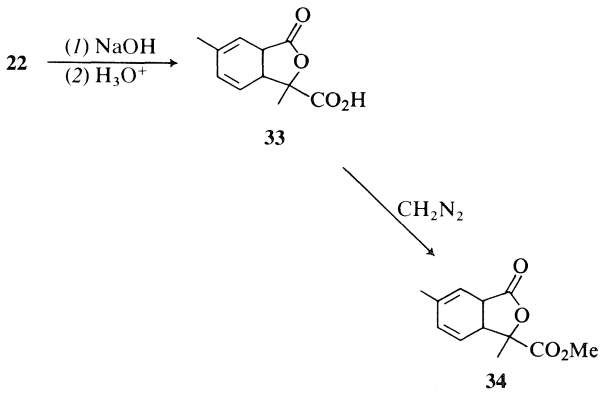

33

34

TABLE 4. ^{1}H nmr spectra of alkyl *exo*-6-hydroxy-4,6-dimethyl-5-oxobicyclo[2.2.2]octa-2,7-diene-2-carboxylates[a]

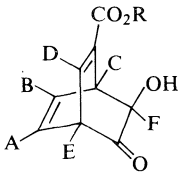

	$^1H\delta^{CDCl_3}$	
	31	**32**
H_A	6.08 (dd, *J* 7, 2 Hz)	6.03 (dd, *J* 7, 2 Hz)
H_B	6.57 (t, *J* 7 Hz)	6.53 (t, *J* 7 Hz)
H_C	4.35 (dt, *J* 7, 2 Hz)	~4.3[b]
H_D	6.98 (d, *J* 2 Hz)	6.93 (d, *J* 2 Hz)
Me_E	1.37 (s)	1.36 (s)
Me_F	1.57 (s)	1.56 (s)
OMe	3.80 (s)	—
OEt	—	1.33 (t, *J* 7 Hz)
	—	4.23 (q, *J* 7 Hz)[b]
OH	2.61 (br s)	2.67 (br s)

[a]The signal intensities are in accord with the assignments.
[b]Overlapping signals.

Hz) with extensive further splitting. The uv spectrum of **33** has maxima at 270 (ε 3300) and 260 nm (ε 3600) consonant with a homoannular conjugated diene. The spectra of **34** are closely similar to those of **33**, *mutatis mutandis*. The presence of a conjugated diene system was corroborated by the formation of a Diels–Alder adduct, **35** (stereochemistry tentative), from **34** and maleic anhydride, and the full structures were confirmed by dehydrogenation of **34** over palladium/carbon to give an aromatic compound whose spectra (see Experimental) are in full accord with the assignment to it of structure **36**; in particular the relationship of its uv spectrum to that of **37**(17) may be noted.

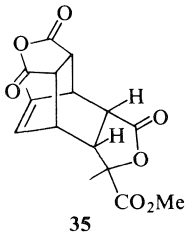

35

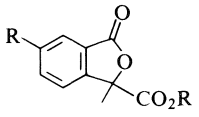

36 R = Me
37 R = H

The formation of **33** from **22** is most simply interpreted as involving a Grob fragmentation (18) of **38**, formed by attack of hydroxide ion on the ketonic carbonyl of **22**. However, hydrolysis of the lactone ring followed by such fragmentation and reclosure of the lactone ring upon acidification would also account for its formation. In either event **33** would be expected to have the relative configuration shown in **33***a*, and this stereochemistry is assigned to the product. Because of the magnitude of the coupling constant ($J \sim 13$ Hz) between the angular methine protons, consideration was given to the possibility that epimerization of **33***a* has occurred in the basic reaction medium and that the product isolated was **33***b*. However, the product is isolated in 95% yield and it seems hardly likely that equilibration of the *cis*-fused **33***a* and the *trans*-fused **33***b* would give the latter exclusively. Furthermore, the appreciable departure from coplanarity of the double bonds required by *trans* fusion would be expected to result in a significant difference between the uv extinction coefficient of the product and that of the *cis*-fused compound **39**,[5] which is not observed. Thus structure **33***a* is assigned to the product.

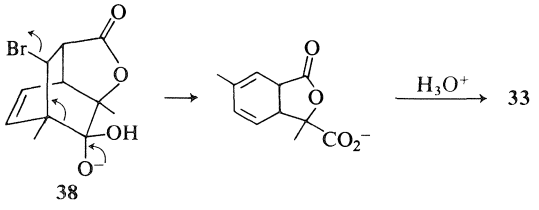

38

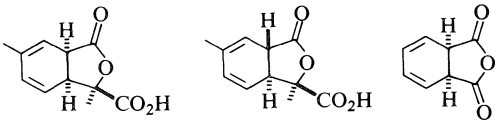

33*a* **33***b* **39**

The alternative base-catalyzed reaction of **22** with alcohols in the presence of 1,1-dimethylhydrazine to give **31** or **32** can be interpreted as involving initial opening of the lactone ring by alkoxide ion to give **40** followed by alkoxide-catalyzed dehydrobromina-

[5]Compound **39** is reported to show λ_{max}^{EtOH} 260 nm (ε 3200), $\lambda_{max}^{CH_3CN}$ 258 nm (ε 3860) (19).

TABLE 5. Infrared, ultraviolet, and ^{1}H nmr spectra of compounds **45** and **47**[a]

Spectrum		**45**	**47**
λ_{max}^{KBr}, μm		3.08 (m), 3.0–3.9, 5.84, 6.33 (br), 7.11	2.90 (m), 2.9–3.5, 5.56 (sh), 5.65, 5.76, 5.81 (sh)
λ_{max}^{MeOH}, nm (ε)		308 (100)	312 (95)
$^H\delta^{D_2O}$	H_A	5.76 (dd, *J* 8, 1.5 Hz)	6.00 (dd, *J* 8, 2 Hz)
	H_B	6.72 (dd, *J* 8, 6.5 Hz)	6.35 (dd, *J* 8, 6.5 Hz)
	H_C	3.1–3.4 (m)	3.60–3.87 (m)
	H_D		3.13–3.33 (m)
	H_E		3.00 (br s)
	Me_F	1.18 (s)	1.43 (s)[b]
	Me_G	1.29 (s)	1.43 (s)[b]
	OMe	3.68 (s)	—

[a]The signal intensities in the ^{1}H nmr spectra are in accord with the assignments.
[b]Superimposed signals.

tion. The latter could proceed directly from **40** via *cis*-elimination or via epimerization of **40** to **41** followed by *trans*-elimination (20). The difference between the hydroxide- and alkoxide-induced reactions of **22** can be attributed to one or more of the following factors: (*i*) readier attack on the sterically hindered ketonic carbonyl carbon by the smaller hydroxide ion, (*ii*) readier dehydrobromination of **40** than of **42**, and (*iii*) readier epimerization of **40** than of **42**.

The formation of **31** and **32** via the intramolecular Diels–Alder product **22** stands in striking contrast to the formation of **43** from the intermolecular Diels–Alder reaction of **11** with propiolic acid (21).[6] Methylation of **43** gives **44**, the regioisomer of **31**.

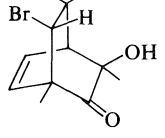

40 X = CO_2R
42 X = CO_2^-

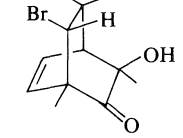

41

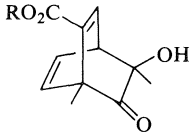

43 R = H
44 R = Me

Thus the modified Wessely oxidation – intramolecular cycloaddition sequence can serve as a source of bicyclo[2.2.2]octane derivatives that differ in their regiochemistry from products obtained by the conventional Wessely oxidation – intermolecular cycloaddition sequence.

Treatment of **23** in water with one equivalent of sodium hydroxide opened the lactone ring and gave the salt **45**, which was isolated as its dihydrate. Its structure follows from its spectra (Table 5) and the fact that on acidification it gave the corresponding hydroxy acid **46**, which could be detected by ^{1}H nmr spectroscopy but could not be isolated because it lactonized rapidly in solution to regenerate **23**. The formation of the latter established that no epimerization occurs in the conversion of **23** to **45**. It is of interest that the uv spectrum of **45** shows a single maximum in the $n \rightarrow \pi^*$ region, while that of **23** shows two maxima. This must reflect the considerable change in the geometry of the system that results upon opening of the lactone ring (*vide supra*). A further point of interest concerning the salt is its solubility in methanol; this can be ascribed to cryptate character in **45**.

Treatment of **23** with two equivalents of sodium hydroxide in boiling water followed by acidification gave the anhydride **47**. Its gross structure is established by its spectra (Table 5) and its stereochemistry follows from the fact that it is different from the *endo* anhydride **48** obtained via intermolecular cycloaddition of maleic anhydride and 2,6-dimethyl-

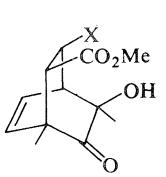

45 X = $CO_2^-Na^+$
46 X = CO_2H

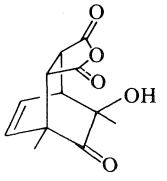

47

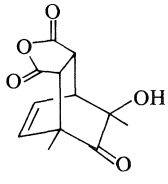

48

[6]The intermolecular reaction is very much slower than the intramolecular reaction, and during its course the acetoxyl group is converted to a hydroxyl group (21).

o-quinol acetate (**11**) (21). Thus in this case the modified Wessely oxidation – intramolecular cycloaddition sequence serves as a source of a bicyclo[2.2.2]octane derivative that differs in its stereochemistry from the product obtained by the conventional Wessely oxidation – intermolecular cycloaddition sequence.

Experimental

Melting points are uncorrected. The ir and uv spectra were recorded for $CHCl_3$ and MeOH solutions, respectively, unless otherwise specified. Proton magnetic resonance spectra (^1H nmr) were recorded for $CDCl_3$ solutions, unless otherwise specified, with Varian HR 220 and T-60 spectrometers; coupling assignments were verified in representative cases by decoupling experiments. Carbon-13 magnetic resonance spectra (^{13}C nmr) were recorded for $CDCl_3$ solutions with Varian CFT-20 and XL-100-15 spectrometers operating in the pulsed Fourier transform mode; both proton-noise decoupled and single frequency off-resonance decoupled spectra were recorded in each case. The chemical shifts (δ) for the ^1H and ^{13}C nmr spectra were measured with reference to internal Me_4Si and are reported in ppm. Spectroscopic data not given in the Experimental section are given in Tables 1–5. Solutions in organic solvents were dried over anhydrous magnesium sulfate.

exo-*6-Hydroxy-4,6-dimethyl-5-oxobicyclo*[*2.2.2*]*oct-7-ene*-exo-*2-carboxylic Acid Lactone* (***12***)[7]

Lead tetraacetate (8.18 g, 18.45 mmol) was dissolved in dry dichloromethane (300 mL). Acrylic acid (4.32 g, 60.0 mmol) was added and the solution was stirred at room temperature for 20 min. A solution of 2,6-dimethylphenol (**9**) (1.83 g, 15.0 mmol) in dry dichloromethane (15 mL) was added dropwise over a 3 min period and stirring was continued at room temperature for an additional 15 min. Ethylene glycol (1 mL) was added to destroy excess Pb(IV). Evaporation gave an orange oil which was taken up in benzene (250 mL); the solution was gravity filtered and extracted with water (2 × 250 mL) and aqueous 1% sodium bicarbonate (250 mL). The organic layer was dried and evaporated to give a yellow oil. This was taken up in benzene (100 mL), and the solution was boiled under reflux for 21 h. Evaporation gave a yellow oil, which on crystallization from chloroform–cyclohexane gave a dark yellow solid (2.4 g). Sublimation at 100°C (0.005 Torr) followed by sublimation at 60°C (0.005 Torr) gave **12** as a white crystalline solid (1.29 g, 45% based on **9**). A further sublimation gave **12**, mp 111.5–112.5°C; *m/e* (relative abundance): 192(4). *Anal.* calcd. for $C_{11}H_{12}O_3$: C 68.73, H 6.29; found: C 68.38, H 6.31.

exo-*6-Hydroxy-4,6-dimethyl-5-oxobicyclo*[*2.2.2*]*octane*-exo-*2-carboxylic Acid Lactone* (***13***)

Compound **12** (304 mg, 1.58 mmol) was dissolved in acetic acid (30 mL), 5% Pd/C (50 mg) was added, and **12** was hydrogenated at room temperature and one atmosphere pressure until uptake of hydrogen ceased. Filtration followed by evaporation gave a colorless oil, which solidified slowly on standing. Sublimation at 80°C (0.005 Torr) gave crystalline **13** (294 mg, 96%), mp 84.5–86°C; ir λ_{max}: 5.63, 5.76 μm; uv λ_{max} (ε): 306 (35) nm; ^1H nmr δ: 1.05 (s, 3H), 1.50 (s, 3H), 1.97 (m, 6H), 2.77 (m, 2H); ^{13}C nmr δ: 208.1 (s), 177.8 (s), 85.2 (s), 43.5 (d), 42.2 (s), 40.1 (d), 33.4 (t), 33.2 (t), 19.8 (q), 15.4 (q), 15.2 (t); *m/e* (relative abundance): 194(9). *Anal.* calcd. for $C_{11}H_{14}O_3$: C 68.02, H 7.27; found: C 67.95, H 7.28.

exo-*6-Hydroxy-4,6-dimethyl-5-oxo*-endo-*3-phenylbicyclo*-[*2.2.2*]*oct-7-ene*-exo-*2-carboxylic Acid Lactone* (***20***)

Lead tetraacetate (23.97 g, 53.8 mmol) and cinnamic acid (42.9 g, 290 mmol) were dissolved in dry dichloromethane (600 mL) and the solution was stirred at room temperature for 30 min. A solution of **9** (5.13 g, 42.0 mmol) in dry dichloromethane was added dropwise over a 5 min period and stirring was continued at room temperature for 45 min. The reaction mixture was worked up as for **12**, except that the benzene solution of the Wessely oxidation product was not boiled. The crude product was a bright orange oil (10.65 g) which crystallized on standing. Three recrystallizations from chloroform–cyclohexane gave **20** (4.79 g) as a white crystalline solid. The washings and filtrates were combined and evaporated to give a deep orange oil which was distilled at 60°C (0.005 Torr). The distillation residue was dissolved in benzene and passed through a Florisil plug (75 g). Evaporation gave a pale yellow solid. Recrystallization from cyclohexane gave 1.87 g of a white crystalline solid which was combined with the first crop to give 6.66 g of **20** (59% based on **9**). Two recrystallizations from cyclohexane gave **20**, mp 160.5–161°C; uv λ_{max} (ε): 310 (100), 270 (200), 265 (270), 263 (280), 259 (315), 252 (290) nm; *m/e* (relative abundance): 268(0.5). *Anal.* calcd. for $C_{17}H_{16}O_3$: C 76.10, H 6.01; found: C 76.01, H 6.02.

cis-β-*Bromoacrylic Acid* (***15***) *and* trans-β-*Bromoacrylic Acid* (***16***)

Propiolic acid (19.7 g, 0.28 mol) and 48% hydrobromic acid (143 g, 0.84 mol) were heated together on a steam bath for 30 min. On cooling 26.9 g of **16** separated as white crystals. The supernatant was concentrated to approximately three-quarters of the original volume, and a second crop (1.02 g) of **16** was deposited when the reaction mixture cooled to room temperature. The filtrate was saturated with sodium chloride and extracted with ether (3 × 100 mL). Evaporation of the extract gave 14.6 g of a clear yellow liquid which crystallized on standing. The yellow solid was taken up in benzene (150 mL) and the solution was stirred with Florisil (2 g). Filtration followed by evaporation gave **15** as a white crystalline solid. Recrystallization from cyclohexane gave 10.4 g, (25%) of **15**. The 66% yield of **16** and 25% yield of **15** contrast with the report that under these reaction conditions only **16** is produced (22).

exo-*3-Bromo*-exo-*6-hydroxy-4,6-dimethyl-5-oxobicyclo*-[*2.2.2*]*oct-7-ene*-exo-*2-carboxylic Acid Lactone* (***21***)

Compound **21** was prepared from lead tetraacetate (9.88 g, 22.3 mmol), **15** (17.08 g, 113 mmol), and **9** (2.44 g, 20.0 mmol) as above. The crude product was obtained as a bright yellow oil which crystallized on standing. Three recrystallizations from chloroform–cyclohexane gave **21** as white crystals (3.38 g, 62% based on **9**). Recrystallization from chloroform–cyclohexane gave **21**, mp 133–134.5°C; *m/e* (relative abundance): 270(0.5), 272(0.5). *Anal.* calcd. for $C_{11}H_{11}BrO_3$: C 48.73, H 4.09, Br 29.47; found: C 48.78, H 4.11, Br 29.58.

[7]The *Chemical Abstracts* name for **12** is 3a,7a-dihydro-6,7a-dimethyl 3,6-methanobenzofuran-2,7(3*H*, 6*H*)-dione. We have preferred to name this and related compounds as bicyclo[2.2.2]octanone derivatives, which better describes their relationship to their parent carbocyclic ring system and, with the following conventions, permits a ready description of their stereochemistry. Substituents are designated as being *exo* or *endo* with respect to the unsaturated bridge of lowest priority, and in saturated compounds to the bridge of lowest priority.

endo-*3-Bromo*-exo-*6-hydroxy-4,6-dimethyl-5-oxobicyclo-[2.2.2]oct-7-ene*-exo-*2-carboxylic Acid Lactone (22)*

Compound **22** was prepared from lead tetraacetate (13.0 g, 29.4 mmol), **16** (17.2 g, 114 mmol), and **9** (3.05 g, 25.0 mmol) as above, except that the benzene solution of the Wessely oxidation product was not boiled. The crude product was obtained as a bright yellow oil (5.03 g). This was taken up in benzene, and the solution was passed through a Florisil column (75 g). Evaporation gave a bright yellow oil which crystallized on standing. Two recrystallizations from chloroform–cyclohexane gave **22** as white crystals (2.33 g, 34% based on **9**). Recrystallization from cyclohexane gave **22**, mp 108–109°C; *m/e* (relative abundance): 273(0.5), 272(0.5), 271(0.5), 270(0.5). *Anal.* calcd. for $C_{11}H_{11}BrO_3$: C 48.73, H 4.09, Br 29.47; found: C 48.81, H 4.12, Br 29.71.

exo-*3-Carbomethoxy*-exo-*6-hydroxy-4,6-dimethyl-5-oxo-bicyclo[2.2.2]oct-7-ene*-exo-*2-carboxylic Acid Lactone (23)*

Compound **23** was prepared from lead tetraacetate (20.2 g, 45.6 mmol), methyl hydrogen maleate (23.7 g, 182 mmol), and **9** (5.25 g, 43.0 mmol) as above. The crude product was obtained as a pale yellow solid (9.61 g). Two recrystallizations from chloroform–cyclohexane gave **23** as a white crystalline solid (3.10 g). The filtrates were combined and evaporated to give a bright yellow oil. Crystallization from ether followed by recrystallizations from ether and chloroform–cyclohexane gave a further 1.30 g of **23** as a white crystalline solid (total 4.40 g, 41% based on **9**). Recrystallization from methanol gave **23**, mp 149–150°C; *m/e* (relative abundance): 251(4) ($M + 1$). *Anal.* calcd. for $C_{13}H_{14}O_5$: C 62.39, H 5.64; found: C 62.23, H 5.63.

endo-*3-Carbomethoxy*-exo-*6-hydroxy-4,6-dimethyl-5-oxo-bicyclo[2.2.2]oct-7-ene*-exo-*2-carboxylic Acid Lactone (24)*

Compound **24** was prepared from lead tetraacetate (7.08 g, 16.0 mmol), methyl hydrogen fumarate (12.5 g, 95.8 mmol), and **9** (1.83 g, 15.0 mmol) as above without boiling in benzene. The crude product was obtained as a bright yellow oil (2.28 g). Three crystallizations from chloroform–cyclohexane gave **24** (1.13 g, 30% based on **9**) as white crystals. Recrystallization from chloroform–cyclohexane gave **24**, mp 122.5–124°C; *m/e* (relative abundance): 250(2). *Anal.* calcd. for $C_{13}H_{14}O_5$: C 62.39, H 5.64; found: C 62.53, H 5.75.

exo-*6-Hydroxy-2*-endo-*3,4,6-tetramethyl-5-oxobicyclo*[*2.2.2*]-*oct-7-ene*-exo-*2-carboxylic Acid Lactone (25)*

Compound **25** was prepared from lead tetraacetate (11.06 g, 24.95 mmol), tiglic acid (5.00 g, 49.9 mmol), and **9** (2.44 g, 20.0 mmol) as above. The crude product was chromatographed on a Florisil column with elution with benzene – 2% ether. Evaporation gave a pale yellow solid which was recrystallized from chloroform–cyclohexane to give **25** (0.57 g, 13% based on **9**) as white crystals. Sublimation at 65°C (0.1 Torr) gave **25**, mp 70–72°C; *m/e* (relative abundance): 220(0.5). *Anal.* calcd. for $C_{13}H_{16}O_3$: C 70.89, H 7.32; found: C 70.83, H 7.32.

endo-*3-Bromo*-exo-*6-hydroxy-6-methyl-5-oxobicyclo*[*2.2.2*]-*oct-7-ene*-exo-*2-carboxylic Acid Lactone (26)*

Compound **26** was prepared from lead tetraacetate (51.6 g, 116 mmol), **16** (63.7 g, 422 mmol), and *o*-cresol (10.8 g, 100 mmol) as above. The benzene solution was evaporated to give a deep red oil (13.75 g) which was distilled at 120°C (10 Torr). The distillation residue was taken up in benzene and passed through a Florisil plug (75 g). Evaporation gave a red oil which was distilled at 120°C (10 Torr). The distillation residue was sublimed at 80°C (0.0005 Torr) and resublimed at 70°C (0.005 Torr) to give a white crystalline solid. Recrystallization from chloroform–cyclohexane gave **26** (3.47 g, 14% based on *o*-cresol). Sublimation at 70°C (0.005 Torr) gave **26**, mp 122–123.5°C; *m/e* (relative abundance): 256(7), 258(7). *Anal.* calcd. for $C_{10}H_9BrO_3$: C 46.72, H 3.53, Br 31.08; found: C 46.87, H 3.63, Br 31.00.

exo-*3-Carbomethoxy*-exo-*6-hydroxy-6-methyl-5-oxobicyclo-[2.2.2]oct-7-ene*-exo-*2-carboxylic Acid Lactone (27)*[8]

o-Cresol (1.00 g, 9.25 mmol) and methyl hydrogen maleate (13.0 g, 100 mmol) were dissolved in dry benzene (100 mL), and the solution was heated to 40°C. Red lead oxide (6.86 g, 10.0 mmol) was added portionwise over a 3 h period. The solution was stirred at 40°C for 12 h and gravity filtered, and the solid residue was washed several times with benzene to bring the volume of the filtrate to 500 mL. The benzene solution was extracted with water (2 × 500 mL) and aqueous 1% sodium bicarbonate (500 mL). The organic layer was dried and evaporated to give a dark oil (1.32 g). The oil was dissolved in methanol (75 mL) and stirred with Florisil (1 g) and activated charcoal (0.5 g) for 30 min. Gravity filtration followed by evaporation gave a red oil which was dissolved in 25% chloroform–cyclohexane (100 mL) and gravity filtered to give a dark yellow solution. The solution was reduced in volume to 25 mL, when a pale yellow solid crystallized. Recrystallization from chloroform–cyclohexane gave **27** (0.76 g, 35% based on *o*-cresol) as white crystals. Recrystallization from methanol gave **27**, mp 145–146.5°C; *m/e* (relative abundance): 236(3). *Anal.* calcd. for $C_{12}H_{12}O_5$: C 61.01, H 5.12; found: C 60.97, H 5.12.

Methyl exo-*6-Hydroxy-4,6-dimethyl-5-oxobicyclo*[*2.2.2*]*octa-2,7-diene-2-carboxylate (31)*

Compound **22** (383 mg, 1.41 mmol) was dissolved in methanol (25 mL) and 1,1-dimethylhydrazine (383 mg, 6.37 mmol) was added. The mixture was boiled under reflux for 21 h and then evaporated to give a yellow oil which was taken up in benzene. The solution was washed with water, dried, and evaporated to give a pale yellow oil (249 mg), which crystallized on standing. Sublimation at 80°C (0.005 Torr) gave **31** as white crystals (231 mg, 75%), mp 118–119°C; ir λ_{max}: 2.87 (w), 5.80, 5.84, 6.10 (w), 6.28 (w) μm; uv λ_{max} (ε): 312 (360), 236 (4,350) nm; *m/e* (relative abundance): 223(0.5) ($M + 1$). *Anal.* calcd. for $C_{12}H_{14}O_4$: C 64.85, H 6.35; found: C 64.77, H 6.35.

Ethyl exo-*6-Hydroxy-4,6-dimethyl-5-oxobicyclo*[*2.2.2*]*octa-2,7-diene-2-carboxylate (32)*

Compound **22** (401 mg, 1.48 mmol) was dissolved in 95% ethanol (100 mL) and 1,1-dimethylhydrazine (200 mg, 3.33 mmol) was added. The mixture was boiled under reflux for 19 h and then evaporated to give a yellow oil which was taken up in benzene (75 mL). The solution was extracted with water (3 × 25 mL). The organic layer was dried and evaporated to yield a pale yellow oil (266 mg), which crystallized on standing. Sublimation at 65°C (0.005 Torr) gave **32** as white crystals (248 mg, 71%). Recrystallization from cyclohexane gave **32**, mp 110–112°C; ir λ_{max}: 3.03 (w), 5.79, 5.85, 6.10 (w), 6.28 (w) μm; uv λ_{max} (ε): 312 (370), 325 (4550) nm; *m/e* (relative abundance): 236(0.5). *Anal.* calcd. for $C_{13}H_{16}O_4$: C 66.08, H 6.83; found: C 66.14, H 6.93.

[8]This procedure represents a variant of the general procedure in which red lead oxide is used in place of lead tetraacetate; its generality is being investigated. Compound **27** was also prepared in lower yield by the standard procedure with lead tetraacetate.

*1,3,3a,7a-Tetrahydro-1,5-dimethyl-3-oxo-1-isobenzofurancarboxylic Acid (**33**)*

Compound **22** (1.13 g, 4.17 mmol) and aqueous sodium hydroxide (0.5 *N*; 20.0 mL, 10.0 mmol) were added to water (10 mL), the mixture was stirred for 6 h and then acidified with concentrated hydrochloric acid, giving a white precipitate (0.62 g). Concentration of the filtrate, evaporation to dryness, and extraction with dichloromethane gave additional product (0.23 g; total 95%). Recrystallization from ethyl acetate gave **33**, mp 163.5–166°C; ir (KBr) λ_{max}: 3.0–4.2 (m), 5.66, 5.88 μm; uv λ_{max} (ε): 270 (3300), 260 (3600) nm; ^{1}H nmr δ: (CD_3OD) 1.71 (s, 3H), 1.77 (t, J = 1.5 Hz, 3H), 3.23 (dm, J = 13 Hz, 1H) 3.70 (dm, J = 13 Hz, 1H), 5.04 (s, 1H, variable), 5.3–5.5 (m, 1H), 5.5–6.1 (m, 2H); ^{13}C nmr (CD_3OD) δ: 179.6 (s), 173.6 (s), 131.9 (s), 129.6 (d), 123.0 (d), 115.5 (d), 90.2 (s), 45.0 (d), 41.6 (d), 24.1 (q), 21.5 (q); *m/e* (relative abundance): 208 (27). *Anal.* calcd. for $C_{11}H_{12}O_4$: C 63.45, H 5.81; found: C 63.20, H 5.91.

*Methyl 1,3,3a,7a-Tetrahydro-1,5-dimethyl-3-oxo-1-isobenzofurancarboxylate (**34**)*

Compound **33** (0.384 g, 1.84 mmol) was dissolved in ether (100 mL) and the solution was titrated with ethereal diazomethane until the yellow color persisted. Evaporation gave a white solid which was sublimed at 65°C (0.005 Torr) to give **34** (0.396 g, 97%), mp 92–92.5°C; ir λ_{max}: 5.60, 5.73 μm; uv λ_{max} (ε): 270 (3650), 260 (3900) nm; ^{1}H nmr δ: 1.73 (s, 3H), 1.78 (t, J = 1.5 Hz, 3H), 3.10 (dd, J = 14, 4 Hz, 1H), 3.4–3.8 (m, 1H), 3.63 (s, 3H), 5.3–5.6 (m, 1H), 5.6–6.0 (m, 2H); ^{13}C nmr δ: 177.4 (s), 171.1 (s), 130.3 (s), 128.7 (d), 121.2 (d), 115.1 (d), 88.9 (s), 52.2 (q), 44.2 (d), 40.9 (d), 23.6 (q), 21.3 (q); *m/e* (relative abundance): 222 (32). *Anal.* calcd. for $C_{12}H_{14}O_4$: C 64.85, H 6.35; found: C 64.97, H 6.48.

*Reaction of **34** with Maleic Anhydride. Formation of **35***

Compound **34** (0.144 g, 0.65 mmol) and maleic anhydride (0.064 g, 0.65 mmol) were dissolved in benzene (50 mL) and the solution was boiled under reflux for 70 h. Evaporation gave a white crystalline solid. Recrystallization from chloroform at −30°C gave **35** (0.187 g, 90%). Sublimation at 130°C (0.005 Torr) gave **35**, mp 226–227°C; ir λ_{max}: 5.36 (w), 5.62, 5.74 (w) μm; ^{1}H nmr δ: 1.65 (s, 3H), 1.80 (d, J = 2 Hz, 3H), 2.57 (dd, J = 4.5, 1.5 Hz, 1H), 3.0–3.4 (m, 3H), 3.4–3.7 (m, 1H), 3.85 (s, 3H), 5.5–5.7 (m, 1H); *m/e* (relative abundance): 320 (24). *Anal.* calcd. for $C_{16}H_{16}O_7$: C 60.00, H 5.04; found: C 60.04, H 5.16.

*Methyl 1,3-Dihydro-1,5-dimethyl-3-oxo-1-isobenzofurancarboxylate (**36**)*

Compound **34** (302 mg, 1.36 mmol) was dissolved in methanol (10 mL), 10% Pd/C (750 mg) was added to the solution, and the mixture was stirred under nitrogen for 10 h. Filtration followed by evaporation gave a white solid which was sublimed at 70°C (0.005 Torr). The sublimate was recrystallized from methanol at −30°C to give **36** as a white crystalline solid (0.210 g, 70%), mp 86.5–88°C; ir λ_{max}: 5.64, 5.75 μm; uv λ_{max} (ε): 290 (1850), 280 (1800), 230 (9500) nm; ^{1}H nmr δ: 1.88 (s, 3H), 2.48 (s, 3H), 3.73 (s, 3H), 7.50 (d, J = 1.5 Hz, 2H), 7.68 (bs, 1H); ^{13}C nmr δ: 169.9 (s), 169.2 (s), 146.6 (s), 140.6 (s), 135.7 (d), 125.8 (d), 125.3 (s), 121.8 (d), 84.7 (s), 53.2 (q), 23.7 (q), 21.3 (q); *m/e* (relative abundance): 220 (2). *Anal.* calcd. for $C_{12}H_{12}O_4$: C 65.44, H 5.49; found: C 65.39, H 5.56.

Sodium exo-*3-Carbomethoxy*-exo-*6-hydroxy-4,6-dimethyl-5-oxo-bicyclo[2.2.2]oct-7-ene*-exo-*2-carboxylate Dihydrate (**45**)*

Compound **23** (1.46 g, 5.85 mmol) and sodium hydroxide (0.232 g, 5.80 mmol) were added to water (60 mL), and the mixture was stirred for 45 min at room temperature. The reaction mixture was extracted with dichloromethane (3 × 50 mL), and the aqueous fraction was evaporated to give 1.77 g of a pale yellow solid. Two recrystallizations from water gave **45** (0.405 g) as a white crystalline solid which decomposed at 280°C. *Anal.* calcd. for $C_{13}H_{15}O_6Na{\cdot}2H_2O$: C 47.86, H 5.86; found: C 47.57, H 5.91.

When an aqueous solution of **45** in D_2O was acidified a solid was deposited, whose ^{1}H nmr spectrum showed signals corresponding to **23** together with signals at δ: 1.25 (s), 1.38 (s), 3.08 (br s), 3.55 (m), 3.75 (s), 5.74 (dd, J = 8, 2 Hz), 6.27 (br s), 6.57 (dd, J = 8, 6 Hz) attributed to **46**.

exo-*6-Hydroxy-4,6-dimethyl-5-oxobicyclo[2.2.2]oct-7-ene*-exo-*2*-exo-*3-dicarboxylic Acid Anhydride (**47**)*

Compound **23** (1.00 g, 4.00 mmol) and sodium hydroxide (0.311 g, 7.77 mmol) were added to water (5 mL) and the mixture was heated on a steam bath for 2 h. The mixture was cooled to room temperature and acidified with concentrated hydrochloric acid to pH 5. Evaporation gave a white solid which was extracted with several portions of ether (125 mL). The ethereal extract was filtered, dried, and evaporated to give a pale yellow oil. This was taken up in chloroform (20 mL), and the solution was allowed to stand at room temperature for 18 h to give crystals (0.349 g). Recrystallization from ether–chloroform gave **47** (0.308 g, 33%) as a white crystalline solid, mp 178–179.5°C; *m/e* (relative abundance): 236 (9). *Anal.* calcd. for $C_{12}H_{12}O_5$: C 61.01, H 5.12; found: C 60.96, H 5.20.

Acknowledgments

We thank the National Research Council of Canada for support of this work and Dr. A. Grey, Canadian 220 MHz NMR Centre, for the 220-MHz ^{1}H nmr spectra.

1. P. Yates and H. Auksi. Chem. Commun. 1016 (1976).
2. F. Wessely and F. Sinwel. Monatsh. Chem. **81**, 1055 (1950).
3. G. W. K. Cavill, E. R. Cole, P. T. Gilham, and D. J. McHugh. J. Chem. Soc. 2785 (1954).
4. F. Wessely and H. Budzikiewicz. Monatsh. Chem. **90**, 62 (1959).
5. K. Holmberg. Acta Chem. Scand. Ser. B, **28**, 857 (1974).
6. D. J. Bichan and P. Yates. J. Am. Chem. Soc. **94**, 4773 (1972); Cah. J. Chem. **53**, 2054 (1975).
7. I. Alfaro, W. Ashton, K. L. Rabone, and N. A. J. Rogers. Tetrahedron, **30**, 559 (1974).
8. H. Labhart and G. Wagniere. Helv. Chim. Acta, **42**, 2219 (1959).
9. R. C. Cookson and S. H. Dandegaonker. J. Chem. Soc. 352 (1955).
10. S. Geribaldi, G. Torri, and M. Azzaro. Bull. Soc. Chim. Fr. 2836 (1973).
11. J. W. ApSimon, W. G. Craig, P. V. Demarco, D. W. Mathieson, L. Saunders, and W. B. Whalley. Chem. Commun. 359 (1966).
12. Guradata and J. B. Stothers, Can. J. Chem. **47**, 3515 (1969).
13. C. M. Cimarusti and J. Wolinsky. J. Am. Chem. Soc. **90**, 113 (1968).
14. J. L. Marshall, S. R. Walter, M. Barfield, A. P. Marchand, N. W. Marchand, and A. L. Segre. Tetrahedron, **32**, 537 (1976).
15. M. Barfield and B. Chakrabarti. Chem. Rev. **69**, 757 (1969).

16. R. C. COOKSON and N. S. WARIYAR. J. Chem. Soc. 2302 (1956); F. KALBERER and H. SCHMID. Helv. Chim. Acta, **40**, 779 (1957).
17. V. N. DOBRYNIN, A. I. GUREVICH, M. G. KARAPETYAN, M. N. KOLOSOV, and M. M. SHEMYAKIN. Tetrahedron Lett. 901 (1962).
18. C. A. GROB and P. W. SCHIESS. Angew. Chem. Int. Ed. Engl. **6**, 1 (1967); C. A. GROB, H. R. KIEFER, H. J. LUTZ, and H. J. WILKENS. Helv. Chim. Acta, **50**, 416 (1967).
19. B. R. LANDAU. Ph.D. Thesis, Harvard University, Cambridge, MA. 1950; M. J. GOLDSTEIN and G. L. THAYER, JR. J. Am. Chem. Soc. **87**, 1925 (1965).
20. S. J. CRISTOL and N. L. HAUSE. J. Am. Chem. Soc. **74**, 2193 (1952); J. SICHER. Angew. Chem. Int. Ed. Engl. **11**, 200 (1972).
21. H. AUKSI. Ph.D. Thesis, University of Toronto, Toronto, Ont. 1978.
22. E. GRYSZKIEWICZ-TROCHIMOWSKI, W. SCHMIDT, and O. GRYSZKIEWICZ-TROCHIMOWSKI. Bull. Soc. Chim. Fr. **15**, 593 (1948).

Etude empirique de la stabilité des hydrocarbures polycycliques non alternants

JEAN PIERRE GASTMANS, DENISE FROMANTEAU GASTMANS ET STÉFANO FERNANDES SLADE
Instituto de Química da Universidade Estadual Paulista, Julio de Mesquita Filho, 14800 Araraquara (SP), Brasil

Reçu le 17 mars 1979

JEAN PIERRE GASTMANS, DENISE FROMANTEAU GASTMANS et STÉFANO FERNANDES SLADE. Can. J. Chem. **57**, 2864 (1979).

Une méthode empirique destinée à prévoir la stabilité des hydrocarbures non alternants est proposée. Cette méthode se base sur les travaux de Krygowski et Randic.

JEAN PIERRE GASTMANS, DENISE FROMANTEAU GASTMANS, and STÉFANO FERNANADES SLADE. Can. J. Chem. **57**, 2864 (1979).

An empirical method for the prediction of the stability of hydrocarbons has been detailed. This method is based on the works of Krygowski and Randic.

Récemment, plusieurs travaux (1–3) ont eu pour but de découvrir des relations simples et empiriques permettant de prévoir le caractere aromatique d'un hydrocarbure insaturé. Comme plusieurs auteurs (*4a*)[1] l'ont remarqué avant nous, la propre notion d'aromaticité est assez confuse et peut recouvrir des comportements les plus divers.

Comme nous nous intéressons au comportement purement chimique d'un composé, nous avons préféré définir deux indices (5); l'indice de stabilité et l'indice d'aromaticité. Le premier sert à prévoir si un hydrocarbure sera stable ou non, le second, s'il est aromatique (au point de vue chimique) ou non.

Le calcul de ces indices se fait de la manière suivante: on calcule systématiquement $\Delta E_{\text{stabilité}}$ pour tous les carbones, la valeur retenue étant la plus basse. On procède de la même manière pour toutes les paires de carbones susceptibles de réagir par addition pour obtenir $\Delta E_{\text{aromaticité}}$.

Nous prétendons, par ce présent travail, énoncer une méthode empirique simple qui permet de prévoir uniquement la stabilité d'un hydrocarbure.

Méthode

Notre méthode se base sur les théories de Kruszewski et Krygowski (1) et Randic (3). Elle en est d'ailleurs la somme.

Le procédé est le suivant:

1. Comme dans la théorie de Krygowsky, on calcule l'indice R:

$$R = S - F$$

où S est le nombre du cycles du type $4N + 3$ et F est le nombre de cycles du type $4N + 1$.

2. On recherche ensuite les cycles de base de grande stabilité qui sont: le naphtalène, l'azulène, le diphenyle et le sesquifulvalène.

Si aucun de ces cycles n'est apparent, on choisit simplement le (ou les) benzène(s).

3. Si $R = 0$ ou ± 1, la stabilité de l'hydrocarbure sera la moyenne arithmétique entre la stabilité des ensembles de carbones restants. Il est utile de rappeler que la stabilité des polyènes (P_n) diminue à mesure que "n" augmente.

Si $R = \pm 2$, la stabilité sera inversement proportionnelle à la moyenne arithmétique entre la stabilité des ensembles restants.

Si $R = \pm 2$ et si aucun cycle de base n'est apparent, l'hydrocarbure sera instable.

Si R est supérieur à 2 ou inférieur à -2, l'hydrocarbure sera problement instable, bien que l'on ne dispose pas de données expérimentales à ce sujet.

Prenons l'acénaphtylène comme exemple (schéma 1):

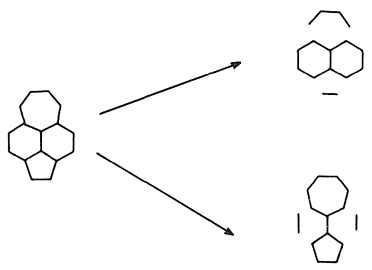

SCHÉMA 1

On peut reconnaître comme cycle de base, respectivement: le naphtalène et le sesquifulvalène. Dans le premier cas, les ensembles restants sont P_4 et P_2 (P_n représente le polyène), dans le second, P_2 et P_2. Dans les deux cas, les polyènes restants sont stables à température ordinaire; l'acénaphtylène sera donc stable, ce que est réellement le cas.

Les cycles de base mentionnés antérieurement ont

[1] On trouvera également une mise au point intéressante dans réf. 4*b*.

0008-4042/79/212864-05$01.00/0

TABLEAU 1. Cycles de base

Composé	IS	REPE (6)[a]	Randic
Benzène	3.47	0.065	0.87
Naphtalène	3.00	0.055	1.32
Diphényle	3.30	0.060	1.74
Sesquifulvalène	2.82	0.022	—
Azulène	2.88	0.023	0.25
Bicyclo(6,2,0)decapentaène	2.07	−0.028	−1.2
Cyclobutadiényl cyclooctatetraène	0.68	−0.08	−2.05

[a]Certaines valeurs de REPE ont été calculées pour ce travail.

été choisis en fonction de leur comportement experimental sur la base des critères suivants:

(*a*) Les cycles de base polycondensés doivent former un circuit conjugué stable R_n, où $n = 1$ ou 2, pour lequel les valeurs de REPE, IS (indice de stabilité) et de l'indice de Randic permettent de prévoir une grande stabilité, comme le montre le tableau 1. Les hydrocarbures formés par la condensation de trois cycles n'ont pas été choisis comme cycle de base. C'est en effet un phénomène bien connu que, généralement, dans une même série, la stabilité diminue à mesure que le nombre de cycles présents augmente. Le bicyclo(6,2,0) décapentaène n'a pas été retenu car ses indices sont trop bas.

(*b*) Les cycles de base polynucléaires linéaires retenus doivent contenir 12 carbones et les valeurs de REPE et IS doivent indiquer une certaine stabilité (l'indice de Randic n'est pas calculable pour tous ces composés). Le cyclobutadiényl cyclooctatétraène n'a pas été retenu à cause de ses indices trop bas.

Dans les tableaux suivants, nous avons reproduit les résultats obtenus pour différents types d'hydrocarbures non alternants.

Il est intéressant de noter le comportement des heptindènes (**D** et **E**). Suivant les théories de Randic et Krygowski, les deux seraient aromatiques. Cependant, tant le REPE que l'IS montrent que l'hydrocarbure angulaire devrait être plus stable. Notre

TABLEAU 2. Hydrocarbures pour lesquels $R = 0$

	Composés	Cycles de base	Résidus	Conclusions	IS	REPE	Exp.	Réf.
A,		**A** + **B** **C** + **D**	P_6 P_6	Stable Stable Stable	2.56	0.033	Stable	7
B,		**A** + **B** **C** + **D**	P_6 P_6	Stable Stable Stable	2.78	0.022	Stable	8
C,		**A** + **D** **B** + **C**	$P_1 + P_3$ $P_3 + P_3$	Instable Instable Instable	2.04	0.018	Instable	9
D,	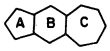	**B**	$P_3 + P_5$	Instable	2.34	0.017	Instable	10
E,		**A** + **C** **A** + **C**	P_2 P_6	Stable Stable	2.59	0.025	Inconnu	
F,		**A** + **D** **B** + **C** **B** + **D**	$P_1 + P_3$ $P_2 + P_4$ P_6	Instable Stable Stable 75% stable	2.45	0.016	Stable	11
G,	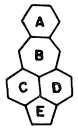	**C** + **D** **B** + **E**	P_2 + o.quinodiméthyde $P_4 + P_2 + P_2$	Instable Stable 50% stable	2.12	0.034	Solution	12

TABLEAU 3. Hydrocarbures pour lesquels $R = \pm 1$

	Composé	Cycles de base	Résidus	Conclusions	IS	REPE	Exp.	Réf.
H,		**B + C**	P_2	Stable	2.66	0.039	Stable	13
I,		**B + C**	P_4	Stable	2.43	0.033	Stable	13
J,		**A + C** **B + C**	P_2 P_2	Stable Stable Stable	2.72	0.018	Stable	14
K,		**A + B** **B + C**	P_4 P_4	Stable Stable Stable	2.54	0.016	Stable	7*a*
L,	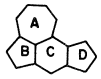	**A + B** **A + D**	Fulvène P_4	± Stable Stable Stable	2.46	0.021	Inconnu	
M,	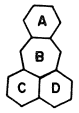	**C + D**	o.quinodi-méthyde	Instable	1.78	0.030	Instable	12
N,		**C + D** **A + D**	Styrène P_6	Stable Stable Stable	2.53	0.030	Stable	15

TABLEAU 4. Hydrocarbures pour lesquels $R = \pm 2$

	Composé	Cycle de base	Résidus	Conclusions	IS	REPE	Exp.	Réf.
O,		**B + C**	$P_2 + P_2$	Instable	2.23	0.018	Solution	16
P,	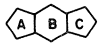	**B**	$P_3 + P_3$	Stable	2.20	0.009	Isolable	17
Q,	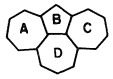	**A + B** **B + C** **B + D**	P_8 P_8 $P_4 + P_4$	Stable Stable Instable 66% stable	2.40	0.009	Isolable	18
R,		—	—	Instable	2.32	−0.018	Instable	19
S,		—	—	Instable	2.25	−0.004	Solution	20
T,	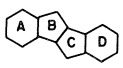	**A, D**	P_4	Instable	2.24	0.031	Isolable	21

NOTE: "Isolable" signifie que le composé peut être isolé, mais qu'il est thermiquement instable ou polymérise facilement.

méthode empirique arrive au même résultat. Expérimentalement, l'heptindène linéaire semble être instable.

Son isomère angulaire n'a pas fait l'objet, à notre connaissance, de tentatives de synthèse. Cette augmentation de stabilité due à la non-linéarité des hydrocarbures est un fait connu dans le cas des hydrocarbures alternants; par exemple, le chrysène angulaire est stable, tandis que le naphtacène linéaire réagit facilement par photooxydation. Il semble que le même phénomène se reproduise pour les hydrocarbures non alternants. Les composés **M** et **N** du tableau 3 constituent un autre exemple.

Lorsque l'on étudie le cas des hydrocarbures pour

TABLEAU 5. Distances de liaison

Composé	Liaison	Distance	Cycle de base
	*a*	1.450 (réf. 22)	**B + C**
	b	1.458	**B + C**
	c	1.398	**A + D**
	d	1.394	**A + D**
	*a*	1.425 (réf. 23)	**A + B**
	b	1.443	**A + B**

TABLEAU 6. Hydrocarbures contenant des cycles 4N

		Cycle de base	Résidus	Conclusions	IS	REPE	Exp.	Réf.
$R = 1$		Cyclobutadiène	Non vide	Instable	0.06	−0.131	Instable	
$R = 0$	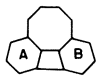	**A, B**	P_4	Stable	2.20	0.003	Stable	24
$R = 1$	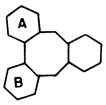	**A + B**	o-quinodiméthyde	Instable	1.46	0.025	Instable	25
$R = 1$	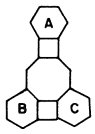	**A, B, C**	P_4	Stable	3.20	0.011	Stable	4*b*

lesquels $R = 2$ ou -2, nous avons observé que la stabilité du composé est inversément proportionnelle à celle des résidus. Ce comportement qui nous semble bien marqué, au vu des données expérimentales, est très curieux. Nous n'avons pas trouvé de raison logique pour expliquer cette inversion.

Lors de l'analyse des résultats du tableau 4, il faut garder de vue qu'il s'agit d'hydrocarbures structuralement instables, tant dans théorie de Randic que dans celle de Krygowski. Dans le cas présent, si l'étude des residus prévoit une stabilité, il faut sous-entendre que l'hydrocarbure en question sera plus stable que ne le laisse prévoir sa structure.

On peut voir que dans tous les cas étudiés, les prévisions empiriques sont très acceptables, sans compter que l'analyse de l'hydrocarbure se fait en quelques secondes. Il peut même paraître curieux qu'une méthode si simple et grossière puisse conduire à des résultats aussi précis.

La méthode que nous proposons n'est, en fait, qu'une image approximative de la réalité; c'est à dire que le composé se comporte comme si, réellement, il pouvait être scindé en cycle de base et un ou plusieurs résidus.

Si nous prenons comme exemple l'acénaphtylène et le cycloheptazulène, dont les distances de liaison sont connues, nous pouvons vérifier, suivant les données du tableau 5, que les liaisons entre les cycles de base et les résidus sont particulièrement longues. Ce fait montre qu'en première approximation, la résonance entre le cycle de base d'une part et les résidus d'autre part est faible. Dans le cas de l'acénaphtylène, on peut voir que la stabilité d'un cycle de base par rapport à l'autre se reflète dans les valeurs de distances. Ainsi les liaisons "*c*" et "*d*" sont plus courtes à cause de la grande stabilité du naphtalène comparée à celle du sesquifulvalène. En conséquence, les cycles de base BC interviennent pour une part plus importante dans la structure et stabilité de l'acénaphtylène.

La méthode que nous avons développée, s'applique principalement aux cycles de 5 et 7 carbones, qui sont d'ailleurs les plus nombreux. Récemment, plusieurs hydrocarbures contenant des cycles de 8 et 4 carbones ont été préparés. Bien que l'on ne dispose pas de données suffisantes pour énoncer, sans risque d'erreur, des lois empiriques concernant leurs stabilités, il nous semble que notre méthode puisse être appliquée en y apportant les modifications suivantes:

1. Les hydrocarbures qui contiennent un cyclobutadiène "non vide" suivant Krygowski sont instables.

2. Pour les autres hydrocarbures, les lois antérieures restent valables, mais R et S représentent maintenant le nombre de cyclobutadiène et cyclooctatétrène respectivement.

A titre d'exemple, nous avons relationné dans le tableau 6, le cas de quelques hydrocarbures connus.

Il faut cependant garder de vue que les lois de Krygowski et Randic, ainsi que les nôtres sont basées essenciellement sur l'équilibre qu'il doit exister entre le nombre de cycles du type $4N + 1$ et celui du type $4N + 3$. Cet équilibre occasionne une migration électronique à partir des cycles de 7 carbones vers ceux de 5 carbones. Dans le cas des cycles de 4 et 8 carbones, qui forment des hydrocarbures alternants, cette migration ne se vérifie pas. De telle sorte que nous ne pouvons considérer les lois énoncées antérieurement que comme des tentatives.

Un autre facteur qui peut invalider ces règles est l'existence de déviation sensibles de la coplanarité, comme c'est le cas pour le cyclooctatétraène.

Remerciements

L'un des auteurs (S.F.S.), boursier de la Fundação de Amparo à Pesquisa do Estado de São Paulo, remercie cet organisme pour la concession d'une bourse d'iniciation scientifique.

1. J. Kruszewski et M. Krygowski. Can J. Chem. **53**, 945 (1975).
2. I. Gutman et N. Trinajstic. Can. J. Chem. **54**, 1789 (1976).
3. N. Randic. J. Am. Chem. Soc. **99**, 44 (1977).
4. (*a*) J. F. Labarre. Bull. Soc. Chim. Fr. 2463 (1977); (*b*) C. F. Wilcox et G. D. Granthan. Tetrahedron, **31**, 2889 (1975).
5. J. P. Gastmans, D. F. Gastmans et R. A. M. de Groote. Tetrahedron Lett. 3339 (1974); J. P. Gastmans, D. F. Gastmans et M. H. M. Ferraz. Tetrahedron, **33**, 2205 (1977).
6. B. A. Hess et L. J. Schaad. J. Org. Chem. **36**, 3418 (1971); J. Am. Chem. Soc. **93**, 305 (1971); **93**, 2413 (1971).
7. (*a*) K. Hafner et G. Schneider. Annalen, **672**, 194 (1964); (*b*) D. H. Reid, W. H. Stafferd et J. P. Ward. J. Chem. Soc. 1193 (1955); J. Am. Chem. Soc. **80**, 143 (1958).
8. A. G. Anderson, Jr, A. A. McDonald et A. F. Montana. J. Am. Chem. Soc. **90**, 2993 (1968).
9. J. M. Pearson, H. A. Sic, D. J. Williams et M. Levy. J. Am. Chem. Soc. **93**, 5034 (1971).
10. D. J. Bertelli. J. Org. Chem. **30**, 891 (1965).
11. K. Hafner, R. Fleischer et K. Fritz. Angew. Chem. Int. Ed. **4**, 69 (1965).
12. M. P. Cava et R. H. Shlessinger. J. Am. Chem. Soc. **85**, 835 (1963); Tetrahedron, **11**, 3051 (1965).
13. V. Boekelheide et G. K. Vick. J. Am. Chem. Soc. **78**, 653 (1956).
14. K. Hafner. Angew. Chem. **71**, 378 (1959); Annalen, **624**, 37 (1959).
15. J. M. Muller, D. Cogniant et P. Cogniant. Tetrahedron Lett. 45 (1971).
16. B. M. Trost, G. M. Brigent, G. Frihart et D. Britelli. J. Am. Chem. Soc. **93**, 737 (1971).
17. K. Hafner *et al.* Angew. Chem. Int. Ed. **2**, 123 (1963).
18. K. Hafner. Pure Appl. Chem. **28**, 153 (1972).
19. R. Bloch, R. A. Marty et P. de Mayo. J. Am. Chem. Soc. **93**, 3072 (1971).
20. H. J. Dauben et D. J. Bertelli. J. Am. Chem. Soc. **83**, 4659 (1961).
21. C. T. Blood et R. P. Linstead. J. Chem. Soc. 2263 (1952).
22. A. W. Hansen. Acta Crystallogr. **13**, 216 (1960); **21**, 97 (1966).
23. R. Qasba, F. Brande, W. Hoppe et R. Huber. Acta Crystallogr. B**25**, 1198 (1969).
24. C. F. Wilcox, J. P. Uetrecht et K. G. Grohmann. J. Am. Chem. Soc. **94**, 2523 (1972).
25. P. Garratt. Aromaticity. McGraw Hill, London. 1971.

Effect of pressure on the Raman spectrum of *s*-trioxane I and II[1]

M. NAKAHARA,[2] P. T. T. WONG, G. J. LEWIS,[3] AND E. WHALLEY
Division of Chemistry, National Research Council of Canada, Ottawa, Ont., Canada K1A 0R9

Received May 17, 1979

M. NAKAHARA, P. T. T. WONG, G. J. LEWIS, and E. WHALLEY. Can. J. Chem. **57**, 2869 (1979).

The Raman spectrum of trioxane II at ~110 K and zero pressure, and the effect of pressure up to 21 kbar on the spectrum of trioxane I and up to 25 kbar on the spectrum of trioxane II, have been measured to determine if the puckered ring of trioxane goes flat. It does not. In trioxane II, many of the bands that are degenerate in the free molecule are split, showing that the C_3 axis of the isolated molecule does not exist. A few volumetric measurements were made on the I–II boundary line.

M. NAKAHARA, P. T. T. WONG, G. J. LEWIS et E. WHALLEY. Can. J. Chem. **57**, 2869 (1979).

On a examiné le spectre Raman du trioxanne II à ~100 K et à pression nulle, et on a mesuré l'effet de la pression, allant jusqu'à 20 kbar, sur le spectre du trioxanne I et jusqu'à 25 kbar, sur le spectre du trioxanne II afin de déterminer si le cycle plissé du trioxanne s'aplatit. Cela ne se produit pas. Dans le trioxanne plusieurs des bandes qui sont dégénérées sont découplées dans la molécule libre montrant ainsi que l'axe C_3 n'existe pas dans la molécule isolée. On a effectué quelques mesures volumétriques à la limite de démarcation entre les trioxannes I et II.

[Traduit par le journal]

1. Introduction

It has been suggested (1) on the basis of the infrared spectrum under pressure that the trioxane molecule becomes flat when squeezed, probably at a phase transition at about 18 kbar from the ordinary phase I to the high-pressure phase II. Trithiane certainly flattens when it is squeezed (2), and the internal rotation angles of 1,2-dichloroethane and 1,2-dibromoethane change significantly towards the *cis* conformation at pressures of a few kilobars (3). However, a detailed analysis of the effect of flattening on the infrared spectrum, which is reported in Section 3.1, showed that the observed (1) effects of pressure are not consistent with flattening. Nevertheless, if trithiane becomes flat, trioxane would be expected to do so, although perhaps at a higher pressure, and evidence for it has been sought in the Raman spectrum. The effect of pressure on the Raman spectra of trioxane I and II at room temperature, and the Raman spectrum of trioxane II recovered at 77 K and zero pressure have been measured.

Preliminary measurements showed that trioxane could not be transformed to phase II at pressures below about 25 kbar. Consequently, a few measurements of the I–II equilibrium line and its hysteresis have been made up to 150°C to help choose the best conditions for the preparation of phase II.

2. Experimental Methods and Results

s-Trioxane was obtained and purified as described in the preceding paper (4).

2.1 Volumetric Measurements

About 4 g of trioxane was melted in a Teflon capsule having 12.5 mm od and 1 mm wall thickness, and the capsule was placed in a 12.5 mm piston-cylinder apparatus (5) lubricated with molybdenum disulphide. The apparatus was heated in an oil bath controlled at ±1°C, and was pressurized by a 100-ton press. The piston displacement was measured 5 min after each change of pressure by an Ames dial gauge graduated to 25 μm. Runs at 50 and 100°C are plotted for both increasing and decreasing pressure in Fig. 1.

The pressures at which the maximum slopes occurred when raising and lowering the pressure differed by 6, 3.4, and 3.2 kbar at 50, 100, and 150°C respectively. The hysteresis in the pressure between up and down runs at the same displacement, when there is little friction in the sample, is about 12% of the pressure, as determined by measuring the ice VI–VII and other transitions (6), and is approximately symmetrical about the transition pressure. This corresponds to a hysteresis of about 2.2 kbar at the I–II transition in trioxane. There is therefore significant friction in the sample even at 150°C. The friction was assumed to be symmetrical about the equilibrium transition pressure, and the transition pressure was taken as the mean of the pressures at which the maximum slopes occurred. They were 16.8, 18.6, and 17.4 kbar at 50, 100, and 150°C respectively, with an uncertainty of about ±1 kbar. Within experimental error the transition pressure is 17.6 ±

[1]NRCC No. 17736.

[2]NRCC Research Associate 1978–1979. Present address: Department of Chemistry, Faculty of Science, Kyoto University, Kyoto 606, Japan.

[3]NRCC Research Associate 1976–1978. Present address: 34 Borough Av., Wallingford, Oxfordshire, England.

0008-4042/79/212869-07$01.00/0

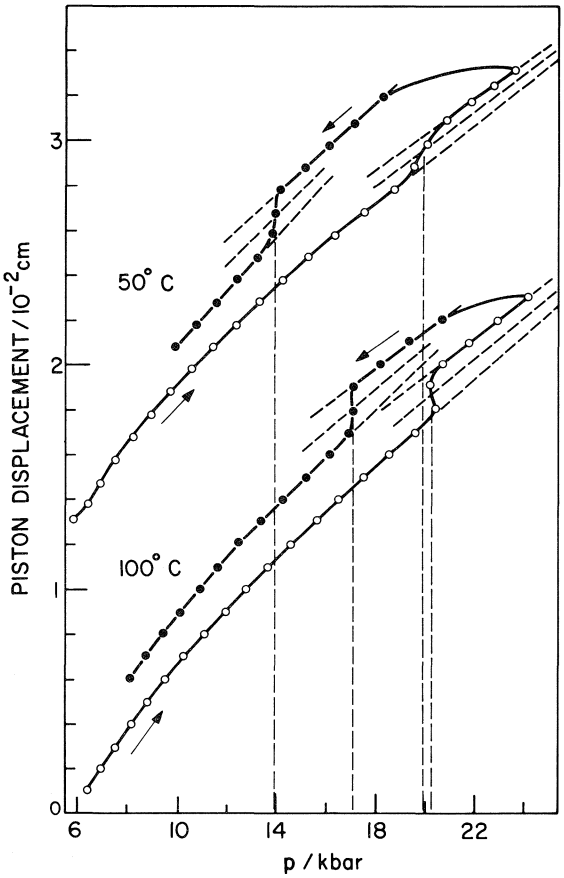

FIG. 1. Graph of piston displacement against pressure for the compression of *s*-trioxane at 50 and 100°C. The dashed lines are extrapolations and interpolations to help estimate the transition pressures and volume changes.

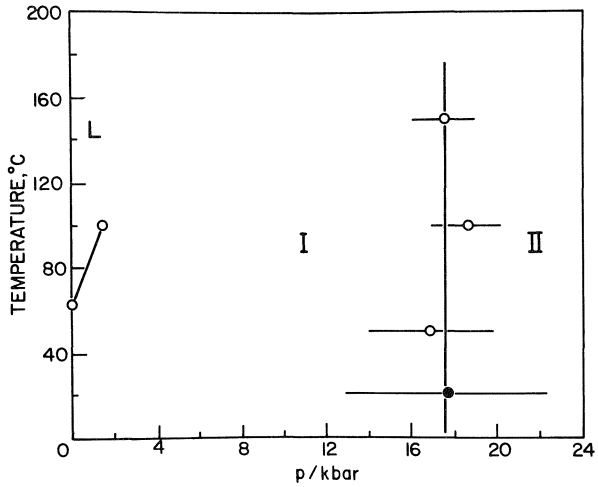

FIG. 2. Phase diagram of trioxane. The ends of the bars indicate the transition pressures for increasing and decreasing pressures. The solid circle at 22°C represents the measurements of Hamann *et al.* (7).

$\sim$1 kbar at all temperatures, which is consistent with the measurement of Hamann *et al.* at 22°C (7).

The volume of transition was determined by extrapolating the apparently straight compression curves well above and well below the transition to the pressures of maximum slope, and the volume changes were determined from the differences in displacement at these pressures. The volume change at the equilibrium pressure was taken as the mean of the apparent volume changes for raising and lowering the pressure. It was $\sim$1.0 and $\sim$1.2 cm^3 mol^{-1} at 50 and 100°C respectively. At 150°C, enough polymer was formed (8) to make the measured volume change unreliable. The melting point was observed at 100°C at 1.4 kbar on decreasing the pressure. By allowing 12% for friction an approximate melting pressure of 1.2 kbar was obtained.

The phase diagram is plotted in Fig. 2, which includes the zero-pressure melting point of 64°C (9). The slope of the melting line near zero pressure is $27 \pm \sim 3$ K kbar^{-1}. The volume of melting at zero pressure from the densities (10, 11) adjusted to 64°C is $12 \pm \sim 1$ cm^3 mol^{-1}, and so the entropy and heat of melting are $44 \pm \sim 6$ J K^{-1} mol^{-1} and $15 \pm \sim 2$ kJ mol^{-1}.

2.2 Raman Spectrum of Recovered Trioxane II

The quenched samples of trioxane II were made by placing a small copper channel in a Teflon capsule, compressing it to make phase II, quenching to 77 K at high pressure, and removing the pressure. The sample held in the copper channel was recovered and mounted on the cold finger of a low-temperature Raman cell, as described elsewhere (12). The recovered sample was opaque, so no polarization measurements could be done. The temperature of the sample was measured with a thermocouple embedded in it and was 110 K. The spectrum is shown in Fig. 3. The frequencies and qualitative relative intensities of the bands are listed in Table 1, along with the frequencies and relative intensities of the spectrum of trioxane I at 110 K taken using a similar technique.

The internal vibrations are similar to those of trioxane I, and most of the bands can be straightforwardly correlated as in Table 1, in which the symmetry species listed (4, 13) are those of the isolated C_{3v} molecule. The species in phase I, which belongs to the space group $R3c$, C_{3v}^6 with two molecules in the primitive cell on sites of symmetry C_3, are the same except that the A_2 vibrations become weakly active as A_1 crystal vibrations. The species in phase II are, of course, not known.

Only a few points deserve comment. Most of the hydrogen-atom vibrations that are degenerate under

the C_{3v} symmetry of phase I split into two bands of approximately equal intensity in phase II. The splitting of the 3033- and 2887-cm^{-1} (at room temperature) bands confirms that the A_1 and E asymmetric and symmetric CH_2 stretches overlap in phase I, as was discussed in an earlier paper (4). Kobayashi's (13) interpretation, in which the components of the asymmetric and of the symmetric stretch are separated by several tens cm^{-1}, seems incorrect. Several new bands occur in phase II. Most are probably combinations, but the bands at 1375 and 1236 cm^{-1} may correspond to the A_2 CH_2 wagging and twisting vibrations of the isolated molecule made active by the distortion. The splitting of the degenerate vibrations shows that the C_3 symmetry which molecules in phase I have is destroyed in phase II. In trithiane, the sulphur analogue of trioxane, there are two molecules in the unit cell of symmetry $Pmn2_1$, C_{2v}^7, and they are on sites of C_s symmetry (14, 15). Trioxane II could have a similar structure.

Brasch *et al.* (1), on the basis of the infrared spectrum under pressure taken in a diamond-anvil apparatus, suggested that trioxane became flat at the I–II transformation. The Raman spectrum shows clearly that trioxane II is not flat at ~110 K and zero pressure. If it were, the A_1 (on the basis of the C_{3v} symmetry of the isolated molecule) asymmetric CH_2 stretch, the A_1 CH_2 rock, and the A_1 ν_3 internal rotation would have lost their Raman intensity. The A_1 asymmetric CH_2 stretch may be present (4, 13) as a weaker band on the low-frequency component of the E asymmetric CH_2 stretch. The A_1 CH_2 rock has been assigned to a very strong infrared band in trioxane I at 1222 cm^{-1} (16), but has not been observed in the Raman spectrum either in ref. 4 or in this work. The A_1 ν_3 internal rotation is also still present as a medium band at 496 cm^{-1}.

2.3 Effect of Pressure on the Raman Spectrum of Trioxane I

The Raman spectra were taken with a 25-kbar hydrostatic optical cell with glass windows (17). The pressure was measured with a manganin gauge calibrated against a 20-kbar pressure balance. The spectral slit widths were 3 cm^{-1}, counting rates 500 s^{-1}, time constant 10 s, and scan speed 10 cm^{-1} min^{-1}. The 514-nm argon line was used at a power of ~1 W. Spectra of phase I were taken at intervals of ~3 kbar at 22°C.

Two sets of spectra were taken. In the first, the trioxane was separated from the naphtha, in which it is soluble, by the apparatus shown in Fig. 4. The sample holder was a quartz tube that was closed at one end except for a 2-mm-diameter hole and was optically flat at the other. The sample was held in

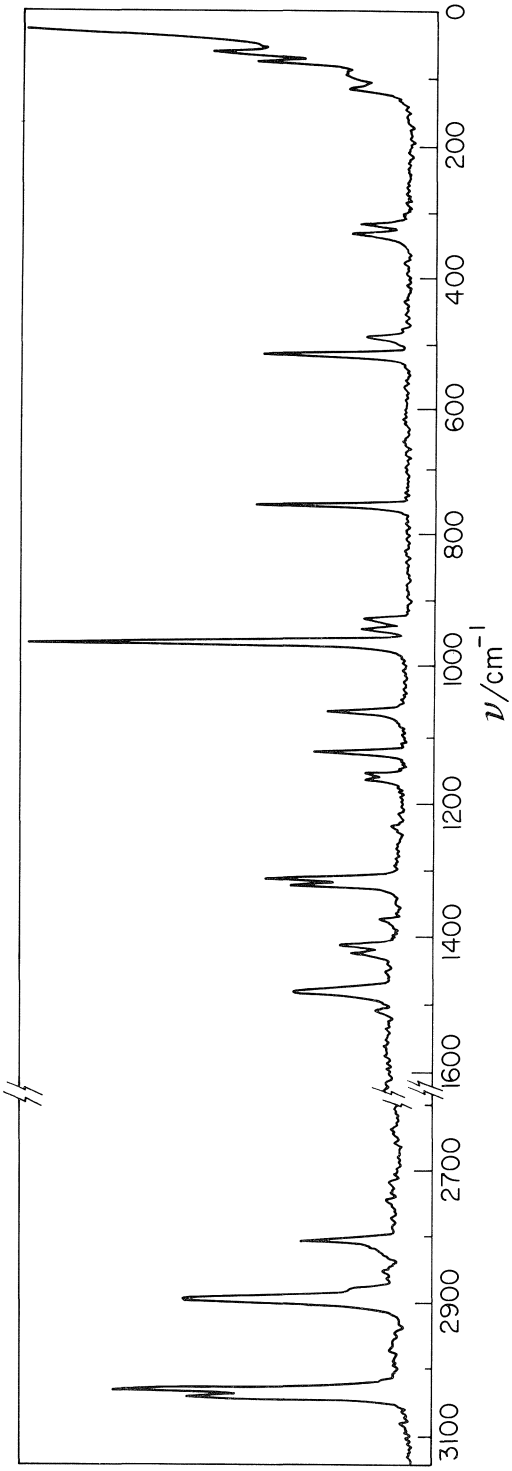

FIG. 3. Raman spectrum of trioxane II at 100 K and zero pressure. The region not shown contained no detected bands.

TABLE 1. Raman spectra of trioxane I and II

Approximate origin[a]	Phase I ν (cm^{-1}) 110 K 0 kbar	Phase I ν (cm^{-1}) 295 K 20 kbar	Phase I ∂ν/∂p (cm^{-1} kbar^{-1})	Species[b]	Phase II ν (cm^{-1}) 110 K 0 kbar	Phase II ν (cm^{-1}) 295 K 25 kbar	Phase II ∂ν/∂p (cm^{-1} kbar^{-1})[d]
CH_2 asymm. st.	3038 vs	3075 vs	1.5[c]	E	3037 s	3060 vs	1.0
				E, A_1	3027 vs		
	3000 vw	—		A_1	~2990 w,b	—	
	~2960 w,b	—		A_1	~2950 w,b	—	
CH_2 symm. st.	2892 vs	2921 s	1.1[c]	A_1, E	2890 vs	2926 s	1.4
				E	2876 w	—	
	2853 w	—		A_1	2851 w	—	
	—	—		—	2823 w	2824 w	
	—	—		—	2815 w	—	
CH_2 symm. st.	2815 s	2840 m	1.0	A_1	2803 m	—	
	2785 vw	—		E	2783 vw		
					2770 vw	—	
	2766 w	—		A_1	2745 w	—	
	2725 w	—		A_1	2715 vw	—	
	2630 vw,b	—		A_1	2635 vw	—	
	—	—			1511 w	—	
CH_2 bend	1487 m	1495 m	0.4	E	1483 m	1488 m	
					1478 m		
CH_2 wag	1419 m	1428 m	0.2	E	1423 m	1423 m	
					1414 m	1414 m	
CH_2 wag	—	—		A_2	1375 w	—	
CH_2 twist	1325 s	1338 m	0.7	E	1324 m	1329 m	
					1313 s		
	1319 sh	—		E	1313[e]	—	
CH_2 twist	—	—		A_2	1236 vw	—	
Ring asymm. st.	1162 m	1168 m	0.4	E	1166 m	1162 m	
					1157 m		
	1077 w	1082 w	0.5	E	1075 vw	—	
	1071 w	—		E	—	—	
Ring symm. st.	1053 m	1062 m	0.6	E	1062 m	1071 m	
	965 sh	—		A_1	—	—	
	952 vs	960 vs	0.3	E	958 vs	969 vs	
CH_2 rock	924 m	937 m	0.4	E	938 m	950 m	
					920 m	928 m	
	919 vw	—		—	928 vw	—	
Ring bend	749 s	756 m	0.3	A_1	750 s	758 m	
Ring bend	520 s	525 s	0.1	E	521 s	526 s	0.3
	492 sh	—		A_1	—	—	
Internal rot., ring bend	484 m	499	0.8	A_1	496 m	518 m	0.4
Internal rot., ring bend	318 m	321 m	0.7	E	339 m	374 m	2.0
	313 m				323 m	342 m	0.9
Intermolecular	96 m	129 m	1.9	E	118 m	172 m	2.0
					98 m	148 m	1.7
					81 s	114 s	1.2
	68 s	84 s	0.9	E	67 s	72 s	0.0

[a]References 4, 13, and 16.
[b]References 4 and 13.
[c]Average value between 10 and 20 kbar.
[d]Average value between 11.4 and 25 kbar.
[e]Probable position by analogy with trioxane I.

the tube by a Viton plug at the closed end and by the window of the high-pressure cell, which the sample cell was wrung to. The assembly was held on the window plug of the Raman cell by a brass holder cushioned with a rubber pad. The holder had apertures for passage of the laser beam. This set-up is particularly suitable for samples that dissolve in the pressure-transmitting fluid, and can be used for liquids that would corrode the Raman cell. It can, of course, be used only for liquids and soft solids. Spectra were measured up to 21 kbar.

In the second set of spectra, naphtha saturated

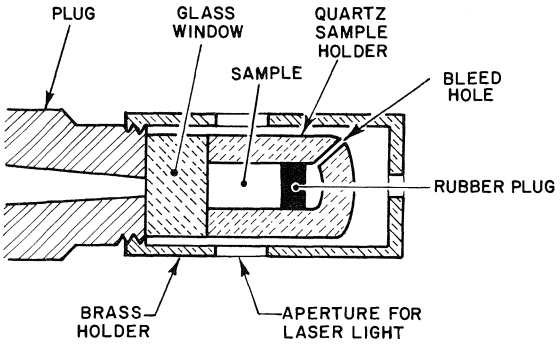

FIG. 4. Sketch of sample holder used to isolate the sample from the pressure-transmitting fluid.

with trioxane was used as the pressure-transmitting fluid, and the samples were either single crystals, clear samples made by cooling the melt slowly, or opaque samples made by cooling the melt rapidly. The clear samples had strong polarization effects characteristic of oriented polycrystals. The relative intensities of the bands of the spectra of both clear samples and single crystals, taken with a linearly polarized exciting beam, changed greatly in the first few kilobars in a way showing that the exciting beam was becoming strongly depolarized. The windows depolarize relatively little even at 20 kbar (18) and it is likely that the depolarization was caused by finely divided trioxane precipitated from the saturated solution by increasing the pressure. To confirm the depolarization, spectra were run with circularly polarized exciting light, which should give the same spectrum as depolarized light and so should be unaffected by the depolarization. The relative intensities were not significantly affected by pressure. Opaque samples behaved similarly, and both these observations confirm the depolarization. Spectra were measured up to 20 kbar.

The changes of intensity due to the depolarization of the exciting light did not significantly affect the frequencies, and so these have been reported. The relative intensities obtained only with either circularly polarized light or with opaque samples were used. They were taken to 16 kbar for all bands and to 21 kbar for the 486- and 520-cm^{-1} bands.

The frequencies of the vibrations changed linearly with pressure, except for the CH_2 stretching vibrations, which were slightly non-linear. Their variation was also non-linear with opaque samples and when circularly polarized exciting light was used, and is undoubtedly real. The slope of the frequency against pressure for each band is listed in Table 1. The results obtained when the sample was held in the quartz tube shown in Fig. 4 or when an opaque polycrystal was held in naphtha saturated with trioxane were essentially the same.

When the trithiane was compressed to 18 kbar, the A_1 ν_3 ring flattening vibration at 309 cm^{-1} lost 75% of its intensity relative to neighboring bands, and it was concluded that the molecule was half way to being flat (2). The corresponding band in trioxane is at 486 cm^{-1} (4). The relative areas of the 486 and 520 cm^{-1} bands and of several other bands were determined by tracing them carefully on high quality paper, cutting them out, and weighing them. There was no significant change in the ratio of the intensity of the 486-cm^{-1} band to the intensity of the 520-cm^{-1} band up to 21 kbar and its ratio to the intensity of the 3033-, 2888-, 1482-, 1319-, 1160-, 951-, 927-, 746-, or 59-cm^{-1} bands up to 16 kbar.

The A_1 asymmetric CH_2 stretch should also lose intensity if the molecule flattens. It is, however, weak compared with the overlapping E asymmetric stretch, and flattening should have only a small effect on the ratio of intensities of the CH_2 asymmetric and symmetric stretches. The data in the preceding paragraph imply that the relative intensity of the 3033- and 2888-cm^{-1} bands was independent of pressure, and a graph of the ratio verified that this is so.

The intensity of the 308-cm^{-1} band (frequency at ambient conditions) (4), relative to the 520-cm^{-1} band, however, appeared to decrease from 0.33 to 0.22 in the range 0–16 kbar, as is clearly evident in the plot in Fig. 5. The intensity of the 308-cm^{-1} band no doubt decreases significantly relative to the rest of the spectrum.

2.4 Effect of Pressure on the Raman Spectrum of Trioxane II

A sample of trioxane II for high-pressure spectroscopy was made in a 25-kbar hydrostatic Raman cell (17) from a single crystal of phase I by heating the cell to 65°C and raising the pressure to 25 kbar.

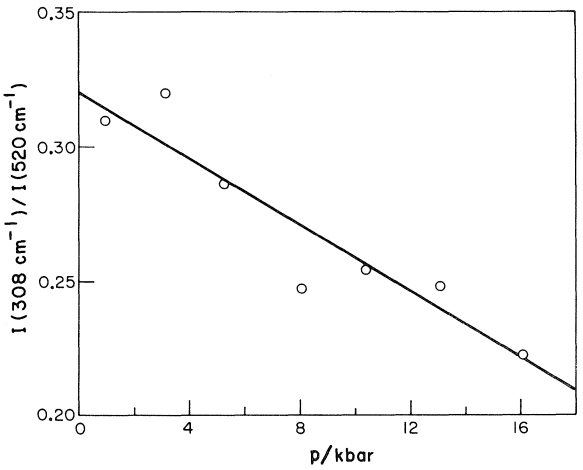

FIG. 5. Pressure dependence of the ratio of the Raman intensities of the 308- and 520-cm^{-1} bands.

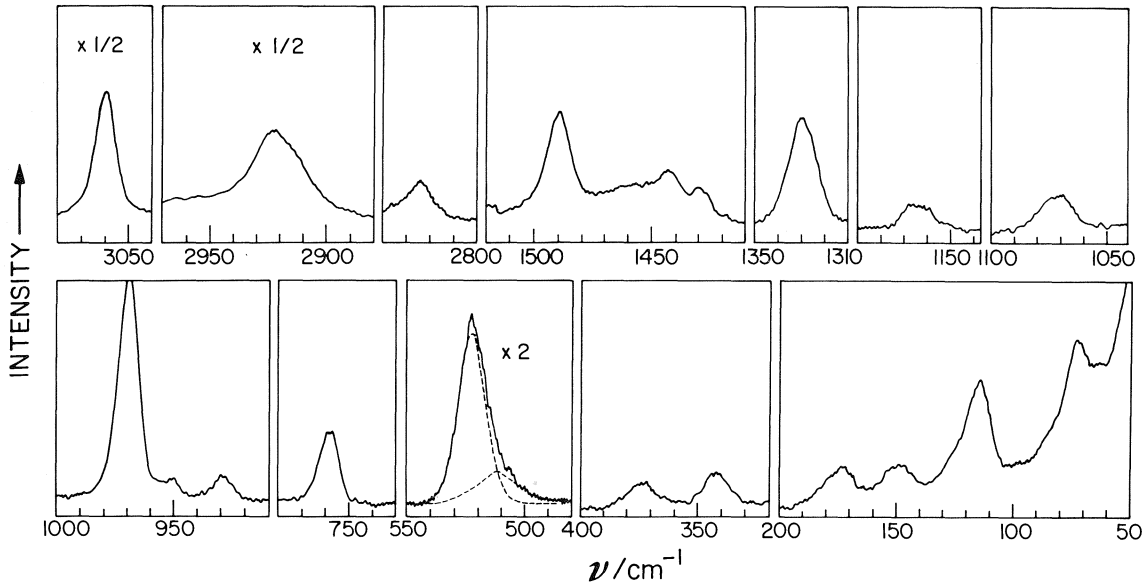

FIG. 6. Raman spectrum of trioxane II at 295 K and 25 kbar. The regions not shown contained no detected bands. An approximate resolution of the 526- and 518-cm^{-1} bands is suggested.

The pressure was determined from the pressure applied to the hydraulic jack, using the experimentally determined intensification ratio. The transformation was monitored by the *c a* Raman spectrum of the band at 3033 cm^{-1}. At the transformation, which occurred at 22.5 kbar, the intensity of the scattered exciting light increased by an order of magnitude because the single crystal was destroyed. The sample was cooled to 22°C and its spectrum was recorded at about 2.5-kbar intervals from 25 kbar to its transformation to phase I. The slit width was 5 cm^{-1}, scan speed 2 or 5 cm^{-1} min^{-1}, and time constant 40 s. The spectrum at 25 kbar is shown in Fig. 6 and the frequencies at 25 kbar are listed in Table 1.

The spectrum is similar to that of phase II at ~110 K except for frequency shifts that can be attributed to the difference of temperature and pressure, a broadening of the bands and a decrease in the splitting of the bands that are degenerate in the isolated molecule. For some bands the splitting disappears. Phase II survived a reduction to 11.4 but not to 8.8 kbar at 22°C. The effect of pressure on the frequencies is summarized in Table 1.

In phase II under pressure at 22°C, the ν_3 internal rotation is a weak low-frequency shoulder of the 525-cm^{-1} band. It should be absent if the molecule is flat. The two bands were resolved by the curve resolver using Gaussian–Lorentzian-product line shapes, and widths that were independent of pressure, as shown in Fig. 6. The relative intensities were about the same as in phase I and did not change significantly with pressure. The molecules in phase II are therefore not significantly flattened at pressures up to 25 kbar.

3. Discussion

3.1 Effect of Pressure on the Spectrum

There is no doubt from the spectra reported in this paper that trioxane does not go flat under the experimental pressures in either phase I or phase II. This is consistent with the reported infrared spectrum (1), as the following arguments show.

As was discussed in connection with the flattening of trithiane (2), the A_1 vibrations that become symmetric to the horizontal plane that is formed on flattening, and so belong to species A_1', and E vibrations that become antisymmetric to the horizontal plane, and so belong to species E'', lose their infrared activity. In the CH stretching region, the A_1 symmetric stretch at 2883 cm^{-1} in phase I and the E asymmetric stretch at 3031 cm^{-1} (the frequencies are those of ref. 15) should lose infrared intensity. Both bands are doublets, but the band that should disappear on flattening is the stronger of both pairs, and is much the stronger of the pair at 3031 cm^{-1}. Neither loses infrared intensity and so there is no evidence for flattening.

The A_1 CH_2 bend at 1494 cm^{-1} should lose infrared intensity on flattening. Brasch *et al.* (1) reported that the 1495-cm^{-1} (their frequency) band was absent from the high-pressure spectrum, although a new band appeared at 1515 cm^{-1}, and the 1420-cm^{-1} band also disappeared. The 1420-cm^{-1} band

was assigned (16) to the E CH_2 wag, which remains active in the planar conformation.

The E CH_2 rock at 918 cm^{-1} and the A_1 ν_1 ring symmetric stretch at 951 cm^{-1} should disappear. In fact, they merge to form "a very intense broad band from 920 to 980 cm^{-1}".

The A_1 ν_2 ring deformation at 744 cm^{-1} and the E ν_8 internal rotation at 305 cm^{-1} should lose infrared intensity. The 744-cm^{-1} band is not reported (1) to lose intensity under pressure, but it was reported by Kobayashi *et al.* (16) to be very weak, and may not have been observed in the high-pressure spectra. The 305-cm^{-1} band is beyond the experimental range. The 480-cm^{-1} band (1), which is the A_1 ν_3 ring flattening vibration at 486 cm^{-1} in the Raman spectrum (4), also disappears, whereas it is predicted to disappear on flattening only in the Raman spectrum. It is clearly present in Raman spectra reported in this paper, but it is merged with the 526-cm^{-1} band in phase II at room temperature in the range 11.4–25 kbar, which explains its disappearance from the infrared spectrum.

3.2 Resistance to Flattening

The potential barrier to flattening the trithiane molecule, according to the potential function

$$V = V_0(1 - \theta^2)^2$$

where V is the potential energy, V_0 the potential energy of the flat relative to the equilibrium conformation, and $\theta = x/x_0$ where x and x_0 are the instantaneous and equilibrium distances between the carbon and oxygen planes, and the flattening frequency at zero pressure of 309 cm^{-1} (2) is about 0.87 perg (picoerg). The force constant that resists flattening is $8V_0/{x_0}^2$, and is 1.6 and 2.8 mdyn $Å^{-1}$ for trithiane and trioxane respectively. The ratio of the volumes of trithiane and trioxane is ~1.4 (11, 14, 15), and so the ratio of surface areas is ~1.25. The ratio of the forces exerted on a molecule by an applied pressure is therefore about 1.25. The force on a molecule divided by the force constant is therefore ~2.2 times larger for trioxane than for trithiane.It should therefore be significantly more difficult to flatten, in agreement with the conclusions of this paper.

Summary

1. The Raman spectrum of trioxane I up to 21 kbar and of trioxane II at ~110 K and zero pressure and at 295 K in the range 11.4–25 kbar have been measured.

2. The spectra show no evidence that the molecules in either trioxane I or trioxane II become flatter in the experimental range.

1. J. W. Brasch, A. J. Melveger, E. R. Lippincott, and S. D. Hamann. Appl. Spectrosc. **24**, 184 (1970).
2. G. J. Lewis and E. Whalley. J. Chem. Phys. **68**, 1119 (1978).
3. H. Takaya, Y. Taniguchi, P. T. T. Wong, and E. Whalley. To be published.
4. M. Nakahara, P. T. T. Wong, and E. Whalley. Can. J. Chem. **57**, 711 (1979).
5. A. K. Kuriakose and E. Whalley. J. Chem. Phys. **48**, 2362 (1968).
6. G. P. Johari, A. Lavergne, and E. Whalley. J. Chem. Phys. **61**, 4292 (1974).
7. S. D. Hamann, M. Linton, and C. W. F. T. Pistorius. High Temp. High Press. **5**, 575 (1973).
8. J. Osugi, K. Hamanoue, and T. Ohtani. Nippon Kagaku Zasshi, **89**, 532 (1968).
9. Dictionary of organic compounds. Vol. 5. Eyre and Spottiswood, London. 1965.
10. J. F. Walker and P. J. Carlisle. Chem. Eng. News, **21**, 1250 (1943).
11. V. Busetti, M. Mammi, and G. Carazzolo. Z. Kristallogr. **119**, 310 (1963); V. Busetti, A. Del Pra, and M. Mammi. Acta Crystallogr. B**25**, 1191 (1969).
12. P. T. T. Wong and E. Whalley. Rev. Sci. Instrum. **43**, 935 (1972).
13. M. Kobayashi. J. Chem. Phys. **66**, 32 (1977).
14. J. E. Fleming and H. Lynton. Can. J. Chem. **45**, 353 (1967).
15. G. Valle, V. Busetti, M. Mammi, and G. Carazzolo. Acta Crystallogr. B**25**, 1432 (1969).
16. M. Kobayashi, R. Iwamoto, and H. Tadokoro. J. Chem. Phys. **44**, 922 (1966).
17. E. Whalley, A. Lavergne, and P. T. T. Wong. Rev. Sci. Instrum. **47**, 845 (1976).
18. H. Takaya, Y. Taniguchi, P. T. T. Wong, and E. Whalley. Unpublished results.

Les oxazolines-4 précurseurs de sels d'iminium fonctionnels. Ouverture en milieu anhydre de ces hétérocycles par des acides protoniques: obtention de sels d'iminium fonctionnels, étude de leur structure

MICHEL VAULTIER, GURBACHAN MULLICK[1] ET ROBERT CARRIÉ

Groupe de Physicochimie Structurale, laboratoire no 3, ERA no 389, 35042 Rennes Cédex, France

Reçu le 26 avril 1979

MICHEL VAULTIER, GURBACHAN MULLICK et ROBERT CARRIÉ. Can. J. Chem. **57**, 2876 (1979).

La protonation des oxazolines-4 en milieu anhydre, à basse température ou à température ambiante, par des acides protoniques conduit généralement à des sels d'iminium fonctionnels acycliques. Lorsque le carbone 4 du cycle oxazoline porte un hydrogène, deux sels d'iminium cycliques diastéréoisomères sont formés. Les conditions d'obtention et la structure de ces espèces sont établies à l'aide de la rmn du proton et du ^{13}C.

MICHEL VAULTIER, GURBACHAN MULLICK, and ROBERT CARRIÉ. Can. J. Chem. **57**, 2876 (1979).

The protonation of 4-oxazolines with protic acids in anhydrous medium, both at low or at room temperature, generally leads to acyclic functional iminium salts. In those cases where the oxazoline ring bears a hydrogen atom in the four position, two diastereoisomeric cyclic iminium salts are obtained. The conditions for preparation of these salts along with the characterization of their structures were determined by the aid of ^{1}H and ^{13}C nmr.

Introduction

Les oxazolines-4 ont été peu étudiées (1). Cependant il a été montré que certains de ces composés sont des ylures d'azométhine potentiels qui peuvent donner des cycloadduits avec divers dipolarophiles (2, 3). L'instabilité des oxazolines-4 en présence d'eau est également connue et les produits d'hydrolyse ont été identifiés (3, 4).

Lors d'une étude sur la réactivité des aziridines, ylures d'azométhine potentiels, vis à vis des réactifs électrophiles et nucléophiles (5), nous avons montré que l'oxazoline-4 **1***a* réagit à température ambiante (*1*) avec les ylures de soufre pour conduire à des azétidines (6). Il n'a pas été clairement établi dans ce cas si la réaction procède par une addition nucléophile sur l'ylure d'azométhine éventuellement en équilibre avec l'oxazoline-4 **1***a* ou par une attaque directe du cycle oxazoline par les ylures du soufre; (*2*) avec certains nucléophiles (5) (phosphite de triméthyle, anions ambivalents . . .) uniquement en présence d'un acide protonique.

Nous avons donc entrepris une étude du comportement des oxazolines-4 en présence d'acides protoniques pour: (*1*) montrer que les oxazolines-4 sont des précurseurs de sels d'iminium fonctionnalisés sur le carbone en α de l'atome d'azote. Ces sels sont d'accès difficile, seule la protonation d'aziridines dans les conditions où elles sont en équilibre avec les ylures d'azométhine correspondants permet de les obtenir (5). L'introduction de fonctions dans cette position ouvre de nouvelles possibilités d'hétérocyclisation; (*2*) établir les conditions d'obtention de ces sels d'iminium et leurs structures, afin de permettre une meilleure compréhension des mécanismes réactionnels et un meilleur choix de conditions expérimentales.

Présentation générale du problème

La schéma 1 donne les diverses possibilités d'évolution d'une oxazoline-4 de formule **1** en présence d'acide protonique AH dans un milieu anhydre.

Ces différentes possibilités résultent de la structure de l'oxazoline-4 qui peut être à la fois considérée comme une énamine, un éther d'énol ou un aminoacétal. Seule la formation des entités de structure **3** et **4** a été observée sauf dans le cas de l'oxazoline **1***e* où deux diastéréoisomères de structure **9** ont été mis en évidence. Les composés **1**, **3** et **4** sont en équilibre. L'ensemble de ces équilibres est complexe et n'a pas été étudié dans le détail, le but de nos recherches étant de dégager les facteurs les plus importants qui interviennent.

Les structures des entités formées ont été établies à l'aide de la rmn du proton et du ^{13}C. Le pourcentage relatif des différents composés est déduit de l'intégration des signaux de leur spectre de rmn ^{1}H.

Protonation à basse température

FSO_3H (−30°C)

L'addition d'un équivalent d'acide fluorosul-

[1]Chercheur associé invité. Adresse actuelle: Explosives Research and Development Laboratory, Pashan, Poona-411021, India.

0008-4042/79/212876-09$01.00/0

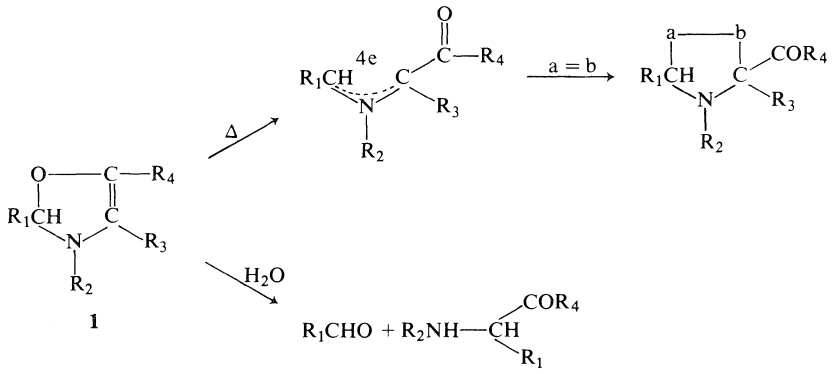

fonique FSO_3H à une solution des oxazolines **1***a–d* dans l'acétonitrile conduit quantitativement aux sels de structure **3**. Les caractéristiques spectroscopiques des composés **1** et **3** figurent dans le tableau 1 et sont en accord avec les structures.

Le déplacement chimique du proton H_a des composés **3** est en accord avec une structure iminium (7) et est comparable aux valeurs que nous avons trouvées pour des structures voisines (5). Il en est de même en ^{13}C pour δC_a et la constante de couplage $J_{C_aH_a}$. L'existence dans chaque cas de 2 carbones sp^2 ne portant pas d'hydrogène, l'un lié à un atome d'azote ($\delta \sim 110$ ppm) l'autre à un atome d'oxygène ($\delta \sim 170$ ppm) montre que **3** est formé (et non la cétone correspondante **4**). Le proton énolique, résonnant à champ relativement fort ($\delta \sim 10$ ppm) il semble logique de penser que le composé n'est pas chélaté. On est donc conduit à attribuer aux sels **3***a*,

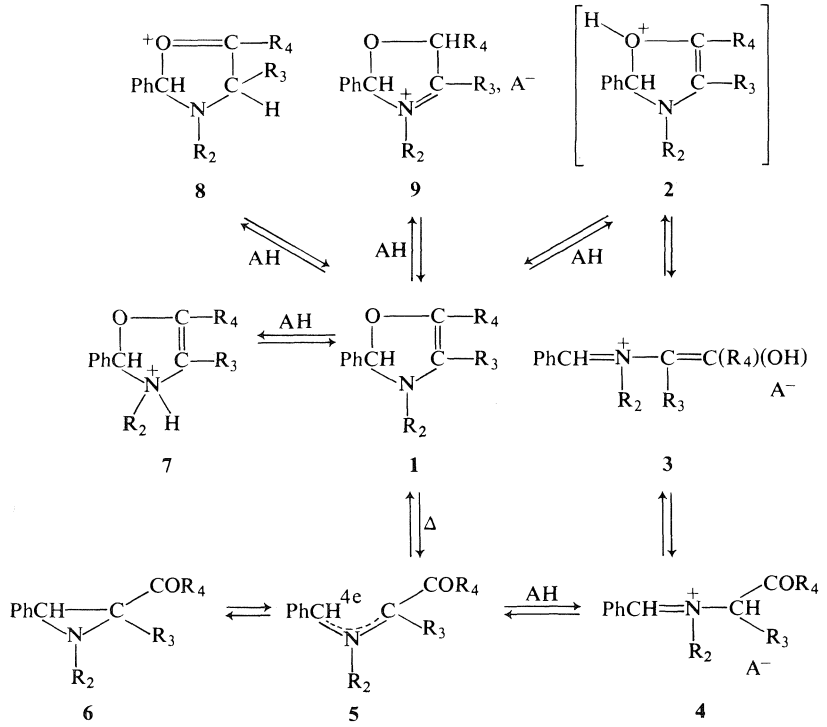

1*a*: R_2 = Ph, R_3 = CO_2Me, R_4 = Me
1*b*: R_2 = Ph, R_3 = CO_2Me, R_4 = Ph
1*c*: R_2 = Ph, R_3 = CN, R_4 = Ph
1*d*: R_2 = Me, R_3 = CO_2Me, R_4 = Ph
1*e*: R_2 = Ph, R_3 = H, R_4 = CO_2Me

SCHÉMA 1

TABLEAU 1. Les résonances magnétiques nucleaires du ^1H et ^{13}C des oxazolines-4 **1***a*, **1***b*, **1***c* et **1***d* et des fluorosulfonates d'iminium correspondants obtenus par addition d'un équivalent d'acide FSO_3H à $-30°C$ dans CD_3CN[a]

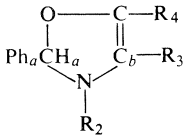

1

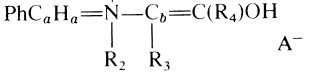

3

Composés	R_2	R_3	R_4	% Relat. 3/3′	^1H rmn δ (ppm/TMS)				^{13}C rmn δ (ppm/TMS), J (Hz)				
					δH_a	δR_3	δR_4	δOH	C_a	$J_{C_aH_a}$	C_b	$=C(R_4)^-$ *	C≡N
1*a*	Ph	CO_2Me	Me		6.60	3.65	2.30		101.3	162	113.7 m	158.2 q[b]	
3*a*	Ph	CO_2Me	Me	100	9.22	3.60	2.65	10.04	174.2	173	110.6 m	170.2 q[b]	
1*b*[c]	Ph	CO_2Me	Ph		6.63	3.59			99.6	161	112.7 d[d]	155.3 (m)	
3*b*	Ph	CO_2Me	Ph	100	9.27	3.36		9.85	175.4	182	111.7 d[e]	167.6	
1*c*[c]	Ph	CN	Ph		6.78				100.8	163	94.6 d[f]	156.0	115.0
3*c*	Ph	CN	Ph	65	9.24			10.91	175.3	184	93.3 m	170.7	115.2
3′*c*	Ph	CN	Ph	35	9.40			10.61	178.3	184	100.0 m	170.6	114.8
1*d*[c]	Me	CO_2Me	Ph		5.83	3.54[g]			100.9	157	119.3 m	153.3	
3*d*	Me	CO_2Me	Ph	100	8.81	3.88[h]		9.66			[i]		

[a]Note: d, doublet; q, quadruplet; m, multiplet.
[b]$^2J(=CCH_3) = 3.8$.
[c]Spectres de ^{13}C enregistrés dans $CDCl_3$ (faible solubilité dans CD_3CN). La différence des déplacements chimiques des différents carbones de **1***a* dans $CDCl_3$ et CD_3CN est inférieure à 1 ppm.
[d]$^3J_{CH_a} = 2.9$.
[e]$^3J_{CH_a} = 5.5$.
[f]$^3J_{CH_a} = 2.0$.
[g]$\delta NCH_3 = 2.64$.
[h]$\delta NCH_3 = 3.48$.
[i]Composé trop instable pour obtenir un enregistrement convenable.

3*b* et **3***d* la structure suivante:

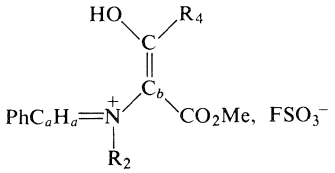

3*a*: R_2 = Ph; R_4 = Me
3*b*: R_2 = R_4 = Ph
3*d*: R_2 = Me; R_4 = Ph

Lorsque R_3 = CN, le résultat est différent, on obtient deux sels d'iminium **3***c* et **3**′*c* dont la stéréochimie n'est pas déterminée. Il faut noter, enfin, que dans ces conditions, la formation de sels d'iminium cétonique **4** n'est pas mise en évidence.

CF_3CO_2H (−40°C)

L'acide trifluoroacétique est beaucoup plus faible que l'acide fluorosulfonique et les oxazolines **1** ne sont pas complètement protonées avec un équivalent d'acide trifluoroacétique. Les caractéristiques spectroscopiques des sels d'iminium **3** et **4** obtenus par addition de 4 équivalents de CF_3CO_2H aux solutions dans $CDCl_3$ des composés **1** figurent au tableau 2. Elles sont en accord avec les structures proposées.

L'analyse de ce tableau montre la diversité du comportement des oxazolines étudiées. L'oxazoline **1***a* conduit à deux couples d'isomères géométriques: un couple d'énols *Z* et *E*, **3***a* et **3**′*a*, et le couple de cétones *Z* et *E*, **4***a* et **4**′*a*. Les hydroxyles de **3***a* et **3**′*a* ne sont pas chélatés avec le groupement ester. Lorsqu'on réchauffe à la température ambiante ces deux composés s'isomérisent en énols chélatés **3**″*a* et **3**‴*a*; il est alors possible, comme nous le verrons, de mettre en évidence, à basse température, le proton énolique à champ faible alors que celui de **3***a* et **3**′*a* est en échange rapide avec l'acide trifluoroacétique en excès (même à 190 K).

L'oxazoline **1***b* conduit au mélange d'un seul énol **3**′*b* dont le proton est chélaté avec le groupement ester (δOH = 13.45 ppm, singulet étroit à 200 K) et d'une seule cétone (80%).

Le comportement de l'oxazoline **1***c* est analogue en présence des acides trifluoroacétique ou sulfonique.

L'addition de quantités croissantes d'acide trifluoroacétique fait disparaître les oxazolines **1** comme le montre le tableau 3. Pour **1***a*, **1***b*, **1***c* la quantité de sels d'iminium formés est toujours inférieure à la quantité d'acide ajoutée. L'existence d'une équilibre entre l'oxazoline-4 de départ et les sels d'iminium est ainsi mise en évidence; elle est confirmée par le fait que les spectres de carbone 13 de l'oxazoline **1***c* additionnée de 4 équivalents de CF_3CO_2H doivent être enregistrés à −90°C pour obtenir des signaux distincts pour **3***c*, **3**′*c* et **1***c* (à −50°C, on observe un signal moyen pour ces trois entités).

La quantité d'acide nécessaire pour faire disparaître l'oxazoline de départ dépend de la basicité relative des composés. Ainsi, comme on pouvait s'y attendre **1***d* est plus basique que **1***a* elle-même plus basique que **1***b* et **1***c*. Il convient également de remarquer que le pourcentage de cétone augmente avec l'acidité du milieu.

L'analyse des résultats de la protonation, à basse température, fait apparaître les points suivants.

Dans des conditions pour lesquelles l'existence d'un équilibre entre l'oxazoline **1** et l'ylure d'azométhine **5** paraît très peu probable, la formation des sels **3** est observée et ne résulterait donc pas de la protonation de l'ylure **5**.

Il semble plus logique d'admettre que le proton se fixe sur l'oxazoline conduisant ainsi à **2** dont l'ouverture est assistée par la paire libre de l'azote (schéma 2). Ce mécanisme est compatible avec la configura-

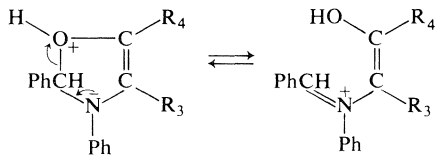

2 **3**

SCHÉMA 2

tion de double liaison carbone–carbone de l'énol formé lors de la protonation de **1***a*, **1***b* et **1***c* avec FSO_3H.

La base conjuguée de l'acide trifluoroacétique, beaucoup moins fort que l'acide fluorosulfonique, est relativement nucléophile. Son utilisation rend les résultats plus complexes et les diverses entités formées sont en équilibre. Dans le cas de l'oxazoline **1***a*, on observe un couple d'énols et un couple de cétones, chaque couple étant composé de deux isomères géométriques au niveau de la fonction iminium. Ce phénomène peut résulter de la nucléophilie de l'ion trifluoroacétate qui par un processus d'addition élimination provoque une isomérisation de l'énol (schéma 3).

La substitution du méthyle en 5 par un phényle modifie considérablement les résultats. L'effet du phényle paraît difficile à analyser, ce groupement modifie non seulement l'acidité des énols mais également les équilibres cétoénoliques et sels d'iminium **3** – amine **10**.

Protonation à température ambiante

Protonation par FSO_3H

L'addition à la température ambiante d'un équivalent d'acide fluorosulfonique à une solution

TABLEAU 2. Les résonances magnétiques nucleaires du ^1H et du ^{13}C des trifluoroacétates d'iminium obtenus par addition de 4 équivalents de CF_3CO_2H à une solution de **1** dans $CDCl_3$ à $-40°C$

$$PhC_aH_a{=}\overset{+}{N}(R_2)\text{—}C_b(R_3){=}C(OH)R_4,\ CF_3CO_2^- \rightleftarrows PhC_aH_a{=}\overset{+}{N}(R_2)\text{—}C_bH_b(R_3)\text{—}COR_4,\ CF_3CO_2^-$$

3 **4**

					^1H rmn δ (ppm/TMS)					^{13}C rmn δ (ppm/TMS), J (Hz)						
No	R_2	R_3	R_4	% Relat.	H_a	R_3	R_4	H_b	OH	C_a	$J_{C_aH_a}$	C_b	$J_{C_bH_b}$	$=C(R_4)^-$ *	R_4	$C{\equiv}N$ $(N\text{—}CH_3)$ *
3*a*	Ph	CO_2Me	Me	49	8.91	3.73	2.69		13.41[a]	173.7	178	110.8		171.7	19.8	
3′*a*	Ph	CO_2Me	Me	25	8.84	3.81	2.65		13.41	174.2		109.1		177.5	18.6	
4*a*	Ph	CO_2Me	Me	21	8.78	4.00	2.49	6.16		178.6	185	82.3	151	195.6	28.5	
4′*a*	Ph	CO_2Me	Me	5	9.05	3.95	2.53	5.90		178.2		74.2	154	193.0	27.9	
3″*b*	Ph	CO_2Me	Ph	20	9.16	3.80			13.45[b]	174.2	179	109.1d[c]		175.1		
4*b*	Ph	CO_2Me	Ph	80	9.24	3.89		6.91		178.1	184	76.8	148[d]	185.1		
3*c*	Ph	CN	Ph	65	9.31				12.66[a]	173.7	176	92.5d[e]		171.0		115.9
3′*c*	Ph	CN	Ph	35	9.01				12.66	177.2	180	99.4d[f]		170.5		115.1
3*d*	Me	CO_2Me	Ph	55	8.66		[g]		12.79[a]	177.4	175	108.5		172.3		45.4
3′*d*	Me	CO_2Me	Ph	15	8.33		[g]		12.79	178.6	[h]	115.6		173.4		[h]
4*d*	Me	CO_2Me	Ph	30	8.79		[g]	6.63		179.5	182	94.3	147	185.9		47.3

[a]En échange avec CF_3CO_2H en excès.
[b]Observé à $-73°C$.
[c]$J_{C_bH_a} = 7.1$ Hz.
[d]Double doublet: $J_{C_bH_a} = 3.3$ Hz.
[e]$J_{C_bH_a} = 8.8$ Hz.
[f]$J_{C_bH_a} = 4.4$ Hz.
[g]Les signaux de NMe et de CO_2Me sont tous compris entre 3.54 et 3.85 ppm et sont indiscernables.
[h]Signaux confondus avec ceux de **3***d*.

TABLEAU 3. Addition de quantités variables d'acide trifluoroacétique à −40°C à des solutions de **1** dans $CDCl_3$

No	R_2	R_3	R_4	Mmol d'acide ajoutées	Mmol d'oxazoline **1** restantes	Espèces formées	%
				1	0.64	**3***a* + **3**′*a*	80/20
1*a*	Ph	CO_2Me	Me	2	0	**3***a* + **3**′*a*	70/30
				3	0	**3***a* + **3**′*a* + **4***a* + **4**′*a*	54/27/13/5
				4	0	**3***a* + **3**′*a* + **4***a* + **4**′*a*	49/25/21/5
				1	0.66	**3**″*b* + **4***b*	25/75
1*b*	Ph	CO_2Me	Ph	2	0.2	**3**″*b* + **4***b*	25/75
				3	0	**3**″*b* + **4***b*	25/75
				4	0	**3**″*b* + **4***b*	20/80
				1	0.8	**3***c* + **3**′*c*	65/35
1*c*	Ph	CN	Ph	2	0.44	**3***c* + **3**′*c*	65/35
				3	0.1	**3***c* + **3**′*c*	65/35
				4	0	**3***c* + **3**′*c*	65/35
1*d*	Me	CO_2Me	Ph	1	0	**3***d* + **3**′*d* + **4***d*	55/15/30

dans CD_3CN des oxazolines **1***a–d* conduit à la formation de sels d'iminium dont les caractéristiques spectroscopiques figurent dans le tableau 4. Il faut noter que ces mêmes résultats sont obtenus si on laisse réchauffer à la température ambiante les solutions étudiées à basse température (par addition également d'un équivalent d'acide FSO_3H). On peut remarquer les points suivants. (*i*) le comportement de l'oxazoline **1***c* est inchangé, les mêmes espèces qu'à basse température sont obtenues; (*ii*) **1***a* donne un mélange de l'énol obtenu à basse température **3***a* (32%), de deux énols à haute température **3**″*a* et **3**‴*a* (60%) pour lesquels l'hydrogène énolique est chélaté (δ = 12.9 ppm) et enfin d'une forme cétonique (8%). Les phénomènes d'isomérisation et de tautomérie céto–énolique se manifestent donc à la température ambiante alors qu'ils étaient inhibés à basse température; (*iii*) **1***b* conduit à un mélange de l'énol

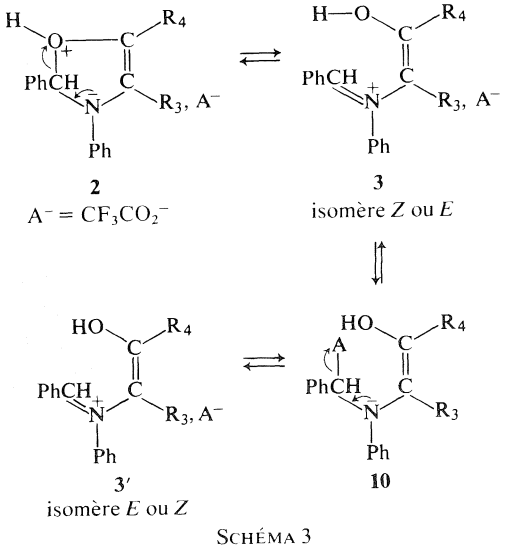

SCHÉMA 3

obtenu à basse température (10%) d'un énol de structure chélatée **3**″*b* (77%) très majoritaire et d'une forme cétonique (13%).

Protonation par l'acide trifluoroacétique

L'addition, à la température ambiante, de 4 équivalents de CF_3CO_2H à des solutions de **1***a*, **1***b* et **1***c* dans $CDCl_3$ et le réchauffage à l'ambiante de solutions préparées à basse température conduisent au même résultat. Les caractéristiques spectroscopiques des espèces formées figurent au tableau 5.

On remarque que le comportement de **1***c* est inchangé. L'oxazoline **1***b* conduit aux mêmes entités qu'à basse température mais, les pourcentages sont inversés, la forme énolique chélatée (δOH = 13.38 ppm) étant devenue majoritaire. L'oxazoline **1***a* conduit au mélange d'un énol chélaté très majoritaire (85%) de structure **3**″*a* (A = $CF_3CO_2^-$) et des deux énols de basse température **3***a* et **3**′*a* (15%). Les formes cétoniques ne sont pas détectables mais, le passage des formes non chélatées **3***a* et **3**′*a* à la forme chélatée **3**″*a* s'effectue sans doute par l'intermédiaire des formes cétoniques.

Cas particulier: protonation de l'oxazoline **1***e*

En raison de l'instabilité des entitées formées l'étude de la protonation de l'oxazoline **1***e* s'est avérée difficile. Cependant, à très basse température, dans SO_2 liquide, et en présence d'acide fluorosulfonique, il a été possible de mettre en évidence la formation des deux sels d'iminium cycliques diastéréoisomères de structures **5**′*e* et **5**″*e*. Leurs caractéristiques spectroscopiques ainsi que celles de l'oxazoline **1***e* figurent dans le tableau 6. Elles sont en accord avec les structures proposées. On notera en particulier la présence d'un carbone de sel d'iminium cyclique (C_β) avec une grande constante de couplage carbone–hydrogène ($J_{C_\beta H_\beta}$ = 207 Hz) caractéristique de ce type de sel (7). De plus, l'existence de 2 carbones sp^3 dans la molécule (C_α, carbone

TABLEAU 4. Les résonances magnétiques nucleaires du ^1H et du ^{13}C des fluorosulfonates d'iminium obtenus par addition à la température ambiante d'un équivalent de FSO_3H à une solution dans CD_3CN des composés **1***a*, **1***b*, **1***c*

					^1H rmn δ (ppm/TMS)					^{13}C rmn δ (ppm/TMS), *J* (Hz)					
No	R_2	R_3	R_4	% Espèces	H_a	R_3	R_4	H_b	OH	C_a	$J_{C_aH_a}$	C_b	$J_{C_bH_b}$	$=\overset{*}{C}-R_4$	R_4
3″*a*	Ph	CO_2Me	Me	50	9.30	3.66	1.97	—	12.9[a]	175.5	181	109.5		176.6	18.9
3*a*	Ph	CO_2Me	Me	32	9.23	3.61	2.62	—	10.04	174.2	173	111.0	—	170.2	19.6
3‴*a*	Ph	CO_2Me	Me	10	9.19	3.80	2.25	—	12.9[a]			[b]			18.1
4*a*	Ph	CO_2Me	Me	8	8.97	3.97	2.60	6.15		178.9	185	84.6	150	193.6	28.8
3″*b*	Ph	CO_2Me	Ph	77	9.21	3.68		—	13.14	175.7	181	110.0[c]		174.4	
3*b*	Ph	CO_2Me	Ph	10	9.34	3.43		—	9.65	175.5	182	111.7[d]		167.6	
4*b* ou **4**′*b*	Ph	CO_2Me	Ph	13	9.41	3.88		7.02	—	179.4	187	78.3	147[e]	187.1	
3*c*	Ph	CN	Ph	65	9.24				10.91[f]				[g]		
3′*c*	Ph	CN	Ph	35	9.40				10.61[f]						

[a]Singulet à −40°C unique pour **3**″*a* et **3**‴*a*.
[b]Difficile à identifier, signaux très peu intenses.
[c]$J_{C_bH_a}$ = 8.8 Hz.
[d]$J_{C_bH_a}$ = 5.5 Hz.
[e]Double doublet $J_{C_bH_a}$ = 3.3 Hz.
[f]Ces signaux sont différenciés à −25°C.
[g]Caractéristiques identiques à celles du tableau 1.

TABLEAU 5. Les résonances magnétiques nucleaires du ^1H et du ^{13}C des trifluoroacétates d'iminium obtenus à température ambiante par addition de 4 équivalents de CF_3CO_2H à des solutions dans $CDCl_3$ de **1***a*, **1***b*, **1***c* et **1***d*

					^1H rmn (ppm/TMS)				^{13}C rmn (ppm/TMS), *J* (Hz)					
Composés	R_2	R_3	R_4	%	H_a	R_3	R_4	H_b ou OH	C_a	$J_{C_aH_a}$	C_b	$J_{C_bH_b}$	$=\overset{*}{C}(R_4)$	R_4
3″*a*	Ph	CO_2Me	Me	85	9.56	3.85	2.07	13.15[a]	173.6	177	108.8	—	176.7	18.5
3*a* + **3**′*a*	Ph	CO_2Me	Me	15	9.18[b]	3.82	2.73	[c]				[d]		
3*b*	Ph	CO_2Me	Ph	70	9.18	3.85	—	13.38[a]	174.2	179	109.1d[e]		175.1	
4*b*	Ph	CO_2Me	Ph	30	9.42	3.94	—	6.88	178.1	184	76.8	148.5d[f]	185.5	
3*c*	Ph	CN	Ph	65										
3′*c*	Ph	CN	Ph	35			[g]					[g]		
3*d*	Me	CO_2Me	Ph	64	8.97		[h]	12.85						
3′*d*	Me	CO_2Me	Ph	14	8.79		[h]	12.85				[g]		
4*d*	Me	CO_2Me	Ph	22	9.33		[h]	6.82						

[a]Singulet à −50°C.
[b]A −40°C ces signaux sont identifiés comme étant ceux des énols **3***a* et **3**′*a* observés lors de la protonation à basse température.
[c]En échange avec CF_3CO_2H.
[d]Les caractéristiques de rmn du ^{13}C figurent au tableau 2.
[e]$J_{C_bH_a}$ = 7.1 Hz.
[f]$J_{C_bH_a}$ = 3.3 Hz.
[g]Ces entités sont identiques à celles formées à basse température.
[h]Les signaux des CO_2CH_3 et des N—CH_3 sont compris entre 3.80 ppm et 4.10 ppm et sont donc difficilement discernables.

TABLEAU 6. Les résonances magnetiques nucleaires du ^1H et du ^{13}C de l'oxazoline-4 **1***e* et des sels d'iminium correspondants obtenus à −100°C avec FSO_3H dans SO_2 liquide (spectres enregistrés à −40°C)

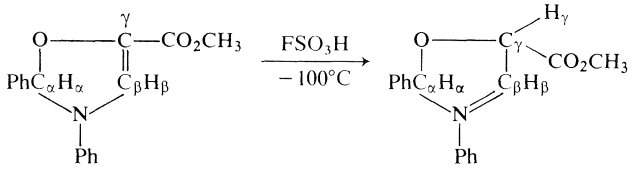

1*e* **5′***e* et **5″***e*

	^1H rmn δ (ppm/TMS)				^{13}C rmn δ (ppm/TMS), *J* (Hz)					
Composés	H_α	H_β	H_γ	CO_2CH_3	C_α	$J_{C_\alpha H_\alpha}$	C_β	$J_{C_\beta H_\beta}$	C_γ	$J_{C_\gamma H_\gamma}$
1*e*[a]	6.90	7.67	—	3.82	97.3	163	121.8	193.4	140.0	—
5′*e* (55%)	[b]	8.95[c]	6.29[d]	4.06	105.7	178[e]	168.9	206.9	85.4	161.1[e]
5″*e* (45%)	[b]	9.10[f]	6.40[g]	4.04	105.9	178[e]	167.9	207.5	85.9	161.1[e]

[a]En solution dans $CDCl_3$.
[b]Masqué par les protons aromatiques (entre 7.10 et 7.75 ppm).
[c]$^4J_{H_\alpha H_\beta}$ = 1.8 Hz; $^3J_{H_\beta H_\gamma}$ = 0.7 Hz.
[d]$^4J_{H_\alpha H_\gamma}$ = 5.9 Hz.
[e]Signaux de 5′*e* et 5″*e* indiscernables.
[f]$^4J_{H_\alpha H_\beta}$ = 1.5 Hz; $^3J_{H_\beta H_\gamma}$ = 1.1 Hz.
[g]$^4J_{H_\alpha H_\gamma}$ = 5.9 Hz (mesuré lors de l'irradiation de Hβ).

acétalique le plus déblindé et C_γ) confirme les structures **5′***e* et **5″***e*.

Le comportement différent de **1***e* comparativement aux autres oxazolines étudiées résulte vraisemblablement de la substitution en 5 par le groupement ester qui modifie la nucléophilie du carbone 5 et contribue à la délocalisation de la paire libre de l'azote la rendant moins disponible pour assister l'ouverture d'une oxazoline protonée sur l'oxygène de type **2**.

Partie expérimentale

Les spectres de rmn du proton ont été enregistrés à 100 MHz sur un appareil JEOL MH 100, ceux du carbone 13 sur un appareil Bruker WP 80 DS à 20 115 MHz. Le TMS est utilisé comme référence interne. Dans le cas du carbone 13, les constantes de couplage ont été mesurées sur des spectres obtenus à l'aide de la technique du découplage en fenêtre ("gated decoupling"), la résolution digitale étant alors d'environ 1 Hz.

Produits de départ

Oxazoline-4 ***1***a

Elle est obtenue quantitativement par thermolyse à sec de la triazoline correspondante à 155°C sous atmosphère d'azote ou d'argon (5). C'est un composé huileux, très facilement hydrolysable, utilisé "in situ".

Oxazoline-4 ***1***b

Elle est préparée selon le mode opératoire décrit par Niklas (3): la *C,N*-diphénylnitrone (1.50 g, 7.6 mmol) et le phénylpropiolate de méthyle (1.22 g, 7.6 mmol) sont dissous dans 20 cm^3 d'acétate d'éthyle anhydre. La solution est maintenue à reflux 15 h sous atmosphère d'azote. L'acétate d'éthyle est distillé sous vide. L'huile résiduelle cristallise au réfrigérateur. La recristallisation dans l'acétonitrile donne 1.5 g de l'oxazoline **1***b*, pf = 115°C, Rdt = 56%.

Oxazoline ***1***c

Elle est préparée selon Texier et Carrié (2). L'α-benzoyl cinnamonitrile (1.86 g, 8 mmol) et le phénylazide (2.86 g, 24 mmol) sont mélangés puis maintenus à 90°C, sous atmosphère d'azote, pendant 18 h à l'aide d'un bain d'huile. Après refroidissement, on additionne de l'éther sec. Les cristaux jaunes d'oxazoline **1***c* sont filtrés, lavés avec un peu d'éther froid. La recristallisation dans l'acétonitrile donne 1.6 g (Rdt = 61.5%), pf = 117°C.

Oxazoline-4 ***1***d

L'isoxazoline-4 correspondante **11** est d'abord préparé

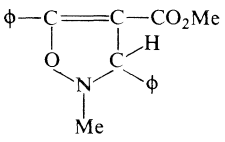

11

selon le mode opératoire de Niklas (3) légèrement modifié. La *C*-phényl *N*-méthylnitrone (1.35 g, 10 mmol) et le phénylpropiolate de méthyle (1.6 g, 10 mmol) sont mélangés puis maintenus à 80°C pendant 3 h à l'aide d'un bain d'huile. L'huile obtenue est alors refroidie et additionnée de méthanol. L'isoxazoline **11** précipite; elle est recristallisée dans le méthanol (1.5 g, Rdt = 50%, pf = 104°C).

L'isoxazoline **11** est dissoute dans le solvant choisi puis la solution transférée dans un tube en verre qui est ensuite scellé sous atmosphère d'azote (par exemple: 295 mg (1 mmol) d'isoxazoline **11** sont dissous dans 0.5 cm^3 de C_6D_6). Le tube scellé est maintenu 3 h à 135–140°C dans un bain d'huile. Le spectre de rmn de la solution indique une transposition totale et quantitative de l'isoxazoline en oxazoline **1***d* (caractéristiques rmn dans le tableau 1).

Oxazoline-4 ***1***e

C,N-diphénylnitrone (2.0 g, 5.08 mmol) et 0.86 g de propiolate de méthyle (5.10 mmol) sont mélangés dans 30 cm^3 de benzène anhydre. La solution est maintenue 3 h à reflux

sous atmosphère d'azote. Le benzène est alors distillé sous vide. Le solide résiduel est recristallisé dans l'acétonitrile conduisant à 1.0 g d'oxazoline-4 **1***e* (Rdt = 40%, pf = 170°C).

Les composés **1***b*, **1***c*, **1***d* et **1***e* doivent être conservés au réfrigérateur sous atmosphère d'azote.

Protonation des oxazolines-4

Les entités observées sont très fragiles. Il est nécessaire de travailler en milieu anhydre sous atmosphère d'argon sec. Les solvants deutériés sont conservés sur tamis moléculaire 4 Å.

D'une façon générale, les analyses à l'aide de la rmn du proton ont été réalisées sur des solutions de 0.5 mmol d'oxazoline-4 dans 0.3 cm^3 de solvant deutérié. Les spectres de rmn du carbone 13 ont été enregistrés sur des solutions de concentration de 1 à 3 mol/L suivant le nombre d'entités formées.

Protonation par l'acide fluorosulfonique FSO_3H dans CD_3CN

Les fluorosulfonates d'iminium obtenus n'étant pas solubles dans $CDCl_3$, nous avons utilisé l'acétonitrile deutérié CD_3CN. Le mode opératoire utilisé est le même pour les oxazolines **1***a–d*: à une solution (ou à une suspension) de 0.5 mmol d'oxazoline-4 dans 0.3 cm^3 d'acétonitrile deutérié, dans un tube de rmn, fermé par un septum, on ajoute sous argon, à l'aide d'une microseringue, lentement, 50 mg de FSO_3H (soit 28.7 μL). La solution est alors agitée et le spectre enregistré. Lors d'une protonation à basse température, la solution d'oxazoline-4 est amenée à −60°C. L'acide lui-même préalablement refroidi est alors ajouté lentement puis la solution agitée. Le même protocole est utilisée pour l'enregistrement des spectres de carbone 13 (2 cm^3 de CD_3CN, 2 mmol d'oxazoline-4 et 2 mmol de FSO_3H (115 μL) lorsqu'une ou deux entités sont formées et 2 cm^3 de CD_3CN, 6 mmol d'oxazoline-4 et 6 mmoles de FSO_3H (345 μL) dans les autres cas).

*Protonation de **1**e par FSO_3H dans SO_2 liquide*

L'oxazoline-4 **1***e* est placée dans un tube de rmn fermé par un septum et purgé à l'argon. Ce tube est refroidi à −40°C et la quantité de SO_2 liquide nécessaire est condensée directement dans le tube à l'aide d'une grande aiguille (140.5 mg de **1***e* et 0.3 cm^3 de SO_2 liquide pour le proton, et 3 mmol de **1***e* (843 mg) et 2 cm^3 de SO_2 liquide pour le carbone 13). La solution est alors congelée à −100°C et l'acide ajouté lentement, le tube étant incliné, de telle façon qu'il n'y ait pas d'échauffement notable lors du contact. On laisse alors revenir lentement à −70°C et on agite à cette température; 10% de C_6D_6 sont ajoutés pour verrouiller le champ de l'appareil de rmn. Les spectres sont enregistrés à −40°C.

Protonation par l'acide trifluoroacétique

Ces études sont réalisées dans $CDCl_3$; 0.3 cm^3 de solution contenant 0.5 mmol d'oxazoline-4 pour le proton et 2 cm^3 de solution contenant de 2 à 6 mmol d'oxazoline pour le carbone 13. Les échantillons sont préparés comme indiqué précédemment (1 mmol de CF_3CO_2H = 76.5 μL).

1. J. A. FRUMP. Chem. Rev. **71**, 483 (1971).
2. F. TEXIER et R. CARRIÉ. Bull. Soc. Chim. Fr. 4119 (1971).
3. J. NIKLAS. Thèse, Munich. 1975.
4. J. E. BALDWIN, R. G. PUDESSERY, A. K. OURESHI et B. SULARZ. J. Am. Chem. Soc. **90**, 5325 (1968).
5. M. VAULTIER. Thèse, Rennes. 1977.
6. M. VAULTIER, R. DANION-BOUGOT, D. DANION, J. HAMELIN et R. CARRIÉ. J. Org. Chem. **40**, 2990 (1975).
7. H. BOHME et H. G. VIEHE. Iminium salts in organic chemistry. Advances in organic chemistry. Vol. 9, tome 1. John Wiley and Sons. 1976. p. 26 et suivantes.

COMMUNICATION

Acid-catalysed cleavage of 4-halonortricyclenes in deuterated medium; evidence that the norbornyl cation is an unsymmetrical species

NICK HENRY WERSTIUK, DALJIT DHANOA, AND GEORGE TIMMINS
Department of Chemistry, McMaster University, Hamilton, Ont., Canada L8S 4M1

Received August 24, 1979

NICK HENRY WERSTIUK, DALJIT DHANOA, and GEORGE TIMMINS. Can. J. Chem. **57**, 2885 (1979).

We have determined the *endo*:*exo* deuterium ratios at C(6) of the *exo*-acetates obtained by D_2SO_4-catalysed cleavage of nortricyclene (**4***a*), 4-chloronortricyclene (**4***b*), 4-bromonortricyclene (**4***d*), and 4-iodonortricyclene (**4***e*). That the ratios are 1.09 ± 0.03, 1.30 ± 0.04, 1.40 ± 0.02, and 1.48 ± 0.02 for ring-opening of **4***a*, **4***c*, **4***d*, and **4***e*, respectively, establishes that the norbornyl cation is an unsymmetrical rapidly-equilibrating species.

NICK HENRY WERSTIUK, DALJIT DHANOA et GEORGE TIMMINS. Can. J. Chem. **57**, 2885 (1979).

Nous avons déterminé les rapports *endo*:*exo* du deutérium au niveau du carbone 6 des acétates obtenus par clivage catalytique à l'aide du D_2SO_4 du nortricylène ayant en position 4 les substituants suivants: Cl (**4***b*), Br (**4***d*), I (**4***e*). Ces rapports qui sont respectivement de 1.09 ± 0.03, 1.30 ± 0.04, 1.40 ± 0.02 et 1.48 ± 0.02 pour l'ouverture des cycles **4***a*, **4***c*, **4***d* et **4***e* établissent que le cation norbornyle est une espèce non symétrique en équilibre rapide.
[Traduit par le journal]

The norbornyl-cation controversy has held the attention of physical organic chemists for the past two and one-half decades (1). We, along with many researchers, were drawn to make a contribution, and thereby provide a solution to the problem (2, 3). The enormous effort which has been expended world-wide to solve the problem has heen documented clearly by Brown (1).[1] As we see it, the central issue of the controversy is stated simply in the following question. Is the symmetrical norbornonium (non-classical) ion (**1***a*) an intermediate or does it best represent the transition state between the rapidly-equilibrating unsymmetrical (classical) ions **2***a* and **3***a*?

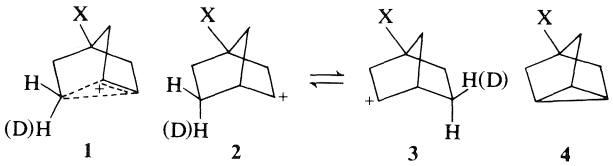

a X = H
b X = F
c X = Cl
d X = Br
e X = I

By employing classical substituent effect studies to ascertain the structure of the norbornyl cation, researchers have introduced substituents on the 2.2.1-framework and thereby destroyed the symmetry of **1***a* and rendered the equilibrating classical ions non-degenerate. Since C(4) is the only site where a single substitution does not destroy symmetry or clutter the front-face of the cation, we reasoned that the critical question (*vide supra*) could be answered if we established whether or not the mass of the substituent at C(4) affects the chemistry of the norbornyl cation. To that end we chose to study the stereochemistry of the acid-catalysed cleavage of 4-halonortricyclenes **4***a*, **4***b*, **4***c*, **4***d*, and **4***e*. If cleavage yields non-classical cations **1***a–e*, then the stereochemistry of the ring-opening, as monitored by the *endo*:*exo* deuterium ratio at C(6), would be unaffected by the mass of the substituent at C(4). However, if cleavage yields classical cations and the ponderal effect[2] (4) of the substituent becomes progressively larger as the mass of the substituent increases, a change in the stereochemical outcome of the reaction would be observed because the rate of rearrangement of ions **2***a–e* to **3***a–e* should decrease through the series. Consequently, reaction of the first-formed 6-*endo*-*d*-cation with solvent should compete more effectively with rearrangement. We wish to report that the *endo*:*exo* deuterium ratio at C(6) of the *exo*-acetate obtained

[1]With comments by P. von R. Schleyer.

[2]de la Mare (4) has suggested that the ponderal effect is derived from non-polar, non-steric, entropy effects which depend on mass.

0008-4042/79/212885-02$01.00/0

TABLE 1. *Endo*:*exo* deuterium ratios at C(6) of norbornyl acetates*

Substrate	*Endo*:*exo* deuterium ratio
4*a*	1.09±0.03
4*c*	1.30±0.04
4*d*	1.40±0.02
4*e*	1.48±0.02

*The errors quoted are the average deviations from the mean that was obtained by analysis of at least three ^{2}Hmr spectra of the deuterated norbornanol obtained from three ring-openings.

TABLE 2. Percent deuterium at C(1) and C(2) of norbornyl acetates

Substrate	Percent deuterium* C(1)	C(2)
4*a*	7.4±0.7	6.8±0.5
4*c*	3.0±0.5	3.1±0.7
4*d*	3.2±0.2	3.9±0.9
4*e*	4.3±0.3	3.9±0.3

*The errors quoted are the average deviations from the mean that was obtained by analysis of at least three ^{2}Hmr spectra.

by D_2SO_4-catalysed[3] ring-opening of nortricyclene (**4***a*), 4-chloronortricyclene (**4***c*), 4-bromonortricyclene (**4***d*), and 4-iodonortricyclene (**4***c*)[4] does indeed become larger as the mass of the substituent at C(4) is increased (Table 1).

To determine the deuterium distribution, we transformed the deuterated acetates into deuterated *exo*-2-norbornanol[5] and recorded at least three FT ^{2}Hmr spectra for each norbornanol complexed with Pr(fod)$_3$. The *endo*:*exo* deuterium ratios of C(6) were derived from the relative peak areas which we obtained from the ^{2}Hmr spectra by means of a computerized curve-fitting routine.

Our value of 1.09 ± 0.03 for the ring-opening of **4***a* agrees well with the ratio of 1.08 ± 0.05 obtained by Nickon and Hammons (7). To check for deuterium scrambling in the products, we determined the deuterium distributions at two stages[6] during the ring-openings of **4***a*, **4***c*, and **4***d*. Within experimental error the distributions were identical at both stages. That optically active *exo*-2-norbornyl acetate does not racemize at a detectable rate under the reaction conditions (7) is further evidence that deuterium-scrambling is not important.

Since the *endo*:*exo* deuterium ratios become larger as the mass of the substituent increases, a ponderal effect contributes to the activation energy of the degenerate rearrangement. Clearly then, the norbornyl cation is an unsymmetrical rapidly-equilibrating species. It is interesting to note also that the $\Delta G^{\neq}$ ($\simeq$ 6 kcal/mole) for the 6,2 hydride shift is also affected by mass of the substituent at C(4) (Table 2).

Acknowledgement

We thank the Natural Sciences and Engineering Research Council of Canada for financial support.

1. H. C. BROWN. *In* The non-classical ion problem. Plenum, New York. 1977.
2. N. H. WERSTIUK, G. TIMMINS, and F. P. CAPPELLI. Can. J. Chem. **51**, 3473 (1973).
3. S. BANERJEE and N. H. WERSTIUK. Can. J. Chem. **54**, 678 (1976).
4. P. B. D. DE LA MARE, L. FOWDEN, E. D. HUGHES, C. K. INGOLD, and J. D. H. MACHIE. J. Chem. Soc. 3200 (1955).
5. A. NICKON and N. H. WERSTIUK. J. Am. Chem. Soc. **94**, 7081 (1972).
6. J. F. CHIANG, C. F. WILCOX, JR., and S. H. SAUER. Tetrahedron, **25**, 369 (1969).
7. A. NICKON and J. H. HAMMONS. J. Am. Chem. Soc. **86**, 3322 (1964).

[3]While **4***a* was cleaved in 0.1 *M* D_2SO_4–CD_3COOD at 25°C, **4***c*, **4***d*, and **4***e* were cleaved at 50°C.

[4]Compound **4***a* was prepared from the tosylhydrazone of 2-norbornanone (5); **4***c* and **4***d* were synthesized from 2-norbornanone by a route which was similar to the synthesis described by Sauer (6); **4***e* was prepared by lithiating **4***c* and quenching the anion with I_2.

[5]The *exo*-acetates were reduced by LAH in ether and the 4-halonorbornanols were reduced by Na in 2-propanol to deuterated *exo*-2-norbornanol.

[6]The deuterium distributions for **4***a* were determined after 14.5 h and 48 h, and for **4***c* and **4***d* analyses were carried out after 70 h and 240 h. The longest interval in each case corresponds to a period equivalent to at least 10 half-lives.

Canadian Journal of Chemistry
Published by
THE NATIONAL RESEARCH COUNCIL OF CANADA

Journal canadien de chimie
Publié par
LE CONSEIL NATIONAL DE RECHERCHES DU CANADA

Volume 57 Number 22 November 15, 1979

Volume 57 numéro 22 15 novembre 1979

Effect of solvent (benzene, ethanol, cyclohexane) on the partial molal volumes of organic compounds

JOHN T. EDWARD, PATRICK G. FARRELL, AND FEREIDOON SHAHIDI[1]
Department of Chemistry, McGill University, 801 Sherbrooke St. W., Montreal, P.Q., Canada H3A 2K6

Received May 11, 1979

JOHN T. EDWARD, PATRICK G. FARRELL, and FEREIDOON SHAHIDI. Can. J. Chem. **57**, 2887 (1979).

The partial molal volumes of *n*-alkanes and *n*-alkanols dissolved in benzene, ethanol, or cyclohexane are given with satisfactory accuracy by the equation previously developed for solutions in carbon tetrachloride, if certain parameters (the covolume, the volume increment for the hydroxyl group, and the volume decrement for some *gauche* interactions) are changed. Additionally, it is necessary to postulate a greater coiling of the alkyl chains when dissolved in cyclohexane.

JOHN T. EDWARD, PATRICK G. FARRELL et FEREIDOON SHAHIDI. Can. J. Chem. **57**, 2887 (1979).

On obtient avec une précision suffisante les volumes molaires partiels des *n*-alcanes et *n*-alcanols dissous dans le benzène, l'éthanol ou le cyclohexane en se servant de l'équation développée antérieurement pour les solutions dans le tétrachlorure de carbone, si on change certains paramètres (comme le co-volume, l'incrément du volume pour le groupe hydroxyle et le décrément du volume pour quelques interactions *gauches*). De plus il est nécessaire de concevoir un plus grand encombrement des chaînes alkyles en solution dans le cyclohexane.

[Traduit par le journal]

Introduction

The partial molal volumes $\bar{V}^0$ of organic solutes reflect not only the intrinsic volumes of the solute molecules, but the extent to which they interact with solvent. Furthermore, when the solute is made up of flexible chain molecules, $\bar{V}^0$ depends on the extent to which the molecules are extended or coiled in solution. In the present paper we report $\bar{V}^0$ values in the three solvents, benzene, ethanol, and cyclohexane, for several *n*-alkanes, which should interact feebly with the solvents, and several *n*-alkanols, which should interact more strongly. Additionally, we compare the $\bar{V}^0$ behaviour of these flexible chain molecules with that of the rigid adamantane and the relatively rigid cycloalkanes.

In previous work we have shown that in carbon tetrachloride at 25°C, $\bar{V}^0$ of straight- and branched-chain alkanes (1), haloalkanes (2), ketones (3), ethers (3), alcohols (3), and of cyclic compounds (4) is given with reasonable accuracy by the equation

$$[1] \quad \bar{V}^0 = V_c + \sum_1^m n^k I^k + \sum_1^n Z_g{}^l \delta^l + C$$

where V_c is a constant covolume of 11.6 mL mol^{-1}, n^k is the number of, and I^k the volume increment associated with, groups of type k, $Z_g{}^l$ is mol fraction of, and δ^l the decrement associated with, *gauche* interactions of type l, and C is a cyclization parameter whose magnitude depends on the number of skeletal atoms in the ring or cage. Z_g was calculated by a method much used by Mann (5), which assumed an enthalpy difference ΔH_g of 700 cal mol^{-1} between an *anti* and *gauche* ($g_{C-C}^{C/C}$) arrangement in a hydrocarbon chain. The I and δ parameters were obtained by systematic study of a large number of compounds (128 chain and 47 ring or cage compounds), including many isomers.

[1]Present address: Lash Miller Chemical Laboratories, University of Toronto, 80 St. George Street, Toronto, Ont., Canada M5S 1A1.

0008-4042/79/222887-05$01.00/0

It would be interesting to test [1] in a similar fashion for solvents other than carbon tetrachloride, but for this to be done with any pretence to thoroughness $\bar{V}^0$ values of large numbers of isomeric compounds must be obtained. Such a project is beyond our means at the moment, and the present paper reports only a brief reconnoitering expedition into unexplored territory. This shows that $\bar{V}^0$ in other solvents can be accommodated by [1], and indicates the desirability of more extensive studies to test [1] in a range of solvents.

Results

Partial molal volumes in benzene and in ethanol are reported in Tables 1 and 5, and in cyclohexane in Tables 4 and 5. Where comparison with data in the literature is possible (6, 7), agreement for the most part is excellent (taking account, where necessary (6), of small differences in temperature of the measurements). The result for methanol in cyclohexane (Table 4) is exceptional, but the value reported in the literature (6) was obtained by extrapolation from higher concentrations than those used by us, and under these conditions the effects of dimerization, trimerization, etc., can be important (8).

A preliminary analysis of these results was made using the equation (9):

$$[2] \quad \bar{V}^0 = 4\pi N(r_w + \Delta)^3/3$$

where N is the Avogadro number, r_w the van der Waals radius (10) of the solute molecule (assumed spherical), and Δ a parameter measuring the void or empty volume (11) associated with the solute molecule. We had expected Δ to diminish in roughly linear fashion with increase in the internal pressure P_i (12) or cohesive energy density (*c.e.d.*) (13) of the solvent, but instead Δ remained approximately constant, as shown in Table 2. It can also be seen in Table 2 that the a parameter for alkanes, defined by the equation (14):

$$[3] \quad \bar{V}^0 = aV_w + b$$

where V_w is the van der Waals volume of N solute molecules, likewise remains roughly constant. This empirical equation holds well for cylindrical molecules such as *n*-alkanes, the parameter a depending on the amount of empty volume associated with the repeating methylene unit (15).

This analysis indicates that about the same empty volume is associated with methyl, methylene, and methine groups in the three solvents under investigation as in carbon tetrachloride. Accordingly, we shall assume (as an approximation) the same values for the increments I for methyl, methylene, and methine in all four solvents. On the other hand, the empty volume associated with the hydroxyl group, which has a substantial dipole moment and hence can interact with solvents by dipole – induced dipole effects, would be expected to vary with polarizability and hence with solvent. For this reason I also would be expected to vary with solvent. We have found the best agreement between experimental and calculated values of $\bar{V}^0$ using the values of I listed in Table 3.

TABLE 1. Partial molal volumes $\bar{V}^0$ (in mL mol^{-1}) of *n*-alkanes and *n*-alkanols in benzene and ethanol at 25°C

	In benzene		In ethanol	
Compound	$\bar{V}^0_{calcd}$	$\bar{V}^0_{exptl}$	$\bar{V}^0_{calcd}$	$\bar{V}^0_{exptl}$
n-Pentane	116.4	117.0±0.1	116.7	116.7±0.5
n-Hexane	133.5	133.8±0.5	133.4	133.9±0.4
n-Heptane	150.6	150.3±0.3	150.1	150.1±0.3
n-Octane	167.7	167.6±0.3	166.7	167.6±0.3
n-Nonane	184.7	184.4±0.3	183.4	182.9±0.3
n-Decane	201.8	201.8±0.3	200.1	199.4±0.3
Methanol	44.0	41.7±0.2[a]	40.5	40.2±0.1[f]
Ethanol	61.4	61.2±0.2[b]	57.9	58.6±0.1[g]
n-Propanol	77.2	77.1±0.2[c]	75.3	75.2±0.1[h]
n-Butanol	94.2	94.6±0.3[d]	91.8	91.7±0.1[i]
n-Pentanol	111.3	111.1±0.4[e]	108.5	108.5±0.1[j]

[a]Reported $\bar{V}^0$ (at 20°C) in ref. 6: 41.3.
[b]60.95.
[c]76.9.
[d]94.1.
[e]111.0.
[f]Reported in ref. 7: 40.20.
[g]58.34.
[h]75.13.
[i]91.75.
[j]108.4.

We now consider the results for solutions of *n*-alkanes and *n*-alkanols in benzene. Values of $\bar{V}^0$ calculated by [1] using the parameters of Table 3, and Z_g values already reported (1, 3) for these solutes in carbon tetrachloride, are shown in Table 1. Agreement with experimental values is almost within the limits of experimental error, except for methanol, a compound aberrant also in carbon tetrachloride.

Values of $\bar{V}^0$ calculated in the same way for these solutes in ethanol also agree well with experimental values. In ethanol (unlike carbon tetrachloride (3)) it was assumed that $Z_{g(C—C)}^{O/C} = 0$ for *n*-propanol and higher alcohols, hydrogen bonding of the hydroxyl group to solvent tending strongly to inhibit the $g_{O—C}^{O/C}$ arrangement.

The accommodation of [1] to the experimental $\bar{V}^0$ values in cyclohexane (Table 4) offers a more serious challenge: $\bar{V}^0$ of *n*-pentane is larger in cyclohexane than in carbon tetrachloride, but $\bar{V}^0$ of *n*-decane is smaller. These results cannot be accommodated if $Z_{g(C—C)}^{C/C}$ values remain the same in the two solvents, but require $Z_{g(C—C)}^{C/C}$ to increase more rapidly with chain length in cyclohexane. This in turn requires the enthalpy difference ΔH_g between *gauche* and *anti* to be smaller in cyclohexane. The calculated

TABLE 2. Solvent parameters

Solvent	v_w[a] (Å^3)	P_i[b] (cal cm^{-3})	c.e.d.[c] (cal cm^{-3})	Δ (Å)	a	b (mL mol^{-1})
Water	20.6	41.0	550.2	0.57	—	—
Ethanol	53.0	69.5	161.3	0.745	1.613	23.5
Benzene	80.4	88.4	83.7	0.745	1.654	20.8
Carbon tetrachloride	84.8	80.6	73.6	0.740	1.627	21.2
Cyclohexane	102.0	~76	66.9	0.755	1.534	28.9

[a]Reference 10.
[b]Reference 12.
[c]Reference 13.

TABLE 3. Parameters for calculation of $\bar{V}^0$ using [1]

Solvent	V_c (mL mol^{-1})	Hydroxyl I (mL mol^{-1})	$\delta^{C/C}_{C-C}$ (mL mol^{-1})	ΔH_g (cal mol^{-1})
Ethanol	12.6	1.1	−2.5	700
Benzene	11.4	5.8	−1.1	700
Carbon tetrachloride	11.6	6.1	−2.5	700
Cyclohexane	13.3	9.7	−2.5	500

values of $\bar{V}^0$ shown in Table 4 have been obtained assuming $\Delta H_g = 500$ cal mol^{-1}. Again, agreement between calculated and experimental values is reasonable, considering the simplicity of the approach; the data at present are too sparse to warrant a more elaborate analysis.

The solute molecules so far considered have been chain molecules existing in solution as mixtures of conformers. In Table 5 we give partial molal volumes of adamantane and cyclohexane, which have fixed or relatively fixed structures, and of several cycloalkanes, most of them existing in one or more mobile conformations. From these values of $\bar{V}^0$, C values have been calculated from [1] using the parameters of Table 3. Trends in C with ring size run parallel in the different solvents. Possible interpretations of C have been given earlier (4).

TABLE 4. Partial molal volumes ($\bar{V}^0$, in mL mol^{-1}) of alkanes and alkanols in cyclohexane at 25°C

Compound	$Z_{g(C-C)}^{C/C}$	$Z_{g(C-C)}^{O/C}$	$\bar{V}^0_{calcd}$	$\bar{V}^0_{exptl}$
n-Pentane	0.79	—	116.3	116.9±0.5
n-Hexane	1.14	—	132.7	133.6±0.6
n-Heptane	1.46	—	149.1	150.0±0.5
n-Octane	1.80	—	165.4	165.6±0.6
n-Nonane	2.13	—	181.7	179.7±0.6
n-Decane	2.46	—	198.0	196.9±0.3
Methanol	—	—	49.8	48.2±0.3[a]
Ethanol	—	—	67.1	67.8±0.4[b]
n-Propanol	—	0.74	83.0	82.0±0.2[c]
n-Butanol	0.46	0.72	100.4	99.6±0.3[d]
n-Pentanol	0.77	0.72	115.3	115.6±0.5[e]
n-Hexanol	1.10	0.72	131.6	131.8[f]
n-Octanol	1.76	0.72	164.2	164.95[f]
n-Decanol	2.42	0.72	196.8	198.4[f]

[a]Reference 6 reports $\bar{V}^0$ at 20°C to be 44.25.
[b]66.5.
[c]81.45.
[d]99.4.
[e]114.7.
[f]Reported by ref. 6 for 20°C.

Discussion

It is apparent that with adoption of the parameters of Table 3, $\bar{V}^0$ in the three solvents under investigation may be calculated from [1] with reasonable accuracy. We now consider whether the relative magnitudes of these parameters accord with the intuitive picture of partial molal volumes developed in our previous papers.

The covolume V_c is the volume of the solvent cavity required to accommodate a point kinetic particle of no intrinsic volume

$$\left(\sum_1^m n^k I^k = 0, \qquad \sum_1^n Z_g{}^l \delta^l = 0, \qquad C = 0\right)$$

It should accordingly be related to the b parameter of Terasawa *et al.* (14) ($\bar{V}^0 = b$ when $V_w = 0$), and this relationship is shown in Fig. 1*A*. We have already given reasons why V_c should be expected to be less than b (1).

There is also an indication (Fig. 1*B*) that V_c may be related to the van der Waals volume v_w of the solvent molecules. Bondi (16) has discussed the effect to be expected from varying particle size on the closeness of packing of spheroids, but without firm conclusions. The present work indicates the desirability of a systematic study of the variation of V_c and b in solvents made up of spherical, aprotic molecules of varying size. The point for the protic solvent, ethanol (not shown), lies far above the straight line

TABLE 5. Partial molal volumes $\overline{V}^0$ and cyclization factors C (both in mL mol^{-1}) for cyclic compounds and adamantane in various solvents

	CCl_4[a]		C_6H_{12}		C_6H_6		EtOH	
Compound	$\overline{V}^0$	C	$\overline{V}^0$	C	$\overline{V}^0$	C	$\overline{V}^0$	C
Cyclopentane	97.8±0.5	−2.2	92.8±0.4	−7.5	—	—	—	—
Cyclohexane	110.9±0.5	−6.0	108.8±0.1	−8.9	111.1±0.3	−4.7	110.6±0.6	−6.4
Cycloheptane	124.0±0.6	−9.7	120.0±0.3	−15.1	—	—	—	—
Cyclooctane	135.4±0.4	−13.6	133.2±0.5	−19.3	—	—	—	—
Cyclodecane	165.3±0.3	−21.0	163.0±0.3	−24.3	—	—	—	—
Adamantane	140.2±0.3	−16.9	137.3±0.5	−21.6	142.7±0.2	−14.3	138.8±0.9	−19.4

[a]From ref. 4.

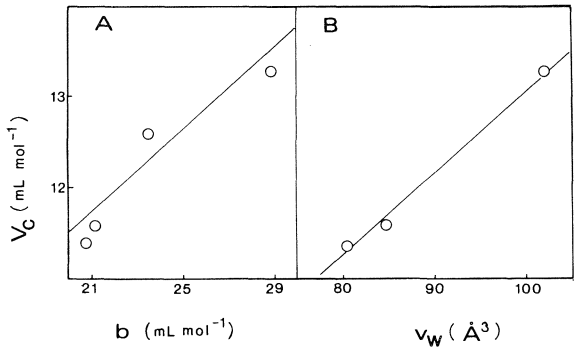

FIG. 1. Relation between V_c and b (A), and between V_c and v_w (B).

of Fig. 1*B*, but the introduction of a partially inert solute molecule into a highly structured, hydrogen-bonded solvent would be expected to break hydrogen bonds and hence to lead to an increase in volume greater than expected from the mere formation of a cavity in the solvent.

We now consider the increment I for the hydroxyl group. If this group interacted with benzene, carbon tetrachloride, or cyclohexane as weakly as do methyl and methylene, it would have $I \simeq 16.6$ mL mol^{-1} (3). The increments in all three solvents are smaller, and reflect the strength of dipole – induced dipole interactions in the order: benzene > carbon tetrachloride > cyclohexane, the order of decreasing polarizability (17). In the protic solvent, ethanol, strong interaction through hydrogen bonding is also possible, and hence I is smallest in this solvent.

Explanations for the differences of $\delta^{C/C}_{C-C}$ (Table 3) and C (Table 5) in the different solvents are less obvious. Variability of δ (e.g., $\delta^{Cl/Cl}_{C-C}$, $\delta^{Br/C}_{C-C}$ (2)) with solvent has been noticed before but with molecules containing polar groups, and for which changes in conformation should result in changes in dipole moment.

The reduction of ΔH_g on changing solvent from carbon tetrachloride to cyclohexane is also remarkable. Latest studies (reviewed in ref. 18) indicate an enthalpy increase of about 900 cal mol^{-1} on going from *anti* to *gauche* butane in the gas phase. This difference is reduced when *n*-butane is in solution, perhaps because the internal pressure exerted by the solvent favours formation of the more compact *gauche* form (19). However, there is no simple correlation, as might be expected (19), between ΔH_g (Table 3) and P_i or *c.e.d.* (Table 2). Possibly a more important parameter is the London dispersion force between the hydrocarbon chain and the solvent molecules, which would favour a more extended chain and closer solvent–solute contacts; this would be weakest in cyclohexane solution.[2] The extent of coiling of polymer chains has been explained in similar fashion (20).

Accepting a smaller ΔH_g in cyclohexane, we can expect *n*-alkane chains to be more coiled in this solvent than in carbon tetrachloride. Hence each successive addition of CH_2 to the chain causes a smaller increase in $\overline{V}^0$ in cyclohexane than in carbon tetrachloride. This explains the smaller a parameter in this solvent (Table 2).

In summary, the present work indicates that [1] will probably prove valid for a variety of organic solvents made up of spherical molecules. It would be desirable to test it more stringently by obtaining $\overline{V}^0$ values for large numbers of isomeric alkanes in each single solvent, and thence obtaining *ab initio* the parameters I and δ, as was done for carbon tetrachloride solutions (1).

Experimental

Solvents and solutes were commercial products, and were purified by methods described earlier (1). The technique for measuring the densities of solutions has also been described (1). In all cases linear variation of the apparent molal volume with concentration was observed over the concentration range (< 0.5% w/w) employed.

Acknowledgments

We are grateful to the Natural Sciences and

[2]This effect would run counter to P_i or *c.e.d.* It is possible that effects of both types are involved.

Engineering Research Council of Canada for financial support, and to the Faculty of Graduate Studies and Research of McGill University for the financial assistance towards the purchase of a precision density meter.

1. J. T. EDWARD, P. G. FARRELL, and F. SHAHIDI. J. Phys. Chem. **82**, 2310 (1978).
2. F. SHAHIDI, P. G. FARRELL, and J. T. EDWARD. J. Phys. Chem. **83**, 419 (1979).
3. J. T. EDWARD, P. G. FARRELL, and F. SHAHIDI. Can. J. Chem. **57**, 2585 (1979).
4. J. T. EDWARD, P. G. FARRELL, and F. SHAHIDI. Can. J. Chem. This issue.
5. G. MANN. Tetrahedron, **23**, 3375 (1967).
6. L. A. K. STAVELEY and B. SPICE. J. Chem. Soc. 406 (1952).
7. M. MANABE and M. KODA. Bull. Chem. Soc. Jpn. **48**, 2367 (1975).
8. J. KREUZER and R. MECKE. Z. Phys. Chem. B**49**, 309 (1941); H. HARMS. Z. Phys. Chem. B**53**, 280 (1943); E. G. HOFFMAN. Z. Phys. Chem. B**53**, 179 (1943).
9. J. T. EDWARD and P. G. FARRELL. Can. J. Chem. **53**, 2965 (1975).
10. A. BONDI. J. Phys. Chem. **68**, 441 (1964); J. T. EDWARD. J. Chem. Educ. **47**, 261 (1970).
11. A. BONDI. J. Phys. Chem. **58**, 924 (1954).
12. J. H. HILDEBRAND and R. L. SCOTT. Solubility of nonelectrolytes. 3rd ed. Reinhold, New York, NY. 1950. Chapt. V.
13. M. R. J. DACK. Chem. Soc. Rev. **4**, 211 (1975).
14. S. TERASAWA, M. ITSUKI, and S. ARAKAWA. J. Phys. Chem. **79**, 2345 (1975).
15. J. T. EDWARD, P. G. FARRELL, and F. SHAHIDI. J. Chem. Soc. Faraday Trans. 1, **73**, 705 (1977).
16. A. BONDI. Physical properties of molecular crystals, liquids, and glasses. John Wiley, New York, NY. 1968. pp. 216, 244–246.
17. O. EXNER. Dipole moments in organic chemistry. G. Thieme, Stuttgart. 1975. p. 21.
18. J. R. DURIG and D. A. C. COMPTON. J. Phys. Chem. **83**, 265 (1975).
19. R. J. OUELLETTE and S. H. WILLIAMS. J. Am. Chem. Soc. **43**, 466 (1971).
20. P. J. FLORY. Principles of polymer chemistry. Cornell University Press, Ithaca, NY. 1953. p. 600.

Partial molal volumes of organic compounds in carbon tetrachloride. V. Cyclic alkanes, ethers, alcohols, ketones, and bromides

JOHN T. EDWARD, PATRICK G. FARRELL, AND FEREIDOON SHAHIDI[1]

Department of Chemistry, McGill University, 801 Sherbrooke St. W., Montreal, P.Q., Canada H3A 2K6

Received May 11, 1979

JOHN T. EDWARD, PATRICK G. FARRELL, and FEREIDOON SHAHIDI. Can. J. Chem. **57**, 2892 (1979).

The partial molal volumes $\overline{V}^0$ or 47 mono- or polycyclic alkanes, ethers, alcohols, ketones, and bromides have been determined in carbon tetrachloride at 25°C. $\overline{V}^0$ of most of these compounds can be calculated with moderate (±1–2%) accuracy using an equation containing parameters previously developed for acyclic compounds, and an additional cyclization parameter C, which is roughly linear with the number n of atoms in the ring, from $n = 3$ ($C = +5.3$ mL mol^{-1}) to $n = 10$ ($C = -21.0$ mL mol^{-1}). Substituted cyclohexanols and some polyfunctional compounds had $\overline{V}^0$ considerably lower than calculated.

JOHN T. EDWARD, PATRICK G. FARRELL et FEREIDOON SHAHIDI. Can. J. Chem. **57**, 2892 (1979).

On a déterminé le volume molaire partiel $\overline{V}^0$ de 47 composés mono ou polycycliques du type: alcanes, éthers, alcools, cétones et bromures, en solution dans le tétrachlorure de carbone à 25°C. Pour la plupart de ces composés, $\overline{V}^0$ peut être calculé avec une précision modérée de (±1–2%) en utilisant une équation contenant les paramètres développés antérieurement pour les composés acycliques et un paramètre additionnel de cyclisation C qui est grossièrement proportionnel au nombre n d'atomes du cycle, à partir de $n = 3$ ($C = +5.3$ mL mol^{-1}) à $n = 10$ ($C = -21.0$ mL mol^{-1}). Les cyclohexanols substitués et quelques composés polyfonctionnels ont des valeurs de $\overline{V}^0$ nettement plus faibles que celles calculées.

[Traduit par le journal]

Introduction

Straight- and branched-chain aliphatic compounds dissolved in carbon tetrachloride exist as mixtures of rapidly equilibrating conformers. If the mole fraction of a conformer is γ, and $z_g{}^l$ represents the number of *gauche* arrangements of type l along the chain, the mole fraction of *gauche* arrangements of this type due to all conformers of the compound is $Z_g{}^l = \sum \gamma z_g{}^l$. γ, and thence $Z_g{}^l$, may be calculated by well-established methods (1, 2). The partial molal volumes $\overline{V}_0$ of aliphatic chains are reduced by an amount linearly related to $Z_g{}^l$ (2–4).

The looping of an extended chain into a ring necessarily involves the creation of a number of *gauche* or eclipsed arrangements, and so might be expected to result in a diminished volume. This indeed has been found true in other additive schemes for molecular volumes (5, 6) which, however, have taken no account of conformational effects and have consequently had only limited usefulness. We shall allow for the effect of cyclization by adding the parameter C to the equation previously employed to account for conformational effects with chain compounds (2–4):

$$[1] \quad \overline{V}^0 = V_c + \sum_1^m n^k I^k + \sum_1^n Z_g{}^l \delta^l + C$$

(see ref. 3 for definition of other symbols). In applying this equation $Z_g{}^l$ will refer only to the mole fraction of *gauche* arrangements of type l due to groups attached to a ring, and not to *gauche* arrangements found within the ring or cage portion of the molecule, for which account is taken in C.

Results

The partial molal volumes of 47 ring and cage compounds in carbon tetrachloride have been determined and are given in Table 1. For 21 of these compounds devoid of side groups or chains ($Z_g = 0$), C has been calculated from [1] using V_c and the other parameters determined in previous work (2–4). A plot of C for these compounds against n, the number of ring atoms, shows a roughly linear relationship changing slope at $n = 10$ (Fig. 1). The values of C given by the two straight lines of Fig. 1 for different values of n are given in Table 2.

Using these values of C, $\overline{V}^0$ has been calculated for 42 of the 47 compounds of Table 1 by [1]. ($\overline{V}^0$ for adamantane and two adamantane derivatives was calculated using C footnoted in Table 2.) For compounds having an atom other than hydrogen or carbonyl oxygen attached to the ring, it was necessary

[1]Present address: Lash Miller Chemical Laboratories, University of Toronto, 80 St. George Street, Toronto, Ont., Canada M5S 1A1.

0008-4042/79/222892-03$01.00/0

TABLE 1. Partial molal volume $\bar{V}^0$ (in mL mol^{-1}) of cyclic compounds in carbon tetrachloride at 25°C

Compound	$\bar{V}^0_{exptl}$	$\bar{V}^0_{calcd}$
1 Cyclopentane	97.8±0.5	96.4
2 Cyclohexane	110.9±0.5	110.0
3 Cycloheptane	124.0±0.6	123.7
4 Cyclooctane	135.4±0.4	137.2
5 Cyclodecane	165.3±0.3	164.6
6 Cyclododecane	198.7±0.5	198.6
7 Adamantane	140.2±0.3	140.3
8 1,1-Diadamantane	240.5±0.5	—
9 2,2-Diadamantane	241.2±0.9	—
10 Propylene oxide	74.2±1.0	75.8
11 Trimethylene oxide	70.0±0.5	69.9
12 Tetrahydrofuran	81.4±0.3	83.4
13 2,5-Dimethyltetrahydrofuran	119.8±0.2	117.8[a]
14 2-5-Dimethoxytetrahydrofuran	128.2±0.3	123.7[b]
15 1,3-Dioxalane	69.7±0.1	73.2
16 Tetrahydropyran	96.4±0.2	97.0
17 1,4-Dioxane	85.0±0.1	86.8
18 *sym*-Trioxane	75.8±0.1	75.2
19 Oxepane	109.6±0.5	110.7
20 1,3-Dioxepane	100.6±0.1	100.5
21 Cyclopropylmethanol	80.3±0.2	82.9[c]
22 Cyclobutanol	80.0±0.2	80.8[d]
23 Cyclopentanol	94.4±0.2	94.3[d]
24 Cyclohexanol	108.1±0.5	107.9[d]
25 Cycloheptanol	121.2±0.6	121.6[d]
26 Cyclohexylmethanol	123.7±0.1	123.5[c,e]
27 *trans*-2-Methylcyclohexanol	118.8±0.1	126.5[f]
28 *trans*-4-Methylcyclohexanol	120.6±0.4	128.7
29 *cis*-4-Methylcyclohexanol	118.9±0.2	124.2[g]
30 Cyclooctanol	133.0±0.5	135.1[d]
31 Methylcyclopropyl ketone	93.6±0.3	92.7[h]
32 Cyclobutanone	75.5±0.1	73.8
33 Cyclopentanone	87.9±0.3	87.3
34 Cyclohexanone	102.6±0.4	100.9
35 Cycloheptanone	115.7±0.2	114.6
36 Cyclooctanone	128.9±0.2	128.1
37 Cyclononanone	142.7±0.2	141.7
38 Cyclodecanone	154.5±0.2	155.5
39 Cycloundecanone	174.2±0.6	172.5
40 Cyclododecanone	190.4±0.4	189.5
41 Cyclopentadecanone	239.4±0.2	240.8
42 1,4-Cyclohexandione	95.0±0.2	91.8
43 1-Bromoadamantane	153.0±0.8	152.9
44 2-Bromoadamantane	149.8±0.4	149.7[i]
45 1-Bromodiamantane	186.3±0.6	—
46 4-Bromodiamantane	188.8±0.3	—
47 2-Bromotriamantane	218.8±0.4	—

[a] $Z_{g(C-C)}^{C/C} = 2$.
[b] $Z_{g(O-C)}^{C/O} = 3.0$, $Z_{g(C-C)}^{O/C} = 2.0$, $Z_{g(O-C)}^{C/C} = 0.6$.
[c] $Z_{g(C-C)}^{O/C} = 1.2$, on the assumption of similarity to 2-methyl-1-propanol (ref. 4).
[d] $Z_{g(C-C)}^{O/C} = 0.5$.
[e] $Z_{g(C-C)}^{C/C} = 0.11$.
[f] $Z_{g(C-C)}^{O/C} = 1$.
[g] $Z_{g(C-C)}^{O/C} = 1.7$, $Z_{g(C-C)}^{C/C} = 0.3$.
[h] Assuming a conformation 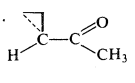 (cf. ref. 8), $Z_{g(C-C)}^{O/C} = 2$.
[i] $Z_{g(C-C)}^{Br/C} = 2$.

to calculate Z_g[l]. When the atom or group is completely or almost completely in the equatorial position, as in 1-bromoadamantane or *trans*-4-methylcyclohexanol (7), $Z_g = 0$. For other compounds the mole ratios of conformers may be calculated by well-established methods (7). For example, cyclohexanol (**24**) can be shown to be made up of two conformers, one ($\gamma = 0.76$) having the hydroxyl group equatorial ($z_{g(C-C)}^{O/C} = 0$), and one ($\gamma = 0.24$) having it axial ($z_{g(C-C)}^{O/C} = 2$), whence $Z_{g(C-C)}^{O/C} = 0.5$. The other cyclic alcohols (**22**, **23**, **25**, **30**) will have the hydroxyl group to some extent in a *quasi-axial* arrangement, and hence a proportion of molecules having arrangements not very different from $g_{(C-C)}^{O/C}$ found in *axial* cyclohexanol. However, information which would enable us to calculate the mole fraction of such arrangements is lacking, and so we have applied [1] to the cyclic alcohols **22**, **23**, **25**, and **30** assuming $Z_{g(C-C)}^{O/C} = 0.5$ for all of them.

These and other values of Z_g are given as footnotes to Table 1. In some cases (e.g., **13**, **14**) these cannot be better than guesses, since not only the shape but also the configuration (*cis* or *trans*) of the molecules is not known.

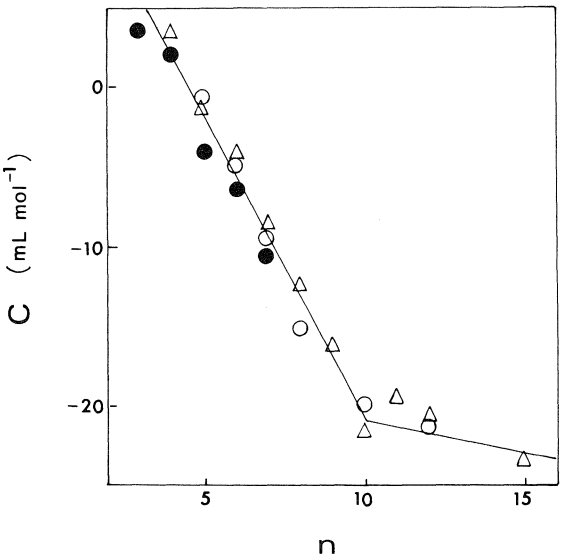

FIG. 1. Plot of cyclization parameter C against number of ring atoms n for alkanes (●), ethers (○), and ketones (△).

TABLE 2. Dependence of cyclization parameter C (in mL mol^{-1}) on number n of skeletal atoms in ring

n	C	n	C	n	C
3	+5.3	8	−13.6	12	−21.8
4	+1.7	9	−17.4	13	−22.2
5	−2.2	10	−21.0[a]	14	−22.6
6	−6.0	11	−21.4	15	−23.0
7	−9.7				

[a] For adamantane ($n = 10$) and derivatives, $C = -16.9$ mL mol^{-1}.

Discussion

The scatter about the straight lines of Fig. 1 shows that the values of C in Table 2 are only rough averages, and so close agreement between calculated and experimental values in Table 1 cannot be expected. However, for many of the cyclic alkanes (**1–5**), alcohols (**22–25**, **30**), and ketones (**32–38**) agreement is within the limits of experimental error. However, for some substituted cyclohexanols (**27–29**) the discrepancy is great. More data on substituted cyclohexanes and substituted cyclohexanols would be desirable.

Some of the polyfunctional compounds (**15**, **17**) also have partial molal volumes appreciably smaller than calculated. Newman and Mackle (9) have pointed out that the polar character of compounds such as **15** is usually greater than that of their acyclic analogues; this should have the effect of making $\overline{V}^0$ of the cyclic compounds less than expected on the basis of I and δ values derived from a study of acyclic compounds. On the other hand, the cyclic ketones (**32–41**) tend to have $\overline{V}^0$ values slightly higher than calculated; it is possible that complexation of the carbonyl group by solvent carbon tetrachloride molecules (4) is slightly less effective in the cyclic than the acyclic compounds. However, such speculations must remain highly tentative until more data have been accumulated.

The central problem raised in this paper is the interpretation of C. The following points should be noted:

(*a*) Cyclization does not necessarily involve a reduction in volume: C for three- and four-membered rings is positive.

(*b*) Similarly, C cannot be explained primarily by a reduction in V_w (and thence in $\overline{V}^0$ (10)). The compression of the van der Waals radii of some hydrogen atoms pointing inwards in medium-sized rings reaches a maximum for $n = 9$–10, and thereafter diminishes (11), while C continues to become more negative after $n = 10$ (Fig. 1).

It seems likely that an explanation of C requires a more profound understanding of the effect of relative size of solute and solvent molecules on the efficiency of packing in the solution. It may be noted that the limited data available for cycloalkanes in other solvents (benzene, cyclohexane) indicate that relationships of the sort shown in Fig. 1 are general, but that for a given n, C becomes larger in solvents having molecules of larger size (12).

Experimental

The compounds investigated were commercial products, except for **28** and **29**, which were the gift of Dr. F. L. Chubb, and **45–47**, the gift of Professor M. A. McKervey. Purification of materials and techniques of measurement were carried out as described previously (2–4).

Acknowledgments

We are grateful to the Natural Sciences and Engineering Research Council of Canada for financial support and to the Faculty of Graduate Studies and Research of McGill University for financial assistance towards the purchase of a precision density meter.

1. G. MANN. Tetrahedron, **23**, 3375 (1967).
2. J. T. EDWARD, P. G. FARRELL, and J. T. EDWARD. J. Phys. Chem. **82**, 2310 (1978).
3. F. SHAHIDI, P. G. FARRELL, and J. T. EDWARD. J. Phys. Chem. **83**, 419 (1979).
4. J. T. EDWARD, P. G. FARRELL, and F. SHAHIDI. Can. J. Chem. **57**, 2585 (1979).
5. S. S. KURTZ and M. R. LIPKIN. Ind. Eng. Chem. **33**, 779 (1941).
6. M. L. HUGGINS. J. Am. Chem. Soc. **63**, 116 (1941).
7. E. L. ELIEL, N. L. ALLINGER, S. J. ANGYAL, and G. A. MORRISON. Conformational analysis. Interscience, New York, NY. 1965. pp. 11, 44.
8. E. M. KOSOWER and M. ITO. Proc. Chem. Soc. 25 (1962).
9. M. S. NEWMAN and R. A. MACKLE. J. Am. Chem. Soc. **94**, 2733 (1972).
10. J. T. EDWARD and P. G. FARRELL. Can. J. Chem. **53**, 2965 (1975); S. TERASAWA, M. ITSUKI, and S. ARAKAWA. J. Phys. Chem. **79**, 2345 (1975).
11. J. SICHER. *In* Progress in stereochemistry. Vol. III. *Edited by* P. B. D. de la Mare and W. Klyne. Butterworths, London. 1962. p. 202.
12. J. T. EDWARD, P. G. FARRELL, and F. SHAHIDI. Can. J. Chem. This issue.

Erratum: Stereoselective synthesis of β-substituted α,β-unsaturated esters by dialkylcuprate coupling to the enol phosphate of β-keto esters

FUK-WAH SUM AND LARRY WEILER
Department of Chemistry, University of British Columbia, Vancouver, B.C., Canada V6T 1W5
(Ref.: Can. J. Chem. **57**, 1431 (1979))
Received July 30, 1979

In Table 4 the enol phosphate from acetylacetone should have the *E* stereochemistry and in the experimental compound **33** should be methyl (*E*)-3-methyl-2-nonenoate.

Erratum: Stannic tetrachloride catalysed glycosylation of 8-ethoxycarbonyloctanol by cellobiose, lactose, and maltose octaacetates; synthesis of α- and β-glycosidic linkages

Erratum: 1,2-Orthoacetate intermediates in silver trifluoromethanesulphonate promoted Koenigs–Knorr synthesis of disaccharide glycosides

JOSEPH BANOUB AND DAVID R. BUNDLE
Division of Biological Sciences, National Research Council of Canada, Ottawa, Ont., Canada K1A 0R6
(Ref.: Can. J. Chem. **57**, 2085 (1979); **57**, 2091 (1979))
Received September 13, 1979

The running heads "Banoub and Bundle: I" and "Banoub and Bundle: II" for the two papers listed above were incorrectly interchanged in the journal, and the two articles should be read in the opposite order to that printed.

Hydrogen exchange and isomerization in *ortho* substituted benzamides. On the question of free rotation in an *N*-protonated amide

ROBERT A. MCCLELLAND AND WILLIAM F. REYNOLDS

Department of Chemistry, University of Toronto, Toronto, Ont., Canada M5S 1A1

Received May 1, 1979

ROBERT A. MCCLELLAND and WILLIAM F. REYNOLDS. Can. J. Chem. **57**, 2896 (1979).

Rate constants have been obtained for the acid-catalyzed N–H exchange of *N*-methyl, 2,*N*-dimethyl, and 2,4,6,*N*-tetramethylbenzamide and the acid-catalyzed isomerization of the three corresponding *N*,*N*-dimethylbenzamides. The ratio $k_{H^+}{}^{ex}/k_{H^+}{}^{iso}$ increases significantly with increased number of *ortho* methyl substituents. This is explained in terms of a suggestion of Perrin, that C—N bond rotation is not completely free in the *N*-protonated amide, since it must compete with a diffusion limited deprotonation reaction. The isomerization reaction, which requires such a rotation, is therefore slowed by *ortho* methyl substituents which hinder rotation, relative to the exchange reaction, which does not require rotation.

ROBERT A. MCCLELLAND et WILLIAM F. REYNOLDS. Can. J. Chem. **57**, 2896 (1979).

On a obtenu les constantes de vitesse de la réaction d'échange N–H, catalysée par les acides, dans le case de trois *N*-méthylbenzamides, soit le produit non substitué et ceux substitués par un méthyle en position 2 ou trois méthyles en 2, 4 et 6 ainsi que dans le cas de l'isomérisation, catalysée par les acides, des trois *N*,*N*-diméthylbenzamides correspondants. Le rapport $k_{H^+}{}^{ex}/k_{H^+}{}^{iso}$ augmente d'une façon importante avec le nombre de substituants méthyles en position *ortho*. Ceci est expliqué à l'aide de la suggestion de Perrin qui veut que la rotation de la liaison C—N ne soit pas complètement libre dans l'amide protoné puisqu'elle doit entrer en compétition avec une diffusion limitée de la réaction de protonation. Par rapport à la réaction d'échange qui n'implique pas de rotation, la réaction d'isomerisation est ralentie par les substituants méthyles en position *ortho*, qui gênent la rotation.

[Traduit par le journal]

Two mechanisms have now been proposed for the acid-catalyzed hydrogen exchange reaction of amides, one involving protonation–deprotonation on the amide nitrogen (1)

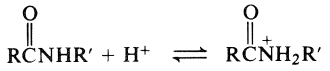

and a second more circuitous route involving an intermediate imidic acid, formed from the oxygen protonated amide (2, 3)

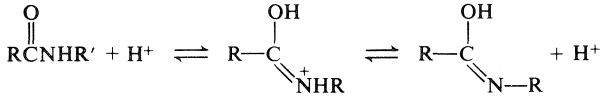

The latter mechanism was based on the observation that rates of exchange of *N*-methyl amides are generally greater than rates of isomerization of corresponding *N*,*N*-dimethyl amides. The isomerization must occur via the nitrogen protonated amide,

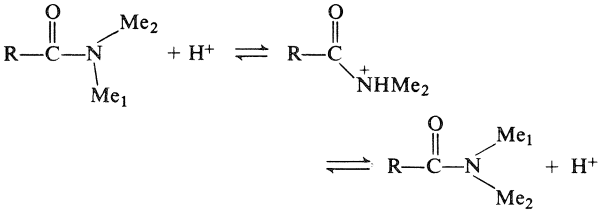

leading to the suggestion that the larger rate of exchange is due to the additional route available to that reaction.

More recently Perrin (4) claims to have ruled out the imidic acid mechanism for the acid-catalyzed exchange of primary amides ($RCONH_2$). This proposal was based on the observation that the two hydrogens undergo exchange at different rates, and the order of reactivity is not that expected for the imidic acid pathway. The diastereotopic hydrogens of amidinium ions (**I** (5) and **II** (6)) also undergo acid-catalyzed exchange at different rates.

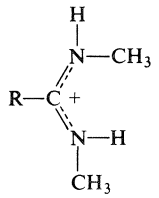

I

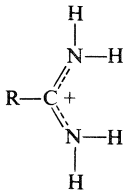

II

Perrin argues (4, 6) that such observations can be explained in terms of intermediate nitrogen protonated species, providing that the hydrogens on the nitrogen in those species do not become equivalent. Perrin points out that although rotation about the C—N single bond in the nitrogen protonated species is

0008-4042/79/222896-06$01.00/0

TABLE 1. Rate constants for the acid-catalyzed exchange and isomerization of *N*-methylated benzamides (33°C)

Benzamide	Δ, cps	$[H^+]^a$	k_{H^+}, M^{-1} s^{-1}	$k_{H^+}^{ex}/k_{H^+}^{iso}$
N-Methyl	5.1	0.016	710 (490, 25°C)[b]	4.4
N,*N*-Dimethyl	7.9	0.110	160 (178, 33°C;[c] 106, 25°C)[b]	
2,*N*-Dimethyl, H_2O	5.1	0.083	137	17
2,*N*-Dimethyl, 33% acetone-d^6	4.9	0.107	102	
2,*N*,*N*-Trimethyl	17.0	5.6	7.0 (9.0)[d]	
2,4,6,*N*-Tetramethyl, H_2O			36, est.[e]	>120
2,4,6,*N*-Tetramethyl, 33% acetone-d^6	4.9	0.41	27	
2,4,6,*N*,*N*-Pentamethyl	19.2		<0.25[e]	

[a][H+] concentration where coalescence occurs.
[b]Reference 3.
[c]Reference 19.
[d]Based on partially coalesced signals in 1 *M* HCl, using method of ref. 20.
[e]See text.

undoubtedly very fast, so is the deprotonation process, which should be very nearly a diffusion limited reaction.

In this paper we consider the question of the mechanism of the exchange and isomerization reactions in *N*-methyl and *N*,*N*-dimethyl amides respectively. Our reasoning was that if C—N single bond rotation is indeed important, the introduction of groups which might hinder this process should show up in the rates. We have therefore measured rates of exchange and isomerization for amides containing one and two *ortho* methyl substituents, and indeed find that there is a pronounced effect.

Experimental Section

Amides were prepared by passing methylamine or dimethylamine through a solution in ether of the appropriate acid chloride. Physical properties of known compounds agreed with literature values. In the case of new compounds satisfactory analyses were obtained.

Spectra were recorded on a Varian T-60 NMR spectrometer, with a probe temperature of 33 ± 0.5°C. Concentrations of amides ranged from 0.04 to 0.2 *M*; rate constants were established to be independent of this concentration. Except where noted, second-order rate constants for the H^+ catalyzed exchange or isomerization were determined by varying the acid concentration until the pair of signals due to the *N*-methyl group or groups was just coalesced into one broad signal with a maximum at the mean position (7). The second-order rate constant was calculated from the formula (3, 7)

$$k = (\pi \cdot \Delta)/(1.41 \cdot [H^+])$$

where Δ ≡ separation in cps of the signals when no acid is present, and $[H^+]$ = concentration of acid.

While more precise values could be obtained by a complete line shape analysis, this approach should yield rate constants which are accurate to ca. 10%, particularly since the line width in the absence of exchange was less than 10% of the doublet splitting and since Δ was insensitive to acidity in the absence of exchange. Rate constants of this accuracy seemed more than sufficient for our purpose.

Results

Table 1 lists second-order rate constants for the acid-catalyzed N–H exchange of three *N*-methyl benzamides ($k_{H^+}^{ex}$) and the acid-catalyzed isomerization ($k_{H^+}^{iso}$) of the three corresponding *N*,*N*-dimethylbenzamides. For the unsubstituted compounds reasonable agreement can be seen between our results and those taken from the literature. In the case of 2,*N*,*N*-trimethylbenzamide, an acid concentration of 5.6 *M* is required to reach the coalescence point. For this compound the rate constant was also calculated from the broadened signals in 1.0 *M* HCl, and the number shows reasonable agreement with that obtained from the coalescence point. The compound 2,4,6,*N*-tetramethylbenzamide was not sufficiently soluble in water to obtain suitable nmr spectra, and we were forced to employ solutions containing 33% acetone-d^6. For 2,*N*-dimethylbenzamide the rate constant for exchange in water is 1.34 times that in 33% acetone-d^6. This factor was used to estimate the rate constant for the exchange of 2,4,6,*N*-tetramethylbenzamide in water alone. With 2,4,6,*N*,*N*-pentamethylbenzamide there is no broadening of the two *N*-methyl peaks in any acid solution. We have placed an upper limit on the second-order rate constant for isomerization in the following way. In any acid solution a first-order rate of isomerization of 1 s^{-1} would result in a 0.3 Hz broadening of the signals in the doublet, and this would have been detectable. Cox (8) has previously shown that rates of isomerization of *N*,*N*-dimethylbenzamide remain reasonably linear in H^+ concentration up to 3–4 *M* HCl, although above this point they reach a maxi-

mum value and then decrease with increasing acidity. Assuming that a 1 s^{-1} rate of isomerization would be observed, and assuming that the rate of isomerization is still linear in H^+ concentration in 4 *M* HCl, the lack of broadening in that acid means that $k_{H^+}{}^{iso}$ is less than 0.25 M^{-1} s^{-1}. (This argument depends very strongly on the pK_a value of the amide, since the levelling-off in the rate observed by Cox (8) is associated with protonation. Some preliminary measurements were carried out to determine the basicity of the pentamethylbenzamide, and suggest that this amide is not substantially protonated (<25%) in 4 *M* HCl. Unfortunately, this compound does not exhibit a predominant spectral change on protonation, and accurate protonation data are therefore difficult to obtain.)

Discussion

The results reported in Table 1 show that successive introduction of *ortho* methyl groups causes a decrease in the rates of both the acid-catalyzed N–H exchange reaction of an *N*-methylbenzamide and the acid-catalyzed isomerization of an *N,N*-dimethylbenzamide, with the effect being considerably more pronounced on the isomerization reaction.

Isomerization of N,N-*Dimethyl Amides*

The dramatic effect on this reaction can be explained in simple terms by recognizing that in order for isomerization to occur there must be a rotation of some sort about the C—N bond of the *N*-protonated intermediate. This suggests that the *ortho* methyl groups are slowing the isomerization by hindering this rotation. The argument can be illustrated in more detailed terms using a scheme such as shown below.

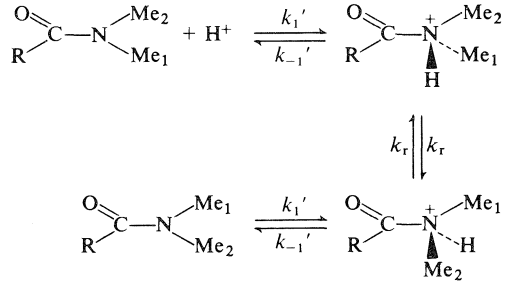

We have drawn for the *N*-protonated amides in this scheme a particular conformational form, the one favored in Perrin's arguments (6), but other conformations also suffice. What is required is (*a*) that the conformation of the *N*-protonated amide which is initially produced be one in which the two methyl groups are not equivalent, and (*b*) that deprotonation occur via the microscopic reverse of protonation or, in other words, from the same or equivalent conformation. With these requirements it can be seen that immediate deprotonation of the initially formed cation can only return the system back to amide with the *N*-methyl groups in their original configuration. For isomerization to occur there must be rotation about the C—N bond, to a conformation of equivalent energy, followed then by deprotonation. Making a stationary state assumption in the two conformations of the *N*-protonated amide, the second-order rate constant for isomerization is given by eq. [1].

$$[1] \quad k_{H^+}{}^{iso} = k_1'k_r/(k_{-1}' + 2k_r)$$

This equation predicts that $k_{H^+}{}^{iso} = k_1'/2$ only when $k_r \gg k_{-1}'$, *but* if the rotation step and the deprotonation step proceed at similar rates, or if rotation is slower, this is not true and $k_{H^+}{}^{iso}$ is less than $k_1'/2$. In fact, the slower the rotation occurs relative to deprotonation the smaller will be the value of $k_{H^+}{}^{iso}$ relative to $k_1'/2$, and, in the limit where $k_{-1}' \gg k_r$ the isomerization can be viewed as involving a pre-equilibrium protonation step, followed by a rate-determining rotation. The *ortho* effect is therefore explained simply in terms of an increasing value of the ratio k_{-1}'/k_r as *ortho* groups are added, attributable to steric hindrance to rotation and decreasing values of k_r.

The various rate constants in eq. [1] cannot be factored out in quantitative terms. We regard the key conclusion to be simply that for the decrease in k_r to have an effect in the first place, the rotation and deprotonation steps *must* occur at comparable rates, even in the compound with no ring substituents. Otherwise, the rate of rotation, regardless what it is, has no influence on the isomerization rate constant, which is simply equal to $k_1'/2$ for all the compounds. In such a case the large rate decreases caused by *ortho* substitution must be explained in terms of a steric effect on k_1', and it seems to us that these rate decreases are too large for such an explanation to be satisfactory.

We should point out that it has not been claimed here that the rotation process is slow, in the sense that it has a high activation barrier. The barrier in fact need not be any greater than that normally found for single bond rotations. The crux of the argument, as we will discuss later, is that the deprotonation reaction is rapid, and that the rotation is only slow compared to this process.

Exchange of N-*Methyl Amides*

Several possibilities exist to explain the smaller effect observed in the rate constants for exchange, and these of course depend on the mechanism assumed for this reaction. In terms of a mechanism involving the *N*-protonated amide, the possibility again arises that rotation is required, if, for example, the incoming proton takes up a position in which it

is not equivalent to the N–H proton already present. This is illustrated below for the *Z* form of the amide, the configuration which is most stable (9).

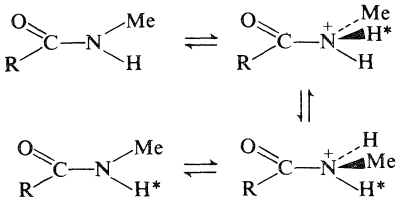

This situation corresponds exactly to that for the isomerization reaction, and the arguments for the slower rate of exchange for the *ortho* substituted benzamides are the same as those just discussed. The major drawback of this interpretation is its prediction of similar effects of *ortho* substituents on both the exchange and isomerization processes, and this clearly is not seen.

Unlike the isomerization process, an exchange mechanism can be written which involves the *N*-protonated amide but does not require carbon–nitrogen bond rotation in this species. As outlined in the equation below, this situation arises when the incoming proton goes into a position in which it is equivalent to the proton already present.

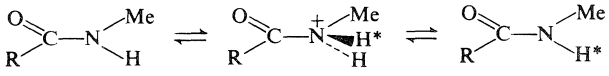

This is the viewpoint expressed by Perrin (6). In this case N–H exchange occurs on every two acts of protonation, so that the rate of exchange is given by eq. [2].

$$[2] \quad k_{H^+}{}^{ex} = k_1/2$$

In terms of such a mechanism the steric effect must be explained only on the rate of *N*-protonation, and it can in fact be argued that a small effect might exist, perhaps of the order of magnitude actually observed. The reasoning is based on the fact that the introduction of *ortho* methyl substituents in an acid–base system generally results in an increase in equilibrium acidity or conversely a decrease in equilibrium basicity. For example, the pK_a values of benzoic acid, *o*-toluic acid, and mesitoic acid are 4.2, 3.9, and 3.4 respectively (10). Another example involves the imidates below whose protonation resembles amide *N*-protonation. Again the 2,4,6-trimethyl compound is more acidic, this time by 1.1 pK_a unit (11).

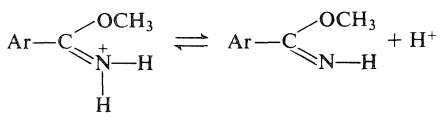

Ar ≡ C_6H_5 or 2,4,6-$(Me)_3C_6H_2$

If such an effect is also in operation for amide *N*-protonation, it should be seen mainly in the protonation rate constant. The *N*-protonation of an amide by the hydronium ion is a proton transfer in the thermodynamically disfavored direction, meaning that the reverse reaction, the deprotonation, will occur at the diffusion limit (12) (see later). Any change in the equilibrium basicity is therefore due to a change in the protonation rate constant k_1. In particular a decrease in basicity caused by the introduction of *ortho* groups would lead to a decrease in k_1. This would appear as a rate retardation for the exchange reaction proceeding by the mechanism of eq. [3].

For the imidic acid mechanism an argument for a small steric rate retardation could be made along similar lines, in terms of a steric effect on the equilibrium basicity of the amide oxygen. This reaction also involves a deprotonation step involving the N–H proton of the *O*-protonated amide, and the effect of steric congestion on the rate of this step must also be considered. All things considered, however, the small rate decreases in the rate constants are compatible with either mechanism for exchange, or even a combination of both.

Question of the Imidic Acid Mechanism

What we like to suggest is that although neither our results nor probably those of Perrin can be taken to rule out the imidic acid mechanism, they do furnish an alternative explanation for the observation which led to the suggestion of that mechanism in the first place — namely, the fact that the rate of N–H exchange in an *N*-methyl amide is generally greater than the rate of isomerization in the corresponding *N*,*N*-dimethyl amide. The imidic acid mechanism accounts for this by providing a second route for the exchange reaction, a route not available to the isomerization process which must proceed through the *N*-protonated amide. An essential part of this argument, however, is that the rate of isomerization is equal to half the rate of *N*-protonation (2, 3). Our results show that this is not necessarily true, the rate of isomerization could be significantly less than half the rate of protonation. The imidic acid argument supposes that it is the exchange reaction which is anomalously fast. We propose that an equally acceptable explanation is that the isomerization reaction is anomalously slow.

Quantitatively we can adapt the following simplified viewpoint by assuming that the rate constants of exchange and isomerization are in fact given by eqs. [2] and [1], so that their ratio becomes

$$\frac{k_{H^+}{}^{ex}}{k_{H^+}{}^{iso}} = \frac{k_1}{k_1'}\left(1 + \frac{k_{-1}'}{2k_r}\right)$$

This equation contains the ratio k_1/k_1', representing

TABLE 2. Relative rate constants for deprotonation and isomerization of *N*,*N*-dimethylbenzamides

	k_{-1}/k_r for		
Ring substituents	$k_1 = k_1'/3$	$k_1 = k_1'$	$k_1 = 3k_1'$
Unsubstituted	24	6.8	2
2-Methyl	100	32	9
2,4,6-Trimethyl	> 720	> 240	> 80

the relative rates of *N*-protonation of an *N*-methylbenzamide and an *N*,*N*-dimethylbenzamide. The protonation of an *N*-methyl aniline and the corresponding *N*,*N*-dimethylaniline can be taken as a model, since this also involves protonation on a nitrogen atom which is strongly conjugated with an adjacent π system. For the parent anilines the order of basicity is unsubstituted < *N*-methyl < *N*,*N*-dimethyl (1:1.7:3.5) (13). There are few other cases in which the basicity of the *N*-methyl compound is known, but it probably lies between the unsubstituted and *N*,*N*-dimethyl derivatives as above. The relative order of these latter two is observed to vary somewhat irregularly, but the difference is never greater than a factor of about three. We have therefore chosen this factor as a limit, and used three values of k_1/k_1' (3, 1, and 1/3) to calculate values of the ratio k_{-1}'/k_r (Table 2). This operation shows that for *N*-protonated *N*,*N*-dimethylbenzamide the rate of C—N rotation is of the same order of magnitude as the rate of deprotonation, *and* cannot be ignored. Thus the rate of isomerization is slower than half the rate of *N*-protonation, although in this case the difference between the two is not that great. However, with the close balance in the rates of rotation and deprotonation in the unsubstituted compound, addition of substituents which retard the rotation has a significant effect. A decrease in k_r by a factor of 4–5 on addition of one *ortho* methyl group followed by a further decrease in k_r by a factor of ten (or greater) for the second *ortho* methyl group is sufficient to explain the decreased $k_{H^+}{}^{ex}/k_{H^+}{}^{iso}$ ratios.

Nitrogen Basicity of Amides

The pK_a value of an *N*-protonated amide can be estimated by assuming that the rate constant in the protonation direction (k_1) is equal to twice the rate of isomerization ($2k_{H^+}{}^{iso}$) and that the rate constant in the deprotonation direction (k_{-1}) is of the order of 10^{10} s^{-1}, that is, that deprotonation is diffusion limited (2, 3, 14). Our results suggest that the first assumption is not completely valid. It is likely however that, with the exception of sterically hindered amides, $k_{H^+}{}^{iso}$ and k_1 differ by less than one order of magnitude, and the pK_a estimates using $2k_{H^+}{}^{iso}$ are at most one log unit too negative, that is, make the nitrogen appear slightly less basic than it actually is. This furthermore does not alter the fact that the pK_a estimates (2, 3, 14) are substantially more negative (by 5–6 pK_a units) than pK_a values obtained from spectroscopic changes, an observation which suggests that the latter values do not refer to the *N*-protonated amide but rather to the *O*-protonated amide. This is, in our opinion, one of the most compelling arguments in favour of predominant *O*-protonation.

This approach could be criticized on the grounds that it has not been proven that the deprotonation reaction is diffusion limited. However, proton transfer reactions to and from nitrogen atoms are generally diffusion limited in the thermodynamically favoured direction (12), even in cases where there is strong resonance interaction between the lone pair being protonated and an adjacent π electron system (15) (as in the case of amides). As noted by Kresge (16), one piece of evidence favouring a deprotonation rate constant near the diffusion limit in the case of amides is that an independent estimate of the nitrogen pK_a value based on a thermodynamic analysis (17) agrees within an order of magnitude with the estimates using the coalescence rate constants and the value of 10^{10} s^{-1} for the deprotonation. Our results provide a second piece of evidence since they suggest that the deprotonation reaction occurs at a rate comparable to (or faster than) that of rotation about a single bond. The latter process is undoubtedly very fast. For example, the rate constant of 10^{10} s^{-1} corresponds to an activation barrier of 4 cal/mol; the sort of barrier normally associated with single bond rotation (18). In order for the estimated pK_a for *N*-protonation to be consistent with the observed spectroscopic pK_a would require a rate constant for deprotonation of the order of 10^4–10^5 s^{-1}. Taking this as an upper limit for the rotational rate constant yields a lower limit for the barrier of rotation of 10–12 kcal/mol, a highly improbable value for single bond rotation. In other words, the assumptions of a diffusion limited deprotonation and a C—N single bond rotation occurring at a similar rate are fully consistent with each other.

In summary, methyl isomerization in *N*,*N*-dimethylbenzamides is slowed more by *ortho* methyl substitution than is the proton exchange rate in *N*-methylbenzamides. Therefore, the observed smaller rate for methyl isomerization than for proton exchange can be explained by assuming that deprotonation of the *N*-protonated amide occurs at a rate comparable to or faster than rotation about the C—N single bond, in agreement with an earlier suggestion of Perrin (4). While the alternative imidic acid route for proton exchange cannot be ruled out, it is clearly unnecessary to postulate this second mechanism to account for the results. In addition,

analysis of the observed rate constants provides further support for the view that amides predominantly *O*-protonate.

NOTE ADDED IN PROOF: Perrin and Johnston (21) have recently presented further arguments for an exchange reaction occurring via an *N*-protonation mechanism.

Acknowledgement

Financial support of the Natural Sciences and Engineering Research Council of Canada is gratefully acknowledged.

1. A. BERGER, A. LOWENSTEIN, and S. MEIBOOM. J. Am. Chem. Soc. **81**, 62 (1959).
2. R. B. MARTIN. J. Chem. Soc. Chem. Commun. 793 (1972).
3. R. B. MARTIN and W. C. HUTTON. J. Am. Chem. Soc. **95**, 4752 (1973).
4. C. L. PERRIN. J. Am. Chem. Soc. **96**, 5628 (1974).
5. R. C. NEUMANN, JR. and G. S. HAMMOND. J. Phys. Chem. **67**, 1659 (1963).
6. C. L. PERRIN. J. Am. Chem. Soc. **96**, 5631 (1974).
7. J. A. POPLE, W. G. SCHEIDER, and H. J. BERNSTEIN. High resolution nuclear magnetic resonance. McGraw-Hill. 1959. Chapt. 10.
8. B. G. COX. J. Chem. Soc. B, 1780 (1970).
9. L. A. LAPLANCHE and M. T. ROGERS. J. Am. Chem. Soc. **86**, 337 (1964).
10. G. KORTUM, W. VOGEL, and K. ANDRUSSOW. Pure. Appl. Chem. **1**, 189 (1960).
11. R. A. MCCLELLAND and N. SHERWIN. Unpublished results.
12. M. EIGEN. Angew. Chem. Int. Ed. Engl. **3**, 1 (1964); J. E. CROOKS. *In* Comprehensive kinetics. Vol. 8. *Edited by* C. H. Bamford and C. F. H. Tipper. Elsevier, New York. 1977. p. 197.
13. D. D. PERRIN. Dissociation constants of organic bases in aqueous solution. Butterworths, London. 1965.
14. R. A. MCCLELLAND and W. F. REYNOLDS. J. Chem. Soc. Chem. Commun. 824 (1974).
15. A. J. KRESGE and G. L. CAPON. J. Am. Chem. Soc. **97**, 1795 (1975).
16. A. J. KRESGE. Acc. Chem. Res. **8**, 354 (1975).
17. A. R. FERSHT. J. Am. Chem. Soc. **93**, 3504 (1971).
18. J. P. LOWE. Prog. Phys. Org. Chem. **6**, 1 (1968).
19. B. G. COX and P. DE MARIA. J. Chem. Soc. Perkin II, 942 (1976).
20. M. T. ROGERS and J. C. WOODBREY. J. Phys. Chem. **66**, 540 (1962).
21. C. L. PERRIN and E. R. JOHNSTON. J. Am. Chem. Soc. **101**, 4753 (1979).

Structural elucidation of the capsular polysaccharide antigen of *Neisseria meningitidis* serogroup Z using ^{13}C nuclear magnetic resonance[1]

HAROLD J. JENNINGS, KARL-GUNNAR ROSELL, AND C. PAUL KENNY

Division of Biological Sciences, National Research Council of Canada, Ottawa, Ont., Canada K1A 0R6 and the Bureau of Biologics, Drugs Directorate, Health and Welfare Canada, Ottawa, Ont., Canada K1A 0L2

Received May 4, 1979

HAROLD J. JENNINGS, KARL-GUNNAR ROSELL, and C. PAUL KENNY. Can. J. Chem. **57**, 2902 (1979).

The capsular polysaccharide antigen from *Neisseria meningitidis* serogroup Z contains equimolar quantities of 2-acetamido-2-deoxy-D-galactose, glycerol, and phosphate. Carbon-13 nuclear magnetic resonance indicates that the polysaccharide is composed by a repeating unit of 1′-*O*-2-acetamido-2-deoxy-α-D-galactopyranosyl-glycerol joined through phosphate diester groups at O-3′ of glycerol and O-3 of the galactosamine residue. Assignments of the signals in the carbon-13 nuclear magnetic resonance spectrum were made by consideration of the previously assigned signals of related monomers and oligomers. When applied to a Karplus type relationship the values of the $^3J(^{13}C–^{31}P)$ coupling constants were consistent with the polysaccharide having an extended conformation.

HAROLD J. JENNINGS, KARL-GUNNAR ROSELL et C. PAUL KENNY. Can. J. Chem. **57**, 2902 (1979).

L'antigène polysaccharide capsulaire du séro-groupe Z de la *Neisseria meningitidis* contient des quantités équimolaires d'acétamido-2 déoxy-2 D-galactose, de glycérol et de phosphate. La résonance magnétique nucléaire du ^{13}C indique que ce polysaccharide est composé d'un motif *O*-1′-acétamido-2 déoxy-2 α-D-galactopyranosyl-glycérol réuni par un groupe diester phosphorique à l'oxygène en position 3′ du glycérol et à l'oxygène en position 3 du résidu galactosamine. On a interprété les signaux des spectres de résonance magnétique nucléaire du ^{13}C en tenant compte des identifications faites antérieurement dans le cas des monomères et des oligomères apparentés. Les valeurs des constantes de couplage, $^3J(^{13}C–^{31}P)$ appliquées à une relation de type Karplus, sont en accord avec celles des polysaccharides ayant une conformation allongée.

[Traduit par le journal]

Introduction

Slaterus first reported the isolation of the new serogroup Z of *Neisseria meningitidis* (1). We now report the structure of the group Z capsular polysaccharide which completes the structural studies on the capsular polysaccharide antigens mainly responsible for the serological group classification of the meningococci (2, 3). Although all the meningococcal polysaccharides are linear, acidic, and contain acetamido groups, they can be divided into two categories based on their acidic components, those containing phosphate diester bonds (4), and those containing 2-keto-3-deoxy acid residues (3, 5, 6). The serogroup Z falls into the former category having a repeating unit of 1′-*O*-2-acetamido-2-deoxy-α-D-galactopyranosyl-glycerol 3′-phosphate, the phosphate linkage to the galactosamine residue being at O-3. Thus it differs from the similarly categorized group A and X polysaccharides (4) in that its phosphate diester moiety is not glycosidically linked to the amino sugar residue. As far as we are aware this is the first reported case of a capsular polysaccharide containing the glycerol phosphate moiety previously associated with some teichoic acid structures (7, 8), although the ribitol phosphate moiety characteristic of other types of teichoic acid (7, 9) has been reported as a structural component of other capsular polysaccharides (10, 11, 12). Like the other meningococcal polysaccharides containing phosphate diester linkages the group Z polysaccharide has an extended conformation as determined from the $^{13}C–^{31}P$ coupling constants measured from its ^{13}C nuclear magnetic resonance spectrum.

Experimental

Materials

The cells of *N. meningitidis* serogroup Z (strain 565) were obtained from the culture collection of the Laboratory Center for Disease Control, Ottawa, and were grown as previously described (13). The capsular polysaccharide was isolated and purified as previously described using an initial Cetavlon precipitation to obtain the crude polysaccharide (13). D-Galactosamine HCl was obtained from Pfansteil Laboratories Inc., Waukegan, IL.

Analytical Methods

Amino sugars were detected using a Technicon auto analyser

[1]NRCC No. 17741

0008-4042/79/222902-06$01.00/0

and their quantitation was carried out by the modified Elson-Morgan method (14), in which the hydrolysate was first incubated with alkaline phosphatase (Worthington Biochemical Corp., Freehold, NJ) in ammonium bicarbonate at pH 8.5. Acid hydrolyses of the polysaccharide were carried out using 4 *M* HCl at 100°C and the amino sugar determinations were carried out at intervals between 4 h and 24 h. The total 2-amino-2-deoxygalactose content was determined by extrapolation to zero time. Phosphorous was determined by the method of Chen *et al.* (15).

Optical rotations were recorded at 23 ± 1°C on a Perkin Elmer 141 polarimeter and all solutions were concentrated below 50°C under diminished pressure.

Periodate oxidations were performed on the Z polysaccharide (10 mg) using a 0.02 *M* sodium metaperiodate solution (10 mL) and the periodate uptake was determined spectrophotometrically (16).

Nuclear Magnetic Resonance Spectroscopy

^{13}C nmr spectra were recorded at 37°C on a Varian XL-100-15 spectrometer operating at 25.16 MHz and a Varian CFT20 spectrometer operating at 20 MHz, both in the pulsed Fourier transform mode with complete proton decoupling. Chemical shifts are reported in parts per million (ppm) downfield from external tetramethylsilane and the ^2H resonance of deuterium oxide was used as the field-frequency lock signal. All the monomers and polysaccharides were run as deuterium oxide solutions at concentrations of 50–100 mg per mL.

^1H nmr spectra were measured at 37°C on a Varian CFT20 spectrometer operating in the pulsed Fourier transform mode. Samples were lyophylised (× 2) from 99.7% D_2O and run in the same solvent. The apparent first-order coupling constants (Hz) were measured directly and the chemical shifts (δ) are expressed relative to internal sodium 3-trimethylsilylpropionate-2,2,3,3-d_4.

Paper Chromatographic Analysis

Whatman No. 1 paper was used for descending paper chromatography using the following solvent systems (A) propan-1-ol – ammonia (specific gravity 0.88) – water (6:3:1), (B) butan-1-ol – ethanol – water (4:1:5), and (C) propan-2-ol – acetic acid – water (54:8:18). Compounds were detected with alkaline silver nitrate (17) and molybdate for sugar phosphates (18).

Hydrolysis of the Z Polysaccharide

Acid hydrolysis of the polysaccharide was carried out at concentrations of 5 mg per mL using 0.1 *N* HCl at 100°C for 2 h. Excess HCl was removed by repeated evaporation with water under vacuum to yield a residue. This residue when applied to a paper chromatogram in solvent (A) gave two major elongated molybdate positive spots indicating the presence of two different phosphorylated components. Dephosphorylation of the residue using alkaline phosphatase with subsequent removal of the NH_4HCO_3 by repeated co-distillations from water yielded only one non-reducing oligosaccharide component as indicated by paper chromatographic analysis.

Gel Filtration

Gel filtration was performed on a Sephadex G-200 column (2.4 cm × 70 cm) with a 0.1 *M* phosphate buffer (pH 7.0). The column was calibrated with blue dextran (MW 2 000 000) and the phosphate content of the eluates was monitored by the method of Chen *et al.* (15).

Gas–Liquid Chromatography

Gas–liquid chromatography (gc) was performed on a Hewlett-Packard 5830 A instrument equipped with a flame ionization detector and a model 18850A electronic integrator. The glass columns (180 cm × 0.15 cm) used contained the following liquid phases on 100–120 mesh Gas Chrom Q (*i*) 3% ECNSS-M at 170°C, (*ii*) 3% OV-1 at 200°C, and (*iii*) 3% OV-17 at 200°C. Combined gas chromatography – mass spectrometry (gc–ms) was carried out on a Finnigan 3100D instrument using the above columns.

Analysis of the Oligosaccharide

Glycose analyses were carried out by the method of Dmitriev *et al.* (19). The oligosaccharide (2 mg) was hydrolysed with 0.5 *M* sulfuric acid (3 mL) at 100°C for 16 h. The solution was neutralized with barium carbonate, filtered, and lyophylised. The residue was treated with water (0.6 mL), 33% aqueous acetic acid (1.0 mL), and 5% sodium nitrite (1.0 mL) at room temperature for 1 h. The solution was then passed through Dowex 50 (H^+) ion-exchange resin and lyophylised, redissolved in water, and treated with sodium borohydride for 2 h at room temperature. Following deionization with Dowex 50 (H^+) ion-exchange resin the solution was evaporated to dryness and methanol was distilled repeatedly from the residue. The final residue was acetylated with pyridine – acetic anhydride (1:1) at 100°C for 15 min and the resulting acetates were analysed by gc–ms using column (*i*) (20).

Methylation of the Oligosaccharide

The oligosaccharide was methylated with methyl iodide in the presence of methyl sulfinyl anion according to the method of Hakomori (21). The methylated product was recovered by partitioning between water and chloroform. The chloroform phase was dried (anhydrous magnesium sulfate), concentrated to small volume, and analysed by gc–ms using column (*ii*).

The permethylated oligosaccharide was treated with 90% formic acid (2 mL) at 100°C for 2 h and then concentrated to dryness. This residue was further hydrolysed with 0.25 *M* H_2SO_4 at 100°C for 16 h, neutralised with barium carbonate, and filtered. The filtrate was treated with sodium borohydride at room temperature for 2 h and excess sodium borohydride was destroyed by the addition of acetic acid. Following evaporation to dryness and several co-distillations of methanol from the residue, the residue was acetylated in pyridine – acetic anhydride (1:1) for 1 h at 100°C. After removal of the reagents by evaporation the residue was dissolved in water and the partially methylated acetate derivatives were extracted into chloroform. The chloroform solution was dried (anhydrous magnesium sulfate), concentrated to small volume, and analysed by gc–ms using column (*iii*) (22).

Results and Discussion

Isolation and Characterisation of 1′-O-2-acetamido-2-deoxy-α-D-galactopyranosylglycerol

Mild acid hydrolysis of the group Z polysaccharide of $[\alpha]_D$ +84° (*c* 0.5 in water), gave two chromatographically separable phosphorylated components both of which on treatment with alkaline phosphatase yielded the same chromatographically pure disaccharide with an optical rotation of $[\alpha]_D$ +59° (*c* 0.7 in water). Hydrolysis of the disaccharide using stronger conditions with subsequent deamination yielded 2,5-anhydro-D-talose, originating from the D-galactosamine residues in the original polysaccharide, and glycerol as determined by gc–ms anal-

ysis; the D-configuration was assigned to the galactosamine residue by virtue of the positive rotation of the original disaccharide. Methylation of the disaccharide and subsequent gc–ms analysis of the permethylated product indicated a single component which gave a fragmentation pattern in its mass spectrum consistent with 1′-*O*-3,4,6-tri-*O*-methyl-2-(*N*-methylacetamido)-α-D-galactopyranosyl-2,3-di-*O*-methyl-glycerol (Fig. 1). The following fragments with their relative intensities (in parentheses) were obtained: 45 (79), 71 (59), 87 (64), 88 (100), 101 (50), 103 (21), 111 (7), 129 (32), 132 (41), 142 (18), 145 (23), 163 (23), 173 (5), 205 (18), 228 (3), and 260 (2). This structure was also confirmed by hydrolysis of the permethylated disaccharide which yielded two methylated sugars identified by gc–ms of their alditol acetate derivatives (22) as 2-deoxy-3,4,6-tri-*O*-methyl-2-(*N*-methylacetamido)-D-galactopyranose and 1,2-di-*O*-methyl-glycerol.

The ^{13}C nmr spectrum of the disaccharide is also consistent with the above structural evidence and the assignments of its individual eleven carbon signals are listed in Table 1. Except for the highly characteristic anomeric signal (C-1) at 98.6 ppm all the other carbons of the galactosamine residue can be readily assigned by comparison with previous assignments made on 2-acetamido-2-deoxy-α-D-galactopyranose (23). Thus the glycosidic linkage is in the α-D-configuration and this was confirmed by ^{1}H nmr studies on the Z polysaccharide which indicated one anomeric doublet at δ 4.95 ppm with a coupling constant of 3.5 Hz, consistent with a *gauche* disposition of the anomeric H-1 and H-2 protons (24). The remaining three signals in the spectrum are assignable to the glycerol moiety and are only consistent with a C-1′ linkage because in comparison with the previously assigned glycerol resonances (11) C-1 experiences a downfield shift of +5.9 ppm whereas the vicinal β-carbon (C-2′) experiences an upfield shift of −1.7 ppm. The magnitude and direction of these shifts are highly characteristic of the linkage being at C-1′ (25).

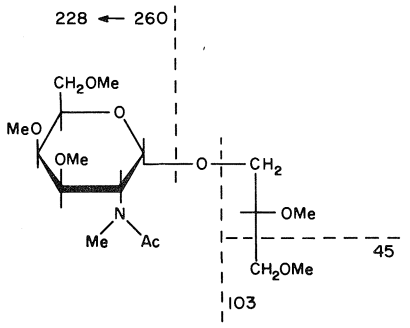

FIG. 1. Methylated oligosaccharide obtained from the group Z polysaccharide with some primary mass fragments.

Structure of the Group Z Polysaccharide

Chemical analyses indicate that the Z polysaccharide contains phosphate in a molar ratio of 1:1 with galactosamine. That glycerol was also present in the same molar ratio could be ascertained from the approximately equal intensities of comparable individual carbon resonances of both the glycerol and galactosamine residues in the ^{13}C nmr spectrum of the Z polysaccharide (Fig. 2). Therefore to complete the structural analysis of the Z polysaccharide it is only necessary to assign the position of the phosphate diester linkages joining the disaccharide repeating units. This proved to be a difficult task using conventional methods. The polysaccharide consumed 0.2 mol periodate per phosphorus atom which could be explained either by the presence of some 6-linked galactosamine in a mixed linked polysaccharide or by end-group oxidation of a 3- or 4-linked galactosamine-containing polysaccharide. The latter explanation is certainly consistent with the finding of large quantities of low molecular weight material in the polysaccharide preparation. However periodate oxidation of the polysaccharide does not discriminate between either the 3- or 4-linkage. Although a modified periodate technique has been devised to accomplish this based on the prior release of the reducing sugar phosphate residues by mild acid hydrolysis (9), it is not applicable to the Z polysaccharide because of the extreme acid-stability of its glycosidic bonds. Therefore the evidence for the presence of 3-linked galactosamine residues in the Z polysaccharide can only be obtained from its ^{13}C nmr spectrum.

The eleven resonance ^{13}C nmr spectrum of the native Z polysaccharide shown in Fig. 2 is only consistent with the polysaccharide having a repeating unit of 1′-*O*-2-acetamido-2-deoxy-α-D-galactopyranosyl-glycerol 3′-phosphate, the phosphate diester linked at C-3 of the galactosamine residue. The ^{13}C chemical shifts for the polysaccharide are listed in Table 1 together with ^{13}C–^{31}P coupling constants. Previous ^{13}C resonance assignments for the disaccharide aided the identification of signals due to carbons in the repeating unit of the polysaccharide. Thus C-1, C-2, C-5, C-6, and the two acetamido carbons were readily assigned. Characteristic shielding of C-2 (−1.1 ppm) by an adjacent phosphate group (25), combined with the observation that the resonance for C-2 is a doublet due to three-bond ^{13}C–^{31}P coupling, places one end of the phosphate linkage on C-3. Geminal coupling to ^{31}P (4.5 Hz) combined with typical deshielding (+5.0 ppm), as in the case of other sugar carbons bearing a phosphate substituent (4, 25), identified the signal for C-3. Previous ^{13}C resonance assignments made on the model compound 1′-*O*-α-D-glucopyranosyl-glycerol 3′-phos-

phate (11) were used to identify the signals for the corresponding carbons in the glycerol residue of the polysaccharide. Thus the signal at 67.4 ppm which was split into a doublet by two bond ^{13}C–^{31}P coupling (3.8 Hz) was assigned to C-3′, the carbon at the other end of the phosphate linkage. The signal at 70.2 ppm was assigned to C-2′ because the corresponding carbon in the model compound had only a slightly different chemical shift, and both of these carbons were similarly three-bond ^{13}C–^{31}P coupled. Conformational considerations discussed below also support this assignment. The remaining signals at 68.9 and 69.4 ppm could not be individually assigned to C-1′ and C-4 on chemical shift grounds alone. Tentative assignment of the signal at 69.4 ppm to C-4 was based on the premise that slight coupling of this carbon to ^{31}P would broaden the resonance and thus reduce its peak height relative to the uncoupled carbon signals. This reduction in peak height of the C-4 signal is not as large as that reported for other unresolved ^{13}C–^{31}P coupled signals (approximately 50%) (25) and indicates that extreme care must be exercised in the indentification of ^{13}C–^{31}P coupled signals on the basis of intensity alone.

The dihedral angle-dependency of ^{13}C–^{31}P coupling constants has been demonstrated in a series of glycose phosphates (4, 26, 27). However only recently using a series of rigid cyclic phosphite ester derivatives has a Karplus-type of relationship between the above two properties been established (28). The maximum and minimum values of the coupling constants used in construction of the curve were 12.2 Hz and 1.8 Hz respectively, although by interpolation of the curve at its base, the probability of even smaller coupling constants (approximately 0.5 Hz) can be envisaged. These would occur when the dihedral angle was in the vicinity of 90° and this situation could readily occur in the phosphate linkage to C-3 of the galactosamine residue of the Z polysaccharide. For rotamers about O—C_3 (Fig. 3) there are two possible positions (P_I and P_{II}) where the dihedral angle between the P—O and C4—C3 bond is approximately 90°. Of these two positions P_I is preferred because an examination of models (Dreiding) indicates the presence of highly unfavourable steric interactions in position P_{II}. This preferred position (P_I) could also be confirmed using the alternate $^3J_{C2,P}$ coupling constant (5.3 Hz) in the Karplus curve which yielded values of approximately 45° and 130°. This latter value is consistent with the theoretical dihedral angle (150°) between the P—O and C3—C2 bonds. Despite the linear non-rigid structure of the Z polysaccharide the extremely small $^3J_{C4,P}$ coupling constant would indicate a fairly restricted disposition of the phosphorus atom (P_I) because any significant contribution of other rotamers

TABLE 1. Carbon-13 chemical shifts of the group Z polysaccharide and relevant monomers[a]

	GalNAc moiety								Glycerol moiety		
	C-1	C-2	C-3	C-4	C-5	C-6	CH_3 ($NHCOCH_3$)	C=O ($NHCOCH_3$)	C-1′	C-2′	C-3′
N. meningitidis group Z	98.5	49.9(5.3)[c]	73.9(4.5)[b]	69.4[e](—)[c,d]	72.0	62.3	23.3	175.6	68.9[e]	70.2(7.8)[c]	67.4(3.8)[b]
α-D-GalNAc(1→1′)-glycerol	98.6	51.0	68.9	69.7	72.2[e]	62.4	23.1	176.0	69.7	71.6[e]	63.6
α-D-GalNAc	92.2	51.4	68.6	69.7	71.6	62.4	23.2	176.1			
Glycerol[f]									63.8	73.3	63.8
α-D-Glue(1→1′)-glycerol 3′-phosphate									70.9	69.5(7.9)[c]	67.5(5.1)[b]

[a]In ppm from external tetramethylsilane.
[b]$^2J(^{31}P–^{13}C)$.
[c]$^3J(^{31}P–^{13}C)$.
[d]Not resolved.
[e]Tentative assignments.
[f]Taken from De Boer *et al.* in ref. 11.

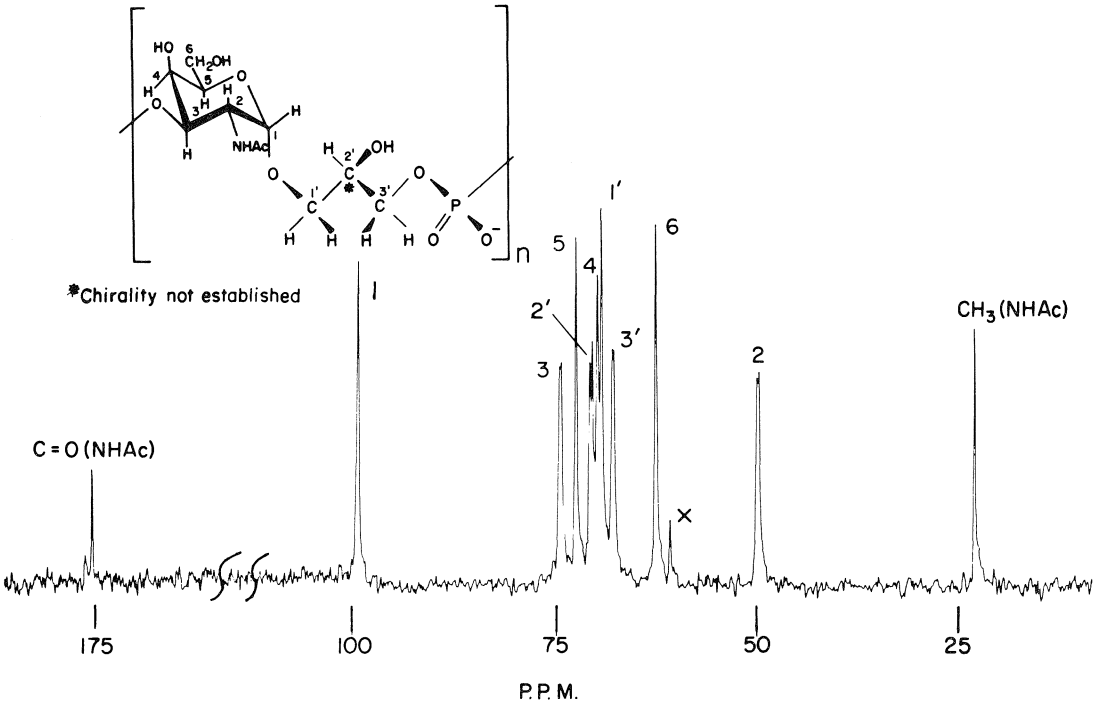

FIG. 2. Fourier-transformed ^{13}C nmr spectrum of the native group Z polysaccharide antigen taken with an acquisition time of 0.4 s, and spectral width 5 kHz. The number of free induction decays was 127 000. Inset: the repeating unit of the group Z polysaccharide.

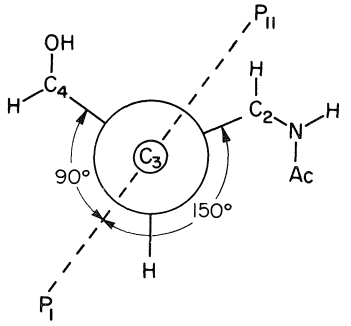

FIG. 3. Classical orientations of the oxygen–phosphorus bond in the group Z polysaccharide looking along the O—C3 bond of the 2-acetamido-2-deoxygalactopyranose residue.

would have resulted in a larger value. Models (Dreiding) also show that this restricted disposition (P_I) could be due to the adverse steric interactions of the phosphate ester group with the proton on C-3, the hydroxyl group on C-4, and the acetamido group on C-2. The $^3J_{C2',P}$ coupling on the glycerol moiety (7.8 Hz) yielded values of approximately 40° and 160° when applied to the Karplus curve. The latter value is compatible with a *trans* disposition of the P—O and C3′—C2′ bonds (Fig. 2) which again could be predicted on steric grounds. Thus the calculated dihedral angles of the phosphorus atom to both the galactosamine and glycerol residues of the Z polysaccharide indicate that it has an extended conformation similar to that found for other linear and highly phosphorylated polysaccharides (4).

Structural features normally associated with teichoic acids have been previously discovered in several bacterial polysaccharide antigens, the most ubiquitous being the ribitol phosphate moiety of the polysaccharide antigens of *H. influenzae* types *a* (12) and *b* (10) and some types of *S. pneumoniae* (29). The Z polysaccharide differs from the above capsular antigens in that it contains glycerol phosphate like some teichoic acids (7). This contrasts with the teichoic acid from *S. lactis* 7944 which has the same structural components as the Z polysaccharide, but has the phosphate group linked exclusively to the glycerol residues (8). It is interesting to note that it should be possible to differentiate between these two structures very easily using ^{13}C nmr. This is because the spectrum of the teichoic acid should manifest only three ^{13}C—^{31}P coupled signals none of which would be associated with the galactosamine residue. This particular case is well illustrated in the ^{13}C nmr spectrum of a related glucose-containing teichoic acid from *B. subtilis* Var. niger (11). Also any alternate structural variation involving glycosidic phosphate linkages as in the teichoic acid from *S. lactis*

I3 (9) would also have been easily recognisable using ^{13}C nmr. This type of structure would give a distinctive ^{13}C nmr spectrum having $^{13}C—^{31}P$ couplings on its highly characteristic and therefore readily assignable anomeric C-1 and C-2 signals.

Acknowledgements

We wish to thank Adèle Martin for valuable technical assistance, Fred Cooper for obtaining the mass spectra, and Dr. I. C. P. Smith for valuable discussions and for the 100 MHz nmr spectra.

1. K. W. Slaterus and Antonie Van Leeuwenhoek. J. Microbiol. Serol. **27**, 304 (1961).
2. H. J. Jennings, A. K. Bhattacharjee, D. R. Bundle, C. P. Kenny, A. Martin, and I. C. P. Smith. J. Infect. Dis. (Suppl.), **136**, S278 (1977).
3. A. K. Bhattacharjee, H. J. Jennings, and C. P. Kenny. Biochemistry, **17**, 645 (1978).
4. D. R. Bundle, I. C. P. Smith, and H. J. Jennings. J. Biol. Chem. **249**, 2275 (1974).
5. A. K. Bhattacharjee, H. J. Jennings, C. P. Kenny, A. Martin, and I. C. P. Smith. J. Biol. Chem. **250**, 1926 (1975).
6. A. K. Bhattacharjee, H. J. Jennings, C. P. Kenny, A. Martin, and I. C. P. Smith. Can. J. Biochem. **54**, 1 (1976).
7. A. R. Archibald and J. Baddiley. Adv. Carbohydr. Chem. **21**, 323 (1966).
8. D. C. Ellwood, M. V. Kelemen, and J. Baddiley. Biochem. J. **86**, 213 (1963).
9. A. R. Archibald, J. Baddiley, J. E. Heckels, and S. Hepinstall. Biochem. J. **125**, 353 (1971).
10. R. M. Crisel, R. S. Baker, and D. E. Dorman. J. Biol. Chem. **250**, 4926 (1975).
11. W. R. De Boer, F. J. Kruyssen, J. T. M. Wouters, and C. Kruk. Eur. J. Biochem. **62**, 1 (1976).
12. P. Branefors-Helander, C. Erbing, L. Kenne, and B. Lindberg. Carbohydr. Res. **56**, 117 (1977).
13. D. R. Bundle, H. J. Jennings, and C. P. Kenny. J. Biol. Chem. **249**, 4797 (1974).
14. J. L. Reissig, J. L. Strominger, and L. F. Leloir. J. Biol. Chem. **217**, 959 (1955).
15. P. S. Chen, J. U. Toriba, and H. Warner. Anal. Chem. **28**, 1756 (1956).
16. G. O. Aspinall and R. J. Ferrier. Chem. Ind. (London), 1216 (1957).
17. W. E. Trevelyan, D. P. Procter, and J. S. Harrison. Nature (London), **166**, 444 (1950).
18. C. S. Haines and F. A. Isherwood. Nature (London), **164**, 1107 (1949).
19. B. A. Dimitriev, L. V. Backinowsky, V. L. Lvov, N. K. Kotchetkov, and I. L. Hoffman. Eur. J. Biochem. **50**, 539 (1975).
20. J. S. Sawardeker, J. H. Sloneker, and A. R. Jeanes. Anal. Chem. **37**, 1602 (1965).
21. S. Hakomori. J. Biochem. (Tokyo), 205 (1964).
22. B. Lindberg. Methods Enzymol. **28B**, 178 (1972).
23. D. R. Bundle, H. J. Jennings, and I. C. P. Smith. Can. J. Chem. **51**, 3812 (1973).
24. R. U. Lemieux, R. K. Kullnig, H. J. Bernstein, and W. G. Schneider. J. Am. Chem. Soc. **80**, 6098 (1958).
25. H. J. Jennings and I. C. P. Smith. Methods Enzymol. **50**, 39 (1978).
26. R. D. Lapper, H. H. Mantsch, and I. C. P. Smith. J. Am. Chem. Soc. **95**, 2878 (1973).
27. J. V. O'Connor, H. A. Nunez, and R. Barker. Biochemistry, **18**, 500 (1979).
28. N. K. Kotchetkov, E. F. Nifantev, M. P. Koroteev, Z. K. Zhane, and A. A. Borisenko. Carbohydr. Res. **47**, 221 (1976).
29. O. Larm and B. Lindberg. Adv. Carbohydr. Chem. **33**, 295 (1976).

Studies on the mass spectrometry of some acyclic nuclear substituted styryl ketoximes and ketones with special reference to the *ortho* effect

P. J. SMITH[1] and C. B. NYATHI

Department of Chemistry and Chemical Engineering, University of Saskatchewan, Saskatoon, Sask., Canada S7N 0W0

AND

J. R. DIMMOCK AND L. M. SMITH

College of Pharmacy, University of Saskatchewan, Saskatoon, Sask., Canada S7N 0W0

Received October 30, 1978[2]

P. J. SMITH, C. B. NYATHI, J. R. DIMMOCK, and L. M. SMITH. Can. J. Chem. **57**, 2908 (1979).

The mass spectra of several ring substituted acyclic styryl ketoximes and analogous ketones have been determined at 70 eV and also at low ionization voltages. The major fragmentation pathways for the oximes are loss of the *ortho* substituent from the parent ion as well as loss of the hydroxyl and hydroxylamine radicals. Other fragmentation pathways include γ- and δ-cleavages as well as the McLafferty rearrangement. While there was a total absence of α-cleavage from the parent ions, the facility of loss of the *ortho* substituents from the oxime molecular ions was compared with the same process occurring in the corresponding acyclic ketones, as well as the related cyclic derivatives, namely the substituted 2-benzylidinecyclohexanones and oximes. Stabilization of the resultant cyclized ion as well as steric factors are considered as factors favouring the cyclization process.

P. J. SMITH, C. B. NYATHI, J. R. DIMMOCK et L. M. SMITH. Can. J. Chem. **57**, 2908 (1979).

On a déterminé les spectres de masse de plusieurs oximes de styril cétones acycliques ayant le cycle substitué, et de cétones analogues en opérant à 70 eV et à de faibles énergies d'ionisation. Le schéma principal de fragmentation implique la perte des substituants en position *ortho* à partir de l'ion moléculaire aussi bien que la perte de radicaux hydroxyle et hydroxylamine. Le clivage en γ et en δ ainsi qu'une transposition de McLafferty ont lieu dans une autre type de fragmentation. La facilité avec laquelle l'ion moléculaire de l'oxime perd ses substituants en position *ortho*, en l'absence totale de clivage α, est comparée au même type de fragmentation que subissent les cétones acycliques et les composés cycliques apparentés comme les benzylidine-2 cyclohexanones substitués et les oximes. On considère la stabilisation de l'ion cyclisé résultant et les facteurs stériques comme étant des éléments qui favorisent la réaction de cyclisation.

[Traduit par le journal]

Introduction

Apart from the early work of Djeressi *et al.* (1), the mass spectra of aliphatic and alicyclic ketoximes have received little attention. In an earlier publication (2) we considered the mass spectra of a series of 2-benzylidenecyclohexanone oximes, while recently the mass spectra of a series of aryl heteryl ketoximes have been studied (3) with the view of investigating a gaseous phase Beckmann rearrangement.

The *ortho* effect as applied to aromatic compounds generally involves the loss of a neutral molecule from a 1,2-disubstituted aromatic derivative (reaction [1]). A less common process is

[1] 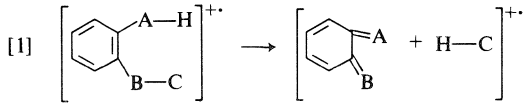

cyclization via the *ortho* effect permitting ring formation. Coutts and Malicky (4) have observed the loss of OCH_3 from *o*-methoxyphenyl-2-propanone oximes via the *ortho* effect, reaction [2].

[2] 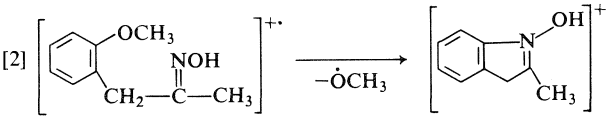

As well, we have studied the cyclization reaction for several styryl ketones (5), reaction [3], and 2-benzylidenecyclohexanones (6), reaction [4].

In order to elucidate the fragmentation directing qualities of the oxime group, the mass spectra of a series of nuclear substituted styryl ketoximes and some deuterated analogs are planned to be investigated in the present study. In addition, the structural and electronic factors involved in the intramolecular aromatic substitution reaction with loss of an *ortho* substituent to give an aromatic species will be considered for several ring substituted styryl oximes and ketones. In order to determine the relative ability of

[1]To whom all correspondence should be addressed.

[2]Revision received July 27, 1979.

0008-4042/79/222908-08$01.00/0

[3] 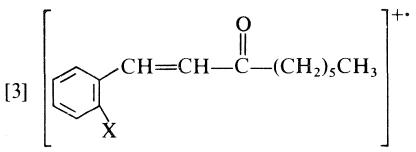

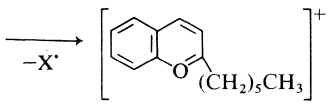

[4] 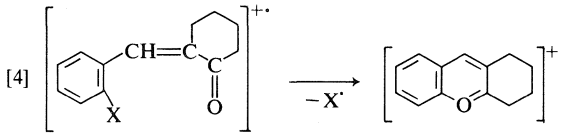

the carbonyl function and the oxime group to promote cyclization, a comparison of the M − H (*ortho*)/M and M − Cl(*ortho*)/M ratios for both the styryl ketone and oxime series and the 2-benzylidenecyclohexanone and corresponding oxime series will be made.

Results and Discussion

The following styryl oximes (**1**–**6**) were prepared and their mass spectra obtained. The mass spectral data for selected ions of these compounds are recorded in Table 1.[3]

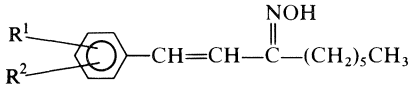

1, $R^1 = R^2 = H$
2, R^1 = 2-Cl; $R^2 = H$
3, R^1 = 4-Cl; $R^2 = H$
4, R^1 = 3-Cl; R^2 = 4-Cl
5, R^1 = 2-Cl; R^2 = 6-Cl
6, R^1 = 4-$N(CH_3)_2$; $R^2 = H$

Several styryl ketones (**7**–**11**) with different *ortho* substituents were examined in addition to the ring chlorinated ketones described earlier (5). Compound **12**, the 2,3,4,5,6-pentafluorostyryl ketone was also investigated. The mass spectral data for selected ions of compounds **7**–**12** are recorded in Table 2.[3]

Due to the paucity in the literature concerning the mass spectra of oximes, it is worthwhile to consider the spectra of oximes **1**–**6** in some detail. A striking feature of the spectra of the six oximes is the total

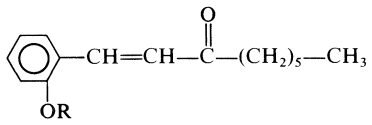

7, R = $-CH_2OCH_3$
8, R = $-CH_2-O-CH_2-CH_3$

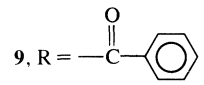

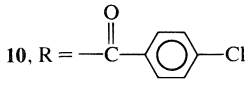

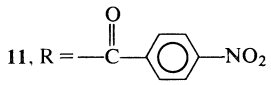

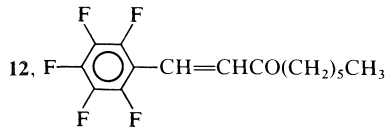

absence of ions corresponding to α-cleavage,

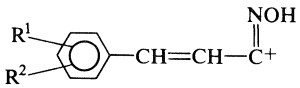

This result is in contrast to the α-cleavage process which occurs in the corresponding ketones leading to the formation of an ion,

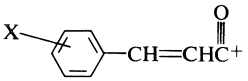

In these acyclic ketones, the α-cleavage process is a major fragmentation pathway and in the case of the unsubstituted compound (X = H), this α-cleavage ion is the base peak.

A significant peak in the mass spectra of compounds **1**–**6** corresponds to the loss of 17 mass units $(M - OH)^+$ from the molecular ion as confirmed by the appropriate metastable peak. This ion has a relative intensity of 73 and 80%, Table 2, in the spectra of the unsubstituted and 4-dimethylamino compounds (**1** and **6**), respectively. The loss of the hydroxyl radical from the molecular ion was further confirmed by high resolution mass spectrometry. When the specifically deuterated oxime,

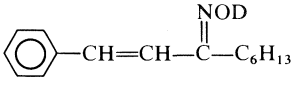

was examined, a loss of 18 mass units from the molecular ion was noted.

[3]A complete listing of the mass spectral peaks for all the compounds down to 2% intensity is available, at a nominal charge, from the Depository of Unpublished Data, CISTI, National Research Council of Canada, Ottawa, Ont., Canada K1A 0S2.

TABLE 1. Relative intensity (r.i.) and m/z values of selected ions observed in the 70 eV spectra of compounds **1** to **6***

1		**2**		**3**		**4**		**5**		**6**	
m/z	r.i.	m/z	r.i.	m/z	r.i.	m/z	r.i.	m/z	r.i.	m/z	r.i.
231(M)	50	265(M)	29	265(M)	55	299(M)	38	299(M)	26	294(M)	100
230(M − 1)	100	264(M − 1)	19	264(M − 1)	100	298(M − 1)	38	298(M − 1)	—	273(M − 1)	20
214(M − 17)	73	248(M − 17)	40	248(M − 17)	74	282(M − 17)	60	282(M − 17)	39	257(M − 17)	80
199(M − 32)	29	233(M − 32)	15	233(M − 32)	30	267(M − 32)	25	267(M − 32)	24	242(M − 32)	13
—	—	230(M − 35)	100	230(M − 35)	—	264(M − 35)	—	264(M − 35)	100	—	—
188(M − 43)	9	222(M − 43)	6	222(M − 43)	8	256(M − 43)	7	256(M − 43)	12	231(M − 43)	—
174(M − 57)	16	208(M − 57)	13	208(M − 57)	18	242(M − 57)	21	242(M − 57)	20	217(M − 57)	—
161(M − 70)	40	195(M − 70)	44	195(M − 70)	45	229(M − 70)	49	229(M − 70)	67	204(M − 70)	3
160	23	194	9	194	32	228	25	228	6	203	3
144	100	178	15	178	34	212	32	212	—	187	46
130	59	164	17	164	36	198	25	198	14	173	13
129	64	163	18	163	60	197	42	197	9	172	19
128	45	162	6	162	11	196	7	196	28	171	20
—	—	160	46	160	30	194	11	194	85	—	—
117	70	151	18	151	36	185	26	185	13	160	6
115	30	149	4	149	7	183	4	183	—	158	8

*The ions used for discussion will be those with m/z values corresponding to the presence of only the ^{35}Cl isotope.

TABLE 2. Relative intensity (r.i.) and m/z values of selected ions observed in the 70 eV spectra of compounds **7** to **12**

7		**8**		**9**		**10**		**11**		**12**	
m/z	r.i.	m/z	r.i.	m/z	r.i.	m/z	r.i.	m/z	r.i.	m/z	r.i.
276(M)	2	290(M)	2	336(M)	0.6	370(M)	0.5	381(M)	0.5	306(M)	5
215(M − OCH_2OCH_3)	3	215(M − $OCH_2OCH_2CH_3$)	6	215(M − OCC_6H_5)	2	215(M − OCC_6H_4p-Cl)	13	215(M − OCC_6H_4p-NO_2)	21	215(M − F)	0
161	10	147	20	105	100	141	35	161	11	236	75
45	100	59	100	77	41	139	100	181	20	221	100
						111	17	150	100	205	9
								145	14	204	19
								120	12	193	39
										143	14
										99	7
										55	13

The M – OH ion could be formed directly from the molecular ion, reaction [5],

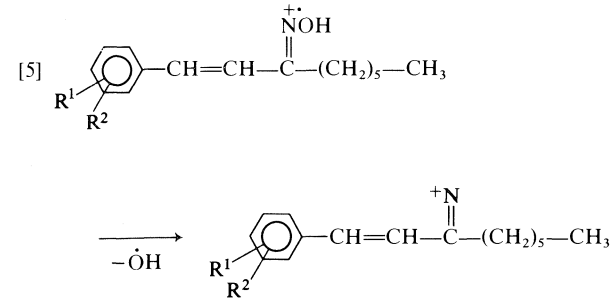

and have a nitrenium ion structure analogous to the ion proposed by loss of the hydroxyl radical from benzophenone oxime (7). Alternatively, the M – 17 ion could result from loss of hydroxyl from an intermediate structure *a* formed by a stepwise hydrogen rearrangement, reaction [6], with the formation of the conjugated cyclic ion in *b*.

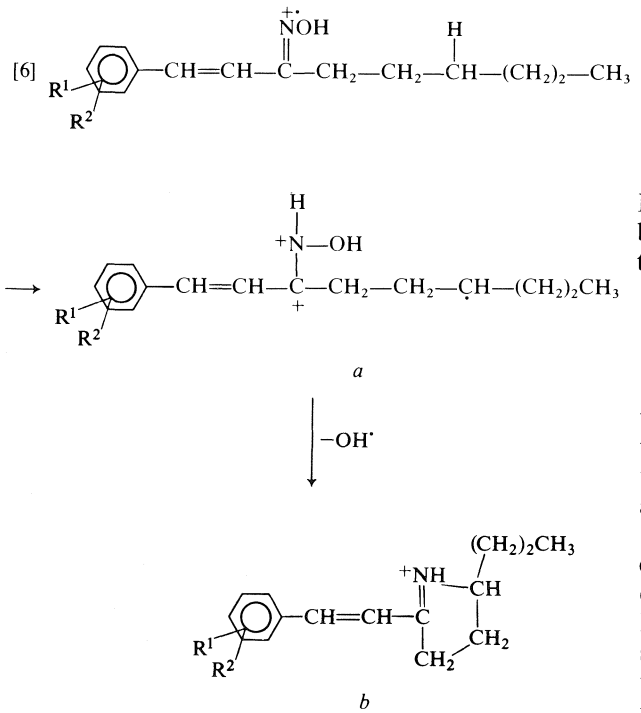

Support for the proposal of an intermediate *a* comes from the observation that the molecular ion of the oximes **1–6** loses 32 mass units, (M – 32), Table 1, as confirmed by the observation of the appropriate metastable peak. High resolution mass spectroscopy indicated that the NHOH radical is lost from the molecular ion. Intermediate *a*, rather than losing solely OH as in reaction [6] could also lose NHOH and after cyclization give ion *c* which would be expected to be stable

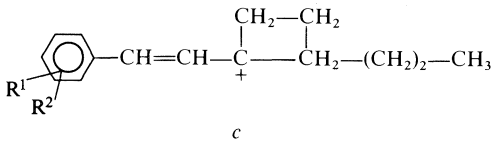

Observation of ions *b* and *c* indicates that *b* would be more stable and, in fact, for all the oximes **1–6** the loss of OH was a preferred fragmentation pathway than the loss of NHOH, Table 1.

An alternative route for the formation of the M – NHOH ion is from the "enol" form of the molecular ion, reaction [7], to give an ion *d*.

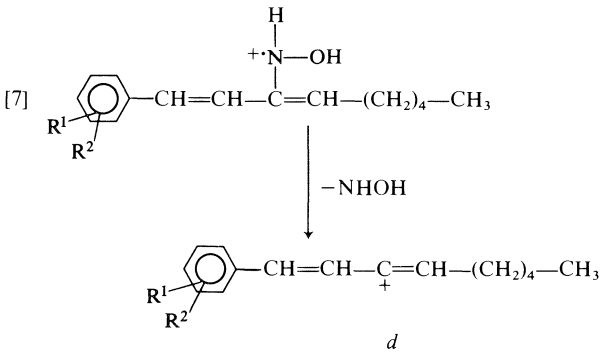

However, the vinylic ion *d* would not be expected to be stable and in order to test this hypothesis, the trideuterated substrate,

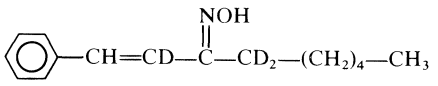

was prepared. It was found that the molecular ion of this substrate lost 32 mass units and not 33 mass units as would be expected if enolization occurred and NDOH were lost from the molecular ion.

It is noted that the molecular ions of all the oximes except **6** lost 57 mass units (γ-cleavage) and to a lesser extent 43 mass units (δ-cleavage), M – 57 and M – 43, Table 1. Oxime **6** does not fragment to the same degree as the other oximes presumably due to the fact that the *para*-dimethylamino group provides increased stabilization to the molecular ion of **6**.[4] The γ- and δ-cleavages presumably occur with cyclization to nitrogen as proposed by Djerassi and co-workers (1).

A major ion *e*, M – 70, Table 1, found in the spectrum of all the oximes except **6** corresponds to the McLafferty rearrangement, reaction [8]. The ion *e*

[4]The molecular ion of oxime **6** is the base peak in the spectrum while the molecular ions of oximes **1–5** range in relative intensity from 26–55%, Table 1.

[8] 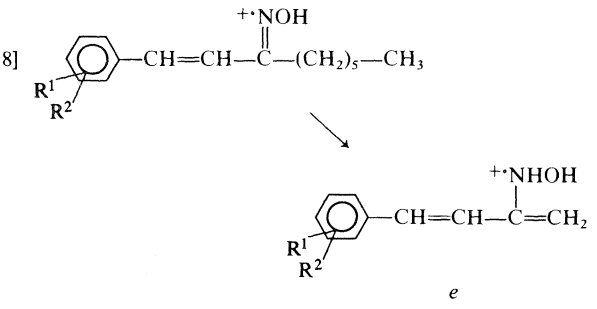

e

could be formed directly from ion *a* proposed as an intermediate for loss of both OH and NHOH from the molecular ion (reaction [6]). In all cases, except for oxime **5**, the McLafferty ion *e* loses OH. In fact, $e - 17$ has a relative intensity of 100% in the spectrum of compound **1** ($m/z = 144$). As well, for all the oximes, an ion corresponding to the loss of NHOH from *e* also was observed. It is noteworthy that in all cases the McLafferty ion *e* loses a hydrogen and, as well, where a chlorine is a ring substituent the loss of a chlorine atom is also observed from *e* as confirmed by the observation of the appropriate metastable peaks.

An examination of the data in Table 1 indicates that the loss of Cl from *e* appears to be more favoured when the chlorine is in an *ortho* position. For example, for the 2,6-dichloro oxime, **5**, ion *e* loses Cl to give an ion with $m/z = 194$ with a relative intensity of 85%. The loss of halogen from the McLafferty rearrangement ion, *e*, could presumably proceed via a combination of either a simple bond cleavage process or via a cyclization similar to that represented in reaction [1], the *ortho* effect, which will be discussed subsequently. It is of interest to note that the McLafferty ions observed in the mass spectra of the corresponding ketones (5) also lose hydrogen and chlorine in a similar fashion with loss not being exclusively restricted to the *ortho* substituent.

As mentioned in the Introduction, the *ortho* effect leading to cyclization has not been studied in detail (8). Since we have examined this process for styryl ketones (5) and for other α,β-unsaturated ketones (6) it was thought of interest to examine whether the reaction is a general one and can be promoted by the oxime function as well as the carbonyl group.

A striking feature of the spectra of the oximes **1–6** is the exclusive loss of an *ortho* substituent from the molecular ion, M − 1 and M − 35, Table 1. A chlorine atom is lost only when it is in an *ortho* position as seen by the data for compounds **2** and **3** and also **4** and **5**. The appropriate metastable peaks were observed for the loss of chlorine from the molecular ions. It was shown that the hydrogen atom which is lost does not come from the oxime function since when the specifically deuterated compound **13** was examined there was no loss of deuterium from the molecular ion. As well, a hydrogen atom is not lost from the molecular ion when *both ortho* positions are substituted with chlorine atoms (compound **5**).

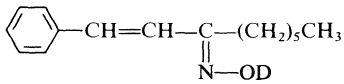

13

A cyclization mechanism identical to that proposed for the corresponding ketones (5) is consistent with the observed loss of only the *ortho* substituent. Nucleophilic attack[5] of the electron rich hetero atom, nitrogen, on the aromatic ring is followed by loss of the *ortho* group (R) to give a stable aromatic system, *f*, reaction [9].

[9] 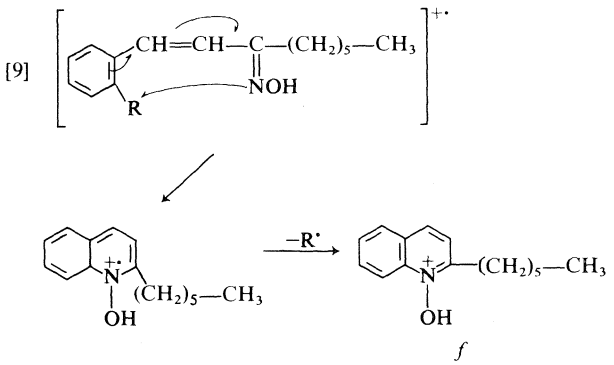

f

Attack of oxygen rather than nitrogen would lead to a less stable fragment ion. It is noteworthy that the cyclization product ion *f* receives stabilization from the oxygen and consequently this ion does not lose the hydroxyl radical.

In order to investigate the factors which affect the cyclization process, it is useful to evaluate this process quantitatively and hence the M − H/M and M − Cl/M ratios were determined at low ionization voltage where the only significant fragmentation process is cyclization with loss of the *ortho* substituent. These ratios are shown in Table 3 for the styryl ketones and corresponding oximes, as well as the 2-benzylidenecyclohexanones (6) and their corresponding oximes (2).

It is noted that for both systems the M − H/M ratios[6] are significantly greater for the oximes than for the corresponding ketones. Thus, in the 2-benzylidenecyclohexanone system, M − H/M = 1.37

[5]Nucleophilic attack on the aromatic ring has been proposed by other workers (9–11) to account for *ortho* rearrangement.

[6]The same trends in M − H/M and M − Cl/M ratios for the oximes as compared with the ketones were observed at 15 eV and 70 eV.

and 0.38 for the ring unsubstituted oxime and ketone, respectively. That the hydrogen which is lost comes from the *ortho* positions is confirmed since the molecular ion of both of the 2,6-dichloro styryl oxime and ketone does not lose a hydrogen.

The preferred formation of the M − H ion in the oximes as compared with the corresponding ketones is probably a result of either the greater availability of electron density, which promotes cyclization, in the C=N bond as compared with the C=O bond or the greater stability of *f* as compared with the product of ketone cyclization.

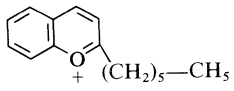

g

A comparison of the M − H/M and M − Cl/M ratios in both the styryl ketones and oximes and benzylidenecyclohexanone and their corresponding oximes shows that the M − Cl/M ratios in all cases are greater than the M − H/M ratios where there is at least one chlorine atom in an *ortho* position. This observation presumably reflects the fact that chlorine is a better leaving group than hydrogen and, thus allows cyclization to be more facile.

The stability of the resultant cyclic ion also partially determines the ease of ring formation. An examination of the M − Cl/M ratios for both the 2-Cl and 2,6-diCl styryl ketones and oximes indicates that the ratio decreases when two chlorines are placed on the aromatic ring; i.e. for the styryl oximes, M − Cl/M = 1.51 and 1.14, for the 2-Cl and 2,6-diCl compounds, respectively. The decrease in M − Cl/M ratio is probably due to greater stability of *f* than *h*,

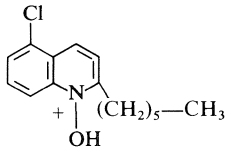

h

which has an electron-withdrawing, destabilizing, chlorine atom on the ring. Consistent with this conclusion is the observation that the mass spectrum of the 2,3,4,5,6-pentafluorostyryl ketone **12** does not lose a fluorine atom. This result can be rationalized either by considering the poor leaving group qualities of fluorine or the considerable deactivation of the cyclic ion due to *five* electron-withdrawing fluorine atoms.

Surprisingly, the trend in the M − Cl/M ratios in both systems from the oximes to the ketones is opposite to that observed for the M − H/M ratios.

TABLE 3. M − H/M and M − Cl/M ratios at 15 eV for a series of substituted 2-benzylidenecyclohexanones* and their corresponding oximes† and a series of substituted 1-phenyl-1-nonen-3-ones‡ (styryl ketones) and their corresponding oximes

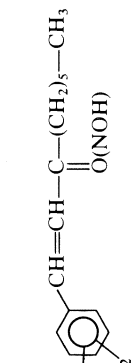

Substituent(s)	Ketone		Oxime		Ketone		Oxime	
	M − H/M	M − Cl/M§	M − H/M	M − Cl/M§	M − H/M	M − Cl/M§	M − H/M	M − Cl/M§
4-H	0.38	—	1.37	—	0.12	—	0.69	—
4-Cl	0.02	—	0.81	—	0.08	0.05	0.52	0.18
2-Cl	0.21‖	11.2‖	1.44‖	5.29‖	0.10	3.29	0.18	1.51
2,6-diCl	—	—	—	—	—	1.81	—	1.14

*Data taken from ref. 6.
†Data taken from ref. 2.
‡Data taken from ref. 5.
§The M − Cl/M ratios were calculated by considering all the ions containing chlorine isotopes.
‖Measured at 70 eV.

TABLE 4. M − OR/M ratios at low ionization voltages for *ortho* substituted ether and benzoate ester styryl ketones

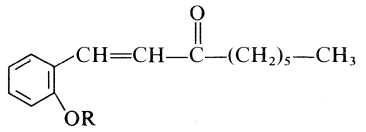

Substituent (R)		eV	M − OR/M
$-CH_2-O-CH_3$	(**7**)	12	0.182
$-CH_2-O-CH_2-CH_3$	(**8**)	10	0.286
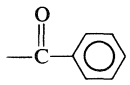	(**9**)	12	2.76
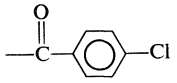	(**10**)	15	1.93
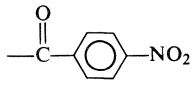	(**11**)	15	8.44

Whereas the M − H/M ratios are greater for the oximes than for the ketones the M − Cl/M ratios are smaller for the oximes compared with the corresponding ketones. This phenomenon may be due to the fact that steric effects are more important in the cyclization process of the oximes than for the ketones. It is more difficult for the bulky oxime function, as compared with the smaller carbonyl group, to attack an *ortho* position containing a large chlorine atom. These effects are unimportant when the *ortho* positions contain the small hydrogen atom.

In order to see whether *ortho* substituents other than hydrogen and chlorine are specifically lost via the ring formation process, several styryl ketones containing ether and ester substituents were examined. The major ions in the mass spectra of **7–11**, Table 2, are as expected with the ethers giving base peaks at $m/z = 45$ and 59 and the benzoate esters giving base peaks for the substituted benzoyl ions.[7]

The M − OR/M ratios were measured at low ionization voltages for compounds **7–11** and are shown in Table 4. It appears that the ethyl ether **8** is a better leaving group than the methyl analog **7** and that the *para*-nitro ester **11** is the best leaving group in the series of esters **9–11**.

Experimental

Mass spectra were determined with an MS-12 mass spectrometer. Source temperatures were varied between 120 and 130°C, depending on the sample. The samples were introduced using the direct probe technique. The high resolution spectra were determined by Dr. A. Boulton, Psychiatric Research Unit, University of Saskatchewan.

The preparation of the oximes **1–6** was by the literature methodology (12) and the styryl ketones **7**, **9–11** by the reported procedures (13).

*1-(2-Ethoxymethoxyphenyl)-1-nonen-3-one (**8**)*

A mixture of 2-octanone (76.9 g, 0.60 mol) and 2-ethoxymethoxybenzaldehyde (0.50 mol) was added to a solution of sodium hydroxide (10 g, 0.25 mol) in 300 mL of water and the resultant mixture was heated under reflux with mechanical stirring for 12 h. On cooling, the two layers were separated and the aqueous layer washed with benzene (3 × 100 mL). The washings were added to the organic layer and the solvent and excess 2-octanone removed under reduced pressure. The product bp 170°C/0.10 mm was prepared in 59% yield. *Anal.* calcd. for $C_{18}H_{26}O_3$: C 74.45, H 9.02; found: C 74.17, H 9.00.

*1-(Pentafluorophenyl)-1-nonen-3-one (**12**)*

To a vigorously stirred solution of 2,3,4,5,6-pentafluorobenzaldehyde (0.13 mol) and 2-octanone (0.15 mol) in dry benzene (200 mL) was added glacial acetic acid (0.13 mol) and piperidine (0.13 mol). The mixture was heated under reflux for 1 h using a condenser attached to a Dean-Stark trap. The benzene solution was cooled, extracted with water, 3 × 100 mL, and the benzene removed *in vacuo* to give a yellow oil, 27%, bp 114°C/1.0 mm. *Anal.* calcd. for $C_{15}H_{15}F_5O$: C 58.82, H 4.94; found: C 58.37, H 4.76.

Oxime of 1-Phenyl-1-nonen-3-one-OD

The oxime of 1-phenyl-1-nonen-3-one, 0.5 g, was dissolved in 10 mL of acetonitrile and 5 mL of D_2O was added. The solvent was removed under reduced pressure and this process was repeated six times. The oxime-OD was recrystallized from 30–60°C petroleum ether and was shown by infrared analysis to be approximately 70% deuterated. The oxime-OD was introduced into the source of the mass spectrometer in a solution of D_2O. This was repeated three times.

Oxime of 1-Phenyl-1-nonen-3-one-α-d_2

The oxime was prepared from 1-phenyl-1-nonen-α-d_2 by the previously published oximation process (12).

1-Phenyl-1-nonen-3-one-α,α,α′-d_3

1-Phenyl-1-nonen-3-one, 0.5 g, was dissolved in CH_3OD, 15 mL, and 1 g of dried sodium acetate was added. The solution was refluxed overnight. The ketone was recovered and the exchange process repeated two more times. The product,

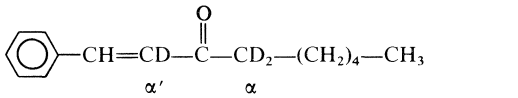

was shown to be completed exchanged at C_α by nmr but there was incomplete exchange at α′.

Acknowledgement

The authors thank the Medical Research Council of Canada for the award of an operating grant to J.R.D. (MA 5538).

1. D. GOLDSMITH, D. BECHER, J. SANPLE, and C. DJERASSI. Tetrahedron Suppl. 7, 145 (1966).
2. P. J. SMITH, J. R. DIMMOCK, and W. A. TURNER. Can. J. Chem. **51**, 1471 (1973).

[7]The corresponding *para* isomers of compounds **7**, **9–11** did not give a loss of the nuclear substituent from the molecular ion.

3. R. K. M. KALLURY and P. L. K. M. RAO. Org. Mass Spectrom. **12**, 411 (1977).
4. R. T. COUTTS and J. L. MALICKY. Org. Mass Spectrom. **7**, 985 (1973).
5. P. J. SMITH, J. R. DIMMOCK, and W. G. TAYLOR. Can. J. Chem. **50**, 871 (1972).
6. P. J. SMITH, J. R. DIMMOCK, and W. A. TURNER. Can. J. Chem. **51**, 1458 (1973).
7. H. BUDZIKIEWICZ, C. DJERASSI, and D. H. WILLIAMS. Mass spectrometry of organic compounds. Holden-Day, San Francisco. 1967. pp. 367–375.
8. H. SCHWARTZ. Fort. Chem. Forsch. **73**, 231 (1978).
9. R. G. COOKS and A. G. VARVOGLIS. Org. Mass Spectrom. **5**, 687 (1971).
10. J. H. BENYON, M. BETRAND, and R. G. COOKS. Org. Mass Spectrom. **7**, 785 (1973).
11. P. C. VIJFHUIZEN, H. VAN DER SCHEE, and J. K. TERLOUW. Org. Mass Spectrom. **11**, 1198 (1976).
12. J. R. DIMMOCK, P. J. SMITH, L. M. NOBLE, and W. J. PANNEKOEK. J. Pharm. Sci. **67**, 1536 (1978).
13. J. R. DIMMOCK, C. B. NYATHI, and P. J. SMITH. J. Pharm. Sci. **67**, 1543 (1978).

Cinétique de la formation de la métalloporphyrine Cu(II)—dérivé tétra éthylènediamino de la protoporphyrine IX (ENP) en milieu aqueux

GUY PAQUETTE[1] ET MIKLOS ZADOR

Département de Chimie, Université de Montréal, C.P. 6210, Succursale A, Montréal (Qué.), Canada H3C 3V1

Reçu le 8 mai 1979

GUY PAQUETTE et MIKLOS ZADOR. Can. J. Chem. **57**, 2916 (1979).

La cinétique de la formation de la métalloporphyrine Cu(II)–ENP est dépendante du pH suite à la protonation des *N* pyrroliques et aussi suite à la protonation des groupes diamines des chaînes latérales. Le degré de protonation de ces chaînes latérales influence également le degré d'association de la porphyrine et de la métalloporphyrine en solution. L'ordre de réaction par rapport à la porphyrine est différent de 1 par suite d'une inhibition par le produit de réaction; cette inhibition s'opère via la formation d'une nouvelle espèce, un complexe mixte porphyrine–métalloporphyrine qui est peu réactif. L'ordre de réaction par rapport au Cu(II) est également différent de 1, dû à la chélation du Cu(II) par les groupes diamines des chaînes latérales. La présence de ligands du Cu(II) influence à la fois la cinétique de la réaction et la nature du produit final de réaction.

GUY PAQUETTE and MIKLOS ZADOR. Can. J. Chem. **57**, 2916 (1979).

The kinetics of formation of the metalloporphyrin Cu(II)–ENP is dependent on the pH due to the protonation of the pyrrol nitrogen atoms and the protonation of the diamino groups of the side chains. The degree of protonation of these side chains also influences the degree of association of the prophyrin and the metalloporphyrin in solution. The order of reaction with respect to the porphyrin is not unity, a consequence of an inhibition by the reaction product; this inhibition operates via the formation of a new species, a mixed complex of porphyrin–metalloporphyrin of low reactivity.

The order of reaction with respect to Cu(II) is also not unity, a consequence of the chelation of Cu(II) by the diamino groups of the side chains. The presence of Cu(II) ligands influence both the reaction kinetics and the nature of the final reaction product.

[Journal translation]

Introduction

Les porphyrines, sous forme de complexes avec des ions métalliques, sont impliquées dans plusieurs systèmes biologiques importants, tels l'hémoglobine, les cytochromes et la chlorophylle. Suite aux nombreux travaux sur le sujet (1–4), il ne semble pas qu'on puisse dégager un mécanisme vraiment général concernant l'incorporation de l'ion métallique à la porphyrine. La nature de la porphyrine et du métal, ainsi que le milieu réactionnel, jouent un rôle important lors de ces réactions. La très faible solubilité de la majorité des porphyrines en milieu aqueux est certainement une cause importante de la diversité des résultats obtenus: les solvants non-aqueux ou mixtes (5–22), de même que les détergents (19) ont été fréquemment utilisés, ce qui implique la présence en solution d'espèces métalliques souvent mal connues et de réactivité différente des espèces aqueuses.

La présente étude porte sur l'interaction du Cu(II) avec une porphyrine synthétique soluble en milieu aqueux, dérivé tétra-éthylènediamino de la protoporphyrine IX (fig. 1). Selon le symbolisme utilisé par White et Plane (20), elle sera désignée par ENP (forme base libre).

Partie expérimentale

Réactifs

La solution stock de Cu(II), sous forme de perchlorate, a été préparée à partir du sel double $CuCO_3 \cdot Cu(OH)_2$ (B.D.H.) et d'acide perchlorique (J. T. Baker).

La force ionique du milieu a été maintenue constante à 0.2 *M* à l'aide de $NaClO_4$. En présence de ligands ajoutés, il a été tenu compte des équilibres de protonation de ceux-ci et des complexes Cu(II)–ligand(s) dans le calcul de la force ionique.

Le dérivé de la protoporphyrine a été synthétisé selon la méthode décrite dans la littérature (20, 21), à partir de l'ester diméthylique de la protoporphyrine IX (Sigma) et d'éthylènediamine (Fischer) préalablement distillé. La pureté du produit a été vérifiée en comparant la position des maximums du spectre uv–visible et les valeurs calculées des absorptivités molaires avec les données publiées (20).

Méthode cinétique

Les réactions ont été étudiées à 25°C par spectrophotométrie en enregistrant la diminution de l'absorption de la bande Soret de la porphyrine dûe à la formation de la métalloporphyrine, dans la région de $\lambda = 360$ à 405 nm. Un spectrophotomètre Zeiss PMQ II, avec un porte-cuvettes thermostaté, a été utilisé. La température à l'intérieur des cuvettes optiques a été mesurée à l'aide d'un thermocouple. Les résultats ont été enregistrés sur un enregistreur logarithmique Sargent-Welsh

[1]Adresse actuelle: Department of Agricultural Chemistry and Physics, MacDonald Campus of McGill University, Ste-Anne de Bellevue (Qué.), Canada H9X 1CO.

0008-4042/79/222916-07$01.00/0

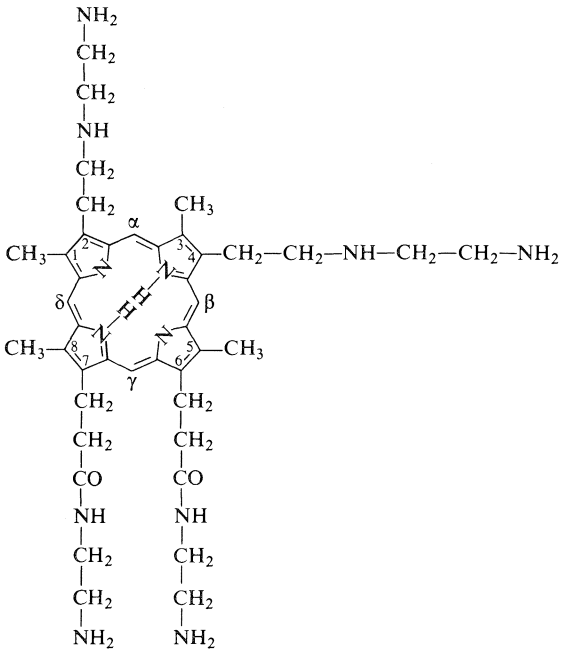

FIG. 1. ENP, forme base libre.

modèle SRLG. La concentration en porphyrine était de 1.0×10^{-5} *M*. Alors que celle du Cu(II) variait de 2.5×10^{-4} à 2.5×10^{-2} *M*. Les constantes de vitesse ont été obtenues à partir de la relation $kt = \ln [A_0 - A_\infty)/(A - A_\infty)]$, où A_0, A et A_∞ représentent les absorbances aux temps de 0, t et infini respectivement. A cause de problèmes particuliers discutés plus loin, la majorité des réactions ont été analysées en cinétique initiale, i.e. sur une période couvrant environ les premiers 25% de réaction. La force ionique a été maintenue constante, puisque des expériences ont montré que la force ionique influence l'état de la porphyrine en solution, de même que la vitesse de réaction.

Résultats et discussion

(a) Etat de la porphyrine en solution

La ENP peut exister en solution sous plusieurs formes (20): la base libre (ENP, fig. 1), le mono et le dication ($HENP^+$ et H_2ENP^{2+}) en milieu acide, sans compter les divers degrés de protonation des chaînes latérales. Les formes dimériques de la base libre et des espèces acides sont également possibles.

L'existence de ces diverses formes de la porphyrine a été proposée suite à une étude spectrale (20), mais l'influence du degré de protonation des chaînes latérales n'a pas été élucidée.

Nos résultats préliminaires indiquaient un rôle probable des chaînes latérales (voir plus loin); il a été décidé alors de réexaminer cette question.

(i) Titrage acide–base

La fig. 2 montre la courbe de titrage obtenue. La solution de pH = 3.3[5] après dissolution de la ENP, a été amenée à pH 2.2 puis titrée par NaOH.

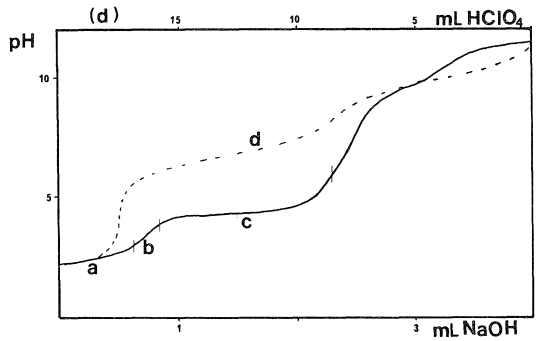

FIG. 2. Courbe de titrage. [ENP] = 2.5×10^{-3} *M*, courbe *a*: excès de $HClO_4$. [NaOH] = 4.7×10^{-2} *M*, courbe *b*: *N* pyrroliques, courbe *c*: chaînes latérales. [En] = 5×10^{-2} *M*; [$HClO_4$] = 5×10^{-2} *M*: courbe *d*.

La courbe se divise en trois parties: (*a*) neutralisation de l'excès d'acide perchlorique ajouté; (*b*) titrage des hydrogènes internes de la forme acide; (*c*) neutralisation des six protons des groupes amines des chaînes latérales.

Deux points particuliers sont à noter. Premièrement, il n'est pas possible de distinguer le départ successif des deux protons de la forme acide, ce qui est fréquent pour les porphyrines (22). Un calcul de la quantité de H^+ impliquée dans la neutralisation des hydrogènes internes indique un rapport 1:1 pour H^+/ENP. Ceci implique la présence soit du monomère monoprotoné, soit du dimère diprotoné comme espèces dominantes. La deuxième possibilité est retenue, en accord avec les constantes publiées (20), à cette concentration élevée de porphyrine (2.5×10^{-3} *M*).

Le point le plus important concerne les chaînes latérales (partie *c*). Dans ce cas, il est également impossible de distinguer le départ des différents protons des groupes amines. Ceci indique que les différences d'acidité entre ces protons sont trop faibles pour être perceptibles dans ces conditions. Le comportement des chaînes éthylènediamines est donc très différent de l'éthylènediamine seule (courbe *d* de la fig. 2).

(ii) Titrage spectrophotométrique

L'évolution des spectres en fonction du pH (fig. 3) fait ressortir deux points importants. D'abord, les spectres 1 à 3 (pH = 1.3 à pH = 2.5) montrent la transformation de la forme acide (λ_{max} = 402 nm) en base libre (λ_{max} = 372 nm) et il semble qu'il n'y ait que deux espèces présentes en solution puisqu'on distingue deux points isobestiques à λ = 386 nm et à λ = 405 nm. Or, comme la bande à λ_{max} = 372 nm a été attribuée au dimère de la base libre (20), ceci indique que la forme acide est très probablement dimérique (20, 21). La réaction acide–base est alors

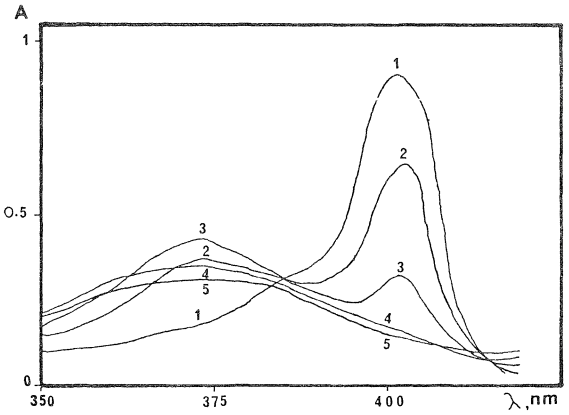

FIG. 3. Evolution des spectres de ENP en fonction de pH. [ENP] = 8×10^{-6} *M*; *1*, pH = 1.3; *2*, pH = 1.9; *3*, pH = 3.5; *4*, pH = 4.9; *5*, pH = 6.4.

représentée par l'équation suivante:

[1] $H_2(ENP)_2^{2+} \rightleftharpoons (ENP)_2 + 2H^+$

Ceci est en accord avec la valeur des constantes d'acidité et de dimérisation obtenues par White et Plane (20) et aussi avec les conclusions tirées de l'analyse de la courbe de titrage acide–base.

A pH $\geq$ 4, les résultats du titrage acide–base, ainsi que les valeurs des constantes d'acidité (20) impliquent, que les azotes internes sont déprotonées; les bases libres subissent alors progressivement la déprotonation des chaînes latérales par l'augmentation du pH.

Les spectres 4 et 5 de la fig. 3 montrent que la bande du dimère de la base libre s'élargit et ne passe plus par les points isobestiques. Les nouvelles espèces qui apparaissent sont probablement des formes oligomériques (trimère etc.). La déprotonation des chaînes latérales a comme effet de diminuer les répulsions électrostatiques des chaînes protonées et d'augmenter les interactions hydrophobes, responsables de la formation d'aggrégats.

L'existence de ces oligomères a été suggérée pour d'autres porphyrines, la protoporphyrine IX et la deuteroporphyrine IX (23), suite à l'analyse de spectres dont les caractéristiques sont semblables à celles des spectres de la fig. 3.

Pour certaines autres porphyrines telle la tetra-*N*-méthylpyridylporphine (TMPyP) il a été démontré que les charges positives périphériques (4^+) empêchent l'association en milieu aqueux (24). C'est le cas contraire de la ENP, qui s'explique par le fait que les substituants *N*-méthylpyridyles de la TMPyP sont joints au noyau porphyrinique aux positions α, β, γ, δ (cf. fig. 1), donc directement liés au système π résonant du noyau. Ce système résonant, responsable de l'association (25), est beaucoup moins influencé par les charges périphériques de la ENP qui sont séparées du noyau par quelques carbones aliphatiques (fig. 1). De plus la longueur des chaînes permet une flexibilité suffisante pour les orienter dans des directions opposées. Les divers groupes chargés sont alors suffisamment éloignés les uns des autres pour permettre la formation du dimère. Cette possibilité n'existe pas chez la TMPyP.

(iii) Cinétique de la réaction en fonction du pH

La fig. 4 montre la variation de la constante de vitesse initiale en fonction du pH. On y remarque les trois points suivants:

(*1*) De pH = 3.75 (point équivalent du titrage acide–base) à pH = 2.0, la vitesse de réaction diminue, selon un ordre approximatif -2 en H^+, ce qui indique une très faible réactivité de la forme acide de la porphyrine par rapport aux formes base libre. Une réaction effectuée à pH = 1.0 est au moins 10^3 fois plus lente qu'à pH = 3.75. C'est le comportement normal des porphyrines dans la région de pH correspondant à la protonation des azotes pyrroliques (9).

(*2*) Aux pH > 3.75, la courbe indique un comportement particulier de la ENP. A ces pH, la plus grande partie de la porphyrine a déjà été transformée en base libre; or la vitesse de réaction continue d'augmenter avec le pH. Par contre, tel que montré par l'étude de White et Plane (20), les caractéristiques spectrales ne changent plus dans le même domaine de pH; il est donc impossible de connaître la nature exacte des espèces, protonées différemment sur les chaînes latérales, dans ces milieux et d'avoir une interprétation quantitative de l'augmentation importante de vitesse observée. Qualitativement, ce phénomène est dû à la réduction de la charge portée par la porphyrine ce qui entraîne la diminution de

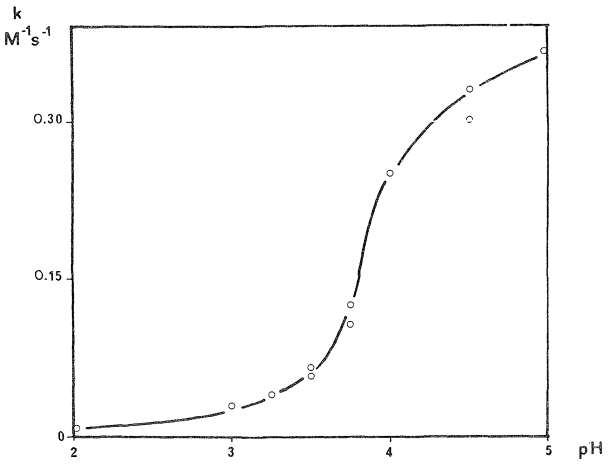

FIG. 4. Variation de la constante de vitesse en fonction du pH. [ENP] = 1×10^{-5} *M*, *T* = 25°C.

l'énergie libre d'interaction électrostatique avec le Cu^{2+}, conduisant à l'augmentation de la constante de vitesse.

De plus, une telle réduction de la charge de la porphyrine, dans le cas des porphyrines substituées en position *méso* (α, β, γ, δ, fig. 1) permet d'accroître la réactivité de la porphyrine en augmentant la densité électronique au centre réactif (24, 26–30). L'effet est probablement moindre dans le cas de la ENP, à cause de la position des groupes chargés sur les chaînes latérales.

(*3*) L'analyse de la fig. 3 a conduit à l'hypothèse de l'existence d'oligomères au pH > 4. La fig. 4 indique la présence de ces oligomères ne diminue pas la réactivité de la porphyrine.

L'évolution des spectres en cours de réaction met également en évidence l'influence de la protonation des chaînes latérales sur l'état des espèces en solution (fig. 5). Dans les deux cas la bande à 380 nm (dimère de la métalloporphyrine (20)) apparaît. A pH = 3.5 (fig. 5*a*) la bande est stable à la fin de la réaction, alors qu'à pH = 4.5 (fig. 5*b*) elle diminue lentement d'intensité et il apparaît éventuellement un précipité dans la cuvette optique. A pH = 3.5, les chaînes latérales protonées maintiennent le dimère en solution, alors qu'à pH = 4.5, les groupes amines commencent à se déprotoner, conduisant à la formation d'oligomères supérieurs qui précipitent éventuellement.

On remarque le même comportement lorsqu'on augmente le pH d'une solution de Cu·ENP formée à pH plus bas.

(b) L'ordre de réaction par rapport à la porphyrine

En supposant un mécanisme simple, l'équation de vitesse s'écrit comme suit:

[2] Vitesse = k[ENP][Cu^{2+}]

Comme dans toutes les réactions effectuées [Cu^{2+}] ≫ [ENP], l'équation se réduit à:

[3] Vitesse = k_{exp}[ENP]

De plus, la vitesse initiale de la réaction varie selon un ordre 1 par rapport à la concentration initiale de porphyrine. Toutefois les graphes de $\ln (A - A_\infty)/(A_0 - A_\infty)$ versus le temps présentent des écarts à la linéarité importants (fig. 6*a*). Il a été vérifié, à l'aide de solutions synthétiques, que ces écarts ne sont pas dus à la méthode expérimentale: l'absorbance mesurée est linéairement reliée au degré d'avancement de la réaction.

Il apparaît donc que seul un "incident" qui se développe au cours même de la réaction puisse être responsable de l'écart à la linéarité, que nous avons attribué à une inhibition par le produit de la réaction.

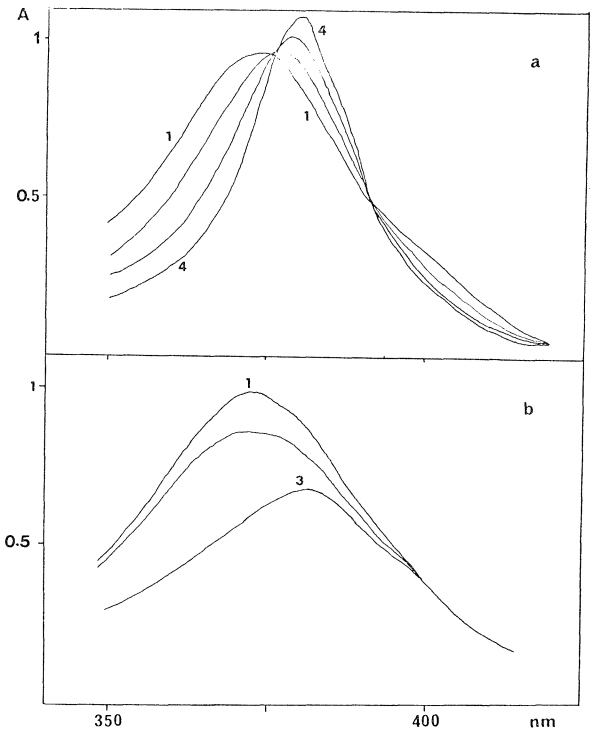

FIG. 5. Evolution des spectres durant la réaction [ENP] = 1×10^{-5} *M*; *T* = 25°C. *a*, pH = 3.5, [Cu(II)] = 2.5×10^{-2} *M*. *b*, pH = 4.5, [Cu(II)] = 5.0×10^{-4} *M*.

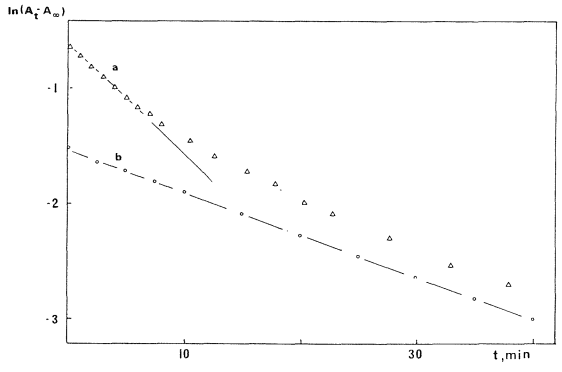

FIG. 6. Courbe d'intégration d'ordre 1. [ENP] = 5×10^{-6} *M*; [Cu(II)] = 5×10^{-2} *M*; pH = 2.0; *T* = 45°C; λ = 408 nm. *a*, [Cu·ENP]$_0$ = 0. *b*, [Cu·ENP]$_0$ = 1.5×10^{-5} *M*.

En effet, l'addition de quantités croissantes du produit entraîne la diminution progressive de la vitesse et, de plus, la courbe cinétique devient alors linéaire (fig. 6*b*). Plus la concentration de Cu·ENP est forte, plus la réaction est ralentie.

Les spectres sont révélateurs de la nature de l'inhibition. L'addition de Cu·ENP à une solution de ENP à pH = 2.0 influence la bande à λ_{max} = 402 nm, i.e. celle de la forme acide de la porphyrine; cet effet est attribué à la formation d'un complexe mixte

ENP–Cu·ENP assez stable pour causer le départ des protons de la forme acide, même à pH = 2.0.

Ce complexe étant moins réactif vis-à-vis l'incorporation du Cu(II), sa formation en fonction du temps entraîne l'allure autoinhibée de la réaction. Lorsque celle-ci est démarrée en présence de Cu·ENP, le complexe mixte est déjà présent en concentration appréciable au départ: la réaction est alors plus lente, mais présente une cinétique d'ordre 1.

C'est la première fois qu'un tel complexe mixte est suggéré, malgré que l'auto-association des porphyrines (1, 2, 23, 24, 31, 32), ainsi que des métalloporphyrines (1, 2, 3, 24, 31, 33, 35) soit bien établie.

Aux autres pH, i.e. 3.5 et 4.5 principalement, l'inhibition par le produit de réaction est aussi présente et elle a été démontrée cinétiquement par la même méthode. Dans ces cas cependant la présence du complexe mixte n'est pas apparente sur les spectres probablement parce que les différences spectrales ne sont pas suffisamment importantes vue l'absence de la forme acide à ces pH.

(c) L'influence de la concentration en Cu(II)

La fig. 7 montre la variation de la constante de vitesse en fonction de [Cu(II)]; le comportement est le même aux divers pH étudiés. Ce type de dépendance est linéaire aux basses concentrations en Cu(II), et semble aussi linéaire, mais de pente différente, aux concentrations plus élevées. Comme la réaction du Zn(II) avec la même porphyrine présente un ordre 1 simple par rapport au Zn(II) (36), les différences constatées avec le Cu(II) sont très probablement liées à la nature de l'ion métallique impliqué.

Il est bien connu que le Cu(II) forme facilement des complexes avec les amines (37). Il est possible que le Cu(II) complexe les groupements diamines des chaînes latérales, ou les chaînes en position 6 et 7 (fig. 1), formant ainsi une espèce complexée moins réactive que la porphyrine seule. Un calcul effectué à partir des constantes d'acidité et de complexation de l'éthylènediamine (*en*) avec le Cu^{2+} indique qu'à pH = 4.5, la proportion de *en* complexée sous forme $Cu{\cdot}en^{2+}$ est de 20 à 30%, avec [Cu(II)] = 2.5×10^{-2} *M*. Or le titrage acide–base de la ENP (fig. 2) a montré que le groupements diamines des chaînes latérales ont des protons plus acides que l'éthylènediamine par un facteur de 10^2–10^3; ils sont donc plus facilement remplacés par Cu^{2+}. De plus, par leur position, les chaînes latérales en position 6 et 7 (fig. 1), permettent la formation d'un tétradentate encore plus stable. Les conditions sont donc favorables à la formation d'un chélate du Cu(II) par les chaînes latérales.

On a alors deux espèces en solution, ENP et

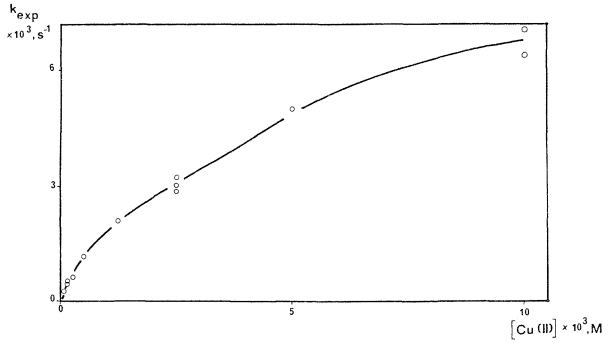

FIG. 7. Influence de la concentration en Cu(II) sur k_{exp} [ENP] = 1×10^{-5} *M*; pH = 3.5; *T* = 45°C.

ENP–Cu. L'équation de vitesse devient ainsi la suivante:

[4] Vitesse = $(k_1[\text{ENP}] + k_2[\text{ENP–Cu}])[\text{Cu(II)}]$

Aux basses concentrations en Cu(II), la concentration en ENP–Cu est faible et le terme correspondant de l'éq. [4] est négligeable devant k_1 ENP; la réaction est alors d'ordre 1 en Cu(II). Aux concentrations plus élevées en Cu(II), le contraire se produit; la vitesse est également d'ordre 1, mais l'espèce complexée ENP–Cu étant moins réactive, la pente de la courbe est plus faible (fig. 7). La courbure représente la transition progressive entre ces deux cas limites.

La réaction du Zn(II) avec ENP montre une cinétique d'ordre 1 par rapport au Zn(II) (36). Or les complexes du Zn(II) avec les polyamines ont des constantes de stabilité plus faibles que ceux du Cu(II) d'un facteur 10^4–10^5 (37). La concentration de l'espèce complexée ENP–Zn est d'autant plus faible, donc négligeable dans ces conditions. Le cas du Zn(II) est ainsi identique à celui du Cu(II) à basses concentrations.

(d) Influence de la présence de ligands du Cu(II)

La présence de faibles concentrations (10^{-4}–10^{-3} *M*) des ligands acétate, pyridine, imadazole et éthylènediamine accélère la réaction d'incorporation du Cu^{2+} à la ENP. La présence des complexes $Cu{\cdot}L^{2+}$, $Cu{\cdot}L_2{}^{2+}$, etc. ouvre de nouvelles voies réactionnelles, selon les équations suivantes:

[5] $Cu^{2+} + \text{ENP} \rightarrow Cu{\cdot}\text{ENP} + 2H^+$ $\quad k_{Cu^{2+}}$

[6] $CuL^{2+} + \text{ENP} \rightarrow Cu{\cdot}\text{ENP} + L + 2H^+$ $\quad k_{CuL^{2+}}$

[7] $CuL_2{}^{2+} + \text{ENP} \rightarrow Cu{\cdot}\text{ENP} + 2L + 2H^+$ $\quad k_{CuL_2{}^{2+}}$

L'équation de vitesse s'écrit alors:

[8] Vitesse = $(k_{Cu^{2+}}[Cu^{2+}] + k_{CuL^{2+}}[CuL^{2+}] + k_{CuL_2{}^{2+}}[CuL_2{}^{2+}])[\text{ENP}]$

A faible concentration en ligand, seules $[Cu^{2+}]$ et

[CuL^{2+}] sont appréciables. Dans ce cas on peut calculer les valeurs de constantes de vitesse individuelles, à 25°C:

$$k_{Cu^{2+}} \simeq 1\ M^{-1}\ s^{-1}$$

$$k_{CuOAc^{+}} \simeq 5\ M^{-1}\ s^{-1}$$

$$k_{Cu.pyr^{2+}} \simeq 16\ M^{-1}\ s^{-1}$$

$$k_{Cu.imz^{2+}} \simeq 6\ M^{-1}\ s^{-1}$$

$$k_{Cu.en^{2+}} \simeq 21\ M^{-1}\ s^{-1}$$

La réactivité accrue des espèces complexées du Cu(II) a déjà été démontrée à quelques reprises (9, 17), de même que pour le Zn(II) (36, 39).

L'analyse cinétiques des réactions à plus fortes concentrations en ligand (10^{-2} à 0.25 *M*) a montré un comportement singulier, inexplicable par les calculs de répartition des espèces du Cu(II) et de constantes de vitesse individuelles. Les spectres enregistrés en cours de réaction (fig. 8) montrent la présence d'un phénomène nouveau à haute concentration. A basse concentration (fig. 8*a*) la transformation du dimère de la base libre (λ_{max} = 372 nm) vers le dimère de la métalloporphyrine (λ_{max} = 382 nm) s'effectue avec une décroissance monotone de

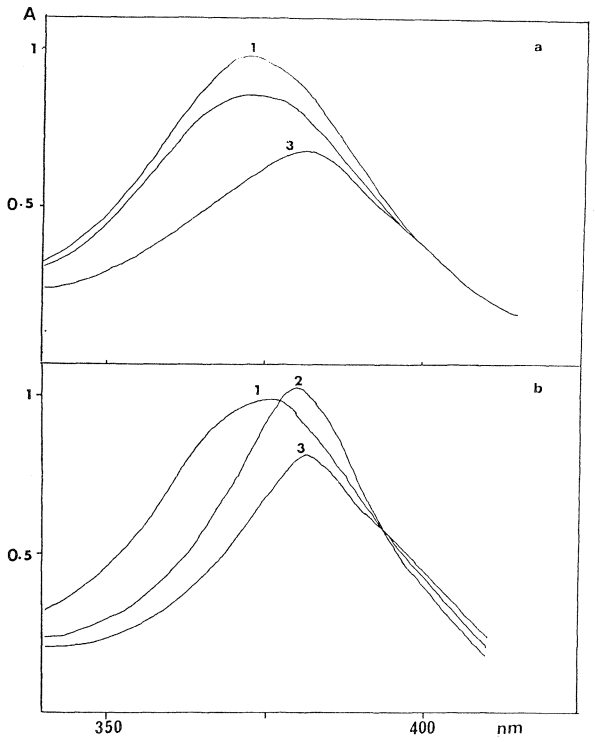

FIG. 8. Evolution des spectres lors de la réaction en présence d'éthylènediamine. [ENP] = 1×10^{-5} *M*; [Cu(II)] = 2.5×10^{-3} *M*; pH = 4.5; *T* = 45°C. *a*, [en] = 5×10^{-4} *M*. *b*, [en] = 5×10^{-2} *M*.

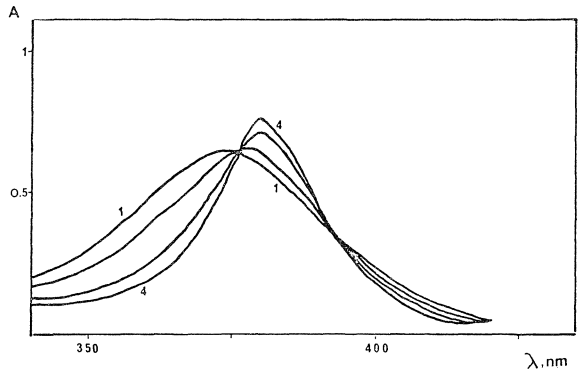

FIG. 9. Evolution des spectres lors de la réaction en présence de forte concentration d'éthylènediamine. [ENP] = 1×10^{-5} *M*; [Cu(II)] = 2.5×10^{-3} *M*; [en] = 2.5×10^{-1} *M*; pH = 4.5, *T* = 25°C, force ionique = 0.75 *M*.

l'intensité. A concentration élevée (fig. 8*b*), il y a d'abord déplacement du maximum vers λ = 382 nm avec augmentation d'intensité; puis l'intensité diminue, quoique moins fortement que dans le premier cas.

On est donc en présence de deux phénomènes consécutifs. On attribue le nouveau phénomène à la complexation, en position axiale, du Cu(II) de la métalloporphyrine par le ligand présent. Les spectres de la réaction en présence de très fortes concentrations de *en* (0.25 *M*) concordent avec cette hypothèse (fig. 9); on y observe uniquement le déplacement de la bande Soret, qui augmente d'intensité. Comme l'élargissement et l'aplatissement du pic à λ_{max} = 382 nm ont été attribués précédemment à la formation d'oligomères supérieurs au dimère, cette bande étroite et plus intense indique l'absence d'oligomères. La Cu·ENP existe donc sous forme de dimère, avec un ligand par métalloporphyrine. C'est essentiellement la même conclusion que celle de MacCragh et coll. qui ont étudié une série de porphyrines du Cu(II) avec des ligands par résonance paramagnétique électronique (38).

Cette idée est confirmée par deux autres faits expérimentaux. D'abord l'addition de fortes concentrations de *en* à une solution de Cu. ENP produit un spectre final semblable à celui de la fig. 9. Deuxièmement, les réactions effectuées en présence de concentrations faibles ou nulle de ligand à ce pH (4.5) montrent un précipité à la fin de la réaction, alors qu'il n'en apparaît pas dans les cas à hautes concentrations, même après plusieurs jours.

Conclusion

La réaction étudiée présente, par rapport aux autres réactions de formation de métalloporphyrines, quelques traits particuliers, dus à la nature des chaînes latérales de la ENP.

La rôle de H^+ y est double: d'une part la protonation des N pyrroliques conduit à des formes acides très peu réactives, ce qui est le cas général; d'autre part, le degré de protonation des chaînes latérales influence les équilibres d'association de la porphyrine et la vitesse d'incorporation du Cu(II).

La formation d'un chélate du Cu(II) par ces mêmes chaînes conduit à une espèce de réactivité moindre que la porphyrine seule.

L'ordre de réaction par rapport à la porphyrine est différent de 1, à cause de la formation d'un complexe mixte ENP–Cu·ENP, peu réactif, au cours de la réaction. C'est la première fois qu'un tel complexe est mis en évidence.

La présence de faibles concentrations de ligands du Cu(II) accélère la réaction d'incorporation du métal, alors qu'à hautes concentrations l'état du produit final est plutôt dimérique qu'oligométrique suite à la complexation du Cu(II) de la métalloporphyrine en position axiale.

Ces particularités du système Cu(II)/ENP soulignent encore une fois la difficulté de proposer un mécanisme vraiment général d'incorporation des ions métalliques aux porphyrines.

Remerciements

Les auteurs remercient le Conseil national de recherches du Canada et le Ministère de l'Education du Québec pour l'aide financière accordée lors de la réalisation de ce travail.

1. F. E. Falk. Porphyrins and metalloporphyrins. Elsevier, New York, NY. 1964.
2. K. M. Smith (*Editeur*). Porphyrins and metalloporphyrins. Elsevier, New York, NY. 1975.
3. A. D. Adler (*Editeur*). The Chemical and physical behavior of porphyrin compounds and related structures. Ann. N.Y. Acad. Sci. **206** (1973).
4. A. D. Adler (*Editeur*). The biological role of porphyrins and related structures. Ann. N.Y. Acad. Sci. **244** (1975).
5. J. P. Macquet et T. Theophanides. Can. J. Chem. **51**, 219 (1973).
6. H. Baker, P. Hambright, L. Wagner et L. Ross. Inorg. Chem. **12**, 2200 (1973).
7. D. A. Brisbin et G. D. Richards. Inorg. Chem. **11**, 2849 (1972).
8. J. James et P. Hambright. Inorg. Chem. **12**, 474 (1973).
9. G. Paquette et M. Zador. Can. J. Chem. **53**, 2375 (1975).
10. B. D. Berezin et A. N. Drobysheva. Russ. J. Phys. Chem. **51**, 11 (1977).
11. D. B. Berezin et O. I. Koifman. Russ. Chem. Rev. **42**, 922 (1973) et références citées.
12. B. D. Berezin, O. A. Golubchikov et O. I. Koifman. Russ. J. Inorg. Chem. **21**, 1070 (1976).
13. B. D. Berezin, N. I. Volkova et E. B. Karavaeva. Russ. J. Inorg. Chem. **20**, 1075 (1975); **22**, 220 (1977).
14. A. D. Adler, F. R. Longo, F. Kampas et J. Kim. J. Inorg. Nucl. Chem. **32**, 2443 (1970).
15. B. Shah, B. Shears et P. Hambright. Inorg. Chem. **10**, 1818 (1971).
16. M. Meot-Ner et A. D. Adler. J. Am. Chem. Soc. **94**, 4763 (1972).
17. S. Sugata et Y. Matsushima. J. Inorg. Nucl. Chem. **39**, 729 (1977); **40**, 1269 (1978); Chem. Pharm. Bull. **26**, 1071 (1978).
18. S. H. Mehdi, D. A. Brisbin et W. A. E. McBryde. J. Chem. Soc. Dalton Trans. 1364 (1976).
19. K. Letts et R. A. Mackay. Inorg. Chem. **14**, 2990 (1975); **14**, 2993 (1975) et références citées.
20. W. E. White et R. A. Plane. Bioinorg. Chem. **4**, 21 (1974).
21. R. R. Das, R. F. Pasternack et R. A. Plane. J. Am. Chem. Soc. **92**, 3312 (1970).
22. P. Hambright et E. B. Fleischer. Inorg. Chem. **9**, 1757 (1970).
23. S. B. Brown, M. Shillcock et P. Jones. Biochem. J. **153**, 279 (1976).
24. R. F. Pasternack, P. R. Huber, P. Boyd, G. Engasser, L. Francesconi, E. Gibbs, P. Fasella, G. Cerio Venturo et L. de C. Hinds. J. Am. Chem. Soc. **94**, 4511 (1972).
25. K. M. Smith (*Editeur*). Porphyrins and metalloporphyrins. Elsevier, New York, NY. 1975. p. 493.
26. W. S. Caughey, W. Y. Fujimoto et B. P. Johnson. Biochemistry, **5**, 3830 (1966).
27. F. A. Walker, E. Hui et J. M. Walker. J. Am. Chem. Soc. **97**, 2390 (1975).
28. F. A. Walker, M.-W. Lo et M. T. Ree. J. Am. Chem. Soc. **98**, 5552 (1976).
29. J. B. Reid et P. Hambright. Inorg. Chem. **16**, 968 (1977).
30. E. W. Baker, C. B. Storm, G. T. McGrew et A. H. Corwin. Bioinorg. Chem. **3**, 49 (1973).
31. J. Turay, P. Hambright et N. Datta-Gupta. J. Inorg. Nucl. Chem. **40**, 1687 (1978) et références citées.
32. J. P. Collman, C. M. Elliot, T. R. Halbert et B. S. Tourog. Proc. Natl. Acad. Sci. U.S.A. **74**, 18 (1977).
33. S. B. Brown et R. F. G. J. King. Biochem. J. **153**, 479 (1976).
34. P. Jones, K. Prudhoe et S. B. Brown. J. Chem. Soc. Dalton Trans. 912 (1974).
35. P. D. W. Boyd, T. D. Smith, J. H. Price et J. R. Pillbrow. J. Chem. Phys. **56**, 1253 (1972).
36. T. P. Stein et R. A. Plane. J. Am. Chem. Soc. **91**, 607 (1969).
37. R. M. Smith et A. E. Martell. Critical stability constants. Vol. 2. Plenum, New York, NY. 1975.
38. A. MacCragh, C. B. Storm et W. S. Koski. J. Am. Chem. Soc. **87**, 1470 (1965).
39. P. Hambright et P. B. Chock. J. Am. Chem. Soc. **96**, 3123 (1974).

The transannular electrophilic reaction of alkenyl nitroso compounds and the stereochemistry of nitrosyl chloride addition

YUAN L. CHOW, K. SOMASEKHARAN PILLAY, AND HERVÉ RICHARD
Department of Chemistry, Simon Fraser University, Burnaby, B.C., Canada V5A 1S6

Received May 1, 1979

YUAN L. CHOW, K. SOMASEKHARAN PILLAY, and HERVÉ RICHARD. Can. J. Chem. 57, 2923 (1979).

Nitrosyl chloride reacted with 1,5-cyclooctadiene and *trans,trans,trans*-1,5,9-cyclododecatriene in methylene chloride by the *cis*-addition to give chloronitroso alkenes with *cis* and *threo* (*trans*) configuration, respectively. These enantiomorphic *C*-nitroso compounds were isolated as a single compound for the former, and a mixture for the latter, of *dl* and (or) *meso* dimers, the presence of which was readily monitored by ^{13}C nmr spectroscopy. The former can assume a conformation to place the π-bonds of the nitroso and olefinic groups in interacting vicinity and undergo an acid catalyzed intramolecular electrophilic cyclization to give bicyclic hydroxylamines which are readily air oxidized to the corresponding nitroxide radicals. Rearrangement in acetic anhydride – methylene chloride afforded good yields of the stable bicyclic hydroxylamine acetates which served as precursors to generate the corresponding nitroxides under mild conditions. Photoaddition of *N*-nitrosopiperidine to 1,5-cyclooctadiene also partly afforded the *cis*-aminonitroso adduct which underwent the intramolecular addition to give hydroxylamines. The *threo*(*trans*)-chloronitroso alkenes failed to cyclize in similar fashion under comparable conditions. Nitrosylchloride added exclusively to the *trans*-double bond of *trans,cis*-1,5-cyclodecadiene without regiospecificity but was believed to follow the stereospecific *cis*-addition; this chloronitroso compound also underwent the acid catalyzed transannular reaction to give similar hydroxylamines that were not isolated in pure states.

YUAN L. CHOW, K. SOMASEKHARAN PILLAY et HERVÉ RICHARD. Can. J. Chem. 57, 2923 (1979).

Par une addition *cis*, le chlorure de nitrosyle dans le chlorure de méthylène se fixe sur le cyclooctadiène-1,5 et le cyclododécatriène-1,5,9 *trans,trans,trans* pour conduire respectivement aux alcènes chloronitrosés *cis* et *thréo* (*trans*). Les composés énantiomorphes *C*-nitrosés sont isolés sous forme de composé unique dans le cas du cyclooctadiène et sous forme d'un mélange de *dl* et/ou de dimères *méso* dans le second cas. La présence de ces derniers a été révélée par l'étude des spectres rmn du ^{13}C. Les composés dérivant du cyclooctadiène-1,5 adoptent une configuration qui place les liaisons π des groupements nitroso et oléfines au voisinage l'un de l'autre. Ceci permet alors une cyclisation électrophile intramoléculaire, catalysée par l'acide, qui conduit aux hydroxylamines bicycliques. Ces derniers s'oxydent facilement à l'air en radicaux nitroso correspondants. La transposition dans un mélange anhydre acétique – chlorure de méthylène fournit avec de bons rendements les acétates d'hydroxylamines bicycliques stables qui dans des conditions douces servent de précurseurs aux nitroxydes correspondants. L'addition photochimique de la *N*-nitroso pipéridine au cyclooctadiène-1,5 fournit aussi en partie l'adduit amino-nitrosé *cis* qui par une addition intramoléculaire conduit aux hydroxylamines. Dans des conditions identiques, les alcènes chloro-nitrosés *thréo* (*trans*) ne se cyclisent pas. Le chlorure de nitrosyle s'additionne exclusivement sur la double liaison *trans* du cyclododécadiène-1,5 *trans,cis*. La réaction n'est pas regiospécifique mais on pense que l'addition se fait stéréospécifiquement de manière *cis*. Ces composés chloronitrosés subissent également une réaction transannulaire catalysée par les acides pour conduire à des hydroxylamines similaires que l'on n'a pas pu isoler à l'état pur.

[Traduit par le journal]

Introduction

In the photoaddition of nitrosamines to olefins (1, 2), the isolated crude products very often exhibited esr signals in the region of the isotropic *g*-factor 2.006–2.007 suggesting the presence of nitroxide radicals. Yet, attempts to isolate these nitroxides by careful chromatography have never been rewarded despite the fact that nitroxides are generally fairly stable; in most cases oximes derived from the *C*-nitroso compounds, the primary photoadducts, are the major product, although certain exceptions have been observed (3, 4). That *C*-nitroso compounds can efficiently trap alkyl, acyl, and alkoxyl radicals during photolysis of nitrites and *C*-nitroso compounds has been well-established by de Boer and co-workers (5) and other groups (6, 7). A similar spin trapping reaction might be invoked to account for the nitroxide formations in photoaddition of

0008-4042/79/222923-13$01.00/0

nitrosamines to olefins but the extent must be very small. In cases where tertiary *C*-nitroso compounds are generated, since tautomerization is blocked, a novel intramolecular electrophilic reaction of the nitroso group with a suitably located labile electron pair occurs to give hydroxylamines which are oxidized to nitroxides (3). Such reactions might be regarded as intramolecular "ene" reactions; examples of intermolecular equivalents have been reported (*vide infra*). Subsequently we became interested in electrophilic reaction of nitroso groups with olefinic bonds.

The chemistry of *C*-nitroso compounds has been reviewed (9–12). Characteristically the *C*-nitroso group is readily reduced to hydroxylamines, oxidized to a nitro group, attacked by radicals to give nitroxides and by nucleophiles to give adducts in addition to tautomerization and dimerization (9). The *C*-nitroso group is electrophilic but hardly powerful enough to react with alkenes, dienes, or acetylene unless the nitroso group is activated by a vicinal electron withdrawing moiety, such as nitrosoarenes (13), trifluoronitrosomethane (13), α-halonitrosoalkanes (9), and nitrosylcyanide (14). Such nitroso compounds act as electrophilic dienophiles (9, 13, 14) to give 1,2-oxazines with dienes (13, 14). A 1,2-cycloaddition reaction with simple olefins is rare unless the nitroso group is powerfully electrophilic as in CF_3NO (13). However, recently nitrosoarenes (15–17) and tertiary nitrosoalkanes (18) have been shown to undergo "ene" reaction with olefinic bonds to give hydroxylamine derivatives, though the yields in the latter cases are not specified. In principle, a nitroso group may be protonated to generate a nitrenium ion intermediate which may react with a strategically located π-electron system. On the basis of this assumption, the reactions of some alkenyl nitroso compounds have been investigated.

Results

Photoaddition of *N*-nitrosopiperidine to 1,5-cyclooctadiene (**1**, 1,5-COD) in methanol in the presence of hydrochloric acid or perchloric acid gives the expected amino oxime **4** which was known to arise from tautomerization of the primary 1,2-addition product (1–4), *C*-nitroso compound **3**. In addition, a second product was isolated in fairly high yield in each photoreaction; this second product was shown to possess no carbon–carbon double bond and oximino moiety but the molecular formulae representing the addition of a molecule of hydrochloric acid or, in the latter case, methanol. Crude or analytically pure samples of these two compounds showed poorly resolved ^1H nmr spectra and a broad esr triplet signal of equal intensity with *g*-value 2.006–2.007 and a_N 15–17 G, typical esr parameters of nitroxide radicals (18, 19). Since the observed esr signal is similar to those of the nitroxides of a flexible bicyclo[3.3.1] system and different from those of the relatively rigid bicyclo[4.2.1] system with well-resolved hyperfine splitting from α and β-hydrogens (19), structures **5** and **6** were assigned to these two products; obviously, the esr signals were due to trace amounts of nitroxides **8** and **9** arising from the air oxidation of **5** and **6** (20). Indeed, hydroxylamine **6** was readily oxidized by alkaline hydrogen peroxide to **9**, which was rigorously characterized with elemental analysis and spectroscopy.

Both hydroxylamines **5** and **6** were difficult to purify by sublimation or recrystallization, though **5** could be recrystallized to give a good analysis by working under nitrogen atmosphere as much as possible. Presumably, oxidation occurred constantly during the operation in normal atmosphere to generate trace amounts of nitroxides **8** and **9**. Likewise,

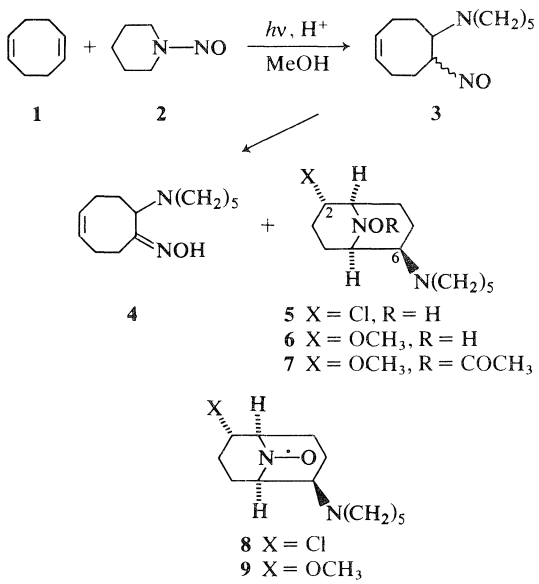

the *O*-acetyl derivatives of hydroxylamines could be prepared only with difficulty, probably for the same reason. By extensive chromatography, hydroxylamine acetate **7** was obtained and showed the typical *N*-acetoxy absorption at 1760 cm^{-1} (3).

Although the ^1H nmr spectra were poorly resolved, it was seen that the C-2 proton in **5** (—C*H*Cl—) had a large coupling constant and that in **6** (—C*H*OCH_3—) had a broad signal; these indicated that the C-6 proton had axial orientation. The narrow signals of the C-6 proton in **5** and **6** indicated the pseudo-equatorial orientation. The configuration will be discussed in detail later.

In the formation of the bicyclic hydroxylamines

shown above, an unisolated nitrosoalkene with a suitable configuration and conformation was assumed to be the precursor. With an aim to clarify the pattern of the transannular reaction the *anti*-dimer of chloronitroso compound **10** was prepared by addition of nitrosyl chloride to 1,5-COD (**1**). The addition gave a good yield of the nitroso dimers. While the purified dimer was very stable, the crude dimeric fractions tautomerized slowly in solution during nmr spectroscopic examinations to give more of oximes **11**, probably catalysed by a trace amount of acids. As the crude or recrystallized dimer showed eight signals in the ^{13}C nmr spectra with the expected chemical shifts, it must be an *anti*-azodioxy compound, either a *meso* (symmetrical) or *dl* (unsymmetrical) dimer (21), arising from a single adduct which was deduced to be the *cis*-adduct, as shown in **10** (*vide infra*). The dimer obviously possessed an *anti*-azodioxy group as shown by uv absorption at 294 nm and strong ir peaks at 1238 and 1208 cm^{-1}. The ^1H nmr spectrum of the dimer exhibited the methine protons at τ 4.57 and 5.48 which were shown to be not coupled to each other. In comparison to a large coupling of the methine protons ($J = 9$ Hz) in *trans*-2-dimethylaminocyclooct-5-ene-1-ol (22), the zero coupling as well as considerations of conformations with Dreiding stereomodels (*vide infra*) suggested that **10** had the *cis*-configuration of the functional groups. The dimer slowly decomposed on storage to give a mixture of *syn*- and *anti*-oximes **11** from which the former, the major product, was isolated. The assignments of the *syn*- and *anti*-configuration were made on the basis of chemical shifts of ^{13}C and the methine protons at the 2-position. The ^{13}C nmr spectrum of the mixture showed two sets of eight signal patterns, one set was relatively more intense than the corresponding signals of the other set. The mixture of oxime **11** was reacted with dimethylamine to give the known *anti*-amino oxime **12** (23).

Decomposition of the dimer of **10** under acidic conditions caused tautomerization to give oximes **11** (and derivatives thereof) and transannular cyclization to hydroxylamines such as **17** and **18**. Generally, in the presence of proton donors the former were formed overwhelmingly, but substantial amounts of the latter were produced in aprotic solvents. Thus, when the dimer was decomposed in a methylene chloride – methanol mixture in the presence of a catalytic amount of perchloric acid, a mixture of *syn*- and *anti*-oxime **11** (70%) and trace amounts of chloro ketone **14** and methoxy ketone **15** were obtained; in addition, by gc–ms, the presence of methoxy oxime **13** was detected. In this reaction, a small amount of hydroxylamine **17** was isolated but could not be crystallized because of the presence of the trace

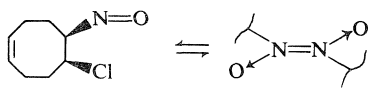

10

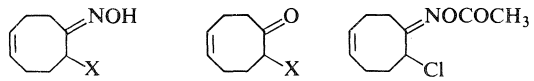

11 X = Cl
12 X = $N(CH_3)_2$
13 X = OCH_3

14 X = Cl
15 X = OCH_3

16

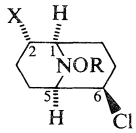

17 X = OCH_3, R = H
18 X = $OCOCH_3$, R = CH_3CO
19 X = OH, R = H

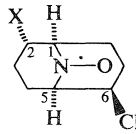

20 X = OCH_3
21 X = $OCOCH_3$
22 X = OH

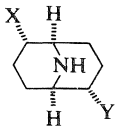

25 X = OAc, Y = Cl
26 X = OH, Y = H
27 X = Y = H

amount of the corresponding nitroxide **20**, as indicated by the esr triplet at $g = 2.0073$ and $a_N = 17.5$ G. Decomposition of the dimer of **10** in methanol – methylene chloride in the presence of hydrochloric acid or dimethylammonium chloride gave similar results, though the relative amounts of the oximes (**11** and **13**) and the ketones (**14** and **15**) varied considerably. Oxime **12** (5%) was also formed in the latter reaction. In these reactions, similar esr signals were always observed with the crude products and the presence of hydroxylamine **17** or related compounds, e.g., X = Cl or $N(CH_3)_2$, were indicated from the crude fractions of chromatography or gc–ms analysis. Many attempts to purify such crude fractions failed, probably due to air oxidation and other decomposition pathways during the operations.

Decomposition of the dimer of *C*-nitroso compound **10** in methylene chloride – acetic anhydride gave hydroxylamine **18** (60%) and oximino acetate **16** (30%), but, in the co-presence of acetic acid or sodium acetate in the same solvent, the yield of **18** was lower and that of **16** increased. Judging from the ten signal pattern of the ^{13}C nmr of oximino acetate **16**, this sample was homogeneous. In view of the chemical shifts of the C-2 at 59.6 ppm and the corresponding methine proton at τ 5.15, this oxime likely possesses the *syn* configuration. The structures of **13**, **14**, and **15** were suggested from their ir, nmr, and mass spectra.

While crude hydroxylamine acetate **18** from chromatography showed an esr triplet due to a trace amount of nitroxide **21** (*vide infra*), the sublimed sample was free of this signal and was characterized rigorously. Both hydroxylamines **17** and **18**, in analogy to hydroxylamines **5** and **6**, exhibited a broad multiplet for the C-2 proton (axial orientation), a narrow one for the C-6 proton (equatorial orientation), and a two proton multiplet for the C-1 and C-5 bridge protons. In particular, the axial orientation of the C-2 proton in **18** was clearly established by the coupling pattern, $J_{2,1} = 5$ Hz, $J_{2,3a} = 11$ Hz and $J_{2,3e} = 7$ Hz, which was obtained by decoupling experiments. From the ^{1}H nmr parameters and considerations based on Dreiding models, **23** and **24** with fairly flattened rings could be the most probable conformations among others for hydroxylamines **5**, **6**, **17**, and **18**. For **17** and **18** and their derivatives, the preferred conformation was most likely **23** because of the narrow signals ($W_{1/2} \approx 10$ Hz) for the protons at C-1 and C-5; it was reported that the corresponding protons in a chair–boat conformation showed much wider signals (≈ 16 Hz) but those in a chair–chair conformation showed narrower signals (9–10 Hz) (24). For a bulky Y = $N(CH_2)_5$ group in **5** and **6**, conformation **24** was more likely since the signal for the corresponding protons was much wider (12–14 Hz).

The mass spectra of these hydroxylamines **5**, **6**, **17**, and **18** indicated the common skeletal features by exhibiting the corresponding mass peaks that might be represented by the ion as shown, among other possibilities. The intensities of these ions varied depending on the group of X, Y, and Z and each compound had other prominent *m/e* peaks than those shown.

Hydroxylamine acetate **18** in methylene chloride showed no esr signal at all but, when shaken in the presence of saturated sodium carbonate solution in the air, it rapidly developed an intense 1:1:1 triplet with *g* value 2.0073 and $a_N = 17.2$ G (line width 4.8 G) within six minutes; the intensity was increased slowly afterward. This signal, as well as those from **5**, **6**, and **17**, persisted for more than a year. Brief reduction of **18** with lithium aluminum hydride gave hydroxylamine **19**, which possessed the expected ms, ^{1}H nmr, and ir spectra and was oxidized with alkaline hydrogen peroxide to give nitroxide **22**, showing a broad esr triplet (1:1:1) with *g* value 2.0078 and $a_N = 17.5$ G (band width 5.4 G).

The structure of hydroxylamine acetate **18** was confirmed by the following chemical transformation. Reduction of **18** with zinc and sodium iodide in acetic acid gave bicyclic amine **25**, which was rigorously characterized by analysis and spectroscopic data. Its ^{1}H nmr spectrum has a very similar pattern to that of **18** in the downfield region; while the C-2 (τ 4.93), C-1, and C-5 (τ 6.90) protons were shifted slightly upfield, the C-6 proton (τ 5.70) remained at the same chemical shift with respect to those of **18**. This suggests that the *N*-acetoxy group orients itself primarily as shown in **23** and **24** exerting long range deshielding effects on protons other than the C-6. The mass spectrum of **25** could be interpreted with a similar fragmentation scheme as shown above. Reduction of **25** with lithium aluminum hydride, followed by tosylation and further reduction with lithium aluminum hydride gave a 6:7 mixture of **26** and **27**; both compounds were identified by their mass spectra from gc–ms analysis. The bicyclic amine **27** was isolated and was tosylated to give known 9-tosyl-9-azabicyclo[3.3.1]nonane (25).

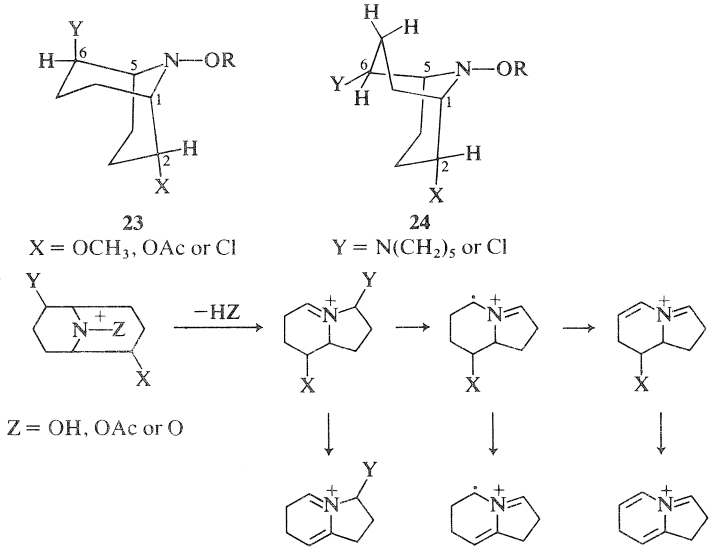

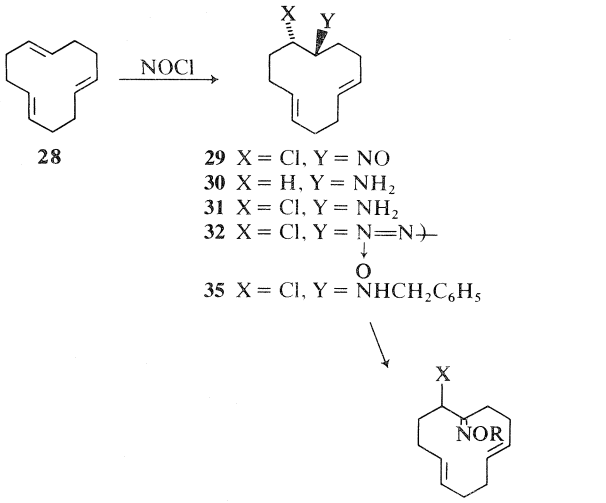

The *anti*-dimer of the chloronitroso compound **29** was obtained in a 94% yield from the addition of nitrosyl chloride to *trans,trans,trans*-1,5,9-cyclododecatriene (**28**, *ttt*CDT) (26, 27); this sample showed one spot on tlc and a sharp melting point. This compound had been prepared previously (26), but its stereochemistry was not reported. Since triene **28** had three-fold axes of symmetry, addition of nitrosyl chloride would not generate regioisomers. The ^{13}C nmr spectrum of the dimer, however, showed 17 lines, some of which were due to superimposed signals. The ^{1}H nmr spectrum of the dimer showed the C-1 (τ 4.16) and C-2 (τ 5.65) protons to be well resolved multiplets; by decoupling of the vicinal protons, the signals were collapsed to two sets of AB quartets. These nmr data indicated that this sample contained two dimers that were shown to be the *dl* and *meso* dimers (21) of *threo* (*trans*) chloronitroso compound **29** by the following transformation. The reduction of this dimeric sample with lithium aluminum hydride gave amine **30** and a minor amount of aziridine **33**, but with a LAH–$AlCl_3$ mixture a single chloro amine **31** in a 65% yield in addition to small amounts of azoxyalkane **32** and amine **30**. Further chloroamine **31** was converted to aziridine **33**.

Azoxyalkane **32** showed a ^{13}C nmr spectrum consisting of two sets of 12 line signals indicating one isomer;[1] it also showed an M^+ ion peak in agreement with the formula. While both amine **30** and chloro amine **31** showed the expected spectral data including ^{13}C nmr spectra containing 12 lines, aziridine **33** exhibited a 6 line ^{13}C nmr spectrum and a simple ^{1}H nmr pattern. This indicated that aziridine **33** must have the *dl*- or *meso*-configuration. Chloro amine **31** exhibited well resolved methine proton signals at τ 5.73 and 7.06 with a coupling constant of 2 Hz. This information did not permit a decision between the *erythro*- or *threo*-configuration. In order to determine the stereochemistry at the C-1 and C-2 positions, aziridine **33** was benzylated to give monobenzylaziridine **34** which could not be bis-benzylated under more vigorous conditions. On treatment with hydrogen chloride, the aziridine ring of **34** was opened up to give monobenzyl chloramine **35**.

The ^{13}C nmr spectrum of monobenzylaziridine **34** exhibited 6 lines for the aziridine portion and 5 lines for the benzyl portion; its ^{1}H nmr spectrum was relatively simple showing a sharp singlet at τ 6.56 for the benzyl protons. These spectroscopic data clearly proved that the aziridines **33** and **34** must possess the plane of symmetry and, therefore, the *meso*-configuration. Should **34** have the *dl*-configuration the aziridine would show 12 line ^{13}C nmr signals and the benzyl protons would be an AB quartet due to their diastereotopic nature. The assignment of the stereochemistry of **33** as *meso* (*cis*)-configuration permits the determination of the stereochemistry of chloronitroso compound **29** as *threo* (*trans*) if the elimination of hydrogen chloride from **31** to give aziridine **33** is assumed to occur by *trans*-elimination as shown below. The stereochemical course of the nitrosyl chloride addition to *ttt*CDT, therefore, must be the *cis*-addition in agreement with that to **1**.

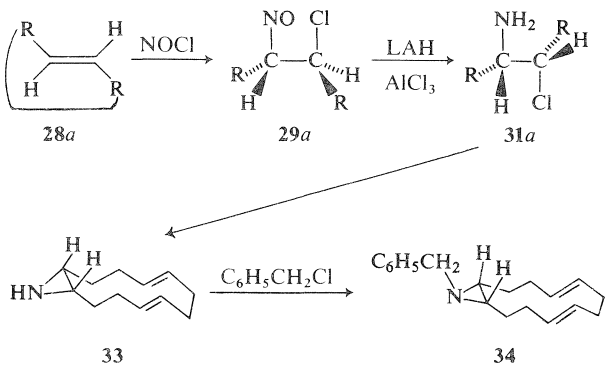

The dimer reacted with pyridine readily to give a nearly quantitative yield of pyridinium chloride **36**, which was further transformed to the known *syn*-dimethylamino oxime **37** (23) on reaction with excess dimethylamine. The treatment of the dimer of **29** with acetic anhydride gave a good yield of oximino acetate **38** and several minor products. Though the minor products could not be obtained, the crude reaction mixture exhibited an esr triplet (1:1:1) with

[1]The isolation of only one azoxyalkane **32** was rather unexpected and may arise by selective reduction of either the *dl* or *meso* isomer of **29** or, alternatively, by stereospecific condensation of one enantiomer of *RR*- or *SS*-**29** with one enantiomer of *RR*- or *SS*-hydroxylamine derived from the reduction of **29**.

$g = 2.0068$ and $a_N = 13.5$ G, typical of a nitroxide. Obviously, if similar transannular electrophilic cyclization as demonstrated with **10** had occurred with **29**, their amounts were fairly small.

The addition of nitrosyl chloride to *trans,cis*-1,5-cyclodecadiene (**39**, *tc*CDD) is able, in theory, to give isomeric chloronitroso adducts arising from attack at different double bonds, from regioselectivity, and from the *cis*- and *trans*-addition pathway; furthermore, the *C*-nitroso dimers would be a complex mixture of *meso* and *dl* isomers (21) arising from all possible combinations of the above enantiomorphic *C*-nitroso isomers. The crude or recrystallized *C*-nitroso dimer showed a surprisingly sharp melting point and also had uv and ir absorptions compatible with the *anti*-azodioxy linkage. This sample was obviously an isomeric mixture as shown by its ambiguous and diffused ^{13}C and ^1H nmr spectra. However, the ir absorption at 770 cm^{-1} and the result from tautomerization products (*vide infra*) indicated that the chloronitroso compounds were a regioisomeric mixture arising from the attack at the *trans* double bond of **39**, i.e., a mixture of **40** and **41** with unknown configurations.

Decomposition of the dimer of *C*-nitroso compounds **40–41** in the presence of hydrochloric acid

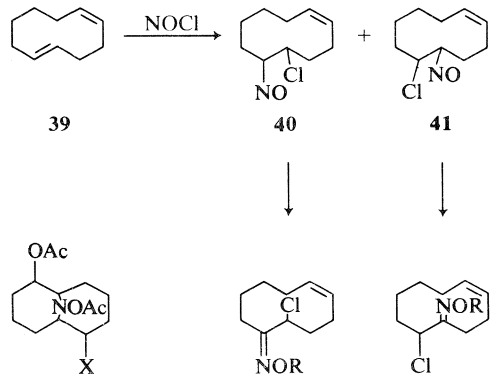

gave a mixture, which showed overlapped esr signals at $g \simeq 2.006$ and two similar nmr signals at τ 5.45 and 5.63, probably due to the C-2 protons of **42** and **43**. As the multiplet at τ 4.7 was changed to broad doublet ($J = 13$ Hz) on irradiation at the τ 8.00 region, the presence of the *cis* double bond was indicated. Chromatography of the mixture afforded one chloro oxime in the pure state and a mixture of cyclized hydroxylamines which could not be purified further. The isolated chloro oxime had pertinent analysis and spectral data for either **42** or **43**. However, structure **42** was favoured for the chloro oxime since decoupling experiments indicated that one C-10 proton at τ 6.93 was coupled with non-allylic protons at τ 8.39. As attempted isomerization of this sample under acidic conditions failed to give the other chloro oxime as shown by nmr monitors, it was concluded that two chloro oximes were positional isomers as in **42** and **43** but not the *syn–anti* isomers of the oxime.

Decomposition of the dimer of **40–41** in the presence of acetic anhydride was slow and gave an oil exhibiting one major esr triplet and two minor ones nearly overlapping in the region $g = 2.007$. The major product was a 1:3 mixture of two oximino acetates (i.e. **44** and **45**) exhibiting two analogous double doublets at τ 5.34 and 5.66 for the C-2 protons; this fraction showed the expected spectral data and analysis, but the assignments of structures to the major and minor components could not be achieved. Two minor compounds obtained in the amount of 8% each were shown to be a chloroacetoxyhydroxylamine acetate, such as **46**, and a diacetoxyhydroxylamine acetate, such as **47**. The spectral data supported the presence of the relevant functional groups in both cases, but their structures could not be confirmed.

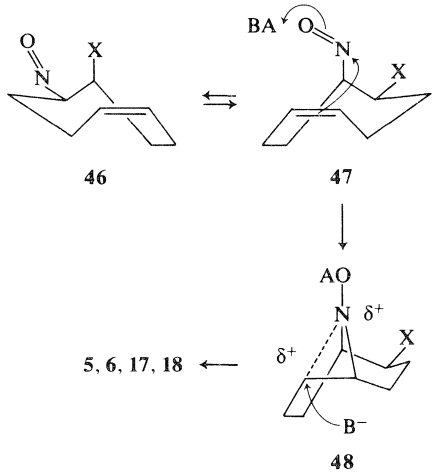

Discussion

From the results described above, two aspects of chemical transformations merit discussion, namely, the transannular electrophilic reaction of nitrosoalkenes and the nitrosyl chloride addition to olefins; both of them are intimately related to stereochemistry.

In spite of the report that the addition of nitrosoarenes to olefins occurs by a free radical (one-electron transfer) mechanism (6, 7) the intramolecular reaction of nitrosoalkenes described above must take place by an ionic mechanism on the basis of the following reasons. Firstly, the reaction is catalyzed by an acid and occurs even in the dark to give hydroxyl-

amines, but not nitroxides, as the primary product. Secondly, the transannular reaction affords six-membered heterocycles rather than five-membered ones; it is well documented that cyclization initiated by nitrogen centred radicals generally gives five-membered compounds as the major or exclusive product (29). The overall pattern of the acid catalyzed electrophilic attack of a *C*-nitroso group is the formation of bridged bicyclic hydroxylamines with the attachment of an anion. Such a reaction may be regarded as an allied reaction of the competing acid catalyzed tautomerization in which the electron pair of the α-CH bond participates in the electron reorganization of the nitroso group, if there are no other readily accessible electrons. The stereochemical requirements for the intramolecular reaction of the nitroso and olefinic groups are, therefore, that the π-orbitals of the interacting groups are capable of overlapping through space; this is related to the conformation of the reacting centres and, in turn, to the mode of addition of nitrosyl derivatives to polyenes.

It is indeed fortunate that nitrosyl chloride addition to 1,5-COD occurs stereospecifically to afford a single chloronitroso compound **10** which should have the *cis*-configuration since a proper conformation is available for the transannular reaction. The ^{1}H nmr results show that the *anti*-dimer of the *C*-nitroso compound **10** preferentially assumes the conformation **46** on the basis that the C-1 (CHNO) and C-2 (CHCl) protons are not coupled and, therefore, have ca. 90° dihedral angle, and that the coupling patterns of the C-1 (J = 11.5 and 4 Hz) and C-2 ($W_{1/2}$ = 11 Hz) indicate pseudo-axial and pseudo-equatorial orientations, respectively, for these protons. Studies of Dreiding stereomodels qualitatively show that **46** and **47** are more stable than other conformations for the *cis*-configuration of **10**. While for the dimer the conformation **46** is preferred owing to the bulky azodioxy group, the monomer **10**, having a much smaller bulk of the nitroso group, may be able to invert readily to **47**, from which a transannular interaction of the nitroso and olefinic π-bonds can occur as shown in **47** and **48**. The attack of an anion Y^- from the opposite side of the nitrogen bridge in the intermediate **48** leads to the observed configuration in **17** and **18**. Thus, the stereochemical consequence of the formation of hydroxylamines **17** and **18** necessitates the *cis*-configuration for **10**. An assumption of the *trans*-configuration for **10** does not readily give a conformation to satisfy the ^{1}H nmr parameters from model studies, nor lead to the observed configuration for hydroxylamines **17** and **18**. Preferential tautomerization of **10** to oxime **11** in protic solvents may be rationalized by the fact that the protonation of the nitroso group is accompanied by enlargement of the bulk of this group through solvation; this raises the conformational energy for **48** which, in turn, makes **10** less likely to undergo the transannular reaction.

The unisolated aminonitroso compounds **3** formed in the photoaddition of nitrosopiperidine to 1,5-COD must have *trans*- as well as *cis*-configurations in agreement with the previous findings (1, 4). Because of the bulky protonated piperidino group, the latter should have the conformation **47** preferentially, from which the transannular reaction can occur efficiently even in protic solvents. The stereochemical requirement of this cyclization is very similar to that discussed in the oxidative photoaddition of nitrosamines to 1,5-COD in which the *cis*-1-amino-2-nitrate, but not the *trans*-isomer, can undergo the transannular reaction to give the oxygen bridged bicyclic compound (22).

Whereas the trapping of radicals with *C*-nitroso compounds is a well established route for direct nitroxide formations (5–8), the present cases showed that for certain nitrosoalkenes, such as **10**, acid catalyzed intramolecular electrophilic reaction can also serve as an efficient route to give nitroxides indirectly via hydroxylamines. The intermolecular analogy of such electrophilic reaction undoubtedly can occur to a small extent, and if reactive olefins and *C*-nitroso compounds, e.g., caryophyllene with an endocyclic *trans* double bond (18) or nitrosobenzene (15–17), are used, isolable yields of hydroxylamines can be obtained. Recently, reactions of α-chloronitrosoalkanes with allenes or 2-phenylpropene have been reported to give good yields of analogous compounds (30).

It follows that chloronitroso compounds **40** and **41** are also capable of assuming conformations in which the reacting nitroso and olefinic π-orbitals can be brought to overlapping proximity but probably with a higher activation energy since the yields of the transannular cyclization are low. Such a conformation is obviously not readily available for chloronitroso compound **29**. The similar type of hydroxylamine, if formed at all as judged by the esr signal, is not present in a significant amount.

Reports on the generation of nitroxides and detection by esr studies are numerous but only in a few cases are nitroxides actually isolated and characterized (18–20), probably due to their low yields and (or) instability. Nitroxides are usually non-crystalline and difficult to purify, as shown previously (3) and in this report. On the other hand, hydroxylamine acetates, such as **18**, can be purified and stored, and further, can be easily hydrolysed under mild conditions, e.g., with aqueous sodium carbonate solution, to give hydroxylamines that are readily oxidized in the

air to generate nitroxide radicals (20). These reactions may explain the detection of the nitroxide esr signal with the crude sample of hydroxylamine acetate **18** isolated in rearrangement in acetic anhydride. Therefore, hydroxylamine acetates can serve as stable precursors to generate nitroxides continuously for a considerable period.

In spite of a large number of reports on nitrosyl chloride addition to olefins (28), the stereochemical course of the addition remains relatively vague mainly because of the fact that enantiomorphic adducts dimerize homospecifically to give the *dl* dimers as well as heterospecifically to give the *meso* dimers (21). This situation has recently been nicely demonstrated by Rogić and co-workers (21), when the confusing claims over the *C*-nitroso dimers derived from the addition to cyclohexene (31, 32) were clearly resolved. The clarification of *C*-nitroso monomer **10** with the *cis*-configuration and that of **29** with the *threo* (*trans*)-configuration proves that the nitrosyl chloride additions to 1,5-COD and *ttt*CDT in methylene chloride occur by the *cis* stereochemical course. These are in agreement with the *cis*-addition of nitrosyl chloride to various olefins in low polarity solvents such as methylene chloride and carbon tetrachloride (21, 31, 33) for which the four-centred addition through a molecular complex has been proposed by Meinwald and co-workers (33). A survey of the literature and unpublished results from our laboratory shows that the addition of nitrosyl chloride (31) or formate (34) to olefins in highly polar solvents, such as sulfur dioxide and formic acid, may preferentially give *trans*-addition products; this may occur by a stepwise attack of the nitrosonium ion stabilized by the highly ionizing media.

In this report ^{13}C nmr spectroscopy has been shown to be a superior method to monitor diastereoisomeric mixtures where ^{1}H nmr spectroscopy is of limited usefulness. In particular, owing to a lability to heat, melting points, gc, and tlc are unsatisfactory criteria as measures of homogeneity for the dimers of *C*-nitroso compounds **29** and **40**–**41**. But ^{13}C nmr spectra unambiguously show that the sample of the dimer of **29** is a mixture of *meso* and *dl* compounds and that of *C*-nitroso compound **10** contains only one diastereoisomer, either *meso* or *dl*. In the latter case, the dimerization process is specifically regulated by the conformational factors associated with *cis*-configuration.

Whereas the addition of nitrosyl chloride to *tc*CDD is non-regiospecific as shown by the tautomerization products **42**–**45**, it is established that the *trans* double bond is more reactive than the *cis* one toward nitrosyl chloride, in agreement with the published results (26–28). In analogy to the addition to other olefins as discussed above, the addition to the *tc*CDD *trans* double bond may also occur by stereospecific *cis* geometry. Unfortunately experiments designed to prove this point have not been successful.

Experimental

General Conditions

Unless specified otherwise, the following conditions prevailed. Nuclear magnetic resonance spectra were measured with a Varian A-56/60 or an XL-100 (with or without a Fourier transform attachment) spectrometer in $CDCl_3$ using TMS as the internal standard, and ir spectra were taken in neat or Nujol mulls with a Perkin-Elmer Model 457. Instruments included an Hitachi-Perkin-Elmer Model RMU-6E, a Cary 14, a Varian E-4, and a Varian 1200 vpc apparatus with a flame ionization detector. The gc–ms measurements used a Varian 1400 (20% SE-30 column) coupled with the mass spectrometer. Melting points were reported as determined with a Fisher-Johns hot stage or a Gallenkamp heating block. Elemental analyses were performed by Mr. M. K. Yang with a Perkin-Elmer microanalyser.

Photoaddition of N-*Nitrosopiperidine to 1,5-Cyclooctadiene*

(*1*) A methanol solution (320 mL) containing 1,5-cyclooctadiene (4.32 g), *N*-nitrosopiperidine (5.47 g), and 70% perchloric acid (6.9 g) was irradiated with a 200 W Hanovia lamp under nitrogen through a Nonex filter for 5 h. The photolysate was treated with sodium carbonate (5.5 g) and stirred. The solution was evaporated to ca. 50 mL and filtered. The filtrate was cooled in a refrigerator to give colorless crystals (450 mg). The crystals were recrystallized from methanol to give the perchlorate of hydroxylamine **6**, mp 202–203°C; ir: 3200, 3080, 1110(s), 1050(s), and 620(s) cm^{-1}; ms *m/e* (%): 255 (M^+, 0.8), 254.1998 (1.6; calcd, for $C_{14}H_{26}N_2O_2$: 254.1994), 238(9), 237.1967 (42, calcd. for $C_{14}H_{25}N_2O$: 237.1967), 155(39), 154.1234 (100, calcd. for $C_9H_{16}NO$: 154.1232), 152(35), 140(29), 124.1127 (52, calcd. for $C_8H_{14}N$: 124.1126), 122(20), 98(26), 84.0815 (93, calcd. for $C_5H_{10}N$: 84.0813). *Anal.* calcd. for $C_{14}H_{26}N_2O_2 \cdot HClO_4$: C 47.39, H 7.67, N 7.89; found: C 47.11, H 7.78, N 7.72. The ^{1}H nmr signals were unresolved and showed a singlet at τ 6.73 and a broad signal at τ 6.3. The crystals were taken up in water and neutralized with a sodium hydroxide solution to afford hydroxylamine **6** (*vide infra*).

The mother liquor was evaporated and the residue was diluted with water. Extraction with methylene chloride (50 mL × 5) and the usual workup gave a solid (8.74 g). This solid (4 g) was chromatographed on silicic acid. Elution with 2.5–5% MeOH in CH_2Cl_2 gave oxime **4** (1.42 g) and with 5–10% MeOH in CH_2Cl_2 gave hydroxylamine **6** (1.57 g). Oxime **4** was recrystallized from methanol to give monoclinic crystals: mp 137–138.5°C; ir: 3170(m), 3020(m), 2700(s), 1505(w), 1100(m), 1095(m), 1032(m), 955(s), 948(s), 895(s), 862(m), 770(s), 730(s) cm^{-1}; ^{1}H nmr τ: 1.12 (1H, D_2O exchangeable), 4.39 (m, 2H), 6.92 (m, 2H), 7.32–9.00 (m, 17H); ms *m/e* (%): 222 (M^+, 6), 206(18), 205(100), 204(14), 164(37), 124(32), 122(14), 111(59), 84(60). ^{1}H nmr decoupling experiments showed that, on irradiation of the big signal at 7.32–9.00, the vinyl signal at τ 4.39 changed to an AB quartet (J = 13 Hz) and the signal at τ 6.92 changed pattern. *Anal.* calcd. for $C_{13}H_{22}N_2O$: C 70.23, H 9.97, N 12.60; found: C 70.20, H 9.88, N 12.68. The oxime **4** was hydrogenated in the presence of platinum black in ethanol to give the known *anti*-2-piperidinocyclooctanone oxime; the ir and nmr spectra were superimposable with those of an authentic sample prepared previously; mp and mixed mp 160–162°C (lit. (33) mp 163–165°C).

The fraction containing hydroxylamine **6** showed the fol-

lowing physical constants; ir: 3500–3000 (broad), 1090(s), 955(m), 900(s) cm^{-1}; ms *m/e* (%): 254 (M^+, 2), 252(1), 237(9), 154(100), 152(15), 124(38), 113(15), 112(15), 98(27), 86(29), 84(49); esr in benzene: $g = 2.0051 \pm 0.0003$ G, $a_N = 17.25$ G (line width 4.5 G). The reduction of the solid with lithium aluminum hydride followed by immediate acetylation gave a complex mixture. This solid (150 mg) was treated in water (2 mL) containing 30% H_2O_2 (2 mL) and 2 drops of 1 *N* NaOH for 1 h. The mixture was extracted with methylene chloride, which was worked up to afford a brown paste (100 mg). This crude product was passed through an alumina column to afford nitroxide **9** as a brown semi-solid; ir: 3150 (bw), 1103(s), 1090(s), 898(m) cm^{-1}; esr in benzene: $g = 2.0067$, $a_N = 17.25$ G (line width 5 G); ms *m/e* (%): 253.1917 (M^+, 12, calcd. for $C_{14}H_{25}N_2O_2$: 253.1917), 238(16), 277.1967 (66, calcd. for $C_{14}H_{25}N_2O$: 237.1967), 205.1701 (16, calcd. for $C_{13}H_{21}N_2$: 205.1705), 155(53), 154.1228 (100, calcd. for $C_9H_{16}NO$: 154.1232), 152(53), 125(29), 124.1130 (77, calcd. for $C_8H_{14}N$: 124.1126), 122.0966 (32, calcd. for $C_8H_{12}N$: 122.0970), 120(30), 111(29), 84(44). *Anal.* calcd. for $C_{14}H_{25}N_2O_2$: C 66.37, H 9.95, N 11.06; found: C 66.65, H 10.02, N 11.47. The yields of oxime **4** and hydroxylamine **6** were 37 and 38%, respectively, based on the amount of *N*-nitrosopiperidine.

Hydroxylamine **6** (516 mg) and acetic anhydride (2 mL) in ether were kept at −15°C for 3 h under hydrogen atmosphere. The reaction mixture was poured into ice-water and worked up in the usual manner to give a solid (467 mg) which was crystallized from pentane twice to afford hydroxylamine acetate **7**; mp 91–92°C (started to decompose at 85°C); ir: 1765(s), 1378(s), 1225(s), 1212(s), 1010(s), 950(s), 932(s), 890(s), 845(m), 790(m) cm^{-1}. *Anal.* calcd. for $C_{15}H_{25}N_2O_2Cl$: C 59.89, H 8.38, N 9.31; found: C 60.10, H 8.48, N 9.30.

(*2*) A solution containing *N*-nitrosopiperidine (7.27 g), 1,5-cyclooctadiene (10 mL) and concentrated hydrochloric acid (7 mL) was photolysed under nitrogen for 1.5 h. The solution (4/5) was evaporated; benzene (100 mL) and ethanol (10 mL) were added to the residue and evaporated. The residue was diluted with acetone to give a white precipitate (9.1 g). The mother liquor was evaporated and diluted with water. The aqueous solution, after being evaporated, was washed with ether and neutralized with sodium carbonate solution. The precipitated solid (2.1 g) was filtered to afford a crude hydroxylamine **5** and recrystallized from methanol twice; recrystallization from cyclohexane gave hydroxylamine **5**; mp 166–167°C (dec.); ir: 3200–2600, 3090(m), 1510(w), 982(m), 948(s), 895, 780(s), 730(s) cm^{-1}; ^1H nmr τ: 2.0(O*H*), 5.19 (m of d, $J = 9$ and 4 Hz, 1H), 6.71 (m, 2H), 7.15 (m, 1H), 7.7 (m, 4H), 8.00 (m); ms *m/e* (%): 243(4), 241(11), 207(2), 205(5), 160(36), 158(100), 124(89), 120(35), 111(19), 98(22), 84(29); ^{13}C nmr: 65.5(d), 60.2(d), 56.6(d), 55.8(d), 51.0(t), 30.0(t), 24.8(t), 23.2(t), 22.8(t), 21.6(t), 17.5(t). *Anal.* calcd. for $C_{13}H_{23}N_2OCl$: C 60.33, H 8.96, N 10.82; found: C 60.30, H 9.11, N 10.90. The crude hydroxylamine fraction showed a triplet esr signal (1:1:1) at $g = 2.006$, $a_N = 16.5$ G in carbon tetrachloride. Irradiation at τ 6.71 or at τ 8.00 region changed the coupling pattern of the signal at τ 5.19. Attempted LAH reduction and acetylation yielded a product showing an ir absorption at 1760 cm^{-1} ($NOCOCH_3$) but could not be purified.

The white precipitate (500 mg) was dissolved in water and neutralized. The precipitate (410 mg) was recrystallized from methanol to afford oxime **4**; mp 134–135°C; the ir and nmr spectra were superimposable with those of the previous sample. The mother liquor was combined and evaporated to give a residue. The residue was a mixture of oxime **4** and hydroxylamine **6**, in a ratio of ca. 3:1 as shown by tlc and ir and nmr spectra.

The Preparation of the Dimer of C-*Nitroso Compound* ***10***

(*1*) A methylene chloride solution (20 mL) of nitrosyl chloride (3.26 g, 0.05 mol) was added dropwise in half an hour to a solution of 1,5-cyclooctadiene (10 g, 0.093 mol) in methylene chloride (20 mL) at −10°C. After 0.5 h hexane (100 mL) was added to the reaction mixture, which was evaporated to 40 mL under vacuum. The solution was cooled to deposit a white solid (2.56 g, mp 99–101°C), which was recrystallized from a 1:4 mixture of $CHCl_3$–hexane to afford the *anti*-dimer of *cis*-1-nitroso-2-chloro-5-cyclooctene (**10**); mp 104.5–105°C; uv λ_{max} (CH_2Cl_2): 294 nm (ε_{max}, 6250); ir: 3020(m), 1238(s), 1208(s), 775(m), 752(m), and 736(s) cm^{-1}; ^1H nmr τ: 4.06–4.40 (m, 2H), 4.57 (dd, $J = 11.5$ and 4.0 Hz, 1H), 5.48 (m, $W_{1/2} = 11$ Hz, 1H), 7.1–8.2 (m, 8H); ^{13}C nmr: 131.0(d), 128.5(d), 67.8(d), 61.0(d), 35.7(t), 27.3(t), 21.8(t), and 21.6(t); ms (110°C) *m/e* (%): 176(1.5), 175(2), 174(3), 173(2), 158(4), 156(9), 138(13), 120(10), 107(42), 91(46), 79(100), 67(42), 53(20), 41(33), and 39(29). *Anal.* calcd. for $(C_8H_{12}NOCl)_2$: C 55.34, H 6.97, N 8.07; found: C 55.23, H 6.93, N 8.07. On irradiation at τ 7.89, the multiplet at 5.48 collapsed to a doublet ($J = 8$ Hz) and that at τ 4.57 was modified. On irradiation at τ 7.78, the double doublet at τ 4.57 collapsed to a singlet and the signal at 5.48 changed slightly. Irradiation at τ 5.48 or at τ 4.57 caused no change in the respective signal nor in the olefinic signal at τ 4.2 area.

The blue mother liquor was washed with sodium carbonate solution and water. The organic phase was dried and evaporated. To the residue, *n*-hexane was added to afford an additional dimer of **10** (564 mg, mp 98–102°C.)

(*2*) A methylene chloride solution of nitrosyl chloride (34% by weight, 0.88 g, 4.63×10^{-3} mol) was added in 15 min to a methylene chloride solution (15 mL) containing COD (0.5 g, 4.63×10^{-3} mol). The solution was stirred at −10°C for 30 min and was diluted with *n*-hexane (50 mL). The mixture was evaporated to ca. 30 mL to afford the first crop (196 mg, 24%, mp 98–101°C). Further evaporation to ca. 10 mL afforded the second crop of solid (165 mg, 20%, mp 95–98°C). The mother liquor was evaporated to afford a dark blue oil (222 mg). These samples were examined with ^{13}C nmr spectroscopy and intensity of comparable peaks was used to estimate the % yield of the products. The first crop contained the dimer of **10** and *syn*-oxime **11** in the ratio of 9:1 and the second crop the dimer of **10** and *syn*- and *anti*-oximes **11** in the ratio of 7:2:1. The blue oil consisted of *syn*- and *anti*-oximes **11**, COD, and the dimer in the ratio of 8:4:4:3. The estimated yield of the dimer of **10** was 43%.

Reactions of the Dimer of ***10***

(*1*) The crude dimer (450 mg) was left at room temperature for two months to give an orange oil which was a mixture of *anti*- and *syn*-oxime **11** showing ir: 3280 (broad), 3020(m), 1640(m), 1155(m), 990(s), 900(s), 755(s) and 680(s) cm^{-1}; ^1H nmr: τ 0.95 (OH), 4.33 (m, 2H), 5.40 (dd, $J = 7.0$ and 5.0 Hz, 2/3 H), 5.68 (dd, $J = 8.0$ and 4.0 Hz, 1/3 H), 7.0–8.1 (m, 8H); ^{13}C nmr: *160.2*(s), 158.8(s), 130.6, 130.1, *129.4*(d), *129.3*(d), *60.2*(d), 55.9(d), *36.9*(t), 33.8(t), 31.8(t) *25.9*(t), *22.8*(t), 22.2, *22.1*(t), 20.9(t). The chemical shifts in italics of ^{13}C nmr were relatively more intense than others. A part of the oil was sublimed to afford a colourless oil of *syn*-1-oximino-2-chloro-5-cyclooctene (**11**); one peak at 17.3 min on a 10% SE-30; ir: 3300 (b), 3020(m), 1645(m), 1225(m), 1215(m), 1165(m), 1155(m), 985(s), 900(s), 755(s), and 670(m) cm^{-1}; ^1H nmr τ: 2.26(OH), 4.33 (m, 2H), 5.40 (dd, $J = 7.0$ and 5.0 Hz, 1H), and 7.0–8.1 (m, 8H); ms (100°C) *m/e* (%): 175 (M^+, 3), 173(5), 158(34), 156(88), 138(94), 120(100), 93(56), 84(66), 74(96), and 67(58). *Anal.* calcd. for $C_8H_{12}NOCl$: C 55.34, H 6.97, N 8.07; found: C 55.50, H 6.97, N 8.38. A mixture of oxime **11** was treated with piperidine to give oxime **4**: mp 135–137°C.

(*2*) A suspension of the dimer of **10** (200 mg) in methylene chloride (5 mL) and methanol (20 mL) containing two drops of perchloric acid (70%) was stirred at 40°C for one day, when the dimer disappeared as shown by tlc. The solution was evaporated and water (20 mL) added. Extraction of the solution with methylene chloride (20 mL × 3) gave a colourless oil (170 mg). By the gc peak matching method, chloro oxime **11** (17.3 min) was shown to be present in 70% yield and 2-chloro-5-cyclooctenone (**14**) and 2-methoxy-5-cyclooctenone (**15**) in trace amounts (23). By gc–ms, the oil was shown to contain the above compounds in addition to a mixture of *syn*- and *anti*-methoxy oxime **13** (16.3 min, 15%): ms *m/e* (%): 169 (M^+, 7), 152(87), 137(49), 120(90), 109(55), 94(72), 79(89), 67(100), and 41(78).

The aqueous phase was adjusted to pH 10 and was extracted with methylene chloride to afford solid hydroxylamine **17** (10 mg); ir: 3200(b), 1265(m), 1102(m), 1088(s), 1050(m), 910(s), 840(m), 725(s), 653(m), 630(m) cm^{-1}; ^1H nmr τ: 5.68 (m, $W_{1/2}$ = 8 Hz, 1H), 6.02 (m, $W_{1/2}$ = 22 Hz, 1H), 6.46–6.76 (m, 2H), 6.64 (s, 3H), and 7.5–8.85 (m, 9H); ms (90°C) *m/e* (%): 207 (M^+, 2), 205 (M^+, 6) 190(39), 188(100), 176(6), 174(20), 170(27), 160(7), 158(22), 120(21), 112(28), 71(46), and 41(41); esr (CH_2Cl_2) triplet (1:1:1): g = 2.0073 ± 0.0006, a_N = 17.5 G (line width = 5.5 G).

When the dimer (200 mg) was treated similarly in the presence of dimethylamine hydrochloride, it gave a neutral fraction (185 mg) consisting of chloro oximes **11** as the major product (81%) and hydroxylamine **17** in a 9% yield. This oil showed the same esr signal as above. The oil was treated with zinc (1 g) and acetic anhydride (1 g). The product was worked up and chromatographed to give acetate of chloro oxime **16** (164 mg) and an oil (32 mg) showing the same esr signal. The basic fraction contained oxime **12** (5%) (23).

(*3*) A solution of the dimer (400 mg), acetic anhydride (2.4 g), and acetic acid (28 mg) in methylene chloride (25 mL) was heated at 40°C under nitrogen for 5 h. The reaction mixture was diluted with water and made basic with saturated sodium carbonate solution. Extraction with methylene chloride followed by the usual workup gave a yellow oil (461 mg) which showed two major and one minor spots on tlc. This mixture was taken up in methylene chloride and chromatographed on a silicic acid column. The four fractions eluted with 0.5–1% CH_3OH in CH_2Cl_2 gave a colourless oil (251 mg, 51%) which was sublimed to afford oximino acetate **16**; ir: 3020(m), 1775(vs), 1625(m), 1370(s), 1200(vs), 1002(s), 980(m), 925(s), 770(m), and 750(m) cm^{-1}; ^1H nmr τ: 4.34 (m, 2H), 5.15 (dd, J = 7.0 and 5.0 Hz, 1H), 6.88–8.10 (m, 8H), 7.83 (s, 3H); ^{13}C nmr: 167.3(s) 166.9(s), 129.7(d), 128.3(d), 59.6(d), 36.2(t), 27.1(t), 21.7(t), 21.3(t), 18.8(q) ppm; ms *m/e* (%): 211(6), 209(8), 175(19), 173(52), 138(37), 120(100), 91(73), 79(96), 67(68), and 43(88). *Anal.* calcd. for $C_{10}H_{14}NO_2Cl$: C 55.69, H 6.54, N 6.50; found: C 55.53, H 6.63, N 6.81. On irradiation at τ 7.85, the double doublet at τ 5.15 collapsed to a sharp singlet. On irradiation at τ 7.50, the olefinic signal at τ 4.34 changed to an AB quartet (J = 12 Hz).

The fractions eluted with 2–4% MeOH in CH_2Cl_2 afforded a yellowish solid (145 mg, 18%) which, in chloroform solution, showed a nitroxide esr triplet (1:1:1), g = 2.0068 ± 0.0006, a_N = 17.2 G (line width 5.7 G). The solid was sublimed to afford white crystals of hydroxylamine acetate **18**; mp 79–83°C; ir: 1768(s), 1726(s), 1370(s), 1246(s), 1232(s), 1213(s), 1200(s), 1032(s), 955(m), 900(m), 880(s), 790(m), 738(m) cm^{-1}; ^1H nmr τ: 4.64 (possibly ddd, J = 11, 7.0, and 5.0 Hz, 1H), 5.70 (m, $W_{1/2}$ = 8 Hz, 1H), 6.41 (m, $W_{1/2}$ = 11 Hz, 2H), 7.59–8.46 (m, 8H), 7.87 (s, 3H), 7.93 (s, 3H); ^{13}C nmr: 169.0(s), 168.4(s), 66.7 (d, C2), 59.4 (d, C1 and C6), 55.2 (d, C5), 27.6(t), 23.3(t), 21.6(t), 20.1(q), 19.4(t), 18.8(q) ppm; ms *m/e* (%): 277.0880 and 275.0903 (M^+, 2 and 6%, calcd. for $C_{12}H_{18}NO_4Cl$: 277.0894 and 275.0925), 235.0815 and 233.0800 (27 and 79, calcd. for $C_{10}H_{16}NO_3Cl$: 235.0789 and 233.0819), 218.0782 and 216.0811 (30 and 88, calcd. for $C_{10}H_{15}NO_2Cl$: 218.0761 and 216.0791), 198(44), 176.0646 and 174.0685 (33 and 100, calcd. for $C_8H_{13}NOCl$: 176.0656 and 174.0685), 158(8), 156(20), 138.0930 (46, calcd. for $C_8H_{12}NO$: 138.0919), 120.0809 (24, calcd. for $C_8H_{10}N$: 120.0813), 96.0576 (29, calcd. for C_6H_8O: 96.0576). On irradiation at τ 6.41, the signal at τ 4.64 became a broad double doublet (J = 10 and 7 Hz) and the pattern at τ 5.70 was changed. *Anal.* calcd. for $C_{12}H_{18}NO_4Cl$: C 52.27, H 6.58, N 5.08; found: C 52.57, H 6.61, N 5.17.

The dimer of **10** (100 mg) dissolved in methylene chloride (5 mL) and acetic anhydride (562 mg) was stirred under nitrogen at 50°C for two days. The usual workup gave an oil which was a mixture of oximino acetate **16** (30%) and hydroxylamine acetate **18** (60%) as judged by the ^1H nmr integration of the methine protons at τ 5.15 and 5.70.

Rearrangement of the dimer in acetic anhydride gave oximino acetate **16** and hydroxylamine acetate **18** in 50 and 42% yields. A similar treatment of the dimer (400 mg) in methylene chloride (15 mL) and acetic anhydride (2.25 g) containing fused sodium acetate (800 mg) gave a 3:2 mixture of **16** and **18**. Column chromatography of the mixture gave oxime acetate **16** (260 mg, 52%) and hydroxylamine acetate **18** (217 mg, 34%).

Reactions of Hydroxylamine 18

(*1*) A methylene chloride solution (4 mL) of **18** (0.5 mg) showed no esr signal. To this solution was added saturated sodium carbonate solution (1 mL) and shaken. Immediately the methylene chloride phase showed the esr signal of the 1:1:1 triplet, g = 2.0073 ± 0.0005, a_N = 17.2 G (line width 4.8 G). The signal increased rapidly for the first six minutes and then slowly afterwards and kept the same intensity for one year.

(*2*) Hydroxylamine acetate **18** (50 mg) in ether (5 mL) was treated with lithium aluminum hydride (200 mg) for five hours at room temperature and was worked up in the usual manner to give a solid (29 mg). Sublimation of the solid gave hydroxylamine **19**; mp 126–129°C; ir: 3300 (s, broad), 1255(s), 1095(s), 1060(s), 1035(s), 990(m), 960(m), 930(m), 905(s), 830(m), and 722(s) cm^{-1}; ^1H nmr τ: 5.48 (m, $W_{1/2}$ = 20 Hz, 1H), 5.67 (m, $W_{1/2}$ = 6 Hz, 1H), 6.64 (m, $W_{1/2}$ = 13 Hz, 2H) and 7.3–8.9 (m, 10H); ms *m/e* (%): 193 (M^+, 2), 191(8), 176(35), 174(100), 157(9), 156(15), 155(22), 140(40), 118(22), 112(22), 98(21), 96(26), 82(23), 80(21), and 67(25).

Hydroxylamine **19** (10 mg) was oxidized in aqueous solution containing 30% hydrogen peroxide (1 mL) and two drops of 1 *N* sodium hydroxide, and was worked up in the usual manner to give a yellow solid (5 mg) of **22**; ir: 1260(m), 1020(m), and 800(m) cm^{-1}; esr (CH_2Cl_2), triplet (1:1:1): g = 2.0078 ± 0.0005, a_N = 17.5 G (line width 5.4 G).

(*3*) A mixture of 80% acetic acid (3.5 mL), sodium iodide (175 mg), hydroxylamine acetate **18** (190 mg), and zinc dust (1.05 g) was stirred at room temperature for 36 h and at 40°C for 2 h. The zinc was filtered and the solution was evaporated. Water was added to the residue and the pH adjusted to 10. Extraction with methylene chloride and the usual workup gave an oil (131 mg, 87%) which was distilled to give **25**; ir: 3300(m), 1735(vs), 1370(s), 1240(vs), 1100(m), 1032(s), 922(s), 895(m), 882(m), 798(m), 775(m), 740(s), 700(s), 575(s) cm^{-1}; ^1H nmr τ: 4.93 (broad quintet, J = 10, 5, and 5 Hz, 1H), 5.70 (m, $W_{1/2}$ = 8 Hz, 1H), 6.9 (m, $W_{1/2}$ = 11 Hz, 2H), 7.4(NH), 7.96 (s, 3H), 7.5–8.4 (m, 8H); ^{13}C nmr: 169.6(s), 71.8(d), 61.9(d), 51.6(d), 47.1(d), 29.1(t), 26.6(t), 24.9(t), 20.8(q), 18.9(t); ms *m/e* (%): 219.0836 and 217.0869 (M^+, 2 and 7, calcd. for $C_{10}H_{16}NO_2Cl$: 219.0840 and 217.0869), 182.1180 (52, calcd. for $C_{10}H_{16}NO_2$: 182.1181), 176(28), 174(79),

159(28), 157(82), 122.0969 (100, calcd. for $C_8H_{12}N$: 122.0969), 96(48), 94(38), 82(40), 80(71). On irradiation of the multiplet at τ 6.90, the signal at τ 4.93 changed to a broad double doublet (J = 10.0 and 5.0 Hz) and the signal at τ 5.70 was modified. *Anal.* calcd. for $C_{10}H_{16}NO_2Cl$: C 55.17, H 7.41, N 6.44; found: C 55.29, H 7.48, N 6.72.

Reactions of Bicyclic Amine ***25***

The bicyclic amine **25** (120 mg) was reduced with lithium aluminum hydride (150 mg) in ether (20 mL) at room temperature for 16 h and was worked up to afford a colourless oil (47 mg); ir: 3300, 1055(s), 1035(s); ms *m/e* (%): 177(1), 175(3), 141(17), 140(12), 123(44), 122(30), 96(34), 94(100), 82(57). The oil (40 mg) was treated with *p*-toluenesulfonyl chloride to give a crude product. This crude product was refluxed with lithium aluminum hydride (150 mg) in ether for one day to afford an oil. By gc–ms analysis, this oil was shown to contain bicyclic amines **27** and **26**; **27**, rt 4.9 min, 43%, *m/e* (%): 125 (M^+, 49), 96(87), 83(41), 82(100), 69(28); **26**, rt 7.2 min, 36%, *m/e* (%): 141 (M^+, 1), 123(62), 122(28), 108(18), 95(25), 94(100), 82(19).

This oil was chromatographed on basic alumina and was eluted with 4–8% CH_3OH–CH_2Cl_2 to afford an oil (7 mg) which was treated with *p*-toluenesulfonyl chloride in pyridine to give a crystalline compound of 9-tosyl-9-azabicyclo[3.3.1]-nonane **27** ($NH{=}NSO_2C_6H_4CH_3$); ms *m/e* (%): 279 (M^+, 8), 236(21), 155(49), 124(11), 95(15), 91(80), 82(57); mp 152–155°C (lit. (25) mp 154–156°C).

Preparation of the Dimer of Chloronitroso Compound ***29***

A solution of nitrosyl chloride (8.3 mL, 0.18 mol) in methylene chloride (50 mL) was added to a solution of *trans,trans,-trans*-cyclododecatriene **28** (32.4 g) in methylene chloride (250 mL) dropwise over 20 min at −10°C. The mixture was allowed to warm to room temperature slowly and methanol was added to give a precipitate (39.02 g, 94%). The precipitate was recrystallized from a 4:1 mixture of ether–CH_2Cl_2 to afford white crystals of the *anti*-dimer of *threo*-1-nitroso-2-chloro-*trans,trans*-5,9-cyclododecadiene (**29**); mp 133–134°C (lit. (26) mp 125–125.5°C); uv (ether): 302 nm (ε, 9400); ir: 3020(m), 1260(s), 1220(s), 1180(s), 1130(m), 990(s), 975(s), 965(s), 770(s), 740(s), and 650(s) cm^{-1}; ^1H nmr τ: 4.16 (m, 1H), 4.70 (m, 4H), 5.65 (m, 1H), 7.7–8.3 (m, 12H); ^{13}C nmr: 133.3, 133.1, 133.0(2C), 129.2, 129.0, 128.9, 128.5, 62.7(d), 62.6(d), 57.5(d), 56.7(d), 33.0 (t, 2C), 31.6 (t, 2C), 31.3 (t, 2C), 28.4(t), 28.1 (t, 4C), 27.7(t); ms (130°C) *m/e* (%): 212(1), 210(2), 161(51), 119(32), 91(60), 79(97), 67(100). On irradiation at the τ 7.8–8.12 region, the multiplet at τ 5.65 collapsed to two nearly superimposed doublets ($J \sim$ 5.0 Hz), the multiplet at τ 4.16 to two doublets at τ 4.11 (J = 5.5 Hz) and 4.21 (J = 4.5 Hz), and the multiplet at τ 4.70 changed its pattern. *Anal.* calcd. for $(C_{12}H_{18}NOCl)_2$: C 63.29, H 7.97, N 6.15; found: C 63.36, H 8.19, N 6.25.

Reduction of the Dimer of ***29*** *with Lithium Aluminum Hydride*

(*1*) A mixture of the crude dimer of **29** (10 g) and lithium aluminum hydride (8.5 g) in ether was refluxed for four days and was treated with 10% potassium hydroxide solution. The usual workup gave basic (5.2 g) negative Beilstein test and neutral (1.05 g) fractions; the latter were shown to be starting triene **28**. The solid base fraction (1.8 g) was chromatographed on silicic acid to afford, with 7% CH_3OH in ether, aziridine **33** (130 mg) as white needles; mp 75–77°C; ir: 3170 (s, b), 3025(m), 970(s), 950(m), and 740(m) cm^{-1}; ^1H nmr τ: 4.78 (m, 4H), 7.77–7.84 (m, 4H), 7.90–8.2 (m, 8H), 8.6–8.9 (m, 2H), and 9.08 (D_2O exchangeable); ^{13}C nmr: 133.1(d), 128.4(d), 37.0(d), 31.6(t), 29.8(t), and 27.9(t) ppm; ms (80°C) *m/e* (%): 177.1499 (M^+, 6, calcd. for $C_{12}H_{19}N$: 177.1517), 176.1448 (17, calcd. for $C_{12}H_{18}N$: 176.1439), 162.1269 (14, calcd. for $C_{11}H_{16}N$: 162.1283), 148(16), 134(17), 122(24), 80(39), 69(100). The solid was sublimed to give white needles, mp 78–78.5°C. *Anal.* calcd. for $C_{12}H_{19}N$: C 81.30, H 10.80, N 7.90; found: C 81.71, H 10.66, N 7.91.

Further elution with 10–20% CH_3OH–ether gave amine **30** (1.03 g) as white needles: mp 93–97°C; ir: 3350, 3280, 3030, 1610(w), 1560 (m, b), 975(s), 970(s), 960(s) cm^{-1}; ^1H nmr τ: 4.90 (m, 4H), 7.23 (bt, $J \simeq$ 10 Hz, 1H), 7.74–9.2 (m, 16H); ^{13}C nmr: 131.9, 131.5, 130.5, 130.0, 45.7(d), 36.6(t), 32.0(t), 31.9(t), 30.3(t), 29.8(t), 29.5(t), 22.6(t) ppm; ms *m/e* (%): 179.1672 (M^+, 31, calcd. for $C_{12}H_{21}N$: 179.1673), 150(28), 136(43), 122(46), 110(43), 96(88), 83(94), 82(92), 70(80), 69(83), 56(100). Sublimation of the solid afforded white needles. *Anal.* calcd. for $C_{12}H_{21}N$: C 80.38, H 11.81, N 7.81; found: C 80.11, H 12.03, N 7.53.

The acetyl derivative of amine **30** was recrystallized from ethanol; mp 120–123°C, ir: 3270(sb), 3080(m), 1635(sb), 1560(s) cm^{-1}; ^1H nmr τ: 4.90 (m, 4H), 6.12 (m, 1H), 7.68–9.10 (m, 16H), 8.04 (s, 3H); ^{13}C nmr: 168.9(s), 131.7 (d, 2C), 130(d), 129.3(d), 44.4(d), 33.7(t), 31.7(t), 31.5(t), 29.4(t), 29.1(t), 27.8(t), 22.8(q), and 22.5(t) ppm; ms *m/e* (%): 221 (M^+, 75), 178(26), 162(100), 133(69), 125(66), 79(76). *Anal.* calcd. for $C_{14}H_{23}NO$: C 75.97, H 10.47, N 6.33; found: C 76.10, H 10.66, N 6.02.

(*2*) The dimer of **29** (500 mg, 1.1×10^{-3} mol) was placed in the thimble of a Soxhlet extractor and leached for 11 h by refluxing a mixture of LAH (274 mg, 7.2×10^{-3} mol) and aluminum chloride (960 mg) in ether. The mixture was worked up by the usual method to afford a crude semi-solid (410 mg); gc analysis showed three peaks at 2.4 (azoxy compound **32**), 3.7 (amine **30**), and 4 (chloroamine **31**) min in 15:10:65 ratio. The mixture was sublimed to afford azoxy compound **32** (85 mg) which was recrystallized from ether; mp 111–113°C; uv (CH_3OH): 354 nm (ε, 26), 290 (sh ε, 21); ir: 1490(s), 1440(s), 1265(s), 1120(sb), 990(s), 970(s), 962(s) cm^{-1}; ^1H nmr τ: 4.84 (m, 8H), 5.46 (m, 1H), 5.65 (bt, $J \simeq$ 6 Hz, 2H), 6.40 (m, 1H), 7.65–8.60 (m, 24H); ^{13}C nmr: 133.6, 133.4, 132.7, 132.4, 130.0, 129.4, 128.5, 78.5, 59.0, 58.7, 57.2(2C), 34.1, 33.8, 31.8(3C), 29.7, 29.5, 29.1, 28.7, 28.2, and 24.5 ppm; ms *m/e* (%): 438.2205, 440.2181, 442.2138 (M^+, 4, 2.5, 1, calcd. for $C_{24}H_{36}N_2OCl_2$: 438.2205, 440.2175, 442.2145). 421, 423, 425 (14, 9, 25), 349.2616 (33, calcd. for $C_{24}H_{33}N_2$: 349.2644), 208(25), 178.1357 (84, calcd. for $C_{12}H_{18}O$: 178.1358), 124(50), 123(59), 109(92), 95(58), 67(100).

The remaining solid showed gc peaks for amine **30** and chloroamine **31** in the 1:7 ratio and a ^{13}C nmr spectrum which showed the peaks for chloroamine **31** with weak peaks for amine **30**. Further sublimation afforded white crystals of chloroamine **31**; ir: 3400–3300(wb), 3015(w), 1600(wb), 990(s), 973(s), 962(s), 760 cm^{-1}; ^1H nmr τ: 4.89 (m, 4H), 5.73 (ddd, J = 7.5, 7, and 2.0 Hz, 1H), 7.06 (ddd, J = 6.5, 6.0, and 2 Hz, 1H), 7.70–8.20 (m, 10H), 8.32–8.50 (m, 2H), 8.33 (bs, D_2O exchangeable); ms *m/e* (%): 213.1295, 215.1252 (M^+, 9 and 3, calcd. for $C_{12}H_{20}NCl$: 213.1284, 215.1255), 178.1601 (43, calcd. for $C_{12}H_{20}N$: 178.1596), 132(5), 130(13), 117.0343, 119.0318 (40 and 14, calcd. for C_5H_8NCl: 117.0345, 119.0316), 96(30), 79(15), 67(14), 56(42), 43(100). On irradiation at τ 8.4 or τ 7.99 the ddd at τ 7.06 and 5.73 collapsed to doublets (J = 2.0 Hz). Irradiation of either of the two signals caused the other to collapse to double doublets with J = 6.5 and 6.0 Hz and J = 7.5 and 7.0 Hz, respectively.

The Base Treatment of Chloroamine ***31***

A 5:1 mixture of chloroamine **31** and amine **30** (51 mg) and sodium methoxide (100 mg) in methanol (3 mL) was kept at room temperature for four hours. The solution was brought to pH 9–10 and extracted with ether to give a crude product

(44 mg). The gc analysis of this oil on a 10% SE 30 column gave the peaks corresponding to amine **30** (4.3 min, 17%), chloroamine **31***a* (5.0 min, 16%), aziridine **33** (5.4 min, 10%), and three unknown peaks. The known compounds were further confirmed by a peak matching method.

Benzylation of Aziridine ***33***

Aziridine **33** (35 mg) and benzylchloride (249 mg) in dry benzene (2 mL) were refluxed for six hours. The residue was treated with ether to give the hydrochloride of **33** (19 mg, 46%), mp 193–197°C (dec.); ir: 2725(m), 2680(m), 2500(w), 966(s) cm^{-1}; ^1H nmr: τ 2.36 (bs, 2H), 4.90 (m, 4H), 7.32 (bd, J = 7 Hz, 2H), 7.6–8.6 (m, 12H). The ether filtrate was evaporated to give an oil of *N*-benzylaziridine **34** (29 mg); ir: 3030(m), 1600(w), 1495(m), 1100(s), 1028(s), 968(s), 692(s) cm^{-1}; ^1H nmr: τ 2.78 (s, 5H), 4.88 (m, 4H), 6.56 (s, 2H), 7.7–9.0 (m, 12H). This oil was slightly contaminated with benzylchloride as shown by the ^1H nmr signals at τ 5.50(s) and 2.74. The oil was refluxed in benzene containing benzylchloride (250 mg) for 12 h. The residue was chromatographed on a silicic acid column to give an oil (22 mg, 42%) showing one spot on a tlc plate corresponding to *N*-benzylaziridine, **35**; ^1H nmr τ: 2.78 (m, 5H), 4.88 (m, 4H), 6.56 (sharp s, 2H); ^{13}C nmr: 139.0, 133.1(2C), 128.1(2C), 127.7(2C), 127.5(2C), 126.7, 65.0 (benzyl), 46.4 (2C, CHN), 31.6(2C), 29.9(2C) and 27.1(2C) ppm; ms (40°C) *m/e* (%): 267.1976 (M^+, 32, calcd. for $C_{19}H_{25}N$: 267.1987), 266(28), 200(13), 187(12), 176.1442 (50, calcd. for $C_{12}H_{18}N$: 176.1439), 172(30), 159(90), 134(43), 91(100), and 41(23).

The above oil taken up in ether (5 mL) was treated with dry hydrogen chloride gas repeatedly to give precipitates (25 mg). This solid was added to a saturated sodium carbonate solution which was extracted with ether to give an oil showing two spots on tlc analysis. Preparative tlc of the oil gave *N*-benzylaziridine **34** (4 mg) and compound **35** (12 mg); ir: 3400 (w, vb), 3025(m), 1580(w), 1260(m), 1080(m), 985(s), 970(m), 958(s), 800(m, b), 750(s), and 698(s) cm^{-1}; ^1H nmr τ: 2.80 (m, 5H), 5.12 (m, 4H), 5.88 (m, $W_{1/2}$ = 18 Hz), 6.24 (AB q, J = 13.5 Hz, $\Delta\delta$ = 28 Hz), 7.50 (m, $W_{1/2}$ = 22 Hz), and 7.8–9.2 (m, 12H), 8.84 (1H, D_2O exchangeable); ^{13}C nmr: 140.3, 132.8, 132.0, 130.5, 129.2, 128.6(2C), 128.1 (2C), 126.9, 63.4, 53.5, 50.3, 33.7, 31.9, 29.5, 29.3, and 28.9; ms (40°C) *m/e* (%): 303.1756 and 305.1729 (M^+, 22 and 8, calcd. for $C_{19}H_{26}NCl$: 303.1754 and 305.1724), 268.2067 (24, calcd. for $C_{19}H_{26}N$: 268.2066), 241(8), 146(26), 133(100), 106(7), 91(61), and 41(8).

Reactions of the Dimer of ***29***

(*1*) A mixture of anhydrous sodium acetate (1 g), the dimer (500 mg, 1.1×10^{-3} mol), and acetic anhydride was stirred under nitrogen at 45°C for 3 days. The solution was adjusted to pH 9 and extracted with methylene chloride (60 mL × 3) to give an oil (481 mg) which showed two major spots (one of them corresponding to the starting material) and several minor spots on tlc. The oil also showed a broad esr triplet (1:1:1) at $g = 2.0068 \pm 0.0008$, a_N = 13.5 G (line width = 6.5 G).

The mixture was chromatographed on silica gel (40 g). The middle fraction eluted with methylene chloride afforded a solid (301 mg) which was recrystallized from methanol to give oximino acetate **38**; mp 49–49.5°C; ir: 3030(w), 1775(s), 1635(m), 1370(s), 1202(s), 996(s), 978(s), 960(s), 950(s), 924(s), 878(m), 803(m), 765, and 718(m) cm^{-1}; ^1H nmr τ: 4.82 (m, 4H), 5.17 (bt, J = 6 Hz, 1H), 6.7–7.4 (m, 1H), 7.6–7.9 (m, 11H), and 7.80 (s, 3H); ^{13}C nmr: 167.9(s), 165.5(3), 132.7, 132.5, 129.6, 129.2, 57.6(d), 31.8(t, 2C), 31.7(t), 29.1(t), 29.0(t), 26.1(t), 19.4(q); ms *m/e* (%): 212(11), 210(32), 192(8), 174(99), 79(63), 67(78), 43(100). On irradiation at τ 7.82, the multiplet at τ 5.17 collapsed to a singlet and the multiplet at τ 4.82 became an AB quartet (J = 16 Hz). *Anal.* calcd. for $C_{14}H_{20}NO_2Cl$: C 62.33, H 7.47, N 5.19; found: C 61.99, H 7.51, N 5.22. An attempt to isolate the minor components of the mixture was unsuccessful.

(*2*) A mixture of the dimer (1 g), methylene chloride (10 mL), methanol (20 mL), and pyridine (500 mg) was stirred under nitrogen at 35°C for one day. The residue after evaporation of solvents was washed with ether to afford crystals of pyridinium chloride **36** (1.23 g); mp 190–194°C (dec.); ir: 3120(s, b), 1625(m), 1290(m), 1140(m), 1010(s), 998(s), 980(s), 970(s), 960(s), 895(m), 820(m), 770(s), 725(s), 690(s) cm^{-1}; ^1H nmr (D_2O) τ: 1.0–2.0 (m, 5H), 4.58 (m, 5H), 6.8–7.35 (m, 2H), 7.5–8.6 (m, 10H). The pyridinium hydrochloride (860 mg) was stirred with an excess of aqueous dimethylamine solution and was worked up in the usual manner to afford amino oxime **37** (645 mg, 91%) as an oil; the ir and nmr spectra were superimposable with those of an authentic sample (23).

(*3*) A solution of the dimer (1 g) in methylene chloride (10 mL) and methanol (10 mL) containing 0.1 mL of concentrated hydrochloric acid was heated at 50°C for 3 days. The reaction was worked up in the usual manner to afford an oil (891 mg) which was chromatographed on alumina. The first fraction eluted with methylene chloride gave the methoxyketone corresponding to **38** (X = OCH_3, R = H, 72 mg) as a colourless volatile oil; ir: 3035(w), 1725(s), 1720(s), 1715(sh), 1130(m), 1098(s), 1080(m), and 970(s) cm^{-1}; ^1H nmr τ: 4.82 (m, 4H), 6.40 (dd, J = 6.5 and 4.0 Hz, 1H), 6.65 (s, 3H), 7.5–8.15 (m, 12H); ms *m/e* (%): 208 (M^+, 93), 176(13), 120(46), 111(47), 81(71), 79(76), 68(100), and 67(100). The second fraction eluted with 0–1% MeOH in CH_2Cl_2 afforded the methoxy oxime **38** (X = OCH_3, R = H, 365 mg); ir: 3330(bs), 3030(w), 1640(w), 1120(m), 1085(vs), 965(s) cm^{-1}; ^1H nmr τ: 1.56(OH), 4.80 (m, 4H), 5.84 (t, J = 5 Hz, 1H), 6.72 (s, 3H), 7.35 (m, 1H), and 7.6–8.3 (m, 11H); ^{13}C nmr: 158.7(s), 131.5(2C), 131.0, 130.6, 78.2(d), 54.5(q), 31.9(t), 31.7(t), 29.9(t), 28.5(t), 27.8(t), 25.4(t); ms *m/e* (%): 223 (M^+, 27), 206(100), 174(41), 169(45), 139(78), 79(71), 67(84). On irradiation at τ 8.20 the triplet at τ 5.84 collapsed to a singlet.

Preparation of the Dimer of C*-Nitroso Compound* ***40–41***

The dimer of **35–36** was prepared in a similar manner to that described above and was recrystallized from methylene chloride as white needles: mp 150–151°C; ir: 3008(m), 1258(s), 1212(s), 1200(s), 1192(s), 1183(s), 1155(m), 770(s), 738(m), 720(s) cm^{-1}; ^1H nmr τ: 4.28 (m, 1H), 4.45 (m, 2H), 5.4 (m, 1H), 7.3–8.1 (m, 4H), 8.4 (m, 4H); uv: 299 nm (ε, 7960); ms *m/e* (%): 203(1), 201(2), 186(13), 184(40), 166(60), 135(90), 93(88), 81(75), 79(70), 67(100). Dissolution of the dimer in dimethylformamide caused decomposition and the ^{13}C nmr could not be taken. *Anal.* calcd. for $(C_{10}H_{16}NOCl)_2$: C 59.55, H 8.00, N 6.95; found: C 59.20, H 7.80, N 6.98.

Reactions of the Dimer of C*-Nitroso Compound* ***40–41***

(*1*) The dimer of **40–41** (500 mg) in a 1:2 mixture of methylene chloride and methanol containing one drop of concentrated hydrochloric acid was refluxed for 36 h. Acid–base extraction of the reaction mixture afforded neutral (464 mg) and basic (33 mg) fractions. The neutral fraction in methylene chloride showed overlapping esr triplets in which the major one was that at $g \simeq 2.0061 \pm 0.0010$, $a_N \simeq 15.2$ G. It also showed ^1H nmr signals at τ 5.45 (dd, J = 11 and 5 Hz), 5.63 (dd, J = 10 and 5 Hz), and two equal intensity singlets at τ 6.71 and 6.81 and two major spots and other minor spots on tlc. The oil (290 mg) was chromatographed on silica gel. The fraction eluted with 0.5–1% MeOH–CH_2Cl_2 gave a solid which was sublimed to give oxime **42**; mp 94–95°C; ir: 3250 (broad), 3005(w), 1620(w), 1433(s), 1000(s), 980(s), 970(s), 910(m), 765(m), 715(m), 625(m) cm^{-1}; ^1H nmr τ: 0.99(OH), 4.70 (m, 2H), 5.45 (dd, J = 11 and 4.5 Hz, 1H), 6.93 (m, 1H), 7.41–8.29 (m, 7H), 8.39 (m, 4H); ^{13}C nmr: 160.2(s), 133.4(d), 128.0(d), 55.6(d), 33.0(t), 29.4(t), 25.3(t), 24.9(t), 24.6(t),

22.5(t); ms *m/e* (%): 203 (M^+, 3), 201(8), 186(20), 184(57), 166(100), 148(55), 91.0546 (51, calcd. for C_7H_7: 91.0547), 79(44), 67(49). On irradiation at τ 8.06 the double doublet at τ 5.45 collapsed to a doublet (J = 11.0 Hz) and the multiplet at τ 4.70 became a poorly resolved doublet (J = 13 Hz). On irradiation at τ 8.39, the multiplet at τ 6.93 became an ill-resolved doublet (J = 14 Hz). *Anal.* calcd. for $C_{10}H_{16}NOCl$: C 59.55, H 8.00, N 6.95; found: C 59.71, H 8.14, N 7.05.

The fraction eluted with 2–4% CH_3OH–CH_2Cl_2 gave a colourless oil which showed a weak nmr signal for olefinic protons and several methoxy singlets, among them, those at τ 6.63, 6.72, and 6.78 had a ratio of 2:1:2; ir: 3300(b), 1710(w), 1650(w), 1090(vs), 945(vs), 915(vs); ms *m/e* (%): 197(21) 180(78), 165(88), 148(100), 123(72). This oil showed strong and complex esr signals at the g = 2.006 region.

(*2*) A methylene chloride (20 mL) solution containing acetic anhydride (2 g) and the dimer of **40**–**41** (403 mg) was stirred under nitrogen at 50°C for 3 days. After the usual workup, the residue (517 mg) was taken up in a 1:1 mixture of methylene chloride – ether from which the starting dimer was precipitated (107 mg). The mother liquor was evaporated and the residue showed three overlapping esr triplet (equal intensity) signals (one major and two minor) in which the major triplet had g = 2.007 ± 0.001, a_N = 14.2 G (line width 4 G). This mixture was chromatographed on silica gel. The first fraction eluted with methylene chloride gave an oil (147 mg, 45%) which was distilled to give a 1:3 mixture of oximino acetate **44** and **45**; ir: 3000(m), 1775(vs), 1630(m), 1260(m), 1205(vs), 1175(s), 1000(s), 935(s), 890(s), 842(m), 780(m), 735(s), 710(m) cm^{-1}; ^1H nmr τ: 4.65 (m, 2H), 5.34 (dd, J = 12.0 and 4.5 Hz, 1/4H), 5.66 (dd, J = 11.0 and 5.0 Hz, 3/4H), 7.2–8.10 (m, 11H), 7.74(s) and 7.76(s) in a 1:3 ratio; ^{13}C nmr: 166.2, 166.1, 131.8, 131.7, 127.5, 127.3, 54.2, 51.5, 34.9, 33.6, 31.3, 28.0, 27.8, 26.5, 24.2, 23.8(2C), 23.5(2C), 21.6, 21.3, and 19.4 ppm; ms (70°C) *m/e* (%): 246 (M^+ +1, 4), 244(10), 243 (M^+, 1), 201(66), 184(65), 166(65), 148(100), 135(85), 93(85). *Anal.* calcd. for $C_{12}H_{18}ClNO_2$: C 59.14, H 7.44, N 5.75; found: C 58.89, H 7.55, N 5.60.

Elution with 0.5–2% CH_3OH–CH_2Cl_2 gave a solid (27 mg, 8%) which showed a single spot on tlc and could not be recrystallized. This solid is assumed to be the bicyclic hydroxylamine acetate **46** (or isomer thereof); ir: 1765(s), 1722(s), 1245(s), 1202(s), 1192(s), 1125(m), 1040(m), 1015(m), 950(m), 850(m), 788(m), 755(m), 730(m), 715(m) cm^{-1}; ^1H nmr τ: 4.70 (bt, J = 9 and 1 Hz, 1H), 5.48 (m, 1H), 6.72 (m, 2H), 7.7–8.6 (m, 12H), 7.83 (s, 3H), 7.96 (s, 3H); ms *m/e* (%): 305.1219 and 303.1237 (M^+, 2 and 7, calcd. for $C_{14}H_{22}NO_4Cl$: 305.1208 and 303.1238), 263(3), 261(8), 246(36), 244(100), 226(96), 220(26), 218(77), 208(31), 184(36), 166(31), 148(43).

The fraction eluted with 2% CH_3OH–CH_2Cl_2 gave an oil (30 mg, 8%) which was sublimed to give **47** (or isomers thereof); ir: 3450(bm), 1765(vs), 1735(vs), 1240(vs), 1190(vs), 1025(s), 940(m), 890(m), 860(m), and 810(m) cm^{-1}; ^1H nmr τ: 4.74 (m, 2H), 5.27 (bq, J = 6.5 Hz, 2H), 7.7–8.8 (m, ca. 12H), 7.90 (s, 3H), 7.93 (s, 6H); ms *m/e* (%): 327 (M^+, 2), 285(33), 268(100), 226(36), 208(22), 166(31), 148(28), 96(25), 67(24); esr major triplet (1:1:1) $g \simeq 2.0089$, a_N = 14.3 G and two minor triplets at $g \simeq 2.0063$ and 2.0045.

1. Y. L. CHOW. Acc. Chem. Res. **6**, 354 (1973).
2. K. S. PILLAY, S. C. CHEN, T. MOJELSKY, and Y. L. CHOW. Can. J. Chem. **53**, 3014 (1975).
3. Y. L. CHOW, K. S. PILLAY, and H. H. QUON. J. Chem. Soc. Perkin Trans. II, 1255 (1977).
4. Y. L. CHOW, S. C. CHEN, and D. W. L. CHANG. Can. J. Chem. **48**, 157 (1970).
5. (*a*) TH. A. J. W. WAJER, A. MACKOR, TH. J. DE BOER, and J. D. W. VAN VOORST. Tetrahedron, **23**, 4021 (1967); (*b*) A. MACKOR, TH. A. J. W. WAJER, TH. J. DE BOER, and J. D. W. VAN VOORST. Tetrahedron Lett. 385 (1967); (*c*) A. MACKOR, TH. A. J. W. WAJER, and TH. J. DE BOER. Tetrahedron, **24**, 1623 (1968).
6. W. B. MOTHERWELL and J. S. ROBERTS. J. Chem. Soc. Chem. Commun. 328 (1972).
7. D. MULVEY and W. A. WATERS. J. Chem. Soc. Perkin Trans. II, 1059 (1978).
8. E. G. JANZEN. Acc. Chem. Res. **4**, 31 (1971).
9. HOUBEN-WEYL. Methoden der Organischen Chemie. Band X/Teil 1. Thieme Verlag, Stuttgart. 1971. Chapts. 3–5.
10. P. A. S. SMITH. The chemistry of open-chain organic nitrogen compounds. Vol. 2. W. A. Benjamin, New York. 1966. Chapt. 13.
11. S. R. SANDLER and W. KARO. Organic functional group preparations. Vol. 2. Academic Press, New York. 1971. Chapt. 16.
12. H. BOYER. *In* The chemistry of the nitro and nitroso groups. Part 1. *Edited by* H. Feuer. Interscience, New York. 1969. p. 15.
13. J. HAMER and M. AHMAD. *In* 1,4-Cycloaddition reaction. *Edited by* J. Hamer. Academic Press, New York, NY. 1967. Chapt. 12.
14. G. W. KIRBY. Chem. Soc. Rev. **6**, 1 (1977).
15. G. T. KNIGHT. J. Chem. Soc. Chem. Commun. 1016 (1970).
16. A. B. SULLIVAN. J. Org. Chem. **31**, 2811 (1966).
17. R. E. BANKS, R. N. HASZELDINE, and P. J. MILLER. Tetrahedron Lett. 4417 (1970).
18. W. B. MOTHERWELL and J. S. ROBERTS. J. Chem. Soc. Chem. Commun. 329 (1972).
19. R. M. DUPEYRE and A. RASSAT. J. Am. Chem. Soc. **88**, 3180 (1966); Bull. Soc. Chim. Fr. 612 (1978); G. D. MENDENHALL and K. U. INGOLD. J. Am. Chem. Soc. **95**, 6395 (1973).
20. F. KLAGES, R. HEINLE, H. SITZ, and E. SPECHT. Chem. Ber. **96**, 2387 (1963); K. ADAMIC, D. F. BOWMAN, T. GILLAN, and K. U. INGOLD. J. Am. Chem. Soc. **93**, 902 (1971).
21. M. M. ROGIĆ, T. R. DEMMIN, R. FUHRMANN, and F. W. KOFF. J. Am. Chem. Soc. **97**, 3241 (1975).
22. K. S. PILLAY and Y. L. CHOW. J. Chem. Soc. Perkin Trans. II, 93 (1977).
23. H. RICHARD. Ph.D. thesis, Simon Fraser University, Burnaby, B.C. 1979.
24. C. Y. CHEN and R. J. W. LE FÈVRE. J. Chem. Soc. 3473 (1965); J. Chem. Soc. B, 539 (1966).
25. H. STETTER and K. KECKEL. Tetrahedron Lett. 801 (1972).
26. G. WILKE. Angew. Chem. **75**, 10 (1963); H. METZGER. Angew. Chem. **75**, 980 (1963).
27. M. OHNO, M. OKAMOTO, and N. NARUSE. Tetrahedron Lett. 1971 (1965).
28. R. C. FAHEY. Top. Stereochem. **3**, 237 (1968).
29. R. A. PERRY, S. C. CHEN, B. C. MENON, K. HANAYA, and Y. L. CHOW. Can. J. Chem. **54**, 2385 (1976).
30. C. SCHENK and TH. J. DE BOER. Tetrahedron, **35**, 147 (1979); C. SCHENK and TH. J. DE BOER. J. Netherland Chem. Soc. **98**, 18 (1979).
31. M. OHNO, M. OKAMOTO, and K. NUKADA. Tetrahedron Lett. 2763 (1965).
32. B. W. PONDER, T. E. WALTON, and W. J. POLLOCK. J. Org. Chem. **33**, 3957 (1968).
33. J. MEINWALD, Y. C. MEINWALD, and T. N. BAKER, III. J. Am. Chem. Soc. **85**, 2513 (1963); **86**, 4074 (1964).
34. H. C. HAMANN and D. SWERN. J. Am. Chem. Soc. **90**, 6481 (1968).

Generation of aminyl and aminium radicals by photolysis of *N*-nitrodialkylamines in solution[1]

YUAN L. CHOW, HERVÉ RICHARD, RODNEY WILLIAMS SNYDER, AND ROBERT W. LOCKHART

Department of Chemistry, Simon Fraser University, Burnaby, B.C., Canada V5A 1S6

Received May 7, 1979

YUAN L. CHOW, HERVÉ RICHARD, RODNEY WILLIAMS SNYDER, and ROBERT W. LOCKHART. Can. J. Chem. 57, 2936 (1979).

Photolysis of nitramines in a neutral solvent generated nitrogen dioxide and aminyl radicals which abstracted a hydrogen but did not add to a π-bond. In dilute acidic solution, the aminyl radicals generated from the photolysis were protonated to the corresponding aminium radicals that preferentially added to π-bonds rather than abstracted a hydrogen. However, complex mixtures of addition products were obtained when nitramines were photolysed in the presence of cyclohexene under nitrogen. The plethora of the products is believed to arise from the complex behavior of nitrogen dioxide in solution; for example, (*i*) nitrogen dioxide may react as *O*- or *N*-radical, (*ii*) nitrogen dioxide exists in equilibrium with nitrogen tetraoxide, and (*iii*) both oxides can react as oxidizing or radical trapping agents. Under oxygen, the oxidative addition of nitramines to cyclohexene gave 1-dialkylamino-2-nitratocyclohexenes which could be treated with lithium aluminium hydride to give good yields of the corresponding amino alcohols. The quantum yields of nitramine disappearance indicated that the photolysis followed short chain processes either in neutral or acidic conditions. The decrease in quantum yield at $> 2\ N\ H_2SO_4$ is believed to be due to a reduced reactivity of aminium radicals in a highly acidic environment. The probable mechanisms of these photolytic radical chain processes are discussed.

YUAN L. CHOW, HERVÉ RICHARD, RODNEY WILLIAMS SNYDER et ROBERT W. LOCKHART. Can. J. Chem. 57, 2936 (1979).

La photolyse des nitramines dans un solvant neutre produit du bioxyde d'azote et des radicaux aminyles qui enlèvent un atome d'hydrogène sans toutefois s'additionner sur la liaison π. En solution diluée d'acide les radicaux aminyles générés sont, par protonation, transformés en radicaux aminiums correspondants qui eux d'additionnent préférentiellement sur la liaison π au lieu d'arracher un atome d'hydrogène. Par ailleurs la photolyse des nitramines en présence de cyclohexane et sous atmosphère d'azote conduit à un mélange complexe de produits d'addition. On pense que la formation de ces produits est due au comportement du dioxyde de l'azote en solution, par exemple (*i*) le dioxyde d'azote peut réagir comme un radical *O* ou *N*, (*ii*) le dioxyde d'azote existe en équilibre avec le tétraoxyde et (*iii*) les deux oxydes peuvent agir soit comme agents oxydants soit comme pièges à radicaux. L'addition oxydante des nitramines sur le cyclohexène sous atmosphère d'azote conduit aux dialkylamino-1 nitrato-2 cyclohexènes qui traités à l'hydrure double d'aluminium et de lithium donnent avec de bons rendements les aminoalcools correspondants. La disparition des rendements quantiques de nitramines indique que la photolyse en milieu neutre ou acide se fait selon un court procédé en chaîne. On croit que la diminution des rendements quantiques, à des concentrations de $H_2SO_4 > 2\ N$, est due à la réactivité réduite des radicaux aminiums en milieu fortement acide. On discute du mécanisme probable de ces réactions de photolyse radicalaire en chaîne.

[Traduit par le journal]

Introduction

Dialkylnitramines (R_2NNO_2) react as neutral compounds (1–4) and exhibit a $\pi \rightarrow \pi^*$ transition absorption at about 240 nm (ε, ~5500) without showing a $n \rightarrow \pi^*$ transition absorption (5–7) commonly observed in nitrosamines (8) in protic solvents. The N—N bond distance of *N*-nitrodimethylamine (NNOD) has been measured crystallographically to be relatively short (9*a*)[2] (ca. 1.3 Å) indicating considerable resonance contribution of the polar form $R_2{}^+N{=}NO_2{}^-$ to the structure (4). The photochemistry of nitramines has been sporadically investigated in the past (10–15). Photolysis of *N*-methyl-*N*-nitro-1-naphthylamine with > 360 nm light has been shown to cause rearrangement to the *o*- and *p*-nitro derivatives by a non-radical mechanism (10).

In contrast to the photostability of nitrosamines in neutral solvents (16, 17), dialkylnitramines undergo photodecomposition in hydrocarbons, alcohols, and acetonitrile to give the corresponding nitrosamines as a major product (11–13). However, photolysis of *N*-nitrodibenzylamine gave *N*-benzylidene benzyl-

[1]Part of the results were published in ref. 1 as a communication.

[2]O. Bastiansen as reported in ref. 9(*b*).

0008-4042/79/222936-08$01.00/0

TABLE 1. Photolysis of nitramines under neutral conditions

Conditions[a]				Percent of products			
Nitramines	Solvent	Olefin	Gas	R_2NNO	R_2NH	R_2NCHO	Remarks
NNOP	MeOH	None or *cyclo*-C_6H_{10}	N_2	Trace	13	7	[b]
NNOP	*n*-Hexane	*cyclo*-C_6H_{10}	CO	33	38	—	[c]
NNOD	*n*-Hexane	*cyclo*-C_6H_{10}	CO	7	28	26	[c]
NNOD	CH_3CN	*cyclo*-C_6H_{10}	CO	22	35	2	[c,d,e]
NNOD	*n*-Hexane	*cyclo*-C_6H_{10}	N_2	6	—	14	[c,f]
NNOD	CH_3CN	Norbornene	CO	55	8	3	[c,f]

[a]More than one equivalent of the olefins was added and the workup of the photolysate was different in each experiment as shown in the Experimental.
[b]The percentages are calculated from the gc peaks; the yields of the crude products were low due to solubility in water.
[c]The amines (R_2NH) were isolated as the nitrate salts and other products were determined by gc and (or) nmr analyses.
[d]In addition, *N*-methylformamide (15%) and 1,3,5-trimethylhexahydro-1,3,5-triazine (10%) were detected by gc–ms.
[e]In the photolysis, $NaHCO_3$ (2 g) was added.
[f]In the photolysis, Na_2CO_3 (2 g) was added.

amine and dibenzylammonium nitrate (12) in addition to the nitrosamine. Thermal decomposition of *N*-nitrodimethylamine in the gas phase was reported to give *N*-nitrosodimethylamine (18). These reactions are generally assumed to occur by the homolytic scission of the N—N bond (12, 14, 15). Photolysis of a 1:1 mixture of doubly ^{15}N-labelled and unlabelled NNOD in the solid phase (13) gave *N*-nitrosodimethylamine with statistically distributed ^{15}N-label but the recovered NNOD showed no mixing of the ^{15}N-label. Although these results do not unambiguously distinguish between N—N or N—O bond scission as the primary photoreaction, the authors favor the latter (13) presumably leading to the generation of oxygen atoms. Our interests in nitrosamine photochemistry (16) have led us to investigate the photoreaction of *N*-nitropiperidine (NNOP) and *N*-nitrodimethylamine (NNOD) which is described in this report.

Results

Nitramines were prepared by oxidation of nitrosamines with 50% hydrogen peroxide. Since 90% hydrogen peroxide used in the original Emmons' method was not available (19), the oxidation was repeated to obtain a better conversion. The unreacted nitrosamines could be removed by passing gaseous hydrochloric acid through a dry ether solution of the crude product. The hydrochlorides of nitrosamines (20) precipitated leaving the much less basic nitramines in the solution.

The photodecomposition of NNOP (**1***a*) and NNOD (**2***a*) under neutral conditions proceeded efficiently and gave similar results regardless of the presence or the absence of cyclohexene or norbornene, e.g., no addition product to the olefins was obtained. The results are summarized in Table 1. In methanol, NNOP was photolysed under nitrogen to give *N*-formylpiperidine (**1***c*), piperidine (as the nitrate salt), and NNP (**1***b*); no formaldehyde was detected. However, in *n*-hexane under carbon monoxide, formamide **1***c* was not formed, indicating that the formyl group was derived from methanol. Photolysis of NNOD under various conditions gave dimethylformamide (**2***c*), *N*-nitrosodimethylamine (**2***b*), and dimethylammonium nitrate, and in one

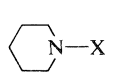

1

$(CH_3)_2N—X$

2

a X = NO_2
b X = NO
c X = CHO

case the trimer of formylidenemethylamine (i.e., 1,3,5-trimethylhexahydro-1,3,5-triazine) and *N*-methylformamide were also obtained. Photolysis of NNOD in acetonitrile in the presence of solid sodium carbonate or bicarbonate yielded considerable amounts (22% and 55%) of nitrosamine **2***b*. Since formamide **2***c* was formed in the absence of methanol, carbon monoxide, or carbonate, the formyl group was not derived from these entities but most probably from the *N*-methyl carbons.

Under dilute acidic conditions the patterns of nitramine photolysis were quite different in the presence or the absence of cyclohexene; in the former case photoaddition of nitramines to the olefin occurred exclusively. In methanol containing hydrochloric acid (ca. 0.05 *N*), NNOP was photolytically decomposed to the piperidinium salt cleanly; formaldehyde was also detected in the distillate. However, under similar conditions but in the presence of cyclohexene, a complex mixture of addition products to cyclohexene was obtained; this mixture consisted of 2-piperidinocyclohexanol (*cis* and *trans*

mixture, **3**, 20%), 2-piperidinocyclohexanone oxime (**9**, 22%), 1-nitro-2-piperidinocyclohexane (**4**, 9%), and two more compounds that were tentatively assigned from gc–ms analysis as piperidinocyclohexene (12%, **11**) and 1-methoxy-2-piperidinocyclohexane (10%, **5**). In a similar manner, NNOD was photolysed in the presence of cyclohexene either under nitrogen or carbon monoxide to give a mixture consisting of dimethylaminocyclohexane (**6**, 15%), 2-dimethylaminocyclohexanol (*cis* and *trans* mixture, **7**, 28%), 2-dimethylaminocyclohexanone oxime (**10**, 24%), and 1-nitro-2-dimethylaminocyclohexane (**8**, 22–24%) in addition to two unknown compounds. In these reactions, piperidine and dimethylamine were also formed but could not be determined quantitatively due to their volatility and solubility. The percentages given above are the relative ones of the gc peaks.

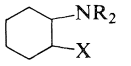

3 $R_2 = -(CH_2)_5-$, X = OH
4 $R_2 = -(CH_2)_5-$, $X = NO_2$
5 $R_2 = -(CH_2)_5-$, $X = OCH_3$
6 $R = CH_3$, X = H
7 $R = CH_3$, X = OH
8 $R = CH_3$, $X = NO_2$

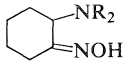

9 $R = -(CH_2)_5-$
10 $R = CH_3$

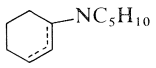

11

Similar photoaddition of nitramines as above, but under oxygen, took place smoothly and gave a crude product which showed strong ir absorptions for nitrate (1620, 1270, 850 cm^{-1}), carbonyl (1710 cm^{-1}), and hydroxyl (3400 and 1100 cm^{-1}) groups (21). The LAH reduction of this crude product from NNOP addition afforded a good yield of an oil which showed two gc peaks corresponding to *cis*- and *trans*-2-piperidinocyclohexanols (**3**) (21) in a 1:2 ratio. The stereoisomers were separated by column chromatography. Similar reduction of the crude product from NNOD photoaddition afforded 64% of a mixture consisting of *cis*- and *trans*-2-dimethylaminocyclohexanol (**7**) (21, 22). A few gc peaks due to side products were also detected but in only minor amounts.

The kinetic disappearance of NNOP in acidic and neutral solutions and under nitrogen or oxygen was shown to follow a zero order in the initial stage of the photolysis. The quantum yields obtained from these studies using the ferric oxalate actinometry (23) are summarized in Table 2. In dilute acidic solutions (<2 *N* H_2SO_4) the quantum yields were higher than those in neutral or in highly acidic (>5 *N* H_2SO_4) solutions, and varied only slightly in the presence or absence of oxygen and (or) olefins in methanol solvent. In acetic acid solutions the quantum yield was slightly higher in the presence of oxygen and noticeably lower in the absence of cyclohexene.

TABLE 2. Quantum yields of *N*-nitropiperidine (0.0077 *M*) photodecomposition[a]

Conditions	ϕ
(*a*) In methanol solution	
Neutral	4.8
0.1 *N* H_2SO_4	7.4; 7.8[b]; 7.8[c]
1.0 *N* H_2SO_4	7.1
2.0 *N* H_2SO_4	7.0
5.0 *N* H_2SO_4	5.2
(*b*) In acetic acid solution	
0.0 *N* H_2SO_4	5.4
0.1 *N* H_2SO_4	5.1
1.0 *N* H_2SO_4	5.4; 4.7[b]
2.0 *N* H_2SO_4	5.7; 4.6[b]; 6.3[c]
5.0 *N* H_2SO_4	3.8
15.0 *N* H_2SO_4	2.4

[a]The photolysis was carried out with a solution containing *N*-nitropiperidine (0.0077 *M*) and cyclohexene (0.02 *M*) under nitrogen unless specified otherwise.
[b]In the absence of cyclohexene.
[c]Under oxygen.

Discussion

In this study, it is shown that the photolyses of dialkylnitramines in neutral solvents form the corresponding dialkylformamides under certain conditions in addition to the reported nitrosamines and ammonium nitrates (11, 12). As already pointed out, the formyl group of formamide **1***c* is derived from methanol and that of formamide **2***c* from the *N*-methyl groups of NNOD. Under dilute acidic methanol solution NNOP is photolytically reduced and methanol is oxidized to formaldehyde. These results can be explained by the homolysis of the N—N bond to form dialkylaminyl radicals and nitrogen dioxide. Under neutral conditions the aminyl radicals abstract hydrogen from methanol or alkenes, or from a dimethylamino moiety if no other suitable H-atom donor is in sight (24). In acidic solutions, aminyl radicals (pK_a 6.5–7.5) (25) are protonated to give the aminium radicals which either add to a π-bond or abstract a hydrogen in the absence of olefins (26). Neither aminyl nor aminium radicals could be trapped by carbon monoxide under our reaction conditions.

The major reaction processes, in a neutral medium, can be summarized by eqs. [1]–[7] and, in acidic methanol, by eqs. [1], [8], [2], [9], and [7]. The disproportionation of the dimethylaminyl radicals to give formylidenemethylamine (eq. [4]) and subsequent trimerization or hydrolysis to formaldehyde

have been proposed previously (24). Under the photolysis conditions the oxidation of $\cdot CH_2OH$ and R_2NCH_2OH (eqs. [3], [6], [9]) can be visualized in a

[1] $R_2NNO_2 \xrightarrow{h\nu} NO_2 + R_2N\cdot$

[2] $2NO_2 \rightarrow N_2O_4$

[3] $R_2N\cdot + CH_3OH \rightarrow R_2NH + \cdot CH_2OH \xrightarrow{ox} CH_2O$

[4] $2(CH_3)_2N\cdot \rightarrow (CH_3)_2NH + CH_3N{=}CH_2 \xrightarrow{H_2O} CH_3NH_2 + CH_2O$ (with $CH_3N{=}CH_2 \rightarrow$ *sym*-triazine)

[5] $R_2NH + N_2O_4 \rightarrow R_2NNO + HNO_3$

[6] $R_2NH + CH_2O \rightarrow R_2NCH_2OH \xrightarrow{ox} R_2NCHO$

[7] $R_2NNO_2 + \cdot CH_2OH \rightarrow R_2N\cdot + ONOCH_2OH \rightarrow HNO_2 + CH_2O$

[8] $R_2N\cdot + H^+ \rightleftarrows R_2NH^+$

[9] $R_2\overset{+\cdot}{N}H + CH_3OH \rightarrow R_2\overset{+}{N}H_2 + \cdot CH_2OH \xrightarrow{ox} CH_2O$

number of ways but may be assumed to use nitrogen dioxide or tetroxide as oxidants (27). *N*-Methylformamide could also be formed from formylidenemethylamine by oxidation. On the basis of the proposed reaction pathways, certain observations can be rationalized. Under acidic conditions, the generated dialkylamines are protonated and, therefore, cannot undergo the hydration and oxidation pathway to form formamides **1***c* and **2***c* as shown in eq. [6]. The formation of high percentages of nitrosamine **2***b* in acetonitrile in the presence of sodium carbonate or bicarbonate suggests a base promoted nitrosation of the amine with nitrogen tetroxide as in eq. [5]. This nitrosation process is a well-known reaction for the preparation of nitrosamines (2). In solution, nitrogen dioxide is expected to be in equilibrium with dinitrogen tetroxide under the reaction conditions; both of them may act as oxidizing agents or radical trapping agents (27). The reactions of nitrogen dioxide with alkanes or alkyl radicals in the gas phase have been shown to follow a complex pattern and also to yield nitric oxide in a late stage from secondary reactions (27). It is possible that nitrosamines might be produced by the combination of the aminyl radicals and nitric oxide. Such a mechanism, even if operative, cannot account for the large percentage yields of nitrosamine **2***b* in the presence of carbonates since it is inconceivable that such bases can catalyse the radical combination.

The quantum yields indicate that nitramine photolysis involves short radical chain processes. The chain transfer step, eq. [7], while difficult to pin down, is also suggested as a possibility in analogy to the nitrosamine photolysis (16, 23). Equation [10] might be another chain transfer step. As in most of free radical chain reactions, the propagation processes in the present case cannot be proven easily. Particularly, in the presence of many radical species in the reaction system, any suggestions of such steps are open to questions.

[10] $R_2NNO_2 + \cdot NO_2 \rightarrow R_2N\cdot + N_2O_4$

In neutral solvents nitrosamines survive as final products because of their photostability under the reaction conditions (16, 17). It might be suggested that, in acidic solution, nitrosamine **1***b* is formed as the primary product by an unknown oxygen transfer mechanism, as suggested to be operative in solid phase photolysis (13), and undergoes photodecomposition. This pathway is not operating since piperidone oxime and the trimer of tetrahydropyridine, the products expected from the nitrosamine photolysis in acidic solution (17, 26), are not obtained. Therefore, while the pattern of photoaddition of nitramines to olefins in acidic solutions is very similar to that of nitrosamines, particularly in the presence of oxygen (*vide infra*), the nitramine photolysis generates the aminium radicals directly in the primary photoprocess and not through the intermediacy of nitrosamines.

The efficient photoaddition of nitramines to cyclohexene under dilute acidic conditions and the failure to do so under neutral conditions clearly demonstrate the reactivity difference between aminium and aminyl radicals. The former shows propensity to attack a π-bond over hydrogen abstraction and the latter undergoes other types of reactions (e.g., dimerization, disproportionation, hydrogen abstraction, etc.) rather than addition. The formation of piperidine and formamide **1***c* in the photolysis of NNOP clearly indicates the pattern of the reactivity of the piperidinyl radicals. We have demonstrated these reactivity patterns by nitrosamine (16) and tetrazene (22, 24) photolyses in recent publications. In the present case, the counter radical in the photoaddition, nitrogen dioxide, can behave as an *O*- as well as an *N*-centered radical to give 2-dialkylaminocyclohexyl nitrites and nitro compounds (21) such as **4** and **8**. It is also conceivable that compounds **4** and **8** are formed by a chain transfer step as shown in eq. [11]. The nitrites may be hydrolysed under the

[11] 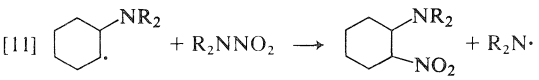

acidic conditions or photolysed (28) to alcohols **3** and **6**, though no effort was made to determine the nature

of these side reactions. It is believed that oximes **9** and **10** are formed via trapping of *C*-radical intermediates by dinitrogen tetroxide as in eq. [12]; tautomeriza-

[12] 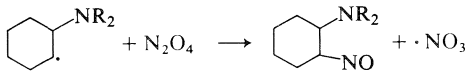

12

tion of *C*-nitroso compounds **12** to oximes is a well-known reaction (16). The other products can be explained by radical mechanisms except the methoxy derivative **5**; its formation may involve an ionic step since there is no precedence for the formation of ether linkages in radical propagation steps involving methanol. While photolysis of nitramines in acidic conditions under an inert gas gave good overall yields of addition products, it gave complex mixtures and cannot be useful for synthetic applications.

The nitramine photolysis in acidic solution under oxygen gives nitrate esters as the primary product and is assumed to proceed via trapping of the *C*-radical intermediates by oxygen as shown in eq. [13],

[13] 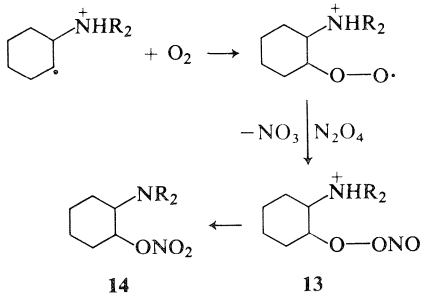

14 **13**

in analogy to nitrosamine photolysis under oxygen (21, 30). Again, dinitrogen tetroxide is assumed to be a nitroso group donor and the NO_3 radical may also combine with the *C*-radical intermediate to form nitrate **14**. The formation of nitroso derivatives during radical reactions of nitrogen dioxide has been known (27), but use of dinitrogen tetroxide as a NO donor has not been proposed previously. The rearrangement of pernitrites to nitrates (e.g., **13** → **14**) has been shown to be spontaneous at about 0°C (29). We have shown that during basic workup nitrate esters can be decomposed to ketones or alcohols (21, 30) which might account for the complexity of the ir spectra of the crude products. An alternative route for the formation of the ketones and alcohols is the decomposition of pernitrite **13** by acid catalysis or photolysis under the reaction conditions. Such reactions are analogous to the decomposition of alkyl hydrogen peroxides (22). However, the treatment of the mixtures with lithium aluminium hydride readily converts them to *cis* and *trans* alcohols **3** and **7** in good yields. The oxidative photoaddition of nitramines to olefins works simply and is an excellent method for preparation of α-aminoalcohols.

It is striking that the quantum yields do not vary significantly within experimental error in the range of 0.1–2 *N* H_2SO_4 either in methanol or acetic acid solution and, also, in the presence or the absence of cyclohexene and oxygen in methanol. This must indicate that the reactivity and concentration of the species propagating the chain processes do not change significantly within this acidity range. Therefore, the drops in the quantum yields above 2 *N* H_2SO_4 could be due to a decrease of the reactivity of the aminium radical at higher acid concentrations as this is known from kinetic esr (31) and flash photolysis studies (32). The causes of the stabilization of aminium radicals at high acidity are not well understood; it may be partly due to screening of the radicals by inert anions, a phenomenon similar to stabilization of carbonium ions in superacid solution (33).

Alternatively, it is tempting to suggest that high acidity might affect the concentration of available nitramines in the solution through protonation and thus also the rates of chain transfer steps such as eqs. [7], [11], and [13]. However, such an acidity effect appears not to be operating since uv spectra of NNOP in methanol are not altered at all in changing acidity from 0–10 *N* H_2SO_4 concentrations. In acetic acid, the optical density difference between λ_{max} 242 nm and λ_{min} 222 nm increases monotonically when the concentration of H_2SO_4 is changed from 0–10 *N*. As there is no abrupt change of the absorption in the vicinity of 2 *N* H_2SO_4 concentration range, the concentration of the nitramine appears to be relatively stable in this acidity range and should not affect the quantum yields.

Experimental

General Conditions and Materials

Unless specified otherwise the following conditions were used. Infrared spectra were recorded with a Perkin-Elmer 457 spectrophotometer using liquid films or Nujol mulls. Ultraviolet spectra were taken with either a Cary 14 or a Unicam SP8000 spectrophotometer. Nuclear magnetic resonance spectra were recorded on a Varian A-56/60 or an XL-100 equipped with a Nicolet 1080 computer in CCl_4 or $CDCl_3$ with Me_4Si as the internal standard. The chemical shifts of ^1H nmr were reported in τ values and those of ^{13}C nmr in parts per million from Me_4Si and coupling constants in hertz (Hz). The decoupling experiments were performed with the XL-100 spectrometer. Mass spectra were recorded with a Hitachi Perkin-Elmer RMU-6E mass spectrometer. High resolution mass spectra were performed at the University of British Columbia, Mass Spectrometric Services. Elemental analyses were carried out by Mr. M. K. Yang using a Perkin-Elmer 240 microanalyzer. Gas chromatographic analyses were performed on a Varian 1200 flame analytical machine using a Varian Aerograph Model 20 recorder equipped with a Model 224 disc

chart integrator. Analyses by gas chromatography – mass spectrometry were performed by Mr. G. Owen to whom we are much indebted. The percentages given in gc analysis were relative ones.

Column chromatography used neutral or basic alumina (Brockman activity 1, 80–200 mesh) or silicic acid (Mallinckrodt, 100 mesh). Acetonitrile (Fisher Scientific) was passed through alumina immediately before use. The commercially available olefins were purified by distillation. Nitrogen supplied in compressed cylinders (Union Carbide of Canada) was purified by passing through a train of a Fieser's solution, concentrated sulfuric acid, and KOH pellets.

The procedure of Emmons (19) was used to oxidize *N*-nitrosodialkylamines to *N*-nitrodialkylamines except that 50% H_2O_2 was used in the place of 90% H_2O_2. The oxidation was repeated to ensure a higher conversion to nitramines. The ether solution of the crude oxidation product was treated with hydrogen chloride to precipitate the unreacted nitrosamines. The ether filtrate was washed with water and dried over magnesium sulfate and evaporated. NNOP distilled at 100–105°C/23 Torr as a clear liquid; ir: 1513, 1388, 1330, 1280, and 1241 cm^{-1}, nmr τ: 6.20 (m, 4H) and 8.33 (m, 6H); uv(MeOH): 249 nm (ε 5500). NNOD was recrystallized from ethanol as white needles (74%); mp 54–55°C (lit. (19) mp 58°C); uv(CH_3OH): 240 nm (ε 6000); ir: 1510(s), 1320(s), 1260(s); nmr τ: 6.56 (t, J = 1.5 Hz); ms *m/e*(%) 91 (M^+, 20), 90(92), 74(8), 44(36), and 42(100); gc retention time on an SE 30 column (150–250°C at 4°/min), 3.6 min.

General Conditions of Photolysis

A solution containing a nitramine and other components in a solvent was placed in a Quartz photolysis apparatus equipped with a Corex filter and was cooled externally with an ice bath. The solution, while purged with a slow stream of a gas, was irradiated with a 200 W Hanovia mercury lamp. The progress of photolysis was followed by recording the absorbancy and the irradiation was terminated when the absorption disappeared. The zero hour sample was kept in the dark to serve as control which showed the absorption peak unchanged. The workup of photolysates varied according to the conditions.

Photolysis of Nitramines Under Neutral or Basic Conditions

N-*Nitropiperidine*

(*a*) NNOP (7.0 g, 0.008 mol) in methanol (200 mL) was photolysed under N_2 for 2.25 h. The solvent was distilled through a Vigreux column and the distillate was trapped (170 mL) in a vessel cooled in Dry Ice. Treatment of the distillate (50 mL) with a 2,4-dinitrophenylhydrazine reagent solution (20 mL) gave no hydrazone. The residue from the photolysate (1.03 g), which exhibited a strong ir band at 1655 cm^{-1} and nmr signals at τ 2.00(s) and 2.90 (m, D_2O exch.), was examined by gc (20% SE30, 130°C) and found to contain two major components and one minor component. Peak matching gc and gc–ms characterized the first component as piperidine (54%; retention time, 1.2 min) and the second component (45%; retention time, 5 min) as *N*-formylpiperidine. The minor component was *N*-nitrosopiperidine. The liquid taken up in ether was extracted with 1 *N* aqueous hydrochloric acid solution. The ether solution was dried and evaporated to afford *N*-formylpiperidine (250 mg); ir: 3400, 1655(s), 1258(w) cm^{-1}; ms *m/e*(%): 113(100), 98(55), 84(57), 70(23), 56(55), and 39(18). The residue from the photolysate exhibited a blue color in the diphenylamine test indicating the presence of nitrate ion.

When the photolysis was carried out under similar conditions but in the presence of one equivalent of cyclohexene, comparable results were obtained in which piperidine and *N*-formylpiperidine were obtained in a 3:2 ratio as shown by gc analysis.

(*b*) A solution of NNOP (1.3 g) and cyclohexene (2.52 g) in *n*-hexane was photolysed under carbon monoxide atmosphere for 16 h. During photolysis, a dark red oil, deposited on the wall, was removed by dissolving it in ethanol every two hours. The combined ethanol solutions were evaporated to give piperidinium nitrate; the ir and nmr spectra were identical with those of an authentic sample. The photolysate was evaporated to give a yellow oil (583 mg) which gave one major gc peak corresponding to *N*-nitrosopiperidine in addition to several weak peaks, none of them corresponding to *N*-formylpiperidine.

N-*Nitrodimethylamine*

(*a*) A mixture of NNOD (1.8 g), cyclohexene (8.4 g), and sodium bicarbonate (2 g) in acetonitrile (200 mL) was photolysed under carbon monoxide for 6 h. The clear photolysate, after filtration, was evaporated and the residue was separated to ether soluble and insoluble parts. The ether solution was evaporated to give a red oil (440 mg) which was shown to contain *N*-nitrosodimethylamine (22%) and *N*,*N*-dimethylformamide (2%) by gc and an nmr estimation; the nmr spectrum showed two pairs of singlets at τ 6.20 and 6.92 and at τ 7.03 and 7.12 in the ratio of 10:1. The ether insoluble oil was stirred with acetonitrile and separated to give a red oil (761 mg, 35%), the ir and nmr spectra were identical with those of dimethylammonium nitrate.

(*b*) A mixture of NNOD (1.8 g), norbornene (18.8 g), and powdered sodium carbonate (2 g) in acetonitrile (190 mL) was irradiated for 6 h. The photolysate was distilled with a Vigreux column and the distillate (170 mL) was treated with dry HCl. The solvent was evaporated to give an oil which was taken up in ether and washed with aqueous sodium carbonate solution and was evaporated, after drying, to afford a yellow oil (423 mg) which exhibited nmr singlets at τ 6.20 and 6.92 in addition to other signals contained in *N*-nitrosodimethylamine (2%) and 2-*endo*-acetamidobicyclo[2.2.1]heptane. The latter was assumed to be formed by an acid catalysed addition of acetonitrile to norbornene and was isolated as white crystals; mp 134–135°C (lit. (34) mp 131–132°C). The photolysate was evaporated to give a residue (1.89 g) which was found to contain the following compounds by the gc peak matching method and estimation from the *N*-methyl singlets of the nmr spectrum: dimethylammonium nitrate (8%), *N*-nitrosodimethylamine (55%), dimethylformamide (3%), and NNOD (6%) in addition to two unidentified minor components.

(*c*) A *n*-hexane solution (200 mL) containing NNOD (0.9 g) and cyclohexene (1.68 g) was photolysed under carbon monoxide for 19 h during which an oil deposited on the wall. The photolysate was evaporated to a residue (153 mg) which showed ir peaks at 1625, 1280, and 870 cm^{-1} for the nitrate group and 1675, 3400, 1065, and 1025 cm^{-1} and weak nmr signals for the cyclohexyl moiety. Since the gc of the residue showed a complex pattern, this was not investigated further. The deposited oil was separated to methylene chloride soluble (340 mg) and insoluble fractions (175 mg). The insoluble fraction was shown to be dimethylammonium nitrate with a small amount of dimethylformamide by its ir and nmr spectra. The soluble fraction was shown to contain *N*-nitrosodimethylamine, dimethylformamide, and dimethylammonium nitrate in the ratio of 1:3:2 by the nmr spectra and gc analysis.

(*d*) A mixture of NNOD (0.9 g, 0.01 mol), cyclohexene (3.36 g, 0.04 mol), and sodium carbonate (2 g) in *n*-hexane (200 mL) was photolysed under nitrogen for 10 h. The photolysate was decanted from the deposited oil and was evaporated to give a yellow oil (322 mg) showing singlets at τ 7.03 and 7.11 for **2***c*, 6.20 and 6.92 for **2***b*, and 6.81 and 7.82 for $(CH_2{=}NCH_3)_3$ (24). Gas chromatographic analysis of the oil

gave the peaks corresponding to **2***b* (6.1 min, 3%) and **2***c* (6.6 min, 30%) and other unidentified peaks.

The insoluble fraction was taken up in methanol and was evaporated to give a dark oil (190 mg); this oil showed a doublet at τ 7.16 (J = 6 Hz, collapsing to a singlet after D_2O exchange) for *N*-methylformamide and singlets at τ 7.03 and 7.11 for **2***c* and 6.20 and 6.92 for **2***b*. The gc analysis of this mixture gave the peaks corresponding to **2***b* (19%), **2***c* (15%), **2***a* (3%), and *N*-methylformamide (58%). The last compound was separated by preparative gc and showed ir, nmr, and ms spectra identical with those of a sample synthesized from methylamine and formic acid.

Photolysis of N-*Nitropiperidine in Acidic Methanol*

NNOP (1.0 g, 0.008 mol) and concentrated HCl (1 mL, 0.06 *N*) in methanol (200 mL) were irradiated under nitrogen for 2 h at which time the reaction mixture was distilled. A mixture of the distillate (50 mL) and 2,4-dinitrophenylhydrazine reagent solution (20 mL) was evaporated to approximately 20 mL and was cooled. The yellow precipitate was recrystallized from methanol to give formaldehyde 2,4-dinitrophenylhydrazone, mp 159–162°C; a mixed melting point with an authentic sample was 161–163°C.

The residue from the photolysate (1.0 g) was dissolved in hot 2-propanol and was cooled to give white crystals (150 mg, mp >200°C) which exhibited identical ir and ms spectra to those of an authentic sample of piperidine hydrochloride; ir: 2520(m), 2420(m), 1590(m), 1160, 1028, 940, and 860(m) cm^{-1}. The mother liquor was evaporated and the residue was diluted with water (50 mL) and worked up in the usual manner. Extraction of the basic fraction with ether gave a crude oil (250 mg) which on gc analysis (20% SE30, 130°C) gave a single peak superimposable with that of piperidine.

In a separate experiment, the photolysate was worked up in the usual manner and the aqueous solution, made basic with sodium carbonate, was extracted with methylene chloride. The methylene chloride solution was dried and evaporated to give an oil (530 mg); ir: 3350(w, br), 2665(w), 2520(w), 2420(w), 1590(w), 1295, 1265, 1160(s), 1130(s), 1035, 862, and 780(m) cm^{-1}; nmr τ: 6.55(m), 7.15(s), 7.57(m), and 8.50(m). Three peaks with retention times of 1.2, 2.4, and 12.7 min were observed when this mixture was examined by gc (20% SE30, 130°C). By peak matching the first and third peaks were shown to be piperidine (37%) and piperidine hydrochloride (21%). The second peak exhibited ms fragments at *m/e* 96(19), 95(100), 94(78), and 67(72) and was characterized as dipiperidinomethane (41%) by comparison with the mass spectrum of an authentic sample prepared from piperidine and methylene chloride.

Photolysis of Nitramines Under Acidic Conditions in the Presence of Cyclohexene

(*a*) A solution of NNOP (1.0 g, 0.008 mol), cyclohexene (0.65 g, 0.008 mol), and concentrated HCl (0.67 mL, 0.04 *N*) in methanol (200 mL) was irradiated under nitrogen for 4.5 h. As the 249 nm band of NNOP in the uv spectra of the photolysate slowly disappeared it was replaced by a new absorption at about 210 nm which subsequently disappeared with further irradiation. The workup gave a neutral fraction (40 mg) and a basic fraction (770 mg); ir: 3300(w), 1550(m), 1155, and 1115(m) cm^{-1}; nmr τ: 4.30(m), 6.70 (d, J = 6 Hz), 7.6(m), and 8.5(m). The complex basic fraction was analyzed by the gc peak matching method and by gc–ms (20% SE30, 110–200°C at 8°/min) and found to be a mixture of eight compounds with the following retention times: 3.0 min, 16%, piperidine; 6.0 min, 5.5%, dipiperidinomethane; 18.3 min, 12%, ms *m/e*: 165(M^+, 42), 164(18), 150(15), 137(100), 124(64), 122(88), 84(50), and 81(48); 20.7 min, 10%, ms *m/e*: 197(M^+, 32), 182(80), 124(100), 98(41), 85(25), and 84(27); 21.2 min, 20%, 2-piperidinocyclohexanol (**3**); 24.6 min, 22%, 2-piperidinocyclohexanone oxime (**9**); 26.1 min, 9%, 1-nitro-2-piperidinocyclohexane (**4**). The above identifications were made by comparison of mass spectra with those of the authentic samples (21, 22, 24). The compounds eluting at 18.3 min and 20.7 min were tentatively identified as a piperidinocyclohexene (**11**) and 1-methoxy-2-piperidinocyclohexane (**5**), respectively, from the mass spectra.

(*b*) A solution of NNOD (0.9 g, 0.01 mol), cyclohexene (1.64 g, 0.02 mol), and concentrated hydrochloric acid (0.9 mL) in methanol (190 mL) was photolysed under nitrogen for 3 h. The photolysate was worked up in the usual manner to give a neutral (160 mg) and basic fraction (790 mg). The basic fraction showed ir peaks at 3350, 1660, 1552, 1160, 1115, and 1048 cm^{-1} and nmr singlets at τ 7.66, 7.70, and 7.80 and was analyzed by gc peak matching and gc–ms (10% SE30, 100–275°C at 6°/min) to give the following compounds: 2.9 min, 15%, dimethylaminocyclohexane (**6**); 4.6 min, 28%, 2-dimethylaminocyclohexanol (**7**); 5.3 min, 8%, unknown, *m/e* (%): 170(22), 142(100), 126(66), 84(68), 71(70), 58(66), 44(38), and 42(44); 6.7 min, 24%, 2-dimethylaminocyclohexanone oxime (**10**), *m/e*(%): 156(M^+, 15), 139(100), 84(80), 71(60), 44(45), and 42(58); 7.5 min, 22%, 1-nitro-2-dimethylaminocyclohexane (**8**); 13.4 min, 3%, unknown, *m/e* (%): 327(2), 222(47), 125(100), 110(75), 84(72), and 58(78).

The neutral fraction showed >30 gc peaks and nmr signals for NNOD at τ 6.6 and for a cyclohexyl moiety at τ 8.00 region. The fraction was not investigated further.

(*c*) The same photoreaction as above was carried out except carbon monoxide instead of nitrogen was used. The photolysate was worked up to give a neutral (176 mg) and basic fraction (680 mg). The basic fraction gave, by gc analysis, **6** (15%), **7** (28.5%), **10** (24.5%), and **8** (24.5%) in addition to the two unknowns. The neutral fraction showed gc and ir spectra similar to that above and was not investigated further.

Oxidative Photoaddition of Nitramine to Cyclohexene in the Presence of Oxygen

(*a*) A solution of NNOP (1 g, 0.008 mol), cyclohexene (0.65 g, 0.008 mol), and concentrated HCl (0.67 mL, 0.04 *N*) in methanol (200 mL) was photolysed under oxygen for 1 h. The photolysate was worked up in the usual manner to yield a small amount of the neutral fraction and the basic extract (1.48 g); ir: 3400(w, br), 1710(w), 1620(s), 1100, and 865(s) cm^{-1}. The basic extract was dissolved in THF (100 mL) and reduced with LAH (1.2 g, 0.03 mol). The usual workup gave an oil (1.01 g, 72%).

The reduced basic extract was chromatographed on alumina (40 g). The first compound (300 mg, 25%) eluted with 0.5% methanol–CH_2Cl_2 gave a solid which was sublimed (25°C/0.5 Torr) to give trans-2-piperidinocyclohexanol (**3**); mp 30.5–32°C (lit. (21) mp 35–36°C); ir (Nujol): 3450(s), 1305, 1195, 1160, 1100(s), 1078(s), 1005, 940, and 870 cm^{-1}; nmr τ: 6.75(m, 1H), 6.75(s, D_2O exch.), 7.80(m, 1H), 7.2–8.2 (unresolved, 5H), 8.50(m, 10H), and 8.80(m, 3H); ms *m/e*(%): 183(13), 166(2), 154(4), 140(6), 125(13), 124(100), 111(16), 98(33), and 84(13). The second compound (150 mg, 12%) was eluted with 1% methanol–CH_2Cl_2 as a crystalline solid which was sublimed twice (25°C/0.5 Torr) to give *cis*-2-piperidinocyclohexanol (**3**); mp 83–85°C; ir (Nujol): 3170(w), 1190, 1105, 985, and 870 cm^{-1}; nmr (CCl_4) τ: 6.10(m, 1H), 7.45(m, 6H), and 7.9–9.0 (unresolved, 14H). Resublimation (25°C/0.5 Torr) gave an analytical sample of the *cis*-alcohol melting at 87–89°C (lit. (21) mp 93–94°C). *Anal.* calcd. for $C_{11}H_{21}NO$: C 72.08, H 11.55, N 7.64; found: C 71.77, H 11.43, N 7.67.

(*b*) A solution of NNOD (0.9 g, 0.01 mol), cyclohexene (1.64 g, 0.02 mol) and concentrated hydrochloric acid in

methanol was irradiated under oxygen for 1.5 h. The photolysate was evaporated and separated to a neutral (105 mg) and a basic fraction (1.52 g); ir: 3420(m), 1715(m), 1625(s), 1275(s), 1040(m), and 870(s) cm^{-1}. The basic fraction was immediately reduced with lithium aluminium hydride (1.5 g) for one day. After usual workup, it gave a 1:3 mixture (1.04 g, 64%) of *cis*- and *trans*-2-dimethylaminocyclohexanols as shown by ir and nmr spectra and gc analysis in comparison with an authentic sample (21, 20).

Quantum Yield Determination

The quantum yields of the photodecomposition of *N*-nitropiperidine under various conditions were determined by the technique described in the previous publications (23). Solutions containing *N*-nitropiperidine (0.01 *M*), cyclohexene (0.02 *M*), and various amounts of acids were placed in quartz tubes and irradiated in a merry-go-round apparatus equipped with a Hanovia 450 W medium pressure mercury lamp. At each five minute interval a tube was removed and frozen in a dark place until making the uv measurements. The decreases of the absorbance of the 245 nm of the nitramine were recorded and plotted against the time. The decreases followed a zero order kinetics up to 30 min irradiation and the slopes gave the amount of nitramine decomposition. After 30 min irradiation, the decreases curved upward indicating that secondary reactions had set in. The zero hour samples were kept in the dark and were found to show no noticeable decrease in the uv absorption. A ferric oxalate actinometry was used and a *correction factor* (23) measuring the light quanta absorbed by the nitramine solution was determined to be 45%. The results are summarized in Table 2.

Acknowledgements

The authors are grateful to the National Research Council of Canada, Ottawa, for generous operation grants for this research project.

1. R. W. Lockhart, R. W. Snyder, and Y. L. Chow. J. Chem. Soc. Chem. Commun. 52 (1976).
2. P. A. S. Smith. Open-chain nitrogen compounds. Vol. 2. W. A. Benjamin, Inc., New York. 1966. Chapt. 15.
3. G. F. Wright. The chemistry of the nitro and nitroso groups. Part 1. *Edited by* H. Feuer. Interscience, New York. 1969. Chapt. 9.
4. I. T. Millar and H. D. Springall. Sidwick's organic chemistry of nitrogen. Clarendon Press, Oxford. 1966. p. 592.
5. J. Stals. Trans. Faraday Soc. **67**, 1739 (1971).
6. R. N. Jones and G. D. Thorn. Can. J. Res. Sect. B, **27**, 823 (1949).
7. C. L. Baumgardner, K. S. McCallum, and J. P. Freeman. J. Am. Chem. Soc. **83**, 4417 (1961).
8. W. S. Layne, H. H. Jaffe, and H. Zimmer. J. Am. Chem. Soc. **85**, 435 (1963); **85**, 1816 (1963).
9. (*a*) W. Costain and E. G. Fox. Nature, **160**, 826 (1947); (*b*) P. W. Allen and L. E. Sutton. Acta Crystallogr. **3**, 46 (1950).
10. D. V. Banthorpe and J. A. Thomas. J. Chem. Soc. 7158 (1965).
11. K. Suryanarayanan and S. Bulusu. U.S. Gov. Res. Dev. Rep. **70** (23), 7 (1970).
12. J. M. Lavanish. Ph.D. Dissertation, Yale University, New Haven, Connecticut. 1966.
13. K. Suryanaryanan and S. Bulusu. J. Phys. Chem. **76**, 496 (1972).
14. J. W. Bodnar and C. Rowell. J. Chem. Phys. **56**, 707 (1972).
15. R. L. Moon. M.Sc. Dissertation, Naval Postgraduate School, Monterey, California. 1972.
16. Y. L. Chow. Acc. Chem. Res. **6**, 354 (1973).
17. Y. L. Chow. Can. J. Chem. **45**, 53 (1967).
18. J. M. Flournoy. J. Chem. Phys. **36**, 1106 (1962); B. L. Korsunskii, F. I. Dubovitskii, and G. V. Sitonina. Dokl. Akad. Nauk, SSSR, **174**, 1126 (1967).
19. W. D. Emmons. J. Am. Chem. Soc. **76**, 3468 (1954).
20. M. P. Lau. Ph.D. Dissertation, Simon Fraser University, Burnaby, B.C. 1970.
21. Y. L. Chow, J. N. S. Tam, C. J. Colon, and K. S. Pillay. Can. J. Chem. **51**, 2469 (1973); K. S. Pillay and Y. L. Chow. J. Chem. Soc. Perkin Trans. II, 93 (1977).
22. L. J. Magdzinski and Y. L. Chow. J. Am. Chem. Soc. **100**, 2444 (1978).
23. T. Mojelski and Y. L. Chow. J. Am. Chem. Soc. **96**, 4549 (1974).
24. L. J. Magdzinski, H. Richard, K. S. Pillay, and Y. L. Chow. Can. J. Chem. **56**, 1657 (1978).
25. R. W. Fessenden and P. Neta. J. Phys. Chem. **76**, 2857 (1972).
26. Y. L. Chow, M. P. Lau, R. A. Perry, and J. N. S. Tam. Can. J. Chem. **50**, 1044 (1972).
27. Y. Rees and G. H. Williams. Adv. Free-Radical Chem. **3**, 199 (1969).
28. R. H. Hesse. Adv. Free-Radical Chem. **3**, 83 (1969).
29. D. H. R. Barton, R. H. Hesse, M. M. Pechet, and L. C. Smith. J. Chem. Soc. Chem. Commun. 754 (1977).
30. K. S. Pillay, K. Hanaya, and Y. L. Chow. Can. J. Chem. **53**, 3022 (1975).
31. V. Malatesta and K. U. Ingold. J. Am. Chem. Soc. **95**, 6400 (1973).
32. R. W. Yip, T. Vidoczy, R. W. Snyder, and Y. L. Chow. J. Phys. Chem. **82**, 1194 (1978).
33. G. A. Olah. Acc. Chem. Res. **4**, 240 (1972).
34. J. A. Berson and D. A. Ben-Efraim. J. Am. Chem. Soc. **81**, 4094 (1959).

Kinetic equations for reactions in concentrated aqueous acids based on the concept of "excess acidity"[1]

ROBIN A. COX AND KEITH YATES

Department of Chemistry, University of Toronto, 80 St. George St., Toronto, Ont., Canada M5S 1A1

Received May 14, 1979

ROBIN A. COX and KEITH YATES. Can. J. Chem. 57, 2944 (1979).

Kinetic equations, applicable to A-1, A-S_E2, and A-2 reactions in concentrated aqueous acids, are derived. The variation in reaction rate with varying acid concentration is treated in terms of the "excess acidity" of the medium (X-function), rather than in terms of Hammett-type acidity functions or the water activity. The parameters obtained are the medium-independent rate constant k_0, in the aqueous standard state, as an intercept, and a slope parameter m^*; hydration parameters (r-values) are also obtained, for A-2 reactions. The equations derived are shown to apply to A-1 acetal hydrolyses, A-S_E2 electrophilic aromatic substitutions, and mixed A-2/A-1 ester hydrolyses. In a general discussion of available methods for analyzing rate data in these media, it is shown that the X-function method encompasses most, if not all, of the others, and that classical acidity functions are no longer necessary.

ROBIN A. COX et KEITH YATES. Can. J. Chem. 57, 2944 (1979).

On a déduit les équations cinétiques applicables aux réactions de type A-1, A-S_E2 et A-2 dans des solutions aqueuses concentrées d'acides. La variation de la vitesse de réaction en fonction de la concentration de l'acide est interprétée en fonction d'un excès d'acidité (fonction de X) plutôt que selon des fonctions d'acidité de type de Hammett ou d'activité de l'eau. On a obtenu les paramètres suivants: la constante de vitesse k_0 indépendante du milieu, dans l'état fondamental aqueux en tant qu'intersection et un paramètre de pente m^* ainsi que les paramètres d'hydratation (valeur conventionnelle) trouvées au cours des réactions de type A-2. On a montré que les équations dérivées s'appliquent aux hydrolyses A-1 d'acétales aux substitutions électrophiles en série aromatique A-S_E2 et aux hydrolyses d'esters mixtes A-2/A-1. Dans une discussion générale sur l'ensemble des méthodes disponibles d'analyse de données de vitesse en milieu acide on a montré que la méthode de la fonction de X englobe la plupart si ce n'est pas toutes les autres méthodes, et que les fonctions classiques d'acidité ne sont plus nécessaires.

[Traduit par le journal]

Introduction

Recently excess acidities, or X-functions, have been determined for 0–99.5% aqueous sulfuric acid and 0–78% aqueous perchloric acid (1). These are derived from ionization ratio data for all types of base in these systems, using a concept developed by Marziano, Passerini, and their associates (2). They have been used to evaluate acid dissociation constants, in the aqueous standard state, for a large number of weak bases in these media (1).

For proton transfer to a base B, eq. [1], the

$$[1] \quad B + H^+ \overset{K_{BH^+}}{\rightleftharpoons} BH^+$$

$$[2] \quad \log (C_{BH^+}/C_B) - \log C_{H^+} = \log (f_B f_{H^+}/f_{BH^+}) + pK_{BH^+}$$

general thermodynamic eq. [2] can be written, from the definition of K_{BH^+}, where C is molar concentration, f molar activity coefficient, and K_{BH^+} is the acid ionization constant of the species BH^+. The assumption is then made that the activity coefficient term in eq. [2] is a linear function of a similar term for a "standard base" B*, slope m^*, which is the previously derived X-function (1), eq. [3].

$$[3] \quad \log (f_B f_{H^+}/f_{BH^+}) = m^* \log (f_{B^*} f_{H^+}/f_{B^*H^+}) = m^* X$$

This assumption has now been extensively tested and found to be obeyed for many different types of base in strong acids (2, 3), and for many types of acid in strongly basic solutions (4, 5). Equation [4] can then be used for the evaluation of pK_{BH^+} values

$$[4] \quad \log I - \log C_{H^+} = m^* X + pK_{BH^+}$$

in the aqueous standard state; the term C_{BH^+}/C_B in eq. [2] is the measured ionization ratio I (1).

In this paper these X-functions are used to develop general kinetic equations, applicable to acid-catalyzed reactions in these and other non-ideal strong acid media, and, by a simple extension (4), to base-catalyzed reactions in strongly basic media (6).

[1]Presented in part at the 2nd Chemical Institute of Canada/American Chemical Society Joint Conference, Montreal, P.Q., May, 1977, No. ORGN 43.

0008-4042/79/222944-08$01.00/0

The accompanying papers test this analysis for several different reactions (7, 8).

Kinetic Analysis

A-1 Mechanism

$$S + H^+ \overset{K_{SH^+}}{\rightleftharpoons} SH^+$$

[5] $$SH^+ \xrightarrow[\text{slow}]{k_0} A^+ \xrightarrow{\text{fast}} P$$

Equation [5] represents a rate-determining unimolecular reaction, with a medium-independent rate constant k_0, of a protonated substrate SH^+ formed from the substrate S in a fast pre-equilibrium proton transfer (K_{SH^+}). The product P may be formed directly, or after subsequent fast step(s) from an intermediate A^+. The observed rate (pseudo-first-order rate constant k_ψ) is then given by eq. [6],

[6] $$dC_P/dt = -d(C_S + C_{SH^+})/dt = k_\psi(C_S + C_{SH^+}) = k_0 a_{SH^+}/f_\ddagger$$

where the substrate concentration is written as the sum of protonated and unprotonated forms (since the extent of protonation is also medium-dependent); a is activity and $f_\ddagger$ is the activity coefficient of the transition state.

Two cases may be considered; one in which the substrate is predominantly unprotonated in the acidity range under study, and the other in which it is mainly protonated.

For case 1 we may write eq. [7], substitute this into eq. [6], take logs and rearrange to give eq. [8].

[7] $$a_{SH^+} = a_S a_{H^+}/K_{SH^+} = C_S C_{H^+} f_S f_{H^+}/K_{SH^+}$$

[8] $$\log k_\psi - \log C_S/(C_S + C_{SH^+}) - \log C_{H^+} = \log (f_S f_{H^+}/f_\ddagger) + \log (k_0/K_{SH^+})$$

Probably the best assumption that can be made about the activity coefficient ratio term in eq. [8] is that it is a linear function of a similar term describing the equilibrium protonation of S, with slope parameter $m^\ddagger$, eq. [9]

[9] $$\log (f_S f_{H^+}/f_\ddagger) = m^\ddagger \log (f_S f_{H^+}/f_{SH^+}) = m^\ddagger m^* X$$

This is an extension of the Kresge α-coefficient assumption (9, 10). Since the second term in eq. [9] is linear in X (eq. [3] above), the slope parameter can be written as the product, $m^\ddagger m^*$, and eq. [8] becomes eq. [10]. (The Bunnett–Olsen treatment (11), in contrast, uses an *additive* combination of slope parameters.)

[10] $$\log k_\psi - \log C_S/(C_S + C_{SH^+}) - \log C_{H^+} = m^\ddagger m^* X + \log (k_0/K_{SH^+})$$

For case 2, $a_{SH^+} = C_{SH^+} f_{SH^+}$ can be substituted into eq. [6]; taking logs and rearranging produces eq. [11]. Addition of $\log f_{SH^+}$ to each side of eq. [9] gives eq. [12], which on substitution into eq. [11] results in the linear equation [13].

[11] $$\log k_\psi - \log C_{SH^+}/(C_S + C_{SH^+}) = \log (f_{SH^+}/f_\ddagger) + \log k_0$$

[12] $$\log (f_{SH^+}/f_\ddagger) = (m^\ddagger - 1) \log (f_S f_{H^+}/f_{SH^+}) = (m^\ddagger - 1) m^* X$$

[13] $$\log k_\psi - \log C_{SH^+}/(C_S + C_{SH^+}) = (m^\ddagger - 1) m^* X + \log k_0$$

Equations [10] and [13] are the appropriate kinetic equations for an A-1 process; values of log C_{H^+} and X for use with these are available (1, 12). If ionization ratio data for the substrate can be obtained, application of eq. [4] gives pK_{SH^+} and m^*, and the terms which correct for differing extents of protonation (the second terms in eqs. [10] and [13]) can also be evaluated, if necessary. If not, either zero or full protonation can be assumed and eq. [10] or eq. [13] used anyway; now, however, the slope and intercept parameters from the straight line plot will be composites, as indicated.

Some A-1 reactions, as attested by much evidence, acidity function and otherwise, involving unprotonated substrates are illustrated in Fig. 1. These are acetal hydrolyses in sulfuric acid at 25°C of methoxymethyl acetate (13), trioxane (14), and paraldehyde (15). In all of these fast pre-equilibrium proton transfer is followed by slow unimolecular breakup of the protonated species, as illustrated for the depolymerization of trioxane (ref. 16, pp. 148–150; ref. 23, pp. 187–189):

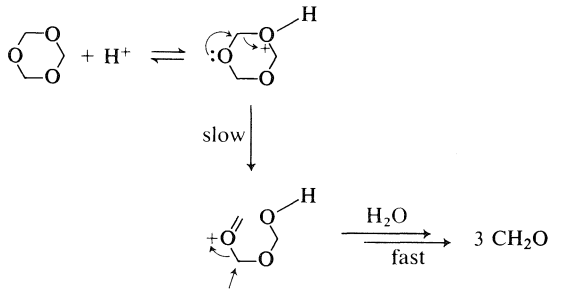

The plots according to eq. [10] show excellent linearity; the data resulting from least-squares analysis are in Table 1. No ionization ratio data for

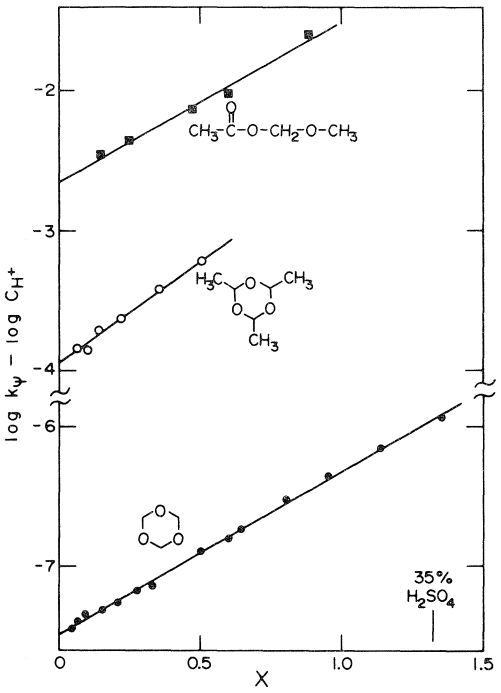

FIG. 1. Some acetal hydrolyses in sulfuric acid at 25°C, plotted according to eq. [10]. Rate data from refs. 13–15; X and log C_{H^+} from ref. 1.

these compounds seem to be available, but it is known that m^* values for typical oxygen protonations are in the range 0.4–0.6 (1), so that $m^{\ddagger}$ is probably in the range 2–3.

A-S_E2 Mechanism

$$[14] \quad S + H^+ \underset{\text{slow}}{\overset{k_0}{\rightarrow}} SH^+ \underset{\text{fast}}{\rightarrow} P$$

Equation [14] represents rate-determining proton transfer to the substrate, with subsequent reaction of SH^+ being fast. The rate is given by eq. [15]; on making the assumptions of eq. [9] and taking logs, eq. [16] results.

$$[15] \quad k_\psi C_S = k_0 a_S a_{H^+}/f_{\ddagger} = k_0 C_S C_{H^+} f_S f_{H^+}/f_{\ddagger}$$

$$[16] \quad \log k_\psi - \log C_{H^+} = m^{\ddagger} m^* X + \log k_0$$

Here the slope parameter $m^{\ddagger}$ is identical to the term α (also called α_A (10)), which has been defined by Kresge *et al.* (9). The value of α is interpretable as the degree of proton transfer at the transition state as shown in eq. [17]; this value varies between zero and one, as the transition state varies between (S + H^+) and SH^+ (9, 10).

$$[17] \quad f_{\ddagger} = (f_S f_{H^+})^{1-\alpha} (f_{SH^+})^{\alpha}$$

Some caution is necessary in using eq. [16] in sulfuric acid and other partially dissociated acids, because in these cases species other than protonated water can act as acid catalysts, in the general acid catalysis mechanism of eq. [14] (17). Kresge and his colleagues have discussed this in connection with aromatic protodetritiation in different acid systems (18), and Cox and Buncel have found catalysis by undissociated H_2SO_4 and protonated $H_3SO_4^+$ for several azoxy rearrangements in strong sulfuric acid (17, 19). In fully dissociated acids such as $HClO_4$ and HCl, these considerations do not apply, however; an equation similar to eq. [16] has been extensively tested by Kresge and co-workers in aqueous $HClO_4$ (10).

Included here are some protodedeuterations (20, 21) and a protodeboronation (22), for substituted benzenes in dilute sulfuric acid, illustrated in Fig. 2. These widely-studied reactions are known to be A-S_E2 (ref. 16, pp. 186–190; ref. 23, pp. 262–274), with the rate-determining step being Wheland intermediate formation:

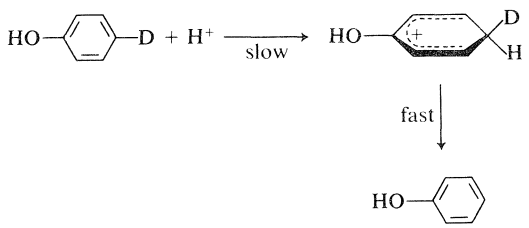

Excellent linearity according to eq. [16] is obtained; the results of least-squares analysis are given in Table 2.

Again the slope parameters are composites, $m^{\ddagger}m^*$; m^* values for typical carbon protonations are large, in the range 1.2–1.6 (1), so $m^{\ddagger}$ probably has a value between 0.5 and 1.0 for these reactions, which seems reasonable.

A-2 Mechanism

$$[18] \quad S + H^+ \underset{\text{fast}}{\overset{K_{SH^+}}{\rightleftharpoons}} SH^+ \qquad SH^+ + Nu \underset{\text{slow}}{\overset{k_0}{\rightarrow}} P$$

The A-2 mechanism of eq. [18] differs from the A-1 mechanism of eq. [5] in the involvement of additional species with protonated SH^+ in the rate-determining transition state. These species, symbolized Nu in eq. [18], may be nucleophiles or bases. Usually one or more water molecules are involved (16, 23, 24); occasionally bisulfate ions in sulfuric

TABLE 1. Results of fitting rate data for some acetal hydrolyses in sulfuric acid at 25°C to eq. [10]

	Depolymerization of paraldehyde (15)	Depolymerization of trioxane (14)	Methoxymethyl acetate hydrolysis (13)
r^a	0.993 (6)	0.999 (14)	0.994 (5)
$m^{\ddagger}m^*$	1.45±0.09	1.16±0.02	1.14±0.08
log (k_0/K_{SH^+})	−3.95±0.02	−7.49±0.01	−2.65±0.04
$\sigma_y{}^b$	±0.033	±0.023	±0.044

[a]Correlation coefficient. Number of points in parentheses.
[b]Root-mean-square deviation between experimental and fitted points.

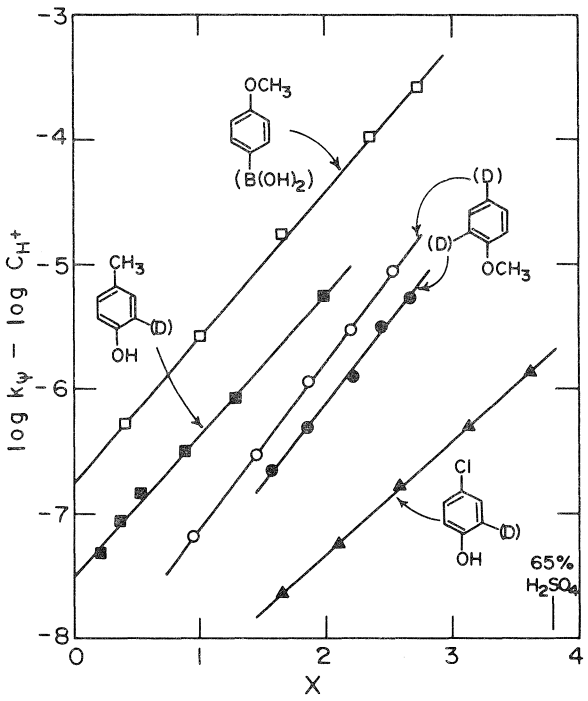

FIG. 2. Some protodedeuterations (20–21) and a protodeboronation (22) of benzene derivatives in sulfuric acid at 25°C. Plotted according to eq. [16], using X and log C_{H^+} from ref. 1.

acid (25, 26), and possibly other species in different acid media (17).

A similar analysis to that for the A-1 case given above results in eq. [19] for mainly unprotonated substrates, and eq. [20] for substrates which exist

$$[19]\quad \log k_\psi - \log C_S/(C_S + C_{SH^+}) - \log C_{H^+} = m^{\ddagger}m^*X + \log a_{Nu} + \log (k_0/K_{SH^+})$$

$$[20]\quad \log k_\psi - \log C_{SH^+}/(C_S + C_{SH^+}) = (m^{\ddagger} - 1)m^*X + \log a_{Nu} + \log k_0$$

predominantly in the protonated form under the reaction conditions. These differ from eqs. [10] and [13] above in the inclusion of an additional nucleophile (or base) activity term. Thus plots of the left-hand side (LHS) of these equations vs. X will curve downward for an A-2 process involving water, the most common case (7). In practice, different log a_{Nu} values can be subtracted from the LHS (one water, two waters, one bisulfate, etc.) until linearity against X is achieved. Alternatively the problem can be treated as a double linear regression with X as one variable and, say, log a_{H_2O} as the other. This procedure gives both $m^{\ddagger}$ and r values, where r is the net number of water molecules involved in forming the transition state (24). This approach is demonstrated in an accompanying paper (7).

For cases in which a mechanism change occurs, as in most ester hydrolyses (24, 27), a non-linear least-squares computer program which fits a combination of (say) eqs. [10] and [19] (i.e., $k_\psi = k_{A-1} + k_{A-2}$) will give all the relevant parameters directly (8).[2] A good illustration of this can be found in the recent work of Edward and Wong (28), who studied the hydrolyses of ethyl benzoate, ethyl thiolbenzoate, and ethyl thionbenzoate in sulfuric acid. They found that all these esters hydrolyzed by an A-2 process in weak acid, with two water molecules involved in the reaction, and switched to an A-1 process in stronger acid, with the position of mechanism change being very substrate-dependent. Detailed mechanisms were given (28), proposed on the basis of the r-parameter (24) and the transition-state activity coefficient (29) criteria. Ample confirmation of these mechanistic proposals can be seen in the excellent agreement of theory with experiment in Fig. 3, where the theoretical curves[2] are calculated assuming that eq. [10] applies to the high acidity A-1 reaction, and eq. [19] to the low acidity A-2 process, with log a_{Nu} taken as 2 log a_{H_2O}. The resulting parameters are given in Table 3. In this case the protonation behaviour is available (1, 28, 30), so $m^{\ddagger}$ and k_0 values can be calculated for the A-2 reactions. The resulting $m^{\ddagger}$ values are closely similar for the three substrates, despite their quite different

[2]A suitable program is given elsewhere (8).

TABLE 2. Least-squares analysis results for some electrophilic aromatic substitutions in sulfuric acid at 25°C, according to eq. [16]

	2-Deutero-4-methylphenol D loss (20)	2,4-Dideuteroanisole		4-Chloro-2-deuterophenol D loss (20)	4-Methoxybenzeneboronic acid $B(OH)_2$ loss (22)
		4-D loss (21)	2-D loss (21)		
r^a	0.998 (6)	0.9999 (5)	0.999 (5)	0.9999 (5)	0.9997 (5)
m^+m^*	1.13±0.03	1.34±0.01	1.29±0.04	0.91±0.01	1.17±0.02
log k_0	−7.51±0.03	−8.48±0.02	−8.70±0.09	−9.15±0.02	−6.75±0.03
σ_y^b	±0.047	±0.012	±0.034	±0.014	±0.031

[a, b] As in Table 1.

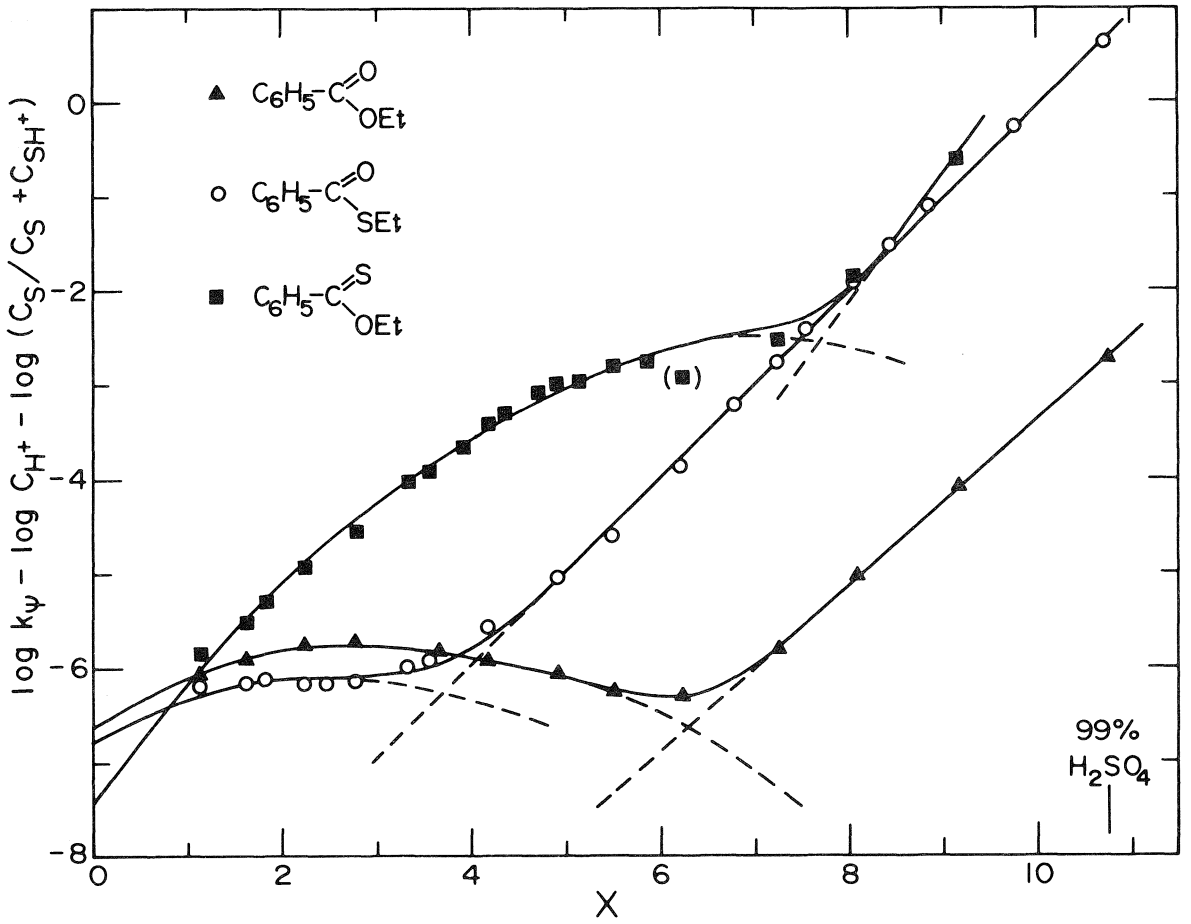

FIG. 3. Hydrolyses of ethyl benzoate, thiolbenzoate, and thionbenzoate in sulfuric acid at 25°C. Points are experimental (28); curves are theoretical, for an A-2 reaction with two water molecules at low acidity, eq. [19], and an A-1 process at high acidity, eq. [10].

protonation behaviour (as exemplified by the m^* values), suggesting similar transition state structures. The k_0 values all refer to the aqueous standard state, and thus are convenient for rate comparisons under standard conditions.

General Discussion

The X-function treatment described above has at least three distinct advantages over the currently available methods, of which there are several.

Firstly, it includes the best parts of all previous

TABLE 3. Data resulting from the application of eqs. [10] and [19] to some ester hydrolyses in sulfuric acid at 25°C[a]

	Ethyl benzoate	Ethyl thiolbenzoate	Ethyl thionbenzoate
pK_{SH^+}[b]	-6.00 ± 0.14[c]	-5.07 ± 0.08[d]	-7.99 ± 0.13[c]
m^*[b]	0.72 ± 0.02[c]	0.65 ± 0.01[d]	1.39 ± 0.03[c]
A-2 Mechanism			
$\log k_0$	-0.63 ± 0.14	-1.70 ± 0.13	0.56 ± 0.14
$m^{\ddagger}$	1.15 ± 0.03	1.15 ± 0.07	1.14 ± 0.02
A-1 Mechanism[e]			
$\log (k_0/K_{SH^+})'$	-12.14 ± 0.09	-9.89 ± 0.10	(-13 ± 1)[f]
$(m^{\ddagger}m^*)'$	0.88 ± 0.01	0.98 ± 0.01	(1.3 ± 0.1)[f]

[a]Reference 28. Errors quoted are standard deviations.
[b]Protonation at the carbonyl or thiocarbonyl function.
[c]Reference 1; using data from ref. 30.
[d]Obtained by applying eq. [4] to log I data from ref. 28.
[e]Terms cannot be separated because protonation at the ether or thioether function is involved. See ref. 8.
[f]Data insufficient for reliable estimation (28).

treatments (except the original Zucker–Hammett hypothesis (31), since discredited on various grounds, for instance the unacceptable activity coefficient behaviour required (24)). It includes the α-coefficient treatment (9), eq. [16], in its entirety. The basis is similar to that for the Bunnett–Olsen method (11),[3] and the parameters derived using the two can be interconverted. It gives the r-parameters (superseding the original w-values (32)) of the hydration parameter treatment (24), but only for those cases in which water really is involved in the reaction; the artificiality of plotting log rate constants against log water activity for cases in which water is not involved, is removed. It offers easy calculation of $f^*_{S\ddagger}$ values from eq. [9], if the necessary f_S values are available (see below), giving the advantages of the transition-state activity coefficient (TSAC) method (29).

Secondly, acidity functions, H_0, H_A, H_0''', etc., are not needed; the activity coefficient cancellation assumption, required to derive them, is not made (1). The only assumption made here is that activity coefficient ratios are linear functions of one another as in eqs. [3] and [9]. This assumption can be tested for equilibria, where it works well (1–5); it cannot be tested directly when transition states are involved, but the results suggest it is valid here too. The similarly-based Bunnett–Olsen method (11, 33) requires in addition the use of H_0, and hence the cancellation assumption used in its derivation;[3] also X-functions are derived using a much larger data base than that used for H_0 (1), and thus should offer higher precision. Nevertheless, at least in sulfuric acid (1), the X-function and Bunnett–Olsen methods are compatible (but see ref. 34), and should lead to the same mechanistic conclusions; detailed kinetic equations for the latter have been given (33). The slope parameters given by the two treatments, m^* and $m^{\ddagger}$, and ϕ_e and $\phi_{\ddagger}$ (33), can be interconverted, approximately, via eq. [21].

$$\begin{aligned} & H_0 + \log C_{H^+} \simeq -X \\ & m^* \simeq 1 - \phi_e \\ & m^{\ddagger} \text{ (or } \alpha) \simeq (1 - \phi_{\ddagger})/(1 - \phi_e) \\ & \phi_{\ddagger} \simeq 1 - m^{\ddagger}m^* \end{aligned} \qquad [21]$$

Thirdly, the nucleophilic or basic species actually involved in the transition state of an A-2 reaction can be determined, using eq. [19] or eq. [20]. Only the hydration parameter treatment (24) has successfully provided this information before, and only for those reactions involving water. The involvement of bisulfate ions in sulfuric acid has been inferred (25, 26), using a treatment which essentially ignored the activity coefficient variations; however, these are unlikely to be negligible in most cases. The TSAC method ignores any explicit involvement of additional species in the derivation of $f^*_{S\ddagger}$ (29), which may therefore contain contributions from (e.g.) the water activity for an A-2 process. This was pointed out by Edward and Wong (28), who use a slightly modified treatment in consequence. The treatment described here, with its ability to deal with additional species activity terms and with mixed mechanisms, probably offers the easiest access to this information.

The major difference between the excess acidity method and the Bunnett–Olsen method (11, 33), apart from the already-mentioned use of H_0 in the latter, lies in eq. [9]. In this work, in common with Kresge (9, 10) a *multiplicative* combination of slope parameters is used, whereas Bunnett and Olsen (11) and their followers (33) prefer an *additive* combina-

[3]This point is discussed in detail in ref. 1.

tion; this work could be regarded as an extension of the Kresge method to include A-1 and A-2 reactions. As Professor Bunnett has remarked, "time will tell which approach is more profitable" (11). There are minor differences; for instance the Bunnett–Olsen method as originally formulated (11) does not include the nucleophile/base activity in A-2 reaction equations, and hence predicts linearity in cases where the X-function method predicts curves (eqs. [19] and [20]). This is easily allowed for, however, as Modena and co-workers have recently begun to do (33); as mentioned, the excess acidity and Bunnett–Olsen methods are essentially compatible.

The X-function method, and the TSAC method (29), provide complementary information regarding reaction mechanisms in strong acid media. Equation [9] can be rearranged to give eq. [22].

$$[22]\quad \log f^*_{S\ddagger} = \log f_S - \log C_{H^+} - m^\ddagger m^* X + \log a^*_{H^+}$$

Of the terms on the right, $\log f_S$ must be measured or estimated (35), $\log C_{H^+}$ is available (1, 12), and $m^\ddagger m^* X$ is obtainable as described in this paper, and $\log a^*_{H^+}$ values have been derived for several acid media (36). The latter are proton activities relative to the standard tetraethylammonium ion, TEA^+, which is assumed to be invariant in its activity coefficient behaviour as the medium composition is changed (the Boyd approximation (37)); the $\log f^*_{S\ddagger}$ values obtained will also be relative to this ion (29).

The TSAC method, which relies on an essentially qualitative comparison of curve shapes, comparing the $\log f^*_{S\ddagger}$ curve as a function of acidity with known activity coefficient curves (29, 35), is probably the better method for distinguishing between different mechanistic possibilities. It can distinguish between A-1 and A-S_E2 mechanisms, for instance (38), which is difficult using any of the other methods. It does, however, require additional data not needed by the X-function method; the activity coefficient of the substrate as a function of acidity must be available or measureable (35).

On the other hand, once the mechanism is known or can reasonably be inferred, the X-function method probably provides the best medium-independent rate constants, k_0, for subsequent analysis. Since these are obtained by extrapolation to the standard state, pure water (where the deviation from ideality, X, is zero), they can be directly compared with those obtained, for instance, in aqueous buffer media, without having to be concerned with activity coefficients or differing acidity function behaviour. Comparison of rate constants obtained in non-ideal solutions has always been a problem; for example, should comparison be made at points of equal weight percent acid, equal molarity, equal H_0, equal substrate acidity function value, or equal water activity? Extrapolation to $H_0 = 0$ is commonly used (39), but this is suspect because different substrates often follow different acidity functions (16). In any case, 1 M acid can hardly be regarded as an ideal solution; the deviation from ideality, expressed as X, is 0.17 for H_2SO_4 and 0.20 for $HClO_4$ at this concentration (1). If rate constants obtained in one of these ways are used to calculate $\Delta H^\ddagger$, $\Delta S^\ddagger$, ρ, etc., it becomes difficult to decide what part of the calculated number represents real substrate behaviour and what part represents deviation from ideality of the medium (19). Using standard state k_0 values from the X-function treatment avoids these problems; they can be used with confidence for calculations of activation parameters, and in LFER plots. This is further demonstrated in the accompanying papers (7, 8).

The slope parameters, $m^\ddagger$, should offer mechanistic information; this has been discussed (in terms of $\phi_\ddagger$) by Lucchini *et al.* (33). Writing eq. [9] in the form of eq. [23],

$$[23]\quad \log f_\ddagger = m^\ddagger \log f_{SH^+} + (1 - m^\ddagger) \log f_S f_{H^+}$$

three possible types of behaviour may be visualized. Firstly, if $m^\ddagger \simeq 1$, $\log f_\ddagger \simeq \log f_{SH^+}$. This is suggestive of an A-2 reaction, where the hydration requirements of SH^+ and of an A-2 transition state should be similar (29); here it is known that $\log f^*_{S\ddagger}$ increases steeply with acidity, as does $\log f_{SH^+}$ (29, 35). Secondly, if $m^\ddagger < 1$, both terms on the right in eq. [23] will be positive, leading to a rise of $\log f_\ddagger$ with acidity; this is characteristic of A-S_E2 reactions (38). Finally, if $m^\ddagger > 1$, the two terms in eq. [23] will tend to cancel, increasingly so as $m^\ddagger$ increases; this leads to $\log f_\ddagger$ values which change only slowly with acidity. This is characteristic of an A-1 reaction (29, 38). The above analysis appears to be borne out experimentally (see Tables 1–3 and the earlier Discussion). In addition, it seems reasonable that similar $m^\ddagger$ values in related reactions would reflect similar transition state structures (see Table 3).

In summary, the major uses of the X-function method appear, at present, to be: confirming or rejecting proposed mechanisms, by producing a linear plot according to one of the equations given in this paper; determining what species are present in the transition states of A-2 reactions; and producing reliable intercept k_0 values for subsequent analysis.

Acknowledgements

We would like to thank the people who discussed this work with us, particularly Professor J. T. Edward and Dr. S. C. Wong. Helpful comments from the referees are also appreciated. Financial support of this research is by the Natural Sciences and Engineering Research Council of Canada.

1. R. A. Cox and K. Yates. J. Am. Chem. Soc. **100**, 3861 (1978).
2. N. C. Marziano, G. M. Cimino, and R. C. Passerini. J. Chem. Soc. Perkin Trans. II, 1915 (1973); N. C. Marziano, P. G. Traverso, A. Tomasin, and R. C. Passerini. J. Chem. Soc. Perkin Trans. II, 309 (1977).
3. N. C. Marziano, P. G. Traverso, and R. C. Passerini. J. Chem. Soc. Perkin Trans. II, 306 (1977).
4. R. A. Cox and R. Stewart. J. Am. Chem. Soc. **98**, 488 (1976).
5. R. A. Cox, R. Stewart, M. J. Cook, A. R. Katritzky, and R. D. Tack. Can. J. Chem. **54**, 900 (1976); M. G. Harris and R. Stewart. Can. J. Chem. **55**, 3800 (1977); R. Stewart and M. G. Harris. Can. J. Chem. **55**, 3807 (1977).
6. D. J. Kroeger and R. Stewart. J. Chem. Soc. B, 217 (1970); R. A. More O'Ferrall. J. Chem. Soc. Perkin Trans. II, 976 (1972).
7. R. A. Cox, C. R. Smith, and K. Yates. Can. J. Chem. **57**, 2952 (1979).
8. R. A. Cox, M. F. Goldman, and K. Yates. Can. J. Chem. **57**, 2960 (1979).
9. A. J. Kresge, R. A. More O'Ferrall, L. E. Hakka, and V. P. Vitullo. J. Chem. Soc. Chem. Commun. 46 (1965).
10. A. J. Kresge, S. G. Mylonakis, Y. Sato, and V. P. Vitullo. J. Am. Chem. Soc. **93**, 6181 (1971).
11. J. F. Bunnett and F. P. Olsen. Can. J. Chem. **44**, 1917 (1966).
12. R. A. Cox, S-O. Lam, R. A. McClelland, and T. T. Tidwell. J. Chem. Soc. Perkin Trans. II, 272 (1979).
13. P. Salomaa. Acta Chem. Scand. **11**, 132 (1957).
14. R. P. Bell, K. N. Bascombe, and J. C. McCoubrey. J. Chem. Soc. 1286 (1956).
15. R. P. Bell and A. H. Brown. J. Chem. Soc. 774 (1954).
16. C. H. Rochester. Acidity functions. Academic Press, London. 1970.
17. R. A. Cox. J. Am. Chem. Soc. **96**, 1059 (1974).
18. A. J. Kresge, S. G. Mylonakis, and L. E. Hakka. J. Am. Chem. Soc. **94**, 4197 (1972).
19. R. A. Cox and E. Buncel. *In* The chemistry of the hydrazo, azo and azoxy groups. *Edited by* S. Patai. Wiley-Interscience, London. 1975. Chapt. 18.
20. V. Gold and D. P. N. Satchell. J. Chem. Soc. 3609 (1955).
21. D. P. N. Satchell. J. Chem. Soc. 3911 (1956).
22. H. G. Kuivila and K. V. Nahabedian. J. Am. Chem. Soc. **83**, 2159 (1961).
23. M. Liler. Reaction mechanisms in sulphuric acid. Academic Press, London. 1971.
24. K. Yates. Acc. Chem. Res. **4**, 136 (1971).
25. R. A. Cox, A. J. Dolenko, and E. Buncel. J. Chem. Soc. Perkin Trans. II, 471 (1975).
26. R. A. Cox and E. Buncel. J. Am. Chem. Soc. **97**, 1871 (1975).
27. K. Yates and R. A. McClelland. J. Am. Chem. Soc. **89**, 2686 (1967).
28. J. T. Edward and S. C. Wong. J. Am. Chem. Soc. **99**, 7224 (1977).
29. T. A. Modro and K. Yates. Acc. Chem. Res. **11**, 190 (1978); R. A. McClelland, T. A. Modro, M. F. Goldman, and K. Yates. J. Am. Chem. Soc. **97**, 5223 (1975).
30. J. T. Edward and S. C. Wong. J. Am. Chem. Soc. **99**, 4229 (1977); J. T. Edward, I. Lantos, G. D. Derdall, and S. C. Wong. Can. J. Chem. **55**, 812 (1977).
31. L. Zucker and L. P. Hammett. J. Am. Chem. Soc. **61**, 2791 (1939).
32. J. F. Bunnett. J. Am. Chem. Soc. **83**, 4956 (1961); **83**, 4968 (1961); **83**, 4973 (1961); **83**, 4978 (1961).
33. V. Lucchini, G. Modena, G. Scorrano, and U. Tonellato. J. Am. Chem. Soc. **99**, 3387 (1977).
34. Ü. L. Haldna, I. A. Koppel, and H. J. Kuura. Reakts. Sposobn. Org. Soedin. **14**, 235 (1977).
35. K. Yates and R. A. McClelland. Prog. Phys. Org. Chem. **11**, 323 (1974).
36. T. A. Modro, K. Yates, and J. Janata. J. Am. Chem. Soc. **97**, 1492 (1975).
37. R. H. Boyd. J. Am. Chem. Soc. **85**, 1555 (1963).
38. T. A. Modro and K. Yates. J. Am. Chem. Soc. **98**, 4247 (1976).
39. S. Clementi and A. R. Katritzky. J. Chem. Soc. Perkin Trans. II, 1077 (1973); V. J. Nowlan and T. T. Tidwell. Acc. Chem. Res. **10**, 252 (1977).

The excess acidity method. The basicities, and rates and mechanisms of enolization, of some acetophenones and acetone, in moderately concentrated sulfuric acid

ROBIN A. COX, CLINTON R. SMITH, AND KEITH YATES

Department of Chemistry, University of Toronto, 80 St. George St., Toronto, Ont., Canada M5S 1A1

Received May 14, 1979

ROBIN A. COX, CLINTON R. SMITH, and KEITH YATES. Can. J. Chem. **57**, 2952 (1979).

The X-function method has been used to evaluate the basicities of six nuclear-substituted acetophenones and acetone, using a combination of new measurements and literature data; the protonation pK_{BH^+} of acetone was found to be -5.37. The same method, which involves the excess medium acidity, when used to analyze the enolization rate constants obtained from the measured bromination rates, shows that most of the acetophenones enolize by an A-2 process involving two water molecules in the rate-determining step. Observed linear free energy relationships for the basicities and the enolization rates imply a relatively early transition state for the enolization. Acetone was found to enolize by a similar mechanism in sulfuric acid solutions more dilute than 81% w/w, but at higher acidities bisulfate ion was the preferred base. The mechanistic behaviour of 4-nitroacetophenone was found to be different, not A-2 but either A-1 or A-S_E2.

ROBIN A. COX, CLINTON R. SMITH et KEITH YATES. Can. J. Chem. **57**, 2952 (1979).

On a utilisé la méthode de l'excès d'acidité (fonction de X) pour évaluer les basicités de six acétophénones substituées et de l'acétone en utilisant une combinaison de nouvelles mesures avec des données de la littérature; on a ainsi trouvé que la protonation pK_{BH^+} de l'acétone est de -5.37. Lorsqu'on utilise la même méthode, qui fait appel à l'excès d'acidité du milieu, pour analyser les constantes de vitesse d'énolisation obtenues à partir des vitesses de bromation, on trouve que la plupart des acétophénones s'énolisent selon un mécanisme A-2 qui implique deux molécules d'eau dans l'étape déterminante de la réaction. Les relations linéaires entre l'énergie libre et les vitesses de basicité et d'énolisation impliquent un état de transition qui se manifeste très tôt au cours de l'énolisation. On a remarqué que le mécanisme d'énolisation de l'acétone ne varie pas dans des solutions d'acide sulfurique à concentration inférieure à 81% (W/W); toutefois à de plus fortes concentrations, l'ion bisulfate est la base préférée. Le mécanisme est différent dans le cas de la nitro-4 acétophénone et n'est pas du type A-2 mais du type A-1 ou A-S_E2.

[Traduit par le journal]

Introduction

Recently an extrapolative technique for obtaining protonation equilibrium constants (pK_{BH^+}) of weak bases has been developed, using ionization ratio (I) measurements in strong acid media (1, 2). Known as the X-function method (1), it involves proton concentrations (C_{H^+}) and the concept of excess medium acidity (X), rather than classical Hammett-type acidity functions, and is summarized as eq. [1] (1).

$$[1] \quad \log I - \log C_{H^+} = m^*X + pK_{BH^+}$$

It has been shown to be both accurate and general (1–3). In this paper the method is used to determine the basicities of six nuclear-substituted acetophenones and acetone.

Excess acidities can also be used in kinetic analysis, as shown in an accompanying paper (4). In that paper rate equations for A-1, A-S_E2, and A-2 processes are derived and tested; these are given here, for reactions involving predominantly unprotonated substrates, as eqs. [2]–[4], respectively,

$$[2] \quad \log k_\psi - \log C_S/(C_S + C_{SH^+}) - \log C_{H^+} = m^{\neq}m^*X + \log (k_0/K_{SH^+})$$

$$[3] \quad \log k_\psi - \log C_{H^+} = m^{\neq}m^*X + \log k_0$$

$$[4] \quad \log k_\psi - \log C_S/(C_S + C_{SH^+}) - \log C_{H^+} = m^{\neq}m^*X + \log a_{Nu} + \log (k_0/K_{SH^+})$$

with symbols as previously defined (4). It is of interest to use this method, eq. [4] in particular, to investigate those A-2 reactions which involve base attack in the rate-determining step, rather than the more commonly studied nucleophilic attack (4–6). This is one of the three possible mechanistic roles for water given by Bunnett, based on the w hydration parameter approach (7). To this end we have studied the enolization of some acetophenones in moderately concentrated sulfuric acid solutions by following their rates of bromination.

The bromination of ketones in acid solution is well known to proceed by the pathway shown in eqs. [5]–[7] (8).

0008-4042/79/222952-08$01.00/0

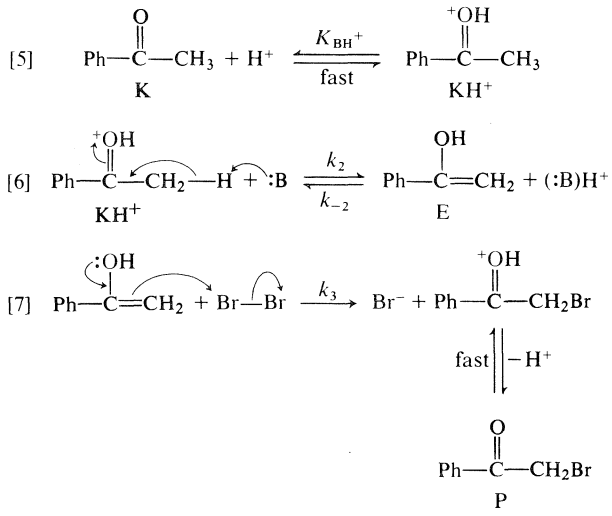

The assumption that the enol is a reactive intermediate, in a steady-state concentration, results in

$$[8] \quad -d[Br_2]/dt = k_3[E][Br_2] = (k_2/K_{BH^+})[K][H^+][B] \times \{1/(1 + k_{-2}[H^+]/k_3[Br_2])\}$$

eq. [8] for the reaction rate, given in terms of the observed variable, the bromine concentration. Provided that the last term in the denominator of eq. [8] is negligible, the observed pseudo-first-order rate constant k_ψ at a given acid concentration (fixed $[H^+]$ and [B]) can be obtained by following the zero-order bromine consumption; the rate-determining step is enolization, eq. [6]. For acetone, k_3 has been shown to be nearly 10^7 (9), so eq. [8] will be well-behaved as long as (*a*) k_{-2} is not large, and (*b*) the bromine concentration is greater than about 10^{-4} *M*. The value of k_{-2} is not expected to be large, since the reverse of eq. [6] involves carbon protonation, known to be comparatively slow (10).

Possible complications to be considered include bromination of the aromatic ring, and polybromination. The latter, troublesome in base-catalyzed enolization (11), is not expected to be a problem because acid-catalyzed bromoketone bromination is known to be slower than reaction of the parent compound (12). Another possible side reaction is condensation, e.g., eq. [9], producing unsaturated compounds which may also consume bromine (13); this has been observed at high ketone concentrations and high acidities (13), but not at uv spectral concentrations (14). It should not be important under the conditions used here.

The compounds involved in this study were 4-methoxy-, 4-methyl-, and 3-methylacetophenone

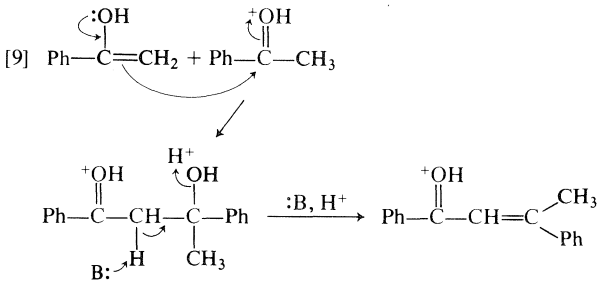

(**1–3**), acetophenone (**4**), 4-bromo-, 3-bromo-, and 4-nitroacetophenone (**5–7**), and acetone.

Experimental

The acetophenones were commercially available, and were recrystallized or redistilled before use. Sulfuric acid concentrations were determined titrimetrically.

Product analyses were performed by allowing equimolar amounts (~0.01 mol) of the acetophenone and bromine to react in 200 mL of 50% sulfuric acid until the bromine was decolourized (~2 h). Neutralization with sodium hydroxide and ether extraction, followed by drying and solvent evaporation, gave product oils which were examined spectrally.

For the basicity measurements, 10 μL of a stock methanolic ketone solution was diluted to 10 mL with the test acid and the uv–visible spectrum recorded. Determinations were in duplicate for each acid concentration. For **2**, **3**, and **6**, absorbances at the wavelength of the unprotonated form were subtracted from those at the wavelength of the protonated form, on the same spectrum (the Davis–Geissman procedure (15)), and the resulting absorbance differences used; this was sufficient to account for the small medium effect observed. For **7** the medium effect was more noticeable, and characteristic vector analysis (CVA) was necessary (16). After this treatment the protonation behaviour as a function of acidity is contained in the resulting coefficients of the first vector (16), and these were used directly. Extinction data for **2** and **5** have been reported by Flexser and Hammett (17); these were also treated by CVA. For **5** the resulting coefficients were used directly; for **2** they were added to our own data, after correcting for scale differences, and both sets used together. The experimental data used are given in Table 1.[1] Davis–Geissman extinction differences were already available for **1** (18), as were pK_{BH^+} and m^* values for **4** (1, 16). For acetone, a combination of uv extinction (14), proton (19) and ^{13}C (20) nmr data, all relating to the protonation, was normalized to a common scale and analyzed by CVA simultaneously.

The reaction kinetics were followed by monitoring the decreasing visible absorption due to bromine at 425 nm as a function of time, as the bromine reacted with an excess of the substrate, at 25°C. The concentration ranges were 10^{-2} to 10^{-3} *M* for bromine, and 1.5×10^{-2} to 10^{-3} *M* for the ketones, depending on reactant and product solubility; the ketone was kept in excess to minimize possible polybromination.

The pseudo-first-order rate constants k_ψ were evaluated as follows. Enolization is first order in ketone (K):

$$[K]_t = [K]_0 \exp(-k_\psi t)$$

[1] Tables 1, 3, and 4 are on deposit and may be obtained, at a nominal charge, from the Depository of Unpublished Data, CISTI, National Research Council of Canada, Ottawa, Ont., Canada K1A 0S2.

TABLE 2. Protonation constants for some acetophenones at 25°C

Compound[a]	ΔA_B (a_1)	ΔA_{BH^+} (a_2)	pK_{BH^+} (a_3)	m^* (a_4)	No.[b]	Error[c]
4-OMe (1)	−1.48 ±0.04[d]	2.29±0.03[d]	−3.76±0.10	0.76±0.03	13	±0.053 (1.2%)
4-Me (2)	−0.73 ±0.01	1.24±0.01	−3.67±0.06	0.60±0.01	23 (1)	±0.018 (0.9%)
3-Me (3)	−0.74 ±0.02	1.45±0.03	−4.09±0.16	0.60±0.03	16	±0.038 (1.7%)
— (4)	—	—	−4.16±0.07[e]	0.60±0.01[e]	—	—
4-Br (5)	−0.52 ±0.04[f]	0.48±0.04[f]	−4.20±0.51	0.56±0.09	7	±0.026 (2.6%)
3-Br (6)	−0.763±0.005	1.51±0.01	−4.86±0.07	0.60±0.01	18	±0.012 (0.5%)
4-NO_2 (7)	−0.24 ±0.01[f]	0.9 ±0.8[f]	−5.00±0.17	0.48±0.08	17	±0.024 (2.0%)

[a]Substituted acetophenone.
[b]Number of points. Any rejected by the program are in parentheses.
[c]Root-mean-square deviation between experimental points and the fitted curve, i.e., σ_y; also given as a percentage of the total change in observed absorbance, $100\sigma_y/(|\Delta A_B| + |\Delta A_{BH^+}|)$.
[d]Extinction × 10^{-4}; data from ref. 18.
[e]Reference 1, from data in ref. 16.
[f]Coefficients of first characteristic vector.

and bromine consumption is generally faster than enolization (see above):

$$[K]_t = [K]_0 - ([Br_2]_0 - [Br_2]_t)$$

Substituting this into the first equation, converting to bromine absorbance (A) at 425 nm (path length l, extinction coefficient ε), and taking logs, gives

$$\log(\varepsilon l[K]_0 - A_0 + A_t) = \log(\varepsilon l[K]_0) - k_\psi t/2.3026$$

Values of the left-hand side of this equation, plotted as a function of time, were accurately linear (correlation coefficients > 0.999) for sulfuric acid solutions more dilute than about 60% w/w. The necessary extinction coefficient ε was obtained from a previously measured calibration curve; the path length and initial ketone concentrations were known, and the initial bromine absorbance was determined, in the absence of added ketone, immediately prior to reaction. Two or more determinations of each rate constant were made, in general; these are given in Tables 3 and 4,[1] together with errors listed as maximum deviations from the mean.

Results

Reaction Products

The enolization reaction, eq. [6], was studied kinetically by following the bromine consumed, as in eq. [7], so it was necessary to establish that this is the only bromine-consuming process involved. To this end the products of large-scale reactions were isolated; ^{1}Hmr spectra provided both convenient identification ($RCOCH_2Br$ and $RCOCHBr_2$ protons are very distinctive (21)) and product ratios, from the peak areas. Observed in most cases were the expected monobrominated compounds and recovered starting material only; dibrominated products, condensation products, etc., were not found. In the case of 4- and 3-methoxyacetophenone considerable ring bromination was observed, as might be expected (anisoles brominate readily (22)), and these compounds were accordingly not studied further.

Basicities

These were determined from the variation of uv–visible spectrum with acid concentration as described in the Experimental. For the acetophenones, values of pK_{BH^+} and m^*, and ΔA_B and ΔA_{BH^+}, were obtained from the Davis–Geissman absorbance differences (ΔA), or the first characteristic vector coefficients (c_1), directly. A non-linear least-squares computer program (23) was used to fit eq. [10]

$$[10]\quad (\Delta A - \Delta A_B)/(\Delta A_{BH^+} - \Delta A) = \text{antilog}(m^*X + pK_{BH^+} + \log C_{H^+})$$

(derived from eq. [1]), since this procedure uses the available data to best advantage (24). Four coefficients were calculated by the program, $a_1 = \Delta A_B$ (or c_{1-B}), $a_2 = \Delta A_{BH^+}$ (or c_{1-BH^+}), $a_3 = pK_{BH^+}$ and $a_4 = m^*$ (see eq. [10]), using values of X and $\log C_{H^+}$ as a function of $\%H_2SO_4$ w/w from ref. 1. The observed absorbance differences or characteristic vector coefficients are given in Table 1, together with $\log I$ values calculated using ΔA_B and ΔA_{BH^+} given by the program.[1] The latter are in Table 2, along with the m^* and pK_{BH^+} values obtained. Figure 1 compares experimental points

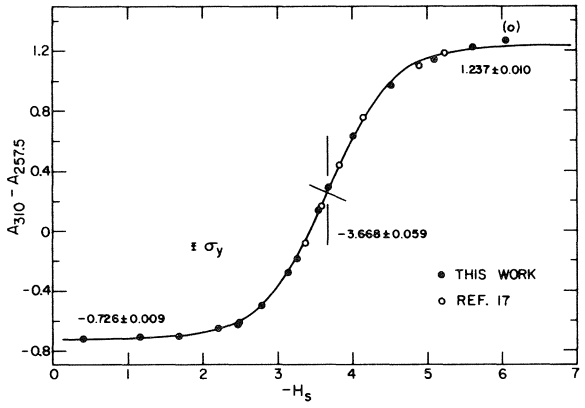

FIG. 1. Absorbance differences for 4-methylacetophenone vs. its substrate acidity function $-H_S$. Points are experimental; the curve is obtained using eq. [10] and the coefficients of Table 2.

with the best regression curve for 4-methylacetophenone (**2**), and Fig. 2 illustrates the excellent log I values obtained for **2**. These two figures use a substrate acidity function (1), $-H_S = m^*X + \log C_{H^+}$, applicable only to **2**, necessitating the exact unit slope shown in Fig. 2.

Acetone is unusual, in that characteristic vector analysis (CVA) produces a second vector (v_2) accounting for some 30% of the observed variability, with the first, v_1, only accounting for about 65%, as against at least 95% in most cases (16). Thus extracting a pK_{BH^+} value for acetone from the data necessitates a more complex analysis.[2]

According to Palm and co-workers (e.g., ref. 25), the protonation of carbonyl compounds, eq. [11], can be regarded as taking place in two stages, eqs. [12] and [13].

$$[11]\quad B + H^+_{aq} \overset{K_{BH^+}}{\rightleftharpoons} BH^+$$

$$[12]\quad B + H^+_{aq} \overset{K_1}{\rightleftharpoons} B\ldots H^+_{aq}$$

$$[13]\quad B\ldots H^+_{aq} \rightleftharpoons BH^+$$

As long as B and B . . . H^+_{aq} do not differ appreciably in their properties (uv spectrum, nmr chemical shift, etc.) the first equilibrium, eq. [12], will not be observable (other than as a slight "medium effect") and the spectral changes observed can be regarded as being due to eq. [11]. This is the case for the acetophenones studied here; even for those requiring CVA v_1 accounted for almost all of the observed systematic (i.e., non-random) variation. However, for a simple compound such as acetone, without a large polarizable phenyl group, association complex formation (eq. [12]) produces a quite noticeable spectral change (14), often mistaken for protonation itself (26), which is reduced here to the observed large variability (30%) due to v_2. In this case we equate v_2 with the eq. [12] process, and v_1 with eq. [13]:

$$I = [BH^+]/[B] \qquad I_1 = [B\ldots H^+_{aq}]/[B]$$

$$I_2 = I/I_1 = [BH^+]/[B\ldots H^+_{aq}]$$

$$\log I - \log C_{H^+} = m^*X + pK_{BH^+}$$

(not directly observable)

$$[14]\quad \log I_1 - \log C_{H^+} = m^*{}_1X + pK_1$$

(observable, v_2)

$$[15]\quad \log I_2 = (m^* - m^*{}_1)X + (pK_{BH^+} - pK_1)$$

(observable, v_1)

[2]The following analysis is based on one due to J. P. Guthrie (personal communication).

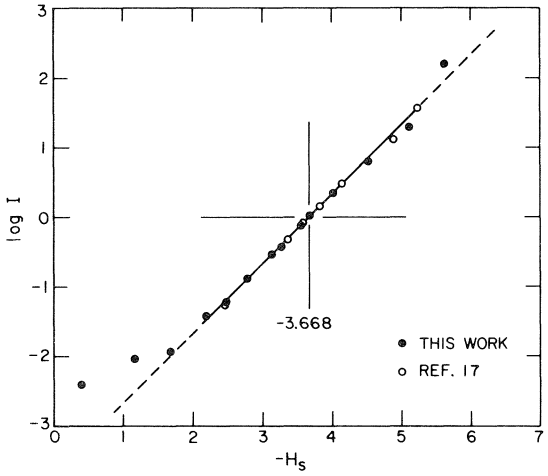

FIG. 2. Log I vs. $-H_S$ for 4-methylacetophenone. The line drawn has the theoretical unit slope.

Equations [14] and [15] were used with the coefficients of the second and first vectors, c_2 and c_1 (rather than ΔA) as described above. *All* of the available data relating to the protonation, uv extinction measurements (14), and proton (19) and ^{13}C (20) nmr chemical shifts, were analyzed simultaneously. For acetone the results obtained were: $pK_1 = -2.02 \pm 0.04$ ($m^*{}_1 = 0.30 \pm 0.01$) for association complex formation, eq. [12]; and $pK_{BH^+} = -5.37 \pm 0.07$ ($m^* = 0.85 \pm 0.02$) for the true protonation equilibrium, eq. [11].

Kinetics

Bromination of the acetophenones **2**, **3**, **4**, **6**, and **7**, as described in the Experimental, resulted in the enolization rate constants given in Tables 3 and 4,[1] and illustrated in Fig. 3. The reactions could not be studied at acidities higher than those cited; above a certain acidity, depending on the substrate basicity, the rates of bromine consumption began to exhibit non-linear behaviour. This is not unexpected; the last term in the denominator of the rate equation used, eq. [8] above, contains a term in $[H^+]$, and above a certain acidity the assumption that this term is negligible will break down. Also possible is the onset of side reactions, such as eq. [9] above.

Except for 4-nitroacetophenone, Fig. 3 shows an initial rate increase, followed by a levelling off. This is similar to the behaviour found for typical A-2 reactions (4–6), and as these are also expected to be A-2 processes (eqs. [5] and [6]), the appropriate kinetic equation to use in analyzing the variation of rate constant with acidity was eq. [4] (4). Required for eq. [4] are values of the protonation correction term, $\log C_S/(C_S + C_{SH^+})$, obtained using eq. [1] and the pK_{BH^+} and m^* values from Table 2; the sub-

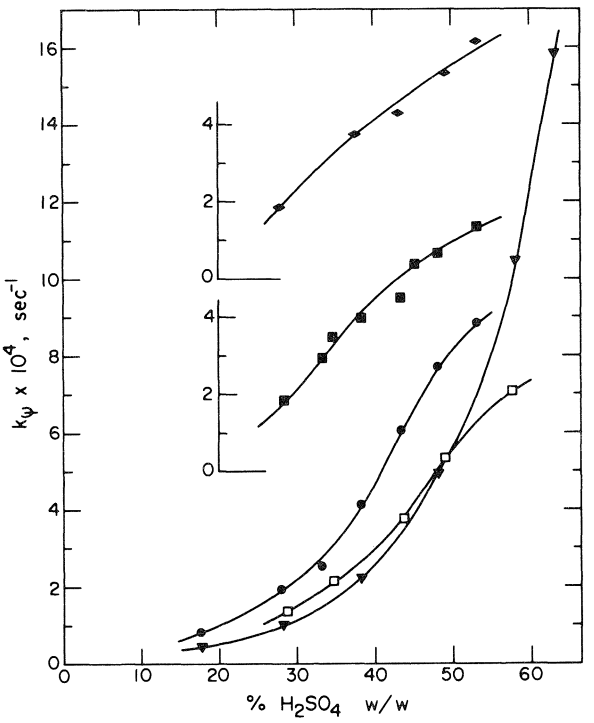

FIG. 3. Observed bromination rate constants vs. percent sulfuric acid, for acetophenone (●), 3-bromoacetophenone (□), 4-nitroacetophenone (▼), 4-methylacetophenone (■), and 3-methylacetophenone (◆). The latter two curves are offset upwards by 5 and 10 scale divisions, respectively, for clarity.

strates (except for acetone) were found to be essentially unprotonated at the acidities studied. The catalyzing base was assumed to be water; water activities in molarity units were calculated using available activities (27) and densities (28).[3] Preliminary studies using double linear regression, with X as one variable and log a_{H_2O} as the other, showed that 1.6–1.7 water molecules were involved on average; i.e., for this reaction $r = 1.6$–1.7 (4, 29). Accordingly 2 log a_{H_2O} was subtracted from the left-hand side of eq. [4] and the result plotted as a function of X. (The value two was used for simplicity; the method can distinguish between 1, 2, and 3 water molecules, but not between 1.5 and 2.5.) An example of the excellent linear plots obtained is shown in Fig. 4, which includes both our results for the enolization of acetophenone obtained by bromination, and Zucker and Hammett's original results (30) obtained by iodination. These two data sets are superimposable and were treated together. Figure 4

[3]Intercept log k_0 values obtained using molarity water activities are true second-order rate constants, i.e., values in 1 M water, allowing convenient comparisons between H_2O and HSO_4^- as bases. Values of log k_0 in pure water, 55.34 M at 25°C, may be obtained from these by adding 2 × 1.743.

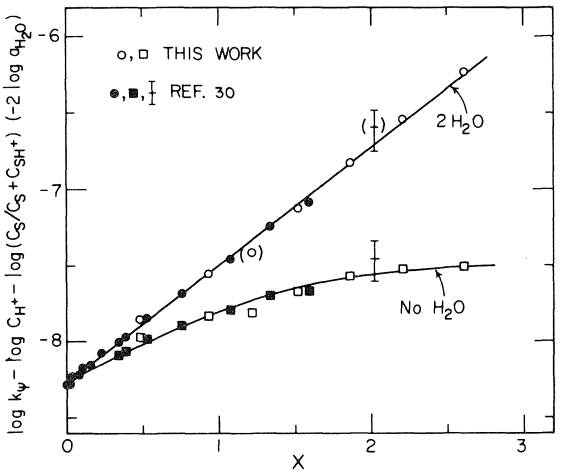

FIG. 4. Plots according to eq. [4] for the enolization of acetophenone in sulfuric acid at 25°C. Assumed are the involvement of two water molecules (circles, line), or none (squares, curve).

also shows the curved plot resulting from the assumption of an A-1 process (eq. [2]) for comparison; plots assuming one or three water molecules, or bisulfate ion, are also curved. The derived $m^{\ddagger}$ and log k_0 data for all the compounds studied are given with the relevant statistical information in Table 5.

The behaviour of 4-nitroacetophenone, as seen in Fig. 3, is clearly different; for this compound, assumption of an A-2 reaction involving two water molecules resulted in a curve, as can be seen from Fig. 5. In fact any A-2 assumption produced a curved plot for this compound, but plots according to either

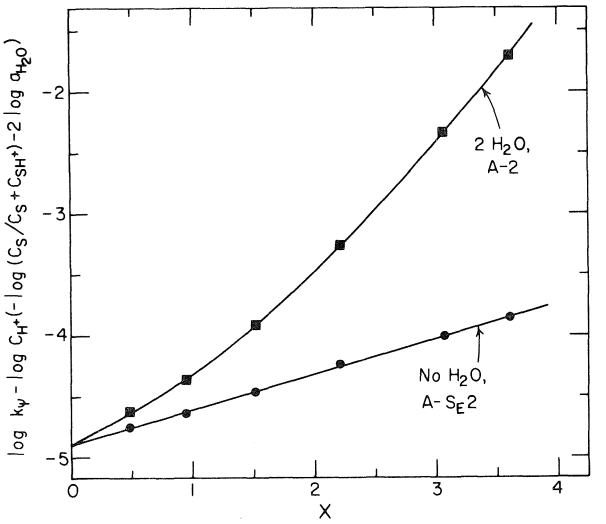

FIG. 5. Plots according to eq. [3] (circles, line), or eq. [4] assuming the involvement of two water molecules (squares, curve), for the enolization of 4-nitroacetophenone in sulfuric acid at 25°C.

TABLE 5. Derived standard-state rate constants for the acid-catalyzed enolization of some acetophenones and acetone at 25°C

Compound[a]	Slope[b]	Intercept[b]	r[c]	No.[d]	σ_y[e]	log k_0	$m^{\ddagger}$
4-Me (2)	0.71 ±0.02	−8.23 ±0.04	0.997	8	±0.032	−4.56±0.07	1.18±0.05
3-Me (3)	0.70 ±0.03	−8.24 ±0.05	0.998	5	±0.035	−4.2 ±0.2	1.16±0.08
— (4)[f]	0.774±0.006	−8.273±0.007	0.999	23 (2)	±0.022	−4.11±0.07	1.30±0.03
3-Br (6)	0.83 ±0.02	−8.55 ±0.04	0.999	5	±0.029	−3.70±0.08	1.37±0.04
4-NO_2 (7)	0.292±0.005	−4.90 ±0.01	0.999	6	±0.013	−4.90±0.01	0.6 ±0.1
Acetone;[g]							
$2H_2O$	0.49 ±0.02	−8.47 ±0.05	0.993	12	±0.113	−3.10±0.09	0.58±0.03
HSO_4^-	0.57 ±0.06	−11.9 ±0.4	0.990	4	±0.092	−6.6 ±0.4	0.67±0.07

[a]Substituted acetophenone. Reaction involving two water molecules unless otherwise stated.
[b]Compounds 2–6, eq. [4]; 7, eq. [3]; acetone, eq. [4] with appropriate base (see text).
[c]Correlation coefficient.
[d]Number of points; any rejected are in parentheses.
[e]Root-mean-square deviation between fitted line and experimental points.
[f]Includes data from ref. 30. See Fig. 4.
[g]Data from ref. 31.

eq. [2] (A-1) or eq. [3] (A-S_E2) were linear. The accurately linear A-S_E2 plot (correlation coefficient 0.999) is shown in Fig. 5.

Acetone enolization has been studied over the whole acidity range by Haldna *et al.* (31); their results were treated according to eq. [4], producing the plots shown in Fig. 6. Acetone also enolizes with the involvement of two water molecules, but only in sulfuric acid solutions less concentrated than about 81%. After this point a change in mechanism occurs, shown by the break in the curve; assuming the involvement of one bisulfate ion as a base after this point, rather than two water molecules, produced the good straight line shown in Fig. 6. Bisulfate ion concentrations were used, obtained from published

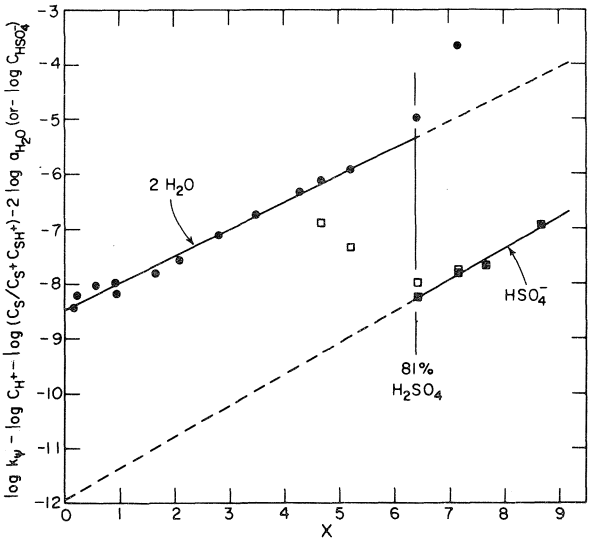

FIG. 6. Plots according to eq. [4] for the enolization of acetone in sulfuric acid at 25°C (31). Circles, assuming the involvement of two water molecules; squares, of one bisulfate ion. Filled squares are points which have been corrected for the reaction involving water.

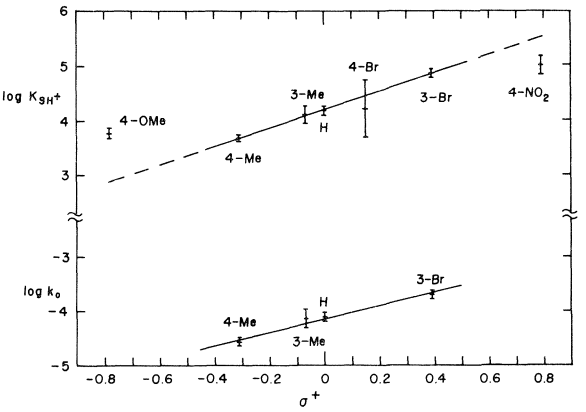

FIG. 7. Linear free-energy relationship plots for acetophenone basicities (upper), and acid-catalyzed enolization rates (lower), both in the aqueous standard state.

sources (32), since the activities were unavailable (33); the rate constants were corrected for the reaction involving water, using $k = k_{H_2O} + k_{HSO_4^-}$.

Linear free energy relationship plots against σ^+ (34), for the pK_{BH^+} values of Table 2 and the log k_0 values of Table 5, are shown in Fig. 7. The resulting ρ values were 1.69 ± 0.13 and 1.24 ± 0.15, respectively.

Discussion

Analysis of equilibrium and rate data obtained in non-ideal strong acid media by the X-function method as described here is capable of providing a considerable amount of mechanistic information.

An advantage of the method is that it enables rate and equilibrium quantities to be compared in the aqueous standard state (i.e. in water) rather than in an arbitrarily chosen acid solution, thus removing medium effects from the comparison (4). Medium effects do occur here; this treatment presents them as values of m^* and $m^{\ddagger}$. Table 2 shows that although

most of the m^* values are around 0.6, normal for carbonyl group protonation (1), methoxy- and nitroacetophenone differ, with values of 0.76 and 0.48, respectively. Slight differences also appear among the $m^{\ddagger}$ values in Table 5.

The standard state pK_{BH^+} and log k_0 values are obtained by an extrapolation, to $X = 0$ (1, 4), which is likely to increase the experimental scatter. Figure 7, which shows two of several possible linear free energy relationships, illustrates this. The scatter is noticeable; even so, the equilibrium and rate plots can be seen to be similar, and reasonable conclusions can still be drawn. A decision to employ σ or σ^+ for the correlation could not be made on the basis of the data, although good correlations with σ^+ have been found before (35).

In the equilibrium plot, the points for the 4-methoxy and 4-nitro substituents can be seen to be well above and below the correlation line, respectively. At least for 4-methoxy, the deviation is well outside the experimental error (given on the plot as $\pm$ one standard deviation, in the error bars). These two substituents are also the ones that deviate considerably, and in opposite directions, from the usual carbonyl protonation m^* of 0.6. It may well be that this treatment has separated the "internal" effect of the substituents, due to resonance, induction, etc., from the "external" effect of charge dispersal into the medium by solvation (measured as m^*). The latter will increase in importance in good solvating media, such as the highly aqueous one used here. For instance, if the oxygen lone pairs in the methoxy substituent are partially "tied up" by solvating water molecules, they are less available for resonance donation into the ring, and can delocalize less positive charge from the *para* position, leading to a less enhanced σ^+ value, as would seem to be required here.

For the various $\rho\sigma$ plots tried, the difference in ρ between equilibrium and rate plots was in the range 0.5–0.6; a Brönsted-type plot of the log k_0 values for **2**, **3**, **4**, and **6** (Table 5) against $-pK_{BH^+}$ for the same compounds (Table 2) is accurately linear (correlation coefficient 0.99) with a slope of 0.71 ± 0.08. This can all be interpreted in terms of a transition state with the proton less than half-transferred to the base; between 50% and 70% of the positive charge present in the protonated ketone is still present in the transition state for enolization.

Insertion of the pK_{BH^+} for acetone, -5.37, into the above Brönsted-type plot produces a predicted log k_0 of -3.30 for the reaction involving water; to this must be added a statistical factor of log 2, since there are two equivalent methyl groups in acetone, giving log $k_0 = -2.99$. This is in good agreement with the observed value of -3.10 ± 0.09. The less readily protonated ketones are more reactive, and reactivities can be adequately predicted from basicities. Less basic ketones react more slowly in a given acid solution because of the lower concentration of the protonated ketone intermediate (36).

Between 1.5 and 2 water molecules act as the "base" in the acid-catalyzed enolization, in sulfuric acid solutions more dilute than about 80%; for simplicity we have assumed $r = 2$ here (e.g., see Fig. 4). Distinctions finer than those between whole numbers are probably possible using the X-function method, but much accurate data over a wide acidity range appears to be necessary. There is no whole-number requirement; r-values should reflect the average situation. In a case like this, with an early transition state without much charge dispersal, fewer than two water molecules should disperse what charge there is reasonably well. More than one appears to be necessary, however, and a transition state like **8** can be visualized for the enolization.

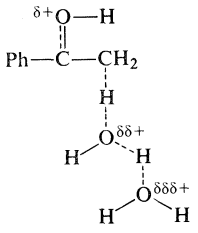

8

Values of r reflect the number of water molecules actually involved in the reaction (the "order" of the reaction in water (29)); solvation changes (if any) between reactant and product should appear in the $m^{\ddagger}$ values. For instance, the acetophenones (excluding 4-nitro-) all have $m^* \simeq 0.6$ and $m^{\ddagger} \simeq 1.3$; acetone has $m^* \simeq 0.8$ and $m^{\ddagger} \simeq 0.6$. This may reflect steric hindrance to solvation of the carbonyl group by the phenyl group, present in the acetophenones and their bromoketone products, but absent in acetone.

In more concentrated sulfuric acid, the base changes and bisulfate ion takes over, as can be seen for acetone in Fig. 6 (31); the reaction involving bisulfate, and that involving water, were found to have the same rate in 81% sulfuric acid. This agrees with the earlier observation of Swain and Rosenberg (37), who studied the racemization of D-α-phenylisocaprophenone in strong sulfuric acid. The change in base is to be expected, since the water activity is decreasing very rapidly as compared to the bisulfate ion concentration in this acidity region (33). The very long extrapolation of Fig. 6 suggests that water is a better base than bisulfate ion *in water* by a factor

of 10^3–10^4. The only previous estimate is the factor of 10^2 given by Swain and Rosenberg, in 85–94% sulfuric acid (37).

4-Nitroacetophenone is anomalous. As shown above (e.g., Fig. 5) the rate-determining step for the enolization of this compound is not an A-2 process at all, but is either A-1 or A-S_E2. Based upon the m^* value of 0.6, an A-S_E2 process ($m^* < 1$) seems much more likely than an A-1 one ($m^* > 1$) (4). In any case, it is difficult to visualize a reasonable A-1 process for this compound. One possible A-S_E2 mechanism may be that the initial protonation, eq. [5], is rate-determining; this seems unlikely, though, because a pK_{BH^+} of -5.0 and a log k_1 of -4.9 (Table 5) lead to a k_{-1} for the reverse of eq. [5] of 1.2. Deprotonation from oxygen is likely to be diffusion-controlled, with a rate constant of 10^9 at least. At this time no firm conclusions can be drawn regarding the reaction mechanism for this compound.

Acknowledgements

Financial support of this research is by the Natural Sciences and Engineering Research Council of Canada.

1. R. A. Cox and K. Yates. J. Am. Chem. Soc. **100**, 3861 (1978).
2. N. C. Marziano, G. M. Cimino, and R. C. Passerini. J. Chem. Soc. Perkin Trans. II, 1915 (1973); N. C. Marziano, P. G. Traverso, A. Tomasin, and R. C. Passerini. J. Chem. Soc. Perkin Trans. II, 309 (1977).
3. R. A. Cox and R. Stewart. J. Am. Chem. Soc. **98**, 488 (1976).
4. R. A. Cox and K. Yates. Can. J. Chem. **57**, 2944 (1979).
5. R. A. Cox, M. F. Goldman, and K. Yates. Can. J. Chem. **57**, 2960 (1979).
6. K. Yates and R. A. McClelland. J. Am. Chem. Soc. **89**, 2686 (1967); T. A. Modro, K. Yates, and F. Beaufays. Can. J. Chem. **55**, 3050 (1977).
7. J. F. Bunnett. J. Am. Chem. Soc. **83**, 4968 (1961).
8. E. S. Gould. Mechanism and structure in organic chemistry. Holt, Rinehart and Winston, London. 1959. p. 372; C. H. Rochester. Acidity functions. Academic Press, London. 1970. p. 169; R. A. Cox. Ph.D. Thesis, McMaster University. 1970.
9. R. P. Bell and G. G. Davis. J. Chem. Soc. 902 (1964).
10. V. J. Nowlan and T. T. Tidwell. Acc. Chem. Res. **10**, 252 (1977); Y. Chiang, A. J. Kresge, and C. I. Young. Can. J. Chem. **56**, 461 (1978).
11. R. A. Cox and J. Warkentin. Can. J. Chem. **50**, 3233 (1972).
12. E. D. Hughes, H. B. Watson, and E. D. Yates. J. Chem. Soc. 3318 (1931); H. B. Watson and E. D. Yates. J. Chem. Soc. 1207 (1932).
13. G. Archer and R. P. Bell. J. Chem. Soc. 2238 (1959).
14. H. J. Campbell and J. T. Edward. Can. J. Chem. **38**, 2109 (1960); H. J. Campbell. Ph.D. Thesis, McGill University. 1961.
15. C. T. Davis and T. A. Geissman. J. Am. Chem. Soc. **76**, 3507 (1954).
16. J. T. Edward and S. C. Wong. J. Am. Chem. Soc. **99**, 4229 (1977).
17. L. A. Flexser and L. P. Hammett. J. Am. Chem. Soc. **60**, 885 (1938).
18. K. Yates. Ph.D. Thesis, University of British Columbia. 1959.
19. A. Levi, G. Modena, and G. Scorrano. J. Am. Chem. Soc. **96**, 6585 (1974).
20. R. A. McClelland and W. F. Reynolds. Can. J. Chem. **54**, 718 (1976).
21. R. A. Cox and J. Warkentin. Can. J. Chem. **50**, 3242 (1972).
22. R. P. Bell and D. J. Rawlinson. J. Chem. Soc. 63 (1961).
23. P. R. Bevington. Data reduction and error analysis for the physical sciences. McGraw-Hill, New York. 1969. p. 237.
24. A. J. Kresge and H. J. Chen. Anal. Chem. **41**, 74 (1969).
25. V. A. Palm, Ü. L. Haldna, and A. J. Talvik. *In* The chemistry of the carbonyl group. *Edited by* S. Patai. Wiley, New York. 1966. p. 439.
26. S. Nagakura, A. Minegishi, and K. Stanfield. J. Am. Chem. Soc. **79**, 1033 (1957); G. Perdoncin and G. Scorrano. J. Am. Chem. Soc. **99**, 6983 (1977).
27. W. F. Giauque, E. W. Hornung, J. E. Kunzler, and T. R. Rubin. J. Am. Chem. Soc. **82**, 62 (1960).
28. International critical tables. Vol. 3. McGraw-Hill, New York. 1930. p. 56.
29. K. Yates. Acc. Chem. Res. **4**, 136 (1971).
30. L. Zucker and L. P. Hammett. J. Am. Chem. Soc. **61**, 2791 (1939).
31. Ü. Haldna, H. Kuura, L. Erreline, and V. Palm. Reakts. Sposobn. Org. Soedin. **2**, 194 (1965); Chem. Abstr. **64**, 3304c (1966).
32. T. F. Young, L. F. Maranville, and H. M. Smith. *In* The structure of electrolyte solutions. *Edited by* W. J. Hamer. Wiley, New York. 1959. p. 35; H. Chen and D. E. Irish. J. Phys. Chem. **75**, 2672 (1971).
33. R. A. Cox. J. Am. Chem. Soc. **96**, 1059 (1974).
34. L. P. Hammett. Physical organic chemistry. 2nd ed. McGraw-Hill, New York. 1970. p. 356.
35. R. Stewart and K. Yates. J. Am. Chem. Soc. **80**, 6355 (1958).
36. N. H. Werstiuk and S. Banerjee. Can. J. Chem. **55**, 173 (1977).
37. C. G. Swain and A. S. Rosenberg. J. Am. Chem. Soc. **83**, 2154 (1961).

The hydrolyses of some sterically crowded benzoate esters in sulfuric acid. The excess acidity method at different temperatures[1,2]

ROBIN A. COX, MALCOLM F. GOLDMAN, AND KEITH YATES

Department of Chemistry, University of Toronto, 80 St. George St., Toronto, Ont., Canada M5S 1A1

Received May 14, 1979

ROBIN A. COX, MALCOLM F. GOLDMAN, and KEITH YATES. Can. J. Chem. 57, 2960 (1979).

The excess acidity method has been used to analyze the observed acid-catalyzed hydrolysis rate constants for methyl benzoate, methyl *para*-toluate, methyl *ortho*-toluate, and methyl 2,6-dimethylbenzoate, over a wide sulfuric acid concentration range, at several different temperatures. Enthalpies and entropies of activation in the aqueous standard state are reported, with slope parameters m^*; also given are the pK_{BH^+} and m^* values found for the protonation of these compounds. The mechanistic changeover from $A_{Ac}2$ to $A_{Ac}1$ hydrolysis occurs at lower acidity with increasing methyl substitution, mainly due to the decrease in activation enthalpy in the transition state for the $A_{Ac}1$ process, caused by release of steric strain and increased mesomeric interaction. The $A_{Ac}2$ hydrolysis involves two water molecules, and is energetically favourable and entropically unfavourable. The $A_{Ac}1$ reaction is difficult energetically, but this is offset by the large positive activation entropies found.

ROBIN A. COX, MALCOLM F. GOLDMAN et KEITH YATES. Can. J. Chem. 57, 2960 (1979).

On a utilisé la méthode de l'excès d'acidité pour analyser les constantes de vitesse observées au cours de l'hydrolyse acide des esters suivants: benzoate de méthyle, *ortho* et *para*-toluate de méthyle et diméthyl-2,6 benzoate de méthyle en faisant varier considérablement la concentration de l'acide sulfurique et la température. On donne les enthalpies et entropies d'activation de l'état fondamental en solution aqueuse, et les paramètres de pente m^*; ainsi que les valeurs de pK_{BH^+} et du m^* trouvées lors de la protonation de ces composés. Le changement du mécanisme de l'hydrolyse de $A_{Ac}2$ à $A_{Ac}1$ se produit à une faible acidité avec l'augmentation des substituants méthyles. Ceci est dû principalement à la diminution de l'enthalpie d'activation dans l'état de transition du mécanisme de type $A_{Ac}1$ provoqué par la décompression stérique et par une augmentation de l'interaction mésomérique. L'hydrolyse du type $A_{Ac}2$ implique deux molécules d'eau et est énergiquement favorisée mais défavorisée du point de vue de l'entropie. Pour la réaction du type $A_{Ac}1$ la grande valeur positive trouvée pour l'entropie compense le fait qu'elle soit énergiquement défavorisée.

[Traduit par le journal]

Introduction

The extrapolative X-function method for the determination of weak base protonation equilibrium constants, eq. [1] (1), can be expanded to provide

$$[1] \quad \log I - \log C_{H^+} = m^*X + pK_{BH^+}$$

$$\Delta G^0 = \Delta H^0 - T\Delta S^0 = -RT \ln K$$

$$= pK_{BH^+}\, RT \ln 10$$

$$[2] \quad \log I - \log C_{H^+} = m^*X + \Delta G^0/RT \ln 10$$

$$= m^*X + \Delta H^0/RT \ln 10 - \Delta S^0/R \ln 10$$

free energies, enthalpies and entropies of ionization, eq. [2], from log ionization ratio (I) measurements as a function of temperature, as long as values for X and log C_{H^+} at the appropriate temperature are available (see Appendix). In this paper this method is used to obtain ΔG^0 values for the substrates, to enable the calculation of pK_{BH^+} values at temperatures other than 25°C.

Excess acidities can also be used in kinetic analysis, as discussed in the previous two papers (2, 3); the appropriate kinetic equations for A-1 and A-2 reactions of predominantly unprotonated substrates are

$$[3] \quad \log k_\psi - \log C_{H^+} - \log C_S/(C_S + C_{SH^+})$$

$$= m^{\ddagger}m^*X + \log (k_0/K_{SH^+})$$

$$[4] \quad \log k_\psi - \log C_{H^+} - \log C_S/(C_S + C_{SH^+})$$

$$= m^{\ddagger}m^*X + \log a_{Nu} + \log (k_0/K_{SH^+})$$

reproduced here as eqs. [3] and [4], with the same nomenclature as that used before (2). If rate measurements at different temperatures are available, values of $\Delta H^{\ddagger}$ and $\Delta S^{\ddagger}$ in the aqueous standard state can be obtained. Expanding the term log (k_0/K_{SH^+}), which contains the medium-independent rate constant k_0, as above using the absolute rate theory (4),

[1]Presented at the 62nd Chemical Conference of the Chemical Institute of Canada, Vancouver, B.C., June, 1979, No. OR-12.

[2]Taken in part from the Ph.D. Thesis of Malcolm F. Goldman, University of Toronto, 1975.

0008-4042/79/222960-07$01.00/0

results in eq. [5], in which the numerical term 10.3188

$$[5] \quad \log (k_0/K_{SH^+}) = (\Delta S^{\ddagger} - \Delta S^0)/R \ln 10 + 10.3188 + \log T - (\Delta H^{\ddagger} - \Delta H^0)/RT \ln 10$$

contains the necessary Boltzmann and Planck constants (4). Substitution of eq. [5] into eqs. [3] and [4] gives the rate equations used in this study.

Previous studies on the mechanism of ester hydrolysis in acid solutions (e.g., the summaries in refs. 5–7) have shown that, after pre-equilibrium protonation, most esters hydrolyze by an A_{Ac}-2 mechanism in dilute acid, eq. [6], and that some switch to an A_{Ac}-1 mechanism in more concentrated acid, eq. [7]. Esters which have R′ substituents capable of forming carbonium ions of reasonable stability can hydrolyze by an A_{Al}-1 mechanism, eq. [8]. Structural and electronic effects in the ester

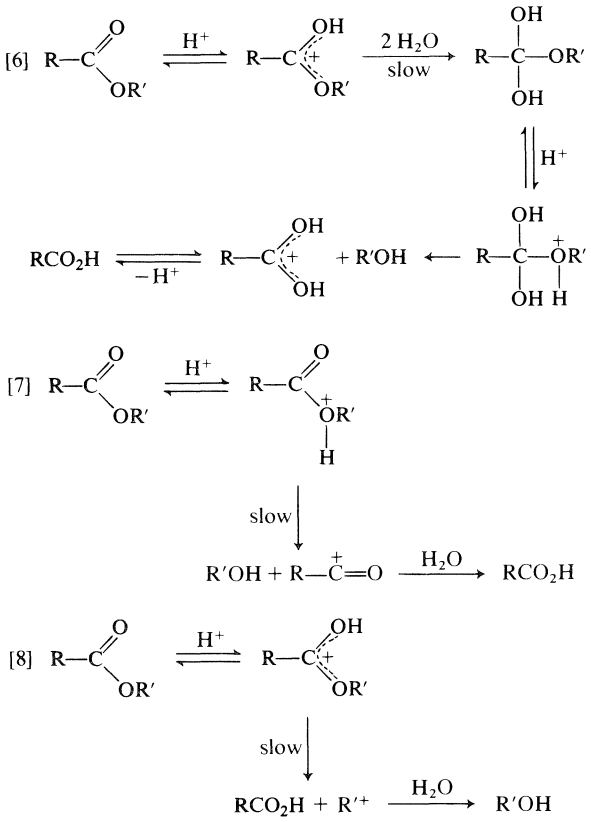

substrate, the medium acidity, and the water activity all help determine which of these mechanisms is followed (5–7).

During the earlier work it was observed that *ortho*-substituted phenyl acetates behaved differently from their *para*-substituted isomers in that the mechanistic changeover from A_{Ac}-2 to A_{Ac}-1 occurred in more dilute acid for the former (8). This appears to be due to a steric effect. Steric effects on acid-catalyzed aromatic ester hydrolyses have received little attention, and in this paper we report on the hydrolyses of the progressively more crowded aromatic esters methyl benzoate (**1**), methyl *para*-toluate (**2**), methyl *ortho*-toluate (**3**), and methyl 2,6-dimethylbenzoate (**4**).

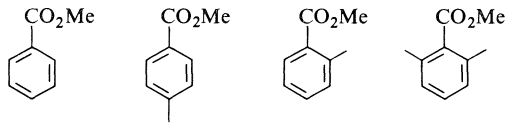

1 **2** **3** **4**

Methyl esters were chosen to minimize A_{Al}-1 hydrolysis, since formation of the unstable carbonium ion CH_3^+ is highly unlikely under conditions in which the more stable acylium species $Ar-\overset{+}{C}=O$ can be formed. The reactions were studied over a wide range of acidities and temperatures in aqueous sulfuric acid, in order to provide accurate acidity dependences and activation parameters, and thus obtain the maximum amount of mechanistic information.

Experimental

Sulfuric acid concentrations were determined from their densities, measured at 25°C using an Anton Paar precision density meter Model No. DMA 02C, by comparison with known densities from the literature (9); these were occasionally checked by titration. Compounds **1**, **2**, and **3** were prepared from the available parent acids and methanol, using a standard acid-catalyzed esterification technique (10); the acylium ion formed by dissolving 2,6-dimethylbenzoic acid in oleum was allowed to react with methanol, according to Newman (11), giving **4**. Upon purification physical properties in agreement with literature values were obtained.

Basicities were obtained from the change in uv spectrum with changing acidity, using a Cary-16 UV spectrophotometer with its cell block thermostatted at 10.0 ± 0.2°C by means of a Neslab PBC-4 bath cooler. The data were analyzed using the Davis–Geissman method (12), and the resulting extinction differences curve-fitted as described previously (3); observed extinction differences and derived log ionization ratios as a function of weight percent sulfuric acid are given in Table 1.[3]

The hydrolysis reaction rates were studied by following uv absorbance changes, using either the sampling method used before (13) for slow reactions, or directly in the thermostatted cell block of a Cary-16, Unicam SP-800, or Unicam SP-1600 UV spectrophotometer, for reactions with half-lives of less than 4–5 hours (14). Pseudo-first-order rate constants were obtained from the slopes of ln $|A_t - A_\infty|$ vs. time plots, or, for very slow reactions, by using the Guggenheim method (14,

[3]Tables 1, 4, and 5 are on deposit and may be obtained, at a nominal charge, from the Depository of Unpublished Data, CISTI, National Research Council of Canada, Ottawa, Ont., Canada K1A 0S2.

TABLE 2. Protonation data for the methyl benzoate esters **1**–**4** at 10°C

Compound	λ_{max} (nm) B	λ_{max} (nm) BH^+	$\Delta\varepsilon_B$[a]	$\Delta\varepsilon_{BH^+}$[a]	pK_{BH^+}	No.[b]	Error[c]
1	232.0	261.5	10.8±0.1	−14.9±0.3	−7.41±0.19	20 (1)	±0.30 (1.2%)
1[d]	232.0	261.5	10.8±0.1	−16.6±0.2	−6.99±0.11	22 (1)	±0.21 (0.8%)
2	242.6	278.0	12.3±0.2	−18.2±0.7	−5.35±0.21	21	±0.52 (1.7%)
3	232.6	265.5	7.2±0.1	−13.7±0.3	−6.40±0.21	19 (1)	±0.28 (1.3%)
4	234.7	269.0	1.7±0.1	−4.8±0.8	−5.51±0.56	16	±0.16 (2.5%)

[a]Obtained using the Davis–Geissman extinction differences of Table 1[3] at the wavelengths cited; × 10^{-3}.
[b]Number of points. Points rejected by the curve-fitting program used are in parentheses.
[c]Root-mean-square deviation between experimental points and the fitted curve, σ_y; also given as a percentage of the total observed change in extinction, $100\sigma_y/(|\varepsilon_B| + |\varepsilon_{BH^+}|)$. Other errors quoted are standard deviations.
[d]Measurements at 25°C.

15). The observed rate constants, means of 2–6 independent kinetic runs, are given as a function of weight percent sulfuric acid and temperature in Table 4,[3] together with the temperature-corrected values of X, log C_{H^+}, log a_{H_2O}, and log $C_S/(C_S + C_{SH^+})$ needed for eqs. [3]–[5]. The temperature correction for X is discussed in the Appendix; temperature-corrected log water activities are available (13) or can be calculated from listed thermodynamic data (16). They were converted to molarity units (from mole fractions) via the densities (9). Temperature-corrected log C_{H^+} values for aqueous sulfuric acid solutions were estimated from available 25°C data (1), densities (9), and the study by Young *et al.* (17), which gives bisulfate ion concentrations in sulfuric acid at 0°, 25°, and 50°C; this temperature correction is quite small, and could reasonably have been ignored without affecting the results.

The wavelengths at which the kinetics were studied were chosen, by preliminary measurements, as those which maximized the observed absorbance differences between reactant and product. In general these were within 2–3 nm of the quite similar reactant and product λ_{max} positions. Even so, the maximum observed change was often very small (0.1–0.2 absorbance units), particularly in dilute acid, and this occasionally resulted in increased scatter amongst the individual determinations. In the stronger acids decarboxylation and (or) sulfonation processes were sometimes noticeable, although these were much slower than the hydrolysis. Apart from this, the spectra of the reaction products were in reasonable agreement with those of authentic samples of the expected product carboxylic acids in the same media.

Activity coefficients of the neutral substrates at different acidities, required for the transition-state activity coefficient method (18), were determined by distribution measurements (19, 20) and are given in Table 5.[3]

Results and Discussion

Basicities

These were obtained from the variation of uv spectrum with acid concentration, using the Davis–Geissman method (12) and direct curve-fitting as described previously (3). The pK_{BH^+} values found for **1**, **2**, **3**, and **4** at 10°C, and a value measured for methyl benzoate at 25°C, are listed in Table 2, together with the relevant statistical information (3). The measurement temperature was 10°C rather than 25°C because of the fast hydrolysis rates of **3** and **4** in strong acid. The site of protonation is the carbonyl oxygen (21), presumably due to the better charge delocalization available, into the ring and onto the other oxygen. The ether-protonated form has no delocalization possibilities.

So that pK_{BH^+} values at 25°C, and at the temperatures at which the kinetic measurements were performed, could be obtained, the values in Table 2 were converted to free energies of protonation, $\Delta G°$, using eq. [2] above. These are listed in Table 3, together with pK_{BH^+} values calculated from them at 10° and 25°C, and the observed m^* values. In order to check the validity of eq. [2], methyl benzoate, which hydrolyzes slowly, was studied at both 10° and 25°C. Both temperatures gave the same ΔG^0; the agreement between the calculated pK_{BH^+} values in Table 3 and the observed ones in Table 2 is excellent. This means that the entropy contribution to the free energy is small, as expected; it is known that as basicities decrease, the enthalpy term becomes the predominant contributor to the free energy, and the entropy term remains approximately constant at its aqueous value, for instance in primary aromatic amines (22), pyridines (23), and azine *N*-oxides (23).

The protonation correction terms, log $C_S/(C_S + C_{SH^+})$, or $-\log(1 + I)$, needed for eqs. [3] and [4], were calculated using temperature-correct pK_{BH^+} values. This can be quite important; as can be seen from Table 3, the pK_{BH^+} for methyl benzoate over only a 15° temperature range varies by nearly 0.4 pK units. Assuming that the same value applied over the 50° range of the kinetic measurements would not have been appropriate. The observed 25°C value for methyl benzoate, −6.99 ± 0.11, agrees very well with the −6.92 which can be derived from the half-

TABLE 3. Free energies of protonation and m^* values for **1**–**4**[a]

Compound	ΔG^0 (kJ/mol)	pK_{BH^+} calculated 10°C	pK_{BH^+} calculated 25°C	m^*
1	−39.97±0.52	−7.37	−7.00	0.83±0.01
2	−29.0 ±1.1	−5.35	−5.08	0.61±0.03
3	−34.7 ±1.1	−6.40	−6.08	0.73±0.03
4	−29.9 ±3.0	−5.51	−5.23	0.58±0.09

[a]Errors are standard deviations.

protonation H_0 of -8.18 and slope vs. $-H_0$ of 0.846 quoted by Lane *et al.* (24), presumably at room temperature. The other esters appear not to have been studied previously.

The pK_{BH^+} values (e.g., Table 3, 25°C) show that a *para*-methyl group is much more efficient at increasing basicity than is an *ortho*-methyl, the pK difference from the unsubstituted case being ~2 units for the former, vs. ~1 unit for the latter. This is probably a manifestation of steric hindrance, making it more difficult to achieve the coplanarity required for full mesomeric (hyperconjugative) delocalization in the *ortho* case (25). Another consequence of "twisting" in the *ortho*-methyl compounds can be seen in the greatly reduced ε_B and ε_{BH^+} values for **3** and **4**, compared to **1** and **2**, in Table 2, as previously observed for hindered azoxybenzenes (25).

Kinetics

Observed pseudo-first-order rate constants, k_ψ, for the substrates **1**–**4** were obtained by following the (sometimes very small) changes in uv absorbance between reactant ester and product carboxylic acid, over an acidity range of 20–90% sulfuric acid, and a temperature range of 50°. These are given in Table 4,[3] and are plotted against X according to eqs. [3] and [4] in Figs. 1–4 (experimental points); for convenience, a percent sulfuric acid concentration scale is also included, at the top of these figures. Methyl benzoate has been previously studied at 25°C by Lane *et al.*, (24); their data and ours are superimposable, and both sets are included in Fig. 1. Other, less comprehensive, studies of the hydrolysis rates of

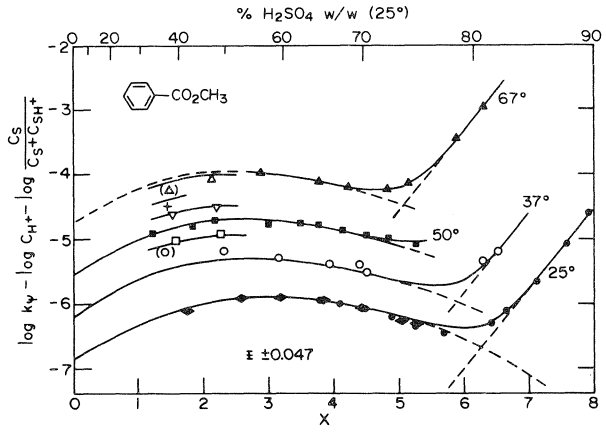

FIG. 1. The hydrolysis of methyl benzoate in aqueous sulfuric acid. Some data at 25°C from ref. 24 (◆); all other data, this work, with the different symbols referring to different temperatures (Table 4).[3] Points are experimental, curves theoretical, assuming an A-2 reaction with two water molecules (eq. [4]) at low acidities, and an A-1 process (eq. [3]) at high acidities. Points not included in the fit are in parentheses.

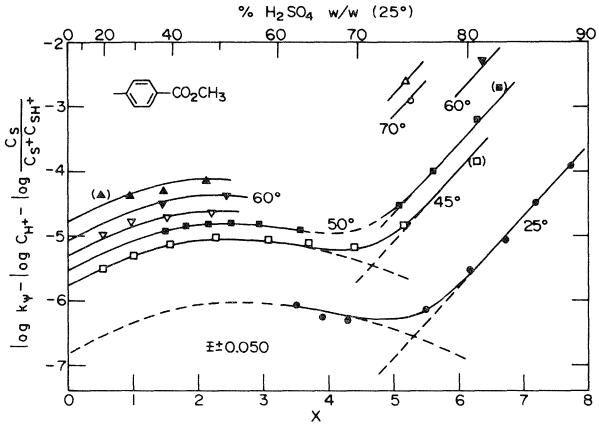

FIG. 2. The hydrolysis of methyl *para*-toluate in aqueous sulfuric acid. See Fig. 1.

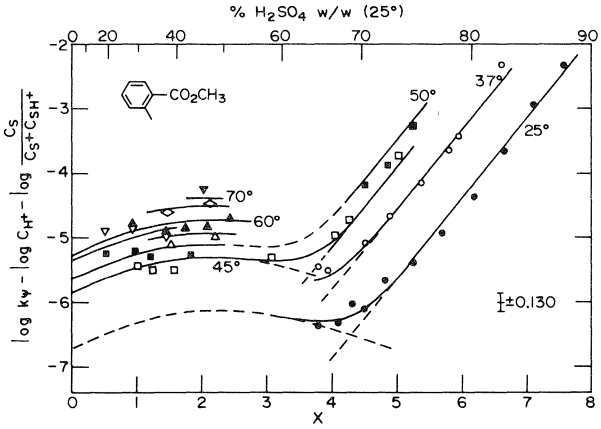

FIG. 3. The hydrolysis of methyl *ortho*-toluate in aqueous sulfuric acid. See Fig. 1.

these compounds are also in adequate agreement (26). All of the data and parameters are fully temperature-corrected.

The graphs for **1**, **2**, and **3** (Figs. 1–3) all exhibit initial downward curvature, typical of an A-2 reaction involving water (2), followed by an upward linear region, typical of an A-1 process (2), like many similar esters (5). Compound **4** (Fig. 4) appears to react almost entirely A-1, but there is noticeable deviation from linearity in the dilute acid region, indicative of a possible A-2 component for this substrate also. Methyl mesitoate (the 2,4,6-trimethyl ester) has been studied previously (27); when treated similarly, exclusive A-1 linear behaviour results for this compound.

The data for **1**–**4**, and that for methyl mesitoate (27), have also been treated using the transition-state activity coefficient (TSAC) method (7, 18). This involves examination of the behaviour of eq. [9] as a

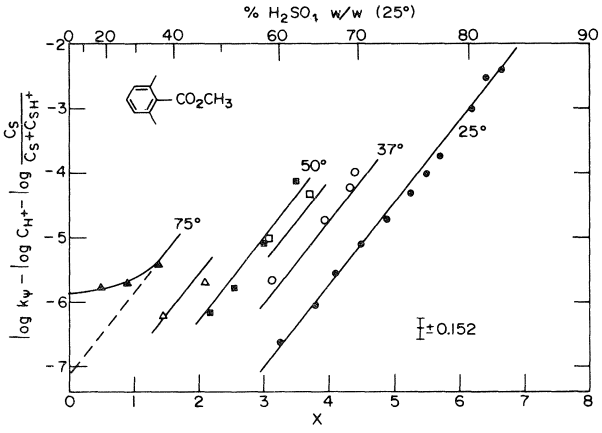

FIG. 4. The hydrolysis of methyl 2,6-dimethylbenzoate in aqueous sulfuric acid. See Fig. 1.

function of acidity; curves of different shapes are

$$[9] \quad \log (f^*_{S^+}/k_0) = \log f_S + \log a^*_{H^+} - \log k_\psi + pK_{SH^+}$$

indicative of different mechanisms (18). The last two terms are given above, and values of $\log a^*_{H^+}$, log proton activities, relative to the activity coefficient of the tetraethylammonium ion, are available (28). The activity coefficients of the neutral substrates **2**, **3**, and **4**, f_S, were measured; activity coefficient data for methyl benzoate and methyl mesitoate are listed (19). The resulting curves have been published (18) and are entirely consistent with the A-2 and A-1 hydrolysis mechanisms, with the changeover A-2 → A-1 taking place in more and more dilute acid as the methyl substitution in the molecule is increased.

With the A-2 → A-1 behaviour established, eqs. [3]–[5] can be used to fit the data, giving activation parameters and slopes. Combining eqs. [4] and [5] yields an equation of the form $y = a + bx_1 + cx_2 + dx_3$, where y consists of the terms on the left in eq. [4], minus $\log T$; the variables are X (x_1), $1/T$ (x_2), and log water activity (x_3), and the constants are $(\Delta S^+ - \Delta S^0)/R \ln 10 + 10.3188$ (a), m^+m^* (b), $(\Delta H^0 - \Delta H^+)/R \ln 10$ (c), and the molecularity of the reaction in water, r (d) (2). Combining eqs. [3] and [5] produces a similar equation (without $r \log a_{H_2O}$) for the A-1 process, and both can be solved using standard multiple linear regression techniques (29). In the overlap region for **1**, **2**, and **3**, however, the observed rate constant k_ψ is given by $k_{A\text{-}2} + k_{A\text{-}1}$, and curve-fitting was necessary, since the k's themselves, not their logarithms, are additive. A standard computer program was used (29); for **4** multiple linear regression could be used directly. It was found that the data did not justify calculating a separate value for r, and so it was assumed to have the fixed value 2, as before (2, 3), this being the average result of preliminary calculations.

The results of this procedure can be seen as the theoretical curves in Figs. 1–4; agreement with experiment is good, as illustrated by the error bars in the figures. The parameters obtained are given in Table 6; these refer to the aqueous standard state, not to any particular acid solution (2).

From the foregoing discussion, the assumption can be made that $\Delta H^0 \simeq \Delta G^0$ and $\Delta S^0 \simeq 0$ for the A-2 reaction, and m^* is available from Table 3, so ΔH^+, ΔS^+, and m^+ can be obtained, as in Table 7. Values of m^+ for a typical A-2 process are around 1.0 (2), as found for **1** and **3**; the m^+ for **2** seems a little high. Since the product m^+m^* values in Table 6 fall in a natural progression, this is probably due to an anomalously low m^*, 0.6, as compared to 0.8 and 0.7 for **1** and **3** (Table 3); a more likely value would be 0.8. The large negative entropies are to be expected from the mechanism (eq. [10]), with the transition state resembling **5**. Steric effects are apparent in the reduced activation energy for the *ortho*-substituted compound **3**, compared to **1** and **2**; delocalization of the positive charge in **5** over the aromatic group R will be more difficult with R twisted out-of-plane, and the carbon will be more electrophilic, lowering ΔH^+. In the protonated substrate, less charge on the ring means more on the two oxygens, with a higher solvation requirement (hence the lowered m^* values for **3** and **4** relative to

TABLE 6. Combined activation data for the hydrolyses of the methyl benzoate esters **1**–**4** in aqueous sulfuric acid[a]

Compound	$\Delta H^+ - \Delta H^0$	$\Delta S^+ - \Delta S^0$	m^+m^*
A-2 reaction with 2 H_2O			
1	94.7±1.1 (22.6)	−126±3 (−30)	0.85±0.01
2	93.0±2.2 (22.2)	−130±6 (−31)	0.79±0.01
3	76.8±6.1 (18.4)	−183±18 (−44)	0.71±0.04
A-1 reaction			
1	168.7±2.9 (40.3)	+44±6 (+11)	1.24±0.04
2	160.2±2.3 (38.3)	+56±6 (+13)	1.10±0.02
3	154.1±7.2 (36.8)	+46±22 (+11)	1.24±0.04
4	143.9±7.3 (34.4)	+31±21 (+7)	1.27±0.04

[a]Enthalpies in kJ/mol (kcal/mol in parentheses), entropies in J/(mol K) (entropy units in parentheses); errors listed are standard deviations.

TABLE 7. Enthalpies and entropies of activation for the A-2 hydrolyses of **1**–**3** in aqueous sulfuric acid[a]

Compound	ΔH^+	ΔS^+	m^+
1	54.7±1.2 (13.1)	−126±3 (−30)	1.02±0.02
2	64.0±2.5 (15.3)	−130±6 (−31)	1.30±0.07
3	42.1±6.2 (10.1)	−183±18 (−44)	0.98±0.07

[a]As in Table 6.

[10] 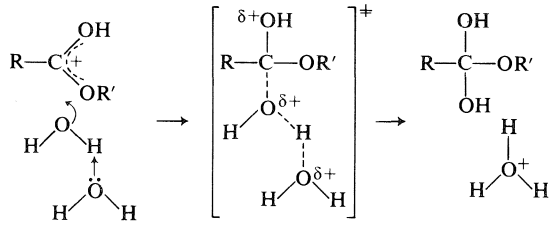

5

1); the resulting increased solvent electrostriction, and the decreased free rotation of R in the crowded transition state **5**, caused by the *o*-methyl, leads to the observed more negative entropy of activation for **3**, compared to **1** and **2**.

$\Delta H^{\ddagger}$, $\Delta S^{\ddagger}$, and $m^{\ddagger}$ cannot be calculated in the same way for the A-1 process, because protonation at the ether oxygen rather than the carbonyl oxygen is involved (eq. [7]), and ΔG^0 for this is not available. Nevertheless, detailed mechanistic information can still be obtained. Two possibilities for the rate-determining step can be visualized, a pre-equilibrium protonation as in eq. [11], or a concerted A-S_E2

[11] 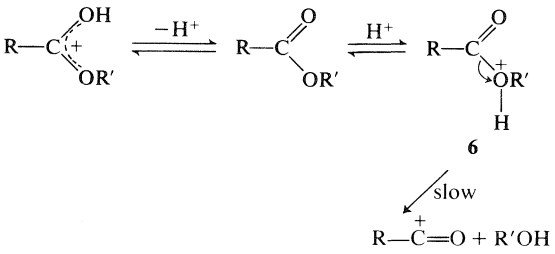

6

[12] 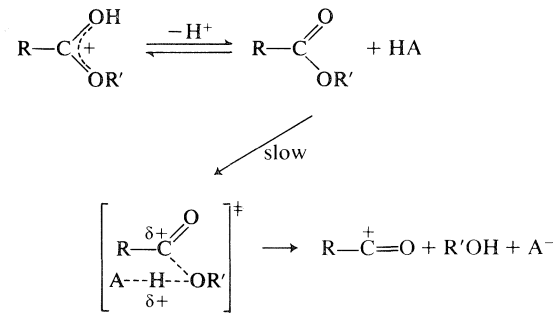

process as in eq. [12]. Kinetic analysis as described before (2) leads to two kinetically indistinguishable rate equations for these mechanisms. Both resemble eq. [3], only now $m^{\ddagger}m^*$ and K_{SH^+} refer to ether oxygen protonation.[4] For eq. [12], H^+ and HA are not easily distinguished below about 90% sulfuric acid (30), so $H^+ \equiv$ HA and the kinetic analysis follows that of eq. [16] in ref. 2, with an intercept containing $\log k_0$ only. However, examination of the $m^{\ddagger}m^*$ values in Table 6, all greater than one for the A-1 reaction, rules the latter possibility out. The ether-protonated structure **6**, with its localized charge, should have a high solvation requirement, with $m^* \simeq 0.5$ (1), giving $m^{\ddagger}$ values of around 2.5. This is quite unreasonable for an A-S_E2 but normal for an A-1 process (2), and hence the A-1 mechanism of eq. [11] is followed.

Although ΔH^0 and ΔS^0 for ether oxygen protonation are not available, reasonable assumptions are that $\Delta S^0 \simeq 0$, as discussed above, and that the ΔH^0 values for **1**, **2**, **3**, and **4** are closely similar, since the R group in **6** has little interaction with the positive charge. Thus the trends in Table 6 can be reasonably discussed. The activation enthalpies show a steady decrease **1** → **4**, presumably due to release of steric strain in the transition state, since this increases **1** → **4**, and to the improved hyperconjugative charge delocalization in the product ion provided by the methyl groups. Overall the enthalpies are much higher for the A-1 than for the A-2 hydrolysis, probably because the ether oxygen is much less basic than the carbonyl oxygen, i.e., most of the $(\Delta H^{\ddagger} - \Delta H^0)$ term is contributed by $-\Delta H^0$; it is difficult to see why the rate-determining step in eq. [11] would need a high $\Delta H^{\ddagger}$. These high enthalpies are offset by the large positive entropies of activation, due to the formation of two species from one, and to the release of solvent molecules resulting from delocalization of the highly solvated charge in **6** into the product acylium ion. Experimentally the entropies of activation for **1**–**4** are all the same; changing methyl substitution in the ring is unlikely to affect either of these factors appreciably. The major factor controlling the earlier mechanistic change A-2 → A-1 in going from **1** to **4** is the relative reduction in activation enthalpy for the A-1 reaction.

[4]Both of these rate equations still contain the term $\log (C_S/(C_S + C_{SH^+}))$ that corrects for *carbonyl* protonation; in this case this represents "locking up" of the substrate in an unreactive form, and the reduced concentration of the substrate that results must be accounted for in the kinetic scheme. This is indicated in eqs. [11] and [12].

Acknowledgements

Financial support of this research is by the Natural Sciences and Engineering Research Council of Canada. The Ontario Government and the Walter Sumner Foundation also provided scholarships for M.F.G.

1. R. A. Cox and K. Yates. J. Am. Chem. Soc. **100**, 3861 (1978).
2. R. A. Cox and K. Yates. Can. J. Chem. **57**, 2944 (1979).
3. R. A. Cox, C. R. Smith, and K. Yates. Can. J. Chem. **57**, 2952 (1979).
4. K. J. Laidler. Theories of chemical reaction rates. McGraw-Hill, Toronto. 1969. Chapt. 3.
5. K. Yates and R. A. McClelland. J. Am. Chem. Soc. **89**, 2686 (1967).

6. K. YATES. Acc. Chem. Res. **4**, 136 (1971).
7. R. A. MCCLELLAND, T. A. MODRO, M. F. GOLDMAN, and K. YATES. J. Am. Chem. Soc. **97**, 5223 (1975).
8. R. A. MCCLELLAND. Ph.D. Thesis, University of Toronto. 1969.
9. International critical tables. Vol. 3. McGraw-Hill, New York. 1930. p. 56.
10. A. I. VOGEL. Practical organic chemistry. 3rd ed. Longmans, London. 1959. p. 781.
11. M. S. NEWMAN. J. Am. Chem. Soc. **63**, 2431 (1941).
12. C. T. DAVIS and T. A. GEISSMAN. J. Am. Chem. Soc. **76**, 3507 (1954).
13. C. R. SMITH and K. YATES. J. Am. Chem. Soc. **93**, 6578 (1971).
14. R. A. COX and E. BUNCEL. J. Am. Chem. Soc. **97**, 1871 (1975).
15. A. A. FROST and R. G. PEARSON. Kinetics and mechanism. 2nd ed. Wiley, New York. 1961. p. 49.
16. W. F. GIAUQUE, E. W. HORNUNG, J. E. KUNZLER, and T. R. RUBIN. J. Am. Chem. Soc. **82**, 62 (1960).
17. T. F. YOUNG, L. F. MARANVILLE, and H. M. SMITH. *In* The structure of electrolyte solutions. *Edited by* W. J. Hamer. Wiley, New York. 1959. p. 35.
18. K. YATES and T. A. MODRO. Acc. Chem. Res. **11**, 190 (1978).
19. K. YATES and R. A. MCCLELLAND. Prog. Phys. Org. Chem. **11**, 323 (1974).
20. M. F. GOLDMAN. Ph.D. Thesis, University of Toronto, Toronto, Ont. 1975.
21. T. BIRCHALL and R. J. GILLESPIE. Can. J. Chem. **43**, 1045 (1965); G. A. OLAH and A. M. WHITE. J. Am. Chem. Soc. **89**, 3591 (1967).
22. P. D. BOLTON, C. D. JOHNSON, A. R. KATRITZKY, and S. A. SHAPIRO. J. Am. Chem. Soc. **92**, 1567 (1970).
23. M. J. COOK, N. L. DASSANYAKE, C. D. JOHNSON, A. R. KATRITZKY, and T. W. TOONE. J. Chem. Soc. Perkin Trans. II, 1069 (1974).
24. C. A. LANE, M. F. CHEUNG, and G. F. DORSEY. J. Am. Chem. Soc. **90**, 6492 (1968).
25. R. A. COX and E. BUNCEL. Can. J. Chem. **51**, 3143 (1973).
26. H. VAN BEKKUM, H. M. A. BUURMANS, B. M. WEPSTER, and A. M. VAN WIJK. Recl. Trav. Chim. Pays-Bas, **88**, 301 (1969); M. L. BENDER and M. C. CHEN. J. Am. Chem. Soc. **85**, 37 (1963); C. A. BUNTON, J. H. CRABTREE, and L. ROBINSON. J. Am. Chem. Soc. **90**, 1258 (1968); J. A. LEISTEN. J. Chem. Soc. 1572 (1956).
27. C. T. CHMIEL and F. A. LONG. J. Am. Chem. Soc. **78**, 3326 (1956); M. L. BENDER, H. LADENHEIM, and M. C. CHEN. J. Am. Chem. Soc. **83**, 123 (1961).
28. T. A. MODRO, K. YATES, and J. JANATA. J. Am. Chem. Soc. **97**, 1492 (1975).
29. P. R. BEVINGTON. Data reduction and error analysis for the physical sciences. McGraw-Hill, New York. 1969. pp. 171–6, 237–40.
30. R. A. COX. J. Am. Chem. Soc. **96**, 1059 (1974).
31. C. D. JOHNSON, A. R. KATRITZKY, and S. A. SHAPIRO. J. Am. Chem. Soc. **91**, 6654 (1969).

Appendix

X-Functions at Temperatures other than 25°C

For the general protonation reaction of eq. [A1], the equilibrium constant K_{BH^+} can be divided into

$$[A1]\quad B + H^+ \rightleftharpoons BH^+ \quad (K_{BH^+})$$

$$[A2]\quad K_{BH^+} = a_B a_{H^+}/a_{BH^+} = (C_B C_{H^+}/C_{BH^+}) \times (f_B f_{H^+}/f_{BH^+})$$

concentration and activity terms as in eq. [A2]. Taking logarithms, and making the assumption that the activity coefficient term $\log (f_B f_{H^+}/f_{BH^+})$ is a linear function of a similar term for a "standard base" B*, abbreviated X, leads directly to the basic excess acidity equation, eq. [1] above, as discussed previously (1). Equation [A2] has the form $K_a = K_C K_f$, and so X can also be expressed as a "combined free energy of transfer", as in eq. [A3].

$$[A3]\quad \Delta G^* = -RT \ln K_f^* = -RTX \ln 10 = -5.708X \text{ kJ/mol at } 25°C$$

It has been found experimentally that eq. [1] above applies to a very wide variety of bases, always giving linear behaviour (see ref. 1 and the references cited there). As might be anticipated, ionization ratios obtained at temperatures other than 25°C also exhibit linear behaviour when plotted against X (using, e.g., the data in ref. 31), giving as intercepts pK_{BH^+} values valid at the temperature of measurement (not at 25°C). Since the extrapolation is to $X = 0$, the reference state (water) at the measurement temperature, these intercept values can be used to derive ΔG^0, ΔH^0, ΔS^0, etc., for the base in question, regardless of any variation in X itself with temperature; the latter is manifested as the different *slopes* obtained at different temperatures. This slope variation can be removed, however; because of the form of eq. [A3] above it is apparent that, if eq. [1] applies, the combined free energies of transfer, $-RT \ln (f_B f_{H^+}/f_{BH^+})$, must be linear functions of one another also. Thus the X-function, expressed as a free energy, is easily corrected from 25°C to T°C via eq. [A4]. Temperature-corrected excess acidities lead to tem-

$$[A4]\quad X_T = X \times 298.15/(273.15 + T)$$

perature independent m^* and $m^\ddagger$ slopes; for this reason eq. [A4] was used in this work throughout.

Etude par résonance magnétique nucléaire de composés organiques contenant des chalcogènes. II.[1] L'éther de diphényle et ses analogues soufré, sélénié et telluré

GABRIEL LLABRÈS ET MARCEL BAIWIR[2]

Laboratoire de Cristallographie, Institut de Physique B5, Université de Liège au Sart Tilman, B-4000 Liège, Belgique

ET

LÉON CHRISTIAENS ET JEAN-LOUIS PIETTE

Laboratoire de Chimie organique hétérocyclique, Institut de Chimie B6, Université de Liège au Sart Tilman, B-4000 Liège, Belgique

Reçu le 1 mai 1979

GABRIEL LLABRÈS, MARCEL BAIWIR, LÉON CHRISTIAENS et JEAN-LOUIS PIETTE. Can. J. Chem. **57**, 2967 (1979).

L'étude par rmn du proton des composés du titre nous a permis de proposer pour ceux-ci une conformation en hélice avec des mécanismes particuliers d'interconversion en accord avec des déterminations de structure cristalline et des calculs théoriques. Comme dans la famille voisine de l'anisole, on observe un certain effet mésomère de l'hétéroatome, partiellement inhibé par des interactions stériques.

La rmn du carbone 13 apporte également dans une certaine mesure des arguments en faveur d'une telle conformation. L'effet de l'hétéroatome sur les déplacements chimiques se discute classiquement en termes d'effet mésomère ou inducteur, un effet d'atome lourd devant cependant être invoqué dans le cas des composés tellurés.

GABRIEL LLABRÈS, MARCEL BAIWIR, LÉON CHRISTIAENS, and JEAN-LOUIS PIETTE. Can. J. Chem. **57**, 2967 (1979).

The ^{1}Hmr study of the title compounds has revealed a screw conformation, with defined interconversion processes, in good agreement with crystal structure determinations and theoretical calculations. The mesomeric effect of the heteroatom is smaller than in the anisole series, due to steric inhibitions.

The ^{13}Cmr enhances, to some extent, these conclusions. In the case of Te compounds, a heavy atom effect adds to the classical mesomeric and inductive effects to account for the experimental observations.

Introduction

Les relations structurelles entre l'éther de diphényle et ses dérivés et les hormones thyroïdiennes (1) ne sont certainement pas étrangères à l'intérêt soutenu porté à ces composés depuis quelques années. De nombreuses techniques expérimentales ont été utilisées pour étudier les conformations préférentielles et les mécanismes d'interconversion des différents conformères stables de ces composés. Le résultat le plus remarquable de tous ces travaux est le manque d'homogénéité des conclusions qui en ont été tirées.

On admet généralement que quatre types de conformation peuvent être considérés (fig. 1). La structure A est plane (2). Dans la structure B, les cycles sont perpendiculaires au plan C—X—C (3). La structure de Marino C est caractérisée par l'orthogonalité des deux cycles (4). Enfin la structure en hélice D est caractérisée par l'angle β fait par le plan C—X—C avec les cycles (5).

Une forme A rigide est stériquement impossible, tandis que la forme B présente un minimum de conjugaison entre les cycles et l'hétéroatome. C'est pourquoi on retient les formes C et D pour interpréter les résultats expérimentaux (voir par exemple (6) et les références y citées).

Les structures cristallines de certains composés étudiés ici ont été déterminées (tableau 1). Dans tous les cas, les composés adoptent la conformation en hélice D, l'angle β variant de 29 à 36°. On remarque également que l'angle C—X—C diminue quand la distance C—X augmente:

$$[1] \quad \text{angle (C—X—C)} = -34.5 \text{ dist (C—X)} + 171.5 \quad (R = 0.99)$$

Enfin, la distance C—O observée (1.28 Å) est significativement plus courte que la liaison simple classique (1.43 Å): elle possèderait donc dans l'éther de diphényle un certain caractère de liaison double.

S'il est évident qu'une seule technique ne peut fournir la somme des résultats expérimentaux nécessaires à la résolution complète du problème con-

[1]Pour la partie I, voir réf. 7.

[2]A qui la correspondance doit être adressée.

0008-4042/79/222967-04$01.00/0

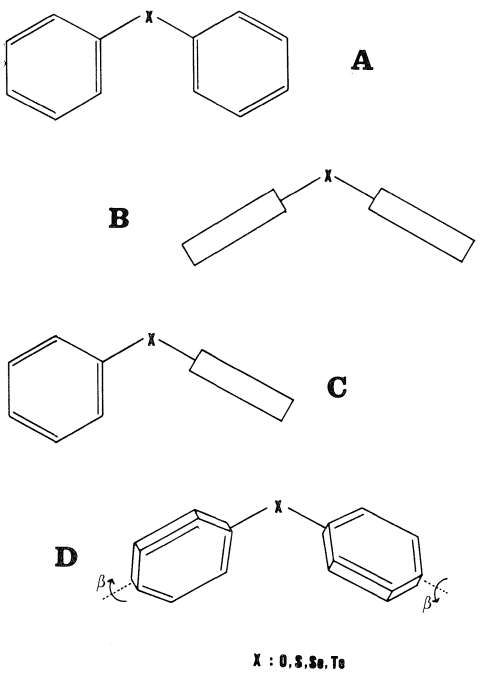

FIG. 1. Les conformations moléculaires de l'éther de diphényle et de ses analogues.

formationnel, nous avons étudié dans quelle mesure la rmn du proton et du carbone 13 fournissait des résultats en accord avec d'autres techniques, et notamment la chimie quantique et l'analyse structurelle par diffraction des rayons X.

Résonance magnétique du proton

On observe pour les quatre composés de la famille de l'éther de diphényle un spectre du type AA'BB'C, ce qui signifie une double équivalence, tant inter- qu'intracyclique. De plus, ce résultat reste qualitativement le même quand on fait varier la température de -80 à $+150$°C.

Les paramètres mesurés sont repris dans le tableau 2.

A cause d'effets stériques et d'anisotropie magnétique entre les cycles, la conformation A est incompatible avec un spectre AA'BB'C. De plus, les paramètres observés devraient différer fortement de ceux de la famille de l'anisole, ce qui n'est manifestement pas le cas (7).

Si de nombreux résultats expérimentaux (8–15) sont en faveur d'une certaine délocalisation de la paire libre de l'hétéroatome, diminuant de l'oxygène au tellure, la rmn du proton n'apporte rien de neuf à ce sujet.

Nous avons utilisé le modèle de Haigh et Mallion (16) pour calculer les effets de l'anisotropie magnétique d'un cycle sur les protons de l'autre. La fig. 2 illustre les résultats de ce calcul dans le cas de l'éther de diphényle. On voit que l'effet calculé peut être assez important, de l'ordre du ppm, pour les deux protons d'un même cycle. C'est pourquoi l'équivalence observée implique un mécanisme particulier d'interconversion, la rotation libre des cycles étant rendue fort improbable par les interactions stériques qu'elle entraînerait.

Galasso *et al.* (17) ont calculé l'énergie de toutes les conformations de Ph—X—Ph (X = O, S et Se). La conformation D est énergétiquement la plus stable, l'interconversion se faisant via la conformation C dans le cas X = O, c'est-à-dire quand l'effet mésomère de l'hétéroatome est le plus important, et via la conformation B dans les autres cas, l'encombrement stérique y étant moindre.

La relation de Penney (18), qui lie l'intégrale de recouvrement de l'hétéroatome et de l'orbitable π du carbone adjacent à l'angle β fait par le cycle avec le plan C—X—C permet de calculer cet angle β à partir des paramètres de rmn observés:

$$[2] \quad I(\beta) = (I(O)/4)(1 + 3\cos 2\beta)$$

Si, comme il paraît raisonnable de le faire, on considère, d'une part, que le déplacement chimique du proton en *para* est proportionnel à l'intégrale $I(\beta)$ et que, d'autre part, l'intégrale $I(\beta)$ est maximum dans la série de l'anisole, où la structure est plane sans effets stériques, [2] se transforme en

$$[3] \quad \cos 2\beta = \frac{1}{3}\left[4\frac{\Delta\delta(\text{Ph—X—Ph})}{\Delta\delta(\text{Ph—X—Me})} - 1\right]$$

TABLEAU 1. Données structurales (p-Y—C_6H_4)$_2$—X

X	O	S		Se	Te
Y	Br	Br	CH_3	CH_3	CH_3
C—X observé	1.28 Å	1.75 Å	1.75 Å	1.93 Å	2.05 Å
C—X liaison simple	1.43 Å	1.81 Å	1.81 Å	1.93 Å	2.14 Å
Angle C—X—C	123°	109.5°	109°	106°	101°
Angle β	29°	36°	35°	35°	30.5°
Réf.	(8)	(9)	(10)	(11)	(12)

TABLEAU 2. Déplacements chimiques (ppm) et constantes de couplage (Hz) dans l'éther de diphényle et ses analogues Ph—X—Ph

X	O	S	Se	Te
δ_o	6.901	7.264	7.370	7.597
δ_m	7.229	7.235	7.182	7.120
δ_p	7.003	7.170	7.177	7.186
J_{23}	8.17	7.87	7.81	7.77
J_{24}	1.11	1.26	1.21	1.27
J_{25}	0.43	0.59	0.55	0.52
J_{26}	2.48	1.94	1.85	1.54
J_{34}	7.41	7.53	7.48	7.58
J_{35}	1.75	1.54	1.56	1.57
RMS	0.108	0.085	0.059	0.098
Solvant	CS_2	CCl_4	CS_2	CS_2

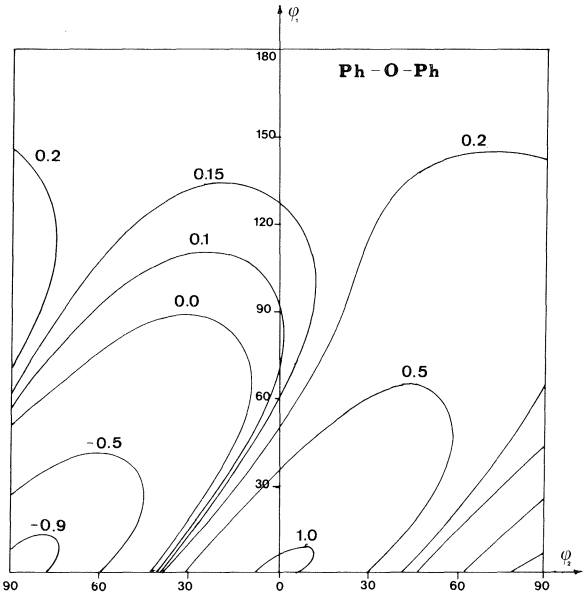

FIG. 2. Contribution de l'anisotropie magnétique d'un cycle sur le déplacement chimique des protons en *ortho* de l'autre cycle. Courbes d'isoécran (ppm). φ_1 = angle de rotation du cycle affecté; φ_2 = angle de rotation du cycle agissant.

L'accord entre les angles β ainsi obtenus et ceux observés expérimentalement est remarquable (tableau 3). Ce résultat justifie *a posteriori* l'hypothèse de planéité de l'anisole et de ses analogues.

Dans les benzènes monosubstitués, il existe d'excellentes relations linéaires entre l'électronégativité du substituant et la constante de couplage J_{23}. Or, bien que l'on accorde généralement au groupement OPh une électronégativité supérieure à celle du groupement OMe, J_{23} a, dans Ph—O—Ph et Ph—S—Ph, des valeurs inférieures à celles mesurées dans Ph—O—Me et Ph—S—Me respectivement.

Cooper (19) a montré que l'effet stérique diminue la constante de couplage d'une fragment —CH=CH—. La fig. 3 montre qu'il existe une bonne

TABLEAU 3. Calcul de l'angle β d'après [3]

	O	S	Se	Te
β calc. (^{1}H)	32.2°	35.8°	35.0°	30.5°
β mesuré	29°	35–36°	35°	30.5°
β calc. (^{13}C)	27.3°	35.7°	33.4°	37.4°

relation linéaire ($R > 0.99$) entre les différentes ΔJ observées entre les familles de l'anisole (sans effets stériques) et de l'éther de diphényle (avec) et la différence Δr entre le contact de van der Waals (3.60 Å) et la distance C—C mesurée.

Dans la famille étudiée ici, un certain effet mésomère existe (20) qui va diminuant de O à Te. Il est inférieur à celui observé dans la famille de l'anisole, la résonance étant partiellement inhibée par des interactions stériques.

Le tableau 4 donne les paramètres mesurés dans quelques composés diparasubstitués. Dans les dérivés méthylés, le déplacement chimique du méthyle augmente de O à Te. L'effet est qualitativement le même que celui mesuré dans la famille de l'anisole, mais moins important (0.15 ppm au lieu de 0.60 ppm). Ce résultat reflète également une certaine inhibition de la résonance par des interactions stériques.

Résonance magnétique du carbone 13

A partir des paramètres du tableau 5, on peut établir d'excellentes relations linéaires ($R > 0.99$) entre les déplacements chimiques des carbones C_1 et C_o des familles de l'éther de diphényle d'une part, et de l'anisole et des halogénobenzènes d'autre part.

Dans ce cas-ci, à nouveau, l'effet déblindant des chalcogènes sur C_1 diminue de O à Se pour devenir blindant pour Te. Pour C_o, l'effet blindant pour O

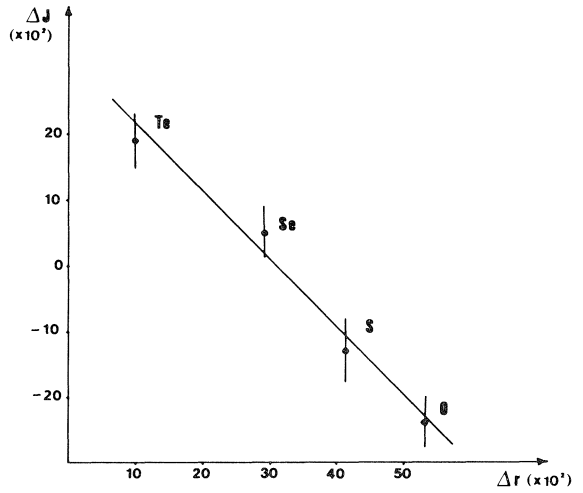

FIG. 3. Relation entre constantes de couplage et contacts stériques (voir texte).

TABLEAU 4. Paramètres rmn des composés diparasubstitués (CCl_4)

X	O		S			Se			Te
Y	Me	Br	Me	Cl	Br	Me	Cl	Br	Me
δ_o	6.803	6.845	7.146	7.23	7.156	7.261	7.338	7.285	7.465
δ_m	7.022	7.406	7.000	7.23	7.400	6.980	7.217	7.375	6.939
δ_{Me}	2.310	—	2.310	—	—	2.315	—	—	2.325
J_{23}	8.22	8.73	7.87	—	8.22	7.85	8.35	8.16	7.79
J_{25}	0.29	0.31	0.33	—	0.24	0.32	0.27	0.14	0.49
J_{26}	2.60	2.75	2.16	—	2.31	1.89	2.36	2.40	1.72
J_{35}	2.33	2.75	2.16	—	2.31	2.10	2.48	2.40	2.12
RMS	0.067	0.028	0.087	—	0.056	0.077	0.084	0.092	0.046

TABLEAU 5. Déplacements chimiques carbone-13

	O	S	Se	Te
C_1	157.2	135.3	130.5	114.8
C_o	118.8	129.0	132.5	137.5
C_m	129.8	130.7	129.3	129.4
C_p	123.3	126.9	127.3	127.6

devient de plus en plus déblindant de S à Te, tandis qu'en C_p, on observe un léger effet blindant qui va en s'atténuant de O à Te.

Par ailleurs, les déplacements chimiques des carbones C_o et C_p sont liés aux déplacements chimiques des protons correspondants par des relations linéaires ($R = 0.99$). Ceci tend à montrer que les effets des chalcogènes sur ces positions seraient de nature essentiellement électronique.

On peut également utiliser la relation de Penney adaptée [3] pour calculer l'angle de rotation β des cycles, à partir des déplacements chimiques de C_p. Le tableau 3 montre que, si l'accord observé est moins bon que celui obtenu avec le proton, il n'en demeure pas moins satisfaisant.

Les résultats obtenus par la résonance magnétique du carbone 13 permettent de conclure à la dualité inducteur–mésomère de l'effet des chalcogènes, la situation se compliquant, dans la cas de Te, d'un effet d'atome lourd (21). Celui-ci explique, en effet, pourquoi l'effet inducteur de O, S et Se sur C_1 devient blindant pour Te. En *ortho*, il ne se manifeste plus et le caractère −I, inférieur au caractère +E pour O, s'impose de plus en plus dans la séquence S, Se, Te. Ce résultat rejoint celui obtenu par Sadekov *et al.* (15). En *para* enfin le caractère mésomère de l'hétéroatome s'exprime légèrement.

Partie expérimentale

Les composés étudiés ici ont été synthétisés dans nos laboratoires suivant une méthode analogue à celle décrite pour la préparation de l'acide phényltelluro-2 benzoïque (22): condensation du diazoïque neutralisé sur le tellurophénolate de sodium obtenu par réduction du noyau de $NaBH_4$ à partir du dimère correspondant.

L'obtention des spectres, le calcul des paramètres de rmn et les conditions expérimentales ont été décrits dans la partie I de la présente série de rapports.

Remerciements

Nous tenons à remercier Messieurs les Professeurs J. Toussaint, M. Renson et A. Van de Vorst pour l'intérêt suivi qu'ils accordent à nos travaux. Nous remercions également le Centre de R.M.N. de l'Université de Liège qui a mis son matériel à notre disposition et, plus spécialement, son Directeur, Monsieur J. Denoel pour son aide technique.

1. P. A. LEHMAN. J. Med. Chem. **15**, 404 (1972).
2. L. E. SUTTON et G. C. HAMPTON. Trans. Faraday Soc. **31**, 945 (1935).
3. C. P. SMYTH et W. S. WALL. J. Am. Chem. Soc. **54**, 3230 (1932).
4. K. HIGASI et S. UYEO. Bull. Chem. Soc. Jpn. **14**, 87 (1939).
5. R. J. W. LE FEVRE, A. SUNDARAM et K. M. S. SUNDARAM. Bull. Chem. Soc. Jpn. **35**, 690 (1962).
6. G. W. BUCHANAN, G. MONTAUDO et P. FINOCCHIARO. Can. J. Chem. **52**, 767 (1974).
7. G. LLABRÈS, M. BAIWIR, L. CHRISTIAENS, J. DENOEL et J. L. PIETTE. Can. J. Chem. **56**, 2008 (1978).
8. J. TOUSSAINT. Mém. Soc. R. Sci. Liège, **12**, 1 (1952).
9. J. TOUSSAINT. Bull. Soc. Chim. Belg. **54**, 319 (1945).
10. W. R. BLACKMORE et S. C. ABRAHAMS. Acta Crystallogr. **8**, 329 (1955).
11. W. R. BLACKMORE et S. C. ABRAHAMS. Acta Crystallogr. **8**, 323 (1955).
12. W. R. BLACKMORE et S. C. ABRAHAMS. Acta Crystallogr. **8**, 317 (1955).
13. M. J. ARONEY, R. J. W. LE FEVRE, R. K. PIERENS et M. G. N. THE. J. Chem. Soc. B, 666 (1966).
14. M. J. ARONEY, R. J. W. LE FEVRE, R. K. PIERENS et M. G. N. THE. J. Chem. Soc. B, 1132 (1971).
15. I. D. SADEKOV, A. Y. BUSHKOV, V. S. YUR'EVA et V. I. MINKIN. Zh. Obshch. Khim. **47**, 2541 (1977).
16. C. W. HAIGH et R. B. MALLION. Org. Magn. Reson. **4**, 203 (1972).
17. V. GALASSO, G. DE ALTI et A. BIGOTTO. Tetrahedron, **27**, 6151 (1971).
18. J. PENNEY. Trans. Faraday Soc. **31**, 734 (1935).
19. M. A. COOPER et S. L. MANATT. J. Am. Chem. Soc. **91**, 6325 (1969).
20. P. A. LEHMANN et L. F. JOHNSON. Org. Magn. Reson. **5**, 61 (1973).
21. G. C. LEVY et G. L. NELSON. Carbon-13 nuclear magnetic resonance for organic chemists. H. Wiley Interscience, New York. 1972.
22. J. L. PIETTE, Ph. THIBAUT et M. RENSON. Tetrahedron, **34**, 655 (1978).

Time-resolved CIDEP in the photoreduction of quinones. A study of the spin lattice relaxation time of semiquinone radicals in solution

JACOBUS W. M. DEBOER, THERESE Y. C. CHAN CHUNG, AND JEFFREY K. S. WAN

Department of Chemistry, Queen's University, Kingston, Ont., Canada K7L 3N6

Received May 18, 1979

JACOBUS W. M. DEBOER, THERESE Y. C. CHAN CHUNG, and JEFFREY K. S. WAN. Can. J. Chem. **57**, 2971 (1979).

The application of time-resolved CIDEP observations to the measurements of T_1 of transient radicals is examined in detail. The importance of proper treatment of the response time is considered theoretically and demonstrated experimentally. By taking into account the variation of response time at high power, a method is described on how to evaluate B_1. At low power levels when the response time does not vary significantly, the extrapolation to zero power will provide a good estimate of T_1. The method was applied to measure T_1 for both the neutral radical and the radical anions of the benzoquinone, tetrachlorobenzoquinone, and duroquinone. It is confirmed that there is no significant difference in T_1 between the neutral radical and the radical anions. The values of the estimated T_1 are 2.2 μs for semibenzoquinone, 2.7 μs for semitetrachlorobenzoquinone, and 3.2 μs for semiduroquinone, all at 10°C and in a 50% isopropanol/toluene solvent.

JACOBUS W. M. DEBOER, THERESE Y. C. CHAN CHUNG et JEFFREY K. S. WAN. Can. J. Chem. **57**, 2971 (1979).

On examine en détail l'application des observations de CIDEP résolues en fonction du temps aux mesures de T_1 des radicaux temporaires. On considère de façon théorique et on démontre expérimentalement l'importance d'un traitement convenable du temps de réponse. On décrit une méthode d'évaluation de B_1 en tenant compte de la variation du temps de réponse à haute puissance. A de faibles niveaux de puissance, quand le temps de réponse ne varie pas de façon significative, l'extrapolation à la puissance zéro fournit une bonne évaluation de T_1. La méthode est appliquée à la mesure de T_1, pour les radicaux neutres et les anions radicalaires de la benzoquinone, de la tétrachlorobenzoquinone et de la duroquinone. L'absence de différence significative de T_1 entre le radical neutre et les anions radicalaires est confirmée. Les évaluations de T_1 sont de 2.2 μs pour la semibenzoquinone, 2.7 μs pour la semitétrachlorobenzoquinone et 3.2 μs pour la semiduroquinone. Ces évaluations sont faites à 10°C dans une solution à 50% d'alcool isopropylique/toluène comme solvant.

[Traduit par le journal]

Introduction

The technique of chemically induced dynamic electron polarization (CIDEP) is now often applied to elucidate the mechanisms and kinetics of free radical reactions in solution (1–3), transient intermediates in photosynthetic systems (4–6), and excited triplet states of organic molecules in crystals (7–9). Perhaps another unique application of CIDEP is the measurement of spin lattice relaxation time T_1 of transient radicals (10–12). Although the electronic T_1 is an important physical parameter which can provide an insight into molecular motions, relatively few other simple methods are available to obtain accurate T_1 of transient radicals.

Two distinctly different types of esr spectrometers have been used in CIDEP studies (13, 14): (*1*) time resolved spectrometers with total response time $\tau < 1\ \mu s < T_1 \ll$ radical half life $t_{1/2}$ where a pulsed electron beam or pulsed laser (on-time < 1 μs) is used to generate the radicals; (*2*) slow response spectrometers ($T_1 < \tau$ (30–500 μs) $< t_{1/2}$) where the radicals are generated by a modulated light source such that the on-time (0.1–20 ms) is sufficiently long for the signal intensity to reach a steady state amplitude. There are a number of advantages in chemical kinetic CIDEP studies to use a slow response spectrometer for initial polarization observations (14, 15) and in the past few years we have devoted our main effort in establishing a method (16) which utilizes an intermittent light source in conjunction with a 100 kHz esr spectrometer to evaluate relative rate parameters of photochemical reactions from the semi-steady-state CIDEP observations. While the steady-state values of the enhancement factor do not depend upon the microwave power level (15), they do have to be corrected for $t_{1/2}$ and T_1 to give the intrinsic value. The parameter $t_{1/2}$, which is obtained directly from the chemical decay part of the computer trace, compensates for changes in light intensity and also any changes in the viscosity of the media. Unfortunately T_1 has to be measured from separate experiments.

0008-4042/79/222971-07$01.00/0

The obvious choice is to take the value of T_1 from a time-resolved CIDEP study. In this paper we examine in detail the advantages and the limits of the application of time-resolved CIDEP technique to the evaluation of T_1 of anthrasemiquinone and other benzosemiquinone radicals in solution.

The situation involved in the time-resolved CIDEP experiment is one when at $t = 0$ suddenly a macroscopic electron magnetization is created. Before $t = 0$ no unpaired electron spins are present in the esr cavity. The sudden creation of magnetization is such that it is much faster than the spectrometer response time τ or T_2 of the spins created, whichever is the longer time. The creation of magnetization, of particular interest here, is produced by photochemical reactions initiated by a laser pulse less than 10 ns duration. Any magnetic polarization is assumed to arise within 10^{-8} s so that the criterion of sudden spin creation is satisfied even when τ, T_2 were as short as 10^{-7} s. If we define the z-axis to be parallel to the static magnetic field B_0, then the magnetization created will be initially along that axis, i.e. the photochemical process produces no coherence in the x,y-plane. Once the magnetization $\boldsymbol{m}$ is produced, the microwave field of magnitude B_1 will exert a torque on $\boldsymbol{m}$ which pulls $\boldsymbol{m}$ away from the z-axis as accompanied by the absorption or emission of microwave energy. At the same time relaxation tends to destroy m_y and restore m_z to the thermal equilibrium value m^∞. In addition, chemical reactions may destroy the spins created independently, although in many of the systems studied the half life of the radicals is considerably longer than T_1. Nevertheless, the observation of the spin using an esr spectrometer is related to m_y, but the response of the spectrometer may obscure the time evolution profile. It is therefore necessary to critically examine the performance of the spectrometer preamplification stages by measuring experimentally the total spectrometer response time and its effect on the determination of T_1.

Theoretical Considerations

Previous work by McLauchlan and co-workers (10) and by Verma and Fessenden (17) has dealt with the theory and technique of using CIDEP to measure T_1 of polarized radicals in solution. The present treatment is an attempt to understand and to underline the difficulties in the experimental measurements and to formulate a practical approach to simulate the experimental observations by a general theoretical treatment. Here, the following assumptions are made in the considerations of the esr spectrometer response in relation to the laser induced magnetization: (*a*) $\boldsymbol{m}(t) = 0$ and $t < 0$; (*b*) $\boldsymbol{m}(0) = (0, 0, m^0)$; (*c*) m^∞ is the steady-state magnetization in the *absence* of microwave field; (*d*) chemical decay of the radical concentration is slow compared to T_1 and T_2; (*e*) the spectrometer response is truly exponential; i.e. the response to a step function is given by a single exponential; (*f*) the observed signal h is proportional to m_y; (*g*) the kinetics of the spin system can be properly described by the Bloch equations.

The Bloch equations in the reference frame rotating with the microwave frequency ω give

$$[1] \quad \dot{m}_x = \delta\omega m_y - R_2 m_x$$

$$[2] \quad \dot{m}_y = -\delta\omega m_x - \omega_1 m_z - R_2 m_y$$

$$[3] \quad \dot{m}_z = \omega_1 m_y - R_1(m_z - m^\infty)$$

where

$$\delta\omega = \omega_0 - \omega$$

$$\omega_0 = \gamma B_0$$

$$\omega_1 = \gamma B_1$$

$$R_1 = (T_1)^{-1}$$

and

$$R_2 = (T_2)^{-1}$$

We shall consider here the on-resonance case, which is $\delta\omega = 0$ and thus m_x and m_y are decoupled:

$$[4] \quad \dot{m}_x = -R_2 m_x \qquad (\text{with } m_x(0) = m_x(\infty) = 0, m_x(t) = 0)$$

$$[5] \quad \dot{m}_y = \omega_1 m_z - R_2 m_y$$

$$[6] \quad \dot{m}_z = \omega_1 m_y - R_1(m_z - m^\infty)$$

where R_2 represents the effective transversal relaxation rate including the inhomogeneous contributions. The initial polarization is given by m^0/m^∞.

Using the initial conditions $m_z(0) = m^0$ and $m_y(0) = 0$, eqs. [5] and [6] can be solved with the method of Laplace transforms to yield

$$[7] \quad \boldsymbol{M}(x) = \int_0^t m(t)\, e^{-xt}\, dt = \mathscr{L}(\boldsymbol{m}) \qquad \mathscr{L}(\boldsymbol{m}) = x\boldsymbol{M}(x) - \boldsymbol{m}(0)$$

$$[8] \quad (x + R_2)M_y = -\omega_1 M_z$$

$$[9] \quad (x + R_1)M_z = \omega_1 M_y + (R_1 m^\infty/x) + m^0$$

or

$$[10] \quad M_y = \frac{-\omega_1(R_1 m^\infty + m^0 x)}{x[(x + R_1)(x + R_2) + \omega_1^2]}$$

It is convenient to include the spectrometer response time at this point. Let the response function be $g(t)$, then the response $h(t)$ to an input $f(t)$ is

$$[11] \quad h(t) = g^*f = \int_{-\infty}^{t} g(t - t')f(t')\,dt'$$

and $\mathscr{L}(h)$ is simply the product of $\mathscr{L}(g)$ and $\mathscr{L}(f)$:

$$[12] \quad H(x) = G(x)F(x)$$

For a true exponential response, g is given by

$$[13] \quad g(t) = \tau^{-1}e^{-t/\tau}$$

thus

$$[14] \quad G(x) = \tau^{-1}/(x + \tau^{-1})$$

The combination of eqs. [10], [12], and [14] gives

$$[15] \quad H(x) = \frac{-\omega_1(R_1m^\infty + m^0x)}{x(x - \lambda_1)(x - \lambda_2)(x + \tau^{-1})}$$

where

$$\lambda_{1,2} = -R \pm (1/2)\sqrt{(R_2 - R_1)^2 - 4\omega_1^2}$$

and

$$R = (1/2)(R_2 + R_1)$$

If $\lambda_1 \neq \lambda_2$, eq. [15] can be written as

$$[16] \quad H(x) = \frac{b_1}{x} + \frac{b_2}{x - \lambda_1} + \frac{b_3}{x - \lambda_2} + \frac{b_4}{x + \tau^{-1}}$$

and therefore

$$[17] \quad h(t) = b_1 + b_2e^{\lambda_1 t} + b_3e^{\lambda_2 t} + b_4e^{-t/\tau}$$

and the b's are found to be

$$[18] \quad b_1 = -\frac{\omega_1R_1m^\infty}{\lambda_1\lambda_2}$$

$$b_2 = \frac{\omega_1m^0 + \omega_1R_1m^\infty\lambda_1^{-1}}{(\lambda_2 - \lambda_1)(1 + \lambda_1\tau)}$$

$$b_3 = -\frac{\omega_1m^0 + \omega_1R_1m^\infty\lambda_2^{-1}}{(\lambda_2 - \lambda_1)(1 + \lambda_2\tau)}$$

$$b_4 = -\tau\frac{\omega_1m^0 - \omega_1R_1m^\infty\tau}{(1 + \lambda_1\tau)(1 + \lambda_2\tau)}$$

If $\omega_1 < (1/2)(R_2 - R_1)$, $\lambda_{1,2}$ are real and the signal h is a sum of decaying exponentials. However, if $\omega_1 > (1/2)(R_2 - R_1)$, the $\lambda_{1,2}$ are complex which lead to oscillatory components with frequency Ω:

$$[19] \quad \Omega = [\omega_1^2 - (1/4)(R_2 - R_1)^2]^{1/2}$$

$$\lambda_{1,2} = -R \pm i\Omega$$

and eqs. [17] and [18] become

$$[20] \quad h(t) = b_1 + (c_2\cos\Omega t + c_3\sin\Omega t)e^{-Rt} + b_4e^{-t/\tau}$$

$$b_1 = -\frac{\omega_1R_1m^\infty}{R^2 + \Omega^2}$$

$$c_2 = \frac{\omega_1m^0\tau - b_1(1 - 2R\tau)}{D}$$

$$[21] \quad c_3 = \frac{-\omega_1m^0(1 - R\tau) + b_1[R(1 - R\tau) + \Omega^2\tau]}{\Omega D}$$

$$b_4 = \tau\frac{-\omega_1m^0 + \omega_1R_1m^\infty\tau}{D}$$

$$D = (1 - R\tau)^2 + (\Omega\tau)^2$$

Note that eqs. [17] to [21] hold true for any ω_1 (except the only case when $\omega_1 = (1/2)(R_2 - R_1)$), but in general the quantities $\lambda_{1,2}$, Ω, and D are complex. However, for two cases (*i*) when $\omega_1 < (1/2) \times (R_2 - R_1)$, all quantities in eqs. [17] and [18] are *real*, and (*ii*) when $\omega_1 > (1/2)(R_2 - R_1)$, all quantities in eqs. [20] and [21] are *real*.

It is clear from the above treatment that the six parameters (ω_1, T_1, T_2, τ, m^0, m^∞) are not determined uniquely and simultaneously by the shape of the response. Since the *absolute* values of m^0 and m^∞ are not measured, only five independent parameters will enter the shape calculation. These are for case (*i*): λ_1, λ_2, τ, ω_1m^0, and $\omega_1R_1m^\infty$; and for case (*ii*): R, Ω, τ, ω_1m^0, and $\omega_1R_1m^\infty$. These conclusions will be tested in the following experimental investigation of anthrasemiquinone radicals in solution and a more limited method will be developed to apply the time-resolved CIDEP observations to estimate the values of T_1.

Experimental

The laser flash photolysis coupled with esr dc detection was first demonstrated by Kim and Weissman (18) and subsequently developed further for CIDEP studies by Trifunac and co-workers (1), by McLauchlan and co-workers (2), and by McIntosh and Bolton (4). Verma and Fessenden (17) have developed earlier a time-resolved esr spectrometer for CIDEP studies of radicals generated by submicrosecond pulses of 2.8 MeV electrons. The experimental design used by Kim and Weissman (18) was essentially duplicated in our present apparatus, which uses a Molectron UV24 N_2 pulsed laser as the light source. The esr spectrometer used is a Varian E3 old model and the dc signal was taken off after the preamplification and fed through a Hewlett Packard 461A 40 dB wide-band amplifier. Additional amplification when required was accomplished by using a Tektronic T922R scope amplifier. The amplified dc signal was digitized by either a Biomation 610 at 100 ns per point or by a Nicolet Explorer III digital scope at 50 ns per point. Both the laser and the digitizer were triggered by an external signal generated from a Hewlett Packard 3325A

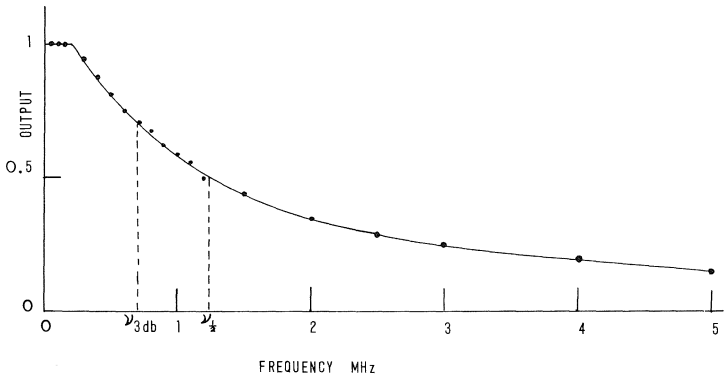

FIG. 1. The frequency response curve of the spectrometer preamplifier.

synthesizer/function generator at 7 Hz. The digitized data were collected and processed by a Nicolet 1180 computer in a synchronous mode.

The microwave cavity of the E3 spectrometer was modified by replacing the front plate with a brass plate having a centered hole of 9 mm diameter for transmission of the laser beam. This modification lowered the cavity Q. However, any further spoiling of Q did not seem to affect the response time.

The initial polarization of the semiquinone radicals studied in this work is so large that the signal-to-noise ratio was excellent even for a single pulse observation. Therefore, it is simple to locate the resonance and its maximum by hand-scanning of the magnetic field slowly while observing the polarization on the scope.

The chemical systems studied were mainly quinones in isopropanol and in the presence of 0.5 *M* phenol. The solution was placed in a 3 mm od Pyrex tube, vacuum degassed, and the tube was then sealed off. In the anthraquinone series, all experiments were done at -7°C with a variation of microwave power between 0.25 and 16 mW. In each experiment observations were monitored both on-resonance and then off-resonance (by shifting the magnetic field about 0.5 kg). In order to eliminate the randomness in the observed signal amplitude 100 scans were collected and time averaged for each measurement, including the off-resonance observation. The reported "time-resolved CIDEP" observation represents the difference between the time averaged on- and off-resonance traces, at a particular power level. In our apparatus some instability in the diode current was observed at a power level of 16 mW or higher.

Results and Discussion

The Measurements of the Spectrometer Response Time

As can be seen from the above theoretical considerations the effect of spectrometer response time is very important unless $\tau^{-1} \gg |\lambda_1|, |\lambda_2|$. When this condition is not met, the shape of the response will depend on the functional form of the spectrometer response function. The total system response in our apparatus is determined by the spectrometer system since the combined response time of the wide-band amplifiers and digitizers is less than 200 ns. We have decided therefore to carry out an independent evaluation of the spectrometer response time by removing the crystal diode and replacing the preamplifier input by a 1 mV signal from the HP3325A synthesizer. In this manner the frequency characteristics of the preamplifier were determined. Figure 1 shows the output voltage as a function of the frequency and Table 1 demonstrates that the actual response is very closely related to a true exponential response.

From the curve in Fig. 1 the response time of the E3 spectrometer preamplifier is estimated to be 230 ns. This is normally short enough for the measurement of T_1 in the microsecond range. However, further experiments (see below) indicate that the total system response time appears to change with microwave power. Moreover, to obtain T_1 directly from the decay curves, B_1 must be small so that $(\gamma B_1)^2 \ll (1/4)(R_2 - R_1)^2$.

The CIDEP Observations of the Anthraquinone/Phenol Photoreduction

The "time-resolved CIDEP" observations of the

TABLE 1. Frequency response of the E3 preamplifier: comparison of the experimental values and the theoretical response calculated as $1/[1 + (2\pi\nu\tau)^2]$ with $\tau = 0.225$ μs

	Output amplitude*	
Frequency ν (MHz)	Experimental (±0.05)	Theoretical
0.05	1.00	1.00
0.10	1.00	0.99
0.15	1.00	0.98
0.20	1.00	0.96
0.30	0.95	0.92
0.40	0.88	0.87
0.50	0.81	0.82
1.00	0.59	0.58
1.50	0.44	0.43
2.00	0.35	0.33
2.50	0.29	0.27
3.00	0.26	0.23
4.00	0.21	0.17
5.00	0.15	0.14

*Normalized to 1.00 at low frequencies.

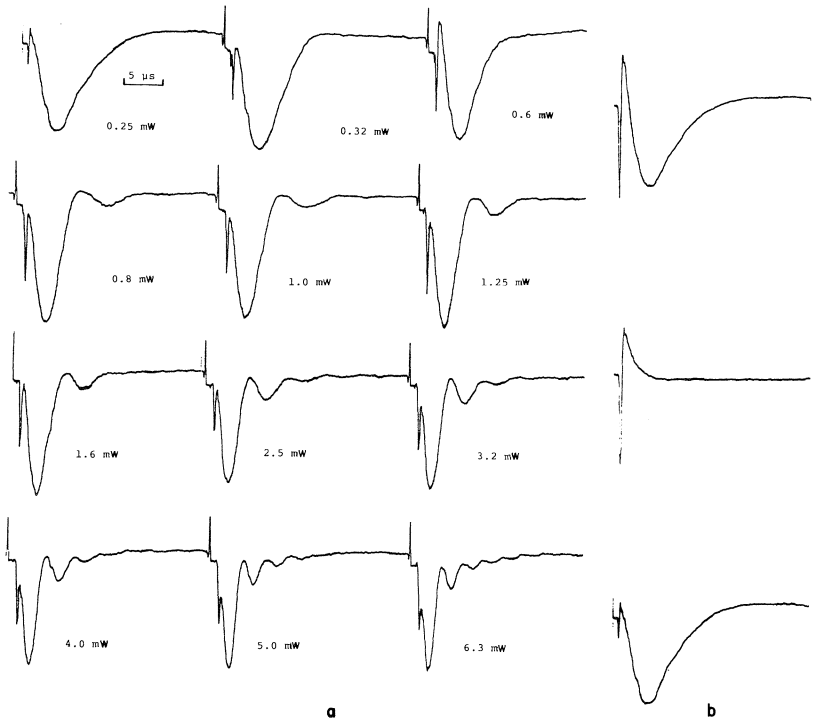

FIG. 2. (*a*) The transient emissive signal decay of the semianthraquinone radicals at −7°C at various microwave power levels. Each curve represents the difference between the on-resonance and off-resonance responses (see *b*). In each trace the first spike represents the laser trigger pulse and the second the laser flash. (*b*) A typical experimental set of observations at 0.25 mW. The upper trace is on-resonance, the middle trace is off-resonance, and the bottom trace is the difference.

anthraquinone/phenol photoreduction are shown in Fig. 2. Each of the traces at a particular power level could be simulated with $m^{\infty} = 0$, $m^{0} < 0$, by using a computer program written for the Nicolet 1180 system. However, it was clear that the simulation of all traces at all different power levels cannot be accomplished by using a unique set of parameters T_1, T_2, and τ, as suggested by the above theoretical considerations. At high power levels a longer response time and a shorter "apparent relaxation time" were required to simulate the experimental shape. The change in τ with power levels seems to be confirmed by a series of off-resonance experiments in which the "pick-up" decayed slower at high power levels. In the determination of T_1 by the method of extrapolation to zero power, it is, therefore, necessary to take into account the change of τ at high power and only data taken at power levels of 1 mW and less should be used for the extrapolation.

On the other hand, experiments carried out at high power levels enable the observation of oscillatory components as defined in eq. [19]. This in turn might be used to measure B_1.

(a) Measurements of B_1

As shown in Fig. 2 oscillatory components began to be visible at power 0.8 mW and higher. However, since the experimental traces at high power cannot be simulated satisfactorily without a detailed correlation to τ, a different approach to determine B_1 was undertaken.

From eq. [19] it is seen that the oscillatory frequency Ω depends upon ω_1 only when $\omega_1 \gg (1/4)(R_2 - R_1)^2$. If we define T to be the oscillation period ($T = 2\pi/\Omega$), then

$$[22] \quad B_1 = 2\pi/\gamma T$$

or

$$B_1\,(\text{mG}) = 356.8/T\,(\mu\text{s})$$

Using this equation the values obtained for B_1 are shown in Fig. 3, and the solid line represents eq. [23]:

$$[23] \quad B_1\,(\text{mG}) = 54 \times (\sqrt{P} - 0.17)$$

where P is the power level read from the spectrometer dial. The B_1 values obtained in this manner give a good fit between the calculated and experimental traces over the entire power range (0.25 to 12.5 mW).

(b) Signal Amplitude at High Power

In many of our experiments the assumption $m^{\infty} = 0$ is valid and the signal amplitude at high

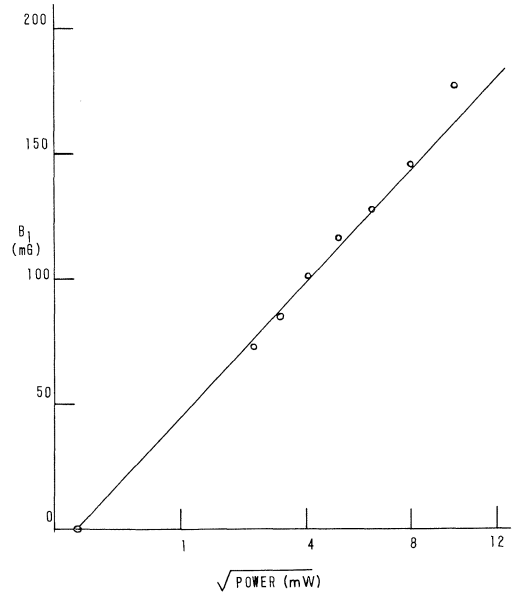

FIG. 3. The plot of B_1 as calculated from the oscillation period versus the square root of microwave power level P as read from the spectrometer dial.

power in eq. [20] can be written as

$$[24]\quad h(t) = [(\omega_1 m^0)/\Omega D][(\Omega\tau \cos \Omega t - (1 - R\tau) \sin \Omega t)e^{-Rt} - \Omega t e^{-t/\tau}]$$

While the shape of [24] is dependent on R_1, Ω, and τ, the signal amplitude is proportional only to ω_1 directly.

The variation of the signal amplitude with B_1 is shown in Fig. 4. Below the saturation point

$$B_1 = (1/\gamma)(1/\sqrt{T_1 T_2})$$

which is indicated by the arrow in Fig. 4, signal amplitude is approximately linear in B_1. As B_1 increases above this point, Ω grows and the maximum signal occurs faster. With a slower response time the signal therefore decreases at higher B_1 since the observation cannot follow the faster oscillation. With a fast response spectrometer the signal will continue to grow but levels off when $\omega_1 \gg R$. Finally in the limit $\tau \ll w_1^{-1} \ll T_1, T_2$, the maximum signal is equal to m^0.

(c) Measurements of T_1

At very low power, i.e. $\omega_1^2 \ll (1/4)(R_2 - R_1)^2$, $\lambda_{1,2}$ are approximately equal to $-R_{1,2} \mp \omega_1^2 \div (R_2 - R_1)$ and the signal decay is dominated by T_1 (for $T_1 > \tau$). Since the Varian E3 is not equipped with a low-power operation configuration, the lowest B_1 usable is about 15 mG and the extrapolation to $B_1 = 0$ only provides *an estimate* of T_1 (10).

To analyze the experimental data we define an

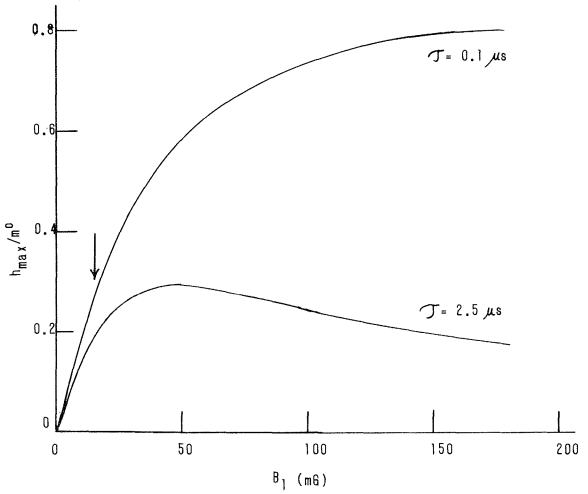

FIG. 4. The signal amplitude expressed as the ratio of h_{max}/m^0 plotted as a function of B_1.

effective decay time T_{eff} as equal to $1/R$ and it is the decay time of the total magnetization. We also define an apparent decay time T_{app} which is obtained from the analysis of the experimental trace assuming it being exponential. The difference between T_{eff} and T_{app} arises from the response time variation and the oscillations. In many of our quinone experiments $T_1 > T_2$. Thus, if $\omega_1 > (1/2)T_2^{-1}$, T_{eff} will be independent of the power but T_{app} will vary with the power. By extrapolation from $B_1 = 15$ mG to $B_1 = 0$, we have in fact reached the limit $T_{eff} = T_{app}$.

Measurements of T_1 *of Semibenzoquinone Radicals and Radical Anions*

(a) The Neutral Semiquinone Radicals

The following semibenzoquinone radicals were generated in the laser flash photolysis of their parent quinones in the presence of 0.5 *M* phenol in a solvent 50% isopropanol in toluene at 10°C: semibenzoquinone, semitetrachlorobenzoquinone, and semiduroquinone. Each radical was studied at various microwave power levels ranging from 0.25 to 1.3 mW, and the apparent decay time T_{app} was obtained from each of the decay traces. The reciprocals of these T_{app} were plotted as a function of the power and extrapolated to zero power to obtain the estimated T_1 (Fig. 5).

(b) The Semiquinone Radical Anions

The same three quinones were photoreduced by 0.5 *M* triethylamine in the same solvent at the same temperature. The CIDEP of each of the radical anions was studied over the same microwave power range and the T_1 was obtained by the same analysis and method as in (*a*). For each of the three different

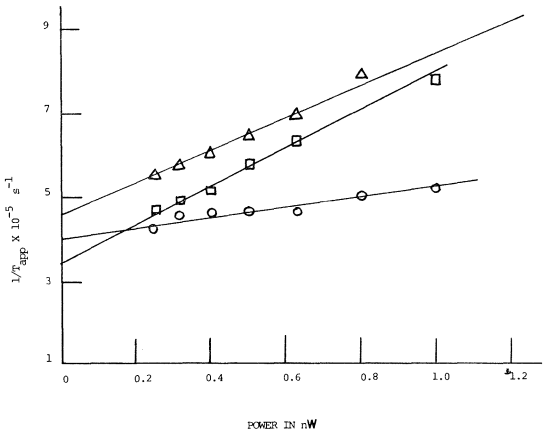

FIG. 5. The plot of $1/T_{app}$ as a function of microwave power. △: Semibenzoquinone radical; ○: semitetrachlorobenzoquinone radical; and □: semiduroquinone radical. The estimated T_1 extrapolated to zero power are 2.2 μs for semibenzoquinone; 2.7 μs for semitetrachlorobenzoquinone; and 3.2 μs for semiduroquinone, all at 10°C and in 50% isopropanol/toluene solvent.

quinones in the same solvent at the same temperature, we found that there is no significant difference outside experimental errors between the T_1 of the neutral radical and the radical anion. In the development of the slow response semi-steady-state CIDEP method using a rotating sector (16), we have made some assumptions by using the literature T_1 values for semibenzoquinone radical anions for the neutral radical systems. The present experiments support such assumptions and the T_1 values of the semiquinone radical anions measured here by the time-resolved CIDEP method agree quite well with those reported in literature using saturation method (19). It also establishes that T_1 has the same value when measured at different hyperfine fields (20).

Conclusions

The importance of proper treatment of the response time in the application of time-resolved CIDEP observations to the measurements of T_1 is demonstrated in detail by comparing the theoretical treatment with the experimental analysis. With spectrometers using either 100 kHz or 2 MHz modulation the intrinsic response time is longer than 800 ns (and much higher with 100 kHz modulation). Any analysis of the time evolution profiles using modulated spectrometers must therefore involve the analysis of the response time in details. Using dc detection method with spectrometers having an intrinsic response time less than 300 ns, T_1 of the transient radicals can be estimated by the extrapolation to zero power method, provided that the response time is known to be approximately constant over the range of power used.

Acknowledgments

This research is supported by the Natural Sciences and Engineering Council of Canada and by the Advisory Research Committee, Queen's University.

1. D. J. NELSON, A. D. TRIFUNAC, M. C. THURNAUER, and J. R. NORRIS. *In* Review of chemical intermediates. To be published.
2. P. J. HORE and K. A. MCLAUCHLAN. *In* Review of chemical intermediates. To be published.
3. J. K. S. WAN and A. J. ELLIOT. Acc. Chem. Res. **10**, 161 (1977).
4. A. R. MCINTOSH and J. R. BOLTON. *In* Review of chemical intermediates. To be published.
5. M. C. THURNAUER. *In* Review of chemical intermediates. To be published.
6. G. C. DISMUKES, A. MCGUIRE, R. BLANKENSHIP, and K. SAUER. Biophys. J. **21**, 239 (1978) and references therein.
7. S. S. KIM and S. I. WEISSMAN. *In* Review of chemical intermediates. To be published.
8. S. S. KIM and S. I. WEISSMAN. Chem. Phys. **27**, 21 (1978).
9. R. FURRER, M. HEINRICH, D. STEHLIK, and H. ZIMMERMAN. Chem. Phys. **36**, 27 (1979).
10. K. A. MCLAUCHLAN, R. C. SEALY, and J. M. WITTMANN. Mol. Phys. **35**, 51 (1978); J. Chem. Soc. Faraday I, **73**, 926 (1977).
11. P. W. ATKINS, A. J. DOBBS, and K. A. MCLAUCHLAN. Chem. Phys. Lett. **29**, 616 (1974).
12. P. W. ATKINS, K. A. MCLAUCHLAN, and P. W. PERCIVAL. Mol. Phys. **25**, 281 (1973).
13. A. J. DOBBS. Mol. Phys. **30**, 1073 (1975).
14. J. K. S. WAN. Adv. Photochem. To be published.
15. A. J. ELLIOT, J. W. M. DEBOER, and J. K. S. WAN. J. Magn. Reson. **32**, 293 (1978).
16. A. J. ELLIOT and J. K. S. WAN. J. Phys. Chem. **82**, 444 (1978).
17. N. C. VERMA and R. W. FESSENDEN. J. Chem. Phys. **65**, 2139 (1976).
18. S. S. KIM and S. I. WEISSMAN. J. Magn. Reson. **24**, 167 (1976).
19. S. K. RENGAN, H. P. KHAKHAR, B. S. PRABHANANDA, and B. VENKATARAMAN. Pramana, **3**, 95 (1974).
20. F. J. ADRIAN, H. M. VYAS, and J. K. S. WAN. J. Chem. Phys. **65**, 1454 (1976).

The reaction of ethyl 3,4,6-tri-*O*-acetyl-2-amino-2-deoxy-β-D-glucoside in acetone

BRIAN CAPON, CECILIA LABBÉ, AND DAVID S. RYCROFT
Department of Chemistry, University of Glasgow, Glasgow, G12 8QQ, Scotland, U.K.

Received April 30, 1979

BRIAN CAPON, CECILIA LABBÉ, and DAVID S. RYCROFT. Can. J. Chem. 57, 2978 (1979).

It is shown by ^1H and ^{13}C nmr spectroscopy that ethyl 3,4,6-tri-*O*-acetyl-2-amino-2-deoxy-β-D-glucoside reacts in acetone to yield a Schiff base, not the hemiorthoamide proposed previously.

BRIAN CAPON, CECILIA LABBÉ et DAVID S. RYCROFT. Can. J. Chem. 57, 2978 (1979).

On a déterminé par la résonance magnétique du ^1H et du ^{13}C que le tri-*O*-acétyl-3,4,6 amino-2 déoxy-2-β-D-éthylglucoside réagit dans l'acétone pour donner une base de Schiff et non l'hémiorthoamide proposé antérieurement.

[Traduit par le journal]

It was reported in 1970 (1) that ethyl 3,4,6-tri-*O*-acetyl-2-amino-2-deoxy-β-D-glucoside (**1**) reacts in acetone solution to yield a compound (**2**) with a hemiorthoamide structure. In view of our interest in tetrahedral intermediates (2) and in the expected instability of hemiorthoamides (3, 4) we have re-investigated this reaction. The optical rotation of a solution of ethyl 3,4,6-tri-*O*-acetyl-2-amino-2-deoxy-β-D-glucoside in acetone changed in a similar manner to that reported previously (1, 5) ($[\alpha]_D - 1.67$ (1 min) → $-31.72°$) and on workup as described previously (1) a product with the same ^1H nmr spectrum as reported previously was obtained (cf. Fig. 2, ref. 1). In this spectrum it was proposed (1) that the two signals at δ = ca. 1.90 separated by ca. 2 Hz were the signals of the methyl of the orthoamide group of **2** which was a doublet because of spin–spin coupling with the NH proton. However in our hands the separation of these two signals was approximately 5/3 times greater when the spectrum was run at 100 MHz (4.8 Hz) than when it was run at 60 MHz (2.8 Hz) and approximately 3/2 times greater when it was run at 90 MHz (3.9 Hz). We therefore conclude that the two signals arise from a difference in chemical shift and not from spin–spin splitting. This conclusion is supported by the effect on the spectrum of shaking with deuterium oxide. In our hands this led to a loss of the NH signal (δ = ca. 1.60, variable) without any alteration of the two peaks at δ = ca. 1.90. However, these experiments are not inconsistent with structure **2** since two diastereoisomers, and hence two methyl signals, are possible.

The reaction of **1** was investigated further in acetone-d_6. The optical rotation changed as in acetone ($[\alpha]_D = -3.15$ (1 min) → $-32.5°$) and a similar product was isolated. The ^1H nmr spectrum of this in $CDCl_3$ lacked the upfield peak at δ = ca. 1.90 (1.89) but the downfield peak (δ = 1.94) was

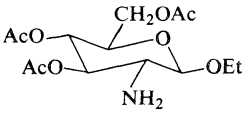

1

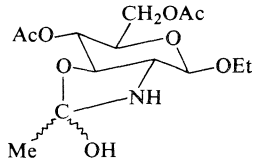

2

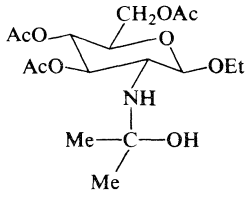

3

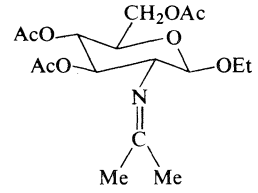

4

unchanged. In addition the peak at δ = 2.01 was of reduced intensity. It was therefore concluded that **1** had reacted with acetone to produce a product in which there were signals at δ = 1.89 and 2.01 which were derived from the acetone. The spectrum of the product from acetone-d_6 also lacked the signal at δ = 2.17 of acetone which was apparent in our spectrum of the product from acetone-h_6 and in Fig. 2 of ref. 1.

Better resolved spectra were obtained with solutions in acetonitrile-d_3. The compound from CH_3COCH_3 showed methyl signals at δ = 1.84, 1.88, 1.91, 1.95, and 2.01. In addition there were small peaks at δ = 2.00 and 1.99 which corresponded to those of the starting material **1** (the third signal of **1** occurs at δ = 1.95 and overlaps with one of those of the product) and at δ 2.08 which corresponded to that of acetone. The product from CD_3COCD_3 lacks the signals at δ = 1.84 and 1.91.

Examination of the ethyl group triplet of the spectra in CD_3CN (or $CDCl_3$) (cf. Fig. 2, ref. 1) indicates that besides the main triplet (δ 1.10,

0008-4042/79/222978-03$01.00/0

CD_3CN; 1.16, $CDCl_3$) there is a second triplet (δ 1.19, CD_3CN; 1.28, $CDCl_3$) of lower intensity which corresponds to the triplet of **1**. Since acetone is also present it is concluded that the product has partially decomposed in both solvents. When D_2O was added to a solution in CD_3CN of the product from **1** and CH_3COCH_3 a spectrum was obtained that corresponded to the sum of the spectra of the starting components. The best spectrum of the product was obtained in CD_3COCD_3 solution after leaving at 35°C for 18 h. This corresponded to ca. 90% conversion but after workup the spectrum taken immediately in $CDCl_3$ indicated that only ca. 80% of the product was present, and on leaving, further decomposition took place. A more stable spectrum was obtained with solutions in CD_3CN.

The two most likely structures were considered to be a carbinolamine **3** or a Schiff base **4**. The latter structure is supported by the fact that the chemical shift of the proton at C2 moves downfield from δ = 2.7 to ca. 3.5 where it overlaps with the protons at C6, C5, and the CH_2 of the ethyl group to form a highly complex multiplet. Further support for the Schiff base structure comes from the ^{13}C nmr spectra (Table 1) and in particular the presence of a signal at δ = 171.7 corresponding to a C=N group (the carbon of the C=N group of Me_2C=NMe has δ = 168(6)). This signal was not observed in the room temperature spectrum of the product from acetone-d_6. However by running spectra at −40°C so that S/N improvement was quicker and decomposition slower a signal from the acetone-d_6 product was seen at δ = 172.16 with ca. 25% of the height of the corresponding signal at δ = 172.29 from the acetone-h_6 product. This loss in height arises partly because of spin-coupling to six deuterium nuclei giving an unresolved 13 line multiplet ($|^2J_{CD}|$ is expected (7) to be ca. 0.5–1 Hz) and partly because of the reduction in the nOe and increase in T_1 attendant on neighbouring deuterium substitution. The geminal deuterium isotope effect on the chemical shift cannot be predicted as such effects have received little study (8) and may be either positive or negative. The effect observed here is very small (−0.13 ppm; cf. +0.32 ppm for acetone-d_6). No signal for a quaternary carbon at δ = 60–80 could be discerned which would be expected if the product had a carbinolamine structure **3**. The signals of the methyl groups derived from the acetone, which occur at δ = 29.4 and 19.5, are also absent in the spectrum of the product from CD_3COCD_3. The large difference in chemical shift that they show is also consistent with the structure **4** (cf. δ = 29.1 and 18.0 for Me_2C=NMe (6)) but would be unexpected for structure **3**. Significant differences in chemical shift in the spectra of **1** and the product were also found for the signals of C1, C2, and C3. Particularly noteworthy is the downfield shift of 8 ppm of the signal of C2.

It is concluded that the change in optical rotation which occurs when **1** is dissolved in acetone arises from formation of the Schiff base **4**, not of the hemiorthoamide **2**.

TABLE 1. ^{13}C nuclear magnetic resonance chemical shifts[a] of ethyl 3,4,6-tri-*O*-acetyl-2-amino-2-deoxy-β-D-glucoside (**1**) and of the product of its reaction in acetone solution

	1	Product
CH_3CH_2	15.5	15.5
CH_3CH_2	66.1	65.8
C6	63.1	63.1
C5	72.4	72.4
C4	70.0	69.8
C3	76.2	75.0
C2	57.1	65.5
C1	104.6	103.2
CH_3—*C*(=O)O	171.3(2)	171.2
	170.7	170.7
		170.4
CH_3—C(=O)O	21.1	20.9(3)
	20.9(2)	
CH_3—*C*=N		171.7
CH_3—C=N		29.4
		19.5

[a]In ppm downfield of internal Me_4Si for solutions in CD_3CN at ca. 25°C.

Experimental

Proton nmr spectra were run at ambient probe temperature on Varian T60 (60MHz), Perkin Elmer R32 (90MHz), and Varian HA100 (100MHz) spectrometers. ^{13}C nmr spectra with a digital resolution of 1.25Hz/data point were run on a Varian XL100 spectrometer at 25.2 MHz in the pulsed FT mode. Off-resonance proton decoupled spectra were used to confirm assignments. Optical rotations were measured on a Perkin Elmer 141 polarimeter.

Ethyl tri-*O*-acetyl-2-amino-2-deoxy-β-D-glucopyranoside (**1**) was allowed to react in acetone as described previously (1) to yield a product with the same ^1H nmr spectrum as reported previously (cf. Fig. 2, ref. 1). In CD_3CN solution the following signals were present: δ = 5.15 (t, *J* = 8.7 Hz, H3 or H4), 4.93 (t, *J* = 8.7 Hz, H4 or H3), 4.56 (d, *J* = 7.3 Hz, H1), 4.4–3.3 (complex multiplet H6, H5, H2, and CH_3CH_2), 2.01, 1.95, 1.91, 1.88, 1.84 (s, CH_3), and 1.10 (t, *J* = 7 Hz, CH_3CH_2). A similar product was obtained from acetone-d_6; the ^1H nmr spectrum was similar to that obtained from CH_3COCH_3 but no signals at δ = 1.84 and 1.91 were present.

Acknowledgement

We thank the U.K. Science Research Council for support.

1. G. FODOR, F. LETOURNEAU, and N. MANDAVA. Can. J. Chem. **48**, 1465 (1970).
2. B. CAPON, J. H. GALL, and D. MCL. A. GRIEVE. J. Chem. Soc. Chem. Commun. 1034 (1976).
3. J. P. GUTHRIE. J. Am. Chem. Soc. **96**, 3608 (1974).
4. P. DESLONGCHAMPS, S. DUBÉ, C. LEBREUX, D. R. PATTERSON, and R. J. TAILLEFER. Can. J. Chem. **53**, 2791 (1975).
5. G. FODOR and L. ÖTVÖS. Chem. Ber. **89**, 702 (1956).
6. N. NAULET, M. L. FILLEUX, G. J. MARTIN, and J. PORNET. Org. Magn. Reson. **7**, 326 (1975).
7. D. F. EWING. Annu. Rep. NMR Spectrosc. **6A**, 389 (1975).
8. F. W. WEHRLI, D. JEREMIĆ, M. LJ. MIHAILOVIĆ, and S. MILOSAVLJEVIĆ. J. Chem. Soc. Chem. Commun. 302 (1978).

Quaternization and sodium borohydride reduction of *N*-(4-pyridylcarbonylamino)-1,2,3,6-tetrahydropyridine. Synthesis of *N*-amino-1,2,3,6-tetrahydropyridines

K. REDDA, L. A. CORLETO, AND E. E. KNAUS[1]

Faculty of Pharmacy and Pharmaceutical Sciences, University of Alberta, Edmonton, Alta., Canada T6G 2N8

Received May 16, 1979

K. REDDA, L. A. CORLETO, and E. E. KNAUS. Can. J. Chem. **57**, 2981 (1979).

Reaction of *N*-(4-pyridylcarbonylamino)-1,2,3,6-tetrahydropyridine (**2***a*) with methyl chloroformate afforded the quaternary salt **3***a* whereas reaction with methyl iodide gave a mixture of **3***b* and **6**. Sodium borohydride reduction of **3***a* using methanol at −65°C gave the *N*-methoxycarbonyl-1,2-dihydropyridine **4***a* whereas reduction using ethanol at 0°C gave the 1,2,3,6-tetrahydropyridine **4***b*. Reduction of **3***b* and **6** gave rise to a mixture of **4***c* and **7**. Catalytic hydrogenation of **4***b* and **4***c* afforded the respective piperidyl derivatives **10** and **11**. The pharmacological activities of the products are presented.

K. REDDA, L. A. CORLETO et E. E. KNAUS. Can. J. Chem. **57**, 2981 (1979).

La réaction de la *N*-(pyridylcarbonylamino-4) tétrahydro-1,2,3,6 pyridine (**2***a*) avec le chloroformate de méthyle fournit le sel quaternaire **3***a* tandis que la réaction avec l'iodure de méthyle fournit un mélange de **3***b* et de **6**. La réduction de **3***a* par le borohydrure de sodium dans le méthanol à −65°C conduit à la *N*-méthoxycarbonyl dihydro-1,2 pyridine **4***a* mais dans l'éthanol à 0°C on obtient le tétrahydro-1,2,3,6 pyridine **4***b*. La réduction de **3***b* et de **6** conduit à un mélange de **4***c* et de **7**. L'hydrogénation catalytique de **4***b* et de **4***c* permet d'obtenir respectivement les dérivés pipéridyles **10** et **11**. On rapporte les propriétés pharmacologiques de ces produits.

[Traduit par le journal]

The sodium borohydride reduction of *N*-carbonyliminopyridinium ylides **1** is a facile procedure for the synthesis of *N*-carbonylamino-1,2,3,6-tetrahydropyridines **2** (1). A broad spectrum pharmacological

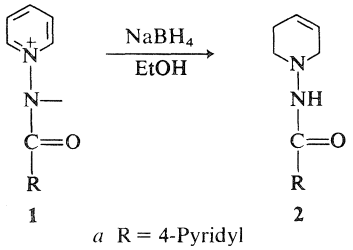

1 2

a R = 4-Pyridyl
b R = 3-Pyridyl
c R = 2-Pyridyl

screen[2] indicated that **2***a–c* exhibited analgesic and anti-inflammatory activities comparable to Aspirin and Indomethacin respectively (2). It was therefore of interest to determine what effect hydrogenation of the 4-pyridyl ring of **2***a* would have on pharmacological activity. We now wish to describe the syntheses and pharmacological activities of reduced pyridyl analogs of *N*-(4-pyridylcarbonylamino)-1,2,3,6-tetrahydropyridine (**2***a*).

The reaction of **2***a* with methyl chloroformate in methanol at −65°C for 30 min affords the quaternary salt **3***a* which on reduction with sodium borohydride also at −65°C for 3 h gave *N*-[4-(1-methoxycarbonyl-1,2-dihydropyridyl)carbonylamino]-1,2,3,6-tetrahydropyridine (**4***a*, 70.5%) (3). On the other hand the same reaction in ethanol at 0°C gave *N*[4-(1-methoxycarbonyl-1,2,3,6-tetrahydropyridyl)-carbonylamino]-1,2,3,6-tetrahydropyridine (**4***b*, 52.7%). Alternatively, reduction of **4***a* using sodium borohydride in ethanol at 0°C also gave **4***b* (58.4%).

Treatment of **2***a* with methyl iodide in methanol followed by sodium borohydride reduction at −65°C afforded a mixture of **4***c* (23.7%), arising from the reduction of **3***c* and **7** (17.1%). The most plausible

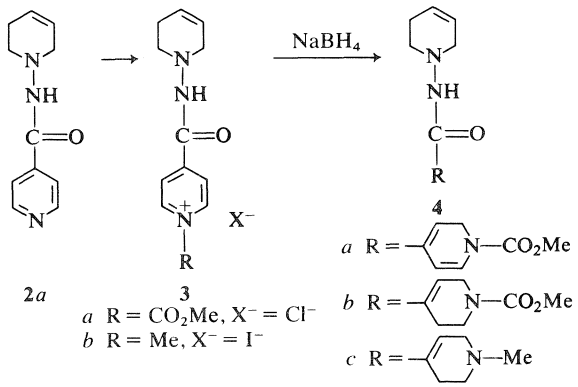

2a 3 4

a R = CO_2Me, X^- = Cl^-
b R = Me, X^- = I^-

[1]To whom all correspondence should be addressed.
[2]The broad spectrum pharmacological screen was performed by Bio-Research Laboratories, Montreal, P.Q.

0008-4042/79/222981-05$01.00/0

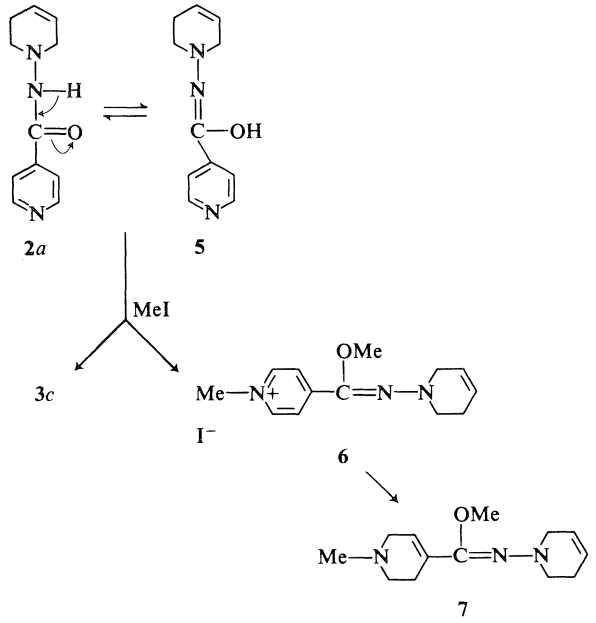

mechanism for the formation of **7** involved methylation of the enolic tautomer **5** to give **6** which on subsequent reduction would yield **7**. A similar O-methylation reaction has been observed for *N*-carbonyliminopyridinium ylides (4).

The mechanism for the reduction of pyridinium salts **3** and **6** likely involves attack by hydride anion at a carbon adjacent to the quaternary nitrogen to give the dienamine **8** which on protonation and subsequent reduction of the immonium species **9** would afford **4** or **7** (5).

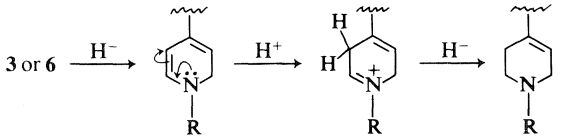

Catalytic hydrogenation of **4***b* and **4***c* using palladium on charcoal and hydrogen gas at 40 psi gave the saturated derivatives **10** (82.8%) and **11** (97.6%) respectively.

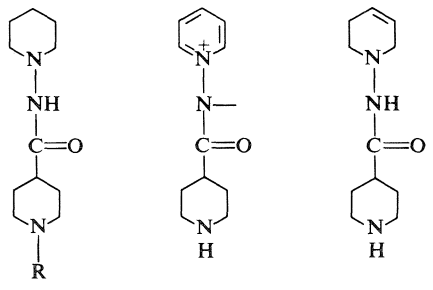

10 R = CO_2Me
11 R = Me
12
13

Reaction of isonipecotic acid hydrazide with 2,4-dinitrophenylpyridinium chloride, using the procedure reported previously (1), gave *N*-(4-piperidylcarbonylimino)pyridinium ylide **12** (10.9%). Reduction of **12** with sodium borohydride in ethanol at 0°C for 4 h afforded *N*-(4-piperidylcarbonylamino)-1,2,3,6-tetrahydropyridine **13** (86%).

The analgesic and anti-inflammatory activities of the *N*-aminocarbonyl-1,2,3,6-tetrahydropyridines were determined.[2]

The compounds were suspended in a solution of physiological saline and Tween 80 (TM) surfactant and administered subcutaneously (S.C.) to Swiss albino mice, before determining their analgesic activity in the phenylquinone writhing test according to the procedure of Collier (6). The analgesic activities of the compounds tested are compared to Aspirin (TM) and Dextropropoxyphene (TM) as illustrated in Table 1. A compound causing a 30–50% reduction is considered to be slightly active whereas one causing a greater than 50% reduction in the number of writhes is an active analgesic agent.

Anti-inflammatory activity was measured using the antagonism of carrageenan induced rat paw edema procedure of Winter (7). The compounds were administered subcutaneously to Sprague–Dawley rats and the anti-inflammatory activities compared to Indomethacin (TM) as shown in Table 2. A compound causing a greater than 30% reduction in edema is considered to be an active anti-inflammatory agent.

Examination of the analgesic test results (Table 1) indicates that elaboration of the 4-pyridyl ring of **2***a* to a 1-methoxycarbonyl-1,2-dihydropyridyl ring **4***a* enhances potency providing a compound with an improved dose-response. Reduction of **2***a* to the *N*-methoxycarbonyl-1,2,3,6-tetrahydropyridyl derivative **4***b* does not change activity whereas the closely

TABLE 1. Analgesic activity of *N*-aminocarbonyl-1,2,3,6-tetrahydropyridines and piperidines tested

Compound	Dose (mg/kg)	Response (% inhibition)
2*a*	128	81[a]
4*a*	16	61[a]
4*b*	128	78[a]
4*c*	256	47[c]
7	128	1.2[c]
10	256	74[b]
13	128	52.5[a]
Standards:		
Aspirin (TM)	50	50[b]
Dextropropoxyphene (TM)	56	50[b]

[a]Active.
[b]Slightly active.
[c]Inactive.

related analog **4***c* exhibits some analgesic activity. The O-methyl iminoether **7** was inactive which suggests the aminocarbonyl moiety is essential for analgesic activity. The fully hydrogenated analog **10** of **4***a* and **4***b* exhibited slight activity. Replacement of the 4-pyridyl ring of **2***a* by a 4-piperidyl ring **13** results in a decrease in activity but the compound is still considered to be an active analgesic.

Elaboration of the 4-pyridyl ring of **2***a* to the 1-methoxycarbonyl-1,2-dihydropyridyl derivative **4***a* results in a small reduction in anti-inflammatory activity whereas conversion to the *N*-methoxycarbonyl-1,2,3,6-tetrahydropyridyl derivative **4***b* provides a slightly active anti-inflammatory agent (see Table 2). Replacement of the 4-pyridyl ring of **2***a* by the *N*-methyl-1,2,3,6-tetrahydropyridyl ring present in **4***c* and **7** or the piperidine ring in **13** provides inactive compounds. The observation that **4***c* causes a 34% reduction in inflammation while **7** is totally inactive indicates that the carbonylamino moiety is essential for anti-inflammatory activity. The fully hydrogenated derivative **10** was found to be a slightly active anti-inflammatory agent.

Other broad spectrum pharmacological screening results indicated that **4***c* inhibited passive cutaneous anaphylaxis in the rat and was found to be an active anti-anaphylactic agent according to the procedure of Goose (8). The *N*-methoxycarbonyl-1,2-dihydropyridyl derivative **4***a* provided a partial block of the response to histamine in the isolated Guinea pig ileum (9) and was considered to be a slightly active antihistaminic agent. None of the compounds prepared exhibited antidepressant, cardiovascular, or hypoglycemic activities.

Experimental

Melting points were determined with a Büchi capillary apparatus and are uncorrected. Nuclear magnetic resonance spectra were determined for solutions in deuterochloroform with TMS as internal standard with a Varian EM-360A spectrometer. Infrared spectra (potassium bromide unless otherwise noted) were taken on a Unicam SP-1000 or Perkin Elmer 267 spectrometer. Mass spectra were measured with an AEI-MS-50 mass spectrometer and these exact mass measurements are used in lieu of elemental analyses. All of the products described gave rise to a single spot on tlc using a solvent system less polar and more polar than the specific solvent system described for purification of the reaction mixture. No residue remained after combustion of the products.

TABLE 2. Anti-inflammatory activity of *N*-aminocarbonyl-1,2,3,6-tetrahydropyridines and piperidines tested

Compound	Dose (mg/kg)	Response (% inhibition) 3 h	Response (% inhibition) 5 h
2*a*	64	25	75[a]
4*a*	128	50	83[a]
4*b*	128	0	50[b]
4*c*	128	0	34[c]
7	128	0	0[c]
10	128	0	50[b]
13	128	0	0[c]
Standard: Indomethacin (TM)	32	17	83[a]

[a]Active.
[b]Slightly active.
[c]Inactive.

N-[*4-(1-Methoxycarbonyl-1,2-dihydropyridyl)carbonylamino*]-*1,2,3,6-tetrahydropyridine* (**4**a)

General Procedure

A solution of methyl chloroformate (0.202 g, 2.15 mmol) in methanol (20 mL) was added dropwise with stirring to a solution of **2***a* (0.218 g, 1.07 mmol) in methanol (20 mL) pre-cooled to −65°C. The reaction was allowed to proceed for 30 min at −65°C with stirring. Sodium borohydride (0.8 g) was added and the reaction was allowed to proceed for an additional 3 h at −65°C. The reaction mixture was then poured onto crushed ice (125 mL) followed by gradual warming to room temperature. Extraction with chloroform (200 mL), drying (sodium sulfate), and removal of solvent *in vacuo* gave a white solid which was purified by elution from a 2.5 cm × 20 cm silica gel column using ether (400 mL) to afford **4***a* (0.199 g, 70.5%); mp 132–134°C; ir: 3200 (m, NH), 1710, and 1670 (s, CO) cm^{-1}; ^1H nmr δ: 7.18 (s, 1H, NH, exchanges with deuterium oxide), 6.84 (d($J_{5,6}$ = 8 Hz), 1H, H-6 (dihydropyridine)), 6.20 (d($J_{2,3}$ = 5 Hz) of d($J_{2',3}$ = 5 Hz) of d($J_{3,5}$ = 2 Hz), 1H, H-3 (dihydropyridine)), 6.00–5.61 (m, 2H, H-4, H-5 (tetrahydropyridine)), 5.45 (d($J_{5,6}$ = 8 Hz) of d($J_{3,5}$ = 2 Hz), 1H, H-5 (dihydropyridine)), 4.51 (d($J_{2,3}$ = 5 Hz), 2H, H-2 (dihydropyridine)), 3.80 (s, 3H, —CH_3), 3.58–3.32 (m, 2H, H-6 (tetrahydropyridine)), 3.08 (t($J_{2,3}$ = 6 Hz), 2H, H-2 (tetrahydropyridine)), 2.52–2.08 (m, 2H, H-3 (tetrahydropyridine)). Exact mass calcd. for $C_{13}H_{17}N_3O_3$: 263.1270; found (high resolution ms): 263.1267.

N-[*4-(1-Methoxycarbonyl-1,2,3,6-tetrahydropyridyl)carbonylamino*]-*1,2,3,6-tetrahydropyridine* (**4**b)

Method A

A solution of methyl chloroformate (0.38 g, 4.02 mmol) was added dropwise to a solution **2***a* (0.40 g, 2.01 mmol) in 95% ethanol (40 mL) pre-cooled to −65°C and the reaction was allowed to proceed for 30 min at −65°C with stirring. Sodium borohydride (0.25 g) was added at once and the reaction allowed to proceed for 4 h at 0°C prior to completion as described under the general procedure. The reaction product was then purified by elution from a 2.5 cm × 17 cm neutral alumina column with ethyl acetate (400 mL) to give **4***b* (0.281 g, 52.7%); mp: 153–155°C; ir: 3180 (m, NH), 1715, and 1675 (s, CO) cm^{-1}; ^1H nmr δ: 7.3–6.88 (m, 1H, H-5 (*N*-tetrahydropyridylcarbonyl)), 6.72 (s, 1H, NH, exchanges with deuterium oxide), 6.0–5.48 (m, 2H, H-4, H-5 (*N*-aminotetrahydropyridine)), 3.80 (s, 3H, —CH_3), 3.80–3.32 (complex m, 4H, H-6 (*N*-tetrahydropyridylcarbonyl), H-6 (*N*-aminotetrahydropyridine)), 3.07 [t($J_{2,3}$ = 6 Hz), 4H, H-2 (*N*-tetrahydropyridylcarbonyl), H-2 (*N*-aminotetrahydropyridine)), 2.50–1.70 (complex m, 4H, H-3 (*N*-tetrahydropyridylcarbonyl), H-3 (*N*-aminotetrahydropyridine)). Exact mass calcd. for $C_{13}H_{19}N_3O_3$: 265.1426; found (high resolution ms): 265.1429. *Anal.* calcd. for $C_{13}H_{19}N_3O_3$: C 58.85, H 7.22, N 15.84; found: C 58.63, H 7.27, N 15.75.

Method B

To a solution of **4***a* (1.172 g, 4.46 mmol) in 95% ethanol (120 mL) pre-cooled to 0°C was added sodium borohydride (0.35 g). The reaction was allowed to proceed for 5 h at 0°C

with continuous stirring and then completed as described under the general procedure. The reaction product was purified by elution from a 2.5 cm × 18 cm neutral alumina column using ethyl acetate (700 mL) to give **4***b* (0.69 g, 58.4%); mp: 153–156°C; identical (ir) to the product prepared under method A.

N-[*4-(1-Methyl-1,2,3,6-tetrahydropyridyl)carbonylamino*]-*1,2,3,6-tetrahydropyridine* (**4***c*) *and* N-[*(1,2,3,6-Tetrahydropyridyl)*]-C-*methoxy*-C-[*4-(1-methyl-1,2,3,6-tetrahydropyridyl)*]*azomethine* (**7**)

Methyl iodide (10 mL) was added to a solution of **2***a* (5.0 g, 24.6 mmol) in dry methylene chloride (120 mL). The reaction was allowed to proceed for 4 h with stirring at 25°C prior to refluxing for an additional 4 h. Removal of the solvent *in vacuo* afforded a hygroscopic intense yellow solid which was dissolved in methanol (120 mL) and the solution cooled to −65°C. Sodium borohydride (1.8 g) was added in one aliquot and the reaction was allowed to proceed for 4 h at −65°C prior to completion as described under the general procedure. The reaction mixture was chromatographed using a 2.5 cm × 18 cm neutral alumina column. Elution with ether–methanol (10:1 v/v) (400 mL) gave **4***c* (1.289 g, 23.7%); mp: 119–122°C, ir: 3200 (m, NH) and 1665 (s, CO) cm^{-1}; ^1H nmr δ: 6.94 (s, 1H, NH, exchanges with deuterium oxide), 6.52 (m, 1H, H-5 (*N*-methyltetrahydropyridine)), 6.00–5.44 (m, 2H, H-4, H-5 (*N*-aminotetrahydropyridine)), 3.72–3.33 (m, 2H, H-6 (*N*-aminotetrahydropyridine)), 3.07 [t($J_{2,3}$ = 6 Hz), 4H, H-2 (*N*-aminotetrahydropyridine), H-6 (*N*-methyltetrahydropyridine)), 2.63–2.08 (complex m, 6H, H-3 (*N*-aminotetrahydropyridine), H-2, H-3 (*N*-methyltetrahydropyridine)), 2.38 (s, 3H, —CH_3). Exact mass calcd. for $C_{12}H_{19}N_3O$: 221.1529; found (high resolution ms): 221.1529.

Further elution with ether–methanol (5:1 v/v) (500 mL) gave a solid which was further purified by preparative tlc using twenty-four 20 cm × 20 cm silica gel GF 254 plates, 0.75 mm in thickness, with ethyl acetate – methanol (1:1 v/v) as development solvent. Extraction with warm methanol (200 mL) of the fraction having R_f 0.30 afforded **7** (0.987 g, 17.1%); mp: 133–136°C; ir: 1655 (s, C=N) cm^{-1}; ^1H nmr δ: 6.55 (m, 1H, H-5 (*N*-methyltetrahydropyridine)), 6.2–5.5 (m, 2H, H-4, H-5 (*N*-aminotetrahydropyridine)), 4.5–4.1 (m, 2H, H-6 (*N*-aminotetrahydropyridine)), 4.10–3.65 (m, 3H, H-6 (*N*-methyltetrahydropyridine)), 3.52 (s, 2H, —OCH_3), 3.11 (t($J_{2,3}$ = 5 Hz), 2H, H-2 (*N*-aminotetrahydropyridine)), 2.78–2.28 (complex m, 6H, H-3 (*N*-aminotetrahydropyridine), H-2, H-3 (*N*-methyltetrahydropyridine)), 2.39 (s, 3H, —N—CH_3). Exact mass calcd. for $C_{13}H_{21}N_3O$: 235.1684; found (high resolution ms): 235.1685.

N-*(1-Methoxycarbonyl-4-piperidylcarbonylamino)piperidine* (**10**)

Catalytic hydrogenation of **4***b* (1.572 g, 5.93 mmol) in methanol (120 mL) was effected using 10% palladium on charcoal (200 mg) and hydrogen gas at 40 psi for 12 h. The charcoal was removed by filtration and the recovered charcoal washed with methanol (30 mL). Removal of the solvent *in vacuo* gave a product which was purified by elution from a 2.5 cm × 20 cm neutral alumina column using ether–methanol (10:1 v/v) (600 mL) to afford **10** (1.321 g, 82.8%); mp: 160–162°C; ir: 3220 (m, NH), 1695, and 1655 (s, CO) cm^{-1}; ^1H nmr δ: 6.6 (s, 1H, NH, exchanges with deuterium oxide), 4.48–4.0 (m, 1H, H-4 (*N*-piperidylcarbonyl)), 3.75 (s, 3H, —OCH_3), 3.35–2.0 (complex m, 8H, H-2, H-6 (*N*-piperidylcarbonyl), H-2, H-6 (*N*-aminopiperidine)), 2.0–1.22 (complex m, 10H, H-3, H-5 (*N*-piperidylcarbonyl), H-3, H-4, H-5 (*N*-aminopiperidine)). Exact mass calcd. for $C_{13}H_{23}N_3O_3$: 269.1740; found (high resolution ms); 269.1744.

N-*(1-Methyl-4-piperidylcarbonylamino)piperidine* (**11**)

Catalytic hydrogenation of **4***c* (0.163 g, 0.738 mmol) in methanol (60 mL) was carried out in the presence of 10% palladium on charcoal (40 mg) and hydrogen gas at 40 psi for 12 h. The charcoal was removed by filtration and the recovered charcoal washed with methanol (30 mL). Removal of the solvent *in vacuo* afforded **11** (0.162 g, 97.6%); mp: (171–174°C; ir: 3215 (m, NH) and 1655 (s, CO) cm^{-1}; ^1H nmr δ: 6.48 (s, 1H, NH, exchanges with deuterium oxide), 3.70 (s, 1H, H-4 (*N*-methylpiperidine)), 3.30–2.37 (complex m, 8H, H-2, H–6 (*N*-methylpiperidine), H-2, H-6 (*N*-aminopiperidine)), 2.27 (s, 3H, —N—CH_3), 2.10–1.15 (complex m, 10H, H-3, H-5 (*N*-methylpiperidine), H-3, H-4, H-5 (*N*-aminopiperidine). Exact mass calcd. for $C_{12}H_{23}N_3O$: 225.1840; found (high resolution ms): 225.1840.

N-*(4-Piperidylcarbonylimino)pyridinium Ylide* (**12**)

To an ice-cooled solution of 2,4-dinitrophenylpyridinium chloride (3.33 g, 11.8 mmol) in methanol (30 mL) was added dropwise isonipecotic acid hydrazide (1.68 g, 11.8 mmol) in methanol (30 mL) and then triethylamine (1.0 mL). The reaction mixture was allowed to stand at room temperature overnight. The solid which precipitated was filtered off and washed in succession with 60 mL each of methanol, water, methanol, and ether. A suspension of the solid obtained above in dioxane–water (4:1) (200 mL) was heated under reflux for 12 h to afford a clear solution. The solvent was removed *in vacuo* below 55°C, water was added to the residue and the insoluble material removed by filtration. The filtrate was concentrated under reduced pressure to give **12**. Chromatography on a neutral alumina column (2.5 cm × 26 cm) using ether–methanol (1:1 v/v) (250 mL) as eluant afforded pure **12** (0.263 g, 10.9%); mp: 65–67°C; ^1H nmr δ: 8.5 (d($J_{2,3}$ = $J_{5,6}$ = 6 Hz) of d($J_{2,4}$ = $J_{4,6}$ = 1.5 Hz), 2H, H-2, H-6 (pyridinium)), 7.72–8.4 (m, 3H, H-3, H-4, H-5 (pyridinium)), 1.4–3.3 (complex m, 9H, piperidyl hydrogens), 3.7 (broad s, 1H, NH, exchanges with deuterium oxide). Exact mass calcd. for $C_{11}H_{15}N_3O$: 205.1136; found (high resolution ms): 205.1134.

N-*(4-Piperidylcarbonylamino)-1,2,3,6-tetrahydropyridine* (**13**)

Sodium borohydride (50 mg) was added to a solution of 95% ethanol (20 mL) pre-cooled to 0°C. A solution of **12** (0.11 g, 0.539 mmol) in 95% ethanol (20 mL) was added dropwise during 20 min. After stirring for 4 h at 0°C the reaction mixture was poured onto crushed ice (75 mL) and allowed to come to room temperature. Extraction with chloroform (4 × 40 mL), drying ($NaSO_4$), and removal of the solvent *in vacuo* gave **13** as a white solid (97 mg, 86.5%); mp: 68–71°C; ir: 3200 (m, NH) and 1665 (s, CO) cm^{-1}; ^1H nmr δ: 5.7 (m, 2H, H-4, H-5 (tetrahydropyridine)), 4.2 (s, 1H, NH, exchanges with deuterium oxide), 1.4–3.8 (complex m, 15H, remaining tetrahydropyridyl and piperidyl hydrogens). Picrate derivative; mp: 82°C. *Anal.* calcd. for $C_{11}H_{19}N_3O$·picrate: C 46.58, H 5.06; found: C 46.36, H 5.02.

Acknowledgements

We are grateful to the Medical Research Council of Canada Grant (MA-4888) for financial support of this work and to the Canadian International Development Agency for a Graduate Scholarship (to K.R.).

1. E. E. KNAUS and K. REDDA. J. Heterocycl. Chem. **13**, 1237 (1976).
2. E. E. KNAUS, K. REDDA, and F. W. WANDELMAIER. U.S. Patent No. 4,088,653 (May 9, 1978).
3. F. W. FOWLER. J. Org. Chem. **37**, 1321 (1972).
4. W. J. MCKILLIP, E. A. SEDOR, B. M. CULBERTSON, and S. WAWZONEK. Chem. Rev. **73**, 255 (1973).
5. R. E. LYLE and P. S. ANDERSON. Adv. Heterocycl. Chem. **6**, 45 (1966).
6. H. O. COLLIER, L. C. DINNEEN, C. A. JOHNSON, and C. SCHNEIDER. Br. J. Pharmacol. Chemother. **32**, 295 (1968).
7. C. A. WINTER. *In* International symposium on non-steroidal antiinflammatory drugs. *Edited by* S. Garattini and M. N. Dukes. Excerpta Medica Foundation, Amsterdam. 1965. p. 190.
8. J. GOOSE and A. M. BLAIR. Immunology, **16**, 749 (1969).
9. W. L. PERRY. Pharmacological experiments on isolated preparations. Livingstone, Edinburgh. 1968. p. 58.

Binuclear palladium complexes of 3,5-disubstituted pyrazoles

J. POWELL[1] AND A. KUKSIS

Lash Miller Chemical Laboratories, University of Toronto, Toronto, Ont., Canada M5S 1A1

Received April 25, 1979

J. POWELL and A. KUKSIS. Can. J. Chem. **57**, 2986 (1979).

A series of binuclear palladium 3,5-disubstituted pyrazole complexes of the general formulation $[(CH_{3-n}X_nCO_2)(pzH)Pd(\mu\text{-}pz)]_2$ where pz = 3,5-dimethyl or 3,5-diphenylpyrazole, X = F, Cl, Br, C_6H_5, n = 0–3, were prepared. These complexes are unique in that they contain both bridging pyrazolyl and monodentate pyrazole groups.

J. POWELL et A. KUKSIS. Can. J. Chem. **57**, 2986 (1979).

On a préparé une série de complexes binucléaires palladium-pyrazoles disubstitués en position 3 et 5 de formule générale $[(CH_{3-n}X_nCO_2)(pzH)Pd(\mu\text{-}pz)]_2$ où pz = diméthyl-3,5 ou diphényl-3,5 pyrazoles, X = F, Cl, Br, C_6H_5, n = 0–3. Ces complexes sont uniques par le fait qu'ils contiennent à la fois un pyrazole agissant comme pont et un pyrazole monodentate.

[Traduit par le journal]

Introduction

Recently much effort has been devoted to the preparation of soluble transition metal complexes which may serve as models for metal surfaces (1). Bimetallic complexes in which two metals are held rigid and close together by bridging ligands are an obvious starting point for this study.

Pyrazole is a thermally and hydrolytically very stable, white crystalline solid. As a ligand it coordinates to metals through the 2-N. When deprotonated, pyrazole becomes the pyrazolide ion which can coordinate through both nitrogens as an exobidentate ligand of C_{2v} symmetry.

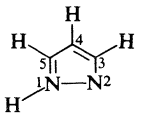

Pyrazole

Pyrazolide ion

Coordination of the nitrogens to a single given metal is impossible because of molecular geometry and as a result metallocycles of general structure **I** are formed (2).

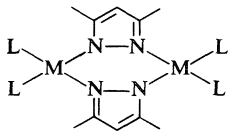

I
M = Rh
L = CO

Since the appearance of Trofimenko's review (3) on the coordination chemistry of pyrazole-derived ligands in 1972, many papers reporting the synthesis of 2-monohaptopyrazole and 1,2-dihaptopyrazolide metal or metalloid complexes have been published. In 1975 Coletta *et al.* (4) reported the synthesis of several compounds of the type $[M(pyrazole)_nX_m]$, where X = univalent anion = Cl, Br, M = Pd or Pt, n = 2, 4, m = 2. In 1971 Trofimenko (2) reported the reaction of 3,5-dimethylpyrazolide ion with $[\pi\text{-}CH_2C(C_6H_5)CH_2PdCl]_2$. A colourless solid was isolated which on the basis of elemental analysis, ^1H nmr spectra, and molecular weight studies was assigned structure **II**. Molecular models indicate the metallocycle ring to be in the puckered boat form rather than planar. Minghetti *et al.* reported the preparation of the trimeric gold(I) pyrazolide, $[Au(\mu\text{-}C_3N_2H_3)]_3$, in 1979 (5).

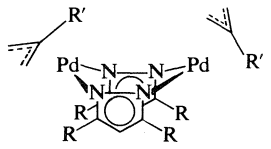

II
R = CH_3
R′ = C_6H_5

In this paper we report the preparation of a series of binuclear palladium 3,5-disubstituted pyrazole complexes believed to have structure **III**. These complexes are unique in that they contain both bridging pyrazolyl and monodentate pyrazole groups.

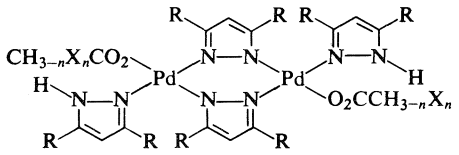

III
R = CH_3, X = F, Cl, Br, n = 0–3
R = C_6H_5, X = Cl, n = 0, 1
R = H, n = 0

[1]To whom all correspondence should be addressed.

0008-4042/79/222986-05$01.00/0

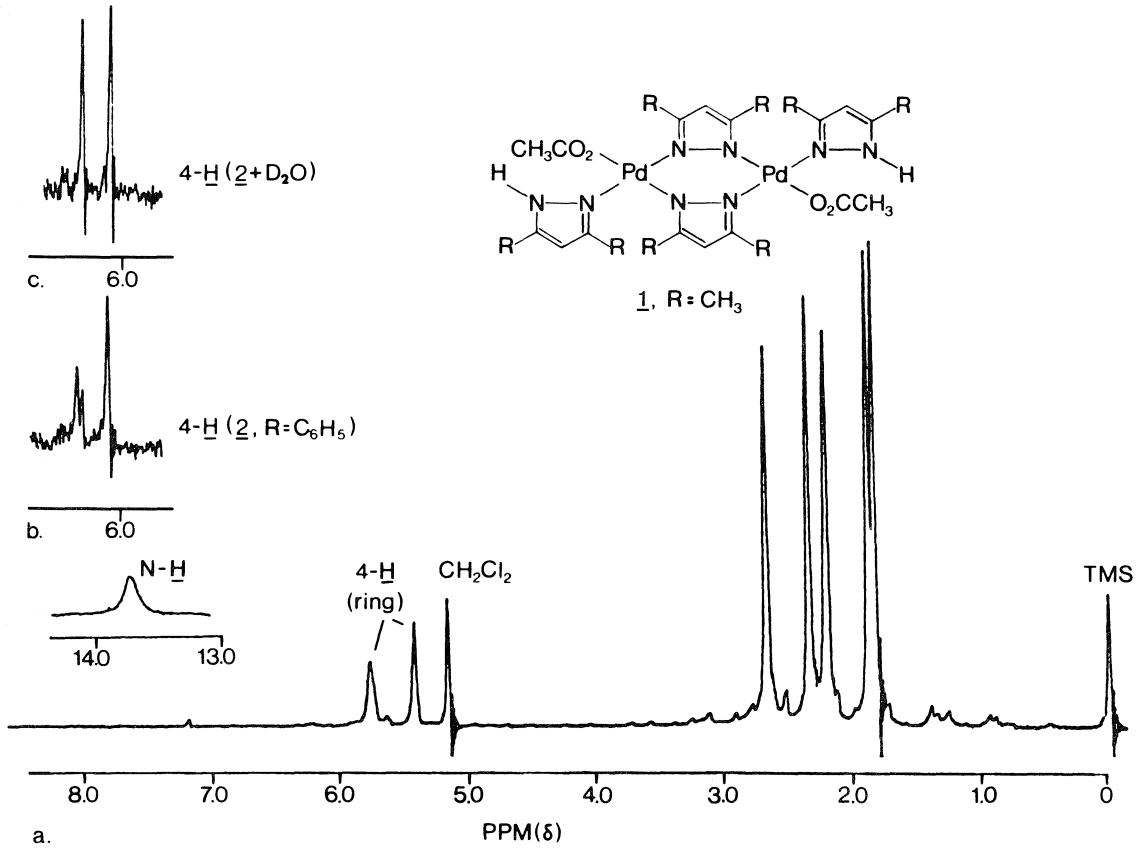

FIG. 1. (*a*) The ^{1}H nmr spectrum of $[(CH_3CO_2)(3,5\text{-dmpH})Pd(\mu\text{-}3,5\text{-dmp})]_2$, **1**, $CDCl_3$ solution. (*b*) The ^{1}H nmr spectrum of $[(CH_3CO_2)(3,5\text{-dppH})Pd(\mu\text{-}3,5\text{-dpp})]_2$, **2**, in the region 6.10–6.35 ppm, $CDCl_3$ solution. The 2:1:1 pattern for the 4-H pyrazole ring protons is more clearly resolved than in the ^{1}H nmr spectrum of **1**. (*c*) Treatment of the $CDCl_3$ solution of **2** with D_2O results in the collapse of the 2:1:1 splitting pattern of the 4-H pyrazole ring protons to two singlets of equal intensity.

Results and Discussion

Addition of 3,5-dimethylpyrazole (3,5-DMP) to a deep orange dichloromethane solution of palladium(II) acetate

$$Pd(O_2CCH_3)_2 + 2(3,5\text{-DMP}) \xrightarrow{CH_2Cl_2} \underset{\mathbf{1}}{\text{yellow powder}}$$

yielded a yellow solution from which a yellow powder, **1**, was isolated. On the basis of ^{1}H nmr, ir spectra, and elemental analysis, a compound having structure **III** is proposed, where R = CH_3, n = 0, a metallocycle, in which the ring is in the puckered boat form rather than planar and the acetate groups are *trans*. Structure **IV** is however a possible alternative.

Both structures would be expected to show five methyl resonances of equal intensity in their ^{1}H nmr spectra and five sharp singlets in the ratio 1:1:1:1:1 are observed in the region 1.80–2.65 ppm (Fig. 1*a*). Structures **III** and **IV** should be distinguishable on the basis of the number of peaks corresponding to the 4-H on the 3,5-dimethylpyrazole ring. One would expect to see two singlets in the ratio 2:2 in the case of structure **III** and three singlets in the ratio 2:1:1 in the case of structure **IV**. Two distinct peaks are

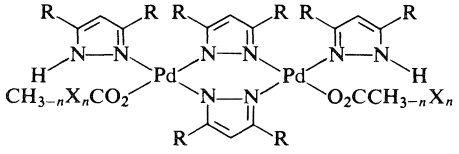

IV

R = CH_3, X = F, Cl, Br, n = 0–3
R = C_6H_5, X = Cl, n = 0, 1
R = H, n = 0

observed in the region 5.20–5.80 ppm, a sharp singlet of relative intensity 2 at 5.40 ppm and a broader,

slightly split peak of relative intensity 2 at 5.75 ppm. A more clearly resolved 2:1:1 pattern for the 4-H pyrazole ring protons is observed in the ^{1}H nmr spectrum of $[(CH_3CO_2)(3,5\text{-dppH})Pd(\mu\text{-dpp})]_2$, **2**, where 3,5-dpp = 3,5-diphenylpyrazole (Fig. 1*b*). On the basis of these observations structure **IV**, having *cis* acetate groups, may be assigned. However, splitting of the peak at 5.75 ppm may be due to long range coupling between the 4-H and the N—H proton of the terminal pyrazole groups. This type of interaction of the N—H proton with the other ring protons has been found to complicate the ^{1}H nmr spectra of substituted pyrroles (6). The ^{1}H nmr spectrum of a D_2O treated $CDCl_3$ solution of **2** showed only two sharp singlets of equal intensity in the region 6.10–6.35 ppm (Fig. 1*b*). Treatment of a $CDCl_3$ solution of **1** with D_2O resulted in a sharpening of the signal at 5.75 ppm. In both spectra the signals due to the N—H protons had disappeared indicating that deuterium–hydrogen exchange had occurred. These observations demonstrate conclusively that the splitting of the 4-H pyrazole ring protons is due to long range coupling with the N—H proton. On the basis of these results compound **1** is assigned structure **III**, the *trans* orientation is presumably favoured on steric grounds. The signal due to the N—H proton occurs much farther downfield at 13.60 ppm as a broad singlet.

The ir spectrum of compound **1** in a KBr pellet shows two strong, broad bands in the 1570–1630 cm^{-1} and 1360–1470 cm^{-1} regions which are assigned to ν(C═O) and ν(C—O), respectively. These carboxyl stretching frequencies are characteristic of unidentate acetate complexes (7). Due to the broad nature of the N—H stretches, it is not possible to determine from the ir spectra whether hydrogen bonds of different types are present.

Reaction of compound **1** with CCl_3COOH, $CHCl_2COOH$, $CH_2ClCOOH$, CBr_3COOH, CF_3COOH, and $(C_6H_5)COOH$ gave complexes **3**–**8** (see Table 1) as yellow powders. In all cases the methyl resonance at 1.80 ppm in the ^{1}H nmr spectrum disappeared. Except for the appearance of the peaks due to ClH_2C—, Cl_2HC—, C_6H_5— and slight shifts in the position of the N—*H* signal, the remainder of the ^{1}H nmr spectra of **3**–**8** is little changed from that of **1**. ^{1}H nmr and ir spectral data for these compounds are given in Table 1.

Compounds **3**–**8** were the products of simple metathetical reactions in which the acetate groups of compound **1** were replaced with other substituted acetate groups. Compounds **3**–**8** should also be attainable from the reaction of 3,5-dimethylpyrazole with the corresponding palladium(II) carboxylate. Reaction of 3,5-DMP with $Pd(O_2C(C_6H_5))_2$ and $Pd(O_2CCH_2Cl)_2$ gave orange oils as products which were not characterized further. When $Pd(O_2CCH_3)_2$ was reacted with pyrazole an insoluble white solid which analysed as $Pd_2C_{16}H_{20}N_8O_4$, $[(CH_3COO_2)(pzH)Pd(\mu\text{-pz})]_2$, **9**, where pz = pyrazole, was obtained. Reaction of $Pd(O_2CCH_3)_2$ with 3,5-diphenylpyrazole gave complex **2** as a yellow powder, structurally analogous to the product of the reaction with 3,5-dimethylpyrazole (see Fig. 1*b*).

The puckered boat form of the metallocycle ring is suggested as the sterically most favourable structure. Binuclear complexes containing coplanar pyrazolide rings have however been reported. The X-ray crystal structure of $[(\eta^5\text{-}C_5H_5)_2Ti(pz)_2]_2$, where pz = pyrazole, shows the compound to have two coplanar pyrazolide anions bridging the two titanium atoms. The four nitrogens from the pyrazolide groups and the titanium atoms form a six membered ring which is in a chair configuration, the metal atoms lying above and below the plane of the pyrazolide rings. The coplanarity of the pyrazolide groups is apparently enforced by the cyclopentadienyl rings which hinder tilting of the pyrazolide groups relative to their observed positions (8).

The metallocycle ring in these palladium complexes is stereochemically rigid. None of the compounds had temperature dependent ^{1}H nmr spectra. Consistent with a rigid boat conformation of the $Pd_2(\mu\text{-}C_5N_2H_7)_2$ ring, the complex $[Pd_2(\mu\text{-}3,5\text{-}dmp)_2Cl_2(PMe_2Ph)_2]$, where PMe_2Ph = dimethylphenylphosphine, exhibits diastereotopic phosphine methyl groups in its ^{1}H nmr spectrum which do not site exchange at temperatures as high as 190°C (9).

The absence of further polymerisation in these compounds (i.e. formation of complexes of the type $[Pd(pyrazole)_2]_n$) may be attributed to hydrogen bonding between N—H and O—$\overset{\overset{O}{\|}}{C}CH_{3-n}X_n$. Without "endcapping" groups on the metal, 1,2-dihapto-pyrazolides of transition metals usually form a polymeric chain (2).

Experimental

All compounds are air stable. Microanalyses were performed by Microanalyses Lab., Toronto and Canadian Microanalytical Service Ltd. Melting points were determined on a Kofler Hotstage and are uncorrected. 3,5-Dimethylpyrazole was purchased from Aldrich Chemical Co. 3,5-Diphenylpyrazole was prepared by a published method (10). Infrared spectra were obtained as KBr pellets using a Unicam SP 1025 Infrared Spectrophotometer. ^{1}H nmr spectra were recorded on a Varian T60 NMR spectrometer.

Method of Preparation

Bis(1,2-dihapto-3,5-dimethylpyrazolido)bis(acetato)bis(3,5-dimethylpyrazole)dipalladium(II), 1

To 0.84 g (3.74 mmol) palladium(II) acetate dissolved in dichloromethane was added 0.74 g (7.48 mmol) 3,5-dimethylpyrazole. The deep orange solution slowly became yellow. After stirring overnight the solution was diluted with hexane

TABLE 1. Physical and analytical data for compounds of structure

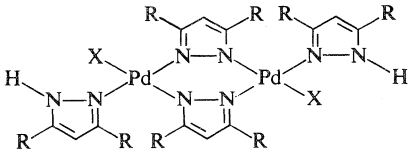

Compound	R	X	Appearance	Mp (°C)	Yield (%)	Infrared spectra[a] ν(C=O)	Infrared spectra[a] ν(C—O)
1	CH_3	CH_3COO	Yellow powder	222–223	70	1570–1630 (b)	1360–1470 (b)
2	C_6H_5	CH_3COO	Deep yellow powder	203–204	82	1575–1615 (b)	1380–1400 (b)
3	CH_3	CBr_3COO	Yellow powder	dec. 290	72	1670–1680	1320–1340
4	CH_3	CH_2ClCOO	Yellow powder	231–232	77	1600–1620 (b)	1370–1390 (b)
5	CH_3	$CHCl_2COO$	Yellow powder	214–215	70	1625–1675	1350–1475
6	CH_3	CCl_3COO	Yellow powder	dec. 288	60	1670–1700	1320–1340
7	CH_3	CF_3COO	Yellow plates	251–252	70	1670–1710	1410–1440
8	CH_3	$(C_6H_5)COO$	Yellow prisms	dec. 250	74	1600–1620	1360–1390 (b)
9	H	CH_3COO	White powder	dec. 279	63	1690–1720	1300
10	C_6H_5	CH_2ClCOO	Fine yellow orange needles	156–157	78	1570–1630 (b)	1350–1390

Compound	^{1}H nmr spectra[b] Methyl groups				Ring proton		N—H	Aromatic	X	Analysis C Calcd	C Found	H Calcd	H Found	N Calcd	N Found
1	1.90	2.25	2.35	2.70	5.45	5.75	13.70		1.80	40.41	40.69	5.09	4.98	15.71	15.61
2					6.15	6.40 (d)	13.85	6.90–8.10 (m)	2.10	63.53	63.32	4.33	4.48	9.26	9.27
3	1.90	2.35	2.45	2.80	5.55	5.85	12.91			24.29	24.40	2.55	2.50	9.44	9.26
4	1.85	2.25	2.35	2.75	5.50	5.85	13.30		3.90	36.85	36.80	4.38	4.28	14.32	13.97
5	1.75	2.15	2.30	2.65	5.40	5.75	12.97		5.75	33.87	33.90	3.79	4.01	13.16	12.88
6	1.85	2.25	2.40	2.70	5.50	5.80	12.85			31.33	31.19	3.29	3.16	12.18	12.09
7	1.90	2.25	2.35	2.70	5.60	5.85	12.70			35.10	35.24	3.68	3.67	13.64	13.67
8	1.90	2.35	2.45	2.85	5.40	5.75	13.90		7.15–7.40	48.76	48.18	4.81	4.81	13.38	13.40
9									7.80–7.90 (m)						
										31.97	31.93	3.35	2.94	18.64	15.59
10					6.10	6.15	13.20	6.80–7.50 8.00–8.10	4.10	60.11	55.36	3.94	3.76	8.76	7.63

[a]Obtained in KBr disks, frequencies given as cm^{-1}, b = broad.
[b]$CDCl_3$ solution; ppm (δ) units; all signals singlets unless otherwise indicated, d = doublet, m = multiplet. Integration supports the assignments given.

and evaporated until solid began to appear. A yellow powder was collected (0.94 g, 70% yield). The solid was reprecipitated from CH_2Cl_2/hexane.

Bis(1,2-dihapto-3,5-diphenylpyrazolido)bis(acetato)bis(3,5-diphenylpyrazole)dipalladium(II), **2**

Prepared as **1** using 3,5-diphenylpyrazole.

Bis(1,2-dihapto-3,5-dimethylpyrazolido)bis(tribromoacetato)bis(3,5-dimethylpyrazole)dipalladium(II), **3**

To 0.17 g (0.24 mmol), **1**, dissolved in dichloromethane was added 0.15 g (0.51 mmol) tribromoacetic acid. After stirring overnight, the solution was diluted with hexane and evaporated until solid began to appear. A yellow powder was collected (0.22 g, 72% yield). The powder was reprecipitated from CH_2Cl_2/hexane.

Compounds **4**–**10** were prepared following the same procedure as that for compounds **1** and **3** using the corresponding pyrazole and carboxylic acid.

Acknowledgement

The financial support of the National Research Council of Canada is gratefully acknowledged.

1. E. L. MUETTERTIES. Bull. Soc. Chim. Belg. **84**, 959 (1975).
2. S. TROFIMENKO. Inorg. Chem. **10**, 1372 (1971) and references therein.
3. S. TROFIMENKO. Chem. Rev. **72**, 497 (1972).
4. F. COLETTA, R. ETTORRE, and A. GAMBARO. J. Inorg. Nucl. Chem. **37**, 314 (1975).
5. G. MINGHETTI, G. BANDITELLI, and F. BONATI. Inorg. Chem. **18**, 658 (1979).
6. R. J. ABRAHAM and H. J. BERNSTEIN. Can. J. Chem. **39**, 905 (1961).
7. K. NAKAMOTO. Infrared and Raman spectra of inorganic and coordination compounds. 3rd ed. Wiley-Interscience, New York. 1977.
8. B. F. FIESELMANN and G. D. STUCKY. Inorg. Chem. **17**, 2074 (1978).
9. T. R. JACK. Ph.D. Thesis, University of Toronto, Toronto, Ont. 1974.
10. J. WISLICENUS. Justus Liebigs Ann. Chem. **308**, 219 (1899).

The photoinitiated isomerization and addition reactions of liquid 2-butenes in the presence of hydrogen sulfide

FRANÇOIS-XAVIER GARNEAU AND IRENEUSZ SZCZEREK

Université du Québec à Chicoutimi, Département des Sciences Pures, Chicoutimi (Qué.), Canada G7H 2B1

Received November 28, 1978[1]

FRANÇOIS-XAVIER GARNEAU and IRENEUSZ SZCZEREK. Can. J. Chem. **57**, 2991 (1979).

The near ultraviolet photolysis ($\lambda > 280$ nm) of liquid *cis*-2-butene in the presence of hydrogen sulfide was shown to result in isomerization and addition reactions. The former was monitored by the formation of *trans*-2-butene as a function of time and hydrogen sulfide concentration. The latter was observed by the presence of *s*-butyl mercaptan and di-*s*-butyl sulfide as products. The total amount of addition products as well as the relative amounts of mercaptan and sulfide were determined as a function of time. Using the foregoing information the extent of the isomerization reaction was shown to be greater than that of the addition reaction during the course of the irradiation at a concentration ratio of H_2S/*cis*-2-butene equal to 0.15.

It was also shown that hydrogen sulfide was a more effective sensitizer than *s*-butyl mercaptan and di-*s*-butyl sulfide but less effective than di-*s*-butyl disulfide in the isomerization of liquid *cis*-2-butene. The extent of isomerization and addition reactions were shown to be greater starting with *cis*-2-butene than with *trans*-2-butene in the presence of hydrogen sulfide.

FRANÇOIS-XAVIER GARNEAU et IRENEUSZ SZCZEREK. Can. J. Chem. **57**, 2991 (1979).

Des réactions d'isomérisation et d'addition ont été observées lors de la photolyse dans le proche uv ($\lambda > 280$ nm) du *cis*-butène-2 avec le sulfure d'hydrogène en phase liquide. L'isomérisation a été suivie par la formation du *trans*-butène-2 en fonction du temps et de la concentration du sulfure d'hydrogène. La formation du mercaptan de butyl-secondaire et du sulfure de di-butyl-secondaire comme produits témoigne d'une réaction d'addition. Les quantités totales des produits d'addition ainsi que leur quantité relative ont été mesurées en fonction du temps. A l'aide de ces données, nous avons montré que l'étendue de la réaction d'isomérisation est plus importante que celle de la réaction d'addition au cours de la photolyse avec un rapport de concentration H_2S/*cis*-butène-2 égal à 0.15.

En outre, le sulfure d'hydrogène s'est avéré un sensibilisateur plus efficace que le mercaptan de butyl-secondaire et le sulfure de di-butyl-secondaire mais moins efficace que le disulfure du dibutyl-secondaire dans l'isomérisation du *cis*-butène-2 liquide. Les réactions d'isomérisation et d'addition sont plus rapides en partant avec le *cis*-butène-2 que le *trans*-butène-2 en présence du sulfure d'hydrogène.

Introduction

The photoinitiated reactions of sulfur compounds with olefins has been the subject of a large number of studies (1). Initially most of the work reported was concerned with the addition reactions of sulfur compounds such as hydrogen sulfide, mercaptans, and disulfides with olefins (2). In these cases fairly high concentrations of the sulfur compounds were used. Subsequently, it was observed that an important isomerization reaction occurred with olefins whose structures permitted the existence of *cis* and *trans* isomers (3). The abstraction of hydrogen atoms by thiyl radicals has also been reported (4).

Collin *et al.* have shown that hydrogen sulfide and mercaptans are indeed very effective sensitizers of isomerization (no addition products were detected) in the far uv gas phase photolysis (5) and, when in low concentrations of hydrogen sulfide, in the liquid phase radiolysis and photolysis of *cis*- and *trans*-2-butene (6). In this paper we report the details of our study on the near uv ($\lambda > 280$ nm) liquid phase photolysis of *cis*- and *trans*-2-butene in the presence of low concentrations of hydrogen sulfide and to a comparison of the extent of isomerization and addition reactions.

Experimental

Chemicals

cis-2-Butene (99.5%), *trans*-2-butene (99.0%), hydrogen sulfide (99.5%), and isobutylene (99.8%) (Matheson of Canada Ltd.) were used as received after being degassed. *cis*-2-Butene contained *trans*-2-butene (0.50%) and 1,3-butadiene ($\simeq$ 110 ppm). *trans*-2-Butene contained *cis*-2-butene (0.35%) and 1,3-butadiene ($\simeq$ 210 ppm). *s*-Butyl mercaptan (bp 84–85°C), di-*s*-butyl sulfide (bp 160–162°C), and di-*s*-butyl disulfide (bp 92–94°C/8 mm) were prepared using the methods described by Vogel (7). Trichloroacetyl isocyanate (Eastman Kodak) was used as received.

Apparatus

The light source was a Hanovia 450 W high pressure mercury-vapor lamp. The samples were prepared in a Pyrex tube fitted with a high-vacuum stopcock using a mechanical – oil

[1]Revision received July 31, 1979.

0008-4042/79/222991-05$01.00/0

diffusion pump system with Teflon stopcocks which was capable of maintaining a vacuum of about 10^{-5} mm mercury. Pressure measurements were made using a metallic membrane manometer (Wallace and Tiernan). The gaseous samples were liquified in the tube using liquid nitrogen. The liquid occupied from 50–75% of the volume of the tube. Only the liquid phase was irradiated.

The irradiations were carried out at room temperature (20°C). Based on the number of moles of *cis*-2-butene and hydrogen sulfide introduced into the tube, the volumes of the liquid and gas phases, and the total pressure of the mixture measured at 20°C, the quantity of hydrogen sulfide in the liquid phase is estimated to be equal to or slightly greater than 90% of the amount added to the tube.

Analysis

The isomerization of *cis*- and *trans*-2-butene was followed by gas chromatography using a 1.5 m × 2.3 mm id *n*-octane/Porasil C "Durapak" column and a hydrogen flame ionization detector.

The presence of hydrogen sulfide after photolysis was detected by the formation of a black precipitate (PbS) with lead acetate and by the formation of sulfur on reaction with a solution of iodine and potassium iodide.

The extent of the addition reaction in the *cis*- and *trans*-2-butenes with hydrogen sulfide system was followed by the disappearance of the hydrogen sulfide. The latter was determined by cooling the reaction mixture in an icebath and allowing the hydrogen sulfide and the 2-butene to pass into a standard acidified iodine – potassium iodide solution (the 2-butene did not react with the KI_3 solution under our conditions). The excess iodine was then titrated with a standard sodium thiosulfate solution.

The two addition products were obtained on evaporation of the gaseous butenes and hydrogen sulfide and were separated from each other by treatment with aqueous sodium hydroxide followed by extraction. They were purified by fractional distillation and were identified by comparison with authentic materials. The structure of the mercaptan was confirmed by the technique of Butler and Mueller (8). A very small amount (~ 0.01% of the addition product mixture) of another substance was detected by gas chromatography and its retention time corresponded to that of di-*s*-butyl disulfide, a possible product in our reaction system.

The variations in the relative amounts of the mercaptan and sulfide formed on irradiation were followed by gas chromatography using 2 m silicone gum 10% UC-W98 column and a hydrogen flame ionization detector.

Results and Discussion

An examination of the reaction mixture resulting from the liquid-phase photolysis ($\lambda > 280$ nm) of *cis*-2-butene and 15% hydrogen sulfide showed the presence of *cis*- and *trans*-2-butenes, *s*-butyl mercaptan, di-*s*-butyl sulfide, and unreacted hydrogen sulfide.

Isomerization Reaction

The isomerization of *cis*-2-butene in the presence of hydrogen sulfide was followed by the variation of the *trans*/(*cis* + *trans*) ratio as a function of time (Fig. 1). The isomerization to *trans*-2-butene occurred rapidly in the initial stages of the photolysis but then decreased in rate as an equilibrium mixture of ca.

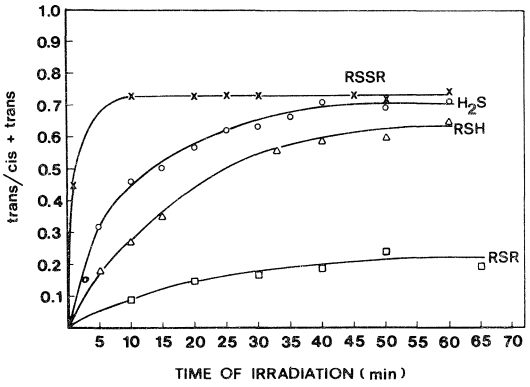

FIG. 1. Photolysis of *cis*-2-butene in the presence of 15% of various sulfur compounds: ×, di-*s*-butyl disulfide; ○, hydrogen sulfide; △, *s*-butyl mercaptan; □, di-*s*-butyl sulfide. The variation of the *trans*/(*cis* + *trans*) ratio vs. the irradiation time. R = *s*-butyl.

70% *trans* and 30% *cis* was approached. An increase in the relative concentration of hydrogen sulfide to *cis*-2-butene was observed to lead to a corresponding increase in the amount of *trans*-2-butene formed (Fig. 2). A concentration ratio of $H_2S/cis\text{-}C_4H_8$ of 0.35 led to the equilibrium mixture in 15 min of irradiation compared to about 40 min with a 0.15 concentration ratio (Fig. 1). That the equilibrium state is reached more rapidly at higher hydrogen sulfide concentrations is clearly shown in Fig. 3 and would be due to an increase of absorption of light by hydrogen sulfide. It is unlikely that the isomerization is due to a photosensitization by the triplet state of hydrogen sulfide for the following reasons: (*1*) hydrogen sulfide is not known to be a good triplet sensitizer of the isomerization *cis–trans* of 2-butenes, (*2*) a mechanism via the triplet state should lead to a photostationary ratio close to 1.0 based on the trends observed in previous studies and the triplet energy of hydrogen sulfide, E_t = 133 kcal/mol (10,

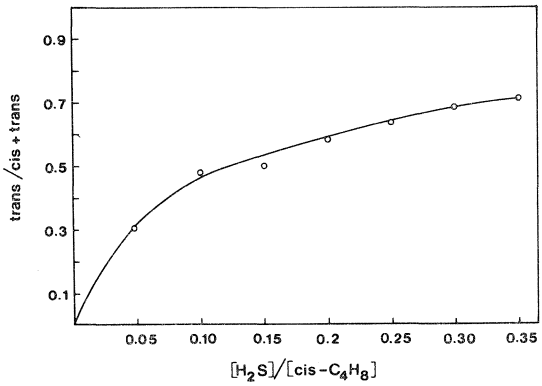

FIG. 2. Photolysis of *cis*-2-butene in the presence of hydrogen sulfide. The variation of the *trans*/(*cis* + *trans*) ratio vs. hydrogen sulfide concentration. Irradiation time 15 min.

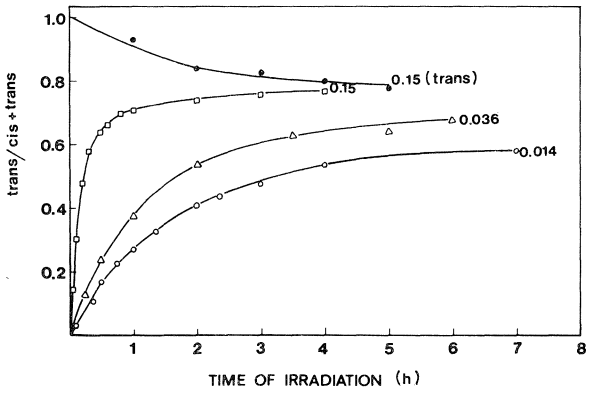

FIG. 3. Photolysis of *cis*- and *trans*-2-butene in the presence of hydrogen sulfide. The variation of the *trans*/(*cis* + *trans*) ratio vs. irradiation time at one concentration ratio (0.15) of hydrogen sulfide (●) in the *trans*-2-butene system and at three concentration ratios of hydrogen sulfide in the *cis*-2-butene system: □, 0.15; △, 0.036; ○, 0.014.

11), and (*3*) even though no actinometry was carried out, the large amount of *trans* isomer formed in our system is indicative of a high quantum yield (> 10) as would be the case in a chain process but would not be the case in a process involving triplet sensitization.

Addition Reaction

The isomerization reaction was accompanied by an addition reaction as shown by the formation of *s*-butyl mercaptan and di-*s*-butyl sulfide as the main products. These two compounds are presumably formed by the addition via thiyl radicals of hydrogen sulfide and mercaptan respectively to the 2-butenes. The extent of the addition reaction was determined by following the disappearance of hydrogen sulfide as a function of time (Fig. 4). As in the isomerization reaction, the addition occurred rapidly in the early stages of the photolysis and then tapered off on continued irradiation and in the presence of decreasing quantities of hydrogen sulfide. After 2 h of irradiation, about 87% of the hydrogen sulfide had disappeared from the reaction system.

The relative quantities of the two main addition products were determined as a function of the time of irradiation for the reaction systems hydrogen sulfide + *cis*-2-butene and *s*-butyl mercaptan + *cis*-2-butene (Fig. 5). The levelling off of the ratio RSH/(RSH + RSR) with increasing time of irradiation indicates that the mercaptan (RSH) can arise at least in part by a secondary pathway. At least two explanations may be suggested for the initial decrease of the *s*-butyl mercaptan (RSH): on the one hand it may absorb the light and decompose to RS + H or R + SH (1), and in addition it may participate in a (some) reaction(s) of the type

[1] $R + RSH \rightarrow RH + RS$

It should be noted that the lower curve (RSH + *cis*-2-butene system) represents experiments where the mercaptan was added to the butene. Thus this lower curve shows its subsequent transformation to sulfide. The upper curve corresponds to experiments where hydrogen sulfide was the added sulfur compound. In this case RSH the mercaptan is a product.

The Radical Nature of the Reactions

The radical nature of the isomerization and addition reactions was shown in the following manner:

(*1*) The absence of isomerization and addition products when a small amount of oxygen, a well-known radical scavenger, was introduced.

(*2*) The increase in the rate of isomerization on addition of acetone (H_2S/acetone: 1/1). After 5 min irradiation, the *trans*/(*cis* + *trans*) ratio was 0.63 and

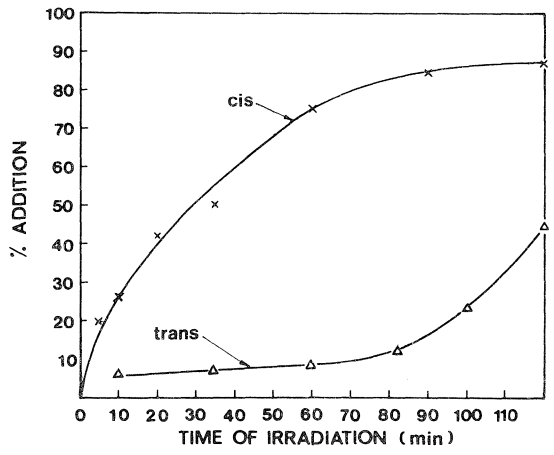

FIG. 4. Photolysis of *cis*- and *trans*-2-butene in the presence of 15% hydrogen sulfide. The variation of the % addition reaction (% hydrogen sulfide reacted) vs. the irradiation time (min).

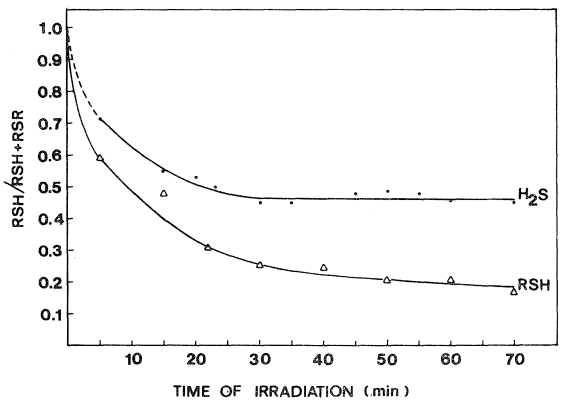

FIG. 5. Photolysis of *cis*-2-butene in the presence of 15% hydrogen sulfide (●) and 15% *s*-butyl mercaptan (△). The variation of the mercaptan/(mercaptan + sulfide) ratio vs. the irradiation time (min). R = *s*-butyl.

TABLE 1. A comparison of the photoinitiated isomerization and addition reactions of hydrogen sulfide with *cis*-2-butene in the liquid phase[a]

Irradiation time (min)	Amount of H_2S reacted (mmol)	% of *trans*-2-butene formed	RSH[b] / RSH + RSR	Amount of butenes remaining (mmol)	Amount of *trans*-2-butene (mmol)	Isomerization / Addition
5	0.20	32	0.70	6.40	2.05	10.25
10	0.26	46	0.64	6.30	2.90	11.15
20	0.42	57	0.50	6.03	3.44	8.19
35	0.51	66	0.45	5.87	3.87	7.59
60	0.75	71	0.45	5.50	3.91	5.21

[a]1 mmol of hydrogen sulfide and 6.66 mmol of *cis*-2-butene.
[b]R = *s*-butyl.

the equilibrium value was reached after 10 min as compared to 40 min in the absence of acetone. This can be explained by the more efficient production of HS radicals due to the greater absorption coefficient of acetone which leads to an increase in the formation of methyl radicals in the following manner:

[2] $CH_3COCH_3 + h\nu \rightarrow CH_3CO + CH_3$

[3] $CH_3 + H_2S \rightarrow CH_4 + HS$

The photostationary ratio of 2.3 observed in our system would militate against acetone triplet sensitization as the only mechanism of isomerization although its partial involvement cannot be excluded (12).

(*3*) The formation of isobutylsulfide (identified by its nmr spectrum) as the only addition product in the photolysis of liquid isobutylene in the presence of hydrogen sulfide under the same conditions. An ionic mechanism would have resulted in the formation of *tert*-butylsulfide, the Markownikoff addition product (1, 2).

Influence of Additives

As the addition products were formed during the course of the isomerization reaction, the influence of the former on the latter was compared to the reaction with hydrogen sulfide (Fig. 1). As expected, considering the dissociation energies of the bonds involved and the absorption coefficients of the compounds (9), the disulfide proved to be the most effective sensitizer for the isomerization reaction under our conditions. *s*-Butyl mercaptan was slightly less effective than H_2S and the sulfide was the poorest sensitizer of the compounds studied.

Comparison of Isomerization and Addition Reactions

The extent of isomerization was compared to that of addition in the reaction system *cis*-2-butene and hydrogen sulfide (Table 1). The extent of the isomerization reaction is slightly more than ten times that of the addition reaction in the early stages of the photolysis and then decreases as the equilibrium mixture of *cis* and *trans* is reached.

Photolysis of trans-*2-Butene*

The isomerization and addition reactions of *trans*-2-butene with hydrogen sulfide were examined as a function of time (Figs. 3 and 4). As in the case of the radiolysis of liquid *trans*-2-butene (6), isomerization occurred at a slower rate than that of *cis*-2-butene. A similar situation was observed in the case of the addition reaction (Fig. 4).

The presence of a larger quantity of 1,3-butadiene as an impurity in the *trans* as compared to the *cis* does not appear to explain the difference in the rate of isomerization as the introduction of maleic anhydride, an often used dienophile in Diels–Alder reactions, to the *trans* + hydrogen sulfide system did not have any significant effect. The rate is either influenced by the rotation barrier of the intermediate formed by the addition of the HS radical to the 2-butene (13) or the limiting step is rather the addition itself of the thiyl radical to the 2-butene (5).

In regard to the addition reaction of *trans*-2-butene with hydrogen sulfide (Fig. 4), an essentially stationary situation was observed to prevail for approximately 1 h after the initial 10 min of irradiation followed by a gradual increase in the extent of addition.

Acknowledgements

We wish to thank the Université du Québec à Chicoutimi and the National Research Council of Canada for financial support. We also thank Professor G. J. Collin for helpful discussions and Jean-Luc Simard for technical assistance.

1. K. GRIESBAUM. Angew. Chem. Int. Ed. **9**. 273 (1970) and references therein.
2. F. W. STACEY and J. F. HARRIS, JR. Org. React. **13**, 165 (1963).
3. C. WALLING and W. HELMREICH. J. Am. Chem. Soc. **81**, 1144 (1959).
4. (*a*) C. SIVERTZ, W. ANDREWS, W. ELSDON, and K. GRAHAM. J. Polym. Sci. **19**, 587 (1956); (*b*) W. A. PRYOR, G. GOJON, and J. P. STANLEY. J. Am. Chem. Soc. **95**, 945 (1973).

5. G. J. COLLIN and P. M. PERRIN. Can. J. Chem. **50**, 2400 (1972).
6. G. J. COLLIN, P. M. PERRIN, and F.-X. GARNEAU. Can. J. Chem. **52**, 2337 (1974).
7. A. I. VOGEL. A textbook of practical organic chemistry. Longmans, Green and Co., London. 1961. pp. 497, 498.
8. P. E. BUTLER and W. H. MUELLER. Anal. Chem. **38**, 1407 (1966).
9. J. G. CALVERT and J. N. PITTS, JR. Photochemistry. John Wiley and Sons, New York. 1967. pp. 489, 490.
10. J. SLATIEL, J. D'AGOSTINO, E. D. MEGARITY, L. METTO, K. R. NEUBERGER, M. WRIGHTON, and O. C. ZAFIRON. Org. Photochem. **3**, 1 (1973) and references therein.
11. A. KUPPERMAN, W. M. FLICKER, and O. A. MOSHER. Chem. Rev. **79**, 77 (1979).
12. J. SALTIEL, K. R. NEUBERGER, and M. WRIGHTON. J. Am. Chem. Soc. **91**, 3658 (1969).
13. K. SUGIMOTO, W. ANDO, and S. OAE. Bull. Chem. Soc. Jpn. **38**, 224 (1965).

Acid catalysis in the gas phase: dissociative proton transfer to formate and acetate esters

A. C. HOPKINSON, G. I. MACKAY, AND D. K. BOHME

Department of Chemistry, York University, Downsview, Ont., Canada M3J 1P3

Received March 16, 1979

A. C. HOPKINSON, G. I. MACKAY, and D. K. BOHME. Can. J. Chem. **57**, 2996 (1979).

The flowing afterglow and selected ion flow tube techniques are employed in gas-phase measurements of the intrinsic kinetics of protonation of methyl formate, *n*-propyl formate, ethyl acetate, and *n*-propyl acetate and subsequent fragmentation according to

$$AH^+ + RCOOR' \rightarrow RCOO(R')H^+ + A \begin{cases} \rightarrow RCO^+ + R'OH \\ \rightarrow RCOOH + R'^+ \end{cases}$$

with R = H and CH_3, R′ = CH_3, C_2H_5, and $(CH_2)_2CH_3$, and A = H_2, CH_4, CO, and H_2O. Protonation by the acids, AH^+, with relative strengths spanning a range of 65 kcal mol^{-1}, is observed to proceed extremely rapidly with rate constants at 299 ± 2 K encompassing values of 2.9 to 8.5 × 10^{-9} cm^3 $molecule^{-1}$ s^{-1}. Fragmentation is observed for $HCOOCH_3$ only with the strongest acid, H_3^+, to produce $CH_3OH_2^+$. For $HCOO(CH_2)_2CH_3$, fragmentation is observed to produce $C_3H_7^+$ with H_3O^+, and also $HCOOH_2^+$ with H_3^+. Little fragmentation of $CH_3COOC_2H_5$ occurs with H_3O^+ but with H_3^+ the major product is $CH_3COOH_2^+$ with smaller amounts of CH_3CO^+ and $C_2H_5^+$. Proton transfer from H_3O^+ to $CH_3COO(CH_2)_2CH_3$ results in considerable dissociation to form $CH_3COOH_2^+$. The fragmentation of these esters is discussed in terms of known reaction energetics and in terms of mechanisms for unimolecular acyl–oxygen, $A_{Ac}1$, and alkyl–oxygen, $A_{Al}1$, fission often invoked for analogous reactions in solution as well as modifications of these mechanisms which have been proposed in the context of recent gas-phase measurements.

A. C. HOPKINSON, G. I. MACKAY et D. K. BOHME. Can. J. Chem. **57**, 2996 (1979).

On a utilisé les techniques de la lueur d'écoulement et du tube à écoulement d'ions pour mesurer en phase gazeuse, la cinétique intrinsèque de la protonation des formates de méthyle et de *n*-propyle des acétates d'éthyle et de *n*-propyle suivi d'une fragmentation se produisant d'après le schéma suivant:

$$AH^+ + RCOOR' \rightarrow RCOO(R')H^+ + A \begin{cases} \rightarrow RCO^+ + R'OH \\ \rightarrow RCOOH + R'^+ \end{cases}$$

dans lequel R = H et CH_3, R′ = CH_3, C_2H_5 et $(CH_2)_2CH_3$, et A = H_2, CH_4, CO et H_2O. On a observé que la protonation par les acides AH^+ ayant une force relative s'étendant sur une échelle de 65 kcal mol^{-1} est extrêmement rapide avec une constante de vitesse à 299 ± 2 K qui englobe des valeurs allant de 2.9 à 8.5 × 10^{-9} cm^3 $molécule^{-1}$ s^{-1}. On observe la fragmentation du CH_3COOH qu'en présence de l'acide le plus fort, H_3^+, et il se produit des $CH_3OH_2^+$. La fragmentation $CH_3(CH_2)_2COOH$ produit du $C_3H_7^+$ lors de la protonation par H_3O^+ et également du $HCOOH_2$ lors de la protonation par H_3^+. Il ne se produit que peu de fragmentation du $CH_3COOC_2H_5$ si on utilise H_3O^+ toutefois avec H_3^+ le produit principal est $CH_3COOH_2^+$ avec des quantités plus faibles de CH_3CO^+ et de $C_2H_5^+$. Le transfert de proton de H_3O^+ à $CH_3(CH_2)_2COOH$ conduit à une dissociation considérable provoquant la formation de $CH_3COOH_2^+$. On discute de la fragmentation de ces esters en termes des énergies connues des réactions et en termes des mécanismes unimoléculaires de fission oxygène–acyle, $A_{Ac}1$, et oxygène–alkyle $A_{Al}1$ auxquels on fait souvent appel pour les réactions analogues en solutions ainsi qu'à des modifications de mécanismes qui ont été proposés dans le contexte de mesures récentes en phase gazeuse.

[Traduit par le journal]

Introduction

We have recently initiated an experimental program designed to explore, in a systematic manner, the kinetics of the gas-phase fragmentation of protonated molecules, BH^+, which have been activated by proton-transfer reactions of the type

[1] $AH^+ + B \rightarrow [BH^+]^* + A$

The flowing afterglow technique employed in these investigations allows the deliberate alteration of the identity of AH^+ and thus the overall exothermicity of this process (1). The ensuing fragmentation

[1*a*] $[BH^+]^* \rightarrow$ products

may thus be followed as a function of the degree of chemical activation of BH^+, at least to the extent to

0008-4042/79/222996-09$01.00/0

which changes in overall exothermicity alter the excess energy deposited in this ion.[1] In an earlier study (3*a*) we reported the intrinsic kinetics of the protonation of formic and acetic acid and the ensuing formation of acylium ions according to dissociative proton transfer of the type

[2] $AH^+ + RCOOH \rightarrow [RCOOH_2^+]^* + A$

[2*a*] $[RCOOH_2^+]^* \rightarrow RCO^+ + H_2O$

with R = H, CH_3, and acids AH^+ whose relative strengths spanned a range of 65 kcal mol^{-1}. These carboxylic acids are members of a larger group of molecules of the type

[3] 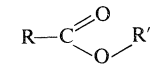

which, when protonated, may undergo heterolysis in one of two ways commonly invoked to explain their cleavage in concentrated acid solutions (4–6): unimolecular acyl–oxygen fission, $A_{Ac}1$, according to

[4] 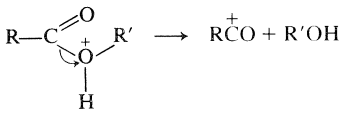

or unimolecular alkyl–oxygen fission, $A_{Al}1$, according to

[5] 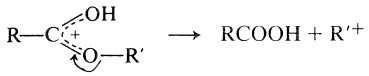

The preferred route of cleavage in solution appears to be sensitive to the nature of R′. In concentrated acid solution the esters of secondary and tertiary alcohols hydrolyse by the $A_{Al}1$ mechanism producing a carboxylic acid and a secondary or tertiary carbonium ion. Esters of primary alcohols would produce the much less stable primary carbonium ions by this mechanism, and consequently cleave by the $A_{Ac}1$ mechanism, except when the carbonium ion is stabilized by an adjacent electron-donating group (e.g. phenyl or methoxy).

The products of both A1 mechanisms have been observed in the gas phase (7, 8). The $A_{Al}1$ mechanism, although the less common in solution reactions, appears to predominate in the gas phase. Two possible explanations of this change in behaviour are (*i*) the $A_{Ac}1$ mechanism requires the energetically less accessible ether-protonated ester as an intermediate (9, 10) and thus, in the absence of solvent, is difficult to obtain or (*ii*) that in the gas phase the internally assisted $A_{Al}1$ mechanism,

[1]For a flowing afterglow study of the fragmentation of $CH_3NO_2H^+$, see ref. 2.

[6] 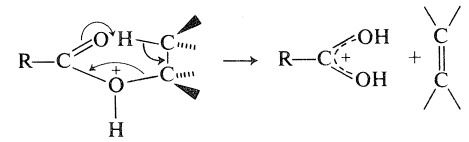

employing a six membered cyclic transition state (reaction [6]) established experimentally (7) by use of deuterium on the β-carbon of the ether group, does not require formation of the unstable primary carbonium ion.

The previous gas phase studies (7, 8) have employed protonated hydrocarbons as the acid (CH_5^+, $C_2H_5^+$, t-$C_4H_9^+$) to initiate the dissociative proton transfer of esters. Here we have used the acids $AH^+ = H_3^+$, CH_5^+, HCO^+, and H_3O^+ which have exothermicities varying over a much wider range (65 kcal mol^{-1}) and we have studied, under the more controlled conditions of the flowing afterglow apparatus, the dissociation mechanisms ([7*a*] and [7*b*])

[7] $AH^+ + RCOOR' \rightarrow [RCOOR'H^+]^* + A$

[7*a*] $[RCOOR'H^+]^* \rightarrow RCOOH + R'^+$

[7*b*] $[RCOOR'H^+]^* \rightarrow RCO^+ + R'OH$

of some formate and acetate esters as a function of the excess energy provided in the proton transfer reaction.

Experimental

The majority of the measurements were carried out in a hydrogen buffer using a conventional flowing plasma mass-spectrometer (flowing afterglow) system which has been described previously (1). A few of the measurements were carried out in a helium buffer with the apparatus in the Selected Ion Flow Tube (SIFT) configuration modelled after the original design reported by Adams and Smith (11). In this configuration a differentially pumped quadrupole mass filter was interposed between the ion production and reaction regions. Ions were extracted from the ion production region through a 1 mm diameter orifice into the quadrupole mass filter which communicated with the flow tube through a 5 mm diameter gas entrainment orifice. The ions were injected into the flow tube at ca. 40 eV and allowed to thermalize by collision at 299 ± 2 K before they entered the reaction region 106 cm further downstream. This procedure eliminated ion types other than the reagent ion and the neutral reagent and buffer gas molecules from the reaction region.

The ions were produced in hydrogen carrier gas in the usual manner according to reactions of the type

[8] $H_3^+ + X \rightarrow XH^+ + H_2$

with k = (2.4 ± 0.5), (2.0 ± 0.4), and (4.3 ± 1.1) × 10^{-9} cm^3 $molecule^{-1}$ s^{-1} for X = CH_4, CO, and H_2O, respectively (unpublished results from this laboratory, refs. 13, 14). We have shown elsewhere that the protonation of CO accomplished in this manner establishes the HCO^+ and not the COH^+ isomer (13).

TABLE 1. Rate constants for proton transfer to methyl- and *n*-propyl formate and ethyl and *n*-propyl acetate at 299 ± 2 K

Reaction	k^a	$k_{ADO}{}^b$	$\Delta H_{298}{}^{0c}$
$H_3O^+ + HCOOCH_3 \rightarrow HCOO(CH_3)H^+ + H_2O$	3.3±0.8 (3)	2.27	−22±5
$HCO^+ + HCOOCH_3 \rightarrow HCOO(CH_3)H^+ + CO$	2.9±0.7 (8)	1.95	−45±3
$CH_5^+ + HCOOCH_3 \rightarrow HCOO(CH_3)H^+ + CH_4$	4.1±1.0 (2)	2.37	−57±3
$H_3^+ + HCOOCH_3 \rightarrow HCOO(CH_3)H^+ + H_2$	7.3±2.2 (3)	5.11	−87±3
$\rightarrow CH_3OH_2^+ + CO$			+15±5
$H_3O^+ + HCOO(CH_2)_2CH_3 \rightarrow HCOO((CH_2)_2CH_3)H^+ + H_2O$	4.6±1.4 (2)	2.48	−26±5
$\rightarrow i\text{-}C_3H_7^+ + HCOOH$			+20±5
$H_3^+ + HCOO(CH_2)_2CH_3 \rightarrow HCOO((CH_2)_2CH_3)H^+ + H_2$	8.5±2.6 (2)	5.77	−91±3
$\rightarrow i\text{-}C_3H_7^+ + HCOOH$			+20±5
$\rightarrow HCOOH_2^+ + C_3H_6$			+22±6
$H_3O^+ + CH_3COOC_2H_5 \rightarrow CH_3COO(C_2H_5)H^+ + H_2O$	2.8±0.7 (3)	2.62	−29±4
$\rightarrow CH_3COOH_2^+ + C_2H_4$			+23±4
$H_3^+ + CH_3COOC_2H_5 \rightarrow CH_3COO(C_2H_5)H^+ + H_2$	5.7±1.4 (4)	6.09	−94±3
$\rightarrow CH_3COOH_2^+ + C_2H_4$			+23±4
$\rightarrow CH_3CO^+ + C_2H_5OH$			+44±2
$\rightarrow C_2H_5^+ + CH_3COOH$			+52±5
$H_3O^+ + CH_3COO(CH_2)_2CH_3 \rightarrow CH_3COO((CH_2)_2CH_3)H^+ + H_2O$	3.8±1.0 (3)	2.85	−32±4
$\rightarrow CH_3COOH_2^+ + C_3H_6$			+25±4

[a]The measured reaction rate constant, k, is given in units of 10^{-9} cm^3 molecule^{-1} s^{-1} along with its estimated accuracy and the number of measurements which is given in parentheses.

[b]The collision rate constant in units of 10^{-9} cm^3 molecule^{-1} s^{-1} calculated using the average-dipole-orientation theory (the $\overline{\cos\theta}$ model) (ref. 16). Permanent dipole moments were taken from ref. 12*a*. Mean polarizabilities of 5.90 Å^3 for $HCOOCH_3$, 8.50 Å^3 for $HCOO(CH_2)_2CH_3$ and $CH_3COOC_2H_5$, and 11.7 Å^3 for $CH_3COO(CH_2)_2CH_3$ were calculated from bond and group polarizabilities taken from ref. 12*b*.

[c]Standard enthalpy change in kcal mol^{-1}, PA(H_2, CH_4, CO, H_2O) = 101 ± 1, 131.5 ± 2.2, 143 ± 1, and 166.4 ± 2.4 kcal mol^{-1}, respectively (ref. 13). PA($HCOOCH_3$, $HCOO(CH_2)_2CH_3$, $CH_3COOC_2H_5$, $CH_3COO(CH_2)_2CH_3$) = 187.8 ± 2, 191.6 ± 2, 195.4 ± 2, and 198 ± 2 kcal mol^{-1} taken from ref. 18*a*. Auxiliary thermodynamic data were taken from ref. 18*b*.

The formates were added into the reaction region as vapors diluted to ca. 10% in helium. The determination of their flows required separate viscosity measurements (15). Reagent and product ions were monitored as a function of addition of the vapor in the range from 5×10^{-5} to 5×10^{-3} mTorr, at total gas pressures, P, between 0.196 and 0.50 Torr, average gas velocities, $\bar{v}$, in the range 7.6 to 8.6×10^3 cm s^{-1}, effective reaction lengths, L, of 48, 59, and 85 cm, and a gas temperature, T, of 299 ± 2 K. Rate constants were determined in the usual manner (1). Branching ratios were obtained by computer fitting and inspection of observed variation in the reactant and product ion signals. This analysis (15) required a knowledge of the mass discrimination, m, between the various ion signals. When a reaction resulted in more than one product ion, m had to be inferred from complementary studies performed under similar experimental conditions. The majority of the uncertainty in the branching ratios (±20%) arose from the error associated with this method of determining the mass discrimination.

The gases used were hydrogen (Linde, Very Dry Grade, 99.95% H_2), methane (Matheson, Ultra High Purity, 99.9% CH_4), helium (Linde, Prepurified Grade, 99.995% He), and carbon monoxide (Matheson, C.P. Grade, 99.5% CO). The vapors were derived from methyl formate and methyl acetate (both from BDH Chemicals), and *n*-propyl formate and *n*-propyl acetate (both from Chem. Service Media). The purities of the esters were checked by conventional gas chromatograph – mass spectrometer assays and, when necessary, redistilled before use.

Results and Discussion

Kinetics of Proton Transfer and Product Distributions

The rate constants measured in this study are listed in Table 1. All of these reactions were observed to be rapid with the rate constant, k, spanning a range in values from 2.8 to 8.5×10^{-9} cm^3 molecule^{-1} s^{-1}. As has been our previous experience with other similar systems, these values are systematically higher by ~50% than the values of the collision rate constants derived from the average-dipole-orientation theory (16) (these are included in Table 1). The implications of such deviations have been discussed elsewhere (16, 17).

For the reactions of H_3O^+, HCO^+, and CH_5^+ with methyl formate only one product ion (m/e = 61) was observed. This ion was identified as protonated methyl formate. There was no measurable evidence for subsequent dissociation. In contrast, the reaction of H_3^+ with methyl formate was observed to produce

predominantly (>90%) $CH_3OH_2^+$ which reacted further by proton transfer to establish $HCOO(CH_3)H^+$ according to the reaction

[9] $CH_3OH_2^+ + HCOOCH_3 \rightarrow HCOO(CH_3)H^+ + CH_3OH$

Figures 1 and 2 provide an indication of the results obtained with *n*-propyl formate. H_3O^+ reacted to produce considerable (~50%) amounts of $C_3H_7^+$ and a small amount (~5%) of $HCOOH_2^+$. Both product ions reacted further with *n*-propyl formate by proton transfer to produce $HCOO((CH_2)_2CH_3)H^+$ in addition to that amount which is produced directly by protonation with H_3O^+. Figure 2 shows that both dissociative channels increased in importance with H_3^+ as the reactant ion, the $C_3H_7^+$ and $HCOOH_2^+$ ions being produced approximately in the ratio of 9:1. The $HCOO((CH_2)_2CH_3)H^+$ appeared to be produced in this case entirely by secondary proton transfer reactions with the weaker

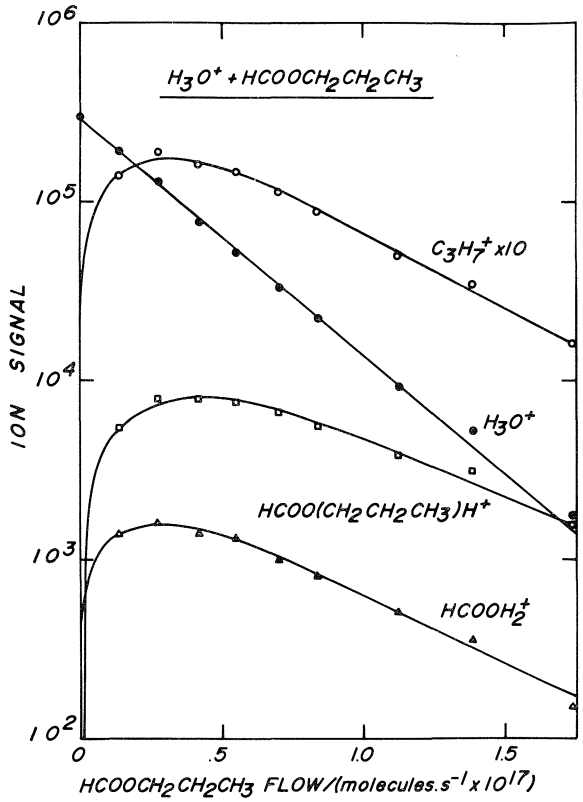

FIG. 1. The variation in major positive ions observed upon the addition of *n*-propyl formate vapour into a flowing H_2O–H_2 plasma in which H_3O^+ is initially the dominant ion. The decay of H_3O^+ provides a rate constant of 4.2×10^{-9} cm^3 molecule^{-1} s^{-1}. $T = 297$ K, $P = 0.363$ Torr, $\bar{v} = 7.8 \times 10^3$ cm s^{-1}, and $L = 45.9$ cm.

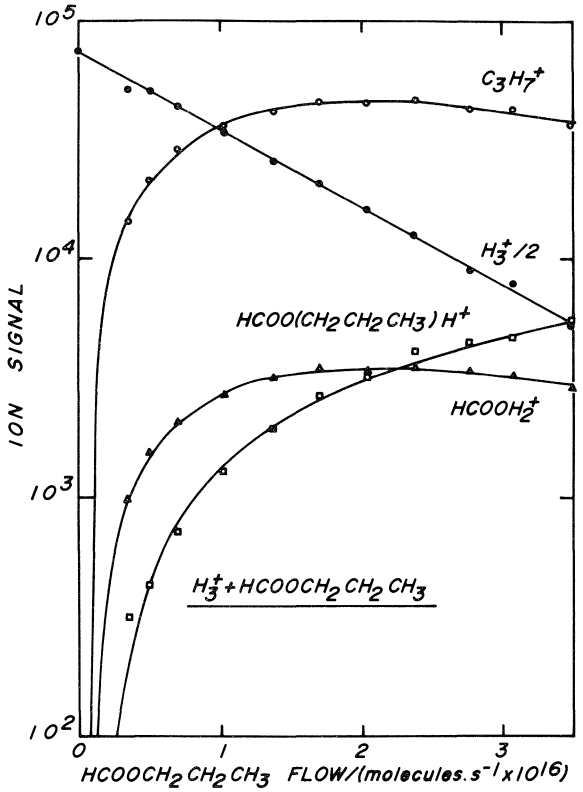

FIG. 2. The variation in major positive ions observed upon the addition of *n*-propyl formate vapour into a flowing H_2 plasma in which H_3^+ is initially the dominant ion. The decay of H_3^+ provides a rate constant of 8.5×10^{-9} cm^3 molecule^{-1} s^{-1}. $T = 299$ K, $P = 0.296$ Torr, $\bar{v} = 8.5 \times 10^3$ cm s^{-1}, and $L = 58.9$ cm.

second-generation acids $C_3H_7^+$ and $HCOOH_2^+$. The subsequent reaction of $HCOO((CH_2)_2CH_3)H^+$ is presumably due to 3-body association with *n*-propyl acetate. The product ion of this association reaction was outside the detection range of the mass spectrometer used in this study.

H_3O^+ was observed to react with ethyl acetate to produce primarily (>90%) an ion ($m/e = 89$) corresponding to protonated ethyl acetate. A concomitant but much smaller (<10%) increase was observed in the signal of an ion at $m/e = 61$, presumably $CH_3COOH_2^+$, which was suggestive of a small dissociative proton transfer channel. In contrast, the results shown in Fig. 3 indicate that dissociative proton transfer predominates in the reaction of H_3^+ with ethyl acetate. $CH_3COOH_2^+$ has become the dominant product (~75%) and two additional products at $m/e = 29$ and 43, identified as $C_2H_5^+$ (~5%) and CH_3CO^+ (~20%), were observed. The shape of the $CH_3COO(C_2H_5)H^+$ signal variation is

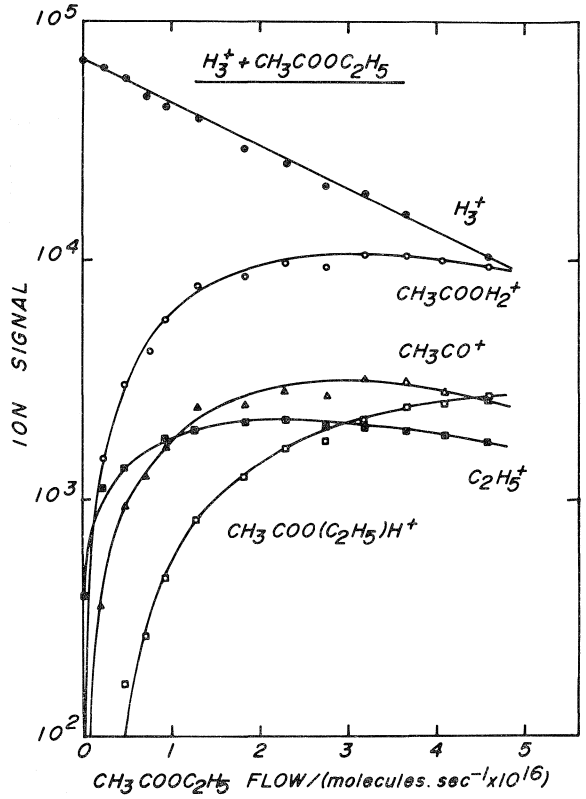

FIG. 3. The variation in the major positive ions observed upon the addition of ethyl acetate vapour into a flowing H_2 plasma in which H_3^+ is initially the dominant ion. The decay of H_3^+ provides a rate constant of 5.0×10^{-9} cm^3 molecule^{-1} s^{-1}. $T = 296$ K, $P = 0.508$ Torr, $\bar{v} = 7.7 \times 10^3$ cm s^{-1}, and $L = 46.9$ cm.

indicative of a secondary product arising entirely from proton transfer reactions with the second-generation acids $CH_3COOH_2^+$, $C_2H_5^+$, and CH_3CO^+.

Finally, H_3O^+ was observed to react with *n*-propyl acetate to form ions corresponding to $CH_3COOH_2^+$ and $CH_3COO((CH_2)_2CH_3)H^+$ in approximately equal amounts. Both ions reacted further, presumably by proton transfer and 3-body association, respectively.

Energetics and Mechanism of Dissociative Proton Transfer

Available thermochemical information enabled us to calculate the relative energies of most of the possible dissociation products of the two protonated formate esters and some of these are shown in Fig. 4. Many combinations of ions and molecules fall within the reaction exothermicities available from the protonation of the esters, particularly by H_3^+, but, in order to simplify the diagram, only products not requiring extensive skeletal rearrangements have been included. For example, the dissociation of $HCOO(CH_3)H^+$ into $CH_3CO^+ + H_2O$, which is only 7 ± 3 kcal mol^{-1} endothermic, has been excluded from Fig. 4.

Methyl Formate

The known energetics indicate that if the majority of the reaction exothermicity from the initial protonation reaction is deposited in $HCOO(CH_3)H^+$ then, in the absence of any barrier to reaction, dissociation of this ion into $CH_3OH_2^+$ and CO should be energetically favorable regardless of which acid (H_3^+, CH_5^+, HCO^+, or H_3O^+) performed the initial protonation.[2] Other plausible reaction products would become accessible with the acids CH_5^+, viz. $HCO^+ + CH_3OH$, and H_3^+, viz. $HCO^+ + CH_3OH$ and $CH_3^+ + HCOOH$. Experimentally, however, only H_3^+ produced measurable dissociation and even with this acid only the most stable products, $CH_3OH_2^+ + CO$, were formed. The absence of $HCO^+ + CH_3OH$ in the dissociation by CH_5^+ and particularly H_3^+ is somewhat surprising, as these species are expected to be formed initially by the $A_{Ac}1$ fission of the C—O bond of the methoxy-protonated tautomer.

[10] 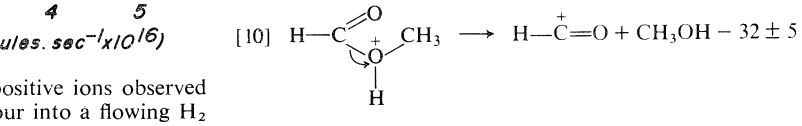

Also, the work of Pesheck and Buttrill (7) has established that protonated methyl acetate dissociates by the $A_{Ac}1$ mechanism to form the acetyl ion and methanol. Furthermore, previous observations made in this laboratory under similar operating conditions indicated that in the dissociative proton transfer reaction of H_3^+ with HCOOH both $HCO^+ + H_2O$, and $H_3O^+ + CO$ were produced with the former, the *less* stable, predominating by a factor of approximately two (3*a*). In this case the production of $H_3O^+ + CO$ from $HCOOH_2^+$ which is analogous to the production of $CH_3OH_2^+ + CO$ from $HCOO(CH_3)H^+$, was viewed to proceed by $A_{Ac}1$ cleavage accompanied by synchronous or near-synchronous transfer of a proton from the carbon atom to the developing water molecule (3*a*).[3] The

[2]At the pressures employed in these measurements collisional stabilization of the excited product ions formed by the initial protonation reaction may be important. The influence of the H_2 or He bath pressure on the observed product spectrum was not investigated systematically in this study.

[3]Sequential proton (deuteron) transfer within a reaction intermediate also has been invoked recently to account for gas-phase observations of hydrogen–deuterium exchange reactions involving hydrogen-containing anions and weak acids such as H_2O (3*b*, 3*c*).

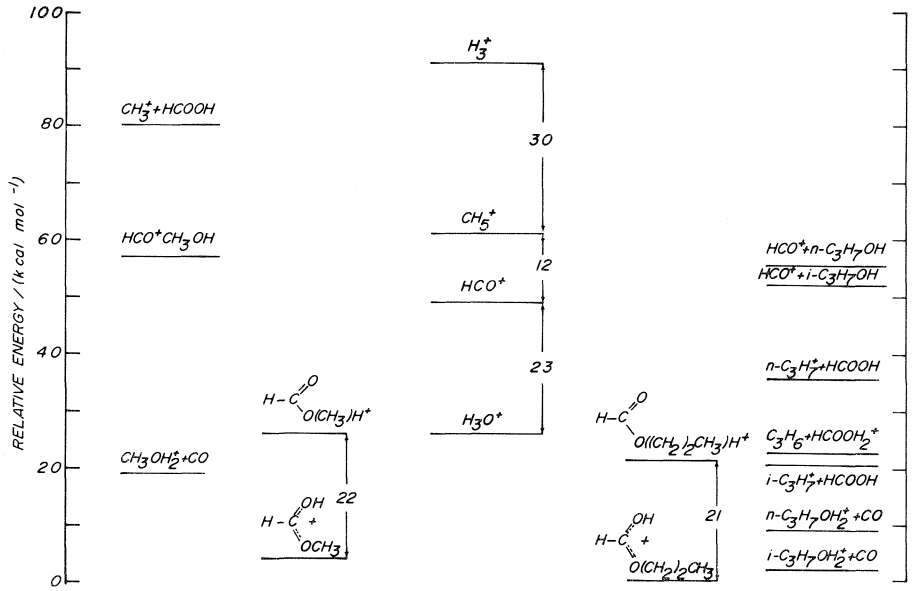

FIG. 4. Relative energies of the acids H_3^+, CH_5^+, HCO^+, and H_3O^+, the two-tautomers of protonated methyl- and *n*-propyl formate, and possible dissociation products of the protonated formates.

analogous route in the decomposition of $HCOO(CH_3)H^+$ would involve proton transfer to the developing methanol molecule according to

[11] 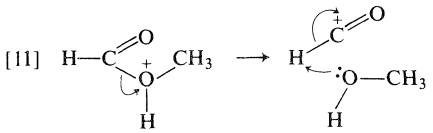

The failure to observe production of any HCO^+ in this case, then, would imply that this intramolecular proton transfer is essentially quantitative. Methanol has a much higher proton affinity than carbon monoxide ($\Delta PA = 38 \pm 4$ kcal mol^{-1}) (13) and we have previously observed rapid proton transfer from HCO^+ to CH_3OH initially at infinite separation (13). The difference in proton affinity between water and carbon monoxide which is relevant in the analogous decomposition of $HCOOH_2^+$ is considerably smaller ($\Delta PA = 23 \pm 3$ kcal mol^{-1}) (13) while proton transfer between the products of the $A_{Ac}1$ fission in protonated methyl acetate, viz. $CH_3CO^+ + CH_3OH$, is actually *endothermic* by 13 ± 4 kcal mol^{-1} for ground states at infinite separation. Although the extent of intramolecular transfer which proceeds according to this model is likely to be sensitive to the total excess energy deposited by the initial protonation reaction which is expected to be different in each of the three protonated species, the trend in dissociation with ΔPA which has been identified for these three species appears to be consistent with this intramolecular proton transfer mechanism invoked originally for this dissociation of $HCOOH_2^+$. The same overall result can be viewed to be achieved by a 1,2-hydride shift from the carbon to the positive oxygen atom with concomitant cleavage of the C—O bond. Such shifts are invoked in many acid-catalysed reactions in solution (19).

n-*Propyl Formate*

In contrast with methyl formate, *n*-propyl formate underwent extensive dissociation, even when the weakest acid, H_3O^+, was used as the protonating agent. If the dissociation is to be exothermic in the latter case, the product, $C_3H_7^+$, must be the isopropyl cation and not the expected *n*-propyl cation:

[12] 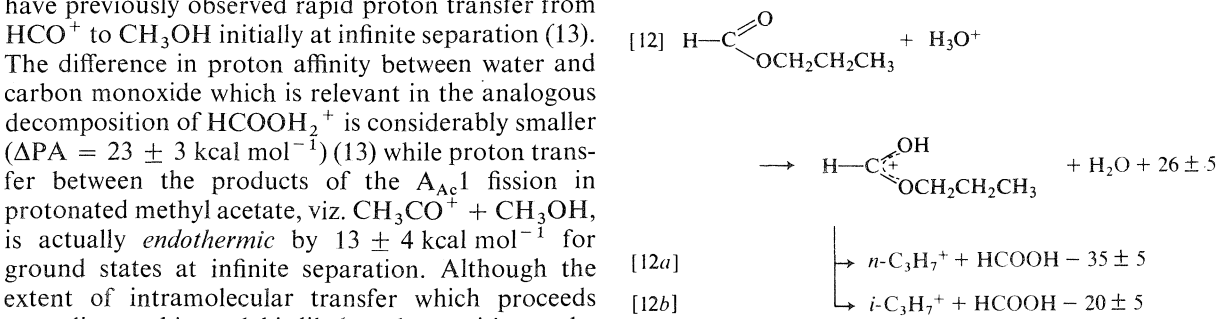

The $A_{Al}1$ cleavage would result in the *n*-propyl

cation and formic acid and if this mechanism is operative it is necessary to postulate that cleavage of the C—O bond is accompanied by a 1,2-hydride shift in the propyl fragment to achieve the more stable isopropyl cation:

[13] 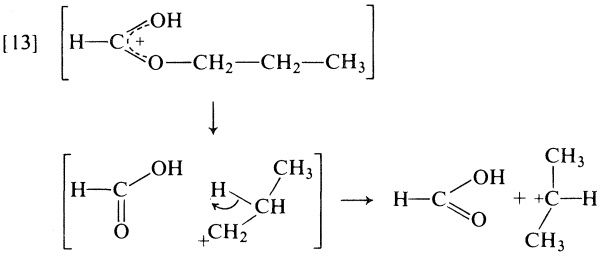

Ab initio molecular orbital calculations have established that $n\text{-}C_3H_7^+$ collapses into $i\text{-}C_3H_7^+$ without a barrier (20, 21). Such a mechanism has been invoked by Pesheck and Buttrill (7) to account for what appeared to be an abnormally large production of $C_4H_{10}^+$ from protonated isobutyl acetate. In this case the *s*-butyl group is conceived to rearrange via a 1,2-hydride shift to the more stable *tert*-butyl group.

A modification of this mechanism, again involving fission of the alkyl–oxygen bond but with concomitant migration of a β-hydrogen of the alkyl group to the carbonyl oxygen has been indicated in the dissociation of protonated ethyl acetate (9). The mechanism requires protonation of the energetically less favourable alkoxy oxygen, which is accessible even in protonation by H_3O^+, and proceeds via a 6-membered cyclic transition state:

[14] 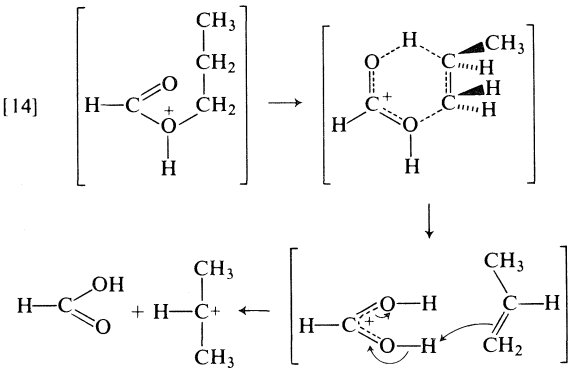

According to this scheme the initial products from protonated *n*-propyl formate are protonated formic acid and propene but proton transfer may again be postulated to occur during the fragmentation to form the isopropyl cation. Propene actually has a slightly higher proton affinity than formic acid ($\Delta PA = 2$ kcal mol^{-1}) (3*a*). Our experimental observations of the dissociative proton transfer with H_3^+ indicated the production of appreciable amounts (~10%) of $HCOOH_2^+$ and this may well be attributed to this internally assisted $A_{Al}1$ mechanism initiated by protonation of the alkoxy oxygen. Protonation at this position by H_3O^+ would require the deposition of at least 80% of the reaction exothermicity as internal energy of the ion so that production of $HCOOH_2^+$ and $C_3H_7^+$ via this mechanism is somewhat less plausible in this case. Production of $C_3H_7^+$ at low reaction exothermicities for the initial protonation may well proceed preferentially by the $A_{Al}1$ cleavage initiated by protonation at the carbonyl oxygen and accompanied by a 1,2-hydride shift. Some support for this viewpoint is provided by recent observations which we have made of the generation of $C_3H_7^+$ from *n*-propanol at exothermicities considerably lower than required for formation of $CH_3CH_2CH_2^+$:

[15] $CH_3CH_2CH_2OH + H_3O^+$

$\rightarrow CH_3CH_2CH_2OH_2^+ + H_2O + 23 \pm 4$

[15*a*] $\rightarrow n\text{-}C_3H_7^+ + H_2O - 33 \pm 4$

[15*b*] $\rightarrow i\text{-}C_3H_7^+ + H_2O - 17 \pm 4$

In this decomposition internal assistance by a carbonyl group of the type suggested for $HCOO(CH_2)_2\text{-}CH_3$ is not available so that C—O cleavage accompanied by a synchronous 1,2-hydride shift is definitely the preferred mechanism in this reaction. This suggests in turn that $C_3H_7^+$ may also not be formed via the 6-membered cyclic transition state in its generation from $HCOO(CH_2)_2CH_3$, at least not at low reaction exothermicities.

Ethyl Acetate

Protonated formic acid does not cleave readily by the $A_{Ac}1$ mechanism to form the acylium ion HCO^+ and it seemed probable that this mechanism should be more competitive with esters of larger carboxylic acids. In fact methyl acetate has been found to react with CH_5^+ mainly by proton transfer but with formation of about 20% CH_3CO^+ and no $CH_3\text{-}COOH_2^+$ (7), indicating that the cleavage of this ester occurs only by the $A_{Ac}1$ mechanism. Ethyl acetate might therefore be expected to form both the acetyl ion, CH_3CO^+, via the $A_{Ac}1$ mechanism and also $CH_3COOH_2^+$ by the internally assisted $A_{Al}1$ mechanism. Experimentally we found that H_3O^+ simply transferred a proton to ethyl acetate and the product of the $A_{Al}1$ mechanism, although slightly exothermic assuming all the reaction exothermicity to be in the protonated ester, occurred only to a small amount (<10%). In the reaction with H_3^+ (Fig. 3), there is sufficient energy to produce dissociation into $CH_3COOH_2^+$ and $C_2H_5^+$, the

products of the internally assisted and unassisted $A_{Al}1$ mechanisms, and also the acetyl ion, the product of the $A_{Ac}1$ mechanism. All three products were observed experimentally, with the relative concentrations in the same order as expected from the exothermicities. The CH_3CO^+ could possibly be generated by secondary dissociation of $CH_3COOH_2^+$ as a result of the excess energy in this ion. However, this interpretation is not substantiated by the results of the reaction of CH_5^+ with ethyl acetate (7) where the ratio of $CH_3COOH_2^+$ to CH_3CO^+ ($\sim 3.5:1$) is approximately the same as with the much stronger acid H_3^+. If the $CH_3COOH_2^+$ were the major primary source of CH_3CO^+ then the amount of dissociation might be expected to be much larger in the reaction initiated by the highly exothermic proton transfer from H_3^+ than in the dissociation initiated by the much weaker acid CH_5^+.

In summary, then, it appears that the dissociation of ethyl acetate, when protonation is accompanied by large exothermicities, can be induced to dissociate by both $A_{Al}1$ and $A_{Ac}1$ mechanisms with the relative frequencies being approximately 4:1.

n-*Propyl Acetate*

Dissociation of *n*-propyl acetate was induced by even the weakest acid, H_3O^+. However, $CH_3COOH_2^+$ was the only dissociation product, in contrast with dissociation of *n*-propyl formate, where $C_3H_7^+$ was the only major product.

$$[16]\quad H_3O^+ + CH_3COO(CH_2)_2CH_3 \rightarrow CH_3COO((CH_2)_2CH_3)H^+ + H_2O + 32 \pm 4$$

$$[16a]\quad \rightarrow CH_3COOH_2^+ + C_3H_6 - 25 \pm 4$$

$$[16b]\quad \rightarrow i\text{-}C_3H_7^+ + CH_3COOH - 32 \pm 4$$

$$[16c]\quad \rightarrow n\text{-}C_3H_7^+ + CH_3COOH - 48 \pm 4$$

$$[16d]\quad \rightarrow CH_3CO^+ + n\text{-}C_3H_6OH - 44 \pm 5$$

Acetic acid has a larger proton affinity than propene ($\Delta PA = 7$ kcal mol^{-1}) and formation of $CH_3COOH_2^+$ is the only dissociative channel requiring less energy than the maximum available from the initial proton transfer between *n*-propyl acetate and H_3O^+. The observed product suggests that only the $A_{Al}1$ mechanism is operative.

The stronger acid, CH_5^+, also yields predominantly the protonated carboxylic acid with *n*-propyl acetate and *n*-propyl propionate but small amounts of further decomposition products were observed for each ester ($\sim 10\%$ of $m/e = 43$, CH_3CO^+ and/or $C_3H_7^+$, for *n*-propyl acetate (7), and 8.8% of $C_7H_5CO^+$ and 1.6% of $C_3H_7^+$ for *n*-propyl propionate (8*b*)). It is not possible to deduce whether the $A_{Ac}1$ mechanism is operative for these two esters, but clearly it is at most a minor pathway for both esters.

Conclusions

Our results, combined with the results of icr and mass spectrometer studies on larger esters, permit certain generalisations about the mechanism of cleavage of esters in the gas phase. For methyl esters the $A_{Ac}1$ mechanism is the only one followed and even this requires high energy to achieve cleavage. For esters containing larger alkyl groups as the ether substituent the $A_{Al}1$ mechanism is dominant and even when the reaction exothermicity is increased and the $A_{Ac}1$ mechanism has become operative for the ethyl and *n*-propyl esters examined here, it never becomes the dominant channel. This behaviour is in marked contrast with the reactions in solution where the $A_{Ac}1$ mechanism is the most common. One possible explanation for this change in behaviour is that the $A_{Ac}1$ mechanism requires protonation on the energetically less accessible ether oxygen and this is more easily achieved in solution where the solvent can assist in accommodating some of the positive charge. In the gas phase the charge on the ether protonated ester is formally localised on the ether oxygen but the hydrogen atoms of the ester group carry considerable positive charge and this can be partly delocalised by forming a hydrogen bond between a hydrogen atom on the β-carbon and the carbonyl oxygen. This "internally solvated" structure then provides the 6-membered ring arrangement which is necessary for the internally assisted $A_{Al}1$ mechanism. Alternatively the normal product of $A_{Al}1$ fission, R^+, may be formed directly from the carbonyl protonated ester, or indirectly by the internally assisted mechanism followed by proton transfer, if this channel is energetically the more favourable.

Acknowledgement

We thank the Natural Sciences and Engineering Research Council of Canada for financial support.

1. D. K. Bohme, R. S. Hemsworth, H. W. Rundle, and H. I. Schiff. J. Chem. Phys. **58**, 3504 (1975).
2. G. I. Mackay and D. K. Bohme. Int. J. Mass Spectrom. Ion Phys. **26**, 327 (1978).
3. (*a*) G. I. Mackay, A. C. Hopkinson, and D. K. Bohme. J. Am. Chem. Soc. **100**, 7460 (1978); (*b*) J. H. Stewart, R. H. Shapiro, C. H. DePuy, and V. M. Bierbaum. J. Am. Chem. Soc. **99**, 7650 (1977); (*c*) G. I. Mackay, M. H. Lien, A. C. Hopkinson, and D. K. Bohme. Can. J. Chem. **56**, 131 (1978).
4. C. K. Ingold. Structure and mechanism in organic chemistry. Cornell University Press, Ithaca, New York, NY. 1953. p. 754.
5. K. Yates and R. A. McClelland. J. Am. Chem. Soc. **89**, 2686 (1967).
6. K. Yates. Acc. Chem. Res. **4**, 136 (1971).
7. C. V. Pesheck and S. E. Buttrill. J. Am. Chem. Soc. **96**, 6027 (1974).
8. (*a*) F. H. Field. *In* Ion–molecule reactions. Vol. 1. *Edited*

by J. L. Franklin. Plenum Press, New York, NY. 1972. p. 261; (*b*) M. S. B. MUNSON and F. H. FIELD. J. Am. Chem. Soc. **88**, 4337 (1966).
9. G. A. OLAH, A. M. WHITE, and D. H. O'BRIEN. *In* Carbonium ions. Vol. IV. *Edited by* G. A. Olah and P. v. R. Schleyer. Wiley-Interscience, New York, NY. 1973. p. 1754.
10. F. M. BENOIT and A. G. HARRISON. J. Am. Chem. Soc. **99**, 3980 (1977).
11. N. G. ADAMS and D. SMITH. Int. J. Mass Spectrom. Ion Phys. **21**, 349 (1976).
12. (*a*) A. L. MCCLELLAND. Tables of experimental dipole moments. W. H. Freeman and Company, London. 1963; (*b*) E. R. LIPPINCOTT and J. M. STUTMAN. J. Phys. Chem. **68**, 2926 (1964).
13. S. D. TANNER, G. I. MACKAY, A. C. HOPKINSON, and D. K. BOHME. Int. J. Mass Spectrom. Ion Phys. **29**, 57 (1979).
14. D. BETOWSKI, J. D. PAYZANT, G. I. MACKAY, and D. K. BOHME. Chem. Phys. Lett. **31**, 321 (1975).
15. G. I. MACKAY, R. S. HEMSWORTH, and D. K. BOHME. Can. J. Chem. **54**, 1624 (1976).
16. (*a*) L. BASS, T. SU, W. J. CHESNAVICH, and M. T. BOWERS. Chem. Phys. Lett. **34**, 119 (1975); (*b*) T. SU, E. C. F. SU, and M. T. BOWERS. J. Chem. Phys. **69**, 2243 (1978).
17. R. A. BARKER and D. P. RIDGE. J. Chem. Phys. **64**, 4411 (1976).
18. (*a*) P. KEBARLE. Ann. Rev. Phys. Chem. **28**, 445 (1977); (*b*) H. M. ROSENSTOCK, K. DRAXL, B. W. STEINER, and J. T. HERRON. J. Phys. Chem. Ref. Data, **6** (1977).
19. E. HEYADE and S. WINSTEIN. J. Am. Chem. Soc. **89**, 1661 (1967).
20. L. RADOM, J. A. POPLE, V. BUSS, and P. v. R. SCHLEYER. J. Am. Chem. Soc. **94**, 311 (1972).
21. P. C. HARIHARAN, L. RADOM, J. A. POPLE, and P. v. R. SCHLEYER. J. Am. Chem. Soc. **96**, 599 (1974).

The allyl and benzyl groups as hydrogen bond acceptors in derivatives of 2-allylphenol and 2-benzylphenol

TED SCHAEFER, RUDY SEBASTIAN, AND TIMOTHY A. WILDMAN

Department of Chemistry, University of Manitoba, Winnipeg, Man., Canada R3T 2N2

Received May 28, 1979

TED SCHAEFER, RUDY SEBASTIAN, and TIMOTHY A. WILDMAN. Can. J. Chem. **57**, 3005 (1979).

The ^{1}H nmr spectra of 2-allylphenol, 2-allyl-6-methylphenol, 2-allyl-6-chlorophenol, and 2-benzyl-4-chlorophenol are analyzed in some detail. It is shown that, relative to a methyl group, the allyl and benzyl moieties, respectively, favor a *cis* orientation by 1570 ± 250 J/mol and 900 ± 220 J/mol in free energy at 305 K in CCl_4 solution. These numbers appear to be independent of the CCl_4 solvent. Coupling parameters within the allyl group in these molecules and in propene and allylbenzene show some regularities but are probably not reliable indicators of the allyl conformational preference, at least in the absence of a model allowing for hindered rotor state populations.

TED SCHAEFER, RUDY SEBASTIAN et TIMOTHY A. WILDMAN. Can. J. Chem. **57**, 3005 (1979).

On a analysé de façon détaillée les spectres rmn du ^{1}H des allyl-2 phénol, allyl-2 méthyl-6 phénol, allyl-2 chloro-6 phénol et benzyl-2 chloro-4 phénol. On a montré que par rapport au groupe méthyle les groupes allyle et benzyle favorisent une orientation *cis* avec respectivement une énergie libre de 1570 ± 250 J/mol et 900 ± 220 J/mol à 305 K en solution dans le CCl_4. Ces valeurs semblent être indépendantes du CCl_4 utilisé comme solvant. Les paramètres de couplage à l'intérieur des groupes allyles dans ces molécules, dans le propène et les allylbenzènes montrent quelques régularités, mais ce ne sont probablement pas des indicateurs surs d'une préférence conformationnelle du groupe allyle, du moins en l'absence de modèle permettant un rotation des différentes populations encombrées.

[Traduit par le journal]

Introduction

A recent direct measurement (1) of the intramolecular equilibrium of the hydroxyl group in 2-methylphenol and in 4-chloro-2-methylphenol shows that the *trans* conformer **2** (X = H, Y = H or

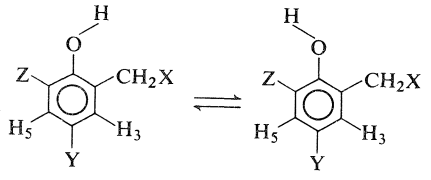

1 **2**

Cl, Z = H) is favored by a free energy of 1600 ± 170 J/mol in CCl_4 solution at 305 K. The measurement depends on the well-established observation (2–5) that $^5J_m^{H,OH}$, the coupling constant over five formal bonds between the hydroxyl proton and the *meta* ring protons, is highly stereospecific. Thus, ^5J_c, the couplings to H-3 in **1** and to H-5 in **2**, approximate to zero; whereas the corresponding ^5J_t couplings over the all-*trans* path are finite. The free energy difference between **1** and **2** follows as $\Delta G^0 = -RT \ln K = -RT \ln {}^5J_3/{}^5J_5$, where it is assumed that in dilute solutions the activity coefficients of **1** and **2** are equal. This procedure has yielded internally selfconsistent results (1–5), as well as agreement with other techniques.

Because the internal barrier to rotation of the hydroxyl group is large compared to thermal energies at ambient temperatures, conformations in which the hydroxyl group deviates from the benzene plane can be ignored to a very good approximation (1). This situation contrasts markedly with that found for the corresponding thiophenol derivatives (5).

In this paper, the conformational preference of the hydroxyl group is investigated for 2-allylphenol, 2-allyl-6-chlorophenol, 2-allyl-6-methylphenol, and 2-benzyl-4-chlorophenol. In addition, all coupling constants for the allyl groups are assessed as indicators of the conformational preferences of the hydrocarbon sidechains in these phenol derivatives, comparing them to propene and allylbenzene as well.

Experimental

Of commercial origin (Aldrich, Parish, and Matheson), the compounds were prepared as dilute solutions (see Tables) and were degassed by the freeze–pump–thaw technique. The samples were flame-sealed into 5 mm od nmr tubes and contained some tetramethylsilane (TMS). The ^{1}H nmr spectra were calibrated in the frequency sweep mode on an HA100 spectrometer at a probe temperature of 305 K. Calibrations of peak positions involved interpolations between frequency markers placed at ca. 5 Hz intervals at sweep rates of 0.2 Hz/s and at a spectral dispersion of 1 Hz/cm of chart paper. The root mean square errors in peak frequencies were typically 0.02 Hz or less. Intermolecular hydroxyl proton exchange was retarded as described (1–5).

0008-4042/79/223005-05$01.00/0

TABLE 1. Proton chemical shifts and spin–spin coupling constants in Hz at 100.001 MHz for 2-allyl-6-chlorophenol and 2-benzyl-4-chlorophenol at 305 K

Parameter	2-Allyl-6-chlorophenol[a]	2-Benzyl-4-chlorophenol	
ν_{OH}	548.261(2)[b]	443.213(2)[c]	400.391(2)[d]
ν_3	695.553(2)	700.694(3)	697.148(2)
ν_4	670.865(2)	—	—
ν_5	709.479(2)	697.946(3)	685.997(2)
ν_6	—	654.871(2)	603.448(2)
$^3J_{34}$	7.609(3)	—	—
$^3J_{45}$	8.046(3)	—	—
$^3J_{56}$	—	8.503(5)	8.523(3)
$^4J_{35}$	1.573(3)	2.588(4)	2.621(3)
$^5J_{36}$	—	0.307(4)	0.311(3)
$^4J_o^{H_6,OH}$	—	−0.140(3)	−0.144(3)
$^5J_m^{H_3,OH}$	0.626(3)	0.368(4)	0.468(3)
$^5J_m^{H_5,OH}$	0.0	0.283(4)	0.245(3)
$^4J_o^{H,CH_2}$	−0.638(3)	−0.640(4)	−0.645(3)
$^5J_m^{H_4,CH_2}$	0.289(3)	—	—
$^5J_m^{H_6,CH_2}$	—	0.328(5)	0.298(3)
$^6J_p^{H,CH_2}$	−0.443(3)	−0.442(4)	−0.428(3)

[a]5 mol% in CCl_4.
[b]Numbers in parentheses are standard deviations in the last significant figure.
[c]3 mol% in CCl_4.
[d]5 mol% in C_6D_6.

Results and Discussion

Spectral Analysis

Performed by means of the computer program LAME (6, 7), the analyses yielded the spectral parameters in Tables 1 to 3. The ^1H nmr spectra of 2-allylphenol, for example, arises from a 10-spin system. However, there is no detectable coupling between the olefinic and ring protons. Accordingly, the ring proton and hydroxyl proton spectra could be analyzed as parts of a 7-spin spectrum and, on the other hand, the olefinic proton spectrum was analyzable as part of a 5-spin system. The methylene protons are coupled to all ring and olefinic protons. The phenyl group ^1H nmr spectrum of the benzyl derivative did not yield to analysis. Figure 1 displays the hydroxyl proton spectra of 2-benzyl-4-chlorophenol in two solvents. Unresolved coupling to the exocyclic phenyl protons causes some broadening; compare spectrum in (1).

Conformational Preference of the Hydroxyl Group

2-Benzyl-4-chlorophenol

According to the assumptions above, it follows that conformation **2** (X = phenyl, Y = Cl, Z = H) has a lower free energy than **1** of $-RT \ln K = -RT \ln {}^5J_3/{}^5J_5 = -RT \ln 0.283/0.368 = 670 \pm 180$ J/mol in CCl_4 solution and 1640 ± 170 J/mol in C_6D_6 solution. The estimated errors assume that the standard deviations in Table 1 are to be multiplied by 4. The greater stability of the *trans* form, **2**, in C_6D_6 has its counterpart in 2-methylphenol (1). Perhaps it arises from intermolecular hydrogen bonding to the π electrons of the solvent molecules, which is more favorable in the *trans* than the *cis* conformations. Preferential solvation near the hydroxyl group is indicated by the large shifts to high field of OH and H-6 resonances relative to the CCl_4 solution (Table 1).

The *trans* form of 2-methyl-4-chlorophenol is more stable than the *cis* form by 1590 ± 250 J/mol in CCl_4 solution. Comparison with 2-benzyl-4-chlorophenol suggests intramolecular hydrogen bonding to the phenyl group in the latter compound accounts for ca. 1 kJ/mol in free energy. The temperature dependence of the stretching band intensities in 2-benzylphenol (8) leads to an enthalpy of 1380 ± 210 J/mol favoring the *cis* form and an entropy difference of -4.4 ± 0.84 J/mol deg so that the free energy difference at 305 K is 40 ± 470 J/mol, *cis* favored. Another infrared investigation implies that the *cis* form is stabilized by a free energy of 450 ± 390 J/mol at 305 K (9). The nmr result of 670 ± 180 J, *trans* favored, is not in striking agreement with the infrared data.

It might be argued that the present data refer to a much more concentrated solution (ca. 0.3 *M*) than do the infrared measurements (ca. 10^{-2} *M*), and that self-association of the solute would favor the *trans* form. This possibility was investigated for 2-methyl-4-chlorophenol (1) and no evidence could be found that self-association drives the intramolecular equilibrium towards the *trans* form, at least for concentrations up to 8 mol% in CCl_4. See also the discussion below on 2-allylphenol and its derivatives. ^{13}C chemical shifts do not throw any light on intramolecular equilibria in benzylphenols (10).

TABLE 2. Proton chemical shifts in Hz at 100.001 MHz and coupling constants for 2-allylphenol and 2-allyl-6-methylphenol at 305 K

Parameter	2-Allyl[a]	2-Allyl-6-Me	Parameter	2-Allyl	2-Allyl-6-Me[b]
ν_{OH}	476.681(2)[c]	468.922(1)	$^4J_o^{H,CH_2}$	−0.630(4)	−0.581(1)
ν_{CH_3}	—	271.701(2)	$^5J_m^{H_4,CH_2}$	0.304(3)	0.303(2)
ν_3	699.773(3)	681.834(2)	$^5J_m^{H_6,CH_2}$	0.336(3)	—
ν_4	676.621(2)	665.556(1)	$^6J_p^{H_5,CH_2}$	−0.427(4)	−0.381(2)
ν_5	700.429(3)	688.856(1)	$^4J_o^{H,CH_3}$	—	−0.762(1)
ν_6	666.670(2)	—	$^5J_m^{H,CH_3}$	—	0.316(1)
$^3J_{34}$	7.487(3)	7.528(2)	$^6J_p^{H,CH_3}$	—	−0.581(1)
$^3J_{45}$	7.433(3)	7.484(2)	$^6J^{CH_2,CH_3}$	—	−0.256(3)
$^3J_{56}$	8.018(4)	—	$^5J_o^{OH,CH_2}$	—	0.000(2)
$^4J_{35}$	1.702(3)	1.703(2)	Root mean square deviation	0.016	0.018
$^4J_{46}$	1.208(3)	—	—	—	—
$^5J_{36}$	0.375(4)	—	Peaks observed	133	85
$^4J_o^{H_6,OH}$	−0.125(3)	—	—	—	—
$^5J_m^{H_3,OH}$	0.327(3)	0.214(2)	Transitions calculated	352	1072
$^5J_m^{H_5,OH}$	0.316(3)	0.409(2)	Transitions assigned	286	892
$^6J_p^{H_4,OH}$	0.0	−0.020(3)			

[a]4 mol% in CCl_4.
[b]5 mol% in CCl_4.
[c]Numbers in parentheses are standard deviations in the last significant figure.

TABLE 3. ^1H nmr spectral parameters[a] for the allyl group in propene and some derivatives at 305 K

Parameter	Propene[b]	Allyl benzene[c]	2-Allyl phenol[d]	2-Allyl-6-chlorophenol[c]	2-Allyl-6-methylphenol[c]
ν_{CH_2}	170.305(4)	333.80	333.5	340.0	332.7_5
ν_α	574.114(4)	590.450(2)	594.864(4)	590.990(3)	594.404(3)
ν_c	496.606(4)	501.538(2)	509.298(4)	503.837(3)	511.915(3)
ν_t	488.482(4)	501.053(2)	503.935(4)	501.866(3)	510.241(3)
$^4J_c^{H,CH_2}$	−1.770(4)	−1.642(3)	−1.740(5)	−1.608(4)	−1.768(4)
$^4J_t^{H,CH_2}$	−1.403(4)	−1.342(3)	−1.482(5)	−1.314(3)	−1.500(4)
^3J_t	16.982(6)	17.007(4)	17.132(7)	17.050(5)	17.162(5)
^3J_c	10.086(6)	10.059(4)	10.086(7)	10.054(5)	10.072(5)
^2J_g	2.164(6)	1.913(3)	1.786(6)	1.865(4)	1.748(5)
$^3J^{H_\alpha,CH_2}$	6.470(4)	6.642(3)	6.365(5)	6.657(3)	6.316(4)
Root mean square error	0.019	0.009	0.015	0.011	0.012
Transitions calculated	104	56	56	56	56
Transitions assigned	104	56	56	56	54
Peaks observed	64	47	47	47	46

[a]In Hz at 100.001 MHz, numbers in parentheses being the standard deviations in the last significant figure.
[b]3.3 mol% in CCl_4.
[c]5 mol% in CCl_4.
[d]4 mol% in CCl_4.

2-Allylphenol, 2-Allyl-6-chlorophenol, and 2-Allyl-6-methylphenol

The chloro derivative exists predominantly as the *trans* form, **2** (X = vinyl, Y = H, Z = Cl), because $^5J_3$ is 0.62_6 Hz and $^5J_5$ <0.03 Hz; 4,6-dichloro-2-methylphenol behaves similarly (footnote 1 in (1)).

Removal of the chlorine substituent to yield 2-allylphenol, gives an equilibrium in which the *trans* form, **2**, is favored by a free energy of 90 ± 190 J/mol; that is, the equilibrium constant is effectively unity. Comparison with 2-methylphenol implies that the allyl group stabilizes the *cis* form, in which the hydroxyl group reputedly hydrogen bonds to the π electrons, by 1500 ± 350 J/mol. The infrared data

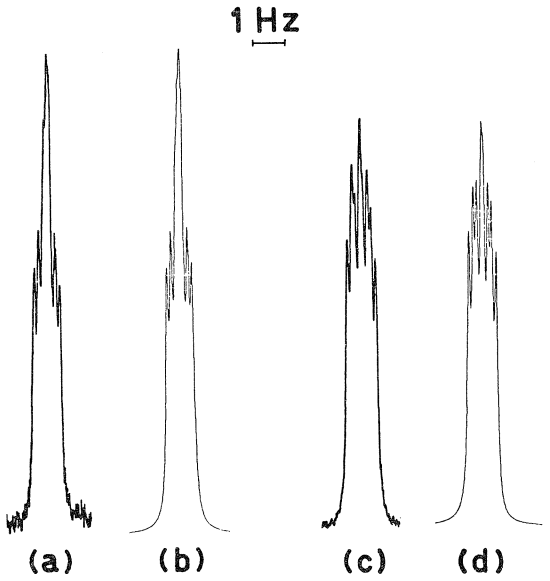

FIG. 1. The hydroxy ^{1}H nmr spectra of 2-benzyl-4-chlorophenol at 100 MHz and 305 K as (*a*) 3 mol% in CCl_4, (*b*) calculated with the parameters in Table 1, (*c*) 5 mol% in C_6D_6, (*d*) calculated with parameters in Table 1. Unresolved coupling to the sidechain protons causes the resolution to be somewhat lower than that in ref. 1, for example.

on enthalpy and entropy yield 760 ± 1100 J/mol as the free energy advantage of the *cis* form of 2-allylphenol (8).

Now, for 2-allyl-6-methylphenol the coupling constants (Table 2) show that **1** (X = vinyl, Y = H, Z = CH_3) has a lower free energy than **2** of 1640 ± 150 J/mol, precisely as would be concluded from a simple comparison of 2-methylphenol and 2-allylphenol. In other words, no solvent or self-association perturbations need be invoked in a comparison of the *cis–trans* equilibria for the latter molecules. In 2-allyl-6-methylphenol, where two *ortho* substituents are present, such associations are expected to be even less significant. Solvent stabilization of those conformers of higher dipole moment is probably not very important in these phenol derivatives (the dipole moments of toluene and allylbenzene differ by less than 0.1 D).

In view of these results, which suggest that a comparison of the *cis–trans* equilibria would yield the same result for the free molecules, a direct comparison with studies of intramolecular photocyclization of the allyl compounds may prove interesting (11). It need not be true that the *cis–trans* equilibria are identical for solvated and free molecules when only one of the *ortho* substituents is present.

A referee has mentioned the possibility of out-of-plane conformations of the hydroxyl group in these compounds. As discussed for phenol itself (12), substantial out-of-plane populations would entail an observable $^6J_p^{H,OH}$. No evidence was found for a $^6J_p^{H,OH}$ of greater than 0.04 Hz in these compounds, indicating that coplanar conformations of the hydroxyl groups are favoured by an energy not significantly less than in phenol, i.e., about 3.5 kcal/mol.

Long-range Coupling Between Methylene Protons and Ring Protons

There exists abundant evidence (13) that coupling between methylene protons and the ring protons depends on the angle of rotation about the sp^2–sp^3 carbon–carbon bond. For example, $^6J_p^{H,CH} \alpha \sin^2\theta$, where θ is the angle by which the C_α—H bond twists out of the benzene plane (13). Of course, unless the barrier to rotation about the exocyclic bond is very large ($\gg$kT), $\sin^2\theta$ must be averaged over the occupied hindered rotor state states (13). The asymmetry of the compounds under consideration here does not allow such a procedure. However, an extensive set of molecular orbital calculations at the PCILO level of approximation suggests that the θ values for the two methylene C—H bonds are 15° and 105° (14), and that such a conformation is stabilized to the extent of 17 kJ/mol. In that event, our previous work (13) predicts $^6J_p^{H,CH}$ as −0.6 Hz, although a further twist of 15°, i.e., to give θ values of 0° and 120°, would yield a ^6J_p of -0.4_6 Hz.

It is interesting that in all of the allyl compounds $^6J_p^{H,CH}$ is −0.41 ± 0.03 Hz and it would be tempting to take this as a rough confirmation of the energy calculations (allowing for small errors in the calculated θ values). In our opinion, however, the only correct approach[1] involves a proper average over all populated states of the hindered sidechain, including the *cis* and *trans* conformers. In the absence of this possibility the magnitudes of $^6J_p^{H,CH}$ for these compounds suggest that the conformational preferences of the allyl and benzyl moieties are very similar.[2]

The Couplings Within the Allyl Group

Their most striking aspect is the small variation from compound to compound in Table 3. Nevertheless, regularities are apparent. In Fig. 2, ^2J_g, and ^3J_t

[1]Such an approach can yield reliable information on preferred conformations and internal rotational barriers for molecules of sufficient symmetry (13).

[2]The decrease in the magnitude of $^6J_p^{H,CH}$ of the allyl group from 0.44 Hz in the 6-chloro derivative (in which the hydroxyl group points away from the allyl group) to 0.38.Hz in the 6-methyl derivative (in which the largest population occurs for the conformer in which the hydroxyl group points towards the allyl group) *is* consistent with reduced freedom of motion of the allyl sidechain for a preferred conformation in which the C_α—C_β bond prefers a plane perpendicular to the benzene plane. The entropy of ionization of 2-allylphenol indicates some restriction of motion of the sidechain in the neutral species (15).

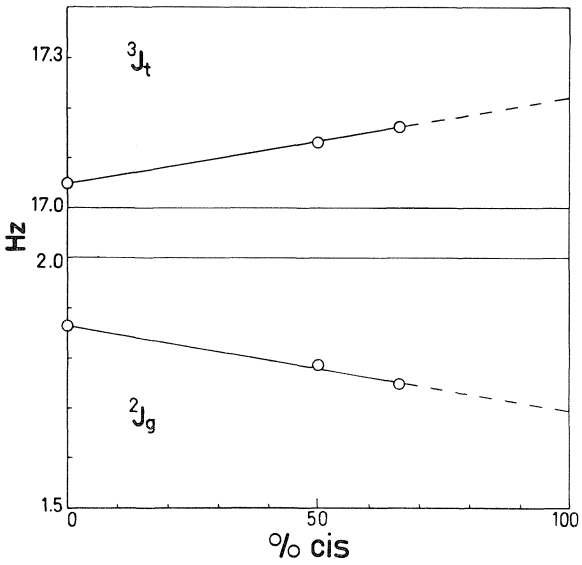

FIG. 2. The coupling constants ^2J_g and ^3J_t in Hz from Table 3 are plotted vs. the population of the conformer in which the hydroxyl group lies *cis* to the allyl group. From left to right, the points refer to 2-allyl-6-chlorophenol, 2-allylphenol, and 2-allyl-6-methylphenol.

are plotted vs. the population of the *cis* conformer, as calculated from $^5J_m^{H,OH}$, for 2-allyl-6-chloro-, 2-allyl-, and 2-allyl-6-methylphenols (four times the standard deviations is ≤ 0.02 Hz for these parameters). In other words, the *cis* conformer of 2-allylphenol has $^3J_t = 17.23 \pm 0.02$ and $^2J_g = 1.69 \pm 0.02$ Hz.

In terms of the Pople and Bothner-By model (16), the decrease of 0.2 Hz in ^2J_g in going from the *trans* to *cis* conformer corresponds to electron withdrawal from antisymmetric orbitals of the $=CH_2$ fragment (hyperconjugative effects), presumably by the polar hydroxyl group. Of course, there occurs a similar drop in ^2J_g between propene and allylbenzene (Table 3), so that conformational changes of the allyl group might also account for the 0.2 Hz decrease.

In principle, the allylic couplings, ^4J_c and ^4J_t, are excellent probes into the conformation of the allyl group in these compounds (17). In practice, the variations are so small (Table 3) that their theoretical values (17) cannot be used to test the calculated (14) high stability of the preferred *cis* conformer of 2-allylphenol. In our opinion, the observed couplings indicate a degree of motional flexibility of the allyl group. A proper treatment would again require a populational average over all the torsional states.

Conclusions

Compared to an *ortho* methyl group, an *ortho* allyl substituent in phenol favours a *cis* orientation of the hydroxyl group by a free energy of 1570 ± 250 J/mol (which is the average of the values obtained from direct comparison and from competition in 2-allyl-6-methylphenol) at 305 K in CCl_4 solution. This value may apply to the gas phase also, probably because *cis* and *trans* conformers have very similar polarities. A similar comparison suggests that the benzyl group favours the *cis* orientation of the hydroxyl group by a free energy of 900 ± 220 J/mol at 305 K in CCl_4.

The coupling parameters within the allyl moiety in propene are rather insensitive to substitution by phenyl or substituted phenyl groups. In our opinion, this means that many hindered rotor (torsion) states are significantly populated at ambient temperatures.

Acknowledgments

We are grateful to the Natural Sciences and Engineering Research Council of Canada for financial assistance.

1. T. SCHAEFER and K. CHUM. Can. J. Chem. **56**, 1788 (1978).
2. J. B. ROWBOTHAM and T. SCHAEFER. Can. J. Chem. **52**, 3037 (1974).
3. J. B. ROWBOTHAM, M. SMITH, and T. SCHAEFER. Can. J. Chem. **53**, 986 (1975).
4. T. SCHAEFER and J. B. ROWBOTHAM. Can. J. Chem. **54**, 2243 (1976).
5. T. SCHAEFER and T. A. WILDMAN. Can. J. Chem. **57**, 450 (1979).
6. S. CASTELLANO and A. A. BOTHNER-BY. J. Chem. Phys. **41**, 3863 (1964).
7. C. W. HAIGH and J. M. WILLIAMS. J. Mol. Spectrosc. **32**, 398 (1969).
8. M. OKI and H. IWAMURA. Bull. Chem. Soc. Jpn. **33**, 717 (1960).
9. A. KANALA and S. KOVAC. Tetrahedron, **31**, 2089 (1975).
10. Y. NAKAI and F. YAMADA. Org. Magn. Reson. **11**, 607 (1978).
11. S. GERESH, O. LEVY, Y. MARKOVITS, and A. SHANY. Tetrahedron, **31**, 2803 (1975).
12. T. SCHAEFER, J. B. ROWBOTHAM, and K. CHUM. Can. J. Chem. **54**, 3666 (1976).
13. T. SCHAEFER, W. NIEMCZURA, and W. DANCHURA. Can. J. Chem. **57**, 355 (1979) and references therein.
14. G. TRINQUIER and J.-P. MALRIEU. J. Mol. Struct. **49**, 155 (1978).
15. W. F. O'HARA, T. HU, and L. G. HEPLER. J. Phys. Chem. **67**, 1933 (1963).
16. J. A. POPLE and A. A. BOTHNER-BY. J. Chem. Phys. **42**, 1339 (1965).
17. M. BARFIELD, A. M. DEAN, C. J. FOLLICK, R. J. SPEAR, S. STERNHELL, and P. W. WESTERMAN. J. Am. Chem. Soc. **97**, 1482 (1975).

Canadian Journal of Chemistry
Published by
THE NATIONAL RESEARCH COUNCIL OF CANADA

Journal canadien de chimie
Publié par
LE CONSEIL NATIONAL DE RECHERCHES DU CANADA

Volume 57 Number 23 December 1, 1979

Volume 57 numéro 23 1 décembre 1979

Kinetics of solvent extraction of metal ions with HEDHP. III. The kinetics and mechanism of solvent extraction of Cr(III) from acidic aqueous solutions with bis-(2-ethyl hexyl) phosphoric acid in benzene

MUHAMMAD FAKHRUL ISLAM AND RANJIT KUMAR BISWAS
Department of Applied Chemistry, University of Rajshahi, Rajshahi, Bangladesh

Received January 10, 1979

MUHAMMAD FAKHRUL ISLAM and RANJIT KUMAR BISWAS. Can. J. Chem. **57**, 3011 (1979).

The rate of solvent extraction of chromium(III) from aqueous sulphuric acid solutions (containing 0.05 mol dm^{-3} sulphate ion and 0.25 mol dm^{-3} acetate buffer, ionic strength, $I = 0.40$ mol dm^{-3}) with bis-(2-ethyl hexyl) phosphoric acid (HDEHP or H_2A_2) in benzene has been measured under various conditions. The rate of backward extraction measurement of Cr(III) from organic phase to aqueous phase is not possible due to the inert property of Cr(III)–DEHP chelate. The forward rate is found to be first-order w.r.t. Cr(III) concentration in the aqueous phase and HDEHP concentration in the organic phase. The order w.r.t. H^+ concentration varies from -1 to 1 over the pH range 1.5 to 5.25. The rate is found to decrease with increasing sulphate and nitrate ions concentrations in the aqueous phase. At (30 ± 1)°C, the rate expression, in the presence of sulphate, acetate, and nitrate ions, is found to be represented by:

$$-dC_{Cr}^{A}/dt = 10^{-0.893} C_{Cr}^{A}[H_2A_2]_{(o)}(500[H^+] + 1 + 10^{-4}[H^+]^{-1})^{-1}(1 + 4.17[SO_4^{2-}])^{-1}(1 + 0.5[NO_3^-])^{-1}$$

In the absence of the anions, the formation of $CrHA_2^{2+}$ intermediate complex ($Cr(OH)^{2+} + H_2A_{2(o)} \rightarrow CrHA_2^{2+} + H_2O$) is the rate determining step at all acidities. The effects of the anions on the rate are discussed.

MUHAMMAD FAKHRUL ISLAM et RANJIT KUMAR BISWAS. Can. J. Chem. **57**, 3011 (1979).

On a mesuré la vitesse d'extraction du chrome(III) à partir de solutions aqueuses d'acide sulfurique (contenant des ions sulfates à 0.05 mol dm^{-3}, tampon acétate à 0.25 mol dm^{-3} d'une force ionique $I = 0.40$ mol dm^{-3}) en utilisant comme solvant l'acide bis(éthyl-2 hexyl) phosphorique (HDEHP ou H_2A_2) en solution dans le benzène et en changeant les conditions. Le caractère inerte du chélate Cr(III)–DEHP ne permet pas de mesurer la vitesse d'extraction en retour de la phase organique à la phase aqueuse. On a trouvé que la vitesse d'extraction directe est du premier ordre par rapport à la concentration du Cr(III) dans la phase aqueuse et à celle du HDEHP dans la phase organique. L'ordre par rapport à la concentration en ions H^+ varie de -1 à 1 sur une échelle de pH allant de 1.5 à 5.25. On a trouvé que la vitesse décroît quand on augmente la concentration en ions sulfate et nitrate de la phase aqueuse. On a trouvé que l'expression de la vitesse, à 30 ± 1°C en présence d'ions sulfate, acétate et nitrate, peut être représentée par la formule suivante:

$$-dC_{Cr}^{A}/dt = 10^{-0.893} C_{Cr}^{A}[H_2A_2]_{(o)}(500[H^+] + 1 + 10^{-4}[H^+]^{-1})^{-1}(1 + 4.17[SO_4^{2-}])^{-1}(1 + 0.5[NO_3^-])^{-1}$$

En l'absence d'anions la formation du complexe intermédiaire $CrHA_2^{2+}$ ($Cr(OH)^{2+} + H_2A_{2(o)} \rightarrow CrHA_2^{2+} + H_2O$) est l'étape déterminante à toutes les acidités. On a discuté de l'effet des anions sur la vitesse d'extraction.

[Traduit par le journal]

0008-4042/79/233011-06$01.00/0

In previous papers of this series, the authors have discussed the kinetics and the mechanism of the solvent extractions of Ti(IV) (1) and V(IV) (2) with HDEHP in benzene. In these papers, it has been reported that the rate of extraction and back extraction of Ti(IV) with HDEHP is slow, whereas that of V(IV) is fast. Taube (3) and Basolo and Pearson (4) noted that the rate of most substitution reactions in Cr(III) complexes in the aqueous solutions was quite slow. The slow behaviour of Cr(III) toward solvent extraction with acetyl acetone was reported by McKaveney and Freiser (5), who noted that no extraction of Cr(III) took place from a sulphate medium into a 1:1 chloroform – acetyl acetone mixture in the pH range of 0 to 6.0 after mixing the phases for 30 min, and this failure to extract was attributed to the extremely slow rate of formation of the metal chelates. Morrison and Freiser (6) reported that the reflux of aqueous Cr(III) solution with acetyl acetone at pH 6.0 for 1 h resulted in complete extraction. On these grounds, Hellwege and Schweitzer (7) studied the extraction kinetics of Cr(III) from perchlorate and chloride media into chloroform containing acetyl acetone. In addition, Sambasiva *et al.* (8) reported the kinetics of extraction of Cr(VI) from HCl solutions by di-*n*-pentyl and di-*n*-octyl sulfoxides.

The extraction equilibrium of Cr(III) from HCl solutions with HDEHP in toluene was reported by Kimura (9) along with 50 other elements. In a previous paper, the authors have reported the extraction equilibrium study of Cr(III) from sulphate–acetate media with HDEHP in benzene (10), in which it has been reported that the time required to reach equilibrium is about 15–30 min at the experimental conditions. This paper discusses the kinetics and mechanism of the extraction of Cr(III) from acidic sulphato–acetato media with HDEHP and compares the result with other results from the literature.

Experimental

Reagents

Reagent grade chemicals were used in the investigations: chromic sulphate (M. C. and Bell), benzene (purified, bp 79–81°C, M. C. and Bell), bis-(2-ethyl hexyl) phosphoric acid (Eastman Kodak), sulphuric acid (98%, BDH), sodium nitrate (99%, BDH), acetic acid (99.4%, BDH), sodium acetate (99%, BDH), sodium azid (99%, E. Merck), potassium permanganate (99%, BDH), etc. All the chemicals were used without further purifications. Regenerated benzene was also used.

Procedures

The stock solution of Cr(III) was prepared by dissolving $Cr_2(SO_4)_3 \cdot 18H_2O$ in sulphuric acid and diluting with water. It was then standardized by titrating with standard ferrous ammonium sulphate (11). The acidity of the stock solution was estimated by titrating with standard Na_2CO_3 solutions. The total sulphate content was then calculated. The test solutions were then prepared by diluting the stock so that the resulting solutions always contained 0.05 mol dm^{-3} sulphate ion (added as Na_2SO_4 or H_2SO_4) and 0.25 mol dm^{-3} acetate ion (added as AcNa or AcH), so that ionic strength $I = 0.40$ mol dm^{-3}, except in the sulphate and acetate ions dependence studies. The pH of the solutions were then adjusted by adding anhydrous Na_2CO_3 only if necessary. The solutions so obtained were kept standing at least for 12 h before extraction. HDEHP was diluted with benzene (pre-equilibrated with water) to obtain the desired strengths.

The details of the procedures were essentially the same as those described in the previous papers (1, 2). pH of the solutions were measured by a Corning-5A-model pH meter. The aqueous phase Cr(III) concentrations were kept at 200 mg dm^{-3} initially in almost all the studies, except in determining the order w.r.t. Cr(III) by differential method.

The initial volume of each phase was always 20 mL. Two phases were taken in a stoppered bottle and agitated at the rate of about 500 shakes min^{-1} at (30 ± 1)°C maintained in a thermostatic water bath by an electrically operated shaking machine. The shaking speed was high enough to give the maximum rate (1). After a certain interval (2–15 s), two phases were separated quickly with a pipette. No emulsification was observed. A certain portion of the aqueous phase was pipetted out, oxidised to dichromate by $KMnO_4$–NaN_3 oxidation method, and its absorbance was measured at 370 nm by spectronic-20 (12) to estimate the Cr(III) content in the aqueous phase. The organic phase Cr(III) concentration was obtained by difference.

Treatments of Data

At high shaking speed and constant temperature and ionic strengths, the rate expression may be expressed as (13–17):

$$[1] \quad -dC_{Cr}^{A}/dt = k_f^* C_{Cr}^{Aa}[H_2A_2]_{(0)}^{b}[H^+]^c$$

where C_{Cr}^{A} = concentration of Cr(III) in the aqueous phase (mg dm^{-3}) and k_f^* = forward rate constant at 0.05 mol dm^{-3} sulphate and 0.25 mol dm^{-3} acetate medium. At constant buffered hydrogen ion concentration (h) and extractant concentration (h_a), eq. [1] becomes:

$$[2] \quad -dC_{Cr}^{A}/dt = qC_{Cr}^{Aa}$$

where q = pseudo first order rate constant = $k_f^* h_a^b (h)^c$. Where $a = 1$ (as found by differential method using both single and multiple runs (18)), the parameter q can be estimated from the slope of log C_{Cr}^{A} vs. time (t) plots.

Since the reaction order w.r.t. H^+ concentration is found to vary between -1 at higher acidities to 1 at lower acidities, q may be represented by:

$$[3] \quad q = k_f^* h_a^b (k_h[H^+] + 1 + k_{h-1}[H^+]^{-1})^{-1}$$

(k_h, k_{h-1} = proportionality constants in the pH dependence of rate at higher and lower acidities respectively) so that, at constant extractant concentration (h_a), where $q = q_{H^+}$, the value of k_h and k_{h-1} may be obtained by the curve fitting of the log q_{H^+} vs. log $[H^+]$ plots. Similarly, at constant h, where $q =$

$q_{H_2A_2}$, the value of b may be obtained from the slope of log $q_{H_2A_2}$ vs. log $[H_2A_2]_{(0)}$ plots. Using the known values of b, k_h, and k_{h-1}, the value of k_f* can be evaluated from the intercepts of the above two plots.

The effects of sulphate, acetate, and nitrate ions on the rate can be represented by the following empirical expression:

$$[4] \quad \log q_L = \log K_f' h_a^b [k_h h + 1 + k_{h-1} h^{-1}]^{-1} - \log (1 + k_{f(L)}[L])$$

where $L = Ac^-$, SO_4^{2-}, or NO_3^- and $k_f' = |k_f^*, k_{f'}^{0*}|$ or k_f^* ($k_{f'}^{0*}$ = forward rate constant at 0.25 mol dm^{-3} acetate medium only) owing to the fact that the reaction order w.r.t. SO_4^{2-} and NO_3^- varies between 0 and -1. For Ac^-, $k_{f(L)} = 0$. The value of $k_{f(L)}$ for other systems may be obtained by the curve fitting method.

Results

In the study of the rate of forward extraction, Cr(III) was present in the aqueous phase. The data used for analysis were only those obtained from the experiments in the early stages of extraction and the effect due to the back extraction may be considered negligible.

(i) Reaction Order w.r.t. Cr(III) Concentrations

Figure 1 shows that the slope of log $(-dC_{Cr}^A/dt)$ vs. log C_{Cr}^A plots are approximately unity in both the methods used (single and multiple runs). Hence, the reaction order w.r.t. Cr(III) is unity.

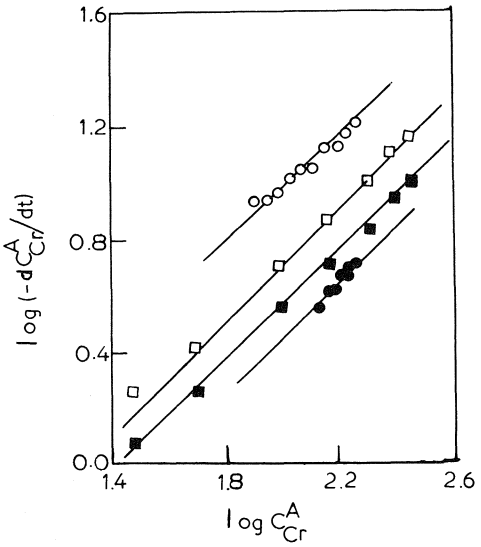

FIG. 1. Determination of the order w.r.t. Cr(III) in the forward extraction. SO_4^{2-} = 0.05 mol dm^{-3}, Ac^- = 0.25 mol dm^{-3}. (○), HDEHP = 0.6 mol dm^{-3}, pH = 4.07, C_{Cr}^A(ini) = 210 mg dm^{-3}, single run. (●), HDEHP = 0.6 mol dm^{-3}, pH = 2.72, C_{Cr}^A(ini) = 200 mg dm^{-3}, single run. (□), HDEHP = 0.6 mol dm^{-3}, pH = 3.5, dt = (5 − 0) s, multiple run. (■), HDEHP = 0.6 mol dm^{-3}, pH = 3.5, dt = (10 − 5) s, multiple run. The slope of all the lines is unity.

(ii) Reaction Order w.r.t. HDEHP Concentrations

The rate has been measured in the HDEHP concentration range of 0.15 to 0.80 mol dm^{-3} and at constant pH values of 2.32, 3.70, and 4.55. The log $q_{H_2A_2}$ vs. log $[H_2A_2]_{(0)}$ plots are given in Fig. 2. Figure 2 shows that the plots are straight lines with a slope of +1, thus, the order w.r.t. HDEHP, i.e. b is 1. From this result, it is concluded that the rate of extraction is proportional to the HDEHP concentrations in the organic phase.

(iii) Reaction Order w.r.t. H^+ Concentrations

The plots of log q_{H^+} vs. log $[H^+]$ are shown in Fig. 3 for constant HDEHP concentrations of 0.2, 0.4, and 0.6 mol dm^{-3} in the pH range 1.5 to 5.25. Figure 3 indicates that the slope of the plot approaches negative unity in the higher log $[H^+]$ region but the value increases with the decrease in log $[H^+]$ until it approaches the value of positive unity. The constants k_h and k_{h-1} in eq. [3] were determined and are listed in Table 1.

(iv) Reaction Order w.r.t. SO_4^{2-} Concentrations

The rates have been measured as a function of sulphate ion concentrations in the aqueous phase containing 0.25 mol dm^{-3} acetate at pH 3.0 (h_a = 0.4 mol dm^{-3}) and 4.5 (h_a = 0.6 mol dm^{-3}). The rate is found to decrease with the increase in the sulphate ion concentrations. Figure 4 represents the log $q_{SO_4^{2-}}$ vs. log $[SO_4^{2-}]$ plots. The experimental points do not fall on straight lines, but curves are obtained which approach a minus unity slope at higher sulphate ion concentrations. The constant $k_{f(L)}$, i.e.

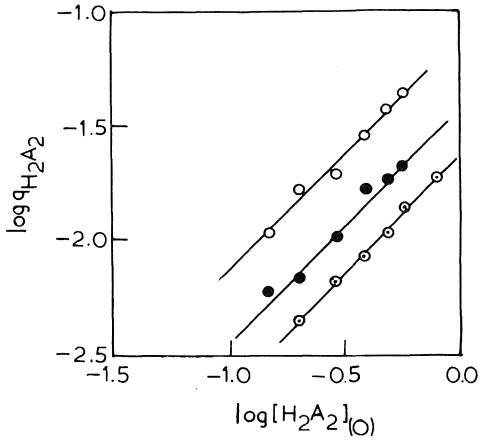

FIG. 2. Determination of the order w.r.t. HDEHP in the forward extraction. SO_4^{2-} = 0.05 mol dm^{-3}, Ac^- = 0.25 mol dm^{-3}. (○), pH = 3.70, slope = 1.00, intercept = −1.14. (●), pH = 2.32, slope = 0.97, intercept = −1.45. (⊙), pH = 4.55, slope = 1.00, intercept = −1.66.

TABLE 1. Value of constants in the rate expression

Rate constant			Other constant			
$\log k_f^*$	$\log k_{f'}{}^{0*}$	$\log k_f{}^{0*}$	k_h	k_{h-1}	$k_{f(SO_4^{2-})}$	$k_{f(NO_3^-)}$
-0.974 ± 0.047	-0.893	-0.893	500	10^{-4}	4.17	0.50

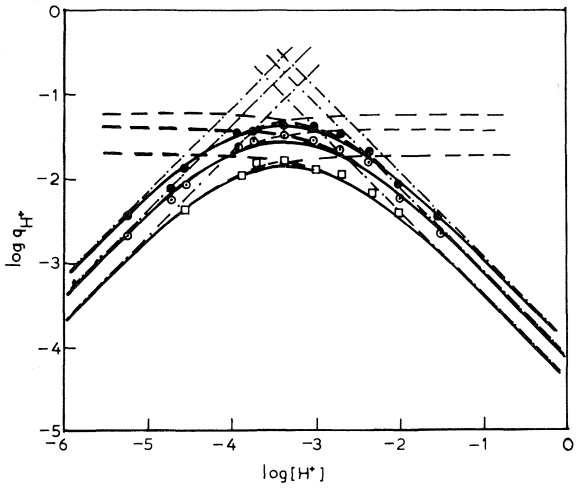

FIG. 3. Determination of the order w.r.t. H^+ in the forward extraction. $SO_4^{2-} = 0.05$ mol dm^{-3}, $Ac^- = 0.25$ mol dm^{-3}. (●), HDEHP = 0.6 mol dm^{-3}; (⊙), HDEHP = 0.4 mol dm^{-3}; (□), HDEHP = 0.2 mol dm^{-3}. The solid thick lines are drawn by: $\log q_{H^+} = \log k_f{}^* h_a{}^b - \log (k_h[H^+] + 1 + k_{h-1}[H^+]^{-1})$, where the value of k_h and k_{h-1} are found to be 500 and 10^{-4} respectively which fit the experimental points best. The thick broken lines are: $\log q_{H^+} = \log k_f{}^* h_a{}^b - \log (1 + k_h[H^+])$ and thin broken lines are: $\log q_{H^+} = \log k_f{}^* h_a{}^b - \log (1 + k_{h-1}[H^+]^{-1})$. The dotted and broken lines represent the asymptotes.

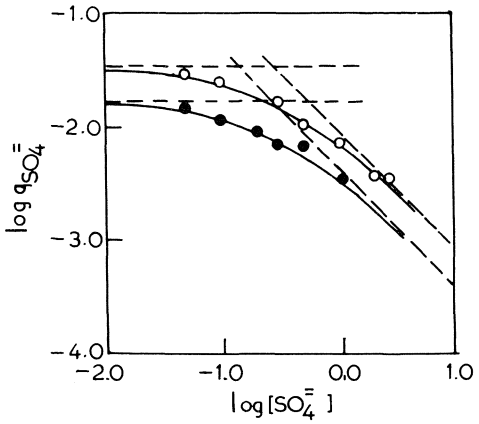

FIG. 4. Determination of the order w.r.t. SO_4^{2-} in the forward extraction. $Ac^- = 0.25$ mol dm^{-3}, (○), pH = 3.0, HDEHP = 0.4 mol dm^{-3}; (●), pH = 4.5, $H_2A_2 = 0.6$ mol dm^{-3}. The solid lines are drawn by $\log q_{SO_4^{2-}} = \log k_{f'}{}^{0*} h_a \times (500h + 1 + 10^{-4}h^{-1})^{-1} - \log (k_{f(SO_4^{2-})}[SO_4^{2-}] + 1)$, where $k_{f(SO_4^{2-})}$ is found to be 4.17, i.e. the value given for $k_{f(SO_4^{2-})}$ that fits the experimental points best is 4.17. The broken lines are two asymptotes: $\log q_{SO_4^{2-}} = \log k_{f'}{}^{0*} \times h_a(500h + 1 + 10^{-4}h^{-1})^{-1} = I$ and $\log q_{SO_4^{2-}} = I - \log k_{f(SO_4^{2-})} - \log [SO_4^{2-}]$.

$k_{f(SO_4^{2-})}$ in eq. [4], for this case, has been determined from the plot by the method of trial, i.e. the value given for $k_{f(SO_4^{2-})}$ that fits the experimental points best and is listed in Table 1. The rate constant $k_{f'}{}^{0*}$ in the presence of 0.25 mol dm^{-3} $[Ac^-]$ is also calculated and listed in the same table.

(v) Reaction Order w.r.t. Ac^- Concentrations

The rate of extraction has been determined when the HDEHP concentration is kept at 0.4 mol dm^{-3} and the acetate ion concentration is changed. The pH of the aqueous phase (containing 0.05 mol dm^{-3} SO_4^{2-}) in these experiments is kept at 3.0. Figure 5 represents the $\log q_{Ac^-}$ vs. $\log [Ac^-]$ plot, where it is found that there is no change of q_{Ac^-} value with the change of $[Ac^-]$, indicating the independence of the acetate ion concentration on the rate of Cr(III) extraction. Acetic acid was found to be partitioned between the benzene and aqueous phase (distribution coefficient, $[AcH]_{(0)}{}^{1/2}/[AcH] = 0.235$ in water/benzene system only and is nearly equal to 0.367 in water/0.2 mol dm^{-3} HDEHP dissolved in benzene). No correction was made for this and in Fig. 5, $[Ac^-]$ indicates the total concentration of acetic acid and sodium acetate, because the rate is found to be independent of acetate ion concentration.

(vi) Reaction Order w.r.t. NO_3^- Concentrations

It is found that the rate of extraction of Cr(III) is decreased to some extent in presence of nitrate ions in the aqueous phase, although the distribution coefficient does not vary with the increase in the nitrate ion concentration (10). For this, the experiments have been conducted from the aqueous solutions containing 0.05 mol dm^{-3} sulphate ion, 0.25 mol dm^{-3} acetate ion and variable amounts of nitrate ions (added as $NaNO_3$). Figure 5 represents the log $q_{NO_3^-}$ vs. log $[NO_3^-]$ plot, which shows that the value of log $q_{NO_3^-}$ decreases with the increase in the nitrate ion concentrations. The experimental points do not fall on a straight line but a curve is obtained which approaches zero slope at lower nitrate ion concentration ranges and -1 slope at higher nitrate ion concentration ranges. The value of the constant $k_{f(NO_3^-)}$ in eq. [4] has been estimated from the plot by the method of trial and error and is listed in Table 1.

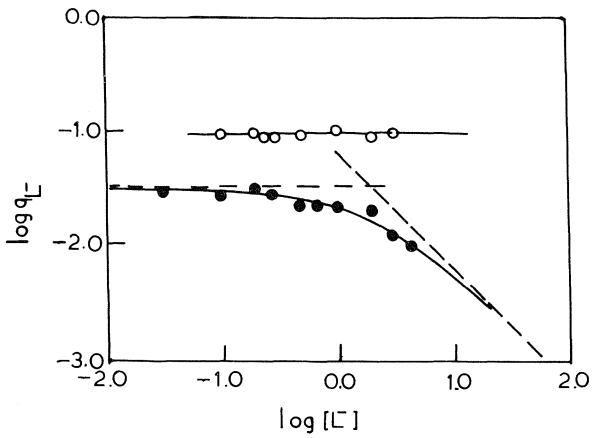

FIG. 5. Determination of the order w.r.t. Ac^- and NO_3^- in the forward extraction. (*a*) (○), [L] = $[Ac^-]$ = $[SO_4^{2-}]$ = 0.05 mol dm^{-3}, pH = 3.0, HDEHP = 0.4 mol dm^{-3}, $k_{f(Ac^-)}$ = 0 (cf. eq. [15]). (*b*) (●), L = $[NO_3^-]$ = $[SO_4^{2-}]$ = 0.05 mol dm^{-3}, pH = 3.0, HDEHP = 0.4 mol dm^{-3}, Ac^- = 0.25 mol dm^{-3}. The solid line is drawn by $\log q_{NO_3^-} = \log k_f^* h_a(500h + 1 + 10^{-4}h^{-1})^{-1} - \log (k_{f(NO_3^-)}[NO_3^-] + 1)$, where $k_{f(NO_3^-)}$ is found to be 0.5. The broken lines are two asymptotes: $\log q_{NO_3^-} = \log k_f^* h_a(500h + 1 + 10^{-4}h^{-1})^{-1} = I$ and $\log q_{NO_3^-} = I - \log (k_{f(NO_3^-)}) - \log [NO_3^-]$.

(vii) Evaluation of the Rate Constants

The forward extraction rate constant, k_f^* at 0.05 mol dm^{-3} sulphate and 0.25 mol dm^{-3} acetate media, has been evaluated from the experimental results. The value of $\log k_f^*$ is quoted in Table 1 with standard deviation.

In this case, the rate constant, $\log k_f^{0*}$ (where k_f^{0*} = forward rate constant in absence of sulphate and acetate ions and $\log k_f^{0*}$ is identical with the $\log k_{f'}^{0*}$ as the rate is independent of acetate ion concentrations) has been evaluated by comparing the relation given by eq. [1] containing H^+ term modified as in eq. [3], which is valid for 0.05 mol dm^{-3} sulphate and 0.25 mol dm^{-3} acetate media, with the following relationships

$$-\frac{dC_{Cr}^{A}}{dt} = \frac{k_f^{0*} C_{Cr}^{A}[H_2A_2]_{(0)}[Ac^-]^0}{(500[H^+] + 1 + 10^{-4}[H^+]^{-1})(1 + 4.17[SO_4^{2-}])}$$

and is tabulated in Table 1.

Discussion

It has been reported early that in the lower acidities Cr(III) is present as hydrolysed and polymerised species. At higher acidities (pH < 2), Cr(III) is present as $[Cr(H_2O)_6]^{3+}$ (19, 20). But as the acidity is decreased, there will appear successively the species like $[Cr(OH)]^{2+}$, $[Cr_2(OH)_2]^{4+}$, $[Cr_4(OH)_4]^{8+}$, $[Cr_2(OH)_3]^{3+}$, $[Cr_4(OH)_8]^{4+}$, $[Cr(OH)_2]^{2+}$, etc. until it precipitates out as $Cr(OH)_3$ at pH around 5.5 (co-ordinated water molecules are not shown) (10, 19, 20). Kobayashi *et al.* reported that the polynuclear chromium compounds contain the non-linear

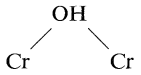

groups (21).

In discussing the results obtained from the rate measurements, i.e. the first order dependence of Cr(III) concentrations on the rate at any pH indicates that the mononuclear Cr(III) species are always involved in the rate determining step. Although there may be present various types of Cr(III) species (mono or polynuclear), only the mononuclear species will be responsible for the rate determinations. The first order dependence of Cr(III) concentration on the rate is in agreement with the general observation that the order w.r.t. the metal ions is found to be unity (2, 7, 13–17, 22, 23), except in the case of extraction of Ti(IV) with HDEHP (1) and of Zn(II) with di-α-naphthyl dithiocarbazone (24). Thus, at lower acidities Cr(III), present as polynuclear form, breaks down rapidly to mononuclear form which then reacts.

The value of the rate constant ($k_f^{0*} = 10^{-0.974}$) obtained for the system may be considered high. It is well known that the substitution reactions in Cr^{3+} species are so slow that it takes a few hours to a few days for completion of the reactions. It is well known that the substitution in $Cr(OH)^{2+}$ is 10–100 times faster than the substitution in Cr^{3+} and the interconversion of Cr^{3+} with $Cr(OH)^{2+}$ is very rapid. As a result, the value of the rate constant suggests that the reactions will proceed via $Cr(OH)^{2+}$ as a primary path instead of via Cr^{3+} in the lower pH ranges at which the experiments were done. At higher pH ranges, the dihydroxypolymerised species may be assumed to be converted rapidly into $Cr(OH)^{2+}$ ions which then react.

The first hydrolysis constant (β_1) for $Cr(OH)^{2+}$ may be given by:

$$[5] \quad [Cr^{3+}] = [Cr(OH)^{2+}][H^+]/\beta_1$$

where β_1 has been estimated to be about 10^{-4} (20, 25), and as a result, the rate expression in absence of sulphate and acetate ion in the low pH range (around pH 2) may be represented by:

$$[6] \quad -dC_{Cr}^{A}/dt = (500\beta_1)^{-1} k_f^{0*}[Cr(OH)^{2+}] \times [H_2A_2]_{(0)}$$

At very low acidities (around pH 4.5, where Cr(III) is supposed to be present entirely as $Cr(OH)_2^+$ or its polymer), the following hydrolysis equilibrium is maintained:

[7] $[Cr(OH)^{2+}] = [Cr(OH)_2{}^{+}][H^+]/\beta_2$

where $\beta_2 = 10^{-6.5}$ (20) and the rate expression becomes:

[8] $-dC_{Cr}{}^{A}/dt = \beta_2 10^4 k_f{}^0 * [Cr(OH)^{2+}][H_2A_2]_{(0)}$

The eqs. [6] and [8] suggest that at both high and low acidities, the step represented by:

[9] $Cr(OH)^{2+} + H_2A_2 \rightarrow CrHA_2{}^{2+} + H_2O$

acts as rate determining in the pH range studied. A similar type of mechanism through the formation of hydroxy species has been suggested for the extraction of Fe(III) with HDEHP by Roddy *et al.* (26).

Similar to the fact that the sulphate ion (10) decreases the distribution ratio of Cr(III), the rate of extraction of Cr(III) is also decreased by the presence of sulphate ion, probably due to the formation of the aqueous Cr^{3+}–$SO_4{}^{2-}$ complex and/or Cr^{3+}–$SO_4{}^{2-}$ ion pairs (27). The sulphate group of such complexes or ion pairs are more slowly replaced by $HA_2{}^{-}$ group or the dissociation of such complexes affects the rate of extraction. Analogous suggestions may be put forward for the effect of nitrate ion on the rate. It is known that Cr(III) also forms complex of the type $[Cr_3O(Ac)_6]^{+}$ with acetate (28). The independence of rate on acetate ion suggests that the complex of Cr(III) with Ac^{-} rapidly breaks down into Cr(III) or such product, in presence of $HA_2{}^{-}$ group which then react with $HA_2{}^{-}$ or no such complex is formed in presence of high sulphate ion concentrations. The exact explanation is not known to us. The acetate independence of Cr(III) on the extraction ratio was also observed and reported (10).

The failure to the backward extraction is expected since a number of metal chelates are known to exhibit refractory character towards the attack by ligands (7, 29). This type of inertness is particularly expected in the case of Cr(III).

Acknowledgement

Authors are grateful to the University Grants Commission (U.G.C.), Dacca, for their financial support to conduct the research.

1. F. Islam and R. K. Biswas. J. Inorg. Nucl. Chem. **40**, 559 (1978).
2. F. Islam and R. K. Biswas. J. Inorg. Nucl. Chem. In press.
3. H. Taube. Chem. Rev. **50**, 69 (1952).
4. F. Basolo and R. G. Pearson. Mechanism of inorganic reactions. Wiley, New York. 1958.
5. J. P. McKaveney and H. Freiser. Anal. Chem. **29**, 288 (1957); **30**, 1965 (1958).
6. G. H. Morrison and H. Freiser. Solvent extraction in analytical chemistry. Wiley, New York. 1957. p. 201.
7. H. E. Hellwege and G. K. Schweitzer. Anal. Chim. Acta, **29**, 46 (1963).
8. R. A. Sambasiva, R. B. Rama Chandra, and S. Y. Sesha. Indian J. Chem. Sect. A, **16**, 80 (1978).
9. K. Kimura. Bull. Chem. Soc. Jpn. **33**, 1038 (1960).
10. F. Islam and R. K. Biswas. J. Inorg. Nucl. Chem. **41**, 229 (1979).
11. A. I. Vogel. A textbook of quantitative inorganic analysis. 3rd ed. Longman-Green, London. 1962. p. 311.
12. G. Charlot. Colorimetric determinations of elements. Elsevier Publishing Co. 1964. p. 226.
13. T. Sekine, Y. Koike, and Y. Komatsu. Bull. Chem. Soc. Jpn. **44**, 1903 (1973).
14. T. Sekine, J. Yumikura, and Y. Komatsu. Bull. Chem. Soc. Jpn. **46**, 2356 (1973).
15. T. Sekine and Y. Komatsu. J. Inorg. Nucl. Chem. **37**, 185 (1975).
16. T. Sekine, Y. Komatsu, and J. Yumikura. J. Inorg. Nucl. Chem. **35**, 3891 (1973).
17. Y. Komatsu, H. Honda, and T. Sekine. J. Inorg. Nucl. Chem. **38**, 1861 (1976).
18. A. A. Frost and R. G. Pearson. Kinetics and mechanism. 2nd ed. Wiley. 1961. p. 45.
19. Y. I. Sannikov, E. I. Krylov, and V. M. Vinogradov. Russ. J. Inorg. Chem. (Eng.), **12**, 1398 (1967).
20. U. V. Mayenburg, O. Siroky, and G. Schwarzenbach. Helv. Chim. Acta, **50**, 1099 (1973).
21. H. Kobayashi, I. Haseda, and E. Kanda. J. Phys. Soc. Jpn. **15**, 1646 (1960).
22. S. M. Karpacheva and L. V. Ilozheva. Radiochimiya (Eng.), **11**, 32 (1969).
23. B. E. McClellan and O. Menis. Anal. Chem. **43**, 436 (1971).
24. B. E. McClellan and H. Freiser. Anal. Chem. **36**, 2262 (1964).
25. J. I. Morrow and J. Levy. J. Phys. Chem. **72**, 885 (1968).
26. J. W. Roddy, C. F. Coleman, and S. Arai. J. Inorg. Nucl. Chem. **33**, 1099 (1971).
27. R. Tsuchiya and A. Umahara. Bull. Chem. Soc. Jpn. **36**, 554 (1963).
28. B. N. Figgis and G. B. Robertson. Nature, **205**, 694 (1965).
29. F. Feigl. Chemistry of specific, selective and sensitive reactions. Academic Press, New York. 1949. pp. 623, 624.

Appendix

Elaborated Mathematical Treatment of eq. [3] to Evaluate the Value of k_h and k_{h-1}

At higher acidities, the contribution due to $k_{h-1}[H^+]^{-1}$ term may be disregarded, and the following equation may be considered to fit the experimental points:

[10] $\log q_{H^+} = \log k_f * h_a{}^b - \log (k_h[H^+] + 1)$

The curve represented by eq. [10] has two asymptotes:

[11] $\underset{[H^+]\rightarrow 0}{\text{Lt}} \log q_{H^+} = \log k_f * h_a{}^b$

[12] $\underset{[H^+]\rightarrow \infty}{\text{Lt}} \log q_{H^+} = \log k_f * h_a{}^b - \log k_h - \log [H^+]$

The asymptote represented by eq. [12] has intercept of value $\log k_f * h_a{}^b - \log k_h$ and hence the value of k_h may be obtained as the value of $\log k_f * h_a{}^b$ is known from the asymptote represented by eq. [11].

Similar treatment at the lower acidities, where the term $k_h[H^+]$ may be neglected, gives the value of k_{h-1}.

The oxidation of ascorbic acid and hydroquinone by perhydroxyl radicals. A flash photolysis study

A. D. NADEZHDIN AND H. B. DUNFORD
Department of Chemistry, University of Alberta, Edmonton, Alta., Canada T6G 2G2

Received May 25, 1979

A. D. NADEZHDIN and H. B. DUNFORD. Can. J. Chem. **57**, 3017 (1979).

The oxidation of ascorbic acid (AH_2) and hydroquinone (QH_2) by photolytically generated $HO_2^{\bullet}$ radicals was studied over a broad range of pH. The rate constants of the following processes were obtained

$$k(AH + HO_2^{\bullet} \rightarrow A^{-\bullet} + H_2O_2) = (1.25 \pm 0.25) \times 10^6\ M^{-1}\ s^{-1}$$

$$k(AH^- + O_2^{-\bullet} \rightarrow A^{-\bullet} + HO_2^-) = (5.75 \pm 0.35) \times 10^4\ M^{-1}\ s^{-1}$$

and

$$k(QH_2 + HO_2^{\bullet} \rightarrow {}^{\bullet}QH + H_2O_2) = \text{either } (0.85 \pm 0.1) \times 10^4$$

$$\text{or } (1.7 \pm 0.2) \times 10^4\ M^{-1}\ s^{-1}$$

depending upon two different possible mechanistic interpretations.

A. D. NADEZHDIN et H. B. DUNFORD. Can. J. Chem. **57**, 3017 (1979).

On a étudié, sur une large échelle de pH, l'oxydation de l'acide ascorbique (AH_2) et de l'hydroquinone (QH_2) par des radicaux $HO_2^{\bullet}$ générés photochimiquement. On a obtenu les constantes de vitesse pour les réactions suivantes:

$$k(AH + HO_2^{\bullet} \rightarrow A^{-\bullet} + H_2O_2) = (1.25 \pm 0.25) \times 10^6\ M^{-1}\ s^{-1}$$

$$k(AH^- + O_2^{-\bullet} \rightarrow A^{-\bullet} + HO_2^-) = (5.75 \pm 0.35) \times 10^4\ M^{-1}\ s^{-1}$$

et

$$k(QH_2 + HO_2^{\bullet} \rightarrow {}^{\bullet}QH + H_2O_2) = \text{soit } (0.85 \pm 0.1) \times 10^4$$

$$\text{ou } (1.7 \pm 0.2) \times 10^4\ M^{-1}\ s^{-1}$$

dépendant des deux différentes interprétations possibles du mécanisme de la réaction.

[Traduit par le journal]

Introduction

The role of perhydroxyl radicals in different oxidadation processes involving oxygen is widely discussed in the literature especially that of biochemistry (1) during the last decade. A large number of elementary reactions of $O_2^{-\bullet}$ (or its acidic form $HO_2^{\bullet}$) have been studied quantitatively. Although most of the processes reported involve perhydroxyl radical as a reducing agent, there are a few studies describing its oxidative ability. In particular, several reactions of $HO_2^{\bullet}$ with one-electron reductants, such as transition metal ions in low oxidation states, Fe^{2+} (2), Cu^+ (3), Ce^{3+} (4) were studied by different techniques. Oxidation of a number of organic reductants like cysteine (5), ascorbic acid (6), and hydroquinone (7) by $HO_2^{\bullet}$ was indicated in γ radiolysis experiments in which an increase of H_2O_2 yield was observed. More recent kinetic studies provide the values of rate constants (8–12). These papers will be discussed in detail later.

In the case of two-electron reductants such as organic molecules one faces several experimental problems. These include possible reactivity of $HO_2^{\bullet}$ radicals with the products of one-electron transfers (semiquinone radicals), and reactions of semiquinones with molecular oxygen which could lead to a chain process (9). Another important problem is the reductive ability of superoxide anions, so the presence of small amounts of products of the two-electron oxidation of initial reagent can cause $O_2^{-\bullet}$ consumption and semiquinone production (see below). This could be a serious misleading factor, when the reaction is studied by following the increase of semiquinone concentration. Therefore, the observation of the initial reductant consumption has to be considered as more direct and reliable than other methods.

In this work we studied the oxidation of ascorbate (AH_2) and hydroquinone (QH_2) by perhydroxyl radicals generated by the flash photolysis of water solutions containing reductant and H_2O_2. As was explained in detail in our initial paper (12), when the ratio of $[H_2O_2]_0$:[reductant] exceeds 10^3, all primary $^{\bullet}OH$ radicals generated by photolysis of H_2O_2

0008-4042/79/233017-06$01.00/0

(13) are scavenged by hydrogen peroxide producing $HO_2^{\bullet}$ radicals within 1/10 of a millisecond after the flash.

Materials and Methods

All the chemicals were of reagent grade used without further purification except ascorbate, which was recrystallized from spectroscopic grade methanol. Buffer solutions for pH regions 3.8–5.8 and 6.0–7.8 were acetic acid – sodium acetate and potassium dihydrogen phosphate – sodium hydroxide; pH values lower than 3.5 were adjusted by adding concentrated $HClO_4$. Several experiments in the neutral pH region were accomplished without any buffer and no dependence of the results on the presence of buffer or its concentration was observed. In the majority of experiments with buffers the ionic strength value was 0.02 *M*. Approximately 10^{-5} *M* EDTA was added to the ascorbate stock solution to prevent AH_2 oxidation on heavy metal residues. Quintuply distilled water was used for all experiments. Control experiments, where optical absorption of the solution was recorded vs. time in the absence of flash light, showed that the spontaneous oxidation of AH_2 and QH_2 by O_2 or H_2O_2 was a negligibly slow process compared to the reductants consumption under irradiation (14).

The flash photolysis apparatus with spectrophotometric registration has been described (12). The limiting error of absorbance was between 5×10^{-5} and 2×10^{-4} absorbance units depending upon the time interval of the experiment. Consumption of ascorbic acid after each flash was followed in the spectral region 260–265 nm where AH_2 absorbs very strongly as is shown in Fig. 1*a* and where dehydroascorbate does not absorb appreciably. Oxidation of hydroquinone was followed at 290 nm where absorption of hydroquinone is about seven times stronger than that of quinone (Fig. 1*b*). H_2O_2 was present in the solutions in a large excess. However, since its molar absorptivity is relatively low ($\sim 2\ M^{-1}\ cm^{-1}$ at 290 nm and $\sim 12\ M^{-1}\ cm^{-1}$ at 265 nm) compared to that of ascorbate or hydroquinone the absorption changes recorded after each flash are totally accounted for by the consumption of reductant. At the wavelength of the photolyzing light (λ = 330 nm) absorption by the reductants was negligibly small compared to that of H_2O_2 and in control flash experiments in the absence of H_2O_2 no change of AH_2 or QH_2 concentrations was observed. The concentration of perhydroxyl radicals formed per flash was measured by the method described in ref. 12 using the $O_2^{-\bullet}$ scavenger, tetranitromethane. All experiments were carried out at 22°C.

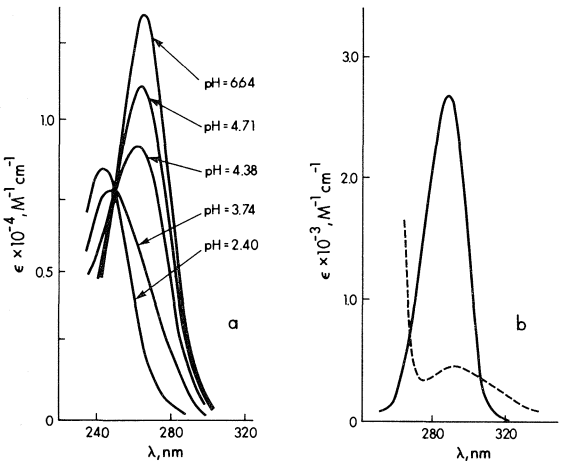

FIG. 1. The ascorbate and hydroquinone absorption spectra. (*a*) Molar absorptivity (ε) of ascorbic acid at different pH values, $\mu = 0.02\ M$, 22°C. (*b*) Solid line: absorption spectrum of hydroquinone at low and neutral pH; broken line represents quinone spectrum.

Results and Discussion

The change of the optical absorption vs. time after each flash in the system $AH_2 + H_2O_2$ obeyed first order kinetics. A typical run is illustrated in Fig. 2. It can be seen from Table 1 that the value of the relaxation time τ_0, is inversely proportional to $[AH_2]$ and did not depend on the initial concentration of perhydroxyl radicals, $[HO_2^{\bullet}]_0$. On the other hand the overall change of AH_2 concentration did not depend on $[AH_2]_0$ and was directly proportional to $[HO_2^{\bullet}]_0$. The stoichiometry of the reaction was $[HO_2^{\bullet}]_0 : \Delta[AH_2] = 2 \pm 0.2$. These facts can be interpreted in terms of two alternative schemes:

Scheme (*a*)

$$[1] \quad HO_2^{\bullet} + AH_2 \rightarrow A^{-\bullet} + H_2O_2 + H^+$$

$$[2] \quad HO_2^{\bullet} + A^{-\bullet} \xrightarrow{H^+} A + H_2O_2$$

or Scheme (*b*)

$$[1] \quad HO_2^{\bullet} + AH_2 \rightarrow A^{-\bullet} + H_2O_2 + H^+$$

$$[3] \quad A^{-\bullet} + A^{-\bullet} \xrightarrow{2H^+} A + AH_2$$

where $A^{-\bullet}$ is the semiquinone radical of ascorbate, studied and chemically characterized in refs. 15–17, and A designates dehydroascorbate.

If reaction [2] is faster in our system than [3] and Scheme (*a*) is valid we can write

$$d[AH_2]/dt = -k_1[AH_2][HO_2^{\bullet}]$$

$$d[HO_2^{\bullet}]/dt = -k_1[AH_2][HO_2^{\bullet}] - k_2[A^{-\bullet}][HO_2^{\bullet}]$$

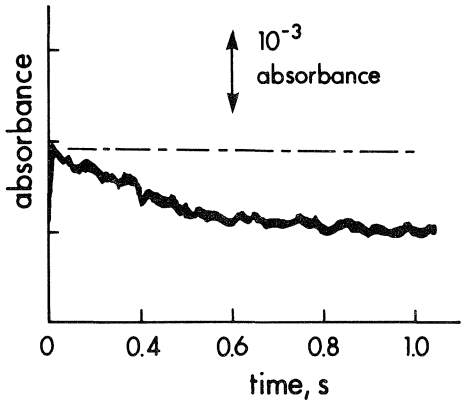

FIG. 2. Absorption change vs. time after flash in the system ascorbate (AH_2) + H_2O_2. $[AH_2]_0 = 1.2 \times 10^{-5}\ M$, $[HO_2^{\bullet}]_0 = 1.2 \times 10^{-7}\ M$, pH = 7.11, $\mu = 0.02\ M$, 22°C.

TABLE 1. Reaction between ascorbic acid and perhydroxyl; $k_{app} = 1/(\tau_0[AH_2])$

pH	$[AH_2]_0 \times 10^5$, M	$[HO_2]_0 \times 10^7$, M	$\Delta[AH_2] \times 10^7$, M	τ_0, s	$k_{app} \times 10^{-6}$, M^{-1} s^{-1}
5.42	0.63	0.5	0.24	0.21	0.76
5.42	0.63	0.8	0.42	0.18	0.89
5.42	0.63	1.1	0.60	0.19	0.84
5.42	0.55	1.0	0.52	0.18	1.01
5.42	1.10	1.0	0.55	0.10	9.10
5.42	2.20	1.0	0.48	0.05	9.10
4.78	0.60	1.1	0.65	0.13	1.30
4.78	1.20	1.1	0.52	0.08	1.10
4.78	1.20	0.8	0.50	0.07	1.19
4.75	0.63	0.8	0.45	0.14	1.14
4.65	0.51	0.9	0.55	0.12	1.53
4.65	1.02	0.9	0.49	0.07	1.40
4.62	0.55	0.8	0.42	0.10	1.81
4.41	0.37	0.9	0.45	0.16	1.70
4.41	0.75	0.9	0.48	0.10	1.34
4.20	0.75	0.9	0.52	0.11	1.20
4.20	0.37	0.9	0.45	0.17	1.58
4.20	0.60	1.1	0.48	0.13	1.28
4.20	0.51	0.9	0.42	0.18	1.10
3.83	0.37	1.2	0.64	0.30	0.90
3.83	0.75	1.2	0.61	0.21	0.63
3.83	0.51	0.9	0.54	0.27	0.73
3.44	1.02	0.9	0.52	0.42	0.47
3.22	0.51	0.9	0.61	0.67	0.29
2.75	1.20	1.1	0.56	0.45	0.19
2.75	1.20	0.8	0.45	0.32	0.13
5.50	0.63	0.8	0.50	0.27	0.59
5.50	1.25	0.8	0.42	0.15	0.53
5.95	1.25	0.5	0.22	0.25	0.32
5.95	2.50	1.1	0.60	0.12	0.33
6.75	1.25	0.8	0.52	0.45	0.18
6.75	1.02	0.9	0.48	0.80	0.12
6.75	2.04	0.9	0.51	0.35	0.14
7.11	1.20	1.2	0.65	0.45	0.17
7.45	1.25	1.1	0.50	0.75	0.12
7.45	2.50	0.8	0.45	0.40	0.11
7.45	3.75	0.8	0.41	0.22	0.13
7.78	1.10	1.0	0.56	0.80	0.11
7.78	2.20	1.0	0.48	0.48	0.14

Using the steady state approximation for the value of $[A^{\cdot}]$ one gets

$$k_1[AH_2][HO_2] = k_2[A^{-\cdot}][HO_2^{\cdot}]$$

and therefore

$$d[HO_2^{\cdot}]/dt = -2k_1[AH_2][HO_2^{\cdot}]$$

Integrating this system of equations and taking into account that $[AH_2] \gg [HO_2^{\cdot}]_0$ we get

$$[4] \quad [AH_2]_0 - [AH_2] = \tfrac{1}{2}[HO_2^{\cdot}]_0\{1 - \exp(-2k_1[AH_2]t)\}$$

Scheme (*b*) after integrating gives

$$[5] \quad [AH_2]_0 - [AH_2] = \tfrac{1}{2}[HO_2^{\cdot}]_0\{1 - \exp(-k_1[AH_2]t)\}$$

Equations [4] and [5] describe the same stoichiometry and kinetic behaviour but the second gives a rate constant two times larger for reaction [1] than the first. Fortunately we were able to distinguish between these two possibilities.

Let us suppose that (*b*) is the correct scheme. According to the steady state approximation for $[A^{-\cdot}]$ relation [6] must be fulfilled:

$$[6] \quad 2k_3[A^{-\cdot}]^2 = k_1[AH_2][HO_2^{\cdot}]$$

The rate constant of the disproportionation of $A^{-\cdot}$ radicals, k_3, is known at different pH values (14). For example at pH = 5 it is $\sim 1.5 \times 10^7$ M^{-1} s^{-1} and at pH 7 it is $\sim 10^6$ M^{-1} s^{-1}. The value of $[A^{-\cdot}]$ in the course of the reaction was estimated by the recording of absorption vs. time at 360 nm where the molar absorptivity of $A^{-\cdot}$ radicals is maximal

and equal to $3 \times 10^3\ M^{-1}\ cm^{-1}$ (15). At least $4 \times 10^{-8}\ M$ of a species with such a molar absorptivity should be easily detected using our registration system. Under typical conditions, $[AH_2]_0 = 10^{-5}\ M$ and $[HO_2^{\cdot}]_0 \simeq 10^{-7}\ M$, we did not observe any change of absorbance at 360 nm in a pH region from 4.2 to 7.5, therefore in the course of AH_2 consumption $[A^{-\cdot}]$ did not exceed $4 \times 10^{-8}\ M$. Using the above mentioned values of k_3 and the experimentally determined k_{app} as k_1 in accordance with Scheme (*b*), one can see that relation [6] is not fulfilled. Therefore reaction [2], Scheme (*a*), must be the main way of $A^{-\cdot}$ radical consumption and k_1 is equal to one half of the k_{app} values in the last column of Table 1.

The dependence of $\log k_1$ vs. pH is shown in Fig. 3. The data can be accounted for quantitatively by considering the acid–base equilibria

[7] $AH_2 \rightleftharpoons AH^- + H^+ \qquad K_7 = [H^+][AH^-]/[AH_2]$

and

[8] $HO_2^{\cdot} \rightleftharpoons O_2^{-\cdot} + H^+ \qquad K_8 = [H^+][O_2^{-\cdot}]/[HO_2^{\cdot}]$

Assuming that the reaction between ascorbate and perhydroxyl radical over the pH region of the study is in fact the sum of two processes

[9] $AH^- + HO_2^{\cdot} \xrightarrow{k_9} A^{-\cdot} + H_2O_2$

[10] $AH^- + O_2^{-\cdot} \xrightarrow{k_{10}} A^{-\cdot} + HO_2^-$

we have

$$[11] \quad \tfrac{1}{2}k_{app} = k_1 = \frac{k_9K_7[H^+] + k_{10}K_7K_8}{([H^+] + K_7)([H^+] + K_8)}$$

Use of a nonlinear least-squares computer program fitting the data to eq. [11] gave the following best fit parameters

$$pK_7 = 4.0 \pm 0.1$$

(compared to the literature value of 4.1 (18))

$$pK_8 = 5.05 \pm 0.1$$

(compared to the literature value 4.9 (19))

$$k_9 = (1.25 \pm 0.15) \times 10^6\ M^{-1}\ s^{-1}$$

and

$$k_{10} = (5.75 \pm 0.35) \times 10^4\ M^{-1}\ s^{-1}$$

The continuous curve in Fig. 3 is numerically simulated using these values. At pH > 7 k_{app} is practically equal to $2k_{10}$, i.e., $1.15 \times 10^5\ M^{-1}\ s^{-1}$. This value is consistent with that obtained by Bielski and Richter (9) ($1.52 \times 10^5\ M^{-1}\ s^{-1}$) and close to the rate constant for $AH_2 + O_2^{-\cdot}$ (8), $2.7 \times 10^5\ M^{-1}\ s^{-1}$ at pH = 7.4. However, the rate constant for the same reaction given in ref. 10, $(0.8 \pm 0.2) \times 10^8\ M^{-1}\ s^{-1}$, is much bigger than our value as well as that listed in refs. 8 and 9.

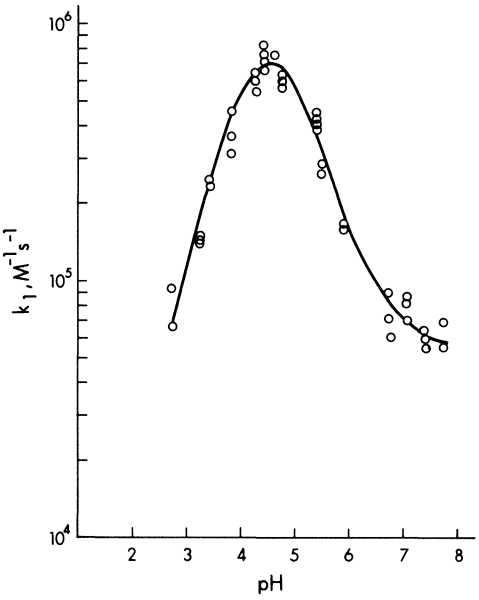

FIG. 3. The pH dependence of k_1. $\mu = 0.02\ M$, 22°C. Points represent experimental data, while the continuous line is numerically simulated using eq. [11] and the best fit parameters.

The results of the flash photolysis study of hydroquinone oxidation are represented in Table 2. We observed the same kind of kinetics as in the $AH_2 + HO_2^{\cdot}$ system and, as it can be seen from Table 2, the value of τ_0 was inversely proportional to $[QH_2]_0$ and did not depend on $[HO_2^{\cdot}]_0$. The overall change of absorption at $\lambda = 290$ nm did not depend on $[QH_2]$ and was proportional to $[HO_2^{\cdot}]_0$, corresponding to the stoichiometry: $[HO_2^{\cdot}]_0 : \Delta[QH_2] = 2 \pm 0.1$. The same two possible mechanisms as in the case of ascorbate oxidation (*a* and *b*) could be suggested for $QH_2 + HO_2^{\cdot}$ interaction, but in the case of hydroquinone we were not able to choose between the two possible ways of semiquinone consumption

[12] $QH^{\cdot} + HO_2^{\cdot} \rightarrow Q + H_2O_2$

or

[13] $QH^{\cdot} + QH^{\cdot} \rightarrow QH_2 + Q$

where $QH^{\cdot}$ is the protonated form of the semiquinone radical ($pK \simeq 4$ (20)) and Q designates *p*-benzoquinone. The rate constant of semiquinone radical disproportionation is extremely high at low pH, $2k_{13} = 1.2 \times 10^9\ M^{-1}\ s^{-1}$ (21) and without knowledge of k_{12} we could not compare the rates of the reactions [12] and [13]. Therefore the elementary rate constant of the reaction

[14] $QH_2 + HO_2^{\cdot} \rightarrow QH^{\cdot} + H_2O_2$

TABLE 2. Reaction between hydroquinone and perhydroxyl radical; $k_{app} = 1/(\tau_0[QH_2]_0)$

pH	$[QH_2]_0 \times 10^4$, M	$[HO_2]_0 \times 10^7$, M	$\Delta[QH_2] \times 10^7$, M	τ_0, s	$k_{app} \times 10^{-4}$, M^{-1} s^{-1}
0.4	0.75	2.5	1.3	0.80	1.67
0.4	1.50	2.5	1.2	0.35	1.90
0.4	1.50	1.2	0.6	0.40	1.67
0.4	0.75	1.2	0.6	0.65	2.05
0.75	1.00	2.0	1.0	0.62	1.61
0.75	2.00	2.0	1.2	0.25	2.00
1.21	1.50	1.6	0.8	0.35	1.90
1.21	1.50	0.9	0.5	0.42	1.58
1.77	0.75	1.6	0.7	0.75	1.78
1.77	1.50	1.6	1.0	0.38	1.75
1.77	2.50	1.3	0.8	0.22	1.82
2.13	2.50	1.6	0.9	0.25	1.60
2.72	1.00	1.6	0.8	0.55	1.82
2.72	2.00	1.3	0.7	0.35	1.45
3.51	0.75	2.5	1.2	0.70	1.90
3.51	1.50	1.2	0.7	0.45	1.48

could be equal to k_{app} from Table 2 or be one half of its value, i.e. k_{14} is either $(1.7 \pm 0.2) \times 10^4$ M^{-1} s^{-1} or $(0.85 \pm 0.1) \times 10^4$ M^{-1} s^{-1}. It is seen from Table 2 that in the pH region from 0.4 to 3.5 k_{app} does not depend on $[H^+]$. At the pH values from 3.5 to 4 the overall change of absorption caused by the flash decreased drastically and a further increase of pH eliminated that change totally. It is possible that traces of quinone could be present as an impurity or even formed slowly in the dark in the solution containing H_2O_2 and hydroquinone. It could compete with hydroquinone for hydroperoxyl radicals at pH values close to the pK of $HO_2^{\cdot}$, 4.88 (19), because of the very high rate constant of the reaction

[15] $Q + O_2^{-\cdot} \rightarrow Q^{-\cdot} + O_2$

$k_{15} = 9.8 \times 10^8$ M^{-1} s^{-1} (11). According to this suggestion quinone should not interfere with hydroquinone oxidation at lower pH values, since $HO_2^{\cdot}$ could be relatively inert as a reductant of Q, and $[O_2^{-\cdot}]$ is small in acidic solutions. The following experiments served to confirm these speculations. Addition of 2×10^{-5} M quinone to the solution containing 2×10^{-4} M QH_2 and 0.2 M H_2O_2 at pH 2.5 totally subdued the hydroquinone consumption normally observed in the absence of quinone after a flash. However, several drops of concentrated $HClO_4$ added to the solution restored the process of QH_2 oxidation under irradiation; the final pH in the system was 1.05. The latter result is relevant to the problem of the drastic disagreement between our value of the rate constant of $QH_2 + HO_2^{\cdot}$ interaction, 1.7×10^4 M^{-1} s^{-1}, and that of the reaction of QH_2 oxidation by $O_2^{-\cdot}$, 1.6×10^7 M^{-1} s^{-1} given in ref. 11 (in spite of the fact that the $HO_2^{\cdot}$ radical is a stronger oxidant than $O_2^{-\cdot}$). In fact we did not observe QH_2 consumption under flash irradiation at neutral pH. The authors of ref. 11 studied the reaction of hydroquinone with $O_2^{-\cdot}$ by following the semiquinone production in the solution of QH_2 where superoxide anions were generated. Taking into account the extremely high rate constant of reaction [15] (see above), one can see that if about 1% of QH_2 is present as quinone, formation of semiquinone could occur via quinone reduction, rather than hydroquinone oxidation. In conclusion we want to stress the necessity of considering all possible ways of intermediate formation when studying superoxide reactions. It is dangerous to assume that $O_2^{-\cdot}$ is acting as an oxidant because of its very strong reducing ability.

According to our data the reactivity of ascorbate in a one-electron oxidation by $HO_2^{\cdot}$ and $O_2^{-\cdot}$ is greater than that of NADH (12), whereas ascorbate radicals, products of the one-electron oxidation of ascorbic acid, are more inert as reductants than NAD$^{\cdot}$ radicals (22). Thus ascorbate has a greater tendency than NADH to react via one-electron steps, whereas with NADH the hydride ion transfer mechanism can compete successfully with the slower initial one electron transfer.

Acknowledgments

This work was supported by the Natural Sciences and Engineering Research Council of Canada. We thank I. M. Ralston for assistance with the computer analysis.

1. A. M. MICHELSON, J. M. MCCORD, and I. FRIDOVICH (*Editors*). Superoxide and superoxide dismutases. Academic Press, New York. 1977.
2. G. G. JAYSON, B. J. PARSONS, and A. J. SWALLOW. J. Chem. Soc. Faraday I, **69**, 236 (1973).

3. YU. N. KOZLOV and V. M. BERDNIKOV. Zh. Fiz. Khim. **47**, 598 (1973).
4. D. MEISEL, Y. A. ILAN, and G. CHAPSKI. J. Phys. Chem. **78**, 2330 (1974).
5. A. J. SWALLOW. J. Chem. Soc. 1334 (1952).
6. N. F. BARR and G. G. KING. J. Am. Chem. Soc. **78**, 303 (1956).
7. T. J. FELLOWS and G. HUGHES. J. Chem. Soc. Perkin, **1**, 1182 (1972).
8. M. NISHIKIMI. Biochem. Biophys. Res. Commun. **63**, 463 (1975).
9. B. H. J. BIELSKI and H. W. RICHTER. J. Am. Chem. Soc. **99**, 3019 (1975).
10. C. L. GREENSTOCK and G. W. RUDDOCK. Int. J. Radiat. Phys. Chem. **8**, 367 (1976).
11. P. S. RAO and E. HAYON. Biochem. Biophys. Res. Commun. **51**, 468 (1973).
12. A. D. NADEZHDIN and H. B. DUNFORD. J. Phys. Chem. **83**, 1957 (1979).
13. YU. N. KOZLOV and V. M. BERDNIKOV. Zh. Fiz. Khim. **47**, 593 (1973).
14. C. LAGERCRANTZ. Acta Chem. Scand. **18**, 562 (1964).
15. M. SCHÖNESHOFER. Z. Naturforsch. **27B**, 649 (1972).
16. B. H. J. BIELSKI, D. A. COMSTOCK, and R. A. BOWEN. J. Am. Chem. Soc. **93**, 5624 (1971).
17. G. R. LAROFF, R. W. FESSENDEN, and R. M. SCHULER. J. Am. Chem. Soc. **94**, 9062 (1972).
18. R. C. WEAST (*Editor*). Handbook of chemistry and physics. CRC Press, Cleveland, OH. 1976. p. D-150.
19. D. BEHAR, G. CHAPSKI, J. RABANI, L. M. DORFMAN, and H. A. SCHWARZ. J. Phys. Chem. **74**, 3209 (1970).
20. G. E. ADAMS and B. D. MICHAEL. Trans. Faraday Soc. **63**, 1711 (1967).
21. P. S. RAO and E. HAYON. J. Phys. Chem. **77**, 2274 (1973).
22. I. YAMAZAKI, K.-N. YOKOTA, and R. NAKAJIMA. *In* Biochemical and medical aspects of active oxygen. *Edited by* O. Hayaishi and K. Asada. University of Tokyo Press, Tokyo/University Park Press, Baltimore. 1977. p. 91.

Magnetic field effect on the fluorescence from γ-irradiated solutions of perfluorocarbons[1]

ROBERT SMITH DIXON AND VINCENT JOHN LOPATA

Atomic Energy of Canada Limited Research Company, Research Chemistry Branch, Whiteshell Nuclear Research Establishment, Pinawa, Man., Canada R0E 1L0

Received May 22, 1979

ROBERT SMITH DIXON and VINCENT JOHN LOPATA. Can. J. Chem. **57**, 3023 (1979).

The effect of an applied magnetic field on the fluorescence from γ-irradiated solutions of perfluorobiphenyl and perfluoronaphthalene has been measured in various solvents. In all the solvents used (cyclohexane, squalane, isooctane) the fluorescence intensity increases with increasing field and tends towards a plateau at high fields (> 0.1 T). At low fields, the fluorescence enhancement is smaller for the perfluorocarbons than for the parent hydrocarbons, due to the larger electron–nuclear hyperfine coupling and broader spread of the hyperfine levels in the radical ions of the perfluorocarbons. At high fields the fluorescence enhancement is also smaller for the perfluorocarbons than for the parent hydrocarbons, indicating a larger relative proportion of prompt (field-independent) fluorescence for the perfluorocarbons than for the parent hydrocarbons.

ROBERT SMITH DIXON et VINCENT JOHN LOPATA. Can. J. Chem. **57**, 3023 (1979).

On a mesuré dans différents solvants l'effet d'un champ magnétique appliqué sur la fluorescence provenant des solutions de perfluorobiphényles et perfluoronaphtalènes irradiées aux rayons γ. Dans tous les solvants utilisés (cyclohexane, squalane, isooctane) l'intensité de la fluorescence augmente avec le champ et tend vers un plateau pour des valeurs élevées du champ (> 0.1 T). Lorsque le champ est faible la fluorescence provenant des perfluorocarbures augmente plus faiblement que celle reliée aux hydrocarbures apparentés. Ceci est dû à un plus grand couplage hyperfin électron–noyau et à un étalement plus vaste des niveaux hyperfins des ions radicalaires des perfluorocarbures. A champs forts l'augmentation de la fluorescence est également plus petite pour les perfluorocarbures que pour les hydrocarbures apparentés indiquant ainsi une plus grande proportion relative de fluorescence rapide (indépendante du champ) dans le cas des perfluorocarbures que dans les cas des hydrocarbures apparentés.

[Traduit par le journal]

Introduction

Large yields of electrons and cations are produced following absorption of ionizing radiation by a liquid. In nonpolar liquids, the major fraction of the ion pairs produced by γ or electron irradiation does not separate completely but undergoes geminate recombination. This produces electronically excited singlet and triplet states, the relative yields of which have been predicted to change in an applied magnetic field (1–3). Such an effect has now been observed in both pulse (4–6) and γ-irradiated (6–8) solutions of aromatic hydrocarbons in alkane solvents. Recently, experiments using the single photon counting technique have confirmed the effect (9–11).

When a pair of solute radical ions M^+ and M^- recombine geminately, loss of spin correlation, i.e., a change from singlet to triplet, occurs because of the isotropic hyperfine interactions between the unpaired electrons and the hydrogen nuclei of M^+ and M^-. A magnetic field was predicted to decrease the rate of loss of spin correlation leading to an increase in singlet production, the effect being time-dependent (1–3). This was confirmed in pulse-irradiated solutions of hydrocarbons in squalane and cyclohexane (4–6). In continuously γ-irradiated solutions (6–8), a smaller magnetic field effect is observed because the prompt emission, which exhibits no field effect, is superimposed on the emission from slower ion recombinations, which does show a magnetic field effect.

To date, the study of the effects of substitution in the solute molecule has been limited to deuteration. Since the magnetic moment of a deuteron is smaller than that of a proton (12, 13) electron–nuclear hyperfine coupling is smaller in deutero radical ions than in the corresponding protiated ions. Thus the rate of loss of spin correlation was calculated to be lower for deuterated compounds (2, 3), leading to a smaller magnetic field effect at high fields. This has been confirmed experimentally with naphthalene and naphthalene-d_8 (8). However, at low fields, the opposite effect was observed, i.e., the enhancement of the fluorescence intensity was higher for naphthalene-d_8 than for naphthalene. Although this appears contradictory, it does, in fact, provide further support for the theory. In order to be effective in preventing mixing between the singlet and triplet states of the geminate ion pair prior to recombination (resulting

[1]AECL No. 6647.

0008-4042/79/233023-05$01.00/0

in a smaller triplet formation in a magnetic field), the Zeeman splitting due to the field must be greater than the spread of the hyperfine levels. This spread is smaller for naphthalene-d_8 because of the smaller coupling constant, so a smaller field is required to produce an initial enhancement in naphthalene-d_8. This hypothesis may be tested further by examining magnetic field effects on compounds with large coupling constants. Radical ions of fluorinated aromatic hydrocarbons have high coupling constants (e.g., 14–16) and we have therefore compared the magnetic field effect on the fluorescence intensity from γ-irradiated naphthalene-f_8 (PFN) and biphenyl-f_{10} (PFB) with that from the corresponding protiated molecules in various solvents.

Experimental

The experimental arrangement is described in detail elsewhere (6–8). The solutions were irradiated in a Suprasil cell which was part of a flow system for ease of sample changing. The Ir-192 γ-ray source gave a dose rate of $\sim 5 \times 10^{-5}$ J g^{-1} s^{-1}, in the solution, as measured by the Fricke dosimeter. The light emitted during radiolysis was focussed by a lens onto an RCA 1P28 photomultiplier tube and the level displayed on a recorder. The cell was positioned between the poles of a small electromagnet which provided a field up to 0.5 T, as measured by a Hall-type gaussmeter. The small residual field ($\sim 10^{-3}$ T) remaining when the magnetic field was turned off was eliminated by passing a reverse current through the magnet until the magnetic field was a minimum in the direction of the Hall crystal. The field at the minimum was $< 10^{-4}$ T. The magnetic field had no effect on the photomultiplier tube or on the emission intensity from a cell containing solvent only, but it was necessary to correct for the current produced in the photomultiplier tube by the γ-source.

Solutions were de-aerated by bubbling with dry ultrahigh purity argon gas (Matheson). Biphenyl (Hinton) and naphthalene (Aldrich) were zone-refined prior to use. Squalane (Eastman) was passed through a silica gel column until the absorption edge, measured spectrophotometrically, remained constant. Biphenyl-f_{10} (Imperial Smelting), naphthalene-f_8 (PCR Inc.), cyclohexane, isooctane, and benzene (Fisher spectroanalyzed) were used without further purification.

Results

In order to determine the emitting species in irradiated solutions of perfluorocarbons, comparisons were made between the spectra obtained by pulse radiolysis and by spectrofluorimetry. The emission spectra from pulse-irradiated 10^{-2} M perfluorobiphenyl (PFB) and perfluoronaphthalene (PFN) in cyclohexane are shown in Fig. 1. Similar spectra were obtained in benzene and the spectra measured during the pulse and following the pulse were the same, within experimental error. The intensity of the PFN spectrum was about twice that of the PFB spectrum, in accordance with their measured fluorescence yields (17). The spectra of both perfluorinated compounds are substantially red-shifted compared to the protiated compounds

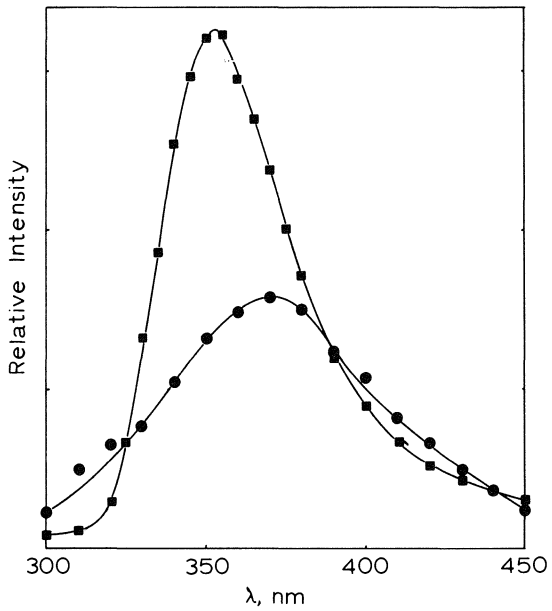

FIG. 1. Fluorescence spectra from pulse-irradiated 10^{-2} M perfluorobiphenyl (○) and perfluoronaphthalene (□) in cyclohexane (corrected for the spectral response of the light detection system).

(18). The maximum of the PFB spectrum occurs at 371 nm, which compared well with spectrofluorimetric measurements of 372 nm in cyclohexane (this laboratory) and 375 nm in petroleum ether (17). The maximum of the PFN spectrum occurs at 353 nm, which is in good agreement with the spectrofluorometric values of 352 nm in cyclohexane, 357 nm in squalane (this laboratory), and 355 nm in petroleum ether (17). However, it is somewhat lower than the values of Singh and Quinn (19) who found a small red shift in λ_{max} with increasing solute concentration. Thus self-absorption, excimer formation, or an impurity effect cannot be excluded completely at high concentrations. Excimer formation appears unlikely since none was seen in photoexcited PFN in methylcyclohexane down to 213 K, though there is evidence for excimer formation in more viscous solvents at low temperatures (20). Nevertheless the similar spectra obtained spectrofluorimetrically and pulse-radiolytically show that the emission from irradiated solutions arises mainly from singlet fluorescence.

The changes in intensity of the fluorescence from γ-irradiated solutions of PFB and PFN (10^{-2} M) in various solvents, viz., cyclohexane, squalane, and isooctane, as a function of magnetic field strength are compared with those of the parent hydrocarbons in Figs. 2 and 3. In all cases the fluorescence intensity increases steadily with increasing magnetic field and tends towards a plateau above ~ 0.1 T, the plateau

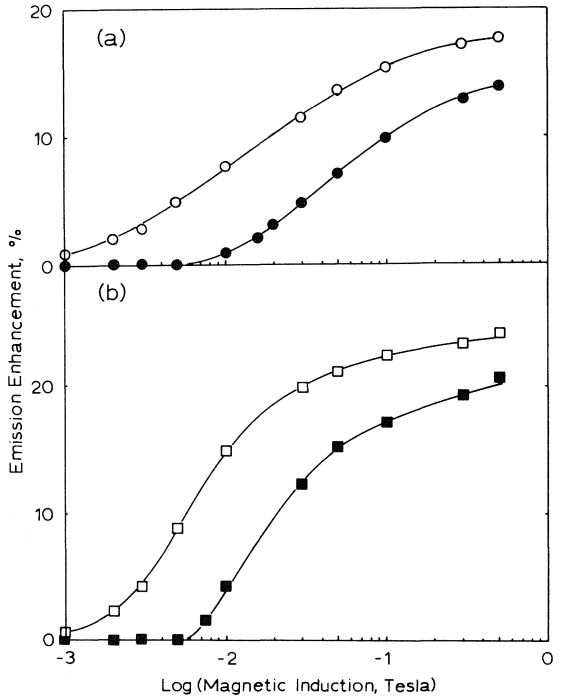

FIG. 2. Increase in fluorescence intensity as a function of applied magnetic field: (*a*) 10^{-2} *M* biphenyl (○) and perfluorobiphenyl (●) in squalane; (*b*) 10^{-2} *M* biphenyl (□) and perfluorobiphenyl (■) in isooctane.

value depending on the solvent. At low fields, the effect of magnetic field on the perfluorinated compounds is much less than on the parent hydrocarbons, and a minimum field of $\gtrsim 0.005$ T is required to produce an initial increase for the perfluorinated compounds. At high fields, the "plateau" value is also smaller for the perfluorinated compounds than the corresponding hydrocarbons in each solvent.

Discussion

In solutions of an aromatic hydrocarbon in an alkane solvent, geminate recombination of solute radical ion pairs is one source of excited states (21–26). For an aromatic hydrocarbon, M, in an alkane solvent, S, the major reactions leading to excited state formation via ion recombination are as follows:

[1] $S \rightsquigarrow S^+ + e^-$

[2] $S^+ + M \rightarrow M^+ + S$

[3] $e^- + M \rightarrow M^-$

[4] $M^+ + e^- \rightarrow M^*$

[5] $S^+ + M^- \rightarrow M^* + S$

[6] $M^+ + M^- \rightarrow M^* + M$

where M* may be an excited singlet or triplet state.

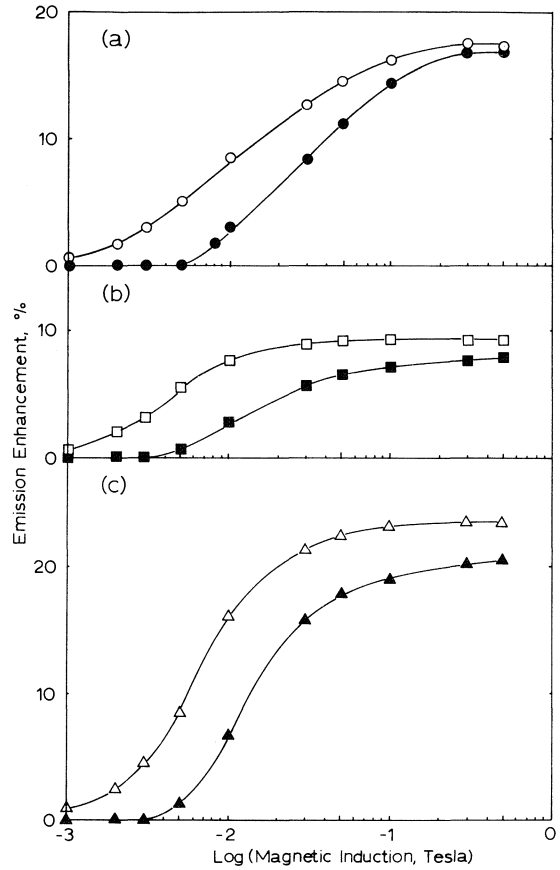

FIG. 3. Increase in fluorescence intensity as a function of applied magnetic field: (*a*) 10^{-2} *M* naphthalene (○) and perfluoronaphthalene (●) in squalane; (*b*) 10^{-2} *M* naphthalene (□) and perfluoronaphthalene (■) in cyclohexane; (*c*) 10^{-2} *M* naphthalene (△) and perfluoronaphthalene (▲) in isooctane.

At high solute concentrations, reaction [6] will probably be the main ion recombination process. Solute excited states may also be formed by energy transfer from excited solvent molecules (21, 22, 24) via reactions [7] and [8].

[7] $S \rightsquigarrow S^*$

[8] $S^* + M \rightarrow M^* + S$

The emission observed in our experiments is the fluorescence from excited singlet PFB and PFN. This may come from direct excitation or from ion recombination of the undissociated solute radical ion pairs (e.g., $PFB^+ + PFB^-$ or, possibly, $S^+ + PFB^-$). PFB appears to attach electrons and a spectrum which is probably that of PFB^- has been observed in acetonitrile and other solvents.[2] The spectrum of PFN^- is not as clearly defined, but addition of PFN to irradiated solutions of PFB in

[2]A. Singh and co-workers, private communication.

acetonitrile reduces the yield of PFB^-.[2] The thermoluminescence seen in frozen solutions of PFB and PFN in polar (27) and non-polar (20) solvents is considered to arise from ion recombination. If the recombining anion were F^- from dissociative electron capture, excited singlets would not be formed (27). Thus, although the extent of dissociative electron capture of PFB or PFN to produce F^- is not known, it appears that the large anions PFB^- and PFN^- have lifetimes long enough to allow their geminate recombination in the non-polar solvents used in the present work.

The increase in fluorescence intensity in a magnetic field was predicted by Brocklehurst (2, 3). The spins of the odd electrons on the recombining ions M^+ and M^- are initially paired in a singlet solvent molecule prior to ionization. If the spins remain correlated, i.e., if their relative orientation and phase do not change, then only singlets will be produced when M^+ and M^- recombine. However, if correlation is lost, triplets may be formed. The theory (2, 3) shows that loss of spin correlation occurs because of the hyperfine interaction between the unpaired electrons and the magnetic nuclei of M^+ and M^-. The loss of correlation is slower in a magnetic field because of the Zeeman effect. At zero field, the degeneracy of the states of the odd electrons in the ion pair, viz., $S = 0$, $M_s = 0$ and $S = 1$, $M_s = 0$, ± 1 (abbreviated to S_0, T_0, T_+, and T_-) allows mixing between the singlet and all three triplet states. At high fields, however, the T_+ and T_- states have different energies because of the Zeeman splitting and appreciable mixing can only take place between the S_0 and T_0 states. This leads to increased singlet formation in a magnetic field. The magnetic field effect is time-dependent (4–6) but is predicted to be zero for ion recombinations which take place in less than ~ 5 ns (2, 3). In pulse-irradiated solutions, the "prompt" emission, which is field-independent, can be separated from the slower ion recombination fluorescence, which is field-dependent. However, in continuously irradiated solutions, the field-independent fluorescence is superimposed on the field-dependent fluorescence, which leads to a smaller overall field effect.

The field effect shown in Figs. 2 and 3 is consistent with the theory (2, 3), and with our earlier results (6–8). The enhancement of the emission intensity increases with increasing magnetic field and approaches a plateau at fields >0.1 T. The high field value varies with solvent in the order cyclohexane < squalane < isooctane for all solutes. The difference between squalane and cyclohexane may be explained in terms of the ion recombination times in the two solvents. In cyclohexane the smaller average ion recombination time will lead to a larger fraction of prompt (field-independent) fluorescence than in squalane, i.e., to a smaller magnetic field effect. The results in isooctane thus indicate a much smaller fraction of prompt fluorescence than in any other solvent which we have studied. The origin of the prompt fluorescence is, however, not unambiguous and the relative contributions of ion recombination and energy transfer to the formation of solute excited states are still being debated (21–26). In cyclohexane, energy transfer from the solvent occurs (24, 25) whereas the lack of fluorescence of isooctane (28) suggests that energy transfer is less likely in this solvent. No data are available to permit an assessment in squalane.

Figures 2 and 3 show that substantially different fields are required to induce the initial effect for the protiated and perfluorinated compounds. For the protiated compounds, a field less than 10^{-3} T is sufficient to cause a small increase in fluorescence intensity, whereas a field greater than $\sim 5 \times 10^{-3}$ T is required to produce an increase with the perfluorinated compounds. This different behaviour provides further support for the theory (2, 3). The rate of loss of spin correlation depends to a large extent on the magnitude of the coupling constant a between the unpaired electrons and the magnetic nuclei of the recombining ions. Fluorination increases the coupling in radical ions of aromatic molecules (14–16) as compared to the parent hydrocarbons (12, 13). Few data are available for the perfluorinated solutes used here, but the cation of PFN has coupling constants of 19 G and 4.78 G, respectively, for the α and β positions (14, 15). These are much higher than the corresponding values of 4.90 and 1.83 G respectively, in naphthalene (29). Coupling constants of anions are generally smaller than those of the corresponding cations, both in hydrocarbons (13) and partly fluorinated hydrocarbons (14). Coupling constants of the anion of PFN are not known; they will presumably be smaller than those of the corresponding cation, but larger than those of the naphthalene radical anion. Thus we expect a larger overall coupling for the PFN ions than for the parent naphthalene ions. Data are unavailable for the radical ions of PFB but comparisons between biphenyl (13) and partly fluorinated biphenyl (14) suggest that the above arguments will also apply to PFB.

The higher electron–nuclear hyperfine coupling in the radical ions of the perfluorocarbons means higher overall spectral widths and a broader spread of the hyperfine levels, and this explains the larger field required to produce an initial effect with the perfluorocarbons (Figs. 2, 3). We have seen earlier that

the magnetic field causes the Zeeman splitting, which prevents mixing between the S_0 and $T_\pm$ states, and this results in higher singlet production. It is clear that, to prevent such S_0–$T_\pm$ mixing and the corresponding singlet increase, the magnetic field must be large enough to prevent overlap of the hyperfine levels, so that mixing of S_0 and $T_\pm$ does not occur. Since the spread of the hyperfine levels is larger for the perfluorinated compounds, a larger field will therefore be required to prevent overlap and to produce an initial singlet increase, as is found. The effect observed at low fields thus provides further support for the theoretical model (2, 3).

At high fields, the magnetic field effect is smaller for the perfluorocarbons than for the hydrocarbons (Figs. 2, 3). Because of the higher coupling constants in the perfluorocarbons, the rate of loss of spin correlation should be higher than for the parent hydrocarbons so that, all other things being equal, the magnetic field effect should be larger for the perfluorocarbons at high fields. The reverse result undoubtedly occurs because of different ratios of field-dependent and field-independent fluorescence in the two sets of compounds. The magnetic field effect in continuously irradiated solutions is an overall effect because the prompt fluorescence (field-independent) is superimposed on the slower ion recombination (field-dependent) fluorescence. Our preliminary results in pulse-irradiated solutions of naphthalene, PFN, biphenyl, and PFB in cyclohexane show that the ratio of in-pulse emission to post-pulse emission is much larger for the perfluoro compounds than for the parent hydrocarbons. This will, in turn, mean a larger fraction of field-independent fluorescence for the perfluoro compounds and a smaller field effect at high magnetic fields, as observed.

Acknowledgements

We would like to thank Dr. E. P. Sargent, Dr. A. Singh, and Dr. B. Brocklehurst for many valuable comments.

1. B. Brocklehurst. Nature, **221**, 921 (1969).
2. B. Brocklehurst. Chem. Phys. Lett. **28**, 357 (1974); **29**, 635 (1974).
3. B. Brocklehurst. J. Chem. Soc. Faraday Trans. II, **72**, 1869 (1976).
4. B. Brocklehurst, R. S. Dixon, E. M. Gardy, V. J. Lopata, M. J. Quinn, A. Singh, and F. P. Sargent. Chem. Phys. Lett. **28**, 361 (1974).
5. F. P. Sargent, B. Brocklehurst, R. S. Dixon, E. M. Gardy, V. J. Lopata, and A. Singh. J. Phys. Chem. **80**, 815 (1977).
6. R. S. Dixon, F. P. Sargent, V. J. Lopata, E. M. Gardy, and B. Brocklehurst. Can. J. Chem. **55**, 2093 (1977).
7. R. S. Dixon, E. M. Gardy, V. J. Lopata, and F. P. Sargent. Chem. Phys. Lett. **30**, 463 (1975).
8. R. S. Dixon, F. P. Sargent, V. J. Lopata, and E. M. Gardy. Chem. Phys. Lett. **47**, 108 (1977).
9. J. Klein and R. Voltz. Phys. Rev. Lett. **36**, 1214 (1976).
10. B. Brocklehurst. Chem. Phys. Lett. **44**, 245 (1976).
11. J. Klein and R. Voltz. Can. J. Chem. **55**, 2102 (1977).
12. N. M. Atherton. Electron spin resonance. Horwood, Chichester. 1973.
13. P. B. Ayscough. Electron spin resonance in chemistry. Methuen, London. 1967.
14. A. Hudson and K. D. J. Root. Adv. Magn. Reson. **5**, 1 (1971).
15. C. Thomson and W. J. MacCulloch. Tetrahedron Lett. **56**, 5899 (1968); Mol. Phys. **19**, 817 (1970).
16. N. M. Bazhin, N. E. Akhmetova, L. V. Orlova, V. D. Shteingarts, L. N. Shchegoleva, and G. G. Yakobson. Tetrahedron Lett. **42**, 4449 (1968).
17. H. M. Rosenberg and S. D. Carson. J. Phys. Chem. **72**, 3531 (1968).
18. I. B. Berlman. Handbook of fluorescence spectra of aromatic molecules. 2nd ed. Academic Press, New York. 1971.
19. A. Singh and M. J. Quinn. J. Photochem. **5**, 167 (1976).
20. M. Al-Jarrah, B. Brocklehurst, and M. Evans. J. Chem. Soc. Faraday Trans. II, **61**, 1921 (1976).
21. J. K. Thomas. Ann. Rev. Phys. Chem. **21**, 17 (1970).
22. A. Singh. Radiat. Res. Rev. **4**, 1 (1972).
23. A. Hummel. *In* Advances in radiation chemistry. Vol. 4. *Edited by* M. Burton and J. L. Magee. Wiley, New York. 1974.
24. J. K. Thomas. Int. J. Radiat. Phys. Chem. **8**, 1 (1976).
25. G. A. Salmon. Int. J. Radiat. Phys. Chem. **8**, 13 (1976).
26. L. Walter, F. Hirayama, and S. Lipsky. Int. J. Radiat. Phys. Chem. **8**, 237 (1976).
27. B. Brocklehurst. Radiat. Res. Rev. **2**, 149 (1970).
28. W. Rothman, F. Hirayama, and S. Lipsky. J. Chem. Phys. **58**, 1300 (1973).
29. A. Carrington, F. Dravnieks, and M. C. R. Symons. J. Chem. Soc. **192**, 947 (1959).

Stereochemical analysis of *exo*-methylenebenzocycloalkanes: evidence from carbon-13 nuclear magnetic resonance chemical shifts, ^{13}C–^{13}C nuclear spin couplings, and force field calculations[1]

GERALD W. BUCHANAN, JOCELYN SELWYN, AND BRIAN A. DAWSON
Department of Chemistry, Carleton University, Ottawa, Ont., Canada K1S 5B6

Received May 25, 1979

GERALD W. BUCHANAN, JOCELYN SELWYN, and BRIAN A. DAWSON. Can. J. Chem. **57**, 3028 (1979).

A series of *exo*-methylenebenzocycloalkanes with ring sizes 5–8 have been prepared, enriched with ^{13}C and also deuterated at the exocyclic position. ^{13}C chemical shifts are found to be influenced by the degree of planarity between the aromatic ring and the exocyclic methylene function. ^{13}C–^{13}C couplings through one, two, and three bonds have been measured. The $^{1}J_{CC}$ values correlate very well with %*S* character calculations. Values of $^{3}J_{CC}$ are found to be influenced by both dihedral angle and valence angle. The relative propensity for these compounds to isomerize to endocyclic material is discussed. Some earlier spectral assignments for the indene derivative are shown to be in error.

GERALD W. BUCHANAN, JOCELYN SELWYN et BRIAN A. DAWSON. Can. J. Chem. **57**, 3028 (1979).

On a préparé une série d'*exo*-méthylènebenzocycloalcanes dont la taille des cycles varie de 5 à 8, enrichis en ^{13}C et également deutérés en position exocyclique. On a trouvé que le degré de planéarité entre le cycle aromatique et la fonction méthylène exocyclique influence les déplacements chimiques du ^{13}C. On a mesuré les constantes de couplage ^{13}C–^{13}C à travers une, deux ou trois liaisons. Les valeurs $^{1}J_{CC}$ correspondent parfaitement aux calculs du % de caractère *S*. On a trouvé que l'angle dièdre et l'angle de valence influencent $^{3}J_{CC}$. On a discuté de la tendance relative qu'ont ces composés à s'isomériser en dérivés endocycliques. On a démontré que certaines interprétations spectrales faites antérieurement pour les dérivés de l'indène sont erronées.

[Traduit par le journal]

Introduction

The dihedral angle dependence of proton–proton vicinal coupling constants is well known (1) and has been widely used for structure determination. In addition, factors such as bond length, valence angle, substituent electronegativity, and substituent orientation are known to affect the magnitude of $^{3}J_{HH}$ (2).

The widespread application of $^{3}J_{HH}$ to stereochemistry has prompted investigations into possible "Karplus-type" relationships in vicinal ^{13}C–^{13}C couplings as well, using single-site ^{13}C-enriched materials. Among systems recently examined are carboxylic acids (3), aliphatic alcohols (4, 5), ketones (6), and esters (7).

To date, few ^{13}C–^{13}C coupling data have been reported for conjugated networks of the type $C{=}C{-}C{=}{}^{13}C\langle{}^{H}_{H}$. The present study presents data for such pathways, present in *exo*-methylenebenzocycloalkanes. These compounds were chosen for study due to unusual behaviour, possibly of conformational origin, observed in the intramolecular Friedel-Crafts acylation reactions leading to the corresponding ketones.[2] No information regarding the geometries of these materials is available from ^{1}H nmr, due to peak overlap in the region $\delta = 1$–3, and the lack of protons vicinal to the *exo*-CH_2 protons.

In addition to the nmr measurements, force-field calculations of the molecular geometries were carried out using the GEMO program (8, 9). The resulting geometries were employed to study the dihedral angle dependence of $^{3}J_{CC}$ and also were used as input for the INDO MO program (10) to calculate the Fermi contact contributions to ^{13}C–^{13}C couplings through one, two, and three bonds.

The ^{13}C chemical shifts for the *exo*-methylene carbon, C-1, and the quaternary aromatic positions are also discussed in detail with respect to the calculated geometries.

Results and Discussion

Chemical Shifts

The ^{13}C shifts for **1–4** are presented in Table 1.

[1]Taken, in part, from the Honours B.Sc. thesis of Jocelyn Selwyn and the Ph.D. thesis of Brian A. Dawson, Carleton University, 1979.

[2]R. H. Wightman. Private communication.

0008-4042/79/233028-06$01.00/0

TABLE 1. ^{13}C chemical shifts (δ_C from TMS ± 0.1)[a]

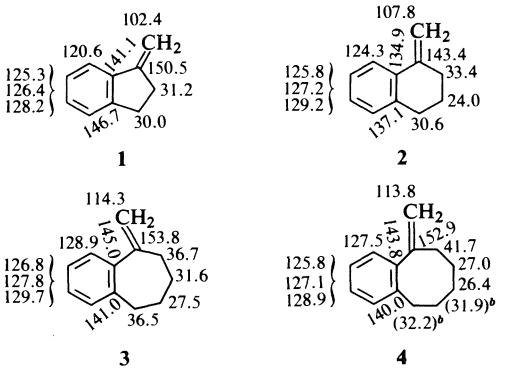

[a]0.1 *M* solutions in $CDCl_3$.
[b]Parentheses denote uncertain assignments.

With the exception of compound **1** (11), no carbon nmr data have been previously reported for these materials. Several techniques were used for peak assignment. Initially, distinction between quaternary, methine, and methylene resonances was made on the basis of their multiplicity in the single frequency off-resonance (SFORD) decoupling experiment. The *exo*-methylene carbons were positively identified by the unambiguous synthesis of the ^{13}C-enriched materials **1***a*–**4***a*. These compounds also permitted clear assignment of the C-1 resonance due to the observation of $^1J_{CC}$ near 70 Hz, a value close to that found in simple disubstituted alkenes (12).

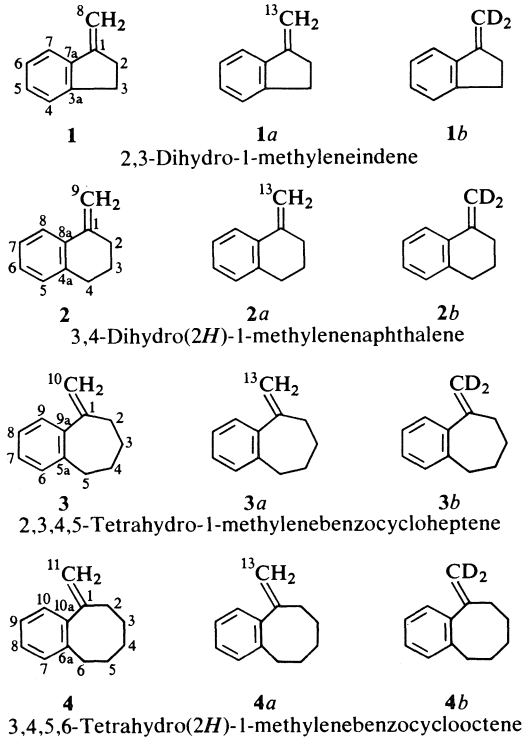

FIG. 1. Structures, IUPAC names, and numbering schemes for materials studied.

Synthesis of the dideuterated compounds **1***b*–**4***b* allowed unambiguous assignment of the C-2 vs. C-3 resonances in **1**–**4** and distinction between the two quaternary aromatic carbon resonances. The presence of deuterium causes small, but resolvable, coupling between deuterium and the vicinal carbon atom (C-2) ($^3J_{CCCD}$ is ca. 0.6–1.5 Hz) (13–16), thereby permitting distinction between C-2 and C-3. The C-3 carbon, being 4 bonds separated from deuterium, is not measurably spin coupled to it. Similarly, C-7a can be distinguished from C-3a in **1***b*, as can C-8a from C-4a in **2***b* etc. In these cases, the quaternary carbons vicinal to the deuterium also show reduced integrated intensities, compared to their protio analogs, due to the less efficient dipole–dipole relaxation of these carbons by the spatially proximate deuterium atom (below), which results in a reduced nOe and a lengthened T_1.

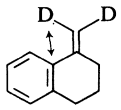

2*b*

For the remaining methylene carbon assignments, the effect of *exo*-CH_2 addition (17) on the ^{13}C shifts of cycloalkanes was considered, in conjunction with the previously published data for benzocycloalkanes (18). With regard to the aromatic methine resonances only the carbon vicinal to the *exo*-methylene carbon could be clearly assigned. This was done on the basis of its upfield "γ" shift (11) in the nearly planar cases of **1** and **2**, and the observation of $^3J_{CC}$ to this position in **1***a*–**4***a*.

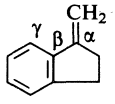

1

It is interesting to note the influence of benzannelation on the carbon shifts of **1**–**4** relative to the methylenecycloalkanes below (17, 19), particularly at the C-1 and *exo*-methylene positions. Our force-field calculations indicate that for **1** and **2**, the *exo*-methylene carbon is nearly coplanar with the benzene ring (Table 2, data for ϕ_1 and ϕ_2), while compounds **3** and **4** are highly non-planar in this region of the molecule.

TABLE 2. Calculated valence (θ) and torsional[a] (ϕ) angles (±0.1°)

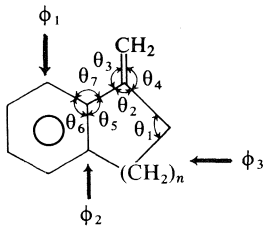

Compound	θ_1	θ_2	θ_3	θ_4	θ_5	θ_6	θ_7	ϕ_1	ϕ_2	ϕ_3
1 (n = 1)	103.2	113.7	123.8	122.5	103.9	121.4	134.5	1.4	178.9	178.2
2 (n = 2)	111.3	119.6	122.8	117.6	119.4	118.3	122.2	1.8	177.1	147.6
3 (n = 3)	114.7	119.4	120.7	119.7	121.0	119.5	119.5	59.0	122.5	109.6
4 (n = 4)	120.1	120.4	120.2	119.4	120.8	119.8	119.4	84.4	96.9	139.5

[a]Defined as the angles which the exocyclic (=CH_2) carbon makes with the carbons denoted by (⟶) as shown on the diagram.

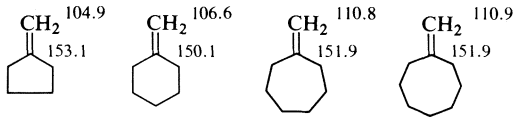

These calculated results are in reasonable agreement with the only experimental data for these materials, those for **1**–**3**, extracted from photoelectron spectra (20).

For the planar cases **1** and **2**, benz-annelation results in substantially increased shielding at C-1, ca. 3–6 ppm. For the non-planar systems **3** and **4**, the C-1 resonance is slightly deshielded relative to the methylenecycloalkane models shown above.

Similarly the *exo*-methylene resonance of **1** is shifted upfield on benz-annelation and those of **3** and **4** experience downfield shifts upon fusion of the aromatic ring. Compound **2** is anomalous in this regard, in that the *exo*-CH_2 resonance is slightly deshielded (ca. 1 ppm) relative to methylenecyclohexane, even though the aromatic ring is nearly coplanar to the $=CH_2$ function.

Our assignments for C-3a and C-7a of **1**, based on deuteration results, are reversed from those reported previously (11). The earlier assignments were made using indane as a model compound and assuming a "β" deshielding effect of the *exo*-methylene group at C-7a. The present work clearly shows that the shifts of the quaternary aromatic carbons cannot be treated on this basis. For **1** and **2**, the shifts of C-7a and C-8a are upfield relative to C-3a and C-4a respectively. In the cases of **3** and **4**, the effect is reversed for the shifts of C-9a and C-10a vs. C-5a and C-6a respectively. Additional support for the present assignments comes from the results of total electron density calculations which are presented in Table 3. The values were calculated from the INDO MO program (10). In each of **1**–**4**, the quaternary aromatic carbon with the higher calculated electron density resonates at higher field, i.e., lower δ_C. We realize that attempts to quantitatively correlate electron densities with chemical shifts are dangerous, but qualitative comparisons are useful.

TABLE 3. Calculated electron densities[a] and ^{13}C shifts (δ_C) for quaternary aromatic carbons

Compound	Carbon	Electron density	$\delta_C \pm 0.1$
1	3a	3.9758	146.6
	7a	3.9883	141.1
2	4a	3.9785	137.1
	8a	3.9857	134.9
3	5a	3.9825	141.0
	9a	3.9795	145.0
4	6a	3.9831	140.0
	10a	3.9715	143.8

[a]Total electron densities in electron units.

Thus, to summarize, the chemical shift trends found at the *exo*-methylene group, C-1, and the quaternary aromatics for **1**–**4** are generally divisible into two categories. The first category is for materials having ϕ_1 and ϕ_2 (Table 2) close to 0° and 180° respectively, i.e., **1** and **2**, while the second category encompasses the non planar materials **3** and **4**, which have ϕ_1 and ϕ_2 values greatly different from 0° and 180° respectively.

^{13}C–^{13}C Couplings

The experimental and INDO MO calculated (10) ^{13}C–^{13}C J values are presented in Table 4. Previously (19), $^1J_{C=CH_2}$ values of 73.2, 72.0, 72.0, and 72.0 Hz were reported for the methylenecycloalkanes of ring sizes 5, 6, 7, and 8 respectively. Data in Table 4 indicate that benz-annelation has little influence on this parameter. The agreement between observed and calculated ^1J values for **1**–**4** is fairly

good, suggesting a dominance of the Fermi contact mechanism for these couplings.[3]

A usual correlation of directly bonded coupling constants is with the product of the *S* character of the bonding orbitals, and the equation below has been proposed (21). In the present work, the % *S* character for the carbons involved was calculated

$$^1J_{C_AC_B} = \frac{7.3(\%S_A)(\%S_B)}{100} - 17 \text{ Hz}$$

from the SCF density matrix, calculated in the coupling constant program. The electron densities in the carbon 2*s*, $2p_x$, and $2p_y$ orbitals were obtained, and from this, the % *S* character can be determined. Using this approach, excellent agreement between observed and calculated $^1J_{CC}$ values was found, the calculated values being 73.7, 73.6, 73.4, and 73.3 Hz for **1**, **2**, **3**, and **4** respectively.

Regarding geminal ^{13}C–^{13}C couplings, no resolvable $^2J_{CC}$ values (i.e. > 0.6 Hz) were observed to the quaternary aromatic carbons 7a, 8a, 9a, and 10a of **1**, **2**, **3**, and **4** respectively. Measurable ^2J values into the aliphatic ring were obtained, however, for **2**, **3**, and **4**. In these instances the calculated couplings exceed the observed by a factor of about five, suggesting that the Fermi contact mechanism is probably not dominant in these interactions.[3] In the previous work on the simple methylenecycloalkanes (19), no $^2J_{CC}$ or $^3J_{CC}$ data were included, perhaps due to the low resolution of the instrument employed.

The vicinal couplings ($^3J_{CC}$) are of particular interest in this work, since for each of **1**–**4**, there are three possible pathways for vicinal coupling, and in every instance, a resolvable $^3J_{CC}$ was obtained experimentally. Agreement between calculated and observed values (Table 4) is considerably better than for geminal couplings, although the calculated couplings are all higher than the observed. Furthermore, it is of interest to attempt to correlate the observed $^3J_{CC}$'s with the calculated torsional (dihedral) angles between the coupled carbons, i.e., ϕ_1, ϕ_2, and ϕ_3 of Table 2. Strictly speaking, it is valid only to examine the dihedral angle dependence of ^3J for couplings occurring via similar types of bonding networks.

If one considers the vicinal couplings to the aromatic carbons, a dihedral angular dependence of $^3J_{CC}$ is obtained as shown in Fig. 2. The single deviation from a "Karplus-type" curve occurs in compound **1** for $^3J_{CC}$ to C-7. In this case, $^3J_{CC}$ is observed

TABLE 4. Experimental and calculated[a] ^{13}C–^{13}C couplings (±0.2 Hz)

Compound	^1J	^2J	^3J							
		Path	Path		Path		Path			
1	73.9	*CH$_2$=C—*CH$_2$	<0.6	*CH$_2$=C—CH$_2$—*CH$_2$	2.1	*CH$_2$=C—C=*C<	4.8	*CH$_2$=C—C=*C<	1.7
	(70.8)		(8.0)		(3.3)	C	(8.8)	H	(4.9)
2	72.6	,,	1.5	,,	2.8	,,	3.6	,,	4.2
	(79.4)		(9.6)		(3.6)	C	(6.0)	C	(6.5)
3	71.0	,,	2.0	,,	1.9	,,	2.4	,,	2.4
	(79.5)		(9.7)		(5.1)	C	(6.3)	C	(6.2)
4	71.1	,,	2.2	,,	2.9	,,	2.2	,,	2.2
	(79.4)		(10.5)		(4.5)	C	(6.0)	C	(6.4)

[a]In parentheses, from the INDO MO program (10).

[3]A referee has pointed out that the INDO scheme may not include all Fermi-dominated mechanisms. Accordingly, one must view the calculated couplings with some caution, in terms of interpreting the results to imply complete dominance or absence of the Fermi-contact coupling mechanism.

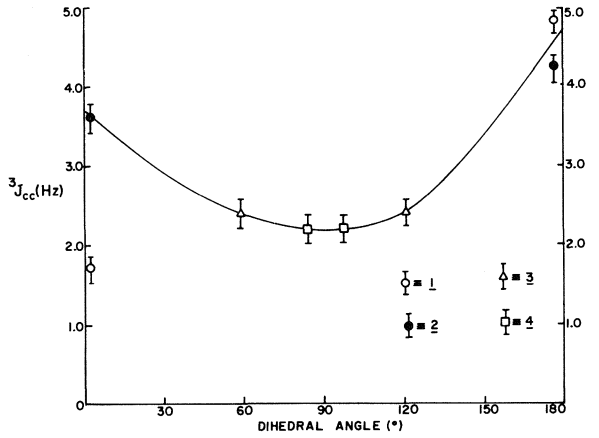

FIG. 2. Dihedral angle dependence of vicinal ^{13}C–^{13}C couplings from the *exo*-methylene carbon to aromatic ring carbons.

to be only 1.7 Hz where the dihedral angle ϕ_1 between the coupled carbons is calculated to be 1.4°. Examination of the other calculated structural data in Table 2, however, shows a marked increase in the *valence* angle θ_7 in **1** compared to **2–4**.

For ^1H–^1H couplings through three bonds, it has been noted (2) that the couplings decrease with increasing C—C 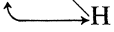 valence angle. This trend is evident in the cyclic alkenes, where $^3J_{HH}$ values for the alkene protons are found to be as follows: cycloheptene (10.8 Hz), cyclohexene (8.8 Hz), cyclopentene (5.1 Hz), cyclobutene (3.0 Hz), and cyclopropene (1.3 Hz). In this series the dihedral angle between the coupled alkene protons is constant. The present findings for **1** suggest that valence angles also influence $^3J_{CC}$. In fact, for the $^3J_{CC}$ to C-3a of **1**, the rather large coupling of 4.8 Hz may be due, in part, to the compressed valence angle θ_5, relative to **2–4**. Clearly, further work is needed to elucidate the valence angle dependence of $^3J_{CC}$ and we are presently synthesizing a series of model compounds to this end.

It is interesting to compare these results with those for 1,3-butadiene (22), enriched with ^{13}C at a terminal methylene position. For this material, $^1J_{CC} = 68.8$, $^2J_{CCC}$ is <1.0, and $^3J_{CCC} = 9.05$ Hz. The latter value, which represents an essentially pure (i.e. >95%) transoid geometry, is considerably larger than any of the ^3J transoid values in Table 4, suggesting that a lower π bond order may be present in **1–4** than in 1,3-butadiene itself.

With respect to the vicinal ^{13}C–^{13}C couplings into the alicyclic ring to C-3, the overall range of $^3J_{CC}$ is small, i.e., 1.9–2.9 Hz. We feel that attempts to correlate such small changes with calculated torsional angles are probably not justified at this stage, since only 4 data points are available. A cursory look at the data, however, suggests that **1** may again be anomalous due to valence angle effects.

Experimental

Spectra

^{13}C spectra were recorded at 25.16 MHz using a Varian XL-100-12 nmr spectrometer equipped with a Nicolet TT-100 Fourier transform data system. For chemical shift measurements on non-labelled compounds, samples were examined as 0.1 *M* solutions in $CDCl_3$ solvent in 5 mm sample tubes. Spectral widths were 5000 Hz.

For measurements of ^{13}C–^{13}C couplings with enriched materials, the sample concentration was 0.04 *M* in $CDCl_3$, and the spectral widths were 500 Hz. A minimum of 8K data points were employed.

Calculations

The initially specified geometries for **1–4**, used as input for the GEMO program (8), were derived from standard parameters (23). Subsequently GEMO carries out a systematic variation of bond lengths, bond angles, and torsional angles to minimize the conformational energy of the molecule. Parameters were iterated until a convergence criterion of 0.01 kcal/mol was met. The barrier to rotation about the bond linking the *exo*-methylene group to the aromatic ring was taken as 2.0 kcal/mol, by analogy with results for styrene (24). Constants for the van der Waals interactions were taken from COMOL, a program written for conformational energy calculations by M. H. J. Koch, Laboratoire de Chimie Physique et de Cristallographie, Université de Louvain, Belgium.

The ^{13}C–^{13}C couplings were calculated using the finite perturbation procedure of Pople *et al.* (10), with a program obtained from Quantum Chemistry Program Exchange #224, Bloomington, IN.

Materials

Compounds **1–4** were synthesized from the corresponding known ketones via Wittig reactions. A typical procedure follows.

Triphenylmethylphosphonium iodide (1.0 g) was placed in a dry 100 mL roundbottom flask fitted with a septum, a gas inlet tube, and a condenser. After flushing with purified nitrogen for 10 min and addition of 25 mL of anhydrous ether, the system was again flushed with nitrogen for 10 min. *N*-Butyllithium (2.0 mL, 1.6 *M* in hexane) was added and the solution was stirred for 20 min. The appropriate ketone (0.003 mol), in 4 mL of anhydrous ether, was added to the reaction flask. After stirring for half an hour 25 mL of water was added and the resulting mixture was vigorously stirred until all the solid particles had dissolved (usually ~1 h). The ether and water layers were separated and the water layer was extracted with ether (4 × 30 mL). The combined ethereal extracts were dried ($MgSO_4$) and the solvent removed under vacuum. The crude product was purified on a neutral aluminum oxide column, eluting with ether. Compound **1**, yield 38%; n_D^{20} 1.5762; ir $\nu_{max}(CDCl_3)$: 1640, 900 cm^{-1}; lit. (25) n_D^{23} 1.5759. Compound **2**, yield 45%; n_D^{20} 1.5558; ir $\nu_{max}(CDCl_3)$: 1642, 900 cm^{-1}; lit. (26) n_D^{20} 1.5560. Compound **3**, yield 40%; n_D^{20} 1.5562; ir $\nu_{max}(CDCl_3)$: 1640, 899 cm^{-1}; lit. (26) n_D^{20} 1.5560. Compound **4**, yield 56%, n_D^{20} 1.5460, ir $\nu_{max}(CDCl_3)$: 1642, 899 cm^{-1}; lit. (26) n_D^{20} 1.5471; ir $\nu_{max}(CCl_4)$: 1642, 899.

Compounds **1–4** also gave ^1H spectra consistent with their structures. It should be noted that **2** undergoes facile isomerization to its endocyclic isomer in $CDCl_3$, a reaction which has

already been followed by ^1H nmr (27). Thus, after the several hours required for a ^{13}C spectrum, **2** had rearranged to approximately a 50:50 mixture of endocyclic and exocyclic material. For **1** and **3**, isomerizations are relatively slow in $CDCl_3$, and **4** does not isomerize, even in the presence of *p*-toluenesulfonic acid (26).

The series of ^{13}C-labelled materials **1***a*–**4***a* and the deuterated compounds **1***b*–**4***b* were prepared in an analogous manner, starting with the appropriately labelled methyl iodide, available from Stohler Isotope Chemicals, Montreal, P.Q.

Acknowledgements

G.W.B. wishes to thank the Natural Sciences and Engineering Research Council of Canada for continuing financial support and the Carleton University President's Computer Fund for generous assistance.

1. M. KARPLUS. J. Chem. Phys. **30**, 11 (1969).
2. J. B. LAMBERT, H. F. SHURVELL, L. VERBIT, R. G. COOKS, and G. H. STOUT. Organic structural analysis. Macmillan Publishing Co. Inc., New York. 1976. pp. 65–71.
3. J. L. MARSHALL and D. E. MÜLLER. J. Am. Chem. Soc. **95**, 8305 (1973).
4. D. DODDRELL, I. BURFITT, J. B. GRUTZNER, and M. BARFIELD. J. Am. Chem. Soc. **96**, 1241 (1974).
5. M. BARFIELD, I. BURFITT, and D. DODDRELL. J. Am. Chem. Soc. **97**, 2631 (1975).
6. P. E. HANSEN, O. K. PAULSEN, and A. BERG. Org. Magn. Reson. **9**, 650 (1977).
7. P. E. HANSEN and A. BERG. Org. Magn. Reson. **8**, 591 (1976).
8. N. C. COHEN. Tetrahedron, **27**, 789 (1971).
9. G. W. BUCHANAN and B. A. DAWSON. Can. J. Chem. **56**, 2200 (1978).
10. J. A. POPLE, J. W. MCIVER, JR., and N. S. OSTLUND. J. Chem. Phys. **49**, 2960 (1968); **49**, 2965 (1968).
11. D. W. HUGHES, B. C. NALLIAH, H. L. HOLLAND, and D. B. MACLEAN. Can. J. Chem. **55**, 3304 (1977).
12. V. J. BARTUSKA and G. E. MACIEL. J. Magn. Reson. **7**, 36 (1972).
13. J. A. SCHWARCZ and A. S. PERLIN. Can. J. Chem. **50**, 3667 (1972).
14. R. U. LEMIEUX, T. L. NAGABUSAR, and B. PAUL. Can. J. Chem. **50**, 773 (1972).
15. L. T. J. DELBEARE, M. N. G. JAMES, and R. U. LEMIEUX. J. Am. Chem. Soc. **95**, 7866 (1973).
16. P. E. HANSEN, J. FEENEY, and G. C. K. ROBERTS. J. Magn. Reson. **17**, 249 (1975).
17. S. H. GROVER and J. B. STOTHERS. Can. J. Chem. **53**, 589 (1975).
18. G. W. BUCHANAN and R. H. WIGHTMAN. Can. J. Chem. **51**, 2357 (1973).
19. H. GUNTHER and W. HERRIG. Chem. Ber. **106**, 3938 (1973).
20. J. P. MAIER and D. W. TURNER. J. Chem. Soc. Faraday Trans. II, **69**, 196 (1973).
21. F. J. WEIGERT and J. D. ROBERTS. J. Am. Chem. Soc. **94**, 6021 (1972).
22. G. BECHNER, W. LÜTTKE, and G. SCHRUMF. Angew. Chem. Int. Ed. Engl. **12**, 339 (1973).
23. J. A. POPLE and D. L. BEVERIDGE. Approximate molecular orbital theory. McGraw-Hill Book Co., New York, NY. 1970.
24. W. J. HEHRE, L. RADOM, and J. A. POPLE. J. Am. Chem. Soc. **94**, 1496 (1972).
25. A. L. GOODMAN and R. H. EASTMAN. J. Am. Chem. Soc. **86**, 908 (1964).
26. H. CHRISTOL and F. PLENOT. Bull. Soc. Chim. Fr. 1325 (1962).
27. A. I. MEYERS and M. E. FORD. Tetrahedron Lett. 2861 (1975).

Synthesis, reactions, and nuclear magnetic resonance spectroscopy of 4-methyl-6*H*-pyrazolo(3,4-b)azepin-7-ones

SURESH CHANDRA SHARMA AND BRIAN MAURICE LYNCH

Department of Chemistry, Saint Francis Xavier University, Antigonish, N.S., Canada B2G 1C0

Received June 5, 1979

SURESH CHANDRA SHARMA and BRIAN MAURICE LYNCH. Can. J. Chem. **57**, 3034 (1979).

Reactions of various 5-aminopyrazoles with ethyl levulinate in acetic acid have been shown to furnish moderate to good yields of the correspondingly substituted 4-methyl-6*H*-pyrazolo-(3,4-b)azepin-7-ones, accompanied by the acetamidopyrazoles. The courses of methylation and of bromination reactions of some of the pyrazoloazepinones have been explored and defined, and conversion of one pyrazoloazepinone into 7-chloropyrazoloazepine and thence by nucleophilic displacements into 7-(substituted amino)pyrazoloazepines has been effected. Structural assignments, tautomeric preferences, and through-space interactions between substituents were established through nuclear magnetic resonance spectroscopy (^{1}H and ^{13}C). Some members of the pyrazoloazepinone series exhibit significant anti-inflammatory and analgesic effects in mice.

SURESH CHANDRA SHARMA et BRIAN MAURICE LYNCH. Can. J. Chem. **57**, 3034 (1979).

Les réactions de différents amino-5 pyrazoles avec le lévulinate d'éthyle dans l'acide acétique fournissent avec des rendements variables les méthyl-4 6*H*-pyrazoloazépine(3,4-b)-ones-7 substituées correspondantes, accompagnés d'acétamidopyrazoles. On a exploré et défini le cours des réactions de méthylation et de bromation de quelques pyrazoloazépinones et on a effectué la transformation d'une pyrazoloazépinone en chloro-7 pyrazoloazépine qui, par des réactions de déplacements nucléophiles conduit aux pyrazoloazépines portant un groupement amino-substitué en position 7. On a établi par la résonance magnétique du proton et du ^{13}C les structures, les préférences tautomériques et les interactions spatiales entre les substituants. Certaines pyrazoloazépinones ont des effets anti-inflammatoire et analgésique significatifs chez les souris.

[Traduit par le journal]

Introduction

3(5)-Aminopyrazoles are useful starting points for syntheses of various pyrazoloazines from sequential condensation and ring-closure reactions involving exocyclic or ring nitrogen atoms and the electron-rich 4-carbon, as exemplified in previous papers from this laboratory (1–3). In view of current interest in the biological activities shown by ring-expanded purines (4–6), we now seek to use the aminopyrazoles as precursors of compounds with analogously fused five and seven membered rings (for example, pyrazoloazepines and pyrazolothiazepines (7)).

Our work involves extension of Makisumi's findings (8) that reactions of 5-amino-1-substituted pyrazoles **1** with ethyl acetoacetate in acetic acid yield 4-hydroxy-6-methyl-1-substituted pyrazolo(3,4-b)pyridines **2**, probably by way of the isolable azomethine/enamine species **3**, **4** (reaction of the parent 1*H*-compound **1***a* furnishes 7-hydroxy-5-methylpyrazolo(1,5-a)pyrimidine **5** in addition to **2***a*). Use of ethyl levulinate rather than ethyl acetoacetate might be expected to yield 1-substituted-7-methyl-5*H*-pyrazolo(3,4-b)azepin-4-ones of general structure **6** if an analogous cyclization pathway is followed, but since Bertho (9) found that reaction of aniline with levulinic acid gave 5-methyl-3*H*-1-benzazepin-2-one **7**, albeit in very low yield, products of general structure **8** (1-substituted-4-methyl-6*H*-pyrazolo(3,4-b)azepin-7-ones) are also possible (see Fig. 1). A further possibility is the independent formation of type **7** and type **8** compounds.

Results and Discussion

We find that reaction of eleven representative aminopyrazoles (**1***a* through **1***m*) with ethyl levulinate in acetic acid furnishes mixtures of the corresponding acetamidopyrazoles and individual molecular species (not pairs of isomers) analysing for types **7** or **8**. Cyclisation competed poorly with simple acetylation where the 1-substituent in the aminopyrazole was strongly electron-attracting (*m*-chlorophenyl, *m*-bromophenyl), but for all other aminopyrazole substrates yields of cyclisation products were higher (see Table 1 for details).

The fine structure of the cyclisation product obtained from 5-amino-1-methylpyrazole **1***b* was established as **8***b* (1,4-dimethyl-6*H*-pyrazolo(3,4-b)-azepin-7-one) through observation of a diagnostic nuclear Overhauser enhancement in the ^{1}H nmr spectrum. The product exhibited a 19% increase in

0008-4042/79/233034-07$01.00/0

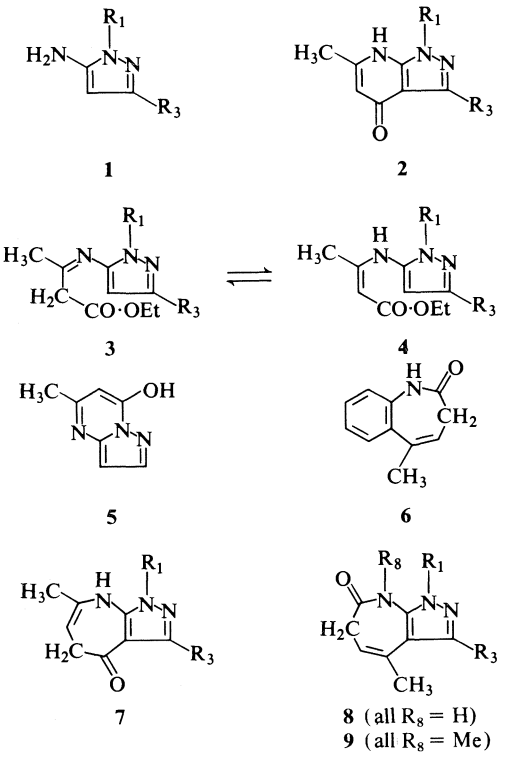

1 **2**

3 **4**

5 **6**

7 **8** (all R_8 = H)
9 (all R_8 = Me)

Key for structures **1** through **4**, **7**, **8**, **9**

	R_1	R_3
a	H	H
b	Me	H
c	Me	Me
d	Ph	H
e	Ph	Me
f	*p*-Br·C_6H_4	H
g	*m*-Br·C_6H_4	H
h	*p*-Cl·C_6H_4	H
k	*m*-Cl·C_6H_4	H
l	*m*-Cl·C_6H_4	Me
m	2,5-Cl_2·C_6H_3	H

signal intensity for the pyrazole ring proton signal (δ 7.48) on irradiation of the *C*-methyl proton signal (δ 2.02) as expected from the spatial proximity of these nuclei in **8***b*. The separation between the *C*-methyl protons and the pyrazole ring proton in **7***b* would preclude any nuclear Overhauser effect enhancement. We similarly assign type **8** structures to all the cyclisation products from the 1-substituted 5-aminopyrazoles **1***c* through **1***m*. Assignments are based upon the close correspondences of the key features of the ^{1}H and ^{13}C nmr spectra of all these products to the proven **8***b* (see Tables 2 and 3, and further discussion below), and also upon evidence

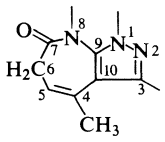

FIG. 1. Ring numbering for 4-methyl-6*H*-pyrazolo(3,4-b)-azepin-7-ones.

of interaction between N-1 and N-8 substituents in the derived type **9** compounds.

For reaction of ethyl levulinate with 1*H*-3(5)-aminopyrazole **1***a*, closure at ring nitrogen to yield either 5-methyl-7*H*-pyrazolo(1,5-a)1,3-diazepin-8-one **10** or 8-methyl-6*H*-pyrazolo(1,5-a)1,3-diazepin-5-one **11** is possible, but these structures for the cyclisation product are excluded by its ^{1}H nmr spectrum, which shows a one-proton *singlet* at δ 7.89 assignable to a pyrazole ring proton. Structures **10** or **11** would give rise to signals for two protons in that spectral region, each split by a vicinal coupling of ca. 2 Hz. In further confirmation, both **10** and **11** have *one* proton bound to nitrogen (and thus expected to exchange rapidly with added deuterium oxide); our product from **1***a* shows *two* low-field one-proton signals (at δ 10.27 and 12.77) disappearing rapidly on addition of deuterium oxide to the perdeuteriated dimethyl sulfoxide solvent. A 4-methyl-6*H*-pyrazolo-(3,4-b)azepin-7-one structure is assigned to the product from aminopyrazole **1***a*, again on the basis of general similarity of the ^{1}H and ^{13}C nmr spectra to those of **8***b* (see Tables 2 and 3), but the tautomeric preference between **8***a* (1*H*,6*H*-4-methyl-pyrazolo(3,4-b)azepin-7-one) and **12***a* (2*H*,6*H*-4-

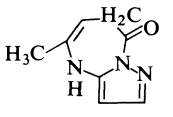

10

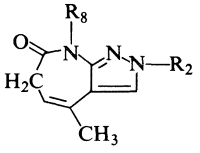

12 *a*, R_2 = R_8 = H
b, R_2 = R_8 = Me

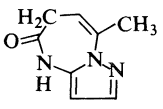

11

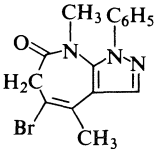

13

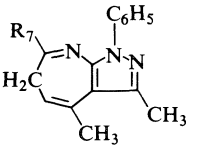

14 R_7 = Cl
15 R_7 = NHCH$_3$
16 R_7 = N(CH$_3$)$_2$
17 R_7 = NH·C_6H_{11}

TABLE 1. Reactions of aminopyrazoles with ethyl levulinate

Reactant: Aminopyrazole No.	Quantity (g*)	Products: Acetamidopyrazoles (g, %)	Pyrazoloazepinones No.	Yield (g, %)	Melting point (°C)	Formula	Analytical data: Calcd. C	H	N	Found C	H	N
1*a*	4.15	1.52, 29	**12***a*	3.67, 45	221–222	$C_8H_9N_3O$	58.88	5.56	25.75	58.61	5.76	25.82
1*b*	10.0	5.75, 40	**8***b*	9.00, 49	163–165	$C_9H_{11}N_3O$	60.99	6.26	23.71	61.37	6.27	24.07
1*c*	6.50	2.32, 27	**8***c*	5.70, 51	196	$C_{10}H_{13}N_3O$	62.80	6.85	21.98	63.07	7.01	21.87
1*d*	8.00	3.25, 32	**8***d*	6.88, 57	146–147	$C_{14}H_{13}N_3O$	70.28	5.48	17.56	70.39	5.31	17.71
1*e*	8.00	3.65, 37	**8***e*	6.28, 54	160–161	$C_{15}H_{15}N_3O$	71.12	5.97	16.59	71.10	5.65	16.65
1*f*	3.42	0.79, 20	**8***f*	2.49, 55	131	$C_{14}H_{12}N_3OBr$	52.84	3.80	13.21	52.66	3.95	13.38
1*g*	1.60	1.67, 89	**8***g*	0.20, 9	215	$C_{14}H_{12}N_3OBr$				52.95	4.23	13.23
1*h*	2.50	0.82, 27	**8***h*	1.98, 56	179	$C_{14}H_{12}N_3OCl$	61.43	4.42	15.35	61.12	4.11	15.48
1*k*	8.08	7.47, 76	**8***k*	0.88, 8	174–176	$C_{14}H_{12}N_3OCl$				61.10	4.16	15.48
1*l*	0.80	0.35, 36	**8***l*	0.46, 41	166–167	$C_{15}H_{14}N_3OCl$	62.61	4.90	14.60	62.41	4.74	14.43
1*m*	2.28	1.39, 51	**8***m*	0.92, 30	129	$C_{14}H_{11}N_3OCl_2$	54.56	3.60	13.64	54.15	3.47	13.90

*This quantity of aminopyrazole was heated under reflux with an equimolar quantity of ethyl levulinate in an amount of acetic acid furnishing a total concentration of 20% w/v, for a period of 18–20 h.

methylpyrazolo(3,4-b)azepin-7-one) is not evident from simple spectroscopic examination of this one species.

However, a study of the products obtained when the various substituted 4-methyl-(6*H*)pyrazolo-(3,4-b)azepin-7-ones were subjected to standard methylation procedures provided evidence concerning the position of equilibrium in the **8***a*–**12***a* system. When the 1-substituted 4-methyl-(6*H*)pyrazolo(3,4-b)-azepin-7-ones **8***b*–**8***f* were reacted, the corresponding 4,8-dimethyl derivatives **9***b*–**9***f* were obtained (see Table 4). However, reaction of the parent compound yielded a trimethyl-6*H*-pyrazolo(3,4-b)azepin-7-one differing from 1,4,8-trimethyl-6*H*-pyrazolo(3,4-b)-azepin-7-one **9***b* in melting point and in its ^1H and ^{13}C nmr spectra (see Tables 2 and 3). The ^{13}C nmr signals from the *N*-methyl carbons fall at δ 35.2 and 37.5 for **9***b*, and at δ 33.6 and 39.4 for the other isomer. By analogy with the pattern observed for the *N*-methyl carbons in 1-methylindazole and in 2-methylindazole (shifts are δ 35.3 and 39.7 respectively (10)), it is proposed that this "other isomer" is 2,4,8-trimethyl-6*H*-pyrazolo(3,4-b)azepin-7-one, **12***b*. The close resemblance of the 3-carbon shift in the parent cyclisation product (δ 127.1) to that for the 2,4,8-trimethyl compound **12***b* (δ 127.3), and the considerable difference from that for the 1,4,8-trimethyl compound **9***b* (δ 135.3) suggests strongly that the preferred tautomeric form of the parent cyclisation product is **12***a*.

There are interesting proximity effects for the methylation products possessing N-1 aryl groups: in these (compounds **9***d*, **9***e*, **9***f*), the N-8 methyl protons are shielded by approximately 0.4 ppm as compared with the 8-methylated species lacking a 1-aryl group. The shielding effect is readily explained if the 1-aryl and pyrazoloazepinone mean ring planes are orthogonal in these 8-methylated species, with the methyl group falling in the diamagnetic zone around the 1-aryl group. Similar, larger shielding effects are observed for the N-8 methyl carbon signals in these species (**9***b*, **9***c* δ 37.5, 37.0; **9***d*, **9***e*, **9***f* δ 35.2, 34.9, 35.1), but these are better rationalised by sterically induced C—H bond polarisations (cf. ref. 11) than anisotropic influences.

Other conversion reactions effected with the azepinone moieties of type **8** and **9** species yielded products of spectroscopic interest or relevant to structure proofs; thus monosubstitution of the compound **9***d* occurred on treatment with bromine. The monosubstitution product has the structure **13** (5-bromo-4,8-dimethyl-1-phenyl-6*H*-pyrazolo(3,4-b)-azepin-7-one), established by the following changes in the ^1H and ^{13}C nmr signal patterns: (*a*) loss of the characteristic H-5 one-proton triplet signal from the δ 5.5 region, (*b*) loss of the J_{5-6} splitting of the two-proton 6-CH_2 signal and an *upfield* shift from δ 3.04 to 2.71, (*c*) a lowered intensity and an upfield shift of the δ 116.6 signal assigned to C-5 to δ 108.0, and (*d*) a downfield shift from δ 36.7 to δ 48.0 for the signal assigned to C-6. The upfield and the downfield shifts in the carbon signals are those to be expected for *ipso*- and vicinally-located bromine (cf. ref. 12), but the upfield shift for the protons attached to C-6 has no precedents, as far as we are aware; a tentative explanation could lie in unfavorable dipole–dipole interactions between the C—Br and C=O bonds in this compound.

TABLE 2. ^{1}H nmr spectra of substituted 4-methyl-6*H*-pyrazolo(3,4-b)azepin-7-ones, **8, 9, 12**

	Chemical shifts, proton counts, and signal multiplicities for protons at positions indicated*							
No.	1	2	3	4	5	6	8	Solvent
12*a*		12.77 (1, s)	7.89 (1, s)	2.03 (3, s)	5.41 (1, t)	2.78 (2, d)	10.27 (1, s)	DMSO-d_6
8*b*	3.70 (3, s)		7.48 (1, s)	2.02 (3, s)	5.27 (1, t)	2.74 (2, d)	10.47 (1, s)	DMSO-d_6
8*c*	3.80 (3, s)		2.36 (3, s)	2.15 (3, s)	5.31 (1, t)	2.84 (2, d)	—	$CDCl_3$
8*d*	7.58 (5, s)		7.86 (1, s)	2.10 (3, s)	5.42 (1, t)	2.89 (2, d)	10.45 (1, s)	DMSO-d_6
8*e*	7.52 (5, s)		2.45 (3, s)	2.20 (3, s)	5.42 (1, t)	2.91 (2, d)	8.17 (1, s)	$CDCl_3$
8*f*	449–460 Hz (4)		7.73 (1, s)	2.18 (3, s)	5.45 (1, t)	2.96 (2, d)	9.13 (1, s)	$CDCl_3$
8*g*	7.48, 7.66 (3, s) (1, s)		7.73 (1, s)	2.15 (3, s)	5.42 (1, t)	2.97 (2, d)	—	$CDCl_3$
8*h*	7.68 (4, s)		7.91 (1, s)	2.09 (3, s)	5.44 (1, t)	2.86 (2, d)	10.53 (1, s)	DMSO-d_6
8*k*	457–475 Hz (4)		7.89 (1, s)	2.13 (3, s)	5.44 (1, t)	2.86 (2, d)	10.51 (1, s)	DMSO-d_6
8*l*	454–468 Hz (4)		2.37 (3, s)	2.16 (3, s)	5.46 (1, t)	2.86 (2, d)	10.47 (1, s)	DMSO-d_6
8*m*	460–470 Hz (3)		7.94 (1, s)	2.12 (3, s)	5.44 (1, t)	2.84 (2, d)	10.65 (1, s)	DMSO-d_6
12*b*		3.93 (3, s)	7.42 (1, s)	2.05 (3, s)	5.46 (1, t)	2.98 (2, d)	3.45 (3, s)	$CDCl_3$
9*b*	3.98 (3, s)		7.54 (1, s)	2.10 (3, s)	5.44 (1, t)	2.89 (2, d)	3.31 (3, s)	$CDCl_3$
9*c*	3.73 (3, s)		2.23 (3, s)	2.09 (3, s)	5.44 (1, t)	2.88 (2, d)	3.18 (3, s)	DMSO-d_6
9*d*	7.61 (5, s)		7.94 (1, s)	2.13 (3, s)	5.53 (1, t)	3.04 (2, d)	2.70 (3, s)	DMSO-d_6
9*e*	7.53 (5, s)		2.35 (3, s)	2.15 (3, s)	5.52 (1, t)	2.94 (2, d)	2.66 (3, s)	DMSO-d_6
9*f*	460–470 Hz (4)		7.89 (1, s)	2.13 (3, s)	5.58 (1, t)	3.06 (2, d)	2.75 (3, s)	DMSO-d_6

*Proton counts and signal multiplicities are shown in parentheses. Envelope dimensions for complex aromatic multiplets are expressed in Hz. J_{56} for all compounds = 7.2 ± 0.2 Hz.

The representative pyrazoloazepinone **8***e* was converted into the unstable, reactive chloro compound **14** on treatment with phosphorus oxychloride. The crude compound was used directly in a series of displacements by nitrogen nucleophiles, providing the 7-(substituted amino) entities **15–17**. The high reactivity of **14** is to be expected from its imidochloride character.

Because our assignments of structure for the pyrazoloazepinones and their derivatives rest almost completely upon pattern resemblances and substituent-induced variations in the ^{1}H and ^{13}C nmr signals for related series of compounds, we wish to provide an account of our reasoning in allocating the nmr signals to specific groups or atoms. We interpreted the features of the ^{1}H nmr spectra assignable to entities present in the uncyclised aminopyrazole (that is, substituents or protons at positions 1, 2, and 3) by direct comparison with the aminopyrazoles, and by general resemblances to other 1- and 1,3-substituted pyrazoles (13–16); the proton signals from the 4-methyl-, 5-methine-, and 6-methylene functions were simply assignable by proton count and by signal multiplicity.

The key compound for signal assignments in the ^{13}C nmr spectra is the species **8***b*, where the nOe

TABLE 3. ^{13}C nmr signals from ring and substituent carbon atoms in substituted 4-methyl-6*H*-pyrazolo(3,4-b)azepin-7-ones, **8, 9, 12**

	Ring carbons at position							Methyl carbons at position					
No.	3	4	5	6	7	9	10	1	2	3	4	8	Solvent
12*a*	127.1	131.4	113.8	36.2	170.1	145.0	112.7				21.0		9:1 $CDCl_3$: DMSO-d_6
12*b*	127.3	130.7	115.8	36.6	169.0	136.7	114.7		39.4		20.8	33.6	$CDCl_3$
8*b*	135.8	132.6	112.2	36.3	170.4	136.7	113.3	35.5			20.4		$CDCl_3$
8*c*	144.7	133.2	113.6	36.1	171.0	136.6	111.1	35.0		14.6	20.7		$CDCl_3$
8*d*	137.7	131.8	113.3	36.2	168.1	—	114.0				20.4		$CDCl_3$
8*e*	138.0	132.5	114.7	36.2	169.2	137.9	112.3			14.8	20.8		$CDCl_3$
8*h*	137.7	131.9	114.2	36.2	167.5	137.4	114.1				19.9		DMSO-d_6
8*k*	137.3	131.4	113.6	36.2	168.1	137.1	112.8				19.9		DMSO-d_6
8*l*	136.0	131.4	115.8	36.2	168.2	—	112.4			14.5	20.3		DMSO-d_6
8*m*	138.2	131.6	113.8	36.2	167.9	136.5	112.8				19.8		DMSO-d_6
9*b*	135.3	131.6	115.9	36.4	169.0	140.6	115.0	35.2			20.0	37.5	$CDCl_3$
9*c*	—	132.3	117.4	36.5	169.9	—	—	35.2		14.5	20.3	37.0	$CDCl_3$
9*d*	137.4	132.0	116.6	36.7	169.5	135.3	—				20.3	35.2	$CDCl_3$
9*e*	139.5	131.8	117.9	36.8	169.1	140.1	114.4			14.7	20.3	34.9	$CDCl_3$
9*f*	137.5	131.1	116.6	36.7	168.2	138.5	116.6				19.9	35.1	DMSO-d_6

TABLE 4. Methylation products from 1-substituted-4-methyl-6*H*-pyrazolo(3,4-b)azepin-7-ones

		Products (1-substituted-4,8-dimethyl-6*H*-pyrazolo(3,4-b)azepin-7-ones)									
						Analytical data					
						Calcd.			Found		
Reactant No.	Reactant quantity (g)	No.	Yield (g, %)	Melting point (°C)	Formula	C	H	N	C	H	N
8*b*	4.00	**9***b*	2.90, 67	119–121	$C_{10}H_{13}N_3O$	62.80	6.85	21.98	62.69	7.14	22.26
8*c*	1.00	**9***c*	0.64, 60	103–104	$C_{11}H_{15}N_3O$	64.36	7.37	20.47	64.31	7.08	20.29
8*d*	1.00	**9***d*	1.00, 95	118–119	$C_{15}H_{15}N_3O$	71.12	5.97	16.59	70.73	6.20	16.75
8*e*	1.00	**9***e*	0.90, 86	182	$C_{16}H_{17}N_3O$	71.88	6.41	15.72	71.69	6.54	15.48
8*f*	1.20	**9***f*	1.16, 93	163–164	$C_{15}H_{14}N_3OBr$	54.23	4.24	12.65	53.84	4.30	12.70

experiment cited above defines the structure. The broadband-decoupled spectrum of this compound gave signals falling into two intensity groupings: δ 20.4, 35.5, 36.2, 112.2, 135.8 (more intense); 113.3, 132.6, 136.7, 170.4 (less intense). Gated decoupling experiments revealed direct $^{13}C—^{1}H$ couplings for all the more intense signals, while the less intense group showed no significant splitting. The δ 20.4 and 35.5 signals were quartets under the gated decoupling conditions, the δ 36.2 signal was a triplet, and the δ 112.2 and 135.8 signals doublets. Since a signal at δ 20.4 ± 0.6 appears in all the pyrazoloazepinones, and a δ ca. 35.5 only for species possessing a 1-methyl substituent (**8***b*, *c*; **9***b*, *c*) it follows that the δ 20.4 signal corresponds to the 4-methyl carbon, and the δ 35.5 to the 1-methyl carbon. The triplet character of the δ 36.2 signal defines it as arising from the 6-methylene carbon. The δ 135.8 doublet signal is assigned to C-3 of the pyrazole ring, by analogy with the chemical shift of C-3 in 1-methylpyrazole (δ 139.4 (17)) and in 5-acetamido-1-methylpyrazole (δ 138.3); the δ 112.2 signal is then assigned by elimination to the methine C-5 (a reasonable analogy for this would be the shift (δ 117.6) for C-3 in 2-methyl-2-butene (18)). Of the family of less intense signals, that at δ 170.4 is immediately assignable as the amide carbonyl, C-7; the δ 132.6 signal, since a signal close to this position appears for all the pyrazoloazepinones, is assigned to C-4 (again, the shift for C-2 (δ 130.1) in 2-methyl-2-butene (18) is an appropriate analogy). Of the two remaining quaternary carbon signals, that at δ 113.3 is assigned to the electron-rich C-10, and the δ 136.7 to C-9. The signal patterns noted in the ^{13}C nmr spectra of compound **8***b* are followed generally for all the type **8** and type **9** compounds, with minor perturbations as a function of the nature of the 1-substituent, and the presence or absence of methyl groups at positions 3 or 8.

Compounds with a *C*-methyl group at the 3 position (**8***c*, *e*, *l*; **9***c*, *e*) exhibit a characteristic signal at around δ 14.5.

Biological Screening Results

The various pyrazoloazepinone derivatives synthesised in this program were evaluated for analgesic activity by monitoring reduction of phenylquinone-induced writhing in mice, using aspirin (50 mg/kg subcutaneous administration) as standard compound (50% reduction is effected by this concentration of aspirin). Compound **8***d* (4-methyl-1-phenyl-6*H*-pyrazolo(3,4-b)azepin-7-one) gave 89% reduction of writhing activity at 32 mg/kg. Compound **12***a* (2*H*,-6*H*-4-methylpyrazolo(3,4-b)azepin-7-one) gave 13% reduction at 128 mg/kg, and also showed anti-inflammatory activity (antagonism of carageenan-induced oedema) at 64 mg/kg in rats.

Conclusions and Comments

The delineated reactions of aminopyrazoles with ethyl levulinate provide a reasonably effective synthetic route to 6*H*-pyrazolo(3,4-b)azepin-7-ones; the yields are far superior to those obtained when aniline is reacted with various γ-keto acids (cf. Bertho (9)). We attribute the increased effectiveness of the cyclisation to the high electron density at the 4-position in the aminopyrazole substrates **1**. The observed cyclisation mode (involving amide formation between ester and amine functions, and electrophilic alkylation at the 4-position) is opposite to that observed in the reactions of aminopyrazoles with ethyl acetoacetate; the preferred reaction course when a ketoester reacts with an aminopyrazole possessing two potential nucleophilic centres (amino-nitrogen and the 4-carbon) is thus not readily predictable Reactions of aminopyrazoles with other γ-dicarbonyl species (such as 2,5-pentanedione (acetonylacetone) or 1,2-diformylhydrazine) were explored briefly as potential routes to other pyrazoloazepines or pyrazolotriazepines, in view of the successful formation of the fused seven-membered ring with ethyl levulinate. However, the products obtained were the unexceptional 5-(2,5-dimethyl-1-pyrrolyl)-1-substituted pyrazoles and 4-(1-substituted-5-pyrazolyl)-1,2,4-triazoles, with preferred cyclisation yielding five-membered rings.

Experimental

General

Melting points were determined using a Fisher-Johns apparatus. Specimens for elemental analysis were dried at 65°C/0.2 Torr for at least 6 h and were analysed using a Hewlett-Packard Model 185 CHN analyser. Most of the ^{1}H nmr measurements were made using a Varian A-60D instrument; the nuclear Overhauser effect experiments used a Varian XL-100. The ^{13}C nmr spectra were obtained using a Bruker WP-80 Fourier transform instrument operating at 20.115 MHz, a 30° pulse of length 3.0 μs, and 16K data points with sweep widths of 5000 Hz. The data assembled in Table 3 were acquired using broadband decoupling, and signal assignments were confirmed using gated decoupling sequences. All chemical shifts are expressed in parts per million from tetramethylsilane (internal reference).

*Standard Synthetic Procedure for Substituted 4-Methyl-6*H*-pyrazolo(3,4-b)azepin-7-ones, **8** and **12***

3(5)-Aminopyrazole **1***a* (4.15 g, 0.05 mol) and ethyl levulinate (7.50 g, 0 05 mol) were heated under reflux in acetic acid (50 mL) for 20 h. The reaction mixture was concentrated under reduced pressure and neutralised with saturated aqueous sodium hydrogen carbonate, yielding a crystalline mixture of 3(5)-acetamidopyrazole and 2*H*,6*H*-4-methylpyrazolo(3,4-b)-azepin-7-one, **12***a*. Separation was effected by preparative thin-layer chromatography on silica using toluene/ethyl acetate/methanol (100:85:15 v/v), yielding the pyrazoloazepinone **12***a*, which was crystallised from ethanol to give 3.67 g (45% yield) of material mp 221–222°C (see Table 1), and 3(5)-acetamidopyrazole, crystallised from ethanol, mp 217–218°C (yield 1.52 g, 29%). ^{1}H nmr (DMSO-d_6) δ: 10.38 (s, 1H, acetamido N*H*), 7.57 (d, 1H, J = 1.6 Hz, H-3(5)), 6.48 (d, 1H, J = 1.6 Hz, H-4), 3.39 (s, 1H, H-1), 2.02 (s, 3H, acetyl H). *Anal.* calcd. for $C_5H_7N_3O$: C 47.99, H 5.64, N 33.58; found: C 48.25, H 5.23, N 33.57.

Similar reactions of other 1-substituted 5-aminopyrazoles **1***b–m* gave mixtures of 1-substituted-4-methyl-6*H*-pyrazolo-(3,4-b)azepin-7-ones **8***b–m* and 1-substituted 5-acetamidopyrazoles, separated as above. Reactant quantities, yields, and analytical data are summarised in Table 1 for the various products of type **8**, and details of the ^{1}H and ^{13}C nmr spectra in Tables 2 and 3. The acetamidopyrazoles were isolated and characterised by ^{1}H and ^{13}C nmr, but were not purified for element analysis. Some of these products contained detectable proportions of the tautomeric 2-acetamido-5-iminopyrazoles.

*Methylations of 4-Methyl-6*H*-pyrazolo(3,4-b)azepin-7-ones*

The following procedure is typical: 1,4-dimethyl-6*H*-pyrazolo(3,4-b)azepin-7-one, **8***b* (4.00 g, 0.0225 mol) was dissolved in 3 *M* aqueous sodium hydroxide and was cooled in ice while a twofold molar proportion of dimethyl sulfate was added dropwise. The reaction mixture was heated to 90°C for 5 min, left to stand at laboratory temperature for 1 h, and extracted with chloroform (3 × 100 mL). The aqueous residue was extracted continuously with a further 200 mL chloroform and the extracts were combined, dried, and evaporated; crystallisation of the residue from ethanol provided 1,4,8-trimethyl-6*H*-pyrazolo(3,4-b)azepin-7-one **9***b*, mp 119–121°C (2.90 g, 67%). Analogous reactions with the compounds **8***c* through **8***f* provided the corresponding 8-methyl derivatives **9***c* through **9***f* (see Table 4).

Methylation of 2*H*,6*H*-4-methylpyrazolo(3,4-b)azepin-7-one **12***a* (0.20 g, 0 0011 mol) under the above conditions provided 0.150 g (70%) of 2,4,8-trimethyl-6*H*-pyrazolo(3,4-b)azepin-7-one **12***b*, mp 92–94°C, differing in ^{1}H and ^{13}C nmr spectra from **9***b* (see Tables 2 and 3).

*Bromination of 4,8-Dimethyl-1-phenyl-6*H*-pyrazolo(3,4-b)-azepin-7-one, **9**d*

The above compound (1.00 g) was dissolved in dichloromethane (3 mL) and treated with bromine (0.70 g) in dichloromethane (1.0 mL) by dropwise addition, and allowed to react at room temperature with continuous stirring for 1 h. Dichlo-

romethane (10 mL) was added, and the resulting solution was washed with saturated aqueous sodium hydrogen carbonate and with water, dried, and concentrated, providing 0.85 g (65%) of 5-bromo-4,8-dimethyl-1-phenyl-6*H*-pyrazolo(3,4-b)-azepin-7-one **13**. An analytical sample, mp 106°C, was obtained by precipitation from dimethyl sulfoxide with water. ^{1}H nmr (DMSO-d_6) δ: 7.84 (s, 1H, H-3), 7.38 (s, 5H, 1-phenyl), 2.71 (s, 5H, 6-CH_2 and 8-CH_3), 2.21 (s, 3H, 4-CH_3). ^{13}C nmr (assignable peaks from overnight accumulation for a 0.2% solution in DMSO-d_6) δ: 165.9 (C-7), 137.9 (C-3), 113.1 (C-10), 107.5 (C-5), 47.8 (C-6), 34.5 (8-CH_3), 20.5 (4-CH_3). *Anal.* calcd. for $C_{15}H_{14}N_3OBr$: C 54.23, H 4.24, N 12.65; found: C 53.84, H 4.16, N 12.91.

*Formation and Nucleophilic Displacements of 7-Chloro-3,4-dimethyl-6*H*-pyrazolo(3,4-b)azepine, **14***

3,4-Dimethyl-1-phenyl-6*H*-pyrazolo(3,4-b)azepin-7-one **8***e* (3.00 g, 0.0125 mol) was heated under reflux in phosphorus oxychloride (10 mL) for 2 h. The reaction mixture was concentrated under reduced pressure, yielding the crude **14**. Attempts at purification resulted in reversion to the starting material. However, successful conversions were effected as follows.

*(a) Into 3,4-Dimethyl-7-methylamino-1-phenyl-6*H*-pyrazolo(3,4-b)azepine **15***

The crude chloro-compound **14** (1.00 g) was dissolved in dichloromethane (10 mL) and cooled in ice. Triethylamine (0.60 g) was added, followed by 40% aqueous methylamine (0.35 g). After stirring for 1 h the solvent was removed under reduced pressure and the residue was crystallised from aqueous methanol, providing 0.85 g (89%) of the methylamino compound **15**, mp 173–174°C. ^{1}H nmr ($CDCl_3$) 430–485 Hz (5H, 1-phenyl), δ: 5.23 (q, 1H, J = 5.0 Hz (disappearing on addition of D_2O), N*H*CH_3), 4.96 (t, J = 7.2 Hz, H-5), 2.76 (d, 3H, J = 5.0 Hz (collapsing to singlet on addition of D_2O), NHCH_3), 2.53 (d, 2H, J = 7.2 Hz, 6-CH_2), 2.47 (s, 3H, 3-CH_3), 2.16 (s, 3H, 4-CH_3). ^{13}C nmr ($CDCl_3$) (phenyl ring signals excluded) δ: 154.3 (C-7), 147.7 (C-9), 140.5 (C-3), 133.2 (C-4), 110.8 (C-5), 109.9 (C-10), 34.0 (C-6), 28.8 (7-NHCH_3), 21.0 (4-CH_3), 15.5 (3-CH_3). *Anal.* calcd. for $C_{16}H_{18}N_4$: C 72.15, H 6.81, N 21.04; found: C 72.25, H 6.73, N 21.00.

*(b) Into 3,4-Dimethyl-7-dimethylamino-1-phenyl-6*H*-pyrazolo(3,4-b)azepine, **16***

The chloro compound **14** (0.50 g) was heated under reflux for 4 h in *N*,*N*-dimethylformamide (5 mL). The reaction mixture was extracted with dichloromethane (3 × 25 mL), washed with water, dried, and concentrated. Separation by preparative thin-layer chromatography gave the 7-dimethylamino derivative **16**, mp 51°C (0.19 g, 36%) and the azepinone **8***e* (0.20 g, 50%). ^{1}H nmr ($CDCl_3$) 440–490 Hz (5H, 1-phenyl), δ: 5.07 (t, 1H, J = 7.2 Hz, H-5), 3.04 (s, 6H, N(CH_3)$_2$), 2.70 (d, 2H, J = 7.2 Hz, 6-CH_2), 2.49 (s, 3H, 3-CH_3), 2.11 (s, 3H, 4-CH_3). *Anal.* calcd. for $C_{17}H_{20}N_4$: C 72.82, H 7.19, N 19.98; found: C 72.59, H 7.01, N 19.56.

*(c) Into 7-Cyclohexylamino-3,4-dimethyl-1-phenyl-6*H*-pyrazolo(3,4-b)azepine, **17***

Cyclohexylamine (0.45 g) was added to the chloro compound **14** (1.00 g). After the exothermic reaction had subsided, benzene (10 mL) was added and the crystalline hydrochloride of **17** was collected by filtration. Yield 1.26 g, 94%, mp 177–178°C. ^{1}H nmr (DMSO-d_6): 440–495 Hz (5H, 1-phenyl), δ: 5.07 (t, 1H, J = 7.2 Hz, H-5), 195–235 Hz (1H, H-1 of cyclohexyl moiety), δ: 2.71 (d, 2H, J = 7.2 Hz, 6-CH_2), 2.35 (s, 3H, 3-CH_3), 2.09 (s, 3H, 4-CH_3). *Anal.* calcd. for $C_{21}H_{27}N_4Cl$: C 68.00, H 7.34, N 15.10; found: C 67.83, H 7.63, N 14.82. Treatment with aqueous sodium hydrogen carbonate gave **17**, mp 81°C. Attempted crystallization from aqueous methanol resulted in reversion to the pyrazoloazepinone **8***e*.

Acknowledgements

The authors wish to thank the National Research Council and the Natural Sciences and Engineering Research Council of Canada for operating and equipment grant support. We also thank Mr. D. G. Smith of the Atlantic Regional Laboratory of the National Research Council of Canada, Halifax, for the nuclear Overhauser effect measurements, and Dr. F. Fried, Bio-Research Limited, Pointe Claire, P.Q., for biological screening through the program of Canadian Patents and Development Limited.

1. M. A. Khan and B. M. Lynch. J. Heterocycl. Chem. **7**, 247 (1970).
2. B. M. Lynch, M. A. Khan, S. C. Sharma, and H. C. Teo. Can. J. Chem. **53**, 119 (1975).
3. I. Chu and B. M. Lynch. J. Med. Chem. **18**, 161 (1975).
4. P. W. K. Woo, H. W. Dion, S. M. Lange, F. F. Dahl, and L. J. Durham. J. Heterocycl. Chem. **11**, 641 (1974).
5. M. Ohno, N. Yagisawa, S. Shibahara, S. Kondo, K. Maeda, and H. Umezawa. J. Am. Chem. Soc. **96**, 4326 (1974).
6. H. Nakamura, G. Koyama, Y. Iitaka, M. Ohno, N. Yagisawa, S. Kondo, K. Maeda, and H. Umezawa. J. Am. Chem. Soc. **96**, 4327 (1974).
7. L. H. Swett and G. H. Aynilian. J. Heterocycl. Chem. **12**, 1135 (1975).
8. Y. Makisumi. Chem. Pharm. Bull. **10**, 612 (1962).
9. A. Bertho. Chem. Ber. **90**, 29 (1957).
10. P. Bouchet, A. Fruchier, G. Joncheray, and J. Elguero. Org. Magn. Reson. **9**, 716 (1977).
11. D. K. Dalling and D. M. Grant. J. Am. Chem. Soc. **94**, 5318 (1972).
12. B. M. Lynch. Can. J. Chem. **55**, 541 (1977).
13. T. J. Batterham. NMR spectra of simple heterocycles. John Wiley, New York. 1973.
14. M. A. Khan and B. M. Lynch. Can. J. Chem. **49**, 3566 (1971).
15. J. J. Bergman and B. M. Lynch. J. Heterocycl. Chem. **11**, 135 (1974).
16. R. N. Butler. Can. J. Chem. **51**, 2315 (1973).
17. R. G. Rees and M. J. Green. J. Chem. Soc. B, 387 (1968).
18. J. J. Becconsall and P. Hampson. J. Mol. Phys. **10**, 21 (1965).

An isokinetic relationship in the oxidation of acetals by ozone. Evidence for rotation before the oxidation of acyclic acetals

ROLAND J. TAILLEFER,[1] SHIRLEY E. THOMAS, YVES NADEAU,[2] AND HELMUT BEIERBECK

Département de chimie, Université de Sherbrooke, Sherbrooke (Qué.), Canada J1K 2R1

Received September 15, 1978[3]

ROLAND J. TAILLEFER, SHIRLEY E. THOMAS, YVES NADEAU, and HELMUT BEIERBECK. Can. J. Chem. **57**, 3041 (1979).

Second order rate constants for the oxidation by ozone of several acyclic acetals of heptaldehyde were determined at several temperatures. An isokinetic relationship is shown to exist for this series of reactions and the isokinetic temperature was found to be below the experimental temperature range, a domain of temperatures where reactivity is dominated by entropy factors. These results are contrasted with those obtained for cyclic acetals of heptaldehyde, where the isokinetic temperature falls above the working temperatures, a domain of temperatures where reactivity depends mainly on enthalpy factors. These results are interpreted in terms of a conformational change before oxidation in the acyclic acetals.

ROLAND J. TAILLEFER, SHIRLEY E. THOMAS, YVES NADEAU et HELMUT BEIERBECK. Can. J. Chem. **57**, 3041 (1979).

Les constantes de vitesse de deuxième ordre pour l'oxydation par l'ozone de plusieurs acétales acycliques du heptaldéhyde ont été déterminées à plusieurs températures. Ceci a permis de mettre en évidence l'existence d'une relation isocinétique pour cette série de réactions. La température isocinétique trouvée est inférieure au domaine de températures expérimentales. Ceci correspond à un domaine de températures où la réactivité dépend essentiellement de $\Delta S^{\ddagger}$. Ces résultats sont en opposition avec ceux de l'oxydation d'acétales cycliques du heptaldéhyde où la température isocinétique est supérieure aux températures expérimentales, donc dans un domaine de températures où la réactivité dépend essentiellement de $\Delta H^{\ddagger}$. Ces résultats sont interprétés en invoquant un changement conformationnel dans les acétales acycliques avant l'étape d'oxydation.

Recently, a new method of oxidation of acetals by ozone (eq. [1]) was discovered (1). The reaction is

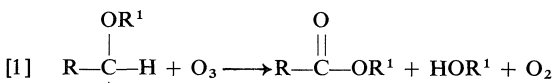

[1] $R-C(OR^1)_2-H + O_3 \longrightarrow R-C(=O)-OR^1 + HOR^1 + O_2$

quite general, giving esters in high yield. The rates at which different acetals are oxidized, however, vary considerably and this led to the proposal of a stereoelectronic theory for the oxidation of acetals by ozone (2). Basically, it was proposed that in order for oxidation to proceed, it is required that one nonbonded electron pair on each oxygen atom of the acetal function lies antiperiplanar to the C—H bond of the acetal function (Scheme 1). This theory was supported by the synthesis of rigid models of every possible gauche conformation that an acetal can adopt and it was found that those conformations which had the stereochemical requirements did in fact undergo oxidation, while those that did not were stable towards ozone. This theory of stereoelectronic control of reactivity was later extended to the breakdown of tetrahedral intermediates formed during the hydrolysis of orthoesters (3, 4), imidate salts (3, 5), esters, and amides (3, 6). In view of the fact that stereoelectronic control of reactivity may be important in many other reactions (3), including reaction of phosphate diesters (7), and reactions of biological interest (8), it seemed important to investigate further the mechanism of oxidation of acetals by ozone.

The mechanism of the reaction[4] can be written as described in Scheme 2. This mechanism is supported by the work of Henry (9). The stoichiometry of the reaction is that shown and the reaction is first-order in ozone and first-order in acetal. Furthermore, nmr

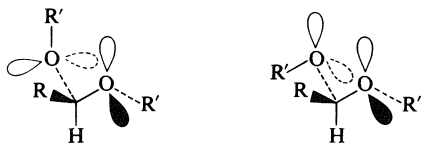

Unreactive conformation Reactive conformation

SCHEME 1

[1]To whom all correspondence should be addressed.
[2]Undergraduate summer student, 1977.
[3]Revision received June 6, 1979.

[4]Evidence for the mechanism of the reaction will be presented in a forthcoming publication.

0008-4042/79/233041-06$01.00/0

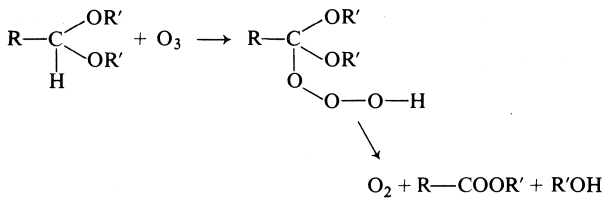

SCHEME 2

evidence was obtained for the intermediacy of the acetal hydrotrioxide (10). This paper describes the kinetic behaviour of acyclic acetals **1** as compared to that of cyclic acetals **2** (Scheme 3).

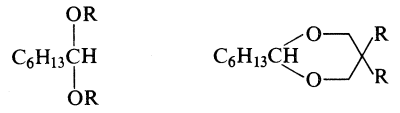

1 R = Me, Et, *n*-Pr, *iso*-Pr

2 R = H, Me

SCHEME 3

Experimental

The acetals used in this study were prepared by standard procedures. Their physical properties corresponded to literature values and their spectra were in accord with their structures. Vapor phase chromatographic analyses were carried out on Varian Aerograph instruments, model 2800 with thermal conductivity detector and temperature programming, or model 600D with flame detector. Columns of various loadings (5%, 10%, 15%) and dimensions (5 ft × 1/8 in., 10 ft × 1/4 in., 15 ft × 1/4 in.) were employed with the liquid phases SE-30, Carbowax-20M, and PPE (OS-138). Ozone was produced from a Welsbach Ozonator model T-816. Low temperature baths were either an acetone – Dry ice mixture (−78°C) or a Neslab low temperature bath, model LTE-9 (−70 to 0°C). The ethyl acetate used was of spectroscopic grade (Fisher Scientific Co., Limited).

General Procedures for Kinetic Runs

Ethyl acetate (50–100 mL) was placed in a reactor together with solid sodium bicarbonate (1–2 g) and cooled to an appropriate temperature. An ozone–oxygen stream (3–5% ozone) was then bubbled through the solvent to achieve a saturated solution in ozone. The sample of acetal (100–200 mg, ca. 1.0 mmol/100 mL) and an internal standard (20–60 mg) were dissolved in 5 mL ethyl acetate, cooled, and added to the ozone solution. The ozone stream was maintained throughout the reaction time to ensure a constant ozone concentration. After ≃2 minutes, the first sample was removed (time = 0), cooled to −78°C while the ozone was displaced by nitrogen, after which samples were removed at convenient intervals. The reaction was followed by vapor phase chromatography. Pseudo-first order rate constants were obtained by following the disappearance of the acetal with respect to the internal standard. The internal standard was a heptanoic acid ester, the vpc response of which was calibrated against the acetal response. All peaks in the vpc spectrum were completely resolved.

Competition Experiments

Relative rates of oxidation of acetals **2** (R = H, CH_3) were also determined by a competition method as described by Hammett (11). The mixture of acetals and internal standard (*n*-propylheptanoate) was reacted with ozone in ethyl acetal at an appropriate temperature. Concentrations were determined as above by vpc analysis.

Concentrations of Ozone in Ethyl Acetate

Ethyl acetate was saturated with ozone at several temperatures ranging from 0°C to −78°C. Aliquots of these solutions were treated at −78°C with acidified potassium iodide solution and the liberated iodine was titrated with standard thiosulfate. The variation of the ozone concentration in ethyl acetate with temperature is shown in Fig. 1.

Results

Tables 1 and 2 list the data obtained for the oxidation of acetals **1** and **2**. Pseudo-first order rate constants were found by following the disappearance of starting acetals. All reactions were carried out at least once to three half-lives or more and all showed good linearity. Second order rate constants were obtained by dividing the pseudo-first order rate constant by the ozone concentration, found for a particular temperature, by interpolation from the graph in Fig. 1. The activation parameters found by plotting ln k/T vs. $1/T$, where k is the second order rate constant, are summarized in Table 3. Relative rates of oxidation of acetals **2** at different temperatures as determined by the competition method are listed in Table 4. The result obtained at −78°C (0.64) compares well with that obtained from separate measurements (0.63).

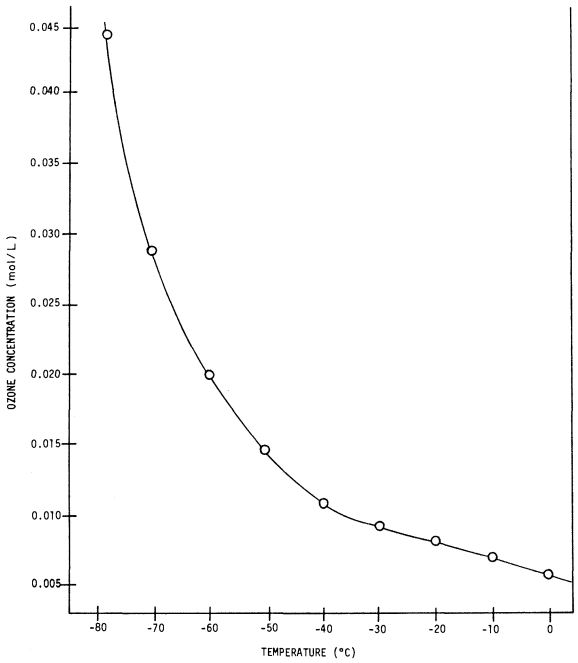

FIG. 1. Concentration of ozone in ethyl acetate.

TABLE 1. Rate constants for the oxidation by ozone of heptaldehyde acetals, $C_6H_{13}CH(OR)_2$

R	T (°C)	k_1 (s^{-1})[a]	Dev (%)[b]	$[O_3]$ (M)[c]	k_2 (L mol^{-1} s^{-1})[d]
CH_3	−33	4.74×10^{-4}	3.6	1.01×10^{-2}	4.69×10^{-2}
	−45	2.21×10^{-4}	2.3	1.26×10^{-2}	1.75×10^{-2}
	−50	2.03×10^{-4}	4.9	1.48×10^{-2}	1.37×10^{-2}
	−58	1.30×10^{-4}	0.6	1.86×10^{-2}	6.99×10^{-3}
	−78	2.82×10^{-5}	0.0	4.40×10^{-2}	6.42×10^{-4}
C_2H_5	−35	9.26×10^{-4}	0.2	1.04×10^{-2}	8.95×10^{-2}
	−40	8.81×10^{-4}	4.4	1.13×10^{-2}	7.83×10^{-2}
	−50	4.62×10^{-4}	0.8	1.48×10^{-2}	3.12×10^{-2}
	−78	6.23×10^{-5}	3.6	4.40×10^{-2}	1.42×10^{-3}
n-C_3H_7	−32	1.52×10^{-3}	0.9	1.00×10^{-2}	1.53×10^{-1}
	−42	9.69×10^{-4}	1.0	1.17×10^{-2}	8.29×10^{-2}
	−52	5.40×10^{-4}	2.3	1.56×10^{-2}	3.46×10^{-2}
	−78	7.58×10^{-5}	0.2	4.40×10^{-2}	1.72×10^{-3}
i-C_3H_7	−45	8.92×10^{-4}	1.3	1.26×10^{-2}	7.08×10^{-2}
	−50	6.15×10^{-4}	3.5	1.48×10^{-2}	4.16×10^{-2}
	−58	3.75×10^{-4}	1.0	1.86×10^{-2}	2.02×10^{-2}
	−78	8.47×10^{-5}	0.8	4.40×10^{-2}	1.93×10^{-3}

[a]Pseudo-first order rate constant for the disappearance of acetal.
[b]Deviation from average of two results.
[c]Ozone concentration, interpolated from Fig. 1.
[d]Second order rate constant = $k_1/[O_3]$.

TABLE 2. Rate constants for the oxidation by ozone of 4-substituted-2-hexyl-1,3-dioxanes, C_6H_{13}—CH(O—R)(O—R)

R	T (°C)	k_1 (s^{-1})[a]	Dev (%)[b]	$[O_3]$ (M)[c]	k_2 (L mol^{-1} s^{-1})[d]
H	−55	1.46×10^{-3}	2.0	1.71×10^{-2}	8.62×10^{-2}
	−59	1.36×10^{-3}	5.0	1.92×10^{-2}	7.11×10^{-2}
	−70	5.98×10^{-4}	5.0	2.79×10^{-2}	2.14×10^{-2}
	−78	3.28×10^{-4}	2.0	4.40×10^{-2}	7.47×10^{-3}
CH_3	−51	2.61×10^{-3}	1.5	1.51×10^{-2}	1.73×10^{-1}
	−60	1.62×10^{-3}	2.0	2.00×10^{-2}	8.12×10^{-2}
	−70	1.01×10^{-3}	1.3	2.79×10^{-2}	3.60×10^{-2}
	−78	5.21×10^{-4}	1.2	4.40×10^{-2}	1.18×10^{-2}

[a]Pseudo-first order rate constant for the disappearance of acetal.
[b]Deviation from average of two results.
[c]Ozone concentration, interpolated from Fig. 1.
[d]Second order rate constant = $k_1/[O_3]$.

TABLE 3. Activation parameters for the oxidation of acetals **1** and **2**

Acetal	R	k_{-78} (L mol^{-1} s^{-1})	$\Delta H^{\ddagger}$ (kJ mol^{-1})	$\Delta S^{\ddagger}$ (J K^{-1})	$\Delta G^{\ddagger}_{-78}$ (kJ mol^{-1})
C_6H_{13}—C(OR)(H)(OR)	Me	6.42×10^{-4}	35.2±1.6	−121± 7.1	58.8
	Et	1.42×10^{-3}	36.6±1.8	−109± 8.0	57.7
	Pr	1.72×10^{-3}	37.0±0.8	−104± 8.4	57.3
	i-Pr	1.93×10^{-3}	38.3±2.2	−96.8± 3.5	57.2
1					
C_6H_{13}, H, dioxane ring, R, R	H	7.47×10^{-3}	36.5±2.2	−94.3±10.5	54.8
	Me	1.18×10^{-2}	33.3±2.5	−106±11.9	54.0
2					

TABLE 4. Relative rate of oxidation by ozone of 4-substituted-2-hexyl-1,3-dioxans,

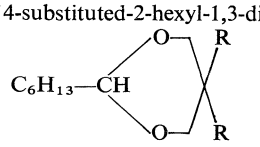

T (°C)	k_H/k_{CH_3}[a]
20	1.16 (0.03)
0	1.03 (0.01)
−78	0.635 (0.05)
−78	0.633[b] (0.01)

[a]Number in parentheses is the standard deviation from at least 3 results.
[b]From separate rate measurements, cf. Table 2.

Discussion

Examination of Table 3 reveals first of all that electron donation in the ether portion of the acetal function increases the rate (−78°C). In fact, the pseudo-first order constants (Table 1) for acetals **1** can be correlated with Tafts σ* constants (12) giving a ρ value of −1.31.[5] Also the entropy of activation for these reactions is very high and negative, indicating a highly ordered transition state.

However the most significant entry in Table 3 is the enthalpy of activation: the slowest reacting acetal **1** (R = Me, $k_{-78} = 6.42 \times 10^{-4}$ L mol^{-1} s^{-1}) has the lowest enthalpy of activation ($\Delta H^{\ddagger} = 35.1$ kJ mol^{-1}) while the fastest reacting acetal **1** (R = *i*Pr, $k_{-78} = 1.93 \times 10^{-3}$ L mol^{-1} s^{-1}) has the highest enthalpy of activation (38.4 kJ mol^{-1}). For cyclic acetals **2** on the other hand, we find the normal situation: the faster the reaction (k), the lower $\Delta H^{\ddagger}$.[6] Clearly then the two different types of acetal show different behavior towards oxidation by ozone.

Leffler has shown (13) that often in a reaction series there is a relationship between $\Delta H^{\ddagger}$ and $\Delta S^{\ddagger}$. This relationship is called the isokinetic relationship (or the compensation effect) and may be written in the form of eq. [2] where β is the isokinetic temper-

$$[2] \quad \Delta H^{\ddagger} = \beta \Delta S^{\ddagger} + h_0$$

ature and h_0 a constant. When such a relationship exists for a particular reaction series, β represents a point of inversion of reactivity.[7] When β is higher than the experimental temperature range, then this represents a domain of temperatures where reactivity depends essentially on $\Delta H^{\ddagger}$. On the other hand, when the isokinetic temperature β is lower than the experimental temperature range, then we have a domain of temperatures where reactivity depends essentially on $\Delta S^{\ddagger}$. When $T = \beta$, then all the compounds in the reaction series react at the same rate.

Proportionality between $\Delta H^{\ddagger}$ and $\Delta S^{\ddagger}$ as determined by plotting eq. [2] however, is not a criterion to prove that an isokinetic relationship holds. Exner (14) and others (15) have criticized the procedure because $\Delta H^{\ddagger}$ and $\Delta S^{\ddagger}$ are determined from the same equation and are therefore necessarily interdependent.

A better way of representing the data, according to Exner (14), is to plot log k against $1/T$ and see if all the lines appear to go through the same point. This is indeed found to be the case for the acyclic acetals **1** (Fig. 2), since the incorporation of the isokinetic constraint left the Arrhenius plot virtually unchanged. The root mean square deviation of fit was found to be 0.0426 when the individual Arrhenius lines were derived in the usual manner. When they were forced through a common point the root mean square deviation increased only insignificantly to 0.0430. The slopes b_i and the coordinates x_0 and y_0 of the isokinetic point were derived by an interactive non-linear least squares minimization (Taylor series expansion) of the function f of the log k values y_{ij} and the inverse temperatures x_{ij} (see for example ref. 16)

$$y_{ij} = b_i(x_{ij} - x_0) + y_0$$

$$f = \sum_i [b_i(x_{ij} - x_0) + y_0 - y_{ij}]^2 = \min$$

$$\partial f/\partial b_i = 0 \qquad i = 1, \ldots, n$$

$$\partial f/\partial x_0 = 0$$

$$\partial f/\partial y_0 = 0$$

The isokinetic temperature, $1/x_0$, found in this way, is 118 K or −155°C. The point of intersection of any two lines varies between −168°C and −92°C, making the error in the isokinetic temperature quite large. Still the limits are below the working temperature range (−78 to −32°C). Therefore, the reactivity in this series of reactions is dominated by *entropy* factors (*vide supra*).

The isokinetic hypothesis cannot be statistically rejected, but considering the large errors in $\Delta H^{\ddagger}$ the hypothesis that the series be isoenthalpic cannot be rejected either. If this were the case however, the reactivity of the series of reactions would still be dominated by *entropy* factors.

The behavior of acyclic acetals **1** can be contrasted with that of cyclic acetals **2**, for which the point of intersection of the two Arrhenius lines falls at a point corresponding to a temperature of −4°C (Fig. 3). Because there are only two lines (hence no statistical test can be made) and the errors in $\Delta H^{\ddagger}$ and $\Delta S^{\ddagger}$ are so large, the value of −4°C for the isokinetic tem-

[5]Log k vs. 2σ* of the R group at −78°C. Correlation coefficient, 0.91.
[6]The errors in the $\Delta H^{\ddagger}$ are rather large and the consequence of that will be discussed later.
[7]For a good lead reference on this subject, see ref. 14.

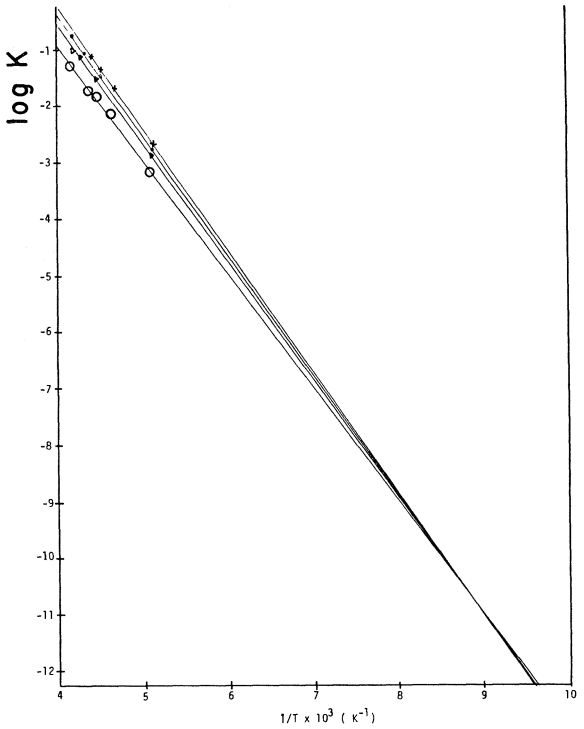

FIG. 2. Arrhenius plots of four acyclic acetals **1**.

perature cannot be accepted from these data alone. That −4°C is about the right value however is confirmed by the results obtained by the competition experiments (Table 4). These data clearly show the point of intersection (inversion of reactivity) of the two lines to be around 0°C: the relative reactivity at −78°C of the two acetals **2** is reversed at 20°C. At 0°C, the relative rate is about 1. The significant point here is that the isokinetic temperature be *above* the working temperature range, hence a range of temperature where reactivity is dominated by *enthalpy* factors.

It appears then that the two types of acetals behave differently. One way of interpreting the results is to consider the preferred conformation of acyclic acetals. It has been shown (17) that the preferred conformation of dimethoxymethane is that represented by structure **I** (Scheme 4). Evidence has been presented (18) for a similar conformation of other acetals (structure **II**, Scheme 4). However, this conformation

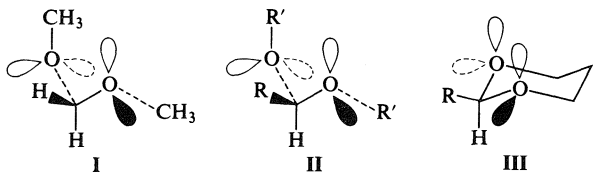

SCHEME 4

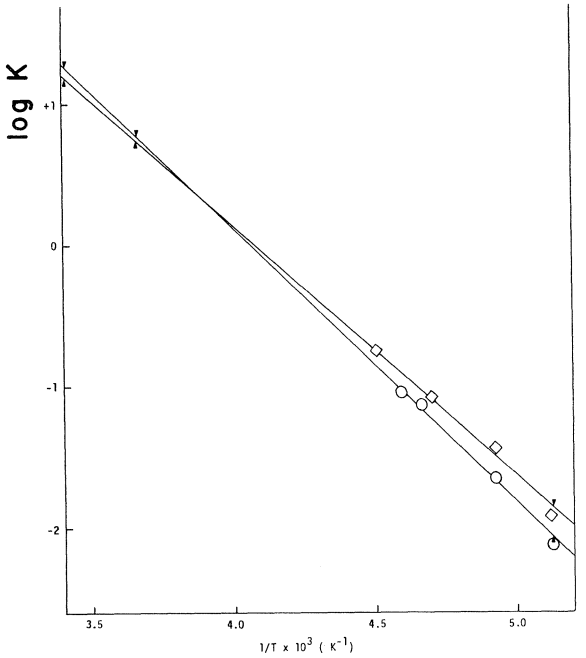

FIG. 3. Arrhenius plots of two cyclic acetals **2**. Log k_{rel} (Table 4) indicated by arrows.

is one which Deslongchamps *et al.* (2, 3) have shown to be unreactive towards ozone. Prior to oxidation, the OR group must rotate (or invert) in order that two non-bonding electron pairs, one on each oxygen atom, lie anti-periplanar to the C—H bond of the acetal function. Thus conformational changes in acyclic acetals are required prior to oxidation by ozone. Since this series of reactions has been shown to be dominated by entropy factors, this suggests that there is a direct relationship between conformational changes and entropy factors. This relationship can be attributed to the reorganization of solvent molecules around the acetal function during the rotation step. Of course, no such conformational changes are required for the cyclic acetals **2** (structure III, Scheme 4) and hence the reactivity of that series of reactions is dominated by enthalpy factors.

Finally, one comment should be added about the fact that the ρ* value found for the oxidation of the acyclic acetals **1**, was −1.31 (−78°C). Previous studies had shown (2, 3, 9) that electron donors accelerate the reaction. However, one consequence of having a reaction series in a domain of temperature where reactivity is dominated by entropy factors, is to reverse the sign of ρ (13). If the rate of a reaction was only a function of $\Delta H^{\ddagger}$, this phenomenon would have been observed. But the variation of $\Delta S^{\ddagger}$ causes the term $T\Delta S^{\ddagger}$ to contribute more than the change in $\Delta H^{\ddagger}$ to the overall $\Delta G^{\ddagger}$ (cf. Table 3).

Acknowledgments

Support for this work by the National Research Council of Canada and by "le Ministère de l'Education", Quebec, is gratefully acknowledged.

1. P. DESLONGCHAMPS and C. MOREAU. Can. J. Chem. **49**, 2465 (1971).
2. P. DESLONGCHAMPS, C. MOREAU, D. FREHEL, and P. ATLANI. Can. J. Chem. **50**, 3402 (1972); P. DESLONGCHAMPS, P. ATLANI, D. FREHEL, A. MALAVAL, and C. MOREAU. Can. J. Chem. **52**, 3651 (1974); P. DESLONGCHAMPS, C. MOREAU, D. FREHEL, and R. CHENEVERT. Can. J. Chem. **53**, 1204 (1975).
3. P. DESLONGCHAMPS. Pure Appl. Chem. **43**, 351 (1975); Tetrahedron, **31**, 2463 (1975); Heterocycles, **7**, 1271 (1977).
4. P. DESLONGCHAMPS, P. ATLANI, D. FREHEL, and A. MALAVAL. Can. J. Chem. **50**, 3405 (1972); P. DESLONGCHAMPS, R. CHENEVERT, R. J. TAILLEFER, C. MOREAU, and J. K. SAUNDERS. Can. J. Chem. **53**, 1601 (1975).
5. P. DESLONGCHAMPS, C. LEBREUX, and R. J. TAILLEFER. Can. J. Chem. **51**, 1665 (1973); P. DESLONGCHAMPS, S. DUBE, C. LEBREUX, D. R. PATTERSON, and R. J. TAILLEFER. Can. J. Chem. **53**, 2791 (1975); P. DESLONGCHAMPS and R. J. TAILLEFER. Can. J. Chem. **53**, 3029 (1975).
6. P. DESLONGCHAMPS, U. O. CHERIYAN, A. GUIDA, and R. J. TAILLEFER. Nouv. J. Chim. **1**, 235 (1977); P. DESLONGCHAMPS, P. GERVAL, U. O. CHERIYAN, A. GUIDA, and R. J. TAILLEFER. Nouv. J. Chim. **2**, 631 (1978).
7. D. G. GORENSTEIN, J. B. FINDLAY, B. A. LUXON, and D. KAR. J. Am. Chem. Soc. **99**, 3473 (1977); D. G. GORENSTEIN, B. A. LUXON, J. B. FINDLAY, and R. MOMII. J. Am. Chem. Soc. **99**, 4170 (1977); D. G. GORENSTEIN, B. A. LUXON, and J. B. FINDLAY. J. Am. Chem. Soc. **99**, 8048 (1977).
8. S. A. BIZZOZERO and B. O. ZWEIFER. FEBS Lett. **59**, 105 (1975); W. L. MOCK. Bioorg. Chem. **5**, 403 (1976).
9. H. HENRY. Ph.D. Dissertation, Université de Montréal, Montréal, P.Q. November 1976.
10. F. KOVAC and B. PLESNICAR. J. Chem. Soc. Chem. Commun. 122 (1978); J. Am. Chem. Soc. **101**, 2677 (1979).
11. L. P. HAMMETT. Physical organic chemistry. McGraw Hill, New York. 1970. p. 91.
12. P. R. WELLS. Linear free-energy relationships. Academic Press, London. 1968.
13. J. E. LEFFLER. J. Org. Chem. **20**, 1202 (1955).
14. O. EXNER. Prog. Phys. Org. Chem. **10**, 411 (1973).
15. J. R. C. PETERSEN. J. Org. Chem. **29**, 3133 (1964); R. R. KRUG, W. G. HUNTER, and R. A. GRIEGER. J. Phys. Chem. **80**, 2335 (1976).
16. P. R. BEVINGTON. Data reduction and error analysis for the physical sciences. McGraw-Hill, New York. 1969.
17. E. E. ASTRUP. Acta Chem. Scand. **25**, 1494 (1971); **27**, 3271 (1973).
18. O. EXNER, V. JEHLICKA, and B. UCHYTIL. Collect. Czech. Chem. Commun. **33**, 2862 (1968).

Kinetic studies on the catalytic reduction of nitrotoluene by hydrazine

N. GOSWAMI AND M. L. RAHMAN[1]

Department of Chemistry, University of Rajshahi, Bangladesh

Received August 9, 1978[2]

N. GOSWAMI and M. L. RAHMAN. Can. J. Chem. **57**, 3047 (1979).

Kinetics of reduction of *p*-nitrotoluene by hydrazine in presence of Raney nickel catalyst have been studied spectrophotometrically. It has been found that the reaction is first order with respect to both hydrazine and nitrotoluene. The influence of solvent, salt, and the amount of catalyst on the reaction rate has been investigated. The rate constant was found to depend on the dielectric constant, the ionic strength, and on the catalyst concentration. The activation energy was estimated to be 103.92 kJ mol^{-1} in 73.58% ethanol in water. This value decreases considerably when the polarity of the solvent increases and when other salts are added. In pure water the value is 32.25 kJ mol^{-1}.

N. GOSWAMI et M. L. RAHMAN. Can. J. Chem. **57**, 3047 (1979).

On a étudié par spectrophotomètrie les cinétiques de réduction du *p*-nitrotoluène par l'hydrazine en présence du nickel de Raney comme catalyseur. On a trouvé que la réaction est d'ordre un par rapport à l'hydrazine et au nitrotoluène. On a étudié l'influence du solvant, du sel, et de la quantité de catalyseur sur la vitesse de réaction. On a trouvé que la constante de vitesse dépend de la constante diélectrique, de la force ionique et de la concentration du catalyseur. On a obtenu une énergie d'activation de 103.92 kJ mol^{-1} pour la réaction dans l'éthanol à 73.58% dans l'eau. Cette valeur décroît considérablement quand la polarité du solvant augmente et quand on ajoute d'autres sels. Dans l'eau pure la valeur est de 32.25 kJ mol^{-1}.

[Traduit par le journal]

Introduction

Hydrazine has been widely used for the reduction of a large number of organic compounds. In the absence of a catalyst the rate of the reaction is very slow and drastic conditions such as heating and refluxing for a long period are required. In the presence of catalysts, however, the reaction rate greatly increases (1–3). The reduction of aromatic nitrocompounds by hydrazine has two advantages. Firstly, as opposed to direct hydrogenation, no pressure apparatus is necessary. Secondly, the catalytic hydrazine reduction method gives yields equal to or better than direct catalytic hydrogenation or other methods (4). Despite the versatility of hydrazine as a reducing agent, most of the work (4) in the field has been aimed at obtaining better yields of the reduction products. Very little seems to have been done on the kinetics and mechanisms of these reactions. The present work has been undertaken to study the kinetics of the reduction of an aromatic nitrocompound (*p*-nitrotoluene) with hydrazine in the presence of a Raney nickel catalyst. This reaction involves two phases, viz. solid and liquid and it would be interesting to study the kinetics of a heterogeneous reaction in solution which, relative to gas phase, has received very little attention.

Experimental

Chemicals

p-Nitrotoluene supplied by the Matheson Coleman and Bell company and hydrazine hydrate by the Merck–Schuchardt company were used without further purification. Rectified spirit was preferred to absolute alcohol as a solvent because the latter might contain traces of benzene. Dioxane was supplied by the Matheson Coleman and Bell company and was used without further purification. Analytical grade potassium chloride and potassium sulphate obtained from Merck AG. Darmstadt were used. When calculating the solvent composition, water from hydrazine hydrate was taken into account.

Raney Nickel

Raney nickel prepared by the method of Mozingo (5) was thoroughly washed with benzene which was removed *in vacuo*. It was heated to about 533 K and then cooled *in vacuo*. The cooled catalyst was stored in xylene. When necessary, an amount of the catalyst was taken in a flask and the xylene was removed *in vacuo*. Heating was then continued to 673 K for 10 h. The degassed catalyst was used within a fortnight of its degasification, which was the period when most reproducible results were obtained. It was observed that catalysts prepared by heating to temperatures lower than 673 K were different in activity and changed their activity rather rapidly.

Kinetic Methods

The reaction vessel was a two-necked round-bottomed flask thermostated to ± 0.1 K. With a definite amount of the catalyst the reactants were thoroughly mixed by an electric stirrer and the aliquots were periodically transferred and filtered off as quickly as possible, the time being recorded by a stop watch. The filtered solutions were analysed for their *p*-nitrotoluene content by measuring the absorbances at 275 nm with the help of a Beckman DB spectrophotometer. For the measurement of the concentration of hydrazine a

[1]To whom all correspondence should be addressed.

[2]Revision received August 2, 1979.

0008-4042/79/233047-06$01.00/0

TABLE 1. *p*-Nitrotoluene decay run in highly concentrated (10.94 *M*) hydrazine at 298 K in ethanol–water system; the initial *p*-nitrotoluene concentration was 5.0×10^{-5} *M* and that of the catalyst (Raney nickel) was 5.0 g dm^{-3}

Time (min)	72.66% ethanol in water, absorbance of *p*-nitrotoluene at 275 nm	53.53% ethanol in water, absorbance of *p*-nitrotoluene at 280 nm	38.23% ethanol in water, absorbance of *p*-nitrotoluene at 280 nm	30.52% ethanol in water, absorbance of *p*-nitrotoluene at 282 nm
0	0.500	0.500	0.500	0.500
3	—	0.300	—	0.100
5	0.470	0.240	0.170	0.000
7	—	0.150	0.100	—
10	0.420	0.000	0.000	—
15	0.390	—	—	—
20	0.350	—	—	—
25	0.320	—	—	—
30	0.260	—	—	—

colouring agent (6) was added and the absorbances were monitored at 458 nm. It was checked that the substances obeyed the Beer–Lambert law and the solvent in the reference cell contained all the components present in the sample cell except the one whose concentration was being determined.

pH

A Coleman model-39 pH meter was used for measuring the pH.

Results

The main product of the reduction of *p*-nitrotoluene by hydrazine in presence of Raney nickel catalyst was found to be *p*-toluidine. In spite of repeated attempts no intermediates or coupled products could be detected. *p*-Toluidine had its maximum absorption at 236 nm at which *p*-nitrotoluene also absorbed significantly. Since it was inconvenient to calculate the concentration of *p*-toluidine from the overlapped absorbance, the kinetics were studied by measuring the rate of decrease of nitrotoluene. It was also observed that quantitative measurement of *p*-toluidine was difficult in the presence of hydrazine which did not seem to behave as a satisfactory solvent at this low wavelength. Table 1 shows the *p*-nitrotoluene decay runs for ethanol–water system.

By keeping the hydrazine concentration and in large excess, the order of the reaction with respect to nitrotoluene was determined and found to be unity in the initial part of each run, but the order approached zero (Fig. 1) or two (Fig. 6) near the end of the run. The transition from first to zero order was observed only when the proportion of ethanol to water was the highest in the medium (73.58%) and in all other cases it was from first to second order. It is interesting to note that with 73.58% ethanol – water medium the first-order behaviour was observed over only 20% of the reaction and that this rose to the extent of about 60% with higher proportion of water (40% and less ethanol). From the slope of the double logarithmic plot of initial rate vs. initial concentration (i.e. initial absorbance), the true order with respect to *p*-nitrotoluene was calculated and found to be unity.[3]

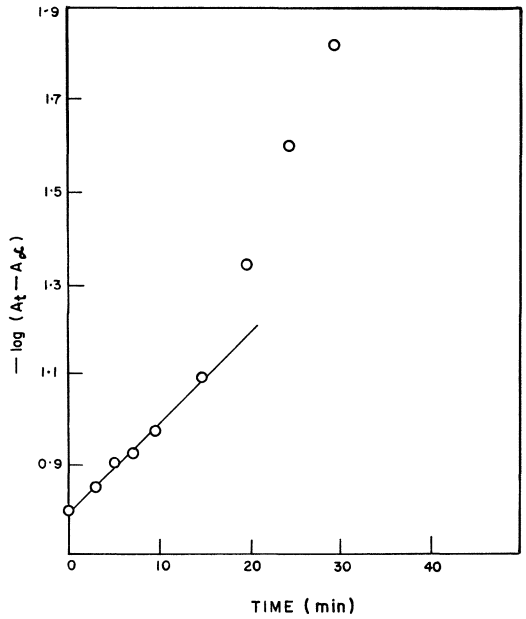

FIG. 1. Variation of $-\log (A_t - A_\infty)$ with time (min); A_t indicates the absorbance at a certain time and A_∞, absorbance at an infinite time; the initial concentration of *p*-nitrotoluene was 5.0×10^5 *M* in 73.58% ethanol in water containing 1 *M* hydrazine; the concentration of the catalyst (Raney nickel) was 5.0 g dm^{-3}; the reaction temperature was 310 K.

Table 1 indicates that the absorbance decreases to

[3]Complete set of data may be obtained, at a nominal charge, from the Depository of Unpublished Data, CISTI, National Research Council of Canada, Ottawa, Ont., Canada K1A 0S2.

zero in some runs but not in others. The zero final absorbance seems to be favoured by high concentrations of hydrazine ($\sim$ 11 M) in a water-rich medium. With low concentrations ($\sim$ 1.0 M) of hydrazine zero absorbance was never obtained.

Under pseudo-first order conditions, the rate can be written as

$$[1] \quad -\frac{d[B]}{dt} = k[Hy]^{n_1}[B] = k'[B]$$

Here [B] stands for the nitrotoluene concentration and [Hy] for the hydrazine concentration. The pseudo-first order rate constant, k', should thus depend on hydrazine concentration. Figure 2 shows that a plot of k' (the rate constants were calculated from first 50% of the reaction) against [Hy] gives a straight line, indicating that the reaction is also first order with respect to hydrazine.

The reaction rate was found to increase linearly with the amount of catalyst up to a certain point after which the rate of increase became slower.[3]

Addition of water to the reaction medium enhanced the rate. The reaction became faster in presence of acids or bases. Effect of dielectric constant on the reaction rate was studied in the dioxane–water and ethanol–water systems and the plots of log k' (the rate constants were calculated from first 30–50% and about 60% of the reaction for the dioxane–water and water–ethanol systems respectively) versus $1/D$ were found to be linear in both systems (Fig. 3). Values of D corresponding to different mixtures of water and ethanol and of dioxane and water were obtained from literature (7).

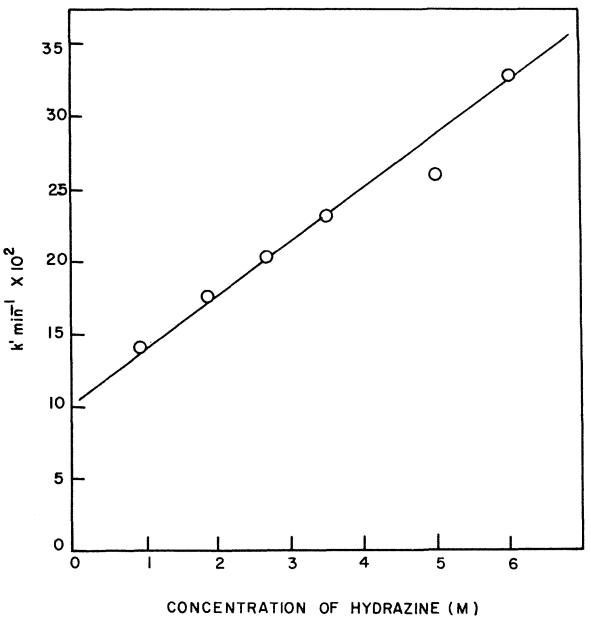

FIG. 2. Variation of rate constant (k' min^{-1}) with the hydrazine concentration (M); the hydrazine concentration was varied keeping the solvent composition constant (50% ethanol in water); the concentration of the catalyst (Raney nickel) was 5.0 g dm^{-3}; the reaction temperature was 313 K. The rate constants were calculated from first 50% of the reaction.

The reaction rate was found to increase with increasing ionic strength of the medium. In the presence of KCl or K_2SO_4, log k' (the rate constants were calculated from first 60–75% of the reaction) was found to vary linearly (Fig. 4) with $\sqrt{\mu}$ (experiments were carried out in 38.23% ethanol – water system).[3] For the calculation of the ionic strength only the concentration of the added electrolyte was taken into account because the concentrations of other ions that might be involved were not known.

The logarithm of the pseudo-first order rate constant was plotted against the reciprocal of temperature when 73.58% alcohol in water was used as the solvent. The result was a straight line (Fig. 5).[3] The slope of the line gave an activation energy of 103.92 kJ mol^{-1}. The activation energy decreased considerably when the proportion of water in the solvent increased and when other salts were added. Table 2 shows the activation energies for various media.

It was thought desirable to compare catalytic reduction by hydrazine with catalytic reduction by

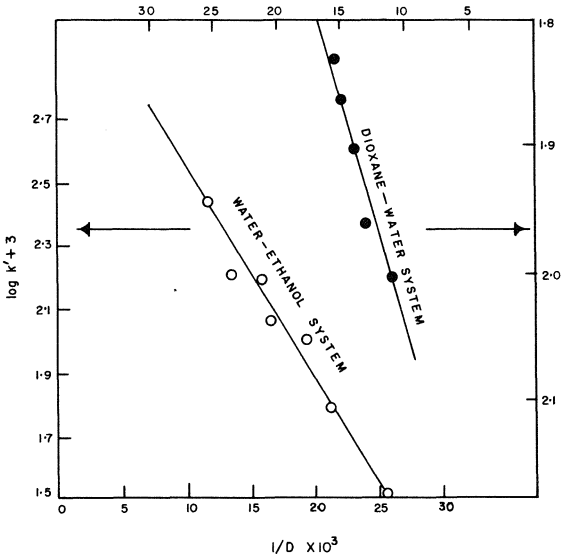

FIG. 3. Variation of logarithm of the rate constant (k' min^{-1}) with the reciprocal of the dielectric constant (D) of the solvent, e.g. ethanol–water system and dioxane–water system containing 1 M hydrazine and 5.0 g dm^{-3} catalyst (Raney nickel); ○, ethanol–water system with the p-nitrotoluene concentration (7.0 × 10^{-5} M) at reaction temperature 298 K; ●, dioxane–water system with the initial p-nitrotoluene concentration (4.0 × 10^{-5} M) at reaction temperature 313 K. The rate constants were calculated from first 30–50% and about 60% of the reaction for the dioxane–water and water–ethanol systems respectively.

TABLE 2. Activation energies for various media

Reaction media vol % ethanol in water	Electrolytes added	Concentration of *p*-nitrotoluene (mol dm^{-3})	Concentration of hydrazine (mol dm^{-3})	Concentration of catalyst (g dm^{-3})	Activation energy (kJ mol^{-1})
73.58	—	5.0×10^{-5}	1.0	5.0	103.92
38.23	—	5.0×10^{-5}	1.0	5.0	50.76
38.23	KCl	5.0×10^{-5}	1.0	5.0	48.72
38.23	K_2SO_4	5.0×10^{-5}	1.0	5.0	41.79
0.0	—	5.0×10^{-5}	1.0	5.0	32.25

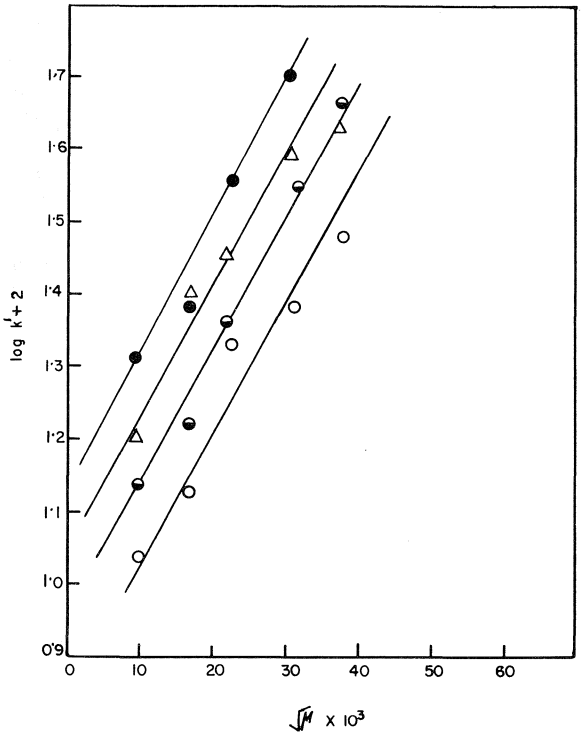

FIG. 4. Variation of logarithm of rate constant (k' min^{-1}) with the square root of the ionic strength ($\sqrt{\mu}$) of KCl and K_2SO_4 in solution with the initial *p*-nitrotoluene concentration 5.0×10^{-5} *M* in 38.23% ethanol – water system containing 1 *M* hydrazine and 5.0 g dm^{-3} catalyst (Raney nickel); ○, in presence of KCl at 298 K; ◒, KCl at 303 K; △, K_2SO_4 at 298 K; ●, K_2SO_4 at 303 K. The rate constants were determined from first 60–75% of the reaction.

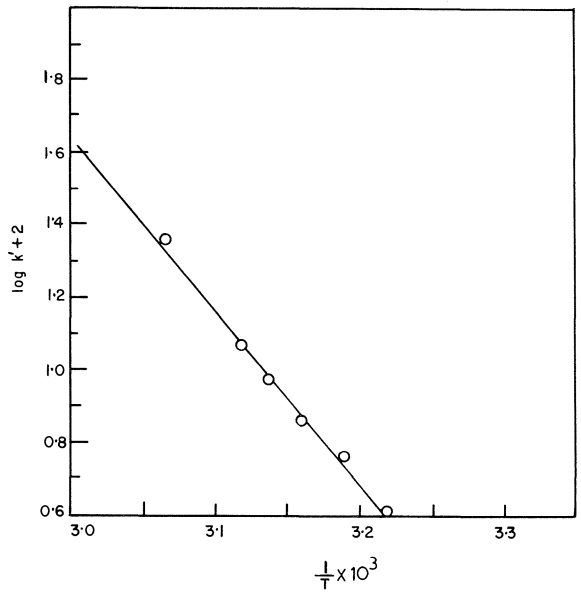

FIG. 5. Variation of logarithm of the rate constant (k' min^{-1}) with the reciprocal of absolute temperature (T); the initial concentration of *p*-nitrotoluene was 5.0×10^{-5} *M* in 73.58% ethanol – water; the hydrazine concentration was 1 *M* and the concentration of the Raney nickel catalyst was 5.0 g dm^{-3}. The rate constants were determined from first 20% of the reaction.

hydrogen. Instead of using hydrogen under pressure, we prepared a type of Raney nickel catalyst that contained a significant amount of adsorbed hydrogen. As mentioned previously, the catalyst in the present work was heated to 673 K to remove hydrogen. This catalyst however was heated only to 533 K and it was able to reduce nitrotoluene at an appreciable rate in absence of hydrazine. The reduction power of this catalyst is clearly due to the adsorbed hydrogen and is therefore similar to catalytic reduction by hydrogen (8). It was found that the rate of reduction was again proportional to the first power of the concentration of nitrotoluene. The effect of dielectric constant and added electrolytes was not so pronounced with this catalyst as in presence of hydrazine and the variation of the rate constant was not very regular.

Discussion

In general a heterogeneous reaction takes place in the following steps: diffusion, adsorption, actual chemical reaction on the surface, desorption, and diffusion again. Of these, diffusion is very fast and is most unlikely to be rate-determining in the present case, because the reaction has a rather high energy of

activation. Besides, an electric stirrer rotating at a constant speed was employed to mix the reactants, thus minimizing the effect of diffusion. The high energy of activation also precludes the possibility of adsorption or desorption being rate-determining. We are thus left with the actual chemical reaction itself on the surface of the catalyst:

[2] S—A + S—B → toluidine + S

Here S stands for surface and A, reducing agent.

The observed kinetics that the reaction is first order with respect to nitrotoluene can be explained according to this scheme if it is assumed that nitrotoluene is sparsely adsorbed on the surface. A very pertinent question in connection with the present reaction is whether hydrazine itself acts as the reducing agent or a product or products of decomposition of hydrazine bring about the reduction. It has been found (9–11) that hydrazine decomposes in the presence of catalysts to give N_2, H_2, and NH_3. Pietra (12), Rottendorf and Sternhell (13) have suggested that the reactivity of hydrazine in the presence of catalysts like Ni, Pd, Pt, Ru, etc. is simply due to the hydrogen liberated. Our observation that the reduction reaction in the presence of Raney nickel alone shows similar behaviour tends to support this hypothesis.

However, it has been observed by repeated experiments that the reaction rate changes considerably if the polarity of the solvent is changed and if foreign electrolytes are added. It is not only the reaction rate that changes, the activation energy also decreases from 103.92 kJ mol^{-1} to about one-third of this value (Table 2). Thus there can be no doubt that the rate-determining step or steps should be ionic in character; we are therefore forced to look for an additional or alternative rate-determining step.

Audrieth and Jolly (11) who worked on the decomposition of hydrazine on Raney nickel found that the reaction was markedly influenced by the presence of water and added salts. Thus there is some parallelism between the present reaction and hydrazine decomposition. Without giving the detailed mechanism of the reaction, the authors mentioned that the products of decomposition were N_2, H_2, and NH_3 and that the kinetics were variable. If, however, one wants to explain the solvent and salt effects, one has to assume that prior to decomposition into the main products hydrazine breaks up into ions. We are thus led to the conclusion that the slow step we are looking for is possibly the breaking up of hydrazine into ions prior to or concurrently with adsorption on the surface.

Addition of salts could have two kinds of effect on such reactions, one of which is called the mass-law effect. This would have an accelerating or a retarding effect on the rate of ionisation, depending on whether the ions formed are being removed or added from outside. The other effect is due to ionic strength. Increase of ionic strength would have an effect analogous to that of making a solvent more polar. In the unimolecular ionisation of a neutral molecule a polar solvent would help stabilise the ions through solvation. Similarly inert salts would provide the ionic atmosphere in which the charged transition-state would be more stable. We have studied the effect of non-common-ion salts. This is not expected to have any mass-action effect and it has been found that the rate constant increases with the ionic strength. However, the ions that are formed from hydrazine may have inhibitory effect on the reaction rate when they have built up to sufficient concentrations. We have observed that after a certain time the rate of reaction decreases and that it no longer remains first order. The phenomenon is even more prominent in the presence of salts (Fig. 6).

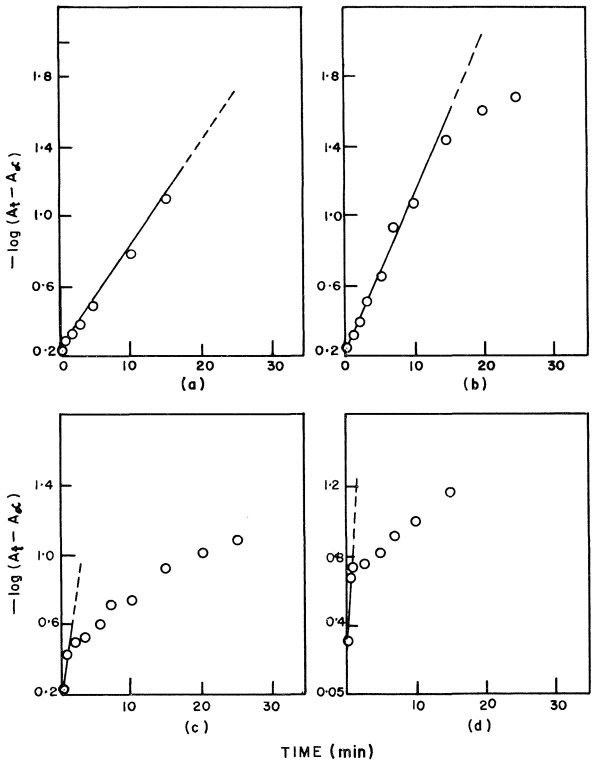

FIG. 6. Variation of $-\log (A_t - A_\infty)$ with time (min) at 298 K; the initial *p*-nitrotoluene concentration was 5.0×10^{-5} *M* in 38.23% ethanol – water containing 1 *M* hydrazine and KCl of different ionic strength; graphs (*a*), (*b*), (*c*), and (*d*) have been obtained with the ionic strengths 1.0×10^{-4}, 5.0×10^{-4}, 30.0×10^{-4}, and 45.0×10^{-4} respectively; the concentration of the catalyst (Raney nickel) was 5.0 g dm^{-3} in each case.

There may be various factors responsible for the decrease in reaction rate some time after the commencement of the reaction. The catalyst may show a poisoning effect and the product or products of reaction may compete for the active sites on the catalyst.

As already mentioned acids and bases have been found to enhance the reaction rate. This also points towards some sort of ionic mechanism. Hydrazine has been reported (4) to exist as hydrazinium positive or hydrazide negative ions depending on the pH of the medium. Addition of a base like $Ba(OH)_2$ is claimed (9) to produce more hydrogen as a decomposition product. A basic medium should, in that case, be more favourable to the reduction reaction. In the present work addition of NaOH has made the reaction faster, but perchloric acid has been found to be even more effective. Acids probably play a dual role in that they produce hydrogen by reaction with the catalyst and may also have catalytic effect.

1. M. J. S. DEWAR and T. MOLE. J. Chem. Soc. 2556 (1956).
2. L. P. KUHN. J. Am. Chem. Soc. **73**, 1510 (1951).
3. D. BALCOM and A. FURST. J. Am. Chem. Soc. **75**, 4334 (1953).
4. A. FURST, R. C. BERLO, and S. HOOTON. Chem. Rev. **65**, 51 (1965).
5. R. MOZINGO. Org. Synth. **3**, 181 (1955).
6. G. W. WATT and J. D. CHRISP. Anal. Chem. **24**, 2006 (1952).
7. (*a*) E. S. AMIS and V. K. LA MER. J. Am. Chem. Soc. **61**, 905 (1939). (*b*) C. V. KING and J. J. JOSEPHS. J. Am. Chem. Soc. **66**, 767 (1944).
8. H. YAO and P. R. EMMETT. J. Am. Chem. Soc. **81**, 4125 (1959).
9. S. N. TANATER. Z. Phys. Chem. A**41**, 37 (1902).
10. A. GUTBIER and K. NEUNDLINGER. Z. Phys. Chem. A**84**, 203 (1904).
11. L. F. AUDRIETH and W. L. JOLLY. J. Phys. Colloid Chem. **55**, 524 (1951).
12. S. PIETRA. Ann. Chim. **47**, 410 (1957).
13. H. ROTTENDORF and S. STERNHELL. Aust. J. Chem. **16**, 647 (1963).

Infrared laser induced decomposition of pentafluoroacetone[1]

M. DROUIN,[2] P. A. HACKETT, C. WILLIS, and M. GAUTHIER
Laser Chemistry Group, National Research Council of Canada, Ottawa, Ont., Canada K1A 0R6

Received April 30, 1979

M. DROUIN, P. A. HACKETT, C. WILLIS, and M. GAUTHIER. Can. J. Chem. **57**, 3053 (1979).

The dissociation of pentafluoroacetone by high power infrared radiation fields is shown to proceed by a free radical mechanism.

M. DROUIN, P. A. HACKETT, C. WILLIS et M. GAUTHIER. Can. J. Chem. **57**, 3053 (1979).

On montre que la dissociation de la pentafluoroacétone, induite par les champs de radiation infrarouge à haute puissance, se produit selon un mécanisme qui implique des radicaux libres.
[Traduit par le journal]

Introduction

Recently we have shown that the molecule hexafluoroacetone undergoes multiphoton decomposition with great facility when it is excited near its ν_{15} band by pulses of ir radiation (1). We have also found that $CF_3{}^{13}COCF_3$ could be directly dissociated at natural abundance leading to product carbon monoxide with over 85% C-13 content (2). The homogenous gas phase pyrolysis had been studied some time ago by Batey and Trenwith (3) who found Arrhenius parameters for the process

[1] $CF_3COCF_3 \rightarrow C_2F_6 + CO$

to be $k_1 = 10^{9.6} \exp(-50\,900/RT)\ s^{-1}$. These authors favoured a molecular rearrangement process involving an activated complex with a three membered carbon ring. In contrast to this the photochemical decomposition of hexafluoroacetone may be interpreted solely in terms of free radical processes (4):

[2] $CF_3COCF_3 \rightarrow CF_3CO + CF_3 \rightarrow 2CF_3 + CO$

However, many examples of multiphoton decomposition have been discovered in which decomposition proceeds by the least endoergic pathway (5). Thus there is no *a priori* reason to favour either pathway. In early attempts to resolve which pathway predominated we tried radical scavenging experiments with O_2 and NO, these were inconclusive (see below) and thus we have resorted to the expedient of studying the multiphoton decomposition of the structurally similar molecule pentafluoroacetone in which the free radical and molecular pathways would give different product arrays. The results, reported below, favour the free radical pathway.

[1]NRCC No. 17768.
[2]NRCC summer student, 1978.

Experimental

Samples were photolysed in 18 cm long, 5 cm diameter Pyrex cells with sodium chloride windows. Radiation from a TEA-CO_2 laser (Lumonics model 101) was focused at the centre of the cell by a focal length = 10 cm germanium lens; incident fluence was monitored by a calibrated pyroelectric detector. The temporal distribution of the laser pulse consisted of an initial spike (FWHM = 150 ns) followed by a tail (τ_D = 1 μs); 80% of the energy was in the initial spike.

After irradiation samples were frozen into glass tubes and analysed by glc using a thermal conductivity detector (6 ft Porapak Q, 6 ft silica gel 80–100 mesh, ¼ in. od copper tube, He carrier gas at 90°C). Typical retention times were C_2F_6 3 min, C_2F_4 3.8 min, CF_3H 4.8 min, C_3F_8 13 min, C_2F_3H 8.4 min, and CF_3CF_2H 15 min. The glc response was calibrated with authentic aliquots of fluoroform, tetrafluoroethylene, hexafluoroethane, carbonyl fluoride, and pentafluoroethane. No authentic sample of trifluoroethylene was available, therefore this product was identified by trapping the glc peak and carrying out mass spectrometric analysis.

During the course of the work a complicating reaction was noted. Although the reaction products were stored in sealed glass ampoules prior to analysis and contacted only clean glass surfaces it was observed that the peaks corresponding to the ethylenes were time dependent. Indeed, reaction mixtures stored for longer than 4 h showed no trace of trifluoroethylene, and tetrafluoroethylene itself disappeared given longer times (10 h). This phenomenon is almost certainly a result of reaction with, or catalysed by, hydrogen fluoride or its reaction products. After this effect was noted all ampoules were stored in liquid nitrogen prior to analysis.

Pentafluoroacetone (Hynes Chemical) was purified by distillation at −160 and −78°C, degassed and stored in blackened bulbs. Analysis by glc failed to reveal any impurities. Oxygen was obtained from Matheson (Research Grade). Nitric oxide (Matheson) was purified by distillation from liquid argon to liquid nitrogen.

Results and Discussion

Irradiations were carried out using the R(34) line of the 00°1–10°0 band of CO_2 at 986 cm^{-1}. This line falls on the red edge of an absorption band of pentafluoroacetone. The infrared absorption spectrum of this molecule has neither been published nor analysed

0008-4042/79/233053-03$01.00/0

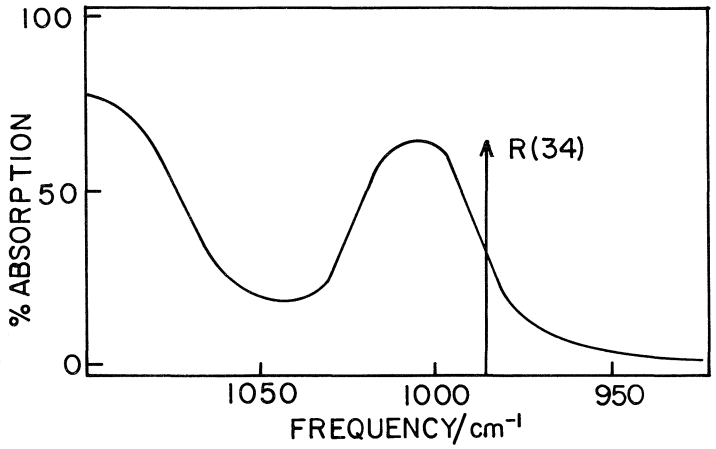

FIG. 1. Low intensity infrared absorption spectrum of pentafluoroacetone; pressure = 46 Torr; pathlength = 10 cm; temperature = 22°C. The arrow indicates the frequency of the CO_2 laser line used.

before, and hence the portion occurring within the gain curve of the CO_2 laser is presented here (Fig. 1). The line used in these experiments probably excited C—C—C skeletal vibrations.

At 0.25 J cm^{-2} incident fluence no decomposition was observed when 0.6 Torr of pentafluoroacetone was photolysed by an unfocused beam. However, decomposition was induced when the beam was focused. Products detected by glc were C_2F_6, C_2F_4, CF_3H, C_2F_3H, C_3F_8, and C_2F_5H. At low conversions all products increased linearly with pulse number. The production rate for the major product detected (C_2F_5H) and the relative production rates for other major products (C_2F_6, C_2F_4, CF_3H, and C_2F_3H) are shown in Fig. 2.

The product array is consistent with the free radical decomposition and recombination mechanism proposed by Pritchard and Perona (6) to explain the one photon photolysis of pentafluoroacetone at 3130 Å; relevant portions are shown below:

[3] $CF_3COCF_2H \xrightarrow{h\nu} CF_3 + CO + CF_2H$

[4] $CF_3 + CF_3 \rightarrow C_2F_6$

[5] $CF_3 + CF_2H \rightarrow CF_3CF_2H^* \rightarrow C_2F_4 + HF$

[6] $CF_3CF_2H^* \xrightarrow{M} C_2F_5H$

[7] $CF_3CF_2H^* \rightarrow CF_2 + CF_3H$

[8] $CF_2H + CF_2H \rightarrow CF_2HCF_2H^* \rightarrow C_2F_3H + HF$

[9] $CF_2HCF_2H^* \xrightarrow{M} C_2F_4H_2$

[10] $CF_2HCF_2H^* \rightarrow CF_2 + CF_2H_2$

[11] $CF_2 + R \rightarrow RCF_2 \xrightarrow{R} RCF_2R$

where R is either CF_2H or CF_3. Free radical attack on pentafluoroacetone to give hydrogen abstraction products has been ignored for the following reasons: (*i*) pentafluoroacetone concentration is low (0.6 Torr), and (*ii*) transient free radical concentrations are high; indeed it is assumed that all pentafluoroacetone molecules within the central focal region are dissociated.

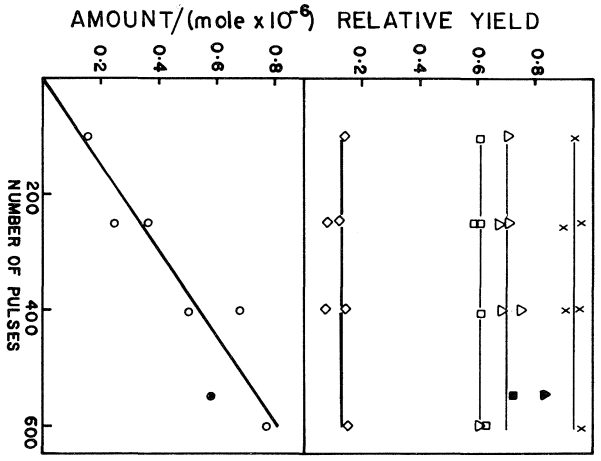

FIG. 2. Product formation in the multiphoton dissociation of pentafluoroacetone as a function of number of pulses. Circles refer to pentafluoroethane. The upper graph displays the relative molar production of other products relative to C_2F_5H: C_2F_4, squares; C_2F_6, triangles; and CF_3H, diamonds. The crosses refer to the peak height ratio C_2F_3H/C_2F_5H from glc. Pressure = 0.6 Torr, cell volume = 330 cm^3; irradiated volume = 14 cm^3; temperature = 23°C; incident fluence = 0.25 J cm^{-2}. The solid symbols are results from irradiation of 0.6 Torr pentafluoroacetone with 0.08 Torr nitric oxide.

We should note at this point that although small amounts of carbon monoxide were not detected by the sampling method its presence was confirmed by pressure measurements above liquid nitrogen and by

mass spectrometry. General support for the proposed mechanism is provided by the value of the ratio of rates of formation

$$\frac{R_f[C_2F_5H] + R_f[C_2F_4] + R_f[CF_3H]}{R_f[C_2F_6]} \approx 2.5$$

A value of 2.0 is expected. Pritchard and Perona (6) find values from 1.80 → 2.40. Furthermore, the ratio of rates of formation is

$$R_f[CF_3H]/(R_f[C_2H_5F] + R_f[C_2F_4]) \approx 0.07$$

which is in good agreement with Pritchard and Perona's estimate for the disproportionation/combination ratio for CF_3 and CF_2H of 0.08. There is, however, one major discrepancy between our results and the one photon study. The earlier workers found $[C_2F_4]/[C_2F_5H] \leq 0.04$, we find values of ~ 0.61. This almost certainly indicates that free radical recombination occurs within a region of high vibrational "temperature"; considering the nature of the excitation this indication is not unexpected. Furthermore, equivalently high yields of C_2F_3H are found. This is not unexpected since the rate of HF elimination from $C_2F_4H_2$* is expected to be at least >20 larger than the rate of elimination from C_2F_5H* (6).

Two experiments with free radical scavengers were performed. In the first 0.6 Torr of pentafluoroacetone was photolysed in the presence of 0.10 Torr of oxygen. The sole product was CF_2O. Clearly vibrationally hot pentafluoroacetone molecules are burned in the presence of oxygen. In the second experiment 0.6 Torr of pentafluoroacetone was photolysed in the presence of 0.08 Torr of NO. No change in either the distribution or the rates of formation of products was observed. Clearly high free radical concentrations and low pressures preclude the effective use of free radical scavengers. We note that the total pressure is limited by dielectric breakdown observed in focused beams.

In conclusion, the product array observed indicates that multiphoton decomposition of pentafluoroacetone proceeds by a free radical mechanism, in which high concentrations of trifluoromethyl and difluoromethyl radicals are formed in a high temperature region. This result makes this molecule relatively unattractive for studies of deuterium atom enrichment in spite of the fact that the molecule contains a single hydrogen atom which may be easily redeuterated by exchange with water through the enol form. Although the free radical mechanism is clearly indicated by the array of products its occurrence could not be proven by classical free radical scavenging experiments. This type of ambiguous behaviour should be general to studies of multiphoton decomposition in focused infrared laser beams in which the decomposition yield is necessarily high and the total pressure is necessarily low.

Acknowledgement

We would like to acknowledge the helpful comments of one referee on the production of trifluoroethylene.

1. P. A. HACKETT, M. GAUTHIER, and C. WILLIS. J. Chem. Phys. **69**, 2924 (1978).
2. P. A. HACKETT, M. GAUTHIER, C. WILLIS, and R. PILON. J. Chem. Phys. **71**, 546 (1979).
3. W. BATEY and A. B. TRENWITH. J. Chem. Soc. 1388 (1961).
4. D. A. WHYTOCK and K. O. KUTSCHKE. Proc. R. Soc. London Soc. A**306**, 503 (1968).
5. F. M. LUSSIER and J. I. STEINFELD. Chem. Phys. Lett. **50**, 175 (1977).
6. G. O. PRITCHARD and M. J. PERONA. Int. J. Chem. Kinet. **1**, 413 (1969).

Entropy changes and structural implications for crystalline phases of pyrazine

ROBERT K. BOYD, JOHN COMPER, AND GEORGE FERGUSON

Guelph–Waterloo Centre for Graduate Work in Chemistry, Guelph Campus, University of Guelph, Guelph, Ont., Canada N1G 2W1

Received May 3, 1979

ROBERT K. BOYD, JOHN COMPER, and GEORGE FERGUSON. Can. J. Chem. **57**, 3056 (1979).

Molar heat capacities of crystalline pyrazine have been measured by adiabatic calorimetry in the range 20–40°C and interpreted to show that in the crystal structures of phases II and III half the molecules must be disordered. Together with previous X-ray studies, this allows possible structures for phase II and phase III to be deduced. Of the eight molecules in the phase III unit cell, four are disordered over two sites so that the point symmetry is effectively *mmm*; the remaining four molecules have 2/*m* symmetry and are not disordered. This structure is consistent with the available spectroscopic evidence. It is likely that the phase II structure is closely related to the phase III structure, for example by the molecules with 2/*m* symmetry adopting a slightly different orientation.

ROBERT K. BOYD, JOHN COMPER et GEORGE FERGUSON. Can. J. Chem. **57**, 3056 (1979).

On a mesuré les capacités calorifiques molaires de la pyrazine cristallisée, à l'aide d'un calorimètre adiabatique dans un intervalle de température de 20–40°C. Les résultats sont interprétés dans le but de montrer que dans les structures cristallines des phases II et III la moitié des molécules doivent être désordonnées. De concert avec les études antérieures de rayons-X, ceci permet de déduire les structures possibles des phases II et III. Des huit molécules dans la maille élémentaire de la phase III, quatre sont désordonnées sur deux sites de telle sorte que le point de symétrie soit effectivement *mmm*. Les quatre molécules restantes ont une symétrie 2/*m* et ne sont pas désordonnées. Cette structure est compatible avec les preuves spectroscopiques disponibles. Il est probable que la structure de la phase II soit reliée de près à celle de la phase III, par exemple par l'intermédiaire des molécules à symétrie 2/*m* adoptant une orientation légèrement différente.

[Traduit par le journal]

The nature of the phase transitions in crystalline pyrazine has been the subject of several investigations incorporating a wide range of techniques; thus, infrared (1) and Raman (2) studies both detected a phase transition at about 29°C. Similarly, an nqr study (3) of the ^{14}N quadrupole coupling constants in pyrazine yielded evidence of a phase transition near 27°C, and also of a second transition near 35°C. Measurements of proton spin–lattice relaxation times (4) (T_1 and T_{1D}) in crystalline pyrazine, on the other hand, resulted in *no* indication of any discontinuity in the appropriate temperature range being detected.

The solid state structure of phase I of pyrazine has been fully defined by X-ray methods at 20°C (5) and at −89°C (6) and more recently (7) an investigation of the phase I–II (28.5°C) and II–III (36.5°C) transitions of pyrazine[1] has been reported in which such techniques as X-ray diffraction, calorimetry, and low-frequency infrared and Raman spectroscopy were used.

In the present work, heat capacities of pyrazine were measured in the range 20–40°C by adiabatic calorimetry; the techniques used have been described previously (8). The pyrazine sample ("Gold Label" brand, Aldrich Chemical Co.) was sublimed from BaO and the heat capacities C_p measured in the 20–40°C range are shown in Fig. 1. The transition centred at about 27.5°C is essentially isothermal and requires an equilibration time of about 1 h if sufficient energy is added to raise the sample temperature from just below the transition to just above it. Two independent measurements of the excess enthalpy of this transition yielded values of 963 J mol^{-1} and 976 J mol^{-1}, in reasonable agreement with the value (954 J mol^{-1}) obtained previously by other means (7). These correspond to values for the excess molar entropy change (ΔS(excess)) for the phase I–II transition of R ln 1.46 to R ln 1.48. The existence of the very weak anomaly (7) centred near 37°C was confirmed in three independent sets of measurements (Fig. 1) in the present work. The excess enthalpy of this transition was 60 ± 10 J mol^{-1}.

The excess entropy of a thermal transition such as that observed for pyrazine near 28°C is frequently interpreted (9) in terms of an order–disorder phe-

[1]The three distinct phases were labelled I, II, III, in order of *increasing* temperature. This is contrary to the usual convention, which uses "Phase I" to describe the highest temperature solid phase. The present work will also use this notation since the possibility of additional transitions between 37°C and the melting point could not be discounted.

0008-4042/79/233056-05$01.00/0

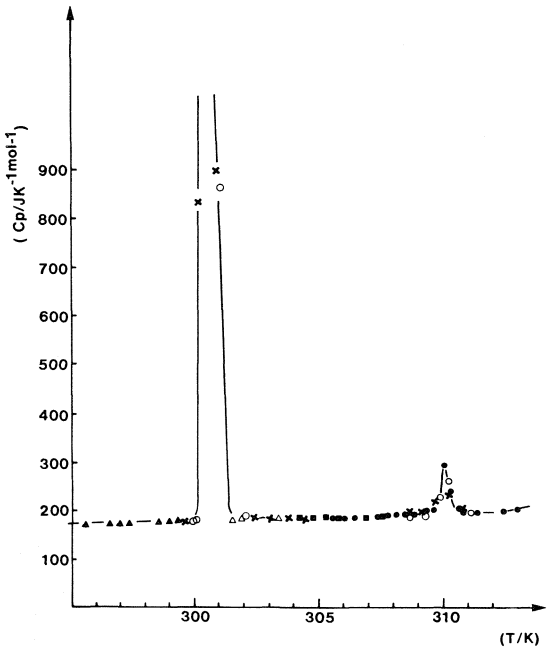

FIG. 1. Heat capacities of pyrazine purified by sublimation. The different symbols used represent independent series of experiments.

nomenon via the equation:

$$\Delta S(\text{excess}) = \Delta S(\text{configuration}) + \Delta S(\text{lattice})$$

where

$$\Delta S(\text{configuration}) = R \ln (W_{II}/W_I)$$

is calculable in terms of the numbers of distinguishable orientations (W) available to molecules in the crystal, above and below the transition. ΔS(lattice) refers to the concomitant change in crystal packing, associated with changes in density, etc. The important point here is that the experimental value of ΔS(excess) is intrinsically an upper limit to ΔS(configuration). Since the baseline heat capacities, above and below the transition, extrapolate reasonably smoothly into one another (Fig. 1), it is expected that ΔS(lattice) should not be large in the present case.

The experimental value of ΔS(excess) (R ln (1.46–1.48)) might correspond to R ln (3/2). However, this would require ΔS(lattice) to be slightly negative. Moreover, the phase I structure is known (5) to be ordered ($W_I = 1$) and it is difficult to understand or interpret a value of $W_{II} = 1.5$. A more reasonable interpretation of the experimental value of ΔS(excess) would involve

$$\Delta S(\text{configuration}) = R \ln (2^{1/2}) = \tfrac{1}{2} R \ln 2 = R \ln (1.414)$$

plus a small positive contribution (approximately 0.3 J K^{-1} mol^{-1}) from ΔS(lattice), as discussed above. This, in turn, implies that the observed transition at 27.5°C corresponds to a process in which an ordered structure ($W_I = 1$) is transformed to a structure in which just *half* of the molecules are disordered over two sites ($W_{II} = 2$). The phase II–III transition (near 37°C) introduces negligible additional excess entropy. Therefore, there can be no gross structural differences between phases II and III, in agreement with previous conclusions (7).

The structural information from the entropy changes, together with the known (5) crystal structure of phase I and the powder and Weissenberg film data (7) for phases II and III, now allow plausible crystal structures for these phases to be deduced.

It is known (7) that the crystal structure of phase III at 38°C is derived from that described (5) for pyrazine phase I at 20°C by a doubling of 9.3 and 5.9 Å unit cell constants, while the third (3.8 Å) was essentially unchanged.[2] The space group of the phase III structure was deduced (7) to be *Cmmm* (D_{2h}^{19}) (the other possible space groups were rejected on the basis of infrared and Raman studies) and while possible symmetry sites of the pyrazine molecules at 38°C were considered (7) no detailed structural model was proposed.

A stereo view of four unit cells of the room temperature phase I structure is shown in Fig. 2. In these cells the molecules are required crystallographically to have 2/*m* symmetry, the two-fold axis coincides with the N· · ·N molecular axis and the molecule lies at an angle of 22.5° to the 5.911 Å axis. The cells are so arranged in Fig. 2 that when all four are considered as a unit, the cell then produced has the approximate dimensions of the phase III structure ($a = 18.57$, $b = 11.31$, $c = 3.85$ Å) (7).

The available evidence (1) indicates that there is no major translational movement of molecules on passing from phases I to II to III. Consequently, the first step in deducing a structure for phase III is to determine if molecules at sites indicated in Fig. 2 could be accommodated into the *Cmmm* space group, and then to decide what different or addi-

[2]The unit cell described (5) for pyrazine has $a = 9.316$, $b = 3.815$, $c = 5.911$ Å in space group *Pmnn*. This is a non-standard setting of *Pnnm* (D_{2h}^{12}. No. 58) which could have $a = 5.911$, $b = 3.815$, $c = 9.316$ Å. Later workers (6, 7) use another non-standard setting of *Pnnm*, which is still correctly labelled *Pmnn* but has the *b* and *c* axes of ref. 5 interchanged. This change produces $a = 9.316$, $b = 5.911$, $c = 3.815$ Å, which allows easy comparison with the *Cmmm* space group of the phase III structure. We also adopt this cell definition in this paper. Non-crystallographers may find these changes from the standard settings confusing.

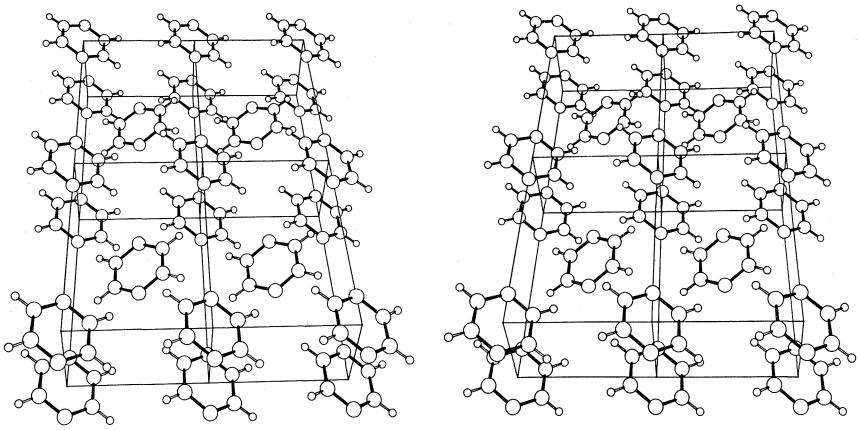

FIG. 2. Stereoview of *four* unit cells of the phase I pyrazine structure (after Wheatley (5)). The 5.9 Å axis is horizontal and the 9.3 Å lies away from the viewer.

tional symmetry requirements are imposed on the molecules by the space group.

Inspection of the symmetry information from International Tables (10) for space group *Cmmm* does indeed show that the molecular centres (as in Fig. 2) could be accommodated in a *Cmmm* lattice.[3] The molecules at the origin (0, 0, 0) of the phase III cell and at ($\frac{1}{2}$, $\frac{1}{2}$, 0) (positions 2*a* in *Cmmm* (10)), and at ($\frac{1}{2}$, 0, 0) and (0, $\frac{1}{2}$, 0) (positions 2*b* in *Cmmm*) are now required to have *mmm* symmetry. The simplest way to achieve this is to require that these molecules be on the mirror planes normal to the 3.8 Å *c*-axis, but this would result in prohibitively short (1.6 Å) H···H intermolecular contacts. The most plausible alternative is to allow the pyrazines at the 2*a* and 2*b* positions to retain the 22.5° orientation found in the phase I structure; the mirror planes normal to the *c*-axis then yield a disordered structure with effective *mirror* symmetry. When *only* this change is made to the four cells of the phase I structure, a structure as shown in Fig. 3 develops.

In Fig. 3 the four molecules situated at ($\frac{1}{4}$, $\frac{1}{4}$, $\frac{1}{2}$), ($\frac{1}{4}$, $\frac{3}{4}$, $\frac{1}{2}$), ($\frac{3}{4}$, $\frac{1}{4}$, $\frac{1}{2}$), and ($\frac{3}{4}$, $\frac{3}{4}$, $\frac{1}{2}$) (originally at ($\frac{1}{2}$, $\frac{1}{2}$, $\frac{1}{2}$) in the smaller phase I cell) have not been moved from, or about, their positions in the phase I cells; the molecular centres are exactly those required for position 4*f* in *Cmmm* (10). These molecules are required by the *Cmmm* space group to have 2/*m* symmetry but in a different manner from that required for phase I. If the molecules are not disordered, the two-fold crystallographic axis which runs parallel to the short 3.8 Å axis will be normal to the ring plane which lies in the crystallographic mirror plane at $z = \frac{1}{2}$. Thus, the only positional uncertainty with these molecules in phase III would be in the precise orientation about the two-fold axis normal to the molecular plane. (An alternative way of obtaining 2/*m* site symmetry is to allow these molecules to retain the orientation found at room temperature and then invoke disorder about the mirror plane at $z = \frac{1}{2}$; the entropy measurements imply that this is not a valid model as it would require *all* those molecules at sites 2*a*, 2*b*, and 4*f* to be disordered.) If the non-disordered molecules in Fig. 3 are simply rotated 22.5° about the N···N molecular axes into the mirror plane at $z = \frac{1}{2}$, the same short (1.6 Å) H···H contacts would be produced as mentioned above for the molecules at the cell corners and edges. Because the entropy data require half the molecules to be non-disordered, the only way to satisfy this and reduce H···H intermolecular interaction in the mirror plane at $z = \frac{1}{2}$ is to rotate the (4*f*) molecules about the crystallographic two-fold axis until such contacts are minimized. A likely orientation is shown in Fig. 4 in which the 4*f* molecules have been rotated 71° about the two-fold axis; this orientation yields H···H intermolecular contacts of approximately 2.4 Å. The atomic coordinates used to produce Fig. 4 were derived from the phase I coordinates by appropriate geometrical manipulations.[4]

This model for the phase III structure is consistent with the results of our entropy studies and available X-ray and spectroscopic data (7). It also has two distinct environments for the nitrogen atoms as required by the nqr results (3).

The arguments presented thus far apply directly to

[3]For details of *Cmmm* (D_{2h}^{19}. No. 65) see p. 154 of ref. 10 and for *Pnnm* (D_{2h}^{12}. No. 58) see p. 146 of ref. 10.

[4]The atomic coordinates are available, at a nominal charge, from the Depository of Unpublished Data, CISTI, National Research Council of Canada, Ottawa, Ont., Canada K1A 0S2.

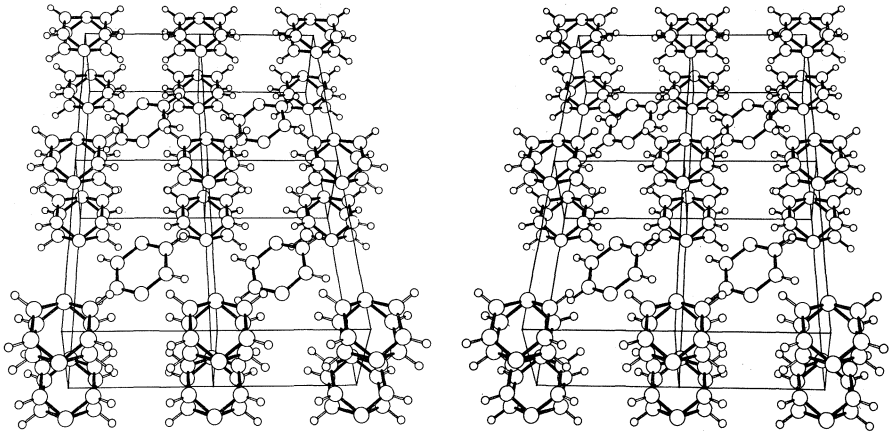

FIG. 3. Stereoview of the same arrangement as in Fig. 2 but with the molecules at the cell edges and corners disordered to yield effective *mmm* site symmetry as would be required in *Cmmm* space group.

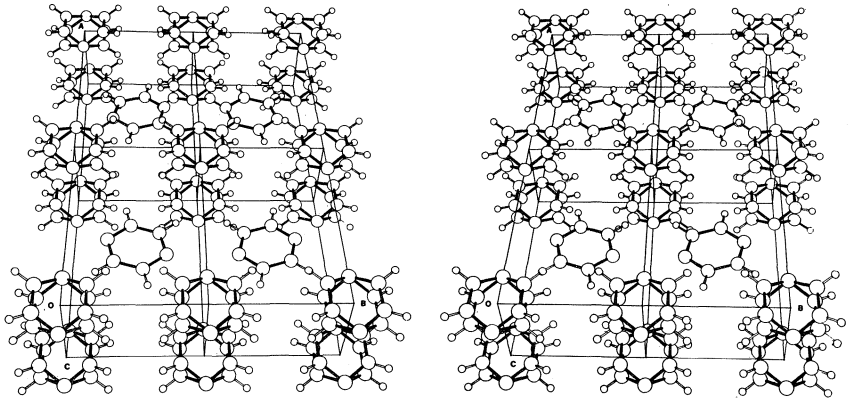

FIG. 4. Stereoview of the postulated phase III structure obtained by modifying the structure shown in Fig. 3. The molecules centred at $(\frac{1}{4}, \frac{1}{4}, \frac{1}{2})$, $(\frac{1}{4}, \frac{3}{4}, \frac{1}{2})$, $(\frac{3}{4}, \frac{1}{4}, \frac{1}{2})$, and $(\frac{3}{4}, \frac{3}{4}, \frac{1}{2})$ now lie in the mirror plane at $z = \frac{1}{2}$ and have been rotated 71° in the plane, about the two-fold symmetry axis to yield an orientation which minimizes intermolecular interactions.

phase III (above 38°C), for which the crystallographic information (7) was more complete than for phase II (28–35°C). However, the thermal transition observed (Fig. 1) (near 38°C) is far too small to correspond to any disordering process or gross change of structure, so that the crystal structures of phases II and III must be very similar. This conclusion is in agreement with all other experimental information (1–7). The most likely process accounting for the II → III transition is a slight change in the orientations of the molecules at the 4*f* sites (2/*m* symmetry). This would be sufficient to account for the accompanying shifts in nqr frequencies (3). In any event, the differences between phases II and III are clearly minor compared to those between phases I and II. The main outstanding problem concerns the nmr data on T_1 and T_{1D} (4), which showed no evidence of either phase transition. The explanation proposed previously (4) is probably still valid in general, viz., the changes in crystal structure are sufficiently subtle as to make only negligible changes in both the dipolar interactions between ^1H nuclei, and in the energy barriers to the molecular reorientations which mediate the spin–lattice relaxation. However, the particular high-temperature structure proposed previously (4) is now known to be wrong, in light of more recent information (7). A more complete understanding of the structure and dynamics of the pyrazine crystal will require accurate crystal structures determined at temperatures above 30°C.

Acknowledgement

Support of this work by the National Research Council of Canada is gratefully acknowledged.

1. V. SCHETTINO, G. SBRANA, and R. RIGHINI. Chem. Phys. Lett. **13**, 284 (1972).
2. G. SBRANA, V. SCHETTINO, and R. RIGHINI. J. Chem. Phys. **59**, 2441 (1973).
3. A. PENEAU, M. GOURDJI, and L. GUIBE. J. Chem. Phys. **60**, 4295 (1974).
4. W. E. SANFORD, R. K. BOYD, and J. A. RIPMEESTER. Mol. Cryst. Liquid Cryst. **46**, 121 (1978).
5. P. J. WHEATLEY. Acta Crystallogr. **10**, 182 (1957).
6. G. DEWITH, S. HORKEMA, and D. FEIL. Acta Crystallogr. B**32**, 3178 (1976).
7. D. BOUGEARD, N. LE CALVE, A. NOVAK, and NGUYEN-BA-CHANH. Mol. Cryst. Liquid Cryst. **44**, 113 (1978).
8. J. A. RIPMEESTER, D. A. WRIGHT, C. A. FYFE, and R. K. BOYD. J. Chem. Soc. Faraday Trans. II, **74**, 1164 (1978).
9. E. F. WESTRUM, JR. and J. P. MCCULLOUGH. Physics and chemistry of the organic solid state. Vol. 1. *Edited by* D. Fox, M. M. Labes, and A. Weissberger. Wiley, New York. 1963. p. 1.
10. International Tables for X-Ray Crystallography. Vol. 1. Kynoch Press, Birmingham. 1965.

Structure of $Ni[Ag(SCN)_2]_2 \cdot 2diox$ and its derivatives

P. P. SINGH, S. A. KHAN, AND J. P. PANDEY[1]

Department of Chemistry, M.L.K. College, Balrampur-271201 (U.P.), India

Received February 7, 1979

P. P. SINGH, S. A. KHAN, and J. P. PANDEY. Can. J. Chem. **57**, 3061 (1979).

$Ni[Ag(SCN)_2]_2 \cdot 2diox$ and its derivatives have been synthesized. Their structures have been given on the basis of infrared spectral, electronic spectral, magnetic moment, and molar conductance studies. These results demonstrate that $Ni[Ag(SCN)_2]_2$ forms two types of complexes: (*i*) cationic–anionic type of general formula $[NiL_x]^{2+}[Ag(SCN)_2]_2^{2-}$ ($x = 3, 4, 6$) and (*ii*) polymeric bridged type having a chain structure consisting of zig-zag thiocyanate bridges between nickel and silver. The cationic–anionic type of complexes are formed by pyridine, nicotinamide, 4-aminopyridine, aniline, *p*-toluidine, thiourea, ethylene thiourea, bipyridine, phenanthroline, pyrazine-2,3-dicarboxamide, and triphenylphosphine, and the polymeric bridged type by dioxane, acetone, and dimethylformamide. All the ligands have been found to prefer to coordinate to nickel instead of silver.

P. P. SINGH, S. A. KHAN et J. P. PANDEY. Can. J. Chem. **57**, 3061 (1979).

On a synthétisé le complexe $Ni[Ag(SCN)_2]_2 \cdot 2diox$ et ses dérivés et on a établi leur structure en se basant sur l'étude des spectres infrarouges et électroniques et sur l'étude du moment magnétique et de la conductance molaire. Ces résultats démontrent que $Ni[Ag(SCN)_2]_2$ forme deux types de complexes (*i*) un complexe du type ionique de formule générale $[NiL_x]^{2+}[Ag(SCN)_2]_2^{2-}$ ($x = 3, 4, 6$), (*ii*) un complexe du type polymère ponté qui a une structure en chaîne consistant en des ponts thiocyanates en zig zag entre les atomes de nickel et d'argent. Les complexes du type ionique sont formés par la pyridine, la nicotinamide, l'amino-4 pyridine, l'aniline, la toluidine, la thiourée, l'éthylène-thiourée, la bipyridine, la phénantroline, la pyrazinedicarboxamide-2,3 et la triphénylphosphine. Le type polymère ponté est formé par le dioxanne, l'acétone et la diméthylformamide. On a trouvé que tous les ligands manifestent une tendance à se coordiner au nickel plutôt qu'à l'argent.

[Traduit par le journal]

Introduction

In $MM'(NCS)_4$, both M[Co(II), Ni(II), Cu(II)] and M'[Zn(II), Cd(II), Hg(II)] are in their preferred coordination geometry, and the compounds are energetically quite stable (1–7). Bimetallic tetrathiocyanate, in which one metal prefers octahedral coordination geometry and the other a linear, viz., Ag(I), Cu(I), Au(I), has not been reported previously. We have synthesized such compounds and have studied their structures and properties, particularly with a view to investigate differences with $MM'(NCS)_4$ types of compounds.

Experimental

Materials and Manipulations

Reagent grade hydrated nickel(II) nitrate, silver(I) nitrate, and potassium thiocyanate (BDH) were used after recrystallization. Nicotinamide (nia), triphenylphosphine (Ph_3P), bipyridine (bipy), 1,10-phenanthroline (phen), thiourea (tu), ethylene thiourea (etu), 4-aminopyridine (apy), and *p*-toluidine (tol) (Aldrich Chemical) were used after recrystallization from ethanol. Acetone (ace), dioxane (diox), dimethylformamide (dmf), pyridine (py), and aniline (ani) (BDH) were purified by known methods. Pyrazine-2,3-dicarboxamide (pzd) (Aldrich Chemicals) was used as such from fresh bottles.

Synthesis of the Complexes

(*i*) $Ni[Ag(SCN)_2]_2 \cdot 2L$ (L = diox, ace, dmf): 5 mmol of Ni(II) thiocyanate and 10 mmol of Ag(I) thiocyanate were mixed together in 50 mL of each of the above solvents (ligands) separately and stirred for 48 h. Light green complexes were formed, filtered, washed with solvents, and dried in vacuum.

(*ii*) $Ni[Ag(SCN)_2]_2 \cdot xL$ ($x = 3, 4, 6$ and L = py, nia, apy, bipy, phen, ani, tol, tu, etu, pzd, and Ph_3P): homogeneous suspensions of 2.5 mmol of $Ni[Ag(SCN)_2]_2$ in ethanol were stirred in a number of 100 mL flasks. To each suspension ethanolic solutions containing excess of different ligands were added and stirred for 24 h. Solid complexes which formed were filtered, washed with ether, and finally dried in vacuum.

Elemental Analysis

Nickel was estimated as dimethylglyoximate, silver as chloride, and sulphur as sulphate gravimetrically. Nitrogen was estimated by Kjeldahl's method. The analytical data are presented in a table deposited as unpublished material.[2]

Physical Measurements

Molar Conductance Measurements

The molar conductance of the only soluble complex of etu was measured in dimethylformamide with a Philip PR-9500 conductivity bridge.

Infrared Spectra

The infrared spectra in the region 4000–200 cm^{-1} were recorded on a Perkin-Elmer 621 model spectrophotometer.

[1]Present address: Degree College, Pratapgarah (U.P.), India.

[2]The set of data is available, at a nominal charge, from the Depository of Unpublished Data, CISTI, National Research Council of Canada, Ottawa, Ont., Canada K1A 0S2.

0008-4042/79/233061-04$01.00/0

Visible and Near Infrared Absorption Spectra

Electronic spectra were recorded on a Cary-14 spectrophotometer in the region 300–2500 nm.

Magnetic Susceptibility Measurements

The measurements were made by the Gouy method at room temperature using $CoHg(SCN)_4$ as standard. Diamagnetic corrections were made using Pascal's constants.

Results and Discussion

All the complexes are insoluble in solvents suitable for molecular weight determination or for growth of single crystal for X-ray analysis. Because of this, we have confined our studies to infrared spectral, electronic spectral, magnetic moment, and molar conductance measurements only. The complexes have been studied under two groups; one with weak bases like diox, dmf, and ace, and the other with strong or medium strong bases viz., py, apy, nia, bipy, phen, tu, etu, pzd, ani, and tol.

(A) $Ni[Ag(SCN)_2]_2 \cdot 2L$ (L = diox, dmf, ace)

(*i*) The analytical results reveal that two ligands molecules are coordinated to each molecule of $Ni[Ag(SCN)_2]_2$.

(*ii*) The positions of infrared spectral bands (Table 1) in the ν_{CN}, ν_{CS}, and δ_{NCS} regions which are diagnostic for the nature of thiocyanate bonding, indicate the presence of only bridged thiocyanate groups (4, 5, 8–10).

(*iii*) The positions of electronic spectral bands, spectral parameters, and magnetic moment values as discussed later, indicate that nickel is in octahedral coordination geometry.

Keeping the above facts and the structure of the reported bimetallic tetrathiocyanates (4, 5, 11) in view, the following two structures can be proposed for $Ni[Ag(SCN)_2]_2 \cdot 2L$

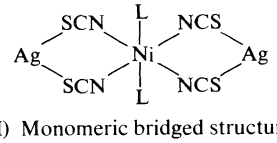

(**I**) Monomeric bridged structure

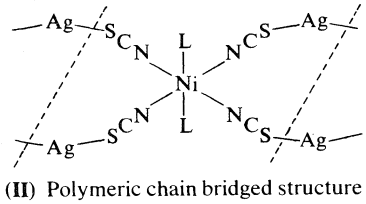

(**II**) Polymeric chain bridged structure

Structure **I** has been proposed on the basis of similarity in the positions of infrared spectral bands in ν_{CN}, ν_{CS}, and δ_{NCS} regions and in electronic spectral band positions with that of $NiHg(SCN)_4 \cdot 2L$ (2, 3, 11). But this structure is energetically unfavourable because Ag(I) prefers a coordination number of two in which it requires linearity along —NCS—Ag—SCN— due to *sp* hybridization. This linearity is not maintained in this structure.

The polymeric chain bridged structure **II** appears to be the most probable structure for $Ni[Ag(SCN)_2]_2 \cdot 2L$ as is supported by the following: (*i*) This structure is based on the crystal structure (12) of AgSCN in which the structural unit is an endless chain formed by the bonds from the silver atom to the S-end of one thiocyanate group and the N-end of another group. The chain has a zig-zag shape and is bent at sulphur (104°) as well as at nitrogen (165°). (*ii*) The preferable coordination number two of Ag(I) is maintained. (*iii*) Octahedral coordination geometry as required by magnetic moment values and electronic spectral studies are also satisfied. (*iv*) The ligands show features of coordination. In the dioxane complex the absorption bands associated with the C—O—C antisymmetric stretch show the expected frequency decrease indicating coordinated dioxane molecules (1, 13). dmf and ace show features of coordination through their carbonyl oxygen as is evidenced by the negative shift in the ν_{CO} mode (14). (*v*) The octahedral coordination geometry of nickel and the presence of a ν_{Ni-L} band in the far infrared region support the linkage of the ligand to nickel. (*vi*) We observed bands due to ν_{Ag-SCN}, ν_{Ni-O}, and ν_{Ni-NCS} modes in the regions 215–220, 370–395, and 235–260 cm^{-1} respectively (3, 15). The presence of bands in these regions indirectly supports our proposed structure.

(B) $Ni[Ag(SCN)_2]_2 \cdot xL$ (x = 3, 4, 6 and L = py, apy, nia, bipy, phen, ani, tol, tu, etu, pzd, and Ph_3P)

(*i*) Analytical data indicate that three molecules of bipy and phen, six molecules of py, apy, nia, ani, tol, pzd, tu, etu, and four molecules of Ph_3P are coordinated to each molecule of $Ni[Ag(SCN)_2]_2$.

(*ii*) The electronic spectral bands, spectral parameters, and magnetic moment values as discussed later show that nickel in all these complexes is in octahedral coordination geometry. The complex of Ph_3P is the only exception; it is diamagnetic indicating the presence of square planar geometry around nickel.

(*iii*) The infrared spectra of these complexes show bands due to ν_{CN}, ν_{CS}, and δ_{NCS} modes in the regions 2060–2130, 710–770, and 430–465 cm^{-1}, respectively. The positions of the bands in these diagnostic regions are indicative of S-bonded thiocyanates (1–3, 6).

(*iv*) The etu complex, whose infrared spectral band positions, magnetic moment values, electronic spectral band positions, values of spectral parameters, mp, etc., are in the range of other complexes of this

TABLE 1. Infrared spectral assignments of thiocyanate vibrations (4000–200 cm^{-1})

Complex	C—N(st)	C—S(st)	NCS(bend)	Ni—L(st)	Ni—NCS(st)	Ag—SCN(st)
$Ni[Ag(SCN)_2]_2 \cdot 2diox$	2160sh, 2140sb	780m, 730b	450s	395sh	255sb, 235m	218m
$Ni[Ag(SCN)_2]_2 \cdot 2ace$	2160sh, 2140sb	785m, 722m	450s	395m	260b, 240w	220w
$Ni[Ag(SCN)_2]_2 \cdot 2dmf$	2160sh, 2125sb	760m, 730m	450s	390sh	265b, 230w	215w
$[Ni(bipy)_3]^{2+}[Ag(SCN)_2]_2^{2-}$	2125s, 2080s	765m, 730s	460w, 450s	280sh	—	218m
$[Ni(phen)_3]^{2+}[Ag(SCN)_2]_2^{2-}$	2130sb, 2090sb	770s, 725s	450m, 442w	285sh	—	215m
$[Ni(nia)_6]^{2+}[Ag(SCN)_2]_2^{2-}$	2138s, 2110s	750b, 720s	460w, 440m	275m	—	216w
$[Ni(py)_6]^{2+}[Ag(SCN)_2]_2^{2-}$	2095s	770sh, 755s	465sh	282sh	—	214m
$[Ni(apy)_6]^{2+}[Ag(SCN)_2]_2^{2-}$	2130s, 2080s	760m, 740m	452m, 445m	274w	—	218m
$[Ni(tol)_6]^{2+}[Ag(SCN)_2]_2^{2-}$	2122s, 2100s	730m, 710m	450s	280s	—	215m
$[Ni(ani)_6]^{2+}[Ag(SCN)_2]_2^{2-}$	2120s	750s, 715m	448m	280s	—	216m
$[Ni(tu)_6]^{2+}[Ag(SCN)_2]_2^{2-}$	2125s, 2105s	765m, 750w	450s, 430s	240sh	—	215w
$[Ni(etu)_6]^{2+}[Ag(SCN)_2]_2^{2-}$	2105s, 2060s	750w, 720sh	455m, 440w	283m	—	215sh
$[Ni(pzd)_6]^{2+}[Ag(SCN)_2]_2^{2-}$	2120s, 2100s	760s, 720s	440w, 430m	284sh	—	218m
$[Ni(Ph_3P)_4]^{2+}[Ag(SCN)_2]_2^{2-}$	2110sh, 2085s	740s, 720m	440w, 430m	—	—	210m

class, is soluble in dimethylformamide, whereas the rest are insoluble. The molar conductance of this complex indicates that it is a 1:1 electrolyte. On the basis of its similarity in other data with this class of compounds, it is thought that all the complexes are 1:1 electrolytes.

(*v*) The pyridine derivative ligands show features of coordination through their ring nitrogen as evidenced by the positive shift in the bands due to ring vibrations (1, 5). Both bipyridine and phenanthroline act as bidentate donors. The nitrogen of NH is the donor site in aniline, *p*-toludine, and ethylene thiourea, and sulphur in thiourea as indicated by the negative shifts in ν_{NH} and ν_{CS} modes respectively (1, 16, 17). The 10 *Dq* of the S-bonded thiourea complex is greater by 1 900 cm^{-1} than the N-bonded ethylene thiourea (Table 2). This difference supports linkage through S in thiourea and through N in ethylene thiourea. The X-sensitive absorption bands at 1092, 705, and 437 cm^{-1} are typical of coordinated triphenylphosphine (1).

On the basis of these results, it can be presumed that the complexes are of the cationic–anionic type as described elsewhere (6) and the possible cations and anions are:

$[NiL_6]^{2+}[Ag(SCN)_2]_2^{2-}$ (L = monodentate donor)

$[Ni(LL)_3]^{2+}[Ag(SCN)_2]_2^{2-}$ (LL = bidentate donor)

The coordination of the ligands to nickel and thiocyanate groups through S to silver can be supported on the following grounds: (*i*) The nickel is in octahedral coordination geometry, which is possible only when the ligands are linked to nickel. (*ii*) The presence of the bands in the regions 275–285 cm^{-1} and at 240 cm^{-1} can more favourably be assigned to ν_{Ni-L} (nitrogen donors) and to ν_{Ni-L} (sulphur donor) respectively (6, 17). The presence of the bands in these regions also supports our proposed structures.

In the case of the triphenylphosphine complex, which is diamagnetic, the cation probably has a square planar geometry and the following structure for this complex may be proposed.

$[Ni(Ph_3P)_4]^{2+}[Ag(SCN)_2]_2^{2-}$

Electronic Spectral Discussion

In order to extend support to the stereochemistry around nickel, we have recorded the electronic spectra of some representative complexes as Nujol mulls (Table 2). In all the complexes we observe bands in the region 27 700 – 24 400 cm^{-1} assigned to ν_3 arising from the transition $^3A_{2g} \rightarrow {}^3T_{1g}(P)$, in the region 17 200 – 14 000 cm^{-1}, ν_2 arising from the transition $^3T_{2g} \rightarrow {}^3T_{1g}(F)$ and in the region 10 500 – 8 400 cm^{-1}, ν_1 arising from the transition $^3A_{2g} \rightarrow {}^3T_{2g}(F)$. Besides these bands, certain low energy bands in the region 8 000 – 5 000 cm^{-1} are also observed in the complexes of dioxane, acetone, and dimethylformamide. They are possibly due to transitions to ^3E_g and $^3B_{2g}$ levels in D_{4h} symmetry. The complex spectra of these complexes may be due to low symmetry affects and thus the *Dq*, *B'*, and β values for these complexes have not been calculated. For the rest of the complexes where nickel is thought to be in O_h symmetry, the ν_2 and ν_3 bands have been selected and various ligand field parameters calculated using the matrices of Tanabe and Sugano (18). Magnetic moment values (2.90–3.22 BM), positions of electronic spectral bands, and the values of spectral parameters indicate an octahedral coordination geometry around nickel (19). *Dq* values of the complexes of pyridine derivatives are higher than the other complexes indicating that pyridine derivatives exert a strong ligand field. Values of the Nephelauxetic parameter β indicate approximately the same degree of covalency in all the complexes.

The spin–orbit coupling constant values ($-\lambda'$) are

TABLE 2. Electronic bands and spectral parameters (cm^{-1})

Complex	ν_3	ν_2	ν_1 $10Dq$ (obs)					$10Dq$ (calcd from ν_2 and ν_3)	B'	β	$-\lambda'$
$Ni[Ag(SCN)_2]_2 \cdot 2diox$	25 000	15 400	9 300	8 300,	7 100,	5 500,	5 100	—			
$Ni[Ag(SCN)_2]_2 \cdot 2ace$	27 700	16 400	10 000	7 100,	5 800,	5 200		—			
$Ni[Ag(SCN)_2]_2 \cdot 2dmf$	24 400	14 700	9 000	6 500,	5 600,	5 000,	4 600	—			
$[Ni(phen)_3]^{2+}[Ag(SCN)_2]_2^{2-}$	26 500	16 500	10 500	—	—	—	—	10 400	770	0.72	270
$[Ni(py)_6]^{2+}[Ag(SCN)_2]_2^{2-}$	27 700	17 200	10 500	—	—	—	—	10 800	890	0.84	300
$[Ni(nia)_6]^{2+}[Ag(SCN)_2]_2^{2-}$	26 300	16 600	9 500	—	—	—	—	10 600	960	0.90	250
$[Ni(ani)_6]^{2+}[Ag(SCN)_2]_2^{2-}$	24 900	14 100	8 400	—	—	—	—	8 500	900	0.85	300
$[Ni(tu)_6]^{2+}[Ag(SCN)_2]_2^{2-}$	26 200	16 400	10 000	—	—	—	—	10 400	840	0.79	170
$[Ni(etu)_6]^{2+}[Ag(SCN)_2]_2^{2-}$	24 700	14 000	8 400	—	—	—	—	8 500	890	0.84	230

lower than the free nickel ion value (315 cm^{-1}) showing delocalization of the *d*-orbitals of nickel and orbital overlap to some extent. Orbital overlap is also suggested by the values of Racah parameter B', which is about 73–90% of the free nickel ion value (1056 cm^{-1}).

Acknowledgements

The authors wish to express their sincere thanks to CSIR, New Delhi, for providing financial assistance and to CDRI, Lucknow, for providing instrumentation facilities.

1. R. MAKHIJA, L. PAZDERNIK, and R. RIVEST. Can. J. Chem. **51**, 438 (1973).
2. R. MAKHIJA, L. PAZDERNIK, and R. RIVEST. Can. J. Chem. **51**, 2897 (1973).
3. R. MAKHIJA and R. RIVEST. Spectrochim. Acta, **30A**, 438 (1974).
4. P. P. SINGH, U. P. SHUKLA, R. MAKHIJA, and R. RIVEST. J. Inorg. Nucl. Chem. **37**, 679 (1975).
5. P. P. SINGH, L. P. PATHAK, and S. A. KHAN. J. Inorg. Nucl. Chem. **38**, 475 (1976).
6. P. P. SINGH and S. A. KHAN. Z. Anorg. Allg. Chem. **423**, 173 (1976).
7. P. P. SINGH, O. P. AGARWAL, and S. A. KHAN. Inorg. Chim. Acta, **33**, 15 (1979).
8. J. L. BURMEISTER. Coord. Chem. Rev. **1**, 205 (1966).
9. A. TURCO and C. PECILE. Nature, **191**, 66 (1961).
10. A. SABATINI and I. BERTINI. Inorg. Chem. **4**, 1665 (1965).
11. C. K. CHAN and M. A. PORAI. Kristallografiya, **5**(3), 462 (1960).
12. I. LINDQVIST. Acta Crystallogr. **10**, 29 (1957).
13. R. J. KERM. J. Inorg. Nucl. Chem. **24**, 1105 (1962).
14. B. B. WAYLAND and R. F. SCHRAMM. Inorg. Chem. **8**, 971 (1969).
15. P. P. SINGH and S. P. YADAVA. J. Inorg. Nucl. Chem. **40**, 1881 (1978).
16. P. P. SINGH and I. M. PANDE. J. Inorg. Nucl. Chem. **34**, 591 (1972).
17. C. D. FLINT and M. GOODGAME. J. Chem. Soc. A, 744 (1966).
18. Y. TANABE and S. SUGANO. J. Phys. Soc. Jpn. **9**, 753 (1954).
19. P. P. SINGH, A. K. SRIVASTAVA, and R. RIVEST. J. Inorg. Nucl. Chem. **38**, 439 (1976).

Substituent and solvent effects on Lewis acidity of *p*-substituted anilines: symmetry of interactions

G. LAUNAY AND B. WOJTKOWIAK

Laboratoire de Spectrochemie Moléculaire, Université de Nantes, Chemin de la Houssiniére, 44072 Nantes Cedex, France

AND

T. M. KRYGOWSKI

Department of Chemistry, The University, 02-093 Warsaw, Pasteura 1, Poland

Received May 3, 1979

G. LAUNAY, B. WOJTKOWIAK, and T. M. KRYGOWSKI. Can. J. Chem. **57**, 3065 (1979).

Symmetrical influences of the solvent and the substituent on NH_2-Lewis acidity of six *p*-substituted anilines studied in a series of six solvents were found. The sensitivity parameter (Hammett reaction constant) estimated for various solvents correlated well with basicity of solvents. The sensitivity parameter of the regression of NH_2-acidity vs. basicity parameters of solvents (slope in eq. [5]) correlated with electron attraction or repulsion as measured by substituent constants σ.

G. LAUNAY, B. WOJTKOWIAK et T. M. KRYGOWSKI. Can. J. Chem. **57**, 3065 (1979).

On a trouvé les influences symétriques du solvant et des substituants sur les acidités de Lewis du groupe NH_2 de six anilines *para* substituées en utilisant une série de six solvants. Les paramètres de sensibilité (constante de la réaction de Hammett) évalués pour plusieurs solvants sont en parfaite corrélation avec la basicité de ces derniers. Le paramètre de sensibilité de la régression d'acidité du NH_2 en fonction des paramètres de basicité du solvant (pente de l'équation [5]) est en corrélation avec une attraction ou une répulsion des électrons telle que mesurée par les constantes de substituants σ.

[Traduit par le journal]

Introduction

Recently Kamlet and Taft (1) have introduced a new scale of solvent basicity making use of the magnitudes of enhanced solvatochromic shifts of the longest wave band in the uv–visible spectrum of *p*-nitroaniline relative to that of *N,N*-diethyl-*p*-nitroaniline. In practice $\tilde{\nu}_{max}$-values for *p*-nitroaniline are plotted against $\tilde{\nu}_{max}^{ref}$-values (1) of its *N,N*-diethyl derivative for measurements carried out in nonpolar solvents, leading to the following regression line:

$$[1] \quad \tilde{\nu}_{max} = a_1\tilde{\nu}_{max}^{ref} + b_1$$

Bathochromic shifts $\Delta\tilde{\nu}$ from this line for *p*-nitroaniline are observed when measurements are carried out in solvents interacting as Lewis bases. The shift is given by:

$$[2] \quad \Delta\tilde{\nu} = \tilde{\nu}_{max}(\text{calcd.}) - \tilde{\nu}_{max}(\text{obs.})$$

and its magnitude increases with increase of the solvent's Lewis basicity. This quantity was taken as a measure of the solvent basicity (1).

Principle of the Method

The aim of this paper is to extend this method to the study of substituent effects in other *p*-substituted anilines. In a given solvent the shift of the first primary band is a measure of the Lewis acidity of the NH_2 group and depends on the effect of the substituent X. It must be noted that, at least for strongly donating substituents, the first primary band is not the lowest frequency band, as it is for the NO_2 substituent. *N,N*-dimethylanilines were preferred to *N,N*-diethylanilines because they are more readily available. The following substituted species were studied: X = $N(CH_3)_2$, CH_3, H, COPh, CN, and NO_2.

Experimental

The anilines and *N,N*-dimethylanilines were commercial products purified by standard methods. Spectroscopic grade solvents were used without further purification. Measurements were carried out at 25°C on a Beckman DK2A spectrophotometer. The wave number accuracy is about $\pm$ 40 cm^{-1}.

Results and Discussion

The wave numbers (cm^{-1}) of the first primary band are collected in Table 1 for *p*-substituted anilines and for their *N,N*-dimethyl derivatives. The parameters a_1 and b_1 obtained for non-polar solvents are compiled in Table 2 for each substituent. The correlation coefficients are also reported. Using these parameters, the shifts $\Delta\tilde{\nu}$ (eq. [2]) were calcu-

0008-4042/79/233065-04$01.00/0

TABLE 1. Wave numbers (cm^{-1}) for the first primary bands of a *p*-substituted aniline and its *N,N*-dimethyl derivative

Solvents	NH_2 / $N(CH_3)_2$	$N(CH_3)_2$ / $N(CH_3)_2$	NH_2 / CH_3	$N(CH_3)_2$ / CH_3	NH_2 / H	$N(CH_3)_2$ / H	NH_2 / COC_6H_5	$N(CH_3)_2$ / COC_6H_5	NH_2 / CN	$N(CH_3)_2$ / CN	NH_2 / NO_2	$N(CH_3)_2$ / NO_2
Perfluoroether $C_8F_{16}O$	40000	38800	42830	40320	43480	40770		[a]	39050	36040		[a]
Pentane	39110	38010	42270	39600	42790	40020	33330	30360	38260	35590	31400	28440
Hexane	38990	37820	42230	39570	42750	39920	33230	30280	38170	35540	31360	28310
Heptane	38960	37780	42230	39530	42720	39860	33210	30230	38150	35540	31270	28290
Cyclohexane	38910	37760	42120	39450	42660	39790	33070	30080	38140	35410	31170	28160
CCl_4	39710	37610	[b]				32400	29580	37540	34410	30300	27540
CH_2Cl_2	38620	37380	31740	38850	42020	38990	31780	28690	37110	34010	28380	25480
Dioxane	38420	37500	41320	39050	41620	39220	31370	29300	36850	34630	28220	26230
Butoxybutane	38770	37810	41560	39310	41930	39730	31770	29880	37090	35200	28750	27330
HMPT	38540	37260	[b]				29100	28560	35060	33770	25280	24910
TMP	38450	37370	41020	39000	41220	39250	30270	28790	36080	34070	26460	25330
DMSO	37910	36510	[b]				29640	28240	35390	33380	25540	24560
CH_3CN	38670	37540	41490	39230	41880	39450	31180	28860	36710	34180	27380	25450

[a]Insoluble in the solvent.
[b]Solvent not transparent.

TABLE 2. Statistical parameters of eq. [1]

Substituent	a_1	b_1	r	n
$N(CH_3)_2$	0.985	1710	0.997	6
CH_3	0.746	12720	0.997	6
H	0.815	10230	0.998	6
COPh	0.952	4400	0.991	6
CN	0.823	9070	0.962	7
NO_2	1.042	1800	0.997	6

lated for each polar solvent and for each substituent (Table 3).

The analysis of the data can be carried out in two different ways. First, the substituent effect can be described in terms of the Hammett equation

$$[3] \quad \Delta\tilde{\nu}(X) = \rho\sigma_X$$

where σ_X is the effect of each substituent X, and ρ is the sensitivity to the substituent effect, called usually the reaction constant.

The application of eq. [3] to the data of Table 3 leads to the results collected in Table 4. The correlation coefficients are rather good, and we are therefore allowed to analyse the ρ values of Hammett plots in terms of solvent effect. The reaction constant ρ in eq. [3] has a physical meaning of the degree of differentiation of NH_2–acidity of *p*-substituted anilines in different solvents due to a fixed kind of structure change (substituent effect). This differentiation becomes greater with increase of a solvent's basicity and hence it would seem reasonable to plot ρ vs. DN, a solvent basicity parameter introduced by Gutmann (cf. ref. 2). The following linear regression was obtained:

$$[4] \quad \rho = 51\mathrm{DN} - 220$$

with a correlation coefficient $r = 0.992$ (Fig. 1).

The data can also be analysed in another way, by considering the influence of the solvent on $\Delta\tilde{\nu}$ values of a given compound using the following equation (3):

$$[5] \quad \Delta\tilde{\nu}\ (\text{solvent}) = K \cdot \mathrm{DN}$$

The regression coefficient K represents the sensitivity of the acidity of the NH_2 group to the solvent basicity for a *p*-substituted aniline with a fixed substituent in the series. The application of eq. [5] to the data of Table 3 leads to the results collected in Table 5. Kamlet *et al.* have very recently drawn a similar conclusion (8). However it was not expressed in a quantitative way as in eq. [5].

When $\Delta\tilde{\nu}$ values are plotted against DN values (eq. [5]) the correlations are satisfactory, except for the first two substituents $N(CH_3)_2$ and CH_3. But,

TABLE 3. Summary of $\Delta\tilde{\nu}$ (eq. [2]) for differently substituted pairs p-$XC_6H_4NH_2$ and p-$XC_6H_4N(CH_3)_2$ in 6 solvents

Solvents[a]	$\Delta\tilde{\nu}$ for X = $N(CH_3)_2$	CH_3	H	COPh	CN[b]	NO_2
Dioxane (14.8)	260	540	570	920	710	900
Butoxybutane	220	490	670	1080	940	1510
Acetonitrite (14.1)	50	500	500	690	480	920
Trimethylphosphate (23.0)	100	800	990	1540	1020	1720
Dimethylsulphoxide (29.8)	−210	—	—	1640	1140	1840
Hexamethylphosphotriamide (38.8)	−100	—	—	2490	1790	2460

[a]DN-values in parentheses (ref. 9).
[b]Due to low precision of eq. [1], see Table 1, Δv for CN are not taken into further consideration. See text and footnote 1.

in these cases, the slope is quite low, hence a low value of the correlation coefficient must be expected.

It is clear that for p-substituted anilines with electron donor substituents there is some kind of π-electron saturation (4), and hence the influence of solvent on NH_2-acidity is rather low or nil. The situation becomes different when substituents are more electron attractive. Then the π-electron system becomes more mobile and hence more sensitive to solvent influences, resulting in an increase of the K-values of eq. [5]. Thus, some relationship between K and σ should be observed. In fact, Fig. 2 shows the correlation between the regression coefficients K and the substituent constant σ. Even though the linearity is not so good as between ρ and DN, there is a clear dependence of K on σ. The point corresponding to the CN derivative should be excluded, since the standard regression line (eq. [1]) is not precise enough[1] for this case. The correlation coefficient now becomes satisfactory ($r = 0.937$) with the following regression equation

$$[6] \quad K = 49\sigma + 35$$

for 5 experimental points. The more detailed physical interpretation of slopes of eqs. [4] and [6] may be obtained as follows. Consider measurements of $\Delta\tilde{\nu}$ for substituted and unsubstituted species carried out in the same solvent. Equation [7a] holds:

$$[7a] \quad \Delta\tilde{\nu}_s - \Delta\tilde{\nu}_{un} = \rho\Delta\sigma$$

When measurements are repeated for the same compounds in another solvent one obtains:

$$[7b] \quad \Delta\tilde{\nu}_s' - \Delta\tilde{\nu}_{un}' = \rho'\Delta\sigma$$

Next consider measurements of $\Delta\tilde{\nu}$ for unsubstituted species carried out in two different solvents. Equation [8a] holds:

$$[8a] \quad \Delta\tilde{\nu}_{un} - \Delta\tilde{\nu}_{un}' = K\Delta DN$$

TABLE 4. Statistics of $\Delta\tilde{\nu}$ vs. σ plot (eq. [3])

Solvent	ρ[a]		r	n	Abbreviation
Dioxane	432	(50)	0.980	5	D
Butoxybutane	785	(116)	0.969	5	B
Acetonitrile	502	(53)	0.983	5	A
Trimethylphosphate	1025	(34)	0.998	5	TMP
Dimethylsulphoxide	1308	(89)	0.998	3	DMSO
Hexamethylphosphotriamide	1700	(287)	0.986	3	HMPT

[a]Standard deviation of the estimate in parentheses.

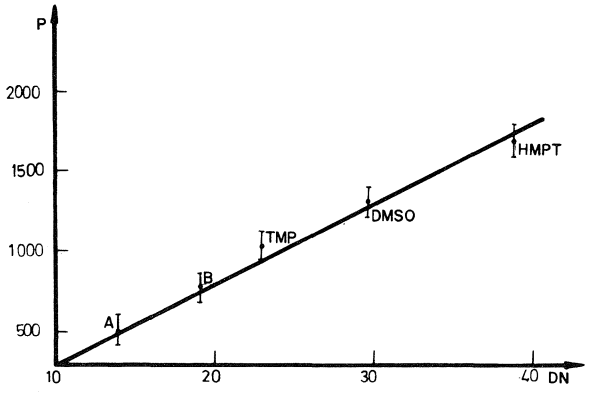

FIG. 1. Plot of ρ of eq. [3] vs. DN.

TABLE 5. Statistics of $\Delta\tilde{\nu}$ vs. DN plot (eq. [5])

Substituent	K[a]	r	n
$N(CH_3)_2$	−14 (6)	0.749	6
CH_3	27 (15)	0.786	4
H	50 (10)	0.962	4
COPh	66 (7)	0.979	6
CN	47 (7)	0.966	5
NO_2	60 (8)	0.974	5

[a]Standard deviation of the estimate in parentheses.

[1]The standard line (eq. [1]) must be estimated with a very high accuracy ($r > 0.99$); otherwise quite erroneous results can be obtained. In this case $r = 0.962$, and hence the point for CN is not taken into account. For details of the problem of the accuracy of a standard line see ref. 5.

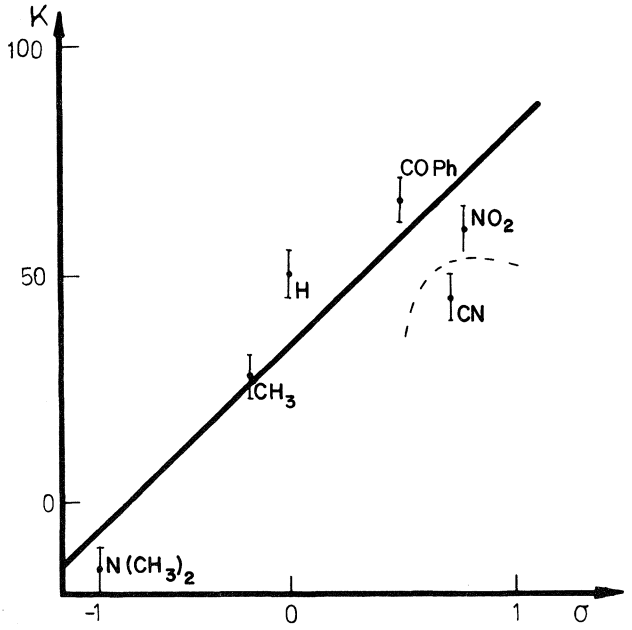

FIG. 2. Plot of K of eq. [5] vs. σ. The line is drawn excluding the point for CN.

When the analogous measurements are carried out for substituted species in the same two solvents one obtains:

[8*b*] $\Delta\tilde{\nu}_s - \Delta\tilde{\nu}_s' = K'\mathrm{DN}$

Combining eq. [7*a*] with eq. [7*b*] and eq. [8*a*] with eq. [8*b*] one obtains eqs. [9] and [10], respectively:

[9] $(\Delta\tilde{\nu}_s - \Delta\tilde{\nu}_{un}) - (\Delta\tilde{\nu}_s' - \Delta\tilde{\nu}_{un}') = \Delta\sigma(\rho - \rho')$

[10] $(\Delta\tilde{\nu}_{un} - \Delta\tilde{\nu}_{un}') - (\Delta\tilde{\nu}_s - \Delta\tilde{\nu}_s') = \Delta\mathrm{DN}(K - K')$

The left sides of eqs. [9] and [10] are set equal, leading to eq. [11].

[11] $\Delta\sigma(\rho - \rho') = \Delta\mathrm{DN}(K - K')$

Further discussion depends upon which slope is to be analysed. For the reaction constant of eq. [3] we obtain, after simple rearrangement, eq. [12]:

[12] $\rho' = \rho + (\Delta K/\Delta\sigma)\mathrm{DN}$

The numerical form of this equation is eq. [4]. The slope of eq. [4] may be interpreted to be $\mathrm{d}K/\mathrm{d}\sigma$, the magnitude describing how the sensitivity of the system to solvent effect depends on the electronegativity of the substituent. On the other hand, if the slope of eq. [6] is to be discussed, after simple rearrangement we obtain eq. [13]:

[13] $K' = K + (\Delta\rho/\Delta\mathrm{DN}) \cdot \sigma$

The numerical form of eq. [13] is eq. [6]. The slope of eq. [6] is assumed to be $\mathrm{d}\rho/\mathrm{dDN}$; the magnitude describing how the sensitivity of the system to the substituent effect depends on the solvent basicity.

Partly similar conclusions were drawn by Kalinowski (6) for the case of solvent effect on ρ for reversible polarographic reduction of substituted nitrobenzenes and azobenzenes, but the complete symmetry of the problems was not discussed there, most probably because of difficulties with liquid-junction potentials. In the case of measurements discussed in this paper no such problem exists.

It can be concluded that solvent and substituent effects on acidity of *p*-substituted anilines are mutually symmetrical; when acidity is correlated with substituent effect, the resulting regression coefficient correlates to solvent basicity.[2] On the other hand, when acidity of NH_2 is correlated with solvent basicity, the regression coefficient now correlates to substituent constant. This property depends on the commutativity of Leffler–Grunwald operators (7), δ_{subst} and δ_{solv}, acting on the measured property $\Delta\tilde{\nu}$. When analysed in columns, the data compiled in Table 2 can be written generally as $\delta_{solv}\Delta\tilde{\nu}$ whereas, when analysed in rows, they can be written as $\delta_{subst}\Delta\tilde{\nu}$. Thus if an element of Table 2 is considered, it can be written as $\delta_{subst}\delta_{solv}\Delta\tilde{\nu}$ or $\delta_{solv}\,\delta_{subst}\Delta\tilde{\nu}$, independent of how it is viewed (row or column).

Finally it seems likely that the symmetrical form of the mutual relation between substituent and solvent effects is quite common even though it has not been systematically investigated. However, due to the complexity of solute–solvent interactions for molecules with different substituents, the above mentioned phenomenon is not often met in a clear form particularly for a longer series of experimental data.

1. M. J. KAMLET and R. W. TAFT. J. Am. Chem. Soc. **98**, 377 (1976).
2. V. GUTMANN. Chem. Br. **7**, 102 (1971).
3. T. M. KRYGOWSKI. J. Electroanal. Chem. **35**, 436 (1972).
4. A. J. HOEFNAGEL, M. A. HOEFNAGEL, and B. M. WEPSTER. J. Am. Chem. Soc. **98**, 6164 (1976).
5. T. M. KRYGOWSKI, E. MIELCZAREK, and P. K. WRONA. In preparation.
6. M. K. KALINOWSKI and B. OSIECKA. Rocz. Chem. **50**, 299 (1976).
7. J. E. LEFFLER and E. GRUNWALD. Rates and equilibria of organic reactions. J. Wiley, New York and London. 1963.
8. M. J. KAMLET, M. E. JONES, R. W. TAFT, and J. L. ABBOUD. J. Chem. Soc. Perkin Trans. II, 342 (1979).
9. V. GUTMANN. The donor–acceptor approach to molecular interactions. Plenum Press, New York and London. 1978.

[2]NOTE ADDED IN PROOF: Such mutual relationships are known as iso-parametric relationships (V. A. Palm, private communication to T.M.K. and lecture at the Euchem Conference on Correlation Analysis in Chemistry. Assisi, Italy. Sept. 10–14, 1979).

^{13}C nuclear magnetic resonance spectra of some halosteroids, 6-ketosteroids, and related compounds

HERBERT L. HOLLAND AND EVERTON M. THOMAS

Department of Chemistry, Brock University, St. Catharines, Ont., Canada L2S 3A1

Received June 14, 1979

HERBERT L. HOLLAND and EVERTON M. THOMAS. Can. J. Chem. **57**, 3069 (1979).

The ^{13}Cmr spectra of 21-haloprogesterones have been assigned, and chemical shifts compared with those of simple α-haloketones. In addition, the ^{13}Cmr spectra of some C-5α and C-6β halosteroids are presented, and long range $^{13}C—^{19}F$ coupling observed between C-19 and the C-6β fluorine in some cases. The spectra of several oxygenated analogues and of a series of 5α-hydroxy-6-ketosteroids are also discussed.

HERBERT L. HOLLAND et EVERTON M. THOMAS. Can. J. Chem. **57**, 3069 (1979).

On a identifié les spectres rmn du ^{13}C des haloprogestérones-21 et on a comparé leurs déplacements chimiques à ceux des α halocétones simples. On présente de plus les spectres rmn du ^{13}C de quelques stéroïdes halogénés en position 5α et 6β, ainsi que les couplages à longue distance $^{13}C—^{19}F$ observés dans certains cas entre le carbone en position C-19 et le fluor en C-6β. On discute également des spectres de plusieurs analogues oxygénés des hydroxy-5α céto-6 stéroïdes.

[Traduit par le journal]

In spite of the widespread use of halosteroids in medicine, there have been few systematic studies of their ^{13}Cmr spectra. In this paper, we report the ^{13}Cmr spectra of some C-5, -6, and -21 fluoro-, chloro-, and bromosteroids. In addition, the spectra of several oxygenated analogues and of a series of 5α-hydroxy-6-ketosteroids are discussed.

Assignments for the 21-haloprogesterones **1***a–c*, together with those of the parent steroid **1***d* (1), are presented in Table 1. Shifts at carbons 17, 20, and 21 are consistent with those of the corresponding carbons of the halo acetones (**7**) and α-halo acetophenones (**8**). The α, β, and γ halogen substituent effects for these compounds and the steroids **1** are listed in Table 1. The magnitudes of these effects are different from those derived for the corresponding alkanes (2), being closer to those reported for α-halocyclohexanones (3). For the latter, interaction between halogen non-bonded orbitals and the π* orbitals of the carbonyl, increasing electron density adjacent to halogen, has been used to explain the observed shifts (3). A similar effect is presumably operating in the simple α-haloketones reported here, and is increased with respect to that in the α-halocyclohexanones by the absence of rigid stereochemistry, allowing maximal orbital overlap to be achieved.

The assignments for a series of C-5α halo and hydroxy substituted androstanes **3** and **4** are listed in Table 2. Carbons of rings C and D of this series are readily assignable by comparison with the spectra of other 17-keto and 17β-hydroxyandrostanes (1). Carbons in rings A and B of the 5α,6β-dichloro

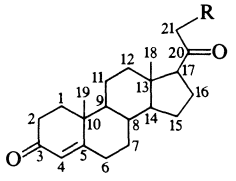

1

a R = F
b R = Cl
c R = Br
d R = H

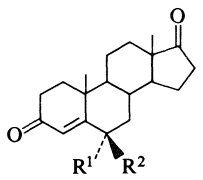

2

a R^1 = H, R^2 = F
b R^1 = H, R^2 = Cl
c R^1 = F, R^2 = H
d R^1 = Cl, R^2 = H
e $R^1 + R^2$ = O

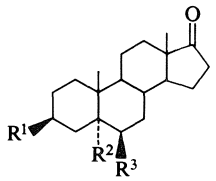

3

a R^1 = OH, R^2 = R^3 = Cl
b R^1 = OAc, R^2 = R^3 = Cl
c R^1 = R^3 = OAc, R^2 = Br
d R^1 = R^2 = OH, R^3 = F
e R^1 = OAc, R^2 = R^3 = OH
f R^1 = OH, R^2 = Cl, R^3 = H

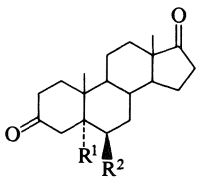

4

a R^1 = OH, R^2 = F
b R^1 = OH, R^2 = H

compounds **3***a* and **3***b* were assigned by comparison with the shifts reported for 5α-hydroxy-6β-chlorocholestanes (4), and are internally consistent with respect to acetylation at C-3. They may also be derived from **3***f* by application of the shift parameters for chlorine at C-6β derived for analogous cholestane derivatives (4).

0008-4042/79/233069-04$01.00/0

TABLE 1. ^{13}C chemical shifts of α-haloketones **1**, **7**, and **8**

	δ (ppm) (Δδ (ppm)) (*J* (Hz))									
Carbon[a]	**1***d*(1)	**1***a*	**1***b*	**1***c*	**7***a*(2)	**7***b*	**7***c*	**7***d*	**8***a*(2)	**8***b*	**8***c*
21(1)[b]	31.3	85.5(54.2)(187.2)	49.4(18.1)	35.7(4.4)	30.2	85.3(55.1)(183.6)	49.2(19.0)	36.0(5.8)	26.4	46.3(19.9)	31.2(4.8)
20(2)	208.3	206.7(−1.6)(17.5)	202.1(−5.2)	201.9(−6.4)	205.1	204.7(−0.4)(18.3)	200.3(−4.8)	200.4(−4.7)	197.4	191.2(−6.2)	191.2(−4.8)
17(3)	63.3	57.8(−5.5)(1.8)	59.9(−3.4)	60.2(−3.1)	30.2	25.4(−4.8)(0)	27.1(−3.1)	27.7(−2.5)	137.4	134.3(−3.1)	133.9(−3.5)
13	43.7	44.9	44.7	44.8							
16	22.8	22.6	23.6	23.8							
18	13.2	13.7	13.6	13.6							

[a]Carbons 1–12, 14, 15, and 19 of **1***a–c* exhibited chemical shifts virtually identical (±0.3 ppm) with those of **1***d* (1).
[b]Numbers in parentheses refer to compounds **7** and the corresponding carbons of compounds **8**.

TABLE 2. ^{13}C chemical shifts of C-5α halo and hydroxyandrostanes **3**, **4**, and **6**[a]

	δ (ppm)						
Carbon	**3***a*	**3***b*	**3***f*	**3***c*	**3***e*	**6**	**4***b*
1	34.6	34.3	31.8*	34.8	32.1	30.9*	32.7
2	30.2	26.2	30.4	26.3	26.7	30.9*	37.9
3	67.7	70.6	67.2	71.4	71.1	67.4	210.5
4	42.9	39.2	45.2	38.0	37.1	44.0	52.0
5	85.1	84.2	84.9	83.0	75.7	75.4	77.4
6	63.3	63.2	36.1	75.3	76.0	34.4	34.3
7	34.6	34.5	25.3	30.7*	33.5	25.6	25.1
8	30.1	30.1	34.3	30.6*	31.6	34.8	34.5
9	46.3	46.1	46.6	47.5	45.5	46.1	45.9
10	41.0	41.0	40.8	40.7	38.6	39.0	39.4
11	20.5	20.5	20.8	20.6	20.4	21.0	20.7
12	31.4	31.4	31.5*	31.3	30.0	36.9	31.6
13	47.8	47.8	47.8	47.8	47.9	43.2	47.8
14	50.5	50.4	51.0	50.8	51.0	50.8	51.1
15	21.7	21.7	21.7	21.7	21.8*	23.3	21.8
16	35.8	35.7	35.8	35.8	35.8	30.6*	35.8
17	220.5	220.1	220.8	220.2	221.1	81.9	220.8
18	13.9	13.9	13.9	14.0	13.9	11.2	13.8
19	19.7	19.5	16.2	17.2	16.5	16.2	15.7
Other		21.3		21.2(2)	21.5*		
		170.4		169.5			
				170.2			

[a]Chemical shifts marked with an asterisk may be interchanged.

The assignment of the rings A and B resonances of **3***c* was again achieved by comparison with the spectra of C-5α and C-6β substituted cholestanes (4). The rings A and B resonances of **3***e*, **6**, and **4***b* were all readily assignable by comparison with the assignments of similarly substituted cholestane derivatives (1). The anticipated upfield γ shift at C-1 caused by the C-5α OH (1, 4) (as in **3***e*, **4***b*, and **6**) is also clearly present with a C-5α chloro substituent (as in **3***f*); it is mitigated in **3***a–c* by the downfield δ shift of the electronegative substituent at C-6β (4).

Chemical shift assignments for the 6-fluorosteroids **3***d*, **4***a*, and **2** (5), and for the 6-chloroan-

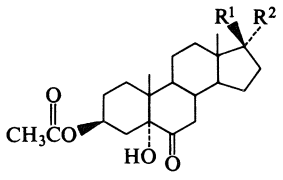

5

a $R^1 + R^2 = O$
b $R^1 = OAc, R^2 = H$
c $R^1 = Ac, R^2 = H$

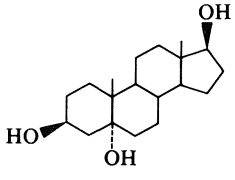

6

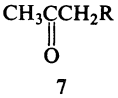

7

a R = H
b R = F
c R = Cl
d R = Br

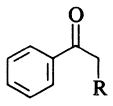

8

a R = H
b R = Cl
c R = Br

TABLE 3. ^{13}C chemical shifts of 6-fluorosteroids **3***d*, **4***a*, **2***a*, and **2***c*, and of 6-chlorosteroids **2***b* and **2***d*

	δ (ppm)					
Carbon	**3***d*[a]	**4***a*	**2***a*	**2***c*	**2***b*	**2***d*
1	30.8	33.4	37.0	36.3	37.7	36.3
2	31.3	37.9	34.2	33.7	34.1	33.7
3	65.0	211.6	199.6	198.4	199.5	198.7
4	39.8	48.9	128.8	120.0	127.8	124.0
5	72.5	76.3	161.2	165.3	164.1	165.0
6	95.1	94.8	93.1	88.0	60.9	58.5
7	30.4	30.8	36.2	37.2	39.1	42.4
8	29.8	30.1	29.8	33.1	29.8	35.7
9	44.2	45.3	53.4	53.7	53.3	53.4
10	37.7	38.9	38.0	39.2	38.3	40.5
11	19.8	20.5	20.3	20.2	20.3	20.4
12	31.3	31.5	31.3	31.1	31.3	31.2
13	47.2	47.8	47.7	47.5	47.7	47.6
14	50.2	50.9	50.9	50.5	50.5	50.5
15	21.2	21.7	21.7	21.7	21.7	21.7
16	35.2	35.8	35.7	35.6	35.7	35.7
17	219.5	220.7	219.8	219.5	219.8	219.5
18	13.4	13.8	13.8	13.7	13.8	13.8
19	15.4	15.5	18.5	18.1	21.1	18.3

[a]Solvent DMSO-d_6.

drostenediones, are presented in Table 3. Assignments of the resonances of **3***d* and **4***a* were made by application of the appropriate C-6β substituent shift parameters (4) to the spectra of **4***b* and **6** (rings A and B only), respectively. The Δ^4-3-ketones **2** were assigned with reference to the spectrum of androst-4-ene-3,17-dione (1, 6). The ^{13}C—^{19}F coupling constants of the fluorosteroids are in Table 4, along with the shift parameters for the 6-halo substituent of **3***d*, **4***a*, and the series **2**. The values of $J(^{13}C—^{19}F)$ for coupling to C-5, -6, -7, and -10 of **3***d* and **4***a* are as expected (4). The couplings to C-4 in **2***a* and **2***c* are due to the presence of the Δ^4-3-keto system; long range $^1H—^1H$ coupling of the C-4 and C-6β hydrogens in Δ^4-3-ketosteroids is well known (7, 8). The coupling to C-8 of **2***c* reflects the presence of an F—C-8 dihedral angle of 180° in this compound.

The striking feature of the spectra of **3***d* and **4***a* is the presence of a significant δ coupling to C-19. The magnitude of this coupling suggests the presence of a through space contribution, an interpretation strengthened by the corresponding value of $^4J \simeq$ zero observed for **2***a* and **2***c*. The internuclear C-19—F distance, estimated from Dreiding models of **3***d* and **4***a* is 2.5 Å; the corresponding distance in **2***a* is 3.0 Å. The former distance is well within the limit established for $^1H—^{19}F$ through space interactions, whereas the latter is close to the limiting value over which such interactions occur (9). A $^4J(^{13}C—^{19}F)$ value of 10 Hz for a 6β-fluorosteroid has been reported, but without comment (4). Long range $^1H—^{19}F$ coupling of the C-19 methyl hydrogens to the C-6 fluorine was observed in **3***d* (J = 4.4 Hz), **4***a* (J = 3.6 Hz), and **2***a* (J = 2.2 Hz) (see ref. 10).

The shift parameters for C-6α and C-6β fluoro and chloro substituents in **2** (Table 4) are indicative of the stereochemistry of substitution at C-6. The axial substituents (as in **2***a* and **2***b*) interact electronically with the π system (7, 8, 11, and references therein), reflected in anomalous shifts, particularly at C-4. Axial (β) substitution also produces the characteristic downfield shifts at C-1 and the upfield shifts at C-8 (4).

Chemical shifts for the last series of compounds to be examined herein, the 6-ketones, are presented in Table 5. The resonances of the Δ^4-3,6,17-trione **2***e* were assigned by application of the shift parameters for a 6-keto function (1) to the spectrum of androst-4-ene-3,17-dione (1, 6), and those of rings A and B of the series **5** by applying the shift parameters for a C-5α OH to the spectrum of 3β-acetyloxy-5α-cholestan-6-one (1). Significant deviation of observed (13.9 ppm) from calculated (16.9 ppm) values occurred only in the case of C-19. The downfield shift (+3.9 ppm) at C-19 normally attributed to the C-5α OH has been fully discussed (12). From our data it is apparent that this shift is absent or severely

TABLE 4. Shift parameters for the 6-halosteroids **3***d*, **4***a*, and **2***a–d*, and $^{13}C—^{19}F$ coupling constants for the 6-fluorosteroids

	Δδ (ppm) (J (Hz))					
Carbon	**3***d*	**4***a*	**2***a*	**2***c*	**2***b*	**2***d*
1	−0.1	+0.7	+1.5	+0.8	+2.2	+0.8
2	−0.4	0	+0.5	0	+0.4	0
3	−2.4	+1.1	+0.7	−0.5	+0.6	−0.2
4	−4.2	−3.1	+4.9 (9)	−3.9 (14.5)	+3.9	+0.1
5	−2.9 (19.3)	−1.1 (23)	−8.9 (12)	−4.8 (11)	−6.0	−5.1
6	+60.7 (178)	+60.5 (179)	+60.8 (167)	+55.7 (185.5)	+28.6	+26.2
7	+4.8 (20.2)	+5.7 (21)	+5.1 (23)	+6.1 (18.3)	+8.0	+11.3
8	−5.0	−4.4	−5.1	−1.8 (11)	−5.1	+0.8
9	−1.9	−0.6	−0.2	+0.1	−0.3	−0.2
10	−1.3 (1.8)	−0.5 (1.8)	−0.4 (2.0)	+0.8 (2.7)	−0.1	+2.1
19	−0.8 (9.2)	−0.2 (9.2)	+1.3[a]	+0.9 (0)	+3.9	+1.1

[a]Some broadening of the C-19 resonance was evident.

TABLE 5. ^{13}C chemical shifts for the 6-ketosteroids **2***e* and **5**[a]

Carbon	δ (ppm)			
	2*e*	**5***a*	**5***b*	**5***c*
1	35.6	29.6	29.6	29.6
2	33.8**	26.3	26.3	26.3
3	199.1	70.8	70.9	70.1
4	126.0	32.2	32.2	32.4
5	160.2	80.1	80.1	80.2
6	201.2	212.0	212.4	212.0
7	45.5	40.5	41.2	41.5
8	33.9**	36.8	37.0	37.2
9	51.6*	44.4	44.2	44.2
10	39.7	42.5	42.5	42.4
11	20.3	20.6	20.9	21.4
12	31.0	31.3	36.6	38.7
13	47.6	48.3	43.2	44.6
14	51.0*	51.3	50.7	56.4
15	21.6	21.6*	23.2	24.1
16	35.6	35.7	27.4	22.8
17	219.2	220.3	82.5	63.5
18	13.7	13.8	12.0	13.4
19	17.7	13.8	13.9	13.9
20				209.3
21				31.4
Other		21.4*		21.4
		171.4		171.1

[a]Chemical shifts marked with asterisks may be interchanged.

mitigated in the presence of a 6-keto function, an observation which supports the electronic origin proposed (12) for the γ antiperiplanar effect.

Experimental

Spectra were recorded and assigned as previously described (13). The following compounds were prepared by published procedures and gave satisfactory physical and analytical data: 21-fluoropregn-4-ene-3,20-dione (**1***a*) (14), 21-chloropregn-4-ene-3,20-dione (**1***b*) (15), 21-bromopregn-4-ene-3,20-dione (**1***c*) (16), 6β-fluoroandrost-4-ene-3,17-dione (**2***a*) (17), 6β-chloroandrost-4-ene-3,17-dione (**2***b*) (18), 6α-fluoroandrost-4-ene-3,17-dione (**2***c*) (17), 6α-chloroandrost-4-ene-3,17-dione (**2***d*) (18), androst-4-ene-3,6,17-trione (**2***e*) (11, 19), 5,6β-dichloro-5α-androstan-3β-ol-17-one (**3***a*) (15), 5,6β-dichloro-5α-androstan-3β-ol-17-one 3-acetate (**3***b*) (15), 5-bromo-5α-androstan-3β,6β-diol-17-one diacetate (**3***c*) (11), 6β-fluoro-5α-androstan-3β,5-diol-17-one (**3***d*) (17), 5α-androstan-3β,5,6β-triol-17-one 3-acetate (**3***e*) (19), 5-chloro-5α-androstan-3β-ol-17-one (**3***f*) (20), 6β-fluoro-5α-androstan-5-ol-3,17-dione (**4***a*) (17), 5-hydroxy-5α-androstan-3,17-dione (**4***b*) (11), 5α-androstan-3β,5-diol-6,17-dione 3-acetate (**5***a*) (21), 5α-androstan-3β,5,17β-triol-6-one 3,17-diacetate (**5***b*) (21), 5α-pregnan-3β,5-diol-6,20-dione 3-acetate (**5***c*) (21), and 5α-androstan-3β,5,17β-triol (**6**) (11). Other compounds used in this study were commercial samples.

Acknowledgements

We thank the Natural Sciences and Engineering Research Council of Canada for financial support, and T. Jones and E. Kelusky for their help in recording the spectra.

1. J. W. BLUNT and J. B. STOTHERS. Org. Magn. Reson. **9**, 439 (1977).
2. J. B. STOTHERS. Carbon-13 NMR spectroscopy. Academic Press, New York, NY. 1972.
3. R. JANTZEN, M. TORDEUX, G. DE VILLARDI, and C. CHACHATY. Org. Magn. Reson. **8**, 183 (1976).
4. J. W. BLUNT. Aust. J. Chem. **28**, 1017 (1975).
5. H. L. HOLLAND. Tetrahedron Lett. 881 (1978).
6. J. R. HANSON and M. SIVERNS. J. Chem. Soc. Perkin Trans. I, 1956 (1975).
7. S. K. MALHOTRA and H. J. RINGOLD. J. Am. Chem. Soc. **87**, 3228 (1965).
8. T. A. WITTSTRUCK, S. K. MALHOTRA, and H. J. RINGOLD. J. Am. Chem. Soc. **85**, 1699 (1963).
9. P. C. MYHRE, J. W. EDMONDS, and J. D. KRUGER. J. Am. Chem. Soc. **88**, 2459 (1966).
10. A. D. CROSS and P. W. LANDIS. J. Am. Chem. Soc. **84**, 1736 (1962).
11. H. L. HOLLAND and P. R. P. DIAKOW. Can. J. Chem. **56**, 694 (1978).
12. W. A. AYER, L. M. BROWNE, S. FUNG, and J. B. STOTHERS. Can. J. Chem. **54**, 3272 (1976).
13. H. L. HOLLAND, P. R. P. DIAKOW, and G. J. TAYLOR. Can. J. Chem. **56**, 3121 (1978).
14. J. E. HERZ, J. FRIED, P. GRABOWICH, and E. F. SABO. J. Am. Chem. Soc. **78**, 4812 (1956).
15. F. L. M. PATTISON and J. E. MILLINGTON. Can. J. Chem. **34**, 757 (1956).
16. N. L. WENDLER, R. P. GRABER, and G. G. HAZEN. Tetrahedron, **3**, 144 (1958).
17. A. BOWERS and H. J. RINGOLD. Tetrahedron, **3**, 14 (1958).
18. J. MORI and J. YAMADA. Chem. Pharm. Bull. **11**, 1418 (1961).
19. H. L. HOLLAND and P. R. P. DIAKOW. Can. J. Chem. **57**, 436 (1979).
20. E. HERSCHBERG, M. RUBIN, and E. SCHWENK. J. Org. Chem. **15**, 292 (1950).
21. L. KNOF. Ann. Chem. **657**, 171 (1962).

Artificial carbohydrate antigens: the synthesis of the tetrasaccharide repeating unit of *Shigella flexneri* O antigen[1]

STAFFAN JOSEPHSON[2] AND DAVID R. BUNDLE

Division of Biological Sciences, National Research Council of Canada, Ottawa, Ont., Canada K1A 0R6

Received June 5, 1979

STAFFAN JOSEPHSON and DAVID R. BUNDLE. Can. J. Chem. **57**, 3073 (1979).

The synthesis of a tetrasaccharide glycoside, 8-methoxycarbonyloctyl *O*-2-acetamido-2-deoxy-β-D-glucopyranosyl-(1→2)-*O*-α-L-rhamnopyranosyl-(1→2)-*O*-α-L-rhamnopyranosyl-(1→3)-α-L-rhamnopyranoside, representing the repeating unit of the *Shigella flexneri* serogroup Y O antigen is reported, together with that of a component trisaccharide. Both oligosaccharide glycosides are functionalised to permit covalent attachment to immunogenic carriers and solid matrices. A key intermediate used to establish α-1,2-rhamnopyranoside linkages was 2-*O*-acetyl-3,4-di-*O*-benzyl-α-L-rhamnopyranosyl chloride (**1**), which was obtained in quantitative yield from 3,4-di-*O*-benzyl-1,2-*O*-(methoxyethylidene)-β-L-rhamnopyranose. Thus 8-methoxycarbonyloctyl 3,4-di-*O*-benzyl-α-L-rhamnopyranoside (**2**) prepared from the rhamnopyranosyl chloride **1** was used in a second Koenigs–Knorr reaction to provide an α-1,2-linked disaccharide. The disaccharide is in turn glycosylated at the C-2′ position with tri-*O*-acetyl-2-deoxy-2-phthalimido-D-glucopyranosyl bromide to provide the trisaccharide glycoside, 8-methoxycarbonyloctyl *O*-2-acetamido-2-deoxy-β-D-glucopyranosyl-(1→2)-*O*-α-L-rhamnopyranosyl-(1→2)-α-L-rhamnopyranoside. Application of the same reaction sequence to a rhamnopyranoside selectively blocked with benzoate esters at C-2 and C-4 gave the *S. flexneri* tetrasaccharide repeating unit. The success of this strategy was dependent upon the ability to use selective transesterification conditions, which permit removal of O acetate groups whilst leaving benzoate esters intact.

STAFFAN JOSEPHSON et DAVID R. BUNDLE. Can. J. Chem. **57**, 3073 (1979).

On décrit la synthèse du glycoside tétrasaccharide méthoxycarbonyloctyl-8 *O*-acétamido-2 déoxy-2 β-D-glucopyrannosyl-(1→2)-*O*-α-L-rhamnopyrannosyl-(1→2) *O*-α-L-rhamnopyrannosyl-(1→3)-α-L-rhamnopyrannoside représentant le monomère de l'antigène O du sérogroupe Y du *Shigella flexneri*; on rapporte aussi la synthèse d'un trisaccharide. Les deux glycosides oligosaccharides sont fonctionnalisés dans le but de les unir par une liaison covalente à des supports immunogènes et à des supports solides. L'intermédiaire clé utilisé pour établir les liaisons α-rhamnopyrannosides-1,2 est le chlorure de *O*-acétyl-2 di-*O*-benzyl-3,4 α-L-rhamnopyrannosyle (**1**) qui est obtenu quantitativement à partir du di-*O*-benzyl-3,4 *O*-(méthoxyéthylidène)-1,2 β-L-rhamnopyrannose. Ainsi le méthoxycarbonyloctyl-8 di-*O*-benzyl-3,4 α-L-rhamnopyrannoside (**2**), préparé à partir du chlorure de rhamnopyrannosyle **1**, est utilisé dans une seconde réaction de Koenigs–Knorr pour obtenir la liaison α-disaccharide-1,2. Le disaccharide est, à son tour, glycosilé en position C-2′ avec le bromure de tri-*O*-acétyl déoxy-2-phtalimido-2 D-glycopyrannosyle pour conduire au glycoside trisaccharide, méthoxycarbonyl-octyl-8 *O*-acétamido-2 déoxy-2 β-D-glucopyrannosyl(1→2)*O*-α-L-rhamnopyrannosyl-(1→2)-α-L-rhamnopyrannoside. L'utilisation de cette même suite de réactions sur un rhamnopyrannoside bloqué sélectivement en positions C-2 et C-4 avec des esters benzoïques donne le monomère du *S. flexneri* tétrasaccharide. Le succès de cette stratégie dépend de la capacité d'utiliser des conditions sélectives de transestérification qui permettent d'enlever le groupe O acétate sans toucher au groupe benzoate.

[Traduit par le journal]

Introduction

The skeletal structure of the *Shigella flexneri* serogroup Y O antigen is a tetrasaccharide of the following structure:

$$\text{-}[\text{-}3)\text{-}\beta\text{-D-GlcNAc}p\text{-}(1\rightarrow2)\text{-}\alpha\text{-L-Rham}p\text{-}(1\rightarrow2)\text{-}\alpha\text{-L-Rham}p\text{-}(1\rightarrow3)\text{-}\alpha\text{-L-Rham}p\text{-}(1\text{-}]_n$$

(1). Much is known about the general serological features of O antigens, particularly with respect to the genus *Salmonella* (2, 3). One of the important features of O antigens is that the "chemical repeating unit" (that isolated by chemical degradation of the intact O chain) does not necessarily coincide with the biological repeating unit (that intact unit which is built up and transferred to the C_{55}-isoprenoid carrier during biosynthesis) (2, 4). Since the biological repeating unit will be important in serological reactions which involve the most distal regions of the O chains (2) such information is relevant to synthesis

[1]NRCC No. 17716.

[2]NRCC Research Associate, 1977–1979.

0008-4042/79/233073-07$01.00/0

of artificial antigens. The biological repeating unit of *S. flexneri* O chains is not known and we have, therefore, synthesised two of the four possible repeating units of the serogroup Y LPS. Our original interest in *S. flexneri* antigens (5) stemmed from a desire to investigate via artificial antigens the possible existence of so-called "conformational determinants" (3). In order to provide a comprehensive range of haptens for such studies and also to raise antibodies (via artificial antigens) of differing specificities we have synthesised several di-, tri-, and tetra-saccharide haptens (5–8). These structures coupled to solid supports provide immunoabsorbents with which to fractionate immune-sera raised against whole-cell vaccines. In this way the various determinants of *S. flexneri* O antigens may be systematically studied. This paper describes the synthesis both of a tetrasaccharide glycoside, 8-methoxycarbonyloctyl *O*-2-acetamido-2-deoxy-β-D-glucopyranosyl-(1→2)-*O*-α-L-rhamnopyranosyl-(1→2)-*O*-α-L-rhamnopyranosyl-(1→3)-α-L-rhamnopyranoside, which represents the repeating unit of the serogroup Y O antigen, and a component trisaccharide hapten, 8-methoxycarbonyloctyl *O*-2-acetamido-2-deoxy-β-D-glucopyranosyl-(1→2)-*O*-α-L-rhamnopyranosyl-(1→2)-α-L-rhamnopyranoside.

Results and Discussion

In order to establish successive 1,2-linkages use was made of a method developed by Garegg and coworkers (9) and elegantly exploited by Lemieux in a synthetic scheme leading to the type 1 blood group H and Lewis-b determinants (10). This method involves the benzylation of 1,2-orthoesters to provide hexopyranose derivatives with "persistent" blocking groups at all positions except C-1 and C-2. In an earlier synthesis of the rhamnose disaccharide glycoside, 8-methoxycarbonyloctyl 2-*O*-(α-L-rhamnopyranosyl)-α-L-rhamnopyranoside, the essential intermediate, a 3,4-di-*O*-benzyl rhamnopyranoside (**2**) was synthesized via a typical orthoester glycoside synthesis (5). The work reported here uses the same 1,2-orthoester, 3,4-di-*O*-benzyl-1,2-*O*-(methoxyethylidene)-β-L-rhamnopyranose, but we have found it more advantageous to convert this compound to 2-*O*-acetyl-3,4-di-*O*-benzyl-α-L-rhamnopyranosyl chloride (**1**) (7). This was achieved in essentially quantitative yield by reaction of the 1,2-orthoester with trimethylchlorosilane at reflux in dichloromethane for 2 h (11). The glycoside **2** was obtained from **1** in 75% yield by a silver trifluoromethanesulphonate (triflate) promoted Koenigs–Knorr reaction. This contrasts with the orthoester method which gives **2** in 63% yield from the 1,2-orthoester (5). We have also shown that 2-*O*-acetyl-3,4-di-*O*-benzyl-α-L-rhamnopyranosyl chloride (**1**) is an excellent building unit for construction of 1,2-linkages (7, 8). In addition this partially benzylated rhamnopyranosyl chloride is a more effective glycosylating intermediate than either the tri-*O*-acetyl-α-L-rhamnopyranosyl chloride or bromide (8). Thus glycosylation of glycoside **2** with **1** in a silver triflate promoted Koenigs–Knorr reaction (12) gave **3** in 71% yield. Following transesterification of **3**, the selectively blocked disaccharide **4** was reacted with tri-*O*-acetyl-2-deoxy-2-phthalimido-D-glucopyranosyl bromide (13) in the presence of silver triflate and 2,4,6-trimethylpyridine (collidine) to provide the blocked trisaccharide **5** in 70% yield. Removal of the blocking groups was performed in two steps. Transesterification, followed by conversion of the amino-sugar residue to the acetamido derivative, gave the partially benzylated trisaccharide **6**, which was then hydrogenated over palladium to give the de-blocked trisaccharide hapten **7**.

Synthesis of the tetrasaccharide repeating unit of *S. flexneri* lipopolysaccharide was begun with an 8-methoxycarbonyloctyl α-L-rhamnopyranoside selectively blocked at positions C-2 and C-4 (7). The preservation of the ester function of 8-methoxycarbonyloctyl glycosides (which is ultimately used to establish covalent linkage to protein or a solid matrix) is a limiting factor when selecting suitable "temporary" and "persistent" blocking groups for sequential chain extension. In addition the "persistent" blocking groups must be sufficiently stable to withstand the partial de-blocking conditions used to reveal the single hydroxyl group, which is the site of the next glycosylation reaction. Previously (7) we used 8-methoxycarbonyloctyl 2,4-di-*O*-benzoyl-α-L-rhamnopyranoside as the starting point for synthesis of a rhamnose trisaccharide glycoside containing a 1,3-linkage. This derivative was used again here since it was shown that the benzoate esters were sufficiently stable to withstand transesterification (by magnesium methoxide in methanol), conditions which remove 2-acetates from contiguous pyranose rings. Thus sequential Koenigs–Knorr reactions using silver triflate, *N*,*N*-tetramethylurea (12), and the selectively blocked rhamnopyranosyl chloride **1** provide first the disaccharide **10**, and following transesterification to yield **11**, the second chain extension step gives the trisaccharide **12**. Removal of the 2″-acetate from the trisaccharide by treatment with magnesium methoxide gave **13** which was reacted with tri-*O*-acetyl-2-deoxy-2-phthalimido-D-glucopyranosyl bromide (13) in the presence of silver triflate and collidine. The fully blocked tetrasaccharide **14** was obtained chromatographically pure in 85% yield. The de-blocking sequence was similar to

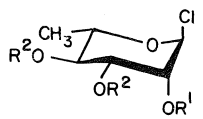

1 R^1 = Ac, R^2 = Bn

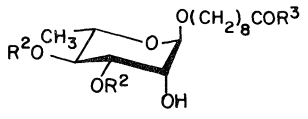

2 R^2 = Bn, R^3 = OCH_3

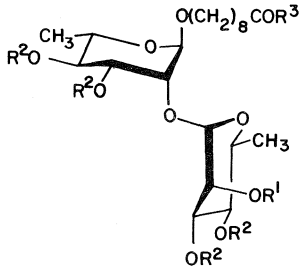

3 R^1 = Ac, R^2 = Bn, R^3 = OCH_3
4 R^1 = H, R^2 = Bn, R^3 = OCH_3

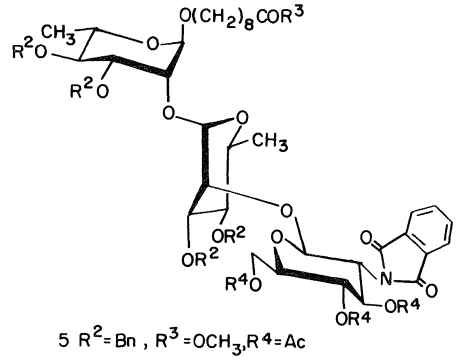

5 R^2 = Bn, R^3 = OCH_3, R^4 = Ac

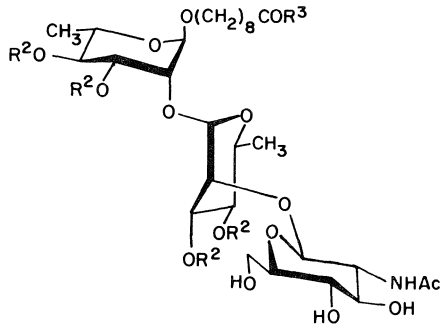

6 R^2 = Bn, R^3 = OCH_3
7 R^2 = H, R^3 = OCH_3
8 R^2 = H, R^3 = $NHNH_2$

Bn = CH_2Ph

that used for trisaccharide **5** with the exception that following hydrogenolysis of the benzyl ethers, a second transesterification step was necessary to completely de-benzoylate the tetrasaccharide. The yield of analytically and chromatographically pure tetrasaccharide **15** from **14** was 67%. Both haptens, the trisaccharide **7** and tetrasaccharide **15**, were converted to the corresponding acyl hydrazide derivatives **8** and **16**, in which form they are used to prepare artificial antigens and immunoabsorbents according to standard procedures (14, 15).

The anomeric purity of both the tri- and tetrasaccharide glycosides and their blocked precursors was confirmed by ^{13}C and ^{1}H nmr. Consideration of the glycosyl halides (13, 16) and reaction conditions (12, 13, 16) employed to synthesize **7** and **15** lead to an expectation of high anomeric purity. This is indeed the case and ^{13}C nmr data for compounds **3–16** require that the compounds possess the desired anomeric configuration and have the structures indicated. In addition single bond $^{1}J_{^{13}C_1,^{1}H_1}$ coupling constants for all four glycosidic linkages of compound **15** confirm the anomeric configurations. This conclusion derives from the observation (17) that aldopyranoses with H-1 in equatorial orientation have ^{1}J values $\simeq$ 170 Hz whilst those that are axial have $^{1}J \simeq$ 160 Hz. The observed coupling constants for compound **15** are consistent with the desired structure.

Proton nmr spectra for the trisaccharide glycoside **7** show three distinct anomeric protons whilst the same trisaccharide attached α-1,3 to another α-L-

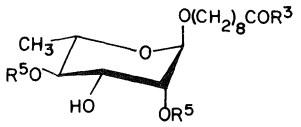

9 R^3=OCH_3, R^5=Bz

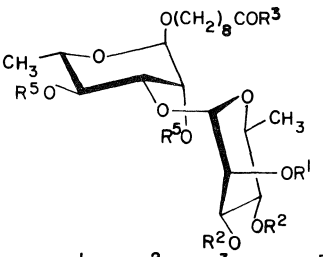

10 R^1=Ac, R^2=Bn, R^3=OCH_3, R^5=Bz
11 R^1=H, R^2=Bn, R^3=OCH_3, R^5=Bz

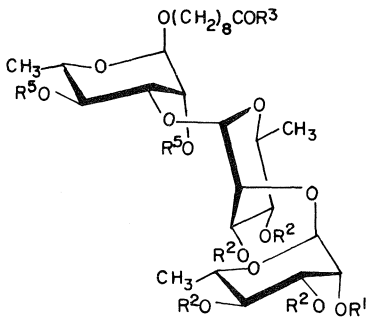

12 R^1=Ac, R^2=Bn, R^3=OCH_3, R^5=Bz
13 R^1=H, R^2=Bn, R^3=OCH_3, R^5=Bz

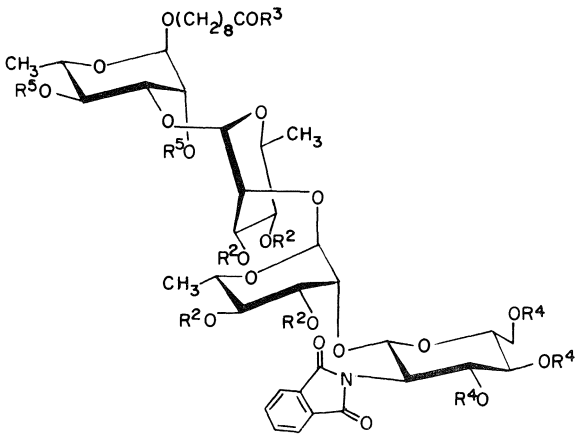

14 R^2=Bn, R^3=OCH_3, R^4=OAc, R^5=Bz

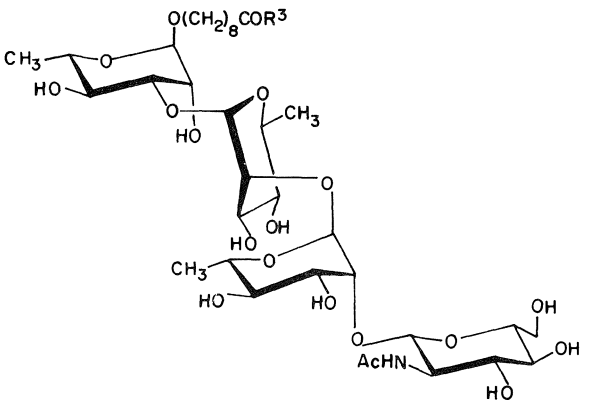

15 R^3=OCH_3
16 R^3=$NHNH_2$

rhamnopyranoside, as in compound **15**, shows two sets of overlapping anomeric signals. One α-linked rhamnopyranoside H-1 resonance is coincident with that due to H-1 of the 2-acetamido-2-deoxy-β-D-glucopyranoside residue. This observation is reminiscent of the ^{1}H nmr spectrum of the serogroup Y O antigen (3) and contrasts sharply with the ^{1}H nmr of 8-methoxycarbonyloctyl *O*-α-L-rhamnopyranosyl-(1→2)-*O*-α-L-rhamnopyranosyl-(1→3)-*O*-α-L-rhamnopyranosyl-(1→3)-*O*-2-acetamido-2-deoxy-β-D-glucopyranoside (8) which shows four distinct and well separated anomeric resonances at 80 MHz. The incremental shift differences due to linkage, sequence, and conformation are receiving further study and will be published separately together with anomeric T_1 evidence which indicates preferred conformations in agreement with the requirements of the *exo*-anomeric effect (18).

In conclusion we have clearly demonstrated that sequential addition, to selectively blocked glycosides,

of suitable monosaccharide building units in conjunction with silver triflate promoted Koenigs–Knorr reactions provides an efficient process for preparing artificial antigens at least as large as tetrasaccharide. Such compounds should prove to be of the utmost value in probing and extending existing serological principles pertaining to oligosaccharide determinants.

Experimental

The materials and methods used here are similar to those employed in previous publications (5–8) with the following exceptions. Preparative high pressure liquid chromatography (hplc) was performed on a Waters 500LC system. A column (25 cm × 1.5 cm) of Sephadex LH20 with methanol as solvent was used to purify acyl hydrazide derivatives. Single bond coupling constants $^1J_{^{13}C_1,^1H_1}$ were determined from ^{13}C spectra recorded in the "gated" decoupling mode (19). Assignments of ^{13}C resonances are tentative.

*2-O-Acetyl-3,4-di-O-benzyl-α-L-rhamnopyranosyl Chloride (**1**)*

Trimethylchlorosilane (10 mL) was added to a solution of 3,4-di-*O*-benzyl-1,2-*O*-(methoxyethylidene)-β-L-rhamnopyranose (8.0 g, 20 mmol) (5) in dichloromethane (50 mL). The reaction was refluxed for 2 h, then evaporated and dried under vacuum to yield a light yellow syrup of **1** (8.1 g, ~100% yield). Proton and ^{13}C nmr indicate the syrup to be at least 95% pure. ^1H nmr ($CDCl_3$) δ: 1.35 (d, $J_{5,6}$ = 6.2 Hz, 3H, H-6), 2.15 (s, 3H, CH_3CO), 3.48 (t, $J_{3,4}$ = 9.5 Hz, 1H, H-4), 3.78–4.32 (m, 2H, H-3 and H-5), 4.57 and 4.65 (AB system, J_{AB} = 10.2 Hz, CH_2Ph), 5.46 (dd, $J_{1,2}$ = 1.7 Hz, $J_{2,3}$ = 2.8 Hz, 1H, H-2), 5.96 (d, $J_{1,2}$ = 1.7 Hz, 1H, H-1), 7.20–7.60 (m, 10H, aromatic); ^{13}C nmr ($CDCl_3$) δ: 90.3 (Cl), 79.4, 76.6 (2C, CH_2Ph), 75.5 (C4), 72.1 (C3), 71.4 (C2), 70.9 (C5), 17.7 (C6).

*8-Methoxycarbonyloctyl 3,4-Di-O-benzyl-α-L-rhamnopyranoside (**2**)*

A solution of **1** (8.1 g, 20 mmol) in dichloromethane (50 mL) was added dropwise to a stirred solution of 8-methoxycarbonyloctanol (4.0 g, 21.3 mmol) (12) silver triflate (6.0 g, 23.3 mmol) and *N,N*-tetramethylurea (10 mL, 83.3 mmol) in dichloromethane (100 mL) at −70°C. The reaction was allowed to warm to room temperature overnight and the solution was then filtered. Following extraction with saturated sodium bicarbonate and water, the concentrated syrup was purified by hplc with Skellysolve B – ethyl acetate (3:1) as solvent. The pure syrup was dissolved in methanol (200 mL) containing a catalytic amount of sodium and stirred overnight. De-ionisation with Rexyn 101 (H^+), concentration, and chromatography by hplc with Skellysolve B – ethyl acetate (2:1) gave pure **2** (7.7 g, 75% yield); $[\alpha]_{589}$ −24.2° (*c* 1.0, $CHCl_3$); R_f 0.20 (solvent same as above); ^1H nmr ($CDCl_3$) δ: 0.90–1.75 (m, 15H, H-6 and —$(CH_2)_6$—), 2.30 (t, 2H, —CH_2CO—), 2.50 (d, 1H, OH), 3.62 (s, 3H, CH_3O), 3.23–4.18 (m, 7H, OCH_2 and ring protons), 4.43–5.01 (m, 4H, OCH_2Ph), 7.23–7.27 (m, 10H, aromatic); ^{13}C nmr ($CDCl_3$) δ: 99.1 (C1), 80.2, 80.1 (2C, CH_2Ph), 75.4 (C4), 71.9 (C3), 68.6 (C2), 67.5 (C5), 67.3 (OCH_2), 17.9 (C6). *Anal.* calcd. for $C_{30}H_{42}O_7$: C 70.01, H 8.23; found: C 69.98, H 8.27.

*8-Methoxycarbonyloctyl 2-O-(2-O-Acetyl-3,4-di-O-benzyl-α-L-rhamnopyranosyl)-3,4-di-O-benzyl-α-L-rhamnopyranoside (**3**)*

Glycoside **2** (4.1 g, 8 mmol) was dissolved in dichloromethane (100 mL) containing silver triflate (3.1 g, 12 mmol) and *N,N*-tetramethylurea (5 mL, 42 mmol). The solution was cooled to −70°C and rhamnopyranosyl chloride **1** (4.0 g, 10 mmol) dissolved in dichloromethane (30 mL) was added dropwise with stirring. The reaction was allowed to warm to room temperature overnight and the solution was then filtered. Following extraction with saturated sodium bicarbonate and water, the concentrated syrup was purified by hplc with Skellysolve B – ethyl acetate (3:1) as solvent. Pure disaccharide **3** (5.0 g, yield 71%) was obtained; $[\alpha]_{589}$ −19.4° (*c* 1.0, $CHCl_3$); R_f 0.34 (same solvent as above); ^1H nmr ($CDCl_3$) δ: 1.20–1.60 (m, 18H, H-6, H-6′ and —$(CH_2)_6$—), 2.12 (s, 3H, CH_3CO), 2.31 (t, 2H, —CH_2CO—), 3.66 (s, 3H, CH_3O), 3.10–4.10 (m, 7H, ring protons and —CH_2O—), 4.30–4.80 (m, 8H, CH_2Ph), 4.85 (d, $J_{1,2}$ = 1.0 Hz, 1H, H-1), 4.99 (bs, 1H, H-1′), 5.52, 5.57 (dd, $J_{1,2}$ = 1.9 Hz, $J_{2,3}$ = 3.3 Hz, 1H, H-2′), 7.31 (bs, 20H, aromatic); ^{13}C nmr ($CDCl_3$) δ: 99.4 (C1), 98.8 (C1′), 80.1 (3C, CH_2Ph), 77.8 (CH_2Ph), 75.4 (2C, C2 and C4), 74.9 (C4′), 72.1 (C3), 71.8 (C3′), 69.1 (C2′), 68.3 (C5), 68.0 (C5′), 67.6 (OCH_2), 18.1 (2C, C6 and C6′). *Anal.* calcd. for $C_{52}H_{66}O_{12}$: C 70.73, H 7.53; found: C 70.50, H 7.61.

*8-Methoxycarbonyloctyl 2-O-(3,4-Di-O-benzyl-α-L-rhamnopyranosyl)-3,4-di-O-benzyl-α-L-rhamnopyranoside (**4**)*

Disaccharide **3** (4.0 g, 4.8 mmol) in methanol (100 mL) containing a catalytic amount of sodium methoxide was left overnight at room temperature. The syrup, obtained after removal of sodium ions with Rexyn 101 (H^+) resin, filtration, and evaporation, was purified by hplc with Skellysolve B – ethyl acetate (2:1) as solvent. This gave pure **4** (3.5 g, 92% yield); $[\alpha]_{589}$ −27.0° (*c* 1.1, $CHCl_3$); R_f 0.46 (solvent same as above); ^1H nmr ($CDCl_3$) δ: 1.20–1.70 (m, 18H, H-6, H-6′ and —$(CH_2)_6$—), 2.32 (t, 2H, —CH_2CO), 2.52 (bs, 1H, OH), 3.67 (s, 3H, CH_3O), 3.20–4.20 (m, 8H, ring protons and —CH_2O—), 4.50–5.00 (m, 8H, CH_2Ph), 4.99 (d, $J_{1,2}$ = 1.0 Hz, 1H, H-1), 5.11 (d, $J_{1,2}$ = 1.6 Hz, 1H, H-1′), 7.30–7.50 (m, 20H, aromatic); ^{13}C nmr ($CDCl_3$) δ: 101.0 (C1′), 98.9 (C1), 80.5 (CH_2Ph), 80.2 (2C, CH_2Ph), 79.6 (CH_2Ph), 75.3 (2C, C2 and C4), 74.9 (C4′), 72.3 (C3), 72.1 (C3′), 68.8 (C2′), 68.0 (2C, C5 and C5′), 67.5 (OCH_2), 18.1 (C6), 18.0 (C6′). *Anal.* calcd. for $C_{50}H_{64}O_{11}$: C 71.40, H 7.67; found: C 71.24, H 7.64.

*8-Methoxycarbonyloctyl O-(3,4,6-Tri-O-acetyl-2-deoxy-2-phthalimido-β-D-glucopyranosyl)-(1 → 2)-O-(3,4-di-O-benzyl-α-L-rhamnopyranosyl)-(1 → 2)-3,4-di-O-benzyl-α-L-rhamnopyranoside (**5**)*

The partially protected glycoside **4** (2.2 g, 2.6 mmol) was dissolved in dichloromethane (30 mL) containing silver triflate (1.4 g, 5.5 mmol) and collidine (0.7 g). The solution was cooled to −70°C and 3,4,6-tri-*O*-acetyl-2-deoxy-2-phthalimido-D-glucopyranosyl bromide (2.5 g, 5.0 mmol) (12) dissolved in dichloromethane (15 mL) was added dropwise with stirring. The reaction was allowed to warm to room temperature overnight and the reaction mixture was then filtered. Following extraction with dilute hydrochloric acid (0.1 *M*), sodium bicarbonate, and water, the product after concentration to a syrup was purified on a silica gel column with Skellysolve B – ethyl acetate (1:1). This gave pure **5** (2.3 g, 70% yield); $[\alpha]_{589}$ 6.1° (*c* 1.0, $CHCl_3$); R_f 0.58 (solvent same as above); mp 117–118°C (recrystallized from ethyl acetate – Skellysolve B); ^1H nmr ($CDCl_3$) δ: 1.00–1.70 (m, 18H, H-6, H-6′ and —$(CH_2)_6$—), 1.90 (s, 3H, CH_3CO), 1.98 (s, 3H, CH_3CO), 2.02 (s, 3H, CH_3CO), 2.28 (t, 2H, —CH_2CO—), 3.65 (s, 3H, CH_3O), 5.32 (d, $J_{1,2}$ = 8.5 Hz, 1H, H-1″), 5.93, 6.06 (dd, $J_{2,3}$ = 10.7 Hz, $J_{3,4}$ = 9.1 Hz, 1H, H-3″), 6.90–7.90 (m, 24H, aromatic), 3.00–5.30 (m, 25H, ring protons and —CH_2Ph); ^{13}C nmr ($CDCl_3$) δ: 101.3 (C′), 100.0 (C1″), 98.7 (C1), 80.7 (CH_2Ph), 79.2 (2C, CH_2Ph), 79.1 (CH_2Ph), 77.8 (C2′), 76.6 (C2), 75.4 (C4), 75.0 (C5″), 72.6 (C4′), 71.4 (2C, C3 and C3′), 70.2 (C4″), 68.9 (C3″), 68.5 (C5), 67.5 (2C, C5′ and

OCH_2), 61.5 (C6″), 54.7 (C2″), 18.1 (C6), 17.7 (C6′). *Anal.* calcd. for $C_{70}H_{83}NO_{20}$: C 66.81, H 6.65, N 1.11; found: C 66.58, H 6.58, N 1.14.

8-Methoxycarbonyloctyl O-*(2-Acetamido-2-deoxy-*β-D-*glucopyranosyl)-(1 → 2)-*O-*(3,4-di-*O-*benzyl-*α-L-*rhamnopyranosyl)-(1 → 2)-3,4-di-*O-*benzyl-*α-L-*rhamnopyranoside (**6**)*

The trisaccharide **5** (1.6 g, 1.3 mmol) was dissolved in methanol (150 mL) containing a catalytic amount of sodium methoxide and was left for 5 h at room temperature. The syrup, obtained after removal of sodium ions with Rexyn 101 (H^+) resin, filtration, and evaporation was dissolved in ethanol (40 mL). Hydrazine hydrate (0.36 g, 85% solution, 6.1 mmol) was added to this solution and the solution was boiled for 2 h. The solution was evaporated and dried under high vacuum to remove traces of hydrazine. The product was then dissolved in methanol–water (3:1, 10 mL), acetic anhydride (3 mL) was added, and the solution was stirred at room temperature overnight. Concentration followed by purification on silica gel with chloroform–methanol (7:1) gave pure trisaccharide **6** (0.95 g, 70% yield); $[\alpha]_{589}$ −5.3° (*c* 1.2, methanol); R_f 0.54 (same solvent as above); ^{1}H nmr (acetone-d_6) δ: 1.00–1.70 (m, 18H, H-6, H-6′ and —$(CH_2)_6$—), 1.70 (s, 3H, CH_3CONH), 2.29 (t, 2H, —CH_2CO—), 3.61 (s, 3H, CH_3O), 7.20–7.60 (m, 20H, aromatic), 3.10–5.30 (ring protons); ^{13}C nmr (CD_3OD) δ: 104.1 (C1″), 102.1 (C1′), 99.7 (C1), 81.3 (CH_2Ph), 79.8 (CH_2Ph), 78.9 (2C, CH_2Ph), 78.2 (C2′), 77.1 (C5″), 76.4 (C2), 76.0 (C4), 75.9 (C4′), 75.5 (C3″), 73.1 (C3), 72.3 (C3′), 71.5 (C4″), 69.4 (C5), 68.6 (C5′), 68.3 (OCH_2), 62.3 (C6″), 57.7 (C2″), 18.4 (C6), 18.1 (C6′). *Anal.* calcd. for $C_{58}H_{77}NO_{16}$: C 66.71, H 7.43, N 1.34; found: C 66.49, H 7.33, N 1.48.

8-Methoxycarbonyloctyl O-*2-Acetamido-2-deoxy-*β-D-*gluco-pyranosyl-(1 → 2)-*O-α-L-*rhamnopyranosyl-(1 → 2)-*α-L-*rhamnopyranoside (7)*

The trisaccharide **6** (900 mg, 0.86 mmol) was dissolved in acetic acid (40 mL) and hydrogenated over 10% palladium on charcoal (0.5 g) at 505 kPa for 3 h. Filtration and evaporation provided a residue which was purified on a silica gel column with ethyl acetate – methanol – water (7:2:1) to give pure **7** (460 mg, 84% yield); $[\alpha]_{589}$ −36.4° (*c* 1.1, methanol); R_f 0.40 (solvent same as above); ^{1}H nmr (D_2O, 85°C) δ: 1.20–1.90 (m, 18H, H-6, H-6′ and —$(CH_2)_6$—), 2.07 (s, 3H, CH_3CONH), 2.37 (t, 2H, —CH_2CO—), 3.71 (s, 3H, CH_3O), 4.74 (d, $J_{1,2}$ = 8.1 Hz, 1H, H-1″), 4.84 (d, $J_{1,2}$ = 0.8 Hz, 1H, H-1), 5.16 (d, $J_{1,2}$ = 1.8 Hz, 1H, H-1′); ^{13}C nmr (D_2O) δ: 103.9 (C1″), 102.3 (C1′), 99.8 (C1), 80.1 (C2), 79.9 (C2′), 77.0 (C5″), 74.9 (C3″), 73.5 (2C, C4 and C4′), 71.5 (C4″), 71.1 (2C, C3 and C3′), 70.4 (C5′), 69.9 (C5), 68.9 (OCH_2), 62.0 (C6″), 57.1 (C2″), 18.1 (2C, C6 and C6′). *Anal.* calcd. for $C_{30}H_{53}NO_{16}$: C 52.70, H 7.81, N 2.05; found: C 52.50, H 7.91, N 2.13.

8-Hydrazinocarbonyloctyl O-*2-Acetamido-2-deoxy-*β-D-*glucopyranosyl-(1 → 2)-*O-α-L-*rhamnopyranosyl-(1 → 2)-*α-L-*rhamnopyranoside (8)*

The de-blocked trisaccharide **7** (53.5 mg, 0.08 mmol) was dissolved in ethanol (3 mL) to which 85% hydrazine hydrate (1.0 g) was added. The solution was stirred for 72 h, then evaporated and dried under high vacuum. Purification on a Sephadex LH20 column with methanol as solvent gave pure hydrazide **8** (49.7 mg, 93% yield); $[\alpha]_{589}$ −35.2° (*c* 1.0, methanol); R_f 0.26 (ethyl acetate – methanol – water 6:3:1); ^{1}H nmr (D_2O, 85°C) δ: 1.10–1.70 (m, 18H, H-6, H-6′ and —$(CH_2)_6$—), 2.10 (s, 3H, CH_3CONH), 2.26 (t, 2H, —CH_2CO—), 4.77 (d, $J_{1,2}$ = 7.8 Hz, 1H, H-1″), 4.87 (bs, 1H, H-1), 5.19 (d, $J_{1,2}$ = 1.7 Hz, 1H, H-1′), 2.10–4.25 (ring protons); ^{13}C nmr (D_2O) δ: 103.9 (C1″), 102.2 (C1′), 99.4 (C1), 80.0 (2C, C2 and C2′), 77.0 (C5″), 74.8 (C3″), 73.4 (2C, C4 and C4′), 71.3 (C4″), 71.0 (2C, C3 and C3′), 70.4 (C5′), 69.9 (C5), 69.2 (OCH_2), 61.8 (C6″), 57.0 (C2″), 17.8 (2C, C6 and C6′). *Anal.* calcd. for $C_{29}H_{53}N_3O_{15}$: C 50.94, H 7.81, N 6.15; found: C 50.90, H 7.98, N 6.30.

8-Methoxycarbonyloctyl O-*(3,4-Di-*O-*benzyl-*α-L-*rhamno-pyranosyl)-(1 → 2)-*O-*(3,4-di-*O-*benzyl-*α-L-*rhamno-pyranosyl)-(1 → 3)-2,4-benzoyl-*α-L-*rhamnopyranoside (13)*

Glycoside **11** (2.2 g, 2.5 mmol) (7) was dissolved in dichloromethane (40 mL) containing silver triflate (1.3 g, 5.2 mmol) and *N,N*-tetramethylurea (2 mL). The solution was cooled to −70°C and the rhamnosyl chloride **1** (2.0 g, 4.9 mmol) dissolved in dichloromethane (15 mL) was added dropwise with stirring. The reaction was allowed to warm to room temperature overnight and was then filtered. Following extraction of the filtrate with saturated sodium bicarbonate and water, the concentrated syrup was purified on a silica gel column with Skellysolve B – ethyl acetate (3:1) as solvent. This gave trisaccharide **12** contaminated with a little disaccharide **11**, both having a R_f 0.32. The syrup was dissolved in a methanol (30 mL)–tetrahydrofuran (10 mL) mixture which was cooled to 0°C and a freshly prepared solution of magnesium methoxide in methanol (15 mL of a 1% solution) was added. The reaction was then stirred for 48 h at 0°C. After removal of magnesium ions with Rexyn 101 (H^+) resin, filtration, and evaporation, the syrup obtained was purified on a silica gel column with the solvent Skellysolve B – ethyl acetate (2:1). This gave pure **13** (1.7 g, 56% yield); $[\alpha]_{589}$ +26.6° (*c* 1.0, chloroform); R_f 0.38 (solvent as above); ^{1}H nmr ($CDCl_3$) δ: 1.03 (d, $J_{5,6}$ = 5.8 Hz, 3H, H-6″), 1.06 (d, $J_{5,6}$ = 5.9 Hz, 3H, H-6′), 1.10–1.80 (m, 15H, H-6 and —$(CH_2)_6$—), 2.10–2.35 (m, 4H, —OH and —CH_2CO—), 3.66 (s, 3H, CH_3O—), 6.85–7.50 (m, 26H, aromatic), 7.80–8.10 (m, 4H, aromatic), 3.00–5.50 (ring protons); ^{13}C nmr ($CDCl_3$) δ: 101.0 (C1′), 100.5 (C1″), 97.4 (C1), 80.1 (CH_2Ph), 79.5 (3C, CH_2Ph), 76.0 (C2′), 75.3 (C3), 74.5 (C4′), 74.1 (C3′), 73.5 (C4″), 72.6 (C2), 72.1 (C4), 71.9 (C3″), 69.0 (C2″), 68.6 (C5′), 68.4 (C5″), 67.9 (C5), 66.7 (OCH_2), 17.8 (3C, C6, C6′ and C6″). *Anal.* calcd. for $C_{70}H_{82}O_{17}$: C 70.33, H 6.91; found: C 70.14, H 6.91.

8-Methoxycarbonyloctyl O-*(3,4,6-Tri-*O-*acetyl-2-deoxy-2-phthalimido-*β-D-*glucopyranosyl)-(1 → 2)-*O-*(3,4-di-*O-*benzyl-*α-L-*rhamnopyranosyl)-(1 → 2)-*O-*(3,4-di-*O-*benzyl-*α-L-*rhamnopyranosyl)-(1 → 3)-2,4-di-*O-*benzoyl-*α-L-*rhamnopyranoside (14)*

The partially blocked trisaccharide **13** (1.3 g, 1.1 mmol) was dissolved in dichloromethane (30 mL) together with collidine (0.35 g, 2.9 mmol) and silver triflate (0.75 g, 2.9 mmol). The solution was cooled to −70°C and the 3,4,6-tri-*O*-acetyl-2-deoxy-2-phthalimido-D-glucopyranosyl bromide (1.3 g, 2.6 mmol) (10) dissolved in dichloromethane (15 mL) was added dropwise with stirring. The reaction was allowed to warm to room temperature overnight and was then filtered. Following extraction of the filtrate with 3% hydrochloric acid, saturated sodium bicarbonate, and water, the concentrated syrup was purified on a silica gel column with Skellysolve B – ethyl acetate (1:1) as solvent. This gave pure tetrasaccharide **14** (1.5 g, 85% yield); $[\alpha]_D$ +48.4° (*c* 1.2, chloroform); R_f 0.56 (same solvent as above); ^{1}H nmr ($CDCl_3$) δ: 0.93 (d, $J_{5,6}$ = 5.9 Hz, 3H, H-6″), 0.99 (d, $J_{5,6}$ = 5.7 Hz, 3H, H-6′), 1.10–1.75 (m, 15H, H-6 and —$(CH_2)_6$—), 1.89 (s, 3H, CH_3CO—), 1.93 (s, 3H, CH_3CO—), 2.01 (s, 3H, CH_3CO—), 3.65 (s, 3H, CH_3O—), 5.90, 6.05 (dd, $J_{2,3}$ = 9.1 Hz, $J_{3,4}$ = 10.8 Hz, 1H, H-3‴), 6.80–8.30 (m, 34H, aromatic); ^{13}C nmr ($CDCl_3$) δ: 100.9 (2C, C1′ and C1‴), 99.8 (C1″), 97.3 (C1), 80.6 (CH_2Ph), 79.8 (CH_2Ph),

78.7 (CH_2Ph), 78.3 (CH_2Ph), 77.9 (C2″), 75.9 (2C, C2′ and C3), 74.9 (C5‴), 74.1 (C4′), 73.4 (C4″), 72.6 (2C, C2 and C4), 71.4 (C3′), 71.0 (C3″), 70.2 (C4‴), 68.9 (C3‴), 68.4 (3C, C5, C5′ and C5″), 66.7 (OCH_2), 61.7 (C6‴), 54.7 (C2‴), 17.8 (2C, C6 and C6′), 17.6 (C6″). *Anal.* calcd. for $C_{90}H_{101}NO_{26}$: C 67.03, H 6.23, N 0.83; found: C 66.96, H 6.31, N 0.87.

*8-Methoxycarbonyloctyl 2-Acetamido-2-deoxy-*β-D-*gluco-pyranosyl-(1 → 2)-*O-α-L-*rhamnopyranosyl-(1 → 2)-*O-α-L-*rhamnopyranosyl-(1 → 3)-*α-L-*rhamnopyranoside (**15**)*

The tetrasaccharide **14** (1.3 g, 0.81 mmol) was dissolved in methanol (100 mL) containing a catalytic amount of sodium and the reaction was stirred overnight. The syrup obtained after removal of sodium ions with Rexyn 101 (H^+) resin, filtration, and evaporation was dissolved in ethanol (40 mL). Hydrazine hydrate (0.30 g, 85% solution, 5.1 mmol) was added to this solution and the solution was boiled for 2 h. The solution was evaporated and dried under high vacuum to remove traces of hydrazine. The product was then dissolved in methanol (20 mL), acetic anhydride (2 mL) was added, and the solution was stirred at room temperature overnight. Concentration gave a syrup which on tlc showed several spots (this due to incomplete de-benzoylation), so no purification was done at this point. The syrup was instead dissolved in acetic acid (40 mL) and hydrogenated over 10% palladium on charcoal (0.5 g) at 505 kPa for 3 h. Filtration and evaporation gave a foam which was again dissolved in methanol (100 mL) containing freshly prepared sodium methoxide. The reaction was then stirred for 48 h. The syrup, obtained after removal of sodium ions with Rexyn 101 (H^+) resin, filtration, and evaporation, was purified on a silica gel column with ethyl acetate – methanol – water (7:2:1) to give pure tetrasaccharide **15** (450 mg, 67% yield); $[\alpha]_{589}$ −54.0° (*c* 1.1, CH_3OH); R_f 0.28 (solvent as above); ^1H nmr (D_2O, 85°C) δ: 1.10–1.85 (m, 21H, H-6, H-6′, H-6″ and —$(CH_2)_6$—), 2.10 (s, 3H, CH_3CONH), 2.32 (t, 2H, —CH_2CO—), 3.71 (s, 3H, CH_3O), 4.75 (d, $J_{1,2}$ = 1.3 Hz, 1H, H-1), 4.76 (d, $J_{1,2}$ = 7.9 Hz, 1H, H-1‴), 5.19 (bd, 2H, H-1′ and H-1″), 3.25–4.25 (ring protons); ^{13}C nmr (D_2O) δ: 103.9 (C1‴, $^1J_{^{13}C_1,^1H_1}$ = 162.8 Hz), 102.3 (C1″, $^1J_{^{13}C_1,^1H_1}$ = 171.0 Hz), 102.0 (C1′, $^1J_{^{13}C_1,^1H_1}$ = 171.0 Hz), 101.1 (C1, $^1J_{^{13}C_1,^1H_1}$ = 168.0 Hz), 80.1 (C2″), 79.7 (C2′), 78.4 (C3), 77.0 (C5‴), 74.9 (C3‴), 73.5 (3C, C4, C4′ and C4″), 71.1 (4C, C2, C3′, C3″, C4‴), 70.4 (C5″), 70.1 (2C, C5 and C5′), 68.9 (OCH_2), 61.9 (C6‴), 57.1 (C2‴), 18.1 (3C, C6, C6′ and C6″). *Anal.* calcd. for $C_{36}H_{63}NO_{20}$: C 52.10, H 7.65, N 1.69; found: C 51.95, H 7.80, N 1.85.

*8-Hydrazinocarbonyloctyl O-2-Acetamido-2-deoxy-*β-D-*glucopyranosyl-(1 → 2)-*O-α-L-*rhamnopyranosyl-(1 → 2)-*O-α-L-*rhamnopyranosyl-(1 → 3)-*α-L-*rhamno-pyranoside (**16**)*

The de-blocked tetrasaccharide **15** (75.0 mg, 0.09 mmol) was dissolved in ethanol (3 mL) to which 85% hydrazine hydrate (1.0 g) was added. The solution was stirred for 72 h, then evaporated and dried under high vacuum. Purification on a Sephadex LH20 column with methanol as solvent gave pure hydrazide **16** (70.1 mg, 93% yield); $[\alpha]_{589}$ −51.0° (*c* 1.1, methanol); R_f 0.25 (ethyl acetate – methanol – water 6:3:1); ^1H nmr (D_2O, 85°C) δ: 1.10–1.80 (m, 21H, H-6, H-6′, H-6″ and —$(CH_2)_6$—), 2.10 (s, 3H, CH_3CONH—), 2.25 (t, 2H, —CH_2CO—), 4.77 (d, $J_{1,2}$ = 7.8 Hz, 1H, H-1‴), 4.79 (d, $J_{1,2}$ = 1.5 Hz, 1H, H-1), 5.20 (bd, 2H, H-1′ and H-1″); ^{13}C nmr (D_2O) δ: 103.9 (C1‴), 102.2 (C1″), 102.0 (C1′), 100.8 (C1), 80.0 (C2″), 79.4 (C2′), 78.6 (C3), 77.0 (C5‴), 74.8 (C3‴), 73.4 (2C, C4 and C4″), 73.0 (C4′), 71.0 (4C, C4‴, C3′, C3″ and C2), 70.4 (2C, C5′ and C5″), 69.9 (C5), 69.2 (OCH_2), 61.9 (C6‴), 57.1 (C2‴), 17.9 (3C, C6, C6′ and C6″). *Anal.* calcd. for $C_{35}H_{63}N_3O_{19}$: C 50.66, H 7.65, N 5.06; found: C 50.54, H 7.70, N 5.12.

Acknowledgements

We wish to thank Mr. J. Christ for technical assistance and Mr. H. Seguin for microanalyses.

1. L. Kenne, B. Lindberg, K. Petersson, and E. Romanowska. Carbohydr. Res. **56**, 363 (1977).
2. O. Lüderitz, A. M. Staub, and O. Westphal. Bacteriol. Rev. **30**, 192 (1966).
3. K. Jann and O. Westphal. *In* The antigens. Vol. 3. *Edited by* M. Sela. Academic Press, New York, NY. 1975. p. 1.
4. O. Lüderitz. Angew. Chem. **9**, 649 (1970).
5. D. R. Bundle and S. Josephson. Can. J. Chem. **57**, 662 (1979).
6. D. R. Bundle and S. Josephson. J. Chem. Soc. Perkin Trans. I. In press.
7. S. Josephson and D. R. Bundle. J. Chem. Soc. Perkin Trans. I. In press.
8. D. R. Bundle and S. Josephson. Carbohydr. Res. In press.
9. H. B. Boren, G. Ekborg, K. Eklind, P. J. Garegg, A. Pilotti, and C-G. Swahn. Acta Chem. Scand. **27**, 25 (1973).
10. R. U. Lemieux. Chem. Soc. Rev. **7**, 423 (1978).
11. T. Ogawa, K. Katano, and M. Matsui. Carbohydr. Res. **64**, C3 (1978).
12. S. Hanessian and J. Banoub. Am. Chem. Soc. Symp. Ser. **39**, 36 (1976).
13. R. U. Lemieux, T. Takeda, and B. Y. Chung. Am. Chem. Soc. Symp. Ser. **39**, 90 (1976)
14. R. U. Lemieux, D. R. Bundle, and D. A. Baker. J. Am. Chem. Soc. **97**, 4076 (1975).
15. R. U. Lemieux, D. A. Baker, and D. R. Bundle. Can. J. Biochem. **55**, 507 (1977).
16. J. Banoub and D. R. Bundle. Can. J. Chem. **57**, 2091 (1979).
17. K. Bock, C. Pedersen, and P. Rasmussen. J. Chem. Soc. Perkin Trans. 1, 1456 (1973).
18. R. U. Lemieux, S. Koto, and D. Voisin. Am. Chem. Soc. Symp. Ser. **87**, 17 (1979).
19. O. A. Gansow and W. Shittenhelm. J. Am. Chem. Soc. **93**, 4294 (1971).

The crystal and molecular structure of *syn*-2,11-dithia[3,3]metacyclophane

WILLEM ANKER, GORDON W. BUSHNELL,[1] AND REGINALD H. MITCHELL[2]

Chemistry Department, University of Victoria, Victoria, B.C., Canada V8W 2Y2

Received June 6, 1979

WILLEM ANKER, GORDON W. BUSHNELL, and REGINALD H. MITCHELL. Can. J. Chem. **57**, 3080 (1979).

The crystal structure of *syn*-2,11-dithia[3,3]metacyclophane, $C_{16}H_{16}S_2$, has been determined by single crystal X-ray diffraction and refined to an *R*-value of 0.049. The crystal is monoclinic with cell dimensions a = 1898.2(5), b = 795.7(3), c = 924.1(4) pm, β = 100.03°(4). The space group is $P2_1/n$ with 4 molecules per cell, D_m = 1.34 g cm^{-3}, D_c = 1.317 g cm^{-3}. Of several possible *syn* conformations, the molecule is found in that with the largest S—S distance of 697.4 pm. The benzenoid rings form a dihedral angle of 20.6°. The distance between the pair of aromatic H atoms which are *ortho* to two methylene groups is 273.0 pm, with 305.2 pm between the carbon atoms to which they are attached. Small angular distortions are observed at these carbon atoms. Mean bond lengths are: C—S 181.0(12), C—C (aromatic) 138.5(8), C—C (bridge) 151.0(11) pm. Mean bond angles are: C—S—C 104°(1), S—C—C 115.4°(9). The C—C—C angles are in the range 117.9–122.7°. The molecule possesses an approximate (non-crystallographic) 2-fold axis of symmetry passing through the midpoints of C(8)—C(18) and C(4)—C(14). The aromatic rings are planar, with the methylene carbons 5–11 pm out of plane on the sulphur side. The S(1) is 171.8(2) pm from plane *1* and 136.8(2) pm from plane *2*, while for S(2) the corresponding values are 136.0(2) and 175.3(2) respectively.

^{1}Hmr data have been re-examined and compared with those obtained for other cyclophanes, together with ^{13}Cmr data and are consistent with the fact that in solution 2,11-dithia[3,3]metacyclophane, **1**, exists as the *syn*-conformer with no appreciable participation of the *anti*-conformer. All related dithia[3,3]metacyclophanes which have internal aryl hydrogens (i.e., no internal substituents) likewise appear to be *syn* from ^{1}Hmr data.

WILLEM ANKER, GORDON W. BUSHNELL et REGINALD H. MITCHELL. Can. J. Chem. **57**, 3080 (1979).

On a déterminé la structure cristalline du dithia-2,11 méta[3,3] cyclophane *syn*, $C_{16}H_{16}S_2$, par diffraction de rayons-X sur un cristal unique et on l'a affinée jusqu'à une valeur conventionnelle de 0.049. Le cristal est monoclinique avec une dimension de maille de a = 1898.2(5), b = 795.7(3), c = 924.1(4) pm, β = 100.03°(4). Le groupe d'espace est $P2_1/n$ avec 4 molécules par maille, D_m = 1.34 g cm^{-3}, D_c = 1.317 g cm^{-3}. Entre plusieurs conformations *syn* possibles, la molécule se classe parmi celles qui ont la plus grande distance S—S soit 697.4 pm. Les cycles aromatiques forment un angle dièdre de 20.6°. Les deux atomes d'hydrogène aromatique en *ortho* des deux groupés méthyléniques sont distants entre eux de 273.0 pm et les atomes de carbone auxquels ils sont attachés sont distants de 305.2 pm. On a observé des petites distorsions angulaires au niveau de ces atomes de carbone. Les longueurs moyennes de liaison sont de: C—S 181.0(2), C—C (aromatique) 138.5(8), C—C (pont) 151.0(11) pm. Les angles moyens de liaison sont de: C—S—C 104°(1), S—C—C 115.4°(9). Les angles C—C—C sont de l'ordre de 117.9–122.7°. La molécule possède approximativement un axe binaire de symétrie (non cristallographique) passant par le point milieu de C(8)—C(18) et C(4)—C(14). Les cycles aromatiques sont plans avec les carbones méthyléniques à 5–11 pm hors du plan du côté du soufre. Le S(1) est à 171.8(2) pm du plan *1* et à 136.8(2) du plan *2* alors que les valeurs correspondantes de S(2) sont respectivement de: 136.0(2) et 175.3(2).

On a réexaminé les données de la rmn du proton et on les a comparées à celles obtenues pour d'autres cyclophanes. Ces données ainsi que celles de la rmn du ^{13}C sont en accord avec le fait que le dithia-2,11 méta[3,3] cyclophane **1** existe en solution sous forme de conformère *syn* sans participation appréciable du conformère *anti*. Les spectres de résonance magnétique du proton révèlent de façon similaire que tous les composés dithia méta[3,3] cyclophanes qui ont des hydrogènes aromatiques internes (i.e. pas de substituants internes) sont sous forme des conformères *syn*.

[Traduit par le journal]

Introduction

2,11-Dithia[3,3]metacyclophane, **1**, was originally prepared in 1968 by two independent groups (1, 2) and was stated to be rapidly equilibrating between various *syn*- and *anti*-conformers. This conclusion was based primarily on the fact that the ^{1}Hmr

[1]Author to whom correspondence concerning X-ray data should be addressed.

[2]Author to whom correspondence concerning nmr data should be addressed.

0008-4042/79/233080-08$01.00/0

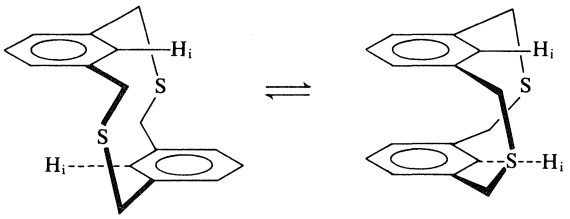

anti-**1** *syn*-**1**

spectrum of **1** showed a single peak at ca. δ 6.6 for the internal aryl hydrogens (H_i) which did not change on cooling. This observed position for H_i was assumed to be an average chemical shift for all contributing conformers, though it was quite clear from these and subsequent papers (3–6) that the *anti*-conformer of **1** was generally thought to be preponderant. This was not unreasonable at that time, since it was known that from ^{1}Hmr (7) and X-ray (8) data that [2,2]metacyclophane only existed in the *anti*-form **2**, and also it was observed (5) that in the

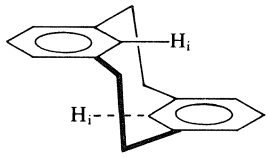

2

coupling reaction of 2,6-bis(bromomethyl)toluene with sodium sulphide, the *anti*-conformer of **3***a* was formed in seven times the amount of *syn*-**3***a*.

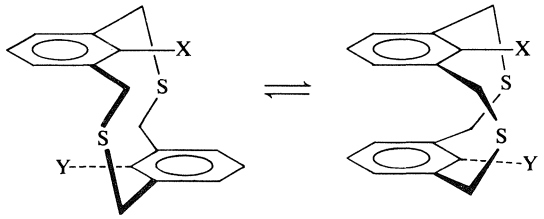

anti-**3** *syn*-**3**

a X = Y = CH_3
b X = H; Y = CH_3
c X = H; Y = NO_2
d X = H; Y = NH_2

As a result of an investigation to attempt to resolve an apparent anomaly (9) of melting points of **1**, we undertook an X-ray crystallographic structure determination of **1**. This paper shows that in the crystalline state **1** exists as the *syn*-conformer, and that this is in fact consistent with the structure of **1** in solution.

Experimental

X-ray Measurements

Approximate cell dimensions from Weissenberg and precession photographs were obtained using CuK_α radiation. The space group $P2_1/n$ was established unequivocally from the systematic absences. The equivalent positions in the second setting are : x, y, z; $\frac{1}{2}+x, \frac{1}{2}-y, \frac{1}{2}+z$; $-x, -y, -z$; $\frac{1}{2}-x, \frac{1}{2}+y, \frac{1}{2}-z$. The cell parameters were refined by least squares using 20 pairs of $\pm 2\theta$ measurements taken on a Picker 4-circle diffractometer using automatic centering routines. Zr filtered MoK_α radiation (λ = 71.069 pm) was used for all diffractometer measurements. The crystal was mounted approximately along the *b*-axis and had a shape and size specified by: 0,0,±1, 0.155 mm; ±1,0,0, 0.085 mm; 0,−1,0, 0.390 mm; 0,1,1, 0.245 mm; 0,1,−1, 0.325 mm. The crystal parameters at 23° are a = 1898.2(5), b = 795.7(3), c = 924.1(4) pm, β = 100.03°(4), molecular formula $C_{16}H_{16}S_2$, mol. wt. = 272.42, cell volume 1.374(1) nm^3, density 1.317 g cm^{-3} calculated, 1.34 g cm^{-3} measured (flotation), Z = 4, absorption coefficient ($MoK_{\bar{\alpha}}$) = 3.57 cm^{-1}, I/I_0 0.94 (max) and 0.90 (min) making absorption corrections unnecessary for conformation determination purposes. The intensity measurements were done automatically up to 2θ = 55° in the octants with k and $l \geq 0$, using a $\theta/2\theta$ scan (ω = 0, bisecting position) with 50 steps of 0.04° in 2θ, counting for 1 s per step. Background measurements were for 25 s before and after the step scan. Three standards 8,0,0; 6,2,0; and 0,0,4 were measured after each set of 50 reflections. Duplicate measurement of the two octants was carried out to improve the counting statistics. The sum of the standards had declined by approximately 8% at the finish, but there was no visual evidence of decomposition. Reflections for which $I < 3\sigma(I)$ were not written out by the diffractometer. The intensities were corrected for Lorentz and polarisation effects, and after the merging process there were 1187 independent reflections in the dataset.

Structure Determination

The structure was solved using the Patterson function. A set of programs supplied by Penfold (10) based on ORFLS, FORDAP, ORTEP, and ORFFE was used throughout. Atomic scattering curves were taken from the International Tables (11). All atoms were assumed to be uncharged and the S atoms were treated as anomalous scatterers (12). The refinement was by full matrix least squares minimization of $\sum w(|F_o| - |F_c|)^2$. The sulphur and carbon atoms were given anisotropic temperature parameters. The hydrogen atom positions were calculated from the carbon coordinates using a C—H length of 97 pm. The hydrogen atoms rode on the C skeleton in the final stages of refinement and were all assigned U_{iso} = 380 pm^2. The final weighting scheme, giving no systematic variation of $w\Delta^2$, was $w = (A + Bx + Cx^2 + Dx^3)^{-1}$ where $x = |F_o|$, A = 2.1134, $B = 4.03 \times 10^{-3}$, $C = 1.028 \times 10^{-2}$, $D = -4.9 \times 10^{-5}$. The final agreement factors were R = 0.049 and R_w = 0.069, where $R_w = (\sum w\Delta^2/\sum w|F_o|^2)^{1/2}$. The final difference map had a maximum of 0.53×10^{-6} e pm^{-3} and a minimum of -0.26×10^{-6} e pm^{-3}. The fractional atomic coordinates for the S and C atoms are given in Table 1. The anisotropic temperature parameters, the calculated hydrogen atom positions, and the structure factor tables have been deposited.[3]

Crystal Structure Description

The packing diagram given in Fig. 1 shows that the crystal structure contains four separate molecules

[3]Copies may be obtained, at a nominal charge, from the Depository of Unpublished Data, CISTI, National Research Council of Canada, Ottawa, Ont., Canada K1A 0S2.

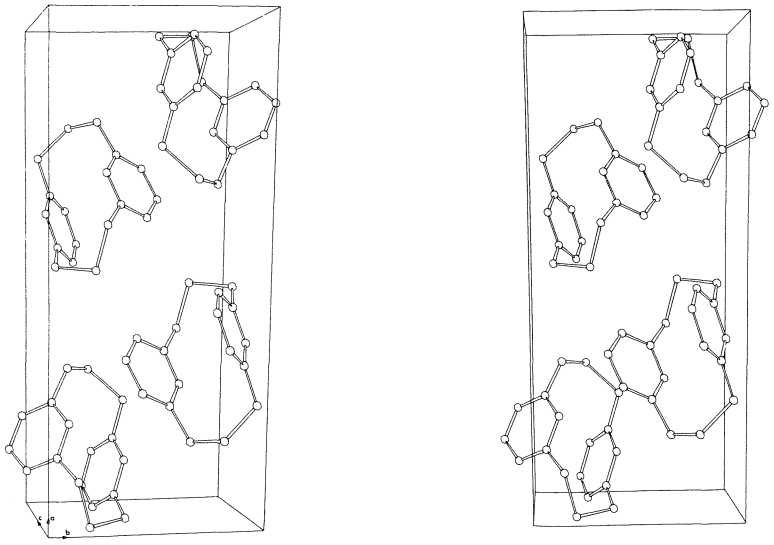

FIG. 1. A stereoscopic view of the unit cell and the molecular packing.

TABLE 1. Fractional atomic co-ordinates* × 10^4

Atom	x	y	z
S(1)	126(1)	2053(3)	915(2)
S(2)	3085(1)	2690(2)	6538(1)
C(1)	193(3)	3859(9)	2114(8)
C(2)	577(3)	3558(8)	3649(7)
C(3)	263(3)	2679(9)	4656(8)
C(4)	636(3)	2338(9)	6048(8)
C(5)	1341(3)	2854(8)	6465(6)
C(6)	1667(2)	3743(6)	5460(6)
C(7)	2442(3)	4296(7)	5839(6)
C(8)	1275(3)	4092(6)	4078(6)
C(11)	1039(3)	1504(9)	842(6)
C(12)	1451(3)	676(7)	2216(5)
C(13)	1177(3)	−686(7)	2851(6)
C(14)	1557(3)	−1389(7)	4147(6)
C(15)	2204(3)	−709(7)	4794(6)
C(16)	2489(2)	645(6)	4163(5)
C(17)	3171(3)	1476(8)	4899(6)
C(18)	2109(3)	1297(6)	2870(5)

*Estimated standard deviations are given in parentheses.

TABLE 2. Bond lengths* (pm)

Bond	Length	Bond	Length
S(1)—C(1)	180.6(7)	S(2)—C(7)	180.8(6)
S(1)—C(11)	180.0(6)	S(2)—C(17)	182.8(6)
C(1)—C(2)	149.7(9)	C(11)—C(12)	152.0(7)
C(7)—C(6)	151.7(7)	C(17)—C(16)	150.6(7)
C(2)—C(3)	138.0(9)	C(12)—C(13)	137.7(8)
C(3)—C(4)	138.3(9)	C(13)—C(14)	140.2(8)
C(4)—C(5)	139.0(8)	C(14)—C(15)	137.9(7)
C(5)—C(6)	139.4(7)	C(15)—C(16)	138.0(7)
C(6)—C(8)	139.0(7)	C(16)—C(18)	138.5(7)
C(2)—C(8)	138.1(7)	C(12)—C(18)	138.1(7)

*Estimated standard deviations are given in parentheses.

per unit cell. Figures 2 and 3 show the molecular structure and atomic labelling scheme. The molecule has an approximate (non-crystallographic) 2-fold axis of symmetry passing through the midpoints of C(8)—C(18) and C(4)—C(14). The bond lengths are given in Table 2. The mean lengths are: S—C, 181.1 pm; exocyclic C—C, 151.0 pm; and aromatic C—C 138.5 pm. There are no very significant deviations from these means and the values are normal. The bond angles are presented in Table 3. The mean angles C—S—C = 103.9°, and S—C—C = 115.4°.

The angles of the first ring in column 1 agree with the corresponding angles of the second ring in column 2 to an extent expected from the standard deviations, assuming the rings to be identical. Deviations from 120° are collectively greater and the angles at C(8) and C(18) are particularly large. Table 4 gives the results of the mean plane calculations. The aromatic rings are planar and the angle between them is 20.6°. Each methylene carbon atom is significantly out (on the S side) of the least squares plane of the ring to which it is attached. The molecular two-fold axis relates the C(1), C(17) displacements 8.9(7), 10.7(6) pm and the C(11), C(7) displacements 6.9(6), 5.2(6) pm, respectively. Similarly the perpendicular distances S(1)—plane *1*, S(2)—plane *2*, S(1)—plane *2*, and S(2)—plane *1* are 171.8(2), 175.3(2), 136.8(2), and 136.0(2) pm, respectively. Figure 2 illustrates the latter point, and Fig. 3 which is projected along the C(8)—C(18) direction shows that the benzene rings do not lie directly one upon the other, but are 7° apart approximately.

Our primary result is the *syn* geometry of the title compound. However, most of the background literature on metacyclophanes is concerned with ring

TABLE 3. Bond angles* (deg)

Atoms	Angle	Atoms	Angle
C(1)—S(1)—C(11)	104.5(3)	C(7)—S(2)—C(17)	103.3(2)
S(1)—C(1)—C(2)	115.1(5)	S(2)—C(17)—C(16)	114.3(3)
S(2)—C(7)—C(6)	116.4(4)	S(1)—C(11)—C(12)	115.6(4)
C(2)—C(8)—C(6)	122.4(5)	C(12)—C(18)—C(16)	122.7(5)
C(3)—C(4)—C(5)	120.8(6)	C(13)—C(14)—C(15)	120.0(5)
C(8)—C(2)—C(3)	117.9(6)	C(18)—C(16)—C(15)	118.2(5)
C(8)—C(6)—C(5)	119.0(5)	C(18)—C(12)—C(13)	118.3(5)
C(2)—C(3)—C(4)	121.0(6)	C(16)—C(15)—C(14)	120.6(5)
C(6)—C(5)—C(4)	118.9(5)	C(12)—C(13)—C(14)	120.1(5)
C(1)—C(2)—C(3)	121.6(6)	C(17)—C(16)—C(15)	121.4(5)
C(7)—C(6)—C(5)	121.2(5)	C(11)—C(12)—C(13)	121.3(5)
C(1)—C(2)—C(8)	120.5(6)	C(17)—C(16)—C(18)	120.2(5)
C(7)—C(6)—C(8)	119.8(5)	C(11)—C(12)—C(18)	120.3(5)

*Estimated standard deviations are given in parentheses.

TABLE 4. (*a*) The mean planes of the aromatic rings; plane *1* is defined by C(2)—C(6) and C(8), plane *2* is defined by C(12)—C(16) and C(18), coefficients of $Ax + By + Cz = D$*

Plane	*A*	*B*	*C*	*D*	χ^2
1	0.3850	−0.8583	−0.3394	−336.71	5.94
2	0.5684	−0.6235	−0.5369	−4.49	14.05

*Angle between planes *1* and *2* = 20.6°.

(*b*) Perpendicular distances to planes (pm)*

Plane	Atom	Distance	Atom	Distance
1	S(1)	171.8(2)	C(1)	8.9(7)
	S(2)	136.0(2)	C(7)	5.2(6)
	C(18)	295.8(5)	C(8)	0.8(5)
	C(14)	391.6(6)		
2	S(1)	136.8(2)	C(11)	6.9(6)
	S(2)	175.3(2)	C(17)	10.7(6)
	C(8)	297.5(5)	C(18)	1.2(5)
	C(8)	393.7(7)		

*The orthogonal system of axes used has *x* along *a*, *y* in the (*a*, *b*) plane, and *z* along the *c** axis. χ^2 is defined as $\Sigma_i(P_i^2/\sigma^2(P_i))$ where the summation is over all atoms, *i*, in the plane. The perpendicular distance of atom *i* from the plane is P_i.

strain. Comparison of our crystal structure with *syn*-**3***a* (13) shows interesting structural changes caused by repulsion between the methyl groups of the latter compound. The crystal structure of *syn*-**3***a* is disordered in the position of one of its sulfur atoms with an 80–20% distribution of conformers in the crystal structure. The most populated conformation of *syn*-**3***a* is quite similar to the conformation of *syn*-**1**, both having the sulfur atoms folded away from the internal aryl positions. The S—S distances are thus at a maximum: *syn*-**1** 697.4 pm and *syn*-**3***a* 695.0 pm. The molecular mechanics of both compounds can be likened to a spring clothes peg, with the $—CH_2—S—CH_2$ bridges acting as pivots for the relatively rigid phenyl groups. *Syn*-**1** has a dihedral angle of 20.6° between the phenyl ring planes, and the distance between the calculated internal hydrogen positions is 273.0 pm, more than twice the van der Waals radius of hydrogen (2 × 120 pm). The π-electron repulsion between C(8) and C(18), 305.2 pm apart, is probably more important than the repulsion between hydrogen atoms. *Syn*-**3***a* has a smaller dihedral angle of 10.3° and is evidence of interaction between the methyl groups which lie 26 and 30 pm from their respective phenyl ring planes on the outer sides. The intramolecular distance between the methyl carbon atoms is 352(1) pm. As expected, *syn*-**3***a* is more strained than *syn*-**1** in its 12-membered ring. The methylene carbon atoms are displaced inwards from the phenyl ring planes by 19 pm in *syn*-**3***a* and 8 pm in *syn*-**1** (averaged values). The $S—CH_2—C$ (aryl) angles average 117.5° in *syn*-**3***a* and 115.4° in *syn*-**1**. The two phenyl rings are not directly above one another in either compound.

Nuclear Magnetic Resonance Spectra

^{1}Hmr spectra were determined as solutions (20 mg of **1** in 0.4 mL solvent) in DMSO-d_6, toluene-d_8, $CDCl_3$, hexachlorobutadiene (HCBD), hexafluorobenzene (HFB), cyclohexane, and CS_2 over a temperature range of −70°C to +150°C on a Perkin-Elmer R32 (90MHz) spectrometer using Me_4Si as internal standard. The results for the internal aryl hydrogens (H_i) are shown in Fig. 4 and full data have been deposited[3] in Table S4. ^{13}Cmr spectra were determined in CD_2Cl_2, DMSO-d_6, THF-d_8, and CS_2 on a Nicolet TT-14 Fourier transform spectrometer operating at 15.1 MHz, and are deposited[3] in Table S5. All chemical shifts are measured in parts per million downfield from Me_4Si.

Discussion

When **1** was first described (1, 2) no other dithiametacyclophanes **3** having defined stereochemistry were known. Mitchell and Boekelheide (5, 14) were

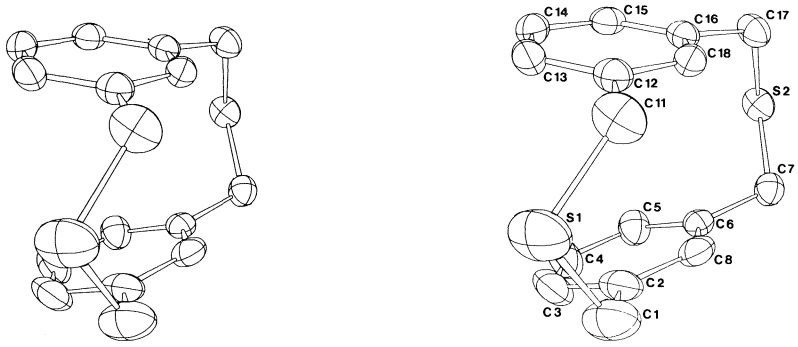

FIG. 2. A stereoscopic view of a single molecule, with the atom labelling scheme and the anisotropic thermal motion shown.

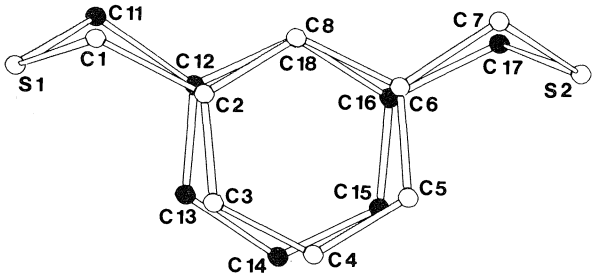

FIG. 3. A single molecule with atom labels, and the carbon atoms of the lower ring blackened.

the first to report the preparation of **3***a* in both *syn* and *anti* forms. *Anti*-**3***a* showed in its ^{1}Hmr spectra the internal —CH_3 hydrogens at δ 1.30, shielded by the adjacent benzene ring, whereas the aryl hydrogens were normal at δ 7.0–7.4. *Syn*-**3***a* showed the aryl hydrogens shielded by the adjacent ring at δ 6.66 and the —CH_3 hydrogens normal for a toluene at δ 2.54. This assignment has been confirmed by X-ray data (13). Since *anti*-**3***a* was obtained in the highest yield (5) it was assumed to be the more stable. For the analogous parent compounds **1** (**3**, X = Y = H) no suitable models existed. The internal aryl hydrogens of [2,2]metacyclophane itself, **2**, appeared (7, 15) at δ 4.25, very highly shielded by the opposite benzene rings. Examination of molecular models would predict that H_i in *anti*-**1** would probably not be shielded as much, since they should not be thrust so far into the opposite benzene ring as those in **2**.

Comparison of **4***a* in which the internal —CH_3 hydrogens appear (16) at δ 0.56, with those of *anti*-**3***a* at δ 1.30 (Δδ = 0.74), might crudely suggest that H_i for *anti*-**1** would appear at ca. δ 5.0. Correspondingly H_i for *syn*-**1** might have been expected to be fairly normal and close to δ 7 (as they were in the higher oligomers (5)). Since H_i for **1** actually appear at δ 6.82 ($CDCl_3$, 10°C) with hindsight, the contribution of the *anti*-conformer might have been calculated as small (<10%).

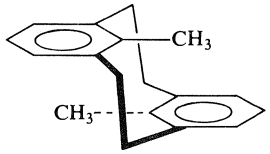

4*a*

Now, however, more suitable models are available for comparison. The *syn*-tris-bridged cyclophane **5**

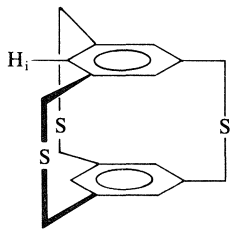

5

has now been reported and for this H_i appeared at δ 6.90 (17) and δ 6.91 (18). This provides an excellent model for H_i of *syn*-**1**. A good model for *anti*-**1** is *anti*-**3***b* (X = H, Y = CH_3) in which H_i appeared at δ 5.50 (19) and δ 5.59 (20). Clearly H_i for **1** are almost identical in chemical shift to those of **5**. Further the remaining aryl hydrogens of **1** at δ 6.91 are clearly shielded from normal benzene hydrogens, consistent with a *syn* structure for **1**. More recently Vögtle *et al.* (21) have reported the ^{1}Hmr spectra of **3***c* (X = H, Y = NO_2) where H_i appears at δ 7.3 and the remaining aryl hydrogens at δ 6.9 consistent with a *syn* structure for **3***c*. On the other hand **3***d* (X = H, Y = NH_2) exists as the *anti*-conformer since H_i appears at δ 5.0 and the remaining aryl hydrogens at ca. δ 7. Finally, Mitchell (22) has reported the variable temperature ^{1}Hmr spectrum of 2,11-diselena[3,3]metacyclophane **6** in which H_i appear (20°C) at δ 6.46. On cooling to −110°C an *anti*-conformer is formed in which H_i appear at δ 4.50.

Taken collectively this evidence points to the fact that at room temperature 2,11-dithia[3,3]metacyclophane **1** exists in solution, as in the crystalline state, as the *syn*-conformer. We can find no evidence for participation of the *anti*-conformer. On cooling no change in shape of any of the ^{1}Hmr peaks occurs down to $-90°C$ (this work and ref. 3). From Fig. 4 it can be seen that in CS_2 the chemical shift of H_i remains invariant with temperature (as does the shift of the other hydrogens (Table S4)). The behaviour in other solvents is normal (23) and does not indicate a change from one conformer to the other. Consistent with results on other aromatic compounds (24), H_i appear at higher field in toluene (δ 6.50) where stronger π–π interactions occur than in more polar solvents such as DMSO (δ 6.98), see Fig. 4.

Since frequency separations observed from ^{13}Cmr spectra are generally much larger than for ^{1}Hmr, and the Gutowsky–Holm equation (25) which is frequently applied to cyclophanes (see for example refs. 1–3, 22, 36) gives the rate of exchange at coalescence as $k' = \pi\Delta\nu/\sqrt{2}$, we hoped that a low temperature ^{13}Cmr spectrum of **1** might provide further information. Somewhat surprisingly the ^{13}Cmr spectra of the simple dithia[3,3]metacyclophanes have not been reported; however, they are relatively easy to assign in comparison to that published (15) for **2** and measured[4] for **5**, and are shown below in Table 5. (Full data in other solvents are given[3] in Table S5.)

For [2,2](2,7)naphthalenophane **7**, both the *syn*- and *anti*-conformers are known (27). By analogy, the chemical shift difference between the internal aryl carbons for *syn*- and *anti*-**1** is thus predicted to be of the order of 3 ppm (~45Hz). Unfortunately this shift is likely to be somewhat smaller than the corresponding predicted proton shift of 1.5 ppm (~135 Hz) and casts doubt on the ability of ^{13}Cmr data for the ring carbons to provide any more information than ^{1}Hmr. However, for **7**, the difference between the ^{13}C shifts for the bridging methylenes is much larger than for the corresponding ^{1}H shifts. We have also verified this to be true in some of our previously (28) prepared thiacyclophanes which have internal methyl substituents and hence where both *syn*- and *anti*-conformers are known. In the event, the ^{13}Cmr signal due to the bridging methylenes of **1** does collapse at ca. $-100°C$ in CD_2Cl_2. Unfortunately, however, we were not able to find a solvent in which **1** retained some solubility at lower temperatures, and hence could not determine whether a freezing out was occurring of either the possible *syn*-**1** ⇄ *anti*-**1** process, or of the wobbling of bridges (shown below) (3, 17), or scissoring of the rings.

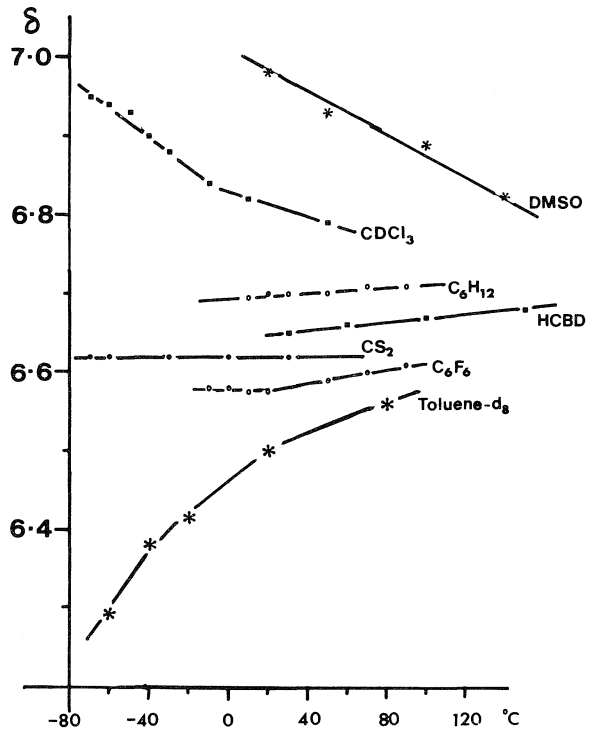

FIG. 4. Chemical shift (δ, ppm) values for H_i of **1** at different temperatures in various solvents.

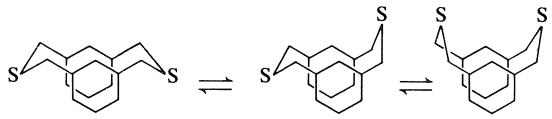

Chemical Reactions of 1

One of the reasons that **1** has been assumed to exist as *syn* ⇄ *anti* conformers is that on Wittig (or Stevens) rearrangement, **1** forms a 4:1, *anti*:*syn* mixture of product isomers **8** (5). It is, in fact, not

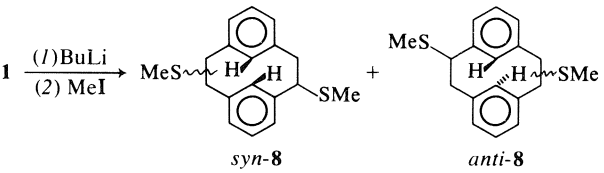

syn-**8** *anti*-**8**

necessary that *anti*-**8** has derived from *anti*-**1**, since it is documented (5) that pure *syn*-**3***a* on Wittig or Stevens rearrangement gives *anti* products. Since to our knowledge (see also ref. 20) *syn*-**3***a* is not convertible to *anti*-**3***a*, it is more likely that an intermediate (possibly open, see ref. 5) is isomerised during the course of the reaction.

[4]We thank Prof. Virgil Boekelheide for kindly supplying us with a sample of **5**.

TABLE 5. ^{13}Cmr data for selected cyclophanes (ppm downfield from Me_4Si)

Compound		Solvent	A	B	C	D	E	Ref.
1	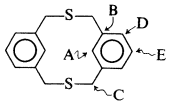	CD_2Cl_2	132.1	137.7	38.3	127.3	128.7	This work
5	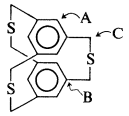	$CDCl_3$	130.4	137.2	38.7	—	—	This work
Anti-**2**	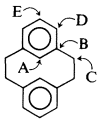	$CDCl_3$	136.3	138.6	41.4	125.1	128.6	(15)
Anti-**7**	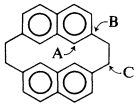	$CDCl_3$	130.8	135.9	38.8			(27)
Syn-**7**	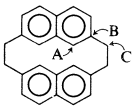	$CDCl_3$	127.2	137.8	35.8			(27)

TABLE 6. ^{1}Hmr data (δ) for selected derivatives of **1**

	H_i	H_{ar}	Ref.
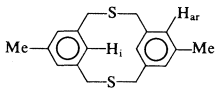	6.58	6.66	29
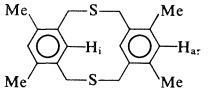	6.50	6.58	3
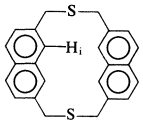	7.13		4
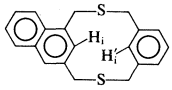	6.73 (H_i':6.95)		This work, 30
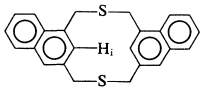	6.95		This work, 29
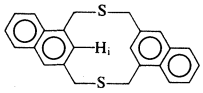	6.95		This work, 29

Other Derivatives of 1

There are several derivatives of **1** in the literature which by ^{1}Hmr comparison to **1** should now *all* be assigned as *syn*-conformers. These are presented in Table 6.

There is one [2,2]cyclophane, **9**, which has recently been assigned (31) to be the *anti*-conformer shown. However, in its ^{1}Hmr spectrum, H_i appear at δ 7.88 and H_{ar} at δ 7.01. Given that S—S (203 pm) and C—S (182 pm) bond lengths are longer than C—C (154 pm), and the fact (32) that in **10**, H_i is only deshielded to δ 5.42 from H_i' at δ 4.41, it seems to us most likely that **9** also exists as the *syn*-conformer.

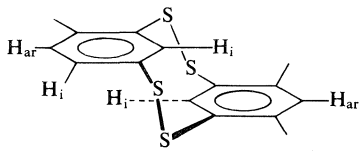

9

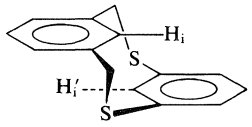

10

Conclusions

In the solid state **1** exists as the *syn*-conformer. In solution, ^{1}Hmr data indicate that **1** and a number of its derivatives also exist as the *syn*-conformer, with no appreciable participation of *anti*-**1** either at room temperature, or on cooling to −90°C.

Acknowledgements

We thank the University of Victoria and the Natural Sciences and Engineering Research Council of Canada for operating grants, Mrs. K. Beveridge for technical assistance, and Mr. Blaine Hawkins for the illustrative photography.

1. T. Sato, M. Wakabayashi, M. Kainosho, and K. Hata. Tetrahedron Lett. 4185 (1968).
2. F. Vögtle and L. Schunder. Chem. Ber. **102**, 2677 (1969).
3. T. Sato, M. Wakabayashi, K. Hata, and M. Kainosho. Tetrahedron, **27**, 2737 (1971).
4. F. Vögtle, R. Schäfer, L. Schunder, and P. Neumann. Ann. **734**, 102 (1970).
5. R. H. Mitchell and V. Boekelheide. J. Am. Chem. Soc. **96**, 1547 (1974).
6. V. Boekelheide and P. H. Anderson. J. Org. Chem. **38**, 3928 (1973).
7. D. J. Wilson, V. Boekelheide, and R. W. Griffin, Jr. J. Am. Chem. Soc. **82**, 6302 (1960).
8. C. J. Brown. J. Chem. Soc. 3278 (1953); P. K. Gantzel and K. N. Trueblood. Acta Crystallogr. **18**, 958 (1965).
9. R. H. Mitchell and V. Boekelheide. J. Am. Chem. Soc. **92**, 3510 (1970).
10. B. R. Penfold. University of Canterbury crystallographic programs. Christchurch, New Zealand.
11. D. T. Cromer and J. T. Waber. International tables for X-ray crystallography. Vol. IV. Kynoch Press, Birmingham. 1974. Table 2.2A. p. 72.
12. D. T. Cromer. International tables for X-ray crystallography. Vol. IV. Kynoch Press, Birmingham. 1974. Table 2.3.1. p. 148.
13. B. R. Davis and I. Bernal. J. Chem. Soc. B, 2307 (1971).
14. R. H. Mitchell and V. Boekelheide. Tetrahedron Lett. 1197 (1970).
15. T. Sato and T. Takemura. J. Chem. Soc. Perkin Trans. II, 1195 (1976).
16. W. S. Lindsay, P. Stokes, L. G. Humber, and V. Boekelheide. J. Am. Chem. Soc. **83**, 943 (1961).
17. V. Boekelheide and R. A. Hollins. J. Am. Chem. Soc. **95**, 3201 (1973).
18. F. Vögtle. Ann. **735**, 193 (1970).
19. V. Boekelheide and C. H. Tsai. J. Org. Chem. **38**, 3931 (1973).
20. F. Vögtle and P. Neumann. Tetrahedron, **26**, 5299 (1970).
21. F. Vögtle, W. Wieder, and H. Förster. Tetrahedron Lett. 4361 (1974).
22. R. H. Mitchell. Tetrahedron Lett. 1363 (1975).
23. J. R. Hanson. J. Chem. Soc. 5036 (1965); A. A. Bothner-By and R. E. Glick. J. Chem. Phys. **26**, 1651 (1957).
24. D. J. Bertelli and C. Golino. J. Org. Chem. **30**, 368 (1965); D. H. Williams and D. A. Wilson. J. Chem. Soc. B, 144 (1966).
25. H. S. Gutowsky and C. H. Holm. J. Chem. Phys. **25**, 1228 (1956); I. C. Calder and P. J. Garratt. J. Chem. Soc. B, 660 (1967).
26. I. Gault, B. J. Price, and I. O. Sutherland. Chem. Commun. 540 (1967).
27. T. Sato, H. Matsui, and R. Komaki. J. Chem. Soc. Perkin Trans. I, 2051 (1976).
28. R. H. Mitchell, R. J. Carruthers, and L. Mazuch. J. Am. Chem. Soc. **100**, 1007 (1978).
29. R. H. Mitchell and R. J. Carruthers. Can. J. Chem. **52**, 3054 (1974).
30. R. H. Mitchell and R. J. Carruthers. Tetrahedron Lett. 4331 (1975).
31. F. Bottino, S. Foti, S. Pappalardo, P. Finocchiaro, and M. Ferrugia. J. Chem. Soc. Perkin Trans. I, 198 (1979).
32. F. Vögtle. Tetrahedron Lett. 3623 (1968).

Comment: 7α-Acetoxydihydronomilin and mexicanolide: limonoids from *Xylocarpus granatum* (Koenig)

ANG S. NG
Department of Chemistry, Nanyang University, Singapore 22
AND
ALEX G. FALLIS
Department of Chemistry, Memorial University of Newfoundland, St. John's, Nfld., Canada A1B 3X7

Received September 7, 1979

ANG S. NG and ALEX G. FALLIS. Can. J. Chem. **57**, 3088 (1979).

A recent report by the present authors (Can. J. Chem. **56**, 1020 (1978)) of the isolation of 7α-acetoxydihydronomilin from the seeds of *Uncaria gambia* (Roxb.) contains a taxonomic error. The seeds were in fact from *Xylocarpus granatum* (Koenig).

ANG S. NG et ALEX G. FALLIS. Can. J. Chem. **57**, 3088 (1979).

Une erreur taxonomique s'est glissée dans notre récente publication concernant l'isolation de la 7α-acétoxydihydronomiline (Can. J. Chem. **56**, 1020 (1978)). Le produit est extrait de semence de *Xylocarpus granatum* (Koenig) et non de semence de *Uncaria gambia* (Roxb.).
[Traduit par le journal]

In Malaysia extracts of at least two different plant species are used as tanning agents called Gambir. We recently reported (1*a*, see also ref. 1*b*) the isolation and structure elucidation of 7α-acetoxydihydronomilin (**1**) from the seeds of one such species *Uncaria gambia* (Roxb.), a member of the Rubiaceae family.[1] This appeared to be the first example of a limonoid from Rubiaceae and as such, was unexpected as previously limonoids had only been found in the related families Rutaceae, Meliaceae, and Cneoraceae.

We wish to point out that the seeds we extracted were misidentified and are in fact from *Xylocarpus granatum* (Koenig), a mangrove of the Meliaceae family,[2] an assignment in keeping with their terpene content. In addition to **1** we have isolated (2) the known limonoid mexicanolide (**2**) (3) from these seeds. Earlier Okorie and Taylor (4) identified the structurally related compounds gedunin (**3**), xylocarpin (**4**), and the corresponding Δ^8 olefin from the petroleum ether extracts of *Xylocarpus granatum* (Koenig) seed. Subsequently, examination of unripe seed (originally reported (5) to be *Xylocarpus molluscensis* but established since (6) as *Xylocarpus granatum* (Koenig)) afforded the bitter principle xylomollin as unusual monoterpenoid secoiridoid possessing hemiacetal and acetal functions.

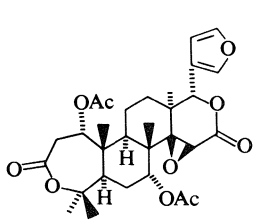

1

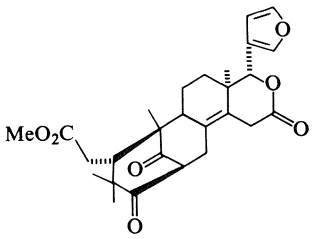

2

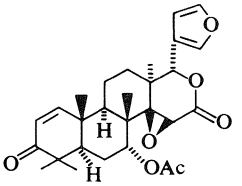

3

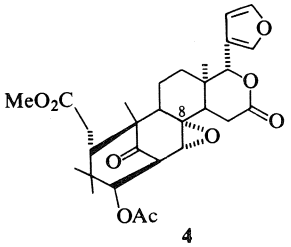

4

[1]7α-Acetoxydihydronomilin has also been isolated from *Cneorum tricoccon* (Linne).

[2]The fruit of *X. granatum* are large, round, and often referred to as "cannon balls." In our sample the largest was similar in size to a soccer ball. One or more tightly packed seeds are contained within this shell or husk. These seeds are easily crushed when fresh but harden and darken upon standing. The dry seeds have a wrinkled appearance and resemble dried prunes in size.

Acknowledgements

We are grateful to Professor D. A. H. Taylor for drawing this taxonomic error to our attention and for a fruitful exchange of correspondence. In addition the National Research Council of Canada is thanked for financial support.

0008-4042/79/233088-02$01.00/0

1. (*a*) F. R. AHMED, A. S. NG, and A. G. FALLIS. Can. J. Chem. **56**, 1020 (1978); (*b*) B. EPE and A. MONDON. Tetrahedron Lett. 2015 (1979).
2. A. S. NG and A. G. FALLIS. Occasional Paper No. 40, Faculty of Graduate Studies, Nanyang University, Singapore. September, 1978.
3. J. D. CONNOLLY, R. MCCRINDLE, and K. H. OVERTON. Tetrahedron, **24**, 1489 (1968); **24**, 1497 (1968); E. K. ADESOGAN and D. A. H. TAYLOR. J. Chem. Soc. C, 1974 (1968).
4. D. A. OKORIE and D. A. H. TAYLOR. J. Chem. Soc. C, 211 (1970).
5. I. KUBO, I. MIURA, and K. NAKANISHI. J. Am. Chem. Soc. **98**, 6704 (1976).
6. D. A. H. TAYLOR. Personal communication.

Neutral pyrazolyl-bridged nickel nitrosyl complexes. Synthesis, structure, and reactivity

KENNETH S. CHONG, STEVEN J. RETTIG, ALAN STORR, AND JAMES TROTTER

Department of Chemistry, University of British Columbia, 2075 Wesbrook Mall, Vancouver, B.C., Canada V6T 1W5

Received June 28, 1979

KENNETH S. CHONG, STEVEN J. RETTIG, ALAN STORR, and JAMES TROTTER. Can. J. Chem. **57**, 3090 (1979).

A series of neutral pyrazolyl-bridged nickel nitrosyl complexes, $[LNi(NO)]_2$ (where L = pyrazolyl, $N_2C_3H_3$; 3,5-dimethylpyrazolyl, $N_2C_5H_7$; or 3,5-di-*tert*-butylpyrazolyl, $N_2C_{11}H_{19}$), is described. The nickel atoms are susceptible to nucleophilic attack and the reactivity of the dimers with neutral donor ligands is reported. In addition to the dimeric molecules a novel trimetallic nickel compound $[(ON)Ni(N_2C_5H_7)_2]_2Ni$ has also been isolated. Crystals of $[Ni(NO)(N_2C_5H_7)]_2$ are monoclinic, $a = 18.925(2)$, $b = 11.012(1)$, $c = 7.037(2)$ Å, $\beta = 100.93(1)°$, $Z = 4$, space group $C2/c$ and crystals of $[(ON)Ni(N_2C_5H_7)_2]_2Ni$ are triclinic, $a = 7.4041(7)$, $b = 9.6331(7)$, $c = 9.7595(8)$ Å, $\alpha = 85.698(9)$, $\beta = 73.174(8)$, $\gamma = 76.109(8)°$, $Z = 1$, space group $P\bar{1}$. Both structures were solved by Patterson and Fourier syntheses and were refined by full-matrix least-squares procedures to $R = 0.035$ and 0.028 for 832 and 2128 reflections with $I \geq 3\sigma(I)$ respectively. Nearly planar centrosymmetric molecules of $[Ni(NO)(N_2C_5H_7)]_2$ contain trigonal planar nickel atoms with Ni—N(pyrazolyl) = 1.880(3) and 1.922(3), Ni—NO = 1.616(4), and N—O = 1.158(4) Å, Ni—N—O = 178.9(4)°. This structure also contains an unusually long N—N bond in the pyrazolyl ring (1.463(4) Å). Centrosymmetric molecules of $[(ON)Ni(N_2C_5H_7)_2]_2Ni$ contain a central square-planar Ni(II) atom bonded to four pyrazolyl nitrogen atoms (mean Ni—N = 1.905(1) Å) and two trigonal planar outer nickel atoms coordinated to two pyrazolyl nitrogen atoms (mean Ni—N = 1.922(3) Å) and to a somewhat bent nitrosyl group (Ni—N = 1.625(3), N—O = 1.153(4) Å, Ni—N—O = 168.9(3)°).

KENNETH S. CHONG, STEVEN J. RETTIG, ALAN STORR et JAMES TROTTER. Can. J. Chem. **57**, 3090 (1979).

On décrit une série de complexes neutres de nitrosyle nickel avec le nickel en position de pont par rapport au pyrazolyle $[LNi(NO)]_2$ (où L = pyrazolyle, $N_2C_3H_3$; diméthyl-3,5 pyrazolyle, $N_2C_5H_7$; ou di-*tert*-butyl-3,5 pyrazolyle, $N_2C_{11}H_{19}$. Les atomes de nickel sont sensibles à une attaque nucléophile et on rapporte la réactivité des dérivés vis-à-vis les ligands donneurs neutres. En plus des molécules dimères, on a également isolé un nouveau composé de nickel trimétallique $[(ON)Ni(N_2C_5H_7)_2]Ni$. Les cristaux de $[Ni(NO)(N_2C_5H_7)]_2$ sont monocliniques: $a = 18.925(2)$, $b = 11.012(1)$, $c = 7.037(2)$ Å, $\beta = 100.93(1)°$, $Z = 4$, groupe d'espace $C2/c$ et les cristaux de $[(ON)Ni(N_2C_5H_7)_2]_2Ni$ sont tricliniques: $a = 7.4041(7)$, $b = 9.6331(7)$, $c = 9.7595(8)$ Å, $\alpha = 85.698(9)$, $\beta = 73.174(8)$, $\gamma = 76.109(8)°$, $Z = 1$, groupe d'espace $P\bar{1}$. On a résolu les deux structures à l'aide de synthèses de Patterson et de Fourier et on les a affinées par la méthode des moindres carrés (matrice complète) jusqu'à des valeurs respectives de $R = 0.035$ et 0.028 pour 832 et 2128 réflexions avec $I \geq 3\sigma(I)$. Les molécules de $[Ni(NO)(N_2C_5H_7)]_2$, sensiblement planes et centrosymétriques, contiennent des atomes de nickel trigonaux plans avec des longueurs de liaisons: Ni—N(pyrazolyle) = 1.880(3) et 1.922(3), Ni—NO = 1.616(4) et N—O = 1.158(4) Å et un angle Ni—N—O = 178.9(4)°. Cette structure contient également une longue liaison N—N dans le cycle pyrazolyle (1.463(4) Å). Les molécules centrosymétriques de $[(ON)Ni(N_2C_5H_7)_2]_2Ni$ contiennent un nickel(II) central quadratique lié aux 4 atomes d'azote du cycle pyrazolyle (i.e. Ni—N = 1.905(1) Å et deux atomes de nickel(II) à l'extérieur trigonaux-plans coordonnés à deux atomes d'azote du cycle pyrazolyle (i.e., Ni—N = 1.922(3) Å et à un groupe nitrosyle légèrement courbé Ni—N = 1.625(3), N—O = 1.153(4) Å, Ni—N—O = 168.9(3)°).

[Traduit par le journal]

Introduction

In our continuing study of pyrazolyl-based ligands (1, 2) our attention has recently been focused on a series of pyrazolyl metal nitrosyl compounds containing bridging bidentate pyrazolyl moieties. The ligating properties of bridging pyrazolyl groups have been reviewed by Trofimenko (3) and recent reports reflecting the current interest in this type of bridging system have included novel η^5-cyclopentadienyl compounds of titanium (4, 5) and nickel (6), binuclear complexes involving palladium and platinum (7), and mono-, bi-, and trinuclear gold derivatives (8). The present paper describes the synthesis of a series of "16-electron" nickel nitrosyl complexes and details their selective acceptor properties towards electron donor molecules. X-ray crystal structures are de-

0008-4042/79/233090-09$01.00/0

scribed for a representative example of the bimetallic complexes prepared and also for the trimetallic compound isolated.

Experimental

Starting Materials

Air-sensitive materials were handled in a glove box under an atmosphere of oxygen-free, dry nitrogen or in a nitrogen-blanketed apparatus. Tetrahydrofuran (THF) was dried by refluxing over sodium/benzophenone and was used immediately following distillation. Benzene was dried by refluxing over molten potassium followed by distillation. Pyrazole and 3,5-dimethylpyrazole (K and K Laboratories) and sodium hydride (Alfa Inorganic) were used as supplied. 3,5-Di-*tert*-butylpyrazole was prepared by a standard route (9). The sodium salts of the three "pyrazole" compounds were prepared by reacting 1:1 mole ratios of sodium hydride and the appropriate pyrazole in THF solution. The solvent was removed and the salts washed with benzene and vacuum dried. Nickel nitrosyl iodide Ni(NO)I was prepared by the method of Haymore and Feltham (10).

Preparation of $[Ni(NO)(N_2C_5H_7)]_2$ *and* $[(ON)Ni(N_2C_5H_7)_2]_2Ni$

Ni(NO)I (2.156 g; 10.0 mmol) and $Na^+N_2C_5H_7^-$ (1.18 g; 10.0 mmol) were mixed together as THF solutions. The resulting blue solution[1] was stirred for 1 h and then the solvent was removed under vacuum. A green solid was isolated and this was soxhlet extracted with benzene solvent for 22 h. The resulting green solution, on cooling, deposited a green crystalline material, $[(ON)Ni(N_2C_5H_7)_2]_2Ni$ (0.05 g; 3.2% yield), which was isolated by filtration and washed with benzene. The filtrate and washings, on removal of solvent by slow evaporation, gave dark green needles of $[Ni(NO)(N_2C_5H_7)]_2$ (1.01 g; 55%).

The $[Ni(NO)(N_2C_3H_3)]_2$ and $[(N_2C_{11}H_{19})Ni(NO)]_2$ dimers were prepared by a similar route using the appropriate sodium "pyrazolide" salt and Ni(NO)I. The yields of these two dimers were 65% and 55% respectively. In these two reactions there was no evidence for the formation of the trimetallic nickel derivatives analogous to the one described above.

Preparation of $[(N_2C_5H_7)Ni(NO)(PPh_3)]_2$

$[Ni(NO)(N_2C_5H_7)]_2$ (0.184 g; 0.5 mmol) was dissolved in THF and solid PPh_3 (0.262 g; 1 mmol) added to the solution. The initial dark green color of the solution gradually changed to a dark blue color. After stirring the reaction mixture overnight the solvent was removed *in vacuo*. The resulting solid was extracted with benzene and the crude material obtained from the benzene solution was recrystallized from benzene/THF to give very dark blue crystals of pure product (0.373 g; 84%).

The $AsPh_3$ complex, $[(N_2C_5H_7)Ni(NO)(AsPh_3)]_2$, was prepared similarly and was isolated as blue–green crystals from benzene solvent in 87% yield. The corresponding compounds containing unsubstituted pyrazolyl bridging moieties, viz. $[(N_2C_3H_3)Ni(NO)(PPh_3)]_2$ and $[(N_2C_3H_3)Ni(NO)(AsPh_3)]_2$, were prepared by analogous reactions and were isolated as purple–blue crystals (yield 47%) and dark blue crystals (yield 52%) respectively.

[1]The blue color at this stage is probably due to the iodide bridged anion $[(ON)Ni(N_2C_5H_7)_2(I)Ni(NO)]^-$ discussed in the following paper.

Preparation of $[Ni(NO)(N_2C_5H_7)]_2 \cdot Ph_2PCH_2CH_2PPh_2$

$[Ni(NO)(N_2C_5H_7)]_2$ dimer (0.202 g; 0.55 mmol) was dissolved in THF and diphos (0.220 g; 0.55 mmol) in the same solvent added to the solution. The dark green solution of the dimer immediately became dark blue. After stirring for about 1 h the solvent was removed *in vacuo*. The dark blue solid obtained was recrystallized from THF/benzene to give the pure product, a blue crystalline material, in high yield.

Reactions of $[Ni(NO)(N_2C_5H_7)]_2$ *with Nitrogen Donor Species*

(a) $N_2C_5H_8$, *3,5-Dimethylpyrazole*

The dimer (0.184 g; 0.50 mmol) reacted with 3,5-dimethylpyrazole (0.096 g; 1.00 mmol) in THF solution to give a blue solution which on work-up gave a blue crystalline solid (0.186 g; 67%). This solid product, $[(N_2C_5H_7)Ni(NO)(N_2C_5H_8)]_2$, appeared indefinitely air-stable at room temperature and solutions, kept under a nitrogen atmosphere, remained blue.

(b) Pyridine, py

A solution (green color) of the dimer, $[Ni(NO)(N_2C_5H_7)]_2$, was treated with an excess of pyridine. The solution turned blue and on removal of solvent and excess ligand a blue solid was obtained. Attempted recrystallization by evaporation of benzene solution gave only the green dimer starting material. Even the crude blue solid out of THF slowly turned green, indicating ready loss of the pyridine ligand. Benzene (^1H nmr) and cyclohexane (ir) solutions of the crude product changed color from blue to green on standing, even under an atmosphere of nitrogen. The ir spectrum of a Nujol mull sample of the "blue solid" showed the presence of coordinated pyridine with characteristic bands at 1600, 635, and 436 cm^{-1} (11–13). The ν_{NO} region showed two bands, a medium shoulder at $\sim$1800 cm^{-1} and a strong main band at 1740 cm^{-1}. The band at 1800 cm^{-1} could well be due to the presence of free dimer in the sample caused by loss of pyridine before and during sample preparation. The ^1H nmr in C_6D_6 showed one signal for the 3,5 Me groups attached to the pyrazolyl moieties but the presence of "free" dimer is again evident from an integration of the various signals. The ready loss of pyridine from the blue solid adduct hampered all attempts to obtain a reasonable analytical analysis for the compound.

(c) Trimethylamine, Me_3N

The $[Ni(NO)(N_2C_5H_7)]_2$ dimer in THF solution displayed a color change from green to blue on treatment with Me_3N at low temperature ($\sim -78°C$). At room temperature the solution turned green and on removal of solvents and volatiles the starting material was recovered. These observations indicate a possible weak coordination of the amine at low temperature in solution.

Attempted Reactions of $[Ni(NO)(N_2C_5H_7)]_2$ *with Other Donors*

Attempted coordination of carbon monoxide or diphenylacetylene to the dimer species did not lead to indicative color changes in THF solutions of the dimer. On removal of solvent and unreacted "ligands" the dimer was quantitatively recovered in both experiments.

Spectra

Mass spectra were recorded on a Varian MAT CH4 mass spectrometer at 70 eV with an ion source temperature of 100–180°C. Infrared spectra were recorded on a Perkin-Elmer 457 spectrophotometer and ^1H nmr spectra on a Varian XL-100 spectrometer. For complexes of low solubility ^1H nmr spectra were obtained using FT techniques. Analytical and spectral data appear in Table 1.

TABLE 1. Analytical data for 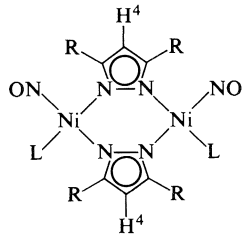 complexes

Compound		Analysis*			ν_{NO} (cm^{-1})		τ (ppm) (C_6D_6 solution)		
R	L	C	H	N	Cyclohexane	Nujol	R	H^4	L
H		23.4 23.1	2.0 1.9	26.5 27.0	1817	1815	1.34d†	3.28t†	
H	PPh_3	60.5 60.3	4.4 4.3	9.8 10.0	1807, 1720	1718	1.88d†	3.55t†	2.52m, 3.06m
H	$AsPh_3$	54.0 54.6	3.9 3.9	9.0 9.1	1816, 1772	1768	1.45d†	3.26t†	2.63m, 2.97m
Me		32.9 32.7	3.9 3.8	22.9 22.9	1800	1800	7.44s	3.59s	
Me	PPh_3	61.9 61.9	5.0 5.0	9.7 9.4	1804, 1758	1728	7.47s	3.46s	2.64m, 2.96m
Me	$AsPh_3$	56.4 56.4	4.5 4.5	8.3 8.6	1805, 1770	1762	7.44s	3.52s	2.61m, 2.93m
t-Bu		49.0 49.3	7.3 7.2	16.0 15.7	1788	1779	8.18s	3.48s	
Me	(1/2)diphos	56.7 56.4	4.9 4.9	10.7 11.0	i	1722	7.51s	3.34s	2.74m, 3.00m, 8.23m
Me	$N_2C_5H_8$	42.5 42.9	5.3 5.4	24.7 25.0	1800, 1756	1755	7.88br	3.88br	4.15s, 7.20s, 7.74s
Me	Pyridine				1805, 1770	1740 1800sh	7.29s	3.41s	3.08br
Trimetallic complex		39.0 39.0	4.7 4.6	22.8 22.7	i	1809		i	

*First rows, found values; second rows, calculated values.
†$J \approx 2$ Hz; d = doublet, s = singlet, t = triplet, m = multiplet, br = broad, sh = shoulder, i = insoluble.

X-ray Crystallographic Analyses

Bis(μ-3,5-dimethylpyrazolyl(N,N′))bis(nitrosylnickel(I))

The crystal chosen was mounted in a general orientation and had dimensions of ca. 0.068 × 0.150 × 0.625 mm. Unit-cell parameters were refined by least squares on 2 sin θ/λ values for 48 reflections measured on a diffractometer with Mo K_α radiation (λ = 0.71073 Å). Crystal data (at 22°C) are:

$C_{10}H_{14}N_6Ni_2O_2$ fw = 367.68

Monoclinic, a = 18.925(2), b = 11.012(1), c = 7.037(2) Å, β = 100.93(1)°, V = 1439.9(4) Å^3, Z = 4, ρ_c = 1.696 g cm^{-3}, $F(000)$ = 752, μ(Mo K_α) = 25.4 cm^{-1}. Absent reflections: hkl, $h + k \neq 2n$, $h0l$, $l \neq 2n$. Space group $C2/c$ (C_{2h}^6, No. 15) from structure analysis.

Intensities were measured with graphite monochromatized Mo K_α radiation on an Enraf-Nonius CAD4-F diffractometer. An ω scan at 0.91–5.03° min^{-1} over a range of (0.65 + 0.35 tan θ) degrees in ω (extended by 25% on both sides for background measurement) was employed. Data were measured to 2θ = 55°. The intensities of 3 check reflections, measured every 3600 s throughout the data collection, remained constant to within ±2.5%. After data reduction, an absorption correction was applied using the Gaussian integration method (14, 15). Transmission factors ranged from 0.634 to 0.852. Of the 1632 independent reflections measured, 852 (52%) had intensities greater than 3σ(I) above background where $\sigma^2(I) = S + 2B + (0.04(S - B))^2$ with S = scan count and B = background count.

Analysis was initiated in the centrosymmetric space group $C2/c$ on the basis of the E-statistics. The coordinates of the Ni atom were determined from the three-dimensional Patterson function and those of the other non-hydrogen atoms from a subsequent difference map. After full-matrix least-squares refinement of the non-hydrogen atoms with anisotropic thermal parameters to R = 0.046, a difference map gave positions for all seven hydrogen atoms which were included in subsequent cycles of refinement with isotropic thermal parameters. The scattering factors of ref. 16 were used for non-hydrogen atoms and those of ref. 17 for hydrogen atoms. Anomalous scattering factors from ref. 18 were used for the Ni atoms. The weighting scheme, $w = 1/\sigma^2(F)$ where $\sigma^2(F)$ is derived from the previously defined $\sigma^2(I)$ gave uniform average values of $w(|F_o| - |F_c|)^2$ over ranges of $|F_o|$ and was employed in the final stages of refinement. Convergence was reached at R = 0.035 and R_w = 0.043 for 852 reflections with $I \geq 3\sigma(I)$. For all 1632 reflections R = 0.095 and R_w = 0.052.

On the final cycle of refinement the mean and maximum parameter shifts corresponded to 0.02 and 0.20σ, respectively. The mean error in an observation of unit weight was 1.1556. The final positional and thermal parameters appear in Tables 2 and 3[2] respectively. Measured and calculated structure factors have been placed in the Depository of Unpublished Data.[2]

Bis[bis(3,5-dimethylpyrazolyl)nitrosylniccolate(I)(N′,N′)]-nickel(II)

Details of the structure analysis are the same as for $[Ni(NO)(N_2C_5H_7)]_2$ except where noted. Crystal dimensions were 0.173 × 0.233 × 0.140 mm. Forty-nine reflections were used in the refinement of the unit-cell parameters. Crystal data are:

$C_{20}H_{28}N_{10}Ni_3O_2$ fw = 616.64
Triclinic, a = 7.4041(7), b = 9.6331(7), c = 9.7595(8) Å, α = 85.698(9), β = 73.174(8), γ = 76.109(8)°, V = 646.8(1) Å^3, Z = 1, ρ_c = 1.583 g cm^{-3}, $F(000)$ = 318, μ(Mo K_α) = 21.9 cm^{-1}. Absent reflections: none. Space group $P\bar{1}$ (C_i^1, No. 2) from structure analysis.

An ω–θ scan at 0.91–5.03 min^{-1} over a range of (0.60 + 0.35 tan θ°) in ω was employed. Of 2925 independent reflections measured (to 2θ = 55°), 2128 (73%) had intensities greater than 3σ(I) above background. The intensities of the check reflections remained constant to within ±1%. An absorption correction was applied, transmission factors ranging from 0.580 to 0.750.

The coordinates of the Ni atoms were determined from the three-dimensional Patterson function and those of the remaining non-hydrogen atoms from a subsequent difference map. Refinement of the non-hydrogen atoms with anisotropic thermal parameters gave R = 0.038. All 14 hydrogen atoms were located from a difference map calculated at this point and were included in subsequent cycles of refinement with isotropic thermal parameters. Convergence was reached at R = 0.028 and R_w = 0.036 for 2128 reflections with $I \geq 3\sigma(I)$. For all 2925 reflections R = 0.051 and R_w = 0.040. The mean and maximum parameter shifts on the final cycle of refinement corresponded to 0.13 and 1.67σ, respectively. The mean error in an observation of unit weight was 1.1405. Final difference maps for both structures were essentially featureless, showing maximum deviations of ±0.3 e Å^{-3}.

The thermal motions of both molecules have been analysed in terms of the rigid-body modes of translation, libration, and screw motion (19) using the computer program MGTLS. For both molecules (rms σU_{ij} = 0.0025 and 0.0013 Å^2 respectively) analysis of all non-hydrogen atoms except the nitrosyl oxygen atoms gave rms ΔU_{ij} = 0.0059 and 0.0045 Å^2 respectively and physically reasonable rigid-body parameters. For $[(ON)Ni(N_2C_5H_7)_2]_2Ni$ some independent motion was noted for the nitrosyl nitrogen and methyl carbon atoms. The appropriate bond distances have been corrected for libration (20), using shape parameters q^2 of 0.08 for all atoms involved. Corrected bond lengths for both molecules appear along with the uncorrected values in Table 4. Corrected bond angles do not differ by more than 1σ from the uncorrected values in Table 5. Torsion angles in the six-membered Ni_2N_4 chelate rings are given in Table 6.

TABLE 2. Final positional parameters (fractional: O, N, and C × 10^4, Ni × 10^5, H × 10^3) with estimated standard deviations in parentheses

Atom	x	y	z
	$[Ni(NO)(N_2C_5H_7)]_2$		
Ni	44663(2)	35966(4)	46722(8)
O	3609(2)	1541(3)	4136(8)
N(1)	5496(1)	3705(2)	5279(5)
N(2)	5911(1)	4826(2)	5547(4)
N(3)	3973(2)	2393(3)	4357(6)
C(1)	5962(2)	2773(3)	5611(6)
C(2)	6649(2)	3217(4)	6014(7)
C(3)	6597(2)	4458(4)	5969(6)
C(4)	5720(3)	1477(5)	5456(13)
C(5)	7194(2)	5396(5)	6331(9)
H(2)	702(2)	290(4)	613(6)
H(4a)	532(4)	133(5)	465(9)
H(4b)	604(3)	94(6)	555(9)
H(4c)	539(3)	131(4)	633(8)
H(5a)	717(2)	596(4)	524(7)
H(5b)	768(2)	504(4)	669(7)
H(5c)	707(2)	588(5)	762(7)
	$[(ON)Ni(N_2C_5H_7)_2]_2Ni$		
Ni(1)	50000	50000	50000
Ni(2)	58198(5)	20107(3)	69813(3)
O	8130(5)	905(4)	8759(4)
N(1)	5707(3)	3152(2)	4168(2)
N(2)	6335(3)	1975(2)	4942(2)
N(3)	2933(3)	4447(2)	6430(2)
N(4)	3352(3)	3354(2)	7366(2)
N(5)	7108(4)	1247(3)	8039(3)
C(1)	6052(3)	2749(3)	2816(3)
C(2)	6913(4)	1286(3)	2711(3)
C(3)	7074(3)	845(2)	4045(3)
C(4)	1035(3)	5080(2)	6908(3)
C(5)	229(4)	4388(3)	8148(3)
C(6)	1716(4)	3328(2)	8415(3)
C(7)	5539(5)	3761(3)	1685(3)
C(8)	7882(4)	−615(3)	4570(4)
C(9)	95(4)	6332(3)	6167(3)
C(10)	1672(6)	2278(3)	9625(3)
H(2)	722(4)	79(3)	193(3)
H(5)	−110(4)	461(3)	871(3)
H(7a)	448(6)	465(4)	208(4)
H(7b)	545(5)	328(4)	86(4)
H(7c)	660(7)	430(5)	120(5)
H(8a)	706(4)	−93(3)	539(3)
H(8b)	895(6)	−77(4)	489(4)
H(8c)	833(6)	−130(5)	388(5)
H(9a)	76(5)	641(4)	513(4)
H(9b)	−107(6)	636(4)	632(4)
H(9c)	18(5)	730(4)	653(4)
H(10a)	243(9)	217(6)	1009(6)
H(10b)	58(9)	261(6)	1038(6)
H(10c)	176(7)	129(6)	927(6)

Results and Discussion

In contrast to nickel nitrosyl iodide, an air-sensitive solid (10), the green crystalline pyrazolyl bridged nickel nitrosyl dimers, the trimetallic nickel complex, and the majority of their adducts formed with neutral donor ligands, are all air-stable solids. However, solutions of both the parent compounds and their adducts are very air-sensitive and rapidly

[2]The structure factor table and Table 3 (thermal parameters) are available, at a nominal charge, from the Depository of Unpublished Data, CISTI, National Research Council of Canada, Ottawa, Ont., Canada K1A 0S2.

TABLE 4. Bond lengths (Å) with estimated standard deviations in parentheses

(a) Non-hydrogen atoms*

Bond	Length		Bond	Length	
	Uncorr.	Corr.		Uncorr.	Corr.
			$[Ni(NO)(N_2C_5H_7)]_2$		
Ni —N(1)	1.917(3)	1.922	N(2)—C(3)	1.338(4)	1.340
Ni —N(2)′	1.874(3)	1.880	C(1)—C(2)	1.368(6)	1.371
Ni —N(3)	1.612(4)	1.616	C(1)—C(4)	1.497(7)	1.500
O —N(3)	1.157(4)	1.158	C(2)—C(3)	1.370(6)	1.376
N(1) —N(2)	1.457(4)	1.463	C(3)—C(5)	1.516(6)	1.521
N(1) —C(1)	1.344(4)	1.348			
			$[(ON)Ni(N_2C_5H_7)_2]_2Ni$		
Ni(1)—N(1)	1.904(2)	1.906	N(3)—C(4)	1.348(3)	1.348
Ni(1)—N(3)	1.902(2)	1.904	N(4)—C(6)	1.345(3)	1.345
Ni(2)—N(2)	1.916(2)	1.919	C(1)—C(2)	1.399(3)	1.399
Ni(2)—N(4)	1.922(2)	1.924	C(1)—C(7)	1.489(4)	1.491
Ni(2)—N(5)	1.623(3)	1.625	C(2)—C(3)	1.369(4)	1.371
O —N(5)	1.153(4)	1.153	C(3)—C(8)	1.504(4)	1.505
N(1) —N(2)	1.376(2)	1.378	C(4)—C(5)	1.385(3)	1.386
N(3) —N(4)	1.379(2)	1.381	C(4)—C(9)	1.490(4)	1.492
N(1) —C(1)	1.338(3)	1.339	C(5)—C(6)	1.382(4)	1.384
N(2) —C(3)	1.353(3)	1.353	C(6)—C(10)	1.494(4)	1.495

*Here and elsewhere primed atoms have coordinates related to those in Table 3 by inversion through the centre of symmetry at 1/2, 1/2, 1/2.

(*b*) Bonds involving hydrogen atoms

Compound	Bond	Length	Mean
$[Ni(NO)(N_2C_5H_7)]_2$	C(sp^2)—H	0.78(4)	
	C(sp^3)—H	0.83–1.12(4–6)	0.96(10)
$[(ON)Ni(N_2C_5H_7)_2]_2Ni$	C(sp^2)—H	0.88(3)	0.92(4)
		0.96(3)	
	C(sp^3)—H	0.80–1.04(3–6)	0.95(8)

lose their color on exposure to the atmosphere with concomitant loss of the ν_{NO} band in their ir spectra and deposition of a white solid.

It is evident from the ^1H nmr results (Table 1) that the dimeric compounds have either a planar central, Ni—(N—N)$_2$—Ni, six-membered ring, or this ring is in a boat conformation. Either arrangement would allow delocalization of six π-electrons in both pyrazolyl groups in the molecule. A planar Ni_2N_4 arrangement has been established for the $[Ni(NO)(N_2C_5H_7)]_2$ dimer in the solid state through a crystal structure analysis (see below).

Infrared Spectra

The ν_{NO} bands for the compounds studied are listed in Table 1. The parent dimers (cyclohexane and Nujol) and the trimetallic compound (Nujol) display one ν_{NO} band in their spectra. With increasing steric crowding on the "pyrazolyl" fragment there is a significant shift in ν_{NO} values to lower wave numbers. This shift could result from increased back-bonding from the Ni atoms to the NO groups as a result of a charge build-up on the Ni atoms caused by an inductive effect from the 3,5 substituents on the "pyrazolyl" moieties.

The adducts display one ν_{NO} band in their Nujol mull spectra but two clearly resolved bands in their ir spectra in cyclohexane solution. This may indicate that the two ligands are occupying a *cis* arrangement in the complexes since a *trans* arrangement would be expected to give one ν_{NO} band in the ir (21, 22). In this case, the most likely arrangement for these adducts is one in which the central Ni_2N_4 ring remains planar, with the two NO groups below this plane and the two donor molecules above this plane. Each Ni atom would then acquire pseudo-tetrahedral geometry.

An alternate explanation is that the adducts dissociate in solution and that the two bands in solution arise from the parent and the adduct.

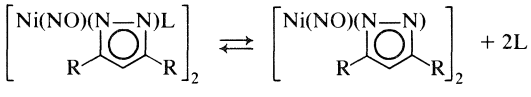

In this case, the adducts would be expected to occupy a *trans* arrangement (one ν_{NO} band due to the ad-

TABLE 5. Bond angles (deg) with estimated standard deviations in parentheses. Non-hydrogen atoms

Bonds	Angle (deg)	Bonds	Angle (deg)
	$[Ni(NO)(N_2C_5H_7)]_2$		
N(1) —Ni —N(2)′	108.4(1)	Ni —N(3)—O	178.9(4)
N(1) —Ni —N(3)	128.3(2)	N(1) —C(1)—C(2)	109.3(3)
N(2)′—Ni —N(3)	123.3(2)	N(1) —C(1)—C(4)	122.3(4)
Ni —N(1) —N(2)	125.6(2)	C(2) —C(1)—C(4)	128.4(4)
Ni —N(1) —C(1)	126.6(2)	C(1) —C(2)—C(3)	106.8(4)
N(2) —N(1) —C(1)	107.7(3)	N(2) —C(3)—C(2)	111.7(3)
Ni′ —N(2) —N(1)	125.9(2)	N(2) —C(3)—C(5)	119.4(4)
Ni′ —N(2) —C(3)	129.6(3)	C(2) —C(3)—C(5)	128.8(4)
N(1) —N(2) —C(3)	104.4(3)		
	$[(ON)Ni(N_2C_5H_7)_2]_2Ni$		
N(1) —Ni(1)—N(3)	89.70(8)	N(3) —N(4)—C(6)	108.2(2)
N(1) —Ni(1)—N(3)′	90.30(8)	Ni(2)—N(5)—O	168.9(3)
N(2) —Ni(2)—N(4)	97.09(8)	N(1) —C(1)—C(2)	108.4(2)
N(2) —Ni(2)—N(5)	131.7(1)	N(1) —C(1)—C(7)	122.7(2)
N(4) —Ni(2)—N(5)	131.1(1)	C(2) —C(1)—C(7)	128.9(2)
Ni(1)—N(1) —N(2)	119.2(1)	C(1) —C(2)—C(3)	106.3(2)
Ni(1)—N(1) —C(1)	131.2(2)	N(2) —C(3)—C(2)	108.9(2)
N(2) —N(1) —C(1)	108.4(2)	N(2) —C(3)—C(8)	121.0(2)
Ni(2)—N(2) —N(1)	122.4(1)	C(2) —C(3)—C(8)	130.0(2)
Ni(2)—N(2) —C(3)	129.1(2)	N(3) —C(4)—C(5)	108.6(2)
N(1) —N(2) —C(3)	107.9(2)	N(3) —C(4)—C(9)	122.4(2)
Ni(1)—N(3) —N(4)	119.3(1)	C(5) —C(4)—C(9)	129.0(2)
Ni(1)—N(3) —C(4)	131.7(2)	C(4) —C(5)—C(6)	106.5(2)
N(4) —N(3) —C(4)	108.0(2)	N(4) —C(6)—C(5)	108.7(2)
Ni(2)—N(4) —N(3)	122.3(1)	N(4) —C(6)—C(10)	122.0(2)
Ni(2)—N(4) —C(6)	129.0(2)	C(5) —C(6)—C(10)	129.3(2)

TABLE 6. Intra-annular torsion angles (deg) six-membered chelate rings

$[Ni(NO)(N_2C_5H_7)]_2$		$[(ON)Ni(N_2C_5H_7)_2]_2Ni$	
Bond	Angle	Bond	Angle
Ni —N(1)	0.7(2)	Ni(1)—N(1)	−64.0(1)
N(1) —N(2)	−0.8(2)	N(1) —N(2)	19.1(1)
N(2) —Ni′	0.7(2)	N(2) —Ni(2)	32.3(1)
Ni′ —N(1)′	−0.7(2)	Ni(2)—N(4)	−32.9(1)
N(1)′—N(2)′	0.8(2)	N(4) —N(3)	−18.1(1)
N(2)′—Ni	−0.7(2)	N(3) —Ni(1)	63.3(1)

duct). The one exception is the diphos complex which is sterically forced to adopt a *cis* arrangement.

^1H Nuclear Magnetic Resonance Spectra

The spectra (Table 1) for the dimers are consistent with a planar Ni_2N_4 ring for these complexes in C_6D_6 solution. The bis-adduct compounds with PPh_3 and $AsPh_3$ gave simple spectra suggestive of very symmetrical structures in solution. A pseudo-tetrahedral arrangement about the nickel atoms **1** rather than a square-planar one **2** is imperative since the latter arrangement, whether *cis* or *trans*, would lead to two signals for the 3,5 substituents on the pyrazolyl groups. On the other hand, a tetrahedral arrangement about the Ni atoms, as in **1**, satisfactorily accounts for the observed spectra, whatever the arrangement of the NO and EPh_3 groups. Thus if the NO groups are *cis* (as suggested by the ir spectra in cyclohexane solution) the spectra could be explained if the central six-membered ring were planar or in a boat conformation which was either static or rapidly inverting on the nmr time scale. If the NO groups are *trans* then again the central Ni_2N_4 ring may be planar or in a boat conformation but, if the latter, then a rapid inversion process on the nmr time scale is a premise necessary to explain the observed spectra.

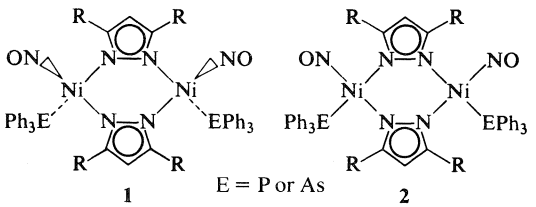

1 E = P or As 2

The ^1H nmr spectrum of the diphos derivative (diphos = $(Ph_2PCH_2)_2$) displays one signal for the 3,5 Me substituents on the pyrazolyl rings, consistent with a very symmetrical structure with a bridging diphos ligand between the two Ni atoms.

The ^1H nmr spectrum of the $[(N_2C_5H_7)Ni(NO)(N_2C_5H_8)]_2$ adduct shows, as expected, one signal for the 3,5 Me substituents on the bridging pyra-

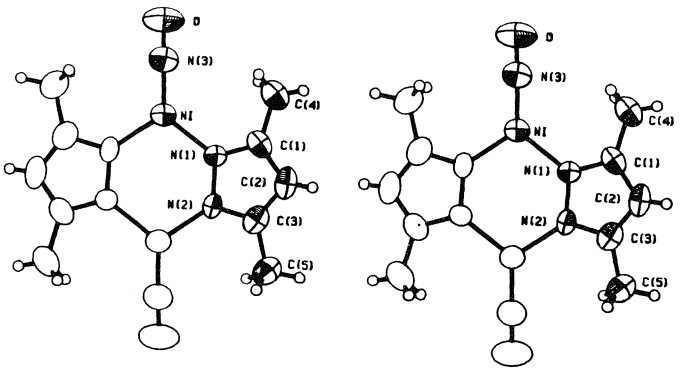

FIG. 1. Stereo view of the bis(μ-3,5-dimethylpyrazolyl(*N*,*N*′))bis(nitrosylnickel(I)) molecule, 50% ellipsoids are shown for the non-hydrogen atoms. Hydrogen atoms have been assigned artificially small thermal parameters for the sake of clarity.

zolyl moieties and two separate signals for the 3,5 Me groups on the donor $N_2C_5H_8$ molecules.

Mass Spectra

The parent dimer complexes all showed strong parent-ion peaks in their mass spectra at about 20% the intensity of the strongest peak due to the parent ion minus two NO groups. The parent ion minus one NO group also gave a prominent signal (35%). The bis-adduct complexes did not display parent ion signals but, rather, gave spectra similar to the parent dimer molecules plus additional signals due to the ligands. Evidently the adducts are not sufficiently thermally stable to withstand the necessary probe temperatures employed (120°C).

The trimetallic compound displayed in its mass spectrum strong signals due to the trimetallic parent ion, parent ion minus one NO group, and parent ion minus two NO groups (strongest signal). In addition a signal corresponding to the doubly charged parent ion minus two NO groups was observed. Noteworthy in this spectrum was the presence of weak signals due to ions from the $[Ni(NO)(N_2C_5H_7)]_2$ dimer. The presence of this dimer must arise from a rearrangement process in the mass spectrometer as there is no evidence for the presence of this compound in the analytically pure trimetallic starting material.

In all the mass spectra the relative intensities of the individual peaks in multi-line signals corresponded closely to those predicted on the basis of the natural isotope composition of elemental nickel.

Crystal Structures of $[Ni(NO)(N_2C_5H_7)]_2$ *and* $[(ON)Ni(N_2C_5H_7)_2]_2Ni$

Both structures provide rare examples of three-coordinate nickel and are the first trigonally coordinated metal nitrosyl complexes to be structurally characterized. The nickel π-complexes $Ni[(CH_3)_3CN{=}C{=}C(CN)_2][(CH_3)_3CNC]_2$ (23), $Ni[P(C_6H_4CH_3)_3]_2(C_6H_5N{=}NC_6H_5)$ (24), and $Ni[P(C_6H_4CH_3)_3]_2(C_6H_5(H)C{=}CHC_6H_5)$(25) have trigonal coordination if the π-donating ligand is considered as being monodentate.

$[Ni(NO)(N_2C_5H_7)]_2$

The crystal structure of $[Ni(NO)(N_2C_5H_7)]_2$ consists of discrete centrosymmetric molecules (Fig. 1) separated by normal van der Waals distances. With the exception of the methyl hydrogen atoms, the molecule is planar within ±0.04 Å and has a Ni. . .Ni′ separation of 3.673(1) Å. Both the central Ni_2N_4 and pyrazolyl rings are slightly, but significantly, non-planar (χ^2 = 8.1 and 20.6, maximum deviations = 0.005(3) and 0.012(4) Å respectively).

The coordination geometry about the nickel is distorted trigonal planar with N—Ni—NO angles of 128.3(2) and 123.3(2)° and an N(1)—Ni—N(2)′ angle of 108.4(1)°. The Ni atom is displaced 0.0061(6) Å from the plane of its substituents. The two Ni—N(pyrazolyl) distances (1.922(3) and 1.880(3) Å) differ by 10σ. Such differences between chemically equivalent bond distances and angles have been noted in other electronically similar tetrahedral $\{NiNO\}^{10}$ complexes (26–28). The nitrosyl group is linearly coordinated (Ni—N—O = 178.9(4)°) and the Ni—NO distance of 1.616(4) Å is intermediate between the values of 1.581(12) Å for the linearly coordinated nitrosyl in the tetrahedral cationic species $Ni(NO)[P(OCH_2)_3CCH_3]^+$ (29) and values of 1.648(5) and 1.686(7) Å for the bent nitrosyls in the tetrahedral complexes $Ni(X)(NO)[P(C_6H_5)_3]_2$ where X = NCS^- (26) and N_3^- (27).

Another unusual feature of the structure of $[Ni(NO)(N_2C_5H_7)]_2$ is the N(1)—N(2) bond length which, at 1.463(4) Å, is considerably longer than the values of 1.33–1.39 Å usually observed for such bonds (refs. 1, 30 and references therein). This may be due to the near planarity of the molecule which allows a *pπ–dπ* interaction between the pyrazolyl π

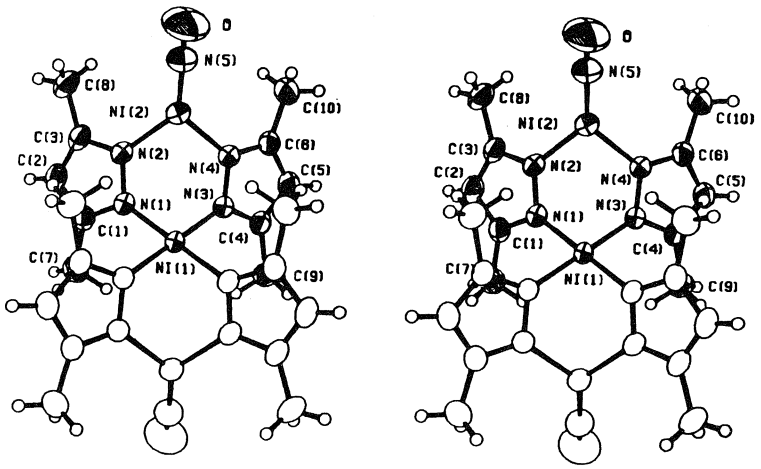

FIG. 2. Stereo view of the bis[bis(3,5-dimethylpyrazolyl)nitrosylniccolate(I)(*N',N'*)]nickel(II) molecule, 50% ellipsoids are shown for the non-hydrogen atoms. Hydrogen atoms have been assigned artificially small thermal parameters for the sake of clarity.

system and filled *d* orbitals on Ni. Back-donation into antibonding π^* orbitals of the pyrazolyl system may be responsible for the observed lengthening of the N—N bond. Other bond lengths in the molecule are normal.

[(ON)Ni($N_2C_5H_7$)$_2$]$_2$Ni

The crystal structure of [(ON)Ni($N_2C_5H_7$)$_2$]$_2$Ni consists of discrete centrosymmetric trinuclear molecules (Fig. 2) separated by normal van der Waals distances. Each molecule contains a central square-planar nickel(II) coordinated to four pyrazolyl nitrogen atoms, and two approximately trigonal planar outer nickel(I) centres coordinated by a nitrosyl group and two pyrazolyl nitrogen atoms. The distorted boat conformation observed for the Ni_2N_4 chelate rings (see Table 6 for torsion angles) and the overall molecular shape is similar to that observed in the complexes [$Me_2Ga(N_2C_3H_3)_2]_2M$, where M = Ni (31) and Cu (32). Attempts to isolate [$Me_2Ga(N_2C_5H_7)_2]_2$Ni failed but a tetrahedral Cu derivative was isolated and its structure has been determined (32). The difference between [(ON)Ni-($N_2C_5H_7$)$_2$]$_2$Ni and the [$Me_2Ga(N_2C_5H_7)_2]_2M$ complexes is the much less restrictive steric requirement of the trigonally coordinated outer Ni atoms as compared to the tetrahedral "$GaMe_2$" groups of the earlier complexes. Thus a square-planar central atom is accommodated in the present structure, with the NO groups extending well away from the central nickel atom and the pyrazolyl methyl groups. Such an arrangement is evidently much less favorable with tetrahedrally coordinated outer atoms as interference with these methyl groups is inevitable.

The central Ni(1) atom has nearly ideal square-planar coordination geometry with unique N—Ni—N angles of 89.70(8) and 90.30(8)°. The mean Ni(1)—N distance of 1.905(1) Å is similar to the value of 1.895(4) Å in [$Me_2Ga(N_2C_3H_3)_2]_2$Ni (31). Trigonally coordinated Ni(2) is displaced 0.0355(3) Å from the plane of its substituents (away from Ni(1)) and has N—Ni—NO angles of 131.1(1) and 131.7(1)° and an N(2)—Ni(2)—N(4) angle of 97.09(8)°. The mean Ni(2)—N(pyrazolyl) bond length of 1.922(3) Å is the same as the longer of the two such bonds in [Ni(NO)($N_2C_5H_7$)]$_2$. The Ni(2)—NO distance of 1.625(3) Å is slightly, but not significantly, longer than the corresponding distance in [Ni(NO)(N_2-C_5H_7)]$_2$ and the nitrosyl grouping is bent (Ni—N—O = 168.9(3)°). The large differences between chemically equivalent bond lengths and angles at the three-coordinate nickel noted for [Ni(NO)(N_2-C_5H_7)]$_2$ are not found in [(ON)Ni($N_2C_5H_7$)$_2$]$_2$Ni. The transition from a nearly planar Ni_2N_4 ring in [Ni(NO)($N_2C_5H_7$)]$_2$ to the distorted boat conformation in [(ON)Ni($N_2C_5H_7$)$_2$]$_2$Ni results in a closer approach of the Ni atoms (Ni(1). . .Ni(2) = 3.3770(3) Å) and a decrease in the intra-annular bond angle at the three-coordinate nickel (from 108.4(1) to 97.09(8)°).

The pyrazolyl ring containing N(1) is planar within experimental error (χ^2 = 2.2) while the second such ring is slightly, but significantly, non-planar (χ^2 = 18.6, maximum deviation = 0.007(3) Å). The Ni atoms are significantly displaced from both pyrazolyl mean planes (Ni(1) by 0.3123(4) and −0.2974(3), Ni(2) by −0.2359(4) and 0.2258(3) Å). The pyrazolyl N—N bonds (mean 1.380(2) Å) are normal and the pyrazolyl planes make angles of 38° with the mean plane of the three-coordinate nickel atom,

effectively eliminating the possibility of $d\pi \rightarrow p\pi$-(pyrazolyl) back donation which may be responsible for the unusually long N—N bond in $[Ni(NO)(N_2C_5H_7)]_2$.

Acknowledgments

We thank the Natural Sciences and Engineering Research Council of Canada for financial support and the University of British Columbia Computing Centre for assistance. We are grateful to Mr. J. Nip for mass spectra; Mr. P. Borda for C, H, N analyses; and to Dr. S. Chan for nmr spectra.

1. K. R. Breakell, S. J. Rettig, D. L. Singbeil, A. Storr, and J. Trotter. Can. J. Chem. **56**, 2099 (1978).
2. K. S. Chong and A. Storr. Can. J. Chem. **57**, 167 (1979).
3. S. Trofimenko. Chem. Rev. **72**, 497 (1972).
4. B. F. Fieselmann and G. D. Stucky. Inorg. Chem. **17**, 2074 (1978).
5. B. F. Fieselmann, D. N. Hendrickson, and G. D. Stucky. Inorg. Chem. **17**, 2078 (1978).
6. A. B. Blake, D. F. Ewing, J. E. Hamlin, and J. M. Lockyer. J. Chem. Soc. Dalton Trans. 1897 (1977).
7. F. Bonati and H. C. Clark. Can. J. Chem. **56**, 2513 (1978).
8. G. Minghetti, G. Banditelli, and F. Bonati. Inorg. Chem. **18**, 658 (1979).
9. J. Elguero, E. Gonzalez, and R. Jacquier. Bull. Soc. Chim. Fr. **2**, 707 (1968).
10. B. Haymore and R. D. Feltham. Inorg. Synth. **14**, 81 (1973).
11. N. S. Gill, R. H. Nuttall, D. E. Scarfe, and D. W. A. Sharpe. J. Inorg. Nucl. Chem. **18**, 79 (1961).
12. R. J. H. Clark and C. S. Williams. Inorg. Chem. **4**, 350 (1965).
13. R. M. Morrison and R. C. Thompson. Inorg. Nucl. Chem. Lett. **12**, 937 (1976).
14. P. Coppens, L. Leiserowitz, and D. Rabinovich. Acta Crystallogr. **18**, 1035 (1965).
15. W. R. Busing and H. A. Levy. Acta Crystallogr. **22**, 457 (1967).
16. D. T. Cromer and J. B. Mann. Acta Crystallogr. Sect. A, **24**, 321 (1968).
17. R. F. Stewart, E. R. Davidson, and W. T. Simpson. J. Chem. Phys. **42**, 3175 (1965).
18. D. T. Cromer and D. Liberman. J. Chem. Phys. **53**, 1891 (1970).
19. V. Schomaker and K. N. Trueblood. Acta Crystallogr. Sect. B, **24**, 63 (1969).
20. D. W. J. Cruickshank. Acta Crystallogr. **9**, 747 (1956); **9**, 754 (1956); **14**, 896 (1961).
21. W. Hieber and I. Bauer. Z. Anorg. Allg. Chem. **321**, 107 (1963).
22. W. Beck and K. Loltes. Z. Anorg. Allg. Chem. **325**, 258 (1965).
23. D. J. Yarrow, J. A. Ibers, Y. Tatsuno, and S. Otsuka. J. Am. Chem. Soc. **95**, 8590 (1973).
24. S. D. Ittel and J. A. Ibers. J. Organomet. Chem. **57**, 389 (1973).
25. S. D. Ittel and J. A. Ibers. J. Organomet. Chem. **74**, 121 (1974).
26. J. H. Enemark. Inorg. Chem. **10**, 1952 (1971).
27. K. J. Haller and J. H. Enemark. Inorg. Chem. **17**, 3552 (1978).
28. J. H. Enemark and R. D. Feltham. Coord. Chem. Rev. **13**, 339 (1974).
29. J. H. Meiners, C. J. Rix, J. C. Clardy, and J. G. Verkade. Inorg. Chem. **14**, 705 (1975).
30. R. T. Baker, S. J. Rettig, A. Storr, and J. Trotter. Can. J. Chem. **54**, 343 (1976).
31. D. F. Rendle, A. Storr, and J. Trotter. J. Chem. Soc. Dalton Trans. 176 (1975).
32. D. J. Patmore, D. F. Rendle, A. Storr, and J. Trotter. J. Chem. Soc. Dalton, 718 (1975).

Anionic pyrazolyl-bridged nickel nitrosyl complexes. Synthesis, structure, and reactivity

KENNETH S. CHONG, STEVEN J. RETTIG, ALAN STORR, AND JAMES TROTTER

Department of Chemistry, University of British Columbia, 2075 Wesbrook Mall, Vancouver, B.C., Canada V6T 1W5

Received June 28, 1979

KENNETH S. CHONG, STEVEN J. RETTIG, ALAN STORR, and JAMES TROTTER. Can. J. Chem. **57**, 3099 (1979).

A series of anionic pyrazolyl-bridged nickel nitrosyl complexes, $M^+[(ON)Ni(\mu\text{-}L_2)(\mu\text{-}X)Ni(NO)]^-$ (where L = pyrazolyl, $N_2C_3H_3$, or 3,5-dimethylpyrazolyl, $N_2C_5H_7$; X = Cl, Br, I, or $N_2C_5H_7$; and M = Na, $(CH_3)_4N$, or $(C_2H_5)_4N$) is described. Crystallographic analyses have been carried out on two of these complexes. Crystals of $[(C_2H_5)_4N]^+[(ON)Ni(\mu\text{-}I)(\mu\text{-}N_2C_5H_7)_2Ni(NO)]^-$ are orthorhombic, $a = 19.910(1)$, $b = 14.0330(7)$, $c = 9.3195(9)$ Å, $Z = 4$, space group $Pn2_1a$ and crystals of $[(C_4H_8O)_2Na][(ON)Ni(\mu\text{-}N_2C_5H_7)_3Ni(NO)]$ are orthorhombic, $a = 19.897(2)$, $b = 19.529(3)$, $c = 15.894(2)$ Å, $Z = 8$, space group $Pbca$. Both structures were solved by Patterson and Fourier syntheses and were refined by full-matrix least-squares procedures to $R = 0.027$ and 0.057 for 2572 and 2168 reflections with $I \geq 3\sigma(I)$ respectively. The structure of $[(C_2H_5)_4N]^+[(ON)Ni(\mu\text{-}I)(\mu\text{-}N_2C_5H_7)_2Ni(NO)]^-$ consists of discrete cations and binuclear anions which have approximate C_{2v} symmetry. The nickel atoms have distorted tetrahedral coordination geometry. Important mean molecular dimensions (distances corrected for libration) are: Ni—I—Ni, 73.67(2)°, Ni—I, 2.765(3), Ni—NO, 1.649(5), Ni—N(pyrazolyl), 1.980(14) Å, and Ni—N—O, 172.5(18)°. The structure of $[(C_4H_8O)_2Na][(ON)Ni(\mu\text{-}N_2C_5H_7)_3Ni(NO)]$ consists of discrete ion-pair units in which the two NiNO moieties are bridged by three $N_2C_5H_7$ ligands, two of which are coordinated to the sodium ion via a novel $\eta^2(N,N)$ π-interaction (mean Na—N = 2.61(3) Å). The sodium is also coordinated to two tetrahydrofuran oxygen atoms to give a distorted tetrahedral coordination geometry about the sodium (Na—O = 2.301(6) and 2.266(5) Å). Except for disordered tetrahydrofuran carbon atoms, the molecular unit has approximate C_{2v} symmetry. The nickel atoms have distorted tetrahedral coordination geometry, the mean distances being Ni—NO, 1.591(6), Ni—N(pyrazolyl), 1.985(2) for the unique pyrazolyl group and 2.016(5) Å for the pyrazolyl nitrogen atoms coordinated to Na. The mean Ni—N—O angle is 176.9(11)°.

KENNETH S. CHONG, STEVEN J. RETTIG, ALAN STORR et JAMES TROTTER. Can. J. Chem. **57**, 3099 (1979).

On décrit une série de complexes anioniques de nickel nitrosyle pyrazolyle avec le Ni en position de pont $M^+[(ON)Ni(\mu\text{-}L_2)(\mu\text{-}X)Ni(NO)]^-$ (où L = pyrazolyle $N_2C_3H_3$ ou diméthyl-3,5 pyrazolyle $N_2C_5H_7$; X = Cl^-, Br, I ou $N_2C_5H_7$ et M = Na, $(CH_3)_4N$ ou $(C_2H_5)_4N$. On a fait des analyses cristallographiques de deux de ces complexes. Les cristaux de $[(C_2H_5)_4N]^+[(ON)Ni(\mu\text{-}I)(\mu\text{-}N_2C_5H_7)_2Ni(NO)]^-$ sont orthorhombiques: $a = 19.910(1)$, $b = 14.0330(7)$, $c = 9.3195(9)$ Å, $Z = 4$, groupe d'espace $Pn2_1a$ et les cristaux de $[(C_4H_8O)_2Na][(ON)Ni(\mu\text{-}N_2C_5H_7)_3Ni(NO)]$ sont orthorhombiques: $a = 19.897(2)$, $b = 19.529(3)$, $c = 15.894(2)$ Å, $Z = 8$, groupe d'espace $Pbca$. On a résolu les deux structures à l'aide des synthèses de Patterson et de Fourier et on les a affinées par la méthode des moindres carrés (matrice complète) jusqu'à des valeurs respectives de $R = 0.027$ et 0.057 pour 2572 et 2168 réflexions avec $I \geq 3\sigma(I)$. La structure de $[(C_2H_5)_4N]^+[(ON)Ni(\mu\text{-}I)(\mu\text{-}N_2C_5H_7)_2Ni(NO)]^-$ consiste en des cations individuelles et des anions binucléaires qui ont une symétrie approximative C_{2v}. La géométrie de coordination des atomes de nickel est de type tétraèdre déformé. Les principales dimensions moléculaires importantes (distances corrigés pour la libration) sont: Ni—I—Ni, 73.67(2)°, Ni—I, 2.765(3), Ni—NO, 1.649(5), Ni—N(pyrazolyle) 1.980(14) Å et Ni—N—O, 172.5(18)°. La structure de $[(C_4H_8O)_2Na][(ON)Ni(\mu\text{-}N_2C_5H_7)_3Ni(NO)]$ consiste en des unités individuelles de paire d'ions dans lesquelles deux fragments NiNO sont en position de pont entre trois ligands ($N_2C_5H_7$). Deux d'entre-eux sont coordonnés à l'ion sodium par l'intermédiaire d'une nouvelle interaction π $\eta^2(N,N)$ (i.e. Na—N = 2.61(3) Å). L'atome de sodium est également coordonné à deux atomes d'oxygène du tétrahydrofuranne pour donner un complexe de coordination de type tétraèdre déformé; au niveau du sodium (Na—O = 2.301(6) et 2.266(5) Å). A l'exception des atomes de carbone désordonnés du tétrahydrofuranne l'unité moléculaire a approximativement une symétrie C_{2v}. Les atomes de nickel ont une coordination tétraédrique déformée. Les distances principales sont: Ni—NO, 1.591(6), Ni—N(pyrazolyle), 1.985(2) pour l'unique groupe pyrazolyle et 2.016(5) Å pour les atomes d'azote coordonnés au sodium. L'angle principal Ni—N—O est de 176.9(11)°.

[Traduit par le journal]

0008-4042/79/233099-08$01.00/0

Introduction

The preceding paper (1) detailed the synthesis of a series of pyrazolyl-bridged nickel nitrosyl dimers and their reactivity towards various types of neutral donor ligands. This account describes the reactivity of these dimeric "16-electron" nickel complexes towards a number of uninegative anions. These anions act as bidentate four-electron bridging ligands and yield stable salts as products. Crystal structure determinations of two of these salts are presented, viz., $[(C_2H_5)_4N]^+[(ON)Ni(\mu\text{-}I)(\mu\text{-}N_2C_5H_7)_2Ni(NO)]^-$ and $[(C_4H_8O)_2Na][(ON)Ni(\mu\text{-}N_2C_5H_7)_3Ni(NO)]$. In the former structure the anion and cation are well-separated entities in the crystal lattice whereas in the latter structure the sodium ion is intimately attached to the anionic part of the salt.

Experimental

The preceding paper detailed the preparation of the pyrazolyl-bridged nickel nitrosyl dimers which were employed as starting materials in this study (1). Their reactivity towards anionic donor species is detailed below.

Preparation of $[(C_2H_5)_4N]^+[(ON)Ni(\mu\text{-}I)(\mu\text{-}N_2C_5H_7)_2Ni(NO)]^-$

A THF solution of $Na^+N_2C_5H_7^-$ (0.236 g; 2.0 mmol) was added to a stirred THF solution of Ni(NO)I (0.431 g; 2.0 mmol). Solid Et_4NCl (0.165 g; 1.0 mmol) was added to the resulting blue solution and the mixture stirred for 24 h. The solution was filtered and the solvent removed *in vacuo*. Extraction with CH_2Cl_2, filtration, followed by evaporation of solvent gave blue crystals of product. These were washed with methanol followed by ether. The yield of pure product was 61%. Elemental analyses and other analytical data for all compounds prepared are presented in Table 1.

Preparation of $Et_4N^+[(ON)Ni(N_2C_5H_7)_2(Cl)Ni(NO)]^-$

The dimer, $[(N_2C_5H_7)Ni(NO)]_2$, (0.184 g; 0.5 mmol) was dissolved in THF and a methanol solution of $Et_4N^+Cl^-$ (0.083 g; 0.5 mmol) added. The green dimer solution immediately turned blue. Evaporation of the solvent gave blue crystals which were washed successively with methanol and ether.

The analogous bromo compound was prepared similarly from the dimer and $Et_4N^+Br^-$. The pyrazolyl $N_2C_3H_3$ bridged halogen derivatives were synthesized utilizing the $[(N_2C_3H_3)Ni(NO)]_2$ dimer as starting material.

Preparation of $Na^+[(ON)Ni(N_2C_5H_7)_3Ni(NO)]^-$

A THF solution of $Na^+(N_2C_5H_7)^-$ (0.354 g; 3.00 mmol) was added to a stirred solution of Ni(NO)I (0.431 g; 2.0 mmol). Solvent was removed *in vacuo* and the oily residue extracted with benzene and filtered immediately. On evaporation of solvent from the resulting solution, lustrous blue crystals of the product formed.

Spectra

Infrared spectra were recorded on a Perkin-Elmer 457 spectrometer and ^1H nmr spectra on a Varian XL-100 spectrometer. For complexes of low solubility ^1H nmr spectra were obtained using FT techniques.

X-ray Crystallographic Analyses

Tetraethylammonium μ-*Iodo-bis(*μ-*3,5-dimethylpyrazolyl-(N,N′))bis(nitrosylniccolate(I))*

The crystal chosen was mounted in a general orientation and had dimensions of ca. 0.20 × 0.66 × 0.43 mm. Unit-cell parameters were refined by least-squares on 2 sin θ/λ values for 46 reflections measured on a diffractometer with Mo K_α radiation (λ = 0.71073 Å). Crystal data (at 22°C) are:

$C_{18}H_{34}IN_7Ni_2O_2$ fw = 624.84

Orthorhombic, $a = 19.910(1)$, $b = 14.0330(7)$, $c = 9.3195(9)$ Å, $V = 2603.8(3)$ Å^3, $Z = 4$, $\rho_c = 1.594$ g cm^{-3}, $F(000) = 1264$, $\mu(Mo\ K_\alpha) = 25.2$ cm^{-1}. Absent reflections: $0kl$, $k + l \neq 2n$; $hk0$, $h \neq 2n$; and $0k0$, $k \neq 2n$. Space group $Pn2_1a$ (non-standard setting of $Pna2_1$, C_{2v}^9, No. 33) from structure analysis.

Intensities were measured with graphite monochromatized Mo K_α radiation on an Enraf-Nonius CAD4-F diffractometer. An $\omega - 1.67\theta$ scan at 0.91–6.71° min^{-1} over a range of (0.55 + 0.35 tan θ) degrees in ω (extended by 25% on both sides for background measurement) was employed. Data were measured to $2\theta = 60°$. The intensities of 3 check reflections, measured every 3600 s throughout the data collection, remained constant to within ±3.5%.

After data reduction, an absorption correction was applied using the Gaussian integration method (2, 3). Transmission factors ranged from 0.424 to 0.702. Of the 3923 independent reflections measured, 2572 (65%) had intensities greater than $3\sigma(I)$ above background where $\sigma^2(I) = S + 2B + (0.04(S - B))^2$ with S = scan count and B = background count.

Systematic absences allow space groups $Pnma$ or $Pn2_1a$, analysis being initiated in the latter on the basis of the E-statistics. The positions of the three heavy atoms were determined from the three-dimensional Patterson function and those of O, N, and C atoms from a subsequent difference map. After full-matrix least-squares refinement of the non-hydrogen atoms with anisotropic thermal parameters to $R = 0.037$, a difference map revealed the positions of 28 of the 34 hydrogen atoms. Ideal positions ($C(sp^2)$—H = 0.95, $C(sp^3)$—H = 0.98 Å) were calculated for all hydrogen atoms, which were assigned isotropic U values 1.1 greater than that of the atom to which they are bonded. Hydrogen atom parameters were kept fixed but their contributions were included in the structure factor calculations. The scattering factors of ref. 4 were used for non-hydrogen atoms and those of ref. 5 for hydrogen atoms. Anomalous scattering factors from ref. 6 were used for the I and Ni atoms. The weighting scheme, $w = 1/\sigma^2(F)$ where $\sigma^2(F)$ is derived from the previously defined $\sigma^2(I)$, gave uniform average values of $w(|F_o| - |F_c|)^2$ over ranges of $|F_o|$ and was employed in the final stages of refinement. An isotropic Type I extinction correction (Thornley–Nelmes definition of mosaic anisotropy with a Lorentzian distribution) was applied (7–9). The final value of q was $3.7(2) \times 10^4$. Convergence was reached at $R = 0.027$ and $R_w = 0.033$ for 2572 reflections with $I \geq 3\sigma(I)$. For all 3923 reflections $R = 0.061$ and $R_w = 0.036$.

On the final cycle of refinement the mean and maximum parameter shifts corresponded to 0.09 and 0.64σ, respectively. The mean error in an observation of unit weight was 0.9374. A final difference map showed maximum fluctuations of ±1.5 e Å^{-3} near I and ±0.20 e Å^{-3} in regions away from the heavy atoms. The final positional and thermal parameters appear in Tables 2 and 3[1] respectively. Measured and calculated structure factors have been placed in the Depository of Unpublished Data.[1]

μ-*(3,5-Dimethylpyrazolyl)*-μ-*[bis(tetrahydrofuran)bis-(*η^2*(N,N)-3,5-dimethylpyrazolyl)sodium(N,N,N′,N′)]bis-(nitrosylnickel(I))*

Details of the structure determination are the same as

[1]The structure factor table and Table 3 (thermal parameters) are available, at a nominal charge, from the Depository of Unpublished Data, CISTI, National Research Council of Canada, Ottawa, Ont., Canada K1A 0S2.

TABLE 1. Analytical data for M^+ 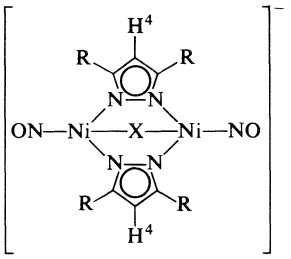 complexes

Compound			Analysis*			%	ν_{NO} (cm^{-1})	τ(ppm) (acetone-d^6 solution)†		
M	X	R	C	H	N	Yield	Nujol	M	H^4	R
Et_4N	I	H	29.5 29.6	4.5 4.6	17.1 17.2	40	1770	6.47q,‡ 8.56t‡§	3.45t‖	1.60d‖
Et_4N	Br	H	31.8 32.2	5.0 4.9	18.8 18.3	60	1762	6.48q,‡ 8.55t‡§	3.43t‖	1.62d‖
Me_4N	Cl	H	28.5 28.5	4.3 4.3	23.0 23.3	45	1754	6.58s	3.43t‖	1.64d‖
Et_4N	I	Me	34.7 34.6	5.5 5.5	15.7 15.7	61	1752	6.52q,‡ 8.57t‡§	3.85s	7.50s
Et_4N	Br	Me	37.6 37.4	6.0 5.9	17.0 17.0	60	1749	6.50q,‡ 8.56t‡§	3.84s	7.52s
Et_4N	Cl	Me	40.5 40.5	6.5 6.4	18.4 18.4	64	1742	6.48q,‡ 8.55t‡§	3.84s	7.54s
Na¶	$N_2C_5H_7$	Me	43.8 43.8	5.9 5.9	17.8 17.8	75	1760	—	3.82s	7.65s

*First row, found values; second row, calculated values.
†τ values refer to (acetone-d^6) = 7.89 ppm.
‡J_{HCCH} = 7 Hz.
§$J_{HC-C-N^{14}}$ = 2 Hz.
‖J_{HCCH} = 2 Hz.
¶2 THF of crystallization τ_{THF} = 6.30 m, 8.15 m; s = singlet; d = doublet; t = triplet; q = quartet.

for $[(C_2H_5)_4N]^+[(ON)Ni(\mu\text{-}I)(\mu\text{-}N_2C_5H_7)_2Ni(NO)]^-$ except where noted. Crystal dimensions were 0.4 × 0.4 × 0.5 mm. Twenty-five reflections were used in the refinement of the unit-cell parameters. Crystal data are:

$C_{23}H_{37}N_8NaNi_2O_4$ fw = 690.07
Orthorhombic, a = 19.897(2), b = 19.529(3), c = 15.894(2) Å, V = 6176.0(8) Å^3, Z = 8, ρ_c = 1.484 g cm^{-3}, $F(000)$ = 2640, μ(Mo K_α) = 12.7 cm^{-1}. Absent reflections: $0kl$, $k \neq 2n$; $h0l$, $l \neq 2n$; and $hk0$, $h \neq 2n$ define uniquely the space group $Pbca$ (D_{2h}^{15}, No. 61).

An $\omega - 1.33\theta$ scan at 0.87–6.71° min^{-1} over a range of 0.55 + 0.35 tan θ° in ω was employed. Of 5442 independent reflections measured (to 2θ = 50°), 2168 (39.8%) had intensities greater than $3\sigma(I)$ above background. No absorption correction was made due to irregularity of the crystal surface but in view of the low value of μ, no serious errors should arise.

The coordinates of the nickel atoms were determined from the three-dimensional Patterson function and those of the remaining non-hydrogen atoms from a subsequent difference map. It was apparent that conformational and orientational disorder of the THF carbon atoms was present. The occupancy factors for the disordered carbon atoms were initially estimated from the relative peak heights on a difference Fourier and were later adjusted to give nearly equal isotropic U values. The disordered carbon atoms were refined with isotropic thermal parameters and the remaining non-hydrogen atoms with anisotropic thermal parameters. In view of the paucity of data, no attempt was made to locate hydrogen atoms. Anomalous scattering factors from ref. 6 were used for the Ni atoms. Convergence was reached at R = 0.057 and R_w = 0.074 for 2168 reflections with $I \geq 3\sigma(I)$. For all 5442 reflections R = 0.158 and R_w = 0.084. The mean and maximum parameter shifts on the final cycle of refinement corresponded to 0.22 and 2.2σ respectively and the mean error in an observation of unit weight was 1.6045. A final difference map showed maximum fluctuations of ±0.50 e Å^{-3} in the vicinity of the Ni atoms and ±0.33 e Å^{-3} elsewhere.

The thermal motion in both structures has been analysed in terms of the rigid-body modes of translation, libration, and screw motion (10) using the computer program MGTLS. For $[(C_2H_5)_4N]^+[(ON)Ni(\mu\text{-}I)(\mu\text{-}N_2C_5H_7)_2Ni(NO)]^-$ (rms σU_{ij} = 0.0038 Å^2) analyses of the cation and of the anion less nitrosyl oxygen atoms (rms ΔU_{ij} = 0.0067 and 0.0042 Å^2 respectively) gave reasonable rigid-body parameters. For $[(C_4H_8O)_2Na][(ON)Ni(\mu\text{-}N_2C_5H_7)_3Ni(NO)]$ (rms σU_{ij} = 0.0057 Å^2 for the ordered atoms) analysis of the entire ordered part of the molecule excluding nitrosyl oxygen and methyl carbon atoms gave rms ΔU_{ij} = 0.0146 Å^2 and physically reasonable results. The appropriate bond distances have been corrected for libration (11), using shape parameters q^2 of 0.08 for all atoms involved. Corrected bond lengths appear in Table 4 along with the uncorrected values. Corrected bond angles are all within 1σ of the uncorrected values in Table 5.

Results and Discussion

The susceptibility of the nickel dimers towards nucleophilic attack is well illustrated by the ease of

TABLE 2. Final positional parameters (fractional; O, N, and C × 10^4, I and Ni × 10^5, H × 10^3) with estimated standard deviations in parentheses

Atom	x	y	z
$[(C_2H_5)_4N]^+[(ON)Ni(\mu\text{-}I)(\mu\text{-}N_2C_5H_7)_2Ni(NO)]^-$			
Equivalent positions: $(x, y, z; 1/2 - x, 1/2 + y, 1/2 + z; -x, 1/2 + y, -z; 1/2 + x, y, 1/2 - z)$			
I	13453(2)	45750	60589(5)
Ni(1)	12686(3)	56490(7)	35897(9)
Ni(2)	11929(3)	64435(6)	69258(8)
O(1)	1264(3)	4693(7)	995(7)
O(2)	1161(4)	6934(6)	9805(7)
N(1)	1290(2)	5051(4)	2066(7)
N(2)	1169(3)	6659(5)	8656(6)
N(3)	461(2)	6341(4)	4254(5)
N(4)	436(2)	6692(3)	5619(6)
N(5)	1944(2)	6591(3)	4278(5)
N(6)	1907(2)	6914(3)	5665(5)
N(7)	1191(2)	9549(4)	2570(5)
C(1)	−113(3)	6566(4)	3587(7)
C(2)	−507(3)	7068(5)	4533(9)
C(3)	−149(3)	7147(4)	5795(7)
C(4)	2481(3)	6979(5)	3663(7)
C(5)	2799(3)	7567(5)	4621(7)
C(6)	2432(3)	7506(4)	5875(6)
C(7)	−250(3)	6260(6)	2083(8)
C(8)	−336(3)	7623(5)	7161(8)
C(9)	2664(3)	6744(7)	2139(9)
C(10)	2525(3)	8002(6)	7272(9)
C(11)	1122(4)	8863(5)	3811(9)
C(12)	758(4)	9219(6)	5110(9)
C(13)	1642(4)	9109(6)	1439(9)
C(14)	1712(4)	9683(10)	69(8)
C(15)	524(3)	9824(6)	1963(8)
C(16)	138(4)	8981(9)	1293(9)
C(17)	1512(4)	10472(5)	3098(8)
C(18)	2192(4)	10317(8)	3836(9)
H(2)	−95	731	436
H(5)	319	794	446
H(7a)	−67	656	175
H(7b)	12	645	146
H(7c)	−30	557	205
H(8a)	−6	737	793
H(8b)	−27	831	705
H(8c)	−81	750	736
H(9a)	227	645	166
H(9b)	279	733	163
H(9c)	304	630	213
H(10a)	246	754	805
H(10b)	298	826	731
H(10c)	220	851	735
H(11a)	158	868	410
H(11b)	88	830	345
H(12a)	102	973	556
H(12b)	32	946	484
H(12c)	71	869	580
H(13a)	145	848	119
H(13b)	208	901	186
H(14a)	213	950	−42
H(14b)	133	956	−57
H(14c)	173	1037	30
H(15a)	60	1031	123
H(15b)	26	1010	274
H(16a)	−21	877	197
H(16b)	−9	921	41
H(16c)	44	847	107
H(17a)	121	1077	379
H(17b)	158	1089	228
H(18a)	233	965	372
H(18b)	253	1074	340
H(18c)	215	1046	486
$[(C_4H_8O)_2Na][(ON)Ni(\mu\text{-}N_2C_5H_7)_3Ni(NO)]$*			
Ni(1)	38345(4)	35500(4)	35336(5)
Ni(2)	37669(4)	53073(4)	34182(5)
Na	2681(1)	4450(1)	4652(2)
O(1)	3917(6)	2143(4)	3501(7)
O(2)	3766(4)	6734(3)	3337(5)
O(3)	2014(3)	3589(3)	5163(4)
O(4)	2014(3)	5312(3)	5096(4)
N(1)	3881(4)	2742(3)	3546(5)
N(2)	3754(3)	6124(3)	3370(4)
N(3)	3004(3)	4030(3)	3134(3)
N(4)	2972(2)	4728(3)	3094(3)
N(5)	3928(2)	4122(3)	4570(3)
N(6)	3932(2)	4829(2)	4517(3)
N(7)	4472(2)	4081(3)	2833(3)
N(8)	4418(2)	4775(3)	2748(3)
C(1)	2437(5)	3738(6)	2829(5)
C(2)	2017(5)	4278(7)	2603(6)
C(3)	2354(4)	4918(6)	2758(4)
C(4)	4108(3)	3959(3)	5363(5)
C(5)	4220(3)	4537(4)	5824(4)
C(6)	4115(3)	5081(4)	5257(4)
C(7)	4984(4)	3858(4)	2319(5)
C(8)	5247(3)	4425(5)	1911(5)
C(9)	4882(4)	5000(4)	2189(4)
C(10)	2350(5)	2963(5)	2781(6)
C(11)	2207(5)	5658(5)	2602(7)
C(12)	4169(4)	3223(4)	5640(5)
C(13)	4197(4)	5849(4)	5424(4)
C(14)	5162(4)	3109(4)	2274(5)
C(15)	4966(4)	5745(4)	1949(5)
C(16)	1298(10)	3665(11)	4986(13)
C(16b)	1539(14)	3172(13)	4582(16)
C(17)	1025(6)	2961(6)	5222(8)
C(18)	1640(13)	2569(13)	5691(18)
C(18b)	1812(22)	2540(23)	5123(31)
C(18c)	1324(10)	2885(10)	5978(12)
C(19)	2251(9)	2978(9)	5490(12)
C(19b)	1943(11)	3291(11)	6008(14)
C(20)	2313(10)	6016(10)	5247(13)
C(20b)	2013(15)	5641(15)	5872(19)
C(21)	1519(8)	6167(7)	5883(9)
C(21b)	1826(11)	6490(11)	5385(13)
C(22)	1098(8)	6040(8)	5303(10)
C(23)	1425(14)	5280(13)	5540(17)
C(23b)	1273(13)	5443(12)	4848(17)
C(23c)	168(2)	602(2)	454(3)

*Occupancy factors for C(16) through C(23c): 0.55, 0.45, 1.00, 0.35, 0.19, 0.46, 0.55, 0.45, 0.58, 0.42, 0.78, 0.42, 0.70, 0.39, 0.39, and 0.22 respectively.

TABLE 4. Bond lengths (Å) with estimated standard deviations in parentheses

(*a*) Non-hydrogen atoms

Bond	Length		Bond	Length	
	Uncorr.	Corr.		Uncorr.	Corr.
	$[(C_2H_5)_4N]^+[(ON)Ni(\mu\text{-}I)(\mu\text{-}N_2C_5H_7)_2Ni(NO)]^-$				
I —Ni(1)	2.755(1)	2.762	N(3) —C(1)	1.337(7)	1.340
I —Ni(2)	2.761(1)	2.767	N(4) —C(3)	1.337(7)	1.340
Ni(1)—N(1)	1.650(6)	1.654	N(5) —C(4)	1.331(7)	1.333
Ni(1)—N(3)	1.979(4)	1.984	N(6) —C(6)	1.350(7)	1.352
Ni(1)—N(5)	1.992(4)	1.997	C(1) —C(2)	1.376(9)	1.379
Ni(2)—N(2)	1.641(5)	1.644	C(1) —C(7)	1.491(9)	1.492
Ni(2)—N(4)	1.970(5)	1.975	C(2) —C(3)	1.379(9)	1.383
Ni(2)—N(6)	1.959(4)	1.964	C(3) —C(8)	1.485(9)	1.487
O(1) —N(1)	1.118(8)	1.119	C(4) —C(5)	1.370(9)	1.373
O(2) —N(2)	1.139(7)	1.140	C(4) —C(9)	1.503(9)	1.505
N(3) —N(4)	1.365(7)	1.370	C(5) —C(6)	1.381(8)	1.384
N(5) —N(6)	1.371(6)	1.375	C(6) —C(10)	1.488(9)	1.490
N(7) —C(11)	1.511(9)	1.529	C(11)—C(12)	1.497(11)	1.505
N(7) —C(13)	1.516(8)	1.528	C(13)—C(14)	1.516(13)	1.530
N(7) —C(15)	1.494(7)	1.509	C(15)—C(16)	1.543(13)	1.555
N(7) —C(17)	1.526(9)	1.544	C(17)—C(18)	1.534(12)	1.544
	$[(C_4H_8O)_2Na][(ON)Ni(\mu\text{-}N_2C_5H_7)_3Ni(NO)]$				
Ni(1)—N(1)	1.580(7)	1.585	N(3) —C(1)	1.354(9)	1.356
Ni(1)—N(3)	2.003(6)	2.014	N(4) —C(3)	1.392(8)	1.394
Ni(1)—N(5)	2.000(5)	2.009	N(5) —C(4)	1.348(7)	1.350
Ni(1)—N(7)	1.980(5)	1.987	N(6) —C(6)	1.326(7)	1.328
Ni(2)—N(2)	1.597(6)	1.597	N(7) —C(7)	1.378(8)	1.379
Ni(2)—N(4)	2.011(5)	2.022	N(8) —C(9)	1.353(7)	1.355
Ni(2)—N(6)	2.008(5)	2.017	C(1) —C(2)	1.393(13)	1.398
Ni(2)—N(8)	1.974(5)	1.983	C(1) —C(10)	1.524(12)	1.527
Na —O(3)	2.292(6)	2.301	C(2) —C(3)	1.440(12)	1.445
Na —O(4)	2.257(6)	2.266	C(3) —C(11)	1.495(11)	1.498
Na —N(3)	2.629(6)	2.638	C(4) —C(5)	1.364(8)	1.368
Na —N(4)	2.600(6)	2.609	C(4) —C(12)	1.509(9)	1.511
Na —N(5)	2.565(5)	2.577	C(5) —C(6)	1.409(8)	1.414
Na —N(6)	2.606(5)	2.617	C(6) —C(13)	1.532(9)	1.535
N(1) —O(1)	1.175(8)	1.175	C(7) —C(8)	1.385(9)	1.389
N(2) —O(2)	1.191(7)	1.191	C(7) —C(14)	1.506(9)	1.508
N(3) —N(4)	1.367(6)	1.377	C(8) —C(9)	1.408(9)	1.414
N(5) —N(6)	1.382(6)	1.391	C(9) —C(15)	1.515(9)	1.518
N(7) —N(8)	1.366(6)	1.375			

formation of anionic complexes with uninegative nucleophiles. In these reactions the formally "16-electron" nickel atoms acquire an 18-electron configuration. However, as reported in the preceding paper (1) for neutral 18-electron complexes formed by reaction of the nickel dimers with suitable donor molecules, the present anionic complexes, although air-stable as solids, are susceptible to atmospheric attack when in solution. The blue color of the (acetone or methylene chloride) solutions is gradually discharged on exposure of the solutions to air, with concomitant loss of the ν_{NO} band in the ir spectrum, and deposition of a white solid.

The order of stability of the anionic complexes with respect to displacement of one bridging moiety by another in the presence of R_4N^+ cations follows the sequence: I > Br > Cl > $(N_2C_5H_7)$. Thus if I^- is available in the reaction mixture this ion displaces any of the others listed to become the third bridging group accompanying the two pyrazolyl moieties already present in the dinuclear anionic complex ion.

Infrared Spectra

Comparison of the ν_{NO} values (Table 1) for the I, Br, and Cl complexes shows a trend which is opposite to that predicted on simple electronegativity arguments. Thus, on electronegativity grounds the Cl compounds should display the highest ν_{NO} values since shift of electron density from the nickel atoms towards Cl should reduce the $d\pi$–π^* back-bonding from Ni to the NO ligand. The reverse trend observed here has also been noted in related series of compounds (12, 13) and may be attributed to the greater π-acceptor ability of the heavier halogen

TABLE 5. Bond angles (deg) with estimated standard deviations in parentheses
Non-hydrogen atoms

Bonds	Angle (deg)	Bonds	Angle (deg)
	$[(C_2H_5)_4N]^+[(ON)Ni(\mu\text{-}I)(\mu\text{-}N_2C_5H_7)_2Ni(NO)]^-$		
Ni(1)—I —Ni(2)	73.67(2)	N(5) —N(6) —C(6)	107.4(4)
I —Ni(1)—N(1)	116.0(2)	C(11)—N(7) —C(13)	109.0(6)
I —Ni(1)—N(3)	93.0(1)	C(11)—N(7) —C(15)	112.0(5)
I —Ni(1)—N(5)	93.2(1)	C(11)—N(7) —C(17)	109.4(5)
N(1) —Ni(1)—N(3)	122.7(2)	C(13)—N(7) —C(15)	111.6(5)
N(1) —Ni(1)—N(5)	126.7(2)	C(13)—N(7) —C(17)	108.8(5)
N(3) —Ni(1)—N(5)	97.0(2)	C(15)—N(7) —C(17)	106.0(6)
I —Ni(2)—N(2)	117.7(2)	N(3) —C(1) —C(2)	108.1(5)
I —Ni(2)—N(4)	94.1(1)	N(3) —C(1) —C(7)	121.7(6)
I —Ni(2)—N(6)	93.7(1)	C(2) —C(1) —C(7)	130.2(6)
N(2) —Ni(2)—N(4)	123.6(2)	C(1) —C(2) —C(3)	107.0(5)
N(2) —Ni(2)—N(6)	123.2(2)	N(4) —C(3) —C(2)	107.9(6)
N(4) —Ni(2)—N(6)	97.2(2)	N(4) —C(3) —C(8)	122.5(6)
Ni(1)—N(1) —O(1)	174.3(6)	C(2) —C(3) —C(8)	129.6(5)
Ni(2)—N(2) —O(2)	170.7(7)	N(5) —C(4) —C(5)	109.7(5)
Ni(1)—N(3) —N(4)	119.9(3)	N(5) —C(4) —C(9)	120.7(6)
Ni(1)—N(3) —C(1)	131.6(4)	C(5) —C(4) —C(9)	129.6(6)
N(4) —N(3) —C(1)	108.5(4)	C(4) —C(5) —C(6)	105.6(5)
Ni(2)—N(4) —N(3)	119.0(3)	N(6) —C(6) —C(5)	109.0(5)
Ni(2)—N(4) —C(3)	132.5(4)	N(6) —C(6) —C(10)	120.8(5)
N(3) —N(4) —C(3)	108.5(5)	C(5) —C(6) —C(10)	130.2(5)
Ni(1)—N(5) —N(6)	119.1(3)	N(7) —C(11)—C(12)	116.8(6)
Ni(1)—N(5) —C(4)	132.5(4)	N(7) —C(13)—C(14)	115.0(7)
N(6) —N(5) —C(4)	108.3(4)	N(7) —C(15)—C(16)	113.4(6)
Ni(2)—N(6) —N(5)	119.5(3)	N(7) —C(17)—C(18)	113.2(7)
Ni(2)—N(6) —C(6)	133.0(4)		
	$[(C_4H_8O)_2Na][(ON)Ni(\mu\text{-}N_2C_5H_7)_3Ni(NO)]$		
N(1) —Ni(1)—N(3)	121.2(4)	Ni(2)—N(6) —C(6)	130.0(4)
N(1) —Ni(1)—N(5)	122.9(3)	N(5) —N(6) —C(6)	108.6(5)
N(1) —Ni(1)—N(7)	119.5(3)	Ni(1)—N(7) —N(8)	121.7(4)
N(3) —Ni(1)—N(5)	94.4(2)	Ni(1)—N(7) —C(7)	130.0(6)
N(3) —Ni(1)—N(7)	96.0(2)	N(8) —N(7) —C(7)	108.2(5)
N(5) —Ni(1)—N(7)	96.4(2)	Ni(2)—N(8) —N(7)	121.3(4)
N(2) —Ni(2)—N(4)	122.5(3)	Ni(2)—N(8) —C(9)	129.1(5)
N(2) —Ni(2)—N(6)	120.6(3)	N(7) —N(8) —C(9)	109.5(5)
N(2) —Ni(2)—N(8)	120.7(3)	N(3) —C(1) —C(2)	105.8(9)
N(4) —Ni(2)—N(6)	95.2(2)	N(3) —C(1) —C(10)	122.1(10)
N(4) —Ni(2)—N(8)	94.7(2)	C(2) —C(1) —C(10)	132.1(10)
N(6) —Ni(2)—N(8)	96.7(2)	C(1) —C(2) —C(3)	109.6(8)
O(3) —Na —O(4)	95.5(3)	N(4) —C(3) —C(2)	104.2(8)
O(3) —Na —X(1)	116.2(4)	N(4) —C(3) —C(11)	119.6(9)
O(3) —Na —X(2)	123.5(4)	C(2) —C(3) —C(11)	136.1(9)
O(4) —Na —X(1)	119.0(4)	N(5) —C(4) —C(5)	110.4(6)
O(4) —Na —X(2)	126.3(4)	N(5) —C(4) —C(12)	121.3(7)
X(1) —Na —X(2)	72.2(4)	C(5) —C(4) —C(12)	128.2(8)
Ni(1)—N(1) —O(1)	175.8(9)	C(4) —C(5) —C(6)	104.9(6)
Ni(2)—N(2) —O(2)	178.0(7)	N(6) —C(6) —C(5)	109.1(6)
Ni(1)—N(3) —N(4)	121.3(4)	N(6) —C(6) —C(13)	123.2(6)
Ni(1)—N(3) —C(1)	127.1(7)	C(5) —C(6) —C(13)	127.7(7)
N(4) —N(3) —C(1)	111.4(7)	N(7) —C(7) —C(8)	107.7(6)
Ni(2)—N(4) —N(3)	120.8(4)	N(7) —C(7) —C(14)	120.6(8)
Ni(2)—N(4) —C(3)	130.0(7)	C(8) —C(7) —C(14)	131.7(8)
N(3) —N(4) —C(3)	109.0(6)	C(7) —C(8) —C(9)	107.2(6)
Ni(1)—N(5) —N(6)	120.5(4)	N(8) —C(9) —C(8)	107.4(6)
Ni(1)—N(5) —C(4)	131.5(5)	N(8) —C(9) —C(15)	123.6(7)
N(6) —N(5) —C(4)	107.0(5)	C(8) —C(9) —C(15)	129.0(8)
Ni(2)—N(6) —N(5)	121.1(4)		

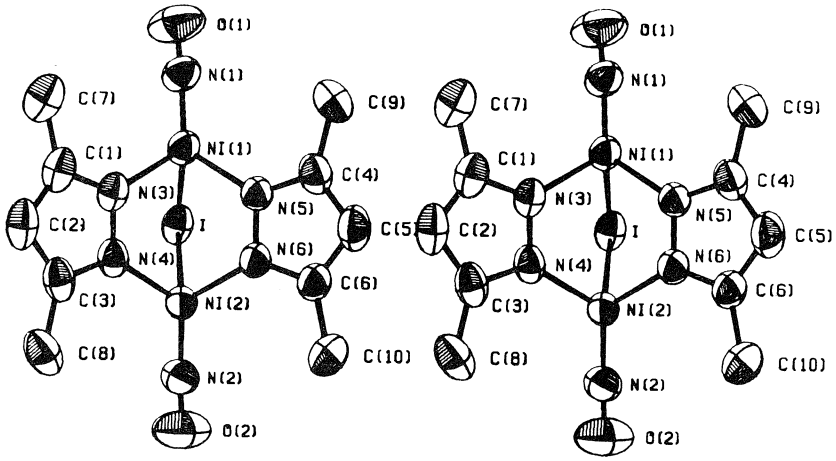

FIG. 1. Stereo view of the $[(ON)Ni(\mu\text{-}I)(\mu\text{-}N_2C_5H_7)_2Ni(NO)]^-$ anion; 50% ellipsoids are shown for the non-hydrogen atoms. Hydrogen atoms have been omitted for the sake of clarity.

ligands, an effect which evidently outweighs the electronegativity effect. There is a noticeable decrease in the ν_{NO} values in going to the 3,5-dimethylpyrazolyl derivatives from the unsubstituted pyrazolyl compounds, presumably caused by an inductive effect of the methyl substituents in the former series of complexes.

^1H Nuclear Magnetic Resonance Spectra

The ^1H nmr spectra of the ionic complexes were recorded in acetone-d^6 solutions. The spectra are entirely in accord with a symmetrically bridged bimetallic anion in solution. Thus the R substituents on the bridging "pyrazolyl" moieties give one sharp signal in the spectra (Table 1). The Et_4N^+ cations give characteristic multiplets with ^{14}N coupling apparent in the CH_3— triplet part of the spectrum but not in the —CH_2— quartet signal.

X-ray Crystallographic Analyses

Tetraethylammonium μ-Iodo-bis(μ-3,5-dimethylpyrazolyl(N,N′))bis(nitrosylniccolate(I))

The crystal structure of $[(C_2H_5)_4N]^+[(ON)Ni(\mu\text{-}I)(\mu\text{-}N_2C_5H_7)_2Ni(NO)]^-$ consists of discrete $(C_2H_5)_4N^+$ cations and binuclear anions (Fig. 1) separated by normal van der Waals distances. The anion contains two NiNO moieties bridged by an iodide and two 3,5-dimethylpyrazolyl ligands and has approximate C_{2v} symmetry. Deviations from ideal C_{2v} symmetry, some of which are significant, are believed to arise primarily from packing forces.

The Ni atoms have distorted tetrahedral coordination geometry, mean[2] angles at Ni (averaged assuming C_{2v} symmetry) being: I—Ni—NO, 116.9(5), I—Ni—N(pz), 93.5(5), N(pz)—Ni—NO, 124.1(8), and N(pz)—Ni—N(pz), 97.1(1)°. The two Ni—I distances of 2.762(1) and 2.767(1) Å are slightly but significantly different and the Ni—I—Ni angle is 73.67(2)°. The Ni---Ni separation is 3.307(1) Å. The four chemically equivalent Ni—N(pz) distances (1.964–1.997(4–5), mean 1.980(14) Å) are significantly different. Such differences between chemically equivalent bonds have been noted in the structures of several other $\{NiNO\}^{10}$ complexes, with both tetrahedral (14, 15 and references therein) and trigonal-planar (1) coordination at Ni. In view of the common observation of this phenomenon, the differences are almost certainly real but, apart from steric factors, no reasonable explanation for this can be given. The mean parameters of the nitrosyl coordination, Ni—N—O = 172.5(18)°, Ni—N = 1.649(5) and N—O = 1.13(1) Å, are near the middle of the observed ranges for these parameters in tetrahedral $\{NiNO\}^{10}$ complexes (14, 15).

Both of the pyrazolyl rings are planar within experimental error (χ^2 = 3.4 and 2.0 for N_2C_3 rings containing N(3) and N(5) respectively) but the nickel and methyl carbon atoms are significantly displaced from both mean planes (N(3) plane: Ni(1), 0.0347(9), Ni(2), −0.0711(8), C(7), −0.031(8), and C(8), 0.016(7) Å; N(5) plane: Ni(1), −0.0706(8), Ni(2), −0.0670(8), C(9), −0.034(8), and C(10), 0.034(8) Å). Other bond lengths and angles are as expected.

μ-(3,5-Dimethylpyrazolyl)-μ-[bis(tetrahydrofuran)-bis(η²(N,N)-3,5-dimethylpyrazolyl)sodium-(N,N,N′,N′)]bis(nitrosylnickel(I))

The structure of $[(C_4H_8O)_2Na][(ON)Ni(\mu\text{-}N_2C_5H_7)_3Ni(NO)]$ consists of discrete ion-pair molecular units (Fig. 2) separated by normal van der Waals distances. If the disordered THF carbon atoms are ignored, the molecule has approximate C_{2v}

[2]Here and elsewhere in this report mean values refer to weighted means with rms deviations from the mean in parentheses.

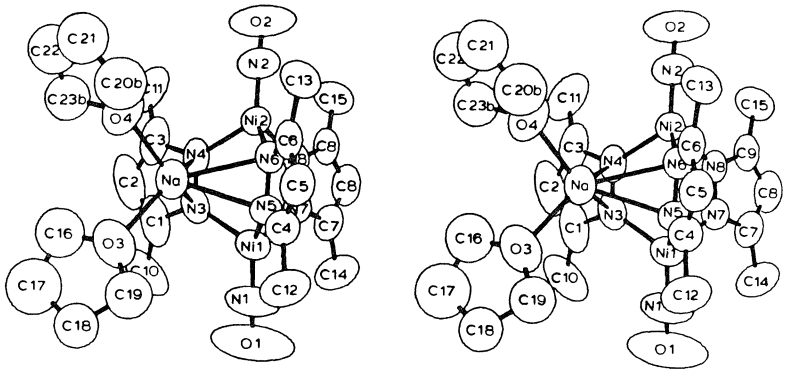

FIG. 2. Stereo view of the μ-(3,5-dimethylpyrazolyl)μ-[bis(tetrahydrofuran)bis(η^2(*N*,*N*)-3,5-dimethylpyrazolyl)sodium-(*N*,*N*,*N*′,*N*′)]-bis(nitrosylnickel(I)) molecule; 50% ellipsoids are shown for the non-hydrogen atoms.

symmetry. The two NiNO moieties are bridged by three 3,5-dimethylpyrazolyl ligands, two of which are also coordinated to sodium via a novel $\eta^2(N,N)$ π-interaction (mean Na—N = 2.61(3), Na—X(1) = 2.531, and Na—X(2) = 2.502 Å, where X(1) and X(2) are the midpoints of the N(3)—N(4) and N(5)—N(6) bonds). Distorted tetrahedral coordination geometry about the sodium is completed by two THF oxygen atoms (Na—O = 2.301(6) and 2.266(5) Å). The shortest Na---C(pz) distance is 3.19(2) Å.

Replacement of the single atom iodide bridge in $[(C_2H_5)_4N]^+[(ON)Ni(\mu\text{-}I)(\mu\text{-}N_2C_5H_7)_2Ni(NO)]^-$ by the two-atom pyrazolyl bridge results in an increase in the Ni---Ni separation from 3.307(1) to 3.439(1) Å in $[(C_4H_8O)_2Na][(ON)Ni(\mu\text{-}N_2C_5H_7)_3Ni(NO)]$. The Ni---Na distances are 3.393(3) and 3.364(3) Å for Ni(1) and Ni(2) respectively. The nickel atoms have distorted tetrahedral coordination geometry with mean angles N(pz)—Ni—NO and N(pz)—Ni—N(pz) of 121(1) and 95.6(9)°. The mean Ni—N(pz) distance involving the pyrazolyl nitrogen atoms coordinated to Na (2.016(5) Å) is significantly longer than the value of 1.985(2) for the other two pyrazolyl nitrogen atoms. The latter distance is in good agreement with the mean Ni—N(pz) distance of 1.980(14) Å in the $[(ON)Ni(I)(N_2C_5H_7)_2Ni(NO)]^-$ anion. The mean parameters of the NiNO group are Ni—N—O = 176.9(11)°, Ni—N = 1.591(6) and N—O = 1.183(8) Å. The short Ni—NO distance is similar to the value of 1.581(12) Å in the $Ni(NO)[P(OCH_2)_3CCH_3]_3^+$ cation (16), which has Ni—N—O = 176.8(2)°.

All three pyrazolyl rings are planar within experimental error (χ^2 = 3.3, 7.3, and 0.2 for N_2C_3 rings containing N(3), N(5), and N(7) respectively). The Ni atoms deviate significantly from all three planes (N(3) plane; Ni(1), 0.0825(8), Ni(2), 0.1273(8); N(5) plane; Ni(1), 0.3042(8), Ni(2) 0.1360(7); N(7) plane; Ni(1), 0.1316(8), Ni(2), −0.0807(7) Å), and the methyl carbon atoms from those planes which interact with the Na (N(3) plane; C(10), 0.04(1), C(11), 0.08(1); N(5) plane; C(12), 0.040(9), C(13), 0.054(7) Å). The deviations of Ni and methyl carbon atoms from the N(3) and N(5) rings are all away from the sodium. Other bond lengths and angles in this structure are as expected.

Acknowledgments

We thank the Natural Sciences and Engineering Council Canada for financial support and the University of British Columbia Computing Centre for assistance. We are grateful to Mr. P. Borda for C, H, N analyses and to Dr. S. Chan for nmr spectra.

1. K. S. CHONG, A. STORR, S. J. RETTIG, and J. TROTTER. Can. J. Chem. **57**, 3090 (1979).
2. P. COPPENS, L. LEISEROWITZ, and D. RABINOVICH. Acta Crystallogr. **18**, 1035 (1965).
3. W. R. BUSING and H. A. LEVY. Acta Crystallogr. **22**, 457 (1967).
4. D. T. CROMER and J. B. MANN. Acta Crystallogr. Sect. A, **24**, 321 (1968).
5. R. F. STEWART, E. R. DAVIDSON, and W. T. SIMPSON. J. Chem. Phys. **42**, 3175 (1965).
6. D. T. CROMER and D. LIBERMAN. J. Chem. Phys. **53**, 1891 (1970).
7. P. J. BECKER and P. COPPENS. Acta Crystallogr. Sect. A, **30**, 129 (1974); **30**, 148 (1974); **31**, 417 (1975).
8. P. COPPENS and W. C. HAMILTON. Acta Crystallogr. Sect. A, **26**, 71 (1970).
9. F. R. THORNLEY and R. J. NELMES. Acta Crystallogr. Sect. A, **30**, 748 (1974).
10. V. SCHOMAKER and K. N. TRUEBLOOD. Acta Crystallogr. Sect. B, **24**, 63 (1969).
11. D. W. J. CRUICKSHANK. Acta Crystallogr. **9**, 747 (1956); **9**, 754 (1956); **14**, 896 (1961).
12. W. BECK and K. LOTTES. Chem. Ber. **98**, 2657 (1965).
13. R. G. COPPERWAITE, R. H. REIMANN, and E. SINGLETON. Inorg. Chim. Acta, **28**, 107 (1978).
14. J. H. ENEMARK and R. D. FELTHAM. Coord. Chem. Rev. **13**, 339 (1974).
15. K. J. HALLER and J. H. ENEMARK. Inorg. Chem. **17**, 3552 (1978).
16. J. H. MEINERS, C. J. RIX, J. C. CLARDY, and J. G. VERKADE. Inorg. Chem. **14**, 705 (1975).

Reactions of Ni(NO)I with pyrazolyl gallate ligands: crystal and molecular structure of $[Me_2Ga(N_2C_5H_7)(OCH_2CH_2NMe_2)]Ni(NO)$

KENNETH S. CHONG, STEVEN J. RETTIG, ALAN STORR, AND JAMES TROTTER

Department of Chemistry, University of British Columbia, 2075 Wesbrook Mall, Vancouver, B.C., Canada V6T 1W5

Received July 3, 1979

KENNETH S. CHONG, STEVEN J. RETTIG, ALAN STORR, and JAMES TROTTER. Can. J. Chem. **57**, 3107 (1979).

Ni(NO)I reacts readily with pyrazolyl gallate ligands Na^+L^- (where L = $MeGa(N_2C_3H_3)_3$, $MeGa(N_2C_5H_7)_3$, and $[Me_2Ga(N_2C_5H_7)(OCH_2CH_2NMe_2)]$) to yield four-coordinate nickel nitrosyl complexes, LNi(NO). In addition, the compound $[Me_2Ga(N_2C_5H_7)(OCH_2CH_2NMe_2)]Ni(N_2C_5H_7)_2Ni(NO)$ has been isolated from one reaction sequence. ^1H nmr data show $[Me_2Ga(N_2C_5H_7)(OCH_2CH_2NMe_2)]Ni(NO)$ to be stereochemically non-rigid at room temperature in solution. Crystals of [dimethyl(*N*,*N*-dimethylethanolamino)(3,5-dimethylpyrazolyl)gallato(*N*(2),*N*(3),*O*)]nitrosylnickel(I) are monoclinic, a = 9.119(1), b = 13.900(2), c = 14.284(2) Å, β = 107.96(1)°, Z = 4, space group $P2_1/c$. The structure was solved by Patterson and Fourier syntheses and was refined by full-matrix least-squares procedures to R = 0.025 and R_w = 0.032 for 1828 reflections with $I \geq 3\sigma(I)$. The coordination about the nickel atom is severely distorted tetrahedral with angles at nickel ranging from 84.4(1) to 133.5(1)°. The nitrosyl group is coordinated in a non-linear fashion with Ni—N—O = 162.3(4)°, Ni—N = 1.632(4) and N—O = 1.147(4) Å. Other important bond lengths (corrected for libration) are: Ni—O, 2.045(2), Ni—N(pyrazolyl), 1.989(3), Ni—N(amino), 2.071(3), Ga—O, 1.922(2), Ga—N, 1.998(3), and Ga—C, two at 1.971(6) Å.

KENNETH S. CHONG, STEVEN J. RETTIG, ALAN STORR et JAMES TROTTER. Can. J. Chem. **57**, 3107 (1979).

Le Ni(NO)I réagit facilement avec les ligands du type gallate de pyrazolyle Na^+L^- (ou L = $MeGa(N_2C_3H_3)_3$, $MeGa(N_2C_3H_7)_3$ et $[Me_2Ga(N_2C_5H_7)(OCH_2CH_2NMe_2)]$) pour donner quatre complexes nitrosylés du nickel tétracoordonnés LNi(NO). On a isolé également le composé $[Me_2Ga(N_2C_5H_7)(OCH_2CH_2NMe_2)]Ni(N_2C_5H_7)_2Ni(NO)$. Les données de la rmn du ^1H montrent que $[Me_2Ga(N_2C_5H_7)(OCH_2CH_2NMe_2]Ni(NO)$ est stéréochimiquement non rigide en solution. Les cristaux de [diméthyl(*N*,*N*-diméthyléthanolamino)(diméthyl-3,5 pyrazolyl)gallato(*N*(2),*N*(3),*O*) nitrosyle nickel sont monocliniques: a = 9.119(1), b = 13.900(2), c = 14.284(2) Å, β = 107.96(1)°, Z = 4, groupe d'espace $P2_1/c$. On a résolu la structure par les synthèses de Patterson et de Fourier et on l'a affinée par la méthode des moindres carrés (matrice complète) jusqu'à une valeur de R = 0.025 et R_w = 0.032 pour 1828 réflexions avec $I \geq 3\sigma(I)$. La coordination autour de l'atome de nickel est distordue grandement en un tétraèdre avec des angles de 84.4(1) à 133.5(1)°. Le groupe nitrosyle est coordonné de façon non linéaire avec Ni—N—O = 162.3(4)°, Ni—N = 1.632(4) et N—O = 1.147(4) Å. D'autres longueurs importantes de liaison (corrigée pour libration) sont: Ni—O, 2.045(2), Ni—N(pyrazolyl), 1.989(3), Ni—N(amino), 2.071(3), Ga—O, 1.922(2), Ga—N, 1.998(3) et Ga—C, deux à 1.971(6) Å.

[Traduit par le journal]

Introduction

Numerous reports (1–4) have described the synthesis and coordination chemistry of bidentate anionic ligands of the type $Me_2Ga(N_2C_3H_3)_2^-$. More recent publications have discussed the preparations and coordinating properties of the tridentate anionic ligands $MeGa(N_2C_3H_3)_3^-$ (5, 6) and $MeGa(N_2C_5H_7)_3^-$ (7). The coordinating abilities of both the bidentate and tridentate ligands, and the properties of their various transition metal complexes, have been compared with similar boron species described earlier by Trofimenko (8). A significant divergence from the pyrazolyl borate type ligands came with the introduction of unsymmetrical tridentate anionic gallate ligands of the type $[Me_2Ga(N_2C_5H_7)(OCH_2CH_2NMe_2)]^-$ (9). These ligands have, as yet, no counterparts in boron chemistry and display unique coordinating properties, very much dependent on the substituents on the pyrazolyl ring and on the amino nitrogen of the ligand (10–12). The present account details our studies on the reactions of Ni(NO)I with the tridentate anionic pyrazolyl gallate ligands $MeGa(N_2C_3H_3)_3^-$, $MeGa(N_2C_5H_7)_3^-$, and $[Me_2Ga(N_2C_5H_7)(OCH_2CH_2NMe_2)]^-$. The solid state structure of $[Me_2Ga(N_2C_5H_7)(OCH_2CH_2NMe_2)]Ni(NO)$ is pre-

0008-4042/79/233107-06$01.00/0

sented and contrasted with the structure of this compound suggested by its room temperature ^1H nmr spectrum in C_6D_6 solution.

Experimental

Starting Materials

Air-sensitive materials were handled in a glove box under an atmosphere of oxygen-free, dry nitrogen or in a nitrogen-blanketed apparatus. Tetrahydrofuran (THF) was dried by refluxing over sodium/benzophenone and was used immediately following distillation. Benzene was dried by refluxing over molten potassium followed by distillation. Ni(NO)I was prepared by the method of Haymore and Feltham (13) and the gallium ligands, Na^+L^-, were prepared as described earlier, L = $MeGa(N_2C_3H_3)_3$ (5), L = $MeGa(N_2C_5H_7)_3$ (7), and L = $[Me_2Ga(N_2C_5H_7)(OCH_2CH_2NMe_2)]$ (9, 10).

Preparation of $[Me_2Ga(N_2C_5H_7)(OCH_2CH_2NMe_2)]Ni(NO)$

Ni(NO)I (0.324 g; 1.5 mmol) was dissolved in THF and a THF solution of $Na^+[Me_2Ga(N_2C_5H_7)(OCH_2CH_2NMe_2)]^-$ (1.63 mmol) was added. The reaction mixture was stirred overnight and the solvent then removed under vacuum. The dark blue residue was extracted with benzene and the mixture filtered. Slow evaporation of the filtrate gave dark blue crystals of the product (0.39 g; 70% yield). An alternate method of purification of this compound was vacuum sublimation at ~80°C. *Anal.* calcd. for $[Me_2Ga(N_2C_5H_7)(OCH_2CH_2NMe_2)]Ni(NO)$: C 35.5, H 6.2, N 15.1; found: C 35.7, H 6.3, N 14.8. ν_{NO} 1770 cm^{-1} (cyclohexane), 1750 br (Nujol), ^1H nmr (C_6D_6): τ = 3.94s (^4H—pz), 6.53t (CH_2, J = 5 Hz), 7.17s (Me—pz), 7.78s (NMe_2), 7.90s (Me—pz), 8.65t (CH_2, J = 5 Hz), 9.88s ($GaMe_2$) (all τ values refer to $\tau_{C_6H_6}$ = 2.84 ppm, pz = pyrazolyl).

Preparation of $[Me_2Ga(N_2C_5H_7)(OCH_2CH_2NMe_2)]Ni(N_2C_5H_7)_2Ni(NO)$

Ni(NO)I (0.324 g; 1.5 mmol) was dissolved in THF and a THF solution of the ligand $Na^+[Me_2Ga(N_2C_5H_7)(OCH_2CH_2NMe_2)]^-$ (1.63 mmol) was added. The reaction mixture was stirred for about 10 min and then approximately 1 mL of water was added. The resultant mixture was heated to reflux and oxygen (air) was admitted periodically until a green tinge appeared in the blue solution. After cooling the mixture to room temperature the solvent was removed *in vacuo*. The blue green residue was extracted with benzene and filtered. After several recrystallizations from benzene/heptane mixtures, dark green air-sensitive crystals were isolated in about 20% yield. *Anal.* calcd. for $[Me_2Ga(N_2C_5H_7)(OCH_2CH_2NMe_2)]Ni(N_2C_5H_7)_2Ni(NO)$: C 40.6, H 6.0, N 18.0; found: C 40.7, H 6.0, N 17.7. ν_{NO} 1790 cm^{-1} (Nujol).

Preparation of $MeGa(N_2C_5H_7)_3Ni(NO)$

Ni(NO)I (0.311 g; 1.44 mmol) was dissolved in THF and an aliquot of $Na^+MeGa(N_2C_5H_7)_3^-$ in THF (1.45 mmol) added with stirring. The mixture was stirred overnight and the solvent then removed *in vacuo*. The blue solid was recrystallized from benzene to give a well formed blue crystalline product (yield ~60%). *Anal.* calcd. for $MeGa(N_2C_5H_7)_3Ni(NO)$: C 41.9, H 5.2, N 21.4; found: C 41.6, H 5.3, N 20.7. ν_{NO} 1785 cm^{-1} (cyclohexane), 1765 cm^{-1} (Nujol), ^1H nmr (C_6D_6) τ = 4.09s (^4H—pz), 7.43s (Me—pz), 8.14s (Me—pz), 9.97s (GaMe).

Preparation of $MeGa(N_2C_3H_3)_3Ni(NO)$

A solution of $Na^+MeGa(N_2C_3H_3)_3^-$ (1.6 mmol) in THF was added dropwise to a stirred solution of Ni(NO)I (0.345 g; 1.6 mmol) in THF at −78°C. After allowing the reaction mixture to warm slowly to room temperature, solvent was removed under vacuum. The solid remaining was extracted with benzene and filtered. Slow evaporation gave blue crystals together with a small amount of orange material. The blue product was separated by vacuum sublimation at 60°C (yield ~60%). *Anal.* calcd. for $MeGa(N_2C_3H_3)_3Ni(NO)$: C 32.1, H 3.2, N 26.29; found: C 32.4, H 3.3, N 23.2. ν_{NO} 1786 cm^{-1} (cyclohexane), 1815 cm^{-1} (Nujol), ^1H nmr (C_6D_6) τ = 1.43d (J = 2 Hz, ^3H—pz), 2.90d (J = 2 Hz, ^5H—pz), 3.77t (J = 2 Hz, ^4H—pz), 10.22s (GaMe).

Mass Spectra

The two compounds $[MeGa(N_2C_3H_3)_3]Ni(NO)$ and $[MeGa(N_2C_5H_7)_3]Ni(NO)$ gave very similar mass spectra. The strongest signal in each spectrum was due to the parent ion minus the nitrosyl group, P—NO^+. All other signals in these two spectra were much weaker (10% or less of the intensity of the P − NO^+ signal) but the P^+ ion and ions due to loss of the methyl group, P − Me^+, and other ions due to loss of "pyrazolyl" moieties were in evidence.

The mass spectrum of the $[Me_2Ga(N_2C_5H_7)(OCH_2CH_2NMe_2)]Ni(NO)$ complex displayed a weak parent ion signal but the strongest signals corresponded to the P − NO^+ and P − NO − Me^+ ions, with the latter giving the slightly stronger signal. The trimetallic complex $[Me_2Ga(N_2C_5H_7)(OCH_2CH_2NMe_2)]Ni(N_2C_5H_7)_2Ni(NO)$ again displayed a weak parent ion signal in its mass spectrum. The strongest signal was due to the P − NO − Me^+ ion with a further strong signal arising from the P − NO^+ ion.

In all four spectra the relative intensities of the individual peaks in multi-line signals corresponded closely to those predicted on the basis of the natural isotope compositions of the contributing metal atoms.

Spectra

Infrared spectra were recorded on a Perkin-Elmer 457 spectrometer and ^1H nmr spectra on a Varian XL-100 spectrometer utilizing FT techniques. Mass spectra were obtained on a Varian MAT CH4 spectrometer at 70 eV with an ion source temperature of 100–180°C.

X-ray Crystallographic Analysis of $[Me_2Ga(N_2C_5H_7)(OCH_2CH_2NMe_2)]Ni(NO)$

The crystal chosen was mounted in a general orientation and had dimensions of ca. 0.12 × 0.29 × 0.39 mm. Unit-cell parameters were refined by least-squares on 2 sin θ/λ values for 43 reflections measured on a diffractometer with Mo K_α radiation (λ = 0.71073 Å). Crystal data (at 22°C) are:

$C_{11}H_{23}GaN_4NiO_2$ fw = 371.76

Monoclinic, a = 9.119(1), b = 13.900(2), c = 14.284(2) Å, β = 107.96(1)°, V = 1722.3(4) Å^3, Z = 4, ρ_c = 1.434 g cm^{-3}, $F(000)$ = 768, μ(Mo K_α) = 25.8 cm^{-1}. Absent reflections: $0k0$, $k \neq 2n$ and $h0l$, $l \neq 2n$ define uniquely the space group $P2_1/c$ (C_{2h}^5, No. 14).

Intensities were measured with graphite monochromatized Mo K_α radiation on an Enraf-Nonius CAD4-F diffractometer. An ω–θ scan at 0.91–5.03° min^{-1} over a range of (0.60 + 0.35 tan θ) degrees in ω (extended by 25% on both sides for background measurement) was employed. Data were measured to 2θ = 50°. The intensities of 3 check reflections, measured every 3600 s throughout the data collection, decreased linearly by 4% during the data collection. After data reduction, an absorption correction was applied using the Gaussian integration method (14, 15). Transmission factors ranged from 0.518 to 0.742. Of the 3001 independent reflections measured, 1828 (60.9%) had intensities greater than 3σ(I) above background where $\sigma^2(I) = S + 2B + (0.04(S - B))^2$ with S = scan count and B = background count.

The positions of the Ga and Ni atoms were determined from the three-dimensional Patterson function and those of the remaining non-hydrogen atoms from a subsequent difference map. After full-matrix least-squares refinement of the non-hydrogen atoms with anisotropic thermal parameters to $R = 0.040$, a difference map gave positions for all 23 hydrogen atoms. Hydrogen positions and isotropic thermal parameters were included in the final stages of the refinement. The scattering factors of ref. 16 were used for non-hydrogen atoms and those of ref. 17 for hydrogen atoms. Anomalous scattering factors from ref. 18 were used for the Ga and Ni atoms. The weighting scheme, $w = 1/\sigma^2(F)$ where $\sigma^2(F)$ is derived from the previously defined $\sigma^2(I)$ gave uniform average values of $w(|F_o| - |F_c|)^2$ over ranges of $|F_o|$ and was employed in the final stages of refinement. Convergence was reached at $R = 0.025$ and $R_w = 0.032$ for 1828 reflections with $I \geq 3\sigma(I)$. For all 3001 reflections $R = 0.066$ and $R_w = 0.039$.

On the final cycle of refinement the mean and maximum parameter shifts corresponded to 0.08 and 0.75σ respectively. The mean error in an observation of unit weight was 0.9911. A final difference map showed maximum fluctuations of ± 0.6 e Å^{-3} near Ga and Ni and ± 0.2 e Å^{-3} elsewhere. The final positional and thermal parameters appear in Tables 1 and 2[1] respectively. Measured and calculated structure factors have been placed in the Depository of Unpublished Data.[1]

The ellipsoids of thermal motion for the non-hydrogen atoms are shown in Fig. 1. The thermal motion has been analysed in terms of the rigid-body modes of translation, libration, and screw motion (19) using the computer program MGTLS. The rms standard error in the temperature factors σU_{ij} (derived from the least-squares analysis) is 0.0030 Å^2. Two successful analyses were carried out, one rigid-group included all non-hydrogen atoms except the nitrosyl oxygen and the six methyl carbon atoms and the other was a five-atom group consisting of Ga and the four atoms bonded to it (rms $\Delta U_{ij} = 0.0064$ and 0.0022 Å^2, respectively). The appropriate bond distances have been corrected for libration (20), using shape parameters q^2 of 0.08 for all atoms involved. Corrected bond distances appear along with the uncorrected values in Table 3. Corrected bond angles are all within 1σ of the uncorrected values given in Table 4. Intra-annular torsion angles defining the conformations of the two five-membered chelate rings appear in Table 5.

TABLE 1. Final positional parameters (fractional; O, N, and C × 10^4, Ga and Ni × 10^5, H × 10^3) with estimated standard deviations in parentheses

Atom	x	y	z
Ga	32503(4)	24437(3)	5418(3)
Ni	67043(5)	15930(3)	8847(3)
O(1)	4420(3)	1484(1)	128(2)
O(2)	8967(5)	632(3)	2291(4)
N(1)	5017(3)	3353(2)	953(2)
N(2)	6467(3)	2988(2)	1082(2)
N(3)	7005(3)	1443(2)	−482(2)
N(4)	7870(4)	965(2)	1764(3)
C(1)	1641(8)	2974(6)	−588(5)
C(2)	2890(8)	1915(5)	1725(4)
C(3)	5181(5)	4292(3)	1215(3)
C(4)	6711(6)	4520(3)	1510(3)
C(5)	7488(5)	3690(3)	1428(3)
C(6)	4201(6)	1381(4)	−898(3)
C(7)	5569(6)	918(4)	−1056(4)
C(8)	3814(9)	4890(5)	1181(5)
C(9)	9192(6)	3513(5)	1642(5)
C(10)	8287(9)	802(6)	−464(6)
C(11)	7163(9)	2357(4)	−950(5)
H(1a)	86(6)	249(3)	−96(4)
H(1b)	207(6)	322(4)	−96(4)
H(1c)	95(8)	329(4)	−52(5)
H(2a)	260(7)	236(4)	198(4)
H(2b)	204(5)	144(3)	158(3)
H(2c)	374(6)	159(4)	208(4)
H(4)	720(4)	511(3)	177(3)
H(6a)	330(5)	112(3)	−117(3)
H(6b)	435(5)	201(4)	−121(4)
H(7a)	573(6)	7(4)	−70(3)
H(7b)	547(5)	102(3)	−183(3)
H(8a)	322(8)	503(5)	73(5)
H(8b)	409(8)	547(5)	163(5)
H(8c)	281(7)	450(4)	105(5)
H(9a)	976(6)	377(4)	212(4)
H(9b)	941(9)	377(5)	97(7)
H(9c)	953(9)	280(5)	191(6)
H(10a)	821(5)	23(3)	−14(3)
H(10b)	831(6)	66(4)	−111(4)
H(10c)	934(9)	126(6)	−9(6)
H(11a)	831(4)	253(2)	−51(3)
H(11b)	622(7)	277(4)	−101(4)
H(11c)	745(7)	218(4)	−153(5)

Results and Discussion

The reactions of nickel nitrosyl iodide with sodium pyrazolide and substituted sodium pyrazolide salts have been reported recently (21). A series of green crystalline pyrazolyl-bridged, "16-electron", nickel nitrosyl dimers was produced which readily interacted with donor species to form blue crystalline adducts in which the nickel atoms attained an 18-electron configuration (21, 22). The present account is concerned with the synthesis of LNi(NO) species in which L is a tridentate chelating ligand (L = $MeGa(N_2C_3H_3)_3$, $MeGa(N_2C_5H_7)_3$, or $[Me_2Ga(N_2C_5H_7)(OCH_2CH_2NMe_2)]$). In the first two complexes a pseudotetrahedral geometry is required as the ligand L cannot occupy a planar set of coordination sites. With L = $[Me_2Ga(N_2C_5H_7)(OCH_2CH_2NMe_2)]$ there is the possibility of a square-planar arrangement of the four donor atoms about the nickel in LNi(NO). The solid state structure of this complex (see below) displays the nickel atom in a distorted tetrahedral environment, but the ^{1}H nmr spectrum, for the compound in C_6D_6 at room temperature, suggests a square-planar geometry in solution. In this spectrum both the —NMe_2 and —$GaMe_2$ moieties display but one sharp signal for their two methyl groups. A tetrahedral structure for the LNi(NO) complex in solution would display two signals for each of the NMe_2 and —$GaMe_2$

[1]The structure factor table and Table 2 (thermal parameters) are available, at a nominal charge, from the Depository of Unpublished Data, CISTI, National Research Council of Canada, Ottawa, Ont., Canada K1A 0S2.

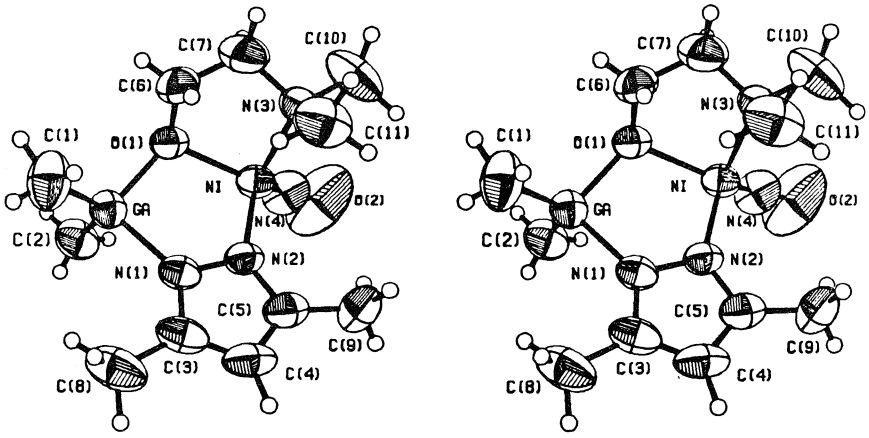

FIG. 1. Stereo view of the [dimethyl(*N*,*N*-dimethylethanolamino)(3,5-dimethylpyrazolyl)gallato(*N*(2),*N*(3),*O*)]nitrosylnickel(I) molecule, 50% ellipsoids are shown for the non-hydrogen atoms.

TABLE 3. Bond lengths (Å) with estimated standard deviations in parentheses

(*a*) Non-hydrogen atoms

Bond	Length		Bond	Length	
	Uncorr.	Corr.		Uncorr.	Corr.
Ga —O(1)	1.912(2)	1.922	N(1)—C(3)	1.354(4)	1.355
Ga —N(1)	1.989(3)	1.998	N(2)—C(5)	1.335(4)	1.337
Ga —C(1)	1.960(6)	1.971	N(3)—C(7)	1.503(5)	1.507
Ga —C(2)	1.962(5)	1.971	N(3)—C(10)	1.463(6)	1.463
Ni —O(1)	2.035(2)	2.045	N(3)—C(11)	1.464(6)	1.467
Ni —N(2)	1.981(3)	1.989	C(3)—C(4)	1.365(6)	1.369
Ni —N(3)	2.063(3)	2.071	C(3)—C(8)	1.487(7)	1.489
Ni —N(4)	1.627(4)	1.632	C(4)—C(5)	1.378(5)	1.381
O(1)—C(6)	1.425(5)	1.428	C(5)—C(9)	1.508(7)	1.510
O(2)—N(4)	1.147(4)	1.147	C(6)—C(7)	1.481(6)	1.485
N(1)—N(2)	1.374(4)	1.381			

(*b*) Bonds involving hydrogen atoms

Bond	Length	Mean
C(sp^2)—H	0.95(4)	
C(sp^3)—H	0.72–1.27(4–9)	0.97(13)

groups. A square-planar arrangement, however, could satisfactorily explain the spectrum. A variable temperature ^{1}H nmr spectrum in toluene-d^8 demonstrated that the room temperature spectrum is due to a rapidly fluxional species, in all probability giving an "average" square-planar environment about the Ni atom. In this experiment the sharp —$GaMe_2$ signal was monitored. On cooling the solution the —$GaMe_2$ signal gradually broadened until at −70°C it became a broad hump and at −80°C (the lowest temperature attainable) the appearance of two signals, one to either side of the position of the original signal, was just discernable. Evidently at these lower temperatures the tetrahedral conformation, observed in the solid state, is becoming established in solution. It is noteworthy that of the two "—CH_2—" "triplets" the upfield one loses resolution first (0°C) and not until −40°C does the resolution in the corresponding low field —CH_2— "triplet" start to collapse. At −80°C both —CH_2— "triplets" have broadened out to the point of disappearing into the background of the spectrum.

In the presence of oxygen, solutions of all three of the Ni(I) complexes lose NO and form Ni(II) derivatives. In the case of the complex [$Me_2Ga(N_2C_5H_7)(OCH_2CH_2NMe_2)$]Ni(NO) it was found possible to effect partial oxidation to give the novel

TABLE 4. Bond angles (deg) with estimated standard deviations in parentheses

Non-hydrogen atoms

Bonds	Angle (deg)	Bonds	Angle (deg)
O(1)—Ga —N(1)	93.2(1)	Ni —N(2)—N(1)	119.0(2)
O(1)—Ga —C(1)	110.8(3)	Ni —N(2)—C(5)	132.4(3)
O(1)—Ga —C(2)	105.2(2)	N(1) —N(2)—C(5)	108.2(3)
N(1)—Ga —C(1)	109.7(3)	Ni —N(3)—C(7)	102.6(2)
N(1)—Ga —C(2)	108.6(2)	Ni —N(3)—C(10)	112.5(3)
C(1)—Ga —C(2)	124.7(3)	Ni —N(3)—C(11)	113.9(3)
O(1)—Ni —N(2)	90.5(1)	C(7) —N(3)—C(10)	105.7(5)
O(1)—Ni —N(3)	84.4(1)	C(7) —N(3)—C(11)	111.4(4)
O(1)—Ni —N(4)	133.5(1)	C(10)—N(3)—C(11)	110.2(5)
N(2)—Ni —N(3)	106.6(1)	N(1) —C(3)—C(4)	109.0(4)
N(2)—Ni —N(4)	119.3(1)	N(1) —C(3)—C(8)	120.7(5)
N(3)—Ni —N(4)	115.5(2)	C(4) —C(3)—C(8)	130.3(5)
Ga —O(1)—Ni	111.2(1)	C(3) —C(4)—C(5)	106.4(3)
Ga —O(1)—C(6)	118.3(2)	N(2) —C(5)—C(4)	109.0(4)
Ni —O(1)—C(6)	110.5(2)	N(2) —C(5)—C(9)	120.9(4)
Ga —N(1)—N(2)	117.6(2)	C(4) —C(5)—C(9)	130.1(4)
Ga —N(1)—C(3)	134.8(3)	O(1) —C(6)—C(7)	110.1(4)
N(2)—N(1)—C(3)	107.4(3)	N(3) —C(7)—C(6)	109.8(4)
Ni —N(4)—O(2)	162.3(4)		

TABLE 5. Intra-annular torsion angles (deg) five-membered chelate rings

Bond	Observed angle	Bond	Observed angle
Ga —O(1)	27.2(2)	Ni —O(1)	−0.8(2)
O(1)—Ni	−27.6(2)	O(1)—C(6)	27.7(4)
Ni —N(2)	17.6(2)	C(6)—C(7)	−51.6(4)
N(2)—N(1)	−1.4(2)	C(7)—N(3)	47.1(3)
N(1)—Ga	−16.7(2)	N(3)—Ni	−24.8(2)

trimetallic complex $[Me_2Ga(N_2C_5H_7)(OCH_2CH_2NMe_2)]Ni(N_2C_5H_7)_2Ni(NO)$ which contains, formally, both a Ni(I) centre and a Ni(II) centre. Full oxidation of this complex, however, leads to the five-coordinate Ni(II) compound $[Me_2Ga(N_2C_5H_7)(OCH_2CH_2NMe_2)]Ni[(N_2C_5H_7)_2GaMe_2]$, a compound which has been prepared by a more conventional route and structurally characterized (23).

Of the two complexes $MeGa(N_2C_5H_7)_3Ni(NO)$ and $MeGa(N_2C_3H_3)_3Ni(NO)$, the former is the more readily prepared and is more stable to NO loss in solution. The latter complex readily loses NO in solution, and its preparation is hampered by the tendency to form $[MeGa(N_2C_3H_3)_3]_2Ni$ (5) and even $[Me_2Ga(N_2C_3H_3)_2]_2Ni$ (4) in the reaction mixture. Both of these compounds are very stable to aerial oxidation and moisture (4, 5). The low temperature synthesis led to much improved yields of the desired $[MeGa(N_2C_3H_3)_3]Ni(NO)$ material. However, facile loss of NO from this compound in the analytical instrument resulted in a low analysis for nitrogen.

The stability of the four complexes reported here should be compared with the stability of the analogous (η^5-C_5H_5)Ni(NO) complex reported some years ago (24, 25). This compound, reportedly highly toxic (26), is a dark red liquid, stable in the pure state and in solution and only slightly decomposed upon distillation. Electron diffraction studies show the Ni—N—O grouping to be linear with a Ni—N distance of 1.58 Å (27). The ν_{NO} value is 1833 cm^{-1} (26).

Crystal Structure of [*Dimethyl(*N,N-*dimethylethanolamino)(3,5-dimethylpyrazolyl)gallato-(*N*(2),*N*(3),*O*)]nitrosylnickel(I)*

The crystal structure of $[Me_2Ga(N_2C_5H_7)(OCH_2CH_2NMe_2)]Ni(NO)$ consists of discrete molecular units, each linked with one other molecule across the centres of symmetry at 1/2, 0, 0 and 1/2, 1/2, 1/2 by C—H---O interactions (O(1)---H(7a) $(1 - x, -y, -z) = 2.33(5)$, O---C = 3.591(6) Å, and O---H—C = 171(3)°) to form weakly associated dimers. All other intermolecular contacts correspond to normal van der Waals interactions.

The molecule (Fig. 1) contains a system of three fused five-membered rings with the central GaONiNN ring being roughly coplanar with the pyrazolyl

ring and perpendicular to the NiOCCN chelate ring. This arrangement of the tridentate gallate ligand is similar to that observed in the octahedral complexes *fac*-$[Me_2Ga(N_2C_3H_3)(OCH_2CH_2NH_2)]_2Ni$ (10) and $[Me_2Ga(N_2C_5H_7)(OCH_2CH_2NH_2)]Mo(CO)_2(\eta^3\text{-}C_4H_7)$ (12). The pyrazolyl ring is planar within experimental error ($\chi^2 = 5.9$, maximum deviation = 0.006(4) Å for N_2C_3) with the metal atoms significantly displaced from the N_2C_3 plane (Ga by 0.1354(4) and Ni by 0.1625(4) Å). The two five-membered chelate rings have "envelope" conformations in which one of the five atoms is displaced from the plane of the other four (O(1) and C(7) from the GaNiNN and NiOCN planes respectively, see torsion angles in Table 5).

The gallium atom has distorted tetrahedral coordination geometry with angles ranging from 93.2(1) to 124.7(3)°. The bond distances and angles in the gallate ligand are in good agreement with those reported for similar structures (1, 3–7, 9, 10, 12, 23).

The coordination about the nickel atom is severely distorted tetrahedral with angles ranging from 84.4(1)° for O(1)—Ni—N(3) to 133.5(1)° for O(1)—Ni—N(4). The nitrosyl group is coordinated in a non-linear fashion with Ni—N—O = 162.3(4)°, Ni—N = 1.632(4) and N—O = 1.147(4) Å. Enemark *et al.* have recently discussed the geometries of a number of four-coordinate nickel nitrosyl compounds (28, 29) and have pointed out that as the stereochemistry of a $\{MNO\}^{10}$ complex changes from tetrahedral towards square-planar, the M—N—O angle decreases from 180° towards the square-planar limit of ~120° with a concomitant increase in the M—N distance. The observed $\{NiNO\}^{10}$ geometry in the present complex is consistent with that observed for other four-coordinate $\{NiNO\}^{10}$ structures which have Ni—N—O = 180(0) → 152.7(7)° and Ni—N = 1.581(12) → 1.686(7) Å (refs. 22, 28, 29 and references therein). The Ni—O(1), Ni—N(2), and Ni—N(3) bond lengths of 2.045(2), 1.989(3), and 2.071(3) Å may be compared to corresponding values of 2.090(3), 2.085(3), and 2.112(3) Å in the octahedral Ni(II) complex *fac*-$[Me_2Ga(N_2C_3H_3)(OCH_2CH_2NH_2)]_2Ni$ (10) which has a similar ligand geometry. The longer distances in the Ni(II) complex probably result from considerably greater steric crowding in the octahedral complex.

Acknowledgments

We thank the Natural Sciences and Engineering Council of Canada for financial support and the University of British Columbia Computing Centre for assistance. We are grateful to Mr. P. Borda for C, H, N analyses and to Dr. S. Chan for nmr spectra.

1. D. F. Rendle, A. Storr, and J. Trotter. J. Chem. Soc. Dalton Trans. 176 (1975).
2. F. G. Herring, D. J. Patmore, and A. Storr. J. Chem. Soc. Dalton Trans. 711 (1975).
3. D. J. Patmore, D. F. Rendle, A. Storr, and J. Trotter. J. Chem. Soc. Dalton, 718 (1975).
4. K. R. Breakell, D. J. Patmore, and A. Storr. J. Chem. Soc. Dalton Trans. 749 (1975).
5. K. R. Breakell, S. J. Rettig, D. L. Singbeil, A. Storr, and J. Trotter. Can. J. Chem. **56**, 2099 (1978).
6. S. J. Rettig, A. Storr, and J. Trotter. Can. J. Chem. **57**, 1823 (1979).
7. K. R. Breakell, S. J. Rettig, A. Storr, and J. Trotter. Can. J. Chem. **57**, 139 (1979).
8. S. Trofimenko. Chem. Rev. **72**, 497 (1972).
9. K. S. Chong, S. J. Rettig, A. Storr, and J. Trotter. Can. J. Chem. **55**, 4166 (1977).
10. K. S. Chong, S. J. Rettig, A. Storr, and J. Trotter. Can. J. Chem. **56**, 1212 (1978).
11. K. S. Chong and A. Storr. Can. J. Chem. **57**, 167 (1979).
12. K. S. Chong, S. J. Rettig, A. Storr, and J. Trotter. Can. J. Chem. **57**, 1335 (1979).
13. B. Haymore and R. D. Feltham. Inorg. Synth. **14**, 81 (1973).
14. P. Coppens, L. Leiserowitz, and D. Rabinovich. Acta Crystallogr. **18**, 1035 (1965).
15. W. R. Busing and H. A. Levy. Acta Crystallogr. **22**, 457 (1967).
16. D. T. Cromer and J. B. Mann. Acta Crystallogr. Sect. A, **24**, 321 (1968).
17. R. F. Stewart, E. R. Davidson, and W. T. Simpson. J. Chem. Phys. **42**, 3175 (1965).
18. D. T. Cromer and D. Liberman. J. Chem. Phys. **53**, 1891 (1970).
19. V. Schomaker and K. N. Trueblood. Acta Crystallogr. Sect. B, **24**, 63 (1969).
20. D. W. J. Cruickshank. Acta Crystallogr. **9**, 747 (1956); **9**, 754 (1956); **14**, 896 (1961).
21. K. S. Chong, A. Storr, S. J. Rettig, and J. Trotter. Can. J. Chem. **57**, 3090 (1979).
22. K. S. Chong, A. Storr, S. J. Rettig, and J. Trotter. Can. J. Chem. **57**, 3099 (1979).
23. K. S. Chong, A. Storr, S. J. Rettig, and J. Trotter. Unpublished results.
24. T. S. Piper, F. A. Cotton, and G. Wilkinson. J. Inorg. Nucl. Chem. **1**, 165 (1955).
25. E. O. Fischer, O. Beckert, W. Hafner, and H. O. Stahl. Z. Naturforsch. **B10**, 598 (1955).
26. R. B. King. Organomet. Synth. **1**, 169 (1965).
27. I. A. Ronova, N. V. Alekseeva, N. N. Veniaminov, and M. A. Kravers. Zh. Strukt. Khim. **16**, 476 (1975).
28. K. J. Haller and J. H. Enemark. Inorg. Chem. **17**, 3552 (1978).
29. J. H. Enemark and R. D. Feltham. Coord. Chem. Rev. **13**, 339 (1974).

Five-coordinate iron and manganese dinitrosyl complexes incorporating tridentate chelating dimethyl(*N*,*N*-dimethylethanolamino)(pyrazolyl)gallate ligands: crystal and molecular structure of $[Me_2Ga(N_2C_5H_7)(OCH_2CH_2NMe_2)]Fe(NO)_2$

KENNETH S. CHONG, STEVEN J. RETTIG, ALAN STORR, AND JAMES TROTTER

Department of Chemistry, University of British Columbia, 2075 Wesbrook Mall, Vancouver, B.C., Canada V6T 1W5

Received July 6, 1979

KENNETH S. CHONG, STEVEN J. RETTIG, ALAN STORR, and JAMES TROTTER. Can. J. Chem. **57**, 3113 (1979).

Novel neutral monomeric five-coordinate manganese and iron dinitrosyl compounds incorporating asymmetric tridentate anionic gallate ligands are described. The crystal structure of the formally "19-electron" iron complex $[Me_2Ga(N_2C_5H_7)(OCH_2CH_2NMe_2)]Fe(NO)_2$ has been determined. Crystals of [dimethyl(*N*,*N*-dimethylethanolamino)(3,5-dimethylpyrazolyl)gallato(*N*(2),*N*(3),*O*)]dinitrosyliron(I) are monoclinic, $a = 7.3079(6)$, $b = 14.274(1)$, $c = 17.076(1)$ Å, $\beta = 91.709(4)°$, $Z = 4$, space group $P2_1/c$. The structure was solved by Patterson and Fourier syntheses and was refined by full-matrix least-squares procedures to $R = 0.034$ and $R_w = 0.046$ for 2848 reflections with $I \geq 3\sigma(I)$. The crystal structure consists of discrete monomeric units. The coordination geometry about the iron atom is distorted trigonal-bipyramidal with the tridentate gallate ligand acting in a meridional fashion, occupying one equatorial and both axial positions. The two nitrosyl groups occupy the other two equatorial sites and both Fe—N—O groupings are considerably bent toward one another in the equatorial plane. Important mean molecular dimensions (distances corrected for libration) are: Fe—O, 2.037(3), Fe—N(pyrazolyl), 2.112(3), Fe—N(amino), 2.279(3), Fe—NO, 1.710(3), N—O, 1.153(5), Ga—O, 1.916(3), Ga—N, 1.975(3), Ga—C, 1.972(6) Å, and Fe—N—O, 158.6(7)°.

KENNETH S. CHONG, STEVEN J. RETTIG, ALAN STORR et JAMES TROTTER. Can. J. Chem. **57**, 3113 (1979).

On décrit un nouveau complexe monomère neutre du manganèse pentacoordonné et des composés du fer dinitrosylé incorporant des ligands anioniques tridentates asymétriques du type gallate. On a déterminé la structure cristalline du complexe de fer comportant formellement "19 électrons" $[Me_2Ga(N_2C_5H_7)(OCH_2CH_2NMe_2)]Fe(NO)_2$. Les cristaux de diméthyle(*N*,*N*-diméthyléthanolamino)(diméthyl-3,5 pyrazolyl) gallato(*N*(2),*N*(3),*O*)dinitrosyle fer(I) sont monocliniques $a = 7.3079(6)$, $b = 14.274(1)$, $c = 17.076(1)$ Å, $\beta = 91.709(4)°$, $Z = 4$, groupe d'espace $P2_1/c$. On a résolu la structure à l'aide des synthèses de Patterson et de Fourier et on l'a affinée par la méthode des moindres carrés (matrice complète) jusqu'à des valeurs de $R = 0.034$ et $R_w = 0.046$ pour 2848 réflexions avec $I > 3\sigma(I)$. La structure cristalline consiste en unités monomères individuelles. La géométrie de coordination autour de l'atome de fer est de type trigonal bipyramidal déformé avec le ligand gallate tridentate agissant de manière méridionale, occupant une position équatoriale et les deux positions axiales. Les deux groupes nitrosyles occupent les deux autres positions équatoriales et les deux groupes Fe—N—C sont considérablement courbés l'un vers l'autre dans le plan équatorial. Les principales dimensions moléculaires importantes (corrigés pour la libration) sont: Fe—O, 2.037(3), Fe—N(pyrazolyl), 2.112(3), Fe—N(amino), 2.279(3), Fe—NO, 1.710(3), N—O, 1.153(5), Ga—O, 1.916(3), Ga—N, 1.975(3), Ga—C, 1.972(6) Å et Fe—N—O, 158.6(7)°.

[Traduit par le journal]

Introduction

Asymmetric tridentate gallate ligands incorporating pyrazolyl and ethanolamino moieties have been the subject of recent publications (1–4). The versatility of these ligands, the stability of their complexes, and their ability to display unique coordination geometries not possible with the related six-electron ligands η^5-$C_5H_5^-$ and $RE(N_2C_3H_3)_3^-$ (where R = H or alkyl and E = B or Ga) has prompted a further expansion of our studies in this area. The present account describes the synthesis and characterization of a series of metal dinitrosyl compounds $LM(NO)_2$ (where M = Mn or Fe and L = $[Me_2Ga(N_2C_5H_7)(OCH_2CH_2NMe_2)]$ or $[Me_2Ga(N_2C_3H_3)(OCH_2CH_2NMe_2)]$) and details the X-ray structural results for the iron complex $[Me_2Ga(N_2C_5H_7)(OCH_2CH_2NMe_2)]Fe(NO)_2$.

Experimental

Starting Materials

Air-sensitive materials were handled in a glove box under an atmosphere of oxygen-free dry nitrogen or in a nitrogen-blanketed apparatus. Tetrahydrofuran (THF) was dried by refluxing over sodium/benzophenone and was used immediately following distillation. Benzene was dried by re-

0008-4042/79/233113-06$01.00/0

fluxing over molten potassium followed by distillation. $Fe(NO)_2I$ was prepared by the method of Haymore and Feltham (5) and $Mn[P(OMe)_3]_2(NO)_2Br$ by the method of Reimann and Singleton (6). The gallium ligands Na^+L^- (where L = $[Me_2Ga(N_2C_3H_3)(OCH_2CH_2NMe_2)]$ or $[Me_2Ga(N_2C_5H_7)(OCH_2CH_2NMe_2)]$) were prepared as described earlier (1, 2).

Preparation of $[Me_2Ga(N_2C_5H_7)(OCH_2CH_2NMe_2)]$-$Fe(NO)_2$

$Fe(NO)_2I$ (0.22 g; 0.91 mmol) was dissolved in THF (20 mL) and $Na^+[Me_2Ga(N_2C_5H_7)(OCH_2CH_2NMe_2)]^-$ (1.0 mmol) in THF (10 mL) added to the resulting solution. After stirring the mixture for 1 h the solvent was removed under vacuum. The solid residue was extracted with several portions of benzene. Following filtration the resulting benzene solution of the product was allowed to evaporate slowly. Shiny black crystals of the product were collected (0.29 g; 81%). *Anal.* calcd. for $[Me_2Ga(N_2C_5H_7)(OCH_2CH_2NMe_2)]$-$Fe(NO)_2$: C 33.1, H 5.8, N 17.5; found: C 33.5, H 6.0, N 17.3. ν_{NO} 1750, 1673 cm^{-1} (cyclohexane), 1740 br, 1668 br cm^{-1} (Nujol).

The corresponding $[Me_2Ga(N_2C_3H_3)(OCH_2CH_2NMe_2)]$-$Fe(NO)_2$ complex was prepared similarly (yield 56%). *Anal.* calcd.: C 29.2, H 5.2, N 18.9; found: C 29.1, H 5.1, N 18.5. ν_{NO} 1750, 1671 cm^{-1} (cyclohexane) 1724 br, 1630 br cm^{-1} (Nujol).

Preparation of $[Me_2Ga(N_2C_5H_7)(OCH_2CH_2NMe_2)]$-$Mn(NO)_2$

$Mn[P(OMe)_3]_2(NO)_2Br$ (0.32 g; 0.72 mmol) was dissolved in THF and solid $AgPF_6$ (0.20 g; 0.80 mmol) added to the resulting solution. The original orange solution immediately turned yellow and a white solid formed. $Na^+[Me_2Ga(N_2C_5H_7)(OCH_2CH_2NMe_2)]^-$ (0.78 mmol) in THF was added and the mixture stirred for 3 h. The dark green solution was filtered and the filtrate evaporated to give a green oil and orange solid. The mixture was washed with MeOH and filtered. The orange solid collected was recrystallized from THF/benzene to give dark red crystals of product (yield 0.093 g, 32%). *Anal.* calcd. for $[Me_2Ga(N_2C_5H_7)(OCH_2CH_2NMe_2)]$-$Mn(NO)_2$: C 33.2, H 5.8, N 17.6; found: C 33.3, H 5.7, N 17.4%. ν_{NO} 1709, 1643 cm^{-1} (cyclohexane), 1705 br, 1648 br cm^{-1} (Nujol). ^1H nmr (C_6D_6) τ = 4.31 s (pz—H^4), 6.27 t (J = 6 Hz, —CH_2—), 7.53 s (pz—Me), 7.92 s (pz—Me), 8.16 t (J = 6 Hz, —CH_2—), 8.20 s (NMe_2), 9.94 s ($GaMe_2$) (τ values refer to $\tau_{C_6H_6}$ = 2.84 ppm, pz = pyrazolyl).

Mass Spectra

The mass spectra of the three complexes were very similar and those of the $[Me_2Ga(N_2C_5H_7)(OCH_2CH_2NMe_2)]$-$M(NO)_2$ (where M = Mn and Fe) compounds were essentially identical. The parent ion in each case was not observed, the highest mass signal arising from the P − Me^+ ion (3%) (P = parent). The strongest signal corresponded to the P − $2NO^+$ ion (100%) with other strong signals arising from the P − NO^+ (40%) and the doubly charged P − 2NO − Me^{2+} ions (20%). The absence of parent ion signals in the mass spectra of organo-gallium complexes, particularly those containing the —$GaMe_2$ moiety, is well documented (7–10).

Spectra

Mass spectra were collected on a Varian MAT CH4 spectrometer at 70 eV with an ion source temperature of 100–180°C. Infrared spectra were recorded on a Perkin-Elmer 457 spectrometer and ^1H nmr spectra on a Varian XL-100 spectrometer using FT techniques.

X-ray Crystallographic Analysis of [*Dimethyl(*N,N*-dimethylethanolamino)(3,5-dimethylpyrazolyl)gallato(*N*(2),*N*(3),*O*)*]*dinitrosyliron(I)*

The crystal chosen was mounted in a general orientation and had dimensions of ca. 0.5 × 0.6 × 0.7 mm. Unit-cell parameters were refined by least-squares on 2 sin θ/λ values for 25 reflections measured on a diffractometer with Mo K_α radiation (λ = 0.71073 Å). Crystal data (at 22°C) are:

$C_{11}H_{23}FeGaN_5O_3$ fw = 398.91

Monoclinic, a = 7.3079(6), b = 14.274(1), c = 17.076(1) Å, β = 91.709(4)°, V = 1780.4(2) Å^3, Z = 4, ρ_c = 1.488 g cm^{-3}, $F(000)$ = 820, μ(Mo K_α) = 22.5 cm^{-1}. Absent reflections: $h0l$, $l \neq 2n$ and $0k0$, $k \neq 2n$ define uniquely the space group $P2_1/c$ (C_{2h}^5, No. 14).

Intensities were measured with graphite monochromatized Mo K_α radiation on an Enraf-Nonius CAD4-F diffractometer. An ω − 2θ scan at 1.26–10.06° min^{-1} over a range of (0.60 + 0.35 tan θ) degrees in ω (extended by 25% on both sides for background measurement) was employed. Data were measured to 2θ = 55°. The intensities of 3 check reflections, measured every 3600 s throughout the data collection, remained constant to within ±2%.

After data reduction, an absorption correction was applied using the Gaussian integration method (11, 12). Transmission factors ranged from 0.331 to 0.408. Of the 4068 independent reflections measured, 2848 (70%) had intensities greater than 3σ(I) above background where $\sigma^2(I) = S + 2B + (0.04(S - B))^2$ with S = scan count and B = background count.

The positions of the gallium and iron atoms were determined from the three-dimensional Patterson function and those of the remaining non-hydrogen atoms from subsequent difference maps. The "ethanolamine" carbon atoms were found to be twofold disordered; site occupancies were estimated from peak heights on a Fourier map to be 0.67 for "*a*" sites and 0.33 for "*b*" sites. Isotropic refinement of the disordered carbons with the occupancy factors fixed gave nearly equal thermal parameters for all of the disordered carbon atoms, thus the site occupancies were kept fixed throughout the refinement. All of the ordered non-hydrogen atoms and the four predominant disordered carbon atoms were refined with anisotropic thermal parameters and the remaining four carbon atoms with isotropic thermal parameters to R = 0.054. A difference map at this point revealed positions for all of the ordered hydrogen atoms which were subsequently refined with isotropic thermal parameters. Ideal positions were calculated for the disordered hydrogen atoms (C—H = 0.98 Å, $U = U_c + 1.1$) which were included as fixed atoms in the final stages of refinement. The scattering factors of ref. 13 were used for non-hydrogen atoms and those of ref. 14 for hydrogen atoms. Anomalous scattering factors from ref. 15 were used for the Ga and Fe atoms. The weighting scheme, $w = 1/\sigma^2(F)$ where $\sigma^2(F)$ is derived from the previously defined $\sigma^2(I)$ gave uniform average values of $w(|F_o| - |F_c|)^2$ over ranges of $|F_o|$ and was employed in the final stages of refinement. An isotropic Type I extinction correction (Thornley-Nelmes definition of mosaic anisotropy with a Lorentzian distribution) was applied (16–18). The final value of g was 2.1(2) × 10^4. Convergence was reached at R = 0.034 and R_w = 0.046 for 2848 reflections with $I \geq 3\sigma(I)$. For all 4068 reflections R = 0.061 and R_w = 0.048.

On the final cycle of refinement the mean and maximum parameter shifts corresponded to 0.24 and 3.9σ (oscillating thermal parameter for H(1b)) respectively. The mean error in an observation of unit weight was 1.5830. A final difference map showed maximum fluctuations of ±0.87 e Å^{-3} near the

heavy atoms and ± 0.22 e Å^{-3} elsewhere. The final positional and thermal parameters appear in Tables 1 and 2[1] respectively. Measured and calculated structure factors have been placed in the Depository of Unpublished Data.[1]

The ellipsoids of thermal motion for the non-hydrogen atoms are shown in Fig. 1. The thermal motion has been analysed in terms of the rigid-body modes of translation, libration, and screw motion (19) using the computer program MGTLS. The rms standard error in the temperature factors σU_{ij} (derived from the least-squares analysis) is 0.0034 Å^2. Three successful analyses were carried out, two five-atoms groups [Ga,O(1),N(1),C(1),C(2) and Fe,N(3),C(7a),C(10a), C(11a)] and a 14-atom group consisting of all non-hydrogen atoms except nitrosyl oxygens, N(3) and Ga methyl carbons and O(1) (which has anomalous thermal parameters as a result of the disorder) gave physically reasonable rigid-body parameters and ΔU_{ij} values of 29, 13, and 57 $\times 10^{-4}$ Å^2 respectively. The appropriate bond distances have been corrected for libration (20), using shape parameters q^2 of 0.08 for all atoms involved. Corrected bond lengths appear along with the uncorrected values in Table 3. Corrected bond angles do not differ by more than 1σ from the uncorrected values given in Table 4. Intra-annular torsion angles defining the conformations of the five-membered chelate rings are listed in Table 5.

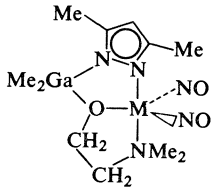

Results and Discussion

The neutral monomeric five-coordinate dinitrosyl complexes $LM(NO)_2$, **1**, (where M = Mn or Fe and L = $[Me_2Ga(N_2C_5H_7)(OCH_2CH_2NMe_2)]$) are the first of their type to be reported. A distorted trigonal bipyramidal arrangement about the "19-electron" iron centre has been proven conclusively through the X-ray crystallographic analysis of the $LFe(NO)_2$ complex. A similar molecular structure is predicted for the manganese derivative, first from the similarity of its mass spectrum and ir spectrum to those of the iron complex, and secondly from its ^{1}H nmr spectrum. The ^{1}H nmr spectrum (see Experimental section) of the manganese complex $[Me_2Ga(N_2C_5H_7)(OCH_2CH_2NMe_2)]Mn(NO)_2$ displays one sharp signal for the —$GaMe_2$ moiety and one sharp signal for the —NMe_2 moiety. A trigonal-bipyramidal structure for the complex in solution with equatorial NO groups and a meridional gallate ligand (see **1**), similar to the solid state structure of the analogous iron compound (see below), satisfactorily explains this spectrum. Attempts to obtain the ^{1}H

[1]The structure factor table and Table 2 (thermal parameters) are available, at a nominal charge, from the Depository of Unpublished Data, CISTI, National Research Council of Canada, Ottawa, Ont., Canada K1A 0S2.

TABLE 1. Final positional parameters (fractional; O, N, and C $\times 10^4$, Ga and Fe $\times 10^5$, H $\times 10^3$) with estimated standard deviations in parentheses

Atom*	x	y	z
Ga	27618(7)	54956(3)	37741(3)
Fe	39386(8)	53814(4)	18308(3)
O(1)	4432(5)	5161(3)	2991(2)
O(2)	2004(7)	4542(3)	566(3)
O(3)	5536(6)	6674(4)	821(3)
N(1)	1373(4)	6264(2)	3007(2)
N(2)	1792(4)	6227(2)	2227(2)
N(3)	6247(5)	4318(2)	1862(2)
N(4)	2663(5)	4746(3)	1168(2)
N(5)	5092(5)	6216(3)	1335(2)
C(1)	4008(12)	6284(6)	4564(4)
C(2)	1343(15)	4396(5)	4054(6)
C(3)	−54(5)	6849(3)	3088(2)
C(4)	−563(6)	7194(3)	2361(3)
C(5)	615(6)	6786(3)	1842(2)
C(6a)′	6099(11)	4716(6)	3256(4)
C(7a)′	7337(10)	4589(5)	2572(5)
C(8)	−810(10)	7041(5)	3876(4)
C(9)	663(11)	6921(5)	974(3)
C(10a)′	5486(11)	3389(5)	1976(7)
C(11a)′	7375(14)	4331(8)	1172(6)
C(6b)″	5212(26)	4095(14)	3124(11)
C(7b)″	5854(27)	3639(14)	2408(11)
C(10b)″	6342(33)	3777(17)	1085(14)
C(11b)″	8050(27)	4793(14)	1971(13)
H(1a)	505(11)	600(5)	472(4)
H(1b)	322(10)	641(5)	483(4)
H(1c)	442(10)	686(6)	439(4)
H(2a)	200(10)	392(6)	430(5)
H(2b)	57(15)	414(8)	360(6)
H(2c)	68(13)	451(6)	438(6)
H(4)	−166(6)	758(3)	222(2)
H(8a)	−177(11)	752(5)	382(4)
H(8b)	−19(10)	680(5)	421(4)
H(8c)	−196(12)	678(7)	388(5)
H(9a)	−16(9)	730(5)	86(4)
H(9b)	170(8)	703(4)	80(3)
H(9c)	70(8)	632(5)	75(4)
H(6a)′	672	510	366
H(6b)′	583	411	349
H(6c)″	624	412	351
H(6d)″	425	372	335
H(7a)′	825	410	270
H(7b)′	799	517	247
H(7c)″	695	326	252
H(7d)″	491	322	218
H(10a)′	648	294	206
H(10b)′	469	339	242
H(10c)′	477	320	150
H(10d)″	737	334	113
H(10e)″	520	343	101
H(10f)″	652	421	66
H(11a)′	839	389	125
H(11b)′	663	415	71
H(11c)′	786	496	110
H(11d)″	903	434	190
H(11e)″	815	530	159
H(11f)″	814	506	250

*Occupancy factor 0.67 for atoms with primes, occupancy factor 0.33 for atoms with double primes.

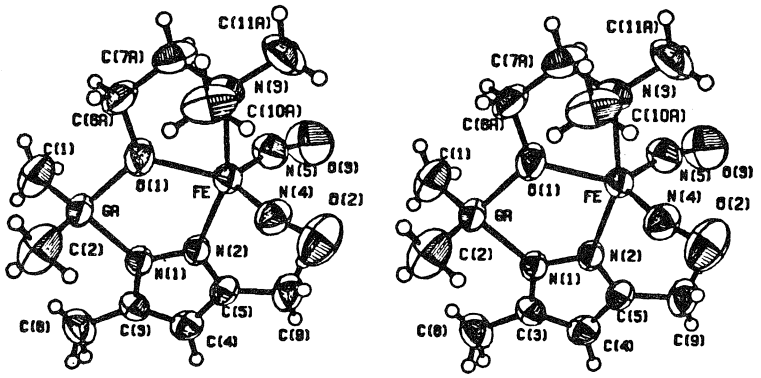

FIG. 1. Stereo view of the [dimethyl(*N*,*N*-dimethylethanolamino)(3,5-dimethylpyrazolyl)gallato(*N*(2),*N*(3),*O*)]dinitrosyliron(I) molecule; 50% ellipsoids are shown for the non-hydrogen atoms. The predominant disordered carbon atoms are shown.

TABLE 3. Bond lengths (Å) with estimated standard deviations in parentheses

(*a*) Non-hydrogen atoms

Bond	Length		Bond	Length	
	Uncorr.	Corr.		Uncorr.	Corr.
Ga —O(1)	1.898(3)	1.916	N(1)—C(3)	1.347(5)	1.350
Ga —N(1)	1.967(3)	1.975	N(2)—C(5)	1.333(5)	1.338
Ga —C(1)	1.960(6)	1.977	N(3)—C(7a)	1.482(9)	1.502
Ga —C(2)	1.949(7)	1.966	N(3)—C(7b)	1.38(2)	
Fe —O(1)	2.028(3)	2.037	N(3)—C(10a)	1.454(8)	1.475
Fe —N(2)	2.106(3)	2.112	N(3)—C(10b)	1.54(2)	
Fe —N(3)	2.268(3)	2.279	N(3)—C(11a)	1.459(9)	1.478
Fe —N(4)	1.706(4)	1.713	N(3)—C(11b)	1.49(2)	
Fe —N(5)	1.700(4)	1.707	C(3) —C(4)	1.376(6)	1.384
O(1)—C(6a)	1.435(7)	1.439	C(3) —C(8)	1.495(7)	1.496
O(1)—C(6b)	1.64(2)		C(4) —C(5)	1.383(6)	1.386
O(2)—N(4)	1.158(5)	1.158	C(5) —C(9)	1.496(7)	1.497
O(3)—N(5)	1.148(5)	1.148	C(6a)—C(7a)	1.51(1)	1.51
N(1)—N(2)	1.377(4)	1.384	C(6b)—C(7b)	1.47(3)	

nmr of the iron compounds were thwarted by their predicted paramagnetic character.

It is interesting to compare analogous uninegative six-electron ligands in this area of chemistry. A very early attempt to prepare the analogous $(\eta^5\text{-}C_5H_5)$-$Mn(NO)_2$ compound by King (21) resulted in an associated material, of the correct empirical formulation, containing both bridging and terminal ν_{NO} bands in its ir spectrum. Various reasons were advanced at that time to explain the absence of the monomeric species. The analogous $(\eta^5\text{-}C_5H_5)Fe$-$(NO)_2$ compound has not been reported. A dimeric complex $[(\eta^5\text{-}C_5H_5)Fe(NO)]_2$ has been described however in which an Fe=Fe double bond and bridging NO groups were postulated to link the monomer units (22). In the case where L = $[RB(N_2C_3H_3)_3]$ (where R = H or alkyl) no compounds of the type $LM(NO)_2$ (where M = Mn or Fe) have been reported and our attempts to prepare such complexes where L = $[MeGa(N_2C_3H_3)_3]$ have so far proven unsuccessful. The previously characterized (23) $[MeGa(N_2C_3H_3)_3]_2Fe$ complex was isolated in attempts to prepare $[MeGa(N_2C_3H_3)_3]$-$Fe(NO)_2$.

A likely explanation for the above observations is the ability of the asymmetrical gallate ligands herein described to occupy a set of three meridional coordination sites about the transition metal atom, an arrangement which appears necessary to stabilize these monomeric species and which is impossible for the ligands $\eta^5\text{-}C_5H_5$ and $[RE(N_2C_3H_3)_3]$ (where E = B or Ga). This is further substantiated in the synthesis of two manganese dinitrosyl derivatives, $[Mn(NO)_2(PPh_3)_2Br]$ (24) and $[Mn(NO)_2\{P(OMe)_2$-$Ph\}_2Cl]$ (25), where unidentate ligands are involved and in the latter compound the halogen atom and phosphine ligands have been shown to occupy meridional coordination sites in the trigonal-bipyramidal molecule, with the two nitrosyl groups equatorial (25–27). The general paucity of

TABLE 4. Bond angles (deg) with estimated standard deviations in parentheses
Non-hydrogen atoms

Bonds	Angle (deg)	Bonds	Angle (deg)
O(1)—Ga —N(1)	90.1(1)	N(1) —N(2) —C(5)	107.2(3)
O(1)—Ga —C(1)	109.5(3)	Fe —N(3) —C(7a)	103.0(3)
O(1)—Ga —C(2)	109.1(4)	Fe —N(3) —C(7b)	108.4(8)
N(1)—Ga —C(1)	111.0(2)	Fe —N(3) —C(10a)	109.1(4)
N(1)—Ga —C(2)	110.2(3)	Fe —N(3) —C(10b)	111.6(9)
C(1)—Ga —C(2)	122.3(4)	Fe —N(3) —C(11a)	114.2(4)
O(1)—Fe —N(2)	83.5(1)	Fe —N(3) —C(11b)	111.7(8)
O(1)—Fe —N(3)	76.3(1)	C(7a)—N(3) —C(10a)	109.1(6)
O(1)—Fe —N(4)	130.1(2)	C(7b)—N(3) —C(10b)	104.2(12)
O(1)—Fe —N(5)	121.3(2)	C(7a)—N(3) —C(11a)	110.8(6)
N(2)—Fe —N(3)	159.4(1)	C(7b)—N(3) —C(11b)	115.8(12)
N(2)—Fe —N(4)	96.9(2)	C(10a)—N(3)—C(11a)	110.3(7)
N(2)—Fe —N(5)	98.3(2)	C(10b)—N(3)—C(11b)	105.9(13)
N(3)—Fe —N(4)	92.9(2)	Fe —N(4) —O(2)	157.9(4)
N(3)—Fe —N(5)	95.8(2)	Fe —N(5) —O(3)	159.3(5)
N(4)—Fe —N(5)	108.1(2)	N(1) —C(3) —C(4)	108.6(3)
Ga —O(1)—Fe	123.4(2)	N(1) —C(3) —C(8)	121.0(4)
Ga —O(1)—C(6a)	116.5(4)	C(4) —C(3) —C(8)	130.5(4)
Ga —O(1)—C(6b)	111.4(7)	C(3) —C(4) —C(5)	105.8(4)
Fe —O(1)—C(6a)	120.1(4)	N(2) —C(5) —C(4)	109.9(4)
Fe —O(1)—C(6b)	109.3(7)	N(2) —C(5) —C(9)	122.1(4)
Ga —N(1)—N(2)	119.8(2)	C(4) —C(5) —C(9)	127.9(4)
Ga —N(1)—C(3)	131.5(3)	O(1) —C(6a)—C(7a)	109.4(5)
N(2)—N(1)—C(3)	108.6(3)	O(1) —C(6b)—C(7b)	114.4(14)
Fe —N(2)—N(1)	121.5(2)	N(3) —C(7a)—C(6a)	110.1(6)
Fe —N(2)—C(5)	131.4(3)	N(3) —C(7b)—C(6b)	109.1(15)

TABLE 5. Intra-annular torsion angles (deg) for five-membered chelate rings

Bond	Observed angle	Bond	Observed angle	
			Conf. "*a*"	Conf. "*b*"
Ga —O(1)	−13.9(1)	Fe —O(1)	15.9(4)	−29.0(7)
O(1)—Fe	12.9(1)	O(1)—C(6)	6.7(6)	15.9(12)
Fe —N(2)	−6.2(2)	C(6)—C(7)	−39.1(6)	21.1(16)
N(2)—N(1)	−1.3(2)	C(7)—N(3)	48.8(5)	−44.9(13)
N(1)—Ga	8.4(2)	N(3)—Fe	−34.4(4)	44.4(8)

structural data on five-coordinate metal dinitrosyl derivatives is evident from the review by Enemark and Feltham (28) in which two such structures were discussed, both square-pyramidal cationic complexes with one linear and one bent nitrosyl group. The above Mn derivative (25–27) is the third such example of a five-coordinate metal dinitrosyl structure but the first where the molecular arrangement is that of a trigonal-bipyramid with equatorial nitrosyl groups and axial phosphine ligands. Enemark and Feltham in their review (28) predicted that the two NO groups in five-coordinate metal dinitrosyls should be *cis* (an arrangement found in all such structures to date) and also that a most favorable arrangement would be a trigonal-bipyramidal arrangement with equatorial NO groups.

The crystal structure of $[Me_2Ga(N_2C_5H_7)(OCH_2CH_2NMe_2)]Fe(NO)_2$ consists of discrete molecules separated by normal van der Waals distances. The molecule (Fig. 1) contains a system of three roughly coplanar fused five-membered rings. This arrangement is typical of meridionally coordinated ethanolamino(pyrazolyl)gallate ligands such as those observed in the square-pyramidal copper complex $(\mu\text{-}N_2C_3H_3)_2[Me_2Ga(N_2C_3H_3)(OCH_2CH_2NMe_2)\text{-}Cu]_2$ (1) and in the octahedral nickel complex *mer*-$[Me_2Ga(N_2C_3H_3)(OCH_2CH_2NH_2)]_2Ni$ in which the ethanolamine chelate ring was also found to be twofold disordered (2). The pyrazolyl group is planar within experimental error ($\chi^2 = 1.0$ for N_2C_5) and both metal atoms deviate slightly but significantly from the N_2C_5 plane (Ga by 0.0545(5) and Fe by 0.0127(6) Å). The central GaOFeNN ring has an "envelope" conformation in which O(1) is displaced from the approximate plane defined by the other four atoms. The Ga- - -Fe separation

is 3.4567(7) Å. As a result of the disorder, there are two conformations for the FeOCCN chelate ring, both of which are puckered (see torsion angles in Table 5). In general the central chelate rings (GaOMNN where M = Ni, Cu, or Fe) are more nearly planar and the deviations of the metal atoms from the pyrazolyl mean planes smaller when this type of ligand is meridionally, rather than facially coordinated (1, 2, 4).

The coordination geometry about the gallium atom is distorted tetrahedral with bond angles at gallium ranging from 90.1(1) to 122.3(4)°. The overall geometry of the ligand is very similar to that reported for related compounds (1, 2).

The structure of $[Me_2Ga(N_2C_5H_7)(OCH_2CH_2NMe_2)]Fe(NO)_2$ is only the second trigonal-bipyramidal metal dinitrosyl structure to be reported (as mentioned earlier) and is the first incorporating a uninegative tridentate chelating ligand. The oxygen and two nitrogen atoms of the $[Me_2Ga(N_2C_5H_7)(OCH_2CH_2NMe_2)]^-$ ligand occupy one equatorial and the two axial coordination sites respectively with the two nitrosyl groups occupying the two remaining equatorial positions. The trigonal-bipyramid is distorted as a result of steric requirements imposed by the gallate ligand. The iron atom is displaced 0.0752(6) Å (towards N(2)) from the plane of the equatorial substituents and the angle between the axial ligands is 159.4(1)°. The equatorial Fe—O distance is 2.037(3) Å and axial Fe—N distances are 2.112(3) (pyrazolyl) and 2.279(3) Å (amino). The difference in the axial bond lengths is considerably greater than that expected on the basis of hybridization differences at nitrogen alone and is probably due to the greater steric hindrance imposed by the amino methyl groups which are nearly eclipsed with the two nitrosyl groups in either of the two disordered sites.

The geometry of the C_{2v} $\{Fe(NO)_2\}^9$ system is of great interest, being the first such system to be structurally characterized. The only comparable structure is that of the $\{Mn(NO)_2\}^8$ complex mentioned earlier in which both nitrosyl groups are bent (Mn—N—O = 165°) towards each other in the equatorial plane. The Mn—N distances are 1.633–1.665(10) Å and the ON—Mn—NO angles are 111.5–113.5(5)° (for two crystal forms, three crystallographically independent molecules). This arrangement for a C_{2v} $\{M(NO)_2\}^8$ system was predicted by Enemark and Feltham (28). The present $\{M(NO)_2\}^9$ system is similar but the extra electron induces some significant changes. The in-plane bending of the nitrosyl groups is more pronounced (mean Fe—N—O = 158.6(7)°) and the angle between the nitrosyl groups decreases to 108.1(2)°. The M—N distance increases to a mean Fe—N of 1.710(3) Å, a sizeable increase considering that for isoelectronic and isostructural Mn and Fe species the M—NO distance is shorter for the iron analog (28).

Acknowledgments

We thank the Natural Sciences and Engineering Research Council of Canada for financial support and the University of British Columbia Computing Centre for assistance. We are grateful to Mr. P. Borda for C, H, N analyses, Dr. S. Chan for nmr spectra, and Mr. J. Nip for mass spectra.

1. K. S. Chong, S. J. Rettig, A. Storr, and J. Trotter. Can. J. Chem. **55**, 4166 (1977).
2. K. S. Chong, S. J. Rettig, A. Storr, and J. Trotter. Can. J. Chem. **56**, 1212 (1978).
3. K. S. Chong and A. Storr. Can. J. Chem. **57**, 167 (1979).
4. K. S. Chong, S. J. Rettig, A. Storr, and J. Trotter. Can. J. Chem. **57**, 1335 (1979).
5. B. Haymore and R. D. Feltham. Inorg. Synth. **14**, 81 (1973).
6. R. H. Reimann and E. Singleton. J. Chem. Soc. Dalton Trans. 841 (1973).
7. A. Arduini and A. Storr. J. Chem. Soc. Dalton Trans. 503 (1974).
8. R. T. Baker, S. J. Rettig, A. Storr, and J. Trotter. Can. J. Chem. **54**, 343 (1976).
9. K. S. Chong, A. Storr, S. J. Rettig, and J. Trotter. Can. J. Chem. **55**, 2540 (1977).
10. K. R. Breakell, S. J. Rettig, A. Storr, and J. Trotter. Can. J. Chem. **55**, 4174 (1977).
11. P. Coppens, L. Leiserowitz, and D. Rabinovich. Acta Crystallogr. **18**, 1035 (1965).
12. W. R. Busing and H. A. Levy. Acta Crystallogr. **22**, 457 (1967).
13. D. T. Cromer and J. B. Mann. Acta Crystallogr. Sect. A, **24**, 321 (1968).
14. R. F. Stewart, E. R. Davidson, and W. T. Simpson. J. Chem. Phys. **42**, 3175 (1965).
15. D. T. Cromer and D. Liberman. J. Chem. Phys. **53**, 1891 (1970).
16. P. J. Becker and P. Coppens. Acta Crystallogr. Sect. A, **30**, 129 (1974); **30**, 148 (1974); **31**, 417 (1975).
17. P. Coppens and W. C. Hamilton. Acta Crystallogr. Sect. A, **26**, 71 (1970).
18. F. R. Thornley and R. J. Nelmes. Acta Crystallogr. Sect. A, **30**, 748 (1974).
19. V. Schomaker and K. N. Trueblood. Acta Crystallogr. Sect. B, **24**, 63 (1969).
20. D. W. J. Cruickshank. Acta Crystallogr. **9**, 747 (1956); **9**, 754 (1956); **14**, 896 (1961).
21. R. B. King. Inorg. Chem. **6**, 30 (1967).
22. H. Brunner. J. Organomet. Chem. **14**, 173 (1968).
23. K. R. Breakell, S. J. Rettig, D. L. Singbeil, A. Storr, and J. Trotter. Can. J. Chem. **56**, 2099 (1978).
24. W. Beck and K. Lottes. Chem. Ber. **98**, 2657 (1965).
25. M. Laing, R. Reimann, and E. Singleton. Inorg. Nucl. Chem. Lett. **10**, 557 (1974).
26. M. Laing, R. Reimann, and E. Singleton. Inorg. Chem. **18**, 324 (1979).
27. M. Laing, R. Reimann, and E. Singleton. Inorg. Chem. **18**, 1648 (1979).
28. J. H. Enemark and R. D. Feltham. Coord. Chem. Rev. **13**, 339 (1974).

Synthesis and structure of 3,5-dimethylpyrazolyl iron and cobalt dinitrosyl dimers

KENNETH S. CHONG, STEVEN J. RETTIG, ALAN STORR, AND JAMES TROTTER

Department of Chemistry, University of British Columbia, 2075 Wesbrook Mall, Vancouver, B.C., Canada V6T 1W5

Received July 23, 1979

KENNETH S. CHONG, STEVEN J. RETTIG, ALAN STORR, and JAMES TROTTER. Can. J. Chem. **57**, 3119 (1979).

The synthesis and characterization of two 3,5-dimethylpyrazolyl metal dinitrosyl dimers $[(N_2C_5H_7)M(NO)_2]_2$ (where M = Fe or Co) are described and their X-ray crystal structures detailed. Both complexes crystallize in the monoclinic space group $C2/c$, a = 23.848(2), 23.722(4), b = 10.7775(7), 10.6888(6), c = 14.764(1), 14.712(2) Å, β = 117.366(6), 117.094(7)°, Z = 8 (for the iron and cobalt complexes respectively). The structure of the iron complex was solved by Patterson and Fourier syntheses. The cobalt complex is isomorphous with the iron analog. Both structures were refined by full-matrix least-squares procedures to R = 0.028 and 0.035 for 4251 and 3376 reflections with $I \geq 3\sigma(I)$ respectively. Both complexes adopt a boat conformation for the central M—(N—N)$_2$—M ring and display significantly non-linear M—N—O groups. The coordination geometry about the metal atoms is distorted tetrahedral. Important molecular dimensions (distances corrected for libration) are: mean Fe—N(pyrazolyl), 2.009(5), mean Fe—NO, 1.696(2) Å, Fe—N—O, 158.5(3)–168.2(2)°, mean Co—N(pyrazolyl), 1.992(7), Co—NO, 1.646(3)–1.680(3) Å, and Co—N—O, 161.6(3)–173.5(3)°. The iron complex is paramagnetic with formally "17-electron" iron atoms. Both structures are compared with similar four-coordinate metal dinitrosyl compounds.

KENNETH S. CHONG, STEVEN J. RETTIG, ALAN STORR et JAMES TROTTER. Can. J. Chem. **57**, 3119 (1979).

On décrit la synthèse et la caractérisation de deux diméthyl-3,5 pyrazolyl métal dinitrosyle $[(N_2C_5H_7)M(NO_2)]_2$ dimères où M = Fe ou Co et on a détaillé leur structure cristalline. Pour les deux complexes les cristaux sont monocliniques, groupe d'espace $C2/c$, a = 23.848(2), 23.722(4), b = 10.7775(7), 10.6888(6), c = 14.764(1), 14.712(2) Å, β = 117.366(6), 117.094(7)°, Z = 8 (pour les complexes de fer et de cobalt respectivement). La structure du complexe de fer est résolue par les synthèses de Patterson et de Fourier. Le complexe de cobalt et l'analogue de fer sont isomorphes. Les deux structures sont affinées par la méthode des moindres carrés (matrice complète) jusqu'à des valeurs de R = 0.028 et 0.035 pour 4251 et 3376 réflexions avec $I \geq 3\sigma(I)$ respectivement. Les deux complexes adoptent une conformation bateau au niveau du cycle central M—(N—N)$_2$—M et montrent de façon significative des groupes M—N—O non linéaires. La géométrie de coordination autour de l'atome de métal est déformée en un tétraèdre. Les dimensions moléculaires importantes (distances corrigées pour la libration) sont: Fe—N(pyrazolyl), 2.009(5), moyen Fe—NO, 1.696(2) Å, Fe—N—O, 158.5(3)–168.2(2)°, moyen Co—N(pyrazolyl), 1.992(7), Co—NO, 1.646(3)–1.680(3) Å et Co—N—O, 161.6(3)–173.5(3)°. Le complexe de fer est paramagnétique avec un atome de fer portant formellement "17 électrons". On compare les deux structures à celles de composés similaires tétracoordonnés de métal dinitrosyle.

[Traduit par le journal]

Introduction

The reactions of Ni(NO)I with sodium pyrazolide and substituted sodium pyrazolide salts have been reported recently (1). Novel "pyrazolyl" bridged dimers were produced and structurally characterized and their reactivity towards electron-donor species examined (1, 2). An extension of our investigations in this area has resulted in the formation of the dimeric complexes $[(N_2C_5H_7)M(NO)_2]_2$ (where M = Fe or Co) in which the transition metal atoms are bridged by 3,5-dimethylpyrazolyl moieties and assume pseudotetrahedral geometry. Considerable attention has been given recently to four-coordinate metal dinitrosyl complexes (3–5) with particular interest being attached to the extent and direction of bending of the M—N—O groupings, and also to possible catalytic activity (6–11). The two structures reported here add further to the structural parameters already available on four-coordinate metal dinitrosyls and also supply some unique features in the area of binuclear complexes.

Experimental

Starting Materials

Air-sensitive materials were handled in a glove box under an atmosphere of oxygen-free dry nitrogen or in a nitrogen-blanketed apparatus. Tetrahydrofuran (THF) was dried by refluxing over sodium/benzophenone and was used immediately following distillation. Benzene was dried by refluxing over molten potassium followed by distillation. $Fe(NO)_2I$ and $Co(NO)_2I$ were prepared by the method of Haymore and Feltham (12). Sodium dimethylpyrazolide $Na^+N_2C_5H_7^-$ was

0008-4042/79/233119-07$01.00/0

prepared from sodium hydride and 3,5-dimethylpyrazole in THF.

Preparation of $[(N_2C_5H_7)Co(NO)_2]_2$

$Co(NO)_2I$ (0.492 g; 2.0 mmol) was dissolved in THF and a solution of $Na^+N_2C_5H_7^-$ (0.236 g; 2.0 mmol) in the same solvent added. After stirring the mixture for 1 h the solvent was removed *in vacuo*. The solid residue was extracted with several portions of benzene and filtered. Evaporation of the benzene solution gave large black crystals which were washed sparingly with heptane (yield 0.2 g; 46%). *Anal.* calcd. for $[(N_2C_5H_7)Co(NO)_2]_2$: C 28.0, H 3.3, N 26.2; found: C 28.2, H 3.3, N 26.0. ν_{NO} 1822 br, 1750 br cm^{-1} (cyclohexane). ^1H nmr (C_6D_6) τ = 4.04 s (^4H—pz), 8.00 s (pz—Me) (τ values refer to $\tau_{C_6H_6}$ = 2.84 ppm, pz = pyrazolyl).

Preparation of $[(N_2C_5H_7)Fe(NO)_2]_2$

This complex was prepared from $Fe(NO)_2I$ and $Na^+N_2C_5H_7^-$ using a similar procedure to that described above for the analogous cobalt complex. Black crystals were again obtained but in this preparation the yield was about 75%. *Anal.* calcd. for $[(N_2C_5H_7)Fe(NO)_2]_2$: C 28.5, H 3.3, N 26.5; found: C 28.5, H 3.3, N 25.8. ν_{NO} 1800, 1785, 1735, 1720 cm^{-1} (cyclohexane); 1802, 1780, 1750, 1710 cm^{-1} (Nujol).

Spectra

Mass spectra were collected on a Varian MAT CH4 spectrometer at 70 eV with an ion source temperature of 100–180°C. Selected mass spectral data for the two complexes are summarized in Table 1. Infrared spectra were recorded on a Perkin-Elmer 457 spectrometer and the ^1H nmr spectrum on a Varian XL-100 spectrometer using FT techniques. The magnetic susceptibility measurement was made on a Faraday magnetic balance.

X-ray Crystallographic Analyses

Bis(μ-3,5-dimethylpyrazolyl)bis(dinitrosyliron(I))

The crystal chosen was mounted in a general orientation and had dimensions of ca. 0.56 × 0.70 × 0.65 mm. Unit-cell parameters were refined by least-squares on 2 sin θ/λ values for 48 reflections measured on a diffractometer with Mo K_α radiation (λ = 0.71073 Å). Crystal data (at 22°C) are:

$C_{10}H_{14}Fe_2N_8O_4$ fw = 421.97

Monoclinic, a = 23.848(2), b = 10.7775(7), c = 14.764(1) Å, β = 117.366(6)°, V = 3369.9(5) Å^3, Z = 8, ρ_c = 1.664 g cm^{-3}, $F(000)$ = 1712, μ(Mo K_α) = 16.8 cm^{-1}. Absent reflections: hkl, $h + k \neq 2n$ and $h0l$, $l \neq 2n$. Space group $C2/c$ (C_{2h}^6, No. 15) from structure analysis.

Intensities were measured with graphite monochromatized Mo K_α radiation on an Enraf-Nonius CAD4-F diffractometer. An ω – 1.67θ scan at 1.34–10.06° min^{-1} over a range of (0.70 + 0.35 tan θ) degrees in ω (extended by 25% on both sides for background measurement) was employed. Data were measured to 2θ = 65°. The intensities of 3 check reflections, measured every 3600 s throughout the data collection, remained constant to within ±3.0%. After data reduction, an absorption correction was applied using the Gaussian integration method (13, 14). Transmission factors ranged from 0.365 to 0.464. Of the 6057 independent reflections measured, 4251 (70.2%) had intensities greater than 3σ(I) above background where $\sigma^2(I) = S + 2B + (0.04(S - B))^2$ with S = scan count and B = background count.

Systematic absences allow space groups Cc or $C2/c$, analysis being initiated in the latter on the basis of the E-statistics and the number of molecules in the unit-cell. The positions of the iron atoms were determined from the three-dimensional Patterson function and those of the remaining non-hydrogen atoms from a subsequent difference Fourier. After full-matrix least-squares refinement of all non-hydrogen atoms with anisotropic thermal parameters to R = 0.039, a difference map gave positions for all 14 hydrogen atoms which were included in all subsequent cycles of refinement with isotropic thermal parameters. The scattering factors of ref. 15 were used for non-hydrogen atoms and those of ref. 16 for hydrogen atoms. Anomalous scattering factors from ref. 17 were used for the Fe atoms. The weighting scheme, $w = 1/\sigma^2(F)$ where $\sigma^2(F)$ is derived from the previously defined $\sigma^2(I)$ gave uniform average values of $w(|F_o| - |F_c|)^2$ over ranges of $|F_o|$ and was employed in the final stages of refinement. An isotropic Type I extinction correction (Thornley–Nelmes definition of mosaic anisotropy with a Lorentzian distribution) was applied (18–20). The final value of g was 1.1(1) × 10^4. Convergence was reached at R = 0.028 and R_w = 0.038 for 4251 reflections with $I \geq 3\sigma(I)$. For all 6057 reflections R = 0.051 and R_w = 0.042.

TABLE 1. Mass spectral data for $[(N_2C_5H_7)M(NO)_2]_2$

	M = ^{56}Fe		M = ^{59}Co	
Assignment	Intensity	m/e	Intensity	m/e
$M_2(N_2C_5H_7)_2(NO)_4^+$	2	422	12	428
$M_2(N_2C_5H_7)_2(NO)_3^+$	63	392	37	398
$M_2(N_2C_5H_7)_2(NO)_2^+$	30	362	18	368
$M_2(N_2C_5H_7)_2(NO)^+$	53	332	34	338
$M_2(N_2C_5H_7)_2^+$	100	302	100	308
$M(N_2C_5H_7)(NO)_2^+$	0	—	3	214
$M(N_2C_5H_7)(NO)^+$	5	181	6	184
$M(N_2C_5H_7)^+$	27	151	21	154
M_2^+	11	112	11	118

On the final cycle of refinement the mean and maximum parameter shifts corresponded to 0.10 and 1.9σ respectively. The mean error in an observation of unit weight was 1.1719. A final difference map showed maximum fluctuations of ±0.40 e Å^{-3} near the metal atoms and ±0.17 e Å^{-3} elsewhere. The final positional and thermal parameters appear in Tables 2 and 3 respectively.[1] Measured and calculated structure factors have been placed in the Depository of Unpublished Data.[1]

Bis(μ-3,5-dimethylpyrazolyl)bis(dinitrosylcobalt(I))

Details of the structure analysis are the same as for $[(N_2C_5H_7)Fe(NO)_2]_2$ except where noted. Crystal dimensions were 0.21 × 0.52 × 0.58 mm and 25 reflections were used in the refinement of the unit-cell parameters. Crystal data are:

$C_{10}H_{14}Co_2N_8O_4$ fw = 428.14

Monoclinic, a = 23.722(4), b = 10.6888(6), c = 14.712(2) Å, β = 117.094(7)°, V = 3321.0(8) Å^3, Z = 8, ρ_c = 1.713 g cm^{-3}, $F(000)$ = 1728, μ(Mo K_α) = 19.4 cm^{-1}. Space group $C2/c$.

An ω–2θ scan at 1.06–6.71° min^{-1} over a range of (0.65 + 0.35 tan θ)° in ω was employed. Of 5994 independent reflections measured (to 2θ = 65°), 3376 (56.3%) had intensities greater than 3σ(I) above background. An absorption correction was applied, transmission factors range from 0.365 to 0.684.

The refinement was initiated using the coordinates of all non-hydrogen atoms taken from the isomorphous iron complex. Refinement with isotropic and then with anisotropic thermal parameters gave R = 0.041. The coordinates of all 14 hydrogen atoms were taken from a difference map calculated at this point. Anomalous scattering factors from ref. 17 were used for the cobalt atoms. Convergence was reached at R = 0.035 and R_w = 0.043 for 3376 reflections with $I \geq 3\sigma(I)$. For all

[1]The structure factor table and Table 3 (thermal parameters) are available, at a nominal charge, from the Depository of Unpublished Data, CISTI, National Research Council of Canada, Ottawa, Ont., Canada K1A 0S2.

TABLE 2. Final positional parameters (fractional × 10^5, H × 10^3) with estimated standard deviations in parentheses

Atom	x	y	z
	$[(N_2C_5H_7)Fe(NO)_2]_2$		
Fe(1)	29729(1)	36351(2)	33281(2)
Fe(2)	43418(1)	22581(2)	48333(2)
O(1)	17902(7)	48291(20)	23117(15)
O(2)	32428(9)	31861(20)	16737(13)
O(3)	54734(11)	11827(26)	62564(25)
O(4)	45554(9)	17826(22)	31263(16)
N(1)	22634(7)	43604(16)	28529(12)
N(2)	31930(7)	33205(15)	24140(12)
N(3)	49896(9)	16649(20)	58266(18)
N(4)	44046(8)	20379(16)	37474(14)
N(5)	29663(6)	20573(13)	40435(11)
N(6)	35366(7)	15158(13)	46888(11)
N(7)	36577(6)	46313(12)	44350(10)
N(8)	42213(6)	40533(13)	50612(10)
C(1)	25021(8)	13826(17)	40885(14)
C(2)	27738(10)	4089(20)	47579(16)
C(3)	34166(10)	5152(17)	51188(14)
C(4)	36890(7)	58109(15)	47644(13)
C(5)	42740(8)	59889(18)	56057(14)
C(6)	45934(7)	48793(16)	57680(12)
C(7)	18209(10)	17030(26)	34996(19)
C(8)	39341(15)	−2790(25)	58737(24)
C(9)	31691(11)	67234(19)	42432(19)
C(10)	52532(8)	45677(23)	65514(14)
H(2)	258(1)	−12(2)	489(2)
H(5)	438(1)	670(2)	588(2)
H(7a)	175(1)	251(3)	362(3)
H(7b)	157(2)	116(3)	361(3)
H(7c)	171(2)	175(3)	285(3)
H(8a)	418(1)	−60(3)	552(2)
H(8b)	374(1)	−92(3)	599(2)
H(8c)	426(2)	17(3)	651(3)
H(9a)	327(2)	736(3)	397(3)
H(9b)	284(2)	644(4)	364(4)
H(9c)	308(2)	707(4)	471(3)
H(10a)	529(1)	392(2)	702(2)
H(10b)	545(1)	517(3)	708(2)
H(10c)	555(1)	444(2)	627(2)
	$[(N_2C_5H_7)Co(NO)_2]_2$		
Co(1)	29504(1)	36879(3)	32766(2)
Co(2)	43768(1)	22351(3)	48360(3)
O(1)	17797(10)	49154(28)	23924(21)
O(2)	32415(12)	32365(28)	16689(18)
O(3)	54788(15)	12238(34)	63781(31)
O(4)	45767(12)	17539(28)	31500(21)
N(1)	22581(10)	44135(24)	28060(18)
N(2)	31980(10)	33615(22)	24072(17)
N(3)	50129(12)	16517(27)	57869(25)
N(4)	44096(10)	20433(23)	37297(20)
N(5)	29901(9)	21573(19)	40707(15)
N(6)	35563(9)	16060(19)	46965(16)
N(7)	36363(8)	45700(18)	44605(14)
N(8)	41985(8)	39899(19)	50723(15)
C(1)	25241(11)	14561(25)	40890(19)
C(2)	27921(14)	4505(28)	47278(22)
C(3)	34358(13)	5604(24)	50901(20)
C(4)	36700(11)	57499(24)	47674(18)
C(5)	42576(12)	59442(27)	55971(21)
C(6)	45771(10)	48249(26)	57586(18)
C(7)	18387(13)	17781(37)	34986(27)
C(8)	39504(20)	−2650(36)	58231(34)
C(9)	31544(16)	66816(31)	42533(29)
C(10)	52422(12)	45273(33)	65250(22)
H(2)	259(1)	−15(3)	491(2)
H(5)	442(1)	661(3)	596(2)
H(7a)	176(2)	260(4)	362(3)
H(7b)	157(2)	113(5)	356(4)
H(7c)	169(2)	163(4)	272(4)
H(8a)	414(2)	−68(4)	539(3)
H(8b)	380(2)	−103(5)	601(3)
H(8c)	426(2)	20(4)	647(3)
H(9a)	335(2)	739(5)	443(4)
H(9b)	298(2)	655(5)	363(4)
H(9c)	283(2)	658(4)	438(3)
H(10a)	526(2)	378(3)	695(3)
H(10b)	544(1)	520(3)	694(2)
H(10c)	553(1)	433(3)	616(3)

5994 reflections $R = 0.090$ and $R_w = 0.048$. The mean and maximum parameter shifts on the final cycle of refinement corresponded to 0.13 and 1.4σ respectively and the mean error in an observation of unit weight was 1.0536. A final difference map showed maximum fluctuations of ± 0.65 e Å^{-3} near the cobalt atoms and ± 0.25 e Å^{-3} elsewhere. The final value of the isotropic extinction parameter g was $0.34(11) \times 10^4$.

The thermal motion in both molecules has been analysed in terms of the rigid-body modes of translation, libration, and screw motion (21) using the computer program MGTLS. For both molecules (rms $\sigma U_{ij} = 0.0009$ and 0.0014 Å^2 for the Fe and Co complexes respectively) analysis of all non-hydrogen atoms except nitrosyl oxygen atoms gave rms $\Delta U_{ij} = 0.0036$ Å^2 (for both complexes) and physically reasonable results. The appropriate bond distances have been corrected for libration (22), using shape parameters q^2 of 0.08 for all atoms involved. Corrected bond lengths appear in Table 4 along with the uncorrected values and corrected bond angles are all within 1σ of the uncorrected values given in Table 5. Intra-annular torsion angles defining the conformations of the central six-membered chelate rings are listed in Table 6.

Results and Discussion

The solid state structures of dinitrosyl iron iodide and dinitrosyl cobalt iodide have been reported (23). The former structure consists of diamagnetic dimeric molecules in which the two $Fe(NO)_2$ moieties are linked by bridging iodine atoms and also by a long (3.05 Å) Fe—Fe bond. The cobalt compound is polymeric with an infinite chain structure with a Co---Co non-bonded distance of 3.864 Å. In both structures the metal atoms are in a pseudotetrahedral environment and both M—N—O groupings are non-linear. A related dimeric iron complex $[Fe(NO)_2(SEt)]_2$ is also diamagnetic with an Fe—Fe single bond (2.72 Å) and bridging SEt groups linking the two $Fe(NO)_2$ moieties (24). In this complex the Fe—N—O groups are again non-linear.

The present structures offer a unique extension to the structural parameters presently available for four-coordinate metal dinitrosyl compounds, particularly

TABLE 4. Bond lengths (Å) with estimated standard deviations in parentheses

(*a*) Non-hydrogen atoms

	Length			
	M = Fe		M = Co	
Bond	Uncorr.	Corr.	Uncorr.	Corr.
M(1)—N(1)	1.696(2)	1.699	1.656(2)	1.659
M(1)—N(2)	1.692(2)	1.695	1.669(2)	1.672
M(1)—N(5)	2.006(1)	2.010	1.987(2)	1.992
M(1)—N(7)	2.009(1)	2.012	1.997(2)	2.000
M(2)—N(3)	1.692(2)	1.695	1.643(3)	1.646
M(2)—N(4)	1.694(2)	1.696	1.677(3)	1.680
M(2)—N(6)	1.999(1)	2.002	1.980(2)	1.983
M(2)—N(8)	2.007(1)	2.011	1.988(2)	1.992
N(1)—O(1)	1.157(2)	1.157	1.147(3)	1.147
N(2)—O(2)	1.162(2)	1.162	1.145(3)	1.145
N(3)—O(3)	1.154(3)	1.154	1.145(3)	1.145
N(4)—O(4)	1.162(2)	1.162	1.135(3)	1.135
N(5)—N(6)	1.381(2)	1.385	1.368(3)	1.373
N(7)—N(8)	1.381(2)	1.385	1.371(3)	1.376
N(5)—C(1)	1.351(2)	1.353	1.346(3)	1.348
N(6)—C(3)	1.347(2)	1.348	1.348(3)	1.349
N(7)—C(4)	1.351(2)	1.352	1.330(3)	1.331
N(8)—C(6)	1.348(2)	1.349	1.340(3)	1.341
C(1)—C(2)	1.382(3)	1.385	1.378(4)	1.382
C(1)—C(7)	1.489(3)	1.490	1.493(4)	1.495
C(2)—C(3)	1.377(3)	1.349	1.374(4)	1.377
C(3)—C(8)	1.494(3)	1.496	1.494(4)	1.495
C(4)—C(5)	1.390(2)	1.392	1.388(3)	1.390
C(4)—C(9)	1.490(3)	1.491	1.489(4)	1.490
C(5)—C(6)	1.379(3)	1.382	1.378(4)	1.381
C(6)—C(10)	1.501(2)	1.504	1.497(3)	1.499

(*b*) Bonds involving hydrogen atoms

Bond	Length	Mean
C(sp^2)—H	0.82(2)–0.91(3)	0.86(4)
C(sp^3)—H	0.83(5)–1.06(3)	0.95(7)

TABLE 5. Bond angles (deg) with estimated standard deviations in parentheses

Non-hydrogen atoms

	Angle (deg)	
Bonds	M = Fe	M = Co
N(1)—M(1)—N(2)	112.26(8)	113.9(1)
N(1)—M(1)—N(5)	111.15(7)	113.8(1)
N(1)—M(1)—N(7)	111.94(7)	113.7(1)
N(2)—M(1)—N(5)	109.30(7)	109.8(1)
N(2)—M(1)—N(7)	108.76(6)	109.61(9)
N(5)—M(1)—N(7)	103.00(6)	94.27(8)
N(3)—M(2)—N(4)	109.0(1)	110.4(1)
N(3)—M(2)—N(6)	113.00(9)	116.0(1)
N(3)—M(2)—N(8)	111.28(9)	113.3(1)
N(4)—M(2)—N(6)	109.96(7)	109.6(1)
N(4)—M(2)—N(8)	112.06(7)	113.1(1)
N(6)—M(2)—N(8)	101.48(6)	93.51(8)
M(1)—N(1)—O(1)	163.4(2)	173.5(3)
M(1)—N(2)—O(2)	168.2(2)	165.1(2)
M(2)—N(3)—O(3)	158.5(3)	173.0(4)
M(2)—N(4)—O(4)	167.0(2)	161.6(3)
M(1)—N(5)—N(6)	118.6(1)	121.3(1)
M(1)—N(5)—C(1)	133.4(1)	130.6(2)
N(6)—N(5)—C(1)	107.9(1)	108.1(2)
M(1)—N(6)—N(5)	119.8(1)	122.7(2)
M(1)—N(6)—C(3)	132.2(1)	128.9(2)
N(5)—N(6)—C(3)	108.0(1)	108.1(2)
M(2)—N(7)—N(8)	118.7(1)	121.4(1)
M(2)—N(7)—C(4)	133.3(1)	130.0(2)
N(8)—N(7)—C(4)	107.9(1)	108.4(2)
M(2)—N(8)—N(7)	119.5(1)	122.2(1)
M(2)—N(8)—C(6)	132.2(1)	129.6(2)
N(7)—N(8)—C(6)	108.2(1)	108.1(2)
N(5)—C(1)—C(2)	108.6(2)	108.7(2)
N(5)—C(1)—C(7)	123.0(2)	123.1(3)
C(2)—C(1)—C(7)	128.4(2)	128.2(3)
C(1)—C(2)—C(3)	106.6(2)	106.5(2)
N(6)—C(3)—C(2)	108.9(2)	108.7(2)
N(6)—C(3)—C(8)	121.9(2)	122.4(3)
C(2)—C(3)—C(8)	129.2(2)	128.9(3)
N(7)—C(4)—C(5)	108.6(1)	108.8(2)
N(7)—C(4)—C(9)	122.7(2)	123.6(2)
C(5)—C(4)—C(9)	128.7(2)	127.6(3)
C(4)—C(5)—C(6)	106.4(2)	106.0(2)
N(8)—C(6)—C(5)	108.9(1)	108.7(2)
N(8)—C(6)—C(10)	122.2(2)	122.7(2)
C(5)—C(6)—C(10)	128.9(2)	128.5(2)

in the area of binuclear complexes. The dimeric iron complex $[(N_2C_5H_7)Fe(NO)_2]_2$ contains, formally, 17-electron Fe centres, and indeed our inability to obtain a proton nmr spectrum for this complex in solution attested to its paramagnetism. A field-independent μ_{eff} value of 1.83 BM per iron atom at 293 K (correction for ligand and metal diamagnetism = 184×10^{-6} cm^3 mol^{-1}) confirmed the absence of any detectable iron–iron interaction in the solid state. An Fe—Fe bond in the complex, similar to that suggested for the $[Fe(NO)_2I]_2$ and $[Fe(NO)_2(SEt)]_2$ dimers, would of course yield a closed-shell configuration about each iron atom. Evidently the distance between the two iron atoms (3.3359(3) Å) in our complex is too large for such an interaction. It is, however, interesting to compare the isoelectronic complex $[Fe(N_2C_5H_7)(CO)_3]_2$ (25, 26). This compound is predicted to have an Fe—Fe single bond in addition to bridging "pyrazolyl" groups on the basis of its diamagnetism indicated by its proton nmr spectrum. No structural details have as yet been reported for this complex, however, and it is difficult to conceive a metal–metal distance close enough to give such a strong interaction. A planar Fe—$(N—N)_2$—Fe ring in this complex might lead to a superexchange phenomenon involving an electron pair coupling of the iron centres via the bridging pyrazolyl moieties.

The crystal structures of $[(N_2C_5H_7)M(NO)_2]_2$ (M = Fe and Co) are isomorphous and both consist of discrete binuclear molecules separated by normal

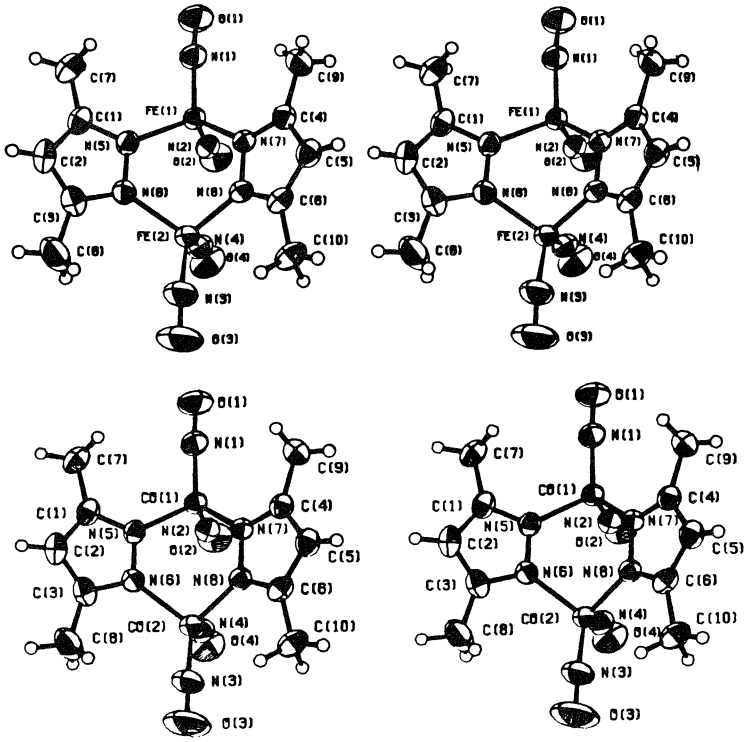

FIG. 1. Stereo view of the bis(μ-3,5-dimethylpyrazolyl)bis(dinitrosyliron(I)) (top) and bis(μ-3,5-dimethylpyrazolyl)-bis(dinitrosylcobalt(I)) (bottom) molecules, 50% ellipsoids are shown for the non-hydrogen atoms.

van der Waals distances. Molecules of both complexes have approximate C_{2v} symmetry (Fig. 1) but packing forces are probably the cause of some small but significant deviations from "ideal" geometry, particularly evident in the differences between corresponding bond angles at the two metal atoms.

The central six-membered M—(N—N)$_2$—M rings in both structures have slightly distorted boat conformations with similar torsion angles (Table 6), the mean magnitude of the torsion angles being 1.0° greater for the cobalt complex. In spite of the similarity of the torsion angles in the central rings, there are some important differences between the fused-ring systems in the two molecules. The cross-ring distances, N(5)---N(7) and N(6)---N(8), are significantly different from one another in both molecules (the latter being shorter) and those in the iron complex (3.142(2) and 3.102(2) Å) are considerably longer than those in the cobalt complex (2.920(3) and 2.890(3) Å). This is closely related to several other notable structural differences between the iron and cobalt complexes. The greater cross-ring distances in the iron analog allow for a closer approach of the metal atoms (Fe---Fe = 3.3359(3), Co---Co = 3.4717(4) Å) even though the M—N(pz) and N—N(pz) bond distances are shorter by an average of 0.01 Å in the cobalt complex. This may indicate some tendency towards an Fe—Fe interaction in the formally electron-deficient complex $[(N_2C_5H_7)Fe(NO)_2]_2$, whereas in $[(N_2C_5H_7)Co(NO)_2]_2$ the cobalt atoms acquire a closed-shell configuration without the necessity of a metal–metal bond.

TABLE 6. Intra-annular torsion angles (deg) for central M—(N—N)$_2$—M rings

Bond	Angle (deg)	
	M = Fe	M = Co
M(1)—N(5)	−43.8(1)	−46.9(1)
N(5)—N(6)	−3.3(1)	−2.1(2)
N(6)—M(2)	48.6(1)	49.6(1)
M(2)—N(8)	−47.1(1)	−48.1(1)
N(8)—N(7)	0.9(1)	−0.1(2)
N(7)—M(1)	45.2(1)	48.1(1)

In the iron complex both pyrazolyl rings are planar within experimental error (χ^2 = 1.4 and 1.2 for N_2C_3 rings containing N(5) and N(7) respectively) while those in the cobalt complex are both slightly, but significantly, non-planar (χ^2 = 8.4 and 10.7, maximum deviations = 0.005(3) and 0.007(3) Å for the N(5) and N(7) rings respectively). The angles between normals to the pyrazolyl mean planes are 57.9(2) and 54.1(2)° for the iron and cobalt structures respectively. The metal atoms are displaced by small but

significant distances from the pyrazolyl mean planes in both structures but these displacements in the cobalt complex are generally of greater magnitude and are all in the opposite direction to those in the iron complex (Fe(1), −0.0993(2), −0.0881(2), Fe(2), −0.0030(3), −0.0594(3), Co(1), 0.0850(3), 0.1310(4), Co(2), 0.0994(3), 0.0975(4) Å from the N(5) and N(7) pyrazolyl mean planes respectively). The methyl carbon atoms are in general slightly but significantly displaced from the pyrazolyl mean planes as well, and since these deviations result from intermolecular steric forces, both the directions and magnitudes of the displacements are essentially the same in both structures (C(7), −0.018(3), −0.005(4), C(8), −0.019(3), −0.018(4), C(9), 0.048(3), 0.061(4), and C(10), 0.051(2), 0.063(3) Å from the appropriate N_2C_3 plane for the iron and cobalt complexes respectively). The geometry of the pyrazolyl groups is as expected with excellent agreement between independent but chemically equivalent parameters.

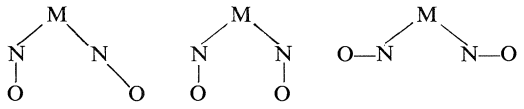

1 **2** **3**

The boat conformation adopted by the central M—(N—N)$_2$—M ring in both structures forces the pseudo-axial NO groups close together such that in both complexes the N(2)---N(4) distances are much shorter than the M---M distances and correspond to van der Waals contacts. The N(2)---N(4) distances in the two complexes are equal within experimental error (2.984(2) and 2.990(3) Å in the iron and cobalt complexes respectively) in spite of the significant difference between the M---M distances. This arrangement leads to the asymmetric type of M(NO) grouping **1** in both complexes in which the two M—N—O moieties are bent toward each other in the MN_2 plane but to significantly different extents. Several four-coordinate $\{M(NO)_2\}^{10}$ complexes have been structurally characterized and usually both M—N—O groupings are bent symmetrically to give what have been termed "attracto", **2**, or "repulso", **3**, conformers (3–5). The attracto conformer is favored for metals of the first transition series and ligands which are good π-acceptors and the repulso conformer for metals of the third transition series and ligands which are poor π-acceptors (3). The exact geometry of this type of complex depends on the relative contributions of the d_{xz} and π^*b_1(NO) orbitals to the $1b_1$ molecular orbital (the highest occupied molecular orbital in the $\{M(NO)_2\}^n$ (n = 9, 10) systems) and is therefore sensitive to the nature of the other ligands as well as to the identity of the central metal (3).

The iron complex $[(N_2C_5H_7)Fe(NO)_2]_2$ is the first $\{M(NO)_2\}^9$ system to be structurally characterized and the geometry of the $M(NO)_2$ grouping shows some significant differences with respect to that observed for the $\{M(NO)_2\}^{10}$ complex $[(N_2C_5H_7)Co(NO)_2]_2$. In the iron complex all four independent Fe—NO distances are equal within experimental error (mean Fe—N = 1.696(2) Å) and all four nitrosyl groups are bent, the pseudo-axial nitrosyl groups being bent significantly less than the pseudo-equatorial nitrosyls (168.2(2) and 167.0(2)° for axial, 163.4(2) and 158.5(3)° for equatorial Fe—N—O). The nitrosyl groups are bent toward one another approximately in the FeN_2 plane with ON—Fe—NO and O---Fe---O angles of 112.26(8) and 100.7(1)° at Fe(1) and 109.0(1) and 95.0(1)° at Fe(2). The N—O distances (mean 1.159(4) Å) are equal within experimental error although the axial N—O distances are slightly longer than the other two (see Table 4). The mean Fe—N(pz) distance is 2.009(5) Å but there are some small but significant differences between individual values, probably a result of hybridization differences at the iron atoms. The coordination geometry about the iron atoms is slightly distorted tetrahedral with all bond angles in the range 101.48(6)–113.00(9)°. In the cobalt complex $[(N_2C_5H_7)Co(NO)_2]_2$ there is considerable variation in the Co—NO distances, the "equatorial" Co—N distances (1.659(2) and 1.646(3) Å) being significantly shorter than the "axial" Co—N distances (1.672(2) and 1.680(3) Å). As in the iron complex all four nitrosyl groups are bent, the pseudo-axial nitrosyl groups being bent significantly more than the pseudo-equatorial nitrosyl groups ((165.1(2) and 161.3(3) for axial vs. 173.5(3) and 173.0(4)° for equatorial), opposite to that observed in the iron complex. The bending is again in the MN_2 plane with ON—Co—NO and O---Co---O angles of 113.9(1) and 105.3(1)° at Co(1), 110.4(1) and 100.2(1)° at Co(2). The N—O distances (mean 1.143(5) Å) are not significantly different but the "axial" N—O distances are slightly shorter than the others, again opposite to that observed for the iron complex. The mean Co—N(pz) distance is 1.992(7) Å and the individual values vary more than in the iron complex. The tetrahedral coordination about the cobalt atoms is somewhat more distorted from "ideal" geometry than in the iron complex, bond angles at Co ranging from 93.51(8) to 116.0(1)°. The observed geometry of the $\{Co(NO)_2\}^{10}$ system in $[(N_2C_5H_7)Co(NO)_2]_2$ is quite similar to that observed in several other such systems (3–5). Two previous examples of significantly different M—N—O bending in four-coordinate $\{M(NO)_2\}^{10}$ complexes are the compounds $[M(NO)_2(PPh_3)_2]$ (where M = Ru (27, 28) and M = Os (29)).

Infrared Spectra

The infrared spectrum of the iron dimer displays four sharp ν_{NO} bands both in the cyclohexane solution spectrum and in the Nujol mull spectrum (see Experimental section). The bands are of roughly equal intensity and must reflect an interaction between the two $Fe(NO)_2$ moieties in the binuclear molecule. Two of the four bands may be due to symmetric and asymmetric vibrations of the pseudo-axial NO groups whilst the remaining two may be assigned to similar vibrations of the pseudo-equatorial NO groups. The ir spectrum of the cobalt dimer $[(N_2C_5H_7)Co(NO)_2]_2$ displayed two broad (unresolved?) ν_{NO} bands in cyclohexane solution and a very broad absorption envelope in the Nujol mull spectrum. The extent of the interaction, if any, between equivalent sets of ligands attached to different metal atoms in polynuclear complexes is difficult to predict (30). Such an interaction might be unexpected in the present complexes, however, particularly in the iron compound since the related complex $[Fe(NO)_2I]_2$ displays but two ν_{NO} bands in its solution ir spectrum (23, 31). In this iodide bridged compound a strong Fe—Fe interaction is indicated (23) and the two NO groups on each Fe atom are inequivalent in the same sense as those in the "pyrazolyl" bridged species $[(N_2C_5H_7)Fe(NO)_2]_2$.

Mass Spectra

Selected mass spectral data are summarized in Table 1. In addition to the data listed other signals due to loss of MeCN and Me groups from the $M_2(N_2C_5H_7)_2^+$ ions were observed. A similar loss of MeCN molecules from the ion $Fe_2(N_2C_5H_7)_2^+$ in the mass spectrum of the related complex $[Fe(N_2C_5H_7)(CO)_3]_2$ has been reported (25). The presence of Fe_2^+ ions in the mass spectrum of this carbonyl complex was taken as partial evidence for the presence of an Fe—Fe bond in the compound. It is interesting therefore that the nitrosyl complexes reported herein also display M_2^+ signals in their mass spectra even though they are not predicted to have M—M bonds. Presumably these ions arise from M—M bonded species formed during fragmentation of the original dimeric species. It is instructive to compare these findings with the mass spectral data discussed earlier for halogen- and sulphur-bridged iron and cobalt dinitrosyl dimers (23, 32).

Acknowledgments

We thank the Natural Sciences and Engineering Research Council of Canada for financial support and the University of British Columbia Computing Centre for assistance. We are grateful to Mr. P. Borda for C, H, N, analyses and to Dr. Robert C. Thompson for performing the magnetic susceptibility measurement.

1. K. S. Chong, S. J. Rettig, A. Storr, and J. Trotter. Can. J. Chem. **57**, 3090 (1979).
2. K. S. Chong, S. J. Rettig, A. Storr, and J. Trotter. Can. J. Chem. **57**, 3099 (1979).
3. J. H. Enemark and R. D. Feltham. Coord. Chem. Rev. **13**, 339 (1974).
4. R. L. Martin and D. Taylor. Inorg. Chem. **15**, 2970 (1976).
5. J. A. Kaduk and J. A. Ibers. Inorg. Chem. **16**, 3283 (1977).
6. B. F. G. Johnson and S. Bhaduri. J. Chem. Soc. Chem. Commun. 650 (1973).
7. B. F. G. Johnson, C. J. Savoy, J. A. Segal, and R. H. Walter. J. Chem. Soc. Chem. Commun. 809 (1974).
8. J. Reed and R. Eisenberg. Science, **184**, 568 (1974).
9. B. L. Haymore and J. A. Ibers. J. Am. Chem. Soc. **96**, 3325 (1974).
10. R. Eisenberg and C. D. Meyer. Acc. Chem. Res. **8**, 26 (1975).
11. J. A. Kaduk and J. A. Ibers. Inorg. Chem. **14**, 3070 (1975).
12. B. Haymore and R. D. Feltham. Inorg. Synth. **14**, 81 (1973).
13. P. Coppens, L. Leiserowitz, and D. Rabinovich. Acta Crystallogr. **18**, 1035 (1965).
14. W. R. Busing and H. A. Levy. Acta Crystallogr. **22**, 457 (1967).
15. D. T. Cromer and J. B. Mann. Acta Crystallogr. Sect. A, **24**, 321 (1968).
16. R. F. Stewart, E. R. Davidson, and W. T. Simpson. J. Chem. Phys. **42**, 3175 (1965).
17. D. T. Cromer and D. Liberman. J. Chem. Phys. **53**, 1891 (1970).
18. P. J. Becker and P. Coppens. Acta Crystallogr. Sect. A, **30**, 129 (1974); **30**, 148 (1974); **31**, 417 (1975).
19. P. Coppens and W. C. Hamilton. Acta Crystallogr. Sect. A, **26**, 71 (1970).
20. F. R. Thornley and R. J. Nelmes. Acta Crystallogr. Sect. A, **30**, 748 (1974).
21. V. Schomaker and K. N. Trueblood. Acta Crystallogr. Sect. B, **24**, 63 (1969).
22. D. W. J. Cruickshank. Acta Crystallogr. **9**, 747 (1956); **9**, 754 (1956); **14**, 896 (1961).
23. L. F. Dahl, E. R. de Gil, and R. D. Feltham. J. Am. Chem. Soc. **91**, 1653 (1969).
24. J. T. Thomas, J. H. Robertson, and E. G. Cox. Acta Crystallogr. **11**, 599 (1958).
25. A. N. Nesmeyanov, V. N. Babin, N. S. Kochetkova, Y. S. Nekrasov, Y. A. Belousov, and S. Y. Sil'vestrova. Dokl. Chem. Proc. Acad. Sci. USSR Chem. Sec. 738 (1974).
26. R. B. King and A. Bond. J. Am. Chem. Soc. **96**, 1343 (1974).
27. A. P. Goughan, B. J. Corden, R. Eisenberg, and J. A. Ibers. Inorg. Chem. **13**, 786 (1974).
28. S. Bhaduri and G. M. Sheldrick. Acta Crystallogr. Sect. B, **31**, 897 (1975).
29. B. L. Haymore and J. A. Ibers. Inorg. Chem. **14**, 2610 (1975).
30. D. M. Adams. Metal-ligand and related vibrations. Edward Arnold Ltd., London. 1967. p. 106.
31. A. Jahn. Z. Anorg. Allgem. Chem. **301**, 301 (1959).
32. B. F. G. Johnson, J. Lewis, I. G. Williams, and J. M. Wilson. J. Chem. Soc. Sect. A, 338 (1967).

Theoretical study of isotropic hyperfine coupling constants in small radicals by MINDO/3 method

PRABHAT K. K. PANDEY AND P. CHANDRA[1]

Department of Chemistry, Banaras Hindu University, Varanasi-221005, India

Received December 11, 1978[2]

PRABHAT K. K. PANDEY and P. CHANDRA. Can. J. Chem. **57**, 3126 (1979).

Isotropic hyperfine coupling constants for ^{1}H, ^{13}C, ^{14}N, ^{17}O, and ^{19}F nuclei in a large number of small radicals as obtained by the SCF-MO-LCAO-UHF-MINDO/3 scheme are presented. It is seen that whereas calculated ^{1}H, ^{13}C, and ^{14}N hyperfine couplings agree fairly well with experiment, the agreement is not so satisfactory for ^{17}O and ^{19}F couplings.

PRABHAT K. K. PANDEY et P. CHANDRA. Can. J. Chem. **57**, 3126 (1979).

On présente les constantes de couplage hyperfin isotropiques des noyaux de ^{1}H, ^{13}C, ^{14}N, ^{17}O et ^{19}F d'un grand nombre de petits radicaux tels qu'obtenus par la combinaison: SCF MO-LCAO-UHF-MINDO/3. On constate que les constantes de couplage hyperfin calculées dans le cas de ^{1}H, ^{13}C et ^{14}N concordent parfaitement avec les valeurs expérimentales, mais la concordance n'est pas aussi satisfaisante dans le cas des couplages du ^{17}O et de ^{19}F.

[Traduit par le journal]

Introduction

A great deal of experimental data is now available on hyperfine coupling constants of various nuclei in free radicals and radical anions (1, 2). The isotropic hyperfine coupling constant, a_N, which is a measure of the extent of the magnetic interaction between the nuclear spin, I, of the nucleus under consideration and the electron spin, S, of the system being investigated, is obtained through the analysis of esr spectra of fluids. These constants are related to the electron spin density distribution in s-orbitals in the radical and consequently serve as a probe for testing various approximate methods used in the theoretical calculation of spin densities.

Most of the earlier calculations (1–4) in this direction employed either VB (valence bond) or MO (molecular orbital) approaches and were limited to π electron systems. In recent years MO theory has been used for both σ and π radicals at *ab initio* (5–13) as well as at semiempirical levels (such as CNDO and INDO (14–19), CNDO/SP (20), NDDO (21)) to calculate spin densities. Bishcof (22) has used the MINDO/3 approximation (23) to calculate proton hyperfine couplings in a few systems employing optimized geometries. In this paper, we have employed the MINDO/3 scheme (23), within the unrestricted Hartree–Fock (UHF) formalism (24), to calculate ^{1}H, ^{13}C, ^{14}N, ^{17}O, and ^{19}F hyperfine couplings in a large number of radicals. This study is a part of our plan to calculate various molecular properties (25) such as dipole moment derivatives (26), magnetic susceptibilities (unpublished results), and nuclear spin–spin coupling constants (27) using the MINDO/3 approximation.

Theory

The relation between the experimentally observed isotropic hyperfine coupling constant, a_N, of a magnetic nucleus N in a paramagnetic system and the theoretically calculated spin density, $\rho(r_N)$, at the site of the nucleus is given by

$$[1] \quad a_N = (4\pi/3)g\beta\gamma_N\hbar\langle S_z\rangle^{-1}\rho(r_N)$$

where the symbols have their usual meanings. The spin density can be obtained from the molecular ground state wavefunction, Ψ

$$[2] \quad \rho(r_N) = \left\langle \Psi \left| \sum_{k}^{\text{electrons}} 2S_{kz}\delta(r_{kN}) \right| \Psi \right\rangle$$

Ψ was obtained as an antisymmetrized product of UHF molecular orbitals which, in turn, were obtained by employing a valence basis set, ϕ, of Slater type orbitals (STO's). In the MINDO/3 scheme, the matrix elements of the Fock matrix (for α electrons) are given by

$$[3] \quad F_{rr}^{\alpha} = U_{rr} + \sum_{t}^{N}(P_{tt}g_{rt} - P_{tt}h_{rt}) + \sum_{N=M}(P_{MM} - Z_M)g_{MM} \qquad \phi_r \text{ on atom } N$$

$$[4] \quad F_{rs}^{\alpha} = (2P_{rs} - P_{rs}^{\alpha})h_{rs} - P_{rs}^{\alpha}g_{rs} \qquad \phi_r \text{ and } \phi_s \text{ both on atom } N$$

[1]To whom all correspondence should be addressed.

[2]Revision received June 11, 1979.

0008-4042/79/233126-09$01.00/0

[5] $F_{rs}^{\alpha} = (I_r + I_s)S_{rs}B_{NM} - P_{rs}^{\alpha}g_{NM}$

ϕ_r on atom N and ϕ_s on atom M

with similar expressions for the β electrons; where U_{rr} is the core integral; g_{rt} and h_{rt} are the coulomb and the exchange integrals between orbitals ϕ_r and ϕ_t, respectively; Z_M is the core charge of the atom M; g_{NM} is the average coulomb integral between orbitals of atom N and atom M; I_r is the valence state ionization potential of orbital ϕ_r; S_{rs} is the overlap integral between orbitals ϕ_r and ϕ_s, and B_{NM} is an empirical parameter for the pair of atoms N and M. The density matrices obtained from eigenvectors (C^{α}) of F^{α} are

[6] $$P_{rs}^{\alpha} = \sum_{i}^{\text{occ}} C_{ri}^{\alpha}C_{si}^{\alpha}; \qquad P_{rs} = P_{rs}^{\alpha} + P_{rs}^{\beta};$$

$$\rho_{rs} = P_{rs}^{\alpha} - P_{rs}^{\beta}$$

and

[7] $$P_{MM} = \sum_{t}^{M} P_{tt}$$

The parameters employed and the procedure used to evaluate various integrals in these equations are given by Bingham, Dewar, and Lo (23). The spin density, $\rho(r_N)$, in terms of atomic spin density matrix, ρ_{rs} at the nucleus N is given by

[8] $$\rho(r_N) = \sum_{rs} \rho_{rs}\phi_r(r)\phi_s(r)$$

It is assumed in eq. [8] that all contributions to summation are negligible unless both ϕ_r and ϕ_s are on the same atom. Since an *s–p* basis is used in the present calculations only *s* orbitals have nonvanishing densities at the respective nuclei and contribute to isotropic hyperfine couplings. With these simplifications, the expression for hyperfine couplings at nucleus N becomes

[9] $$a_N = [(4\pi/3)g\beta\gamma_N\hbar\langle S_z\rangle^{-1}|\phi_{s_N}(r_N)|^2]\rho_{s_Ns_N}$$

where the subscript s_N denotes the *s*-orbital of atom N. The quantity in the angular brackets has been treated as an adjustable parameter between calculated spin densities and experimental coupling constants in a least-squares sense. The single determinantal UHF wavefunction, however, is not an eigenfunction of the S^2 operator and contains contaminating contributions from higher multiplicities. The annihilation of the largest contaminant leads to a good approximation to a pure spin state and this has been done here by a procedure suggested by Amos and Hall (28). In the parameter fitting in expression [9], annihilated spin densities have been used. The values for these parameters (hereafter called Hyperfine Magnetic Nucleus Constant 'HMNC') for different magnetic nuclei are presented in Table 1 along with corresponding INDO values for comparison.

Results and Discussion

In all 29 radicals have been studied and the experimental geometry was employed wherever available (29–32). In other cases the geometry used in earlier calculations, either from *ab initio* or semi-empirical methods, has been employed (5, 6, 9, 10, 14, 15, 17, 19, 33–36).

Columns 2 and 3 of Table 2 list $\langle S^2\rangle_{sd}$ and $\langle S^2\rangle_{asa}$, the unannihilated and annihilated $\langle S^2\rangle$ values for various systems studied (column 1). In columns 5 and 6 we list annihilated spin densities and calculated hyperfine couplings, respectively, for nuclei given in column 4. The last column of this table contains experimental data (37–56).

It is seen from this table that $\langle S^2\rangle_{sd}$ is invariably much higher than 0.75, the expected value for a doublet radical. We have, therefore, used annihilated spin densities in the least-squares fitting between experimental couplings and spin densities to obtain the HMNC value (listed in Table 1), for $\langle S^2\rangle_{asa}$ is almost always seen to be very close to 0.75, the exact value for a doublet radical. In the following we discuss the calculated MINDO/3 couplings for each nucleus separately and compare the results with those of other calculations.

Proton Hyperfine Couplings

An examination of Table 2 reveals that MINDO/3 proton hyperfine couplings are in fair agreement with the experimental data. In order to understand the details of hyperfine coupling mechanisms we have studied the spin density distributions in a few radicals. Table 3 gives the annihilated spin densities in the different atomic orbitals of π-radicals CH_3 and NH_3^+.

It is interesting to note that the π-orbital ($2p_z$ atomic orbital) has a spin density of 1.0 in both these systems and there is finite, though small, spin density

TABLE 1. MINDO/3 and INDO parameters, $(4\pi/3)g\beta\gamma_N\hbar\langle S_z\rangle^{-1}|\phi_{s_N}(r_N)|^2$, used to calculate isotropic hyperfine couplings

Nucleus	MINDO/3 (G)	INDO* (G)
^{1}H	516.39	539.86
^{13}C	757.63	820.10
^{14}N	335.41	379.34
^{17}O	−888.68	−888.68
^{19}F	48244.22	44829.20

*Reference 14.

TABLE 2. Calculated $\langle S^2 \rangle_{sd}$, $\langle S^2 \rangle_{asa}$, spin densities, and hyperfine couplings*

Radical	$\langle S^2 \rangle_{sd}$	$\langle S^2 \rangle_{asa}$	Atom	Spin density	Hyperfine coupling (G)	Experimental coupling (G) (ref.)
CH	0.75244	0.75000	H	−0.0236	−12.17	—
			C	0.0048	3.65	—
OH	0.75233	0.75000	H	−0.0259	−13.37	−22.7 37
			O	0.0960	−8.53	—
CN	0.75643	0.74998	C	0.0713	54.01	210.0 38
			N	0.0669	22.43	4.5 38
NO	0.75392	0.74999	N	0.0163	5.46	—
			O	0.0301	−2.67	—
HBO^-	0.78085	0.74987	H	0.3896	201.16	94.0 39
			O	0.1029	−9.14	—
HBF	0.78301	0.74997	H	0.5431	280.44	—
			F	0.8814	425.22	—
HC^1C^2	0.84837	0.74610	H	0.1566	80.84	16.1 40
						15.7 41
			C^1	0.2682	203.23	321.9 41
			C^2	−0.0062	−4.66	55.7 41
HCN^-	0.75854	0.74999	H	0.2203	113.76	137.0 42
			C	0.1426	108.07	74.3 42
			N	0.0119	3.99	6.5 42
HCO	0.75731	0.74998	H	0.2687	138.75	137.0 43
						127.0 44
			C	0.1868	141.52	131.0 44
			O	0.0235	−2.08	—
HNF	0.93856	0.74882	H	−0.0475	−24.52	—
			N	−0.0109	−3.66	—
			F	0.1345	64.87	—
HO^1O^2	0.75250	0.75000	H	−0.0325	−16.79	−10.2 45
			O^1	0.0771	−6.84	—
			O^2	0.0869	−7.72	—
BH_2	0.76016	0.74997	H	0.1967	101.56	—
BF_2	0.76078	0.74998	F	0.5531	266.82	190.0 46
NH_2	0.75851	0.74998	H	−0.0330	−17.04	−23.9 47
			N	0.0301	10.08	10.3 48
NF_2	0.86974	0.74511	N	−0.0201	−6.74	—
			F	0.0375	18.11	—
CO_2^-	0.76247	0.74995	C	0.1800	136.39	166.7 49
			O	−0.0083	0.74	32.1 49
NO_2	0.75739	0.74998	N	0.1642	55.06	54.8 50
			O	−0.0071	0.63	16.3 50
FCO	0.76477	0.74993	F	0.5771	278.40	325.5 51
			C	0.2879	218.13	288.7 51
			O	−0.0403	3.58	—
FO^1O^2	0.75227	0.75000	F	0.0266	12.81	12.84 52
			O^1	0.1561	−13.87	—
			O^2	0.0679	−6.04	—
BH_3^-	0.80100	0.74884	H	−0.0859	−44.34	−16.5 39
CH_3	0.76617	0.74988	H	−0.0476	−24.56	−23.04 53
			C	0.0503	38.11	38.5 53
NH_3^+	0.76660	0.74989	H	−0.0469	−24.24	−25.9 47
			N	0.0577	19.34	19.5 47

TABLE 2 (*Concluded*)

Radical	$\langle S^2\rangle_{sd}$	$\langle S^2\rangle_{asa}$	Atom	Spin density	Hyperfine coupling (G)	Experimental coupling (G) (ref.)
H_2CN	0.82257	0.74885	H	0.1061	54.79	92.1 54
			C	−0.0312	−23.61	—
			N	0.0287	9.61	9.5 54
H_2NO	0.75609	0.74999	H	−0.0163	−8.44	11.9 55
			N	0.0832	27.91	11.9 55
			O	0.0584	−5.15	—
H_2CF	0.75924	0.74997	H	0.0286	14.76	21.1 56
			C	0.1818	137.73	54.8 56
			F	0.2559	123.43	64.3 56
HCF_2	0.75455	0.74999	H	0.1457	75.25	22.2 56
			C	0.3066	232.28	148.8 56
			F	0.2677	129.12	84.2 56
CF_3	0.76818	0.74987	C	0.4048	306.67	271.6 56
			F	0.2086	100.64	142.4 56
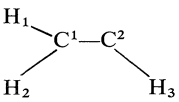	0.95175	0.74690	H_1	0.0220	11.37	13.4 53
			H_2	0.1146	59.18	65.9 53
			H_3	0.0434	22.40	37.0 53
			C^1	−0.0221	−16.70	−8.55 53
			C^2	0.1907	144.51	107.57 53
$H_3{}^2C^2C^1H_2{}^1$	0.76622	0.74987	H^1	−0.0550	−28.42	−22.38 53
			H^2	0.0491	25.36	26.87 53
			C^1	0.0567	42.92	39.07 53
			C^2	−0.0139	−10.51	−13.57 53

*All radicals were not used in parametrization. Actual oxygen and fluorine spin densities are obtained by multiplying the figures reported here by 10^{-1} and 10^{-2}, respectively.

transmitted to the σ framework. These spin densities successfully reproduce both the magnitude and the sign of the observed α-proton hyperfine couplings. Thus, like INDO and *ab initio* methods, MINDO/3 can also accommodate the exchange polarization effects which are invoked to account for α-proton hyperfine couplings. Similar arguments can be put forward for CH and OH π-radicals where the calculated values agree fairly well with experimental values.

The observed large proton hyperfine couplings in σ-radicals are also well accounted for by MINDO/3 calculations. Table 4 lists the annihilated spin density distributions in HCN, HCO, H_2CN, and vinyl radicals. From this table it is seen that the spin density in the π-orbitals of HCN, HCO, and H_2CN is very small (π-orbitals are linear combinations of $2p_z$ atomic orbitals where the z axis is perpendicular to the molecular plane). The excess spin density is shifted to the σ framework in these systems. In H_2CN, the highest occupied molecular orbital is of b_2 symmetry and most of the spin density is localized in the $2p_y$ orbital of nitrogen in the molecular plane, which has the same symmetry as the group orbital $(1s_{H_1}-1s_{H_2})$. Thus, in this molecule protons acquire a large spin density due to hyperconjugation. This is supported by *ab initio* calculation (9). The spin density results of HCN^- and HCO are also similar to that of the *ab initio* calculation due to Claxton (9) and the large proton hyperfine couplings in these systems can be accounted for by following his explanations. In these molecules, the ^{13}C, ^{14}N, and ^{17}O couplings also agree fairly well with *ab initio* and experimental data, and indeed in all these cases MINDO/3 results are better than the INDO results of Thomson (18) who employed the INDO optimized geometries in his calculations.

The MINDO/3 calculated proton hyperfine couplings in the vinyl radical agree fairly well with the experimental data, but the ordering of MO's does not agree with that of *ab initio* calculations (9). If we imagine the formation of vinyl radical as a result of removal of one hydrogen atom from ethylene, the resulting free radical is expected to be a σ radical, since the odd electron is most likely to be in one of the sp^2 hybrids at the carbon (or in a rehybridized orbital in the radical plane). This conclusion is supported by *ab initio* calculations where the highest occupied MO is seen to be of σ type and most of the spin density is in atomic orbitals in the radical plane. Although the

TABLE 3. Spin density distribution in CH_3 and NH_3^+ radicals*

Radical	Atomic orbital	Unannihilated spin density (sd)	Annihilated spin density (asa)	Observed hyperfine couplings (G)
CH_3	H_1 1s	−0.07135	−0.04756	−23.04
	H_2 1s	−0.07135	−0.04756	−23.04
	H_3 1s	−0.07135	−0.04756	−23.04
	C 2s	0.07542	0.05031	38.5
	C $2p_x$	0.06931	0.04619	$\langle S^2\rangle_{sd} = 0.76617$
	C $2p_y$	0.06931	0.04619	$\langle S^2\rangle_{asa} = 0.74988$
	C $2p_z$	1.00000	1.00000	
NH_3^+	H_1 1s	−0.07039	−0.04694	−25.9
	H_2 1s	−0.07039	−0.04694	−25.9
	H_3 1s	−0.07039	−0.04694	−25.9
	N 2s	0.08637	0.05767	19.5
	N $2p_x$	0.06240	0.04157	$\langle S^2\rangle_{sd} = 0.76660$
	N $2p_y$	0.06240	0.04157	$\langle S^2\rangle_{asa} = 0.74989$
	N $2p_z$	1.00000	1.00000	

*The z axis is perpendicular to the plane of the radical.

TABLE 4. Annihilated spin density distribution in HCN^-, HCO, H_2CN, and vinyl radicals*

Atomic orbitals	HCN^-	HCO	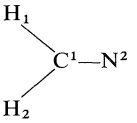	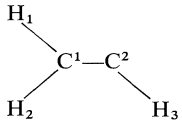
H_1 1s	0.22029	0.26870	0.1061	0.02202
H_2 1s			0.1061	0.11461
H_3 1s				0.04338
2s (1)	0.14264	0.18680	−0.03117	−0.02205
$2p_x$ (1)	0.12993	0.06906	−0.04910	−0.00424
$2p_y$ (1)	0.02406	0.21301	−0.06118	−0.04019
$2p_z$ (1)	0.01026	0.02909	−0.19596	−0.36261
2s (2)	0.01191	0.00234	0.02865	0.19074
$2p_x$ (2)	0.11892	0.08170	0.01548	0.21950
$2p_y$ (2)	0.35225	0.17839	0.88510	0.47624
$2p_z$ (2)	−0.01026	−0.02909	0.19596	0.36261
$\langle S^2\rangle_{sd}$	0.75854	0.75731	0.82257	0.95175
$\langle S^2\rangle_{asa}$	0.74999	0.74998	0.74885	0.74690

*The z axis is perpendicular to the plane of the radical.

MINDO/3 calculations show a total spin density in the π framework of the radical to be zero, the highest occupied and next to highest occupied MO's (Table 5) are seen to be of π symmetry (orbital energies −0.362 and −0.373 au respectively). The highest occupied MO of σ symmetry has an energy of −0.378 au. These MO's are fairly close in energy and the calculations indicate that when this is the case, the assumption that the occupation of MO's is in order of their increasing orbital energies breaks down. The total energy of the radical is given by

$$[10] \quad E = \frac{1}{2}\sum_{i=1}^{occ} E_i^{\alpha} + \frac{1}{2}\sum_{i=1}^{occ} E_i^{\beta}$$

where

$$E_i^{\alpha} = H_{ii}^{\alpha} + \varepsilon_i^{\alpha}$$

$$H_{ii}^{\alpha} = \int \Psi_{i\alpha}^{*}(1) H^{core}(1) \Psi_{i\alpha}(1)\, d\tau$$

$\Psi_{i\alpha}$ being the ith molecular orbital for α electrons with orbital energy ε_i^{α}. Thus each electron of the radical contributes an amount $\frac{1}{2}E_i$ to total energy. The values of E_i for $5\sigma_\alpha$, $1\pi_\alpha$, and $1\pi_\beta$ orbitals of vinyl radical are calculated to be −3.633, −3.765, and −3.798 au respectively. Based on these values, the occupation of MO's should occur in the order $1\pi_\beta$, $1\pi_\alpha$, $5\sigma_\alpha$, thus giving it a configuration (. . . . $1\pi_\beta 1\pi_\alpha 5\sigma_\alpha$) (rather than the configuration ($5\sigma_\alpha 1\pi_\alpha 1\pi_\beta$) based on orbital energies) and consequently predicting the most loosely bound electron of vinyl radical to be in a σ-molecular orbital, in conformity with the experimental as well as the spin density data.

It is seen from Table 5 that whenever the energy separation of the highest occupied and next to the highest occupied molecular orbitals is large, the MINDO/3 procedure predicts both the symmetry of highest occupied molecular orbital, as well as the

TABLE 5. Symmetry, spin and orbital energy of the two highest occupied MO's of some planar σ and π radicals

Radical	Highest occupied MO			Next highest occupied MO		
	Symmetry	Spin	Energy (au)	Symmetry	Spin	Energy (au)
5-electrons						
CH	π	α	−0.3415	σ	β	−0.3873
BH_2	σ	α	−0.3709	σ	β	−0.4115
7-electrons						
OH	π	β	−0.4774	π	α	−0.5084
NH_2	σ	β	−0.3846	σ	α	−0.4262
BH_3^-	π	α	−0.0500	σ	β	−0.1375
CH_3	π	α	−0.3546	σ	β	−0.4908
NH_3^+	π	α	−0.8062	σ	β	−0.9093
9-electrons						
CN	σ	α	−0.3836	π	β	−0.4319
HCC	π	β	−0.3871	π	β	−0.3871
11-electrons						
HBO^-	σ	α	−0.0617	σ	β	−0.0852
HBF	σ	α	−0.3823	σ	β	−0.4191
H_2CCH	π	β	−0.3620	π	α	−0.3734
HCN^-	σ	α	0.0394	σ	β	−0.0155
H_2CN	σ	β	−0.3619	σ	α	−0.3631
HCO	σ	α	−0.3431	σ	β	−0.4604
NO	π	α	−0.3385	σ	β	−0.4062
13-electrons						
HNF	σ	β	−0.4024	π	α	−0.4205
HOO	σ	β	−0.3790	π	α	−0.3914
17-electrons						
BF	σ	α	−0.4111	σ	β	−0.4146
CO_2^{2-}	σ	α	−0.0733	σ	β	−0.1287
NO_2	σ	α	−0.3878	σ	β	−0.4466
FCO	σ	α	−0.3947	σ	β	−0.4468
19-electrons						
NF_2	π	α	−0.4359	σ	α	−0.4402
FOO	σ	β	−0.3923	π	α	−0.3964

hyperfine coupling correctly. The predicted symmetries of the highest occupied molecular orbitals, based on orbital energies are wrong, whenever the orbital energies of highest and next to highest molecular orbitals are very close (~1 eV). In such situations configuration based on E_i values are generally in agreement with experimental as well as the spin density data. Such is the situation in NH_2 and FOO radicals, which (Table 5) have orbital energies of highest occupied molecular orbitals very close. Thus, the π-radicals NH_2 and FOO based on orbital energy data are seen to have the highest occupied MO's of σ-symmetry, contrary to expectation (configurations $(1\pi_\alpha 3\sigma_\alpha 3\sigma_\beta)$ and $(\ldots 4\sigma_\alpha 4\sigma_\beta 5\sigma_\alpha 5\sigma_\beta 2\pi_\alpha 2\pi_\beta 6\sigma_\alpha 6\sigma_\beta 7\sigma_\alpha 7\sigma_\beta 3\pi_\alpha)$ respectively). Employing the E_i values, we get the configurations $(\ldots 3\sigma_\alpha 3\sigma_\beta 1\pi_\alpha)$ and $(\ldots 4\sigma_\alpha 5\sigma_\alpha 5\sigma_\beta 6\sigma_\alpha 2\pi_\beta 2\pi_\alpha 6\sigma_\beta 4\sigma_\beta 7\sigma_\alpha 7\sigma_\beta 3\pi_\alpha)$ for the NH_2 and FOO radicals where the highest occupied molecular orbital is of π-symmetry as expected.

The HOO and HNF radicals from Table 5 are seen to have very similar orbital energies and both ε_i and E_i values predict the wrong symmetry for the highest occupied molecular orbital. In these cases, the use of MINDO/3 optimized geometries and imposition of symmetry in construction of the ground state eigenfunction might yield a lower value of total energy for the configuration, with the highest occupied molecular orbitals of right symmetry, but we have not attempted it. In any case, the orbital energies are so close, that the new calculation is not likely to alter the spin densities significantly.

In the case of the HCC radical, the calculated couplings do not agree with the available experimental data (41) or *ab initio* results (11, 13). In this system the odd electron is found to be in a pair of degenerate orbitals (energy = −0.387 au), thus correctly predicting that the radical is of σ type (total spin density in π_x and π_y being zero). The lack of agreement between calculated and experimental

couplings is probably due to the poor geometry (13) employed by us which may account for the slow convergence of the calculated energy in our computations.

The nonplanar radicals in which proton couplings have been studied are H_2NO, H_2CF, HCF_2, and C_2H_5. In H_2NO, the calculated proton couplings (8.44 G) are in fair agreement with experimental result (11.9 G). The highest occupied MO of this radical belongs to the a' irreducible representation of the C_s point group. The small spin density at the protons comes from $2p_z$ orbitals of nitrogen and oxygen through exchange polarization. Since the next highest occupied MO (a'') is much lower in energy, no spin density is transferred to protons through hyperconjugation. Small proton hyperfine couplings in H_2CF also follow the same pattern. However, the proton couplings in HCF_2 are not reproduced satisfactorily and the failure may be attributed to inappropriate MINDO/3 parametrization for fluorine.

For the ethyl radical, the computations were performed in two conformations (14) and the resultant average values of the couplings for methyl and methylene protons and also for the carbons agree fairly well with experiment. It is found that the odd electron is almost completely localized in the $2p\pi$ orbital (perpendicular to methylene group) of methylene carbon. The methylene protons which are in the nodal plane of this orbital acquire a small spin density because of exchange polarization. The positive spin density at the methyl protons arises through a combination of exchange polarization and hyperconjugation mechanisms.

Following the procedure of Pople and Beveridge (14) and using MINDO/3 spin densities, we estimate the relative importance of hyperconjugation and exchange polarization to be 93% and 7% in transferring the spin density to methyl protons in ethyl radical. Incidentally the same figures were arrived at by Pople and Beveridge who employed INDO spin densities.

The notable success of the annihilated MINDO/3 spin densities is that the π and the σ radicals do not need separate treatments, e.g. the same set of parameters give hyperfine couplings which are close to experimental values both in CH_3 (π radical) and HCO (σ radical). In most other semiempirical schemes, it is seen that a set of parameters which is good for π systems fails for σ systems and vice versa. In general MINDO/3 proton hyperfine couplings are comparable to INDO (14–19) and CNDO/SP (20) values.

^{13}C *Hyperfine Couplings*

A glance at Table 2 shows that the overall trend of MINDO/3 calculated ^{13}C hyperfine couplings is fairly satisfactory, both π and σ radicals being well accounted for. Particularly for CH_3 and HCO, MINDO/3 results are better than either INDO (43.08 G, 146.7 G) (18) or *ab initio* (52 G, 148.4 G) (12) results. In FCO, the MINDO/3 value (218.3 G), though poorer than the *ab initio* value of 290.3 G (10), is better than the corresponding INDO figure of 199.6 G (20). The geometry of FCO which we employed was due to Thomson and Brotchie (10*a*) and is in excellent agreement with UHF optimized geometry of Bleicher and Botschwina (10*b*). The slight disagreement between the calculated and experimental couplings might be attributed to fluorine parameters. The CO_2^- radical is bent in the ground state (35) and ^{13}C coupling is expected to be positive. MINDO/3 predicts a value of 136.4 G whereas the experimental value is 166.7 G. The value for the carbon coupling in HCN is not so good but is far better than the corresponding INDO value (156.1 G) (18). In H_2CN, only proton and nitrogen couplings are known experimentally (50) but Brivati *et al.* (57) have indicated a negative value for carbon coupling in this case. MINDO/3 calculations support this idea with magnitude fairly close to the *ab initio* value of 18.73 G (9). Experimental couplings at carbons in the vinyl radical are considerably different both in sign and magnitude. MINDO/3 accommodates both the sign and the relative magnitude although the absolute magnitudes of couplings are larger than their experimental counterparts. In the ethyl radical too, the magnitude and the sign are well accounted for at both carbons which has already been discussed.

Fluorination of the methyl radical considerably increases the *s*-character of the carbon orbitals which is reflected in increase of couplings on carbon atoms in these radicals. For example, the experimental values of hyperfine couplings in CH_3 and CF_3 are 38.5 G and 271.6 G, respectively. Calculated couplings reflect this feature in the same order (including H_2CF and HCF_2 as intermediate radicals). The magnitudes of individual couplings are not so satisfactory. We have used the INDO optimized geometry (14), which gives an increased pyramidal structure at carbon atom with increase in the number of fluorines in the radical. The less satisfactory aspect of couplings (magnitude) in these systems can be attributed to both geometry and fluorine parameters. Perhaps MINDO/3 optimized geometry might yield better results but we did not attempt it. The values of carbon couplings in CN and HCC radicals are rather poor.

^{14}N *Hyperfine Couplings*

The results of the application of the theory to the

nitrogen couplings are also given in Table 2 for a set of ten radicals. Except for CN and H_2NO, the present calculated couplings are better than any other calculations either *ab initio* or semiempirical. It is particularly interesting to note that in the NH_2, NH_3^+, and NO_2 radicals almost identical (compared to experiment) results are obtained. Despite employing *ab initio* geometrical model (9) in HCN and INDO model (17) in H_2CN the theory predicts very satisfactory ^{14}N coupling constants. The H_2NO case is interesting. It is generally agreed in experimental studies (58) that the spin density of X (X = N, O) is almost entirely localized in the π orbitals of nitrogen or oxygen atoms. However, there is no agreement concerning the spin density distribution between nitrogen and oxygen atoms. The reported values of nitrogen $2p$ spin densities range from 0.23 (59) to 0.9 (60). The calculated (annihilated) spin densities in the $2p\pi$ orbitals of nitrogen and oxygen are 0.3542 and 0.3540, respectively. As have been mentioned earlier, the spin density increases with the increase of s character at particular nucleus, so the pyramidal model employed here might not be very appropriate and MINDO/3 optimized geometry might yield better results.

^{17}O and ^{19}F Hyperfine Couplings

The ^{17}O couplings given in Table 2 are without any least-squares fitting. The HMNC value for ^{17}O is the INDO value due to Pople and Beveridge (14). The fitting was not done because the experimental couplings are not known for most of the systems studied here. Unlike the proton, carbon, and nitrogen couplings the calculated oxygen couplings are seen to be rather poor and do not exhibit any well defined trend. For example, in the case of CO_2^- and NO_2 where the calculated carbon and nitrogen coupling values are satisfactory, the ^{17}O couplings are too small. On the other hand, in H_2NO the calculated coupling is much larger than the experimental value. Peroxy radicals (ROO), which are intermediates in many reactions including those of biochemical interest, have been subjected to many theoretical as well as experimental studies (19, 47, 52, 61, 62). INDO (19) studies have shown that most of the spin density resides in $2p\pi$ orbitals of oxygens (79% on terminal and 21% on central) and is independent of the nature of the substituent R. Present calculations do not show such sharp difference between terminal and central oxygen atom $2p\pi$ spin densities. In HO^1O^2 the $\rho_{2p\pi_{12}}(O^1)$ and $\rho_{2p\pi}(O^2)$ are 0.3833 and 0.6167, respectively; in FOO, $\theta_{2p\pi}$ for O^1 and O^2 and F are 0.4902, 0.4486, and 0.0613, respectively. Table 5 shows in both of these two cases the energy difference between the highest and next highest occupied MO's is very small and reversal of MO's takes place, and consequently interpretation of couplings cannot be based upon MINDO/3 wavefunctions. From the point of view of the sign of spin densities in these systems, MINDO/3 and INDO results agree.

The ^{19}F hyperfine couplings have been studied in a set of 9 systems and are given in Table 2. The calculated couplings are not as satisfactory as the ^1H, ^{13}C, and ^{14}N couplings but are much better than ^{17}O couplings. In FCO, the MINDO/3 gives better matching with experiment (51) than the *ab initio* value of 196.8 G (10*a*). It is also noteworthy that as the number of fluorines in a radical increases, the calculated couplings start getting worse, e.g., in the H_2CF, HCF_2, and CF_3 radicals, whereas experiment shows ^{19}F couplings are smallest in H_2CF and largest in CF_3, the MINDO/3 predicts the largest value for HCF_2. A similar worsening of ^1H and ^{13}C hyperfine couplings with increase of number of fluorines can be seen from Table 2 in several radicals. This worsening of the calculated hyperfine couplings with increasing number of fluorines could be attributed to the fact that the spatial interactions due to fluorine lone pairs are likely to be fairly important and thus sensitive to the assumed geometry of the radical and MINDO/3 optimized geometries might improve the results, but we have not attempted these yet.

Conclusions

In conclusion, it is worthwhile to comment on the use of annihilated spin densities in our calculations. Our calculations indicate, just as those of some other workers (5–10, 17, 18), that annihilation of contaminants improves the results considerably, contrary to the observation of Pople and Beveridge (14). In fact it has been shown by separating UHF spin densities, as suggested by Yonezawa *et al.* (63), into spin delocalization and spin polarization parts that whereas spin polarization contributions are reduced to one-third by annihilation (63, 64), the delocalization contribution remains unaffected (63). The use of a mixture of annihilated and unannihilated spin densities in the ratio of 3:1 has been suggested by Amos and Burrows (65) which again shows a preference for annihilated spin densities.

In the preceding sections results and discussions of isotropic hyperfine couplings for ^1H, ^{13}C, ^{14}N, ^{17}O, and ^{19}F isotopes have been presented for various radicals. We conclude that MINDO/3 coupling constants as obtained by annihilated spin densities are fairly satisfactory in most of the radicals for ^1H, ^{13}C, and ^{14}N. This is also borne out by the correlation coefficients between calculated and experimental couplings of 0.9279, 0.7859, and 0.9988, for these nuclei respectively. Nothing can be said with certainty about ^{17}O results but the ^{19}F couplings seem to be less satisfactory.

Acknowledgements

Financial assistance from C.S.I.R., New Delhi, is gratefully acknowledged. Thanks are also due to one of the referees for making some valuable suggestions.

1. N. M. ATHERTON. Electron spin resonance. John Wiley, New York. 1973.
2. J. E. WERTZ and J. R. BOLTON. Electron spin resonance, elementary theory and practical applications. McGraw-Hill, New York. 1972.
3. M. BERSOHN and J. C. BAIRD. An introduction to electron paramagnetic resonance. Benjamin, New York. 1966.
4. F. J. ADRIAN and M. KARPLUS. J. Chem. Phys. **41**, 56 (1964); M. RAIMONDI, M. SIMONETTA, and G. F. TANTARDINI. J. Chem. Phys. **56**, 509 (1972) and references cited therein.
5. T. A. CLAXTON. Chem. Phys. Lett. **4**, 469 (1969).
6. T. A. CLAXTON, D. MCWILLIAMS, and N. A. SMITH. Chem. Phys. Lett. **4**, 505 (1970).
7. T. A. CLAXTON. Trans. Faraday Soc. **66**, 1537 (1970); **66**, 1540 (1970).
8. T. A. CLAXTON. Int. J. Quantum Chem. **4**, 337 (1970).
9. T. A. CLAXTON. Trans. Faraday Soc. **67**, 897 (1970).
10. (*a*) C. THOMSON and D. A. BROTCHIE. Int. J. Quantum Chem. Symp. **8**, 277 (1970); (*b*) W. BLEICHER and P. BOTSCHWINA. Mol. Phys. **30**, 1029 (1975).
11. I. H. HILLIER, J. KENDRICK, and M. F. GUEST. Mol. Phys. **30**, 1133 (1975).
12. (*a*) D. A. BROTCHIE and C. THOMSON. Chem. Phys. Lett. **22**, 338 (1973); (*b*) F. DRIESSLER, R. AHLRICHS, V. STAEMMLER, and W. KUTZELNIGG. Theor. Chim. Acta, **30**, 315 (1973).
13. W. A. LATHAN, W. J. HEHRE, and J. A. POPLE. J. Am. Chem. Soc. **93**, 808 (1971).
14. J. A. POPLE and D. L. BEVERIDGE. Approximate molecular orbital theory. McGraw-Hill, New York. 1970.
15. D. L. BEVERIDGE and J. W. MCIVER, JR. J. Chem. Phys. **54**, 4681 (1971).
16. H. G. BENSON and A. HUDSON. Mol. Phys. **20**, 185 (1971).
17. M. F. CHIU, B. C. GILBERT, and B. T. SUTCLIFFE. J. Phys. Chem. **76**, 553 (1972).
18. C. THOMSON. Theor. Chim. Acta, **17**, 320 (1970).
19. S. BISKUPIC and L. VALKO. J. Mol. Struct. **27**, 97 (1975).
20. G. M. ZHIDOMIROV and N. D. CHUVYLKIN. Theor. Chim. Acta, **30**, 197 (1973).
21. P. K. MEHROTRA. Ph.D. Thesis. I.I.T., Madras, India. 1976.
22. P. BISCHOF. J. Am. Chem. Soc. **98**, 6844 (1976).
23. R. C. BINGHAM, M. J. S. DEWAR, and D. H. LO. J. Am. Chem. Soc. **97**, 1285 (1975).
24. J. A. POPLE and R. K. NESBET. J. Chem. Phys. **22**, 571 (1954).
25. P. K. K. PANDEY. Ph.D. Thesis. Banaras Hindu University, India. 1977.
26. P. K. K. PANDEY, P. CHANDRA, P. L. PRASAD, and S. SINGH. Chem. Phys. Lett. **49**, 353 (1977).
27. P. K. K. PANDEY and P. CHANDRA. Theor. Chim. Acta, **50**, 211 (1978).
28. A. T. AMOS and G. G. HALL. Proc. R. Soc. London, A**263**, 483 (1961).
29. G. R. BIRD. J. Chem. Phys. **25**, 1040 (1956).
30. J. A. AUSTIN, D. H. LEVY, C. A. GOTTLIEB, and H. E. RADORD. J. Chem. Phys. **60**, 207 (1974).
31. G. HERZBERG. Molecular spectra and molecular structure. I. Spectra of diatomic molecules. D. Van Nostrand, Princeton. 1950.
32. G. HERZBERG. Molecular spectra and molecular structure. III. Electronic spectra and electronic structure of polyatomic molecules. D. Van Nostrand, Princeton. 1966.
33. M. D. HARMONY, R. J. MYERS, L. J. SCHOEN, D. R. LIDE, JR., and D. E. MANN. J. Chem. Phys. **35**, 1129 (1961).
34. C. W. WOODMAN. J. Mol. Spectrosc. **33**, 311 (1970).
35. H. M. MCCONNELL. J. Chem. Phys. **24**, 764 (1956).
36. T. D. DAVIS, R. E. CHRISTOFFERSEN, and G. M. MAGGIORA. J. Am. Chem. Soc. **97**, 1347 (1975).
37. K. TORIYAMA and M. IWASAKI. J. Chem. Phys. **55**, 1890 (1971).
38. W. C. EASLEY and W. WELTNER, JR. J. Chem. Phys. **52**, 197 (1970).
39. C. R. CATTON, M. C. R. SYMONS, and W. H. WARDALE. J. Chem. Soc. A, 2622 (1969).
40. E. L. COCHRAN, F. J. ADRIAN, and V. A. BOWERS. J. Chem. Phys. **40**, 213 (1964).
41. W. R. M. GRAHAM, K. I. DISMUKE, and W. WELTNER, JR. J. Chem. Phys. **60**, 3817 (1974).
42. K. D. J. ROOT, M. C. R. SYMONS, and B. C. WEATHERLEY. Mol. Phys. **11**, 161 (1968).
43. E. L. COCHRAN, F. J. ADRIAN, and V. A. BOWERS. J. Chem. Phys. **36**, 1661 (1962).
44. R. W. HOLMBERG. J. Chem. Phys. **51**, 3255 (1969).
45. F. J. ADRIAN, E. L. COCHRAN, and V. A. BOWERS. J. Chem. Phys. **47**, 5441 (1967).
46. W. NELSON and W. GORDY. J. Chem. Phys. **51**, 4710 (1969).
47. T. COLE. J. Chem. Phys. **35**, 1169 (1961).
48. S. FONER, E. L. COCHRAN, V. A. BOWERS, and C. JEN. Phys. Rev. Lett. **1**, 91 (1958).
49. S. SCHLICK, B. L. SILVER, and Z. LUZ. J. Chem. Phys. **54**, 867 (1971).
50. Z. LUZ, A. REUVENI, R. W. HOLMBERG, and B. L. SILVER. J. Chem. Phys. **51**, 4017 (1969).
51. E. L. COCHRAN, F. J. ADRIAN, and V. A. BOWERS. J. Chem. Phys. **44**, 4626 (1966).
52. F. J. ADRIAN. J. Chem. Phys. **46**, 1543 (1967).
53. R. W. FESSENDEN and R. H. SCHULER. J. Chem. Phys. **39**, 2147 (1963); R. W. FESSENDEN. J. Phys. Chem. **71**, 74 (1967).
54. M. C. R. SYMONS. J. Chem. Phys. **55**, 1493 (1971).
55. J. Q. ADAMS, S. W. NICKSIC, and J. R. THOMAS. J. Chem. Phys. **45**, 654 (1966).
56. R. W. FESSENDEN and R. H. SCHULER. J. Chem. Phys. **43**, 2704 (1965).
57. J. A. BRIVATI, K. D. J. ROOT, M. C. R. SYMONS, and D. J. A. TINGLINGS. J. Chem. Soc. A, 1942 (1969).
58. H. HAYAT and B. L. SILVER. J. Phys. Chem. **77**, 72 (1973).
59. O. KIKUCHI. Bull. Chem. Soc. Jpn. **42**, 1187 (1969).
60. C. L. HAMILTON and H. M. MCCONNELL. Structural chemistry and molecular biology. *Edited by* A. Rich and N. Davidson. W. H. Freeman, San Francisco. 1968.
61. J. GOLE and E. F. HAYES. J. Chem. Phys. **57**, 360 (1972).
62. D. H. LISKOW, H. F. SCHAEFER III, and C. F. BENDER. J. Am. Chem. Soc. **93**, 6734 (1971).
63. T. YONEZAWA, H. NAKATSUJI, T. KAWAMURA, and H. KATO. J. Chem. Phys. **51**, 669 (1969).
64. W. MARSHALL. Proc. R. Soc. London, A**78**, 113 (1961).
65. A. T. AMOS and B. L. BURROWS. J. Chem. Phys. **52**, 3072 (1972).

Thermodynamic properties of binary mixtures containing thiaalkanes. II. Thermal pressure coefficients of pure compounds at 298.15 K

R. PHILIPPE, Z. FERHAT-HAMIDA, AND J. C. MERLIN

Université de Lyon I, Laboratoire de Chimie Analytique I, 43 boulevard du 11 Novembre 1918, 69621 Villeurbanne, France

Received May 16, 1979

R. PHILIPPE, Z. FERHAT-HAMIDA, and J. C. MERLIN. Can. J. Chem. **57**, 3135 (1979).

An apparatus for the measurement of thermal pressure coefficients of pure compounds is described. The thermal pressure coefficient β of *n*-thiaalkanes R_2S (R = CH_3, C_2H_5, *n*-C_3H_7, *n*-C_4H_9, *n*-C_7H_{15}) and of dithiaalkanes R_2S_2 (R = CH_3, C_2H_5, iso-C_3H_7) were measured at 298.15 K and at zero pressure. These experimental results in conjunction with data from literature for other compounds are compared using the reduced parameter of pressure P^* proposed by Flory. The P^* do not have regular values for the lower members of thiaalkanes series. One explanation of these irregularities is the different size of the molecules.

R. PHILIPPE, Z. FERHAT-HAMIDA et J. C. MERLIN. Can. J. Chem. **57**, 3135 (1979).

Nous décrivons un appareil utilisé pour la mesure des coefficients de pression thermique. Nous avons mesuré, à 298.15 K et à pression nulle, le coefficient de pression thermique β de *n*-thiaalcanes R_2S (R = CH_3, C_2H_5, *n*-C_3H_7, *n*-C_4H_9 et *n*-C_7H_{15}) et de dithiaalcanes R_2S_2 (R = CH_3, C_2H_5 et iso-C_3H_7). Ces résultats expérimentaux sont comparés avec d'autres résultats de la littérature en utilisant le paramètre de réduction de la pression P^* proposé par Flory. Les valeurs de P^* pour les premiers membres de la série des thiaalcanes n'ont pas des valeurs régulières. Ces irrégularités peuvent s'expliquer par la différence de taille deces molécules.

Introduction

The present work is a part of a research programme aimed at the correlation of H^E and V^E for different binary mixtures, and it is a continuation of research on thermodynamic properties of thiaalkanes + alkanes mixtures (1, 2). The knowledge of thermal pressure coefficient of pure components is required for comparison of the excess function of the mixtures with the predictions of various theories (3, 4) and provide useful information about the nature of liquid and about the forces between molecules. Many accurate measurements have been made on alkanes (5, 6) and branched alkanes (7), cycloalkanes (8), aromatic and polar compounds (9), polymers (10), and differently sterically hindered (DSH) compounds (11) but, apparently, no measurements have been done on the thiaalkanes series. Here we present measurements on pure compounds at 298.15 K: the thermal pressure coefficient of five *n*-thiaalkanes and the thermal expansivity and thermal pressure coefficient of three dithiaalkanes.

The thermal expansivity α defined by

$$[1] \quad \alpha = V^{-1}(\partial V/\partial T)_p$$

was measured from density ρ according to the relation

$$[2] \quad \alpha_T = \rho_T{}^{-1}[\rho_1(T_1) - \rho_2(T_2)/(T_2 - T_1)]$$

where the temperature T is defined by $T = (T_1 + T_2)/2$ and the thermal pressure coefficient β, defined by

$$[3] \quad \beta = (\partial P/\partial T)_V$$

was measured directly by static method.

Experimental

Solvents

Cyclohexane was a Fisher product (purity > 99 mol%) and *n*-hexadecane was a Merck product (purity > 99 mol%) and were used without further purification.

The thiaalkanes were "chemically pure" products (all obtained from S.N.P.A., Paris, except 2-thiapropane which was a Prolabo product) and were used without further purification. Their densities were used as criteria of purity; the values found for the lower homologues agree with accepted literatures values (Table 1). No reliable data are available for the higher homologues.

Thermal Expansion Coefficients

The thermal expansion coefficient α was determined according to the formula [2] from the densities ρ measured at three temperatures: T_1 = 297.15 K, T_2 = 299.15 K, and $(T_1 + T_2)/2$. The densities ρ were determined by the pycnometric technique by the same method as described before (1). The pycnometers were made of Pyrex glass and had an internal volume of about 22 cm^3. The temperature was measured with a Leeds and Northrup calibrated strain-free platinum resistance thermometer (8163 B type) associated wth a Leeds and Northrup high precision resistance Mueller bridge (G2 type). The calibration of thermometer was checked at the triple point temperature of water. The magnitude of $T_2 - T_1$ (about 2 K), close to 298.15 K, allows a linear interpolation to determine α.

0008-4042/79/233135-05$01.00/0

TABLE 1. Densities ρ at 298.15 of compounds

Compound	ρ/kg m^{-3} This work	Literature	Reference
2-Thiapropane	—	842.28	12
3-Thiapentane	831.5	831.18	12
4-Thiaheptane	832.6	833.12	12
5-Thianonane	834.5	—	
8-Thiapentadecane	839.4	—	
2,3-Dithiabutane	1054.7	1056.9	12
3,4-Dithiahexane	988.4	988.1	12
2,5-Dimethyl-3,4-dithiahexane	937.9	938.1	13

Thermal Pressure Coefficients

Thermal pressure coefficients were determined according to the procedure of Westwater *et al.* (14). The apparatus is similar to that previously described (11) and the schematic diagram of this is presented in Fig. 1. The thermal pressure cell containing the sample is a slightly modified version of that described in literature (6, 7), the volume was within 8 cm^3 and a platinum wire with a sharpened tip was centered in the 0.8 mm capillary. The pressure vessel built by the Prolabo Co. (Paris) was made of stainless steel with a 1 L capacity and could withstand a pressure within 4 MPa at 335.15 K. The hydraulic pressure generator is of screw-capstan type from Hight Pressure Equipment (Erie, U.S.A.). It displaces 60 cm^3 up to a pressure of 35 MPa. Pressure measurements are performed with a strain gauge supplied by Schaevitz Em Ltd. (P 703.0001 type) giving a 0.001 MPa resolution and an accuracy of 0.38% of the full range output. The temperature was measured with a 50 Ω platinum resistance thermometer (Thermo Est S.A.) and a Mueller bridge from Leeds and Northrup Co. (8163 B type, No. 161939). The resistance element section of the thermometer was located close to the bulb of thermal pressure cell and was enclosed in a stainless steel cylinder. The thermometer was calibrated by means of a water triple-point cell. The overall precision of temperature measurement was found to be within ±1 mK. We believe the temperatures measured were within 2 mK. The pressure vessel was immersed in a water thermostat (Lauda, NBS type) and the temperature of water was controlled to within ±0.01 K. Let us notice that the large mass of the pressure vessel minimizes temperature fluctuations of the thermoregulated bath, and at the equilibrium the temperature in the pressure vessel is regulated within ±0.5 mK.

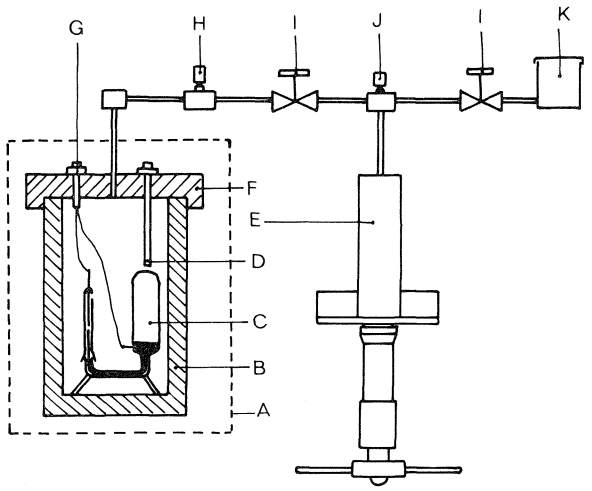

FIG. 1. Schematic diagram of the equipment used in the measurement of thermal pressure coefficient: *A* thermoregulated water bath, *B* pressure vessel, *C* Pyrex glass cell, *D* temperature probe, *E* pressure generator, *F* pressure vessel cap, *G* leads for the constant volume checking circuit, *H* strain pressure gauge, *I* high pressure valve, *J* safety head assembly, *K* reservoir for pressure fluid.

The liquid sample, about 7 cm^3, is placed in the Pyrex glass cell and degassed by repeated freezing with liquid nitrogen and melting under vacuum. The cell was then removed from vacuum line, inverted rapidly over degassed mercury, and the mercury level adjusted at the extremity of the platinum wire for the desired temperature. After positioning in the pressure vessel the whole apparatus is then connected to the pressure line and placed in the water thermostat. The temperature is increased and the pressure adjusted to restore the liquid to its initial volume indicated by the pilot light connected in series with the mercury and the platinum wire. Pressure over 0.5 MPa was used and at equilibrium the contact was sensitive to an increment of 0.001 MPa. The total temperature interval for one run is not larger than 2 K.

The plot of applied pressure against temperature was always linear within experimental error and the slope of this line, computed by a least-squares fitting procedure, gave β_{obs} and the temperature at zero pressure.

A correction is necessitated by the fact that the volume of the glass vessel is not strictly constant. During the experimental process, when the temperature is increased by ΔT and the pressure by ΔP_{obs}, the change in internal volume of the glass is:

$$[4] \quad \Delta V_g = V_g \alpha_g \Delta T - V_g K_g \Delta P_{obs}$$

where α_g is the thermal coefficient of expansion of the Pyrex (9.9×10^{-6} K^{-1} (6)), K_g is the isothermal compressibility of Pyrex ($2.96\ 10^{-7}$ MPa^{-1} (5*b*)) and $V_g = V_l + V_{Hg}$ is the volume of the cell. The volume of liquid sample (V_l) and mercury (V_{Hg}) in the cell were computed from their respective weights.

Similarly the change in volume of mercury is:

$$[5] \quad \Delta V_{Hg} = V_{Hg} \alpha_{Hg} \Delta T - V_{Hg} K_{Hg} \Delta P_{obs}$$

where α_{Hg} is the thermal coefficient of expansion of mercury (1.81×10^{-4} K^{-1} (6)) and K_{Hg} the isothermal compressibility of mercury, represented as a function of the temperature by the equation (23):

$$[6] \quad K_{Hg} = 3.921 \times 10^{-7} + 4.7 \times 10^{-10} (T - 273.15) + 3.5 \times 10^{-15} (T - 273.15)^3 \text{ MPa}^{-1}$$

TABLE 2. Thermal pressure coefficient at zero pressure β of cyclohexane and *n*-hexadecane

Compounds	*T*/K	β/MPa K^{-1} This work	Literature	Reference
Cyclohexane	298.15	1.069±0.002	1.068	15
			1.072	8*b*
			1.075	16
n-Hexadecane	296.61	1.049±0.002	1.042	6
	298.17	1.031±0.002	1.033	6
	299.31	1.016±0.002	1.026	6

TABLE 3. Parameters for the pure compounds at 298.15 K

Compound	α 10^3/K^{-1}	β/MPa K^{-1}	P^*/J cm^3	μ/D	s_1 10^{10}/m^{-1}
2-Thiapropane	1.414[a]	1.121[b]	588.5	1.40[e]	1.225
3-Thiapentane	1.200[a]	0.923[b]	455.3	1.60[e]	1.081
4-Thiaheptane	1.090[a]	0.906[b]	432.8	1.55[e]	1.012
5-Thianonane	1.015[a]	1.007[b]	469.8	1.57[e]	0.971
8-Thiapentadecane	0.953[a]	1.084[b]	495.5	—	0.907
2,3-Dithiabutane	1.052[b]	1.314[b]	620.1	1.95[f]	1.134
3,4-Dithiahexane	0.991[b]	1.207[b]	558.7	1.99[g]	1.039
2,5-Dimethyl-3,4-dithiahexane	0.965[b]	1.071[b]	491.2	—	0.930
3-Oxapentane	1.650[c]	0.869[d]	484.4	1.22[e]	1.111
4-Oxaheptane	1.300[c]	0.945[d]	480.7	1.20[e]	1.027

[a]Reference 1.
[b]This work.
[c]Calculated from ρ_1 (293.15 K) and ρ_2 (298.15 K) data reported in ref. 17 using the formula $\alpha = [(\rho_1/\rho_2) - 1]/5$.
[d]Reference 5.
[e]Reference 18.
[f]At 303.15 K, ref. 19.
[g]Reference 20.

The change in volume of liquide ΔV_l corresponds with an extra pressure ΔP such as

$$[7] \quad \Delta V_l = (\Delta P - \Delta P_{obs}) V_l K_l$$

where $K_l = \alpha_l/\beta_l$ is the isothermal compressibility of the liquid. Taking relations [4], [5], and [7] into account and dividing through by ΔT, one obtains

$$[8] \quad \beta = \beta_{obs} \frac{\alpha_l V_l}{\alpha_l V_l + (\alpha_{Hg} - \beta_{obs} K_{Hg}) V_{Hg} - (\alpha_g - \beta_{obs} K_g) V_g}$$

The overall performance of the apparatus was checked by measurement of the thermal pressure coefficient of cyclohexane and *n*-hexadecane. The results are shown in Table 2 where they are compared with literature values. As these data have not been obtained by the same method, our results are in excellent agreement with the data obtained by the direct method.

Results and Discussion

In the course of some experiments a slow reaction was found to occur between thiaalkanes and mercury, as shown by a film of black solid material which formed on mercury–liquid interface in the cell and causing a change in the cell volume of about 5×10^{-6} cm^3 found by dilatometric measurements. It therefore appears that any reaction with mercury was insufficient to introduce any significant errors into the data obtained. After 12 h, indeed, no change in internal volume of the cell was detected, and two consecutive sets of measurements on the same sample agree within our estimated experimental uncertainties.

The experimental thermal pressure coefficient β of thiaalkanes is given in Table 3 together with the thermal expansivity α, the pressure reduction parameter P^*, the dipole moment μ, and the molecular surface/volume ratio *s*.

As pointed out previously (11), discussion of these results will be made with the values of pressure reduction parameter P^* representative of cohesive energy of the compounds rather than on β, since β also reflects the state of expansion which varies considerably along the series. The parameter P^* is obtained from the Flory model (3) with experimental values of α and β by the equation:

$$[9] \quad P^* = \beta \tilde{v}^2 T$$

where the reduced volume $\tilde{v}$ is calculated by:

$$[10] \quad \tilde{v}^{1/3} = [(4/3)\alpha T + 1]/(\alpha T + 1)$$

These values are reported on Fig. 2 together with

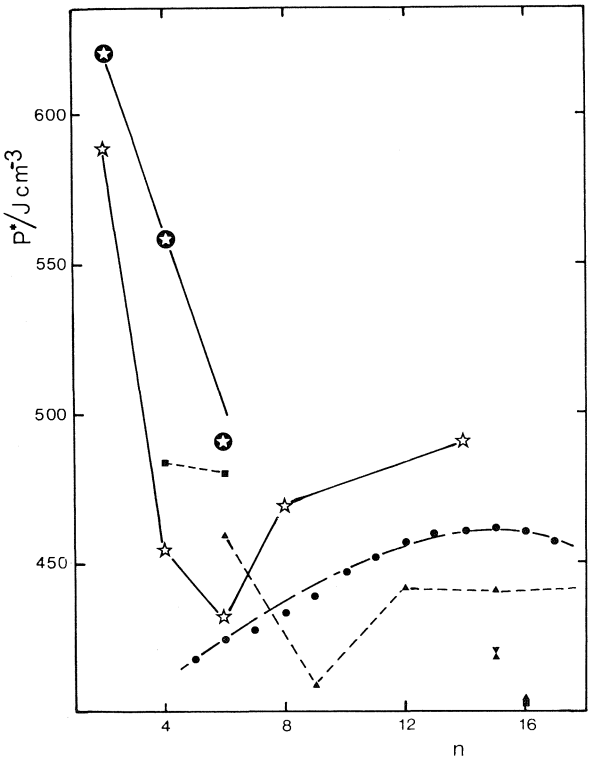

FIG. 2. Pressure reduction parameter P^* plotted versus n the total number of carbon atoms for dithiaalkanes (✪), n-thiaalkanes (☆), n-ethers (■), trialkylamines (▲), n-alkanes (●), diisopentylamine (⧗), and 2,2,4,4,6,8,8-heptamethylnonane (⬟).

the values obtained for other series of compounds (7, 11) for comparison.

These values are higher than those of other series. As for n-trialkylamine series, the P^* values for the lower members of the n-thiaalkanes series do not vary smoothly with molecular weight, and a minimum is found for 4-thiaheptane. The influence of chain length is less perceptible but it seems that the P^* values tend towards a limiting value when the molecular weight increases. The limiting value for this series is higher than for the "DSH" series (11) and the order appears to be $R_2S > n\text{-}Cn > R_3N > R_4Sn > (OR)_4Si$.

For dithiaalkane series, the number of compounds studied is not sufficient to obtain comprehensive conclusions. Nevertheless, by comparison with the n-thiaalkane series, it is quite possible that the larger values found for 2,3-dithiabutane and 3,4-dithiahexane are related to the polarity of these compounds, and by comparison with the branched alkanes and the branched amines (11), the branched dithiaalkane (2,5-dimethyl-3,4-dithiahexane) seems to have slightly lower value of P^*. We do not think that the high values found for the lower members of n-thiaalkanes and dithiaalkanes series can be explained solely by the more polar character of these molecules. Table 3, indeed, shows that molecules of same shape, the aliphatic ethers, have a dipole moment lower than the homomorphic n-thiaalkanes and have a higher P^* value. The size effect prevails over this polarity effect as it can be seen on molar volume:

Compound	V_m (298.15 K) (10^{-6} m^3 mol^{-1})
$(C_2H_5)_2S$	108.5
$(C_2H_5)_2O$	104.7
$(C_3H_7)_2S$	141.7
$(C_3H_7)_2O$	137.7

As interactions of molecules take place between molecular surfaces, we think that the comparison of energies by unit surface is more meaningful than those of energies by unit volume P^*. Energy by unit surface may be determined from the ratio P^*/s where s is the molecular surface/volume ratio. The s values depend on the shape of the molecule and were computed assuming the thiaalkanes to be right cylinders of core volume V^* as n-alkanes (21). This assumption is proved by the fact that the Van der Waals volumes (22) of S atom (10.8×10^{-6} m^3 mol^{-1}) and CH_2 group (10.2×10^{-6} m^3 mol^{-1}) are fairly close. Accordingly s is given by:

$$[11] \quad s = \frac{4}{D} + \frac{\pi D^2 N_A}{2 \times 10^{23} V^*}$$

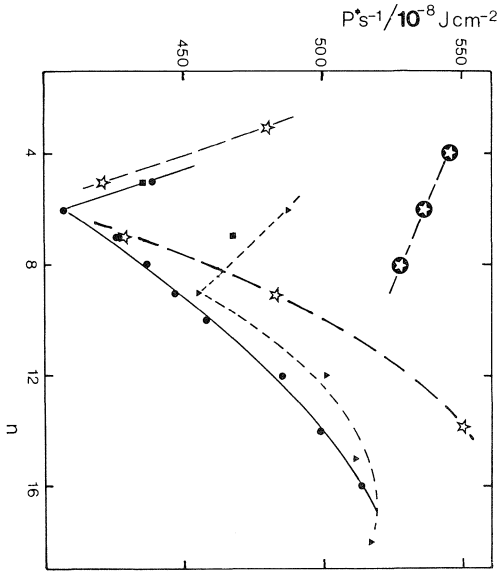

FIG. 3. P^*s^{-1} plotted versus n the total number of atoms of the compounds for dithiaalkanes (✪), n-thiaalkanes (☆), n-ethers (■), triaalkylamines (▲), and n-alkanes (●).

where D is the cylinder diameter equal to 4.98×10^{-10} m (21*b*) for linear alkane chain and 6.96×10^{-10} m (21*a*) for branched alkane chain to that of the 2,5-dimethyl, 3,4-dithiahexane, and $N_A = 6.02 \times 10^{23}$ is the Avogadro constant.

The s values are reported in Table 3 and the P^*s^{-1} values are plotted on Fig. 3 (versus n, the total number of atoms of the compounds because S atom has been considered equivalent to a carbon atom). Figure 3 shows that the P^*s^{-1} values of the n-thiaalkanes are quite comparable to those of n-alkanes. Nevertheless, for dithiaalkanes the P^*s^{-1} values are somewhat higher than those of the n-alkanes or n-thiaalkanes and it is not possible to decide the proportion of increased polarity (Table 3) and that of molecular model in these higher values.

These results will be used for a detailed theoretical interpretation of excess thermodynamic properties (H^E, V^E) of binary mixtures of thiaalkanes with n-alkanes in a later paper.

Acknowledgements

We would like to thank the Franco-Algerian Scientific Corporation Service for a research fellowship to one of us (Z.F.H.). The donation of samples of thiaalkanes from S.N.P.A. is acknowledged.

1. Z. FERHAT-HAMIDA, R. PHILIPPE, J. C. MERLIN, and H. V. KEHIAIAN. J. Chim. Phys. **76**, 130 (1979).
2. Z. FERHAT-HAMIDA, R. PHILIPPE, J. C. MERLIN, and H. V. KEHIAIAN. J. Chim. Phys. To be published.
3. (*a*) P. J. FLORY. J. Am. Chem. Soc. **87**, 1833 (1965); (*b*) A. ABE and P. J. FLORY. J. Am. Chem. Soc. **87**, 1838 (1965).
4. D. PATTERSON and G. DELMAS. Discuss. Faraday Soc. **49**, 1 (1970).
5. (*a*) G. ALLEN, G. GEE, and G. J. WILSON. Polymer, **1**, 456 (1960); (*b*) G. ALLEN, G. GEE, D. MANGARAJ, D. SIMS, and G. J. WILSON. Polymer, **1**, 467 (1960).
6. R. A. ORWOLL and P. J. FLORY. J. Am. Chem. Soc. **89**, 6814 (1967).
7. J. M. BARDIN. Ph.D. thesis, McGill University, Montréal, P.Q. 1972.
8. (*a*) E. D. BAGLEY, T. P. NELSON, J. W. BARLOW, and S. A. CHEN. Ind. Eng. Chem. Fundam. **9**, 93 (1970); (*b*) E. D. BAGLEY, T. P. NELSON, S. A. CHEN, and J. BARLOW. Ind. Eng. Chem. Fundam. **10**, 27 (1971).
9. C. F. LAU, G. N. MALCOM, and D. V. FENBY. Aust. J. Chem. **22**, 855 (1969).
10. U. BIANCHI, G. AGABIO, and A. TURTTURRO. J. Phys. Chem. **69**, 4392 (1965).
11. R. PHILIPPE, G. DELMAS, and M. COUCHON. Can. J. Chem. **56**, 370 (1978).
12. R. R. DREISBACH. Physical properties of chemical compounds. Chem. Soc., Washington. 1959.
13. D. T. MCALLAN, T. V. CULLUM, R. A. DEAN, and F. A. FILDER. J. Am. Chem. Soc. **73**, 3627 (1951).
14. W. WESTWATER, N. W. FRANTZ, and J. H. HILDEBRAND. Phys. Rev. **31**, 135 (1928).
15. G. C. BENSON, S. MURAKAMI, V. T. LAM, and J. SINGH. Can. J. Chem. **48**, 211 (1970).
16. M. B. EWING, K. N. MARSH, and R. H. STOKES. J. Chem. Thermodyn. **4**, 637 (1972).
17. J. TIMMERMANS. Physico-chemical constants of pure organic compounds. Elsevier Publishing Company, London. 1965.
18. C. P. SMYTH. Dielectric behavior and structure. McGraw-Hill Book Company Inc., New York. 1955.
19. L. M. KUSHNER, G. GORIN, and C. P. SMYTH. J. Am. Chem. Soc. **72**, 477 (1950).
20. H. E. WESTLAKE, H. L. LAQUER, and C. P. SMYTH. J. Am. Chem. Soc. **72**, 436 (1950).
21. B. E. EICHINGER and P. J. FLORY. Trans. Faraday Soc. (*a*) **64**, 2053 (1968); (*b*) **64**, 2066 (1968).
22. A. BONDI. Physical properties of molecular crystals, liquids and gases. John Wiley, New York. 1968.
23. K. E. BETT, K. E. WEALE, and D. M. NEWITT. Br. J. Appl. Phys. **5**, 243 (1954).

The synthesis of oligoribonucleotides V.[1] The stepwise synthesis of the 3′-terminal heptanucleotide sequence of $tRNA^{fMet}$ from *E. coli*

KELVIN K. OGILVIE AND NICOLE Y. THERIAULT

Department of Chemistry, McGill University, 801 Sherbrooke St. W., Montreal, P.Q., Canada H3A 2K6

Received June 6, 1979

KELVIN K. OGILVIE and NICOLE Y. THERIAULT. Can. J. Chem. **57**, 3140 (1979).

The stepwise synthesis of a heptaribonucleotide GpCpApApCpCpA corresponding to the 3′-terminus of $tRNA^{fMet}$ from *E. coli* is described. The procedure takes advantage of the ease of obtaining ribonucleoside units bearing a *tert*-butyldimethylsilyl group on the 2′-position. These units, bearing a 5′-methoxytrityl group are phosphorylated at the 3′-position and coupled to the free 5′-position of the growing nucleotide chain using the chlorophosphite coupling procedure. Yields varied from 87 to 50% over the entire sequence.

KELVIN K. OGILVIE et NICOLE Y. THERIAULT. Can. J. Chem. **57**, 3140 (1979).

On décrit la synthèse par étapes de l'heptaribonucléotide GpCpApApCpCpA correspondant à l'extrémité 3′ de l'ARN de transfert (FMet) provenant du *E. coli*. Cette méthode profite de l'obtention facile des unités ribonucléosides ayant un groupement *tert*-butyldiméthylsilyle en position 2′. Les unités portant un groupement méthoxytrityle-5′ sont phosphorylées en position 3′ et couplés à la position 5′ libre de la chaîne nucléotide en croissance en utilisant le procédé de couplage au chlorophosphite. Les rendements pour la séquence complète varient de 87 à 50%.

[Traduit par le journal]

The chemical synthesis of oligonucleotides involves two principal problems: the availability of suitably protected nucleosides and methods to condense these units to form nucleotides. In the deoxynucleotide area adequate protecting groups have long been available and most attention has been applied to the question of phosphorylation procedures (1–9). In the ribonucleotide area developments have lagged well behind the deoxy series largely because of the difficulties of finding suitable procedures for protecting the 2′-hydroxyl group.

Reese extensively explored the problem of protection of ribonucleosides (for review see ref. 10) and essentially settled on tetrahydropyranyl-type protection for the 2′-position. Khorana and co-workers also investigated this area (11) and Smrt and co-workers made important contributions (12, 13) to the protecting groups for ribonucleosides. Neilson was the first to combine the tetrahydropyranyl protecting groups with the triester technology to make important ribonucleotide chains of significant length. In 1974 Neilson and Werstiuk (14), using a block-condensation triester approach, synthesized a nonanucleotide corresponding to the anticodon loop from the fMet tRNA from *E. coli*. They later improved on the synthesis of this same sequence (15). Neilson and England also prepared two tetranucleotides and a pentanucleotide using a single addition (stepwise) procedure (16). The latter is, until now, the longest reported ribonucleotide prepared by a stepwise triester approach. Ikehara and co-workers assembled a pentanucleotide (17) using a stepwise diester approach. They have been experimenting with photochemical protecting groups (18), enzymatic coupling (19), and have recently reported a chemical block – triester synthesis of a heptanucleotide corresponding to units 53–59 from fMet tRNA from *E. coli* (20). Van Boom *et al.* have made the tetradecaribonucleotide $(UA)_7$ by a block-assembly triester procedure (21*a*). They have also prepared hexanucleotides corresponding to naturally occurring sequences by block-condensations (21*b*). Wiewiorowski and co-workers (22) have also used a block-condensation triester approach to prepare a heptanucleotide sequence from the anticodon loop of an initiator tRNA.

We wish to describe in this report the synthesis of the heptaribonucleotide GCAACCA corresponding to the 3′-terminus of fMet tRNA from *E. coli*. The chain was assembled in a stepwise fashion to prove the efficiency of the silyl protecting groups combined with the dichlorophosphite condensation procedure for the synthesis of oligoribonucleotides. The synthesis of all of the protected ribonucleosides has been previously described (23, 24). The present synthesis is outlined schematically in Scheme 1.

The questions which arise most naturally in connection with any new proposal for nucleotide syn-

[1]This article is also considered as Part X in a series on alkylsilyl protecting groups. For the previous article in these series see K. K. Ogilvie and N. Y. Theriault, Tetrahedron Lett. 2111, 1979.

0008-4042/79/233140-05$01.00/0

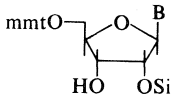

1*a*, B = *N*-benzoylcytosine
1*b*, B = adenine
1*c*, B = *N*-benzoylguanine

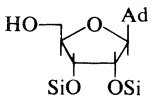

1*d*
mmt = monomethoxytrityl
Si = tertbutyldimethylsilyl

1*a* —(*1*) TCEOPCl$_2$ (*2*) **1***d* (*3*) I$_2$, H$_2$O→ RO—C$^{Bz^{Si}_p}$(TCE)A$^{Si}_{Si}$ **2**

Compounds **2**–**7**, *a* series R = mmt
b series R = H

1*a* —(*1*) TCEOPCl$_2$ (*2*) **2***b* (*3*) I$_2$, H$_2$O→ ROC$^{Bz^{Si}_p}$(TCE)C$^{Bz^{Si}_p}$(TCE)A$^{Si}_{Si}$ **3**

1*b* —(*1*) TCEOPCl$_2$ (*2*) **3***b* (*3*) I$_2$, H$_2$O→ ROA$^{Si}{}_p$(TCE)C$^{Bz^{Si}_p}$(TCE)C$^{Bz^{Si}_p}$(TCE)A$^{Si}_{Si}$ **4**

1*b* —(*1*) TCEOPCl$_2$ (*2*) **4***b* (*3*) I$_2$, H$_2$O→ ROA$^{Si}{}_p$(TCE)A$^{Si}{}_p$(TCE)C$^{Bz^{Si}_p}$(TCE)C$^{Bz^{Si}_p}$(TCE)A$^{Si}_{Si}$ **5**

1*a* —(*1*) TCEOPCl$_2$ (*2*) **5***b* (*3*) I$_2$, H$_2$O→ ROC$^{Bz^{Si}_p}$(TCE)A$^{Si}{}_p$(TCE)A$^{Si}{}_p$(TCE)C$^{Bz^{Si}_p}$(TCE)C$^{Bz^{Si}_p}$(TCE)A$^{Si}_{Si}$ **6**

1*c* —(*1*) TCEOPCl$_2$ (*2*) **6***b* (*3*) I$_2$, H$_2$O→ ROG$^{Bz^{Si}_p}$(TCE)C$^{Bz^{Si}_p}$(TCE)A$^{Si}{}_p$(TCE)A$^{Si}{}_p$(TCE)C$^{Bz^{Si}_p}$(TCE)C$^{Bz^{Si}_p}$(TCE)A$^{Si}_{Si}$ **7**

SCHEME 1

thesis include: (*a*) Do yields fall off significantly with increasing chain length and/or is it necessary to go to higher and higher ratios of reagents to ensure adequate yields? (*b*) Is it necessary to extend the time for condensation as the chain length increases? A positive answer to either or both of these questions can severely limit the practicality of a procedure.

In the early diester work on deoxynucleotides it was often necessary to use high ratios of one reagent to another. For example in the condensation (25) of Tr-(Tp)$_4$T with pT-OAc to form a hexanucleotide a 15-fold excess of pT-OAc was necessary to insure a 60% yield after 3 days of condensation. However, in Neilson's stepwise synthesis of the pentanucleotide ApCpCpUpC (16) the ratio of monomer to growing chain varied slightly from about 1.4 to 1 at the dinucleotide level to 2 to 1 at the pentanucleotide level while the yields decreased moderately from 73 to 45%. However, even though Neilson's work employed mesitylenesulfonyl triazole, considered to be a rapid condensing agent (6), the time of reaction varied from 3 days at the dinucleotide level to 10 days to form the penta. In Ikehara and co-workers' stepwise synthesis of UpAp^{m2}GpCpC (17) using a diester approach, ratios of reacting nucleotide units varied from 1 to 1 at the trinucleotide to 1 to 4 at the pentanucleotide stage. Yields ranged from 38 to 21% over this sequence and all condensation steps required 5 days. It is of course important to note that these procedures did indeed work and the desired nucleotide products were formed.

In Table 1 we have summarized the important observations in connection with the synthesis of the heptanucleotide GpCpApApCpCpA. Three points are worth noting. (*1*) The total reaction time remained constant at 2 h and 45 min over the entire sequence. (*2*) Yields decreased moderately from 87% at the dinucleotide to 50% at the heptanucleotide stage. (*3*) The ratio of monomer to oligomer increased from 1.7 to 1 at the trinucleotide stage to 3.3 to 1 at the heptanucleotide stage. Most of the shorter chains were synthesized several times and the yield ranges are also indicated in Table 1.

All of the nucleotides produced in this work were obtained after thick layer chromatography of the reaction products. The important by-products include the 3′–3′-linked dimers produced during the initial phosphorylation of compounds **1**. Since these

TABLE 1. Summary of condensation* and detritylation† reactions

Nucleoside mmol (mg)	Nucleotide chain (5-OH unprotected) mmol (mg)	Product mmol (mg)	Yield (%)	Yield range (%)	Product on detritylation No.	Yield (%)
1*a* 0.475 (348)	**1***d* 0.429 (215)	**2***a* 0.372 (530)	87	72–94	**2***b*	76
1*a* 0.48 (352)	**2***b* 0.288 (331)	**3***a* 0.234 (487)	81	70–81	**3***b*	75
1*b* 0.239 (157)	**3***b* 0.119 (215)	**4***a* 0.094 (250)	79	62–88	**4***b*	83
1*b* 0.237 (155)	**4***b* 0.118 (281)	**5***a* 0.077 (247)	65	63–65	**5***b*	88
1*a* 0.237 (174)	**5***b* 0.117 (348)	**6***a* 0.065 (253)	55	50–55	**6***b*	74
1*c* 0.182 (140)	**6***b* 0.0554 (200)	**7***a* 0.027 (125)	50	—	**7***b*	74

*A solution of nucleoside unit **1** in THF (0.75 *M*) was added dropwise to a solution of trichloroethylphosphorodichloridite in THF (0.75 *M*) containing collidine (4 equiv.) at −78°C. The solution was maintained at −78°C for 45 min. The nucleotide unit (5′-OH free component, series *b*) in THF (0.25 *M*) was added to the solution and stirring was continued at −78°C for 1 h. The solution was allowed to warm to room temperature and was kept there for 1 h. At this point the mixture was treated with iodine/water and this and all further steps were as previously described (23, 24).
†Conditions for this step were 80% HOAc at room temperature for 20 h.

TABLE 2. Chromatographic properties* of protected oligoribonucleotides

Compound	R_f	Melting point† (°C)	λ_{max} (95% EtOH) (nm)
2*a*	0.32[a]; 0.71[b]; 0.89[c]; 0.64[d]	129–134	237, 261, 305
2*b*	0.14[a]; 0.55[b]; 0.86[c]; 0.46[d]	138–144	261, 303
3*a*	0.27[a]; 0.75[b]; 0.89[c]; 0.68[d]	145–150	260, 304, shoulder: 238
3*b*	0.17[a]; 0.75[b]; 0.88[c]; 0.57[d]	172–176	260, 304
4*a*	0.33[b]; 0.86[c]; 0.38[d]	137–142	261, 304, shoulder: 238
4*b*	0.17[b]; 0.86[c]; 0.23[d]	162–166	261, 305
5*a*	0.12[b]; 0.88[c]; 0.19[d]	181–186	261, 305, shoulder: 236
5*b*	0.05[b]; 0.82[c]; 0.07[d]	183–188	261, 305
6*a*	0.14[b]; 0.90[c]; 0.18[d]	189–194	261, 305
6*b*	0.05[b]; 0.91[c]; 0.08[d]	199–205	261, 305
7*a*	0.10[b]; 0.87[c]; 0.32[d]	201–206	260, 303, shoulder: 238
7*b*	0.0[b]; 0.81[c]; 0.17[d]	202–207	260, 303

*R_f values are reported for Brinkman Polygram sheets in solvents (*a*) ether, (*b*) ethyl acetate, (*c*) tetrahydrofuran and (*d*) ether/chloroform/methanol (5:4:1).
†Fisher–Johns melting point apparatus, uncorrected.

dimers contain two methoxytrityl groups they nearly always have higher R_f values than the desired reaction product and are easily separated. Problems occasionally arise when the tritylated oligomer $n + 1$ has similar chromatographic mobility to the untritylated starting oligomer n. This problem seems to occur largely when the monomer that is being added does not contain a protecting group on the amino function of the base. For example, the tetranucleotide mmt-A^{Si}_{p}(TCE)C^{BzSi}_{p}(TCE)C^{BzSi}_{p}(TCE)A^{Si}_{Si} (**4***a*) had only slightly different chromatographic properties from the starting trimer C^{BzSi}_{p}(TCE)C^{BzSi}_{p}(TCE)A^{Si}_{Si} (**3***b*). This problem is easily overcome since on treating a mixture of **4***a* and **3***b* with 80% acetic acid, compound **4***a* loses a trityl group to produce **4***b* which has chromatographic properties different from **3***b* (Table 2) and separation is easily obtained in this fashion. The yields reported in Table 1 are from reactions where none of the *b*-oligomers (e.g. **3***b*) remained at the end of the reaction. In any event the similarity of desired product and *b*-series starting material occurred for **2***a*, **4***a*, and **5***a* where purity of product was easily verified by detritylation as described. All of the *a*-series compounds (**2***a*–**7***a*) were detritylated with 80% acetic acid at room temperature for 20 h. Isolated yields are reported in Table 1.

Several of the protected nucleotide products were completely deprotected to the free nucleotides for identification. Thus **2***b*, **3***b*, **4***b*, **5***b*, and **7***b* were treated successively with (*1*) Zn–Cu couple in DMF at 55°C for an average of 5 h; (*2*) half-saturated methanolic ammonia at room temperature for two days, and finally (*3*) tetrabutylammonium fluoride (TBAF) for 30 min (Scheme 2).

The properties of the deprotected oligonucleotides are recorded in Table 3. The di- through pentanucleotides were all completely degraded by phosphodiesterases to give the monomer units in the correct ratios. The heptanucleotide GpCpApApCpCpA was degraded first by ribonuclease A to give GpCp, ApApCp, Cp, and A. The GpCp unit was then degraded by ribonuclease T_1 to give Gp and Cp.

The work described in this manuscript clearly

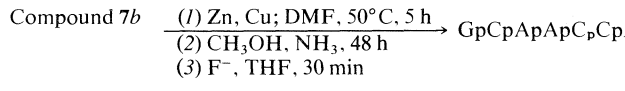

SCHEME 2

demonstrates that the silyl protecting groups combined with the chlorophosphite condensation procedure presents a very effective method for the synthesis of oligoribonucleotides. The protected nucleosides are obtained by rapid and practical synthetic procedures. The chlorophosphite condensation procedure is short ($2\frac{3}{4}$ h). The products are isolated by silica gel chromatography. The synthesis of a heptaribonucleotide by a stepwise procedure clearly demonstrates the facility of the method. We will soon describe the use of these basic procedures along with block condensations in the chemical synthesis of the sequence corresponding to the $tRNA^{fMet}$ from *E. coli*.

Experimental

General Methods

All general procedures including the preparation of all starting materials have been previously described (23, 24). The procedures used for the synthesis of oligonucleotides are as previously described (23, 24) and the ratio of reactants used are summarized in Table 1. The solvents used to isolate the nucleotides **2***a*–**7***a* are listed in Table 4. The procedures used for completely deprotecting the nucleotides **2***a*–**7***a* have also been previously described along with the enzymatic procedures used to characterize the free oligonucleotides (23, 24). Yields (determined spectrophotometrically) for complete deprotection of oligonucleotides are generally in the 30–60% range. The only change in enzymatic procedures was that the products of enzyme degradation were characterized and quantitated on a Spectrophysics Model SP8000 Microprocessor-based HPLC unit. The column used was a Lichrosorb H2-10A (aminobonded phase) column. The solvent consisted of 10% 0.2 *M* $NH_4H_2PO_4$ (pH 3.3) and 90% H_2O. The column was maintained at 30°C with a flow rate of 2 mL/min.

TABLE 3. Properties of free oligonucleotides

Compound	R_f^{A}*	R_f^{F}*	R_m^{Tp}†	$\lambda_{max}(H_2O)$‡ (nm)
CpA	0.23	0.52	0.22	261
CpCpA	0.05	0.37	0.56	261
ApCpCpA	0.01	0.24	0.59	260
ApApCpCpA	0.00	0.20	0.66	258
GpCpApApCpCpA	0.00	0.07	0.67	257

*Descending paper chromatography (Whatman 3MM) values for solvent A, isopropyl alcohol – concentrated ammonium hydroxide – water (7:1:2); solvent F, *n*-propanol – concentrated ammonium hydroxide – water (55:10:35).
†Paper electrophoresis (Whatman 3MM) at pH 7.5 (triethylammonium bicarbonate buffer).
‡Cary 17 recording spectrophotometer.

TABLE 4. Solvents used during isolation of protected oligonucleotides by thick layer chromatography

Product	Solvent sequence (developments)
2*a*	Et_2O (2)
2*b*	Et_2O (1); 1:1 Et_2O–EtOAc (1)
3*a*	Et_2O (2)
3*b*	Et_2O (1); 29:1 $CHCl_3$–MeOH (2)
4*a*	Et_2O (1); 3:1 Et_2O–EtOAc (1)
4*b*	5:4:1 Et_2O–$CHCl_3$–MeOH (1 or 2)
5*a*	5:4:1 Et_2O–$CHCl_3$–MeOH (1)
5*b*	5:4:1 Et_2O–$CHCl_3$–MeOH (2)
6*a*	5:4:1 Et_2O–$CHCl_3$–MeOH (2)
6*b*	5:4:1 Et_2O–$CHCl_3$–MeOH (2)
7*a*	5:4:1 Et_2O–$CHCl_3$–MeOH (2)
7*b*	5:4:1 Et_2O–$CHCl_3$–MeOH (2)

Acknowledgements

We gratefully acknowledge financial support from the Natural Sciences and Engineering Research Council of Canada and from the Quebec Education Ministry. We would also like to acknowledge the valuable technical assistance of Douglas Entwistle in developing HPLC procedures for determining the results of enzyme degradations.

1. A. M. MICHELSON and A. R. TODD. J. Chem. Soc. 2632 (1955).
2. P. T. GILHAM and H. G. KHORANA. J. Am. Chem. Soc. **80**, 6212 (1958).
3. R. L. LETSINGER and K. K. OGILVIE. J. Am. Chem. Soc. **89**, 4801 (1967).
4. F. ECKSTEIN and I. RIZK. Angew. Chem. **79**, 939 (1967).
5. C. B. REESE and R. SAFFHILL. Chem. Commun. 767 (1968).
6. N. KATAGIRI, K. ITAKURA, and S. A. NARANG. J. Am. Chem. Soc. **97**, 7352 (1975).
7. J. V. VAN BOOM and P. M. J. BURGERS. Tetrahedron Lett. 4875 (1976).
8. F. RAMIREZ, E. EVANGELIDOU-TSOLIS, A. JANKOWSKI, and J. R. MARECEK. J. Am. Chem. Soc. **99**, 3144 (1977).
9. R. L. LETSINGER and W. B. LUNSFORD. J. Am. Chem. Soc. **98**, 3655 (1976).
10. C. B. REESE. Phosphorus Sulfur, **1**, 245 (1976).
11. M. SMITH, D. H. RAMMLER, I. H. GOLDBERG, and H. G. KHORANA. J. Am. Chem. Soc. **84**, 430 (1962).
12. A. HOLY and J. SMRT. Collect. Czech. Chem. Commun. **31**, 3800 (1966).
13. J. SMRT and F. SORM. Collect. Czech. Chem. Commun. **32**, 3169 (1967).
14. T. NEILSON and E. S. WERSTIUK. J. Am. Chem. Soc. **96**, 2295 (1974).
15. E. S. WERSTIUK and T. NEILSON. Can. J. Chem. **54**, 2689 (1976).
16. T. E. ENGLAND and T. NEILSON. Can. J. Chem. **54**, 1714 (1976).
17. E. OHTSUKA, K. FUJIYAMA, M. OHASHI, and M. IKEHARA. Chem. Pharm. Bull. **24**, 570 (1976).

18. E. OHTSUKA, S. TANAKA, and M. IKEHARA. Chem. Pharm. Bull. **25**, 949 (1977).
19. E. OHTSUKA, S. NISHIKAWA, R. FUKUMOTO, S. TANAKA, A. F. MARKHAM, M. IKEHARA, and M. SUGIURA. Eur. J. Biochem. **81**, 285 (1977).
20. E. OHTSUKA, S. TANAKA, and M. IKEHARA. J. Am. Chem. Soc. **100**, 8210 (1978).
21. (*a*) J. H. VAN BOOM and P. M. J. BURGERS. Recl. Trav. Chim. Pays-Bas, **97**, 73 (1978); (*b*) J. H. VAN BOOM, P. M. J. BURGERS, R. CREA, G. VAN DER MAREL, and G. WILLE. Nucleic Acids Res. **4**, 747 (1977).
22. R. W. ADAMIAK, E. BIALA, K. GRZESKOWIAK, R. KIERZEK, A. KRASZEWSKI, W. T. MARKIEWICZ, J. OKUPNIAKM, J. STAWINSKI, and M. WIEWIOROWSKI. Nucleic Acids Res. **5**, 1889 (1978).
23. K. K. OGILVIE, A. L. SCHIFMAN, and C. L. PENNEY. Can. J. Chem. **57**, 2230 (1979).
24. K. K. OGILVIE, S. L. BEAUCAGE, A. L. SCHIFMAN, N. Y. THERIAULT, and K. L. SADANA. Can. J. Chem. **56**, 2768 (1978).
25. T. M. JACOB and H. G. KHORANA. J. Am. Chem. Soc. **87**, 368 (1965).

The chemistry of thujone. II.[1] Insect juvenile hormone analogues via acid dianion coupling. The β lactone route

JAMES P. KUTNEY, MICHAEL J. MCGRATH, ROBERT N. YOUNG, AND BRIAN R. WORTH
Department of Chemistry, University of British Columbia, 2075 Wesbrook Place, Vancouver, B.C., Canada V6T 1W5

Received May 25, 1979

JAMES P. KUTNEY, MICHAEL J. MCGRATH, ROBERT N. YOUNG, and BRIAN R. WORTH. Can. J. Chem. **57**, 3145 (1979).

Several stereoselective syntheses of (*E*)-2-ethyl-6-methyl-5-octenoic acid (**17**) are described. The dianion of pure **17** was subsequently coupled with (*E*)-β-thujaketonic acid methyl ester (**5**), derived from thujone (**1**), to give the β-lactones **45** and **46** which were then epoxidized and pyrolyzed exemplifying a route to juvenile hormone analogues such as **51** and **54**.

JAMES P. KUTNEY, MICHAEL J. MCGRATH, ROBERT N. YOUNG et BRIAN R. WORTH. Can. J. Chem. **57**, 3145 (1979).

On décrit plusieurs synthèses stéréosélectives de l'acide (*E*)-éthyl-2 méthyl-6 octène-5 oïque. Le dianion pur de **17** couplé à l'ester méthylique de l'acide (*E*)-β-thujacétonique (**5**) provenant de la thujone (**1**) conduit aux β lactones **45** et **46**. Ces derniers sont alors transformés en époxyde qui, par pyrolyse, permettent d'accéder aux analogues **51** et **54** de l'hormone juvénile.
[Traduit par le journal]

The steam distillate from the slash (waste) of the western red cedar is an excellent source of the monoterpenoid ketone, thujone (**1**) (1, 2). In an effort to further exploit the ready availability and interesting functionality of **1**, its utility in a general route to a series of insect juvenile hormone (JH) analogues was investigated. Permanganate oxidation (2) of thujone[2] had provided α-thujaketonic acid (**2**) which could be ring opened, thermally to give (*E*)-β-thujaketonic acid (**4**), or via base catalysed cleavage of the ester (**3**) to give (*Z*)-β-thujaketonic acid methyl ester (**7**) (1). The gross structural similarities between the synthetic units, **3**, **5**, and **7** and the "right hand" portion of the juvenile hormones **I**, **II**, and **III** (**8**–**10**) pointed to a potential usage of thujone derived intermediates. In fact an earlier report (1) described the coupling of these keto-acids and esters with C8-units, via Wittig olefination, to give analogues such as **11**, **12**, and **13**. This method was, however, limited to the preparation of derivatives with a trisubstituted internal double bond, thus limiting the series of analogues available for biological screening. A further detriment to this route lay in the difficulty experienced in separating the *E*- and *Z*-isomers (at C6) formed during the coupling.

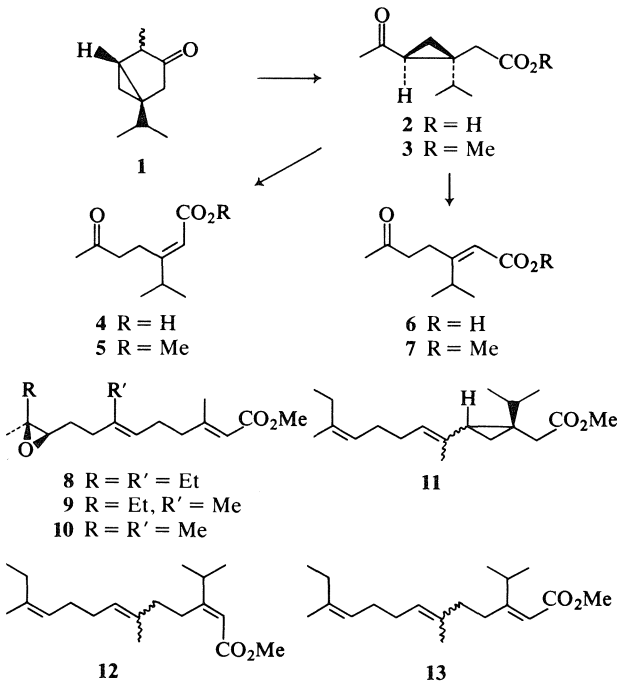

SCHEME 1

Thus, in order to circumvent these difficulties it was necessary to devise an alternative route which, ideally, would fulfill four important requirements: (*i*) the ability to generate tri- and tetrasubstituted internal unsaturations, (*ii*) a mode of coupling that would allow at least selective *trans*-isomer formation, (*iii*) facile separation of the isomeric alkenes, (*iv*) specific protection of the internal double bond so as to allow specific epoxidation at C10(11). Of the various methods available (3–10), that involving coupling between a carboxylic acid dianion and a ketone to give a β-hydroxy acid, generation of di-

[1]For Part I, see ref. 1.

[2]Although thujone exists in two epimeric forms at C4, oxidative cleavage to **2** destroys this chiral centre thus allowing crude thujone to be used for this work.

0008-4042/79/233145-10$01.00/0

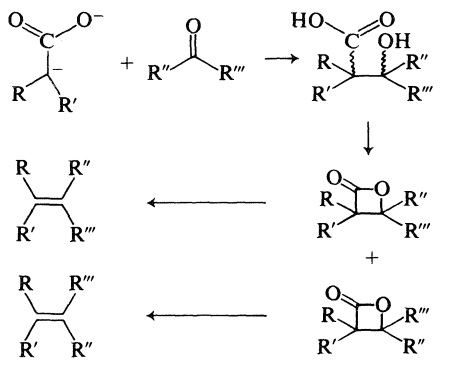

SCHEME 2

astereomeric β-lactones, and subsequent thermal elimination of carbon dioxide (Scheme 2) seemed the most suitable (4, 11, 12).

To determine the suitability of the thujone-derived ketoesters for the proposed route, the dianion from cyclohexane carboxylic acid was reacted with (*E*)-β-thujaketonic acid methyl ester (**5**). The required adduct **14** was formed in 60% yield. Subsequent reaction with benzenesulphonyl chloride in pyridine provided the β-lactone **15** as evidenced by characteristic infrared absorption at 1810 cm^{-1}. Pyrolysis of **15** at 140°C gave a 68% yield of the expected tetrasubstituted alkene **16**.

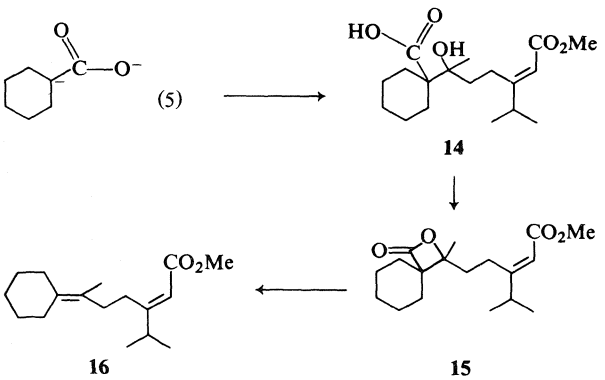

SCHEME 3

With the success of the model sequence, the preparation of prerequisite acid units representing the "left hand" portion of juvenile hormones **8**–**10** was necessary. Initially, the more troublesome targets **17** and **18**, related to the C18 cecropia juvenile hormones (**8** and **9**), were chosen since successful application of the proposed scheme with these units would effectively guarantee a route to the analogue related to **10**.

An efficient synthesis of a mixture of the *E*- and *Z*-octenoic acids **17** and **18** was available, based on the known cyclopropylcarbinol–homoallyl rearrangement (13–16), as shown in Scheme 4. Grignard reaction on methyl cyclopropyl ketone afforded the known carbinol **19** (13) which on reaction with magnesium bromide (17, 18) in ether gave a mixture of the *E*- and *Z*-homoallylic bromides **20**. Initially this mixture was used to alkylate (19) the α-anion of methylbutanoate giving only a low yield of the esters **21** admixed with the Claisen product (20), methyl-2-ethyl-3-oxohexanoate. Similar alkylation of the anion **22**, of the oxazoline (21, 22) formed by reaction between butanoic acid and 2-amino-2-methyl-1-propanol, gave only a 44% yield of the adducts **23**. Direct, acid catalysed hydrolysis of **23** was not successful; however, methylation using iodomethane and subsequent aqueous base catalysed hydrolysis gave the esters **24**. Reaction of **24** in aqueous ethanolic sodium hydroxide solution at 50°C did provide a route, albeit inefficient, to the required acids. Reaction of the dianion of butanoic acid (23) with the bromides **20** in a mixture of tetrahydrofuran (THF) and hexamethylphosphortriamide (HMPA) provided the *E*- and *Z*-acids **17** and **18** directly. Best results were obtained by analogous alkylation with the relatively unstable iodides **25**, formed by reaction of the mixture **20** with sodium iodide in acetone or more efficiently by ring opening of **19** with magnesium iodide in ether (17, 18). In this manner an 80% yield (from **19**) of the acids **17** and **18** was obtained. Separation of the isomeric acids **17** and **18** was not possible by glc or by tlc methods. Accurate determination of the ratio of these products was however possible from areas of the resonances due to C5 in the ^{13}Cmr spectrum (24). In this manner, the composition was determined as 80% *E*- (**17**), 20% *Z*- (**18**).

Although this route provided a fast and efficient means of obtaining the octenoic acids for developing the efficiency of subsequent reactions, in order to ensure the integrity of juvenile hormone analogues for biological screening a stereospecific route to **17** or **18** was necessary.

Initially, the synthesis outlined in Scheme 5 was investigated. Horner reaction between 2-butanone and the sodium salt of trimethylphosphonoacetate afforded *E*- and *Z*-methyl-3-methyl-2-pentenoates which were separated by spinning band distillation as described earlier (1, 25). The major, *E*-isomer was elaborated by standard means to the pure *E*-allylic chloride **26** (1). Alkylation of ethyl-3-oxopentanoate (26) with **26** in 1,2-dimethoxyethane (DME) gave pure *E*-β-ketoester **27**. For each intermediate in this route (Scheme 5) the respective *E*- and *Z*-isomers were not separable by either tlc or conventional glc systems. Therefore *E*-, *Z*- mixtures of the intermediates up to and including **27** were initially prepared as described above from a mixture (ca. 2:1) of *E*- and *Z*-methyl-3-methyl-2-pentenoates. In each case the differences in chemical shift for the vinylic methyl signals in 270 MHz ^{1}Hmr proved satisfactory

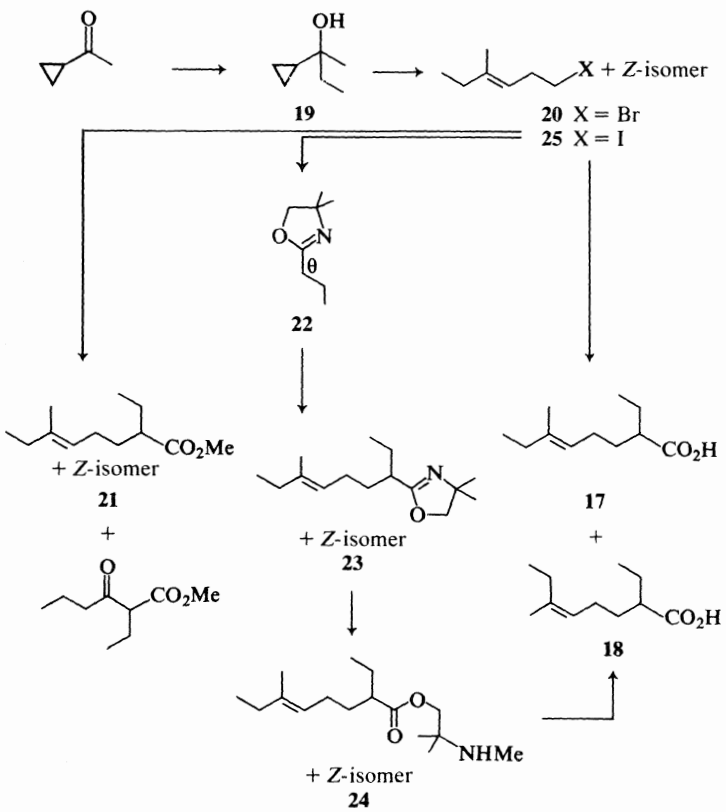

SCHEME 4

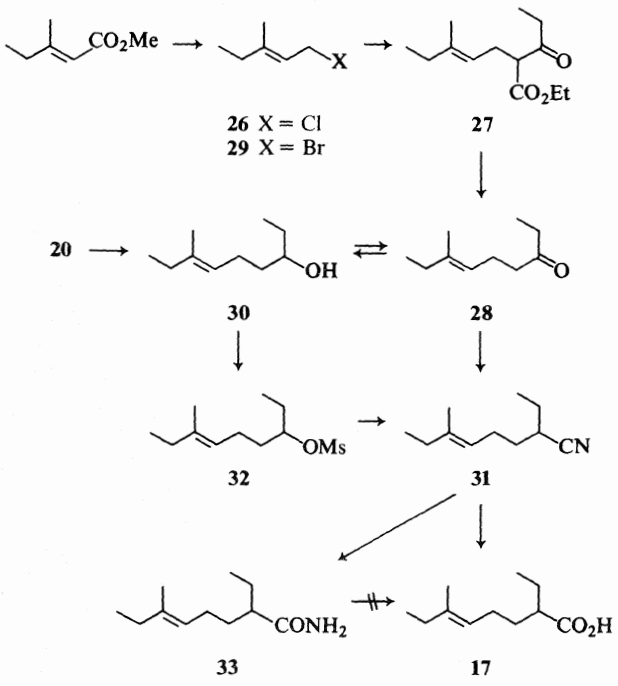

SCHEME 5

for the determination of isomer ratios. These chemical shift values were then used to determine the integrity of subsequent purity of compounds within the *E* series. Examination of **27** (derived from pure *E*-methyl-3-methyl-2-pentenoate) by 270 MHz ^{1}Hmr spectroscopy did not show detectable *Z*-isomer (1). An *E*-, *Z*- mixture of the ketone **28** was prepared from a mixture of isomeric bromides **20** via reaction of the derived Grignard reagent with propanal and oxidation of the alcohol **30** with pyridinium chlorochromate. The ^{1}Hmr spectrum of this mixture of ketones was used to determine the isomeric purity of subsequent batches of the ketone **28**, and to optimize conditions for further transformations. Optimum conditions for the conversion of pure **27** to pure *E*-γ,δ-unsaturated ketone **28** were attained using barium hydroxide in aqueous ethanol under reflux. Thus a 75% yield of **28**, of >98% isomeric purity, was obtained (1). Homologation of **28** was accomplished via the nitrile **31** for which two routes were investigated. Firstly reduction of **28** (>98% *E*) with sodium borohydride in methanol gave **30** which was readily converted to the mesylate **32**. Reaction of the latter with sodium cyanide in HMPA gave a 60%

overall yield of **31** contaminated with ca. 9% *Z*-isomer as determined from the 270 MHz ^{1}Hmr spectrum. The obvious isomerization of *E* to *Z* in the sequence **28** → **30** → **32** → **31** dictated an alternative method of preparation of **31**. Success was achieved when **28** (>98% *E*) was reacted with potassium hydride and tosylmethylisocyanide (TOSMIC) (27–29) in DME. The nitrile **31** of ca 98% isomeric purity was isolated in 75% yield. Analogous reaction using potassium *tert*-butoxide in *tert*-butanol and DME gave nitrile of 95% isomeric purity. Hydrolysis of **31** (98% *E*) required heating to 180°C in a sealed tube with potassium hydroxide in aqueous methanol, and under these conditions acid **17** of ca. 87% isomeric purity (determined as above using ^{13}Cmr spectroscopy) was obtained in 74% yield. Treatment of **31** with powdered potassium hydroxide in refluxing dry *tert*-butanol (30) gave a 62% yield of the crystalline primary amide **33** (ca. 93% *E*, 7% *Z*). Although recrystallization of **33** may have improved the isomeric purity, attempts to convert **33** to the acid **17** under mild conditions (aqueous sodium peroxide (31)) were unsuccessful. Thus although this route (Scheme 5) provided the required acid **17**, the subsequent conversion of a substrate of ca. 93% isomeric purity to juvenile hormone analogues was considered unsatisfactory.

An alternative route to the *E*-acid **17** is outlined in Scheme 6. In this regard, pure *E*-allylic chloride (1) **26** was reacted with phenylthiomethylcopper (32–35) in THF to give a mixture of the thioether **34** (75% by glc) and thioanisole **35** (20% by glc). This mixture was generally used as such for subsequent conversions. An analytical sample of **34** (94% *E* by 270 MHz ^{1}Hmr) was obtained by preparative glc. Another sample obtained by fractional distillation of the mixture, however, was similarly shown to be 98% *E*-isomer. Reaction of the mixture of **34** and **35** with iodomethane and sodium iodide in dimethylformamide (DMF) in the presence of metallic mercury and calcium carbonate (35) at 70°C gave, after dilution with ether, the precipitated salts **36** and **37** together with an ethereal solution of the unstable iodide **25**, thioanisole **35**, and the thioether **34** in the ratio 38:50:12 (as determined by glc). Separation of the iodide from the above mixture either by distillation or by preparative glc was not possible. Therefore the mixture was treated, as such, with the dianion from *n*-butanoic acid in THF and HMPA to give the acid **17** and a mixture of **34** and **35**. The separated neutral fraction was combined with the salts from the previous reaction and the cycle repeated. The ^{13}Cmr spectrum of **17** obtained via this route indicated 95% *E*-, 5% *Z*-isomer (24).

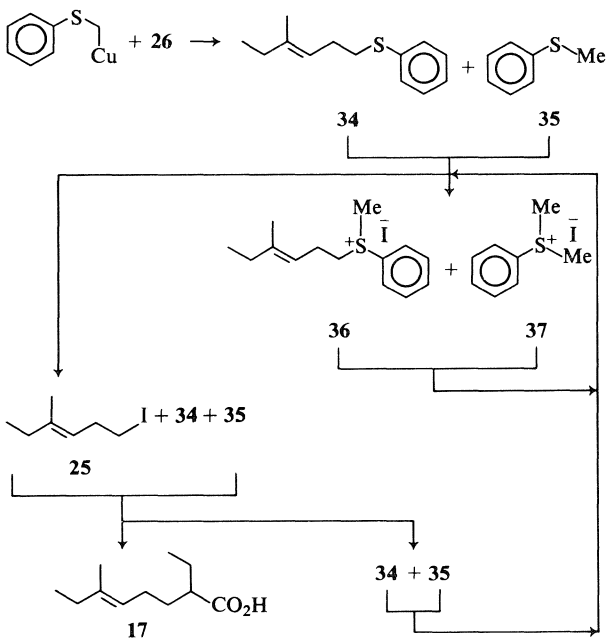

SCHEME 6

Although this synthesis had allowed generation of the acid **17** with high stereoselectivity, it was decided that for the purposes of biological screening of subsequently derived JH analogues, a higher isomer integrity was desirable. Therefore various methods of purification of **17** were investigated. A derivative of the acid was sought such that purification would enable separation of pure *E*-isomer and such that efficient regeneration of acid could be accomplished without concomitant alkene isomerisation. The crystalline amide **33** was also available via the acid chloride **38** but, as mentioned above, regeneration of **17** under mild conditions was not possible. The methyl ester was a liquid, as expected, and separation of the *E*- and *Z*-isomers using glc or conventional chromatographic methods (including silver nitrate impregnated silica gel (36)) was not accomplished. Imidizolides were reported (37) to generally exhibit good crystalline properties; however, the derivative **39** derived from **17** was a liquid. Both the ammonium and dimethylammonium salts were crystalline but relatively unstable, each liberating the acid **17** and the respective amine on standing. The crystalline diisopropylammonium salt was stable but recrystallization even from *n*-hexane at −78°C was quite inefficient. The derivative of choice proved to be the dicyclohexylammonium salt **40**, which could be readily formed and which quantitatively liberated the acid **17** on treatment with cold, dilute hydrochloric acid in methanol solution without

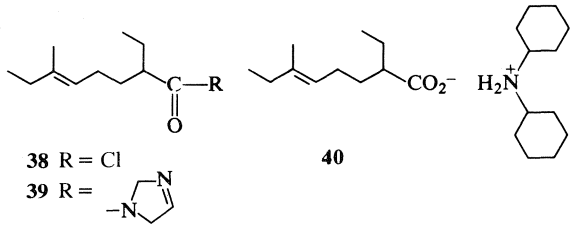

38 R = Cl
39 R =

40

observable *E*-/*Z*- isomerisation. This salt was obtained in stable crystalline form and could be recrystallised from ethyl acetate, 2-butanone, or, more efficiently, from acetone.

A sample of **17** (95% *E*, 5% *Z*) prepared via the route depicted in Scheme 6 was converted to the salt **40** and this derivative recrystallized four times from acetone to give a sample of mp 81.5–82°C. Regeneration of the acid **17** (48% recovery overall) gave a sample of 98% isomeric purity (as determined by ^{13}Cmr). A sample of acid **17** (80% *E*, 20% *Z*), derived as indicated in Scheme 4, was purified as described above, with seven recrystallizations of the intermediate salt, to give a sample of 95% *E* purity. Severe losses of material in this procedure precluded the use of this latter route to the *E*-acid **17**.

Of the methods examined, that involving the thioether **34** seemed to offer the best route to large quantities of **17** of suitable isomeric purity. Now with the chemistry to pure *E*-acid **17** in hand, its application to the corresponding *Z*-isomer **18** and to the acids **41** and **42**, related to the hormones **8**, **9** and **10**, is assured.

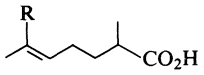

41 R = Et
42 R = Me

Prior to attempting the coupling reaction, several experiments were carried out to determine optimum conditions for formation of the acid dianion. Two bases were examined, lithium diisopropylamide (LDA) and lithium 2,2,6,6-tetramethylpiperidide (LTMP) (38). The extent of α-anion formation was determined by quenching with D_2O and measuring the decrease in area related to the α-H resonance at δ 2.31 in the 270 MHz ^{1}Hmr spectrum of **17**. ^{13}Cmr spectroscopy was used to evaluate any concomitant *E*-/*Z*- isomerisation. In this manner optimum conditions were found (up to 79% dianion formation without detectable stereoisomerisation) using LDA in THF at 50°C for four hours, followed by quenching at 0°C. These conditions were subsequently used for the coupling reaction.

In the event, coupling of pure *E*-acid **17** with the more readily available (*E*)-β-thujaketonic acid methyl ester (**5**) gave a mixture of diastereomeric β-hydroxyacids **43** which was characterized as the methyl esters

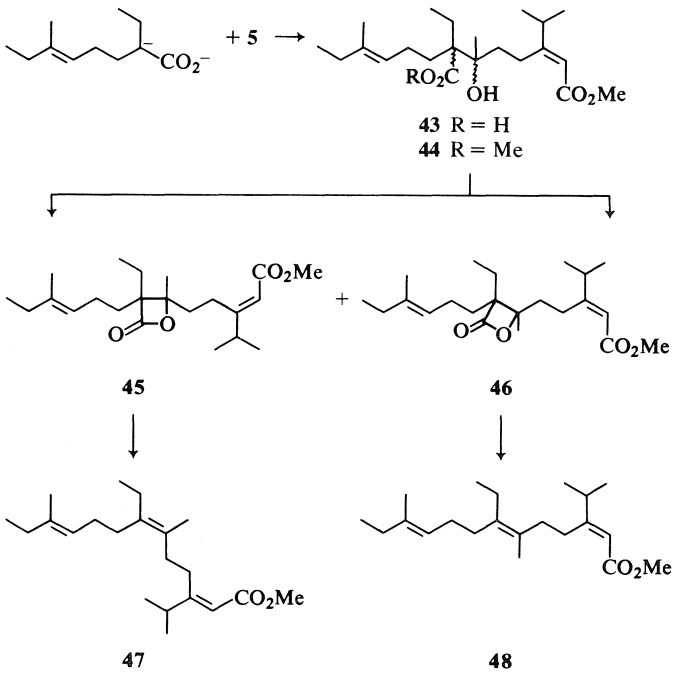

43 R = H
44 R = Me

45 **46**

47 **48**

SCHEME 7

44 obtained by reaction with diazomethane in ether at 0°C. Alternatively reaction of the crude hydroxy-acids with benzenesulphonyl chloride at 0°C in pyridine gave a mixture of the two diastereomeric β-lactones **45** and **46** in the ratio 45:55 (i.e., ratio of the corresponding trienes **47** and **48** formed by pyrolytic cleavage during glc examination). Chromatographic separation on silica gel afforded the individual isomeric lactones. Subsequent pyrolysis of **45** in refluxing methylcellusolve gave the less polar triene-ester **47**. Similarly **46** was efficiently converted to **48**. The coupling reaction was then repeated on a mixture of *E*- and *Z*-acids **17** and **18** (ratio 80:20) and the product converted to a mixture of the isomeric β-lactones. Analysis of this four component mixture both by tlc and glc showed only two components (viz. **45** and **46**) thus confirming the necessity for pure *E*- (or *Z*-) acid as substrate.

Although a variety of methods have appeared for the selective epoxidation (39–47) of trisubstituted alkenes near the terminus of a polyene chain, here the extra activity of an internal tetrasubstituted double bond was expected to preclude any such selection. These suspicions were justified as shown by a trial epoxidation of the triene-ester **47**. Reaction of **47** with one equivalent of *meta*-chloroperbenzoic acid (*m*CPBA) at 0°C gave a mixture of **47**, the bis-epoxide **49**, and a mixture (70:30) of the mono-epoxides **50** and **51**.

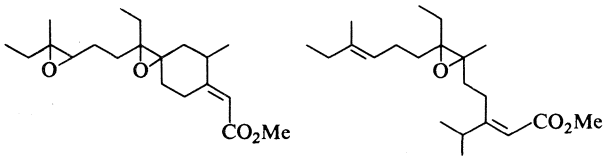

49

50

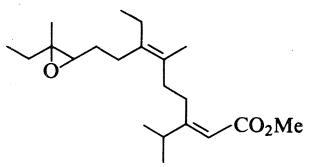

51

The dividends from the choice of the acid dianion coupling mode were now apparent as similar epoxidation of the separated β-lactones **45** and **46** gave a high yield of epoxy-lactones **52** and **53** respectively. Pyrolysis of **52** in refluxing methylcellusolve gave **51**. Similarly **53** gave the juvenile hormone analogue **54** in high yield.

Experimental

Uncorrected melting points were determined on a Reichert micro hot stage. Boiling points are uncorrected. Infrared spectra were recorded on either a Perkin–Elmer 710 or 457 spectrophotometer. ^{1}Hmr spectra were recorded on a Varian T-60, HA-100, or XL-100, or a 270-MHz spectrometer in $CDCl_3$ solution, with tetramethylsilane as internal standard. Isomer ratios were determined by weighing respective peaks of an expanded spectrum run at 270 MHz. Mass spectra were recorded on an Atlas CH-4B or AEI MS-902 instrument. Microanalyses were carried out by Mr. P. Borda, Microanalytical Laboratory, University of British Columbia. ^{13}Cmr spectra were measured on a Varian CFT-20 instrument. Analytical glc separations were carried out on a Hewlett Packard 5830A gas chromatograph. Preparative glc separations utilized a Varian model 90-P gas chromatograph. Column chromatography utilized Merck silica gel 60 (70–230 mesh) or Merck aluminum oxide 90 (neutral). Preparative and thin layer chromatography utilized Merck silica gel GF_{254}.

As a matter of routine, all reagents and solvents were recrystallized or distilled prior to use.

The Hydroxyacid ***14***

A solution of cyclohexane carboxylic acid (93 mg) in dry tetrahydrofuran (5 mL) was added at −78°C to a solution of lithium diisopropylamide (2 equiv.) in dry tetrahydrofuran (2 mL) and the mixture warmed to 50°C for 1.5 h under an atmosphere of dry nitrogen. The solution was cooled to ca. 20°C and then added slowly to a solution of (*E*)-β-thujaketonic acid methyl ester (**5**) (150 mg) in dry tetrahydrofuran at −78°C. The solution was stirred at this temperature for 30 min, warmed to ca. 20°C and neutralized with methanolic hydrochloric acid. The mixture was diluted with water and extracted with dichloromethane. The extract was washed with 5% sodium bicarbonate solution, the washings acidified and extracted with dichloromethane. This extract was dried ($MgSO_4$) and evaporated to give the hydroxy acid **14** (150 mg, 64%) as a colourless oil; ir ν_{max}: 3350, 3300–2400, 1700, 1640; ^{1}H nmr δ: 8.3 (2H, broad envelope, D_2O exchangeable, —CO_2H and —OH), 5.66 (1H, s, —C=C$H$$CO_2CH_3$), 3.70 (3H, s, —$CO_2CH_3$), 1.25 (3H, s, —C(OH)C$H_3$), 1.10 (6H, d, J = 7 Hz, —CH(CH_3)$_2$); ms *m/e*: 311 (M^+ − CH_3), 283, 199, 167, 139.

The β*-Lactone* ***15***

Benzenesulphonyl chloride (200 mg) was added to a solution of the hydroxyacid **14** (110 mg) in dry pyridine (5 mL) at −5°C. The mixture was allowed to stand at ca. 0°C overnight, poured into ice-water and extracted with ether. The extract was washed with 5% sodium bicarbonate solution, dried ($MgSO_4$), and evaporated. Chromatography of the residue on silica gel gave the β-lactone **15** (65 mg, 65%) as a colourless oil; ir ν_{max}: 1810, 1710, 1650; ^{1}H nmr δ: 5.70 (1H, s, —C=C$H$$CO_2CH_3$), 3.70 (3H, s, —$CO_2CH_3$), 1.78 (3H, s, —C(OR)C$H_3$), 1.10 (6H, d, J = 7 Hz, —CH(CH_3)$_2$); ms *m/e*: 264 (M^+ −CO_2), 233, 221, 142.

The Ester ***16***

The β-lactone **15** (60 mg) was heated to 140°C for 1.5 h in a nitrogen atmosphere. Chromatography on silica gel gave the olefin **16** (35 mg, 68%) as a colourless oil; ir ν_{max}: 1710, 1640; ^{1}H nmr δ: 5.70 (1H, s, —C=C$H$$CO_2CH_3$), 3.70 (3H, s, —O$CH_3$), 1.75 (3H, s, —$CH_3$), 1.10 (6H, d, J = 7 Hz, —CH-(CH_3)$_2$); ms *m/e*: 264 (M^+), 233, 221, 142, 123.

The Alcohol ***19***

Ethyl bromide (26 g) in dry ether (25 mL) was added to magnesium turnings (7.51 g) in dry ether (75 mL) under dry nitrogen, and the mixture refluxed for 1.5 h. The solution was cooled to ca. 0°C and cyclopropyl methyl ketone (17 g) added during 30 min. The mixture was stirred at ambient temperature for 16 h, diluted with cold, saturated ammonium chloride solution, and extracted with ether. The extract was washed with brine, dried (K_2CO_3), and concentrated at atmospheric pressure. The crude product was distilled between 43 and 67°C at 60 Torr to give pure (glc, 7% Carbowax 1500 on 90–100 mesh Anakrom ABS) carbinol **19** (18.34 g, 80%); ir (film) ν_{max}:

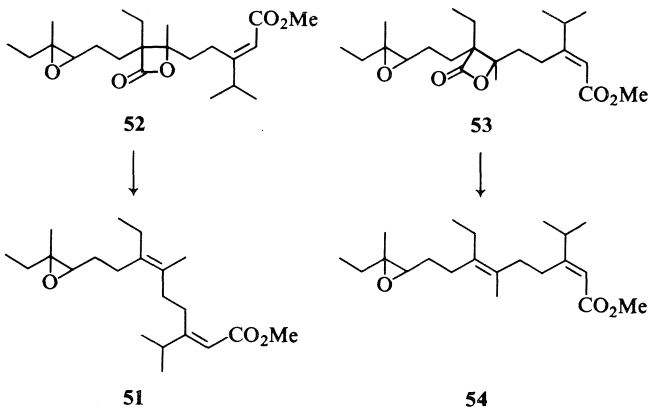

SCHEME 8

3400, 3080; ^{1}Hmr δ: 1.57 (2H, q, J = 7.4 Hz, —CH_2CH$_3$), 1.09 (3H, s, —CH$_3$), 0.98 (3H, t, J = 7.4 Hz, —CH$_2$CH_3), 0.35 (m, cyclopropyl —H); ms m/e: 99 (M − 15), 85.

(E)- *and* (Z)-*6-Bromo-3-methyl-3-hexene (**20**)*

A solution of 1,2-dibromoethane (18.2 mL) in dry ether was added slowly, at 0°C, to magnesium turnings (5.63 g) in ether (100 mL). After complete addition (1.5 h) the mixture was heated to reflux for 1 h, then stirred at ambient temperature for 16 h. A solution of the alcohol **19** (6.16 g) in dry ether (25 mL) was added and the mixture refluxed for 1.5 h, then stirred at ambient temperature for 6 h. The mixture was cooled and carefully washed with brine. The ethereal layer was dried (Na_2SO_4) and evaporated to give an oil (9.46, g, 98%) which appeared homogeneous by tlc and by glc. This product was distilled at 75°C, 10 Torr to give *E*- and *Z* homoallylic bromides **20**; ir ν_{max}: 2970, 2930, 2880, 1670, 1460, 1380, 1275; ^{1}Hmr ($CDCl_3$) δ: 5.16 (1H, complex multiplet, C4-H), 3.36 (2H, t, J = 7 Hz, —CH_2Br), 2.58 (2H, q, J = 7 Hz, C5-H2), 2.04 (2H, q, J = 7 Hz, C2-H2), 1.64 (3H, bs, C3-CH$_3$), 1.00 (3H, t, J = 7 Hz, —CH$_2$CH_3). An *E*/*Z* ratio of 3:1 was determined from the areas under the vinylic methyl signals for the *E*- (δ 1.64) and *Z*- (δ 1.72) isomers.

*The Esters **21***

n-Butyllithium (0.6 mL of a 2.83 M solution in pentane) was added to a solution of diisopropylamine (0.17 g, 0.24 mL) in dry THF (1.7 mL) at 4°C. The solution was stirred at this temperature for 15 min and then cooled to −78°C. Methyl butanoate (0.173 g) was added and the mixture stirred for 40 min at −78°C. A solution of the bromides **20** (0.36 g) in HMPA (0.15 mL) was added and the mixture stirred at −78°C for 30 min, then at ambient temperature for 1.5 h, poured onto ice cold 1 M HCl and extracted with ether. The ethereal extract was dried (Na_2SO_4) and evaporated. Chromatography on alumina gave the esters **21** (0.08 g, 20%); ir ν_{max}: 1720; ^{1}Hmr ($CDCl_3$) δ: 5.10 (1H, bm, C5-H), 3.72 (3H, s, —OCH$_3$).

*The Oxazolines **23***

n-Butyllithium (0.48 mL of 2.7 M solution in *n*-pentane) was added slowly to a solution of the propyloxazoline **22** (172 mg) in dry THF at −78°C. The yellow solution was stirred at this temperature under a nitrogen atmosphere for 30 min and then treated with the bromides **20** (255 mg). The mixture was kept at −78°C for 30 min and then allowed to attain ambient temperature. The mixture was partitioned between brine and ether, the ethereal layer dried (Na_2SO_4), and evaporated. The residue was distilled at 70°C, 0.1 Torr to give the oxazolines **23** (322 mg, 94%); ^{1}Hmr ($CDCl_3$) δ: 5.17 (1H, bm, vinylic —H), 3.94 (2H, bs, —O—CH$_2$—), 1.64 (3H, bs, vinylic —CH$_3$), 1.33 (6H, bs, >C(CH$_3$)$_2$), 1.03 (3H, t, J = 7 Hz, —CH$_2$CH_3), 0.97 (3H, t, J = 7 Hz, —CH$_2$CH_3), plus small signals attributable to the *Z*-isomer; ms m/e: 237 (M$^+$), 222, 181, 154, 142, 126.

*The Aminoester **24***

A mixture of the oxazolines **23** (70 mg) and iodomethane (1 mL) was allowed to stand at ambient temperature for 20 h, the solvent was removed *in vacuo*, and the residue triturated with ether to afford the methiodide salt. This solid was dissolved in 1 M NaOH (5 mL) and the solution stirred at ambient temperature for 20 h. The mixture was diluted with water and extracted with petroleum ether. The organic layer was dried and concentrated to give **24** (60 mg); ir ν_{max}: 3300, 1725; ^{1}Hmr ($CDCl_3$) δ: 5.00 (1H, bm, vinylic —H), 3.82 (2H, s, —OCH$_2$—), 2.31 (3H, s, —NCH$_3$), 1.51 (3H, bs, vinylic —CH$_3$), 1.08 (6H, s, —C(CH$_3$)$_2$).

*The Acids **17** and **18***

*From **24***

The ester **24** was heated to 50°C for 17 h in a mixture of 6 M NaOH and ethanol. The mixture was acidified with 1 M HCl and extracted with ether to give (48%) the acids **17** and **18** (see below).

*From **20***

n-Butyllithium (2.0 mL of 2.82 M solution in pentane) was added to a cold (−15°C) solution of diisopropylamine (0.8 mL, 0.58 g) in dry THF (4.5 mL) and the mixture stirred for 15 min. Dry *n*-butyric acid (0.25 mL, 0.24 g) was added and the mixture stirred at ca. 0°C for 20 min. The *E*/*Z*-bromides **20** (0.5 g) in dry HMPA (1 mL) were added and the solution stirred at 0°C for 10 min, then at ambient temperature for 30 min. The mixture was carefully acidified and partitioned between ether and brine. The ether extracts were washed with brine (×2), dried and concentrated. Distillation of the residue (115°C, 0.3 Torr) gave the acids **17** and **18** (0.25 g, 48%), (see below).

*The Iodides **25***

*From **20***

The bromides **20** (0.366 g) and dry sodium iodide (0.150 g) in dry acetone (1 mL) were heated to reflux in the presence of $CaCO_3$ and mercury (35). After 30 min the mixture was cooled, filtered, and concentrated *in vacuo*. Distillation of the residue at 30°C/0.1 Torr gave the iodides **25** (0.254 g, 55%).

*From **19** (17, 18)*

The carbinol **19** (11.8 g) in dry ether (200 mL) was added slowly to a solution of magnesium iodide (4 equiv.) in dry ether and the mixture refluxed for 5 h under a nitrogen atmosphere. After a further 16 h at ambient temperature, the reaction was carefully quenched with cold water and then extracted

with petroleum ether (30–60°C). The organic extract was washed with brine. dried (Na_2SO_4), and concentrated *in vacuo* to give the *E*-/*Z*-iodides **25** (23 g, 100%) homogeneous by glc (5% OV 17), bp 40°C/0.1 Torr; ^{1}Hmr ($CDCl_3$) δ: 0.97 (3H, t, J = 7.5 Hz, —CH_2CH_3 *Z*-isomer), 0.99 (3H, t, J = 7.5 Hz, —CH_2CH_3 *E*-isomer), 1.60 (3H, s, —CH_3 *E*-isomer), 1.68 (3H, d, J = 1.1 Hz, —CH_3 *Z*-isomer), 2.0 (2H, m, —CH_2CH_3), 2.57 (2H, m, —CH_2CH_2I), 3.09 (2H, m, —CH_2I), 5.08 (1H, m, vinylic —H). Ratio by ^{1}Hmr (methyl group resonances) *E*/*Z* ca. 3:1.

*The Acids **17** and **18** from **25***

A solution of *n*-butyllithium in hexane (75.2 mL of 1.72 *M*) was added to a mixture of anhydrous diisopropylamine (11.9 g) and dry THF (96 mL) at −78°C under a nitrogen atmosphere. The mixture was stirred at −78°C for 30 min and then warmed to −23°C. At this temperature, *n*-butyric acid (4.71 g) was added and the mixture stirred for 30 min. The temperature was raised to 0°C and dry HMPA (10.5 g) added. After 40 min, the iodides **25** (6.1 g) were added and the solution stirred for 20 h at ambient temperature. The mixture was acidified with cold 1 *N* HCl and extracted with petroleum ether (30–60°C). The organic layer was then extracted with ice cold 1 *N* NaOH, the alkaline layer neutralised with 1 *N* HCl, and extracted with petroleum ether. This organic extract was washed with brine, dried (Na_2SO_4), and concentrated *in vacuo*. Distillation of the residue at 90°C/0.1 Torr gave the isomeric acids **17** and **18** (3.88 g, 79%), homogeneous by glc (5% OV 17); ir ν_{max}: 3400–2400, 1705; ^{1}Hmr ($CDCl_3$) δ: 5.09 (1H, m, C5-H), 2.31 (1H, m, C2-H), 2.00 (4H, m, C7-H2 and C4-H2), 1.60 (4H, m, C3-H2 and C2-CH_2CH_3), 1.66 (3H, s, vinylic —CH_3, *Z*-isomer), 1.58 (3H, s, vinylic —CH_3, *E*-isomer), *E*/*Z* ratio by vinylic —CH_3 signals ca. 3:1; ^{13}Cmr (^{1}H, noise decoupled) ($CDCl_3$) δ: 182.9 (C1), 138.1 (C6, *Z*-isomer), 137.9 (C6, *E*-isomer), 123.3 (C5, *Z*-isomer), 122.0 (C5, *E*-isomer), *E*/*Z* ratio by C5 signal = 4:1; ms *m*/*e*: 184.1454 (M^+, $C_{11}H_{20}O_2$ requires 184.1463), 183, 166, 155, 138, 109. *Anal.* calcd. for $C_{11}H_{20}O_2$: C 71.70, H 10.94; found: C 71.92, H 10.86. NB the discrepancy in the ratios derived by ^{13}C and ^{1}Hmr was apparently due to overlap of the vinylic —CH_3 signals with a broad multiplet. The ratio derived from the ^{13}Cmr spectrum utilised signals with clean, baseline separation.

*The Alcohol **30***

The bromides **20** (3.19 g) and magnesium turnings (0.46 g) were allowed to stir in dry ether (2 mL) for 5 h. Propanal (0.966 g) was added and the stirring continued for 12 h at ambient temperature. The mixture was carefully quenched with water, dried (Na_2SO_4), and concentrated *in vacuo* to give **30** (2.16 g, 83%), identical (by glc) with an authentic sample (1).

*The Ketone **28** from **30***

Oxidation of **30** according to the literature (48) procedure gave the ketone **28** (71%) identical with an authentic sample (1).

*The Mesylate **32***

The alcohol **30** (200 mg) and methanesulphonyl chloride (900 mg) were stirred in dry pyridine (2 mL) at 0°C for 18 h. The mixture was poured into ice-water and extracted with dichloromethane. The extract was washed with brine, dried ($MgSO_4$), and evaporated to give the crude mesylate **32** (450 mg); ir ν_{max}: 1350, 1170; which was used without further purification.

*The Nitrile **31***

*From **32***

The crude mesylate **32** (450 mg) and sodium cyanide (300 mg) were stirred in dry hexamethylphosphortriamide (1 mL) under a nitrogen atmosphere for 15 h. The mixture was diluted with water and extracted with ether. The extract was washed with 1 *N* hydrochloric acid, water and brine, dried ($MgSO_4$), and evaporated. Chromatography on silica gel afforded the nitrile **31** (210 mg, 60% from **30**); ir (film) ν_{max}: 2230, 1668; ms *m*/*e*: 165 (M^+), 150, 137, 122. High resolution molecular weight determination calcd. for $C_{11}H_{19}N$: 165.1517; found: 165.1525. *Anal.* calcd. for $C_{11}H_{19}N$: C 79.94, H 11.59; found: C 80.20, H 11.52.

*From **28***

TOSMIC (29) (0.377 g) in dry DME (4 mL) was added to potassium hydride/mineral oil suspension (0.39 g, 4.99 mmol KH/g of suspension) in dry DME (4 mL) at −46°C under a nitrogen atmosphere. The mixture was stirred at this temperature for 10 min, then at 0°C for 10 min to give a bright yellow solution. Pure *E*-enone **28** (1) (0.175 g) in DME (4 mL) was added at 0°C and the solution stirred for 45 min. Anhydrous methanol (0.079 mL) was added and stirring continued for 1 h (0–5°C). The solution was then allowed to attain ambient temperature and methanol (0.21 mL) added. Stirring was continued for a further 88 h. The mixture was then diluted with water and extracted with *n*-pentane. The extract was washed with brine, dried (Na_2SO_4), and the solvents removed *in vacuo*. Chromatography of the residue on silica gel gave the *E*-cyanide **31** (0.14 g, 75%); bp 67–73°C/0.1 Torr; ^{1}Hmr ($CDCl_3$) δ: 5.08 (1H, t, J = 7.6 Hz, vinylic —H) 2.48 (1H, m, —CHCN i.e., C2-H), 1.63 (3H, s, vinylic —CH_3): ^{13}Cmr ($CDCl_3$) δ: 139.2 (C6), 122.25 (C1), 120.8 (C5). The *E*/*Z* ratio was 98:2 from signals due to the vinylic methyl groups in the 270 MHz ^{1}Hmr spectrum and by signals due to C5 in the ^{13}Cmr spectrum as before. A sample of **31** prepared similarly from the ketones (*E*/*Z* ratio 19:6) was likewise shown to contain the *E*- and *Z*-isomers in the ratio ca. 19:6 indicating no observable double bond isomerisation during this step.

*The Acids **17** and **18** from **31***

A sample of the nitrile **31** (0.054 g, 98% *E*-) and potassium hydroxide (0.09 g) in methanol (1 mL) and water (0.3 mL) were heated at 180°C (sealed tube) for 48 h. Usual work-up gave the acids **17** and **18** (0.042 g, 74%) in the ratio 87:13 determined as above by ^{13}Cmr spectroscopy.

*The Amide **33***

The nitrile **31** (98% *E*-, 0.05 g) and powdered, dry potassium hydroxide (0.06 g) were heated in refluxing, dry *tert*-butanol (0.5 mL) for 10 h. The usual work-up procedure gave the amide **33** (0.034 g, 62%); ^{1}Hmr ($CDCl_3$) δ: 6.22 (1H, s, —NH), 5.60 (1H, s, —NH), 1.66 (3H, s, vinylic —CH_3, *Z*-isomer), 1.58 (3H, s, vinylic —CH_3, *E*-isomer). *E*/*Z* ratio from vinylic methyl signals was 93:7.

*The Sulphide **34***

Pure *E*-chloride **26** (1) (3.6 g) was added to a solution of phenylthiomethylcopper (from 3.7 g of thioanisole) (32–34) in dry THF (28 mL) at −50°C under an atmosphere of nitrogen. The mixture was stirred at −50°C for 30 min, at −23°C for 3 h, then at ambient temperature for 60 h. The solution was diluted with water and extracted with petroleum ether (30–60°C). The extract was washed with brine, dried (Na_2SO_4), and concentrated *in vacuo*. The crude product (4.62 g) was shown (glc, 5% OV17) to comprise thioanisole (20%) and product (75%). An analytical sample of **34** was obtained by preparative glc; ir ν_{max}: 3060, 3045, 1660, 1580, 735, 688; ^{1}Hmr ($CDCl_3$) δ: 7.22 (5H, m, Ar —H), 5.16 (1H, m, vinylic —H), 2.90 (2H, t, J = 6.5 Hz, —$CH_2SC_6H_5$), 1.68 (3H, s, vinylic —CH_3, *Z*-isomer), 1.57 (3H, s, vinylic —CH_3, *E*-isomer), *E*/*Z* ratio: 47:3; ms *m*/*e*: 206.1124 (M^+, $C_{13}H_{18}S$ requires 206.1129), 136, 123. *Anal.* calcd. for $C_{13}H_{18}S$: C 75.69, H 8.80; found: C 75.86, H 8.70.

A small sample obtained by distillation (85°C/0.1 Torr) was similarly shown to have an *E*/*Z* ratio of 49:1.

*The Iodide **25** from **34***

The crude thioether **34** (containing thioanisole, 4.1 g), dry

sodium iodide (10.7 g), calcium carbonate (0.156 g), and mercury (1 drop) were mixed in dry DMF (42 mL). Iodomethane (32.3 mL) was added and the mixture heated at 60–75°C for 28 h under an atmosphere of dry argon. The mixture was then cooled to ca. 20°C, diluted with ether, and cooled to ca. 0°C. The crystalline material was removed by filtration, dried, and reserved for recycling. The filtrate was washed with brine, dried (Na_2SO_4), and the solvents removed by distillation at atmospheric pressure (60–70°C). Gas–liquid chromatographic analysis (5% OV17) of the residue (0.68 g) indicated iodide **25** (38%), thioanisole (49%), and thioether **34** (12%). The iodide thus obtained was not purified but used as such for the next step.

*The Acid **17** from **25***

The dianion of *n*-butyric acid (1.4 g) was alkylated, as described earlier, with the crude **25** (1.8 g) to give (**17**) (0.924 g). The *E*/*Z* ratio in this product was found to be 95:5 by ^{13}Cmr as before. The neutral fraction (2.7 g) from the work-up of this reaction, shown by glc to contain thioanisole (56%) and the thioether (42%), was reserved for recycling.

*Purification of **17** via **40***

Dicyclohexylamine (2.98 g, 3.28 mL) was added to a solution of the acid **17** (95% *E*-, 2.88 g) in *n*-hexane. The mixture was cooled to −78°C and the crystalline product **40** collected by filtration. The salt was recrystallized (× 5) from acetone to give material with mp 81.5–82°C.

The salt **40** was then dissolved in methanol containing ca. 10% HCl at 0°C. The mixture was stirred for 5 min, diluted with ice cold water, and extracted with petroleum ether (30–60°C). The extract was washed with brine, dried (Na_2SO_4), and concentrated *in vacuo*. Distillation of the residue gave **17** (1.38 g). The *E*/*Z* ratio was determined as 49:1 by ^{13}Cmr spectroscopy.

*The Hydroxyacid **43***

n-Butyllithium (5.9 mL, 1.70 *M*) was added to a solution of diisopropylamine (0.922 g, 1.28 mL) in dry THF (6.3 mL) at −78°C under a nitrogen atmosphere, and the mixture stirred for 1 h at this temperature, then at −23°C for 20 min. A solution of the *E*-acid **17** (0.763 g) in dry THF (1 mL) was added and the solution stirred at −23°C for 30 min, then at 0°C for 10 min. The mixture was heated to 50°C for 4 h, and then cooled to −78°C. A solution of the ketoester **5** (0.827 g) in dry THF (1 mL) was added slowly, and the mixture warmed (over 2 h) to 0°C, poured into ice-water, and extracted with petroleum ether (30–60°C). The extract was dried and concentrated to give **5** (0.293 g). The aqueous layer was adjusted to pH 1 with ice cold 1 *N* HCl and then extracted with petroleum ether (30–60°C). This extract was washed with brine, dried, and concentrated to give the hydroxyacid **43** (1.37 g); ir ν_{max}: 3450–2600, 1710, 1700, 1640; ^{1}Hmr ($CDCl_3$) δ: 8.0 (2H, bs, —OH and —CO_2H), 5.60 (1H, s, C=C*H*CO_2Me), 5.05 (1H, bt, vinylic —H), 3.65 (3H, s, —OCH_3), 1.6 (3H, s, vinylic —CH_3), 1.3 (3H, s, —CH_3); ms *m*/*e*: 382.2717 (M^+, $C_{22}H_{38}O_5$ requires 382.2719), 381, 269, 251, 219, 199, 184, 167, 96.

*The Ester **44***

A sample of the crude **43** (60 mg) was esterified with diazomethane in ether to give, after chromatography on silica gel, the ester **44** (27 mg, 44%); ir ν_{max}: 3470, 1715, 1640, 1170; ^{1}Hmr ($CDCl_3$) δ: 5.60 (1H, s, C=C*H*CO_2Me), 5.06 (1H, bt, vinylic —H), 3.63 (3H, s, —OCH_3), 3.60 (3H, s, —OCH_3), 3.50 (1H, bs, —OH), 1.60 (3H, s, vinylic —CH_3), 1.23 (3H, s, —CH_3), 1.08 (6H, d, J = 7 Hz, —CH(CH_3)$_2$); ms *m*/*e*: 396 (M^+), 381, 315, 283, 251, 218, 167, 166. *Anal.* calcd. for $C_{23}H_{40}O_5$: C 69.66, H 10.17; found: C 69.93, H 10.33.

*The β-Lactones **45** and **46***

The crude hydroxyacid **43** (1.37 g) and benzenesulphonyl chloride (0.27 g) were stirred in dry pyridine (3 mL) at 0–5°C for 18 h. The mixture was poured into ice-water and extracted with dichloromethane. The extract was washed with sodium bicarbonate solution, brine, dried (Na_2SO_4), and concentrated *in vacuo*. Chromatography on silica gel at ca. 5°C gave the lactone **46** (0.51 g, 39%); ir ν_{max}: 1810, 1715, 1640, 1170; ^{1}Hmr ($CDCl_3$) δ: 5.68 (1H, s, —C=C*H*CO_2CH_3), 5.09 (1H, bt, vinylic —H), 3.64 (3H, s, —OCH_3), 1.59 (6H, s, 2 × —CH_3), 1.07 (6H, d, J = 7 Hz, —CH(CH_3)$_2$); and the lactone **45** (0.49 g, 38%); ir ν_{max}: 1810, 1715, 1640, 1170; ^{1}Hmr ($CDCl_3$) δ: 5.67 (1H, s), 5.07 (1H, bt), 3.63 (3H, s), 1.57 (6H, s), 1.07 (6H, d, J = 7 Hz). Each isomer was homogeneous by glc (OV17).

*The Triene **47***

The lactone **45** (0.49 g) was heated in refluxing 2-methoxyethanol (20 mL) for 1 h under a nitrogen atmosphere. The solvent was removed *in vacuo* to give, after distillation at 120°C/0.1 Torr, the triene ester **47** (0.39 g, 91%); ir ν_{max}: 1720, 1640, 1175; ^{1}Hmr ($CDCl_3$) δ: 5.66 (1H, s, —C=C*H*CO_2CH), 5.16 (1H, bs, vinylic —H), 3.70 (3H, s, —OCH_3), 1.73 (3H, s, —CH_3), 1.57 (3H, s, —CH_3), 1.10 (6H, d, J = 7 Hz, —CH(CH_3)$_2$); ^{13}Cmr ($CDCl_3$) δ: 170.3 (C1), 167.2 (C3), 136.7 (C11), 135.3 (C7), 127.9 (C6), 123.2 (C10), 112.8 (C2), 50.8 (—O*C*H_3); ms *m*/*e*: 320.2708 (M^+, $C_{21}H_{36}O_2$ requires: 320.2715); *Anal.* calcd. for $C_{21}H_{36}O_2$: C 78.69, H 11.32; found: C 78.97, H 11.06.

*The Triene **48***

Similarly, the lactone **46** gave **48** (90%); ir ν_{max}: 1720, 1640, 1175; ^{1}Hmr ($CDCl_3$) δ: 5.62 (1H, s, —C=C*H*CO_2CH_3), 5.11 (1H, bs, vinylic —H), 3.65 (3H, s, —OCH_3), 1.71 (3H, s, —CH_3), 1.59 (3H, s, —CH_3), 1.07 (6H, d, J = 7 Hz, —CH(CH_3)$_2$); ^{13}Cmr ($CDCl_3$) δ: 170.2 (C1), 167.3 (C3), 136.8 (C11), 135.3 (C7), 127.9 (C6), 123.1 (C10), 112.8 (C2), 50.8 (—O*C*H_3); *Anal.* calcd. for $C_{21}H_{36}O_2$: C 78.69, H 11.32; found: C 78.79, H 11.40.

In the ^{13}Cmr spectra of the trienes **47** and **48** signals for C10 of the 10(11) *Z*-isomers (δ 124.3) were not observable. Furthermore each was homogeneous by glc (5% OV17, 180°C) analysis.

*The Epoxides **49**, **50**, and **51** from **47***

The triene ester **47** (0.05 g) and *m*CPBA (0.027 g) were stirred in chloroform (3 mL) at 0°C for 5 h. Chromatography on silica gel gave triene ester **47** (0.019 g) and a mixture (0.014 g) of **50** and **51**; ir ν_{max}: 1710, 1640; ^{1}Hmr ($CDCl_3$) δ: 5.65 (1H, s, —C=C*H*CO_2CH_3), 5.12 (1H, bt, vinylic —H for **50**), 3.68 (3H, s, —OCH_3), 1.60 (3H, s, vinylic —CH_3 for **50**), 1.41 (3H, s, —CH_3 for **50**), 1.09 (6H, d, J = 7.5 Hz, —CH(CH_3)$_2$ for **51**), 1.12 (6H, d, J = 7.5 Hz, —CH(CH_3)$_2$ for **50**); ratio of **50**/**51** ca. 7:3 from signals at δ 1.12 and 1.09 ppm; ms *m*/*e* 336.2641 (M^+, $C_{21}H_{36}O_3$ requires: 336.2664); and the bisepoxide **49** (0.016 g); ir ν_{max}: 1720, 1640; ^{1}Hmr ($CDCl_3$) δ: 5.65 (1H, s, —C=C*H*CO_2CH_3), 3.67 (3H, s, —OCH_3), 1.41 (3H, s, C6-CH_3), 1.24 (3H, s, C11-CH_3), 1.07 (6H, d, J = 7 Hz, —CH(CH_3)$_2$); ms *m*/*e* 352.2615 (M^+, $C_{21}H_{36}O_4$ requires: 352.2614).

*The Lactone **52***

Reaction of **45** with *m*CPBA (1.5 equiv.) in dichloromethane below 0°C gave, after chromatography on silica gel, the epoxide **52** in 92% yield; ir ν_{max}: 1810, 1710, 1640; ^{1}Hmr ($CDCl_3$) δ: 5.72 (1H, s, C2-H), 3.69 (3H, s, —OCH_3), 1.62 (3H, bs, C6-CH_3), 1.24 (3H, bs, C11-CH_3), 1.09 (6H, d, J = 7.5 Hz, C3-CH(CH_3)$_2$), 0.95 (6H, two overlapping triplets, —CH_2CH_3); homogeneous by glc (5% OV17, 180°C).

*The Lactone **53***

Similarly, **46** gave (91%) the lactone **53**; ir ν_{max}: 1810, 1710, 1640; ^{1}Hmr ($CDCl_3$) δ: 5.73 (1H, s, C2-H), 3.71 (3H, s,

—OCH_3), 1.64 (3H, s, C6-CH_3), 1.27 (3H, s, C11-CH_3), 1.10 (6H, d, J = 7.5 Hz, C3-CH(CH_3)$_2$), 0.97 (6H, two overlapping triplets, —CH_2CH_3); homogeneous by glc (5% OV17, 180°C).

The Epoxide 51

The lactone **52** was heated in refluxing 2-methoxyethanol under a nitrogen atmosphere for 2 h. The solvent was evaporated *in vacuo* and the residue purified by molecular distillation at 130°C, 0.5 Torr to give a quantitative yield of the epoxide **51**; ir ν_{max}: 1710, 1640; ^{1}Hmr ($CDCl_3$) δ: 5.64 (1H, s, C2-H), 3.68 (3H, s, —OCH_3), 2.74 (1H, t, J = 6 Hz, C10-H), 2.40 (1H, quintet, J = 7.5 Hz, —$CH(CH_3)_2$), 1.73 (3H, s, C6-CH_3), 1.22 (3H, s, C11-CH_3), 1.09 (6H, d, J = 7.5 Hz, —CH(CH_3)$_2$), 0.95 (3H, t, J = 7.5 Hz, —CH_2CH_3), 0.94 (3H, t, J = 7.5 Hz, —CH_2CH_3); ms *m/e* 336 (M^+), 318, 304, 289, 218, 202, 177, 121, 109. High resolution molecular weight determination, calcd. for $C_{12}H_{36}O_3$: 336.2664; found: 336.2660. *Anal.* calcd. for $C_{21}H_{36}O_3$: C 74.95, H 10.78; found: C 75.10, H 10.81.

The Epoxide 54

Similarly, **53** gave the epoxide **54**; ir ν_{max}: 1710, 1640; ^{1}Hmr ($CDCl_3$) δ: 5.64 (1H, s, C2-H), 3.68 (3H, s, —OCH_3), 2.72 (1H, t, J = 6 Hz, C10-H), 2.39 (1H, quintet, J = 7.5 Hz, —$CH(CH_3)_2$), 1.74 (3H, s, C6-CH_3), 1.24 (3H, s, C11-CH_3), 1.08 (6H, d, J = 7.5 Hz, —CH(CH_3)$_2$), 0.98 (3H, t, J = 7.5 Hz, —CH_2CH_3), 0.94 (3H, t, J = 7.5 Hz, —CH_2CH_3); ms *m/e* 336 (M^+), 318, 304, 289, 275, 218, 203, 177, 121, 109, 57. High resolution molecular weight determination, calcd. for $C_{21}H_{36}O_3$: 336.2664; found: 336.2676. *Anal.* calcd. for $C_{21}H_{36}O_3$: C 74.95, H 10.78; found: C 74.74, H 10.64.

Acknowledgements

Financial aid from the National Research Council of Canada is gratefully acknowledged. The authors would also like to thank MacMillan Bloedel Limited for generous supplies of thujone.

1. J. P. Kutney, J. Balsevich, R. Carruthers, Arie Markus, M. J. McGrath, R. N. Young, and B. R. Worth. Bioorg. Chem. **7**, 289 (1978).
2. J. Werner and M. T. Bogert. J. Org. Chem. **3**, 578 (1939).
3. N. Kornblum, S. D. Boyd, H. W. Pinnick, and R. G. Smith. J. Am. Chem. Soc. **93**, 4316 (1971).
4. A. P. Krapcho and E. G. E. Jahngen. J. Org. Chem. **39**, 1322 (1974); **39**, 1650 (1974).
5. M. Julia and J. M. Paris. Tetrahedron Lett. 4833 (1973).
6. G. H. Posner, G. L. Loomis, and H. S. Sawaya. Tetrahedron Lett. 1373 (1975).
7. S. Hara, H. Taguchi, H. Yamamoto, and H. Nozaki. Tetrahedron Lett. 1545 (1975).
8. J. E. McMurray and L. R. Krepski. J. Org. Chem. **41**, 3929 (1976).
9. W. Dumont and A. Krief. Angew. Chem. Int. Ed. Engl. **15**, 161 (1976).
10. N. Kornblum and L. Cheng. J. Org. Chem. **42**, 2944 (1977).
11. G. W. Moersch and A. R. Burkett. J. Org. Chem. **36**, 1149 (1971).
12. D. J. Humphreys and C. E. Newall. J. Chem. Soc. Perkin Trans. I, 33 (1978).
13. J. P. McCormick and D. L. Barton. J. Chem. Soc. Chem. Commun. 303 (1975).
14. M. Julia and J. M. Paris. Tetrahedron Lett. 3445 (1974).
15. M. Julia, S. Julia, and R. Guégan. Bull. Soc. Chim. Fr. 1072 (1960).
16. M. Julia, S. Julia, and S. Y. Tchen. Bull. Soc. Chim. Fr. 1849 (1961).
17. E. C. Ashby and R. C. Arnott. J. Organomet. Chem. **14**, 1 (1968).
18. L. F. Fieser and M. Fieser. Reagents for organic synthesis. Vol. 1. J. Wiley & Sons. 1967.
19. J. A. MacPhee and J. E. Dubois. J. Chem. Soc. Perkin Trans. I, 694 (1977).
20. D. F. Sullivan, R. P. Woodbury, and M. W. Rathke. J. Org. Chem. **42**, 2038 (1977).
21. A. I. Meyers and E. D. Mihelich. Angew. Chem. Int. Ed. Engl. **15**, 270 (1976).
22. A. I. Meyers, D. L. Temple, R. L. Nolen, and E. D. Mihelich. J. Org. Chem. **39**, 2778 (1974).
23. P. E. Pfeffer, L. S. Silbert, and J. M. Chirinko, Jr. J. Org. Chem. **37**, 451 (1972).
24. J. W. Blunt and M. H. G. Munro. Aust. J. Chem. **29**, 975 (1976).
25. H. Roller, K. H. Dahm, C. C. Sweeley, and B. M. Trost. Angew. Chem. **79**, 190 (1967); Angew. Chem. Int. Ed. Engl. **6**, 179 (1967).
26. G. W. Anderson, I. F. Halverstadt, W. H. Miller, and R. O. Roblin, Jr. J. Am. Chem. Soc. **67**, 2197 (1945).
27. O. H. Oldenziel and A. M. van Leusen. Tetrahedron Lett. 1357 (1973).
28. U. Schöllkopf and R. Schröder. Angew. Chem. Int. Ed. Engl. **12**, 407 (1973).
29. O. H. Oldenziel, D. van Leusen, and A. M. van Leusen. J. Org. Chem. **42**, 3114 (1977).
30. J. H. Hall and M. Gisler. J. Org. Chem. **41**, 3769 (1976).
31. H. L. Vaughn and M. D. Robbins. J. Org. Chem. **40**, 1187 (1975).
32. E. J. Corey and D. Seebach. J. Org. Chem. **31**, 4097 (1966).
33. R. L. Sowerby and R. M. Coates. J. Am. Chem. Soc. **94**, 4758 (1972).
34. E. J. Corey and G. H. Posner. J. Am. Chem. Soc. **89**, 3911 (1967).
35. E. J. Corey and M. Jautelat. Tetrahedron Lett. 5787 (1968).
36. A. S. Gupta and S. Dev. J. Chromatogr. **12**, 189 (1963).
37. H. A. Staab and W. Rohr. *In* Newer methods of preparative organic chemistry. Vol. 5. *Edited by* W. Foerst. Academic Press. 1968. p. 61.
38. R. A. Olofson and C. M. Dougherty. J. Am. Chem. Soc. **95**, 582 (1973).
39. P. A. Grieco, Y. Yo, S. Gilman, and M. Ni. J. Org. Chem. **42**, 2034 (1977).
40. E. J. Corey, J. A. Katzenellenbogen, N. W. Gilman, S. A. Roman, and B. W. Erickson. J. Am. Chem. Soc. **90**, 5618 (1968).
41. E. E. Van Tamelin, M. A. Schwartz, E. Hessler, and A. Stone. J. Chem. Soc. Chem. Commun. 409 (1966).
42. E. E. Van Tamelin and T. J. Curphey. Tetrahedron Lett. 121 (1962).
43. K. Mori, B. Stalla-Bourdillon, M. Ohki, M. Matsui, and W. S. Bowers. Tetrahedron, **25**, 1667 (1969).
44. J. A. Findlay and W. D. MacKay. J. Chem. Soc. Chem. Commun. 733 (1969).
45. R. Breslow and L. M. Maresca. Tetrahedron Lett. 887 (1978).
46. K. H. Dahm, B. M. Trost, and H. Roller. J. Am. Chem. Soc. **89**, 5292 (1967).
47. W. S. Johnson, T. Li, D. J. Faulkner, and S. F. Campbell. J. Am. Chem. Soc. **90**, 6225 (1968).
48. E. J. Corey and J. W. Suggs. Tetrahedron Lett. 2647 (1975).

Ring forming reactions of some amineimides with a note on electrophilic bromination

IAN D. BRINDLE AND MARTIN S. GIBSON

Department of Chemistry, Brock University, St. Catharines, Ont., Canada L2S 3A1

Received June 28, 1979

IAN D. BRINDLE and MARTIN S. GIBSON. Can. J. Chem. **57**, 3155 (1979).

Allylic and propargylic amineimides react with bromine to form 4*H*-1,3,4-oxadiazinium salts in accord with recent studies of electrophilic brominations. A novel synthesis of 5,6-dihydro-4,4-dimethyl-6-hydroxymethyl-2-phenyl-4*H*-1,3,4-oxadiazinium bromide by the reaction of *N'N'*-dimethylbenzohydrazide and epibromohydrin is reported.

IAN D. BRINDLE et MARTIN S. GIBSON. Can. J. Chem. **57**, 3155 (1979).

Les amineimides allyliques et propargyliques réagissent avec le brome pour former les sels de 4*H* oxadiazinium-1,3,4 en accord avec les récentes études sur les bromations électrophiliques. On rapporte une nouvelle synthèse du bromure de dihydro-5,6 diméthyl-4,4 hydroxyméthyl-6 phényl-2 4*H* oxadiazinium-1,3,4 obtenue par la réaction de la *N'N'*-diméthylbenzohydrazine avec l'épibromohydrine.

[Traduit par le journal]

During the course of a study of the thermolysis of allyldimethylamine-benzimide **1** (1), we noted that both this compound and the related propargyldimethylamine-benzimide **2** underwent ring closure on the addition of bromine to give salts. The ambident nature of the imido group in such amine-imides has been well documented by Wawzonek and Yeakey who noted that methylation occurs at the imide oxygen in 1,1-dimethyl-1-*p*-nitrobenzylamine-acetimide (2) and by Brindle and Gibson who showed that allylic migration occurs to the imide nitrogen on thermolysis under conditions which preclude a prior rearrangement to oxygen (1). Alternative formulations have thus to be considered for the salts derived from bromination of **1** and **2**; that from **1** might be **3** or **5** whilst that from **2** might be **4** or **6**.

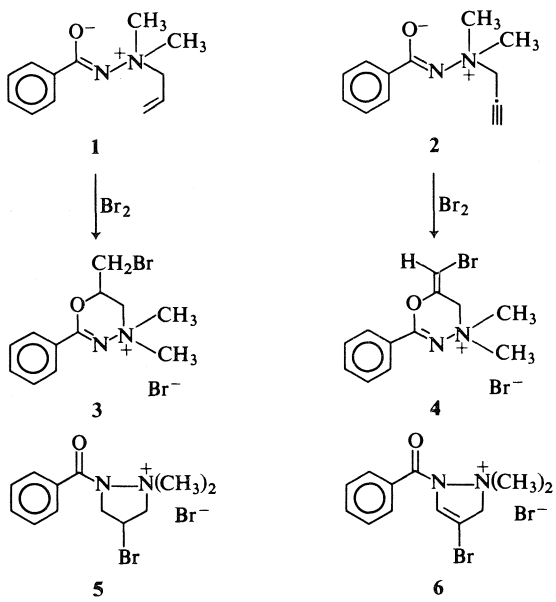

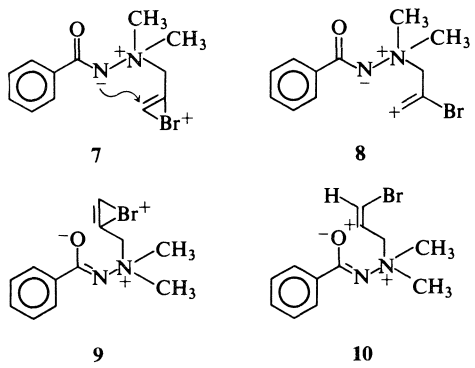

Initially we were disposed to formulae **5** and **6** respectively (3) by analogy with such reactions as the conversion of *N*-2-bromomethyl-*N'*-phenylurea to 1-phenyl-2-imidazolone by ethoxide ion, in which nitrogen rather than oxygen is the nucleophilic centre (4, 5). However the only band in the ir spectrum near the carbonyl region was in each case at 1625 cm^{-1} which seemed more in line with a C=N stretching mode. This matter has now been resolved by a single crystal X-ray study on the salt from bromination of **2** which verifies the structure as the oxadiazinium salt **4** (see following paper); by extension, **3** is the structure assigned to the bromination product of **1**.

These conclusions are consistent with the results of recent studies of electrophilic halogenation by McManus *et al.* (6). Thus formation of salt **6** would involve either the *fused* (*endo*) mode of attack on the halonium intermediate **7** or the even more unlikely prior formation of the carbocation **8**. However,

0008-4042/79/233155-02$01.00/0

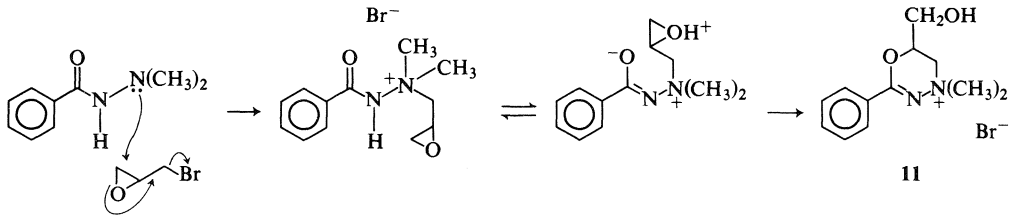

SCHEME 1

oxygen attack is actually observed, presumably via the preferred *spiro* (*exo*) configuration **9** or possibly via the more stable carbocation **10**; spiro attack by nitrogen (leading to a four membered ring) was considered unlikely and was not observed.

We have extended the argument to a related system in which a protonated epoxide is the likely intermediate. The reaction of *N'N'*-dimethylbenzohydrazide with epibromohydrin yields the hydroxymethyl 4*H*-1,3,4-oxadiazinium salt **11**. We view this process (Scheme 1) as also involving attack in the *spiro* mode.

Experimental

(E)-6-(Bromomethylene)-5,6-dihydro-4,4-dimethyl-2-phenyl-4H-1,3,4-oxadiazinium Bromide ***4***

Bromine (3.2 g, 0.02 mol) in chloroform was added during 30 min to a solution of compound **2** (1) (4.0 g, 0.02 mol) in chloroform (25 mL). Evaporation and crystallization from 2-propanol gave the *salt* **4** (4.2 g, 58%), mp 173–174°C (dec., sample inserted at 165°C); ν_{max}: 1625 cm^{-1}. *Anal.* calcd. for $C_{12}H_{14}Br_2N_2O$: C 39.78, H 3.87, Br 44.20; found: C 39.99, H 3.93, Br 44.28.

6-(Bromomethyl)-5,6-dihydro-4,4-dimethyl-2-phenyl-4H-1,3,4-oxadiazinium Bromide ***3***

Compound **1** (3.0 g, 0.015 mol) was treated with bromine in chloroform in the same way as **2** above. The crude product solidified on trituration with hexane and crystallized from 2-propanol to give the *salt* **3** (4.1 g, 76%), mp 200–202°C (dec.); ν_{max}: 1625 cm^{-1}. *Anal.* calcd. for $C_{12}H_{16}Br_2N_2O$: C 39.56, H 4.40, Br 43.96; found: C 39.53, H 4.50, Br 44.01.

5,6-Dihydro-4,4-dimethyl-6-hydroxymethyl-2-phenyl-4H-1,3,4-oxadiazinium Bromide ***11***

A solution of *N'N'*-dimethylbenzohydrazide (1.64 g, 0.01 mol) and epibromohydrin (5.0 g, 0.036 mol) in chloroform (10 mL) deposited the *bromide* **11** (0.45 g, 15%) after standing for 2 days at room temperature, followed by trituration with a small amount of methanol. Crystallization from 2-propanol gave hygroscopic microcrystals, mp 182–184°C; ν_{max}: 1610 cm^{-1}. *Anal.* calcd. for $C_{12}H_{17}BrN_2O_2$: C 47.85, H 5.69, Br 26.53; found: C 47.93, H 5.69, Br 26.40.

Acknowledgement

The authors wish to thank Dr. Kurt L. Loening, Nomenclature Director of Chemical Abstracts Service for the naming of compound **4**.

1. I. D. BRINDLE and M. S. GIBSON. J. Chem. Soc. Perkin Trans. I, 517 (1979).
2. S. WAWZONEK and E. YEAKEY. J. Am. Chem. Soc. **82**, 5718 (1960).
3. I. D. BRINDLE and M. S. GIBSON. Chem. Commun. 803 (1969).
4. B. CAPON. Q. Rev. Chem. Soc. London, **18**, 71 (1964).
5. F. L. SCOTT and D. F. DENTON. Tetrahedron Lett. 1681 (1964).
6. S. R. MCMANUS, D. W. WARE, and R. A. HAMES. J. Org. Chem. **43**, 4288 (1978), and references cited; see also J. E. BALDWIN. Chem. Commun. 734 (1976), and subsequent papers.

The crystal and molecular structure of a compound containing a novel ring system: (*E*)-6-(bromomethylene)-5,6-dihydro-4,4-dimethyl-2-phenyl-4*H*-1,3,4-oxadiazinium bromide

DORIS MARGARET THOMPSON,[1] IAN DAVID BRINDLE, AND MARY FRANCES RICHARDSON[2]

Chemistry Department, Brock University, St. Catharines, Ont., Canada L2S 3A1

Received June 28, 1979

DORIS MARGARET THOMPSON, IAN DAVID BRINDLE, and MARY FRANCES RICHARDSON. Can. J. Chem. **57**, 3157 (1979).

The crystal structure of (*E*)-6-(bromomethylene)-5,6-dihydro-4,4-dimethyl-2-phenyl-4*H*-1,3,4-oxadiazinium bromide has been determined by single crystal X-ray diffraction methods. The crystals are monoclinic, space group $P2_1/c$, with $a = 12.002(5)$, $b = 6.414(4)$, $c = 17.881(7)$ Å, $\beta = 101.42(7)°$, and $Z = 4$ formula units of $C_{12}H_{14}N_2OBr_2$. The structure was refined by full-matrix least-squares analysis to a conventional *R*-factor of 0.0491 for 1019 observed reflections.

The oxadiazinium ring is in the half-chair form, with the methylene group out of the plane defined by the other five atoms. The C—O bond distances in the ring are somewhat shorter than the distance observed for a carbon–oxygen single bond, suggesting that some delocalization of electron density occurs over part of the ring.

DORIS MARGARET THOMPSON, IAN DAVID BRINDLE et MARY FRANCIS RICHARDSON. Can. J. Chem. **57**, 3157 (1979).

On a déterminé la structure cristalline du bromure de (*E*) (bromométhylène)-6 dihydro-5,6 diméthyl-4,4 phényl-2 4*H* oxadiazinium-1,3,4 en utilisant les méthodes de diffraction de rayons X sur un cristal unique. Les cristaux sont monocliniques, groupe d'espace $P2_1/c$ avec $a = 12.002(5)$, $b = 6.414(4)$, $c = 17.881(7)$ Å, $\beta = 101.42(7)°$ et $Z = 4$ unités de formule $C_{12}H_{14}N_2OBr_2$. On a affiné la structure par une analyse des moindres carrés (matrice complète) jusqu'à un facteur conventionnel *R* de 0.0491 pour 1019 réflexions observées. Le cycle oxadiazinium a une forme de demi-chaise avec le groupe méthylène hors du plan défini par les cinq autres atomes. Les longueurs de liaison C—O sont un peu plus courtes que celles observées pour la simple liaison carbone–oxygène. Ceci suggère qu'une certaine délocalisation de densité électronique se produit sur une partie du cycle.

[Traduit par le journal]

The addition of bromine to propargyl-dimethylaminebenzimide results in a product whose structure is not readily determined by ir and nmr spectroscopy (1). This crystal structure determination has established that an oxadiazinium salt **1** is produced, and contains the first detailed report on the structural parameters of an oxadiazinium ring.

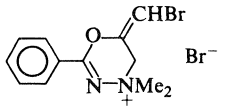

1

Experimental

The compound was prepared as described previously (1), and a single crystal 0.10 × 0.15 × 0.75 mm was mounted on a glass fibre with epoxy glue. Oscillation and Weissenberg photographs showed systematic absences consistent with space group $P2_1/c$. The crystal was transferred to a Picker manual four-circle diffractometer and accurate cell dimensions were obtained from scans of the axial and selected $h\,0\,l$ reflections out to 2θ values of 60°. Crystal data are as follows:

$C_{12}H_{14}N_2OBr_2$ fw = 362.07
Monoclinic, $P2_1/c$, $a = 12.002(5)$, $b = 6.414(4)$, $c = 17.881(7)$ Å, $\beta = 101.42(7)°$, $V = 1349.2$ Å^3, $\rho_c = 1.782$ g cm^{-3}, $Z = 4$, μ(MoKα) = 63.4 cm^{-1}, λ(MoKα) = 0.7107 Å.

Data were measured by the θ–2θ scan technique at a scan speed of 2°/min and a scan range of 2°, to a maximum 2θ of 40°. The background was measured for 10 s at both ends of the scan. A standard reflection was monitored after every 25–50 reflections; its value decreased steadily throughout the course of the data collection, reaching a value of ~80% of the original intensity by the time the data collection was finished. The crystal had become yellow and slightly opaque by the time data collection was completed.

The data were corrected for the declining intensity of the standard, as well as for Lorentz and polarization effects. No absorption correction was made. Of 1258 reflections measured in the independent quadrant, 1019 had $F_o \geq 3\sigma(F_o)$ and were classified as observed. The SHELX-76 set of computer programs was used in structure determination and refinement (2).

The Patterson map yielded the locations of the bromine atoms and subsequent electron-density difference maps revealed the remaining atoms, including hydrogens. Refinement

[1]Present address: Department of Chemistry, Austin College, Sherman, TX.

[2]To whom all correspondence should be addressed.

0008-4042/79/233157-03$01.00/0

was carried out by full-matrix least-squares analysis. The function minimized was $\sum w(|F_o| - |F_c|)^2$, where F_o and F_c are the observed and calculated structure factors, respectively, $w = k/(\sigma^2(F) + gF^2)$, $\sigma(F)$ is based on counting statistics, and k and g are refinable parameters in the least-squares analysis. The final values of k and g were 2.14 and 8.58×10^{-4}, respectively.

The scattering factors of the neutral C, H, N, O, and Br atoms were taken from the International tables for X-ray crystallography (3). Individual hydrogen atom parameters were not refined. The methyl groups were treated as rigid rotors. The positions of the remaining eight hydrogen atoms were calculated, and these atoms were included as fixed contributions to F_c. The thermal parameters of the hydrogen atoms were fixed at values 20% greater than those of the carbon atoms to which they were bonded.

Several cycles of refinement were carried out on 85 parameters (scale factor, positional parameters of all non-hydrogen atoms, anisotropic thermal parameters for bromine, isotropic thermal parameters for the remaining non-hydrogen atoms, and three parameters for each methyl group). For the 1019 observed reflections the final conventional $R = \sum ||F_o| - |F_c||/\sum |F_o| = 0.049$; the weighted $R_w = [\sum w(|F_o| - |F_c|)^2/w|F_o|^2]^{1/2} = 0.052$. The corresponding R and R_w for all reflections were 0.068 and 0.057.

A final difference map revealed scattered small peaks near the bromine atoms but no other significant peaks. A table of observed and calculated structure factors is available.[3]

TABLE 1. Atomic positional and thermal parameters for $C_{12}H_{14}N_2OBr_2$, estimated standard deviations in parentheses

Atom	10^4x	10^4y	10^4z	10^3U
C(1)	3157(9)	−801(16)	4904(6)	50(3)
C(2)	2687(7)	224(15)	4297(5)	39(3)
C(3)	1585(7)	−65(16)	3763(5)	43(3)
C(4)	582(7)	2508(16)	4408(5)	42(3)
C(5)	−43(7)	1826(16)	3063(5)	39(3)
N(1)	958(6)	1930(12)	3684(4)	32(2)
N(2)	1664(6)	3672(11)	3492(4)	35(2)
O	3321(5)	1853(10)	4069(4)	49(2)
C(6)	2738(7)	3448(14)	3671(5)	32(2)
C(7)	3479(7)	5053(15)	3466(5)	35(3)
C(8)	3080(8)	6416(14)	2867(5)	38(3)
C(9)	3761(8)	8031(16)	2697(6)	49(3)
C(10)	4867(9)	8171(18)	3090(6)	57(3)
C(11)	5287(8)	6803(16)	3673(6)	47(3)
C(12)	4598(8)	5246(16)	3861(6)	44(3)
Br(1)	1455.4(9)	1915(2)	1409.1(6)	
Br(2)	2454.2(9)	−2984(2)	5333.5(6)	

Atom	10^4U_{11}	10^4U_{22}	10^4U_{33}	10^4U_{12}	10^4U_{13}	10^4U_{23}
Br(1)	672(8)	496(9)	450(8)	7(6)	249(6)	−63(6)
Br(2)	563(8)	471(8)	619(8)	6(6)	135(6)	159(6)

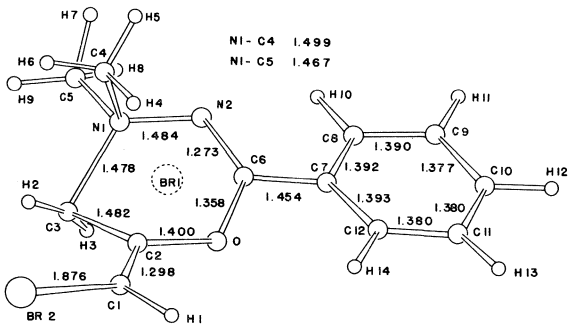

FIG. 1. Perspective view and bond distances for $C_{12}H_{14}N_2OBr_2$. The Br(1) ion lies below the oxadiazinium ring. Standard deviations range from 0.010 Å to 0.014 Å.

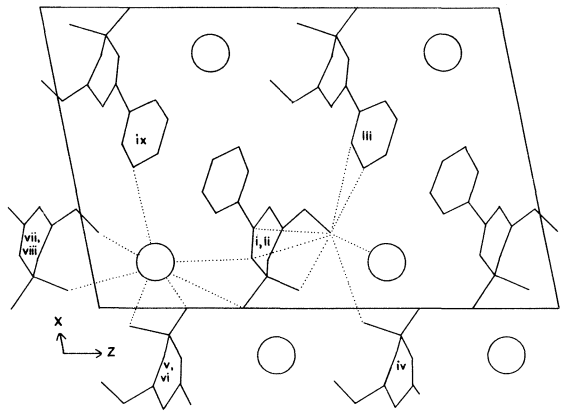

FIG. 2. Molecular packing of $C_{12}H_{14}N_2OBr_2$ as viewed down the y-axis. The large circles represent Br(1) ions. The dotted lines show contacts about Br(1) and Br(2) which are less than 4.0 Å. The Roman numerals are keyed to the symmetry transformations in the table of short contact distances (see footnote 3).

Results and Discussion

Table 1 lists the refined atomic parameters.[3] Figure 1 shows a view of the molecule and the associated bond lengths; the bond angles may be found in Table 2.

The oxadiazinium ring exists in the half-chair form. Five of the six atoms in the ring lie in the same plane (Table 3), whereas the methylene group (C(3)) lies below this plane. The phenyl, alkene, and imide moieties are also planar (Table 3). The *exo*-bromomethylene group is twisted about the C(1)—C(2) bond so that Br(2) lies above the oxadiazinium ring. This feature would appear to be due to steric crowding between Br(2) and the C(3) methylene group, an interpretation which is supported by the expanded C(1)—C(2)—C(3) angle of 131.3(9)° and an H(2)—Br(2) contact (2.86 Å) which is ~0.2 Å shorter than the sum of the van der Waals radii (4).

Most of the bond distances (Fig. 1) are close to

[3]Lists of structure factors, hydrogen positions, and short contact distances in the structure are available, at a nominal charge, from the Depository of Unpublished Data, CISTI, National Research Council of Canada, Ottawa, Ont., Canada K1A 0S2.

TABLE 2. Bond angles in degrees

Bonds	Angle	Bonds	Angle
Br(2)—C(1)—C(2)	124.4(8)	N(2)—C(6)—C(7)	119.8(8)
C(1)—C(2)—C(3)	131.3(9)	N(2)—C(6)—O	127.4(8)
C(1)—C(2)—O	116.8(8)	C(7)—C(6)—O	112.8(7)
C(3)—C(2)—O	111.8(8)	C(2)—O—C(6)	117.5(7)
C(2)—C(3)—N(1)	109.0(8)	C(6)—C(7)—C(8)	120.3(8)
C(3)—N(1)—N(2)	111.7(6)	C(6)—C(7)—C(12)	120.7(9)
C(3)—N(1)—C(5)	111.0(7)	C(8)—C(7)—C(12)	119.0(9)
C(3)—N(1)—C(4)	111.5(7)	C(7)—C(8)—C(9)	120.6(9)
C(4)—N(1)—C(5)	108.9(6)	C(8)—C(9)—C(10)	119.1(10)
C(4)—N(1)—N(2)	107.3(7)	C(9)—C(10)—C(11)	121.0(11)
C(5)—N(1)—N(2)	106.2(6)	C(10)—C(11)—C(12)	119.8(10)
N(1)—N(2)—C(6)	117.0(7)	C(11)—C(12)—C(7)	120.3(9)

TABLE 3. Unweighted least-squares planes and deviations of the atoms from the planes (in Å)[a]

Atom	Deviation	Atom	Deviation
Phenyl ring: $0.4476X - 0.6093Y - 0.6545Z = -4.619$			
C(7)	0.012	C(10)	−0.007
C(8)	−0.023	C(11)	−0.005
C(9)	0.020	C(12)	0.002
C(6)[b]	0.050		
Oxadiazinium ring: $0.2011X - 0.4694Y - 0.8598Z = -6.185$			
C(2)	0.016	C(1)[b]	0.551
O	−0.008	Br(2)[b]	0.741
C(6)	−0.016	C(7)[b]	−0.034
N(2)	0.029	C(3)[b]	−0.649
N(1)	−0.021		
Alkene group: $0.5390X - 0.6447Y - 0.5421Z = -3.249$			
C(1)	−0.027	O	0.011
C(2)	0.009	Br(2)	0.015
C(3)	−0.008	C(6)[b]	0.594
Imide group: $0.1941X - 0.4690Y - 0.8616Z = -6.198$			
N(1)	−0.023	C(6)	−0.003
N(2)	0.032	C(7)	−0.016
O	0.010		

[a]The equation of the plane has the form $AX + BY + CZ = D$, where X, Y, and Z are orthogonal coordinates (in Å) of the atoms in a system where the x, y, and z axes are parallel to the a^*, b, and c axes of the unit cell, respectively.
[b]Not used in the plane calculation.

accepted values (5–8). The shortness of the C(6)—O and C(6)—C(7) bonds and the C(2)—O—C(6) angle of 117.5° suggest that there is some electron delocalization between the oxadiazinium and phenyl moieties. The planes of the oxadiazinium and phenyl rings intersect at an angle of 20°.

The molecular packing diagram is shown in Fig. 2. The bromide ions (Br(1)) alternate with oxadiazinium cations. The packing is governed by contacts with Br(1) and Br(2), there being several contacts to these atoms on the order of 3.75 Å. The only other intermolecular distance less than 4.0 Å (other than those involving some of the hydrogen atoms) is from C(3) to C(8) at $(x, 1 + y, z)$; the distance is 3.47(1) Å.

Acknowledgement

We are grateful to the National Research Council of Canada for their generous support of this research.

1. I. D. BRINDLE and M. S. GIBSON. Can. J. Chem. This issue.
2. G. SHELDRICK. SHELX-76 program for crystal structure determination. 1976.
3. International tables for X-ray crystallography. Vol. IV. The Kynoch Press, Birmingham. 1974. pp. 99, 100, 149.
4. A. BONDI. J. Phys. Chem. **68**, 441 (1964).
5. International tables for X-ray crystallography. Vol. III. The Kynoch Press, Birmingham. 1968. pp. 275, 276.
6. F. GARBASSI and L. GIARDA. Acta Crystallogr. B**29**, 1190 (1973).
7. A. PRAKASH, C. CALVO, A. M. CAMERON, and J. WARKENTIN. J. Cryst. Mol. Struct. **3**, 71 (1973).
8. C. S. HUBER. Acta Crystallogr. B**29**, 1046 (1973).

Isotopically-enriched carbohydrates: The preparation of [^{2}H]-enriched aldoses by catalytic hydrogenolysis of cyanohydrins with $^2H_2$[1]

ANTHONY STEPHEN SERIANNI AND ROBERT BARKER[2]

Department of Biochemistry, Michigan State University, East Lansing, MI 48824, U.S.A.

Received June 5, 1979

ANTHONY STEPHEN SERIANNI and ROBERT BARKER. Can. J. Chem. **57**, 3160 (1979).

A procedure is described for the preparation of aldoses and aldose phosphates enriched with ^{2}H by hydrogenolysis of aldononitriles and aldononitrile phosphates over palladium using $^2H_2$. Aldoses, aldose phosphates, and derivatives prepared with ^{13}C and (or) ^{2}H enrichment and characterized by ^{1}H and ^{13}C nmr were: DL-[1-^{14}C, ^{2}H]glyceraldehyde, D-[1-^{13}C, ^{2}H]-erythrose, D-[1-^{13}C, ^{2}H]threose, D-[2-^{13}C, ^{2}H]ribose, D-[2-^{13}C, ^{2}H]arabinose, methyl α-D-[2-^{13}C, ^{2}H]ribofuranoside, methyl β-D-[2-^{13}C, ^{2}H]ribofuranoside, DL-[3-^{2}H]erythrose, DL-[3-^{2}H]threose, DL-[1-^{13}C, ^{2}H]glyceraldehyde 3-phosphate, and D-[1-^{13}C, ^{2}H]ribose 5-phosphate. ^{13}C isotope shifts, ^{1}H and ^{13}C chemical shifts, and homo- and heteronuclear coupling constants are reported.

ANTHONY STEPHEN SERIANNI et ROBERT BARKER. Can. J. Chem. **57**, 3160 (1979).

On décrit une méthode de préparation des aldoses et des phosphates d'aldose enrichis en ^{2}H par hydrogénolyse, à l'aide de ^{2}H/Pd, des aldonitriles et des phosphates d'aldonitrile. On a caractérisé par la rmn du ^{13}C et du ^{2}H les aldoses, les phosphates d'aldoses et les autres dérivés suivants: DL-[^{14}C-1-^{2}H] glycéraldéhyde, D-[^{13}C-1-^{2}H] érythrose, D-[^{13}C-1-^{2}H] thréose, D-[^{13}C-2-^{2}H] ribose, D-[^{13}C-2-^{2}H] arabinose, α-D-[^{13}C-2-^{2}H] ribofurannoside de méthyle, β-D-[^{13}C-2-^{2}H] ribofurannoside de méthyle, DL-[^{2}H-3] érythrose, DL-[^{2}H-3] thréose, phosphate-3 de DL-[^{13}C-1-^{2}H] glycéraldéhyde et phosphate-5 de D-[^{13}C-1-^{2}H] ribose. On a rapporté les déplacements isotopiques du ^{13}C, les déplacements chimiques du ^{1}H et du ^{13}C ainsi que les constantes de couplage homo- et hétéronucléaires.

[Traduit par le journal]

Introduction

Configurational and conformational analysis of carbohydrates and their derivatives in solution by nuclear magnetic resonance spectroscopy is greatly facilitated by the use of isotopically enriched compounds. Assignments of ^{13}C chemical shifts have been made using [^{2}H]-enriched carbohydrates based on the disappearance of the resonance arising from the carbon directly bound to the deuteron and on the upfield shifts experienced by carbon nuclei β and γ to the deuteron (1–4). The interpretation of complex ^{1}Hmr spectra can also be aided by deuteration (5, 6). The use of [^{13}C]-enriched aldoses, aminoaldoses, and aldose phosphates permitted the unequivocal assignment of carbon chemical shifts, determination of ^{13}C–H and ^{13}C–^{13}C coupling constants, and the *in vitro* monitoring of enzyme-catalyzed conversions (7–12). In certain circumstances, the use of [^{13}C, ^{2}H]-enriched aldoses and their biologically-important phosphate esters would permit the examination of chemical and biochemical proton exchange – transfer reactions (isomerizations, epimerizations) by ^{13}C and ^{1}Hmr. A simple method of ^{2}H-enrichment is described in this paper and is applied to the preparation of doubly-enriched [^{13}C, ^{2}H] compounds.

The preparation of [^{2}H]-enriched carbohydrates is most often accomplished by reduction of carbonyl derivatives with NaB^2H_4 (4, 5). This approach is limited by the availability of the appropriate carbonyl. Balza *et al.* (13) have prepared deuterated glycosides by ^{1}H–^{2}H exchange in ^2H_2O on a Raney nickel catalyst. In this paper, we describe a simple method for the incorporation of ^{2}H into the simple aldoses and aldose phosphates in 70–80% yields. An aldose is condensed with cyanide at pH 8.0 ± 0.5 to produce the 2-epimeric cyanohydrins, which are stabilized by lowering the pH to 4.0. The cyanohydrins are hydrogenolyzed in ^2H_2O solution with $^2H_2$ over palladium to yield the [1-^{2}H]-enriched 2-epimeric aldoses having one more carbon than the parent compound. The aldoses can be separated as described previously (14, 15). [^{2}H]-enriched aldose phosphates can be prepared from aldononitrile phosphates in a similar fashion.

The utility of this method lies in the ease with which isotopes of carbon, hydrogen, and oxygen (16)

[1]Supported in part by a grant (GM-21731) from the National Institute of General Medical Sciences and by a program of the Stable Isotope Resource of the Los Alamos National Laboratory, supported jointly by the Department of Energy and the National Institutes of Health (RR00962). Michigan Agricultural Experiment Station Journal Article No. 9189.

[2]Author to whom correspondence may be addressed at Division of Biological Sciences, Cornell University, Ithaca, NY 14853.

0008-4042/79/233160-08$01.00/0

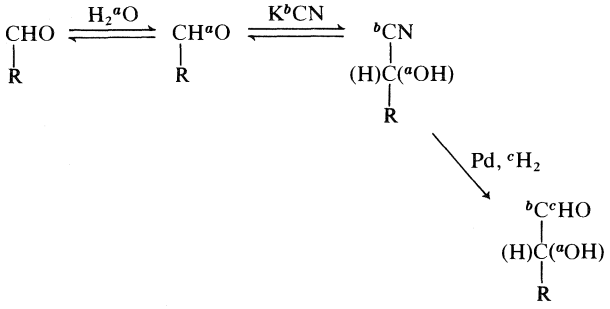

SCHEME 1

can be incorporated either independently or simultaneously into the carbohydrate molecule, as shown in Scheme 1.

We have prepared several singly and multiply-enriched aldoses, aldose phosphates, and derivatives, and characterized them by ^{1}H and ^{13}Cmr. ^{1}Hmr parameters were confirmed and refined by computer simulation of the spectra. ^{13}C isotope shifts, ^{1}H and ^{13}C chemical shifts, and homo- and heteronuclear coupling constants are reported.

Results and Discussion

Carbohydrates via the Catalytic Hydrogenolysis of Cyanohydrins

The synthetic route described in this and earlier reports (9–11) utilizes the condensation of cyanide with an aldose or aldose derivative, as first described by Kiliani (17). In this classical reaction, a cyanide salt and aldose are mixed in aqueous solution at high pH to produce cyanohydrins which, in the alkaline solution, hydrolyze to aldonic acid salts (18). We have observed (19), however, that cyanohydrins can be formed rapidly and essentially quantitatively at pH 8.0 $\pm$ 0.5 with minimal hydrolysis, and that they are stable at pH 4.0. As described by Kuhn and Bister (20) for the preparation of 2-amino-2-deoxy-aldoses from 2-benzylamino-2-deoxyaldononitriles, we find that aldononitriles can be hydrogenolyzed to aldoses in 70–80% yield. Furthermore, condensation with $K^{13}CN$ provides a convenient route for the preparation of [^{13}C]-enriched derivatives of all the aldoses (9, 10) and of the C_3 to C_5 aldose phosphates (11). The mixed aldononitrile epimers produced from cyanide condensation are reduced without purification and the product epimeric aldoses purified by chromatography (14, 15). Aldononitrile phosphate epimers can be separated prior to reduction by chromatography at pH 3.9 (11), illustrating the stability of cyanohydrins and the absence of cyanide exchange at low pH values.

Hydrogen pressure, pH, and the structure of the nitrile all affect the ease of hydrogenolysis of cyanohydrins (9–11). Hydrogenolysis occurs smoothly in the absence of excess cyanide, which appears to poison the catalyst. In the course of this study it was observed that chloride ion promotes "over-reduction" to aminoalditols. Sulfuric acid rather than HCl is preferred since sulfate ion does not inhibit hydrogenolysis, gives higher yields of aldose, and can be removed more easily than chloride ion. Iodate ion, at low concentrations, inhibits reduction completely (11).

In addition to the introduction of carbon isotopes, the catalytic hydrogenolysis of cyanohydrins provides a route to carbohydrates enriched with hydrogen and oxygen isotopes. The technique permits the separate or simultaneous incorporation of carbon and hydrogen isotopes at C-1 and H-1, respectively, and oxygen isotopes at O-2 for each cycle of cyanide addition and catalytic reduction (Scheme 1). Successive application of condensation and reduction permits the synthesis of derivatives enriched at sites other than C-1 and C-2. A wide variety of selectively-enriched carbohydrates and their derivatives, which were difficult to prepare previously, are now accessible.

For the incorporation of ^{2}H, cyanide condensation and hydrogenolysis are carried out in $^{2}H_2O$ instead of H_2O solutions to avoid exchange of ^{1}H for ^{2}H on the catalytic surface. This exchange decreases the incorporation of ^{2}H at H-1. Under the conditions used for hydrogenolysis, ^{1}H–^{2}H exchange did not occur at other positions, as determined by ^{1}Hmr. In several cases, nitrile (~15%) remained in the reduction mixtures after 10 h of hydrogenolysis. Complete conversion to products was achieved by adding new catalyst and continuing the reduction.

Nuclear Magnetic Resonance Parameters

^{13}C nmr Spectra

Substitution of ^{2}H for ^{1}H permits the assignment of ^{13}C resonances of the directly-bound and nearby carbons due to decreased nuclear Overhauser effects and characteristic isotope shifts. In addition ^{13}C–^{2}H coupling can be measured. The effect of ^{2}H substitution for ^{1}H on the ^{13}C chemical shift of the derivatized carbon is shown in Table 1 for several carbohydrates. The values observed are similar to those observed by Gorin (1) and Gorin and Mazurek (4). The use of [^{13}C, ^{2}H]-enriched compounds facilitates the observation of the deuterated carbon and the evaluation of $^{1}J_{^{13}C,^{2}H}$ (Fig. 1). The ^{13}Cmr spectrum of D-[1-^{13}C] threose in aqueous solution shows the presence of three major tautomeric forms, namely, the α- and β-furanoses, and a linear *gem*-diol (hydrate) (Fig. 1A). The proton-decoupled ^{13}Cmr spectrum of D-[1-^{13}C, ^{2}H]threose (Fig. 1B) shows four lines for

TABLE 1. ^{13}C chemical shifts, ^{13}C–^{1}H and ^{13}C–^{2}H coupling constants for several [^{13}C, ^{2}H] enriched carbohydrates and derivatives

Compound	$^{1}J_{C,^{1}H}$[b] (Hz)	$^{1}J_{C,^{2}H}$[c] (Hz)	Carbon chemical shift (ppm)[a] ^{13}C–^{1}H	Carbon chemical shift (ppm)[a] ^{13}C–^{2}H	$\Delta\nu$[d] (Hz)	ΔJ[e] (± 5.3)
α-D-[1-^{13}C, ^{2}H]threose	172.3	26.0	103.5	103.2	5.9	2.9
β-D-[1-^{13}C, ^{2}H]threose	173.8	26.4	98.0	97.7	5.1	1.8
D-[1-^{13}C, ^{2}H]threose, hydrate	162.8	24.9	91.0	90.8	4.8	0.6
α-D-[1-^{13}C, ^{2}H]erythrose	172.3	26.8	96.9	96.5	5.1	−2.3
β-D-[1-^{13}C, ^{2}H]erythrose	172.3	26.0	102.5	102.1	5.9	2.9
D-[1-^{13}C, ^{2}H]erythrose, hydrate	164.2	25.3	90.8	90.5	5.1	−0.6
Methyl α-D-[2-^{13}C, ^{2}H]ribofuranoside		22.5	72.5	72.1	5.1	
Methyl β-D-[2-^{13}C, ^{2}H]ribofuranoside		23.8	75.7	75.3	5.1	
α-D-[2-^{13}C, ^{2}H]arabinopyranose		22.4	73.4	72.9	6.6	
β-D-[2-^{13}C, ^{2}H]arabinopyranose		22.0	70.0	69.6	5.9	
α-D-[1-^{13}C, ^{2}H]ribose 5-phosphate	173.6	26.8	97.6	97.3	4.4	−1.0
β-D-[1-^{13}C, ^{2}H]ribose 5-phosphate	173.0	26.0	102.3	102.0	4.4	3.6
DL-[1-^{13}C, ^{2}H]glyceraldehyde 3-phosphate	159.8	24.9	90.8	90.5	5.1	−2.4

[a]Chemical shifts are given relative to external Me_4Si and are accurate to ± ppm. Carbon spectra were obtained with broad-band proton decoupling at 30°C.
[b]$^{1}J_{C,^{1}H}$ couplings for unphosphorylated and phosphorylated aldoses were taken from refs. 10 and 11, respectively, and are accurate to ±0.7 Hz.
[c]Coupling constants are accurate to ±0.7 Hz.
[d]$\Delta\nu = \nu_{(^{1}H)} - \nu_{(^{2}H)}$, where $\nu_{(^{1}H)}$ and $\nu_{(^{2}H)}$ are equal to the resonance frequencies of the protonated and deuterated carbons, respectively. $\Delta\nu$ is positive since the observed isotope shifts upon deuteration are upfield from the protonated homologue.
[e]$\Delta J = {}^{1}J_{^{13}C,^{1}H} - \gamma_{^{1}H}\,{}^{1}J_{^{13}C,^{2}H}/\gamma_{^{2}H}$, where $\gamma_{^{1}H}$ and $\gamma_{^{2}H}$ are the magnetogyric ratios for ^{1}H and ^{2}H, respectively.

each tautomeric form, three arising from ^{13}C–^{2}H coupling, and one from the residual protonated carbon. The ^{13}C–^{2}H isotope shift can be estimated from the difference in resonance position between the protonated carbon and the center of gravity of the deuterated carbon triplet. The percent isotopic incorporation is not reflected in peak areas since nuclear Overhauser enhancement is smaller for deuterated than for protonated methine carbons (21). For example, the ^{1}Hmr spectrum of the same preparation of D-[1-^{13}C, ^{2}H]threose shows no resonance for H-1, indicating deuterium enrichment of at least 97%, whereas the proton-decoupled ^{13}Cmr spectrum (Fig. 1B) gives the appearance of a significant proportion of ^{1}H at H-1.

In Table 1, $^{1}J_{^{13}C,^{2}H}$ coupling constants are listed for several carbohydrates and derivatives. The data indicate that $^{1}J_{^{13}Cl-^{2}H1}$ is larger when OH-1 and OH-2 are *cis* in the furanose ring, and that this coupling is larger in the ring forms than in the acyclic hydrates. The same relationships were observed for $^{1}J_{^{13}C,^{1}H}$ (11) (Table 1). Colli *et al.* (22) have shown for several non-carbohydrate compounds that the ratio $^{1}J_{^{13}C,^{1}H}:{}^{1}J_{^{13}C,^{2}H}$ is very close to the value predicted from the magnetogyric ratios for ^{1}H and ^{2}H. The value of ΔJ indicates the extent of variation between observed and predicted values of $^{1}J_{^{13}C,^{2}H}$ and is zero for perfect agreement. As shown in Table 1, values for ΔJ are within the error of the determinations.

^{1}H nmr Spectra

Replacement of ^{1}H with ^{2}H often simplifies ^{1}H spectra, facilitating the assignment of chemical shifts and coupling constants. For example, whereas the 180 MHz ^{1}Hmr spectrum of D-erythrose is essentially first-order, that of D-threose is complex (Fig. 2A). The complexity was eliminated in the spectrum of DL-[3-^{2}H]threose and it was shown that in D-threose the ^{1}Hmr spectrum is complicated by the near magnetic equivalence of H-3α and H-4α which perturbs the resonances of these nuclei and produces a complex multiplet for H-4′α.

Substituting ^{2}H for ^{1}H at H-3 in threose removes three vicinal ^{1}H–^{1}H couplings and the resonances due to H-3 from the spectrum, greatly simplifying assignment and analysis. D-Threose exists primarily as three tautomeric forms in aqueous solution in the ratio α-furanose/β-furanose/hydrate of 4.2 : 3.1 : 1 (10) (Fig. 1A). Although H-2 can be identified by selective homonuclear decoupling of H-1 or by ^{13}C-enrichment at C-2, neither technique permits the unequivocal assignment of H-3, H-4, and H-4′ for each tautomer. Figure 2B shows the H2-H4 region of the 180 MHz ^{1}Hmr spectrum of DL-[3-^{2}H]threose. The H-2, H-4, and H-4′ resonances are easily identified for the furanose forms on the basis of their proportions in solution. In addition, the spectrum is essentially first-order, permitting direct determination of several geminal and vicinal ^{1}H–^{1}H coupling constants. The H-2 resonance of the hydrate is at 3.46 ppm, but resonances due to H-3, H-4, and H-4′ for this form are not readily assigned. However, from the ^{1}Hmr spectrum of the 3-^{2}H derivative (Fig. 2B), it is clear that H-4 and H-4′ for the linear hydrate lie in the same region as H-4′ for the β-furanose, per-

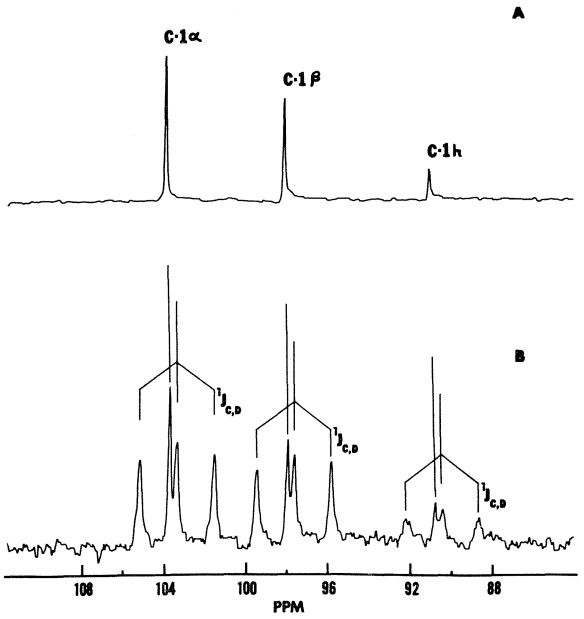

FIG. 1. ^{13}C–^2H coupling and isotope shift in a [^{13}C, ^2H]-enriched carbohydrate. (A) The 15.08 MHz proton-decoupled ^{13}Cmr spectrum of the enriched region of D-[1-^{13}C]threose. The three predominant tautomeric forms in aqueous solution are α- and β-furanose (103.4 and 97.9 ppm, respectively) and acyclic hydrate (91.1 ppm) (10). (B) The 15.08 MHz proton-decoupled ^{13}Cmr spectrum of the enriched region of D-[1-^{13}C, ^2H]threose, showing the splitting of C-1 of each form by the directly-bound deuteron. Isotope shift is shown for each species as the difference in the positions between the protonated C-1 and the center of gravity of the triplet arising from the deuterated C-1.

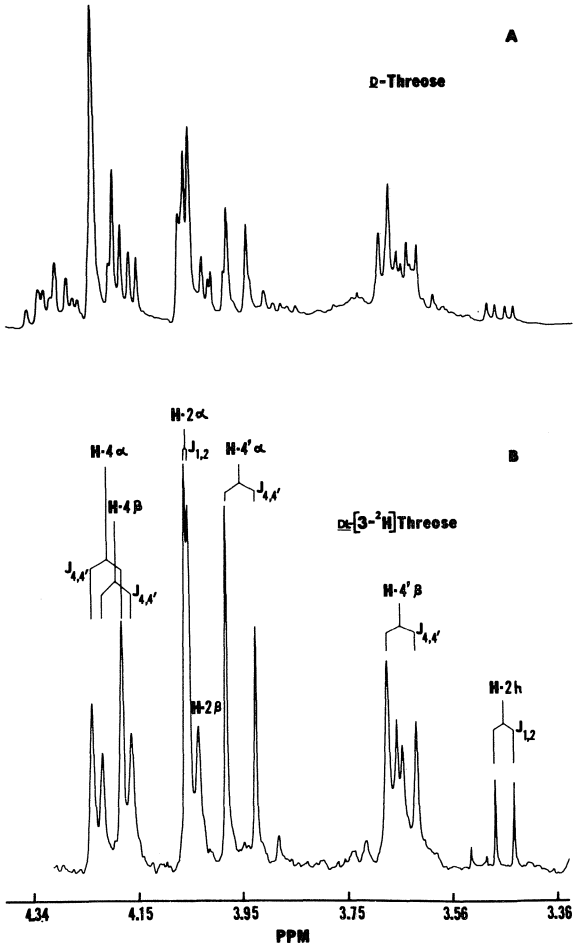

FIG. 2. (A) The 180.04 MHz ^1Hmr spectrum of the H2-H4 region of D-threose. (B) The 180.04 MHz ^1Hmr spectrum of the same region of DL-[3-^2H]threose. Deuteration at C-3 simplifies the spectrum so that assignment of resonances can be made as shown. The upfield half of the doublet from H-2β (due to coupling to H-1β) is observed, with the other half hidden by the H-2α doublet. The magnitude of this coupling is confirmed by observation of H-1β (not shown). The chemical shifts of H-3α and H-3β ,determined by computer simulation, are 4.20 ppm and 4.30 ppm, respectively. Lines between the resonances due to H-4′β appear to arise from H-4 and H-4′ of the acyclic hydrate. H-4′ was arbitrarily designated as the more shielded H-4 of each form.

mitting the position of these resonances to be estimated by computer simulation. Chemical shifts for H-3 for the cyclic forms of D-threose were estimated by comparison of the normal and deuterated compounds and refined by computer simulation. Apparent and intrinsic proton chemical shifts and ^1H–^1H coupling constants for the tetroses are given in Tables 2 and 3.

In both tetroses, H-1 of the hydrate is more shielded than H-1 for the furanoses, while H-2 of the hydrate is the most shielded nucleus.

Heteronuclear ^2H–^1H coupling has been observed in both high resolution ^1H and ^2Hmr spectra (22, 23). However, the ^1Hmr spectra of DL-[3-^2H]threose (Fig. 2B) and DL-[3-^2H]erythrose at 180 MHz do not exhibit ^2H–^1H couplings. Only vicinal or long range ^1H–^2H coupling pathways would be expected in these compounds. Since ^1H–^2H coupling constants are about 15% (1/6.5144) of their ^1H–^1H analogs, the triplets with $^3J_{^1H,^2H}$ values of 0.15–0.77 Hz would be difficult to resolve. As discussed by Mantsch *et al.* (24), ^1H spectra often exhibit an average ^1H–^2H coupling because the remaining ^1H–^1H couplings are considerably larger than the ^1H–^2H couplings or the ^2H-induced isotope shifts in the ^1H spectrum, and the ^1H spectrum is consequently deceptively simple (25). Line broadening (~0.7 Hz) due to pseudorotation of the furanose ring also hinders observation of the smaller ^1H–^2H couplings.

Specific deuteration has been useful in establishing long-range ^1H–^1H coupling in the furanose ring. For example, deuteration of D-erythrose at either H-1 or

TABLE 2. Apparent and intrinsic ^1H chemical shifts for the tetroses and some methyl pentofuranosides in ^2H_2O

Compound	Chemical shifts (ppm)[a]							
	H1	H2	H3	H4	H4′	H5	H5′	CH_3
α-D-Erythrose	5.27[b]	4.10	4.28	4.03	3.92			
				(4.02)				
β-D-Erythrose	5.25	4.02	4.39	4.20	3.79			
D-Erythrose, hydrate	5.09	3.54		3.79	3.64			
α-DL-Threose	5.24	4.05		4.20	3.95			
			(4.20)					
β-DL-Threose	5.40	4.04		4.18	3.65			
			(4.30)					
DL-Threose, hydrate	5.02	3.46		3.67[c]	3.63[c]			
Methyl α-D-ribofuranoside	4.99	4.11	4.02	4.09		3.74	3.64	3.43
			(4.03)			(3.73)	(3.66)	
Methyl β-D-ribofuranoside	4.88	4.02	4.14	3.99		3.79	3.59	3.38
				(4.00)		(3.78)		
Methyl α-D-arabinofuranoside	4.91	4.04	3.92	4.02		3.81	3.68	3.40
			(3.93)			(3.80)	(3.69)	
Methyl β-D-arabinofuranoside	4.89	4.13	4.00	3.88		3.76	3.60	3.41
							(3.61)	

[a]Chemical shifts are given relative to internal sodium 3-(trimethylsilyl)-1 propanesulfonate and are accurate to ±0.01 ppm. Spectra of reducing sugars and glycosides were taken at pH 6.5 and 8.0, respectively. Intrinsic chemical shifts determined by computer simulation are given in parentheses when they are significantly different from experimental values. Assignments of H4, H4′ and H5, H5′ are arbitrary.
[b]Assignment aided by 360 MHz ^1Hmr spectrum obtained at the Purdue Biochemical Magnetic Resonance Laboratory, Department of Chemistry, Purdue University.
[c]Values accurate to ±0.02 ppm.

TABLE 3. Apparent and intrinsic geminal and vicinal ^1H–^1H coupling constants for the tetroses and some methyl pentofuranosides in ^2H_2O

Compound	Coupling constant (Hz)[a]							
	1,2	2,3	3,4	3,4′	4,4′	4,5	4,5′	5,5′
α-D-Erythrose	4.7	5.0[b]	5.0[b]	3.1	−10.0			
	(4.7)	(5.2)	(5.1)	(3.0)	(−10.1)			
β-D-Erythrose	3.4	4.8	5.0	3.4	−9.7			
	(3.4)	(4.8)	(4.9)	(3.5)	(−9.7)			
D-Erythrose, hydrate	4.0	6.6		7.6	−12.1[b]			
α-DL-Threose	1.2	1.8			−10.1			
	(1.2)	(1.8)	(5.6)[b]	(2.6)[b]	(−10.1)			
β-DL-Threose	4.2	4.1			−9.6			
	(4.0)	(4.0)	(5.3)	(3.6)	(−9.6)			
DL-Threose, hydrate	6.2	2.7						
Methyl α-D-ribofuranoside	4.2	6.2	3.1			3.4	4.4	−12.3
	(4.3)	(6.2)	(3.3)			(3.1)	(4.8)	(−12.4)
Methyl β-D-ribofuranoside	1.2	4.7	6.8			3.7	6.4	−12.3
	(1.2)	(4.6)	(6.9)			(3.1)	(6.6)	(−12.2)
Methyl α-D-arabinofuranoside	1.7	3.3	5.8			3.4	5.6	−12.2
	(1.7)	(3.3)	(5.9)			(3.1)	(6.1)	(−12.2)
Methyl β-D-arabinofuranoside	4.5	7.9	6.7			3.4	6.7	−12.1
	(4.6)	(8.0)	(7.1)			(3.2)	(7.4)	(−12.0)

[a]Coupling constants are accurate to ±0.15 Hz. Values found in parentheses are intrinsic coupling constants (±0.2 Hz) determined by computer simulation. Assignments of H4, H4′ and H5, H5′ are arbitrary.
[b]Values are accurate to within ±0.3 Hz.

H-3 simplifies the H-3 or H-1 multiplets, respectively, for the β-anomer, indicating that a small (~0.6 Hz) coupling exists between these nuclei. The α-anomer shows no such coupling. Interestingly, methyl α-D-arabinofuranoside has $^4J_{H1,H3} = 0.5$ Hz, whereas the β-anomer shows no coupling (26).

Heteronuclear spin–spin coupling between ^{13}C and ^1H is valuable in examining conformations of carbohydrates in solution. Generally, two- and three-bond ^{13}C–H coupling constants are difficult to obtain from ^1H-coupled ^{13}Cmr spectra, even when [^{13}C]-enriched compounds are used. These studies are greatly facilitated at high fields (67.89 MHz for carbon) as demonstrated recently (27), but, even in this case, deuterated analogues and heteronuclear selective ^1H decoupling were used to confirm assignments. An alter-

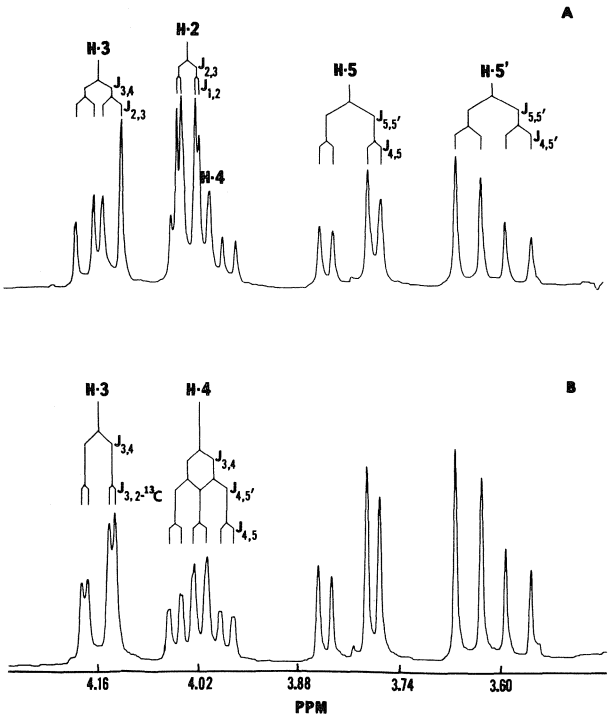

FIG. 3. (A) The 180.04 MHz ^{1}Hmr spectrum of the H-2 to H-5 region of methyl β-D-ribofuranoside, showing the assignment of multiplets. H-5′ was arbitrarily designated as the more shielded H-5. (B) The 180.04 MHz ^{1}Hmr spectrum of the same region of methyl β-D-[2-^{13}C, ^{2}H]ribofuranoside, showing the loss of the H-2 multiplet and coupling of H-3 to ^{13}C-2. The H-4 multiplet is broadened while H-5 and H-5′ are unchanged. Residual [2-^{13}C, ^{1}H] compound would produce two H-2 multiplets split by $^1J_{C2,H2} \simeq 154$ Hz (11). One of these multiplets would appear at approximately 3.59 ppm in this spectrum. It is not observed.

native approach has been to analyze ^{13}C-enriched compounds by ^{1}Hmr (28–34). In cases where ^{1}Hmr spectra are complex, the synthesis of compounds with ^{2}H- and (or) ^{13}C-enrichment may aid interpretation. For example, Fig. 3A shows the 180 MHz ^{1}Hmr spectrum of the H2 to H5 region of methyl β-D-ribofuranoside. The spectrum of the [2-^{13}C, ^{2}H]-enriched derivative (Fig. 3B) is simplified by the loss of a quartet at 4.02 ppm due to H-2. The multiplet centered at 4.14 ppm is altered. In Fig. 3A, $^3J_{H3,H4}$ and $^3J_{H2,H3}$ can be assigned. Inspection of the coupling patterns for H-1 (not shown) and H-2 confirms the assignment of the multiplet at 4.14 ppm to H-3. In Fig. 3B, the H-3 multiplet contains $^3J_{H3,H4}$ and a new coupling, $^2J_{C2,H3} = 1.6$ Hz. Loss of the H-2 multiplet in this spectrum permits H-4 to be assigned and $^3J_{H4,H5}$ and $^3J_{H4,H5'}$ to be evaluated from the H-4 multiplet. Note that H-4 is slightly broadened in the [^{13}C]-enriched compound, suggesting a small three-bond coupling of this nucleus to C-2. This broadening probably does not arise from ^{1}H–^{2}H coupling (see above). Resonances due to H-5 and H-5′ are quartets centered at 3.79 and 3.59 ppm, respectively. In [2-^{13}C, ^{2}H] methyl α-D-ribofuranoside, $^2J_{C2,H3}$ is small, producing a broadening of the H-3 doublet.

The apparent and intrinsic ^{1}H chemical shifts and ^{1}H–^{1}H coupling constants for methyl *ribo* and *arabino* furanosides determined from the experimental and computer-simulated data, respectively, are listed in Tables 2 and 3. Although in several instances the use of [^{2}H]-enriched compounds was not required to make these assignments, there is no doubt of the value of multiply-enriched derivatives for use in more complex instances.

Experimental

Materials and Instrumentation

D-Glyceraldehyde was prepared from D-fructose by oxidation with lead tetraacetate (35) and quantitated with Nelson's reagent (36) using DL-glyceraldehyde (Sigma Chemical Co) as a standard. D-Erythrose and D-threose were prepared as described by Perlin (37) and Ball (38), respectively. Potassium [^{13}C] cyanide (K^{13}CN) was supplied by the Los Alamos Scientific Laboratory, University of California, Los Alamos, NM, with 99.64% purity and 90.7 atom% ^{13}C enrichment. Potassium [^{14}C] cyanide (K^{14}CN) was purchased from New England Nuclear with a specific activity of 46 mCi/mmol. Palladium barium sulfate (5%) and deuterium oxide (^2H_2O) (99.8 atom%) were purchased from Sigma Chemical Co. Lead tetraacetate, deuterium chloride (^{2}HCl) (20%,99 atom%), and sodium deuteroxide (NaO^{2}H) (30%, 99 atom%) were obtained from Aldrich Chemical Co. Acetic acid-$^2H_4$ (99.5 atom%) and deuterium gas ($^2H_2$) (99.5 atom%) were obtained from Merck Sharpe and Dohme Canada Limited.

Dowex 1-X2 (200–400 mesh) was obtained from Sigma Chemical Co. and converted to the hydroxide form with 2 *M* NaOH.

^{13}Cmr spectra were obtained using a Bruker WP-60 15.08-MHz Fourier transform spectrometer equipped with quadrature detection. Spectra were obtained at 30°C with 4K spectral points and the spectrometer was locked to the resonance of ^2H_2O in a capillary. Chemical shifts are given relative to external tetramethylsilane (Me_4Si) and are accurate to ±0.1 ppm.

^{1}Hmr spectra were obtained at 30°C in ^2H_2O on a Bruker WH-180 equipped for Fourier transform operation using a 400 Hz sweep width and 8K spectral points. Chemical shifts are reported in ppm downfield from internal sodium 3-(trimethylsilyl)-1-propanesulfonate and are accurate to ±0.01 ppm. Complex spectra were analyzed by computer simulation as described previously (11,39). The rms error between a simulated and experimental spectrum was typically 0.15 Hz. ^2H_2O solutions were treated with ^2H_2O-washed Chelex resin (Sigma Chemical Co) to remove paramagnetic species (40) prior to analysis by ^{1}Hmr.

pH Measurements in ^2H_2O solutions were corrected using the equation pH = pD − 0.4 (41). Phosphate assays were carried out according to Leloir and Cardini (42) and radioactivity (^{14}C) was assayed as described previously (9).

General Method For the Preparation of Deuterated Carbohydrates. Preparation of D-[*1-*^{13}*C,* ^{14}*C,* ^{2}*H*]-*Erythrose and Threose*

A solution of K^{13}CN (2 mmol, 13 mL ^2H_2O) at 20°C con-

taining $K^{14}CN$ (10^7 cpm) was added to a 25 mL sealed flask (9) and adjusted to pH 8.0 ± 0.1 with 0.7 *M* acetic acid-$^2H_4$. D-Glyceraldehyde (2 mmol) was concentrated from 3 mL of ^2H_2O several times at 30°C *in vacuo*. The residual gum was dissolved in 4–5 mL ^2H_2O and added to the solution of $K^{13}CN$. The pH of the reaction mixture was maintained between 8.0 and 8.3 with additions of 0.7 *M* acetic acid-$^2H_4$ and (or) 1.0 *M* NaO^2H. After 20–25 min, the pH was lowered to 4.0 ± 0.2 with 17 *M* acetic acid-$^2H_4$. A further adjustment of pH to 1.7 ± 0.2 was made with 3 *M* ^2HCl.

Palladium-barium sulfate (5%, 62 mg per mmol of nitrile) was weighed into a 50 mL side-arm flask, 5 mL ^2H_2O was added, and the system was evacuated and charged three times with N_2. After the last evacuation, the system was charged with $^2H_2$ and the catalyst reduced for 15–20 min at atmospheric pressure and 25°C with efficient stirring. The ballast containing $^2H_2$ was filled with light mineral oil to prevent entry of H_2O into the reduction apparatus (10). The [^{13}C]-enriched aldononitriles were then added and the reduction was continued for 10 h, or until the nitriles were completely reduced as determined by gas-chromatography (10). The product epimeric aldoses were deionized and separated as described previously (10). Products were characterized by ^{1}H and ^{13}Cmr yield: 70% based on product weight as gums and on the recovery of radioactivity after separation.

Preparation of D-[2-^{13}C, ^{14}C, ^2H]*Ribose and Arabinose*

D-[2-^{13}C, ^{14}C, ^{2}H]ribose and arabinose were prepared from D-[1-^{13}C, ^{14}C, ^{2}H]erythrose according to a modified procedure described for the preparation of the [1-^{13}C] compounds (9). The condensation reaction with KCN in H_2O was carried out at pH 7.8–8.0 for 9 min. The solution was adjusted to pH 4.0 with acetic acid and then to pH 3.0 ± 0.1 with HCl. The epimeric nitriles were reduced with Pd/H_2 at 20 psi and 25°C in a Parr apparatus, and the product aldoses were purified and analyzed by ^{13}C and ^{1}Hmr. Yield as dry gums: 78% after separation.

Preparation of Methyl α-D-[2-^{13}C, ^{14}C, ^2H]*Ribofuranoside and Methyl* β-D-[2-^{13}C, ^{14}C, ^2H]*Ribofuranoside*

D-[2-^{13}C, ^{14}C, ^{2}H]ribose was converted to the methyl furanosides by the procedure of Barker and Fletcher (43). The reaction mixture was neutralized by passage through a 1.2 cm × 5 cm column of Dowex 1-X8 (200–400 mesh) in the acetate form and elution with deionized water. The resulting solution was concentrated at 30°C *in vacuo* and applied to a 1.5 cm × 23 cm column of Dowex 1-X8 (200–400 mesh) in the hydroxide form (44) and developed with decarbonated distilled H_2O with a flow rate of 0.25 mL/min. Fractions (3 mL) were collected and assayed with phenol–sulfuric acid (45.) The α-anomer eluted between fractions 25–35 and the β-anomer eluted between fractions 60–80. Fractions were pooled, concentrated at 30°C *in vacuo*, and analyzed by ^{13}C and ^{1}Hmr. Anomers were identified by comparison of ^{13}C chemical shifts for C-2 with those reported previously (46).

Methyl-D-arabinofuranosides were prepared by the procedure of Augestad and Berner (47) and the α- and β-anomers were separated by the method of Austin *et al.* (44). Anomers were identified by ^{13}Cmr using chemical shifts reported previously (46).

DL-[2-^{14}C, 3-^{2}H]erythrose and threose were prepared from [1-^{2}H]glycolaldehyde by successive condensations of the C_2 and C_3 deuterated aldoses with KCN ($K^{14}CN$) and reduction with Pd/H_2 (10). The two condensations with KCN were modified by using H_2SO_4 rather than HCl to adjust the pH of the reaction mixtures from 4.0 to 1.7 ± 0.1 prior to reduction. Catalyst was removed by filtration through sintered glass and the reduction products were deionized with $BaCO_3$. The solution was filtered through Celite to remove the $BaSO_4$ precipitate and residual $BaCO_3$, the filter pad was washed well with H_2O, and the filtrate and washings were treated batchwise with Dowex 1 × 8 (OAc^-) and Dowex 50 × 8 (H^+) sucessively. The clear, colorless solution was concentrated to 2 mL at 30°C *in vacuo* and the mixture separated as described previously on Dowex 50 × 8 (200–400) (Ba^{++}) (10).

DL-[1-^{14}C, ^{2}H]glyceraldehyde was prepared from DL-[1-^{14}C,]-glyceronitrile by reduction with $^2H_2$ and purified as described previously (10). Yield after purification, 82%. ^{13}Cmr: 75.5 ppm (C-2, hydrate) and 63.4 ppm (C-3, hydrate).

D-[1-^{14}C]erythrose 4-phosphate (E4P) was prepared from D-[1-^{14}C]erythrononitrile 4-phosphate by reduction with H_2 (11). D-[1-^{14}C] E4P was converted to D-[1-^{13}C, ^{2}H, 2-^{14}C]-ribose 5-phosphate by reduction with $Pd/^2H_2$. DL-[1-^{13}C, ^{14}C, ^{2}H]glyceraldehyde 3-phosphate was prepared from DL-[1-^{13}C, ^{14}C]glyceronitrile 3-phosphate and purified as described previously (11). Yield based on recovery of phosphate and radioactivity after chromatography, 69% with 5% inorganic phosphate.

1. P. A. J. Gorin. Can. J. Chem. **52**, 458 (1974).
2. H. J. Koch and A. S. Perlin. Carbohydr. Res. **15**, 403 (1970).
3. D. R. Bundle, H. J. Jennings, and I. C. P. Smith. Can. J. Chem. **51**, 3812 (1973).
4. P. A. J. Gorin and M. Mazurek. Can. J. Chem. **53**, 1212 (1975).
5. R. U. Lemieux and J. D. Stevens. Can. J. Chem. **44**, 249 (1966).
6. S. J. Angyal and G. S. Bethell. Aust. J. Chem. **29**, 1249 (1976).
7. T. E. Walker, R. E. London, T. W. Whaley, R. Barker, and N. A. Matwiyoff. J. Am. Chem. Soc. **98**, 5807 (1976).
8. T. E. Walker, R. E. London, R. Barker, and N. A. Matwiyoff. Carbohydr. Res. **60**, 9 (1978).
9. A. S. Serianni, H. A. Nunez, and R. Barker. Carbohydr. Res. **72**, 71 (1979).
10. A. S. Serianni, E. L. Clark, and R. Barker. Carbohydr. Res. **72**, 79 (1979).
11. A. S. Serianni, J. Pierce, and R. Barker. Biochemistry, **18** (7), 1192 (1979).
12. H. A. Nunez, T. E. Walker, R. Fuentes, J. O'Connor, A. Serianni, and R. Barker. J. Supramol. Struct. **6**, 535 (1977).
13. F. Balza, N. Cyr, G. K. Hamer, A. S. Perlin, H. J. Koch, and R. S. Stuart. Carbohydr. Res. **59**, C7 (1977).
14. J. K. N. Jones and R. A. Wall. Can. J. Chem. **38**, 2290 (1960).
15. O. Samuelson. Methods Carbohydr. Chem. **6**, 65 (1972).
16. E. Clark and R. Barker. Unpublished results.
17. H. Kiliani. Ber. **20**, 339 (1887).
18. R. Varma and D. French. Carbohydr. Res. **25**, 71 (1972).
19. A. Serianni, H. Nunez, and R. Barker. Unpublished results.
20. R. Kuhn and W. Bister. Ann. **602**, 217 (1957).
21. J. B. Stothers. ^{13}C NMR studies of reaction mechanisms and reactive intermediates. Topics in carbon-13 NMR spectroscopy. Vol. 1. *Edited by* G. C. Levy. John Wiley & Sons, New York. 1974. p. 229.
22. H. N. Colli, V. Gold, and J. E. Pearson. J. Chem. Soc. Chem. Commun. 408 (1973).
23. H. J. Bernstein and N. Sheppard. J. Chem. Phys. **37**, 3012 (1962).
24. H. H. Mantsch, H. Saito, and I. C. P. Smith. Prog. Nucl. Magn. Reson. Spectrosc. **11**, 211 (1977).
25. R. J. Abraham. Analysis of high resolution NMR spectra. Elsevier, London. 1971. p. 268.

26. J. D. STEVENS and H. G. FLETCHER. J. Org. Chem. **33**, 1799 (1968).
27. K. BOCK and C. PEDERSEN. Acta Chem. Scand. Ser. B, **31**, 354 (1977).
28. A. S. PERLIN and B. CASU. Tetrahedron Lett. 2921 (1969).
29. R. U. LEMIEUX, T. L. NAGABHUSHAN, and B. PAUL. Can. J. Chem. **50**, 773 (1972).
30. J. A. SCHWARCZ and A. S. PERLIN. Can. J. Chem. **50**, 3667 (1972).
31. R. U. LEMIEUX. Ann. N.Y. Acad. Sci. **222**, 915 (1973).
32. A. S. PERLIN, N. CYR, R. G. S. RITCHIE, and A. PARFONDY. Carbohydr. Res. **37**, C1 (1974).
33. J. A. SCHWARCZ, N. CYR, and A. S. PERLIN. Can. J. Chem. **53**, 1872 (1975).
34. R. G. S. RITCHIE, N. CYR, and A. S. PERLIN. Can. J. Chem. **54**, 2301 (1976).
35. A. S. PERLIN. Methods Carbohydr. Chem. **1**, 61 (1962).
36. J. CLARK, JR. and R. L. SWITZER. Experimental biochemistry. 2nd ed. W. H. Freeman and Company, San Francisco. 1977. p. 166.
37. A. S. PERLIN. Methods Carbohydr. Chem. **1**, 64 (1962).
38. D. H. BALL. J. Org. Chem. **31**, 220 (1966).
39. J. V. O'CONNOR, H. A. NUNEZ, and R. BARKER. Biochemistry, **18**, 500 (1979).
40. H. PEARSON, D. GUST, I. M. ARMATAGE, H. HUBER, J. D. ROBERTS, R. E. STARK, R. R. VOLD, and R. L. VOLD. Proc. Natl. Acad. Sci. U.S.A. **72**, 1599 (1975).
41. R. LUMRY, E. L. SMITH, and R. R. GRANT. J. Am. Chem. Soc. **73**, 4330 (1951).
42. L. F. LELOIR and C. E. CARDINI. Methods Enzymol. **3**, 840 (1957).
43. R. BARKER and H. G. FLETCHER, JR. J. Org. Chem. **26**, 4605 (1961).
44. P. W. AUSTIN, F. E. HARDY, J. G. BUCHANAN, and J. BADDILEY. J. Chem. Soc. 5350 (1963).
45. J. E. HODGE and B. T. HOFREITER. Methods Carbohydr. Chem. **1**, 380 (1962).
46. R. G. S. RITCHIE, N. CYR, B. KORSCH, H. J. KOCH, and A. S. PERLIN. Can. J. Chem. **53**, 1424 (1975).
47. I. AUGESTAD and E. BERNER. Acta Chem. Scand. **8** (2), 251 (1954).

Carbon-13 nuclear magnetic resonance spectra of oxazoles

HENK HIEMSTRA, HENDRIK A. HOUWING, OKKO POSSEL, AND ALBERT M. VAN LEUSEN
Department of Organic Chemistry, Groningen University, Nijenborgh 16, 9747 AG Groningen, The Netherlands

Received June 14, 1979

HENK HIEMSTRA, HENDRIK A. HOUWING, OKKO POSSEL, and ALBERT M. VAN LEUSEN. Can. J. Chem. **57**, 3168 (1979).

The ^{13}C nmr spectra of oxazole and eight mono- and disubstituted derivatives have been analyzed with regard to the chemical shifts and the various carbon–proton coupling constants of the ring carbons. The data of the parent oxazole are compared with thiazole and 1-methylimidazole.

HENK HIEMSTRA, HENDRIK A. HOUWING, OKKO POSSEL et ALBERT M. VAN LEUSEN. Can. J. Chem. **57**, 3168 (1979).

On a analysé les spectres rmn du ^{13}C de l'oxazole et de huit dérivés mono ou bisubstitués du point de vue des déplacements chimiques et des différentes constantes de couplage C—H des atomes de carbone du cycle. Les données relatives à l'oxazole parente sont comparées à celles du thiazole et du méthyl-1 imidazole.

[Traduit par le journal]

In the course of our work on a new synthesis of azoles (1) we were confronted with a lack of ^{13}C nmr data of oxazoles. Thus far, only the spectrum of benzoxazole (2) and the ^1J (C, H) coupling constants of 4-methyloxazole (3) have been reported.[1] It became, therefore, worthwhile to carry out a ^{13}C nmr analysis of the oxazole ring system.

We here present the data of a series of nine oxazoles, i.e., the chemical shifts of the ring carbons (Table 1) and coupling constants (Table 3). Furthermore, these data of the parent oxazole are compared with thiazole and 1-methylimidazole (Tables 2 and 3).

Experimental

The oxazoles **4**, **6**, **7**, and **8** (Table 1) were recently prepared in our laboratory by reaction of tosylmethyl isocyanide (TosMIC) or derivatives thereof, and aromatic aldehydes (1). Samples of the oxazoles **1**, **2**, **3**, and **5** were prepared according to the literature referred to in Table 1.

The ^{13}C nmr spectra were measured in $CDCl_3$ solution at 35°C on a Varian XL 100 apparatus using the FT technique and an internal deuterium lock. The $CDCl_3$ absorptions were used as internal reference; chemical shifts were corrected to δ_{TMS} with $\delta_{TMS} = \delta_{CDCl_3} + 77.0$ ppm. Coupled spectra were recorded using the gated noise decoupling technique.

In the measurements in which the methyl protons were selectively decoupled, the low power decoupling transmitter was employed in the hetero mode. To that end the proton spectrum of the sample was recorded first (also with ^2H lock and in the CW mode) to determine the exact setting of the decoupler offset, i.e., the setting that gives a zero beat at the position of the singlet of the methyl protons.

Results and Discussion

^{13}C Chemical Shifts

Chemical shift data of the parent oxazole (**1**), three monosubstituted derivatives (**2**–**4**), and five disubstituted ones (**5**–**9**) are given in Table 1. The chemical shifts of the ring carbons have been assigned by making use of the (absence of) one-bond C—H coupling constants (^1J), and known substituent effects of aryl, methyl, methoxy, and tosyl (1*g*, 4, 5).

From this assignment the following generalizations can be made. (*1*) In all cases C(2), located between two electronegative hetero atoms, resonates at the lowest field; at ca. 150 ppm when unsubstituted, and about 10 ppm lower when substituted with methyl, methoxy, or phenyl. (*2*) The chemical shifts of C(4) and C(5), at ca. 126 and 138 ppm, respectively, when both carbons are unsubstituted, show a downfield shift of 10–15 ppm upon substitution with one aryl group and, simultaneously, an upfield shift of about 5 ppm for the other (unsubstituted) carbon.

In Table 2 the chemical shifts of the ring carbons of oxazole (**1**) are compared with thiazole **10** (5) and *N*-methylimidazole **11** (6). The highest field absorption of **1** belongs to C(4) rather than to C(5) as in **10** and **11**, which may be a reflection of the higher electronegativity of oxygen. In **10** the C(4) absorption is shifted ca. 18 ppm to lower field as compared with **1** and **11**; an almost identical difference is observed for the C(β) of thiophene with respect to furan and pyrrole (11).

Coupling Constants

All one-bond coupling constants (^1J) and most of the long range coupling constants (^2J, ^3J) of the oxazole ring atoms were easily obtained from the coupled ^{13}C spectra[2] (see Table 3). The oxazoles

[1] After this paper was submitted for publication, ^{13}C nmr spectra of a large number of benzoxazoles and oxazole were published (12). The spectral data of oxazole were almost identical to our results.

[2] The splitting patterns of the oxazole ring atoms were first order both in ^1H and ^{13}C nmr.

0008-4042/79/233168-03$01.00/0

TABLE 1. ^{13}C nuclear magnetic resonance chemical shifts of the ring carbons of a series of oxazoles

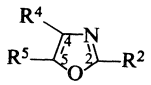

Compound	Substituents R²	R⁴	R⁵	Chemical shifts[a] (ppm) C(2)	C(4)	C(5)	Other absorptions	Ref.
1	H	H	H	150.6	125.4	138.1		7
2	Ph	H	H	160.9	127.6	137.7	125.4, 126.7, 127.8, 129.3	8
3	H	Tos	H	152.1	142.6	141.8	21.5, 128.2, 129.9, 136.2, 145.2	9
4	H	H	*p*-ClPh	150.1	121.3	149.8	124.9, 125.6, 128.5, 133.7	1*a*
5	Me	Ph	H	161.0	140.1	132.6	13.0, 124.7, 127.1, 128.0, 130.7	10
6	Me	H	*p*-ClPh	160.3	121.7	149.3	13.1, 124.3, 125.9, 128.2, 132.8	1*e*
7	MeO	H	*p*-ClPh	162.1	121.1	145.3	57.9, 124.1, 126.3, 128.7, 133.0	1*k*
8	H	Me	*p*-ClPh	148.5	131.0	143.8	13.2, 125.7, 126.6, 128.2, 132.8	1*j*
9	H	Benzo		152.6	140.1	150.0	110.8, 120.5, 124.4, 125.4	2

[a]Estimated errors are within ±0.3 ppm.

TABLE 2. ^{13}C nuclear magnetic resonance chemical shifts (ppm) of oxazole (**1**), thiazole (**10**), and 1-methylimidazole (**11**)

Compound	C(2)	C(4)	C(5)	CH_3
1	150.6	125.4	138.1	—
10[a]	153.6	143.3	119.6	—
11	135.8	126.7	118.3	30.7

[a]Data obtained from ref. 5.

5, **6**, **8**, and 1-methylimidazole (**11**) gave more complex signals because of additional long range coupling with the methyl hydrogens. The additional coupling could be eliminated, however, by selective irradiation of the methyl protons. For the oxazoles **5**, **6**, and **8** this decoupling did not affect the other coupling constants; only 1-methylimidazole (**11**) showed a slight reduction of the coupling constants. The ^2J and ^3J coupling constants of **11** listed in Table 3 were obtained by multiplying the measured coupling constant (J reduced) with a factor derived from the ^1J's of the selectively decoupled and the gated noise decoupled spectra of **11**, assuming a constant ratio J reduced/J for each proton.[3]

$^1J(C,H)$

In all oxazoles (**1–9**) the various ^1J's have about the same values: 230 Hz for C(2)—H(2), 194 Hz for C(4)—H(4), and 210 Hz for C(5)—H(5). This leads to the following sequence for oxazoles ^1J C(2),-H(2) > ^1J C(5),H(5) > ^1J C(4),H(4), whereas for thiazole (**10**) and 1-methylimidazole (**11**) was found ^1J C(2),H(2) > ^1J C(5),H(5) ≃ ^1J C(4),H(4). The

TABLE 3. The ^{13}C—H coupling constants (J, Hz) of the ring atoms of oxazoles **1–8**, thiazole (**10**), and 1-methylimidazole (**11**)[a]

Compound[b]	J between C(2) and H(2)	H(4)	H(5)	J between C(4) and H(2)	H(4)	H(5)	J between C(5) and H(2)	H(4)	H(5)
1	231.1	10.7	7.9	8.9	195.3	16.5	4.1	18.9	209.1
2		[c]	[c]		193.8	16.2		18.6	207.6
3	236.2		9.0	9.3		13.7	4.0		217.2
4	230.9	11.3		8.4	194.3		4.2	17.4	
5			8.1			14.3			205.6
6		11.3			192.3			17.0	
7		12.5			193.0			15.6	
8	229.0			8.2			5.6		
10[d]	213.0	15.2	6.0	15.2	187.0	7.1	≃0	16.2	190.6
11[f]	205.9	10.6	7.0	10.7[e]	188.0	10.3[e]	3.5	16.6	188.6

[a]Estimated errors within ±0.6 Hz.
[b]For substituents of oxazoles **1–8** see Table 1.
[c]Not determined because of further coupling with the phenyl protons.
[d]Values obtained from ref. 5.
[e]Assignment might be the reverse.
[f]Values are in close analogy to data in ref. 6.

[3]See ref. 4, p. 66 ff.

greater electronegativity of oxygen causes a larger difference between the ^1J's of the oxazoles.

^{2}J (C, H)

The two-bond coupling constants of the oxazoles ^2J C(4),H(5) and ^2J C(5),H(4) have values of about 16 Hz and 18 Hz, respectively. Comparison with **10** and **11** shows that ^2J C(5),H(4) is almost independent of the nature of ring atom 1 (O, S, or N), whereas ^2J C(4),H(5) appears to increase with a larger electronegativity of atom 1 (5).

^{3}J (C, H)

In oxazoles the three-bond coupling constants are smaller than the ^2J's. The sequence in magnitude of the ^3J's for the three ring systems is for oxazole ^3J C(2),H(4) > ^3J C(4),H(2) $\simeq$ ^3J C(2),H(5) > ^3J C(5),H(2), and for thiazole and imidazole: ^3J C(2),H(4) $\simeq$ ^3J C(4),H(2) > ^3J C(2),H(5) > ^3J C(5),H(2).

The data in Table 3 show that the magnitude of the coupling constants of the oxazole nucleus is only slightly affected by substituents. This observation can be of use in structural assignments in oxazole chemistry.

1. (*a*) A. M. VAN LEUSEN, B. E. HOOGENBOOM, and H. SIDERIUS. Tetrahedron Lett. 2369 (1972); (*b*) O. H. OLDENZIEL and A. M. VAN LEUSEN. Tetrahedron Lett. 2777 (1972); (*c*) A. M. VAN LEUSEN, H. SIDERIUS, B. E. HOOGENBOOM, and D. VAN LEUSEN. Tetrahedron Lett. 5337 (1972); (*d*) A. M. VAN LEUSEN and H. E. VAN GENNEP. Tetrahedron Lett. 627 (1973); (*e*) H. A. HOUWING, J. WILDEMAN, and A. M. VAN LEUSEN. Tetrahedron Lett. 143 (1976); (*f*) A. M. VAN LEUSEN and J. SCHUT. Tetrahedron Lett. 285 (1976); (*g*) A. M. VAN LEUSEN, B. E. HOOGENBOOM, and H. A. HOUWING. J. Org. Chem. **41**, 711 (1976); (*h*) A. M. VAN LEUSEN, J. WILDEMAN, and O. H. OLDENZIEL. J. Org. Chem. **42**, 1153 (1977); (*i*) A. M. VAN LEUSEN and J. WILDEMAN. Synthesis, 501 (1977); (*j*) O. POSSEL and A. M. VAN LEUSEN. Heterocycles, **7**, 77 (1977); (*k*) H. A. HOUWING and A. M. VAN LEUSEN. To be published.
2. R. F. JOHNSON and W. C. JANKOWSKI. Carbon-13 nmr spectra. Wiley, New York, NY. 1972. p. 227.
3. P. HAAKE, L. P. BAUSHER, and W. B. MILLER. J. Am. Chem. Soc. **91**, 1113 (1969).
4. F. W. WEHRLI and T. WIRTHLIN. Interpretation of carbon-13 nmr spectra. Heyden, London. 1976. p. 36 ff.
5. R. FAURE, J.-P. GALY, E. J. VINCENT, and J. ELGUERO. Can. J. Chem. **56**, 46 (1978).
6. (*a*) M. BEGTRUP. J. Chem. Soc. Perkin Trans. II, 736 (1976); (*b*) M. BEGTRUP, R. M. CLARAMUNT, and J. ELGUERO. J. Chem. Soc. Perkin Trans. II, 99 (1978).
7. H. BREDERECK and R. BANGERT. Chem. Ber. **97**, 1414 (1964).
8. P. G. FERRINI and A. MARXER. Angew. Chem. **75**, 165 (1963).
9. J. R. BULL and A. TUINMAN. Tetrahedron, **31**, 2151 (1975).
10. M. LEWY. Chem. Ber. **20**, 2576 (1887).
11. J. B. STOTHERS. ^{13}C nmr spectroscopy. Academic Press, New York, NY. 1972 . p. 253.
12. J. LLINARES, J.-P. GALY, R. FAURE, E.-J. VINCENT, and J. ELGUERO. Can. J. Chem. **57**, 937 (1979).

COMMUNICATION

The formation and structure of a 1,5-disubstituted S_4N_4 ring, $(Ph_3P{=}N)_2S_4N_4$, from the reaction of triphenylphosphine with tetrasulphur tetranitride

JOSEF BOJES, TRISTRAM CHIVERS,[1] GREG MACLEAN, AND RICHARD T. OAKLEY
Department of Chemistry, University of Calgary, Calgary, Alta., Canada T2N 1N4
AND
A. WALLACE CORDES
Department of Chemistry, University of Arkansas, Fayetteville, AR 72701, U.S.A.

Received September 6, 1979

JOSEF BOJES, TRISTRAM CHIVERS, GREG MACLEAN, RICHARD T. OAKLEY, and A. WALLACE CORDES. Can. J. Chem. **57**, 3171 (1979).

Two novel products, $(Ph_3P{=}N)_2S_4N_4$ and $(Ph_3P{=}N)_3S^+S_4N_5^-$, have been isolated from the reaction of triphenylphosphine with S_4N_4; an X-ray structural determination of $(Ph_3P{=}N)_2S_4N_4$ shows it to consist of a 1,5-disubstituted S_4N_4 ring with the exocyclic substituents in an *axial, equatorial* configuration.

JOSEF BOJES, TRISTRAM CHIVERS, GREG MACLEAN, RICHARD T. OAKLEY et A. WALLACE CORDES. Can. J. Chem. **57**, 3171 (1979).

On a isolé deux nouveaux produits de la réaction de la triphénylphosphine avec S_4N_4: $(Ph_3P{=}N)_2S_4N_4$ et $(Ph_3P{=}N)_3S^+S_4N_5^-$. La détermination de la structure de $(Ph_3P{=}N)_2S_4N_4$ à l'aide de rayons-X montre que ce composé est formé d'un cycle S_4N_4 disubstitué en positions 1 et 5 avec des substituants exocycliques ayant une configuration *axiale équatoriale*.
[Traduit par le journal]

The formation (1, 2) and structure (3) of $Ph_3P{=}N{-}S_3N_3$ have been known for some time. As a part of our studies on the nucleophilic degradation of S_4N_4 (4) we have reinvestigated the reaction of S_4N_4 with triphenylphosphine, the original method used to prepare $Ph_3P{=}N{-}S_3N_3$ (1). Consistent with our earlier results (4), we find that the $S_4N_5^-$ ion is also formed in this reaction, as a salt of the novel sulphonium ion, $(Ph_3P{=}N)_3S^+$. More significant, however, is the formation of $(Ph_3P{=}N)_2S_4N_4$ (**1**) as the major product when the reaction is carried out in acetonitrile. In this Communication we describe the formation and structure of **1**, the first example of a 1,5-disubstituted S_4N_4 ring, and the isolation and characterization of $(Ph_3P{=}N)_3S^+S_4N_5^-$ (**2**).

Reaction of triphenylphosphine (2.85 g, 10.0 mmol) and S_4N_4 (1.00 g, 5.43 mmol) in acetonitrile (60 mL) at 23°C produces a salmon-pink precipitate. After washing this precipitate with diethyl ether (to remove Ph_3PS), extraction with acetonitrile (5 × 100 mL) yields, upon evaporation of the solvent, pale yellow needles of $(Ph_3P{=}N)_3S^+S_4N_5^-$ (**2**) (0.47 g), which exhibit uv–visible (in CH_2Cl_2, λ_{max}: 345 nm(sh), $\varepsilon \sim 3.3 \times 10^3$ L mol^{-1} cm^{-1}, and ~290 nm) and ir (in Nujol, excluding cation bands: 956 s, 916 m, 665 vw, 647 w, 600 w, 438 m, and 300 w cm^{-1}) bands characteristic of the $S_4N_5^-$ ion (4, 5).[2] We found that **2** is also produced in 23% yield from triphenylphosphine and S_4N_4 in benzene at 23°C; it is surprising that no mention of this compound has been made before (1, 2).

We believe the formation of **2** involves $Ph_3P{=}N{-}S{-}N{=}PPh_3$ as an intermediate which immediately disproportionates to $[(Ph_3P{=}N)_3S^+]_2S^{2-}$. The subsequent reaction of sulphide ion with S_4N_4 is known to produce $S_4N_5^-$ (4*b*). In support of this belief we showed that the reaction of $Ph_3P{=}N{-}SiMe_3$ with SCl_2 yields $(Ph_3P{=}N)_3S^+Cl^-$ (85%) (6).[3] Final confirmation of the identity of **2** was obtained by cation exchange between $(Ph_3P{=}N)_3S^+Cl^-$ and *n*-$Bu_4N^+S_4N_5^-$ (4*a*, 5*a*) in acetonitrile.

[1]Author to whom correspondence may be addressed.

[2]The identity of the new sulphonium ion, $(Ph_3P{=}N)_3S^+$, has been confirmed by an X-ray crystal structure determination of **2** performed by Dr. M. Extine, Molecular Structure Corporation, Texas. The important structural parameters are as follows: d(S—N) = 1.635(4), d(P—N) = 1.597(4) Å; NSN = 102.1(2)°, SNP = 119.2(3)°.

[3]A related compound $[(Ph_3P{=}N)_3S^{3+}][3Cl^-]$ (based on analytical data), with a red color, was previously claimed to be one of the products of the reaction of triphenylphosphine with S_4N_3Cl.

0008-4042/79/233171-02$01.00/0

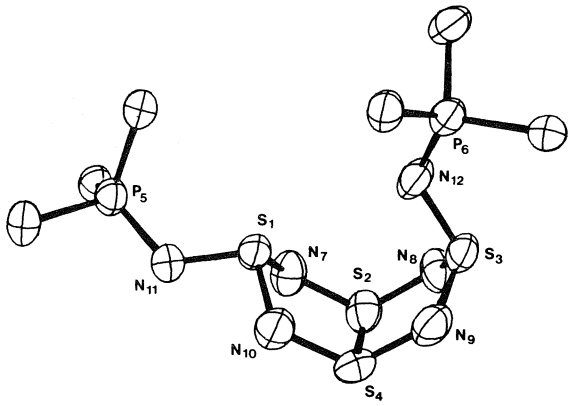

FIG. 1. ORTEP drawing of the $(Ph_3P{=}N)_2S_4N_4$ structure (the phenyl rings are omitted for clarity). Principal structural parameters are (e.s.d's in parentheses): S(1)—N(7), 1.675(4); S(1)—N(10), 1.666(4); S(3)—N(8), 1.630(4); S(3)—N(9), 1.632(4); S(2)—N(7), 1.588(4); S(2)—N(8), 1.605(4); S(4)—N(9), 1.613(4); S(4)—N(10), 1.583(4), S(1)—N(11), 1.599(4); S(3)—N(12), 1.621(4); S(1)—S(3), 3.727(2); S(2)—S(4), 2.452(2); P(5)—N(11) and P(6)—N(12), 1.592(4) Å. N(7)—S(1)—N(10), 101.0(2); N(8)—S(3)—N(9), 104.0(2); N(7)—S(2)—N(8), 120.6(2), N(9)—S(4)—N(10), 120.2(2), S(1)—N(7)—S(2), 118.8(1); S(1)—N(10)—S(4), 118.6(1); S(2)—N(8)—S(3), 120.9(2); S(3)—N(9)—S(4), 120.5(2)°.

The acetonitrile-insoluble solid from the Ph_3P/S_4N_4 reaction (1.09 g) can be recrystallized from CH_2Cl_2/CH_3CN to give pale yellow blocks of $(Ph_3P{=}N)_2S_4N_4$ (**1**) (dec. > 120°C). The structure of **1** has been determined by X-ray diffraction methods. Crystal data are as follows:

$(Ph_3P{=}N)_2S_4N_4$ mw = 736.86
Monoclinic, space group $P2_1/c$, a = 10.306(1), b = 19.473(5), c = 17.804(1) Å, β = 94.03(1)°, V = 3564 Å^3, Z = 4, ρ_c = 1.373 g cm^{-3}.

A total of 3303 reflections [$I \geq 3\sigma(I)$] were collected with a manual GE XRD-5 diffractometer using θ-2θ scans and Cu-K_α radiation. The structure was solved by direct methods and the final full-matrix least-squares refinement, which included anisotropic thermal parameters for all non-hydrogen atoms, gave an unweighted R-factor of 0.043.

The structure of **1** (see Fig. 1) consists of a ruptured S_4N_4 cage in which one cross-ring S—S interaction is replaced by bonds to two exocyclic triphenylphosphinimino ligands. The presence of the two exocyclic groups and the different orientation of the *exo*-S—N bonds (axial and equatorial) cause the endocyclic S—N bond distances to range from 1.583 to 1.675 Å. Nonetheless, the mean SN bond distance (1.62 Å) is similar to that found in S_5N_6 (1.61 Å) (7) and S_4N_4 (1.62 Å) itself (8). The S—S distance between the S atoms bonded to exocyclic groups is opened up to 3.727 Å and the remaining S—S interaction is considerably contracted (2.452 Å), as in S_5N_6 (2.43 Å) (7), in comparison to the two S—S distances of 2.59 Å found in S_4N_4 (8). The mean exocyclic S—N distance (1.61 Å) is similar to that found in $Ph_3P{=}N{-}S_3N_3$ (3), but the mean P=N distance (1.59 Å) is significantly shorter (1.65 Å in $Ph_3P{=}N{-}S_3N_3$).

The only known disubstituted derivatives of S_4N_4 are $S_4N_4O_2$ (9), in which both exocyclic oxygens are attached to the same sulphur atom, and the recently isolated $S_4N_4Cl_2$ (10) of undetermined structure. Thus the X-ray crystallographic study of $(Ph_3P{=}N)_2S_4N_4$ represents the first structural determination of a 1,5-disubstituted S_4N_4 ring. The structure of $S_4N_4Cl_2$, an important intermediate in the chlorination of S_4N_4 may well be related to that of **1**.

Acknowledgements

We thank the Natural Sciences and Engineering Council of Canada, the University of Calgary, and the University of Arkansas Research Committee for financial support, and Janet Cordes for help with diffractometer data collection.

1. (*a*) E. FLUCK, M. BECKE-GOEHRING, and G. DEHOUST. Z. Anorg. Allg. Chem. **312**, 60 (1961); (*b*) H. L. KRAUSS and H. JUNG. Z. Naturforsch. Teil B, **16**, 624 (1961).
2. I. RUPPERT, V. BASTIAN, and R. APPEL. Chem. Ber. **107**, 3426 (1974).
3. E. M. HOLT, S. L. HOLT, and K. J. WATSON. J. Chem. Soc. Dalton Trans. 1990 (1974).
4. (*a*) J. BOJES and T. CHIVERS. Inorg. Chem. **17**, 318 (1978); (*b*) J. BOJES, T. CHIVERS, I. DRUMMOND, and G. MACLEAN. Inorg. Chem. **17**, 3668 (1978).
5. (*a*) O. J. SCHERER and G. WOLMERHÄUSER. Angew. Chem. Int. Ed. Engl. **14**, 485 (1975); (*b*) W. FLUES, O. J. SCHERER, J. WEISS, and G. WOLMERHÄUSER. Angew. Chem. Int. Ed. Engl. **15**, 379 (1976).
6. H. PRAKASH and M. M. SISLER. Inorg. Chem. **7**, 2200 (1968).
7. T. CHIVERS and J. PROCTOR. J. Chem. Soc. Chem. Commun. 642 (1978); T. CHIVERS and J. PROCTOR. Can. J. Chem. **57**, 1286 (1979).
8. (*a*) B. D. SHARMA and J. DONOHUE. Acta Crystallogr. **16**, 891 (1963); (*b*) M. L. DELUCIA and P. COPPENS. Inorg. Chem. **17**, 2336 (1978).
9. H. W. ROESKY, W. SCHAPER, O. PETERSEN, and T. MÜLLER. Chem. Ber. **110**, 2695 (1977).
10. L. ZBORILOVA and P. GEBAUER. Z. Anorg. Allg. Chem. **448**, 5 (1979); Z. Chem. **19**, 76 (1979).

Canadian Journal of Chemistry
Published by
THE NATIONAL RESEARCH COUNCIL OF CANADA

Journal canadien de chimie
Publié par
LE CONSEIL NATIONAL DE RECHERCHES DU CANADA

Volume 57 Number 24 December 15, 1979 Volume 57 numéro 24 15 décembre 1979

Infrared multiphoton chemistry of fluoroform-*d*[1]

M. GAUTHIER, R. PILON, P. A. HACKETT, AND C. WILLIS
Laser Chemistry Group, Division of Chemistry, National Research Council of Canada, Ottawa, Ont., Canada K1A 0R6

Received June 7, 1979

M. GAUTHIER, R. PILON, P. A. HACKETT, and C. WILLIS. Can. J. Chem. **57**, 3173 (1979).

The infrared multiphoton chemistry of CF_3D has been investigated in the ν_2 and ν_5 bands. The primary dissociation step forms DF and CF_2. The major sink for the biradical is dimerization to form C_2F_4; this process preserves the $^{13}C/^{12}C$ isotopic selectivity which is reasonably high ($\alpha \approx 20$). The isotopic selectivity for $^2H/^1H$ is impaired by some scrambling reaction involving excited substrate. The possible nature of this scrambling reaction is discussed. In comparison with other CF_3X systems (X = I, Br, Cl), CF_3D is difficult to decompose, having low dissociation probability, and appears to decompose only after collisional activation.

M. GAUTHIER, R. PILON, P. A. HACKETT et C. WILLIS. Can. J. Chem. **57**, 3173 (1979).

On a étudié la chimie multiphoton dans l'infrarouge du CF_3D dans la région des bandes ν_2 et ν_5. La première étape de la dissociation conduit à DF et CF_2. Le principal affaiblissement du diradical est dû à une réaction de dimérisation qui donne du C_2F_4; cette réaction protège la sélectivité isotopique $^{13}C/^{12}C$ qui est raisonnablement grande ($\alpha \approx 20$). La sélectivité isotopique $^2H/^1H$ est affaiblie par une réaction désordonnée qui implique un substrat activé. On discute de la nature possible de cette réaction. Par comparaison aux autres systèmes du type CF_3X (X = Br, I, Cl), CF_3D est difficile à décomposer; il a une faible probabilité de dissociation et semble se décomposer seulement après une activation par collisions.

[Traduit par le journal]

Introduction

In earlier papers (1–3), we have reported details of the infrared multiphoton chemistry of the trifluoromethyl halides, CF_3I, CF_3Br, and CF_3Cl. The present work was undertaken in order to extend the CF_3X series to include CF_3D for two reasons. In the first case, the $^2H/^1H$ isotope shift is large for the ν_5 band of fluoroform (4) which should assure facile selective excitation of CF_3D molecules, a process of obvious practical importance. Secondly, the substitution of halogen by deuterium significantly increases the vibrational frequencies of the molecules, this increase results in a concomitant decrease in the density of vibrational states at any particular internal energy and should lead to a decrease in the efficiency of the multiphoton absorption process (5).

In the halides the primary dissociation step observed is the bond scission, reaction [1]

[1] $CF_3X \rightarrow CF_3 + X$

This reaction is favoured on thermodynamic grounds (6) being some 30 kcal mol^{-1} lower than the molecular elimination, reaction [2]

[2] $CF_3X \rightarrow CF_2 + FX$

However, for CF_3D the situation is reversed. The endothermicity for the molecular elimination, reaction [3]

[3] $CF_3D \rightarrow CF_2 + DF$

is +64.8 kcal mol^{-1} (6) which is over 30 kcal mol^{-1} lower than that for the carbon–deuterium bond scission. Furthermore, the observed activation energy for CF_2 production in the pyrolysis of CF_3H is +69 kcal mol^{-1} (7).

Experimental

All irradiations were performed with a line tunable TEA CO_2 laser (Lumonics Research Ltd., model 103). The temporal distribution of the laser pulse was monitored by a

[1]NRCC No. 17783.

0008-4042/79/243173-05$01.00/0

photon drag detector (Rofin, model 7415). The distribution was bimodal; a short "spike" (FWHM = 80 ns) was followed by a long tail (FWHM = 600 ns). About 70% of the incident energy was contained in the initial "spike". Samples of CF_3D (97%D, 3%H; Merke, Sharpe and Dohme), purified by distillation at −160°C, were irradiated in a Pyrex cell (18 cm long, 5 cm diameter) equipped with sodium chloride windows (Harshaw, laser grade). The laser beam passed through a 1.8 cm aperture and was focussed at the centre of the cell by a $f = 10$ cm germanium lens.

Analysis of all products determined was achieved directly by mass spectrometry. This method is unsatisfactory by comparison with others but was necessitated by (*a*) the inefficiency of the decomposition, *vide infra*, and (*b*) the low sensitivity of available gas chromatographs to the highly fluorinated compounds present. However, many calibrations of both single compounds and binary mixtures were performed in order to check the precision of the method. Moreover, possible interfering compounds were tested in order to improve the reliability of the assignment of *m/e* peaks to constituents of the photolysed mixture. C_2F_4 was determined from peaks at 81, 82, and 83, CF_3D from peak 52, and CF_3H from peak 51. Isotopic selectivities for carbon-13 were determined from the C_2F_4 product peaks and are reported as α values:

$$\alpha = \frac{^{13}C/^{12}C \text{ (product } C_2F_4)}{^{13}C/^{12}C \text{ (substrate } CF_3D)}$$

Results and Discussion

(a) Kinetics

The kinetics of the multiphoton chemistry of CF_3D can be described in terms of the following set of reactions

$$[3]\quad CF_3D \xrightarrow[M]{nh\nu} CF_2 + DF$$

$$[4]\quad CF_2 + CF_2 \rightarrow C_2F_4$$

$$k_4 = 2.5 \times 10^8 T^{1/2} \exp(-200/T) \text{ L mol}^{-1} \text{ s}^{-1} \quad \text{(refs. 8, 9)}$$

$$[5]\quad CF_2 + C_2F_4 \rightarrow c\text{-}C_3F_6$$

$$k_5 = 8.7 \times 10^4 T^{1/2} \exp(-3200/T) \text{ L mol}^{-1} \text{ s}^{-1} \quad \text{(refs. 7, 9)}$$

$$[6]\quad CF_2 + DF \rightarrow CF_3D$$

The only product observed at low conversions, at all pressures, temperatures, and irradiation wavelengths studied was C_2F_4, which is presumably formed with an equivalent amount of DF which did not survive through to analysis in our experiments. However, SiF_4 was detected in experiments carried to higher conversions.

However, it is not clear that the only fate of CF_2 is dimerization to form C_2F_4. Secondary reactions, of the type of reaction [5], are unlikely to be significant, even allowing for reaction at the potentially higher temperatures of the focal region. Indeed no higher products were observed. The importance of reaction [6], the back reaction, is difficult to assess in the absence of appropriate rate data. Smail and Rowland (10) have studied the equivalent reactions involving HI, HBr, and HCl. They report $k_{6(HI)} = 70 \times k_{6(HBr)} = 3500 \times k_{6(HCl)}$. More recent work suggests this trend continues to include HF (11). Accepting this trend and placing $k_{6(HI)}$ at close to the collisional limit gives an upper limit of $k_6 \leq 5 \times 10^4$ L mol^{-1} s^{-1}. For the conversions used in the present series of experiments, even allowing that DF survives as a free gas phase product, one can safely neglect reaction [6] on the grounds that its rate is too low. Further support of this conclusion was gained by irradiating a mixture of 0.5 Torr CF_3D and 0.10 Torr HBr. The observed yields of C_2F_4 and CF_2HBr were approximately equal. A simple analysis of the pulsed kinetics yields $k_{6(HBr)} = 5 \times 10^7$ L mol^{-1} s^{-1} which is in reasonable agreement with the estimate used above.

The above analysis indicates that measurement of C_2F_4 serves as an acceptable surrogate for the yield of primary dissociations as there appear to be no back reactions. Figure 1 shows the pressure dependence of this parameter. It is seen that the dissociation probability is proportional to pressure. There are many explanations for this behaviour; collisions may increase the rate of multiphoton absorption by removing "rotational bottlenecks" (12); the primary dissociation may be the result of bimolecular "energy pooling" reactions of two vibrationally activated molecules (13); or the observed dissociation may be a bulk pyrolysis of the irradiated gas, increased pressure would decrease the rate of cooling of the irradiated volume increasing the yield of dissociation (14). The latter explanation may be rejected on the grounds that the process is isotopically selective for carbon isotopes. Experiments to distinguish between the two remaining possibilities are in progress.

No evidence was found for reaction products arising from carbon–deuterium bond scission. This result confirms the conclusions of an earlier study of multiphoton decomposition of pentafluoroethane (15). That is that for "small" molecules only the lowest thermodynamic exit channel will be observed whereas as the volume of vibrational phase space increases the spontaneous dissociation rate of unimolecular dissociation decreases so that large molecules should show evidence for multichannel dissociation. A simple RRK calculation (16) reveals that the spontaneous dissociation rate for CF_3D reaches 2×10^8 s^{-1} at internal energies 14 kcal mol^{-1} above the threshold for molecular elimination which is well below the threshold for the free radical process. Hence for the methane it is unlikely that

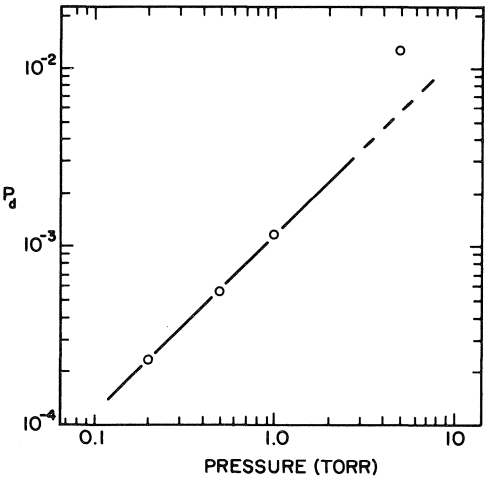

FIG. 1. Pressure dependence of dissociation probability. P_d, the probability that an irradiated molecule will decompose, is plotted against CF_3D pressure. Irradiation wavelength 9797 cm^{-1}; incident fluence (energy density) = 1.04 J cm^{-2}; temperature = 22°C.

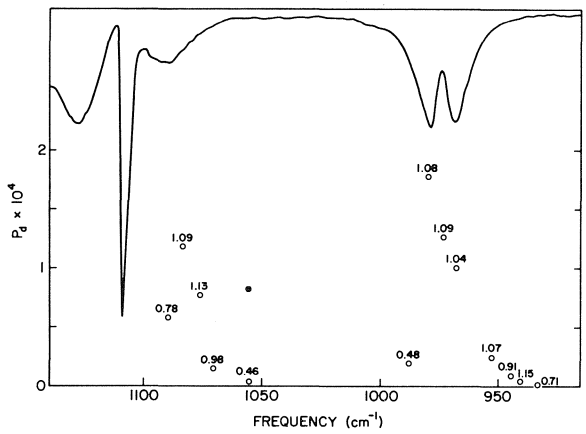

FIG. 2. Excitation frequency dependence of reaction dissociation probability. The parameter above each point refers to the incident fluence in J cm^{-2}. CF_3D pressure = 0.5 Torr, temperature = 22°C. Open circles refer to $^{12}CF_3D$ and the filled ones to $^{13}CF_3D$. The one photon absorption spectrum is shown for reference (solid line).

internal energies greater than 83 kcal mol^{-1} will be reached whereas for the ethane internal energies of 130 kcal mol^{-1} are surpassed in similar radiation fields.

It is obvious from the preceding discussion that fluoroform does not undergo multiphoton decomposition with great facility, indeed it is apparent that collisions are essential. The spectral dependence of the probability of dissociation was investigated at a pressure of 0.5 Torr. The results are shown in Fig. 2 together with the incident fluence used in each irradiation, the threshold fluence convention (14) was not used as the dissociation yield is not pressure independent. This "action spectrum" shows the normal features of multiphoton excitation in focussed beams; that is the multiphoton action spectrum is red shifted from and broader than the one photon absorption spectrum. These are consequences of molecular anharmonicity and the large Rabi frequencies required to overcome that anharmonicity. As noted in the Introduction one expects this problem to be more significant in CF_3D than in CF_3Cl, CF_3Br, and CF_3I, a consequence of the lower density of vibrational states at any particular internal energy. More directly the "quasicontinuum", region II (6), will lie at higher levels for CF_3D than for the halides. The effect of this can be seen from Table 1 which compares dissociation probabilities measured at the centre of the action spectrum for multiphoton decomposition of the four compounds in similar radiation fields. It can be seen that neither the threshold dissociation energies nor the integrated oscillator strengths of the one photon transitions provide sufficient means to correlate the observed dissociation probabilities, without invoking anharmonicity and the quasi continuum relaxation. It is beyond the scope of this work and all current theories of multiphoton absorption to provide an intimate description of the sequential absorption process but the general conclusions of Table 1 provide a useful insight into this area.

(b) Isotopically Selective Excitation and Dissociation

The one photon infrared absorption spectrum of fluoroform has been well studied (4, 17, 18). The bands which fall within the 9–11 μm region where the CO_2 laser has strong output are the $\nu_2(a_1)$ band and the $\nu_5(e)$ band. The former corresponds to a C—F stretch and the latter to a D—C—F bend. In $^{12}CF_3D$ the vibrational frequencies are ν_2 = 1111 cm^{-1}, ν_5 = 975 cm^{-1} (17). The ν_2 band shows well developed PQR structure but restrictions of available laser output allow photolysis only on the tail of the P branch below 1100 cm^{-1}.

In $^{12}CF_3H$ the vibrational frequencies are ν_2 = 1141 cm^{-1} and ν_5 = 1157 cm^{-1} (17), for $^{13}CF_3H$ ν_2 = 1116 cm^{-1} and ν_5 = 1132 cm^{-1} (18). Thus the isotope shift for carbon-13 substitution in CF_3D is expected to be of the order of 35 cm^{-1} for both vibrational bands studied. Fluoroform-*d* may be selectively excited in the ν_5 band at 975 cm^{-1}, 100 cm^{-1} away from any absorption transition in fluoroform-*h*.

Isotopically selective chemistry was verified for carbon-13 by selectively dissociating $^{13}CF_3D$ at

TABLE 1. Multiphoton dissociation of CF_3X species[a]

Compound	Threshold energy[i] (kcal/mol)	Normalised band intensity[b]	Dissociation probability[c] (P_d)
CF_3D	64.8	1.0	1.78×10^{-4}[d]
CF_3D	64.8	Complex band	1.19×10^{-4}[e]
CF_3Cl	81.0	8.4	$>5.1 \times 10^{-4}$[f]
CF_3Br	66.2	8.3	$>2.0 \times 10^{-3}$[g]
CF_3I	49.4	10.5	$>8.8 \times 10^{-2}$[h]

[a]All results are from experimental setup reported in this paper; temperature = 22°C; pressure = 0.5 Torr, irradiation near maximum of "action spectrum".
[b]Integrated band intensity normalised to CF_3D ν_5 band; obtained from infrared absorption spectra measured under standard conditions.
[c]P_d = (number of molecules dissociated)/(number of molecules irradiated).
[d]Irradiation frequency = 979.7 cm^{-1}; incident fluence = 1.08 J cm^{-2}; this work.
[e]1083.5 cm^{-1}; 1.09 J cm^{-2}; this work.
[f]For the three halides the P_d values are lower limits since work in ref. 3 concentrated on ^{13}C decomposition: 1081.1 cm^{-1}; 1.12 J cm^{-2}; ref. 3.
[g]1057.3 cm^{-1}; 1.0 J cm^{-2}; ref. 3.
[h]1053.9 cm^{-1}; 0.68 J cm^{-2}; ref. 3.
[i]Reference 6.

natural abundance in the ν_2 band at 0.46 J cm^{-2} incident fluence of 1055.6 cm^{-1} radiation. The fluoroform-*d* pressure was 0.5 Torr and the cell was at ambient temperature. An α value of 25 was obtained.

The problem of hydrogen isotope selectivity is more complex, however. The hydrogen product is carried as DF which rapidly exchanges with cell walls, therefore only depletion experiments were possible. Such experiments are inherently less sensitive and must be carried to higher conversions. Mixtures of CF_3D and CF_3H in ratios of 32:1 and 1:1 were photolysed in the ν_5 band at 0.5 Torr initial pressure. CF_3D and CF_3H concentrations were monitored from peaks at $m/e = 52$ and 51. However, although CF_3D decreased and C_2F_4 increased with time it was observed that m/e 51 and presumably $[CF_3H]$ increased with time. It was verified that this peak did not arise from other chemical products, e.g., C_2F_6, C_2F_5H, $C_2F_4H_2$, none of which could be detected. Furthermore, the possibility of a contribution of $^{13}CF_2$ from C_2F_4 was discounted by examining m/e peaks at 81, 82, and 83. Hence, we have to conclude that an exchange reaction between CF_3D and HF is induced by the radiation field. The exchange reaction was equally prevalent when the cell walls were held at −90°C and appears to proceed at a rate equal to the rate of C_2F_4 production in our experiments. Quantitative analysis of the peak height time dependence showed that a carbon atom balance was maintained throughout the experiments but offered no positive indication to the nature of the exchange reaction. The problem of selective dissociation of deuterium bearing fluoroform is therefore intractable in the present cell and with the presently available irradiation fluences.

In conclusion, the present study has demonstrated the importance of molecular complexity and vibrational state density in determining the rate and level of multiphoton absorption. CF_3D seems to fit into place with predictions based on studies of other systems. Selective dissociation of carbon-13 at natural abundance has been demonstrated, but the demonstration of selective dissociation of deuterium bearing molecules awaits the control of complicating exchange reactions.

We note that other authors have recently reported the infrared multiple dissociation with application to deuterium enrichment (19). No mention of the complicating side reaction was made. If by suitable cell design the side reaction may be overcome then fluoroform-*d* may become a viable substrate for deuterium enrichment. Furthermore, the side reaction may offer a useful laser based redeuteration pathway.

1. M. GAUTHIER, P. A. HACKETT, M. DROUIN, R. PILON, and C. WILLIS. Can. J. Chem. **56**, 2227 (1978).
2. M. DROUIN, M. GAUTHIER, R. PILON, P. A. HACKETT, and C. WILLIS. Chem. Phys. Lett. **60**, 16 (1978).
3. M. GAUTHIER, P. A. HACKETT, and C. WILLIS. Chem. Phys. In press.
4. S. R. POLO and M. K. WILSON. J. Chem. Phys. **21**, 1129 (1953).
5. J. G. BLACK, E. YABLONOVITCH, N. BLOEMBERGEN, and S. MUKAMEL. Phys. Rev. Lett. **38**, 1131 (1977).
6. J. L. FRANKLIN, J. G. DILLARD, H. M. ROSENSTOCK, J. T. HERRON, K. DRAXL, and F. H. FIELD. Natl. Bur. Stand. NSRDS-NBS **26** (1969).
7. S. F. POLITANSKI. Kinet. Catal. **10**, 410 (1969).
8. W. J. R. TYERMAN. Trans. Faraday Soc. **65**, 1188 (1969).
9. F. W. DALBY. J. Chem. Phys. **41**, 2297 (1964).
10. T. SMAIL and F. W. ROWLAND. J. Phys. Chem. **74**, 1866 (1970).
11. B. E. HOLMES, D. W. SETSER, and G. O. PRITCHARD. Int. J. Chem. Kinet. **8**, 215 (1976).

12. N. V. CHEKALIN, V. S. LETOKHOV, V. N. LOKHMAN, and A. N. SHIBANOV. Chem. Phys. **36**, 415 (1979).
13. P. A. HACKETT, M. GAUTHIER, and C. WILLIS. J. Chem. Phys. **69**, 2924 (1978).
14. P. A. HACKETT, C. WILLIS, and M. GAUTHIER. J. Chem. Phys. **71**, 2682 (1979).
15. P. A. HACKETT, M. DROUIN, and C. WILLIS. J. Phys. Chem. To be published.
16. S. W. BENSON and G. HAUGEN. J. Phys. Chem. **69**, 3898 (1965).
17. N. J. FYKE, P. LOCKETT, J. K. THOMPSON, and P. M. WILT. J. Mol. Spectrosc. **58**, 87 (1975).
18. H. F. CHAMBERS, R. W. KIRK, J. K. THOMPSON, M. J. WARNER, and P. M. WILT. J. Mol. Spectrosc. **58**, 76 (1975).
19. I. P. HERMAN and J. B. MARLING. Chem. Phys. Lett. **64**, 75 (1979).

Pyrolysis of triethylgallium by the toluene carrier technique

MICHELLENE C. PAPUTA AND STANLEY JAMES W. PRICE[1]

Department of Chemistry, University of Windsor, Windsor, Ont., Canada N9B 3P4

Received June 4, 1979

MICHELLENE C. PAPUTA and STANLEY JAMES W. PRICE. Can. J. Chem. **57**, 3178 (1979).

The pyrolysis of triethylgallium has been studied in a toluene carrier gas system in the temperature range of 464.7 to 700.7 K and a pressure range of 0.82 to 3.73 kPa. From the data obtained from this work, the following mechanism for the thermal decomposition of the metal alkyl is proposed:

[1] $Ga(C_2H_5)_3 \rightarrow Ga(C_2H_5)_2 + C_2H_5$

[2] $Ga(C_2H_5)_2 \rightarrow Ga(C_2H_5)H + C_2H_4$

[3] $Ga(C_2H_5)H \rightarrow GaH_2 + C_2H_4$

[4] $nGaH_2 \rightarrow \frac{n}{2}H_2 + (GaH)_n$

[5] $(GaH)_n \rightarrow Ga + \frac{n}{2}H_2$

where [1] is the rate determining step. After runs below 606 K were corrected for the contribution of a concurrent residual reaction, a least-squares analysis of experimental results from 567 to 651 K based on both product and residual alkyl analysis gave

$$\log k_1 = 15.7 - (194\,600/2.303RT)$$

at 1.60 kPa.

The rate constant, k_1, is very slightly pressure-dependent as revealed by tests at 648.0 K (80% and 45% decomposition). Studies indicate there is no detectable surface catalysis effect. Similarly, no effect was observed for changes in concentration or contact time.

The mechanism for the formation of polymeric gallium hydride in reaction [4] is not clearly defined and may consist of more than one step. Reaction [5] is slow but based on the C_2H_4:H_2 ratio must occur to a significant extent (40–80%) during a run. Further decomposition occurs between runs, causing a build-up of H_2 in the reaction vessel.

Experimental data for the hydrogen abstraction by ethyl radicals from toluene

$$C_2H_5^{\cdot} + C_6H_5CH_3 \rightarrow C_2H_6 + C_6H_5CH_2^{\cdot}$$

yield the equation

$$\log k_9 = 11.08 - (40\,200/2.303RT)$$

MICHELLENE C. PAPUTA et STANLEY JAMES W. PRICE. Can. J. Chem. **57**, 3178 (1979).

On a étudié la pyrolyse du triéthyle gallium dans un système utilisant le toluène comme gaz porteur, à des températures allant de 464.7 à 700.7 K et à des pressions variant de 0.82 à 3.73 kPa. A partir des résultats obtenus on propose, pour la décomposition thermique du métal alkylé, le mécanisme suivant:

[1] $Ga(C_2H_5)_3 \rightarrow Ga(C_2H_5)_2 + C_2H_5$

[2] $Ga(C_2H_5)_2 \rightarrow Ga(C_2H_5)H + C_2H_4$

[3] $Ga(C_2H_5)H \rightarrow GaH_2 + C_2H_4$

[4] $nGaH_2 \rightarrow \frac{n}{2}H_2 + (GaH)_n$

[5] $(GaH)_n \rightarrow Ga + \frac{n}{2}H_2$

où [1] est l'étape déterminante. Après avoir corrigé les essais faits en dessous de 606 K pour tenir compte de la contribution d'une réaction résiduelle concourante, une analyse, par la méthode des moindres carrés, des résultats expérimentaux entre 567 et 651 K basés sur les produits de la réaction et sur le métal alkylé résiduel donne l'équation:

$$\log k_1 = 15.7 - (194\,600/2.303RT)$$

à 1.60 kPa.

La constante de vitesse k_1 varie très légèrement avec la pression comme le révèlent les essais

[1]To whom all correspondence should be addressed.

0008-4042/79/243178-04$01.00/0

à 648 K (80% et 45% de décomposition). Les études indiquent qu'il n'y a pas d'effet détectable de la surface du catalyseur. De même, on n'observe pas d'effets dus au changement de concentration ou du temps de contact. Le mécanisme de formation de l'hydrure de gallium polymère dans la réaction [4] n'est pas clairement défini et peut comprendre plus d'une étape. La réaction [5] est lente, mais si on se base sur le rapport $C_2H_4:H_2$, elle peut se produire d'une façon importante (40–80%) au cours d'une réaction. Une décomposition plus poussée se produit entre les essais provoquant un dégagement d'hydrogène dans le vase réactionnel. Les données expérimentales concernant la réaction d'enlèvement d'un hydrogène du toluène par le radical éthyle

$$C_2H_5^{\cdot} + C_6H_5CH_3 \rightarrow C_2H_6 + C_6H_5CH_2^{\cdot}$$

conduisent à l'équation

$$\log k_9 = 11.08 - (40\,200/2.303RT)$$

[Traduit par le journal]

Introduction

The present paper is the fourth in a series in the pyrolysis of ethyl metallic alkyls by the toluene carrier method and is related to previous studies on methyl metallic alkyls. The toluene carrier study of diethylmercury (1) gave $\log A\ (s^{-1}) = 15.4$ and $E = 191.2$ kJ mol^{-1}, in excellent agreement with values proposed by Benson and O'Neal (2). Three previous studies of this compound (3–5) all gave slightly lower $\log A$ and E values but all four studies showed a reasonable degree of agreement when rate constants were compared. The toluene carrier work on diethylzinc (6) showed marked catalysis by zinc oxide. In the absence of zinc oxide $\log A\ (s^{-1}) = 14.3$ and $E = 205.0$ kJ mol^{-1}. These are the only Arrhenius parameters for this compound. Similarly, for tetraethyltin $\log A\ (s^{-1}) = 16.0$ and $E = 248.3$ kJ mol^{-1} (7).

From a mechanistic viewpoint the previous study of trimethylgallium is of considerable importance (8). This study indicated that the A factor of the second step in the decomposition

$$Ga(CH_3)_2 \rightarrow GaCH_3 + CH_3$$

was limited by the time required for the return of $4p$ electron to the $4s$ state. In the case of triethylgallium it was expected that either a similar effect would be observed or that an alternate mode of decomposition would be followed.

Previous studies of $Ga(C_2H_5)_3$ by differential thermal analysis (9) and in a hydrogen carrier system (10) showed first traces of decomposition at approximately 473 K. In the DTA studies ethane and ethylene were produced in roughly equal quantities at 523 K but at 773 K ethylene was the major product. The hydrogen study used the infrared band at 2940 cm^{-1} to monitor the concentration of $Ga(C_2H_5)_3$ as a function of temperature. Bands at 948 cm^{-1} and 2995 cm^{-1} were monitored to follow ethylene and ethane production respectively. The main region of decomposition occurred between 623 K and 723 K. Ethylene was the major product and from the spectra given a very approximate activation energy of 175 kJ mol^{-1} can be estimated.

In conjunction with the development of semiconductor films, two studies of the heat of formation of $Ga(C_2H_5)_3$ have also been carried out (11, 12). These studies gave $\Delta H_{f298}^{0}(Ga(C_2H_5)_3, g) = -60.3$ kJ mol^{-1} and -75.3 kJ mol^{-1}, respectively. This corresponds to a mean Ga—C bond dissociation energy of 217–222 kJ mol^{-1}.

Experimental

Materials

(i) Toluene

The toluene employed was toluene from sulfonic acid, number X325 as supplied by Eastman Organic Chemicals. It was dried by refluxing under vacuum at least 24 h over freshly pressed sodium ribbon and then degassed by bulb-to-bulb distillation.

(ii) Triethylgallium

This was prepared by slowly adding triethylaluminum (25% hexane solution) to freshly prepared gallium tribromide (13). Hexane was distilled off and the fraction boiling at 68–70°C at 8.0 kPa was collected. A 91.2% yield was obtained.

Apparatus and Procedure

The experiments were carried out in a system similar to that used in previous work (14). The reaction vessel had a volume of 160 cm^3. To test for surface effects a vessel was packed with small quartz tubes. This vessel had a volume of 101 cm^3 and a surface-to-volume ratio twenty times that of the unpacked vessel. Both vessels were treated with hot concentrated nitric acid before use. The residual acid was baked out under vacuum after the vessels were installed in the reaction system.

The gaseous products were analyzed using a Perkin-Elmer model 154 gas chromatograph equipped with a 6 mm × 2 m silica gel column. The column was maintained at 80°C, and a helium flow rate of 20 cm^3 per min was used. For hydrogen analysis nitrogen was used in place of helium.

The liquid products were analyzed on a Perkin-Elmer model 900 gas chromatograph equipped with flame ionization detectors. The analyses were done on a 2 mm id × 2 m column packed with 80–100 mesh *n*-octane/porasil C (chemically bonded Durapak). The column and injection port temperatures were 120 and 150°C, respectively. A digital integrator was used and all analyses and standardizations were based on peak areas.

The preparation of gas chromatographic standards and the

TABLE 1. Experimental parameters and product distribution for selected runs

T (K)	t_c (s)	Initial alkyl concentration ($M \times 10^6$)	Products (mol × 10^4) C_2H_6	C_2H_4	C_4H_{10}	*n*-Propyl benzene	% Decomposition (product analysis)*	% Undecomposed (atomic emission Ga residue)
700.7	1.44	8.91	4.00	18.10	5.51	0.36	94.6	—
651.0p	1.31	4.02	6.19	13.50	1.62	0.24	79.2	14.9
649.7	1.60	8.03	1.16	31.80	2.83	0.19	77.0	19.4
637.7	1.56	4.98	1.15	15.40	1.17	0.12	59.2	39.4
628.6	1.68	12.18	1.29	13.30	1.50	0.04	42.3	58.6
628.2	1.57	2.96	1.33	9.15	0.61	0.07	43.5	55.3
628.2	0.83	2.99	0.36	5.11	0.81	—	34.2	68.6
609.9	1.71	4.76	0.74	5.17	0.62	—	25.5	74.9
608.2†	1.43	4.28	0.86	3.98	—	—	19.0	78.6
605.7	1.60	4.33	0.40	3.89	0.24	—	17.6	85.5
593.4	1.71	3.73	0.33	2.07	—	—	10.9	90.1
519.4	1.94	10.2	0.42	0.28	—	—	1.9	—
467.7	2.32	12.6	0.30	0.02	—	—	0.8	—

*Based on release of all three C_2 groups per molecule (i.e. that for reactions [1]–[3], [1] is the rate controlling step).
†Runs in packed reaction vessel. Total pressures 1.5–1.7 kPa.

method of analysis for butane dissolved in toluene have been previously described (6).

Analysis for residual $Ga(C_2H_5)_3$ was performed by atomic flame emission spectroscopy. An Instrument Laboratory Atomic Absorption/Emission Spectrometer, Model IL 251, was operated in the Flame Emission mode at 417.2 nm and a slit width of 160 μm.

Results and Discussion

Selected experimental results are given in Table 1. They may be discussed in terms of the following mechanism.

[1] $Ga(C_2H_5)_3 \rightarrow Ga(C_2H_5)_2 + C_2H_5$

[2] $Ga(C_2H_5)_2 \rightarrow Ga(C_2H_5)H + C_2H_4$

[3] $Ga(C_2H_5)H \rightarrow GaH_2 + C_2H_4$

[4] $nGaH_2 \rightarrow \frac{n}{2}H_2 + (GaH)_n$

[5] $(GaH)_n \rightarrow Ga + \frac{n}{2}H_2$

[6] $2C_2H_5 \rightarrow C_2H_4 + C_2H_6$

[7] $2C_2H_5 \rightarrow C_4H_{10}$

[8] $C_2H_5 \rightarrow C_2H_4 + H$

[9] $C_2H_5 + C_6H_5CH_3 \rightarrow C_2H_6 + C_6H_5CH_2$

[10] $C_2H_5 + C_6H_5CH_2 \rightarrow C_6H_5CH_2CH_2CH_3$

[11] $H + C_6H_5CH_3 \rightarrow H_2 + C_6H_5CH_2$

[12] $H + C_6H_5CH_3 \rightarrow CH_3 + C_6H_6$

[13] $CH_3 + C_6H_5CH_3 \rightarrow CH_4 + C_6H_5CH_2$

The analytical data given in Table 1 indicate that each time reaction [1] occurs it is rapidly followed by reactions [2] and [3] or some other processes that release the remaining two C_2 groups as ethylene. Reaction [2] rather than reaction [2*a*]

[2*a*] $Ga(C_2H_5)_2 \rightarrow GaC_2H_5 + C_2H_5$

is expected because of the limiting effect of the $4p \rightarrow 4s$ electron pairing that would be concurrent with reaction [2*a*] (8).

Reactions [4] and [5] are suggested overall reactions. Reaction [4] is sufficiently fast that all gallium other than that in undecomposed $Ga(C_2H_5)_3$ is found in the reaction zone.

Taking reactions [2], [3], [4], [6], [7], and [8] the expected $[C_2H_4]/[H_2]$ ratio is about 3.5. The ratio found experimentally, approximately 2.1–3.0, indicates that although reaction [5] does not go to completion during the course of a run, it does occur

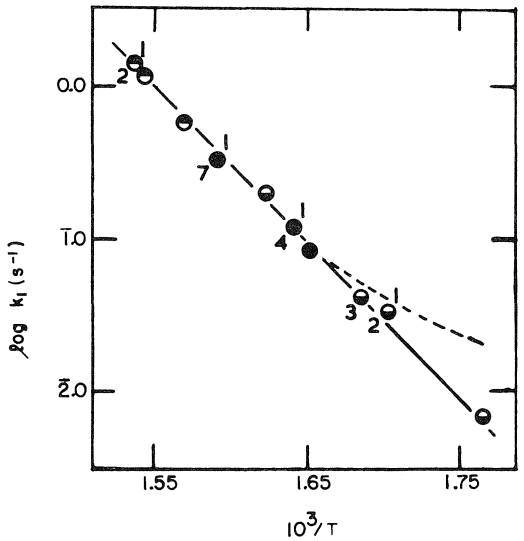

FIG. 1. Arrhenius plot for the decomposition of triethylgallium: ◓, k_m based on analysis for undecomposed $Ga(C_2H_5)_3$; ◒, k_g based on product analysis; ●, k_m and k_g. Number of runs in packed reaction vessel above the circles and number of runs averaged to obtain the given point below the circles. The dotted curve indicates the plot that would be obtained below 606 K if correction for the residual reaction was not made.

TABLE 2. Effect of $Ga(C_2H_5)_3$ concentration on k_1

T (K)	Concentration ($M \times 10^6$)	k_1 (s^{-1})
649	7.45	1.17
649	3.85	1.26
649	0.92	1.21
628	14.4	0.300
629	4.5	0.376
628	3.0	0.325
628	1.5	0.358
610	4.8	0.148
610	1.8	0.148

to a significant extent. The remaining $(GaH)_n$ continues to decompose between runs leading to the observed build-up of H_2 in the reaction vessel.

The values of k_1 used to plot Fig. 1 were calculated from the usual first order equation. The values in Table 2 indicate that the assumption of first order seems valid within the limits of experimental error. Of the 33 values of k_1 used in Fig. 1, 14 are based on atomic emission analysis of residual alkyl, 19 on product analysis, and nine on both methods. No detectable heterogeneous contribution to k_1 was noted and only a very slight dependence on total pressure was observed. Below 606 K the Arrhenius plot showed a distinct curvature. Below 540 K this plot again became linear with an apparent activation energy of about 32 kJ mol^{-1}. The values of k_1 were corrected for this residual reaction before Fig. 1 was constructed.

A weighted linear least-squares analysis of the points in Fig. 1 gives

$$\log k_1\ (s^{-1}) = 15.7 \pm 0.2 - (194\,600 \pm 2\,400/2.303RT) \text{ at } 1.60 \text{ kPa}$$

The errors quoted are twice the standard deviation. The weighting scheme used was related to the expected effect of the accuracy of the analytical procedures on the values of k_1. Points based on residual alkyl analysis were given weightings from 4 to 0 from high decomposition to low decomposition. Points based on product analysis were correspondingly weighed from 0 to 3. The low weighting for values based on product analysis at high decomposition is largely due to the difficulty of recovering the butane dissolved in the toluene for reliable quantitative analysis.

The A factor is very close to that observed for the decomposition of $Ga(CH_3)_3$. Accepting the activation energy as a reasonable measure of $D[(C_2H_5)_2Ga—C_2H_5]$ gives

$$D[C_2H_5Ga—C_2H_5] + D[Ga—C_2H_5] = 465 \pm 15 \text{ kJ mol}^{-1}$$

By analogy with $Ga(CH_3)_3$ then $D[C_2H_5Ga—C_2H_5]$ would be expected to be approximately 160 kJ mol^{-1} and log A_{2a} about 8. At the maximum temperature used in the present work (700 K) this leads to an estimated $\log k_{2a} = -4$ and indicates clearly that reaction [2a] should not be significant in the present study.

It is also possible from the present data to obtain rate constants for the abstraction of hydrogen from toluene by the C_2H_5 radicals released in reaction [1]. The method of calculation has been published previously (6). The Arrhenius equation obtained

$$\log k_9\ (\text{cm}^3\ \text{mol}^{-1}\ \text{s}^{-1}) = 11.08 - (40\,200 \pm 5\,000/2.30RT)$$

is in good agreement with previous results (1, 6, 7).

It is also possible to estimate very approximately the rate of ethyl radical decomposition from the expression

$$d[C_2H_4{}^t - 2(\text{mol } Ga(C_2H_5)_3 \text{ decomposed}) - C_2H_4{}^*]/dt = k_8[C_2H_5]$$

where $C_2H_4{}^t$ = total C_2H_4 and $C_2H_4{}^*$ is the C_2H_4 from disproportionation. The rate constants obtained are somewhat scattered but are in the general range 2–20 s^{-1} and give an activation energy of 134 kJ mol^{-1} at 1.6 kPa in general agreement with previous toluene carrier work (6).

Acknowledgement

This work has been supported by an operating grant from the Natural Sciences and Engineering Research Council of Canada.

1. A. C. LALONDE and S. J. W. PRICE. Can. J. Chem. **49**, 3367 (1971).
2. S. W. BENSON and H. E. O'NEAL. Kinetic data on gas phase unimolecular reactions. NSRDS-NBS21. 1970. p. 520.
3. H. V. CARTER, E. I. CHAPPELL, and E. WARHURST. J. Chem. Soc. 106 (1956).
4. W. PASTFIELD. Diss. Abstr. **15**, 1325 (1955).
5. C. HEITZ. J. Organomet. Chem. **8**, 401 (1967).
6. A. A. KOSKI, S. J. W. PRICE, and B. C. TRUDELL. Can. J. Chem. **54**, 482 (1976).
7. M. DALY and S. J. W. PRICE. Can. J. Chem. **54**, 1814 (1976).
8. M. G. JACKO and S. J. W. PRICE. Can. J. Chem. **41**, 1560 (1963).
9. N. N. TRAVKIN, B. G. GRIBOV, V. P. RUMYANTSEVA, I. G. TONOYAN, and E. N. ZORINA. Zh. Obshch. Khim. **45**, 316 (1975).
10. E. P. BOCHKAREV, L. I. ZAKHARKIN, YU. V. YUSHKOV, L. S. IVANOV, N. P. FATYUSHIA, V. V. GAVRILENKO, YU. S. DEMENTEV, A. G. PETRIK, and V. A. L'VOVA. Nauch. Tr., Nauch-Issled. Proekt. Inst. Redkometal Prom. **46**, 6 (1973).
11. YU. KH. SHAVLOV, V. G. GENCHEL, R. M. AIZATULOVA, and G. S. PESOTSKII. Zh. Fiz. Khim. **46**, 2379 (1972).
12. G. M. KOL'YAKOVA, I. B. RABINOVICH, and E. N. ZORINA. Dokl. Akad. Nauk SSSR, **209**, 616 (1973).
13. J. J. EISCH. J. Am. Chem. Soc. **84**, 3605 (1962).
14. M. KRECH and S. J. W. PRICE. Can. J. Chem. **41**, 224 (1963).

Theoretical study of the X^2B_1, A^2A_1, $^2B_2$ valence-shell and the first $\pi_u{}^2 3s$-type doublet and quartet Rydberg states of NH_2

S. D. PEYERIMHOFF

Lehrstuhl für Theoretische Chemie, Universität Bonn, Wegelerstraße 12, D-5300 Bonn 1, West-Germany

AND

R. J. BUENKER

Lehrstuhl für Theoretische Chemie, Gesamthochschule Wuppertal, Gaußstraße 20, D-5600 Wuppertal, West-Germany

Received May 24, 1979

S. D. PEYERIMHOFF and R. J. BUENKER. Can. J. Chem. **57**, 3182 (1979).

The angular potential energy curves of the X^2B_1, A^2A_1, B^2B_2 valence-shell and $^4\Sigma_g^-$, $^2\Sigma_g^-$ (2^2B_1), $^2\Delta_g$ (2^2A_1, 3^2B_1), and $^2\Sigma_g^+$ Rydberg states arising from $\pi_u{}^2$ $3s$ configurations are calculated by configuration interaction techniques. The data obtained reproduce very satisfactorily all X^2B_1 and A^2A_1 characteristics deduced from experiments; they support the previous theoretical prediction of a small-angle $^2B_2$ state but find a very low $|R_{e'e''}|^2$ value for the $^2B_2$–A^2A_1 transition. The $^4\Sigma_g^-$ as well as three of the above four doublet Rydberg multiplets are found to prefer linear (or nearly linear) geometry and larger NH separations (in the symmetric structure) than NH_2 in its ground state. A relatively large electronic transition moment for combination with both X^2B_1 and A^2A_1 is calculated for the lowest Rydberg multiplet which lies roughly 5.3 eV above the A^2A_1 state, while the intensity of transitions of the higher $3s$ states is found to be considerably smaller. Finally it is pointed out that the former Rydberg transition fits in well with recent emission experiments in this wavelength region recently reported by Herzberg.

S. D. PEYERIMHOFF et R. J. BUENKER. Can. J. Chem. **57**, 3182 (1979).

On a calculé par les techniques d'interaction de configuration les courbes d'énergie potentielle angulaire des électrons de valence X^2B_1, A^2A_1, B^2B_2 et $^4\Sigma_g^-$, $^2\Sigma_g^-$ (2^2B_1), $^2\Delta_g$ (2^2A_1, 3^2B_1) et des états de Rydberg $^2\Sigma_g^+$ provenant des configurations $\pi_u{}^2$ $3s$. Les données recueillies reproduisent de façon très satisfaisante toutes les caractéristiques X^2B_1 et A^2A_1 déduites expérimentalement. Ces données confirment les prédictions théoriques faites antérieurement au sujet du petit angle de l'état $^2B_2$ mais elles fournissent une très faible valeur $|R_{e'e''}|^2$ pour la transition $^2B_2$–A^2A_1. On a trouvé que le $^4\Sigma_g^-$ aussi bien que trois des 4 doublets précédents des multiplets de Rydberg préfèrent une géométrie linéaire (ou presque linéaire) et de plus grandes séparations du NH (dans la structure symétrique) que celles du NH_2 dans l'état fondamental. Pour le plus petit multiplet de Rydberg on a calculé un moment de transition électronique relativement grand pour la combinaison avec X^2B_1 et A^2A_1 qui se situe grossièrement à 5.3 eV au dessus de l'état A^2A_1 alors que l'intensité des transitions des états les plus élevés $3s$ sont considérablement plus petits. Finalement on a montré que la première transition de Rydberg s'accorde avec les récentes expériences d'émission dans cette région de longueur d'onde récemment mentionnée par Herzberg.

[Traduit par le journal]

Introduction

The first two electronic states X^2B_1 and A^2A_1 of NH_2 have been studied quite extensively over a number of years by various experimental and theoretical techniques (1); these states are degenerate ($^2\Pi_u$) in the linear arrangement of nuclei and thus the Renner–Teller interaction produces a number of interesting perturbations in the fine structure of the associated A^2A_1–X^2B_1 spectrum. The equilibrium angles have been determined (1) as 103.3° (X^2B_1) and 144° (A^2A_1), while a third NH_2 valence-shell state B^2B_2 has recently been predicted by *ab initio* SCF and CI studies (2) with an energy minimum occurring at the very small bond angle of 47.5°.

To our knowledge no study has been undertaken thus far in order to identify the Rydberg states of NH_2. The lowest-energy configuration of Rydberg type $\pi_u{}^2 3s$ leads to three doublet states $^2\Sigma_g^-$, $^2\Delta_g$, and $^2\Sigma_g^+$ which all are allowed to combine with the $^2\Pi_u$ (X^2B_1, A^2A_1) states according to the dipole selection rules. If the standard guidelines (3) are applied which place the $3s$ member roughly 29 000 cm^{-1} below its corresponding IP, the lowest vertical Rydberg feature in the NH_2 absorption spectrum is expected to lie quite high (in the 7.5–8 eV region given the fact that the first IP is at 11.4 eV (4)), so that Rydberg states seem to be ruled out as being of importance in the lower-energy part of the NH_2 spectrum. On the other hand, recent *ab initio* CI calculations on the NH_2^+ ion (5) show the lowest states $^3\Sigma_g^-$, $^1\Delta_g$ ($^1B_1$

0008-4042/79/243182-08$01.00/0

component), and $^1\Sigma_g^+$ all to be linear or nearly linear, so that a substantial difference of 0.7 eV is calculated between the first vertical and adiabatic IP, and it is expected that such a difference is carried over to the NH_2 Rydberg states, which are expected to possess potential energy surfaces which run nearly parallel to those of the ionic species. Furthermore if emission from a linear (or nearly linear) Rydberg state to the weakly bent A^2A_1 component of the lower $^2\Pi_u$ species (favored by the Franck–Condon principle) would be a possibility, the Rydberg states might already appear in the NH_2 emission spectrum below 6 eV, and on this basis the features seen between 5 and 6 eV (6) which are indicative of a linear transition, whereby the carrier seems likely to be either NH_2 or NH_2^+, might conceivably involve NH_2 Rydberg transitions.

It is thus the goal of the present work to determine the location as well as the geometrical characteristics of the $\pi_u^2 3s$ Rydberg states of NH_2. At the same time the three known NH_2 valence-shell states will be treated, and intensities for transitions between the various valence-shell and Rydberg species will be calculated in order to aid in the experimental assignment of the NH_2 spectrum in the region above that of the well-known A^2A_1–X^2B_1 band. The theoretical treatment will be quite analogous to that employed in the earlier study (5) of the NH_2^+ system in order to allow for a direct comparison with the results of these calculations as well.

Details of the Calculations

The AO basis set employed in the present work comprises 56 contracted cartesian gaussian functions. It is basically the same as that used in the prior study of NH_2^+ (5) but it has been extended to include one Rydberg-type s ($\alpha = 0.02$) and a set of Rydberg p ($\alpha = 0.02$) functions. Thus it consists of a $(6s,4p,2d)$ set on nitrogen, a $(2s,1p)$ set on each hydrogen, and two s and two p functions in both of the NH bonds; details concerning the values of exponents and contraction coefficients may be found in ref. 5.

The configuration interaction treatment is of the general MRD-CI type (7, 8), with configuration selection and energy extrapolation (8). A core of one orbital corresponding to the $1s$ inner shell is kept doubly occupied in all configurations and one MO representing the inner-shell complement is disregarded entirely in the treatment; all other 54 orbitals in the basis are allowed variable electron occupation according to the MRD-CI procedure. The SCF solutions are obtained for the X^2B_1, A^2A_1, B^2B_2, $^2A_1$, and $^4B_1$ states indicated in Table 1 and these MO's are then employed as the basis for the CI calculations; additional SCF wavefunctions corresponding to $3p$ Rydberg states are also obtained (Table 1) at the X^2B_1 ground state equilibrium geometry. Details of the CI treatment employed, i.e. MO orbital basis, number of reference configurations from which single and double excitations are generated, number of roots according to which selection is carried out, orders of secular equations actually solved (selected configurations) and size of configuration space for which the CI energy has been extrapolated, are collected in Table 2. All configurations which contribute more than 0.25% (on a c^2 basis) are thereby included in the reference set. Finally, an estimate of the full CI energy in the AO basis employed is undertaken (5) according to a generalization of the formula given by Davidson (9) for the contribution of higher than double-excitation configurations. In all cases the sum of the squares of the expansion coefficients for the reference configurations is found to lie between 92% and 96%.

The electronic transition moments $\boldsymbol{R}_{e'e''}$ between two states $\Psi_{e'}$ and $\Psi_{e''}$ are always evaluated in an orthogonal MO basis. Hence in these cases additional CI calculations (listed in the lower part of Table 2) are carried out for the lower-energy species $\Psi_{e''}$ employing the same MO's as are used for the upper state $\Psi_{e'}$; in order to maintain the same accuracy as in the standard treatment this procedure sometimes requires inclusion of additional reference configurations for the lower state in the less suitable MO basis (Table 2).

Results and Discussion

The calculated potential energy curves as a function of the internuclear angle are given in Fig. 1 for the three valence states and the various Rydberg species of NH_2 arising from the $\pi_u^2 3s$ electronic configuration; the NH distance is thereby held fixed at the ground state equilibrium value (10, 11) of $R_0 = 1.935a_0$ (1.024 Å).

The $^2\Pi - X^2B_1$, A^2A_1 *States*

The two lowest states are obtained for 11 different internuclear angles between 180° and 45°. A polynomial fit to these data points gives an angle of 103.0° and 141.4° for the X^2B_1 and A^2A_1 minima respectively, in excellent agreement with the experimentally derived values of 103.3° (11, 12) and 144 ± 5° (13). The SCF and MRD-CI energies are −55.58063 and −55.77367 hartrees, respectively, at the experimental ground state equilibrium (103.3°, 1.024 Å), while the corresponding estimate for the full CI limit in the present AO basis lies at −55.78432 hartree. These values are similar to those obtained by Bell and Schaefer (2) in an earlier SCF and CI treat-

TABLE 1. SCF states of NH_2 and corresponding electronic configurations treated in the present work

State	No.	Configuration	Correlation with linear NH_2
X^2B_1	1	$\ldots 1b_2^2 3a_1^2 1b_1$	$\ldots 1\sigma_u^2 \pi_u^3\ ^2\Pi_u$
A^2A_1	2	$\ldots 1b_2^2 3a_1 1b_1^2$	
B^2B_2	3	$\ldots 1b_2 3a_1^2 1b_1^2$	$\ldots 1\sigma_u \pi_u^4\ ^2\Sigma_u^+$
$^4B_1$	4	$\ldots 1b_2^2 3a_1 1b_1 3s(a_1)$	$\ldots 1\sigma_u^2 \pi_u^2 3s\ ^4\Sigma_g^-$
$^2A_1$	5	$\ldots 1b_2^2 3a_1^2 3s(a_1)$	$(^2\Delta_g + {}^2\Sigma_g^+)$
$^2B_2$		$\ldots 1b_2^2 3a_1^2 3p(b_2)$	$\ldots 1\sigma_u^2 \pi_u^2 \sigma_u\ (^2\Delta_u + {}^2\Sigma_u^+)$
$^4A_2$		$\ldots 1b_2^2 3a_1 1b_1 3p(b_2)$	$\ldots 1\sigma_u^2 \pi_u^2 \sigma_u\ ^4\Sigma_u^-$
$^4A_1$		$\ldots 1b_2^2 3a_1 1b_1 3p(b_1)$	$\ldots 1\sigma_u^2 \pi_u^2 \sigma_u\ ^4\Pi_u$

TABLE 2. Technical details of the CI treatment undertaken for the various states of NH_2

State	MO set[a]	No. reference configs/ No. of roots selected[b]	Secular equations generated/solved
		Standard treatment	
X^2B_1	1	1M/1R	9715/2284–3357
A^2A_1	2	1M/1R	8925/2333–3230
B^2B_2	3	1M/1R	9029/2207–3194
$^4B_1$	4	1M/1R	16926/2865–3166
2^2B_1, 3^2B_1	4	3M/2R	44388/3514–3780
2^2A_1, 3^2A_1	4	5M/2R	35382/3163–5507
		Lower-state treatment for $\boldsymbol{R}_{e'e''}$ calculations	
X^2B_1	2	1M/1R	9715/3050–3145
	4	5M/1R	55015/2424–3254
A^2A_1	3	1M/1R	8925/2512–3083
	4	5M/1R	59207/2500–3248

[a]Numbering refers to SCF calculation of Table 1.
[b]The notation mM/nR refers to m main (or reference) configurations and an n-root selection process.

ment employing a double-ζ basis with one d polarization function; they obtain -55.573448 hartree for the SCF solution (103.3°, 1.024 Å) and -55.734014 hartree for their CI value, i.e. an energy lowering of 0.16057 hartree (compared to the 0.19304 hartree value in the present work) as a result of using a smaller number of configurations (991) and a somewhat smaller AO set than in the present work.

A variational treatment (14) for the vibrational part of the Schrödinger equation (based on 30 Hermite polynomials and the angular CI potential) yields a zero-point (bending) energy for the X^2B_1 ground state of 773 cm^{-1} corresponding to $\bar{\nu}_0 = 1546$ cm^{-1}, i.e. roughly 50 cm^{-1} higher than the spectroscopic value of 1497.3 cm^{-1} (1, 11, 15) obtained for this quantity. This discrepancy seems to remain (16) even if the CI treatment is upgraded (to correlate all electrons and not only the valence shells) or if the AO basis set is extended even further (to include f functions) with a reduction ensuing only when the effects of bond length variation with bending are taken into account (16). An even larger change has been found in N_2H_2, for example (17), in comparing results from a direct coupling of all three symmetric vibrational modes ν_1(NH), $\nu_2(\theta)$, and ν_3(NN) with those of the corresponding uncoupled one-dimensional treatments. The calculated zero-point bending energy for the A^2A_1 state (again on the basis of the angular CI potential at fixed $R = 1.024$ Å) is 451 cm^{-1}, but this value cannot be compared directly (16) to the experimental frequency $\bar{\nu}_0$ which is based on an extrapolation to $v = 0$ from higher vibrational quantum numbers.

The calculated ΔE_e value between the two states is 12 148 cm^{-1} (at fixed $R = 1.024$ Å), but this is lowered by approximately 1100 cm^{-1} if the proper distance of $1.855a_0$ for the upper state is employed (see Fig. 2); usage of the calculated zero-point frequencies places the present T_0 value (under the assumption of equal frequencies for the two NH stretching modes) just slightly below the corresponding experimental result of 11 140 cm^{-1} (1). Since, however, the main emphasis in the present work is not placed on obtaining a potential energy surface as accurate as possible for the two $^2\Pi$ components no further geometry optimizations are undertaken. This topic will be taken up in another study employing an even larger AO basis and a more extensive CI treatment in order to obtain an accurate *ab initio* description of the vibrational–rotational structure of the

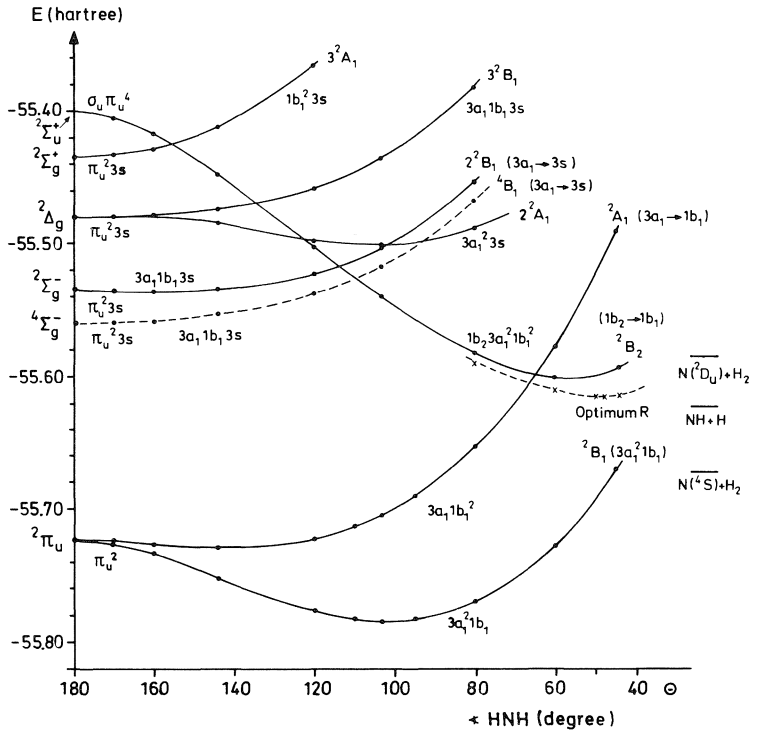

FIG. 1. Calculated CI angular potential energy curves for NH_2 in ground and various excited states (R = 1.024 Å); plotted are the estimates for the full CI energy in the AO basis employed. The corresponding energies for the separated fragments N + H_2 and NH + H are also indicated, whereby the value for $N(^4S)$ + H_2 is calculated while the two other levels are determined from experimental data. The dotted line below the solid $^2B_2$ curve refers to the structure at optimum NH distance.

X^2B_1–A^2A_1 band (16). The calculated $^2A_1$ barrier to linearity is considerably larger (1178 cm^{-1} at the estimated full CI level, R = 1.024 Å) than the value of 777 ± 100 cm^{-1} deduced by Dixon (13) or the more recent value of 730 cm^{-1} calculated by Jungen *et al.* (18) to fit the experimental spectrum; in accordance with the work of Bell and Schaefer (2) it is found that correlation energy effects are quite important for the barrier description since the corresponding SCF barrier is found to be as high as 1442 cm^{-1}. Finally the present calculations confirm the experimental finding that only a single vibrational bending level is found below the barrier maximum.

In summary then the present calculations are seen to represent the geometrical characteristics of the two lowest NH_2 states as well as their relative energy spacing to high accuracy; from this information it is concluded that the other NH_2 states, not yet characterized spectroscopically, should be predicted at approximately the same level of reliability, since the theoretical treatment employed for these species is fully equivalent to that of the X^2B_1 and A^2A_1 states.

The $^2B_2$ *State*

The $^2B_2$ state of NH_2 has been predicted (2) to possess a very small bond angle of 47.5° and the present calculations (Fig. 1) support this finding. In order to ascertain whether the small-angle structure is a real minimum the energy has been obtained for a number of C_{2v} grid points (θ and NH distances) as shown in Fig. 3. It is seen that although there is a strong interdependence between bond angle and bond distance (for smaller distances the larger-angle structure is preferred and for a structure of 180° (Fig. 2) the optimal bond separation is only $2.035a_0$ according to the SCF treatment), the calculations do find a genuine minimum for the symmetric NH_2 structure, just as has been predicted in the previous theoretical work (2). The optimum structure according to the present calculations is θ = 50° and NH = $2.135a_0$ (MRD–CI energy of −55.60267 hartree), although it should be noted that the energy at the neighboring points θ = 50°, NH = $2.195a_0$ and θ = 47.5°, NH = $2.195a_0$ is only higher by 0.0002 hartree and 0.00014 hartree at the MRD-CI level;[1] the optimized structure of ref. 2 is θ = 47.5° and NH = $2.196a_0$. The present energy minimum is

[1]The optimization yields the lowest energy (−55.615230 hartree) at θ = 50° and NH = $2.195a_0$ if the full CI estimate is taken, whereby the increase in energy to θ = 47.5° at the same bond length is 0.00002 hartree while that to NH = $2.135a_0$ for θ = 50° is 0.00018 hartree.

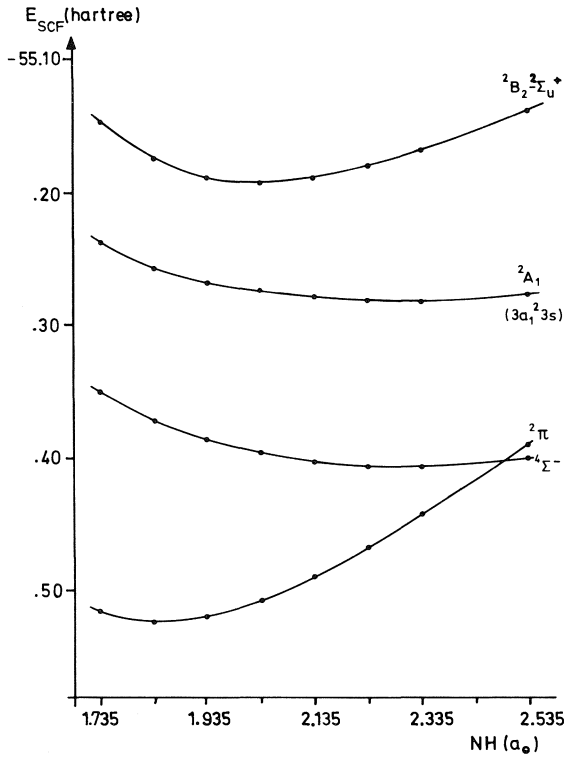

FIG. 2. Calculated SCF energies as a function of the NH distance (assuming C_{2v} symmetry) for various states at $\theta = 180°$.

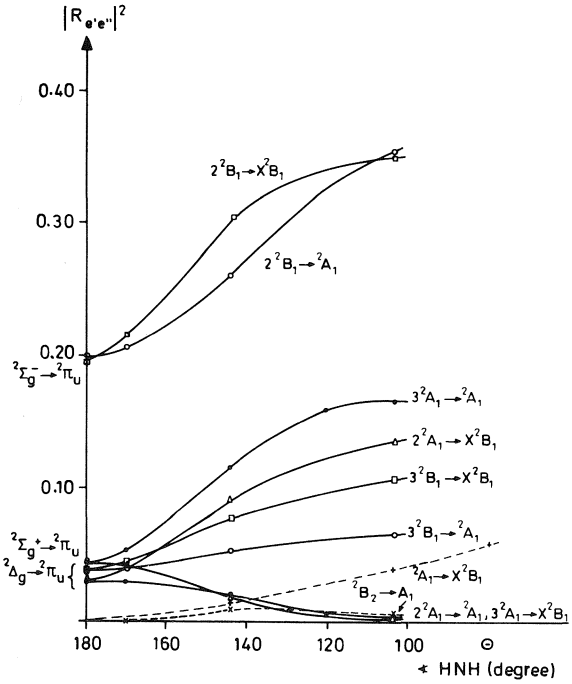

FIG. 3. Calculated CI potential energy curves (full CI estimate) for the $^2B_2$ state showing the relatively large coupling of the geometrical variables ∠HNH and NH distance.

found to lie 4.60 eV (full CI level, or 4.66 eV in the MRD-CI treatment) above that of the X^2B_1 ground state equilibrium structure, in close agreement with the 4.79 eV value predicted earlier for this quantity (2).

In order to have a comparison between the stability of this small-angle structure and the separated species N + H_2 additional CI calculations are carried out for the system (N—H_2) separated at $10a_0$, whereby the equilibrium H_2 bond length of $1.4a_0$ is employed to best represent the N(^4S) + $H_2(^1\Sigma_g^+)$ products. The energy obtained is −55.66536 hartree (MRD-CI) or −55.67200 hartree (full CI estimate), which result lies 39.3 kcal (or 35.6 kcal) *below* that of the $^2B_2$ state. Similarly the energy for the system NH + H is also somewhat below that of the $^2B_2$ minimum based on the difference in binding energies (H_2 = 4.747 eV and NH = 3.40 eV) of 31 kcal/mol between H_2 and NH. A direct fragmentation of $^2B_2$ into N(^4S) + $H_2(^1\Sigma_g^+)$ is not possible, however, so that the lowest C_{2v} products would be N(^2D_u) + $H_2(^1\Sigma_g^+)$, whereby N(^2D_u) is known to lie 2.38 eV (55 kcal) above the lowest ^4S nitrogen state. If all this information is taken together the depth of the minimum in the C_{2v} structure should be in the order of 15–20 kcal, while the NH + H dissociation limit should be approximately 5–10 kcal below the present calculated C_{2v} minimum. According to the present calculations it also seems clear that perturbation in the A^2A_1 state because of the presence of the B^2B_2 state will occur only for very high vibrational energy levels since the calculated adiabatic crossing of states occurs 3.3 eV above the energy of the A^2A_1 minimum.

The $\pi_u{}^2 3s$ Rydberg States

Excitation from the ground state $\pi_u{}^3$ configuration to the first member of the Rydberg *s* series gives rise to one quartet $^4\Sigma_g^-$ ($^4B_1$) and three states $^2\Sigma_g^-$ ($^2B_1$), $^2\Delta_g$ ($^2A_1$, $^1B_1$), and $^2\Sigma_g^+$ ($^2A_1$) of doublet multiplicity. A proper SCF treatment has not been carried through for each of these states (Table 1), however, but rather MO's of the quartet state are employed exclusively in the ensuing MRD-CI calculations for all such Rydberg species (Table 2).

The geometrical characteristics of the various Rydberg states (Fig. 1) are wholly parallel to those of their ionic counterparts investigated earlier (5), for which internuclear angles of 150° ($^3B_1$–$^3\Sigma_g^-$), 107.6° and 155.2° ($^1A_1$, $^1B_1$–$^1\Delta_g$), and 180° ($^1\Sigma_g^+$–$^1A_1$) have been obtained from analogous MRD-CI calculations. Thus the present study finds that three of the four possible Rydberg 3*s* members prefer the linear (or almost linear) geometry (Fig. 1 and Table 3) while only the 2^2A_1 component of the $^2\Delta_g$ state is most stable in a decidedly bent nuclear arrangement.

TABLE 3. Energies (in eV) of the various states contained in Fig. 1 at $\theta = 180°$, $\theta = 103.3°$, and their respective optimum angle ($R = 1.024$ Å throughout)

State	Energy		
	$\theta = 180°$	$\theta = 103.3°$	θ = opt.
$^2\Pi_u \begin{cases} X^2B_1 \\ A^2A_1 \end{cases}$	1.652	0.0[a]	0.0[a] (103.3°)
		2.161	1.506 (141.4°)
$^4\Sigma_g^- - ^4B_1$	6.108	7.241	6.108 (180°)
$^2\Sigma_g^- - 2^2B_1$	6.800	7.633	6.764 (154°)
$^2\Delta_g \begin{cases} 2^2A_1 \\ 3^2B_1 \end{cases}$	8.272	7.690	8.272 (180°)
		9.456	7.68 (≈100°)
$^2\Sigma_g^+ - 3^2A_1$	9.512	12.57	9.512 (180°)
$^2\Sigma_u^+ - B^2B_2$	10.42	6.639	4.93 (55°)
			4.60 (50°, $R = 2.135a_0$)

[a]All energies are given relative to X^2B_1. The MRD-CI energy of this state is −55.77367 hartree, while the energy estimate corresponding to a full CI treatment in the present AO basis is −55.78432 hartree.

In a similar manner the relative splitting between the various components of the $\pi_u{}^2 3s$ configuration is nearly identical to that found for the NH_2^+ ion, for which splittings between $^3\Sigma_g^-$ and the two other components $^1\Delta_g$ and $^1\Sigma_g^+$ of 2.03 eV and 3.45 eV respectively (at $\theta = 180°$ and NH = 1.027 Å) have been calculated (5). On the other hand the preferred bond lengths seem to be larger in the Rydberg states (Fig. 2) than in the ion (approximately $1.934a_0$ (5)), an observation which is consistent with a general tendency for the Rydberg species to dissociate into the lower-energy fragments NH + H (Fig. 1). A further study of this effect might also be of interest in connection with the photodecomposition of NH_3, which process yields (in addition to NH_2 in its X^2B_1 and A^2A_1 states) NH species in various electronic states at relatively high incident energies, whereby it is not yet clear whether such products occur from primary or secondary reaction steps (19, 20).

The lowest members of the Rydberg p series are forbidden to combine directly with the $^2\Pi_u$ ground state (at least in linear symmetry, which should be preferred by most of these states as well as by the corresponding $3s$ members) and have thus not been treated directly in the present work. A few SCF calculations have been carried out ($\theta = 144°$), however, and these place the $^4\Pi_u$ and $^4\Sigma_u^-$ states 1.85 eV and 1.48 eV respectively above the corresponding $^4\Sigma_u^-$ $3s$ species of otherwise identical electronic configuration (Table 1). Splittings of this magnitude are seen to be quite in line with standard Rydberg $3s$–$3p$ energy separations (3).

Calculated Intensities

The square of the electronic transition moments involving the various states treated so far are collected in Fig. 4 as a function of the internuclear angle; transitions to both components of the $^2\Pi_u$ state are considered thereby.

The A^2A_1–X^2B_1 transition is not allowed in the linear arrangement of nuclei but the corresponding $|R_{e'e''}|^2$ value climbs fairly rapidly with bending to a calculated value of 0.039 at 103°, and increases still further for smaller internuclear angles. Apparently the only experimental information which is available for comparison comes from the measurement of Halpern *et al.* (21), who obtain a radiative life-time of 10 μs for the Σ (0, 9, 0) level of the A^2A_1 state. Under the simple assumption that the life-time can be obtained from

$$\tau_{1/e} = 1.5/\bar{\nu}^2 f_e q_{v'v''}$$

(whereby the present calculations give $f_e = 0.00196$),[2] a value for τ of 5.4 μs results if the Franck–Condon factor $q_{v'v''}$ is taken to be 0.5 for this vibrational transition of peak intensity in the band. The latter assumption is not unreasonable, so that the correlation between the theoretical and experimental data seems to be quite adequate. In order to obtain a more direct comparison vibrational wavefunctions χ_v would need to be generated and the integral $|\langle\chi_{v'}|R_{e'e''}(\theta)|\chi_{v''}\rangle|^2$ would have to be evaluated directly rather than simply employing the Franck–Condon approximation.

The $^2\Sigma_u^+$–$^2\Pi_u$ transition is also forbidden in $D_{\infty h}$ symmetry and only the $^2B_2$–$^2A_1$ component becomes dipole-allowed in the bent nuclear arrangement. In contrast to the $^2A_1$–$^2B_1$ electronic transition moment, however, this quantity remains rather small (0.006 at 103°) for the $^2B_2$–$^2A_1$ transition (Fig. 4) so that the unfavorable Franck–Condon region together with the smallness of the $|R_{e'e''}|^2$ value leads one to expect the $^2B_2$–$^2A_1$ bands to be of very low intensity. Asymmetric vibrations will remove the forbidden-

[2]The oscillator strengths are obtained as $f_e = (2/3)|R_{e'e''}|^2 \Delta E$, whereby ΔE is in atomic units; ΔE is 2.161 eV (Table 3) in the calculations, i.e. a value which is quite close to the measured results of 16725 cm^{-1} = 2.0735 eV (21).

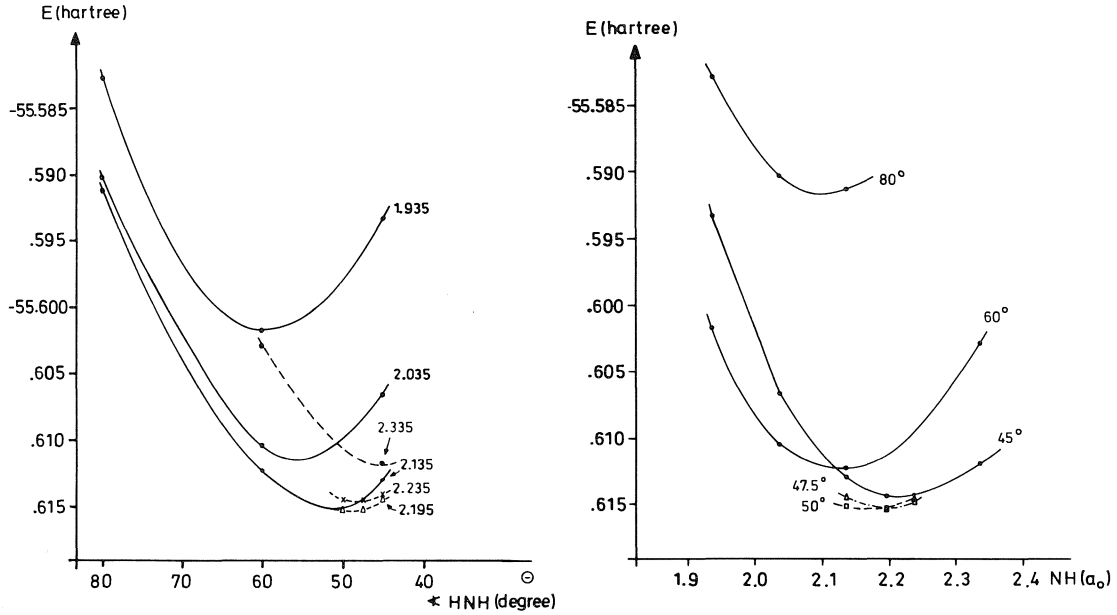

FIG. 4. Calculated transition moments $|R_{e'e''}|^2$ (in au^2) between various electronic states of NH_2 (R = 1.024 Å).

ness to the lower X^2B_1, but even then strong transitions would not appear likely. All these facts taken together then suggest that the $^2B_2$ state will not be easily accessible for direct spectroscopic investigation.

By contrast transitions from the first allowed Rydberg state $^2\Sigma_g^-$–$^2B_1$ to both $^2\Pi_u$ components are calculated to be relatively strong (Fig. 4). For example, a value of $f_e = 0.034$ is deduced for the 2^2B_1–A^2A_1 transition ($|R_{e'e''}|^2 = 0.26$, $\Delta E = 5.29$ eV, $\theta = 144°$), whereby the greatest portion of this intensity should appear in the favored Franck–Condon region, i.e. at linear or near-linear geometries corresponding to a transition energy of roughly 5.30 eV. The pattern in the vibrational structure for the corresponding transition favoring the small-angle $^2B_1$ ground state region might be somewhat complicated by the fact that in this range of internuclear angle ($\sim$103°) and energy the influence of the 2^2A_1 species should also be important (Fig. 1). Intensities of transitions from the Rydberg 3s states to the two $^2\Pi_u$ components are of intermediate strength between that of the well-characterized A^2A_1–X^2B_1 system and what is predicted in the present calculations for the first Rydberg band. Finally additional overlapping features might appear in the corresponding energy range because of the presence of the lower multiplets of the 4s (and some 4p) members not treated in the present work.

Summary and Conclusion

The present study has attempted to describe the NH_2 molecule in a variety of its low-lying electronic states while maintaining C_{2v} symmetry. Very good agreement has been found between the calculated data and the measured characteristics of the first two (X^2B_1 and A^2A_1) states, including details regarding geometrical structure, relative energetics, and transition intensity. A third valence state (B^2B_2), which has been predicted by earlier theoretical work (2), has been confirmed to be a very small-angle species, but computed electronic transition moments indicate very low intensity for a $^2B_2$–$^2A_1$ combination (with the corresponding $^2B_2$–$^2B_1$ species being dipole-forbidden). The calculations thus suggest a relatively long life-time for this species once it is formed, provided radiationless conversion (via an asymmetric vibration) to the $^2A_1$ state is not a much more favored route of deexcitation in this case.

The geometrical behavior of the various multiplets of the 3s Rydberg members parallels very closely that of the respective ionic states, as is to be expected. The calculations predict appreciable (an order of magnitude larger than that of the A^2A_1–X^2B_1 band) intensity for transitions between the first doublet state $^2\Sigma_g^-$–2^2B_1 of this nature and each of the A^2A_1 and X^2B_1 lower states. In particular they indicate that a rather strong $^2\Sigma_g^-$ (2^2B_1)–A^2A_1 band will be found in the 5.0–5.3 eV spectral region, provided appreciable population of one of the states involved is possible, thereby providing a possible assignment for a band system recently observed by Herzberg (6) which has been thought to have either NH_2 or its positive ion as its carrier. The vertical transition

between the X^2B_1 ground state and the first Rydberg member is found to occur around 7.6 eV and it is concluded that observation of such a band system in this energy region might well be hindered because of the presence of overlapping bands involving other $3s$ multiplets and/or those of the lowest $4s$ Rydberg species. Finally preliminary calculations find rather large NH separations in the above Rydberg states, which finding is thought to be an indication for the occurrence of dissociation processes involving fragments such as NH + H which are energetically more stable than is NH_2 in any state lying above its first two ($^2A_1$ and X^2B_1) valence-shell species.

Acknowledgments

The authors wish to thank Professor G. Herzberg for valuable discussions in initiating this work. The services and computer time made available by the University of Bonn Computer Center (RHRZ) have been essential to the present study and are gratefully acknowledged.

1. J. W. C. Johns, D. A. Ramsay, and S. C. Ross. Can. J. Phys. **54**, 1804 (1976).
2. S. Bell and H. F. Schaefer III. J. Chem. Phys. **67**, 5173 (1977).
3. M. B. Robin. *In* Chemical spectroscopy and photochemistry in vacuum ultraviolet. *Edited by* C. Sandorfy, P. J. Ausloos, and M. B. Robin. ASI Series C8. D. Reidel, Dordrecht, Holland. 1974.
4. G. Herzberg. Electronic spectra of polyatomic molecules. D. Van Nostrand Inc., New York, NY. 1966.
5. S. D. Peyerimhoff and R. J. Buenker. Chem. Phys. **42**, 167 (1979).
6. G. Herzberg. Private communication.
7. R. J. Buenker, S. D. Peyerimhoff, and W. Butscher. Mol. Phys. **35**, 771 (1978).
8. R. J. Buenker and S. D. Peyerimhoff. Theor. Chim. Acta, **35**, 33 (1974); **39**, 217 (1975).
9. E. R. Davidson. *In* The world of quantum chemistry. *Edited by* R. Daudel and B. Pullmann. Reidel, Dordrecht, Holland. 1974. p. 17; S. R. Langhoff and E. R. Davidson. Int. J. Quant. Chem. **8**, 61 (1974).
10. D. A. Ramsay. J. Chem. Phys. **25**, 188 (1956).
11. P. B. Davis, D. K. Russel, and B. A. Thrush. Proc. R. Soc. London A, **353**, 299 (1977).
12. K. Dressler and D. A. Ramsay. Philos. Trans. R. Soc. London, **251**, 553 (1959).
13. R. N. Dixon. Mol. Phys. **9**, 357 (1965); **10**, 1 (1965).
14. R. J. Buenker, S. D. Peyerimhoff, and M. Perić. ASI Series. Excited states in quantum chemistry. *Edited by* C. A. Nicolaides and D. R. Beck. Reidel, Dordrecht, Holland. 1978. p. 63; M. Perić, R. Runau, J. Römelt, S. D. Peyerimhoff, and R. J. Buenker. J. Mol. Spectrosc. In press.
15. M. Vervloet, M. F. Merienne-Lafore, and D. A. Ramsay. Chem. Phys. Lett. **57**, 5 (1978).
16. M. Perić, R. Runau, R. J. Buenker, and S. D. Peyerimhoff. To be published.
17. M. Perić, R. J. Buenker, and S. D. Peyerimhoff. Mol. Phys. **35**, 1495 (1978).
18. Ch. Jungen, K.-E. Hallin, and A. J. Merer. Private communication.
19. K. H. Becker and K. H. Welge. Z. Naturforsch. A**17**, 676 (1962); **19**, 1006 (1964); F. Stuhl and K. H. Welge. Z. Naturforsch. A**18**, 900 (1963). H. Okabe and M. Lenzi. J. Chem. Phys. **47**, 5241 (1967). J. Masanet, A. Gilles, and C. Vermeil. J. Photochem. **3**, 417 (1974/75).
20. R. Runau, S. D. Peyerimhoff, and R. J. Buenker. J. Mol. Spectrosc. **68**, 253 (1977).
21. J. B. Halpern, G. Hancock, M. Lenzi, and K. H. Welge. J. Chem. Phys. **63**, 4808 (1975).

Solvent extraction of monothioacetylacetone chelates of zinc(II) and nickel(II)[1]

MARZIO LEBAN, DAVID JEFFRIES, AND JAMES FRESCO
Department of Chemistry, McGill University, Montreal, P.Q., Canada H3A 2K6

Received July 12, 1979

MARZIO LEBAN, DAVID JEFFRIES, and JAMES FRESCO. Can. J. Chem. **57**, 3190 (1979).

The formation constants of nickel(II) and zinc(II) monothioacetylacetonates have been determined as 2.95×10^{12} and 6.46×10^{10} respectively. These are about 700 times more stable than the corresponding acetylacetonates. Both monothioacetylacetonates were more than 99% extracted into chloroform and ligand hydrolysis was not significant before completion of metal ion extraction.

MARZIO LEBAN, DAVID JEFFRIES et JAMES FRESCO. Can. J. Chem. **57**, 3190 (1979).

On a déterminé les constantes de formation des monothioacétylacétonates de Ni(II) et de Zn(II); leurs valeurs sont de 2.95×10^{12} et 6.46×10^{10} respectivement. Ces composés sont environ 700 fois plus stables que les acétylacétonates correspondants. L'extraction des deux monothioacétylacétonates dans le chloroforme était complète à plus de 99% l'hydrolyse de la ligande n'etait pas significative avant la fin de l'extraction de l'ion métallique.

Introduction

In contrast to results obtained in earlier studies of monothiobenzoylacetone and monothiodibenzoylmethane (1, 2, 3), more recent studies (4, 5) of β-mercaptocinnamamides and monothiodibenzoylmethane have shown the stability of zinc chelates is greater than nickel chelates. This is in accord with the observation (6) that ligands with both oxygen and sulphur basic centres show a reversal of the Irving–Williams order with respect to these two metals.

Data to be presented for monothioacetylacetone show the zinc chelate is less stable than the nickel chelate. Conformity to the Irving–Williams order has been assigned previously to exceptional structural differences between the zinc and nickel chelates of certain sulphur-containing ligands (7).

Disregard of the instability of monothio-β-diketone solutions was suggested (8) as a probable source of error in early measurements. Leban's investigation (9) of the kinetics of decomposition of aqueous solutions of monothioacetylacetone and related compounds was verified subsequently for mixed aqueous solutions (10). Results reported here have been corrected on the basis of these studies.

Experimental

Materials

2-Mercapto-pent-2-en-4-one (**1**) was prepared by a base-catalysed reaction of acetylacetone with hydrogen sulfide (11). The sodium salt (**2**) was then prepared by reacting **1** with alcoholic sodium followed by addition of anhydrous ether to precipitate **2**. The crystals were purified by recrystallization. *Anal.* calcd. for C_5H_7OSNa: C 43.47, H 5.11, S 23.20, equiv. wt. 137.9; found: C 42.28, H 5.10, S 23.31, equiv. wt. 138.2.

1,1,1-Trifluoro-4-mercapto-pent-3-en-2-one (**3**) was prepared according to the procedure described by Ho, Livingstone, and Lockyer (12). Prior to isolation of **3** the reaction mixture was allowed to reach room temperature and the sodium salt (**4**) prepared by reaction with alcoholic sodium and precipitation by addition of petroleum ether. The salt purified by recrystallization from anhydrous ether solution by addition of petroleum ether.

Zinc-65 and nickel-63 were obtained from Amersham-Searle as the dichlorides in dilute HCl solution and were diluted prior to use. The concentration of the zinc-65 stock solution was $< 3 \times 10^{-5}$ *M* (below the detection limit by EDTA titration). The concentration of the nickel-63 stock solution was determined gravimetrically with dimethylglyoxime, to be $3.28\ (\pm 0.02) \times 10^{-2}$ *M*. Radiochemical purity was checked by γ-ray spectroscopy and decay measurements. All other chemicals used were of reagent grade.

Extraction of Monothio-β-diketones

Stock solutions of the monothio-β-diketones were basic in sodium hydroxide. Aliquots of 5 mL stock solution were transferred to separatory funnels containing 25 mL chloroform and 20 mL of buffer solution at ionic strength 0.1 *M*. For **1**, extractions were carried out over the pH range 2 to 9 and for **3** extractions were performed over the pH range 0.6 to 8. To minimize the effect of decomposition of the ligands in the most acidic aqueous phases the time of attainment of extraction equilibrium was crucial. For **1** and **3** it was less than 2 min and 30 s respectively Aliquots of equilibrated aqueous phases were immediately made basic by addition of 5 mL 2 *M* NaOH.

The concentration of monothio-β-diketone in the aqueous phase was recorded using a Beckman DB spectrophotometer. In the case of **3** it was necessary to correct for decomposition in the samples at pH < 4. This was accomplished by measuring the elapsed time from addition of the stock solution of **4** to the separatory funnel to the addition of the 5 mL of 2 *M* NaOH after sampling the equilibrated aqueous phase. This time, together with the first order rate constant reported previously (9), was the basis for decomposition corrections.

Extraction of Metal Chelates

All solutions were thermostatted at 25.0°C. Aliquots of the metal stock solutions were added to buffer solutions previously delivered to separatory funnels. Ionic strength of the aqueous phase was kept constant at 0.1 *M*. Ligand was intro-

[1]Taken in part from the M.Sc. thesis of Marzio Leban, McGill University, Montreal, P.Q. 1970.

0008-4042/79/243190-03$01.00/0

duced just prior to extraction and achievement of equilibrium was verified by parallel experiments.

Values for metal distribution ratios were determined by comparison of the counting rates of aqueous phase aliquots with that of a standard. The zinc-65 activity was measured using a Nuclear Supplies EA-14 gamma well scintillation counter coupled with a Nuclear Supplies SA-250 scaler. For nickel-63 counting a Nuclear-Chicago Type 79180 1.4 mg/cm^2 mica end window Geiger tube connected to a Nuclear-Chicago Type 8770 scaler was used.

The pH values of the equilibrated aqueous phases were measured with a Metrohm pH meter calibrated with Fisher standard buffers at pH 4.00 and 7.00.

Results and Discussion

Ligand Partition Coefficients and Acid Dissociation Constants

The pH dependence of monothioacetylacetone extraction was consistent with the extraction of a weak acid. The data were fitted to a line drawn according to the formula $\log D = \log K_{D_R} - \text{pH} - \log([H^+] + K_a)$. Here D, K_{D_R}, and K_a represent the distribution ratio, partition coefficient, and dissociation constant, respectively. The value of $\log K_{D_R} = 2.52 \pm 0.03$ was obtained by averaging the values of $\log D$ at low pH values. The value of $pK_a = 6.47 \pm 0.06$ was determined from a least squares analysis of the data in the high pH region.

The solvent extraction behaviour of trifluoromonothioacetylacetone was similar to that of the previous species. The values of $\log K_{D_R}$ and pK_a were determined as 2.29 ± 0.01 and 5.04 ± 0.05 respectively. Since fluoromethylacetylacetones are strongly hydrated (13), a lower value of K_{D_R} for **3** with respect to **1** could be expected. Both **1** and **3** have K_{D_R} values one order of magnitude larger than that of acetylacetone ($\log K_{D_R} = 1.37$) (14). This effect may possibly be associated with the replacement of oxygen by sulfur and a resultant decrease in hydrogen bonding sites.

The pK_a value obtained for **1** in this study is in agreement with a value, $pK_a = 6.40 \pm 0.02$, found by potentiometric titration of **2** with HCl.[2] The lower value of pK_a for **1** relative to that of acetylacetone, $pK_a = 8.8$ (14), would be in accord with the sulfur–oxygen electronegativity difference. Thiols are usually stronger acids than the corresponding alcohols and phenols. The increased acidity of **3** as compared to **1** is consistent with the electron withdrawing effect of the —CF_3 group.

Metal Chelate Stability Constants and Partition Coefficients

The extraction of nickel(II) and zinc(II) into chloroform as a function of monothioacetylacetonate concentration showed an initial rapid rise followed by approach to a constant value. The relationship between the distribution ratio of a divalent metal chelate and aqueous free ligand concentration, $[A^-]$, can be shown to be

$$[1]\quad \frac{1}{D} = \frac{1}{K_{D_C}} + \frac{1}{K_{D_C}K_2}\left(\frac{1}{[A^-]}\right) + \frac{1}{K_{D_C}K_1K_2}\left(\frac{1}{[A^-]}\right)^2$$

where K_{D_C}, K_1, and K_2 are the chelate partition coefficient and first and second step-wise formation constants, respectively.

The free ligand concentration is obtained from the initial concentrations of ligand, $[A^-]_i$ and metal ion, $[M]_i$ according to

$$[2]\quad [A^-] = ([A^-]_i - 2[M]_i)K_a/\{[H^+](K_{D_R} + 1) + K_a\}$$

For the case of Zn(II) where $[M]_i \ll [A^-]_i$ eq. [2] may be simplified to

$$[3]\quad [A^-] = [A^-]_iK_a/\{[H^+](K_{D_R} + 1) + K_a\}$$

The calculated value for the free ligand concentration was then substituted in eq. [1] for each extraction and the resulting data matrix solved for the coefficients $1/K_{D_C}$, $1/K_{D_C}K_2$ and $1/K_{D_C}K_1K_2$ using a computer programme which evaluated the coefficients by von Holdt's Matrix Method for Least Squares (15). These values for nickel were $1/K_{D_C} = (9.03 \pm 0.61) \times 10^{-4}$, $1/K_{D_C}K_2 = (1.23 \pm 0.35) \times 10^{-9}$, and $1/K_{D_C}K_1K_2 = (3.08 \pm 0.98) \times 10^{-16}$. For zinc the values were $1/K_{D_C} = (8.82 \pm 0.87) \times 10^{-3}$ and $1/K_{D_C}K_1K_2 = (1.37 \pm 0.05) \times 10^{-13}$. The chelate partition coefficients and stability constants obtained from these appear in Table 1. Successive stability constants could not be resolved from the zinc results.

The stability constants for nickel and zinc acetylacetonates determined under comparable solution conditions (16) are smaller by 2.81 and 2.89 log units respectively than the corresponding monothioacetylacetonates. The greater stability of nickel

TABLE 1. Stability constants and partition coefficients for monothioacetylacetonate chelates of Ni(II) and Zn(II) at 25°C

Metal	$\log K_1$	$\log K_2$	$\log \beta_2$	$\log K_{D_C}$
Ni	$6.60^{+0.19}_{-0.20}$	$5.86^{+0.24}_{-0.27}$	$12.47^{+0.17}_{-0.12}$	$3.04^{+0.03}_{-0.02}$
Zn			$10.81^{+0.01}_{-0.02}$	$2.05^{+0.05}_{-0.04}$

[2]O. Siimann. Unpublished results. McGill University.

monothioacetylacetonate is supported by comparing the shorter nickel–oxygen bond distances of this chelate (17) with those reported for nickel acetylacetonate (18, 19).

Data obtained for the extraction of the zinc chelate of **3** show the stability of the chelate is less than that of the corresponding zinc monothioacetylacetonate. In the presence of pyridine the extraction of the zinc chelate of **3** is enhanced and the formation of a 1:1 pyridine adduct was demonstrated from the extraction data.

The difference between K_{D_C} values for the nickel and zinc monothioacetylacetonates suggests that adduct formation with monothioacetylacetone could have occurred more favorably with the nickel chelate. Also in Table 1 it may be noted that the nickel chelate is 40 times more stable than the zinc chelate and is in conformity with the Irving–Williams order.

In marked contrast with the slow attainment of extraction equilibrium and final incomplete extraction of nickel acetylacetonate (20) the corresponding monothioacetylacetonate extraction achieved equilibrium within 2 min and was virtually quantitative in the region of pH independence.

Acknowledgment

We are grateful to the National Research Council of Canada for financial support of this work.

1. S. H. H. Chaston and S. E. Livingstone. Aust. J. Chem. **19**, 2035 (1966).
2. S. E. Livingstone and E. A. Sullivan. Aust. J. Chem. **22**, 1363 (1969).
3. E. Uhlemann, P. Thomas, G. Klose, and K. Arnold. Z. Anorg. Allg. Chem. **364**, 153 (1969).
4. M. Chikuma, A. Yokoyama, and H. Tanaka. Chem. Pharm. Bull. **22**, 1378 (1974).
5. M. Chikuma, A. Yokoyama, Y. Ueda, and H. Tanaka. Chem. Pharm. Bull. **23**, 473 (1975).
6. A. Corsini, Q. Fernando, and H. Freiser. Anal. Chem. **35**, 1424 (1963).
7. K. S. Math, Q. Fernando, and H. Freiser. Anal. Chem. **36**, 1762 (1964).
8. A Yokoyama, M. Chikuma, and H. Tanaka. Chem. Pharm. Bull. **20**, 2000 (1972).
9. M. Leban. M.Sc. Thesis, McGill University, Montreal, P.Q. 1970; M. Leban, J. Fresco, and S. E. Livingstone. Aust. J. Chem. **27**, 2353 (1974); M. Leban, J. Fresco, M. Das, and S. E. Livingstone. Aust. J. Chem. **27**, 2357 (1974).
10. S. Harada, M. Sawada, M. Chikuma, A. Yokoyama, and H. Tanaka. Chem. Pharm. Bull. **25**, 158 (1977).
11. R. Mayer, G. Hiller, M. Nitzche, and J. Jentzsch. Angew. Chem. Int. Ed. Engl. **2**, 370 (1963).
12. R. K. Y. Ho, S. E. Livingstone, and T. N. Lockyer. Aust. J. Chem. **19**, 1179 (1966).
13. J. C. Reid and M. Calvin. J. Am. Chem. Soc. **72**, 2948 (1950).
14. J. Rydberg. Svensk. Kem. Tidskr. **65**, 37 (1953).
15. P. C. Stevenson. Processing of counting data. NAS-NS-3109. University of California, Livermore, CA. 1966. pp. 61–63.
16. G. Gutnikov and H. Freiser. Anal. Chem. **40**, 39 (1968).
17. O. Siimann, D. D. Titus, C. D. Cowman, J. Fresco, and H. B. Gray. J. Am. Chem. Soc. **96**, 2353 (1974).
18. H. Montgomery and E. C. Lingafelter. Acta Crystallogr. **17**, 1481 (1964).
19. G. J. Bullen, R. Mason, and P. Pauling. Inorg. Chem. **4**, 456 (1965).
20. J. Stary. Anal. Chim. Acta, **28**, 227 (1963).

Sulfides as precursors for sulfonyl chloride synthesis

RICHARD FRANCIS LANGLER,[1] ZOPITO ALESSIO MARINI, AND EDWARD SOMMERS SPALDING

Chemistry Department, Dalhousie University, Halifax, N.S., Canada B3H 4J3

Received April 16, 1979

RICHARD FRANCIS LANGLER, ZOPITO ALESSIO MARINI, and EDWARD SOMMERS SPALDING. Can. J. Chem. **57**, 3193 (1979).

Sulfides are advanced as sulfonyl chloride precursors. S_N2 cleavage of the intermediate sulfonium ions is discussed in conjunction with both the sulfohaloform pathway and our previous hypothesis that asymmetric chlorosulfonium chloride salts undergo Pummerer rearrangements which exhibit regioselectivity that can be anticipated on the basis of substituent electronegativity difference (ΔX_p). Thioglycolic acid is developed as a new sulfur transfer agent for sulfonyl chloride synthesis.

RICHARD FRANCIS LANGLER, ZOPITO ALESSIO MARINI et EDWARD SOMMERS SPALDING. Can. J. Chem. **57**, 3193 (1979).

On propose les sulfures comme précurseurs des chlorures de sulfonyles. On discute du clivage des ions sulfoniums intermédiaires selon un mécanisme S_N2 conjointement avec le cheminement du sulfohaloforme et de notre hypothèse antérieure. Cette dernière stipule que les chlorhydrates de chlorosulfonium asymétriques subissent des transpositions de Pummerer qui montrent une régiosélectivité et qui peuvent être prévus à partir de la différence d'électronégativité des substituants (ΔX_p). On a mis en évidence l'acide thioglycolique comme un nouvel agent de transfert de soufre dans la synthèse du chlorure de sulfonyle.

[Traduit par le journal]

Introduction

Our previous studies of the chlorinolysis of sulfur compounds (1–8) have been directed toward the development of new synthetic methods for the preparation of sulfonyl chlorides (2, 4, 5). Sulfonyl chlorides can furnish a variety of functionalities (9–17) and may be prepared with well established methods (2, 9, 18, 19). A widely employed approach involves the aqueous chlorinolysis of sulfur-containing substrates viz. sulfenyl chlorides (20, 21), mercaptans, disulfides, thiolesters, Bunte salts (22), isothioureas (23), thiocyanates (24), sulfinyl chlorides (25), thiolsulfonates (26), and sulfinic acids (2, 27). We have been developing the aqueous chlorinolysis of sulfides as an approach to the preparation of sulfonyl chlorides (4, 5, 7).

An excellent review of methods for the preparation of sulfides has recently become available (28). The most general approach to sulfide synthesis involves nucleophilic substitution by mercaptide anions on carbon bearing a suitable leaving group. This reaction has been extended to include simple aromatic substrates with a leaving group attached directly to a phenyl ring (29). A simple general scheme for sulfonyl chloride synthesis is shown in eq. [1].

$$[1]\quad R'SH + X{-}R'' \xrightarrow{\bar{\bar{B}}} R'SR'' \xrightarrow[HOAc]{Cl_2/H_2O} R''SO_2Cl$$

[1]Enquiries should be directed to Dr. R. F. Langler, Chemistry Department, Mount Allison University, Sackville, N.B., Canada E0A 3C0.

The conversion of sulfides into sulfonyl chlorides requires a cleavage step in the chlorinolysis reaction. These reactions proceed, in general, by chlorosulfonium cation intermediacy so that cleavage[2] may occur in either S_N1 or S_N2 fashion as shown in Scheme 1. We have previously reported the application of benzylic sulfides to the synthesis of sulfonyl chlorides (5). We believe that the cleavage step in these reactions involves an S_N1 mechanism.

Extensions of the approach which utilizes sulfides in which one substituent attached to sulfur will form a carbocation during chlorinolysis are readily envisioned. In particular, in cases where the desired sulfonyl chloride requires a carbon substituent which would itself form a stable carbocation, one would choose a sulfide in which the group to be lost would give rise to a carbocation of superior stability to that expected for the group to be retained. Unfortunately, extensions of this approach have very little utility since sulfonyl chlorides in which the carbon substituent can form a particularly stable carbocation are themselves unstable[3] and cannot be prepared (12, 15, 30); e.g., aqueous chlorinolysis of 1-naphthylmethyl mercaptan affords 1-chloromethyl naphthalene and not the expected sulfonyl chloride (15).

The detailed pathway by which alkyl sulfides are

[2]Evidence that these reactions are ionic and not free radical has been presented previously (4).

[3]We have suggested that the mode of decomposition is a unimolecular ionic process (15) whereas Kice has suggested a radical mechanism (12) or a cyclic transition state formed by attack of chlorine on the α carbon as it leaves from sulfur.

0008-4042/79/243193-07$01.00/0

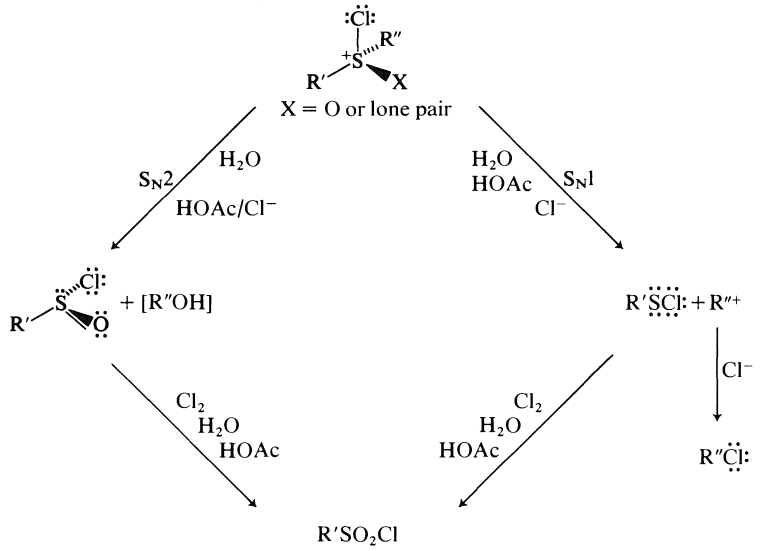

SCHEME 1

transformed into sulfonyl chlorides without the intermediacy of carbocations in the cleavage step (the sulfohaloform reaction) has been reported recently (4). (See Scheme 2.)

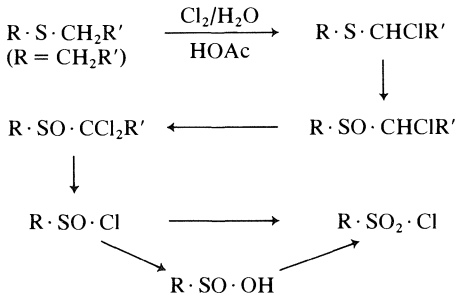

SCHEME 2. The sulfohaloform reaction

The cleavage step in the sulfohaloform reaction appears to proceed by an S_N2 mechanism (4). Several recognized complications may arise which interfere with the cleavage step: (*i*) steric crowding may preclude the existence of the desired product,[4] (*ii*) steric crowding in the intermediate α-polychloro-oxochlorosulfonium chloride can shift preferred nucleophilic attack by H_2O (4) to chloride ions with a consequent reduction in overall reaction rate and some concomitant shift in the electrophilic site attacked (1*a*), and (*iii*) carbocation formation prior to formation of the requisite α-polychlorosulfoxide intermediate can give rise to a sulfonyl chloride in which the carbon α to the sulfonyl group bears chlorine atoms (6).

Application of the sulfohaloform pathway to the analysis of asymmetric sulfide chlorinations requires that one be able to predict which of the first formed α-chlorosulfides will predominate. The substituent which incorporates the first chlorine atom is the one which will be ultimately cleaved. We have previously (1*a*) reported that asymmetric sulfide chlorinations in aprotic media introduce chlorine more readily on the α-carbon bearing the more electronegative substituent. If this postulate holds in protic media, the major sulfonyl chloride formed will be the one which retains the sulfide substituent having the α-carbon atom with the less electronegative group(s). Mercaptans could then be assessed as sulfur transfer agents for sulfonyl chloride synthesis by choosing R′ (in eq. [1]) so that $X_p(R') > X_p(R'')$.

TABLE 1. Group electronegativities*

Group	Pauling electronegativity (X_p)	*a*	*b*
H—	2.20	—	—
CH_3—	2.27	—	—
CH_3CH_2—	2.28	—	—
$ClCH_2^-$	2.47	—	—
$PhCH_2$—	2.44	7.90	0.94
$CH_3OC(O)CH_2$—	2.73	8.75	1.38
HO_2C—	3.52	—	—
$CH_3(CH_2)_2$	2.27	7.40	1.29
$CH_3(CH_2)_3$—	2.27	7.40	0.99
$CH_3(CH_2)_4$—	2.27	7.40	0.80
$CH_3(CH_2)_5$—	2.27	7.40	0.67
$CH_3SO_2(CH_2)_2$—	2.71	8.70	1.02
$PhSO_2(CH_2)_2$—	2.68	8.60	0.66

*Group electronegativities without *a* and *b* values are taken from Huheey's data (32, 33). Group electronegativities where *a* and *b* values are supplied were calculated using Huheey's method.

[4]Reference 31 gives a possible example.

TABLE 2. Exhaustive chlorinations of asymmetric sulfides in aqueous acetic acid

Sulfide substrates ($R_1CH_2SCH_2R_2$)	Sulfonyl chlorides		ΔX_p ($X_{R_1} - X_{R_2}$)
	Major (% yield)	Minor (% yield)	
$CH_3CH_2SCH_3$	CH_3SO_2Cl (62)	$CH_3CH_2SO_2Cl$ (38)	0.07
$CH_3CH_2CH_2SCH_3$	CH_3SO_2Cl (55)	$CH_3CH_2CH_2SO_2Cl$ (45)	0.08
$ClCH_2CH_2SCH_2CH_3$ (15)	$CH_3CH_2SO_2Cl$ (100)	—	0.20
$PhCH_2CH_2SCH_3$	CH_3SO_2Cl (100)	—	0.24
$ClCH_2CH_2SCH_3$ (15)	CH_3SO_2Cl (100)	—	0.27
$CH_3OC(O)CH_2CH_2SCH_3$	CH_3SO_2Cl (100)	—	0.53
$ClCH_2SCH_3$*	CH_3SO_2Cl (100)	—	0.74
$CH_3CHClSCH_2CH_3$*	$CH_3CH_2SO_2Cl$ (100)	—	0.74
n-C_3H_9CHClS-*n*-C_4H_9*	*n*-$C_4H_9SO_2Cl$ (100)	—	0.74

*Exhaustive chlorinations of last 3 cases were reported previously (4).

Results and Discussion

In order to test these proposals, a simple series of sulfides was subjected to exhaustive chlorination in aqueous acetic acid. The appropriate substituent electronegativities are shown in Table 1. Results of the chlorinations with appropriate ΔX_p values are presented in Table 2. These results are consistent with the outcomes expected on the basis of ΔX_p and sulfohaloform reaction arguments as presented above.

Inspection of the substituent electronegativities tabulated by Huheey (32, 33) led to the conclusion that thioglycolic acid would be an excellent sulfur transfer agent for sulfonyl chloride synthesis as depicted in eq. [1]. We have prepared a series of sulfides from a variety of halides and thioglycolic acid as shown in eq. [2].

$$[2]\quad R{-}X + HSCH_2CO_2H \xrightarrow[CH_3ONa]{CH_3OH} RSCH_2CO_2H \quad \mathbf{1}$$

The first problem is that of delineating the pathway by which the sulfide acids **1** are transformed into sulfonyl chlorides upon exhaustive chlorination in aqueous acetic acid. The pathway study was carried out on the sulfide acid **1***a* (R = CH_3).

Chlorinolysis of **1***a* in aqueous acetic acid for a short time furnished 1,1,1-trichloro-2-thiapropane-2-oxide (**2**) in 75% yield. Since we have previously established (4) that 1,1-dichloro-2-thiapropane-2-oxide reacts[5] under these conditions to furnish methanesulfonyl chloride in 60% yield without proceeding through the trichlorosulfoxide, it follows that the dichlorodimethyl sulfoxide is not the principal intermediate giving rise to **2**. Furthermore, we have shown (1*a*, 4) that sulfides with strongly electron-withdrawing groups on a carbon α to the sulfur atom furnish chlorosulfonium chloride salts which hydrolyze to furnish the corresponding sulfoxides rather than Pummerer rearranging to the corresponding α-chlorosulfides. Therefore the sulfide acid **1***a* must react as shown in Scheme 3. Details for the mechanisms have been given previously (1*a*, 3, 4).

The pathway elaborated for the transformation of the sulfide acid **1***a* into a sulfonyl chloride mixture presents a problem. Namely, there is no Pummerer rearrangement of a chlorosulfonium chloride salt anywhere in the pathway. Since the first step very likely produces a sulfoxide, all Pummerer rearrangements are occurring from oxochlorosulfonium chloride salts. In order that substituent electronegativity be a useful basis for evaluating mercaptans as sulfur transfer agents vis-à-vis sulfonyl chloride synthesis, sulfoxide chlorinations must also exhibit regioselectivity which correlates with substituent electronegativity difference (ΔX_p). Table 3 presents the asymmetric sulfoxide chlorinations which are presently known. The data in Table 3 suggest that ΔX_p may very well continue as a useful basis for

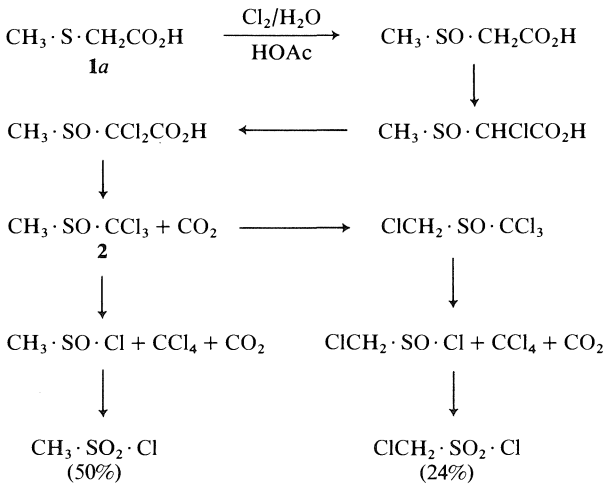

SCHEME 3

[5]The dichlorosulfoxide is converted to the trichlorosulfoxide in 16% yield under these conditions (4).

TABLE 3. Regioisomeric chlorosulfoxides from sulfoxide chlorinations

Sulfoxide substrate ($R_1CH_2SOCH_2R_2$)	Chlorosulfoxide products (% yield)	ΔX_p ($X_{R_1} - X_{R_2}$)	Reference
$CH_3(CH_2)_3S(O)CHCl(CH_2)_2CH_3$	$CH_3(CH_2)_3S(O)CCl_2(CH_2)_2CH_3$ (100)	0.74	34
$CH_3S(O)(CH_2)_3CH_3$	$CH_3S(O)CHCl(CH_2)_2CH_3$ (100)	0.07	34
$PhCH_2S(O)CH_3$*	$PhCHClS(O)CH_3$ (100)	0.29	34
$CHCl_2S(O)CH_2Cl$	$Cl_3CS(O)CH_2Cl$ (100)	0.74	4
$ClCH_2S(O)CH_3$	$Cl_2CHS(O)CH_3$ (100)	0.74	4
$Cl_2CHS(O)CH_3$	$Cl_3CS(O)CH_3$ (100)	1.48	4

*There has been a report that benzyl methyl sulfoxide chlorinates with little or no regioselectivity when iodobenzene dichloride is employed as the chlorinating agent (35).

TABLE 4. Yields* of sulfonyl chlorides obtained via sulfide acids **1**

Substrate	Product	Overall yield (%)
CH_3CH_2Br	$CH_3CH_2SO_2Cl$	70
$CH_3(CH_2)_2Br$	$CH_3(CH_2)_2SO_2Cl$	65
$CH_3(CH_2)_3Cl$	$CH_3(CH_2)_3SO_2Cl$	60
$CH_3(CH_2)_4Br$	$CH_3(CH_2)_4SO_2Cl$	80
$CH_3(CH_2)_5Br$	$CH_3(CH_2)_5SO_2Cl$	78
$CH_3SO_2(CH_2)_3Cl$	$CH_3SO_2(CH_2)_3SO_2Cl$ (**3***a*)	50
$PhSO_2(CH_2)_3Cl$	$PhSO_2(CH_2)_3SO_2Cl$ (**3***b*)	60

*Yields are reported for sulfonyl chlorides after purification by distillation or recrystallization.

assessing mercaptans as sulfur transfer agents whether chlorinolyses of the sulfide intermediates follow the sulfohaloform pathway or the closely related pathway shown in Scheme 3.

We have chlorinated a series of sulfide acids **1** which furnished the expected sulfonyl chlorides in good yields as shown in Table 4. The sulfonyl chlorides **3***a* and **3***b* were prepared as examples of more interesting substrates which can be accessed with this new method. The complete route for the preparation of their precursors **7***a* and **7***b* appears in Scheme 4.

All of the substrates examined for the development of both the present method and our previously published method (5) for the synthesis of sulfonyl chlorides have substituents attached to sulfur via primary carbon atoms. Consequently we have examined a secondary system in order to compare the two methods. The results are shown in eqs. [3] and [4].

$$[3]\quad \underset{\mathbf{1}b}{(CH_3)_2CHSCH_2CO_2H} \xrightarrow[HOAc]{Cl_2/H_2O} \underset{46\%}{(CH_3)_2CHOAc} + \underset{54\%}{(CH_3)_2CHSO_2Cl} + \underset{46\%}{Cl_2CHSO_2Cl}$$

$$[4]\quad (CH_3)_2CHSCH_2Ph \xrightarrow[HOAc]{Cl_2/H_2O} (CH_3)_2CHSO_2Cl + PhCH_2Cl$$

The results shown in eq. [3] indicate that chlorinolyses of the sulfide acids **1** are subject to complication by S_N1 dissociation prior to formation of the α-polychlorosulfoxide intermediates necessary to obtain S_N2 cleavage. However, as shown in eq. [4], benzylic sulfides are not susceptible to such a complication since S_N1 cleavage of the benzyl group occurs very early in the reaction pathway (5). The pathway for the chlorinolysis of **1***b* appears in Scheme 5.

We have now successfully developed two sulfur transfer agents for sulfonyl chloride synthesis i.e. phenylmethanethiol (5) and thioglycolic acid. While yields are generally higher and reaction times shorter for chlorinolyses of benzylic sulfides, there is a drawback in their application to the synthesis of smaller sulfonyl chlorides. When benzylic sulfides are exhaustively chlorinated in aqueous media the

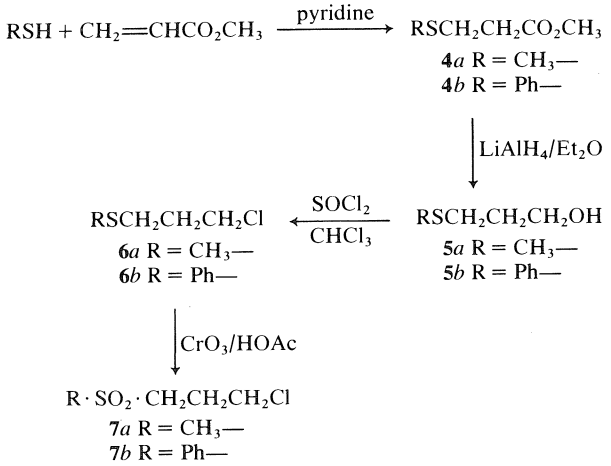

SCHEME 4

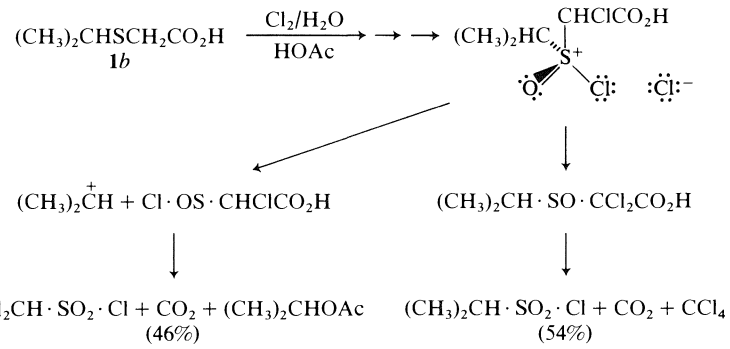

SCHEME 5

sulfonyl chloride product is contaminated with approximately one equivalent of benzyl chloride and a small amount of benzyl acetate (5). When the desired sulfonyl chloride has a volatility comparable to that of benzyl chloride, purification is tedious and time consuming. In contrast, the chlorinolysis of sulfide acids **1** produces the desired sulfonyl chlorides carbon dioxide and carbon tetrachloride and the sulfonyl chlorides are therefore isolated in good purity directly from the reaction mixtures. Thus thioglycolic acid is a superior sulfur transfer agent for the preparation of small sulfonyl chlorides where the carbon bearing the chlorosulfonyl group in the product will not be a suitable carbocationic centre. Phenylmethanethiol is a superior transfer agent for the preparation of crystalline or non-volatile sulfonyl chlorides or systems in which the carbon bearing the chlorosulfonyl group can bear positive charge with some facility.

In conclusion, we have developed thioglycolic acid as a new sulfur transfer reagent for sulfonyl chloride synthesis. Sulfonyl chloride synthesis requires substrate analysis in terms of (*i*) stability of carbocations which could be formed by S_N1 dissociation of intermediate chlorosulfonium and oxochlorosulfonium cations, (*ii*) ΔX_p for asymmetric sulfides for which neither carbon attached to sulfur is a potential carbocationic centre, and (*iii*) steric factors which may complicate the cleavage of α-polychloro-oxochlorosulfonium chloride intermediates.

Experimental

General

The ir spectra were recorded on a Perkin-Elmer 237B spectrophotometer. The nmr spectra were obtained on a Varian T-60 instrument using TMS as the internal standard. The mass spectra were recorded on a Dupont-CEC model 21-104 mass spectrometer. The samples were directly introduced using an all glass probe and the spectra run at 30 eV with a source temperature of 150°C. Melting points were determined on a Fisher-Johns melting point apparatus and are uncorrected.

Exhaustive Chlorinations In Aqueous Medium

The sulfide substrate was dissolved in glacial acetic acid (25 mL) and water (3 mL). Chlorine (ca. 200 mL/min) was bubbled into the reaction mixture for 2.5 h with ice/water cooling as necessary to maintain the temperature of the reaction mixture between 20 and 30°C. Water (50 mL) was added and the resultant mixture washed with methylene chloride (100 mL). The organic layer was washed with 2.5% w/v NaOH (two 50 mL aliquots), dried ($MgSO_4$), filtered, and the solvent evaporated. The residue was distilled or recrystallized before yield was determined.

Preparation of $PhCH_2CH_2SCH_3$

Sodium metal (0.851 g) was dissolved in absolute ethanol (100 mL). Methanethiol (5 mL) was slowly distilled into the cooled ethoxide solution. 2-Phenyl-1-chloroethane (5.021 g) in ethanol (10 mL) was added dropwise over 15 min and the reaction mixture stirred at ambient temperature for 48 h. Water (100 mL) was added and the resultant mixture washed with chloroform (three 100 mL aliquots). The combined organic layers were dried and concentrated. The crude concentrate was rectified at reduced pressure affording the sulfide (4.572 g, bp 96°C/5 Torr), nmr ($CDCl_3$) δ: 7.70 (5H, s), 3.00 (4H, m), and 2.10 (3H, s); ms *m/e*: 152 ($M^{\ddagger}$, 28%), 91 (53%), and 61 (100%).

Preparation of $CH_3SCH_2CH_2C(=O)OCH_3$ **4**a

Sodium metal (4.210 g) was dissolved in methanol (200 mL) and the solution cooled. Methanethiol (10 mL) was distilled into the reaction mixture and methyl acrylate (15.691 g) added. The reaction mixture was refluxed 1 h. Water (250 mL) was added and the resultant mixture washed with chloroform (four 200 mL aliquots). The combined organic layers were dried and concentrated. The residue was distilled at reduced pressure yielding the sulfide ester (8.586 g, bp 106–108°C/100 Torr), ir ($CHCl_3$): 1740 cm^{-1}; nmr ($CDCl_3$) δ: 3.76 (3H, s), 2.73 (4H, m), and 2.13 (3H, s); ms *m/e*: 134 ($M^{\ddagger}$, 64%), 74 (98%), and 61 (100%).

Chlorination of Asymmetric Sulfides

A series of asymmetric sulfides were subjected to aqueous chlorinolysis as described under "Exhaustive Chlorinations". The relative yields were determined by integration of the nmr spectrum of the crude product. Results are shown in Table 2.

Preparation of $CH_3SCH_2CH_2CH_2OH$ **5**a

Lithium aluminum hydride (1.701 g) was covered with THF (15 mL) and the mixture refluxed for 0.5 h. The mixture was cooled to room temperature and a solution of CH_3S-

$(CH_2)_2CO_2CH_3$ (6.000 g) in THF (10 mL) added dropwise over 10 min. The reaction mixture was refluxed for 0.5 h. Upon completion of the reflux ethyl acetate (2.5 mL) was added dropwise; 10% HCl (30 mL) was added dropwise, the layers separated, and the organic layer dried and concentrated. The residue was fractionated at reduced pressure furnishing the sulfide alcohol (4.238 g, bp 136°C/100 Torr), ir ($CHCl_3$): 3620 and 3450 cm^{-1}; nmr ($CDCl_3$) δ: 3.76 (2H, t), 2.60 (2H, t), 2.33 (1H, s), 2.13 (3H, s), and 1.90 (2H, m); ms *m/e*: 106 (M^+, 100%), 88 (67%), and 73 (40%).

Preparation of $PhS(CH_2)_3Cl$ ***6***b *and $CH_3S(CH_2)_3Cl$* ***6***a

$CH_3S(CH_2)_3OH$ or $PhS(CH_2)_3OH$ (15) (10 g) was dissolved in chloroform (40 mL) and the solution brought to gentle reflux. Thionyl chloride (1 equiv.) in chloroform (20 mL) was added dropwise to the reaction mixture over 10 min. Upon completion of the addition the reaction mixture was refluxed.

After 4.5 h reflux the solvent was removed and the residue distilled affording $PhS(CH_2)_3Cl$ (4.876 g, bp 130°C/2.2 Torr), nmr ($CDCl_3$) δ: 7.20 (5H, s), 3.60 (2H, t), 3.03 (2H, t), and 2.00 (2H, m); ms *m/e*: 188 (19%), 186 (M^+, 57%), 123 (100%), and 110 (82%).

After 24 h reflux the solvent was removed and the residue rectified yielding $CH_3S(CH_2)_3Cl$ (8.309 g, bp 114–116°C/100 Torr), nmr ($CDCl_3$) δ: 3.70 (2H, t), 2.70 (2H, t), 2.13 (5H, m); ms *m/e*: 126 (4.4%), 124 (M^+, 13.3%), 88 (42%), and 61 (100%).

Preparation of $PhSO_2(CH_2)_3Cl$ ***7***b *and $CH_3SO_2(CH_2)_3Cl$* ***7***a

Chromium trioxide (2.5 equiv.) was covered with glacial acetic acid (140 mL) and a solution of the appropriate chlorosulfide (5.00 g) in glacial acetic acid (10 mL) added. The reaction mixture was *vigorously stirred* and the temperature maintained at 90–100°C for 0.5 h. Water (150 mL) was added and the resultant mixture washed with methylene chloride (four 100 mL aliquots). The combined organic layers were washed with 5% NaOH (100 mL aliquots) until the aqueous layer remained basic. The organic layer was dried, concentrated, and the residue distilled.

$CH_3SO_2(CH_2)_3Cl$ (3.816 g, bp 168–170°C/4 Torr) had ir ($CHCl_3$): 1325 and 1145 cm^{-1}; nmr ($CDCl_3$) δ: 3.80 (2H, t), 3.26 (2H, t), 3.00 (3H, s), and 2.20 (2H, m); ms *m/e*: 158 (3.1%), 156 (M^+, 9.3%), 94 (60%), and 41 (100%).

$PhSO_2(CH_2)_3Cl$ (3.139 g, bp 180–182°C/1.9 Torr) had ir ($CHCl_3$): 1325 and 1150 cm^{-1}; nmr ($CDCl_3$) δ: 7.80 (5H, m), 3.60 (2H, t), 3.30 (2H, t), and 2.20 (2H, m); ms *m/e*: 220 (2.7%), 218 (M^+, 8.1%), 77 (100%), and 41 (57%).

Preparation of Sulfide Acids ***1***

The preparations of the sulfide acids were all carried out in the same manner as illustrated for the preparation of the methyl system **1***a*. The crude samples were checked to confirm that the expected product had formed. Sodium metal (0.407 g) was dissolved in methanol (25 mL) and thioglycolic acid (0.807 g) added. A solution of methyl iodide (1.216 g) in methanol (10 mL) was added dropwise and the reaction mixture stirred at ambient temperature for 24 h. The solvent was evaporated and the residue *thoroughly dried*. Water (5 mL) was added, followed by concentrated HCl (1 mL). Chloroform (250 mL) was added, the solution dried ($MgSO_4$), filtered, and concentrated affording crude sulfide acid.

Preparation of $CH_3CH_2SCH_2CO_2CH_3$

Crude sulfide acid was prepared from ethyl bromide (4.264 g), thioglycolic acid (3.614 g), and sodium metal (1.866 g) in methanol (60 mL) as described for the sulfide acids **1**.

The crude acid was covered with methanol (5 mL) and concentrated HCl (6 mL). The reaction mixture was stirred at ambient temperature for 5 min. Chloroform (250 mL) was added and the mixture dried ($MgSO_4$), filtered, and concentrated. The residue was rectified at reduced pressure affording the sulfide acid methyl ester (1.820 g, bp 106–108°C/100 Torr); ir ($CHCl_3$): 1730 cm^{-1}; nmr ($CDCl_3$) δ: 3.73 (3H, s), 3.23 (2H, s), 2.66 (2H, q), and 1.26 (3H, t); ms *m/e*: 134 (M^+, 38.0%), 75 (100%), and 74 (60%). *Anal.* calcd. for $C_5H_{10}O_2S$: C 44.75, H 7.51; found: C 44.25, H 7.73.

$CH_3SCH_2CO_2H$ **1***a* had ir ($CHCl_3$): 3000 and 1720 cm^{-1}; nmr ($CDCl_3$) δ: 11.53 (1H, s), 3.23 (2H, s), and 2.26 (3H, s); ms *m/e*: 106 (M^+, 44%) and 61 (100%).

$CH_3CH_2SCH_2CO_2H$ had ir ($CHCl_3$): 3000 and 1720 cm^{-1}; nmr ($CDCl_3$) δ: 11.50 (1H, s), 3.26 (2H, s), 2.70 (2H, q), and 1.26 (3H, t).

$CH_3(CH_2)_2SCH_2CO_2H$ had ir ($CHCl_3$): 2990 and 1720 cm^{-1}; nmr ($CDCl_3$) δ: 11.09 (1H, s), 3.26 (2H, s), 2.66 (2H, t), 1.73 (2H, m), and 1.00 (3H, t); ms *m/e*: 134 (M^+, 50%), 75 (100%), and 47 (86%).

$CH_3(CH_2)_3SCH_2CO_2H$ had ir ($CHCl_3$): 3000 and 1720 cm^{-1}; nmr ($CDCl_3$) δ: 11.10 (1H, s), 3.50 (2H, s), 2.70 (2H, t), 1.60 (4H, m), and 1.00 (3H, t); ms *m/e*: 148 (M^+, 51%), 89 (78%), 61 (51%), and 47 (100%).

$CH_3(CH_2)_4SCH_2CO_2H$ had ir ($CHCl_3$): 3000 and 1720 cm^{-1}; nmr ($CDCl_3$) δ: 11.23 (1H, s), 3.23 (2H, s), 2.66 (2H, t), 1.40 (6H, m), and 0.90 (3H, t); ms *m/e*: 162 (M^+, 37%), 103 (80%), and 69 (100%).

$CH_3(CH_2)_5SCH_2CO_2H$ had ir ($CHCl_3$): 3000 and 1720 cm^{-1}; nmr ($CDCl_3$) δ: 11.37 (1H, s), 3.23 (2H, s), 2.66 (2H, t), 1.40 (8H, m), and 0.90 (3H, t); ms *m/e*: 176 (M^+, 34%), 117 (100%), and 83 (64%).

$CH_3SO_2(CH_2)_3SCH_2CO_2H$ had ir ($CHCl_3$): 3000 and 1720 cm^{-1}; nmr ($CDCl_3$) δ: 11.30 (1H, s), 3.30 (2H, s), 2.96 (7H, m), and 2.16 (2H, m); ms *m/e*: 195 (27%), 121 (27%), and 73 (100%).

$PhSO_2(CH_2)_3SCH_2CO_2H$ had ir ($CHCl_3$): 3000 and 1720 cm^{-1}; nmr ($CDCl_3$) δ: 11.45 (1H, s), 7.90 (5H, m), 3.26 (4H, m), 2.83 (2H, t), and 2.13 (2H, m); ms *m/e*: 256 (50%), 143 (82%), and 77 (100%).

$(CH_3)_2CHSCH_2CO_2H$ **1***b* had ir ($CHCl_3$): 3000 and 1720 cm^{-1}; nmr ($CDCl_3$) δ: 11.25 (1H, s), 3.33 (3H, m), and 1.30 (6H, d); ms *m/e*: 134 (M^+, 55%), 92 (42%), and 75 (100%).

Chlorinolysis of ***1***a

Crude sulfide acid **1***a* (0.93 g) was chlorinated for 10 min employing the procedure outlined under "Exhaustive Chlorinations". Trichloromethyl methyl sulfoxide (1.212 g) was obtained. After purification by column chromatography employing silica gel and chloroform elution, the product was shown to be identical to authentic material by nmr, ir, and tlc.

Chlorination of Sulfide Acids

The desired alkyl sulfide acid (5 g) was chlorinated as described under "Exhaustive Chlorinations" and the alkane sulfonyl chloride products distilled. In each case the product had the known ir, nmr, and bp. Overall yields for conversion of the alkyl halides into the corresponding sulfonyl chlorides are given in Table 4.

$CH_3SO_2(CH_2)_3SO_2Cl$ **3***a* was recrystallized from chloroform and had mp 62–65°C; ir ($CDCl_3$): 1380, 1310, 1170, and 1145 cm^{-1}; nmr ($CDCl_3$) δ: 3.96 (2H, t), 3.26 (2H, t), 2.96 (3H, s), and 2.56 (2H, t); ms *m/e*: 143 (6.8%), 141 (20.4%), 79 (13.3%), and 41 (100%). *Anal.* calcd. for $C_4H_9ClO_4S_2$: C 21.76, H 4.11; found: C 21.35, H 4.18.

$PhSO_2(CH_2)_3SO_2Cl$ **3***b* was recrystallized from chloroform and shown to be identical to previously prepared material (15) by ir, nmr, mp, and mixture mp.

Chlorination of $(CH_3)_2CHSCH_2CO_2H$ ***1***b

The sulfide acid (4.71 g) was subjected to the procedure outlined under "Exhaustive Chlorinations". The crude product contained 2-acetoxypropane (1.499 g), 2-propanesulfonyl chloride (2.284 g), and dichloromethanesulfonyl chloride (2.509 g) as determined by a method described previously (4). The identity of the constituents in the mixture was confirmed by the addition of authentic samples of each compound which resulted in the change of the intensities of the appropriate signals in the nmr spectrum of the mixture.

Chlorination of $(CH_3)_2CHSCH_2Ph$

The benzylic sulfide (5.84 g) was subjected to the procedure outlined under "Exhaustive Chlorinations". The crude product contained 2-propanesulfonyl chloride (4.281 g). The identity of the sulfonyl chloride and benzyl chloride were confirmed by the addition of authentic samples to the crude which resulted in the change in intensities of the appropriate signals in the nmr spectrum of the mixture. No isopropyl acetate was present in the crude.

Acknowledgements

The authors are indebted to Mr. T. P. Ahern for some technical assistance and to Dr. J. H. Kim for running the mass spectra. We are grateful to Dalhousie University for financial support in the form of a grant from the Research Development Fund.

1. (*a*) T. P. Ahern, D. G. Kay, and R. F. Langler. Can. J. Chem. **56**, 2422 (1978); (*b*) D. G. Kay, R. F. Langler, and J. E. Trenholm. Can. J. Chem. **57**, 2185 (1979).
2. R. F. Langler, Z. A. Marini, and J. A. Pincock. Can. J. Chem. **56**, 903 (1978).
3. J. S. Grossert, W. R. Hardstaff, and R. F. Langler. Can. J. Chem. **55**, 421 (1977).
4. J. S. Grossert and R. F. Langler. Can. J. Chem. **55**, 407 (1977).
5. R. F. Langler. Can. J. Chem. **54**, 498 (1976).
6. W. R. Hardstaff, R. F. Langler, J. Leahy, and M. J. Newman. Can. J. Chem. **53**, 2664 (1975).
7. J. S. Grossert, W. R. Hardstaff, and R. F. Langler. Chem. Commun. 50 (1973).
8. J. S. Grossert and R. F. Langler. Chem. Commun. 49 (1973).
9. J. March. Advanced organic chemistry. McGraw-Hill, New York, NY. 1968. pp. 373, 374.
10. J. F. King. Acc. Chem. Res. **8**, 10 (1975).
11. W. E. Truce and A. M. Murphy. Chem. Rev. **48**, 69 (1951).
12. J. L. Kice. *In* The chemistry of organic sulfur compounds. *Edited by* N. Kharasch and C. Y. Meyers. Pergamon, NY. 1966. pp. 120, 121.
13. M. Asscher and D. Vofsi. J. Chem. Soc. 4962 (1964).
14. F. G. Bordwell and H. M. Andersen. J. Am. Chem. Soc. **75**, 6019 (1953).
15. H. O. Fong, W. R. Hardstaff, D. G. Kay, R. F. Langler, R. H. Morse, and D. N. Sandoval. Can. J. Chem. **57**, 1206 (1979).
16. G. Olah. Friedel-Crafts and related reactions. Vol. 3. Part 2. Interscience, NY. 1964. p. 1319.
17. H. Burton and W. A. Davy. J. Chem. Soc. 528 (1948).
18. E. E. Gilbert. Sulfonation and related reactions. Interscience, NY. 1965. pp. 84 and 126.
19. L. A. Paquette and R. B. Houser. J. Am. Chem. Soc. **91**, 3870 (1969).
20. H. Brintzinger, H. Koddebusch, K. Kling, and G. Jung. Ber. **85**, 455 (1952).
21. I. B. Douglass, V. Simpson, and A. Sawyer. J. Org. Chem. **14**, 272 (1949).
22. I. B. Douglass and T. B. Johnson. J. Am. Chem. Soc. **60**, 1486 (1938).
23. T. B. Johnson and J. M. Sprague. J. Am. Chem. Soc. **58**, 1348 (1936).
24. T. B. Johnson and I. B. Douglass. J. Am. Chem. Soc. **61**, 2548 (1939).
25. I. B. Douglass, B. S. Farah, and E. G. Thomas. J. Org. Chem. **26**, 1996 (1961).
26. I. B. Douglass and C. E. Osborne. J. Am. Chem. Soc. **75**, 4582 (1953).
27. R. Otto. Ann. Chem. **145**, 323 (1868).
28. W. Tagaki. *In* Organic chemistry of sulfur. *Edited by* S. Oae. Plenum Press, New York, NY. 1977. p. 231.
29. J. R. Campbell. J. Org. Chem. **29**, 1830 (1964).
30. M. S. Kharasch, E. N. May, and F. R. Mayo. J. Org. Chem. **3**, 189 (1940).
31. J. Butler and R. M. Kellogg. J. Org. Chem. **42**, 973 (1977).
32. J. E. Huheey. J. Phys. Chem. **69**, 3284 (1965).
33. J. E. Huheey. J. Phys. Chem. **70**, 2086 (1966).
34. (*a*) K. C. Tin and T. Durst. Tetrahedron Lett. 4643 (1970); (*b*) T. Durst, K. C. Tin, and M. J. V. Marcil. Can. J. Chem. **51**, 1704 (1973).
35. M. Cinquini and S. Colonna. J. Chem. Soc. Perkin Trans. I, 1883 (1972).

The biosynthesis of caerulomycin A in *Streptomyces caeruleus*. Incorporation of ^{14}C- and ^{13}C-labeled precursors and analyses of labeling patterns by ^{13}C nmr[1]

A. GAVIN MCINNES, DONALD G. SMITH, AND JOHN A. WALTER

Atlantic Regional Laboratory, National Research Council of Canada, Halifax, N.S., Canada B3H 3Z1

AND

LEO C. VINING AND JEFFREY L. C. WRIGHT[2]

Biology Department, Dalhousie University, Halifax, N.S., Canada B3H 4J1

Received July 3, 1979

A. GAVIN MCINNES, DONALD G. SMITH, JOHN A. WALTER, LEO C. VINING, and JEFFREY L. C. WRIGHT. Can. J. Chem. **57**, 3200 (1979).

Carbon-13 nuclear magnetic resonance spectroscopy of caerulomycin A (**1**) produced by cultures of *Streptomyces caeruleus* has shown that [1-^{13}C]acetate labels C-2, C-4, and C-4′, whilst [1,2-^{13}C]acetate enriches these carbons plus C-2′, C-3, C-3′, C-5′, and C-6′. The results establish that acetate is incorporated with little dilution at C-3 and C-4 in the substituted ring of **1**, whereas C-2, and C-2′ to C-6′ of the unsubstituted ring, are assembled from lysine via the symmetrical intermediate 2*S*,6*S*-diaminopimelic acid. The methoxyl carbon incorporates label from DL-[3-^{13}C]serine, but this precursor does not enrich C-5, C-6, or C-7 of the substituted ring, and the origins of these carbons remain undetermined.

A. GAVIN MCINNES, DONALD G. SMITH, JOHN A. WALTER, LEO C. VINING et JEFFREY L. C. WRIGHT. Can. J. Chem. **57**, 3200 (1979).

La résonance magnétique nucléaire du ^{13}C de la caerulomycine A (**1**) produit par les cultures de la *Streptomyces caeruleus* a montré que l'acétate [^{13}C-1] marque les carbones en positions 2,4 et 4′ tandis que l'acétate [^{13}C-1,2] enrichi ces même carbones avec en plus ceux en positions 2′, 3, 3′, 5′ et 6′. Ces résultats indiquent que l'acétate est incorporé avec très peu de dilution en positions C-3 et C-4 du cycle substitué de **1** tandis que les carbones C-2 et C-2′ à C-6′ du cycle non substitué proviennent de la lysine via un intermédiaire symétrique l'acide diaminopimélique 2*S*,6*S*. Le carbone du métoxy est marqué à partir de la DL[^{13}C-3] serine, mais ce précurseur n'enrichit par les carbones 5, 6 ou 7 du cycle substitué dont l'origine rest indéterminé.

[Traduit par le journal]

Introduction

Streptomyces caeruleus produces a unique group of metabolites containing the 2,2′-dipyridyl ring system (1–4). Caerulomycin A (**1**), the first of these compounds to be isolated (1), is an antibiotic and is the main component of the mixture produced under the usual conditions of culture. We have investigated its biosynthesis by measuring the incorporation of isotope from potential ^{13}C- and ^{14}C-labeled precursors.

Experimental

Culture

Streptomyces caeruleus Baldacci HLX 877 was supplied by Dr. P. V. Divekar, Hoechst Pharmaceuticals Ltd., Bombay. Slants prepared from it showed variations in morphology, and successive subculture on agar medium led to a marked decrease in caerulomycin production. Single-colony isolates of the parent strain varied in pigmentation, sporulation, and ability to produce caerulomycin; a non-pigmented sporulating isolate, strain 4/2, was selected for this work. Stock cultures were lyophilized and stored at −20°C; slant cultures were maintained on modified Czapek agar with the following composition (g/L): soluble starch (20), nutrient agar (20), $NaNO_3$ (2.0), $CaCO_3$ (2.0), K_2HPO_4 (1.0), yeast extract (1.0), $MgSO_4 \cdot 7H_2O$ (0.5), KCl (0.5). The pH was adjusted to 8.9 with NaOH before autoclaving. This medium, without nutrient agar, was also used to prepare a vegetative inoculum for cultures producing caerulomycin. The inoculum was grown in two stages. In the first, spores and surface growth from a slant were dispersed in 10 mL of medium and transferred to an additional 40 mL of medium in a 250-mL Erlenmeyer flask. The culture was incubated for 10–12 days at 26°C on a rotary shaker (220 rpm, 3.8 cm eccentricity), then blended, and 4 mL was used to inoculate a second flask containing 50 mL of inoculum medium. The secondary inoculum culture was incubated as before for 4 days.

Cultures for producing caerulomycin A were grown in 250-mL Erlenmeyer flasks containing 50 mL of nutrient medium. In most of the experiments where ^{14}C-labeled compounds were added to the cultures, medium 1 was used. It contained (g/L): soluble starch (20), $NaNO_3$ (2.0), $CaCO_3$ (2.0), K_2HPO_4 (1.0), KCl (0.5), and $MgSO_4 \cdot 7H_2O$ (0.5). The pH value was adjusted to 8.9 with NaOH before autoclaving. In the remaining experiments with ^{14}C-labeled compounds, and where ^{13}C-labeled supplements were added to cultures, medium 2 was used. It contained (g/L): sorbitol (25), KNO_3 (2.0), $CaCO_3$ (2.0), K_2HPO_4 (1.0), $MgSO_4 \cdot 7H_2O$ (0.5), and NaCl (0.5). The pH was adjusted to 8.9 with KOH before autoclaving. Each flask received 2 mL of secondary inoculum and was incubated under the same conditions as the inoculum

[1]NRCC No. 17742.

[2]Present address: Atlantic Regional Laboratory, National Research Council of Canada, Halifax, N.S., Canada B3H 3Z1.

0008-4042/79/243200-05$01.00/0

cultures. Harvest times and the medium used are given with the results of each experiment.

Labeled Supplements

Radioactive compounds were obtained from New England Nuclear Corporation, Boston, MA; DL-[3-^{13}C]serine as well as sodium [1-^{13}C]- and sodium [1,2-^{13}C]acetate, all 90% enriched, were obtained from Merck Sharp and Dohme, Pointe Claire, P.Q. Supplements were prepared as aqueous solutions; those containing sodium acetate were sterilized by autoclaving; all other solutions were filtered through a 0.45 μm pore size membrane. Where the supplement was added in portions to a culture, it was subdivided equally. Times of addition varied; for radioactive supplements they are noted in Table 1. Carbon-13 labeled supplements were added on the 1st, 4th, 7th, and 10th days after inoculation. Radioactive supplements were added in cumulative amounts corresponding to 1 mmol per liter of culture. Sodium [1-^{13}C]acetate (total 934 mg; 11.3 mmol), sodium [1,2-^{13}C]acetate (882 mg; 10.5 mmol) and DL-[3-^{13}C]serine (108 mg; 1.02 mmol) were each added to 1 liter of culture. Cultures were harvested on the 14th day, except those receiving sodium [1,2-^{13}C]acetate which were harvested on the 15th day and yielded 61 mg of enriched metabolite.

Isolation of Caerulomycin A

Cultures were harvested by filtration and the filtrate, adjusted to pH 7 if acidic, was extracted with three half-volumes of ether. Basic products were then transferred from the ether to *N* HCl and recovered by neutralizing with excess $NaHCO_3$, then reextracting into ether. The product from 1-liter cultures, after removal of solvent, was chromatographed on a column (2.6 cm × 90 cm) of cross-linked dextran (Sephadex G-25 fine, Pharmacia Limited, Uppsala), equilibrated with the solvent system benzene – ethyl acetate – acetic acid – water (1:12:4:12). Caerulomycin A was collected at an elution volume of 340–450 mL during development with the organic phase. It was crystallized from ethanol and sublimed in high vacuum at 120–150°C as colourless needles, mp 175–176°C. The purity of the sample was checked by thin-layer chromatography (3) and by scanning the chromatogram for radioactivity where appropriate.

Instrumentation

Radioactivity was measured in a liquid scintillation counter. On thin-layer chromatograms it was detected with a gas-flow Geiger-Mueller detector.

^{13}C nmr spectra were recorded with Varian XL-100/15 and Varian FT-80A Fourier-transform spectrometers. Conditions were: XL-100/15 (FT-80A): frequency 25.16 MHz (20.0 MHz), spectral width 5120 Hz (4132 Hz), acquisition time 3.2 or 0.8 s (0.99 s), delay between acquisitions 2.2 s for high-resolution spectrum, 1.0 s for suppression of nuclear Overhauser enhancement when chromium acetylacetonate ($Cr(acac)_3$) was used as a relaxation reagent, flip angle 33°, 40° (40°), 90°, pulse length 40 μs (11 μs), time constant for exponential weighting of free induction decay −0.4 s or −1.0 s (−0.4 s), strength of ^{1}H-decoupling field $\gamma H_2/2\pi$ ca. 3800 Hz (ca. 4000 Hz), broad-band decoupling by 0°–180° phase modulation effective over 1000 Hz bandwidth, sample concentration ca. 140 mg/mL, solvent DMSO-d_6, solution volume 0.25 to 0.4 mL, $Cr(acac)_3$ concentration (when used) 10 mg/mL, 5 mm diameter sample tubes, internal lock to ^{2}H in solvent, reference to internal $(CH_3)_4Si$.

Enrichments from singly ^{13}C-labeled precursors were calculated as described previously (5) from spectra of the ^{13}C-enriched and natural-abundance material recorded under identical conditions. In the case of enrichment with [3-^{13}C]-serine, $Cr(acac)_3$ was added to the caerulomycin A solutions and the nmr measurements repeated, with suppression of the nuclear Overhauser enhancement (nOe) by switching off the ^{1}H-decoupling field between data acquisition periods. This technique and method of calculation was also used to obtain absolute ^{13}C enrichments from the sample labeled by [1,2-^{13}C]acetate. In this latter product many resonances consisted of doublet (intensity I_d) and multiplet (I_m; usually quartet) components due to the presence of ^{13}C—^{13}C and ^{13}C—^{13}C—^{13}C or ^{13}C—^{13}C—^{13}C—^{13}C units, superimposed on a central singlet (I_c) resonance arising from ^{13}C not directly bonded to other ^{13}C atoms. The relative intensities I_c, I_d, I_m should be proportional to the amounts of ^{13}C nuclei in each of the above situations, since ^{13}C—^{13}C contributions to spin–lattice relaxation have a negligible effect when a relaxation reagent is used in conjunction with a suppressed nOe technique.

Results

^{14}C-Labeled Substrates

The incorporation of radioactivity into caerulomycin A from a variety of ^{14}C-labeled compounds is summarized in Table 1. Labeled compounds were fed to *S. caeruleus* in two groups, with different growth and feeding conditions being used for each group. L-[U-^{14}C]alanine was included in each group as a reference compound. The results show that tryptophan and glycine are ineffective as precursors and that, although the antibiotic contains a methoxyl group, formate does not contribute to the one-carbon pool from which this part of the caerulomycin A structure is drawn. On the other hand, radioactivity was incorporated efficiently from L-[U-^{14}C]lysine and DL-[3-^{14}C]serine. The direct comparison between L-[U-^{14}C]alanine, sodium [1-^{14}C]acetate, D-[U-^{14}C]glucose, DL-[1-^{14}C]aspartate, and DL-[4-^{14}C]aspartate shows acetate to be the most readily incorporated whereas [1-^{14}C]aspartate is a relatively poor precursor. Higher yields of product and lower dilutions of isotope were obtained when the culture developed slowly, with sorbitol as a carbon source, and with successive small supplements of the precursor during the prolonged period of antibiotic production (see Table 1, cultures grown in medium 2). These conditions were chosen for studies with ^{13}C-labeled compounds.

^{13}C-Labeled Substrates

The ^{13}C nmr spectrum of caerulomycin A has been assigned previously (3). The spectrum of material labeled from [1-^{13}C]acetate showed enrichments of $<0.2\%$ at all positions except C-2 ($6.7 \pm 0.9\%$), C-4 ($19.6 \pm 2.5\%$), and C-4′ ($12.5 \pm 1.6\%$).

Similar feeding conditions were used to examine the incorporation of sodium [1,2-^{13}C]acetate. Values of $^1J_{CC}$ and the following quantities, calculable for

TABLE 1. Incorporation of radioactivity into caerulomycin A from ^{14}C-labeled compounds

Compound administered*		Caerulomycin A	
	(μCi/mmol)	(μCi/mmol)	Dilution
Sodium [1-^{14}C]acetate	12.3	0.467	26.3
D-[U-^{14}C]glucose	10.2	0.331	30.8
DL-[4-^{14}C]aspartate	6.13	0.142	43.2
L-[U-^{14}C]alanine	7.28	0.132	55.2
DL-[1-^{14}C]aspartate	17.9	0.164	109
L-[β-^{14}C]tryptophan	9.94	0.063	158
DL-[*benzene ring*-^{14}C]tryptophan	9.37	0.017	551
Sodium [^{14}C]formate	7.47	0.010	747
L-[U-^{14}C]lysine†	20.9	8.50	2.46
DL-[3-^{14}C]serine†	28.4	3.42	8.30
L-[U-^{14}C]alanine†	21.0	0.97	21.7
[1-^{14}C]glycine†	21.7	0.13	167

*Carrier was added to each radioactive compound so that the total supplement was 1 mmol per litre.
†These cultures were grown in medium 2. Radioactive supplements were subdivided equally and added on the 1st, 4th, 8th, and 12th days after inoculation. Cultures were harvested on the 16th day. All other cultures were grown in medium 1; a single radioactive supplement was added on the 2nd day and cultures were harvested on the 7th day.

TABLE 2. Caerulomycin A enriched with [1,2-^{13}C] acetate: contributions to the average ^{13}C probability (p_A) at labeled sites from natural abundance material (p_{NA}), from the precursor (p_p), and from ^{13}C scrambling (p_s); mole fraction (x) of ^{13}C originating from the precursor; S and T values and one-bond ^{13}C—^{13}C spin–spin couplings ($^1J_{CC}$)*

Carbon	p_A	p_{NA}	p_p	p_s	x	S	T	$^1J_{CC}$†(Hz)
C-3	0.164 ±0.031	0.009	0.148	0.007	0.172 ±0.04	0.82 ±0.01	0.06 ±0.01	C-2, C-3; 63.7±1.0
C-4	0.166 ±0.031	0.009	0.142	0.015	0.174 ±0.04	0.77 ±0.01	<0.01	C-3, C-4; 65.9±0.3
C-2	0.065 ±0.012	0.010	0.034	0.021	0.061 ±0.011	0.47 ±0.02	‡	C-2, C-2′; 71.7±0.3
C-2′	0.060 ±0.010	0.010	0.032	0.018	0.055 ±0.010	0.48 ±0.02	‡	C-2′, C-3′; 64±1
C-3′	0.060 ±0.011	0.011	0.037	0.012	0.055 ±0.010	0.55 ±0.01	0.21 ±0.02	C-3′, C-4′; 54.2±0.3
C-4′	0.134 ±0.025	0.010	0.080	0.044	0.138 ±0.025	0.54 ±0.01	0.04 ±0.02	C-4′, C-5′; 53.9±0.3
C-5′	0.058 ±0.011	0.011	0.036	0.011	0.053 ±0.010	0.56 ±0.01	0.23 ±0.04	C-5′, C-6′; 54.0±0.3
C-6′	0.060 ±0.011	0.011	$p_p + p_s$ 0.049		0.055 ±0.010	0.237 ±0.009	0.0	

*$x = (p_A - 0.0111)/(B - 0.0111)$, $p_{NA} = 0.0111(1 - x)$, $p_p = Sp_A/B$, $p_s = p_A - p_{NA} - p_p$, $S = (I_d + I_m)/(I_c + I_d + I_m)$ and $T = I_m/(I_d + I_m)$ where $(1 - x)$ is the mole fraction of natural abundance ^{13}C, B(= 0.9) is the ^{13}C probability at sites in [1,2-^{13}C] acetate, and I_c, I_d, and I_m are the integrated intensities of singlet, doublet, and multiplet resonances for individual carbons, respectively.
†$^1J_{CC}$ values were also obtained from the spectrum of the metabolite enriched with [1-^{13}C]acetate, where high ^{13}C enrichments at C-4 and C-4′ allowed the following measurements: C-3, C-4, 65.1±1.0 Hz; C-4, C-5, 66.5±1.0 Hz; C-3′, C-4′, 54.0±1.0 Hz; C-4′, C-5′, 53.4±1.0 Hz.
‡Intensity of broad multiplet not measurable.

each labeled site from the intensities of resonance components in the ^{13}C nmr spectrum of caerulomycin A obtained in this experiment, are given in Table 2: p_A (^{13}C probability), x (mole fraction of ^{13}C originating from labeled precursor), S (probability that the ^{13}C atom is directly bonded to one or more ^{13}C atoms), T (probability of incorporation of a third ^{13}C atom adjacent to a ^{13}C—^{13}C unit). Pairs of coupled carbons were matched from one-bond ^{13}C—^{13}C spin–spin couplings. Table 2 shows that C-2′ through C-6′ plus C-2, C-3, and C-4 are enriched by doubly labeled acetate. Since only C-2, C-4, and C-4′ are enriched by [1-^{13}C]acetate it follows that C-2′, C-3, C-3′, C-5′, and C-6′ originate from the methyl group of acetate. The enrichments ($100(p_A - 0.0111)$) in the [1,2-^{13}C]acetate experiment are not uniform (C-3, C-4 ≈ 15 ± 3%; C-2, C-2′, C-3′, C-5′, C-6′ ≈ 5 ± 1%; C-4′ ≈ 12 ± 2%) but for C-2, C-4, and C-4′ are consistent with those obtained with [1-^{13}C]acetate.

The $^1J_{CC}$ values, enrichments, and the intensity distribution of resonance components for the individual carbons establish unequivocally that pairs of carbons are incorporated as $^{13}C—^{13}C$ units from doubly labeled acetate at the following positions: C-3, C-4; C-2, C-2′; C-3′, C-4′; C-4′, C-5′. It is apparent from both the overlap of pairs and from the positions labeled by each acetate carbon that C-3′, C-5′, and C-6′ are derived from the methyl group of the precursor, preceded or accompanied by scission of the $^{13}C—^{13}C$ bond. This is borne out by an examination of singlet, doublet, and multiplet resonance intensities for individual carbons. Substantially higher enrichment at C-3 and C-4 (see p_A and x values Table 2) indicates that these two carbons are incorporated from acetate as a separate biogenetic unit. It is also apparent (Table 2) that x is the same (0.056 ± 0.005) for C-2, C-2′, C-3′, C-5′, and C-6′. The value of x is about half that for C-4′ (0.138 ± 0.025). The higher enrichment at C-4′ is explained by the contribution from two different $^{13}C—^{13}C$ units, one at C-3′, C-4′ and the other at C-4′, C-5′. The S-values for C-2 and C-2′ through C-5′ are uniform (0.52 ± 0.05) and C-2′ through C-6′ are symmetrically labeled, both in origin and amount about an axis through N-1′ and C-4′. Furthermore the S-value for C-6′ and the T-value for C-3′ and C-5′ coincide (0.23 ± 0.02) indicating that they represent the probability of ^{13}C being present in the precursor pool during assembly of C-2 and C-2′ through C-6′. Subsequent dilution with natural abundance material has reduced p_A for these carbons to 0.062 ± 0.005. Satellites accompanying the C-6′ resonances are, therefore, due to random incorporation of ^{13}C at C-6′ when the ^{13}C probability for C-5′ was about 0.23. They are not due to an intact $^{13}C—^{13}C$ unit at C-5′, C-6′ derived from doubly labeled acetate. The combined evidence at this stage is consistent with C-2 plus C-2′ through C-6′ being derived from the symmetrical intermediate 2*S*,6*S*-diaminopimelic acid as illustrated in Fig. 1.

The value $T = 0.04$ for the C-4′ resonance shows that when this carbon is part of the $^{13}C—^{13}C$ unit C-4′, C-5′ (or C-4′, C-3′), the probability (0.04) of incorporating a single ^{13}C label at the adjacent C-3′ (or C-5′), is about 1/6th the probability (0.23) of incorporating ^{13}C at C-2′ (or C-6′) adjacent to the unit C-3′, C-4′ (or C-4′, C-5′). This is consistent with the single labels at C-3′ and C-5′ originating from the acetate–methyl group via pyruvate (see Fig. 1) and undergoing dilution of ^{13}C to 1/6th the level in the $^{13}C—^{13}C$ pairs derived via oxalacetate and aspartate.

It is also noteworthy that the value $T = 0.06$ for the C-3 resonance is equal to p_A for C-2. Consequently C-2 and C-3 are linked after the monosubstituted pyridine ring, comprising C-2 and C-2′ through C-6′, has been constructed and diluted with natural abundance material.

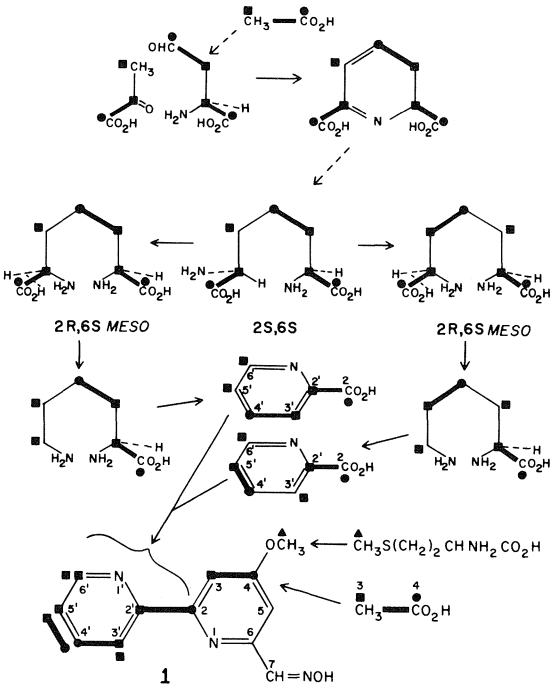

FIG. 1. The portion of the biosynthetic pathway to caerulomycin A involving 2*S*,6*S* diaminopimelic acid and acetate.

Some scrambling of the labels in doubly labeled acetate has occurred prior to incorporation and this has increased the proportion of single label at each site in enriched caerulomycin A. As expected, sites originating from the carboxyl group of acetate were affected to a greater extent than those derived from the methyl group (6).

^{13}C nmr analysis of caerulomycin A labeled from DL-[3-^{13}C]serine showed enrichment of the methoxyl carbon ($2.6 \pm 0.6\%$), confirming the expected origin of this substituent from the one-carbon pool of the organism, derived via the serine–glycine conversion (7). Lesser enrichment ($1.0 \pm 0.4\%$) was observed at C-3′ and C-5′. This is accounted for by conversion of serine to pyruvate through the action of serine dehydratase (7), and is supporting evidence for the participation of pyruvate in forming the unsubstituted pyridine ring of caerulomycin A.

None of the precursors discussed above labeled C-5, C-6, or C-7.

Discussion

The pattern of ^{13}C incorporation from [1-^{13}C]- and [1,2-^{13}C]acetate indicates that the unsubstituted pyridyl ring of caerulomycin A is derived from three-

and four-carbon precursors assembled in the manner characteristic of lysine biosynthesis in bacteria. The pathway must include at least one symmetrical intermediate such as 2*S*,6*S*-diaminopimelic acid. Since L-[U-^{14}C]lysine was incorporated with high efficiency and its formation from diaminopimelic acid is virtually irreversible (8), we conclude that lysine is a direct precursor of the antibiotic. Lysine is also a precursor of the pyridine ring in proferrorosamine A (**2**), an iron-complexing metabolite produced by

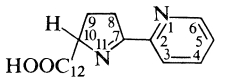

2

Pseudomonas roseus fluorescens (9). Picolinic acid was also found to be efficiently incorporated into proferrorosamine and it is tempting to suggest that it is also an intermediate in the biosynthesis of caerulomycin A.

While C-2 of the substituted pyridyl ring is contributed by lysine and carbons 3 and 4 enter from acetate by a route which, to judge from the relatively low dilution, is a fairly direct one, the source of the three remaining carbons is uncertain. Serine has been eliminated by direct test, and the possibility that they might come from alanine or pyruvate can be discounted because C-5, C-6, and C-7 should then have been labeled from acetate or serine to an extent similar to that observed for the positions contributed by the three-carbon precursor of lysine. None of the ring carbons was labeled by one-carbon donors and since [1-^{14}C]glycine was a very poor precursor of the antibiotic, a $C_2 + C_1$ unit derivation is unlikely. The most plausible explanation is that a three-carbon glycolytic pathway intermediate, such as dihydroxy acetone phosphate, reacts, either directly or after conversion to methylglyoxal, with a picolinyl-C_2 intermediate to supply the balance of the structure. Helbling and Viscontini (10) have reported that cultivation of *P. roseus fluorescens* on asparagine and [1-^{14}C]glycerol (which would be expected to form [1,3-^{14}C]dihydroxyacetone phosphate) yielded proferrorosamine A in which 75% of the radioactivity was distributed between C-8, C-9, C-10, and C-12. About one-third was located at C-12.

Acknowledgements

We thank John Berrigan and Erich Sperker for invaluable technical help. The work was supported by research grants (to LCV) from the National Research Council of Canada and from Merck–Frosst Laboratories, Pointe Claire, P.Q.

1. A. Funk and P. V. Divekar. Can. J. Microbiol. **5**, 317 (1959).
2. P. V. Divekar, G. Read, and L. C. Vining. Can. J. Chem. **45**, 1215 (1967).
3. A. G. McInnes, D. G. Smith, J. L. C. Wright, and L. C. Vining. Can. J. Chem. **55**, 4159 (1977).
4. A. G. McInnes, D. G. Smith, J. A. Walter, J. L. C. Wright, L. C. Vining, and G. P. Arsenault. Can. J. Chem. **56**, 1836 (1978).
5. J. L. C. Wright, L. C. Vining, A. G. McInnes, D. G. Smith, and J. A. Walter. Can. J. Biochem. **55**, 678 (1977).
6. W. B. Turner. *In* Fungal metabolites. Academic Press, Inc., New York, NY. 1971. p. 280.
7. A. L. Lehninger. *In* Biochemistry. Worth Publishers, Inc., New York, NY. 1976. p. 568.
8. H. E. Umbarger. Ann. Rev. Biochem. **47**, 543 (1978); **47**, 557 (1978).
9. M. Pouteau-Thouvenot, J. Padikkala, M. Barbier, A. Helbling, and M. Viscontini. Helv. Chim. Acta, **55**, 2295 (1972).
10. A. M. Helbling and M. Viscontini. Helv. Chim. Acta, **59**, 2284 (1976).

Gas phase ion equilibria: $RCO^+ + OH_2 \rightleftharpoons RC(OH)_2^+$; heats of formation of acylium ions RCO^+ and protonated acids $RC(OH)_2^+$; gas phase catalysis of proton shift $RC(OH)_2^+ \rightarrow RCO(OH_2)^+$

W. R. DAVIDSON, S. MEZA-HÖJER,[1] AND P. KEBARLE[2]

Chemistry Department, University of Alberta, Edmonton, Alta., Canada T6G 2G2

Received June 27, 1979

W. R. DAVIDSON, S. MEZA-HÖJER, and P. KEBARLE. Can. J. Chem. **57**, 3205 (1979).

The equilibria [2]: $RCO^+ + OH_2 \rightleftharpoons RC(OH)_2^+$ for R = CH_3, C_2H_5, and C_6H_5 were studied in a pulsed electron beam high ion source pressure mass spectrometer. van't Hoff plots led to ΔH_2 values: (CH_3), 24.6; (C_2H_5), 22.7; (C_6H_5), 21.9 kcal/mol. $\Delta H_f(RC(OH)_2^+)$ were obtained from gas phase basicity ladders combined with the new $\Delta H_f(t\text{-butyl}^+)$ = 163 kcal/mol (Beauchamp). The $\Delta H_f(RC(OH)_2^+)$ were: (CH_3), 71.3; (C_2H_5), 63.6; (C_6H_5), 95.5 kcal/mol. Combination of ΔH_2 with $\Delta H_f(RC(OH)_2^+)$ leads to $\Delta H_f(RCO^+)$: (CH_3), 153.7; (C_2H_5), 144; (C_6H_5), 174.6 kcal/mol. These results are in agreement with selected data from appearance potentials. The energies and structures of the participants in reaction [2] were calculated by MINDO/3 and STO-3G. MINDO/3 gave good agreement with ΔH_2. The establishment of the equilibria [2] was unusually slow. A study of the kinetics revealed that k_{2f} is approximately third order, unusually small, and has an unusually large negative temperature coefficient. Furthermore, reaction [2] was found to be catalyzed by RCOOH. An explanation of these observations is given by assuming that the proton shift $RCO(OH_2)^+ \rightarrow RC(OH)_2^+$ has a large activation energy barrier in the gas phase. This barrier is removed by formation of a hydrogen bonded complex with RCOOH.

W. R. DAVIDSON, S. MEZA-HÖJER et P. KEBARLE. Can. J. Chem. **57**, 3205 (1979).

On a étudié l'équilibre 2: $RCO^+ + OH_2 = RC(OH)_2^+$ où R = CH_3, C_2H_5 et C_6H_6 à l'aide d'un spectromètre de masse utilisant comme source d'ions à haute pression un faisceau d'électrons produit par pulsations. Les courbes de van't Hoff conduisent à des valeurs de ΔH_2: (CH_3) 24.6, (C_2H_5) 22.7, (C_6H_5) 21.9 kcal/mol. On a obtenu les valeurs de $\Delta H_f(RC(OH)_2^+)$ à partir des échelles de basicité de la phase gazeuse combinées avec la nouvelle valeur pour $\Delta H_f(tert\text{-butyl}^+)$ de 163 kcal/mol (Beauchamp). Les valeurs sont les suivantes: (CH_3) 71.3, (C_2H_5) 63.6 et (C_6H_5) 95.5 kcal/mol. La combinaison de ΔH_2 avec $\Delta H_f(RC(OH)_2^+)$ conduit aux valeurs suivantes de $\Delta H_f(RCO^+)$ (CH_3) 153.7, (C_2H_5) 144, (C_6H_5) 174.6 kcal/mol. Les résultats sont en accord avec des données choisies à partir des potentiels d'apparition. Les énergies et les structures des substances participant à la réaction 2 sont calculées par MINDO/3 et STO-3G. Les calculs faits par MINDO/3 donnent des résultats qui s'accordent bien avec les valeurs de ΔH_2. La réaction [2] atteint l'équilibre lentement ce qui est inhabituel. Une étude des cinétiques révèle que k_{2f} est approximativement du troisième ordre, qu'elle est anormalement faible et qu'elle est dôtée d'un coefficient de température anormalement grand. On a trouvé de plus que la réaction [2] est catalysée par RCOOH. On donne une explication de ces observations en faisant l'hypothèse que le déplacement du proton $RCO(OH_2)^+ \rightarrow RC(OH)_2^+$ a une barrière d énergie d'activation dans la phase gazeuse. Cette barrière est supprimée par la formation d'un complexe d'hydrogène lié à RCOOH.

[Traduit par le journal]

Introduction

Recent reports from this laboratory (1–5) described studies of gas phase equilibria [1] involving the reactions of carbo cations A^+ ($C_2H_5^+$, $C_3H_7^+$, $t\text{-}C_4H_9^+$) with the compounds B:

[1] $A^+ + B \rightleftharpoons AB^+$

where B = H_2 (1), CH_4 (1), OH_2 (2), CO (3), ClR′ (4). Process [1] may be considered as a Lewis acid–base reaction between the Lewis acid A^+ and the $\sigma(H_2, CH_4)$, $\pi(CO)$, and $n(OH_2, ClR')$ donor bases B.

The present work deals with equilibria [2] in which the Lewis acids are the acylium ions RCO^+ and the base is water. Earlier work (3) showed that the product of the addition of water to the acylium ions in the gas phase is the protonated acid $RC(OH)_2^+$.

[2] $RCO^+ + OH_2 \underset{r}{\overset{f}{\rightleftharpoons}} RC(OH)_2^+$

Since RCO^+ can be produced by carbonylation of R^+ by CO (3) these gas phase reactions are analogous to the Koch–Haaf (6) synthesis of acids in con-

[1]Visiting professor 1977–1978 from Chemistry Department, National University of Mexico, Mexico City, Mexico.

[2]To whom all correspondence should be addressed.

0008-4042/79/243205-11$01.00/0

densed media. The gas phase reaction [2] is in principle similar to the Lewis acid–base additions [1]. However, to obtain the final product, the proton shift [3] is required.

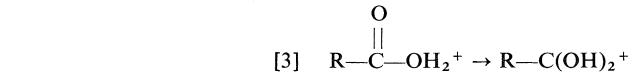

[3] $R-\overset{\overset{O}{\|}}{C}-OH_2^+ \rightarrow R-C(OH)_2^+$

The structure on the left is the hydroxyl protonated acid, while that on the right is the more stable carbonyl protonated acid. The necessity for the 1,3 proton shift [3] introduces some complications in the gas phase kinetics of the equilibria [2]. As will be seen these complications are of considerable interest.

In the present work, measurements of the equilibria with R = C_2H_5 and C_6H_5 could be made. van't Hoff plots of the equilibrium constants K_2 lead to ΔH_2^0 and ΔS_2^0. The enthalpies of formation of $RC(OH)_2^+$ can be obtained from the known proton affinities of the acids RCOOH. Therefore one can calculate $\Delta H_f(RCO^+)$ from ΔH_2 and $\Delta H_f(RC(OH)_2^+)$ since the enthalpies of formation of the neutrals involved in [2] are known. The present results combined with earlier data for R = CH_3 (5) and R = H provide ΔH_f values for HCO^+, CH_3CO^+, $C_2H_5CO^+$, and $C_6H_5CO^+$.

It was considered of interest to compare the experimentally determined ΔH_2 with theoretically calculated ΔE_2. Accordingly the electronic energies of the reactants entering process [2] were calculated using MINDO/3 and STO-3G for R (H, CH_3, C_2H_5, and C_6H_5). The theoretical results are also of interest because they provide information on the geometries of RCO^+ and $RC(OH_2)_2^+$. Information is also obtained on the energetics of the proton shift [3], i.e. the energy difference between the hydroxy and carbonyl protonated acids, and the activation energy barrier between these two structures.

Experimental

The kinetics and the equilibria of reaction [2] were studied with a pulsed electron beam high ion source pressure mass spectrometer of design similar to that commonly used in our laboratory (7). However, in the present instrument the electron gun was mounted on the ion source as described earlier, see Fig. 1 (8). The reactant gas mixture at a known pressure between 1.5–4 Torr is passed in slow flow through the thermostated ion source. In the present work equilibria [2] were measured with water vapor as the major gas. The water vapor carried small amounts (~0.1%) of the acid RCOOH. Some of the kinetic measurements were made with methane or isobutane as major gas. The major gas carried small amounts (~0.1%) of the acid RCOOH. The gas mixtures were prepared at 1 atm total pressure in a 5 L storage bulb kept at 170°C. The flow through the ion source was obtained by bleeding the reaction mixture from the storage bulb into the flow system.

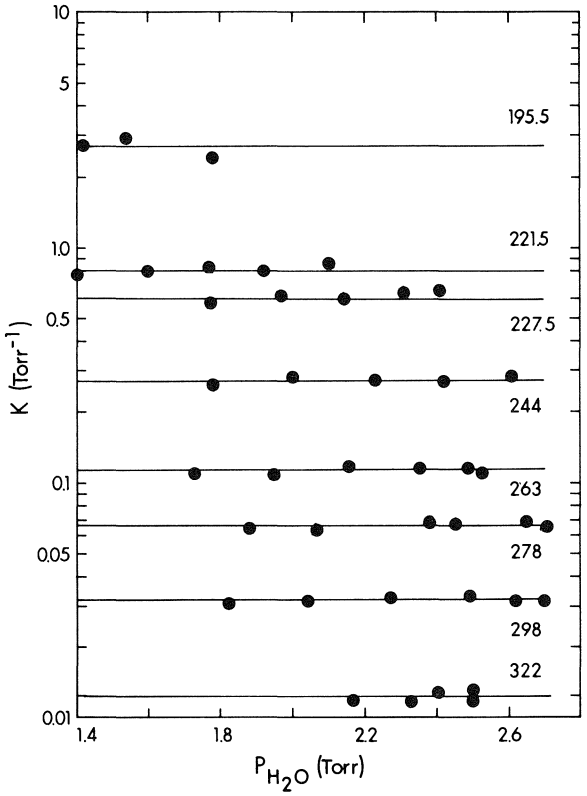

FIG. 1. Plot of equilibrium constants K for reaction $C_2H_5CO^+ + OH_2 \rightleftharpoons C_2H_5C(OH)_2^+$, obtained at different temperatures (°C) versus water pressure.

Results and Discussion

(a) Kinetics and Equilibria of $RCO^+ + OH_2 \rightleftharpoons RC(OH)_2^+$

Equilibrium [2] was measured in experiments where the major gas passed through the ion source was water (1.5–3 Torr). The water vapor contained some 0.1% RCOOH. The positive ions produced by electron impact and subsequent ion–molecule reactions in water vapor are (7) the protonated water clusters $H^+(H_2O)_n$.

[4] $H^+(H_2O)_n + RCOOH \rightleftharpoons RC(OH)_2^+(OH_2)_k + (n-k)H_2O$

In the present system, as expected, the initial ions observed where $H^+(H_2O)_n$, which disappeared within microseconds while ions of mass corresponding to $RC(OH)_2^+$, were formed. The proton transfer [4] is exothermic (9) and fast. At lower temperatures the hydrated protonated acid resulting from [4] added more water molecules, thus rapidly reaching equilibrium. When the ion source temperature was raised, the equilibrium hydrates of the protonated acid con-

tained less and less water molecules. Above a given temperature, the bare protonated acid formed by [4], with $k = 0$, could be observed to decompose via reaction [2r]

[2r] $RC(OH)_2^+ \rightarrow RCO^+ + OH_2$

In a given temperature interval the ions RCO^+ and $RC(OH)_2^+$ were observed to reach stationary concentrations after several hundreds of microseconds. The constant ion intensity ratio at long reaction times was assumed to be the equilibrium concentration ratio for reaction [2] and was used for the evaluation of the equilibrium constant K_2. Plots of K_2 versus water pressure are shown in Figs. 1 and 2 for $R = C_2H_5$ and $R = C_6H_5$. These figures show the pressure range covered and the extent to which K_2 was invariant with water pressure. The equilibrium constants K_2 were also found to be independent of the concentration of the RCOOH. van't Hoff plots of the K_2 from Figs. 1 and 2 are shown in Fig. 3. This figure also includes the van't Hoff plot of reaction [2] with $R = CH_3$ obtained earlier in this laboratory (5). The ΔH_2^0 and ΔS_2^0 obtained from the van't Hoff plots are given in Table 1. The thermochemical significance of the data obtained from the van't Hoff plots will be considered in the next section. The observation that equilibrium [2] required several hundred microseconds to establish, even when pure water at a few Torr pressure was used, is unusual. For example, the clustering equilibria

$$H^+(H_2O)_{n-1} + H_2O \rightleftharpoons H^+(H_2O)_n$$

establish only after some 10 μs under the same temperature and pressure conditions (7).

Rate measurements were made with the hope that they might lead to an understanding as to why equilibrium [2] is so slow. All kinetic runs were done with benzoic acid, i.e. R = Ph. First the time dependence of $PhC(OH)_2^+$ and $PhCO^+$ was examined with water as major gas at pressures between 1.5 to 3 Torr in the temperature range 194–260°C. Addition reactions like [2f] are generally third order, which means that the reverse reaction [2r] must be second order (7, 10, 11). The order of [2r] was examined and found consistent with second order dependence; however, the experimentally accessible pressure change, by a factor of 2, was not really sufficient to prove the order conclusively. As expected, the rate constants were found to be very small. Thus, $k_{2f} \approx 7.5 \times 10^{-31}$ cm^6 molecules^{-2} s^{-1} and $k_{2r} \approx 4.4 \times 10^{-14}$ cm^3 molecule^{-1} s^{-1} (205°C, benzoic acid, third body water vapor). The temperature dependence of k_{2r} and k_{2f} was also examined. It was found that k_{2f} had an extremely large negative temperature coefficient: $k_{2f} = cT^{-n}$ where $n > 13$. The conditions for kinetic studies, with water as

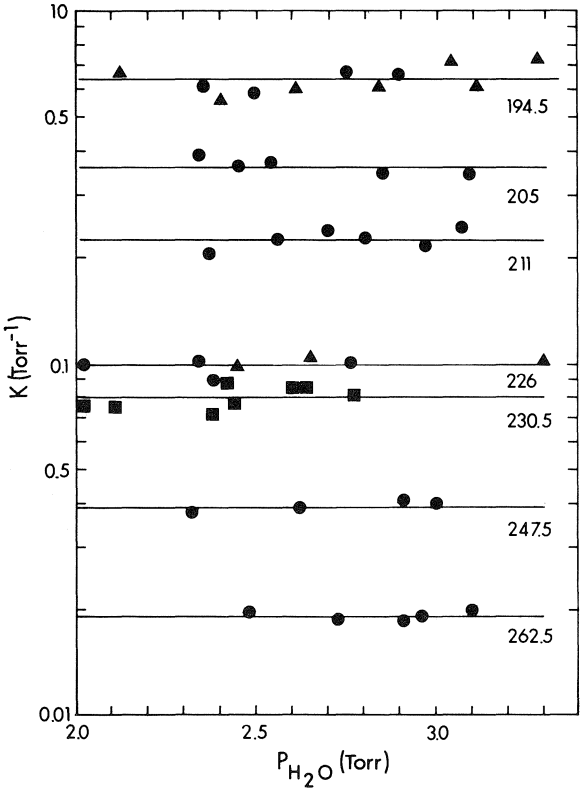

FIG. 2. Plot of equilibrium constants K for reaction $C_6H_5CO^+ + OH_2 \rightleftharpoons C_6H_5C(OH)_2^+$ obtained at different temperatures (°C) versus water pressure.

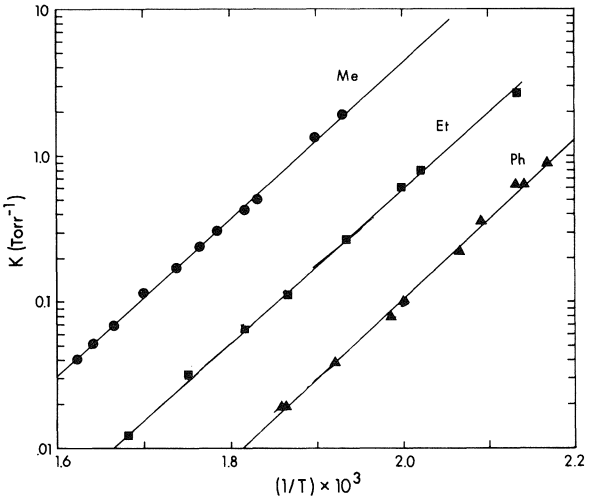

FIG. 3. van't Hoff plot of equilibrium constants for reaction $RCO^+ + OH_2 \rightleftharpoons RC(OH)_2$ for R = Me, Et, and Ph.

TABLE 1. Thermochemical data[a] for: $RCO^+ + OH_2 \rightleftharpoons RC(OH)_2^+$

R	ΔH_2^0(exp)[a]	ΔS_2^{0} [b]	ΔG_2^0(525)[c]	ΔH_2(imp)[d]	ΔH_2(MINDO/3)[e]	ΔE_2(STO-3G)[f]
H	—	—	—	(49.3)[q] (44.0)[r]	−46.0	—
CH_3	−24.6	−33.1(−33.1)	−7.2	−24.6	−27.6	−64.5
C_2H_5	−23.7	−35.1(−33.1)	−5.3	−22.7	−22.0	−56.8
C_6H_5	−25.8	−42.9(−35.5)	−3.3	−21.9	−19.1	−56.3

R	ΔH_f(RCOOH)[g]	PA(RCOOH)[h]	$\Delta H_f(RC(OH)_2^+)$[i]	$\Delta H_f(RCO^+)$	$\Delta H_f(RCO^+)$lit
H	−90.5	181.9	93.2	(200.3)[k]	195[l]
CH_3	−103.3	191.1	71.3	153.7[j]	152.3[m] 154.7[n] 153.4[p]
C_2H_5	−108.3	193.8	63.6	144.1[j]	~144[l]
C_6H_5	−70.1	200.0	95.5	174.6[j]	~173[l]

[a]Enthalpy change (kcal/mol) for reaction [2]: $RCO^+ + OH_2 \rightleftharpoons RC(OH)_2^+$ obtained from slopes of van't Hoff plots Fig. 3.
[b]Entropy change in (cal/deg) for reaction [2]. Values without parentheses from van't Hoff plots Fig. 3, values in parentheses from estimates of the third law entropy changes (see text).
[c]Free energy change (kcal/mol) for reaction [2] at 525 K from van't Hoff plot Fig. 3.
[d]Improved enthalpy changes for reaction [2] obtained from $\Delta G_2^0(525)$ and evaluated ΔS_2^0, see section *a*.
[e]Enthalpy changes for reaction [2] (kcal/mol) predicted by MINDO/3 calculated ΔH_f of reactants.
[f]Energy change for reaction [2] (kcal/mol) predicted by STO-3G calculated energies of the reactants.
[g]From Cox and Pilcher (15).
[h]ΔH for deprotonation reaction $RC(OH)_2^+ \rightleftharpoons RCO_2H + H^+$ from proton affinity ladder by Yamdagni and Kebarle (16) and Lau and Kebarle (17). Based on $PA(NH_3) = 208$ kcal/mol from new $\Delta H_f(t\text{-}C_4H_9^+) = 163$ kcal/mol, Houle and Beauchamp (18) and $\Delta H_f(H^+) = 365.7$ kcal/mol (19, 20).
[i]From PA(RCOOH) (see footnote *h*) and ΔH_f(RCOOH) given in first column, lower half of table.
[j]From $\Delta H_f(RC(OH)_2^+)$ (preceding column), ΔH_2(imp) and $\Delta H_f(H_2O) = -57.8$ kcal/mol.
[k]From $PA(HCO^+) \approx 139$ kcal/mol (Bohme (21) and Kebarle (22)) and $\Delta H_f(CO) = -26.4$ kcal/mol (15).
[l]From appearance potentials (19).
[m]From appearance potential of CH_3CO^+ from CH_3COCH_3 (23, 24).
[n]From $\Delta H = 1$ kcal/mol for reaction $CH_3CO^+ + i\text{-}C_4H_8 \rightleftharpoons CH_2CO + t\text{-}C_4H_5^+$ (based on basicity ladder (18) at 600 K and $\Delta H_f(t\text{-}C_4H_9^+) = 163$ kcal/mol (18)).
[o]Estimated error in all enthalpies from ion equilibria ±2 kcal/mol.
[p]Value quoted by Lias (20) based on basicity ladder at 300 K and $\Delta H_f(t\text{-}C_4H_9^+) = 163$ kcal/mol (18).
[q]Calculated from $\Delta H_f(HCO^+) = 200.3$ kcal/mol (see footnote *k*) and $\Delta H_f(HC(OH)_2^+) = 93.2$ kcal/mol (see footnote *i*).
[r]Calculated from $\Delta H_f(HCO^+) = 195$ kcal/mol (see footnote *e*) and $\Delta H_f(HC(OH)_2^+) = 93.2$ kcal/mol.

third gas, were not very favorable since the proton transfer reaction [4] at lower temperatures led to hydrates of the protonated acid, which complicated the initial kinetic stage. Therefore an investigation was conducted using methane or isobutane as the major gas. The ions produced by electron impact and subsequent ion molecule reactions in methane are CH_5^+ and $C_2H_5^+$ while in isobutane the final ion is $t\text{-}C_4H_9^+$ (12, 13). When benzoic acid is present these ions engage in rapid proton transfer. For example $t\text{-}C_4H_9^+$ leads to the fast reaction [5].

[5] $t\text{-}C_4H_9^+ + PhCOOH \rightleftharpoons i\text{-}C_4H_8 + PhC(OH)_2^+$

At suitably elevated temperatures one can observe that the protonated benzoic acid formed by [5], subsequently decomposes by [2r]. The time dependence of the ions in such a run with CH_4 as major gas is shown in Fig. 4. The $PhC(OH)_2^+$ is seen to decompose forming $PhCO^+$. The side reaction [6] involving formation of the proton held dimer from the protonated acid is also observed.

[6] $PhC(OH)_2^+ + PhCOOH \rightleftharpoons (PhCOOH)_2H^+$

The ion ratio $[A^+]/[C^+]$, where A^+ is $PhC(OH)_2^+$ and C^+ is $(PhCOOH)_2H^+$ is seen to become constant after about 150 μs. This must mean that the forward and reverse rates of [6] are relatively faster than [2r] such that A^+ and C^+ reach equilibrium in spite of the reactant drain caused by [2r]. It is easy to show that when A^+ and C^+ are in equilibrium $d[A^+]/dT = -\nu_{2r}[A^+]$, where ν_{2r} is the reaction frequency, i.e., pseudo first order rate constant for reaction [2r].

Plots of $\log [A^+]$ versus t for $t > 200$ μs, where the proton transfer [5] was complete, gave good straight lines whose slopes provided values for ν_{2r}. Experiments at different major gas pressures showed that ν_{2r} was pressure dependent. One such plot is given in Fig. 5*A*. It is seen that ν_{2r} is proportional to the pressure of the major gas M. This means: $\nu_{2r} \approx k_{2r}[M]$, i.e., the rate constant k_{2r} is second order and consequently k_{2f} is third order. The pressure dependence of [2r] with methane as third gas was also examined. It was found that methane is three times less efficient as third body than isobutane.

Interestingly k_{2r} was found to be also approximately proportional to the pressure of benzoic acid. For example, changing the benzoic acid from 1.2 to 2.4 mTorr increased k_{2r} from 1.2×10^{-13} to 2×10^{-13} cm^3 $molecule^{-1}$ s^{-1} (isobutane major gas, 260°C). Considering the very low benzoic acid pressure, this is a very large effect. This must mean that benzoic acid does not act as a very efficient third body but as a homogeneous catalyst. This important point

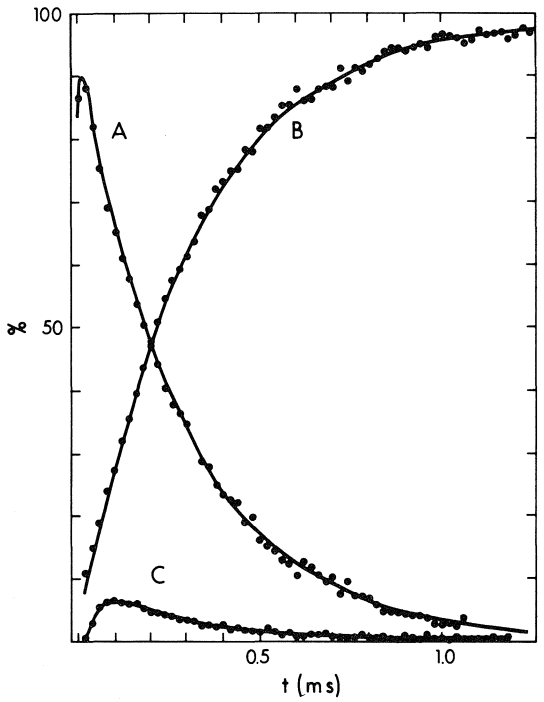

FIG. 4. Dissociation of protonated benzoic acid A = $PhC(OH)_2^+$ to B = $PhCO^+$, by reaction $PhC(OH)_2^+ \rightleftharpoons PhCO^+ + OH_2$. Formation of proton held dimer C = $(PhCOOH)_2H^+$ is also observed. After some 100 μs intensity ratio A/C is constant which means equilibrium A = C is rapid in comparison to decomposition of A to B. $p(CH_4) = 3.5$ Torr, $p(PhCOOH) \approx 3 \times 10^{-3}$ Torr, $T = 266°C$.

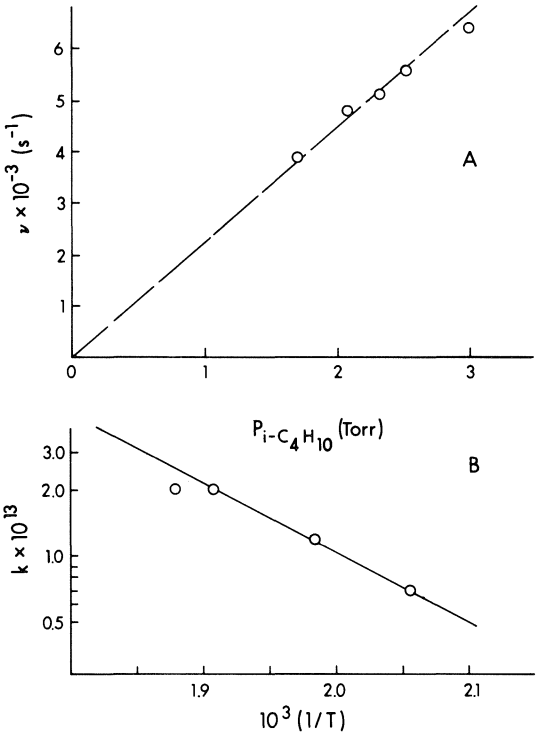

FIG. 5. (*A*) Plot of the reaction frequency ν_{2r} (s^{-1}) versus pressure of the major gas, M = *i*-C_4H_{10}. Increase of ν_{2r} (pseudo first order rate constant) with isobutane pressure shows that decomposition: $PhC(OH)_2^+ \rightleftharpoons PhCO^+ + OH_2$ is approximately second order, i.e. $k_{2r} \approx \nu_{2r}[M]$. All runs at 260°C and $P(PhCOOH)/P(i\text{-}C_4H_{10}) \approx 6 \times 10^{-4}$. (*B*) Arrhenius plot of k_{2r} (cm^3 $molecule^{-1}$ s^{-1}), major gas *i*-butane containing 0.1% benzoic acid. Line obtained gives $k_{2r} = A \exp(-E_A/RT)$ with $A \approx 10^{-6.5}$ cm^3 $molecule^{-1}$ s^{-1} and $E_A = 14.5$ kcal/mol.

will be examined later (see section *c*) in connection with the activation barrier for the proton shift [3].

The temperature dependence of k_{2r} was examined in several runs in which the pressure of the major gas and of the benzoic acid was kept constant. An Arrhenius plot of k_{2r} is shown in Fig. 5*B*. The line obtained provides the equation $k_{2r} \approx A \exp(-E_A/RT)$ with $A \approx 10^{-6.5}$ (cm^3 $molecule^{-1}$ s^{-1}) and $E_A \approx 14.5$ kcal/mol. Unfortunately the temperature range covered is rather short and the data points not quite sufficient. Therefore it is hard to estimate the error in the activation energy. Since catalysis by benzoic acid is also present, the value of the activation energy cannot be directly associated with the endothermicity of reaction [2r].

Combining the k_{2r} obtained above with the equilibrium constants K_2, for benzoic acid (see Fig. 3), one obtains k_{2f}, from $K = k_{2f}/k_{2r}$. For example $k_{2r} = 7 \times 10^{-14}$ (cm^3 $molecule^{-1}$ s^{-1}) (for $T = 486.5$ K, major gas isobutane, see Fig. 5*B*) can be combined with $K_2 = 0.2$ ($Torr^{-1}$) or $= 1 \times 10^{-17}$ (cm^3 $molecule^{-1}$) (for $T = 486.5$ K, see Fig. 3) to obtain $k_{2f} = K_2 k_{2r} = 7 \times 10^{-31}$ cm^6 $molecule^{-2}$ s^{-1}. The third order rate constant k_{2f} is indeed very small, when compared to the value for the forward clustering reaction $H_3O^+ + H_2O + CH_4 \rightleftharpoons H^+(H_2O)_2 + CH_4$ at the same temperature which is 5×10^{-28} cm^6 $molecule^{-1}$ s^{-1}, i.e. three orders of magnitude larger. From $\Delta H_2^0 = -25.8$ kcal/mol and the activation energy $E_{A2r} = 14.5$ kcal/mol one obtains a negative "activation energy" of about 11 kcal/mol for reaction [2f]. Converting this "negative activation energy" to the form $k_{2f} = CT^{-n}$ one obtains the relationship $k_{2f} \approx 6 \times 10^{14} T^{-10.4}$ cm^6 $molecule^{-2}$ s^{-1} (experimental temperature range 485–586 K, third body isobutane). We notice that the negative temperature exponent *n* is very large although not quite as large as the *n* for the same reaction but with water as third body, quoted above. While third body dependent reactions usually have negative temperature coefficients, the value of *n* is usually (7, 10, 11) small, i.e., in the range 1 to 3. A discussion of the mechanism and the possible causes for the unusual behavior of reaction [2f] and [2r] will be given in section *c*.

(b) Thermochemical Information from Equilibria [2]: $RCO^+ + OH_2 \rightleftharpoons RC(OH)_2^+$ and Theoretical Calculations of Energies and Geometries of Compounds Entering Reaction [2]

The ΔG_2^0 values for reaction [2] in the experimentally accessible temperature range can be obtained from the van't Hoff plots in Fig. 3. From the position of the van't Hoff lines, at a given constant temperature, the order for the $-\Delta G_2^0$ is $CH_3CO > C_2H_5CO > C_6H_5CO$. The $-\Delta G_2^0$ at 525 K are given as an example in Table 1. The above order shows that the stabilization of the acyl cation RCO^+ increases in the order R: $CH_3 < C_2H_5 < C_6H_5$. This is the expected order on the basis of increasing polarizability in CH_3, C_2H_5, and C_6H_5, and the stabilization by π donation in $C_6H_5CO^+$. Since the stabilization by R is an electronic effect, the order observed for the ΔG_2^0 changes can be expected to hold also for the ΔH_2^0 changes, obtained from the slopes of the van't Hoff plots. Unfortunately, this is not the case, the $-\Delta H_2^0$ values change little and in an irregular manner (see Table 1). The regular change of the ΔG_2^0 values is reflected not in the ΔH_2^0 results but in the ΔS_2^0 results, which are seen to increase regularly in the order: methyl, ethyl, phenyl: 33, 35, 43 cal/deg. There seems to be no meaningful physical reason for this large entropy increase. The entropy situation may be examined on the basis of reaction [7].

[7] $$CH_3CO^+ + C_6H_5C(OH)_2^+ \rightleftharpoons CH_3C(OH)_2^+ + C_6H_5CO^+$$

$$A + B \rightleftharpoons C + D$$

From the above quoted ΔS_2^0 values, one can evaluate $\Delta S_7^0 = 43 - 33 = 10$ cal/deg. The translational and rotational symmetry entropy changes are easily evaluated from the well known eq. [8].

[8] $$\Delta S_7(\text{trans}) = R \ln M_C M_D / M_A M_B = 0.6 \text{ cal/deg}$$

$$\Delta S_7(\text{rot. sym}) = R \ln \sigma_A \sigma_B / \sigma_C \sigma_D = R \ln \tfrac{3}{2} = 0.8 \text{ cal/deg}$$

The symmetry numbers σ are based on the geometries of the cations given in Fig. 6. The combined contribution of these entropy changes is 1.4 kcal/deg. The only other significant contribution to ΔS_7^0 can come from a change of internal rotations. The acyl cations, being linear, are devoid of internal rotations. The protonated acids have three internal rotations, two around the C—OH bonds and one for the $C—C(OH)_2^+$ bond. The C—OH rotations may be expected to be similar for the two protonated acids, however, the $C—C(OH)_2^+$ rotation in benzoic acid may be more hindered than that in acetic acid since one expects some stabilization of the protonated benzoic acid by the resonance structure **I** and the corresponding ortho resonance structures.

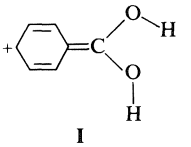

I

Assuming a barrier of 10 kcal/mol (14) for the C—C internal rotation in the protonated benzoic acid and no barrier for the protonated acetic acid, one can estimate (14) the entropy change for the internal rotations $\Delta S_7(\text{int. rot}) \approx 1$ cal/deg. The reduced moments of inertia required for the calculation (14) were obtained from the structures given in Fig. 6. Combining the above contributions to ΔS_7^0 one obtains $\Delta S_7^0 \approx 2.4$ cal/deg which is considerably smaller than the experimental result $\Delta S_7^0 \approx 10$ cal/deg. We believe that the error lies in the experimental entropies. A similar estimation of ΔS for

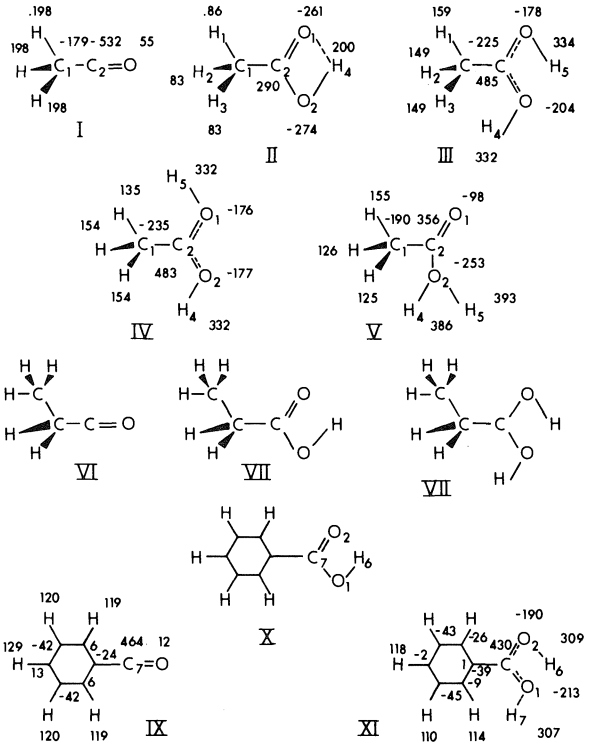

FIG. 6. Structures from STO-3G calculations, bond distances, and bond angles which were optimized in Table 2. Energies from STO-3G and MINDO/3 are also given in Table 2. Numbers besides atoms shown above correspond to STO-3G net atomic charges from Mulliken population analysis given in thousands of an elementary positive charge. Structures **II**, **VII**, **X** are the acids, which are uncharged. All other structures are singly charged positive ions.

reaction [7] but involving propionic rather than benzoic acid leads to a $\Delta S_7^0 \approx 0$ since in this case the properties of the reactants are even more similar.

As discussed in the preceding section, equilibrium [2] is unusually slow. For example the time required to approach 90% of the equilibrium concentrations could be as long as 1 ms. The slowness is deleterious to the accuracy of the equilibrium measurements since other processes affecting the concentrations of the ions RCO^+ and $RC(OH)_2^+$, like diffusion to the wall, and slow side reactions, can be neglected only when they are relatively slow compared to the equilibrium forward and reverse rates. This condition is not fully present in the above measurements. We believe that a set of improved ΔH_2 values can be obtained by using the calculated ΔS_7^0 obtained above. In the earlier publication (5) dealing with equilibrium [2] for R = CH_3, the van't Hoff derived $\Delta H_2 = -24.6$ kcal/mol was found to be in good agreement with the ΔH_2 value calculated from the thermodynamic cycle shown below.

$$\Delta H_2 = \Delta H_f(CH_3COOH) - \Delta H_f(H_2O) - \Delta H_f(CH_2CO) + PA(CH_2CO) - PA(CH_3COOH) = 25.6 \text{ kcal/mol}$$

Assuming that $\Delta H_2 = -24.6$ kcal/mol is correct for R = CH_3 we calculate ΔH_2 for R = C_2H_5 and C_6H_5 by using the ΔG_2^0 at 525 K (Fig. 3 and Table 1) which falls in the middle of the experimental range. Setting $\Delta S_2^0(C_2H_5) = \Delta S_2^0(CH_3)$ and $\Delta S_2^0(C_6H_5) = \Delta S_2^0(CH_3) + 2.4$ cal/deg in accordance with the evaluated ΔS_7^0 one obtains from $\Delta H = \Delta G + T\Delta S$ the improved ΔH_2 values shown in Table 1 as ΔH_2(imp). Related thermochemical literature data (15–24) are also given in Table 1.

It is of some interest to compare the ΔH_2 values with results from theoretical calculations. For this purpose calculations were made with STO-3G and MINDO/3. The electronic energies of all compounds entering reaction [2] with R = H, CH_3, C_2H_5, C_6H_5 were calculated using the Gaussian 70 (STO-3G) program (25). The structures obtained are shown in Fig. 6. The bonds and angles of the ions $RC(OH)_2^+$ and RCO^+ that were optimized are shown in Table 2. The same type bonds and angles were optimized for the corresponding neutrals. The remaining geometry was taken from the standard geometries outlined by Pople and Gordon (26). The electronic energies obtained are shown in Table 2. The MINDO/3 calculations used, for the neutral compounds, distances and angles from Dewar's (27) work when those were available (HCOOH, CH_3-COOH). For the other neutral compounds suitable distances and angles were selected from Dewar's compilation (27) and then some geometry optimization was performed (see Table 2). The geometries of the ions were based on the geometries of the corresponding neutrals plus the geometry optimizations given in Table 2.

The most stable structures predicted by STO-3G and MINDO/3 were the same. Both STO-3G and MINDO/3 predicted for the acids and protonated acids the internally hydrogen bonded structures as being the most stable (see Fig. 6 structure **II** for acetic acid and structure **III** for protonated acetic acid). The hydrogen bonded cisoid structure **III** of $CH_3C(OH)_2^+$ was predicted by STO-3G and MINDO/3 to be more stable by $\sim$8 kcal/mol than the transoid structure **IV** (see Fig. 6 and Table 2). This rotational barrier occurring in all the protonated acids may be responsible for the somewhat larger ΔS_2 of $\sim$33 cal/deg observed for reaction [2] involving the protonated acids as compared to other association reactions: $R^+ + B \rightleftharpoons RB^+$. The carbonyl protonated acid $CH_3C(OH)_2^+$ was predicted by STO-3G to be more stable than the hydroxy protonated isomer $CH_3COOH_2^+$ (see structures **III** and **V** Fig. 6 and Table 2) by 20.6 kcal/mol, MINDO/3 gave a very similar result: 18.8 kcal/mol (see fully optimized structures in Table 2). It is interesting to note that Benoit and Harrison (28), on the basis of a correlation of proton affinities with oxygen 1*s* ionization energies, have estimated a difference of about 24 kcal/mol for the proton affinities for carbonyl and hydroxyl protonation of acetic acid. Since the theoretical calculations are of limited accuracy and the correlation of the oxygen 1*s* ionization energies with the proton affinities is also only approximate, the agreement between the two results must be considered quite good.

The energy changes for reaction [2] can be calculated from the energies of the reactants E(STO-3G) or the ΔH_f(MINDO/3) of the reactants are given in Table 1. The results from MINDO/3 are seen to be very close to the ΔH_2(imp) also given in Table 1. On the other hand, ΔE_2(STO-3G) are found to be roughly two times larger than the ΔH_2(imp). Process [2] is a reaction in which an electron pair bond is formed. STO-3G does not give good results for the energy change in such situations, because of the very limited basis set used (29). Also included in Table 1 is an experimental value for ΔH_2 with R = H, i.e., the formation of protonated formic acid from the formyl cation and water. This result is not based on equilibrium measurements of reaction [2] but was calculated from the proton affinity of CO (21, 22) which leads to $\Delta H_f(HCO^+) = 200.3$ kcal/mol (see Table 1). The proton affinity of HCOOH (16, 17) leads to $\Delta H_f(HC(OH)_2^+)$ and a

TABLE 2. Results from STO-3G and MINDO/3 calculations for reactants in reaction: $RCO^+ + OH_2 \rightleftharpoons RC(OH)_2^+$, for R = H, CH_3, C_2H_5, C_6H_5

Compound[a]	Parameters optimized[b]		Energy (au) STO-3G	ΔH_f(kcal/mol) MINDO/3[c]
	Bond distances	Bond angles		
H_2O	All	All	−74.96334	−53.6[d] (−57.8)
HCO^+	HC (1.09) CO (1.115)			184.6[d]
HCOOH				−88.8 (−90.5)
$HC(OH)_2^+$	HC (1.12) CO (1.27) OH (0.958)	HCO (122) HCO (111)		85.1
CH_3CO^+ **(I)**	C_1C_2 1.51 (1.42) C_2O 1.14 (1.13)		−150.143858	136.9[d]
CH_3COOH **(II)**			−224.80297	−104.5 (−103.3)
$CH_3C(OH)_2^+$ **(III)**	C_1C_2 1.53 (1.51) CO 1.31 (1.28) OH 1.00 (0.95)	CCO 121.9 (125) COH 110.9 (122)	−225.20994	55.7[d]
$CH_3C(OH)_2^+$ **(IV)**			−225.19719	66.4
$CH_3CO(OH_2)^+$ **(V)**	C_1C_1 1.536 C_2O_1 1.20 C_2O_2 1.448 OH 0.989	$C_1C_2O_1$ 133.8 $C_1C_2O_2$ 112.7 COH 115.1	−225.17714	76.5
$C_2H_5CO^+$ **(VI)**	C_1C_2 (1.52) C_2C_3 1.54 (1.44) C_3O 1.14 (1.13)	$C_1C_2C_3$ 109 (119)	−188.73188 −263.38249	128.8 −108.3 (−108.3)
C_2H_5COOH **(VII)**				
$C_2H_5C(OH)_2^+$ **(VIII)**	C_2C_3 1.5 (1.51) C_3O 1.35 (1.29) OH 1.02 (0.95)	$C_1C_2C_3$ 112.9 (122) C_2C_3O 122.7 (120) C_3OH 109.2 (124)	−263.78578	53.2
$C_6H_5CO^+$ **(IX)**	C_1C_7 1.44 (1.42) C_7O 1.19 (1.13)		−338.34185	159.9
C_6H_5COOH **(X)**			−412.97650	−59.4 (−70.1)
$C_6H_5C(OH)_2^+$ **(XI)**	C_1C_7 1.50 (1.49) C_7O 1.36 (1.29) OH 1.00 (0.95)	COH 108.8 (124)		

[a]Roman numeral beside structure refers to structure shown in Fig. 6.
[b]Bond angles in degrees, bond distances in Å given only for ionic species. Results from STO-3G without parentheses, from MINDO/3 with parentheses.
[c]Numbers in parentheses are the accurately known experimental enthalpies of formation of the neutral molecules (15).
[d]Energies given correspond to fully geometry optimized structures.

combination of the values provides $\Delta H_2 = -49.3$ kcal/mol. An older value $\Delta H_f(HCO^+) = 195$ kcal/mol (19) based on appearance potentials when combined with $\Delta H_f(HC(OH)_2)^+$ leads to $\Delta H_2 = -44.0$ kcal/mol. The MINDO/3 calculation gives $\Delta H_2 = -46$ kcal/mol which is in between the two experimental values and thus is a good theoretical prediction.

A comparison of the enthalpies of formation of RCO^+ obtained from the present ΔH_2(imp) with $\Delta H_f(RCO^+)$ from appearance potentials is shown in the lower half of Table 1. The evaluation of $\Delta H_f(RCO^+)$ from ΔH_2 also requires $\Delta H_f(RC(OH)_2^+)$ which was obtained from gas phase basicity ladders (16, 17). The gas phase basicity ladder was put on an absolute basis by using the new value of $\Delta H_f(t\text{-butyl}^+) = 163$ kcal/mol, due to a redetermination of the ionization potential of the *t*-butyl radical by Houle and Beauchamp (18). This change brings $\Delta H_f(RCO^+)$ obtained from ΔH_2 and $\Delta H_f(RC(OH)_2^+)$ in better agreement with results for $\Delta H_f(RCO^+)$ from appearance potentials. For example: $\Delta H_f(CH_3CO^+) = 153.7$ kcal/mol (from ΔH_2 and $\Delta H_f(CH_3C(OH)_2^+)$ while $\Delta H_f(CH_3CO^+) = 152.3$ kcal/mol from the appearance potential of CH_3CO^+ from CH_3COCH_3 (23, 24). In our earlier

publication (5) dealing with the same ΔH_2 (R = CH_3) agreement with the above appearance potential $\Delta H_f(CH_3CO^+)$ was not obtained. The gas phase basicity of ketene recalculated to the new heat of formation of t-$C_4H_9^+$ leads to a $\Delta H_f(CH_3CO^+)$ = 154.7 kcal/mol (5, 17) or 153.4 kcal/mol (20), both values being in agreement with the appearance potential result.

The relatively good agreement of the $\Delta H_f(C_2H_5CO^+)$ and $\Delta H_f(C_6H_5CO^+)$ results based on ΔH_2 and $\Delta H_f(RC(OH)_2^+)$ with the appearance potential results (see Table 1) is encouraging although the appearance potential data (19) come, in this case, from the more questionable determinations. On the whole, one can conclude that the present results lend support to the new $\Delta H_f(t\text{-}C_4H_9^+)$ = 163 kcal/mol and the corresponding new PA(NH_3) = 208 kcal/mol (18).

(c) Homogeneous Gas Phase Catalysis of the 1,3 Proton Shift $RCO(OH_2)^+ \rightarrow RC(OH)_2^+$

The kinetics of reaction [2] were described in section (*a*), where the following salient features emerged. The third body dependent rate constant in the forward direction was unusually small. The negative temperature coefficient of the same reaction was extremely large, the reaction was catalyzed by the presence of acid RCOOH. These unusual features can be explained if one assumes that the 1,3 proton shift from the hydroxy protonated acid $RCO(OH_2)^+$ to the carbonyl protonated and $RC(OH_2)_2^+$, i.e. reaction [3], has an appreciable *potential energy barrier*. This situation is represented in Fig. 7. In the preceding section results of STO-3G and MINDO/3 calculations showed that $CH_3CO(OH_2)^+$ (structure **V**, Fig. 6) had an energy of ~20 kcal/mol higher than that of $CH_3C(OH)_2^+$ (structure **III**, Fig. 6), a similar result had been predicted by Benoit and Harrison (28) on the basis of a correlation 1*s* oxygen core electron energies with proton affinities. These data, together with the total endothermicity of the dissociation: $CH_3C(OH_2)^+ \rightarrow CH_3CO^+ + OH_2$ ($-\Delta H_2$ = 24.5 kcal/mol, Table 1), were used in the approximate potential energy diagram shown in Fig. 7. In order to explore the approximate size of the barrier for the 1,3 proton shift leading from $CH_3CO(OH_2)^+$ (**III**) to $CH_3C(OH)_2^+$ (**V**), we performed STO-3G calculations of some 20 structures with geometries intermediate between **III** and **V**. Unfortunately these were not sufficient to provide the path requiring the minimum energy, i.e., the reaction coordinate. They did, however, indicate that the barrier is substantial. This result is in agreement with recent work by Middlemiss and Harrison (30). These authors, by measuring the kinetic energy of

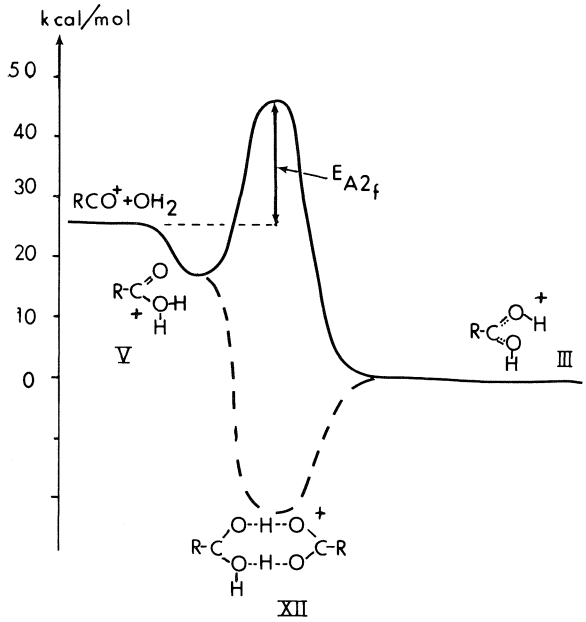

FIG. 7. Schematic potential energy diagram of reaction coordinate of reaction: $RCO^+ + OH_2 \rightleftharpoons RC(OH)_2^+$. $RC(OH)_2^+$ corresponds to carbonyl protonated acid, while $RCO(OH_2)^+$ to hydroxy protonated acid. Energy values are given in diagram from experiment and calculation (see text). Dashed line gives potential energy for catalyzed proton shift: $RCO(OH_2)^+ \rightarrow RC(OH)_2^+$ by formation of an intermediate complex with the acid RCOOH.

RCO^+ produced by dissociation of internally excited protonated acids, deduced that there are two different protonated acid species which they assumed to be $RC(OH)_2^+$ and $RCO(OH_2)^+$. The structure of lower energy, presumably $RC(OH)_2^+$, dissociated to $RCO^+ + OH_2$ with kinetic energy release. As pointed out by Middlemiss and Harrison, this kinetic energy probably originates from the presence of an energy barrier of the type illustrated in Fig. 7. From the amount of kinetic energy present in RCO^+, the authors estimated that the barrier indicated by E_{A2f} in Fig. 7 is approximately 20 kcal/mol. The barrier E_{A2f} in Fig. 7 was drawn to scale, assuming this value to be correct.

Assuming that Fig. 7 represents at least approximately the true situation, it becomes clear that the equilibrium [7] could not have been measured at the conditions of our experiments in the absence of catalysis. For example, the activation energy barrier $E_{A2r} \approx 40$ kcal/mol for the dissociation of $RC(OH)_2^+$ to $RCO^+ + OH_2$ could not have been overcome at the low temperatures employed. Also in the absence of catalysis k_{2f} would have had a positive temperature coefficient due to the presence of E_{A2f}. The catalytic effect of the acid RCOOH observed in section *a* can be explained by reaction [9].

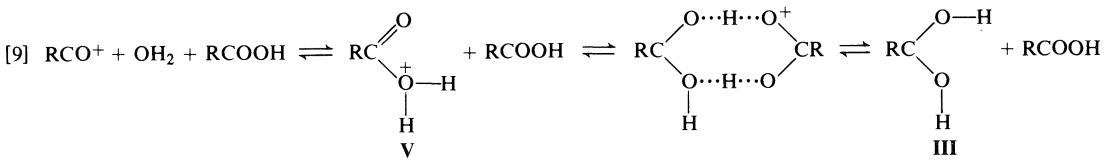

Here the proton is not "transferred" by a 1,3 shift but the catalyst supplies one proton to position 3 and takes one away from position 1. The likely potential energy diagram for this process is indicated in Fig. 7. The observed very large negative temperature coefficient for k_{2f} can be explained on the basis of the mechanism given in [9]. **V** is much more weakly bonded than **III**. The temperatures used are high enough to cause dissociation of **III**. For these conditions **V** will be nearly completely dissociated to $RCO^+ + OH_2$. One expects a rapid equilibrium $RCO^+ + OH_2 \rightleftharpoons$ **V**, shifted very much to the left side. The concentration of **V** should then be given by eq. [10] where $\Delta H(\mathbf{V})$ and $\Delta S(\mathbf{V})$ represent the enthalpy and entropy changes for: $\mathbf{V} \rightleftharpoons RCO^+ + OH_2$. The MINDO/3 result indicates $\Delta H(\mathbf{V}) \approx 7$ kcal/mol (see Table 2). Therefore one may expect the concentration of **V** to decrease with temperature with the exponential factor exp (7 (kcal/mol)/RT).

$$[10] \quad [\mathbf{V}] = \frac{\exp[-\Delta S(\mathbf{V})/R] \exp[\Delta H(\mathbf{V})/RT]}{[RCO^+][H_2O]}$$

The conversion of **V** to **III**, which occurs via **XII**, will also have a negative temperature coefficient. The very special geometry of **XII** means that **XII** is a low entropy species, i.e. a tight complex. Therefore species **V**, when colliding with the catalyst RCOOH, will form **XII** more frequently at low temperatures, while at high temperatures back dissociation to **V** and RCOOH will be favored. The addition of this negative temperature coefficient to the term exp ($\Delta H(\mathbf{V})/RT$) predicts for k_{2f} a negative temperature coefficient, which when expressed as negative "activation energy" will have a value larger than ~7 kcal/mol. It will be recalled that the negative "activation energy" measured in section *a* (for $R = C_6H_5$) was approximately 11 kcal/mol. Thus mechanism [9] and Fig. 7 do provide a semiquantitative prediction of very large negative temperature coefficient for the rate constant k_{2f} as observed.

It is interesting to note that in protic solvents the 1,3 proton shift required for reaction [2] will be easily catalyzed by the solvent molecules in a manner similar to that indicated by eq. [9], i.e., one given solvent molecule removes the proton from **V** while a second solvent molecule provides a new proton to the carbonyl oxygen of **V**.

Acknowledgements

We are thankful to Professor A. G. Harrison who graciously supplied us with a preprint of his work (30). The STO-3G calculations for the intermediates between $CH_3CO(OH_2)^+$ and $CH_3C(OH)_2^+$ were performed by Dr. P. P. S. Saluja.

This work was supported by the Natural Sciences and Engineering Research Council of Canada.

1. K. Hiraoka and P. Kebarle. J. Am. Chem. Soc. **98**, 6119 (1976).
2. K. Hiraoka and P. Kebarle. J. Am. Chem. Soc. **99**, 360 (1977).
3. K. Hiraoka and P. Kebarle. J. Am. Chem. Soc. **99**, 366 (1977).
4. D. K. Sen-Sharma and P. Kebarle. J. Am. Chem. Soc. **100**, 5826 (1978).
5. W. R. Davidson, Y. K. Lau, and P. Kebarle. Can. J. Chem. **56**, 1016 (1978).
6. H. Koch and W. Haaf. Angew. Chem. **70**, 311 (1958); H. Hogeveen. Advances in physical organic chemistry. Vol. 10. *Edited by* V. Gold. Academic Press, New York, NY. 1973.
7. A. J. Cunningham, J. D. Payzant, and P. Kebarle. J. Am. Chem. Soc. **94**, 2627 (1972).
8. M. French and P. Kebarle. Can. J. Chem. **53**, 2268 (1975).
9. P. Kebarle. Ann. Rev. Phys. Chem. **28**, 445 (1977).
10. A. Good. Trans. Faraday Soc. **67**, 3495 (1971).
11. M. Meot-Ner and F. H. Field. J. Chem. Phys. **61**, 3642 (1974).
12. F. H. Field. J. Am. Chem. Soc. **91**, 2827 (1969).
13. F. H. Field. *In* Ion–molecule reactions. Vol. 2. *Edited by* J. L. Franklin. Plenum Press, New York, NY. 1972.
14. J. B. Cumming and P. Kebarle. Can. J. Chem. **56**, 1 (1978).
15. J. D. Cox and G. Pilcher. Thermochemistry of organic and organometallic compounds. Academic Press, London and New York. 1970.
16. R. Yamdagni and P. Kebarle. J. Am. Chem. Soc. **98**, 1320 (1976).
17. Y. K. Lau and P. Kebarle. Can. J. Chem. To be published.
18. F. A. Houle and J. L. Beauchamp. J. Am. Chem. Soc. In press.
19. H. M. Rosenstock, K. Draxl, B. W. Steiner, and J. T. Herron. Energetics of gaseous ions. J. Phys. Chem. Ref. Data, Vol. 6. 1977. Suppl. 1.
20. S. G. Lias. *In* Kinetics of ion molecule reactions. *Edited by* P. Ausloos. Plenum Press. 1978.
21. D. K. Bohme. *In* Interactions between ions and molecules. *Edited by* P. Ausloos. Plenum Press. 1974.
22. P. Kebarle. Ann. Rev. Phys. Chem. **28**, 445 (1977).
23. E. Murad and M. G. Inghram. J. Chem. Phys. **41**, 404 (1964).

24. R. H. STALEY, R. D. WIETING, and J. L. BEAUCHAMP. J. Am. Chem. Soc. **99**, 5964 (1977).
25. W. J. HEHRE, W. A. LATHAM, R. DITCHFIELD, M. D. NEWTON, and J. A. POPLE. GAUSSIAN 70, Quantum Chemistry Program Exchange, Indiana University, Bloomington, IN.
26. J. A. POPLE and M. GORDON. J. Am. Chem. Soc. **89**, 4253 (1967).
27. R. C. BINGHAM, M. J. S. DEWAR, and D. H. LO. J. Am. Chem. Soc. **97**, 1285 (1975); **97**, 1294 (1975); **97**, 1302 (1975).
28. F. M. BENOIT and A. G. HARRISON. J. Am. Chem. Soc. **99**, 3580 (1977).
29. W. A. LATHAM, W. J. HEHRE, and J. A. POPLE. J. Am. Chem. Soc. **93**, 808 (1971); K. HIRAOKA, P. P. S. SALUJA, and P. KEBARLE. Can. J. Chem. **57**, 2159 (1979).
30. N. E. MIDDLEMISS and A. G. HARRISON. Can. J. Chem. **57**, 2827 (1979).

Synthèse et amination réductrice de phosphonopyruvates : préparation d'acides amino-2 carboxy-2 alkylphosphoniques (β-phosphonoalanine)

JEAN-MARIE VARLET ET NOËL COLLIGNON

Laboratoire de chimie organique, Institut National Superieur de Chimie Industrielle de Rouen, B.P. 0876130 Mont-Saint-Aignan, France

ET

PHILIPPE SAVIGNAC

Equipe Centre National de la Recherche Scientifique-Institut de Recherche Chimique Appliquée 2-8 Rue Henry Dunant, B.P. No 2894320 Thiais, France

Reçu le 7 juin 1979

JEAN-MARIE VARLET, NOËL COLLIGNON et PHILIPPE SAVIGNAC. Can. J. Chem. **57**, 3216 (1979).

La réaction des α-cupro(I)alkanephosphonates avec les chlorures de méthoxalyle et d'éthoxalyle conduit aux phosphonopyruvates de dialkyle qui soumis à l'amination réductrice dans l'éthanol à pH 6–7 en présence de $NaBH_3CN$, d'acétate d'ammonium ou d'amines primaires fournissent les aminoesters phosphoniques; leur hydrolyse par l'acide chlorhydrique dilué conduit aux aminoacides phosphoniques (phosphonoalanine). L'ensemble de ces trois réactions constitue une méthode générale d'accès à la phosphonoalanine et aux structures apparentées.

JEAN-MARIE VARLET, NOËL COLLIGNON, and PHILIPPE SAVIGNAC. Can. J. Chem. **57**, 3216 (1979).

The reaction of α-copper(I)alkanephosphonates with methyl and ethyl oxalyl chlorides gives methyl or ethyl dialkylphosphonopyruvates which, submitted to reductive amination in ethanol at pH 6–7 with sodium cyanohydridoborate ($NaBH_3CN$) and ammonia, or primary amines, lead to phosphonic amino esters; hydrolysis with diluted HCl gives phosphonic amino acids. These three reactions constitute a general way to β-phosphonoalanine and β-alkyl β-phosphonoalanine.

Introduction

Bien qu'il soit l'acide phosphonique le plus répandu, l'acide amino-2 éthylphosphonique (AEPA ou ciliatine) n'est cependant pas le seul phosphonate naturel; d'autres phosphonates de structure apparentée ont été identifiés tel l'acide amino-2 carboxy-2 éthylphosphonique ou phosphonoalanine qui fut isolé par Kittredge et coll. (1) en 1964 et synthétisé par Chambers et Isbell la même année (2).

L'intervention de la phosphonoalanine au cours de la biosynthèse de l'AEPA postulée par Kittredge et coll. (1) a été démontrée par Horiguchi et Rosenberg (3) qui distingue deux voies métaboliques à partir de l'acide phosphonopyruvique provenant du réarrangement intramoléculaire du phosphoénol pyruvate (4). Dans la première (*a*) l'acide phosphonopyruvique après décarboxylation conduit au phosphonoacétaldéhyde converti par transamination en AEPA; dans la seconde (*b*) la transamination de l'acide phosphonopyruvique donne la phosphonoalanine dont la décarboxylation conduit à l'AEPA.

Nous avons montré dans une précédente étude (5) qu'il était possible synthétiquement de réaliser l'amination réductrice du phosphonoacétaldéhyde et des oxo-2 alkanephosphonates en général dans de bonnes conditions (milieu protique, pH 6–7) avec des rendements élevés.

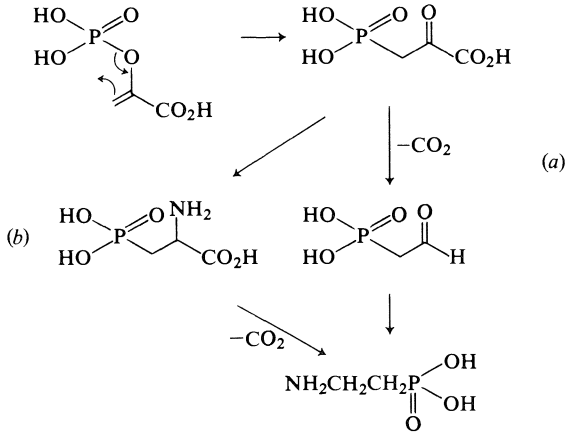

La réalisation à l'échelle préparative de la seconde voie était plus délicate; elle nécessitait l'obtention de dialkylphosphonopyruvates, composés non connus, dont l'amination réductrice constituait un cas intéressant puisque les produits de réaction sont des aminoesters phosphoniques précurseurs d'aminoacides phosphoniques naturels. La séquence réactionnelle suivie ainsi que l'ensemble des structures préparées sont décrites dans la fig. 1.

Préparation des dialkylphosphonopyruvates 1

Les procédés classiques de phosphonylation ne

0008-4042/79/243216-05$01.00/0

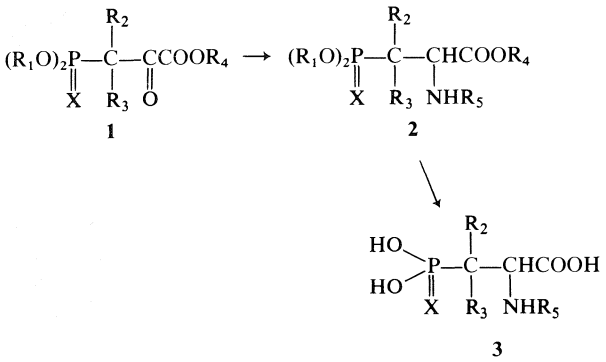

	R_1	R_2	R_3	R_4	R_5	X
a	Me	H	H	Me		O
b	Me	H	H	Et		O
c	Et	H	H	Me	H	O
d	Et	H	H	Et	H	O
e	*i*Pr	H	H	Et	H	O
f	Et	Me	H	Et	H	O
g	Et	Et	H	Et	H	O
h	Et	Me	Me	Et	H	O
i	Et	H	H	Me	Et	O
j	Et	H	H	Et	Me	O
k	Me	H	H	Et	H	S
l	Et	H	H	Et	H	S

FIG. 1. Séquence réactionnelle suivie.

sont pas applicables aux phosphonopyruvates. L'isomérisation de Michaelis–Arbuzov entre un trialkylphosphite et l'α-bromopyruvate conduit exclusivement au phosphoénol pyruvate (réaction de Perkow), dont le réarrangement intramoléculaire en phosphonopyruvate a été postulé mais non démontré.

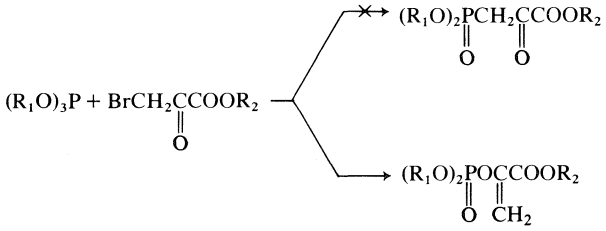

La mobilité des hydrogènes de l'α-bromopyruvate ne permet pas davantage d'envisager sa réaction avec un phosphite sodé (réaction de Michaelis–Becker), la réaction d'un α-lithioalkanephosphonate (6) sur l'oxalate d'éthyle est également à écarter pour des raisons analogues.

Devant l'échec de ces procédés, nous avons développé une réaction originale qui est la phosphonoalkylation des chlorures de méthoxalyle et d'éthoxalyle. Cette réaction qui utilise le couplage d'un α-cuproalkanephosphonate et d'un chlorure d'acide (7) est très souple et permet d'accéder à une grande variété de structures ainsi qu'en témoigne le Tableau 1.

Les phosphonopyruvates sont sensibles à la basicité du milieu; il est indispensable d'employer la quantité stoéchiométrique de butyllithium préalablement dosé et exempt de lithine; le temps de réaction est limité à cinq heures à −30°C. Les substituants liés au phosphore ni le remplacement de l'oxygène par le soufre n'ont d'effets importants. L'introduction sur le carbone en position α de substituants (Me, Et) perturbe la formation du carbanion phosphonate α-lithié dont l'échange et la condensation sont incomplets; dans ces essais les rendements n'excèdent pas 55%. Il est à remarquer également que le chlorure de méthoxalyle, étant donné sa fragilité, donne toujours des résultats inférieurs.

Les phosphonopyruvates sont des composés fragiles qui se dégradent partiellement à la distillation et lentement à température ambiante. Les dérivés soufrés sont plus stables que les dérivés oxygénés.

Les dérivés oxygénés non substitués sur la position α présentent un pourcentage (20%) de forme énolique décelable en rmn du ^1H et du ^{13}C (voir partie expérimentale).

Amination réductrice des phosphonopyruvates 1 → 2

L'agent aminant est l'acétate d'ammonium ou une amine primaire, l'agent réducteur est le cyanoborohydrure de sodium commercial dans l'éthanol (pH 6–7) à 25°C (8, 9). L'ensemble des résultats est réuni dans le Tableau 2. La réduction a d'abord été étudiée sur les phosphonopyruvates oxygénés ou soufrés non substitués sur la position α (essais **2***c–l*). La fonction carbonyle dans ces structures présente une réactivité inférieure à celle des β-cétophosphonates. Dans des conditions expérimentales équivalentes, le pourcentage d'aminoester pur, contrôlé par rmn et ir n'excède jamais 55%. Une telle désactivation de la molécule attribuable à la présence du groupe ester a été constatée par

TABLEAU 1. Phosphonopyruvates **1**

Essais	pé/Torr (°C)	Rdt (%)
1*a*	100–105/1	10
1*b*	121–125/0.9	52
1*c*	115–120/1	33
1*d*	127–131/0.6	72
1*e*	115–120/0.5	64
1*f*	117–121/0.8	54
1*g*	113–117/0.3	56
1*h*	115–119/0.4	52
1*k*	110–114/0.5	63
1*l*	131–135/1	67

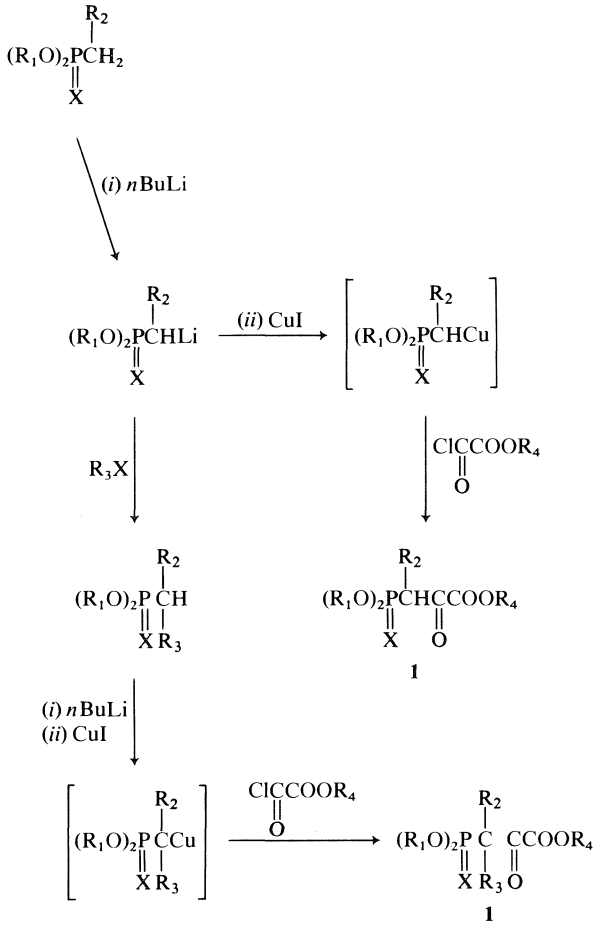

Borch *et al.* qui n'obtiennent que 21% d'amination réductrice avec la cyclohexanone substituée en 2 par le carboxylate d'éthyle, 50% avec l'acide pyruvique et 47% avec l'acide phénylpyruvique (8). L'emploi de bromure d'ammonium, au lieu d'acétate (essai **2***d'*) n'apporte pas d'amélioration; dans cet essai, on isole parallèlement l'aminoester (ν: 1735 (CO) cm^{-1}) et l'aminoamide (ν: 1675 (CO) cm^{-1}).

$(EtO)_2PCH_2CHCOOEt$ (NH$_2$) $\qquad$ $(EtO)_2PCH_2CHCONH_2$ (NH$_2$)

Les substituants R_1 liés au phosphore n'ont pas d'influence, par contre, le remplacement de l'oxygène par le soufre provoque une chute nette du rendement attribuable très certainement à une gêne stérique, l'aminoréduction des cétones décroissant régulièrement avec leur encombrement (5, 8).

L'importance du facteur stérique est confirmé par les essais réalisés avec des phosphonopyruvates substitués sur la position α. Le rendement de l'amination décroît régulièrement à mesure que croît le degré de substitution ou que grossit le substituant (essais **2***f*, **2***g*, **2***h*).

L'extension de la réaction aux amines primaires (méthylamine, éthylamine) fait l'objet des essais **2***i* et **2***j*. Les résultats sont tout à fait comparables aux précédents. Cependant dans ces deux cas on isole toujours un mélange d'aminoester phosphonique et d'aminoamide décelé en ir et confirmé par rmn ^1H.

L'emploi de la diméthylamine a été un échec; il confirme une observation précédemment signalée lors de l'amination réductrice de l'oxo-2 propylphosphonate de diéthyle (5) pour lequel nous avions constaté la séquence réactionnelle suivante $NH_3 > R_1NH_2 > R_1R_2NH$.

Pour tous les exemples du Tableau 2, les aminoesters phosphoniques sont isolés en milieu acide après double extraction; la fraction recueillie dans la phase éthérée est constituée par l'α-hydroxyéther phosphonique provenant de la réduction des phosphonopyruvates. Cette réaction est confirmée par la réduction directe du phosphonopyruvate **1***d* par le cyanoborohydrure seul dans l'éthanol en présence d'agent protonant. L'α-hydroxyester phosphonique est obtenu avec un rendement de 59%; sa structure est vérifiée par rmn de ^1H et spectrométrie de masse.

$(EtO)_2PCH_2CCOOEt$ (O, O) $\xrightarrow[HCOOH/EtOH]{NaBH_3CN}$ $(EtO)_2PCH_2CHCOOEt$ (O, OH) 59%

Hydrolyse des aminoesters phosphoniques 2 → 3

La libération des fonctions acides carboxyliques et phosphoniques est réalisée par l'acide chlorhydrique 6 *N* porté au reflux pendant une nuit. Les résultats sont rassemblés dans le Tableau 3. Tous les composés sont hydrolysés sans signe apparent de dégradation. Les rendements maximum sont atteints

TABLEAU 2. Aminoesters phosphoniques **2**

Essais	Temps de réaction (h)	Rdt (%)[a]
2*c*	48	47
2*d*, *d'*	48, 72	54, 55[b]
2*e*	48	40
2*f*	60	44
2*g*	72	29
2*h*	72	13
2*i*	72	53[b,c]
2*j*	72	64[b]
2*k*	72	21
2*l*	48	22

[a]Rendement en produit brut contrôlé par ^1H rmn et ir.
[b]Il s'agit dans ce cas d'un mélange d'aminoester phosphonique et d'aminoamide.
[c]La réaction a été faite dans le méthanol.

TABLEAU 3. Aminoacides phosphoniques **3**

Essais	Rdt (%)[a]
3*d*	70
3*f*	43
3*g*	34
3*h*	24
3*i*	53
3*j*	54
3*l*	71[b]

[a]Rendement en produit pur cristallisé.
[b]Produit hygroscopique.

pour les composés non substitués en α porteurs d'une fonction amine primaire ou secondaire; les rendements minimum sont obtenus pour les composés substitués en α. Nous avons déjà constaté dans une précédente étude l'effet protecteur des substituants en α du phosphore qui contrarient l'attaque nucléophile du phosphoryle (10).

Le brut d'hydrolyse après concentration est passé sur résine Dowex 50WX8 (50–100 mesh) préalablement mise sous forme H^+; on élue à l'eau et recueille la fraction comprise entre pH 2 et pH 7. Cette fraction fournit les aminoacides phosphoniques cristallisés purs par analyse élémentaire et dont la structure est confirmée par rmn ^1H. Les composés isolés fondent avec décomposition aux environs de 230–260°C à l'exception de **3***j* pour lequel le point de décomposition se situe vers 134°C.

Conclusion

L'ensemble de nos résultats montre que les phosphonopyruvates sont des réactifs prometteurs qui représentent une source potentielle originale d'aminoacides phosphoniques malgré l'importance des effets stériques qui représentent les facteurs limitatifs les plus influents.

Partie expérimentale

Les spectres rmn ^1H sont enregistrés à 60 MHz sur Perkin-Elmer R 24 A ou Varian T 60; les solvants sont $CDCl_3$, CCl_4 ou D_2O; le Me_4Si sert de référence interne; les abréviations suivantes sont utilisées: s = singulet, d = doublet, t = triplet, m = multiplet, bl = bande large. Les spectres rmn ^{13}C sont enregistrés à 20 MHz sur Varian CFT 20 ($CDCl_3$, Me_4Si interne). Les spectres ir sont tracés sur Beckman Acculab TM 2 (liquide pur ou pastilles de KBr). Les spectres de masse sont enregistrés à 75 eV (300 μA) sur JEOL JMS D 100 (couplage CPG). Les points de fusion sont déterminés sur banc Kofler et ne sont pas corrigés. La purification des acides aminophosphonocarboxyliques est réalisée sur résine Dowex 50 WX 8 (50–100 mesh). Les analyses élémentaires (C, H, N Technicon) sont en accord avec les formules brutes à ±0.3% près.

Preparation des phosphonopyruvates (Tableau 1)

Exemple-type: essai **1***c*

Dans un ballon à quatre tubulures équipé d'un agitateur mécanique, d'un thermomètre plongeant, d'une ampoule isobare et d'un réfrigérant, on place sous argon 5×10^{-2} mol de *n*-butyllithium dans l'hexane, préalablement dosé (≃ 1.45 *M*); on refroidit à −20°C et introduit un volume égal de tétrahydrofuranne (≃ 35 cm³). Le méthanephosphonate de diéthyle (7.6 g, 5×10^{-2} mol) dans 20 cm³ de THF est introduit goutte à goutte à −65°C. La solution devient rapidement trouble; après 10 min à −65°C, on ajoute l'iodure de cuivre (I) (5×10^{-2} mol + 10%) et élève graduellement la température jusqu'à −30°C. Après 60 min à −30°C, le chlorure de méthoxalyle (6.7 g, 5.5×10^{-2} mol) dans 35 cm³ d'éther est ajouté goutte à goutte; la solution se décolore lentement. Après addition, on maintient la température 5 h à −30°C puis revient lentement à 20°C. On hydrolyse par 40 cm³ d'eau, favorise la précipitation des sels, puis filtre sur fritté garni de Célite, lave le fritté 3 fois par 60 cm³ de CH_2Cl_2, puis repasse la totalité du filtrat sur le même fritté. La solution limpide est décantée et la phase aqueuse extraite une fois à CH_2Cl_2. La phase organique séchée est évaporée et le résidu distillé, pé 115–120°C/1 Torr (rdt = 33%); rmn ^1H (CCl_4) δ(ppm): 1.28 (t, 6H), 3.36 (d, 2H, $^2J_{H-P}$ = 22 Hz), 3.8 (s, 3H), 4.0 (m, 6H), 5.23 (d, $^2J_{H-P}$ = 11 Hz); rmn ^{13}C ($CDCl_3$) δ (ppm): 16.30 (d, CH_3—CH_2—O, $^3J_{P-C}$ = 5.8 Hz), 38.25 (d, CH_2—P, $^1J_{P-C}$ = 127.9 Hz), 53.25 (s, CH_3—O), 62.82 (d, CH_3—CH_2—O, $^2J_{P-C}$ = 5.5 Hz), 89.41 (d, P—CH=C, $^1J_{P-C}$ = 179 Hz), 159.6 (d, C=O, $^2J_{P-C}$ = 49.8 Hz).

Essai **1***g*

Dans le même appareillage que précédemment, on place 5×10^{-2} mol de *n*-butyllithium (≃ 1.45 *M* dans l'hexane), refroidit à −20°C et ajoute un volume équivalent de THF. Le méthanephosphonate de diéthyle (7.6 g, 5×10^{-2} mol) dans 20 cm³ de THF est introduit à −65°C; la solution se trouble. Après 10 min à −65°C, on ajoute l'iodure d'éthyle (7.95 g, 5.1×10^{-2} mol) lentement et laisse la température remonter peu à peu à 20°C. Après 10 min à 20°C, on refroidit à nouveau à −55°C et ajoute 5×10^{-2} mol de *n*-butyllithium. Le mélange est agité 30 min à −55°C. Après addition de CuI à −55°C, la suite des opérations est identique à l'exemple précédent; on distille 7.8 g (rdt = 56%) de phosphonopyruvate, pé 113–117°C/0.3 Torr; rmn ^1H (CCl_4) δ (ppm): 0.93 (t, 3H), 1.33 (m, 9H), 1.86 (m, 2H), 4.13 (m, 7H).

Essai **1***h*

Même appareillage que précédemment et mêmes quantités de *n*-butyllithium et de THF. L'éthanephosphonate de diéthyle (8.3 g, 5×10^{-2} mol) est métallé à −55°C pendant 30 min. L'iodure de méthyle (7.24 g, 5.1×10^{-2} mol) est ajouté à −70°C, puis la température ramenée lentement à 20°C. Après 10 min à 20°C, on refroidit à nouveau à −50°C et ajoute 5×10^{-2} mol de *n*-butyllithium. Après 90 min à −50°C, l'iodure de cuivre (I) est introduit et les opérations poursuivies comme précédemment; pé 115–119°C/0.4 Torr (rdt = 52%); rmn ^1H (CCl_4) δ (ppm): 1.33 (m, 9H), 1.43 (d, 6H, $^3J_{H-P}$ = 16 Hz), 4.13 (m, 6H).

Amination réductrice des phosphonopyruvates (Tableau 2)

En présence d'acétate d'ammonium. Exemple-type: essai **2**d

Un mélange de *O,O*-diéthylphosphono-3 pyruvate d'éthyle (1 g, 3.79×10^{-3} mol), d'acétate d'ammonium sec (3.1 g, 3.97×10^{-2} mol), de cyanoborohydrure de sodium (0.175 g, 2.78×10^{-3} mol) et de tamis moléculaire 4 Å (≃ 0.5 g) dans 25 cm³ d'éthanol absolu est agité magnétiquement 48 h à 25°C dans un flacon hermétiquement clos. Après filtration du tamis, le mélange réactionnel est acidifié à pH 2 par HCl concentré. L'éthanol est évaporé et le résidu dilué par 20 cm³ d'eau. La phase aqueuse est lavée à l'éther (3 × 25 cm³), alcalinisée à pH 9 par KOH en pastilles, saturée avec NaCl et extraite à CH_2Cl_2 (4 × 25 cm³). L'extrait séché et évaporé

donne 0.54 g (54%) d'une huile identifiée à l'amino-2 *O,O*-diéthylphosphono-3 propionate d'éthyle; ir (liq. pur) ν: 3370 et 3290 (NH_2), 1735 (CO), 1240 et 1025 (O—P(O)) cm^{-1}; rmn ^1H ($CDCl_3$) δ (ppm): 1.3 (2t, 9H), 2.4 (s, 2H), 2.9 (m, 2H), 3.3 à 4.6 (m, 7H).

En présence de bromure d'ammonium: essai **2**d′

Une solution équimolaire de NH_4Br et de NH_3 est préparée comme suit. Dans 50 cm^3 d'éthanol absolu, on dissout 2.5×10^{-2} mol de Na, puis ajoute 5×10^{-2} mol de NH_4Br sec; NaBr précipite. Au mélange obtenu, on ajoute le *O,O*-diéthylphosphono-3 pyruvate d'éthyle (1.26 g, 5×10^{-3} mol) et le tamis moléculaire 4 Å (≃ 0.5 g). Après traitement analogue au précédent, on recueille 0.69 g (55% brut) d'un mélange d'amino-2 *O,O*-diéthylphosphono-3 propionate d'éthyle (en particulier ir ν: 1735 (CO) cm^{-1}) et de *O,O*-diéthylphosphono-3 propionamide (en particulier ir ν: 1675 (CO) cm^{-1} et rmn ^1H δ: 7.4 (bl, C(O)—NH_2) ppm).

En présence d'une amine primaire. Exemple-type: essai **2**j *($R_5 = CH_3$)*

Un mélange de *O,O*-diéthylphosphono-3 pyruvate d'éthyle (0.99 g, 3.93×10^{-3} mol), de méthylamine (2.2 g de la solution à 33% dans l'éthanol, 2.36×10^{-2} mol), de $NaBH_3CN$ (0.175 g, 2.78×10^{-3} mol) et de tamis moléculaire 4 Å (≃ 0.5 g), dans 12 cm^3 d'éthanol absolu est ajusté à pH 7 par addition d'acide acétique, puis agité pendant 72 h à 25°C dans un flacon fermé. Le mélange, traité comme précédemment donne 0.67 g (64% brut) d'un mélange de *N*-méthylamino-2 *O,O*-diéthylphosphono-3 propionate d'éthyle majoritaire (en particulier ir ν: 1730 (CO) cm^{-1} et rmn ^1H δ: 2.4 (s, CH_3—N) ppm et de *O,O*-diéthylphosphono-3 *N*-méthylpropionamide (en particulier ir ν: 1670 (CO) cm^{-1}).

Réduction du phosphonopyruvate **1**d

Un mélange de *O,O*-diéthylphosphono-3 pyruvate d'éthyle (3.12 g, 1.23×10^{-2} mol), de $NaBH_3CN$ (0.77 g, 1.23×10^{-2} mol) et de 1 cm^3 d'acide formique pur dans 30 cm^3 d'éthanol absolu est agité pendant 96 h à 25°C dans un flacon bouché. Le mélange est acidifié à pH 2 par HCl concentré. L'éthanol est évaporé; le résidu repris à l'eau est alcalinisé à pH 9 par KOH en pastilles. L'extraction par CH_2Cl_2 (4×25 cm^3) donne 1.87 g (59%) d'hydroxy-2 *O,O*-diéthylphosphono-3 propionate d'éthyle, ir (liq. pur) ν: 3150 (OH), 1740 (CO), 1240 et 1025 (O—P(O)) cm^{-1}; rmn ^1H ($CDCl_3$) δ (ppm): 1.3 (m, 9H), 2.3 (m, 2H), 3.8 à 4.9 (m, 8H); sm: 255 ($M + 1$), 209 (M − OEt), 181, pic de base (M − C(O)OEt), 153 (181 − C_2H_4), 125 (153 − C_2H_4).

Hydrolyse d'un aminoesterphosphonocarboxylique (Tableau 3)

Exemple-type: essai **3**d

L'amino-2 *O,O*-diéthylphosphono-3 propionate d'éthyle (0.43 g, 1.7×10^{-3} mol) est porté au reflux pendant 12 h dans 5 cm^3 d'HCl aqueux 6 *M*. La solution refroidie est extraite par CH_2Cl_2 (2×6 cm^3) et évaporée; le résidu repris à l'eau est évaporé à nouveau (2 fois), puis dissous dans 30 cm^3 d'eau bouillante et décoloré au noir animal. La solution refroidie, incolore (pH ≃ 1), est passée sur colonne chargée de résine Dowex 50 × W 8 (50–100 mesh) préalablement régénérée en cycle H^+. La colonne est éluée à l'eau. Après élution des ions Cl^-, la fraction de pH 2 à 7 est collectée (≃ 80 cm^3); évaporée, elle donne 0.20 g (70%) d'acide amino-2 phosphono-3 propionique (phosphonoalanine) cristallisé pur, pf 225–230°C (déc.) (lit. (2) pf 228°C); rmn ^1H (D_2O) δ (ppm): 2.2 (m, 2H), 4.2 (m, 1H). *Anal.* calc. pour $C_3H_8NO_5P$: C 21.31, H 4.77, N 8.28; trouvé: C 21.65, H 4.84, N 8.24.

1. J. S. KITTREDGE et R. R. HUGHES. Biochemistry, **3**, 991 (1964); L. D. QUIN. Topics in phosphorus chemistry. Vol. 4. Grayson and Griffith, New York, NY. 1966; J. S. KITTREDGE et E. ROBERTS. Science, **164**, 37 (1969).
2. J. R. CHAMBERS et A. F. ISBELL. J. Org. Chem. **29**, 832 (1964); M. K. RHO et Y. J. KIM. Daeham Hwahak Hwoejee, **17**, 135 (1973); Chem. Abstr. **79**, 5552 (1973).
3. M. HORIGUCHI. Biochim. Biophys. Acta, **261**, 102 (1972); M. HORIGUCHI et H. ROSENBERG. Biochim. Biophys. Acta, **404**, 333 (1975).
4. W. A. WARREN. Biochim. Biophys. Acta, **156**, 340 (1968); C. R. LIANG et H. ROSENBERG. Biochim. Biophys. Acta, **156**, 437 (1968).
5. J. M. VARLET, N. COLLIGNON et P. SAVIGNAC. Synth. Commun. **8**, 335 (1978).
6. E. J. COREY et G. T. KWIATKOWSKI. J. Am. Chem. Soc. **88**, 5654 (1966).
7. P. COUTROT, P. SAVIGNAC et F. MATHEY. Synthesis, 36 (1978).
8. R. F. BORCH, M. D. BERNSTEIN et H. D. DURST. J. Am. Chem. Soc. **93**, 2897 (1971); R. F. BORCH. Org. Synth. **52**, 124 (1972).
9. U. H. DOLLING, A. W. DOUGLAS, E. J. J. GRABOWSKI, E. F. SCHOENEWALDT, P. SOHAR et M. SLETZINGER. J. Org. Chem. **43**, 1634 (1978).
10. J. BLANCHARD, N. COLLIGNON, P. SAVIGNAC et H. NORMANT. Tetrahedron, **32**, 455 (1976).

Proton and carbon-13 nuclear magnetic resonance studies of the conformational properties of seven-membered heterocycles. 2,4-Benzodithiepin and its derivatives

F. SAURIOL-LORD AND M. ST-JACQUES

Département de Chimie, Université de Montréal, C.P. 6210, Montréal (Qué.), Canada H3C 3V1

Received June 28, 1979

F. SAURIOL-LORD and M. ST-JACQUES. Can. J. Chem. **57**, 3221 (1979).

The conformational properties of 1,3-dithia-5,6-benzocycloheptene (**7**) (2,4-benzodithiepin), three 2,2-dialkyl derivatives, and two monosubstituted derivatives (2-CH_3 and 2-OCH_3) have been investigated by ^1H and ^{13}C dnmr methods. It is reported that the most stable conformation of the seven-membered ring is a chair on which, in the case of the monosubstituted compounds, the 2-CH_3 group adopts an equatorial position while the 2-OCH_3 group takes the axial position. Only for the 2,2-pentamethylene derivative (**10**) was a minor amount (13%) of TB form detected. These results are markedly different from those found previously for the oxygen analogs and the conformational effect of the cyclic heteroatoms will be discussed in terms of the anomeric and steric effects.

F. SAURIOL-LORD et M. ST-JACQUES. Can. J. Chem. **57**, 3221 (1979).

On a étudié les propriétés conformationnelles du dithia-1,3 benzo-5,6 cycloheptène (benzo-2,4 dithiépine) (**7**), de trois dérivés dialkyl-2,2 et de deux dérivés monosubstitués (CH_3-2 et OCH_3-2) en utilisant les méthodes de la rmn dynamique du ^1H et du ^{13}C. Dans le cas des composés monosubstitués on note que la conformation la plus stable des cycles à 7 est la forme chaise dans laquelle le groupe CH_3 en position 2 occupe la position équatoriale tandis que le groupe OCH_3 est axial. On a détecté de faibles quantités (13%) de forme bateau tordu seulement dans le cas du dérivé pentaméthylène-2,2 (**10**). Ces résultats sont très différents de ceux obtenus antérieurement pour les analogues oxygénés et l'effet conformationnel des hétéroatomes dans ces molécules sera discuté en termes d'effets anomériques et stériques.

[Traduit par le journal]

Recently results from ^1H and ^{13}C nmr studies (1) of seven-membered heterocyclic compounds containing the —O—CR_2—O— and —O—CHR—O— moieties such as in 2,4-benzodioxepin, its monosubstituted, and its disubstituted derivatives (i.e. **1–6**), have revealed that the ring conformations were determined by the nature and pattern of substitution. Thus were observed: a mixture of chair (C) and twist-boat (TB) forms for **1**, a TB conformation for the dialkyl derivatives **2**, **3**, and **4**, a C form for the 2-methyl derivative **5**, and a TB form for the 2-methoxy derivative **6**; that is, two different ring conformations were observed for the monosubstituted compounds.

It is of obvious interest to extend such observations to ring systems containing other heteroatoms, such as S and N, in order to delineate all of the factors governing the conformational features of seven-membered heterocycles.

The current interest in the properties of 1,3-dithianes (2) suggests that a study of seven-membered heterocycles containing the —S—CR_2—S— and —S—CHR—S— fragments such as for compounds **7–12** ought to yield valuable complementary information useful in characterizing the fundamental differences between the conformational properties of similar families of six and seven-membered heterocycles.

Compounds **7–12** were consequently prepared and studied by ^1H and ^{13}C nmr under experimental conditions similar to those used for compounds **1–6** and the results reported herein show that the sulfur atoms lead to strikingly different conformational properties from those reported for the corresponding oxygen heterocycles **1–6**. Furthermore the observations made are helpful to understand some of the conformational consequences of the anomeric effect (3) in the seven-membered ring.

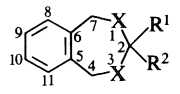

1, X = O	**7**, X = S	$R^1 = R^2 = H$
2, X = O	**8**, X = S	$R^1 = R^2 = CH_3$
3, X = O	**9**, X = S	R^1, R^2 = tetramethylene
4, X = O	**10**, X = S	R^1, R^2 = pentamethylene
5, X = O	**11**, X = S	$R^1 = H, R^2 = CH_3$
6, X = O	**12**, X = S	$R^1 = H, R^2 = OCH_3$

Results

Compounds **7**, **8**, **9**, and **10** gave ^1H nmr spectral changes at low temperatures whereas ^{13}C nmr spectral modifications were observed only for compounds

0008-4042/79/243221-09$01.00/0

9 and **10**. Spectral and dynamic results will be presented successively as observations from the spectra of each nucleus investigated.

In this work, instead of calling **7** by its systematic name (1,5-dihydro-3*H*-2,4-benzodithiepin), it will be referred to as a derivative of benzocycloheptene and therefore called 1,3-dithia-5,6-benzocycloheptene (1) in order to facilitate comparisons with benzocycloheptene and 1,3-dithianes. Consequently substituents in **8**–**12** are located on C-2.

^1H Nuclear Magnetic Resonance Spectra

Compounds **7**–**12** were not sufficiently soluble in CHF_2Cl, the solvent used for compounds **1**–**6**, and consequently most of the spectra were recorded for solutions in tetrahydrofuran; methylene chloride was also used for **10**. Because signals of the aromatic protons do not provide useful conformational information, only the signals of the aliphatic protons will be analysed in detail in this section.

The 100 MHz ^1H nmr room temperature spectrum of the unsubstituted parent compound **7** shows two singlets, one at δ 3.979 (H(2); methylene protons on C-2) and the other at δ 4.000 (H(4,7); methylene protons on C-4 and C-7). Each signal splits at lower temperature (coalescence temperature $T_c \approx -34°C$ for the most intense signal) to give two overlapping AB quartets at −90°C which are easily assignable from intensity arguments. It is pertinent to point out here that the H(2) signal was not reported to split in an earlier communication (4). At −90°C, the upfield lines of each AB pattern are observed to be broader than the downfield lines, most likely because of unresolved long range coupling (5). A free energy of activation ($\Delta G^{\neq}$) of 11.0 kcal/mol at T_c is calculated for the dynamic process using standard equations (6) with a transmission coefficient of one-half (*vide infra*). This value is comparable to the 10.9 kcal/mol reported earlier (4) from spectral observations at 60 MHz on a solution of **6** in $CHCl_3$/*m*-F-toluene. Table 1 contains a summary of the pertinent parameters.

The ^1H nmr spectrum of **8** (2,2-dimethyl) at room temperature shows two aliphatic singlets at δ 3.944 (H(4,7) and at δ 1.675 (CH_3)). At lower temperature the methyl signal gives a doublet while the H(4,7) line splits into an AB quartet. The pertinent spectral and dynamic parameters are given in Table 1.

The H(4,7) methylene protons at δ 3.960 of **9** (2,2-tetramethylene) also showed the typical singlet to quartet spectral change at low temperatures as summarized in Table 1.

The ^1H nmr spectra of compound **10** (2,2-pentamethylene) have been recorded in both THF-d_8 and CD_2Cl_2. Thus the room temperature spectrum in CD_2Cl_2 shows an H(4,7) singlet at δ 3.912 which splits to give two overlapping AB patterns of equal intensity at −90°C whose components were assigned from intensity patterns. The pertinent data is reported in Table 1 where $\Delta G^{\neq}$ is calculated at −32°C for the AB pattern with the larger chemical shift difference.

The ^1H nmr spectrum of **10** dissolved in THF-d_8 revealed, in addition to the two equally intense AB patterns for H(4,7), two other peaks located at 4.11 and 3.99 ppm and originating from a minor conformation. Because one of the THF-d_8 residual proton signals falls in this region, further ^1H nmr studies of this compound were not carried out since detailed information could be obtained more easily from ^{13}C nmr spectra as reported next.

Finally, compounds **11** (2-methyl) and **12** (2-methoxy) showed temperature independent ^1H nmr spectra as indicated in Table 1.

^{13}C Nuclear Magnetic Resonance Spectra

Only compounds **9** and **10** (the 2,2-tetramethylene and 2,2-pentamethylene derivatives respectively) gave rise to temperature dependent ^{13}C nmr spectra.

Table 2 contains the pertinent ^{13}C chemical shift data for compounds **7**, **8**, **11**, and **12** at high and low temperatures for purpose of comparison with the corresponding data determined for **9** and **10** above and below coalescence of the modified signals.

The assignment of the various carbon signals is relatively straightforward and was made from symmetry arguments which distinguished between the C-2 and the more intense C-4,7 signals. The C-5,6 signal is the least intense of the three aromatic lines owing to relaxation effects on these non-protonated carbon atoms. The remaining two aromatic signals belonging to the two different aromatic carbon pairs left were assigned by analogy with previous conclusions for benzocycloheptene (7).

The spectral modification observed for compound **9** is limited to the C-2′,5′ signals (δ 43.63) of the five-membered ring which splits into a doublet below −34°C (T_c) whose equally intense components are separated by 14.6 Hz at −90°C. A $\Delta G^{\neq}$ value of 11.9 kcal/mol was calculated at T_c. The pertinent shift data is summarized in Table 2.

The ^{13}C nmr spectral investigation of **10** (2,2-pentamethylene) was carried out at two frequencies (22.63 and 75.4 MHz) in three different solvents (tetrahydrofuran, methylene chloride-d_2, and diethyl ether).

Firstly, the simplest spectral behavior was observed in methylene chloride-d_2 at 22.63 MHz whereby at low temperatures only the C-2′,6′ and the C-3′,5′ signals each split into doublets with equally intense

TABLE 1. ^{1}H nuclear magnetic resonance spectral and dynamic parameters[a] for compounds **7** to **12**

Compound	Temperature (°C)	δ_A	δ_{av}	δ_B	$^2J_{AB}$(Hz)[b]	T_c(°C)	$\Delta G^{\ddagger}$(kcal/mol)[c]
7	25		4.00				
	−90	4.44		3.66	15.0	−34	11.0
	25		3.98[d]				
	−90	4.70		4.00	14.2		
8	25		3.94				
	−90	4.42		3.59	15.5	−23	11.6
	25		1.67[e]				
	−90	1.97		1.44		−27	11.6
9	25		3.96				
	−90	4.39		3.65	15.2	−13	12.1
10[f]	25		3.91				
	−90	4.43[g]		3.51	15.3		
		4.11		3.58	15.3	−32	11.3
11	25	4.11		3.85	14.4		
12	25	~4.7		[h]	14.8		

[a]At 100 MHz for solutions in THF-d_8 unless mentioned otherwise and containing internal Me_4Si. Unless otherwise mentioned, the data refer to the signals of the benzylic methylene protons on C-4 and C-7.
[b]The estimated uncertainty in coupling constants is ±0.5 Hz. Absolute values of couplings are given.
[c]Calculated at T_c using a transmission coefficient of one-half. The errors in $\Delta G^{\ddagger}$ are estimated to be 0.5 kcal/mol for 7 and **10** and 0.3 for **8** and **9**.
[d]This signal arises from the methylene protons H(2).
[e]This signal belongs to the methyl protons.
[f]The solvent is CD_2Cl_2 instead of THF-d_8. Owing to overlap of THF lines with the upfield components of the AB patterns at −90°C complete analysis was not possible at 100 MHz.
[g]The chemical shifts for two overlapping AB quartets are reported here.
[h]The upfield part of the AB quartet overlapped with signals from the solvent and was not further analysed.

TABLE 2. ^{13}C nuclear magnetic resonance chemical shift data for compounds **7** to **12** at high and low temperatures[a]

Compound	Temperature (°C)	C-2	C-4,7	C-5,6	C-8,11	C-9,10	Substituents on C-2		
7	25	39.23	36.94	140.59	129.72	128.08			
	−90	41.56	37.76	142.41	129.63	127.78			
8	25	53.12	33.57	140.72	129.24	127.65	31.29 (CH_3)		
	−80	52.99	32.49	141.24	129.07	127.78	31.16		
9	25	63.74	35.13	141.37	129.42	127.69	43.63 (C-2′,5′)	25.24 (C-3′,4′)	
	−100	63.48	34.35	141.71	129.33	127.78	43.54[b]	[c]	
							42.89		
10[d]	25	58.39	32.15	140.25	129.11	127.60	38.54 (C-2′,6′)	22.48 (C-3′,5′)	26.15 (C-4′)
	−80	57.48	31.63	140.38	128.81	127.86	39.27[e]	22.22[f]	25.98
							36.55	21.23	
10[g]	25	58.88	32.59	140.37	129.52	127.58	39.13	23.20	26.53
	−90 Mj[h]	57.15	31.59	141.13	129.03	127.73	39.57	22.50	26.53
			31.43				37.03	21.43	
	−90 Mn[h]	60.86	32.81	138.43	130.16	127.22	38.79	24.22	25.95
			32.08	138.31	130.08				
11	25	50.92	36.55	140.55	129.42	128.04	21.58 (CH_3)		
	−80	52.69	36.77	141.46	129.29	127.86	22.05		
12	25	87.34	30.55	141.89	129.59	127.82	56.92 (CH_3)		
	−80	85.70	29.43	142.15	129.59	127.95	56.75		

[a]At 22.63 MHz for solutions in THF (unless mentioned otherwise) containing internal Me_4Si and CD_2Cl_2 (13%) for field locking purpose.
[b]The indicated signal has undergone a splitting into two lines of equal intensities at low temperatures due to the non equivalence of C-2′ and C-5′. Signals not assigned.
[c]Due to strong overlap with a solvent signal, the assignment could not be made unambiguously.
[d]Solution in CD_2Cl_2; spectra taken at 22.63 MHz.
[e]Two equally intense lines arising from the non equivalence of C-2′ and C-6′. Signals not assigned to the respective carbons.
[f]Two equally intense lines arising from C-3′ and C-5′. Signals not assigned to the respective carbons.
[g]Solution in diethyl ether; spectrum at −90°C taken at 75.4 MHz.
[h]The symbols Mj and Mn stand for: Mj = major conformer and Mn = minor conformer.

lines. The C-2′ and C-6′ lines coalesce at −34°C and the $\Delta G^{\ddagger}$ value calculated is 11.2 kcal/mol. Furthermore it was observed that several lines (C-2 and C-5,6) broaden somewhat at intermediate temperatures and then sharpen up at lower temperatures. Such an observation is compatible with the existence of a mixture of conformers, one of which is less abundant than 5% (8).

The 22.63 MHz ^{13}C nmr spectra of **10** in THF showed, in addition to the above splitting, the presence at −80°C of lesser intense lines belonging to a minor conformation (about 13%). In fact the C-2 and C-5,6 lines clearly show a splitting into two unequal lines. Thus the C-2 line (δ_c 58.73) splits into two lines located at 57.48 and 61.05 ppm (the latter being less intense), whereas the C-5,6 line (δ 140.59) splits into two lines located at 138.61 and 141.46 ppm (the former being less intense).

Because some overlap was observed between one of the THF signals and some signals belonging to **10**, the spectra was also recorded in diethyl ether at 22.63 MHz. It showed results similar to those reported for the THF solution with the advantage that all the signals of **10** were clearly visible at room temperature. On the other hand, the low temperature spectra showed obstruction from the solvent lines of diethyl ether as was the case in THF. More satisfactory spectra were obtained only at higher field (75.4 MHz) for both solvents but since the diethyl ether solution gave less overlapping, the data obtained for this solvent is summarized in Table 2.

The assignment of the signals of **10** was made through comparison with the shifts of the other disubstituted derivatives **8** and **9**. For the spectrum of **10** in methylene chloride-d_2, the signals of the six-membered ring carbon atoms observed at room temperature were assigned from intensity arguments (C-4′ being least intense) and substituent effects predicted (1) to shift the C-2′ and C-5′ signals more downfield than C-3′ and C-5′.

The assignment of the signals of the two conformers of **10** in diethyl ether was also carried out through comparisons. The signals of the major conformer appeared at chemical shifts very similar to those observed in methylene chloride-d_2. The weaker signals (labeled Mn in Table 2) could also be assigned readily; in this case relative intensities permitted the assignment of the less intense line at 25.95 ppm to C-4′ and the more intense line at 24.22 ppm to C-3′,5′.

Discussion

Conformations of the Seven-membered Rings

Previously published (4) low temperature 60 MHz ^1H nmr spectra of **7** showed a spectral change for the H(4,7) signals but apparently not for H(2). Consequently the nature of its most stable conformation could not be deduced with absolute certainty. On the other hand, the 100 MHz data reported in Table 1 show that the methylene protons on C-2 are non-equivalent at −90°C thus ruling out the TB form (**15**; $R^1 = R^2 = H$) as the major conformation. The absence of a ^{13}C nmr spectral change indicates that only one conformation can be detected by nmr. Because TB is less energetic than B (**14**), then the most stable conformation of **7** must be the chair (**13**) as was the case (1) for the oxygen analog of **7**, namely **1** which, in contrast, was found to exist as a mixture of conformations involving a minor amount of TB in addition to C.

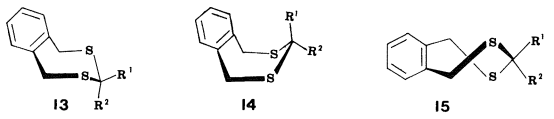

The 2,2-dimethyl derivative **8** is found to exist only in the C form in agreement with the nonequivalence of the methyl ^1H nmr signals at −90°C as reported in Table 1. Interestingly the ^{13}C methyl signals were found to be accidentally equivalent at low temperatures contrary to the proton signals. Our data therefore confirm earlier 60 MHz ^1H nmr observations (4).

In the case of **9** (2,2-tetramethylene), the ^{13}C signals of C-2′ and C-5′ (of the five-membered ring) show non-equivalence in agreement with axial and equatorial positions of the chair conformation. Thus, it is seen that the most stable conformations of the seven-membered ring of **8** and **9** are different from those of the oxygen analogs **2** and **3** for which only the TB form was detected by nmr (1).

For compound **10** (2,2-pentamethylene) it is the ^{13}C nmr data which are most revealing. They provide clearcut evidence for the existence of a mixture of conformations in both tetrahydrofuran and diethyl ether. Table 2 and Fig. 1 show that the ^{13}C chemical shift of the C-5,6 signals is most informative and, as was the case (1) for **2**, **3**, and **4**, suggest that C is the major conformer while TB is the minor conformer. Furthermore, in methylene chloride-d_2, the amount of TB form decreases beyond the minimum detectable limit of ^{13}C nmr. These observations are to be contrasted with earlier ones for **4** which showed that only the TB form was detected (1).

The absence of spectral changes for **11** (2-methyl) is compatible with a single conformation which is most clearly established to be the chair with an equatorial methyl group from argument based on the ^{13}C chemical shift of C-4,7 given in Table 2 and shown in Fig. 1. Thus the absence of a significant upfield γ-shift (*vide infra*) relative to the parent compound **7** argues most convincingly in favor of the chair form

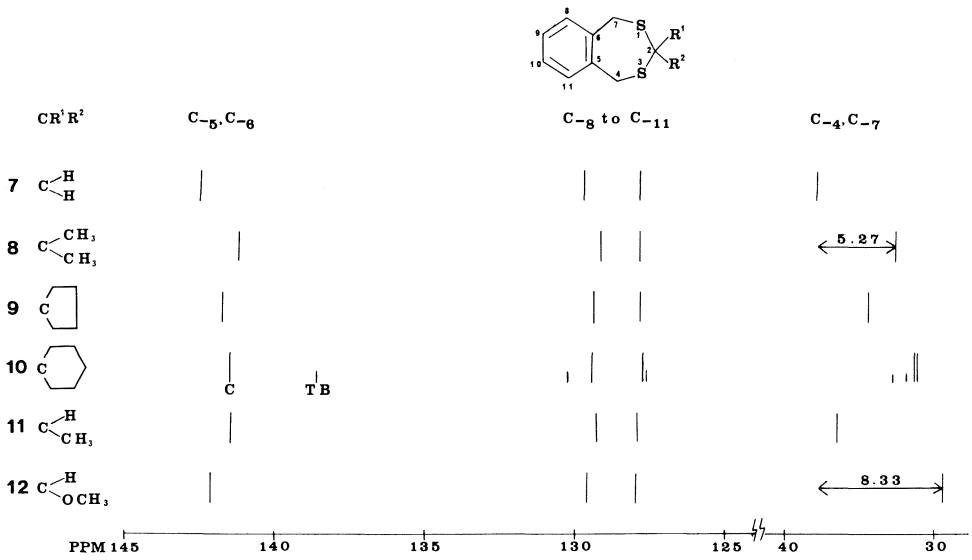

FIG. 1. Diagram comparing the carbon-13 chemical shifts at low temperature of compounds **7** to **12** summarized in Table 2.

which is also the conformation adopted by the oxygen analog **5**.

Compound **12** (2-methoxy) is also characterized by the absence of spectral changes unlike observations reported for its analog **6**. The ^{13}C chemical shift of the C-5,6 signal shown in Fig. 1 is in agreement (1) with C rather than TB. Furthermore the strong upfield γ-shift (8.33 ppm) of the C-4,7 signal suggests that the 2-methoxy group must be located at the C-2 axial position of the chair form.

Conformational Consequences of the Anomeric and Steric Effects

The conclusion that the chair form is the most stable for all sulfur heterocycles **7–12** differs radically from results reported previously (1) for the series of compounds **1–6** and summarized earlier in the text.

The differences brought about by the change of the ring heteroatoms can be explained quite well in terms of the so-called "anomeric effect" modulated by differences in steric interactions.

First introduced in the carbohydrate field to explain the axial preference of polar substituents in pyranose sugars (9), the anomeric effect has later been generalized to systems containing the R—X—C—Y moiety where X and Y have at least one unshared electron pair (10). As a consequence it was shown that a gauche arrangement about the X—C bond was most stable.

Although explained in several ways (3, 10), the anomeric effect is essentially the manifestation of electronic interactions which stabilize those conformations possessing the geometrical features favoring the interactions.

Two cases must be examined with respect to our work. The first one involves the two heteroatoms of the seven-membered ring, while the second case is concerned with the additional effect caused by the oxygen atom of the methoxy substituent in **6** and **12**.

The analysis of the acetal bond sequence —O(1)—C—O(3)— of **1** can best begin with results for dimethoxymethane for which it was established that the g^+g^+ (TB-like) conformation is more stable than the g^+g^- (C-like) arrangement (11). Furthermore, the solvent effect observed (1) for **1** whereby the proportion of the TB form increases with decreasing polarity of the solvent (21% in CHF_2Cl (1.48 *D*) to 33% in dimethyl ether (1.30 *D*)) is in line with the trend expected from consideration of predictions made from the generalized anomeric effect (10). Thus, the preferential stabilization of TB with respect to C for **1** reduces the free energy difference (ΔG^0) between these two conformations to 0.57 kcal/mol in CHF_2Cl at $-130°C$ or 0.40 kcal/mol in dimethyl ether at $-128°C$ and consequently signals for both C and TB forms of **1** are detected by nmr. In contrast only chair signals were detected for benzocycloheptene (12).

The origin of the anomeric effect has been attributed to the participation of an *anti* lone pair of electrons in a stabilizing n–σ^* interaction (13). In addition, it has been suggested that a distinction should be made between the two lone pairs of a given oxygen atom whereby one is 2*p*-like and a better donor than the other lone pair which is sp^2-like and a poorer donor (14).[1]

The analysis of the relative electronic stabilization in the C and TB forms is consequently dependent on the model selected. Firstly, when it is assumed that

[1]See also ref. 13, p. 167.

both lone pairs are equivalent, it is difficult to conclude that C should not be as stabilized as TB because each C—O bond of the C form as well as of TB contains an *anti* lone pair. If, on the other hand, the oxygen lone pairs are considered to be different, then the *anti* lone pairs in C are sp^2-like whereas in TB one *anti* lone pair is 2*p*-like while the other is sp^2-like. The second model therefore appears to predict a greater stabilization of TB.

It is also conceivable that a greater steric interaction may exist in the C form of **1**, between the axial protons on C-2, C-4, and C-7, than for the C form of benzocycloheptene. This factor could then contribute partially to the smaller energy difference between the C and TB forms of **1**. Considering that a solvent change is expected to alter electronic effects but not steric effects (15), the observed solvent effect on the C:TB ratio (3.8 in CHF_2Cl and 2.0 in dimethyl ether) may be useful to assess the relative importance of the various factors. This observation argues in favor of an electronic origin and it is in line with predictions made through consideration of the stereoelectronic effect, but most likely is not solely due to it because other electronic effects related to the dipole and quadrupole moments of the whole molecule may also be significant. It therefore appears unrealistic to select one of the orbital models for the stereoelectronic effect from the results for **1**.

Contrastingly, our results for **7** indicate that the energy difference between C and TB is too large to permit detection of both conformations by nmr. This observation is no doubt related to the longer C—S bond length (16) (C—S = 1.82 Å, C—O = 1.43 Å, and C—C = 1.54 Å) either through its effect on the degree of stabilization by the anomeric effect for the S—C—S fragment and/or its consequence on steric repulsion between the axial protons in C.

It is interesting to note that for the simplest model, 2,4-dithiapentane, vibrational analysis suggested that the g^+g^- arrangement (or GG′, C-like) is the least energetic (17) and that a mixture of three other conformations was thought to exist in the liquid phase. Another report (18), in contrast, concluded in favor of a single planar form on the basis of photoelectron spectroscopy data.

Systematized information from theoretical origin has suggested that the lone pairs of S are better intrinsic donors than those of O in a $n \rightarrow \sigma^*$ interaction and furthermore that the C—S bond is a better acceptor than C—O.[2] The extent of orbital overlap in the S—C—S fragment is expected to be weaker than for the O—C—O moiety (19) because of the longer S—C bond. The result of these opposing effects appears to have escaped sufficient quantification for application to compound **7**.

Our experimental results for **7** are therefore significant in that they show that the C form, with a g^+g^- arrangement about the —S—C—S— bonds, is most stable and that TB, with a g^+g^+ arrangement, is not detected by either ^1H or ^{13}C nmr. Furthermore, our observation that C is the most stable conformation for the 2,2-disubstituted compounds **8**, **9**, and **10** shows that the longer C—S bonds attenuate the effect of steric repulsion in these compounds. Such steric effects were strongly destabilizing for **2**, **3**, and **4** which were reported to exist only in the TB form (1).

Nevertheless, the observation of a minor amount of TB ($\sim$13% in THF at $-90°C$) for **10** indicates that the free energy difference between the C and TB forms of the seven-membered ring is not very large and that seemingly small differences as exist between **8**, **9**, and **10** are sufficient to lead to detectable amounts of the minor TB conformation. Furthermore, the solvent effect noted for **10** is rationalizable in terms of electronic effects of which the stereoelectronic $n \rightarrow \sigma^*$ effect could be dominant.

The presence of the 2-methoxy substituent in **6** and **12** further complicates the evaluation of the stereoelectronic stabilization for the various possible conformations of each of these compounds.

Let us begin with the examination of 2-methoxy-1,3-dioxane (**16**) which can serve as a model for **6**. It has recently been observed[3] that **16** exists as a mixture of conformers in CHF_2Cl whereby, at $-148°C$, 30% of chair with the substituent in the axial position (represented by C-a) and 70% of chair with an equatorial methoxy group (represented by C-e) were observed. Because steric interactions should be strong in the C-a conformation of **6** as a consequence of the somewhat greater puckering of the seven-membered ring (12), this form is not expected to be more dominant than for **16**. But instead of a mixture of C-a (minor) and C-e (major) forms, only the TB form was detected for **6** in CHF_2Cl.

The assessment of the relative importance of stereoelectronic interactions in the various conformations of orthoformates is more complex than in acetals. Results published for trimethoxymethane (20), the simplest model compound, revealed that it exists as a mixture of two conformers, called TGG and TGG′, in solution and in the vapor phase. It was also suggested that TGG′ is more stable by about 0.6 kcal/mol. The spatial arrangements about the three C—O bonds for these two conformations are very similar to those characterizing two of the three possible TB conformations of **6** which arise from

[2]Reference 13, p. 154.

[3]F. Sauriol. Unpublished results.

different rotational positions of the methoxy group. Thus the TB_2 (X = O) form is equivalent to TGG and TB_3 (X = O) is equivalent to TGG′.

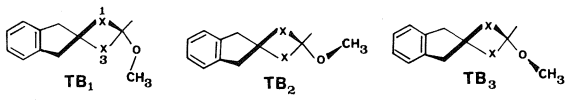

Rotation of the methoxy group is expected (21) to be rapid at −150°C on the nmr time scale so that it is not possible to determine whether or not a mixture of rotational forms actually exists for **6**. Nevertheless, results for the simple model fit very well with our identification of TB as the most stable ring conformation for **6**. It therefore appears that a steric interaction destabilizes C-a and that TB becomes the most stable conformation of **6** because it is stabilized by the stereoelectronic interactions whereas C-e is not.

With regard to compound **12**, the longer C—S bonds should attenuate the importance of steric repulsion in the C-a form as was found to be the case for the disubstituted derivatives **8**, **9**, and **10**. Consequently the anomeric effect, which is expected to stabilize C-a at least as much as TB, best explains the observation of the single C-a form for **12**. It is interesting to point out that the analogous six-membered heterocycle 2-methoxy-1,3-dithiane has also been found[3] to exist solely in the C-a form in CHF_2Cl and in $CBrF_3$.

Conformational Dynamics

The conformational inversion of the chair form of benzocycloheptene and its derivatives is known to involve a rate-determining chair-to-boat step (1, 22, 23). Consequently the $\Delta G^{\ddagger}$ values reported in Table 1 characterize this interconversion process for compounds **7** to **9**. Thus it is seen that the substitution of a *gem*-dimethyl group on C-2 affects $\Delta G^{\ddagger}$ only slightly as was observed to be the case for analogous substitution on 1,3-dithiane (24).

The complete description of the averaging processes responsible for the spectral changes observed for **10** must focus on the inversion processes of both the six- and seven-membered rings. Considering that 1,1-dialkyl cyclohexanes are characterized by $\Delta G^{\ddagger}$ values in the range 10–11 kcal/mol,[4] it can be concluded that at −90°C the ring inversion of the chair form of both rings is slow on the nmr time scale. But because $\Delta G^{\ddagger}$ for chair inversion of the seven-membered ring is expected to be slightly higher than for the six-membered ring, then the spectral change of the benzylic protons of **10** yields a $\Delta G^{\ddagger}$ value characteristic of the larger ring. Furthermore, the ^{13}C nmr spectral change observed for **10** in tetrahydrofuran and diethyl ether, which provides direct information on the chair-to-boat step, is compatible with the above conclusion.

Finally, no dynamic information was obtained for **11** and **12** because of the absence of a spectral change as a consequence of the existence of only one conformation detectable by nmr. Nevertheless it is expected that $\Delta G^{\ddagger}$ for chair inversion ought to be comparable to the values determined for compounds **7**–**10**.

^1H and ^{13}C Chemical Shifts

Table 1 reveals that the chemical shifts of the individual methylene protons on C-4 (and C-7) determined at low temperatures are very similar for compounds **7**, **8**, and **9** for which the chemical shift differences are 0.78, 0.83, and 0.74 ppm respectively. In addition, the shift differences of 0.92 and 0.53 ppm determined for **10** are also comparatively large.

The upfield halves of the AB patterns of the H(2) and H(4) methylene protons of **7** were observed to be broader than the lower field halves in accord with long range coupling (5) expected for equatorial protons. Consequently the axial H(2) and H(4) protons are downfield from the equatorial protons as was reported for the methylene protons α to the sulfur atom in thiane and 1,3-dithiane (25, 26). This specific effect of sulfur has been explained in terms of the C—S bond anisotropy (25).

The particularly large chemical shift differences in **7**, **8**, **9**, and **10** arise because in the parent benzocycloheptene the benzylic methylene protons are separated by −0.106 ppm (12) compared to 0.48 ppm for cyclohexane (27), where the negative sign indicates that for benzocycloheptene the axial protons absorb at lower field contrary to the observation for cyclohexane. The contribution from the C—S bond anisotropy therefore adds on to these basic reference values.

The ^{13}C chemical shifts also show certain characteristics of importance. Firstly the C-2 signal of **7** appears about 7 ppm downfield from that for 1,3-dithiane (2*b*); this difference is too large to be caused by the different solvents and must arise as a consequence of ring size. Methyl and dimethyl substitution produce a downfield shift of the C-2 signal by 11.7 and 13.9 ppm respectively at room temperature; these values are very close to the 10.2 and 13.1 ppm determined for the six-membered analogs (2*b*). Table 2 further shows that lowering the temperature affects the C-2 chemical shift of **7** and **11** about equally but that **8** is perturbed only slightly. Consequently the substituent effects determined at low temperatures are slightly different (i.e. 11.4 and 11.1 ppm).

The trend of C-2 substitution effects for the di-

[4]Reference 6, p. 582.

substituted compounds **8**, **9**, and **10** (+13.9, +24.5, and +19.2 ppm at room temperature) is similar to that observed for analogously substituted cyclohexane derivatives (+3.2, +15.5, and +5.5 ppm) (28).

Probably the most important ^{13}C substituent parameter is the so-called γ-effect because of its utility in providing stereochemical information (29). Thus for the series **8–12** the chemical shift of the carbons 4 and 7 are governed by this effect. Table 2 reveals that for **8** the C-4,7 upfield shift is −3.37 ppm at room temperature; this value is somewhat comparable to the −2.89 ppm determined for 2,2-dimethyl-1,3-dithiane (2*b*). It is interesting to note that the γ-effect for **8** determined at −80°C becomes −5.27 ppm as shown in Fig. 1. Furthermore, the trend observed for the C-4,7 shifts in **8**, **9**, **10** (Mj) as depicted in Fig. 1 is similar to that observed for analogously substituted derivatives of cyclohexane (28) as well as for **2**, **3**, and **4** (1).

The very small γ-shift observed for **11** indicates the absence of an axial substituent (29) and is compatible with a chair conformation with an equatorial group. In contrast, the C-4,7 signal of **12** is shifted upfield by −6.39 ppm at room temperature (−8,33 ppm at low temperature as shown in Fig. 1). This large upfield shift is in accord with substitution at the axial position so that **12** exists as a chair with OCH_3 located solely in the axial position within the limits of detection by nmr. The corresponding upfield shift for 2-methoxy-1,3-dithiane is −5.66 at low temperature.[3]

It is interesting to note that the axial and equatorial methyl ^{13}C signals of **8** are accidentally equivalent at low temperature whereas two C-2′,5′ signals are observed for **9** and two C-2′,6′ signals for **10**. The particularity effect of sulfur on ^{13}C chemical shifts has been noted previously (26).

The aromatic signals of the chair conformations are somewhat similar for all compounds as seen in Fig. 1. Furthermore, in the case of **10**, the C-5,6 TB signal is most different from that of the C form; a separation of 3.7 ppm is observed. A similar upfield shift of the C-5,6 TB signal was also reported (1) for **1**.

Distinct TB signals are also observed for the other aromatic carbons as well as for C-4,7 and other carbons. However, the fact that only chair signals are observed for **7**, the reference compound, makes it difficult to attempt to rationalize the chemical shifts characteristic of the TB form. As was shown for **1**, proper reference parameters are required for a convincing explanation of substituent effects on the chemical shifts for a given conformation (1). Moreover, the different effects noted previously as a result of substitution of O by S suggest that extrapolations from one series to the other is dangerous (26).

Experimental

Melting points are uncorrected and were determined using a Büchi melting point apparatus. High-resolution mass spectra at 70 eV were recorded using an Associated Electrical Industries Model MS-902 spectrometer.

The variable temperature ^1H nmr spectra at 100 MHz were obtained using a JEOL JNM-4H-100 spectrometer equipped with a temperature control unit Model JES-VT-3 under conditions described earlier (1).

The variable temperature ^{13}C nmr spectra were recorded in the FT mode with a Bruker WH-90 spectrometer operating at 22.63 MHz and equipped with the Bruker variable temperature accessory as described elsewhere (1). The pulse repetition was normally set equal to the acquisition time, except for the integration of the signals of **10** at −90°C, when a pulse repetition time of 5 s was used.

The rate constants were determined at the coalescence temperature using the equation $k = \Pi\Delta\nu\sqrt{2}$ for singlet to doublet splitting in ^{13}C nmr spectra (i.e., for **9** and **10**; in the case of **10** where the lines are of unequal intensity the equation provides an acceptable estimate (30) and the equation $k = \Pi(\Delta\nu^2 + 6J^2)^{1/2}/\sqrt{2}$ for singlet to AB splitting (31) in ^1H nmr spectra (i.e., for **7** to **10**). The free-energy barriers (ΔG^+) were calculated from standard equations (6) using a transmission coefficient of one-half which is most appropriate to describe the chair-to-boat step of the chair inversion.

Syntheses

Compounds **7** to **12** were prepared from 1,2-benzenedimethanethiol (32) (**17**) used as starting material based on a procedure published by Shahak and Bergmann (33). The starting dithiol **17** was prepared from 1,2-benzenedimethanol (Aldrich) using standard reactions involving a transformation into the dichloro derivative with hydrochloric acid and zinc dichloride (34) followed by conversion into the dithiol using thiourea.[5]

*1,3-Dithia-5,6-benzocycloheptene (**7**)*

Compound **7** was prepared by a procedure already published (33). Its ^1H nmr spectrum was identical to that published (4) and its ^{13}C nmr chemical shifts reported in Table 2 confirmed the structure of **7**.

*2,2-Dimethyl-1,3-dithia-5,6-benzocycloheptene (**8**)*

A mixture of 2.2 g of the dithiol **17**, 1 mL of acetone, 60 mL of isopropanol, and 5 mL of a solution of 30% sulfuric acid in methanol was refluxed using a Dean–Stark apparatus to collect about 30 mL of distillate. The reddish solution remaining in the reaction flask was then cooled and a solid compound precipitated; it was filtered and recrystallized from isopropanol A white solid (mp 134–135°C) was thus obtained in about 40% yield. Its ^1H nmr spectrum was identical to that published (4) for **8** and the ^{13}C nmr data reported in Table 2 confirmed the structure.

*2,2-Tetramethylene-1,3-dithia-5,6-benzocycloheptene (**9**)*

This compound was prepared by a procedure identical to that used for **8** from 0.91 g of the dithiol **17**, 25 mL of isopropanol, 0.48 mL of cyclopentanone, and 2.1 mL of 30% sulfuric acid in methanol. After recrystallization from methanol about 47% of **9** was obtained (mp 125–126°C). This product was characterized by its ^1H and ^{13}C nmr spectra (Tables 1 and 2) and by its high-resolution mass spectrum. *Mol. Wt.* calcd. for $C_{13}H_{16}S_2$: 236.0692; found (ms 70 eV): 236.0773.

*2,2-Pentamethylene-1,3-dithia-5,6-benzocycloheptene (**10**)*

This compound was prepared by a procedure similar to that

[5]Reference 34, p. 497.

used for **8** and **9** from 1.5 g of **17**, 30 mL of isopropanol, 0.88 g of cyclohexanone, and 2.6 mL of 30% sulfuric acid in methanol. Recrystallization from methanol gave 42% of compound **10** (mp 97.5–98°C) which was characterized by its ^1H and ^{13}C nmr spectra (Tables 1 and 2) and by its mass spectrum. *Mol. Wt.* calcd. for $C_{14}H_{18}S_2$: 250.0849; found (ms 70 eV): 250.0847.

*2-Methyl-1,3-dithia-5,6-benzocycloheptene (**11**)*

This compound was prepared by the same procedure as **8** using 1.6 g of **17**, 0.54 mL of acetaldehyde, 30 mL of isopropanol, and 0.55 mL of concentrated hydrochloric acid. Recrystallization in isopropanol gave 40% of **11** (mp 118–119°C) which was characterized by its ^1H and ^{13}C nmr spectra (Tables 1 and 2) and by its mass spectrum. *Mol. Wt.* calcd. for $C_{10}H_{12}S_2$: 196.0380; found (ms 70 eV): 196.0382.

*2-Methoxy-1,3-dithia-5,6-benzocycloheptene (**12**)*

The preparation of this compound involved a procedure recently published for six-membered rings (35).

A solution of 15 mL of *n*-butyllithium in hexane (0.018 mol) and 25 mL of anhydrous THF were placed in a 50 mL flask which was maintained at 0°C under a nitrogen atmosphere. A solution of 1.7 g (10 mmol) of **17** in 10 mL of dry THF was then added dropwise. After the addition and 5 min of stirring, 1.15 g (10 mmol) of dichloromethylmethyl ether were added dropwise. The reaction mixture was then stirred at room temperature for 2 h. Evaporation of the solvent gave an orange oil. The addition of chloroform dissolved most of the product. The solution was then filtered and the chloroform evaporated, after which 15 mL of methanol were added to the residue. The methanol was decanted from the viscous product and the washing procedure was repeated. Chromatography on silica gel (elution with ether) gave pure **12** as a white crystalline compound which sublimed at about 95°C in a sealed capillary. The pure compound was characterized by its ^1H and ^{13}C nmr spectra (Tables 1 and 2) and by its mass spectrum. *Mol. Wt.* calcd. for $C_{10}H_{12}S_2O$: 212.0329; found (ms 70 eV): 212.0832.

Acknowledgments

We wish to acknowledge the contribution of Mr. A. Blanchette for the preparation of some of the compounds studied, the technical assistance of Mr. R. Mayer, and financial assistance from the National Research Council of Canada.

1. A. Blanchette, F. Sauriol-Lord, and M. St-Jacques. J. Am. Chem. Soc. **100**, 4055 (1978).
2. (*a*) J. B. Lambert, E. Vulgaris, S. I. Featherman, and M. Majchrzak. J. Am. Chem. Soc. **100**, 3269 (1978); (*b*) E. L. Eliel, V. S. Rao, and F. G. Riddell. J. Am. Chem. Soc. **98**, 3583 (1976); (*c*) K. Pihlaja and B. Björkqvist. Org. Magn. Reson. **9**, 533 (1977); (*d*) E. L. Eliel. Angew. Chem. Int. Ed. Engl. **11**, 739 (1972).
3. N. S. Zefirov and N. M. Shekhtman. Russ. Chem. Rev. **40**, 315 (1971).
4. H. Friebolin, R. Mecke, S. Kabuss, and A. Luttringhaus. Tetrahedron Lett. 1929 (1964).
5. S. A. Khan, J. B. Lambert, O. Hernandez, and F. A. Carey. J. Am. Chem. Soc. **97**, 1468 (1975).
6. L. M. Jackman and F. A. Cotton. Dynamic nuclear magnetic resonance spectroscopy. Academic Press, New York, NY. 1975.
7. (*a*) W. Adock, B. D. Gupta, T. C. Khor, D. Doddrell, and W. Kitching. J. Org. Chem. **41**, 751 (1976); (*b*) H. Gunther, G. Jikeli, H. Schickler, and J. Prestien. Angew. Chem. Int. Ed. Engl. **12**, 762 (1973).
8. F. A. L. Anet and V. J. Basu. J. Am. Chem. Soc. **95**, 4424 (1973).
9. J. T. Edwards. Chem. Ind. London, 1102 (1955); for a review see also R. U. Lemieux and S. Koto. Tetrahedron, **30**, 1933 (1974).
10. W. F. Bailey and E. L. Eliel. J. Am. Chem. Soc. **96**, 1798 (1974), and references cited therein.
11. E. E. Astrup. Acta Chem. Scand. **25**, 1494 (1971).
12. M. St-Jacques and C. Vaziri. Org. Magn. Reson. **4**, 77 (1972).
13. N. D. Epiotis, W. R. Cherry, S. Shaik, R. L. Yates, and F. Bernardi. Top. Curr. Chem. **70**, 1 (1977), and references cited therein.
14. (*a*) S. David, O. Eisenstein, W. J. Hehre, L. Salem, and R. Hoffman. J. Am. Chem. Soc. **95**, 3806 (1973); (*b*) L. Radom, W. J. Hehre, and J. A. Pople. J. Am. Chem. Soc. **94**, 2371 (1972).
15. M. K. Kaloustian. J. Chem. Ed. **51**, 777 (1974), and references cited therein.
16. E. L. Eliel. Acc. Chem. Res. **3**, 1 (1970).
17. M. Ohsaku, Y. Shiro, and H. Murata. Bull. Chem. Soc. Jpn. **45**, 113 (1972).
18. C. Guimon, M-F. Guimon, and G. Pfister-Guillouzo. Tetrahedron Lett. 1413 (1975).
19. S. Wolfe. Paper presented at the 2nd Joint Conference CIC/ACS, Montreal, May 30, 1977, and private communication.
20. H. Lee and J. K. Wilmshurst. Spectrochim. Acta, **23A**, 347 (1967).
21. F. A. L. Anet and I. Yavari. J. Am. Chem. Soc. **99**, 6752 (1977).
22. N. L. Allinger and J. T. Sprague. J. Am. Chem. Soc. **94**, 5734 (1972).
23. M. St-Jacques and C. Vaziri. Can. J. Chem. **51**, 1192 (1973).
24. H. Friebolin, H. G. Schmid, S. Kabuss, and W. Faisst. Org. Magn. Reson. **1**, 67 (1969).
25. J. B. Lambert and J. E. Goldstein. J. Am. Chem. Soc. **99**, 5689 (1977).
26. E. L. Eliel, V. S. Rao, F. W. Vierhapper, and G. Z. Juaristi. Tetrahedron Lett. 4339 (1975).
27. F. A. L. Anet and A. J. R. Bourn. J. Am. Chem. Soc. **89**, 760 (1967).
28. D. Zimmermann, R. Ottinger, J. Reisse, H. Christol, and J. Brugidou. Org. Magn. Reson. **6**, 346 (1974).
29. F. W. Wehrli and T. Wirthlin. Interpretation of carbon-13 nmr spectra. Heydon, New York, NY. 1976.
30. D. Kost, E. H. Carlson, and M. Raban. Chem. Commun. 565 (1971), and references cited therein.
31. R. J. Kurland, M. B. Rubin, and W. E. Wise. J. Chem. Phys. **40**, 2426 (1964).
32. V. J. Traynelis. *In* 7-Membered heterocyclic compounds containing oxygen and sulfur. Heterocyclic Compounds. Vol. 26. *Edited by* A. Rosouisky. Wiley-Interscience, New York, NY. 1972. Chapt. 11.
33. I. Shahak and E. D. Bergmann. J. Chem. Soc. C, 1005 (1966).
34. A. I. Vogel. A text-book of practical organic chemistry. 3rd ed. John Wiley and Sons, Inc., New York, NY. 1956. p. 272.
35. P. Stütz and P. A. Stadler. Helv. Chim. Acta, **55**, 75 (1972).

The preparation and Raman spectra of $SeBr_3AsF_6$, $SeBr_3SbF_6$, $TeBr_3AsF_6$, and normal coordinate analyses of the tribromosulphur(IV), tribromoselenium(IV), and tribromotellurium(IV) cations

W. V. F. BROOKS, JACK PASSMORE, AND E. KEITH RICHARDSON

Department of Chemistry, University of New Brunswick, P.O. Box 4400, Fredericton, N.B., Canada E3B 5A3

Received June 4, 1979

W. V. F. BROOKS, JACK PASSMORE, and E. KEITH RICHARDSON. Can. J. Chem. **57**, 3230 (1979).

$SeBr_3AsF_6$ and $TeBr_3AsF_6$ were prepared from the elements and an excess of bromine and arsenic pentafluoride, as well as from $Se_4(AsF_6)_2$ and $Te_4(AsF_6)_2$ with excess bromine. $SeBr_3SbF_6$ was prepared from $Se_4(SbF_6)_2$ and bromine, and $TeBr_3AsF_6$ from tellurium tetrabromide and arsenic pentafluoride. Br_3AsF_6 was found to oxidize arsenic trifluoride and sulphur dioxide to arsenic pentafluoride and SO_2BrF respectively. Reaction pathways to the tribromochalcogen cations are discussed. Raman spectra of the tribromochalcogen salts were obtained. Assignments were confirmed, and force constants derived from normal coordinate analyses and compared with those derived for SBr_3^+, PBr_3, $AsBr_3$, and $SbBr_3$.

W. V. F. BROOKS, JACK PASSMORE et E. KEITH RICHARDSON. Can. J. Chem. **57**, 3230 (1979).

On a préparé l'hexafluoroarsenate de tribromosélénium et l'hexafluoroarsenate de tribromotellure à partir de leurs éléments et d'un excès de brome, ainsi qu'à partir du $Se_4(AsF_6)_2$ et du $Te_4(AsF_6)_2$ et d'un excès de brome. Le $SeBr_3S_6F_6$ est préparé à partir du $Se_4(SbF_6)_2$ et du brome, et le $TeBr_3AsF_6$ est obtenu à partir du tétrabromure de tellure et du pentafluorure d'arsenic. On a trouvé que le Br_3AsF_6 oxyde le trifluorure d'arsenic et le bioxyde de soufre respectivement en pentafluorure d'arsenic et en SO_2BrF. On discute des schémas de réaction des cations tribromochalcogènes. On a obtenu les spectres Raman des sels de tribromochalcogènes. Les attributions sont confirmées et les constantes de forces dérivées des analyses normales de coordonnées sont comparées à celles obtenus pour SBr_3^+, PBr_3, $AsBr_3$ et $SbBr_3$.
[Traduit par le journal]

Salts of MF_3^+ and MCl_3^+ (M = S, Se, and Te) (1–6) have been prepared and characterized. These species are of interest as simple chalcogen halogen cations, and as species that may be given on autoionisation of the neutral chalcogen tetrahalides. Trihalochalcogen cations have been prepared as salts of very weakly basic anions, where the tetrahalochalcogen has not been reported, e.g. SBr_3AsF_6 and SeI_3AsF_6 are stable whereas SBr_4 and SeI_4 are as yet unknown (7, 8). The 1:1 adduct $TeBr_4 \cdot AlBr_3$ has been prepared (9, 10) and assigned an ionic formulation on the basis of nqr spectra (11). On completion of this work the preparation of $SeBr_3AlCl_4$ and $SeBr_3AlBr_4$ were reported, and ionic formulations assigned on the basis of Raman spectra (12).

The preparations and Raman spectra of $SeBr_3AsF_6$, $SeBr_3SbF_6$, and $TeBr_3AsF_6$, briefly referred to in an earlier publication (7), are reported below.

Experimental

Except where stated, apparatus, reagents, and techniques are the same as those described (7, 8, 13). Elemental analyses were by Alfred Bernhardt, West Germany.

Literature methods (14) were used to prepare $Te_4(AsF_6)_2$ and $Se_4(AsF_6)_2$. Tellurium tetrabromide was prepared from the elements, and Br_3AsF_6 and Br_3SbF_6 by the method of Glemser and Smalc (15) via the corresponding O_2^+ salt. The preparation of $Se_4(SbF_6)_2$ was a modification of that used to prepare $Se_4(Sb_2F_{11})_2$ (16). Selenium (Se_8 3.28 mmol) and SbF_5 (27.3 mmol) were refluxed at 110°C for 2 days in SO_2 (6.3 g). Removal of the volatiles left 8.007 g of a pale yellow solid consisting of what was presumed to be $Se_4(SbF_6)_2$ and a reduced antimony fluoride, however, it probably contained $Se_4^{2+}(Sb_2F_{11})_2^-$ as well. This mixture was used in subsequent reactions.

Preparation of $SeBr_3AsF_6$

Reactions involving selenium, or tellurium, bromine, and arsenic pentafluoride went to completion within a few minutes of reaching room temperature. The chalcogen and bromine were allowed to react in the solvent before the addition of arsenic pentafluoride. The soluble product was filtered through the sintered glass frit, followed by condensing the solvent (AsF_3 or SO_2) back onto the solid and refiltering in the closed system. This process was repeated until the soluble product was extracted, unless otherwise specified.

In a typical reaction Se (2.216 mmol) and Br_2 (4.06 mmol) were reacted with AsF_5 (4.00 mmol) in SO_2 (8.26 g) solution. A copious yellow precipitate formed that had some solubility in SO_2. Following filtration traces of insoluble unreacted selenium and a pale yellow soluble crystalline solid (1.1097 g or 2.16 mmol assuming $SeBr_3AsF_6$) were obtained on removal of the volatiles SO_2, AsF_3, unreacted AsF_5 and Br_2. *Anal.* calcd. for $SeBr_3AsF_6$: Se 15.55, Br 47.22, As 14.76, F 22.45; found: Se 15.28, Br 47.10, As 14.33, F 22.58.

$Se_4(AsF_6)_2$ (1.58 mmol) was reacted with Br_2 (12.33 mmol) in SO_2 (10 g), yielding 3.11 mmol of the soluble highly crystalline $SeBr_3AsF_6$ and 2.93 mmol of $SeBr_4$, the identity of which was inferred from its physical properties (17, 18). $Se_4(AsF_6)_2$ (1.96 mmol) and Br_2 (24.34 mmol) were reacted

0008-4042/79/243230-07$01.00/0

TABLE 1. Various preparations

Reactants	Quantity of SO_2	Products
1, $Se_4(AsF_6)_2$ (0.79 mmol) Cl_2 (3.81 mmol)	11.7 g	$SeCl_3AsF_6$ (1.49 mmol)[a] $SeCl_4$
2, $Te_4(AsF_6)_2$ (0.79 mmol) Br_2 (6.69 mmol)	5 g	$TeBr_3AsF_6$ (1.46 mmol) $TeBr_4$[b] (1.87 mmol)
3, $Te_4(AsF_6)_2$ (2.33 mmol) Br_2 (15.26 mmol) AsF_5[c] (9.58 mmol)	10 g	$TeBr_3AsF_6$ (7.48 mmol)
4, $TeBr_4$ (3.82 mmol) AsF_5 (7.65 mmol)	11.3 g	$TeBr_3AsF_6$[d] (3.62 mmol) Br_2, AsF_3

[a]Solution (SO_2) and solid Raman spectra identified the soluble solid as $SeCl_3AsF_6$ (5) and the insoluble solid as $SeCl_4$ (12, 19). Each component showed small impurity peaks due to the other since $SeCl_4$ is slightly soluble in SO_2.
[b]Contained some $TeBr_3AsF_6$.
[c]AsF_5 added last.
[d]SO_2BrF (20) was not observed in any of the infrared spectra taken of the volatiles reaction products.

in SO_2 (8 g) followed by addition of AsF_5 (6.58 mmol) to give $SeBr_3AsF_6$ (7.05 mmol).

Preparation of $SeBr_3SbF_6$

In a typical reaction $Se_4(SbF_6)_2$ (0.527 g mixture, calculated ca. 0.47 mmol $Se_4(SbF_6)_2$) was reacted with Br_2 (2.00 mmol) in SO_2 (5.5 g) solution. Filtration and slow evacuation of the volatiles gave 0.595 g (1.07 mmol assuming $SeBr_3SbF_6$) of soluble pale yellow crystals (single) and 0.252 g of insoluble yellow solid, containing a reduced antimony fluoride and some $SeBr_4$.

Preparation of Another Bromoselenium Cation

Se (14.16 mmol) and Br_2 (17.83 mmol) were reacted with AsF_5 (17.65 mmol) in SO_2 (5.75 g) and gave 5.70 g (7.64 mmol assuming $Se_2Br_5AsF_6$) deep purple crystals (soluble in SO_2). In another experiment Se (36.34 mmol), Br_2 (38.42 mmol), and AsF_5 (20.65 mmol) yielded 10.08 g (13.50 mmol assuming $Se_2Br_5AsF_6$) purple crystals and 1.262 g grey–purple insoluble solid (which probably contains elemental selenium and $SeBr_4$).

The same purple crystals were also prepared by pouring Br_2 (5.25 mmol) in SO_2 (8.34 g) onto $Se_4(AsF_6)_2$ (1.23 mmol). Filtration followed by evacuation of the volatiles (SO_2 and Br_2) left 1.68 g (2.25 mmol assuming $Se_2Br_5AsF_6$) solid.

X-ray powder photographs of this material, from a variety of different preparations, were the same and did not contain lines attributable to $SeBr_3AsF_6$. X-ray photographs of a single crystal obtained at -5°C and also showed the material was different from $SeBr_3AsF_6$. *Anal.* calcd. for $Se_2Br_5AsF_6$: Se 21.16, Br 53.53, As 10.03, F 15.27; found: Se 21.06, Br 53.42, As 9.87, F 15.00. An independent determination of selenium and arsenic by atomic absorption methods supported this formulation. Crystals decomposed slowly at room temperature, in the X-ray beam, and under irradiation in the laser beam.

Preparation of $TeBr_3AsF_6$

In a typical reaction, tellurium (9.01 mmol) and Br_2 (20.6 mmol) were reacted with AsF_5 (15.5 mmol) in SO_2 (7 g) solution. Filtration and two washings, followed by evacuation of the volatiles yielded 4.29 g (7.71 mmol assuming $TeBr_3AsF_6$) of a soluble, beige, highly crystalline solid containing single crystals, and 0.68 g of a less soluble beige solid containing $TeBr_3AsF_6$ and $TeBr_4$ (19). *Anal.* calcd. for $TeBr_3AsF_6$: Te 22.94, Br 43.09, As 13.47, F 20.49; found: Te 23.10, Br 42.81, As 13.07, F 20.68. Other reactions leading to $TeBr_3AsF_6$ are given in Table 1.

Stability of $SeBr_3AsF_6$, $SeBr_3AsF_6$, and $TeBr_3AsF_6$

Yellow crystalline $SeBr_3AsF_6$ (mp 144–152°C) and white crystalline $TeBr_3AsF_6$ (mp 175–185°C) were stored under dry nitrogen in sealed Pyrex glass vessels at 0°C for a year without detectable signs of decomposition. Yellow crystalline $SeBr_3SbF_6$ (decomposes at 100°C) showed purple discolouration after 4 months.

Reaction of Br_3AsF_6 with AsF_3

Solid Br_3AsF_6 (1.19 mmol) was reacted with AsF_3 (22.62 mmol), yielding two immiscible liquids. Volatiles (0.3164 g or 1.81 mmol assuming AsF_5) were distilled from the vessel held at -78°C, and identified by its infrared spectrum as AsF_5. The remainder (3.1832 g) contained AsF_3 and bromine. Involatile material was not observed.

Reaction of Br_3AsF_6 with SO_2

Sulphur dioxide (5.15 mmol) was condensed into Br_3AsF_6 (2.09 mmol), giving AsF_5, Br_2, SO_2, and SO_2BrF. The intensities of the SO_2 and SO_2BrF bands in the infrared were about the same indicating comparable quantities of both were present. Involatile material was not observed. SO_2BrF was also a product of the reaction of Br_3SbF_6 and SO_2.

Reactions of KBr with AsF_5 in SO_2

KBr (5.49 mmol) and AsF_5 (13.94 mmol) were reacted in SO_2 (4.6 g). The products consisted of SO_2, traces of SO_2BrF and AsF_5 (combined weight 5.35 g) volatile at -78°C; Br_2 and AsF_3 (combined weight 0.75 g) volatile at room temperature; as well as 1.524 g of solid, the Raman spectrum and powder diffraction photograph of which were identical to that of $KAsF_6$ (21). In addition to the bands attributable to AsF_3 and Br_2, the Raman spectrum of the material volatile at room temperature showed peaks at 436 cm^{-1}, 872 cm^{-1}, and 1309 cm^{-1} using the 5145 Å (green) exciting wavelength. The intensity decreased and the peak broadened in the order 436 > 872 > 1309 cm^{-1}.

Results and Discussion

Preparation of Tribromoselenium(IV) and Tribromotellurium(IV) Hexafluoroarsenate(V)

$SeBr_3AsF_6$ and $TeBr_3AsF_6$ were prepared es-

sentially quantitatively from the respective element, bromine, and a slight excess of arsenic pentafluoride in arsenic trifluoride or sulphur dioxide solution according to reaction [1].

[1] $2M + 3Br_2 + 3AsF_5 \rightarrow 2MBr_3AsF_6 + AsF_3$

(M = Se or Te)

The tellurium salt was also prepared quantitatively from tellurium tetrabromide and arsenic pentafluoride according to reaction [2].

[2] $2TeBr_4 + 3AsF_5 \rightarrow 2TeBr_3AsF_6 + AsF_3 + Br_2$

The polyatomic cations Se_4^{2+} and Te_4^{2+} have been well characterized; however, their chemistry has not been intensively studied (14*b*, 23, 24). These cations with excess bromine readily formed the corresponding tribromochalcogen(IV) salt and chalcogen tetrabromide according to reaction [3].

[3] $M_4^{2+}(AsF_6)_2^- + 7Br_2 \rightarrow 2MBr_3AsF_6 + 2MBr_4$

(M = Se or Te)

The addition of arsenic pentafluoride to the products led to complete conversion of selenium and tellurium to the corresponding tribromochalcogen(IV) salt. $SeBr_3SbF_6$ was prepared from $Se_4(SbF_6)_2$ and bromine. Excess chlorine reacts with $Se_4(AsF_6)_2$ to give $SeCl_3AsF_6$ and $SeCl_4$.

A different selenium bromine cation was prepared by the reaction of $Se_4(AsF_6)_2$ and Br_2 in a molar ratio of 1:5, and in the reaction of selenium, bromine, and arsenic pentafluoride in the ratio $Se:Br_2:AsF_5$ of 4:5:3. Preparative and analytical evidence points to $Se_2Br_5AsF_6$ as the formulation of the salt.

Reaction Pathways to MBr_3^+ (M = S, Se, and Te), Salts

A bromine polyatomic cation cannot be an intermediate in reactions leading to MBr_3^+ (M = S, Se, and Te) salts as Br_3AsF_6 reacts rapidly with both AsF_3 and SO_2 according to reactions [4] and [5], and SO_2BrF was not detected in reactions using sulphur dioxide solvent.

[4] $2Br_3AsF_6 + AsF_3 \rightarrow 3AsF_5 + 3Br_2$

[5] $Br_3AsF_6 + SO_2 \rightarrow AsF_5 + Br_2 + SO_2BrF$

Chalcogen polyatomic cations, however, may be intermediates, and both Se_4^{2+} and Te_4^{2+} react with bromine to yield chalcogen tribromide cations, probably via species related to $Se_2Br_5^+$ and/or $S_2Br_3^+$ (25, 26). A number of bromochalcogen cation species may be relatively stable and include species related to $(S_7I)^+$ (27, 28). Bromine and chalcogen lead to chalcogen bromide. Tellurium tetrabromide and arsenic pentafluoride may react according to reaction [6], however, $TeBr_3AsBrF_5$ itself is not detected as a product but $TeBr_3AsF_6$ and Br_2 (reaction [2]). Potassium chloride and SbF_5 give related products (29, 30).

[6] $TeBr_4 + AsF_5 \rightarrow TeBr_3AsBrF_5$

The resonance Raman spectrum observed in SO_2 and AsF_3 solutions of SBr_3AsF_6 (7) is also observed in a Raman spectra of the volatile products of KBr and AsF_5 in SO_2. The species responsible for this resonance Raman spectrum is therefore not a sulphur–bromine species, and not an intermediate, in the formation of SBr_3^+ salts.

Raman Spectra

Raman spectra of $SeBr_3AsF_6$ and $TeBr_3AsF_6$ in the solid state and in SO_2 or AsF_3 solution are given in Fig. 1. Table 2 lists the frequencies and assignments by comparison with the corresponding anions (21), $AsBr_3$ (22), and $SbBr_3$ (31, 32). The assignments

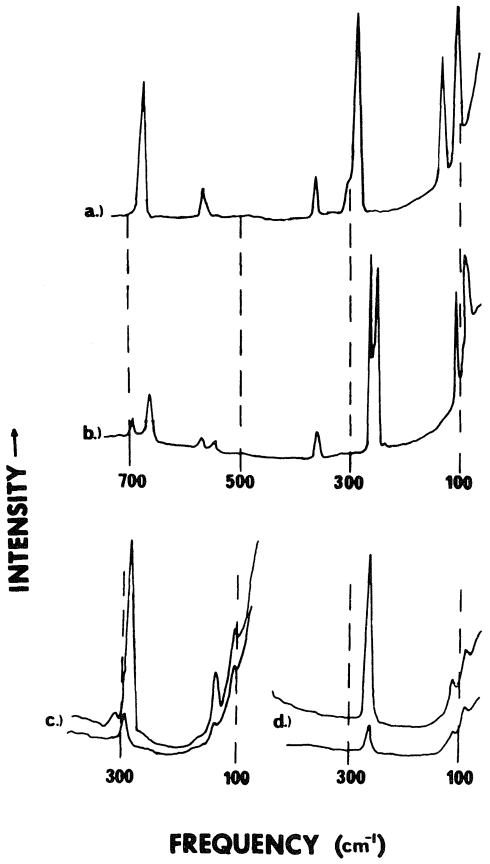

FIG. 1. Raman spectra of $SeBr_3^+$ and $TeBr_3^+$ cations. (*a*) Solid $SeBr_3AsF_6$; (*b*) solid $TeBr_3AsF_6$; (*c*) $SeBr_3AsF_6$ in SO_2 solution; (*d*) $TeBr_3AsF_6$ in SO_2 solution. For (*c*) and (*d*) the upper spectra are with parallel polarization and the lower with perpendicular polarization. Slit width = 4 cm^{-1} using 5145 Å line in all cases.

TABLE 2. Assignments of the Raman spectra[a] of $SeBr_3AsF_6$, $SeBr_3SbF_6$, and $TeBr_3AsF_6$

Raman spectra												
$SeBr_3AsF_6$		$SeBr_3SbF_6$		$TeBr_3AsF_6$		$AsBr_3$[b]		$SbBr_3$				
Solid	SO_2 soln	Solid	SO_2 soln	Solid	SO_2 soln	Cryst.	Melt	Solid[c]	CCl_4[d]	$CsAsF_6$[e]	$LiSbF_6$[e]	Assignment[f]
		693?		699						699	669	$\nu_3(MF_6)^-$[g]
677	676p	645		668	674p					685	668	$\nu_1(MF_6)^-$
570, 560				575, 552						576	558	$\nu_2(MF_6)^-$
366		277		365						372	294	$\nu_5(MF_6)$
303, 298	303[i], 298dp	310, 300	301dp	267, 261(sh)	266dp	285, 262	287dp	234, 229, 223	245dp			ν_3[h]$(MBr_3)^+$
292	291p	292	289p	256	265p	272	272p	246, 243	254p			$\nu_1(MBr_3)^+$
136	138p	138	136p	110	112p	133	128p	113	101p			$\nu_2(MBr_3)^+$
109	108dp	110.5	108dp	96	92dp	106, 96	99dp	98, 92, 89	81dp			$\nu_4(MBr_3)^+$

[a]Frequencies (in cm^{-1}) accurate to ca. ± 3 cm^{-1}. Solvent peaks have been omitted.
[b]See ref. 22.
[c]See ref. 31.
[d]See ref. 32.
[e]See ref. 21.
[f]Tentative assignment assuming O_h symmetry for AsF_6^- and SbF_6^- and C_{3v} symmetry for $SeBr_3^+$ and $TeBr_3^+$.
[g]Infrared active only for O_h symmetry.
[h]Corresponds to $\nu_3(AsBr_3)$, $\nu_3(SbBr_3)$, $\nu_3(SeBr_3)^+$, or $\nu_3(TeBr_3)^+$ in appropriate column.
[i]Impurity?

TABLE 3. Structural parameters for group V tribromides and group VI tribromide cations

Compound	r_e (nm)	α_e (deg)	Cation	r_e (nm)	α_e (deg)
PBr_3[a]	0.2220	101.0	SBr_3^+[d]	0.215	101
$AsBr_3$[b]	0.2324	99.6	$SeBr_3^+(C_{3v})$[e]	0.2263	100.9
$SbBr_3$[c]	0.2490	98.2	$SeBr_3^+(C_{2v})$[f]	(0.227, 0.227, 0.225)	(103, 99.5, 99.5)
			$TeBr_3^+(C_{3v})$[e]	0.243	97.9

[a]Reference 38.
[b]Reference 39.
[c]Reference 40.
[d]Estimated.
[e]Average of observed parameters from ref. 35.
[f]Angles and bond distances approximately those found from ref. 35.

TABLE 4. Force constants (Newton m^{-1}) of group V tribromides and group VI tribromide cations

Force constant	Value						
	PBr_3	SBr_3^+	$AsBr_3$	$SeBr_3^+(C_{3v})$	$SeBr_3^+(C_{2v})$	$SbBr_3$	$TeBr_3^+$
F_r	170.8(2)	201.1(2)	164.2(2)	168.1(1)	166.4(1)	151.9(1)	186.2(2)
F_α	25.9(1)	27.7(1)	19.4(1)	25.6(2)	26.1(2)	15.3(2)	18.1(2)
$F_{\alpha\alpha'}$	5.4(1)	4.9(1)	2.7(1)	5.6(2)	5.3(2)	2.3(1)	2.1(1)
$F_{r\alpha}$	2.4(1)	6.2(2)	−0.6(2)	−6.0(2)	−6.3(1)	−7.7(2)	5.9(3)

and frequencies of $SeBr_3^+$ are essentially in agreement with those recently reported (12) for $SeBr_3 \cdot AlCl_4$ and $SeBr_3AlBr_4$.

The spectra support an essentially ionic formulation for the salts. The peaks attributed to $SeBr_3^+$ are similar in solution and in the solid state, with the exception of $\nu_3(SeBr_3)^+$ which is split in the solid state. The four Raman active bands (two polarized and two depolarized) expected for $(SeBr_3)^+$ are observed and, as expected (7, 33, 34), are at higher frequencies than the corresponding bands for the isoelectronic molecule $AsBr_3$.

The Raman spectra of solid $TeBr_3AsF_6$ and the solution are similar in the bending region but differ in the TeBr stretching region. Peaks in the stretching region are similar to those in the Raman spectrum of $SbBr_3$ (solid) (32), $TeCl_3AsF_6$, $SeCl_4$, $TeCl_4$, and $TeBr_4$ (19). The symmetry of $SeBr_3^+$ in $SeBr_3AsF_6$, and $SeBr_3SbF_6$ and $TeBr_3^+$ in $TeBr_3AsF_6$ is C_1 (35). Therefore, the origin of the complexity of the solid state spectra is most likely due to the low symmetry of the tribromochalcogen ion in the solid state, as has been proposed for $AsBr_3$ (22) and $SbBr_3$ (31). In solution the complex peaks collapse into one broad partially polarized band. The broad peak in the stretching region shifts slightly to higher wavenumbers under perpendicular polarization suggesting that $\nu_3(TeBr_3)^+$ is at slightly higher wavenumbers. The four Raman bands expected for $TeBr_3^+$ are at higher frequencies than their $SbBr_3$ counterparts.

$TeBr_4$ is isomorphous with $TeCl_4$ (36); the structure is a tetramer with $TeCl_3^+$ and Cl^- ions at the apexes of a distorted cube, and therefore can be regarded as $(TeCl_4)_4$ or $[(TeCl_3)^+Cl^-]_4$ with strong anion–cation interaction (37). The Raman spectrum of $TeBr_3^+$ in the solid state in the tellurium bromine stretching region is similar to that of $TeBr_4$ (250(s), 226(s), 220(s)) (19), but at somewhat higher wavenumbers. It is therefore reasonable to suppose that $TeBr_4$ is $[(TeBr_3)^+Br^-]_4$ with stronger anion–cation interaction than that in $TeBr_3AsF_6$. Similar conclusions were reached from an nqr study (11) and by earlier workers on the basis of vibrational spectra of $TeBr_4$ (9, 19). A comparison of Raman data for $SeBr_3^+$ in $SeBr_3AsF_6$ and $SeBr_3SbF_6$ with infrared data for $SeBr_4$ (9, 19) allows a weaker but similar conclusion to be made concerning $SeBr_4$.

Normal Coordinate Analysis

In order to compare force constants of isoelectronic group V tribromides with the tribromochalcogen cations and to check their assignments, we did a normal coordinate analysis and force constant determination on the six species: SBr_3^+, $SeBr_3^+$, $TeBr_3^+$, PBr_3, $AsBr_3$, and $SbBr_3$. Frequencies (Table 2 and ref. 7) were taken from liquid phase or solution (SO_2 for $SeBr_3AsF_6$ and $TeBr_3AsF_6$ and AsF_3 for SBr_3AsF_6) Raman spectra. The symmetry of all tribromo species was assumed to be C_{3v} and parameters are given in Table 3. The Wilson **F** and **G** matrix method (41) was used with a harmonic valency force field including off diagonal

terms. The frequencies were calculated for all the principal isotopic species so that means of isotopic frequencies were compared to observed frequencies. The calculated isotopic splittings are all too small to be observed in solution spectra. The force constants were determined by a least-squares fitting procedure (42).

A pyramidal XY_3 molecule with C_{3v} symmetry has six independent harmonic force constants; these are the diagonal stretching, the diagonal bending, and the four off diagonal interactions (stretch–stretch′, bend–bend′, adjacent stretch–bend, and opposite stretch–bend). Most vibrational analyses of pyramidal trihalides have followed Howard and Wilson (43) in setting the two stretch–bend interaction terms to zero. We found this choice unsatisfactory for the PBr_3 and SBr_3^+ cases; there are strong correlations and the maximum observed minus calculated frequency differences were more than 10 cm^{-1}. We found that setting the stretch–stretch and opposite stretch–bend interaction constants to zero and adjusting the remaining four constants gave good results in all cases (calculated and observed frequencies differing by less than 1 cm^{-1}). The derived force constants are listed in Table 4. As expected the force constants for the tribromochalcogen cations are higher than that of the corresponding group V tribromides. To study the effects of the lowered symmetry in the crystalline state, we repeated the calculations with a C_{2v} geometry of $SeBr_3^+$. Keeping the three stretching constants and the three bending constants equal, the geometric change from C_{3v} to lower symmetry introduced an effect comparable to the isotopic shifts; thus the C_{3v} model should be a reasonable approximation for the solid phase. However, the geometric change must be accompanied by a significant change in force constants, which most likely accounts for the complications in the solid state spectra.

Exact comparisons with the force fields reported elsewhere for these and similar molecules are not possible because of the different assumptions mentioned above. However, the diagonal constants show the trends observed in comparable treatments. Thus, the group V trichlorides (5, 44) and bromides show a decrease in both constants, from PX_3 to SbX_3; however, the stretching force constants for SeX_3^+ (5) are smaller than those for SX_3^+ and TeX_3^+ (X = Cl, Br) while the bending constants for SX_3^+, SeX_3^+, and TeX_3^+ show a steady decrease. The reason for the low stretching constant for SeX_3^+ is not altogether clear.

Acknowledgement

We are grateful to the Natural Sciences and Engineering Council of Canada for financial support and for a scholarship (E.K.R.).

1. A. J. Edwards and P. Taylor. J. Chem. Soc. Dalton, 2150 (1973) and references therein.
2. B. Krebs, B. Buss, and D. Altena. Z. Anorg. Allg. Chem. **386**, 257 (1971).
3. B. A. Stork-Blaisse and C. Romers. Acta Crystallogr. B**27**, 386 (1971).
4. A. J. Edwards. J. Chem. Soc. Dalton. In press.
5. W. Sawodny and K. Dehnicke. Z. Anorg. Allg. Chem. **349**, 169 (1967).
6. V. Gutmann and H. J. Emeléus (*Editors*). Inorganic chemistry series two. Butterworths University Park Press, London. 1975. p. 85 and 137 and references therein.
7. J. Passmore, E. K. Richardson, and P. Taylor. Inorg. Chem. **17**, 1681 (1978).
8. J. Passmore and P. Taylor. J. Chem. Soc. Dalton, 804 (1976).
9. Gmelin Handbuch der Anorganischen Chemie. 8th ed. Tellurium Supplement, B3. Springer-Verlag, Berlin. 1978 and references therein.
10. E. Montignie. Z. Anorg. Allg. Chem. **315**, 102 (1962).
11. T. Okuda, K. Yamada, Y. Furukawa, and H. Negita. Bull. Soc. Jpn. **48**, 392 (1975).
12. A. Finch, P. N. Gates, and D. R. Netherton. Inorg. Chim. Acta, **32**, L91 (1979).
13. C. Lau and J. Passmore. J. Chem. Soc. Dalton, 2528 (1973).
14. (*a*) J. Barr, R. J. Gillespie, G. P. Pez, P. K. Ummat, and O. C. Vaidya. Inorg. Chem. **10**, 362 (1971); (*b*) R. J. Gillespie and J. Passmore. Advances in inorganic chemistry and radiochemistry. Vol. 17. *Edited by* H. J. Emeléus and A. G. Sharpe. Academic Press, New York, NY. 1975. p. 49 and references therein.
15. O. Glemser and A. Smalc. Angew. Chem. Int. Ed. Engl. **8**, 517 (1969).
16. J. Barr, D. B. Crump, R. J. Gillespie, R. Kapoor, and P. K. Ummat. Can. J. Chem. **46**, 3607 (1968).
17. D. M. Yost and J. B. Hatcher. J. Am. Chem. Soc. **53**, 2549 (1931).
18. N. W. Tideswell and J. D. McCullough. J. Am. Chem. Soc. **78**, 3026 (1956).
19. (*a*) G. C. Hayward and P. J. Hendra. J. Chem. Soc. A, 643 (1967); (*b*) J. W. George, N. Katsaros, and K. J. Wynne. Inorg. Chem. **6**, 903 (1967).
20. P. R. Reed, Jr. and R. W. Lovejoy. Spectrochim. Acta, **24A**, 1795 (1968).
21. G. M. Begun and A. C. Rutenberg. Inorg. Chem. **6**, 2212 (1967).
22. J. E. D. Davies and D. A. Long. J. Chem. Soc. A, 1273 (1971) and references therein.
23. C. D. Desjardins and J. Passmore. Can. J. Chem. **55**, 3136 (1977).
24. J. Passmore. Homatomic rings, chains and macromolecules of main-group elements. *Edited by* A. L. Rheingold. Elsevier Scientific, New York. 1977. p. 539 and references therein.
25. A. Bali and K. C. Malhotra. Aust. J. Chem. **28**, 983 (1975).
26. R. C. Paul, R. D. Sharma, R. K. Verma, and K. C. Malhotra. Indian J. Chem. **10**, 737 (1972).
27. J. Passmore, P. Taylor, T. K. Whidden, and P. White. J. Chem. Soc. Chem. Commun. 689 (1976).
28. G. Sutherland and J. Passmore. Unpublished results.

29. L. KOLDITZ and W. REHAK. Z. Anorg. Allg. Chem. **341**, 100 (1965).
30. L. KOLDITZ. Halogen chemistry. Vol. 2. *Edited by* V. Gutmann. Academic Press, New York, NY. 1967. pp. 121, 132, 133.
31. E. CHEMOUNI. J. Inorg. Nucl. Chem. **33**, 2317 (1971).
32. J. C. EVANS. J. Mol. Spectrosc. **4**, 435 (1960).
33. D. D. GIBLER, C. J. ADAMS, M. FISCHER, A. ZALKIN, and N. BARTLETT. Inorg. Chem. **11**, 2325 (1972).
34. C. LAU, H. LYNTON, J. PASSMORE, and P. Y. SIEW. J. Chem. Soc. Dalton, 2535 (1973).
35. J. PASSMORE, E. K. RICHARDSON, T. K. WHIDDEN, and P. WHITE. Can. J. Chem. In press.
36. K. W. BAGNALL. *In* Comprehensive inorganic chemistry. Vol. 2. *Edited by* J. C. Bailar *et al*. Pergamon Press, New York. 1973. p. 935 and references therein.
37. B. BUSS and B. KREBS. Inorg. Chem. **10**, 2795 (1971).
38. K. KUCHITSU, T. SHIBATA, A. YOKOZEKI, and C. MATSUMURA. Inorg. Chem. **10**, 2584 (1971).
39. S. SAMDAL, D. M. BARNHART, and K. H. HEDBERG. J. Mol. Struct. **35**, 67 (1976).
40. S. KONAKA and M. KIMURA. Bull. Chem. Soc. Jpn. **46**, 413 (1973).
41. E. B. WILSON, JR., J. C. DECIUS, and P. C. CROSS. Molecular vibrations. McGraw-Hill, New York. 1955.
42. J. H. SCHACHTSCHNEIDER and R. H. SNYDER. Spectrochim. Acta, **19**, 117 (1963).
43. J. B. HOWARD and E. B. WILSON, JR. J. Chem. Phys. **2**, 630 (1934).
44. P. W. DAVIS and R. A. OETJEN. J. Mol. Spectrosc. **2**, 253 (1958).

Metal derivatives of azoles. Part V. Platinum(II) and palladium(II) pyrazolates as a new type of neutral bidentate ligands

ANNA LAURA BANDINI, GUIDO BANDITELLI, AND GIOVANNI MINGHETTI

CNR Center, Istituto di Chimica Generale dell'Università, Via Venezian 21, 20133 Milano, Italy

AND

FLAVIO BONATI

Istituto Chimico dell'Università, Camerino, 62032, Italy

Received June 4, 1979

ANNA LAURA BANDINI, GUIDO BANDITELLI, GIOVANNI MINGHETTI, and FLAVIO BONATI. Can. J. Chem. **57**, 3237 (1979).

The complexes (L—L)M(pz)$_2$ {(L—L) = $(Ph_2PCH_2)_2$, M = Pt, Pd; (L—L) = 2,2′-dipyridine, M = Pt} and (L—L)M(pz′)$_2$ {(L—L = $(Ph_2PCH_2)_2$, M = Pt; (L—L) = 2,2′-dipyridine, M = Pt, Pd} where pzH = pyrazole and pz′H = 3,5-dimethylpyrazole, behave as ligands towards suitable acceptors affording 1:1 or 1:2 adducts.

The 1:1 adducts are obtained by reaction with group IIB metal halides, cobalt(II) chloride, copper(II), or zinc(II) sulphate and are likely to be binuclear complexes, (ligand)MX_2, with two pyrazolato anions bridging the different metals.

The nature of the 1:2 adducts [(ligand)$_2$M′][BF_4]$_2$ (M′ = Zn, Ni, Co) as well as of the adduct (dipy)Pt(pz)$_2$·2Rh(CO)$_2$Cl, are discussed.

ANNA LAURA BANDINI, GUIDO BANDITELLI, GIOVANNI MINGHETTI et FLAVIO BONATI. Can. J. Chem. **57**, 3237 (1979).

Les composés (L—L)M(pz)$_2$ {(L—L) = $(Ph_2PCH_2)_2$, M = Pt, Pd; (L—L) = 2,2′-dipyridine, M = Pt} et (L—L)M(pz′)$_2$ {(L—L) = $(Ph_2PCH_2)_2$, M = Pt; (L—L) = 2,2′-dipyridine, M = Pt, Pd} où pzH = pyrazole et pz′H = 3,5-diméthylpyrazole, peuvent complexer sur des accepteurs convenables en conduisant à des composés d'addition 1:1 ou 1:2.

Les complexes 1:1 sont obtenus pour réaction avec des alogenures des metaux du deuxième groupe B, avec cobalt dichlorure et avec les sulfates de cuivre(II) ou de zinc(II). Ils peuvent être, raisonnablement, regardés comme des complexes binucléaires où les deux anions pyrazolate se conduisent comme des ligands pontés entre les differents metaux.

On discute de la nature des composés d'addition 1:2 [(ligand)$_2$M′][BF_4]$_2$ (M′ = Zn, Ni, Co) aussi que du complex (dipy)Pt(pz)$_2$·2Rh(CO)$_2$Cl.

Introduction

In a preceding paper of ours (1) a series of palladium(II) and platinum(II) azolates, (L—L)M(az)$_2$, were described, where L—L is a chelating ligand and azH is a 1-unsubstituted azole. In any of these square planar complexes, the azolato anions are coordinated to the metal through one of the nitrogen atoms; the uncoordinated nitrogens, which are basic and can be protonated, are still available as donor sites, so that the complexes can be thought of as potentially bidentate ligands.

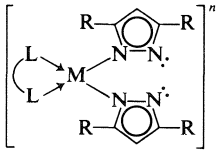

	A	B	C	D	E	F	G	H
M	Pt	Pt	Pt	Pt	Pd	Pd	B	Ga
R	Me	H	Me	H	Me	H	H	H
L—L	dpe	dpe	bipy	bipy	bipy	dpe	2H	2Me
n	0	0	0	0	0	0	−1	−1

The behaviour of these molecules as ligands towards selected acceptors is described in this paper. The chelating ligand, L—L, is either 1,2-bis(diphenylphosphine)ethane or the less flexible 2,2′-dipyridyl; the azole is either pyrazole, (pzH), or the more sterically demanding 3,5-dimethylpyrazole (pz′H); the metal is palladium(II) or platinum(II), so that the resulting molecules do not bear any formal charge and, especially in the case of platinum, are kinetically inert. These last points had been already exploited by us (2) in another type of platinum(II) containing bidentate ligands, i.e. (L)(L′)Pt–C(OR)=NR′]$_2$, while the lack of charge constitutes one notable difference between the species A—F and the anionic dihydrobis(1-pyrazolyl)borate(III), G (3), dimethylbis(1-pyrazolyl)gallate(III), H (5), and its (2-*N*,*N*-dimethylamino)ethoxy analogue (6).

Discussion

By reaction of the ligands A—F with Lewis acids, stable 1:1 or 2:1 adducts were obtained (see Table 1). The 2:1 adducts formed when an aquo-cation was employed and the anion was a very weak nucleophile

0008-4042/79/243237-06$01.00/0

TABLE 1. Analytical and other data

Compound[a]	Melting point	Analyses C Found	C Calcd.	H Found	H Calcd.	N Found	N Calcd.	Other data
I, A·$ZnSO_4$	ca. 300 d	46.11	45.76	4.43	4.02	5.84	5.93	[b]
II, A·$CuSO_4$	286–290 d	45.85	45.85	4.13	4.03	5.78	5.93	[b,c]
III, A·$ZnCl_2$	195–200	46.56	47.01	3.86	4.15	6.01	6.09	[b,d]
IV, A·$CdBr_2$	315–318	41.09	40.95	3.39	3.60	5.51	5.31	[b,e,g]
V, A·CdI_2	295–300 d	38.14	37.60	3.36	3.31	4.83	4.87	[b,f]
VI, A·$HgCl_2$	243–254	41.72	40.98	3.67	3.61	5.32	5.31	Insol.[g]
VII, A·$HgBr_2$	260–265	37.56	37.80	3.23	3.32	5.02	4.90	Insol.[g]
VIII, $[A_2Zn][BF_4]_2$	300–305	47.00	47.88	4.29	4.21	5.94	6.20	[h]
IX, B·$CdCl_2$	237–241	42.00	42.18	3.37	3.29	5.64	6.15	
X, B·$HgCl_2$	198–201 d	38.91	38.46	3.20	3.00	5.56	5.61	[b]
XI, $[B_2Ni][BF_4]_2$	>270	45.48	45.56	3.57	3.56	6.60	6.64	[j]
XII, C·CdI_2	>300	26.30	26.46	2.38	2.42	10.17	9.26	[b]
XIII, C·CdI_2·CH_2Cl_2	>300	24.75	25.41	2.30	2.41	8.41	8.46	[b]
XIV, C·$CoCl_2$	295–300 d	35.56	35.79	3.24	3.28	12.20	12.51	[b]
XV, C·$CoCl_2$·CH_2Cl_2		33.20	33.36	3.12	3.17	11.11	11.11	
XVI, C·$PdCl_2$	>280	32.80	33.42	2.87	3.06	11.28	11.69	Insol.
XVII, $[C_2Ni][BF_4]_2$·H_2O	>300	36.12	36.04	3.46	3.45	12.62	12.60	
XVIII, D·$CoCl_2$	>240	31.50	31.24	2.35	2.28	13.83	13.65	[i]
XIX, D·$[Rh(CO)_2Cl]_2$		27.45	27.48	1.72	1.60	9.58	9.61	
XX, E·CdI_2·0.4Me_2CO	260–275 d	30.25	30.24	2.75	2.90	10.22	9.98	[f]
XXI, E·$ZnBr_2$	200 d	35.68	35.42	3.30	3.25	12.25	12.40	[i]
XXII, E·$CoCl_2$	255 d	41.22	41.24	3.78	3.78	14.56	14.42	[i]
XXIII, E·$PdCl_2$·0.5H_2O	>300	37.59	37.58	3.57	3.60	12.85	13.15	Insol.
XXIV, $[E_2Co][BF_4]_2$·2H_2O	260 d	40.98	40.93	3.87	4.09	14.21	14.31	
XXV, $[(bipy)_2Pd_2(pz')_2][BF_4]_2$	>280 d	39.37	40.54	3.35	3.37	12.01	12.60	
XXVI, $[(bipy)Co(pz'H)_2][BF_4]_2$	>230 d	40.46	41.36	4.17	4.13	14.68	14.46	
XXVII, F·CdI_2	180–185 d	38.15	38.24	3.07	2.98	4.97	5.57	[b]

[a]A = (dpe)Pt(pz')$_2$; B = (dpe)Pt(pz)$_2$; C = (bipy)Pt(pz')$_2$; D = (bipy)Pt(pz)$_2$; E = (bipy)Pd(pz')$_2$; F = (dpe)Pd(pz)$_2$, pzH being pyrazole and pz'H 3,5-dimethylpyrazole.
[b]Not electrolyte in dichloromethane.
[c]Oxygen: found 6.68, calcd. 6.79.
[d]Molecular weight: found 954 (osmometry in $CHCl_3$), calcd. 919.7.
[e]Cadmium: found 10.80, calcd. 10.63; platinum: found 19.22, calcd. 18.48.
[f]Not electrolyte in acetone.
[g]Soluble in nitromethane, with decomposition.
[h]Molecular weight: found 2109 (osmometry in $CHCl_3$), calcd. 1805.8.
[i]Not electrolyte in acetonitrile.
[j]Platinum: found 23.20, calcd. 23.15; nickel: found 3.38, calcd. 3.48.

as in the case of the complexes $[\{(dpe)Pt(pz')_2\}_2Zn](BF_4)_2$, **VIII**, $[\{(dpe)Pt(pz)_2\}_2Ni](BF_4)_2$, **XI**, $[\{(bipy)Pt(pz')_2\}_2Ni](BF_4)_2$·$H_2O$, **XVII**, and $[\{(dpe)Pd(pz')_2\}_2Co](BF_4)_2$·2$H_2O$, **XXIV**. Their formulae were established by elemental analyses, spectra, and by the value of the electrical conductivity in solution. The ionic nature of these compounds in the solid state was evidenced by the presence of only one strong and broad vibration due to the BF_4^- ion with tetrahedral symmetry at ca. 1050 cm^{-1}, thus ruling out more complicated structures. The ir spectra also gave evidence on the presence (or absence) of the water molecules. The proton nmr spectra of the compounds **XI** and **XVII** showed the required bands due to the chelating ligand and to the pyrazolato groups. The ^4J(Pt—H) = 7 Hz was quite evident in the spectrum of the compound **XVII** (Table 2), thus allowing the methyl signal having the ^{195}Pt satellites to be assigned to the 5-Me and the other methyl signal to the 3-Me group.

In the adducts, coordination around the platinum(II) or palladium(II) atom is reasonably assumed to be square planar; in the zinc adduct, **VIII**, coordination around the zinc atom is likely to be tetrahedral, while various possibilities arise for the nickel(II) and cobalt(II) derivatives, especially if the molecule(s) of water is inside the coordination sphere.

The observed diamagnetism and electronic spectrum of **XI**, both in acetonitrile solution and in the solid state, suggest square planar nickel(II) (7). Similar evidence, also in acetonitrile, suggests the same coordination for the compound **XVII**. Here, if the water molecule is not far away from the nickel atom, a strongly elongated square pyramidal coordination (8) cannot be excluded completely, but is unlikely since other pyrazolates, e.g. [Me_2Ga-

TABLE 2. Proton magnetic resonance data[a]

Compound	Solvent	Chelating ligand	Pyrazole ring protons: 3- and 5-substituents	Pyrazole ring protons: 4-substituent	
A[d]	$CDCl_3$	2.7–2.1m, Ph 7.5–7.9m, CH_2	8.25s, 5-Me, ^4J = 4 Hz 8.12s, 3-Me	4.54br, ^4J = 9 Hz	
$[AH_2]^{2+}$[d]	$CDCl_3$	2.4m, Ph 7.0–7.5m, CH_2	8.19s, 5-Me, ^4J = 5 Hz 7.89s, 3-Me	4.27s, br	−1.4br NH
V	CD_2Cl_2	2.0–3.0m, Ph [b], CH_2	8.05s, 5-Me, ^4J = 4.5 Hz 7.85s, 3-Me	4.37br	
E[d]	CD_3OD	1.5–2.0m and 2.2–2.7m bipy	8.01s, 7.78	4.34s	
$[EH_2]^{2+}$[d]	CD_2Cl_2	1.5–3.0m bipy	7.78s, 7.50s, 7.30s	3.92s, br 3.82s, br	−2.0br NH
XX	$(CD_3)_2CO$	1.3–1.8m and 2.0–2.7m, bipy	7.58s, 7.38s	4.12s	
XXI	CD_3CN	1.3–2.0m and 2.1–2.5, bipy	7.79s, 7.57s	4.07s, 3.89s	
XVII	CD_3CN	1.25–1.75m and 2.0–2.2m, bipy	7.75s, 5-Me, ^4J = 7 Hz 7.63s, 3-Me	4.26s, ^4J = 13 Hz	
B[d]	$CDCl_3$	2.0–2.8m, Ph + 5-CH 7.5–8.0m, CH_2	3.20d, ^3J = 9 Hz ^3J(H—H) = 2 Hz, 3-CH[c]	4.05t, ^4J = 7 Hz ^3J(H—H) = 2 Hz	
XI	CD_3CN	1.85–2.70m, Ph [b], CH_2	3.69–3.89m, br	[b]	
X	$CDCl_3$	1.83–3.0m, Ph 7.0–8.5m, CH_2	3.22s, br [c]	4.13s, br	
XIX	$CDCl_3$	1.95–2.0m and 2.30–2.55m, bipy	1.49d, ^3J = 16, ^3J(H—H) = 2.5 0.75s and 0.83s, 3-CH	3.54t, ^3J(H—H) = 1.5 Hz	
F[d]	$CDCl_3$	1.8–2.9m, Ph + 5-CH	3.40s, br [c]	3.85s, br	
XXVII	CD_3CN	1.8–2.8m, Ph + 5-CH 7.2–7.8m, CH_2	2.88s [c]	3.98s	

[a]τ units; Varian NEVA, 60 MHz operating at room temperature; s = singlet, d = doublet, t = triplet, m = multiplet, br = broad.
[b]Not observed owing to insufficient solubility.
[c]The 5-CH is probably covered by absorptions due to the aromatic protons.
[d]These data are reported for comparison (ref. 1).

$(pz)_2]_2Ni$ (4*b*) or $[Me_2B(pz)_2]_2Ni$ (9) were found to contain square planar nickel(II).

On the other hand, a tetrahedral coordination may be suggested for the violet paramagnetic cobalt(II) derivative, **XXIV**, on the evidence of the visible spectrum and on the assumption that the two water molecules are outside the cobalt coordination sphere. By comparison, the related mononuclear $[Co(pz'H)_4]^{2+}$ ion was shown (9*b*) to contain tetrahedrally coordinated cobalt(II). The reaction leading to the compound **XXIV** afforded also two other products in small yields. One of them is white and cobalt-free, the other is blue and paramagnetic; on the basis of elemental analyses, electrical conductivity, ir, and electronic spectra, formulae like $[(bipy)_2Pd_2(\mu\text{-}pz')_2]\ (BF_4)_2$, **XXV**, and $[(bipy)Co(pz'H)_2]\ (BF_4)_2$, **XXVI**, are suggested.

The 1:1 adducts (see Table 1) were obtained when the ligands A—F were reacted with a metal halide or a metal sulphate, generally in methanol solution or in ether suspension. In the case of $(dpe)Pd(pz)_2 \cdot CdI_2$, **XXVII**, ether had to be used, since in methanol scrambling of the ligands occurred and $(dpe)PdI_2$ was isolated.

The 1:1 adducts are thermally stable solids and are sparingly soluble in organic solvents, which have a remarkable tendency to be included in the crystals. In particular, the compounds, $(bipy)Pt(pz')_2CdI_2$, **XII**, and $(bipy)Pt(pz')_2CoCl_2$ could be isolated with (**XIII** and **XV**) or without (**XII** and **XIV**) 1 mol of clathrated dichloromethane; solvent molecules can probably fit into the holes of a crystal lattice in which the bulky and rather unflexible bipyridine or 3,5-dimethylpyrazolato ligands have to be accommodated.

When the solubility was sufficient, e.g. **III**, the determinations of the molecular weight and of the molar conductivities showed the complexes to be monomeric, ruling out dimeric, ionic formulae such as $[(dpe)Pt(\mu\text{-}pz')_2Zn(\mu\text{-}pz')_2Pt(dpe)]^{2+}[ZnCl_4]^{2-}$. The very limited, although not negligible solubility of the 1:1 adducts **I** and **II**, between zinc(II) or copper(II) sulphate and $(dpe)Pt(pz')_2$, did not allow a reliable molecular weight determination but argues against a polymeric structure. These two compounds, which

are not electrolytes in CH_2Cl_2, are likely to be either monomers, (dpe)Pt(μ-pz′)$_2$M(SO_4), or dimers, (dpe)Pt(μ-pz′)$_2$M(μ-SO_4)$_2$M(μ-pz′)$_2$Pt(dpe).

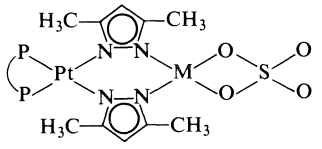

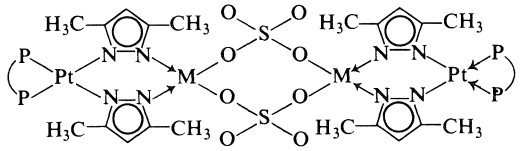

No distinction is possible on the basis of the infrared spectrum for the sulphate group, which has C_{2v} symmetry in both cases; moreover, strong vibrations due to the Pt-containing ligands are present in the regions typical for sulphate adsorptions. Related (pyrazole)$_2$M(SO_4) species have been reported and were assumed to be mononuclear (8*b*).

The complexes [(bipy)Pd(pz′)$_2$·$PdCl_2$·0.5H_2O]$_n$, **XXIII**, and [(bipy)Pt(pz′)$_2$·$PdCl_2$]$_n$, **XVI**, are insoluble, so that polymeric structures where the ligands bridge two $PdCl_2$ moieties are more likely.

The infrared spectra (4000–250 cm^{-1}) of these 1:1 adducts show all the vibrations due to the metal-containing ligand, thus suggesting that the gross structure of the latter is unaltered after the reaction. In the low-frequency region, where metal–halogen stretching frequencies are expected, a rather complicated pattern is present owing to ligand vibrations. This precludes any safe assignment.

The proton nmr spectra (Table 2) were recorded for those compounds which were sufficiently soluble. The 3,5-dimethylpyrazolates showed always two sets of methyl groups; of these the one at higher field should be assigned to the set nearer to the transition element because, when this is platinum, coupling with ^{195}Pt can be observed. The actual value of the ^4J(Pt—H) is 4.5 Hz in (dpe)Pt(pz′)$_2$·CdI_2 and is quite similar to that recorded for the ligand itself or the protonated species [(dpe)Pt(pz′H)$_2$]$^{2+}$ (4 or 5 Hz respectively).

Although also the proton in the 4 position of the pyrazolato ring was coupled to the platinum in the parent molecule, (dpe)Pt(pz′)$_2$ (J = 4 Hz), only a broadening of the signal was recorded in the case of its CdI_2 derivative, as had already been observed for the related [(dpe)Pt(pz′H)$_2$]$^{2+}$ cation (1). No such coupling was observed in the adducts of the palladium containing ligands; however, two 4-CH signals instead of one, together with the required two methyl signals, were recorded for a CD_3CN solution of (bipy)Pd(pz′)$_2$·$ZnBr_2$. Two magnetically non-equivalent 4-CH groups can presently be explained only if the two pyrazolato ligands cannot occupy symmetrical positions, owing perhaps to steric crowding.

In the blue, paramagnetic (nmr criterion) and non-electrolyte cobalt(II) compounds, the transition metal atom is surrounded pseudo-tetrahedrally by the ligands. Such an arrangement of the ligands was proposed on magnetic and spectral evidence for the blue bimetallic species (dpe)Pt⊣C(OR)=N(Ar)→]$_2$$CoCl_2$ (2), for the blue bis(3,5-dimethylpyrazole)- or bis(1,3,5-trimethylpyrazole) dichlorocobalt(II) (10*a*) and is now supported by an X-ray structure carried out for bis(3,5-dimethyl-4-ethylpyrazole)dichlorocobalt(II) (10*b*).

The reaction of dimeric dicarbonylchlororhodium(I) was carried out with the complex (bipy)-Pt(pz)$_2$ and a 2:1 adduct was isolated, for which the following structures are possible

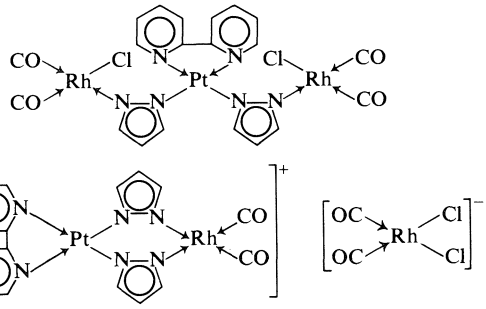

plus a more complicated one, analogous to that proposed for an adduct between a porphyrin and [(CO)$_2$RhCl]$_2$ (11), involving a pentacoordinated rhodium(I). The value of the electric conductance, both in acetone and in dichloromethane solution, supports the ionic structure, which may be present even in the solid state since the pattern of the infrared absorptions in the ν_{CO} region does not change from solid state (Nujol) to solution (CH_2Cl_2) spectra.

The behaviour of the ligand (bipy)Pt(pz)$_2$, therefore, is different from that of the (dpe)Pt⊣C(OMe)=N—Ar]$_2$ or (Ph$_3$P)(ArNC)Pt⊣C(OMe)=N—Ar]$_2$ ligands which give non-ionic adducts where they act as exo-bidentate ligands. In addition another difference lies in the stability of the solution, which is very limited in the case of (dpe)Pt⊣C(OMe)=N(Ar)→Rh(CO)$_2$Cl]$_2$. Both adducts are decomposed by reaction with a classical ligand, such as Ph_3P, according to the reactions:

$$\text{(bipy)Pt(pz)}_2\cdot[\text{Rh(CO)}_2\text{Cl}]_2 + 4\text{Ph}_3\text{P} \rightarrow \text{(bipy)Pt(pz)}_2 + 2\text{(CO)(Ph}_3\text{P)}_2\text{RhCl} + 2\text{CO}$$

$$\text{(dpe)Pt⊣C(OMe)=NAr]}_2[\text{Rh(CO)}_2\text{Cl}]_2 + 4\text{Ph}_3\text{P} \rightarrow \text{(dpe)Pt⊣C(OMe)=NAr]}_2 + 2\text{(CO)(Ph}_3\text{P)}_2\text{RhCl} + 2\text{CO}$$

TABLE 3. Electronic spectra

Compound	Solvent	λ_{max} (ε)
II, A·$CuSO_4$	CH_2Cl_2	650 (94) 350 (744) 270 (14 600) 265 (15 050) 254 (15 350) 247 (17 000) 245 (21 500) 237 (25 500)
XI, $[B_2Ni][BF_4]_2$	CH_3CN	440 (90); the same λ_{max} upon reflectance
C	$CHCl_3$	410 (2290)
	CH_3OH	384 (1280)
XII, C·CdI_2	$CHCl_3$	410 (2250)
XIV, C·$CoCl_2$	CH_3CN	642 (395) 612 (465) 576 (350) 376 (1260)
D	$CHCl_3$	390 (2000) 360 (2200) 320 (9000) 300 (10 500) 250 (21 700)
XVIII, D·$CoCl_2$	CH_3CN	640 (350) 600 (380) 570 (310) 350 (2300) 315 (12 900) 250 (30 400)
	CH_3OH	500 (39) 360 (2250) 320 (11 850) 307 (11 100) 270 (15 200) 237 (14 100)
E	CH_3OH	306 (6200) 236 (6050)
XX, E·CdI_2·0.4Me_2CO	CH_3CN	315sh (11 750) 306 (12 970) 236 (34 450)
XXII, E·$CoCl_2$	CH_3CN	642 (370) 616 (405) 580 (300) 315 (13 530) 236 (26 250) 215 (33 260)
XXIV, $[E_2Co][BF_4]_2$·$2H_2O$	$(CH_3)_2CO$	606 (298) 570 (375) 524 (285) 308 (27 990) 236 (50 265) 215 (54 795)
XXVI, [(bipy)Co(pz′H)$_2$][BF_4]$_2$	CH_3CN	616 (325) 598 (300) 308 (11 170) 236 (19 800) 215 (22 840)

TABLE 4. Conductivity data

Compound	Temperature (°C)	Solvent	Concentration (10^{-4} *M*)	Conductivity (ohm^{-1} cm^2 mol^{-1})
VIII	24	$(CH_3)_2CO$	2.5	295
VIII	24	CH_2Cl_2	2.8	75
XVII	20	$(CH_3)_2CO$	2.1	296
XXIV	20	$(CH_3)_2CO$	5.5	211
XXIV	20	CH_3CN	6.4	299
XIX	23	CH_2Cl_2	3.8	26
XIX	23	$(CH_3)_2CO$	2.3	87

Experimental

The starting materials, A—F, were prepared as described in our preceding paper (1). General techniques and spectroscopic methods have been described previously (2). Analytical and other data are given in Table 1, nmr data in Table 2, spectroscopic data in Table 3, and conductivity data in Table 4. All the analytical samples were pumped to constant weight (ca. 0.1 Torr, 25°C). Evaporation was always carried out under reduced pressure (water aspirator).

Preparation of the Adducts

A·$CdBr_2$, **IV**. To a stirred methanol suspension (40 mL) of the compound A (202 mg; 0.26 mmol), a solution of $CdBr_2$·$4H_2O$ (90 mg; 0.26 mmol) in warm methanol was added. After stirring for 15 min, the solution was evaporated to dryness and the residue was extracted with dichloromethane (40 mL). Diethyl ether (50 mL) was added to the extract and the crude compound crystallized out upon concentration. Recrystallization was achieved by concentrating a solution in CH_2Cl_2/Et_2O (70 + 70 mL). The colourless compound is sparingly soluble in CH_2Cl_2 and is insoluble in chloroform, acetone, benzene, or acetonitrile. The preparation of A·CdI_2, **V**, A·$ZnCl_2$, **III**, A·$ZnSO_4$, **I**, green A·$CuSO_4$, **II**, and of $[A_2Zn][BF_4]_2$, **VIII**, was carried out similarly from CdI_2, $ZnCl_2$, $ZnSO_4$·$7H_2O$, $CuSO_4$·$5H_2O$, and $Zn(BF_4)_2$·$6H_2O$; the crude products were crystallized from CH_2Cl_2/Et_2O (between 1/1 to 1/4 volume ratio).

A·$HgCl_2$, **VI**. A solution of mercury(II) chloride (86 mg; 0.316 mmol) in diethyl ether (25 mL) was added to a stirred suspension of the compound A (216 mg; 0.275 mmol) in the same solvent. After stirring for 1 h the colourless precipitate was filtered and washed with ether. The white compounds A·$HgBr_2$, **VII**, B·$HgCl_2$, X, B·$CdCl_2$, **IX**, and yellow E·$ZnBr_2$, **XXI**, were obtained similarly from the appropriate reagents, sometimes with longer reaction times (6 h for **X** and **XXI**, 24 h for **IX**), and were then crystallized twice from CH_2Cl_2/Et_2O or CH_3CN/dry Et_2O.

C·CdI_2, **XII**, and C·CdI_2·CH_2Cl_2, **XIII**. Cadmium(II) iodide (105 mg; 0.28 mmol) in methanol (2 mL) was added to a solution of the compound C (149 mg; 0.27 mmol) in the same solvent (30 mL) whereupon a yellow precipitate formed at once. In this case the reaction mixture was evaporated to dryness and the residue was extracted with dichloromethane (40 mL). Addition of petroleum ether gave a yellow precipitate, which did not dissolve again completely in dichloromethane (0.25 L), affording the yellow compound **XIII** (60 mg). From the clear extract the orange yellow compound **XII** (110 mg) precipitated upon concentration to a small volume.

The compounds C·$CoCl_2$, **XIV**, $[C_2Ni][BF_4]_2$·$2H_2O$, **XVII**, and C·$PdCl_2$, **XVI**, were obtained similarly from C and anhydrous $CoCl_2$, $Ni(BF_4)_2$·$6H_2O$ or $(PhCN)_2PdCl_2$ in methanol solution. The emerald-green (cobalt), pale pink (nickel), or pale yellow (palladium) precipitates were purified by crystallization from acetonitrile/diethyl ether or, in the last

case, by washing with methanol and ether. The emerald-green compound **XV** was obtained by washing **XIV** with dichloromethane.

D·$[Rh(CO)_2Cl]_2$, **XIX**. Compound D (197 mg; 0.407 mmol), $[Rh(CO)_2Cl]_2$ (158 mg; 0.407 mmol), and ether (50 mL) were stirred 4 h. The orange yellow precipitate was filtered and crystallized by concentration from CH_2Cl_2/Et_2O. Infrared carbonyl stretching frequencies at 2080, 2065, 2020, and 1990 (CH_2Cl_2 solution) and at 2070, 2050, 2010, 1990, 1970, and 1940 cm^{-1} (Nujol mull).

D·$CoCl_2$, **XVIII**. After 10 min a methanol solution (50 mL) of the compound D (199 mg; 0.41 mmol) and of anhydrous cobalt(II) chloride (70 mg; 0.54 mmol) in the same solvent (20 mL) gave a blue precipitate (152 mg); additional precipitate (66 mg) was obtained upon concentration of the blue mother liquor. The combined precipitates were extracted with acetonitrile and the blue product (200 mg) was obtained by concentrating the extract in the presence of ether. The compound is sparingly soluble in acetonitrile with a blue colour, which becomes yellow upon addition of methanol and gives back the blue colour upon addition of ether or of hexane; it dissolves in methanol with a yellow colour, while in ethanol, where it is sparingly soluble, only a blue colour was observed for the solution.

E·$CoCl_2$, **XXII**. The blue precipitate which formed upon addition of dry $CoCl_2$ (30 mg; 0.23 mmol) to a methanol solution (20 mL) of E (100 mg; 0.22 mmol) was crystallized from acetonitrile/ether. The pale pink $[B_2Ni][BF_4]_2$, **XI**, was obtained and purified similarly from B and $Ni(BF_4)_2·6H_2O$.

F·CdI_2, **XXVII**. Cadmium(II) iodide (80 mg; 0.22 mmol), compound F (139 mg; 0.22 mmol), and diethyl ether (40 mL) were stirred for 1 day under nitrogen. The pale yellow compound (200 mg) was filtered and washed with ether; it could not be crystallized from CH_2Cl_2/Et_2O. The same product could not be obtained by carrying out the reaction in methanol.

Acknowledgment

The financial support by the Consiglio Nazionale delle Ricerche (ROMA) is gratefully acknowledged.

1. G. Minghetti, G. Banditelli, and F. Bonati. J. Chem. Soc. Dalton Trans. In press.
2. G. Minghetti, F. Bonati, and G. Banditelli. Inorg. Chem. **15**, 2649 (1976).
3. S. Trofimenko. Chem. Rev. **72**, 497 (1972); A. G. Shaver. J. Organomet. Chem. Library, **3**, 157 (1977).
4. (*a*) K. R. Breakell, D. J. Patmore, and A. Storr. J. Chem. Soc. Dalton Trans. 749 (1975); (*b*) D. F. Rendle, A. Storr, and J. Trotter. J. Chem. Soc. Dalton Trans. 176 (1975).
5. K. S. Chong, S. J. Rettig, A. Storr, and J. Trotter. Can. J. Chem. **56**, 1212 (1978).
6. S. Chong, S. J. Rettig, A. Storr, and J. Trotter. Can. J. Chem. **55**, 4166 (1977).
7. F. A. Cotton and G. Wilkinson. Advanced inorganic chemistry. 3rd ed. Interscience Publisher, New York. 1972. p. 897.
8. (*a*) L. Sacconi. Coord. Chem. Rev. **8**, 351 (1972) and references therein; (*b*) M. S. Barvinok and L. K. Lukina. Zh. Neorg. Khim. **23**, 2406 (1978); Chem. Abstr. **89**, 208312*y* (1978).
9. (*a*) S. Trofimenko. J. Am. Chem. Soc. **89**, 6288 (1977); G. F. Herring, D. J. Patmore, and A. Storr. J. Chem. Soc. Dalton Trans. 711 (1975); (*b*) A. V. Nikolaev, L. G. Laurenova, S. V. Larionov, and Z. A. Grankina. Koord. Khim. **4**, 1574 (1978); Chem. Abstr. **89**, 225340*y* (1978).
10. (*a*) M. J. Bagley, D. Nicholls, and B. A. Warburton. J. Chem. Soc. A, 2694 (1970); (*b*) V. M. Agre, I. A. Krol, V. K. Trunov, O. V. Ivanov, and V. M. Dziomko. Koord. Khim. **4**, 1603 (1978); Chem. Abstr. **90**, 32258*q* (1979).
11. H. Ogoshi, T. Omura, and Z. Yoshida. J. Am. Chem. Soc. **95**, 1666 (1973).

Contribution to the solution chemistry and polarographic behaviour of anthrapurpurin complexan

F. CAPITAN,[1] A. GUIRAUM, AND J. L. VILCHEZ
Department of Analytical Chemistry, Faculty of Sciences, Granada, Spain
AND
J. F. ARENAS
Department of Physical Chemistry, Faculty of Sciences, Granada, Spain

Received June 15, 1979

F. CAPITAN, A. GUIRAUM, J. L. VILCHEZ, and J. F. ARENAS. Can. J. Chem. **57**, 3243 (1979).

The reduction of the 1,2,7-trihydroxyanthraquinone-3-methylamino-*N*,*N*-diacetic acid at dropping mercury electrode has been investigated. The reduction involves two electrons as well as either one or two hydrogen ions depending on the pH. Two alternative reaction mechanisms are proposed. Five acid-dissociation constants have been determined by potentiometric and spectrophotometric methods. A sequence for the dissociation of the protons is proposed. Thermal gravimetric and differential analysis of the anhydrous and dihydrated reagent are reported.

F. CAPITAN, A. GUIRAUM, J. L. VILCHEZ et J. F. ARENAS. Can. J. Chem. **57**, 3243 (1979).

La réduction de l'acide 1,2,7-trihydroxyanthraquinone-3-méthyle-amino-*N*,*N*-diacétique a été etudiée à l'électrode à goutte de mercure à differents valeurs du pH avec un tampon acétique. La réduction se fait avec l'intervention de deux électrons ainsi que d'un ou deux ions H^+ selon que le pH soit au-dessous de 7.76 ou au-dessus de cette valeur là respectivement. Deux mécanismes de réaction ont été établis. On a fait la détermination potentiométrique et spectrophotométrique de cinq constantes de dissociation et on a proposé une séquence pour la dissociation des protons. On a étudié également l'analyse thermique du composé anhydre et hydraté.

Introduction

Prior to this work, several analytical applications of anthrapurpurin complexan (1,2,7-trihydroxyanthraquinone-3-methylamino-*N*,*N*-diacetic acid) were studied (1, 2).

There are only a few data in the literature concerning dissociation constants of anthraquinone complexans. To our knowledge, only those of alizarin complexan (3) and sulphonated alizarin complexan (4) have been reported. Likewise, few data have been reported concerning the polarographic behaviour of anthraquinonic derivatives (5–7) but no attention has yet been paid to their complexans. In this work, we have determined five dissociation constants of anthrapurpurin complexan by potentiometric and spectrophotometric methods and investigated the reduction of the reagent at the dropping mercury electrode at different values of pH in some acetic–acetate buffers. The reaction mechanism has been established and one of the pK values has been determined from the polarographic data and found to be in good agreement with that determined by potentiometric and spectrophotometric methods. Accordingly, the order of dissociation of the protons has been established.

The thermal behaviour of the reagent has also been investigated and the solubility in distilled water determined.

Experimental

Anthrapurpurin complexan was synthesized according to Belcher's method (8). The infrared spectrum of the solid in KBr pellets was recorded on a Beckman 4240 spectrophotometer. The nmr spectrum of the reagent dissolved in dimethyl sulfoxide was recorded on a Perkin Elmer R20 spectrometer. To increase the solubility of the sample we synthesized the acetic triester methyl diester derivative by consecutive esterification of the three phenolic groups and the two carboxylic groups. The elemental analysis of this derivative agrees with the empirical formula $C_{27}H_{25}NO_{10}$. Its nmr spectrum was recorded in deuterated chloroform. The mass spectrum of the reagent could not be recorded because of its low volatility, thus the spectrum of the pentamethylic derivative was recorded on a Hewlett-Packard 5930 A spectrometer. Thermal analyses were carried out with a Setaram GDTD thermoanalyzer fitted with a B70 thermobalance using Pt/Pt–Rh thermocouples. Analyses were always performed in a static air atmosphere using 20 mg samples in platinum melting pots of 5 mm inner diameter and heating at the rate of 10°C/min. Calcinated alumina with the same particle size as the sample was used to record TDA diagrams. A Beckman Research potentiometer was used to perform potentiometric titrations and a Beckman ACTA 3 spectrophotometer was used for the spectrophotometric determination of dissociation constants.

Polarograms were recorded on a Sargent XVI polarograph and an AMEL 471 multipurpose unit. Controlled-potential coulometric reactions were carried out on a Metrohm-Herisau

[1]To whom all correspondence should be addressed.

0008-4042/79/243243-04$01.00/0

E-524 potentiostat and pH was measured with a Radiometer pH-29 pH-meter. The sce was used as reference electrode in all cases, a water-jacketed cell through which water was circulated from a thermostat was used to control temperature at 25°C and oxygen was removed by bubbling nitrogen of 99.997% of purity through the solutions. Different acetic–acetate buffers were used as supporting electrolytes in the pH range of 3.75 to 8.70. Capillaries were calibrated at pH = 4.60. Drop time as well as flow of mercury was determined as a function of the height of the mercury column (a lineal dependence between m and h being observed). Samples for polarography were prepared in all cases starting with a bulk solution 10^{-3} M of anthrapurpurin complexan and diluting with the supporting electrolyte up to the required concentration.

Results

The ir spectrum of anthrapurpurin complexan has been recorded in the range 4000–250 cm^{-1}, the most significant features being the following: the broad band at 3460 cm^{-1} must be assigned to ν(OH), that at 1743 cm^{-1} must be assigned to ν(C=O), and that at 1295 cm^{-1} is probably due to a C—N stretching vibration. None of these bands are recorded in the ir spectrum of 1,2,7-trihydroxyanthraquinone (6).

Only signals from aliphatic protons have been recorded in the nmr spectrum of the reagent. That at 3.67 ppm corresponds to the methylenic —CH_2—COOH protons and that at 4.10 ppm corresponds to the methylamino —CH_2—N< protons. No additional signal could be observed. In the nmr spectrum of the esterified derivative the following signals have been recorded: 2.34 ppm corresponding to the methylic protons CH_3—COO— in positions 2- and 7-, 2.45 ppm corresponding to CH_3—COO— in position 1-, 3.53 ppm corresponding to the methylenic protons —CH_2—COO^-, 3.67 ppm corresponding to methylic protons —COO—CH_3, and 4.03 ppm corresponding to methylamino protons —CH_2—N<. A complex signal is recorded in the range 7.5–8.3 ppm originated by the aromatic protons in positions 4-, 5-, 6-, and 8-.

The mass spectrum of the pentamethylic derivative of the reagent shows the molecular peak at 471 m/e which agrees wth the expected molecular weight for this compound.

The solubility of the reagent in distilled water has been determined by the Rose method (9) and found to be 0.19 g/L.

Thermal gravimetric and differential analyses of the anhydrous and dihydrated compound have been performed. The anhydrous reagent, Fig. 1, shows an endothermic effect at 184°C which is followed by an exothermic effect at 190°C. The loss of mass amounts to nearly 10.9% and may correspond to a decarboxylation, the calculated loss being 11%. The elemental analysis of a sample of the reagent heated up to

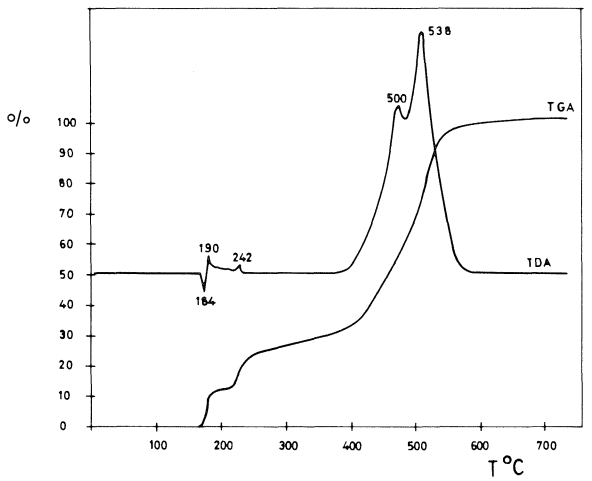

FIG. 1. Thermal analysis of anhydrous anthrapurpurin complexan.

184°C for half an hour is in accordance with this hypothesis. An additional exothermic effect is observed at 242°C with a loss of mass amounting again to nearly 10.9%. Such loss may be caused by a further decarboxylation. The ir spectrum of a sample of the reagent heated up to 245°C for 1 h does not show bands assignable neither to ν(C=O) nor to ν(OH) vibrations. This observation agrees with the proposed interpretation. Finally, two large exothermic effects are observed at 500°C and 530°C which should correspond to the combustion of the sample. The hydrated compound shows the same effects as the anhydrous one but two additional endothermic effects can be seen at 87°C and 140°C with a loss of mass amounting to nearly 4% for each one. The first effect may correspond to the loss of one molecule of lattice water and the second one to the loss of one molecule of strongly hydrogen-bonded water.

Only one polarographic wave has been observed in the polarograms recorded from aqueous solutions of anthrapurpurin complexan at different concentrations, temperatures, and pH. Figure 2 shows a representative polarogram at pH = 4.60. First of all, we investigated the dependence of i_d on the height of the mercury column as well as on pH. The results were obtained from a 10^{-4} M solution at pH = 4.60. The plot of i_d vs. $h^{1/2}$ shows a linear dependence which proves that the wave height is diffusion-controlled. The temperature coefficient of i_d has been investigated in the range between 20°C and 85°C with 2.5×10^{-4} M solutions at pH = 4.60. The temperature coefficient is found to be $d(\log i_d) \div dT = 0.0063$ (close to the theoretical value 0.007) confirming the diffusion-controlled nature of the

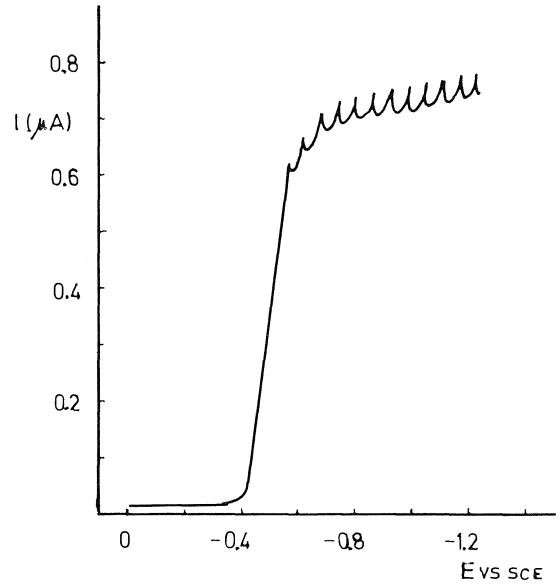

FIG. 2. Polarographic wave of anthrapurpurin complexan at pH = 4.60.

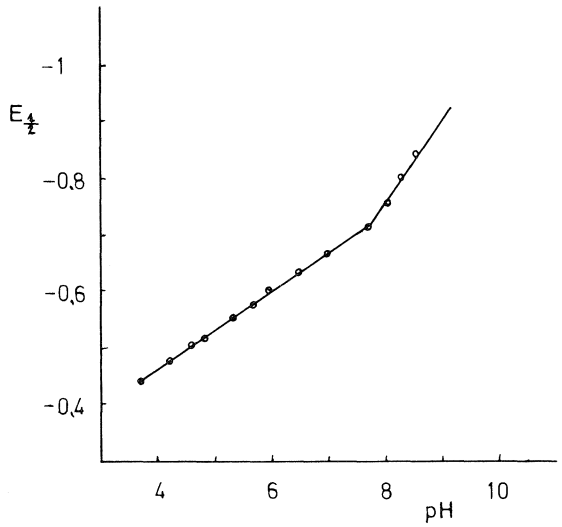

FIG. 3. Dependence of half-wave potential on pH.

polarographic wave. Then, we studied the dependence of the half-wave potential on pH to determine how many hydrogen ions are involved in the reduction. Polarograms were recorded from 2.5×10^{-4} M solutions in the range of pH between 3.75 and 8.70. Values of $E_{1/2}$ as well as those of $n\alpha$ were calculated in each case. Figure 3 shows the plot of $E_{1/2}$ vs. pH. One can observe two straight lines the slopes of which are 0.0697 and 0.12 depending on whether pH is lower or higher than 7.76. Accordingly, the number of hydrogen ions involved in the reduction must be either $p = 1$ or $p = 2$ respectively. The intersection point at pH = 7.76 defines the value of a pK which agrees with that of pK_3 determined by potentiometric and spectrophotometric methods.

On the other hand, we checked that the diffusion current is proportional to the solute concentration, i.e., that Ilkovic's equation holds in the concentration range between 6×10^{-6} M and 5×10^{-4} M at pH = 4.60. In all cases we also calculated $E_{1/2}$ which was independent of concentration. There is a linear dependence of i_d on concentration. The slope of i_d vs. concentration was found to be 2.708 μA cm^3/mol. Hence, the diffusion current constant is $I = i_d/m^{2/3} \cdot t^{1/6} c = 607 D^{1/2} n = 2.41$ and the diffusion coefficient $D = 3.9 \times 10^{-6}$ cm^2/s, where $n = 2$, $m = 0.68$ mg/s, and $t = 9.7$ s. Such values for I and D agree with those previously published for some anthraquinones (5). Finally, we carried out a controlled-potential coulometry to determine n, i.e., the number of electrons involved in the reduction. A mercury pool was used as the cathode and a platinum wire as the auxiliary electrode, the reference electrode was a sce. The concentration of the sample before and after the electrolysis was measured polarographically to ensure that reduction reached completion. The electrolyzed samples contained 0.1640 g of solute in 100 mL of solution, a continuous stream of nitrogen was passed during the electrolysis at the end of which the wave at $E_{1/2} = -0.5$ V had disappeared but a new one did appear at $E_{1/2} = -1.22$ V. Therefore, it appears that the reduction involves two electrons in the range of pH investigated.

Finally, the acid-dissociation constants of anthrapurpurin complexan have been determined by potentiometric (10–12) and spectrophotometric methods (13) at ionic strength $\mu = 0.1$. A maximum of five dissociation constants have been determined in the range of pH investigated and their pK values are collected in Table 1 together with that obtained fron the polarographic method.

Discussion

Taking into account the above results we have proposed a mechanism for the reduction of anthrapurpurin complexan at the dme.

The reduction of any anthraquinone may proceed along two different pathways depending on the substituents, pH and supporting electrolyte (5–7): (*a*) by

TABLE 1. Selected pK values of anthrapurpurin complexan

Method	pK_1	pK_2	pK_3	pK_4	pK_5
Potentiometric	3.0	5.3	7.6	10.0	11.0
Spectrophotometric	—	5.5	7.6	—	—
Polarographic	—	—	7.76	—	—

pH lower than 7.76

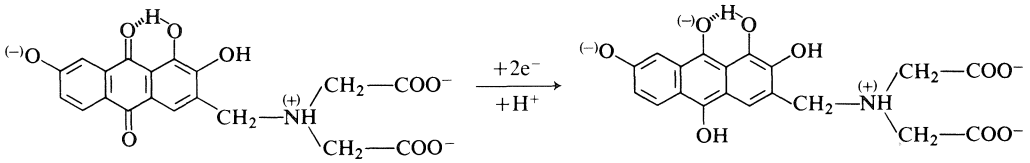

pH higher than 7.76

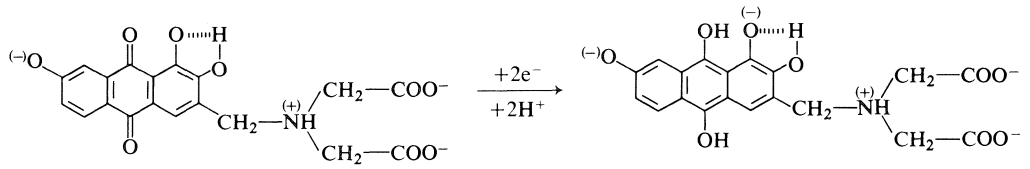

capturing one electron to form a semiquinone system, or (*b*) by capturing two electrons to form a hydroquinone. In this case the number of electrons involved in the reduction has been two in the whole range of pH we have investigated. Therefore, it seems reasonable to assume that the product of the reduction is the hydroquinone derivative. However, the number of hydrogen ions involved is either one or two depending on pH. It seems possible to explain these mechanisms by assuming that the —OH substituent in position 1 is not dissociated at pH lower than 7.76. Accordingly, the quinone oxygen in position 9 is reduced to $—O^-$ and hydrogen-bonded to —OH in position 1. At pH higher than 7.76 the —OH group in position 1 is dissociated and may be hydrogen-bonded to —OH in position 2; therefore, the second hydrogen ion is captured to form the hydroquinone derivative.

Consequently, the order of dissociation of the protons seems to be as follows: (*a*) the second carboxyl group proton (the first one is transferred to the nitrogen atom during the dissolution of the reagent, (*b*) the phenolic proton in position 7), (*c*) idem in position 1, (*d*) idem in position 2, and (*e*) the proton at the imino group. The phenolic proton in position 7 seems to dissociate before those in positions 1 and 2 provided that it is not linked by any intramolecular hydrogen bond.

1. F. Capitan, M. Roman, and A. Guiraum. An. R. Soc. Esp. Fis. Quim. B**67**, 147 (1971); B**68**, 989 (1972).
2. F. Capitan, M. Roman, and A. Guiraum. Quim. Ind. **18**, 13 (1972).
3. F. Ingman. Talanta, **20**, 135 (1973).
4. M. A. Leonard. Analyst, **100**, 275 (1975).
5. N. H. Furman and K. G. Stone. J. Chem. Soc. 3055 (1948).
6. H. Bloom, L. H. Briggs, and B. Cleverley. J. Chem. Soc. 178 (1959).
7. R. Jones and T. M. Spotswood. Aust. J. Chem. **15**, 942 (1962).
8. R. Belcher, M. A. Leonard, and T. S. West. J. Chem. Soc. 2390 (1958).
9. J. Rose. Advanced physicochemical experiments. Pitman, London. 1961.
10. J. Bjerrum. Metal ammine formation in aqueous solution. P. Haase, Conpenhagen. 1941.
11. H. Irving and H. S. Rossotti. J. Chem. Soc. 2904 (1954).
12. M. Otomo, K. Fukui, and K. Kodama. Bull. Chem. Soc. Jpn. **42**, 455 (1974).
13. R. F. Wilson and G. W. Lester. Talanta, **10**, 319 (1963).

Coefficients *B* de viscosité dans les systèmes ternaires aqueux. III. Halogénures alcalins – alcool *tert*-butylique – eau à 25°C

MARC PALMA ET JEAN-PIERRE MOREL

Laboratoire d'Etudes des Interactions Solutés-Solvants, Groupe de Chimie Physique, Université de Clermont, Bât. 6 Chimie, B.P. 45, 63170 Aubiere, France

Reçu le 12 juillet 1979

MARC PALMA et JEAN-PIERRE MOREL. Can. J. Chem. **57**, 3247 (1979).

Nous avons mesuré, à 25°C, le coefficient *B* de viscosité de HCl, LiCl, NaCl, KCl, RbCl, KI et KBr dans les mélanges hydroorganiques contenant de $X = 10$ à 40% en poids d'alcool *tert*-butylique, les concentrations en électrolyte variant entre 0.1 et 0.3 *M*.

Les courbes $B = f(X)$ présentent des points d'inflexion et des minimums dont la position peut s'expliquer par les propriétés structurales du solvant mixte.

On observe, dans l'eau, une relation linéaire entre l'entropie d'hydratation et le coefficient *B* des ions. De la même façon, on peut mettre en évidence, pour tous les mélanges étudiés, une corrélation linéaire entre l'entropie de solvatation et le coefficient *B* des électrolytes.

Ces corrélations permettent de caractériser deux zones distinctes ($X < 20\%$ et $X > 20\%$) dans la gamme des mélanges eau–*tert*-BuOH.

MARC PALMA and JEAN-PIERRE MOREL. Can. J. Chem. **57**, 3247 (1979).

We have measured the coefficient of viscosity *B* at 25°C of HCl, LiCl, NaCl, KCl, RbCl, KI, and KBr in the mixtures of aqueous organic solvents containing from 10 to 40% *tert*-butyl alcohol by weight (X), the concentration of electrolyte varying from 0.1 to 0.3 *M*.

Plots of $B = f(x)$ show points of inflexion and minima whose positions can be explained by the structural properties of the mixed solvent.

In water, a linear relationship between the entropy of hydration and coefficient *B* of the ions is observed. In the same way, it can be shown that a linear correlation exists between the entropy of solvation and coefficient *B* of the electrolytes for all the mixtures studied.

These correlations lead to the characterization of two distinct zones ($X < 20\%$ and $X > 20\%$) for the range of *tert*-butyl alcohol – water mixtures.

[Journal translation]

Introduction

Nous avons abordé l'étude de la viscosité des solutions ternaires aqueuses contenant un électrolyte et un nonélectrolyte par le système NaCl – alcool *tert*-butylique – eau (1). Ces premiers résultats nous ont conduit ensuite à examiner les systèmes MX–*t*-BuOH–eau (MX: halogénure alcalin, *t*-BuOH: alcool *tert*-butylique) pour des concentrations en électrolyte et en alcool dans l'eau inférieures à 2 *M* (2); dans cette approche, MX et *t*-BuOH étaient considérés comme des solutés dans l'eau. Les résultats que nous présentons ici concernent les mêmes systèmes où MX reste un soluté alors que la concentration en *t*-BuOH devient assez grande pour qu'on puisse considérer cet alcool comme un co-solvant de l'eau. Il s'agira donc, en fait, de déterminer de façon classique le coefficient *B* de la loi de Jones–Dole des halogénures alcalins dans les mélanges eau–*t*-BuOH.

Depuis quelques années, nous avons étudié nombre de propriétés thermodynamiques de divers solutés, en particulier celles des halogénures alcalins (3–5) dans les mélanges aqueux contenant jusqu'à 40% en poids d'alcool *tert*-butylique; ce co-solvant nous paraissait le plus typique de ce qu'il est convenu d'appeler les "promoteurs hydrophobes de la structure de l'eau". Les nombreux résultats obtenus ont mis en évidence des relations entre: propriétés à dilution infinie du soluté et propriétés structurales du solvant. La difficulté de rendre compte quantitativement de ces dernières fait qu'il est cependant difficile de proposer des modèles précis de solvatation.

Le coefficient *B* de la loi de Jones–Dole (6) est une grandeur caractéristique des interactions ion–solvant particulièrement parlante. Aussi, l'étude de la viscosité des solutions aqueuses d'électrolyte a-t-elle donné lieu à de nombreux travaux (6–9). Si l'on considère des petits ions comme ceux des halogénures alcalins dont la taille est de l'ordre de grandeur de la taille d'une molécule d'eau, l'effet de volume de type Einstein (10) sur la viscosité du solvant peut-être négligé; on peut alors considérer que l'effet observé rend essentiellement compte de l'interaction ion–solvant, c'est-à-dire de la modification du solvant dans la cosphère de l'ion. Aucune théorie ne permet la prévision du coefficient *B* de viscosité; cependant on peut dire que ce paramètre, qui chiffre l'augmentation ou la diminution de viscosité d'un solvant provoquées par la présence d'un électrolyte, rend compte

0008-4042/79/243247-06$01.00/0

TABLEAU 1. Coefficients B (L mol^{-1}) des halogénures alcalins dans les mélanges eau–t-BuOH

	B							
Composé	0%	10%	15%	20%	25%	30%	35%	40%
HCl	0.062	0.027	0.010	0.016	0.027	0.038	0.050	0.053
LiCl	0.138	0.130	0.128	0.124	0.122	0.146	0.176	0.214
NaCl	0.079	0.059	0.035	0.009	0.002	0.023	0.037	0.047
KCl	−0.014	−0.035	−0.065	−0.096	−0.100	−0.086	−0.067	−0.053
RbCl	−0.037	−0.061	−0.090	−0.124	−0.128	−0.119		−0.084
CsCl	−0.050	−0.075	−0.110	−0.141	−0.144	−0.135		−0.104
KI	−0.083	−0.143	−0.180	−0.194	−0.198	−0.192	−0.186	−0.178
KBr	−0.049	−0.079	−0.117	−0.139	−0.142	−0.135		−0.119

en fait de la modification des degrés de liberté des molécules d'eau dans la zone perturbée par l'ion. Deux relations empiriques importantes justifient ce point de vue: la relation linéaire entre B et l'entropie d'hydratation des ions, d'abord proposée par Frank et Evans (11), puis développée par Nightingale (12); la relation linéaire entre B et un coefficient analogue qui traduit les variations de l'inverse du temps de relaxation longitudinale, T_1, du proton des molécules d'eau en rmn, avec la concentration en électrolyte; cette corrélation a été mise en évidence par Engel et Hertz (13).

Les mesures de coefficient B d'électrolyte dans les mélanges hydroorganiques sont peu nombreuses. Les plus significatives sont celles de Feakins et coll. (14), pour les halogénures alcalins dans les mélanges eau–méthanol. Les variations de B sont cependant assez faibles lorsque varie le pourcentage en poids de méthanol ajouté dans l'eau. Notre projet est d'examiner ce qu'il en est dans les mélanges eau–t-BuOH; les résultats obtenus nous permettront de vérifier si les corrélations établies dans l'eau se conservent dans ces milieux.

Partie expérimentale

Appareillage

Sa description détaillée a déjà été faite précédemment (1, 15). Il s'agit d'un dispositif automatique réunissant un ensemble viscosimétrique Fica (avec viscosimètre à tube capillaire de diamètre = 0.5 mm de type Ubbelohde), un densimétre digital Anton Paar et une burette à dilution.

Produits

Les halogénures alcalins sont des produits purs pour analyses "Merck". Ils ont été maintenus pendant 48 h dans une étuve à 150°C avant utilisation. L'alcool *tert*-butylique a été purifié au laboratoire selon la méthode habituelle (16). L'eau est tridistillée dans un appareil en quartz, les solvants et les solutions sont filtrés sur verre fritté de porosité no 4.

Traitement des données et choix du domaine de concentration

Nous avons vu ailleurs (1) que la méthode de détermination du coefficient B de Jones–Dole consiste à représenter la droite $F = (\eta_r - 1 - A\sqrt{c})/c$ en fonction de c, A étant la valeur calculée de ce coefficient à l'aide de la formule de Falkenhagen et Vernon (17). Le coefficient B se détermine en extrapolant cette droite à concentration nulle. Le calcul théorique de l'incertitude relative $\Delta F/F$ montre que celle-ci peut s'écrire sous la forme suivante:

$$[1] \quad \frac{\Delta F}{F} = \frac{\Delta \eta_r}{|\eta_r - 1 - A\sqrt{c}|} + \left| 1 + \frac{A/2\sqrt{c}}{\eta_r - 1 - A\sqrt{c}} \right| \frac{\Delta c}{c}$$

Quand la concentration devient suffisamment faible, la précision sur F peut devenir très mauvaise. Par ailleurs, l'expérience montre que F peut s'écrire sous la forme:

$$[2] \quad F = B + Dc + Ec^2 + \ldots$$

Au-delà d'une certaine concentration, Ec^2 devient grand devant ΔF, et la méthode de détermination de B citée plus haut n'est plus valable. La mesure du coefficient B doit donc s'effectuer à l'interieur d'un domaine de concentration relativement étroit. L'importance du choix de ce domaine s'illustre bien lorsqu'on examine dans la littérature les déterminations connues des coefficients B(2).

Les mesures ont été effectuées ici pour des molarités comprises en général entre 0.1 et 0.3.

Résultats

Les valeurs des coefficients B des électrolytes dans les différents mélanges eau–t-BuOH sont rassemblées dans le tableau 1.[1]

Discussion

1. Variations des coefficients B *avec la composition du solvant*

Les variations du coefficient B des différents halogénures alcalins avec le pourcentage X de t-BuOH dans le mélange hydroorganique sont représentées par les courbes des figs 1 et 2. On a porté sur celles-ci la grandeur de transfert ΔB_t, différence entre la valeur de B dans un mélange donné et la valeur de B dans l'eau. Pour tous les électrolytes étudiés, sauf HCl, on peut faire les constations suivantes: B passe par un minimum pour un solvant contenant entre 20 et 25% en poids de t-BuOH; pour les chlorures

[1]On peut obtenir la série complète des données expérimentales, à un prix nominal, en s'adressant au Dépôt de données non publiées, ICIST, Conseil national de recherches du Canada, Ottawa (Ont.), Canada K1A 0S2.

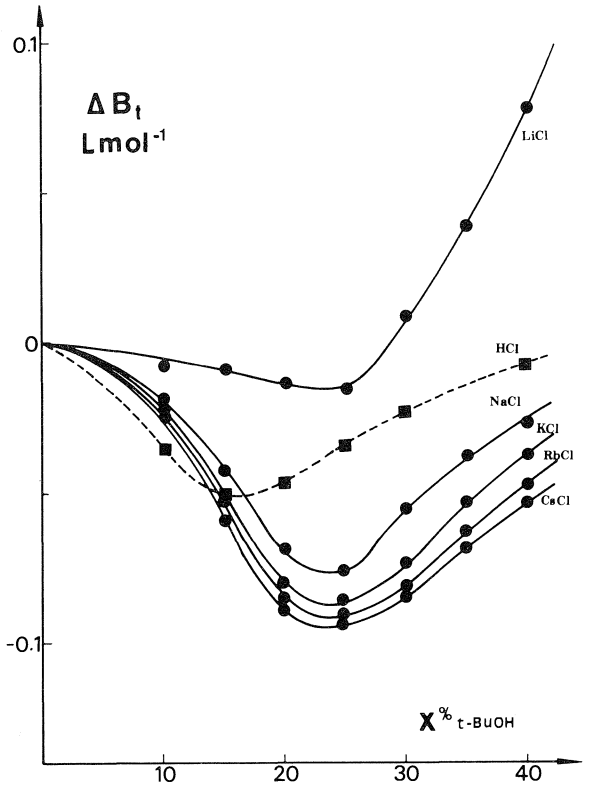

FIG. 1. Coefficients B de transfert des chlorures alcalins de l'eau aux mélanges eau – alcool *tert*-butylique.

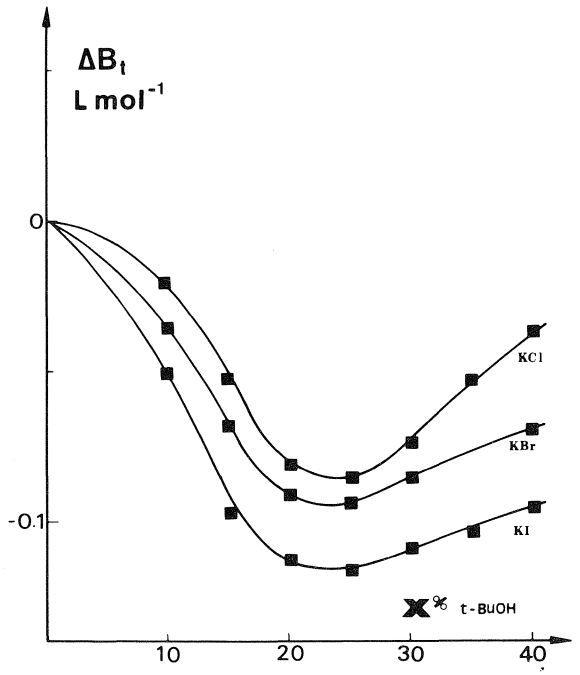

FIG. 2. Coefficients B de transfert des halogénures de potassium de l'eau aux mélanges eau – alcool *tert*-butylique.

alcalins, la profondeur du minimum augmente quand croît le rayon du cation, de même pour les halogénures de potassium, celle-ci augmente quand croît le rayon de l'anion; les courbes présentent un point d'inflexion marqué pour une composition de l'ordre de 15% en poids de *t*-BuOH.

La courbe représentative du coefficient B de HCl se différencie des autres courbes par la position de son minimum déplacée vers $X = 15\%$.

Si, sans chercher à distinguer le rôle respectif des zones A et B de Frank (18), on admet que l'électrolyte est globalement promoteur de la structure du solvant si $B > 0$ et briseur si $B < 0$, on peut énoncer la conclusion qualitative suivante: les électrolytes étudiés sont, soit moins promoteurs, soit plus briseurs, dans les mélanges étudiés que dans l'eau.

Ceci peut s'expliquer si l'on admet que ces mélanges sont plus structurés que l'eau pure: dans ces milieux, l'action des ions promoteurs qui induisent autour d'eux une structure de symétrie centrale (zone A) est moins marquée que dans l'eau ($B > 0$ mais plus petit que dans l'eau); au contraire, les ions briseurs dont l'influence est déterminée par celle de leur zone B, ont une action d'autant plus efficace que le milieu est plus structuré ($B < 0$ mais plus petit que dans l'eau). Ces conclusions doivent, à notre avis, être fortement nuancées. Le raisonnement ci-dessus

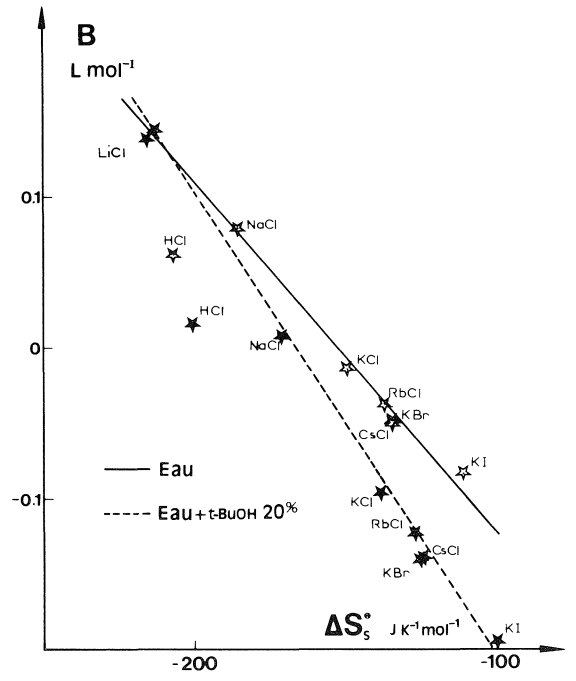

FIG. 3. Variation des coefficients B de viscosité des halogénures alcalins en fonction de leurs entropies de solvatation dans l'eau et dans un mélange eau – alcool *tert*-butylique à 20%.

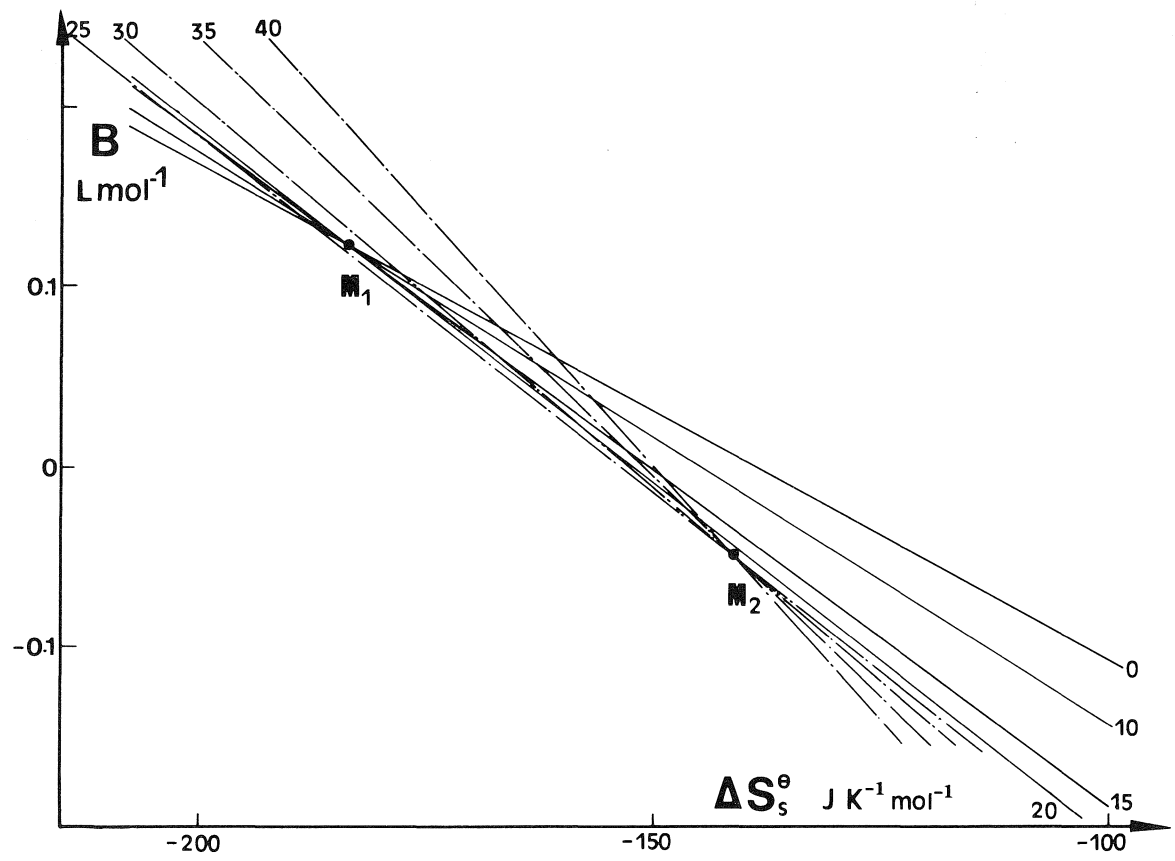

FIG. 4. Variation des coefficients B de viscosité des halogénures alcalins en fonction de leurs entropies de solvatation dans les mélanges eau – alcool *tert*-butylique.

est au mieux valable dans les mélanges très riches en eau où seule cette dernière intervient dans la cosphère des ions; quand on atteint des pourcentages assez élevés de *t*-BuOH dans le solvant, les molécules d'alcool sont elles aussi impliquées dans la solvatation des ions et sans doute même dans la zone A. Ce phénomène peut expliquer la croissance de B pour les fortes valeurs de X, et le fait que le minimum est d'autant moins prononcé que le cation ou l'anion est petit, c'est-à-dire comporte une zone A importante. Du fait de la superposition des deux effets: modification de la structure de l'eau et intervention des molécules d'alcool dans la solvatation, il est probable que le minimum des courbes $B = f(X)$ ne correspond pas au mélange de structure maximum; celui-ci se traduirait plutôt par la présence du point d'inflexion situé vers $X = 15\%$, point significatif d'un changement de tendance. Les derniers travaux relatifs à la structure des mélanges eau–*t*-BuOH montrent d'ailleurs que la composition en question correspond à la possibilité de formation d'un quasi-clathrate $(H_2O)_{21}$–*t*-BuOH, structure privilégiée dont la présence a pu être mise en évidence (19, 20).

2. Relations coefficient B — *entropie*

L'interprétation des courbes $\Delta B_t = f(X)$ reste assez délicate, tout comme celle des courbes relatives aux grandeurs thermodynamiques des électrolytes à dilution infinie dans les mélanges eau–*t*-BuOH. Il est cependant remarquable de constater la similitude des courbes des figs 1 et 2, avec celles représentant les variations de l'entropie de transfert ΔS_t^θ des mêmes électrolytes entre l'eau et les mêmes mélanges (3): au minimum de ΔB_t correspond un maximum de ΔS_t^θ et la présence du point d'inflexion pour la même valeur de X se trouve dans les deux familles de courbes. Il est donc probable qu'une relation précise existe entre les valeurs de B et l'entropie des ions dans les milieux étudiées.

Dans l'eau, Nightingale (12) a montré l'existence d'une corrélation linéaire entre B et l'entropie d'hydratation ΔS_h^θ des ions (grandeur thermo-

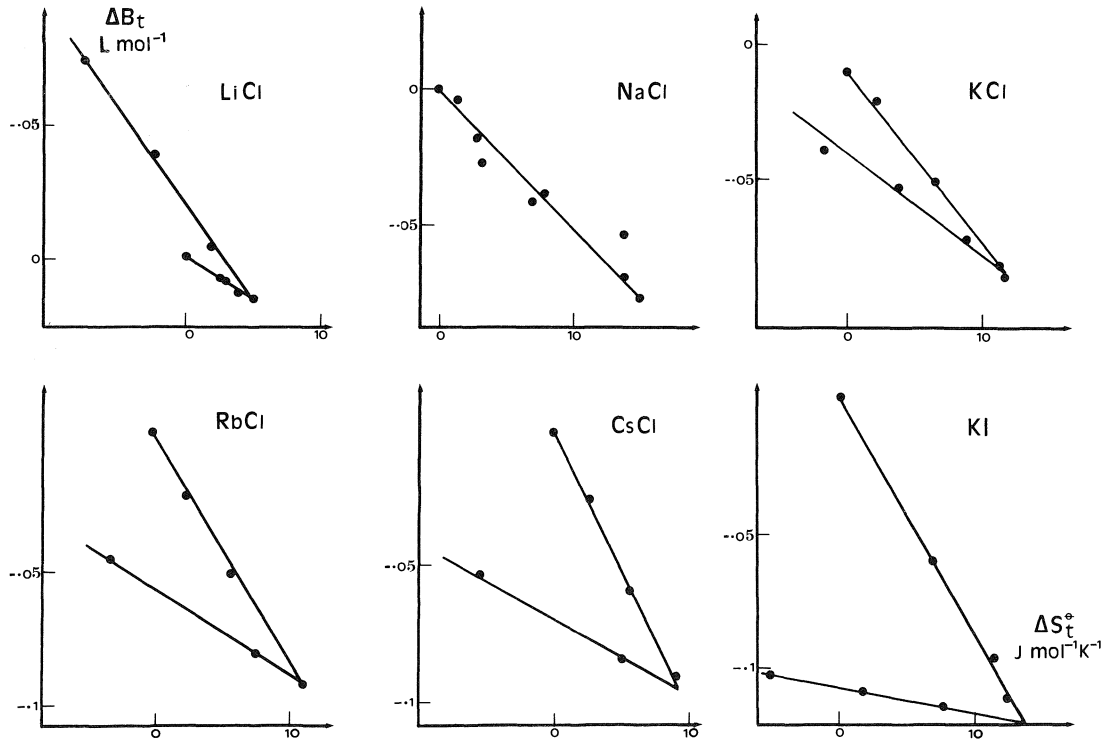

FIG. 5. Coefficients B de transfert des halogénures alcalins en fonction de leurs entropies de transfert de l'eau aux mélanges eau – alcool *tert*-butylique.

dynamique relative au passage de la phase gazeuse à l'état standard dans l'eau). Il nous est facile de calculer les entropies de solvatation ΔS_s^θ des différents électrolytes:

$$[3] \quad \Delta S_s^\theta = \Delta S_h^\theta + \Delta S_t^\theta$$

les valeurs de ΔS_h^θ étant celles données par Desnoyers et Jolicoeur (21).

Nous ne chercherons pas à attribuer leurs valeurs propres aux ions, ni pour B, ni pour ΔS_s^θ; le choix arbitraire que nous pourrions faire n'apporterait rien aux conclusions que nous allons tirer.

La fig. 3 montre que dans le cas où $X = 20\%$, la corrélation linéaire qui existe dans l'eau est conservée. (HCl ne se place pas sur la droite ni dans un cas, ni dans l'autre.) Il en est de même dans tous les mélanges c'est-à-dire pour toutes les valeurs de X étudiées. Sur la fig. 4, nous avons simplement tracé les droites moyennes traduisant toutes ces corrélations. Analytiquement, si l'on écrit:

$$[4] \quad B(MX) = a\Delta S_h^\theta(MX) + b \text{ dans l'eau}$$

on peut alors écrire, pour tous les mélanges de composition X:

$$[5] \quad B(MX) = (a' + \alpha X)\Delta S_s^\theta(MX) + (b' + \beta X)$$

relation qui traduit l'existence des deux faisceaux de droites de la fig. 4. Le traitement des valeurs numériques par la méthode des moindres carrés, avec B en mol^{-1} L et ΔS_s^θ en J K^{-1} mol^{-1} dans l'échelle des molarités, conduit aux valeurs suivantes:

Pour $X = 10, 15, 20$:

$$a' = a = -2.3 \times 10^{-3}$$
$$\alpha = 3.5 \times 10^{-5}$$
$$b' = b = 0.3$$
$$\beta = -0.8 \times 10^{-2}$$

Pour $X = 25, 30, 35, 40$:

$$a' = -1.8 \times 10^{-3} \neq a$$
$$\alpha = 5.0 \times 10^{-5}$$
$$b' = -0.3 = -b$$
$$\beta = -0.8 \times 10^{-2}$$

Ces deux groupes de valeurs traduisent nettement l'évolution différente de la même corrélation suivant

la zone de composition des mélanges que l'on considère, la frontière entre ces zones se situant vers la composition qui correspond au minimum des courbes $B = f(X)$, soit entre 20 et 25% en poids de *t*-BuOH. La signification précise des différents paramètres est naturellement difficile à donner; ceux-ci ont toutefois le mérite de faire apparaître clairement l'existence de deux types de milieux solvants dans le domaine que nous avons étudié: de l'eau pure jusqu'à un pourcentage un peu supérieur à 20% en poids de *t*-BuOH, le mélange se comporte essentiellement comme l'eau même si ses propriétés structurales évoluent, c'est donc une structure de type essentiellement aqueux qui détermine les grandeurs thermodynamiques et de transport qui traduisent la solvatation; pour des pourcentages en alcool allant de 25 à 40%, il s'agit d'un autre type de milieu où les caractéristiques de la structure aqueuse ont disparu.

Les courbes de la fig. 5 où est porté ΔB_t en fonction de ΔS_t^{θ}, c'est-à-dire les fonctions de transfert, traduisent de façon encore plus spectaculaire la discontinuité entre les deux types de milieu: il apparait ici deux corrélations linéaires distinctes suivant la zone de composition pour un électrolyte donné.

Conclusion

Des variations importantes ont été observées pour les valeurs des coefficients *B* des halogénures alcalins dans les mélanges eau–*t*-BuOH; celles-ci peuvent s'interpréter en admettant que l'alcool ajouté augmente la structure de la phase aqueuse, au moins dans les milieux les plus riches en eau. Nous considérons comme plus interessantes les observations suivantes.

Dans tous les solvants mixtes étudiés, il existe, comme dans l'eau, une relation de proportionnalité entre l'entropie de solvatation des ions et leur coefficient *B* de viscosité. Ces deux grandeurs macroscopiques traduisent donc, d'une façon semble-t-il assez générale, les mêmes phénomènes au niveau moléculaire: le bilan global de la modification des degrés de liberté du solvant due à la présence de l'ion.

De plus l'étude des corrélations entre ΔS^{θ} et *B* permet de mettre en évidence, dans les mélanges étudiés, deux zones bien définies: celle des mélanges riches en eau au comportement déterminé par leur structure de type aqueux, et, pour des pourcentages en alcool supérieurs à 20%, des mélanges hydro-organiques qui ne recélent sans doute plus rien de la structure tridimensionnelle de l'eau.

1. M. Palma et J. P. Morel. Can. J. Chem. **55**, 1521 (1977).
2. M. Palma et J. P. Morel. J. Solution Chem. A paraître.
3. Y. Pointud, J. Juillard, J. P. Morel et L. Avedikian. Electrochim. Acta, **19**, 229 (1974).
4. Y. Pointud, J. Juillard, L. Avedikian, J. P. Morel et M. Ducros. Thermochim. Acta, **8**, 423 (1974).
5. L. Avedikian, G. Perron et J. E. Desnoyers. J. Solution Chem. **4**, 331 (1975).
6. G. Jones et M. Dole. J. Am. Chem. Soc. **51**, 2950 (1929).
7. W. M. Cox et J. H. Wolfenden. Proc. R. Soc. Ser. A, **145**, 475 (1934).
8. M. Kaminsky. Z. Phys. Chem. **5**, 154 (1955); **8**, 173 (1956); **12**, 206 (1957).
9. J. E. Desnoyers et G. Perron. J. Solution Chem. **1**, 199 (1972).
10. A. Einstein. Ann. Phys. Leipzig. **19**, 289 (1906).
11. H. S. Frank et M. W. Evans. J. Chem. Phys. **13**, 507 (1945).
12. E. R. Nightingale, Jr. J. Phys. Chem. **63**, 1381 (1959).
13. G. Engel et H. G. Hertz. Ber. Bunsenges. Phys. Chem. **72**, 808 (1968).
14. D. Feakins, D. J. Freemantle et K. G. Lawrence. J. Chem. Soc. Faraday Trans. 1, **70**, 795 (1974).
15. M. Palma et J. P. Morel. J. Chim. Phys. **73**, 645 (1976).
16. J. P. Morel et J. Morin. J. Chim. Phys. **67**, 2018 (1970).
17. H. Falkenhagen et E. L. Vernon. Phys. Z. 33 (1932).
18. H. S. Frank et Y. Wen. Discuss. Faraday Soc. **24**, 133 (1957).
19. C. de Visser, G. Perron et J. E. Desnoyers. Can. J. Chem. **55**, 856 (1977) et autres références citées dans cet article.
20. K. Iwasaki et T. Fujiyama. J. Phys. Chem. **81**, 1908 (1977); **83**, 463 (1979).
21. J. E. Desnoyers et C. Jolicoeur. *Dans* Modern aspects of electrochemistry. n° 5. *Edité par* J. O'M. Bockris et B. E. Conway. Butterworths, London. 1969.

A ^1H and ^{13}C nuclear magnetic resonance study of silicon and germanium chalcogenide derivatives

JOHN E. DRAKE, BORIS M. GLAVINĆEVSKI, ROBYN HUMPHRIES, AND ABDUL MAJID

Department of Chemistry, University of Windsor, Windsor, Ont., Canada N9B 3P4

Received June 28, 1979

JOHN E. DRAKE, BORIS M. GLAVINĆEVSKI, ROBYN HUMPHRIES, and ABDUL MAJID. Can. J. Chem. **57**, 3253 (1979).

This paper reports the ^1H and ^{13}C nmr parameters of the disilyl- and digermyl-chalcogenide species $(Me_nH_{3-n}M)_2E$, where M = Si, Ge; E = O, S, Se, Te and n = 0 to 3. The general pattern of changing shifts is markedly influenced by methyl substitution.

JOHN E. DRAKE, BORIS M. GLAVINĆEVSKI, ROBYN HUMPHRIES et ABDUL MAJID. Can. J. Chem. **57**, 3253 (1979).

On rapporte les paramètres rmn du ^{13}C et du ^1H des espèces chalcogénides disylilés et digermylés $(Me_nH_{3-n}M)_2E$ ou M = Si, Ge; E = O, S, Se, Te et n = 0 à 3. Le schéma général des changements des déplacements chimiques est fortement influencé par la substitution du méthyle.

[Traduit par le journal]

Introduction

In a recent study of bis(methylgermyl) and bis(dimethylgermyl) chalcogenides, a comprehensive table was presented of their ^1H nmr parameters along with other spectroscopic data (1). We report herein similar data for the silicon analogues along with ^{13}C nmr shift data for both the silicon and germanium counterparts. Despite claims to the contrary, the theoretical principles and molecular parameters affecting ^{13}C nmr parameters, at least for organometallic compounds, are still not well understood (2) and it is difficult to advance beyond empirical correlations to rationalise trends in such parameters as chemical shifts or coupling constants (3–6).

Experimental

The species $(Me_nH_{3-n}Si)_2E$ were prepared by methods developed in our laboratory for the analogous germanium compounds (1).

The natural abundance carbon-13 spectra were obtained on a Bruker CPX 100 (FT model) spectrometer operating at a resonance frequency of 22.639 MHz, at a probe temperature of 35°C. All spectra were recorded under ^1H noise-decoupling conditions. The samples were sealed in capillaries as neat liquids and the capillaries were placed coaxially in 5 mm tubes containing $CDCl_3$ which served as a lock and TMS as standard.

The proton spectra were recorded on a JEOL C-60HL spectrometer operating at a resonance frequency of 60 MHz at room temperature. Chemical shifts are in ppm ($\delta \pm 0.02$ ppm) to low field of internal TMS in CCl_4 solution (5% v/v). Chemical shifts of the tellurides were measured relative to cyclohexane. Deviations for coupling constants of neat liquids are J(HH) ± 0.05 Hz, J(SiH) ± 1.0 Hz, and J(CH) ± 0.2 Hz.

Results and Discussion

The ^1H nmr parameters for the whole series of $(Me_nH_{3-n}Si)_2E$ compounds ($n = 0 \rightarrow 3$; E = O, S, Se, Te) are presented in Table 1, along with their ^{13}C chemical shifts, as well as those of their germanium analogues.

α-^1H and α-^{13}C Chemical Shifts

It is a general trend in methyl-hydrido-silane (3) and -germane (7) derivatives of the type $Me_nH_{3-n}MX$ (M = Si, Ge; X = F, Cl, Br, I; n = 0, 1, 2) that the α-proton shifts are principally controlled by the inductive effect. The same is also true for the series of chalcogermanes (1) of the type $(Me_nH_{3-n}Ge)E$ (E = O, S, Se, Te) and for the series $(H_3Si)_2E$, a distinctive trend in the α-proton chemical shifts (δ(SiH)) shows a steady up-field shift as the chalcogen changes from O → S → Se → Te (see Table 1 and Fig. 1(*a*)). Thus, the less electron-withdrawing chalcogens are expected to leave the α-protons more shielded. The trend is relatively large with the total shift (Δ^1H, O → Te) from oxygen to tellurium being 0.90, but considerably less than in the $(H_3Ge)_2E$ series where Δ^1H, O → Te, is 1.69 (1) (Fig. 1(*b*)). This difference mainly arises because of the much higher shifts of the oxides of germanium, suggesting that oxygen is not as effectively electronegative relative to silicon as it is to germanium. This is expected if $(p$–$d)\pi$ bonding is more important in the silanes. The trend persists but is less marked (Δ^1H, O → Te, = 0.41) for the series $(MeH_2Si)_2E$ (Fig. 1(*c*)) again reflecting what was found for $(MeH_2Ge)_2E$ (Fig. 1(*d*); Δ^1H, O → Te, = 1.06 (1)). An examination of the corresponding α-^{13}C chemical shifts for the monomethylated series (Fig. 1(*c*) and (*d*)) confirms similar progressive high field shifts ($\Delta^{13}C$, O → Te, = 3.45 (Si) and 3.48 (Ge)). However, as can be seen from

0008-4042/79/243253-04$01.00/0

TABLE 1. The ^1H and ^{13}C nmr parameters of $(Me_nH_{3-n}Si)_2E$ species[a]

Compound	$^1H\delta$(Me)	$^{13}C\delta$(Me)	$^1H\delta$(SiH)	$\lvert J_{HH}^{vic}\rvert$	$\lvert J^{29}SiH\rvert$	$\lvert J^{13}CH\rvert$	$^{13}C\delta$(Me)Ge
$(H_3Si)_2O$[b]	—	—	4.61	—	221.5	—	—
$(MeH_2Si)_2O$[c]	0.28	−1.23	4.66	3.33	213.0	121.5	−0.48
$(Me_2HSi)_2O$[c]	0.14	−0.58	4.69	2.85	204.9	120.0	1.03
$(Me_3Si)_2O$[c,d]	0.06	0.97	—	—	—	118.0	3.25
$(H_3Si)_2S$[b]	—	—	4.35	—	223.7	—	—
$(MeH_2Si)_2S$[b]	0.49	−3.51	4.47	3.83	214.7	123.0	−0.91
$(Me_2HSi)_2S$[c]	0.38	0.58	4.63	3.39	205.1	121.2	2.18
$(Me_3Si)_2S$[c,d]	0.31	3.77	—	—	—	119.3	5.65
$(H_3Si)_2Se$[d]	—	—	4.12	—	224.0	—	—
$(MeH_2Si)_2Se$	0.59	−3.64	4.43	3.98	215.8	124.5	−1.23
$(Me_2HSi)_2Se$	0.51	0.59	4.73	3.54	205.5	121.4	2.27
$(Me_3Si)_2Se$[d]	0.42	4.81	—	—	—	120.6	5.98
$(H_3Si)_2Te$[e]	—	—	3.71	—	224.4	—	—
$(MeH_2Si)_2Te$	0.73	−4.68	4.25	4.14	216.2	125.3	−3.96
$(Me_2HSi)_2Te$	0.63	0.47	4.82	3.74	206.0	122.7	2.06
$(Me_3Si)_2Te$[b,f,g]	0.58	6.24	—	—	—	121.5	7.08

[a] ^1H nmr parameters of $(Me_nH_{3-n}Ge)_2E$ can be found in ref. 1. ^1H and ^{13}C nmr parameters referenced to external TMS as standard.
[b] Reference 4.
[c] Reference 3.
[d] Reference 11.
[e] Reference 18.
[f] Reference 19.
[g] Compare with $^1H\delta$(Me) of $(Me_3Si)_2Te$ (C_6H_{12} solution) of 0.67 ppm in ref. 19 and 0.60 ppm (CCl_4 solution) in ref. 17.

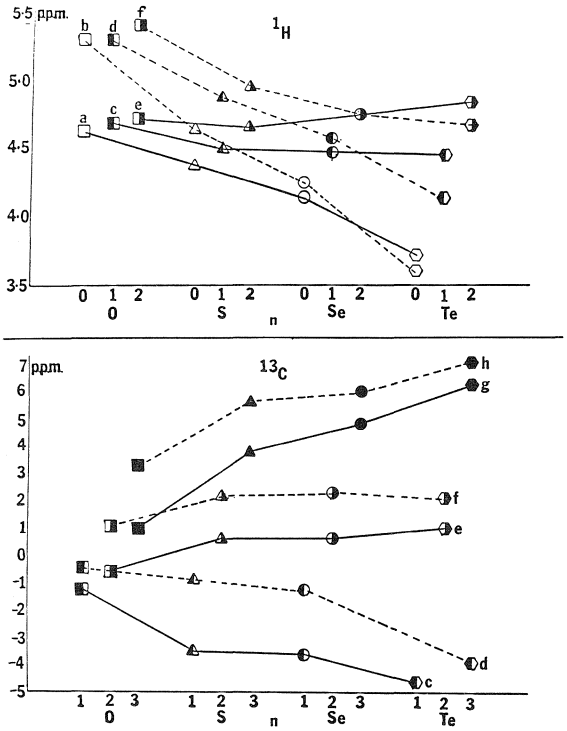

FIG. 1. Change in α-^1H and α-^{13}C chemical shifts with changing number of methyl groups and chalcogens in the series $(Me_nH_{3-n}M)_2E$ drawn to emphasize result of chalcogen changes. $(H_3Si)_2E$ = *a*; $(H_3Ge)_2E$ = *b*; $(MeH_2Si)_2E$ = *c*; $(MeH_2Ge)_2E$ = *d*; $(Me_2HSi)_2E$ = *e*; $(Me_2HGe)_2E$ = *f*; $(Me_3Si)_2E$ = *g*; and $(Me_3Ge)_2E$ = *h*. Oxides □; sulfides △; selenides ○; tellurides ⬡; silicon series —; germanium series

Fig. 1(*e*, *f*, *g*, *h*) there is a reversal in the direction of the trend for both the silicon and germanium $(Me_2HM)_2E$ compounds ($\Delta^{13}C$, O → Te, = −1.49 (Si) and −1.03 (Ge)) which is more marked for the $(Me_3M)_2E$ derivatives ($\Delta^{13}C$, O → Te, = −5.27 (Si) and −3.83 (Ge)). The α-proton shifts in the $(Me_2HSi)_2E$ series also show a slight overall downfield shift (Fig. 1(*e*)) although the $(Me_2HGe)_2E$ series still maintains the upfield shift. Nevertheless, the general trends imply that the factors resulting in an overshadowing of the inductive effect influence both the α-^1H and α-^{13}C chemical shifts and have a similar effect on both the silicon and germanium derivatives.

The effect of successive substitution of protons by methyl groups within the $(Me_nH_{3-n}M)_2E$ series where the chalcogen is unchanged is illustrated in Fig. 2 for the α-^1H and ^{13}C shifts respectively. In general, (*i*) increasing methylation results in a decreased shielding of the α-carbons (8) as well as the α-protons; (*ii*) the effects are much more marked in the $(Me_nH_{3-n}M)_2Te$ compounds ($\Delta^{13}C$, *n* = 1 to 3, = −10.92 (Si) and −11.04 (Ge); Δ^1H, *n* = 0 to 2, −1.11 (Si) and −1.06 (Ge) (1)), becoming progressively less marked through the selenium and sulfur series and being relatively small in the $(Me_nH_{3-n}M)_2O$ compounds ($\Delta^{13}C$, *n* = 1 to 3, = −2.20 (Si) and −3.25 (Ge); Δ^1H, *n* = 0 to 2, −0.08 (Si) and −0.12 (Ge) (1)); (*iii*) the general pattern of changing shifts is similar on silicon and germanium compounds.

β-^1H *Chemical Shifts*

The trends in the CH_3 resonance shifts are typical

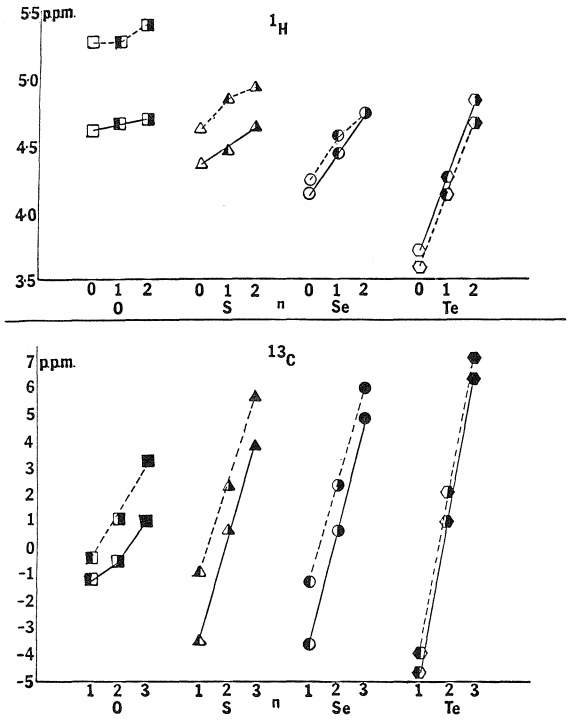

FIG. 2. Change in the α-^{1}H and α-^{13}C chemical shifts drawn to emphasize changes in number of methyl groups. Symbols as in Fig. 1.

of observation on the related halogeno-silanes (3) and halogeno- (7) and chalco- (1, 9) germanes. Thus, there is a shift to higher field with increasing methyl substitution and a shift to lower field as the chalcogen changes from the more electronegative but smaller oxygen atom through to the less electronegative but bulkier tellurium atom. β-Proton shifts are generally assumed to be related to anisotropic rather than inductive effects and this is also apparently the case with these $(Me_nH_{3-n}Si)_2E$ species.

Coupling Constants

The ^{13}C- and ^{29}Si-proton coupling constants were evaluated from the well-resolved satellites of the β- and α-proton resonances. Satellites were also observed that arose from long-range spin–spin coupling involving ^{77}Se and ^{125}Te suggesting that exchange, if any, of silyl groups must be slow.

The largest trend in changing values of coupling constants arises in the decrease in $J(^{29}SiH)$ as methyl groups substitute for protons. Assuming that the lower value indicates a decrease in *s*-character (6, 10) and that Bent's rule is operative (11), then the methyl group is behaving as a less-electronegative group than hydrogen. This further suggests that the "methyl-effect" is not one primarily associated with an inductive contribution. On the other hand, the increase, albeit very slight, in the value of $J(^{29}SiH)$ along the series O → S → Se → Te, implies an increasing electronegativity from oxygen to tellurium which violates chemical sense. However, as with the α-chemical shifts, the effect of methyl substitution is more pronounced than the change of chalcogen. A comparison of the values of $J(^{13}CH)$ in the silicon series with those of the corresponding germanium series (1) shows the consistent feature of decrease with methyl-substitution and increase along the series O → S → Se → Te. The trends are small but, in contrast to $J^{29}SiH$, of about the same magnitude. The absolute values are about 8 Hz higher for the germanes than for the silanes, implying that the silicon moieties are less electronegative than their germanium counterparts, which is consistent with the findings of others (12).

By contrast, the values of the vicinal coupling constants $J(_{HH}{}^{vic})$ are consistently higher in the silanes than in germanes (1), although trends related to changes in the number of methyl groups and the nature of the chalcogen are identical. This is not unexpected for compounds that are presumably structurally similar with a slightly longer H—C—M—H distance for the germanes (7, 13). The long range *J*(H—Si—Te—Si—H′) coupling is observed and its value of 0.59 Hz fits into the general series of similar compounds that have been studied (14–16) and in particular, finishes the sequence of $H_3SiESiH_3$ compounds where *J*(HH′) is 0.70, 0.63, and 0.59 Hz for S, Se, and Te, respectively.

Acknowledgement

We thank the Natural Sciences and Engineering Research Council of Canada for financial support.

1. J. E. DRAKE, B. M. GLAVINCEVSKI, H. E. HENDERSON, and R. T. HEMMINGS. Can. J. Chem. **56**, 465 (1978).
2. G. A. MACIEL. Substituent effects on ^{13}C chemical shifts. Topics in C-13 n.m.r. spectroscopy. Vol. 1. *Edited by* G. C. Levy. Wiley and Sons, New York, NY. 1974.
3. E. A. V. EBSWORTH and S. G. FRANKISS. Trans. Faraday Soc. 1574 (1967); 1518 (1963).
4. E. A. V. EBSWORTH and J. J. TURNER. J. Phys. Chem. **67**, 805 (1963).
5. E. A. V. EBSWORTH. Physical basis of the chemistry of the group IV elements. Organometallic compounds of the group IV elements. Vol. 1. *Edited by* A. G. MacDiarmid. Marcel Dekker, Inc., New York, NY. 1968.
6. C. JUAN and H. S. GUTOWSKY. J. Chem. Phys. **37**, 2198 (1962).
7. G. K. BARKER, J. E. DRAKE, and R. T. HEMMINGS. Can. J. Chem. **52**, 2622 (1974); J. E. DRAKE and R. T. HEMMINGS. Can. J. Chem. **51**, 302 (1973); J. E. DRAKE, R. T. HEMMINGS, and C. RIDDLE. J. Chem. Soc. A, 3359 (1970).
8. J. B. STOTHERS. Carbon-13 NMR spectroscopy. Academic Press, New York, NY. 1972.
9. J. E. DRAKE, R. T. HEMMINGS, and H. E. HENDERSON. J. Chem. Soc. Dalton Trans. 366 (1976).

10. N. MULLER and D. E. PRITCHARD. J. Chem. Phys. **31**, 768 (1959); **31**, 1471 (1959).
11. H. A. BENT. J. Chem. Educ. **37**, 616 (1960); J. Chem. Phys. **33**, 1258 (1960); **33**, 1259 (1960); **33**, 1260 (1960); Chem. Rev. **61**, 275 (1961).
12. J. E. HUHEEY. Inorganic chemistry: principles of structure and reactivity. Harper and Row, New York, NY. 1972. pp. 622–625.
13. C. H. VAN DYKE and A. G. MACDIARMID. Inorg. Chem. **3**, 1071 (1964).
14. E. A. V. EBSWORTH. Volatile silicon compounds. Pergamon Press, Inc., New York, NY. 1963.
15. J. E. DRAKE and C. RIDDLE. Inorg. Nucl. Chem. Lett. **6**, 713 (1970); J. Chem. Soc. A, 3134 (1970).
16. J. T. WANG and C. H. VAN DYKE. Chem. Commun. 612 (1967).
17. K. A. HOOTON and A. L. ALLRED. Inorg. Chem. **4**, 671 (1965).
18. H. BURGER and U. GOETZE. Inorg. Nucl. Chem. Lett. 549 (1967).
19. H. BURGER and U. GOETZE. Spectrochim. Acta, 2003 (1968).

The synthesis of cyclic peptides by the four component condensation (4 CC)

AMADEO FAILLI, HANS IMMER, AND MANFRED GÖTZ

Department of Chemistry, Ayerst Research Laboratories, P.O. Box 6115, Montreal, P.Q., Canada H3C 3J1

Received November 1, 1978

This paper is dedicated to Prof. Karel Wiesner on the occasion of his 60th birthday

AMADEO FAILLI, HANS IMMER, and MANFRED GÖTZ. Can. J. Chem. **57**, 3257 (1979).

Since cyclic peptides constitute a group of natural and synthetic products of considerable practical and theoretical significance, model experiments were carried out to explore the scope of the four component condensation for the synthesis of these structures.

AMADEO FAILLI, HANS IMMER et MANFRED GÖTZ. Can. J. Chem. **57**, 3257 (1979).

Depuis que les peptides cycliques ont été reconnus comme groupe de composés naturels et synthétiques d'une importance théorique et pratique considérable, des expériences pilotes ont été réalisées dans le but d'explorer la portée de la condensation à quatre constituants lors de la synthèse de ces peptides cycliques.

[Traduit par le journal]

Introduction

In spite of the remarkable versatility of the four component condensation (4 CC) (1), the reaction has not been widely applied to the solution of problems in medicinal chemistry. Notable exceptions are the synthesis of a penam derivative (2), work towards the preparation of an oxacepham derivative (3), and reports from our laboratories dealing with the synthesis of *N*-amino-peptides (4, 5) and the potential anti-Parkinson drug pareptide (6).

Cyclic peptides constitute a group of natural and synthetic products of considerable practical and theoretical significance (7, 8); they act as hormones, antibiotics, toxins, and also affect membrane function. Hence our interest in synthetic approaches to cyclic peptides by the 4 CC.

Results

The preparation of cyclic tripeptides by traditional methods is only successful if *N*-substituted amino acids are employed, for instance proline or sarcosine, since the *cis* configuration of the amide bonds in the linear tripeptide is sufficiently stable to allow ring closure (9, 10). On the other hand, a few syntheses of cyclic tetrapeptides containing exclusively *N*-unsubstituted amino acids as building blocks have been reported (11*a*, *b*). The preparation of *N*-unsubstituted cyclic tripeptides by the 4 CC appears feasible since the primary addition product **A** constitutes a 12-membered ring, which then collapses to the strained cyclic tripeptide, similar to the formation of a strained β-lactam from a 7-membered ring (2, 3).

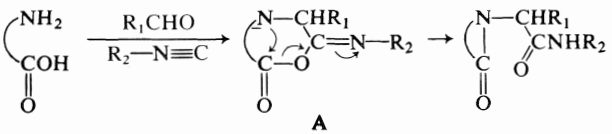

A

To test this hypothesis, triglycine was used as a model compound in the 4 CC. Disappointingly, the two products isolated turned out to be substituted cyclic hexaglycines, resulting from a doubling reaction (11*b*, 12) (Scheme 1). It follows that **A** was either never formed or the collapse of **A** to the desired 9-membered ring was disfavoured in comparison to the intermolecular reaction of two molecules of **A**. An intermolecular 4 CC and a subsequent intramolecular 4 CC could also account for the products isolated, and similarly the collapse of a 24-membered ring, initially created by a double 4 CC. Since two asymmetric centres are present in **1** or **2** both a racemate and the *meso* form are obtained in each case.

The facile formation of cyclic hexapeptides by a doubling reaction in the course of a 4 CC indicates that similar compounds should be generated by a single 4 CC, provided a suitable linear hexapeptide is employed as starting material. In a model experiment hexaglycine underwent the 4 CC in the presence of isobutyraldehyde and cyclohexyl isonitrile to yield the desired racemic cyclic hexapeptide **3** (Scheme 2).

This result encouraged us to attempt the ring closure of a slightly modified C-terminal eledoisin hexapeptide. In view of the blood pressure lowering effect of eledoisin and many of its shortened analogs (13), these molecules were modified in a variety of ways in an attempt to prolong their biological half-life (5, 14–17). A hitherto unreported ring closed eledoisin derivative would be less prone to attack by

[1]I. Vavra, Department of Pharmacology, Ayerst Research Labs. Private communication.

0008-4042/79/243257-05$01.00/0

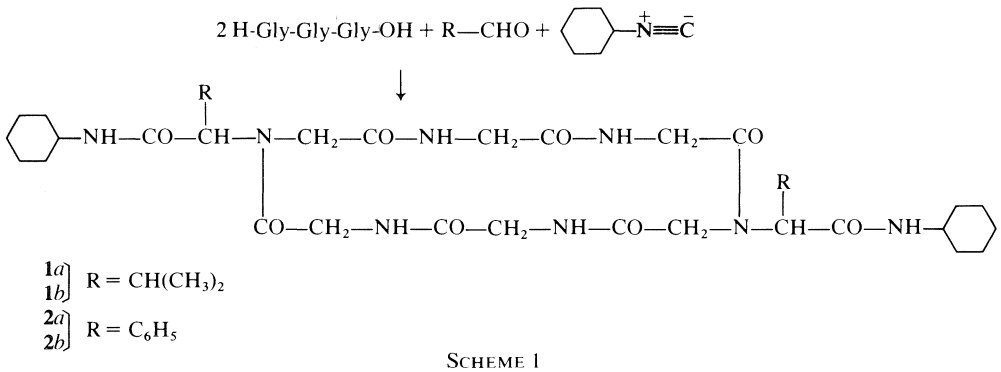

SCHEME 1

exopeptidases. The starting material **4** (H-Ala-Phe-Val-Gly-Leu-Met-OH) has not been described previously and it was obtained by conventional methods as shown in Scheme 3.

On cyclization of **4** with isobutyraldehyde and cyclohexyl isocyanide the diastereomeric mixture **5***a*, *b* was isolated (Scheme 4). On chromatography **5***a*, *b* could readily be separated. The combined yield of cyclic material amounted to 33%, comparable to yields achieved by other cyclization reactions (18, 19). It should be noted that none of the yields reported in this communication was maximized.

Compounds **5***a* and **5***b* were without effect on the cardiovascular system.[1]

In the type of cyclization described in this paper a new substituent is introduced as side chain in the original amino acid sequence. It should be noted that appropriate choice of the aldehyde (20) will lead to substituents which can be removed after cyclization. Experiments towards this goal are in progress.

Experimental

The nmr spectra were obtained on a Varian A-60A spectrometer, mass spectra on an LKB 9000S spectrometer, and ir spectra on a Perkin Elmer 225 infrared spectrophotometer.

Synthesis of **1**a *and* **1**b

Isobutyraldehyde (2.16 g, 30 mmol) was added under stirring to a suspension of glycyl-glycyl-glycine (1.7 g, 9 mmol) in dry ethylene glycol (15 mL). The ice cold mixture was treated dropwise with cyclohexyl isonitrile (0.97 g, 9 mmol) and left at room temperature for 5 days. After dilution with water the precipitate was collected, washed with water, and chromatographed on silica gel. On elution with $CHCl_3$/CH_3OH (95:5) isomers **1***a* and **1***b* were isolated. Isomer **1***a*: recrystallized from $CHCl_3$/CH_3OH; mp 286–287°C (dec.); yield: 380 mg (12%); ir (Nujol) ν: 3350, 3290, 1692, 1640, 1550; nmr ($CDCl_3$/CD_3OD 4:1): 1.00 and 1.05 (2d, J = 7 Hz, 12H, $(CH_3)_2CH$) ppm; ms (*m*/*e*: 704(M^+), 686, 668. *Anal.* calcd. for $C_{34}H_{56}N_8O_8 \times 0.94\%$ H_2O (K. Fischer): C 57.30, H 8.04, N 15.75; found: C 57.05, H 8.04, N 15.45. Isomer **1***b*: recrystallized from acetone; mp 210°C (dec.); yield: 230 mg (8%); ir (Nujol) ν: 3530, 3350, 3060, 1680, 1640, 1540; nmr ($CDCl_3$/CD_3OD 4:1): 1.04 (2d, J = 7 Hz, 12H, $(CH_3)_2CH$) ppm; ms (*m*/*e*): 704(M^+), 686, 668. Isomers **1***a* and **1***b* were homogenous on tlc (system: $CHCl_3$/CH_3OH 92:8; charring with H_2SO_4). *Anal.* calcd. for $C_{34}H_{56}N_8O_8 \times 0.84\%$ H_2O (K. Fischer): C 57.44, H 8.03, N 15.76; found: C 56.83, H 7.85, N 15.34.

Synthesis of **2**a *and* **2**b

Benzaldehyde (10.6 g, 100 mmol) was added under stirring to a suspension of glycyl-glycyl-glycine (5.67 g, 30 mmol) in dry ethylene glycol (50 mL). The ice cold mixture was treated dropwise with cyclohexyl isonitrile (3.27 g, 30 mmol) and left at room temperature for 9 days. H_2O (100 mL) and $CHCl_3$ (150 mL) were added, followed by traces of CH_3OH to prevent formation of a gum. On standing a colorless solid separated (800 mg, **2***a*). The aqueous phase was exhaustively extracted with $CHCl_3$; the combined organic layers were dried and evaporated to dryness. The residue was triturated with acetone and the separated solid collected (842 mg, **2***b*). On silica gel chromatography of the mother liquor additional quantities of both isomers were isolated. Isomer **2***a*: recrystallized from $CHCl_3$/CH_3OH; mp 330–333°C (dec.); yield: 1.309 g (11.3%); ir (Nujol) ν: 3340, 3270, 3220, 3050, 1670, 1650, 1632, 1574, 1546; ms (*m*/*e*): 772(M^+), 754, 736. *Anal.* calcd. for $C_{40}H_{52}N_8O_8 \times 0.22\%$ H_2O (K. Fischer): C 62.02, H 6.78, N 14.45; found: C 61.52, H 6.86, N 14.30. Isomer **2***b*: recrystallized from $CHCl_3$/CH_3OH; mp 341–343°C (dec.); yield: 579 mg (5%); ir (Nujol) ν: 3340, 3250, 3090, 1665, 1650,

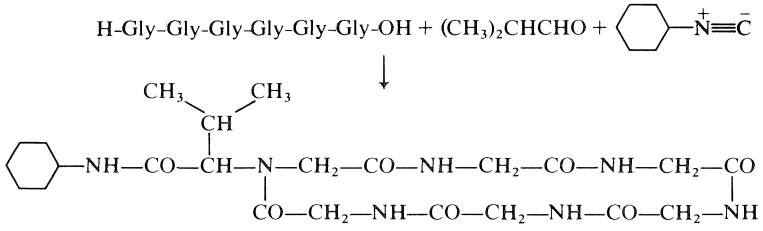

3

SCHEME 2

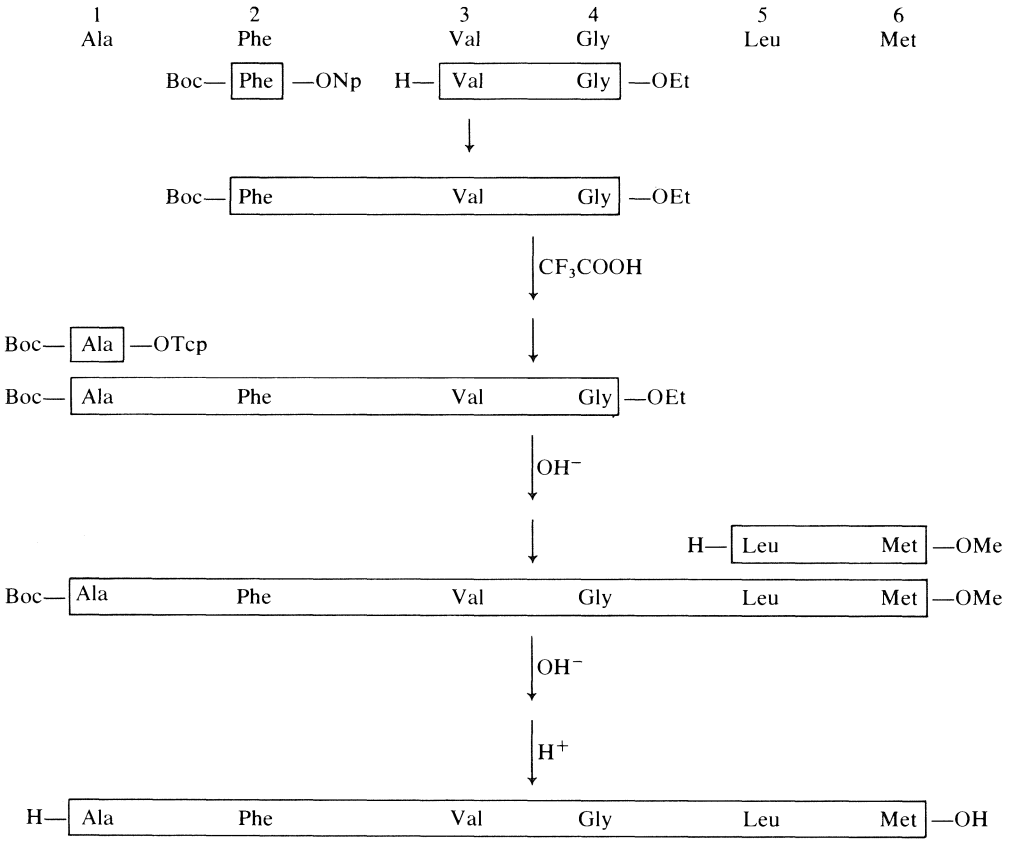

4

SCHEME 3

1562, 1520. The sample was not volatile enough to give a useful mass spectrum. Isomers **2***a* and **2***b* were homogenous on tlc (system: $CHCl_3/CH_3OH$ 92:8; charring with H_2SO_4). *Anal.* calcd. for $C_{40}H_{52}N_8O_8$: C 62.10, H 6.77, N 14.35; found: C 62.09, H 6.83, N 14.28.

Hexaglycine Trifluoroacetate

A mixture of *N*-benzyloxycarbonyl hexaglycine (21) (3.6 g, 7.28 mmol) and anhydrous CF_3COOH (12 mL) was refluxed for 90 min under stirring. The solvent was removed *in vacuo*, the residue treated with H_2O and neutralized with cold

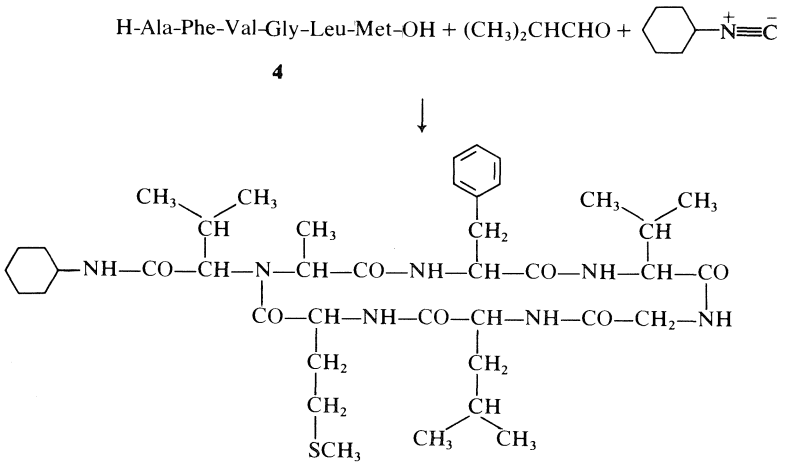

5*a*, *b*

SCHEME 4

NH_4OH. The solid was collected, washed with H_2O and C_2H_5OH, dissolved in hot, dilute NH_4OH, charcoalized, and filtered. The solution was concentrated *in vacuo*, the precipitate collected and washed with H_2O, followed by C_2H_5OH; mp dec. >240°C; yield: 2.47 g (60%); nmr (TFA): 4.25 (s, CH_2) ppm. *Anal.* calcd. for $C_{12}H_{20}N_6O_7$: C 39.96, H 5.55, N 23.33; found: C 40.06, H 5.56, N 22.82. A suspension of hexaglycine (2.24 g, 6.24 mmol) was stirred with CF_3COOH (8 mL) until complete solution was achieved. The excess acid was removed *in vacuo*, the residue triturated with ether, the solid collected and washed with ether; mp 227°C (dec.). Homogenous on electrophoresis (pH 1.6; Ninhydrin).

Synthesis of **3**

In the course of 8 h, a warm solution of hexaglycine trifluoroacetate (2.94 g, 6.19 mmol) in dry DMSO (5 mL) was added dropwise to a vigorously stirred solution of isobutyraldehyde (1.52 g, 20.64 mmol), cyclohexyl isonitrile (0.68 g, 6.19 mmol), and triethylamine (0.620 g, 6.19 mmol) in dry DMSO (15 mL). The pH was adjusted to 7 with pyridine and the mixture was stirred at room temperature for 5 days. The solvent was removed *in vacuo* and the residue chromatographed on silica gel ($CHCl_3/CH_3OH$, 9:1). The desired fractions were combined, evaporated, and triturated with acetone/ether/hexane. Yield: 624 mg (19%); mp 317–320°C (dec.); ir (Nujol) ν: 3300, 1670, 1540; nmr (DMSO): 0.94 (d, J = 7 Hz, 6H, $(CH_3)_2CH$) ppm; ms (*m/e*): 523(M^+), 505. Homogenous on tlc (system: $CHCl_3/CH_3OH$ 85:15; I_2 and charring with H_2SO_4). *Anal.* calcd. for $C_{23}H_{37}N_7O_7$: C 52.76, H 7.12, N 18.72; found: C 52.93, H 7.24, N 18.55

Boc-Phe-Val-Gly-OEt

$(C_2H_5)_3N$ (3.03 g, 30 mmol) was added to a cold solution of H-Val-Gly-OEt × HCl (22) (7.14 g, 30 mmol) in dry DMF (65 mL). The mixture was filtered into a cold solution of Boc-Phe-ONp (22) (11.6 g, 30 mmol) in dry DMF (33 mL). After 3 days at 0°C the solution was poured into ice/H_2O, the product collected, washed with H_2O, and dried. The material was recrystallized from CH_3OH/IPE; mp 160–162°C; yield: 11.94 g (88%); $[\alpha]_D^{25} = -13.9°$ (*c* 1.0 in DMF); nmr ($CDCl_3$): 0.84, 0.97 (2d, J = 3 Hz, 6H, $(CH_3)_2CH$), 1.24 (t, J = 7 Hz, 3H, CH_3CH_2O), 1.36 (s, 9H, $(CH_3)_3C$), 7.21 (s, 5H, arom) ppm; ms (*m/e*): 449(M^+). Homogenous on tlc (system: C_6H_6/EtOAc 50:50; charring with ammonium molybdate). *Anal.* calcd. for $C_{23}H_{35}N_3O_6$: C 61.43, H 7.84, N 9.34; found: C 61.44, H 8.05, N 9.26.

Boc-Ala-Phe-Val-Gly-OEt

Boc-Phe-Val-Gly-OEt (11.2 g, 25 mmol) was deprotected with cold CF_3COOH in the usual way. The H-Phe-Val-Gly-OEt × CF_3COOH obtained was dissolved in dry DMF (45 mL) and $(C_2H_5)_3N$ (35 mL) was added at 0°C, followed by Boc-Ala-OTcp (23, 24) (9.2 g, 25 mmol) in dry DMF (59 mL). After 24 h at 0°C the solution was poured into ice/H_2O, the product was collected, washed with H_2O, dried, and recrystallized from CH_3OH/IPE; mp 207–209°C; yield: 11.96 g (90%); $[\alpha]_D^{25} = -24.3°$ (*c* 1.0 in DMF). Homogenous on tlc (system: MeOH/EtOAc 2:98; charring with ammonium molybdate). *Anal.* calcd. for $C_{26}H_{40}N_4O_7$: C 59.98, H 7.74, N 10.76; found: C 60.18, H 7.94, N 10.73.

Boc-Ala-Phe-Val-Gly-OH

NaOH (1 *N*, 24.4 mL) was added in the course of 15 min to Boc-Ala-Phe-Val-Gly-OEt (10.4 g, 19.8 mmol) suspended in CH_3OH (57 mL) and $CH_3OCH_2CH_2OH$ (57 mL) at 0°C under stirring. After 2 h at room temperature the solution was poured into ice/H_2O and acidified with 1 *N* HCl (24.4 mL) and 15 drops of AcOH. The product was collected, washed with H_2O, and dried. Yield: 8.95 g (88%); nmr (DMSO): 0.87 (d, J = 7 Hz, 6H, $(CH_3)_2CH$), 1.13 (d, J = 7 Hz, 3H, CH_3CH), 1.35 (s, 9H, $(CH_3)_3C$), 7.24 (s, 5H, arom) ppm; $[\alpha]_D^{25} = -22.6°$ (*c* 1.0 in DMF). *Anal.* calcd. for $C_{24}H_{36}N_4O_7$ × 0.3% H_2O (K. Fischer): C 58.33, H 7.36, N 11.33; found: C 58.07, H 7.30, N 11.32.

Boc-Ala-Phe-Val-Gly-Leu-Met-OCH_3

H-Leu-Met-OCH_3 × CF_3COOH (2.08 g, 5.32 mmol), obtained from Boc-Leu-Met-OCH_3 (25) by deprotection with CF_3COOH, was dissolved in dry DMF (10 mL) and mixed with $(C_2H_5)_3N$ (0.8 mL) at 0°C. The mixture was added under stirring at −15°C to Boc-Ala-Phe-Val-Gly-OH (2.62 g, 5.32 mmol) and CDI (0.862 g, 5.32 mmol) in dry DMF (10 mL). After stirring overnight at room temperature the solvent was removed *in vacuo*, the residue triturated with 5% $NaHCO_3$ solution, collected by filtration, washed with H_2O, and dried. Recrystallized from CH_3OH/H_2O; mp 254–255°C; yield: 3.13 g (78%); $[\alpha]_D^{25} = -31.3°$ (*c* 2.0 in DMF); nmr (DMSO): 0.90 (d, J = 6 Hz, 6H, $(CH_3)_2CH$), 1.30 (d, J = 7 Hz, 3H, CH_3CH), 1.48 (s, 9H, $(CH_3)_3C$), 2.05 (s, 3H, CH_3S), 3.65 (s, 3H, CH_3O), 7.25 (s, 5H, arom) ppm. Homogenous on tlc (system: $CHCl_3/CH_3OH$, 95:5; charring with ammonium molybdate). *Anal.* calcd. for $C_{36}H_{58}N_6O_9S$: C 57.58, H 7.78, N 11.19; found: C 57.92, H 7.89, N 10.89.

Boc-Ala-Phe-Val-Gly-Leu-Met-OH

A mixture of Boc-Ala-Phe-Val-Gly-Leu-Met-OCH_3 (3.65 g, 4.86 mmol) in hot $CH_3OCH_2CH_2OH$ (97 mL) and CH_3OH (97 mL) was added to cold H_2O (25 mL) with vigorous stirring. The suspension was cooled to 5°C, treated with 1 *N* NaOH (9.7 mL) and stirred for 24 h at room temperature. The solution was poured into ice/brine containing 1 *N* HCl (10.7 mL) and AcOH (5 drops). The collected solid was washed with water and recrystallized from CH_3OH/H_2O; mp 252–281°C (dec.); yield: 3.43 g (95%); $[\alpha]_D^{25} = -26.5°$ (*c* 2.0 in DMF); nmr (DMSO): 1.36 (s, 9H, $(CH_3)_3C$), 2.06 (s, 3H, CH_3S) ppm. *Anal.* calcd. for $C_{35}H_{56}N_6O_9S$: C 57.04, H 7.66, N 11.44; found: C 57.03, H 7.62, N 10.93.

*H-Ala-Phe-Val-Gly-Leu-Met-OH (***4***)*

Boc-Ala-Phe-Val-Leu-Met-OH (4.14 g, 5.63 mmol) was deprotected by treatment with CF_3COOH. The CF_3COOH was removed *in vacuo* and the residue triturated with ether. The solid was collected, washed with ether, and dried *in vacuo*; mp 260–263°C (dec.); yield: 4.23 g (100%). The free base was prepared by treatment of the salt with 2 *N* NH_4OH. The solid was collected, washed with H_2O and EtOH, and dried *in vacuo*. The material is insoluble in DMF; mp 262–264°C (dec.); yield 1.56 g (44%). *Anal.* calcd. for $C_{30}H_{48}N_6O_7S$ × 1.07% H_2O (K. Fischer): C 55.97, H 7.63, N 13.05; found: C 55.30, H 7.59, N 12.85.

Synthesis of **5**a, b

In the course of 5.5 h H-Ala-Phe-Val-Gly-Leu-Met-OH × CF_3COOH (2.14 g, 2.85 mmol) in dry DMF (37 mL) was dropped into a stirred solution of $(CH_3)_2$ CHCHO (0.684 g, 9.5 mmol), cyclohexylisonitrile (0.314 g, 2.85 mmol), and dry $(C_2H_5)_3N$ (0.288 g, 2.85 mmol) in dry DMF (7 mL). The pH was adjusted to 7 with pyridine and the clear solution remained at room temperature for 65 h. The solvent was removed *in vacuo* and the residue chromatographed on silica gel. The isomers were separated by elution with C_6H_6/IPA (95:5). Both isomers were separately rechromatographed and triturated with hexane.

Isomer ***5a***: mp 158–175°C (dec.); yield: 319 mg (14%); $[\alpha]_D^{25} = -182°$ (*c* 1.0 in DMF); ms (*m/e*) = 799 (M^+). *Anal.* calcd. for $C_{41}H_{65}N_7O_7S$: C 61.55, H 8.19, N 12.25, S 4.00;

found: C 61.27, H 8.26, N 11.81, S 4.12. Amino acid analysis: Gly 1, Val 1.02, Met 0.98, Leu 0.96, Phe 1.0. Isomer ***5b***: mp 155°C (dec.); yield: 424 mg (18.6%); $[\alpha]_D^{25} = -77°$ (*c*1.0 in DMF); ms (*m/e*) = 799 (M^+). *Anal.* calcd. for $C_{41}H_{65}N_7O_7S$: C 61.55, H 8.19, N 12.25, S 4.00; found: C 60.57, H 8.13, N 11.76, S 3.87. Amino acid analysis: Gly 1, Val 0.97, Met 0.95, Leu 0.94, Phe 0.97.

Acknowledgments

We would like to thank Dr. G. Schilling and his staff for providing analytical and spectral data.

1. I. Ugi. Angew. Chem. **74**, 9 (1962).
2. I. Ugi and E. Wischöfer. Chem. Ber. **95**, 136 (1962).
3. G. Just, B. Y. Chung, and K. Grozinger. Can. J. Chem. **55**, 274 (1977).
4. A. Failli, V. Nelson, H. Immer, and M. Götz. Can. J. Chem. **51**, 2769 (1973).
5. H. Immer, V. Nelson, W. Robinson, and M. Götz. Justus Liebigs Ann. Chem. 1789 (1973).
6. A. Failli, K. Sestanj, H. Immer, and M. Götz. Arzneim. Forsch. 27 (II), 12, 2296 (1977).
7. Yu. A. Ovchinnikov and V. T. Ivanov. Tetrahedron, **31**, 2177 (1975).
8. C. M. Deber, V. Madison, and E. R. Blout. Acc. Chem. Res. **9**, 106 (1976).
9. M Rothe, K.-D. Steffen, and I. Rothe. Angew. Chem. Int. Ed. Engl. **4**, 356 (1965).
10. J. Dale and K. Titlestad. Chem. Commun. 656 (1969).
11. (*a*) R. O. Studer. Experientia, **25**, 899 (1969); (*b*) R. Schwyzer, B. Iselin, W. Rittel, and P. Sieber. Helv. Chem. Acta, **39**, 872 (1956).
12. R. Schwyzer, J. P. Carrion, B. Gorup, H. Nolting, and Aung Tung-Kyi. Helv. Chim. Acta, **47**, 441 (1964).
13. E. Schröder and R. Lübke. The peptides. Vol. 2. Academic Press, New York and London. 1966. p. 127.
14. R. L. Huguenin and R. A. Boissonas. Helv. Chim. Acta, **44**, 213 (1961).
15. K. Jost, J. Rudinger, and F. Sorm. Collect. Czech. Chem. Commun. **26**, 2496 (1961).
16. M. M. Shemyakin, L. A. Shchukina, E. I. Vinogradova, G. A. Ravdel, and Y. A. Ovchinnikov. Experientia, **22**, 535 (1966).
17. P. Oehme, J. Bergmann, H. G. Müller, R. Grupe, H. Niedrich, W. A. Vogt, and F. Jung. Acta Biol. Med. Ger. **28**, 121 (1972).
18. E. Schröder and R. Lübke. The peptides. Vol. 1. Academic Press, New York and London. 1966. p. 271.
19. K. Kopple. J. Pharm. Sci. **61**, 1345 (1972).
20. I. Ugi, H. Aigner, B. Beijer, D. Ben-Efraim, H. Burghard, P. Bukall, G. Eberle, H. Eckert, D. Marquarding, D. Rehn, R. Urban, L. Wackerle, and H. Von Zychlinsky. Peptides 1976. *Edited by* A. Loffet. Editions de l'Université de Bruxelles. 1976. p. 166.
21. F. Weygand and W. Steglich. Chem. Ber. **93**, 2983 (1960).
22. J. C. Sheehan and V. J. Grenda. J. Am. Chem. Soc. **84**, 2417 (1962).
23. Ed. Sandrin and R. A. Boissonas. Helv. Chim. Acta, **46**, 1637 (1963).
24. P. H. Bentley, H. Gregory, A. H. Laird, and J. S. Morley. J. Chem. Soc. 6130 (1964).
25. K. Lübke, E. Schröder, R. Schmiechen, and H. Gibian. Justus Liebigs Ann. Chem. **679**, 195 (1964).

Hydrolysis of cyclic unsymmetrical *anti* imidate salts. New evidence for stereoelectronic control

PIERRE DESLONGCHAMPS, UKKEN OUSEPH CHERIYAN, AND ROLAND J. TAILLEFER

Laboratoire de Synthèse Organique, Département de Chimie, Université de Sherbrooke, Sherbrooke (Qué.), Canada J1K 2R1

Received February 27, 1979

This paper is dedicated to Prof. Karel Wiesner on the occasion of his 60th birthday

PIERRE DESLONGCHAMPS, UKKEN OUSEPH CHERIYAN, and ROLAND J. TAILLEFER. Can. J. Chem. **57**, 3262 (1979).

The synthesis and the hydrolytic behavior of the cyclic imidate salts **7**, **8**, and **9** is reported. Under acidic conditions, the salt **7** gives the ester ammonium salt **21** and the salt **9** gives a 1:1 mixture of the ester ammonium salt **22** and the amide alcohol **23** as the rotamer **23***B* only. Under basic conditions, the salt **7** (or **8**) gives a 2:8 (or 1:9) mixture of the amide alcohol rotamers **25***A* and **25***B* (or **27***A* and **27***B*) under kinetically controlled conditions. The salt **9** gives, as the kinetic product, the amide alcohol rotamer **23***B* only. These results can be rationalized on the basis of the stereoelectronic theory for the cleavage of tetrahedral intermediates and by taking into account that the nitrogen in tetrahedral intermediates must be either protonated under acidic conditions, or hydrogen bonded with the solvent under basic conditions, in order to observe the cleavage of a C—N bond.

PIERRE DESLONGCHAMPS, UKKEN OUSEPH CHERIYAN et ROLAND J. TAILLEFER. Can. J. Chem. **57**, 3262 (1979).

La synthèse et l'hydrolyse des imidates cycliques **7**, **8** et **9** sont rapportées. En milieu acide, l'imidate **7** se transforme en sel d'ammonium ester **21** et l'imidate **9** donne un mélange (1:1) du sel d'ammonium ester **22** et d'amide alcool **23** sous la forme du rotamère **23***B* seulement. En milieu basique, l'imidate **7** (ou **8**) donne un mélange dans le rapport 2:8 (ou 1:9) des rotamères **25***A* et **25***B* (ou **27***A* et **27***B*) de l'amide alcool **25** (ou **27**). L'imidate **9** conduit à l'amide alcool **23** sous forme du rotamère **23***B* seulement. Ces résultats peuvent etre expliqués en utilisant la théorie de controle stéréoélectronique pour le bris des intermédiaires tétraédriques, et en tenant compte du fait que l'azote de l'intermédiaire tétraédrique doit être protoné en milieu acide ou doit former un pont hydrogène avec le solvant lors du bris d'un lien C—N.

In the course of our studies (1, 2) on the ^{18}O carbonyl–oxygen exchange in the basic hydrolysis of tertiary amides, we have shown (2) that the nitrogen of tetrahedral intermediates in the T^- ionic form (cf. **2** in Scheme 1) must be hydrogen bonded with

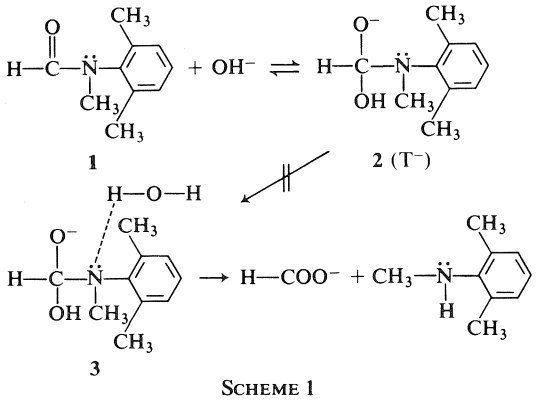

SCHEME 1

the solvent in order to observe a cleavage of the C—N bond. More specifically, we have shown that *N*-2,6-dimethylphenyl-*N*-methylformamide (**1**) is completely resistant to hydrolysis but undergoes extensive carbonyl–oxygen exchange under basic conditions (Scheme 1). This result was interpreted in the following way: compound **1** must form the tetrahedral intermediate **2** so that carbonyl–oxygen exchange can take place, but **2** cannot yield the hydrolysis products because the presence of the two methyl groups on the phenyl ring prevents the formation of a hydrogen bond between the tertiary nitrogen and water (**2** ⇸ **3**).

We have also observed a similar result in our recent studies (3) on the hydrolysis of *syn* imidate salts derived from unsymmetrical tertiary formamides. We have shown that the basic hydrolysis of the two unsymmetrical imidate salts **4***A* and **4***B* derived from *N*-2,6-dimethylphenyl-*N*-methylformamide (**1**) (Scheme 2) gave only the amide alcohol products under basic conditions. This result was again explained by taking into account that the nitrogen in the resulting tetrahedral intermediate **5** cannot become hydrogen bonded (**5** ⇸ **6**) with the solvent. Consequently, the C—N bond cleavage to yield the ester amine products cannot take place, while the carbon–oxygen bond cleavage to yield the amide alcohol products takes place readily. These findings were further confirmed by our study on the isomerization of salts **4***A* and **4***B* with methanol (3).

0008-4042/79/243262-10$01.00/0

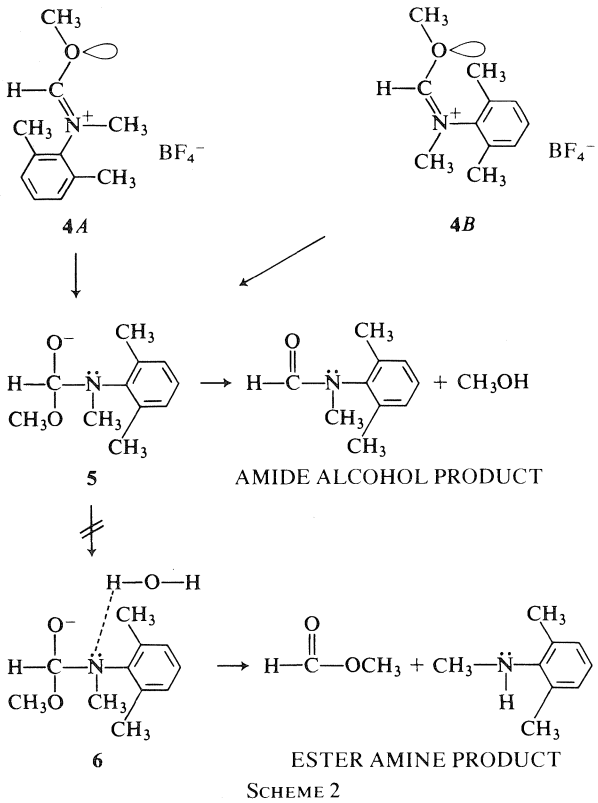

SCHEME 2

We have also undertaken a study of the hydrolysis of unsymmetrical imidate salts which have an *anti* configuration. We wish now to report this work.

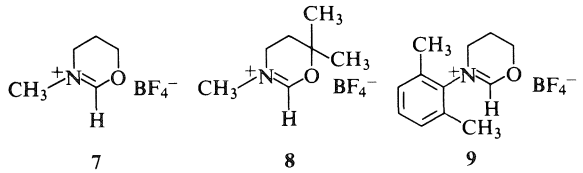

Synthesis

We have selected the cyclic imidate salts **7**, **8**, and **9** for this study. Due to their cyclic nature, these salts are *anti* imidate salts.[1] The synthesis of these three salts is described in Scheme 3 and the details of these procedures can be found in the experimental section.

Acid Hydrolysis

The hydrolytic behavior of imidate salts **7** and **9** was first studied under acidic conditions by the action of water in acetonitrile.[2] Under those conditions, the imidate salt **7** was slowly hydrolyzed to yield the ester ammonium salt **21** exclusively (Scheme 4). The imidate salt **9** behaved in a completely different manner giving a $\simeq$1:1 mixture of the ester ammonium salt **22** and the amide alcohol **23** and some fluoroboric acid (Scheme 5). Again, the hydrolysis is a slow process, and it could be observed that at the beginning of the reaction, the amide alcohol **23** was first formed as the least stable rotamer **23***B* only, which then slowly isomerized to give an equilibrium mixture of **23***A* (67%) and **23***B* (33%).[3]

The configuration of the two rotamers **23***A* and **23***B* was determined by nmr comparison with the two rotamers **24***A* and **24***B* whose configuration was rigorously established (3).[4]

Basic Hydrolysis

The hydrolytic behavior of the imidate salts **7**, **8**, and **9** was also studied under basic conditions. The hydrolysis of salt **7** with excess sodium hydroxide in water–acetonitrile (1:5) at room temperature is an instantaneous reaction which gave the amide alcohol **25** exclusively, as an equilibrium mixture of the two amide rotamers **25***A* (40%) and **25***B* (60%) (Scheme 4).[5]

When the same reaction was carried out at 0°C, the amide alcohol **25** was again the only product formed, but the ratio of the rotamers was found to be 23% (**25***A*) and 77% (**25***B*). The equilibrium ratio of 40:60 was then reached on standing. The slow rate of equilibration of the two rotamers at 0°C (Table 1) indicates that the rotamers **25***A* and **25***B*, in the ratio of 23:77, were the direct products of hydrolysis. This finding was further confirmed by repeating the experiment at −10°C and at 10°C. Again, it gave only the amide alcohol and the isomeric ratio was essentially the same (20:80 and 25:75 respectively).

We have also treated the ester ammonium salt **21**

[1]In *anti* imidate salts, derived from formamide, the C—H bond is *anti* to the O—alkyl bond (cf. **7**, **8**, **9**). In *syn* imidate salts, the C—H bond is *syn* to the O—alkyl bond (cf. **4***A* and **4***B*) (4).

[2]The hydrolysis of imidate salt **8** was not studied under those conditions.

[3]We have also observed that the equilibrium ratio of the two amide alcohol rotamers **23***A* and **23***B* varies considerably with the solvent used. In pure water, the ratio is 25% (**23***A*) and 75% (**23***B*). In water–acetonitrile (2:5), it is 55% and 45%. In water–acetonitrile (1:5), it is 67% and 33% and in pure acetonitrile, the ratio is 74% to 26%.

[4]The formamide hydrogen in **24***A* and **24***B* appears at 8.11 and 8.47 ppm in acetonitrile. The formamide hydrogen in **23***A* and **23***B* appears at 8.13 and 8.49 ppm respectively in the same solvent.

[5]The configuration of the amide rotamers was established by nmr spectroscopy. The N—methyl resonance appears at a higher field in the rotamer *B* (5): amide alcohol **25**:**25***A* (2.93 ppm, N—CH_3) and **25***B* (2.77 ppm, N—CH_3); amide alcohol **27**:**27***A* (2.91 ppm, N—CH_3) and **27***B* (2.78 ppm, N—CH_3). Also, the coupling constant of the N—CH_3 group is larger in the rotamers **B** (rotamers **A** $\simeq$ 0.4 Hz and rotamers **B** $\simeq$ 0.8 Hz in acetonitrile).

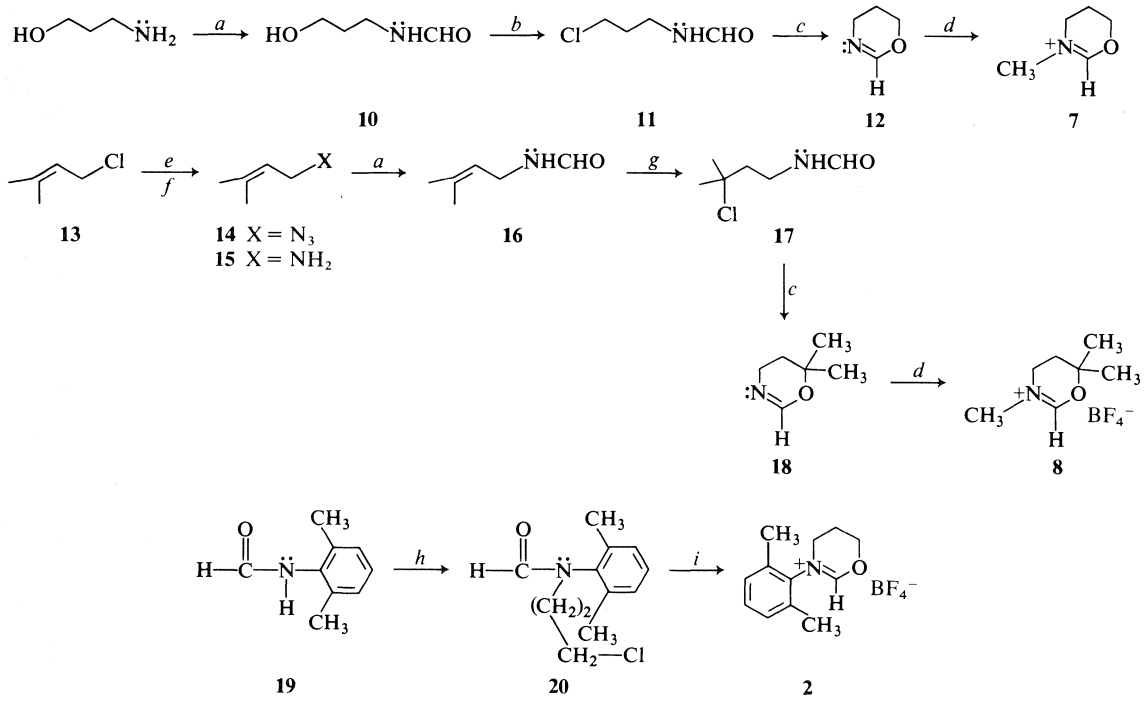

SCHEME 3. (*a*) $HCOOC_2H_5$, heat; (*b*) $(C_6H_5)_3P$, CCl_4; (*c*) $AgBF_4$; NaOH; (*d*) $(CH_3)_3O^+BF_4^-$; (*e*) NaN_3; (*f*) $LiAlH_4$; (*g*) HCl, 0°C; (*h*) NaH–THF–$ClCH_2CH_2CH_2Br$; (*i*) $AgBF_4$.

under the same basic conditions at 0°C. There is again an instantaneous reaction which gave only the amide alcohol **25** with the same ratio of amide rotamers **25***A* (20%) and **25***B* (80%).

The hydrolysis of the imidate salt **8** gave similar results. Basic hydrolysis of **8** at 0°C gave only the amide alcohol product as a mixture of the two rotamers **27***A* and **27***B* in a 1:9 ratio. On standing, the equilibrium mixture of the two amide rotamers was then obtained (**27***A* (41%) and **27***B* (59%)). The slow rate of equilibration of the two rotamers (Table 2) shows that the rotamers **27***A* and **27***B* in the 1:9 ratio were the direct product of hydrolysis.

The basic hydrolysis of the imidate salt **9** gave a different result. Treatment of the salt **9** with sodium hydroxide in water–acetonitrile (1:5) led to an instantaneous reaction yielding exclusively the amide alcohol **23** in the form of the least stable rotamer **23***B* only (Scheme 5). On standing, isomerization of **23***B* took place to give the equilibrium mixture of **23***A* (67%) and **23***B* (33%).

When the 1:1 mixture of the ester ammonium salt

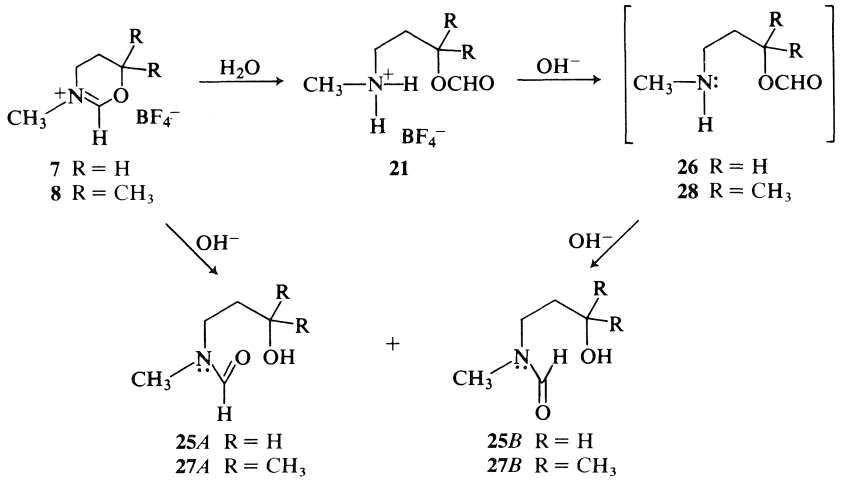

SCHEME 4

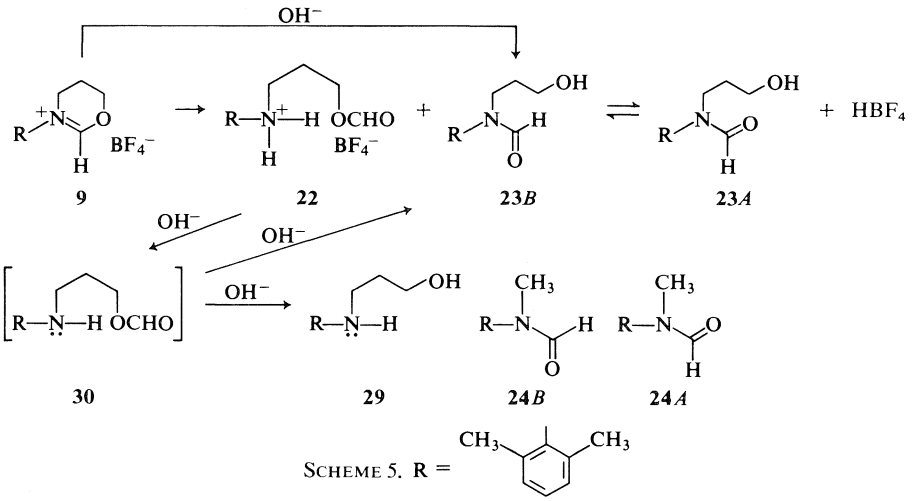

SCHEME 5. R =

22 and the amide alcohol **23** (**23***A* (67%) and **23***B* (33%)) (obtained by hydrolysis of **9** with water in acetonitrile) was treated with excess sodium hydroxide at room temperature, it gave 70% of the amide alcohol **23** (**23***A* (67%) and **23***B* (33%)) and 30% of the amine alcohol **29**.

TABLE 1. Isomerization of **25***A* into **25***B* at 0°C[a]

Time (min)	% **25***A*	% **25***B*
1	24	76
6	23	77
18	24	76
33	25	75
55	28	72
92	31	69
134	32	68
Equilibrium	41	59

[a]Imidate salt **7** was hydrolyzed with NaOD in CD_3CN/D_2O. The hydrolysis was instantaneous giving amide alcohol **25** only. The interconversion of **25***A* and **25***B* was followed by nmr spectroscopy (cf. Experimental).

TABLE 2. Isomerization of **27***A* into **27***B* at 0°C[a]

Time (min)	% **27***A*	% **27***B*
2	10	90
9	10	90
16	12	88
23	15	85
39	17	83
64	18	82
95	24	76
144	28	82
173	30	70
233	33	67
Equilibrium	41	59

[a]Imidate salt **8** was hydrolyzed with NaOD in CD_3CN/D_2O. The hydrolysis was instantaneous giving amide alcohol **27** only. The interconversion of **27***A* and **27***B* was followed by nmr spectroscopy (cf. Experimental).

Hydrolysis of salt **9** was also carried out with sodium hydroxide in water only. The reaction is instantaneous and also gave the amide alcohol **23** in the form of the rotamer **23***B* only. Then, isomerization took place to give an equilibrium mixture of **23***A* (25%) and **23***B* (75%). The salt **9** was then hydrolyzed with water only giving 28% of the amide alcohol **23** and 72% of the ester ammonium salt **22**. The hydrolysis was slow and, again at the beginning, **23** appeared in the form of **23***B* only, slowly equilibrating to a mixture of **23***A* (25%) and **23***B* (75%).[3] When sodium hydroxide was added to the above aqueous solution, we obtained 28% of the amide alcohol **23** and 72% of the amine alcohol **29**.

Discussion

Acidic Hydrolysis

The result obtained with the imidate salt **7** under acidic conditions is the predicted result for *anti* imidate salts (4), i.e., 100% of the ester ammonium salt **21**, and it can be readily explained in the following way. Water reacts with the salt **7** (Scheme 6) with stereoelectronic control (6) to yield the tetrahedral intermediate **31** which is then rapidly protonated by the fluoroboric acid produced, to give the T^+ ionic form **32**. Then the intermediate **32**, which has an electron pair on each oxygen properly oriented to eject the amino group (6), can break down to yield the corresponding amine ester **26** which is then rapidly protonated to give the ester ammonium salt **21**.

The difference in behavior of the imidate salt **9** can be explained by the presence of the two methyl groups on the phenyl ring. The salt **9** (Scheme 6) must first react with water to form the tetrahedral intermediate **33** in the neutral form T^0. However, it is difficult to protonate the nitrogen in **33** to give **34** (T^+) because of the presence of the two methyl groups on the phenyl ring (2, 3). Consequently **33**, as well as giving

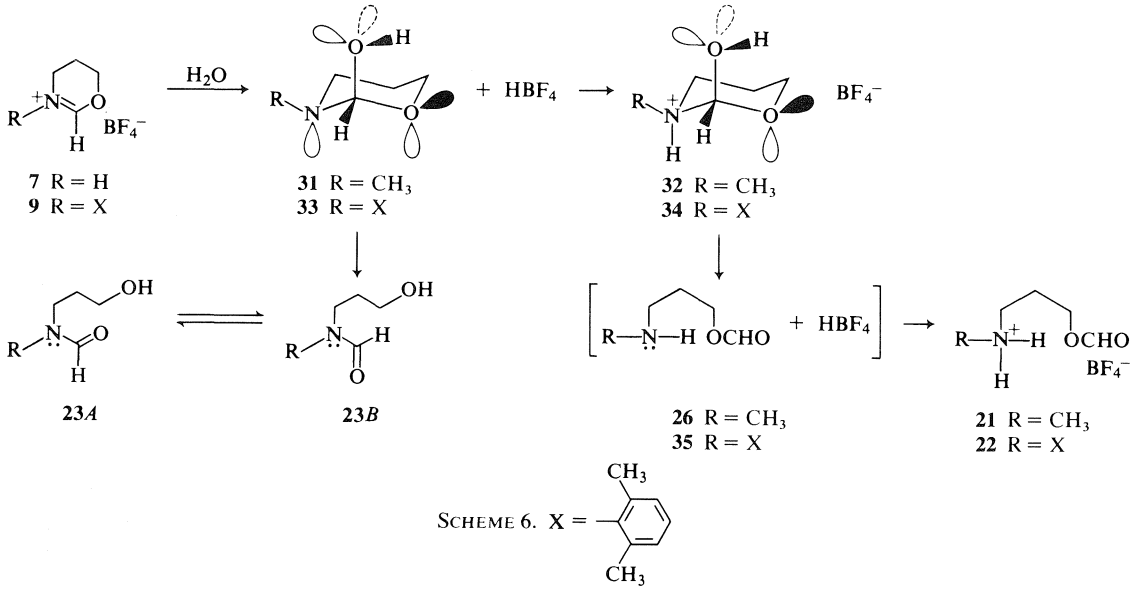

34 (T^+) which leads to the ester ammonium salt **22** via **35**, would also cleave to give the amide alcohol product as the rotamer **23***B* only. The precise manner by which **33** can yield the rotamer **23***B* will be discussed later.

Basic Hydrolysis

Imidate Salts 1 and 8

In resume, the basic hydrolysis of imidate salt **7** gives a mixture (2:8) of the amide alcohol rotamers **25***A* and **25***B* as the kinetic products of the reaction. Isomerization follows to yield the equilibrium ratio (4:6) of **25***A* and **25***B*. The basic hydrolysis of the ester ammonium salt **21** gives an identical result (Scheme 4).

The above results suggest that the amine ester **26** is likely to be an intermediate in the hydrolysis of the imidate salt **7**. The exclusive formation of the amine ester product **26** first is not surprising (Scheme 7). We have previously shown that *anti* imidate salts always give, under basic conditions, the amine ester product under kinetically controlled conditions (4). Indeed, reaction of hydroxide ion on salt **7** with stereoelectronic control must give the intermediate **31**, which after removal of a proton on the hydroxyl group (T^-) and after hydrogen bonding with the solvent (→**36**), breaks down to yield the amine ester **26**. Then this amine ester **26**, being a reactive ester would recyclize rapidly to give new tetrahedral intermediates which then yield the amide rotamers **25***A* and **25***B* in the 2:8 ratio.

The amide rotamers **25***A* and **25***B* must be formed respectively from the stereoelectronically controlled cleavage of the tetrahedral intermediates **38** and **39** and the formation of these two intermediates is the result of the attack of the amino group on the *Z* (**26***A*) and the *E* (**26***B*) forms (7) of the ester function in the amine ester **26**. The results show that the route **26***B* → **39** → **25***B* is preferred over the route **26***A* → **38** → **25***A*. However, on the basis of the present knowledge, it is difficult to rationalize the observed preference for one pathway.

The basic hydrolysis of the imidate salt **8** gave a result similar to that observed with the imidate salt **7**. It can therefore be interpreted in the same manner. The salt **8** must have first produced the amine ester **28** via **33** and **37**. The amine ester **28** was then transformed into a 1:9 mixture of the amide rotamers **27***A* and **27***B* via the routes **28***A* → **40** → **27***A* and **28***B* → **41** → **27***B*.

Imidate Salt 9

The basic hydrolysis of imidate salt **9** takes a different course from salts **7** and **8**, yielding first the amide rotamer **23***B* only, which is then isomerized to the equilibrium mixture of **23***A* and **23***B* (Scheme 5). The basic hydrolysis of the corresponding ester ammonium salt **22** gives either a mixture of **23***A* and **23***B* plus the amine alcohol **29** (in acetonitrile–water) or only the amine alcohol **29** (in water). These results show that the amine ester **30** is not an intermediate in the hydrolysis of **9**. The formation of the amide rotamer **23***B* is therefore the result of the direct fragmentation of a tetrahedral intermediate which is formed from **9**. The hydrolysis of salt **9** is particularly interesting as it shows a complete transmission of stereochemistry from the reactant to the product of the reaction (**23***B*).

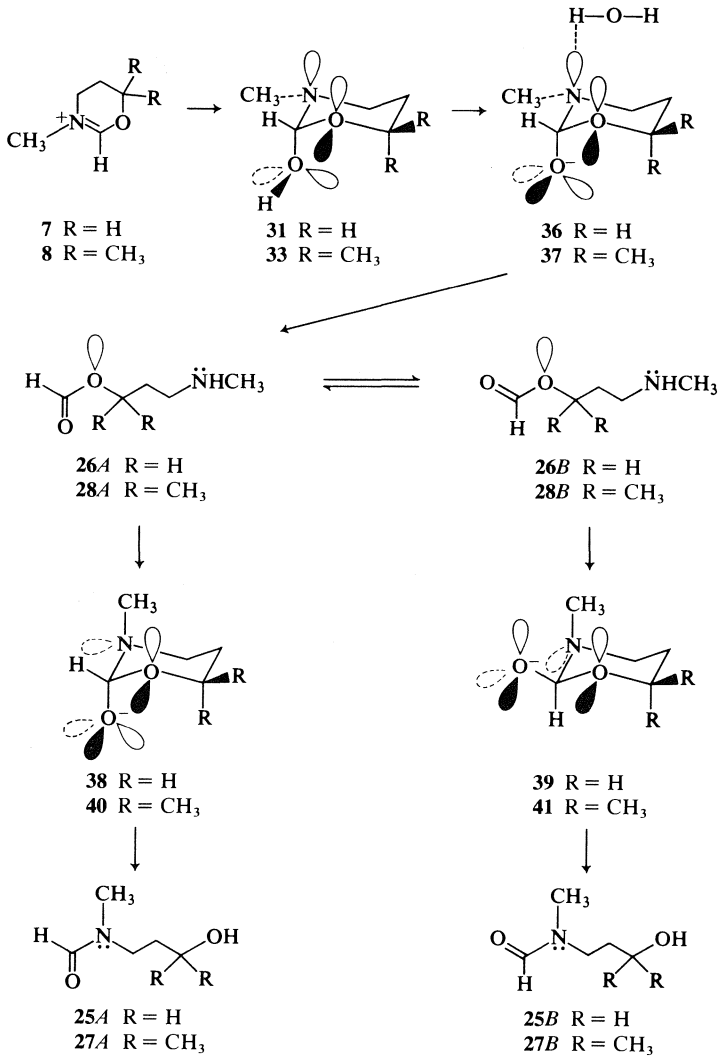

SCHEME 7

The reaction of hydroxide ion on **9** with stereoelectronic control should give **42** (Scheme 8). However, **42** cannot break down with stereoelectronic control to give either the amide alcohol rotamer **23***A* or **23***B*. Furthermore, the intermediate **42** cannot yield the amine ester **30** because the tertiary nitrogen cannot be hydrogen-bonded to the solvent (1–3).

If the intermediate **42** could break down without stereoelectronic control, it would yield first **43** which would then be transformed into both the rotamers **23***A* and **23***B*. Indeed, **43** is an intermediate during the thermal isomerization of **23***A* and **23***B*. This hypothesis must therefore be eliminated.

The intermediate **42** could, however, undergo conformational changes to give either the intermediate **44** (by nitrogen inversion) or the intermediate **45** by chair inversion. Since **44** and **45** can break down with stereoelectronic control to give **23***A* and **23***B*, respectively, this means that the conversion of **42** into **44** would not occur, while that of **42** into **45** would take place readily. In both intermediates **44** and **45** the bulky 2,6-dimethylphenyl group becomes axially oriented; it would therefore be quite surprising that one process would be favored energetically and this rationalization must be rejected.

The specific formation of rotamer **23***B* from **9** can, however, be explained in the following way. The reaction of hydroxide ion with **9** would occur with stereoelectronic control to yield the intermediate **42**. This intermediate would then be converted into the half-boat conformer **46** which has the proper orbital orientation to give the amide alcohol rotamer **23***B* only.

In **42**, the hydroxyl group and the 2,6-dimethyl-

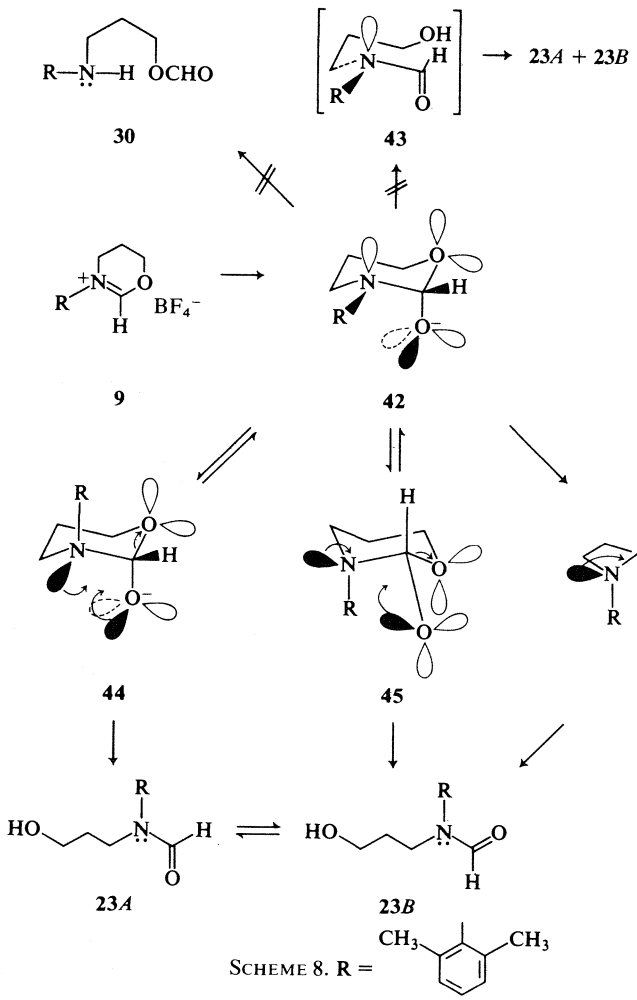

SCHEME 8. R =

phenyl group undergo very severe steric interactions. This steric interaction can, however, be lessened on going from **42** to **46**, and it would therefore be the driving force for the specific conversion of **42** into the half-boat **46**. This can be seen by the examination of the conversion of **42** into **46** with space filling molecular models. Thus, **9** would first give **42** which would then generate **46**, which would break down to the amide rotamer **23***B*. The half-boat **46** would not be converted into **44** and **45** because these conversions would involve more energy than the breakdown of **46** with stereoelectronic control to give the amide rotamer **23***B*.

Experimental

Vapor-phase chromatographic (vpc) analyses and separations were carried out on a Varian aerograph instrument model 2800 with a thermal conductivity detector. The ir spectra were taken on a Perkin-Elmer 257 spectrophotometer. Proton nmr spectra were recorded on a Varian A-60 or a Bruker WP-60 instrument. Chemical shifts are reported in δ values relative to tetramethylsilane as internal standard. Mass spectral assays were obtained using a Hitachi-Perkin-Elmer RMU-6-A instrument at 70 eV.

Syntheses

N-*(3-Hydroxypropyl)formamide (**10**)*

A mixture of 3-amino-1-propanol (10 g, 0.13 mol) and ethyl formate (10 g, 0.135 mol) was refluxed overnight. Fractional distillation yielded pure amide **10** (10 g, 75%); bp 138–139°C/0.7 Torr; ir ν_{max} ($CHCl_3$): 3430 and 1680 cm^{-1}; nmr ($CDCl_3$) δ: 1.8 (2H, m), 3.7 (4H, m), 8.3 (1H, b s); ms *m/e*: 103 (M^+). An analytical sample was prepared by vpc (5 ft. $\frac{1}{4}$ in., 10% SE-30, 150°C). *Anal.* calcd. for $C_4H_9NO_2$: C 46.59, H 8.80; found: C 47.03, H 8.92.

N-*(3-Chloropropyl)formamide (**11**)*

A mixture of *N*-(3-hydroxypropyl) formamide **10** (5.15 g, 0.05 mol) and triphenylphosphine (13.2 g, 0.05 mol) was refluxed in a mixture of carbon tetrachloride (75 mL) and dichloromethane (50 mL) for 18 h. The solvents were then removed by distillation at atmospheric pressure. The residual liquid on distillation gave pure chloroamide **11** (2.4 g, 40%); bp 120–122°C/0.5 Torr; ir ν_{max} ($CHCl_3$): 3440, 3300, and 1690 cm^{-1}; nmr ($CDCl_3$) δ: 2.15 (2H, m), 3.7 (4H, m), 8.5 (1H); ms *m/e*: 121, 123 (M^+). An analytical sample was prepared by

vpc (5 ft, ¼ in., 10% SE-30, 100°C). *Anal.* calcd. for C_4H_8NOCl: C 39.52, H 6.63; found: C 39.83, H 7.01.

Iminoether ***12***

To a solution of the chloroamide **11** (1.62 g, 13.3 mmol) in nitromethane (25 mL) in a flask covered with aluminium foil, silver tetrafluoroborate (2.6 g, 13.3 mmol) was added and stirred overnight. The reaction mixture was then filtered and the filtrate concentrated to give a white solid that was only sparingly soluble in dichloromethane. Hydrogen chloride gas was bubbled into a suspension of the product in dichloromethane for 1 h. It was then filtered and the residue was dissolved in acetonitrile and again filtered. The latter filtrate on concentration yielded the fluoroborate salt of **12** (2 g); nmr (CD_3CN) δ: 2.3 (2H, m), 3.6 (2H, t), 4.8 (2H, t), 8.5 (1H, b s).

The crude salt (1.65 g, 9.5 mmol) was suspended in dichloromethane (50 mL) and cooled to 0°C in an ice bath. A cold solution of sodium hydroxide (15 mL, 1 *N*) saturated with sodium chloride was added with stirring. The organic layer was separated and the aqueous layer was extracted with dichloromethane. The extracts were combined, washed with brine, and dried over sodium sulfate. Fractional distillation yielded pure iminoether **12** (8) (400 mg); bp 120–121°C; ir ν_{max} (CH_2Cl_2): 1660 cm^{-1}; nmr ($CDCl_3$) δ: 2.0 (2H, m), 3.2 (2H, t), 4.3 (2H, t), and 7.2 (1H, b).

Imidate Salt ***7***

To a suspension of trimethyl oxonium fluoroborate (167 mg, 1.13 mmol) in dichloromethane (15 mL), a solution of the iminoether **15** (96 mg, 1.13 mmol) in dichloromethane (5 mL) was added dropwise and stirred overnight. The solvent was then distilled off to give a viscous liquid (220 mg) insoluble in dichloromethane. This product was used without further purification; ir ν_{max} (CH_3CN): 1695 and 1030 cm^{-1}; nmr (CD_3CN) δ: 2.3 (2H, m), 3.3 (3H, s), 3.5 (2H, t), 4.5 (2H, t), and 8.21 (1H, s).

1-Chloro-3-methyl-2-butene ***13***

Dry lithium chloride (2.47 g, 0.058 mol) was dissolved in a minimum amount of dimethylformamide (35 mL). This was mixed with collidine (7.62 g, 0.063 mol, distilled over calcium hydride) and 3-methyl-2-butene-1-ol (5.01 g, 0.058 mol). The reaction mixture was then cooled in an ice bath with stirring. Methane sulfonyl chloride (7.21 g, 0.063 mol) was added dropwise under an atmosphere of nitrogen (9). After the addition was complete, the stirring was continued for 1½ h at 0°C. It was then poured over 300 g of crushed ice and extracted with ice-cold 1:1 pentane/ethyl ether (3 × 200 mL). The extracts were then combined and washed four times with 50 mL each of saturated copper nitrate solution, followed by water. They were then dried over anhydrous sodium sulfate and the solvent was fractionally distilled off to give a liquid residue (4 g). The nmr spectrum of the liquid showed it to be the desired allylic chloride (95%) containing the mesylate of the saturated alcohol as an impurity. Attempted distillation resulted in decomposition. This crude product was used without further purification.

1-Azido-3-methyl-3-butene ***14***

The allyl chloride **20** (1.8 g, 18 mmol) was dissolved in pentane (100 mL) and stirred with a solution of sodium azide (3.2 g, 50 mmol) and tetrabutyl ammonium hydrosulfate (680 mg, 2 mmol) in water (20 mL) overnight at room temperature. The pentane layer was then separated, washed with brine, dried over sodium sulfate, and fractionally distilled to give the azide **14** (10) (1 g, 52%); ir ν_{max} ($CHCl_3$): 2350 cm^{-1}; nmr ($CDCl_3$) δ: 1.72 (3H), 1.9 (3H), 3.1 (2H, d), and 5.3 (1H, m); ms *m/e*: 111 (M^+). An analytical sample was prepared by vpc (5 ft, ¼ in., 10% SE-30, 80°C). *Anal.* calcd. for $C_5H_9N_3$: C 54.03, H 8.16; found: C 53.85, H 8.05.

1-Amino-3-methyl-2-butene ***15***

A solution of the azide **14** (600 mg, 5.4 mmol) in ether was added dropwise to lithium aluminium hydride (500 mg, excess) suspended in ether (25 mL) with stirring. The stirring was continued overnight after the addition was complete. The reaction mixture was cooled to 0°C and decomposed with saturated sodium sulfate solution (3 mL). It was then filtered, dried over Na_2SO_4, and fractionally distilled to give the amine **15** (360 mg, 78%); ir ν_{max} (CH_3CN): 3500 cm^{-1}; nmr (CD_3CN) δ: 1.7 (6H), 3.1 (3H, d), and 5.2 (1H, m); ms *m/e*: 85 (M^+). Hydrochloride salt: mp 197–200°C (lit. (11) mp 201°C).

1-Formamido-2-methyl-2-butene ***16***

1-Amino-3-methyl-2-butene **15** (210 mg, 2.47 mmol) was refluxed in ethyl formate (10 mL) overnight. Removal of solvent yielded the amide **16** (220 mg) which was purified by vpc (5 ft, ¼ in., 10% SE-30, 110°C); ir ν_{max} ($CHCl_2$): 3440, 1680 cm^{-1}; nmr ($CDCl_3$) δ: 1.6 (6H), 3.9 (2H, t), 5.2 (1H, m), and 8.2 (1H, s); ms *m/e*: 113 (M^+).

Chloroformamide ***17***

The amide **16** (110 mg, 1 mmol) was dissolved in dry dimethoxyethane (15 mL) and cooled at 0°C. Dry hydrogen chloride gas was bubbled through this solution for 30 min. The reaction mixture was then stirred overnight. Removal of the solvent at reduced pressure yielded the crude chloroformamide **17** (145 mg) which was used without purification; ir ν_{max} ($CHCl_3$): 3440 and 1685 cm^{-1}; nmr ($CDCl_3$) δ: 1.6 (6H), 2.0 (2H, m), 3.5 (2H, m), and 8.2 (1H); ms *m/e*: 149, 151 (M^+).

Iminoether ***18***

Silver tetrafluoroborate (162 mg, 0.83 mmol) was suspended in nitromethane (10 mL) and cooled to 0°C. The chloroformamide **17** (125 mg, 0.83 mmol) dissolved in nitromethane (10 mL) was then added dropwise with stirring. After the addition was complete, the stirring was continued overnight. The silver chloride formed was filtered off and the filtrate was evaporated to dryness to give the hydrofluoroborate salt of **18** (160 mg); nmr (CD_3CN) δ: 1.4 (6H, s), 2.15 (2H, m), 3.7 (2H, t), and 8.3 (1H).

This salt (160 mg) was dissolved in dichloromethane (20 mL) and cooled to 0°C. This solution was then shaken with sodium hydroxide (2 mL, 2 *N*) saturated with sodium chloride. The organic layer was separated and the aqueous layer was extracted with dichloromethane. The combined extracts were washed with brine and dried over sodium sulfate. The residual liquid obtained after fractional distillation of the solvent was purified by vpc (5 ft, ¼ in., 10% SE-30, 100°C) to give the iminoether **18** (12) (25 mg); nmr ($CDCl_3$) δ: 1.45 (6H, s), 1.9 (2H, t), 3.5 (2H, t), and 8.0 (1H).

Imidate Salt ***8***

The iminoether **18** (12.8 mg, 0.11 mmol) and trimethyloxonium tetrafluoroborate (15 mg, 0.1 mmol) were mixed in dichloromethane (10 mL) and the mixture was stirred overnight. Removal of the solvent yielded crude **8** (21 mg) as a solid which was recrystallized from ether–dichloromethane; mp 109–110°C; ir ν_{max} (CH_2Cl_2): 1680 and 1040 cm^{-1}; nmr (CD_3CN) δ: 1.5 (6H, s), 2.2 (2H, m), 3.4 (3H, s), 3.6 (2H, m), and 8.1 (1H). *Anal.* calcd. for $C_7H_{14}NOBF_4$: C 39.10, H 6.56; found: C 38.05, H 6.94.

N-(2,6-Dimethylphenyl)-N-(3-chloropropyl)formamide ***20***

Sodium hydride (16 g, 57%, 0.033 mol) washed with dry hexane was suspended in dry tetrahydrofuran and cooled in an ice bath. *N*-(2,6-Dimethylphenylformamide) **19** (4.2 g, 0.028 mol) was then added with stirring. A brisk effervescence took place and a white voluminous precipitate was formed immediately. The reaction mixture was then allowed to warm up to room temperature and stirred for 3 h. 1-Bromo-3-chloro-

propane (4.47 g, 0.028 mol) was then added dropwise followed by dimethylsulfoxide (50 mL). The stirring was continued overnight and it was poured into cold water (100 mL). The organic layer was separated and the aqueous layer was extracted with dichloromethane. The extracts were combined, washed with water, and dried over sodium sulfate. The removal of the solvent and fractional distillation of the residue under reduced pressure yielded the amide **20** (4.4 g, 65%); bp 132°C/0.2 Torr; ir ν_{max} ($CHCl_3$): 1675 cm^{-1}; nmr ($CDCl_3$) δ: 2.0 (2H, m), 2.25 (6H, s), 3.75 (4H, m), 7.35 (3H, m), and 8.25, 8.53 (1H); ms *m/e*: 225, 227 (M^+). *Anal.* calcd. for $C_{12}H_{16}NOCl$: C 63.85, H 7.14; found: C 63.78, H 7.41.

Imidate Salt ***9***

A solution of the amide **20** (702 mg, 3.12 mmol) dissolved in nitromethane (30 mL) was added to silver tetrafluoroborate (608 mg, 3.12 mmol) in a flask covered with aluminium foil and the mixture was stirred overnight. The reaction mixture was then filtered and the solvent was distilled off under reduced pressure. The residue was dissolved in dichloromethane and hydrogen chloride gas was bubbled until the precipitation of silver chloride was complete. It was then filtered and the residue obtained on concentrating the filtrate was crystallized from dichloromethane to give pure imidate salt **9** (600 mg, 75%); mp 181–182°C; ir ν_{max} (CH_2Cl_2): 1660 cm^{-1}; nmr (CD_3CN) δ: 2.4 (6H, s), 2.6 (2H, m), 4.0 (2H, t), 5.0 (2H, t), 7.5 (3H), and 8.6 (1H, s). *Anal.* calcd. for $C_{12}H_{16}NOBF_4$: C 52.02, H 5.82; found: C 51.88, H 5.71.

Acidic Hydrolysis

Imidate Salt ***7***

The imidate salt **7** (6 mg, 0.03 mmol) was dissolved in CD_3CN (500 μL) and D_2O (40 μL). After 4 h, only ester ammonium salt **21** could be detected; nmr (CD_3CN/D_2O) δ: 8.1 (1H, s, formyl proton), 4.15 (3H, t, OCH_2), 3.1 (3H, s, $\overset{+}{N}CH_3$). The solution was then cooled in ice-water, ice-cold deuterated sodium hydroxide (1 *N* NaOD, 100 μL) was added and an nmr spectrum was immediately recorded. Only amide **25** could be detected (20% **25***A*, 80% **25***B*).

Imidate Salt ***9***

The imidate salt **9** (4 mg, 0.015 mmol) was dissolved in CD_3CN (500 μL) and D_2O (50 μL) and the hydrolysis was followed by nmr. The hydrolysis was complete in about 18 h to give amide alcohol **23** and ester ammonium salt **22** in the ratio of 1:1. After 4 h of reaction, only conformer **23***B* of the amide product had begun to appear. The ratio of the two conformers after 29 h was **23***A*:**23***B* = 2:1.

Basic Hydrolysis

Imidate Salt ***7***

Imidate salt **7** (24 mg, 0.12 mmol) was dissolved in CD/CN (500 μL), deuterated sodium hydroxide (1 *N* NaOD)D_2O, 200 μL, 0.2 mmol) was added at room temperature, and an nmr spectrum was immediately recorded. Only amide **25***A* (40%) and **25***B* (60%) could be detected. In a separate experiment, imidate **7** (45 mg, 0.24 mmol) was dissolved in acetonitrile (1 mL) and shaken with sodium hydroxide (500 μL, 1 *N*, 0.5 mmol). The solution was then extracted with dichloromethane to give amide **25** (19 mg) which was purified by vpc (5 ft, ¼ in., 10% SE-30, 140°C); ir ν_{max} ($CHCl_3$): 3425, 1670 cm^{-1}; nmr ($CDCl_3$) δ: 1.8 (2H, m, CH_2—CH_2CH_2), 2.83, 2.91 (3H, two s, N—CH_3), 3.5 (4H, m, N—CH_2, OCH_3), 8.0 (1H, s, formyl proton); ms *m/e*: 117 (M^+).

In another experiment, imidate salt **7** (15 mg, 0.08 mmol) was dissolved in CD_3CN and cooled to 0°C, ice-cold deuterated sodium hydroxide (100 μL of 2 *N* NaOD/D_2O, 0.2 mmol) was added, and an nmr spectrum was immediately recorded at 0°C. The only product formed was amide alcohol **25***A* and **25***B* in the ratio 23:77. The conversion of **25***A* into **25***B* was then followed by nmr spectroscopy (Table 1) until equilibration.

In another experiment, imidate salt **7** (5 mg, 0.03 mmol) was dissolved in CD_3CN (500 μL) and cooled to −10°C in the nmr probe. Ice-cold deuterated sodium hydroxide (100 μL of 1 *N* NaOD/D_2O, 0.1 mmol) was added and the spectrum recorded immediately. The spectrum showed 20% of **25***A* and 80% of **25***B*. The same experiment was repeated at +10°C and the spectrum revealed 25% of **25***A* and 75% of **25***B*.

Imidate salt **7** (6 mg, 0.03 mmol) was dissolved in CD_3CN (500 μL) and D_2O (40 μL). The hydrolysis was followed by nmr spectroscopy and it was complete after 4 h giving only ester ammonium salt **21**. The solution was then cooled to 0°C and ice-cold deuterated sodium hydroxide (100 μL of 1 *N* NaOD/D_2O) was added. A spectrum was immediately recorded at 0°C showing 20% of **25***A* and 80% of **25***B*.

Imidate Salt ***8***

Imidate salt **8** (6 mg, 0.03 mmol) was dissolved in CD_3CN (500 μL) and cooled to 0°C. Ice-cold deuterated sodium hydroxide (100 μL, 1 *N* NaOD/D_2O, 0.1 mmol) was added and an nmr spectrum was immediately recorded. The only product formed was amide alcohol **27***A* and **27***B* in the ratio of 1:9. The conversion of **27***A* into **27***B* was followed by nmr spectroscopy (Table 2) until equilibration.

In a separate experiment, imidate salt **8** (8 mg, 0.04 mmol) was shaken with sodium hydroxide (1 *N*, 500 μL). The solution was then saturated with sodium chloride and extracted with dichloromethane. The organic extracts were combined, washed with brine, and dried over anhydrous sodium sulfate. Distillation of solvent gave a viscous liquid; ir ν_{max} ($CHCl_3$): 3600 (sharp), 3420 (broad), 1670, and 1020 cm^{-1}; nmr (CD_3Cl_3) δ: 1.20 (6H, s, *gem*-dimethyl group), 1.70 (2H, m, CH_2), 2.82, 2.93 (3H, two s, N—CH_3), 3.45 (2H, m, N—CH_2), 7.91, 8.00 (1H, two s, formyl proton); ms *m/e*: 145 (M^+).

Imidate Salt ***9***

Imidate salt **9** (40 mg, 0.14 mmol) was dissolved in CD_3CN (500 μL) and placed in an nmr tube. Deuterated sodium hydroxide (300 μL, 1 *N* NaOD/D_2O, 0.3 mmol) was added and the spectrum was immediately recorded. The hydrolysis was instantaneous and gave only the amide alcohol in the conformation **23***B*. It slowly isomerized to give an equilibrium mixture of **23***A* (67%) and **23***B* (33%) when kept for more than 73 h; nmr (CD_3CN/D_2O/NaOD) δ: **23***A*: 2.0 (m), 2.35 (s), 3.7 (m), 7.32 (s), 8.1 (s); **23***B*: 2.0 (m), 2.5 (s), 4.0 (m), 7.4 (s), 8.5 (s).

In a separate experiment, imidate **9** (155 mg, 0.56 mmol) was dissolved in acetonitrile (1 mL) and shaken with sodium hydroxide (800 μL, 1 *N*, 0.8 mmol). The solution was immediately treated with acetic anhydride and pyridine (20 mL, 1:1). The solution was kept overnight and then concentrated under vacuum. The residue was dissolved in dichloromethane and washed with water. Solvent evaporation gave a yellow oil, the spectra of which corresponded to the acetate of amide alcohol **23**. It was purified by chromatography on silica gel; ir ν_{max} ($CHCl_3$): 1740, 1675 cm^{-1}; nmr ($CDCl_3$) δ: 2.0 (2H, m), 2.1 (3H, s), 2.3 (6H), 3.7 (2H, m), 4.15 (2H, t), 7.3 (3H), 8.16, 8.5 (1H); ms *m/e*: 249 (M^+), 189 (M^+ − 60). Purification by preparative vpc gave an analytical sample. *Anal.* calcd. for $C_{14}H_{19}NO_3$: C 67.45, H 7.68; found: C 67.65, H 7.54.

The imidate salt **9** (4 mg, 0.015 mmol) was dissolved in CD_3CN (500 μL) and D_2O (50 μL) and the hydrolysis was followed by nmr spectroscopy. After 30 h, the hydrolysis was complete (50% amide alcohol **23** and 50% ester ammonium salt **22**) and the amide alcohol was at equilibrium (67% **23***A*, 33% **23***B*). Deuterated sodium hydroxide (50 μL, 1 *N*

NaOD/D_2O, 0.05 mmol) was then added and a spectrum recorded immediately. The reaction mixture contained 70% amide alcohol **23** at its equilibrium concentration (67% **23***A*, 33% **23***B*) and 30% of amine alcohol **30**. In a separate experiment, imidate salt **9** (10 mg, 0.94 mmol) was dissolved in water (500 μL) and kept overnight. The solution was then treated with sodium hydroxide (1 *N*, 100 μL), saturated with sodium chloride, and extracted with ether. The combined ether extracts were washed with brine, dried over anhydrous sodium sulfate, and filtered. Solvent evaporation gave a viscous oil (6 mg). Thin layer chromatographic analysis (ethyl acetate) indicated two products which were separated by thick layer chromatography to give amide alcohol **23**, identified by comparison with authentic material, and amine alcohol **29**; ir ν_{max} (CH_2Cl_2): 3360, 1470, and 1020 cm^{-1}; nmr (CD_3CN) δ: 1.76 (3H, m), 2.27 (6H, s), 3.05 (2H, t), 3.66 (2H, t), 7.13 (3H, m); ms *m/e*: 179 (M^+).

Imidate salt **9** (5 mg, 0.02 mmol) was dissolved in deuterium oxide (500 μL). After 4 h the hydrolysis was complete, giving ester ammonium salt **22** (72%) and amide alcohol **23** (28%).[6] Deuterated sodium hydroxide (100 μL, 1 *N* NaOD/D_2O, 0.1 mmol) was then added and an nmr spectrum was immediately recorded to reveal the presence of amide alcohol **23** (28%) and amine alcohol **29** (72%). No *trans* acylation reaction was detected.

Acknowledgements

This research has been supported by the Hoffmann-La Roche Foundation, the National Research Council of Canada, and the Ministère de l'Education of Québec.

[6]The amide alcohol **23** first appears as conformer **23***B* only. The same experiment was repeated and the equilibration of the amide was followed by nmr spectroscopy. The equilibrium was attained in ca. 72 h (**23***A* 25%, **23***B* 75%).

1. P. DESLONGCHAMPS, U. O. CHERIYAN, A. GUIDA, and R. J. TAILLEFER. Nouv. J. Chim. **1**, 235 (1977).
2. P. DESLONGCHAMPS, P. GERVAL, U. O. CHERIYAN, A. GUIDA, and R. J. TAILLEFER. Nouv. J. Chim. **2**, 631 (1978).
3. P. DESLONGCHAMPS, U. O. CHERIYAN, J.-P. PRADÈRE, P. SOUCY, and R. J. TAILLEFER. Nouv. J. Chim. In press.
4. P. DESLONGCHAMPS, C. LEBREUX, and R. J. TAILLEFER. Can. J. Chem. **51**, 1665 (1973); P. DESLONGCHAMPS, S. DUBÉ, C. LEBREUX, D. R. PATTERSON, and R. J. TAILLEFER. Can. J. Chem. **53**, 2791 (1975); P. DESLONGCHAMPS and R. J. TAILLEFER. Can. J. Chem. **53**, 3029 (1975).
5. B. A. LAPLANCHE and M. T. ROGERS. J. Am. Chem. Soc. **85**, 3728 (1963).
6. P. DESLONGCHAMPS. Pure Appl. Chem. **43**, 351 (1975); Tetrahedron, **31**, 2463 (1975); Heterocycles, **7**, 1271 (1977).
7. R. HUISGEN and H. OTT. Tetrahedron, **6**, 253 (1959).
8. F. BECKE and P. PAESSLER. Badische Anilin- und Soda-Fabrik AG. Ger. Patent No. 1,923,022 (November, 1970); Chem. Abstr. **74**, 22818c (1971).
9. E. W. COLLINGTON and A. J. MEYERS. J. Org. Chem. **36**, 3044 (1971).
10. A. GAGNEUX, S. WINSTEIN, and W. G. YOUNG. J. Am. Chem. Soc. **82**, 5956 (1960).
11. G. DESVAGES and M. OLOMUCKI. Bull. Soc. Chim. Fr. **9**, 3229 (1969).
12. V. W. SEELIGER and W. DIAPERS. Justus Liebigs Ann. Chem. **697**, 171 (1966).

Thermal decomposition of ozonides. A complementary method to the Baeyer–Villiger oxidation of hindered ketones

RICHARD LAPALME, H.-JÜRG BORSCHBERG, PIERRE SOUCY, AND PIERRE DESLONGCHAMPS

Laboratoire de Synthèse Organique, Département de Chimie, Université de Sherbrooke, Sherbrooke (Qué.), Canada J1K 2R1

Received March 5, 1979

This paper is dedicated to Prof. Karel Wiesner on the occasion of his 60th birthday

RICHARD LAPALME, H.-JÜRG BORSCHBERG, PIERRE SOUCY, and PIERRE DESLONGCHAMPS. Can. J. Chem. **57**, 3272 (1979).

Treatment of vinyl acetate with ozone yields the mixed anhydride of acetic and formic acids and formaldehyde oxide. The formaldehyde oxide can be trapped by reaction with ketones yielding the corresponding ozonides. Thermal decomposition of these ozonides gave the corresponding lactone and (or) the corresponding olefin carboxylic acid. The ozonides were also prepared by the ozonolysis of the corresponding olefins.

RICHARD LAPALME, H.-JÜRG BORSCHBERG, PIERRE SOUCY et PIERRE DESLONGCHAMPS. Can. J. Chem. **57**, 3272 (1979).

L'ozonolyse de l'acétate de vinyle donne l'anhydride mixte des acides acétique et formique ainsi que l'oxyde du formaldéhyde. Ce dernier peut être piégé par des cétones pour conduire aux ozonides correspondants. La décomposition thermique de ces ozonides donne les lactones ou les acides oléfines carboxyliques correspondants. Les ozonides ont aussi été préparés par l'ozonolyse des oléfines correspondants.

In connection with our investigation toward the total synthesis of ryanodine (1), it became important to find a complementary method to the Baeyer–Villiger oxidation of sterically hindered ketones. We wish to report a study which shows that the thermal decomposition of ozonides is a method which can replace the Baeyer–Villiger reaction in some cases.

Ozonolysis of vinyl acetate (CH_2Cl_2, $-78°C$) gave acetic–formic mixed anhydride and an insoluble white solid which is the result of the polymerization (2) of the carbonyl oxide of formaldehyde (formaldehyde oxide (**1**)) (3) (Scheme 1). Filtration gave a dichloromethane solution of practically pure acetic–formic mixed anhydride which was characterized further by a reaction with cyclohexylamine, yielding *N*-cyclohexylformamide (90%) and *N*-cyclohexylacetamide (10%) (4). The *dry* peroxide polymer of **1** is explosive (shock sensitive); it can be reduced with bisulfite or dimethylsulfide.[1]

Ozonolysis of vinyl acetate (7 equiv., $-78°C$, CH_2Cl_2) in the presence of camphor (**2**) (1 equiv.) gave in high yield an ozonide, characterized by nmr at $-78°C$ (two broad singlets at 5.22 and 5.12 ppm). Decomposition of the ozonide started upon warming to room temperature. After reflux in benzene for 1 h, the lactone **4** (5) was isolated in 63% yield after purification. The isomeric lactone **5** (5) was not detected. Thus, formaldehyde oxide (**1**) produced from vinyl acetate has reacted with camphor to form an ozonide. The configuration of the ozonide must correspond to structure **3** which is the result of the attack of **1** on the least hindered face of the carbonyl group in camphor. Since, only one lactone (**4**) was obtained, the decomposition of the ozonide **3** is completely specific.

We have studied also the ozonolysis of 2-methylenebornane (**6**) at $-78°C$ followed by reflux in benzene. It gave a $\simeq 1:1$ mixture of the isomeric lactones **4** and **5** in a low yield of 14% and camphor (9%). This result can be rationalized in the following way. Ozonolysis of **6** gives first the molozonide **7** which can decompose into the two carbonyl oxides **1** and **8** plus camphor and formaldehyde. Recombination yields a mixture of the isomeric ozonides **3** and **9**. The thermal decomposition of the ozonide **3** would produce only the lactone **4** while that of the ozonide **9** could either produce only the lactone **5** or a mixture of **4** and **5**. The low yield can be explained by the difficulty of recombination of the two carbonyl oxides **1** and **8** with camphor and formaldehyde respectively to give the ozonides **3** and **9**. Therefore, most of the carbonyl oxides would have produced dimeric or polymeric peroxides, which would be stable at the boiling point of benzene (6). It is also possible that both ozonides **3** and **9** gave only the lactone **4** and the formation of the isomeric lactone **5** would come from the decomposition of another unidentified "peroxide" species.

The tricyclic ketone **10** (7) was also treated with vinyl acetate and ozone to give the ozonide **11** iso-

[1]At any time, this explosive polymeric peroxide should be handled with all precautions.

0008-4042/79/243272-06$01.00/0

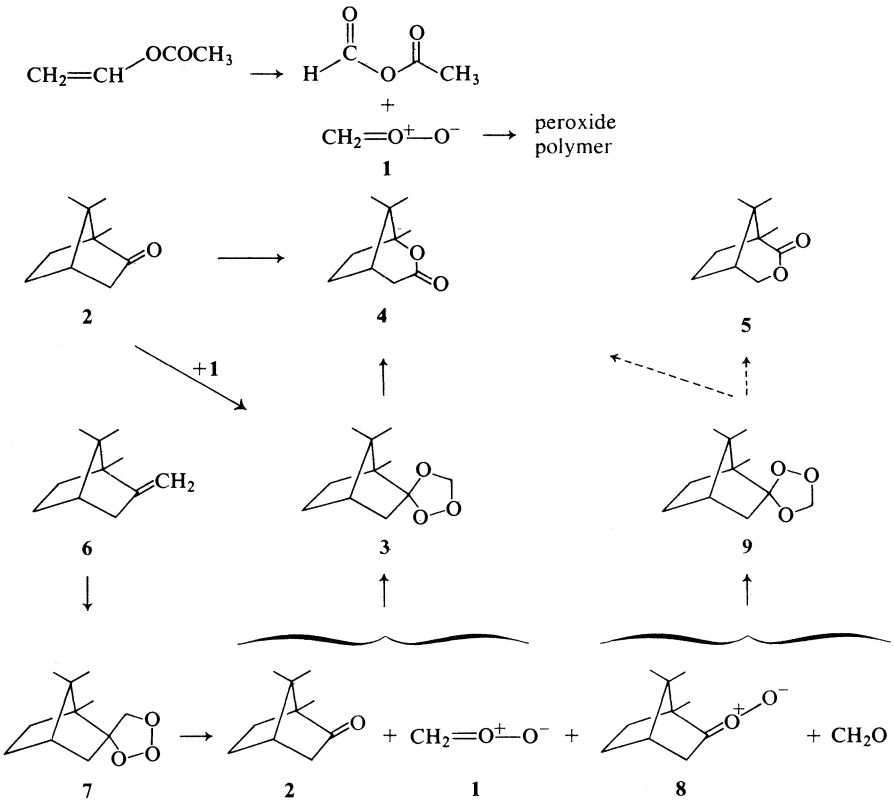

SCHEME 1

lated in 48% yield (Scheme 2). This stable ozonide is not reduced with dimethylsulfide at 20°C but it can be reduced with triphenylphosphine giving the ketone **10** in quantitative yield. The stereochemistry assigned to **11** is again based on the expectation that formaldehyde oxide **1** will prefer to react with the least hindered face of the carbonyl group in **10**. Thermal decomposition (benzene reflux, 4 h) gave the starting ketone **10** (40%) and the unsaturated olefin carboxylic acid **12** (15%, identified with an authentic sample of the corresponding methyl ester **13** (7)).

2-Norbornanone (**14**) was also treated with vinyl acetate – ozone followed by a reflux in benzene. It gave a complex mixture of unidentified olefin carboxylic acids and the lactone **16** (20%) (8). The olefin carboxylic acid **15** was not found in the mixture. The olefins **17**–**20** were also treated with ozone and the presumed ozonides were decomposed thermally by reflux in benzene. Compound **17** gave a mixture of **14** (8%), **15** (30%), and **16** (16%). Compound **18** gave **14** (16%) and **16** (10%) plus benzaldehyde (58%). The adamantane unsaturated ester **19** gave a small quantity of adamantanone (2%) and a mixture (62%) of lactone **21** (9) and olefin acid **22**. The relative percentage of **21** and **22** was not determined. On heating in the presence of *p*-toluenesulfonic acid, the olefin acid **22** was converted into the lactone **21**. 2-Methyleneadamantane (**20**) gave 15% of adamantanone and about 30% of a mixture of compounds **21** and **22**.

We have also found in the literature (10) that the ozonolysis of camphene (**23**) does not give a stable ozonide, and the compounds **24** and **25** are isolated in high yield. Similarly, 2,3,3-trimethyl-1-butene (**26**) gives an unstable ozonide which rearranges to *tert*-butyl acetate (**27**) (11).

The product formation from the thermal decomposition of the ozonides can be explained in the following manner. On heating, the weak peroxide bond of an ozonide such as **28** (Scheme 3) must cleave to give first a diradical such as **29** (12) which can either give the original ketone **30** and the diradical **31**, or formaldehyde and the diradical **32** which can fragment further to form the diradical **33**. The diradical **33** (R = H) can then either abstract a hydrogen to yield the corresponding olefin carboxylic acid **34** or form the lactone **35** (R = H). The diradical **33** (R = CH_3) would give the lactone **35** (R = CH_3).

We prefer the above mechanism to the one where

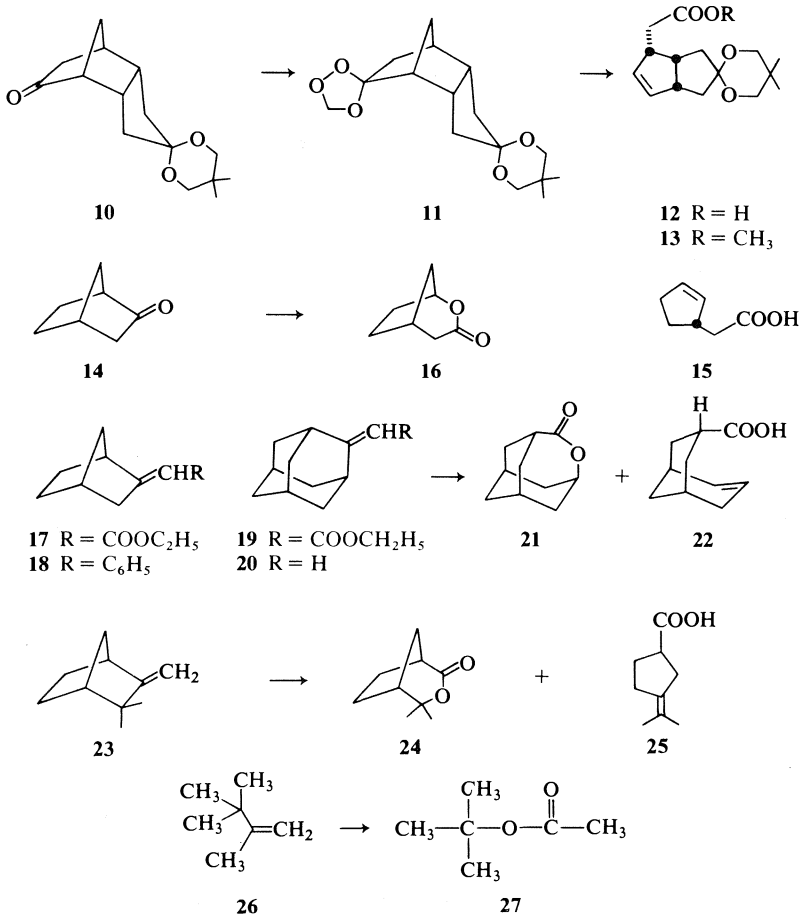

SCHEME 2

the rearragement would occur via the direct transformation of the carbonyl oxide (**28** → **36** → **37** → **38** → **35**) (see p. 747 in ref. 13).

This preliminary exploratory work shows that the thermal decomposition of ozonides gives products which are identical or equivalent to those obtained in the Baeyer–Villiger oxidation of ketones. It shows also that the vinyl acetate – ozone procedure is an interesting method to produce ozonides. However, this method has two important disadvantages: (*a*) the formaldehyde oxide (**1**) reacts with itself to yield an explosive insoluble peroxide polymer, and (*b*) the polymerization of formaldehyde oxide (**1**) competes with the reaction of **1** with ketones, a large excess of vinyl acetate being essential.

It would be interesting to find a carbonyl oxide which would be either slow to polymerize or at least would give a soluble polymer (less explosive). This carbonyl oxide reagent could be useful as a complementary method for the Baeyer–Villiger reaction in some specific cases.

We have tried the ozonolysis of ethyl vinyl ether in the presence of camphor. After heating in benzene, we have isolated camphor (70%) and the lactone **4** (30%). Formation of an insoluble polymer was not observed and we did not experience an explosion. The reaction of ozone with ethyl vinyl ether must have given first formaldehyde and the expected "stabilized" carbonyl oxide **39** (Scheme 4). Some of the carbonyl oxide **39** produced must have been trapped by camphor; however, most of **39** must have reacted with the formaldehyde produced.

We have treated the ryanodine synthetic intermediate **40** (1) with ozone in the presence of excess of either vinyl acetate or ethyl vinyl ether on a small scale. We have recovered compound **40** quantitatively; the anticipated conversion **40** → **41** did not take place. This result indicated that the dimerization or polymerization process of carbonyl oxide was faster than its reaction with the ketone functions of compound **40**.

Experimental

The ir spectra were taken on a Perkin-Elmer 257 spectrophotometer. Vapor phase chromatographic (vpc) analyses were carried out on a Varian aerograph instrument model 90-P. Proton nmr spectra were recorded on a Varian A-60 or a

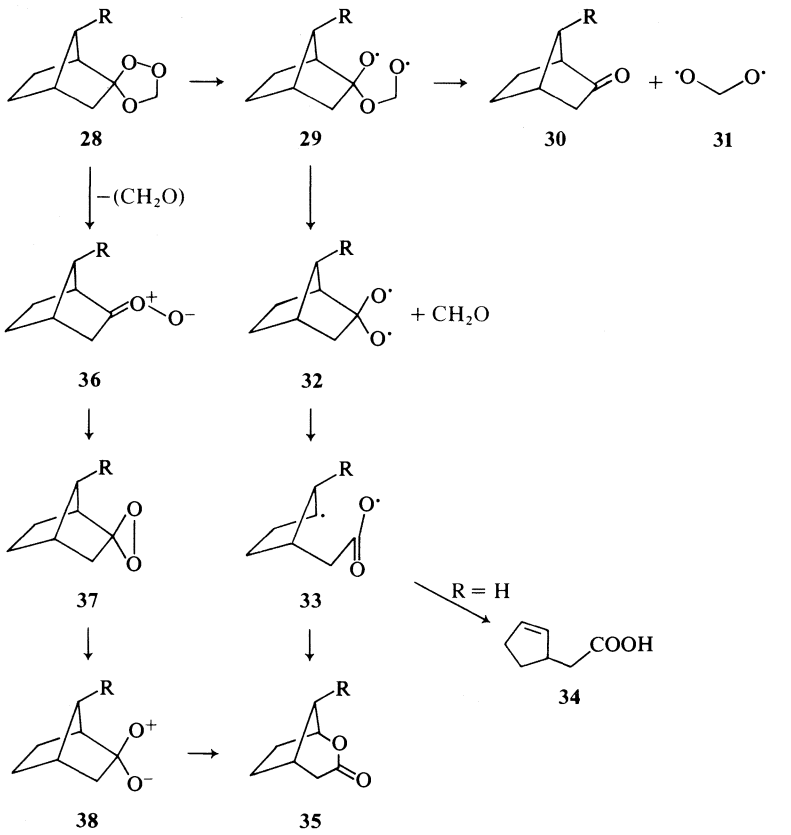

SCHEME 3

Brüker WP-60 instrument, Chemical shifts are reported in δ values relative to tetramethylsilane as internal standard (A-60) or relative to chloroform (WP-60). The carbon nmr spectrum was recorded on a Brüker HX-90 instrument. The ozonolysis reactions were carried out using a Welsbach Ozonator, model T-816. The mass spectra were taken on a Hitachi-Perkin-Elmer RMU-6 mass spectrometer. Anhydrous magnesium sulfate was used as the drying agent in working up reactions. Low boiling petroleum ether (bp 30–60°C) was used as solvent. Thin layer chromatography (tlc), both analytical and preparative, was carried out on silica gel. Adamantanone, 2-cyclopentaneacetic acid, and 2-norbornanone are commercial products (Aldrich Chemical Co.).

2-Methylenebornane **6**

2-Methylisoborneol (14) was prepared by the reaction of a large excess of methyl magnesium bromide on camphor in ether. Thionyl chloride (2.2 mL, 3 equiv.) was added dropwise to a cold solution (0°C) of 2-methylisoborneol (1.83 g, 10.9 mmol) in dry pyridine (75 mL). After 0.5 h, the reaction mixture was poured on ice and extracted with ether. The organic phase was washed with hydrochloric acid (2 *N*), water, and

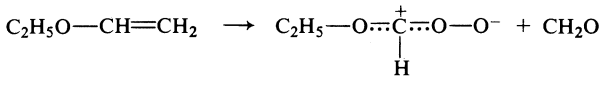

39

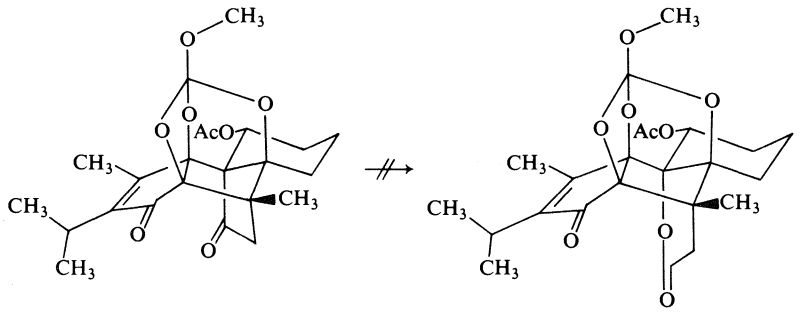

SCHEME 4

sodium bicarbonate (5%). After drying, the volume of ether was reduced (to ≃10 mL) by distillation. The vpc analysis showed a mixture of 2-methylenebornane **6** (67%) and the corresponding isomeric *endo* olefin (33%). Pure 2-methylenebornane **6** (15) was obtained by vpc; ir ($CHCl_3$)$_3$): 1650 cm^{-1}; nmr ($CDCl_3$) δ: 4.7 (2H, m, olefinic hydrogens), 0.92 (3H, s, CH_3), 0.90 (3H, s, CH_3), and 0.77 (3H, s, CH_3).

*Ethyl 2-Norbornylidene Acetate **17***

The compound **17** was prepared by the reaction of the lithium salt of trimethylsilyl ethyl acetate on 2-norbornanone in anhydrous tetrahydrofuran (16). Ethyl 2-norbornylidene acetate **17** was isolated in 26% yield by vpc as a mixture of the two geometrical isomers; ir ($CHCl_3$): 1703 and 1658 cm^{-1}; nmr ($CDCl_3$) δ: 5.7 (0.2H, m, olefinic hydrogen), 5.5 (0.8H, m, olefinic hydrogen), 4.1 (2H, q, J = 7 Hz), and 1.28 (3H, t, J = 7 Hz).

*2-Benzylidene Norbornane **18***

2-Benzyl-2-*endo*-hydroxynorbornane (17) (mp 61–63°C; nmr ($CDCl_3$) δ: 7.48 (5H, s, aromatic hydrogens) and 2.87 (2H, s, benzylic hydrogens)) was prepared by the reaction of benzyl magnesium chloride on 2-norbornanone in ether.

2-Benzyl-2-*endo*-hydroxynorbornane (313 mg, 1.55 mmol) was dehydrated with pyridine (20 mL) and thionyl chloride (0.7 mL) by following a procedure similar to the one described for the preparation of 2-methylenebornane (**6**). A mixture was obtained (230 mg) which contained the desired *exo* olefin **18** (80%) and the corresponding isomeric *endo* olefin (20%).

The above mixture (230 mg) was heated for 2 h at 120°C in dimethylsulfoxide containing potassium *tert*-butoxide (250 mg). The cooled reaction mixture was poured on ice and extracted with a mixture of ether and petroleum ether (1:3). The organic phase was washed with water, dried, and evaporation of the solvent under reduced pressure gave a yellow oil which was filtered through a short column of silica gel (petroleum ether). The olefin **18** (215 mg, ≃95% yield) was obtained pure as a mixture of two geometrical isomers (4:1 ratio); i.r. ($CHCl_3$): 1660, 1600, 1490, and 1442 cm^{-1}; nmr ($CDCl_3$) δ: 7.43 (5H, b s, aromatic hydrogens), 6.43 (0.8H, t, J = 2.5 Hz, olefinic hydrogen), and 6.26 (0.2H, m, olefinic hydrogen).

*Ethyl 2-Adamantylidene Acetate **19***

The compound **19** was prepared in 45% yield by the reaction of the lithium salt of trimethylsilyl ethyl acetate on adamantanone in anhydrous tetrahydrofuran (16;) ir ($CHCl_3$): 1705, 1655, 1445, and 1230–1195 cm^{-1}; nmr ($CDCl_3$) δ: 5.58 (1H, s, olefinic hydrogen), 4.13 (2H, q, J = 7 Hz), and 1.27 (3H, t, J = 7 Hz).

*2-Methyleneadamantane **20***

2-Methyl 2-adamantanol (mp 212–213°C; nmr ($CDCl_3$) δ: 1.4 (3H, s)) was prepared by the reaction of methyl magnesium bromide on admantanone in ether (18). Thionyl chloride (0.3 mL) was added dropwise to a cold solution (0°C) of 2-methyl 2-adamantanol (502 mg, 3.0 mmol) in dry pyridine (0.7 mL). After 45 min, the reaction mixture was poured on ice and extracted with ether. The organic phase was washed with hydrochloric acid (2 *N*), water, and sodium bicarbonate (5%). Drying and evaporation of the solvent gave a waxy solid (430 mg). Preparative tlc (hexane) gave pure 2-methyleneadamantane **20** (19); nmr ($CDCl_3$) δ: 4.6 (2H, s, olefinic hydrogens), 2.55 (2H, m), and 2.1–1.8 (12 H, m).

Ozonolysis of Vinyl Acetate

A stream of ozone in oxygen was passed through a cold solution (−78°C) of freshly distilled vinyl acetate (989 mg, 11.6 mmol) in dry dichloromethane (15 mL) until a light blue color appeared. Excess ozone was removed by bubbling nitrogen while the solution was allowed to warm up to room temperature. The white explosive polymer was removed by filtration through cotton. Proton nmr of the solution showed two singlets at 8.9 (1H) and 2.2 (3H) δ indicating the presence of acetic formic mixed anhydride. The solution was cooled to 0°C and cyclohexyl amine (2.9 g, 30 mmol) was added. After 1 h at room temperature, dichloromethane was added. The organic phase was then washed with hydrochloric acid (*N*) and sodium bicarbonate (5%). Drying and evaporation gave a mixture (1.36 g) of *N*-cyclohexylformamide (90%) and *N*-cyclohexylacetamide (10%) which were identified by nmr and vpc comparison with an authentic sample (4).

*Oxidation of Camphor (**2**)*

(a) O_3/Vinyl Acetate

A stream of ozone in oxygen was passed through a cold solution (−78°C) of camphor (154 mg, 1 mmol) and freshly distilled vinyl acetate (550 mg, 6 mmol) in dry dichloromethane (10 mL) until a light blue color appeared. Excess ozone was then removed by bubbling nitrogen. Proton nmr at −78°C showed two singlets at 5.22 and 5.12 δ indicating the presence of the ozonide **3**. The solution was then allowed to warm up to room temperature. Thin layer chromatography with ether hexane (1:1) showed one non-polar compound. Removal of the white explosive polymer by filtration through cotton gave a colorless solution. Dichloromethane (50 mL) was added and the resulting solution was washed with sodium bicarbonate (0.1 *N*, 3 × 10 mL). Drying and evaporation of the solvent under reduced pressure was followed by the addition of benzene (10 mL), and the solution was refluxed for 1 h. The crude product was shown to contain lactone **4** only by tlc analysis. Preparative tlc with ether/hexane (1:1) gave pure lactone **4** as a waxy solid (107 mg, 63%). Compound **4** was shown to be identical (ir and nmr) with the major product obtained from the Baeyer–Villiger oxidation of camphor with peracetic acid (5).

(b) O_3/Ethyl Vinyl Ether

A stream of ozone in oxygen was passed through a cold solution (−78°C) of camphor (50 mg, 7 mmol) and freshly distilled ethyl vinyl ether (720 mg, 70 mmol) in dry dichloromethane. Excess ozone was removed as before. Benzene was added and the dichloromethane was removed by distillation. The benzene solution was refluxed for 1 h and cooled to room temperature. Analysis by ir, nmr, and tlc showed that a mixture of camphor and lactone **4** was obtained, vpc measurement indicating 70% camphor and 30% lactone **4**.

*Oxidation of 2-Methylenebornane (**6**)*

A stream of ozone in oxygen was passed through a cold solution (−78°C) of 1-methylenebornane (91 mg, 0.6 mmol) in dichloromethane (20 mL) until a light blue color developed. Thin layer chromatographic analysis in ether/hexane (1:1) indicated two non-polar compounds which did not correspond to either the isomeric lactones **4** and **5** or camphor. A work-up similar to the one carried out for the oxidation of camphor was done. The mixture was then refluxed for 1 h in benzene. Analysis by ir, nmr, vpc, and tlc showed the presence of the isomeric lactones **4** and **5** (14% yield, in a ≃1:1 ratio) and camphor (9%).

*Oxidation of the Tricyclic Ketal Ketone **10***

A stream of ozone in oxygen was passed through a cold solution (−70°C) of tricyclic ketone **10** (60 mg, 0.24 mmol) and freshly distilled vinyl acetate (80 μL) in dry dichloromethane (5 mL) until a light blue color developed. The solution was allowed to warm up slowly to 0°C while nitrogen was passed through it until it was reduced to ≃0.5 mL. Preparative tlc with ether/hexane (1:1) gave the ozonide **11** (30 mg,

48%); ir ($CHCl_3$): 1112, 1089, 1075, and 992 cm^{-1}; nmr ($CDCl_3$) δ: 5.15 (1H, s), 5.03 (1H, s), 3.49 (4H, s), and 0.96 (6H, s); ms *m/e*: 296 (M^+); ^{13}C nmr ($CDCl_3$) δ: 115 (s), 111.5 (s), 94.2 (t), 73.1 (t), 71.1 (t), 46.9 (d), 41.1 (t), 40.3 (d), 39.7 (d), 33.9 (t), 33.2 (t), 32.6 (t), 29.7 (s), and 25.6 (q, one signal for both methyl groups). Analysis by ^{13}C nmr showed only one product. Analysis by ^1H nmr showed two equal singlets for the methylene group of the ozonide ring. There is at least one example in the literature of a methylene dioxy group (OCH_2O) where the two hydrogens have different chemical shifts but no coupling ($J = 0$ Hz) between the two of them (20)

A solution of the ozonide **11** (27 mg, 0.09 mmol) in dry benzene was refluxed during 4 h. After concentrating the solution to about 3 mL, an excess of ethereal diazomethane was added. The solvent was then evaporated. Separation by preparative tlc gave tricyclic ketal ketone **10** (10 mg, 40%) and the olefin ester **13** (13 mg, 51%) which was found identical (ir, nmr) with an authentic sample (7).

*Oxidation of 2-Norbornanone (**14**)*

2-Norbornanone (125 mg, 1.14 mmol) was oxidized with ozone and vinyl acetate (592 mg, 6.82 mmol) in dichloromethane (10 mL) by following the procedure described for camphor. After reflux with benzene for 18 h, the solution was evaporated and ether was added. The solution was treated with an excess of diazomethane and evaporated to dryness. Column chromatography with silica gel using ether gave the bicyclic lactone **16** (28 mg, ≃20%) (identified by ir and nmr) and a complex mixture of methyl ester products (120 mg). The vpc and tlc analyses showed the absence of the methyl ester of the olefin carboxylic acid **15** by comparison with an authentic sample.

*Oxidation of Ethyl 2-Norbornylidene Acetate **17***

A stream of ozone in oxygen was passed through a cold solution (−78°C) of ethyl 2-norbornylidene acetate (**17**) (154 mg, 0.86 mmol) in a mixture of dichloromethane and pentane (1:1, 15 mL) until a light blue color developed. Excess ozone was removed by bubbling nitrogen. Benzene (20 mL) was added, most of the dichloromethane and pentane were removed by distillation, and the mixture was refluxed for 3 h. The solution was concentrated to about 3 mL and treated with excess ethereal diazomethane. Comparison with standard solutions by vpc analysis showed a mixture of 2-norbornanone **14** (8%), the methyl ester of cyclopentaneacetic acid **15** (30%), and the lactone **16** (16%). These compounds were further identified by ir and nmr comparison with authentic samples.

*Oxidation of 2-Benzylidenenorbornane (**18**)*

2-Benzylidenenorbornane (**18**) (115 mg, 0.62 mmol) was oxidized by ozone following the procedure described for compound **17**. A mixture of 2-norbornanone (**14**) (16%), lactone **16** (10%), and benzaldehyde (58%) was obtained (vpc and nmr).

*Oxidation of Ethyl 2-Adamantylidene Acetate **19***

Ethyl 2-adamantylidene acetate (**19**) (208 mg, 0.94 mmol) was oxidized by ozone following the procedure described for compound **17**. After reflux in benzene, tlc analysis showed the presence of adamantane lactone **21** and the olefin carboxylic acid **22**. A few crystals of *p*-toluenesulfonic acid were added and the mixture was refluxed for 4 h. Comparison with standard solutions by vpc analysis showed a mixture of adamantanone (2%) and adamantanelactone (**21**) (62%). The reaction product **21** was shown to be identical by nmr with authentic adamantanelactone (9).

*Oxidation of 2-Methyleneadamantane (**20**)*

2-Methyleneadamantane (**20**) (69 mg, 0.46 mmol) was oxidized by ozone following the procedure described for compound **17**. After reflux in benzene for 3 h, *p*-toluenesulfonic acid (3 mg) was added and refluxing was continued for 1 h. Vapor phase chromatographic and nmr analyses showed a mixture of adamantanelactone **21** (30%) and adamantanone (15%).

Acknowledgements

Support for this work by the Natural Sciences and Engineering Research Council of Canada (NSERCC) and by the Ministère de l'Education (Québec) is gratefully acknowledged. We are indebted to Professor J. K. Saunders for the interpretation of the carbon nmr spectrum of the ozonide **11**.

1. P. Deslongchamps. Pure Appl. Chem. **49**, 1329 (1977).
2. K. Hayashi, H. Ochi, M. Nishii, Y. Miyake, and S. Okamura. J. Polym. Sci. B, **1**(8), 427 (1963).
3. L. A. Hull. J. Org. Chem. **43**, 2780 (1978) and references therein.
4. C. D. Hurd and A. S. Roe. J. Am. Chem. Soc. **61**, 3355 (1939).
5. (*a*) R. R. Sauers. J. Am. Chem. Soc. **81**, 925 (1959); (*b*) R. R. Sauers and G. P. Ahearn. J. Am. Chem. Soc. **83**, 2759 (1961).
6. P. R. Story and J. R. Burgess. Tetrahedron Lett. 1287 (1967).
7. P. Deslongchamps, U. O. Cheriyan, Y. Lambert, J.-C. Mercier, L. Ruest, R. Russo, and P. Soucy. Can. J. Chem. **56**, 1687 (1978).
8. J. Meinwald and E. Frauenglass. J. Am. Chem. Soc. **82**, 5235 (1960).
9. (*a*) P. Soucy, T.-L. Ho, and P. Deslongchamps. Can. J. Chem. **50**, 2047 (1972); (*b*) A. C. Udding, H. Wynberg, and J. Strating. Tetrahedron Lett. 5719 (1968).
10. P. S. Bailey. Chem. Ber. **88**, 795 (1955).
11. R. Criegee, A. Kerckow, and H. Zinke. Chem. Ber. **88**, 1878 (1955).
12. P. R. Story, T. K. Hall, W. H. Morrison III, and J. C. Farine. Tetrahedron Lett. 5397 (1968).
13. R. Criegee. Angew. Chem. Int. Ed. Engl. **14**, 745 (1975).
14. M. L. Capman, W. Chodkiewiez, and P. Cadiot. Bull. Soc. Chim. Fr. **8**, 3233 (1968).
15. H. H. Zeiss and F. R. Zwanzig. J. Am. Chem. Soc. **79**, 1733 (1957); M. Chaykovsky and E. J. Corey. J. Org. Chem. **28**, 1128 (1969); G. E. Gream, C. F. Pincombe, and D. Wege. Aust. J. Chem. **27**, 603 (1974).
16. K. Shimoji, H. Taguchi, K. Oshima, H. Yamamoto, and H. Nozaki. J. Am. Chem. Soc. **96**, 1620 (1974).
17. K. Stack, W. Winter, and W. Schaumann. Ger. Patent No. 1,108,684 (June, 1961); Chem. Abstr. **57**, 4593h (1962).
18. P. v. R. Schleyer and R. D. Nicholas. J. Am. Chem. Soc. **83**, 182 (1961).
19. R. C. Fort, Jr. and P. v. R. Schleyer. J. Org. Chem. **30**, 789 (1965).
20. P. Yates and R. S. Dewey. Tetrahedron Lett. 847 (1962).

Organic sulfur mechanisms. 21. The reaction of arylsulfenes with sulfur dioxide[1]

JAMES FREDERICK KING AND MOHAMMAD ASLAM

Department of Chemistry, University of Western Ontario, London, Ont., Canada N6A 5B7

Received April 6, 1979

This paper is dedicated to Prof. Karel Wiesner on the occasion of his 60th birthday

JAMES FREDERICK KING and MOHAMMAD ASLAM. Can. J. Chem. **57**, 3278 (1979).

Phenylsulfene and diphenylsulfene (**2**), obtained by reaction of 2,6-lutidine with appropriate precursors, react with sulfur dioxide to give, respectively, benzaldehyde and benzophenone, in confirmation of the suggestion of Staudinger and Pfenninger that the benzophenone formed in the reaction of diphenyldiazomethane (**1**) with sulfur dioxide arises from reaction of the latter with the sulfene (**2**). The reaction of sulfenes with sulfur dioxide would appear to have only limited scope, all known examples occurring with a sulfene having at least one aryl group attached to the sulfene carbon atom; even with these sulfenes the reaction is apparently readily precluded in the presence of most other sulfene traps. ^{18}O-Labelling experiments in the reaction of diphenylsulfene (**2**) with sulfur dioxide indicate that the oxygen atoms in about two-thirds of the benzophenone molecules come from the sulfur dioxide, whereas **2** itself supplies the oxygen atoms for the remaining third. Previously suggested mechanisms predict that the benzophenone oxygens come only from the sulfur dioxide. General processes that could lead to the observed labelling pattern are discussed and specific examples presented. The available evidence, including reported labelling studies on the related reaction of sulfur dioxide with sulfur trioxide, provides a basis for excluding certain possible mechanisms and for preferring some over others, but is not sufficient to establish a single mechanism for the reaction of arylsulfenes with sulfur dioxide.

JAMES FREDERICK KING et MOHAMMAD ASLAM. Can. J. Chem. **57**, 3278 (1979).

Le phénylsulfène et le diphénylsulfène (**2**) obtenus par la réaction de la lutidine-2,6 avec des précurseurs appropriés, réagissent avec le bioxyde de soufre pour conduire respectivement à la benzaldéhyde et à la benzophénone. Ceci est en accord avec la suggestion de Staudinger et Pfenninger qui stipule que la benzophénone obtenue lors de la réaction du diphényldiazométhane (**1**) avec le bioxyde de soufre provient de la réaction de ce dernier avec le sulfène (**2**). La réaction des sulfènes avec le bioxyde de soufre semblerait avoir une étendue limitée puisque tous les exemples connus se rapportent à des sulfènes ayant au moins un groupement aryle attaché à l'atome de carbone du sulfène: même avec ces sulfènes, la réaction apparemment est empêchée facilement en présence de la plupart des pièges à sulfènes. Les expériences de marquage isotopique à l'^{18}O dans la réaction du diphénylsulfène (**2**) avec le bioxyde de soufre indiquent que les atomes d'oxygène des molécules de benzophénone dans la proportion de 2/3 environ proviennent du bioxyde de soufre alors que le composé **2** lui-même fournit le 1/3 des oxygènes restants. Les mécanismes suggérés antérieurement prédisent que les atomes d'oxygène de la benzophénone proviennent seulement du bioxyde de soufre. Tout en présentant des exemples spécifiques, on discute des techniques générales qui conduiraient au type de marquage isotopique observé. Les preuves disponibles, incluant les études de marquage isotopique publiées sur la réaction apparentée du bioxyde de soufre avec le trioxyde de soufre, fournissent un point de départ pour exclure certains mécanismes possibles et pour préférer quelques uns à d'autres, mais ce n'est pas suffisant pour établir un mécanisme approprié pour la réaction des sulfènes aromatiques avec le bioxyde de soufre.

[Traduit par le journal]

Introduction

The reaction of a diazoalkane with sulfur dioxide was first reported in 1916 by Staudinger and Pfenninger (1), whose observations and proposed mechanisms may be summarized by Scheme 1. Since episulfones such as **3** very readily lose sulfur dioxide to form the olefin, the sequence **1** → **2** → **3** followed by the desulfonylation provides a useful synthesis of symmetrical alkenes,[2] though the general applicability of this route is considerably reduced by the incursion of two other reactions. One of these leads to Δ^3-1,3,4-thiadiazoline 1,1-dioxides (**7**), and thence, sometimes apparently spontaneously, to the azine

[1]Part 20: Can. J. Chem. **55**, 2323 (1977).

[2]For a review of sulfene to episulfone (or olefin) reactions see ref. 2. The intermediacy of the sulfene in this sequence follows from the observation by Opitz and Fischer (3, 4) of the characteristic adduct in the reaction of diazomethane and sulfur dioxide in the presence of 1-pyrrolidinoisobutene. Further examples of this experiment have recently been cited by Tanabe *et al.* (5, 6) as evidence for sulfene formation in the reaction of diazoalkanes and sulfur dioxide; these authors neglect, however, to acknowledge the prior work of Opitz and Fischer.

0008-4042/79/243278-14$01.00/0

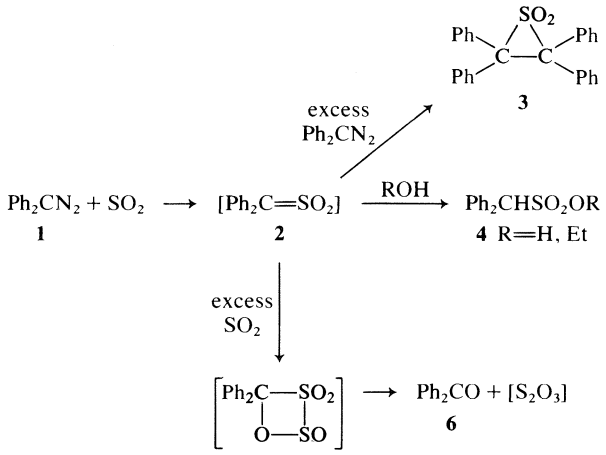

SCHEME 1

$R^1R^2C{=}N{-}N{=}CR^1R^2$ (7–9). The other competitive process is the reaction which forms the subject of the present paper, namely the formation of the simple carbonyl compound, e.g., benzophenone (**6**), originally suggested by Staudinger and Pfenninger (1) as arising from reaction of the sulfene (**2**) with sulfur dioxide. In studying this reaction our primary aim was to obtain further knowledge of sulfenes, as part of our continuing investigation of the chemistry of these species (10); we also hoped perhaps to learn something that would be helpful in improving the Staudinger–Pfenninger alkene synthesis.

What little information that was available at the start of this work showed that the formation of benzophenone was not unique. Tokura and coworkers had reported formation of (*a*) up to 22%

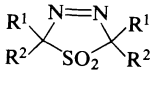

7

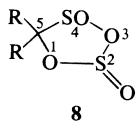

8

yields of benzaldehyde in the reaction of sulfur dioxide with phenyldiazomethane (11), (*b*) increasing amounts of 1,4-dibenzoylbenzene with increase in solvent polarity from the reaction with 1,4-bis[α-diazobenzyl]-benzene (12), and (*c*) a small amount of benzil from the reaction with azibenzil (13). Recently Brophy *et al.* (9) have described the formation of some substituted pivalophenones and related compounds from the corresponding diazoalkanes and sulfur dioxide; these authors suggested that the ketones might arise from the five-membered ring intermediate **8**, rather than the analogue of Staudinger and Pfenninger's four-membered ring intermediate (**5**) (in the mechanistic discussion which follows we shall refer to these routes, which are shown in Scheme 2, as the "BCHS" and "SP" mechanisms, respectively). Even more recently Tanabe and Nagai have reported the formation from bis(*p*-methoxyphenyl)diazomethane of up to 67% yields of 4,4′-dimethoxybenzophenone as well as smaller amounts of the corresponding tetraphenylethylene and bis(*p*-methoxyphenyl) sulfide, and also of the observation of a small amount of *p*-tolualdehyde from *p*-tolyldiazomethane (14).

Our initial aims were to define the scope of the reaction and to find if, in fact, the reaction really does involve a sulfene, and, if so, by what mechanism. In this paper we describe our findings (*a*) that sulfur dioxide indeed reacts with some sulfenes to form the ketone (or aldehyde), (*b*) that the reaction is apparently favoured when at least one of the substituents of the sulfene ($RR^1C{=}SO_2$) is an aryl group, and (*c*) that the reaction of **2** cannot be proceeding exclusively via the simplest SP or BCHS mechanisms and may well be occurring by a quite different route.

Results and Discussion

Sulfene Intermediacy and the Scope of the Reaction

The obvious experiment to ascertain if sulfenes and sulfur dioxide react as proposed, is simply to generate a sulfene by a known route in the presence of sulfur dioxide, and to determine if any of the ketone (or aldehyde) is formed. Though the action of tertiary amines on alkanesulfonyl halides and related compounds provides the most generally useful route to sulfenes, the requirement that sulfur dioxide be present creates a problem arising from the tendency of sulfur dioxide and amines to form complexes (15):

$$R_3N + SO_2 \rightleftharpoons R_3N{\cdot}SO_2$$

The result is that with pyridine or triethylamine, for example, the above equilibrium is evidently sufficiently far to the right that it is difficult to maintain simultaneously a sufficiently high concentration of the base to form the sulfene at a reasonable rate while having a high enough concentration of sulfur dioxide to test if it actually reacts with the sulfene. 2,6-Lutidine, however, presumably because the two methyl groups decrease the tendency for complex formation, was found to react with phenylmethanesulfonyl chloride in the presence of excess sulfur dioxide to give a small amount (~10%) of benzaldehyde. The fate of the major part of the phenylmethanesulfonyl chloride was not determined, but in view of the known tendency for phenylsulfene to react with chloride ion leading (in the absence of sulfur dioxide) ultimately to the thiobenzoyl chloride

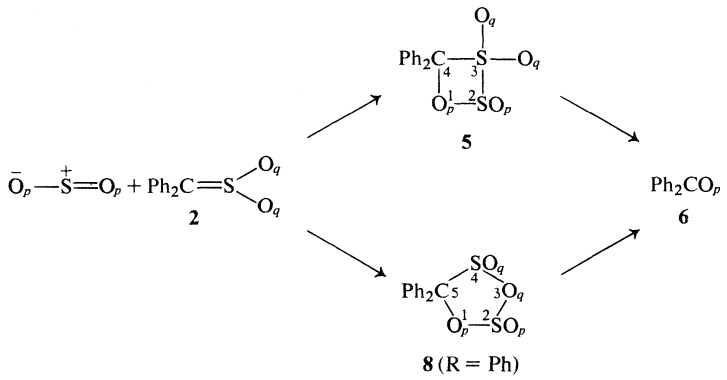

Staudinger–Pfenninger (SP) mechanism: **2** → **5** → **6**
Brophy–Collins–Hobbs–Sternhell (BCHS) mechanism: **2** → **8** → **6**
p = ^{18}O content of the starting SO_2
q = ^{18}O content of the sulfonyl group in the ester (**9***c*)

SCHEME 2

S-oxides (16, 17), we tried the reaction of phenylmethanesulfonic anhydride instead of the chloride and obtained a much improved yield of benzaldehyde (50%, isolated as the 2,4-dinitrophenylhydrazone). In the absence of sulfur dioxide no benzaldehyde was formed; use of pyridine instead of 2,6-lutidine led to a lower (10%) yield of benzaldehyde. In our hands further variation of reaction conditions or reagents did not increase the yield of benzaldehyde. This result should perhaps be viewed in the light of the observation of Tokura *et al.* (11) that even in liquid sulfur dioxide the reaction with phenyldiazomethane gives mainly the products of the episulfone route and at most only a minor amount (22%) of benzaldehyde.

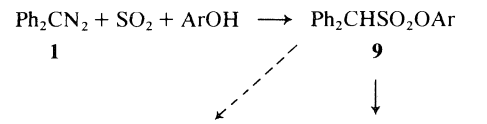

a Ar = *p*-nitrophenyl
b Ar = 2,4-dinitrophenyl
c Ar = 2-chloro-4-nitrophenyl

SCHEME 3

We then turned to the reaction of sulfur dioxide with **2** (generated, of course, by a route other than reaction of **1** with SO_2). Such a system was expected also to be useful for our planned ^{18}O-labelling experiments (see the next section), owing to the greater ease with which small quantities of benzophenone may be handled as compared with benzaldehyde. The obvious starting materials, i.e., diphenylmethanesulfonyl chloride or the anhydride, were unfortunately unavailable; neither the chloride nor the anhydride have to our knowledge been described, and all attempts in our laboratory to make the chloride have failed. This difficulty is general to the synthesis of any sulfonyl derivative RSO_2Z in which the corresponding cation, R^+, is relatively stable and Z is a good leaving group; instead of RSO_2Z one simply obtains R—Z.[3]

We have achieved partial success by adjusting the leaving group tendency of Z by varying the substituents in the esters **9**, prepared as shown in Scheme 3. The *p*-nitrophenyl ester (**9***a*) was found to be unreactive to 2,6-lutidine, whereas **9***b* underwent ready desulfonylation to **10**, perhaps as indicated by the broken arrows in Scheme 3. Ester **9***c*, however, was found to react with 2,6-lutidine and sulfur dioxide in methylene chloride to give benzophenone in 15–25% yields; the only other identified product (other than 2-chloro-4-nitrophenol) was the ether (**10***c*). As evidence that diphenylsulfene (**2**) is formed under these conditions, we found that the ester (**9***c*) with 2,6-lutidine reacts with sulfene trapping reagents to form the appropriate products: i.e., with *p*-toluidine we obtained the *p*-toluidide[4] (Ph_2CHSO_2NH—*p*-Tol), and with 1-morpholino-2-methylpropene the characteristic sulfene–enamine cycloadduct (5, 6).

The extent of conversion of diphenylsulfene (**2**) to

[3]For example, diphenylmethanesulfonic acid with thionyl chloride gives benzhydryl chloride, presumably by a mechanism analogous to that shown by the broken arrows in Scheme 3.

[4]Notwithstanding a contrary report (18) it was found originally by Dr. D. R. K. Harding in these laboratories (see ref. 10) that Ph_2CHSO_2NH—*p*-Tol is also readily prepared from **1** and SO_2 in the presence of *p*-toluidine. Another error in the same paper has also been corrected by Harding (private communication). He found that hydrolysis of diphenylmethanesulfonpiperide with aqueous HCl gives no sign of diphenylmethane as originally reported (18), but rather a good yield of benzhydryl chloride, formed presumably via the benzhydryl cation in a manner related to the conversion of **9** to **10** in Scheme 3.

benzophenone (**6**) can be seen to be roughly comparable to that of phenylsulfene to benzaldehyde, the mediocre yield in the overall conversion of **9***c* to **6** being partly due to the formation of **10***c*, a separate, "non-sulfene" reaction. In practice the best yields of benzophenone were obtained using a limited amount of sulfur dioxide. With a larger amount of sulfur dioxide such that it became the major solvent component, the ratio of **6** to **10***c* was distinctly reduced. In view of the greater ionizing power of sulfur dioxide as compared with methylene chloride,[5] this observation is consistent with the ionization mechanism, **9** → Ph_2CH^+ → **10** shown in Scheme 3. As a further test of this mechanism we treated benzhydryl chloride, which would be expected (21) to give the benzhydryl cation under these conditions, with the same mixture of 2,6-lutidine, 2-chloro-4-nitrophenol, sulfur dioxide, and methylene chloride as used in most of the above experiments. The only product (in 70% yield) was the ether (**10***c*), without any sign of either benzophenone (**6**) or the ester (**9***c*). This result (*a*) serves to confirm our earlier conclusion that benzophenone (**6**) and the ether (**10***c*) are formed by quite different routes, and (*b*) indicates that the fragmentation of **9***c* to the benzhydryl cation, sulfur dioxide, and the aryloxide anion is essentially irreversible under these conditions.

The above results confirm the original suggestion of Staudinger and Pfenninger that sulfenes react with sulfur dioxide to form the carbonyl analogue. It is clear, however, that sulfur dioxide is an inefficient sulfene trap, failing to compete with diphenyldiazomethane, *p*-nitrophenol, 2,4-dinitrophenol, 2-chloro-4-nitrophenol, 1-morpholino-2-methylpropene, *p*-toluidine, and probably chloride ion, often apparently when these other sulfene traps are present in relatively small amounts. This conclusion is borne out by our experience in trying to observe reaction of other sulfenes with sulfur dioxide. 1-Phenyldiazoethane gave a 5% yield of acetophenone, and reaction of methanesulfonic anhydride with 2,6-lutidine and sulfur dioxide gave no sign of formaldehyde. Apart from the original report (1) of benzophenone formation (in 80% yield) the only high yield conversions of sulfenes to ketones are those reported by Brophy *et al.* (9) in reactions of diazoalkanes of the general formula $ArRCN_2$ in which R is a bulky group such as *t*-butyl or 1-adamantyl; successively lower yields of the ketone were obtained on changing R to an isopropyl or methyl group, the major products in the latter case being derived presumably from the episulfone and Δ^3-1,3,4-thiadiazoline (**7**) routes.

^{18}O-Labelling and the Mechanisms of the Sulfene – Sulfur Dioxide Reaction and the Sulfur Dioxide – Sulfur Trioxide Exchange

In the simplest form of the SP or BCHS mechanisms,[6] the oxygen of benzophenone comes entirely from the sulfur dioxide with none whatever from the sulfene (**2**) (see Scheme 2). Obviously this suggestion may be tested by an ^{18}O-labelling experiment if one has a method of providing labelled sulfur dioxide in the presence of unlabelled sulfene (and preferably vice versa as well). Whereas the original Staudinger–Pfenninger procedure would not do for such an experiment because it does not allow different levels of labelling for the sulfene and the sulfur dioxide, the reaction of ester **9***c* with 2,6-lutidine and sulfur dioxide is well-suited. Although the ready desulfonylation (**9***c* → **10***c*) is inconvenient because it lowers the yield of benzophenone, there is a compensating advantage in that it is particularly easy to determine the ^{18}O content of the sulfonyl function simply by heating a sample of the ester (**9***c*) in a flask attached directly to the mass spectrometer and determining the composition of the sulfur dioxide produced. In addition, the ^{18}O-labelled ester is readily obtained using ^{18}O-labelled sulfur dioxide in the synthesis shown in Scheme 3.

Preliminary ^{18}O-labelling experiments indicated that our determinations of the ^{18}O contents of the starting sulfur dioxide and of the benzophenone product were subject to considerable uncertainty, deriving perhaps from the ability of these compounds (particularly the sulfur dioxide) to exchange oxygen atoms with water. It is evident from the data in Table 1 that even when the ^{18}O contents of the sulfur dioxide were determined just before and just after the reaction they must be regarded as only approximate values; note particularly the differences between the "initial" and "final" values in runs 1 and 2. Control experiments with labelled ester (**9***c*) and labelled benzophenone (**6**) show that they undergo little or no ^{18}O exchange during the reaction. In addition, with the workup and analysis used there is no extensive loss of label from the benzophenone, although it seems likely that the accumulation of a sequence of small effects leads to low values for the determined ^{18}O contents of **6**; a rough estimate of the accumulated loss of about 1% (or rather less for the smaller

[5]Since data directly comparing the polarity of liquid sulfur dioxide and methylene chloride seem scarce, we adduce the following. Empirical methods (19) indicate that the polarity of methylene chloride is comparable to (or slightly less than) that of nitrobenzene, which in turn may be inferred to be much less polar than sulfur dioxide from Lichtin's estimate (20) that the ionization constants for triarylmethyl chlorides are about 10^{10} times greater in liquid sulfur dioxide than in nitrobenzene.

[6]We assume in this discussion that O-1, S-2, and its sulfinyl oxygen in **5** and **8** (as formed initially, at least) derive from the sulfur dioxide, and the sulfur bonded to carbon and the attached oxygens come from the sulfene (**2**).

TABLE 1. ^{18}O-labelling in the reaction of ester **9***c* with 2,6-lutidine and sulfur dioxide in methylene chloride[a]

	^{18}O percentage			
	Sulfur dioxide			
Run No.	Initial[b]	Final[b]	Ester **9***c*[c]	Benzophenone
1	13.2	10.1	(0.2)[d,e]	5.5 (6±0.5)[f]
2	13.6	15.8	(0.2)[d,e]	5.6 (6±0.5)
3	0.3[d]	[e]	19.3	5.7 (6±0.5)
4	0.3[d]	0.7	15.0	3.1 (3.5±0.5)

[a]The molar ratio of **9***c*: base: SO_2 was 1:26:34.
[b]"Initial" refers to a sample taken just prior to sealing the ampoule and "final" to one taken immediately upon opening (see Experimental).
[c]Refers to the ^{18}O content of the oxygens of the sulfonyl group only, as determined on the thermally extruded sulfur dioxide. Control experiments showed only natural abundance levels of ^{18}O in the other oxygens.
[d]Natural abundance.
[e]Not determined.
[f]Values without parentheses are obtained directly from ms; those in parentheses are estimated from these taken with control experiment data (see text).

^{18}O content in run 4) leads to the values given in parentheses in Table 1. Taking both the variability in determining the ^{18}O content of the labelled sulfur dioxide used as the starting material and the above correction for the ^{18}O content of the product (**6**), we estimate that starting with sulfur dioxide containing about 13 ± 3% ^{18}O we obtain benzophenone with ~6 ± 1% ^{18}O, i.e., that perhaps 50 ± 20% of the original label from the sulfur dioxide appears in the benzophenone (**6**). Similarly it would appear from runs 3 and 4 that about 30 ± 10% of the label originally in the sulfonyl groups of the ester (**9***c*) shows up in the benzophenone.

Rough though these results are, they show clearly that the oxygen of the benzophenone cannot come *exclusively* from either the sulfur dioxide or from the ester (**9***c*). This in turn requires that the reaction cannot proceed exclusively via a simple formation and decomposition of either **5** or **8** (R = Ph) (or both), since such a mechanism must give the same ^{18}O content in the benzophenone as in the sulfur dioxide used, i.e., ~13% in runs 1 and 2 and natural abundance in runs 3 and 4 (or slightly higher owing to the very small ^{18}O enrichment of the excess sulfur dioxide by introduction of labelled SO_2 from the process **9***c* → **10***c* + SO_2).

It would appear from the above results that this system, in which a portion of the label comes from one starting material and the remainder from the other, illustrates an interesting and potentially general problem which would appear, rather surprisingly, not to have been previously observed in labelling experiments with the heavier elements (i.e., those which show small isotope effects). The more usual circumstance is that all of the label of the product comes from one starting material only, in which case it is readily seen that in the absence of labelling losses and of any isotope effects, the extent of labelling in the product must be the same as that in the starting material. In fact, this was observed in the present study in the preparation of a sample of [^{18}O]benzophenone by hydrolysis of diphenyldichloromethane with ^{18}O-enriched water; the ^{18}O contents were the same within experimental error (~20%). When the potentially labelled atoms derive from *two* starting materials, only one of which is labelled, it is obvious that the extent of the labelling in the product cannot be as great as that of the labelled starting material since a portion of the potentially labelled atoms must come from an unlabelled source. If (taking for illustrative purposes the present case which uses ^{18}O-labelling) we define

$$f_1 = \frac{^{18}O \text{ content of product}}{^{18}O \text{ content of the first starting material}}$$

then (in the absence of labelling losses and isotope effects) the fraction f_1 is simply the fraction of the potentially labelled (i.e., oxygen) atoms in the product that derive from the starting material with the label. If there are only two starting material sources for the potentially labelled atoms, then f_2, the fraction of these atoms that derive from the second starting material, is simply $1 - f_1$. In other words, if one carries out two labelling experiments, the first with (only) one starting material labelled and the second with (only) the other labelled, then $f_1 + f_2 = 1$ (or, if expressed as percentages must add up to 100). By extension, if a product has three (or four, etc.) sources of the potentially labelled atom, the three (or four, etc.) labelling experiments would give three (or four, etc.) f values summing to unity.

In the example at hand we note that the sum of 50 ± 20% and 30 ± 10% is 80 ± 30%, i.e., the labelling experiments comply with the requirement of

complementarity for *two* label sources only if we take the values in the upper range of the error limits, say ~65% and ~35%, respectively. An alternative possibility is that there is a third oxygen source in these reactions, but this is not in accord with our observation that diphenyldiazomethane reacted with labelled sulfur dioxide (17.0% ^{18}O) to give benzophenone with essentially the same (16.9%) ^{18}O content. If there are only two sources of the potentially labelled atom, it would appear that about two of every three benzophenone oxygens derive from sulfur dioxide and one of every three from the sulfene (**2**) formed from the ester (**9***c*).

Having concluded earlier that neither the simple SP or BCHS routes accounts for this result we should now provide one which does. It rapidly becomes apparent, however, that there is no shortage of possible mechanisms but rather of information for distinguishing the correct one. Our present discussion will therefore merely illustrate, with examples, the general ways of accounting for our results, and mention some experiments in this and the related sulfur trioxide – sulfur dioxide system which may be helpful in limiting the problem. We follow Staudinger and Pfenninger's lead in pointing to sulfene – sulfur dioxide cycloadducts as possible key intermediates[7] and list the other possible simple cycloadducts (**11**, **12**, and **13**), which, in addition to **5** and **8** (R = Ph) have (*a*) the sulfur atoms at either the sulfonyl or sulfinyl oxidation levels, and (*b*) the sulfene carbon tetracoordinated. In addition we note the cyclic esters **14** and **15**, which by desulfinylation and desulfonylation, respectively, could give benzophenone (**6**). *A propos* of these species we point out that desulfinylation of an intermediate α-sultine (like **14**) has been suggested to account for the thermal conversion of sulfenes to their carbonyl analogues (24), and in the oxidation of sulfines to their carbonyl analogues (25, 26); semi-empirical calculations on the sulfene – α-sultine interconversion have led to the prediction that it is an "allowed" pathway (27). The corresponding desulfonylation of an α-sultone (**15**) would be expected from the known behaviour of episulfones (1, 2) to occur readily. Mixed sulfinic–sulfonic anhydrides (whether cyclic, like **11**, or acyclic) have not, to our knowledge, been isolated, though such a species has been suggested as an intermediate in the formation of the thiobenzoyl chloride *S*-oxides (17, 28).

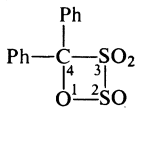

5

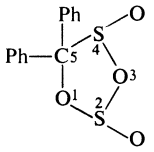

8 (R = Ph)

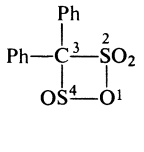

11

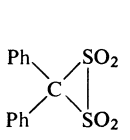

12

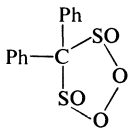

13

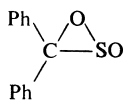

14

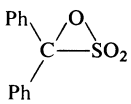

15

We perceive two general categories of mechanisms by which the benzophenone oxygen may come from either of the two sources

I. *Competition* between two reactions, with the oxygen of the benzophenone (**6**) coming in one reaction from the sulfur dioxide and in the other from the sulfonyl group of the ester (**9***c*).

II. *Equilibration* of oxygens.

In the simplest case of competition, or Category I, process, the fractions f_1 and f_2 (defined above) merely indicate the relative rates of the two competing reactions. With equilibrium (Category II) reactions there are two possibilities, (A) a *partial* exchange involving *all* of the sulfur dioxide and sulfene oxygens, and (B) *complete* exchange of *some* of these oxygens. Note that *complete* exchange of *all* of these oxygens would, because of the large excess of the sulfur dioxide employed, simply give a product (**6**) with essentially the same ^{18}O content as the original sulfur dioxide, contrary to experiment. The fractions f_1 and f_2 with Category IIA reflect the relative rates of exchange vs. product formation, and with Category IIB, the number of oxygen atoms from each source undergoing equilibration.

Scheme 4 illustrates a possible Category I mechanism. In addition to the BCHS process, **2** → **8** → **6**, there is a second (minor) mode of decomposition of **8** to give **14** (as indicated by the horizontal broken line), which then would desulfinylate to give **6** in which the oxygen derives from the sulfene (**2**) rather than from the sulfur dioxide. If we designate the ^{18}O content of each oxygen atom of the original sulfur dioxide by *p*, and that of each oxygen of the sulfonyl group of the ester (**9***c*), and hence of the sulfene (**2**), by *q*, then ^{18}O contents at various positions as the reaction proceeds are as shown in Scheme 4. To account for the observed ^{18}O content of the final product (**6**), one merely has to postulate that the "major" cleavage of **8** is twice as fast as the "minor".

An example of a Category IIA process is shown in Scheme 5, the (partial) equilibration occurring by way of the symmetrical α-disulfone (**12**) (note that **13** would also serve). The requisite labelling in the product (**6**), would arise if k_1 (leading to **12**) were *four* times k_2 (leading to **8**), since half of the disulfone (**12**)

[7]See also the discussions of the thermal (22) and photochemical (23) reactions of sulfur dioxide with ketene, the carbonyl analogue of sulfene.

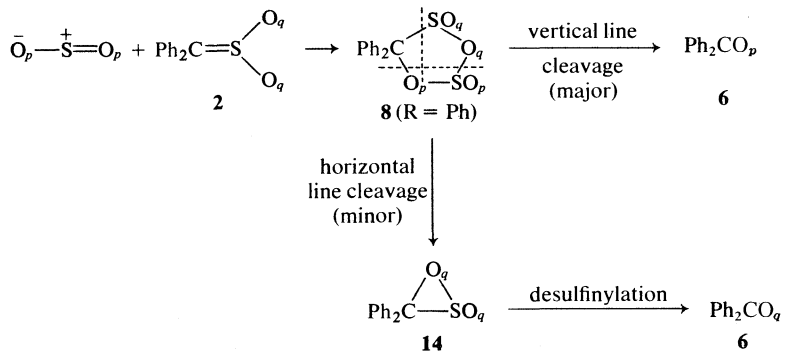

SCHEME 4. An example of a Category I process.

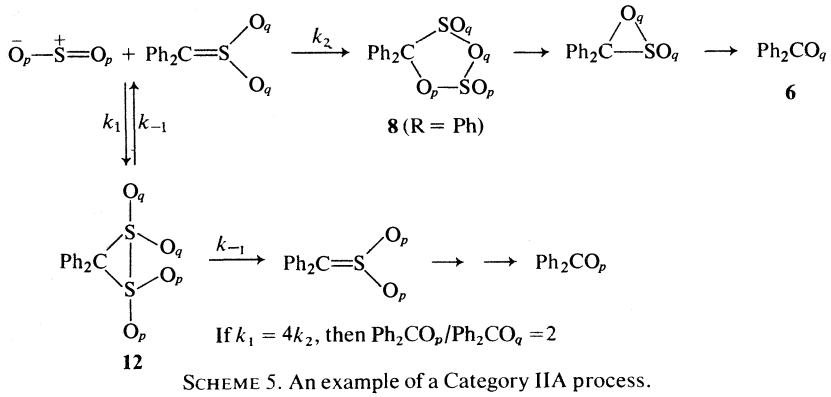

SCHEME 5. An example of a Category IIA process.

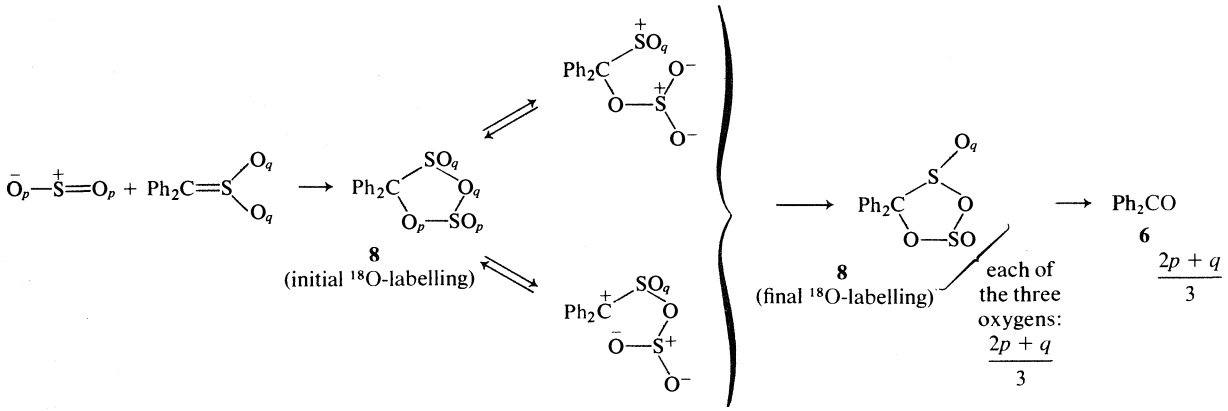

SCHEME 6. One example of a Category IIB process.

would have to return to the original sulfene (**2**) and sulfur dioxide.

Perhaps the most interesting of these categories is that labelled IIB, which, in the present system, would require *two* sulfur dioxide oxygens to equilibrate with *one* sulfene oxygen and then have one of these oxygens incorporated into the benzophenone (**6**). Scheme 6 shows one way by which this might occur. A rapid equilibration as shown would give the labelling pattern indicated by "**8** (final ^{18}O-labelling)", which by either of the decomposition modes shown in Scheme 4 would give **6** with ^{18}O content $(2p + q)/3$, i.e., in which the benzophenone had 2/3 of the ^{18}O content of the sulfur dioxide and 1/3 of that of the sulfonyl group of the original ester (**9***c*), as required by experiment.

Scheme 7 summarizes two other possible routes. These involve **11**, which could conceivably be formed from the sulfene (**2**) and sulfur dioxide in either of two ways, the "normal" route (i.e., without change

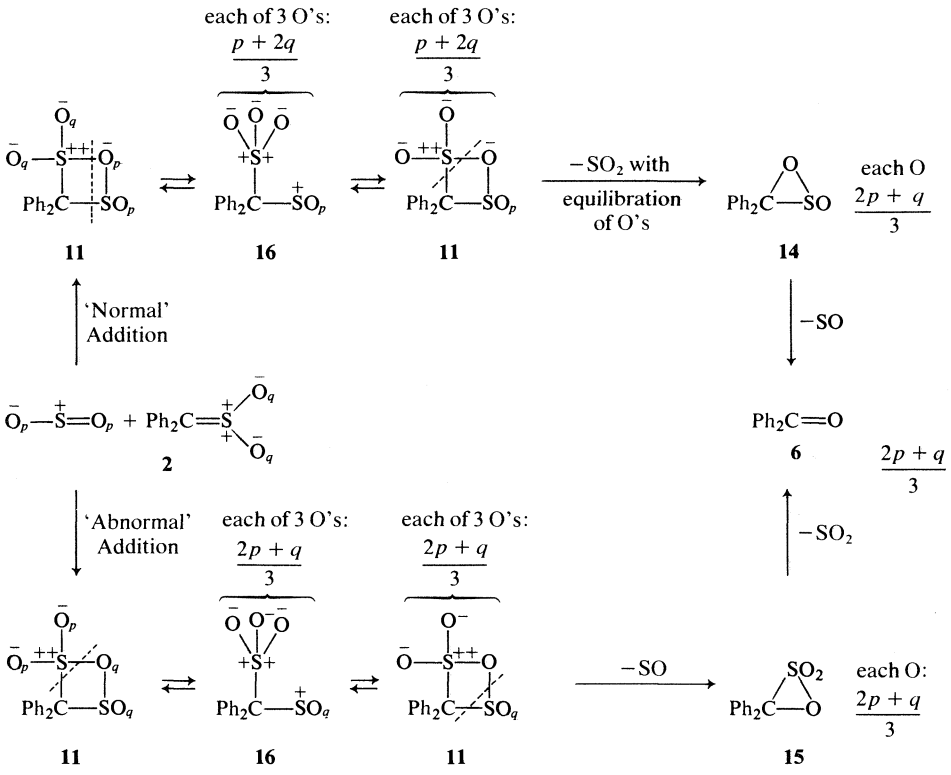

SCHEME 7

of formal oxidation levels of the sulfur atoms) or the "abnormal" route (i.e., with reduction of the sulfene sulfur and oxidation of the sulfur of the sulfur dioxide).[8] After equilibration of some of the oxygens as shown, the ^{18}O content of the benzophenone is $(2p + q)/3$, in agreement with experiment.

One feature of the "normal" addition route (**2** + SO_2 → **11** → **14** → **6**) which perhaps requires further explanation is the formation of **14** from **11** with equilibration of the oxygen atoms (as noted in Scheme 7). One possible way for this to arise could be by way of **17**, itself formed from **11**, perhaps in the conformation having a quasi-equatorial sulfinyl oxygen. Zwitterion **17** must be distinguished from the sulfene (**2**), which in principle may be obtained from **17** by rotating about the C—S bond and rehybridizing the sulfur; obviously postulation of **17** in this scheme implies the hypothesis that the cyclization **17** → **14** is faster than conversion to the sulfene (**17** → **2**).

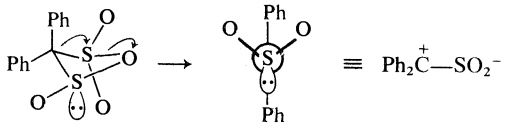

11 **17**

In this context we point out that **18**, a species obviously analogous to **11**, may be proposed to account for the remarkable observation (29) that *ready ^{18}O exchange but no ^{35}S exchange is observed between sulfur dioxide and sulfur trioxide*. Simple cycloaddition–cycloreversion via the "normal" route through **18** accounts for these observations in a

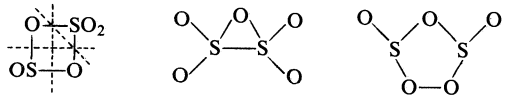

18 **19** **20**

simple fashion and at the same time affords a parallel for **11**, the species derived by cycloaddition to a carbon analogue of sulfur trioxide, i.e., the sulfene (**2**). Again we refer to the reaction in which the sulfur atoms retain their original oxidation levels as "normal" (the two modes of this are shown by the horizontal and vertical broken lines in **18**) and that (shown by the oblique broken line in **18**) involving oxidation–reduction as "abnormal". Note that simple "abnormal" cycloaddition–cycloreversion leads to no exchange, whereas either "normal" addition followed by "abnormal" reversion (or the

[8] "Normal" and "abnormal" reactions of sulfenes are defined and discussed elsewhere (17).

complementary "abnormal" followed by "normal" sequence) would lead to exchange of *both* oxygen and sulfur, contrary to the reports (29).

Another process which is excluded by the absence of sulfur exchange is the formation of the symmetrical cyclic anhydrides **19** and **20**. In view of the analogy between sulfenes and sulfur trioxide one might question the likelihood of the formation of the sulfene analogues **12** and **13**; the available data, however, do not allow a definite exclusion of the exchange via **12** or **13**. In an attempt to ascertain if the sulfene (**2**) and sulfur dioxide were, in fact, exchanging oxygen atoms, we carried out the reaction of labelled **9***c* with 2,6-lutidine and sulfur dioxide in the presence of *p*-toluidine as a sulfene trap. We found that the ^{18}O content of the *p*-toluidide so obtained (11.3%) was nearly that of the starting ester (12.5%); a control experiment in which the *p*-toluidide was formed from **9***c* (^{18}O content 5.4%) without sulfur dioxide gave essentially the same ^{18}O content (5.3%) in the product. The above experiment, though it indicates the absence of a *rapid* ^{18}O exchange between sulfur dioxide and the sulfene (**2**), does not exclude a slow reaction; the failure to observe extensive loss of ^{18}O may simply reflect the ease of trapping of the sulfene by *p*-toluidine before exchange can occur.

A final possibility which can apparently be excluded experimentally is a cycloreversion from **11** to give thiobenzophenone *S*-oxide (**21**) and sulfur trioxide, with **21** going to benzophenone (**6**) under the

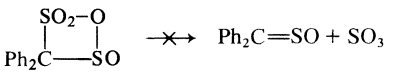

11 **21**

reaction conditions.[9] We found that treatment of **21** with either sulfur dioxide or sulfur trioxide gave no benzophenone, and also that the presence of added **21** in a reaction of **1** with sulfur dioxide gave merely unreacted **21** and no additional **6**. It seems likely that **21** is not converted to **6** under these conditions and therefore cannot be a precursor of **6** in the reaction of diphenylsulfene (**2**) with sulfur dioxide.

Concluding Summary

In view of the experimental and mechanistic complexity of the foregoing, it would seem useful to summarize the points which emerge from this study.

(1) The formation of a ketone or aldehyde in the reaction of a diazoalkane with excess sulfur dioxide very probably proceeds via the sulfene, since, in addition to previous work (3, 4) consistent with the formation of sulfenes from those starting materials, we find that the same sulfene generated by another route in the presence of sulfur dioxide gives the same ketone or aldehyde.

(2) To date the reaction of sulfur dioxide with sulfenes has been observed only with sulfenes bearing at least one aryl group on the sulfene carbon; it appears as the major reaction only with diaryl sulfenes or with certain arylalkyl sulfenes with a bulky alkyl group.

(3) An array of experiments, including ^{18}O-labelling studies, have been carried out to shed some light on the mechanism of the reaction, and though the ^{18}O-labelling results are only approximate, our experiments allow certain conclusions to be drawn.

(*a*) Neither the simple Staudinger–Pfenninger mechanism (via **5**) nor a variant process by way of **8** can be the *only* process operating.

(*b*) A *complete* exchange of oxygen atoms between sulfur dioxide and the sulfene (**2**) is similarly excluded.

(*c*) Mechanistic categories capable of accounting for the ^{18}O results are classed according to whether they involve (I) competition between two routes giving different labelling, or (II) equilibration of oxygen atoms, with the latter category subdivided into processes in which there is (A) competition between an oxygen exchange and a route to **6**, or (B) a complete exchange of a limited number of oxygens. Examples of each of the categories are given in Schemes 4–7.

(*d*) Cycloadduct **18** is pointed to as a species which may be formed from reaction of sulfur dioxide with sulfur trioxide and which accounts particularly easily for the reported ready exchange of oxygen atoms and lack of exchange of sulfur atoms between the two compounds. If we may argue from the analogy of sulfur trioxide with sulfenes we would favour the route involving "normal" formation of **11** (see Scheme 7) over reactions proceeding via **12**, **13**, or the "abnormal" route to **11**.

(*e*) An attempt to detect sulfene – sulfur dioxide oxygen exchange showed little or no exchange.

(*f*) From experiments with thiobenzophenone *S*-oxide (**21**) we conclude that **21** is probably not a precursor of benzophenone (**6**) in the diphenylsulfene – sulfur dioxide reaction.

Experimental

Spectra were determined using the following instruments: nmr, Varian T-60, HA-100 or XL-100; ir, Beckman Acculab 4 using 0.1 mm NaCl cells; ms, Varian MAT 311A mass spectrometer. The nmr and ir spectra refer to solutions in $CDCl_3$ and $CHCl_3$, respectively. Melting points were obtained with a Kofler Hot Stage and are uncorrected. Methylene

[9]Photodecomposition of the analogous ketene – sulfur dioxide cycloadduct is postulated to give sulfine (CH_2=SO) as well as carbon dioxide, which is directly observed (23). Thermolysis (at 130°C) or photolysis of thiobenzophenone *S*-oxide (**21**) forms benzophenone in good yield (30).

chloride and 2,6-lutidine were dried by distillation from calcium hydride and stored over molecular sieves (Fisher 4Å). Methylene chloride extracts were dried over anhydrous magnesium sulfate. Solvents were evaporated using a rotary evaporator under reduced pressure. Anhydrous ether was that supplied by Fisher Scientific Co. Ltd., phenylmethanesulfonyl chloride was Eastman White Label material (sold as α-toluenesulfonyl chloride). Diphenyldiazomethane was obtained by yellow mercuric oxide oxidation of benzophenone hydrazone (Aldrich) (31). Thick layer chromatography was carried out with MN-Kieselgel G/UV_{254}.

Reaction of Phenylmethanesulfonyl Chloride with Sulfur Dioxide and 2,6-Lutidine

Liquid sulfur dioxide (10 mL) was collected in a flask. After addition of phenylmethanesulfonyl chloride (0.38 g, 2 mmol) in methylene chloride (10 mL) and 2,6-lutidine (2.32 mL, 20 mmol) the flask was sealed with a glass stopper held firmly in place with masking tape. The reaction mixture was stirred for 3 h and then diluted with methylene chloride (40 mL) and washed with dilute HCl (2 × 50 mL) and water (50 mL). Drying of the solution followed by evaporation of the methylene chloride gave the product (30 mg). The ir and nmr spectra showed the presence of benzaldehyde and some extraneous peaks apparently due to the lutidine. In a separate experiment an acidified solution of 2,4-dinitrophenylhydrazine in absolute alcohol was added directly to methylene chloride layer. On cooling, benzaldehyde 2,4-dinitrophenylhydrazone separated out as an orange-red crystalline solid (58 mg, 10%); this was recrystallized from absolute alcohol, mp 237–238°C; mixed mp with an authentic sample 236–238°C.

Phenylmethanesulfonic Anhydride

Phenylmethanesulfonyl chloride (20 g, 0.1 mol) was dissolved in a mixture of dioxane (80 mL) and water (20 mL) and the solution cooled in an ice bath. Triethylamine (20 g, 0.20 mol) was added dropwise during 10 min and the solvent evaporated under reduced pressure. The residue was dissolved in the minimum amount of water, and the solution poured through a column of Rexyn 101 resin (H^+ form) suspended in water. The water was removed first by evaporation under reduced pressure and then by azeotropic distillation with benzene using a Dean–Stark apparatus. Evaporation of the benzene gave phenylmethanesulfonic acid (13 g) as a dark brown, oily liquid.

The acid was converted to the anhydride by dissolving in dry benzene (60 mL) and treating with *N,N'*-di-*p*-tolylcarbodiimide (8.9 g, 0.04 mol) in benzene (35 mL) for 1 h as described by Khorana (32). Removal of the *N,N'*-di-*p*-tolylurea by filtration followed by evaporation of the benzene gave the crude anhydride (12.0 g, 98%). Recrystallization from $CHCl_3$–ether (with decolorizing charcoal) gave phenylmethanesulfonic anhydride (10.2 g, 83% yield) as a white solid, mp 110–112°C; nmr δ: 7.38 (5H, s) and 4.7 (2H, s) ppm; ir ν_{max}: 1405 and 1190 (vs) cm^{-1}. *Anal.* calcd. for $C_{14}H_{14}O_5S_2$: C 51.53, H 4.32, S 19.61; found: C 51.51, H 4.39, S 19.44.

Reaction of Phenylmethanesulfonic Anhydride with Sulfur Dioxide and Tertiary Amines

Phenylmethanesulfonic anhydride (320 mg, 1 mmol) and 2,6-lutidine (1.16 mL, 10 mmol) in methylene chloride (10 mL) was added to sulfur dioxide (30 mL) as above and the reaction mixture allowed to stand at room temperature for 3 h. Addition of 2,4-dinitrophenylhydrazine solution as above gave benzaldehyde 2,4-dinitrophenylhydrazone (71 mg, 50%) mp 237–241°C, identified by ir and nmr spectra, as above.

When a mixture of phenylmethanesulfonic anhydride (326 mg, 1.0 mmol) and 2,6-lutidine (1.16 mL, 10 mmol) in methylene chloride (50 mL) without sulfur dioxide was allowed to stand for 3 h at room temperature and then worked up by washing with dilute hydrochloric acid and water, the ir and nmr spectra showed no sign of benzaldehyde, the recovered material (105 mg) consisting largely of unchanged phenylmethanesulfonic anhydride.

When pyridine (1.61 mL, 20 mmol) was mixed with the anhydride (652 mg, 2.0 mmol) in methylene chloride (20 mL), and sulfur dioxide bubbled into the mixture and the product treated with 2,4-dinitrophenylhydrazine as described above, benzaldehyde 2,4-dinitrophenylhydrazone was obtained in 10% yield (30 mg). In the absence of sulfur dioxide the reaction of the anhydride with pyridine gave after workup a mixture of *cis*- and *trans*-stilbenes with no sign of any benzaldehyde visible in either the ir or the nmr spectrum.

*Preparation of the Aryl Diphenylmethanesulfonates (**9**)*

*(a) 2-Chloro-4-nitrophenyl Diphenylmethanesulfonate (**9**c)*

Diphenyldiazomethane (1 g, 5.2 mmol) in anhydrous ether (15 mL) was mixed with 2-chloro-4-nitrophenol (1 g, 6 mmol) also in anhydrous ether (25 mL) and the mixture cooled in an ice bath. Triethylamine (0.5 mL) was added from a dropping funnel and sulfur dioxide simultaneously bubbled in until the purple colour of the diphenyldiazomethane had disappeared. Dilute HCl (20 mL) was added immediately and the yellowish-white solid collected by filtration, dissolved in methylene chloride (30 mL), and washed first with dilute HCl and then with water. Evaporation of the solvent gave the crude ester (1.45 g, 69%). Recrystallization from methylene chloride–hexanes gave yellowish-white crystals of **9***c*, mp 123–125°C (with evolution of gas); nmr δ: 5.89 (1H, s), a pair of multiplets centered at 7.4 and 7.6 (total 10H) characteristic of the geminal diphenyl groups, and the characteristic pattern of the 2-chloro-4-nitrophenyl group from 7.0 to 8.3 (3H) ppm; ir ν_{max}: 1350 (s) and 1175 (s) cm^{-1}. *Anal.* calcd. for $C_{19}H_{14}ClNO_5S$: C 56.51, H 3.49, N 3.46, S 7.94, Cl 8.78; found: C 56.62, H 3.46, N 3.34, S 7.88, Cl 8.59.

*(b) p-Nitrophenyl Diphenylmethanesulfonate (**9**a)*

Treatment of diphenyldiazomethane (1.0 g, 5.2 mmol) and *p*-nitrophenol (1.45 g, 10.4 mmol) in ether and triethylamine (0.5 mL) and sulfur dioxide as above, gave, after recrystallization from chloroform–ether, **9***a* as a yellowish crystalline solid (0.8 g, 42%), mp 128–130°C; nmr δ: 5.79 (1H, s), a pair of multiplets centered at 7.4 and 7.6 (10H) characteristic of the two phenyl groups, a pair of doublets centered at 7.0 (2H) and 8.2 (2H) ppm due to the *p*-nitrophenyl group; ir ν_{max}: 1525 (s), 1350 (s), 1150 (s) cm^{-1}. *Anal.* calcd. for $C_{19}H_{15}NO_5S$: C 61.78, H 4.09, N 3.79, S 8.68; found: C 61.68, H 4.00, N 3.69, S 8.64.

*(c) 2,4-Dinitrophenyl Diphenylmethanesulfonate (**9**b)*

Diphenyldiazomethane (0.5 g, 2.6 mmol) and 2,4-dinitrophenol (2.37 g, 13 mmol) in ether (115 mL) were treated with triethylamine (0.25 mL) and sulfur dioxide and, subsequently, dilute HCl (50 mL), as above. The reaction mixture was transferred to a separatory funnel. The ether layer was separated and washed with saturated sodium bicarbonate solution (4 × 50 mL) and finally with water (50 mL). Evaporation of the ether under reduced pressure at room temperature gave the crude ester (**9***b*) (0.76 g, ~70% yield), contaminated with about 20% 2,4-dinitrophenyl diphenylmethyl ether (**10***b*) as judged from the peak at 6.51 ppm (presumed to be due to **10***b*). Recrystallization from chloroform–ether gave the ester (**9***b*) as yellowish crystals (still containing about 20% of **10***b*), mp 87–88°C (with bubbling), nmr δ: 6.03, (s, 1H), a pair of multiplets centered at 7.39, 7.64 ppm characteristic of the 2,4-dinitrophenyl system; ir ν_{max}: 1540 (m), 1345 (s) 1170 (s) cm^{-1}. Because of the apparent ease with which **9***b* loses SO_2 to give **10***b*, no serious attempt was made to obtain the pure ester (**9***b*).

Preparation of Diphenylmethanesulfonyl p-*Toluidide*

Diphenyldiazomethane (1.0 g, 5.2 mmol) was dissolved in anhydrous ether (15 mL) and a solution of *p*-toluidine (1.0 g, 10.4 mmol) in anhydrous ether (25 mL) added and the mixture cooled in an ice bath. Sulfur dioxide was bubbled in until the purple colour of diphenyldiazomethane disappeared. The reaction mixture was washed with dilute HCl (50 mL); drying and evaporation of the ether gave a gummy solid which was recrystallized from ether–pentane to yield a white crystalline solid (0.75 g, 43% yield), mp 132°C; nmr δ: 2.18 (3H, s), 5.28 (1H, s), 6.35 (1H, s, NH-band which disappeared on shaking with D_2O), 6.84 (4H, m), two multiplets centered at 7.23, 7.43 (10 H) ppm characteristic of the diphenyl system; ir ν_{max}: 3380 (w), 1385 (s), 1340 (s), 1150 (s) cm^{-1}; ms *m/e*: calcd. M^+ 337.1136; found M^+ 337.1135.

*Reaction of 2-Chloro-4-nitrophenyl Diphenylmethanesulfonate (***9c***) with 2,6-Lutidine in the Presence of* p-*Toluidine*

2-Chloro-4-nitrophenyl diphenylmethanesulfonate (**9***c*) (200 mg, 0.5 mmol) was dissolved in methylene chloride (1.0 mL), *p*-toluidine (106 mg, 1 mmol) and 2,6-lutidine (1.5 mL) were added, and the reaction mixture stirred for 48 h. The reaction was worked up by diluting it with methylene chloride (50 mL) and washing this layer first with dilute HCl (2 × 25 mL), saturated sodium bicarbonate solution (3 × 25 mL), and finally with water (25 mL). Drying of the solution and evaporation of the methylene chloride gave the product (156 mg). The nmr and ir spectra showed it to be diphenylmethanesulfonyl *p*-toluidide (90% yield). The spectra showed no sign of any diphenylmethyl 2-chloro-4-nitrophenyl ether in the reaction product.

*Reaction of 2-Chloro-4-nitrophenyl Diphenylmethanesulfonate (***9c***) with 2,6-Lutidine in the Presence of 2-Methyl-1-morpholinopropene*

2-Chloro-4-nitrophenyl diphenylmethanesulfonate (**9***c*) (200 mg, 0.5 mmol) was dissolved in methylene chloride (1.0 mL). 2,6-Lutidine (1.5 mL) and 2-methyl-1-morpholinopropene (33) (77 mg, 0.55 mmol) were added and the reaction mixture stirred for 48 h. The reaction was worked up by diluting the mixture with methylene chloride (50 mL) followed by washing this solution with dilute HCl (2 × 25 mL), saturated sodium bicarbonate solution (4 × 25 mL), and finally with water (25 mL). Drying of the solution and evaporation of the methylene chloride gave the crude product (179 mg, 96%) which contained about 15% of starting material. Separation of the crude product with thick-layer chromatography using ether–pentane (4:1) gave 2,2-diphenyl-3-morpholino-4,4-dimethylthietane 1,1-dioxide (130 mg, 70%). Recrystallization from methylene chloride – hexanes gave a product melting at 150–153°C; mixed mp with an authentic sample (6), 151–153°C; ms: M^+ calcd. 371.1555; found 371.1547. The nmr and ir spectra were identical to those of the authentic sample (ms: M^+ found 371.1547). Though the reported mp (136–137°C) differs from that given here, the above evidence clearly shows (*a*) that the products obtained by the two routes are identical, and (*b*) that our materials and that made by Tanabe *et al.* (6) are identical and have the assigned structure; it is unclear whether the lower mp reported by these authors derives from polymorphism or impurity, or is merely a misprint.

*Reaction of 2-Chloro-4-nitrophenyl Diphenylmethanesulfonate (***9c***) with Sulfur Dioxide and 2,6-Lutidine*

Liquid sulfur dioxide (0.75 mL) was collected in a seal-off ampoule (13 mm OD with a 7 mm neck, 14 cm long after sealing) cooled in a dry ice – acetone bath. The ester (**9***c*) (200 mg, 0.5 mmol) in methylene chloride (1 mL) and 2,6-lutidine (1.5 mL, 13 mmol) were added and the ampoule sealed, allowed to come to room temperature, and shaken for 48 h. The ampoule was then cooled and opened, the sulfur dioxide allowed to evaporate, and the reaction mixture diluted with methylene chloride (50 mL). The methylene chloride layer was washed with dilute HCl (2 × 20 mL), several times with saturated sodium bicarbonate solution and finally with water, and dried. Evaporation of the solvent gave the product (80 mg) estimated to consist of ~16 mg of benzophenone and ~64 mg of the ether (**10***c*) (38% yield) by comparison of the ir spectrum with spectra of authentic mixtures. Acidification and extraction of the combined $NaHCO_3$ washes gave a material shown by ir to be 2-chloro-4-nitrophenol mixed with a little benzophenone; tlc gave the phenol (34 mg, 43%) and benzophenone (5 mg), total benzophenone yield 21 mg (23%). In another experiment the crude product (65 mg) on thick-layer chromatography using pentane–ether (4:1) gave benzophenone (15 mg, 17%) and diphenylmethyl 2-chloro-4-nitrophenyl ether (**10***c*) (30 mg, 18%). The ir and nmr spectra of both materials were identical to those of authentic samples.

When the reaction was carried out identically except that methylene chloride was omitted from the reaction mixture, the crude product was estimated by ir spectra comparisons to contain about 5 mg of benzophenone (6% yield).

*Thermal Desulfonylation of 2-Chloro-4-nitrophenyl Diphenylmethanesulfonate (***9c***)*

The ester (**9***c*) (0.25 g, 0.62 mmol) was dissolved in chloroform (25 mL) and the solution refluxed on a steam bath for 3 h. Evaporation of the solvent followed by recrystallization from chloroform–hexanes gave 2-chloro-4-nitrophenyl diphenyl ether (**10***c*) (0.15 g, 71%), mp 125–126°C; nmr δ: 6.35 (s, 1H), and multiplets in the ranges 7.15–7.55 and 6.88–8.25 ppm characteristic of the diphenyl and 2-chloro-4-nitrophenyl systems respectively; ir ν_{max}: 1520 (m), 1480 (m), 1340 (s), 1265 (s) cm^{-1}; ms: M^+ calcd. 339.0662; found 339.0663.

Reaction of 1-Phenyl-1-diazoethane with Sulfur Dioxide

A solution of 1-phenyl-1-diazoethane (~2.0 g, 15 mmol) in ether (50 mL) was prepared by HgO oxidation of acetophenone hydrazone in the presence of KOH and CaO following the procedure of Day *et al.* (34) for the preparation of 4-diazooctane; the solution showed a strong band at 2060 cm^{-1}. This solution was added dropwise with stirring to liquid sulfur dioxide (50 mL). When the addition was complete the sulfur dioxide was evaporated. A white solid which separated out was removed by filtration; nmr and mass spectra indicated the solid to be 1,2-dimethyl-1,2-diphenylethene. To the filtrate an acidified solution of 2,4-dinitrophenylhydrazine was added and an orange-red crystalline precipitate of acetophenone 2,4-dinitrophenylhydrazone separated out (225 mg, 5%). Recrystallization from absolute ethanol gave a material melting at 239°C; mixed mp with an authentic specimen, 239–240°C.

Reaction of Methanesulfonic Anhydride with Sulfur Dioxide and 2,6-Lutidine

A solution of 2,6-lutidine (1.16 mL, 10 mmol) in methylene chloride (10 mL) was cooled in dry ice and saturated with sulfur dioxide. Methanesulfonic anhydride (35) (174 mg, 1 mmol) was added, the flask was sealed with a stopper (held firmly with masking tape), allowed to come to room temperature, and held there for 3 h. The reaction mixture was extracted with water (2 × 10 mL) and to this extract a saturated solution of dimedone (20 mL) in 10% alcohol added. No sign of any of the dimedone derivative of formaldehyde was observed.

^{18}O-Labelling Analyses

Water–^{18}O purchased from Merck, Sharp and Dohme Canada Limited was the ^{18}O source for these experiments; the ^{18}O contents given herein for the ^{18}O-labelled water used in these experiments are taken directly from the labels. Our ^{18}O analyses were carried out on a Varian MAT 311A mass spectrometer using 25 ev and inlet temperature 100°C for the SO_2 analyses and 20 ev and probe temperature 18°C for benzophenone samples. With each set of analyses a natural abundance sample of the compound was run and the values of the $M + 1$ and $M + 2$ peaks found to agree satisfactorily with expected values, i.e., Δ (found % − calcd. %) $\leq \pm 0.3\%$. Relative abundances of the peaks were obtained by averaging values from three or more concurring traces. In calculating the abundance of ^{18}O-containing species, correction was made for the ^{34}S content of SO_2 (4.4368% relative to $^{32}S = 100$) and the ^{13}C satellite contribution to the $M + 2$ peak of benzophenone (0.98%) (36). The value quoted in the tables for percentage ^{18}O for the sulfur dioxide is the average of the values calculated from the percentages of $S^{16}O_2$ and $S^{16}O^{18}O$, i.e., from the expressions

$$100 - 10\sqrt{\%\, S^{16}O_2} \quad \text{and} \quad 50 - 5\sqrt{100 - 2 \times (\%S^{18}O^{16}O)}$$

respectively. Whereas these values were invariably in good agreement, that from the percentage of $S^{18}O_2$, i.e., $10\sqrt{\%\, S^{18}O_2}$, was sometimes rather different and was discarded, since the error in measuring the comparatively small $S^{18}O_2$ peak rendered this value much the least reliable.

^{18}O-Labelled Sulfur Dioxide

^{18}O-Labelled water (0.5 g, 96.5 at.% ^{18}O) was introduced into a 20 cm long, 16 mm OD thick-walled tube closed at one end and with an Ace Glass 0-4 Teflon vacuum stopcock with O-rings, at the other end. The tube was cooled in a dry ice – acetone bath and sulfur dioxide (~2 mL, Matheson anhydrous) condensed from a lecture bottle. The stopcock was closed, the mixture was allowed to come to room temperature, and the tube shaken for 48 h. The tube was then connected to a short drying train consisting of a small gas wash bottle containing concentrated H_2SO_4 followed by a tube lightly packed with glass wool; the (Tygon) tubing leading from this was connected to an ampoule (13 mm OD with 7 mm neck, total length 14 cm when subsequently sealed) cooled in a dry ice – acetone bath, and the ^{18}O-labelled sulfur dioxide allowed to condense in the ampoule. The tubing was then clamped, disconnected from the drying train, and immediately connected to the inlet of the mass spectrometer. A typical mass spectrum showed the following relative intensities for the *m/e* 64, 66, and 68 peaks: 100, 34.92, and 3.54, corresponding to $S^{16}O_2$, $S^{16}O^{18}O$, and $S^{18}O_2$ percentages of respectively 75.37, 22.98, and 1.65; these in turn (from the equations given above) yield values of 13.2, 13.2, and 12.8% ^{18}O, respectively.

2-Chloro-4-nitrophenyl Diphenylmethanesulfonate ^{18}O-Labelled at the Sulfonyl Group

A mixture of diphenyldiazomethane (0.75 g, 3.9 mmol) and 2-chloro-4-nitrophenol (1.5 g) in ether containing triethylamine was treated with ^{18}O-labelled sulfur dioxide (20.5% ^{18}O) as described above for the unlabelled ester. The recrystallized product melted at 120–123°C; the nmr and ir spectra were identical to those of unlabelled **9***c* except that the band at 1175 cm^{-1} had diminished and two additional bands at 1155 (m) and 1135 (m) cm^{-1} had appeared.

To determine the ^{18}O content of the sulfonyl group, the ester (200 mg) was placed in a round-bottomed flask attached directly to the heated inlet of the mass spectrometer. The flask was evacuated and heated gently with a stream of hot air. The mass spectrum of the evolved SO_2 showed 19.3% ^{18}O.

*Reaction of 2-Chloro-4-nitrophenyl Diphenylmethanesulfonate (**9***c*) with ^{18}O-Labelled Sulfur Dioxide and of the Labelled Ester with Unlabelled Sulfur Dioxide*

The labelled liquid sulfur dioxide (0.75 mL) was collected in an ampoule and its mass spectrum obtained as described above. The ^{18}O content thus obtained is given as the "initial" value in Table 1. The ester (**9***c*) (200 mg, 0.5 mmol) in methylene chloride (1 mL) and 2,6-lutidine (1.5 mL, 13 mmol) were added and the ampoule sealed and shaken at room temperature for 48 h. The ampoule was then cooled in a dry ice – acetone bath, the neck scratched with a file near the sealed tip, and the neck attached to the inlet system of the mass spectrometer with rubber tubing pushed onto the neck of the ampoule well below the scratch. The neck of the ampoule was then broken at the scratch and the mass spectrum obtained from the sulfur dioxide thus admitted to the instrument; the ^{18}O content so obtained is the "final" value in Table 1.

The crude benzophenone was isolated as described above for the unlabelled ester. Control experiments, however, indicated that the chromatographic purification led to loss of most of the ^{18}O and the following procedure for partial removal of the ether (**10***c*) was used. The crude product was extracted with mixed hexanes (5 mL, Fisher Spectranalyzed) and the solvent evaporated. The residue after evaporation was further extracted with hexanes and the extract evaporated, and this residue subjected to the extraction–evaporation procedure a further time to give a mixture estimated by comparison of the ir spectrum with those of authentic mixtures to contain in a typical run about 18 mg (20% yield) of benzophenone and about 10 mg of **10***c*. The ^{18}O contents of the benzophenone samples are given in Table 1.

In another experiment, which gave benzophenone with 5.5% ^{18}O, the $NaHCO_3$ layers were combined, acidified with HCl, and extracted with CH_2Cl_2. The ratios of the *m/e* 173, 174, 175, and 176 peaks of the 2-chloro-4-nitrophenol so obtained were identical to those of authentic natural abundance material. The ether (**10***c*) obtained from the hexane extractions was similarly found to show peaks at *m/e* 339, 340, 341, and 342 identical to those found with the natural abundance ether.

The same quantities and procedure were used for the reaction of natural abundance SO_2 with the ester **9***c* labelled at the sulfonyl group, to give a mixture containing, typically, 14 mg of benzophenone and 8 mg of **10***c*; Table 1 gives the ^{18}O contents of the benzophenone samples.

To determine if the presence of the ether (**10***c*) affected the ms determination of ^{18}O content, samples of labelled benzophenone (15 mg) were mixed with the ether (**10***c*) (10 mg) and dissolved in methylene chloride. The solvent was then evaporated and the ^{18}O contents of the "unmixed" and "mixed" samples determined. The respective values were as follows: 24.6 and 23.6%, 8.7 and 8.6%, 7.7 and 7.2%, 6.0 and 5.9%, i.e., the "mixed" samples showed slightly lower ^{18}O contents (in somewhat varying measure).

The following experiments were carried out to determine the extent (if any) to which benzophenone underwent ^{18}O exchange under the conditions of the reaction and workup. (*1*) ^{18}O-Enriched sulfur dioxide (0.5 mL, 5.5% ^{18}O) was collected in an ampoule and benzophenone (80 mg) and **10***c* (25 mg) in methylene chloride (1 mL), and 2,6-lutidine (1.5 mL) added, and the tube sealed and shaken overnight. The ms of the benzophenone obtained following the usual workup showed no sign of any incorporation of ^{18}O. (*2*) Liquid sulfur dioxide (0.75 mL) was collected in an ampoule and ^{18}O-labelled benzophenone (50 mg, 21.5% ^{18}O), 2-chloro-4-nitrophenone (60 mg)

and **10***c* (50 mg) in methylene chloride (1 mL), and 2,6-lutidine (1.5 mL) added and the tube sealed and shaken at 25°C for 48 h. The benzophenone obtained after the usual workup showed 20.9% ^{18}O. (*3*) Reaction of labelled ester (**9***c*) (200 mg, 18.9% ^{18}O) precisely as before except that the reaction was stopped after 6 h gave unreacted ester (**9***c*) (along with benzophenone and **10***c*). Analysis of the ester (as above) showed 18.6% ^{18}O. (*4*) Reaction of **9***c* (200 mg) as before except for the addition of labelled benzophenol (25 mg, 21.5% ^{18}O) to the initial reaction mixture gave after workup a product (45 mg) containing benzophenone with 15.3% ^{18}O. With the usual 14–20% yield of benzophenone (10–15 mg) and no exchange (but merely dilution of the label) the calculated range for the ^{18}O content of the benzophenone would be 13.5–15.4%.

^{18}O-Enriched Benzophenone

(a) *From Diazomethane and Labelled Sulfur Dioxide*

Liquid sulfur dioxide (0.5 mL, 17.0% ^{18}O) was collected in a cooled flask and a solution of diphenyldiazomethane (**1**) (65 mg, 0.34 mmol) in methylene chloride (1.5 mL) added dropwise with stirring. After addition was complete and the purple colour of **1** had disappeared the sulfur dioxide was evaporated and the product dissolved in methylene chloride and washed with water. Drying of the methylene chloride layer and evaporation of the solvent gave an oil which was extracted with hexanes to give a product (50 mg, 82%) the ir spectrum of which was identical to that of benzophenone except for an additional peak at 1642 ($>C=^{18}O$) cm^{-1}. Mass spectrometric analysis showed 16.9% ^{18}O.

(b) *From Diphenyldichloromethane and ^{18}O-Labelled Water*

Diphenyldichloromethane (37) (1.5 g, 6.3 mmol) was mixed with ^{18}O-labelled water (0.5 g, ~20% ^{18}O) in 1,2-dimethoxyethane (5 mL) and the reaction mixture heated at reflux overnight. The dimethoxyethane was evaporated and the aqueous residue extracted with methylene chloride (5 mL). The methylene chloride layer was washed with water (5 mL), dried, and evaporated giving an oil which on addition of hexanes and cooling gave [^{18}O]benzophenone as a white, crystalline solid (0.7 g, 61%). The ir spectrum except for the peak at 1642 ($>C=^{18}O$) cm^{-1} was identical to that of ordinary benzophenone. Mass spectral analysis showed 21.5% ^{18}O.

Reaction of Benzhydryl Chloride with 2,6-Lutidine and 2-Chloro-4-nitrophenol in Sulfur Dioxide and Methylene Chloride

A solution of benzhydryl chloride (200 mg, 1 mmol), prepared by refluxing benzhydrol in excess thionyl chloride (the method of Gilman and Kirby (38) but without the toluene), and 2-chloro-4-nitrophenol (175 mg, 1 mmol) in methylene chloride (1 mL) was added to an ampoule containing liquid sulfur dioxide (0.75 mL), and the tube sealed and shaken at room temperature for 24 h. Upon workup diphenylmethyl 2-chloro-4-nitrophenyl ether (**10***c*) (236 mg, 70%) was obtained. The nmr and ir spectra were identical to those of authentic **10***c*; spectra of the crude product showed no sign of any benzophenone or 2-chloro-4-nitrophenyl diphenylmethanesulfonate (**9***c*).

Attempted Reactions of Thiobenzophenone S-*Oxide (**21**)*

(a) *With Sulfur Trioxide*

Thiobenzophenone *S*-oxide (**21**) (39) (90 mg, 0.42 mmol) was dissolved in methylene chloride (10 mL) and liquid sulfur trioxide (Sulfan, Allied Chemical) (5 drops) was added. The reaction mixture was stirred for 15 min and then worked up by pouring onto ice (50 g), separating the methylene chloride layer, and washing it with water. Evaporation of the solvent gave back thiobenzophenone *S*-oxide (60 mg), identified by ir spectrum, with no sign of benzophenone.

(b) *With Sulfur Dioxide*

Thiobenzophenone *S*-oxide (**21**) (100 mg) in ether was mixed with liquid sulfur dioxide (5 mL). After 15 min the mixture was worked up giving unreacted **21** (90%).

Reaction of Diphenyldiazomethane with Sulfur Dioxide in the Presence of Thiobenzophenone S-*Oxide*

A solution of diphenyldiazomethane (**1**) (100 mg, 0.55 mmol) in anhydrous ether (15 mL) was added dropwise with stirring to a mixture of liquid sulfur dioxide (10 mL), thiobenzophenone *S*-oxide (110 mg, 0.52 mmol), and anhydrous ether (5 mL). Stirring was continued a further 5 min and the sulfur dioxide and ether evaporated to give an oil (215 mg), which was extracted with anhydrous ether (25 mL). Evaporation of the ether gave a product (164 mg), the ir spectrum of which, by comparison with authentic mixtures, showed it to be a roughly equimolar mixture of benzophenone and thiobenzophenone *S*-oxide.

*Reaction of ^{18}O-Labelled 2-Chloro-4-nitrophenyl Diphenylmethanesulfonate (**9c**) with 2,6-Lutidine and* p-*Toluidine*

(a) *In the Absence of Sulfur Dioxide*

Reaction of ^{18}O-labelled **9***c* (64 mg, 0.16 mmol, 5.4% ^{18}O) with *p*-toluidine (35 mg, 0.32 mmol) and 2,6-lutidine (0.5 mL) in methylene chloride as described above for the unlabelled ester (**9***c*) gave labelled diphenylmethanesulfonyl *p*-toluidide (47 mg, 88%) which on recrystallization from ether–pentane melted at 132–134°C. The nmr and ir spectra (except for an additional band at 1130 cm^{-1} in the latter) were identical to those of the unlabelled amide. The ^{18}O content of the sulfur dioxide evolved on heating (to ~120°C) essentially as already described for the ester (**9***c*) was found to be 5.3%.

(b) *In the Presence of Sulfur Dioxide*

^{18}O-Labelled ester (**9***c*) (200 mg, 0.5 mmol, 12.5% ^{18}O) in methylene chloride (1 mL), *p*-toluidine (~524 mg, 4.9 mmol), and 2,6-lutidine (1.5 mL, 13 mmol) were added to liquid sulfur dioxide (0.75 mL) in an ampoule which was then sealed and shaken at room temperature for 48 h. Workup as described for the experiment without *p*-toluidine gave a crude product (90 mg) which on thick-layer chromatography using pentane–ether (4:1) gave benzophenone (7.5 mg, 8%), diphenylmethyl-2-chloro-4-nitrophenyl ether (**10***c*) (7 mg, 4%), and diphenylmethanesulfonyl *p*-toluidide (50 mg, 29%). The *p*-toluidide was recrystallized from ether–pentane, mp 132–133°C; the nmr and ir spectra (except for the added peak at 1130 cm^{-1}) were identical to those of the natural abundance amide; ^{18}O content (obtained as described above) 11.3%.

*Partial Reaction of ^{18}O-Labelled 2-Chloro-4-nitrophenyl Diphenylmethanesulfonate (**9c**) with Sulfur Dioxide*

Liquid sulfur dioxide (0.75 mL) was collected in an ampoule. The ester (**9***c*) (18.9% ^{18}O, 200 mg, 0.5 mmol) in methylene chloride (1 mL) and 2,6-lutidine (1.5 mL) were added and the ampoule sealed and shaken for 6 h. The product (140 mg) obtained after the usual workup was shown by its ir and nmr spectra to consist of unreacted ester (>75%) plus some benzophenone (**6**) and the ether (**10***c*). Determination of the ^{18}O content as above showed 18.6% ^{18}O in the recovered ester (**9***c*).

Acknowledgements

We are particularly indebted to Mr. Doug Hairsine for the mass spectrometric determinations of ^{18}O content and to Dr. S. K. Wong for valuable sugges-

tions regarding their interpretation. We are grateful to the National Research Council of Canada for financial support of this work.

1. H. STAUDINGER and F. PFENNINGER. Ber. **49**, 1941 (1916).
2. N. H. FISCHER. Synthesis, 393 (1970).
3. G. OPITZ and K. FISCHER. Z. Naturforsch. B, **18**, 775 (1963); G. OPITZ and K. FISCHER. Angew. Chem. Int. Ed. Engl. **4**, 70 (1965).
4. G. OPITZ. Angew. Chem. Int. Ed. Engl. **6**, 107 (1967).
5. T. TANABE, T. SHINGAKI, and T. NAGAI. Chem. Lett. 679 (1975).
6. T. TANABE and T. NAGAI. Bull. Chem. Soc. Jpn. **50**, 1179 (1977).
7. G. HESSE and E. REICHOLD. Chem. Ber. **90**, 2101 (1957).
8. H. H. INHOFFEN, R. JONAS, H. KRÖSCHE, and U. EDER. Justus Liebigs Ann. Chem. **694**, 19 (1966).
9. G. C. BROPHY, D. J. COLLINS, J. J. HOBBS, and S. STERNHELL. Aust. J. Chem. **28**, 151 (1975).
10. J. F. KING. Acc. Chem. Res. **8**, 10 (1975).
11. N. TOKURA, T. NAGAI, and S. MATSUMURA. J. Org. Chem. **31**, 349 (1966).
12. T. NAGAI, H. NAMIKOSHI, and N. TOKURA. Tetrahedron, **24**, 3267 (1968).
13. M. TANAKA, T. NAGAI, and N. TOKURA. J. Org. Chem. **37**, 4106 (1972).
14. T. TANABE and T. NAGAI. Tetrahedron Lett. 1545 (1978); Bull. Chem. Soc. Jpn. **51**, 1459 (1978).
15. J. A. MOEDE and C. CURRAN. J. Am. Chem. Soc. **71**, 852 (1949); D. VAN DER HELM, J. D. CHILDS, and S. D. CHRISTIAN. J. Chem. Soc. Chem. Commun. 887 (1969).
16. J. F. KING and T. DURST. J. Am. Chem. Soc. **85**, 2676 (1963); Can. J. Chem. **44**, 819 (1966).
17. J. F. KING, R. P. BEATSON, and J. M. BUCHSHRIBER. Can. J. Chem. **55**, 2323 (1977).
18. H. KLOOSTERZIEL, M. H. DEINEMA, and H. J. BACKER. Recl. Trav. Chim. Pays-Bas, **71**, 1228 (1952).
19. C. REICHARDT and K. DIMROTH. Fortschr. Chem. Forsch. **11**, 1 (1968).
20. N. LICHTIN. Prog. Phys. Org. Chem. **1**, 75 (1963).
21. L. C. BATEMAN, E. D. HUGHES, and C. K. INGOLD. J. Chem. Soc. 1011 (1940).
22. A. DE S. GOMES and M. M. JOULLIÉ. J. Heterocycl. Chem. **6**, 729 (1969); J. M. BOHEN and M. M. JOULLIÉ. J. Org. Chem. **38**, 2652 (1973); E. TEMPESTI, L. GIUFFRE, M. FORNAROLI, and G. AIROLDI. Chem. Ind. London, 183 (1973).
23. I. R. DUNKIN and J. G. MACDONALD. J. Chem. Soc. Chem. Commun. 1020 (1978).
24. C. L. MCINTOSH and P. DE MAYO. Chem. Commun. 32 (1969); J. F. KING, P. DE MAYO, C. L. MCINTOSH, K. PIERS, and D. J. H. SMITH. Can. J. Chem. **48**, 3704 (1970); H. HIRAOKA. J. Chem. Soc. Chem. Commun. 1014 (1974).
25. A. BATTAGLIA, A. DONDONI, G. MACCAGNANI, and G. MAZZANTI. J. Chem. Soc. Perkin Trans. II, 609 (1974).
26. W. WALTER and O. H. BAUER. Justus Liebigs Ann. Chem. 305 (1975); 1584 (1976).
27. L. CARLSEN and J. P. SNYDER. J. Org. Chem. **43**, 2216 (1978).
28. J. F. KING and D. R. K. HARDING. Can. J. Chem. **54**, 2652 (1976).
29. T. H. NORRIS. J. Phys. Chem. **63**, 383 (1959); J. L. HUSTON. J. Phys. Chem. **63**, 389 (1959) and references cited in each of these papers; see also T. C. WADDINGTON *in* Non-aqueous solvent systems. *Edited by* T. C. Waddington. Academic Press, London and New York. 1965. p. 275.
30. L. CARLSEN, N. HARRIT, and A. HOLM. J. Chem. Soc. Perkin Trans. I, 1404 (1976); L. CARLSEN, A. HOLM, E. KOCH, and B. STILKERIEG, Acta Chem. Scand. Ser. B, **31**, 679 (1977).
31. L. I. SMITH and K. L. HOWARD. Org. Synth. Coll. Vol. III, 351 (1955).
32. H. G. KHORANA. Can. J. Chem. **32**, 227 (1954).
33. E. BENZING. Angew. Chem. **71**, 521 (1959).
34. A. C. DAY, P. RAYMOND, R. M. SOUTHAM, and M. C. WHITING. J. Chem. Soc. C, 467 (1966).
35. L. N. OWEN and S. P. WHITELAW. J. Chem. Soc. 3723 (1953).
36. M. C. HAMMING and N. G. FOSTER. Interpretation of mass spectra of organic compounds. Academic Press, New York, NY. 1972.
37. H. STAUDINGER and H. FREUDENBERGER. Org. Synth. Coll. Vol. II, 573 (1943).
38. H. GILMAN and J. E. KIRBY. J. Am. Chem. Soc. **48**, 1733 (1926).
39. B. ZWANENBURG, L. THIJS, and J. STRATING. Recl. Trav. Chim. Pays-Bas, **86**, 577 (1967).

Derivatives of fused 3-hydroxymethyl-pyran-4-ones as a mobile keto–allyl system

ADOLF PHILIPP AND IVO JIRKOVSKY[1]

Ayerst Laboratories, P.O. Box 6115, Montreal, P.Q., Canada H3C 3J1

Received May 9, 1979

This paper is dedicated to Prof. Karel Wiesner on the occasion of his 60th birthday

ADOLF PHILIPP and IVO JIRKOVSKY. Can. J. Chem. **57**, 3292 (1979).

Syntheses of 3-hydroxymethyl-4*H*,5*H*-pyrano(3,4-c)(1)benzopyran-4-one, **7**, and 3-hydroxymethyl-4*H*,5*H*-(1)benzothiopyrano(4,3-b)pyran-4-one, **8**, from 2,2-difluoro-4-methyl-5*H*-(1)benzopyrano- and (1)benzothiopyrano(3,4-e)-1,3,2-dioxaborins, **3** and **4**, are reported. Upon treatment with a solution of sodium cyanide, the corresponding mesylates **9** and **10** as well as the chloromethyl derivatives **11** and **12** yielded 3-methyl-4-oxo-4*H*,5*H*-pyrano(3,2-c) (1)benzopyran-2-carbonitrile, **13**, and 3-methyl-4-oxo-4*H*,5*H*-(1)benzothiopyrano(4,3-b)pyran-2-carbonitrile, **14**, respectively; these nitriles were converted to carboxylic acids **21** and **22** via methyl esters **19** and **20**. Reaction of the mesylate **10** with dimethylamine afforded a normal displacement product **23**. A similar reaction of **12** required longer time and led to the vinylogous amide **24**.

ADOLF PHILIPP et IVO JIRKOVSKY. Can. J. Chem. **57**, 3292 (1979).

On décrit la synthèse de la hydroxyméthyl-3-4*H*,5*H*-pyrano (3,4-c) benzo(1) pyranone-4, **7**, et la hydroxyméthyl-3-4*H*,5*H*-benzo(1) thiopyrano(4,3-b) pyranone-4, **8**, à partir des difluoro-2,2-méthyl-4-5*H*-benzo(1) pyrano et benzo(1) thiopyrano (3,4-e)-dioxaborines-1,3,2, **3** et **4**. Les mésylates correspondants **9** et **10** aussi bien que les dérivés chlorométhylés **11** et **12** traités par une solution de cyanure de sodium conduisent respectivement aux méthyl-3-oxo-4-4*H*,5*H*-pyrano(3,2-c) benzo(1)-pyrannecarbonitrile-2, **13**, et méthyl-3-oxo-4-4*H*,5*H*-benzo(1) thiopyrano(4,3-b)pyrannecarbonitrile-2, **14**; ces nitriles sont transformés via les esters méthyliques **19** et **20** en acides carboxyliques **21** et **22**. Le mésylate **10** réagit avec la diméthylamine pour conduire par un déplacement normal au produit **23**. Une réaction semblable du composé **12** requiert un temps plus long et conduit à l'amide vinylogue **24**.

[Traduit par le journal]

Current interest in the chemistry of fused pyran-4-ones is due largely to their potential antiallergic activity (1). Two synthetic approaches are being used for the construction of condensed systems with a pyran-4-one ring: the classical Kostanecki reaction (2) involving acylation of aromatic *o*-hydroxyketones or their condensation with diethyl oxalate, and the dual formylation of fused 2,2-difluoro-4-methyl-1,3,2-dioxaborins with the Vilsmeier reagent (3). The former method provides annelated pyran-4-ones with a 2-substituent, whereas the latter affords analogous 3-formyl-pyran-4-ones. A reaction sequence connecting these two routes would be clearly of synthetic value.

Using 4*H*,5*H*-pyran(3,2-c) (1)benzopyran-4-one[2] and 4*H*,5*H*-(1)benzothiopyrano(4,3-b)pyran-4-one as model systems, we now wish to describe the conversion of 3-hydroxymethyl derivatives to their 3-methyl analogs functionalized in position 2.

The treatments of chroman-4-one **1** and thiochroman-4-one **2** with boron trifluoride – acetic anhydride – acetic acid (4, 5) afforded dioxaborins **3** and **4** respectively (Scheme 1). The action of phosphorus oxychloride and dimethylformamide (3) on these complexes produced aldehydes **5** and **6** in high yields and the subsequent reductions with sodium borohydride in methanol at 0°C gave the desired alcohols **7** and **8**. The mesylations were carried out by adding mesyl chloride to a solution of **7** or **8** in methylene chloride and triethylamine at −5°C. The same reaction yielded the chloromethyl derivatives **11** and **12** when carried out at room temperature for a longer period of time. The latter conversions were monitored by tlc to demonstrate an intermediacy of the mesylates. Treatment of **11** and **12** with sodium cyanide in aqueous tetrahydrofuran afforded nitriles **13** and **14** in a 50% yield. A similar reaction of **9** and **10** with sodium cyanide resulted in decreased yields of **13** and **14**. Alkaline hydrolysis of the nitriles furnished the enol-lactones **17** and **18**; the proposed intermediacy of **15** and **16** plausibly accounts for the loss of the cyano group. The nitriles **13** and **14** were converted to the methyl esters **19** and **20** via the corresponding imino esters (6); hydrolysis of **19** and **20** with methanolic sodium hydroxide produced carboxylic acids **21** and **22** respectively.

On treatment with an excess of cold 40% aqueous

[1]Author to whom correspondence should be addressed.

[2]The incentive for the first synthesis of this heterocyclic system stemmed from a desire to obtain direct evidence for the structure of a fungal metabolite citromycetin and its degradation product di-*O*-methylcitromycin (4).

0008-4042/79/243292-04$01.00/0

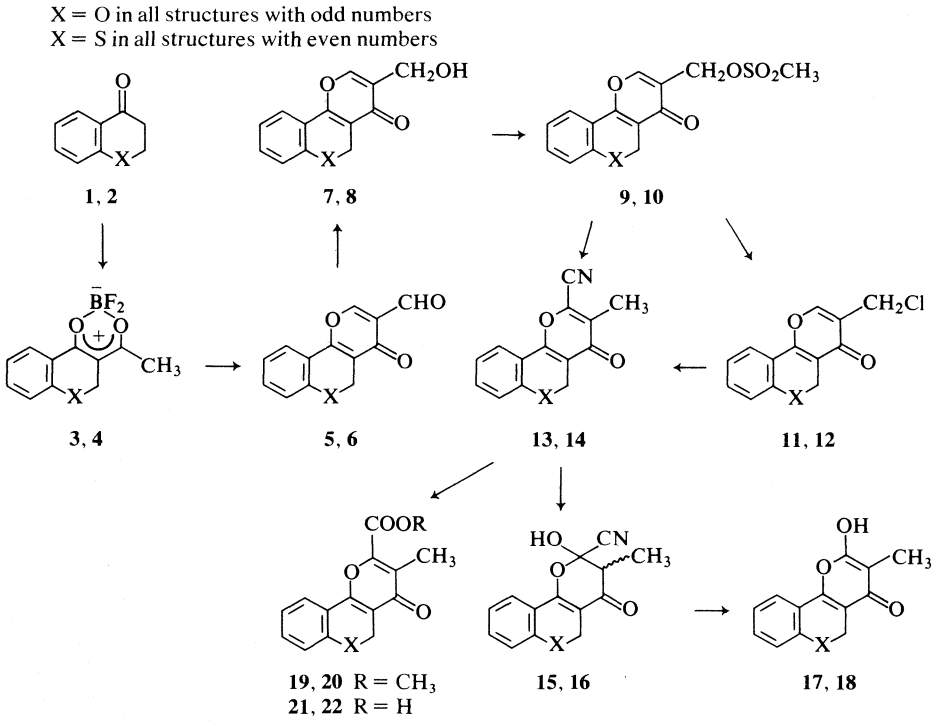

SCHEME 1

dimethylamine, the mesylate **10** was readily transformed into the amine **23** (Scheme 2). Attempts to prepare this amine from the chloro-derivative **12** yielded the vinylogous amide **24**. A prolonged reaction of **23** with aqueous dimethylamine in tetrahydrofuran resulted also in the formation of **24**. The *trans* configuration of this compound is apparent from its ^{1}Hmr spectrum (the coupling constant of the olefinic protons J = 12 Hz, cf. ref. 7). The generation of **24** from **23** can be explained in terms of a Michael addition of dimethylamine in position 2 followed by a retro-Mannich reaction and opening of the pyranone ring (8).

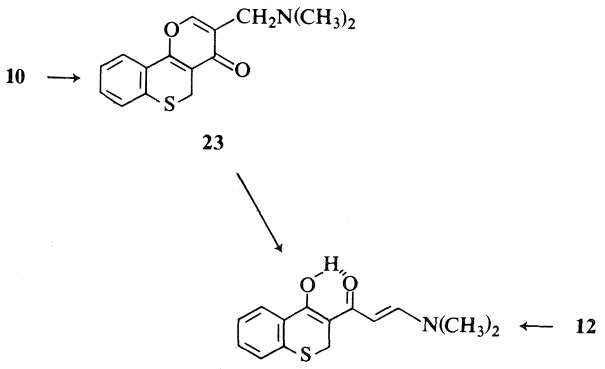

SCHEME 2

In view of the above reactions, it appears that the present systems function as typical Michael acceptors. The mode of formation of the nitriles **13** and **14** presumably involves an attack of CN^- at position 2 which may initiate an addition–elimination sequence or an S_N2' reaction. In any event, the subsequent isomerization of the C=C bond leads to a resonance-stabilized product which is not the case in the comparable reaction with dimethylamine, where only a normal displacement product can be isolated.

Experimental

Melting points are uncorrected. The infrared spectra were obtained with a Perkin-Elmer 225 spectrometer. Proton magnetic resonance (^{1}Hmr) spectra were determined with a Varian CFT-20 instrument using deuteriochloroform as solvent, unless otherwise stated. Chemical shift values are expressed on the δ scale (ppm), relative to tetramethylsilane internal standard. Mass spectra were recorded on an LKB 9000 S spectrometer.

*Preparation of Dioxaborins **3** and **4***

A stream of boron trifluoride gas was passed through a cooled solution of chroman-4-one **1** (9) (35.6 g) in glacial acetic acid (106 mL) and acetic anhydride (71 mL) until the mixture turned deep red and precipitation occurred. After standing overnight at room temperature, the product was collected on a filter, washed with a small amount of cold acetic acid, and air dried to yield 43 g (75%) of crude 2,2-difluoro-4-methyl-5*H*-(1)benzopyrano(3,4-e)-1,3,2-dioxaborin **3**. Analytically pure material was obtained by recrystallization from chloroform–ether; lemon yellow crystals, mp

196–197°C (lit. (*4b*) mp 196–197°C, yield 26%); ^{1}Hmr (DMSO-d_6) δ: 2.42 (s, 3H, CH_3), 5.23 (s, 2H, CH_2). *Anal.* calcd. for $C_{11}H_9BF_2O_3$: C 55.51, H 3.81; found: C 55.75, H 3.87.

Similarly, thiochroman-4-one **2** (10) was converted to **4** in 60% yield; orange-yellow crystals, mp 183–185°C; ^{1}Hmr δ: 2.50 (s, 3H, CH_3), 3.81 (s, 2H, CH_2). *Anal.* calcd. for $C_{11}H_9BF_2O_2S$: C 52.00, H 3.57; found: C 51.82, H 3.56.

*Preparation of Aldehydes **5** and **6***

Phosphorus oxychloride (23 g) was slowly added to dry dimethylformamide (79 g) at 5°C. The mixture was stirred for 15 min, the dioxaborin **4** (18.9 g) was added, and the resultant solution was heated at 100°C for 90 min. After cooling, the mixture was poured onto crushed ice, stirred for 2 h, and a brownish precipitate was collected by filtration. The crude product was washed with water, dried, and recrystallized from benzene to give 15.5 g (85%) of 4-oxo-4*H*,5*H*-(1)benzothiopyrano(4,3-b)pyran-3-carboxaldehyde **6**: mp 141–143°C; ir($CHCl_3$): 1700 and 1640 cm^{-1}; ^{1}Hmr δ: 3.99 (s, 2H, CH_2), 8.38 (s, 1H, O—CH═), 10.26 (s, 1H, CH═O); *m/e*: 244. *Anal.* calcd. for $C_{13}H_8O_3S$: C 63.91, H 3.30; found: C 64.00, H 3.42.

Using the same procedure, 4-oxo-4*H*,5*H*-pyrano(3,2-c)(1)-benzopyran-3-carboxaldehyde **5** was prepared from **3** in 70% yield: mp 192–194°C (benzene); ir(Nujol): 1705 and 1660 cm^{-1}; ^{1}Hmr (DMSO-d_6) δ: 5.15 (s, 2H, CH_2), 8.77 (s, 1H, O—CH═), 10.03 (s, 1H, CH═O); *m/e*: 228. *Anal.* calcd. for $C_{13}H_8O_4$: C 68.42, H 3.53; found: C 68.51, H 3.53.

*Preparation of Alcohols **7** and **8***

To a stirred solution of **6** (47.9 g) in methanol (4400 mL) was added over 15 min sodium borohydride (9.9 g) at 0°C. The mixture was stirred at room temperature for 2 h, then evaporated under reduced pressure, and the residue was partitioned between water and chloroform. The organic layer was washed with saturated brine, dried over anhydrous magnesium sulfate, filtered, and the solvent was removed on a Rotavapor leaving a brownish residue. Trituration of this solid with ether afforded 35.4 g (73%) of **8**, mp 143–145°C. Recrystallization from methanol provided an analytical specimen, mp 147–149°C; ir(Nujol): 3300 and 1655 cm^{-1}; ^{1}Hmr (DMSO-d_6) δ: 3.92 (s, 2H, CH_2S), 4.41 (dd, J_1 = 5.5 Hz, J_2 = 1 Hz, 2H, CH_2O, upon deuteration collapses into narrow doublet), 5.18(t, J_1 = 5.5 Hz, 1H, OH), 8.19(m, 1H, O—CH═). *Anal.* calcd. for $C_{13}H_{10}O_3S$: C 63.35, H 4.09; found: C 63.26, H 4.07.

In an identical manner, **5** was reduced to **7** in 55% yield: mp 188–189°C (methanol); ir(Nujol): 3380 and 1670 cm^{-1}; ^{1}Hmr (DMSO-d_6) δ: 4.32(dd, J_1 = 5 Hz, J_2 = 1 Hz, 2H, CH_2OH, upon deuteration collapses into narrow doublet), 5.15 and 5.17(s + t, J_1 = 5 Hz, 2H + 1H, CH_2O and OH), 8.15(m, 1H, O—CH═); *Anal.* calcd. for $C_{13}H_{10}O_4$: C 67.82, H 4.38; found: C 67.66, H 4.51.

*Preparation of Mesylates **9** and **10***

To a stirred suspension of the alcohol **8** (2.64 g) in methylene chloride (150 mL) was added triethylamine (2.1 mL) followed by methanesulfonyl chloride (0.9 mL) at −5°C. The mixture was stirred in an ice bath for 20 min, and then washed successively with cold water, 3 *N* HCl, 10% $NaHCO_3$, and again with water. Customary work-up of the organic phase afforded 3.4 g (98%) of **10**: mp 138–139°C (chloroform–ether); ir($CHCl_3$): 1655, 1365, and 1175 cm^{-1}; ^{1}Hmr δ: 3.15 (s, 3H, CH_3), 3.98 (s, 2H, CH_2S), 5.13(s, 2H, CH_2O), 8.12(s, 1H, O—CH═). *Anal.* calcd. for $C_{14}H_{12}O_5S_2$: C 51.83, H 3.73; found: C 51.75, H 3.59.

Under similar conditions, the alcohol **7** was converted to the mesylate **9** (yield 75%): mp 167–168°C (chloroform–ether); ir(Nujol): 1657, 1350, and 1175 cm^{-1}; ^{1}Hmr(DMSO-d_6) δ: 3.24(s, 3H, CH_3), 5.01 and 5.16 (s + s, 4H, CH_2O), 8.52 (s,1H, O—CH═). *Anal.* calcd. for $C_{14}H_{12}O_6S$: C 54.54, H 3.92; found: C 54.60, H 3.81.

*Preparation of Chloromethyl Compounds **11** and **12***

To a stirred suspension of the alcohol **8** (35.3 g) in methylene chloride (1000 mL) was added triethylamine (34 mL) followed by methanesulfonyl chloride (12.2 mL) at 5°C. The mixture was stirred overnight at ambient temperature, evaporated on a Rotavapor, and the residue was chromatographed on a silica gel column. Elution with chloroform afforded 26.3 g (69%) of **12**; yellow crystals, mp 151–153°C (benzene); ^{1}Hmr δ: 3.95(s, 2H, CH_2S), 4.47(s, 2H, CH_2Cl), 8.05(s, 1H, O—CH═); *m/e*: 266 and 264. *Anal.* calcd. for $C_{13}H_9ClO_2S$: C 58.98, H 3.42; found: C 59.00, H 3.65.

From a similar reaction of **7**, compound **11** was obtained in 75% yield; mp 163–165°C (benzene–ether); ^{1}Hmr(DMSO-d_6) δ: 4.48(s, 2H, CH_2Cl), 5.15(s, 2H, CH_2O), 8.52(s, 1H, O—CH═); *m/e*: 250 and 248. *Anal.* calcd. for $C_{13}H_9ClO_3$: C 62.79, H 3.65; found: C 62.80, H 3.67.

*Preparation of Nitriles **13** and **14***

A mixture of **12** (28 g), tetrahydrofuran (800 mL), sodium cyanide (10.4 g), and water (800 mL) was stirred overnight at room temperature, concentrated under reduced pressure, and extracted with chloroform. Evaporation of the extracts gave a paste which was chromatographed on silica gel. Elution with chloroform yielded 13.6 g (50%) of **14**; yellow crystals, mp 144–145°C (chloroform–ether); ir($CHCl_3$): 2240 and 1635 cm^{-1}; ^{1}Hmr δ: 2.25(s, 3H, CH_3), 3.95(s, 2H, CH_2S); *m/e*: 255. *Anal.* calcd. for $C_{14}H_9NO_2S$: C 65.86, H 3.55, N 5.53; found: C 65.85, H 3.65, N 5.79.

Essentially the same procedure was used for the transformation of **11** to **13** (column chromatography of the crude product over silica gel was carried out using 5% ethyl acetate – benzene eluent), yield 50%; mp 179–181°C (chloroform–ether); ir($CHCl_3$): 2230 and 1640 cm^{-1}; ^{1}Hmr δ: 2.25(s, 3H, CH_3), 5.20(s, 2H, CH_2O); *m/e*: 239. *Anal.* calcd. for $C_{14}H_9NO_3$: C 70.29, H 3.79, N 5.86; found: C 70.52, H 3.71, N 5.86.

*Alkaline Hydrolyses of Nitriles **13** and **14***

A mixture of **13** (100 mg), methanol (5 mL), and 10% sodium hydroxide (4 mL) was refluxed for 2 h, diluted with water, washed with ether, and acidified with hydrochloric acid. The precipitate was collected and recrystallized from ethyl acetate to afford 35 mg (36%) of **17**; mp 279–281°C; ir(Nujol): 3100 and 1653 cm^{-1}; ^{1}Hmr(DMSO-d_6) δ: 1.93(s, 3H, CH_3), 5.15(s, 2H, CH_2O); *m/e*: 230. *Anal.* calcd. for $C_{13}H_{10}O_4$: C 67.82, H 4.38; found: C 67.54, H 4.19.

Similar treatment of **14** (100 mg) produced 28 mg (29%) of **18**: mp 275–277°C (methanol); ir(Nujol): 3100–2900 and 1650 cm^{-1}; ^{1}Hmr(DMSO-d_6) δ: 1.95(s, 3H, CH_3), 3.89(s, 2H, CH_2S); *m/e*: 246. *Anal.* calcd. for $C_{13}H_{10}O_3S$: C 63.40, H 4.09; found: C 63.68, H 4.22.

*Preparation of Methyl Esters **19** and **20***

A suspension of the above nitrile **14** (1.41 g) in dry methanol (200 mL) was saturated with hydrogen chloride and left at ambient temperature overnight. The resultant solution was refluxed for 4 h, evaporated, and the residue was partitioned between 10% sodium bicarbonate and chloroform. Usual work-up of the organic phase yielded 1.28 g (80%) of **20**; mp 148–150°C (methanol); ir($CHCl_3$): 1735 and 1640 cm^{-1}; ^{1}Hmr δ: 2.35(s, 3H, CH_3), 3.94, and 3.96(s + s, 5H, CH_2S and CH_3O). *Anal.* calcd. for $C_{15}H_{12}O_4S$: C 62.48, H 4.20; found: C 62.58, H 4.11.

In a similar manner, **13** was converted to **19** in 60% yield; mp 119–120°C (methanol); ir($CHCl_3$): 1735 and 1650 cm^{-1};

^{1}Hmr(DMSO-d_6) δ: 2.21(s, 3H, CH_3), 3.92 (s, 3H, CH_3O), 5.10(s, 2H, CH_2O). *Anal.* calcd. for $C_{15}H_{12}O_5$: C 66.17, H 4.44; found: C 66.14, H 4.50.

*Preparation of Carboxylic Acids **21** and **22***

To a solution of sodium hydroxide (0.5 g) in methanol (50 mL) was added **20** (1.6 g), and the mixture was refluxed for 2 h. The solvent was removed on a Rotavapor, the residue was dissolved in water and washed with ether. The aqueous solution was then added to 3 *N* hydrochloric acid (25 mL) upon stirring. The precipitate was collected by filtration, washed with water, and dried to give 1.5 g (98% of 3-methyl-4-oxo-4*H*,5*H*-(1)benzothiopyrano(4,3-b)pyran-2-carboxylic acid **22**, mp 300–301°C. An analytical sample was crystallized from aqueous dimethyl sulfoxide; mp 302–303°C; ir(Nujol): 2800 and 1728 cm^{-1}; ^{1}Hmr(DMSO-d_6) δ: 2.21(s, 3H, CH_3), 3.91(s, 2H, CH_2S); *m/e*: 274. *Anal.* calcd. for $C_{14}H_{10}O_4S$: C 61.30, H 3.68; found: C 61.60, H 3.64.

In a similar experiment starting with **19**, 3-methyl-4-oxo-4*H*,5*H*-pyrano(3,2-c) (1)benzopyran-2-carboxylic acid **21** was obtained in 85% yield; mp 270–272°C (aqueous dimethyl sulfoxide); ir(Nujol): 2900–2800 and 1725 cm^{-1}; ^{1}Hmr (DMSO-d_6) δ: 2.25(s, 3H, CH_3), 5.18(s, 2H, CH_2O); *m/e*: 258. *Anal.* calcd. for $C_{14}H_{10}O_5$: C 65.12, H 3.90; found: C 65.30, H 3.95.

*3-(*N,N-*Dimethylaminomethyl)-4*H,5H-*(1)benzothiopyrano-(4,3-b)pyran-4-one **23***

A solution of **10** (2.09 g) in tetrahydrofuran (40 mL) and 40% aqueous dimethylamine (2.5 mL) was stirred at room temperature for 15 min, diluted with brine, and extracted with chloroform. The combined extracts were concentrated and chromatographed on basic alumina. Elution with 5% ethyl acetate – benzene afforded 1.31 g (77%) of **23**: mp 82.5–84.5°C (benzene–ether): ^{1}Hmr δ: 2.32 (s, 6H, CH_3N), 3.49(s, 2H, CH_2N), 3.99(s, 2H, CH_2S), 7.95(s, 1H, O—CH═); *m/e*: 273. *Anal.* calcd. for $C_{15}H_{15}NO_2S$: C 65.91, H 5.53, N 5.12; found: C 65.89, H 5.59, N 5.05.

*3-[3-(Dimethylamino)-1-oxo-2-propen-1-yl-]thiochroman-4-one **24***

A solution of **12** (265 mg) in tetrahydrofuran (9 mL) and 40% aqueous dimethylamine (0.9 mL) was kept at room temperature and monitored by tlc. After 15 and 60 min, the chromatograms showed that the major component of the mixture was unchanged **12**. The mixture was allowed to stand 24 h, evaporated, and chromatographed over silica. Elution with chloroform afforded 132 mg (50%) of **24**; mp 153–155°C (benzene); ir(Nujol): 1627 cm^{-1}: ^{1}Hmr δ: 3.01(s, 6H, CH_3N), 3.75(s, 2H, CH_2S), 5.09, and 7.80(doublets, J = 12Hz, 1H + 1H, CH═CH). *Anal.* calcd. for $C_{14}H_{15}NO_2S$: C 64.34, H 5.79, N 5.36; found: C 64.17, H 5.95, N 5.30.

In another experiment, to a solution of amine **23** in tetrahydrofuran was added an excess of 40% aqueous dimethylamine, and the mixture was kept at room temperature for several days. Customary work-up and chromatography afforded **24**, identical with the material obtained by the foregoing procedure in every respect; yield 55%.

1. (*a*) J. B. Wright and H. G. Johnson. J. Med. Chem. **16**, 861 (1973); (*b*) A. Nohara, H. Kuriki, T. Saijo, K. Ukawa, T. Murata, M. Kanno, and Y. Sanno. J. Med. Chem. **18**, 34 (1975); (*c*) J. R. Bantick, H. Cairns, A. Chambers, R. Hazard, J. King, T. B. Lee, and R. Minshull. J. Med. Chem. **19**, 817 (1976); (*d*) J. P. Devlin, K. Freter, and P. B. Stewart. J. Med. Chem. **20**, 205 (1977).
2. (*a*) S. von Kostanecki and A. Rozycki. Chem. Ber. **34**, 102 (1901); (*b*) S. von Kostanecki, L. Paul, and J. Tambor. Chem. Ber. **34**, 2475 (1901).
3. (*a*) G. A. Reynolds and J. A. van Allan. J. Heterocycl. Chem. **6**, 375 (1969); (*b*) A. Nohara, T. Umetani, and Y. Sanno. Tetrahedron Lett. **22**, 1995 (1973).
4. (*a*) F. M. Dean, S. Murray, and W. Taylor. J. Chem. Soc. Chem. Commun. 440 (1974); (*b*) F. M. Dean, K. B. Hindley, S. Murray, and W. Taylor. J. Chem. Soc. Perkin Trans. I, 2444 (1976).
5. C. L. Mao, F. C. Frostick, Jr., E. H. Man, R. M. Manyik, R. L. Wells, and C. R. Hauser. J. Org. Chem. **34**, 1425 (1969).
6. J. B. Cloke, E. C. Knowles, and R. J. Anderson. J. Am. Chem. Soc. **58**, 2547 (1936).
7. C. Kashima, H. Aoyama, Y. Yamamoto, and T. Nishio. J. Chem. Soc. Perkin Trans. II, 665 (1975).
8. F. Eiden and C. Herdeis. Arch. Pharm. (Weinheim), **310**, 573 (1977).
9. S. G. Powell. J. Am. Chem. Soc. **45**, 2708 (1923).
10. F. Krollpfeiffer and H. Schultze. Chem. Ber. **56**, 1819 (1923).

The synthesis of 5,6-dihydro-3,3-dimethyl-4,1-benzoxazonine-2,7(1*H*,3*H*)dione and its conversion into 1,3-dihydro-3,3-dimethylfuro[3,4-*b*] quinolines

CHRISTOPHER A. DEMERSON AND LESLIE G. HUMBER

Ayerst Research Laboratories, Montreal, P.Q., Canada H3C 3J1

Received June 11, 1979

This paper is dedicated to Prof. Karel Wiesner on the occasion of his 60th birthday

CHRISTOPHER A. DEMERSON and LESLIE G. HUMBER. Can. J. Chem. **57**, 3296 (1979).

Periodate oxidation of 1,1-dimethyl-1,3,4,9-tetrahydropyrano[3,4-*b*]indole **1** gave 5,6-dihydro-3,3-dimethyl-4,1-benzoxazonine-2,7(1*H*,3*H*)dione **2**, a member of the novel 4,1-benzoxazonine ring system. Its conversion into 1,3-dihydro-3,3-dimethylfuro[3,4-*b*]quinolines is described.

CHRISTOPHER A. DEMERSON et LESLIE G. HUMBER. Can. J. Chem. **57**, 3296 (1979).

L'oxydation du diméthyl-1,1 tétrahydro-1,3,4,9 pyrano[3,4-*b*] indole **1** par le periodate donne la dihydro-5,6 diméthyl-3,3 benzoxazonine-4,1(1*H*,3*H*) dione 2,7 (**2**) un membre du nouveau système cyclique benzoxazonine-4,1. On décrit sa transformation en dihydro-1,3 diméthyl-3,3 furo[3,4-*b*] quinolines.

[Traduit par le journal]

During the past few years a number of reports from these laboratories have centred on the 1,3,4,9-tetrahydropyrano[3,4-*b*]indole ring system. Our investigations have led to the preparation of derivatives that are pharmacologically active as antiinflammatory (1, 2) and antidepressant (3) agents. As part of our continuing studies we now wish to report on the conversion of 1,3,4,9-tetrahydropyrano[3,4-*b*]indoles to novel 4,1-benzoxazonines, and subsequently into furo[3,4-*b*]quinolines.

The oxidative cleavage of indolic double bonds has been well documented. Witkop and co-workers have studied a variety of methods such as ozonolysis (4, 5), oxidation by peracids (6), and autoxidation (7). In 1966 Dolby and Booth reported the sodium periodate cleavage of a number of indoles (8). Since this latter method was reported to be facile and afford good yields we applied it to the oxidation of pyrano-[3,4-*b*]indoles. Periodate treatment of compound **1** in methanol–water afforded 5,6-dihydro-3,3-dimethyl-4,1-benzoxazonine-2,7(1*H*,3*H*)dione **2**, the first example of a 4,1-benzoxazonine, in an 85% yield. This compound was converted to a number of other 4,1-benzoxazonine derivatives, shown in Scheme 1, which is self-explanatory.

When the 4,1-benzoxazonine **2** was stirred with sodium hydride in tetrahydrofuran for a short interval and then made neutral, 3,4-dihydro-3,3-dimethylfuro[3,4-*b*]quinoline-9(1*H*)-one **12** (Scheme 2) precipitated out in an 86% yield. The structure was established by ^{1}Hmr spectroscopy. That the compound did not exist in its tautomeric quinolinol form was clear from the infrared spectrum. Also, the uv spectrum had maxima at 239, 314, and 326 nm, typical for quinolones (9).

Reaction of the furo[3,4-*b*]quinoline-9-one **12** with phosphorus oxychloride gave the chloro compound **13**. Replacement of the chlorine atom occurred readily on treatment with a variety of primary alkylamines to produce the compounds **14**–**20** listed in Table 1. The reactions were done in hot phenol, and as a consequence the 9-phenoxy derivative **21** (Scheme 2) was a by-product.

The 9-aminoalkyloxy derivatives (**21**–**24**, Table 1) were formed in one step by the action of the appropriate amino-alkanol on the intermediary sodium furo[3,4-*b*]quinolate, which was prepared either from the 4,1-benzoxazonine **2** or from the quinolone **12**. Compound **25** was obtained from the epoxide **24** by reaction with isopropylamine.

The furo[3,4-*b*]quinoline ring system is not novel (10). However a general method for the preparation of substituted derivatives has not previously been available. The approach described in this report utilizes, as starting material, pyrano[3,4-*b*]indoles, of which a large number of substituted derivatives are readily attainable (1–3). Thus, a wide variety of 4,1-benzoxazonines and furo[3,4-*b*]quinolines are now accessible.

The furo[3,4-*b*]quinolines were evaluated in the Ayerst Pharmacology Department for their ability to decrease the blood pressure of spontaneously hypertensive rats, using the protocol described by Vavra *et al.* (11). While some representatives of this class possessed weak antihypertensive properties, none was of sufficient interest to be considered a candidate for further development.

Experimental

Melting points were taken on a Thomas-Hoover apparatus

0008-4042/79/243296-05$01.00/0

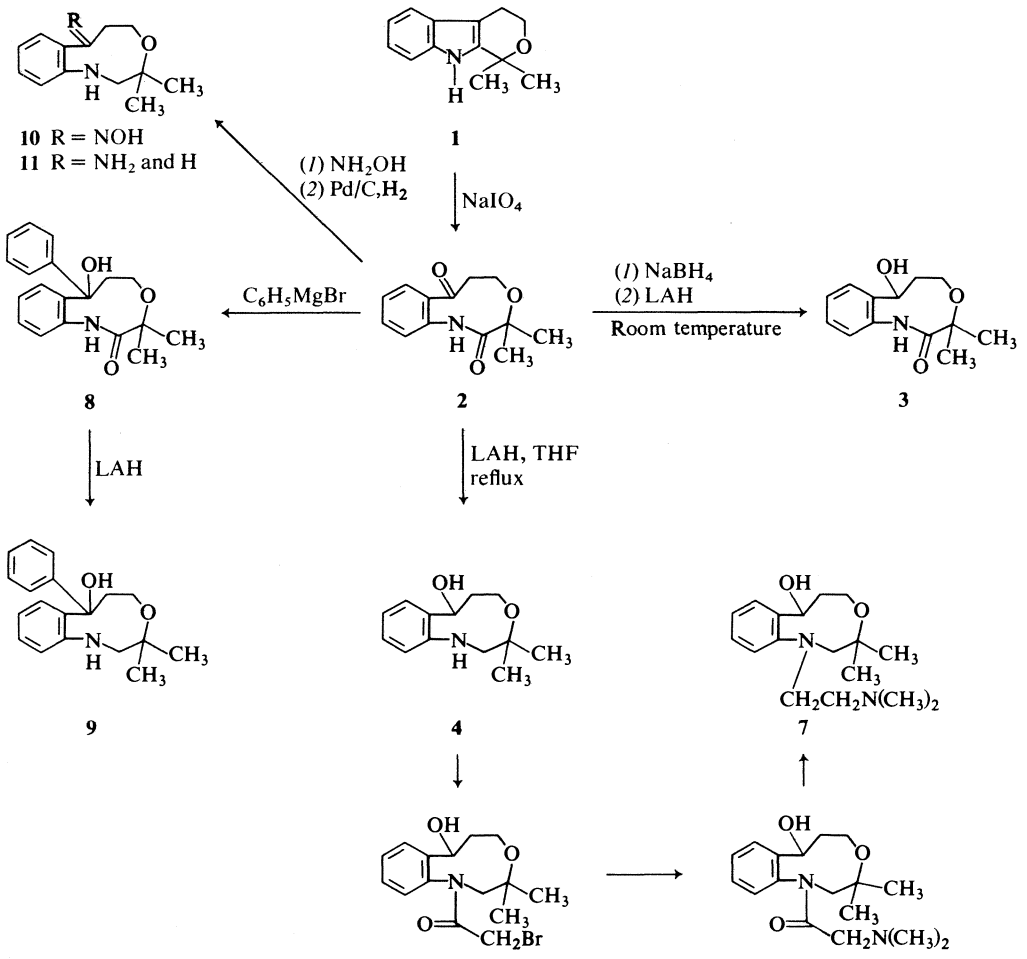

SCHEME 1

and need no correction. The ^{1}Hmr spectra were determined using a Varian A-60A spectrometer and the chemical shifts (δ) are reported in parts per million downfield from TMS. Analyses were performed by Dr. G. Schilling and staff of our laboratories.

*5,6-Dihydro-3,3-dimethyl-4,1-benzoxazonine-2,7(1*H*,3*H*)dione* **2**

A solution of the pyrano[3,4-*b*]indole **1** (3) (25.7 g, 0.127 mol) in methanol (600 mL) was added dropwise to sodium metaperiodate (60.6 g, 0.28 mol) in water (300 mL). After stirring at 22°C for 24 h, the resulting precipitate was filtered off and washed with methanol. The filtrate was concentrated *in vacuo*, water added, and the product filtered off. Extraction of the aqueous filtrate with dichloromethane, drying (Na_2SO_4), and concentrating *in vacuo* afforded more solid. The combined materials were recrystallized from acetone to give the 4,1-benzoxazonine **2** (25 g, 85%), mp 146–148°C; ir ($CHCl_3$): 3360, 1675 (b) cm^{-1}; ^{1}Hmr ($CDCl_3$) δ: 1.45 (6H, s, *gem* dimethyl), 2.80 (2H, bm, CH_2CO), 4.06 (2H, bm, CH_2O), 7.42 (4H, m, aromatic), 8.17 (1H, bs, NH). *Anal.* calcd. for $C_{13}H_{15}NO_3$: C 66.93, H 6.48, N 6.01; found: C 66.60, H 6.52, N 6.01.

*3,3-Dimethyl-7-hydroxy-1,5,6,7-tetrahydro-4,1-benzoxazonin-2(3*H*)-one* **3**

The 4,1-benzoxazonine **2** (20 g, 0.086 mol) was added portionwise to a cooled mixture of sodium borohydride (20 g, 0.53 mol) in methanol (500 mL). After stirring at 22°C for 2 h, the reaction was concentrated *in vacuo*, and the residue partitioned between chloroform and water. The chloroform phase was washed with water, dried (Na_2SO_4), and evaporated *in vacuo* to give a solid. Recrystallization from acetonitrile afforded the alcohol **3** (10 g, 49%), mp 141–142°C; ir ($CHCl_3$): 3310, 3200, 3080, 1655 cm^{-1}. *Anal.* calcd. for $C_{13}H_{17}NO_3$: C 66.36, H 7.28; found: C 66.00, H 7.29.

Alternatively the alcohol **3** can be prepared in a comparable yield by stirring the 4,1-benzoxazonine **2** with a 5-fold excess of lithium aluminium hydride in ether at 22°C for 2 h.

3,3-Dimethyl-1,2,3,5,6,7-hexahydro-4,1-benzoxazonin-7-ol **4**

A solution of the 4,1-benzoxazonine **2** (15 g, 0.064 mol) in tetrahydrofuran (300 mL) was added dropwise to a cooled stirring mixture of lithium aluminium hydride (12.16 g, 0.32 mol) in tetrahydrofuran (250 mL). After 20 h of refluxing the

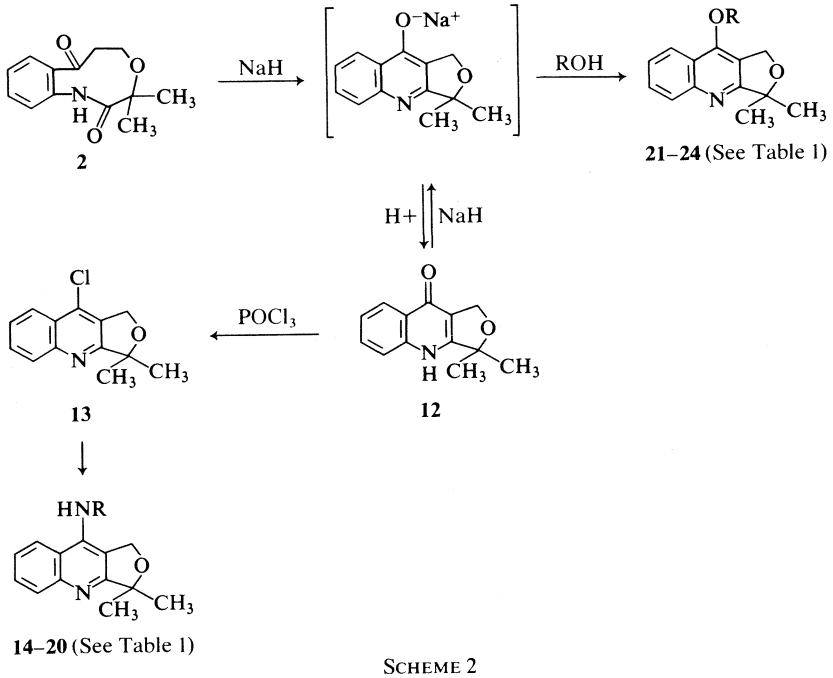

SCHEME 2

TABLE 1. 9-Substituted-1,3-dihydro-3,3-dimethylfuro[3,4-*b*]quinolines

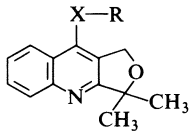

No.	X	R	Melting point (°C)	Recrystallizing solvent[a]	Formula[b]	Yield (%)[c]
14	NH	$(CH_2)_2N(CH_3)_2$	126–127	A	$C_{17}H_{23}N_3O$	92
15	NH	$(CH_2)_3N(CH_3)_2$	87–88	B	$C_{18}H_{25}N_3O$	88
16	NH	$(CH_2)_2C_6H_5$	151–153[d]	C	$C_{21}H_{22}N_2O{\cdot}HCl$[e]	63
17	NH	$CH_2CH(OH)CH_2N(C_2H_5)_2$	oil[f]	—	$C_{20}H_{29}N_3O_2$	57
18	NH	$CH(CH_3)CH_2CH_2CH_2N(C_2H_5)_2$	oil	—	$C_{22}H_{33}N_3O$	29
19	NH	$(CH_2)_3C_4H_8NO$[h]	96–98	D	$C_{20}H_{27}N_3O_2$	79
20	NH	$(CH_2)_3C_5H_{11}N_2$[h]	245–250[d]	C	$C_{21}H_{30}N_4O{\cdot}4HCl$[e]	60
21	O	C_6H_5	101–102	E	$C_{19}H_{17}NO_2$	—[g]
22	O	$(CH_2)_2N(CH_3)_2$	92–93	F	$C_{17}H_{22}N_2O_2$	90
23	O	$(CH_2)N(CH_3)_2$	71–72	F	$C_{18}H_{24}N_2O_2$	81
24	O		133–134	G	$C_{16}H_{17}NO_3$	68
25	O	$CH_2CH(OH)CH_2NHCH(CH_3)_2$[i]	175–177[e]	C	$C_{19}H_{26}N_2O_3.HCl$[e]	48

[a]A = ethyl acetate, B = hexane, C = ethanol, D = benzene – petroleum ether (bp 60–90°C), E = water, F = acetonitrile, G = cyclohexane.
[b]All compounds were analysed for C, H, and N and results were within ±0.4% except for C of **16**, calcd. 71.07, found 71.53; C of **20**, calcd, 50.41, found 50.82.
[c]Yields of **14** to **20** are calculated from **13**, of **22** and **23** from **2**, **24** from **12**, and **25** from **24**.
[d]Melting point of the hydrochloride.
[e]Characterized as the hydrochloride.
[f]Boiling point was 233–235°C (0.03 Torr).
[g]Obtained as a by-product in various yields (see Experimental).
[h]C_4H_8NO = morpholino, $C_5H_{11}N_2$ = *N*-methylpiperazino.
[i]Prepared from the reaction of compound **24** with isopropylamine (see Experimental).

excess hydride was destroyed with tetrahydrofuran–water (2:1). The addition of 20% sodium hydroxide solution (12 mL), filtration, and concentration *in vacuo* gave an oil. This was partitioned between water and chloroform, the chloroform phase washed with water, dried (Na_2SO_4), and concentrated *in vacuo* to afford the alcohol **4** (12.8 g, 90%) as a solid, mp 148–151°C (acetone); ^{1}Hmr ($CDCl_3$) δ: 1.13 (6H, s, *gem* dimethyl), 1.85 (2H, m, CH_2), 3.09 (2H, d, J = 2.5 Hz), 3.15 (2H, m, CH_2O), 3.75 (2H, bs, NH, OH), 5.13 (1H, 2d, J_1 = 7.5 Hz, J_2 = 5 Hz), 7.08 (4H, m, aromatic). *Anal.* calcd.

for $C_{13}H_{19}NO_2$: C 70.55, H 8.65, N 6.33; found: C 70.79, H 8.73, N 6.30.

1-Bromoacetyl-1,2,3,5,6,7-hexahydro-3,3-dimethyl-4,1-benzoxazonin-7-ol ***5***

Bromoacetyl bromide (14 g, 0.069 mol) was added to a stirring mixture of the alcohol **4** (14 g, 0.064 mol), benzene (400 mL), and 2 *N* sodium hydroxide (45 mL) at 0°C. After 1 h, more 2 *N* sodium hydroxide (20 mL) was added and stirring continued for a further 40 min. The phases were separated and the benzene layer washed with 2 *N* hydrochloric acid, water, dried (Na_2SO_4), and evaporated to give the product **5** (12.6 g, 56%); ^{1}Hmr ($CDCl_3$) δ: 1.09 (3H, s, CH_3), 1.35 (3H, s, CH_3), 1.5 (2H, m, CH_2), 2.5 (2H, m, OCH_2), 3.09 (1H, d, J = 15 Hz, CH_2Br), 4.38 (1H, d, J = 15 Hz, CH_2Br), 5.64 (1H, d, J = 4 Hz, CHO), 7.2 (4H, m, aromatic).

*1-(*N,N*-Dimethylglycyl)-1,2,3,5,6,7-hexahydro-3,3-dimethyl-4,1-benzoxazonin-7-ol* ***6***

A mixture of the bromo compound **5** (12.65 g, 0.037 mol), 40% aqueous dimethylamine (175 mL), and tetrahydrofuran (250 mL) was stirred at 22°C for 2 h. Most of the solvent was evaporated off *in vacuo*, the residue diluted with water, and extracted (× 3) with chloroform. Concentration of the extracts gave a solid that was crystallized from ethyl acetate – petroleum ether (bp 30–60°C) to afford the amine **6** (9.6 g, 83%), mp 113–115°C; ir ($CHCl_3$): 3600, 3420, 1655 cm^{-1}; ^{1}Hmr ($CDCl_3$) δ: 1.1 (3H, s, CH_3), 1.38 (3H, s, CH_3), 2.18 (6H, s, $N(CH_3)_2$), 2.66 (1H, s, OH), 3.65 (2H, q, J = 7 Hz, $COCH_2N(CH_3)_2$), 5.53 (1H, m, CHO), 7.2 (4H, m, aromatic). *Anal.* calcd. for $C_{17}H_{23}N_2O_3$: C 66.64, H 8.55, N 9.15; found: C 66.55, H 8.53, N 9.00.

1-[2-(Dimethylamino)ethyl]-1,2,3,5,6,7-hexahydro-3,3-dimethyl-4,1-benzoxazonin-7-ol hydrochloride ***7***

A mixture consisting of the dimethylamino compound **6** (5.2 g, 0.018 mol), lithium aluminium hydride (5.0 g, 0.13 mol), and tetrahydrofuran (150 mL) was refluxed for 18 h. The excess hydride was decomposed with tetrahydrofuran–water (2:1), the reaction filtered, and the filtrate evaporated *in vacuo*. The residue was partitioned between water and chloroform, and the chloroform phase concentrated *in vacuo* to yield the amino alcohol **7** (5.13 g) as an oil. It was converted into the hydrochloride (3.14 g, 50%), mp 253–254°C; ^{1}Hmr (DMSO-d_6) δ: 0.88 (3H, s, CH_3), 1.23 (3H, s, CH_3), 2.42 (6H, s, $N(CH_3)_2$), 5.6 (1H, m, CHO), 7.3 (4H, m, aromatic). *Anal.* calcd. for $C_{17}H_{28}N_2O_2 \cdot HCl$: C 62.08, H 8.89, N 8.52, Cl 10.78; found: C 61.98, H 8.89, N 8.43, Cl 10.59.

*3,3-Dimethyl-7-hydroxy-7-phenyl-1,5,6,7-tetrahydro-4,1-benzoxazonin-2(3*H*)-one* ***8***

Bromobenzene (31.4 g, 0.2 mol) in dry diethyl ether (30 mL) was added dropwise to magnesium turnings (4.8 g, 0.2 g-at.) in diethyl ether (50 mL). After 10 min of refluxing, the 4,1-benzoxazonine **2** (11.7 g, 0.05 mol) in tetrahydrofuran (100 mL) was added and refluxing continued for 2 h. Saturated aqueous ammonium chloride solution was added and the solution extracted with chloroform. The extract was dried (Na_2SO_4), evaporated *in vacuo*, and the residue crystallized from benzene–acetonitrile to afford the alcohol **8** (4.5 g, 30%), mp 131–132°C; ^{1}Hmr (DMSO-d_6) δ: 1.17 (3H, s, CH_3), 1.33 (3H, s, CH_3), 2.2 (2H, m, CH_2), 3.8 (1H, bs, OH), 8.0 (9H, m, aromatic). *Anal.* calcd. for $C_{19}H_{21}NO_3$: C 73.96, H 6.79, N 4.49; found: C 74.03, H 6.87, N 4.34.

3,3-Dimethyl-1,2,3,5,6,7-hexahydro-7-phenyl-4,1-benzoxazonin-7-ol ***9***

The alcohol **8** (8 g, 0.026 mol) and lithium aluminium hydride (8 g, 0.2 mol) in tetrahydrofuran (200 mL) was refluxed for 24 h. The excess hydride was destroyed with tetrahydrofuran–water (2:1), and the resulting slurry filtered. The filtrate was concentrated *in vacuo* and the product crystallized from ethanol to afford the amine **9**, (5.0 g, 65%), mp 147–148°C; ir ($CHCl_3$): 3580, 3350 cm^{-1}; ^{1}Hmr ($CDCl_3$) δ: 1.0 (3H, s, CH_3), 1.2 (3H, s, CH_3), 2.0 (2H, m, CH_2), 3.1 (2H, s, NCH_2), 3.3 (2H, t, J = 5 Hz, OCH_2), 4.15 (2H, bs, OH, NH), 7.1 (9H, m, aromatic). *Anal.* calcd. for $C_{19}H_{23}NO_2$: C 76.73, H 7.80, N 4.71; found: C 76.95, H 7.81, N 4.71.

*3,3-Dimethyl-5,6-dihydro-4,1-benzoxazonine-2,7(1*H*,3*H*)-dione oxime* ***10***

A solution consisting of sodium acetate (37.5 g, 0.46 mol), hydroxylamine hydrochloride (31.5 g, 0.45 mol), and the 4,1-benzoxazonine **2** (50 g, 0.214 mol) in 1.2 L of ethanol was stirred at 22°C for 2 days. Filtration gave the oxime **10** (30 g, 57%), mp 205–206°C (ethanol); ^{1}Hmr (DMSO-d_6) δ: 1.32 (6H, bs, *gem* dimethyl), 2.7 (2H, m, CH_2), 3.96 (2H, m, CH_2O), 7.35 (4H, m, aromatic), 9.4 (1H, bs, NH), 11.2 (1H, bs, NOH). *Anal.* calcd. for $C_{13}H_{16}N_2O_3$: C 62.88, H 6.50, N 11.28; found: C 62.35, H 6.63, N 11.27.

*7-Amino-3,3-dimethyl-1,5,6,7-tetrahydro-4,1-benzoxazonin-2(3*H*)-one* ***11***

The oxime **10** (1 g, 0.004 mol) in ethanol (100 mL) containing concentrated hydrochloric acid (0.4 mL) and 5% palladium on carbon (0.2 g) was hydrogenated at atmospheric pressure for 18 h. Filtration, concentration *in vacuo*, and crystallization from ethanol afforded the amine **11** as its hydrochloride (0.67 g, 60%), mp 165–167°C; ir (Nujol): 3400, 1665 cm^{-1}; ^{1}Hmr (D_2O) δ: 1.15 (3H, s, CH_3), 1.38 (3H, s, CH_3), 2.15 (2H, m, CH_2), 3.9 (2H, m, CH_2O), 4.9 (1H, m, CHO), 7.5 (4H, m, aromatic).

*3,4-Dihydro-3,3-dimethylfuro[3,4-*b*]quinolin-9(1*H*)-one* ***12***

The 4,1-benzoxazonine **2** (11.66 g, 0.05 mol) in tetrahydrofuran (250 mL) was added dropwise to a stirring mixture of sodium hydride (4.8 g of a 55% dispersion, 0.1 mol) in tetrahydrofuran (220 mL). After 0.5 h at 22°C the reaction was neutralized with glacial acetic acid. The resulting precipitate was filtered, triturated with water, and dried to afford furo[3,4-*b*]quinolinone **12** (9.3 g, 86%), mp 335–340°C (dec.) (methanol); ir (Nujol): 3220, 3180, 3100, 1610, 1580, 1504 cm^{-1}; uv λ_{max}: 326 (14 000), 314 (12 800), 239 (33 000); ^{1}Hmr (DMSO-d_6) δ: 1.54 (6H, s, *gem* dimethyl), 4.92 (2H, s, CH_2O), 7.4 (3H, m, aromatic), 8.19 (1H, m, aromatic), 11.9 (1H, bs, NH). *Anal.* calcd. for $C_{13}H_{13}NO_2$: C 72.54, H 6.09, N 6.51; found: C 72.30, H 6.15, N 6.45.

*9-Chloro-1,3-dihydro-3,3-dimethylfuro[3,4-*b*]quinoline* ***13***

Powdered furo[3,4-*b*]quinoline **12** (6.5 g, 0.03 mol) was added portionwise to vigorously stirring phosphorus oxychloride (26 mL) at 22°C. After 1 h the reaction was poured into crushed ice (340 mL). A small amount of residue was filtered off after the ice melted and the filtrate made alkaline with 50% sodium hydroxide solution (75 mL). Filtration gave the chloro compound **13** (5.96 g, 85%), mp 108–110°C (petroleum ether, bp 60–80°C); uv: λ_{max}: 320 (6280), 306 (5060), 294 (4740), 225 (31 800); ^{1}Hmr ($CDCl_3$) δ: 1.62 (6H, s, *gem* dimethyl), 5.22 (2H, s, CH_2), 7.67 (2H, m, aromatic), 8.15 (2H, m, aromatic). *Anal.* calcd. for $C_{13}H_{12}ClNO$: C 66.81, H 5.18, N 5.99; found: C 67.01, H 5.43, N 5.71.

*9-Substituted-1,3-dihydro-3,3-dimethylfuro[3,4-*b*]quinolines* ***14–20*** *(Table 1)*

A mixture of the chloro compound **13** (0.05 mol), the appropriate alkylamine (0.12 mol), and phenol (20 g) was heated at 150°C for 20 h. The reaction was taken into chloroform, washed with 10% sodium hydroxide solution, and extracted with 5% aqueous hydrochloric acid. The acid extract was washed with diethyl ether and then made alkaline with 10% aqueous sodium hydroxide. Extraction with diethyl

ether, followed by drying (Na_2SO_4) and concentration afforded the title compounds.

1,3-Dihydro-3,3-dimethyl-9-phenoxyfuro[3,4-b]quinoline ***21***

Silica gel chromatography of the products **14**–**20** described above using benzene–acetone–triethylamine (7:2:1) afforded compound **21** as a solid in yields of 5–40% (calculated from the chloro compound **13**).

9-Substituted-1,3-dihydro-3,3-dimethylfuro[3,4-b]quinolines ***22*** *and* ***23***

A solution of 4,1-benzoxazonine **2** (10 g, 0.043 mol) in tetrahydrofuran (100 mL) was added dropwise over a 1 h period to a stirring suspension of sodium hydride (5 g of a 55% dispersion in mineral oil, 0.11 mol). After stirring for a further 1 h at 22°C the appropriate aminoalkyl chloride (0.15 mol) was added and the reaction refluxed for 18 h. Filtration and concentration *in vacuo* afforded the title compounds.

9[(2,3-Epoxy)propyloxy]-3,4-dihydro-3,3-dimethylfuro[3,4-b]quinoline ***24***

This compound was prepared as described above except that the intermediate sodium furo[3,4-*b*]quinolate (see Scheme 2) was obtained by the treatment of the furo[3,4-*b*]quinolone **12** with excess sodium hydride.

1-(1,3-Dihydro-3,3-dimethylfuro[3,4-b]quinolin-9-yloxy)-3-(isopropylamino)-2-propanol ***25***

A mixture consisting of the epoxide **24** (0.5 g, 0.0018 mol), isopropylamine (10 mL), and benzene (10 mL) in a pressure bottle was heated at 100°C for 18 h. Concentration *in vacuo* afforded the amine **25**, mp 132–135°C (cyclohexane).

1. C. A. Demerson, L. G. Humber, T. A. Dobson, and R. R. Martel. J. Med. Chem. **18**, 189 (1975).
2. C. A. Demerson, L. G. Humber, and A. H. Philipp. J. Med. Chem. **19**, 391 (1976).
3. L. G. Humber, C. A. Demerson, A. A. Asselin, M. P. Charest, and K. Pelz. Eur. J. Med. Chem. **10**, 215 (1975).
4. B. Witkop and S. Goodwin. J. Am. Chem. Soc. **75**, 337 (1953).
5. B. Witkop and J. Patrick. J. Am. Chem. Soc. **74**, 3855 (1952).
6. B. Witkop. J. Am. Chem. Soc. **72**, 1428 (1950).
7. B. Witkop and J. Patrick. J. Am. Chem. Soc. **73**, 2196 (1951).
8. L. J. Dolby and D. L. Booth. J. Am. Chem. Soc. **88**, 1049 (1966).
9. E. Winterfeldt. Justus Liebigs Ann. Chem. **745**, 23 (1971).
10. E. Tamate. Nippon Kagaku Zasshi, **78**, 1293 (1957); I. K. Korobitsyna, C. Yin, and Yu. K. Yurev. Zh. Obsch. Khim. **31**, 836 (1961); E. A. Fehnel, J. A. Deyrup, and M. B. Davidson. J. Org. Chem. **23**, 1996 (1958).
11. I. Vavra, H. Tom, and E. Greselin. Can. J. Physiol. Pharmacol. **51**, 727 (1973).

Solvent effects on the photocycloaddition and photoenolisation reactions of isophorone

JANICE DEBORAH SHILOFF AND NORMAN ROBERT HUNTER[1]

Department of Chemistry, University of Manitoba, Winnipeg, Man., Canada R3T 2N2

Received June 18, 1979

This paper is dedicated to Prof. Karel Wiesner on the occasion of his 60th birthday

JANICE DEBORAH SHILOFF and NORMAN ROBERT HUNTER. Can. J. Chem. **57**, 3301 (1979).

The influence of solvent on two photochemical reactions of isophorone has been investigated. The photocycloaddition of isopropenyl acetate to isophorone (3,5,5-trimethylcyclohex-2-en-1-one) (**1**) is best achieved using methanol as solvent. Photodeconjugation of isophorone (**1**) to the exocyclic methylene isomer **2** proceeds most efficiently in ethyl acetate.

JANICE DEBORAH SHILOFF et NORMAN ROBERT HUNTER. Can. J. Chem. **57**, 3301 (1979).

On a étudié l'influence du solvant sur deux réactions photochimiques de l'isophorone. La photocycloaddition de l'acétate d'isopropényle sur l'isophorone (triméthyl-3,5,5 cyclohexèn-2-one-1) (**1**) se produit plus facilement si on utilise le méthanol comme solvant. La photodéconjugaison de l'isophorone en l'isomère **2** possédant un méthylène exocyclique se produit avec un meilleur rendement lorsqu'on utilise l'acétate d'éthyle comme solvant.

[Traduit par le journal]

Introduction

In a recent review on the photocatalyzed enolisation process Sammes (1) indicated that the general utility of the photoisomerisation of α,β-unsaturated ketones to their β,γ-isomers is restricted by the many competing photoreactions which α,β-enones undergo. Earlier Dauben *et al.* (2) had reported the effects of alkyl substitution on the photochemistry of 2-cyclohexenones and summarized the known photodeconjugation reactions of β-alkyl α,β-cyclohexenones. More recently Chapman and Weiss (3) and Nakanishi and Sato (4) have provided short reviews on photodeconjugation of enones and Tada and Miura (5) reported on the photoenolisation of four β-methyl α,β-enones.

The only systematic investigation of the effect of solvent on the photodeconjugation reaction is Jennings' study of isophorone photochemistry (6). In that report Jennings indicated that solvent polarity played a very important role in the competition between isophorone photodimerisation and photodeconjugation. In very polar solvents the yield of dimer was highest and decreased to zero in very non-polar solvents. Jennings also reported that irradiation of isophorone (**1**) in heptane at −13°C gave a single, unstable, product which was proven by chemical and spectroscopic methods to be the deconjugated enone 3-methylidene-5,5-dimethylcyclohexanone (**2**) (Scheme 1) which probably arises via the transient enol.

Our interest in the photodeconjugation reaction was aroused when we repeated the photocycloaddition of isopropenyl acetate to isophorone according to the procedure of Valenta and Liu (7) (Scheme 2). In the literature procedure, a 0.5 *M* solution of isophorone in benzene was irradiated for four days in the presence of a 20-fold molar excess of isopropenyl acetate to give the photoadduct **3** which could not be distilled because of the presence of polymeric by-products.

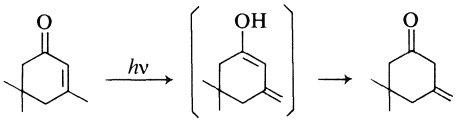

1 **2**

SCHEME 1

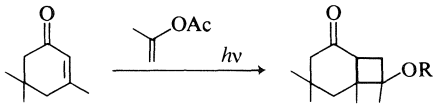

1

3 R = Ac
4 R = H

SCHEME 2

When we monitored this reaction by gas chromatography, we observed that one important competing reaction was the photodeconjugation of isophorone to the exomethylene compound **2**. Compound **2** slowly isomerized back to **1** on standing in the photolysis solution. It was our feeling that by a judicious choice of solvent, the yield of both the photodeconjugation and the photocycloaddition reactions could be substantially improved. The results of our investigation are described below.

Results and Discussion

At the outset of our investigation, we laid down

[1]To whom enquiries should be addressed.

0008-4042/79/243301-03$01.00/0

several criteria to be met for the two reaction types. Firstly, both reactions must proceed with complete selectivity on the basis of solvent change only. Secondly, both reactions should be amenable to scale-up and thirdly, the products must be readily isolable in high yield and purity. The small-scale reactions which were carried out to determine appropriate solvent choices are described in the Experimental.

The deconjugated enone **2** was prepared by irradiation of a 0.1 *M* solution of isophorone (**1**) in ethyl acetate. After 14 h of irradiation gc analysis indicated a greater than 95% conversion of **1** to **2**. Careful evaporation of the solvent yielded a colourless liquid which gave spectral data in agreement with that recorded by Jennings (6) for compound **2**. The ethyl acetate solution of **2** obtained after photolysis could be stored at 0°C for several weeks without appreciable reversion to **1**.[2]

We next turned our attention to the photocycloaddition of isopropenyl acetate to isophorone. Many of the earlier studies of photocycloaddition reactions (7–9) are characterized by the use of non-polar solvents and a large excess of alkene. In this study we have used methanol as solvent and only a four-fold excess of the alkene relative to isophorone. These modifications allow the preparation of photoadduct **3** in 71% yield after distillation. In order to effect comparison of this photoproduct with that reported (7), the ketoacetate **3** was hydrolyzed to the known ketoalcohol **4** (7) in 88% yield after distillation. Our procedure provides improvement over the literature procedure in terms of reaction time, ease of purification, and increased yield.

The dramatic effect of solvent in the course of isophorone photoreactions reported in this paper can be understood in terms of the reported dualistic nature of the triplets arising from enone photolysis (10) and the effect of solvent upon these triplet states (4). Our results indicate that many enone photoreactions may be profoundly affected by the appropriate choice of solvent.

Experimental

Infrared spectra were recorded with a Pye Unicam SP1000 infrared spectrometer using a neat film or in CCl_4 as solvent. Proton magnetic resonance spectra were recorded with a Varian EM-360 spectrometer using CCl_4 as solvent and tetramethylsilane as internal standard. Mass spectra were measured with a Finnigan-1015 quadrupole mass spectrometer. Gas chromatographic analyses were done on a 10% SE-30 column using an Hewlett-Packard 700 chromatograph with flame ionization detection.

All photoreactions were carried out using a Photochemical Research Associate PRA-R400 photoreactor after purging the solvent with dry N_2 gas. Solvents were used as obtained from commercial sources. Isopropenyl acetate was used as obtained from J. T. Baker Chemical Co. and isophorone (Aldrich Chemical Co. Inc.) was distilled prior to use.

Small-scale Reactions

The small-scale reactions were set up in Pyrex test-tubes in a "merry-go-round" assembly using a 0.25 *M* solution of isophorone (0.35 g per 10 mL of solvent) and a 1.0 *M* solution of isopropenyl acetate (1.0 g per 10 mL of solvent) for each of the solvents studied. The reactions were monitored at two hour intervals by gas chromatography. All the photoadducts have longer reaction times than isophorone while the deconjugated isomer **2** had a shorter retention time. In methanol as solvent, exclusive photoadduct formation was observed. In ethyl acetate, exclusive deconjugation was observed. Benzene and hexane gave mixtures of deconjugation and cycloaddition products as well as extensive polymerization of isopropenyl acetate.

3-Methylidene-5,5-dimethylcyclohexane (2)

Isophorone (4.50 mL, 4.15 g, 0.03 mol) in ethyl acetate (300 mL) was irradiated through a Pyrex filter in a PRA-R400 photoreactor for 14 h at which time gc indicated greater than 95% conversion of isophorone into the deconjugated isomer **2**. Careful evaporation of a 10 mL aliquot of the ethyl acetate solution, at less than 30°C, gave a clear colourless liquid (0.135 g, 98% of theoretical) which had the following spectral data: mass spectrum, $C_9H_{14}O$ requires *m/e* 138; *m/e* found: 138 (fragmentation pattern identical to isophorone); infrared (neat): 1720 ($\rangle C{=}O$) and 1640 ($\rangle C{=}CH_2$) cm^{-1}; ^{1}Hmr indicated that the sample contained less than 10% isophorone. The ^{1}Hmr peaks due to **2** are δ: 4.75 (2H, bs, $\rangle C{=}CH_2$), 2.93 (2H, bs, H's on C-2), 2.15 (2H, bs), and 2.27 (2H, bs) due to H's on C-4 and C-6, and 0.98 (6H, sharp singlet, CH_3's on C-5). The ^{1}Hmr spectrum was in agreement with the spectrum published in the literature (6).

7-Acetoxy-4,4,6,7-tetramethylbicyclo[4.2.0]octan-2-one (3)

The PRA-R400 photoreactor, equipped with a Pyrex filter system, was charged with isophorone (10.0 g, 0.072 mol, 0.24 *M*), 300 mL of methanol, and isopropenyl acetate (30.0 g, 0.30 mol) and cooled in an ice-water bath. After 6.5 h of irradiation gc analysis indicated essentially total consumption of the isophorone, no deconjugation, and no polymerization of the isopropenyl acetate. The reaction was worked up by evaporation of the solvent and unconsumed isopropenyl acetate followed by addition of 100 mL of toluene and evaporation of the toluene to give the crude product (16.27 g, 0.068 mol, 94%). The crude product was distilled at 1.5 Torr in a Kugelrohr (130°C air bath temperature) to yield, as the major fraction collected, 12.21 g (0.051 mol, 70.8%) of pure **3** as a mixture of diastereomers. Mass spectrum for $C_{14}H_{22}O_3$ requires *m/e* 238; *m/e* found: 238 (M^+), 196 (loss of $CH_2{=}C{=}O$), base peak 43 ($CH_3{-}C{\equiv}O^+$). Infrared (CCl_4): 1705 ($\rangle C{=}O$) and 1730 ($CH_3{-}\underset{\underset{O}{\|}}{C}{-}O{-}$) cm^{-1}; ^{1}Hmr: complex absorption pattern showing acetate methyl peaks at 1.93 and 1.97 δ and saturated methyl singlets (eight peaks) in the region 0.87 to 1.30 δ.

7-Hydroxy-4,4,6,7-tetramethylbicyclo[4.2.0]octane-2-one (4)

7-Acetoxy-4,4,6,7-tetramethylbicyclo[4.2.0]octan-2-one (11.90 g, 0.05 mol) was dissolved in methanol (125 mL) with

[2]This process affords, for the first time, a ready source of **2** for further chemical studies. The results of these studies, as well as kinetic studies of the photodeconjugation reaction, will be reported in a future communication.

slight warming on the steambath. After the solution had cooled to ambient temperature, anhydrous potassium carbonate (20.7 g, 0.15 mol) was added. The resulting mixture was stirred for 6 h and then worked up by pouring into 300 mL of H_2O and extracting the organic product with methylene chloride (3 × 75 mL). The organic extracts were washed with water (2 × 50 mL), dried, and evaporated. The resulting oil was distilled at 1.2 Torr in a Kugelrohr (120–140°C air bath temperature) to give the keto alcohol **4** (8.62 g, 0.044 mol, 88%). Mass spectrum for $C_{12}H_{20}O_2$ requires *m/e* 196; *m/e* found: 196. Infrared (neat): 3450 (OH) and 1700 ($\diagdown\!\!\diagup$C=O) cm^{-1}; ^{1}Hmr (CCl_4): complex pattern showing OH absorption at 3.98 δ and at least five methyl singlets in the region 0.9 to 1.23 δ.

Acknowledgments

The financial assistance of the Natural Sciences and Engineering Research Council of Canada and the Research Board, University of Manitoba, is gratefully acknowledged.

1. P. G. SAMMES. Tetrahedron, **32**, 405 (1976).
2. W. G. DAUBEN, G. W. SHAFFER, and N. D. VIETMEYER. J. Org. Chem. **33**, 4060 (1968).
3. O. L. CHAPMAN and D. S. WEISS. Organic photochemistry. Vol. 3. *Edited by* O. L. Chapman. Marcel Dekker, Inc., New York, NY. 1973. Chapt. 3.
4. K. NAKANISHI and H. SATO. Natural products chemistry. Vol. 2. *Edited by* K. Nakanishi, T. Goto, S. Itô, S. Natori, and S. Noyoe. Kodanska Ltd., Tokyo. Academic Press, Inc., New York, NY. 1975. Chapt. 12.
5. M. TADA and K. MIURA. Bull. Chem. Soc. Jpn. **49**, 713 (1976).
6. P. W. JENNINGS. Ph.D. Dissertation, University of Utah. 1965; Diss. Abstr. **26**, 698 (1965).
7. Z. VALENTA and H.-J. LIU. Org. Synth. **57**, 113 (1977).
8. N. R. HUNTER, G. A. MACALPINE, H.-J. LIU, and Z. VALENTA. Can. J. Chem. **48**, 1436 (1970).
9. P. G. BAUSLAUGH. Synthesis, 287 (1970) and references quoted therein.
10. T. TEZUKA. Tetrahedron Lett. 5677 (1968).

Claisen rearrangement of allyloxyanthraquinones

C. M. WONG, R. SINGH, AND K. SINGH

Department of Chemistry, University of Manitoba, Winnipeg, Man., Canada R3T 2N2

AND

H. Y. P. LAM

Manitoba Institute of Cell Biology, Winnipeg, Man., Canada R3E 0V9

Received July 3, 1979

This paper is dedicated to Prof. Karel Wiesner on the occasion of his 60th birthday

C. M. WONG, R. SINGH, K. SINGH, and H. Y. P. LAM. Can. J. Chem. **57**, 3304 (1979).

Allyloxyanthraquinones showed unusual behaviour during the Claisen rearrangement. Thus, 1-allyloxyanthraquinone **9** rearranged very readily in the presence of benzylamine while 2-allyloxyanthraquinone **13** refused to do rearrangement even under very drastic conditions. On the other hand, 1,2-diallyloxyanthraquinone rearranged with the loss of the 2-allyloxy group as the result of a retro-ene reaction which has not been previously observed[1] while 1,4-di(2′-chloro-2′-propenyloxy)anthraquinone **18** rearranged to give, as a major product, the unsymmetrically substituted anthraquinone **19** which is useful in the synthesis of anthracycline aglycones.

C. M. WONG, R. SINGH, K. SINGH et H. Y. P. LAM. Can. J. Chem. **57**, 3304 (1979).

Les allyloxyanthraquinones ont un comportement inhabituel pendant la transposition de Claisen. Alors que l'allyloxy-1 anthraquinone **9** se transforme très facilement en présence de la benzylamine, l'allyloxy-2 anthraquinone **13** au contraire est réfractaire, même dans des conditions très drastiques. D'un autre côté, la diallyloxy-1,2 anthraquinone se transpose en perdant le groupement allyle en position 2; c'est le résultat d'une réaction ène-rétro qui n'a pas été observée antérieurement,[1] tandis que la di(chloro-2′ propényloxy-2′)-1,4 anthraquinone **18** se transpose pour donner comme produit principal l'anthraquinone **19** substituée d'une façon non symétrique et qui est utile à la synthèse des aglycones anthracyclines.

[Traduit par le journal]

Introduction

The Claisen rearrangement of aryl allyl ethers, generally known as a form of [3,3]-sigmatropic rearrangement, can be used synthetically as a substitute for the Fries rearrangement or Friedel–Crafts reaction for functionalizing an aromatic ring, including deactivated ring systems. Information concerning the mechanistic studies, yields of ortho- and para-rearrangement products, effects of the solvent polarity, and the use of bases as catalysts have been compiled and discussed by Rhoads and Paulins (1). Its exploitation in natural product synthesis was also reviewed in a recent article by Ziegler (2). Furthermore, the use of transition metal salts and acidic solvents as catalysts, and acid anhydrides as trapping agents, has been reported to show favorable results in some isolated cases of Claisen rearrangement (2–6). However, not much work has been reported on anthraquinone systems, except some short publications such as those by Kende *et al.* (7*a*), Roberts and Rutledge (7*b*), and Sheinmann and co-workers (7*c*), which prompted us to report our results in this area of studies.

In connection with our synthetic and structure–activity relationship studies of antitumor anthracyclines (8) such as 4-demethoxydaunomycin (**1**), adriamycin (**2**), daunomycin (**3**), and carminomycin (**4**), an unsymmetrically functionalized anthraquinone such as **22** would be of great interest as an intermediate for the construction of the tetracyclic aglycones of **1**, **2**, **3**, **4**, and other rhodomycinones (9). Conversion of **22** to **5** followed by Michael addition and Claisen condensation between **5** and methyl vinyl ketones **6** could furnish the tetracyclic compound **7** in a one step process.

Another aspect in our design of this group of antibiotics is to select an inexpensive starting material and convert it in a simple way to a potentially useful intermediate such as **5**. The ready availability of the very inexpensive quinizarin (**8**) makes it attractive although many attempts to functionalize its phenolic ring properly by Friedel–Crafts or Reimer–Tiemann type reactions were un-

[1]This result was reported as part of the author's presentation to the symposium of anthracycline antitumor antibiotics at the 61st conference of the Chemical Institute of Canada, Winnipeg, Man., June, 1978. A similar result was also reported by Scheinmann and co-workers (7*c*).

0008-4042/79/243304-04$01.00/0

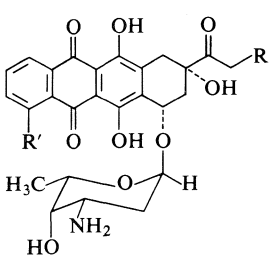

1 R = R′ = H
2 R = OH, R′ = OCH_3
3 R = H, R′ = OCH_3
4 R = H, R′ = OH

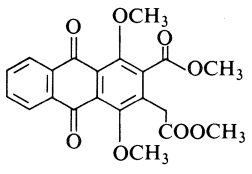

5

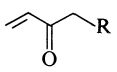

6 R = H, or $-OCH_2C_6H_5$

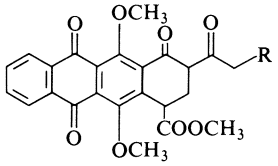

7 R = H, or $-OCH_2C_6H_5$

successful or unsatisfactory. This paper reports some of our studies on the Claisen rearrangement of anthraquinones with structures similar to that of **8**.

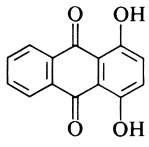

8

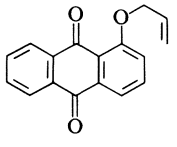

9

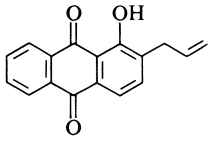

10

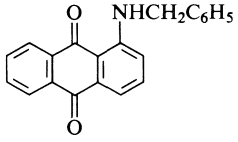

11

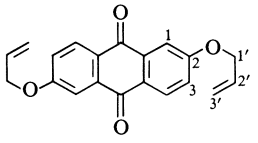

12

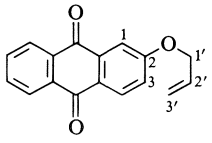

13

Results and Discussion

When 1-allyloxyanthraquinone (**9**) was heated in a sealed tube immersed in an 180°C oil bath for 12 h, 1-hydroxy-2-allylanthraquinone (**10**) was isolated in about 70% yield. However, when the rearrangement was carried out in *o*-xylene solution containing 5% of benzylamine in a 150°C oil bath for 4 h, **10** was isolated in 88% yield together with a trace of 1-(*N*-benzylamino)anthraquinone (**11**) which became the only product (4% yield) when the *o*-xylene solution was heated at 105°C for 72 h. In the absence of benzylamine, less than 10% of **10** was isolated after 120 h of heating at 150°C. Other reagents such as *N*,*N*-dimethylaniline, acid anhydrides, and titanium chloride (3–6) gave inferior yields or isomerization of the allyl double bond or decomposition of both products and starting material. It is evident that benzylamine is a superior basic catalyst in the Claisen rearrangement of simple allyloxyanthraquinones. However, when 2,6-diallyloxyanthraquinone (**12**) or 2-allyloxyanthraquinone (**13**) was heated in 1,2,4-trimethylbenzene in a sealed tube for as long as 96 h, in the presence of a variety of catalysts and with temperatures up to 240°C, no rearrangement was observed.

Kinetics and the stereochemistry requirement of Claisen rearrangement have been quite thoroughly studied and a negative entropy has been proposed as a reflection of the high degree of order in the transition state which favors the chairlike transition over the boatlike transition (2). Furthermore, selective migration of the allyl group has been reported. Thus, 2-allyloxynaphthalene gave only 1-allyl-2-hydroxynaphthol, while 2-allyloxyphenanthrene gave only 1-allyl-2-hydroxyphenanthrene and 3-allyloxyphenanthrene gave only 4-allyl-3-hydroxyphenanthrene (10). The rationale for such specificity is the localization of the double bonds in the aromatic nucleus during the transition state, in the form having, in the case of 2-allyloxynaphthalene, the double bond at C1—C2 positions and in the case of 2-allyloxyphenanthrene and 3-allyloxyphenanthrene, the double bonds at C1—C2, C3—C4 positions, respectively.

However, no Claisen rearrangement of 2-allyloxyanthraquinone or similar compounds has been reported and our finding indicated that such a system is extremely resistant to rearrangement. Explanation in terms of the stereochemistry requirement and localization of double bonds as in the cases of 2-allyloxynaphthalene and 2-allyloxyphenanthrene is unsatisfactory because there is no obvious interference with the formation of the chairlike transition nor is there any severe steric interaction that completely retards the rearrangement. Furthermore, localization of double bonds of anthraquinones should allow 2-allyloxyanthraquinone to form 1-allyl-2-hydroxyanthraquinone. Thus, it is very likely that the great reluctance is due to the electronic effect of the quinone structure. Although this kind of electronic effect has not been indicated as a decisive factor in sigmatropic rearrangement, its influence can be seen easily in the case of an *endo* versus *exo*- $\pi^4s + \pi^2s$ cycloaddition process involving quinone or other dienophiles.

Considering the C2 and C3 positions of anthraquinone as equally electron-deficient, it is discernible that the C2 of **9**, being electron deficient, can easily overlap with the C3, π orbital. On the other hand, the C1 position of **12** or **13**, having higher electronic density than the C2 of **9**, will be less ready to overlap with the C3, π orbital. Furthermore, the contribution of the C2=$\overset{+}{O}$—$^{-2}$ resonance form of **12** or **13** will definitely shorten the C1′—O bonds as compared to the corresponding C1′—O bond of **9** making the

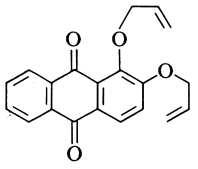

14

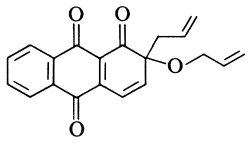

15

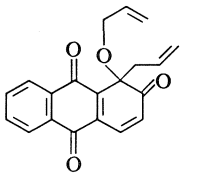

16

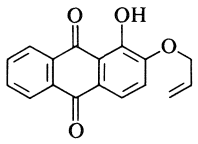

17

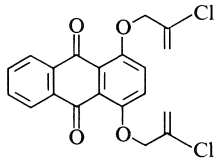

18

former bonds stronger and more resistant to the rearrangement.

It is possible that there could be other factors influencing the rearrangement process. The explanation advanced above can account for, at least in part, the great reluctance of 2-allyloxyanthraquinone and its analogues toward the concerted [3,3]-sigmatropic rearrangement.

To look further into the inert nature of the 2-allyloxyanthraquinone, 1,2-diallyloxyanthraquinone (**14**) was heated in *o*-xylene solution containing 5% benzylamine with the hope that the dienone **15** or **16** could be isolated. Instead, the only major identifiable product in about 40% yield was 1-hydroxy-2-allylanthraquinone (**10**) plus a trace of 1-hydroxy-2-allyloxyanthraquinone (**17**). A similar result was obtained when the reaction was carried out in the absence of benzylamine.

The formation of **10** could only be explained if **15** instead of **16** was formed as a product of [3,3]-sigmatropic rearrangement followed by a retro-ene process (Eq. [1]).

[1]

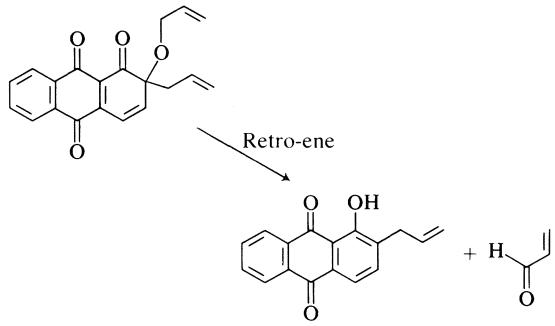

Further investigation of sigmatropic rearrangement on anthraquinones revealed some practical applications toward the preparation of **5** which would be an important intermediate to anthracyclines starting from the inexpensive quinizarin **8**.

When 1,4-di(2′-chloro-2′-propenyloxy) anthraquinone (**18**) was refluxed for 60 h in *o*-xylene solution containing 10% *N*,*N*-dimethylbenzylamine, the major product, isolated in 40% yield, was the unsymmetrically functionalized anthraquinone **19**. The other major products were the pentacyclic compound **20** in about 15% yield and the uncyclized anthraquinone **21** in about 5% yield. Isomerization of the chloropropenyl groups under this condition was negligible.

The formation of **19** enables the differentiation of two identical groups which can be easily introduced

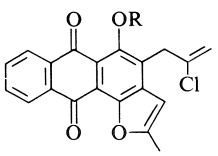

19 R = H
22 R = CH_3

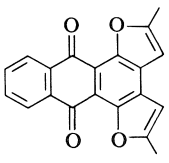

20

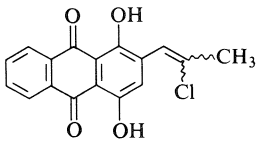

21

unsymmetrically into a deactivated aromatic system. The successful conversion of the methyl ether **22** to **5** via ozonolysis and the development of **5** into tetracyclic aglycones of anthracycline antitumor antibiotics are in progress and will be reported later.

Experimental

All infrared spectra (cm^{-1}) were recorded on a Perkin-Elmer infrared 710A spectrophotometer using methylene chloride as solvent. Nuclear magnetic resonance spectra (δ) were recorded on a Varian A56/60A MHz spectrometer using deuterated chloroform as solvent and tetramethylsilane as internal standard. Mass spectra were recorded on a Finnigan Model 1015 mass spectrometer. High resolution mass spectra

2. 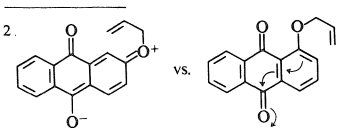

were recorded on an A.E.I. MS9 spectrometer. Melting points were measured on a Fisher-Johns apparatus and were uncorrected. Microanalyses were performed by Dr. Daessle of Montreal.

*Preparation of 1-Allyloxyanthraquinone (**9**)*

An acetone solution (300 mL) containing 1-hydroxyanthraquinone (5 g), pulverized potassium carbonate (15 g), and allyl bromide (8 mL) was refluxed for 24 h with vigorous stirring under anhydrous conditions. The acetone solution was cooled, filtered, and evaporated to dryness under reduced pressure and the residue was redissolved in chloroform (150 mL). The insoluble potassium carbonate residue was removed by filtration and the chloroform solution was evaporated to dryness under reduced pressure to give a solid yellow residue which was purified by recrystallization from chloroform–ether, mp 138–140°C; ir: 1675, 1592; nmr: 4.75 (t of d, 2H, J = 4 Hz and 15 Hz, —O—CH_2—CH=CH_2), 5.39 (m, 1H, CH=CH_2), 5.65 (m, 1H, —CH=CH_2), 6.22 (m, 1H, —O—CH_2—CH=CH_2). Mass spectrum m/e^+: 264.

*Preparation of 2-Allyl-1-hydroxyanthraquinone (**10**)*

An *o*-xylene solution (50 mL) containing 5% benzylamine and 1-allyloxyanthraquinone (3.7 g) (**9**) was heated under a nitrogen atmosphere in an oil bath at 145–150°C for 4 h with stirring. The *o*-xylene solution was evaporated under reduced pressure and the semi-solid residue was crystallized from ether to give, after filtration, a yellow crystalline product (3.3 g), mp 114–116°C; ir: 1670 (ketone), 1635 (hydrogen bonded ketone), 1595 (aromatic); nmr: 12.90 (s, 1H, —OH), 8.40–7.20 (m, 6H's, aromatic), 6.70–5.50 (m, 3H's, —CH=CH_2), 3.50 (d, 2H's, allylic H's). *Anal.* calcd. for $C_{17}H_{12}O_3$: C 77.27, H 4.55; found: C 77.12, H 4.32.

*The Preparation and Sigmatropic Rearrangement of 1,2-Diallyloxyanthraquinone (**14**)*

1,2-Diallyloxyanthraquinone (**14**) was prepared from the corresponding 1,2-dihydroxyanthraquinone under similar conditions to those described for the preparation of **9** and was purified by recrystallization from chloroform–ether, mp 114–116°C; ir: 1670, 1590; nmr: 4.64 (d, 4H, —O—CH_2—CH=CH_2), 5.20–6.70 (m, 6H, —CH=CH_2), 7.10–8.40 (m, 6H's, aromatic); mass spectrum m/e^+: 320.

An *o*-xylene solution (50 mL) containing the 1,2-diallyloxyanthraquinone (**14**) was refluxed under a nitrogen atmosphere for 96 h. The dark brown solution was evaporated to dryness under reduced pressure and the residue was separated by preparative tlc on silica. The major product in about 38% yield was isolated and characterized as 1-hydroxy-2-allylanthraquinone (**10**).

*Preparation of 1,4-Di-(2′-chloro-2′-propenyloxy)anthraquinone (**18**)*

An acetone solution (1 L) containing quinizzarin (24 g), pulverized potassium carbonate (50 g) and potassium iodide (5 g), and 2,3-dichloro-1-propene (44 g) was refluxed for 56 h or until the colour of the solution changed from blue to orange. The cooled solution was filtered and then evaporated to dryness under reduced pressure and the residue was dissolved in chloroform (1 L) which was filtered once more to remove the small amount of potassium carbonate residue. Evaporation of the chloroform solution to dryness under reduced pressure gave the 1,4-di(2′-chloro-2′-propenyloxy)anthraquinone (**18**) (20.4 g) which could be purified by recrystallization from chloroform–ether, mp 145–147°C; ir: 1670 (ketone), 1630 (allyl), 1595 and 1585 (aromatic); nmr: 4.65 (broad s, 4H, allylic H), 5.50 (m, 2H, CCl=CH(E)), 5.92 (m, 2H, CCl=CH(Z)), 7.20–8.40 (m, 6H, aromatic); mass spectrum m/e^+: 388.

*Preparation of 2-Methyl-5-(2′-chloro-2′-propenyl)-6-hydroxyfura(a)anthraquinone (**19**), 2,7-Dimethyldifura(a,c)anthraquinone (**20**), and 1,4-Dihydroxy-2,3-di(2′-chloro-2′-propenyl)anthraquinone (**21**)*

An *o*-xylene solution (200 mL) containing 10% of *N*,*N*-dimethylbenzylamine and 1,4-di-(2′-chloro-2′-propenyloxy)-anthraquinone (15 g) was refluxed for 60 h in an oil bath kept at 170°C under a nitrogen atmosphere which was maintained by fitting a nitrogen balloon over the condenser. The xylene solution was evaporated to dryness under reduced pressure and the residue was redissolved in chloroform (300 mL). The chloroform solution was filtered to remove the *N*,*N*-dimethylbenzylamine hydrochloride. The filtrate was washed with 0.1 *N* hydrochloric acid (2 × 100 mL), dried over anhydrous magnesium sulfate, and was evaporated to dryness under reduced pressure. The products were separated by pressurized (15 lb/in^2) column chromatography over DSF-5 Kieselgel (Camag, Switzerland) with chloroform as eluting solvent.

Fractions that contained 1,4-dihydroxy-2,3-di(2′-chloro-1′-propenyl)anthraquinone (**21**) were combined and evaporated to dryness. Recrystallization of the residue from chloroform gave **21** as red crystals (800 mg), mp 176–178°C; ir: 3600–2800 (broad), 1630, 1595; nmr: 2.42 (d, 3H, J = 1Hz, C=CHClCH_3), 6.89 (q, 1H, J = 1 Hz, HC=CClCH$_3$), 7.74–8.5 (m, 5H, aromatic), 12.9 (s, 1H, —OH), 13.60 (s, 1H, —OH). Mass spectrum m/e^+: 314.

2-Methyl-5-(2′-chloro-2′-propenyl)-6-hydroxy fura(*a*)-anthraquinone (**19**) was isolated as above and was crystallized from chloroform–ether to give yellow crystals (5.8 g), mp 194.5–196°C; ir: 3600–2800 (broad), 1680, 1640, 1605; nmr: 2.58 (s, 3H, C=C—CH_3), 3.90 (s, 2H, benzylic), 5.08–5.24 (m, 2H, Cl—C=CH_2), 6.46 (broad s, 1H, Ph—CH=C), 7.55–8.40 (m, 4H, aromatic); high resolution mass spectrum, m/e^+ calcd. for $C_{20}H_{13}O_4Cl$: 352.0499; found: 352.0501. *Anal.* calcd. for $C_{21}H_{15}O_4Cl$ (methyl ether): C 68.85, H 4.13, Cl 9.56; found: C 68.86, H 4.27, Cl 9.36.

Similarly, 2,7-dimethyl difura(*a.c*)anthraquinone (**20**) was isolated from the eluent as yellow crystals (2.0 g) after recrystallization from chloroform–ether, mp 295°C (dec); ir: 1670, 1570; nmr: 2.65 (d, 6H, J = 1.5 Hz, C=C—CH_3), 5.80 (m, 2H, C=CH), 7.60–8.40 (m, 4H, aromatic); mass spectrum m/e^+: 316.

1. S. J. Rhoads and N. R. Raulins. Organic reactions. Vol. 22. *Edited by* W. G. Dauben. John Wiley and Son, New York, NY. 1975. p. 1.
2. E. Ziegler. Acc. Chem. Res. **10**, 227 (1977).
3. H. F. Stewart and R. P. Seibert. J. Org. Chem. **33**, 4560 (1968).
4. K. Narasaka, E. Bald, and T. Mukaiyama. Chem. Lett. Jpn. 1041 (1975).
5. U. Svanholm and V. D. Parker. J. Chem. Soc. Perkin Trans. II, 169 (1974).
6. D. S. Karanewsky and Y. Kishi. J. Org. Chem. **41**, 3026 (1976).
7. (*a*) A. S. Kende, J. L. Belletire, and E. L. Hume. Tetrahedron Lett. **31**, 2935 (1973); (*b*) J. L. Roberts and P. S. Rutledge. Aust. J. Chem. **30**, 1743 (1977); (*c*) K. A. Bell, I. J. Flatman, P. Golborn, A. Pachl, and F. Scheinmann. J. Chem. Soc. Chem. Commun. 900 (1978).
8. (*a*) C. M. Wong, D. Popien, R. Schwenk, and J. TeRaa. Can. J. Chem. **49**, 2712 (1971); (*b*) C. M. Wong, R. Schwenk, D. Popien, and T. L. Ho. Can. J. Chem. **51**, 466 (1973).
9. H. Brockmann, H. Brockmann, Jr., and J. Niemeyer. Tetrahedron Lett. 4719 (1968).
10. S. Marcinkiewicz, J. Green, and P. Mamalis. Tetrahedron, **14**, 208 (1961).

Total synthesis of steroids. Part 1. Ring A aromatic compounds. Regiocontrol in diene additions with 6-methoxy-1-vinyl-3,4-dihydronaphthalene

JAGABANDHU DAS, RUDOLF KUBELA, GERALD A. MACALPINE, ŽARKO STOJANAC, AND ZDENEK VALENTA

Department of Chemistry, University of New Brunswick, Fredericton, N.B., Canada E3B 5A3

Received July 13, 1979

This paper is dedicated to Prof. Karel Wiesner on the occasion of his 60th birthday

JAGABANDHU DAS, RUDOLF KUBELA, GERALD, A MACALPINE, ŽARKO STOJANAC, and ZDENEK VALENTA. Can. J. Chem. **57**, 3308 (1979).

A total synthesis of ring A aromatic *D*-homosteroids and the conversion of one of them to estrone and its derivatives are described. The key reaction is a catalysed addition of 6-methoxy-1-vinyl-3,4-dihydronaphthalene to 2,6-dimethyl-1,4-quinone which proceeds with orientation inversion compared to the thermal addition. Reactions with several other quinones are described. The synthetic sequence includes a hydride reduction in which an apparently more hindered carbonyl group of an enedione system is reduced preferentially. Cyclization of a 1,6-keto aldehyde under acidic conditions gives the desired acetyl cyclopentene derivative, while a predominant formation of cycloheptenones is observed when the same cyclization is performed with base.

JAGABANDHU DAS, RUDOLF KUBELA, GERALD A. MACALPINE, ŽARKO STOJANAC et ZDENEK VALENTA. Can. J. Chem. **57**, 3308 (1979).

On décrit une synthèse totale de stérodides *D*-homo dont le cycle A est aromatique ainsi que la transformation de l'un d'entre eux en estrone et en ses dérivés. La réaction fondamentale consiste en une addition catalysée du méthoxy-6 vinyl-1 dihydro-3,4 naphtalène sur la diméthyl-2,6 quinone-1,4 et dont l'orientation est l'inverse de celle d'une addition thermique. On décrit également des réactions impliquant plusieurs autres quinones. La série de réactions comprend entre autres une réduction par un hydrure où apparemment le groupe carbonyle le plus encombré d'un système ènedione est réduit préférentiellement. La cyclisation du cétoaldéhyde-1,6 en milieu acide conduit au dérivé acétylcyclopentène désiré; mais en milieu basique la même réaction permet d'obtenir des cyclohepténones comme produit principal.

[Traduit par le journal]

Introduction

Since the first reported total synthesis of a steroid, that of equilenin in 1939 (1), the development and refinement of synthetic strategies involved in the efficient preparation of more complex steroids[1] has contributed significantly to the increasing sophistication of organic synthesis. In the 1940's and 1950's, the total synthesis of any steroid with three or more chiral centers presented a major challenge and this was taken up by some of the leading laboratories in the world. As a consequence of their pioneering and successful development of new synthetic tools and of new methods required to achieve regio- and stereocontrol, even relatively complex steroids are reasonably accessible by total synthesis in the 1970's.

There are, however, at least two important reasons why studies of steroid total synthesis should continue. Because of the varied and important biological activities of steroids, it is of interest to prepare new compounds in order to find new biological agents. For this purpose, total synthesis is often more versatile than a partial synthesis. The second reason concerns synthetic strategy. In spite of the dramatic developments during the past forty years, the efficiency of the synthetic pathways can still be greatly improved. This can lead, at the same time, to the discovery of new general strategies or to the refinement of known methods.[2]

In this and subsequent articles, we wish to report on our study of several years belonging to the second category. The general scheme for a synthesis of steroids shown in Fig. 1 not only has, as its crucial step, a reaction already observed (as a dimerization) eighty-two years ago by Ipatief (4) and elaborated into a synthetically useful form by Diels and Alder in 1928 (5), but involves a general strategy, the elaboration of steroid ring C by a Diels–Alder reaction, proposed soon after this reaction was discovered and attempted many times since (6). However, the scheme did not work efficiently because the regio- and stereochemistry of the addition was not controlled.

Apart from this problem, this approach has the

[1]For comprehensive reviews of steroid total synthesis, see ref. 2.

[2]For some recent examples in these two categories, see ref. 3.

0008-4042/79/243308-12$01.00/0

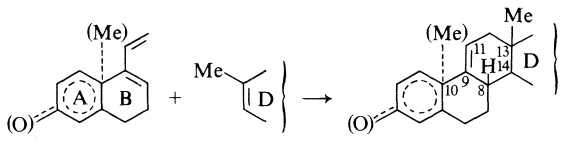

FIG. 1. General scheme for steroid synthesis.

following synthetic advantages. (*1*) Many required AB dienes should be readily available by synthesis. (*2*) A large number of relatively simple dienophiles, with or without preformed ring D, should be suitable. (*3*) The method should work for ring A aromatic as well as for C(10)-methylated steroids. (*4*) The C(9)—C(11) double-bond, useful for the introduction of important C(11)-functionality, is formed automatically. (*5*) The required *cis* relationship of C(8)—H and C(13)—CH_3 is established in an addition in which the potential ring D atoms lie *endo* (7) (i.e., the C(13)-methyl group is *exo*). With a suitable functionality in ring D, it should subsequently be possible to establish either stereochemistry at C(14). (*6*) For C(10)-methylated steroids, the desired *cis* relationship of the methyl groups at C(10) and C(13) would be a consequence of a preferred addition of the dienophile from the direction *anti* to the C(10)-methyl group of the diene.

This paper deals with the preparation of ring A aromatic *D*-homosteroids in which 1,4-quinones are used as dienophiles. One of the adducts is then converted into estrone and its derivatives. Subsequent papers describe the solution of stereochemistry in the synthesis of C(10)-methylated steroids, the synthesis of progesterone derivatives, and the use of simpler (non-quinonoid) dienophiles. In this progression, an increasing understanding of the addition has permitted an approach to more complex steroids by a series of synthetic pathways of improving efficiency.

Diels–Alder Additions

Readily available (8) diene **1** is the starting material suitable for the synthesis of ring A aromatic steroids by the method shown in Fig. 1. Previous studies indicated that mixtures of regioisomers, often in relatively poor yield, are obtained in additions of **1** to such a priori suitable dienophiles as citraconic anhydride (**15**) (9) and various cyclopentenones (6). In the absence, at the initiation of our work, of any simple dienophiles whose addition could be reliably controlled, we decided to use suitably substituted quinones (10, 11).

Table 1 summarizes the results of thermal and catalysed additions. Reaction of 2,6-dimethyl-1,4-benzoquinone (**2**) with diene **1** in boiling benzene gives a good yield of adduct **3**. No trace of the regioisomer **4** could be found in crystallization mother-liquors. In contrast, the same addition in ether with 1.3 mol equivalents of boron trifluoride etherate at −15°C gives adduct **3** in 10–15% yield and the desired adduct **4** in 69% yield (11). Since diene **1** alone is very unstable under acidic conditions, the good yield of the addition testifies to the high rate of the catalysed reaction (12). Structures of **3** and **4** were proven in the following simple way. The two compounds gave the corresponding (and different) C(8)—C(9) double-bond isomers **16** on treatment with acid. Compound **16** obtained from **4** instantaneously gave a dark purple color in alcoholic solution after addition of sodium hydroxide, indicating the extended chromophore **17**. A similar treatment of **16** obtained from **3** led to no chromophore change. Treatment of adduct **4** with sodium bicarbonate in boiling methanol gave a 94% yield of the desired isomer **18**.[3] In contrast, compound **3** proved stable to these (and stronger) basic conditions. As expected, the *syn-cis* isomer is thus converted into the more stable *anti–trans* isomer **18** in the case of adduct **4**, while the *syn–cis* isomer is more stable than the *syn–trans* isomer in the case of adduct **3**.

The complete stereochemistry of adduct **4** and its isomer **18** also follows rigorously from their conversion into estrone described below. It should be noted that only *endo* adducts (quinone ring *endo* to the diene) are obtained. This is reasonable since a greater effect by secondary attractive interactions (13) can be expected with quinones. During our extensive study of thermal and catalysed additions of quinones, described in this and subsequent publications, we have not encountered a single case in which the *exo*-product is formed even in minor quantities. This clearly constitutes an additional synthetic advantage in the use of quinones as dienophiles.

While the preparation of **18** was sufficient for the completion of the planned steroid synthesis, it was decided to explore the observed and unusual orientation reversal further. The addition of 2,5-dimethyl-1,4-benzoquinone (**5**) to **1** under thermal conditions also leads to the exclusive formation of the *endo*-"ortho"-adduct **6**, while the catalyst again reverses orientation, giving the "meta"-adduct **7** as the major product.[4] As shown in Table 1, three addi-

[3]Its structure is supported by the 220 MHz nmr spectrum in which the C(14)—H atom appears as a clean doublet (J = 18 Hz) at δ 2.63. The assignment of this signal was confirmed by a base catalysed deuterium exchange.

[4]Throughout, the term "ortho" is used for compounds in which the angular substituent (methyl, acetyl, or methoxycarbonyl) is at C(14) (steroid numbering) and thus next to the ring B methylene group. This substituent is at C(13) in the "meta"-adducts.

TABLE 1. Thermal and catalysed additions of diene **1** to quinones

Dienophile	Catalyst	Solvent	Temperature	Time	Total yield (%)	"Ortho"-adduct[4] (% of total yield)	"Meta"-adduct[4] (% of total yield)
2	—	C_6H_6	Boiling	24 h	82	100 (**3**)	0 (**4**)[a]
2	$BF_3 \cdot Et_2O$ (1.3 mol equiv.)	Et_2O	−15°C	30 min	80	14 (**3**)	86 (**4**)[a]
5	—	C_6H_6	Boiling	15 h	64	100 (**6**)	0 (**7**)[a]
5	$BF_3 \cdot Et_2O$ (1.05 mol equiv.)	Et_2O	0°C	25 min	52	24 (**6**)	76 (**7**)[a]
8	—	C_6H_6	20°C	30 min	>90	88 (**9**)	12 (**10**)[b]
8	—	C_6H_6	Boiling	3 min	>90	83 (**9**)	17 (**10**)[b]
8	$AlCl_3$ (1.05 mol equiv.)	CH_2Cl_2	−78°C	20 min	>90	25 (**9**)	75 (**10**)[b]
11	—	Et_2O	−20 to +20°C	3 h	88	100 (**12**)	0[a]
13	—	C_6H_6	Boiling	15 h	48	100 (**14**)	0[a]
13	$BF_3 \cdot Et_2O$ (2.1 mol equiv.)	Et_2O	0°C	20 min	31	100 (**14**)	0[a]

[a]Yields and ratios determined by product isolation.
[b]Yields and ratios determined by comparison of nmr spectra of crude and analytically pure products.

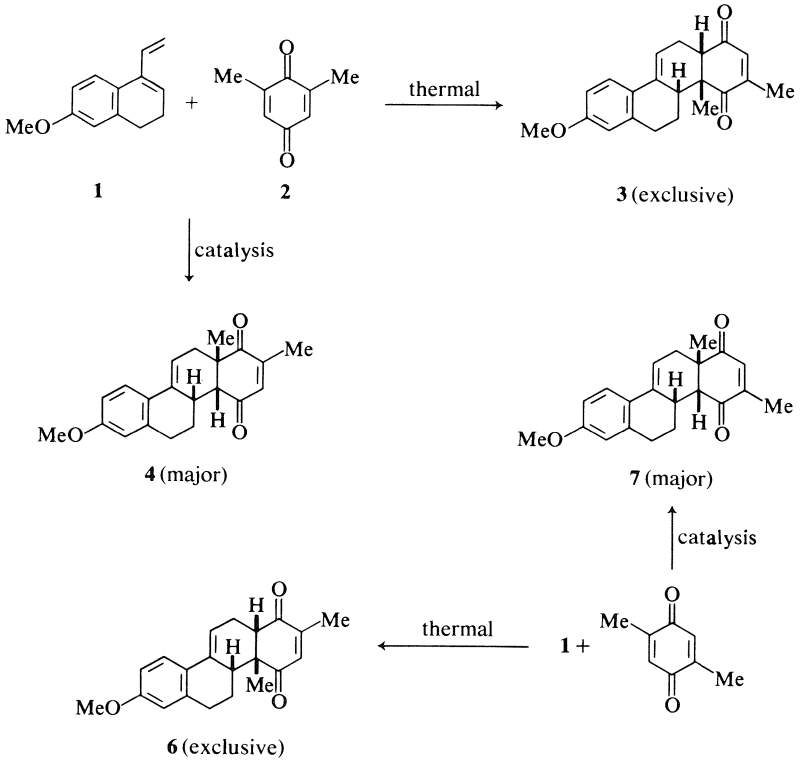

tional quinones, 2-acetyl-1,4-benzoquinone (**8**), 2-carbomethoxy-6-methyl-1,4-benzoquinone (**11**), and 6-methoxy-1,4-toluquinone (**13**), were examined. It should be noted that, in thermal additions, only quinone **8** gives any "meta"-adduct and that in a minor quantity. In catalysed additions, quinone **13** forms a clear exception to the general "meta"-adduct dominance. Structure, including stereochemistry, of all adducts was determined by methods similar to those used for compounds **3** and **4** (see Experimental).

Orientation

From a purely synthetic standpoint, these results clearly create a very favourable situation. Catalysed additions leading to compounds **4**, **7**, and **10** provide *D*-homosteroids with suitable C(13)-substituents in a simple manner. At the same time, all the thermal

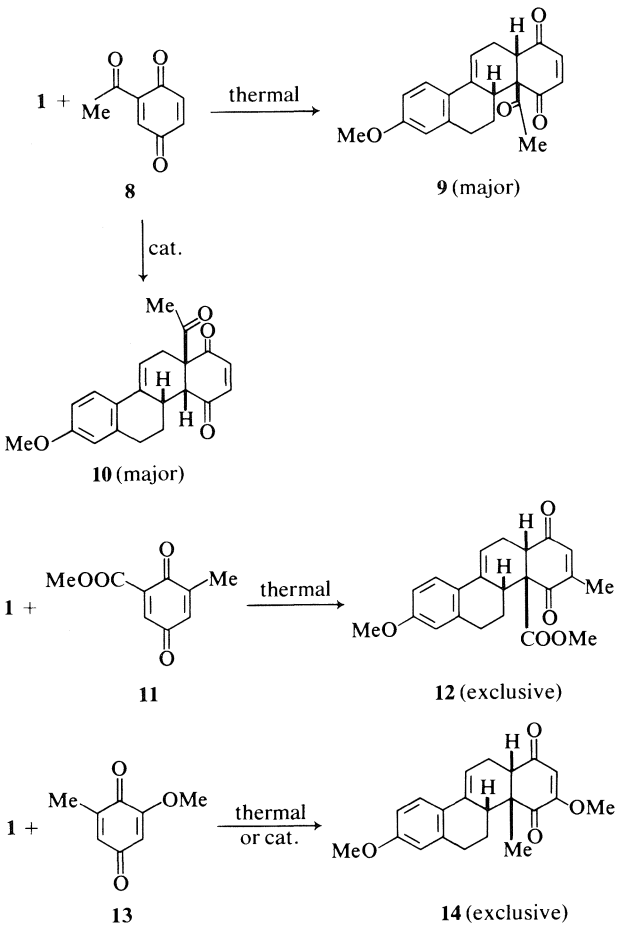

additions give fair to good yields of C(14)-substituted compounds available for other purposes. In contrast to this simple picture of synthetic strategy based on products obtained, the mechanistic questions concerning these orientation reversals are very complex.

The results of the thermal additions alone are unusual. In order to assess the general orientation tendencies of diene **1**, we have repeated its addition to citraconic anhydride (**15**) (9) and have extensively studied its thermal addition to such simple dienophiles as methyl acrylate, acrylonitrile, and methyl *trans*-crotonate.[5] In all these cases, the "ortho"- and "meta"-adducts are formed in approximately equal quantities, with a slight preference (if any) for "meta"-addition up to a maximum product ratio of 2:1! Diene **1** is thus an interesting "orientation probe" for which the sum of all factors favouring "ortho"- addition is almost exactly equal to the sum of effects favouring "meta"-adducts in additions to non-quinonoid dienophiles including **15**. Considering the strong "ortho"-preference shown by quinones (Table 1), what is then, for example, the nature of the difference between citraconic anhydride (**15**) and the two dimethyl quinones **2** and **5**? Superficially, they clearly have structural similarities. The situation is all the more remarkable since the observed "ortho"-preference is largely independent of the nature of the quinone substituent. The activating methoxycarbonyl group in **11** and acetyl group in **8** show an orientation effect comparable to that of the deactivating methyl group in **2** and **5** in thermal additions.

It would be inappropriate to include an exhaustive discussion of this problem[6] in this presentation of a steroid synthesis. One aspect of the present study must, however, be mentioned since it is relevant to results and conclusions recently reached elsewhere. In an important experimental study of methyl quinone additions, Bohlmann *et al.* (16*b*) suggested that a steric effect is necessary to explain the *ortho*-predominance in thermal additions in which the frontier molecular orbital (FMO) theory in its presently applied form (14) fails to make the correct predictions. Houk *et al.* (17), using a perturbation

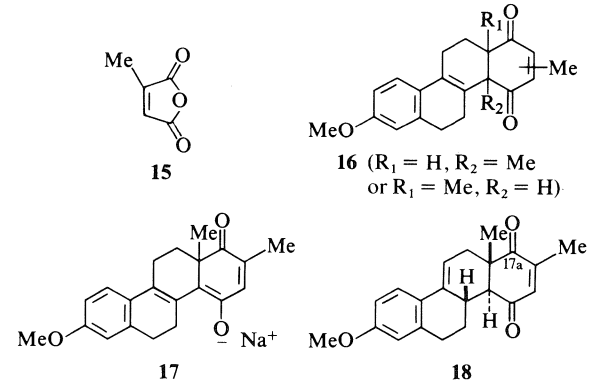

[5]Dr. Jagabandhu Das. Unpublished experiments in this Department (Ph.D. Dissertation, University of New Brunswick, 1978).

[6]This requires the consideration of *all* thermal and catalysed additions of diene **1** to various dienophiles and of the used quinones to many dienes and a consideration of the complicating fact that thermal additions of **1** to non-quinonoid dienophiles do not lead exclusively to *endo* adducts. At the present time, we are studying two aspects of the problem. Dr. Masatoshi Kakushima of our Department is calculating the molecular properties of appropriate model dienes and dienophiles in order to establish whether a qualitative explanation of the results can be provided by molecular orbital theory (13, 14). In addition, we have experiments in progress which are designed to probe the question whether the transition state geometries of thermal quinone additions and of all catalysed additions (15) are similar to or significantly different from those of thermal additions of non-quinonoid dienophiles. Any such possible geometric differences involving unsymmetrical transition states (16) would clearly have to be taken into account in a complete rationalization of the orientation results.

approach, explained these and similar results by postulating that a methyl group situated on the reacting double-bond of a dienophile can assume acceptor properties via the π^* CH_3 orbital (in addition to its deactivating donor properties), and thus direct a nucleophilic attack to the remote alkene terminus.

Our results indicate that the quinones are indeed "anomalous" compared to other (simpler) dienophiles, and that a more exact definition of the role of a methyl group situated on the dienophile double-bond (17) will not be sufficient to explain the pronounced "ortho"-effect observed in thermal additions of quinones. (*1*) Citraconic anhydride (**15**) and dimethyl quinones **2** and **5** all possess a reacting methyl alkene moiety, yet **15** reacts with diene **1** to give an *ortho*:*meta* ratio of adducts of ~1:1,[5] comparable to that observed in additions of methyl acrylate, acrylonitrile, and methyl *trans*-crotonate to **1**. In contrast, **2** and **5** give exclusively the "ortho"-adduct. (*2*) Quinones **8** and **11**, containing the activating acetyl and methoxycarbonyl groups, respectively, (instead of a methyl group) on their reacting double-bonds, also show a pronounced "ortho" preference in their thermal additions.

The comparable results of thermal additions of diene **1** to the two dimethyl quinones, **2** and **5**, furthermore show that the strong *ortho*-preference is independent of the position of a methyl group on the non-reacting double-bond of the quinone. This clearly constitutes a serious limitation to any postulates of an electronic non-identity of the two quinone carbonyl groups, at least in the ground state. An analysis of this problem is in progress.[6]

The complete rationalization of the results of the catalysed reactions is also difficult and should clearly not be undertaken before the thermal reactions are understood.[6] The ease of the catalysed reactions is no doubt due to the complexing of the Lewis acid with the dienophiles (12) and the consequent lowering of their LUMO energy (15*c*). Concerning the question of the reacting complex (or complexes)[7] in the catalysed reactions described here, our previous

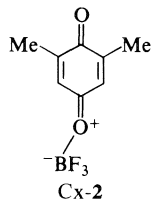

Cx-**2**

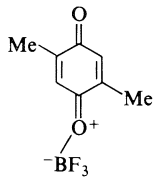

Cx-**5**

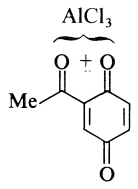

Cx-**8**

work with simpler dienes (10) indicates that quinone **2** probably adds exclusively in the form shown in formula Cx-**2** (= complexed **2**). The postulate of Cx-**2** as the reacting species is, for example, sufficient to explain the exclusive formation of the "meta"-adduct in a reaction with *trans*-1,3-pentadiene (10). Because of the symmetry of **5**, its two carbonyl groups are identical and its reacting form must thus be Cx-**5**, the only uncertainty being the attachment of the catalyst *syn* or *anti* to the neighbouring methyl group. Finally, there is little doubt that, for electronic reasons, acetyl quinone **8** will complex at one (or both) carbonyl groups indicated in formula Cx-**8**. Since only one addition of the methoxy quinone **13** has been studied and since it is, furthermore, not a priori obvious which of the carbonyl groups in **13** could be expected to possess greater Lewis basicity, it would be unwise to speculate on the nature of the reacting complex of **13** at the present time.

Ring D Contraction

Dione **18**, prepared from diene **1** in two steps in a 65% yield, contains the number of carbon atoms and an arrangement of groups in ring D suitable for the creation of a 5-membered ring D with an acetyl group at C(17). Two methods were available in principle: a 1,2-rearrangement of a suitably reduced derivative leading directly to a 5-membered ring or a ring opening of a derivative by double-bond cleavage followed by ring closure. The latter proved more efficient.

Reduction of **18** with lithium aluminum tri-*tert*-butoxyhydride in tetrahydrofuran at room temperature gave alcohol **19**[8] in a 94% yield of isolated

[7]We have so far not succeeded in the determination of any of the quinone ⇌ complex equilibria by spectroscopic methods, mainly because of the apparent predominance of uncomplexed species. It should, furthermore, be noted that the "reacting complex" will be determined not only by these equilibria, but also by the relative rates of subsequent additions. A serious uncertainty concerns the form of diene **1** in these catalysed reactions. Since diene **1** polymerizes readily under acidic conditions (in the absence of dienophile), it proved impossible to examine **1** + Lewis acid spectroscopically. We assume that a large number of molecules of **1** are complexed (presumably on —OCH_3) under the reaction conditions, but that the more reactive uncomplexed molecules of **1** react with complexed quinone.

[8]The site of the reduction (but not the stereochemistry) follows rigorously from spectroscopic data. The stereochemical assignment is supported by a hydrogenation study (see Experimental).

crystalline product. Since ring D of **18** contains four trigonal carbon atoms, it is unlikely that this remarkable specificity arises simply from a preferred axial attack by hydride ion from the less hindered α-side. The situation is reminiscent of preferential hydride reductions of unsymmetrically substituted anhydrides at the apparently "more hindered" carbonyl group (18) and the observed result may be explicable by an electronic difference between the two carbonyl groups (19) and/or by the postulate that the angle of attack (20) by the reducing agent is such that the path to the C(17a)-carbonyl group is, in fact, less hindered.

Since alcohol **19** and the corresponding acetate prepared from it could not be reduced cleanly, **19** was converted to the unstable mesylate **20** which was, without purification, treated with zinc dust in boiling benzene–methanol (1:1) (21). The resulting mixture of α,β- and β,γ-unsaturated ketones was then equilibrated by treatment with sodium carbonate in boiling aqueous methanol to give pure ketone **21**. An 81% overall yield of crystalline **21** was obtained in the five steps from adduct **4** in a run in which intermediates were not purified.

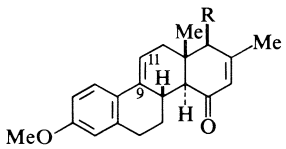

19 R = OH
20 R = OMs
21 R = H

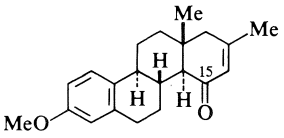

22

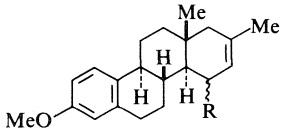

23 R = OH
24 R = OAc
25 R = H

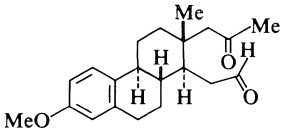

27

Catalytic hydrogenation of **21** with palladium on calcium carbonate in glacial acetic acid gave an 84% yield of crystalline **22**. An ir spectrum of the mother liquors showed no appreciable signal corresponding to a saturated carbonyl group, but the nmr spectrum indicated a second product, presumably isomeric at C(9). This reduction to **22** stabilized rings B and C and simplified subsequent transformations. It should be noted that, should C(11)-oxygenated derivatives be required in an application of this sequence, the appropriate electrophilic attack at C(11) could be performed using **21**.

The following three-step sequence proved most efficient for the conversion of the C(15)-carbonyl group in **22** into a methylene group. Reduction of **22** with sodium bis(2-methoxyethoxy)aluminum hydride (22) in dry ether gave the mixture of epimeric alcohols **23** efficiently. In contrast, reductions with sodium borohydride and lithium aluminum hydride gave complex mixtures of products. Acetylation then led to acetate mixture **24**. Compounds **23** and **24** were not purified due to instability. Since the reported method using lithium in ethyl amine (23) not only reductively removed the acetoxyl function, but also reduced the anisol ring, the following milder modification was developed. Treatment of acetate mixture **24** with excess lithium in refluxing liquid ammonia and tetrahydrofuran led to crystalline olefin **25**, obtained in a 78% overall yield for the three steps from enone **22**.

The synthetic strategy used required that the ring D double-bond remain at C(16)—C(17) during the conversion **18** → **25**. While the method described above achieves this in high yield, it does involve six synthetic steps. All attempts, both at the enedione stage **18** and with enone **22**, to shorten the sequence by double reductions and by more vigorous reductions led to complex mixtures and to double-bond migrations. For example, treatment of **22** with zinc amalgam in boiling benzene–ethanol and concentrated hydrochloric acid gave a good yield of an olefin with two olefinic hydrogen atoms.

Olefin **25** has the functionality suitable for its conversion into a C(17)-acetyl derivative of estrone by a sequence involving double-bond cleavage and aldol condensation. Treatment of **25** with osmium tetroxide in dry pyridine (24) gave a mixture of two isomeric vicinal diols **26** which was converted by lead tetraacetate in tetrahydrofuran into oily keto aldehyde **27**, homogeneous in thin-layer chromatography. Finally, treatment of **27** with equal volumes

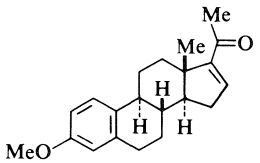

28

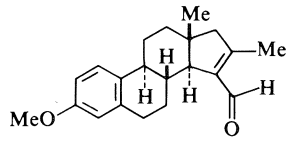

29

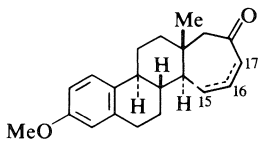

30 C_{15}—C_{16} olefin
31 C_{16}—C_{17} olefin

of tetrahydrofuran and 5% hydrochloric acid at 75°C for 40 h gave the desired crystalline enone **28** in a 60% yield based on olefin **25**. The nmr spectrum of mother liquors clearly indicated the formation of

a small amount of the alternative 5-membered ring D product, **29**.

The overall conversion **1** + **2** → **28** involves thirteen steps and is achieved in a 22% yield. This is a minimum yield since recrystallized intermediates were used at several stages.

The cyclization of keto aldehyde **27** deserves further comment. In contrast to previously reported results with similar systems (25), treatment of **27** with aqueous potassium hydroxide and tetrahydrofuran at reflux temperature for 16 h gave a mixture of three products, **28**, **30**, and **31**, in an approximate ratio of 1:3:1 and a total yield of 71%. No trace of cycloheptenones **30** and **31** could be detected in crystallization mother liquors from acidic cyclization of **27** described above. Basic treatment of pure **30** gave an equilibrium mixture of **30** and **31**. Basic treatment of **28** did not give any cycloheptenone products, while acidic treatment of **30** did not lead to any detectable amounts of cyclopentenes **28** and **29**. While these data do not reveal all details of the two cyclizations, they do indicate that the base catalysed condensation is probably governed by the preferential formation of the primary enolate ion (formed from **27**), while the reaction with acid proceeds via the more substituted enol. Depending on conditions used, a reasonable yield of five-membered or seven-membered ring D derivatives of keto aldehyde **27** can thus be obtained.

Enone **28** was converted to *d,l*-estrone methyl ether by the reported Beckmann rearrangement of the corresponding oxime and the subsequent hydrolysis of the resulting *N*-acetyl enamine (26). *d,l*-Estrone was then obtained by demethylation with pyridine hydrochloride (27). A detailed comparison of the synthetic compounds with natural estrone and with literature data is described in the Experimental.

For the synthesis of estrone itself and that of its simple derivatives, the strategy described above clearly does not match the elegant simplicity of the approach (28) based on an original discovery by Ananchenko and Torgov (29). It is longer and the direct preparation of optically active compounds would require a chiral induction in the catalysed Diels–Alder step **1** + **2** itself. However, it has certain advantages. (*1*) The C(9)—C(11) double-bond in intermediates **18**–**21** offers possibilities for the functionalization of ring C. (*2*) It automatically provides a C(17)-acetyl sidechain and a possibility of a nucleophilic attack at C(16) in enone **28**. (*3*) Formation of adduct **10** indicates that it should be possible to introduce a wide variety of C(13)-substituents. (*4*) Finally, as will be described in subsequent publications of this series,[9] the method works well with dienes possessing the C(10)-methyl group and with both quinonoid and non-quinonoid dienophiles. This provides opportunity for the direct total synthesis of C(10)-alkylated steroids for which, in our opinion, additional synthetic strategies are needed.

[9]See also refs. 11 and 30.

Experimental

Melting points were determined on a Kofler hot stage and are uncorrected. Ultraviolet (uv) spectra were recorded on a Perkin–Elmer 402 spectrophotometer in ethanol solution. The wavelengths are reported in nanometers (nm) with ε values in parentheses. Infrared (ir) spectra were determined on a Perkin–Elmer 457 instrument in chloroform solution. Values are given in wave-numbers (cm^{-1}) calibrated to the polystyrene band at 1601 cm^{-1}. Proton magnetic resonance (^{1}Hmr) spectra were obtained on a Varian T-60 spectrometer using deuterochloroform as solvent; chemical shift values are given in δ (ppm) scale relative to tetramethylsilane (TMS) used as internal reference. High resolution ^{1}Hmr spectra were recorded by the Canadian 220 MHz NMR Centre, Department of Medical Genetics, University of Toronto. Low resolution mass spectra (ms) were measured on a Hitachi Perkin–Elmer RMU-6D mass spectrometer. High resolution mass spectra were measured by Dr. A. M. Hogg, University of Alberta, Edmonton. Microanalyses were performed by Dr. F. Pascher, Mikroanalytisches Laboratorium, Bonn, West Germany. The following abbreviations have been used: s, singlet; d, doublet; dd, double doublet; t, triplet; m, multiplet; sh, shoulder; dec., decomposition; Et_2O, ethyl ether; Ac_2O, acetic anhydride.

Thermal Addition of 2,6-Dimethyl-1,4-benzoquinone. Adduct 3

Diene **1** (8) (680 mg, 5.0 mmol) and 2,6-dimethyl-1,4-benzoquinone (31) (950 mg, 5.1 mmol) were reacted in dry benzene (25 mL) under reflux for 24 h. The solvent was removed *in vacuo* and the residue crystallized from ethyl acetate to give **3** (1.323 g, 82.3%), mp 164–167°C; ir ν_{max}: 1680, 1610; ^{1}Hmr δ: 1.5 (3H, s, C(14)—CH_3), 2.1 (3H, d, J = 2 Hz, C(16)—CH_3), 3.8 (3H, s, CH_3O), 6.0 (1H, m, C(11)—H); ms *m/e*: 322 (M^+). *Mol. Wt.* calcd. for $C_{21}H_{22}O_3$: 322.1569; found (high resolution ms): 322.1575.

No isomer of **3** could be detected in the ^{1}Hmr spectrum of mother liquors. Compound **3** was unchanged after 1 h treatment with $NaHCO_3$ in boiling methanol.

Catalysed Addition of 2,6-Dimethyl-1,4-benzoquinone

A solution of diene **1** (2.380 g, 12.7 mmol) in Et_2O (5 mL) was added to a solution of quinone **2** (1.680 g, 12.4 mmol) and BF_3 etherate (2.320 g, 16.5 mmol) in 20 mL of Et_2O at −15°C. Light tan crystals of **4** began to form almost immediately. After 30 min, the crystals were collected by filtration and washed with Et_2O. Recrystallization from ethyl acetate gave adduct **4** (2.720 g, 69%), mp 194–196°C; ir ν_{max}: 1680 (broad), 1635, 1610; ^{1}Hmr δ: 1.4 (3H, s, C(13)—CH_3), 2.0 (3H, d, J = 2 Hz, C(17)—CH_3), 3.1 (1H, d, J = 5 Hz, C(14)—H), 3.8 (3H, s, CH_3O), 6.1 (1H, m, C(11)—H); ms *m/e*: 322 (M^+). *Mol. Wt.* calcd. for $C_{21}H_{22}O_3$: 322.1569; found (high resolution ms): 322.1570.

Adduct **3** (0.459 g, 11.4%) was obtained from concentrated ethyl acetate mother liquors.

Approximately the same yield and the same ratio of the two isomers was obtained in reactions at −20°C, 0°C, and at ambient temperature using 1.3, 2.0, and 2.3 mol equiv. of BF_3 etherate. The reaction was much slower with less than 1.0 mol equiv. of BF_3 etherate.

*Isomerization of Adduct **4** to **18***

Adduct **4** (1.610 g, 5.0 mmol) and $NaHCO_3$ (322 mg, 3.8

mmol) were suspended in dry methanol (100 mL). The mixture was stirred and heated under reflux until all of **4** had dissolved (30 min). About one half of the methanol was evaporated *in vacuo* and water (50 mL) was added. The light yellow precipitate was filtered and crystallized from methanol to give **18** (1.521 g, 94%), mp 148–149°C; ir ν_{max}: 1680, 1625, 1605; ^{1}Hmr δ: 1.2 (3H, s, C(13)—CH_3), 2.0 (3H, d, J = 2 Hz, C(17)—CH_3), 3.8 (3H, s, CH_3O), 6.1 (1H, m, C(11)—H); ms *m/e*: 322 (M^+). *Anal.* calcd. for $C_{21}H_{22}O_3$: C 78.23, H 6.88, O 14.89; found: C 78.39, H 6.92, O 14.86.

*Acidic Isomerization of Adducts **3** and **4***

Compound **4** (100 mg) was treated with Dowex 50-X in boiling ethanol (10 mL) for 15 h. The resin was removed by filtration and the solvent was evaporated *in vacuo* to give **16** (C(13)—CH_3, C(14)—H) (88 mg, 88%), mp 103–105°C (methanol). The yellow alcoholic solution of **16** (C(13)—CH_3, C(14)—H) instantaneously turns dark purple (enolate **17**) on addition of aqueous NaOH: ir ν_{max}: 1675, 1610; ^{1}Hmr δ: 1.3 (3H, s, C(13)—CH_3), 2.0 (3H, d, J = 2 Hz, C(17)—CH_3), 3.4 (1H, broad s, C(14)—H), 3.8 (3H, s, CH_3O), no signal in the 5.0–6.3 region; ms *m/e*: 322 (M^+).

Compound **3** (100 mg) was heated under reflux in glacial acetic acid (5 mL) for 30 min. Water (40 mL) was added and the product was extracted with Et_2O to give **16** (C(13)—H, C(14)—CH_3) (99 mg) obtained as a hard resin. Attempts to crystallize the compound were unsuccessful; similar results were obtained when **3** was treated with Dowex 50-X in methanol or with *p*-toluenesulfonic acid in benzene. Alcoholic solution of **16** (C(13)—H, C(14)—CH_3), did not change color on treatment with aqueous NaOH; ir ν_{max}: 1680, 1610; ^{1}Hmr δ: 1.5 (3H, s, C(14)—CH_3), 2.0 (3H, d, J = 2 Hz, C(16)—CH_3), 3.8 (3H, s, CH_3O), no signal in the 5.0–6.3 region; ms *m/e*: 322 (M^+).

*Thermal Addition of 2,5-Dimethyl-1,4-benzoquinone. Adduct **6***

Diene **1** (372 mg, 2.0 mmol) and 2,5-dimethyl-1,4-benzoquinone (32) (272 mg, 2.0 mmol) were reacted in dry benzene (10 mL) under reflux for 15 h. The solvent was evaporated *in vacuo* and the residue crystallized from Et_2O to give **6** (410 mg, 64%), mp 166–169°C (ethyl acetate). The mother liquor did not contain any amount of **7** or another isomer of **6** detectable by ^{1}Hmr spectroscopy; ir ν_{max}: 1680 (very broad), 1630, 1615; ^{1}Hmr δ: 1.5 (3H, s, C(14)—CH_3), 2.0 (3H, d, J = 2 Hz, C(17)—CH_3), 3.8 (3H, s, CH_3O), 6.0 (1H, m, C(11)—H); ms *m/e*: 322 (M^+). *Anal.* calcd. for $C_{21}H_{22}O_3$: C 78.23, H 6.88, O 14.89; found: C 78.00, H 6.85, O 14.82.

Catalysed Addition of 2,5-Dimethyl-1,4-benzoquinone

Diene **1** (372 mg, 2.0 mmol) and 2,5-dimethyl-1,4-benzoquinone (272 mg, 2.0 mmol) were dissolved in dry Et_2O (10 mL). A solution of BF_3 etherate (300 mg, 2.10 mmol) in dry Et_2O (5 mL) was added and the mixture was maintained at 0°C for 25 min. Addition of triethyl amine (1 mL) was followed by addition of water (25 mL), the organic layer was separated, dried, and evaporated *in vacuo*. The methyl region of the ^{1}Hmr spectrum of the crystalline residue indicated the presence of only two adducts in an ~3:1 ratio. Crystallization from ethanol gave **7** (257 mg, 40%), mp 151–152°C; ir ν_{max}: 1680 (broad), 1635, 1615; ^{1}Hmr δ: 1.4 (3H, s, C(13)—CH_3), 2.0 (3H, d, J = 2 Hz, C(16)—CH_3), 3.1 (1H, d, J = 5 Hz, C(14)—H), 3.8 (3H, s, CH_3O), 6.1 (1H, m, C(11)—H); ms *m/e*: 322 (M^+). *Anal.* calcd. for $C_{21}H_{22}O_3$: C 78.23, H 6.88, O 14.89; found: C 77.76, H 6.86, O 15.15.

A second crystallization crop (78 mg, 12.1%) was mainly **6** containing a small amount of **7** (^{1}Hmr spectrum). The actual yields in this catalysed addition are much higher than those given. The combined mother liquors contain only **6** and **7** as ^{1}Hmr detectable compounds.

*Reactions of Adducts **6** and **7***

Compound **6** was found to be stable to $NaHCO_3$ in boiling methanol. Treatment of **6** (100 mg) in boiling acetic acid (5 mL) for 30 min, followed by addition of H_2O (30 mL), extraction with $CHCl_3$, drying of the organic layer, and evaporation *in vacuo* gave a residue which was crystallized from methanol to give the $\Delta^{8,9}$-isomer of **6** (75 mg, 75%), mp 108–111°C. An alcoholic solution of this compound did not change color on treatment with aqueous NaOH; ir ν_{max} (CCl_4): 1685, 1640, 1615; ^{1}Hmr δ: 1.5 (3H, s, C(14)—CH_3), 2.0 (3H, d, J = 2 Hz, C(17)—CH_3), 3.8 (3H, s, CH_3O), no signal in the 5.0–6.3 region; ms *m/e*: 322 (M^+).

Adduct **7** (30 mg) was treated with $NaHCO_3$ (5 mg) in boiling methanol (5 mL) for 3 min. Water (15 mL) was added, the mixture was neutralized with dilute HCl, the solid was collected by suction and recrystallized from methanol to give 14-iso **7** (28 mg, 93%) mp 170–172°C; ir ν_{max}: 1680, 1630, 1610; ^{1}Hmr δ: 1.2 (3H, s, C(13)—CH_3), 2.1 (3H, d, J = 2 Hz, C(16)—CH_3), 3.8 (3H, s, CH_3O), 6.1 (1H, m, C(11)—H); ms *m/e*: 322.

Treatment of **7** (50 mg) in boiling acetic acid (3 mL) for 30 min, followed by addition of H_2O (15 mL), extraction with $CHCl_3$, drying of the organic layer, and evaporation *in vacuo* gave a yellow crystalline residue which was recrystallized from Et_2O to give the $\Delta^{8,9}$-isomer of **7** (45 mg, 90%), mp 141–144°C. Its alcoholic solution gave a dark purple color after addition of a drop of aqueous NaOH; ir ν_{max} (CCl_4): 1690, 1640, 1615; ^{1}Hmr δ: 1.3 (3H, s, C(13)—CH_3), 2.0 (3H, d, J = 2 Hz, C(16)—CH_3), 3.4 (1H, broad s, C(14)—H), 3.8 (3H, s, CH_3O), no signal in the 5.0–6.3 region; ms *m/e*: 322 (M^+).

Thermal Addition of 2-Acetyl-1,4-benzoquinone

Diene **1** (353 mg, 1.92 mmol) was dissolved in dry benzene (20 mL) at ambient temperature and 2-acetyl-1,4-benzoquinone (33) (240 mg, 1.60 mmol) was added in one portion. The reaction mixture at once became dark (π-complex), but after several min the colour disappeared and the reaction was completed. After 30 min, the solvent was evaporated *in vacuo* and yellow crystals (520 mg, 97%) were collected by filtration. The methyl region of the ^{1}Hmr spectrum (at 220 MHz) revealed the presence of only two adducts (singlets at δ 2.17 and 2.28) in a ratio of 1:7 (**10**:**9**). Recrystallization from Et_2O gave pure **9**, mp 139–140°C; ir ν_{max}: 1690 (broad), 1610; ^{1}Hmr δ: 2.3 (3H, s, C(14)—acetyl), 3.7 (1H, t, J = 7 Hz, C(13)—H), 3.8 (3H, s, CH_3O), 6.1 (1H, m, C(11)—H); ms *m/e*: 336 (M^+). *Mol. Wt.* calcd. for $C_{21}H_{20}O_4$: 336.1362; found (high resolution ms): 336.1359.

Reactions in dry Et_2O or in acetone at ambient temperature gave a comparable yield and ratio of products (1:7) as determined by ^{1}Hmr spectra. A reaction in which **1** (353 mg, 1.92 mmol) in boiling benzene (10 mL) was added rapidly to a boiling solution of quinone **8** (240 mg, 1.60 mmol) in benzene (10 mL) and in which the solution was evaporated *in vacuo* after 3 min gave a crystalline product (535 mg, ~100%) which according to the 220 MHz ^{1}Hmr spectrum contained adducts **10** and **9** in a ratio of 1:5.

Adduct **9** (84 mg, 0.25 mmol) was treated with concentrated HCl (2 drops) in $CHCl_3$ (10 mL) at ambient temperature for 30 min. Dilution with $CHCl_3$ (20 mL), washing with saturated $NaHCO_3$ solution and then H_2O, drying and evaporation *in vacuo* gave the crude $\Delta^{8,9}$-isomer of **9** (84 mg) as yellow foam; ir ν_{max}: 1710, 1680, 1610; ^{1}Hmr δ: 2.3 (3H, s, C(14)—acetyl), 3.5 (1H, dd, J = 6 and 4 Hz, C(13)—H), 3.8 (3H, s, CH_3O), no signal in the 5.0–6.3 region; ms *m/e*: 336 (M^+).

Pure adduct **10** was obtained in the following experiment.

Catalysed Addition of 2-Acetyl-1,4-benzoquinone

$AlCl_3$ (230 mg, 1.7 mmol), freshly sublimed in a stream of dry HCl gas, was added to a solution of quinone **8** (240 mg,

1.6 mmol) in dry CH_2Cl_2 (20 mL) cooled in a Dry Ice – acetone bath to −78°C. A cooled solution of diene **1** (350 mg, 1.9 mmol) in CH_2Cl_2 (5 mL) was added rapidly, the mixture stirred at −78°C for 20 min and poured into ice-water. Separation of the CH_2Cl_2 layer, Et_2O extraction of the aqueous layer, washing and drying of combined organic layers, and evaporation to a small volume *in vacuo* gave a yellow crystalline product (535 mg, ~100%). Its ^{1}Hmr spectrum established the **9**:**10** ratio to be approximately 1:3. The mixture was dissolved in boiling Et_2O (15 mL); on cooling, yellow crystals of pure **9** (130 mg), mp 139–140°C, separated. Concentration of the mother liquor to about 5 mL and cooling to −15°C gave crystals which on recrystallization under the same conditions gave pure adduct **10** (363 mg), mp 188–205°C dec.; ir ν_{max}: 1685 (broad); ^{1}Hmr δ: 2.2 (3H, s, C(13)—acetyl), 3.8 (3H, s, CH_3O), 3.9 (1H, d, one branch covered by CH_3O, C(14)—H), 6.0 (1H, m, C(11)—H); ms *m/e*: 336 (M^+). *Mol. Wt.* calcd. for $C_{21}H_{20}O_4$: 336.1362; found (high resolution ms): 336.1366.

Isomerization of **10** (84 mg, 0.25 mmol) with HCl was done in the same way as with adduct **9** (see above). The resulting yellow foam (84 mg) crystallized from Et_2O to give pure $\Delta^{8,9}$-isomer of **10**, mp 131–132°C; ir ν_{max}: 1710 (sh), 1675, 1600; ^{1}Hmr δ: 2.3 (3H, s, C(13)—acetyl), 3.8 (3H, s, CH_3O), 4.0 (1H, broad s, C(14)—H), no signal in the 5.0–6.3 region; ms *m/e*: 336 (M^+).

*Thermal Addition of 2-Carbomethoxy-6-methyl-1,4-benzoquinone (**11**)*

A solution of quinone **11** (34) (1.800 g, 10.0 mmol) in dry Et_2O (50 mL) was added to diene **1** (1.953 g, 10.5 mmol) in dry Et_2O (50 mL) cooled in an ice–salt bath to −20°C. Crystalline product started to separate immediately. The mixture was stirred at −20°C for 1 h and at ambient temperature for 2 h. Filtration gave adduct **12** (3.220 g, 88%) as yellow crystals, mp 192–195°C (ethyl acetate); ir ν_{max}: 1750, 1730, 1715, 1685, 1615; ^{1}Hmr δ: 2.1 (3H, d, J = 2 Hz, C(16)—CH_3), 3.6 (1H, t, left branch covered by CH_3O, J = 8 Hz, C(13)—H), 3.8 (6H, s, $2CH_3O$), 6.1 (1H, m, C(11)—H); ^{1}Hmr (220 MHz) δ: clear t at 3.6 (1H, J = 8 Hz, C(13)—H); ms *m/e*: 366 (M^+). *Anal.* calcd. for $C_{22}H_{22}O_5$: C 72.11, H 6.05, O 21.83; found: C 71.99, H 5.96, O 21.84.

The same result and yield of crystalline **12** (88%) was also obtained in reactions in Et_2O at −20°C for 60 min, and in Et_2O or benzene at 22°C for 60 min.

*Reactions of Adduct **12***

Adduct **12** remained unchanged on treatment with $NaHCO_3$ in boiling methanol.

Adduct **12** (366 mg, 1.0 mmol) was treated with sodium acetate (100 mg) in boiling Ac_2O (10 mL) for 75 min. The solvent was removed *in vacuo*, the residue treated with dry Et_2O (50 mL), sodium acetate removed by filtration, and Et_2O evaporated to give the $\Delta^{13,17a}$-enol acetate of **12** (316 mg, 77%) as dark yellow crystals, mp 218–220°C; ir ν_{max}: 1760 (broad), 1650, 1610; ^{1}Hmr δ: 2.0 (3H, d, J = 2 Hz, C(16)—CH_3), 2.3 (3H, s, O-acetyl), 3.7 (3H, s, CH_3O), 3.8 (3H, s, CH_3O), 5.7 (1H, m, C(11)—H); ms *m/e*: 408 (M^+).

The **12**-enol acetate (100 mg, 0.25 mmol) was treated with dry Na_2CO_3 (100 mg) in boiling methanol (5 mL) for 30 min. After stirring at ambient temperature for an additional 2 h, H_2O (5 mL) was added and the precipitate recrystallized from ethyl acetate to give pure **12** (72 mg, 79%).

The above hydrolysis of **12**-enol acetate was repeated using CH_3OD and D_2O to give **12** deuterated at C(13), mp 190–192°C; ^{1}Hmr δ: no signal at 3.6, m at 2.4–2.7 narrower; ms *m/e*: 367 (M^+).

Adduct **12** (100 mg) was treated with Dowex-50X resin (50 mg) in boiling 95% ethanol (10 mL) for 6 h. Removal of the resin by filtration and evaporation of the solvent *in vacuo* gave a yellow solid which could not be crystallized. Precipitated from hot methanol, it melted at 101–115°C dec.; ir ν_{max} (CCl_4): 1750, 1690, 1615; ^{1}Hmr δ: 2.0 (3H, d, J = 2 Hz, C(16)—CH_3), 3.7 (1H, m, C(13)—H), 3.8 (6H, s, $2CH_3O$), no signal in the 5–6.3 region; ms *m/e*: 366 (M^+). This $\Delta^{8,9}$-isomer of **12** did not give an extended chromophore on treatment of its ethanolic solution with NaOH.

Thermal Addition of 6-Methoxy-1,4-toluquinone

Diene **1** (93 mg, 0.50 mmol) was treated with quinone **13** (35) (76 mg, 0.50 mmol) in boiling benzene for 15 h. Evaporation of solvent *in vacuo* and crystallization from ethyl acetate gave **14** (81 mg, 48%), mp 165–167°C; ir ν_{max}: 1710, 1670, 1610; ^{1}Hmr δ: 1.5 (3H, s, C(14)—CH_3), 3.8 (6H, s, $2CH_3O$), 5.9 (1H, s, C(17)—H), 6.0 (1H, m, C(11)—H), the 1.7–3.0 region similar to that of **3** and different from that of **4**; ms *m/e*: 338 (M^+). *Mol. Wt.* calcd. for $C_{21}H_{22}O_4$: 338.1518; found (high resolution ms): 338.1516. *Anal.* calcd. for $C_{21}H_{22}O_4$: C 74.50, H 6.55, O 18.95; found: C 74.15, H 6.57, O 19.21.

No isomeric adduct was detectable in crystallization mother liquors.

Catalysed Addition of 6-Methoxy-1,4-toluquinone

A solution of diene **1** (186 mg, 1.0 mmol) in dry Et_2O (5 mL) was added to a solution of **13** (152 mg, 1.0 mmol) and BF_3 etherate (300 mg, 2.1 mmol) in dry Et_2O (5 mL) at 0°C. After 20 min, triethylamine (1 mL) and then H_2O (20 mL) was added, Et_2O layer separated, washed, dried, and evaporated. Crystallization from ethyl acetate gave **14** (105 mg, 31%), mp 163–166°C. No isomeric adduct was detectable in the total reaction product and in crystallization mother liquors.

*Reduction of Enedione **18***

A solution of **18** (1.530 g, 4.72 mmol) and lithium aluminum tri-*tert*-butoxyhydride (2.000 g, 7.88 mmol) in dry tetrahydrofuran (50 mL) was stirred at ambient temperature for 15 min. Dilution with H_2O, extraction with $CHCl_3$, drying of the organic extract with $MgSO_4$, and evaporation *in vacuo* gave a white solid which was filtered and washed with Et_2O to give **19** (1.433 g, 94%), mp 211–213°C (ethanol–Et_2O); ir (KBr) ν_{max}: 1650 (broad), 1610, 1575; ^{1}Hmr δ: 0.9 (3H, s, C(13)—CH_3), 2.0 (3H, narrow m, C(17)—CH_3), 3.8 (3H, s, CH_3O), 4.3 (1H, m, C(17a)—H), 5.9 (2H, m, C(11)—H and C(16)—H); ms *m/e*: 324 (M^+). *Mol. Wt.* calcd. for $C_{21}H_{24}O_3$: 324.1726; found (high resolution ms): 324.1731.

*Reactions of Alcohol **19**. Catalytic Hydrogenation of **18** and **19** (R = O-acetyl)*

A mixture of **19** (R = OH) (180 mg), sodium acetate (50 mg), and Ac_2O (10 mL) was refluxed for 2 h. Ac_2O was removed *in vacuo*, the residue was dissolved in benzene, sodium acetate filtered off, solvent evaporated, and the residue crystallized from ether to give **19** (R = O-acetyl) (178 mg, 84%), mp 182–184°C; ir (KBr) ν_{max}: 1750, 1680, 1655, 1640, 1615; ^{1}Hmr δ: 1.0 (3H, s, C(13)—CH_3), 1.9 (3H, narrow m, C(16)—CH_3), 2.2 (3H, s, acetyl), 3.8 (3H, s, CH_3O), 5.9 (3H, dm, C(11)—H, C(16)—H and C(17a)—H); ms *m/e*: 366 (M^+).

Acetate **19** (R = O-acetyl) (70 mg) was dissolved in hot ethanol (15 mL), solution cooled to ambient temperature, PtO_2 (5 mg) added, and the mixture stirred in H_2 atmosphere at normal pressure for 60 min. The catalyst was filtered, washed with hot $CHCl_3$, the solvent was removed *in vacuo* and the residue was crystallized from $CHCl_3$–Et_2O to give tetrahydro-**19** (R = O-acetyl) (64 mg, 90%), mp 172–175°C; ir (KBr) ν_{max}: 1740, 1720, 1615; ^{1}Hmr δ: 0.9 (3H, s, C(13)—CH_3), 1.0 (3H, d, J = 7 Hz, C(17)—CH_3), 2.2 (3H, s, acetyl), 3.8 (3H, s, CH_3O), 5.1 (1H, d, J = 5 Hz, C(17a)—H); ms *m/e*: 370 (M^+).

Since a single isomer was obtained in high yield in this hydrogenation, it is assumed that the newly introduced H-atoms at C(9) and C(17) are both α.

A mixture of enedione **18** (100 mg) and PtO_2 (10 mg) in methanol (10 mL) was stirred in H_2 atmosphere at normal pressure. Three mol equivalents of H_2 were absorbed in 10 min, The usual workup gave a residue which on crystallization from Et_2O–hexane afforded hexahydro-**18** (99 mg, ~98%), mp 173–176°C; ir ν_{max}: 3610, 3480 (broad), 1720, 1615, 1580; ^{1}Hmr δ: 0.8 (3H, s, C(13)—CH_3), 1.0 (3H, d, J = 7 Hz, C(17)—CH_3), 3.8 (3H, s, CH_3O), 3.9 (1H, d, J = 5 Hz, C(17a)—H); ms *m/e*: 328 (M^+).

Acetylation of this hexahydro-**18** compound (100 mg) in boiling Ac_2O (5 mL), followed by crystallization of the residue from $CHCl_3$–Et_2O gave a compound (98 mg, 86%), mp 172–175°C, identical in all respects with tetrahydro-**19** (R = O-acetyl) described above. The fact that the same C(17a)-epimer is obtained as the only product by catalytic hydrogenation and by hydride reduction of the C(17a)-carbonyl group in **18** provides strong support for the stereochemistry assigned to **19**.

*Conversion of **19** to **21***

Alcohol **19** (1.433 g, 4.42 mmol) was reacted with mesyl chloride (1.140 g, 10 mmol) in dry pyridine (20 mL) at 0°C for 16 h. The solution was diluted with H_2O (80 mL) and extracted with $CHCl_3$. Combined $CHCl_3$ extracts were washed with 5% HCl and brine and dried over $MgSO_4$. Removal of the solvent *in vacuo* and crystallization of the residue from Et_2O–hexane gave crude **20** (1.420 g, 78%); ir ν_{max}: 1680, 1660 (sh), 1640 (sh), 1610; ^{1}Hmr δ: 0.9 (3H, s, C(13)—CH_3), 2.0 (3H, narrow m, C(17)—CH_3), 3.2 (3H, s, mesyl), 3.8 (3H, s, CH_3O), 5.5 (1H, m, C(17a)—H), 6.0 (2H, m, C(11)—H and C(16)—H).

Crude mesylate **20** (1.420 g, 3.53 mmol) was refluxed in benzene–methanol (1:1, 100 mL) for 12 h with freshly activated Zn dust. Fresh portions of Zn were added every few hours; the total of Zn used was 6 g. The mixture was filtered, the solid washed with benzene, the combined filtrate extracted with H_2O, and the organic layer dried over $MgSO_4$ and evaporated *in vacuo* to give a crystalline residue (1.176 g, ~100%) showing two spots on tlc and consisting of **21** and its β,γ-unsaturated isomer (nmr, ir).

The mixture was treated with Na_2CO_3 (0.5 g) in boiling methanol (100 mL) and H_2O (5 mL) for 30 min. Dilution with H_2O (200 mL), extraction with benzene, drying over $MgSO_4$, evaporation *in vacuo*, and crystallization of the residue from benzene–hexane gave **21** (900 mg, 83%), mp 174–176°C; ir (KBr) ν_{max}: 1670, 1650 (sh), 1640 (sh), 1610; ^{1}Hmr δ: 0.9 (3H, s, C(13)—CH_3), 1.9 (3H, broad s, C(17)—CH_3), 3.8 (3H, s, CH_3O), 5.9 (2H, m, C(11)—H and C(16)—H). *Mol. Wt.* calcd. for $C_{21}H_{24}O_2$: 308.1776; found (high resolution ms): 308.1777.

*Conversion of Adduct **4** to **21** without Purification of Intermediates*

Adduct **4** (1.610 g, 5.0 mmol) was isomerized with $NaHCO_3$ (322 mg) in methanol (100 mL). Partition of the product between H_2O and $CHCl_3$ and evaporation of solvent *in vacuo* gave crude **18** which was reduced with lithium aluminum tri-*tert*-butoxyhydride (2.000 g, 7.88 mmol) in dry tetrahydrofuran (50 mL). Partition of the product between H_2O and $CHCl_3$ and evaporation of $CHCl_3$ *in vacuo* gave crude **19** from which mesylate **20** was prepared as described above. The crude mesylate was reduced with Zn dust (6 g) in boiling benzene–methanol (1:1, 100 mL). After solid material was removed by filtration, K_2CO_3 (2.0 g) in H_2O (5 mL) was added, the mixture refluxed for 30 min, and the product obtained by partition between H_2O and benzene. Drying over $MgSO_4$, evaporation *in vacuo*, and crystallization from benzene–hexane gave light tan needles of **21** (1.254 g, 81% for the 5 steps), mp 174–176°C.

*Catalytic Reduction of **21***

Enone **21** (930 mg, 3.0 mmol) was hydrogenated in glacial acetic acid (20 mL) containing 10% Pd on $CaCO_3$ (100 mg) at normal pressure until 1 mol of H_2 was taken up. After filtration and washing of the catalyst with benzene, the filtrate was neutralized with aqueous $NaHCO_3$ and the product extracted with benzene. Drying over $MgSO_4$, evaporation *in vacuo* and crystallization from benzene–hexane gave **22** (785 mg, 84%), mp 142–144°C; ir (KBr) ν_{max}: 1675, 1640, 1600, 1580; ^{1}Hmr δ: 0.9 (3H, s, C(13)—CH_3), 1.9 (3H, broad s, C(17)—CH_3), 3.8 (3H, s, CH_3O), 3.8 (1H, narrow m, C(16)—H). *Mol. Wt.* calcd. for $C_{21}H_{26}O_2$: 310.1933; found (high resolution ms): 310.1930.

*Conversion of Enone **22** to Olefin **25***

Sodium bis(2-methoxyethoxy)aluminum hydride (0.84 mL of 70% benzene solution, 6.0 mmol) was added dropwise to a solution of **22** (752 mg, 2.42 mmol) in dry Et_2O (20 mL) at ambient temperature. The mildly exothermic reaction was completed in ~10 min. The complex was destroyed with a small quantity of 2.5% aqueous KOH, product extracted with Et_2O, solution washed with brine, dried over $MgSO_4$, and evaporated *in vacuo* (20°C) to give crude **23** (755 mg): two spots in tlc; ir (CCl_4) ν_{max}: 3620, 1610; ^{1}Hmr δ: 0.9 and 1.0 (total 3H, two s in 1:4 ratio, C(13)—CH_3), 1.7 (3H, narrow m, C(17)—CH_3), 3.8 (3H, s, CH_3O), 4.3 (1H, broad m, C(15)—H), 5.7 (1H, m, C(16)—H). Compound **23** slowly decomposed on chromatography and on heating its solutions above 20°C.

Crude **23** (755 mg, 2.42 mmol) was treated with freshly distilled Ac_2O (15 mL) in dry pyridine (15 mL) at ambient temperature for 72 h. Dilution with Et_2O, neutralization with aqueous $NaHCO_3$, repeated extraction with Et_2O, washing of combined extracts with 5% aqueous HCl and brine, drying over $MgSO_4$, and evaporation *in vacuo* (all operations at or below 20°C) gave crude **24** (~800 mg); ir (CCl_4) ν_{max}: 1730, 1610; ^{1}Hmr δ: 0.9 and 1.0 (total 3H, two s, C(13)—CH_3), 1.7 (3H, broad s, C(17)—CH_3), 2.0 (3H, s, acetyl), 3.8 (3H, s, CH_3O), 5.3–5.7 (2H, two m, C(16)—H and C(15)—H).

Crude **24** from above was dissolved in dry tetrahydrofuran (50 mL) and added to liquid NH_3 (200 mL). The solution was allowed to reflux (−33°C) and Li metal (100 mg, 14.5 mmol) was added; deep blue color persisted during the reaction. After 30 min, small portions of solid NH_4Cl were added until color had discharged, NH_3 allowed to evaporate, residue in Et_2O washed with 5% aqueous HCl and brine, dried over $MgSO_4$, solvent evaporated *in vacuo*, and residue crystallized from Et_2O–methanol to give platelets of **25** (557 mg, 78% from **22**), mp 96–97°C (lit. (36) mp 96°C); ir (KBr) ν_{max}: 1610, 1580; ^{1}Hmr δ: 0.8 (3H, s, C(13)—CH_3), 1.7 (3H, broad s, C(17)—CH_3), 3.8 (3H, s, CH_3O), 5.4 (1H, m, C(16)—H). *Mol. Wt.* calcd. for $C_{21}H_{28}O$: 296.2141; found (high resolution ms): 296.2141.

*Formation of Keto Aldehyde **27***

A solution of olefin **25** (500 mg, 1.69 mmol) in dry pyridine (17 mL) containing OsO_4 (476 mg, 1.87 mmol) was stirred at ambient temperature for 2 h. $NaHSO_3$ (1.02 g, 9.8 mmol) in H_2O (10 mL) was added and the solution was stirred at 20°C for 30 min. The light red solution was poured into brine, extracted with $CHCl_3$, combined $CHCl_3$ extracts were washed with 5% aqueous HCl, dried over $MgSO_4$, and evaporated *in vacuo* to give crude diol **26** (~560 mg) showing two spots in tlc.

Crude **26** (560 mg, 1.69 mmol) in dry tetrahydrofuran (15 mL) was treated with lead tetraacetate (914 mg, 2.06 mmol)

at 0°C for 5 min. Partition between $CHCl_3$ and a saturated $NaHCO_3$ solution, washing of organic layer with 5% aqueous HCl, drying over $MgSO_4$, and evaporation *in vacuo* gave oily **27** (550 mg, ~99%), homogeneous in tlc; ir (CCl_4) ν_{max}: 2710, 1720 (broad), 1610; ^{1}Hmr δ: 0.9 (3H, s, C(13)—CH_3) 2.0 (2H, s, —CH_2—C=O), 2.3 (3H, s, CH_3—C=O), 3.7 (3H, s, CH_3O), 9.7 (1H, narrow t, —CH=O); ms *m/e*: 328 (M^+). Due to instability, **27** was not purified further.

Cyclization to ***28***

Crude **27** (550 mg, 1.68 mmol) was heated in tetrahydrofuran (20 mL) and 5% aqueous HCl (20 mL) at 75°C for 40 h. The solution was poured into brine, extracted with $CHCl_3$, organic extracts dried over $MgSO_4$, and evaporated *in vacuo* to give crude product (520 mg) which was crystallized from methanol yielding yellowish needles of **28** (317 mg, 60.5%), mp 160–161.5°C (acetone–methanol) (lit. (36) mp 161–163°C); ir (KBr) ν_{max}: 1660, 1610, 1585; uv λ_{max}: 229 (14 000), 277 (2 700), 287 (2 380); ^{1}Hmr δ: 0.9 (3H, s, C(13)—CH_3), 2.3 (3H, s, CH_3—C=O), 3.8 (3H, s, CH_3O), 6.8 (1H, m overlapping with aromatic protons, C(16)—H). *Mol. Wt.* calcd. for $C_{21}H_{26}O_2$: 310.1933; found (high resolution ms): 310.1927.

The ^{1}Hmr spectrum of the residue (~200 mg) from crystallization of **28** indicated the presence of aldehyde **29** (signal at δ 10.0, s) and of additional **28**.

Base Catalysed Condensation of ***27***

A solution of **27** (80 mg, 0.24 mmol) in tetrahydrofuran (1 mL) and 2.5% aqueous KOH (5 mL) was heated to reflux under N_2 for 16 h. Extraction with $CHCl_3$, washing of combined extracts with 5% aqueous HCl and brine, drying over $MgSO_4$, and evaporation *in vacuo* gave a residue which was purified by preparative tlc (silica gel, Et_2O – petroleum ether, 3:7) to give:

28 (10 mg, 13%), mp 159–161°C;

30 (32 mg, 40%), mp 151–153°C (methanol); ir (CCl_4) ν_{max}: 1710, 1670 (small), 1610; ^{1}Hmr δ: 1.0 (3H, s, C(13)—CH_3), 3.8 (3H, s, CH_3O), 5.8 (2H, m, C(15)—H and C(16)—H); ms *m/e*: 310 (M^+);

31 (14 mg, 18%), oily; ir (CCl_4) ν_{max}: 1665 (broad), 1610; uv λ_{max}: 220 (10 800); ^{1}Hmr δ: 1.0 (3H, s, C(13)—CH_3), 2.5 (2H, s, —CH_2—C=O), 3.8 (3H, s, CH_3O), 6.0 (1H, dm, $J \simeq 12$ Hz, C(17)—H), 6.5 (1H, m, overlapping with aromatic protons, C(16)—H); ms *m/e*: 310 (M^+).

d,l-*Estrone Methyl Ether*

A solution of **28** (242 mg, 0.78 mmol) in pyridine (4 mL) and ethanol (20 mL) containing $NH_2OH \cdot HCl$ (139 mg, 2.20 mmol) was heated under reflux for 45 min. Solution in $CHCl_3$, washing with 5% aqueous HCl and brine, drying over $MgSO_4$, and evaporation *in vacuo* gave crude oxime (270 mg), mp 178–184°C.

The oxime was reacted with methanesulfonyl chloride (0.4 mL, 5.2 mmol) in dry pyridine (12 mL) at 0°C for 30 min and at 20°C for 3 h. Water was added and the product was extracted with $CHCl_3$. The solvent was removed *in vacuo* and the residue dissolved in methanol (20 mL) containing 5% aqueous NaOH (5 mL). This solution was refluxed for 3 h, partitioned between H_2O and $CHCl_3$, and the combined extracts dried over $MgSO_4$ and evaporated *in vacuo*. Crystallization of the residue gave *d,l*-estrone methyl ether (90 mg) and additional product (28 mg) was obtained by preparative tlc on silica gel for a total yield of 53%, mp 140–143°C (acetone–methanol) (lit. (27) mp 143–144°C); ir ν_{max}: 1730, 1610, 1570; (KBr) 1740, 1710, 1680; ^{1}Hmr δ: 0.9 (3H, s, C(13)—CH_3), 3.8 (3H, s, CH_3O).

The synthetic material was found identical in ir spectra ($CHCl_3$ and KBr), ^{1}Hmr spectra, and ms with the methyl ether prepared (27) from natural *d*-estrone. The synthetic and natural materials were also found identical on tlc with several solvent systems.

d,l-*Estrone*

The methyl ether (35 mg, 0.12 mmol) was mixed with freshly prepared pyridine hydrochloride (1.0 g) and heated at 210°C under N_2 for 40 min. The cooled mixture was dissolved in $CHCl_3$, the solution washed with 5% aqueous HCl and brine, dried over $MgSO_4$, and the solvent evaporated *in vacuo*. The residue was dissolved in Et_2O and the product extracted with 17% aqueous KOH. Acidification of the aqueous layer, extraction with ether, drying over $MgSO_4$, removal of solvent *in vacuo*, and crystallization of the residue from methanol gave *d,l*-estrone (13 mg, 59%), mp 249–253°C (acetone) (lit. (27) mp 251–254°C); ir ν_{max}: 3610 (sharp), 3340 (broad), 1735, 1610; ms *m/e*: 242 (M^+).

Synthetic *d,l*-estrone was found to be identical with natural estrone in ir ($CHCl_3$), ms, and tlc.

Acknowledgements

Support of this work by the National Research Council of Canada in the form of operating grants and of fellowships to R.K. and G.A.M. is gratefully acknowledged. A generous quantity of quinone **2** was kindly donated by the Hoffmann-La Roche Co., Nutley, N.J. We thank Professor Pierre Deslongchamps, Université de Sherbrooke, for many discussions in which, several years ago, the orientation problem in general and the possibility of steroid syntheses by a guided Diels–Alder reaction in particular received thorough attention.

1. W. E. Bachmann, W. Cole, and A. L. Wilds. J. Am. Chem. Soc. **61**, 974 (1939).
2. A. A. Akhrem and Yu. A. Titov. Total steroid synthesis. Am. ed. Plenum Press, New York, NY. 1970; K. Nakanishi, T. Goto, S. Itô, S. Natori, and S. Nozoe (*Editors*). Natural products chemistry. Vol. 1. Academic Press, New York, NY. 1974; R. T. Blickenstaff, A. C. Ghosh, and G. C. Wolf. Total synthesis of steroids. Academic Press, New York, NY. 1974; R. Pappo. *In* The chemistry and biochemistry of steroids. Intra-Science Research Foundation, Santa Monica, CA. Research Reports Vol. 3, Nos. 1 and 2, 123 (1969); G. Saucy and N. Cohen. MTP Int. Rev. Sci. Ser. One, **8**, 1 (1973); N. Cohen. Acc. Chem. Res. **9**, 412 (1976).
3. G. Stork and J. E. McMurry. J. Am. Chem. Soc. **89**, 5461 (1967); **89**, 5464 (1967); N. Cohen, B. L. Banner, J. E. Blount, M. Tsai, and G. Saucy. J. Org. Chem. **38**, 3229 (1973); A. R. Daniewski and M. Kocor. J. Org. Chem. **40**, 3135 (1975); S. Danishefsky and P. Cain. J. Am. Chem. Soc. **98**, 4975 (1976); W. S. Johnson, S. Escher, and B. W. Metcalf. J. Am. Chem. Soc. **98**, 1039 (1976); W. Oppolzer, M. Petrzilka, and K. Bättig. Helv. Chim. Acta, **60**, 2964 (1977); R. L. Funk and K. P. C. Vollhardt. J. Am. Chem. Soc. **99**, 5483 (1977); T. Kametani, H. Nemoto, M. Tsubuki, and M. Nishiuchi. Tetrahedron Lett. 27 (1979); W. S. Johnson, L. R. Hughes, and J. L. Carlson. J. Am. Chem. Soc. **101**, 1281 (1979); A. R. Daniewski, P. S. White, and Z. Valenta. Can. J. Chem. **57**, 1397 (1979).
4. V. Ipatief. J. Russ. Physiochem. Soc. **29**, 171 (1897).
5. O. Diels and K. Alder. Ann. **460**, 98 (1928).
6. A. S. Onishchenko. Diene synthesis. Translated by Israel

Program for Scientific Translations, Jerusalem. Oldbourne Press, London. 1964. p. 423.
7. K. ALDER and G. STEIN. Angew. Chem. **50**, 510 (1937); J. G. MARTIN and R. K. HILL. Chem. Rev. **61**, 337 (1961); J. SAUER. Angew. Chem. Int. Ed. Engl. **6**, 16 (1967).
8. D. A. ROBINS and J. WALKER. J. Chem. Soc. 3249 (1956).
9. J. HEER and K. MIESCHER. Helv. Chim. Acta, **31**, 219 (1948); W. E. BACHMANN and J. M. CHEMERDA. J. Am. Chem. Soc. **70**, 1468 (1948).
10. Ž. STOJANAC, R. A. DICKINSON, N. STOJANAC, R. J. WOZNOW, and Z. VALENTA. Can. J. Chem. **53**, 616 (1975).
11. R. A. DICKINSON, R. KUBELA, G. A. MACALPINE, Ž. STOJANAC, and Z. VALENTA. Can. J. Chem. **50**, 2377 (1972).
12. A. WASSERMANN. J. Chem. Soc. 618 (1942); P. YATES and P. EATON. J. Am. Chem. Soc. **82**, 4436 (1960); SIR ROBERT ROBINSON and G. I. FRAY. J. Am. Chem. Soc. **83**, 249 (1961); H. WOLLWEBER. Methoden der organischen Chemie. Vol. V/1c. Houben-Weyl. Georg Thieme Verlag, Stuttgart. 1970. p. 1092; K. N. HOUK and R. W. STROZIER. J. Am. Chem. Soc. **95**, 4094 (1973).
13. R. B. WOODWARD and R. HOFFMANN. J. Am. Chem. Soc. **87**, 4388 (1965); W. C. HERNDON and L. H. HALL. Theor. Chim. Acta, **7**, 4 (1967); K. N. HOUK. Tetrahedron Lett. 2621 (1970); P. V. ALSTON and R. M. OTTENBRITE. J. Org. Chem. **40**, 1111 (1975).
14. K. N. HOUK. Acc. Chem. Res. **8**, 361 (1975); P. V. ALSTON and R. M. OTTENBRITE. J. Org. Chem. **40**, 1111 (1975); O. EISENSTEIN, J. M. LEFOUR, N. T. ANH, and R. F. HUDSON. Tetrahedron, **33**, 523 (1977); I. FLEMING. Frontier orbitals and organic chemical reactions. John Wiley and Sons, Toronto. 1978.
15. (*a*) H. M. WALBORSKY, L. BARASCH, and T. C. DAVIS. Tetrahedron, **19**, 2333 (1963); (*b*) K. L. WILLIAMSON and Y. F. L. HSU. J. Am. Chem. Soc. **92**, 7385 (1970); (*c*) K. N. HOUK and R. W. STROZIER. J. Am. Chem. Soc. **95**, 4094 (1973).
16. (*a*) R. B. WOODWARD and T. J. KATZ. Tetrahedron, **5**, 70 (1959); (*b*) F. BOHLMANN, W. MATHAR, and H. SCHWARZ. Chem. Ber. **110**, 2028 (1977).
17. K. N. HOUK, L. N. DOMELSMITH, R. W. STROZIER, and R. T. PATTERSON. J. Am. Chem. Soc. **100**, 6531 (1978).
18. J. J. BLOOMFIELD and S. L. LEE. J. Org. Chem. **32**, 3919 (1967); D. M. BAILEY and R. E. JOHNSON. J. Org. Chem. **35**, 3575 (1970); M. KAYSER and P. MORAND. Can. J. Chem. **56**, 1524 (1978).
19. M. KAYSER. Ph.D. Dissertation. University of Ottawa, Ottawa, Ont. 1979. p. 42.
20. H. B. BURGI, J. D. DUNITZ, J. M. LEHN, and G. WIPFF. Tetrahedron, **30**, 1563 (1974); N. T. ANH and O. EISENSTEIN. Nouv. J. Chim. **1**, 61 (1977); J. E. BALDWIN. Chem. Commun. 738 (1976).
21. A. J. SPEZIALE, J. A. STEPHENS, and Q. E. THOMPSON. J. Am. Chem. Soc. **76**, 5011 (1954).
22. M. CAPKA, V. CHVALOVSKY, K. KOCHLOEFL, and M. KRAUS. Coll. Czech. Chem. Commun. **34**, 118 (1969).
23. A. S. HALLSWORTH, H. B. HENBEST, and T. I. WRIGLEY. J. Chem. Soc. 1957 (1969).
24. J. S. BARAN. J. Org. Chem. **25**, 257 (1960).
25. W. F. JOHNS. J. Am. Chem. Soc. **80**, 6456 (1958).
26. G. ROSENKRANZ, O. MANCERA, F. SONDHEIMER, and C. DJERASSI. J. Org. Chem. **31**, 520 (1956).
27. W. S. JOHNSON, D. K. BANERJEE, W. P. SCHNEIDER, C. D. GUTSCHE, W. E. SHELBERG, and L. F. CHINN. J. Am. Chem. Soc. **72**, 1426 (1950); **74**, 2832 (1952).
28. S. N. ANANCHENKO and I. V. TORGOV. Tetrahedron Lett. 1553 (1963); D. J. CRISPIN and J. S. WHITEHURST. Proc. Chem. Soc. London, 22 (1963); T. MIKI, K. HIRAGA, and T. ASAKO. Proc. Chem. Soc. London, 139 (1963); H. SMITH, G. A. HUGHES, and G. H. DOUGLAS. Experientia, **19**, 394 (1963); T. B. WINDHOLZ, J. H. FRIED, and A. A. PATCHETT. J. Org. Chem. **28**, 1092 (1963).
29. S. N. ANANCHENKO and I. V. TORGOV. Dokl. Akad. Nauk SSSR, **127**, 553 (1959).
30. N. COHEN, B. L. BANNER, W. F. EICHEL, Z. VALENTA, and R. A. DICKINSON. Synth. Commun. **8**, 427 (1978).
31. M. F. ANSELL, B. W. NASH, and D. A. WILSON. J. Chem. Soc. 3028 (1963).
32. W. T. SUMERFORD and D. N. DALTON. J. Am. Chem. Soc. **66**, 1330 (1944); H. J. TEUBER and G. JELINEK. Chem. Ber. **85**, 95 (1952).
33. M. C. KLOETZEL, R. P. DAYTON, and P. Y. ABADIR. J. Org. Chem. **20**, 38 (1955).
34. W. NUDENBERG, A. M. GADDIS, and L. W. BUTZ. J. Org. Chem. **8**, 500 (1943).
35. T. KUSAKA. J. Pharm. Soc. Jpn. **62**, 490 (1942).
36. S. J. DAUM. Diss. Abstr. **24**, 4992 (1964); Chem. Abstr. **61**, 8357g (1964).

Pyridazino[3,4,5-de]phthalazines. I. Synthesis of the heterocyclic system and key intermediates

JOHN E. FRANCIS,[1] KARL J. DOEBEL, PAULA M. SCHUTTE, EDGAR C. SAVARESE, STEPHEN E. HOPKINS, AND ERNST F. BACHMANN

Research Department, Pharmaceuticals Division, CIBA-GEIGY Corporation, Ardsley, NY 10502, U.S.A.

Received August 9, 1979

This paper is dedicated to Prof. Karel Wiesner on the occasion of his 60th birthday

JOHN E. FRANCIS, KARL J. DOEBEL, PAULA M. SCHUTTE, EDGAR C. SAVARESE, STEPHEN E. HOPKINS, and ERNST F. BACHMANN. Can. J. Chem. **57**, 3320 (1979).

1*H*-Pyridazino[3,4,5-de]phthalazine (**4**) and 3-hydrazino-1(or 9)*H*-pyridazino[3,4,5-de]-phthalazine (**6**) represent intramolecular hydrazones of the drugs hydralazine and dihydralazine, respectively. These novel heterocycles were synthesized by several different routes starting from 2,6-dimethylbenzoic acid, 3-methylphthalic anhydride, or hemimellitic acid. Tetrabromination of 2,6-dimethylbenzoic acid with bromine and carbon tetrachloride under free radical conditions followed by treatment with dilute aqueous hydrazine hydrate produced pure **4** in yields up to 58%. Treatment of 3-methylphthalic anhydride with 2 mol of *N*-bromosuccinimide under radical conditions followed by reaction of the dibromo compound with hydrazine hydrate in methyl Cellosolve produced 3-oxo-3*H*-2,9(or 1,2)-dihydropyridazino[3,4,5-de]phthalazine in 60% yield. This intermediate was converted to the 3-thiono compound or 3-chloro-1(or 9)*H*-pyridazino[3,4,5-de]phthalazine from which the hydrazine **6** was generated by hydrazine hydrate treatment. This hydrazine was further characterized by conversion with acid chlorides to novel tetracyclic condensed triazoles or by nitrous acid to a tetracyclic condensed tetrazole. The unsubstituted heterocycle **4** was uninteresting in pharmacological screens but the hydrazine **6** resembled hydralazine by lowering blood pressure in several animal test models and in limited clinical trials.

JOHN E. FRANCIS, KARL J. DOEBEL, PAULA M. SCHUTTE, EDGAR C. SAVARESE, STEPHEN E. HOPKINS et ERNST F. BACHMANN. Can. J. Chem. **57**, 3320 (1979).

Les composés suivants: 1*H*-pyridazino[3,4,5-de] phtalazine (**4**) et hydrazino-3 1*H* ou 9*H*-pyridazino[3,4,5-de] phtalazine (**6**) représentent des hydrazones intramoléculaires dans les drogues hydralazine et dihydralazine respectivement. Ces nouveaux hétérocycles sont synthétisés selon différentes méthodes en partant de l'acide diméthyl-2,6 benzoïque, de l'anhydride méthyl-3 phtalique ou de l'acide hémimellitique. La tétrabromation de l'acide diméthyl-2,6 benzoïque par le brome dans le tétrachlorure de carbone sous forme de radical libre suivi du traitement par l'hydrate d'hydrazine diluée produit le composé **4** à l'état pur avec des rendements pouvant atteindre 58%. Le traitement de l'anhydride méthyl-3 phtalique avec 2 mol de *N*-bromosuccinimide dans des conditions radicalaires suivi de la réaction du composé dibromé avec l'hydrate d'hydrazine dans le méthyl Cellosolve conduit au dérivé: oxo-3 3*H*-dihydro-2,9 (ou 1,2) pyridazino[3,4,5-de] phtalazine avec un rendement de 60%. Cet intermédiaire est transformé en composé thiono-3 ou chloro-3 1 (ou 9) *H* pyridazino[3,4,5-de] phtalazine qui traité par l'hydrate d'hydrazine conduit à l'hydrazine **6**. Cet hydrazine est de plus caractérisé par sa transformation en triazoles tétracycliques condensés à l'aide de chlorures d'acides ou en tétrazoles tétracycliques condensés. L'hétérocycle **4** non substitué n'est pas intéressant du point de vue pharmacologique mais l'hydrazine **6** ressemble à l'hydralazine en ce sens qu'elle fait baisser la pression sanguine lors de plusieurs tests chez les animaux et dans des essais cliniques limités.

[Traduit par le journal]

The antihypertensive drug hydralazine (**1**) synthesized by Druey more than thirty years ago (1) has staged a comeback recently (2) because the disturbing side effects produced by the body's reaction to the arteriolar dilating mechanism of action are counteracted by co-administration of a diuretic agent and a β-adrenergic blocking drug (3). Although the combination of a diuretic and a β-blocker is effective in the treatment of many patients with high blood pressure, the addition of an arteriolar dilating agent is effective for the treatment of a further population of resistant cases (4).

Druey prepared many modifications of the hydralazine structure, including dihydralazine (**2**), marketed in Europe. He also defined the most important structure–activity relationships in this class of compounds and suggested that the hydrazones of hydralazine could be useful prodrugs of the active principle (5). This concept is supported by a report on the investigational drug budralazine (**3**) (6) that

[1]Author to whom correspondence should be addressed.

0008-4042/79/243320-12$01.00/0

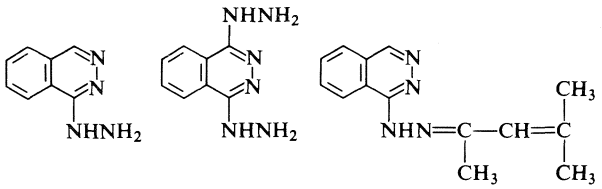

1 2 3

describes the metabolic pattern of this drug as similar to that of hydralazine (7, 8). Hydrazones of hydralazine derived from acetone, pyruvic acid, and α-ketoglutaric acid were identified in the serum and urine of patients taking hydralazine and these compounds may contribute significantly to the action of the parent drug (8).

On the basis of Druey's hypothesis, we investigated a novel heterocyclic system that is formally an internal hydrazone of hydralazine, namely, 1*H*-pyridazino[3,4,5-de]phthalazine (**4**),[2] the intramolecular cyclization product of the hitherto unknown 1-hydrazinophthalazine-8-carboxaldehyde (**5**). In the course of this work, we prepared a similar structure related to dihydralazine, namely, the hydrazino compound **6**, a second important target.

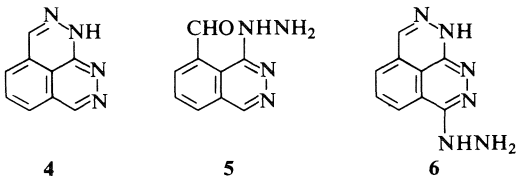

4 5 6

Since portions of this work have appeared only in the patent literature (9, 10) and in reviews (11, 12), we wish to describe the synthesis of the target compounds, some of the properties of this novel heterocyclic system, and the biological results related to the rationale for this project.

In designing the synthesis of these compounds, we saw that all nine carbon atoms could be derived from an oxidized 1,2,3-trimethylbenzene, in which the 2-methyl group is at the highest oxidation stage (carboxylic acid or equivalent) and the 1- and 3-substituents are at the aldehyde stage or the carboxylic acid stage. The nitrogen atoms could then be introduced by the use of hydrazine. Therefore, the heterocycle **4** would be prepared from 2,6-diformylbenzoic acid (**7**) or an equivalent synthon, whereas the hydrazine **6** would be generated from 3-formylphthalic acid (**8**) or equivalent. A hemimellitic acid derivative, such as the triester **9**, seemed another likely starting material as it could be reacted with hydrazine and then reduced to the desired product. In fact, we carried out all of these proposed schemes successfully.

The unsubstituted heterocycle was prepared first by a straightforward approach. 2,6-Dimethylbenzoic acid (**10**) (13) was converted to 2,6-bis(dibromomethyl)benzoic acid (**11**) smoothly with 4 mol of

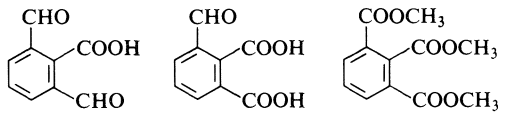

7 8 9

bromine in carbon tetrachloride at reflux under tungsten lamp illumination. The tetrabromo compound crystallized directly from the reaction, usually in high yield and good purity. The reaction was unsuccessful when *N*-bromosuccinimide was tried. Treatment of **11** with aqueous base followed by aqueous acid gave the desired intermediate, assigned structure **12** rather than **7** based on infrared spectral data indicating a hydroxyphthalide structure (14, 15). Either **11** or **12** on prolonged reflux in a 10–15% solution of hydrazine hydrate (99–100%) in water yielded the desired heterocycle **4**. When the reaction was worked up after an hour or hydrazine hydrate in ethanol was used as the reaction medium, the hydrazone of 1(2*H*)-phthalazinone-8-carboxaldehyde (**13**) was the only product isolated. Attempted purification of **13** by recrystallization from water, methyl Cellosolve, acetic acid, or attempted derivatization with benzaldehyde or acetic anhydride yielded only the highly insoluble azine **14** on workup. Attempted intramolecular cyclization of **13** in hot dimethylformamide or dimethylacetamide produced some of the desired tricyclic product but contaminated by starting material and unidentified impurities. The dry hydrazone could be sublimed unchanged but attempted aqueous acidic hydrolysis or treatment with aqueous sodium hydroxide produced the azine. Attempted cyclization in 10% aqueous organic bases such as piperidine or pyridine produced largely the azine and only traces of the desired heterocycle. However, when the hydrazone was heated at reflux in 10% aqueous hydrazine hydrate for a day, the tricyclic structure was obtained in good yield. The aldehyde **12** was reacted with more concentrated aqueous hydrazine hydrate in attempts to improve the yield and reduce the amount of solvent. Up to a strength of 40% hydrazine hydrate, the yield of **4** was still acceptable although contamination increased, but with 60 or 85% aqueous hydrazine hydrate, the hydrazone **13** was the only isolable product after

[2]In previous publications and patents, compounds with this ring system were called 1,2,8,9-tetraazaphenalenes. The text name is preferred by Chemical Abstracts.

three days at reflux. After one week at reflux, the only isolable product, surprisingly, was the Wolff–Kishner product 8-methyl-1(2*H*)-phthalazinone (**15**). A small amount of this same material was isolated as the only identifiable product from the reaction of **11** with hydrazine hydrate in refluxing methyl Cellosolve.

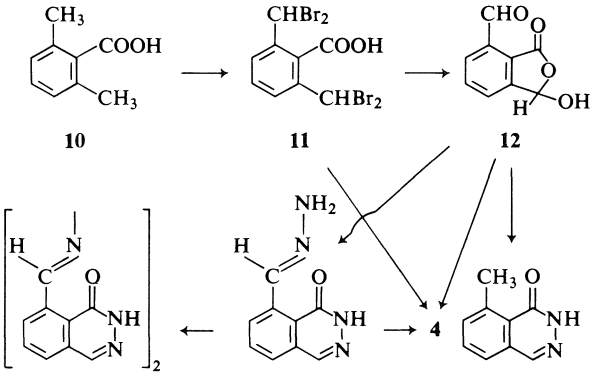

10 **11** **12**

14 **13** **15**

The tricyclic product **4** was obtained in bright yellow crystals from ethanol or water and was very stable up to its decomposition point just below 300°C. It was stable to aqueous acid and base and formed salts with methanesulphonic, hydrochloric, and maleic acids. This stability contrasts sharply with that of 1*H*-benzo[de]quinoline **16** (16) even though both heterocycles have the required number of π electrons to satisfy the Huckel rule for aromaticity (17). The ^{1}Hmr spectrum of **4** at room temperature showed a seven peak multiplet in the aromatic region (A_2B pattern) corresponding to three protons. The protons at positions 3 and 7 appeared as a singlet and the exchangeable proton on nitrogen was visible downfield as a broad singlet in deuterated dimethylsulphoxide. Thus, although the structure **4** is written for convenience as if hydrogen were localized at N-1, the molecule behaves as a tautomeric hybrid symmetrical about the line joining carbons at positions 9a, 9b, and 5. The ^{13}Cmr spectrum also agrees with this structure, although the carbon at position 9b could not be located in the spectrum. Treatment of **4** with fuming nitric acid in sulphuric acid gave the 4,6-dinitro derivative **17** in 49% yield. Attempted reduction of **17** to a mono- or diamino compound gave only intractable material.

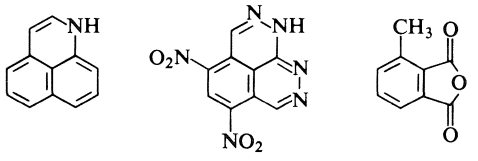

16 **17** **18**

A more versatile intermediate for preparing all of the pyridazino[3,4,5-de]phthalazines unsubstituted at positions 4, 5, and 6 was derived from 3-methylphthalic anhydride (**18**) (17). Bromination of this anhydride with 2 mol of *N*-bromosuccinimide in carbon tetrachloride, heated and illuminated by an immersion-type Mercury vapour lamp, gave the dibromomethyl compound **19**. This was converted by aqueous base followed by acid to the cyclized form of **8**, the hydroxyphthalide structure **20**. This valuable intermediate combined excellent shelf life with sufficient reactivity for our purposes although we explored other reactive intermediates with a similar oxidation state. For example, treatment of **20** with methanol and sulphuric acid gave mainly the reactive *pseudo*-ester **21**.

Another route to reactive intermediates involved a two-stage oxidation. Monobromination of **18** yielded the bromomethyl compound **22** (19) which was converted by aqueous base followed by acid to phthalide-7-carboxylic acid (**23**) (20). Conversion to the acid chloride **24** (20) followed by bromination

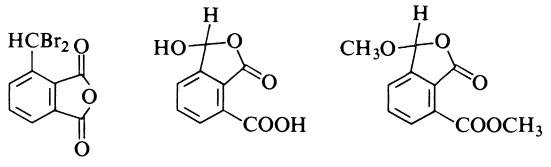

19 **20** **21**

under radical conditions gave the highly reactive intermediate **25**. Alternatively, **24** was converted to the ethyl ester **26** and then brominated to intermediate **27**.

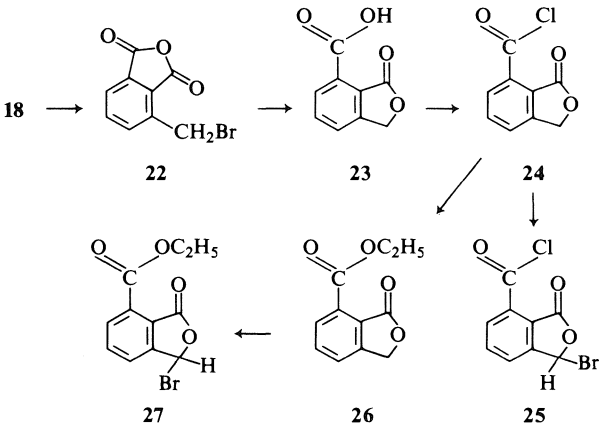

22 **23** **24**

27 **26** **25**

The work of Bird and Turner on the selective esterification of 3-chlorophthalic acid (21) encouraged our similar approach with 3-methylphthalic acid. Treatment of the diacid with methanol and sulphuric acid gave the desired half ester **28** in 65% yield along with 26% of the diester **29** (22). Careful saponifica-

tion of **29** produced the alternate half ester, 2-carbomethoxy-3-methylbenzoic acid (**30**). Free radical bromination of **28** produced the dibromomethyl derivative **31**, which was now at the desired oxidation

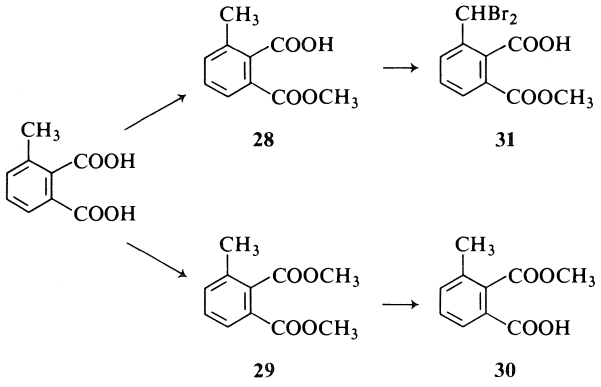

stage. The structure of the half ester **28** was elucidated unambiguously by a classical approach. Reduction of the sodium salt of **28** with sodium borohydride and aluminum chloride in diglyme followed by an acid workup yielded 7-methylphthalide (**32**) (23). Treatment of **32** with *N*-bromosuccinimide followed by ethanolic hydrazine hydrate yielded 8-methyl-1-(2*H*)-phthalazinone (**15**). Methylation of **15** gave the 2-methyl derivative **33** which was smoothly brominated to the tribromo compound **34**. Aqueous alkaline treatment of **34** followed by neutralization produced 1(2*H*)-phthalazinone-8-carboxaldehyde (**35**), not obtained previously. This aldehyde was converted smoothly by 10% hydrazine hydrate to the tricyclic compound **4**. This sequence proved the structure of the intermediates, as well as that of the half ester **30**, over which there is some uncertainty in the literature (24, 25). This also completed another synthesis of the main target structure.

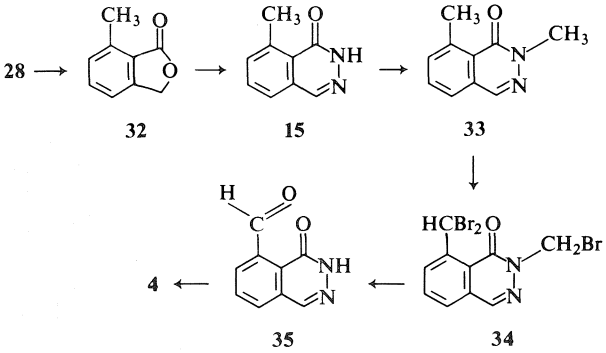

Regrettably, other attempts to use the bulk of the methyl group in preparing key intermediates were unsuccessful. Reduction of 3-methylphthalic anhydride with zinc – cupric sulphate in acid gave a 53:47 mixture of 4-methylphthalide (**36**) and 7-methylphthalide (**32**) as determined by a combination of vapour phase chromatographic separation and infrared spectral analysis. Reduction of the anhydride with 0.5 mol of lithium aluminum hydride in tetrahydrofuran gave a methylphthalide mixture only slightly richer in the desired 7-methylphthalide (59:41). Unknown to us at the time, Newman and Leegwater carried out a variation of this reduction leading to 7-methylphthalide in 69% yield (23). Conversion of **18** to 3-methylphthalimide **37***a* (26) followed by treatment with zinc – cupric sulphate in alkali gave a phthalide mixture so enriched in the undesired isomer (91:9) that it served as a method for preparing 4-methylphthalide. Another promising route was suggested by the work of Horii *et al.* (27) on the reduction of phthalimides to hydroxyphthalimidines. Accordingly, 3-methylphthalimide (**37***a*), the *N*-phenyl compound **37***b*, and the *p*-nitrophenyl derivative **37***c* were each reduced with methanolic sodium borohydride to the corresponding hydroxyphthalimidine (**38***a–c*). Each of these compounds, on treatment with ethanolic hydrazine hydrate, gave the undesired 5-methyl-1(2*H*)-phthalazinone **39**.

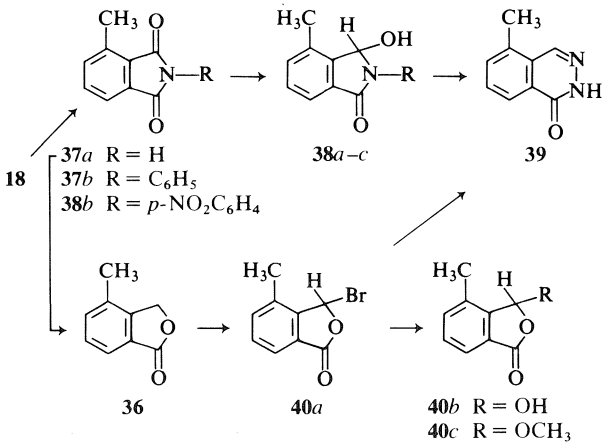

This same phthalazinone was prepared by bromination of 4-methylphthalide with *N*-bromosuccinimide followed by ethanolic hydrazine hydrate. The bromo compound **40***a* was further characterized by conversion to 3-hydroxy-4-methylphthalide **40***b* and its methyl ether **40***c*. No attempt was made to determine how much of the desired intermediates could be gleaned from the mother liquors of **38***a–c* once it became obvious that this approach was unsuitable for large scale preparations, especially since more viable routes were discovered.

The intermediates **19**, **20**, **21**, **25**, and **31** were all converted in one or two stages to 3-oxo-3*H*-2,9(or 1,2)-dihydropyridazino[3,4,5-de]phthalazine **41**, a versatile intermediate for many derivatives with this ring

system (9, 10). The shortest route, treatment of **19** with hydrazine hydrate in methyl Cellosolve at reflux for 24 h or more, produced **41** in 75–80% yields. Milder treatment of intermediates **19** or **20** with hydrazine hydrate gave 3,4-dihydro-4-oxo-5-phthalazinecarboxylic acid (**42***a*) which was further reacted with 85% hydrazine hydrate over 3½ days to produce **41** in 65% yield. The intermediate **27** was converted in ethanolic hydrazine hydrate to the ester **42***b* which was used for other purposes, but the methyl ester **42***c* was prepared from the acid **42***a* either by treatment with diazomethane or by reaction with thionyl chloride followed by methanol, and this ester was converted to **41** in refluxing ethanolic hydrazine hydrate.

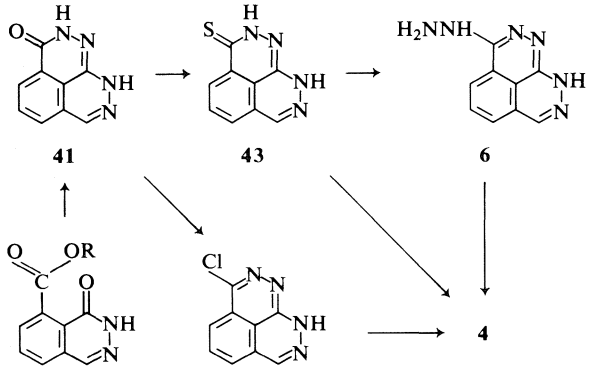

42*a* R = H
42*b* R = C_2H_5
42*c* R = CH_3

The cyclic hydrazide **41** was converted to the thiohydrazide **43** with phosphorous pentasulphide in pyridine which was then reacted with hydrazine hydrate, preferably in boiling methyl Cellosolve, to produce the second major synthetic target **6**. This was characterized as a dihydrochloride or a dimesylate but was most conveniently purified by conversion to its benzylidene hydrazone which was recrystallized and then boiled with hydrochloric acid until the benzaldehyde steam distilled out of the mixture and the dihydrochloride of **6** remained. Alternatively, **41** was converted to the chloro compound **44** with phosphoryl chloride from which **6** was prepared with hydrazine hydrate. Compounds **43** and **44** were converted to the parent heterocycle **4**, although in poor yield, by the use of Raney nickel in ethanol – methyl Cellosolve and red phosphorous in hydriodic acid, respectively. The hydrazine **6** was converted to **4** rather well with cupric sulphate at neutral pH in the presence of oxygen or, even better, by warming in phosphate buffer at pH 7.2. When the reaction was carried out in deuterium oxide, 3-deuterio-1(or 9)*H*-pyridazino[3,4,5-de]phthalazine was obtained.

Finally, the tricyclic system was synthesized from trimethyl hemimellitate **9** (28) or dimethyl-3-carboxyphthalate **45** (20). Each of these esters was reacted with hydrazine hydrate in methyl Cellosolve at prolonged reflux to form a bright orange high melting solid believed to be 7-hydroxy-3-oxo-3*H*-2,9-dihydropyridazino[3,4,5-de]phthalazine **46**, or a tautomer, which was converted with phosphorous pentachloride – phosphoryl chloride to the 3,7-dichloro compound **47**, as its hydrochloride from which **4** was obtained after treatment with red phosphorous and hydriodic acid.

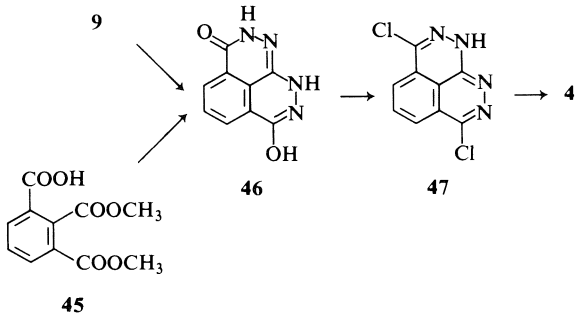

The hydrazine **6** was further derivatized in different ways. Reaction with aromatic aldehydes generally yielded coloured high melting solids (see Experimental). With benzoyl or acetyl chloride or trifluoroacetic acid, three examples of a new heterocyclic system **48***a–c*, were obtained. Nitrous acid treatment of **6** produced yet another new heterocycle, the condensed tetrazole **49**.

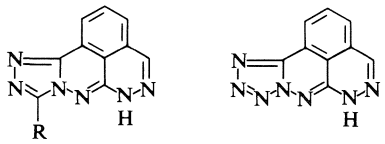

48*a* R = C_6H_5
48*b* R = CH_3
48*c* R = CF_3

49

Biological Results

The target compounds **4** and **6** were investigated for antihypertensive activity. Compound **4** was tested intravenously in the anaesthetized cat and the Nembutal anaesthetized dog. Impressive falls in blood pressure were observed with increased intensity and duration of action as the dose was increased. The compound also caused a fall in blood pressure with tachycardia in the normotensive rat. In the Goldblatt dog (29), it caused hypotension of short duration i.v. but only marginal oral activity. In the neurogenic hypertensive dog (30), the compound was inactive. Acute LD_{50} studies indicated an insufficient therapeutic index to warrant further study.

The dihydrochloride of **6**, under the code number *GPA 1595*, caused pronounced and prolonged blood pressure depression i.v. in the anaesthetized cat with increased coronary and femoral artery flow and increased cardiac contractile force. In DOCA rats it caused a substantial blood pressure fall when given orally. In the Goldblatt dog, *GPA 1595* given i.v. produced a pronounced drop in blood pressure within thirty minutes and a gradual drop in blood pressure by the oral route. The peak effect at $4\frac{1}{2}$ h was accompanied by pronounced tachycardia. Good activity in this model was demonstrated even at low oral doses. Based on acute and chronic toxicity studies, this drug was much less toxic than **4** and was recommended for clinical trial. In limited trials, *GPA 1595* caused hypotension in man accompanied by tachycardia and a high incidence of headache as one might expect of a peripheral vasodilator. Since no advantage over hydralazine could be demonstrated, the compound was not further pursued clinically. The benzylidene hydrazone of **6** was inactive in the anaesthetized cat i.v. but showed significant blood pressure activity orally in the Goldblatt dog after $3\frac{1}{2}$ h, possibly as it was acting as a pro-drug of *GPA 1595*. None of the other derivatives of **6** were of pharmacological interest.

Key intermediates in the synthesis of **4** and **6** proved to be valuable sources of many other tricyclic compounds and these will be reported in later publications.

Experimental

Melting points (uncorrected) were determined on a Thomas-Hoover capillary apparatus or, if above 220°C, on a Reichart hot stage apparatus. Infrared spectra (ir) reported in wave numbers (cm^{-1}) for the principal peaks in Nujol (N), potassium bromide (KBr), or chloroform ($CHCl_3$), were measured on a Perkin-Elmer model 137 calibrated with respect to the 1602 cm^{-1} band of polystyrene or on a model 457 grating instrument. Proton magnetic resonance spectra (^{1}Hmr) were measured on a Varian A-60D or a Varian EM-390 spectrometer in DMSO-d_6 unless otherwise stated, with peaks reported in ppm relative to tetramethylsilane as internal standard. Ultraviolet spectra (uv) were recorded on a Cary 14B spectrophotometer in nanometers with ε values in parentheses.

*2,6-Bis(dibromomethyl)benzoic Acid (**11**)*

In a 3 L, 3-necked Pyrex flask equipped with magnetic stirrer, dropping funnel, and upright condenser, a solution of 2,6-dimethylbenzoic acid **10** (17 g) (13) in carbon tetrachloride (1200 mL) was heated to incipient reflux under close range illumination with a 250 W tungsten lamp. Bromine (75 g) in CCl_4 (350 mL) was added dropwise rather rapidly to maintain vigorous reflux. During this period of about 30 min, HBr was evolved vigorously and a white precipitate formed. When evolution ceased, the mixture was cooled, filtered, and the precipitate washed with fresh solvent and oven dried at reduced pressure. The yield of **11** was 90% of theory and required no further purification, mp 203–206°C; ir (N): 1675; ^{1}Hmr ($CDCl_3$): 7.6–8.6 (m, 3*H*, aryl + C*H*Br_2). *Anal.* calcd. for $C_9H_6Br_4O_2$: C 23.21, H 1.30, Br 68.64; found: C 23.49, H 1.07, Br 68.69.

*3-Hydroxyphthalide-7-carboxaldehyde (**12**)*

The acid **11** (37.2 g) was added gradually to a stirring solution of 5% aqueous Na_2CO_3 (600 mL), heated on a steam bath until a clear solution was obtained, and then cooled and acidified with concentrated HCl. The white precipitate was collected (9.12 g) and combined with a second crop (2.57 g) obtained from the mother liquor by continuous chloroform extraction over 24 h. Recrystallization from benzene–hexane yielded a colourless solid, mp 127–133°C, unchanged by further recrystallizations; ir (N): 3250, 1740, 1690, 1590. *Anal.* calcd. for $C_9H_6O_3$: C 60.67, H 3.40; found: C 60.62, H 3.25.

*1(2H)-Phthalazinone-8-carboxaldehyde Hydrazone (**13**)*

(*a*) The aldehyde **12** (6.0 g) was added to a stirring solution of hydrazine hydrate (99–100%, 100 mL) in water (65 mL) and heated at reflux for 30 min. The hot solution was filtered free of a little solid and refrigerated overnight. The off-white solid was collected, washed with water, and dried *in vacuo* at 40°C for 66 h, mp 235–237°C. A portion was sublimed at 120°C/0.05 Torr for microanalysis, mp 235–237°C; ir (KBr): 3380, 3275, 3175, 1635, 1560; ^{1}Hmr: 7.3 (br s, NH_2), 7.8–8.4 (m, 3*H*, aryl + —C*H*=N—), 9.6 (s, vinyl ring *H*), 12.5 (br s, N*H*). *Anal.* calcd. for $C_9H_8N_4O$: C 57.43, H 4.29, N 29.77; found: C 57.28, H 4.23, N 30.04.

(*b*) A mixture of 50% hydrazine hydrate (4 mL), ethanol (10 mL), and the acid **11** (466 mg) was stirred at reflux for 18 h. The clear solution was evaporated at reduced pressure, triturated with water, and filtered. The precipitate (240 mg) was identical to the product obtained in method (*a*).

*Azine **14***

A mixture of the hydrazone **13** (4.7 g) and 0.1 *N* NaOH (550 mL) was heated under reflux for 24 h, cooled, and the white precipitate collected, washed with water, and oven dried *in vacuo*. Yield: 17.4 g (37%), mp > 350°C; ir (N): 3250, 1670. *Anal.* calcd. for $C_{18}H_{12}N_6O_2$: C 62.78, H 3.52, N 24.41; found: C 62.71, H 3.57, N 24.47.

*3-(Dibromomethyl)phthalic Anhydride (**19**)*

A mixture of 3-methylphthalic anhydride (81 g) (**18**), *N*-bromosuccinimide (182 g), benzoyl peroxide (140 mg), and carbon tetrachloride (1.5 L) was irradiated and heated at reflux in a Pyrex vessel with a 100 W Hanovia insertion-type ultraviolet lamp under magnetic stirring and moisture exclusion. The mixture turned brick red and an additional 140 mg of peroxide were added. The reaction was continued for 16.5 h, cooled, filtered free of succinimide and evaporated to dryness at reduced pressure. The residual solid was dissolved in hot ether, decolourized with charcoal, and the filtrate reduced in volume on a steam bath as *n*-hexane was gradually added to incipient crystallization. After refrigeration over 18 h the white solid was collected, washed with *n*-hexane, and dried *in vacuo*. The product (120 g, 75%), mp 93–94.5°C, was used without further purification. Another sample, recrystallized from ether–hexane, gave colourless needles, mp 93–95°C; ir (N): 1850, 1790, 1755; ^{1}Hmr: 7.6–8.6 (m, 3*H*, aryl + C*H*Br_2). *Anal.* calcd. for $C_9H_4Br_2O_3$: C 33.78, H 1.26, Br 49.92; found: C 33.66, H 1.20, Br 49.41.

*3-Hydroxyphthalide-7-carboxylic Acid (**20**)*

The anhydride **19** (40 g) was added in portions to a hot solution of 2 *N* NaOH (500 mL) under stirring. The clear solution was acidified with concentrated HCl, heated at 80°C for 0.5 h, and evaporated to dryness at reduced pressure. The residue was dissolved in hot water (600 mL), treated with

charcoal, and filtered. After 3 days at 5°C, the filtrate yielded colourless blocks (21.3 g, 88%), mp 163.5–166°C. Two recrystallizations from water raised the mp to 165.5–168.5°C; ir (N): 3320, 2800–2200 (broad), 1720, 1590; ^{1}Hmr: ~7.0 (br s, OH), 7.7–8.1 (m, 3*H*, aryl + benzylic *H*). *Anal.* calcd. for $C_9H_6O_5$: C 55.68, H 3.12; found: C 55.98, H 2.99.

*Methyl-3-methoxyphthalide-7-carboxylate (**21**)*

A mixture of hydroxyphthalide **20** (19 g), absolute methanol (167 mL), and concentrated H_2SO_4 (10 mL) was heated at reflux under moisture exclusion for 5 h. The mixture was distilled to remove ca. 100 mL of liquid, poured into ice-water (350 mL), and extracted with $CHCl_3$ (3 × 100 mL). The extract was washed with 5% Na_2CO_3, dried (Na_2SO_4), and concentrated to dryness at reduced pressure. The residue was triturated with ether to obtain the first crop (6.6 g), mp 94–97°C. Concentration of the mother liquor and gradual treatment with *n*-hexane gave two additional crops of solid (4.7 g). The first crop was twice recrystallized from ether to afford colourless needles, mp 94–97°C; ir (CCl_4): 1790, 1735; ^{1}Hmr ($CDCl_3$): 3.7 (s, CH_3O), 4.1 (s, CH_3O), 6.4 (s, —CH—), 7.7–8.0 (m, 3*H*, aryl). *Anal.* calcd. for $C_{11}H_{10}O_5$: C 59.48, H 4.54; found: C 59.66, H 4.35.

*Phthalide-7-carboxylic Acid (**23**)*

Crude 3-bromomethylphthalic anhydride (**22**, prepared according to ref. 19) (47.6 g, mp 74–87°C) was suspended in ethanol (100 mL) and aqueous 2 *N* NaOH (500 mL) and stirred at 80°C for 15 min. The pale yellow solution was cooled, acidified with concentrated HCl, heated 1 h at 80°C, and then refrigerated overnight. The crystalline product (35 g, 100%), mp 166–169°C, was twice recrystallized from methanol to give the pure sample as colourless blocks, mp 168.5–171°C (lit. (20) mp 170–172°C); ir ($CHCl_3$): 2750–2600 (broad), 1740, 1715, 1290. *Anal.* calcd. for $C_9H_6O_4$: C 60.66, H 3.40; found: C 60.41, H 3.35.

*Phthalide-7-carbonyl chloride (**24**)*

The acid **23** was converted to the acid chloride **24** in refluxing benzene–$SOCl_2$ after 3 h. One recrystallization from benzene – *n*-hexane gave the pure product (73%), mp 92–96.5°C; ir ($CHCl_3$): 1770, 1720, 1290.

*Ethyl Phthalide-7-carboxylate (**26**)*

Acid chloride **24** (30.8 g) was heated at reflux in absolute ethanol (184.5 mL) for 30 min, cooled, and the first crop of ester collected. Evaporation of the mother liquor and trituration with cold ethanol gave the second crop. Recrystallization of the combined material from benzene yielded white crystals (23.1 g, 65%), mp 89.5–92.5°C. Recrystallization from ethanol gave the pure ester, mp 90.5–92°C; ir ($CHCl_3$): 1770, 1720; ^{1}Hmr ($CDCl_3$): 3.1 (t, CH_3), 4.45 (q, CH_2—CH_3), 5.3 (s, benzylic CH_2), ~7.7 (m, 3*H*, aryl). *Anal.* calcd. for $C_{11}H_{10}O_4$: C 64.07, H 4.89; found: C 64.10, H 4.88.

*2-Carbomethoxy-6-methylbenzoic Acid (**28**)*

3-Methylphthalic acid was obtained by dissolution of the anhydride **18** in dilute aqueous NaOH at 80°C within 0.5 h, acidification with HCl, and recrystallization of the resulting precipitate from ethyl acetate – *n*-hexane, mp 156.5°C (lit. (26) mp 154°C). A mixture of 3-methylphthalic acid (18 g), methanol (180 mL), and concentrated H_2SO_4 (10 mL) was heated at reflux for 6 h under moisture exclusion. It was concentrated at reduced pressure to one-third volume, poured into ice-water, and extracted with chloroform. The chloroform solution was extracted with 10% aqueous Na_2CO_3 and the carbonate layer acidified with concentrated HCl, whereupon the crude ester crystallized (12.7 g, mp 85–98°C). Three recrystallizations from benzene–hexane yielded the pure product (8.0 g, 41%), mp 110.5–111.5°C; ir ($CHCl_3$): 2700–2300 (broad), 1720. *Anal.* calcd. for $C_{10}H_{10}O_4$: C 61.85, H 5.19; found: C 61.97, H 5.08.

The chloroform layer containing the diester **29** was dried (Na_2SO_4) and concentrated at reduced pressure to a pale yellow oil (5.5 g) which gradually crystallized. It was recrystallized from benzene–hexane, mp 40–44°C (lit. (22) mp 42.5–44°C); ir ($CHCl_3$): 1720.

*2-Carbomethoxy-3-methylbenzoic Acid (**30**)*

Dimethyl 3-methylphthalate (**29**, 20.79 g) in ethanol (25 mL) was added to a solution of KOH (5.61 g) in water (75 mL) and the mixture heated 2 h at reflux on the steam bath. The pH was adjusted to 8 with a few drops more of alkali and the solution extracted with ether. The ether extract was washed with brine, dried over Na_2SO_4, and concentrated to dryness to recover 3.8 g of diester. The alkaline solution was cooled and acidified with concentrated HCl to produce the crude monoester (15.05 g), mp 66–84°C. It was twice recrystallized from benzene–hexane with charcoal, twice from methanol–water, and again from benzene–hexane to yield the pure half ester (7.05 g), mp 114–115°C; ir (N): 2700–2300 (broad), 1720, 1690 (shoulder). *Anal.* calcd. for $C_{10}H_{10}O_4$: C 61.85, H 5.19; found: C 62.05, H 4.95. Mixed mp with **28**: 67–84°C.

*7-Methylphthalide (**32**)*

(*a*) Sodium methoxide (16.7 g) in methanol (500 mL) was reacted with 2-carbomethoxy-6-methylbenzoic acid (**28**, 58.6 g) in methanol (500 mL) and the clear solution evaporated to dryness *in vacuo*. The dry powder was kept in a desiccator over P_2O_5 until ready to be used. This sodium salt (54 g) was treated with 1 *M* $NaBH_4$ in dry diglyme (distilled over CaH_2 and then $LiAlH_4$) (500 mL). Under vigorous stirring and moisture exclusion, 2 *M* $AlCl_3$ in dry diglyme (200 mL) was added dropwise. The exotherm was controlled with an ice bath during addition, stirred at 75°C for 1 h, cooled, and then quenched in ice (500 mL) containing concentrated HCl (200 mL). The mixture was heated 1 h at 60–80°C, allowed to stand overnight, and extracted with chloroform. The dried (Na_2SO_4) chloroform solution was distilled at the water pump to remove chloroform and diglyme and the residual oil distilled at high vacuum. The fraction bp 106–120°C/0.8 Torr (21.4 g, 58%) solidified in the receiver and was recrystallized from benzene–hexane, methanol–water, and again from benzene–hexane to afford pure 7-methylphthalide, mp 86–87.5°C (lit. (23) mp 83–85°C); ir ($CHCl_3$): 1750; ^{1}Hmr ($CDCl_3$): 2.6 (s, CH_3), 5.2 (s, CH_2), ~7.3 (m, 3*H*, aryl). *Anal.* calcd. for $C_9H_8O_2$: C 72.96, H 5.44; found: C 72.92, H 5.28.

(*b*) 7-Methylphthalide was also prepared from 2,6-dimethylbenzoic acid essentially as described by Newman and Leegwater (23) except that the acid was brominated rather than the methyl ester.

*8-Methyl-1(2H)phthalazinone (**15**)*

A mixture of 7-methylphthalide (14.8 g), *N*-bromosuccinimide (18 g), benzoyl peroxide (50 mg), and carbon tetrachloride (200 mL) was heated to incipient reflux under moisture exclusion and then illuminated externally by a 1000 W tungsten lamp. A vigorous reaction occurred, the mixture turned dark orange, and gradually it became colourless. The mixture was cooled, filtered free of succinimide, and concentrated to dryness at reduced pressure. The pale yellow oil (22.85 g), ir ($CHCl_3$): 1780, thought to be 3-bromo-7-methylphthalide, was used directly without further purification. The bromophthalide (18 g), absolute ethanol (200 mL), and hydrazine hydrate (20 mL) were stirred at reflux 18 h. The solution was evaporated to one-half its volume and the crystalline material collected. Addition of water to the filtrate gave a

second crop. The combined product (11.3 g, 87%), mp 184–187.5°C, was recrystallized from ethanol with charcoal and twice from 1:1 ethanol – 0.05 *N* HCl to afford white crystals, mp 191–192.5°C; ir (N): 3120, 1650, 1565; ^{1}Hmr: 2.9 (s, C*H*$_3$), 7.5–7.9 (m, 3*H*, aryl), 8.3 (s, vinyl *H*), 12.6 (s, N*H*). *Anal.* calcd. for $C_9H_8N_2O$: C 67.49, H 5.04, N 17.48; found: C 67.34, H 4.95, N 17.25.

*2,8-Dimethyl-1(2*H*)-phthalazinone (**33**)*

A mixture of 8-methyl-1(2*H*)-phthalazinone (1.6 g), 4 *N* NaOH (2.5 mL), methyl iodide (1 mL), and methanol (25 mL) was heated at reflux for 1 h, quenched in ice-water and the precipitate washed with water and air dried. This material (1.0 g), mp 98–101°C, was combined with 1.5 g from a second run and recrystallized from cyclohexane to afford the pure material (1.6 g), mp 98–101°C; ir (N): 1640, 1575; ^{1}Hmr: 2.86 (s, C*H*$_3$), 3.68 (s, N—C*H*$_3$), ~7.4 (m, 3*H*, aryl), 7.83 (s, vinyl *H*). *Anal.* calcd. for $C_{10}H_{10}N_2O$: C 68.94, H 5.79, N 16.09; found: C 68.72, H 5.66, N 16.20.

*2-Bromomethyl-8-dibromomethyl-1(2*H*)-phthalazinone (**34**)*

A mixture of 2,8-dimethyl-1(2*H*)-phthalazinone (400 mg), benzoyl peroxide (20 mg), and carbon tetrachloride (50 mL) was raised to reflux and bromine (0.5 mL) in CCl_4 (50 mL) added dropwise. The mixture was heated and illuminated externally 3 h longer with a 250 W infrared lamp. The solution was evaporated to dryness and the residual solid (600 mg), mp 124–140°C, recrystallized from benzene–hexane to give the pure compound (400 mg), mp 156–159°C; ir (N): 1650; ^{1}Hmr: 5.97 (s, N—C*H*$_2$—Br), 7.4–8.5 (m, 3*H*, aryl), 8.2 (s, vinyl *H*), 8.86 (s, C*H*Br$_2$). *Anal.* calcd. for $C_{10}H_7Br_3N_2O$: C 29.23, H 1.72, N 6.82, Br 58.34; found: C 29.16, H 1.80, N 6.87, Br 58.27.

*1(2*H*)-Phthalazinone-8-carboxaldehyde (**35**)*

A mixture of **34** (6.3 g) and 5% aqueous Na_2CO_3 (200 mL) was heated 1 h on a steam bath, filtered hot, cooled, and the pH adjusted to 7 with HCl. The resulting white precipitate (1.0 g), mp 251–253°C, was recrystallized from water to give the pure aldehyde, mp 252–254°C. *Anal.* calcd. for $C_9H_6N_2O_2$: C 62.06, H 3.48, N 16.09; found: C 61.84, H 3.38, N 16.23.

*Reduction of 3-Methylphthalimide(**37**a): 4-Methylphthalide (**36**)*

Zinc dust (72 g) and cupric sulphate solution (400 mg of the salt in 14 mL of water) were stirred into a paste and treated with 20% NaOH solution (160 g). The mixture was cooled to 4°C and 3-methylphthalimide (**37***a*, 58.8 g) (26) added gradually over 0.5 h under stirring and external cooling and then 0.5 h longer at 5–8°C. It was diluted with water (100 mL) and stirred vigorously on a steam bath for 3 h. The mixture was filtered free of inorganic insolubles, acidified with concentrated HCl, heated 1 h on a steam bath, cooled, and extracted with chloroform. The extracts were dried (Na_2SO_4), concentrated, and the residual oil (48 g) distilled *in vacuo*. The fraction bp 124–131°C/1–0.9 Torr (27 g, 50%) was crystallized from benzene–*n*-hexane. The product (19.2 g), mp 66.5–68.5°C, was pure by vpc analysis and identical to a sample from another run purified by alumina chromatography (Woelm, neutral, activity I) and recrystallized from benzene–*n*-hexane, mp 69–70.5°C; ir ($CHCl_3$): 1750; ^{1}Hmr ($CDCl_3$): 2.4 (s, C*H*$_3$), 5.2 (s, C*H*$_2$), ~7.4 (m, 3*H*, aryl). *Anal.* calcd. for $C_9H_8O_2$: C 72.95, H 5.44; found: C 72.96, H 5.36.

In another run, the concentrated $CHCl_3$ extract was distilled and the fraction bp 118–132°C/0.3 Torr (45%) subjected to vpc analysis directly. The ratio of 4-methylphthalide to 7-methylphthalide was 91:9.

*3-Bromo-4-methylphthalide (**40**a)*

4-Methylphthalide (14.8 g) was brominated as described for 7-methylphthalide (**32**) but without external illumination. The product was obtained as a solid (14.7 g), mp 86–90°C, analytically pure, from the reaction after 50 min, ir ($CHCl_3$): 1790. *Anal.* calcd. for $C_9H_7BrO_2$: C 47.61, H 3.11, Br 35.20; found: C 47.59, H 2.85, Br 35.07.

*3-Hydroxy-4-methylphthalide (**40**b)*

A mixture of 3-bromo-4-methylphthalide (5.0 g) and water (8.2 mL) was heated 35 min at reflux, the solid broken up with a spatula, water (20 mL) added, and reflux continued 25 min longer. The mixture was filtered hot and a white solid (1.2 g), mp 276.5–280°C, collected. This was thought to be *bis*(4-methyl-3-phthalidyl) ether. The filtrate was cooled and white needles (2.15 g), mp 115–116.5°C, twice recrystallized from benzene–hexane to give the pure compound, mp 117.5–119°C; ir (N): 3550, 1765. *Anal.* calcd. for $C_9H_8O_3$: C 65.85, H 4.92; found: C 65.68, H 4.84.

*3-Methoxy-4-methylphthalide (**40**c)*

A mixture of **40***a* (4.0 g), methanol (25 mL), and concentrated HCl (5 drops) was heated 1.5 h at reflux, cooled, filtered free of white solid (0.9 g, 281–291°C, ir identical to high melting solid in previous reaction), and evaporated at reduced pressure to a yellow syrup (2.5 g). Three crystallizations from methanol–water gave the pure sample, mp 61–63.5°C; ir ($CHCl_3$): 1765; ^{1}Hmr: 2.4 (s, C*H*$_3$), 3.5 (s, C*H*$_3$O), 6.6 (s, C*H*, benzylic), 7.5–7.8 (m, 3*H*, aryl). *Anal.* calcd. for $C_{10}H_{10}O_3$: C 67.40, H 5.66; found: C 67.21, H 5.57.

Reduction of 3-Methylphthalic Anhydride

(*a*) Lithium aluminum hydride (1.82 g) in dry tetrahydrofuran (THF) (150 mL) was added gradually to a stirring solution of 3-methylphthalic anhydride (13 g) in dry THF (300 mL) at 0°C under moisture exclusion. The milky white suspension was stirred 1.5 h longer, excess hydride destroyed with ethyl acetate, and the mixture poured into ice and HCl. It was extracted with ether, the ether dried (Na_2SO_4), concentrated to a pale yellow oil (11.9 g), and distilled *in vacuo*. The product bp 114–123°C/0.9 Torr (8.86 g, 75%) was a mixture of 4-methylphthalide and 7-methylphthalide in the ratio 41:59, as shown by vpc/ir analysis.

(*b*) A slurry of 3-methylphthalic anhydride (13 g), glacial acetic acid (40 g), and concentrated HCl (29 g) was treated gradually with a paste of zinc dust (17.8 g) in cupric sulphate (95 mg) in water (3.5 mL) at 25–30°C. It was heated 5 h on a steam bath under vigorous stirring, allowed to stand 16 h, filtered free of solid, diluted with water (75 mL), adjusted to pH 5 with K_2CO_3, heated 1 h and then cooled. The white solid which formed was dried over P_2O_5 (9.9 g) and vacuum distilled. The fraction bp 134–145°C/1 Torr (8.22 g, 70%) was a 53:47 mixture of 4-methyl- and 7-methylphthalide (vpc/ir analysis).

*3-Methyl-*N*-phenylphthalimide (**37**b)*

A mixture of 3-methylphthalic anhydride (24.3 g), aniline (13.7 mL), and glacial acetic acid (100 mL) was heated 16 h at reflux, quenched in ice (200 mL), and the resulting precipitate washed with water and recrystallized from ethanol to give the pure product (26.7 g, 75%), mp 143.5–146°C; ir ($CHCl_3$): 1760, 1710. *Anal.* calcd. for $C_{15}H_{11}NO_2$: C 75.95, H 4.68, N 5.91; found: C 75.84, H 4.69, N 6.01.

Similarly, 3-methyl-*N*-(*p*-nitrophenyl)phthalimide (**37***c*) was prepared in 81% yield, mp 273–276°C. Recrystallized from dimethylformamide, white crystals, mp 274–276°C, were obtained. Infrared (KBr): 1775, 1730. *Anal.* calcd. for $C_{18}H_{10}N_2O_4$: C 63.83, H 3.58, N 9.92; found: C 64.19, H 3.71, N 10.02.

*3-Hydroxy-4-methylphthalimidine (**38**a)*

Sodium borohydride (3.8 g, 0.1 mol) in methanol (90 mL) was added dropwise under vigorous stirring at 25–30°C to a suspension of 3-methylphthalimide (8.05 g, 0.05 mol) in 9:1 methanol–water (60 mL). It was stirred 16 h, treated with glacial acetic acid until a clear solution was obtained, and evaporated to dryness at reduced pressure. The residue was triturated with water and the solid, mp 155–179°C, recrystallized from methanol (30 mL) to give a white solid (1.35 g, 17%), mp 187–189.5°C, which showed a major spot in tlc and only a trace impurity; ir (N): 3250, 1675. *Anal.* calcd. for $C_9H_9NO_2$: C 66.23, H 5.56, N 8.58; found: C 65.89, H 5.56, N 8.48.

By a similar route 3-methyl-*N*-(*p*-nitrophenyl)phthalimidine (**37***c*) was converted to 4-hydroxy-3-methyl-*N*-(*p*-nitrophenyl)-phthalimidine (**38***c*) after 66 h reaction in 70% yield, mp 233–236°C. Recrystallization from glacial acetic acid gave one spot material in tlc, mp 232–235°C; ir (N): 3350, 1675. *Anal.* calcd. for $C_{15}H_{12}N_2O_4$: C 63.37, H 4.25, N 9.85; found: C 63.24, H 4.38, N 10.01.

Similarly, except that a 4:1 ratio of borohydride to substrate was used, 4-hydroxy-3-methyl-*N*-phenylphthalimidine (**38***b*) was prepared from **37***b* in 26% pure yield, mp 152.5–154°C; ir ($CHCl_3$): 3520, 1700; ^{1}Hmr: 2.45 (s, CH_3), 6.59 (s), 6.63 (s, O*H*, benzylic *H*), 7.2–7.9 (m, 8*H*, aryl). *Anal.* calcd. for $C_{15}H_{13}NO_2$: C 75.29, H 5.47, N 5.86; found: C 75.16, H 5.49, N 6.04.

*5-Methyl-1(2*H*)phthalazinone (**39**)*

(*a*) A mixture of **38***a* (8.15 g), water (50 mL), and hydrazine hydrate (50 mL) was heated 16 h at reflux, cooled, and filtered. The white solid (7.75 g, 97%), mp 213.5–215°C was recrystallized from methanol to give the pure product (6.2 g), mp 214–216°C; ir (N): 3120, 1645, 1595, 1550; ^{1}Hmr: 2.7 (s, CH_3), ~7.6 (m, 2*H*, aryl), ~8.2 (m, *H* at C-8), 8.6 (s, vinyl *H*), 12.8 (s, N*H*). *Anal.* calcd. for $C_9H_8N_2O$: C 67.48, H 5.04, N 17.49; found: C 67.40, H 5.02, N 17.49.

(*b*) A suspension of **40***a* (23.9 g) in ethanol (250 mL) was reacted with hydrazine hydrate (25.2 mL) at reflux for 16 h. Water (100 mL) was added, the solution evaporated to one-half volume, cooled, and the yellow precipitate (11.3 g, 71%), mp 151.5–167°C, recrystallized from ethanol – 0.05 *N* HCl to afford the pure product, mp 209–213°C, with an identical ir spectrum to that from method (*a*).

(*c*) Reaction of **38***b* (1.5 g), ethanol (50 mL), and hydrazine hydrate (5 mL) after 18 h at reflux was incomplete. The whole was concentrated to dryness and reacted with 50% hydrazine hydrate (40 mL) at reflux over 18 h, cooled, and the white precipitate (770 mg) mp 208–211°C, recrystallized from methanol to give the pure product, mp 213.5–215.5°C, identical (ir) to that of method (*a*).

(*d*) By the same route, **38***c* was converted to the phthalazinone derivative, mp 212.5–213.5°C, identical (ir) to that from method (*a*).

*1*H*-Pyridazino[3,4,5-de]phthalazine (**4**)*

(*a*) To a suspension of 2,6-bis(dibromomethyl)benzoic acid (46.5 g) in water (1150 mL) was added hydrazine hydrate (173 mL) and the mixture rapidly raised to reflux and stirred 64 h. The hot mixture was filtered and the filtrate allowed to cool to about 10°C. The yellow precipitate (13.3 g, 78%) was recrystallized from ethanol in sparkling yellow crystals (10.4 g). In several other runs, the product was recrystallized from boiling water. On the hot stage apparatus, the product changed crystal form in the range 190–240°C and melted with decomposition in the range 294–298°C; ir (KBr): (region 3500–800, principal peaks): 3200, 3120, 3030, 2800–2200 (broad), 1620, 1610, 1590, 1550, 1490, 1450, 1425, 1375, 1340, 1170, 980, 900, 860, 850. ^{1}Hmr: 7.45–7.9 (m, 3*H*, aryl), 8.3 (s, 2*H*, vinyl), 12.5 (s, N*H*); uv (neutral 3A ethanol): 250 (7900); 330 (11250); (acidic 3A ethanol): 243 (9600), 251 (8300), 311 (9250), 335 (5400), 350 (5600), 367 (2850); (alkaline 3A ethanol): 349 (12150), 367 (15100), 378 (16450); ^{13}Cmr (Varian CFT-20): 121.55 (C-4, C-6), 134.04 (C-5), 126.68 (C-3a, C-6a), 140.73 (C-3, C-7), 180.92 (C-9a). (C-9b could not be detected.) Mass spectra (A.E.I. MS-9) *m/e*: 170 (mol. ion), 142 (—N_2), 115 (—N_2, —HCN), 114 (—$2N_2$).

(*b*) Hydrazine hydrate (122 mL) was added to a suspension of 3-hydroxyphthalide-7-carboxaldehyde (**12**) (30.2 g) in water (1040 mL) and the mixture stirred 66 h at reflux. The solution was filtered hot and then allowed to cool overnight to room temperature. The yellow solid (22.14 g, 77%) was recrystallized from ethanol to give a sample (16.9 g), mp 293–298°C dec., identical (ir) to that of method (*a*).

(*c*) A mixture of 1(2*H*)-phthalazinone-8-carboxaldehyde hydrazone (**13**) (940 mg), hydrazine hydrate (10 mL), and water (100 mL) yielded after 24 h reflux crude **4**, mp 279–288°C dec., in 82% yield. Recrystallization from ethanol gave the product identical (ir) to that of method (*a*).

(*d*) Under similar conditions, 1(2*H*)-phthalazinone-8-carboxaldehyde (**35**) was converted to **4**, mp 291–296°C dec., in 58% yield.

*4,6-Dinitro-1*H*-pyridazino[3,4,5-de]phthalazine (**17**)*

Fuming nitric acid (100 mL) was added dropwise at 10°C to a stirring solution of concentrated H_2SO_4 (100 mL) and **4** (17.0 g) was added gradually at a rate to maintain a temperature of 15–23°C. It was stirred 15 min longer and then quenched in ice-water. A small amount of solid was filtered off and the filtrate adjusted to pH 8 with 20% NaOH. The dark red precipitate was dissolved in boiling water (3 L), filtered, and the filtrate acidified with acetic acid and cooled overnight. The red precipitate which formed (12.8 g) was twice recrystallized from dimethylformamide–water (6:1) to give the pure product, mp > 350°C; ir (N): 3100, 1640, 1615, 1565, 1535, 1340; ^{1}Hmr: 9.24 (s, *H* at C-5), 9.5 (s, 2*H*, vinyl), 10.1 (broad s, N*H*). *Anal.* calcd. for $C_9H_4N_6O_4$: C 41.53, H 1.55, N 32.30; found: C 41.53, H 1.76, N 32.28.

*Reaction of **12** with 60% Hydrazine Hydrate: 8-Methyl-1(2*H*)-phthalazinone (**15**)*

Hydrazine hydrate (45 mL) was added to a suspension of 3-hydroxyphthalide-7-carboxaldehyde (1.78 g) in water (30 mL) to afford a clear solution. After 30 min at reflux, an aliquot (3 mL) was cooled, filtered, and the precipitate identified (ir) as the hydrazone **13**. After 6 h at reflux, the aliquot was mainly **13** with some **4** present (ir, tlc). This mixture appeared to remain unchanged after 23 h and 48 h, but after 166 h at reflux, the remainder was cooled and the product (840 mg), mp 197–199°C, identified (ir) as largely 8-methyl-1(2*H*)-phthalazinone (**15**). Recrystallization from ethanol – 0.05 *N* HCl gave the pure product, mp 188–191°C. The same result was observed with 85% hydrazine hydrate as the reaction medium.

*3,4-Dihydro-4-oxo-5-phthalazine Carboxylic Acid (**42**a)*

A mixture of 3-hydroxyphthalide-7-carboxylic acid (**20**) (30.2 g), hydrazine hydrate (50 mL), and water (100 mL) was stirred at reflux for 16 h, cooled, acidified with dilute HCl, and the off-white product (32.2 g), mp 300–306°C, recrystallized from glacial acetic acid, mp 303.5–306°C; ir (N): 2700–2200 (broad), 1700, 1655, 1585. *Anal.* calcd. for $C_9H_6N_2O_3$: C 56.84, H 3.18, N 14.73; found: C 57.02, H 3.15, N 14.65.

The same product was obtained from 3-(dibromomethyl)-phthalic anhydride in 50% hydrazine hydrate and ethanol at reflux or hydrazine hydrate – chloroform at reflux.

*Ethyl-3,4-dihydro-4-oxo-5-phthalazinecarboxylate (**42**b)*

Ethyl phthalide-7-carboxylate **26** was converted to the 3-bromo compound **27** as described for 7-methylphthalide and obtained in quantitative yield as a pale yellow oil, ir (CH_2Cl_2): 1800 and 1720. The oil (25.2 g) was dissolved in absolute ethanol (172 mL), whereupon some white solid formed. Hydrazine hydrate (17.25 mL) in ethanol (172 mL) was added cautiously and the mixture stirred 16 h at reflux. It was filtered hot and the filtrate evaporated to dryness at reduced pressure, suspended in 1 *N* HCl, and extracted with chloroform. The dried (Na_2SO_4) extract was filtered through Woelm neutral alumina, grade II (100 g), concentrated to dryness and recrystallized from ethanol to give the pure ester (8.3 g, 43%), mp 169.5–171.5°C; ir ($CHCl_3$): 1730, 1670, 1600. *Anal.* calcd. for $C_{11}H_{10}N_2O_3$: C 60.54, H 4.62, N 12.84; found: C 60.54, H 4.62, N 12.62.

*Methyl-3,4-dihydro-4-oxo-5-phthalazinecarboxylate (**42**c)*

A mixture of the acid **42***a* (100 g) and thionyl chloride (250 mL) was stirred at reflux under moisture exclusion for 2.5 h. It was concentrated at reduced pressure, taken up in benzene (50 mL), filtered, and the precipitate (96.9 g, 88%, calculated as the acid chloride) kept in a desiccator until ready for use. The acid chloride (232.5 g) in absolute methanol (2 L) was stirred 18 h at reflux and then refrigerated. The ester crystallized in colourless needles (220.1 g, 97%), mp 210–212°C.

The original sample of this ester was obtained by reaction of **42***a* with ethereal diazomethane in methanol in 82% yield. Recrystallized from methanol, it melted at 207–209°C; ir (N): 1730, 1670; ^{1}Hmr: 4.0 (s, C*H*$_3$O), 7.8–8.3 (m, 3*H*, aryl), 8.6 (s, vinyl *H*), 13.0 (s, N*H*). *Anal.* calcd. for $C_{10}H_8N_2O_3$: C 58.82, H 3.95, N 13.72; found: C 58.77, H 3.99, N 13.86.

*3-Oxo-3*H*-2,9(or 1,2)-dihydropyridazino[3,4,5-de]phthalazine (**41**)*

(*a*) A mixture of 3-(dibromomethyl)phthalic anhydride (**19**) (95.26 g), hydrazine hydrate (120 mL), and methyl Cellosolve (490 mL) was stirred 24 h at reflux, cooled, and the yellow solid washed with water, methanol, and oven dried *in vacuo*. The crude product (45.0 g, 80%), mp > 350°C, was recrystallized from dimethylformamide to give a microcrystalline powder, mp > 350°C; ir (N) (range 3500–800, principal peaks): 3260 (sh), 3180, 2850, 1655, 1630, 1610, 1590, 1200, 870, 840; ^{1}Hmr (CD_3COOD): ~7.9 (m, 3*H*, aryl), 8.4 (s, vinyl *H*). *Anal.* calcd. for $C_9H_6N_4O$: C 58.06, H 3.25, N 30.09; found: C 57.92, H 3.58, N 30.28.

(*b*) A mixture of **21** (1.11 g), hydrazine hydrate (4 mL), and absolute ethanol (10 mL) was stirred 94 h at reflux. It was filtered hot and the precipitate washed with water, methanol, and recrystallized from dimethylformamide to give the pure product (0.82 g, 88%), mp > 350°C, identical (ir) to that from method (*a*).

(*c*) Phthalide-7-carbonyl chloride **24** was converted to the 3-bromo compound **25** as described in the bromination of 7-methylphthalide. It was obtained as a solid which fumed in air, ir ($CHCl_3$): 1800 and 1720 in 67% yield. The crude **25** (28.7 g), ethanol (279 mL), and hydrazine hydrate (50 mL) after 18 h reflux with the usual workup and purification gave 2.2 g (11%) identical to that from method (*a*).

(*d*) The half ester **28** (9.7 g) was converted to the dibromo compound **31** as described for the synthesis of **11**. The crude **31** was obtained as an oil (ir (N): 2700–2300 (broad) and 1720), dissolved in cold ethanol (100 mL), treated cautiously with 50% aqueous hydrazine hydrate (40 mL), and stirred 72 h at reflux. Hot filtration yielded a first crop (1.54 g) of yellow solid and the filtrate was concentrated to dryness and heated in glacial acetic acid for 66 h, evaporated to dryness, and triturated with methanol to produce a second crop (1.8 g). Recrystallization from dimethylformamide gave pure **41** (1.29 g, 14%) identical (ir) to that of method (*a*).

(*e*) A mixture of **42***a* (3.16 g), hydrazine hydrate (170 mL), and water (30 mL) was stirred 84 h at reflux, cooled, poured into excess 5% aqueous Na_2CO_3, and the yellow product collected, washed, and dried. The yield was 2.4 g (65%), mp > 350°C, identical (ir) to that from method (*a*).

*3-Thiono-3*H*-2,3(or 9)-dihydropyridazino[3,4,5-de]phthalazine (**43**)*

A mixture of **41** (44.14 g), phosphorous pentasulphide (58.29 g), and pyridine (356 mL) was stirred 2.5 h at reflux, cooled, and poured into a stirring solution of ice-cold saturated brine (1 L). After 1.5 h stirring, the orange-red product was collected, suspended in water, refiltered, and dried at 100°C *in vacuo*. The crude product (35.0 g, 73%), mp 298–320°C, was suitable for further experiments. A portion was recrystallized from methyl Cellosolve – water (insoluble material removed), and then dimethylformamide–water to give the analytical sample, mp 318–322°C (stage preheated to 250°C); ir (N) (3500–800 principal peaks): 3230 (sh), 3130, 1615, 1580, 1550, 1370, 1330, 1230, 1210, 1182, 840; ^{1}Hmr: 7.8–8.8 (m, 4*H*, aryl + vinyl), 5.3 (br s, 2N*H*). *Anal.* calcd. for $C_9H_6N_4S$: C 53.45, H 2.99, N 27.71; found: C 53.37, H 3.00, N 27.85.

*3-Chloro-1(or 9)*H*-pyridazino[3,4,5-de]phthalazine (**44**)*

A mixture of phosphoryl chloride (60 mL), water (10 drops), and **41** (9.3 g) was stirred 20 h at reflux, evaporated at reduced pressure to a brown foam, triturated with cold ethanol, and a yellow solid (8.6 g), mp ~270°C dec., collected. On standing, a second and third crop of solid precipitated from the ethanol solution. The combined material (11.1 g) was dissolved as well as possible in excess hot 1 *N* HCl, filtered, and the filtrate cooled and made basic with 20% aqueous Na_2CO_3. The resulting tan precipitate was washed with water and dried *in vacuo*. This material **44** was pure enough for further work.

A second sample of **44** (12.0 g) was suspended in dry methanol (200 mL), methanesulphonic acid (4.6 mL) added, and the solution refrigerated at −8°C. The precipitate (11.0 g, 37%), mp 244–246°C dec., was twice recrystallized from methanol, the first with charcoal, to give the pure sample, mp 246–249°C dec.; ir (N): 2800–2200 (broad), 1630, 1595, 1555; ^{1}Hmr: 2.6 (s, C*H*$_3$—S), 8.1–8.6 (m, 3*H*, aryl), 9.2 (s, vinyl *H*), 13.0 (s, 2N*H*). *Anal.* calcd. for $C_9H_5ClN_4 \cdot CH_4O_3S$: C 39.94, H 3.02, N 18.63, Cl 11.79, S 10.66; found: C 39.98, H 3.09, N 18.73, Cl 11.62, S 10.56.

*3-Hydrazino-1(or 9)*H*-pyridazino[3,4,5-de]phthalazine Dihydrochloride (**6**)*

A mixture of 85% hydrazine hydrate (500 mL) and **43** (30 g) was stirred vigorously at reflux for 20 h. It was cooled, filtered, and the yellow precipitate washed with water and dried *in vacuo*. The free base (21.0 g) was suspended in excess 3 *N* HCl, filtered free of insoluble material, and the filtrate concentrated to dryness at reduced pressure. The residue was taken up in a minimal quantity of water and crystallized by addition of cold concentrated HCl. A second crystallization by this method gave the analytical sample, mp 245–248°C dec.; ir (N): (3500–800, principal peaks): 2700–1900 (broad), 1620, 1600, 1575, 1550, 1525, 1320, 1160, 955, 850, 813; ^{1}Hmr (D_2O, sodium 3-(trimethylsilyl)-1-propane sulphonate as internal standard): 8.0–8.45 (m, 3*H*, aryl), 8.6 (s, vinyl *H*); uv (H_2O): 228 (19100), 269 (9550), 311 (7050), 367 (4770). *Anal.* calcd. for $C_9H_6N_2 \cdot 2HCl$: C 39.57, H 3.69, N 30.77, Cl 25.97; found: C 39.68, H 4.34, N 30.78, Cl 25.65.

The dimethane sulphonate was prepared in ethanol and recrystallized from methanol–ether, mp 235–237°C dec. *Anal.* calcd. for $C_9H_8N_6 \cdot 2CH_4O_3S$: C 33.67, H 4.11, N 21.42; found: C 33.94, H 4.40, N 21.46.

Benzylidene Hydrazone of ***6***

To a stirring solution of the dihydrochloride of **4** (14.4 g) in water (150 mL) and ethanol (100 mL) was added at 50°C a solution of benzaldehyde (5.5 mL) in ethanol (50 mL). A thick mass quickly formed and water (100 mL) was added to aid stirring. After 5 min, 1 *N* $NaHCO_3$ (130 mL) was added, whereupon the precipitate turned from yellow to orange. The mixture was stirred another 10 min at 50–55°C, cooled, filtered, and the product washed with water, then ethanol, and dried *in vacuo*. The crude product (14.9 g, 98%), mp 260–265°C, resolidified and remelted at 325–335°C, was recrystallized three times from methyl Cellosolve to give bright orange needles, mp 268–270°C/336–340°C dec.; ir (N): (3500–1500 region): 3250, 3050, 1625, 1595, 1560, 1545, 1525. *Anal.* calcd. for $C_{16}H_{12}N_6$: C 66.65, H 4.20, N 29.15; found: C 66.49, H 4.25, N 29.06.

The following hydrazones, prepared similarly, had C, H, and N analyses within 0.3. The aldehyde, colour of hydrazone, recrystallization solvent, and mp are indicated: 3-nitrobenzaldehyde, red, DMF, 305–308/ > 350°C; 3,4-dichlorobenzaldehyde, orange, DMF, 313–320/ > 350°C; *p*-acetamidobenzaldehyde, orange, methyl Cellosolve – water, mp 213–217/ ~330°C dec.; veratraldehyde, orange, DMF–H_2O, mp 235–237°C; 4-cyanobenzaldehyde, reddish-orange, DMF, mp 305–310/ > 350°C; 3,4,5-trimethoxybenzaldehyde, orange, methyl Cellosolve – water, mp 265–267°C; *trans*-cinnamaldehyde, red, DMF, mp 243–247/ > 350°C; 2-pyridinecarboxaldehyde, orange, DMF, mp 257–258°C; indole-3-carboxaldehyde, orange, DMF–H_2O, mp 305–310/ > 350°C.

*3-Deuterio-1(or 9)*H*-pyridazino[3,4,5-de]phthalazine*

A mixture of **6** (1 g), deuterium oxide (99.5%, 100 mL), and $CuSO_4$ crystals (20 mg) was adjusted to pH 8 with a little anhydrous Na_2CO_3. It was stirred at room temperature while air was bubbled in over 18 h. The mixture was filtered free of dark solid, concentrated to dryness at reduced pressure, and extracted with chloroform (4 × 50 mL). Evaporation of the chloroform left a yellow solid (0.2 g), mp 257–262°C dec., which was recrystallized from ethanol to give 0.14 g, mp 268–270°C dec.; ir (KBr) (3000–800, principal peaks): 2850 (broad), 1657, 1620, 1610, 1585, 1450, 1368, 1170, 850; ^{1}Hmr: 7.2–7.6 (m, 3*H*, aryl), 8.2 (s, 1*H*, vinyl), 11.8 (broad s, N*H*).

*9-Phenyl-6*H*-pyridazino[3,4,5-de][1,2,4]triazolo[3,4-a]-phthalazine (****48****a)*

The dihydrochloride of **6** (14.0 g) was added gradually to a stirring solution of benzoyl chloride (6.5 mL) in pyridine (100 mL). After the initial exotherm, it was stirred 2 h at reflux, poured into ice-water, and stirred 16 h. The precipitate was washed with water and ethanol thoroughly and the crude **48***a* (13.0 g, 89%) mp 298–338°C dec., was recrystallized twice from methyl Cellosolve, once with charcoal, to give pale yellow crystals, mp 332–342°C dec.; ir (N): 3020, 1625, 1600, 1530; uv (CH_3OH): 279.5 (28500), 348 (6200). *Anal.* calcd. for $C_{16}H_{10}N_6$: C 67.11, H 3.53, N 29.36; found: C 66.99, H 3.68, N 29.52.

By the use of acetyl chloride in pyridine, the 9-methyl derivative **48***b*, mp > 355°C, was obtained. Infrared (N): 3020, 1625, 1600, 1520. *Anal.* calcd. for $C_{11}H_8N_6$: C 58.92, H 3.60, N 37.48; found: C 58.65, H 3.74, N 37.60.

*9-Trifluoromethyl-6*H*-pyridazino[3,4,5-de][1,2,4]triazolo-[3,4-a]phthalazine (****48****c)*

The dihydrochloride of **6** (65.7 g) in trifluoroacetic acid (200 mL) was stirred 20 h at reflux, poured into ice-water (600 mL), and the precipitate (64.3 g) recrystallized twice from dimethylformamide to afford the pure **48***c*, mp 314–315°C; ir (N): 3110, 1630, 1608, 1595, 1530, 1278, 1188, 1178, 1135. *Anal.* calcd. for $C_{11}H_5F_3N_6$: C 47.49, H 1.81, N 30.21, F 20.49; found: C 47.38, H 1.96, N 30.13, F 20.17.

*6*H*-Pyridazino[3,4,5-de]tetrazolo[5,4-a]phthalazine (****49****)*

A solution of **6**·2HCl (44 g) in water (900 mL) cooled to 0°C was treated dropwise with $NaNO_2$ (10.65 g) in water (150 mL) to maintain a temperature of 0–5°C. A tan solid gradually precipitated during addition. It was stirred 30 min longer and the precipitate washed with water and air dried. The crude tetrazole **49** (34 g, 100%) was recrystallized three times from DMSO (once with charcoal), washed thoroughly with ethanol, and dried *in vacuo*, mp > 350°C; ir (N): 3050, 1620, 1600, 1580, 1530. *Anal.* calcd. for $C_9H_5N_7$: C 51.18, H 2.39, N 46.43; found: C 51.02, H 2.35, N 46.13.

Preparation of ***4*** *from Hemimellitic Esters*

A mixture of trimethyl hemimellitate (**9**) (28) (2.52 g), hydrazine hydrate (20 mL), and methyl Cellosolve (80 mL) was stirred 46 h at reflux, cooled, and the yellow-orange precipitate washed well with water and methanol and dried *in vacuo*. Crude **46** (1.6 g), mp > 350°C, ir (N): 3500, ~3200, 2700–2200 (broad), 1630, 1585, 1565, 1530 was also obtained in 37% yield from dimethyl-3-carboxyphthalate (**45**) in refluxing 50% aqueous hydrazine hydrate after 47 h.

Crude **46** (10 g), phosphorous pentachloride (25 g), and phosphoryl chloride (125 mL) were heated at reflux under moisture exclusion for 22 h. The dark mixture was cooled, quenched in ice-water and filtered. The product (2.75 g), mp > 330°C was combined with a second crop (2.85 g) obtained by evaporation of the mother liquor to 100 mL, (ir (N): 2800–2200 (broad), 1615, 1565, 1540) and used without purification. A portion (500 mg), red phosphorous (8 g), and 47% hydriodic acid (120 mL) was stirred at reflux 18 h, cooled, filtered, and the filtrate concentrated to one-half volume, neutralized with 5% aqueous Na_2CO_3 and concentrated to dryness. The residue was taken up in hot ethanol (200 mL), filtered free of residual solid, and again concentrated to dryness. The residue was taken up in water, treated with $NaHSO_3$ (1 g) and acetic acid (5 drops), and extracted with hot chloroform. The dried chloroform extract was concentrated to dryness and identified as **4** by ir and tlc in four different solvent systems compared to authentic **4**.

Preparation of ***4*** *from* ***43***

A mixture of **43** (4.04 g), ethanol (200 mL), and methyl Cellosolve (200 mL) was treated with Raney nickel (about 20 g), heated 4 h on a steam bath, filtered hot, cooled, and again filtered. The filtrate was concentrated to dryness, taken up in boiling ethanol (500 mL), filtered free of solid, and again concentrated to dryness. The residue was taken up in boiling water (800 mL), filtered, and cooled. The product formed from the filtrate (0.4 g) was identical to authentic **4**, as shown by ir and tlc.

Preparation of ***4*** *from* ***44***

Crude **44** (4.82 g), 47% hydriodic acid (60 mL), and red phosphorous (4 g) were stirred 18 h at reflux, poured into ice-water, filtered, and the filtrate concentrated to dryness at reduced pressure. The residual yellow solid was suspended in water, made alkaline with Na_2CO_3, washed with water, and dried. The product (1.3 g, 38%) was identical (ir) to authentic **4**.

Preparation of ***4*** *from* ***6***

The dihydrochloride of **6** (60 mg) was suspended in 1 *M* sodium phosphate buffer, pH 7.2 (30 mL), and heated at 80°C

for 20 h. It was evaporated to dryness, washed with ether, and the residual solid suspended in warm ethanol and filtered. The ethanol extract was concentrated to dryness and the yellow crystalline residue (32 mg, 94%) was pure by tlc and identical (ir) to **4**.

Acknowledgements

The authors are grateful to Dr. J. Schneller, Dr. J. Schulze, and Mr. D. Spiegel for microanalytical, vpc, special ir, uv, and ^{1}Hmr studies, to Dr. R. Rodebaugh for ^{13}Cmr and Mr. C. Shimanskas for ms studies in the Analytical Department. We thank Miss C. Signor, Mrs. L. Raabis, Mrs. M. MacDonald, Miss L. Samoyedna, and Mr. J. Belanger for ir, uv and ^{1}Hmr spectra. Drs. R. Tanz, R. Lee, and S. Ehrreich supplied the cardiovascular test results, Drs. R. Katz and I. Fratta the toxicology data, and Dr. M. Weiner, the clinical information. We also thank Dr. V. Boekelheide for helpful discussions.

1. J. Druey and A. Marxer. J. Med. Pharm. Chem. **1**, 1 (1959).
2. J. Koch-Weser. Am. Heart J. **95**, 1 (1978).
3. R. Zacest, E. Gilmore, and J. Koch-Weser. N. Engl. J. Med. **286**, 617 (1972).
4. M. Moser, J. R. Guyther, F. Finnerty, Jr., D. W. Richardson, H. Langford, H. M. Perry, Jr., D. E. Wood, I. Krishan, G. C. Branche, Jr., and W. M. Smith. J. Am. Med. Assoc. **237**, 255 (1977).
5. J. Druey and J. Tripod. *In* Antihypertensive agents. *Edited by* E. Schlittler. Academic Press, New York. 1967. Chapt. 6.
6. R. Moroi, K. Ono, T. Saito, M. Sano, and T. Akimoto. Chem. Pharm. Bull. Tokyo, **24**, 2850 (1976).
7. J. Wagner, J. W. Faigle, P. Imhof, and G. Liehr. Arzneim. Forsch. **27**, 2388 (1977).
8. K. D. Haegele, A. J. McLean, P. duSouich, K. Barron, J. Laquer, J. L. McNay, and O. Carrier. Br. J. Clin. Pharmacol. **5**, 489 (1978).
9. K. J. Doebel and J. E. Francis. U.S. Patents 3,422,105 (1·14·69); 3,429,882 (2·25·69); 3,479,355 (11·18·69); 3,524,878 (8·18·70); 3,535,320 (10·20·70); 3,539,567 (11·10·70); 3,539,594 (11·10·70); 3,560,499 (2·2·71); 3,560,500 (2·2·71); 3,562,268 (2·9·71); 3,562,271 (2·9·71); 3,575,976 (4·20·71); 3,578,665 (5·11·71); 3,624,108 (11·30·71); 3,691,165 (9·12·72); 3,711,473 (1·6·73); 3,761,493 (9·25·73).
10. J. E. Francis. U.S. Patents 3,524,777 (11·24·70); 3,629,251 (12·21·71).
11. N. R. Patel. *In* The chemistry of heterocyclic compounds. Vol. 27. *Edited by* R. N. Castle. John Wiley & Sons, New York. 1973. Chapt. 6.
12. J. E. Francis. Proc. 6th Int. Symposium on Medicinal Chemistry, Brighton, U.K. Sept. 4–7, 1978.
13. G. Berger and S. C. J. Olivier. Recl. Trav. Chim. Pays-Bas, **46**, 600 (1927).
14. D. D. Wheeler, D. C. Young, and D. S. Erley. J. Org. Chem. **22**, 547 (1957).
15. L. J. Bellamy. The infra-red spectra of complex molecules. John Wiley & Sons, Inc., New York. 1964.
16. S. O'Brien and D. C. C. Smith. J. Chem. Soc. 2907 (1963).
17. E. Huckel. Z. Phys. **70**, 204 (1931).
18. M. S. Newman and C. D. McCleary. J. Am. Chem. Soc. **63**, 1542 (1941).
19. C. Albisetti, Jr., A. Barney, T. Cairns, and H. Winberg. U.S. Patent 2,729,622 (1·3·56).
20. E. Wenkert, D. Johnston, and K. Dave. J. Org. Chem. **29**, 2534 (1964).
21. R. F. Bird and E. E. Turner. J. Chem. Soc. 5050 (1952).
22. E. D. Parker and L. A. Goldblatt. J. Am. Chem. Soc. **72**, 2151 (1950).
23. M. S. Newman and A. L. Leegwater. J. Am. Chem. Soc. **90**, 4410 (1968).
24. M. Hayashi, S. Tsuruoka, I. Morikawa, and H. Namikawa. Bull. Chem. Soc. Jpn. **11**, 184 (1936); Chem. Abstr. **30**, 5965 (1936).
25. N. Rabjohn and H. H. Farmer. J. Am. Chem. Soc. **77**, 760 (1955).
26. V. Jurgens. Chem. Ber. **40**, 4409 (1907).
27. Z. Horii, C. Iwata, and Y. Tamura. J. Org. Chem. **26**, 2273 (1961).
28. C. Graebe and M. Leonhardt. Ann. **290**, 217 (1896); C. Graebe and F. Bossel. Chem. Ber. **26**, 1797 (1898).
29. H. Goldblatt. J. Exp. Med. **59**, 347 (1934).
30. K. S. Grimson. Arch. Surg. London, **43**, 284 (1941).

Metabolites of bird's nest fungi. Part 11.[1] Diterpenoid metabolites of *Cyathus earlei* Lloyd

WILLIAM A. AYER AND SING PING LEE

Department of Chemistry, University of Alberta, Edmonton, Alta., Canada T6G 2G2

Received May 23, 1979

This paper is dedicated to Prof. Karel Wiesner on the occasion of his 60th birthday

WILLIAM A. AYER and SING PING LEE. Can. J. Chem. **57**, 3332 (1979).

The bird's nest fungus *Cyathus earlei* Lloyd produces new diterpenoid metabolites of the cyathin type. Cyathatriol is shown to have structure **1** and has been correlated with cyathin A_3. 11,15-*O*,*O*-Diacetylcyathatriol (**2**), 15-*O*-acetylcyathatriol (**3**), and 11-*O*-acetylcyathatriol (**4**) have also been isolated. The first cyathins containing only two oxygens, cyathin B_2 (**19**) and allocyathin B_2 (**12**), are also described.

WILLIAM A. AYER et SING PING LEE. Can. J. Chem. **57**, 3332 (1979).

Les champignons des nids d'oiseau *Cyathus earlei* Lloyd produisent deux nouveaux métabolites diterpéniques du type cyatine. On a montré que le cyathatriol a la structure **1** et on l'a relié à la cyathyne A_3. On a également isolé les composés suivants: *O*,*O*-diacétyl 11,15 cyathatriol (**2**), *O*-acétyl-15-cyathatriol (**3**) et le *O*-acétyl-11-cyathatriol (**4**). On a également décrit les premières cyathines contenant seulement deux oxygènes, soient la cyathine B_2 (**19**) et l'allocyathine B_2 (**12**).

[Traduit par le journal]

Cyathus earlei Lloyd is a tropical or subtropical species of bird's nest fungus (family Nidulariaceae) which is known to occur in Cuba, Puerto Rico, Mexico, and Hawaii (2). As part of our investigation of the nature of the metabolites of various bird's nest fungi[2] we have examined the metabolites formed when *C. earlei* is grown in liquid culture. Extraction with ethyl acetate of the mycelium obtained after sixty-five days growth on Brodie medium (ref. 2, p. 36) gave six new compounds belonging to the "cyathin" group (4) of diterpenoids. The compounds were separated by chromatography over silica gel. First eluted was a compound $C_{20}H_{28}O_2$ (cyathin B_2)[3] followed by an isomeric substance (allocyathin B_2). The next three substances eluted are acetyl derivatives of the most polar compound, $C_{20}H_{32}O_3$, for which we propose the name cyathatriol. Cyathatriol is shown below to possess structure **1**, and the intermediate compounds are 11,15-*O*,*O*-diacetylcyathatriol (**2**), 15-*O*-acetylcyathatriol (**3**), and 11-*O*-acetylcyathatriol (**4**).

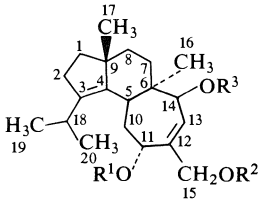

1 $R^1 = R^2 = R^3 = H$
2 $R^1 = R^2 = Ac, R^3 = H$
3 $R^1 = H, R^2 = Ac, R^3 = H$
4 $R^1 = Ac, R^2 = R^3 = H$
5 $R^1 = R^2 = R^3 = Ac$
10 $R^1 = R^3 = H, R^2 = —CH_2Ph$

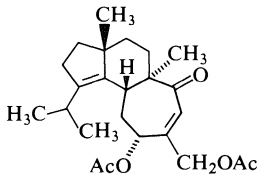

6

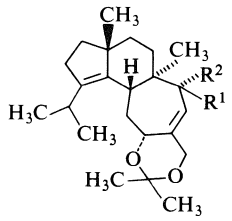

7 $R^1 = OH, R^2 = H$
8 $R^1, R^2 =$ Carbonyl
9 $R^1 = H, R^2 = OH$

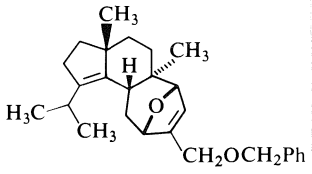

11

Acetylation (Ac_2O, pyridine) of cyathatriol (**1**) provided *O*,*O*,*O*-triacetylcyathatriol (**5**). Acetylation of 15-*O*-acetylcyathatriol (**3**) and 11-*O*-acetylcyathatriol (**4**) under similar conditions produce the same triacetyl derivative **5**, and hydrolysis of **3** and **4** gave cyathatriol (**1**). Acetylation of 11-*O*-acetylcyathatriol **4** under mild conditions gave 11,15-*O*,*O*-diacetylcyathatriol (**2**). Oxidation of **2** with manganese dioxide gave *O*,*O*-diacetylcyathin A_3 (**6**), identical in all respects with an authentic sample (4). Cyathatriol was also correlated with cyathin A_3 via its acetonide **7** which on oxidation with Collins' reagent furnished cyathin A_3 acetonide (**8**). These experiments define the structure of cyathatriol except for the configuration of the hydroxyl group at C-14.

The positions of the acetyl groups in **2**, **3**, and **4** were apparent from the ^{1}Hmr spectra of these com-

[1]For part 10, see ref. 1.
[2]For a review of earlier work, see ref. 3.
[3]For the system of trivial nomenclature, see ref. 4.

0008-4042/79/243332-06$01.00/0

pounds. Thus **2** shows a multiplet at δ 5.85 for the hydrogen at C-11 (the reason for the very low chemical shift is discussed below) and a two proton AB quartet at δ 4.44 for the C-15 methylene group. The signal for the hydrogen on C-14 appeared at δ 3.70 as a doublet spin coupled (J = 6 Hz) to the olefinic proton at C-13. The assignment also follows from the oxidation of **2** to *O*,*O*-diacetylcyathin A_3 (**6**). In compound **3** the signal for the C-15 methylene group appears at δ 4.60, and in **4** the C-11 hydrogen is shifted downfield to δ 5.95.

The low field position of the C-11 hydrogen in cyathatriol (δ 4.85) and the acetyl derivatives, some of which are mentioned above, provided the first indication that the hydroxyl group at C-14 is β-oriented since a hydroxyl group proximate in space to a hydrogen is strongly deshielding (5).

Further evidence for the stereochemistry at C-14 was obtained by a study of the lithium aluminum hydride (LAH) reduction of cyathin A_3 acetonide (**8** = **8***a*) illustrated in Scheme 1. Study of Dreiding models clearly indicated that LAH reduction of the carbonyl group should occur predominantly from the less hindered β-face of the molecule and indeed the unnatural epimer **9** (= **9***a* in Scheme 1) was the major product of the reduction (ratio **9**:**7** = 7:1). Both ^{1}Hmr and ^{13}Cmr support the assigned structures and stereochemistry (it is assumed that ring C exists in the chair form indicated). Thus the C-11 hydrogen which appears at δ 4.80 in **7***a* (deshielded by C-14 β-OH) appears at δ 4.15 in **9***a*. The coupling between the olefinic hydrogen at C-13 and the hydrogen at C-14 is ca. 6 Hz in **7***a*, consistent with a dihedral angle approaching 0°, and less than 1 Hz in **9***a*, as expected for a dihedral angle approaching 90° (6). In the ^{13}Cmr spectrum[4] of **7***a* the methyl group at C-6 resonates at δ 17.6, whereas in **9***a* it resonates at δ 12.1, demonstrating the γ-gauche relationship (7) of the hydroxyl and methyl groups in the latter compound. Conversely, C-5 is upfield in **7***a* (δ 39.1) relative to **9***a* (δ 45.0).

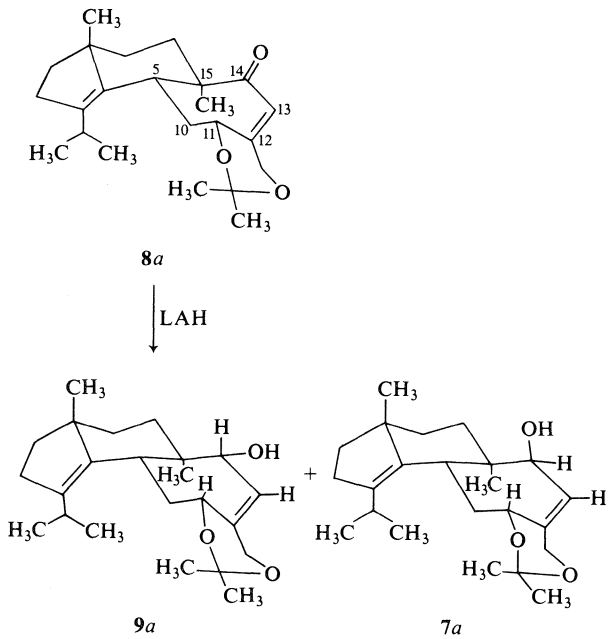

SCHEME 1

In order to demonstrate chemically the *trans*-relationship between the hydroxyls at C-11 and C-14 we decided to attempt the formation of an internal ether. It was first necessary to block the C-15 oxygen function. The use of 15-*O*-acetylcyathatriol (**3**) was not possible since it is rapidly isomerized to 11-*O*-acetylcyathatriol (**2**) in the presence of bases such as pyridine or triethylamine. However, treatment of cyathatriol with a limited amount of sodium hydride and benzyl bromide gave the C-15 benzyl ether **10**. When **10** was treated briefly with an ethereal solution of methanesulfonyl chloride and triethylamine the ether **11** was obtained in low yield. The orientation of the ethereal oxygen is not clearly defined by the ^{1}Hmr spectrum, however we favor the β-orientation since the hydrogen at C-5 has an unusually low chemical shift (δ 3.20), attributed to the deshielding effect of the ethereal oxygen. This assignment is also consistent with mesylation of the less hindered C-11 hydroxyl followed by backside displacement by the hydroxyl group at C-14.

Allocyathin B_2, assigned structure **12**, was obtained as a pale yellow oil and showed a very informative uv spectrum. The spectrum (λ_{max}: 266 nm (ε 5150) and 325 nm (ε 12 100)) is very similar to that of anhydrocyathin B_3 (**13**), previously obtained from cyathin B_3 (8). The ^{1}Hmr was also similar to that of **13** except that the hydrogen *vicinal* to the hydroxyl group in **12** gives rise to absorption at δ 3.63 (dd, J's 6 and 1 Hz). The ir spectrum of **12** shows hydroxyl absorption and only one carbonyl absorption (1675 cm^{-1}). Oxidation of allocyathin B_2 with Collins' reagent gave anhydrocyathin B_3 (**13**), confirming structure **12** except for the configuration at C-14. Reduction of anhydrocyathin B_3 (**13**) with LAH provided a mixture of diols **14** and **15** in a ratio of ca. 2:1. Oxidation of **14** with MnO_2 gave allocyathin B_2 (**12**). Similar oxidation of **15** provided 14-epiallocyathin B_2 (**16**). The assignment of con-

[4]For a discussion of the ^{13}Cmr spectra of the cyathins, see ref. 1. Complete assignments for cyathatriol and its derivatives are detailed in the accompanying paper discussing the biosynthesis of these compounds.

figuration in **12** and **16** is based on application of Brewster's benzoate rule (9). Thus $[M]_D$**17** − $[M]_D$**12** = +78.1° indicating the *S* configuration at C-14 in **12**, and $[M]_D$**18** − $[M]_D$**16** = −26.5° indicating the *R* configuration in **16**. It thus appears that allocyathin B_2 has the same configuration at C-14 as cyathatriol.

Cyathin B_2 is assigned structure **19** on the basis of the following evidence. The infrared spectrum shows the presence of a unconjugated ketone (1710 cm^{-1}) and an α,β-unsaturated aldehyde (2710, 1698, 1645 cm^{-1}). The unsaturated aldehyde gives rise to absorption in the uv at 228 nm (ε 6100). The ^{1}Hmr spectrum also shows the unsaturated aldehyde system (δ 9.38 (s) and 6.60 (m)) and, in addition shows an AB quartet (J = 14 Hz) at δ 3.32 and 3.64 for the protons of the C-13 methylene group. A similar set of signals (δ 3.09, 3.69, J = 11 Hz) appears for the C-13 methylene protons in anhydrocyathin B_3 (**13**). In an attempt to correlate cyathin B_2 with cyathin B_3 (**20**) cyathin B_2 was treated with alkaline hydrogen peroxide in methanol. A mixture of products was obtained, none of which corresponded to cyathin B_3. The least polar component of the mixture, however, was anhydrocyathin B_3 (**13**). A possible mechanism for the transformation of **19** into **13** is illustrated in Scheme 2, where an initially formed epoxide **A** undergoes β-elimination to give **B**, which in turn undergoes nucleophilic addition and subsequent β-elimination (for brevity, written as one step in **B**) to give **C** which undergoes vinylogous β-elimination (to **D**) followed by tautomerization to the fully conjugated triene system in **13**. This transformation establishes most of the features of structure **19** and together with the spectroscopic data provides strong evidence for the structure of cyathin B_2 (**19**).

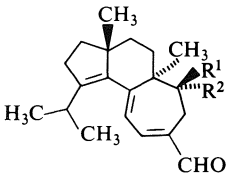

12 R^1 = OH, R^2 = H
13 R^1 = R^2 = Carbonyl
16 R^1 = H, R^2 = OH
17 R^1 = OBz, R^2 = H
18 R^1 = H, R^2 = OBz

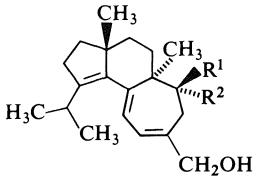

14 R^1 = OH, R^2 = H
15 R^1 = H, R^2 = OH

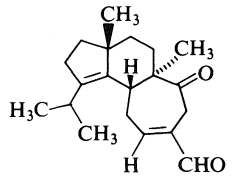

19

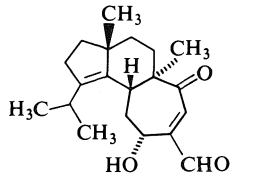

20

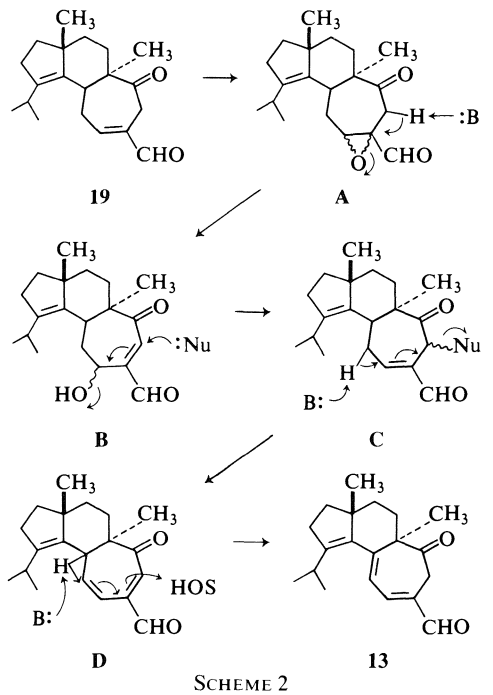

SCHEME 2

All six compounds described herein show moderate antibiotic activity against *Staphyloccocus aureus*.

Experimental

High resolution mass spectra were recorded on an AEI MS-50 mass spectrometer, coupled to a DS 50 computer. Infrared spectra were recorded on a Unicam SP 1000 or a Nicolet 7199 FT spectrometer and uv spectra on a Cary model 14 M spectrometer. ^{1}Hmr spectra were determined on a Varian HA-100 spectrometer with TMS as internal standard. Melting points were recorded on a Fisher-Johns melting point apparatus and are uncorrected. Specific rotations at the D line were determined using a Perkin-Elmer 141 automatic polarimeter.

Silica gel tlc plates were 0.5 mm silica gel G (E. Merck, Darmstadt) containing 1% electronic phosphor (General Electric, Cleveland). Compounds were detected by viewing under uv light or by spraying with 30% sulfuric acid and charring. All solvents were reagent grade and were distilled prior to use. Unless otherwise specified, anhydrous magnesium sulfate was used as a drying agent for organic solutions and silica gel 60 (BDH Chemicals) as absorbant for column chromatography. Skellysolve B refers to Skelly Oil Company light petroleum, bp 62–70°C.

Growth of Cyathus earlei *Lloyd and Isolation of Metabolites*

Slant tubes of *Cyathus earlei* Lloyd ATCC 38343 were obtained from H. J. Brodie (strain 1286). The fungus was grown in liquid still culture at room temperature on Brodie medium (2) in 2.8 L Fernbach flasks (1 L medium/flask, total 18 L). After 30 days growth the broth was decanted and the mycelium reflooded with fresh sterile Brodie medium. Five weeks later the mycelium was removed by filtration and placed in Soxhlet thimbles and extracted with ethyl acetate for 4 days. The ethyl acetate extract was washed with water, dried over sodium sulfate, and concentrated to a viscous brown oil (7.7 g). A portion (4 g) of the crude extract was subjected to column chromatography over silica gel (200 g). Progress of the separation was

monitored by thin layer chromatography (tlc). Elution with Skellysolve B – benzene (1:9) gave *cyathin* B_2 (51 mg). Elution with benzene afforded *allocyathin* B_2 (210 mg). Elution with ether–benzene (1:9) gave *15-O-acetylcyathatriol* (310 mg) followed by *11,15*-O,O-*diacetylcyathatriol* (46 mg). Elution with ether–benzene (1:4) gave *11*-O-*acetylcyathatriol* (132 mg). Finally, elution with ether–benzene (2:3) gave cyathatriol (22 mg).

Cyathin B_2 (**19**)

Cyathin B_2 was obtained as a viscous syrup; ir (CCl_4): 2710, 1710, 1698, 1645 cm^{-1}; uv (CH_3OH) λ_{max}: 228 nm (ε 6100); ^{1}Hmr (CCl_4) δ: 0.99 (s, 3H), 1.02 (d, J = 6 Hz, 6H), 1.10 (s, 3H), 3.32 (d, J = 14 Hz, 1H on C-13), 3.64 (dd, J's 14 and 1 Hz, 1H on C-13), 6.60 (m, C-11, H), 9.38 (s, 1H). *Exact mass* calcd. for $C_{20}H_{28}O_2$: 300.2090; found (ms): 300.2092.[5]

Allocyathin B_2 (**12**)

Allocyathin was obtained as a yellow syrup which showed a single spot on tlc, $[\alpha]_D^{25}$ +87.1° (*c* 0.95, CH_3OH); ir (CCl_4): 3600, 2720, 1675, 1570 cm^{-1}; uv (hexane) λ_{max}: 266 (ε 5150), 325 nm (ε 12 100); ^{1}Hmr (CCl_4) δ: 0.96 and 1.05 (each 3H, d, J = 6 Hz), 0.97 (s, 3H), 1.01 (s, 3H), 2.80 (heptet, J = 6 Hz, H on C-18), 3.09 (dd, J's 18 and 6 Hz, 1H on C-13), 3.63 (dd, J's 6 and 1 Hz, H on C-14), 5.84 (d, J = 8 Hz, H on C-10), 6.68 (dd, J's 8 and 1 Hz, H on C-11), 9.37 (s, 1H). *Exact mass* calcd. for $C_{20}H_{28}O_2$: 300.2090; found (ms): 300.2092. *Anal.* calcd. for $C_{20}H_{28}O_2$: C 80.02, H 9.40; found: C 80.04, H 9.70.

11,15-O,O-*Diacetylcyathatriol* (**2**)

11,15-*O,O*-Diacetylcyathatriol crystallized from Skellysolve B – ether, mp 123–124°C; ir (CCl_4): 3600, 3500, 1745 cm^{-1}; ^{1}Hmr (CCl_4) δ: 0.70 (s, 3H), 0.95 (d, J = 6 Hz, 6H), 1.10 (s, 3H), 1.98 (s, 3H), 2.00 (s, 3H), 2.90 (heptet, J = 6 Hz, H on C-18), 3.00 (dd, J's 10 and 1 Hz, 1H at C-5), 3.70 (d, J = 6 Hz, 1H), 4.34 (dd, J's 14 and 1 Hz, 1H on C-15), 4.54 (dd, J's 14 and 1 Hz, 1H on C-15), 5.82 (dd, J's 6 and 1 Hz, 1H on C-13), 5.85 (m, 1H on C-11). *Anal.* calcd. for $C_{24}H_{36}O_5$: C 71.25, H 8.96; found: C 70.96, H 9.07. The highest peak in the mass spectrum corresponded to the molecular ion – H_2O. *Exact mass* calcd. for $C_{24}H_{34}O_4$ ($M^+ - H_2O$): 386.2457; found: 386.2454.

15-O-*Acetylcyathatriol* (**3**)

15-*O*-Acetylcyathatriol was obtained as a viscous oil showing a single spot on tlc; ir (CCl_4): 3600, 3500, 1745 cm^{-1}; ^{1}Hmr (CCl_4) δ: 0.75 (s, 3H), 0.98 (d, J = 6 Hz, 6H), 1.07 (s, 3H), 2.05 (s, 3H), 3.00 (m, 2H, H's on C-5 and C-18), 3.82 (d, J = 6 Hz, H on C-14), 4.60 (s, 2H on C-15), 4.70 (m, H on C-11), 5.65 (d, J = 6 Hz, H on C-13). *Exact mass* calcd. for $C_{22}H_{34}O_4$: 362.2457; found: 362.2479. *Anal.* calcd. for $C_{22}H_{34}O_4$: C 72.87, H 9.45; found: C 72.58, H 9.48.

11-O-*Acetylcyathatriol* (**4**)

11-*O*-Acetylcyathatriol crystallized from ether, mp 165–166°C; ir (CCl_4): 3500, 1710 cm^{-1}; ^{1}Hmr ($CDCl_3$) δ: 0.80 (s, 3H), 0.97 (d, J = 6 Hz, 6H), 1.10 (s, 3H), 2.10 (s, 3H), 3.02 (br d, J = 10 Hz, H on C-5), 3.90 (d, J = 6 Hz, H on C-14), 4.06 (s, 2H on C-15), 5.86 (dd, J's 6 and 1 Hz, H on C-13), 5.95 (m, H on C-11). *Exact mass* calcd. for $C_{22}H_{34}O_4$: 362.2457; found: 362.2496. *Anal.* calcd. for $C_{22}H_{34}O_4$: C 72.87, H 9.45; found: C 72.51, H 9.54.

[5]Where combustion analysis is not reported, molecular formulas were determined by high resolution mass spectrometry. Eventual correlation with compounds of established molecular formula validates the deductions made in this manner.

Cyathatriol (**1**)

Cyathatriol was obtained as a white powder which crystallized from acetone, mp 172–173°C; ir (film): 3300 cm^{-1}; ^{1}Hmr (acetone-d_6) δ: 0.80 (s, 3H), 0.94 (d, J = 6 Hz, 3H), 0.95 (d, J = 6 Hz, 3H), 1.07 (s, 3H), 3.00 (m, H's on C-5 and C-18), 3.76 (d, J = 6 Hz, H on C-14), 4.12 (s, 2H on C-15), 4.85 (ddd, J's 8, 4, and 1 Hz, H on C-11), 5.87 (dd, J's 6 and 1 Hz, H on C-13). *Exact mass* calcd. for $C_{20}H_{32}O_3$: 320.2351; found: 320.2336. *Anal.* calcd. for $C_{20}H_{32}O_3$: C 74.94, H 10.07; found: C 74.67, H 10.14.

Cyathatriol (**1**) *from* **3** *and* **4**

15-*O*-Acetylcyathatriol (20 mg) in methanol (2 mL) containing potassium carbonate (20 mg) was stirred at room temperature for 16 h. The reaction mixture was diluted with water (10 mL) and extracted with ether (3 × 50 mL). The ether extract was dried and evaporated to give crystalline cyathatriol (16 mg).

11-*O*-Acetylcyathatriol was hydrolyzed under the same conditions to give cyathatriol.

Preparation of 11,14,15-O,O,O-*Triacetylcyathatriol from* **3**, **4**, *and* **1**

To a solution of 15-*O*-acetylcyathatriol (**3**, 20 mg) in pyridine (1 mL) there was added acetic anhydride (30 μL). The solution was left at room temperature for 24 h, then diluted with ether (50 mL) and washed successively with 1*M* HCl, saturated $NaHCO_3$, and brine. The organic solution was worked up in the usual manner to give an oil (32 mg). Purification by column chromatography yielded 11,14,15-*O,O,O*-triacetylcyathatriol (**5**, 24 mg) as a colorless oil; ir (CCl_4): 1735 cm^{-1}; ^{1}Hmr ($CDCl_3$) δ: 0.85 (s, 3H), 0.98 (d, J = 6 Hz, 3H), 0.99 (d, J = 6 Hz, 3H), 1.09 (s, 3H), 2.10 (s, 6H), 2.14 (s, 3H), 2.90 (heptet, H on C-18), 4.41 (d, J = 14 Hz, H on C-15), 4.68 (d, J = 14 Hz, H on C-15), 4.87 (d, J = 6 Hz, H on C-14), 4.90 (m, H on C-11), 5.84 (dd, J's 6 and 1 Hz, H on C-13). The highest peak in the mass spectrum corresponded to loss of acetic acid from the molecular ion. *Exact mass* calcd. for $C_{24}H_{36}O_4$ ($M^+ - CH_3COOH$): 386.2463; found: 386.2465.

In a similar fashion both 11-*O*-acetylcyathatriol (**4**) and cyathatriol (**1**) were transformed to the same triacetyl derivative.

11,15-O,O-*Diacetylcyathatriol* (**2**) *from 11*-O-*Acetylcyathatriol* (**4**)

A solution of 11-*O*-acetylcyathatriol (**4**, 10 mg) in methylene chloride (1 mL) was cooled to 0°C and pyridine (50 μL) and acetic anhydride (30 μL) added. After 18 h at 0°C the reaction mixture was worked up in the usual manner to give a product which was purified by chromatography over silica gel using benzene as eluant to give 11,15-*O,O*-diacetylcyathatriol (7 mg), identical (mp, ir, ^{1}Hmr, ms) with an authentic sample.

O,O-*Diacetylcyathin* A_3 (**6**) *from 11,15*-O,O-*Diacetylcyathatriol* (**2**)

A mixture of **2** (13 mg) and activated (10) manganese dioxide (100 mg) in CH_2Cl_2 was stirred at room temperature for 1.5 h. The reaction mixture was filtered and the filter cake washed thoroughly with ether. Concentration of the filtrate gave an oil (13 mg) which was chromatographed using benzene–ether (4:1) to give *O,O*-diacetylcyathin A_3 (**6**), identical (ir, ^{1}Hmr ms) with an authentic sample.

Cyathatriol Acetonide (**7**)

Cyathatriol (**1**, 30 mg) was dissolved in 2,2-dimethoxypropane (2 mL) at 35°C and *p*-toluenesulfonic acid (3 mg) added. After 5 min water (10 mL) was added and the solution was extracted with ether. Evaporation of the ether gave **7** as a white solid (31 mg), mp 189–190°C from ether, $[\alpha]_D^{25}$ −21.4°

(MeOH); ir ($CHCl_3$): 3600, 3500 cm^{-1}; ^{1}Hmr ($CDCl_3$) δ: 0.76 (s, 3H), 0.97 (d, J = 6 Hz, 6H), 1.09 (s, 3H), 1.38 (s, 6H), 3.05 (heptet, H on C-18), 3.22 (dd, J's 10 and 1 Hz, H on C-5), 3.65 (d, J = 6 Hz, H on C-14), 3.80 (d, J = 12 Hz, H on C-15), 4.48 (ddd, J's 12, 1, and 1 Hz, H on C-15), 4.70 (m, H on C-11), 5.60 (dd, J's 6 and 1 Hz). *Exact mass* calcd. for $C_{23}H_{36}O_3$: 360.2665; found: 360.2676. *Anal.* calcd. for $C_{23}H_{36}O_3$: C 76.60, H 10.07; found: C 76.70, H 10.35.

Compound **7** was further characterized as its 14-*O*-benzoyl derivative, mp 151–153°C (from Skellysolve B – ether), $[\alpha]_D^{25}$ −1.7° (*c* 0.35, MeOH).

*Cyathin A_3 Acetonide (**8**) from Cyathatriol Acetonide (**7**)*

Chromium trioxide (21 mg) was added to a stirred solution of pyridine (32 μL) in CH_2Cl_2 (2 mL). After 10 min a solution of **7** (14 mg) in CH_2Cl_2 (0.5 mL) was introduced and the reaction mixture was stirred at room temperature for a further 5 min. After work-up in the usual manner and purification of the product by chromatography over silica gel (eluant benzene–ether 9:1), cyathin A_3 acetonide (**8**, 11 mg) was obtained, identical (ir, ^{1}Hmr, ms) with an authentic sample.

*Reduction of Cyathin A_3 Acetonide (**8**)*

To a solution of **8** (50 mg) in ether (6 mL) at 0°C was added $LiAlH_4$ (10 mg). The reaction mixture was stirred for 20 min, then a solution of 10% aqueous $NaHCO_3$ was added and the mixture was extracted with ether. The extract was dried and concentrated and the residue chromatographed over silica gel to give cyathatriol acetonide (**7**, 4.2 mg) and *14-epicyathatriol acetonide* (**9**, 28.1 mg), mp 186–187°C, $[\alpha]_D^{25}$ −17.0° (*c* 0.27, MeOH); ir (CCl_4): 3600 cm^{-1}; ^{1}Hmr ($CDCl_3$) δ: 0.79 (s, 3H), 0.99 (d, J = 6 Hz, 6H), 1.10 (s, 3H), 1.40 (s, 6H), 2.65 (dd, J's 10 and 1, H on C-5), 3.00 (heptet, H on C-18), 3.82 (d, J = 13 Hz, 1H on C-15), 4.10 (broad s, H on C-14), 4.21 (m, H on C-11), 4.40 (ddd, J's 13, 1, 1 Hz, 1H on C-15), 5.27 (broad s, H on C-13). *Exact mass* calcd. for $C_{23}H_{36}O_3$: 360.2665; found: 360.2676.

14-Epicyathatriol acetonide (**9**) was further characterized as its 14-*O*-benzoyl derivative, mp 157–158°C (from Skellysolve B – ether), $[\alpha]_D^{25}$ +12.2° (*c* 0.35, MeOH).

*15-O-Benzylcyathatriol (**10**)*

A solution of cyathatriol (**1**, 6.8 mg) in ether (2 mL) was treated with sodium hydride (6 mg) and benzyl bromide (10 μL) and then heated under reflux for 24 h. The reaction mixture was poured into ice water (10 mL) and extracted with ether (3 × 50 mL). The extract was dried and concentrated to give an oil (5.4 mg) which was purified by chromatography over silica gel (eluant benzene) to give the ether **10** (4.5 mg) as a colorless oil; ir ($CHCl_3$): 3500; ^{1}Hmr ($CDCl_3$) δ: 0.80 (s, 3H), 0.98 (d, J = 6 Hz, 6H), 1.10 (s, 3H), 3.00 (heptet, H on C-5), 3.85 (d, J = 6 Hz, H on C-14), 4.12 and 4.25 (AB quartet, J = 12 Hz, H's on C-15), 4.59 (s, 2H benzyl methylene), 4.85 (m, H on C-11), 5.80 (dd, J's 6 and 1 Hz, H on C-13), 7.35 (s, 5H). The highest peak in the mass spectrum was for $M^+ - H_2O$. *Exact mass* calcd. for $C_{27}H_{36}O_2$ ($M^+ - H_2O$): 392.2712; found: 392.2713.

*Formation of Cyclic Ether **11***

The benzyl ether **10** (6 mg) in ether (2 mL) at 0°C was treated with triethylamine (15 μL) and methanesulfonyl chloride (7 μL). After 5 min the reaction mixture was diluted with ether (20 mL) and washed with dilute HCl. Evaporation of the ether gave a crude oil (6 mg) which was chromatographed on silica gel to give the ether **11** as a colorless oil (2 mg); ir, no OH absorption; ^{1}Hmr ($CDCl_3$) δ: 0.97 (d, J = 6 Hz, 3H), 0.98 (d, J = 6 Hz, 3H), 1.00 (s, 3H), 1.12 (s, 3H), 2.85 (heptet, H on C-18), 3.20 (dd, J's 7 and 4 Hz, H on C-5), 3.72 (br s, H on C-14), 3.80 (s, 2H), 4.27 (d, J = 12 Hz, 1H on C-15), 4.30 (m, 1H, H on C-11?), 4.39 (d, J = 12 Hz, 1H on C-15), 5.50 (br s, H on C-13), 7.20 (s, 5H). *Exact mass* calcd. for $C_{27}H_{36}O_2$: 392.2715; found: 392.2731.

*Oxidation of Allocyathin B_2 (**12**)*

Chromium trioxide (36 mg) was added to a stirred solution of pyridine (57 μL) in CH_2Cl_2 (3 mL). After 15 min a solution of **12** (18 mg) in CH_2Cl_2 (0.5 mL) was added and the mixture was stirred for 5 min. The precipitated material was filtered off and washed with ether. The organic solutions were combined and evaporated. The residue was purified by ptlc to give anhydrocyathin B_3 (**13**, 16 mg), identical (tlc, ir, ^{1}Hmr, uv, ms) with an authentic sample (9).

*Attempted Epoxidation of Cyathin B_2 (**19**)*

Cyathin B_2 (12.5 mg) was dissolved in ice cold methanol (1 mL) and 1 *M* NaOH (80 μL) and 30% H_2O_2 (5 μL) were added. The solution was kept at 0°C for 24 h, then diluted with water (10 mL) and extracted with ether, to yield an oil (12 mg) which was subjected to ptlc to give anhydrocyathin B_3 (**13**, 2 mg), which could be followed by its yellow color, identical with an authentic sample.

*Reduction of Anhydrocyathin B_3 (**13**)*

A mixture of **13** (42 mg), LAH (20 mg), and ether (6 mL) was stirred at room temperature for 15 min, then excess hydride was destroyed by addition of saturated $NaHCO_3$. Extraction with ether and the usual work-up provided an oil which was separated into two components by ptlc (triple elution with ether) to give diols **14** (25 mg) and **15** (13 mg). *Diol **14*** showed the following properties: ir ($CHCl_3$): 3500; ^{1}Hmr ($CDCl_3$) δ: 0.98 (s, 3H), 0.99 (d, J = 6 Hz, 6H), 1.05 (s, 3H), 2.84 (heptet, H on C-18), 3.60 (dd, J's 5 and 2 Hz, H on C-14), 4.10 (s, 2H on C-15), 5.59 (d, J = 8 Hz, H on C-10), 6.05 (dd, J's 8 and 1 Hz, H on C-11). *Exact mass* calcd. for $C_{20}H_{30}O_2$: 302.2246; found: 302.2242. *Diol **15*** had the following properties: ir ($CHCl_3$): 3500 cm^{-1}; ^{1}Hmr ($CDCl_3$) δ: 0.96 (d, J = 6 Hz, 3H), 0.96 (s, 3H), 1.00 (d, J = 6 Hz, 3H), 1.10 (s, 3H), 3.75 (dd, J's 10 and 2 Hz, H on C-14), 4.12 (s, 2H on C-15), 5.45 (d, J = 8 Hz, H on C-10), 5.86 (dd, J's 8 and 2 Hz, H on C-11). *Exact mass* calcd. for $C_{20}H_{30}O_2$: 302.2246; found: 302.2242.

*Oxidation of Diols **14** and **15***

Activated MnO_2 (50 mg) was added to a solution of diol **15** (9 mg) in CH_2Cl_2 (2 mL) and the mixture stirred for 15 min, then filtered and the filter cake washed thoroughly with ether. Concentration of the filtrate gave the hydroxyaldehyde **16** (8.2 mg) as a colorless oil $[\alpha]_D^{25}$ +97.5° (*c* 0.6, MeOH); ir ($CHCl_3$): 3600, 2720, 1675, 1570 cm^{-1}; ^{1}Hmr ($CDCl_3$) δ: 0.96 (s, 3H), 0.96 (d, J = 6 Hz, 3H), 1.00 (d, J = 6 Hz, 3H), 1.10 (s, 3H), 3.67 (dd, J's 10 and 2 Hz, H on C-14), 5.58 (d, J = 8 Hz, H on C-10), 6.64 (dd J's 8 and 2 Hz, H on C-11), 9.48 (s). *Exact mass* calcd. for $C_{20}H_{28}O_2$: 300.2090; found: 300.2092.

Oxidation of diol **14** in the same manner provided allocyathin B_2 (**12**).

*Benzoates **17** and **18***

Allocyathin B_2 (**12**, 10 mg) in $CHCl_2$ (1 mL) was treated with pyridine (0.1 mL) and benzoyl chloride (0.05 mL) and the solution kept at room temperature for 6 h, then diluted with ether and washed with dilute HCl. Work-up gave an oil which was purified by chromatography over silica gel (eluent, benzene) to give benzoate **17** as a colorless syrup (10 mg), $[\alpha]_D^{25}$ +84.5° (*c* 0.7, MeOH); ir ($CHCl_3$): 1710, 1665 cm^{-1}; ^{1}Hmr ($CDCl_3$) δ: 0.96 (s, 3H), 1.01 (d, J = 6 Hz, 6H), 1.12 (s, 3H), 2.90 (heptet, H on C-18), 3.34 (dd, J's 18 and 6 Hz, 1H on C-13), 5.23 (dd, J's 6 and 1 Hz, H on C-14), 6.00 (d, J = 8 Hz, H on C-10), 6.80 (dd, J's 8 and 2 Hz, H on C-11), 7.40 (m, 3H

aromatic), 7.90 (m, 2H aromatic), 9.40 (s, 1H). *Exact mass* calcd. for $C_{27}H_{32}O_3$: 404.2351; found: 404.2352.

Under the same conditions 14-epiallocyathin B_2 (**16**) was benzoylated to give **18** as a colorless oil, $[\alpha]_D^{25}$ +71.0° (*c* 0.50, MeOH); ir ($CHCl_3$): 1710, 1665 cm^{-1}; ^{1}Hmr ($CDCl_3$) δ: 0.96 (s, 3H), 0.99 (d, *J* = 6 Hz, 3H), 1.01 (d, *J* = 6 Hz, 3H), 1.26 (s, 3H), 2.80 (heptet, 1H), 3.06 (dd, *J*'s 18 and 2 Hz, 1H on C-13), 5.18 (dd, *J*'s 11 and 2 Hz, H on C-14), 5.84 (d, *J* = 8 Hz, C-10H), 6.70 (dd, *J*'s 8 and 2 Hz, H on C-11), 7.50 (m, 3H, aromatic), 8.02 (m, 2H, aromatic), 9.42 (s, 1H). *Exact mass* calcd. for $C_{27}H_{32}O_3$: 404.2351; found: 404.2352.

Acknowledgements

We wish to thank Dr. H. J. Brodie for the slant cultures and Dr. Lois M. Browne for help in maintaining and growing the cultures. We gratefully acknowledge the financial support of the Natural Sciences and Engineering Research Council of Canada.

1. W. A. AYER, T. T. NAKASHIMA, and D. E. WARD. Can. J. Chem. **56**, 2197 (1978).
2. H. J. BRODIE. The bird's nest fungi. University of Toronto Press, Toronto, Ont. 1975. p. 156.
3. W. A. AYER, L. M. BROWNE, S. FERNÁNDEZ, D. E. WARD, and T. YOSHIDA. Rev. Latinoam. Quim. **9**, 177 (1978).
4. W. A. AYER and H. TAUBE. Can. J. Chem. **51**, 3842 (1973).
5. J. B. CARR and A. C. HUITRIC. J. Org. Chem. **29**, 2506 (1964).
6. L. M. JACKMAN and S. STERNHELL. *In* Application of nuclear magnetic resonance spectroscopy in organic chemistry. 2nd ed. Pergamon Press, Toronto. 1969. pp. 294–298.
7. S. H. GROVER and J. B. STOTHERS. Can. J. Chem. **52**, 870 (1974).
8. W. A. AYER and L. L. CARSTENS. Can. J. Chem. **51**, 3157 (1973).
9. J. H. BREWSTER. Tetrahedron, **13**, 106 (1961).
10. I. M. GOLDMAN. J. Org. Chem. **34**, 1979 (1969).

Metabolites of bird's nest fungi. Part 12.[1] Studies on the biosynthesis of the cyathins

WILLIAM A. AYER, SING PING LEE, AND THOMAS T. NAKASHIMA
Department of Chemistry, University of Alberta, Edmonton, Alta., Canada T6G 2G2

Received August 8, 1979

This paper is dedicated to Prof. Karel Wiesner on the occasion of his 60th birthday

WILLIAM A. AYER, SING PING LEE, and THOMAS T. NAKASHIMA. Can. J. Chem. **57**, 3338 (1979).

The cyathins are a group of diterpenoids of unique structure which are produced by bird's nest fungi of the family *Cyathus*. Biosynthetic studies utilizing [1-^{13}C], [2-^{13}C], and [1,2-$^{13}C_2$]acetate indicate that 11-*O*-acetylcyathatriol, produced by the fungus *C. earlei*, is formed from acetate via the isoprenoid pathway. The labelling experiments are consistent with a route involving cyclization–rearrangement of geranylgeranyl pyrophosphate as shown in Schemes 1 and 3.

WILLIAM A. AYER, SING PING LEE et THOMAS T. NAKASHIMA. Can. J. Chem. **57**, 3338 (1979).

Les cyathines forment un groupe de diterpénoides à structure spéciale qui sont produits par les champignons de la famille *Cyathus* que l'on trouve dans les nids d'oiseaux. Les études biosynthétiques utilisant un acétate marqué au ^{13}C en positions [^{13}C-1], [^{13}C-2] et [$^{13}C_2$-1,2] indiquent que le *O*-acétyl-11 cyathatriol produit par le champignon *C. earlei* est formé à partir de l'acétate par l'intermédiaire d'un mécanisme isoprénoide. Les expériences de marquage sont en accord avec un cheminement impliquant une transposition accompagnée d'une cyclisation du phosphate de géranylgéranyle tel qu'indiqué dans les schémas 1 et 3.

[Traduit par le journal]

The cyathins are a unique type of diterpenoid produced by several species of bird's nest fungi of the genus *Cyathus* (family *Nidulariaceae*). They all possess the carbon skeleton **1** which we have named cyathane (2) although the parent hydrocarbon **1** is unknown.[2] In the preceding paper (1) we have described the metabolites isolated from the mycelium of liquid cultures of *Cyathus earlei* Lloyd. Since cyathatriol (**2**) and its derivatives 11-*O*-acetylcyathatriol (**3**), 15-*O*-acetylcyathatriol (**4**), and 11,15-*O*,*O*-diacetylcyathatriol (**5**) are produced in good yield and are easily isolated, it seemed an appropriate species for the study of some of the details of the biosynthesis of the cyathins. Since the cyathins appear to be diterpenoid in nature (2) and may thus be derived from acetate via mevalonic acid, "active isoprene," and geranylgeranyl pyrophosphate,[3] we have undertaken a study of the incorporation of ^{13}C-labelled acetate by *C. earlei* into cyathatriol and its derivatives, utilizing carbon-13 nuclear magnetic resonance (^{13}Cmr) to trace the biosynthetic pathway.[4]

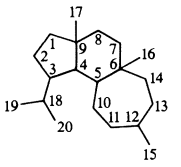

1

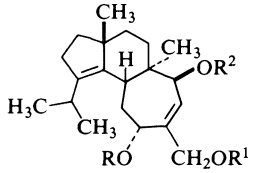

2 R = R^1 = R^2 = H
3 R = Ac, R^1 = R^2 = H
4 R = R^2 = H, R^1 = Ac
5 R = R^1 = Ac, R^2 = H
6 R = R^1 = R^2 = Ac

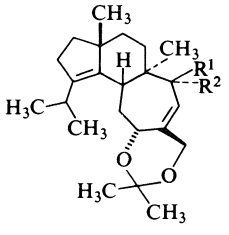

8 R^1 = OH, R^2 = H
9 R^1 = H, R^2 = OH

In order to follow the labelling pattern it was first necessary to assign the chemical shifts of the carbons in cyathatriol and its derivatives. The ^{13}C chemical shifts of compounds **2** to **5** as well as those of *O*,*O*,*O*-triacetylcyathatriol (**6**) are summarized in Table 1. The assignments of the individual carbon resonances to specific carbon atoms are based largely on selective (**3**) and off-resonance (**3** and **4**) proton decoupling

[1]For part 11, see ref. 1.
[2]For a compilation of the various cyathins which have been isolated, see ref. 3.
[3]For a review of terpenoid biosynthesis, see ref. 4.
[4]For a review of the use of ^{13}Cmr in biosynthetic studies see ref. 5.

0008-4042/79/243338-06$01.00/0

TABLE 1. Carbon-13 chemical shifts[a] of some cyathins

Carbon	2	3	4	5	6	8	9
1	38.5[b]	38.1 (0.3)[c]	38.1 (0.2)	38.0	38.0	37.9	37.7
2	28.9	28.7 (0.2)	28.6 (0.2)	28.6	28.7	28.9	28.7
3[d]	139.8	139.7 (0.5)	139.6 (0.5)	139.5	140.4[e]	140.2	140.5
4	139.5	138.5 (0.3)	138.6 (0.3)	138.3	137.6	139.2	138.5
5	40.4	40.1 (1.3)	40.0 (0.6)	39.8	40.8[f]	39.1	45.0
6	42.6	42.1 (0.9)	42.0 (0.7)	42.0	41.0	42.5	43.0
7	33.1	33.2 (0.6)	32.8[f] (0.7)	32.7[g]	33.5	34.6	33.6
8	37.0	37.0 (0.5)	37.0 (0.3)	36.9	36.6	36.8	36.4
9	49.8	49.4 (0.3)	49.4 (0.3)	49.3	49.3	49.7	49.9
10	37.4	33.9 (1.3)	36.6 (1.1)	33.1	33.7	34.8	33.9
11	72.1	73.8 (3.2)	71.3 (4.6)	72.8	72.7	71.9	72.9
12	145.7	143.5 (1.6)	141.6 (2.0)	138.1	136.5	144.9	138.8
13	126.9	127.9 (3.4)	129.5 (1.9)	131.5	126.2	122.9	127.0
14	76.4	76.1 (2.7)	76.1 (1.9)	75.8	77.6	76.6	78.2
15	65.4	63.9 (8.5)	66.0 (2.8)	65.2	64.3	63.3	62.6
16	17.1	16.7 (0.8)	16.8 (0.7)	16.5	16.4	17.6	12.1
17	24.5	24.4 (0.2)	24.4 (0.2)	24.3	24.2	24.4	24.3
18	27.3	26.9 (0.4)	26.8 (0.4)	26.8	26.9	26.9	27.2
19[d]	22.0	21.9 (0.1)	22.0 (0.1)	21.8	21.9	22.2	22.0
20	21.8	21.8 (0.2)	21.7 (0.2)	21.7	21.7	22.0	21.8
* —OCCH$_3$ O		171.0 (0.4)	171.1 (0.4)	170.6, 170.3	2×170.4, 170.1	100.4[h]	100.1[h]
O * —OCCH$_3$		21.2 (1.6)	21.1 (1.4)	21.0, 20.9	21.1, 2×20.9	27.1[i,j], 24.1[i,k]	27.1[i,j], 24.1[i,k]

[a]All values from internal TMS; accurate to ±0.1 ppm;
[b]C-1, C-8 and C-10 may be interchanged.
[c]Values in parentheses indicate Eu(fod)$_3$ induced shifts.
[d]C-3, C-4 and C-19, C-20 may be interchanged.
[e]C-3, C-4, C-12 may be interchanged.
[f]C-5, C-6 may be interchanged.
[g]C-7, C-10 may be interchanged.
[h]Acetonide carbon.
[i]Acetonide methyls.
[j]May be interchanged with C-18.
[k]May be interchanged with C-17.

experiments, and by comparison with our previously assigned ^{13}C spectra of related cyathins (6). Figure 1 shows a comparison of the ^{13}Cmr shifts observed for the previously assigned (6) *O,O*-diacetylcyathin A_3 (**7**) and for 11,15-*O,O*-diacetylcyathatriol (**5**) reported herein. The only difference in structure between the compounds in Fig. 1 is the replacement of the C-14 carbonyl group in **7** with a β-hydroxyl group in **5**. The changes in shielding should occur only in the proximity of the structural change. Using an additivity approach for this change (OH vs. carbonyl (7, 8)) reproduces the shielding changes observed.

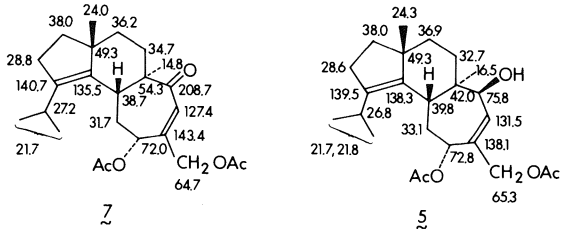

FIG. 1. Comparison of ^{13}Cmr data for *O,O*-diacetylcyathin A_3 (**7**) and 11,15-*O,O*-diacetylcyathatriol (**5**).

For all of the compounds the chemical shift of C-10 is very similar to that of C-7 and C-8. In order to distinguish between these carbons a Eu(fod)$_3$ shift study was undertaken with **3** and **4**. It was expected that complexation would be favored at C-11, C-15 rather than at C-14 and indeed in both cases C-11 shows a larger shift than C-14. Consequently, the signal in the δ 32–37 region which shows the largest Eu(fod)$_3$ shift is assigned to C-10.

Table 1 also includes the shift values for cyathatriol acetonide (**8**) and 14-epicyathatriol acetonide **9** (1). The shift values for **8** agree well with those of **2**–**6** whereas the C-16 methyl signal in **9** appears at δ 12.1, reflecting the γ-*gauche* effect of the C-14 hydroxyl. The C-5 signal moves downfield to δ 45.0 in **9** (δ 39.1 in **8**), reflecting the fact that the C-14 hydroxyl is no longer γ-*gauche* to C-5.

The cyathane skeleton **1** is unique among the diterpenoids. We have earlier noted that the carbon

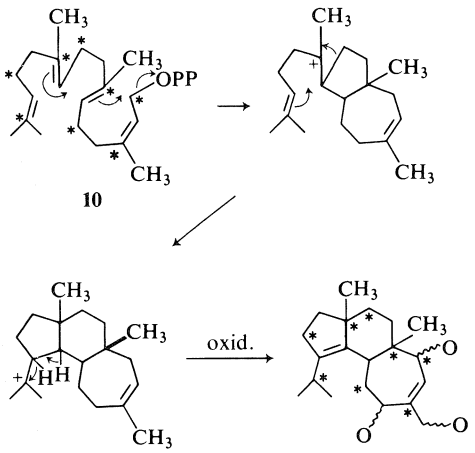

SCHEME 1

skeleton of the cyathins may be formed by cyclization–rearrangement of geranylgeranyl pyrophosphate (**10**) as shown in Scheme 1 (2). Recently, Faulkner and co-workers (9) have isolated from sea hares compounds with the carbon skeleton **11**

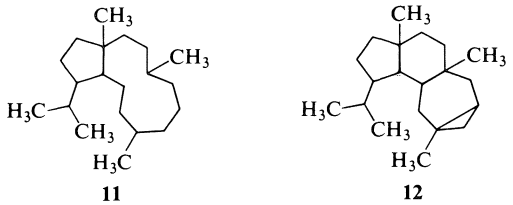

(dolabellane), which differ only in that they are bicyclic and the C-12 methyl group of cyathane appears at C-11 (cyathane numbering) in dolabellane. This same skeleton appears, in tetracyclic form, in compounds of the newly discovered verrucosane (**12**) class (10). This latter type of skeleton may be derived from geranylgeranyl pyrophosphate (**10**) as illustrated in Scheme 2 for the dolabelladiene cation **11***a*. Subsequent C-5 to C-6 bond formation and migration of the C-11 methyl to C-12 leads to the cyathane skeleton.

Incorporation of [^{13}C-1]-labelled acetate into the cyathins via mevalonic acid and geranylgeranyl pyrophosphate as shown in Scheme 1 would result in labelling at the asterisked carbons (C-2, C-6, C-8, C-9, C-10, C-12, C-14, C-18) whereas incorporation via Scheme 2 would result in a partly different distribution (C-2, C-5, C-6, C-8, C-9, C-11, C-13, C-18) as indicated in the scheme. In the first case C-10, C-12, and C-14 of ring C are labelled, in the second case it is C-5, C-11, and C-13.

Cyathus earlei was grown in liquid culture in the presence of sodium [1-^{13}C]acetate as described in the Experimental and 11-*O*-acetylcyathatriol (**3**) was isolated by chromatography. Figure 2 shows the ^{13}Cmr spectrum of the resulting enriched 11-*O*-acetylcyathatriol (spectrum A), the natural abundance spectrum and assignments (spectrum B), and the computer derived subtraction of B from A (curve C). The latter curve clearly shows that carbons 2, 6, 8, 9, 10, 12, 14, and 18 as well as the acetyl carbonyl carbon are derived from the carboxyl carbon of [1-^{13}C]acetate, in agreement with the biosynthetic pathway shown in Scheme 1. When sodium [2-^{13}C]acetate was added to growing *C. earlei*, 11-*O*-acetylcyathatriol enriched at the remaining carbons (2, 5, 6, 8, 9, 11, 13, and 18, and the acetyl methyl) was obtained. Figure 3 shows the

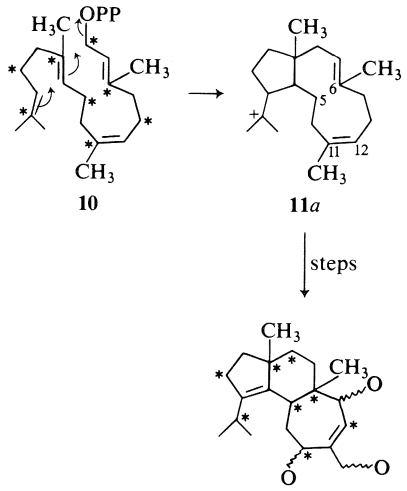

SCHEME 2

spectrum of the enriched as well as the natural abundance sample and the computer subtraction (curve C) identifies the enriched carbons. These experiments serve to eliminate from consideration the dolabellane route (Scheme 2) to the cyathins and are consistent with the pathway shown in Scheme 1.

The pathway shown in Scheme 1 involves a molecular rearrangement which may be detected using doubly-labelled sodium acetate (ref. 5, p. 164). The intact acetate units in geranylgeranyl pyrophosphate (**10***a*) derived via mevalonate are shown as heavy lines in **10***a* (Scheme 3). As illustrated in Scheme 3, the postulated rearrangement involves a scission of one of the acetate units (C-4, C-8) which will eliminate the ^{13}C—^{13}C coupling between C-4 and C-8, and these two carbons, along with C-1, C-7, C-11, and C-19, should appear as singlets in the proton-decoupled spectrum of 11-*O*-acetylcyathatriol (**3**) derived from [1,2-^{13}C]acetate if the C-4 to C-9 bond migration does occur. Figure 4 shows a comparison of the natural abundance spectrum (curve A) and the 100 MHz spectrum of **3** obtained by feeding experiments utilizing [1,2-^{13}C]acetate.

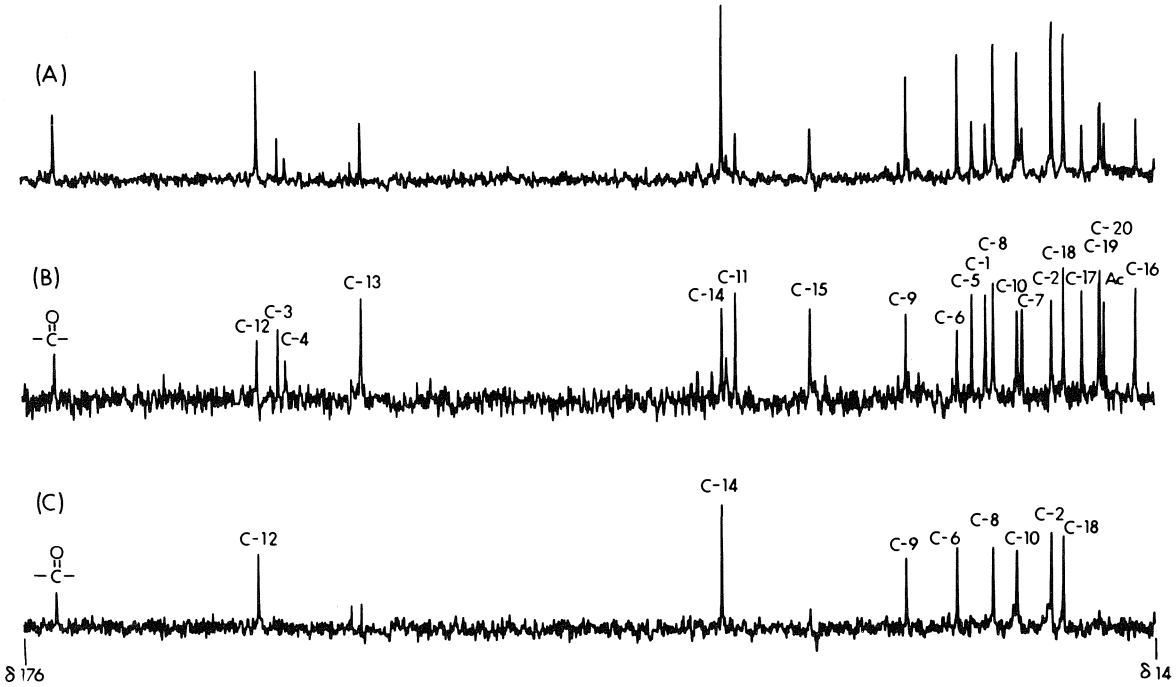

FIG. 2. Proton decoupled ^{13}Cmr spectra (22.6 MHz) of: (A) 11-*O*-acetylcyathatriol (**3**) from [1-^{13}C]acetate enrichment; (B) natural abundance spectrum of **3**; (C) computer derived subtraction of curve B from curve A.

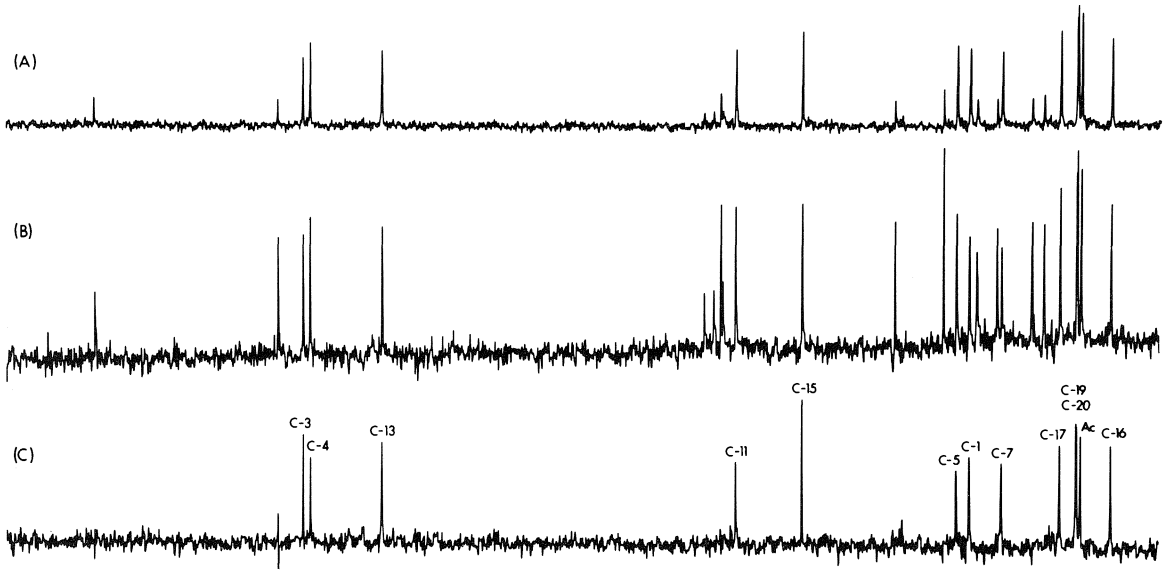

FIG. 3. Proton decoupled ^{13}Cmr spectra (22.6 MHz) of: (A) 11-*O*-acetylcyathatriol (**3**) from [2-^{13}C]acetate enrichment; (B) natural abundance spectrum of **3**; (C) computer derived subtraction of curve B from curve A.

Clearly C-4 and C-8 do not show ^{13}C—^{13}C coupling, consistent with the molecular rearrangement shown in Schemes 1 and 3.

In summary, the results reported herein indicate that the cyathins are biosynthesized from acetate, presumably via mevalonic acid, "active isoprene", and geranylgeranyl pyrophosphate, and the results are consistent with a cationic cyclization–rearrangement sequence of the type shown in Schemes 1 and 3.

Experimental

Instrumentation

The ^{13}Cmr spectra were determined in chloroform-d_1 (5% tetramethylsilane as standard) at a concentration of approximately 5–20% (w/v) in 5 or 10 mm sample tubes using a

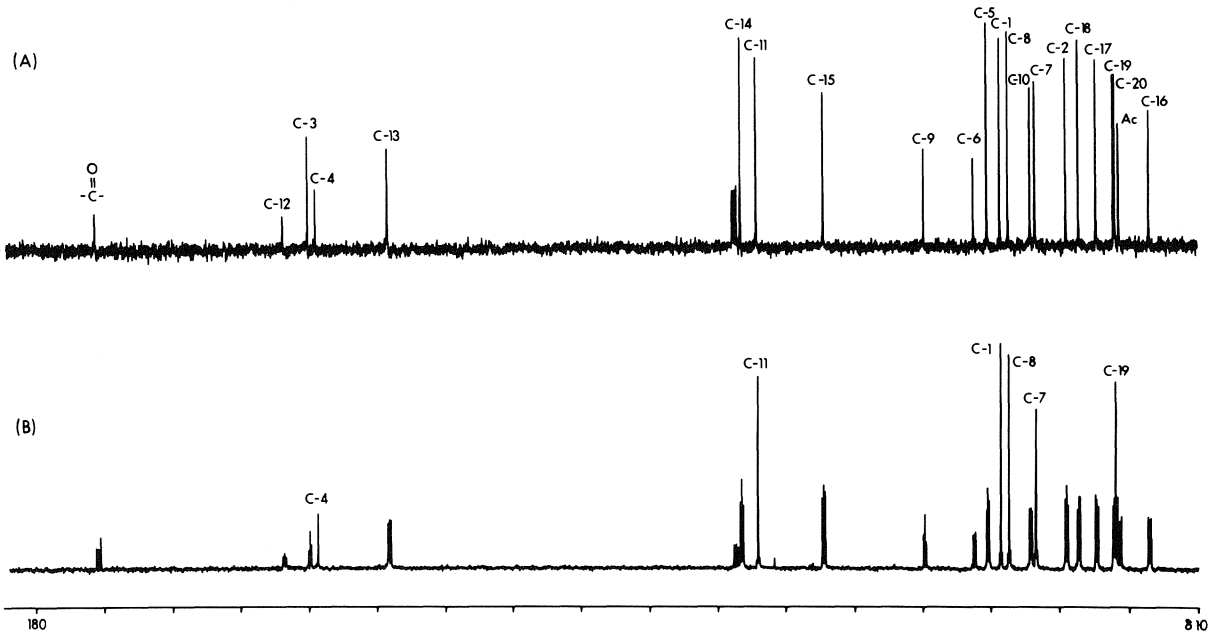

FIG. 4. Proton decoupled ^{13}Cmr spectra (100.6 MHz) of: (A) 11-*O*-acetylcyathatriol (**3**), natural abundance; (B) 11-*O*-acetylcyathatriol from [1,2-$^{13}C_2$]acetate enrichment.

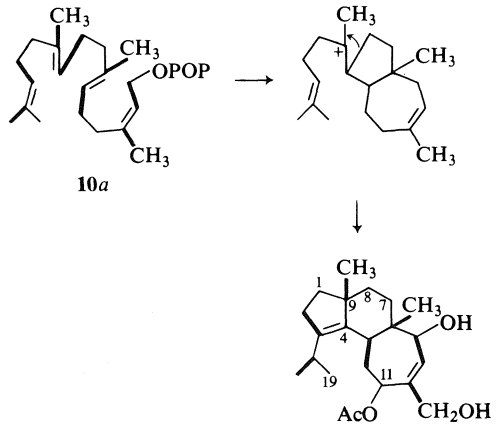

SCHEME 3

Bruker WP-60, HFX-90, or WH-400 spectrometer operating in the Fourier transform mode. A few drops of methanol-d_4 were added to the solutions of **2** and **5** to increase solubility. Because of the limited amount of material, **8** was dissolved in ca. 10 μL of methanol-d_4 and the spectrum determined in a 1.7 mm microprobe. For the shift study, a solution of Eu(fod)$_3$ in chloroform-d_1 was added dropwise to a solution of the substrate in chloroform-d_1 until approximately a 1:1 weight ratio was obtained. ^{1}Hmr spectra were recorded on a Varian HA-100-12 in. system or on a Varian HA-100-15 in. system interfaced to a Digilab FTS/NMR-3 data system.

Materials

Sodium [1-^{13}C]acetate and sodium [2-^{13}C]acetate (90% enriched) were purchased from Merck Sharp and Dohme Canada Ltd. Sodium [1,2-$^{13}C_2$]acetate was obtained from Prochem US Services Ltd. Brodie medium was prepared in the usual manner (11) and sterilized before use. Silica gel refers to E. Merck Silica Gel 60. Compounds **2–6, 8,** and **9** were obtained as previously described (1).

Incorporation of ^{13}C-labelled Acetate into 11-O-Acetylcyathatriol (3)

Cyathus earlei Lloyd ATCC 38343 (1) was grown in liquid still culture at room temperature in Brodie medium in 2 2.8-L Fernback flasks (1 L medium/flask). After fourteen days growth sodium [1-^{13}C]acetate (1.00 mmol/L) in water (5 mL, sterilized) was added to each flask. One week later a further 1.00 mmol was added to each flask. Two weeks later the culture broth was decanted and the mycelium was reflooded with fresh sterilized Brodie medium. Seven days after the reflood, sterilized sodium [1-^{13}C]acetate solution (2 mmol per flask) was again added. Three weeks later the mycelium was harvested by filtration, dried, and extracted with ethyl acetate in a Soxhlet apparatus. The crude extract (ca. 0.5 g) was subjected to chromatography over silica gel (25 g) as previously described (1). Elution with ether–benzene (3:7) afforded 11-*O*-acetylcyathatriol (40 mg) which was crystallized from ether, mp 165–166°C (1). The experiments with sodium [2-^{13}C]acetate and sodium [1,2-$^{13}C_2$]acetate were conducted in exactly the same way as described for sodium [1-^{13}C]acetate.

Acknowledgements

We thank Professor H. J. Brodie for slant cultures of *C. earlei* and the Natural Sciences and Engineering Research Council of Canada for financial support.

1. W. A. AYER and S. P. LEE. Can. J. Chem. **57**, 3332 (1979).
2. W. A. AYER and H. TAUBE. Can. J. Chem. **51**, 3842 (1973).
3. W. A. AYER, L. M. BROWNE, S. FERNÁNDEZ, D. E. WARD, and T. YOSHIDA. Rev. Latinoamer. Quim. **9**, 177 (1978).

4. D. V. BANTHORPE and B. V. CHARLWOOD. *In* Chemistry of the terpenes and terpenoids. *Edited by* A. A. Newman. Academic Press, New York, NY. 1972. p. 337.
5. A. G. MCINNES, J. A. WALTER, J. L. C. WRIGHT, and L. C. VINING. *In* Topics in carbon-13 nmr spectroscopy. Vol. 2. *Edited by* G. C. Levy. John Wiley and Sons, New York, NY. 1976. p. 125.
6. W. A. AYER, T. T. NAKASHIMA, and D. E. WARD. Can. J. Chem. **56**, 2197 (1978).
7. G. E. MACIEL. J. Phys. Chem. **69**, 1947 (1965).
8. L. M. JACKMAN and D. P. KELLEY. J. Chem. Soc. B, 102 (1970).
9. C. IRELAND and D. J. FAULKNER. J. Org. Chem. **42**, 3157 (1977), and references therein.
10. A. MATSUO, H. NOZAKI, M. NAKAYAMA, S. HAYASHI, and D. TAKAOKA. J. Chem. Soc. Chem. Commun. 198 (1978).
11. H. J. BRODIE. The bird's nest fungi. University of Toronto Press, Toronto, Ont. 1975. p. 36.

Total synthesis of barbatane sesquiterpenes: α- and β-barbatenes, gymnomitrol, and isogymnomitrol

MITSUAKI KODAMA, TOSHIO KURIHARA, JINKO SASAKI, and SHÔ ITÔ

Department of Chemistry, Faculty of Science, Tohoku University, Sendai 980, Japan

Received July 30, 1979

This paper is dedicated to Prof. Karel Wiesner on the occasion of his 60th birthday

MITSUAKI KODAMA, TOSHIO KURIHARA, JINKO SASAKI, and SHÔ ITÔ. Can. J. Chem. **57**, 3343 (1979).

A total synthesis of the barbatenes and a formal total synthesis of gymnomitrol and isogymnomitrol were achieved through a common intermediate utilizing a cycloaddition reaction and skeletal rearrangements.

MITSUAKI KODAMA, TOSHIO KURIHARA, JINKO SASAKI et SHÔ ITÔ. Can. J. Chem. **57**, 3343 (1979).

On a réalisé la synthèse totale des barbatènes et une synthèse totale formelle du gymnomitrol et de l'isogymnomitrol à partir d'un intermédiaire commun en utilisant une réaction de cycloaddition et des transpositions moléculaires.

[Traduit par le journal]

Barbatenes (gymnomitrene, isogymnomitrene, pompenes), **1** and **2**, and gymnomitrol **3**, are sesquiterpenes isolated from certain liverwort species together with some oxygenated congeners (1–6), and isogymnomitrol **4** is the isomerization product of **3**. All of these compounds have the novel tricyclo-[5.3.1.$0^{2,6}$]undecane framework which is biogenetically related to the carbon skeleton of the trichothecanes.

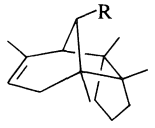

1 R = H *a*-barbatene
4 R = OH isogymnomitrol

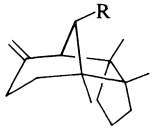

2 R = H β-barbatene
3 R = OH gymnomitrol

This unique carbon skeleton should be accessible by stereospecific skeletal rearrangement of bicyclo-[2.2.2]octane derivatives, e.g., **5**, which in turn would be readily available by Diels–Alder reaction of an appropriate dihydrobenzene and an activated cyclopentene derivative. In this communication we wish to report the stereospecific total synthesis of these four compounds according to this strategy via a common intermediate.

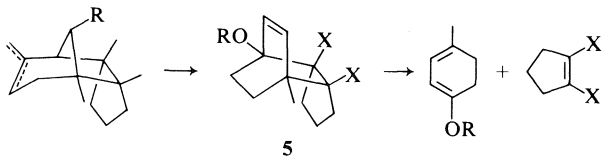

5

SCHEME 1

*Synthesis of the Common Intermediate (Type **5**)*

When cyclopentene-1,2-dicarboxylic anhydride **6** (7, 8) and two molar equivalents of 4-methylcyclohexa-1,4-dienyl methyl ether **7** (9) were heated in refluxing toluene in the presence of a catalytic amount of *p*-toluenesulfonic acid under a nitrogen atmosphere, the *endo*-adduct **8**,[1] mp 104–105°C, was formed exclusively in 93% yield. The *endo* relationship of the double bond and anhydride grouping in **8**

[1]All compounds were adequately characterized by spectroscopic methods (ir, nmr, and ms) and by correct elemental analysis.

0008-4042/79/243343-03$01.00/0

4. D. V. BANTHORPE and B. V. CHARLWOOD. *In* Chemistry of the terpenes and terpenoids. *Edited by* A. A. Newman. Academic Press, New York, NY. 1972. p. 337.
5. A. G. MCINNES, J. A. WALTER, J. L. C. WRIGHT, and L. C. VINING. *In* Topics in carbon-13 nmr spectroscopy. Vol. 2. *Edited by* G. C. Levy. John Wiley and Sons, New York, NY. 1976. p. 125.
6. W. A. AYER, T. T. NAKASHIMA, and D. E. WARD. Can. J. Chem. **56**, 2197 (1978).
7. G. E. MACIEL. J. Phys. Chem. **69**, 1947 (1965).
8. L. M. JACKMAN and D. P. KELLEY. J. Chem. Soc. B, 102 (1970).
9. C. IRELAND and D. J. FAULKNER. J. Org. Chem. **42**, 3157 (1977), and references therein.
10. A. MATSUO, H. NOZAKI, M. NAKAYAMA, S. HAYASHI, and D. TAKAOKA. J. Chem. Soc. Chem. Commun. 198 (1978).
11. H. J. BRODIE. The bird's nest fungi. University of Toronto Press, Toronto, Ont. 1975. p. 36.

Total synthesis of barbatane sesquiterpenes: α- and β-barbatenes, gymnomitrol, and isogymnomitrol

MITSUAKI KODAMA, TOSHIO KURIHARA, JINKO SASAKI, and SHÔ ITÔ

Department of Chemistry, Faculty of Science, Tohoku University, Sendai 980, Japan

Received July 30, 1979

This paper is dedicated to Prof. Karel Wiesner on the occasion of his 60th birthday

MITSUAKI KODAMA, TOSHIO KURIHARA, JINKO SASAKI, and SHÔ ITÔ. Can. J. Chem. **57**, 3343 (1979).

A total synthesis of the barbatenes and a formal total synthesis of gymnomitrol and isogymnomitrol were achieved through a common intermediate utilizing a cycloaddition reaction and skeletal rearrangements.

MITSUAKI KODAMA, TOSHIO KURIHARA, JINKO SASAKI et SHÔ ITÔ. Can. J. Chem. **57**, 3343 (1979).

On a réalisé la synthèse totale des barbatènes et une synthèse totale formelle du gymnomitrol et de l'isogymnomitrol à partir d'un intermédiaire commun en utilisant une réaction de cycloaddition et des transpositions moléculaires.

[Traduit par le journal]

Barbatenes (gymnomitrene, isogymnomitrene, pompenes), **1** and **2**, and gymnomitrol **3**, are sesquiterpenes isolated from certain liverwort species together with some oxygenated congeners (1–6), and isogymnomitrol **4** is the isomerization product of **3**. All of these compounds have the novel tricyclo-[5.3.1.$0^{2,6}$]undecane framework which is biogenetically related to the carbon skeleton of the trichothecanes.

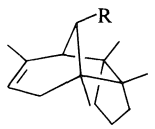

1 R = H *a*-barbatene
4 R = OH isogymnomitrol

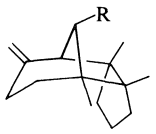

2 R = H β-barbatene
3 R = OH gymnomitrol

This unique carbon skeleton should be accessible by stereospecific skeletal rearrangement of bicyclo-[2.2.2]octane derivatives, e.g., **5**, which in turn would be readily available by Diels–Alder reaction of an appropriate dihydrobenzene and an activated cyclopentene derivative. In this communication we wish to report the stereospecific total synthesis of these four compounds according to this strategy via a common intermediate.

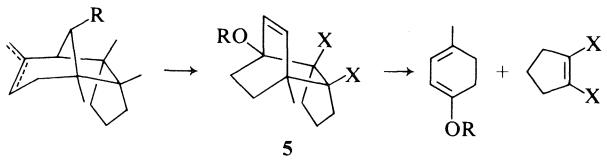

5

SCHEME 1

*Synthesis of the Common Intermediate (Type **5**)*

When cyclopentene-1,2-dicarboxylic anhydride **6** (7, 8) and two molar equivalents of 4-methylcyclohexa-1,4-dienyl methyl ether **7** (9) were heated in refluxing toluene in the presence of a catalytic amount of *p*-toluenesulfonic acid under a nitrogen atmosphere, the *endo*-adduct **8**,[1] mp 104–105°C, was formed exclusively in 93% yield. The *endo* relationship of the double bond and anhydride grouping in **8**

[1]All compounds were adequately characterized by spectroscopic methods (ir, nmr, and ms) and by correct elemental analysis.

0008-4042/79/243343-03$01.00/0

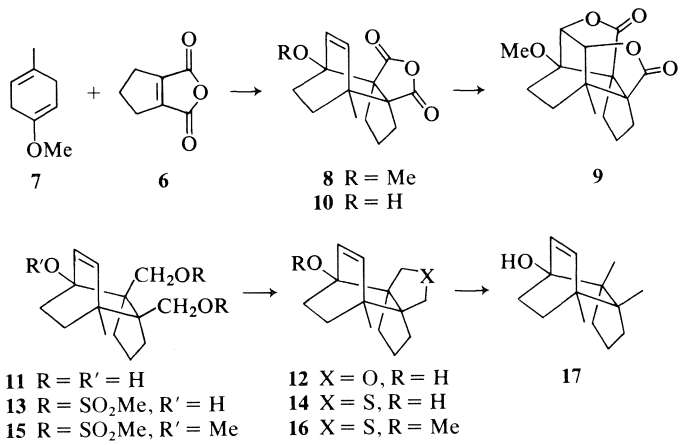

SCHEME 2

was confirmed by the formation of the bis-lactone **9**, mp 198–198.5°C, on alkaline bromination. After some preliminary experiments, **8** was first demethylated by boron tribromide in dichloromethane to the alcohol **10**, mp 264–265°C, in 96% yield. For the conversion of the anhydride group to two methyl groups, **10** was first reduced with lithium aluminum hydride in refluxing THF to give triol **11**, mp 230°C (dec.), in 84% yield. Although the attempted tosylation of **11** afforded mainly ether **12**, mp 206–208°C, mesylation (MsCl/Py) yielded dimesylate **13** as a colorless oil in 93% yield, and the latter was converted to sulfide **14**, mp 203–205°C, in 45% yield with anhydrous Na_2S in HMPA at 120°C (10).[2] Desulfurization of **14** with lithium in ethylamine at −20°C in the presence of 2-propanol yielded the desired olefin **17**, mp 188–190°C; *m/e* 206 (M^+), 110 (base peak); δ 0.81 (3H, s), 0.91 (3H, s), 1.01 (3H, s), 5.76 (1H, d, J = 8.5), 6.07 (1H, d, J = 8.5), in 87% yield.

Skeletal Rearrangement

The possibility of the rearrangement from tricyclo[5.2.2.$0^{2,6}$]undecane system to tricyclo[5.3.1.$0^{2,6}$]undecane was investigated utilizing the ether **12** as a model compound; **12** was treated with dry HI in dichloromethane to afford two iodides **18**, mp 121–123°C (58%), and **19**, mp 113.5–114.5°C (37%). The configuration of iodine was verified by the presence of W-type coupling (J = 2.5 Hz) in the signals due to H(8) (δ 4.72 ppm) in **18** and due to H(9) (δ 4.97 ppm) in **19**.

While **18** reverted to ether **12** when treated with diazabicycloundecane in refluxing benzene, **19** underwent smooth rearrangement to give ketone **20**, mp 132–135°C, ν 1702 cm^{-1}, quantitatively on treatment with potassium *tert*-butoxide in THF at room temperature. The structure of **20** was further confirmed by its conversion to the diosphenol **21**, mp 180–183°C, λ_{max} 273 nm (ε 5500) on alkaline oxidation (O_2, *t*-BuOK). Thus, the rearrangement to the barbatane carbon skeleton was achieved.

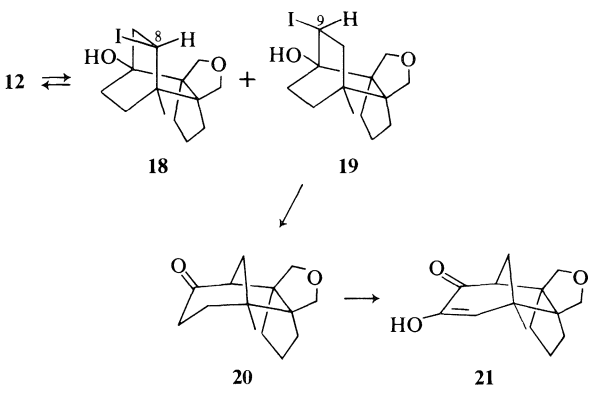

SCHEME 3

Synthesis of α- and β-Barbatenes (1 and 2)

Similar reaction of the hydrocarbon **17** with HI yielded two iodides, one of which was unstable and underwent the rearrangement upon contact with silica gel. Thus, chromatographic separation (SiO_2) of the products afforded the ketone **23**, mp 208–211°C, ν 1703 cm^{-1}, in 45% yield along with the iodide **22**. While Grignard reaction (MeMgI) and subsequent dehydration with $SOCl_2$ in pyridine yielded α-barbatene exclusively, dehydration using $POCl_3$ in pyridine afforded a ca. 1:1 mixture of α- and β-barbatenes. Separation of the products follows the known procedure (2) and the products are identified by comparison of their ir and nmr spectra with those of authentic specimens.

[2]In the same reaction using the corresponding methyl ether **15**, the sulfide **16** was obtained in over 65% yield.

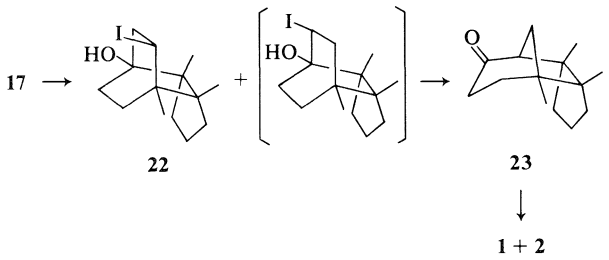

SCHEME 4

Formal Synthesis of Gymnomitrol 3 and Isogymnomitrol 4

The unsaturated alcohol **17** was oxidized with *m*-chloroperbenzoic acid (0°C, 6 h) to give the epoxy alcohol **24**, mp 93–95°C, quantitatively, which on alumina chromatography underwent skeletal rearrangement to the ketoalcohol **25**, mp 228°C, in 61% yield. Jones' oxidation of **25** yielded the diketone **26**, amorphous solid, ν 1745, 1710 cm^{-1}. The nmr and ir spectra match the reported data for the same compound derived from natural gymnomitrol (6) and also match the complete spectra of a sample of **26** supplied by Coates (11*a*). Since **26** has been synthesized by Coates[3] and converted in three steps to gymnomitrol **3** and isogymnomitrol **4**, the acid-catalyzed rearrangement product of **3**, the present study completes the formal total synthesis of these alcohols in a completely different strategy.

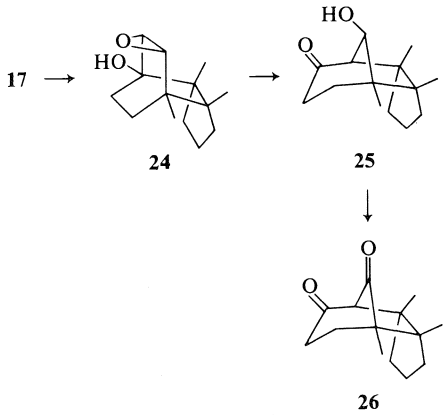

SCHEME 5

Acknowledgements

Our sincere thanks are due to Prof. S. Hayashi and Dr. A. Matsuo, Hiroshima University, for the spectra of the barbatenes, to Prof. J. D. Connolly, University of Glasgow, for the authentic sample and an nmr spectrum of gymnomitrol, to Prof. R. M. Coates, University of Illinois, for the spectra of the diketone **26**, and to Suntory Company for generous financial support.

1. N. H. ANDERSEN and S. HUNECK. Phytochemistry, **12**, 1818 (1973).
2. N. H. ANDERSEN, C. R. COSTIN, C. M. KRAMER, JR., Y. OHTA, and S. HUNECK. Phytochemistry, **12**, 2709 (1973).
3. A. MATSUO, T. MAEDA, M. NAKAYAMA, and S. HAYASHI. Tetrahedron Lett. 4131 (1973).
4. A. MATSUO, H. NOZAKI, M. NAKAYAMA, Y. KUSHI, S. HAYASHI, and N. KAMIJO. Tetrahedron Lett. 241 (1975).
5. J. D. CONNOLLY, A. E. HARDING, and I. M. S. THORNTON. J. Chem. Soc. Chem. Commun. 1320 (1972).
6. J. D. CONNOLLY, A. E. HARDING, and I. M. S. THORNTON. J. Chem. Soc. Perkin Trans. II, 2487 (1974).
7. S. C. SEN-GUPTA. J. Indian Chem. Soc. **17**, 183 (1940).
8. R. E. WINGARD, JR., R. K. RUSSELL, and L. A. PAQUETTE. J. Am. Chem. Soc. **96**, 7474 (1974).
9. H. H. INHOFFEN, K. WEISSERMEL, and G. QUINKERT. Chem. Ber. **88**, 1313 (1955).
10. L. A. PAQUETTE, J. M. PHOTIS, and R. P. MICHELI. J. Am. Chem. Soc. **99**, 7899 (1977).
11. (*a*) R. M. COATES, R. MASON, and S. K. SHAHI. J. Am. Chem. Soc. To be published. (*b*) L. A. PAQUETTE. *In* Topics in current chemistry. Vol. 79. Springer-Verlag, Berlin. 1979. p. 41.

[3]We thank Professor Coates for information regarding his synthesis. This work is also quoted in ref. 11*b*.

A synthetic approach to quassin. Synthesis of a ring A *seco* derivative

NADA STOJANAC, ŽARKO STOJANAC, PETER S. WHITE, AND ZDENEK VALENTA

Department of Chemistry, University of New Brunswick, Fredericton, N.B., Canada E3B 5A3

Received August 9, 1979

This paper is dedicated to Prof. Karel Wiesner on the occasion of his 60th birthday

NADA STOJANAC, ŽARKO STOJANAC, PETER S. WHITE, and ZDENEK VALENTA. Can. J. Chem. **57**, 3346 (1979).

Synthesis of compound **16**, a ring A *seco* derivative of quassin (**1**), is described. The overall strategy consists of manipulations within a rigid system established by a Diels–Alder reaction, followed by unfolding of the molecule. The sequence includes a cyclization of a 1,5-bromoketone with Zn and a selective oxidation of one carbonyl group in a tricyclic diketo diester with peracetic acid.

NADA STOJANAC, ŽARKO STOJANAC, PETER S. WHITE et ZDENEK VALENTA. Can. J. Chem. **57**, 3346 (1979).

On décrit la synthèse du composé **16**, un dérivé cyclique A *seco* de la quassine (**1**). La stratégie globale consiste en des manipulations à l'intérieur d'un système rigide produit par une réaction de Diels–Alder suivie du déplissement de la molécule. La suite de réaction comprend une cyclisation de la bromocétone-1,5 à l'aide de zinc et une oxydation sélective du groupe carbonyle du dicéto ester tricyclique par l'acide peracétique.

[Traduit par le journal]

Some time ago, we reported a synthetic approach to quassin (**1**), the bitter principle of *Quassia amara* (1, 2), in which all but two skeletal carbon atoms (C(2) and C(3)) were introduced by reaction **2** + **3** → **4** proceeding in a regio- and stereospecific[1] manner (3). It was based on the expectation that the relatively complex stereochemistry of **1** could more readily be established in a rigid system. We now wish to report one sequence which exploits this strategy, and includes an unconventional formation of the C(14)—C(15) bond and an unfolding of the caged molecule to the *seco*-quassin derivative **16**.

Triketone **5**, mp 68–70°C, prepared from **4** in ~80% yield by reduction with Zn in acetic acid (3) followed by hydrolysis with concentrated HCl in CH_3OH at 20°C and an oxidation of the resulting mixture of two epimeric alcohols, mp's 120–121°C and 107–108°C, with Collins' reagent (4), was equilibrated with anhydrous K_2CO_3 in dry CH_3OH to give a 3 : 2 mixture of **5** and **6**.[2,3] Isomer **6**, mp 138–140°C, purified by chromatography (hexane–EtOAc 5 : 1),[3] gave **7**, mp 150–152°C, on treatment with ethoxyethynyl magnesium bromide. Aqueous oxalic acid in EtOH converted **7** into oily **8** which yielded the saturated ester **9**,[4] mp 140–142°C, on hydrogenation with PtO_2 in ethanol. Compound **9** contains all the skeletal C-atoms of quassin and all nonepimerizable chiral centres in quassin (C*'s in structure **1** and **5**–**9**) are established.

To form the C(14)—C(15) bond (see structure **1** and **11**), **9** was treated with *N*-bromosuccinimide in CCl_4 at 80–85°C in the presence of $(CH_3)_3COOH$ or benzoyl peroxide to give **10**, mp 110–112°C,[5] which on reaction with OsO_4 in benzene and a catalytic amount of pyridine for 10 days, followed by treatment of the osmate ester with Zn in acetic acid at 20°C for 2 days and by decomposition with H_2S in $CHCl_3$ at 0°C, gave the desired foamy triol **11** (acetonide, mp 156–158°C). The yield of **11** purified by chromatography (hexane–EtOAc 2 : 3)[3] was 40% based on **10**. OsO_4 added stereospecifically and the addition led to a geometry of the CH_2Br and C=O groups particularly suitable for the coupling.[6]

[1]Diene **2** and adduct **4** are mixtures of diastereomers at C—OAc. All synthetic compounds reported in this Communication are racemic.

[2]A longer sequence in which the equilibration at this centre goes quantitatively in the desired sense is reported in ref. 3.

[3]All reactions were performed under N_2. All reported chromatographic purifications involved short column chromatography on Silica Gel G.

[4]Chromatographic purification of **9** (hexane–EtOAc 4:1)[3] removed minor quantities of its side-chain C—CH_3 diastereomer. Yield of **9** was 50% for the three steps from **6**.

[5]Yields of this reaction varied considerably and unpredictably, the best yields being almost quantitative.

[6]The sequence could also be performed, less efficiently, by initial osmate decomposition and by subsequent treatment of the resulting diol or its cyclic carbonate with Zn. We have not been able to achieve this Zn—HOAc coupling in model open-chain systems. Similar bond formations in halo ketones with Na (5) and R_2CuLi (6) and in a halo epoxide with Li (7) are reported; it should be noted, however, that the additional functionality and the danger of 1,2-eliminations in our system demand an exceptionally mild treatment.

0008-4042/79/243346-03$01.00/0

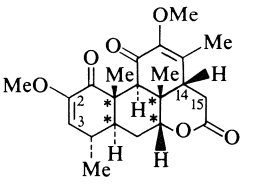

1

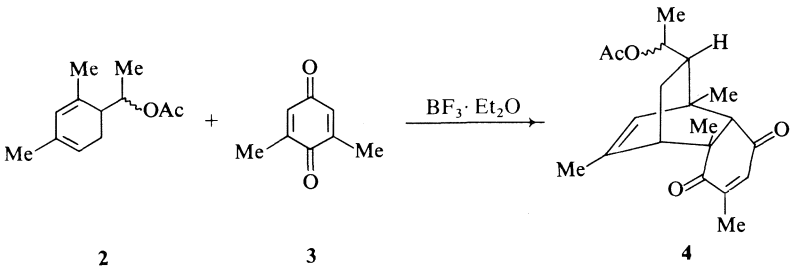

2 3 4

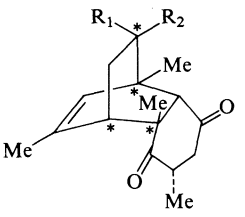

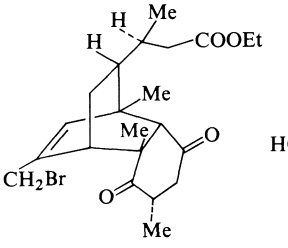

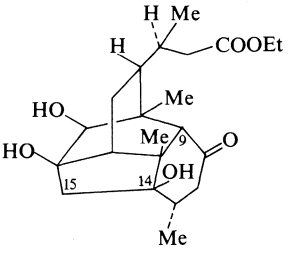

10 11

5 R_1 = acetyl; R_2 = H
6 R_1 = H; R_2 = acetyl

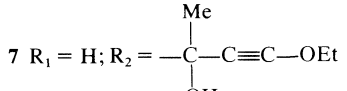

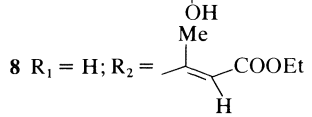

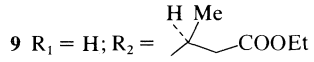

Cleavage of the *vic*-diol in **11** with H_5IO_6 in ether led to an unstable enol hemiacetal[7] which was immediately oxidized to lactone **12**, ν_{max} ($CHCl_3$) 3600, 3450, 1800 cm^{-1}, with Collins' reagent (4). Treatment of **12** with Ac_2O in pyridine at 100°C gave enone **13**, mp 166–167°C, λ_{max} (EtOH) 226 nm (ε 6880), ν_{max} 1800 cm^{-1}, ^{1}Hmr δ 6.00 (1H, s); its structure was established by X-ray diffraction. Hydrogenation of **13** with PtO_2 in EtOH gave ketone **14**, mp 141–142°C, ν_{max} 1800 cm^{-1}, no vinylic H in ^{1}Hmr spectrum, as the only product. Reaction of **14** with $NaOCH_3$ (10% in CH_3OH) under reflux for 20 h followed by treatment with ethereal diazomethane gave diketo diester **15**, mp 181–182°C. Finally, oxidation of **15** with 40% peracetic acid in HOAc–NaOAc at 65°C for 8 h gave the desired lactone **16**,[8] mp 144–145°C, ν_{max} 1735, 1720 (sh) cm^{-1}. The carbonyl

[7] ^{1}Hmr spectrum indicated a keto aldehyde ⇌ enol hemiacetal equilibrium.

[8] Relative configuration at C(4), C(5), C(8), C(10), and C(13) in **16** follows rigorously from the X-ray study of **13** and from previously reported transformations (3). The configuration at C(7) is clearly established by the position and shape of the ^{1}Hmr signal of the C(7)—H atom (δ 4.23, unresolved t, $W_{1/2}$ = 6 Hz), comparable to that in quassin (**1**). The configuration at C(14) must be as indicated because (*a*) the quantitative conversion **13** → **14** must involve a hydrogenation from the (less hindered) convex side and (*b*) for thermodynamic reasons, the two H-atoms at C(7) and C(14) can confidently be expected to be *cis* after the equilibrating conversion **14** → **15**. Several arguments (including thermodynamic stability) establish the configuration at C(9) (^{1}Hmr signal for C(9)—H at δ 3.15, s), the simplest being the fact that *an isomer* of **15** (β C(7)—H, β C(9)—H) was obtained in a sequence in which the secondary OH group in a derivative of **11** was first oxidized to a ketone which was subsequently cleaved without the use of equilibrating conditions.

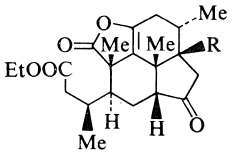

12 R = OH
14 R = H

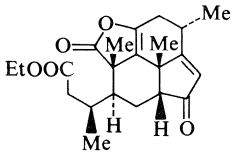

13

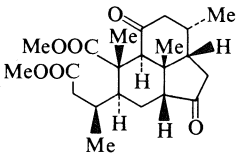

15

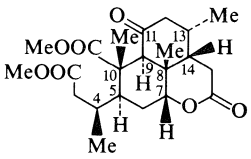

16

group at C(11) proved inert to these oxidation conditions.

The overall yield of the sequence **11** → **16** was 60–70%, the lowest single step yield (~80%) being for the conversion **14** → **15**.

Six of the seven chiral centres of quassin are established in **16**. The seventh, C(4), has the incorrect configuration. Since quassin derivatives equilibrate at C(4) to give, quantitatively, compounds with the equatorial CH_3-group (1), it should prove possible to correct this after ring A formation, provided that the cyclization will be successful in spite of the juxtaposition of the two CH_3 groups at C(4) and C(10) in **16** and its derivatives.

Acknowledgements

Support of this work by the National Research Council of Canada, Ottawa, a generous gift of quinone **3** by the Hoffmann-La Roche Co., Nutley, NJ, and technical assistance by Ms. Pierrette Pheeney are gratefully acknowledged.

1. Z. Valenta, S. Papadopoulos, and C. Podešva. Tetrahedron, **15**, 100 (1961); Z. Valenta, A. H. Gray, D. E. Orr, S. Papadopoulos, and C. Podešva. Tetrahedron, **18**, 1433 (1962).
2. R. M. Carman and A. D. Ward. Tetrahedron Lett. 317 (1961); Aust. J. Chem. **15**, 805 (1962).
3. N. Stojanac, A. Sood, Ž. Stojanac, and Z. Valenta. Can. J. Chem. **53**, 619 (1975).
4. J. C. Collins, W. W. Hess, and F. J. Frank. Tetrahedron Lett. 3363 (1968).
5. S. Danishefsky and D. Dumas. Chem. Commun. 1287 (1968).
6. E. J. Corey and I. Kuwajima. J. Am. Chem. Soc. **92**, 395 (1970).
7. R. R. Sauers, R. M. Hawthorne, and B. I. Dentz. J. Org. Chem. **32**, 4071 (1967).

Total synthesis of ryanodol[1,2]

André Bélanger,[3] Daniel J. F. Berney,[3,4] H.-Jürg Borschberg,[6] Robert Brousseau,[3] Alain Doutheau,[6] Robert Durand,[8] Hajime Katayama,[6] Richard Lapalme,[7] Dominique M. Leturc,[4,5] Chun-Chen Liao,[6] Fred N. MacLachlan,[7] Jean-Pierre Maffrand,[8] Fabrizio Marazza,[6] Robert Martino,[8] Claude Moreau,[8] Louiselle Saint-Laurent,[6] Roger Saintonge,[3] Pierre Soucy,[6] Luc Ruest,[9] and Pierre Deslongchamps

Laboratoire de Synthèse Organique, Département de Chimie, Faculté des Sciences, Université de Sherbrooke, Sherbrooke (Qué.), Canada J1K 2R1

Received August 30, 1979

This paper is dedicated to Prof. Karel Wiesner on the occasion of his 60th birthday

André Bélanger, Daniel J. F. Berney, H.-Jürg Borschberg, Robert Brousseau, Alain Doutheau, Robert Durand, Hajime Katayama, Richard Lapalme, Dominique M. Leturc, Chun-Chen Liao, Fred N. MacLachlan, Jean-Pierre Maffrand, Fabrizio Marazza, Robert Martino, Claude Moreau, Louiselle Saint-Laurent, Roger Saintonge, Pierre Soucy, Luc Ruest, and Pierre Deslongchamps. Can. J. Chem. **57**, 3348 (1979).

The total synthesis of (+)-ryanodol (**1**) is described.

André Bélanger, Daniel J. F. Berney, H.-Jürg Borschberg, Robert Brousseau, Alain Doutheau, Robert Durand, Hajime Katayama, Richard Lapalme, Dominique M. Leturc, Chun-Chen Liao, Fred N. MacLachlan, Jean-Pierre Maffrand, Fabrizio Marazza, Robert Martino, Claude Moreau, Louiselle Saint-Laurent, Roger Saintonge, Pierre Soucy, Luc Ruest et Pierre Deslongchamps. Can. J. Chem. **57**, 3348 (1979).

La synthèse totale du (+)-ryanodol (**1**) est décrite.

0008-4042/79/243348-07$01.00/0

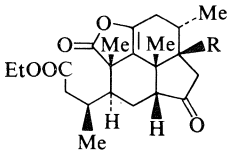

12 R = OH
14 R = H

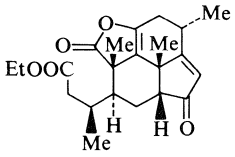

13

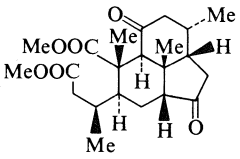

15

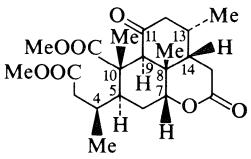

16

group at C(11) proved inert to these oxidation conditions.

The overall yield of the sequence **11** → **16** was 60–70%, the lowest single step yield (~80%) being for the conversion **14** → **15**.

Six of the seven chiral centres of quassin are established in **16**. The seventh, C(4), has the incorrect configuration. Since quassin derivatives equilibrate at C(4) to give, quantitatively, compounds with the equatorial CH_3-group (1), it should prove possible to correct this after ring A formation, provided that the cyclization will be successful in spite of the juxtaposition of the two CH_3 groups at C(4) and C(10) in **16** and its derivatives.

Acknowledgements

Support of this work by the National Research Council of Canada, Ottawa, a generous gift of quinone **3** by the Hoffmann-La Roche Co., Nutley, NJ, and technical assistance by Ms. Pierrette Pheeney are gratefully acknowledged.

1. Z. Valenta, S. Papadopoulos, and C. Podešva. Tetrahedron, **15**, 100 (1961); Z. Valenta, A. H. Gray, D. E. Orr, S. Papadopoulos, and C. Podešva. Tetrahedron, **18**, 1433 (1962).
2. R. M. Carman and A. D. Ward. Tetrahedron Lett. 317 (1961); Aust. J. Chem. **15**, 805 (1962).
3. N. Stojanac, A. Sood, Ž. Stojanac, and Z. Valenta. Can. J. Chem. **53**, 619 (1975).
4. J. C. Collins, W. W. Hess, and F. J. Frank. Tetrahedron Lett. 3363 (1968).
5. S. Danishefsky and D. Dumas. Chem. Commun. 1287 (1968).
6. E. J. Corey and I. Kuwajima. J. Am. Chem. Soc. **92**, 395 (1970).
7. R. R. Sauers, R. M. Hawthorne, and B. I. Dentz. J. Org. Chem. **32**, 4071 (1967).

Total synthesis of ryanodol[1,2]

André Bélanger,[3] Daniel J. F. Berney,[3,4] H.-Jürg Borschberg,[6] Robert Brousseau,[3] Alain Doutheau,[6] Robert Durand,[8] Hajime Katayama,[6] Richard Lapalme,[7] Dominique M. Leturc,[4,5] Chun-Chen Liao,[6] Fred N. MacLachlan,[7] Jean-Pierre Maffrand,[8] Fabrizio Marazza,[6] Robert Martino,[8] Claude Moreau,[8] Louiselle Saint-Laurent,[6] Roger Saintonge,[3] Pierre Soucy,[6] Luc Ruest,[9] and Pierre Deslongchamps

Laboratoire de Synthèse Organique, Département de Chimie, Faculté des Sciences, Université de Sherbrooke, Sherbrooke (Qué.), Canada J1K 2R1

Received August 30, 1979

This paper is dedicated to Prof. Karel Wiesner on the occasion of his 60th birthday

André Bélanger, Daniel J. F. Berney, H.-Jürg Borschberg, Robert Brousseau, Alain Doutheau, Robert Durand, Hajime Katayama, Richard Lapalme, Dominique M. Leturc, Chun-Chen Liao, Fred N. MacLachlan, Jean-Pierre Maffrand, Fabrizio Marazza, Robert Martino, Claude Moreau, Louiselle Saint-Laurent, Roger Saintonge, Pierre Soucy, Luc Ruest, and Pierre Deslongchamps. Can. J. Chem. **57**, 3348 (1979).

The total synthesis of (+)-ryanodol (**1**) is described.

André Bélanger, Daniel J. F. Berney, H.-Jürg Borschberg, Robert Brousseau, Alain Doutheau, Robert Durand, Hajime Katayama, Richard Lapalme, Dominique M. Leturc, Chun-Chen Liao, Fred N. MacLachlan, Jean-Pierre Maffrand, Fabrizio Marazza, Robert Martino, Claude Moreau, Louiselle Saint-Laurent, Roger Saintonge, Pierre Soucy, Luc Ruest et Pierre Deslongchamps. Can. J. Chem. **57**, 3348 (1979).

La synthèse totale du (+)-ryanodol (**1**) est décrite.

0008-4042/79/243348-07$01.00/0

This communication describes the stereocontrolled synthesis of the complex diterpene, (+)-ryanodol (**1**) (3, 4) (Scheme 1).

This compound exists in nature in the form of the α-pyrrole carboxylate ester derivative **2** known as ryanodine (3).

The two starting materials used in this construction are the readily available 5,6-dimethoxyindane (**3**) (5) and (+)-carvone (**4**) which were converted respectively into the two key building blocks, the *o*-spirolactone dienone **10** and the optically active (+)-isopropyl vinylketone acetal **15** (Scheme 2).

5,6-Dimethoxyindane (**3**) was first converted (CH_3OCHCl_2, $TiCl_4$, CH_2Cl_2) (6) into the corresponding aromatic aldehyde **5**[10,11] (mp 52°C) which was then cleaved (BBr_3, CH_2Cl_2) (7) to 4-formyl-5,6-dihydroxyindane (**6**, mp 130–131°C, 80% yield from **3**). Selective esterification of **6** ($BrCH_2COBr$, C_5H_5N, benzene) gave the monobromoacetate **7** (mp 110°C) which was cyclised (Na_2CO_3, THF, reflux) into lactone aldehyde **8** (mp 131–132°C, 80% yield from **6**). On Wolff–Kishner reduction of

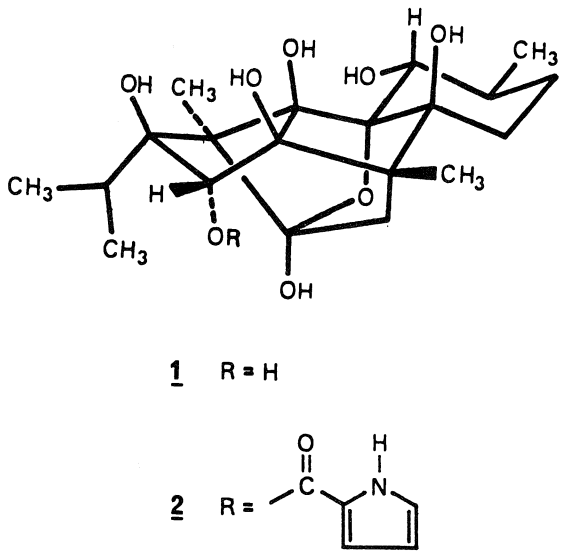

SCHEME 1

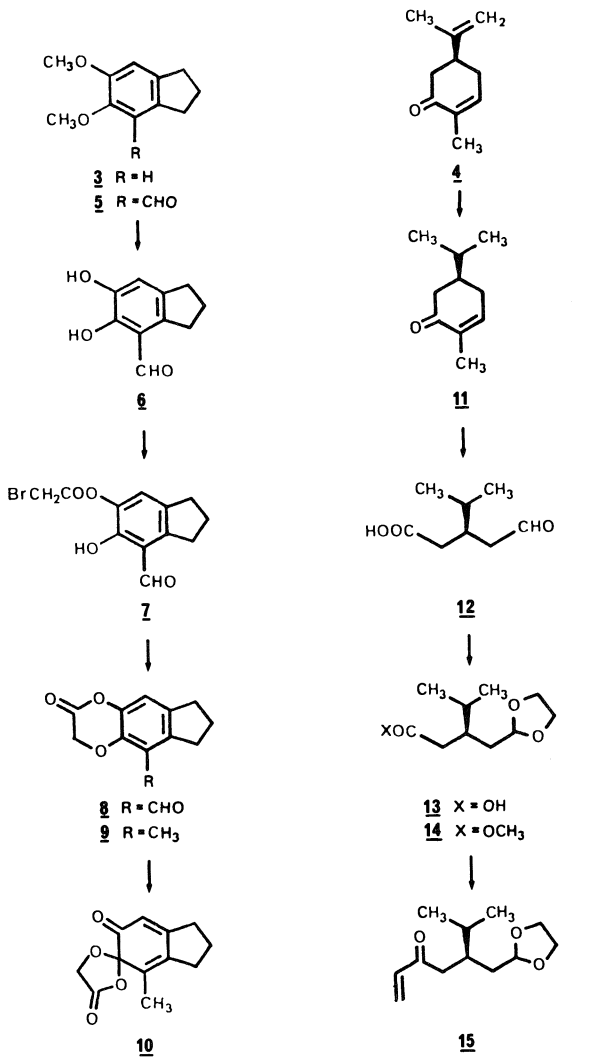

SCHEME 2

[1]Portions of this work have been presented on several occasions, in particular at the 10th I.U.P.A.C. Symposium of Natural Products, New Zealand, August 1976 (see ref. 2). The completed synthesis was presented at the Symposium on Synthesis and Bioorganic Chemistry of Natural Products, American Chemical Society–Chemical Society of Japan Meeting, Honolulu, April 1979.

[2]For previous publications on some aspects of this work, see refs. 1 and 2.

[3]Taken in part from Ph.D. theses. Université de Sherbrooke. (A.B., 1974; D.J.F.B., 1969; R.B., 1972; R.S., 1977.)

[4]Taken in part from M.Sc. theses. D.J.F.B., 1967, Université de Montréal, and D.M.L., 1972, Université de Sherbrooke.

[5]Deceased, March 29th, 1979.

[6]Post-doctoral collaborator.

[7]NRCC Postdoctorate Fellow. (R.L., 1977–78; F.N.M., 1977–78.)

[8]Coopérant militaire. Service de la Coopération Technique, France.

[9]Agrégé de Recherche, Département de Chimie, Université de Sherbrooke.

[10]For all substances, the spectra (ir, ^1H nmr, ms, and in selected cases ^{13}C nmr) were in agreement with the assigned structures. Satisfactory microanalyses were obtained for crystalline substances. All rotations are for chloroform solution unless stated otherwise.

[11]In some cases, where the yield of a reaction is not quantitative (>95%), minor products have been isolated and the structure determined. This information will appear in the detailed account.

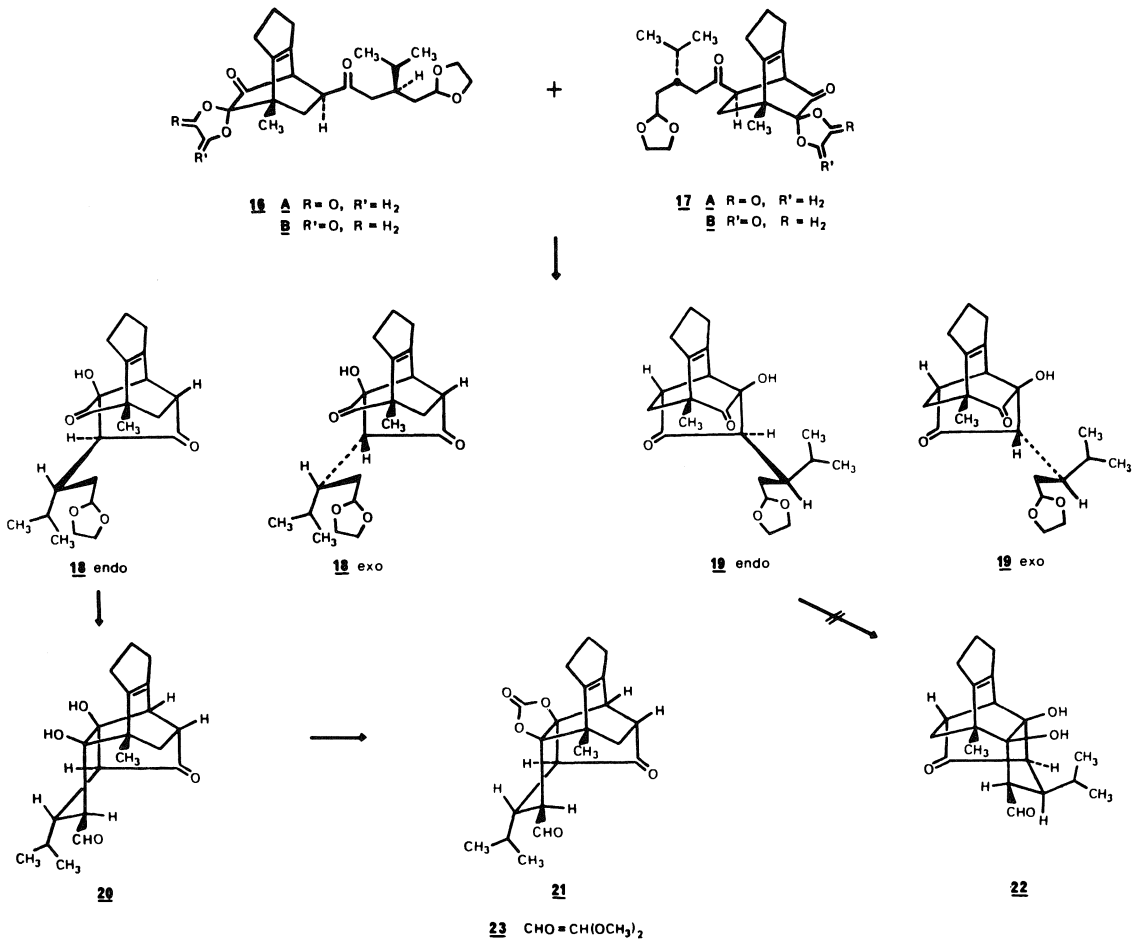

SCHEME 3

lactone aldehyde **8**, the aromatic lactone **9** (mp 75–76°C, 80% yield) was formed and then transformed (NaOH (1 equiv.), H_2O, CH_3CN; NBS) (8) to the *o*-spirolactone dienone **10** (mp 97–98°C, ≥95% yield).

d-Carvone (**4**) was reduced (Pt/H_2, ether) (9) to the dihydro derivative **11** which was then oxidized (O_3, $CH_3COOC_2H_5$; $Pd/C–H_2$) to yield the aldehyde carboxylic acid **12**. Acetalization ($(CH_2OH)_2$, *p*-TsOH, benzene; NaOH in CH_3OH) of **12** gave **13** which was then esterified (CH_3I, K_2CO_3, acetone) (10) and the resulting methyl ester **14** was purified by distillation (70% yield from carvone). The purified methyl ester **14** was hydrolysed (NaOH, CH_3OH) to the acetal carboxylic acid **13** which was finally converted (LiH, THF; CH_2=CHLi) into optically active isopropyl vinylketone acetal **15** ($[\alpha]_{578}$ +0.6°; 75% yield from **13**). Compound **15** was more conveniently prepared on a large scale by the following procedure: reduction ($LiAlH_4$, ether) of the methyl ester function in **14** (≃100% yield) to the corresponding primary alcohol followed by oxidation ($C_5H_5\overset{+}{N}HCrO_3Cl^-$, $NaHCO_3$, CH_2Cl_2, room temperature, 2.5 h), (11) to the expected aldehyde (93% yield). A Grignard reaction (CH_2=CHBr, Mg, ether) on this aldehyde followed by Jones oxidation (0°C) (12) gave isopropyl vinylketone acetal **15**.

Diene **10** was reacted (benzene, reflux, 1 h) with a slight excess of the dienophile **15** to give a 1:1 mixture of adducts **16** *A*, *B* and **17** *A*, *B* in quantitative yield (Scheme 3). This crude product was then converted (1 *N* NaOH, THF, room temperature) into a mixture of four diastereoisomers **18** and **19** (*exo* and *endo*) in which the *endo* epimers are the major isomers (*endo*/*exo* ≃ 3:1). This crude mixture was then treated under acidic (CH_3CO_2H—H_2O (7:3), 75°C, 2 h), followed by basic conditions (1 *N* NaOH, THF, room temperature) to yield the crude dihydroxyketoaldehyde **20**, which on further treatment ($COCl_2$, C_5H_5N, benzene) afforded the five-membered cyclic carbonate **21** (mp 186–188°C; $[\alpha]_D$ +121.3°), isolated by chromatography in 27% yield

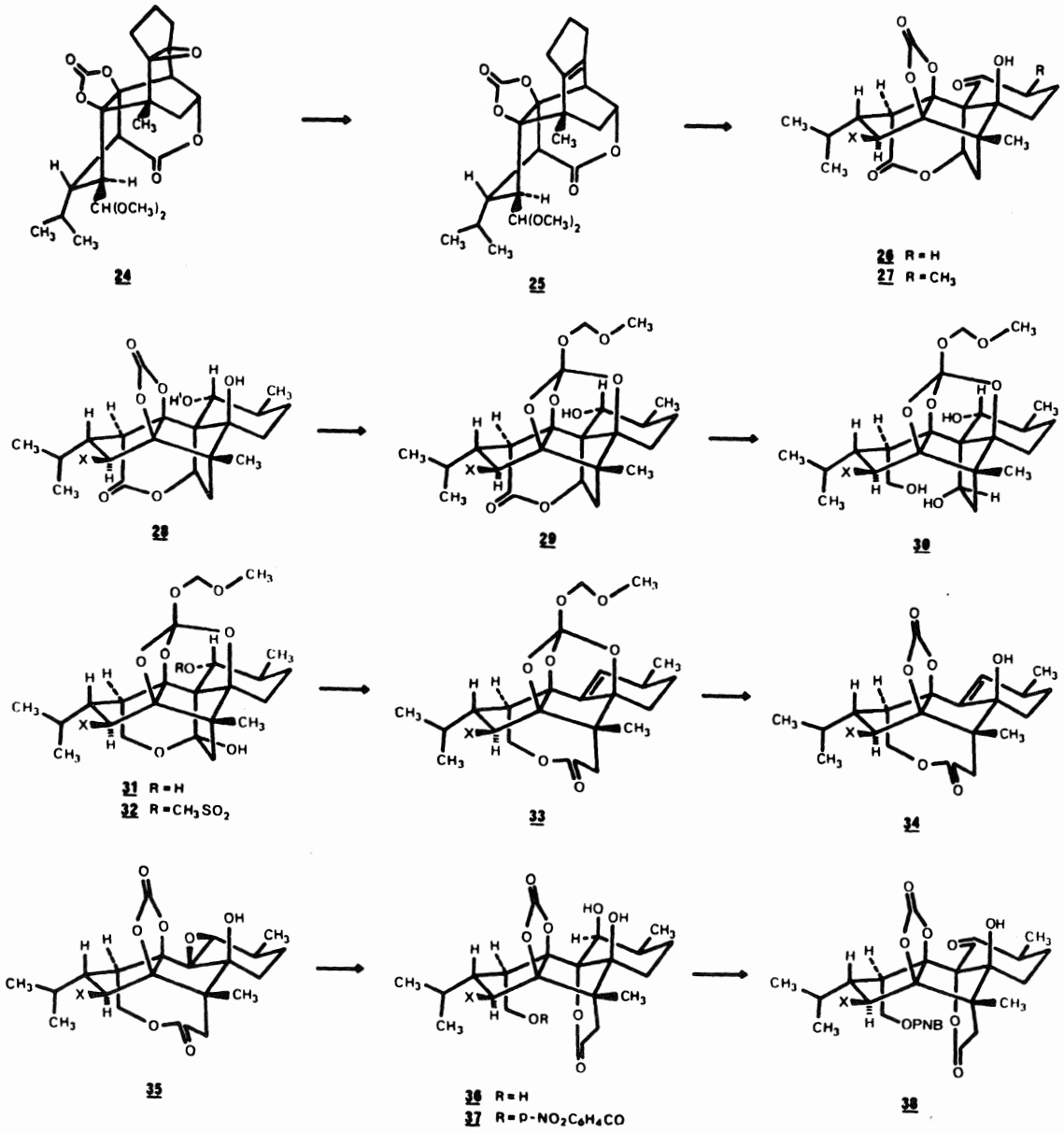

SCHEME 4. X = $CH(OCH_3)_2$

from **10**.[12,13,14] Compound **21** was further transformed (CH_3OH, $(CH_3O)_3CH$, *p*-TsOH) into the dimethoxyacetal derivative **23** (mp 114.7–115.2°C, $[\alpha]_D$ +121.3°).

Baeyer–Villiger oxidation (40% CH_3CO_3H, CH_3CO_2Na, room temperature, 15 h; 80°C, 1 h) of **23** gave the desired epoxylactone **24** (85%) accompanied by a small quantity (15%) of an isomeric lactone (Scheme 4). Retroepoxidation (WCl_6, *n*-BuLi (2 equiv.), THF, −78°C) (13) was carried out on this mixture and the olefin lactone **25** (mp 179–181°C, $[\alpha]_D$ −10.9°) was obtained pure by chromatography (80% yield from **23**). Ozonolysis of olefin lactone **25**

[12]The theoretical yield (**10** → **21**) is 50%, therefore this 27% represents 54% of the theoretical yield.

[13]The diastereoisomers **18** *endo* and **19** *endo* have been isolated by chromatography. Pure **18** *endo* was converted into **20** in quantitative yield, whereas **19** *endo* gave a complex mixture from which the expected isomeric pentacyclic compound **22** could not be isolated.

[14]The relative configuration of the isopropyl group in compounds **20** and **21** was determined by nmr on a derivative of **21** (see ref. 2, p. 1342).

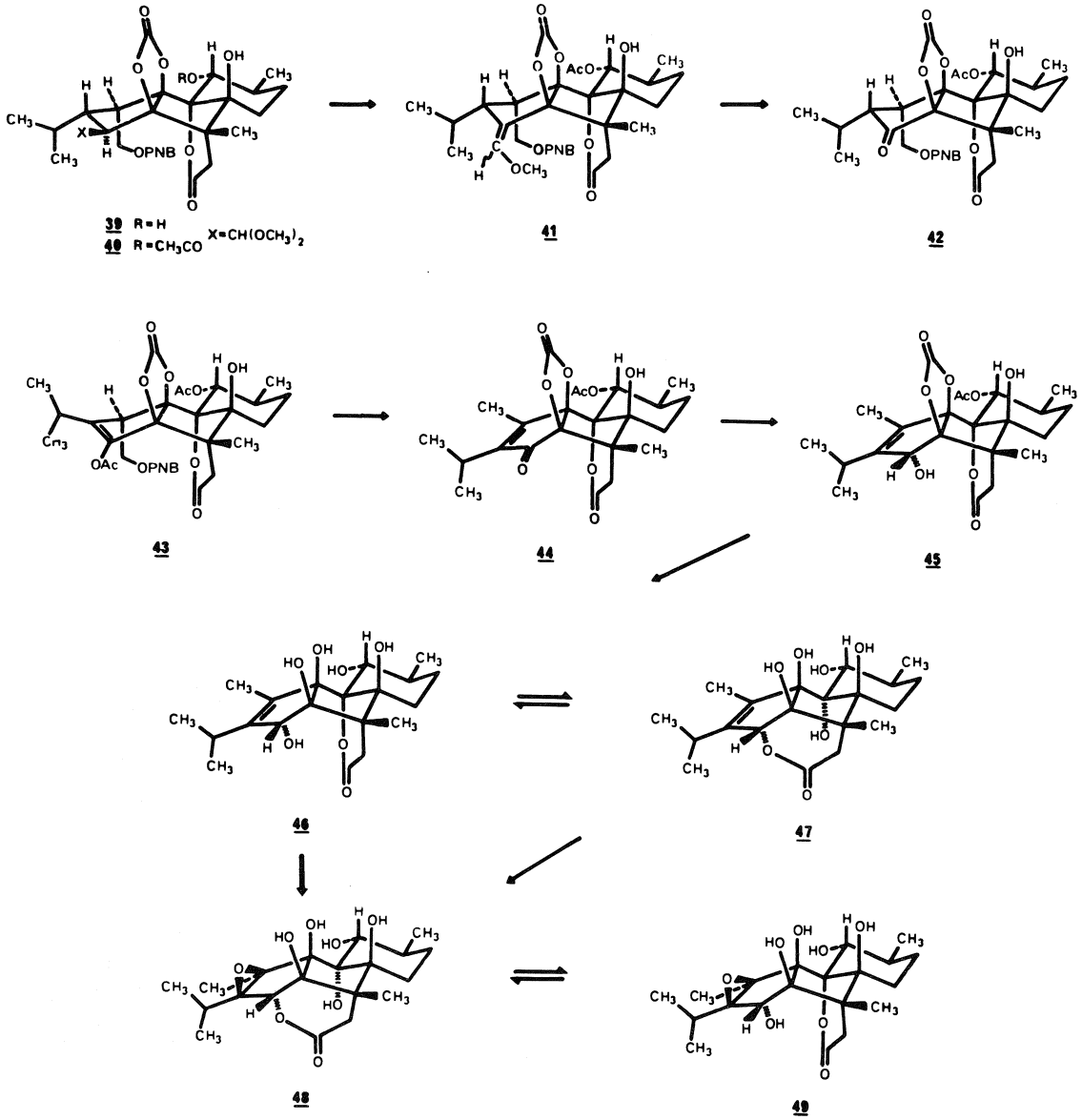

SCHEME 5

(O_3, $CH_3COOC_2H_5$, *p*-TsOH; $(CH_3)_2S$) (14) resulted in the desired aldol condensation product **26** (mp 238–238.5°C, $[\alpha]_D$ −48.0° (THF), ≥90% yield) which was then converted (lithium diisopropylamide in THF, −78°C; $(C_2H_5)_3B$, −25°C, 3 h; CH_3I) (15) into the equatorial monomethylated derivative **27** (mp 245.5–254°C (dec.), $[\alpha]_D$ −56.6° (THF), 70% yield).

The ketone function in **27** was selectively reduced ($NaBH_4$, CH_3OH, THF, 0°C) to the equatorial alcohol product **28** (mp 257–267°C; >95% yield) which was further characterized ($(CH_3CO)_2O$, C_5H_5N) as the acetate derivative **28** (H′ = CH_3CO) (mp 244–246°C, $[\alpha]_D$ −34.7°). Compound **28** was then transformed (NaH, THF, $ClCH_2OCH_3$, room temperature) into the methoxymethylorthocarbonate hydroxylactone dimethoxyacetal **29** (mp 169.5–170°C, $[\alpha]_D$ −12.1°, 80% yield plus 13% recovery of **28**). The product **29** was further reduced ($LiAlH_4$, THF) to the triol **30** (foam, $[\alpha]_D$ −40.1°, 95% yield) which underwent a highly selective oxidation ($CrO_3 \cdot (C_5H_5N)_2$, CH_2Cl_2, −45 to −22°C, 1 h) (16) to give the hemiketaldiol **31** (mp 121–123°C, $[\alpha]_D$ −39.2°, 76% yield). The secondary alcohol of **31** was mesylated (CH_3SO_2Cl, C_5H_5N, 0°C, 1 h) to yield hemiketal mesylate **32** (89% yield).

Compound **32** underwent a high yield fragmentation under basic conditions (CH_3SOCH_3, CH_3SOCH_2Li, room temperature, 30 min) to furnish the large ring lactone olefin methoxymethylorthocarbonate dimethoxyacetal **33** which was immediately converted by mild acid hydrolysis ($\simeq$0.3 *N* HBF_4, THF, 0°C, 3 h) into the lactone olefin hydroxycarbonate dimethoxyacetal **34** (mp 220–223°C, $[\alpha]_D$ −126°, 97.5% yield from **32**).

Epoxidation of compound **34** (CF_3CO_3H, Na_2HPO_4, $ClCH_2CH_2Cl$, 4°C, 15 h) afforded the β-epoxide **35** (mp 173–175°C, $\simeq$98% yield). Treatment of the β-epoxide **35** under basic conditions (0.1 *N* NaOH (0.4 mol equiv.), $CH_3OCH_2CH_2OCH_3$, 5.5 h, room temperature) gave after chromatography the desired lactone triol carbonate dimethoxyacetal **36** (mp 246–248°C, $[\alpha]_D$ −32.9°, 77% yield from **34**). Compound **36** was converted (p-$O_2NC_6H_4COCl$, C_5H_5N, 0°C, 25 min) into the primary p-nitrobenzoate derivative **37** (mp 130–131°C, $[\alpha]_D$ −33.0°, uv (CH_3OH) λ_{max}: 259 nm (ε: 12 184), 95% yield) which was then oxidized ($CrO_3 \cdot 2C_5H_5N$, CH_2Cl_2, 25°C) (16) to yield the hydroxyketone lactone carbonate p-nitrobenzoate dimethoxyacetal **38** (foam, $[\alpha]_D$ −30.3°, 78% yield). Reduction of **38** ($LiBH_4$, THF, −30 to −20°C, 1.5 h) resulted in a mixture of the desired equatorial alcohol **39** (foam, $[\alpha]_D$ −15.3°, 73% yield) and the previously described axial alcohol product **37** which were separated by chromatography (Scheme 5). Compound **39** was then acetylated ($(CH_3CO)_2O$, C_5H_5N) to yield the equatorial acetate derivative **40** (mp 318–319°C (dec.), $[\alpha]_D$ −20.6°).

Degradation of ring *A* of compound **40** led to the carbonate acetate derivative **44** of oxoanhydroryanodol. Compound **40** was first converted (p-TsOH, benzene, reflux) to a mixture of enol ethers **41** which was then oxidized (O_3, CH_2Cl_2, −78 to −55°C; $(CH_3)_2S$) to the cyclopentanone product **42**. Compound **42** was transformed ($(CH_3CO)_2O$, CH_3CO_2Na, 100°C, 15 h) into the enolacetate **43** (mp 316–318°C (dec.)). The enol acetate **43** under basic conditions (DBN, benzene, 75°C, 2.5 h) gave the carbonate–acetate derivative **44** of oxoanhydroryanodol (mp 301–302°C, $[\alpha]_D$ +150.6°, uv (CH_3OH) λ_{max}: 238 nm (8775), 50% yield from **40**).[15]

Compound **44** was reduced ($NaBH_4$, THF, CH_3OH, 0°C, 2 h) to the *endo* allylic alcohol **45** (mp 300–301°C (dec.), $[\alpha]_D$ +89.6° (CH_3OH), $\geq$90% yield). Basic hydrolysis of **45** (1 *N* NaOH, THF, room temperature, 24 h) gave a mixture (ratio 3:1) of anhydroryanodol **46** (mp 148–150°C, $[\alpha]_D$ +54.3° (CH_3OH)) and epianhydroryanodol **47** (mp 227–228°C, $[\alpha]_D$ −97.8° (CH_3OH)) which were separated and identified with authentic samples.[16]

Epoxidation (CF_3CO_3H, Na_2HPO_4, $ClCH_2CH_2Cl$, room temperature) of either synthetic anhydroryanodol (**46**) or synthetic epianhydroryanodol (**47**) gave the β-epoxide **48** of epianhydroryanodol[17] (foam, $[\alpha]_D$ −41.7°). Finally, reductive cyclization of **48** yielded totally synthetic ryanodol (**1**) (mp 267–268°C, $[\alpha]_D$ +38.5°, $\geq$60% yield) which was found identical (^1H nmr, tlc, and mixed mp 266.5–267.5°C) with an authentic sample (mp 266–267°C, $[\alpha]_D$ +40.0°) of ryanodol (**1**) obtained from the basic hydrolysis of ryanodine (**2**) (3). The chemical reactivity of totally synthetic ryanodol (**1**) was also verified: treatment of totally synthetic **1** with p-toluenesulfonic acid in dioxane at room temperature during 24 h yielded the expected mixture of anhydroryanodol (**46**) and epianhydroryanodol (**47**).

This communication will be followed by a detailed account which will include the necessary investigative studies which led to the final solution described above.

Acknowledgements

This research was supported by the Natural Sciences and Engineering Research Council of Canada and by the Ministère de l'Education of Québec.

1. D. Berney and P. Deslongchamps. Can. J. Chem. **47**, 515 (1969).
2. P. Deslongchamps. Pure Appl. Chem. **49**, 1329 (1977).
3. K. Wiesner. Adv. Org. Chem. **8**, 295 (1972); K. Wiesner, Z. Valenta, and J. Findlay. Tetrahedron Lett. 221 (1967).
4. S. N. Srivastava and M. Przybylska. Can. J. Chem. **50**, 1882 (1972).
5. R. Granger, P. F. G. Nau, and C. François. Bull. Soc. Chim. Fr. 496 (1958).
6. A. Ritchie, H. Gross, and E. Höft. Org. Synth. **47**, 1 (1967).
7. F. L. Benton and T. E. Dillon. J. Am. Chem. Soc. **64**, 1128 (1942).

[15]The experimental conditions for the conversion **40** → **44** have not been optimized.

[16]Basic hydrolysis of ryanodine (**2**) gives ryanodol (**1**) which can be transformed under acidic conditions into anhydroryanodol (**46**) (mp 150–151°C, $[\alpha]_D$ +53.3° (CH_3OH)) (3). Basic equilibration (1 *N* NaOH, THF, room temperature) of anhydroryanodol (**46**) resulted in a mixture (ratio 3:1) of **46** and epianhydroryanodol (**47**) (mp 225–226.5°C, $[\alpha]_D$ −103.2° (CH_3OH)).

[17]Utilizing **46** and **47** derived from the natural product, the following experiments were carried out: (*a*) epoxidation (Na_2HPO_4, CF_3CO_3H) of either **46** or **47** yielded the β-epoxide **48** (foam, $[\alpha]_D$ −43.2°, 85% yield) of epianhydroryanodol, (*b*) basic equilibration (1 *N* NaOH, THF) of **48** produced a mixture (ratio 3:2) of **48** and the β-epoxide **49** (mp 232–234°C (dec.), $[\alpha]_D$ +29.9° (CH_3OH)) of anhydroryanodol, and (*c*) reductive cyclization (Li, NH_3, THF) of either **48** or **49** furnished ryanodol ($\simeq$60% yield).

8. G. L. SCHMIR, L. A. COHEN, and B. WITKOP. J. Am. Chem. Soc. **81**, 2228 (1959); E. J. COREY and L. F. HAEFELE. J. Am. Chem. Soc. **81**, 2225 (1959).
9. A. S. HALLSWORTH, H. B. HENBEST, and T. I. WRIGLEY. J. Chem. Soc. 1969 (1957).
10. R. E. IRELAND, D. A. EVANS, D. CLOVER, G. M. RUBOTTOM, and H. YOUNG. J. Org. Chem. **34**, 3717 (1969).
11. E. J. COREY and J. W. SUGGS. Tetrahedron Lett. 2647 (1975).
12. K. BOWDEN, I. M. HEILBRON, E. R. H. JONES, and B. C. L. WEEDON. J. Chem. Soc. 39 (1946).
13. K. B. SHARPLESS, M. A. UMBREIT, M. T. NIEH, and T. C. FLOOD. J. Am. Chem. Soc. **94**, 6538 (1972).
14. J. J. PAPPAS, W. P. KEAVENEY, E. GAUCHER, and M. BERGER. Tetrahedron Lett. 4273 (1966).
15. M. W. RATHKE and A. LINDERT. Synth. Commun. **8**, 9 (1978); E. NEGISHI and M. J. IDACAVAGE. Tetrahedron Lett. 845 (1979).
16. R. RATCLIFFE and R. RODEHORST. J. Org. Chem. **35**, 4000 (1970).

Total synthesis of (±)-5β,8α-androst-9(11)-ene-3,17-dione

MASATOSHI KAKUSHIMA, LEONARD ALLAIN, ROBERT A. DICKINSON, PETER S. WHITE, AND ZDENEK VALENTA

Department of Chemistry, University of New Brunswick, P.O. Box 4400, Fredericton, N.B., Canada E3B 5A3

Received September 10, 1979

MASATOSHI KAKUSHIMA, LEONARD ALLAIN, ROBERT A. DICKINSON, PETER S. WHITE, and ZDENEK VALENTA. Can. J. Chem. **57**, 3354 (1979).

A total synthesis of (±)-5β,8α-androst-9(11)-ene-3,17-dione is described. The key step is a ring C forming $SnCl_4$-catalyzed Diels–Alder reaction in which the geometry of the diene controls *syn–anti* stereochemistry while the catalyst guides the addition to the desired *endo* orientation. A preparation of ethyl *E*-2-methyl-4-oxo-2-butenoate and the dehydration of a tertiary allylic alcohol by the pyrolysis of the corresponding tosyl carbamate are also described.

MASATOSHI KAKUSHIMA, LEONARD ALLAIN, ROBERT A. DICKINSON, PETER S. WHITE et ZDENEK VALENTA. Can. J. Chem. **57**, 3354 (1979).

On décrit une synthèse totale de la (±)5β,8α androstène-9(11)dione-3,17. L'étape clé de cette synthèse est la formation du cycle C par une réaction de Diels–Alder catalysée par le $SnCl_4$. Dans cette réaction, la géométrie du diène contrôle la stéréochimie *syn–anti* tandis que le catalyseur oriente l'addition vers la position *endo* désirée. On décrit également la préparation du méthyl-*E*-2 oxo-4 buten-2 oate d'éthyle et la déshydratation d'un alcool tertiaire allylique par pyrolyse du carbamate de tosyle correspondant.

[Traduit par le journal]

In a continuation of our study of regio- and stereocontrol of the Diels–Alder reaction by Lewis acid catalysis (1–3),[1] we have investigated the potential of simple bifunctional dienophiles (2) for the construction of the steroid C-ring. We now wish to report a synthesis of the 8-epiandrostane derivative **13** in which the key step is a stannic chloride catalyzed addition of **4** to **8**. The accompanying communication describes the application of the method to the synthesis of steroids with normal C8-configuration.

Allyl alcohol **2** was prepared by the reported (5) treatment of **1**[2] with lithium acetylide followed by hydrogenation in pyridine (8). Reaction of **2** with *p*-toluenesulfonyl isocyanate (9*a*) in benzene at 20°C gave **3**, mp 138–145°C, which on bulb to bulb vacuum distillation (9*b*) at 170°C (1 Torr) yielded **4**, bp 140°C (1 Torr), in 58% yield from **2**.

Dienophile **8** was prepared from ethyl crotonate in a four step sequence in 65% overall yield. Deconjugative methylation (10) of ethyl crotonate gave **5**, bp 80°C (15 Torr), which was converted to **6** by a reaction with *m*-chloroperbenzoic acid. Epoxide **6** was briefly heated in absolute EtOH with anhydrous K_2CO_3 to give **7** which yielded oily dienophile **8**[3] on treatment with active MnO_2 or with pyridinium chlorochromate (11) followed by

[1]For earliest studies and recent reviews, see ref. 4.

[2]Racemic **1** was used for the synthesis reported here. Chiral **1** is accessible from methyl vinyl ketone and 2-methylcyclohexane-1,3-dione in an asymmetric synthesis using (*S*)-proline (6, 7).

[3]Treatment of **8** with $SnCl_4$ in CH_2Cl_2 for 4 days at 0°C gave a mixture of **8** (^{1}Hmr signal for olefinic H at δ 6.80) and its *Z*-isomer (^{1}Hmr signal for olefinic H at δ 6.15) in a ratio of 3.5:1.

0008-4042/79/243354-03$01.00/0

8. G. L. SCHMIR, L. A. COHEN, and B. WITKOP. J. Am. Chem. Soc. **81**, 2228 (1959); E. J. COREY and L. F. HAEFELE. J. Am. Chem. Soc. **81**, 2225 (1959).
9. A. S. HALLSWORTH, H. B. HENBEST, and T. I. WRIGLEY. J. Chem. Soc. 1969 (1957).
10. R. E. IRELAND, D. A. EVANS, D. CLOVER, G. M. RUBOTTOM, and H. YOUNG. J. Org. Chem. **34**, 3717 (1969).
11. E. J. COREY and J. W. SUGGS. Tetrahedron Lett. 2647 (1975).
12. K. BOWDEN, I. M. HEILBRON, E. R. H. JONES, and B. C. L. WEEDON. J. Chem. Soc. 39 (1946).
13. K. B. SHARPLESS, M. A. UMBREIT, M. T. NIEH, and T. C. FLOOD. J. Am. Chem. Soc. **94**, 6538 (1972).
14. J. J. PAPPAS, W. P. KEAVENEY, E. GAUCHER, and M. BERGER. Tetrahedron Lett. 4273 (1966).
15. M. W. RATHKE and A. LINDERT. Synth. Commun. **8**, 9 (1978); E. NEGISHI and M. J. IDACAVAGE. Tetrahedron Lett. 845 (1979).
16. R. RATCLIFFE and R. RODEHORST. J. Org. Chem. **35**, 4000 (1970).

Total synthesis of (±)-5β,8α-androst-9(11)-ene-3,17-dione

MASATOSHI KAKUSHIMA, LEONARD ALLAIN, ROBERT A. DICKINSON, PETER S. WHITE, AND ZDENEK VALENTA

Department of Chemistry, University of New Brunswick, P.O. Box 4400, Fredericton, N.B., Canada E3B 5A3

Received September 10, 1979

MASATOSHI KAKUSHIMA, LEONARD ALLAIN, ROBERT A. DICKINSON, PETER S. WHITE, and ZDENEK VALENTA. Can. J. Chem. **57**, 3354 (1979).

A total synthesis of (±)-5β,8α-androst-9(11)-ene-3,17-dione is described. The key step is a ring C forming $SnCl_4$-catalyzed Diels–Alder reaction in which the geometry of the diene controls *syn–anti* stereochemistry while the catalyst guides the addition to the desired *endo* orientation. A preparation of ethyl *E*-2-methyl-4-oxo-2-butenoate and the dehydration of a tertiary allylic alcohol by the pyrolysis of the corresponding tosyl carbamate are also described.

MASATOSHI KAKUSHIMA, LEONARD ALLAIN, ROBERT A. DICKINSON, PETER S. WHITE et ZDENEK VALENTA. Can. J. Chem. **57**, 3354 (1979).

On décrit une synthèse totale de la (±)5β,8α androstène-9(11)dione-3,17. L'étape clé de cette synthèse est la formation du cycle C par une réaction de Diels–Alder catalysée par le $SnCl_4$. Dans cette réaction, la géométrie du diène contrôle la stéréochimie *syn–anti* tandis que le catalyseur oriente l'addition vers la position *endo* désirée. On décrit également la préparation du méthyl-*E*-2 oxo-4 buten-2 oate d'éthyle et la déshydratation d'un alcool tertiaire allylique par pyrolyse du carbamate de tosyle correspondant.

[Traduit par le journal]

In a continuation of our study of regio- and stereocontrol of the Diels–Alder reaction by Lewis acid catalysis (1–3),[1] we have investigated the potential of simple bifunctional dienophiles (2) for the construction of the steroid C-ring. We now wish to report a synthesis of the 8-epiandrostane derivative **13** in which the key step is a stannic chloride catalyzed addition of **4** to **8**. The accompanying communication describes the application of the method to the synthesis of steroids with normal C8-configuration.

Allyl alcohol **2** was prepared by the reported (5) treatment of **1**[2] with lithium acetylide followed by hydrogenation in pyridine (8). Reaction of **2** with *p*-toluenesulfonyl isocyanate (9*a*) in benzene at 20°C gave **3**, mp 138–145°C, which on bulb to bulb vacuum distillation (9*b*) at 170°C (1 Torr) yielded **4**, bp 140°C (1 Torr), in 58% yield from **2**.

Dienophile **8** was prepared from ethyl crotonate in a four step sequence in 65% overall yield. Deconjugative methylation (10) of ethyl crotonate gave **5**, bp 80°C (15 Torr), which was converted to **6** by a reaction with *m*-chloroperbenzoic acid. Epoxide **6** was briefly heated in absolute EtOH with anhydrous K_2CO_3 to give **7** which yielded oily dienophile **8**[3] on treatment with active MnO_2 or with pyridinium chlorochromate (11) followed by

[1]For earliest studies and recent reviews, see ref. 4.

[2]Racemic **1** was used for the synthesis reported here. Chiral **1** is accessible from methyl vinyl ketone and 2-methylcyclohexane-1,3-dione in an asymmetric synthesis using (*S*)-proline (6, 7).

[3]Treatment of **8** with $SnCl_4$ in CH_2Cl_2 for 4 days at 0°C gave a mixture of **8** (^{1}Hmr signal for olefinic H at δ 6.80) and its *Z*-isomer (^{1}Hmr signal for olefinic H at δ 6.15) in a ratio of 3.5:1.

0008-4042/79/243354-03$01.00/0

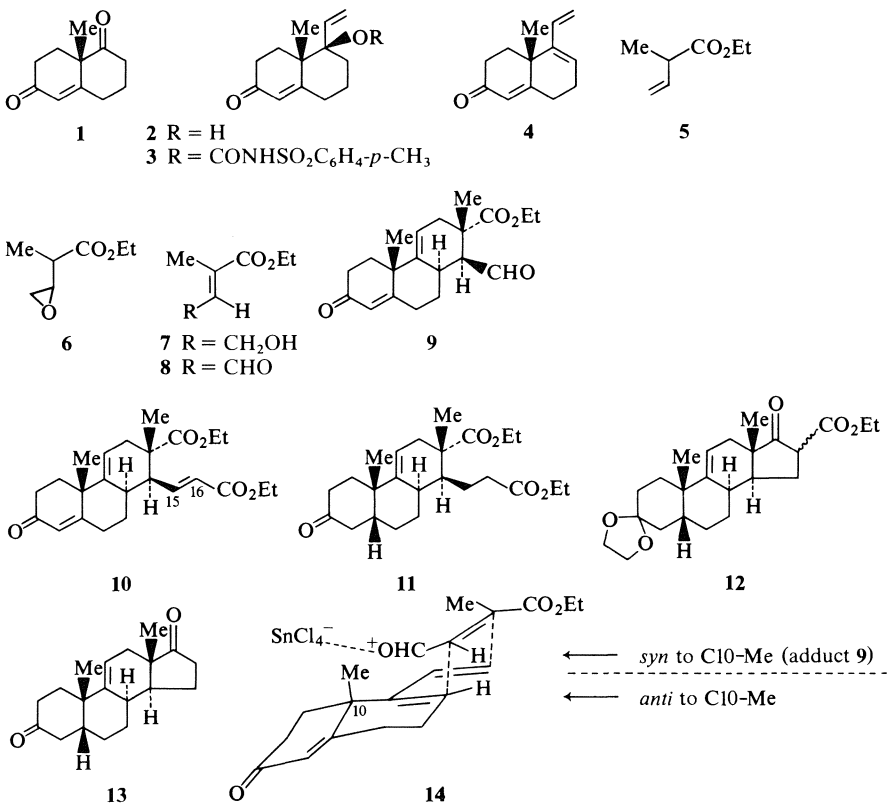

chromatography on Kieselgel (100 mesh, Herrmann).

Reaction of **4** with **8** and anhydrous $SnCl_4$ (2) (1.6:1:0.8) in CH_2Cl_2 at 0°C for 4 days gave a mixture of at least four aldehydic adducts[4] in which one adduct strongly predominated (55–65%) as revealed by the inspection and integration of aldehydic proton signals in the 220 MHz ^{1}Hmr spectrum of the crude product. The use of excess **8** in this addition results in the formation of undesired dihydropyran derivatives (2, 12). A rigorous proof of structure and stereochemistry of the major adduct **9** is given below.

Reaction of the above mixture[5] with the sodium salt of triethyl phosphonoacetate in monoglyme followed by column chromatography[6] on Silica gel H (type 60) gave crude **10**[5,7] which was hydrogenated on 5% Pd–$BaSO_4$ in EtOH to give oily **11** in 48% overall yield from **4**. Hydrogenation of **10** (in quantities smaller than 100 mg) with $[(C_6H_5)_3P]_3RhCl$ (13) selectively reduces the 15,16-double bond. Blocking of the keto group in **11** with ethylene glycol and *p*-toluenesulfonic acid in boiling benzene, followed by Dieckmann condensation with excess potassium *tert*-butoxide (14) in boiling benzene gave crude[5] oily **12**. Finally, alkaline hydrolysis of **12** (0.25 *N* NaOH, 100°C, 3 h) followed by treatment with oxalic acid in H_2O–acetone[8] and column chromatography on Silica gel H (type 60) gave **13**, mp 198–199°C, ir (KBr) ν_{max}: 1730 and 1705 cm^{-1}; ^{1}Hmr ($CDCl_3$) δ: 0.97 (3H, s), 1.50 (3H, s), and 5.70 (1H, m). Structure of **13** was established by X-ray diffraction. The overall yield of the conversion **4** → **13** was 24%.[5]

[4]Both the dienophile **8**[3] and any aldehydic adduct are susceptible to equilibration at the position α to the formyl group during the long reaction time required. (See also footnote 9.) $AlCl_3$ and $BF_3 \cdot Et_2O$ proved less suitable as catalysts for this and any other addition involving aliphatic bifunctional dienophiles (2).

[5]Due to instability of the aldehydes to oxidation and isomerization, a separation proved impractical. For efficiency, the entire sequence **4** + **8** ↠ **13** was performed with crude materials. Diester **10**[7] and the final product **13** were obtained in analytical purity for characterization and for the determination of the overall yield of the synthesis.

[6]Excess diene **4** and one of the minor adducts (16% of aldehydic adducts) were recovered unchanged.

[7]Crystallization from pentane – diisopropyl ether gave pure **10**, mp 89–90°C.

[8]Decarboethoxylation of **12** in wet dimethyl sulfoxide (15) gave **13** directly, but in a lower yield.

The formation of **9** as the major adduct is in agreement with our finding that catalyzed additions to diene **4** invariably proceed preferentially from the direction *syn* to the C10-methyl group.[9] Preferred complexation of the formyl group in dienophile **8** then controls orientation and *endo* stereochemistry (2) to give **9** as indicated in structure **14**. Details on *syn–anti* stereoselectivity in catalyzed additions to **4** and related dienes[9] will be reported shortly. The accompanying communication describes an efficient addition *anti* to the C10-methyl group of an appropriate diene.

Acknowledgements

The support of this work by the Natural Sciences and Engineering Research Council of Canada, in the form of operating grants and a fellowship (R.A.D.) is gratefully acknowledged. We wish to thank Professor G. Stork, Columbia University, N.Y., for drawing our attention to Dr. A. M. Hudrlik's dissertation.

1. R. A. DICKINSON, R. KUBELA, G. A. MACALPINE, Ž. STOJANAC, and Z. VALENTA. Can. J. Chem. **50**, 2377 (1972); N. COHEN, B. L. BANNER, W. F. EICHEL, Z. VALENTA, and R. A. DICKINSON. Synth. Commun. **8**, 427 (1978); J. DAS, R. KUBELA, G. A. MACALPINE, Ž. STOJANAC, and Z. VALENTA. Can. J. Chem. **57**, 3308 (1979).
2. M. KAKUSHIMA, J. ESPINOSA, and Z. VALENTA. Can. J. Chem. **54**, 3304 (1976).
3. Ž. STOJANAC, R. A. DICKINSON, N. STOJANAC, R. J. WOZNOW, and Z. VALENTA. Can. J. Chem. **53**, 616 (1975); N. STOJANAC, A. SOOD, Ž. STOJANAC, and Z. VALENTA. Can. J. Chem. **53**, 619 (1975).
4. A. WASSERMANN. J. Chem. Soc. 618 (1942); P. YATES and P. EATON. J. Am. Chem. Soc. **82**, 4436 (1960); SIR ROBERT ROBINSON and G. I. FRAY. J. Am. Chem. Soc. **83**, 249 (1961); H. WOLLWEBER. Methoden der organischen Chemie. Vol. V/1c. *Edited by* Houben-Weyl. Georg Thieme Verlag, Stuttgart. 1970. p. 1092; I. FLEMING. Frontier orbitals and organic chemical reactions. John Wiley & Sons, Toronto. 1978.
5. I. N. NAZAROV and I. A. GURVICH. Zh. Obshch. Khim. **25**, 956 (1955); M. S. NEWMAN, S. RAMACHANDRAN, S. K. SANKARAPPA, and S. SWAMINATHAN. J. Org. Chem. **26**, 727 (1961).
6. W. Ger. Patent No. 2102623. Priority date Jan. 21, 1970; Z. G. HAJOS and D. R. PARRISH. J. Org. Chem. **39**, 1615 (1974); J. GUTZWILLER, P. BUCHSCHACHER, and A. FÜRST. Synthesis, 167 (1977).
7. W. Ger. Patent No. 2014757. Priority date March 20, 1970; U. EDER, G. SAUER, and R. WIECHERT. Angew. Chem. Int. Ed. Engl. **10**, 496 (1971).
8. S. SWAMINATHAN, J. P. JOHN, and S. RAMACHANDRAN. Tetrahedron Lett. 729 (1962).
9. (*a*) H. ULRICH and A. A. R. SAYIGH. Angew. Chem. Int. Ed. Engl. **5**, 704 (1966); (*b*) L. C. ROACH and W. H. DALY. Chem. Commun. 606 (1970).
10. J. L. HERRMANN, G. R. KIECZYKOWSKI, and R. H. SCHLESSINGER. Tetrahedron Lett. 2433 (1973).
11. E. J. COREY and J. W. SUGGS. Tetrahedron Lett. 2647 (1975).
12. A. M. HUDRLIK. Ph.D. Dissertation, Columbia University, New York, N.Y. 1967.
13. J. F. YOUNG, J. A. OSBORN, F. H. JARDINE, and G. WILKINSON. Chem. Commun. 131 (1965); F. H. JARDINE, J. A. OSBORN, G. WILKINSON, and J. F. YOUNG. Chem. Ind. 560 (1965).
14. W. S. JOHNSON, B. BANNISTER, and R. PAPPO. J. Am. Chem. Soc. **78**, 6331 (1956).
15. A. P. KRAPCHO and A. J. LOVEY. Tetrahedron Lett. 957 (1973).

[9]This *syn* preference is, however, not quantitative. *Syn–anti* ratios in the range of 2:1 to 4:1 are observed in catalyzed additions of diene **4** to quinones and to aliphatic bifunctional dienophiles. There is, therefore, no doubt that an *anti* adduct (isomeric with **9** at C8, C13, and C14) is present in a minor quantity in the mixture of aldehydes resulting from the addition **4** + **8** + $SnCl_4$ described here.

Total synthesis of androstanes

MASATOSHI KAKUSHIMA, JAGABANDHU DAS, GARY R. REID, PETER S. WHITE, AND ZDENEK VALENTA

Department of Chemistry, University of New Brunswick, P.O. Box 4400, Fredericton, N.B., Canada E3B 5A3

Received September 10, 1979

MASATOSHI KAKUSHIMA, JAGABANDHU DAS, GARY R. REID, PETER S. WHITE, and ZDENEK VALENTA. Can. J. Chem. **57**, 3356 (1979).

A total synthesis of androstane derivatives is described. The desired configuration at C8 and at C13 is achieved in a ring C forming $SnCl_4$-catalyzed Diels–Alder reaction. The preparation of methyl *Z*-2-methyl-4-oxo-2-pentenoate and the cyclization of a keto ester to a steroid 15,17-dione are also reported.

0008-4042/79/243356-03$01.00/0

The formation of **9** as the major adduct is in agreement with our finding that catalyzed additions to diene **4** invariably proceed preferentially from the direction *syn* to the C10-methyl group.[9] Preferred complexation of the formyl group in dienophile **8** then controls orientation and *endo* stereochemistry (2) to give **9** as indicated in structure **14**. Details on *syn–anti* stereoselectivity in catalyzed additions to **4** and related dienes[9] will be reported shortly. The accompanying communication describes an efficient addition *anti* to the C10-methyl group of an appropriate diene.

Acknowledgements

The support of this work by the Natural Sciences and Engineering Research Council of Canada, in the form of operating grants and a fellowship (R.A.D.) is gratefully acknowledged. We wish to thank Professor G. Stork, Columbia University, N.Y., for drawing our attention to Dr. A. M. Hudrlik's dissertation.

1. R. A. DICKINSON, R. KUBELA, G. A. MACALPINE, Ž. STOJANAC, and Z. VALENTA. Can. J. Chem. **50**, 2377 (1972); N. COHEN, B. L. BANNER, W. F. EICHEL, Z. VALENTA, and R. A. DICKINSON. Synth. Commun. **8**, 427 (1978); J. DAS, R. KUBELA, G. A. MACALPINE, Ž. STOJANAC, and Z. VALENTA. Can. J. Chem. **57**, 3308 (1979).
2. M. KAKUSHIMA, J. ESPINOSA, and Z. VALENTA. Can. J. Chem. **54**, 3304 (1976).
3. Ž. STOJANAC, R. A. DICKINSON, N. STOJANAC, R. J. WOZNOW, and Z. VALENTA. Can. J. Chem. **53**, 616 (1975); N. STOJANAC, A. SOOD, Ž. STOJANAC, and Z. VALENTA. Can. J. Chem. **53**, 619 (1975).
4. A. WASSERMANN. J. Chem. Soc. 618 (1942); P. YATES and P. EATON. J. Am. Chem. Soc. **82**, 4436 (1960); SIR ROBERT ROBINSON and G. I. FRAY. J. Am. Chem. Soc. **83**, 249 (1961); H. WOLLWEBER. Methoden der organischen Chemie. Vol. V/1c. *Edited by* Houben-Weyl. Georg Thieme Verlag, Stuttgart. 1970. p. 1092; I. FLEMING. Frontier orbitals and organic chemical reactions. John Wiley & Sons, Toronto. 1978.
5. I. N. NAZAROV and I. A. GURVICH. Zh. Obshch. Khim. **25**, 956 (1955); M. S. NEWMAN, S. RAMACHANDRAN, S. K. SANKARAPPA, and S. SWAMINATHAN. J. Org. Chem. **26**, 727 (1961).
6. W. Ger. Patent No. 2102623. Priority date Jan. 21, 1970; Z. G. HAJOS and D. R. PARRISH. J. Org. Chem. **39**, 1615 (1974); J. GUTZWILLER, P. BUCHSCHACHER, and A. FÜRST. Synthesis, 167 (1977).
7. W. Ger. Patent No. 2014757. Priority date March 20, 1970; U. EDER, G. SAUER, and R. WIECHERT. Angew. Chem. Int. Ed. Engl. **10**, 496 (1971).
8. S. SWAMINATHAN, J. P. JOHN, and S. RAMACHANDRAN. Tetrahedron Lett. 729 (1962).
9. (*a*) H. ULRICH and A. A. R. SAYIGH. Angew. Chem. Int. Ed. Engl. **5**, 704 (1966); (*b*) L. C. ROACH and W. H. DALY. Chem. Commun. 606 (1970).
10. J. L. HERRMANN, G. R. KIECZYKOWSKI, and R. H. SCHLESSINGER. Tetrahedron Lett. 2433 (1973).
11. E. J. COREY and J. W. SUGGS. Tetrahedron Lett. 2647 (1975).
12. A. M. HUDRLIK. Ph.D. Dissertation, Columbia University, New York, N.Y. 1967.
13. J. F. YOUNG, J. A. OSBORN, F. H. JARDINE, and G. WILKINSON. Chem. Commun. 131 (1965); F. H. JARDINE, J. A. OSBORN, G. WILKINSON, and J. F. YOUNG. Chem. Ind. 560 (1965).
14. W. S. JOHNSON, B. BANNISTER, and R. PAPPO. J. Am. Chem. Soc. **78**, 6331 (1956).
15. A. P. KRAPCHO and A. J. LOVEY. Tetrahedron Lett. 957 (1973).

[9]This *syn* preference is, however, not quantitative. *Syn–anti* ratios in the range of 2:1 to 4:1 are observed in catalyzed additions of diene **4** to quinones and to aliphatic bifunctional dienophiles. There is, therefore, no doubt that an *anti* adduct (isomeric with **9** at C8, C13, and C14) is present in a minor quantity in the mixture of aldehydes resulting from the addition **4** + **8** + $SnCl_4$ described here.

Total synthesis of androstanes

MASATOSHI KAKUSHIMA, JAGABANDHU DAS, GARY R. REID, PETER S. WHITE, AND ZDENEK VALENTA

Department of Chemistry, University of New Brunswick, P.O. Box 4400, Fredericton, N.B., Canada E3B 5A3

Received September 10, 1979

MASATOSHI KAKUSHIMA, JAGABANDHU DAS, GARY R. REID, PETER S. WHITE, and ZDENEK VALENTA. Can. J. Chem. **57**, 3356 (1979).

A total synthesis of androstane derivatives is described. The desired configuration at C8 and at C13 is achieved in a ring C forming $SnCl_4$-catalyzed Diels–Alder reaction. The preparation of methyl *Z*-2-methyl-4-oxo-2-pentenoate and the cyclization of a keto ester to a steroid 15,17-dione are also reported.

0008-4042/79/243356-03$01.00/0

MASATOSHI KAKUSHIMA, JAGABANDHU DAS, GARY R. REID, PETER S. WHITE et ZDENEK VALENTA. Can. J. Chem. **57**, 3356 (1979).

On décrit une synthèse totale de dérivés de l'androstane. On a obtenu la configuration désirée au niveau des carbones en position 8 et 13 en réalisant la synthèse du cycle C selon une réaction de Diels–Alder catalysée par $SnCl_4$. On rapporte également la préparation du méthyl-2 oxo-4 pentène-2 oate de méthyle (*Z*) ainsi que la préparation d'un stéroide dione-15,17 obtenu par cyclisation d'un ester cétonique.

[Traduit par le journal]

In the preceding communication (1), we have described the $SnCl_4$-catalyzed addition of diene **1** to ethyl *E*-2-methyl-4-oxo-2-butenoate in which the geometry of **1** favors an addition *syn* to the C10-methyl group while a preferential complexing of the formyl group in the dienophile (2) determines orientation and *endo* stereochemistry. The resulting adduct then leads to 8-epi-androstanes by further transformations (1). We now wish to report the controlled addition of enol acetate **2** to the *Z*-dienophile **4** in which the side *anti* to the C10-methyl group of **2** is strongly favored and which therefore, via adduct **6**, leads to a facile synthesis of steroids with the desired configuration at C8 and at C13.

Oily enol acetate **2**, ir ($ChCl_3$) ν_{max}: 1750 and 1665 cm^{-1}, was prepared efficiently on treatment of **1** (1) with HBr in acetic anhydride at 20°C for 10 h. In a less convenient preparation, the reflux of **1** in isopropenyl acetate with *p*-toluenesulfonic acid first led mainly to the isomeric 3-acetoxy-2,4-diene (~24 h) which was converted to **2** under the same conditions in 130 h. The dienophile **4**, bp 62°C (20 Torr), ir (CCl_4) ν_{max}: 1740 and 1705 cm^{-1}; ^{1}Hmr ($CDCl_3$) δ: 2.00 (3H, d, J = 2 Hz), 2.23 (3H, s), 3.80 (3H, s), 6.17 (1H, q, J = 2 Hz), was obtained in 88% yield by the treatment of **3** with CH_3I and K_2CO_3 in dry acetone at 20°C for 28 h; **3** is available in one step from a reaction of pyruvic acid, acetone, and 85% H_3PO_4 (3).

Reaction of **2** with **4** and anhydrous $SnCl_4$ (1:2:1.5) in CH_2Cl_2 at 0°C for 1 h gave **6**, mp 155–156°C, ir (CCl_4) ν_{max}: 1735, 1715, and 1680 cm^{-1}, in 70% yield based on consumed **2**.[1] The structure of **6** was established by X-ray diffraction.

To complete the steroid synthesis, **6** was simply converted into **7**, mp 150–158°C, in 85% yield by a reaction with ethylene glycol and *p*-toluenesulfonic acid in boiling benzene and **7** was then treated with dimsyl sodium (4)[2] to give dione **9**, mp approx. 191°C (dec.), uv λ_{max} (MeOH): 262 nm (ε 17 700), (MeOH–KOH): 264 nm (ε 22 100), (MeOH–HCl): 247 nm (ε 13 300); ir (KBr) ν_{max}: 3650–2250, 1645, and 1560 cm^{-1}, along with acid **10** which could be separated from **9** by fractional crystallization. The yield of the conversion **7** → **9** is at least 41% as determined by subsequent methylation described below.

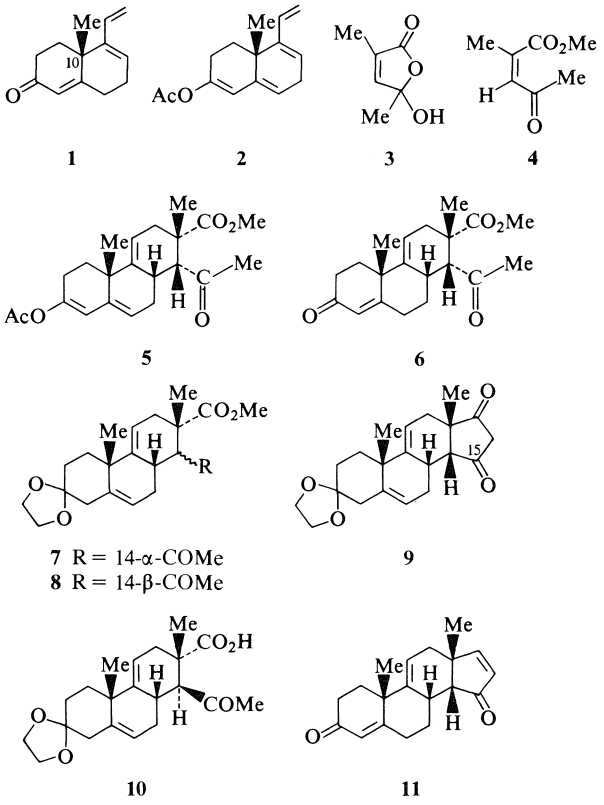

Thus, steroid **9** was prepared from 2-methyl-

[1]The uncorrected yield of crystalline **6** after purification on a column of Silica gel H (type 60) was 55%. No other adduct was detected. Unused diene was recovered in the form **1**; the starting material **2** and the adduct **5** decompose to **1** and **6**, respectively, during the reaction. The primary adduct **5**, mp 129–131°C, could be isolated in a low yield (15–20%) under scrupulously anhydrous conditions and was found to give **6** on mild acid hydrolysis. The reaction of **1** with **4** and $SnCl_4$ is very slow under the conditions used.

[2]Dry dimethyl sulfoxide (10 equiv., 1 volume) was first reacted with NaH (2 equiv.) at 80°C for 30 min. Toluene (2 volumes) was then added at 110°C and, when distillation started, **7** (1 equiv.) in toluene (20 volumes) was slowly added while distillation continued. Additional toluene (20 volumes) was added during the distillation. We thank Professor R. H. Schlessinger, University of Rochester, N.Y., for valuable advice on this capricious cyclization.

cyclohexane-1,3-dione, methyl vinyl ketone, acetylene, acetone, and pyruvic acid in eleven synthetic steps; six to prepare **2**,[3] two to prepare **4**, and three to convert them into **9**. It should be noted that the conversion **2** → **6** → **9** is formally equivalent to a controlled addition of 2-methyl-2- cyclopentene-1,4-dione to diene **2**.

To determine the ring D cyclization yield and to characterize dione **9** further, crude cyclization product (**9** + **10**) was treated with CH_2N_2 in ether. Column chromatography on Silica gel H (type 60) then gave ester **8**, mp 207–208°C (21% yield from **7**), and the two ring D enol ethers of **9** (2:1 ratio, 41% yield from **7**). The major one (MeO at C15) was converted in 58% yield to enone **11**, mp 125–127°C, ir (CCl_4) ν_{max}: 1710, 1675, 1620, and 1595 cm^{-1}; ^{1}Hmr ($CDCl_3$) δ: 5.70 (1H, m, C11—H), 5.78 (1H, broad s, C4—H), 6.00 (1H, d, J = 6 Hz, C16—H), and 7.23 (1H, d, J = 6 Hz, C17—H), by reduction with sodium bis(2-methoxyethoxy) aluminum hydride (Ventron Co.) followed by spontaneous dehydration of the alcohol in CCl_4 at 20°C and by hydrolysis of the resulting 15-methoxy-14,16-diene, ^{1}Hmr ($CDCl_3$) δ 6.34 (2H, sharp s, C16 and C17—H's), with 1 *N* HCl in acetic acid at 20°C for 20 h. The ring D structure of **11** and its precursors follows most clearly from the ^{1}Hmr signal corresponding to both ring D H-atoms of the above diene; the spectrum of the alternative 17-methoxy-14,16-diene would show two widely separated signals for the C16—(enol ether H) and C15—H atoms. The δ and J values for the two ring D H-atoms in **11** are in good agreement with data reported for a similar system (5).

Clearly, an addition *anti* to the C10-methyl group is favored by the geometry of diene **2** in this case; a preferred complexation on the oxygen atom

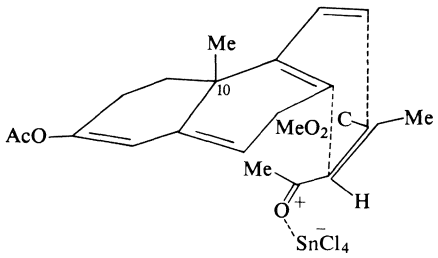

12

of the keto group in **4** (1, 2) then achieves the desired orientation and *endo* stereochemistry as shown in structure **12**.[4] The regioselectivities and the *syn–anti* and *endo–exo* stereoselectivities achieved by the use of bifunctional dienophiles in catalyzed additions as described in this and the preceding communications (1, 2) should prove of general use for the controlled construction of carbon frameworks.

Acknowledgements

The support of this work by the Natural Sciences and Engineering Research Council of Canada in the form of operating grants and a bursary (G.R.R.) is gratefully acknowledged.

1. M. KAKUSHIMA, L. ALLAIN, R. A. DICKINSON, P. S. WHITE, and Z. VALENTA. Can. J. Chem. **57**, 3354 (1979).
2. M. KAKUSHIMA, J. ESPINOSA, and Z. VALENTA. Can. J. Chem. **54**, 3304 (1976).
3. R. SCHEFFOLD and P. DUBS. Helv. Chim. Acta, **50**, 798 (1967).
4. J. J. BLOOMFIELD. J. Org. Chem. **26**, 4112 (1961).
5. I. M. CLARK, W. A. DENNY, SIR E. R. H. JONES, G. D. MEAKINS, A. PENDLEBURY, and J. T. PINLEY. J. Chem. Soc. Perkin Trans. I, 2765 (1972).

[3]For preparation of diene **1**, see ref. 1 and references cited therein.

[4]The conformation of the complexed carbonyl group during addition is unknown; the one given in **12** is arbitrarily chosen. It is also not known whether $SnCl_4$ forms more than one bond during the reaction. (It is, for example, tempting to speculate that Sn also interacts with the 5,6-double bond of **2**.)